Russian Chemical Reviews, Volume 73 (2004)

Contents of Volume

Number 1

Institute of Physical Chemistry, Russian Academy of Scienes 1
A Yu Tsivadze

Supramolecular metal complex systems based on crown-substituted tetrapyrroles 5
A Yu Tsivadze

Surface forces and physicochemistry of surface phenomena 25
N V Churaev

Physicochemical dynamics of disperse systems 37
N B Uriev

Phase equilibria and phase structures of polymer blends 59
A E Chalykh, V K Gerasimov

Physicochemical aspects of metal corrosion inhibition in aqueous solutions 75
Yu I Kuznetsov

Cation—cation interaction in crystalline actinide compounds 89
N N Krot, M S Grigoriev

Kinetics, mechanism and intermediates of some radiation-induced reactions in aqueous solutions 101
B G Ershov

Number 2

Self-assembly of nanoparticles at interfaces 115
V I Roldughin

Self-propagating high-temperature synthesis of nanomaterials 147
A E Sytschev, A G Merzhanov

Acetylenic derivatives of quinones 161
M S Shvartsberg, I I Barabanov, L G Fedenok

Chemical transformations of chlorophyll and its application in the design of a new generation of environmentally safe dyes 185
B D Berezin, S V Rumyantseva, A P Moryganov, M B Berezin

Quantitative estimation of the reactivity of the surface of solids on the basis of inductive constants 195
Yu K Ezhovskii

Number 3

Crystal chemistry, properties and synthesis of microporous silicates containing transition elements 205
N V Chukanov, I V Pekov, R K Rastsvetaeva

State-of-the-art in the studies of three-dimensional radical copolymerisation 225
V P Roshchupkin, S V Kurmaz

Methods of calculation of the critical conversion in the formation of network polymers 251
V I Irzhak

Polyketones as alternating copolymers of carbon monoxide 267
G P Belov, E V Novikova

The mechanism of thermal decomposition of secondary nitramines 293
Yu Shu, B L Korsunskii, G M Nazin

Number 4

Phosphapalladacycles: preparation routes 309
V V Dunina, O N Gorunova

The theory of formation of surface complexes and its application to the description of multicomponent dynamic sorption systems 351
W H Höll, A I Kalinichev

Lead difluoride and related systems 371
I I Buchinskaya, P P Fedorov

Disaccharide nucleosides 401
E V Efimtseva, S N Mikhailov

Number 5

A.N.Nesmeyanov Institute of Organoelement Compounds of the Russian Academy of Sciences 415
Yu N Bubnov

Cationic and neutral transition metal complexes with a tetramethylfulvene or trimethylallyldiene ligand 417
A Z Kreindlin, M I Rybinskaya

Substitution reactions at boron atoms in metallacarboranes 433
V I Bregadze, S V Timofeev, I B Sivaev, I A Lobanova

Chemical crystallography of fullerenes 455
I S Neretin, Yu L Slovokhotov

Trends in the development of polycondensation and condensation polymers 487
S V Vinogradova, V A Vasnev

Nanostructured polymeric systems as nanoreactors for nanoparticle formation 501
L M Bronstein, S N Sidorov, P M Valetsky

Number 6

Metallacyclopentadienes: structural features and coordination in transition metal complexes 517
F M Dolgushin, A I Yanovsky, M Yu Antipin

The structure of X-ray photoelectron spectra of light actinide compounds 541
Yu A Teterin, A Yu Teterin

Chiral 1,3,2-oxazaborolidines in asymmetric synthesis: recent advances 581
V A Glushkov, A G Tolstikov

Oxy acids of halogens HOHal 609
I V Nikitin

Number 7

Synthesis of allylic alcohols from alkenes and their derivatives 621
A K Banerjee, P S Poon, M S Laya, W J Vera

Chemistry and biological activities of 1,8-naphthyridines 637
V P Litvinov

Chiral phosphites as ligands in asymmetric metal complex catalysis and synthesis of coordination compounds 671
K N Gavrilov, O G Bondarev, A I Polosukhin

Nucleosides and oligonucleotides containing 2'-reactive groups: synthesis and applications 701
T S Zatsepin, E A Romanova, T S Oretskaya

Number 8

Department of Chemistry of the Kyiv National Taras Shevchenko University 735
N S Slobodyanik

Various types of metal complexes based on chelating β-diketones and their structural analogues 737
V V Skopenko, V M Amirkhanov, T Yu Sliva, I S Vasilchenko, E L Anpilova, A D Garnovskii

Phosphate tungsten bronzes 753
V V Skopenko, V V Lisnyak, N V Stus, N S Slobodyanik

Pyrido- and pyrimidoisoindoles: methods of synthesis and properties 771
A A Pokholenko, Z V Voitenko, V A Kovtunenko

Conformationally rigid cyclic α-amino acids in the design of peptidomimetics, peptide models and biologically active compounds 785
I V Komarov, A O Grigorenko, A V Turov, V P Khilya

Graft copolymers with chemically complementary components as a special class of high-molecular-weight compounds 811
T B Zheltonozhskaya, N E Zagdanskaya, O V Demchenko, L N Momot, N M Permyakova, V G Syromyatnikov, L R Kunitskaya

Number 9

Development of inorganic chemistry as a fundamental for the design of new generations of functional materials 831
Yu D Tretyakov

Complex manganese oxides with the brownmillerite structure: synthesis, crystal chemistry and properties 847
A M Abakumov, M G Rozova, E V Antipov

The role of heteroepitaxy in the development of new thin-film oxide-based functional materials 861
A R Kaul, O Yu Gorbenko, A A Kamenev

Structural and microstructural features of functional materials based on cuprates and manganites 881
Yu D Tretyakov, E A Goodilin, D V Peryshkov, D M Itkis

Synthesis of functional nanocomposites based on solid-phase nanoreactors 899
Yu D Tretyakov, A V Lukashin, A A Eliseev

Semiconducting clathrates: synthesis, structure and properties 923
K A Kovnir, A V Shevelkov

Number 10

Inorganic structures as materials for gas sensors 939
R B Vasiliev, L I Ryabova, M N Rumyantseva, A M Gaskov

Olefination of carbonyl compounds: modern and classical methods 957
V N Korotchenko, V G Nenajdenko, E S Balenkova, A V Shastin

Oxide materials as positive electrodes of lithium-ion batteries 991
E V Makhonina, V S Pervov, V S Dubasova

Modelling of chemical conversion processes in multicomponent reciprocal salt systems 1003
E S Gryzlova, N A Kozyreva

Number 11

Spin catalysis as a new type of catalysis in chemistry 1033
A L Buchachenko, V L Berdinsky

Metal oxoalkoxides. Synthesis, properties and structures 1041
N Ya Turova

The tris(trimethylsilyl)silyl group in organic, coordination and organometallic chemistry 1065
A N Kornev

Physicochemical aspects of isomerisation of free radicals 1091
E T Denisov, T G Denisova

Chemical physics of decomposition of energetic materials. Problems and prospects 1121
L P Smirnov

Number 12

Modern analytical thermooptical spectroscopy 1143
M A Proskurnin, M Yu Kononets

The central chirality of the metal atom and configurational relations in asymmetric reactions catalysed by metal complexes 1173
V A Pavlov

Methodological, applied and thermodynamic aspects of hydrogen sorption by graphite and related carbon nanostructures 1211
Yu S Nechaev, O K Alekseeva

© 2008, No Rights Reserved.

 © 2004 Russian Academy of Sciences and Turpion Ltd

DOI 10.1070/RC2004v073n01ABEH000863

Institute of Physical Chemistry of the Russian Academy of Sciences

This issue of the Journal comprises reviews written by researchers of the Institute of Physical Chemistry of the Russian Academy of Sciences (IPC RAS), one of the leading chemical research establishments of the Russian Academy of Sciences.

In 1929, Academician V A Kistyakovsky, a renowned physicochemist and a specialist in the field of complex colloid-electrochemical problems, was entrusted with the task of organising a colloid-electrochemical laboratory (CELA) under the aegis of the USSR Academy of Sciences. In 1934, the laboratory was granted the status of the Colloid-Electrochemical Institute (CEIN) of the USSR Academy of Sciences. Many prominent scientists, such as Academicians P A Rebinder, A N Frumkin, M M Dubinin, V I Spitsyn, B V Derjaguin, Corresponding Members of RAS G V Akimov, K V Chmutov, A K Pikaev, N A Izgaryshev, S Z Roginsky and Professors A D Gelman, Yu N Golovanov, I L Rozenfeld, N D Tomashev, N E Brezhneva, B A Zaitsev, A T Vagramyan, K M Gorbunova, *etc*., have worked at the Institute at different times. The development of many promising research areas in IPC RAS, such as physicochemical mechanics; physicochemistry of disperse systems and surface forces; sorption and adsorption processes; thin liquid and polymeric layers; corrosion of metals and alloys; electrochemistry and electrocrystallisation; radiochemistry and radiation chemistry as well as chromatography is associated with the names of these distinguished scientists.

At present, the multi-disciplinary fundamental and applied investigations carried out at the Institute are developing along the following lines:

— colloid-surface phenomena and adsorption;

— physicochemistry of nano- and supramolecular systems;

— radiochemistry and chemistry of high energy;

— physicochemical aspects of corrosion, electrochemistry, protective coatings and crystallisation.

The Institute has unique experimental facilities. In 2002, a centre for joint use of physical methods including electron microscopy and X-ray microanalysis, oscillation and electron spectroscopy, positron annihilation, ellipsometry, X-ray diffraction analysis, chromatoionic and mass spectrometry and atomic absorption analysis was organised within the structure of the Institute. The Institute possesses its own corrosion stations for conducting full-scale field tests in Moscow, Zvenigorod, Murmansk and Vladivostok and performs similar tests through a network of stations functioning within the structure of the Tropical Research Centre of RAS and located in different climatic zones of Russia. The Institute has at its disposal complex technological equipment for conducting accelerated tests and possesses a database on atmospheric resistance of various materials with different types of protection created on the basis of long-term observations. Other equipment includes a system for continuous monitoring and computer processing of meteorological data and corrosion parameters of tested materials, a computerised laboratory for static and dynamic autoclave testing of non-strained and mechanically strained materials in aqueous solutions at high temperatures and high pressures, four linear accelerators and four gamma-ray sources.

The Institute has in its structure a research-and-education centre consisting of two main departments (Inorganic, radio- and radiation chemistry and Physicochemistry of surface phenomena and colloid systems) and several research-and-education departments, such as 'Physical chemistry of polymers', 'Physicochemistry of supramolecular systems', 'Physicochemical basis of technology of composite materials', 'Adsorption and adsorbents', 'Chromatography and chromatographic instruments', 'Corrosion and protection of metals', 'Ion-exchange chromatography' and 'Physicochemical mechanics'. Postgraduate courses and four dissertation boards of the Higher Attestation Commission also function at the Institute.

The Institute collaborates successfully with national academies of sciences, universities and research establishments in the USA, Canada, Great Britain, France, FRG, Sweden, Finland, Japan, Korea, Australia and Italy. Researchers of the Institute take an active part in international symposia and conferences; their works are translated and published in many countries of the world. The Institute maintains close ties with large enterprises affiliated to the Ministry for Atomic Energy and the Ministry of Defense of the Russian Federation and some other state-owned institutions and carries out contract work for many manufacturing companies and research centres in France, Germany, USA, India, Korea and other countries.

At present, the Institute comprises proud of several scientific schools with rich traditions and great research experience in all the fields mentioned above.

The staff of the Institute is 920 people including two Academicians and three Corresponding Members of RAS, 70 D.Sci. and 295 Ph.D.'s.

Within the framework of the Programme 'Colloid-surface phenomena and adsorption processes', the Institute carries out in-depth studies on surface forces, stability of colloids and liquid films, adhesion phenomena and physicochemical mechanics of disperse structures and solids and develops theories of gas and vapour adsorption by microporous sorbents.

Some of the most recent achievements of the Institute are as follows: the development of a novel method for measuring parameters of porous structures of adsorbents; the proposal of a methodology for computation of contact angles of aqueous solutions of electrolytes on charged solid surfaces of various degrees of hydrophilicity allowing prediction of the stabilities and thicknesses of wetting films; the development of a new in principle technology for investigations into structure formation and flow processes of concentrated nanodispersed systems; preparation of carbon-based sorbents that allow purification of solutions of organic substances and aqueous media and ultimate purification of drinking water from dioxins and monitoring of the dioxin content in air, water and soil; elaboration of fundamentals of non-linear preparative multicomponent chromatography; development of novel procedures for studying structures of liquids in thin layers. An automatic unit for measuring surface and interphase tensions of liquids and wetting angles under static and dynamic regimes and for determination of critical concentrations of micelle formation developed at the Institute was awarded a diploma and a Gold Medal at the International Exhibition of Innovations, Investigations and Technologies (Brussels, 2001). Yet another development of IPC RAS, *viz.,* a unit for the conversion of a polarised light, was awarded a Silver Medal (Brussels, 2002).

A detailed description of this area of research is given in the reviews by N V Churaev, 'Surface forces and physicochemistry of surface phenomena', and N B Uriev, 'Physicochemical dynamics of disperse systems'.

The fundamental and applied investigations into the structures, phase equilibria, surface and diffusion phenomena in polymeric, polymeric-monomeric and filled systems are carried out within the framework of the Programme 'Physicochemistry of nano- and supramolecular systems' aimed at the elaboration of physicochemical principles for preparation, modification and stabilisation of polymeric coatings, adhesive mixtures and composite binding materials. Strategies for supramolecular design of planar systems are being developed; the effect of dimensional selectivity has been predicted and realised for the first time; two-dimensional polymeric networks with functional molecules and nanoparticles integrated into them have been prepared; the dependence of parameters of nanopores in novel optoelectronic materials based on porous silicon (both before and after oxidation) and artificial opals on the temperature of their processing has been investigated; a theory of colloid interactions of elastic surfaces and a theory of, and a method for, dynamic measurements of forces using atomic-force microscopy have been developed. The principles of the design of a novel class of 'two-dimensional' nanocomposite materials (polymer/metal) have been developed and realised and their feasibility as efficient catalytic systems, which represent elements of planar solid sensors, has been demonstrated.

Physicochemistry of polymers is discussed in the review by A E Chalykh and V K Gerasimov, 'Phase equilibria and phase structures of polymer blends' and physicochemistry of supramolecular systems, in the review by A Yu Tsivadze, 'Supramolecular metal complex systems based on crown-substituted tetrapyrroles'.

As regards physicochemistry of corrosion processes, electrochemistry, protective coatings and crystallisation, studies on kinetics and mechanisms of metal corrosion under natural (atmospheric, marine, subterranean) conditions are currently under way. Also being studied are mechanisms of controlled synthesis and effects of volatile and contact inhibitors of metal corrosion and saturation with hydrogen. A theory of acid resistance, passivity and local violations of the passive state of non-strained and mechanically strained construction alloys is being developed; elaboration of protective coatings against specific corrosion of rocket engine nozzles and thermal-power metallic equipment in the atmosphere of combustion products and in aqueous and gaseous heat carriers as well as studies on multifunctional metallic and composite coatings, hydrogen saturation and hydrogen-induced embrittlement of metals are being carried out.

These studies have led to the development of novel coating technologies for corrosion protection of metals under natural conditions and elaboration of theoretical and practical principles of corrosion-resistant doping of alloys with cathodic additives. Technologies for the production of stainless steels and alloys with optimised compositions, aluminium, copper, nickel, titanium and zirconium, and possessing high corrosion resistance have been developed. A series of novel highly refractory compounds and their heat-conducting compositions with protective (including diamond-like) coatings have been developed. Novel technologies for applying protective and functional galvanic and chemically reduced metallic coatings onto diverse articles have been devised. The mechanism of hydrogen-induced embrittlement upon application of electrolytic coatings has been established and methods for elimination of this defect in aircraft and rocket engineering have been developed. Fundamentals of vapour-phase protection of metals with organic corrosion inhibitors have been elaborated and a new industrial technology for the preparation of protective materials for rocket-and-space engineering has been proposed. A database of the interaction of hydrogen isotopes with thermonuclear reactor materials contacting with plasma has been formed.

This line of research is considered in the review by Yu I Kuznetsov, 'Physicochemical aspects of metal corrosion inhibition in aqueous solutions'.

In the field of theoretical radiochemistry, the following topics are being developed: quantum chemistry of transuranium elements and their derivatives; studies on various valence forms of radioactive elements in aqueous and organic solutions, salt melts, gas and solid phases; redox reactions involving ions of actinides; systematic studies into the synthesis of novel derivatives of radioactive elements, determination of their structures and the most essential properties; elaboration of the scientific basis of extraction and sorption processes for the isolation and purification of radioactive elements, studies of isotope effects in reactions of heavy elements, and physicochemistry of radioactive and irradiated solids.

In the field of applied radiochemistry, the following studies should be mentioned: elaboration of the physicochemical basis for safe disposal of radioactive wastes from nuclear-power energetics, burial of liquid radioactive wastes and safe operation of underground storage pits; development of novel and improvement of existing extractive, sorptive, *etc*., procedures for the isolation of pure radioactive elements; solution of miscellaneous radioecological problems and a search for radioactive sources for medicinal and other applications.

The main investigations in the field of theoretical radiation chemistry include an analysis of primary processes of interactions of the ionising radiation with various substances; studies of fast and superfast reactions in the condensed phase using pulse radiolysis; development of scientific principles for the application

of ionising radiation for modification of various materials; studies on radiation-chemical processes occurring in laser, optoacoustic and superconducting materials and polymeric media and the development of methods for predicting radiation stabilities of various materials and compositions.

The work in the field of applied radiation chemistry is directed to the use of radiation chemistry for solution of environmental problems (*e.g.,* decomposition of toxic substances, *etc.*) and to the development of methods for protecting structural materials from radiation corrosion. Novel radiation-resistant materials and compositions based on them are being developed and advanced radiation-chemical methods for preparation of novel materials for medicine, biotechnology and membrane technology and dosimetric systems for radiation control are being designed.

This line of research is covered in the reviews by N N Krot and M S Grigoriev, 'Cation – cation interactions in crystalline actinide compounds', and B G Ershov, 'Kinetics, mechanisms and intermediates of some radiation-induced reactions in aqueous solutions'.

Needless to say, the size of this issue cannot encompass the whole range of investigations carried out at IPC RAS. Therefore, all those who are interested in more detailed information about the Institute are invited to visit our web-site: http://www.ipc.rssi.ru.

Academician A Yu Tsivadze,
Director of IPC RAS

Russian Chemical Reviews **73** (1) 5 – 23 (2004) © 2004 Russian Academy of Sciences and Turpion Ltd

DOI 10.1070/RC2004v073n01ABEH000862

Supramolecular metal complex systems based on crown-substituted tetrapyrroles

A Yu Tsivadze

Contents

I.	Introduction	5
II.	Crown-substituted porphyrins	7
III.	Crown-substituted monophthalocyaninates	10
IV.	Supramolecular aggregation of crown-substituted monophthalocyaninates	13
V.	Sandwich-like double- and triple-decker crown-substituted phthalocyaninates	18
VI.	Supramolecular systems based on double- and triple-decker crown-substituted phthalocyaninates	20
VII.	Conclusion	21

Abstract. The characteristic features of the structures and properties of crown-substituted porphyrinates and phthalocyaninates are considered. Interactions of these compounds with alkali metal salts yield supramolecular ensembles. The factors determining the architecture of such ensembles are described. The bibliography includes 97 references.

I. Introduction

Over many years, the development of coordination chemistry was associated with a search for ligands able to form stable complexes with metal ions. It is polydentate chelate ligands that proved to be these ligands, among which macrocyclic compounds occupy a special place.[1–13] Such macrocyclic ligands as crown ethers, azacrown ethers and thiacrown ethers, cryptands, podands, phthalocyanines, porphyrins and other polyazacyclic compounds have received especially wide acceptance in coordination chemistry.

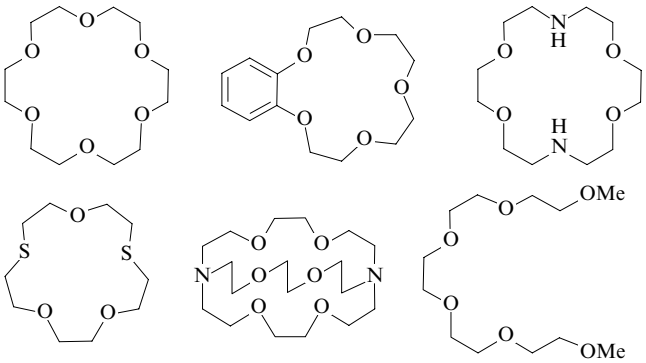

A Yu Tsivadze Institute of Physical Chemistry, Russian Academy of Sciences, Leninsky prosp. 31, Moscow 119991, Russian Federation. Fax (7-095) 952 53 08. Tel. (7-095) 952 04 62. E-mail: phyche.ac.ru

Received 3 Yule 2003
Uspekhi Khimii **73** (1) 6 – 25 (2004); translated by R L Birnova

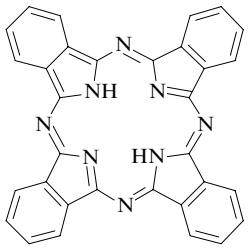

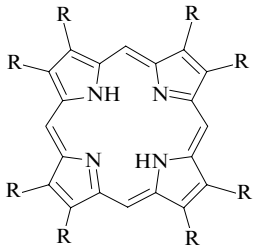

Natural porphyrins and their synthetic analogues, *viz*., phthalocyanines, which are the most spectacular representatives of polyazacyclic compounds, are related to the class of conformationally rigid macrocyclic ligands. With metal ions in the oxidation state 2+, these ligands form intramolecular planar tetragonal complexes where two protons of the ligand are replaced by metal ions. Formally, the central metal ion in such complexes forms two typically covalent and two typically coordination bonds with the nitrogen atoms of the polyazacycle, which actually become equivalent as a result of complexation.

Metal complexes with crown ethers contain neither typically covalent, nor typically coordination metal—ligand bonds. Crown ethers form surprisingly stable complexes even with ions of alkali metals, which until recently were not considered as metals that form complexes.

In contrast to porphyrins and phthalocyanines, crown ethers represent conformationally flexible ligands. In the free state, the distribution of donor heteroatoms in crown compounds is random; however, after penetration of the cation into the cavity of the macrocycle the latter adopts a crown-shaped conformation. For example, 12-crown-4 (12-C-4) can exist in different conformations depending on the nature of the substituents, solvent, temperature and other factors (Fig. 1).

Flexible crown ligands are specifically adapted to the complexation conditions to yield various types of complexes (Fig. 2). Depending on the sizes of the cations and of the cavities of crown ethers, such complexes are divided into three main types, *viz*., complexes in which the size of a cation is comparable with that of the macrocyclic ligand cavity (complexes of the type **A** or **B**); complexes in which the size of a cation is smaller than that of the crown ligand cavity (compounds **C** or **D**) and complexes in which the size of a cation is larger than that of the macrocyclic ligand cavity (compounds **E** – **G**).

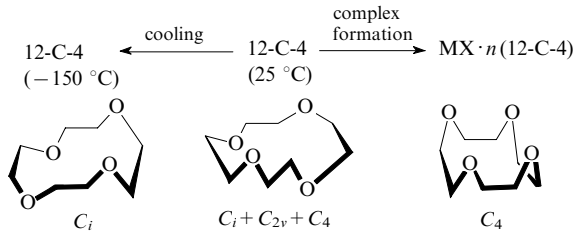

Figure 1. Conformations of 12-crown-4.

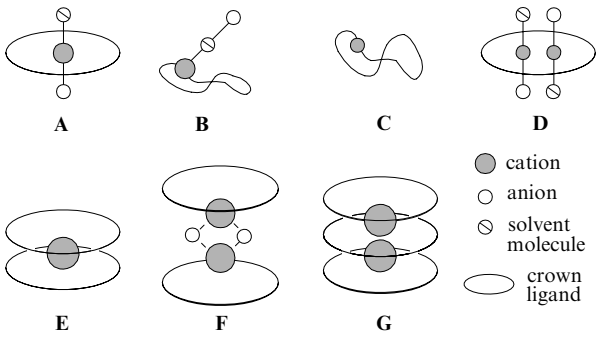

Figure 2. Various types of metal complexes with crown ligands (according to the Punia classification).
A, an encapsulated ion pair (the cation – anion pair remains to be a contact pair, M : L = 1 : 1); **B,** a partly encapsulated ion pair (the cation forms a solvent-separated pair with the anion, M : L = 1 : 1); **C,** enveloping encapsulation (M : L = 1 : 1); **D,** a compound with M : L = 2 : 1; **E,** a sandwich-like compound (M : L = 1 : 2); **F**, dimers linked by bridging ligands (M : L = 1 : 1); **G**, a triple-decker sandwich compound (M : L = 2 : 3).

The progress in conformational analysis [6] and, particularly, in spectral conformational analysis † has made it possible to investigate, by the example of a vast (several hundreds) number of complexes, the conformational changes occurring in crown ligands under the influence of diverse factors (*e.g.*, peripheral substituents, metal that represents complexing agent, anions, solvent, *etc.*). This has led to elaboration of a fundamentally new conformational approach to modification of properties of macroheterocyclic compounds based on directed changes in the conformational equilibrium and hence in the complex-forming and ion-selective properties of the crown ligands. Thus an idea appeared to fix, with the help of peripheral substituents, those crown-ether conformations which are especially suitable for selective interactions with the target metal ion. Such a preorganisation of the ligand allows a purposeful choice of crown compounds that bind selectively specific cations.[1–13] At the same time, it should be remembered that rigid fixation of crown ethers deprives them of flexibility, which enables surprisingly effective adaptation to the existing conditions. Therefore, the choice of side substituents should be a reasonable compromise between the rigidity and flexibility of the ligands formed.‡

There are numerous examples of the violation of the Pedersen geometrical correspondence principle [2,3,6,12–15] according to which stable complexes are formed provided the size and shape of the macrocyclic ligand cavity match the size and shape of the complex-forming cation; these can be accounted for by the diversity of the conformational forms of the crown ethers. This principle is violated in those cases where the anion, solvent or intermolecular interactions force the ligand to adopt a conformation where the coordination with a cation (the size of which is larger or smaller than that expected based on the geometrical correspondence principle) is more favourable.

In this case, we deal with dimensional effects characteristic of nanochemistry and nanotechnology. For example, if the size of a metal cation exceeds that of the macrocyclic cavity to such an extent that the cation can by no means occupy the central position in the macrocycle, sandwich-like dimers and trimers (**E** and **G**) are formed; the metal cations in these aggregates are located between the neighbouring crown-ether molecules. The formation of such supramolecular aggregates ensures stability of the complex, but ordered architectures of the molecular ensembles.

The principles of the molecular stereodesign of crown compounds developed allow a purposeful search for highly selective extraction systems for isotope separation. In the choice of a particular system, it is important to know how a concrete crown extractant adapts to specific extraction and reextraction conditions by respective conformational changes. This approach has led to the development of a physicochemical basis of technological processes for the separation of lithium, magnesium, calcium, potassium and boron isotopes.[16]

It is known that porphyrins and phthalocyanines form stable metal complexes possessing unique electrophysical and optical properties;[17–19] however, poor solubility of such complexes in organic solvents and water prevents their wide utilisation. Many problems related to practical realisation of these unique properties of phthalocyaninates could be circumvented through the introduction of peripheral substituents. Some of these substituents ensured the required solubility on the complexes, while others conferred entirely new properties on them. Dimensional effects also play an important role. For example, metal ions with the sizes allowing them to occupy the central position in the macrocycle form monophthalocyaninates (compounds **1**, **2**), whereas bulkier ions (*e.g.,* rare-earth elements) form sandwich-like double- (compound **3**) and triple-decker complexes.

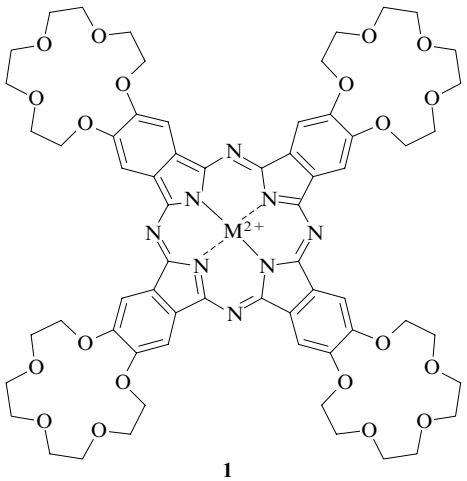

1

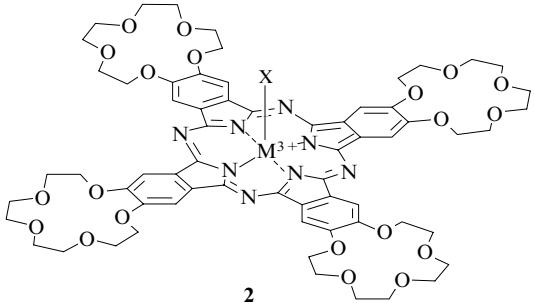

2

† Spectral conformational analysis combines oscillation spectroscopy, quantum-chemical calculations and theoretical analysis of normal molecular oscillations.

‡ In the case of porphyrins, nature itself has solved the problem through the selection of appropriate substituents.

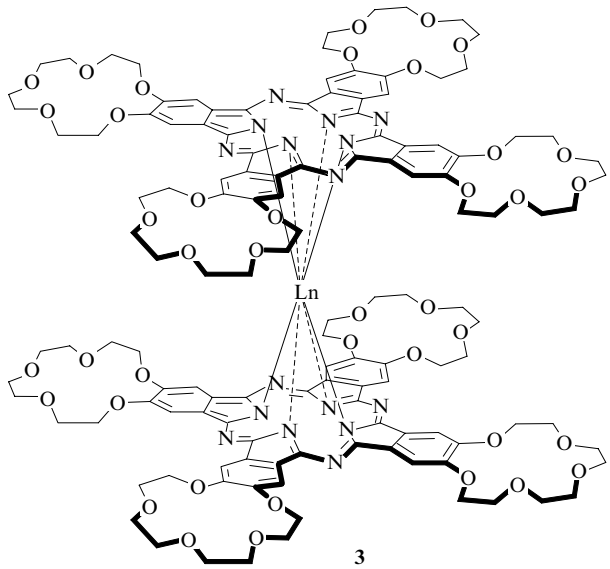

3

It is noteworthy that peripheral substituents do not disturb the rigidity of the macrocycle, but influence the mutual arrangement of the phthalocyanine molecules, which, in turn, determines the type of $\pi-\pi$-interactions between the aromatic systems and the formation of supramolecular stacking or liquid crystalline systems. In this respect, crown-ether substituents differ favourably from all other substituents in their ability to provide the required solubility and ordering of complex supramolecular architectural ensembles and to confer novel properties on the phthalocyaninate complexes owing to the formation of additional ion conductivity side channels along with the central semiconducting channel.

A series of crown-substituted phthalocyanines have recently been synthesised which are readily soluble in the majority of solvents and do not form isomeric mixtures like unsubstituted phthalocyanines. Reactions of metal complexes of such tetracrown phthalocyanines with alkali metal salts yield heteronuclear supramolecular aggregates.[20–24] Proneness of crown substituents to form complexes with alkali metals and the tendency of phthalocyanines for stacking interactions of aromatic rings favour the formation of such aggregates.

Although porphyrins and phthalocyanines belong to macrocyclic ligands, it was not until the discovery of crown ethers that the remarkable stability of the metal complexes of the former was associated with the macrocyclic effect. Nor did the elucidation of the mechanism of reversible binding of oxygen to hemoglobin lead to the introduction of the term 'supramolecular chemistry', although the non-linear cooperative effect observed thereupon was undoubtedly associated with the formation of supramolecular systems as follows from the sigmoidal shape of the titration curve. The necessity for the introduction of the term 'supramolecular chemistry' arose only in 1978 in the consideration of the unusual selectivity of the complexes formed by alkali metal cations and crown ethers.[1,4,5]

Supramolecular chemistry studies supramolecular systems formed as a result of noncovalent intermolecular interactions.[1–6] The main concepts of supramolecular chemistry are fixation (binding), recognition and coordination. The stability of alkali metal complexes with crown ligands is provided by the recognition of geometrically complementary species and the multiplicity of their interactions due to the increase in the interaction surface. A main goal of supramolecular chemistry is the design of ordered functional units having molecular sizes and that could receive, store, transmit and read information like chemical-and-biological 'machines'[§] responsible for skilful regulation of vital processes in nature.[1]

§ Photosynthesis performed by chlorophyll, one of the most typical representatives of natural porphyrins, is an example.

The uniqueness and remarkable efficiency of chemical processes occurring in living organisms have always been a subject of admiration for chemists. The more mysteries of nature that are unravelled by chemists the more new enigmas and undisclosed mechanisms of control over various chemical processes in biological systems emerge. Recently, it has become evident that the unusual controllability and selectivity of vital processes cannot be explained in terms of covalent interactions. The ability to exert flexible control over chemical processes is one of the common features of biological and supramolecular processes realised at the molecular level. The ease of the control over chemical processes mediated by synthetic analogues of macrocyclic natural compounds is reached owing to their selectivity and extreme sensitivity to low-energy influences.

Synthesis of crown-substituted porphyrins and that of phthalocyanines are based on different approaches. This is due to differences in the modes of attachment of crown-ether substituents to porphyrins and phthalocyanines. Thus, crown-ether substituents are fused to phthalocyanines to form a fused tetracyclic system (structure **A**), while these are linked to porphyrins through a C—C bond between the carbon atoms of the benzene ring and the methine group (structure **B**) about which free rotation is possible. These differences are reflected in the supramolecular organisation of these systems.

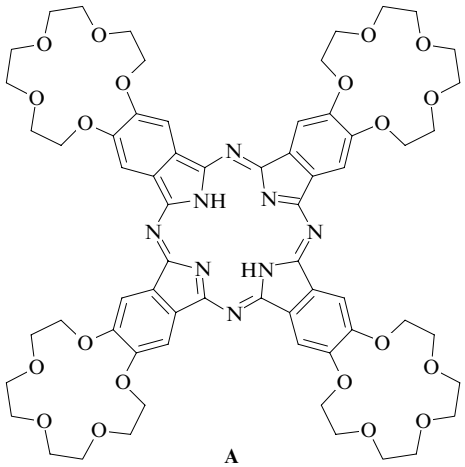

A

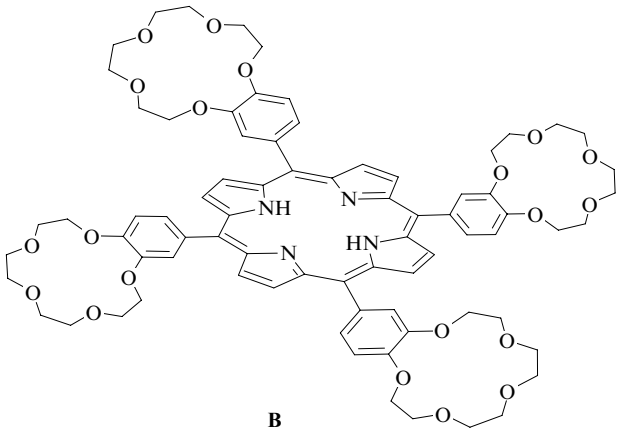

B

II. Crown-substituted porphyrins

Functionalised porphyrins present interest as models for the study of various biological processes, such as heme oxygenation, cytochrome activity and photosynthetic electron transport.[25–29] Thus it was tempting to use porphyrins containing macrocyclic substituents able to recognise cations for the study of sodium-potassium transport across biological membranes. The ionophoric behaviour of such substituted porphyrins can easily be

monitored by following fluorescence changes.¶ The methods for the synthesis of this class of model compounds depend on the nature and position of side substituents. Earlier, substituted pyrroles containing ester, amide or alkyl groups were used for the synthesis of substituted porphyrins;[30–32] however, compounds thus prepared did not possess ionophoric properties. The first attempt to synthesise crown-substituted porphyrins from 4′-formylbenzo-15-crown-5, pyrrole and benzaldehyde (Scheme 1) was undertaken in 1982 by Thanabal and Krishnan.[33] Depending on the ratio of the reactants, tetra- (**A**), tri- (**B**), di- (**C**) or mono-15-crown-5-substituted (**D**) porphyrins were obtained. If the porphyrin molecule is presented as a circle and 15-crown-5 as an ellipse, the resulting compounds will appear as shown in Scheme 1.

Scheme 1

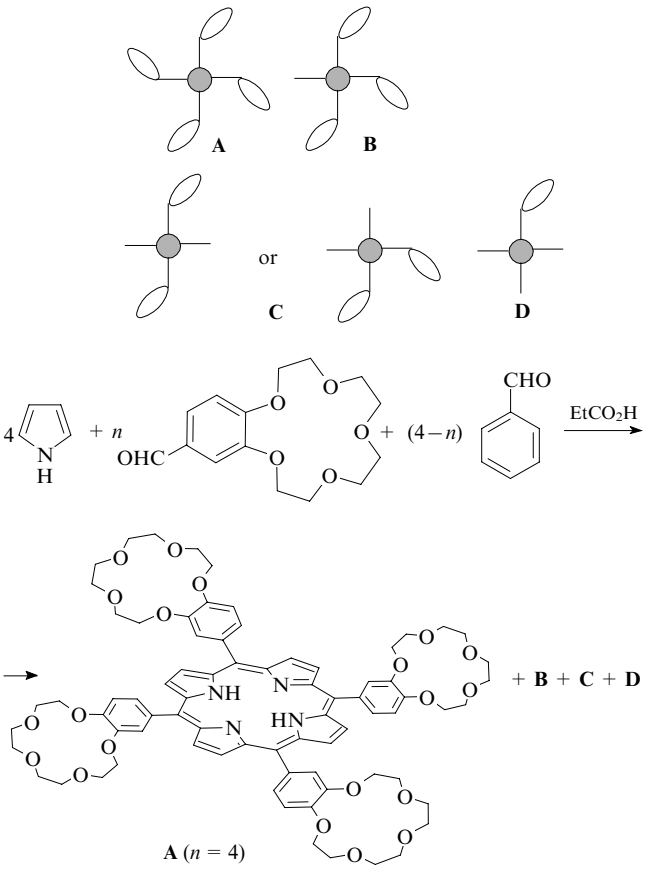

$n = 1-4$.

Interactions of these crown-substituted porphyrins with metal salts (Co, Cu, Zn) yield chelate compounds. The addition of sodium, magnesium and calcium salts to solutions of tetra- and tricrown-substituted porphyrinates did not cause any changes in the electronic spectra of the complexes, whereas the addition of potassium, ammonium and barium salts resulted in a decrease in their intensities, changes in both Q-bands (broadening and shift by *ca.* 10 nm towards the long wavelength region) (a bathochromic shift) and Soret bands (a hypsochromic shift).†

Such changes can be attributed to specific complexation of crown-substituted porphyrins with these cations. The difference in the behaviour of these cations with respect to crown-substituted porphyrins is due to the formation of M : L = 1 : 1 complexes of benzo-15-crown-5 with sodium, magnesium and calcium cations, whereas potassium, ammonium and barium cations form sandwich complexes with the composition M : L = 1 : 2 (compound **4**). In the latter case, it is dimerisation of the macrocycles induced by a specific behaviour of potassium, ammonium and barium cations that causes changes in their electronic spectra.

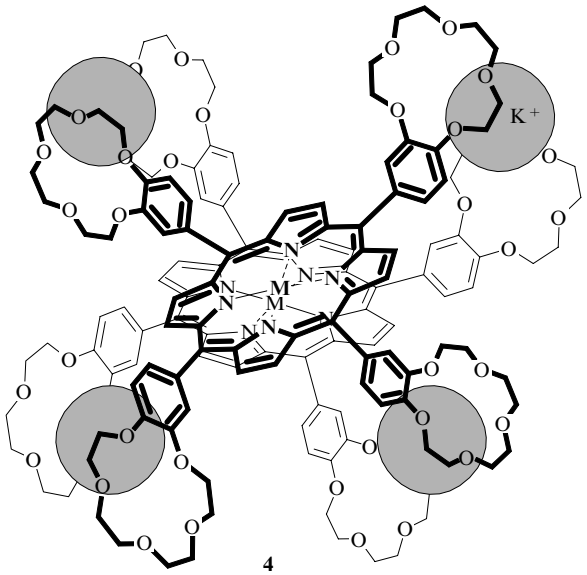

M = 2H, Co, Zn, Cu.

The reaction of crown-substituted porphyrins (P) with potassium cations can schematically be presented as:

$$2P + 4K^+ \longrightarrow P_2(K^+)_4.$$

It was suggested [33] that the addition of potassium ions first induces the formation of the dimer P_2, which is followed by complexation, potassium cations filling all the unoccupied positions in the macrocyclic cavities of the peripheral crown-ether substituents. It should be noted that saturation is reached even at very low concentrations of potassium cations (10^{-5} mol litre^{-1}). The stability constant of the complex $P_2(K^+)_4$ is equal to 10^{23} litre^5 mol^{-5}, *i.e.*, it is by several orders of magnitude greater than the corresponding constants of the K^+ complexes with crown ethers.

It was found that the addition of even very small amounts of potassium ions (10^{-5} mol litre^{-1}) to a zinc complex with tetracrown porphyrin ($\sim 10^{-5}$ mol litre^{-1}) in the presence of an excess of sodium ions ($\sim 10^{-2}$ mol litre^{-1}) results in dimerisation as can be evidenced from the significant changes in the electronic absorption spectra of ZnTCP (TCP is tetracrown porphyrin) in ethanol. Such a selectivity of ZnTCP with respect to potassium cations enables its application for quantitation of low concentrations of potassium ions. No such selectivity is observed for ammonium and barium cations: the presence of even very small amounts of sodium ions leads to disaggregation of complexes $P_2(NH_4^+)_4$ and $P_2(Ba^{2+})_4$.

The addition of potassium ions to a CuTCP complex results in significant changes in the ESR spectra due to the formation of $(CuTCP)_2(K^+)_4$ complexes. ESR spectroscopic data suggest that copper ions occupy a position in the centre of the porphyrin ring cavity. The Cu–Cu distance in the dimer reaches ~ 4.20 Å, which is in favour of coaxial symmetry of the complex.[33] The porphyrin rings in the dimer $(CuTCP)_2(K^+)_4$ are turned by 45° relative to one another.

¶ The changes in the porphyrin fluorescence can be conjugated, *e.g*, to the inhibition of oxidative phosphorylation in respiratory mitochondrial systems.

† It is known that Q and Soret bands are extremely sensitive to structural changes.

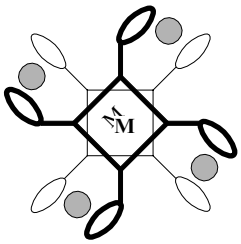

X-Ray diffraction analysis of a potassium complex $K(B\text{-}15\text{-}C\text{-}5)_2I$ (B-15-C-5 is benzo-15-crown-5) revealed that the crown-ether ligands in this compound are at a distance of ~ 3.8 Å from one another and the plane passing through the oxygen atoms is parallel to the plane of the benzene ring.[34]

The formation of highly ordered systems is yet another specific feature of the tri- and disubstituted copper complexes $(CuTriCP)_2(K^+)_3$ and $(CuDCP)_2(K^+)_2$.[33] However, the Cu—Cu distance in these complexes is greater than that in the corresponding tetrasubstituted complex $(CuTCP)_2(K^+)_4$.

The addition of methanolic solutions of sodium, magnesium and calcium salts to solutions of free tetracrown porphyrin and its ZnTCP complex (5×10^{-5} mol litre^{-1}) in $CHCl_3$ does not bring about changes in their fluorescence spectra, while the addition of potassium salts induces significant changes due to dimerisation. (It is of note that the fluorescence spectra of the complexes appeared to be more sensitive to potassium ions than their absorption spectra). In the case of free tetracrown porphyrin, the dimerisation effect is insignificant.[33]

A detailed analysis of the ESR and optical spectra of a zinc complex with tetracrown porphyrin revealed [35] that the cavities of the porphyrin rings in the dimer are parallel and turned by 23° relative to one another.

Potassium, caesium, ammonium and barium cations induce the formation of porphyrin dimers in the case of vanadyl complexes, the dimerisation constant decreases on going from tetracrown-substituted vanadyl porphyrinate to tri- and disubstituted complexes. The constant of cation-induced dimerisation of vanadyl tetracrown porphyrinate decreases in the following order: $K^+ > Ba^{2+} > Cs^+ \approx NH_4^+$. According to data from ESR spectroscopy, the V—V distance in these dimeric complexes is equal to ~ 4.70 Å.

Magnesium, nickel and manganese(III) complexes with tetracrown porphyrin also yield dimers upon interaction with potassium salts.[36] An electrochemical analysis of redox properties of these metal complexes revealed that the oxidation of the porphyrin ring in dimers occurs at lower anodic potentials than in the corresponding monomers. The electronic absorption and emission spectra of the electrochemically oxidised and reduced states of these dimers were interpreted based on the changes in their electronic structures.[36] The ESR spectra of the oxidised dimeric radical show that the unpaired electron is localised on one of the porphyrin π-systems unlike chlorophyll molecules in bacterial photosynthetic systems.

Synthesis of dioxocyclam- and diaza-18-crown-6-substituted porphyrins (**5a**,**b**) and metal complexes based on them (**5c**,**d**) has been described.[37–39]

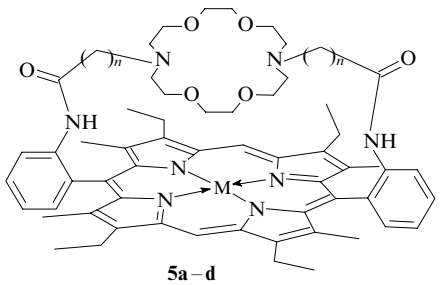

5a–d

5a: M = 2 H, n = 1;
5b: M = 2 H, n = 2;
5c: M = Zn(II), n = 1;
5d: M = Co(II), n = 2.

X-Ray diffraction analysis of compounds **5b** and **5c** [38] confirmed the presence in these compounds of a bridging diaza-18-crown-6 ligand binding two peripheral benzene rings attached to the porphyrin macrocycle. The cavity of diaza-18-crown-6 is coaxial with that of the macrocyclic ring of porphyrin (an analogous position of the rings was observed in a structurally similar 5,15-di(2-alkylamidophenyl)etioporphyrin complex with dioxocyclam [37]). Cobalt and zinc ions enter the cavity of the porphyrin ring. Electrochemical studies of these compounds revealed that cobalt complexes undergo oxidation in an atmosphere of nitrogen. In PhCN, the addition of oxygen is reversible, and irreversible in CH_2Cl_2. Oxidation of the cobalt complex in an atmosphere of carbon monoxide yields a compound in which the cobalt ion is linked to the carbonyl group.

A monomeric zinc complex with bis(benzo-15-crown-5)porphyrin was prepared starting from dipyrrolylmethane, 4′-formylbenzo-15-crown-5 and zinc acetate (Scheme 2).[40] Treatment of the complex **6** with $AgPF_6$ yielded a diporphyrin zinc complex **7** containing two covalently (*meso-meso*) linked porphyrin rings.

Scheme 2

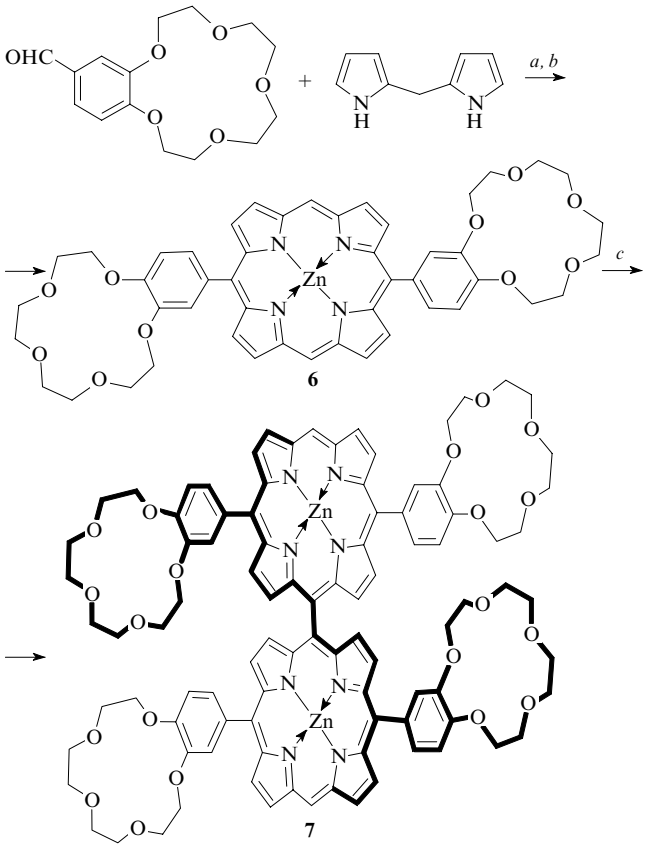

a — $BF_3 \cdot OEt_2$, $CHCl_3$, 2,3-dichloro-5,6-dicyano-1,4-benzoquinone;
b — $Zn(OAc)_2 \cdot 2\,H_2O$, $CHCl_3$ – MeOH;
c — $AgPF_6$, $CHCl_3$ – MeOH – MeCN.

The addition of sodium salts to the monomeric complex **6** in $CHCl_3 - CH_3CN$ (2 : 1) did not cause any changes in the electronic absorption spectra of the complex, whereas the addition of potassium ions caused a shift in the Soret band from 415 to 396 nm (with an isosbestic point at 404 nm) and a decrease in the fluorescence intensity. It was suggested [40] that these changes are due to the formation of a diporphyrin dimer similar to the dimers **4** described above. The changes in the NMR spectrum of the complex **6** following addition of cations K^+ provide additional evidence in favour of formation of a dimer of the type **4**. The addition of a potassium salt to the covalently linked dimeric zinc

complex **7** results in more complicated changes in the electronic absorption spectra.

In the absence of alkali metal ions, the Soret band in the electronic absorption spectrum of compound **7** appears as a doublet at 421 and 453 nm. The splitting of this band is attributed to an exciton interaction. Upon addition of a potassium salt to a solution of the complex **7**, the intensities of the bands at 421 and 453 nm first decrease, and when the concentration of potassium ions reaches 1.0×10^{-5} mol litre^{-1}, the Soret band is shifted towards 423 nm and its intensity increases. These changes are accompanied by an appearance of a shoulder with an isosbestic point at 408 nm on the high-energy side of the Soret band.‡

The fluorescence intensity of the dimer **7** also changes with the concentration of potassium ions. At first, potassium cations ($[K^+] \leqslant 1.0 \times 10^{-5}$ mol litre^{-1}) cause a decrease in the intensity of the fluorescence band; however, the fluorescence increases with increasing concentration of potassium ions. Similar changes in the electronic absorption and fluorescence spectra were observed upon addition of rubidium ions, but not in the case of caesium and sodium ions. These findings are in conflict with the data on the behaviour of the monomeric complex **6** under identical conditions. It may thus be assumed that the intermolecular interactions of the crown-ether fragments of the monomeric (**6**) and dimeric (**7**) zinc complexes with potassium ions have the same character, but the molecular ensembles formed by these complexes differ. Coaxial dimerisation of the monomeric zinc complex upon interaction with potassium ions (the formation of 'face-to-face' dimers) is probable, while self-complementary dimerisation of the covalently bound zinc complex is impossible and linear extended aggregation is more preferable (Fig. 3). The complex character of changes in the electronic absorption and luminescence spectra suggest a multistage equilibrium resulting in the formation of a linear ensemble. The decrease in the fluorescence intensity in the initial step points to the formation of a coaxial diporphyrin, while its subsequent increase may result from interactions of the crown-ether groups of the linear aggregates with alkali metal ions. The polymeric nature of the aggregates is confirmed by light scattering studies: the molecular weight of the aggregate may amount to 10^5, *i.e.,* the linear ensemble is made up of 50 aggregated molecules. It is suggested[40] that the methodology of the supramolecular organisation of porphyrins described above can successfully be used in the design of novel molecular architectural ensembles and new generations of highly efficient materials.

‡ The appearance of a shoulder on the high-energy side of the Soret band is interpreted as the formation of a stacking diporphyrin of the coaxial type (a 'face-to-face' dimer).[40]

III. Crown-substituted monophthalocyaninates

Unlike porphyrins, the pyrrole fragments of phthalocyanines (Pc) forming the macrocyclic cavity are linked by four nitrogen atoms of the azamethine groups. Although these four additional nitrogen atoms are not directly involved in the complexation due to remoteness from the cavity centre, they create quite different

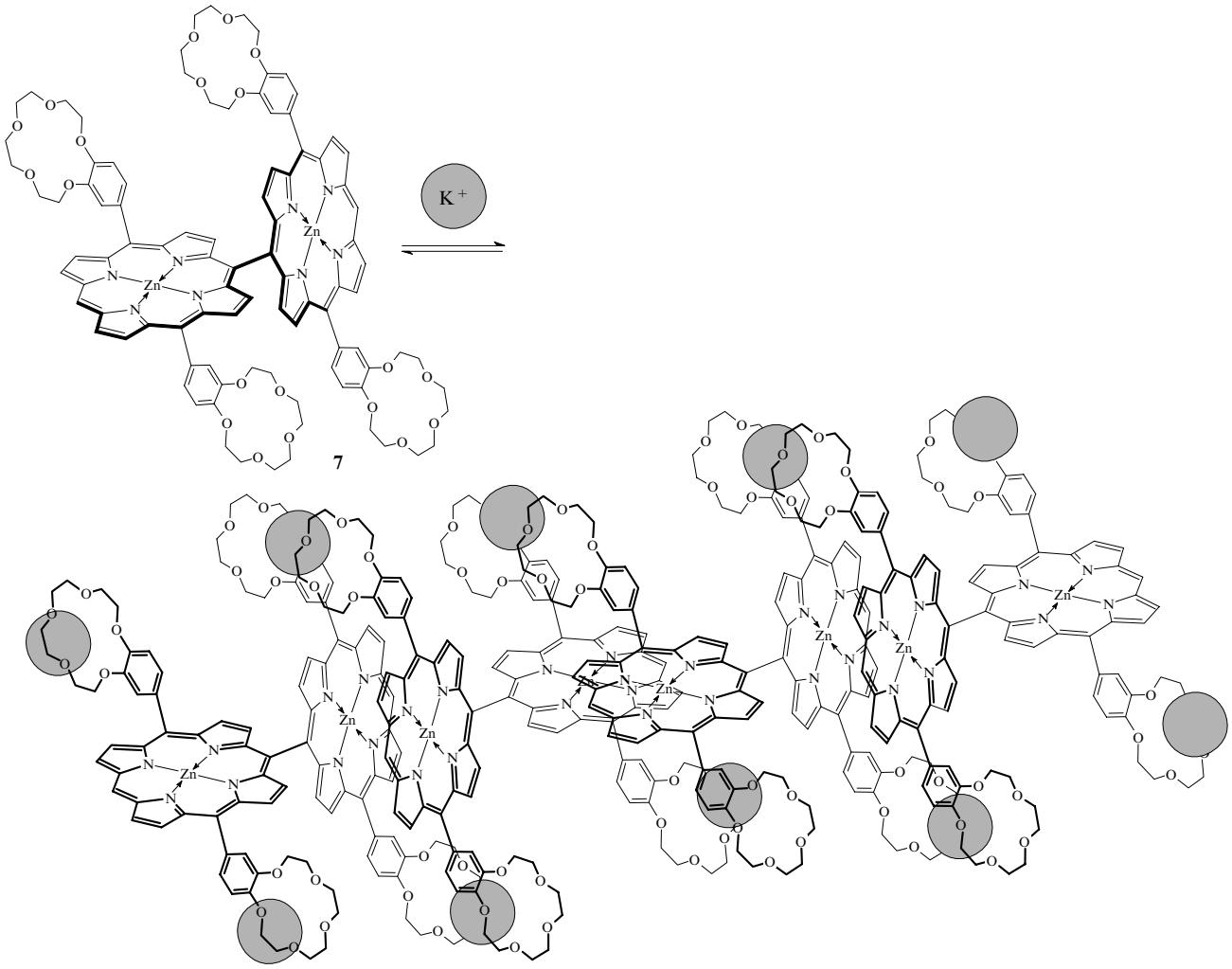

Figure 3. Supramolecular aggregation of dimeric zinc bis(benzo-15-crown-5)porphyrinates **7**.

conditions for the interaction with metal salts. Because of the peculiar electronic structure of the aromatic system, metal phthalocyanines manifest high chemical and thermal stability and possess unique optical, electrical and photochemical properties, which opens up new opportunities for their wide application as semiconductors, catalysts, sensors, pigments and biologically active compounds.

Phthalocyanines are conformationally rigid ligands; therefore, their complexation is accompanied by forced planar-tetragonal coordination of the central metal ion, which ensures high kinetic stability of the corresponding phthalocyaninates.

The first phthalocyanine complex (CuPc) was obtained by accident in 1927 during the synthesis of 1,2-dicyanobenzene from *o*-dibromobenzene and CuCN in pyridine at 200 °C (see Ref. 41). The nitrile-based and urea-based template syntheses of metallophthalocyanines were developed later. The former approach is based on the reaction of phthalonitrile with various metal salts.[42] At present, phthalocyanines are synthesised in different ways, but the template method is still the most popular.

Metallophthalocyanines have limited application due to their poor solubility in organic solvents and water, which prevents the preparation of chemically pure substances and high-quality films based on them. Numerous substituted phthalocyanines have been synthesised in order to improve their solubility. Thus the introduction of bulky substituents (*e.g.*, *tert*-butyl, naphthyl or crown-ether substituents) into the benzene rings of the phthalocyanine molecule increases their solubility in organic solvents,[41,42] whereas sulfation of benzene rings increases the solubility of phthalocyanines in water.

The introduction of a crown-ether fragment into a phthalocyanine molecule as a substituent in the benzene ring of the isoindole fragment not only increases its solubility, but also favours the formation of heterometal complexes upon interaction of phthalocyaninates with alkali and alkaline earth metal salts. Syntheses of such complexes have been described.[20–24,43–46] Tetracrown-substituted phthalocyanines were prepared from benzo-15-crown-5, which was converted into dicyanobenzo-15-crown-5. The latter was used as a starting reagent in the nitrile template synthesis of tetracrown-substituted phthalocyanine (CR-Pc) (Scheme 3).

Interactions of dicyanobenzo-15-crown-5 with divalent metal salts yield chelate complexes M(CR-Pc) [M = Co(II), Ni(II), Zn(II), Cu(II), *etc*.]. With trivalent metals (M = Al), metal complexes are formed with extra ligands occupying an axial position. In contrast to the synthesis of crown-substituted porphyrins where mono-, di-, tri- and tetracrown-substituted derivatives are formed, in the case of phthalocyanines, tetracrown-substituted complexes are always formed as the reaction products. Data from various physicochemical methods have made it possible to postulate a symmetrical structure for the compounds formed. No direct evidence for such symmetry was available until recently due to a lack of X-ray data; however, a comparison of the vibrational spectra of tetracrown-substituted copper phthalocyaninate in a conformationally sensitive region of the IR and Raman spectra (600–1600 nm) (Fig. 4) revealed that these spectra did not coincide either in frequencies, or in relative intensities of the bands over the whole spectral region. This suggests that the IR and Raman spectra of this compound follow the alternative exclusion principle, *viz*., the frequencies that appear in the IR spectra are absent from the Raman spectra and *vice versa*. It is well known that these regularities are characteristic of highly symmetrical compounds.[6] Thus, the symmetrical structure of the above compound was deduced from its vibrational spectra.

An attempt to synthesise an aluminium complex with tetracrown phthalocyanine by the nitrile template method failed.[47] The interaction of aluminium chloride with dicyanobenzo-15-crown-5 (DCB15C5) in quinoline (the nitrile method) at 170 °C was accompanied by degradation of DCB15C5 and the complex was not formed. The yield of the corresponding Al(CR-Pc)(SO_4H) complex (**8**) synthesised from $Al_2(SO_4)_3$ and DCB15C5 in the melt

Scheme 3

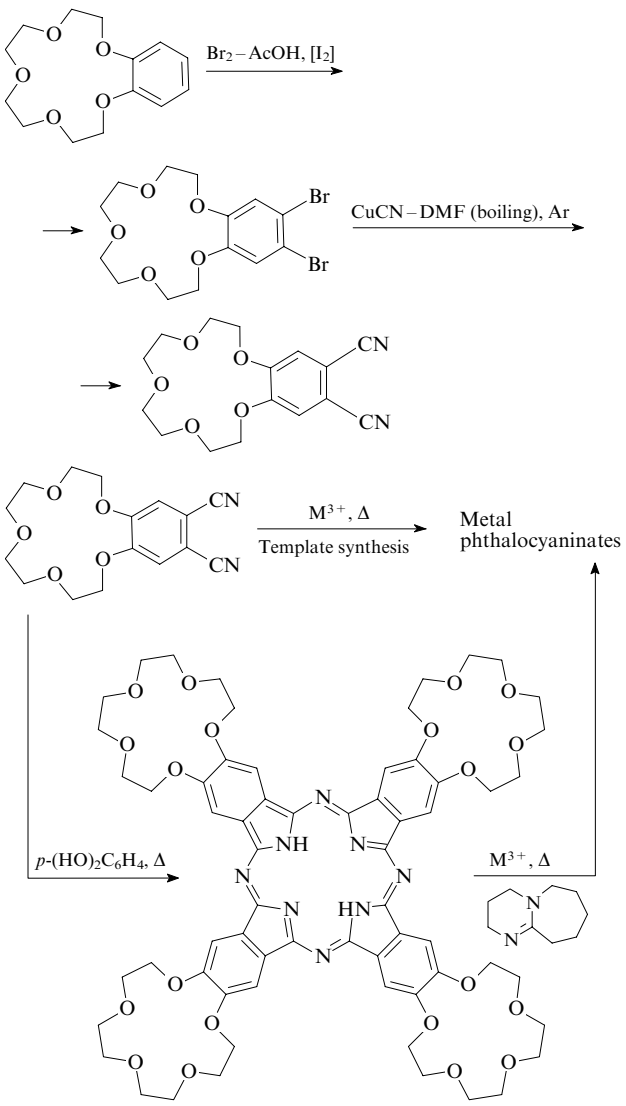

was very low due to hydrolysis of the cyano groups. In order to exclude this undesirable effect, the reaction of $Al_2(SO_4)_3$ with DCB15C5 was carried out in urea as in the urea-based version of the template synthesis which is employed for the preparation of

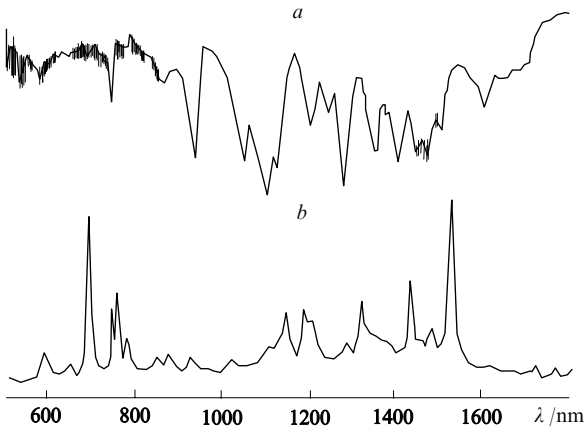

Figure 4. IR- (*a*) and Raman spectra (*b*) of copper tetra(15-crown-5)-phthalocyaninate.

phthalonitriles from phthalimide, phthalic acid or its derivatives and urea. Urea, which decomposes at 130 °C in the presence of a catalyst (ammonium molybdate) with evolution of ammonia, serves as an aminating reagent for the conversion of the phthalic acid derivative into phthalonitrile directly in the course of the synthesis.

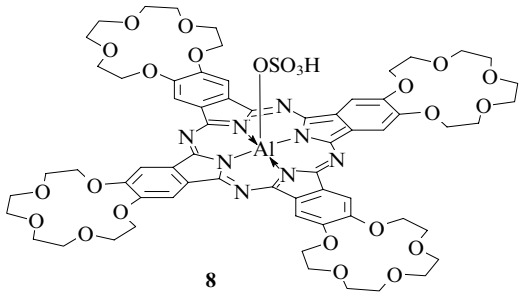

8

It was found that the Al(CR-Pc)(SO_4H) complex is soluble in both organic solvents (*e.g.*, chloroform, acetone, pyridine, ethanol, dimethyl sulfoxide, *N*,*N*-dimethylformamide) and in water. The aqueous solution of this complex is stable in neutral and weakly acidic media. At pH > 7, complex **8** is hydrolysed into Al(CR-Pc)OH.

The synthesis of a zinc complex with a crown-substituted phthalocyanine by the nitrile template method is also difficult due to the necessity of prolonged heating of the reagents and relative instability of zinc phthalocyanine complexes.[48] Therefore, the direct method, *viz.*, the reaction of zinc acetate with H_2(CR-Pc), was used for the synthesis of the crown-substituted zinc monophthalocyaninate Zn(CR-Pc).[49] This reaction was carried out either in the presence of an excess of lithium hydroxide in a chloroform–ethanol mixture or in the presence of a stoichiometric amount of BuLi in dimethyl sulfoxide. In the latter case, the yield of the Zn(CR-Pc) complex reached 95%.

Similar problems were observed in the template synthesis of crown-substituted monophthalocyaninates of rare-earth elements (REE). Because of the large radii of lanthanide ions, it is much more difficult to prepare REE monophthalocyaninates than sandwich bisphthalocyaninates.[50–54] An analysis of known methods for the synthesis of crown-substituted REE monophthalocyaninates revealed [55] that the protonated ligand H_2(CR-Pc) is the most suitable starting material. However, reactions of REE acetates with H_2(CR-Pc) occur only in the presence of strong bases, *e.g.*, 1,10-phenanthroline (Phen) and 1,8-diazabicyclo[5.4.0]undec-7-ene (DBU).[55] Boiling of lutetium acetate and H_2(CR-Pc) in dichlorobenzene in the presence of an excess of DBU gives crown-substituted lutetium monophthalocyaninate.

$$H_2(\text{CR-Pc}) + Lu(OAc)_3 \xrightarrow[\Delta]{\text{DBU, } o\text{-}Cl_2C_6H_4} Lu(\text{CR-Pc})(\text{DBU})OAc.$$

In the presence of 1,10-phenanthroline, the reaction proceeds in a similar way. In the compound Lu(CR-Pc)$(Phen)_2X$ formed, phenanthroline acts both as the base and the chelating ligand for lutetium ions. Both lutetium complexes possess sufficiently high solubilities in organic solvents of various polarity (*e.g.,* chloroform, dichloromethane, dimethyl sulfoxide, acetone) and in water (the concentration of a saturated aqueous solution of the DBU complex is 1.7×10^{-4} mol litre^{-1}).

Until recently, data on the synthesis of crown-substituted phthalocyaninates of platinum metals were absent from the literature. At the same time, complexes of platinum metals with such ligands present substantial interest because of the great diversity of coordination properties of both the ligands and the central metal atoms. The synthesis of a complex of ruthenium(II) with tetra(15-crown-5)phthalocyanine has been described.[56]

The template synthesis is mainly used in the preparation of ruthenium complexes with unsubstituted phthalocyanine from phthalonitrile (or cyanobenzamide) and ruthenium trichloride is the main procedure.[57–60] The ruthenium(II) monophthalocyaninate 'PcRu' reacts with various ligands to give complexes with the composition $PcRuL_2$ (L = Py, DMF, DMSO, *etc.*).[60,61] This approach was also used in the synthesis of tetraalkyl-substituted ruthenium phthalocyaninates (yield 95%).[62]

There are still no unambiguous literature data on the structure of the 'PcRu' complex prepared by the template synthesis. Using LAXS and EXAFS methods, Ercolani and co-workers [60,63] have demonstrated that the 'PcRu' complex represents a dimer the length of the Ru–Ru bond in which is equal to 2.40 Å. The molecular formula of this complex can be written as $[(PcRu)_2]_6$. The Ru···Ru distance between the neighbouring dimers (4.30–4.40 Å) exceeds significantly that in the dimer. In the crystal structures of $[(Ru(Py)Pc)_2(\mu\text{-}C)]$ [64] and $(Bu^n_4N)[Ru(CN)(Py)Pc]$,[65] the ruthenium atoms deviate from the plane of the macrocycle by ~0.05 Å. The distance between the neighbouring pyrrole planes, $(Np)_4$,§ is 3.65 Å.[64,65]

The template method was also used for the synthesis of ruthenium tetra(15-crown-5)phthalocyaninate (Scheme 4).[56] It is of note that one complex, Ru(CR-Pc)(CO)CH_3OH (**9**), containing an axial carbonyl group is formed irrespective of the starting ruthenium compound, *viz.*, $RuCl_3 \cdot n H_2O$ or $Ru_3(CO)_{12}$. The formation of a Ru(CR-Pc)(CO)CH_3OH complex was expected in the case of $Ru_3(CO)_{12}$, the formation of a complex with the same composition from $RuCl_3$ was rather unexpected. However, considering that the attachment of CO to the Ru atom occurred in the template synthesis of unsubstituted ruthenium phthalocyanine complexes in an atmosphere of CO with ruthenium chloride as a starting reagent,[66] the formation of a complex of this composition can hardly be called unexpected.

Scheme 4

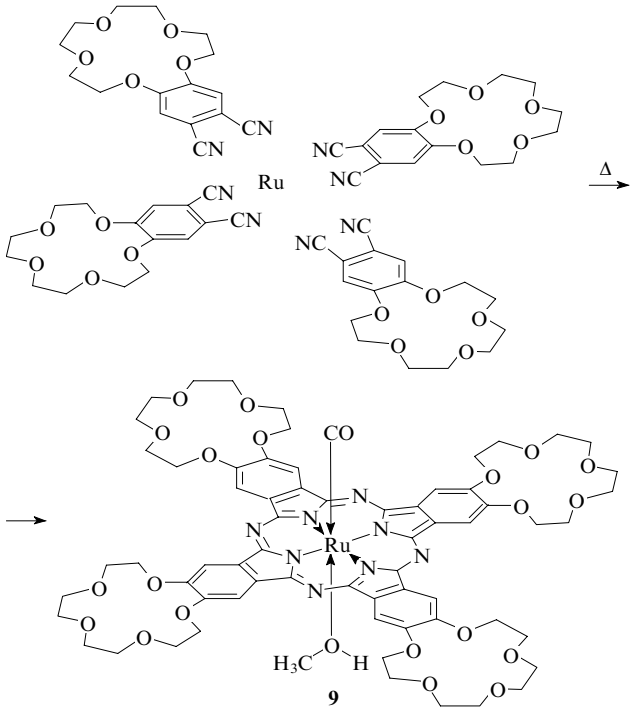

9

Ru = $RuCl_3 \cdot n H_2O$; $Ru_3(CO)_{12}$.

The IR spectra of two Ru(CR-Pc)(CO)CH_3OH complexes prepared from $RuCl_3$ (α-form) and $Ru_3(CO)_{12}$ (β-form) differ in the region around 1000–1300 cm^{-1} which contains characteristic bands corresponding to ν(COC) of the crown-ether groups. This suggests that crown-ether substituents in the α- and β-forms of Ru(CR-Pc)(CO)CH_3OH have different conformations.[56]

§ $(Np)_4$ is a plane passing through four nitrogen atoms of the pyrrole rings.

It can thus be concluded that Co, Ni, Zn and Cu cations in the oxidation state 2+ form chelate monophthalocyaninate complexes with crown-substituted phthalocyanines, whereas REE and aluminium cations in the oxidation state 3+ and ruthenium cations in the oxidation state 2+ form monophthalocyaninates with various axial ligands.

IV. Supramolecular aggregation of crown-substituted monophthalocyaninates

Crown-substituted metal monophthalocyaninates can form various supramolecular polymeric ensembles by noncovalent interactions. The stability of such ensembles in solution is determined by the multiplicity and dynamism of weak interactions of the $\pi-\pi$-stacking type.[67, 68] These interactions govern packaging of molecules into crystals and, correspondingly, such important characteristics of materials as electron transport. Modification of phthalocyanines by crown-ether substituents creates the necessary prerequisites for preparation of pillar-type structures with C_4, symmetry and high electroconductivity.

Crown-substituted phthalocyanines and their metal complexes form rigid stable coaxial dimers in the presence of alkali and alkaline earth metal ions for which the crown-ether fragments represent chelating ligands. The main prerequisite for the formation of such dimers is a large diameter of the cation which significantly exceeds that of the crown-ether ligand cavity. The formation of heteronuclear supramolecular dimers in the presence of potassium halides or acetate (KX) was studied [20–23, 43–46] using bivalent transition metal complexes (Cu, Ni, Co, Zn) as examples. These studies have demonstrated the possibility of formation of rigid coaxial dimers with the composition $2\,M(CR\text{-}Pc)\cdot 4\,K^+$ (M = Cu, Ni, Co, Zn). It was found also that the aggregation strongly depends on the nature of the solvent and the type of anion.

The electronic absorption spectra, which are highly sensitive to any changes in the complexes in the course of their aggregation, were selected as a tool for dimerisation studies. These spectra are very informative and demonstrate, in the most illustrative way, the characteristic changes in the structure of supramolecular aggregates under the influence of various factors.[20, 21]

In contrast to the aggregation of crown-substituted phthalocyanines, which occurs upon an increase in their concentration in solution and does not result in changes in their absorption spectra, the dimerisation induced by alkali metal cations has well-defined spectral manifestations. Thus it was found that the short-wavelength shift of the major absorption bands (*i.e.*, the Q-band and the Soret band) suggest the formation of rigid coaxial dimers in the system, the so-called H-dimers. The magnitude of the Q-band shifts depends on the distance between the interacting transient dipoles that appear as a result of an electron transfer in the phthalocyanine ligands.

The presence of a Q-band at 670 nm with a half-width of 500 cm^{-1} and a vibrational satellite at 610 nm and of a Soret band around ~ 350 nm with a shoulder in the short-wavelength region is characteristic of electronic absorption spectra of solutions of monophthalocyanines. Absorption around ~ 420 nm, which corresponds to the $n \rightarrow \pi^*$-transition due to the presence of crown-ether substituents, is represented by a broad low-intensity symmetrical band.

In addition to the aforementioned shifts of the major bands, interactions of alkali metal cations with crown-substituted metal phthalocyaninates are accompanied by broadening and a decrease in intensity of Q-bands. For example, the decrease in the intensity of the Q-band of $(15\text{-C-}5)_4$PcCu and $(18\text{-C-}6)_4$PcCu complexes depends on the concentration of the alkali metal salt: the corresponding dependence is linear and reaches a plateau at the stoichiometry 2 : 1 (four cations per two ligands) indicating the formation of the sandwich dimers **10** (Fig. 5).

If the diameter of the alkali metal cation (d_{M^+}) is larger than the size of the cavity of the crown-ether substituent (d_{CR}), highly

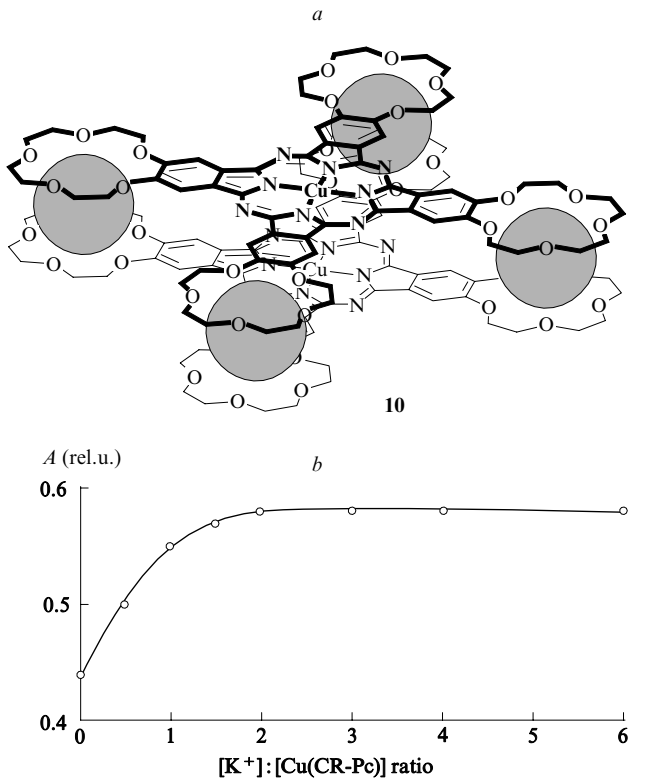

Figure 5. The structure of a sandwich-like supramolecular dimer $K_4[Cu(CR\text{-}Pc)]_2$ (**10**) (*a*) and a spectrophotometric titration curve of the Cu(CR-Pc) complex with potassium thiocyanate (*b*).

symmetrical sandwich complexes with the composition $4\,MX\cdot 2\,M(CR\text{-}Pc)$ are formed, while for $d_{M^+} < d_{CR}$, monophthalocyanine complexes $4\,MX\cdot M(CR\text{-}Pc)$ are formed.

Studies of formation of Co(CR-Pc) complexes with sodium and potassium thiocyanates (Scheme 5) (d_{K^+} = 2.66 Å; d_{Na^+} = 1.94 Å; d_{CR} = 1.7–2.2 Å) by the molar ratio method revealed [69] that the increase in the $[M^+]$: [Co(CR-Pc)] ratio results in changes in the electronic absorption spectra typical of phthalocyanine aggregation, *viz.*, a significant decrease in the intensity of Q-bands up to $[M^+]$: [Co(CR-Pc)] = 2 (nearly twofold for KSCN and threefold for NaSCN) with a simultaneous broadening of the Q-bands characteristic of complex formation and an appearance of an additional absorption band around 626 nm (for M = K) or 737 nm (for M = Na) (Fig. 6). Further increase in the metal : ligand ratio leads to precipitation.

The interaction of sodium thiocyanate with Co(CR-Pc) occurs in two steps.[69] Initially, an increase in the $[Na^+]$: [Co(CR-Pc)]

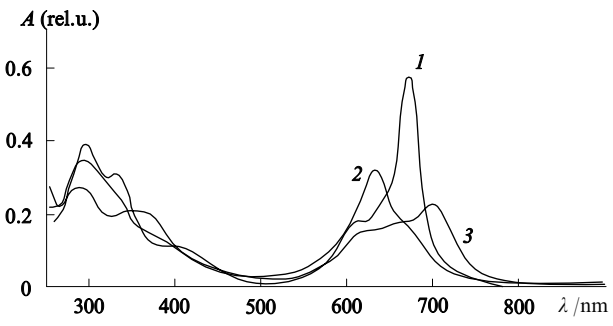

Figure 6. Electronic absorption spectra of Co(CR-Pc) (curve *1*) and its complexes with potassium (curve *2*) and sodium ions (curve *3*) in a chloroform – ethanol mixture (80 : 20, by volume).

Scheme 5

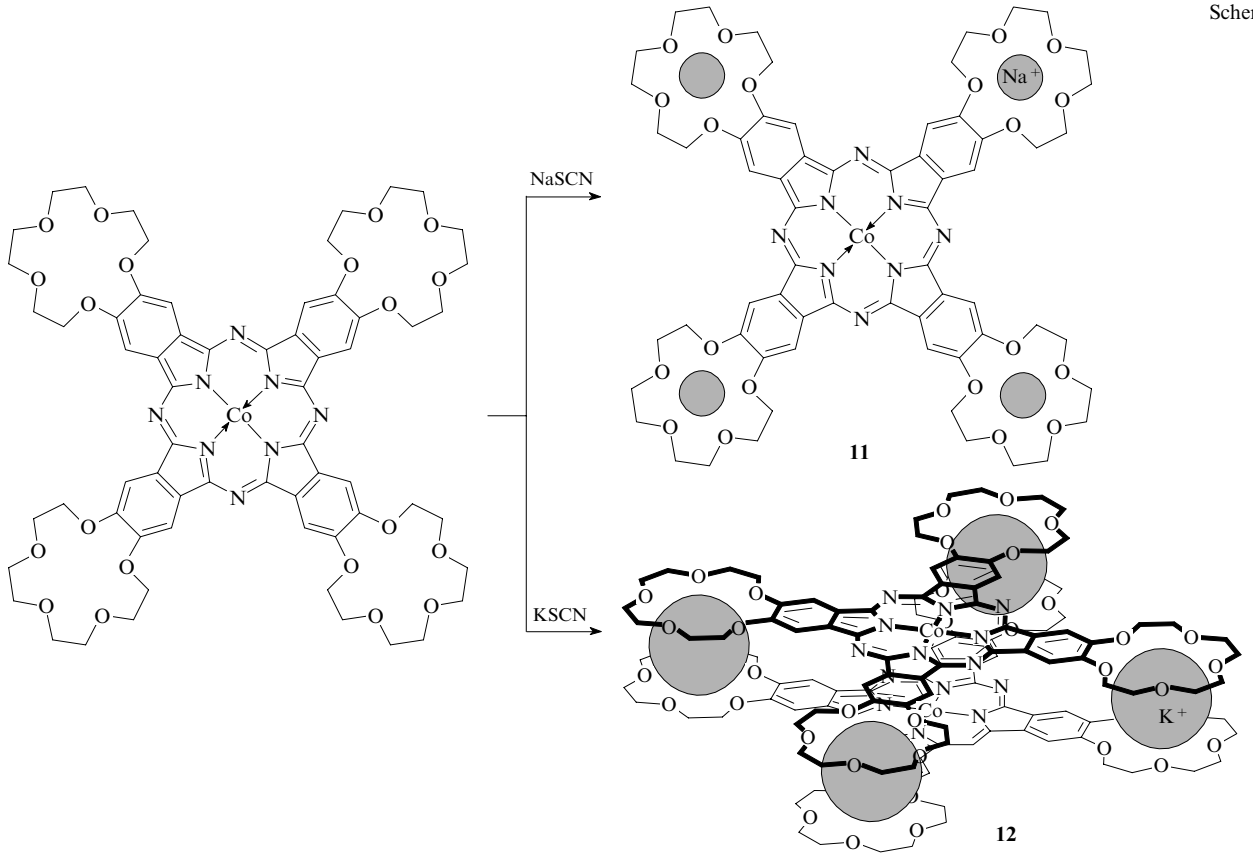

ratio from 0 to 2 results in a decrease in absorption intensity at 668 nm and an increase at 629 nm. Then in the interval of $[Na^+]:[Co(CR\text{-}Pc)]$ ratios from 2 to 4, the intensity of absorption at 629 nm decreases with a simultaneous increase in the absorption intensity around 700 nm, which suggests the formation of a complex with the composition $4\,NaSCN\cdot Co(CR\text{-}Pc)$ (**11**) (see Fig. 6). At a metal : ligand ratio of 4, the complex is precipitated as a solid phase. The complex with the composition $4\,NaSCN\cdot Co(CR\text{-}Pc)$ is characterised by $\lambda_{max} = 737$ nm and $\varepsilon = 2.90\times10^4$ litre mol^{-1} cm^{-1}, whereas the corresponding parameters for the complex with the composition $4\,KSCN\cdot 2\,Co(CR\text{-}Pc)$ (**12**) established by the molar ratio method are $\lambda_{max} = 626$ nm and $\lambda = 4.28\times10^4$ litre mol^{-1} cm^{-1}. The difference between the λ_{max} equal to 111 nm is sufficient for simultaneous detection of sodium and potassium ions in a solution using the Co(CR-Pc) complex (Figs 6–8). Other known crown-containing phthalocyaninates do not manifest such specific sodium–potassium selectivity.

The form of crown-containing phthalocyaninates present in a solution often plays a crucial role as regards their practical applications. Thus successful application of crown-containing phthalocyaninates as photosensitisers in the photodynamic therapy of malignant tumours requires that these were present in the monomeric form. Contrariwise, the synthesis of liquid crystals demands that soluble crown-containing phthalocyaninates formed the so-called stacks characteristic of unsubstituted phthalocyaninates.[70]

Similar sodium–potassium selectivity was observed for Co(CR-Pc) solutions in chloroform,[69] since the Co(CR-Pc) complex is poorly soluble in water. In order to detect sodium and potassium ions in biological systems with the help of the Co(CR-Pc) complex, it seemed important to characterise the behaviour of the complex in solvents of different polarity and their mixtures with the aim to search for an optimum system where the Co(CR-Pc) complex existed in the monomeric form and manifested sodium–potassium selectivity. It was shown[71] that in a chloroform–ethanol mixture containing $\leqslant 20$ vol.% ethanol

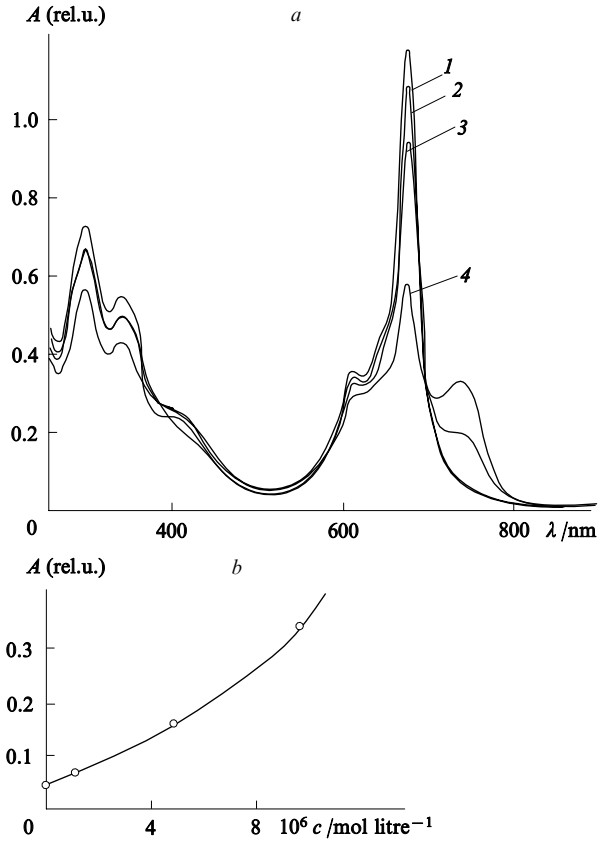

Figure 7. Absorption spectra (*a*) and the calibration curve (*b*) of the $n\,NaSCN\cdot Co(CR\text{-}Pc)$ complex ($n = 0-4$). Concentrations of the Na^+ cations /mol litre^{-1}: (*1*) 0, (*2*) 1×10^{-6}, (*3*) 5×10^{-6}, (*4*) 1×10^{-5} ($\lambda_{max} = 737$ nm).[72]

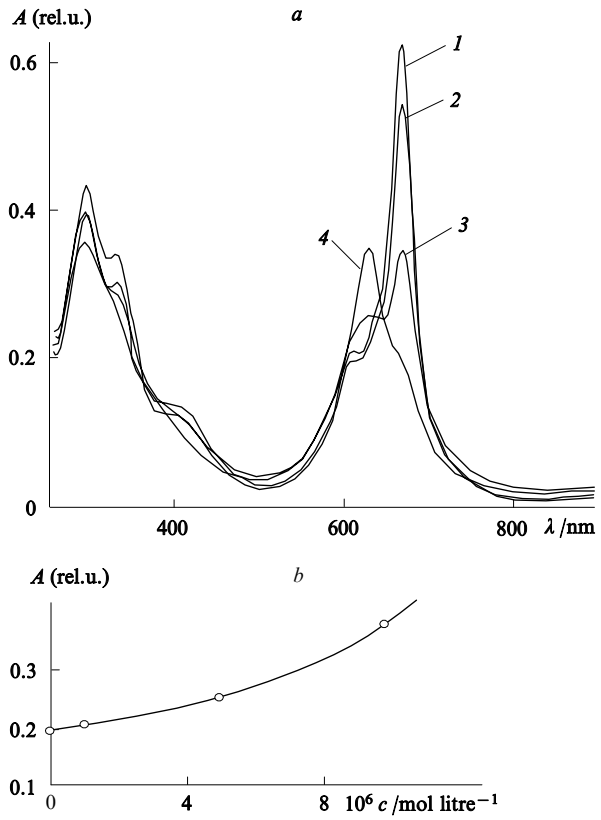

Figure 8. Absorption spectra (*a*) and the calibration curve (*b*) of the nKSCN·Co(CR-Pc) complex ($n = 0-2$). Concentration of the K^+ cations, mol litre^{-1}: (*1*) 0, (*2*) 1×10^{-6}, (*3*) 5×10^{-6}, (*4*) 1×10^{-5} (λ_{max} = 626 nm).[72]

the Co(CR-Pc) complex existed almost completely in the monomeric state. This makes it possible to rule out the effect of the solvent on the interaction of this complex with alkali metal ions. A chloroform–water mixture can be used for the study of biological fluids. However, it cannot be used as a model system because of the limited solubility of water in chloroform.

The kinetics of formation of heteronuclear complexes of Co(CR-Pc) with sodium and potassium cations in a chloroform–ethanol–water mixture was studied in order to apply the effect of differently directed shifts of the Q-band in the absorption spectrum of this compound under the influence of sodium and potassium salts for analytical purposes.[72]

The time dependence of the optical density of the absorption band of Co(CR-Pc) at 626 nm in the presence of an equimolar amount of KSCN suggests that the Co(CR-Pc) complex with potassium is formed at a sufficiently high rate (the equilibrium is reached within 3–5 min). A similar time dependence of the optical density of the absorption band at 737 nm upon addition of NaSCN suggests that the complexation with sodium ions proceeds at a much lower rate than with potassium ions and is complete only after 20–30 min. As a consequence, Co(CR-Pc) complexes with K^+ and Na^+ are formed at different rates, presumably due to differences in their structures, *viz.*, the 'sandwich' complex **12** with K^+ is formed from the starting compounds practically instantaneously, while the formation of the planar sodium complex **11** proceeds through the formation of an intermediate complex with a stoichiometric composition 2M·L. A comparison of the spectral data suggests that both complexes are characterised by a strong dependence of the optical density on the concentration of the metal ions, which enables their application for quantitative determination of Na^+ and K^+ present in a solution simultaneously (Figs 7 and 8).[72]

It is of note that the sodium–potassium selectivity of the Co(CR-Pc) complex is observed only in the case of sodium and potassium thiocyanates and is not manifested in the presence of anions other than NCS^- (*e.g.*, Cl^-, Br^-, I^-, AcO^-). Presumably, ambident thiocyanate ions play a crucial role in the complexation of Co(CR-Pc) with K^+ and Na^+ cations. If sodium ions were located in the centre of the crown-ether cavity, as it normally occurs, to form monomeric complexes, no changes in their electronic spectra would have been observed. In all probability, thiocyanate ions favour the rearrangement of the supramolecular aggregates based on heteronuclear (Co,Na)-monomeric complexes due to the formation of the Co–SCN bonds.

Interactions of alkali metal cations with crown-containing phthalocyaninates of trivalent metal ions with axial ligands occur differently. Thus the Al(CR-Pc)(SO_4H) complex in chloroform interacts with K^+ ions, which is confirmed by a decrease in the intensity of the Q-band; however, the dimer is not formed as can be evidenced from the absence of the corresponding absorption band.[47] This suggests that in contrast to the bivalent metal chelate complexes M(CR-Pc) (M = Cu, Co, Zn, *etc.*), the Al(CR-Pc)(SO_4H) complex does not form 'sandwich' molecules. Apparently, a coordinated extra ligand (SO_4H^-) prevents this process. Even such polar solvents as MeOH and EtOH are incapable to induce the dimerisation of the complex **8**. The electronic absorption spectra indicate that the aluminium complex in chloroform is aggregated to a larger extent than that in the $CHCl_3$–EtOH mixture. Nevertheless, the absorption spectra of the complex **8** depend on the nature of the solvent (Fig. 9).

The aggregation of Al(CR-Pc)(SO_4H) molecules strongly depends on the type of the anion; the corresponding electronic absorption spectra provide an illustrative example (Fig. 10).

As can be seen from Fig. 10, no changes in the Q-band at ~ 691 nm occur upon the interaction of Al(CR-Pc)(SO_4H) with sodium chloride despite the appearance of low-intensity bands at ~ 657 nm characteristic of dimers. The interactions of the complex **8** with sodium bromide and sodium iodide result in the disappearance of the band at ~ 691 nm and an appearance of less intense bands characteristic of aggregated forms around ~ 652 and ~648 nm. However, more significant spectral changes manifested in the appearance of a narrow intense band at ~ 639 nm are observed in the interaction of Al(CR-Pc)(SO_4H) with sodium fluoride: the band intensity is comparable to that at ~ 691 nm. It may thus be concluded that in this case we deal with

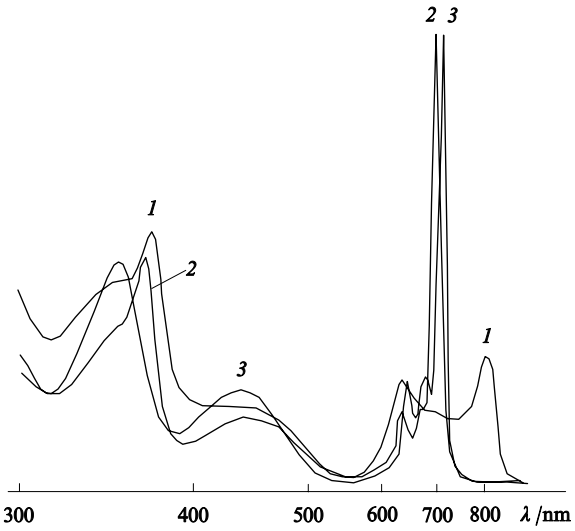

Figure 9. Electronic absorption spectrum of Al(CR-Pc)(SO_4H) in different solvents.
(*1*) Water, (*2*) dimethyl sulfoxide, (*3*) chloroform.

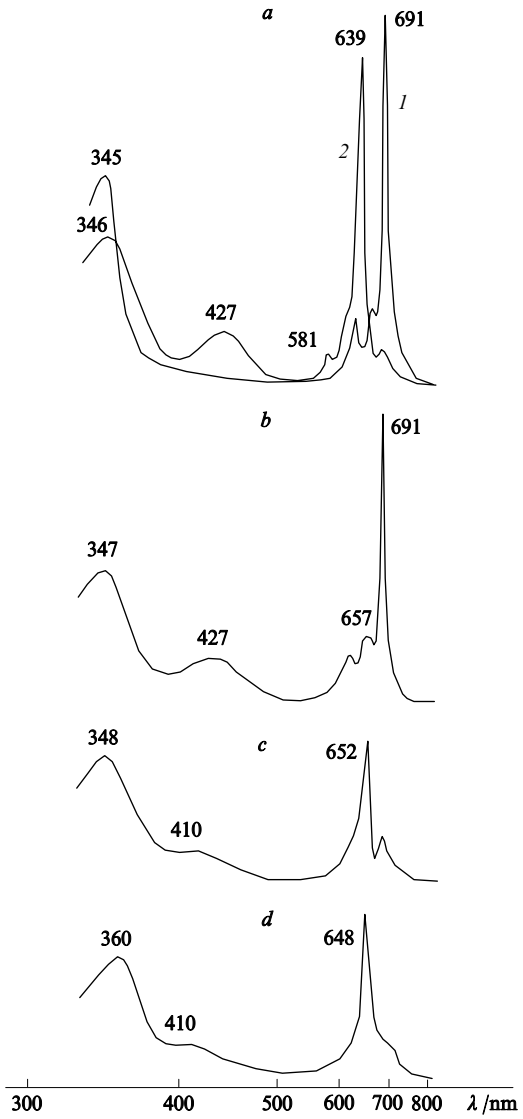

Figure 10. Electronic absorption spectra of Al(CR-Pc)(SO_4H) complexes with NaX where X = F (*a*), Cl (*b*), Br (*c*), I (*d*), in $CHCl_3$.
The concentration of the Al(CR-Pc)(SO_4H) complex in chloroform is 2.5×10^{-6} mol litre^{-1}.
(*1*) Al(CR-Pc)(SO_4H), (*2*) Al(CR-Pc)(SO_4H)$\cdot 4\,Na^+$.

the formation of highly ordered supramolecular ensembles which involve fluoride bridges.

Supramolecular aggregation occurs upon dissolution of Al(CR-Pc)(SO_4H) in water as can be evidenced from significant changes in the electronic absorption (see Fig. 9) and luminescence spectra (Fig. 11). Lowering of the intensity of the luminescence band of complex **8** in water limits its application in the photodynamic therapy of cancer despite its easy solubility in water and normally high quantum yields of luminescence of aluminium phthalocyaninates.

The photodynamic activity of crown-containing phthalocyaninates is manifested in those cases where they are present in aqueous solutions as monomers.[73] However, the majority of crown-containing phthalocyaninates form aggregates in water due to dispersion interactions between aromatic systems.[74] If the charge of the central metal ion is three, a charge-compensating ligand is required for partial separation of the macrocycles, which favours the existence of crown-containing phthalocyaninates in water as monomers.

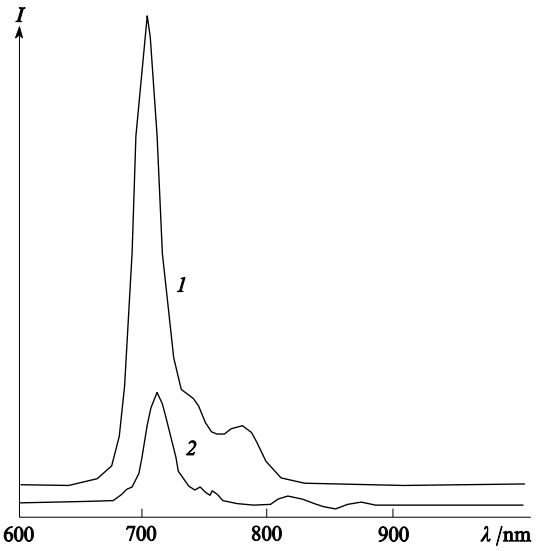

Figure 11. Luminescence spectra of Al(CR-Pc)(SO_4H) solutions in chloroform (λ_{max} = 696 nm) (*1*) and water (λ_{max} = 705 nm) (*2*).

It has been shown[75] that depending on the mutual arrangement of macrocyclic π-aromatic systems in the aggregates their electronic spectra exhibit a short- or a long-wavelength shift of the absorption band in the visible region of the spectrum relative to its position in the corresponding spectrum of the monomer. Aggregates of the first type usually contain a small number of molecules with strong π-interactions between each other. These include, in particular, coaxial dimers also referred to as H-aggregates. In the second type of aggregates termed as J-aggregates, the molecules are strongly displaced relative each other. Here, another type of interaction between electronic π-systems of the molecules results in a long-wavelength shift with a simultaneous narrowing of the absorption band.[75] These changes in the electronic absorption spectra are observed only in aggregates consisting of 4–9 monomers. The mutual arrangement of molecules in such aggregates differs from that in J-dimers which are spectrally indistinguishable from monomers.[75]

A compound with the composition Lu[(15-C-5)$_4$Pc](OAc)$_2\cdot$ 2 Phen, the phenanthroline molecules in which play the role of chelating ligands, has been synthesised[55,76] in order to obtain phthalocyaninates which normally do not form aggregates in aqueous solutions (as is required of preparations used in the photodynamic therapy of cancer). It was suggested[76] that such axial chelate ligands prevent the aggregation. Indeed, this compound was found to exist in aqueous solutions (pH 5.5) in the monomeric state.

Since physiological solutions contain sodium and potassium salts, it is important to elucidate the behaviour of this compound in aqueous solutions containing NaCl and KCl. It was found that NaCl does not induce any aggregation of the Lu(CR-Pc)(OAc)$\cdot$ 2 Phen complex. When the latter is used in the concentration 2×10^{-5} mol litre^{-1} and NaCl is used in the concentrations < 2.0 mol litre^{-1}, no significant changes are observed in the Lu(CR-Pc)(OAc)$\cdot$ 2 Phen complex within the pH range 3.5–9.0 and J-aggregates are formed only upon alkaline hydrolysis.

The interaction of the lutetium complex with potassium chloride in aqueous solutions is accompanied by the formation of H-dimers, however, only if the electrolyte is used in a large excess.

The interaction of the Lu(CR-Pc)(OAc)$\cdot 2\,H_2O$ complex with sodium and potassium acetates was studied using spectrophotometry and ^{1}H NMR spectroscopy.[77] It was found that potassium ions favour the formation of 2[Lu(CR-Pc)(OAc)$\cdot 2\,H_2O$]$\cdot 4\,K^+$ dimers in a $CHCl_3$ – DMSO mixture. It was thus assumed that the

complex represents a coaxial dimer of the 'guest – host' type and has an eclipsed conformation.

The interaction of the ruthenium complex **9** containing CO and CH_3OH molecules as axial ligands with sodium and potassium thiocyanates presents substantial interest. The cation-induced supramolecular aggregation of this complex was studied by electronic absorption spectroscopy (Fig. 12).[78] An analysis of changes in the absorption intensity of the Q-band of the complex **9** *vs.* the $[M^+]:[\mathbf{9}] = n$ ratio revealed that the interactions of the complex **9** with K^+, Rb^+ and Cs^+ thiocyanates yield supramolecular aggregates of the composition $n\mathbf{9}\cdot 2n$MNCS in the form of 'brickwork' (Fig. 13).

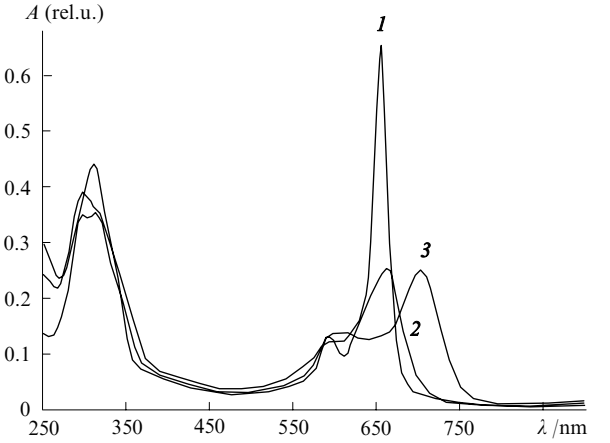

Figure 12. Electronic absorption spectra of (CR-Pc)Ru(CO)(CH_3OH) (**9**) and its complexes with KSCN and NaSCN in $CHCl_3$.
(*1*) **9**, (*2*) **9** + 2 KSCN, (*3*) **9** + 2 NaSCN (after 8 days).

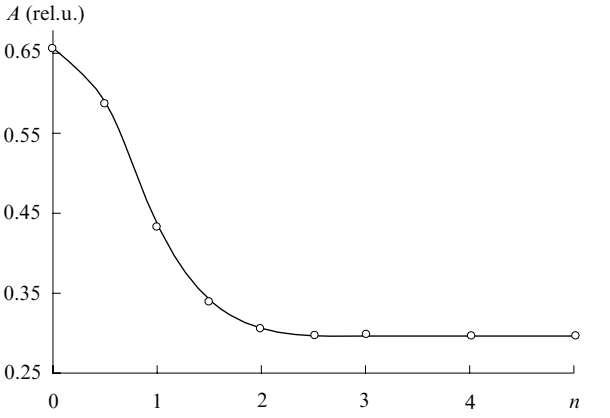

Figure 13. Dependence of the intensity of the absorption Q-band in the electronic absorption spectra of complex **9** in $CHCl_3$ on n ($n = [KSCN]:[\mathbf{9}]$). Similar dependencies are also observed for Rb^+ and Cs^+.

The interaction of the complex **9** with NaSCN is more complicated. In contrast to the cations K^+, Rb^+ and Cs^+, the diameter of the Na^+ cation coincides with the size of the cavity of 15-crown-5, which favours the encapsulation of Na^+ into the crown ether.[6] At the initial moment of time, the interaction of the complex **9** with NaSCN causes a bathochromic shift of the Q-band from 655 to 679 nm, which is followed by more complex reaction kinetics: after 30 min, the Q-band is shifted to 690 nm, after 2 days, to 698 nm, after 4 days, to 701 nm and after 8 days, to 704 nm (see Fig. 12, curve *3*). Such a complex kinetic behaviour and a simultaneous strong shift of the absorption Q-band can be attributed to the formation of a coordination bond between the thiocyanate ions, sodium cations present in the cavities of the crown ethers and ruthenium(II) ions. This can occur upon substitution of the thiocyanate ion for an axially coordinated methanol molecule.

Elucidation of structural specificities of supramolecular aggregates formed upon interaction of the ruthenium complex with sodium thiocyanate required the use of data from vibrational spectra, since it is well known that vibrational frequencies change considerably depending on the mode of coordination of the NCS groups.[79] The NCS^- group can coordinate a metal through a nitrogen or a sulfur atom as well as through a bridging structure. The type of coordination depends on the nature of the metal. The type of bonding of the NCS group in metal complexes is determined on the basis of empirical criteria.[80] Thus the stretching vibration frequencies ν(CN) in N-bonded complexes lie around 2070 cm^{-1} and are lower than those in S-bonded complexes (around 2100 cm^{-1}). The vibration frequencies ν(CN) in the bridged $M-NCS-M'$ complexes lie above 2100 cm^{-1}. The ν(CN) values for thiocyanate alkali metal complexes with crown ethers are usually lower than those for thiocyanate complexes with transition metals.[10, 11, 79] The IR spectra of ruthenium complexes before and after interaction with potassium and sodium thiocyanates are shown in Figs 14 and 15, respectively.

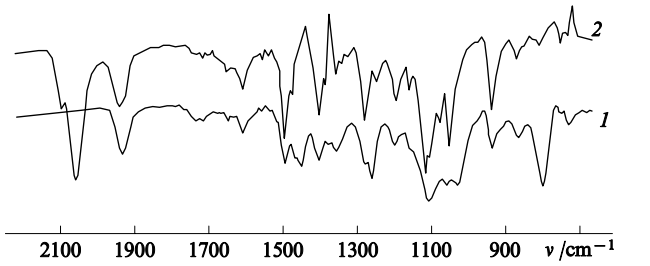

Figure 14. IR spectra of Ru(CR-Pc)(CO)(CH_3OH) (*1*) and its complex with KSCN (*2*).

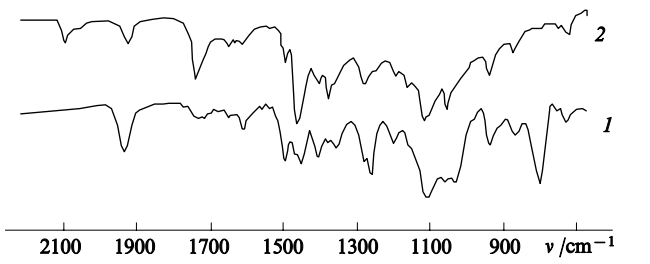

Figure 15. IR spectra of Ru(CR-Pc)(CO)(CH_3OH) (*1*) and its complex with NaSCN (*2*).

The IR spectra of ruthenium crown-containing phthalocyaninates contain all the bands characteristic of metal complexes with crown-containing phthalocyanines. The most intense bands lie around 900 – 1300 cm^{-1}, *i.e.*, in the region where complex stretching-deformation vibrations of the CO, CC and HCH fragments of the crown ether are manifested. It is in this region that the conformational changes associated with the complexation of crown ethers with alkali metals are displayed.[6]

Analysis of the IR spectra of ruthenium phthalocyaninate **9** and its complexes with KSCN and NaSCN allows certain conclusions to be drawn concerning the effect of complexation of alkali metals with crown-substituted ruthenium(II) phthalocyaninate on the conformational state of the crown-ether substituent. The IR spectra of alkali metal complexes with Ru(CR-Pc)(CO).(CH_3OH) in the conformation-sensitive region (900 –

1400 cm^{-1}) differ essentially from the IR spectrum of the original complex, which points to conformational rearrangements in the crown ethers.

Analysis of changes in the IR spectra around 2000–2150 cm^{-1} points also to a strong effect of the nature of the substrate anion on the architecture of the supramolecular ensembles formed. The IR spectrum of the Ru(CR-Pc)(CO)(CH_3OH) complex with potassium thiocyanate contains a stretching vibration band [ν(CN)] at 2060 cm^{-1} (see Fig. 14), which suggests that the NCS group represents an outer-sphere ligand [6, 79] which is not involved in the formation of a supramolecular aggregate. The IR spectrum of the Ru(CR-Pc)(CO)(CH_3OH) complex with sodium thiocyanate contains two stretching vibration bands [ν(CN)] at 2097 cm^{-1} and 2060 cm^{-1} (Fig. 16), which points to coordination of sodium ion with the nitrogen atom of the NCS group. At the same time, the increase in the vibration frequency [ν(CN)] of complex **9** with NaCNS is so significant in comparison with the vibration frequency of the free NCS^- ion and sodium thiocyanate complexes with benzocrown ethers that it may lead to coordination of the sulfur atoms by the ruthenium atom resulting in the formation of bridged complexes.[6, 79] The changes in the IR spectrum of complex **9** with NaSCN (by analogy with the electronic absorption spectra) occurring during several days testify to further rearrangements of the architecture of the aggregate associated with coordination of the NCS group by the ruthenium atom of the macrocycle. This is confirmed by changes in the relative intensities of the absorption bands at 2097 and 2060 cm^{-1}. The band at 2060 cm^{-1} in the IR spectrum of the completely formed supramolecular aggregate is transformed into a shoulder, while the band at 2097 cm^{-1} is transformed into the major band (Fig. 16). This suggests that the NCS^- anion makes the most weighty contribution to the formation of a supramolecular ensemble in the interaction of the Ru(CR-Pc)(CO)(CH_3OH) complex with the NaSCN anion. The hypothetical structures of the supramolecular ensembles formed upon interaction of ruthenium complexes **9** with potassium (*a*) and sodium thiocyanate (*b*), respectively, are shown in Fig. 17.

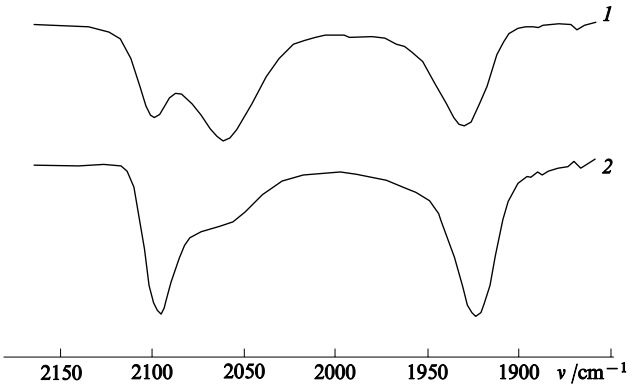

Figure 16. IR spectra of the Ru(CR-Pc)(CO)(CH_3OH) complex with NaSCN around 1900–2150 cm^{-1} recorded after 30 min (*1*) and 8 days (*2*).

V. Sandwich-like double- and triple-decker crown-substituted phthalocyaninates

The size of lanthanide cations exceeds the diameter of the phthalocyanine ligand cavity; therefore, their interactions yield predominantly sandwich-like structures (the so-called double- and triple-decker complexes). Depending on synthetic conditions, differently coloured ('green' and 'blue') forms of REE diphthalocyaninates are formed.

Until recently, the architectures of 'green' and 'blue' forms of diphthalocyaninates were open to discussion. Based on the ESR data for the 'green' form of the diphthalocyaninates $LnPc_2$, the structure of the radical paramagnetic complex was postulated as the most probable.[51–54, 81–83] The 'blue' form was often associated with the protonated diamagnetic structure $HLnPc_2$.[51, 81] Based on data from X-ray diffraction spectroscopy and ESR, it was proposed [84] that the central metal atom is in the oxidation state 4+. According to other authors,[52–54] intramolecular electron transfer is possible in the 'green' form as a result of which the degree of oxidation of the central metal atom changes from Ln^{3+} to Ln^{4+} and a 'blue' form is formed instead.

For the first time, diphthalocyaninates of REE were prepared by fusion of metal acetates with phthalonitrile.[51] Later, it was found [52–54] that this reaction occurs in several steps and depends on the nature of the central metal atom. Monophthalocyanine is formed in the first step of the synthesis of *tert*-butyl-substituted diphthalocyaninates of REE, it is further converted into a 'green' and then into a 'blue' form.

The synthesis of tetra(15-crown-5)-substituted lutetium diphthalocyaninate Lu(CR-Pc)$_2$ was carried out by boiling dicyanobenzo-15-crown-5 as a starting reagent in hexanol for 20 h.[85] A simpler and more convenient method for the template synthesis of a sandwich green form of Lu(CR-Pc)$_2$ has been proposed which consists in the fusion of lutetium acetate with dicyanobenzo-15-crown-5 in a sealed evacuated tube. [86] The optimum conditions for the synthesis of the 'green' and 'blue' forms of crown-substituted lutetium diphthalocyaninates were established by varying the

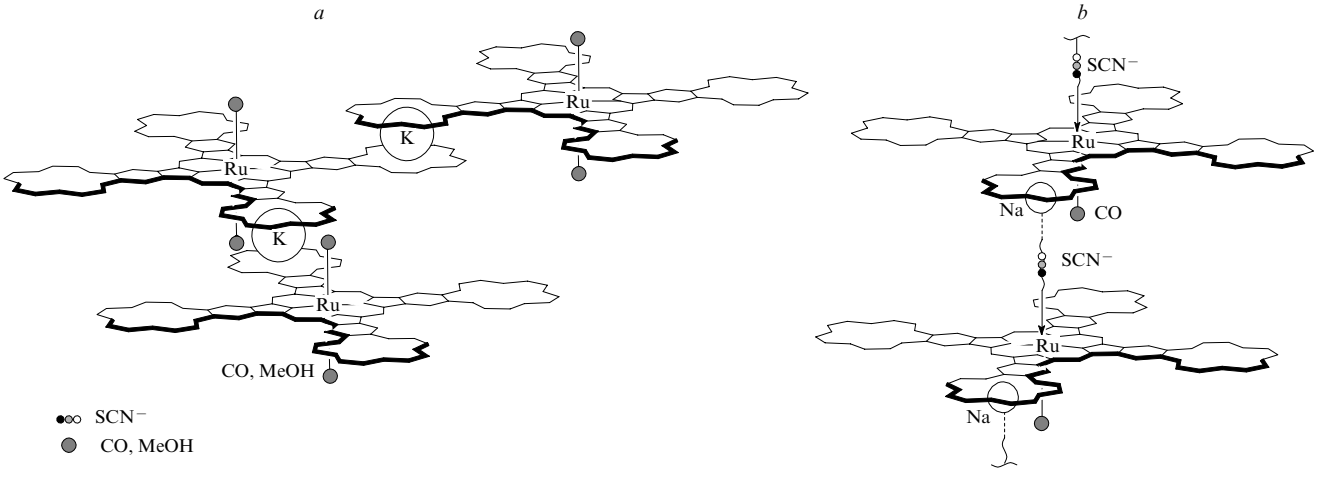

Figure 17. Tentative structures of the supramolecular ensembles based on the Ru(CR-Pc)(CO)(CH_3OH) complexes with KSCN (*a*) and NaSCN (*b*).

temperature (200 – 290 °C), molar ratios of the reagents (from 1 : 1 to 1 : 8) and reaction time (from 30 min to 5 h).

For a long time, the data on X-day diffraction analysis of crown-substituted metal phthalocyaninates were absent due to significant difficulties in growing of single crystals of this class of compounds. Recently, the molecular crystal structure of the 'blue' form of the $Lu_2(CR\text{-}Pc)_3$ complex (**13**) was established using X-ray diffraction spectroscopy.[87] Prismatic dark-blue crystals were obtained by slow crystallisation of complex **13** from a mixed solvent ($DMSO - CHCl_3$, 2 : 1). This compound was found to have a triple-decker structure (Fig. 18).

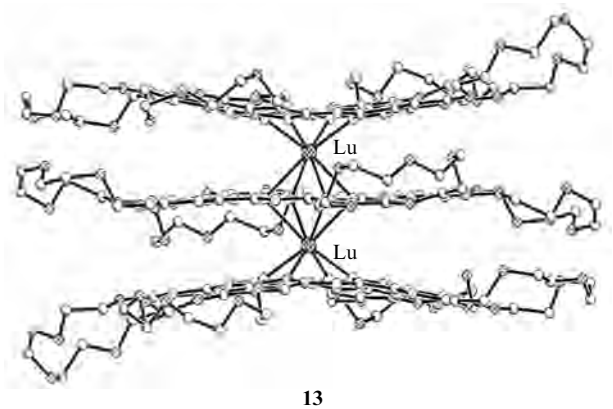

13

Figure 18. Structure of the triple-decker complex $Lu_2(CR\text{-}Pc)_3$.

The lutetium atoms in compound **13** are localised between the planes of the phthalocyanine ligands. Two outer phthalocyanine rings have similar orientations with respect to the internal ring which is turned by 43.7° relative to these rings.

The neighbouring macrocycles are not equidistant from the lutetium ion; the distances between the lutetium atoms and the planes of the outer phthalocyanine ligands passing through the donor atoms of the pyrrole ring nitrogens are equal to 1.218 Å, while the corresponding distances from the central ligand are much greater (1.703 Å). This fact agrees with a significant increase in the metal – bridging ligand distance characteristic of all presently known triple-decker molecules with tetrapyrrole macrocyclic ligands.[88,89] The lutetium atom in the double-decker molecule of $LuPc_2$ occupies a practically symmetrical position: for the average metal – ligand distance equal to 1.34 Å, the difference in the distances does not exceed 0.01 Å.[90].

The coordination polyhedron of the lutetium ion represents a distorted tetragonal antiprism. The Lu – Lu distance is 3.406 Å. The Ln – Ln distances in structurally similar Ce_2P_3 (see Ref. 88) and Nd_2Pc_2P[89] complexes (P is porphyrin) exceed the sum of the corresponding lanthanide atomic radii by 0.1 and 0.06 Å, respectively.[91]

The intramolecular interplanar distance between two neighbouring ligands is 2.923 Å [in $LuPc_2$, the ligands are even closer to one another (2.69 Å)[90]], *i.e.*, the distance between them is less than the van der Waals distance (3.34 Å) between two aromatic systems. Minimisation of the non-bonding interactions is achieved due to a turn of the central macroligand relative to the outer ligands. The atoms in the crown-ether rings protrude above the plane passing through the nitrogen atoms of the pyrrole rings to a greater extent than other atoms constituting the phthalocyanine backbone.

Compound **13** is the first example of a substituted phthalocyanine complex with the established crystal structure.

Double-decker phthalocyaninates of REE are neutral compounds, which represent stable free radicals $[Pc^{2-}M^{3+}Pc^{2-\bullet}]^0$. They undergo reversible redox conversions:

$$\underset{\text{Blue form (anionic)}}{[Pc^{2-}M^{3+}Pc^{2-}]^-} \underset{e}{\overset{-e}{\rightleftharpoons}} \underset{\text{Green form (neutral)}}{[Pc^{2-}M^{3+}Pc^{-\bullet}]^0} \underset{e}{\overset{-e}{\rightleftharpoons}} \underset{\text{Red form (cationic)}}{[Pc^{-\bullet}M^{3+}Pc^{-\bullet}]^+}.$$

The data on double- and triple-decker crown-substituted phthalocyaninates of REE are mainly available for lutetium complexes. Other authors describe the synthesis of double- and triple-decker ytterbium and gadolinium complexes with tetra(15-crown-5)phthalocyanine.[92] $Yb(CR\text{-}Pc)_2$ [but not $Yb_2(CR\text{-}Pc)_3$], $Gd_2(CR\text{-}Pc)_3$ or $Gd(CR\text{-}Pc)_2$ could be prepared by template synthesis,[92] but the yields of the target products were extremely low. Direct interaction of the protonated ligand $H_2(CR\text{-}Pc)$ with ytterbium and gadolinium acetates in the presence of a strong base (DBU) yields the same complexes, *viz.*, $M(CR\text{-}Pc)_2$ and $M_2(CR\text{-}Pc)_3$ [M = Gd, Yb, CR-Pc = (15-C-5)$_4$Pc]. This approach affords sufficiently high yields and a high degree of purity and was also used in the synthesis of the lanthanum complex **14**.[93]

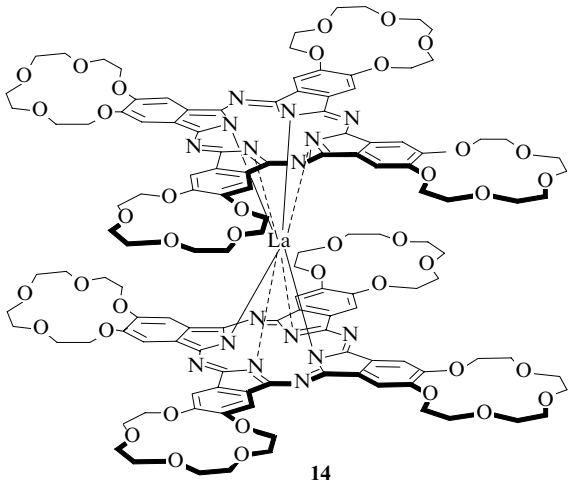

14

$$H_2(CR\text{-}Pc) \xrightarrow{a \text{ or } b} [La(CR\text{-}Pc)_2]^- + [La(CR\text{-}Pc)_2]^0$$

a — $H_2(CR\text{-}Pc) : [La(OAc)_3 \cdot 1.5\,H_2O] : DBU = 1 : 10 : 200$, boiling *o*-dichlorobenzene (b.p. 180 °C), 3 h;
b — $H_2(CR\text{-}Pc) : [La(OAc)_3 \cdot 1.5\,H_2O] : DBU = 1 : 1.5 : 10$, boiling 1-chloronaphthalene (b.p. 250 °C), 2 h.

However, the reaction products represented a radical-neutral form $[(CR\text{-}Pc)^{2-}La^{3+}(CR\text{-}Pc)^{-\bullet}]^0$ and a single-electron-reduced form $[La^{3+}(CR\text{-}Pc)_2^{2-}]^-$; DBU, which is commonly used as a deprotonating reagent in organic synthesis, stabilises the reduced form of crown-substituted lanthanum diphthalocyaninate.

This is the first reaction where a single-electron-reduced form of diphthalocyaninate is prepared in the course of synthesis. The neutral form of the $M(CR\text{-}Pc)_2$ complex represents a stable free radical. Its stability in the case of the terminal elements of the lanthanide series can be attributed to delocalisation of the unpaired electron over two phthalocyanine ligands. In complex **14,** the delocalisation of the electron is much more difficult, since the phthalocyanine rings in this compound are at a much greater distance from one another than, *e.g.*, in the stable complex $[(CR\text{-}Pc)^{2-}Lu^{3+}(CR\text{-}Pc)^{-\bullet}]^0$. For this reason, the electronic state of the two ligands in the $La(CR\text{-}Pc)_2$ complex is levelled off giving rise to the anionic form $[La(CR\text{-}Pc)_2]^-$.

The reaction of $H_2(CR\text{-}Pc)$ with Gd, Yb and Lu acetates in boiling *o*-dichlorobenzene yields the corresponding monophthalocyaninates, whereas boiling of these reagents in chloronaphthalene yields double- and triple-decker complexes. Sandwich-like double-decker lanthanum complexes are formed even upon boiling in *o*-dichlorobenzene. This can be explained by the fact that the larger radius of La (1.061 Å) in comparison with Gd (0.938 Å), Yb (0.858 Å) and Lu (0.848 Å) results in an increase in the

distance between the phthalocyanine ligands, which in turn stabilises the sandwich-like structure of the phthalocyaninate due to the weakening of $\pi-\pi$-interactions.

VI. Supramolecular systems based on double- and triple-decker crown-substituted phthalocyaninates

As mentioned above, crown-substituted metal monophthalocyaninates interact with bulky alkali metal cations to form supramolecular dimers as a result of binding of alkali metal cations to the crown-ether fragments of the neighbouring ligands. The crown-containing phthalocyanine ligands in double- and triple-decker complexes are separated by REE ions which prevent the penetration of alkali metal cations between two neighbouring phthalocyanine fragments of the sandwich complex. However, alkali metals can coordinate with the 'top' and 'bottom' crown-substituted phthalocyanine ligands of the sandwich-like dimers to give pillar-like structures (Scheme 6).

The complexes of 15-crown-5-substituted diphthalocyaninates of REE with alkali metal salts are more stable than the benzo-15-crown-5 itself.[45, 94, 95] The authors point to a positive cooperative effect in the reaction of crown-substituted lutetium diphthalocyaninates with alkali metal cations. This can be explained by the fact that the insertion of the first cation between the two ligands is more difficult in comparison with the insertion of the second and subsequent cations due to prearrangement of the structure. The nature of these positive non-linear cooperative interactions has been studied in detail. The curves of spectrophotometric titration of transition-metal monophthalocyaninates by alkali and alkaline earth metal salts have a common linear shape, whereas the titration curve of octa(18-crown-6)-substituted lutetium diphthalocyaninate by rubidium salts is sigmoidal and resembles that observed in the interaction of hemoglobin with molecular oxygen. This suggests that in this case we deal with a non-linear cooperative effect which is not typical of triple-decker complexes and monophthalocyaninates. Based on the results of light scattering studies, a mechanism for the formation of supramolecular oligomers containing up to 260 building blocks of the $Lu(CR\text{-}Pc)_2$ complex with KSCN has been proposed.[45] Such supramolecular aggregates have pillar-like and tubular shapes where one-dimensional transport of electrons and ions is possible (Fig. 19). It was suggested that these structures can be used in ionic and molecular electronics as well as in the design of new generations of functional materials.[45, 94, 95]

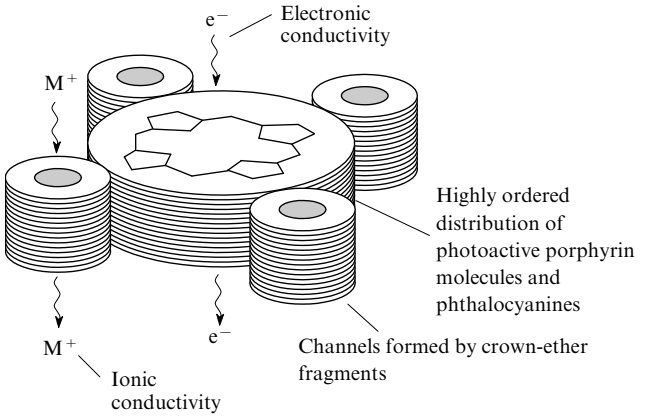

Figure 19. A schematic representation of an ordered supramolecular ensemble based on metal crown phthalocyaninates.

The supramolecular assembly of single-electron-reduced forms of octa(15-crown-5)diphthalocyaninates of the REE series $[Ln(CR\text{-}Pc)_2]^-$ (Ln = Y, Gd, Yb, Lu) has been studied.[96] It was found that the single-electron-reduced form is generated upon dissolution of the radical form in the presence of DBU or by titration of the radical form with DBU in chloroform. The addition of K^+, Rb^+ or Cs^+ thiocyanates to a solution of $[Ln(CR\text{-}Pc)_2]^-$ induces similar spectral changes manifested in a bathochromic shift with a simultaneous decrease in the half-width

Scheme 6

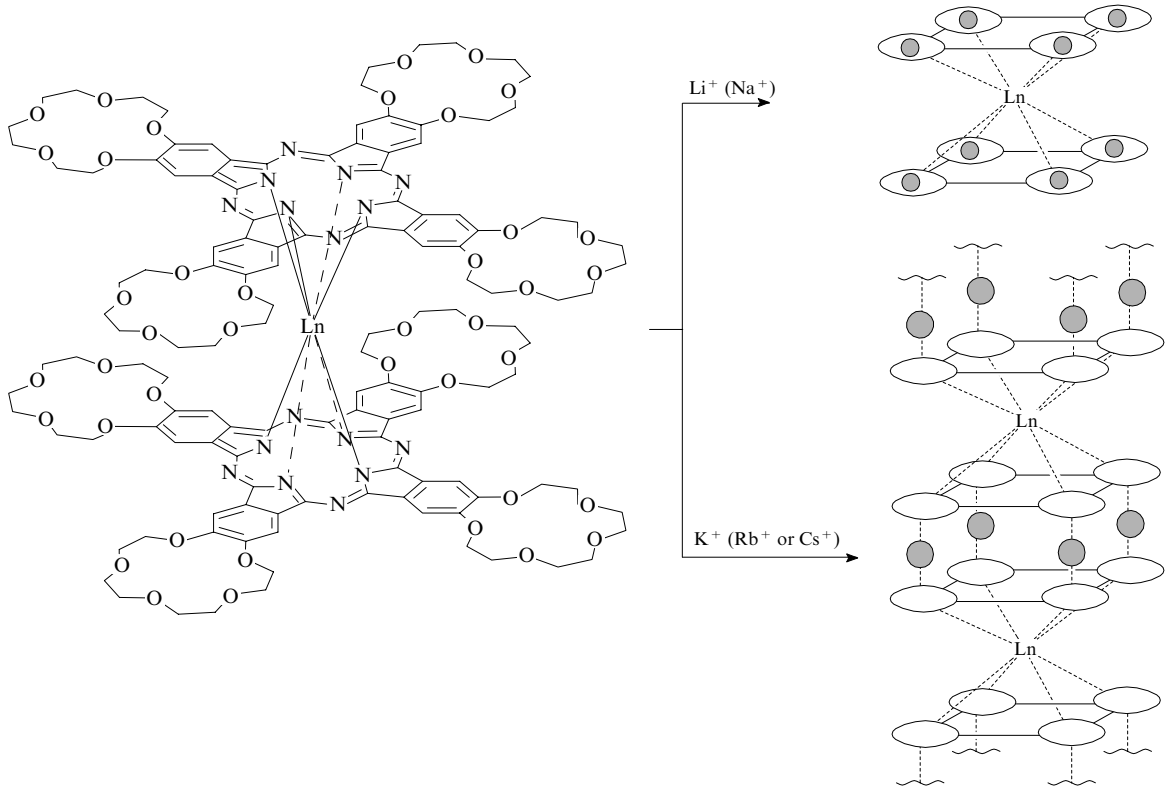

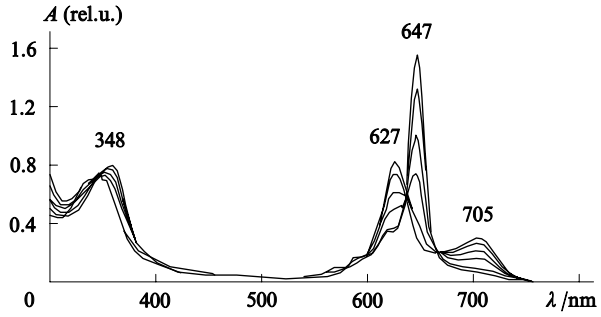

Figure 20. Changes in the electronic absorption spectra of the $[Lu(CR\text{-}Pc)_2]^-$ complex ($c = 6.0 \times 10^{-6}$ mol litre^{-1}) with potassium cations as a function of K^+ concentration.
The concentration of KSCN varied from 0 to 4.8×10^{-5} mol litre^{-1}.

of the Q_1-band (Fig. 20). The splitting of the band of the reduced form also disappears. Analysis of the electronic absorption spectra and spectrophotometric titration curves of the $[Ln(CR\text{-}Pc)_2]^-$ complexes by alkali metal thiocyanates prompted a conclusion about the formation of polymeric coaxial supramolecular aggregates $[(Ln(CR\text{-}Pc)_2)\cdot 4\,MSCN]_n$ ($n > 20$). The radical form of the complex $Lu(CR\text{-}Pc)_2$ interacts differently with potassium and rubidium picrates, whereas the single-electron-reduced form of the complex is arranged into supramolecular 'host–guest' structures on interaction with K^+, Rb^+ and Cs thiocyanates in the same manner. Non-linear cooperative effects are manifested in all the three cases (Fig. 21). No such effect of the anion on the assembly was observed for other potassium salts (acetate, bromide).

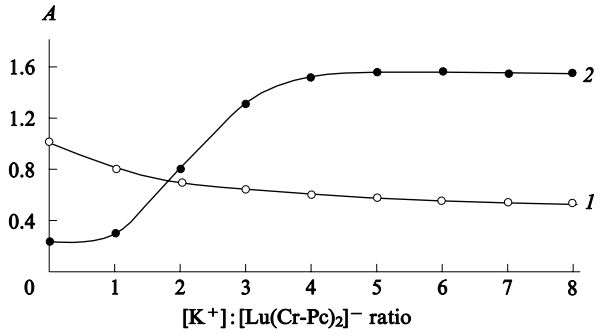

Figure 21. Spectrophotometric titration curves of the $[Lu(CR\text{-}Pc)_2]^-$ complex with potassium cations. The optical densities of the bands at 627 (*1*) and 647 nm (*2*) are given at various $[K^+]:[Lu(CR\text{-}Pc)_2]^-$ ratios. The sigmoidal shape of the titration curve points to a non-linear cooperative effect of the complex formation.

It was shown that interactions of $[La(CR\text{-}Pc)_2]^-$ with cations K^+, Rb^+ and Cs^+ are also accompanied by a non-linear positive cooperative effect (Fig. 22) and yield highly ordered polymeric aggregates.[97] The reduced form of sandwich double-decker crown phthalocyaninates of REE were shown to represent a common sensor for the cations K^+, Rb^+ and Cs^+.

VII. Conclusion

Attachment of crown-ether fragments to porphyrins and phthalocyanines not only improves the inherent properties of crown ethers, porphyrins and phthalocyanines, but also confers novel properties on them. Thus the selectivity of crown-substituted porphyrins and phthalocyanines with respect to alkali metal ions and the stability of the corresponding complexes markedly

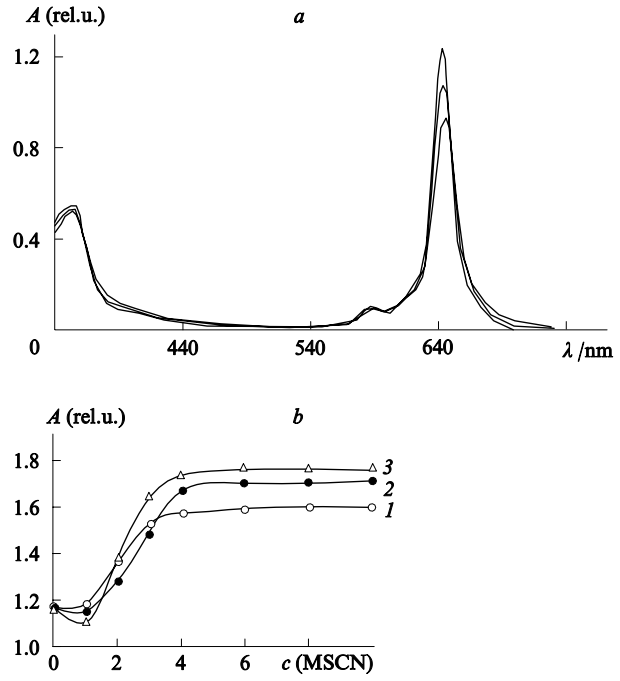

Figure 22. Electronic absorption spectra of the $[La(CR\text{-}Pc)_2]^-$ complex with potassium thiocyanate at different concentrations of K^+ (*a*) and spectrophotometric titration curves (*b*) of the $[La(CR\text{-}Pc)_2]^-$ complex with potassium (*1*), rubidium (*2*) and caesium thiocyanates (*3*).

exceeds the corresponding parameters of crown ethers and their complexes. The solubilities of crown-substituted porphyrins and phthalocyanines are also higher than those of unsubstituted compounds. Some representatives of this class are soluble even in water and thus acquire amphiphilic properties. The ability of crown-substituted porphyrins and phthalocyanines to form heteronuclear supramolecular architectural ensembles upon interaction with alkali metal salts is their characteristic feature.

Crown-ether fragments are linked to porphyrins and phthalocyanines in different fashions. Benzocrown-ether fragments are attached to porphyrins by a C–C bond to produce flexible structures, whereas bonding of crown-ether fragments to phthalocyanines is rigid. In contrast to crown-containing phthalocyanines, porphyrins form tetracrown-substituted analogues along with mono-, di- and tricrown-substituted derivatives. Crown-substituted porphyrins and phthalocyanines differ also in the type of supramolecular heteronuclear architectural ensembles formed upon their interaction with alkali metal salts.

Interactions of potassium, ammonium and barium salts with tetra- and tricrown-substituted porphyrins and metal complexes based on them result in the formation of supramolecular dimers (interactions with sodium, magnesium and calcium salts occur by a different mechanism).

Treatment of the monomeric zinc–bis(benzo-15-crown-5)-porphyrin complex with $AgPF_6$ yields a dimer in which two porphyrin rings are linked by a covalent *meso-meso* bond. Although intermolecular contacts between the neighbouring crown-ether fragments in the monomeric and dimeric zinc complexes interacting with potassium ions are similar, the supramolecular architectural ensembles formed differ from one another. Coaxial ('face-to-face') dimerisation of monomeric zinc complexes is possible upon interaction with potassium ions, whereas linear extended aggregation is more preferable for covalently bonded dimeric zinc complexes.

The nature of the central metal atom in porphyrinates strongly affects the structure of the complexes formed upon their interaction with alkali metal salts. According to the ESR data, the porphyrin rings in the dimeric potassium complex with copper

tetracrown monoporphyrinate are turned by 45° relative to one another, whereas in an analogous zinc complex they are turned by 23°.

The mode of interaction of alkali metal salts with crown-substituted monophthalocyaninates of d-elements differs significantly from that with analogous double- and triple-decker complexes of REE. In the former case, monomeric or dimeric heteronuclear complexes are formed depending on the size of the alkali metal cations; in the latter case, oligomeric supramolecular ensembles are formed.

The stucture of the complexes formed also depends on the nature of the anion. For example, the reaction of the Al(CR-Pc)(SO_4H) complex with sodium chloride is not accompanied by changes in the electronic spectra of the complex, which points to the formation of monomeric heteronuclear complexes. On the other hand, interactions with sodium bromide and iodide afford dimers and the interaction with sodium fluoride yields polymeric supramolecular aggregates.

The optical sodium–potassium selectivity observed in reactions of tetracrown-substituted cobalt monophthalocyaninates with potassium and sodium thiocyanates is manifested in an oppositely directed shift of the Q-band: towards the long-wavelength region (λ_{max} = 737 nm) in the case of sodium thiocyanate and towards the short-wavelength region (λ_{max} = 626 nm) in the case of potassium thiocyanate. The difference in the Q-band shift in the case of a ruthenium complex with tetra(15-crown-5)phthalocyanine is 75 nm. Such a great difference enables the use of this effect for selective photometric measurements of sodium and potassium ions.

The ordered supramolecular aggregates formed upon interaction of sandwich-like phthalocyanine complexes of REE with alkali metals have pillar-like and tubular shapes, where one-dimensional transport of electrons, energy and ions is possible. The electric conductivity of these pillar-like and 'nanotubular' structures strongly depends on the orderliness of the giant supramolecular architectural ensembles formed. It is believed that such ensembles can be used as a starting material in the design of new generations of functional materials for ionic and molecular electronics.

This review has been written with the financial support of the Russian Foundation for Basic Research (Project Nos. 03-03-33160 and 02-03-08013).

References

1. J-M Lehn *Supramolecular Chemistry. Concepts and Perspectives* (Weinheim: VCH, 995)
2. C J Pedersen *J. Am. Chem. Soc.* **89** 2495 (1967)
3. C J Pedersen *J. Am. Chem. Soc.* **92** 391 (1970)
4. Yu A Ovchinnikov, V T Ivanov, A M Shkrob *Membranno-Aktivnye Kompleksony* (Membrane-Active Complexones) (Moscow: Nauka, 1974)
5. M Hiraoka *Crown Compounds. Their Characteristics and Applications* (Amsterdam: Elsevier, 1982)
6. A Yu Tsivadze, A A Varnek, V E Khutorskii *Koordinatsionnye Soedineniya Metallov s Kraun-Ligandami* (Coordination Compounds of Metals with Crown Ligands) (Moscow: Nauka, 1991)
7. N K Dalley *Synthetic Multidentate Macrocyclic Compounds* (New York: Academic Press, 1978) p. 209
8. Van F P Rerworlere, F P Boer *Inorg. Chem.* **13** 2071(1975)
9. P P Power, Xu Xiaojie *J. Chem. Soc., Chem. Commun.* 358 (1984)
10. I K Kireeva, V A Trofimov, N B Generalova, A Yu Tsivadze *Koord. Khim.* **15** 463 (1989) [a]
11. V A Trofimov, I K Kireeva, N B Generalova, A Yu Tsivadze *Koord. Khim.* **16** 1458 (1990) [a]
12. A Yu Tsivadze, N B Generalova, E N Pyatova, I Ya Kachkurova, V A Popova, I V Podgornaya *Zh. Neorg. Khim.* **33** 1649 (1988) [b]
13. L Kh Minacheva, N B Generalova, I K Kireeva, V G Sakharova, A Yu Tsivadze, M A Porai-Koshits *Zh. Neorg. Khim.* **38** 1666 (1993) [b]
14. P E Ane, F J Dederog *Acta Crystallogr.* **35** 1215 (1979)
15. P Groth *Acta Chem. Scand. Ser. A* **36** 109 (1982)
16. A Yu Tsivadze, V I Zhilov, S V Demin *Koord. Khim.* **22** 243 (1996) [a]
17. K A Askarov, B D Berezin, R P Evstigneeva *Porfiriny: Spektroskopiya. Elektrokhimiya. Primenenie* (Porphyrins: Spectroscopy. Electrochemistry. Applications) (Moscow: Nauka, 1987)
18. B D Berezin, O I Koifman *Usp. Khim.* **49** 2389 (1980) [*Russ. Chem. Rev.* **49** 1188 (1980)]
19. B D Berezin *Koordinatsionnye Soedineniya Porfirinov i Ftalotsianina* (Coordination Compounds of Porphyrins and Phthalocyanine) (Moscow: Nauka, 1978)
20. V Ahsen, E Yilmazer, M Ertas, Q J Bekaroglu *J. Chem. Soc., Dalton Trans.* 401 (1988)
21. N Kobayashi, A B P Lever *J. Am. Chem. Soc.* **109** 7433 (1987)
22. O E Sielcken, M M van Tilborg, M F M Rock, R Hendriks, W Drenth, R J M Nolte *J. Am. Chem. Soc.* **109** 4261 (1987)
23. A Yu Tsivadze, in *Strukturoobrazovanie i Mezhfaznye Yavleniya v Sistemakh Zhidkost'–Zhidkost'* (Structure Formation and Phase Boundary Effects in Liquid–Liquid Systems) (Moscow: Russian Chemical Technology University, 2000) p. 11
24. A Yu Tsivadze *Ross. Khim. Zh.* **40** (4–5) 43 (1996) [c]
25. F P Schwarf, M Gouterman, Z Mulijiani, D H Dolphin *Bioinorg. Chem.* **2** 1 (1972)
26. J P Collman, R R Gagne, T R Halbert, J-C Marchon, C A Reed *J. Am. Chem. Soc.* **95** 7868 (1973)
27. J P Collman, J I Brauman, K M Doxsee, T R Halbert, E Bunnenberg, R E Linder, G N LaMar, J D Gaudio, G Lang, K Spartalian *J. Am. Chem. Soc.* **102** 4182 (1980)
28. I Tabushi, N Koga, S Yanagita *Tetrahedron Lett.* 257 (1979)
29. A L Moore, G Dirks, D Gust, J A Moore *Photochem. Photobiol.* **32** 691 (1980)
30. J B Pain, D Dolphin *Can. J. Chem.* **56** 1710 (1978)
31. C K Chang *J. Am. Chem. Soc.* **99** 2819 (1979)
32. R Malini, V Krishnan *J. Phys. Chem.* **84** 551 (1980)
33. V Thanabal, V Krishnan *J. Am. Chem. Soc.* **104** 3643 (1982)
34. P R Mallinson, M R Truter *J. Chem. Soc., Perkin Trans. 2* 1818 (1972)
35. T K Chandrashekar, H van Willigen, M H Ebersole *J. Phys. Chem.* **89** 3453 (1985)
36. M G Bhaskar, V Krishnan *Inorg. Chem.* **27** 3253 (1985)
37. C Comte, C P Gros, R Guilard, R G Khoury, K M Smith *J. Porphyr. Phthalocyan.* **2** 377 (1998)
38. C Comte, C P Gros, S Koeller, R Guilard, D J Nurco, K M Smith *New J. Chem.* **22** 621 (1998)
39. K M Kadish, J-G Shao, Z-P Ou, C Comte, C P Gros, R Guilard *J. Porphyr. Phthalocyan.* **4** 639 (2000)
40. H Shinmori, A Osuka *Tetrahedron Lett.* **41** 8527 (2000)
41. K Kasuga, M Tsutsui *Coord. Chem. Rev.* **32** 67 (1980)
42. J Rosental *Photochem. Photobiol.* **53** 859 (1991)
43. Z Gasyna, N Kobayashi, M Sailman *J. Chem. Soc., Dalton Trans.* 2397 (1989)
44. N Kobayashi, M Togashi, T Osa, K Ishii, S Yamauchi, H Hino *J. Am. Chem. Soc.* **118** 1073 (1996)
45. T Toupance, H Benoit, D Sarazin, J Simon *J. Am. Chem. Soc.* **119** 9191 (1997)
46. R J M Nolte, W W Drenth *Inorganic and Organometallic Polymers with Special Properties* (Ed. R M Laine) (Netherlands: Kluwer Academic, 1992) p. 223
47. E O Tolkacheva, L I Demina, A Yu Tsivadze, Sh G Bitiev, V I Zhilov *Zh. Neorg. Khim.* **20** 449 (1995) [b]
48. P A Barren, C E Dent, R P Linsteed *J. Chem. Soc.* **12** 1719 (1936)
49. E O Tolkacheva, S V Selivanova, O Yu Komarova, L A Lapkina, V E Larchenko, S V Meshkov, A Yu Tsivadze *Zh. Neorg. Khim.* **43** 263 (1998) [b]
50. N B Subbotin, L G Tomilova, N A Kostromina, E A Luk'yanets *Zh. Obshch. Khim.* **56** 397 (1986) [d]
51. I S Kirin, P N Moskalev, Yu A Makashov *Zh. Neorg. Khim.* **10** 1951 (1965) [b]

52. L G Tomilova, E V Chernykh, N T Ioffe, E A Luk'yanets *Zh. Obshch. Khim.* **53** 2594 (1983) [c]
53. L G Tomilova, E V Chernykh, E A Luk'yanets *Zh. Obshch. Khim.* **55** 2631 (1985) [d]
54. L G Tomilova, E V Chernykh, E A Luk'yanets *Zh. Obshch. Khim.* **57** 2368 (1987) [d]
55. L A Lapkina, V E Larchenko, E O Tolkacheva, K I Popov, N Yu Konstantinov, V M Nosova, A Yu Tsivadze *Zh. Neorg. Khim.* **43** 987 (1998) [b]
56. Yu Yu Enakieva, Yu G Gorbunova, S G Sakharov, A Yu Tsivadze *Zh. Neorg. Khim.* **47** 1973 (2002) [b]
57. N P Farrell, A J Murray, J R Thornback *Inorg. Chim. Acta* **28** 144 (1978)
58. D Dolphin, B R James, A J Murray, J R Thornback *Can. J. Chem.* **58** 1123 (1980)
59. G Rossi, M Gardini, G Pennesi, C R Ercolani, V L Goedken *J. Chem. Soc., Dalton Trans.* 193 (1989)
60. A Capobianchi, G Pennesi, A M Paoletti, G Rossi, R Caminiti, C Sadun, C Ercolani *Inorg. Chem.* **35** 4643 (1996)
61. L Alagna, A Capobianchi, P Marovino, A M Paoletti, G Pennesi, T Prosperi, G Rossi *Inorg. Chem.* **38** 3688 (1999)
62. M Hanack, S Kamenzin, C Kamenzin, L R Subramanian *Synth. Met.* **110** 93 (2000)
63. R Caminiti, M P Donzello, C Ercolani, C Sadun *Inorg. Chem.* **38** 3027 (1999)
64. A Kienast, C Bruhn, H Homborg *Z. Anorg. Allg. Chem.* **623** 967 (1997)
65. M Weidemann, H Huckstadt, H Homborg *Z. Anorg. Allg. Chem.* **624** 846 (1998)
66. S Omiya, M Tsutsui, E F Meyer, I Bernal, D L Cullen *Inorg. Chem.* **19** 134 (1980)
67. N Ishikawa, Y Kaizu *Chem. Phys. Lett.* **203** 472 (1993)
68. N Ishikawa, Y Kaizu *Chem. Lett.* **2** 183 (1998)
69. E O Tolkacheva, A Yu Tsivadze, Sh G Bitiev *Zh. Neorg. Khim.* **38** 1694 (1993) [b]
70. C Sirlin, I Basio, J Simon *Chem. Phys. Lett.* **139** 362 (1987)
71. Yu G Gorbunova, P S Sin'ko, V I Zhilov, A Yu Tsivadze, V I Dvorkin *Koord. Khim.* **25** 840 (1999) [a]
72. V I Dvorkin, Yu G Gorbunova, V I Zhilov, G Yu Sitnikova, A Yu Tsivadze *Zh. Anal. Khim.* **57** 661 (2002) [e]
73. D Verle, A Vendt, A Vaitemeier, I Shtark, V Shpiller, G Shnaider, S Myuller, U Mikhel'son, Kh Klish, A Khoierman, A Ardeshirpur *Izv. Akad. Nauk, Ser. Khim.* 2071 (1994) [f]
74. E W Abel, J M Pratt, R Whelan *J. Chem. Soc., Dalton Trans.* **6** 509 (1976)
75. K Ya Burshtein, A A Bagatur'yants, M V Alfimov *Izv. Akad. Nauk, Ser. Khim.* 67 (1997) [f]
76. L A Lapkina, V E Larchenko, K I Popov, A Yu Tsivadze *Zh. Neorg. Khim.* **43** 1876 (1998) [b]
77. L A Lapkina, V E Larchenko, K I Popov, A Yu Tsivadze *Zh. Neorg. Khim.* **46** 92 (2001) [b]
78. Yu Yu Enakieva, Yu G Gorbunova, L I Demina, A Yu Tsivadze *Zh. Neorg. Khim.* **48** 1986 (2003) [b]
79. A Yu Tsivadze *Zh. Vses. Khim. O-va im D I Mendeleeva* **2** 166 (1985) [c]
80. K Nakamoto *Infrared and Raman Spectra of Inorganic and Coordination Compounds* (New York: Wiley, 1986)
81. G A Corker, B Grant, N J Clevak *J. Electrochem. Soc.* **126** 1339 (1979)
82. M Moussavi, A De Cian, J Fisher, R Weiss *Inorg. Chem.* **27** 1287 (1988)
83. A N Darovskikh, O V Frank-Kamenetskaya, V S Fundamenskii, O A Galinskaya *Kristallografiya* **30** 1085 (1985) [g]
84. A N Darovskikh, O V Frank-Kamenetskaya, V S Fundamenskii, A M Golubev *Kristallografiya* **31** 279 (1986) [g]
85. M Bardin, E Bertounesque, V Plichan *J. Electroanal. Chem.* **271** 173 (1989)
86. E O Tolkacheva, A Yu Tsivadze, Sh G Bitiev, Yu G Gorbunova, V I Zhilov, V V Minin *Zh. Neorg. Khim.* **40** 984 (1995) [b]
87. S I Troyanov, L A Lapkina, V E Larchenko, A Yu Tsivadze *Dokl. Akad. Nauk* **367** 644 (1999) [h]
88. J W Buchler, A De Cian, J Fisher, M Kihn-Botulinsli, H Paulus, R Weiss *J. Am. Chem. Soc.* **108** 3652 (1986)
89. M Moussavi, A De Cian, J Fisher, R Weiss *Inorg. Chem.* **25** 2107 (1986)
90. A De Cian, J Fisher, R Weiss *Inorg. Chem.* **24** 3162 (1985)
91. K Saito *Chemistry and Periodic Table (Iwanami Modern Chemistry Series)* No. 5 (Tokyo: Iwanami Shaten, 1979)
92. L A Lapkina, E Niskanen, H Ronkomaki, V E Larchenko, K E Popov, A Yu Tsivadze *J. Porphyr. Phthalocyan.* **4** 587 (2000)
93. A G Martynov, Yu G Gorbunova, I V Khrapova, S G Sakharov, A Yu Tsivadze *Zh. Neorg. Khim.* **47** 1616 (2002) [b]
94. T Toupance, V Ahsen, J Simon *J. Am. Chem. Soc.* **116** 5352 (1994)
95. T Toupance, V Ahsen, J Simon *J. Chem. Soc., Chem. Commun.* 75 (1994)
96. L A Lapkina, Yu G Gorbunova, V E Larchenko, A Yu Tsivadze *Zh. Neorg. Khim.* **48** 1164 (2003) [b]
97. A G Martynov, I V Biryukova, Yu G Gorbunova, A Yu Tsivadze *Zh. Neorg. Khim.* **49** (2004) (in the press) [b]

[a] — *Russ. J. Coord. Chem. (Engl. Transl.)*
[b] — *Russ. J. Inorg. Chem (Engl. Transl.)*
[c] — *Mendeleev Chem. J. (Engl. Transl.)*
[d] — *Russ. J. Gen. Chem (Engl. Transl.)*
[e] — *J. Anal. Chem. (Engl. Transl.)*
[f] — *Russ. Chem. Bull., Int. Ed. (Engl. Transl.)*
[g] — *Crystallogr. Rep. (Engl. Transl.)*
[h] — *Dokl. Chem. (Engl. Transl.)*

Russian Chemical Reviews **73** (1) 25 – 36 (2004) © 2004 Russian Academy of Sciences and Turpion Ltd

DOI 10.1070/RC2004v073n01ABEH000867

Surface forces and physicochemistry of surface phenomena

N V Churaev

Contents

I. Surface forces 25
II. The influence of electrolytes, surfactants and polymers on the surface forces 28
III. Surface forces in wetting phenomena 32

Abstract. The results of modern theoretical and experimental studies of components of the long-range surface forces which determine the properties of dispersions and wetting liquid films are generalised. The bibliography includes 113 references.

I. Surface forces

During the last 10 – 15 years, numerous studies dealing with the interactions of interfaces through thin liquid films have been carried out as applied to colloids including nanoparticles and asymmetrical systems, *i.e.,* wetting films. This line of research forms the basis for solving a number of engineering problems such as control of the properties of dispersions, wetting, flotation and water treatment and the problems of environmental protection.

The physicochemistry of the surface phenomena considers the components of the surface forces and their change upon modification of the interfaces due to the adsorption of ions, surfactants and polymers including polyelectrolytes.

We shall start the discussion of the state-of-the-art of this field of physicochemical science with consideration of the results of fundamental studies of the surface forces which play the key role when the distances between the interacting particles or surfaces are comparable with the radius of action of these forces.

1. General remarks

Attractive or repulsive forces whose radius of action is much greater than the length of chemical bonds arise between condensed phases separated by a thin gas or liquid interlayer. The physical nature of such long-range forces can be different. They may be due to the electric fields of charged surfaces, fluctuating electromagnetic fields related to the movement of electrons in atoms and molecules, and structural forces arising upon the overlap of the boundary layers of the liquids with a changed structure.[1] The radius of action of these forces has the same order of magnitude as the correlation length in the liquid bulk (usually, this makes several nanometres). For solutions of polymers or surfactants, it is necessary, in addition, to take into account the steric forces which appear when the adsorption layers approach each other and overlap.[2]

N V Churaev Institute of Physical Chemistry, Russian Academy of Sciences, Leninsky prosp. 31, 119991 Moscow, Russian Federation. Fax (7-095) 952 53 08. Tel (7-095) 955 46 28

Received 3 July 2003
Uspekhi Khimii **73** (1) 26 – 38 (2004); translated by Z P Bobkova

The surface forces and the thermodynamic properties of thin liquid interlayers between two planar surfaces of solids are described conventionally by the disjoining pressure (Π), which was introduced by Derjaguin.[3] This value is equal to the difference between the pressure P acting on a planar liquid interlayer with thickness h and the pressure P_0 in the bulk of the same liquid outside the thin interlayer under equilibrium

$$\Pi = P - P_0 . \quad (1)$$

However, it should be borne in mind that the pressure Π does not always 'disjoin' the interlayer; depending on the direction of action of the surface forces, it can also attract the surfaces of different phases.

In the case of wetting films adjoining the gas phase, the P value in expression (1) is atmospheric pressure and the P_0 value characterises the pressure in the bulk region of the meniscus which is in equilibrium with the film.

The disjoining pressure $\Pi(h)$ is a very important thermodynamic parameter of the thin interlayer (film). Let us consider reversible changes in the state of the interlayer taking place upon the change in its thickness by ∂h, while the temperature T, the chemical potentials μ_i of the dissolved substances and the pressure P remain constant. As this takes place, the external forces which are necessary to ensure the equilibrium of the thin film do work equal to the increment of the Gibbs thermodynamic potential ∂G. Thus, it can be written that

$$\Pi(h) = -\left(\frac{\partial G}{\partial h}\right)_{T,P,\mu} . \quad (2)$$

The $\Pi(h)$ dependence which characterises the contribution of various components of the surface forces to the interaction of the surfaces is called the disjoining pressure isotherm. It contains full information on the state of the system at specified temperature, pressure and the composition of the bulk solution.

The surface forces are manifested first of all in disperse systems containing suspended particles that are involved in thermal Brownian motion. Upon the collision of particles, depending on the surface forces that act between them, the system can either remain stable, or alternatively, form weakly bound floccules or stable aggregates. Larger particles settle (or float to the surface) in a gravitational field to give porous precipitates whose structure depends on the forces that act between the particles.

In recent years, in view of a number of practical applications, special attention has been attracted by disperse systems with particle size of the order of several nanometres.

Wetting films, which model asymmetric systems, deserve special attention. These thin liquid films have the condensed

phase on one side and the phase of their own vapour or a different immiscible liquid on the other side.

The theory of several constituents of the surface forces has been developed in relation to a rather simple case of planar interlayers and films. Transition to calculations of the interaction of spherical (or other) particles is done using the Derjaguin approximation based on the integration of the local forces acting between the opposing 'planar elementary sections' of the curved surfaces.[4] For example, in this approximation, the force F that acts between two identical spherical particles with the radius r is given by

$$F = \pi r G(h), \tag{3}$$

where $G(h)$ is the free energy of interaction between planar interlayers with the thickness h,

$$G(h) = \int_h^\infty \Pi(h)\mathrm{d}h\,. \tag{4}$$

However, it should be borne in mind that the scope of applicability of the Derjaguin approximation is limited to interlayer thicknesses much smaller than the particle radius. Therefore, for calculation of the forces and energy for the interaction of particles smaller than 0.1 μm, more complex procedures are employed.[5–9]

2. Dispersion forces

The macroscopic theory of dispersion forces was first developed by Lifshits[10] for the simple case of attraction of identical planar surfaces in vacuum. Subsequently, it was extended to more complex systems in his joint work with Dzyaloshinsky and Pitaevsky.[11] The expression obtained for the disjoining pressure of thin interlayers ($h < 15$ nm) has the following form:

$$\Pi_\mathrm{m} = -\frac{A_{132}}{6\pi h^3}\,, \tag{5a}$$

where

$$A_{132} = \frac{3\hbar}{4\pi}\int_0^\infty \frac{(\varepsilon_1-\varepsilon_3)(\varepsilon_2-\varepsilon_3)}{(\varepsilon_1+\varepsilon_3)(\varepsilon_2+\varepsilon_3)}\mathrm{d}\xi. \tag{5b}$$

Here, the subscripts 1 and 2 refer to the phases that confine the thin film of liquid 3; $\hbar$ is Planck's constant. The frequency dependences of the dielectric constant of the medium $\varepsilon(\mathrm{i}\xi)$ are taken on an imaginary frequency axis.

A qualitatively equivalent solution was obtained earlier by Hamaker[12] in terms of a microscopic approach. Therefore, the constant A_{132} is still called the Hamaker constant, although calculation of this constant from Eqn (5b) gives a markedly different value.

For interlayers with a thickness of $>40-50$ nm, where the electromagnetic retardation effect, first taken into account by Casimir and Polder,[13] is manifested, the disjoining pressure decreases more sharply with an increase in the interlayer thickness h

$$\Pi_\mathrm{m} = -\frac{B}{h^4}\,. \tag{6}$$

In the case of dielectrics, the parameter B depends on the difference between the dielectric constants ε_0 of the interacting bodies and the interlayer separating them and amounts to $\sim 10^{-25}$ J m. For metals, the values of B are higher by approximately an order of magnitude.[1]

To calculate the dispersion forces for the intermediate range of distances, computer programmes are required.[14–17] In this case, the calculation gives the functions $A(h)$ rather than the Hamaker constants, which extends the scope of applicability of Eqn (5a).

Positive A and B values correspond to attractive forces, while negative values imply repulsive forces. The values of these constants and the functions $A(h)$ were reported in monographs[1,2] and in some papers (see, for example, Refs 18–20). In one study,[18] the functions $A(h)$ were calculated using corrected spectral data for water interlayers. Dagastine *et al.*[19] reported the A values for the dispersion attractive forces through water interlayers for a number of solids such as silicon, quartz, diamond, mica, TiO_2, MgO, Al_2O_3, CaF_2, LiF, NaCl, KBr and CdS. The values of A for some other inorganic materials were also documented.[20]

Various methods have been developed for experimental verification of the theory of dispersion forces; the methods make use of model objects such as lens–plane, sphere–sphere and crossed cylinders whose movement towards each other simulates the contact of dispersion particles.

The commercially manufactured instruments (for example, Mark) for direct measurement of the surface forces use glass cylinders crossed at an angle of 90° and coated by mica sheets.[21] The measurements give the dependences of F/R on the shortest distance H between the surfaces of the crossed cylinders with the radius R.

Direct verification of the theory of dispersion forces has been carried out only for the interaction of model bodies in vacuum through interlayers of gases and nonpolar liquids. In the case of aqueous solutions as interlayers, comparison with the theory is hampered because the results of measurements depend not only on the dispersion forces but also on electrostatic and structural forces.

In recent years, atomic force microscopy (AFM) has been used more and more often to study the surface forces. This method allows one to measure the forces between a rounded tip or a small spherical particle (5–10 μm) and a planar surface. The interaction force is found from the deformation of a planar cantilever spring with a test particle attached to the spring end. The number of publications devoted to the use of this method is rapidly increasing. However, it is used most often not merely to verify the theory of dispersion forces but in more complex cases where several components of surface forces act simultaneously, including electrostatic forces, which cover the longest distances.

3. Electrostatic forces

The theory of interaction of charged particles can now be considered as being well developed.[1,2,21] Solutions for the cases of a constant potential (ψ) or a constant charge (σ) of planar surfaces approaching each other have been obtained. Subsequently, the theory has been corrected because, as the surfaces approach each other, the potential-determining ions can be desorbed under the action of the electric field of the opposite surface. This effect, which has been called charge regulation, is often taken into account when analysing the results of direct measurements of electrostatic forces.[22]

The electrostatic repulsion forces between likely charged surfaces are often calculated using the approximation of small surface potentials. The disjoining pressure isotherm has the following form:

$$\Pi_\mathrm{e}(h) = (2\varepsilon\varepsilon_0\kappa^2\psi^2)\exp(-\kappa h), \tag{7}$$

where ε is the dielectric constant of the dispersion medium, ε_0 is the electric constant, κ is the reciprocal Debye radius depending on the ionic strength of the solution.

To pass to the interaction forces between identical particles, relation (1) is used. In the case of small particles where relation (1) is inapplicable, more complex solutions should be used.[5] A strict estimation of the electrostatic interaction requires taking into account other effects, namely, polarisation of the electric double layers (EDL) and the possible redistribution of the surface charge as the particles approach each other. The role of these nonequilibrium phenomena has been considered in a review.[23] The influence of the image forces on the ion distribution near a charged wall and the effects of ion correlation and the finite volume of ions on the electrostatic interaction have been analysed.[24]

However, direct AFM measurements of the electrostatic repulsion forces[25–27] showed that, except for the region of small

distances, rather good agreement is observed between the experimental data and simple solutions of the theory. At least, the calculated ζ-potentials (which are usually equivalent to the surface potentials ψ) are close to the values measured by independent methods. However, it has also been found by AFM [28] that the measured forces depend on the velocity (v) at which the tip moves towards the planar mica surface when $v > 10$ μm s^{-1}. The relaxation times of the EDL were roughly estimated as 5–6 ms. The nature of slow relaxation of the dense part of the EDL has been considered by Dukhin and Liklema.[29] This effect is especially pronounced for high rates of particle movement towards each other, for example, in the case of vigorous stirring or turbulent flow of the dispersion.

In a dispersion consisting of two types of particles which differ in the sign of the ψ-potential, the electrostatic forces become attractive forces, which results in so-called heterocoagulation.[1] If the particle potentials differ only in magnitude, the particles may repel at large distances. The sign of the electrostatic forces changes when they approach each other to the critical distance

$$h_c = \kappa^{-1} \ln \frac{\psi_1}{\psi_2},$$

where ψ_1 and ψ_2 are the potentials of the interlayer surfaces. Coagulation takes place after overcoming a potential barrier formed upon the mutual effect of the electrostatic and dispersion forces.

The publications devoted to the theory of heterocoagulation and the results of experimental studies of the stability of dispersions with a predominantly aqueous dispersion medium have been analysed.[30] The researchers noted an important role of heterocoagulation in the technology of disperse materials.

4. Structural forces

Even the first direct measurements of the forces acting between crossed mica-coated glass threads or cylinders showed that at a distance of $H < 2-3$ nm between the surfaces, the results deviate from the Derjaguin–Landau–Verwey–Overbeek (DLVO) theory, which takes into account only dispersion and electrostatic forces.

This is exemplified in Fig. 1, which shows the results of measurements of the dependence of the repulsive force F/R of molecularly smooth glass surfaces in a 1.1×10^{-2} M aqueous solution of NaCl on the shortest distance H between the surfaces.[31] Small glass plates several micrometers thick cut out of the wall of a rapidly blown bubble were coated with silver from the inside (to obtain the fringe pattern which serves for measuring the interlayer thickness) and attached to the surface of glass cylinders with the radius $R = 1$ cm. The continuous and dashed curves in Fig. 1 correspond to DLVO theory calculations in the constant charge and constant potential approximations, respectively. The experimental points in the region of interlayer thicknesses of $H < 3$ nm lie above the calculated curves, indicating an additional participation of structural repulsion forces. These forces arise upon the overlap of the structurally changed boundary layers of water that exist near the hydrophilic surface of glass. Qualitatively the same results were obtained for solutions of NaCl with other concentrations (10^{-3} and 10^{-1} mol litre^{-1}).[31]

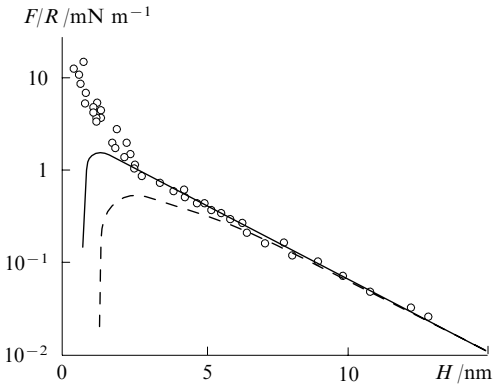

Figure 1. Dependences of the repulsion forces F/R on the distance H between smooth glass surfaces in a 1.1×10^{-2} M aqueous solution of NaCl.[31] For explanation, see the text.

The modified structure of the boundary layers of water was confirmed by a number of independent methods. For instance, recording of the IR spectra of water near the hydrophilic surface with the use of a laser excitation source [32] showed that water dipoles are oriented at a right angle to the surface. If the surface is charged, this orientation extends to 3–5 molecular layers.

It is known that near hydrophilic surfaces, the mobility of water molecules is retarded and the time of dielectric relaxation is an order of magnitude longer than that in the water bulk. Changes in the structure of the boundary layers of water are accompanied by strengthening of intermolecular bonds.[33]

Statistical mechanics calculations have shown that in aqueous solutions of electrolytes, the structural repulsion force between hydrophilic surfaces appears when the interlayer thickness is < 2 nm and increases exponentially as the interlayer becomes thinner.[34]

The experimental isotherms for the structural component of the disjoining pressure for water interlayers between the hydrophilic surfaces are approximated by the exponential dependence

$$\Pi_s(h) = K \exp\left(-\frac{h}{\lambda}\right), \tag{8}$$

where the parameter K describes the magnitude of the forces, and the parameter λ describes the long-range action. The parameters K and λ determined in experiments with thin interlayers of aqueous solutions between various hydrophilic surfaces can be found in monographs.[1, 21, 35]

The first attempts to develop a theory of structural forces were based on the Landau theory of second order phase transitions and the use of the order parameter η. This parameter was defined in such a way that it was zero in the isotropic bulk phase and nonzero (either a positive or a negative value) in the ordered phase. For small interlayer thicknesses, the calculations resulted in expression (8), where λ has the meaning of the correlation length and the parameter K, according to this approach, depends on the degree of surface ordering of water dipoles. The first estimates of these parameters were obtained in experiments with thin interlayers.[1] Subsequently, several versions of this approach have been used, including those taking into account the inhomogeneity of the orientational state of water molecules near the surfaces that confine the interlayer.[36, 37]

In a study devoted to the theory of structural forces,[38] the effects of excluded volume, dipole orientation, and the finite volume of water molecules were taken into account. This theory also predicts an exponential growth of structural forces with a decrease in the interlayer thickness. In addition, it was found that the period of oscillations of structural forces is close to the size of water molecules. The results of calculations are in good agreement with experimental data for a 10^{-3} M aqueous solution of KCl between mica surfaces.[21] The parameters K and λ for interlayers with a thickness of < 3 nm were found to be 3×10^6 N m^{-2} and 1 nm, respectively.

However, it should be borne in mind that the values of the parameters of structural forces presented here were obtained for hydrophilic molecularly smooth surfaces of glass and mica. Real surfaces are chemically heterogeneous and irregular and can be loosened or coated by adsorption layers of surfactants or polymers. Therefore, the quantitative determination of structural forces can only be used as rough estimates.

5. Hydrophobic forces

Some studies have shown that pronounced attractive forces act between the hydrophobic surfaces in water.[1,21,35] Their dependence on the interlayer thickness is described by the same equation (8), but the K values are negative in this case. The hydrophobic surfaces for measurements were usually produced by adsorption of a cationic surfactant or polyelectrolyte on glass or mica. It was found that hydrophobic forces have a greater radius of action than hydrophilic repulsion forces and the range of action increases with an increase in the degree of hydrophobicity of the surfaces. The measured λ values were 1 to 65 nm, depending on the experimental conditions.

The hydrophobic attraction detected in some cases when the distance between the surfaces is up to 100 nm is attenuated with a decrease in H according to a binomial exponential law with $\lambda = 13-15$ nm at long distances and with $\lambda = 1-2$ nm at short distances.

The physical nature of the hydrophobic attractive forces still remains unclear. Once it was assumed that this effect can be attributed, by analogy with the hydrophilic repulsion forces, to the structural changes of the boundary layers of water. Indeed, computations have shown[39,40] that the density of water decreases near a hydrophobic surface, unlike a hydrophilic one. However, the thickness of such boundary layers does not exceed 2–3 nm, which does not suffice to explain the observed long-range action.

It has been shown[41] that a correlation between hydrophobic attraction forces and the contact angles of water can be followed only at small distances. Due to the sharp increase in the attractive forces at short distances, no force oscillations, involved in the case of hydrophilic repulsion, can be detected experimentally.

Apparently, the long-range attraction is related to evolution of bubbles of the gas dissolved in water on the hydrophobic surfaces and the subsequent coalescence of the bubbles[42] or to thermal oscillations of the surfaces of such bubbles.[43,44] The role of the bubbles was confirmed, in particular, by the fact that the hydrophobic attraction forces decrease as water is being degassed.[45–47] Numerous nanobubbles were detected by atomic force microscopy on the quartz surface hydrophobised by octadecyltrichlorosilane.[48] It was concluded that the bubbles are formed before the contact of the tip of the atomic force microscope with the substrate. If the long-range hydrophobic attraction forces are caused by coalescence of the bubbles, their size should be 10–50 nm, which is consistent with experimental observations.

The solvophobic attraction of the surfaces coated by a film of amorphous Teflon with 0.5-nm high surface irregularities was observed not only in water but also in many organic liquids (except for n-alkanes and n-alkanols).[49] The results obtained are in line with the hypothesised formation of submicrometre air bubbles on the interacting surfaces.

The experimental values of the parameters K and λ present in Eqn (8) in the case of the hydrophobic forces for various objects have been summarised in a review.[42]

It can be assumed that the proper hydrophobic attraction exists only in degassed water, *i.e.*, in the absence of gas bubbles. Thus the nature of structural forces can be interpreted from a unified standpoint by relating them to changes in the structure of boundary layers — an increase in the water density and the normal orientation of dipoles in the case of hydrophilic repulsion forces and a density decrease and a tangential orientation of dipoles in the case of hydrophobic attraction forces. In any case, the λ values for hydrophilic and hydrophobic forces are similar and amount to 1–2 nm, which corresponds to the correlation length in the water bulk. This permits inclusion of both types of short-range structural forces in the overall isotherm of the disjoining pressure.

II. The influence of electrolytes, surfactants and polymers on the surface forces

1. Electrolytes

The effect of the electrolyte composition and concentration shows itself through a change in the surface charge as a result of both ion exchange and the change in the Debye radius

$$\kappa^{-1} = (\varepsilon\varepsilon_0 kT)^{1/2} (8\pi z^2 e^2 c)^{-1/2}, \qquad (9)$$

where k is the Boltzmann constant, z is the charge number, e is the charge of an electron, c is the concentration of the solution (in mol cm^{-3}).

It can be seen from Eqn (9) that with an increase in the electrolyte concentration, the Debye radius decreases and, according to Eqn (7), this reduces the range of action of the electrostatic forces. The repulsive forces also decrease, due to the more pronounced influence of the change in the κh in the exponential quantity on the disjoining pressure Π_e. The calculated repulsive forces may increase due to the increase in the charge and the potential ψ of the surfaces, but to only a limited extent, because Eqn (7) was derived with the assumption of small ψ.

Several mechanisms of formation of the surface charge are known. The most important of these are dissociation of the ionogenic surface groups and ion exchange. Therefore, the surface charge is controlled most often by varying the pH, the ionic composition, and the concentration of the solutions.

Usually, the surface charge and potential are determined experimentally. This is done most often using methods based on the measurement of the streaming potential of the solution in a slot or a capillary and on the measurement of the rate of electrophoresis of dispersion particles.

This is exemplified in Fig. 2, which shows the results of measurements of the ζ-potential in 50–150 μm thick planar cells formed by polished glass surfaces.[50] These data provide an idea of the range of possible variation of the surface charge of glass. The calculations were performed using the Smolukhovsky equation with the Dukhin correction for the surface conductivity.

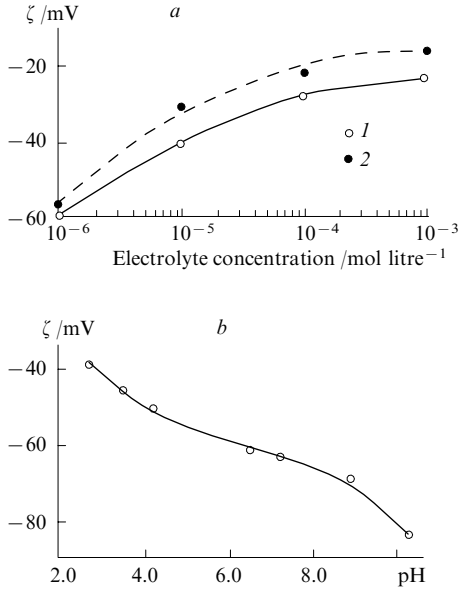

Figure 2. Dependences of the ζ-potential of the surface of glass plates[50] on the concentration of electrolytes (*a*) and on the pH (*b*).
Electrolyte: (*1*) NaCl, (*2*) $AlCl_3$

For quartz capillaries with molecularly smooth surfaces, the absolute values of the ζ-potential are much greater. This confirms the importance of the state of the surfaces, even if they are similar in chemical composition. In addition, the composition of the solution also plays a role. For example, at a constant ionic strength of a 10^{-3} M solution of KCl + HCl (or KOH), the ζ value at pH 10 reaches -140 mV, while at pH 2, it tends to zero.[51]

In the case of high surface potentials ($|\psi| > 100$ mV), electrostatic forces no longer depend on the surface charge and depend only on the electrolyte concentration and the κ^{-1} value.[52]

Atomic force microscopy measurements of the forces of interaction of the TiO_2 particles with a face of a rutile crystal in an electrolyte solution have shown [53] that for electrolyte concentrations of $< 10^{-2}$ mol litre^{-1}, the shielding length κ^{-1} is in good agreement with the value calculated from Eqn (9). At pH 5.6, only dispersion attraction forces corresponding to the Hamaker constant $A = 6 \times 10^{-20}$ J, close to the theoretical value, acted in the isoelectric point.

For spherical polystyrene particles with a diameter of 2 μm, long-range electrostatic repulsion was observed at KCl concentrations smaller than 10^{-2} mol litre^{-1} (see Ref. 54). For a 10^{-3} M solution, the experimental data were in good agreement with those calculated using the Derjaguin approximation (3) and the surface potential $\zeta_1 = 87$ mV was close to a value measured independently (83 mV).

In the interaction of a ZnS sphere of diameter 5 μm with a planar surface of mica with different ζ-potentials (-100 and -90 mV, respectively), the experimental dependence of the repulsive forces on the interlayer thickness was in better agreement with the condition of constant charge.[55] The researchers concluded that the solution of the Poisson – Boltzmann equation should be supplemented by a condition of charge control on both surfaces.

Dependences of the forces of interaction of spherical cellulose particles with a size of 20 – 30 μm on the distance H between them in aqueous solutions of electrolytes have been obtained by AFM.[56] These dependences were used to model some processes of the pulp-and-paper industry. In solutions with low concentrations of KBr (10^{-4} mol litre^{-1}), electrostatic repulsion is the main force at long distances; at $H < 20$ nm, steric repulsion predominates. With an increase in the pH, both forces grow due to an increase in the degree of ionisation of the COOH groups and swelling of cellulose. The observed dynamic effects were attributed to slow establishment of the equilibrium in the polymer – solution system.

Glass and fused quartz can swell in water, which gives rise to a surface gel layer.[57] Therefore, the results of measurements of surface forces can depend on the contact time between the surfaces and water. The diffusion structure of the surface layer can markedly decrease the Hamaker constant and complicate the calculation of electrostatic forces.

The surface roughness can also influence the attractive or repulsive forces. Comparative calculations were carried out for the case of interaction of a rough and a planar surface in a solution of a 1 – 1-electrolyte with ionic strength of 10^{-2} mol litre^{-1}. It was assumed that the ζ-potentials are 25 mV and the Hamaker constant is 10^{-20} J.[58] The roughness was specified by a random distribution of bulges and pits of a hemispherical shape and different radii. Roughness was found to influence substantially the shape of potential curves, especially for short distances between the surfaces. In particular, both the height of the potential barrier and the depth of the potential well can considerably decrease.

By direct microscopic examination,[59] stability of mixed dispersions of silica (SiO_2) and small crystals of NaCl in a saturated salt solution was detected; this cannot be explained in terms of the DLVO theory. The AFM measurements of interaction forces showed that short-range repulsive forces exist between a spherical silica particle and a planar surface of a NaCl crystal in a saturated solution of NaCl, whereas with KCl in place of NaCl, attractive forces appear. These effects were attributed to the action of structural (polar) forces caused by different orientation of the dipoles of water molecules.

2. Surfactants

Adsorption of ionogenic surfactants can change appreciably both the magnitude and the sign of the surface charge. For example, the initial negative charge of the quartz surface is strongly affected by adsorption of a cationic surfactant. Figure 3 shows the dependence of the ζ-potential on the concentration of the cetyltrimethylammonium bromide (CTAB) in a supporting electrolyte solution (5×10^{-4} mol litre^{-1} of NaCl) at pH 6.5 obtained by the streaming potential method. An increase in the content of CTAB results in charge reversal. When the surfactant concentration is close to the critical micelle concentration (CMC) (10^{-3} mol litre^{-1}), ζ-potential increases to $+140$ mV, and the surface charge increases to $+4$ μC cm^{-2} (see Ref. 60). On the basis of the two-layer adsorption theory,[61] it was shown that the adsorption potentials for the first and second layer of CTAB are $15\,kT$ and $11\,kT$, respectively. The curve in Fig. 3, plotted using the equations of this theory, is in satisfactory agreement with experimental data (dots).

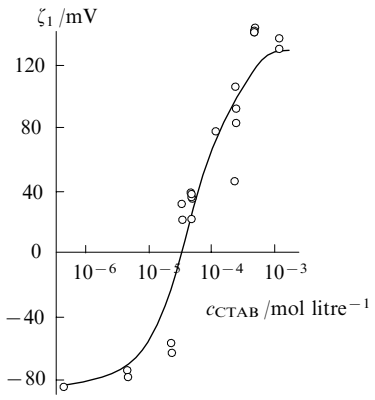

Figure 3. Results of measurements of the ζ_1-potentials of the surface of quartz capillaries for different concentrations of CTAB in a 5×10^{-4} M solution of NaCl (pH 6.5).[60] The curve corresponds to calculations in terms of two-layer adsorption.[61]

The same type of dependence of the surface charge on the surfactant concentration was obtained by direct measurements of the forces of interaction between mica surfaces in CTAB solutions.[62] When the CTAB concentration is low, electrostatic repulsion forces prevail over the dispersion attraction forces; upon neutralisation of the surface charge, the former are replaced by hydrophobic attraction forces.

It has been established [63] that the adsorption mechanism changes at pH 3 where no charged centres remain on the quartz surface. In this case, the bilayer adsorption of the surfactant becomes impossible. Processing of the resulting dependence of the charge on the CTAB concentration in terms of the monolayer adsorption model showed that the adsorption potential is $11\,kT$.

Subsequently, it has been found by AFM [64] that at a CTAB concentration higher than 2 CMC, cylindrical micelles are formed on the mica surface; over a period of 24 h, they are transformed into a planar bilayer structure.

In an alkaline medium, the formation of a second layer on the surface of glass takes place at a CTAB concentration below the CMC and the density of this layer is much lower than the density of the layer on the mica surface. By removing the second layer, it is possible to bring the glass surfaces in a tight hydrophobic contact.[65] The researchers cited suggested that the second layer

consists of separate bunches of surfactant molecules or surface aggregates.

Anionic surfactants influence the charge of the quartz surface into a much lesser extent. After the addition of 5×10^{-5} mol litre^{-1} of sodium dodecyl sulfate to the background solution of NaCl (10^{-4} mol litre^{-1}), the ζ-potential of the quartz surface slightly increased in magnitude (from -125 to -150 mV) and did not change upon further increase in the concentration of sodium dodecyl sulfate in the solution by an order of magnitude.[66]

The adsorption of nonionic surfactants on the hydrophilic surface up to the formation of a full monolayer leads to gradual hydrophobisation of the surface. The formation of the second layer in which the polar groups of the surfactant molecules are directed toward the solution makes the surface hydrophilic again. However, the ζ-potential does not change noticeably; its decrease has been noted only in the case of adsorption of nonionic surfactants whose molecules are capable of forming hydrogen bonds with the surface hydroxy groups.

Note that the influence of surfactant adsorption on the charge and hydrophilicity of the surface, which determine the electrostatic and structural forces, was analysed only for silicate surfaces; however, the key conclusions are valid at a qualitative level for the surfaces of other natural materials, because most of them are negatively charged.

3. Polymers

We shall start with a simpler case of noncharged polymers and then consider polyelectrolytes.

Nikologorskaya *et al.*[67] have employed dynamic light scattering to measure the Brownian diffusion coefficients of the particles of monodisperse silicasols Ludox-SM with the radius $r = 19$ nm and Syton-W50 ($r = 69$ nm) before and after the adsorption of polyethylene oxide (PEO) with a molecular mass of 4×10^4 and estimated the thickness of the adsorbed layers on the basis of the results obtained. At a low electrolyte concentration, the sols were stable due to the action of electrostatic repulsion forces. However, with an increase in the NaCl concentration to 10^{-2} mol litre^{-1} when the Debye radius became smaller than the length of the unfolded PEO molecule, flocculation of the sols took place in the presence of even small amounts of the polymer, as a result of binding of two particles to the same macromolecule (so-called bridging). As the PEO concentration increases and a filled adlayer is formed, the sols become stable once again due to the arising steric repulsion of the particles.

A study of the interaction of mica surfaces in aqueous solutions of ethylhydroxyethylcellulose showed[68] that the adsorbed macromolecules could be easily squeezed out of the interlayer space at 20 °C. This attests to a low adsorption energy. When the temperature was raised to 60 °C, the adsorption of the polymer increased, apparently due to a decrease in the hydrophilicity of the surface, and squeezing out of the molecules became difficult. Upon preliminary hydrophobisation of the mica surface, the adsorption of cellulose sharply increased and long-range steric repulsion was observed.

In aqueous solutions of a triblock copolymer (polyethylene oxide – polytetrahydrofuran – polyethylene oxide) with a molecular mass of 11 900 at a concentration below the CMC, steric repulsion force was detected between the surfaces of quartz spheres; the force increased monotonically as the spheres approached each other.[69] However, after long-term keeping of the spheres in a 10^{-4} % solution of the copolymer, thinning of the interlayer down to 10 nm gave rise to bridging bonds between the surface aggregates of the macromolecules. The steric repulsion was replaced by weak adhesive forces. In an electrolyte solution (NaBr, 0.2 mmol litre^{-1}) without a copolymer, only electrostatic repulsion forces corresponding to a quartz surface potential equal to -75 mV acted between the quartz spheres.

The interaction of mica surfaces in solutions of phospholipid, polyglycerol, and their mixtures in triolein has been studied by the Mark-4 device.[70] Ordering of liquid triglyceride molecules results in the bridging of surfaces and gives rise to two barriers related to structural forces. Conversely, the adsorption of polyglycerol induces the appearance of a steric repulsion barrier at a distance of 12 nm. The adsorption of a phospholipid/polyglycerol mixture on the mica surface results in the formation of complexes, which brings about long-range repulsive forces.

The interaction forces between a spherical particle (15 – 25 μm in diameter) of regenerated cellulose and the planar surface of the same polymer were measured by AFM.[71] The long-range repulsion was due to electrostatic forces corresponding to low potentials of regenerated cellulose surfaces. When the surfaces are brought into contact, adhesive forces are detected between the swelled surface layers of cellulose, which represent a viscoelastic gel. The interaction at short distances is reversible. Upon an increase in the electrolyte concentration, the adhesion strength is enhanced.

If the polymer is not adsorbed on the surfaces that confine the interlayer, attractive forces may arise due to the decrease in the osmotic pressure in the solution film between the particles. This effect was observed experimentally by examining the interaction of a glass sphere with a radius of 38 μm with a glass substrate using an atomic force microscope. Both surfaces were precoated with n-octadecyl alcohol layers. The measurements were carried out in solutions of polydimethylsiloxane in cyclohexane.[72] The distance between the surfaces where the attractive forces are manifested is comparable with the radius of gyration of the polymer macromolecule. When the sphere and the plane are brought to a shorter distance, the steric repulsion forces between the overlapping adlayers of n-octadecanol begin to be detectable.

Costello, Luckham and Tadros[73] studied the interaction forces between the mica surfaces with chemically grafted methyl methacrylate/ethylene oxide copolymer using the method of crossed cylinders. In Fig. 4, the dots correspond to experimental values minus the contribution of the electrostatic repulsion forces. The obtained dependences proved to be fully reversible. The continuous curve was constructed using the de Gennes equation[74]

$$\Pi_{st} = \frac{kT}{l^3}\left[\left(\frac{2L}{h}\right)^{9/4} - \left(\frac{h}{2L}\right)^{3/4}\right], \tag{10}$$

where Π_{st} is the steric repulsion force, l is the average distance between the grafting sites of molecules, L is the thickness of the equilibrium grafted layer of the polymer, h is the thickness of the interlayer between the surfaces.

The first term in the right-hand part of Eqn (10) takes into account the effect of the increasing osmotic pressure caused by accumulation of the polymer in the mutually penetrating layers, while the second term corresponds to the elastic forces that tend to restore the initial linear shape of the macromolecules. As can be seen from Fig. 4, the calculated and experimental results are in good agreement with the assumption that $L = 10$ nm.

For polyethylene oxide adsorbed on the mica surface from aqueous solutions, the steric interaction is not reversible, unlike that for grafted polymers.[75] Figure 5 shows the results of measurements of the interaction of crossed mica cylinders in a 0.1 M background solution of KNO_3. In the absence of the polymer, only weak electrostatic repulsion forces can be detected (curve *I*). After keeping the surfaces for 16 h in an aqueous solution of PEO with a molecular mass of 1.6×10^5 (the concentration is 1.5×10^{-4} g ml^{-1}), the repulsive forces follow curve *II*. The same law of variation of the steric forces is obeyed during the repeated bringing together of the surfaces, but only when they have been kept apart for 1 h. Curve *III* corresponds to the repeated compression of the adlayers (bringing the surfaces together), 5 min after the preceding drawing them apart, and to the subsequent fast drawing apart. This short (5 min) period the surfaces are kept far from each other is insufficient for the initial structure of the adsorption layers to be restored. Similar slow rearrangement effects are involved in the case of PEO with a lower molecular weight (1.4×10^4), which is shown by the corresponding

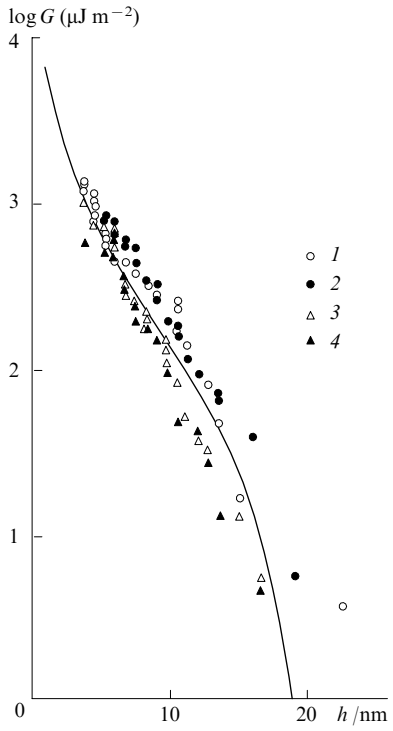

Figure 4. Steric repulsion energy of methyl methacrylate/ethylene oxide copolymer layers grafted to a mica surface in an aqueous 10^{-2} M solution of KNO_3 *vs.* the interlayer thickness.[73]

$$G(h) = \int_h^\infty \Pi_{st}(h)\mathrm{d}h$$

Experimental points: (*1*) the first compression of the grafted copolymer layers, (*2*) the first drawing of the surfaces apart, (*3, 4*) data obtained in the second series of experiments; the curve corresponds to the calculations in terms of the de Gennes theory.[74]

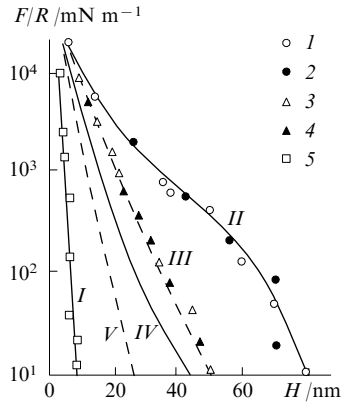

Figure 5. Steric repulsion forces of polyethylene oxide layers adsorbed on mica surfaces *vs.* the distance between the surfaces.[75]
Experimental points: (*1*) the first moving of the surfaces toward each other, (*2*) slow drawing of the surfaces apart after the contact, (*3*) repeated compression of the adlayers 5 min after their preceding separation, (*4*) subsequent fast separation, (*5*) moving of the surfaces toward each other in a 0.1 M solution of KNO_3; (*I – V*) see the text.

curves *IV* and *V*. Thus, the steric forces for grafted and adsorbed polymer molecules are substantially different.

The results of investigations of the interaction forces between various biological objects (cells, lipid bilayers, *etc.*) have been surveyed.[76]

Polyelectrolytes are widely used in modern applied chemistry. This is due to the fact that the charge of the polyelectrolyte chains can be controlled by varying the ion composition and the concentration of the background electrolyte.

The particles of most dispersions used in industry bear a negative charge; therefore, cationic polyelectrolytes (CPE) are used most often for practical purposes. Their influence on the surface interaction was studied by direct measurements of the forces of these interactions in solutions of CPE of various concentrations. It was shown [77] that the electrostatic adsorption of polyethoxylated dodecylamine on a negatively charged mica surface ($\zeta_1 = -105$ mV) takes place at pH < 8 to give a monolayer which shields the surface charge and hydrophobises the surface. This gives rise to molecular attraction forces between the surfaces, which are replaced by steric repulsion forces as the surfaces come closer together. Since the CPE structure contains oxyethyl chains, the hydrophobic attraction forces are not manifested. A decrease in the pH results in reversible structural rearrangement of the adlayer.

Similar results have been obtained for a highly charged cationic polyelectrolyte, poly(2-acryloxyethyl)trimethylammonium chloride with a molecular mass of 1.5×10^6 (see Ref. 78). At a low concentration of the background electrolyte, the molecules of the given CPE were adsorbed on a mica surface as a planar conformation. An increase in the CPE concentration results in gradual shielding of the surface charge of mica and in a decrease in the electrostatic repulsion forces until they completely disappear in the vicinity of the charge reversal point (Fig. 6). The results of measurements (dots) are in good agreement with the results of calculations in terms of the DLVO theory (curves) where the Hamaker constant was taken to be 2.2×10^{-20} J. A further increase in the concentration of poly(2-acryloxyethyl)trimethylammonium chloride induced a slight increase in the adsorption and gave rise to steric forces.

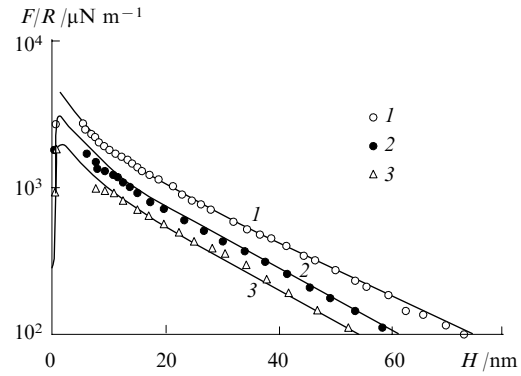

Figure 6. Repulsion force between mica surfaces in aqueous solutions of poly(2-acryloxyethylene)trimethylammonium chloride with a concentration of 1 (*1*), 5 (*2*) and 10 ppm (*3*) containing 0.1 mmol litre^{-1} of KBr *vs.* the distance between them.[78] The curves correspond to the calculation in terms of the DLVO theory.

In dilute solutions of poly(2-vinylpyridine), the interaction forces measured by AFM during moving together of a glass bead and a flat glass substrate also corresponded to analogous forces found in terms of the DLVO theory.[79] However, the adhesion strength at tearing off of the bead was much greater, which is due to the formation of bridging bonds between the surfaces not filled by CPE adlayers with participation of adsorbed CPE molecules. At higher concentrations of CPE and the salt, steric interaction appears and adhesion markedly decreases, which points to a looser state of the adlayer.[79]

It has been reported [80] that at a relatively low concentration of poly(2-vinylpyridine), the AFM-measured interaction remained purely electrostatic. This implies a planar conformation of the

molecules in the adlayer. However, the materials of the bead (quartz) and the substrate (mica) were different; therefore, the surface potentials differed in magnitude, which resulted in switching of the sign of electrostatic forces following a decrease in the solution interlayer thickness. Both the adsorbed CPE molecules and the residual charge of the incompletely shielded substrate contributed to the surface charges formed.

Measurements of the streaming potential of aqueous solutions of the styrene/dimethylaminopropylmaleimide copolymer of various concentrations in thin quartz capillaries with a molecularly smooth surface showed that the isotherm of the electrostatic adsorption of CPE follows the Langmuir equation with an adsorption potential of 25.4 kT (see Ref. 81). This corresponds to the formation of the first layer of planar-oriented molecules. After charge reversal of the solid surface, hydrophobic adsorption of macromolecules takes place to give the second layer. The calculations showed that the hydrophobic adsorption potential is much lower, being equal to 17.7 kT.

Berndt *et al.* [82] have studied the influence on the surface forces of the adsorption of an anionic polyelectrolyte (APE), polystyrenesulfonate with different molecular masses (10^4 to 5×10^5), on positively charged mica surfaces coated by a monolayer of the dioctadecyldimethylammonium cations. For the maximum coverage of the APE monolayer, the interaction forces decrease by an order of magnitude due to the complete neutralisation of the surface charge. The lack of structural forces indicates a planar orientation of the adsorbed APE macromolecules. Thus, these results do not differ qualitatively from those obtained for CPE on negatively charged surfaces.

Using the Mark-4 device, the interaction forces between mica surfaces in sodium polyacrylate solutions, including those containing calcium atoms, have been measured.[83] In the absence of Ca^{2+} ions, no noticeable adsorption of the polymer molecules in mica has been detected. The adsorption started at a $CaCl_2$ concentration higher than 3×10^{-3} mol litre^{-1} due to the formation of bonds between the COO^- groups of the polyelectrolyte and mica with participation of the Ca^{2+} ions. The adhesion strength of the contacting adlayers increased with an increase in the pH.

The same technique was used to measure the interaction forces between mica surfaces in a solution containing 0.2 mg ml^{-1} of proteoglycan (PG) sulfate, which is a part of cellular membranes.[84] The adsorption of PG from a 10^{-4} M solution of NaCl on a hydrophobised mica surface is irreversible. The interaction of the anionic PG adlayers is caused by electrostatic and steric repulsion forces, which show themselves at a distance of less than 10 nm between the surfaces and do not depend on the electrolyte concentration.

The measurement of the interaction forces between the 'brushes' of highly charged diblock copolymer grafted to mica surfaces (hydrophobised by a cationic surfactant) has shown [85] that only electrostatic and short-range steric repulsion can be found between these surfaces. In a salt-free solution, the brushes were straightened under the action of polyelectrolyte counterions. After the addition of a salt, the electrostatic interactions were partially shielded and the polymeric brushes acquired again their flexibility. The region where the interaction is observed depends only slightly on the salt concentration and, when the surfaces move towards each other, it is described adequately by the Pincus scaling theory.[85]

In a number of studies (see, for example, Refs 86–88), osmotic attraction of glass or quartz surfaces in solutions of non-adsorbable polyelectrolytes was detected. The attraction is due to a decrease in the polyelectrolyte concentration in the interlayer between the surfaces whose charge has the same sign as the charge of the polymer.

III. Surface forces in wetting phenomena

1. Wetting films

Wetting films are asymmetrical systems. The surface forces involved in these films can be described using the Derjaguin heterocoagulation theory developed for colloids. Unlike the symmetrical system considered in terms of the DLVO theory, in the wetting films, the field of electrostatic forces is no longer symmetrical as the potentials ψ_1 and ψ_2 of the film surfaces differ in magnitude and, in some cases, also in sign. That is why more diverse combinations of the individual components of the surface forces can be realised in this case. Unlike the symmetrical liquid interlayers between identical surfaces, in the case of wetting films, electrostatic forces often become attractive forces, while dispersion forces are repulsive. The latter is due to the fact that the difference between the dielectric permeabilities $(\varepsilon_2-\varepsilon_3)$ in the equation (5b) for dispersion forces becomes negative in the case of wetting films adjacent to air, because for air, $\varepsilon_2 = 1$.

The thickness h of wetting films formed on planar solid substrates is measured by the method of film-reflected light microinterference or by ellipsometry.[89] The disjoining pressure is specified by the hydrostatic pressure

$$\Pi = \rho g H_h ,$$

where ρ is the density of the liquid, g is the acceleration of gravity and H_h is the difference between the liquid levels in a planar horizontal film and in the vessel it communicates with. By varying the film thickness through specifying different hydrostatic pressures H_h, one can obtain the disjoining pressure isotherms $\Pi(h)$ for wetting films.

It was shown by experiment that the thickness of wetting films of nonpolar liquids is mainly determined by the action of dispersion forces and the isotherm $\Pi(h)$ can be described by Eqn (5a) with the constant A_{130} where subscripts 1, 3 and 0 refer to the substrate, the liquid in the film, and air, respectively.

For volatile liquids, it is possible to obtain the isotherms $\Pi(h)$ by measuring the thickness of polymolecular adsorption films at different relative vapour pressures p/p_s in a preliminary evacuated chamber. In this case, the disjoining pressure in the film is equal to

$$\Pi(h) = -\frac{RT}{\upsilon_m}\ln\frac{p}{p_s}, \qquad (11)$$

where υ_m is the molar volume of the liquid.

Agreement of experimental data with the results of calculation (5a) was obtained for 1–4 nm thick films of alkanes (from pentane to octane) on the surface of quartz.[90] The values of A_{130} thus found were similar for all alkanes — the molecules in the films were mainly oriented parallel to the surface and their different lengths did not affect the result. The possibility of this layered orientation was later confirmed by the Monte Carlo method for n-hexadecane near the gold surface.[91]

Good agreement with the theory of dispersion forces was attained in experiments with cyclohexane, which wets the silicon surface, for thicknesses from 1 to 12 nm.[92] The involvement of other components of surface forces can also be expected in experiments with wetting films of polar liquids.

This is exemplified in Fig. 7, which shows the results of ellipsometric measurements of the thickness of wetting water films on quartz surfaces with different degrees of hydrophilicity. The $h(p/p_s)$ isotherms were obtained for a fully hydroxylated surface of crystalline quartz (curve *1*) and a thermally dehydroxylated surface of the same quartz (curve *4*).[93] The degrees of hydrophilicity of these surfaces are described by water contact angles $\theta = 2-3^\circ$ and 43°, respectively. Isotherms *2* and *3* measured for a polished surface of fused quartz ($\theta = 5-10^\circ$ and 20°, respectively) occupy an intermediate position.[94]

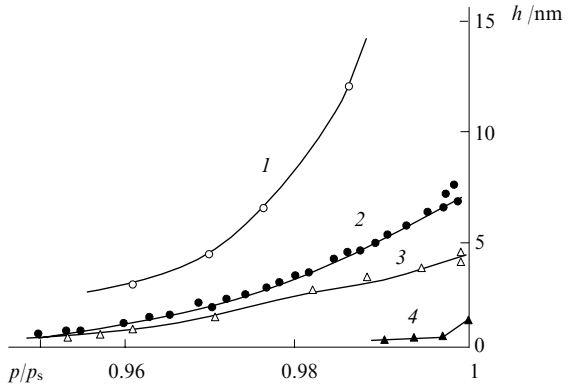

Figure 7. Isotherms of polymolecular adsorption of water vapour on quartz surfaces with different degrees of hydrophilicity. (*1*–*4*) see the text.

The disjoining pressure isotherms obtained for water are consistent with Eqn (8) for structural forces. The influence of electrostatic forces was insignificant, as shown by rough calculations. The involvement of dispersion forces could be expected only for isotherm *4*.

However, it has been shown [95] that isotherms obtained for water films with a thickness of less than 2 nm on mica are not consistent with the isotherms of the theory of dispersion forces. For other polar liquids such as methanol and n-propanol, the isotherms $\Pi(h)$ of thin films (at $p/p_s < 0.8$) are in line with the theory of dispersion forces.[96] However, at a higher vapour pressure, the film thickness exceeds the calculated value due to the additional contribution of electrostatic forces.

Electrolyte solutions form much thicker wetting films, but the region of their existence is limited to a vapour pressure close to saturation. Therefore, the stabilities of these films are studied using the methods described at the beginning of the Section, according to which the disjoining pressure is specified by the hydrostatic pressure (the difference between the liquid levels) or by the capillary pressure of the meniscus.[35, 89] Since electrostatic forces are the longest-range ones, most often, they determine the stability of thick films of aqueous solutions of electrolytes.

The isotherms of the disjoining pressure of the wetting films of aqueous solutions of electrolytes have a characteristic S-shape (Fig. 8). Thick β-films are metastable and at some critical thickness, they break, leaving thinner, thermodynamically stable α-films on the surface. Such films resemble in many aspects the films of pure water on a quartz surface (see Fig. 7).

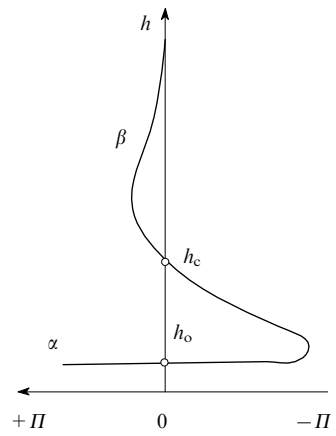

Figure 8. General view of the S-shaped isotherm of disjoining pressure of wetting films including the regions of metastable β-films and thin stable α-films.

The theoretical isotherm for the electrostatic component of the disjoining pressure of water films with the potentials ψ_1 for the boundary with a substrate and ψ_2 for the interface with air has the form

$$\Pi_e(h) = \left(\frac{RTc}{\mathrm{sh}^2(\kappa h)}\right)[2\Phi_1\Phi_2\mathrm{ch}(\kappa h) - (\Phi_1)^2 - (\Phi_2)^2], \qquad (12)$$

where c is the concentration of the solution, mol ml^{-1}, $\Phi = ze\psi/kT$ is the dimensionless potential of the interface.

Using Eqn (12), one can obtain a quantitative interpretation of the upper section of the S-shaped isotherm shown in Fig. 8 and explain the possibility of rupture of β-films upon thinning, namely, switching from the electrostatic repulsion forces, which maintain the stability of thick β-films, to electrostatic attraction forces takes place as the film thickness reaches the critical value

$$h_c = \kappa^{-1}\ln\left(\frac{\psi_1}{\psi_2}\right). \qquad (13)$$

The dependence of the thickness of wetting films on a planar quartz surface on the concentration and pH of an electrolyte (KCl) solution at a constant ionic strength equal to 10^{-3} mol litre^{-1} has been studied by microinterference.[97] The experimental data obtained for thicknesses of about 100 nm were consistent with theoretical results provided that the potentials ψ_1 and ψ_2 of the film surfaces were constant. The potentials ψ_1 and ψ_2 known from electrokinetic measurements and data for foam films were used. According to the theory, the loss of stability occurs at pH < 8 and at an electrolyte concentration of $> 10^{-3}$ mol litre^{-1}. After rupture of the β-films, drops of the bulk solution forming contact angles of 10–25° (which correspond to incomplete wetting) with the remaining thin α-film were left on the surface.

The known analytical solutions for electrostatic forces were obtained for two limiting cases, namely, constant potentials (ψ = const) or constant charges (σ = const) for both film surfaces upon the change in the film thickness. McCormack *et al.*[98] considered cases where different boundary conditions may be fulfilled on the interfaces of the film. In particular, for a constant potential of the surface of the solid substrate (ψ_1 = const) and a constant charge (σ_2 = const) of the film–gas interface, the expression for the electrostatic component of the disjoining pressure assumes the form [94]

$$\Pi(h) = nkT\left[\frac{\Phi_1}{\mathrm{ch}(\kappa h)} + \Phi_2\mathrm{th}(\kappa h)\right]^2 - \Phi_{2\infty}^2, \qquad (14)$$

where n is the concentration of ions; the potential ψ_1 is taken to be independent of the film thickness, and the $\psi_{2\infty}$ potential is taken for $h \to \infty$. As the film thickness decreases, the ψ_2 values start to depend on the thickness, which corresponds to a constant charge σ_2 of the film–gas interface.

The film rupture under the conditions described above takes place at a critical thickness h_c, which can be determined from Eqn (14) using the known criterion for film stability, $d\Pi/dh = 0$

$$\mathrm{sh}(\kappa h_c) = \frac{\Phi_{2\infty}}{\Phi_1}. \qquad (15)$$

This expression has been used [99] to explain the stability of 45-nm films of a 10^{-4} M solution of KCl formed between the surface of a thin quartz capillary (r = 4.5 μm) and a gas bubble.

A clear idea of the properties of wetting films of aqueous solutions of electrolytes at different boundary conditions can be gained from Fig. 9. Here curve *1* is the disjoining pressure isotherm calculated from Eqn (14) with dimensionless surface potentials $\Phi_1 = 8$ and $\Phi_{2\infty} = 2$; for comparison, the Figure shows isotherms *2* and *3* calculated for identical boundary conditions at both interfaces of the film (σ = const or ψ = const, respectively). The Figure demonstrates how different electrostatic boundary conditions influence the thickness and stability of wetting films of aqueous solutions of electrolytes. When the charge is constant on both surfaces of the film (curve *2*), the

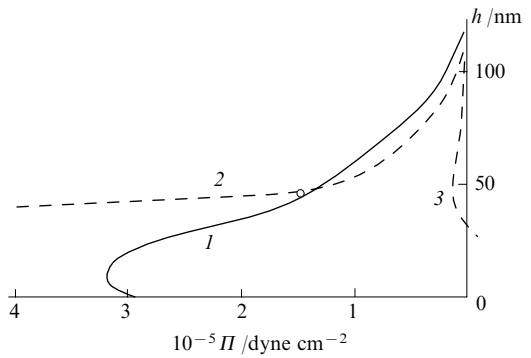

Figure 9. Disjoining pressure isotherms of wetting films calculated for various boundary conditions:
(*1*–*3*) see the text.

films remain stable over a broad range of disjoining pressures, while in the case of constant potentials (curve *3*), the films lose stability even at low pressures when the film thickness approaches the critical value [see Eqn (13)].

The presence of surfactants in aqueous solutions influences considerably the thickness and stability of wetting films. Nonionic surfactants influence the degree of hydrophilicity of the film surfaces; this can change the magnitude and the sign of the short-range structural forces. The influence of the adsorption of ionic surfactants is more pronounced, as it changes the magnitude and the sign of electrostatic long-range forces.

Gee *et al.*[93] have measured the thickness of wetting films on a polished quartz surface as a function of the concentration of aqueous solutions of CTAB by ellipsometry and microinterference. Unlike the preceding studies, the potentials of the film surface ψ_1 and ψ_2 were measured by independent methods.[95] The measurements showed that in the region of $c_{\mathrm{CTAB}} < 10^{-7}$ mol litre^{-1}, the films were metastable, because the surface potentials, though having like signs, still differed in magnitude. On further increase in the surfactant concentration, the films lost stability, and the contact angles they formed with the substrate had a maximum ($\theta \approx 50-60^{\circ}$) at $c_{\mathrm{CTAB}} = 10^{-5}$ mol litre^{-1}. The film stability was restored on approaching the CMC ($c_{\mathrm{CTAB}} \approx 10^{-3}$ mol litre^{-1}) where both film surfaces acquired equal positive charges. The observation of the charge reversal for quartz surfaces in solutions of CTAB has been used, in particular, to evaluate the efficiency of flotation.[100]

The rupture of wetting films of aqueous solutions of another cationic surfactant, dodecylamine, has been observed at concentrations below the CMC.[101] The effect of an anionic surfactant, sodium dodecyl sulfate, on the stability of water wetting films is less pronounced, because its presence increases only slightly the negative charge of the quartz surface.[102] Upon adsorption of sodium dodecyl sulfate, the negative charge of the second surface of the film also increases; therefore, film stability is enhanced.

Comparative analysis of the results obtained for wetting and foam films of surfactant solutions has provided an explanation for the difference in their stability mechanisms.[103, 104]

The same experimental methods were employed to study films of aqueous solutions occurring between a solid surface and a liquid immiscible with water (*e.g.*, oil).[105, 106] Such systems can model emulsion films.

The thickness of a water film formed between quartz and silicone oil (with a molecular mass of 2400) was $\approx 50-60$ nm at a concentration of the background electrolyte (KCl) of 10^{-4} mol litre^{-1} (see Ref. 105); this was much smaller than the thickness of a wetting film adjacent to air. Similar results have been obtained for films of aqueous solutions of CTAB with a concentration from 4×10^{-4} to 10^{-3} mol litre^{-1} in contact with silicon oil or tetradecane. Under these conditions, either an oil-in-water or a water-in-oil emulsion is formed in quartz capillaries, depending on the direction of movement of the oil–water meniscus.[107]

Stable water films were also observed between quartz and xylene,[105] in particular, with solutions containing nonionic surfactants.[106]

Let us consider how the presence of a polymer in the solution influences the wetting film stability. A substantial additional contribution can be expected from steric repulsion forces, caused by the deformation of the polymer adsorption layers when they are brought into contact. The radius of action of these forces depends on the length of the macromolecule and its conformation in the adsorbed state.

Gasanov *et al.*[108] have obtained disjoining pressure isotherms for wetting films of aqueous solutions of polyethylene oxide with a molecular mass of 6×10^5 on a planar quartz surface. However, the thickness of the adsorption layer of the polymer on quartz (20 nm) was much smaller than the thickness of the films studied (50–100 nm). Therefore, the role of the polymer was only to decrease somewhat the film thickness (by 5–10 nm) due to shielding of a part of the surface charge of quartz by the macromolecules adsorbed due to the formation of hydrogen bonds with the surface hydroxy groups.

In wetting films of aqueous solutions of the triblock copolymer F108 with a molecular mass of 1.4×10^4 whose molecules are composed of the central hydrophobic polypropylene oxide block and two terminal hydrophilic PEO blocks, adsorption took place on both interfaces.[109] As the adsorption layers approached each other and finally overlapped, stable (due to steric repulsion forces) 30–40-nm thick films were formed.

The use of cationic polyelectrolytes also allows one to stabilise wetting films. In solutions of the highly charged styrene/dimethylaminopropylmaleimide polymers, the major effect is due to electrostatic forces.[110] In this case, the stability of wetting films can be controlled by varying the composition and chain length of the polymer and the charge and conformation of molecules in solutions with different ion compositions.

2. Wetting control

The use of disjoining pressure isotherms of wetting films makes it possible to estimate the contact angles θ formed by liquids on solid substrates. The corresponding expression is derived from combination of the Frumkin–Derjaguin theory of free surface energy γ_{sv} of a solid substrate coated by an equilibrium wetting film with the thickness h_0,

$$\gamma_{\mathrm{sv}} = \gamma_{\mathrm{sl}} + \gamma_{\mathrm{lv}} + G(h_0), \tag{16}$$

where $G(h_0)$ is the free Gibbs energy of the equilibrium film

$$G(h_0) = \int_{h_0}^{\infty} \Pi(h)\mathrm{d}h,$$

on the one hand, and the known Young equation

$$\gamma_{\mathrm{lv}} \cos\theta = \gamma_{\mathrm{sv}} - \gamma_{\mathrm{sl}}, \tag{17}$$

where γ_{lv} is the surface tension of the liquid, γ_{sl} is the free energy of the solid–liquid interface, on the other hand. By combining the two equations, we get [110–112]

$$\cos\theta = 1 + \frac{G(h_0)}{\gamma_{\mathrm{sl}}}. \tag{18}$$

The equilibrium film thickness h_0 can be found by solving the equation of the overall isotherm, which includes the dispersion, electrostatic, structural and steric forces

$$\Pi(h) = \Pi_{\mathrm{m}}(h) + \Pi_{\mathrm{e}}(h) + \Pi_{\mathrm{s}}(h) + \Pi_{\mathrm{ster}}(h) = 0\,. \tag{19}$$

The equilibrium film thickness h_0 is determined as the smallest root of Eqn (19), which corresponds to intersection of the isotherm with the axis of thicknesses (see Fig. 8). This method of calculation can be used for macroscopic drops and meniscuses

where the equilibrium vapour pressure above the film is close to the saturation pressure.

Examples of calculations of the dependences of contact angles on the magnitude and sign of the surface charge, the Hamaker constants and the structural repulsion and hydrophobic attraction forces have been reported.[111–113] Comparison of the results of calculations with experimental data showed that the effect of hydrophilic repulsion forces can be detected at contact angles of $\theta < 15-20^\circ$, while the effect of hydrophobic attraction forces, at $\theta > 50-60^\circ$. In the intermediate region of θ values, wetting can be described using the DLVO theory.

The proposed calculation methods can be used to predict wetting and to select the optimal composition of solutions that ensure the required process conditions, for example, for flotation, dust extraction and capillary impregnation.

This work was written with partial financial support of the Russian Foundation for Basic Research (Project No. 01-03-32112).

References

1. B V Derjaguin, N V Churaev, V M Muller *Poverkhnostnye Sily* (Surface Forces) (Moscow: Nauka, 1987)
2. W B Russel, D A Saville, W R Schowalter *Colloidal Dispersions* (Cambridge: Cambridge University Press, 1989)
3. B V Derjaguin *Kolloid. Zh.* **17** 207 (1955)
4. B V Derjaguin *Zh. Fiz. Khim.* **6** 1306 (1935)
5. L N McCartney, S Levine *J. Colloid Interface Sci.* **30** 345 (1969)
6. D J Mitchell, B V Ninham *J. Chem. Phys.* **56** 1117 (1972)
7. J E Kiefer, V A Parsegian, G H Weiss *J. Colloid Interface Sci.* **67** 140 (1978)
8. J Chen, A Anandarajan *J. Colloid Interface Sci.* **180** 519 (1996)
9. L Beloni, O Spalla *Ber. Bunsen-Ges. Phys. Chem.* **100** 905 (1996)
10. E M Lifshits *Zh. Eksp. Teor. Fiz.* **29** 94 (1955)
11. I E Dzyaloshinskii, E M Lifshits, L P Pitaevskii *Zh. Eksp. Teor. Fiz.* **37** 229 (1959)
12. H C Hamaker *Physica* **4** 1058 (1937)
13. H B Casimir, D Polder *Phys. Rev.,* **73** 36 (1948)
14. J Visser *Adv. Colloid Interface Sci.* **3** 331 (1972)
15. D B Hough, L R White *Adv. Colloid Interface Sci.* **14** 3 (1980)
16. M K Chaudhury, R J Good *J. Colloid Interface Sci.* **94** 292 (1983)
17. Ya I Rabinovich, N V Churaev *Kolloid. Zh.* **46** 69 (1984) [a]
18. R R Fernandez-Varea, R Garcia-Molina *J. Colloid Interface Sci.* **231** 394 (2000)
19. R R Dagastine, D C Prieve, L R White *J. Colloid Interface Sci.* **231** 351 (2000)
20. L Bergstrom *Adv. Colloid Interface Sci.* **70** 125 (1997)
21. J N Israelachvili *Intermolecular and Surface Forces* (New York: Academic Press, 1985)
22. D Y C Chen, R M Pashley, R L White *J. Colloid Interface Sci.* **77** 283 (1980)
23. S S Dukhin *Adv. Colloid Interface Sci.* **44** 1 (1993)
24. R Kjellander *Ber. Bunsen-Ges. Phys. Chem.* **100** 894 (1996)
25. G Toikka, R A Hayes *J. Colloid Interface Sci.* **191** 102 (1997)
26. I Larson, C J Drummond, D Y C Chen, F Grieser *Langmuir* **13** 2109 (1997)
27. B V Zhmud, A Meurk, L Bergstrom *J. Colloid Interface Sci.* **207** 332 (1998)
28. O Teschke, E F de Souza, G Ceotto *Langmuir* **15** 4935 (1999)
29. S S Dukhin, J Lyklema *Kolloid. Zh.* **53** 466 (1991) [a]
30. A M Islam, B Z Chowdhry, M J Snowden *Adv. Colloid Interface Sci.* **62** 109 (1995)
31. R G Horn, D T Smith *J. Non-Cryst. Solids* **120** 72 (1990)
32. Q Du, E Freysz, Y R Chen *Science* **264** 826 (1994)
33. N V Churaev *Kolloid. Zh.* **58** 725 (1996) [a]
34. G A Martynov *Zh. Fiz. Khim.* **73** 1744 (1999) [b]
35. N V Churaev *Fizikokhimiya Protsessov Massoperenosa v Poristykh Telakh* (Physical Chemistry of Mass Transfer Processes in Porous Solids) (Moscow: Khimiya, 1990)
36. A A Kornyshev, S Leikin *Phys. Rev. A* **40** 6431 (1989)
37. V S Mitlin, M M Sharma *J. Colloid Interface Sci.* **157** 447 (1993)
38. A Trokhimchuk, D Henderson, D T Wasan *J. Colloid Interface Sci.* **210** 320 (1999)
39. R Winkler, A Gerstmair, P Reineker, N Matsuda, D Y Yoon *Int. J. Quantum Chem.* **52** 437 (1994)
40. J Forsman, B Jonsson, C E Woodward *J. Phys. Chem. B* **101** 4253 (1997)
41. M Hato *J. Phys. Chem.* **100** 18530 (1996)
42. H K Christenson, P M Claesson *Adv. Colloid Interface Sci.* **91** 391 (2001)
43. W A Ducker, Z Xu, J N Israelachvili *Langmuir* **10** 3279 (1994)
44. E Ruckenstein, N Churaev *J. Colloid Interface Sci.* **147** 535 (1991)
45. V S J Craig, B W Ninham, R M Pashley *Langmuir* **15** 1562 (1999)
46. L Meagher, V S Craig *Langmuir* **10** 2736 (1994)
47. N Ishida, M Sakamoto, M Miyahara, K Higashitani *Langmuir* **16** 5681 (2000)
48. N Ishida, T Inoue, M Miyahara, K Higashitani *Langmuir* **16** 6377 (2000)
49. R F Considine, C J Drummond *Langmuir* **16** 631 (2000)
50. Y Gu, D Li *J. Colloid Interface Sci.* **226** 328 (2000)
51. Z M Zorin, T Kolarov, N E Esipova, D Platikanov, I P Sergeeva *Kolloid. Zh.* **52** 666 (1990) [a]
52. E D Shchukin, A V Pertsov, E A Amelina *Kolloidnaya Khimiya* (Colloid Chemistry) (Moscow: Moscow State University, 1982) p. 176
53. I Larson, C J Drummond, D Y C Chan, F Grieser *J. Am. Chem. Soc.* **115** 11885 (1993)
54. Y Q Li, N J Tao, J Pan, A A Garsia, S M Lindsay *Langmuir* **9** 637 (1993)
55. D T Atkins, R M Pashley *Langmuir* **9** 2232 (1993)
56. A Carambassis, M W Rutland *Langmuir* **15** 5584 (1999)
57. V V Yaminsky, B W Ninham, R M Pashley *Langmuir* **12** 3223 (1998)
58. S Bhattacharjee, C-H Ko, M Elimelech *Langmuir* **14** 3365 (1998)
59. E Veeramasunneni, Y Hu, M R Yalamanchili, J D Miller *Langmuir* **188** 473 (1997)
60. I P Sergeeva, V M Muller, M A Zakharova, V D Sobolev, N V Churaev *Kolloid. Zh.* **57** 400 (1995) [a]
61. V M Muller, I P Sergeeva, N V Churaev *Kolloid. Zh.* **57** 368 (1995) [a]
62. P Kekicheff, H K Christenson, B W Ninham *Colloids Surf.* **40** 31 (1989)
63. I P Sergeeva, V D Sobolev, N V Churaev, H-J Jakobasch, P Veidenkhammer, F I Shmitt *Kolloid. Zh.* **60** 645 (1998) [a]
64. W A Ducker, E J Wanless *Langmuir* **15** 160 (1999)
65. M W Ruthland, J L Parker *Langmuir* **10** 1110 (1994)
66. Z M Zorin, E K Gasanov, N E Esipova, I N Kornil'ev *Kolloid. Zh.* **53** 25 (1995) [a]
67. E N Nikologorskaya, V A Kosaikin, N V Churaev *Kolloid. Zh.* **52** 502 (1990) [a]
68. I Pezron, E Pezron, P M Claesson, M Malmsten *Langmuir* **7** 2248 (1991)
69. K Eskilsson, B W Ninham, F Tiberg, V V Yaminsky *Langmuir* **14** 7287 (1998)
70. A Dedinaite, B Campbell *Langmuir* **16** 2248 (2000)
71. S Zauscher, D J Klingenberg *J. Colloid Interface Sci.* **229** 457 (2000)
72. A Milling, S Biggs *J. Colloid Interface Sci.* **170** 604 (1995)
73. B A Costello, P F Luckham, Th F Tadros *Colloids Surf.* **34** 301 (1989)
74. P G de Gennes *Adv. Colloid Interface Sci.* **27** 189 (1987)
75. J Klein, P Luckham *Nature (London)* **300** 429 (1982)
76. P F Luckham, P G Hartley *Adv. Colloid Interface Sci.* **49** 341 (1994)
77. A Waltermo, M Sjoberg, B Anhede, P M Claesson *J. Colloid Interface Sci.* **156** 365 (1993)
78. M A G Dahlgren, P M Claesson, R Audebert *J. Colloid Interface Sci.* **166** 343 (1994)
79. S Biggs, A D Proud *Langmuir* **13** 7202 (1997)
80. P G Hartley, P J Scales *Langmuir* **14** 6948 1998
81. I P Sergeeva, T B Ermakova, V D Sobolev, N V Churaev *Kolloid. Zh.* **65** 662 (2003) [a]
82. P Berndt, K Kurihara, T Kunitake *Langmuir* **8** 2486 (1992)

83. J M Berg, P M Claesson, R D Neuman *J. Colloid Interface Sci.*, **161** 182 (1993)
84. M Malmsten, P Claesson, G Siegel *Langmuir* **10** 1274 (1994)
85. T Abraham, S Giasson, J F Gohy, R Jerome *Langmuir* **16** 4286 (2000)
86. E S Pagac, R D Tilton, C Prieve *Langmuir* **14** 5106 (1998)
87. A J Milling, K Kendall *Langmuir* **16** 5106 (2000)
88. S Biggs, J L Burns, Y-de Yan, G J Jameson *Langmuir* **16** 9242 (2000)
89. B V Derjaguin, N V Churaev *Smachivayushchie Plenki* (Wetting Films) (Moscow: Nauka, 1984)
90. M L Gee, T W Healy, L R White *J. Colloid Interface Sci.* **131** 19 (1989)
91. S Balasubramanian, M L Klein, J I Siepman *J. Chem. Phys.* **103** 3184 (1995)
92. I M Tidswell, T A Rabedeau, P S Pershau *Phys. Rev. B* **49** 10869 (1991)
93. M L Gee, T W Healy, L R White *J. Colloid Interface Sci.* **140** 450 (1990)
94. N V Churaev *Kolloid. Zh.* **62** 581 (2000) [a]
95. D Beaglehole, E Z Radzinska, B W Ninham, H K Christenson *Phys. Rev. Lett.* **66** 2084 (1991)
96. M L Gee, T W Healy, L R White *J. Colloid Interface Sci.* **133** 514 (1989)
97. I N Kornil'ev, Z M Zorin, N V Churaev *Kolloid. Zh.* **46** 892 (1984) [a]
98. D McCormack, S L Carnie, D Y C Chan *J. Colloid Interface Sci.* **169** 177 (1995)
99. A P Ershov, Z M Zorin, V D Sobolev, N V Churaev *Kolloid. Zh.* **63** 179 (2001) [a]
100. L Alexandrova, R J Pugh, F Tiberg, L Grigorov *Langmuir* **15** 7464 (1999)
101. P Somasundaran, S Simpson, I Ivanov, R K Jain, D Sarkar *Langmuir* **15** 7658 (1999)
102. Z M Zorin, E K Gasanov, N E Esipova, I N Kornil'ev *Kolloid. Zh.* **53** 25 (1991) [a]
103. T Kolarov, R Yankov, N E Esipova, D Exerova, Z Zorin *Colloid Polym. Sci.* **271** 519 (1993)
104. D Exerova, N V Churaev, T Kolarov, N E Esipova, N Panchev, Z M Zorin *Adv. Colloid Interface Sci.* **104** 1 (2003)
105. N P Hankins, J A Haynes, S D Lubetkin, in *Chemical Colloids and Interfaces in Oil Production* (Paris: Technip, 1992) p. 59
106. B P Binks, W S Cho, P D I Fletcher *Langmuir* **13** 7180 (1997)
107. A P Ershov, N E Esipova, M A Zakharova, Z M Zorin, G A Iskandyar, E A Madzharova, I P Sergeeva, V D Sobolev, T F Svitova, N V Churaev *Kolloid. Zh.* **56** 53 (1994) [a]
108. E K Gasanov, I P Sergeeva, V D Sobolev, Z M Zorin, N V Churaev *Kolloid. Zh.* **53** 617 (1991) [a]
109. N E Esipova, S V Itskov, N V Churaev *Kolloid. Zh.* **64** 775 (2002) [a]
110. I P Sergeeva, T B Ermakova, N V Churaev, K Grundke, O Yudin *Kolloid. Zh.* **64** 531 (2002) [a]
111. N V Churaev *Kolloid. Zh.* **56** 707 (1994) [a]
112. N V Churaev, V D Sobolev *Kolloid. Zh.* **57** 888 (1995) [a]
113. N V Churaev, V D Sobolev *Kolloid. Zh.* **62** 278 (2000) [a]

[a] — *Colloid. J. (Engl. Transl.)*
[b] — *Russ. J. Phys. Chem. (Engl. Transl.)*

Russian Chemical Reviews **73** (1) 37 – 58 (2004) © 2004 Russian Academy of Sciences and Turpion Ltd

DOI 10.1070/RC2004v073n01ABEH000861

Physicochemical dynamics of disperse systems

N B Uriev

Contents

I.	Introduction	37
II.	Main conditions for structure formation in disperse systems	37
III.	Destruction of disperse systems in dynamic conditions	41
IV.	Conclusion	56

Abstract. Results of studies of physicochemical dynamics of disperse systems, which is a new and rapidly developing field of physical chemistry, are generalised. Most attention is given to frequently occurring disperse systems composed of a solid phase and a liquid dispersion medium. The dynamics of contact interactions between particles of disperse solid phases is a key element of the dynamics of such systems. The physicochemical factors responsible for contact interactions are considered in relation to the bulk structural – rheological properties of disperse systems. The bibliography includes 114 references.

I. Introduction

Among disperse systems, highly dispersed systems characterised by a highly developed interface are of most interest. These are first and foremost structured systems [1, 2] in which dispersed structures form spontaneously through intermolecular interactions due to contacts between particles. Traditionally, the properties of these systems were studied primarily under static conditions.[3] The present review is devoted to problems associated with the behaviour of such systems in dynamic conditions typical of both various chemical engineering processes and many natural phenomena.

Such fields of science as molecular and Brownian dynamics have been extensively developed.[4, 5] The case in point is physicochemical dynamics of microheterogeneous systems [6] containing particles, whose sizes can be substantially (by 2 – 3 orders of magnitude) larger than the sizes of colloidal particles. This area of physical chemistry of disperse systems borders on physicochemical hydrodynamics,[7] which deals with processes occurring in the vicinity of the surface of an individual particle of a solid phase (or a solid – liquid interface), as well as on physicochemical hydrodynamics of capillary systems.[8]

Physicochemical dynamics of disperse systems treats predominantly dynamic processes taking place in ensembles of particles of dispersed phases linked in a spatial structural network through dispersion forces, the mechanism of decomposition of such systems under dynamic exposure conditions to form aggregates, their evolution, interactions with each other and a dispersion medium (up to decomposition into individual particles to release a dispersion medium immobilised in these aggregates). Within the framework of physicochemical dynamics, not only destruction of aggregates but also reverse processes of structure formation under conditions of dynamic action on a dispersion medium are considered.

Physicochemical dynamics includes dynamics of contact interactions between particles as the major component,[9 – 13] which determines the characteristic features of destruction and the mechanism of structure formation in disperse systems in dynamic conditions.

The present review is devoted to the following problems: conditions and the mechanism of structure formation in disperse systems, criteria for their destruction under dynamic conditions, verification of the type and intensity of dynamic actions on structured disperse systems, the dynamics of contact interactions between particles of dispersed phases, including those in the presence of a surfactant adsorption layer on their surface, the flow mechanism for structured disperse systems (fundamentals of the flow theory) in dynamic conditions with substantiation of ways and procedures for achieving the maximum fluidity upon complete deaggregation.

The maximum fluidity is required for creating the optimum dynamic state of disperse systems corresponding to the main condition for optimisation and intensification of various heterogeneous chemical engineering processes in such systems as well as processes for the production of a broad spectrum of dispersed composition materials.

The main concepts in physicochemical dynamics of disperse systems were finally developed in the last 10 – 15 years. However, since some fundamental aspects in this field of physical chemistry of disperse systems have been published before that time, the earlier studies are also briefly considered and analysed in the present review.

II. Main conditions for structure formation in disperse systems

1. Types of contacts between particles in disperse systems

In spite of an enormous variability in the chemical composition and physical properties of disperse systems, most of them are characterised by a combination of two major features: the presence of a highly developed interface and a high concentration of a dispersed phase in a liquid (or gaseous) dispersion medium. As a consequence, these systems have a high interface free energy (F^*). The free energy of systems always tends to decrease. Hence, processes accompanied by a decrease in this energy (ΔF^*) can occur spontaneously in disperse systems.[14]

N B Uriev Institute of Physical Chemistry, Russian Academy of Sciences, Leninsky prosp. 31, 119991 Moscow, Russian Federation.
Fax (7-095) 335 17 78. Tel. (7-095) 955 46 42.
E-mail: uriev@phyche.ac.ru

Received 3 July 2003
Uspekhi Khimii **73** (1) 39 – 62 (2004); translated by T N Safonova

The free energy can decrease due to formation of contacts between particles on coagulation, which proceeds particularly extensively in lyophobic aggregation-unstable disperse systems. When a certain critical concentration of particles of dispersed phases in liquid or gaseous dispersion media (φ_c) is achieved, this process leads to the spontaneous formation of a spatial structural network. The major components of the latter are the contacts between the particles and the particles as such, which form spatial cells in the bulk of the disperse system. In this case, the disperse system becomes structured, *i.e.*, is transformed from a free dispersed state to a bound dispersed (aggregated) state.

The formation of three-dimensional structures leads to radical changes in the main structural and mechanical properties of such systems. These systems completely lose aggregation stability but become stable with respect to sedimentation, because a structural network prevents particles of immobilised dispersed phases from precipitating. At the same time, such systems lose fluidity and high mobility. Their viscosity continuously increases as the dispersity increases (and, correspondingly, as the size and concentration of particles in dispersion media decrease). Structured disperse systems are characterised by the modulus of elasticity and the ultimate strength τ_p (or P_m). These are only the most typical features of such systems.

Of numerous factors responsible for the properties of structured disperse systems, two main groups are associated with the following fundamental parameters:[9–13,15–17] first, the cohesive force f_c and the cohesive (interaction) energy E_c in contacts between particles of dispersed phases; second, the number of contacts n between particles per unit volume.

The strength and energy of interactions in contacts between particles depend on the type (nature) of contacts (Fig. 1, Table 1). The characteristic feature of relatively unstable structures with contacts of the first and second types is their complete reversibility with respect to strength. A consideration of direct (atomic) and coagulation contacts as two different types is somewhat tentative. For example, in the case of strong lyophobic interactions between particles, a liquid in coagulation structures can be completely displaced from the interspace between the particles, and the difference between these types of contacts disappears. After cessation of external mechanical actions, contacts in the destroyed structure can be spontaneously restored to the initial level. This property (so-called thixotropy) is typical of various powder- and paste-like dispersions. Structures with strong phase contacts do not possess this property at all. Such structures (so-called condensation structures) are formed in disperse systems, in which contacts are reversible with respect to strength as a result of phase and/or chemical transformations, for example, upon crystallisation from supersaturated solutions or melts (on their cooling), polymerisation, sintering, plastic deformation on pressing, removal of a liquid dispersion medium, *etc*. The minimum phase

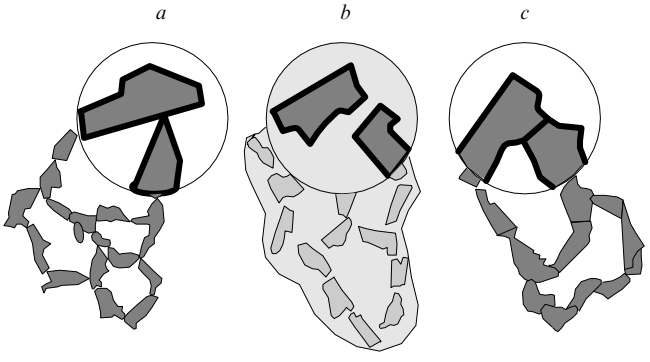

Figure 1. Main types of contacts between particles of dispersed phases according to Rehbinder.[1]
Contacts: (*a*) direct (atomic), (*b*) coagulation, (*c*) phase.

Table 1. Types and characteristics of contacts between particles.

Contacts	f_c/N	E_c/J	Note
Direct (atomic)	10^{-8}–10^{-9}	10^{-17}–10^{-16}	contacts occur in finely dispersed powders
Coagulation	10^{-10}–10^{-8}	10^{-19}–10^{-18}	contacts occur in pastes (suspensions) or emulsions through a thin liquid interlayer
Phase	$\geqslant 10^{-7}$–10^{-6}	$\geqslant 10^{-17}$–10^{-16}	strong contacts typical of condensation structures of dispersed materials

contact corresponds to $\sim 10^2$ interatomic bonds. This contact is essentially no different from an atomic contact typical of finely dispersed powders. Since the contact surface area is only $\sim 10^{-16}$ m^2, the probability of occurrence of a defect is very low, and the strength of the contact approaches that of an ideal solid body. As the area of the phase contact increases, the force f_c generally reaches $\sim 10^{-3}$ N.

The mechanical properties of disperse structures appeared in different steps of structure formation depend on the force f_c for an individual contact determined by its nature as well as on the number of such contacts per unit volume. Coagulation structures play an important role in the properties of disperse systems and (particularly) dispersed materials. It is their formation that is the first step in the synthesis of structured disperse systems and materials.

2. Criteria for the formation of dispersed structures

a. Characteristic critical particle size

Dispersed structures can be generated if two conditions, which determine the critical particle size of a dispersed phase d_c and their critical concentration in liquid or gaseous dispersion media, are fulfilled.

To a first approximation, these conditions can be described as follows.

1. Depending on the type of contacts, systems have a particular characteristic critical particle size; if $d < d_c$ (d is the characteristic particle size), the structure can form and exist; if $d > d_c$, the structure becomes unstable in a gravitational field, *i.e.*, can be self-destructed under gravity forces of the particles involved in this structure.

2. At the critical concentration of particles of dispersed phases in a dispersion medium, a spatial structure with the strength $\tau_p > 0$ can form spontaneously.

Let us consider successively the quantitative values of these criteria.

According to the first conditions, the criterion for aggregability characterising the possibility of formation of dispersed structures is based on a simple principle: a coagulation structure in disperse systems can appear if the cohesive forces between particles are comparable to the particle weight (or larger than this weight in a particular dispersion medium [2])

$$f_c \geqslant G^*, \tag{1}$$

where

$$G^* = \rho_{ef}\, d^3 g, \tag{2}$$

G^* is the particle weight, ρ_{ef} is the effective density of the particle in a dispersion medium ($\rho_{ef} = \rho_0 - \rho_1$, where ρ_0 is the density of the solid phase and ρ_1 is the density of the dispersion medium), g is the gravitational acceleration.

For structures with direct atomic contacts (the coordination number of the particle $z = 1$),[1,2,15]

$$d_c \sim \left(\frac{f_c}{\rho_{ef} g}\right)^{1/3}. \quad (3)$$

For dispersions with a liquid medium (pastes, suspensions), which have lyophobic coagulation contacts [15–18] and contain particles in a short-range potential well ('short-range' coagulation: $h \approx h_2$, h is the distance between the particles),[17]

$$\overline{d}_c \sim \frac{k}{h_2}\left(\frac{A^*}{\rho_{ef} g}\right)^{1/2}, \quad (4)$$

where k is the dimensionless coefficient equal to ≈ 0.2 and A^* is the Hamaker constant.

For coagulation structures containing particles in a long-range potential well ('long-range' coagulation, $h \approx h_1$),[15]

$$\overline{d}_c \sim \frac{1}{h_1}\left(\frac{\pi}{2}\frac{B}{h_1 \rho_{ef} g}\right)^{1/2}, \quad (5)$$

where B is the Lifshits constant.

An important result of calculations of d_c for the typical values $A^* \sim 10^{-19}-10^{-20}$ J, $B \approx 10^{-28}$ J m and $\rho_{ef} \sim 2$ is that $d_c \gg 1$ μm and can amount up to 100 μm. This value is several orders of magnitude larger than the size of colloidal particles. Relations (3)–(5) are given with respect to one contact between two particles. This is a hypothetical limiting case characteristic of the initial step of formation of aggregates from particles.

In actuality, the coordination number of particles in the structure is $z \geqslant 2$. Hence, d_c for each of the above-considered structural types can be larger than those calculated by Eqns (3)–(5).

In the general form, the criterion for aggregation in the case of solid phase — liquid medium dispersions can be determined from the condition that the potential energy of interaction between particles in a contact must be comparable to the energy of external actions on the disperse system.[19]

Let us assume that the potential energy of interaction between two spherical particles of radius $r = d/2$ is expressed by the equation

$$U(r, h) = r\,[C_1(h) + C_2(h)], \quad (6)$$

where C_1 describes the contribution of the molecular attractive forces [18]

$$C_1(h) = -\frac{B}{h^2} \quad \text{at } h \gg h_k, \quad (7)$$

$$C_1(h) = -\frac{A^*}{12h} \quad \text{at } h \ll h_k, \quad (8)$$

$h_k \cong 10^{-8}$ m corresponds to the characteristic wavelength of the line in the absorption spectra of atoms and molecules of the contacting particles; $A^* \cong 10^{-19}$ J, $B \cong 10^{-27}-10^{-28}$ J m; $C_2(h)$ reflects the contribution of the Coulombic repulsion forces.[18, 20, 21]

Let us write $C_2(h)$ as follows

$$C_2(h) = 64\pi \frac{NT}{k^2}\gamma^2 e^{-\kappa_1 h}, \quad (9)$$

where N is the concentration of the electrolyte, T is the temperature expressed in terms of energy,

$$\gamma = \text{th}\frac{U_1}{4},\ U_1 = q\frac{\Psi}{T},$$

Ψ is the electrical potential on the particle surface, q is the charge on ions of the electrolyte,

$$\kappa_1 = \left[8\pi q^2 N(\varepsilon T)\right]^{1/2},$$

ε is the dielectric constant.

A sequence of transformations of Eqn (9) gives the following expressions for low ($U_1 \ll 1$) and high ($U_1 \gg 1$) energy potentials at $\kappa_1 h \ll 1$: [21]

$$C_2(h) = A_0\,|\ln \kappa_1 h|, \quad (10)$$

where

$$A_0 = \frac{\delta \varepsilon T^2}{q^2},$$

$$\delta = \begin{cases} \dfrac{\pi^2}{4} & \text{at } U_1 \gg 1, A_0 \sim 10^{-11} \text{ J m}^{-1} \\ 2U_\infty^2 & \text{at } U_1 \ll 1, A_0 < 10^{-11} \text{ J m}^{-1}. \end{cases}$$

Here, U_∞ is the value of U_1 with $h \to 0$.

From Eqns (6)–(8) and (10), it follows that h_{max} corresponding to the maximum of the barrier separating the short- and long-range potential wells can be calculated as follows:

$$h_{max} = \frac{A^*}{12A_0}. \quad (11)$$

In the case of short- and long-range coagulation, the equations for the binding energy of the particles in the structure are as follows:

for short-range coagulation

$$U_2 = z[U(h_{max}) - U(h_2)] = -zA_0 \ln\frac{h_{max}}{h_2} + \frac{zA^* r}{12}\left(\frac{1}{h_2} - \frac{1}{h_{max}}\right), \quad (12)$$

for long-range coagulation

$$U_1 = -zU(h_1) = z\frac{Br}{h_1^2}\left(1 - \frac{2}{\kappa_1 h_1}\right). \quad (13)$$

If the potential energy of interactions between particles (6) is represented as a model function composed of two potential wells taking the shape of parabolic curves of depth U_2 and U_1, the stability (or aggregation) criterion for static conditions is expressed in the general form as follows:

$$U_i > \frac{4}{3}\pi \rho_{ef} r^3 g h_i, \quad (14)$$

The index $i = 1$ corresponds to long-range coagulation, and $i = 2$ corresponds to short-range coagulation. Equation (14) serves as the energy criterion for stability of the structure with respect to sedimentation, *i.e.*, to destruction followed by sedimentation of the particles under their own weight.

A combination of Eqn (14) and the condition for stability of the structure with respect to Brownian motion [3, 15] gives an equation, which determines the range of the critical sizes of particles capable of forming structures stable in static conditions,[19]

$$\frac{d_i}{2} = r_i = \left[\frac{U_i}{r}\left(\frac{4}{3}\pi \rho_{ef} g h_i\right)^{-1}\right]^{1/2}. \quad (15)$$

Assuming that $A^* = 10^{-19}$ J, $A_0 = 10^{-11}$ J m^{-1}, $B = 10^{-27}$ J m, $h_1 \sim 5 \times 10^{-8}$, $h_2 = 10^{-9}$ m, $\rho_0 \sim (1-2) \times 10^3$ kg m^{-3} and $z = 6$, one obtains $d_c/2 \sim 10^{-7}-10^{-5}$ m for systems with long-range coagulation of particles and $d_c/2 \sim 5 \times 10^{-5}-10^{-4}$ m for systems with short-range coagulation.

The maximum values of $d_c/2$ correspond to the criteria for aggregability (4) and (5).

Therefore, calculations of the criterion for aggregability according to Eqns (4), (5) and (15) give analogous results. The values of d_c demonstrate that coagulation structures can form spontaneously in dispersions with particle sizes of tens or even hundreds of micrometers. This indicates that the surface phenomena, contact interactions and structure formation are to a large extent responsible for the properties and characteristic features of most natural disperse systems, which were traditionally assigned to coarsely dispersed materials (for this reason, these materials were treated within the framework of mechanics of continua and hydrodynamics). The following systems belong to such materials: various powdered materials,[2, 22] for example, mineral binders (cements, lime, gypsum); fillers for varnishes and dyes, resins and

polymers; powdered fuels; mineral fertilisers, powders for fire extinction; nutritive disperse systems (flour, sugar powder), paste systems and suspensions, including slurries of chemical industries, suspensions of cellulose fibres used in the production of paper and cartons, suspensions and pastes for the production of porcelain, faience and ceramics; heterogeneous fuels; powdered and paste-like by-products and wastes from manufacturing, in particularly, from concentration plants; numerous natural disperse systems (grounds and soils); bottom sediments of rivers, lakes, seas and oceans.

At the same time, particles in these systems cannot participate in thermal Brownian motion, because their characteristic size is several orders of magnitude larger than the colloidal particle sizes. Hence, the conditions for the creation of a dynamic state of particles in such systems (*i.e.*, the movement of these particles necessary for various chemical engineering processes, for example, mass transfer processes) cannot be achieved through thermal motion. To produce a dynamic state analogous to Brownian motion in dilute aggregation-stable (lyophilic) colloids, it is necessary to deliver energy from external sources with an acceleration of no smaller than g.

b. Concentration factor and strength of coagulation structures

Let us consider quantitative estimates of the concentration factor, which determines the possibility of formation of dispersed structures. In essence, the minimum strength of a structural network, which can hold its constituent particles in a gravitational field, can serve as this criterion. Eventually, it is the strength of the structure that is responsible for its stability in dynamic conditions.

The theories of strength developed in the studies [23–26] are based on an additive approximation, which can be represented in the general form as follows:[3]

$$P_m \sim \chi f_c,$$

where χ is the number of contacts between particles per unit surface.

The corresponding plot of the structure strength *vs.* the concentration of a dispersed phase in a dispersion medium is shown in Fig. 2 *a*. A series of additional parameters characterising the degree of an increase in the strength depending on the concentration can be proposed: $\tan\alpha = dP_m/d\varphi$ for $\varphi_0 < \varphi < \varphi_c$ and $\tan\beta'$ for $\varphi > \varphi_c$, where φ_0 and φ_c are the minimum concentrations at the beginning of structure formation and at the beginning of a sharp strengthening, respectively.[2,26]

Assuming the irregular random particle distribution in the bulk (unlike the distribution assumed in the studies [23–26] and the regular particle distribution in the bulk [27–29]),[30] a more general dependence of the strength on the porosity of dispersed structures was obtained. This approach is based on the concepts of the percolation theory.[31,32]

An earlier attempt to solve this problem [33] was based on the use of a simplified model of the Bethe lattice,[34] which is far from real coagulation structures formed in disperse systems.

A model of a lattice of randomly packed spheres [27] used in the study [30] made it possible to take into account the possibility of the formation of dispersed structures characterised by various particle distributions in a broad range of the coordination numbers from 3 to 9.

When developing a theory for the description of the dependence of the structure strength on its relative porosity $v = \varphi/\varphi_0$ by analogy with the dependence of the conductivity on the porosity of the structure consisting of current-conducting spheres,[30–35] the authors proposed the parameter C, which reflects a particular topological property of a disperse system and is determined by the equation

$$C = \frac{P_m(v)}{P_m(I')}, \tag{16}$$

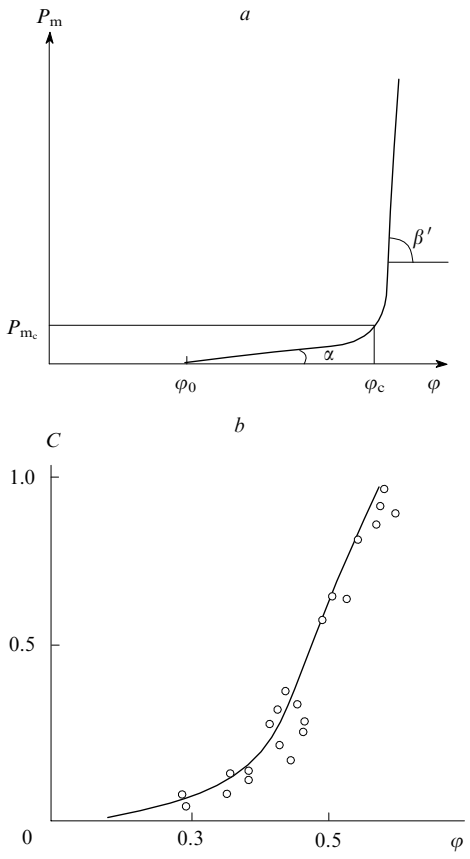

Figure 2. Plots of the strength of dispersed structures *vs.* the concentration (porosity) of a dispersed phase in a dispersion medium.
(*a*) The general character of the dependence,[24] (*b*) the dependence found using the percolation theory; the experimental data are shown by circles.[26]

where $P_m(v)$ is the strength of the porous structure with any effective porosity, $P_m(I')$ is the strength of the system at the maximum volume concentration of the particles (φ_{max}) in the dispersion medium.

The critical relative porosity $v_c = \varphi_0/\varphi_{max}$ corresponds to the maximum porosity at which a structural network is formed in the bulk of a dispersion.

At $v < v_c$,

$C(v) = 0$;

at $v > v_c$ (or $v \to v_c$),

$C(v) = (v - v_c)^{\mu}$,

where μ is determined by the dimensionality of the space (for a three-dimensional space, $\mu \approx 1.8$);[35,36]

at $v \to 1$,

$$C(v) = 1 - K(1 - v), \tag{17}$$

the coefficient K, in turn, depends on the coordination number z

$$K = \frac{2z - 2}{z - 2}. \tag{18}$$

The latter equation allows one to find the dependence of $C(v)$ on the coordination number in the range from 3 to 9, *i.e.*, virtually for all types of quasi-lattices. From Eqns (17) and (18) taking into account the values of K for various z, one has

$$C(\Pi) = 1 - K\left(1 - \frac{1 - \Pi}{1 - \Pi_0}\right) \approx 2.7 - 4.2\,\Pi \tag{19}$$

where $\Pi = 1 - \varphi$, $\Pi_0 = 1 - \varphi_0$.

The experimental data obtained for a model porous structure formed from monodispersed spherical particles of polystyrene and the theoretical dependence (19) are presented in Fig. 2 *b*. It can be seen that there is a good agreement between the theoretical and experimental results.

Based on this theory, the dependences of the strength on the porosity of spatial structures formed in finely dispersed structured systems consisting of clusters and particles and, in a more general case, of aggregates of primary particles (at $d \ll d_c$), were found.

The strength of structures consisting of aggregates can be described by the following equation:[30, 37]

$$C(\varphi) \sim \left(\frac{\varphi}{\varphi_{max}}\right)^{\gamma} \tag{20}$$

where

$$\gamma = 3 + \frac{f/f_a}{3-f},$$

f is the fractal dimensionality of the structure and f_a is the fractal dimensionality of the cluster (aggregate).[38]

This equation is true at $f < 3$. In particular, for percolation clusters, $f_a = 1.8$ at $f = 2.5$, and then $\gamma = 8.8$. For branched clusters, $f_a = 1.5$ at $f = 2$, and then $\gamma = 4.3$.[38–40]

Therefore, Eqns (17), (19) and (20) derived with the use of the percolation theory made it possible to describe the dependence of the strength on the porosity for a random distribution of particles and aggregates in the bulk of the structure. This is the most general case corresponding to real conditions.[41]

III. Destruction of disperse systems in dynamic conditions

1. Dynamic state of disperse systems

Due to the spontaneous formation of a spatial structural network at $d \leqslant d_c$ and $\varphi > \varphi_0$, both a disperse system as a whole and its constituent phases completely lose mobility, *i.e.*, the possibility of relative movement, under static conditions, which is accompanied by the corresponding increase in the viscosity, strength and modulus of elasticity. These structural and rheological characteristics particularly sharply increase at $\varphi > \varphi_c$, whereas φ_c (as well as φ_0) substantially decrease as the dispersity (S) increases at $d \leqslant d_c$. This is also favoured by an increase in the degree of particle anisometry and the occurrence of lyophobic-lyophilic mosaicity on the particle surface, particularly, if the particle surface is predominantly lyophobic. If there are no conditions for easy mobility (fluidity) and, hence, for the possibility of movement of the particles of dispersed phases with respect to each other and relative to a dispersion medium, there is no possibility to carry out various chemical engineering processes and control structural and rheological properties.

For highly concentrated and, particularly, finely disperse systems, this problem is much more difficult to solve because of a spontaneous increase in the number of contacts between particles per unit volume. The line of attack on this problem consists in going from static conditions, in which highly viscous and stable dispersed structures are formed (particularly, at $\varphi \geqslant \varphi_c$ and $d \ll d_c$), to dynamic conditions, in which these structures can be efficiently destroyed due to breaking of coagulation contacts between particles of dispersed phases. These conditions can be achieved by creating an isotropic dynamic state in a disperse system such that an equally probable degree of destruction occurs throughout the bulk of the disperse system. In the limit, coagulation structures are completely destroyed and all coagulation contacts are broken (Fig. 3). It is these conditions that could provide the maximum fluidity and the corresponding lowest viscosity level of the ultimately and isotropically destroyed structure. The dynamic aggregation stability of a disperse system corresponds only to this 'limiting' isotropic dynamic state produced by delivering an energy higher than the cohesive energy to each particle.

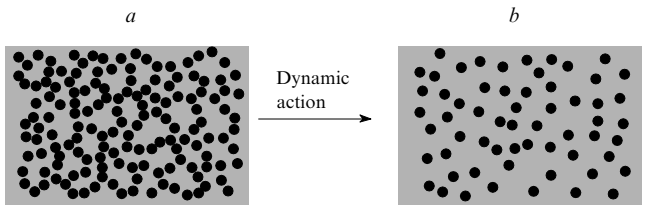

Figure 3. Scheme illustrating conditions for the creation of the optimum dynamic state of disperse systems.
(*a*) A structured dispersion, (*b*) complete ultimate deaggregation.

The type of this energy, its values and conditions of energy delivery to a system depend on the particle size of a dispersed phase, the number of the particles per unit volume, the binding energy between particles (lyophilic or lyophobic interactions) and the viscosity of a dispersion medium.

To determine the main parameters of actions (or their combination) on a disperse system with the aim of creating a controlled dynamic state, it is necessary to determine responses of both individual particles of dispersed phases and the disperse system as a whole to various actions. The responses of particles of dispersed phases to various actions can be described using the characteristic times (τ) of the following microprocesses, which were determined using the dimension theory:[6, 9]

interparticle interactions ($f_{c,\mu}$) through surface forces (molecular attractive forces f_c and Coulombic repulsive forces f_μ)

$$\tau_{f_{c,\mu}} \sim \frac{\eta d^2}{f_{c,\mu}};$$

thermal motion due to the internal energy of molecules of a dispersion medium

$$\tau_B \sim \frac{\eta d^3}{kT};$$

inertial motion of particles under external forces

$$\tau_i \sim \frac{\rho_{ef} d^2}{\eta};$$

sedimentation under gravitational forces

$$\tau_s \sim \frac{\eta}{\rho_{ef} d^2 g},$$

where η is the viscosity of the dispersion medium.

The dependences of the inverse relaxation times of various microprocesses on the particle size are shown in Fig. 4. It can be seen that the contribution of each of the actions on particles to τ (and, correspondingly, to $\dot{\varepsilon} = 1/\tau$) changes substantially (by orders of magnitude) with changes in the particle size; correspondingly, the conditions for producing a dynamic state of disperse systems change.

A combination of the factors responsible for a dynamic state of finely disperse colloidal systems, which are classical objects of physical chemistry of disperse systems and surface phenomena, have been studied in most detail.

For such systems, the main characteristic times of microprocesses of a dynamic state are determined by the ratio between $\tau_{fc,\mu}$ and τ_B. For such systems, the contributions of the inertial effects and sedimentation processes are insignificant due to small masses and sizes of particles.

The possibility of formation of dispersed structures or their self-destruction (deaggregation) in the case of colloidal dispersions is determined by the known criterion [3]

$$U_c \sim \frac{\beta^* kT}{(1/2)z}, \tag{21}$$

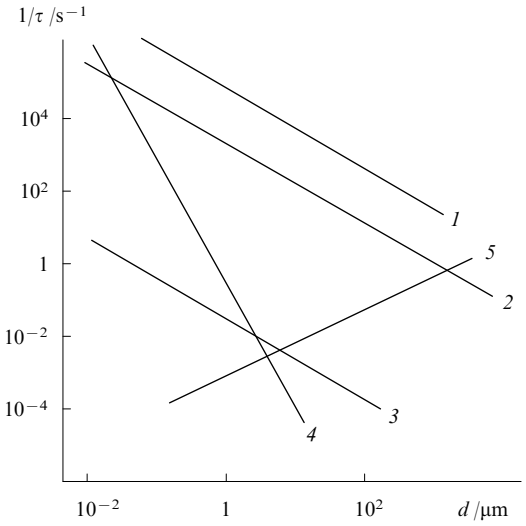

Figure 4. Dependence of the characteristic times of microprocesses on the particle size of a dispersed phase.[9, 30]
(*1*) Inertial effects, (*2*) molecular attraction, (*3*) Coulombic repulsion, (*4*) Brownian motion, (*5*) sedimentation. The results were obtained at $A^* \sim 5 \times 10^{-20}$ J, $\eta \sim 1$ mPa s, $\rho = 2 \times 10^3$ kg m^{-3}.

where U_c is the energy of molecular interactions between the particles in a structural network, β^* is the coefficient

$$\beta^* = \ln \frac{n_a}{n_p},$$

(n_a is the number of particles in the aggregated state, n_p is the number of particles in the deaggregated (peptised) state) and z is the coordination number of particles in a loose aggregate (~ 2).

The coagulation structure in a colloidal disperse system is stable if the energy of molecular interactions between particles is higher than that calculated by Eqn (21). If this energy is lower than the energies of thermal motion and random Brownian oscillations of the particles of dispersed phases, this structure undergoes self-destruction.

In essence, Eqn (21) determines the conditions for the creation of an isotropic dynamic state in colloidal systems. However, if $U_c > (10-15)\,kT$, such systems lose aggregation stability and become also unstable with respect to sedimentation. The dynamic state of such systems loses an isotropic character. When the size of aggregates formed from colloidal particles is larger than 1 μm, the possibility of the creation of a dynamic state under the action of thermal energy of molecular oscillations in a dispersion medium is very low, if at all.

For disperse systems with a particle size larger than 1 μm, the occurrence of an isotropic dynamic state is determined primarily by the relation between $\tau_{fc,\mu}$, τ_i and τ_s.

Based on the above-considered facts, the conditions (criteria) for the attainment of an isotropic dynamic state in disperse systems can be represented in the general form:

for a region of colloidal systems ($d_c < 1$ μm)

$$U_c \geqslant (10-15)\,kT,$$

$$\frac{1}{\tau_B} > \frac{1}{\tau_{f_{c,\mu}}};$$

for a region of microheterogeneous structured disperse systems (1 μm, $< d_c < 100$ μm)

$$E_c = \frac{mV^2}{2} > U_c,$$

$$U_c \sim \frac{k^* d}{h^n},$$

where E_c is the kinetic energy imparted to a particle from an external source of mechanical power, m is the mass of the particle, V is its relative velocity, U_c is the total energy of molecular interactions in contacts between a particle and the adjacent particles, k^* is the constant of molecular interactions between condensed phases, n is the coefficient;

for the region of coarsely disperse systems

$$A > g,$$

where A is an acceleration imparted to a particle from an external source.

Taking into account these criteria, the conditions for the creation of an isotropic dynamic state in structured disperse systems ($\varphi > \varphi_0$ and $d \ll d_c$) are determined by a combination of macroscopic ($\eta_{ef} = \eta_{min}$, where η_{ef} is the effective viscosity) and microscopic parameters.

The conditions for the delivery of energy to a disperse system from an external source depend on the nature of a disperse system. In two-phase systems, such as solid dispersed phase – liquid dispersion medium (pastes, suspensions), liquid – liquid and liquid – gas (foam), the energy is supplied predominantly in the course of their deformation

$$\dot{\varepsilon} = \frac{d\varepsilon}{dt},$$

where $\dot{\varepsilon}$ is the deformation rate, ε is the relative deformation, t is the time. In two-phase systems, such as solid phase – gaseous medium (powders), and three-phase systems, such as solid phase – liquid medium – gaseous medium, the energy is supplied in a combined way by changing both the volume and shape.

However, the choice of the type of action on disperse systems is not limited to only changes in their volume and shape. The determining factor is the possibility of the creation of a controlled isotropic dynamic state in a system under conditions of the chosen type of action.

The main problem in the description of the dynamic state of disperse systems is to reveal the relationship between the contact interactions of the particles of dispersed phases and the bulk properties of the dispersion. For static conditions, this problem was, in essence, solved. The functional relationship between the strength of individual contacts of the particles and the strength of the structure as a whole was found in the context of the theories of strength of dispersed structures. For dynamic conditions, this problem is substantially complicated already because the formation and breaking of individual contacts between the particles occur in non-equilibrium conditions with a simultaneous change in the distance (interspace) between the particles and a manifestation of the hydrodynamic factor associated with leakage of a dispersion medium inside and outside the interspace. Therefore, let us consider the characteristic features of contact interactions between particles of dispersed phases under such conditions prior to analysis of the conditions for the creation of a dynamic state of disperse systems.

2. Dynamics of contact interactions in disperse systems

a. Non-equilibrium as an important feature of the dynamics of contact interactions

To describe the behaviour of most disperse systems in the course of various heterogeneous chemical engineering processes,[41] which proceed under conditions of forced convective diffusion of dispersed phases, as well as of many natural phenomena involving natural disperse systems, it is necessary to go from a consideration of contact interactions in static conditions to non-equilibrium dynamic conditions.

For such processes, a non-equilibrium dynamic state of disperse systems prevails. Interactions between particles to form contacts or, on the contrary, the breaking of contacts can occur at high particle velocities. Therefore, it is incorrect to consider the conditions for their coagulation (breaking of contacts) without regard for the dynamics of their movement toward or away from

each other.† For example, in real heterogeneous processes, $\dot{\varepsilon}$ is as high as 10^2-10^3 s^{-1} under deformation of disperse systems. An analogous situation is observed also when a deformable disperse system is subjected to orthogonally directed oscillation. In the study,[9] it was demonstrated that the relative particle velocities reach 1–1.5 m s^{-1} at the oscillation frequency $f_v = 50$ Hz and the amplitude of $10^{-2}-10^{-3}$ m. The non-equilibrium is even more pronounced in the case of oscillations of polydisperse systems and also in the presence of anisometric particles. As the oscillation frequency increases (particularly, when such dispersions are subjected to low-frequency mechanical oscillation in combination with high-frequency ultrasonic oscillation region), the velocity can substantially exceed 10^3 s^{-1}.

Below are considered the basics of the dynamics of contact interactions predominantly in systems composed of a solid phase and a liquid dispersion medium. The preparation of such dispersions is generally preceded by dynamic processes in solid phase–gas (S–G) systems. In the case of the addition of a liquid medium, the preparation is also preceded by dynamic processes in intermediate solid phase–liquid–gas (S–L–G) systems. Hence, this section of the review deals with certain aspects of the dynamic theory of contact interactions in powders and three-phase systems.

b. Dynamics of contact interactions in two-phase dispersions composed of a solid phase and a liquid dispersion medium

Consideration of the Coulombic component of the disjoining pressure and the slip of a dispersion medium. The solution of problems of dynamic coagulation of particles and, correspondingly, the determination of the conditions for the formation of coagulation contacts are based on calculations of dependences of the force F, which prevents two particles from approaching each other, on the initial velocities, the distance between the particles h and the viscosity of a dispersion medium η.[9–11]

For $h \gg r$ (where r is the particle radius) and the initial velocity V, this force is determined by the equation:

$$F(V,h) = -6\pi\eta r\frac{\mathrm{d}h}{\mathrm{d}t} \equiv \sigma\pi\eta r V. \tag{22}$$

In the case of interaction between two particles in concentrated dispersions, $h \ll r$. Then, taking into account the slip effect of a liquid determined by the coefficient β, the force $F(V,h)$ is given by the expression [9]

$$F(V,h) = \frac{\pi V r^2}{12\beta^2\eta}\left[(h+6\beta\eta)\ln\left(1+6\frac{\beta\eta}{h}\right)-\right.$$
$$\left.-(r+6\beta\eta)\ln\left(1+6\frac{\beta\eta}{r}\right)\right]. \tag{23}$$

In the case of strong slip over the surface of lyophobic particles ($6\beta\eta \gg r$),[47,48] Eqn (23) is simplified

$$F(V,h) = \frac{\pi V r^2}{2\beta}\ln\frac{r}{h}, \tag{24}$$

In the case of weak slip (lyophilic systems, $6\beta\eta \ll r$), $F(V,h)$ is given by the following equation:[9]

$$F(V,h) = \frac{3\pi}{2}\eta\frac{Vr^2}{\beta}. \tag{25}$$

The solution of the problem of inertial coagulation (dynamic conditions) for lyophilic systems in the presence of a high ($U_1 \gg 1$) and low ($U_1 \ll 1$) potential barriers between particles (U_1 is the potential barrier in units of kT) consists in determining the initial critical velocity at which particles approach each other (V_{c_0}), *i.e.*, the maximum velocity above which the particles undergo coagulation,[9]

$$V_{c_0} = V_1\left[\frac{|\ln(A^*kr/12A_0)|}{krA^*/A_0}\right] + V_2\ln\left(12\frac{h_0A_0}{rA^*}\right), \tag{26}$$

where

$$V_1 = \left(\frac{A^*rk'}{6m}\right)^{1/2},$$
$$V_2 = \frac{3}{2}\frac{\pi\eta r^2}{m}, \tag{27}$$

h_0 is the distance between the particle surfaces at the start time ($h_0 \sim r$), m is the effective mass of the particle and k' is the inverse Debye radius.

If the velocity V, at which particles approach each other under an external action, is higher than that calculated by Eqn (26), the particles undergo coagulation.

Analysis of stability in dynamic conditions showed that the Coulombic factor is of importance only in the case of relatively low-intensity external actions. The contribution of this factor decreases, for example, as the deformation rate increases and in the case of deformation of polydisperse systems (particularly, in the presence of strongly anisometric particles). The slip effect of a dispersion medium over the particle surface of a dispersed phase increases substantially as the relative particle velocity increases and the distance between the particles decreases.[9,11–13]

The slip effect is most pronounced when particles with a hydrophobic surface approach each other in a polar liquid.[11] For water, this effect can be attributed, in particular, to the fact that the dipoles of water molecules are parallel to the hydrophobic surface, which substantially facilitates their mobility in the tangential direction and, apparently, decreases the viscosity in a wall boundary layer.[47,48] For example, the slip coefficient β of water relative to hydrophobised quartz can be as high as $\sim 10^{-4}$ m^3 N^{-1} s^{-1} (see Ref. 48). In this case, the contribution of the slip effect is much larger than that for hydrophilic particles. Hence, the corresponding critical velocities will also be substantially different. In the case of weak and strong slip of particles, the critical velocities at which particles approach each other are calculated by the equations [10]

$$V_{c_0} > \frac{9\eta}{4\rho r}\ln\frac{h_2}{h_0}, \tag{28}$$

$$V_{c_0} > \frac{3}{4\beta\rho}\frac{h_0}{r}\gamma, \tag{29}$$

where h_2 is the distance between the particle surfaces at which they are fixed due to dynamic coagulation and γ is the coefficient

$$\gamma = 1 + \ln\frac{r}{h_0}.$$

According to the results of the study,[10] the distance h_2 corresponds to the distance at which the potential energy of interactions between particles has a positive maximum. It should be noted that, due to lyophobic–lyophilic mosaicity of the particle surfaces in real dispersions, the critical coagulation rates are determined by the probability of pair collisions between particles at lyophobic, lyophilic or both lyophobic and lyophilic regions.[49] Taking into account the above three types of collisions, the probability of particle coagulation under dynamic conditions is given by the expression [50]

$$E^* = \alpha(1-\Theta)^2 + \beta^*\Theta + \gamma^*\Theta(1-\Theta), \tag{30}$$

where E^* is the probability of the formation of a bond between two particles, α and β^* are the probabilities of coagulation and

† Strictly speaking, the breaking of a contact even as a result of very slow detachment of particles, *i.e.*, in 'static' conditions, cannot, in essence, be considered as an equilibrium process because the transformation from the 'contact-is-present' state to the 'contact-is-broken' state is accompanied by a series of non-equilibrium phenomena (for example, in a double electrical layer).[42–46]

flocculation, respectively, Θ is the fraction of a modified particle surface, γ^* corresponds to the probability of binding as a result of a contact between a stabiliser immobilised on the surface of one particle and the surface of another particle.

Consideration of the particle shape factor. The consideration of the particle shape is an important problem in the dynamic theory of contact interactions, which was solved in the general case in the studies.[9,10] Below are considered two typical cases. In one of them, the possibility of coagulation of strongly anisometric particles with a very small radius of curvature of the frontal surface (for example, as extended needle-like rods) was taken into account. In another case, the conditions for collision between two disk-like particles in the case of both parallel and 'edge – plane' orientations were considered. The critical rates of dynamic coagulation are expressed by the following equations, respectively:

$$V_{01} = \frac{9\eta}{\rho r_{\max}} \left(\frac{r_1}{r_{\max}}\right)^2, \tag{31}$$

$$V_{02} = 12\frac{\eta}{\rho r_0}\left(\frac{r_2}{r_0}\right)^{1/2} = 12\frac{\eta}{\rho r_{\max}}\left(\frac{3}{2}\right)^{3/4}\left(\frac{r_2}{r_{\max}}\right)^{5/4}, \tag{32}$$

where r_1 is the local radius of curvature of particles of linear size

$$r_{\max} = \left(\frac{3m}{4\pi\rho}\right)^{1/3},$$

m is the mass of particles, ρ is their density, r_0 is the radius of the disk-like particle with thickness $2r_2$, r_2 is the radius of curvature of its frontal surface, $r_2 \ll r_0$. In Eqns (31) and (32), r_1 and $r_2 > 0$.

The plots of the critical coagulation rate *vs*. the particle radius are shown in Fig. 5. It can be seen that the shape factor has a strong effect on the critical coagulation rate. For anisometric particles with a size ratio of 1 : 100, the rate decreases by an order of magnitude. Hydrophobisation of the surface, particularly, of anisometric particles, also leads to a decrease in the critical rate of dynamic coagulation by several orders of magnitude.

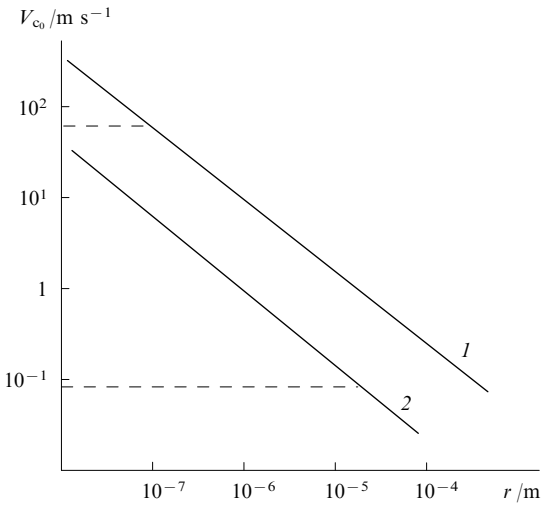

Figure 5. Plots of the coagulation rate *vs*. the particle radius r.[3,10,30] (*1*) For spherical particles ($r = r_0$), (*2*) for anisometric particles ($r_1/r_0 = 0.01$). Dashed lines correspond to particles with a hydrophobic surface.

Role of elastic properties of particles and the structure-mechanical barrier produced by a surfactant adsorption layer. Dynamic particle coagulation is preceded by the approach of the particles to each other accompanied by the displacement of a liquid medium from the interspace between their surfaces. This process is attended by an excess pressure in the interspace and corresponding particle deformation, whose value depends on the outflow rate of the liquid, its viscosity and modulus of elasticity of the particles.[51,52] The contribution of the structural component of the disjoining pressure should be taken into account if the particles are separated by a very small distance ($h_c \sim 2-3$ nm). The range of action of the structural component of the disjoining pressure is $h_c \geqslant 2$ nm.[3,18] For inertial coagulation of particles with a rough surface, the consideration of the roughness leads to an increase in h_c to 100 nm.

As mentioned above, the attainment of the critical coagulation rate V_{c_0} is a prerequisite for the formation of a 'dynamic' contact between particles. If V_{c_0} is higher than a particular value, elastic rebound of particles becomes possible because elastic 'recoil' exceeds the viscous resistance of a liquid to motion. Taking into account this factor, the range of the critical coagulation rates should satisfy the condition determined by the relation

$$\frac{10^2\zeta^2\eta}{\rho r_{\max}} \ll V_{c_0} \ll \frac{10^2\zeta^2\eta}{\rho r_{\max}E}\left(\frac{\eta}{\rho r_{\max}}\right)^2\zeta^4\left[\frac{1}{\zeta}\left(\frac{r_{\max}}{h_c}\right)^5\right]^{4/7}. \tag{33}$$

Here, $\zeta = r_1/r_{\max}$ and E is the modulus of elasticity of the particles. Inertial coagulation of particles under dynamic conditions can take place only in a particular range of the rates V_{c_0}, which depends on the elastic properties, the shape (the degree of anisometry), the density of the particles and the liquid viscosity.

The conditions of aggregation dynamic stability are substantially influenced by the presence of a surfactant adsorption layer on the particle surface and the properties of this layer, *viz*., the binding energy with the particle surface, the elasticity and the degree of lyophilicity of radicals exposed to a dispersion medium. The criterion for loss of aggregation stability under dynamic conditions in the presence of a surfactant adsorption layer on the particle surface can be expressed by the following equation:

$$V_{c_0}^2 - 9\frac{\eta}{\rho r_{\max}}\left(\frac{r}{r_{\max}}\right)^2\lambda^*\ln\left(\frac{h_0}{L}\right)V_{c_0} - \frac{E_L}{2\rho}\left(\frac{L}{r_{\max}}\right)^2\frac{r}{r_{\max}}(\lambda^*)^2\left(\frac{P_L}{E_L}\right)^3 > 0, \tag{34}$$

where r is the local radius of curvature of the particle surface with a surfactant adsorption layer, λ^* is the particle shape coefficient, L is the thickness of the surfactant adsorption layer, P_L and E_L are the strength and the modulus of elasticity of this layer, respectively.

The structure-mechanical barrier is an essential factor of aggregation dynamic stability of a system, if

$$E_L > E_{L_c} \equiv \left(\frac{E_L}{P_L}\right)^3 2\rho\left(\frac{r}{r_{\max}}\right)^3\left(\frac{r_{\max}^2}{L}\right)\left(9\rho\frac{\eta}{r_{\max}}\ln\frac{h_0}{L}\right)^2, \tag{35}$$

where E_{L_c} corresponds to the critical modulus of elasticity, below which a 'breakdown' of the adsorption layer is possible.

c. Aspects of dynamics of contact interactions in finely dispersed powders

A knowledge of the parameters of formation and breaking of direct (according to Rehbinder [1]) contacts between particles under dynamic conditions is necessary for the description of the macrorheological characteristics and properties of powders in processes of flow, compaction or creation of an air-boiling or vibroboiling layer.[53–55]

Contact interactions between particles of solid phases in air and various media under static conditions have been studied extensively (see, for example, Refs 3, 15–17 and 56). The extension of the views of contact interactions, which are based on results of static measurements, to dynamic conditions appeared to be incorrect for dynamic actions on dispersed powders.[9] In particular, this follows from the dependence of the work of detachment on the detachment rate of contacting solid phases.[57–59] The differences in the works of detachment in static and dynamic conditions can be as high as two or even more orders of magnitude. The available methods (even their advanced mod-

ifications) for high-precision measurements of the cohesive forces in contacts allow one to take into account the influence of the detachment rate only at very low values of the latter, which differ from the real values corresponding to conditions of flow, boiling or compaction of powders by several orders of magnitude.

In this connection, approaches were developed,[58–62] which enable one to determine the strength and energy of interactions between particles from the results of dynamic (vibration) measurements with the use of apparatus and methods described in the studies.[58, 59, 61, 62] These approaches involve measurements of the structural and rheological properties of powders (effective shear stresses and viscosities) in the course of compaction or transformation of a powder from the vibrofluidisation state to the vibroboiling state accompanied by breaking of contacts between particles. The developed theory of this process allows one to calculate the energy and strength of interparticle interactions from the results of rheological measurements under vibration.

Equations derived in the studies [58, 61] can be used for determining the characteristics of contact interactions under vibration in powders with the rigorously characterised parameters of the particles (monodispersed spherical particles). As an example, let us give one of these formulas

$$f_{cv}C_v = \frac{\pi a^2 \omega \eta_v^0}{\zeta^*(r^{*2} - r_1^2)\ln(r_2^*/r_1^*)}\,. \tag{36}$$

Here, f_{cv} is the average autohesive force in the contact under dynamic conditions, C_v is the number of autohesive contacts per unit volume in the vibroboiling state, a and ω are the amplitude and circular frequency of vibrations, respectively, r_1^* and r_2^* are the radii of coaxial cylinders of a viscosimeter, ζ^* is the distance of autohesion, whose minimum value is 0.4 nm, η_v^0 is the largest value of the effective vibroviscosity [59] determined by extrapolating the rate of shear deformation to $\dot{\varepsilon} \to 0$.

Calculations using Eqn (36) demonstrated that the cohesive forces under dynamic conditions depend on the rate and acceleration of vibrations. For a number of polymer powders [poly(vinyl chloride), Fluoroplast, polyethylene] in dynamic conditions, f_{cv} is 2–4 orders of magnitude larger than f_c determined in static measurements on an adhesiometer.[15, 16] For glassy particles, these forces differ by no more than a factor of 6–7 (Table 2). The disagreement between the results of static and dynamic measurements increases as the detachment rate of particles increases.

Table 2. Autohesive characteristics of powders in static (f_c) and dynamic (f_{cv}) conditions (at the harmonic vibrational frequency of 200 Hz).

Powder	$\bar{d}$ /μm	$10^8 f_c$ /N	η_k /Pa s	f_{cv} /N
Ion-exchange resin KB-4P2	250	40	–	–
Polystyrene	50	100	40	2×10^{-3}
Poly(vinyl chloride)	20	4	10	3×10^{-3}
Glass	10	30	20	2×10^{-6}
Fluoroplast F30P	5	5	10	9×10^{-5}
Polyethylene	5	2	3	1×10^{-4}

Upon elimination of physicochemical inhomogeneity (lyophilic–lyophobic mosaicity) due to formation of a saturated adsorption monolayer of a surfactant on the particle surface, the cohesive forces in contacts between particles not only sharply decrease (because the particles move away from each other to a distance equal to twice the thickness of the hydrocarbon fragment of the surfactant molecule) but also become virtually independent of the prehistory of the structure formation of a finely dispersed powder (Table 3). Correspondingly, the autohesion level in contacts between particles changes.

To describe the macrorheological and mechanical properties of finely dispersed powders,[62, 63] one should use the characteristics of autohesion determined not in static (as is often the case) but in adequate dynamic conditions.

Table 3. Autohesive forces in contacts between particles of SiO_2 and $CaCO_3$ powders.

φ	$f_{c1}/10^{-5}$ N (without surfactants)	$f_{c2}/10^{-5}$ N (surfactant monolayer)	f_{c1}/f_{c2}
Powder of SiO_2 ($s = 1\times10^3$ m^2 kg^{-1}), surfactant — octadecylamine			
0.45	6.8	2.61	2.6
0.5	22.5	2.25	10.0
0.536	114.0	2.86	40.0
Powder of $CaCO_3$ ($s = 3\times10^3$ m^2 kg^{-1}), surfactant — stearic acid			
0.3	0.645	0.55	1.26
0.35	1.22	0.425	2.88
0.38	1.93	0.48	4.0

Note. Specific surfaces (s) were determined by low-temperature adsorption of nitrogen [Brunauer–Emmett–Teller (BET) method].

d. Dynamics of contact interactions in three-phase systems

The formation of three-phase structures under dynamic conditions in the course of their transformation into two-phase S–L systems (in particular, under conditions of mixing under vibration) proceeds as follows.

Contacts between solid-phase particles in powders are the first to be broken,[62, 63] then a liquid dispersion medium penetrates between the particles [62] to form microgranules, which act as kinetic units. The final step of this process involves association ('coalescence') of granules upon their collisions accompanied by the transformation of the disperse S–L–G system into the S–L system. Let us consider the kinetics of this process.

The structure in a powder is destroyed under vibration if the following condition is fulfilled:

$$a\omega^2 \geqslant \frac{f_c}{\rho d^3}\,, \tag{37}$$

where ρ and d are the density and diameter of the particles, respectively.

If a liquid medium penetrates into a vibroboiling layer consisting of powder particles and wets their surface,[64, 65] a capillary meniscus appears [15] and a granular structure forms. Subsequent interactions between the granules can lead to either their coalescence or recoil.

It can be assumed that the average kinetic energy produced by collisions between granules is determined by the equation

$$\overline{E}_a = D^3\rho_a\left[\overline{(V_a + a\omega\cos\omega t)^2 - V_a^2}\right] \sim D^3\rho_a(a\omega)^2, \tag{38}$$

where D is the diameter of granules, ρ_a is their density, V_a is the granule velocity prior to collisions, the overline denotes the averaging over time.

'Coalescence' of granules occurs if the energy determined by Eqn (38) is smaller than the energy required for the rupture of the meniscus formed between the granules. The energy required for breaking of the contact between two granules linked through a capillary meniscus is equal to $D^2\sigma$, where σ is the surface tension of the liquid phase. From this, the first condition for coalescence of granules can be obtained

$$D \leqslant \frac{\sigma}{\rho_a(a\omega)^2}\,. \tag{39}$$

This inequality determines the condition for cohesion of not-too-large granules (or individual particles), whose collisions can be considered as purely elastic. As the granules grow, their rheological properties become increasingly important. The condition for 'coalescence' of large granules can be obtained by comparing the collision time t of elastic spheres with diameter D (see Ref. 66) and the time of stress relaxation in the granule τ

$$t \sim \frac{D}{C_1^*}\left(\frac{C^*}{V}\right)^{1/5}, \qquad (40)$$

$$\tau \sim \frac{\eta_a}{E_a},$$

where

$$C_1^* \equiv \left(\frac{E_a}{\rho_a}\right)^{1/2},$$

V is the vibrational rate, η_a is the viscosity of the granule, E_a is the modulus of elasticity of the granules.

From this, it follows that the second condition for 'coalescence' of granules is described by the relation

$$D > \eta_a\left(\frac{V}{\rho_a^2 E_a^3}\right)^{1/5}. \qquad (41)$$

By comparing Eqns (39) and (41) on the assumption that $V \sim a\omega$, the following condition, which provides association of the particles to form granules and their subsequent growth, can be written as

$$a\omega < (C_1^*)^{6/11}(C_2^*)^{5/11}, \qquad (42)$$

where

$$C_2^* = \frac{\sigma}{\eta_a}.$$

In simplified form, Eqn (42) can be written as follows:

$$a\omega \leqslant (C_1^* C_2^*)^{1/2} \equiv \left[\frac{\sigma}{\eta_a}\left(\frac{E_a}{\rho_a}\right)^{1/2}\right]^{1/2}. \qquad (43)$$

Conditions (37) and (42) define the range of vibrational rates at which the 'old' S–G structure is destroyed and the 'new' S–L structure is formed in the system:

$$\frac{f_c}{\omega\rho d^3} \leqslant a\omega \leqslant \left[\left(\frac{E_a}{\rho}\right)^{1/2}\left(\frac{\sigma}{\eta_a}\right)\right]^{1/2}. \qquad (44)$$

Hence, in particular, it follows that this range of rates $a\omega$ exists only under high-frequency vibrations.

It should be noted that Eqn (44) was derived on the assumption that the S–G structure is completely destroyed (up to primary particles). However, this process occurs rarely in real highly disperse systems ($d \sim 1$ μm). Therefore, the size of the microaggregates D and their cohesive force F_c should be substituted for d and f_c, respectively, into expressions (37) and (44). In this case, expression (44) takes the form

$$\frac{F_c}{\omega\rho_a D^3} \leqslant a\omega \leqslant \left[\frac{\sigma}{\eta_a}\left(\frac{E_a}{\rho_a}\right)^{1/2}\right]^{1/2}. \qquad (45)$$

In particular, from this it follows that this rate range exists at a relatively high frequency of vibrations, whose value can be calculated by the formula

$$\omega \geqslant \frac{F_c}{\rho_a D^3}\left[\frac{\eta_a}{\sigma}\left(\frac{\rho_a}{E_a}\right)^{1/2}\right]^{1/2}. \qquad (46)$$

As an example, let us consider a model system consisting of a quartz powder ($d \approx 1$ μm) and calcium bentonite serving as a binder. At $A^* \approx 10^{-20}$ J and $h_1 \sim 10^{-8}$ mm, the binding force f_c of particles is $\approx 10^{-11}$ N. Assuming that the modulus of elasticity of granules is of the same order of magnitude as their strength, E_a is taken to be approximately 10^6 N m^{-2}. The viscosity of granules is close to that of the structure formed upon their 'coalescence' $\eta_a \approx 10^2$ Pa s, $\sigma \approx 0.1$ N m^{-1}. Let us assume that the size of inhomogeneities in the structure after granule coalescence is no larger that 30 μm. According to Eqn (46), the minimum vibrational frequency providing the formation of this structure is higher than 100 Hz. From this it follows that the allowable vibrational rate at which an S–L–G system is transformed into an S–L system is ~ 1 m s^{-1}, which is consistent with the experimental data.[2]

All the above have the following important consequences.

The energies and strength of contact interactions between particles in dynamic conditions differ substantially (in some cases, by several orders of magnitude) from the corresponding values measured or calculated in static conditions. This difference depends on the chemical nature and physical properties of dispersed phases and the intensity of external mechanical actions on disperse systems.

The inertial effects and hydrodynamic resistance of a medium[66] as well as the particle shape and lyophobic–lyophilic mosaicity of the particle surface are important factors determining the critical parameters corresponding to conditions of formation or breaking of contacts between particles in liquid media.

Under dynamic conditions, the structure-mechanical barrier (according to Rehbinder) formed by surfactant adsorption layers on the particle surface and the properties of these layers play an essential role in achieving dynamic aggregation stability of dispersions. Micelles in solutions of surfactants can serve an analogous function.[67]

In the case of finely dispersed powders, the energy and strength of interparticle interactions depend substantially on the intensity of external actions.

The dynamics of contact interactions in three-phase disperse systems is determined by a combination of complex processes of formation and breaking of coagulation and direct point contacts between particles, capillary meniscuses between the aggregates and their structural and mechanical properties.

At the same time, the kinetics of structure formation under dynamic conditions and the properties of the resulting structures also depend on the intensity of external actions, in particular, on the frequency and amplitude of oscillations.

3. Dynamic state of two-phase disperse systems of the solid phase – liquid medium type under continuous shear

The method most commonly used for describing the properties of S–L structured disperse systems under continuous shear deformation consists in constructing complete rheological flow curves.[68–73] These curves characterise the dependence of the effective shear viscosity η_{ef} on the shear rate $\dot{\varepsilon}$ or the shear stress P under the necessary condition of isotropic destruction‡ of a dispersion located in the interspace between the surfaces of coaxial cylinders or in a measuring cell of rotational viscosimeters. It is assumed that the shear at a given rate is extended throughout the interspace (or throughout the cell),[69,74] thus providing the isotropic character of destruction.

The complete flow curve of structured dispersions with viscosity drop $\eta_{ef} = f(\dot{\varepsilon},P)$ of up to 8–10 orders of magnitude on the assumption that the above conditions are fulfilled, *i.e.*, under purely homogeneous shear (according to Rehbinder), was first reported in the study.[75] The authors of the cited study introduced the notions of the highest viscosity of a virtually non-destroyed structure (η_0), which corresponds to the upper plateau in the flow curve, and the lowest Newtonian viscosity of an ultimately destroyed structure (η_{min} or η_∞).

‡ For the same degree of destruction in the bulk of the disperse system under consideration.

It was assumed that each level of the measured effective viscosity corresponds to a particular equilibrium level of isotropic destruction characterised by a certain ratio between the broken and acting coagulation contacts between particles of dispersed phases.

Consequently, the minimum level of the lowest Newtonian viscosity and, accordingly, the maximum fluidity should correspond to the limiting isotropic dynamic state. This interpretation of the flow mechanism of structured dispersions under continuous shear was embodied in studies of the rheological properties of various disperse systems.[68, 69, 71, 74] These notions were developed, primarily, by elaborating the idea of the aggregation (cluster) mechanism of destruction with complete deaggregation at $\eta_{ef} = \eta_{min}$ (Refs 76–81) as well as by introducing Krieger's correction (d^3/kT),[82] which takes into account the contribution of Brownian motion. This contribution is essential for dispersions containing particles of characteristic size $\ll 1$ μm (Fig. 6).

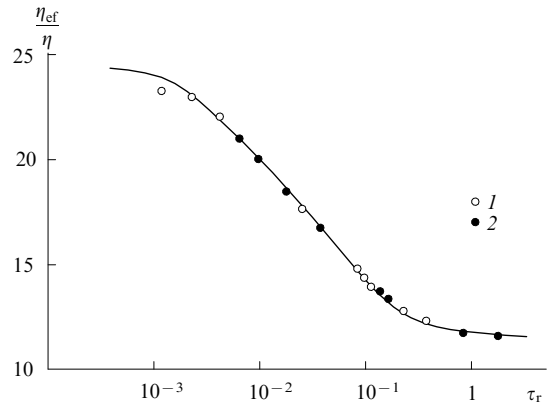

Figure 6. Plot of the relative viscosity *vs*. the effective shear stress τ_r for a suspension of polystyrene particles taking into account Krieger's correction.[82]
(*1*) In benzyl alcohol, (*2*) in cresol.

According to these views, the flow mechanism of structured dispersions as successive destruction under the action of the increasing shear rate $0 < \dot{\varepsilon} < \dot{\varepsilon}_\infty$ (or increasing shear stress P) is as follows: breaking of the bonds followed by their virtually complete recovery in a flow ($\eta_{ef} \approx \eta_0$ with $\dot{\varepsilon} \to 0$), destruction first into superaggregates and then into aggregates with the possible formation of new aggregates through inertial coagulation (at $\eta_\infty < \eta_{ef} < \eta_0$ and $0 < \dot{\varepsilon} < \dot{\varepsilon}_\infty$) and, finally, complete deaggregation at $\eta_{ef} \approx \eta_{min}$ and $\dot{\varepsilon} \geqslant \dot{\varepsilon}_\infty$.

The known flow theories involving this mechanism can be arbitrarily divided into two groups.[30, 76] The theories of one group are based on the concept of the 'average field',[77, 78] which assumes that particles linked in poorly deformable spherical aggregates exist in a homogeneous medium with viscosity η_i. These theories are applicable primarily to dilute and moderately concentrated structured dispersions.

The effective viscosity of thixotropic systems can be estimated according to the equation [9, 30]

$$\frac{\eta_{ef}}{\eta_1} = 1 + \frac{1}{\eta_{ef}/\eta_2 + (\dot{\varepsilon}\tau)^n}, \tag{47}$$

where $\eta_1 \equiv \eta_{ef}(\dot{\varepsilon} \to 0)$, τ is the relaxation time of the major process of interactions between particles through surface forces

$$\tau = \frac{\eta_1 d^2}{f_c},$$

the exponent n depends on the type of the structural model (for weakly aggregated systems, $n \sim 1/2$).

The results of calculations using Eqn (47) and by analogous expressions [71, 83–86] are in good agreement with the experimental data for monodisperse suspensions containing spherical particles, if their concentration (φ) is lower than 60% (this concentration corresponds to a random cubic packing φ_c). For dispersions with $\varphi \sim \varphi_c$ and $\varphi > \varphi_c$, the calculated data differ substantially from the experimental results, and these differences increase with $\dot{\varepsilon} \to 0$, *i.e*., as the highest viscosity of the virtually non-destroyed structure (according to Rehbinder) is approached.

For structured dispersions, this viscosity level $\eta_{ef} \sim \eta_0$ is adequately described in a broad concentration range ($\varphi < \varphi_c$) relying on the concepts of the quasi-crystalline character of the structure on the assumption of its continuity.[87–89] In the general form, this viscosity level is determined by the equation [87]

$$\frac{\eta_{ef}}{\eta_1} \sim C_1 \exp\left[\frac{h}{d}\left(\frac{\tau_B}{\tau_{f_c}} - \frac{\tau_B P}{\eta_1}\right)\right], \tag{48}$$

where

$$C_1 \equiv \lambda\left(\frac{d\tau_1}{h\tau_{f_c}}\right)^{1/2},$$

$$\lambda \equiv \left\{1 + \left[\frac{d}{h}\left(\frac{\eta_0}{\tau_i}\right)^2 \frac{\tau_{f_c}}{\tau_i}\right]^2\right\}^{1/2} - \frac{d}{h}\left(\frac{\eta_0}{\eta_1}\right)^2 \frac{\tau_{f_c}}{\tau_i}. \tag{48a}$$

Here, τ_B, τ_{fc} and τ_i are the characteristic times of the corresponding microprocesses (see above), h is the distance between the particle surfaces in the quasi-lattice, $\eta_1 = \eta$ at $\varphi = 0$.

If $h = d$, this equation is transformed into the expression reported in the studies.[88, 89] It should be noted that at $\eta_{ef} \sim \eta_0$, the general expression (48) and its special analogues (see Refs 87 and 89) provide a satisfactory description of the dependence $\eta_{ef}(\dot{\varepsilon})$ with $\dot{\varepsilon} \to 0$ regardless of the concentration, whereas at $\dot{\varepsilon} > 0$, the deviation of the theoretical curve described by Eqn (47) from the experimental data increases with increasing φ. As $\dot{\varepsilon}$ and φ increase, the $\Delta\eta_{ef}/\Delta\dot{\varepsilon}$ ratio sharply increases. This fact is taken into account in the theory developed in the studies.[30, 62] According to this theory, the effective viscosity depends on the rate as follows:

$$\frac{\eta_{ef}}{\eta_1} \sim \frac{1}{(\tau\dot{\varepsilon})^n}. \tag{49}$$

This formula describes satisfactorily all steps of destruction of an aggregated suspension with increasing $\dot{\varepsilon}$ (or P), which was confirmed by comparing the calculated and experimental data for dispersions formed by monodispersed particles of poly(methyl methacrylate) in decalin stabilised by a monolayer of dihydrostearic acid (Fig. 7, curve *1*). Each step of destruction has a particular prevailing characteristic time of a microprocess τ and the corresponding Debora number [30, 62, 76]

$$D^* = \dot{\varepsilon}\tau.$$

For the region A in Fig. 7 (curve *1*),

$$\eta_{ef} \sim \eta_0,\ \dot{\varepsilon} < \frac{1}{\tau_\mu \exp(-\tau_B/\tau_\mu)},\ D^* \sim \dot{\varepsilon}\tau_B,\ \dot{\varepsilon}\tau_\mu.$$

For the region B corresponding to destruction into superaggregates,

$$\eta_{ef} < \eta_0,\ \frac{\eta_{ef}}{\eta_1} \sim \frac{1}{(\dot{\varepsilon}\tau_B)^{3/5}};\ \frac{1}{\tau_\mu} \ll \dot{\varepsilon} \ll \frac{1}{\tau_B};\ D^* \sim \dot{\varepsilon}\tau_B,\ D^* = \dot{\varepsilon}\tau_{f_c}.$$

For the region C corresponding to destruction of superaggregates into aggregates,

$$\eta_{ef} \ll \eta_0,\ \frac{\eta_{ef}}{\eta_1} \sim \frac{1}{(\dot{\varepsilon}\tau_B)^{1/2}};\ \frac{1}{\tau} \ll \dot{\varepsilon} \ll \frac{1}{\tau_\mu},\ D^* = \dot{\varepsilon}\tau_\mu.$$

For the region D corresponding to complete deaggregation,

$$\eta_{ef} \sim \eta_1\left(\frac{1}{\tau_B}, \frac{1}{\tau_\mu} \ll \dot{\varepsilon} \ll \frac{1}{\tau_1}\right);\ D^* \sim \dot{\varepsilon}\tau_i.$$

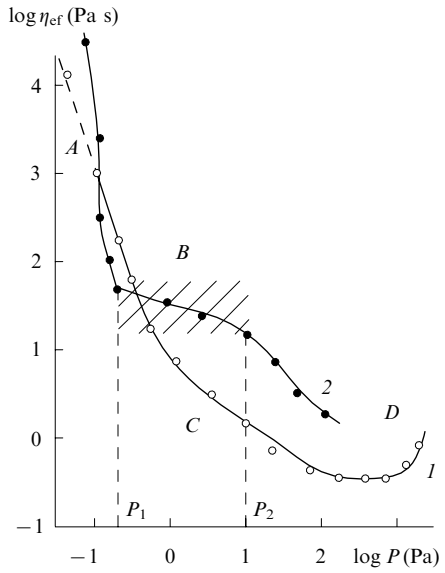

Figure 7. Complete flow curve of a suspension of poly(methyl methacrylate) in decalin.[68]
The solid curve represents the results of calculations by Eqn (49), the points correspond to the experimental values; the concentration of the suspension (%): (*1*) 59.5, (*2*) 60.1; the portion of the flow curve corresponding to a plateau, which is not exactly reproduced, is dashed.

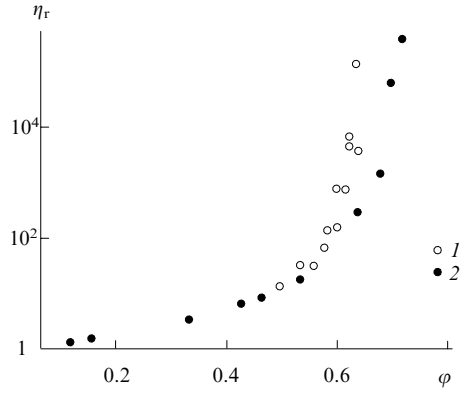

Figure 8. Dependence of the relative viscosity η_r on the concentration of a dispersed phase [monodispersed particles with a diameter of 129 (*1*) and 84 nm (*2*) of poly(methyl methacrylate) in decalin].[69]

Finally, in going to the dilatancy region accompanied by percolation of an adsorption layer,

$$\frac{\eta_{ef}}{\eta_1} \sim \dot{\varepsilon}\tau_i,\ \dot{\varepsilon} \gg \frac{1}{\tau_i},\ P > \frac{r^* h_i}{d^2} P_L\ ,$$

where r^* is the local radius of curvature in the zone of contacts between particles with diameter d, h_i is the thickness of the adsorption layer on their surface, P_L is the strength of the adsorption layer.

Therefore, for lyophilic disperse systems formed by monodispersed spherical particles at a concentration $\varphi < \varphi_c$, destruction of a coagulation structure is isotropic in character; at $\dot{\varepsilon} \sim \dot{\varepsilon}_\infty$, complete deaggregation and the corresponding limiting isotropic dynamic state with maximum fluidity are achieved.

When creating a controlled isotropic dynamic state in dispersions under continuous shear deformation, it should be taken into account that flow curves are completely reversible. The reversibility was confirmed by the fact that the effective viscosity levels and the corresponding degrees of isotropic destruction depending on $\dot{\varepsilon}$ and P throughout the range of their changes in rheological measurements are the same irrespective of whether these levels are attained with increasing or decreasing $\dot{\varepsilon}$ and P (*i.e.*, when moving in upward or downward directions). This indicates that rheological flow curves obtained under purely homogeneous shear are completely reversible.

However, in attempting to construct flow curves for the same systems at concentrations $\varphi > \varphi_c$ (*i.e.*, at $\varphi > 60\%$) in compliance with all the above-mentioned conditions and, correspondingly, to use Eqn (49) for their theoretical description, it was found that the calculated data differ substantially from the experimental results and the flow curves, which were measured in upward and downward directions (see Fig. 7, curve *2*), were poorly reproduced. The degree of these deviations, which is manifested in the presence of a plateau in the flow curve $\eta_{ef} = f(P)$, increases as φ increases in the region $\varphi > \varphi_c$.[89,90]

Such plateaus in the flow curves were found, in particular, in the studies.[71,90] However, the reasons for their appearance were considered to be an artefact[91] or were not discussed at all. The fact that the flow curves are irreproducible in the plateau region is unambiguously indicative of the violation of the isotropic character of a dispersion flow in this region.

At the same time, analysis of theoretical dependences of the strength of a dispersed structure on its porosity (see Fig. 2)[23,24] and experimental data[92,93] on the dependence of the relative viscosity on the effective concentration of a dispersed phase for monodispersed spherical particles of poly(methyl methacrylate) in decalin (Fig. 8) demonstrated that the region $\varphi = \varphi_c \approx 60\%$ corresponds to the onset of a sharp increase in the strength and viscosity with increasing φ. It is this limit, where the inhomogeneity of the structure becomes observable.

An analogous phenomenon, which takes place in going to the region $\varphi \geqslant \varphi_c$, was reported in monograph.[94] Apparently, the authors of the cited monograph were the first to interpret the anomaly of the flow process, which is characterised by a sharp jump (drop) of the shear stress P when its critical value is reached with increasing $\dot{\varepsilon}$, and an ambiguous dependence of the viscosity on the shear stress as a consequence of the appearance of local discontinuity.

This phenomenon, its possible variations and reasons for its occurrence both in well-characterised disperse systems and systems formed by polydispersed (in some cases, anisometric) particles of dispersed phases in liquid media were analysed in-depth.[2,76]

The interpretation assuming discontinuity at $\varphi > \varphi_c$ is supported by the results of studies of dispersions formed by monodispersed spherical particles with lyophilic surfaces (see, for example, Refs 90, 91 and 95).

The theoretical description of this phenomenon[30,62,68] was based on the comparison of the following three relaxation times of the processes, which together determine the discontinuity condition: τ_1, the time of elastic energy release under deformation; τ_2, the time of formation of a new surface due to the development of a macroscopic crack, *i.e.*, a slip zone with an inhomogeneous structure; τ_3, the time of mass transfer to the discontinuity zone as a result of vacancy drift, *i.e.*, the time of the possible 'healing' of the structure under shear deformation.

The structural discontinuity occurs if the following inequality is fulfilled:

$$\frac{1}{\tau_1} \gg \frac{1}{\tau_2} + \frac{1}{\tau_3}\ . \tag{50}$$

The discontinuity can take place in a broad range limited by the initial (P_1) and final (P_2) shear stresses

$$P_1 \sim P_c \left(\frac{d}{\varepsilon_i}\right)^{1/2},$$

$$P_2 \sim P_c - \frac{d\eta}{h\tau_B} \ln \frac{d}{\lambda h}, \quad (51)$$

where P_c is the flow limit of a disperse system, ε_i is the size of the structure inhomogeneity, λ is the parameter determined from Eqn (48a) and h is the average distance between the particles in the structure.

From a comparison of the available experimental[90,91] and calculated[30,90,91] data, it follows that a change from $\varphi = 59\% - 60\%$ to higher concentrations is accompanied by substantial changes in the flow mechanism of dispersions. The threshold concentration corresponds to a random cubic packing,[27,28] in the case of which the flow of a dispersion consisting of monodispersed spherical particles is isotropic in character under conditions of purely homogeneous shear. However, at concentrations higher than this threshold value, islands, *viz*., elements with a denser hexagonal packing, appear inside dispersions with a random cubic packing. As φ increases in the region $\varphi > 60\%$, the concentration of such islands increases, which is equivalent to the appearance and an increase in the number of inhomogeneity elements of the structure. Their coalescence gives rise to macroinhomogeneities, when a particular critical concentration is reached in the course of deformation. Apparently, a concentration jump in the vicinity of macroinhomogeneity boundaries is responsible for the appearance of local slip zones, which are equivalent to discontinuity, under shear in the range $P_1 \leqslant P_i \leqslant P_2$. The higher the concentration of a dispersed phase in a dispersion medium at $\varphi > \varphi_c$, the higher is the probability of this flow mechanism.

This mechanism of formation and development of discontinuities was confirmed in a computer simulation of the behaviour of an ensemble of monodispersed spherical particles in a Newtonian liquid under shear (Fig. 9).

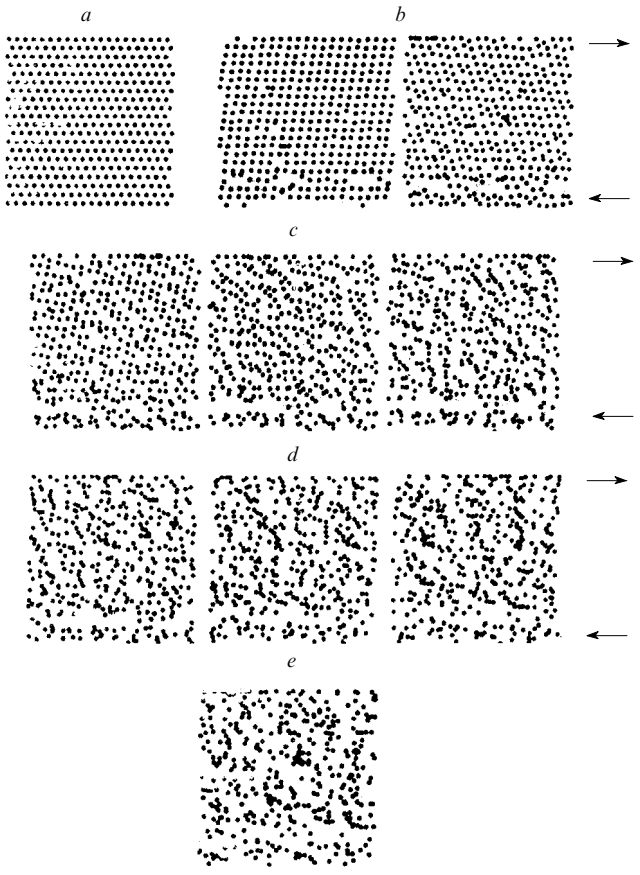

Figure 9. Results of computer simulation of the flow process for suspensions of monodispersed quartz particles with a diameter of 1 μm in water with discontinuity[96] in static conditions (*a*) and under continuous shear at different rates (*b*–*e*).
$\dot{\varepsilon}$ /s^{-1}: (*b*) 10^{-1}, (*c*) 50, (*d*) 100, (*e*) 150.

It can be assumed that this flow mechanism is even more probable for real disperse systems containing polydispersed and anisometric particles, because there are more possibilities for a local increase in the concentration of a dispersed phase in a dispersion medium, particularly, on going to $\varphi > \varphi_c$. This was shown by analysis of the complete rheological flow curve of aqueous dispersions of bentonite at a concentration $\varphi = 20\%$ (for this system, it is higher than φ_c).

The S-shaped flow curve shown in Fig. 10 *a* illustrates an ambiguous dependence of the viscosity η_{ef} on the shear stress P. Such a curve is characteristic of structured dispersions, whose deformation is accompanied by discontinuities.[76]

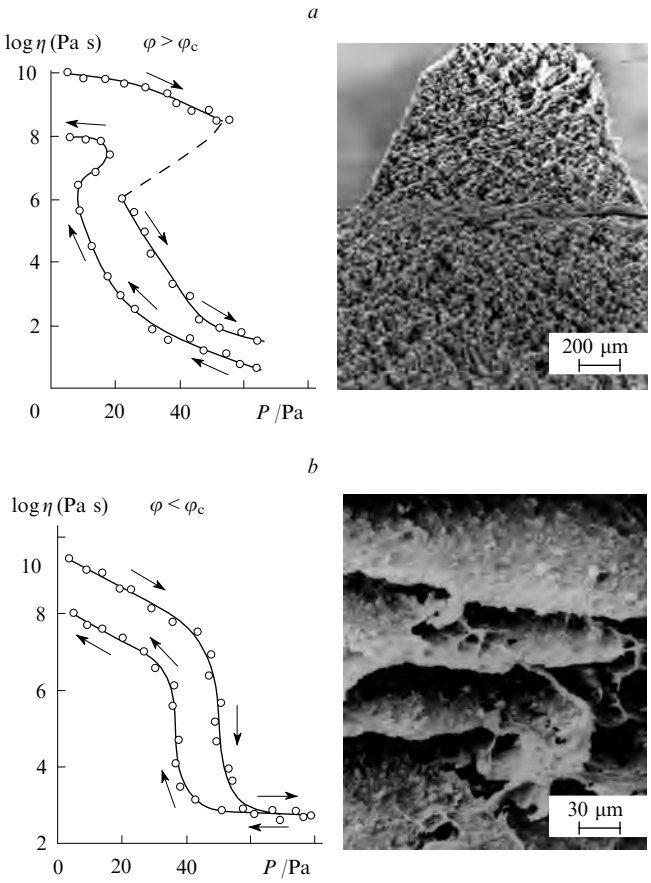

Figure 10. Complete rheological flow curves for aqueous dispersions of calcium bentonite (S_{BET} = 70 m^2 g^{-1}).[68,76]
(*a*) For a system with $\varphi = 20\%$ ($\varphi > \varphi_c$), (*b*) for a system with $\varphi = 11\%$ ($\varphi < \varphi_c$). Solid and dashed lines represent the results of measurements under increasing and decreasing shear stress, respectively; scanning electron micrographs were taken using a specially designed procedure.[62,95]

The hypothesis of discontinuity is supported by photomicrographs taken in the course of deformation of these dispersions (to the right of Fig. 10 *a*,*b*). It can be seen that the discontinuity is developed inside the structure subjected to deformation ($\varphi > \varphi_c$). Its appearance and subsequent development under shear deformation excludes shear propagation in the bulk of the structure outside the discontinuity zone.

All subsequent measurements at an increasing shear rate lead to complete violation of the isotropic character of destruction and a distortion of the results of measurements. Hence, it is impossible to construct flow curves under continuous shear. This is confirmed also by the fact that the flow curves measured in downward and upward directions are irreproducible.

The measured shear stress describes, in essence, only friction between layers bounded by discontinuity zones and the possible partial destruction in the regions adjacent to the discontinuity surfaces.

Taking into account the above notions, it could be assumed that the bulk character of destructions without discontinuities would be observed at lower concentrations of a dispersed phase in the region $\varphi < \varphi_c$. This assumption is supported by the shape of the flow curve of a dispersion at $\varphi = 11\%$, which reflects an unambiguous dependence of η_{ef} on P (Fig. 10*b*). However, the photomicrographs of the structure (to the right of Fig. 10*b*) are indicative of the opposite phenomenon: the appearance of not one (like at $\varphi > \varphi_c$), but even numerous discontinuities with the formation of periodically repeating dense structured layers, which are oriented along the shear direction and are separated by a dispersion medium. It should be noted that the concentration of a dispersed phase in these layers is as high as 60%, *i.e.*, is several times higher than the volume-average concentration before deformation (11%). Correspondingly, the strength and viscosity of the structure should increase many-fold [see Eqns (19) and (20); Figs 2 and 8]. The flow curves for the same compositions as those reported in the studies [1, 75] were reproduced in experiments.

The possible mechanism of such a sharp increase in the density of a structure in solid-like layers is associated with the effect of inertial coagulation of anisometric particles, the probability of which increases as the rate of movement of the layers with respect to each other increases [see Eqns (28) – (32)].

As mentioned above, the critical rate of inertial coagulation for anisometric particles can be many times lower than that for spherical particles. This is also favoured by the slip of a liquid with respect to the particle surface,[48] which was taken into account in the study.[12]

Therefore, inertial coagulation can give rise to structures stable to an extent that they cannot be destroyed even at high shear rates corresponding to $\dot{\varepsilon}_\infty$. This becomes even more favourable if the particle surfaces have lyophobic regions with a small radius of curvature, at which selective inertial coagulation with fixation of particles in the short-range potential well is substantially facilitated.[50]

Consequently, the commonly accepted notions of the attainment of the lowest viscosity level of an 'ultimately destroyed structure' $\eta_{ef} \approx \eta_{min}$ at $\dot{\varepsilon} \to \dot{\varepsilon}_\infty$ (see Refs 1, 75 and 97) can be assigned not to the structure as a whole but only to low-concentration (in essence, structureless) layers oriented along the shear direction. Moreover, it can be assumed that it is this portion of the flow curve corresponding to $\eta_{ef} \approx \eta_{min}$, where high-viscosity and dense (and, hence, particularly stable) structures can form, which is very typical of systems containing anisometric particles.

Periodically repeated structure layering was revealed (from a change in the density) in the course of sedimentation in highly disperse systems formed by particles, whose surface is characterised by lyophobic – lyophilic mosaicity (Fig. 11). This was demonstrated [62, 98] using an annihilation gamma probe. Apparently, layered sediments are formed according to this mechanism. This mechanism is responsible for natural phenomena, such as landslides and landslips of bottom sediments of rivers, lakes, *etc*.

Under dynamic conditions, the formation of layered structures is favoured by possible changes in the sedimentation rate V_1 and the rate of increase in the sediment density (V_s) depending on the shear rate in a flow and, hence, on the effective viscosity.

The drops of the shear rate $\Delta\dot{\varepsilon}$, which are characteristic of both natural phenomena and a series of industrial processes (chemical engineering and pipeline transportation) involving structured dispersions, inevitably lead to changes in V_1 and V_s and variations in the sediment density $\Delta\rho$. In the theoretical study,[9] this dependence was revealed on assumption of the aggregation mechanism of destruction of a coagulation structure under shear and the dependences of the size D and the density of aggregates ρ_a on $\dot{\varepsilon}$. The above dependence is expressed by the equation

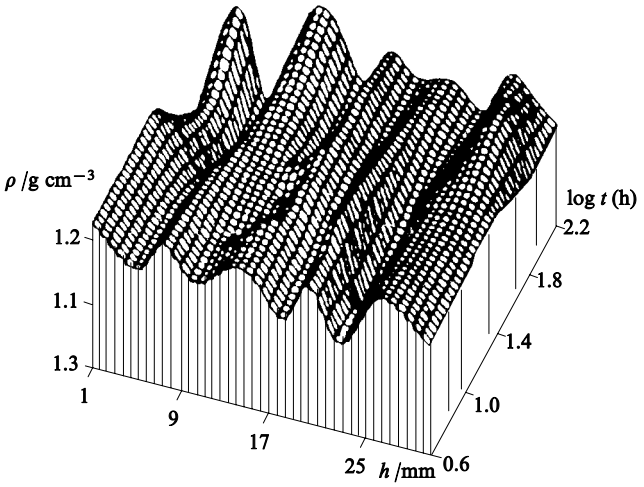

Figure 11. Periodic layers of different densities formed in the course of sedimentation in an aqueous suspension of technical carbon (d = 42 nm, φ = 28%).[98]

$$V_1 = \frac{(1-\varphi_{max})D^2 g \Delta\gamma_1}{12\lambda z \eta_1 \varphi_{ext}} \left(\frac{\eta_1 \varphi_{ext} \dot{\varepsilon}}{2.7 P_m}\right)^{1/2}, \qquad (52)$$

where φ_{max} is the maximum concentration of the dispersion in a sediment, η_1 is the viscosity of the dispersion in an interaggregate space, φ_{ext} is the concentration of the dispersed phase in an interaggregate space, $\Delta\gamma_1$ is the difference between the average densities of the aggregates and the suspension between the aggregates, λ is the dimensionless parameter, P_m is the strength of the aggregate structure

$$P_m = z_1 \frac{4 f_c}{n d^2},$$

z_1 is the number of bonds per particle on the aggregate surface, n is the number of particles in the aggregate.

According to Eqn (52), the rate V_1 is proportional to $(\dot{\varepsilon})^{1/2}$. The rate of sediment growth is related to V_1 by a simple equation

$$V_s = V_1 \varphi_{max}.$$

Hence it follows that any change in $\dot{\varepsilon}$ leads to changes in the rates of these processes. Since $\Delta\gamma_1$ also varies with V_1, the probability of the formation of layered sediments increases as $\Delta\dot{\varepsilon}$ and the frequency of its change increase. This is illustrated in Fig. 12, which displays the dependence of V_1 on $\dot{\varepsilon}$ and the corresponding change in η_{ef} for a concentrated aqueous carbon suspension.

An analogous result for suspensions of monodispersed spheres was obtained in the study.[98] The effect of layering of dispersions was mentioned in the studies.[99, 100]

Therefore, the appearance of structure macroinhomogeneities under dynamic conditions (including discontinuities, along which shears occur in structured disperse systems) results from the fact that the critical concentrations of not only a dispersed phase in a dispersion medium φ_c but also, in a more general case, of microinhomogeneity elements in the bulk of the structure are attained and exceeded. What this means is discontinuities in disperse systems formed by anisometric particles with lyophobic – lyophilic surface mosaicity can appear at concentrations $\varphi < \varphi_c$ (see Fig. 10*b*).

As a consequence, the limiting isotropic dynamic state and the corresponding condition for true ultimate destruction, *i.e.*, η_{ef} (with $\dot{\varepsilon} \to \dot{\varepsilon}_\infty$) = η_{min} in the bulk of the system subjected to deformation, cannot be attained under shear deformation.

Let us consider the mechanism of destruction of disperse systems with $\varphi < \varphi_c$ and analyse the data obtained for a model

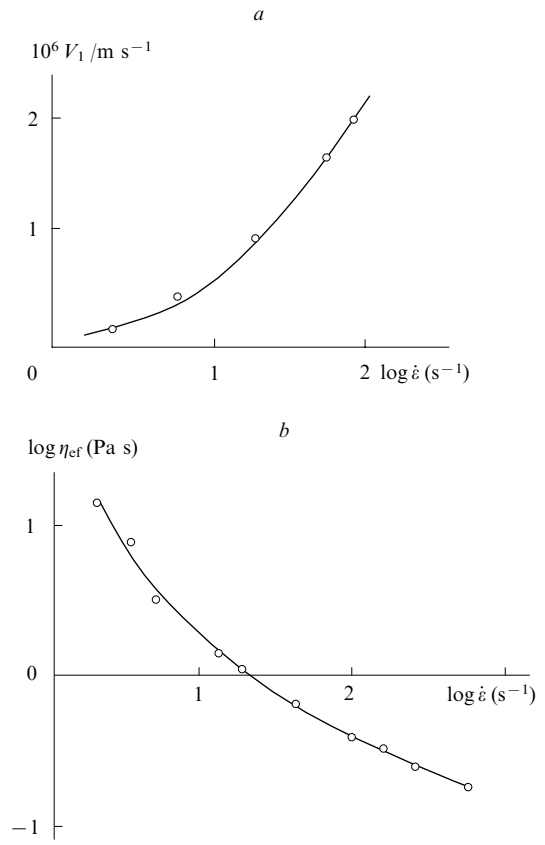

Figure 12. Plots of the sedimentation rate (*a*) and effective viscosity (*b*) *vs.* the shear rate for an aqueous carbon suspension ($\varphi_m \approx 60\%$).[68]

system of a dispersion of spherical polystyrene particles ($d = 70$ nm) in a gelatin gel in the presence of stabilisers [additives of a NaCl electrolyte and an anionic surfactant, *viz.*, aliphatic alcohol (Fig. 13)].

Destruction of a coagulation structure under shear leads to its decomposition into aggregates, which appear when the yield stress

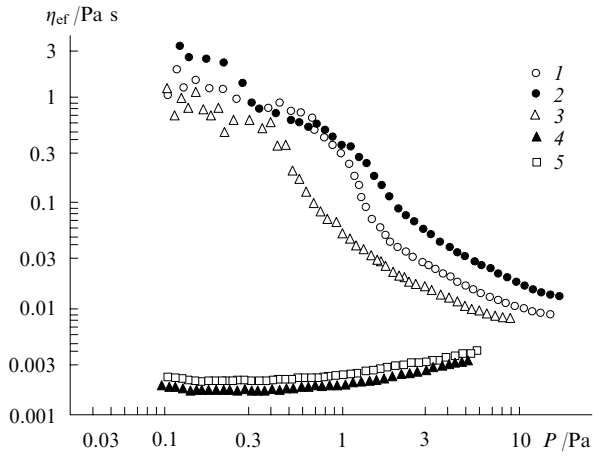

Figure 13. Complete flow curves for a suspension of polystyrene particles in gelatin gel ($\varphi = 4.8\%$).[101]
(*1*) A suspension of particles without additives, (*2*) a suspension of particles with an NaCl additive (0.02%), (*3*) a suspension of particles with an additive of an aliphatic alcohol (0.1%), (*4*) a liquid dispersion medium, (*5*) a theoretical curve under the condition of complete deaggregation.

P_c of the system is reached with increasing shear stress.[2] The characteristic size of aggregates in this region can be calculated by the equation [68]

$$D_a = \left(\frac{\alpha A^* z r^2}{16 P_c h^2 \varphi}\right)^{1/3}, \qquad (53)$$

where $A^* \approx 7 \times 10^{-20}$ J; h was varied from 60 to 100 nm, $r = 35$ nm and $z = 3$. The calculated values D_a varied with the temperature of the system from 300 to 1000 nm. The measurements of the rheological properties of these dispersions showed that even in the region of very high shear rates (as high as $\dot{\varepsilon} \approx 1300$ s^{-1}), the level $\eta_{ef} \approx \eta_{min}$ is more than 30 times higher than that found from the condition of complete destruction for $\varphi = 4.8\%$ according to Batchelor's formula [102]

$$\eta_{ef} \approx \eta_1(1 + 2.54 + 6.25\varphi^2),$$

where η_1 is the viscosity of a dispersion medium. Hence, not individual particles but their aggregates, whose effective concentration is 35% – 60% (*i.e.*, is approximately an order of magnitude higher than the concentration of polystyrene particles), serve as kinetic units at $\eta_{ef} \approx \eta_{min}$.

The above-described mechanism of destruction is even more strongly supported by the results of analysis of the structural and rheological properties of a dilute dispersion formed by monodispersed spherical SiO_2 nanoparticles ($d = 14$ nm) in ester.[103]

Lyophobic interactions in this dispersion give rise to a fractal structure formed by aggregates of particles. The complete flow curve (Fig. 14) shows two pronounced Newtonian viscosity levels, *viz.*, the highest level $\eta_0 \approx 10^8$ Pa s and the lowest level $\eta_{min} \simeq 10^{-1}$ Pa s. Therefore, the effective viscosity drop is nine orders of magnitude. Taking into account that the level attained at $P = 10$ Pa remains virtually the same as P increases to 100 Pa, it can be assumed that this level should actually correspond to the lowest viscosity of the ultimately destroyed structure.[1]

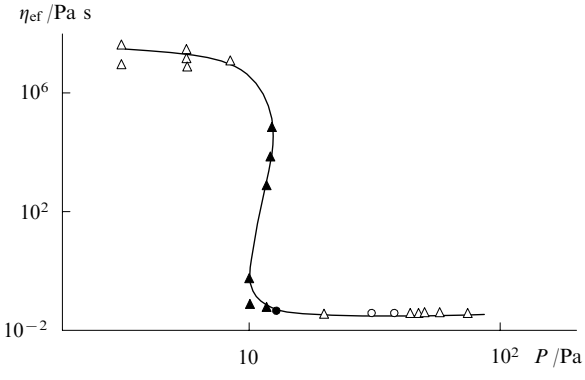

Figure 14. Complete flow curve for a suspension of SiO_2 ($d = 14$ nm) in ester ($\varphi_{ef} = 2.5\%$).[103]
Different triangles and circles correspond to different geometries of a measuring cell.

The validation of this assumption is substantially facilitated by the fact that the dispersed phase consists of monodispersed spherical particles and its volume content in the dispersion medium is < 3%. Therefore, the Einstein equation can be used for the description of the region $\eta \approx \eta_1(1 + 2.5\varphi)$ (see Refs 104 and 105) on condition that complete deaggregation of the dispersion in this region is attained.

However, a comparison of η and η_{ef} demonstrated that the latter values are tens of times larger. Consequently, the experimental values of η_{ef} do not correspond to the condition of true ultimate destruction, but they correspond to bulk thickening of a dispersion medium with kinetic structural elements ($\varphi_{ef} \gg 3\%$) retained at $\eta_{ef} \approx \eta_{min}$. Therefore, the Einstein equation is inappli-

cable for the estimation of the real volume concentrations of these elements, and the equations derived by Patel and Russel[78] or Frankel and Acrivons[86,106] should be used. According to these equations, φ_{ef} for aggregates is $\sim 49\%$. The initial size of these aggregates at the shear stress $P = P_c = 10$ Pa, which corresponds to the onset of a sharp decrease in the effective viscosity, can be determined by Eqn (53). The value calculated by Eqn (53) is 1500 nm, which was confirmed by direct measurements of the average size of aggregates by neutron diffraction ($D_a \approx 1560$ nm).[68]

As a further development of the concepts reported in the study,[107] it was demonstrated that the flow process of such colloidal disperse systems as fractal gels analogous to those described above can be considered as a flow of a system consisting of 'solid-like' and 'liquid-like' components, whose viscosities differ by many orders of magnitude ($\eta_{ef1} \sim 10^8$ Pa s and $\eta_{ef2} \sim 10^{-1}$ Pa s, respectively), and the corresponding relaxation times are $\tau_1 \sim 10^5$ s and $\tau_2 \sim 10^{-4}$ s.

It should be noted that the flow giving rise to alternating 'solid-like' and 'liquid-like' quasi-phases, which form layers oriented along the shear direction, was interpreted[107] as the most probable process in the context of thermodynamics of non-equilibrium processes.

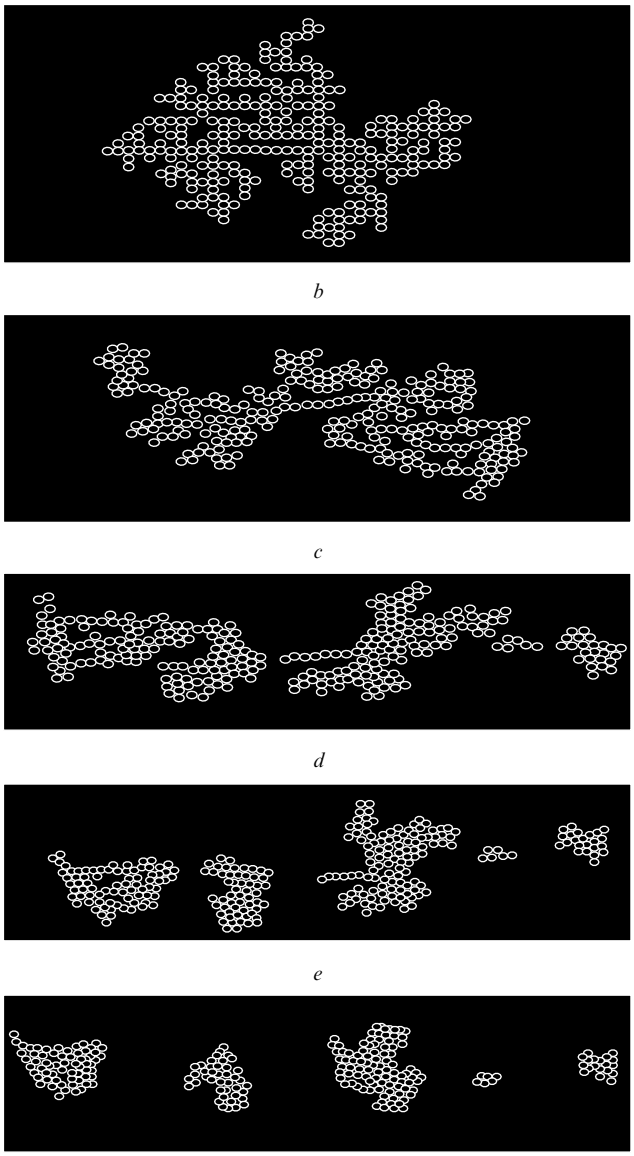

Figure 15. Evolution of a superaggregate in the course of shear deformation (computer experiment).[68]
$\dot{\varepsilon}$ /s^{-1}: (*a*) 0, (*b*) 0.3, (*c*) 1, (*d*) 10, (*e*) 50.

The results of computer simulation of the structure evolution of aggregated disperse systems with increasing shear rate (Fig. 15) are also indicative of the formation of smaller aggregates, which are characterised by an increasing density and, correspondingly, increasing strength and viscosity, against the background of destruction of superaggregates under deformation. This effect follows from the theory of destruction of aggregated dispersions under shear deformation. The aggregate radius R_a is related to the particle radius by the equation[19,30,62]

$$\frac{R_a}{r} \sim n^{1/f}, \tag{54}$$

where n is the number of particles involved in the aggregate and f is its fractal dimensionality. Then, the concentration of particles in the aggregate φ_{int} also increases with increasing shear rate $\dot{\varepsilon}$

$$\frac{\varphi_{int}}{\varphi_{max}} \sim \left(\frac{r}{R_a}\right)^{3-f}, \tag{55}$$

where φ_{max} is the maximum particle concentration in a particular disperse system.

Aggregates form a chain (layer) oriented along the shear direction. It can be stated that this mechanism, which combines destruction and formation of dispersed structures with a higher strength, excludes the possibility of attaining the true and complete destruction, and, hence, the limiting dynamic state even at very high $\dot{\varepsilon} \to \dot{\varepsilon}_\infty$ in the region of $\eta_{ef} \approx \eta_{min}$.

4. Dynamic state of disperse solid phase – liquid medium systems under combined action of shear and orthogonal oscillation

Anisotropic destruction of dispersed structures oriented along the shear direction, which is accompanied by decomposition into aggregates and formation of new more stable aggregates through inertial coagulation, excludes the attainment not only of an isotropic dynamic state but also of equivalent aggregation dynamic stability of disperse systems.

Consequently, to attain the limiting isotropic dynamic state, it is necessary to subject a disperse system to action in such a way as to either exclude the formation of structure inhomogeneity elements as aggregates and structured layers or achieve their ultimate destruction. For this purpose, the energy delivered to a disperse system and imparted to particles fixed in a structural network should be higher than the binding energy with adjacent particles.

As mentioned above, until the binding energy of a particle (whose size is smaller than 1 μm) in contact with adjacent particles is lower than $(10-15)kT$, the structure can be destroyed through thermal motion (random Brownian oscillations) of particles. In all cases of lyophobic interactions between particles, the total energy of their binding with adjacent particles in a structure is, generally, much higher than $(10-15)kT$, and destruction *via* Brownian motion becomes impossible.

Besides, it can be suggested that just as particles of sizes larger than 1 μm in aggregation-stable colloidal disperse systems undergo random oscillations under the action of thermal impacts of molecules of a dispersion medium, so can such particles in structured dispersions if they are subjected to forced oscillations using an external source. The necessary condition for the attainment of aggregation dynamic stability of such systems in the case of their complete deaggregation is that the energy of forced oscillations should be higher than the total energy (U_c) of binding of particles with adjacent particles in a structural network (taking into account z). It can also be assumed that forced oscillations play a decisive role in destruction under combined action of continuous shear and oscillations, whereas the mass transfer of elements of the destroyed structure proceeds under continuous shear.

The destruction under shear involves two main steps, *viz.*, destruction of a continuous structural network to form layers and/or aggregates of particles and destruction of aggregates as such. Correspondingly, the results of an external oscillation action first on a continuous structure and then on the aggregate structure should be considered with the aim of determining the parameters necessary for complete destruction of a coagulation structure. Various aspects of this problem were considered in-depth.[2, 30, 62]

Assuming that particle oscillations are excited with an external source through a medium, the rate of particle motion in the vicinity of the aggregate surface can be taken as

$$V(t) = V_0 a \sin \omega t.$$

Here, V_0 is the maximum rate of particles under oscillation, a is the oscillation amplitude and ω is the oscillation frequency. In the case of such harmonic oscillations, a particle undergoing forced oscillations with a frequency ω comparable to the eigenmode frequency can escape from a structural network. The eigenmode frequencies at which the particle can escape from long-range ($i = 1$) and short-range ($i = 2$) coagulation sites are determined, respectively, by the equations

$$\omega_1 \sim \frac{1}{r}\left(\frac{B}{\rho h_2^4}\right)^{1/2} \sim \frac{10}{r}, \qquad \omega_2 \sim \frac{1}{r}\left(\frac{A^*}{10\rho h_1^3}\right)^{1/2} \sim \frac{10^2}{r}. \tag{56}$$

For a comparative numerical analysis, let us assume that $\eta_1 \sim \eta = 10^{-1}$ Pa s, $A^* \sim 10^{-19}$ J, $B = 10^{-28}$ J m, $h_2 \sim 5 \times 10^{-8}$ m, $h_1 \sim 10^{-9}$ m, $\rho = 1000$ kg m^{-3}.

As expected, the results of numerical estimates differ sharply (by several orders of magnitude) and depend on r and h. Thus, the frequency increases by five orders of magnitude as r decreases from 10^{-4} to 10^{-7} m and, particularly, as h_i decreases from 5×10^{-8} to 10^{-9} m.

From this it follows that it is worthwhile to combine low-frequency mechanical oscillations and ultrasonic oscillations, particularly, in the case of destruction of colloidal disperse systems. It should be emphasised that it is technically quite possible to expose dispersed structures to oscillations with such parameters. This was demonstrated, in particularly, in the studies,[7, 62, 108] where structures were destroyed in the course of compaction of finely dispersed powders as well as of highly filled suspensions containing ultra-dispersed aerosil particles ($s_{BET} \approx 400$ m^2 g^{-1}).[62]

The effect of oscillations on a disperse system at $\eta_{ef} \to \eta_0$ can be expressed by the simple equation

$$\frac{\eta_{ef}}{\eta_0} \sim e^{U_c/\Theta} \tag{57}$$

where

$$\Theta = kT + m(a\omega)^2.$$

The first term of the latter equation takes into account the possible contribution of thermal motion. The second term accounts for the kinetic energy imparted to a system subjected to oscillation with an amplitude a and a circular frequency ω.

This approach to estimations of oscillation action on disperse systems was also used in the study.[109]

The second step of destruction of dispersions is associated with aggregate disintegration under combined action of oscillation and shear. In these conditions, the effective viscosity of a dispersion consisting of aggregates can be expressed as follows:[30, 61]

$$\eta_{ef} \sim \eta_{ef}^0 \frac{L}{d^*} \sim \eta_{ef}^0 \left[1 + \frac{1}{a\omega L/z_a\eta + (\dot{\varepsilon}/\dot{\varepsilon}_a)^{1/2}}\right]. \tag{58}$$

Here, η_{ef}^0 is the highest effective viscosity, d^* is the average distance between the aggregates, L is the distance between the centres of the aggregates ($L = D + d^*$, D is the diameter of the aggregate) and z_a is the coordination number of the aggregate,

$$\dot{\varepsilon} \approx \frac{z_a P_c}{\eta_{ef}^0}.$$

Equation (58) was derived from the condition that the parameter L/d^* is expressed as follows

$$\frac{L}{d^*} \sim \frac{z_a \eta}{\rho a \omega L},$$

where ρ is the density of particles of a solid phase.

It is worthwhile to represent the dependence of the effective viscosity on the oscillation intensity

$$I \approx a^2\omega^3.$$

This parameter determines the oscillation power per unit oscillating mass. In essence, this parameter can be considered as a 'vibrotemperature',[30] an increase of which leads to an increase in the intensity of motion of kinetic units (particles or aggregates), much as an increase in the temperature in colloidal systems leads to intensification of Brownian motion.

The dependence of the effective viscosity on this parameter can be described by the following equation:[30, 62]

$$\eta_{ef} \sim \eta_1 \left(\frac{z_a h}{a\omega\rho D} + 1\right) \sim \eta_1 \left[\frac{z_a \eta}{\rho L}\left(\frac{\omega}{I}\right)^{1/2} + 1\right], \tag{59}$$

where h is the distance between particles in an aggregate.

It was demonstrated[62, 68] that the results of calculations by Eqns (57)–(59) are in good agreement with the results of studies of the rheological properties of concentrated suspensions of aluminosilicates in water subjected to oscillation. The selected parameters of these suspensions are as follows: $\varphi \sim 0.46$–0.6; $A^* \sim 10^{-20}$ J; $h = 1$–10 nm; $(R/r)_{min} \sim 10$. Under conditions of continuous shear, irreversible macroscopic discontinuities appear at $P = P_c$ or $\dot{\varepsilon} \approx \dot{\varepsilon}_c$. The possibility of the occurrence of these discontinuities is completely eliminated under combined action of continuous shear and orthogonally directed oscillation with a frequency $f_v^* = 50$ Hz ($\omega = 2\pi f_v^* = 300$ s^{-1}) and with increasing intensity (Fig. 16). In particular, this is evidenced by a relatively

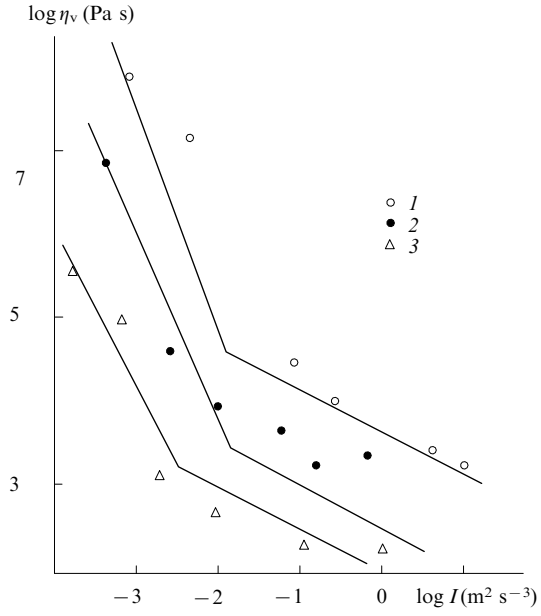

Figure 16. Vibrorheological curves of aqueous suspensions of aluminosilicates.
Circles and triangles represent experimental data;[2] curves show the results of calculations by Eqns (58) and (59); $\varphi = 0.6$ (*1*), 0.53 (*2*), 0.46 (*3*).

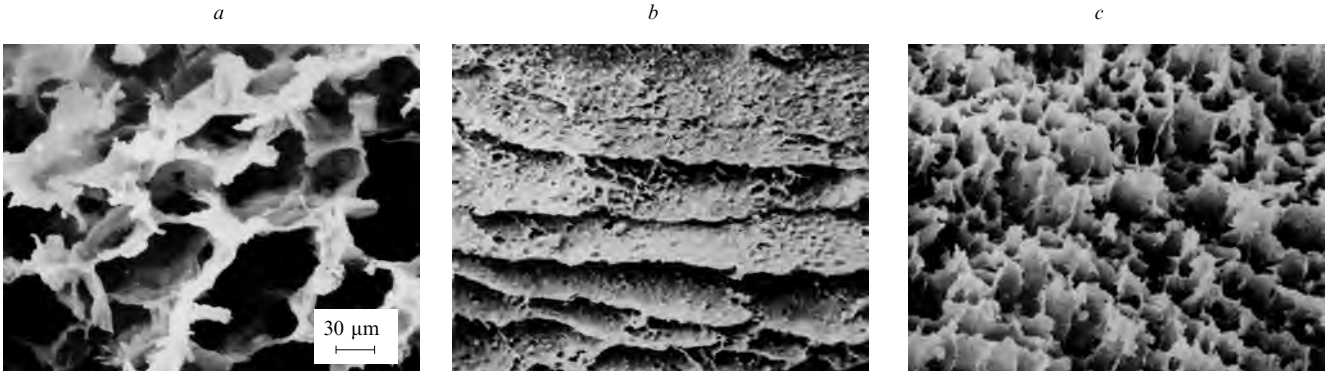

Figure 17. Characteristic features of destruction and formation of coagulation structures for aqueous dispersions of CaB, $\varphi_{max} = 11\%$ ($\times 1000$). (*a*) A structure before deformation (static conditions), (*b*) a structure under conditions of continuous shear ($\dot{\varepsilon} = 0.3\ s^{-1}$), (*c*) a structure under combined action of continuous shear ($\dot{\varepsilon} = 0.3\ s^{-1}$) and orthogonal oscillation ($f_v^* = 50$ Hz, $a = 10^{-3}$ m)

high reproducibility of vibrorheological flow curves (with slight deviations within several percentage) in viscosity measurements in going both from the minimum to the maximum values of I and in the reverse direction.

The flow curves have two main portions characterising various steps of destruction of a coagulation structure (see Fig. 16): the first sharp decrease in the viscosity corresponds to decomposition of a continuous structure into aggregates, whereas the second decrease corresponds to destruction of the latter into aggregates of smaller sizes and individual particles. At the same time, these curves reflect some essential features of destruction under oscillation.

Although eliminating discontinuity and destroying the structure, oscillation does not lead to complete destruction of aggregates, as evidenced by retention of substantial differences in the level of η_v (up to an order of magnitude) at $I \geqslant 1$. Destruction of aggregates of very small sizes is a very energy-consuming process. This is confirmed by the fact that an increase in I by 3–4 orders of magnitude in lower portions of the flow curves leads to a small decrease in the viscosity.

Analogous results were obtained for aqueous suspensions of calcium bentonite (CaB) both for systems with $\varphi > \varphi_c$ and suspensions at concentrations $\varphi \leqslant \varphi_c$. Figure 17 presents scanning electron micrographs of dispersed structures taken with the use of a procedure described in the studies.[62,95] The photomicrographs show successive structural transformations. It can be seen that discontinuities, which appear under continuous shear, are completely eliminated under orthogonally directed oscillation. This important result indicates that a combination of continuous shear and orthogonal oscillation allows one, in principle, to control an isotropic dynamic state. However, the destruction under oscillation and shear is not limiting (although is close to the limiting value) but is characterised by the presence of aggregates throughout the range of changes in $\eta_{ef} = \eta_v$, where η_v is the effective viscosity under oscillation.

Vibrations destroy structures predominantly at weak contacts thus initiating the formation of dense microaggregates, in which particles are fixed in a short-range potential minimum due to inertial coagulation. This fact complicates substantially the attainment of ultimate destruction. In combination with continuous shear, oscillation facilitates mutual dynamic scanning of the surfaces of contacting particles and, in the presence of lyophobic–lyophilic mosaicity of these surfaces in most real disperse systems, leads to a 'manifestation' of mosaicity and selective formation of new strong contacts predominantly in lyophobic regions.[2] This spontaneous formation of microaggregates, in which particles are fixed in sites of short-range coagulation, is manifested as the effect of strengthening of the structure under oscillation.[2] This phenomenon resides in the fact that after cessation of exposure to orthogonal oscillation, the effective viscosity η_{ef} (the effective stress P at $\dot{\varepsilon} = \text{const}$) sharply increases compared to its equilibrium value in a steady shear flow at the same value of $\dot{\varepsilon}$ prior to exposure to oscillation (Fig. 18). Hence it follows that the limiting isotropic dynamic state and, correspondingly, aggregation dynamic stability of disperse systems can be attained only if both inertial (short-range) coagulation and the effect of strengthening due to oscillation (this effect is associated with coagulation and lyophobic–lyophilic mosaicity of the particle surface) are excluded.

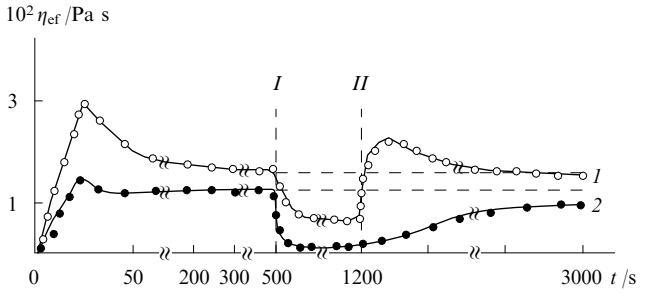

Figure 18. Dependence of the effective viscosity of an aqueous dispersion of CaB ($s_{BET} = 70\ m^2\ g^{-1}$, $\varphi = 0.33$) on the time under continuous shear deformation $\dot{\varepsilon} = 0.3\ s^{-1}$ (see Ref. 2).
(*1*) a dispersion in the absence of surfactant additives, (*2*) a dispersion of particles whose surface was modified with a monolayer of oxyethylated alkylphenol (OP-10); (*I*) the onset of oscillation orthogonal to continuous shear ($f_v^* = 50$ Hz, $a = 5 \times 10^{-4}$ m), (*II*) cessation of oscillation.

It was demonstrated[94] that an efficient way for solving this problem consists in combining the exposure of a disperse system to oscillation and the introduction of surfactant additives, which lyophilise the particle surface and create a structure-mechanical barrier (according to Rehbinder). Therefore, inertial coagulation under dynamic conditions is hindered in the presence of a surfactant adsorption layer, which serves as a structure-mechanical barrier. From Eqn (35) it follows, in particular, that the attainment of aggregation stability of dispersions under dynamic conditions requires an increase in the strength of an adsorption layer, particularly, in the presence of asperities with a small radius of curvature on the particle surface. The modulus of elasticity of the layer can be decreased by increasing the thickness of the layer L, the particle size and the distance between their surfaces.

In the presence of an adsorption layer, the critical coagulation rate can be determined by Eqn (34) or from the following relation:

$$V_c^* > \lambda_i \frac{L}{r_{max}} \left(\frac{P_L}{E_L}\right)^{3/2} \left(\frac{E_L\, r^*}{2\rho r_{max}}\right)^{1/2}, \qquad (60)$$

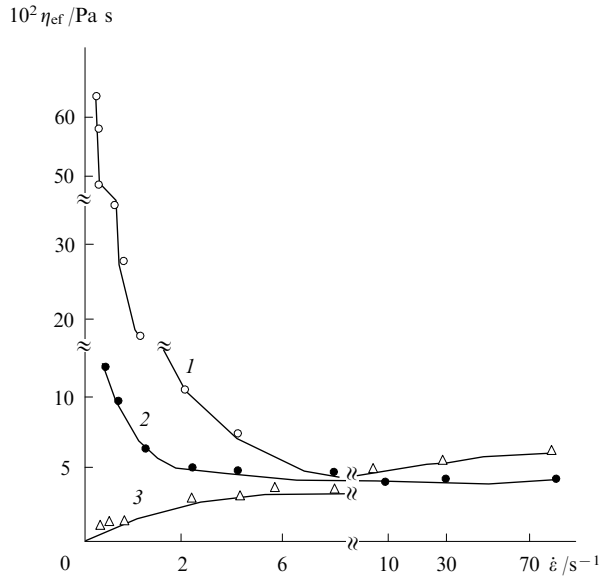

Figure 19. Dependence of the effective viscosity of highly concentrated aqueous carbon suspensions (φ = 72.5%) on the shear rate.[111]
(*1*) In the absence of oscillation action; (*2*) in the absence of oscillation action with an additive of an anion-active surfactant, *viz*., a sulfonation product of oil tars (1% of the mass of the solid phase); (*3*) under conditions analogous to those used in run (*2*) combined with orthogonal oscillation with a frequency of 50 Hz and acceleration $A = 2.5g$.

where the parameter λ_i determines the curvature of the particle surface in the contact zone: for spheres, $\lambda_i = 1$; for particles with a radius of curvature $r^* < r_{max}$, in particular, for two disk-like particles, which collide perpendicular to one another, $\lambda_i = 2(r_{max}/r^*)^{3/4}$. Assuming $L \sim 10^2$ nm for disk-like particles with $r^* \sim 3 \times 10^2$ nm and $r_{max} = 10$ μm, the aggregation stability in dynamic conditions will take place at $E_L \sim P_L > E_{Lc} \sim 10^5$ Pa. For polyvinyl alcohol, this condition is fulfilled [110] at a rather high rate $V_c^* \sim 0.5$ m s^{-1}. The same condition is obviously fulfilled for a polyfunctional anion-active surfactant of a new type, which was prepared starting from dehydrated liquid products of hydrocarbon pyrolysis, which were mixtures of water-soluble salts of sulfonic acids of bicyclic aromatic hydrocarbons (sulfonation product of oil tars).[111] When choosing surfactants, which satisfy the above-mentioned conditions, one should take into account the characteristic features of their micellar structures, because micelles formed in solutions of surfactants can produce a structure-mechanical barrier.[67]

The results of experimental test of the efficiency of a combined action of orthogonally directed oscillation and the presence of surfactants, which create a structure-mechanical barrier on the surface of particles of dispersed phases are presented in Figs 18 and 19.

Upon modification of the CaB particle surface with oxyethylated alkylphenol OP-10, both the depth and the destruction rate under oscillation (a decrease in η_{ef}) increase (see Fig. 18, curve *2*) compared to the analogous values observed under oscillation but in the absence of surfactants (curve *1*). This fact can be attributed to a substantial decrease in the strength and energy of interparticle interactions under oscillation. At the same time, the vibrostrengthening effect completely disappears in the presence of surfactants, and the rate of thixotropic recovery of a structure decreases sharply, which is indicative of the absence of 'breakdown' of the adsorption layer under oscillation and the retention of a structure-mechanical barrier in the course of prolonged (for more than 10 min) high-intensity oscillation.

An analogous effect of a combination of orthogonal oscillation and surfactant additives was revealed in a shear flow of highly concentrated aqueous carbon suspensions (see Fig. 19). A particularly sharp decrease in η_{ef} (by two orders of magnitude) was observed at low shear rates ($\dot{\varepsilon} \leqslant 2$ s^{-1}). The viscosities calculated by the equations reported in the study [30] had close values in this region, which indicates that the ultimate destruction was reached. A slight increase in the viscosity with increasing $\dot{\varepsilon} > 2$ s^{-1} is not associated with the structural effects, but apparently results from turbulisation of a flow under oscillation ('vibrodilatancy'). This is confirmed by full reversibility of the effect. Thus, the viscosity reaches the initial minimum level when $\dot{\varepsilon}$ decreases to 2 s^{-1}. The effect of a decrease in the vibroviscosity and oscillation intensity in concentrated cement aqueous dispersions as a result of the surface modification of cement particles with surfactant additives is illustrated in Fig. 20. This effect is noticeable in the presence of OP-10 (curve *2*) and, particularly, of sodium methylsiliconate (curve *3*). In the latter case, a decrease in η_{ef} amounts to as much as four orders of magnitude and a decrease in the oscillation intensity necessary for the attainment of η_{ef} ranges up to three orders of magnitude.[68] It should be emphasised that both these effects are

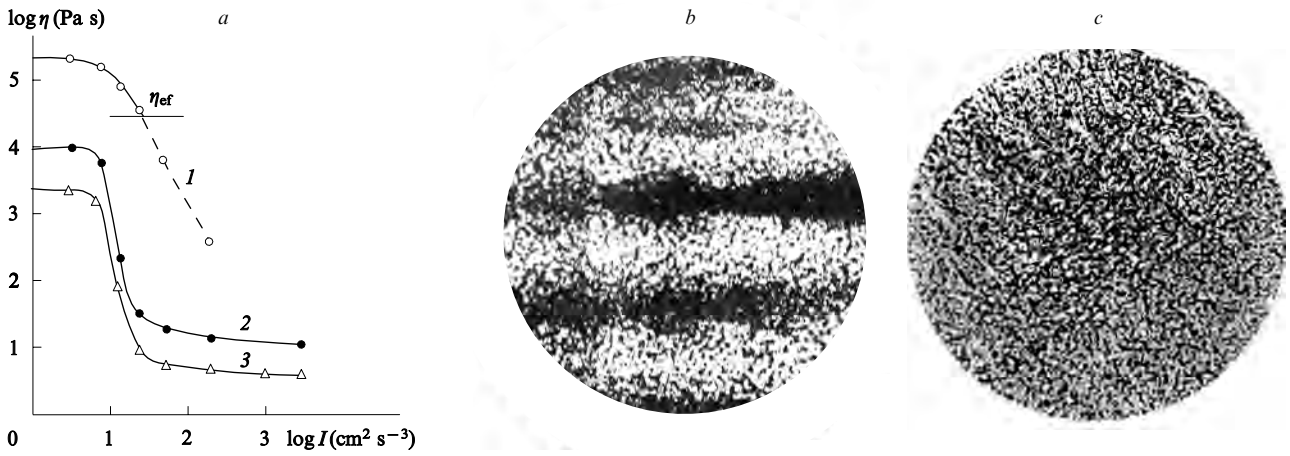

Figure 20. Effect of combined action of shear deformation, orthogonal oscillation and surfactant additives.[68]
The model dispersion is a mixture of tricalcium hydrosilicate and tricalcium hydroaluminate in water (φ = 0.48).
(*a*) rheological flow curves: (*1*) under shear without oscillation (η_{ef}), (*2*) a combination of continuous shear ($\dot{\varepsilon}$ = 0.3 s^{-1}) and oscillation with increasing intensity, (*3*) under conditions analogous to those used in run (*2*) in combination an additive of sodium methylsiliconate (0.3%). Photomicrographs of the structure formed under dynamic conditions: (*b*) under continuous shear for 600 s, (*c*) under combined action of continuous shear, orthogonal oscillation and a surfactant additive (15 s).

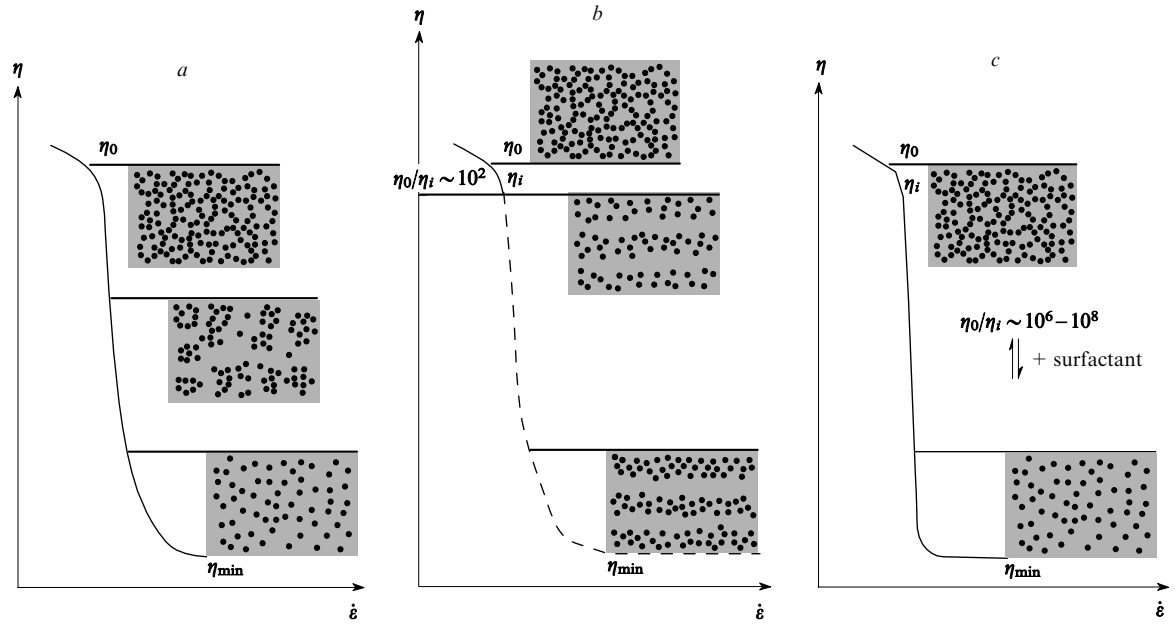

Figure 21. Scheme illustrating the destruction mechanism of coagulation structures in disperse systems under dynamic conditions.[68]
(*a*) Under continuous shear deformation with increasing shear rate (commonly accepted views), (*b*) the real pattern of destruction of dispersions under continuous shear, (*c*) spontaneous ultimate destruction with the attainment of the true maximum fluidity and complete ultimate deaggregation under conditions of an optimum combination of continuous shear and orthogonally directed oscillation in the presence of surfactant additives.

most pronounced in the region of the lowest vibroviscosity levels. This indicates that oscillations suppress the formation of dense and stable microaggregates as a result of inertial coagulation, which is typical of destruction under oscillation in the absence of surfactants. At the same time, this fact is also indicative of isotropic destruction, *i.e.*, of the attainment of the limiting dynamic state in the case of both highly concentrated aqueous carbon suspensions and cement aqueous dispersions.

A combination of orthogonal oscillation and the introduction of surfactant additives can be considered as an efficient way of intensifying processes of wetting and flowing of non-Newtonian structured high-viscosity dispersions as a result of their transformations into low-viscosity Newtonian liquids.[64,65] This phenomenon is of considerable importance in the preparation of composition materials with a binder as a structured dispersion.[62]

The main steps of the generation of a controlled dynamic state of two-phase structured disperse systems of the solid phase – liquid dispersion medium type are illustrated in Fig. 21. The main step involves the construction of complete rheological flow curves describing the overall range of changes in dynamic states, which are determined by the effective viscosity levels corresponding to a given deformation rate. When constructing these curves, it was assumed that a certain equilibrium degree of isotropic destruction (degree of deaggregation) corresponds to each viscosity level, and complete deaggregation corresponds to the lowest Newtonian viscosity level η_{min} (see Fig. 21 *a*). In actuality, the destruction is often anisotropic in character and gives rise to solid-like layers, which are strengthened as the deformation rate increases, are separated by an interlayer of a dispersion medium and are oriented along the shear direction (see Fig. 21 *b*). Consequently, contrary to the commonly accepted views of the flow mechanism of structured dispersions, the true ultimate destruction as well as the maximum fluidity of dispersions are not achieved.

The use of the above-described approaches and methods for creating of the optimum dynamic state in structured dispersions actually allows one to achieve the complete and isotropic destruction with complete spontaneous deaggregation and, correspondingly, to attain true maximum fluidity (Fig. 21 *c*).

IV. Conclusion

The dynamic state of structured disperse systems depends on the degree and conditions of destruction of dispersions. Depending on the type and intensity of external actions, disperse systems in dynamic conditions are characterised by the presence of macroscopic quasi-phases as aggregates consisting of particles and solid-state layers, which are oriented along the direction of the high-intenisty continuous action (for example, shear). The sizes and densities of aggregates and layers depend on the state of the surface, the shape of primary particles and the degree of destruction. The same factors are responsible for the effective viscosity of disperse systems under dynamic conditions. Methods for the creation of a controlled dynamic state of such systems are based on the following two main factors: first, the modification of particle surfaces (their lyophilisation) to form a surfactant adsorption layer serving as a structure-mechanical barrier, which hinders inertial coagulation of particles; second, the complex exposure of a disperse system to continuous shear and orthogonally directed oscillation, whose intensity (in combination with the modification of the particle surface) corresponds to the condition of complete (ultimate) deaggregation.

This level of the limiting isotropic dynamic state corresponds to dynamic aggregation stability and maximum fluidity of structured disperse systems. In essence, the views of the characteristic features and methods for creating a dynamic state and controlling the properties of disperse systems under dynamic conditions provide the basis for physicochemical dynamics of structured disperse systems.

The attainment of the true maximum fluidity of structured disperse systems with complete deaggregation allows one to radically change the conditions for performing various chemical engineering processes, including those for the preparation of dispersed composition materials. It is known that the rate of heterogeneous processes carried out under conditions of forced convective diffusion is inversely proportional to the viscosity. Hence, the attainment of complete destruction, deaggregation of a system and the true lowest Newtonian viscosity by decreasing the effective viscosity of dispersions by 5 – 7 orders of magnitude

provides the possibility of accelerating many heterogeneous chemical engineering processes to the same extent.

Liberation of an immobilised dispersion medium from a structural network and a sharp increase of the 'operating' active interface due to complete deaggregation make it possible to increase the rate and degree of completion of a series of heterogeneous processes by several orders of magnitude.

In the case of complete deaggregation under conditions of attainment of the optimum dynamic state of dispersions, both the dispersity of the solid phase S and its concentration φ increase and, hence, it is possible to pass to the previously 'forbidden' (due to a sharp increase in the viscosity and the limiting shear stress) region of highly concentrated ($\varphi > \varphi_c$) and finely disperse systems, which also allows one to accelerate sharply heterogeneous processes, whose rates are proportional to the areas of operating interfaces.

By attaining the highest degree of homogeneity of phase distribution with a simultaneous increase in their dispersity and concentration in dispersion media, one can prepare both traditional and new types of highly filled dispersed composition materials possessing the desired properties and structures.

Numerous examples of various applications of the principles of the creation of a controlled dynamic state in disperse systems lie at the basis of new methods and high-performance technologies for the production and procession of disperse systems and composition materials.[2, 54, 55, 105, 112–114]

In conclusion, let us formulate briefly the main results of studies carried out in the last 10–15 years, which provide the basis for physicochemical dynamics of disperse systems:

— the dynamic theory of contact interactions was devised;

— the theory of complete rheological flow curves taking into account discontinuities was developed;

— foundations of the theory of the creation of the limiting dynamic state of disperse systems and their maximum fluidity were laid;

— the mechanism of a combined action of oscillation and the introduction of surfactant additives in flow processes of dispersions for the attainment of their maximum fluidity was revealed.

In addition, new characteristic features of sedimentation processes both under static and dynamic conditions were found. The results of these fundamental studies were supported by experimental investigations and have found practical applications in various fields of technology and engineering. Among new promising lines of physicochemical dynamics, let us note the elucidation of the mechanism of flowing of structured dispersions, investigations of the dynamics of three-phase disperse systems and the development of theoretical foundations of new methods for performing various chemical engineering processes in highly concentrated and finely disperse systems.

This review has been written with the financial support of the Russian Foundation for Basic Research (Project No. 03-03-32237).

References

1. P A Rehbinder *Izbrannye Trudy. Poverkhnostnye Yavleniya v Dispersnykh Sistemakh. Fiziko-Khimicheskaya Mekhanika* (Selected Works. Surface Effects in Disperse Systems. Physicochemical Mechanics) (Moscow: Nauka, 1979)
2. N B Uriev *Vysokokontsentrirovannye Dispersnye Sistemy* (High-Concentrated Disperse Systems) (Moscow: Khimiya, 1980)
3. E D Shchukin, A V Pertsov, E A Amelina *Kolloidnaya Khimiya* (Colloid Chemistry) (Moscow: Vysshaya Shkola ,1992)
4. R M Mazo *Brownian Motion: Fluctuations, Dynamics and Applications* (Oxford: Oxford University Press, 2002)
5. M Kollmann *Dynamics and Microstructure of Interacting Brownian Particle Systems: Electrokinetic Effects, (Quasi)-two-Dimensional Systems and Sphere Caging Imprint* (Constantsa: Constantsa University, 2001)
6. N B Uriev *Priroda* **10** 20 (2000)
7. V G Levich *Fiziko-Khimicheskaya Gidrodinamika* (Physicochemical Hydrodynamics) (Moscow: Nauka, 1959)
8. V V Krotov, A I Rusanov *Physicochemical Hydrodynamics of Capillary Systems* (London: Imperial College Press, 1999)
9. N B Uriev, A A Potanin, in *Uspekhi Kolloidnoi Khimii* (Progress in Colloid Chemistry) (Tashkent: FAN, 1987)
10. A A Potanin, N B Uriev, V M Muller *Kolloid. Zh.* **49** 915 (1987) [a]
11. A A Potanin, N B Uriev, V M Muller *Kolloid. Zh.* **50** 493 (1988) [a]
12. O I Vinogradova *Kolloid. Zh.* **56** 39 (1994) [a]
13. O I Vinogradova *Kolloid. Zh.* **58** 590 (1996) [a]
14. J W Gibbs *The Scientific Papers of J Willard Gibbs* (New York: V I Dover, 1961)
15. V V Yaminskii, V A Pchelin, E A Amelina, E D Shchukin *Koagulyatsionnye Kontakty v Dispersnykh Sistemakh* (Coagulation Contacts in Disperse Systems) (Moscow: Khimiya, 1982)
16. J N Israelachvili *Intermolecular and Surface Forces* (London: Academic Press, 1991)
17. E D Shchukin *J. Colloid Interface Sci.* **256** 114 (2002)
18. B V Derjaguin, N V Churaev, V M Muller *Poverkhnostnye Sily* (Surface Forces) (Moscow: Nauka, 1985)
19. A A Potanin, N B Uriev *Teor. Osnovy Khim. Tekhnol.* **22** 529 (1988) [b]
20. B V Derjaguin *Acta Physicochim. URSS* **10** 333 (1939)
21. V M Muller, in *Issledovanie v Oblasti Poverkhnostnykh Sil* (Investigation in the Field of Surface Forces) (Moscow: Nauka, 1967) p. 270
22. F D Zimon, E I Andrianov *Autogeziya Sypuchikh Materialov* (Autohesion of Loose Materials) (Moscow: Metallurgiya, 1978)
23. P A Rehbinder, E D Shchukin, L Ya Margolis *Dokl. Akad. Nauk SSSR* **154** 695 (1964) [c]
24. E D Yakhnin, A B Taubman *Dokl. Akad. Nauk SSSR* **155** 179 (1964) [c]
25. E D Yakhnin. *Kolloid. Zh.* **60** 717 (1998) [a]
26. V G Babak, A Langenfeld, M J Stebe *Prog. Colloid Polym. Sci.* **118** 216 (2001)
27. M J Powell *Phys. Rev.* **20** 4194 (1979)
28. H Rumpf *Chem. Ing. Techn.* **90** 144 (1958)
29. I M Yaglom *Problema Trinadtsati Sharov* (The Problem of Thirteen Spheres) (Kiev: Vishcha Shkola, 1975)
30. N B Uriev, A A Potanin *Tekuchest' Suspenzii i Poroshkov* (Fluidity of Suspensions and Powders) (Moscow: Khimiya, 1992)
31. D Stauffer *Phys. Rep.* **54** 1 (1979)
32. F C Hapensteadt *Analysis and Simulation of Chaotic Systems* (New York: Springer, 2000)
33. A S Makarov, V A Sushko *Kolloid. Zh.* **41** 735 (1979) [a]
34. M F Fisher, J W Essam *Math. Phys.* **2** 608 (1961)
35. M Ottavi, J Clevc, G Girand, J Rousseng *J. Phys.* **11** 1311 (1978)
36. S Kirpatrik *Rev. Mod. Phys.* **45** 577 (1973)
37. A A Potanin, N B Uriev *Kolloid. Zh.* **50** 70 (1988) [a]
38. R Lullien, R Botel *Aggregation and Fractal Aggregates* (Singapur: World Scientific, 1987)
39. S Havlin *Fractals in Physics* (Amsterdam: North Holand, 1986)
40. R Buscall, P Mills, J Goodwin *J. Chem. Soc., Faraday Trans. 1* **84** 4249 (1988)
41. R Turton, R C Bailie, W B Whiting, J A Shaewitz *Analysis, Synthesis and Design of Chemical Processes* (Englewood Cliffs, NJ: Prentice-Hall RTR, 2002)
42. B V Derjaguin, N A Krotova, V P Smilga *Adgeziya Tverdykh Tel* (Adhesion of Solids) (Moscow: Nauka, 1973)
43. B V Derjaguin *Izv. Akad. Nauk SSSR, Ser. Khim.* **5** 1153 (1937) [d]
44. B V Derjaguin *Acta Physicochim. URSS* **14** 633 (1941)
45. B V Derjaguin, L D Landau *Zh. Eksp. Teor. Fiz.* **11** 802 (1941)
46. B V Derjaguin, L D Landau *Zh. Eksp. Teor. Fiz.* **15** 662 (1945)
47. B V Derjaguin, N V Churaev *Langmuir* **3** 607 (1987)
48. N V Churaev, V D Sobolev, A N Somov *J. Colloid Interface Sci.* **97** 577 (1984)
49. E D Yakhnin *Dokl. Akad. Nauk SSSR* **178** 152 (1968) [c]
50. S Yu Kuznetsov, N B Uriev *Kolloid. Zh.* **53** 755 (1991) [a]
51. A A Potanin, N B Uriev *Kolloid. Zh.* **50** 712 (1988) [a]
52. J M Serayssol, R Davis *J. Colloid Interface Sci.* **114** 54 (1986)
53. M Leva *Psevdoozhizhenie* (Fluidisation) (Moscow: Gostoptekhizdat, 1961)
54. V A Chlenov, N V Mikhailov *Vibrokipyashchii Sloi* (Vibro-Fluidised Bed) (Moscow: Nauka, 1972)

55. I I Blekhman *Vibratsionnaya Mekhanika* (Vibration Mechanics) (Moscow: Nauka, 1994)
56. E D Shchukin, E A Amelina *Adv. Colloid Interface Sci.* **11** 235 (1979).
57. B V Derjaguin, V M Muller, A M Mikhowich, Yu P Toporov *J. Colloid Interface Sci.* **118** 553 (1987)
58. N B Uriev *Structural and Mechanical Properties of High-Disperse Powder under Dynamic Conditions* (Washington, DC: Particulate Science and Technology Hemisphere Publ. Co., 1989) p. 283
59. E L Vinogradov, L I Godunova, M A Makar'ev, A N Kozlov *Kolloid. Zh.* **45** 313 (1983) [a]
60. M R Spasskii, E D Shchukin *Kolloid. Zh.* **35** 897 (1973) [a]
61. M A Makar'ev, Candidate Thesis in Chemical Sciences, Institute of Physical Chemistry, Academy of Sciences of the USSR, Moscow, 1984
62. N B Uriev, in *Fiziko-Khimicheskie Osnovy Tekhnologii Dispersnykh Sistem i Materialov* (Physicochemical Foundations of the Technology of Disperse Systems and Materials) (Moscow: Khimiya, 1988)
63. K Rietema *The Dynamics of Fine Powders* (Amsterdam: Elsevier, 2002)
64. B D Summ, Yu V Goryunov *Fiziko-Khimicheskie Osnovy Smachivaniya i Rastekaniya* (Physicochemical Foundations of Wetting and Spread) (Moscow: Khimiya, 1976)
65. B D Summ, N B Uriev *Kolloid. Zh.* **58** 92 (1996) [a]
66. L D Landau, E M Lifshits *Mekhanika Sploshnykh Sred* (Mechanics of Continuum) (Moscow: GITTL, 1954)
67. A I Rusanov *Mitselloobrazovanie v Rastvorakh Poverkhnostno-aktivnykh Veshchestv* (Micelle-Formation in Solutions of Surfactants) (St Petersburg: Khimiya, 1992)
68. N B Uriev *Colloids Surf. A* **87** 1 (1994)
69. C W Macosko *Rheology Principles, Measurements and Applications* (London, New York: VCH, 1994)
70. M Reiner *Deformatsiya i Techenie.* (*Deformation and Flow*) (Moscow: GNTI Neft. Gorno-Topl. Lit., 1963)
71. W J Frith Ph.D. Thesis, Katholicke Universiteit Leuven, Belgium, 1996
72. G N Ourieva Ph.D. Thesis, Katholicke Universiteit Leuven, Belgium, 1999
73. J Mewis *J. Non-Newtonian Fluid Mech.* **6** 1 (1979)
74. G V Vinogradov, A Ya Malkin *Reologiya Polimerov* (Rheology of Polymers) (Moscow: Khimiya, 1977)
75. L A Abduragimova, P A Rehbinder, N N Serb-Serbina *Kolloid. Zh.* **27** 184 (1955) [a]
76. N B Uriev, S V Choi *Kolloid. Zh.* **55** 183 (1993) [a]
77. W B Russel *Powder Technol.* **51** 15 (1987)
78. P D Patel, W B Russel *Colloids Surf.* **31** 355 (1988)
79. E E Bibik *Reologiya Dispersnykh Sistem* (Rheology of Disperse Systems) (Leningrad: Leningrad State University, 1981)
80. P F Ovchinnikov *Vibroreologiya* (Vibrorheology) (Kiev: Naukova Dumka, 1983)
81. W N Hunt, C F Zukoski *J. Colloid Interface Sci.* **210** 343 (1999)
82. I M Krieger *Adv. Colloid Interface Sci.* **3** 111 (1972)
83. C E Chaffey *Colloid Polym. Sci.* **3** 111 (1977)
84. A A Potanin, N B Uriev *J. Colloid Interface Sci.* **142** 385 (1991)
85. G Schoukens, J Mewis *J. Rheology* **22** 381 (1978)
86. N A Frankel, A Acrivons *Chem. Eng. Sci.* **23** 847 (1967)
87. I Ree, H Eyring *J. Rheology* **2** 83 (1958)
88. G M Bartenev, N V Ermilova, in *Fiziko-Khimicheskaya Mekhanika Dispersnykh Struktur* (Physicochemical Mechanics of Disperse Structures) (Moscow: Nauka, 1965) p. 371
89. N V Churaev *Kolloid. Zh.* **50** 108 (1988) [a]
90. W J Frith, T A Strivens, J Mewis *J. Colloid Interface Sci.* **53** 358 (1975)
91. W J Frith, P d'Haene, R Buscall, J Mewis *J. Rheol.* **40** 531 (1996)
92. B Ouriev Ph.D. Thesis, ETH, Zurich, 2000
93. H M Laun, in *Proceedings of the 10th International Congress on Rheology, Sydney, 1988* Vol. 5, p. 37
94. N B Uriev, N V Mikhailov *Kolloidnyi Tsementnyi Klei i Ego Primenenie v Stroitel'stve* (Colloid Cement Glue and Its Use in Construction) (Moscow: Stroiizdat, 1967)
95. E D Shchukin, N V Pertsov, V I Osipov, R I Zlochevskaya (Eds) *Fiziko-Khimicheskaya Mekhanika Prirodnykh Dispersnykh Sistem* (Physicochemical Mechanics of Natural Disperse Systems) (Moscow: Moscow State University, 1985)
96. N B Uriev, A V Cheremisov, A Yu Tkachev *Kolloid. Zh.* **61** 413 (1999) [a]
97. V A Fedotova, K A Khadzhaeva, P A Rehbinder *Dokl. Akad. Nauk SSSR* **170** 1133 (1966) [c]
98. N B Uriev, I I Bardyshev *Colloids Surf., A* **225** 25 (2003)
99. R Buscall, I J Mcgowan *Faraday Disc. Chem. Soc.* **76** 277 (1983)
100. A E Hosoi, T F Dupont *J. Fluid Mech.* **328** 297 (1996)
101. Yu Ngotan, N B Uriev, S N Battacharia *Kolloid. Zh.* **57** 220 (1975) [a]
102. G K Batchelor *J. Fluid Mech.* **83** 97 (1977)
103. E van der Aershot, J Mewis *Colloids Surf.* **69** 15 (1992)
104. A Einstein *Ann. Phys.* **19** 289 (1906)
105. A Einstein *Ann. Phys.* **34** 591 (1911)
106. J Happel, H Brenner *Low Reynold Number Hydrodynamics* (2nd Ed.) (Leyden, The Netherlands: Noordhoff, 1973)
107. N B Uriev, I Ya Ladyzhinsky *Colloids Surf.* **108** 1 (1996)
108. I G Shatalova, N S Gorbunov, V I Likhtman *Fiziko-Khimicheskie Osnovy Vibratsionnogo Uplotneniya Poroshkovykh Materialov* (Physicochemical Foundations of Vibration Compacting of Powder Materials) (Moscow: Nauka, 1965)
109. R I Nigmatulin *Dinamika Mnogofaznykh Sred* (Dynamics of Multiphase Media) Pt. I, II (Moscow: Nauka, 1987)
110. V N Izmailova, P A Rehbinder *Strukturoobrazovanie v Belkovykh Sistemakh* (Structure Formation in Protein Systems) (Moscow: Nauka, 1974)
111. N B Uriev, V V Saskovets, S V Choi, L I Peregudova, A P Izhik, L G Vinogradova, N P Krut'ko *Kolloid. Zh.* **57** 83 (1995) [a]
112. N B Uriev, Ya P Ivanov *Strukturoobrazovanie i Reologiya Neorganicheskikh Dispersnykh Sistem i Materialov* (Structure Formation and Rheology of Inorganic Dispersion Systems and Materials) (Sofia: Bulgarian Academy of Sciences, 1991)
113. N B Uriev, M A Taleisnik *Pishchevye Dispersnye Sistemy* (Food Dispersion Systems) (Moscow: Pishchevaya Prom-st, 1980)
114. N B Uriev, I S Dubinin *Kolloidnye Tsementnye Rastvory* (Colloid Cement Slurries) (Moscow: Stroiizdat, 1980)

[a] — *Colloid. J. (Engl. Transl.)*
[b] — *Theor. Found. Chem. Eng. (Engl. Transl.)*
[c] — *Dokl. Chem. (Engl. Transl.)*
[d] — *Russ. Chem. Bull., Int. Ed. (Engl. Transl.)*

Russian Chemical Reviews **73** (1) 59 – 74 (2004) © 2004 Russian Academy of Sciences and Turpion Ltd

DOI 10.1070/RC2004v073n01ABEH000859

Phase equilibria and phase structures of polymer blends

A E Chalykh, V K Gerasimov

Contents

I.	Introduction	59
II.	Methods of construction of phase diagrams	59
III.	State-of-the-art studies of phase equilibria	61
IV.	Theoretical analysis	66
V.	Non-equilibrium and metastable states	69
VI.	Conclusion	71

Abstract. Experimental, methodical and theoretical studies dealing with phase equilibria and phase structures of polymer blends are generalised. The general and specific features of the change in solubility of polymers with changes in the molecular mass and copolymer composition and upon the formation of three-dimensional cross-linked networks are described. The results of the effect of the prehistory on the phase structure and the non-equilibrium state of polymer blends are considered in detail. The bibliography includes 125 references.

I. Introduction

The problem of phase equilibria and phase structures of polymer systems is one of the central problems in physical chemistry of polymers. This problem combines surprisingly interests of fundamental science and requirements of practice, polymer materials science and technology of polymer processing, the thermodynamics of polymer solutions and blends, the kinetics of phase decomposition and structure formation. This field of science has been extensively studied, and each investigation concerned different aspects of this problem to a lesser or greater extent.

Studies of phase equilibria of polymers can be divided into two periods. The first period can be tentatively called the 'period of compatibility'. In studies of this period, phase structures of particular polymer composites prepared under certain blending conditions were examined by various methods (mechanical, relaxation, thermochemical and sorption). Based on these results, conclusions were drawn about the polymer compatibility or incompatibility without regard for the temperature and concentration conditions for the preparation of composites.[1–9]

The second period of studies is being continued. It can be called the period of 'phase diagrams'. In investigations of this period, particular attention is given not to estimation of the polymer compatibility based on indirect data,† but to the directed construction of phase diagrams in broad ranges of temperature, compositions and molecular weights of the components. A comparative analysis of the monographs and reviews of the first and second periods shows that phase diagrams of binary, ternary or multicomponent systems were reported in virtually all modern large studies dealing with the properties of polymer and oligomer blends.[11–15]

However, the available extensive experimental data, which have partially been surveyed in the monographs,[15,16] demonstrate that, in spite of obvious progress, many results concerning phase structures and phase diagrams are contradictory with respect to both compositions of co-existing phases and positions of critical points. Besides, radically different phase diagrams were obtained for a number of systems by different researchers with the use of various methods of investigation and procedures for the preparation of blends. For example, diagrams with an upper critical solution temperature (UCST), a lower critical solution temperature (LCST) or two critical temperatures were reported for the same systems in different studies.

The paradox of the situation in this area of physical chemistry of polymers is that some researchers ignore results inconsistent with their point of view, other researchers believe that discrepancies in the experimental results are associated with the specificity of the methods used, whereas yet other researchers explain the contradictory results in the context of particular theories of polymer solutions.[16–24]

In our opinion, investigations of polymer blends have now come to a new stage. The main aim of such investigations is to obtain balanced non-contradictory information on phase equilibria and thermodynamic parameters of polymer blending. We consider the published data on phase compositions and characteristics of polymer blends from this standpoint. A detailed analysis of all experimental results is beyond the scope of our brief review. We focussed our attention on the most prominent examples, analysed the reasons for the above-mentioned contradictions and made attempts to find ways of resolving these contradictions.

II. Methods of construction of phase diagrams

The classification of methods which are used or will be used for constructing phase diagrams (rather than for estimating compatibility between components of polymer systems or the phase composition of materials) should be based not on methods of measurement, as suggested in the studies,[7,16,23,25] but on phenomena occurring in the system under study in the course of

A E Chalykh, V K Gerasimov Institute of Physical Chemistry, Russian Academy of Sciences, Leninsky prosp. 31, 119991 Moscow, Russian Federation. Fax (7-095) 952 53 08. Tel. (7-095) 955 44 63.
E-mail: chalykh@mail.ru (A E Chalykh).
Tel. (7-095) 955 44 42. E-mail: vladger@mail.ru (V K Gerasimov)

Received 3 July 2003
Uspekhi Khimii **73** (1) 63 – 78 (2004); translated by T N Safonova

† It should be noted that such studies are still published.[10]

measurements. Within the framework of this approach, all available and newly developed methods for the construction of phase diagrams can be divided into three groups.

Methods of determining critical points in the temperature–concentration field of polymer systems from the appearance and/or dissolution of particles of a dispersed phase of a particular nature belong to the first group. The second group includes methods associated with the determination of the compositions of co-existing phases. Calculation (semiempirical) methods for the construction of boundary lines in phase diagrams comprise the third group.

Two ways of performing experiments are used in the first group of methods. In one case, the composition of a solution, melt or blend remains constant throughout the experiment, and the figurative point (*A* in Fig. 1) moves along the temperature scale in response to changes in external conditions. In the second approach, phase decomposition or homogenisation of a polymer system initiated by forced changes in the composition of the system is performed under isothermal conditions. In this case, the figurative point of the system (*B* in Fig. 1) moves over the isotherm along the axis of compositions. It should be noted that in the first approach, measurements for a given composition are carried out continuously and the periodicity appears only on going from one composition of the system to another, whereas periodic measurements are almost always carried out in the second approach. This is associated with the procedure for changing the composition: a particular component is either additionally introduced into or removed from the mixture. In polymer–solvent or polymer(1)–polymer(2)–solvent systems, this is achieved by either dilution of the mixture or evaporation of a low-molecular-weight component.[1,8,26–28] In the case of polymer blends, all operations associated with the preparation (blending, pressing, thermal annealing, quenching) are carried out, but each time for blends of different compositions.[3,5,12] Evidently, to obtain reproducible results, particularly in the latter case, conditions under which components are mixed and samples for analysis are prepared should be rigorously constant, which is often impossible to achieve.

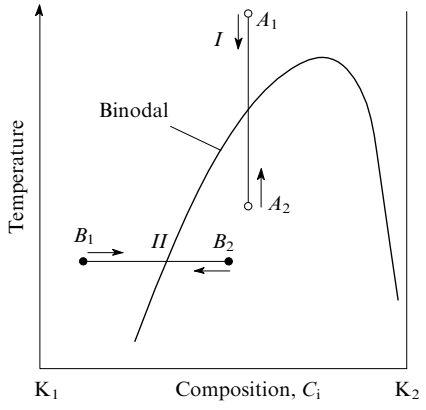

Figure 1. Scheme for performing experiments on the construction of phase diagrams (K_1 and K_2 are components of the system). Method *I*, the figurative point *A* moves along the temperature scale. Method *II*, the figurative point *B* moves along the composition axis.

In both approaches, the temperature $T_{ph.s}$ (at a given composition) or the composition $C_{ph.s}$ (at a given temperature), at which the phase state of the system changes, is determined from one of the chosen parameters (optical or electron density, intensity of light or neutron scattering, refractive index, thermal effect or changes in the local mobility of macromolecules and their fragments, labels, viscosity of the system as a whole, *etc.*). Particles of a dispersed phase either appear, if a true solution or melt is used as the starting system, or dissolve, if the starting state of the system corresponds to a heterogeneous region in the phase diagram.[29–37]

Methods belonging to the second group allow one to determine compositions of co-existing phases at different temperatures. These methods also employ different techniques for performing experiments. One of these techniques is based on interdiffusion. In this case, the phases of the starting components are brought into contact and then the character of the concentration distribution in the region of their spontaneous diffusion mixing is studied *in situ* by a particular local method.[38,39] Numerous experiments demonstrated[15,40–42] that there is a pronounced relationship between the character of the concentration distribution in the region of interdiffusion of semi-infinite phases and the phase diagram, which reflects the essence of processes of their spontaneous mixing. If phase conjugation is carried out at a temperature higher than UCST (or lower than LCST), $T > T_m$ or at a temperature higher than the isotropisation temperature, the formation of a concentration profile accompanied by a continuous change in the composition from one component to another is observed in the region of interdiffusion (Fig. 2 *a*).

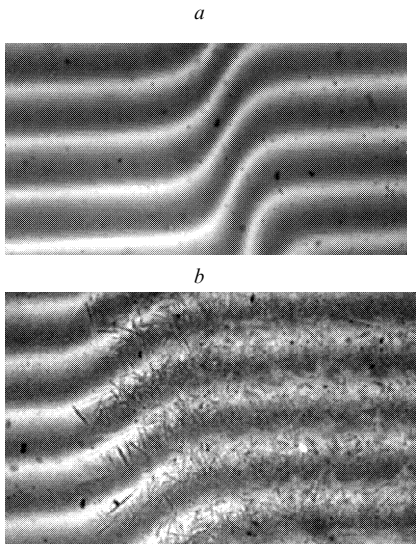

Figure 2. Concentration profiles of the CS ($M_w = 5.1 \times 10^4$)–PDMS ($M_w = 1.8 \times 10^3$) system above (*a*) and below (*b*) the isotropisation temperature of CS. The diffusion time is 4 min.[43]

If phase conjugation is performed at a temperature lower than UCST (or higher than LCST), $T < T_m$ or below the isotropisation temperature, the interface which separates the regions of diffusion mixing of components appears in the region of interdiffusion (Fig. 2 *b*). For systems with amorphous layering, these are regions of true solutions (to the right and left of the binodal curve) but with a variable composition. For crystalline or liquid-crystalline equilibrium systems,‡ these are the region of solutions to the left of the liquidus line in phase diagrams and the region of dissolution of an amorphous component in an amorphous phase of a crystalline or liquid-crystalline component (region below the liquidus line).

In all cases, the concentrations of solutions corresponding to compositions of co-existing phases are established on each side of the interface. Therefore, information required for the construction of phase diagrams can be obtained by performing interdiffusion at different temperatures and determining the compositions of co-existing phases in each experiment.

‡ In our review, we restrict ourselves to the consideration of thermotropic liquid-crystalline systems. Phase equilibria for lyotropic liquid-crystalline systems have been described in sufficient detail in the monograph.[44]

It should be borne in mind that in systems characterised by rather high diffusion mobility of components ($10^{-10} < D < 10^{-5}$ cm^2 s^{-1}), the above-described measurements are carried out *in situ*, which enables one to obtain phase diagrams on modern diffusiometers [45] within very short periods of time.

For systems characterised by low translational mobility of components ($D < 10^{-10}$ cm^2 s^{-1}), steps of formation of the diffusion zone and studies of the concentration distribution in this zone are, as a rule, separated in temperature and time. For example, interdiffusion in such systems [most often, these are polymer(1) – polymer(2) systems] is generally carried out at high temperatures ($T \geqslant T_g + 50°$; T_g is the glass transition temperature) over a long period of time. This process is followed by quenching of the gradient structure, the preparation of a sample and investigation of the concentration profile. If these conditions are met, the measured concentration profiles and the compositions of co-existing phases should be assigned to the annealing temperature of the system under study.

Another method of performing experiments involves an examination of swelling. In the practice of investigation of phase equilibria, this method is named the 'method of limited swelling' [25] and is recommended for determining the right branch of the binodal.[28] However, the traditional version (weight or volumetric determination of the equilibrium degree of swelling [1] followed by the calculation of the composition of the sample) of this method can be used only in the case of strictly limited swelling, *i.e.*, when the left branch of the diagram is actually absent. Apparently, this requires not only special preliminary measurements of the kinetics of polymer swelling but also the simultaneous determination of the composition of the liquid in which swelling occurs. These measurements can be used for the construction of a fragment of the binodal curve only if the composition of the liquid remains unchanged in the course of swelling. One must verify experimentally that the degree of swelling determined for the same sample is reproduced when moving along the temperature axis. In all other cases, this method can be recommended only as a preliminary step.

The third group of methods involves semiempirical calculation methods. These methods are based not on direct experimental data on phase decomposition of systems but on concentration dependences of the thermodynamic characteristics of solutions, whose extrapolation provides estimates of the positions of binodal or spinodal curves. Methods of measuring excess light scattering,[23] calculations of the thermodynamic correction $(\partial \ln a_i / \partial \ln \varphi_i$, where a_i are the activities of components, φ_i are their bulk concentrations) in experiments on self-diffusion and interdiffusion [31, 46, 47] or evaluation of the effective parameter of interaction from the results of inverse gas chromatography [1, 48] are used most extensively.

Most of the above-mentioned methods in combination with differential scanning calorimetry,[24, 49] static sorption,[50] relaxation spectroscopy,[51, 52] X-ray microanalysis,[39] electronic and atomic force microscopy [53] or photoelectron spectroscopy [54] are used for studying phase structures and compositions of polymer blends. The specificity of these studies is associated not with the organisation of experiments or interpretation of the results but with the determination of the position of the figurative point for the sample under investigation in the temperature – concentration field of the phase diagram.

As an example, we refer to the results of structural – morphological studies of blends of poly(vinyl chloride) (PVC) and poly(methyl methacrylate) (PMMA) prepared according to different methods: using a common solvent, polymerisation of methyl methacrylate in PVC, extrusion and pressing.[55, 56] It should be noted that investigations of the phase structures of these materials were carried out either at room temperature (static sorption of tetrahydrofuran and X-ray microanalysis) or using continuous heating to determine the glass transition temperatures and rheological parameters at temperatures higher than their flow temperatures. The results of measurements for this system are summarised in Fig. 3 (ω is the weight concentration) as isoconcentration lines in the temperature – concentration field of the phase diagram, because the assignment to temperatures is ambiguous. All these lines are located in a heterogeneous metastable or labile region of the diagrams,[58] and the compositions of co-existing phases measured for these blends (in the study,[57] these lines are called the compatibility boundaries) differ substantially from equilibrium values. Evidently, these structures are unstable in spite of the fact that the free energies of mixing (to be more precise, the free energies of formation of the phase structure) for some of these structures have negative values, and heating to temperatures higher than the glass transition temperature leads to secondary phase decomposition accompanied by changes in the composition of co-existing phases and their dispersion characteristics.

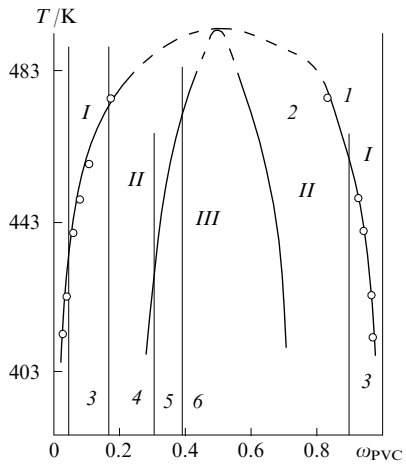

Figure 3. Phase diagram of the PVC – PMMA system.
(*1*) Binodal, (*2*) spinodal; vertical lines correspond to the compatibility limits for blends prepared by different methods: extrusion (*3*), pressing (*4*), using a common solvent (*5*), polymerisation of methyl methacrylate in PVC (*6*);[50, 57 – 59]
(*I*, single-phase solution; *II*, metastable region; *III*, region of labile solutions.)

We are sure that structural methods can also be used for the construction of phase diagrams, if special studies confirming the reversibility and equilibrium of the compositions of co-existing phases determined by a particular method are carried out and the phase transition temperature is identified.

III. State-of-the-art studies of phase equilibria

As mentioned above, the characteristic feature of the state-of-the-art studies of polymer blends is that researchers seek to obtain balanced non-contradictory data on phase equilibria and phase structures. When solving this problem, it is necessary to take into account the following facts:

— different research teams obtain experimentally reliable and adequate information on phase structures and properties of polymer blends using various methods;

— interpretation of the results is the subjective opinion of researchers, and different conclusions can be drawn based on the same experimental data;

— analysis of phase equilibria should be uniform [§] for all regions of phase diagrams and for all possible types of phase equilibria rather than being restricted to particular fragments of boundary curves (sometimes, of an unidentified phase nature);

§ Taking into account the temperature and concentration dependences, for example, for pair interaction parameters, the effect of the molecular mass, the composition of a copolymer, *etc*.

— experimental information on the phase state of particular polymer blends carries, among other things, information on the thermal prehistory of blends, conditions of preparation, thermal stability and reactivities of the components.

Polymer systems with amorphous layering are, as a rule, characterised by the following features.

1. An increase in the molecular mass (MM) of one of the components in systems with UCST generally leads to an increase in the critical temperature, extension of the two-phase region and a shift of the critical point in accordance with the Flory – Huggins theory (Fig. 4 – 6). Recall that the dependence of the solubility of polymers and oligomers on their MM (Fig. 7) served as the starting information for the development of the concept of segmental solubility of polymers in interface layers.[5] In the studies,[14, 42, 60] the dependence of the solubility on the molecular weight at a constant temperature was demonstrated to be described by linear equations on the $\varphi - (1/M)$ coordinates in a broad MM range (Figs 8, 9). These equations, in turn, can be used for the determination of critical molecular masses and compositions.

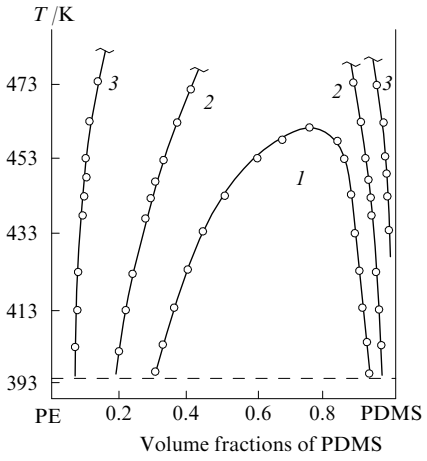

Figure 4. Phase diagrams[60] of the PE (5×10^3) – PDMS system. (Hereinafter, M_n are given in parentheses)
Molecular masses of PDMS: (*1*) 310; (*2*) 400; (*3*) 1200.

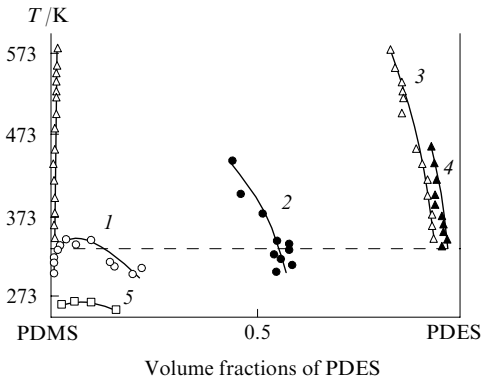

Figure 5. Phase diagrams of the polydiethylsiloxane (PDES) (3×10^5) – PDMS systems.
Molecular masses of PDMS: (*1*) 1×10^3, (*2*) 2.5×10^3, (*3*) 5.5×10^3, (*4*) 8.1×10^3 (see Ref. 42), (*5*) 1×10^3 (see Ref. 61).

Systems with LCST (Fig. 10) are characterised by somewhat different features. For these systems, an increase in the molecular mass leads to a decrease in the critical temperature, extension of the two-phase region and a shift of the critical point toward a higher-molecular-mass component.

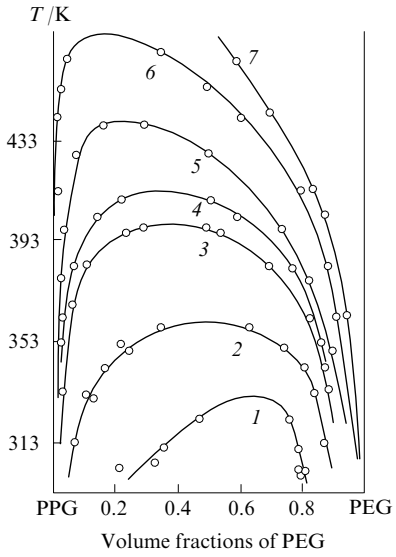

Figure 6. Phase diagram of the PPG (1×10^3) – PEG systems with different molecular masses.[15]
Molecular masses of PEG: (*1*) 600, (*2*) 1000, (*3*) 3000, (*4*) 4000, (*5*) 6000, (*6*) 15000.

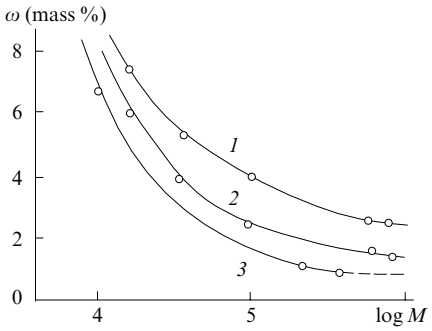

Figure 7. Solubilities of PS in PMMA (*1*, *3*)[5, 62] and PMMA in PS (*2*)[62] as functions of the molecular mass of PMMA.

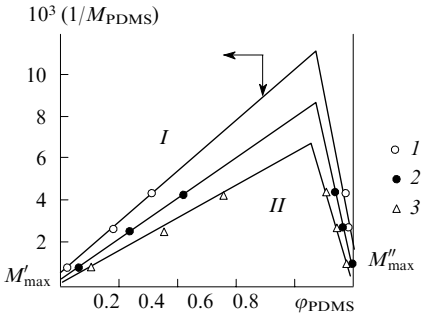

Figure 8. Isothermal sections of binodals on the $\varphi - (1/M)$ coordinates for the PE – PDMS systems at 398 (*1*), 428 (*2*) and 453 K (*3*) (*I*, one-phase region; *II*, two-phase region).[60]

2. For blends of statistical copolymers with homopolymers, the influence of the change in the molecular mass is consistent with the above-described effects. A change in the composition of a copolymer (in the case of constant molecular masses of the components) fulfils the following unified rule: the closer is the composition of the copolymer to that of the homopolymer (which is identical to a decrease in the difference in the solubility parameters of the copolymer and homopolymer), the lower is the

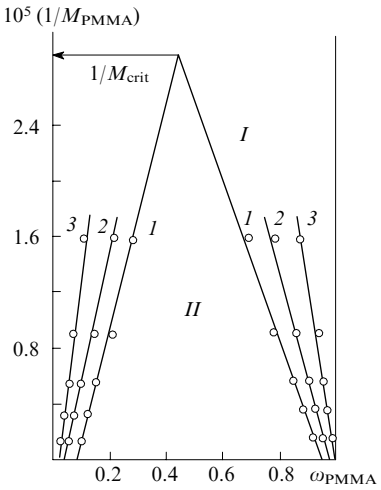

Figure 9. Isothermal sections of binodals on the $\omega-(1/M)$ coordinates for the PVC–PMMA systems at 473 (*1*), 453 (*2*) and 433 K (*3*) (*I*, one-phase region; *II*, two-phase region).[58]

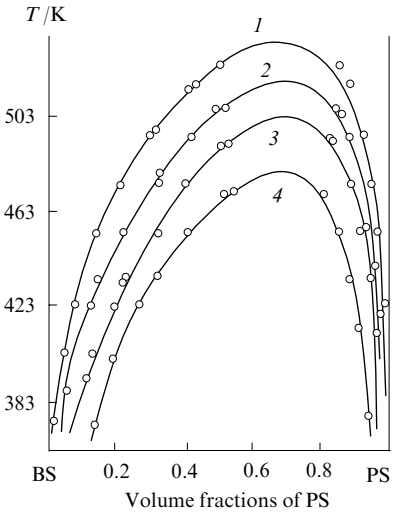

Figure 11. Phase diagrams of the PS (7.7×10^3) – BS (1.8×10^5) systems.[15] The composition of the copolymer [number of styrene units (%)]: (*1*) BS-25, (*2*) BS-65, (*3*) BS-75, (*4*) BS-85.

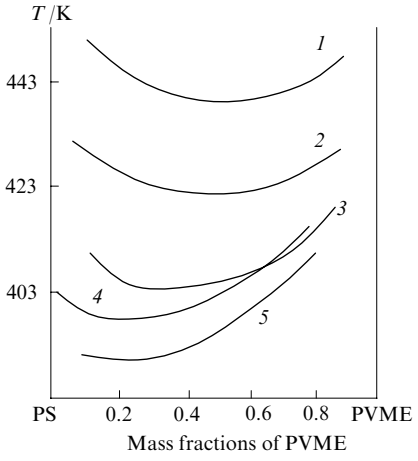

Figure 10. Phase diagrams of the PS – PVME (5.4×10^4) systems.[63] Molecular masses of PS: (*1*) 2×10^4, (*2*) 3.57×10^4, (*3*) 6.7×10^4, (*4*) 10.6×10^4; (*5*) 23.3×10^4.

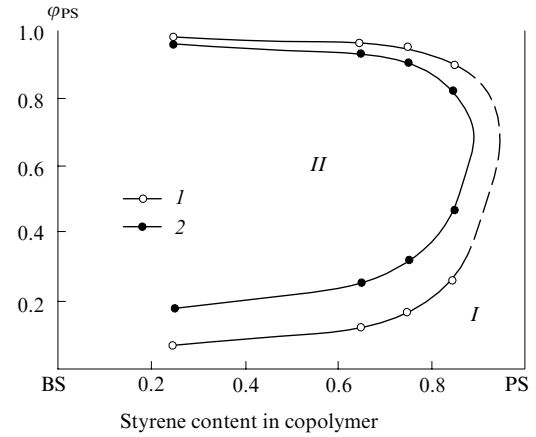

Figure 12. Isothermal sections of binodals of the PS – BS system at 423 (*1*) and 463 K (*2*) depending on the composition of the copolymer (*I*, one-phase region; *II*, two-phase region).

critical temperature of mixing (for systems with UCST) and the smaller is the region of the heterogeneous state, *i.e.*, the binodal curve as a whole is shifted downward along the temperature axis with retention of the position of the critical point. An example is a system of polystyrene (PS) and butadiene–styrene random copolymers (BS) (Fig. 11). It should be noted that the construction of isothermal sections of binodal curves allows one (as can be seen from Fig. 12) to determine the critical compositions of copolymers and the critical concentration of a blend containing components with particular molecular masses at a particular temperature. For example, in the PS–BS system with MM $\approx10^5$, the critical composition of the copolymer above which the system is compatible corresponds to 90 mass % and 95 mass % of polystyrene units in the copolymer chain at 463 and 423 K, respectively.

3. The formation of a three-dimensional cross-linked network in one of the components leads to extension of the two-phase region, a shift of the branch of the binodal curve corresponding to solubility of the sol fraction toward the axis of the linear homopolymer (and its degeneration at high degrees of conversion) and location of UCST in the region of thermal destruction of the material.[64,65]

It should be noted that a series of systems described in the literature are not characterised by the above features. For example, the solubility in the PMMA–poly(ethylene glycol) (PEG) system (Fig. 13), unlike that in poly(propylene glycol) (PPG) (Fig. 14), increases with increasing molecular mass of PEG in spite of the fact that the former system has UCST. At MM (PEG) $>3\times10^3$, UCST is lower than the melting point of PEG, and the dome of the binodal is located under the liquidus line of high-molecular-mass PEG. In this case, the position of the critical point, as expected, is shifted to the middle of the composition region. It should be noted that a phase diagram reported in the studies[22,67] for the same system but with another ratio between the molecular weights of the components has both a binodal and a liquidus line (Fig. 15). This behaviour is not specific to the above systems. Analogous results were obtained in the studies[14,68,69] for the following systems: butadiene–acrylonitrile random copolymers (BAN) and acrylated oligoesters (AOE), PVC–AOE and polyethylene (PE)–saturated alcohols, respectively. For these systems, unusual dependences of isothermal sections of phase diagrams on the molecular masses of the components were obtained. As can be seen from Fig. 16, the polyisoprene (PI)–acrylated oligoester system is completely compatible if the number of methylene groups (*n*) in the hydrocarbon frag-

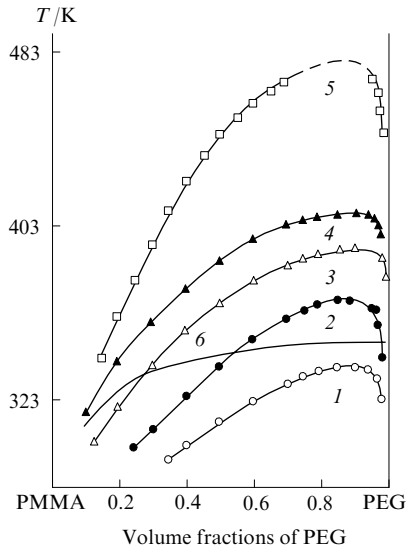

Figure 13. Phase diagrams [66] of the PMMA (2×10^5) – PEG systems: (*1*) PEG-600, (*2*) PEG-400, (*3*) tetraethylene glycol, (*4*) triethylene glycol, (*5*) ethylene glycol, (*6*) liquidus line for PEG (2×10^4).

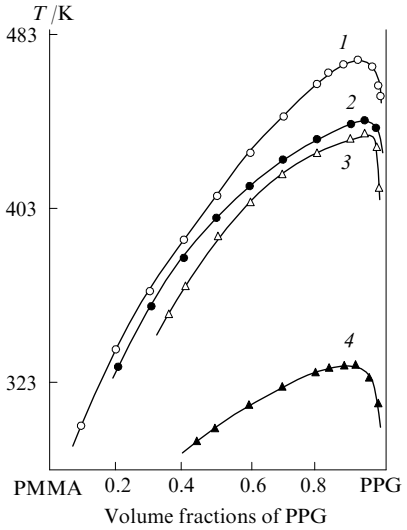

Figure 14. Phase diagrams [66] of the PMMA (2×10^5) – PPG system with different molecular masses.
Molecular masses of PPG: (*1*) 2025, (*2*) 1200, (*3*) 1025, (*4*) 425.

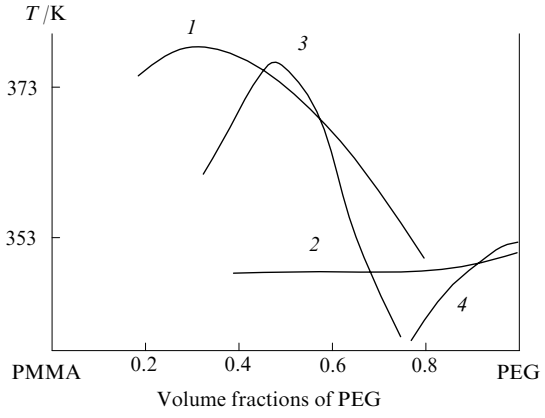

Figure 15. Phase diagrams of the PMMA – PEG system.
(*1*, *3*) Binodal curves, (*2*, *4*) liquidus lines. Curves (*1*, *2*),[22] curves (*3*, *4*).[67]

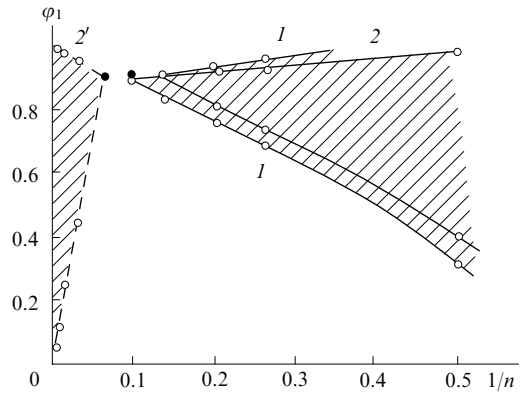

Figure 16. Isothermal sections of binodals [70] for the *cis*-PI – *p*-methylene dimethacrylate (*1*, *2*) and *cis*-PI – low-molecular-mass PE (*2′*) systems at 313 (*1*) and 323 K (*2*, *2′*) (φ_1 is the solubility of the low-molecular-mass component). Black points indicate UCST calculated according to Eqn (1).

ment is 10, whereas this system is only partially compatible at $n > 15$. This effect should be related to the influence of the terminal groups on the solubility parameter of oligomers.

Other examples of the anomalous behaviour of polymer – polymer systems are substantial differences in UCST (Fig. 17) with retention of the critical concentration, the presence of two critical temperatures in the same temperature – concentration region [PVC – PMMA, Fig. 18; poly(vinyl methyl ether) (PVME) – PS, Figs 10 and 19; PE – polyisobutylene melt],[60, 73] substantial differences in the shape of the binodal curve in the vicinity of the critical temperature (PS – PI) [74, 75] and independence of the critical concentration of the molecular mass of the components with retention of the usual dependence of the critical temperature in the polycarbonate (PC) – epoxide oligomer (EO) systems (Fig. 20).[76]

The results of studies of polymer systems containing crystallisable components are also often contradictory. Generally, liquidus curves for polymer – solvent systems obtained by different researchers by various experimental methods are identical or close to each other,[77, 78] the melting point depressions being in satisfactory quantitative agreement in a broad composition range for a homologous series of solvents (Fig. 21),[79] whereas there is no

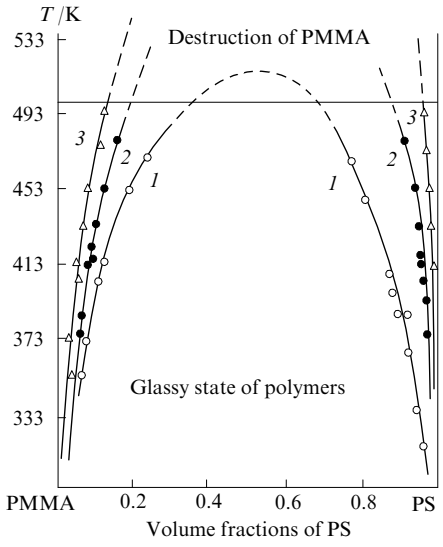

Figure 17. Phase diagrams of the PMMA – PS (800) system.[15]
Molecular masses of PMMA: (*1*) 1.5×10^3, (*2*) 3.3×10^4, (*3*) 8.9×10^4.

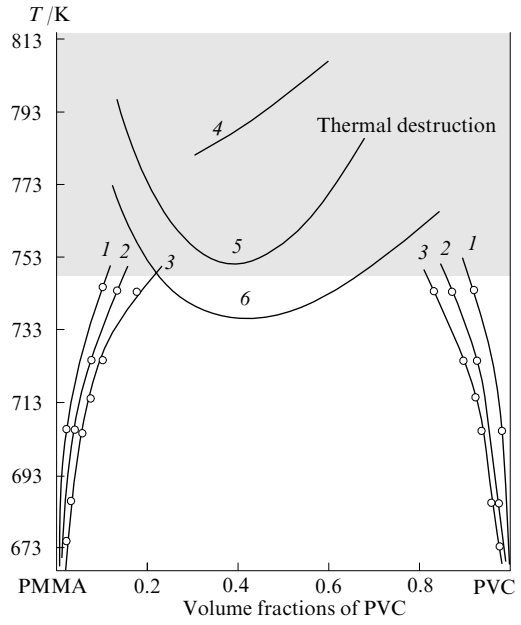

Figure 18. Phase diagrams of the PVC – PMMA system with the following molecular masses: $1.4 \times 10^5 - 7.3 \times 10^5$ (*1*), $1.4 \times 10^5 - 3 \times 10^5$ (*2*), $1.4 \times 10^5 - 1.9 \times 10^5$ (*3*), $1.6 \times 10^4 - 8 \times 10^4$ (*4*), $5.5 \times 10^4 - 8 \times 10^4$ (*5*), $5.5 \times 10^4 - 6 \times 10^4$ (*6*). Curves (*1–3*),[55] (*4–6*).[71]

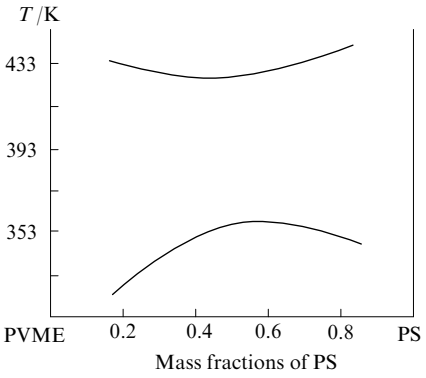

Figure 19. Phase diagrams of the PS (3.7×10^4) – PVME (4.6×10^4) system.[72]

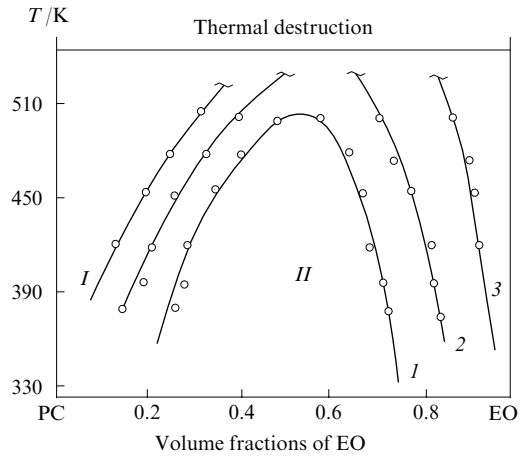

Figure 20. Phase diagrams of the PC – EO system.[76]
Molecular masses of EO: (*1*) 380, (*2*) 600, (*3*) 2750 (*I*, one-phase region; *II*, two-phase region).

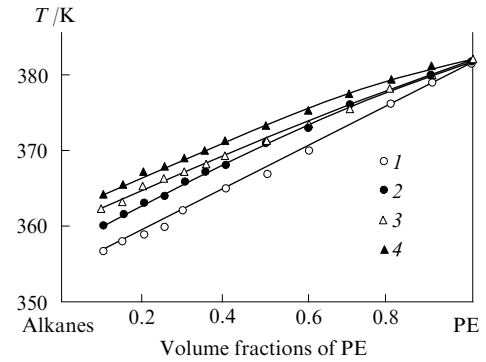

Figure 21. Melting point depressions of PE (3×10^4) in the presence of alkanes: heptane (*1*), decane (*2*), tridecane (*3*), hexadecane (*4*).[79]

quantitative agreement between the melting point depressions for polymer – polymer systems even if extrapolations to the equilibrium melting temperatures are used.[24, 80–82] Unfortunately, the preliminary experimental data on liquidus curves rather than equilibrium melting temperatures were reported in most studies.[24] Besides, the results of these measurements were often considered as the most suitable data for calculations of pair interaction parameters (χ) of the components.[83, 84]

Fragments of the diagrams for crystalline equilibrium in the PMMA – PEG system are shown in Fig. 22. It can be seen that the melting point decreases in all cases, which is consistent with the general thermodynamic relations.[85, 86] However, different researchers reported substantially different melting point depressions. For example, it was found [67] that a change in the composition by 20% led to depression of 10 – 15 K, whereas this value was estimated at 1 – 5 K in the studies.[22, 87, 88] The estimates of χ obtained from these data in the context of the approach proposed by Nishi and Wang [84] demonstrate a scatter from -5.0 to -0.5, which cannot evidently be ignored.

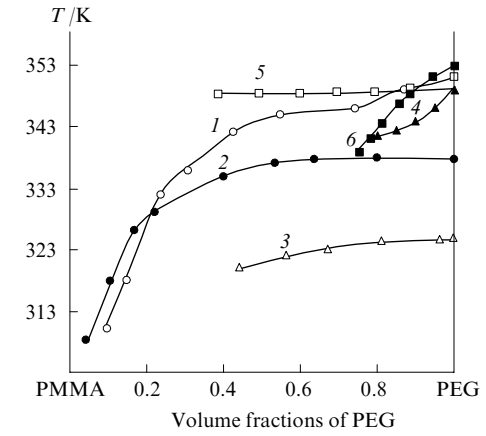

Figure 22. Curves of melting point depressions for PEG in a mixture with PMMA according to the results obtained by different researchers: (*1*, *2*),[88] (*3*),[87] (*4*),[89] (*5*),[22] (*6*).[67]

The same problems arise in the analysis of data on liquid-crystalline equilibrium in blends of thermotropic polymers. Data on blends of polydimethylsiloxane (PDMS) and cyclolinear siloxanes (CS) [40] are exemplified in Fig. 23. Interestingly, the isotropisation temperature depression (ΔT_{iso}) is substantially larger than the melting point depression (ΔT_m). In the system presented in Fig. 23, $\Delta T_m \approx 5^\circ$, whereas $\Delta T_{iso} \approx 30^\circ$ at the same concentration of amorphous PDMS.

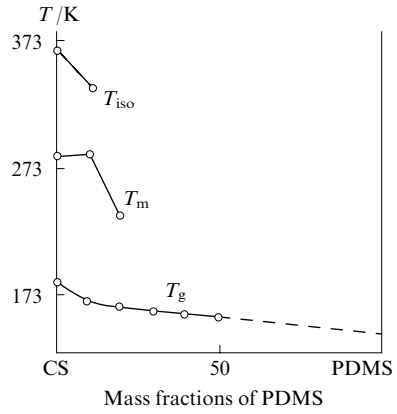

Figure 23. Phase diagram of the CS (4.4×10^4) – PDMS (600) system.[40]

The equilibrium in the poly(butylene terephthalate) (PBTF) – liquid cristalline polyether (PET) system belongs to complex equilibria (Fig. 24)[41] involving liquid-crystalline components, which undergo the mesomorphic transition. The problem of the equilibrium mesomorphic transition was virtually not discussed, *i.e.*, it was implicitly assumed that the mesomorphic component passes completely into a liquid-crystalline phase. However, this assumption requires structural validation.

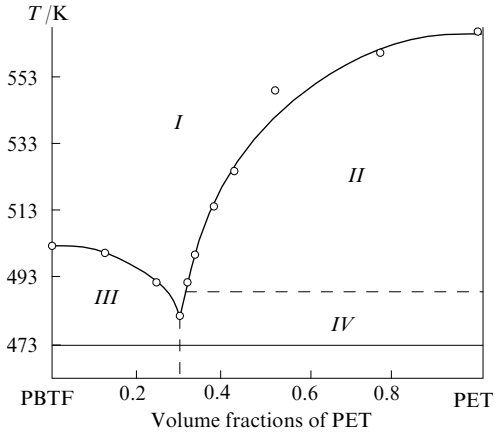

Figure 24. Phase diagram of the PBTF – PET system.[41]
(*I*) Region of isotropic solutions, (*II*) region of the liquid-crystalline state of PET, (*III* and *IV*) regions of the crystalline state of PBTF and PET, respectively.

Since all the above-described diversity in the phase behaviour of polymer blends seems to be a rule rather than the exception, the questions arise of whether it is possible to obtain a balanced general picture of phase equilibria in the context of the physico-chemical concepts and which parameters and/or conditions should be additionally used to obtain information on equilibrium and non-equilibrium states of the compositions of co-existing phases.

IV. Theoretical analysis

Although there are several theories of polymer solutions, we believe that it is possible to use the simplest and most widely accepted one, *viz.*, the classical version of the Flory – Huggins theory,[90] for several reasons. First, it was demonstrated[6,12] that the predictive ability of this theory is no worse than that of the new Flory theory, the Prigogine – Patterson theory, the Sanchez – Lacombe theory and the new Huggins theory. Second, the basic concepts of this theory are simple and evident. Third, we are sure that this theory has a high undisclosed potential.

Recall that the Flory – Huggins theory, as applied to polymer – polymer systems, gives the following expressions[91–93] for the free energy of mixing ¶

$$\Delta G_m = RT\left[\frac{\varphi_1 \ln(\varphi_1)}{r_1} + \frac{\varphi_2 \ln(\varphi_2)}{r_2} + \chi\varphi_1\varphi_2\right],$$

the chemical potentials of components

$$\Delta\mu_1 = RT\left[\frac{\ln(\varphi_1)}{r_1} + \left(\frac{1}{r_1} - \frac{1}{r_2}\right)\varphi_2 + \chi\varphi_2^2\right],$$

$$\Delta\mu_2 = RT\left[\frac{\ln(\varphi_2)}{r_2} + \left(\frac{1}{r_2} - \frac{1}{r_1}\right)\varphi_1 + \chi\varphi_1^2\right],$$

the parameters of critical points

$$\chi_{crit} = \frac{1}{2}\left(\frac{1}{\sqrt{r_1}} + \frac{1}{\sqrt{r_2}}\right)^2,$$

$$\varphi_{2,crit} = \frac{\sqrt{r_1}}{\sqrt{r_1} + \sqrt{r_2}}, \qquad (1)$$

the spinodal concentration

$$\frac{1}{r_1\varphi_{1,s}} + \frac{1}{r_2\varphi_{2,s}} - 2\chi = 0,$$

the melting point depression[77,84]

$$\Delta T_m = \frac{\Delta\mu_{2,cr} T_m^\circ}{\Delta H_m}$$

and the isotropisation temperature depression[94]

$$\Delta T_{iso} = \frac{\Delta\mu_{2,meso} T_{meso}^\circ}{\Delta H_{meso}},$$

where ΔG_m is the molar free energy of mixing, φ_1 and φ_2 are the volume concentrations of the components, r_1 and r_2 are the ratios of the molar volumes to the reference volume, which are approximately equal to the degrees of polymerisation of the components, χ is the pair interaction parameter, $\Delta\mu_1$ and $\Delta\mu_2$ are the chemical potentials of the components in the amorphous state, χ_{crit} and $\varphi_{2,crit}$ are the parameters of the critical point, $\varphi_{1,s}$ and $\varphi_{2,s}$ are the spinodal concentrations, ΔT_m is the melting point depression, T_m° is the melting point of a pure component, ΔH_m is the enthalpy of melting, $\Delta\mu_{2,cr}$ is the chemical potential of the crystallisable component in the crystalline state, ΔT_{iso} is the isotropisation temperature depression, T_{iso}° is the isotropisation temperature of a pure component, ΔH_{meso} is the enthalpy of the mesomorphic transition and $\Delta\mu_{2,meso}$ is the chemical potential of a component in the liquid-crystalline state.

The following conclusions can be drawn from these equations:

— the isotropisation temperature depression is larger than the melting point depression $\Delta T_{iso} = \Delta T_m \Delta H_m / \Delta H_{meso}$ in the case of equal chemical potentials and phase transition temperatures of a pure component;

— the position of the critical point is always determined by the molecular mass ratio; hence, if the molecular mass of one component is known, the mass of another component can be calculated from the experimentally determined positions of critical points;

¶ All thermodynamic potentials are excessive with respect to the standard state (pure components).

— this theory allows one to analyse the region of true solutions from the viewpoint of the existence of concentration fluctuations, which are considered as clusters by Zimm and Lundberg:[95–97]

$$\frac{G_{11}}{v_1} = -(1-\varphi_1)\left[\frac{\partial(a_1/\varphi_1)}{\partial a_1}\right] - 1\,,$$

$$\frac{G_{11}}{v_1} = \frac{1}{\varphi_1}\left[\frac{1}{\varphi_1(1/r_1\varphi_1 + 1/r_2\varphi_2 - 2\chi)} - 1\right],$$

$$N_c = \frac{\varphi_1 G_{11}}{v_1} + 1 = \frac{1}{\varphi_1(1/r_1\varphi_1 + 1/r_2\varphi_2 - 2\chi)},$$

where G_{11}/v_1 is the integral of clusterisation and N_c is the number of molecules in the cluster.

It can be seen that the integral of clusterisation is determined by the distance to the spinodal curve. Hence, traditional phase diagrams can be supplemented with regions in the vicinity of binodal curves, where the appearance of heterophase fluctuations and cluster structures would be expected.[98] The results of NMR spectroscopy using pulsed gradient magnetic field (Fig. 25)[32] provide direct evidence for the existence of such heterophase fluctuations and cluster structures.

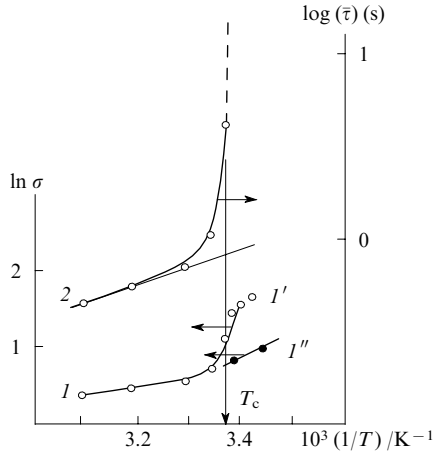

Figure 25. Temperature dependences of the spectral width (σ), the self-diffusion coefficients (*1*, *1′*, *1″*) and the average lifetime ($\bar{\tau}$) of macromolecular associates (*2*) in the PS – cyclohexane system.[32] $\varphi_{PS} = 0.15$; (*1′*) microlayering, (*1″*) macrolayering of the system.

Phase diagrams not only contain information on temperature – concentration regions of co-existence of phases, miscibility of components and the ratio between the dispersed phase and dispersion medium but also enable one to obtain information on the thermodynamic parameters of interaction, in particular, on the pair interaction parameter.

Figure 26 exemplifies the temperature dependence of the parameter χ for the PMMA – PEG system. It can be seen that χ for systems characterised by one critical temperature (UCST or LCST) depends linearly on $1/T$. Consequently, χ can be divided into the enthalpy (χ_H) and entropy (χ_S) components,[99] and the critical temperature can be estimated by extrapolating to χ_{crit}. For systems possessing two critical temperatures, the dependence takes the form shown in Fig. 27. For these systems, both critical temperatures (Fig. 28) can be estimated by extrapolating χ to χ_{crit}.

The thermodynamic parameters of mixing determined from analysis of complex equilibria should be characterised by similar dependences on the concentration, temperature and molecular mass. If the boundary curves of different types intersect at a single point (see, for example, Figs 15 and 22), the thermodynamic parameters should be equal in magnitude. In many cases, this condition is not fulfilled. For example, according to the results of

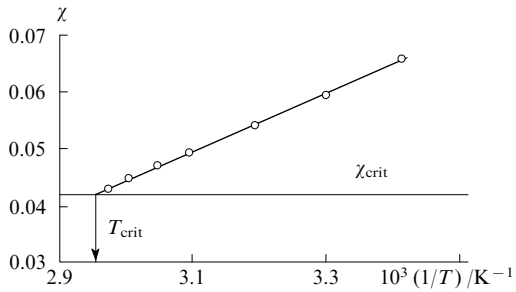

Figure 26. Plot of the pair interaction parameter *vs.* the inverse temperature for the PMMA (2×10^5) – PEG-600 system. (The phase diagram of this system is shown in Fig. 13.)

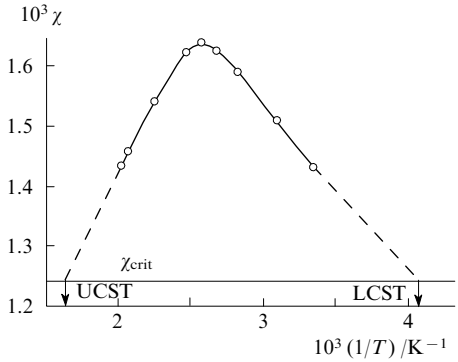

Figure 27. Plot of the pair interaction parameter[100] *vs.* the inverse temperature for the PCP (1.2×10^5) – BAN-26 (2.3×10^5) system.

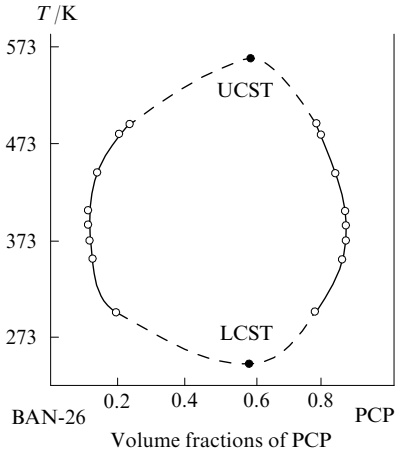

Figure 28. Phase diagram[100] of the BAN-26 (2.3×10^5) – PCP (1.2×10^5) system; UCST and LCST are extrapolated.

the study,[22] the parameter χ for the PMMA – PEG system, which was calculated from the crystalline equilibrium state at the point of tangency of the binodal and liquidus curves, is -0.584, whereas, according to the results of another study,[67] this parameter for the same system at the same tangency point is -4.97. At the same point, the parameters χ calculated from the data on amorphous equilibrium are 2.7×10^{-4} and 2.5×10^{-4}, respectively. Evidently, these facts require a more thorough thermodynamic and structural analysis.

In the study,[60] it was demonstrated that the phase behaviour of a polymer system can be predicted based not only on the pair interaction parameter but also on the solubility parameters of components (δ_1 and δ_2), which are related to χ by the following equation

$$\chi = \frac{z\Delta\omega_{12}}{kT} = \frac{z(\delta_1 - \delta_2)^2}{kT}, \qquad (2)$$

where z is the coordination number of the system and $\Delta\omega_{12}$ is the exchange energy.

The positions of the boundary curves of the miscibility region of a particular polymeric component and any other component can be calculated according to Eqn (2). For PMMA and a PE melt, these regions are presented in Figs 29 and 30, respectively. As can be seen from these figures, the higher is the molecular mass of the component, the smaller is the hypothetical region of mutual compatibility of this component and other components, which agrees with the Flory – Huggins theory.

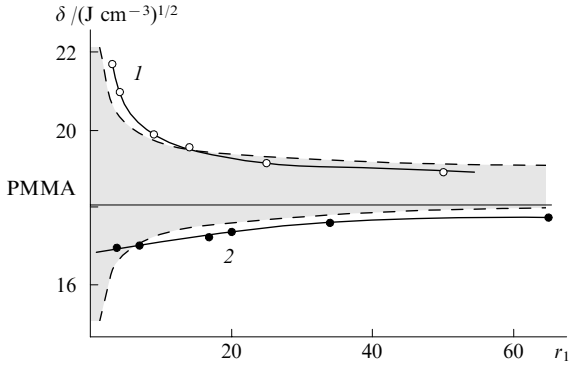

Figure 29. Plots of the solubility parameters of PEG (*1*) and PPG (*2*) *vs.* the degree of polymerisation (r_1) of oligoglycol.[88] The region of compatibility with PMMA is shaded.

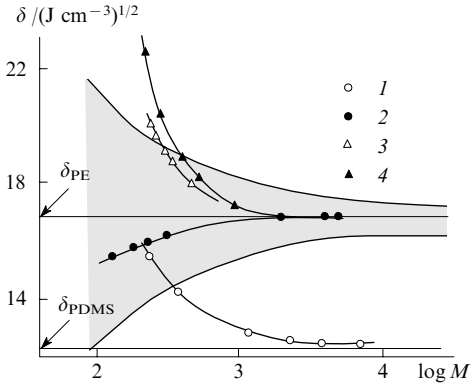

Figure 30. Plots of the solubility parameters of PDMS (*1*), saturated hydrocarbons (*2*), *p*-methylene dimethacrylates (*3*) and phthalic esters (*4*) *vs.* their molecular masses. The region of complete compatibility of oligomers with polyethylene is shaded.[60]

The position of the figurative point of the second component, which is determined by the degree of its polymerisation, the solubility parameter and the nature of the terminal groups and monomer units, shows how the compatibility between components changes with the molecular mass. This representation of the data on miscibility enables one to reveal the influence of the terminal groups, which generally differ in nature from monomer units, and, correspondingly, differ in the local solubility parameter, on the compatibility between components. As the molecular mass increases, this influence decreases and the trajectory of motion of the figurative point of the second component on the $\delta - \log M$ coordinates becomes flatter.

Let us consider the trajectories of motion of the figurative points for PEG and PPG (Fig. 29) in more detail. As the molecular mass of PEG increases, its figurative point goes from the two-phase region into the one-phase region and then again passes into the two-phase region at very high MM ($\sim 100\,000$). For PPG, the situation is simpler and more traditional: the figurative point is initially located in the one-phase region and then leaves this region and moves farther and farther away as the molecular mass of PPG increases. Based on Fig. 29, one can predict how the compatibility between the components will change depending on the nature of the terminal group of polyglycol or on going from a homopolymer to copolymers of ethylene glycol and propylene glycol. Analogous changes in the compatibility are observed in blends of PE with low- and high-molecular mass compounds.[101] Therefore, information on the influence of the terminal groups on the compatibility between components is also indirectly present in the Flory – Huggins theory of polymer solutions.

In conclusion of this section, it should be noted that knowing the temperature dependence of χ (experimentally determined or calculated)[12] and the starting phase state of the components, the possible phase states can be estimated in a broad temperature range and the full concentration range. The generalised phase diagram of the PDMS – CS system[94] is exemplified in Fig. 31.

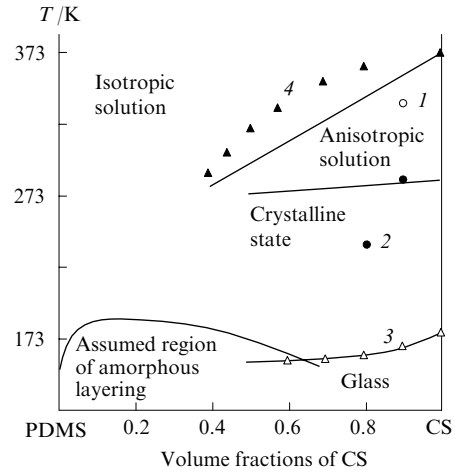

Figure 31. Generalised diagram of phase and physical states[94] of the PDMS (600) – CS (5.1×10^4) system.
Calculated curves are indicated by solid lines. Circles and triangles represent the experimental temperatures of the mesomorphic transition (*1*)[40] and (*4*),[94] crystallisation temperature (*2*)[40] and glass transition temperatures (*3*).[40]

The above-considered facts lead to the following important conclusions.

1. If data obtained for a polymer system by different researchers using various methods are consistent with each other, the results would be expected to be equilibrium or close to equilibrium. The thermodynamic parameters calculated from these data should demonstrate self-consistent behaviour depending on external parameters and do not contradict the major theoretical conclusions.

2. If there is a discrepancy between data obtained by different researchers with the use of various methods, one cannot say with certainty which experimental data are close to equilibrium or how much they differ from equilibrium without resorting to additional structural and, sometimes, kinetic studies. In this case, one can speak only about trends in changes in the boundary curves. The thermodynamic parameters of the compounds with the same phase structure may, for good reason, differ from each other, but their changes depending on external parameters should be of the same character. In our opinion, it is this requirement that is the distinguishing feature of the present stage of investigation of phase equilibria in polymer systems.

The results [71] (see Fig. 18) for the PVC – PMMA system, which has been studied many times and in sufficient detail, provide a prominent example of a fundamental contradiction in the experimental data on phase structures and phase equilibria. It can be seen that the binodals with LCST are located in the region of active thermal destruction of PVC, and the observed turbidity is, most likely, attributable to a change in the chemical structure of the macromolecular chain (formation of polyene sequences [102]) and the appearance of gaseous destruction products. This problem was discussed in detail in the study.[103] A change in the phase state of the system under changes in the chemical nature of the components is of its own interest. At present, theoretical aspects of this problem are in their developmental stage and the required experimental data are being accumulated.[14, 20, 64, 104]

V. Non-equilibrium and metastable states

In a general way, the non-equilibrium state of any system, including polymer systems, can be determined as a deviation from equilibrium. This deviation can be estimated from one of the following parameters: the density, compositions of co-existing phases, the presence of the concentration gradients, dispersion and interface characteristics, *etc*. The metastable state of a system is a special case of a non-equilibrium state in which phase decomposition of the system is hindered or does not occur at all. It should be noted that the location of the figurative point of a system in metastable or labile regions of the phase diagram is necessary but insufficient evidence for the assignment of a material with a particular composition to a metastable state or to materials with a spinodal structure. It is more probable that this is the initial state of a blend, which is responsible for the trajectory of further structural transformations as the system approaches equilibrium.[105 – 107]

Right there the simplicity and obviousness of characterisation of a non-equilibrium state end, because it is necessary to determine experimentally and characterise the equilibrium state and its parameters for each particular system under study; otherwise, one cannot speak about the equilibrium or non-equilibrium state of a particular sample or material prepared under certain conditions.

Non-equilibrium states of polymer blends occur much more frequently than the equilibrium state.[108] However, the thermodynamic description of materials, which is presently used in physical chemistry of polymers and polymer materials science, is based on theories of polymer systems belonging to equilibrium states of blends, solutions and melts.[109] The reasons for this fact are known and have been discussed in many monographs.[14, 15, 110]

In one of his publications, Prigogine [110] determined the place of equilibrium thermodynamics within the framework of non-equilibrium thermodynamics as a limiting case of non-equilibrium thermodynamics with energy fluxes tending to zero. Based on this opinion, we believe that the non-equilibrium state of polymer blends can be described, but only on condition that the time of experiment is much shorter than the time it takes for the structure to be noticeably changed, *i.e*., shorter than the time it takes for the non-equilibrium state of the mixture to be essentially changed.[31]

In studies of particular polymer systems by various methods, the temperature dependences of the compositions of co-existing phases are found, the structure and morphology of blends are determined and the thermodynamic potentials of mixing are calculated. Evidently, to compare experimental data and reveal possible contradictions, it is necessary that the thermodynamic parameters under consideration should have the same physical sense. For this purpose, we interpreted [100] results using the following sequences.

1. Phase diagrams → calculation of the temperature dependence of the pair interaction parameters → construction of the generalised diagram → calculation of the concentration dependence of the free energy of mixing.

2. Sorption isotherms of a common solvent → determination of the chemical potential of the polymeric component → calculations of partial free energies of pure polymers and their mixtures → calculation of the free energy of mixing of a polymer blend with a particular composition possessing a certain processing prehistory.

3. Phase structure → determination of the compositions of co-existing phases (from results of X-ray spectral analysis) → determination of the medium size of the dispersed phase and its size distribution → calculation of the interface surface energy → calculation of the total free energy of a particular sample.

Therefore, all experimental evidence reduces to the only comparable characteristic, *viz*., the free energy of mixing of a particular object possessing a certain processing prehistory.

The phase diagram of the polychloroprene (PCP) – BAN-18 system [100, 111] is shown in Fig. 32. Processing of this diagram gave the temperature dependence of the pair interaction parameter and the concentration dependence of the free energy of mixing for the isotherm corresponding to the temperature at which sorption measurements were carried out (Fig. 33). The dashed line links the free energies of co-existing phases, *i.e*., the free energies of mixing of a completely equilibrated two-phase system. The solid line located between the binodal concentrations corresponds to a non-equilibrium one-phase solution. The difference between these lines

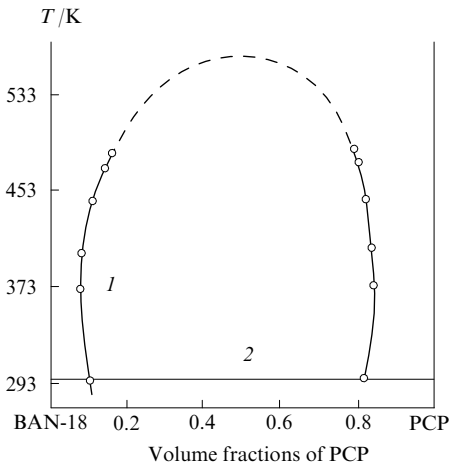

Figure 32. Phase diagrams [15] of the PCP (1.2×10^5) – BAN-18 (2.2×10^5) system.
(*1*) Binodal, (*2*) isotherm corresponding to the temperature at which sorption measurements were carried out.

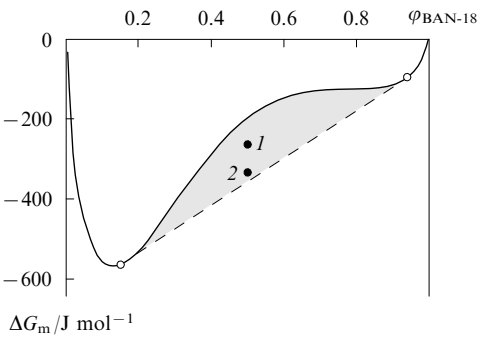

Figure 33. Dependence of the free energy of mixing [112] for the PCP (1.2×10^5) – BAN-18 (2.2×10^5) system.
The common tangent is shown by a dashed line. The compositions of co-existing phases are represented by empty circles. Solid circles indicate $\Delta G_{m,sorp}$ for samples prepared by milling (*1*) and using a common solvent (*2*).

is equal to a gain in energy achieved on going from the one-phase non-equilibrium state to the two-phase equilibrium state.

A traditional thermodynamic analysis of sorption isotherms [113] of tetrahydrofuran on the same polymer blends using the Gibbs–Duhem equation [114] and the Hess cycle [1] allows one to determine free energies of mixing of polymer blends (points *1* and *2* in Fig. 33). As can be seen from Fig. 33, calculated $\Delta G_{m,sorp}$ have negative values in spite of the fact that the systems under study are heterogeneous, and the experimental values for samples of materials prepared under particular conditions of mixing of polymers differ from each other as well as from the theoretical values for equilibrium and non-equilibrium states of the system. The free energies of polymer materials, which were determined from sorption measurements, are located in the shaded region some distance from the equilibrium state.

We believe that with a knowledge of these thermodynamic data, it is possible to characterise quantitatively the non-equilibrium state of a particular material by determining the degree of non-equilibrium (α) as follows

$$\alpha = \frac{\Delta G_{object} - \Delta G_{sep}}{\Delta G - \Delta G_{sep}}. \qquad (3)$$

The notations are explained in Fig. 34.

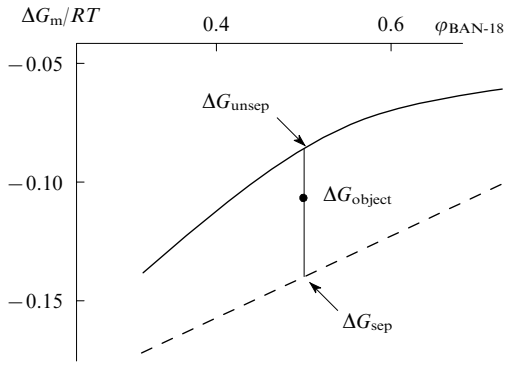

Figure 34. Fragment of the dependence (Fig. 33) of ΔG_m on the composition of the blend; ΔG_{sep} and ΔG_{unsep} correspond to the layered and non-layered systems, respectively.

It should be noted once again that the degree of non-equilibrium calculated according to this equation characterises all non-equilibria (with respect to compositions, particle size, the state of interfaces, *etc*.) resulting in a deviation of the position of the figurative point of the sample from its projection onto the common tangent line.

Analysis of the structural and morphological organisation of blends and estimations of interface surface energies revealed the reasons for the appearance of non-equilibrium in this system in more detail.[115, 116] It was demonstrated [100] that the compositions of co-existing phases in materials subjected to sorption studies (Fig. 35) correspond to binodal concentrations, and the samples differ from each other in the particle size distribution. Therefore, the non-equilibrium state of these materials is associated with an excess interface surface and, correspondingly, with the excess Gibbs free energy

$$\Delta G_m = \varphi \Delta G' + (1 - \varphi)\Delta G'' + \sigma S,$$

where $\Delta G'$, $\Delta G''$ are the free energies of mixing of each phase, φ is the fraction of a dispersed phase and σS is the interface energy.

Taking into account the latter expression for ΔG_m, the numerator of Eqn (3) is σS. The average sizes of phases estimated from structural and morphological data are in satisfactory agreement with the estimates based on thermodynamic data.[100]

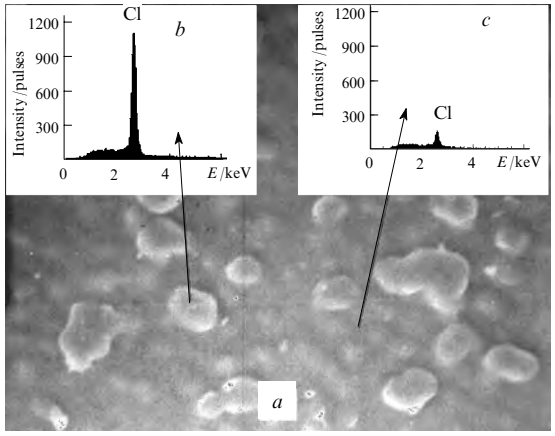

Figure 35. Surface morphology of a low-temperature chip of the PCP (1.2×10^5) – BAN-26 (2.3×10^5) blend obtained by scanning electron microscopy (*a*). The spectra of characteristic X-ray radiation of the dispersed phase (*b*) and the dispersion medium (*c*) are shown in insets.

Other systems also show analogous non-equilibrium behaviour upon the formation of polymer blends in solution in a common solvent.

In the study,[112] the above-described approach and the results of structural–morphological investigation were used for calculating free energies of mixing for equilibrium, non-equilibrium and real systems. As can be seen from Fig. 36, the character of changes in the free energy of mixing upon the formation of a binary polymer blend from a three-component solution is analogous to that described above. Using Eqn (3), it is also possible to estimate quantitatively the degree of non-equilibrium for various composites, which is associated with the excess Gibbs free energy located in interface layers of co-existing phases. It should be noted that the figurative points of particular samples are remote from non-equilibrium curves. It was demonstrated [112] that this effect may be attributed to the energy spent for nucleation of a dispersed phase.[117]

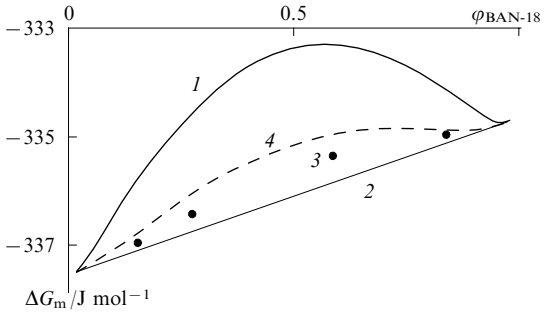

Figure 36. Plot of the free energy of mixing *vs*. the concentration of one of the polymers for the PVC – BAN-18 – dichloroethane system.
(*1*) Non-equilibrium one-phase system, (*2*) equilibrium two-phase system, (*3*) (circles) free energies of materials taking into account the total interface energy, (*4*) free energies of materials taking into account the total interface energy of critical nuclei.

A more complex situation is observed for the PVC – PMMA system. Analysis of the experimental data on the prehistory of the preparation of polymer blends shows that the largest discrepancy in the results is observed when THF or ethyl methyl ketone is used as a common solvent. As can be seen from Fig. 37, a change in the composition of solutions on going from a ternary system to a binary one gives rise to a region of stable phase structures in the

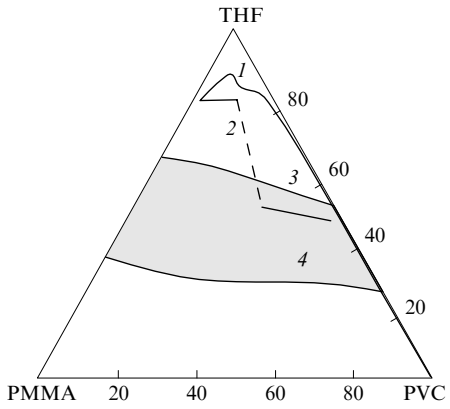

Figure 37. Diagram of phase and physical states[118] for the PVC – PMMA – THF system at 293 K.
(*1*) Binodal, (*2*) line of stabilisation of the phase structure, (*3*) line of critical viscosity, (*4*) glass transition.

middle region of the phase diagram.[118] The structure formed in this region remains unchanged upon removal of the solvent and going to a binary system.

Such materials are characterised by several types of non-equilibrium: first, the deviation of the compositions of co-existing phases of particular composites from equilibrium values (see Fig. 3); second, high dispersity and, as a consequence, a high excess surface energy; third, a large excess free volume because evaporation of the solvent is accompanied by the glass transition of the system and the latter is rather far removed from the glass transition temperature.

All the above-mentioned types of non-equilibrium are most pronounced when a binary polymer blend is prepared with the use of a common solvent and are much less pronounced in the case of mixing in a melt or polymerisation of the MMA monomer in the PVC matrix.

Direct structural – morphological studies[39, 119, 120] demonstrated that annealing of non-equilibrium structures led to secondary phase decomposition resulting in degeneration of the first and third types of non-equilibrium. In the phase diagram, the character of the binodal curve in the vicinity of the critical point is noteworthy. It should be noted that the double-hump shape of the curve is reversible and highly reproducible, depends only slightly on the molecular mass of PMMA and is observed only in experiments with the use of a limited range of common solvents.

Detailed IR spectroscopic studies of the conformational states of macromolecular chains of PVC in solutions, melts and starting powders prepared under various conditions of suspension polymerisation revealed[121, 122] three stable conformational states of PVC characterised by different glass transition temperatures, melting points and supramolecular organisation. The first state has regular helical TGTGTGT conformations of the chain with an isotactic sequence as well as long planar TGTG conformations in a syndiotactic configuration and appears in the synthesis of PVC. This state corresponds to a supramolecular structure of the fringed-micelle type. The second state is formed from solution and is characterised by short TT sequences and the micellar folded morphology. The third (intermediate) type is characterised by a set of conformers of the first and second types.

Following the principle of independence of phase equilibria proposed by Papkov,[28] it can be assumed that the double-hump shape of the binodal curve results from the presence of two conformational states of PVC in the system; the ratio between these states varies depending on the nature of the solvating agent.

Based on the aforementioned facts, a new type of non-equilibrium, which is associated with the possible existence of the temperature – concentration region of stable conformers of macromolecular chains, should be taken into account. In this case, the appearance of LCST (see Fig. 18) is, presumably, caused by a change in the set of conformations.

An analogous effect of the change in the character of the phase equilibrium under the influence of the solvent and the appearance of UCST (see Fig. 19) were observed in the PS – PVME system characterised by LCST.[62]

This complex phase behaviour is typical of many systems containing PVC as a component. Examples are provided by the PVC – dioctyl phthalate[105] and PVC – BAN-40 – solvent systems.[123]

Pseudobinodal curves, which are not reproduced in heating – cooling cycles, were also observed. In a number of studies, two glass transition temperatures and melting points were detected.[124] The influence of the nature of the solvent on the phase state of a system was also reported.[125] Interestingly, all these anomalous phenomena are correlated to the position of the region of conformational rearrangements.

VI. Conclusion

The main characteristic features of the influence of the molecular-mass characteristics on phase equilibria in polymer – polymer systems were revealed and confirmed in studies of many binary and ternary systems. The deviations from these features described in original studies reflect the specificity of the behaviour of particular polymers rather than argue against these general features. The development of polymer materials science is associated with both further accumulation of experimental data, primarily, on phase diagrams, and elucidation and classification of specific features of the behaviour of polymer systems.

We believe that the notions 'system' and 'material' should be distinguished for a more clear understanding of experimental and theoretical data. Systems are characterised by a phase equilibrium and a phase diagram, equilibrium and reproducible thermodynamic parameters, parameters determining the translational characteristics, the identity of the intermediate region of conjugated phases and the interface, the minimum interface surface.

Materials are characterised by a specific phase structure, which depends on the thermal and processing prehistory, and a set of non-equilibria of various types. The interface is only a part of the intermediate region of conjugated phases. Both the translational and thermodynamic characteristics depend on the prehistory of the material and can vary with time.

This classification seems to be necessary and fruitful for the development of the concept of the determination of equilibrium characteristics and the degree of non-equilibrium of particular materials.

In our opinion, the following conditions should be met to solve the problem of non-equilibrium states of binary and ternary polymer systems.

— Researchers must overcome the psychological barrier associated with the identification of the thermodynamic parameters for particular materials (thermal capacity and its temperature dependence, free energy of mixing, interaction parameters) with the thermodynamic parameters of equilibrium systems. For example, the results of determination of ΔG_m for polymer blends from sorption measurements[1] or by inverse gas chromatography[48] characterise not ΔG_m for the equilibrium state but the free energy of mixing of a particular sample with a particular phase structure prepared under particular conditions.

— Further investigation of the mechanism of formation of the non-equilibrium structural – morphological organisation of materials is required. It is customary to assume that materials in which mutual dissolution or structure formation and establishment of the thermodynamic equilibrium are complicated by the glass transition of solutions, melts and blends, should be assigned to non-equilibrium materials. However, in a number of studies,[5, 62, 118] it was demonstrated that the structural – morphological organisation of a sample is stabilised also in highly elastic and plastic states, if partial coefficients of translational diffusion of

components, which are responsible for nucleation of a new phase and nucleus growth, amount to as much as 10^{-12} cm^2 s^{-1}.

Within the framework of the proposed approach, a number of important problems remain to be solved and call for special systematic studies.

1. For amorphous equilibrium systems, the most important aims are to study experimentally and elucidate the behaviour of the composites of co-existing phases in the vicinity of a dome of double-hump binodals, find the number and positions of critical points and determine the spinodal curve.

2. Based on the available experimental data, polymers can be considered as sets of stable conformers. Evidently, in this case, the phase diagram should be constructed in another concentration – temperature field.

3. Partially crystalline polymers are, generally, non-equilibrium primarily with respect to their supramolecular and phase structures. This initial non-equilibrium state of a material has a determining effect on the thermodynamic characteristics of polymer solutions and blends and complicates seriously calculations of the thermodynamic parameters of mixing for crystalline equilibrium systems.

4. The observed changes in the positions of boundary curves in the temperature – concentration field of phase diagrams under mechanical effects of various types call for interpretation from the structural, conformational and thermodynamic standpoints.

In the future, fundamental investigations of phase equilibria and phase structures of polymers can be applied to prediction problems in materials science, *i.e.*, predictions of processing conditions, efficiency and service life of polymer materials. However, theoretical predictions are years in the future. At present, semiempirical methods are used. For these methods, information on phase diagrams is of most importance. One of the major aims is still to improve methods for the empirical and semiempirical prediction of equilibrium states of polymer systems.

This review has been written with the financial support of the Russian Foundation for Basic Research (Project No. 02-03-32991).

References

1. A A Tager *Fizikokhimiya Polimerov* (The Physical Chemistry of Polymers) (Moscow: Khimiya, 1978)
2. R F Gold (Ed.) *Multicomponent Polymer Systems* (Washington, DC: American Chemical Society, 1971)
3. E Martuscelli, R Palumbo, M Kryszewsky (Eds) *Polymer Blends* (New York: Plenum, 1980)
4. L H Sperling *Interpenetration Polymer Networks and Related Materials* (New York: Plenum, 1981)
5. V N Kuleznev *Smesi Polimerov* (Polymer Blends) (Moscow: Khimiya, 1980)
6. D Poul, S Newman (Eds) *Polymer Blends* Vol. 1 (New York: Academic Press, 1978)
7. O Olabisi, L M Robeson, M T Shaw *Polymer – Polymer Miscibility* (New York: Academic Press, 1979)
8. E A Bekturov *Troinye Polimernye Sistemy v Rastvorakh* (Ternary Polymer Systems in Solutions) (Alma-Ata: Nauka, 1975)
9. A E Nesterov, Yu S Lipatov *Termodinamika Rastvorov i Smesei Polimerov* (Thermodynamics of Polymer Solutions and Blends) (Kiev: Naukova Dumka, 1984)
10. S AVshivkov, E V Rusinova, A P Safronov, I V Zarudko, A L Nadol'skii *Vysokomol. Soedin., Ser. A* **42** 1397 (2000) [a]
11. T Araki, Q Tran-Cong, M Shibayama (Eds) *Structure and Properties of Multiphase Polymer Materials* (New York: Marcel Dekker, 1998)
12. D R Paul, C B Bucknall (Eds) *Polymer Blends* (New York: Wiley-Interscience, 2000)
13. S A Vshivkov, E V Rusinova *Fazovye Perekhody v Polimernykh Sistemakh, Vyzvannye Mekhanicheskim Polem* (Phase Transitions in Polymer Systems Induced by Mechanical Field) (Ekaterinburg: Urals State University, 2001)
14. S M Mezhikovskii *Fizikokhimiya Reaktsionnosposobnykh Oligomerov* (Physical Chemistry of Reactive Oligomers) (Moscow: Nauka, 1998)
15. A E Chalykh, V K Gerasimov, Yu M Mikhailov *Diagrammy Fazovogo Sostoyaniya Polimernykh Sistem* (Diagrams of Phase State of Polymer Systems) (Moscow: Yanus-K, 1998)
16. A E Nesterov, Yu S Lipatov *Fazovoe Sostoyanie Rastvorov i Smesei Polimerov* (Phase State of Polymer Solutions and Blends) (Kiev: Naukova Dumka, 1987)
17. I B Rabinovich, A N Mochalov, L Ya Tsvetkova, T B Khlyustova, E M Moseeva, V A Maslova *Acta Polym.* **34** 482 (1983)
18. K R Shull, E J Kramer *Macromolecules* **23** 4769 (1990)
19. D G Bucknall, Ph.D. Thesis, Imperial College, London, 1991
20. R J J Williams, B A Rozenberg, J-P Pascault *Adv. Polym. Sci.* **128** 95 (1997)
21. Z Q Cao, F Mechin, J-P Pascault *Adv. Chem. Ser.* **252** 177 (1996)
22. A I Suvorova, I S Tyukova, A Kh Khasanova, A L Nadol'skii *Vysokomol. Soedin., Ser. A* **42** 35 (2000) [a]
23. V I Klenin *Termodinamika Sistem s Gibkotsepnymi Polimerami* (Thermodynamics of Systems with Flexible-Chain Polymers) (Saratov: Saratov State University, 1995)
24. Yu K Godovskii *Teplofizika Polimerov* (Thermal Physics of Polymers) (Moscow: Khimiya, 1982)
25. S A Vshivkov *Metody Issledovaniya Fazovogo Ravnovesiya Rastvorov Polimerov* (Investigation Methods of Phase Equilibrium of Polymer Solutions) (Sverdlovsk: Sverdlovsk State University, 1991)
26. V N Kuleznev, L S Krokhina *Usp. Khim.* **42** 1278 (1973) [*Russ. Chem. Rev.* **42** 570 (1973)]
27. S P Papkov *Fiziko-Khimicheskie Osnovy Pererabotki Rastvorov Polimerov* (Physicochemical Foundations of Processing of Polymer Solutions) (Moscow: Khimiya, 1971)
28. S P Papkov *Ravnovesie Faz v Sisteme Polimer – Rastvoritel'* (Phase Equilibrium in Polymer – Solvent Systems) (Moscow: Khimiya, 1981)
29. J S Higgins, H C Benoit *Polymers and Neutron Scattering* (Oxford: Clarendon Press, 1994)
30. D G Bucknall, V Arrighi, in *Polymer Blends* Vol. 1 (Eds D R Paul, C B Bucknall) (New York: Wiley-Interscience, 2000) p. 349
31. A E Chalykh *Vysokomol. Soedin., Ser. C* **43** 2304 (2001) [a]
32. A I Maklakov, V D Skirda, N F Fatkullin *Samodiffuziya v Rastvorakh i Rasplavakh Polimerov* (Self-Diffusion in Polymer Solutions and Melts) (Kazan': Kazan' State University, 1987)
33. A L Kovarskii *Molecular Dynamics of Additives in Polymers, Utrecht, 1997*
34. A M Vasserman, A L Kovarskii *Spinovye Zondy i Metki v Fizikokhimii Polimerov* (Spin Probes and Labels in the Physical Chemistry of Polymers) (Moscow: Nauka, 1986)
35. E V Anufrieva, T N Nekrasova, T V Sheveleva, M G Krakovyak *Vysokomol. Soedin., Ser. A* **36** 449 (1994) [a]
36. K S Kazanskii, G V Rakova, S A Dubrovskii, V I Kuznetsov, N V Antoshchenko *Osobennosti Struktury Gidrogelei, Obrazuyushchikhsya pri Trekhmernoi Radikal'noi Polimerizatsii Makroionomerov Polietilenoksida. Preprint* (Characteristics of Hydrogel Structure Formed upon Three-Dimensional Radical Polymerisation of Polyethylene Oxide Macroionomers. Preprint) (Chernogolovka: Institute of Problems of Chemical Physics, Russian Academy of Sciences, Chernogolovka, 1997)
37. V G Kulichikhin *Mol. Cryst. Liq. Cryst.* **169** 51 (1989)
38. A Ya Malkin, A E Chalykh *Diffuziya i Vyazkost'. Metody Issledovaniya* (Diffusion and Viscosity. The Methods of Investigation) (Moscow: Khimiya, 1979)
39. A E Chalykh, A D Aliev, A E Rubtsov *Elektronno-Zondovyi Mikroanaliz v Issledovanii Polimerov* (Electron Probe Microanalysis in Polymer Investigation) (Moscow: Nauka, 1990)
40. I A Volegova, E V Konyukhova, Yu K Godovskii, H Berghmans *Vysokomol. Soedin., Ser. A* **39** 1492 (1997) [a]
41. V G Kulichikhin, N N Avdeev, A V Semakov, N A Plate *Izv. Akad. Nauk, Ser. Khim.* 1862 (1994) [b]
42. E M Chaika, A E Chalykh, V K Gerasimov, V S Papkov *Izv. Akad. Nauk, Ser. Khim.* 1268 (2003) [b]

43. F A Avgonova, Candidate Thesis in Physical and Mathematical Sciences, Institute of Physical Chemistry, Russian Academy of Sciences, Moscow, 2000
44. N A Plate (Ed.) *Zhidkokristallicheskie Polimery* (Liquid-Crystalline Polymers) (Moscow: Khimiya, 1988)
45. A E Chalykh, A I Zagaitov, V V Gromov, D P Korotchenko *Opticheskii Diffuziometr ODA-2. Preprint* (Optical Diffusiometer ODA-2. Preprint) (Moscow: Institute of Physical Chemistry, Russian Academy of Sciences, 1996
46. R Haase *Thermodynamik der Irreversiblen Prozesse* (Darmstadt: Dietrich Steinkopff Verlag, 1963)
47. A E Chalykh *Diffuziya v Polimernykh Sistemakh* (Diffusion in Polymer Systems) (Moscow: Khimiya, 1987)
48. A E Nesterov, Yu S Lipatov *Obrashchennaya Gazovaya Khromatografiya v Termodinamike Polimerov* (Reverse Phase Gas Chromatography in Thermodynamics of Polymers) (Kiev: Naukova Dumka, 1976)
49. V A Bershtein, V M Egorov *Differentsial'naya Skaniruyushchaya Kalorimetriya v Fizikokhimii Polimerov* (Differential Scanning Calorimetry in the Physical Chemistry of Polymers) (Leningrad: Khimiya, 1990)
50. A A Tager, T I Sholokhovich, M V Tsilipotkina *Vysokomol. Soedin., Ser. A* **14** 1423 (1972) [a]
51. G M Bartenev, A G Barteneva *Relaksatsionnye Svoistva Polimerov* (Relaxation Properties of Polymers) (Moscow: Khimiya, 1992)
52. P G Babaevskii, S G Kulik *Treshchinostoikost' Otverzhdennykh Polimernykh Kompozitsii* (Resistance to Cracks of Cured Polymer Compositions) (Moscow: Khimiya, 1991)
53. H-J Guntherodt, R Wiesendanger (Eds) *Scanning Tunnelling Microscopy* (Berlin: Springer, 1994)
54. V I Povstugar, V I Kodopov, S S Mikhailova *Stroenie i Svoistva Poverkhnosti Polimernykh Materialov* (Structure and Properties of the Surface of Polymer Materials) (Moscow: Khimiya, 1988)
55. A E Chalykh, I N Sapozhnikova *Usp. Khim.* **53** 1827 (1984) [*Russ. Chem. Rev.* **53** 1062 (1984)]
56. D J Walsh, J G McKeown *Polymer* **21** 1330 (1980)
57. I N Razinskaya, B P Shtarkman, L I Batueva, B S Tyves, M N Shlykova *Vysokomol. Soedin., Ser. A* **21** 1852 (1979) [a]
58. I N Sapozhnikova, Candidate Thesis in Chemical Sciences, Institute of Physical Chemistry, Academy of Sciences of the USSR, Moscow, 1983
59. J Schurer, A de Boer, G Challa *Polymer* **16** 201 (1975)
60. A E Chalykh, N N Avdeev *Vysokomol. Soedin., Ser. A* **27** 2467 (1985) [a]
61. T M Radzhabov, Yu D Shibanov, Yu K Godovskii *Vysokomol. Soedin., Ser. A* **30** 1667 (1988) [a]
62. A E Chalykh, N I Prokopov, I A Gritskova, V K Gerasimov *Vysokomol. Soedin., Ser. A* **38** 1888 (1996) [a]
63. J L Halary, J M Ubrich, J M Nunzi, L Monnerie, R S Stein *Polymer* **25** 956 (1984)
64. A E Chalykh, V K Gerasimov, A E Bukhteev, A V Shapagin, G Kh Kudryakova, T V Brantseva, Yu A Gorbatkina, M L Kerber *Vysokomol. Soedin., Ser. A* **45** 1148 (2003) [a]
65. S A Nenakhov, Candidate Thesis in Chemical Sciences, Institute of Physical Chemistry, Academy of Sciences of the USSR, Moscow, 1977
66. A E Chalykh, O V Dement'eva, V K Gerasimov *Vysokomol. Soedin., Ser. A* **40** 815 (1998) [a]
67. A B Burdin, A A Tager *Vysokomol. Soedin., Ser. B* **37** 850 (1995) [a]
68. A V Kotova, A E Chalykh, N N Avdeev, S M Mezhikovskii *Vysokomol. Soedin., Ser. A* **24** 460 (1982) [a]
69. A Nakajima, H Fujiwara, F Hamada *J. Polym. Sci., Part A-2* **4** 507 (1966)
70. A E Chalykh, N N Avdeev, A A Berlin, S M Mezhikovskii *Dokl. Akad. Nauk SSSR* **238** 893 (1978) [c]
71. H Jager, E J Vorenkamp, G Challa *Polym. Commun.* **24** 290 (1983)
72. D D Davis, T K Kwei *J. Polym. Sci., Polym. Phys. Ed.* **18** 2337 (1980)
73. V M Andreeva, I S Tyukova, A A Tager, N A Glazovskaya, L V Zaitseva *Vysokomol. Soedin., Ser. B* **27** 526 (1985) [a]
74. D G Welygan, C M Burns *J. Polym. Sci., Polym. Lett. Ed.* **11** 339 (1973)
75. A E Chalykh, R R Khasbiullin, S Parandoosh, in *Proceedings of the 4th International Symposium on Molecular Order and Mobility in Polymer Systems, St Petersburg, 2002* P-119
76. A E Bukhteev, Candidate Thesis in Chemical Sciences, Institute of Physical Chemistry, Russian Academy of Sciences, Moscow, 2003
77. L Mandelkern *Crystallization of Polymers* (New York: McGraw-Hill, 1966)
78. J B Jackson, P J Flory, R Chiang *Trans. Faraday Soc.* **59** 1906 (1963)
79. L N Mizerovskii, K V Pochivalov, V V Afanas'eva, N I Lytkina *Khim. Volokna* **2** 30 (2000)
80. M Takahashi, J Hasegawa, S Shimono, H Matsuda *Netsu Sokutei* **22** 2 (1995); *Chem. Abstr.* **123** 113 849 (1995)
81. M Takahashi, K Umezaki, K Fujiwara, H Matsuda *Netsu Sokutei* **22** 16 (1995); *Chem. Abstr.* **123** 113 850 (1995)
82. B Wunderlikh *Macromolecular Physics* Vol. 3 (New York: Academic Press, 1980)
83. E V Rusinova, S A Vshivkov *Vysokomol. Soedin., Ser. B* **45** 823 (2003) [a]
84. T Nishi, T T Wang *Macromolecules* **8** 909 (1975)
85. I Prigogine, R Defay *Chemical Thermodynamics* (London: Longman, 1954)
86. Ya I Gerasimov, V A Geiderikh *Termodinamika Rastvorov* (Thermodynamics of Solutions) (Moscow: Moscow State University, 1980)
87. Yu S Lipatov, V P Privalko, K D Petrenko *Kompozits. Polim. Mater.* **30** 49 (1986)
88. O V Dement'eva, Candidate Thesis in Chemical Sciences, Institute of Physical Chemistry, Russian Academy of Sciences, Moscow, 1998
89. E Martuscelli, G B Demma, in *Polymer Blends* (Eds E Martuscelli, R Palumbo, M Kryszewski) (New York: Plenum, 1980) p. 101
90. P J Flory *Principles of Polymer Chemistry* (New York: Cornell University Press, 1953)
91. R L Scott *J. Chem. Phys.* **17** 279 (1949)
92. H Tompa *Polymer Solutions* (London: Butterworth, 1956)
93. V N Kuleznev, in *Multicomponent Polymer Systems* (Ed. R F Gold) (Washington, DC: American Chemical Society, 1971)
94. V K Gerasimov, A E Chalykh, A Avgonov *Vysokomol. Soedin., Ser. A* **45** 409 (2003) [a]
95. B H Zimm *J. Chem. Phys.* **21** 934 (1953)
96. B H Zimm, J L Lundberg *J. Phys. Chem.* **60** 425 (1956)
97. H W Starkweather *J. Polym. Sci., Part B: Polym. Lett.* **1** 133 (1963)
98. Ya I Frenkel' *Kineticheskaya Teoriya Zhidkostei* (Kinetic Theory of Liquids) (Leningrad: Nauka, 1975)
99. P J Flory, H Höcker *Trans. Faraday Soc.* **67** 2258 (1971)
100. V K Gerasimov, N F Chugunova, A D Aliev, T I Chalykh *Izv. Vyssh. Uchebn. Zaved., Khim. Khim. Tekhnol.* **43** (2) 133 (2000)
101. N N Avdeev, Candidate Thesis in Chemical Sciences, Institute of Physical Chemistry, Academy of Sciences of the USSR, Moscow, 1990
102. K S Minsker, S V Kolesov, G E Zaikov *Starenie i Stabilizatsiya Polimerov na Osnove Vinilkhlorida* (Ageing and Stabilisation of Polymers Based on Vinyl Chloride) (Moscow: Nauka, 1982)
103. A E Chalykh, I N Sapozhnikova *Acta Polym.* **35** 592 (1984)
104. A E Chalykh, Z A Kochnova, E S Zhavoronok *Vysokomol. Soedin., Ser. A* **43** 2147 (2001) [a]
105. V G Chertkov, Candidate Thesis in Chemical Sciences, Institute of Physical Chemistry, Academy of Sciences of the USSR, Moscow, 1987
106. A I Zagaitov, Candidate Thesis in Chemical Sciences, Institute of Physical Chemistry, Russian Academy of Sciences, Moscow, 2000
107. V I Gerasimov, S N Chvalun, A E Chalykh, V K Gerasimov, L A Kazarin, A V Gaponenko, V I Mashchenko *Russ. Polym. News* **8** 27 (2003)

108. L A Utracki *Commercial Polymer Blends* (London: Chapman and Hall, 1998)
109. A E Nesterov, Y S Lipatov *Thermodynamics of Polymer Blends* (Lancaster: Technomic, 1997)
110. I Prigogine *Introduction to Thermodynamics of Irreversible Processes* (2nd Ed.) (New York: Wiley, 1962)
111. A E Chalykh, A E Rubtsov, A Avgonov, A D Aliev, V V Gromov *Vysokomol. Soedin., Ser. A* **40** 596 (1998) [a]
112. V K Gerasimov, A E Chalykh *Izv. Vyssh. Uchebn. Zaved., Khim. Khim. Tekhnol.* **46** (1) 5 (2003)
113. T I Kirillova, A A Tager, R Sh Frenkel' *Vysokomol. Soedin., Ser. A* **26** 1584 (1984) [a]
114. A E Chalykh, V K Gerasimov, V G Chertkov *Vysokomol. Soedinen., Ser. B* **36** 2077 (1994) [a]
115. V B Busygin, V Yu Stepanenko, A E Chalykh *Poverkhnostnye Energeticheskie Svoistva Polimerov* (Surface Energetic Properties of Polymers); article deposited at the VINITI, Moscow, 2001, No. 1709-V2001
116. S Wu, in *Polymer Blends* Vol. 1 (Eds D Poul, S Newman) (New York: Academic Press, 1978)
117. M Fol'mer *Kinetika Obrazovaniya Novoi Fazy* (Kinetics of Formation of a New Phase) (Moscow: Nauka, 1986)
118. A E Chalykh, I N Sapozhnikova, L I Medvedeva, V K Gerasimov *Vysokomol. Soedin., Ser. A* **28** 1895 (1986) [a]
119. A D Aliev, Candidate Thesis in Physical and Mathematical Sciences, Institute of Physical Chemistry, Academy of Sciences of the USSR, Moscow, 1984
120. A E Rubtsov, Candidate Thesis in Chemical Sciences, Institute of Physical Chemistry, Russian Academy of Sciences, Moscow, 1994
121. A E Chalykh, I N Sapozhnikova, R A Bulgakova, N P Sokolova *Vysokomol. Soedin., Ser. A* **29** 1749 (1987) [a]
122. A E Chalykh, I N Sapozhnikova, L I Medvedeva *Dokl. Akad. Nauk SSSR* **288** 939 (1986) [c]
123. G Kh Kudryakova, A E Chalykh, V K Gerasimov, N F Chugunova, in *Struktura i Dinamika Molekulyarnykh Sistem* (Structure and Dynamics of Molecular Systems) (Ufa: Institute of Physics of Molecules and Crystals, Urals Sciences Centre, Russian Academy of Sciences, 2002) Vol. 9, p. 290
124. M Theodorou, B Jasse *J. Polym. Sci., Polym. Phys. Ed.* **21** 2263 (1983)
125. A P Safronov, T V Somova *Vysokomol. Soedin., Ser. A* **44** 2014 (2002) [a]

[a] — *Polym. Sci. (Engl. Transl.)*
[b] — *Russ. Chem. Bull., Int. Ed. (Engl. Transl.)*
[c] — *Dokl. Chem. (Engl. Transl.)*

Russian Chemical Reviews **73** (1) 75 – 87 (2004)
© 2004 Russian Academy of Sciences and Turpion Ltd

DOI 10.1070/RC2004v073n01ABEH000864

Physicochemical aspects of metal corrosion inhibition in aqueous solutions

Yu I Kuznetsov

Contents

I.	Introduction	75
II.	Oxidising inhibitors	75
III.	Adsorption inhibitors	77
IV.	Complexation-type inhibitors	80
V.	Polymeric inhibitors	84

Abstract. The state-of-the-art of research dealing with the development and perfection of metal corrosion inhibitors in aqueous solutions is analysed. The main mechanisms involved in formation of protective layers on metals by inhibitors are discussed. Ways of creating mixed corrosion inhibitors with high protective properties are considered. The bibliography includes 150 references.

I. Introduction

The method of prevention of metal corrosion based on the use of corrosion inhibitors (henceforth referred to as inhibitors), *i.e.*, chemical compounds or compositions 'which, when present in a system at sufficient concentrations, decrease the corrosion rate without causing considerable changes in the concentration of any corrosive reagent', has been known for several centuries.[1] However, it was only in the middle of the twentieth century that a scientific concept about the mechanism of the inhibitor action was created and first achievements in the directed synthesis of inhibitors appeared after that. Corrosion inhibitors are used in numerous systems, from water supply systems and virtually any power plants to the protection of microelectronics and contemporary military equipment. Considering that losses from metal corrosion exceed 5% of the gross national product in industrial countries, the development and application of inhibitors, which is one of the main methods of corrosion protection, should be considered as a scientific and engineering task of current interest.

The action of inhibitors is always associated with changes in the state of the surface being protected due to adsorption or formation of poorly soluble compounds with metal cations. Such compounds decrease the area of active metal surface and/or increase the corrosion activation energy; as a rule, corrosion is of electrochemical nature in aqueous media. It is no wonder that the first classification of inhibitors was based on their ability to slow down cathodic or anodic (or both) electrochemical reactions. Later, a group of inhibitors capable of suppressing corrosion by accelerating rather than slowing down cathodic reactions was added to this classification.[2] In the latter case, the action of an inhibitor is based on its electrochemical conversion, *viz.*, reduction. This process provides conditions for the thermodynamic stability of a thin protective oxide film, which, in turn, slows down the anodic reaction. A modern classification includes oxidants as well as adsorption, complexation and polymeric inhibitors.[3] Such a division suggests that inhibition mechanisms are diverse and that achievements in different fields of chemistry can be utilised for corrosion protection.

Only inhibitors used in aqueous solutions are considered in this review. The use of inhibitors in other systems has specific features which, from a chemist's viewpoint, deserve a separate discussion. However, the action of inhibitors is almost always based on their ability to prevent metal corrosion caused by the presence of water in a system, hence the leading role rightfully belongs to water-soluble corrosion inhibitors.

II. Oxidising inhibitors

Salts of chromic acid are the best-known oxidising inhibitors; they show protective properties toward many metals in a broad pH range. An important role in the mechanism of their action belongs to the reduction of chromate ions, *e.g.*, according to the reaction

$$CrO_4^{2-} + 4H_2O + 3e \longrightarrow Cr(OH)_3 + 5OH^-, \; E^0_{cor} = -0.13 \text{ V}.^{\dagger} \qquad (1)$$

Judging by the values of its standard potential and the free corrosion potential of iron in water (E_{cor} is -0.3 to -0.4 V), this reaction can occur even in neutral aqueous solutions. However, chromate undergoes reduction only at the initial instant when a metal contacts with the solution; after a film of hardly soluble chromium and iron hydroxides has been formed on its surface, reaction (1) virtually ceases [2] and a kind of equilibrium between Cr^{3+} compounds and adsorbed chromate ions is established. If a defect appears in the passivating film for some reason, chromate migrates into such a defect, undergoes reduction and 'heals' the film. This is one of the main reasons for the continuing use of chromates in conversion and protective paint coatings in spite of serious environmental restrictions.[4, 5]

Naturally, chromates manifest their oxidising properties more readily in acid solutions, especially on those metals whose E_{cor} is more negative than E_{cor} of iron, *e.g.*, on aluminium. However, acceleration of the cathodic reaction can also stimulate corrosion if an oxidant cannot create conditions for the formation of a passive film on a metal surface. The effect of oxidants is consid-

Yu I Kuznetsov Institute of Physical Chemistry, Russian Academy of Sciences, Leninsky prosp. 31, 119991 Moscow, Russian Federation. Fax/Tel. (7-095) 334 85 90. E-mail: kuznetsov@ipc.rssi.ru

Received 3 July 2003
Uspekhi Khimii **73** (1) 79 – 93 (2004); translated by S S Veselyi

† Hereinafter, the electrode potentials are presented *versus* the standard hydrogen electrode.

erably affected by the solution pH (especially in the case of aluminium due to its amphoteric properties). At certain stoichiometric ratios of components involved in electrochemical reactions, conditions can be created such that only foreign or mixed oxide layers are formed on the aluminium surface, whereas other oxoanion reduction products capable of loosening the oxide structure are absent.[6] Judging by the changes in the corrosion inhibition coefficient

$$\gamma = \frac{K_0}{K_{in}}$$

(where K_0 and K_{in} are the corrosion rates in a reference solution and in a solution containing the additive under study), chromate acts as a corrosion activator at $2.0 < pH < 6.0$ (Fig. 1), whereas its inhibiting effect is more pronounced in more acidic (or more alkaline) solutions.

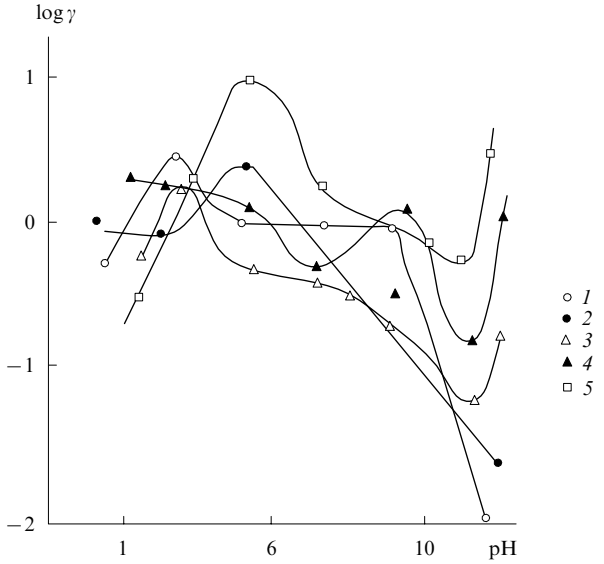

Figure 1. Effect of pH in a solution containing 0.01 N SO_4^{2-}, 0.1 N Cl^-, 0.1 N F^- and oxoanion additives on the inhibition coefficient of aluminium corrosion.[6]
Additive: (*1*) 0.1 N $Cr_2O_7^{2-}$, (*2*) 0.1 N MnO_4^-, (*3*) 0.05 N VO_4^{3-}, (*4*) 0.05 N WO_4^{2-}, (*5*) 0.05 N MoO_4^{2-}.

It has long been an important problem to find inhibitors that are less environmentally hazardous than toxic chromates. Most commonly, molybdates are used as substitutes; their oxidising properties are inferior to those of chromates (see Fig. 1). Thermodynamic calculations showed[7] that molybdate forms a barely soluble salt at potentials of active dissolution of iron in weakly acidic solutions (at $pH < 6.0$),

$$Fe + HMoO_4^- = FeMoO_4 + H^+ + 2e,\ E = E^0 - 0.0295\,pH. \quad (2)$$

The oxidising properties of molybdate with respect to steel do not manifest themselves in neutral media, so efficient protection of the steel surface requires the presence of yet another oxidant.[8] Black MoO_2 films are formed at $pH < 5$, which suggests that reduction of molybdate or, more accurately, isopolymolybdate compounds occurs. However, passivation phenomena manifest themselves only slightly even at pH 3. On metals whose free corrosion potentials are more negative than that of steel, the effect of molybdate is also observed in neutral media, let alone in weakly acidic solutions. In fact, the protective properties of molybdate with respect to zinc attain a maximum in solutions with pH 5.0; however, the following reaction is possible at pH 7:

$$MoO_4^{2-} + 2H_2O + 2e = MoO_2 + 4OH^-. \quad (3)$$

Corrosion inhibition occurs due to the formation of a thin layer of a molybdate reduction product on the zinc surface.

In the past, molybdates have attracted the attention of researchers as compounds that can prevent pitting of various steels, including stainless steels. The effect of MoO_4^{2-} as a corrosion inhibitor is even compared with the effect of molybdenum as an alloying component of ferrite iron–chromium alloys.[9,10] However, MoO_4^{2-} acts as an adsorption inhibitor rather than an oxidant, since the nucleation and development of pits occur in the passive region of potentials where molybdenum can, in fact, be oxidised into MoO_4^{2-}.

In a discussion of molybdates, tungstates and similar salts, one cannot neglect their ability to form heteropoly compounds.[11] Many of them are stronger oxidants than molybdate, hence they can be regarded as suitable compounds for the protection of metals in highly corrosive media. For example, salts of phosphomolybdic acid have long been known as corrosion inhibitors in hot brines, but some specific features of their protection mechanism have been revealed only recently.[12] It was proven that phosphomolybdic acid is an efficient corrosion inhibitor of steel in acid brines (65% LiBr) only at temperatures above 120 °C. Its addition to brine accelerates the cathodic reaction on steel and thus increases E_{cor} by 0.1–0.15 V. In weakly alkaline brines (pH 8.5), this acid can decrease the corrosion rate of steel by an order of magnitude in a broad temperature range (80–220 °C). The effect of phosphomolybdic acid on the effective activation energy of corrosion (ΔG^*_{ef}) depends on the solution pH: the value of ΔG^*_{ef} decreases at pH 5.0 but increases at pH 8.5; this suggests that the mechanism changes due to decomposition of the acid and incorporation of its fragments into the oxide film. Thus, the mechanism of steel protection is not limited to the increase in the oxidative properties of the solution upon addition of phosphomolybdic acid; to a considerable extent, it results from changes in the composition of oxide films resulting in an increase in their corrosion resistance.

Inhibition of metal corrosion in solutions of acids by inhibitor reduction products is typical of weaker oxidants, too. Iron protection by phenylarsonic acid ‡ is believed to occur according to this mechanism.[13]

Oxidants that do not form oxides (hydroxides) upon reduction can also be efficient inhibitors.§ Organic nitro compounds that are reduced at high rates even in neutral media can serve as examples. For example, the current density in the reduction of 3,5-dinitrobenzoate (> 10 mA cm^{-2}) exceeds considerably the passivation current density (i_p) of iron in borate buffer solution.[2] An oxidant of this kind does not affect directly the anodic reaction of iron dissolution, but it can increase the pH of the near-electrode layer due to generation of hydroxyl anions, which favours passivation. The efficiency of this type of inhibitor (*e.g.*, derivatives of benzoic acid, phenol, naphthol, *etc.*) was proven in numerous studies generalised in a monograph by Rozenfeld and Persiantseva.[15]

Trabanelli[16] correctly noted that reduction of organic inhibitors in acids can give chemical compounds some of which can protect metal surfaces whereas others can stimulate metal dissolution. Reduction of sulfoxides to organic sulfides, which are more efficient inhibitors, is a typical example of secondary inhibition.

‡ However, this acid inhibits the corrosion of titanium for a different reason, *viz.*, due to the formation of insoluble complex compounds with its cations.

§ The reference to steel protection by sodium nitrite leaves room for discussion. Some authors ascribed its protective effect in neutral solutions solely to adsorption of the NO_2^- anion on the metal, relating passivation in acid media only to the oxidation properties of nitrite.[2] However, it has already been proven that the oxidation properties of nitrite may not be ignored in the former case, near the free corrosion potential, as well.[14]

III. Adsorption inhibitors

If a protective layer is formed by adsorption-type inhibitors, adsorption is not only the first but also the main step. Obviously, it can play an important role in mechanisms of action of other inhibitors as well, but their interactions with metals are not limited to adsorption.

The kinetics of metal corrosion depends on many factors (local phase and chemical equilibria, surface tensions and activities of components in interphase layers), but the most important role belongs to the electric and energy characteristics of the surface. It is not surprising that one can slow down metal corrosion by affecting the adsorption of a medium component, since adsorption can change the above characteristics considerably. On the other hand, the majority of studies were performed with polycrystalline metal surfaces where it is difficult to detect the reconstructing effect of an inhibitor on the near-surface layer and on the electronic structure of the adsorbent. Therefore, though admitting the importance of studies on such effects,¶ let us limit ourselves to consideration of the 'macro effects' of an inhibitor that is adsorbed, *i.e.*, how it affects the rates of electrode reactions and the metal corrosion itself. If an adsorption-type inhibitor is used, an exceptionally important role belongs to the redox properties of the medium components and their adsorptivity.

The processes of adsorption and formation of protective layers on a metal substantially depend on the charges of the surface and inhibitor species. As a rule, cation-active inhibitors slow down cathodic reactions and active metal dissolution. Local corrosion is more efficiently prevented by anion-active inhibitors. However, the electrostatic interaction of an inhibitor with a metal surface is not the only motive force of adsorption. Some contributions to it can made by 'squeezing-out' of inhibitor species from the interionic space [18] and by hydrophobic interaction of non-polar inhibitor fragments with water.[19] Donor–acceptor interactions between a metal and an inhibitor can result in a stronger chemisorption binding of the latter to the surface.

If a metal is dissolved from the active state, which is usually the case in acids, then, for moderate metal surface coverages (θ), it is possible to single out two main contributions to the corrosion inhibition coefficient, *viz.*, related to changes in the ψ_1-potential and to surface blocking:

$$\log\gamma = \text{const} \times \Delta\psi_1 - \log(1-\theta). \qquad (4)$$

Even this simplified approach proposed by Antropov back in the 1970s [20] proved to be useful for formulating the concept of inhibitor action. However, it does not answer the important question: what structure should a compound have in order to be an efficient inhibitor?

Other approaches are required to establish the inhibitor structure–efficiency relationship. The majority of adsorption inhibitors are organic compounds; that is why many researchers used the linear free energy (LFE) relationship to reveal the role of the inhibitor structure.[14, 21–25]

Grigoriev and Ekilik [21] studied this problem in most detail in relation to acid corrosion, which usually occurs in the active dissolution region of potentials. They showed that if the inhibitor species are small and their adsorption increases the corrosion activation energy ($\Delta G^{\neq}$) due to charge redistribution in the double electric layer, the following equation is valid:

$$\log\gamma_R = \log\gamma_H + \rho\sigma, \qquad (5a)$$

where ρ is the reaction parameter, which is assumed to be equal to unity for a standard reaction series and which depends on the nature of the reaction being studied and on the conditions under which it occurs; σ is a constant of a substituent R, which accounts for its electron-donor ($\sigma < 0$) or electron-acceptor ($\sigma > 0$) effect on the reaction centre in comparison with hydrogen. In the general case of inhibitors capable of partial blocking of the active sites, equation (5a) assumes the form

$$\log\left(\frac{\gamma_R}{\gamma_H}\right) = \rho\sigma - \log\left(\frac{\theta_R}{\theta_H}\right), \qquad (5b)$$

where θ_H and θ_R are the degrees of coverage of the metal surface by the non-substituted and substituted inhibitor of the given reaction series, respectively. Similar regularities were also observed by many authors, not only in acidic but also in other media. For example, the efficiency of *N*-benzylideneaminoethanol derivatives in neutral medium containing hydrogen sulfide increases linearly with an increase in the electron-donor effect of the substituent R taken into account by its Wepster's σ^n-constant (Fig. 2).[24] According to Eqn (5b), substituents affect the protective properties of organic compounds solely by increasing the inhibitor adsorption; as a result, the value $\Delta G^{\neq}$ increases, whereas the surface area of the metal that undergoes corrosion decreases. For example, if the inhibitor being adsorbed is an electron donor, the inhibitor–surface binding strengthens with an increase in the electron density on the reaction site. Other mechanisms of inhibitor adsorption are also possible (see, *e.g.*, the monographs [14, 20]).

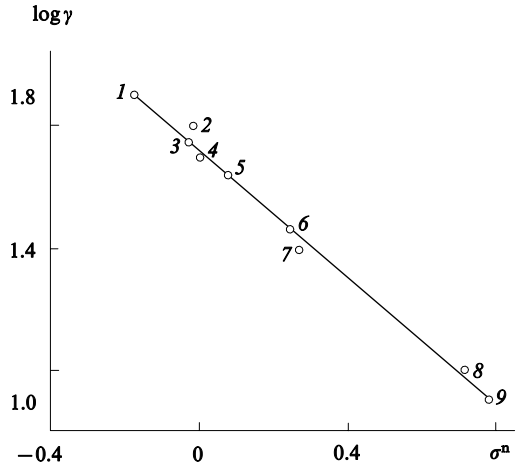

Figure 2. Dependence of the inhibition coefficient of steel corrosion in aqueous solution (0.5% NaCl, 0.25 g litre^{-1} CH_3COOH, 0.4 g litre^{-1} H_2S, pH 6.0) by substituted *N*-benzylidenaminoethanols with general formula $HO(CH_2)_2N=CH-C_6H_4-R$ on Wepster's constants of substituents.[24]
Substituents: (*1*) *p*-$N(CH_3)_2$; (*2*) *m*-OH, *p*-OCH_3; (*3*) *m*-OCH_3, *p*-OCH_3; (*4*) H; (*5*) *m*-OCH_3; (*6*) *p*-Br; (*7*) *p*-Cl; (*8*) *m*-NO_2; (*9*) *p*-NO_2. The inhibitor concentration is 0.004 mol litre^{-1}.

The approach considered above can also be applied for describing the effect of organic compounds on the passivation current density of metals, though the surface blocking in the active–passive transition region can be caused by oxide formation to a greater extent than by the inhibitor adsorption. Both linear and more complex dependences of $\log\gamma_p$ (here, $\gamma_p = i_p^0/i_p$, i_p^0 and i_p are the current densities in the reference and inhibited solutions, respectively) on substituent σ-constants were obtained for acidic [21] and neutral [14] media.

Studies of the effect of the organic anion structure on iron passivation in neutral solutions made it possible to find [14] new efficient adsorption-type inhibitors. Benzoate (**1**) hinders passivation; however, by introducing various substituents in the benzene ring, it was found that anthranilates (**2**) facilitate passivation. In the series of *N*-substituted anthranilates **2**, sodium *N*-phenyl-

¶ An attempt to generalise them was undertaken previously.[17]

anthranilate (SPA) **3** is notable for its passivating capability. It is in an aqueous solution of this corrosion inhibitor that the possibility of iron passivation without the formation of an oxide film was shown for the first time.[26] The discovery of this phenomenon, which was called adsorption passivation,[14,27] inspired a search for novel, even more efficient passivators; of the compounds tested, salts of mefenamic acid **4** (MEF) and isodiftorant **5** are noteworthy.

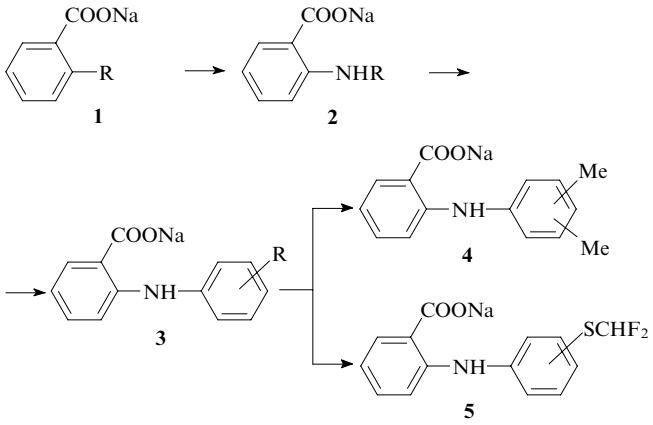

The linear free energy relationship principle was successfully used to describe the inhibition of local corrosion of metals, which is an even more complex process. In this case, the displacement of the electrode local depassivation potential [or the potential of the formation of the first pit (E_{pit})] to more positive values

$$\Delta E = E_{\text{pit}} - E_{\text{pit}}^{\text{background}}$$

was used as the inhibitor efficiency criterion. This value is determined from potential–time dependences or from anodic polarisation curves. In many cases, V-shaped dependences of ΔE on substituent σ-constants were observed, *i.e.*, the value of ρ changed its sign within a reaction series; this is caused by a change in the rate-determining step of the process. For example, this is typical of passive state stabilisation of the D16T aluminium alloy by *o*-substituted benzoates.[3] In this case, the branches corresponding to electron-donor and electron-acceptor substituents can have different sensitivities to the nature of the corrosive anion,† pH and solution temperature.

If solvation effects for a reaction series in question and a standard reaction series differ considerably, it is worthwhile to take into account, aside from the substituent σ-constant, its hydrophobicity π- or *f*-constants calculated from distribution factors of compounds in an octanol–water system

$$P = \exp\frac{\Delta G_{\text{o-w}}}{RT},$$

where $\Delta G_{\text{o-w}}$ is the distribution free energy for a compound.[28] This approach, which takes into account the electronic and hydrophobic properties of a substituent simultaneously, was originally used in biochemical studies; however, it also proved to be useful for description of efficient inhibitors.

Using quantitative prediction methods, it was shown that the efficiency of metal protection is limited if adsorption inhibitors that are individual chemical compounds are only used. This is connected with the tightening of environmental requirements. In many systems, the best protection is achieved by surfactants with high hydrophobicity ($\log P > 3$), *i.e.*, compounds poorly soluble in water and therefore unsafe ecologically.[29] In view of this, it becomes ever more urgent to develop inhibitor mixtures from components that could improve metal protection more efficiently than any of its components.

† Not only Cl^- but also other anions (I^-, Br^-, NCS^-) can cause depassivation in the system studied.[3]

The majority of such inhibitors for acidic media were created on the basis of the double electric layer recharging effect by some anions discovered back in the 1950s. The essence of this effect is as follows: an anion adsorbed on a surface that was initially charged positively gives some negative charge to that surface. Large organic cations that have considerable shielding effects can be adsorbed on such a surface; this improves the metal protection. There are many examples of successful corrosion inhibition by this method in complex systems. Schmitt *et al.*,[30] who considered the synergism and antagonism of various inhibitors of carbon dioxide-induced corrosion of steels, found that, though the surfaces to be protected contain carbonate deposits, the inhibition efficiency is largely determined by cooperative adsorption of anions and alkylammonium cations. According to results obtained by Shikai and Yufen,[31] the activity of anions in mixed inhibitors containing organic cations depends on the nature of the acid and decreases in the following series:

H_2SO_4	$I^- > SCN^- > HS^- > Br^- > Cl^-$;
HCl	$I^- > HS^- > Cl^- > SCN^- > Br^-$;
HF	$SCN^- > I^- > HS^-$;
CH_3COOH	$HS^- > SCN^- > I^- > Br^- > Cl^-$.

The mutual effects of components in a mixed inhibitor are usually evaluated by comparing the product of their corrosion inhibition coefficients ($\Pi\gamma_i$) with a similar value measured in the presence of the corresponding mixture (γ_{mix}). If the mutual effect coefficient *m* of the components

$$\kappa_m = \frac{\gamma_{\text{mix}}}{\Pi\gamma_i} \tag{6}$$

is larger than 1, one can say that their protective effect is enhanced, whereas if it is lower than 1, the protective effect is weakened.

A similar criterion was suggested [32] for the analysis of the concentration dependences γ of individual and mixed inhibitors. For example, if *n* portions of an individual inhibitor Δc_i are introduced successively (with its zero initial concentration), the overall concentration effect coefficient is expressed by the formula

$$\kappa_c = \frac{\gamma_{\Sigma c}}{(\gamma_{\Delta c_i})^n}, \tag{7a}$$

where the subscripts show whether the measured values reflect the effect of the total inhibitor amount (Σc) or of its certain portion (Δc_i). In the case of the power-law dependence common for adsorption inhibitors

$$\gamma = \gamma_0 c^{\beta},$$

where γ_0 and β are constants, Eqn (7a) assumes the form

$$\kappa_{\Sigma c} = \gamma_0^{1-n} n^{\beta} (\Delta c_i)^{\beta(1-n)}. \tag{7b}$$

For *m* inhibitors in a mixture and a variable concentration (c_i) of one inhibitor, designating the $\gamma_{\Delta ci}$ for the mixed inhibitor as $\gamma_{\Delta ci,\Sigma}$, the following equation is obtained:[32]

$$\kappa_m = \frac{\kappa_{\Sigma c}(\gamma_{\Delta c_i,\Sigma})^n}{\Pi\gamma_i}. \tag{8}$$

Ekilik and Ekilik [32,33] analysed the equation they derived for the inhibition of iron corrosion in 1 M H_2SO_4 by 2-(2-pyridyl)-benzoimidazole, NaCl, NaF, NaSCN and their binary and ternary mixtures. They concluded that the effect of chloride on the protective action of the azole exceeds the mutual effect coefficients for all other combinations studied. It was also shown that evaluation of mutual effects of mixture components in the case of iron acid corrosion inhibition requires that not only the kinetic equations of partial electrode reactions but also the free corrosion potential be taken into account. If changes in E_{cor} are ignored, erroneous conclusions about the mutual enhancement of mixture components can be drawn.

It is in much more rare cases that the presence of certain cations increases the protective effect of organic anions. For example, local depassivation of iron in weakly alkaline solutions is more strongly inhibited by phenylanthranilic acid if this inhibitor is combined with hexamethylenediamine.[34] However, this kind of synergy of protective effects of inhibitors is not versatile. Selective dissolution of binary alloys (45% Ni + 55% Zn, 70% Cu + 30% Zn, 90% Cd + 10% Zn, 97% Sn + 7% In) in weakly acidic solutions of mixtures of cation-active organic compounds (acridine, substituted pyrylium salts, 2-aminobenzoimidazole) and halides [35] was found to involve mainly an antagonism of the mutual effects of inhibiting mixture components caused by their competitive adsorption.

The approach based on the linear free energy relationship is also used to study the mutual effects of inhibitors and to search for more efficient inhibitor mixtures.[36–38] For a mixture of inhibitors corresponding to the same reaction series and at their constant total concentration

$$c_1 + c_2 + \ldots + c_i = \text{const}$$

the following relationship is valid:

$$\log\gamma = a + \rho\sum_{i=1}^{n} N_i\sigma_i\,, \qquad (9)$$

where a is a constant and N_i is the molar fraction of the ith compound in the mixture (*i.e.*, $\Sigma N_i = 1$). If the inhibitors present in the system and corresponding to m different reaction series are designated by the left subscript 1, 2, ..., m, then for an ideal system, *i.e.*, a system where no mutual effects of the inhibitors exist, one can write:

$$\log_m\gamma_c = $$

$$= \sum_{1}^{m} a + {}_1\rho\sum_{i=1}^{{}_1n}\left({}_1N_i \times {}_1\sigma_i\right) + \ldots + {}_m\rho\sum_{i=1}^{{}_mn}\left({}_mN_i \times {}_m\sigma_i\right). \qquad (10)$$

In a similar equation for real corrosion systems, the first term and the coefficients do not match those in Eqn (10). Taking this into account, Grigoriev *et al.*[38] assumed that, provided that the concentrations of the components are unchanged, *i.e.*, N = const, the ρ values, which are different for different reaction series, become equal for mixtures of these compounds. In such a case, the following equation is valid:

$$\log_m\gamma_{\text{mix}} = $$

$$= {}_m a_{\text{mix}} + {}_m\rho\left[\sum_{i=1}^{{}_1n}\left({}_1N_i \times {}_1\sigma_i\right) + \ldots + \sum_{i=1}^{{}_mn}\left({}_mN_i \times {}_m\sigma_i\right)\right]. \qquad (11)$$

In fact, Eqn (11) is well obeyed for mixtures of azomethine **6**, imidazobenzoimidazole **7** and pyrimidobenzoimidazole **8** derivatives

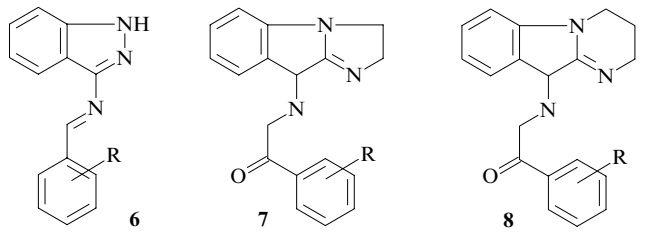

in 1 M H_2SO_4 + 0.25 M NaCl solution at different temperatures and with different numbers of components (m). It was found that the concentration of a mixed inhibitor (consisting of representatives of the above reaction series) ensuring the required corrosion inhibition coefficient ($_{\text{mix}}c$) can also be found using substituent σ-constants and taking the molar fractions of each mixture component into account

$$\log {}_{\text{mix}}c = a + \rho\sum N_i\sigma_i. \qquad (12)$$

To optimise the composition of inhibitor mixtures, it is necessary to establish the reasons for deviations of their action from 'additivity'. This requires additional studies, primarily on joint adsorption of mixture components on metal surfaces. In this respect, attention should be paid to effects of mutual enhancement of inhibiting effects and adsorption of organic anions.

For example, experiments on corrosion protection of steel by mixtures of hydroxynaphthoates (HNP) with substituted anthranilates showed [39] the synergistic effect of these inhibitors, which is only observed if the anion of the aromatic amino acid has high hydrophobicity, *e.g.*, in mixtures with MEF anions (Fig. 3). Ellipsometric studies showed that the synergism results from the ability of one of the anions (at its low concentration) to initiate the adsorption of the other anion. In this case, the free adsorption energy ΔG_a° increases, *i.e.*, the bond between the inhibitor and the oxidised iron surface strengthens. This effect is expressed even more clearly for SPA – sodium oleate mixtures; however, in this case an adduct, which interacts with the surface through chemisorption, is formed in the solution bulk; the ΔG_a° value reaches 40 ± 4 kJ mol^{-1} (see Ref. 40), which is more than two times higher than $\Delta G_a^\circ = 16.8 \pm 0.3$ kJ mol^{-1} for SPA.

The hard – soft acid – base (HSAB) principle is widely used to estimate possible interactions involved in joint adsorption of inhibitors.[14, 31, 41–46] This approach mainly relies on the nature of the reaction centres rather than on the nature of the substituent.

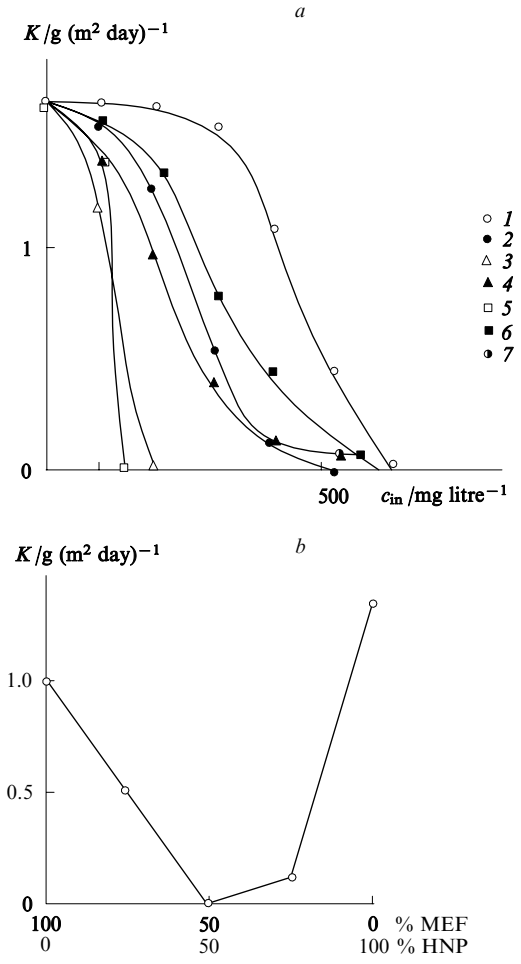

Figure 3. Dependence of the corrosion rate of St.3 steel in water containing 30 mg litre^{-1} NaCl and 70 mg litre^{-1} Na_2SO_4 on the inhibitor concentration (*a*) and on the component ratio in HNP – MEF mixtures at c_{in} = 200 mg litre^{-1} (*b*).[39]
Inhibitor: (*1*) SPA, (*2*) HNP, (*3*) sodium *N*-methylanthranilate (SMA), (*4*) MEF – HNP mixture (1 : 1), (*5*) MEF, (*6*) SMA, (*7*) SPA.

The surfaces of metals, primarily d-metals, are comparatively 'soft' reagents; however, they become 'hard' reagents upon oxidation, at least when Fe_2O_3, Al_2O_3 or MgO is formed. In the former case, strong adsorption can be expected for compounds with readily polarisable (soft) reaction centres; in the latter case, adsorption is mainly determined by electrostatic (*i.e.*, hard) interaction of the adsorbate with the surface.

In corrosion studies, estimation of hard and soft properties of reagents became possible owing to the use of the equation for nucleophile reactivity [14]

$$S = \alpha \log \mathrm{MR} + \beta \mathrm{H} + \gamma\pi, \tag{13a}$$

where S is a kinetic parameter of the process reflecting the relative change in the activation energy due to changes in the nucleophile nature; α, β, and γ are coefficients; MR is the molar refraction of the nucleophile's reaction centre,‡ and H is its relative basicity

$$H = \mathrm{p}K_\mathrm{a} + 1.74.$$

The parameter π characterises the hydrophobicity of an atom or a group of atoms with respect to the hydrogen atom; this is calculated from distribution coefficients,

$$\pi = \log P_{\mathrm{C_6H_5R}} - \log P_{\mathrm{C_6H_6}}.$$

The effect of the nucleophile basicity on the reactivity is weak; therefore, it is possible to use only two parameters, *viz.*, molar refraction and hydrophobicity

$$S = \alpha \lg \mathrm{MR} + \beta + \gamma\pi, \tag{13b}$$

which certainly simplifies the verification of this equation and its use for interpretation of mechanisms of complex heterogeneous reactions, such as corrosion, anodic dissolution of metals, *etc*. For example, the increase in polarisability of halides in the series $F^- < Cl^- < Br^- < I^-$ should increase the degree of charge transfer in the adsorbed complex, which facilitates covalent binding and blocking of the electrode surface. Taking into account that the hydrophobicity of anions increases in the same series, it becomes clear why not only Cl^- and Br^- but also I^- (to an even greater extent) being adsorbed on the iron surface from acidic solutions slow down its dissolution. It is important that the highest protective effect in acids is shown by organic cations combined with soft bases, *viz.*, I^- and CNS^-. The F^- anion, which is a hard base, is weakly adsorbed by the non-oxidised iron surface (which can be considered as a soft acid) and therefore does not enhance the protective effects of organic cations.

However, such a joint corrosion inhibition results not only from surface recharging. It was noted a long time ago that a metal surface can undergo partial hydrophobisation upon chemisorption of anions and can become somewhat 'softer' upon adsorption of soft bases.[3] Both factors can facilitate subsequent adsorption of large organic molecules or ions on a metal; those molecules or ions which are capable of covalent interactions through π-electrons of an aromatic ring or unsaturated bonds are the most efficient inhibitors.

The application of the HSAB principle to metal dissolution and corrosion inhibition processes has been considered in detail in a number of reviews.[43–46] It will only be noted here that the use of this principle is especially efficient if medium components interact with a metal surface more strongly than in the case of physical adsorption. Self-assembling molecules that chemically modify a metal surface can serve as an example. It is no coincidence that the use of alkanethiols for the protection of iron [49–52] or copper [50, 53] requires special surface cleaning to remove oxides and enable soft interaction of the SH group with the metal. Except for specific cases where surface preparation is performed *in vacuo* or using the Langmuir–Blodgett technique, alkanethiols are inefficient as corrosion inhibitors since chemisorption of these molecules only occurs on non-oxidised surfaces.[54] It is possible that the use of alkanethiols combined with other corrosion inhibitors can improve protective properties of self-assembling surface layers, as shown for dodecane-1-thiol and Schiff's bases (*N*-2-hydroxyphenyl- or *N*-2-octadecyl-3-methoxysalicylideneimine);[55] however, practical implementation of this kind of inhibition could be hampered considerably by the toxicity of alkanethiols.

Less toxic alkylphosphonates deserve attention in this connection: they can form oriented layers on oxidised surfaces of aluminium [56] and iron.[57, 58] However, metal surface modification by this method has been studied insufficiently. Further studies in this direction are needed to reveal advantages of adsorption of alkylphosphonates in comparison with that of more common inhibitors, *e.g.*, dialkyl phosphates that are also capable of irreversible adsorption on an oxidised iron surface.[59]

IV. Complexation-type inhibitors

It is not easy to draw a border between adsorption-type and complexation-type inhibitors, since inhibition by a single compound can involve different mechanisms depending on the metal to be protected and the pH of the medium. On the other hand, taking complexation into account, it is often possible to explain corrosion inhibition that is inexplicable within the adsorption theory. The antagonism of action of two depassivators, which was originally discovered on nickel and then on other metals and alloys,[60–62] can serve as an example. For example, the E_pit of nickel in solutions of corrosive sodium caproate ($C_5H_{11}COONa$) does not depend any more on the activator concentration if the concentration of the first anion is $c_{\mathrm{an},1} > c_\mathrm{c}$.[60] Seemingly, the addition of as little as 10^{-8} mol litre^{-1} of NaCl, which is less corrosive under these conditions, to a comparatively concentrated (0.05 M) $C_5H_{11}COONa$ solution should not affect E_pit; however, this value does increase, *i.e.*, nickel depassivation is hindered. Chloride cannot activate nickel at such a low concentration (c_Cl); furthermore, adsorptive displacement of caproate by chloride is impossible at the ratio $c_{\mathrm{an},1}/c_\mathrm{Cl} = 5 \times 10^6$. As c_Cl is increased to 0.1 mol litre^{-1}, the inhibition effect becomes obvious, since the E_pit values in the individual solutions of both activators are lower than those in mixed solutions. The effect of low Cl^- concentrations can be explained as follows: although chloride cannot displace caproate, it can prevent hydration of the complex by replacing a weaker nucleophile, *viz.*, water, in this complex. The changes in the complex composition probably decrease its solubility, which can result in a change in the rate-determining step of depassivation and in the blocking of some of the active sites; as a result, E_pit increases. As the chloride concentration is increased, the inhibiting effect increases until chloride becomes capable of displacing caproate. In such a case, depassivation is inhibited by caproate until c_Cl becomes sufficiently high to displace $C_5H_{11}COO^-$ completely, and E_pit becomes equal to that in pure chloride solutions. This effect was also observed with other carboxylates, $RCOO^-$, where R = H, C_nH_{2n+1} ($n = 1–9$), $HC{\equiv}C$, $CClH_2$ and CF_3. The inhibiting effect of Cl^- increases with an increase in the substituent hydrophobicity expressed through its f-constant,

$$\Delta E = E_{(\mathrm{an}+\mathrm{Cl})\,\mathrm{pit}} - E_{(\mathrm{an})\,\mathrm{pit}} = 0.05 + 0.17f, \tag{14}$$

which does not contradict the explanation proposed for such an unusual inhibiting effect.

Two groups of complexation-type inhibitors can be distinguished. The first group comprises heterocyclic compounds that can form insoluble complexes with copper, zinc and other metals in aqueous solutions. The second group includes complexones (chelating reagents) and their complexes with metal cations.

In the first group, the widely used azoles (imidazoles, triazoles, thiazoles, *etc*.) are notable for their efficiency. Azoles, particularly

‡ Equation (13a) differs from the widely known Edwards equation, which was considered in detail in a number of publications,[14, 47, 48] by the third term. Like in Edwards' calculations, it is legitimate here to use the MR of the entire nucleophile, rather than its reaction centre, for comparatively small nucleophiles.

benzotriazole and its derivatives, have almost no competitors for protection of copper and copper alloys. Their recent uses include the protection of electronic equipment,[63,64] in cooling systems (inhibitors resistant to chlorine have been developed [65]) as well as in brines,[66] for modification of conversion coatings on copper,[67] steel,[68] zinc [69] and silver.[70]

The mechanisms of action of these inhibitors differ considerably from those considered above; they are discussed in several reviews.[71–73] In most cases, azoles form thin insoluble surface films of complex compounds with cations of those metals that are often present on oxidised surfaces.[74–76] The interest in azoles has not weakened during the past decade; their ability to form thin self-assembling layers on copper, observed, *e.g.*, for 2-mercaptobenzoxazole [77] or *N*-vinylcarbazole,[78] opens new prospects for corrosion prevention by these compounds.

Other heterocyclic inhibitors that can form insoluble metal complexes, *e.g.*, certain macrocyclic compounds (porphyrins, phthalocyanines), are also worthy of attention.[79] The number of publications dealing with this group of inhibitors is growing steadily, and they should probably be reviewed in a separate paper. It will only be noted here that the efficiency of copper and zinc protection with azoles is closely related to the ability of these metals to form different bonds in complexes and can be estimated using the linear free energy relationship approach.[71] The increase in the electron density on the reaction centre in 2-substituted benzoimidazoles (BI), which is reflected by substituent induction constants (Fig. 4), strengthens the σ-bond in protective zinc complexes and increases the protection efficiency. In contrast, copper, which can act as an electron donor owing to its low ionisation potential and high electronegativity, forms π-complexes with BI; therefore, electron-acceptor substituents enhance copper protection.

The leading position in the second group of inhibitors belongs to phosphorus-containing complexones, such as 1-hydroxyethanediyldiphosphonic acid (HEDP), nitrilotri(methylphosphonic acid) (NTP), ethylenediamine-*N*,*N*,*N*′,*N*′-tetra(methylphosphonic acid) (EDTP) and 2-phosphonobutane-1,2,4-tricarboxylic acid (PBTC) as well as their metal complexes. The mechanism of their protective action is rather complex. It is possible to distinguish (maybe, somewhat arbitrarily), as has been done elsewhere,[80] three types of systems 'metal–solution of a complex-forming reagent' with the following features:

(1) ligands are hydrophilic, and their complexes are highly soluble in the corrosive medium;

(2) ligands are rather hydrophobic, while their complexes are either poorly soluble or insoluble;

(3) metal corrosion is controlled by interaction with complexes (soluble in the medium) of the same or some other metal.

In the former case, complexones often accelerate corrosion; if it occurs at potentials of the active metal dissolution range, carboxyl-containing complexones are most dangerous, whereas phosphonic acids are most dangerous for oxidised metal as they can cause the formation of small pits.[14,81] If the value of E_{cor} is outside the potential range where metal ionisation with formation of a soluble complex is thermodynamically possible, adsorption of a suitable ligand can block the corroding surface (at least partially), change the ψ_1 potential of the electrode, *etc.* Furthermore, many phosphonic complexones form barely soluble polynuclear complexes at high metal/ligand activity ratios

$$m = [M^{n+}]:L$$

Since *m* should be high in the near-electrode layer at low complexone concentrations and active metal dissolution, it is such complexonates that can be formed on the surface. This results in corrosion inhibition, though the inhibition is unlikely to be highly efficient because mononuclear highly soluble complexes, in particular those with iron, are formed as *m* decreases.[82] In fact, the i_p of iron in a borate buffer (pH 7.36) initially decreases and then increases with an increase in the concentrations of many complexones.[14] It was noted [83] that HEDP, NTP and similar complexones show no passivating properties for steel even in oxygen-saturated neutral solutions.

However, more hydrophobic phosphorus-containing complexones do not cause pitting on iron, *i.e.*, they can be attributed to the second type of the systems in question. For example, pits on iron were not formed up to oxygen evolution potentials in a borate buffer containing 10^{-3}–10^{-6} mol litre^{-1} hexamethylenediamine-*N*,*N*,*N*′,*N*′-tetra(methylphosphonic acid) (HMDTP).[81] In comparison with HNP and EDTP, the HMDTP complexone is less hydrophilic and more surface-active; it can even hinder iron depassivation by chlorides: at equimolar NaCl : HMDTP ratio and their concentrations equal to 0.01 mol litre^{-1}, the E_{pit} increases by 0.08 V. This effect is comparable to the action of the

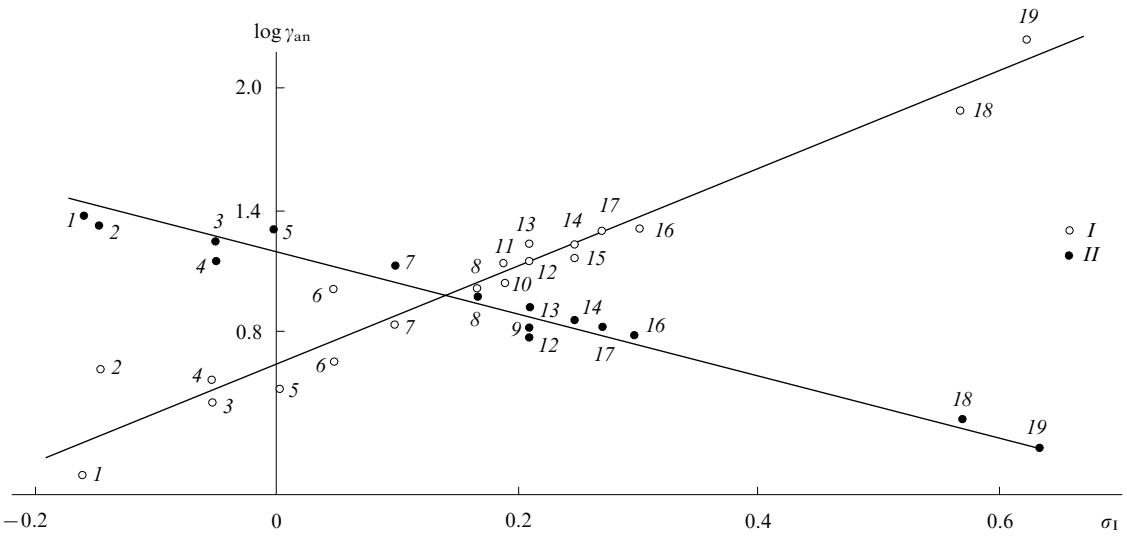

Figure 4. Effect of the inhibition coefficient of anodic dissolution of copper (*I*) and zinc (*II*) in 0.5 M phosphate solution at pH 11.4 on the induction constants of substituents in benzoimidazole.[71]
(*I*) $c_{in} = 5 \times 10^{-4}$ mol litre^{-1}, $E = -0.14$ V; (*II*) $c_{in} = 5 \times 10^{-3}$ mol litre^{-1}, $E = 1.0$ V.
Substituent: (*1*) OH, (*2*) COO^-, (*3*) C_2H_5, (*4*) CH_3, (*5*) H, (*6*) CH_2SCH_3, (*7*) NH_2, (*8*) NHC_2H_5, (*9*) $CH_2SO_2C_4H_9$, (*10*) $NHCH_3$, (*11*) SCH_3, (*12*) $SCH=CH_2$, (*13*) $CH_2SO_2C_6H_5$, (*14*) SH, (*15*) SC_6H_5, (*16*) OCH_3, (*17*) OC_3H_5, (*18*) CN, (*19*) NO_2.

caproate anion, but it is lower than that in the case of higher alkanecarboxylates [14] or dialkyl phosphates.[59]

In acid solutions (0.5 M H_2SO_4), nitrilotri(methylphosphonic acid) does not act as a corrosion inhibitor with respect to iron, (2-hydroxyethyl)iminodi(methylphosphonic acid) shows weak protective properties, whereas the more hydrophobic diethylenetriamine-*N*,*N*,*N*′,*N*″-penta(methylphosphonic acid) (DTPP) and (2-hydroxyethyl)iminodi(methylphosphonic acid) are rather good inhibitors.[84] It is of note that the addition of small amounts of iodide anions, as well as of ethylenediamine or diethylenetriamine, enhances the protective properties of aminophosphonic acids. These complexones probably behave as cation-active adsorption-type inhibitors in acidic media.

It was shown [85] that DTP and EDTP taken at optimum concentrations passivate steel in weakly alkaline carbonate solutions (pH 9.8) but do not hinder its pitting in the presence of chloride ions.

Complexones become rather good corrosion inhibitors of steel in hard water due to the presence of Ca^{2+} and Mg^{2+} ions. Probably, these cations partially neutralise the negative charge of complexones and thus decrease the adsorbate hydrophilicity and increase adsorption.[14,41] It is likely that these systems correspond to the third type of system, metal–solution of a complex-forming reagent, though calcium complexonates are usually characterised by the lowest stability constants among similar complexes of divalent metals. It was found [86,87] that even small Ca^{2+} concentrations strongly affect the efficiency of steel protection with HEDP or hydroxyphosphonoacetic acid (HPA), but not with PBTC. In fact, the efficiency increases from 64% to 88% as the Ca^{2+} : HPA concentration ratio increases from 0 to 1.0 due to stronger inhibition, first of the cathodic reaction and then of the anodic reaction as well. It was shown [88] that in stirred aqueous solution with low concentrations of corrosive anions (8.2 and 14 mg litre^{-1} Cl^- and SO_4^{2-}, respectively) but with a comparatively high content (130.2 mg litre^{-1}) of calcium ions, HEDP displays protective properties for low-carbon steel at as low a concentration as 1 mg litre^{-1}. The protection efficiency increases up to the concentration of 50 mg litre^{-1}; however, HEDP accelerates corrosion at concentrations $\geqslant$ 100 mg litre^{-1}. This fact was explained by decomposition of the protective oxide film. The best protection of steel in 0.5 M $NaClO_4$ solution (pH 7) is achieved with the molar ratio Ca : HEDP = 0.5. Using an atomic force microscope, the formation of a relatively uniform protective film was observed on the surface under these conditions.[89]

Neagle [86] analysed steel surfaces after exposure to hard water in the presence of HPA as the inhibitor. It was concluded that Ca^{2+} facilitates HPA transport and adsorption and is incorporated in the thin (20–40 nm) protective film that almost does not weaken heat transfer. In an alkaline solution [$Ca(OH)_2$, pH 12.5] simulating the concrete pore-filling liquid, the presence of calcium facilitates steel protection by NTP.[90] Studies of a steel surface by FT-IR spectroscopy and XPS revealed the formation of an NTP film with polymeric structure, in which Ca^{2+} is bound with three phosphonic groups.

Important information about the mechanism of steel protection by complexonates can be obtained by studying the dependence of the inhibitor concentration, which provides the maximum degree of protection, on the stability constant (K_s). It was shown [14,91] that in water containing no hardness salts (*i.e.*, in soft water), Ca^{2+} and especially Mg^{2+} phosphonate complexes are often more efficient corrosion inhibitors than the corresponding acids themselves. For example, complexes of NTP with magnesium or calcium can prevent completely the corrosion of steel in soft water. Complexes of HEDP, 1-carboxy-1-hydroxypropane-3-aminodi(methylphosphonic acid) (CHADP) or EDTP with these metals are more efficient than the acids themselves.[92,93] However, HMDTP and PBTC are more efficient than their complexes with Ca^{2+}, and complexes of HMDTP with Ca^{2+} and Mg^{2+} maintain the ability to suppress the corrosion of steel in water completely. In contrast, although imino-*N*-acetic-*N*,*N*-di(methylphosphonic acid) is more efficient than its magnesium complex, its protective efficiency is lower than that of its calcium complex.[81]

In order to explain the entire data on the efficiency of complexonates, one should take into account that the stability constants of magnesium and calcium phosphonates are usually lower than those of the corresponding iron complexonates, hence electrophilic substitution of the complex-forming agent is thermodynamically favourable.[91] It results in the precipitation of barely soluble hydroxides

$$MH_kL^{2-a} + Fe^{2+} = FeH_kL^{2-a} + M^{2+} \xrightarrow{2OH^-} M(OH)_2, \qquad (15)$$

which, along with the inhibitor adsorption, facilitates steel protection. However, if the stability constant is low, the complexonate is dissociated to a considerable extent and its actual concentration in solution is lower. It is no wonder that the left branch of the $\log c - \log K_s$ dependence (Fig. 5) is ascending, which indicates that the inhibitor efficiency increases with an increase in the complexonate stability to a certain threshold. If it is exceeded, the inhibitor efficiency decreases, probably due to the kinetic hindrance of electrophilic substitution of complex-forming cations by iron.

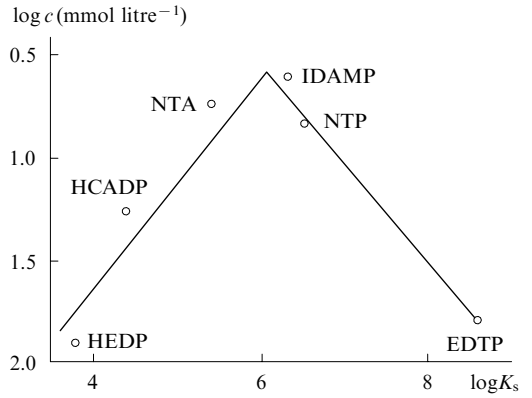

Figure 5. Dependence of the concentration of calcium complexonates providing the maximum protection of steel in water containing 30 mg litre^{-1} NaCl + 70 mg litre^{-1} Na_2SO_4 on their stability constants.[81]
IDAMP is imino-*N*,*N*-diacetic-*N*-methylphosphonic acid.

The presence of hardness salts in water can decrease the inhibiting effect of complexones, therefore zinc phosphonates are often used as inhibitors. The effect of mutual enhancement of the protective action of zinc salts and phosphonic acids has been known for a long time,[14,41] but studies of this effect are still under way for different complexones and metals to be protected.

The zinc–HEDP complex can passivate steel not only in pure water but also in a borate buffer (pH 7.4) containing 0.03 mol litre^{-1} Na_2SO_4.[14] According to XPS data, washing of a steel surface with water after its exposure for 16 h to a solution of this complex (200 mg litre^{-1}, pH 7.6) did not completely remove the inhibitor from the film. The film was rather thin, as the X-ray photoelectron spectrum recorded before ion etching of the sample clearly displayed a signal of metallic iron. The film contained phosphorus in the outer layer only, whereas zinc, which has been in excess with respect to its content in the inhibitor, was still detected during layer-by-layer argon etching of the sample. Probably, the complex is decomposed, at least partially, during the initial stages of film formation, *e.g.*, due to displacement of Zn^{2+} by iron ions. The zinc ions that are released react with hydroxyl ions generated in the cathodic reaction to give barely soluble $Zn(OH)_2$, which shields the surface and slows down corrosion. As the corrosion rate decreases, the deposition of $Zn(OH)_2$ slows down, and

predominant adsorption of the inhibiting complex on the surface starts.

It was found [89] that zinc salts synergistically enhance steel protection by an inhibitor such as HEDP in 0.5 M $NaClO_4$ solution; the strongest effect was observed with the molar ratio Zn : HEDP = 3. It was shown that $Zn(OH)_2$ deposition is responsible to a considerable extent for the higher effect of zinc on the protective properties of HEDP in comparison with calcium. This fact agrees with results of earlier studies.[14,91] The ability of HEDP – Zn^{2+} mixtures to hinder the anodic dissolution of steel was also confirmed for aqueous solutions containing up to 0.01% Cl^- (see Ref. 94). For static conditions, it is recommended to use a binuclear complex with Zn : HEDP = 2, since HEDP anions themselves are corrosive with respect to steel. On the other hand, an excess of zinc ions favours hindering of the cathodic reaction of oxygen reduction.

In sea water, HEDP itself has poor protective properties, whereas its complex with zinc protects steel more efficiently, especially at high flow rates ($V = 3$ m s^{-1}).[95] In this case, high degrees of protection ($\geqslant 95\%$) are reached at a complex concentration equal to 0.1 mmol litre^{-1} (this value is by an order lower than that at $V = 1$ m s^{-1}).

The synergistic effect of components in mixtures of zinc salts with NTP used for steel protection was observed by different researchers.[91,96] The inhibitor forms a thin compact film on the metal surface, which comprises both $Zn(OH)_2$ and NTP – zinc complexes. It was shown [97] that the NTP – zinc complex prevents pit corrosion of Kh18N9T steel in chloride-containing water, though it does not suppress it completely.

Enhancement of the protection of low-carbon steel due to synergism was also found for mixtures or complexes of zinc with EDTP,[92] CHADP,[93] PBTC,[98] *N*,*N*-di(phosphonomethyl)glycine,[99] ethyl- and chloroethylphosphonic,[100] phenylphosphonic,[101] 2-dimethylamino-2-hydroxypropylenediphosphonic and benzyliminodi(methylphosphonic) acids.[14] A similar effect was observed [101] for protection of brass [14,102] and aluminium alloys.[103]

Thus, the mechanism of metal protection by complexonates involves not only adsorption but also surface reactions of electrophilic substitution of complex-forming cations, deposition of barely soluble hydroxides and formation of hetero- and polynuclear complexes. No wonder that the dependences of their efficiency on chemical composition are rather complex in many cases. For example, the concentration of a complexonate-type inhibitor required to manifest protective properties depends on its stability constant: if the nature of the complex-forming cation is the same, *e.g.*, for zinc complexes (Fig. 6 *a*), this value increases with an increase in the stability constant, since the possibility of the formation of zinc hydroxide decreases. If the complex-forming cation is varied while the complexone remains the same, the dependence of the inhibitor efficiency on the solubility product of the hydroxide formed upon electrophilic substitution passes through a maximum (Fig. 6 *b*).[3] The protective properties of phosphonates of divalent metals are enhanced with a decrease in the solubility of their hydroxides and an increase in the stability of their complexonates, until their stability constants exceed those of iron(II) phosphonates. The mechanism of protection by more stable complexonates also involves the electrophilic substitution of a divalent metal ion, but probably due to the formation of more stable iron(III) complexonates.

The protection mechanism considered above, which we proposed and described in detail previously,[14,91] is also valid for complexonates of metals other than divalent ones. Cations of rare-earth metals (REM), which are recommended as metal corrosion inhibitors more and more often due to environmental problems,[104–107] are worthy of attention. The mechanism of steel protection by REM phosphonates was first studied for NTP derivatives.[108] Electrophilic substitution of REM by Fe^{2+} cations is thermodynamically unfavorable due to the high stability of the phosphonates [their stability constants are 4 – 8 orders larger than

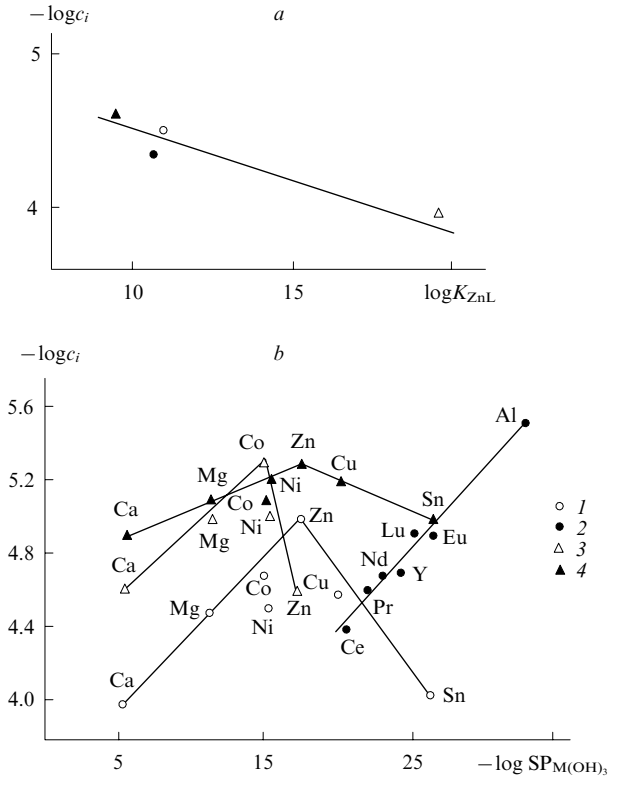

Figure 6. Effect of the stability constants of zinc complexes with phosphonic acids (*a*) and of the solubility products of hydroxides of complex-forming metals in phosphonate corrosion inhibitors (*b*) on their protective concentrations for St.3 in water containing 30 mg litre^{-1} NaCl and 70 mg litre^{-1} Na_2SO_4. The speed of solution movement relative to steel cylinders is 0.8 m s^{-1}.
Phosphonic acids: (*1*) HEDP, (*2*) NTP, (*3*) EDTP, (*4*) CHADP.

that of the similar iron(II) complex]. However, in neutral solutions, the Fe^{2+} ion is readily oxidised to Fe^{3+}; the latter forms a complexonate whose stability is comparable to that of the yttrium – NTP complex, which is the most stable of all REM – NTP complexes. Hence, in this case, electrophilic substitution can occur according to the following scheme:

$$MH_kL^{3-a} + Fe^{3+} = FeH_kL^{3-a} + M^{3+} \xrightarrow{2OH^-} M(OH)_3. \qquad (16)$$

Simultaneously, competing formation of $Fe(OH)_3$ occurs; the latter is characterised by weak protective properties. Thus, reaction (15), which, at least partially, prevents Fe^{2+} oxidation, does not occur, and the protective effects of REM complexonates are appreciably inferior to those of NTP complexes with divalent metals. Auger electron spectroscopic studies of the surface film on iron formed in water containing a cerium – NTP complex showed that the film was enriched with cerium. The Ce : Fe ratio was close to 1.0 throughout the film thickness and even somewhat higher in the inner layer. On the other hand, P : Ce $\leqslant$ 0.6 (this ratio equals 3.0 in the inhibitor); it is smaller in deeper layers, which are less accessible to washing water, than in the outer layers. This suggests that hydroxides play an important role; it is therefore not surprising that the efficiency of NTP complexes with trivalent metals increases with a decrease in the solubility product of $M(OH)_3$ (see Fig. 6 *b*).

It is of note that the protective film formed by the less stable aluminium(III) complexonate, which can undergo reaction (15), is more perfect and probably free of the adverse effect of $Fe(OH)_3$. Therefore, the NTP – aluminium complex is one of the most efficient inhibitors in soft water with low chloride content.

Metal complexonates are used in the reagent-based treatment of aqueous systems,[14, 109] in acid washing solutions, in cutting fluids, *etc*. Small additions of such complexonates facilitate the cathodic protection of steel in sea water [110] and improve the protective properties of magnetite coatings when added to oxidising nitrate solutions.[111] The nature of complex-forming cations is also important in magnetite coatings modified by complexonates. Complexonates which form barely soluble hydroxides are preferable; yet another condition should be met, *viz*., complexonates should not be too large, otherwise the structure of a magnetite coating can be violated and its defectiveness can increase.

The comparatively high cost of reagents and the tightening of environmental requirements for the content of phosphorus in water restrict the usage of phosphonate inhibitors in water consumption systems. To decrease the concentration of phosphonates, it was recommended to use them as mixtures with inexpensive additives, *e.g*., adsorption-type inhibitors (aliphatic amines,[112] phthalic anhydride,[113] and other compounds [14]), complex-forming reagents (tartrates,[114] gluconates [115]) or extracts from certain plants.[116]

The combined use of phosphonates and oxidants is justified by their mechanism of action. Since reduction of some oxidants can increase pH of the near-surface solution layer, metal phosphonates are destabilised: in effect, nucleophilic substitution of the ligand by hydroxyl groups occurs, which results in the deposition of $M(OH)_x$ hydroxides poorly soluble in water. Furthermore, it is known that the addition of nitrite enhances steel protection by complexones (HEDP [117] or PBTC [118]); at elevated temperatures, small amounts of sodium *m*-nitrobenzoate (SNB) act similarly. It was shown [119] that both oxidants can also enhance the inhibiting effect of the HEDP–zinc complex in hot water (80 °C). This is only possible at a certain ratio of the complexonate and oxidant concentrations, which depends on the nature of the oxidant. Although SNB is a stronger oxidant than $NaNO_2$, its inhibiting effect is weaker. Both oxidants play an auxiliary role, that is, they only provide better conditions for the protective layer formation by the phosphonate.

However, though numerous patents on mixed inhibitors based on complexonates have been issued, the scientific grounds for formulating such mixtures are still poorly explored. Aside from the methods for improving the efficiency of complexonate inhibitors considered above, yet another promising method should be noted, *viz*., their joint use with water-soluble polymers.

V. Polymeric inhibitors

It was known back in the 1930s that the addition of polyphosphates to water (a few milligrams per liter) inhibits not only scaling but also steel corrosion. However, while the anti-scaling effect of polyphosphates results from their adsorption and dispersing ability, their inhibiting properties are associated with the ability to form poorly soluble compounds with metal cations. Polyphosphates are most efficient in mixtures with Zn^{2+}, Ca^{2+} or Ni^{2+}; steel corrosion is mainly hindered due to inhibition of the cathodic reaction. The use of water-soluble polymers, along with polyphosphates, for the anti-scaling protection of aqueous systems started in the 1970s; these polymers containing COOH and OH groups (and mostly based on derivatives of acrylic and maleic acids) had high hydrolytic stability. Water treatment with mixtures of zinc phosphates or phosphonates with such polymers became popular 10–15 years later; a short time after that, the ability of polymers to inhibit metal corrosion was also discovered. In the early 1980s, the first 'phosphorus-free' (zinc-polymeric) water treatment programmes were developed in Japan due to restrictions on the content of phosphates (even non-toxic ones) in waste water. Suzuki and Kawamura [120] presented a brief review of these programmes and concluded that, despite certain achievements, 'phosphate-free' water treatment still cannot be widely used.

Studies on the mechanism of action of an acrylic acid–2-hydroxyethyl methacrylate–methyl methacrylate copolymer (MM = 3000) showed that adsorption of the polymer on a calcium phosphate film slows down the film growth, makes it less porous and thinner, and improves its protective properties. Presumably, in order to improve the efficiency of polymeric reagents that can eventually become leaders in scaling and corrosion prevention in cooling systems, it is necessary to study the dependence of their efficiency on the most important characteristics of polymers (molecular mass, number of functional groups, *etc*.). Analysis of the results of such studies has led to the conclusion [121] that polymers with molecular masses not exceeding 10 000–12 000 are most efficient for scaling inhibition. Unfortunately, these polymers have been little studied in application to metal corrosion inhibition, though numerous publications are available on the properties of new polymeric inhibitors.

Zinc salts are added in almost all cases to carboxylic [29] or sulfonate [122] polymers in order to confer on them corrosion-inhibiting properties with respect to steel in water, while phosphonate polymers do not require such addition. On the contrary, the efficiency of steel corrosion inhibition in water without stirring with polyvinylpyrrolidone (MM = 40 000) decreases in the presence of Zn^{2+} (see Ref. 123), suggesting that the activities of the polymers' functional groups differ considerably. Certain bipolar polypeptides, primarily polyasparaginates with MM = 1000–2000, are efficient inhibitors of carbon dioxide corrosion of steel [124] and scaling.[125] Reaction products of polysuccinic acid with aliphatic amines, particularly poly(succinimides) and poly(dodecyl-succinamides), proved to be rather efficient inhibitors of hydrogen sulfide-induced corrosion of steel. Owing to low toxicity, such polymers are likely to have considerable promise for application in oil-extracting and petrochemical industries.[126]

Apart from the nature of a polymer's functional groups and molecular mass, its protective properties can be affected by the presence of hydrophobic radicals. For example, in weakly alkaline solutions (pH 8–10), the efficiency of aluminium protection with a maleic acid–styrene–acrylic ester copolymer increases with an increase in the number of carbon atoms in the ester alkyl chain.[127]

Polymers containing acid groups are more commonly used as scaling inhibitors, whereas cation-active polymers are used to prevent the metal corrosion. It was shown, for example,[128] that the ultra-thin film (70 nm) obtained by layer-by-layer deposition of poly(diallyldimethylammonium chloride) or poly(*N*-octyl-4-vinylpyridinium iodide) and poly(styrenesulfonate) inhibits considerably the dissolution of 316L steel in 0.6–0.7 M NaCl solution and suppresses pitting on its surface, despite the high water content in the film and its high ionic permeability.

Even thinner conductive polyaniline films (which can be obtained not only by chemical techniques but also by anodic polarisation of a metal) show passivating properties toward stainless steels in acids. This was originally shown by De Berry [129] and then confirmed by many researchers. Protective polyaniline films were also obtained on aluminium,[130, 131] copper [132, 133] and titanium.[134] However, for a long time, similar protective films could not be obtained on low-carbon steel in aqueous solutions, partially due to the corrosion of the anode. To avoid corrosion, Yagova *et al*.[135, 136] applied films from a 0.4 M aniline solution containing arenecarboxylate inhibitors, *e.g*., 0.08 M solution of salicylic acid. As a result, they obtained a film that protected steel in 0.05 M H_2SO_4 and in humid atmosphere. Polyaniline films on iron were also obtained in the presence of phosphates and 3-aminobenzenesulfonic acid (ABSA).[137, 138] The protective properties of the film increased in both cases; however, whereas ABSA formed a copolymer with polyaniline, phosphates were just incorporated in the passivating layer of iron oxides but did not react with the polymer. However, some researchers do not acknowledge the protective properties of films based on polyaniline, polypyrrole, *etc*. on iron or steel, and discussions on this subject continue.[139, 140]

Polyhexamethyleneguanidinium (PHMG) $-[(CH_2)_6-NH-C(=NH^+)-NH]_n-$ is also a polymeric cation worthy of note, as well as its salts synthesised by Antonik *et al.*[141] and Tomin *et al.*[142] At $n = 10-100$, PHMG is a strong base and a biocide; its anticorrosion properties depend strongly on the counter-ion. PHMG phosphate mixed with small amounts of sodium nitrite and tetraborate provides good protection of steel in non-stirred aqueous solutions but is inefficient against scaling. The PHMG–HEDP salt shows both protective and technological properties required for its usage in cooling systems of oil refineries. Tomin *et al.*[142] also reported good protective properties of a polymer synthesised by the reaction of hexamethylenediamine with phosphoric acid and urea in the presence of glycerol.

Yet another group of this class of inhibitors includes hydrophilic monomers that can polymerise upon adsorption on a metal surface rather than polymers. This kind of polymerisation can decrease the solubility of the adsorption layer, increase the protective effect and make adsorption irreversible. Acetylene derivatives known since the 1940s as corrosion inhibitors of steel in acids are examples of such compounds. Brief reviews on the mechanism of action of these inhibitors, starting from the first experiments with iron powder, which showed that corrosion inhibition in HCl with acetylene results from the formation of a hydrophobic film of a hydrogenation and polymerisation product, are known.[2, 3, 143]

Aliphatic acetylenic alcohols in protonated form are relatively stable in acids and undergo various reactions only in the presence of an electrochemically active metal surface. There is no doubt at present that alkynols first undergo reduction and then dehydration and polymerisation, and that protective films formed by them consist of products of not only polymerisation but also other chemical transformations. It was shown [144, 145] that the susceptibility of alkynols to electrochemical reduction correlates with their ability to undergo polymerisation on iron in acids. According to Frignani *et al.*,[146] the inhibiting effects of alkynols can be enhanced by replacing the acetylenic hydrogen by a halogen. Small anodic polarisation of iron in a 1 M HCl solution facilitates the formation of a chemisorption layer, whereas cathodic polarisation accelerates the growth of a polymeric film.[147]

Aromatic acetylenic alcohols are reactive in acids.[148] They form products that are also efficient inhibitors and that undergo further reactions; as a result, steel is coated with a poly(phenyl ketone) protective film.

It was shown in a number of studies that preliminary application of certain monomers on a metal surface from aqueous solution can protect it in a corrosive medium owing to the formation of a polymeric structure. For example, immersion of aluminium samples for 15 min in 0.5% solution of methacryloyloxypropylmethoxysilane (at 80 °C) results in an alumosiloxane film stable even in 3.5% NaCl solution.[149]

The results of these studies give a reason to assume that the achievements of polymer chemistry, especially if they are used to search for ways of controlling the polymerisation of inhibitors in thin adsorption layers, will make it possible to create a new approach for efficient protection of metals by inhibitors. However, the currently known inhibitors of this type, *viz.*, acetylenic alcohols or alkenals, have a noticeable toxicity (the maximum permissible concentrations of propynol and acrolein are 1.0 and 0.7 mg m^{-3}, respectively); besides, they present fire and explosion hazards. In view of this, attention should be paid to the less toxic cinnamaldehyde, which is adsorbed on steel and protects it from acid corrosion by forming a polymeric film.[29] Probably, the efficiency of protection of monomers can be increased by using them together with polymerisation initiators, as was observed for methacrylonitrile and potassium persulfate used to protect steel in 1 M HCl solution.[150]

* * *

Intense studies on the mechanism of metal corrosion inhibition and its dependence on the composition and properties of inhibitors have continued in the past decade. Unfortunately, it is impossible to discuss all physicochemical aspects of corrosion inhibition within a single paper. Achievements of the quantum-chemical approach to the description of this complex process undoubtedly deserve a special discussion. The development of the theory of action of quite specific volatile inhibitors and the mechanisms of metal protection in organic solvents, paint and conversion coatings were also left outside the scope of this review. However, the author hopes that the presented material on the current state of corrosion inhibitor science, whose development has been one of the most important fields of research at the Institute of Physical Chemistry, will attract the attention of not only physicochemists already working in this field but also researchers in other fields of chemistry.

References

1. Standart ISO 8044-1989
2. I L Rozenfeld *Ingibitory Korrozii* (Corrosion Inhibitors) (Moscow: Khimiya, 1977)
3. Yu I Kuznetsov *Zashch. Met.* **38** 122 (2002) [a]
4. J H W De Wit, in *Corrosion Mechanisms in Theory and Practice* (Eds P Marcus, J Oudar) (New York: Marcel Dekker, 1995) p. 581
5. C J E Smith, S L Erricker, V M Evans, in *Proceedings of the 9th European Symposium on Corrosion Inhibitors* Vol. 1 (Ferrara: Ferrara University, 2000) p. 415
6. Yu N Mikhailovskii, G A Berdzenishvili *Zashch. Met.* **22** 699 (1986) [a]
7. K Kurosawa, T Fukushima *Corros. Sci.* **29** 1103 (1989)
8. M S Vukasovich, in *Reviews on Corrosion Inhibitor Science and Technology* (Eds A Raman, P Labine) (Houston: NACE, 1993) II-12-1
9. G S J Frankel *J. Electrochem. Soc.* **145** 2186 (1998)
10. W J Tobler, S Virtanen, in *Corrosion and Corrosion Protection* (Eds J D Sinclair, R P Frankenthal, E Kalman, W Plieth) (Pennington: The Electrochemical Society, 2001) p. 341
11. M T Pop *Geteropoli- i Izopolioksometallaty* (Heteropoly- and Izopolyoxometalates) (Novosibirsk: Nauka, 1990)
12. S V Oleinik, Yu I Kuznetsov, A R Vartapetyan *Zashch. Met.* **39** 16 (2003) [a]
13. M A Pletnev, S M Reshetnikov *Zashch. Met.* **38** 132 (2002) [a]
14. Yu I Kuznetsov *Organic Inhibitors of Corrosion of Metals* (New York: Plenum, 1996)
15. I L Rozenfeld, V P Persiantseva *Ingibitory Atmosfernoi Korrozii* (Inhibitors of Atmospheric Corrosion) (Moscow: Nauka, 1985)
16. G Trabanelli, in *Reviews on Corrosion Inhibitor Science and Technology* (Eds A Raman, P Labine) (Houston: NACE, 1993) I-2-1
17. G V Khaldeev *Ingibirovanie Rastvoreniya Metallov* (Inhibition of Metal Dissolution) (Moscow: Nauka, 1993)
18. B B Damaskin, E V Stenina *Elektrokhimiya* **22** 315 (1986) [b]
19. B N Afanas'ev, Yu P Akulova, N A Charykov *Zashch. Met.* **34** 303 (1998) [a]
20. L I Antropov, E M Makushin, V F Panasenko *Ingibitory Korrozii Metallov* (Inhibitors of Metal Corrosion) (Kiev: Tekhnika, 1981)
21. V P Grigoriev, V V Ekilik *Khimicheskaya Struktura i Zashchitnoe Deistvie Ingibitorov Korrozii* (Chemical Structure and Protective Action of Corrosion Inhibitors) (Rostov-on-Don: Rostov State University, 1978)
22. D L Kuznetsov, O Yu Podkopaeva, S M Shevchenko, in *Proceedings of the 9th European Symposium on Corrosion Inhibitors* Vol. 2 (Ferrara: Ferrara University, 2000) p. 1075
23. E Stupnisek-Lisak, D Kasunic, J Vorkapic-Furac *Corrosion (Houston)* **55** 617 (1995)
24. Yu I Kuznetsov, R K Vagapov *Zashch. Met.* **37** 238 (2001) [a]
25. V S Sastri, J R Perumareddi *Corrosion (Houston)* **57** 617 (1997)
26. Yu I Kuznetsov *Zashch. Met.* **30** 341 (1994) [a]
27. N I Podobaev, N V Chukhareva *Zashch. Met.* **36** 211 (2000) [a]

28. C Hansch, A Leo *Correlation Analysis in Chemistry and Biology* (New York: Willey, 1981)
29. W W Frenier, in *Proceedings of the 9th European Symposium on Corrosion Inhibitors* Vol. 1 (Ferrara: Ferrara University, 2000) p. 415
30. G Schmitt, B N Labus, H Sun, in *Proceedings of the 8th European Symposium on Corrosion Inhibitors* Vol. 2 (Ferrara: Ferrara University, 1995) p. 1113
31. Nie Shikai, Li Yufen, in *Proceedings of the 8th European Symposium on Corrosion Inhibitors* Vol. 1 (Ferrara: Ferrara University, 1995) p. 353
32. V V Ekilik, G N Ekilik *Zashch. Met.* **34** 162 (1998) [a]
33. V V Ekilik, G N Ekilik *Zashch. Met.* **33** 264 (1997) [a]
34. Yu I Kuznetsov, N P Andreeva *Zashch. Met.* **31** 289 (1995) [a]
35. V V Ekilik, A G Berejnaja, E N Balakshina, G N Ekilik, M N Svetaya, in *Proceedings of the 9th European Symposium on Corrosion Inhibitors* Vol. 1 (Ferrara: Ferrara University, 2000) p. 543
36. V P Grigoriev, S P Shpan'ko, A F Nassar *Zashch. Met.* **36** 371 (2000) [a]
37. V P Grigoriev, S P Shpanko, V M Kravchenko, I M Gershanova, A F Nassar, O V Dymnikova, in *Proceedings of the 9th European Symposium on Corrosion Inhibitors* Vol. 1 (Ferrara: Ferrara University, 2000) p. 149
38. V P Grigoriev, S P Shpan'ko, A F Nassar, V A Anisimova *Zashch. Met.* **39** 27 (2003) [a]
39. Yu I Kuznetsov, N N Andreev, N P Andreeva *Zashch. Met.* **34** 5 (1998) [a]
40. Yu I Kuznetsov, N P Andreeva, N P Sokolova, R A Bulgakova *Zashch. Met.* **39** 511 (2003) [a]
41. E A Kalman, in *Working Party Report on Corrosion Inhibitors* (London: The Institute of Materials, 1994) p. 12
42. I S Pogrebova, in *Proceedings of the 8th European Symposium on Corrosion Inhibitors* Vol. 2 (Ferrara: Ferrara University, 1995) p. 691
43. Yu I Kuznetsov, S V Oleinik, A V Khaustov *Zashch. Met.* **39** 352 (2003) [a]
44. Yu I Kuznetsov *Zashch. Met.* **31** 229 (1995) [a]
45. Yu I Kuznetsov *Zashch. Met.* **33** 117 (1997) [a]
46. Yu I Kuznetsov *Zashch. Met.* **35** 229 (1999) [a]
47. V A Pal'm *Osnovy Kolichestvennoi Teorii Organicheskikh Reaktsii* (Foundations of the Quantitative Theory of Organic Reactions) (Leningrad: Khimiya, 1977)
48. A D Garnovskii, A P Sadimenko, O A Osipov, G V Tsintsadze *Zhestko-Myagkie Vzaimodeistviya v Koordinatsionnoi Khimii* (Hard – Soft Interactions in Coordination Chemistry) (Rostov-on-Don: Rostov State University, 1986)
49. Sh Zhang, T Shibata, T Haruna *Corros. Sci.* **42** 1071(2000)
50. M Stratmann, W Furbeth, G Grundmeier, in *Corrosion Mechanisms in Theory and Practice* (Eds P Marcus, J Oudar) (New York: Marcel Dekker, 1995) p. 373
51. K Nozara, H Nishihara, K Aramaki *Corros. Sci.* **39** 1625 (1997)
52. G Grundmeier, C Reinarts, M Rohwerder *Electrochim. Acta* **43** 165 (1998)
53. M Itoh, H Nishihara, K Aramaki *J. Electrochem. Soc.* **141** 2018 (1994)
54. E Kalman *Electrochim. Acta* **46** 3607 (2001)
55. Z Quan, S Chen, X Cui *Corros. Sci.* **44** 703 (2002)
56. I Maege, E Jaehne, A Henke *Prog. Org. Coat.* **34** 1 (1998)
57. I Felhosi, Z Keresztes, E Kalman, in *Corrosion and Corrosion Protection* (Eds J D Sinclair, R P Frankenthal, E Kalman, W Plieth) (Pennington: The Electrochemical Society, 2001) p. 387
58. I Felhosi, E Kalman, P Pochik *Elektrokhimiya* **38** 265 (2002) [b]
59. Yu I Kuznetsov, N P Andreeva, G Yu Kazanskaya *Zashch. Met.* **36** 390 (2000) [a]
60. Yu I Kuznetsov, O A Luk'yanchikov *Elektrokhimiya* **23** 1225 (1987) [b]
61. I I Reformatskaya, Ya M Kolotyrkin, L I Freiman, in *Trudy Vsesoyuz. Konf. po Elektrokhimii, Chernovtsy, 1988* (Proceedings of All-Union Conference on Electrochemistry, Chernovtsy, 1988) p. 229
62. Yu I Kuznetsov, O A Luk'yanchikov *Zashch. Met.* **27** 64 (1991) [a]
63. V O Brusic, in *Reviews on Corrosion Inhibitor Science and Technology* Vol. 2 (Eds A Raman, P Labine) (Houston: NACE, 1996) XIII-1
64. E Stupinicek-Lisac, V Cinotti, D Reichenbach *J. Appl. Electrochem.* **29** 117 (1999)
65. R A Holliday, B Renda, S F Zullo, in *Proceedings of the 9th European Symposium on Corrosion Inhibitors* Vol. 2 (Ferrara: Ferrara University, 2000) p. 617
66. O V Volkova *Kholod. Tekh.* **8** 14 (2001)
67. H Baba, T Kodama *Corros. Sci.* **41** 1987 (1999)
68. Yu I Kuznetsov, L P Podgornova, D B Vershok *Zashch. Met.* **35** 22 (1999) [a]
69. S Manov, F Noli, A M Lamazouere, L Aries *J. Appl. Electrochem.* **29** 995 (1999)
70. C Lan-kun, Z Dong-shu, Z Hong-fan, Z Hao. *J. China Univ. Sci. Technol.* **28** 263 (2002)
71. Yu I Kuznetsov, L P Podgornova, in *Korroziya i Zashchita ot Korrozii (Itogi Nauki i Tekhniki)* [Corrosion and Corrosion Protection (Advanced in Science and Engineering Series)] (Moscow: Izd. VINITI, 1989) p. 132
72. O Hollander, in *Reviews on Corrosion Inhibitor Science and Technology* (Eds A Raman, P Labine) (Houston: NACE, 1993) II-13-1
73. C Fiaud, in *Proceedings of the 8th European Symposium on Corrosion Inhibitors* Vol. 2 (Ferrara: Ferrara University, 1995) p. 929
74. W Qafsaoui, C Blanc, N Pébère, in *Corrosion and Corrosion Protection* (Eds J D Sinclair, R P Frankenthal, E Kalman W Plieth) (Pennington: The Electrochemical Society, 2001) p. 467
75. M J Graham, in *Reviews on Corrosion Inhibitor Science and Technology* (Eds A Raman, P Labine) (Houston: NACE, 1993) I-8-1
76. M Hepel, E Cateforis *Electrochim. Acta* **46** 3801 (2001)
77. V D Castro, F Allegretti, C Baldachini *Surface Sci.* **507**–**510** 7 (2002)
78. C-T Wang, Sh-H Chen, H-Y Ma *J. Serb. Chem. Soc.* **67** 685 (2002)
79. V S Agarwala, in *Reviews on Corrosion Inhibitor Science and Technology* (Eds A Raman, P Labine) (Houston: NACE, 1993) I-5-1
80. Yu I Kuznetsov, in *Proceedings of the 7th European Symposium on Corrosion Inhibitors* Vol. 1 (Ferrara: Ferrara University, 1990) p. 1
81. Yu I Kuznetsov, G Yu Kazanskaya, N V Tsirul'nikova *Zashch. Met.* **39** 141 (2003) [a]
82. N M Dyatlova, V Ya Temkina, K I Popov *Kompleksony i Kompleksonaty Metallov* (Complexones and Metal Complexonates) (Moscow: Khimiya, 1988)
83. A Veres, G Reinhard, E Kalman *Br. Corros. J.* **27** 147 (1992)
84. T Khorvat, E Kal'man *Elektrokhimiya* **36** 1229 (2000) [b]
85. Kuang Yafei, Huang Shaoling *J. Hunan Univ. Natur. Sci.* **24** 44 (1997)
86. W Neagle, in *Surface and Interface Characterisation in Corrosion* (Ed. S Shah) (Houston: NACE, 1994) p. 239
87. T Galkin, V A Kotenev, M Arponen, in *Proceedings of the 8th European Symposium on Corrosion Inhibitors* Vol. 1 (Ferrara: Ferrara University, 1995) p. 475
88. L Hubert, C Garcia, N Kohler, in *Proceedings of the 9th European Symposium on Corrosion Inhibitors* Vol. 2 (Ferrara: Ferrara University, 2000) p. 835
89. I Felhosi, Z Keresztes, F H Karman *J. Electrochem. Soc.* **146** 961 (1999)
90. N Nakayama *Corros. Sci.* **42** 1897 (2000)
91. Yu I Kuznetsov, in *Progress in the Understanding and Prevention of Corrosion* Vol. 2 (Cambridge: Cambridge University Press, 1993) p. 845
92. Yu I Kuznetsov, G Yu Kazanskaya *Zashch. Met.* **33** 234 (1997) [a]
93. S G Ermolenko, Yu I Kuznetsov *Zashch. Met.* **31** 341 (1995) [a]
94. H S Awad, S Turgoose *Corrosion (Houston)* **58** 505 (2002)
95. Yu I Kuznetsov, Yu A Popkov *Zh. Prikl. Khim.* 1042 (1990) [c]
96. Y Gonzalez, M C Lafont, N Pebere *J. Appl. Electrochem.* **26** 1259 (1996)

97. S Kuczkowska, I Drela, P Falewicz, in *Proceedings of the 9th European Symposium on Corrosion Inhibitors* Vol. 2 (Ferrara: Ferrara University, 2000) p. 861
98. Ju I Kuznetsov, V A Isaev, G Ju Kazanskaja, in *Materialy V Ogolnopolskiego Sympozium Naukowo Technicznego, Poraj (Polska) 1998* p. 75
99. J Telegdi, M M Shaglouf, A Shaban *Electrochim. Acta* **46** 3791 (2001)
100. S Rajendran, B V Apparao, N Palaniswamy *Anti-Corros. Meth. Mater.* **47** 294 (2000)
101. S Rajendran, B V Apparao, N Palaniswamy, in *Proceedings of the 8th European Symposium on Corrosion Inhibitors* Vol. 1 (Ferrara: Ferrara University, 1995) p. 465
102. B B Bofardi, in *Reviews on Corrosion Inhibitor Science and Technology* (Eds A Raman, P Labine) (Houston: NACE, 1993) I I-6-1
103. Yu I Kuznetsov, T I Bardasheva *Zh. Prikl. Khim.* **66** 1100 (1993) [c]
104. B R W Hinton, in *Reviews on Corrosion Inhibitor Science and Technology* (Eds A Raman, P Labine) (Houston: NACE, 1993) I-11-1
105. F Mansfeld, Y Wang *Br. Corros. J.* **29** 194 (1994)
106. M Bethencourt, F J Botana, J J Calvino, M Marcos, M A Rodriquez-Chacon *Corros. Sci.* **40** 1803 (1998)
107. F Blin, S G Leary, K Wilson, in *EUROCORR-2003* (Budapest: EFC, 2003) Paper No. 336
108. Yu I Kuznetsov, A F Raskol'nikov, I V Starobinskaya, V N Alekseev *Zh. Prikl. Khim.* **66** 745 (1993) [c]
109. Yu V Balaban-Irmenin, V M Lipovskikh, A M Rubashov *Zashchita ot Vnutrennei Korrozii Truboprovodov Vodyanykh Teplovykh Setei* (Protection from Internal Corrosion of Water Heat Pipelines) (Moscow: Energoatomizdat, 1999)
110. Yu I Kuznetsov, in *Reviews on Corrosion Inhibitor Science and Technology* Vol. 2 (Eds A Raman, P Labine) (Houston: NACE, 1996) II-1
111. Yu I Kuznetsov, in *Proceedings of the 9th European Symposium on Corrosion Inhibitors* Vol. 1 (Ferrara: Ferrara University, 2000) p. 375
112. G Baril, F Moran, N Pébère In *Proceedings of the 9th European Symposium on Corrosion Inhibitors* Vol. 2 (Ferrara: Ferrara University, 2000) p. 849
113. J Kubicki, P Falevicz, S Kuczkowska, in *Proceedings of the 8th European Symposium on Corrosion Inhibitors* Vol. 1 (Ferrara: Ferrara University, 1995) p. 521
114. G Gunasekharan, B V Apparao, N Palaniswamy *Corrosion Sci.* **43** 1615 (2001)
115. G Gunasekharan, B V Apparao, N Palaniswamy, in *Proceedings of the 8th European Symposium on Corrosion Inhibitors* Vol. 1 (Ferrara: Ferrara University, 1995) p. 435
116. I H Faroogi, H Aqbal, M A Guraishi *Anti-Corros. Meth. Mater.* **46** 328 (1999)
117. Yu I Kuznetsov, V I Isaev *Zashch. Met.* **27** 753 (1992) [a]
118. A Marshal, B Greaves, in *Reviews on Corrosion Inhibitor Science and Technology* (Eds A Raman, P Labine) (Houston: NACE, 1993) II-9-1
119. Yu I Kuznetsov, G V Zinchenko *Korr.: Mater. Zashch.* **1** (3) 26 (2003)
120. T Suzuki, T Kawamura, in *Reviews on Corrosion Inhibitor Science and Technology* (Eds A Raman, P Labine) (Houston: NACE, 1993) II-10-1
121. J S Gill *Development of Scale Inhibitors. Corrosion/96* (Houston: NACE, 1996) Paper 229
122. S Patel, in *A Investigation of Sulfonated Polymers for Deposit and Corrosion Control. Corrosion/98* (Houston: NACE, 1998) Paper 225
123. A J Amalraj, M Sundaravadivelu, A P P Regis, in *Proceedings of the 9th European Symposium on Corrosion Inhibitors* Vol. 1 (Ferrara: Ferrara University, 2000) p. 407
124. A J McMahon, D Harrop, in *Green Corrosion Inhibitors: An Oil Company Perspective. Corrosion/95* (Houston: NACE, 1996) Paper 32
125. W Hater, B Mayer, M Schweinsberg, in *Proceedings of the 9th European Symposium on Corrosion Inhibitors* Vol. 1 (Ferrara: Ferrara University, 2000) p. 39
126. G Shmitt, A O Saleh, in *Evaluation of Environmentally Friendly Corrosion Inhibitors for Sour Service. Corrosion/95* (Houston: NACE, 2000) Paper 335
127. B Muller, M Shubert, C Oughourlian *in Proceedings of the 9th European Symposium on Corrosion Inhibitors* Vol. 1 (Ferrara: Ferrara University, 2000) p. 427
128. R F Terek, B J Schlenoff *Electrochem. Solid-State Lett.* **5** B13 (2002)
129. D W De Berry *J. Electrochem. Soc.* **132** 1022 (1985)
130. R Racicot, R Brown, S C Yang *Synth. Met.* **85** 1263 (1997)
131. D Huerta, S R de Moraes, A J Motheo, in *Corrosion and Corrosion Protection* (Eds J D Sinclair, R P Frankenthal, E Kalman W Plieth) (Pennington: The Electrochemical Society, 2001) p. 611
132. V Brusic, M Angelopoulos, T Graham *J. Electrochem. Soc.* **144** 436 (1997)
133. N Tabakowa, N Petkowa, J Stejskal *J. Appl. Electrochem.* **28** 1083 (1998)
134. L D Arsov Jr *J. Solid-State Electrochem.* **2** 266 (1998)
135. I V Yagova, S S Ivanov, V V Yagov *Zashch. Met.* **34** 59 (1998) [a]
136. I V Yagova, S S Ivanov, I V Bykov *Zashch. Met.* **34** 157 (1998) [a]
137. M C Bernard, A Hugot-Le Goff, S Joiret *J. Electrochem. Soc.* **148** B299 (2001)
138. M C Bernard, A Hugot-Le Goff, S Joiret, in *Substituted Polyanilin for Iron Protection (International Corrosion Congress), Granada, (Spain) 2002* Paper 135
139. U Ramelt, P T Nguen, W Plieth *Electrochim. Acta* **48** 1257 (2003)
140. I Yu Sapurina *Korr.: Mater. Zashch.* **1** (5) 2 (2003)
141. L M Antonik, V A Lopyrev, N A Korchevin *Zh. Prikl. Khim.* **75** 266 (2002) [c]
142. V P Tomin, N A Korchevin, V Ya Badennikov *Problemy Ratsional'nogo Vodopol'zovaniya i Korrozionnoi Zashchity Teploobmennogo Oborudovaniya v Neftepererabatyvayushchei Promyshlennosti* (The Problems of Rational Water Use and Corrosion Protection of Heat-Exchange Equipment in Oil-Refining Industry) (Irkutsk: Irkutsk State Technology University, 1998)
143. W W Frenier, F B Growcock, in *Reviews on Corrosion Inhibitor Science and Technology* (Eds A Raman, P Labine) (Houston: NACE, 1993) II-10-1
144. N I Podobaev, Ya G Avdeev *Zashch. Met.* **37** 19 (2001) [a]
145. N I Podobaev, Ya G Avdeev *Zashch. Met.* **38** 51 (2002) [a]
146. A Frignani, C Monticelli, G Trabanelli, in *Proceedings of the 9th European Symposium on Corrosion Inhibitors* Vol. 2 (Ferrara: Ferrara University, 2000) p. 749
147. G Lendvay-Gyorik, G Meszaros, B Lengyel, in *Proceedings of the 9th European Symposium on Corrosion Inhibitors* Vol. 2 (Ferrara: Ferrara University, 2000) p. 725
148. F B Growcock, V R Lopp, R J Jasinski *J. Electrochem. Soc.* **135** 823 (1988)
149. A M Beccaria, L Chiaruttini *Corros. Sci.* **41** 885 (1999)
150. G Mengoli, M M Musiani, C Pagura, in *Proceedings of the 6th European Symposium on Corrosion Inhibitors* Vol. 1 (Ferrara: Ferrara University, 1985) p. 61

[a] — *Prot. Met. (Engl. Transl.)*
[b] — *Russ. J. Electrochem. (Engl. Transl.)*
[c] — *Russ. J. Appl. Chem. (Engl. Transl.)*

 © 2004 Russian Academy of Sciences and Turpion Ltd

DOI 10.1070/RC2004v073n01ABEH000852

Cation – cation interaction in crystalline actinide compounds

N N Krot, M S Grigoriev

Contents

I. Introduction 89
II. Crystal structures of Np(V) compounds with cation – cation bonds 90
III. Influence of the cation – cation interactions on the properties of Np(V) compounds 94
IV. Cation – cation interactions in compounds of other actinide ions 97
V. Comparison of cation – cation interactions in solutions and crystals of actinide compounds 98

Abstract. The published data on the structures and properties of crystalline actinide compounds having mutually coordinated AnO_2^+ or AnO_2^{2+} cations as structural elements are surveyed. This cation – cation interaction is an important structure-forming factor for many crystalline compounds of Np(V) and U(VI). It strongly affects their UV-Vis and IR spectra as well as other properties. Differences and similarities between the cation – cation interactions of actinide ions in solutions and crystals are discussed. The bibliography includes 114 references.

I. Introduction

The specific complexation of AnO_2^+ and AnO_2^{2+} ions with certain cations commonly referred to as cation – cation (CC) interaction has been observed for the first time [1] in a study of behaviour of Np(V) in solutions of uranyl perchlorate. Later, the CC interactions were also revealed in NpO_2^+ solutions containing such cations as Th(IV), Cr(III), Fe(III), Al(III), Ga(III), Sc(III), In(III), Bi(III), Pb(II), Hg(II), Hg(I) (see Ref. 2) and Rh(III).[3] As for sodium, magnesium and some lanthanide [*e.g.*, La(III), Ce(III) and Y(III)] cations, they are inactive with respect to NpO_2^+.[1,2] Apart from Np(V), CC interactions are characteristic of U(V),[4,5] Pu(V) [6] and Am(V) [7] ions.

Different aspects of the CC interaction in solutions of pentavalent actinides have been considered in numerous publications.[1–41] For its characterisation, traditional spectrophotometry in visible and nearest IR regions as well as other techniques, such as potentiometry,[1] IR,[28] Raman,[31,34,36] Mössbauer,[24] ESR,[26] NMR [33] spectroscopies, large-angle X-ray scattering (LAXS) [32,35] and laser-induced photoacoustic spectroscopy [41] have been used. Special attention has been paid to the elucidation of the nature of the CC interactions in solutions. The principal results of these studies are considered below (Section V).

The kinetics of formation [2,3,9,12,17] and stability [1,3,9,29,34,36,40,41] of CC complexes have been studied in numerous publications. In particular, it has been shown that the complexation rate is defined primarily by the nature of highly charged cations interacting with the AnO_2^+ ions. This process proceeds very fast (*viz.*, during mixing of the components) with cations that have labile coordination spheres. In contrast, such cations as Cr_{aq}^{3+} (see Refs 2, 9, 12 and 17) and Rh_{aq}^{3+} (see Ref. 3) behave differently. In those cases, the formation and dissociation of CC complexes proceed quite slowly which is typical of substitution of water molecules by other ligands in the inner coordination spheres of aforementioned hydrated ions. The kinetic stability of AnO_2^+ CC complexes with Cr(III) and Rh(III) ions makes possible the utilisation of strongly basic cation-exchange resins for their isolation and purification by means of consecutive sorption, washing and desorption avoiding a significant decomposition.[2,3,6,24]

The stability of actinide CC complexes is relatively low but it increases substantially with an increase in the ionic strength (μ) of solutions or with a change from aqueous to organic solutions.[14,39] Neptunoyl cation [NpO_2^+, also referred to as neptunyl (V)] forms most stable complexes with such 'active' cations as UO_2^{2+} (see Refs 40 and 41), Cr(III) [9] and Rh(III).[3] The respective stability constants at 25 °C and $\mu = 6-10$ lie in the range of 2 – 4 litre mol^{-1}. The stability of An(V) CC complexes with a specific 'active' cation decreases in the series $UO_2^+ > NpO_2^+ > PuO_2^+ > AmO_2^+$.[29,41] The activity of AnO_2^{2+} ions as coordinating centres in the CC interactions decreases in the same series:[29] $UO_2^{2+} > NpO_2^{2+} > PuO_2^{2+} > AmO_2^{2+}$. These regularities correlate well with decreases in the effective positive and negative charges localised on the actinide atom and oxygen atoms of the corresponding dioxocations, respectively.[37,42] Therefore, it may be soundly assumed [3] that the electrostatic forces play a crucial role in the CC interactions though an involvement of other factors, such as the energy difference between donor and acceptor orbitals of the dioxocations, cannot also be ruled out.[37]

As has been established by numerous studies, the CC interactions strongly affect the rates of various redox reactions [6,8,11,16–19,23,26] and the isotope exchange [12] involving the AnO_2^+ ions. Typically, the reactivity of AnO_2^+ ions is reduced in the presence of 'active' cations. For instance, a complex of PuO_2^+ with a hydrated Cr(III) cation reacts with Cr(VI), Np(VI) and Ce(IV) more slowly by several orders of magnitude than hydrated PuO_2^+ under identical conditions.[6]

The CC interaction or CC bond in solid compounds was revealed for the first time in the $Rh(H_2O)_5NpO_2F_4$ complex.[3] However, this compound has not been isolated in the individual form and its structure has remained obscure. The existence of CC bonds in the crystal structures of several Np(V) compounds was first established by X-ray diffraction in the mid 1980s.[43–46]

N N Krot, M S Grigoriev Institute of Physical Chemistry, Russian Academy of Sciences, Leninsky prosp. 31, 119991 Moscow, Russian Federation. Fax (7-095) 335 17 78. Tel. (7-095) 335 20 05.
E-mail: krot@ipc.rssi.ru (N N Krot). Tel. (7-095) 429 93 77.
E-mail: grigoriev@ipc.rssi.ru (M S Grigoriev)

Received 27 May 2003
Uspekhi Khimii **73** (1) 94 – 106 (2004); translated by Ya V Zubavichus

Subsequently CC bonds have been revealed in many (more than 20) actinide compounds, whose crystal structures have been determined. This made it possible to analyse some general features of the CC interactions in crystalline compounds of actinides and compare them with the known data for the corresponding solutions. This is the aim of the present review, which surveys the results of studies published prior to 2001 inclusive and, partly, in 2002. Some aspects of the CC interactions in An(V) compounds are discussed elsewhere.[47–49]

II. Crystal structures of Np(V) compounds with cation–cation bonds

To date, there are 23 compounds whose crystal structures involve CC bonds as confirmed by single-crystal X-ray diffraction studies (Table 1). It would be helpful to precede the discussion of the above compounds with a brief description of their structural features. More detailed information may be found elsewhere.[43–46,49–68]

The most striking structural peculiarity of double Np(V)-sodium mellitate $Na_4[(NpO_2)_2C_6(COO)_6]\cdot 8H_2O$ (**1**) is the presence of dimeric groups composed of two mutually coordinated NpO_2^+ ions (see Refs 43 and 44). Therein, both neptunoyl ions act as coordinating centres and ligands simultaneously (Fig. 1). Such a coordination type is not found in structures of other Np(V) compounds listed in Table 1. It is characterised by a relatively short distance between neighbouring Np atoms (*ca.* 3.48 Å). The neptunoyl ions within the dimers are additionally linked by two bridging bidentate carboxyls of different mellitate ions. Two other mellitate anions are bound to NpO_2^+ through adjacent monodentate carboxy groups.

The crystal structure of double Np(V)-ammonium pyromellitate $(NH_4)_3[(NpO_2)_5\{C_6H_2(COO)_4\}_2]\cdot 7H_2O$ (**2**) is quite complicated.[45] It includes five crystallographically nonequivalent NpO_2^+ ions forming the CC bonds (Fig. 2*a*). Two of them may be considered as bidentate ligands, which both act as coordination centres for an oxygen atom of an adjacent neptunoyl group. Therefore, they both form three CC bonds though they differ from each other in the origin of oxygen atoms in the equatorial planes and the Np–O bond lengths. Two other NpO_2^+ ions also form three CC bonds but they act as monodentate ligands and coordinate two adjacent neptunoyl groups. The fifth NpO_2^+ ion forms only two CC bonds. It acts as a monodentate ligand and a coordinating centre for one neighbouring neptunoyl ion.

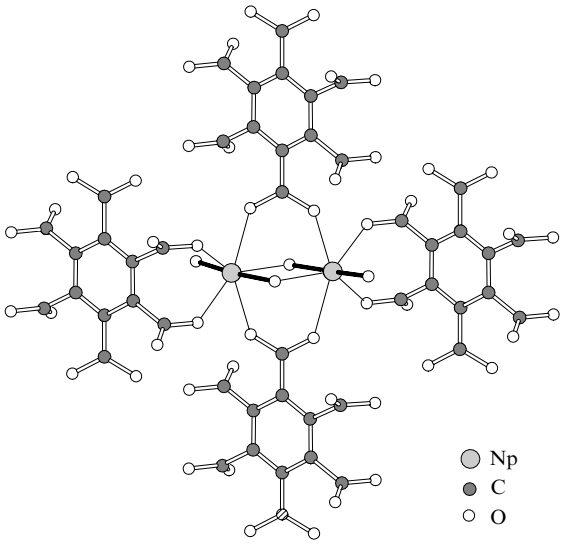

Figure 1. The CC interaction in the crystal structure of **1**.[44]

The crystal structure of $Cs_4[(NpO_2)_2Cl_4NpO_2Cl_2(NO_3)H_2O]$ (**3**) also contains nonequivalent NpO_2^+ ions, which however differ

Table 1. Np(V) compounds with known crystal structures containing CC bonds.

Compound	Coordination polyhedron [a]	Np–O bond length /Å [b,c]			Ref.
		l_1	l_2	l_3	
$Na_4[(NpO_2)_2C_6(COO)_6]\cdot 8H_2O$ (**1**)	PBP	1.91	1.85	2.48	43, 44
$(NH_4)_3[(NpO_2)_5\{C_6H_2(COO)_4\}_2]\cdot 7H_2O$ (**2**)	PBP	1.832–1.876	1.806–1.843	2.373–2.481	45
$Cs_4[(NpO_2)_2Cl_4NpO_2Cl_2(NO_3)(H_2O)]$ (**3**)	PBP	1.85	1.80	2.37	46
$[(NpO_2)_2SO_4(H_2O)_2]$ (**4**)	PBP	1.829–1.854		2.426–2.443	50
$[(NpO_2)_2SO_4(H_2O)]$ (**5**)	PBP, SBP	1.848–1.874		2.354–2.466	51
$[NpO_2Cl(H_2O)]$ (**6**)	PBP	1.83–1.85		2.36–2.50	52
$K_4(H_5O_2)[(NpO_2)_3(MoO_4)_4]\cdot 4H_2O$ (**7**)	PBP, TBP	1.900	1.844–1.846	2.393–2.394	53
$Na_2[(NpO_2)_2(MoO_4)_2H_2O]\cdot H_2O$ (**8**)	PBP	1.88	1.81–1.83	2.54	54
$[NpO_2ClO_4(H_2O)_4]$ (**9**)	PBP	1.860	1.810	2.396	55
$[(NpO_2)_2(NO_3)_2(H_2O)_4]\cdot H_2O$ (**10**)	PBP, HBP	1.837–1.846	1.812	2.419–2.481	56
$[La(H_2O)_6][(NpO_2)_3(NO_3)_6]\cdot 4H_2O$ (**11**)	HBP	1.852		2.417	57
$[NpO_2HCOO(H_2O)]$ (**12**)	PBP	1.846–1.850		2.388–2.434	58
$[NpO_2HCOO]$ (**13**)	PBP	1.857–1.915		2.363–2.434	58
$[NpO_2CH_2(OH)COO(H_2O)]$ (**14**)	PBP	1.828	1.801	2.442	59
$[NpO_2C_6H_5COO(H_2O)]\cdot 0.75H_2O$ (**15**)	PBP	1.82–1.87		2.40–2.50	60
$[(NpO_2)_2(CH_3COO)_2(H_2O)]\cdot CH_3CN$ (**16**)	PBP, SBP	1.811–1.874		2.334–2.473	61
$NH_4[NpO_2C_2O_4]\cdot 2.67H_2O$ (**17**)	PBP	1.886	1.824	2.364	62
$[(NpO_2)_2C_2O_4(H_2O)_4]\cdot 2H_2O$ (**18**)	PBP	1.858	1.830	2.392	63
$[(NpO_2)_2CH_2(COO)_2(H_2O)_3]\cdot H_2O$ (**19**)	PBP	1.840–1.842	1.828	2.436–2.477	64
$[(NpO_2)_2CH_2(COO)_2(H_2O)_2]\cdot H_2O$ (**20**)	PBP	1.840–1.870		2.420–2.502	65
$[(NpO_2)_2(DMSO)_7(H_2O)_2](ClO_4)_2\cdot H_2O$ (**21**)	PBP	1.86	1.82	2.49	66
$[(NpO_2)_2\{o\text{-}C_6H_4(COO)_2\}(H_2O)_3]\cdot H_2O$ (**22**)	PBP	1.841–1.852		2.373–2.437	67
$[NpO_2NO_3(CH_3CONH_2)_2]$ (**23**)	PBP	1.859	1.821	2.379	68

[a] Notations: PBP, SBP, HBP and TBP stand for pentagonal, special (see text, Fig. 3*b*), hexagonal and tetragonal bipyramids, respectively; [b] $O\overset{l_2}{=}Np\overset{l_1}{=}O\overset{l_3}{\cdots}Np$; [c] estimated standard deviations of Np–O bond lengths lie in the range of 0.003–0.01 Å except for **3**, for which it amounts to 0.03 Å.

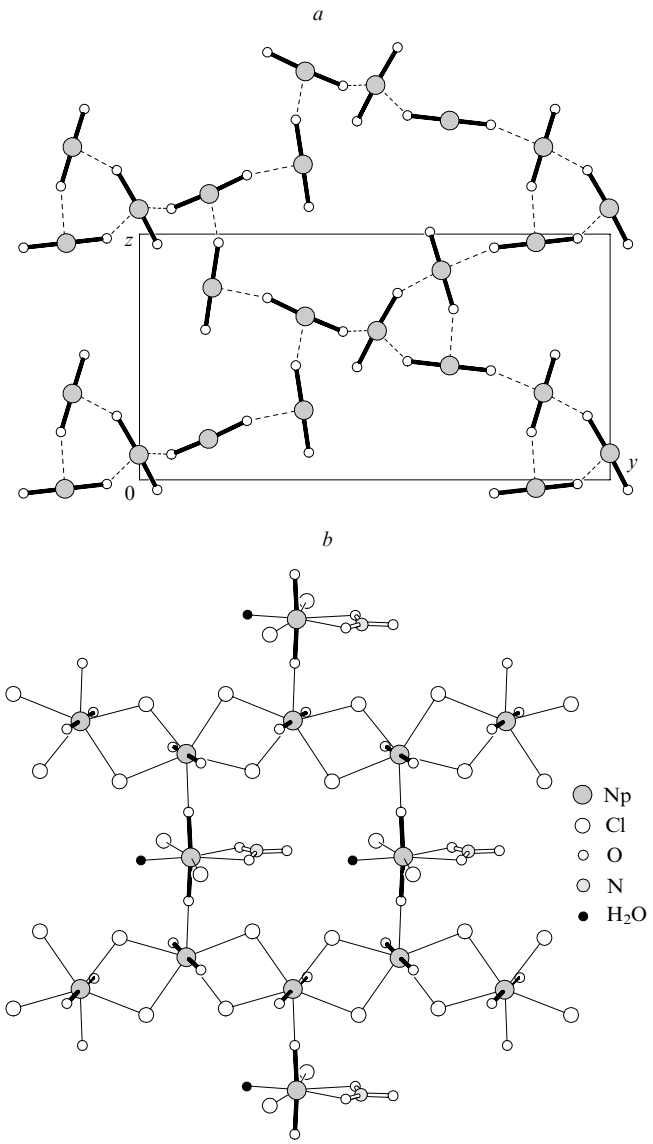

Figure 2. The CC interaction in the crystal structures of **2** (*a*)[45] and **3** (*b*).[46]

in the CC interactions from **2**.[46] One third of the NpO_2^+ ions is coordinated to adjacent Np atoms through both oxygen atoms and does not form other CC bonds (Fig. 2 *b*). In the equatorial plane, each ion of that type is coordinated by two Cl^- ions, two oxygen atoms of the NO_3^- ligand and a water molecule. The remaining neptunoyl groups form only single CC bonds acting as coordinating centres. Their equatorial coordination numbers are also equal to 5: an oxygen atom of an adjacent NpO_2^+ ion and four bridging Cl^- ions are located in their equatorial planes. The Np···Np interatomic distance corresponding to the CC interaction is 4.222 Å.

The pattern of CC bonds in $[(NpO_2)_2SO_4(H_2O)_2]$ (**4**)[50] is of particular interest since it is often found in the crystal structures of other Np(V) compounds. It may be represented as a distorted square net built up of two crystallographically nonequivalent NpO_2^+ ions (Fig. 3 *a*). All neptunoyl ions act as bidentate ligands and at the same time coordinate two adjacent neptunoyls. As a result, each Np atom is involved in four CC bonds. The square nets are linked through tetradentate bridging SO_4^{2-} anions, which are bound to four Np atoms. For both types of NpO_2 ion, the coordination polyhedra (CP) of the central atoms are pentagonal bipyramids though the Np – O bond lengths are slightly different. The equatorial planes of both coordination polyhedra include,

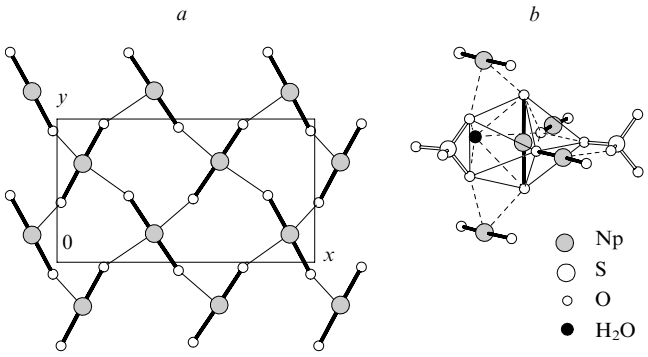

Figure 3. The CC interaction in the crystal structures of **4** (*a*)[50] and **5** (*b*).[51]

apart from oxygen atoms of the SO_4^{2-} anions and adjacent NpO_2^+ ions, one water molecule.

A similar type of CC interaction is also revealed in the crystal structures of $[NpO_2Cl(H_2O)]$ (**6**),[52] $[NpO_2HCOO(H_2O)]$ (**12**),[58] $[NpO_2C_6H_5COO(H_2O)]\cdot 0.75\,H_2O$ (**15**),[60] $[(NpO_2)_2CH_2.(COO)_2(H_2O)_2]\cdot H_2O$ (**20**)[65] and $[(NpO_2)_2\{o\text{-}C_6H_4(COO)_2\}.(H_2O)_3]\cdot H_2O$ (**22**).[67] Nevertheless, nets of cations in these compounds have some distinctions. For example, the crystal structure of **6** includes NpO_2^+ cations of two types differing from each other in numbers of bridging Cl^- ions (1 *vs.* 3) and H_2O molecules (2 *vs.* 0) in their coordination spheres. In contrast, all neptunoyl groups in the crystal structure of **12** are equivalent: in the equatorial plane, they contain two oxygen atoms of adjacent NpO_2^+ groups, two oxygen atoms of bridging carboxy groups and a water molecule. The net of cations in the crystal structure of **15** is formed by neptunoyl ions of four nonequivalent types though in all cases, the central atom CP is a pentagonal bipyramid. The equatorial planes of the coordination polyhedra revealed in **15** are similar to those in **12**. They differ only in the interatomic distances and the dispositions of oxygen atoms from various ligands. The crystal structures of **20** and **22** reveal two nonequivalent NpO_2^+ ions, which are characterised by the coordination number 5 and contain oxygen atoms of various origins in their equatorial planes. In compound **20**, the first type of neptunoyl ions bind two oxygen atoms of adjacent neptunoyls, one oxygen atom of a carboxy group and two water molecules. In the case of the second type of neptunoyl ions, the equatorial plane is built up of two oxygen atoms of adjacent NpO_2^+ ions and three oxygen atoms of two carboxy groups. In compound **22**, the CP of neptunoyl ions of the first type is analogous to that in **20**. Another type of NpO_2^+ ions in **22** coordinates one water molecule, two oxygen atoms of adjacent NpO_2^+ cations and two oxygen atoms of carboxy groups. The shortest Np···Np distances within the cation nets of **4**, **6**, **12**, **15**, **20** and **22** lie in the range of 3.776 – 4.238 Å.

The pattern of the CC bonds in the crystal structure of $[(NpO_2)_2SO_4(H_2O)]$ (**5**) is substantially more complex than in **4** though NpO_2^+ ions in both cases act as bidentate ligands and coordinate two adjacent neptunoyl ions.[51] In the crystal structure of **5**, the CC interactions give rise to a spatial net involving two types of CP. The first one is a pentagonal bipyramid and the second one is a special polyhedron type, which has not hitherto been observed (Fig. 3 *b*). It can be represented as a pentagonal bipyramid with one of the equatorial vertices occupied by two oxygen atoms, which are situated above and below the equatorial plane. The two oxygen atoms belong to one SO_4^{2-} anion. Other oxygen atoms in the equatorial plane come from two NpO_2^+ ions, H_2O and SO_4^{2-}. The equatorial plane of the normal pentagonal bipyramid is composed of three oxygen atoms of different bridging sulfates and two O atoms of the NpO_2^+ ions. The distances between neighbouring Np atoms involved in the CC interaction lie in the range of 3.923 – 4.253 Å. The layered structure of **16** reveals CC interactions and coordination polyhedra of a similar charac-

ter.[61] Nevertheless, the pattern of CC bonds therein differs from that in **5**. The pattern may be described as a distorted square net resembling the structure of **4**.

In the crystal structure of $K_4(H_5O_2)[(NpO_2)_3(MoO_4)_4]\cdot H_2O$ (**7**), neptunium atoms have two types of coordination polyhedra, *viz*., pentagonal and tetragonal bipyramids, in the ratio 2 : 1, respectively.[53] The former polyhedra are linked by molybdate ions to form layers. In those layers, NpO_2^+ ions act as monodentate ligands for neptunoyl ions of the latter type, which have four oxygen atoms in their equatorial planes and are located between the layers (Fig. 4 *a*). Therefore, NpO_2^+ ions of the latter type (with equatorial coordination number 4) form two CC bonds without involvement of their own oxygen atoms. The Np···Np distance responsible for the CC interaction is 4.130 Å.

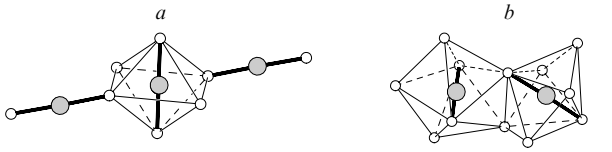

Figure 4. The CC interaction in the crystal structures of **7** (*a*)[53] and **8** (*b*).[54] Notations are the same as in Fig. 3.

The crystal structure of $Na_2[(NpO_2)_2(MoO_4)_2(H_2O)]\cdot H_2O$ (**8**)[54] includes two types of NpO_2^+ ions with coordination numbers 5. Ions of the two types are bound in pairs by virtue of the CC interaction and bridging ligands (Fig. 4 *b*). In the pairs, one of the NpO_2^+ ions acts as a monodentate ligand, while the second one acts only as a coordinating centre. The Np···Np distance within the dimers is 3.727 Å. Equatorial planes of both types of NpO_2^+ ions are occupied by oxygen atoms of bridging MoO_4^{2-} ions, which thus link the neptunoyl dimers into a three-dimensional framework. A similar type of CC interaction giving rise to formation of neptunoyl dimers was revealed in the crystal structure of $[(NpO_2)_2(DMSO)_7(H_2O)_2](ClO_4)_2\cdot H_2O$ (**21**) (see Ref. 66). In this compound, the dimers may be considered as complex cations occupying sites of an ionic crystal lattice. They are composed of two CP (pentagonal bipyramids) linked by an oxygen atom of one of the NpO_2^+ ions. For the latter NpO_2^+ ion, which acts as a ligand, the equatorial plane includes one water molecule and four DMSO molecules. The second neptunoyl ion of the dimer binds one water molecule, three DMSO molecules and one oxygen atom of the adjacent NpO_2^+ ion. The Np···Np distance within the dimer (4.252 Å) is noticeably longer than that in the structure of **8**. The reason for this difference relates to the different ways of assembling the Np coordination polyhedra in the CC interaction. In the crystal structure of **21**, the polyhedra have a shared vertex, which is apical for one of the CP and equatorial for another. In contrast, in the crystal structure of **8**, the Np atoms involved in the CC interaction are linked through one of the oxygen atoms of a molybdate ion so the polyhedra have a shared edge. In one of the polyhedra, this edge connects an apical and an equatorial vertex, while in the other one, it connects two equatorial vertices.

The crystal structure of $[NpO_2ClO_4(H_2O)_4]$ (**9**) (see Ref. 55) reveals particular zigzag chains formed by NpO_2^+ ions owing to the CC interaction (Fig. 5 *a*). Each neptunoyl group in the chains is involved in two CC bonds acting as a monodentate ligand and a coordinating centre simultaneously. The equatorial planes of the CP of Np atoms consist of an oxygen atom of an adjacent NpO_2^+ ion and four water molecules. Similar zigzag chains are also present in the crystal structures of $[NpO_2CH_2(OH)COO(H_2O)]$ (**14**) (see Ref. 59), $[(NpO_2)_2C_2O_4(H_2O)_4]\cdot 2H_2O$ (**18**) (see Ref. 63), and $[NpO_2NO_3(CH_3CONH_2)_2]$ (**23**) (see Ref. 68). In the crystal structure of **14**, the equatorial plane of NpO_2^+ ions consists of a water molecule, an oxygen atom of an adjacent NpO_2^+ ion, two oxygen atoms of a carboxy group and a hydroxy group. Meanwhile, in the crystal structure of **18**, the equatorial plane includes two H_2O molecules, two O atoms of a tetradentate bridging oxalate group and an oxygen atom of an adjacent neptunoyl. In the crystal structure of **23**, the equatorial plane is formed by an oxygen atom of an adjacent neptunoyl, two oxygen atoms of an NO_3^- ion and two oxygen atoms of two acetamide molecules. The shortest Np···Np interatomic distances within the neptunoyl chains revealed in the crystal structures of **9**, **14**, **18** and **23** lie in the range of 4.075 – 4.207 Å.

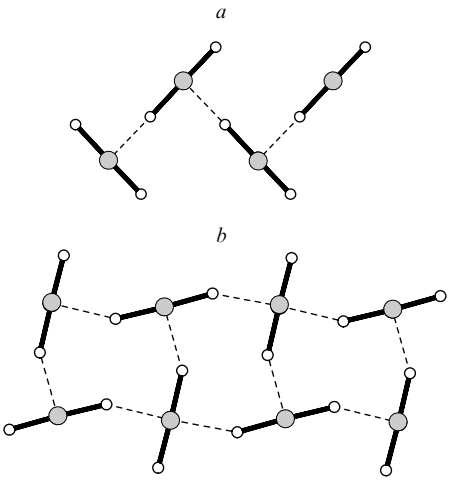

Figure 5. The CC interaction in the crystal structures of **9** (*a*)[55] and **10** (*b*).[56] Notations are the same as in Fig. 3.

In the crystal structure of $[(NpO_2)_2(NO_3)_2(H_2O)_4]\cdot H_2O$ (**10**) (see Ref. 56), the system of CC bonds may be described as ribbons formed by NpO_2^+ cations with two types of coordination polyhedra, *viz*., pentagonal and hexagonal bipyramids (Fig. 5 *b*). Neptunoyl cations of the former type act as bidentate ligands and coordinate four water molecules and one NpO_2^+ cation of the latter type. Neptunoyl cations of the latter type are involved in three CC bonds acting as monodentate ligands. Their equatorial planes contain two oxygen atoms of adjacent NpO_2^+ cations and four oxygen atoms of two NO_3^- ions. The Np···Np interatomic distances lie in the range of 4.130 – 4.200 Å.

The crystal structure of $[La(H_2O)_6][(NpO_2)_3(NO_3)_6]\cdot 4H_2O$ (**11**) (see Ref. 57) is characterised by the presence of a highly symmetrical net of mutually coordinated NpO_2^+ cations acting as bidentate ligands (Fig. 6 *a*). Equatorial planes of the neptunoyl ions contain four O atoms of two bidentate NO_3^- ligands and two oxygen atoms of adjacent NpO_2^+ cations, which occupy *trans*-positions with respect to each other. The shortest Np···Np distances are 4.058 Å and 4.159 Å.

In the crystal structure of $[NpO_2HCOO]$ (**13**) (see Ref. 58), each NpO_2^+ is involved in four CC bonds, similarly to many other Np(V) compounds. Nevertheless, the pattern of CC bonds in **13** is peculiar. Indeed, it combines neptunoyl ions to form a diamond-like framework (Fig. 6 *b*). The coordination polyhedra of the Np atoms are pentagonal bipyramids containing two O atoms of adjacent NpO_2^+ ions and three carboxylic oxygen atoms of two bidentate chelate bridging $HCOO^-$ anions. The distances between neighbouring Np atoms within the framework of cations are 3.783 Å and 4.003 Å.

The crystal structure of $NH_4[NpO_2C_2O_4]\cdot 2.67H_2O$ (**17**) (see Ref. 62) reveals trimers of neptunoyl ions that are coordinated to each other as monodentate ligands (Fig. 7 *a*). As a consequence, each NpO_2^+ ion is involved in two CC bonds. The coordination polyhedra of the Np atoms are pentagonal bipyramids, whose equatorial planes contain one O atom of an adjacent NpO_2^+ ion and four carboxylic oxygen atoms of two tetradentate bridging oxalate ions. The Np···Np distance within such a cyclic trimer is 4.093 Å.

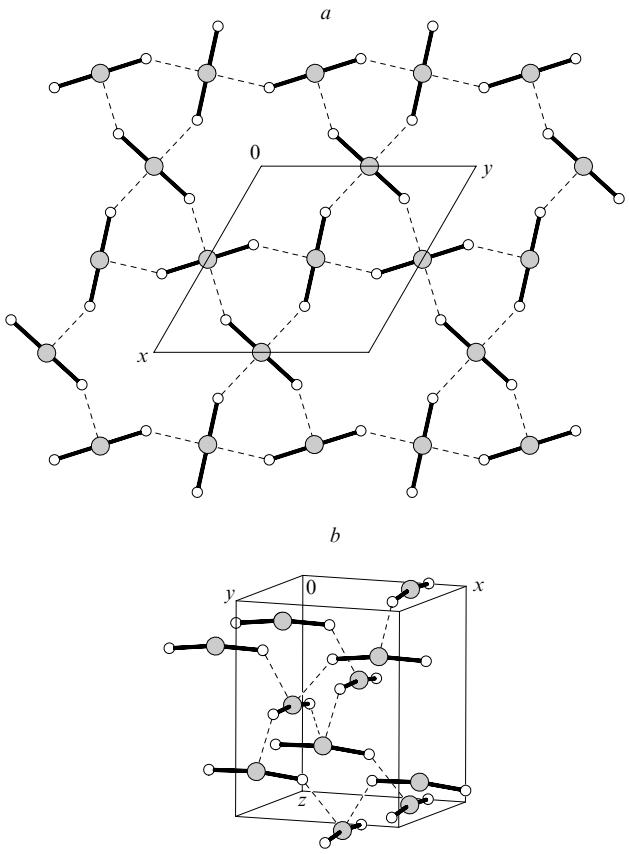

Figure 6. The CC interaction in the crystal structures of **11** (*a*)[57] and **13** (*b*).[58] Notations are the same as in Fig. 3.

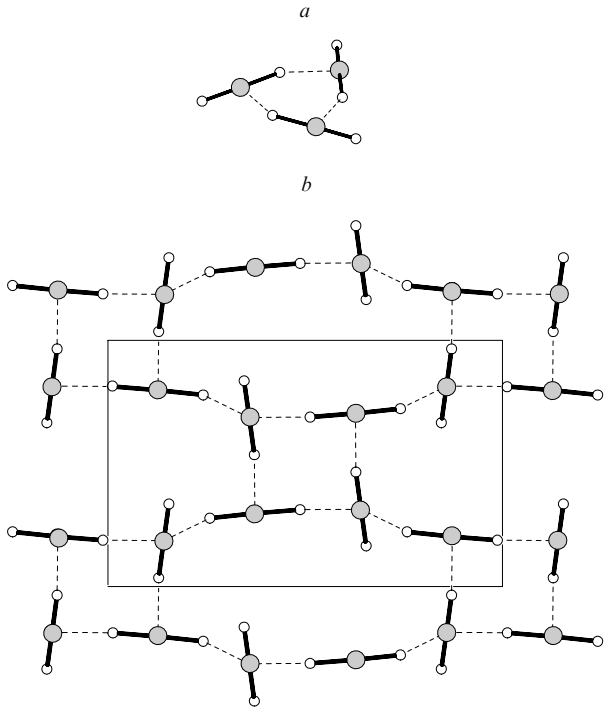

Figure 7. The CC interaction in the crystal structures of **17** (*a*)[62] and **19** (*b*).[64] Notations are the same as in Fig. 3.

Finally, in the crystal structure of $[(NpO_2)_2CH_2(COO)_2.(H_2O)_3]\cdot H_2O$ (**19**) (see Ref. 64), there is a planar net of cations composed of four- and eight-membered rings due to the CC interaction (Fig. 7 *b*). One half of the NpO_2^+ ions within the net acts as monodentate ligands coordinating at the same time two adjacent neptunoyl ions, a water molecule, and two oxygen atoms of two malonate ions. The remaining NpO_2^+ ions act as bidentate ligands and contain one O atom of NpO_2^+, two carboxylic O atoms of one $CH_2(COO)_2^{2-}$ anion and two water molecules in the equatorial planes of their CP. The shortest Np···Np distances within the net of cations lie in the range of 4.182 – 4.234 Å.

The data outlined above clearly demonstrate that the CC interaction is a widespread phenomenon in crystalline compounds of Np(V), which often governs their crystal structures. Below, we summarise some general regularities which characterise the CC interaction.

1. In the crystal structures of all Np(V) compounds studied, the CC bonds are always formed through the bridging oxygen atom, which belongs to one of the interacting neptunoyl groups. However, the identity of NpO_2^+ ions forming a CC bond is not lost since the corresponding Np – O bond lengths are significantly different ($l_1 \ll l_3$, for notations, see Note [b] to Table 1). This conclusion is supported by the fact that the geometry of the coordination environment of NpO_2^+ ions as regards their equatorial planes is only slightly modified by the formation of the CC bond.

2. The formation of the CC bond is accompanied by a significant change in the Np – O bond lengths within the NpO_2^+ ions. It is due to the electrostatic forces: the effective negative charge localised on the oxygen atom causes its attraction to the coordinating centre, which possesses a high positive charge. This positive charge, in turn, determines the repulsion of the Np atoms involved in the CC bond. As a result, the l_1 distance within the NpO_2^+ ion becomes noticeably longer than l_2. According to Table 1, the mean $l_1 - l_2$ difference is 0.04 Å. The fluctuation of this difference may be explained by effects of composition and structures of specific compounds on the distribution of the effective charges within NpO_2^+.

3. The bond length between the oxygen atom of the NpO_2^+ cation and the coordinating centre (denoted l_3 in Table 1) lies in the range of 2.33 – 2.54 Å. The respective mean value of 2.45 Å is close to typical bond lengths between an Np atom and O atoms of various ligands coordinated in the equatorial plane.

4. Neptunium atoms involved in a CC bond may have different coordination polyhedra though pentagonal bipyramids occur most frequently (see Table 1).

5. Neptunoyl ions may be involved in one or more (up to four) CC bonds. According to this criterion, they can be classified into eight types shown schematically in Fig. 8. Those types occur in Np(V) compounds in various combinations. For instance, the types *a* and *b* NpO_2^+ ions are present as dimers in the crystal structures of **8** and **21**. The type *c* mutual coordination of ions ensures the formation of dimers in **1**, cyclic trimers in **17** and

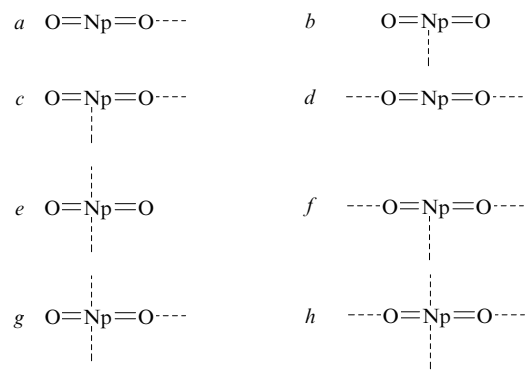

Figure 8. Types of NpO_2^+ ions depending on the number and character of the CC bonds formed.

zigzag chains in **9**, **14**, **18** and **23**. A mutual combination of the type *h* NpO_2^+ ions produces planar (**4**, **11**, **12**, **15**, **16**, **20** and **22**) or three-dimensional (**5** and **13**) cationic nets. The types *d* and *e* neptunoyl ions were found only in the crystal structures of **3** and **7**, respectively. Combinations of the types *f* and *g* NpO_2^+ ions were revealed in the crystal structures of **2** and **10**.

The formation of a specific pattern of CC bonds in the crystal structures of Np(V) compounds depends upon a number of factors, among which the following are of major importance:

— the nature of anionic or molecular ligands in the equatorial planes of NpO_2^+ ligands involved in the formation of the CC bonds;

— the number and the nature of outer-sphere cations in the case of double salts of Np(V);

— the number of water molecules in the crystal structure;

— preparation conditions.

The influence of the nature of ligands in the equatorial plane of NpO_2^+ ions on the CC pattern can be clearly illustrated with the crystal structures of Np(V)-sodium double mellitate [43, 44] and pyromellitate.[69] Despite the similar character of the ligand coordination in the two structures, CC bonds are present in the former compound and are absent in the latter. This can be due to different charges localised on the respective ions. A typical effect of the ligand nature on the CC interaction between neptunoyl ions is also observed in the crystal structures of **16** and **14**. Both compounds, *viz*., Np(V) acetate and glycolate, are characterised by similar compositions whereas planar nets composed of the *h* type of the NpO_2^+ ions as opposed to zigzag chains of the *c* type of the neptunoyl ions are revealed in the crystal structures of the former and the latter, respectively.

In double salts of Np(V), the CC interaction between NpO_2^+ cations is generally weaker than in monocationic derivatives. Probably, this is caused by the electrostatic interactions of NpO_2^+ ions with outer-sphere cations, which impedes a mutual coordination of neptunoyls. The effect of monovalent cations (M^+) on the CC interaction of the NpO_2^+ ions decreases in the series $Na^+ > NH_4^+ \approx K^+ > Cs^+$, in agreement with expectations. For instance, CC bonds are absent in the crystal structure of the $Na[NpO_2C_2O_4(H_2O)]\cdot 2H_2O$ double salt [70] although cyclic trimers of NpO_2^+ ions are revealed in the structure of a closely related compound $NH_4[NpO_2C_2O_4(H_2O)]\cdot 2.67H_2O$ (**17**).

The CC interaction in double salts of Np(V) strongly depends not only on the nature of the cations M^+ but on their number, *i.e*., on the $M^+ : NpO_2$ ratio as well. An increase in this ratio increases saturation of the coordination sphere of NpO_2^+ ions with anionic ligands, which evidently hampers the formation of the CC bonds. This effect can be illustrated with the crystal structure of $Cs_3[NpO_2(SO_4)_2]\cdot 2H_2O$ (see Ref. 71), which contains no CC bonds.

An increase in the number of water molecules in an Np(V) compound generally results in a substantial weakening of the CC interaction. For example, in the crystal structure of **20**, every NpO_2^+ ion is involved in four CC bonds whereas only two CC bonds are formed by neptunoyl ions in the crystal structure of **18**. This effect may be explained by the formation of H-bonds between oxygen atoms of NpO_2^+ ions and water molecules, which interfere with the CC interaction.

Synthetic conditions often have a definitive influence on the composition of Np(V) compounds and thus on the occurrence and the character of the CC bonds in their crystal structures. For instance, compounds **12** and **13** are crystallised from formate solutions under hydrothermal conditions at 120 °C and 160 °C, respectively. As has been mentioned above, these compounds have totally different patterns of the CC bonds.

Unfortunately, the regularities formulated above are only qualitative and do not allow an unambiguous prediction of patterns of the CC interaction in the crystal structures of novel Np(V) compounds. Meanwhile, they provide valuable assistance in suggesting occurrence and the type of the CC bonds in compounds of a known composition but unknown crystal structure.

III. Influence of the cation – cation interactions on the properties of Np(V) compounds

1. Crystallisation and dissolution

The cation – cation interactions in crystalline compounds of Np(V) have a strong influence on their properties. In particular, many compounds possessing CC bonds behave abnormally on dissolution and crystallisation. Probably, it is due to the involvement of the CC bonds in the formation of infinite fragments of the crystal structure. This conclusion can be illustrated with several examples. The solubility of Np(V) double oxalates with the common stoichiometry $MNpO_2C_2O_4\cdot nH_2O$, where M^+ is ammonium or alkali metal ion, decreases noticeably upon their storage for several days.[72] As has been shown,[73] this decrease is explained by slow conversion of the above compounds into simple oxalate $(NpO_2)_2C_2O_4\cdot 6H_2O$. The low solubility and slow formation of the latter compound relate evidently to the infinite chain-like system of the CC bonds revealed therein.[63]

A typical trend in the solubility change due to formation of an infinite system of the CC bonds is also observed in the precipitation of simple Np(V) formates.[58, 74] Solutions of NpO_2OH with the concentration $[NpO_2^+] = 0.1 - 0.3$ mol litre^{-1} in an excess of HCOOH remain transparent for several hours. Then, slow crystallisation of $NpO_2HCOO\cdot 2H_2O$ begins. The latter is characterised by a solubility of 5.32×10^{-2} mol litre^{-1} at 23 °C and [HCOOH] = 0.2 mol litre^{-1}. With an increase in temperature up to 65 °C, the solubility does not change significantly. Nevertheless, upon heating of the saturated solution in a boiling water bath, crystals of **12** precipitate. This compound is characterised by a solubility of 2.42×10^{-2} mol litre^{-1} at 100 °C and [HCOOH] = 0.3 mol litre^{-1}. At temperatures above 140 °C, the monohydrate **12** converts into anhydrous salt **13**, which leads to a further decrease in the concentration of Np(V) in the liquid phase.

Similar trends in the crystallisation of various hydrates are observed in the preparation of Np(V) simple salts with sulfate,[50, 51, 75] acetate,[76] benzoate [60, 77] and other carboxylate [59, 78, 79] anions. In general, slow formation and dissolution of precipitates as well as relatively low solubility in water and organic solvents are characteristic of Np(V) compounds with infinite nets of CC bonds. Such compounds are typically nonhygroscopic.

2. UV-Vis absorption spectra

The cation – cation interaction specifically affects optical properties of Np(V) compounds. This is confirmed by an analysis of the UV-Vis absorption spectra of more than 30 simple and complex neptunoyl salts with known crystal structures.[55, 56, 77 – 87] A comparison of UV-Vis spectra of crystalline compounds with CC bonds and those without CC bonds, on the one hand, and of the respective solutions, on the other hand, revealed several important regularities.[81, 88, 89] One of them concerns correlations between the symmetry of the CP of Np atoms in a compound and the general shape of its UV-Vis spectrum. As has been noted above, pentagonal bipyramid and, less frequently, hexagonal bipyramid are the major types of coordination polyhedra occurring in neptunoyl compounds. According to extensive experimental studies, UV-Vis spectra of all crystalline salts of Np(V) characterised by the pentagonal-bipyramidal coordination of the central atom (D_{5h} symmetry) manifest narrow and intense absorption bands in the region of 970 – 1050 nm similar to the dominant band in the spectra of hydrated NpO_2^+ ions (Fig. 9 *a*). In contrast, such narrow absorption bands are absent in the case of compounds with hexagonal bipyramids (D_{6h} symmetry) as the coordination polyhedra of the Np atoms (Fig. 9 *b*). This can easily be rationalised.[90] According to the Laporte selection rules, *f*–*f* transitions are forbidden in a centrosymmetric ligand field (including the case of D_{6h} symmetry). For CP without an inversion centre (such as the pentagonal bipyramid), the probability of such transitions

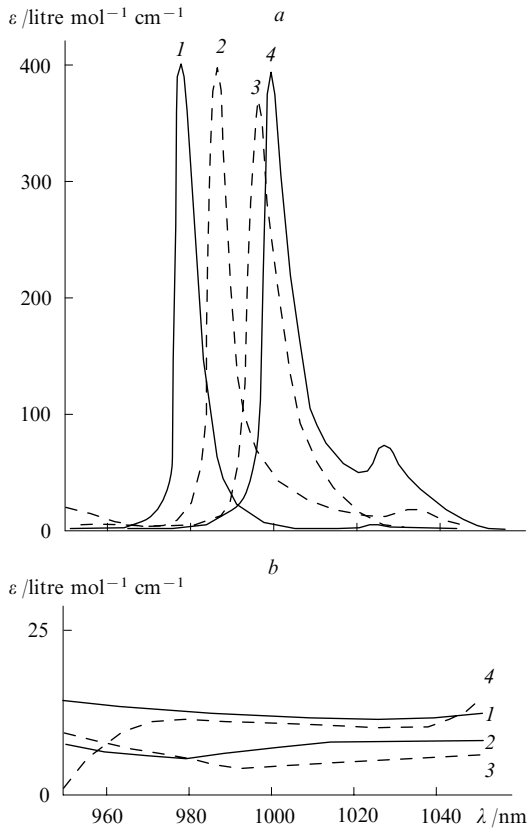

Figure 9. The UV-Vis absorption spectra of hydrated Np(V) ions and different neptunoyl compounds: (*a*) NpO_2^+ (aq) (*1*), **24** (*2*), **28** (*3*),[84] **12** (*4*);[82] (*b*) $NH_4[NpO_2(HCOO)_2]$ (*1*),[74] $K[NpO_2CO_3]$ (*2*),[81] $Cs_2[NpO_2.(CH_3COO)_3]$ (*3*),[82] **11** (*4*).[57]

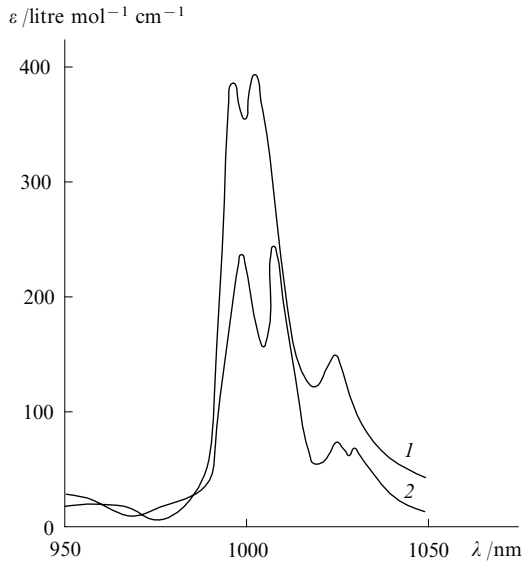

Figure 10. The UV-Vis absorption spectra of **4** (*1*) and **6** (*2*).[62]

becomes appreciable giving rise to narrow and fairly intense absorption bands in the UV-Vis spectra.

UV-Vis spectra of crystalline compounds and respective solutions are normally characterised by similar values of the molar extinction (ε_m) at the absorption maxima. Somewhat reduced ε_m values are observed only for amorphous, such as Np(V) hydroxide, or poorly crystalline substances.[89]

Based on the resemblance of the UV-Vis spectra of neptunoyl derivatives in aqueous solutions to those of crystalline compounds characterised by the D_{5h} symmetry of the coordination polyhedron of the neptunium atoms, one may assume that the hydration number (h) of NpO_2^+ ions in dilute aqueous solutions is 5. Suggestions that $h = 6$ or 4 adopted by several authors[33,77,91] are most probably erroneous.[92] A similar conclusion is also valid for AmO_2^+ ions, since the UV-Vis spectra of the respective aqueous solutions manifest narrow and fairly intense bands assigned to f–f transitions. Furthermore, the effects of the CP symmetry on the UV-Vis spectra established for neptunoyl ions are also applicable to PuO_2^{2+} ions as confirmed by the UV-Vis spectra of a series of Pu(VI) double oxalates (see Ref. 93). Thus, plutonoyl like other actinoyl ions are characterised by the hydration number 5 in aqueous solutions.

In the UV-Vis spectra of some crystalline compounds with D_{5h} symmetry of the Np coordination polyhedra, the main absorption band is split (Fig. 10).[66,78,80,85] This suggests the presence of several nonequivalent neptunoyl groups in the crystal structure. However, an unsplit UV-Vis band does not necessarily imply the crystallographic equivalency of all NpO_2^+ ions. For example, in the crystal structure of **15**, there are four types of neptunoyl ions despite the major absorption band in the UV-Vis spectrum of this compound being only slightly broadened rather than split.[77]

The position of the major absorption maximum in the UV-Vis spectrum of a crystal is normally red-shifted with respect to the corresponding solution provided that the CP of the Np(V) atoms in the crystal structure of this compound have no inversion centres. The magnitude of this shift ($\Delta\lambda_m$) depends on the nature of ligands in the equatorial plane of the NpO_2^+ ions and the occurrence of the CC bonds. For compounds without CC bonds, the positions of absorption maxima in the UV-Vis spectra of crystalline samples are quite close to those of the respective solutions with the shift not exceeding $\pm$ 5 nm (Table 2).

Table 2. UV-Vis spectral parameters of crystalline Np(V) compounds with known crystal structures without CC bonds.

Compound	λ_m /nm	$\Delta\lambda_m$ /nm	Ref.
$Na[NpO_2C_2O_4(H_2O)]\cdot 2H_2O$ (**24**)	989	2	70, 84
$Cs_3[NpO_2(SO_4)_2]\cdot 2H_2O$ (**25**)	986	1	71, 80
$[Co(NH_3)_6][NpO_2(SO_4)]\cdot 2H_2O$ (**26**)	989	4	80, 94
$[Co(NH_3)_6][NpO_2(C_2O_4)_2]\cdot 4H_2O$ (**27**)	1000	4	84, 95
$[Co(NH_3)_6][NpO_2(C_2O_4)_2]\cdot 3H_2O$ (**28**)	992	−4	84, 95
$[Co(NH_3)_6][NpO_2\{o\text{-}C_6H_4(COO)_2\}_2]\cdot 2H_2O$ (**29**)	996	4	86

The situation changes dramatically if the crystal structure of an Np(V) compound involves CC bonds. In those cases, the absorption band in the UV-Vis spectrum of the crystal is quite strongly shifted towards longer wavelengths with respect to the spectra of the corresponding complex in a solution. The magnitude of this shift depends on the character of the CC bonds. For compounds that contain neptunoyl ions acting as monodentate ligands, $\Delta\lambda_m$ lies in the range of 8 – 17 nm (Table 3). In the case of a bidentate coordination of NpO_2^+ ions, the shift amounts to 15 – 39 nm (Table 4). Crystal structures of some compounds contain both mono- and bidentate neptunoyl ions simultaneously. The major absorption bands in the UV-Vis spectra of such compounds are split into two components with distinctly different red shifts. The UV-Vis spectrum of **19** may be taken as a striking example of such a situation.

In the course of systematic UV-Vis studies of NpO_2^+ crystalline compounds, several unusual facts have been revealed. In particular, the spectra of Np(V) chromates[83,96–98] manifest intense broad bands strongly (> 40 nm) shifted towards longer wavelengths. According to X-ray crystallographic data,[96–98] this

Table 3. UV-Vis spectral parameters of crystalline compounds with the monodentate coordination of NpO_2^+.

Compound	λ_m /nm	$\Delta\lambda_m$ /nm	Ref.
$[NpO_2ClO_4(H_2O)_2]$ (**9**)	991	10	55
$[NpO_2CH_2(OH)COO(H_2O)]$ (**14**)	1004	16	59, 79
$NH_4[NpO_2C_2O_4]\cdot 2.67\,H_2O$ (**17**)	997	8	62, 84
$[(NpO_2)_2C_2O_4(H_2O)_4]\cdot 2\,H_2O$ (**18**)	1002	17	63
$[(NpO_2)_2CH_2(COO)_2(H_2O)_3]\cdot H_2O$ (**19**)	999	14	64
$[(NpO_2)_2(DMSO)_7(H_2O)_2](ClO_4)_2\cdot H_2O$ (**21**)	995	11	66
$[NpO_2NO_3(CH_3CONH_2)_2]$ (**23**)	1002	—	68

Table 4. UV-Vis spectral parameters of crystalline compounds with the bidentate coordination of NpO_2^+.

Compound	λ_m /nm	$\Delta\lambda_m$ /nm	Ref.
$[(NpO_2)_2SO_4(H_2O)_2]$ (**4**)	999; 1005	17; 23	50, 80
$[(NpO_2)_2SO_4(H_2O)]$ (**5**)	1007; 1021	25; 39	51, 80
$[NpO_2Cl(H_2O)]$ (**6**)	1000; 1009	19; 28	52, 85
$[(NpO_2)_2(NO_3)_2(H_2O)_4]\cdot H_2O$ (**10**)	996	15	56
$[NpO_2HCOO(H_2O)_2]$ (**12**)	1003	21	58, 82
$[NpO_2HCOO]$ (**13**)	1008	26	58, 82
$[NpO_2C_6H_5COO(H_2O)]\cdot 0.75\,H_2O$ (**15**)	1009	27	60, 77
$[(NpO_2)_2CH_2(COO)_2(H_2O)_3]\cdot H_2O$ (**19**)	1007	22	64, 78
$[(NpO_2)_2CH_2(COO)_2(H_2O)_2]\cdot H_2O$ (**20**)	1006; 1015	25; 37	65, 78
$[(NpO_2)_2\{o\text{-}C_6H_4(COO)_2\}(H_2O)_3]\cdot H_2O$ (**22**)	1007	23	67, 87

shift is not induced by the CC interaction. Probably, a partial charge transfer from the Np atoms to the CrO_4^{2-} due to a strong oxidising ability of the latter is responsible for the phenomenon.

Yet another anomaly, *viz*., a broad irregularly shaped band characterised by a strong red shift, was observed in the spectrum of crystalline Np_2O_5[99] (Fig. 11). Apparently, the neptunoyl moiety is substantially weakened or totally absent in the crystal structure of Np_2O_5.

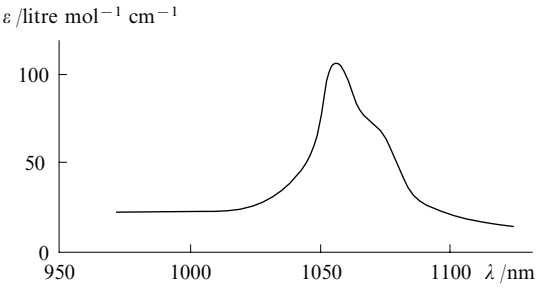

Figure 11. The UV-Vis absorption spectra of crystalline Np_2O_5.[99]

Finally, we note that the aforementioned regularities often allow reliable predictions of the occurrence and the character of the CC bonds in the crystal structures of novel Np(V) compounds on the basis of their UV-Vis spectra. Such predictions were made for a number of compounds including neptunoyl chloride,[87] oxalates,[84] malonates,[78] benzoates[77] and phthalates.[87] Afterwards, all of these predictions proved correct through direct determinations of the crystal structures of the respective compounds by means of single-crystal X-ray diffraction.[52, 60, 62–65, 67] Definitely, these predictions are only of qualitative character. The UV-Vis absorption spectroscopy of crystalline Np(V) compounds and conclusions based on the spectral results should not be taken as a substitute for other techniques. It should rather be considered as the first step in the structural study of newly prepared Np(V) compounds.

3. Infrared and other spectra

It has been demonstrated[100,101] that IR spectra of a number of simple Np(V) salts are characterised by intense broad bands of antisymmetric (ν_{as}) vibrations of the neptunoyl moiety. This observation was first explained by formation of H-bonds between water molecules and oxygen atoms of the neptunoyl ions. However, systematic structural studies have recently established that simple Np(V) salts usually contain CC bonds. Therefore, one may suggest that it is the CC interaction that is responsible for the intense broad vibrational bands of NpO_2^+ observed in these compounds. This suggestion is supported by IR spectroscopic studies of many Np(V) compounds with known crystal structures.[58, 66, 68, 75–79, 87] The distinct difference in the ν_{as} band between IR spectra of neptunoyl salts with (*a*) and without (*b*) the CC bonds is illustrated in Fig. 12 for a few typical cases.

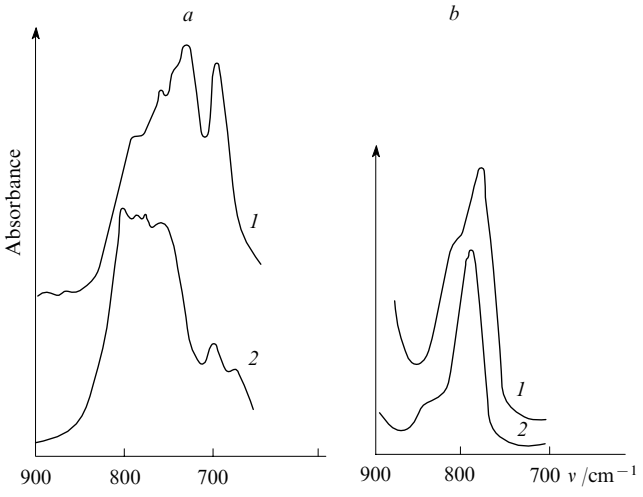

Figure 12. The IR spectra of some Np(V) compounds (see Ref. 78): (*a*) **20** (*1*) and **19** (*2*), which involve CC bonds; (*b*) $NH_4[NpO_2CH_2(COO)_2]$ (*1*) and $Cs[NpO_2CH_2(COO)_2]$ (*2*) without CC bonds.

Yet another distinctive feature of the IR spectra of Np(V) compounds possessing CC bonds in their crystal structures is a pronounced shift of the ν_{as} bands towards lower frequencies. The magnitude of this shift depends upon the number and the character of the CC bonds. In particular, it correlates to a certain extent with the changes in the Np–O bond lengths resulting from the CC interaction as well as with the red shift of bands in the UV-Vis spectra (Table 5). Unfortunately, this correlation bears only a qualitative character, partially due to ambiguities in the determination of precise positions of maxima for broad irregularly shaped ν_{as} vibrational bands in the IR spectra of compounds with the CC bonds. On the other hand, Np–O bond lengths change within a relatively narrow range and the precision of their determination is not sufficiently high.

Several publications[24, 43, 49, 58, 87, 93, 102] have reported on the Mössbauer spectra of Np(V) compounds, crystal structures of which reveal the CC interaction. However, no suggestions of spectral effects attributable exclusively to the CC interaction have been made.

An interesting result has been obtained in a study of magnetic properties of compound **14**.[103] According to the low-temperature magnetic susceptibility measurements, this salt (note that its crystal structure reveals a distorted planar square net of CC bonds[58]) undergoes a ferromagnetic transition at 12 K. It is the first observation of ferromagnetism for Np(V) compounds. We

Table 5. Correlations between the UV-Vis band position, Np – O bond length and ν_{as} vibrational frequencies in the IR spectra of Np(V) compounds with CC bonds.

Compound	λ_m /nm	$\Delta\lambda_m$ /nm	Np – O /Å	ν_{as} /cm^{-1}	Ref.
$[(NpO_2)_2SO_4(H_2O)_2]$ (**4**)	999; 1005	17; 23	1.830; 1.851 [a]	768; 760	50, 75
$[NpO_2Cl(H_2O)]$ (**6**)	1000; 1009	19; 28	1.835; 1.840 [a]	768	52
$[NpO_2ClO_4(H_2O)_4]$ (**9**)	991	10	1.810; 1.860	808; 776	55
$[NpO_2HCOO(H_2O)]$ (**12**)	1003	21	1.846; 1.850	764	58
$[NpO_2HCOO]$ (**13**)	1008	26	1.857; 1.915	740	58
$[NpO_2CH_2(OH)COO(H_2O)]$ (**14**)	1004	16	1.828; 1.801	802	59, 79
$[NpO_2C_6H_5COO(H_2O)]\cdot 0.75\,H_2O$ (**15**)	1009	27	1.82 – 1.87 [a]	745	60, 67
$NH_4[NpO_2C_2O_4]\cdot 2.67\,H_2O$ (**17**)	997	8	1.825; 1.887	794	62, 84
$[(NpO_2)_2CH_2(COO)_2(H_2O)_3]\cdot H_2O$ (**19**)	1007	22	1.840; 1.828 [a]	805; 765	64, 78
$[(NpO_2)_2CH_2(COO)_2(H_2O)_2]\cdot H_2O$ (**20**)	1006; 1015	25; 37	1.840; 1.870 [a]	760; 725	65, 78
$[(NpO_2)_2(DMSO)_7(H_2O)_2](ClO_4)_2\cdot H_2O$ (**21**)	995	11	1.86	800	66
$[(NpO_2)_2\{o\text{-}C_6H_4(COO)_2\}(H_2O)_3]\cdot H_2O$ (**22**)	1007	23	1.850; 1.843 [a]	755	67, 87
$[NpO_2NO_3(CH_3CONH_2)_2]$ (**23**)	1002	–	1.859	790; 778	68

[a] Np – O bond lengths are averaged for different types of NpO_2^+ ions.

believe that further investigations into the magnetic properties of Np(V) compounds will lead to new important findings.

IV. Cation – cation interactions in compounds of other actinide ions

The mutual coordination of UO_2^{2+} ions has been observed for the first time in a crystallographic study of UO_2Cl_2 (**30**) by means of neutron diffraction.[104] In the orthorhombic crystal lattice of this compound, the uranyl ions form infinite zigzag chains through the CC bonds, which is similar to the pattern of NpO_2^+ ions in the crystal structures of compounds **9**, **14**, **18** and **23**. Each UO_2^{2+} ion is involved in two CC bonds acting as a monodentate ligand with respect to the adjacent ion.

Similar infinite zigzag chains were revealed in the crystal structure of UO_2MoO_4 (**31**).[105] Furthermore, it has to be taken into account that all anhydrous salts with the common stoichiometry UO_2EO_4, where E = S, Se, Cr, Mo or W, are isostructural according to powder X-ray diffraction data.[106–108] Thus, their crystal structures contain identical chain-like patterns of the CC bonds.

Quite another pattern of the CC bonds was revealed in uranyl hexafluoroacetylacetonate $UO_2(C_5HF_6O_2)_2$ (**32**).[109] Its crystal structure, like that of compound **17**, contains trimers of uranyl ions. Nevertheless, in this compound all UO_2^{2+} ions in the trimers are crystallographically nonequivalent. According to some indirect evidence,[110, 111] CC bonds may also be formed in other uranyl β-diketonates though the corresponding crystal structures have not been determined so far.

The formation of CC bonds has been confirmed for a rather complicated and structurally uncommon oxothiolate uranyl complex $(HNEt_3)_2[(UO_2)_4(\mu_3\text{-}O)_2(SC_5NH_4)_6]\cdot Me_2CO$ (**33**). The crystal structure of this compound reveals tetranuclear anions composed of two identical fragments $(UO_2)_2(SC_5NH_4)_3^-$, in which uranyl ions form CC bonds of the O=U=O···U type. These fragments are bound to each other through two bridging O atoms. Therefore, as regards the pattern of the CC bonds within the complex anion, the two UO_2^{2+} ions act as monodentate ligands whilst two other ions act exclusively as coordinating centres.

No other uranyl derivatives possessing CC bonds have been reported so far. Nevertheless, we assume that CC bonds may well be revealed in further structural studies of a number of anhydrous uranyl salts containing anions of low coordination capacity as ligands.

The character of the CC bonds and their influence on the properties of uranyl compounds are similar to those discussed above for neptunoyl compounds. In both cases, the CC bonds are formed through bridging oxygen atoms, which are characterised by different An – O bond lengths ($l_1 \ll l_3$, Table 6). The formation of the CC bonds is also accompanied by a significant increase in the U – O bond length within the uranyl ions. The mean value of the $l_1 - l_2$ difference is 0.06 Å. The U – O distance to the oxygen atom of an adjacent uranyl ion coordinated in the equatorial plane is 2.51 Å on average, which is slightly longer than values typical of uranyl complexes with various oxygen ligands. Thus, UO_2^{2+} ions behave as relatively weak ligands in the formation of the CC bonds.

Table 6. U – O bond lengths (Å) in the crystal structures of uranyl compounds with CC bonds.[a]

Compound	l_1	l_2	l_3	Ref.
UO_2Cl_2 (**30**)	1.78	1.73	2.52	104
UO_2MoO_4 (**31**)	1.808	1.758	2.508	105
$UO_2(C_5HF_6O_2)_2$ (**32**)	1.79	1.72	2.47	109
	1.72	1.68	2.54	
	1.81	1.71	2.48	
$(HNEt_3)_2[(UO_2)_4(\mu_3\text{-}O)_2(SC_5NH_4)_6]\cdot$ $\cdot Me_2CO$ (**33**)	1.838	1.771	2.488	112

[a] $O\overset{l_2}{=}U\overset{l_1}{=}O\overset{l_3}{\cdots}U$.

Apart from the aforementioned Np(V) and U(VI) derivatives, no other An(V) or An(VI) compounds exhibiting CC bonds have been reported. Attempts to synthesise NpO_2MoO_4 and NpO_2EO_4, where E = S, Cr or W, which are presumably isostructural to UO_2MoO_4, failed due to reduction of Np(VI) to the pentavalent state. Nevertheless, the possibility of an occurrence of CC bonds in some anhydrous neptunyl compounds cannot be totally ruled out.

Several attempts to prepare Am(V) compounds analogous to Np(V) salts with known crystal structures have been undertaken. It was established that the isolation conditions and the crystal structures of $[Co(NH_3)_6][AmO_2(SO_4)_2]\cdot 2H_2O$ and $[Co(NH_3)_6]\cdot[NpO_2(SO_4)_2]\cdot 2H_2O$ devoid of CC bonds are virtually identical.[113] Meanwhile, it turned out that $(AmO_2)_2SO_4\cdot nH_2O$ is not isostructural to any of the known simple Np(V) sulfates with CC bonds. Moreover, Am(V), in contrast to Np(V), is not precipitated from concentrated formate solutions as $AmO_2HCOO\cdot nH_2O$ but rather is slowly converted into poorly soluble $Am(HCOO)_3$.[114] With a high level of confidence, we may assume that these results suggest a significant weakening of the CC bonds upon transition from NpO_2^+ to AmO_2^+. However, preparation of Am(V) com-

pounds with CC bonds should not be judged as completely impossible. Indeed, AmO_2^+ ions in solutions can serve as weak ligands in the CC interactions with highly charged cations, although uranyl ions do not manifest this ability. At the same time, as has been noted above, some crystalline compounds of U(VI) reveal CC bonds.

Since Pu(V) and, in particular, U(V) are prone to the CC interaction in solutions, one should expect the occurrence of CC bonds in crystal structures of some of their compounds. Most probable candidates in the search for such compounds are salts of suitable anions with kinetically stable cationic complexes of PuO_2^+ or UO_2^+ with Cr^{3+} or Rh^{3+} like $Rh(H_2O)_5NpO_2F_4$ (see Ref. 5). Preparation of compounds with a mutual coordination of PuO_2^+ or UO_2^+ ions is hardly possible taking into account their easy disproportionation.

V. Comparison of cation – cation interactions in solutions and crystals of actinide compounds

As has been noted in the Introduction, different aspects of the CC interaction have been considered in numerous publications. Special attention has been paid to the elucidation of the nature of this phenomenon. Several authors suggested that the CC interaction can be reduced to a special type of incomplete redox reaction between the AnO_2^+ cation and an 'active' cation.[7, 13, 14, 19, 20, 22, 23, 25] A series of arguments have been adduced in support. In particular, according to several reports, kinetics of formation of complexes owing to the CC interaction of NpO_2^+ with U(VI), Fe(III), Th(IV) or In(III) and of AmO_2^+ with U(VI) does not obey the law of mass action. Moreover, the UV-Vis spectra of NpO_2^+ (see Refs 14 and 20) and AmO_2^+ (see Ref. 7) in the presence of some 'active' cations manifest broad bands in the region of 600 – 900 nm attributed to the exciton absorption. The experimentally established weakening of the CC interaction in the series $UO_2^+ > NpO_2^+ > AmO_2^+$ was explained [7, 25] by an increase in the redox potentials of the corresponding An(VI)/An(V) pairs. These and some other arguments [14, 15] have been consistently rebutted in a series of studies,[26, 29 – 35] which at the same time substantiated an alternative suggestion stating that the CC interaction in a solution originates from complexation between the AnO_2^+ ions and the 'active' cations. However, the character of this complexation remains disputable. Two alternative concepts of the nature of the CC interaction in solutions have been formulated based on numerous experimental results.[2, 29, 32 – 35] The first concept states that the CC interaction may be considered as a process of substitution of water molecules within the coordination sphere of the 'active' cation by oxygen atoms of the actinoyl ion. The second concept suggests an outer-sphere interaction mediated by such ligands as H_2O or ClO_4^-. The following arguments may be adduced in favour of the first concept:

1. The formation of CC complexes of AnO_2^+ with Cr_{aq}^{3+} (see Refs 2 and 9) and Rh_{aq}^{3+} proceeds slowly, which is typical of inner-sphere substitution of water molecules by various ligands in 'active' cations mentioned.

2. The NMR data [33] on the CC interaction between NpO_2^+ and UO_2^{2+} support the hypothesis of the formation of a T-shaped inner-sphere complex (two linear AnO_2^{n+} groups arranged perpendicularly to each other).

3. The major band in the UV-Vis absorption spectra of hydrated NpO_2^+ ions at 980 nm is shifted in the presence of 'active' cations by 9 – 17 nm towards longer wavelengths.[1 – 3, 8] Such a large shift may be induced by either direct involvement of oxygen atoms of the neptunoyl groups into chemical bonds or incorporation of sufficiently strong ligands into the equatorial plane of the NpO_2^+ ions. Note that H_2O molecules and ClO_4^- anions are generally considered as weak ligands.

4. According to IR [28, 100, 101] and Raman [31, 34] spectra, vibrational frequencies of NpO_2^+ change substantially due to the CC interaction. The character of these changes is similar to that in the UV-Vis spectra.

5. The An···An interatomic distance in CC complexes of NpO_2^+ with UO_2^{2+} is 4.2 Å,[32, 35] which is surprisingly close to the sum of the Np – O bond length within neptunoyl (*ca.* 1.8 Å) and a typical distance between the U atom of uranyl and oxygen atoms of ligands coordinated in the equatorial plane (*ca.* 2.4 Å).

The above arguments strongly assume that the outer-sphere model of the CC interaction is hardly probable although these are not sufficient to rule it out decisively. In this respect, we note rather unexpected negative values of enthalpy and entropy of the CC interaction determined for NpO_2^+ complexes with Rh(III) (see Ref. 3), Cr(III) (see Ref. 9) and U(VI) (see Ref. 40). Though the negative values are normally typical of the outer-sphere complexation of actinides, these results can be rationalised taking into account higher hydration energy of the CC complex with respect to the starting species due to formation of a binuclear complex, which is characterised by a high specifically distributed charge.

Convincing evidence in favour of the inner-sphere nature of the CC interaction involving AnO_2^+ ions comes from results of the characterisation of the CC complexes in crystalline compounds of Np(V) summarised above. Indeed, in all crystalline structures discussed, the CC bonds are formed by direct incorporation of an oxygen atom of a neptunoyl ion into the coordination sphere of the adjacent NpO_2^+ ion. On the other hand, there is a close analogy between the CC interaction formed by AnO_2^+ ions in solutions and in crystals. This analogy becomes apparent if the UV-Vis spectra of NpO_2^+ CC complexes in solutions are compared with the spectra of the respective compounds in the crystalline state. As has already been mentioned, upon formation of CC complexes in solutions, the UV-Vis absorption band of Np(V) ions shifts by 9 – 17 nm. Crystalline compounds with a monodentate mutual coordination of NpO_2^+ ions (see Table 3) are characterised by virtually the same shift. Besides, the Np···Np interatomic distances between CC-interacting neptunoyl ions in perchloric acid solutions [32, 35] and in crystalline $[NpO_2ClO_4(H_2O)_4]$ (see Ref. 55) are close to each other being both equal to ~ 4.2 Å. Therefore, there is sufficient evidence that the CC interactions of actinoyl ions in solutions and in crystals are realised in similar ways. Notwithstanding, the two cases have distinctive features due to the following factors:

1. In solutions, the CC interaction is usually limited to formation of binuclear complexes. Trimeric and larger (*i.e.*, higher-nuclearity) species have been detected only in very concentrated ($c > 0.5$ mol litre^{-1}) solutions of Np(V) perchlorate.[31, 34] In contrast, formation of infinite systems of CC bonds (*viz.*, chains, ribbons, planar nets or three-dimensional frameworks) is typical of crystalline neptunoyl compounds. Dimeric ions have been revealed in the crystal structures of only two out of twenty-three compounds listed in Table 1, namely, in **1** and **21**.

2. Neither mutual coordination of AnO_2^+ ions nor their CC interaction with other 'active' ions (apart from AnO_2^+) in solutions has been observed. Meanwhile, the crystal structures of a number of uranyl compounds (see Table 6) contain CC bonds. This may be explained by a rather small effective charge localised on oxygen atoms within the AnO_2^+ ions. As a result, they cannot substitute water molecules in the coordination spheres of 'active' cations in aqueous media. Nevertheless, some U(VI) compounds with CC bonds can be crystallised from organic solutions or prepared by solid state methods.

3. Systematic structural studies of crystalline compounds of Np(V) have shown that the incorporation of a large number of water molecules in the crystal structure results in a weakening of the CC bonds and a prevalence of the monodentate coordination of NpO_2^+ ions. Upon transition from crystals to aqueous solution, this tendency becomes more pronounced. This may be explained by the formation of hydrogen bonds between oxygen atoms of the neptunoyl ions and H_2O molecules. This suggestion is supported by the fact that the CC interaction is intensified provided that a weaker proton donor is taken as a solvent instead of water.[14, 39]

The absence of infinite systems of CC bonds and their weakening in aqueous solutions result in a relatively low influence

of the CC interaction on the UV-Vis spectra of Np(V) compounds in concentrated aqueous solutions.[32, 35] Probably, the same factors along with the larger $l_3 - l_1$ difference are responsible for some peculiarities of the Raman spectra of Np(V) compounds in solutions.[31, 34, 36]

Therefore, one may conclude that the CC interaction of actinoyl ions both in solutions and in crystals is realised through the inner-sphere coordination of AnO_2^+ by the 'active' ions. The only difference for the two cases consists of the intensity of the processes.

* * *

According to the experimental data summarised above, the CC interaction of NpO_2^+ ions is a common phenomenon occurring in many Np(V) compounds with known crystal structures. It strongly affects physicochemical properties of compounds under consideration, such as precipitation and dissolution kinetics, UV-Vis and IR spectra, *etc*. The number of Np(V) compounds in which the presence of the CC bond has been confirmed constantly increases. Meanwhile, structural data for other pentavalent actinides, in particular, PuO_2^+ are lacking. Therefore, the development of preparative chemistry of Pu(V), which is immature as yet, is an urgent task. Undoubtedly, the accomplishment of this task will make a significant contribution to coordination chemistry of actinides.

References

1. J C Sullivan, J C Hindman, A J Zielen *J. Am. Chem. Soc*. **83** 3373 (1961)
2. J C Sullivan *J. Am. Chem. Soc*. **84** 4256 (1962)
3. R K Murmann, J C Sullivan *Inorg. Chem*. **6** 892 (1967)
4. T W Newton, F B Baker *Inorg. Chem*. **1** 368 (1962)
5. G Gordon *Inorg. Chem*. **2** 1277 (1963)
6. T W Newton, M J Burkhart *Inorg. Chem*. **10** 2323 (1971)
7. A G Rykov, A A Frolov *Radiokhimiya* **17** 187 (1975) [a]
8. T W Newton, F B Baker *J. Phys. Chem*. **67** 1425 (1963)
9. J C Sullivan *Inorg. Chem*. **3** 315 (1964)
10. T W Newton, F B Baker *Inorg. Chem*. **4** 1166 (1965)
11. J C Sullivan, R C Thompson *Inorg. Chem*. **6** 1795 (1967)
12. J C Sullivan, M J Burkhart *J. Phys. Chem*. **72** 2675 (1968)
13. A G Rykov, A A Frolov *Radiokhimiya* **14** 709 (1972) [a]
14. A G Rykov, A A Frolov *Radiokhimiya* **14** 717 (1972) [a]
15. A Ekstrom, Y Farrar *Inorg. Chem*. **11** 2610 (1972)
16. C Lavallee, T W Newton *Inorg. Chem*. **11** 2616 (1972)
17. A Ekstrom *Inorg. Chem*. **12** 2455 (1973)
18. A Ekstrom *Inorg. Chem*. **13** 2237 (1974)
19. A G Rykov, A A Frolov *Radiokhimiya* **16** 803 (1974) [a]
20. A G Rykov, A A Frolov *Radiokhimiya* **16** 556 (1974) [a]
21. E J Hinderberger, R C Thompson *Inorg. Chem*. **14** 784 (1975)
22. A A Frolov, A G Rykov *Radiokhimiya* **17** 287 (1975) [a]
23. A G Rykov, A A Frolov *Radiokhimiya* **18** 58 (1976) [a]
24. D G Karraker, J A Stone *Inorg. Chem*. **16** 2979 (1977)
25. A A Frolov, A G Rykov *Radiokhimiya* **21** 329 (1979) [a]
26. C Madic, B Guillaume, J C Morisseau, J P Moulin *J. Inorg. Nucl. Chem*. **41** 1027 (1979)
27. A A Frolov, A G Rykov *Radiokhimiya* **21** 598 (1979) [a]
28. V A Vodovatov, L G Mashirov, D N Suglobov *Radiokhimiya* **21** 830 (1979) [a]
29. B Guillaume, D E Hobart, J Y Bourges *J. Inorg. Nucl. Chem*. **43** 3295 (1981)
30. B Guillaume, G M Begun, R L Hahn, A H Narten, in *'11èmes Journées des Actinides' (Proceedings), Jesolo Lido, Italy, 1981* p. 91
31. B Guillaume, G M Begun, R L Hahn, in *Abstracts of Reports of the International Conference 'Actinides-81', Pacific Grove, USA, 1981* p. 102
32. B Guillaume, A H Narten, R L Hahn, in *Abstracts of Reports of the International Conference 'Actinides-81', Pacific Grove, USA, 1981* p. 105
33. V A Glebov, M F Tikhonov *Koord. Khim*. **8** 48 (1982) [b]
34. B Guillaume, G M Begun, R L Hahn *Inorg. Chem*. **21** 1159 (1982)
35. B Guillaume, R L Hahn, A H Narten *Inorg. Chem*. **22** 109 (1983)
36. C Madic, G M Begun, D E Hobart, R L Hahn *Radiochim. Acta* **34** 195 (1983)
37. G V Ionova, V G Pershina, V I Spitsyn *Zh. Neorg. Khim*. **28** 3113 (1983) [c]
38. V A Vodovatov, L G Mashirov *Radiokhimiya* **26** 264 (1984) [a]
39. V P Shilov, T N Bukhtiyarova *Radiokhimiya* **33** (5) 87 (1991) [a]
40. B E Stout, G R Choppin, F Nectoux, M Pagès *Radiochim. Acta* **61** 65 (1993)
41. N J Stoyer, D C Hoffman, R J Silva *Radiochim. Acta* **88** 279 (2000)
42. G V Ionova, V G Pershina, N I Suraeva *Radiokhimiya* **31** (1) 11 (1989)
43. A Cousson, S Dabos, H Abazli, F Nectoux, J Jové, M Gasperin, M Pagès, in *Abstracts of the 1st International Conference on Chemistry and Technology of Lanthanides and Actinides, Venice, 1983* p. 99
44. A Cousson, S Dabos, H Abazli, F Nectoux, M Pagès, G Choppin *J. Less-Common Met*. **99** 233 (1984)
45. A Cousson *Acta Crystallogr., Sect. C* **41** 1758 (1985)
46. S V Tomilin, Yu F Volkov, R F Melkaya, V I Spiryakov, I I Kapshukov *Radiokhimiya* **28** 304 (1986) [a]
47. S V Tomilin, Yu F Volkov, V I Spiryakov, I I Kapshukov *Stereokhimiya Koordinatsionnykh Soedinenii Pyativalentnykh Aktinidov* (Stereochemistry of Coordination Compounds of Pentavalent Actinides) (Moscow: TsNII Atominform, 1988)
48. N N Krot, D N Suglobov *Radiokhimiya* **31** (6) 1 (1989) [a]
49. M S Grigoriev, Doctoral Thesis in Chemical Sciences, Institute of Physical Chemistry, Russian Academy of Sciences, Moscow, 1995
50. M S Grigoriev, A I Yanovskii, A M Fedoseev, N A Budantseva, Yu T Struchkov, N N Krot, V I Spitsyn *Dokl. Akad. Nauk SSSR* **300** 618 (1988) [d]
51. M S Grigoriev, N A Baturin, N A Budantseva, A M Fedoseev *Radiokhimiya* **35** (2) 29 (1993) [a]
52. M S Grigoriev, A A Bessonov, N N Krot, A I Yanovskii, Yu T Struchkov *Radiokhimiya* **35** (4) 17 (1993) [a]
53. M S Grigoriev, I A Charushnikova, A M Fedoseev, N A Budantseva, N A Baturin, L L Regel' *Radiokhimiya* **33** (4) 19 (1991) [a]
54. M S Grigoriev, N A Baturin, A M Fedoseev, N A Budantseva *Koord. Khim*. **20** 552 (1994) [b]
55. M S Grigoriev, N A Baturin, A A Bessonov, N N Krot *Radiokhimiya* **37** 15 (1995) [a]
56. M S Grigoriev, I A Charushnikova, N N Krot, A I Yanovskii, Yu T Struchkov *Zh. Neorg. Khim*. **39** 179 (1994) [c]
57. I A Charushnikova, M S Grigoriev, N N Krot, A I Yanovski, Yu T Struchkov, in *'24èmes Journées des Actinides' (Proceedings), Oberburgl, Austria, 1994* p. 32
58. M S Grigoriev, A I Yanovskii, Yu T Struchkov, A A Bessonov, T V Afonas'eva, N N Krot *Radiokhimiya* **31** (4) 37 (1989) [a]
59. M S Grigoriev, I A Charushnikova, N A Baturin, N N Krot *Zh. Neorg. Khim*. **40** 732 (1995) [c]
60. N N Krot, I A Charushnikova, M S Grigoriev, in *'22èmes Journées des Actinides' (Program and Abstracts), Méribel, France, 1992* p. 35
61. I A Charushnikova, V P Perminov, S B Katser *Radiokhimiya* **37** 493 (1995)
62. M S Grigoriev, A A Bessonov, A I Yanovskii, Yu T Struchkov, N N Krot *Radiokhimiya* **33** (5) 46 (1991) [a]
63. M S Grigoriev, I A Charushnikova, N N Krot, A I Yanovskii, Yu T Struchkov *Zh. Neorg. Khim*. **41** 539 (1996) [c]
64. M S Grigoriev, I A Charushnikova, N N Krot, A I Yanovskii, Yu T Struchkov *Radiokhimiya* **35** (4) 24 (1993) [a]
65. M S Grigoriev, I A Charushnikova, N N Krot, A I Yanovskii, Yu T Struchkov *Radiokhimiya* **35** (4) 31 (1993) [a]
66. I A Charushnikova, N N Krot, Z A Starikova *Radiokhimiya* **42** 397 (2000) [a]
67. I A Charushnikova, N N Krot, Z A Starikova *Radiokhimiya* **43** 434 (2001) [a]

68. G B Andreev, N A Budantseva, M Yu Antipin, N N Krot *Koord. Khim.* **28** 465 (2002) [b]
69. F Nectoux, H Abazli, J Jové, A Cousson, M Pagès, M Gasperin, G Choppin *J. Less-Common Met.* **97** 1 (1984)
70. S V Tomilin, Yu F Volkov, G I Visyashcheva, I I Kapshukov *Radiokhimiya* **26** 734 (1984) [a]
71. M S Grigoriev, A I Yanovskii, A M Fedoseev, N A Budantseva, Yu T Struchkov, N N Krot *Radiokhimiya* **33** (2) 17 (1991) [a]
72. A D Gel'man, V I Blokhin, T N Bukhtiyarova, N N Krot *Zh. Neorg. Khim.* **15** 1899 (1970) [c]
73. V G Zubarev, N N Krot *Radiokhimiya* **23** 857 (1981) [a]
74. A I Logvis', A A Bessonov, N N Krot *Radiokhimiya* **36** 6 (1994) [a]
75. N A Budantseva, A M Fedoseev, M S Grigoriev, T I Potemkina, T V Afonas'eva, N N Krot *Radiokhimiya* **30** 607 (1988) [a]
76. A A Bessonov, M S Grigoriev, T V Afonas'eva, N N Krot *Radiokhimiya* **31** (4) 33 (1989) [a]
77. I A Charushnikova, T V Afonas'eva, V P Perminov, N N Krot *Radiokhimiya* **34** (6) 7 (1992) [a]
78. N N Krot, I A Charushnikova, T V Afonas'eva, M S Grigoriev *Radiokhimiya* **35** (2) 14 (1993) [a]
79. I A Charushnikova, T V Afonas'eva, N N Krot *Radiokhimiya* **37** 9 (1995) [a]
80. A A Bessonov, N A Budantseva, A M Fedoseev, V P Perminov, T V Afonas'eva, N N Krot *Radiokhimiya* **32** (5) 24 (1990) [a]
81. N N Krot, A A Bessonov, V P Perminov *Dokl. Akad. Nauk SSSR* **312** 1402 (1990) [d]
82. A A Bessonov, T V Afonas'eva, N N Krot *Radiokhimiya* **32** (5) 31 (1990) [a]
83. A M Fedoseev, N A Budantseva, M S Grigoriev, V P Perminov *Radiokhimiya* **33** (4) 7 (1991) [a]
84. A A Bessonov, N N Krot *Radiokhimiya* **33** (3) 35 (1991) [a]
85. A A Bessonov, T V Afonas'eva, N N Krot *Radiokhimiya* **33** (3) 47 (1991) [a]
86. I A Charushnikova, N N Krot, Z A Starikova *Radiokhimiya* **43** 438 (2001) [a]
87. M Saeki, M Nakada, T Yamashita, T Nakamoto, N N Krot *Radiochim. Acta* **80** 89 (1998)
88. N N Krot, A A Bessonov, M S Grigoriev, in *'21èmes Journées des Actinides' (Program and Abstracts), Montechoro, Portugal, 1991* p. 169
89. A A Bessonov, Candidate Thesis in Chemical Sciences, Institute of Physical Chemistry, Russian Academy of Sciences, Moscow, 1991
90. J L Ryan, in *MTP International Review of Science* Vol. 7 (Ed. K W Bagnall) (London: Butterworth; Baltimore: University Park Press, 1972) p. 323
91. V A Glebov, T M Nikitina, M F Tikhonov *Radiokhimiya* **19** 277 (1977) [a]
92. A Yu Garnov, N N Krot, A A Bessonov, V P Perminov *Radiokhimiya* **38** 428 (1996) [a]
93. A A Bessonov, N N Krot, N A Budantseva, T V Afonas'eva *Radiokhimiya* **38** 223 (1996) [a]
94. M S Grigoriev, A M Fedoseev, N A Budantseva, A I Yanovskii, Yu T Struchkov, N N Krot *Radiokhimiya* **33** (3) 54 (1991) [a]
95. M S Grigoriev, N A Baturin, L L Regel', N N Krot *Radiokhimiya* **33** (2) 19 (1991) [a]
96. M S Grigoriev, T E Plotnikova, N A Baturin, N A Budantseva, A M Fedoseev *Radiokhimiya* **37** 102 (1995) [a]
97. M S Grigoriev, N A Baturin, A M Fedoseev, N A Budantseva *Radiokhimiya* **33** (5) 53 (1991) [a]
98. M S Grigoriev, T E Plotnikova, N A Baturin, N A Budantseva, A M Fedoseev *Radiokhimiya* **38** 136 (1996) [a]
99. A A Bessonov, N A Budantseva, A M Fedoseev, in *'24èmes Journées des Actinides' (Proceedings), Oberburgl, Austria, 1994* p. 67
100. V A Vodovatov, V B Kolokoltsov, T V Kovaleva, L G Mashirov, D N Suglobov, V G Sles, in *Transplutonium 1975* (Amsterdam: North-Holland, 1976) p. 247
101. V A Vodovatov, L G Mashirov, D N Suglobov *Radiokhimiya* **17** 900 (1975) [a]
102. M Saeki, M Nakada, N M Masaki,T Yamashita, in *Abstracts of Reports of the International Conference 'Actinides-97', Baden-Baden, 1997* T3-P20
103. T Nakamoto, M Nakada, A Nakamura, Y Haga, Y Onuki *Solid State Commun.* **109** 77 (1999)
104. J C Taylor, P W Wilson *Acta Crystallogr., Sect. B* **29** 1073 (1973)
105. V N Serezhkin, V K Trunov, L G Makarevich *Kristallografiya* **25** 858 (1980) [e]
106. L M Kovba, V K Trunov, A I Grigoriev *Zh. Strukt. Khim.* **6** 919 (1965) [f]
107. V N Serezhkin, L M Kovba, V K Trunov *Kristallografiya* **17** 1127 (1972) [e]
108. N P Brandenburg, B O Loopstra *Acta Crysallogr., Sect. B* **34** 3734 (1978)
109. J C Taylor, A Ekstrom, C H Randall *Inorg. Chem.* **17** 3285 (1978)
110. G V Sidorenko, R B Dushin, E K Legin, D N Suglobov *Radiokhimiya* **24** 75 (1982) [a]
111. A A Belyaeva, R B Dushin, G V Sidorenko, D N Suglobov *Radiokhimiya* **27** 534 (1985) [a]
112. D Rose, Y-D Chang, Q Chen, J Zubieta *Inorg. Chem.* **33** 5167 (1994)
113. A M Fedoseev, N A Budantseva *Radiokhimiya* **31** (5) 14 (1989) [a]
114. A V Anan'ev, V P Shilov *Radiokhimiya* **26** 807 (1984) [a]

[a] — *Radiochemistry (Engl. Transl.)*
[b] — *Russ. J. Coord. Chem. (Engl. Transl.)*
[c] — *Russ. J. Inorg. Chem. (Engl. Transl.)*
[d] — *Dokl. Chem. (Engl. Transl.)*
[e] — *Crystallogr. Rep. (Engl. Transl.)*
[f] — *J. Struct. Chem. (Engl. Transl.)*

Russian Chemical Reviews **73** (1) 101 – 113 (2004) © 2004 Russian Academy of Sciences and Turpion Ltd

DOI 10.1070/RC2004v073n01ABEH000865

Kinetics, mechanism and intermediates of some radiation-induced reactions in aqueous solutions

B G Ershov

Contents

I.	Introduction	101
II.	Radiation chemical formation of oxidising and reducing reagents	101
III.	Oxidation of halide ions	102
IV.	Reactions of metal atoms and metal ions in unusual oxidation states	107
V.	Reactions of actinides	108
VI.	Reactions of organic radicals	109
VII.	Conclusion	111

Abstract. The results of pulse radiolysis studies of the kinetics and mechanism of fast one-electron redox reactions of halide ions, metal ions, actinides and other compounds with hydrated electrons, hydroxyl and other radicals and hydrogen atoms and the properties of intermediates formed in these reactions are analysed. The oxidation of a mixture of chloride and bromide ions yields mixed radical anions $ClBr^{-\bullet}$. Data on the formation of metal atoms and ions in unusual and unstable oxidation states by the reduction of metal ions in aqueous solutions and on the reactions involving such ions are presented. It is shown that the reduction of compounds in aqueous solutions with organic radicals takes place through outer- or inner-sphere electron transfer. The bibliography includes 116 references.

I. Introduction

The use of pulse radiolysis has made a considerable contribution to the studies of the kinetics and mechanism of redox reactions and the nature and properties of the short-lived intermediates thus arising. This technique was implemented into the research practice at the Institute of Physical Chemistry of the USSR Academy of Sciences in the early 1970s by initiative and with all-round support from Academician V I Spitsyn and Corresponding member of the Academy A K Pikaev. The description of the method and the results obtained using this method by Russian and foreign researchers before 1980 are considered in detail in a monograph.[1] Data on the properties of metal atoms and metal ions in unusual oxidation states formed upon one-electron reduction or oxidation of metal ions in stable oxidation states in aqueous solutions and on the small clusters formed upon their aggregation are presented in recent reviews.[2–4] The results of pulse radiolysis study of the redox reactions of actinides have been summarised.[5]

This review is a discussion of the results of pulse radiolysis studies of one-electron redox reactions involving diverse inorganic and organic compounds in aqueous solutions obtained mainly during the last 15 years. To cover the problem comprehensively and to provide substantiated interpretation of the data, earlier publications are also considered. Particular attention is paid to the oxidation of halide ions in aqueous solutions. The redox reactions involving chlorine, bromine and iodine are frequently encountered in nature and are used in practice. Thus water disinfection by chlorination still remains the main method for potable water treatment. The production processes involving halogens are widely used in industry. Therefore, considerable attention in the review is paid to the latest advances in the kinetic and mechanistic studies of halogen reactions. Owing to the use of modern investigation techniques for fast redox processes, the formation of mixed short-lived radical anions of the $ClBr^{-\bullet}$ type was detected.[6,7] In addition, characteristic features of a number of one-electron redox reactions of hydrated electrons, hydroxyl radicals, and other inorganic and organic radicals with various compounds in aqueous solutions are analysed.

B G Ershov Institute of Physical Chemistry, Russian Academy of Sciences, Leninsky prosp. 31, 119991 Moscow, Russian Federation.
Fax (7-095) 335 17 78. Tel. (7-095) 333 95 67, (7-095) 333 73 77.
E-mail: ershov@ipc.rssi.ru

Received 3 July 2003
Uspekhi Khimii **73** (1) 107 – 120 (2004); translated by Z P Bobkova

II. Radiation chemical formation of oxidising and reducing reagents

When investigating by pulse radiolysis the kinetics and mechanism of one-electron reduction or oxidation of compounds in aqueous solutions and the nature and the properties of the arising intermediates, radical ion species formed upon radiolysis of the solution are taken as the reagents. These species are formed upon ionisation of water molecules on exposure to radiation and in secondary reactions with dissolved compounds. The chemical stage of water radiolysis yields hydrated electrons (e_{aq}^-), hydrogen atoms, protons, and hydroxyl radicals ($OH^\bullet$) as well as hydrogen and hydrogen peroxide molecules. In the general form, the process of water radiolysis can be represented as follows:

$$H_2O \rightsquigarrow e_{aq}^- (2.7) + H^\bullet (0.6) + OH^\bullet (2.9) + \\ + H_2 (0.5) + H_2O_2 (0.7) + H^+ (2.7). \quad (1)$$

The values in parentheses are the initial radiation chemical yields of the products formed in the radiolysis of water and dilute aqueous solutions per 100 eV of absorbed energy for light types of radiation (γ-rays or accelerated electrons for which the linear transfer of energy is insignificant), recorded 10^{-7} s after the action of ionising radiation when the reactions at the sites of local formation of these species ('tracks' and 'spurs') have been completed. The hydrated electrons and hydrogen atoms behave as effective reducing agents. The standard reducing potentials of the

H_2O/e_{aq}^- and $H^+/H^\bullet$ pairs are -2.87 and -2.3 V, respectively.[8] The hydroxyl radical, conversely, is a strong oxidant; its redox potentials in water depend on the pH and amount to 1.9 and 2.73 V for the $OH^\bullet/OH^-$ and $OH^\bullet, H^+/H_2O$ pairs, respectively. These species are used to study one-electron reduction and/or oxidation. However, their simultaneous presence in an aqueous solution initiates the occurrence of both processes and markedly hampers study of the kinetics and the mechanism of redox reactions. Therefore, researchers use such compositions of aqueous solutions which ensure the predominant formation of either oxidising or reducing species. The oxidising radicals $OH^\bullet$ are produced most easily by saturating the solution with nitrous oxide. In a neutral solution, the limiting concentration of the gas under normal conditions equals approximately 0.05 mol litre^{-1}. The exposure to ionising radiation initiates the reaction

$$N_2O + e_{aq}^- + H_2O \longrightarrow N_2 + OH^\bullet + OH^-, \quad (2)$$

whose rate constant equals 9×10^9 litre mol^{-1} s^{-1} (see Ref. 9). As a consequence, hydroxyl radicals are formed in the solution almost alone. It is noteworthy that in the reaction with N_2O, the hydrogen atoms can also be converted into $OH^\bullet$ radicals; however, the rate constant for this reaction is only 1.3×10^4 litre mol^{-1} s^{-1} (see Ref. 9).

Conversely, to create a reducing medium in an aqueous solution, it is necessary to remove the hydroxyl radicals. This is done using solutions containing organic compounds acting as traps for $OH^\bullet$ radicals, *e.g.*, alcohols or salts of organic acids. These compounds also allow binding of hydrogen atoms. For example, upon the addition of isopropyl alcohol or formate ions, the reactions

$$(CH_3)_2CHOH + OH^\bullet\,(H^\bullet) \longrightarrow (CH_3)_2C^\bullet OH + H_2O\,(H_2), \quad (3)$$

$$HCO_2^- + OH^\bullet\,(H^\bullet) \longrightarrow CO_2^{-\bullet} + H_2O\,(H_2), \quad (4)$$

initiated by ionising radiation give rise only to reducing species, namely, hydrated electrons and organic radicals, $(CH_3)_2C^\bullet OH$ or $CO_2^{-\bullet}$. The standard reducing potentials (E°) of some organic radicals used most often are given below.[8]

Species	$CO_2^{-\bullet}$	$(CH_3)_2C^\bullet OH$	$CH_3CH^\bullet OH$	$^\bullet CH_2OH$
E°/V	-1.9	-1.39	-1.25	-1.18

The hydrated electron, the hydroxyl radical, the hydrogen atom, and organic radicals are highly reactive species, and, as a rule, the rates of their interaction with dissolved compounds are controlled by diffusion, the rate constants of the corresponding reactions being about $10^9 - 10^{10}$ litre mol^{-1} s^{-1}. The products of one-electron reduction or oxidation (most often, of a radical nature) are also highly reactive species. Therefore, they are generated and studied in aqueous solutions using a technique of fast processes, first of all, pulse radiolysis with optical or conductometric recording of short-lived products.[1]

III. Oxidation of halide ions

We have already noted that redox reactions involving chlorine, bromine, and iodine are widely used in practice. Therefore, the kinetics and the mechanisms of these reactions are under comprehensive research. Upon photolysis, radiolysis, or other types of physicochemical treatment of aqueous solutions containing halide ions, these ions are oxidised to give first halogen atoms. Subsequently, the process goes through a number of intermediate stages and affords halogen molecules and halogen compounds and the subsequent hydrolysis affords oxygen-containing compounds. The use of pulse radiolysis allows one to study the kinetics and the mechanism of oxidation of halide ions, to establish the nature of the intermediates, in particular, the possibility of formation of mixed radical anions containing atoms of different halogens.

1. Oxidation of Cl^- ions by $OH^\bullet$ radicals

The $OH^\bullet$ radicals are used as the reagent in the kinetic and mechanistic studies of the one-electron oxidation of Cl^- ions in aqueous solutions. In a neutral aqueous solution, Cl^- ions are not oxidised as the reaction is endothermic. Oxidation takes place only in acidic solutions to give $Cl_2^{-\bullet}$ radical anions. The UV spectra of the latter species exhibit an absorption band with a maximum at $\lambda = 340$ nm, the extinction coefficient (ε) at this wavelength being $(8.8 \pm 0.5) \times 10^3$ litre mol^{-1} cm^{-1}. The most detailed pulse radiolysis study of the reaction mechanism has been reported by Jayson *et al.*[10] The process includes the following reversible reactions:

$$Cl^- + OH^\bullet \rightleftharpoons ClOH^{-\bullet}, \quad (5)$$

$$ClOH^{-\bullet} + H^+ \rightleftharpoons Cl^\bullet + H_2O, \quad (6)$$

$$Cl^- + Cl^\bullet \rightleftharpoons Cl_2^{-\bullet}. \quad (7)$$

The $Cl_2^{-\bullet}$ radical anions disappear according to second-order reactions

$$Cl_2^{-\bullet} + Cl_2^{-\bullet} \longrightarrow Cl_2 + 2\,Cl^-, \quad (8)$$

$$OH^\bullet + Cl_2^{-\bullet} \longrightarrow OH^- + Cl_2. \quad (9)$$

It is worth noting that reactions (6) and (8), important in the redox transformations of chlorides, involve charged species, and, hence, they should depend on the ionic strength of the solution. The rate constants for reactions (6), (8) have been measured by pulse radiolysis and their dependences on the ionic strength have been elucidated.[11] In addition, some other reactions involving $Cl_2^{-\bullet}$ radical anions have been studied. This was done using N_2O-saturated weakly acidic (5×10^{-4} M HCl) aqueous solutions of NaCl after a 20-ns pulse of accelerated electrons [the absorbed dose per pulse was $(1.5 \pm 0.3) \times 10^{17}$ eV ml^{-1}]. It was found that after the pulse, optical absorption at $\lambda = 340$ nm passes through a maximum and then diminishes with time. This is due to the formation and subsequent decay of the $Cl_2^{-\bullet}$ radical anions. With an increase in the salt concentration, the rate of disappearance of $Cl_2^{-\bullet}$ increases, which is due to the increase in the ionic strength.

The rate constants for reactions (6), (8), and (9) at different ionic strengths of the solution have been determined by comparing the experimental data with the results of computations performed with the assumption of simultaneous reactions between the products of radiolysis of pure water.[11] The rate constant for reaction (6) increases with an increase in the salt concentration, whereas the rate constant for reaction (8) decreases. This result is consistent with the expected influence of the ionic strength on the rate of reactions between likely and oppositely charged species. Note that high concentrations of dissolved substances in water and the ionic strength of the solution have a pronounced influence on the yields of radiolysis products formed by reaction (1).[12] This must be taken into account when performing calculations. Figure 1 shows the dependences of the rate constants for reactions (6) and (8) on the solution ionic strength both experimental and calculated taking into account the dependence of the reaction rate constant on the activity of the charged species involved in the reaction. The last-mentioned type of dependence can be written as follows (the activity coefficient of the intermediate complex is taken to be unity according to the Brønsted – Bjerrum theory):

$$k = k_0\,\gamma_1^{\nu_1}\gamma_2^{\nu_2} = k_0\gamma_\pm^{\nu}, \quad (10)$$

where k and k_0 are the reaction rate constants for nonzero and zero ionic strengths of the solution, respectively; γ_1 and γ_2 are the activity coefficients of species 1 and 2; $\gamma_\pm$ is the average molal coefficient of activity of the electrolyte; ν_1 and ν_2 are the numbers of particles 1 and 2 involved in the reaction ($\nu = \nu_1 + \nu_2$).

The change in the $\gamma_\pm$ coefficient in the concentration range from 0 to 1 mol litre^{-1} is described adequately by the Debye – Hückel equation:[13]

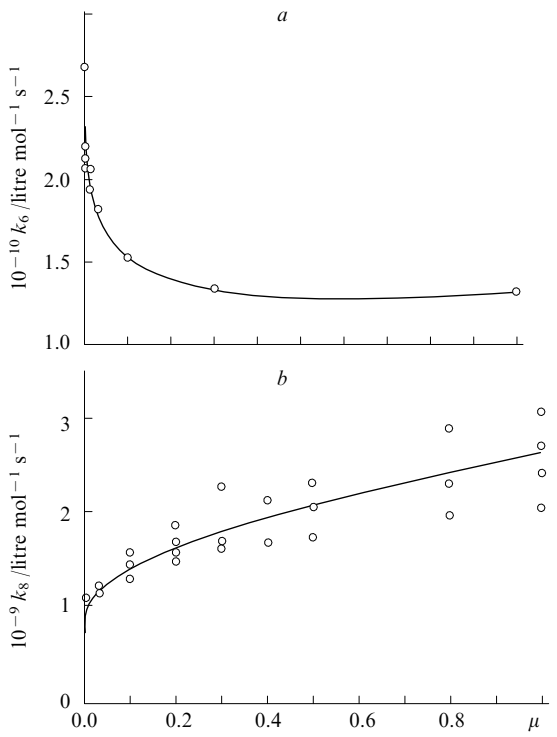

Figure 1. Rate constants for reactions (6) and (8) (k_6 and k_8 , respectively) *vs.* ionic strength of the solution (μ).
The dots correspond to experimental results and the curves, to the calculation from Eqns (10), (11): (*a*) reaction (6); (*b*) reaction (8). The calculation parameters are given in the text.

$$\log \gamma_{\pm} = \frac{A_1 z_1 z_2 \mu^{1/2}}{1 + Ba\mu^{1/2}} + b\mu, \qquad (11)$$

where A and B are coefficients that are constant for the given temperature and solvent; z_1 and z_2 are the charges of the reactants; μ is the ionic strength of the solution for concentrations expressed in mol litre^{-1}; and a and b are experimental parameters.

As can be seen from Fig. 1, the rate constants for reactions (6) and (8) as functions of the solution ionic strength found by optimisation are well described by the Debye–Hückel theory. This fact made it possible to determine their magnitudes for zero ionic strength.[11] For reaction (6), the value $k_6 = 8.3 \times 10^8$ litre mol^{-1} s^{-1} was obtained and the parameters a and b in relation (11) are equal to 0.46 nm and 4.8×10^{-2} litre mol^{-1}, respectively. The value $k_6 = 1.6 \times 10^9$ litre mol^{-1} s^{-1} calculated for an ionic strength of 0.2 is in satisfactory agreement with the rate constant measured in another study,[14] which is equal to 2.0×10^9 litre mol^{-1} s^{-1}. McElroy[15] has studied recombination of the $Cl_2^{-\bullet}$ radical anions produced in the photochemical reaction of $SO_4^{-\bullet}$ with the Cl^- ions. On extrapolation to zero ionic strength, the estimated rate constant for this reaction is 7×10^8 litre mol^{-1} s^{-1}, which is in rather good agreement with the value found in another publication.[11]

For reaction (8) and $\mu = 0$, the value $k_8 = 2.5 \times 10^{10}$ litre mol^{-1} s^{-1} was found; the calculated parameters a and b are 0.42 nm and 0.77 litre mol^{-1}, respectively. The constant $k_8 = 1.4 \times 10^{10}$ litre mol^{-1} s^{-1} calculated for $\mu = 1$ proved to be somewhat lower than the value 2.1×10^{10} litre mol^{-1} s^{-1} reported in another publication.[10]

The rate constant for reaction (9) (k_9) does not depend on the ionic strength of the solution, being equal to 9.2×10^9 litre mol^{-1} s^{-1}. A study of flash photolysis of chloride ions in water[15] gave a value of 1×10^9 litre mol^{-1} s^{-1} for the same rate constant. However, McElroy[15] used conductometry as a technique for recording the variation of the electrical conductivity of the solution, which is not selective in the presence of other reactions involving charged species.

Studies of the kinetics and the mechanism of the oxidation of Cl^- ions with the $OH^\bullet$ radicals made it possible to measure once again the rate constant for a very important reaction between hydrogen atoms and hydrogen peroxide:

$$H^\bullet + H_2O_2 \longrightarrow OH^\bullet + H_2O. \qquad (12)$$

The reported[16] value of 9.0×10^7 litre mol^{-1} s^{-1} did not correspond to the results of computer simulation of the radiation-induced chemical transformations of pure water and water containing added hydrogen and/or hydrogen peroxide and appeared clearly overestimated.[17] Therefore, systematic research into the radiation-induced transformations of argon-saturated chloride solutions (0.1 M HCl) containing hydrogen peroxide has been carried out.[18] Analysis of the kinetics of the additional formation of $Cl_2^{-\bullet}$ radical anions for short radiolysis times (5 μs), caused by the additional generation of the $OH^\bullet$ radicals by reaction (12) allowed Ershov *et al.*[18] to determine the rate constant for this reaction $k_{12} = 3.5 \times 10^7$ litre mol^{-1} s^{-1}. This value is consistent with the constant found for the decay of hydrogen atoms by EPR.[19] For long radiolysis times (250 μs), recombination of the $Cl_2^{-\bullet}$ radical anions and their reaction with H_2O_2 are the predominant processes

$$H_2O_2 + Cl_2^{-\bullet} \longrightarrow 2\,HCl + O_2^{-\bullet}. \qquad (13)$$

The role of reaction (13) increases with an increase in the concentration of hydrogen peroxide. When the H_2O_2 content is $\geqslant 5 \times 10^{-2}$ mol litre^{-1}, the kinetics of the decay of $Cl_2^{-\bullet}$ absorption is better described by a pseudo-first-order equation, which indicates that these radical anions mainly disappear by reaction (13). Modelling of the kinetic curves for the decay of the $Cl_2^{-\bullet}$ species allowed Ershov *et al.*[11] to determine the rate constant for reaction (13): $k_{13} = 9.5 \times 10^5$ litre mol^{-1} s^{-1}. For solutions containing hydrogen peroxide, it was necessary to include additional steps taking into account the reactions of $H^\bullet$ and $OH^\bullet$ with H_2O_2 and with the $HO_2^\bullet$ radical.

The results of a kinetic study of the redox reactions of Cl^- ions in aqueous solutions induced by ionising radiolysis are summarised in Table 1.

Table 1. Rate constants (k) for the oxidation of the Cl^- and Br^- ions.

Reaction	k /litre mol^{-1} s^{-1}	Ref.
$OH^\bullet + Cl^- \longrightarrow ClOH^{-\bullet}$	4.3×10^9	10
$ClOH^{-\bullet} \longrightarrow OH^\bullet + Cl^-$	6.1×10^9 (see [a])	10
$H^+ + ClOH^{-\bullet} \longrightarrow Cl^\bullet + H_2O$	2.5×10^{10}	10
$Cl^- + Cl^\bullet \longrightarrow Cl_2^{-\bullet}$	8.0×10^9	20
$Cl_2^{-\bullet} \longrightarrow Cl^\bullet + Cl^-$	1.1×10^5 (see [a])	10
$Cl_2^{-\bullet} + Cl_2^{-\bullet} \longrightarrow Cl_3^- + Cl^-$	8.3×10^8	11
$H^\bullet + Cl_2^{-\bullet} \longrightarrow Cl^- + HCl$	7.0×10^9	14
$OH^\bullet + Cl_2^{-\bullet} \longrightarrow OH^- + Cl_2$	9.2×10^9	11
$H_2O_2 + Cl_2^{-\bullet} \longrightarrow 2\,HCl + O_2^{-\bullet}$	9.5×10^5	11
$Cl_2^{-\bullet} + Br^- \longrightarrow ClBr^{-\bullet} + Cl^-$	4.0×10^9	7
$ClBr^{-\bullet} + Cl^- \longrightarrow Cl_2^{-\bullet} + Br^-$	1.1×10^2	7
$ClBr^{-\bullet} \longrightarrow Cl^- + Br^\bullet$	8.5×10^7 (see [a])	7
$Cl^- + Br^\bullet \longrightarrow ClBr^{-\bullet}$	1.0×10^{10}	7
$ClBr^{-\bullet} + Br^- \longrightarrow Br_2^{-\bullet} + Cl^-$	8.0×10^9	7
$Br_2^{-\bullet} + Cl^- \longrightarrow ClBr^{-\bullet} + Br^-$	4.3×10^6	7
$Br_2^{-\bullet} \longrightarrow Br^\bullet + Br^-$	4.6×10^4 (see [a])	21, 22
$Br^\bullet + Br^- \longrightarrow Br_2^{-\bullet}$	1.0×10^{10}	21, 22
$Br_2^{-\bullet} + Br_2^{-\bullet} \longrightarrow Br_3^- + Br^-$	3.4×10^9	7

[a] The rate constant is expressed in s^{-1}.

2. Oxidation of Br^- ions by $Cl_2^{-\bullet}$ radical anions and the formation of $ClBr^{-\bullet}$ radical anions

Most often, chlorine is accompanied by bromine and/or iodine impurities. Therefore, the redox reactions with chlorine are accompanied by chemical transformations of these halogens. Indeed, chlorination of water yields bromate ion BrO_3^- (see Ref. 21), which is carcinogenic. Lots of other examples can also be cited. This underlines the topicality of comprehensive investigation of the influence of bromine and iodine impurities on the oxidation of chlorine.

Radiation-induced or photochemical oxidation of Br^- ions in aqueous solutions is known [22] to give $Br_2^{-\bullet}$ radical anions [$\lambda_{max} = 360$ nm, $\varepsilon = (9.9\pm0.6)\times10^3$ litre mol^{-1} cm^{-1}]. However, their spectra, unlike the spectra of the $Cl_2^{-\bullet}$ radical anions, exhibit also a weak optical absorption in the region of 650–700 nm. The standard reduction potentials of the $Cl_2^{-\bullet}$ and $Br_2^{-\bullet}$ radical anions are as follows: $E^\circ(Cl_2^{-\bullet}/2\,Cl^-) = 2.30$ V; $E^\circ(Br_2^{-\bullet}/2\,Br^-) = 1.66$ V;[8] hence, these species behave as rather strong oxidants. The rate constants for many reactions of one-electron oxidation of organic and inorganic compounds involving these radical anions have been measured by pulse radiolysis and photolysis.[23] Comparison of the $E^\circ(Cl_2^{-\bullet}/2\,Cl^-)$ value with $E^\circ(Br_2^{-\bullet}/2\,Br^-)$ and also with $E^\circ(Br^\bullet/Br^-) = 2.0$ V may indicate that the $Cl_2^{-\bullet}$ radical anions are able to oxidise Br^- ions in an aqueous solution to give $Br_2^{-\bullet}$ radical anions.

Recently, oxidation of the Br^- ions by $Cl_2^{-\bullet}$ radical anions [6, 7, 24] has been studied by pulse radiolysis. The interest in this important reaction was stimulated not only by fundamental but also by practical problems. First of all, this was due to the need to study the oxidation of bromine during water chlorination and the radiation-induced chemical reactions in natural water near sites of nuclear waste disposal, first of all, in salt mines (see for example, Refs 25–27). Apart from substantial amounts of chlorides, this water contains bromides. Chemical transformations of the latter initiated by ionising radiation can substantially influence the ultimate composition of the obtained products and, hence, the safety of waste storage. The studies showed that in N_2O-saturated concentrated solutions of chlorides (1 M NaCl, pH 3.3) containing 1.0×10^{-3} mol litre^{-1} of bromine, oxidation of Br^- ions by $Cl_2^{-\bullet}$ radical anions proceeds at a high rate and ends in the formation of the $Br_2^{-\bullet}$ radical anions.[6, 7] At $[Br^-] \leqslant 1.0\times10^{-4}$ mol litre^{-1}, mixed radical anions $ClBr^{-\bullet}$ are produced. Similar mixed intermediates ($ClSCN^{-\bullet}$ and $BrSCN^{-\bullet}$ radical anions) have been detected previously by pulse radiolysis upon oxidation of chloride [28] and bromide ions,[29] respectively, in the presence of small amounts of the SCN^- ions added. The $ClBr^{-\bullet}$ radical anions arise and coexist in an equilibrium with the $Cl_2^{-\bullet}$ and $Br_2^{-\bullet}$ species, in accordance with the reactions

$$Cl_2^{-\bullet} + Br^- \rightleftharpoons ClBr^{-\bullet} + Cl^-, \quad (14)$$

$$ClBr^{-\bullet} + Br^- \rightleftharpoons Br_2^{-\bullet} + Cl^-. \quad (15)$$

Redox reactions (14) and (15) can be written in the following way:
reaction (14),

$$Cl_2^{-\bullet} + e^- \longrightarrow Cl^- + Cl^-,$$

$$Cl^- + Br^- \longrightarrow ClBr^{-\bullet} + e^-;$$

reaction (15),

$$ClBr^{-\bullet} + e^- \longrightarrow Br^- + Cl^-,$$

$$Br^- + Br^- \longrightarrow Br_2^{-\bullet} + e^-.$$

The corresponding redox potentials are $\Delta E_{14}^\circ = E^\circ(Cl_2^{-\bullet}/2\,Cl^-) - E^\circ(ClBr^{-\bullet}/Cl^-,Br^-)$ and $\Delta E_{15}^\circ = E^\circ(ClBr^{-\bullet}/Cl^-,Br^-) - E^\circ(Br_2^{-\bullet}/2\,Br^-)$. The ΔE° value can be expressed *via* the equilibrium constant (K) as $\Delta E^\circ = 0.059 \log K$. By using the known values, $E^\circ(Br_2^{-\bullet}/2\,Br^-) = 1.66$ V and $E^\circ(Cl_2^{-\bullet}/2\,Cl^-) = 2.3$ V, one can find [2, 4] $K_{14}\times K_{15} = 7.0\times10^{10}$.

Optimisation of the time dependence observed in the optical spectra for the intensity of the signal at 700 nm, which is composed of the absorption of the $ClBr^{-\bullet}$ and $Br_2^{-\bullet}$ radical anions, has given [7] the following values: $K_{14} = 3.78\times10^7$, $K_{15} = 1.85\times10^3$, $\varepsilon_{ClBr^{-\bullet}} = 110$ litre mol^{-1} cm^{-1} (for $\lambda =$ 700 nm). The K_{14} and K_{15} values were used to calculate the oxidation potential for the $ClBr^{-\bullet}/Cl^-,Br^-$ pair, which proved to be 1.85 V. As was to be expected, this value is intermediate between the potentials of $Br_2^{-\bullet}$ (1.66 V) and $Cl_2^{-\bullet}$ (2.30 V).

For the equilibria,

$$ClBr^{-\bullet} \rightleftharpoons Br^\bullet + Cl^- \quad (16)$$

and

$$Br_2^{-\bullet} \rightleftharpoons Br^\bullet + Br^-, \quad (17)$$

the relation $K_{15} = K_{16}/K_{17}$ is valid. Using the known [30, 31] $K_{17} = 4.6\times10^{-6}$ mol litre^{-1} and the equilibrium constant $K_{15} = 1.85\times10^3$ determined by Ershov *et al.*,[7] we get $K_{16} = 8.5\times10^{-3}$ mol litre^{-1}. Similarly, for the equilibria,

$$ClBr^{-\bullet} \rightleftharpoons Cl^\bullet + Br^- \quad (18)$$

and

$$Cl_2^{-\bullet} \rightleftharpoons Cl^\bullet + Cl^-, \quad (19)$$

it can be written that $K_{14} = K_{19}/K_{18}$. Using the above-indicated value $K_{14} = 3.78\times10^7$ and the reported [20] constant $K_{19} = 5.3\times10^{-6}$ mol litre^{-1}, one can calculate the value $K_{18} = 1.4\times10^{-13}$ mol litre^{-1}. Comparison of the values of K_{16} and K_{18} shows that the probability of the decay of the $ClBr^{-\bullet}$ species according to reaction (18) is low compared to that by reaction (16).

Computer simulation of the experimental data on the oxidation kinetics of the Br^- ions by the $Cl_2^{-\bullet}$ radical anions has been reported.[7] The calculated rate constants for the formation of the $Cl_2^{-\bullet}$ radical anions and for their reaction with Br^- ions and the known rate constants of other reactions are presented in Table 1. It was found [7] that the set of reactions proposed describes

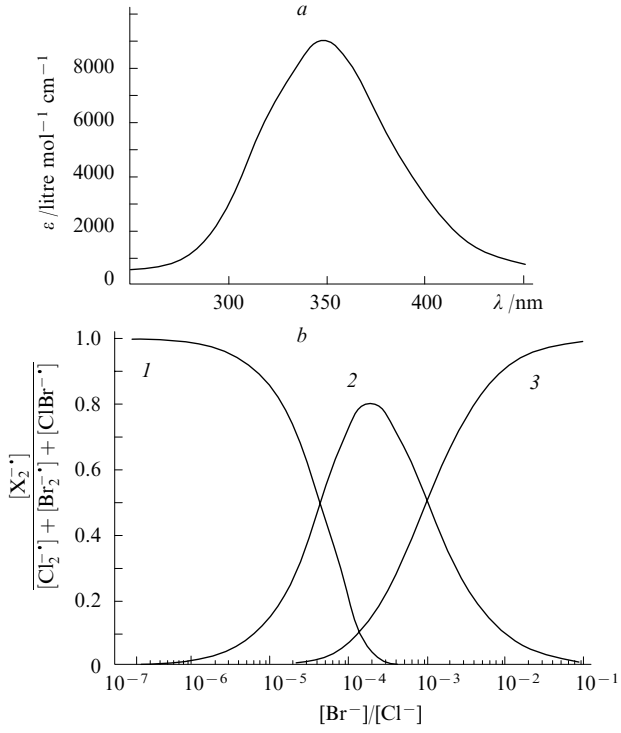

Figure 2. (*a*) Absorption spectrum of the $ClBr^{-\bullet}$ radical anion. (*b*) Equilibrium concentrations of the $X_2^{-\bullet} = Cl_2^{-\bullet}$ (*1*), $ClBr^{-\bullet}$ (*2*) and $Br_2^{-\bullet}$ (*3*) radical anions in solution *vs.* $[Br^-]/[Cl^-]$ [7, 24] ratio.

adequately the kinetics of variation of the optical absorption generated by an electron pulse at all wavelengths. For each wavelength, known [9,22] extinction coefficients were used for the $Cl_2^{-\bullet}$, $ClOH^{-\bullet}$ and $Br_2^{-\bullet}$ radical anions, while the $\varepsilon_{ClBr^{-\bullet}}$ values were calculated.

Figure 2*a* shows the absorption spectrum of the $ClBr^{-\bullet}$ radical anions obtained by matching the experimental data to the calculations in terms of the set of chemical reactions indicated in Table 1.[7] The spectrum is a broad absorption band with a maximum at $\lambda = 350\pm3$ nm and with the coefficient ε at this wavelength equal to 9300 ± 200 litre mol^{-1} cm^{-1}. Thus, the optical characteristics of $ClBr^{-\bullet}$ prove to be intermediate between the corresponding characteristics of the $Cl_2^{-\bullet}$ ($\lambda_{max} = 340$ nm and $\varepsilon = 8800$ litre mol^{-1} cm^{-1}) [10] and $Br_2^{-\bullet}$ radical anions ($\lambda_{max} = 360$ nm and $\varepsilon = 9900$ litre mol^{-1} cm^{-1}).[32]

Figure 2*b* presents an illustration of the dependence of the ratio of the equilibrium concentrations of the $Cl_2^{-\bullet}$, $ClBr^{-\bullet}$, and $Br_2^{-\bullet}$ radical anions on the concentration ratio of the Cl^- and Br^- ions.[7,24] The $Cl_2^{-\bullet}$ radical anions oxidise the Br^- ions to give $ClBr^{-\bullet}$ and $Br_2^{-\bullet}$ radical anions. As the concentration of Br^- increases, the equilibrium shifts towards $Br_2^{-\bullet}$.

3. Decay of the $Cl_2^{-\bullet}$ radical anions and the formation of molecular chlorine and the Cl_3^- anions

The oxidation of chloride ions in water gives rise to molecular chlorine as a result of recombination of the $Cl_2^{-\bullet}$ radical anions arising at an intermediate stage

$$Cl_2^{-\bullet} + Cl_2^{-\bullet} \longrightarrow Cl_3^- + Cl^- \qquad (20a)$$

or

$$Cl_2^{-\bullet} + Cl_2^{-\bullet} \longrightarrow Cl_2 + 2\,Cl^-. \qquad (20b)$$

The Cl_3^- ion exists in equilibrium with molecular chlorine

$$Cl_3^- \rightleftharpoons Cl_2 + Cl^-. \qquad (21)$$

Zimmerman and Strong [33] have measured the absorption spectra of Cl_3^- and Cl_2 in neutral and acidic aqueous solutions containing dissolved chlorine. The spectrum of Cl_3^- ions is a broad optical band with a maximum at $\lambda \approx 220$ nm and $\varepsilon = 1\times10^4$ litre mol^{-1} cm^{-1}. These data were confirmed by more advanced investigation techniques.[34] It was found that for Cl_3^-, the extinction coefficient at $\lambda = 220$ nm equals 1.04×10^4 litre mol^{-1} cm^{-1}; the spectrum also exhibits a weak peak at 320 nm ($\varepsilon = 180$ litre mol^{-1} cm^{-1}). The value of ε at 330 nm for chlorine does not exceed 70 litre mol^{-1} cm^{-1}. The stability constant of the Cl_3^- ions (K_{21}) was found to be 0.18 ± 0.02 mol litre^{-1} (see Ref. 34). Hence, the equilibrium of reaction (21) shifts towards the trichloride ions Cl_3^- only when the content of the Cl^- ions in solution is very high.

Until recently, trichloride ions have not been detected as products of photochemical or radiation chemical oxidation of Cl^- ions or transformations of $Cl_2^{-\bullet}$ radical anions in aqueous solutions. It was not clear which species, Cl_3^- or Cl_2, arises as the primary product of the transformations of the $Cl_2^{-\bullet}$ radical anions by reactions (20a) and (20b), respectively. This and some other questions were answered by Ershov *et al.*,[24] who suggested, proceeding from the value $K_{21} = 0.18\pm0.02$ mol litre^{-1}, that Cl_3^- can be found in relatively concentrated ($\geqslant 1$ M) solutions of Cl^-. This conclusion was confirmed experimentally.[24] A weak absorption with a maximum at 220 nm was found to appear in the spectrum of a 1 M solution of NaCl during the decay of the $Cl_2^{-\bullet}$ radical anions, the signal intensity being higher for higher concentrations of the salt. A rather clear-cut optical absorption was detected in the spectra of a 5 M solution of NaCl. It seemed reasonable to relate the appearance of the signal at 220 nm to the formation of Cl_3^- ions upon the decay of $Cl_2^{-\bullet}$. The rate of disappearance of the signal increased with an increase in the absorbed dose per pulse. The kinetics of the decay of the $Cl_2^{-\bullet}$ radical anions was well described by a second-order equation and the $\tau_{1/2}$ value decreased in proportion with the dose per pulse. Unlike the decay of the $Cl_2^{-\bullet}$ species, the appearance of Cl_3^- ions depended only little on the dose per pulse and could not be described by simple first- or second-order kinetics. The $\tau_{1/2}$ values did not change much upon variation of the absorbed dose per pulse. All this indicated that the formation of the signal from Cl_3^- ions is not limited by the decay of the $Cl_2^{-\bullet}$ radical anions but is limited by another process, which is slower. It was found [24] that the slow process of establishing the equilibrium in reaction (21) is the rate-limiting step in the formation of Cl_3^- ions. Analysis of the kinetics of appearance of the Cl_3^- ions allowed the researchers to determine the rate constants for the forward (the subscript f) and back (the subscript b) reactions (21) to be $k_{21f} = 1.1\times10^5$ s^{-1}, $k_{21b} = 2.0\times10^4$ litre mol^{-1} s^{-1}. The equilibrium constant of reaction (21) obtained by this optimisation, $K_{21} = k_{21b}/k_{21f}$, amounts to 0.18 litre mol^{-1}, which is in full agreement with the value measured previously.[33,34] Thus, the reaction between two $Cl_2^{-\bullet}$ species is most likely to afford the Cl_2 molecule. Apparently, the like charges of the radical anions prevent these species from approaching each other and the reaction occurs at a certain distance between them upon an electron transfer by reaction (20b). The subsequent appearance of the Cl_3^- ion is due to establishment of equilibrium (21).

4. Oxidation of the Br^- ions and formation of the Br_3^- anions

The radiation-induced oxidation of Br^- ions by $OH^\bullet$ radicals in acidic aqueous solutions gives rise to $Br_2^{-\bullet}$ radical anions.[22,32] The oxidation mechanism is similar to the mechanism considered above for chlorides. The pattern of transformations of bromide ions includes the following reactions:

$$Br^- + OH^\bullet \rightleftharpoons BrOH^{-\bullet}, \qquad (22)$$

$$BrOH^{-\bullet} + H^+ \rightleftharpoons Br^\bullet + H_2O, \qquad (23)$$

$$Br^- + Br^\bullet \rightleftharpoons Br_2^{-\bullet}, \qquad (24)$$

$$Br^\bullet + OH^- \rightleftharpoons BrOH^{-\bullet}, \qquad (25)$$

$$BrOH^{-\bullet} + Br^- \longrightarrow Br_2^{-\bullet} + OH^-. \qquad (26)$$

The mechanism of recombination of $Br_2^{-\bullet}$ radical anions has been studied.[31] It was found that disappearance of $Br_2^{-\bullet}$ absorption, which was observed 1 μs after the action of an electron pulse on a 0.1 M solution of NaBr (N_2O, pH 3.3), is accompanied by the formation of a new band with a maximum at 265 nm. This is due to the formation of Br_3^- ions in accordance with the reactions:

$$Br_2^{-\bullet} + Br_2^{-\bullet} \longrightarrow Br_2 + 2\,Br^-, \qquad (27)$$

$$Br_2 + Br^- \rightleftharpoons Br_3^-. \qquad (28)$$

For bringing the experimental data in correspondence with the results of computation, the following rate constants for reactions (22)–(26) were used:[22,35] (the subscripts f and b refer to the forward and back reaction, respectively): $k_{22f} = 1.06\times10^{10}$ litre mol^{-1} s^{-1}; $k_{22b} = 3.3\times10^7$ s^{-1}; $k_{23f} = 4.4\times10^{10}$ litre mol^{-1} s^{-1}; $k_{23b} = 1.4$ s^{-1}; $k_{24f} = 1.0\times10^{10}$ litre mol^{-1} s^{-1}; $k_{24b} = 4.6\times10^4$ s^{-1}; $k_{25f} = 1.3\times10^{10}$ litre mol^{-1} s^{-1}; $k_{25b} = 4.2\times10^6$ s^{-1}; $k_{26} = 1.9\times10^8$ litre mol^{-1} s^{-1}. The values of k_{27}, k_{28f} and k_{28b} were varied during optimisation. It was found [32] that the formation and disappearance of the $Br_2^{-\bullet}$ radical anions is described adequately using the values $\varepsilon_{Br_2^{-\bullet}} = 9900$ litre mol^{-1} cm^{-1} (see Ref. 22) and $k_{27} = 3.0\times10^9$ litre mol^{-1} s^{-1}. The resulting k_{27} value is in good agreement with the experimental rate constant measured for dilute solutions of Br^- ions, which is equal to 2.2×10^9 litre mol^{-1} s^{-1} (see Ref. 23). The agreement for the kinetics of appearance of the Br_3^- anions is attained for $k_{28f} = 9.6\times10^8$ litre mol^{-1} s^{-1}, $k_{28b} = 5.5\times10^7$ s^{-1} and $\varepsilon_{Br_3^-} = 4.4\times10^4$ litre mol^{-1} cm^{-1}. The equilibrium constant for reaction (28) calculated using the k_{28f} and k_{28b} as $K_{28} = k_{28f}/k_{28b}$ amounts to 17.4 litre mol^{-1}. Thus, the obtained values of $\varepsilon_{Br_3^-}$ and K_{28} are in good agreement with the extinction coefficient and the equilibrium constant determined [34] in a study of reaction (28)

in slightly acidic solutions of molecular bromine and Br^- ions, which are equal to 4.1×10^4 litre mol^{-1} cm^{-1} and 16.1 litre mol^{-1}, respectively.

5. Chlorine and bromine mixed trihalide ions

It was established [24, 36] that the presence of even very small amounts ($\geqslant 10^{-6}$ mol litre^{-1}) of Br^- ions in concentrated (1–5 M) solutions of NaCl results in substantial changes in the oxidation mechanism of chloride ions. During the decay of $Cl_2^{-\bullet}$ radical anions, Cl_3^- ions are no longer formed but, instead, the reaction gives a new intermediate characterised by an intense absorption band. As the bromine concentration increases (up to 10^{-3} mol litre^{-1} NaBr), new products responsible for intense optical bands with maxima at 230 and 245 nm are formed successively. On a further increase in the bromine content in the solution, an absorption band with a maximum at 265 nm corresponding to the Br_3^- ion appears in parallel with the disappearance of the $Cl_2^{-\bullet}$, $ClBr^{-\bullet}$ and $Br_2^{-\bullet}$ radical anions.

Analysis of the variation of the spectral pattern in the UV region demonstrates the complexity of the chemical transformations involved, in particular, transition from Cl_3^- ($\lambda_{max} = 220$ nm) to Br_3^- ($\lambda_{max} = 265$ nm) through consecutive formation of mixed chlorine/bromine oxidation products. It was shown [24, 36] that the absorption bands with maxima at 230 and 245 nm refer to mixed trihalide ions, Cl_2Br^- and $ClBr_2^-$, respectively. It has been noted previously [34] that these species are also formed in the reactions of Cl_2 and ClBr molecules with Cl^- and Br^- ions in acidified aqueous solutions.

A reaction scheme for the formation of Cl_2Br^- ions upon radiation-induced chemical oxidation of chloride ions in slightly acidic aqueous solutions has been proposed.[24] First, it includes reactions (20a) and (21) we considered above (with the rate constants found for them), which give rise to molecular chlorine and Cl_3^-. Second, it is supplemented [34] by steps yielding mixed compounds of chlorine and bromine upon reactions of Cl_2 molecules with Br^- ions:

$$Cl_2 + Br^- \longrightarrow Cl_2Br^-,\ k_{29f} = 6.0 \times 10^9 \text{ litre mol}^{-1}\text{ s}^{-1}; \quad (29f)$$

$$Cl_2Br^- \longrightarrow Cl_2 + Br^-,\ k_{29b} = 9.0 \times 10^3\ \text{s}^{-1}; \quad (29b)$$

$$ClBr + Cl^- \longrightarrow Cl_2Br^-,\ k_{30f} = 1.0 \times 10^6 \text{ litre mol}^{-1}\text{ s}^{-1}; \quad (30f)$$

$$Cl_2Br^- \longrightarrow ClBr + Cl^-,\ k_{30b} = 1.7 \times 10^5\ \text{s}^{-1}; \quad (30b)$$

$$Cl_2Br^- + Br^- \longrightarrow ClBr_2^- + Cl^-,\ k_{31} = 3.0 \times 10^8 \text{ litre mol}^{-1}\text{ s}^{-1}. \quad (31)$$

Previously, the rate constant for the reaction of Cl_2 with Br^- ions in 1 M HCl (k_{29f}) was measured to be $(7.7 \pm 1.3) \times 10^9$ litre mol^{-1} s^{-1}. The order of magnitude of the constant shows that this reaction is controlled by diffusion. By modelling in terms of this set of reactions, the constants $k_{29b} = (6.0 \pm 1.0) \times 10^9$ litre mol^{-1} s^{-1} and $K_{29} = k_{29f}/k_{29b} = (6.7 \pm 1.3) \times 10^5$ litre mol^{-1} were determined.[24] The ratio of the constants for the forward and back reactions (30) was selected proceeding from the known $K_{30} = k_{30f}/k_{30b}$ value, equal to (6.0±0.3) litre mol^{-1} (see Ref. 34). The partial transformation of Cl_2Br^- into $ClBr_2^-$ upon the reaction with Br^- ions has also been taken into account (the extinction coefficient of the last-mentioned trihalide at $\lambda = 230$ nm is 1.8×10^4 litre mol^{-1} cm^{-1}). The proposed set of reactions [24] describes adequately the radiation-induced oxidation of chloride ions in aqueous solutions containing some bromide ions. The extinction coefficients of the Cl_2Br^- (230 nm) and Br_2Cl^- (245 nm) trihalide ions were calculated to be $\varepsilon = (3.6 \pm 0.4) \times 10^4$ and $(2.2 \pm 0.3) \times 10^4$ litre mol^{-1} cm^{-1}, respectively. These values are in good agreement with the values 3.27×10^4 and 2.49×10^4 litre mol^{-1} cm^{-1} measured in another study,[34] where the trihalides Cl_2Br^- and Br_2Cl^- were prepared by reactions of Cl_2 and ClBr with Br^- ions.

Table 2. Rate constants (k) and equilibrium constants (K) for the formation of trihalide ions X_3^- (X = Cl, Br) and optical characteristics of the X_3^- ions [24, 36]

Reaction	k (see [a])	K (see [b])	X_3^-	λ_{max} /nm	ε (see [c])
$Cl_2 + Cl^- \longrightarrow Cl_3^-$	2.0×10^4	0.18	Cl_3^-	220	1.3×10^4
$Cl_3^- \longrightarrow Cl_2 + Cl^-$	1.1×10^5 (see [d])				
$Cl_2 + Br^- \longrightarrow Cl_2Br^-$	6.0×10^9	6.7×10^5	Cl_2Br^-	230	3.6×10^4
$Cl_2Br^- \longrightarrow Cl_2 + Br^-$	9.0×10^3 (see [d])				
$ClBr + Cl^- \longrightarrow Cl_2Br^-$	1.0×10^6	6.0			
$Cl_2Br^- \longrightarrow ClBr + Cl^-$	1.7×10^5 (see [d])				
$Cl_2Br^- + Br^- \longrightarrow ClBr_2^- + Cl^-$	3.0×10^8		$ClBr_2^-$	245	2.2×10^4
$Br_2 + Br^- \longrightarrow Br_3^-$	9.6×10^8	17.5	Br_3^-	265	4.4×10^4
$Br_3^- \longrightarrow Br_2 + Br^-$	5.5×10^7 (see [d])				

[a] The rate constant is expressed in litre mol^{-1} s^{-1}; [b] the equilibrium constant is expressed in litre mol^{-1}; [c] the extinction coefficient is expressed in litre mol^{-1} cm^{-1}; [d] the constant is in s^{-1}.

Table 2 presents the reactions responsible for the formation of anionic and molecular products in aqueous solutions containing Cl^- and Br^- ions and the corresponding equilibrium constants.

Thus, the results of pulse radiolysis studies attest to an important role of admixtures of Br^- ions in the oxidation mechanism of the Cl^- ions. At an early radical ion step, in the presence of Br^- ions, the $Cl_2^{-\bullet}$ radical anions tend to be converted into $ClBr^{-\bullet}$ and $Br_2^{-\bullet}$. The subsequent decay of these species gives rise to a large number of molecular (Cl_2, ClBr, Br_2) and ionic (Cl_3^-, Cl_2Br^-, $ClBr_2^-$, Br_3^-) products which occur in equilibrium. It is noteworthy that this behaviour is caused by the fact that bromine is a weaker oxidant than chlorine. Therefore, it is reasonable to expect that iodine, whose oxidative properties are even less pronounced, would also tend to produce mixed radical anions and molecular products in the redox processes in aqueous solutions in the presence of Cl^- and Br^- ions.

6. The reactivity of $X_2^{-\bullet}$ radical anions

The $Cl_2^{-\bullet}$, $Br_2^{-\bullet}$ and $I_2^{-\bullet}$ radical anions behave as fairly strong oxidants. Table 3 lists the reduction potentials for these species and for halogen atoms (the values were taken from a paper by Stanbury,[37] who summarised the data on theoretical and experimental determination of the potentials of inorganic radicals). It can be seen that the oxidising properties of the radical anions and atoms diminish in the sequence Cl, Br, I. On passing from a halogen atom to the radical anion, the potential also decreases, which is due to complexing of the halogen atom by the halogen ion.

Table 3. Reduction potentials (E°) of some inorganic radicals.[37]

Pair	E° /V	Pair	E° /V
$Cl^\bullet/Cl^-$	2.41	$SO_4^{-\bullet}/SO_4^{2-}$	2.43
$Br^\bullet/Br^-$	1.92	$SO_3^{-\bullet}/SO_3^{2-}$	0.63
$I^\bullet/I^-$	1.33	$NO_3^\bullet/NO_3^-$	~2.5
$Cl_2^{-\bullet}/2\,Cl^-$	2.09	$CO_3^{-\bullet}/CO_3^{2-}$	~1.5
$Br_2^{-\bullet}/2\,Br^-$	1.62	$(CSN)_2^{-\bullet}/2\,CSN^-$	1.32
$I_2^{-\bullet}/2\,I^-$	1.03	$SeO_3^{-\bullet}/SeO_3^{2-}$	1.68

Note. The error of determination of the potential does not exceed ±(0.05–0.10) V.

A multitude of publications have been devoted to the reactivity of the $Cl_2^{-\bullet}$, $Br_2^{-\bullet}$, and $I_2^{-\bullet}$ radical anions. This interest points to an important role of these species in the oxidation processes involving halogens. Selected values of the rate constants for the reactions of radical anions with some organic and inorganic ions and compounds in an aqueous solution are presented in Table 4. For most of reactions, the constants decrease in the sequence $Cl_2^{-\bullet}$, $Br_2^{-\bullet}$, $I_2^{-\bullet}$ in parallel with weakening of the oxidising properties of radical anions. The rate constants for one-electron oxidation are, most often, rather high; however, they are substantially lower than those for the $OH^{\bullet}$ radicals,[9] which can be attributed to lower potentials of the $Cl_2^{-\bullet}$, $Br_2^{-\bullet}$ and $I_2^{-\bullet}$ radical anions compared to the potentials of $OH^{\bullet}$. Most of the constants given in Table 4 are lower than the values typical of diffusion-limited reactions. The rate of these reactions may be expected to depend substantially on the free energy [or the difference between the reduction potentials (ΔE°)] of the reacting species]. Indeed, for reactions of the same type between Np^{III} or Pu^{III} and $Cl_2^{-\bullet}$, $Br_2^{-\bullet}$ or $I_2^{-\bullet}$, one can follow the expected linear dependences of the logarithm of the rate constant on the ΔE°.[5] The review [5] describes in detail features of the kinetics and the mechanism of the reactions of halogen radical anions (and other inorganic radical anions) with actinides.

Table 4. Rate constants (k) for one-electron oxidation of a number of compounds by the $X_2^{-\bullet}$ radical anions [23, 38–50]

Compound	k /litre mol^{-1} s^{-1}		
	$Cl_2^{-\bullet}$	$Br_2^{-\bullet}$	$I_2^{-\bullet}$
$X_2^{-\bullet}$ (see [a])	2.2×10^9	2.2×10^9	3.2×10^9
Cr^{2+}	2.4×10^9	1.9×10^9	1.5×10^9
Fe^{2+}	1.4×10^7	3.6×10^6	3.6×10^6
NO_2^-	2.5×10^8	6.7	–
H_2O_2	1.4×10^5	$<1\times10^3$	–
U^{3+}	4.2×10^9	3.4×10^9	1.2×10^9
Ascorbic acid	6.0×10^8	1.1×10^8	$\leqslant6\times10^5$
Cysteine	8.5×10^8	1.8×10^8	–
$(CH_3)_2S$	3.0×10^9	3.2×10^9	–
4-Hydroxybenzoate	2.8×10^8	2.3×10^8	–
Tryptophan	2.6×10^9	7.0×10^8	$<1\times10^6$

[a] Recombination reaction: X = Cl, Br, I.

IV. Reactions of metal atoms and metal ions in unusual oxidation states

The hydrated electron and the hydrogen atom have high reduction potentials, whereas the $OH^{\bullet}$ radical, conversely, is an effective oxidant. Therefore, when these species react with metal ions, one-electron reduction or oxidation occurs provided that the ratio of the potentials meets the requirement of decreasing the free energy of the system. In the case of Pb^{2+} ions, both processes can take place

$$Pb^{2+} + e_{aq}^- \longrightarrow Pb^+,$$

$$Pb^{2+} + OH^{\bullet} \longrightarrow Pb^{3+} + OH^-.$$

This gives rise to Pb^{3+} and Pb^+ ions in unusual and unstable oxidation states; their electronic configurations are $d^{10}s^1$ and $d^{10}s^2p^1$, respectively. Due to the presence of one electron in the outer s or p orbital, this metal ion or atom is extremely reactive. These species can be compared to radicals having an unpaired electron. The lifetimes of these species in aqueous solutions are determined by kinetic factors and, as a rule, they are measured in micro- or milliseconds.

Many metals thermodynamically able to exist in water in unusual oxidation states have now been studied by pulse radiolysis. Data on the rate constants for the formation of metal ions in unusual oxidation states upon the reduction of stable metal ions with hydrated electrons and hydrogen atoms or their oxidation by means of $OH^{\bullet}$ radicals have been reported in the book.[9] The rate constants for some reactions involving metal atoms and ions in unusual and unstable oxidation states are documented.[51] The properties of these short-lived species are considered in most detail in reviews.[2, 3]

Table 5 presents characteristics of optical absorption and electrochemical potentials of metal atoms and ions in unusual oxidation states with the structure of aqua complexes. It can be seen that species with the electron configuration $d^{10}s^1$ exhibit one intense absorption band in the UV region. It was found [2, 3] that the energies of optical transitions in the absorption maxima ($E_{\lambda max}$) increase linearly with an increase in the ion charge (z). Within a Subgroup, the energy increases with an increase in the Period number. The pattern of optical absorption of the metal aqua complexes with other electronic configurations proves to be more complex. However, for metal ions with the electron configuration $d^{10}s^2p^1$, the longer-wavelength absorption band shifts to the UV region in the sequence Tl^0, Pb^+, Bi^{2+}, and the $E_{\lambda_{max}}$ value increases linearly with an increase in z, as for ions with the electron configuration $d^{10}s^1$.

Comparison of the potentials presented in Table 5 shows that copper, silver and gold atoms are effective reductants. This is due to the presence of one electron in their outer s orbitals. In isoelectronic series of metals, the potential tends to decrease with an increase in the charge of the metal ion. Within a single Subgroup (*i.e.*, for ions with the same charge), the potential increases with an increase in the Period number.

Metal atoms and metal ions in unusual oxidation states are highly reactive and, depending on the potential, they can either reduce or oxidise organic and inorganic compounds. The rate

Table 5. Optical characteristics and reduction potentials of metal atoms and aqua complexes of metal ions in unusual oxidation states (see the studies [1–3, 52–54] and references cited therein).

Metal	λ_{max} /nm	ε /litre mol^{-1} cm^{-1}	E° /V
Cu^0	380	5.6×10^3	−2.6
Cu^{3+}	265	1.1×10^3	~1.8
Zn^+	310	1.8×10^4	−2.3
Ga^{2+}	270	–	−0.63
Ag^0	360	1.6×10^4	−1.8
Ag^{2+}	275	5.4×10^3	–
Cd^0	240	2.0×10^4	−0.81
Cd^+	295	1.8×10^4	−1.8
In^0	500	$\geqslant1.8\times10^3$	−1.05
In^{2+}	250	2.0×10^4	−0.45
Sn^{3+}	~215	–	~0.7
Au^0	260	4.2×10^3	−1.5
Au^{II}	270,	6.3×10^4,	–
	440	2.0×10^3	–
Hg^0	254	2.8×10^3	0.68
Hg^+	250	1.4×10^4	−1.0
Tl^{2+}	~225	–	0.3
Tl^0	260,	9.0×10^3,	−1.9
	450	5.0×10^3	–
Pb^0	300	1.2×10^4	−0.96
Pb^{3+}	$\leqslant$210	–	1.8
Pb^+	320	2.5×10^3	~(−1.0)
Bi^{2+}	285	2.4×10^4	–
Mn^+	~300	–	–
Co^+	310,	4.4×10^3,	−1.8
	370	4.8×10^3	–
Ni^+	300	5.5×10^3	~(−2.7)
Ir^{II}	280	1.7×10^3	–
Pd^+	290	6.4×10^3	–

Table 6. Rate constants (k) for some reactions of metals in unusual oxidation states.[51]

Compound	k /litre mol^{-1} s^{-1}					
	Ag^0	Cr^{2+}	Zn^+	Ni^+	Cd^+	Co^+
O_2	5.0×10^9	1.6×10^8	–	2.2×10^9	1.0×10^{10}	3.2×10^9
H_2O_2	3.5×10^9	7.1×10^4	2.5×10^9	3.2×10^8	2.2×10^9	1.5×10^9
MnO_4^-	1.2×10^{10}	4.0×10^9	–	7.2×10^9	7.8×10^9	1.0×10^{10}
NO_3^-	–	–	2.1×10^9	1.4×10^6	3.5×10^8	1.8×10^9
BrO_3^-	–	–	2.1×10^9	–	1.3×10^8	–
CCl_4	1.1×10^9	–	–	–	–	$\leqslant6\times10^5$
$ClCH_2CO_2^-$	1.5×10^8	–	–	–	–	–
1,4-Benzoquinone	1.5×10^8	3.5×10^9	3.0×10^9	–	3.9×10^9	–

constants for some reactions involving metal atoms and ions in unusual oxidation states are summarised in Table 6. (This Table was compiled using data from the book.[51]) The reaction rate constants are usually fairly high; in some cases (for example, for reactions of Ag^0, Cd^+ and Co^+ with O_2, H_2O_2 and inorganic anions), they correspond to the diffusion limits. Apparently, the electron transfer occurs by an outer-sphere mechanism. Among the reactions not controlled by diffusion of the reactants, no reactions can be found for which the rate constant would follow a clear-cut dependence on the reduction potential of the metal ion.

Some metal atoms and metal ions in unusual oxidation states tend to add more metal ions to yield small clusters.[3,55–57] This ability is especially characteristic of atoms that can attach an additional metal cation with a σ_s-bond (Ag, Cu) or a σ_{sp}-bond (In, Tl), thus forming small homoelement clusters consisting of two to about ten atoms.[3,54–56] It was also found[58,59] that silver atoms, Ag_2^+ cations and, perhaps, Ag_3^{2+} cations form complexes with cyanide anions, ethylenediaminetetraacetic acid or ammonia. The optical properties, the redox potentials and the kinetic characteristics of such clusters differ appreciably from analogous properties of the clusters having a hydration shell. The nucleation processes of silver in polymeric membranes,[59–62] in gelatin[63] and on the surface of colloidal silica[64] follow similar mechanisms, *i.e.*, they include the intermediate formation of the same clusters as those formed in homogeneous aqueous solutions of silver ions, which have been described in detail in our review.[3]

The possibility of formation of short-lived mixed (heteroelement) clusters has also been established.[65–69] These arise upon the reactions of metal ions in unstable oxidation states, in particular Co^+ ion, with other metal ions in stable oxidation states, for example, with the Ag^+ ion. Under these conditions, a short-lived $(CdAg)^{2+}$ cluster is formed.[65,68] A similar approach has been used[66] to obtain mixed clusters, $(CdTl)^{2+}$, $(TlAg)^+$ and $(TlCd)^{2+}$.

A metal ion in an unusual oxidation state can not only react with a different metal ion to give a mixed cluster; it can also reduce or oxidise a different ion. For instance, Zn^+ ions obtained upon the reduction of Zn^{2+} with hydrated electrons, unlike Cd^+ ions, enter into electron transfer reactions with silver, thallium and cadmium ions, no mixed clusters being formed.[65,66,68] In addition, the Tl_2^+ ions reduce Pb^{2+} ions. By using metal ions with various reduction potentials and various electron structures, the conditions that favour one or another reaction were identified.[3] It was found that mixed clusters are formed in those cases where the potentials of reacting metal ions either coincide or do not differ much. This also requires the possibility of formation of a bonding molecular orbital between the atomic orbitals of the reacting metal ions. Fast electron transfer between metal ions takes place when the standard potentials of the ions are appreciably different.

V. Reactions of actinides

During recent years, a substantial contribution has been made to the study of the kinetics and mechanisms of one-electron redox reactions involving actinides. A specific feature of these elements is the diversity of stable oxidation states depending on the pH value and the presence of diverse ligands. The reduction of tetra-, penta-, hexa- and heptavalent actinides with hydrated electrons has very high rate constants ($\sim2\times10^9$ to 1×10^{11} litre mol^{-1} s^{-1}, see Refs. 70–78). As in the case of other diffusion-controlled one-electron redox reactions, no clear-cut correlation can be followed between the rate constants and the reduction potentials (E°) of the corresponding pairs of actinide ions. The rate constants for the reactions of actinides with hydrogen atoms which occur predominantly in acidic media are much lower (10^7–10^9 litre mol^{-1} s^{-1}).[79–81] This difference can hardly be explained by the fact that the reduction potential of a hydrogen atom (−2.3 V) is less negative than the potential of the electron (−2.87 V). The researchers cited attributed this to different reduction mechanisms. In the case of the hydrated electron, the reaction occurs as an outer-sphere electron transfer. The reaction of actinides with hydrogen is apparently an inner-sphere reaction, which includes the insertion of an H$^\bullet$ atom into the hydration shell to give the $H_3O^\bullet$ complex with subsequent transfer of an electron from this complex to the central ion. The logarithms of the rate constants for the reactions between a hydrogen atom and AnO_2^{2+} ions (An = U, Pu, Am, Np) were found to follow a nearly linear dependence on the reduction potential.[5] Thus, the mechanisms of reactions for them are identical and are not controlled by diffusion. Hydrogen atoms act as one-electron oxidants with respect to the U^V, Np^{III} and Pu^{III} ions. Apparently, this is due to the formation of hydride complexes of these actinides at an intermediate stage of the reaction.[80,82]

The rate constants for the actinide reactions with the OH$^\bullet$ radicals are 10^8–10^9 litre mol^{-1} s^{-1}, their values being markedly dependent on the acidity of the aqueous solution.[83–87] The reactions follow an inner-sphere mechanism involving either detachment of a hydrogen atom from a water molecule by the OH$^\bullet$ radical or the replacement of the OH^- ion in the hydration shell of the actinide ion by this radical.[5]

The oxidation of halide ions in aqueous solutions by hydroxyl radicals giving rise to the $X_2^{-\bullet}$ radical anions has been described above in detail. In aqueous solutions containing SO_4^{2-}, NO_3^- or CO_3^{2-} ions, similar processes give $SO_4^{-\bullet}$, $NO_3^\bullet$ or $CO_3^{-\bullet}$ radical anions, respectively. In recent years, systematic research of the kinetics and mechanism of one-electron redox reactions of actinides involving these species has been carried out. It was found that their reduction potentials are commensurate with the potential of the OH$^\bullet$ radical in the pH region of 1–13 and they tend to oxidise actinides. Moreover, the rate constants for the $SO_4^{-\bullet}$ radical anion,[81,84] $NO_3^\bullet$ radical[84,88,89] and $CO_3^{-\bullet}$ radical anion[77,87] usually do not differ much from those for the OH$^\bullet$ radical. In the case of noncharged $NO_3^\bullet$ radical, the reaction rates are most likely controlled by diffusion, as for the $HSeO_3^\bullet$ radical.[90]. The rate constants for the reactions of Np^V and Np^{VI} with the ozonide $O_3^{-\bullet}$ radical anions are as low as 2×10^6 and 2×10^5 litre mol^{-1} s^{-1}, respectively.[91]

The reactions with halogen radical anions usually have lower rate constants than the reactions with sulfate and nitrate radicals.[84,88,89,92–94] As has already been noted, for the reactions of Np^{III} or Pu^{III} with $Cl_2^{-\bullet}$, $Br_2^{-\bullet}$ or $I_2^{-\bullet}$, the logarithm of the rate constant obeys a linear dependence on the difference between the reduction potentials (ΔE°) of the reacting species. Similar correlations can be followed for reactions of $CO_3^{-\bullet}$ with the carbonate complexes of Am^{III}, Np^{III} and Pu^{III} (see Ref. 77) or U^V, Np^V and Pu^V (see Ref. 95). Thus, if the reaction rate is not controlled by diffusion, it often depends on the reduction potentials of actinide ions and the inorganic radicals they react with. For example, the

reactivity in redox processes decreases in the following sequence: $SO_4^{-\bullet} > NO_3^{\bullet} > OH^{\bullet} > Br_2^{-\bullet} > Cl_2^{-\bullet} > I_2^{-\bullet} > O_3^{-\bullet}$ (see Ref. 5). The reactivity of actinides towards the $OH^{\bullet}$ radical and the inorganic radical anions listed above is appreciably affected by their charge and complexation state. This is due to the inner-sphere mechanism of the reactions involved.

Reactions of actinides with organic radicals are discussed in the following Section.

VI. Reactions of organic radicals

A large body of experimental data (mainly obtained by pulse radiolysis) concerned with the reactivity of organic radicals towards the one-electron reduction of organic and inorganic compounds in aqueous solutions has been accumulated to date. The measured rate constants have been summarised in a book.[96] Table 7 presents the rate constants for the reduction of a number of organic and inorganic compounds with various organic radicals and with hydrogen atoms. These particular constants were chosen [97–103] among the multitude of known rate constants because they allow one to follow the requlrities of their variation in a series of related organic radicals. These are 1-hydroxyalkyl radicals formed upon pulse radiolysis of aqueous solutions of alcohols in reactions of type (3). It is reasonable to expect that the reactivity of organic radicals in the one-electron reduction of organic and inorganic compounds should depend, most of all, on the reaction mechanism and limiting step. The reduction potential of the hydrogen atom is −2.3 V; the rate constants for the reductions involving the hydrogen atom are usually very high and are restricted by the rate of diffusion. In the case of organic radicals, the constants are also fairly high,[96] but they are still markedly lower than those for hydrogen. The rate constants for a large number of redox reactions involving organic radicals, including alkyl radicals ($^{\bullet}CH_3$, $CH_3C^{\bullet}H_2$, *etc.*) formed upon abstraction of a hydrogen atom from the α- or β-position of mono- or polyhydric alcohols, amines, nitro derivatives and other organic compounds, have now been measured. Most of these species react at high rates (10^6–10^9 litre mol^{-1} s^{-1}) with organic and inorganic compounds, mainly as reducing agents. The reduction of nitro, sulfo and halogen compounds and other organic compounds containing electronegative substituents and the reduction of various quinones, dyes, and their derivatives proceed at high rates, their rate constants reaching the values normally observed for diffusion-controlled reactions. Unfortunately, the reduction potentials of organic radicals are not always known, which restricts the possibility of comparison of rate constants and hampers elucidation of the reaction kinetics. However, the potentials of 1-hydroxyalkyl radicals $^{\bullet}CH_2OH$, $CH_3C^{\bullet}HOH$ and $(CH_3)_2C^{\bullet}OH$ have been determined; they decrease along the given series as follows: −1.18, −1.25 and −1.39 V.[8] Thus, the reducing ability of the radicals is enhanced in this sequence. It appeared of interest to find the relationship between the reactivity and the reducing capacity and the size of the radicals. Analysis of the reactivity (see Table 7) showed that the rate constants for the reactions of 1-hydroxyalkyl radicals with metal ions (Cu^{2+} and Cr^{2+}) decrease, while those for reactions with organic compounds (nitrobenzene, RNO, PNAF and NF), conversely, increase in the sequence $^{\bullet}CH_2OH$, $CH_3C^{\bullet}HOH$, $(CH_3)_2C^{\bullet}OH$. It is worth mentioning that for some other compounds,[96] it is not always possible to distinguish a clear-cut regularity in the variation of the constant as a function of the potential or the size of the radical. It should be borne in mind that determination of the rate constants of reactions involving organic radicals by pulse radiolysis with optical recording is faced with some experimental difficulties, which are caused by the following reasons. Organic radicals absorb in the far UV region and the extinction coefficients are relatively low. This hampers the measurement of the rate constants of reactions involving such radicals directly by following their absorption. The rate of appearance of the absorption of the reaction product is not always measurable. Therefore, many constants have not been determined by the direct method but were found by comparing the reactivity of the compound under study with a known reactivity of a different compound, the product of whose reduction has optical characteristics suitable for the measurements. These difficulties have been taken into account by Ershov *et al.*[104–106] They performed a systematic pulse radiolysis study of the reactivity of hydrogen atoms and a series of 1-hydroxyalkyl radicals $^{\bullet}CH_2OH$, $CH_3C^{\bullet}HOH$ and $(CH_3)_2C^{\bullet}OH$ towards the reduction of Hg^{2+} ions and I_2 molecules. These radicals differ in size and in the values of known redox potentials. The reagents (Hg^{2+} and I_2) differ appreciably in the outer-sphere and electronic structures. Therefore, different reduction mechanisms could be expected. The products of reduction of the radical acceptors (Hg^{+} and $I_2^{-\bullet}$) have appropriate optical characteristics which allow the rate constants of these reactions to be measured with high accuracy.

The reactions were carried out in acidic (pH 1.0–2.0, $HClO_4$) aqueous solutions of $Hg(ClO_4)_2$ and I_2 containing small amounts of an alcohol (methanol, ethanol or 2-propanol). Under these conditions, hydrated electrons reacted with H^+ to give hydrogen atoms

$$e_{aq}^- + H^+ \longrightarrow H^{\bullet}. \quad (32)$$

The hydrogen atoms, like $OH^{\bullet}$ radicals, entered into a reaction of type (3) with alcohols, which were thus converted almost entirely into alcohol radicals ($R^{\bullet}$).

Then the alcohol radicals reacted with the Hg^{2+} ions or I_2 molecules:

$$R^{\bullet} + Hg^{2+} \longrightarrow Hg^{+} + X + H^{+}, \quad (33)$$

$$R^{\bullet} + I_2 \longrightarrow I_2^{-\bullet} + X + H^{+}, \quad (34)$$

where X is CH_2O, CH_3CHO and $(CH_3)_2CO$ in the case of CH_3OH, CH_3CH_2OH and $(CH_3)_2CHOH$, respectively.

The rate of the reaction of the alcohol radicals with the Hg^{2+} ions was measured based on the appearance of absorption bands with maxima at $\lambda = 225$ and 255 nm corresponding to the Hg^{+} ion formed in reaction (33).[107, 108] The reaction with I_2 was monitored by following the absorption at $\lambda = 725$ nm due to the the $I_2^{-\bullet}$ radical anion produced in reaction (34).[109, 110]

Table 7. Rate constants (k) for some reactions involving hydrogen atoms and organic radicals.

Atom, radical	E°/V	k /litre mol^{-1} s^{-1}							
		Hg^{2+} (see [103]) (pH 2)	Cu^{2+} (see [95, 96]) (pH 5–6)	Cr^{2+} (see [97]) (pH 1)	I_2 (see [104–106])	RNO (see [98])	NF (see [99])	PNAF (see [100])	$C_6H_5NO_2$ (see [101])
$H^{\bullet}$	−2.30	2.0×10^9	–	–	3.5×10^{10}	–	–	–	–
$^{\bullet}CH_2OH$	−1.18	7.0×10^8	1.6×10^8	1.6×10^8	5.0×10^9	7.9×10^8	8.0×10^8	1.0×10^8	3.2×10^9
$CH_3C^{\bullet}HOH$	−1.25	3.8×10^8	9.0×10^7	7.9×10^7	6.5×10^9	2.4×10^9	1.5×10^9	8.0×10^8	3.9×10^9
$(CH_3)_2C^{\bullet}OH$	−1.39	3.1×10^8	5.0×10^7	5.1×10^7	8.0×10^9	3.2×10^9	3.3×10^9	3.8×10^9	5.0×10^9

Note. RNO is *N*,*N*-dimethyl-4-nitrosoaniline; NF is *anti*-5-nitro-2-furaldoxime; PNAF is *p*-nitroacetophenone.

The data on the formation of the Hg^+ cation were analysed in terms of the reaction scheme composed of the following reactions with known rate constants:[9,96]

$$R^\bullet + R^\bullet \longrightarrow \text{product},$$

$$H^\bullet + H^\bullet \longrightarrow H_2,$$

$$Hg^+ + Hg^+ \longrightarrow Hg^0 + Hg^{2+},$$

$$H^\bullet + Hg^{2+} \longrightarrow Hg^+ + H^+.$$

The rate constants for the recombination of alcohol radicals are 2.4×10^9, 1.5×10^9 and 1.1×10^9 litre mol^{-1} s^{-1} for $^\bullet CH_2OH$, $CH_3C^\bullet HOH$ and $(CH_3)_2C^\bullet OH$, respectively.[111] Computer simulation gave the following rate constants for reaction (33) with the $^\bullet CH_2OH$, $CH_3C^\bullet HOH$ and $(CH_3)_2C^\bullet OH$ radicals: 7.0×10^8, 3.8×10^8 and 3.1×10^8 litre mol^{-1} s^{-1}, respectively. Thus, the rate constants for the reactions of the alcohol radicals with the Hg^{2+} ions decrease in the above sequence.

A similar approach has been used to calculate the rate constants for reactions (34) between the alcohol radicals and I_2 on the basis of the kinetics of the appearance of $I_2^{-\bullet}$ absorption. The following reactions were taken into account:

$$H^\bullet + I_2 \longrightarrow I_2^{-\bullet} + H^+,$$

$$I_2^{-\bullet} + I_2^{-\bullet} \longrightarrow I_3^- + I^-,$$

$$I^\bullet + I^- \rightleftharpoons I_2^{-\bullet},$$

$$I_2 + I^- \rightleftharpoons I_3^-,$$

$$I^\bullet + I^\bullet \longrightarrow I_2.$$

In this case, the rate constants for the forward and back reactions and the extinction coefficients of the reactants and the products are known.[109,110] The rate constants for the reduction of iodine in reaction (34) by the $^\bullet CH_2OH$, $CH_3C^\bullet HOH$ and $(CH_3)_2C^\bullet OH$ radicals are 5.0×10^9, 6.5×10^9 and 8.0×10^9 litre mol^{-1} s^{-1}, respectively. Thus, the rate constants for the reactions of alcohol radicals with I_2, unlike reactions with Hg^{2+}, increase in this sequence. It is also noteworthy that an increase in the values of constants with an increase in the size of the radical definitely indicates that the reactions involving these radicals are not controlled by diffusion.

The rate constants for the alcohol radicals and hydrogen atoms with I_2 increase with an increase in the reduction potentials (see Table 7). Moreover, a good linear dependence of $\log k$ on the reduction potential of the reagent can be followed (Fig. 3 *a*). Therefore, it can be concluded that the efficiency of the outer-sphere transfer of an electron from the alcohol radicals to the I_2 molecule is determined by their reducing capacity. It is of interest that the hydrogen atom fits well in this series of radicals as regards the reduction mechanism and the variation in the potential.

The rate constants for reactions of the Hg^{2+} ions with the hydrogen atoms and alcohol radicals increase with a decrease in the size of the reducing agent (see Table 7). Therefore, it can be suggested that the reaction of the radicals $R^\bullet$ with Hg^{2+} gives initially the short-lived $[Hg^{2+} \cdots R^\bullet]$ complex; this is followed by an inner-sphere electron transfer and separation of the reaction products. Note that the formation of relatively stable complexes in similar reactions is typical of many metals, most often, transition metals.[2,3] Due to steric hindrance, which becomes more pronounced with an increase in the size of the radical, the rate of formation of the intermediate complex should limit the rate of reduction; this is actually observed in experiments. The tendency of transition metals to form unstable hydride complexes upon reactions with hydrogen atoms has been confirmed experimentally in some cases.[1,2,53] It is also assumed that the reactions of hydrogen atoms proceed with participation of water present in the hydration shell of the ion; this may give intermediately the $H_3O^\bullet$ species, an electron from which passes to the central metal ion.

The conclusions drawn from the study of the reactivity of alcohol radicals with respect to the Hg^{2+} ion and with I_2 can be extended to the reactions of these radicals with other metals and compounds (see Table 7). Indeed, for the Cu^{2+} and Cr^{2+} ions, as for Hg^{2+}, the rate constants for reactions with alcohol radicals regularly decrease in the sequence $^\bullet CH_2OH$, $CH_3C^\bullet HOH$ and $(CH_3)_2C^\bullet OH$, which can also be attributed to the steric hindrance involved in the reactant interaction. Conversely, in the reactions with organic compounds (nitro- and nitrosobenzene, RNO and NF), the rate constants increase in the given sequence (see Table 7). This is due to the fact that the efficiency of the electron transfer to a molecule of the organic compound is determined by the reduction potential of the radical. In this case, as in the case of iodine, the logarithm of the rate constant follows a linear dependence on the potential (see Fig. 3 *b*).

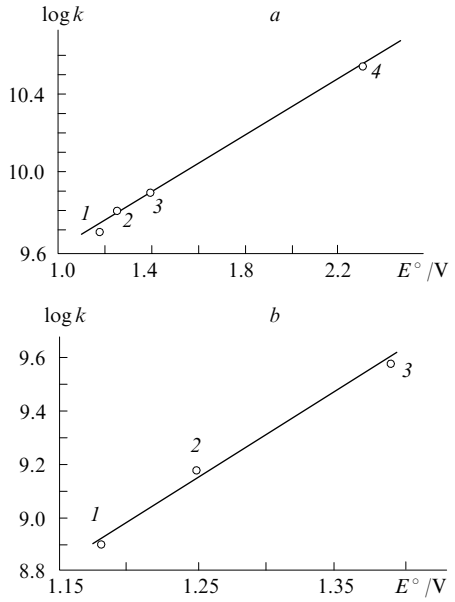

Figure 3. Dependence of $\log k$ on the potential (E°) in the reactions of $^\bullet CH_2OH$ (*1*), $CH_3C^\bullet HOH$ (*2*) and $(CH_3)_2C^\bullet OH$ (*3*) radicals and hydrogen atom (*4*) with I_2 (*a*) and with *N*,*N*-dimethyl-4-nitrosoaniline (*b*).

However, the conclusion concerning the inner-sphere mechanism of the reduction of transition metal ions, Hg^{2+}, Cu^{2+} and Cr^{2+}, with organic radicals is not universal and it cannot be extended to all other ions. For example, the alcohol radicals reduce the Fe^{3+} cations, their reactivity increasing in the sequence $^\bullet CH_2OH$, $CH_3C^\bullet HOH$ and $(CH_3)_2C^\bullet OH$ ($k = 8 \times 10^7$, 3.8×10^8 and 5.8×10^8 litre mol^{-1} s^{-1}, respectively).[96] This fact rather attests in favour of a mechanism with outer-sphere electron transfer in which the reducing properties of the radical are of crucial importance. Note that reactions of the alcohol and many other organic radicals with transition metal complexes [$Fe(CN)_6^{3-}$, $IrCl_6^{2-}$, *etc.*] are diffusion-controlled, the rate constants reaching $\sim 5 \times 10^9$ litre mol^{-1} s^{-1} and depending only slightly on the type of the reducing radical used.[96]

The rates of reactions of organic radicals with oxygen are also controlled by diffusion; they are characterised by constants of $\sim 10^9 - 10^{10}$ litre mol^{-1} s^{-1}. These reactions yield the $RO_2^\bullet$ radicals or the $O_2^{-\bullet}$ peroxide radicals. Conversely, the reactions with H_2O_2 are very slow ($\sim 1 \times 10^5$ litre mol^{-1} s^{-1}) and seem to be accompanied by the formation of the $OH^\bullet$ radicals.

The reactions of the $CO_2^{-\bullet}$ radical anion with various inorganic and organic compounds have been studied in detail. The reduction potential of this radical anion is -1.9 V; as a reducing agent, it markedly surpasses other radicals, being inferior only to the hydrated electron and the hydrogen atom. Therefore, this species tends to enter into electron transfer reactions with various compounds and the rate constants of such reactions approach the diffusion limit.[96]

Comparison of the reduction potentials of metal ions in unusual oxidation states and organic radicals (see Tables 5 and 7) shows that some metal ions, for example, Zn^+, Cd^+, *etc*., surpass organic radicals in reducing ability. Therefore, in those radiation-induced chemical reactions where they arise simultaneously [for example, in the reduction of metal ions, Zn^{2+}, Cd^{2+}, *etc*., by hydrated electrons or in dehydrogenation of organic compounds by reaction (3)], organic radicals are reduced by metal ions. Conversely, for higher potentials of metal ions (for ions like Pb^+, Hg^+ and, probably, Pd^+ and Pt^+), the radicals reduce the ions to give metal atoms.

In the studied reactions of actinides with organic radicals, the latter behave as reducing agents.[5,112–115] It is noteworthy that data on the reactivity of organic radicals towards actinides and on the nature of the products are important for evaluation of the radiation stability of organic extractants used in the radiochemical industry and for predicting the efficiency of actinide separation. According to publications,[112–115] the rates of the reactions of the $^{\bullet}COOH$ and $(CH_3)_2C^{\bullet}OH$ radicals and *o*-phenanthrolinium, 2,2′-bipyridinium and some other electron adducts with actinide ions can be fairly high and, most likely, they are controlled by diffusion. This is supported by calculation of the diffusion-limited rate constant for the reaction of Np^{VI} with $(CH_3)_2C^{\bullet}OH$ using the Smolukhovsky equation.[115] The value calculated theoretically proved to be rather close to the experimental value. In addition, it was found that the activation energies for the reaction of U^{VI} with the *o*-phenanthrolinium and 2,2′-bipyridinium electron adducts are equal to 10 and 16.7 kJ mol^{-1}, respectively. These values do not differ much from the activation energy of water diffusion and are usual for reactions whose rates are controlled by diffusion or approach the diffusion limit.

It is worth mentioning that the electronic structure of organic radicals has a considerable influence on the rates of their reactions with actinides. It was found [116] that reactions of uranium, neptunium, plutonium and americium ions with the *o*-phenanthrolinium and 2,2′-bipyridinium H-adducts proceed much more slowly than reactions with the electron adducts of the same compounds. This is attributable to the fact that the electron adduct arises upon protonation of the nitrogen atoms in the molecules, whereas the H-adduct is produced upon incorporation of the hydrogen atom into the aromatic rings. Therefore, in the electron adducts, the unpaired electron is delocalised over the aromatic π-system, whereas in the H-adducts, the system of conjugation is violated due to the formation of a cyclodienyl type radical. The electron transfer proceeds more easily from the electron adduct than from the H-adduct due to the difference between their electronic structures.

Thus, it can be concluded that, at least for some reduction reactions involving organic radicals, the redox process follows a classical pattern, according to which the reaction proceeds either in the outer or in the inner sphere. For the former type, the interaction between the oxidant and the reductant is not significant during the electron transfer and, most likely, it does not affect the coordination spheres of the reactants. As has been shown, for these reactions, a clear-cut dependence of the reactivity of organic radicals on their reducing potential can be observed. A necessary condition for reactions of the latter type is the presence of a strong bond between the reductant and the oxidant during the electron transfer, which is implemented by the formation of a short-lived intermediate complex. In this case, the rate of electron transfer is limited by this step and depends more appreciably on steric factors.

VII. Conclusion

The results of investigation of a number of redox reactions in aqueous solutions initiated by exposure to ionising radiation indicate that development of this line of research is quite promising. The pulse radiolysis method provides broad opportunities for the study of the kinetics, the mechanism and the nature of the short-lived intermediates of fast one-electron redox reactions. By the early 1990s, a great amount of information had been accumulated on the reactivity of hydrated electrons, hydrogen atoms, hydroxyl radicals and $HO_2^{\bullet}$ radicals,[8] diverse inorganic [23] and organic [96] radicals, metal ions in unusual oxidation states [51] and actinides.[5] During the last 15 years, new data have been obtained, which are largely summarised in this review. Of these, mention should be made first of all of the studies of the redox processes involving halide ions. The rate and equilibrium constants for many reactions have been measured for the first time and the tendency of halogens for the formation of mixed products of not only molecular but also radical nature has been established. The $ClBr^{-\bullet}$ radical anion is probably only the first representative of this series. The research along these lines, important from not only a theoretical but also a practical standpoint, will undoubtedly be continued.

In our opinion, the theoretical analysis of the data on the reactivity of diverse one-electron oxidants and reductants of radical nature towards various compounds still receives inadequate attention. Systematic analysis of these data would be useful for the development of chemical kinetics and for extension of the knowledge on the mechanisms of chemical reactions.

References

1. A K Pikaev, S A Kabakchi, I E Makarov, B G Ershov *Impul'snyi Radioliz i Ego Primenenie* (Pulse Radiolysis and Its Applications) (Moscow: Atomnaya Energiya, 1980)
2. B G Ershov *Usp. Khim.* **66** 103 (1997) [*Russ. Chem. Rev.* **66** 93 (1997)]
3. B G Ershov *Izv Akad. Nauk, Ser. Khim.* 1 (1999) [a]
4. B G Ershov *Zh. Neorg. Khim.* **4** 644 (2002) [b]
5. A K Pikaev, V P Shilov, A V Gogolev *Usp. Khim.* **66** 845 (1997) [*Russ. Chem. Rev.* **66** 763 (1997)]
6. B G Ershov, M Kelm, E Janata, A V Gordeev, in *Proceedings of the 8th International Conference on Chemistry and Migration Behaviour of Actinides and Fission Products in Geosphere (MIGRATION'01), Bregenz, 2001* p. 140
7. B G Ershov, M Kelm, A V Gordeev, E Janata *Phys. Chem. Chem. Phys.* **4** 1872 (2002)
8. P Wardman *J. Phys. Chem. Ref. Data* **18** 1637 (1989)
9. G V Buxton, C L Greenstock, W P Helman, A B Ross, W Tsang *J. Phys. Chem. Ref. Data* **17** 513 (1988)
10. G G Jayson, B J Parsons, A J Swallow *J. Chem. Soc., Faraday Trans. 1* **69** 1597 (1973)
11. B G Ershov, M Kelm, A V Gordeev, E Janata *Radiat. Phys. Chem.* (2004) (in the press)
12. V M Byakov, F G Nichiporov, in *Vnutritrekovye Khimicheskie Protsessy* (Intratrack Chemical Processes) (Moscow: Energoatomizdat, 1985) p. 111
13. R A Robinson, R H Stokes *Electrolyte Solutions* (London: Butterworths, 1955) p. 226
14. S Navaratnam, B Parsons, F J Swallow *Radiat. Phys. Chem.* **15** 159 (1980)
15. W J McElroy *J. Phys. Chem.* **94** 2435 (1990)
16. J P Sweet, J K Thomas *J. Phys. Chem.* **68** 1363 (1964)
17. A V Gordeev, S A Kabakchi, B G Ershov, V A Grishkin, V L Bugaenko *Dokl. Akad. Nauk SSSR* **296** 1388 (1987) [c]
18. B G Ershov, M Kelm, A V Gordeev, E Janata *Radiat. Phys. Chem.* **67** 613 (2003)
19. S P Mezyk, D M Bartels *J. Chem. Soc., Faraday Trans. 1* **91** 3127 (1995)
20. V Nagarajan, R F Fessenden *J. Phys. Chem.* **89** 2330 (1985)
21. L Raphael, in *Bromine Compounds Chemistry and Applications*. (Eds D Price, B Iddon, B J Wakefield) (New York: Elsevier, 1988) p. 369
22. D Zehavi, J Rabani *J. Phys. Chem.* **76** 312 (1972)
23. P Neta, R E Huie *J. Phys. Chem. Ref. Data* **17** 1027 (1988)
24. B G Ershov, M Kelm, E Janata, A V Gordeev *Radiochem. Acta* **90** 617 (2002)
25. S Sunder, H Christensen *Nucl. Technol.* **104** 403 (1993)
26. M Kelm, E Bohnert *Nucl. Technol.* **129** 119 (2000)

27. M Kelm, E Bohnert *Nucl. Technol.* **129** 123 (2000)
28. M Schoneshofer, A Henglein *Ber. Bunsen-Ges. Phys. Chem.* **73** 289 (1969)
29. M Schoneshofer *Int. J. Radiat. Phys. Chem.* **1** 505 (1969)
30. M S Matheson, W A Mulac, J L Weeks, J Rabani *J. Phys. Chem.* **70** 2092 (1966)
31. B Cercek, M Ebert, L W Gilbert, A J Swallow *Pulse Radiolysis* (London, New York: Academic Press, 1965) p. 83
32. B G Ershov, A V Gordeev, E Janata, M Kelm *Mendeleev Commun.* 149 (2001)
33. G Zimmerman, F C Strong *J. Am. Chem. Soc.* **79** 2063 (1957)
34. T X Wang, M D Kelley, J N Cooper, R C Beckwith, D W Margerum *Inorg. Chem.* **33** 5872 (1994)
35. U K Klaning, T Wolf *Ber. Bunsen-Ges. Phys. Chem.* **89** 243 (1985)
36. B G Ershov, E Janata, M Kelm, A V Gordeev *Mendeleev Commun.* 55 (2002)
37. D M Stanbury *Adv. Inorg. Chem.* **33** 69 (1989)
38. K Hasegawa, P Neta *J. Phys. Chem.* **82** 854 (1978)
39. H M Khan, W L Waltz, R J Woods *Int. J. Radiat. Appl. Instrum., Part C, Radiat. Phys. Chem.* **27** 41 (1986)
40. B J Parsons, M Al-Hakim, G O Phillips, A J Swallow *J. Chem. Soc., Faraday Trans. 1* **82** 1575 (1986)
41. A Harriman, P Neta, M C Richoux *J. Phys. Chem.* **90** 3444 (1986)
42. R E Huie, P Neta *J. Phys. Chem.* **90** 1193 (1986)
43. P Hambright, P Neta, M C Richoux, Z Abou-Gamza, A Harriman *J. Photochem.* **36** 255 (1987)
44. S V Jovanovic, A Harriman, M G Simic *J. Phys. Chem.* **90** 1935 (1986)
45. M Bonifacic, K-D Asmus *J. Chem. Soc., Perkin Trans. 2* 1805 (1986)
46. X Shen, J Lind, G Merenyi *J. Phys. Chem.* **91** 4403 (1987)
47. H M Novais, S Steenken *J. Phys. Chem.* **91** 426 (1987)
48. M Brandys, R E Sassoon, J Rabani *J. Phys. Chem.* **91** 953 (1987)
49. Z B Alfassi, A Harriman, R E Huie, S Mosseri, P Neta *J. Phys. Chem.* **91** 2120 (1987)
50. Z B Alfassi, R E Huie, S Mosseri, P Neta *J. Phys. Chem.* **91** 3888 (1987)
51. G V Buxton, Q G Mulazzani, A B Ross *J. Phys. Chem. Ref. Data* **24** 1055 (1995)
52. B G Ershov, N L Sukhov, G V Ionova, V I Spitsyn *Zh. Neorg. Khim.* **31** 1363 (1986) [b]
53. B G Ershov *Usp. Khim.* **50** 2137 (1981) [*Russ. Chem. Rev.* **50** 1119 (1981)]
54. G V Buxton *Radiation Chemistry. Principles and Applications* (Eds M A J Rogers, M Farhataziz) (New York: VCH, 1987)
55. B G Ershov, E Janata, A Henglein, A Fojtic *J. Phys. Chem.* **97** 4589 (1993)
56. E Janata, A Henglein, B G Ershov *J. Phys. Chem.* **98** 10 888 (1994)
57. B G Ershov, E Janata *Izv. Akad. Nauk, Ser. Khim.* 2367 (1999) [a]
58. M Mostafavi, S Remita, M O Delcourt, J Belloni *J. Chim. Phys.* **93** 1828 (1996)
59. S Remita, M Mostafavi, M O Delcourt *J. Chim. Phys.* **93** 1837 (1996)
60. O Platzer, J Amblard, J L Marignier, J Belloni *J. Phys. Chem.* **96** 2334 (1992)
61. J Amblard, O Platzer, J Ridard, J Belloni *J. Phys. Chem.* **96** 2341 (1992)
62. M Mostafavi, M O Delcourt, J Belloni *J. Imaging Sci. Technol.* **38** 54 (1994)
63. S Kapoor, D Lawless, P Kennepohl, D Meisel, N Serpone *Langmuir* **10** 3018 (1994)
64. D Lawless, S Kapoor, P Kennepohl, D Meisel, N Serpone *J. Phys. Chem.* **98** 9619 (1994)
65. B G Ershov, E Janata, A Henglein *J. Phys. Chem.* **98** 7619 (1994)
66. B G Ershov, E Janata, A Henglein *J. Phys. Chem.* **98** 10 891 (1994)
67. N L Sukhov, B G Ershov *Khim. Vys. Energ.* **30**171 (1996) [d]
68. B G Ershov, E Janata, A Henglein *Radiat. Phys. Chem.* **47** 59 (1996)
69. B G Ershov, E Janata *Khim. Vys. Energ.* **33** 89 (1999) [d]
70. A K Pikaev, A V Gogolev, V P Shilov, A M Fedoseev *Isotopenpraxis* **26** 465 (1990)
71. A K Pikaev, A V Gogolev, V P Shilov, A M Fedoseev *Radiat. Phys. Chem.* **37** 531 (1991)
72. A K Pikaev, A V Gogolev, V P Shilov, A M Fedoseev *Khim. Vys. Energ.* **28** 302 (1994) [d]
73. A M Koulkes-Pujo, D Folcher *Nouv. J. Chim.* **6** 571 (1981)
74. A V Gogolev, V P Shilov, A M Fedoseev, A K Pikaev *Radiokhimiya* **32** 121 (1990) [e]
75. A K Pikaev, V P Shilov, A M Fedoseev *Dokl. Akad. Nauk SSSR* **260** 1407 (1981) [c]
76. A K Pikaev, V P Shilov, A M Fedoseev *Izv. Akad. Nauk SSSR, Ser. Khim.* 1947 (1980) [a]
77. A V Gogolev, V P Shilov, A M Fedoseev, A K Pikaev *Izv. Akad. Nauk SSSR, Ser. Khim.* 28 (1990) [a]
78. A K Pikaev, G N Pirogova, I M Kosareva, A V Gogolev, V P Shilov *Khim. Vys. Energ.* **37** 90 (2003) [d]
79. V P Shilov, A K Pikaev *Khim. Vys. Energ.* **16** 468 (1982) [d]
80. A V Gogolev, V P Shilov, A M Fedoseev, A K Pikaev *Radiokhimiya* **32** 123 (1990) [e]
81. A V Gogolev, V P Shilov, A M Fedoseev, A K Pikaev *Khim. Vys. Energ.* **25** 472 (1991) [d]
82. V P Shilov, A V Gogolev, A M Fedoseev, A K Pikaev *Khim. Vys. Energ.* **28** 114 (1994) [d]
83. A V Gogolev, V P Shilov, A M Fedoseev, I E Makarov, A K Pikaev *Radiokhimiya* **30** 761 (1988) [e]
84. A V Gogolev, V P Shilov, A M Fedoseev, A K Pikaev *Izv. Akad. Nauk SSSR, Ser. Khim.* 456 (1986) [a]
85. V P Shilov, A M Fedoseev, A K Pikaev *Radiokhimiya* **27** 127 (1985) [e]
86. Ch Lierse, K H Schmidt, J C Sullivan *Radiochim. Acta* **44**/**45** 71 (1988)
87. A V Gogolev, V P Shilov, A K Pikaev *Izv. Akad. Nauk SSSR, Ser. Khim.* 20 (1989) [a]
88. A V Gogolev, A M Fedoseev, A K Pikaev *Khim. Vys. Energ.* **21** 478 (1987) [d]
89. A V Gogolev, I E Makarov, A K Pikaev, in *Proceedings of the VIth Tihany Symposium on Radiation Chemistry* (Ed. P Hedvig) (Budapest: Akademia Kiado, 1987) p. 161
90. A V Gogolev, V P Shilov, A M Fedoseev, A K Pikaev *Mendeleev Commun.* 155 (1993)
91. A V Gogolev, V P Shilov, A K Pikaev *Radiokhimiya* **31** 124 (1989) [e]
92. C Lierse, J C Sullivan, K H Schmidt *Inorg. Chem.* **26** 1408 (1987)
93. A V Gogolev, A M Fedoseev, in *Tez. Dokl. 1-oi Moskovskoi Konferentsii po Radiokhimii* (Abstracts of Reports of the 1st Moscow Conference on Radiochemistry) (Moscow: Institute of Physical Chemistry, Russian Academy of Sciences, 1986) p. 23
94. A V Gogolev, V P Shilov, A M Fedoseev, I E Makarov, A K Pikaev *Izv. Akad. Nauk SSSR, Ser. Khim.* 1248 (1987) [a]
95. W A Mulac, S Gordon, K H Schmidt, D Wester, J C Sullivan *Inorg. Chem.* **23** 1639 (1984)
96. B Ross, P Neta *Natl. Stand. Ref. Data Ser.* 70 (1982)
97. M Freiberg, D Meyerstein *J. Chem. Soc., Faraday Trans. 1* **76** 1825 (1980)
98. M Freiberg, W A Mulac, K H Schmidt, D Meyerstein *J. Chem. Soc., Faraday Trans. 1* **76** 1838 (1980)
99. H Cohen, D Meyerstein *Inorg. Chem.* **13** 2434 (1974)
100. J H Baxendale, A A Khan *Int. J. Radiat. Phys. Chem.* **1** 11 (1969)
101. C L Greenstock, I Dunlop *Radiat. Res.* **56** 428 (1973)
102. G E Adams, R L Willson *J. Chem. Soc., Faraday Trans. 1* **69** 719 (1973)
103. K D Asmus, G Beck, A Henglein, A Wigger *Ber. Bunsen-Ges. Phys. Chem.* **70** 869 (1966)
104. B G Ershov, E Janata *Chem. Phys. Lett.* **372** 195 (2003)
105. B G Ershov, E Janata *Radiat. Phys. Chem.* **69** 55 (2004)
106. B G Ershov, E Janata, A V Gordeev *Mendeleev Commun* (2) (2004) (in the press)
107. S Fujita, H Horii, S Taniguchi *J. Phys. Chem.* **77** 2868 (1973)
108. S Fujita, H Horii, T Mori, S Taniguchi *J. Phys. Chem.* **79** 960 (1975)
109. H A Schwarz, B H J Bielski *J. Phys. Chem.* **90** 1445 (1986)

110. A J Elliot *Can. J. Chem.* **70** 1658 (1992)
111. M S Alam, B S M Rao, E Janata *Phys. Chem. Chem. Phys.* **3** 2622 (2001)
112. A V Gogolev, V P Shilov, A K Pikaev *Khim. Vys. Energ.* **30** 388 (1996) [d]
113. A V Gogolev, V P Shilov, A M Fedoseev, A K Pikaev *Khim. Vys. Energ.* **28** 94 (1994) [d]
114. S S Pippin, G R Choppin, D Meisel, J C Sullivan *J. Less-Common Met.* **149** 193 (1989)
115. A V Gogolev, V P Shilov, A M Fedoseev, A K Pikaev *Khim. Vys. Energ.* **28** 402 (1994) [d]
116. J Teply, I Janovsky, R Mehnert, O Brede *Radiat. Phys. Chem.* **12** 169 (1980)

[a] — *Russ. Chem. Bull., Int. Ed. (Engl. Transl.)*
[b] — *Russ. J. Inorg. Chem. (Engl. Transl.)*
[c] — *Dokl. Chem. (Engl. Transl.)*
[d] — *High Energ. Chem. (Engl. Transl.)*
[e] — *Radiochemistry (Engl. Transl.)*

Russian Chemical Reviews **73** (2) 115 – 145 (2004) © 2004 Russian Academy of Sciences and Turpion Ltd

DOI 10.1070/RC2004v073n02ABEH000866

Self-assembly of nanoparticles at interfaces †

V I Roldughin

Contents

I.	Introduction	115
II.	Periodic colloid structures	116
III.	Self-assembly of nanoparticles at interfaces	120
IV.	Template methods	126
V.	Physicochemical properties of ensembles of nanoparticles	129
VI.	Conclusion	139

Abstract. Various approaches to the formation of ordered structures of colloid particles are described. The emphasis is placed on the formation of such structures by nanoparticles at interfaces. A number of processes involving the so-called self-assembly of particles are considered. Examples of the formation of ordered structures (two- and three-dimensional colloid crystals) are given. The driving forces of the self-assembly of nanoparticles and the salient features of the physicochemical properties of ordered ensembles of such nanoparticles are analysed. The bibliography includes 502 references.

I. Introduction

Studies on the properties of nanoparticles and nanoscale structures have attracted increasing interest of researchers in the last fifteen years. Extensive literature on various methods of producing nanoparticles and fabricating nanostructured materials has been published. This was accompanied by the development of experimental techniques for studying the processes occurring in nanoscale systems.

The results obtained were reviewed and summed up (see, *e.g.*, Refs 1 – 11) and the main fields of research on nanoscale systems were pointed out. The new research avenues, which are rapidly developing at present, were in the early stage of development five or six years ago. They include investigations into the self-assembly of nanoparticles at interfaces.

Interest in the self-assembly of particles is due to some reasons. First, research on such processes gives an insight into the laws governing the behaviour of nanoscale objects under different conditions. Second, self-organised ensembles of nanoparticles exhibit new (and often quite unexpected) properties. Third, if nanoparticles themselves are mainly of interest for basic research, the ensembles of nanoparticles are considered to be a kind of working element in certain devices. Fabrication of such devices implies targeted arrangement of particles on solid substrates. Because of this, investigations on the behaviour of nanoparticles at interfaces are to a great extent governed by practical demands. This opens up the possibility of creating a new generation of nanoscale devices with a multilevel architecture based on an intrinsic property of nanoparticles, namely, on their ability to spontaneously form ordered ensembles. Attempts at simulating self-organisation processes observed in real biological systems also give an impetus to research in this field.

In this review we will describe various approaches to the formation of ordered structures at interfaces. The emphasis is placed on self-assembly of colloid systems and on the methods facilitating this process. The major part of our review will be dedicated to the so-called colloid crystals that are the most interesting and promising objects. The most important properties of self-assembled structures and the conditions for their formation will also be considered.

We will not dwell on the problems concerning self-assembly of nanoscale systems in the broad sense, because this is beyond the scope of the review. We can only point to recent attempts at fabricating nanomechanical devices that are based on nanotubes and fullerenes and operate following a certain algorithm (see Ref. 12). Investigations in this field are in the early stage of development and the models and schemes proposed are to a great extent hypothetical ones despite good reproducibility in computer experiments.

We will also consider some problems concerning the formation of ordered ensembles of particles in the bulk of colloid dispersions. At the same time, the formation of disordered composite materials based on nanoparticles (in particular, using silica matrices [13 – 18]) will be left out of consideration despite the fact that in some cases this process results in the formation of quite interesting structures [14, 19] possessing unique optical and catalytic properties. This research avenue has been intensively developing and deserves detailed consideration elsewhere.

We will leave essentially untouched the problems concerning changes in the properties of the particles deposited on solid substrates. The interaction between the particles and the substrate can result in significant changes in the characteristics of the former.[20] This is due to distortion of the crystal lattice of nanoparticles,[21] which is probably responsible for, *e.g.*, the enhanced catalytic activity and the changes in the optical characteristics of nanoparticles on solid substrates.

V I Roldughin Institute of Physical Chemistry, Russian Academy of Sciences, Leninsky prosp. 31, 119991 Moscow, Russian Federation. Fax (7-095) 952 53 08. Tel. (7-095) 955 46 47.
E-mail: roldugin@phyche.ac.ru

Received 3 July 2003
Uspekhi Khimii **73** (2) 123 – 156 (2004); translated by A M Raevsky

† This is the last publication in the series of reviews concerning the main avenues of research carried out at the Institute of Physical Chemistry, Russian Academy of Sciences [see *Russ. Chem. Rev.* **73** (1) 2004].

Ordered ensembles of molecular clusters[22,23] will also be excluded from consideration. The advantage of such systems is that the corresponding 'building blocks' are of the same size. However, these systems belong to molecular crystals rather than colloid systems. Because of this, both the mechanisms of formation and the physical properties of such ordered structures are strongly different from those typical of colloids.

Yet another problem left out of consideration is self-assembly of macroscopic particles, which is similar to that of microparticles. It should only be noted that revealing self-assembly processes at microscopic level gave an impetus to studies on self-assembly of millimetre-scale particles.[24,25] To this end, such particles of various shape were specially treated (*e.g.*, different faces of cubic polyurethane particles were coated with different materials). Using particles of different geometry and different conditions for modification of their surfaces, it is possible to cause aggregation of particles to give a variety of ordered structures.

II. Periodic colloid structures

The title of this section is exactly the same as that of a book by Efremov, which was published more than three decades ago.[26] Numerous examples in this book showed that it is possible to form ensembles of particles with ordered structures (the so-called colloid crystals) in the colloid systems. These examples can be divided into two groups. The first group comprised highly ordered structures (at that time, they were observed only in natural objects, in particular, opals). The second group comprised the systems that exhibited a trend to formation of ordered structures (it included colloid dispersion prepared under laboratory conditions).

Considerable progress towards fabrication of ordered structures has been achieved since the publication of the above-mentioned book.[26] This was provided by the high level of the development of methods for the synthesis of monodisperse colloid particles, which became the subject of routine studies. Currently, search for the procedures suitable for forming colloid crystals with desired properties is carried out.[27–30] Considerable advances towards the formation of colloid crystals with perfect structure (Fig. 1) have also been achieved.

1. The interparticle interaction

Ordered ensembles of colloid particles (colloid crystals) can serve as model systems in the studies of the gas–liquid and liquid–crystal phase transitions, because they allow the processes to be visualised. The properties of the colloid structures formed in such experiments and the laws of the phase transitions in these systems are governed by the forces of the interparticle interaction. These forces are of various nature and are determined by the properties of the dispersion medium, by the state of the particle surface and by the presence of additives in the colloid system. Consider now several expressions for the potentials of the interparticle interaction, which are most often used in theoretical description of colloids. The potential of the dispersion or van der Waals interaction, which occurs in virtually all systems,[31] is given by

$$U_{\mathrm{d}}(r) = -\frac{\mathrm{A}}{12}\left\{\frac{4r^2}{(2R)^2 - 4r^2} + \frac{4r^2}{(2R)^2} + 2\ln\left[\frac{(2R)^2 - 4r^2}{(2R)^2}\right]\right\}, \qquad (1)$$

where r is the distance between the centres of the particles, A is the Hamaker constant and R is the radius of the particles.

Yet another widely used potential describes an electrostatic interparticle interaction, which is due to the overlap of ionic atmospheres that form in electrolyte solutions near the surfaces of the charged particles. Theoretical analysis usually employs a simplified model of this interaction,[31] which is described by the modified Yukava potential

$$U(r_{ij}) = \frac{Z_i Z_j e^2}{4\pi\varepsilon_0\varepsilon r_{ij}}\left(\frac{\mathrm{e}^{\kappa R_i}}{1+\kappa R_i}\right)\left(\frac{\mathrm{e}^{\kappa R_j}}{1+\kappa R_j}\right)\mathrm{e}^{-\kappa r_{ij}}, \qquad (2)$$

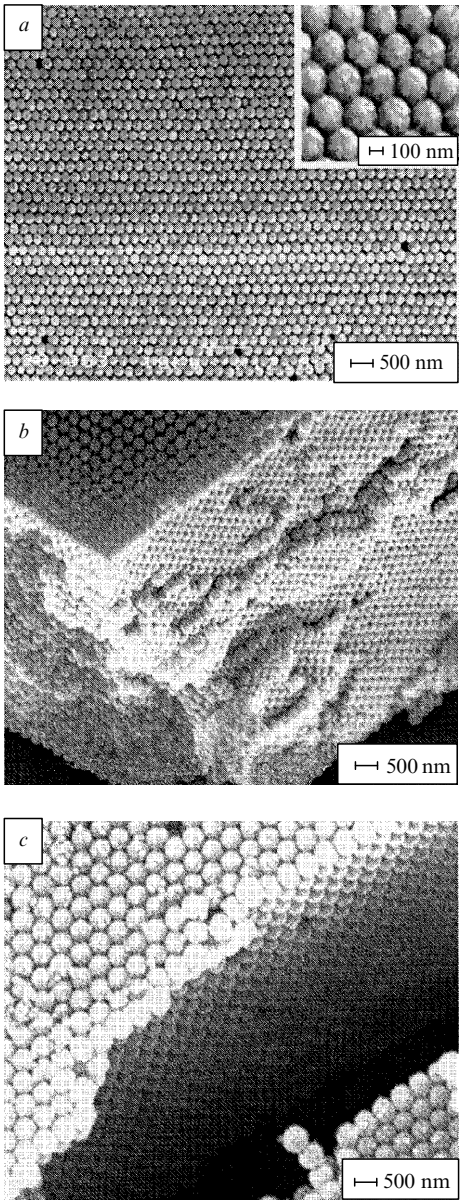

Figure 1. SEM images of three-dimensional crystalline ensembles of polystyrene beads in 12 μm-thick packs.[27]
Particle size: 220 nm for the surface of the crystal (*a*) and for the cleaved facet (*b*) and 480 nm (*c*).

where r_{ij} is the distance between the particles of the sorts i and j; Z_i and Z_j are the corresponding particle charges; e is the charge of electron; ε_0 is the electric constant; ε is the dielectric permittivity of the medium; e is the base of natural logarithm; R_i and R_j are the radii of the particles of the sorts i and j, respectively; and κ is the reciprocal Debye radius defined as follows:

$$\kappa^2 = \frac{e^2}{\varepsilon_0\varepsilon kT}\sum_i n_i z_i^2, \qquad (3)$$

where n_i is the concentration of ions of the sort i in the solution and z_i is the charge of these ions.

If particles are stabilised sterically rather than electrostatically (steric forces are due to the presence of adsorption layers of polymers or surfactants), the interparticle interaction can be quite correctly described by the repulsive potential of dense monolayers in a good solvent [32]

$$E_{st} = \frac{100R\delta_s^2}{(r-2R)\pi\sigma_{th}^3} kT \exp\left[\frac{-\pi(r-2R)}{\delta_s}\right], \quad (4)$$

where δ_s is the monolayer thickness and σ_{th} is the surface area per molecule in the monolayer.

When considering the interparticle interaction, one should take into account two potentials, *viz*., the attractive potential and the repulsive potential, which are in essence some combinations of the potentials mentioned above. Often, numerical calculations are simplified using certain model potentials, *e.g*. a rectangular potential well

$$\frac{U(r)}{kT} = \begin{cases} \infty & \text{at} \quad r < 2R \\ -\dfrac{E_0}{kT} & \text{at} \quad 2R < r < (1+\delta_w)2R \\ 0 & \text{at} \quad r > (1+\delta_w)2R, \end{cases} \quad (5)$$

where E_0 and δ_w are the depth and width of the potential well, respectively. The stick sphere potential is given by

$$\frac{U(r)}{kT} = \lim_{\Delta \to 0} \begin{cases} \infty & \text{at} \quad r < 2R \\ \ln\left(\dfrac{12\psi\Delta}{2R+\Delta}\right) & \text{at} \quad 2R < r < (1+\Delta)2R, \\ 0 & \text{at} \quad r > (1+\Delta)2R, \end{cases} \quad (6)$$

where ψ is the parameter determining the adhesive binding energy and Δ is the variable parameter. The Lennard-Jones potential (its exponents are sometimes chosen arbitrarily) has the form

$$U(r) = 4E_{LD}\left[\left(\frac{\delta_{LD}}{r}\right)^{12} - \left(\frac{\delta_{LD}}{r}\right)^{6}\right], \quad (7)$$

where E_{LD} and δ_{LD} are the energy and spatial parameters, respectively.

The potentials listed above can be used to calculate various characteristics of colloid dispersions, *viz*., the osmotic pressure, second virial coefficient, particle solubility, phase diagram, *etc*. By comparing the calculated and experimental data it is possible [33] not only evaluate the parameters of a particular potential but also determine which of them is more convenient for the description of a given colloid dispersion. If not only the thermodynamic characteristics but also the structure factor is known, one can reconstruct the pair potential of the interparticle interaction even for polydisperse colloid systems.[34]

2. Simple systems

The development of methods for the synthesis of nearly monodisperse colloid particles permitted the growth of rather large colloid crystals with a high degree of crystallinity under laboratory conditions.[35] Initially, high-quality colloid crystals were formed from electrically stabilised latex particles. The stabilisation of the particles was enhanced due to deionisation of the aqueous dispersion medium. In this medium, the interparticle interaction involves the screened Coulombic potential (2), which causes a strong repulsion between particles at long distances due to a large Debye radius. Because of this, the transition to the crystalline state occurs at a volume fraction of the particles of less than 0.01, resulting in the formation of both face-centred cubic (f.c.c.) and body-centred cubic (b.c.c.) crystals.[36, 37] Ordered structures comprised of sterically stabilised colloid particles were obtained much later.[38, 39] The steric stabilisation provided a strong repulsion between particles at short distances so the transition of the colloid dispersion from the liquid to the crystalline state occurred at a volume fraction of particles of nearly 0.5 (as a rule, the f.c.c. structure was formed). Then, more complex systems and phase transitions in them have become the focus of research activity in the field of colloid crystals.

As mentioned above, colloid systems can serve as models for studying the behaviour of atomic and molecular systems. Colloids offer some obvious advantages. In particular, their parameters, *viz*., the size, shape and potential of the interparticle interaction can be measured and varied with ease. The properties of the medium in which colloid particles are dispersed can also be controlled and measured. Because of this, a wide variety of phase states of colloid systems, namely, the gaseous, liquid-like (including glassy state) and crystalline states is observed. Even the existence of a quasi-crystal structure in the single-component colloid system was predicted.[40] Such a structure (icosahedral quasi-crystal) is typical of some binary and ternary metal alloys. It is formed at a rather high osmotic pressure in a specific concentration range.

Various models [41, 42] including those predicting the existence of the glassy state of a colloid fluid [43] were proposed to describe the phase behaviour of colloid systems. Such models are employed in the analysis of the phase transitions in colloid dispersions.[44, 45]

Under particular conditions, sterically stabilised colloid particles behave as a system of hard spheres.[39] To enhance this similarity, particles are coated with a thin adsorption layer of a polymer and then dispersed in a medium characterised by the same refractive index to weaken the van der Waals interaction. Not only the solidification transitions but also the glass transitions were observed in such systems at a volume fraction of particles of about 0.58.[39] At higher particle concentrations, no homogeneous nucleation of crystals was observed and long-range diffusion displacements of particles were suppressed (this was indicated by the shape of the fluctuation correlation function of the particle concentration).[46] Heterogeneous nucleation under the same conditions resulted in large plate-like colloid crystals. This points out that the glassy state is thermodynamically unstable and exists due to the inability of a concentrated homogeneous colloid liquid to go to the crystalline state (for this transition to occur, long-range particle diffusion must be possible). The existence of glassy colloid systems was confirmed by Speedy [47] who also showed that the equation of state of the hard-sphere fluid has singularities indicating some implicit phase transitions. These results were tested [48] and it was shown that larger (compared to those observed in Ref. 47) hard-sphere particles always crystallised at a volume fraction of 0.63 to 0.64. These values are close to the volume fraction of hard-sphere particles in a random close packing (0.644). A series of experiments with 1.03 μm poly(methyl methacrylate) particles stabilised by poly(12-hydroxystearic) acid was carried out to determine the limiting volume fraction of particles at which crystallisation of a dispersion of hard-sphere particles is possible.[49] The results obtained show that at a volume fraction of particles of 0.63 crystallisation still takes a reasonably short time; if the volume fraction of particles exceeded a value of 0.64, no crystals were formed.

Experiments with nanoparticles have opened yet another possibility of controlling the parameters of a colloid system. The nanoparticle size is comparable with the thickness of the protective shell. Experiments show that the structure of colloid crystals depends on the ratio of the chain length, L, of the ligand shell molecules to the particle radius. For saturated linear hydrocarbons, the chain length (in nanometres) is related to the number of monomeric units, n, as follows

$$L = 0.154 + 0.1265\,n. \quad (8)$$

Because of this, it is possible to obtain particles with a prescribed L/R ratio. Depending on the value of this parameter, the structures with the f.c.c. lattice (at small L/R ratios) or the b.c.c. packing of particles (at large L/R ratios) are formed. This is probably due to the fact that it is the f.c.c. lattice that is the most preferable in the case of hard spheres,[50] while the b.c.c. lattice is formed [51] if the potential of the interparticle interaction has a repulsive term (*e.g*., the Yukava potential) or some contribution that decreases in proportion to r^{-n} ($n < 6$). The mechanism of formation of ordered structures with the b.c.c. lattice from sterically stabilised nanoparticles is still to be clarified, because in this case the range of action of the repulsive potential is too short.

Korgel and Fitzmaurice [34] varied the size of gold nanoparticles stabilised by dodecanethiol or octanethiol and observed the f.c.c. – b.c.c. transition at $L/R = 0.59$ and 0.60, respectively. These values differ from that obtained for polymer micelles [52] but are close to the value determined for electrostatically stabilised colloids. [51] Calculations [34] of changes in the free energy upon the f.c.c. – b.c.c. transition were carried out assuming the Lennard-Jones potential of the interaction between nanoparticles and showed that this transition corresponds to $L/R = 0.65$ for the dodecanethiol-stabilised nanoparticles.

3. Coulombic systems

Dispersions of charged colloid particles behave as liquid metals. Such particles can be treated as ions, while the co-ions and counter-ions in solution can be considered as electrons. This is not a complete analogy because the size of colloid particles can be three orders of magnitude larger than the size of ions in liquid metals. Mixing of colloid particles of two different sizes significantly complicates the situation as compared to that in the single-component systems, because two new parameters appear, which determine the structure of the colloid dispersion, *viz*., the ratio of the particle diameters and the fraction of particles of a given sort in the mixture.

Experiments showed that if the particle diameters are close, a homogeneous crystalline solid solution is formed at any component ratio in the mixture. The solid solution is characterised by a finite shear modulus and the Bragg diffraction pattern, which is similar to that observed in the case of disordered substitutional alloys. At large differences between the particle sizes in the binary mixture, the system is either in the glassy state or in the crystalline state depending on the time interval available to reach the equilibrium state. For instance, it was found [53] that the dispersion of a mixture of polystyrene latex particles of sizes 110 and 54.5 nm is a disordered solid characterised by a finite shear modulus and non-Bragg diffraction pattern at the volume fraction of the particles of the minor fraction of greater than 5%. At the same time, the crystal structure is formed almost without no exception if the volume fraction of the minor fraction is less than 5%.

Disordered phases are also formed in dispersions of the mixtures of larger particles. For instance, the formation of a disordered phase in the system of particles of sizes 5 and 7 μm at the volume fractions of the larger particles between 10% and 90% was reported.[54] In these experiments, the disordered structure existed over a period of short observation time. If the colloid solution is allowed to stay for a rather long time, a crystal structure typical of intermetallic compounds is formed. However, the transition to crystalline state can take more than a year.[53] Four different intermetallic structures (of the $NaZn_{13}$, AlB_2, $CaCu_5$ $MgCu_2$ types) of binary mixture of spherical particles whose sizes varied from 200 to 800 nm were observed.[55, 56] The type of the crystal structure depends on the ratio of the particle diameters, on the volume fractions of different particles and on the total particle concentration. The attainment of equilibrium in such systems is a slow process and can take several years.

Thus, it does not always happen that the equilibrium in colloid systems can be achieved after passage of a reasonably short time. For this reason, conventional model experiments usually deal with metastable structures. Therefore, the glassy state of colloid dispersions rather than the formation of ordered structures similar to intermetallic compounds has been the subject of a rather large number of publications. Formally, the glassy state region of a colloid can be determined theoretically as the region corresponding to the existence of an intermetallic alloy in the equilibrium phase diagram.[57]

The thermodynamic parameters of colloid crystals can be calculated in a rather simple way. For instance, if the interparticle interaction is given by the pair potential (2), the free energy, F, of a binary system has the form

$$F = \frac{1}{2N}\sum_{i,j}\left\langle \frac{Z_i Z_j e^2}{4\pi\varepsilon_0\varepsilon r_{ij}}\left(\frac{e^{\kappa R_i}}{1+\kappa R_i}\right)\left(\frac{e^{\kappa R_j}}{1+\kappa R_j}\right)e^{-\kappa r_{ij}}\right\rangle + E_k - TS, \quad (9)$$

where $N = N_1 + N_2$ is the total number of particles in the system; the angular brackets denote the averaging over the canonical ensemble and summation is carried out over the lattice sites of the colloid crystal; E_k is the kinetic energy of the particles and the entropy, S, can be calculated using the known relationship [58]

$$S = 3k\sum_{i=1}^{2} x_i\left(1 - \ln\frac{\theta_i}{T}\right), \quad (10)$$

where $x_i = N_i/N$, $\theta_i = 2\pi\hbar\omega_i/k$ is the Einstein temperature [58] determined assuming that the particles of the first and second sorts execute oscillations at their eigenfrequencies ω_i.

The so-called dusty plasmas provide yet another group of examples of electrostatically stabilised colloid systems capable of forming ordered structures. These objects became the subject of research interest in the last decade. Dusty plasma is a sort of low-temperature plasma containing mesoscopic particles whose sizes range from a hundredth of micrometre to several tens of micrometres. Such plasmas are formed in the course of plasma etching and sputtering and in the combustion products, as well as existing near the space objects. Large plasma particles acquire a rather large charge (up to 10^5 e per particle), which is responsible for their strong, long-range repulsion. As a result, such particles form structures that are similar to those observed in liquids and solids.[59–63] In contrast to colloid systems, the mechanism of formation of ordered structures in dusty plasmas is still to be clarified. A feature of dusty plasmas is simultaneous action of the forces typical of the equilibrium systems and the forces due to the nonequilibrium state of the system. For instance, nonuniform temperature fields produce thermophoretic forces [64, 65] that are comparable in magnitude [66] with the electrical forces exerted on particles. Thermophoretic forces to a great extent govern the conditions for the formation, shape and geometry (arrangement) of the dusty plasma structures. Various models of such structures have been proposed.[67, 68] They are mainly based on the non-equilibrium state of dusty plasmas and predict realistic values of the parameters of crystals (they are close to those observed in the experiments) but sometimes include unsubstantiated admissions, which prevents the dusty plasma problem from being considered as solved. At the same time, numerical simulation of dusty plasmas is usually carried out assuming only the screened Coulombic potential of the type (2) for the interparticle interaction. Even with this limited set of the interaction parameters it is possible to predict [69] the existence of various structures in plasma.

4. Mixtures of sterically stabilised particles

Mixtures of sterically interacting colloid particles of different shape are characterised by a wide variety of the phase states and serve as well-defined models in studies of a broad spectrum of phenomena. The mixtures can be prepared in such a way that the major contribution will come from the interaction of particles considered as hard bodies (the thermodynamics of the system is governed by the entropy effects). Considerable attention is given to the systems prepared by adding various admixtures to monodisperse hard spheres. Smaller spherical particles,[70] globular non-adsorbable polymers [71] or rod-like colloid particles [72] are used as the second component. In most cases, the admixture is considered as an agent affecting the interparticle interaction. Such admixtures usually initiate attraction between particles, which is due to the presence of 'depleted layers.' The interaction following this mechanism can be explained with ease. We will consider it taking non-adsorbable polymers as an example (these are most often used for controlling the interaction between colloid particles).

Polymer molecules are separated from the surface of colloid particles by a distance of the order of the radius of gyration. The near-surface region free from the polymer molecules (more exactly, from the centres of mass of the macromolecules) is called

the depleted layer. As the colloid particles bring closer together, their depleted layers are overlapped and the volume accessible to the polymer molecules decreases. As a result, an excess external pressure is produced and applied to the particles; this is equivalent to the action of attractive forces.

The behaviour of mixtures of colloid particles and polymers (see, *e.g.*, Ref. 73) has been the subject of extensive literature concerning the corresponding theoretical models.[74] The phase diagrams constructed using the experimental data show the presence of the gas–liquid, gas–solid and liquid–solid transitions. The transition of the system to the nonequilibrium glassy state was also pointed out.[75]

The interaction due to the presence of depleted layers is typical of not only the mixtures of colloid particles and polymers but also the mixtures of colloid spherical particles of different sizes as well as the mixtures of spherical and rod-like particles. The potential of the interaction between large spherical particles dipped in a medium containing small spherical particles is given by the following approximate expression [76]

$$U(h) = -3kT\varphi\frac{R}{\sigma}\left(1-\frac{h}{\sigma}\right)^2, \tag{11}$$

where h is the distance between the surfaces of large spherical particles, φ is the volume fraction of small spherical particles, R is the radius of large spherical particles and σ is the diameter of small spherical particles. In the case of spherical particles of radius R (and rods of length L and diameter D) the depletion force potential has the form

$$U_{\mathrm{r}}(h) = -\frac{3}{2}kT\varphi\frac{L}{D}\frac{R}{D}\left(1-\frac{h}{L}\right)^3. \tag{12}$$

As can be seen, rod-like particles more efficiently 'tighten' large spheres. This was also confirmed in the experiments. The phase diagram of a mixture of spherical and rod-like colloid particles was constructed based on simple statistical considerations.[77] The results of experiments with the mixtures of 370 nm spherical silica particles and boehmite particles of length 230 nm and diameter 9 nm showed good agreement with the calculated phase diagram which included the gas–liquid, gas–solid and liquid–solid transitions. What is more, a two-step phase transition was observed. Namely, particle aggregation to give hard-sphere clusters was followed by a slower process of the formation of ordered arrangement of the clusters. In this case it is possible to draw an analogy to the phase transitions in the mixtures of hard-sphere particles of different diameters.[78] It was pointed out [77] that it was impossible to consider all the phase states of the system studied, because yet another, orientational, phase transition must be observed for the colloid dispersion of rod-like particles.[79] Calculations of thermodynamic parameters of the mixtures of spherical and rod-like particles should be carried out on the microscopic level [80] because of the key role of many body interactions. Relevant information can be found in the literature.[81,82]

Summing up, mention may be made that not only highly ordered structures but also liquid-crystalline phases can also be observed in colloid systems. The liquid-crystalline phases are formed in the dispersions of rod-like or plate-like particles as the dispersion concentrations increase. Onsager explained the transition between the isotropic and nematic phases occurring with an increase in the particle concentrations based on the entropy considerations [83] taking the phase transition in dispersions of plate-like clay particles, which was observed by Langmuir.[84] Then, analogous phase transitions were observed for many colloid systems; however, almost all experiments were carried out with rod-like particles (see, *e.g.*, Refs 85–88). New plate-like particles [gibbsite, $Al(OH)_3$, particle of thickness 20 nm and diameter 170 nm], in which the transition between the isotropic and nematic phases was observed, were obtained only recently [89] (the transition occurred even in the systems characterised by high polydisperse indices [90]). In polydisperse systems, the dispersions separated into two zones. In one zone, the isotropic phase was formed, while the nematic phase was formed in the other zone. The relative arrangement of the phases along the vertical axis (in the gravitational field) was determined by the dispersion composition. The experimental data are in qualitative agreement with the results of numerical simulation,[91] which gives the following conditions for the coexistence of the isotropic and nematic phases:

$$n_{\mathrm{i}}D^3 \cong 3.8,$$

$$n_{\mathrm{n}}D^3 \cong 3.9,$$

$$\frac{\Pi D^3}{kT} \cong 32,$$

where n_{i} and n_{n} are the particle concentrations in the isotropic and nematic phases, respectively, D is the particle diameter and Π is the osmotic pressure.

It should be noted that the matrix (dispersion medium) can also favour the formation of ordered structures (colloid and liquid crystals); here the matrix can be either a thermotropic [92] or lyotropic [93–96] liquid crystal.

5. Nonequilibrium processes

Recently, the focus of research activity in the field of colloid crystals has moved towards the investigations on the kinetics of phase transitions. In particular, the effect of the thickness of the stabilising shell on the growth rate of a colloid crystal was analysed.[97] Experiments were carried out with nearly 170 nm silica particles using various surfactants as stabilisers. This allowed the thickness of the adsorption layer to be varied from 2 to 50 nm. Colloid crystals were formed by centrifugation of dispersions. An increase in the thickness of the stabilising layer was accompanied by a dramatic increase in the rate of crystallisation. This can be explained by a decrease in the work done to form a seed crystal. The introduction of a non-adsorbable polymer into the system also led to a significant change in the rate of crystallisation. The depleted layers caused the interparticle attraction to strengthen, which favoured faster formation of colloid crystals.

Quantitative studies on the kinetics of the growth of colloid crystals were carried out taking electrostatically stabilised particles as examples.[98,99] It was found that the growth rate obeys the classical Wilson–Frenkel law

$$\upsilon^* = 1 - \exp\left(-\frac{\Delta\mu}{kT}\right), \tag{13}$$

where $\upsilon^* = \upsilon/\upsilon_\infty$ is the relative growth rate, υ_∞ is the growth rate at infinite supersaturation ($\Delta\mu = \infty$) and $\Delta\mu$ can be expressed through the chemical potential difference between the liquid and solid phases of the colloid dispersion at a given pressure p and temperature T

$$\Delta\mu = \mu_{\mathrm{f}}(p,T) - \mu_{\mathrm{s}}(p,T).$$

Theoretical estimates of the kinetic parameters of the crystal growth have been reported.[100] Calculations were carried out assuming the Yukava potential of the interparticle interaction [see Eqn (2)]. The phase coexistence curves obtained are in good agreement with the experimental data and the results of numerical simulation (see Ref. 101).

Taking into account an ordered arrangement of particles, the nonequilibrium macrocharacteristics of colloid crystals can also be calculated with ease. This was demonstrated taking calculations of the viscosity of colloid crystals as an example.[102] The viscosity was determined by numerically solving the system of hydrodynamic equations using the mapping method assuming a Newtonian fluid. Calculations were carried out for three cubic (simple, b.c.c. and f.c.c.) lattices. In this case, the viscosity is a

function of two parameters and the viscosity tensor takes the form (no summation over the repeating subscripts is performed):

$$(\eta_c)_{ijkl} = \frac{1}{2}\eta(1+\beta)\left(\delta_{ik}\delta_{jl} + \delta_{il}\delta_{jk} - \frac{2}{3}\delta_{ij}\delta_{kl}\right) + \eta(\alpha-\beta)\left(\delta_{ij}\delta_{jl}\delta_{lk} - \frac{1}{3}\delta_{ij}\delta_{kl}\right).$$

At low volume fractions, φ, of particles, the coefficients α and β can be expressed by the following series expansions

$$\alpha = \frac{5}{2}\varphi\left[1 + A_\alpha\varphi + B_\alpha\varphi^{5/3} + O(\varphi^{10/3})\right]^{-1},$$

$$\beta = \frac{5}{2}\varphi\left[1 + A_\beta\varphi + B_\beta\varphi^{5/3} + O(\varphi^{10/3})\right]^{-1}.$$

The parameters A_α , B_α and A_β, B_β are listed in Table 1.

Table 1. Parameters determining the viscosity of a colloid crystal at low particle concentrations.

$-A_\alpha$	B_α	A_β	B_β
Simple cubic lattice			
3.78699	3.42673	0.85800	−2.286
b.c.c. lattice			
0.14079	−1.07874	−1.57281	0.71916
f.c.c. lattice			
−0.23611	−0.82315	−1.50926	0.54877

At large φ values, the viscosity depends on the volume fraction of particles in another manner. The coefficients α and β can be approximated as follows:

for the simple cubic lattice

$$\alpha = \frac{3}{16}\pi\chi^{-1} + \frac{27}{80}\ln\chi^{-1} + C_\alpha + D_\alpha\chi\ln\chi^{-1} + O(\chi),$$

$$\beta = \frac{1}{4}\pi\ln\chi^{-1} + C_\beta + D_\beta\chi\ln\chi^{-1} + O(\chi);$$

for the b.c.c. lattice

$$\alpha = \frac{1}{4}\sqrt{3}\pi\ln\chi^{-1} + C_\alpha + D_\alpha\chi\ln\chi^{-1} + O(\chi),$$

$$\beta = \frac{1}{8}\sqrt{3}\pi\ln\chi^{-1} + \frac{37}{120}\sqrt{3}\pi\ln\chi^{-1} + C_\beta + D_\beta\chi\ln\chi^{-1} + O(\chi);$$

and for the f.c.c. lattice

$$\alpha = \frac{3}{32}\sqrt{2}\pi\ln\chi^{-1} + \frac{87}{160}\sqrt{2}\pi\ln\chi^{-1} + C_\alpha + D_\alpha\chi\ln\chi^{-1} + O(\chi),$$

$$\beta = \frac{3}{16}\sqrt{2}\pi\ln\chi^{-1} + \frac{47}{80}\sqrt{2}\pi\ln\chi^{-1} + C_\beta + D_\beta\chi\ln\chi^{-1} + O(\chi),$$

here

$$\chi = 1 - \left(\frac{\varphi}{\varphi_c}\right)^{1/3},$$

and φ_c is the volume fraction of particles, corresponding to the dense packing of spheres. The values of the corresponding constants are given in Table 2.

The results obtained (dependences of the viscosity on the packing density of spherical particles) are in reasonable agreement with the experimental data.

Table 2. Parameters determining the viscosity of a colloid crystal at high particle concentrations.

$-C_\alpha$	D_α	$-C_\beta$	D_β
Simple cubic lattice			
2.85	−1.3	0.604	−0.30
b.c.c. lattice			
1.83	−12.0	7.5	6.0
f.c.c. lattice			
9.54	14.0	7.4	−9.0

III. Self-assembly of nanoparticles at interfaces

1. Solid substrates

Nanoparticles possess the ability to form ordered self-assemblies both in the bulk of the dispersion [4, 103] and at interfaces.[4] Ordered layers of nanoparticles exhibit unique optical, electric, magnetic and catalytic properties.[104, 105] Recently, highly ordered colloid structures have been considered as candidates for optoelectronic devices,[106] photonic materials,[107] biosensors [108] and a new generation of memory devices. With nanoparticles it is possible to significantly shorten the time necessary for fabrication of nanoscale devices compared to, *e.g.*, electron-beam lithography (the ion-beam and X-ray lithography usually require massive equipment). Nanostructured surfaces are also required in studies of the interaction between cells and surfaces.

Depending on the character of the interparticle interaction (electrostatic, capillary, or van der Waals forces, biospecific recognition) and on the goal of a particular study, various methods of fabrication of ordered ensembles of nanoparticles are employed. It is possible to form two-dimensional and three-dimensional (3D) [24, 109, 110] ordered arrays of particles, as well as mesoporous structures and particle aggregates of specific shape. The properties of the systems obtained depend on both the characteristics of the particles (size, shape, composition) and the architecture of the ensembles (interparticle distance, structural hierarchy, *etc*.).

The simplest method of formation of ordered structures comprised of nanoparticles (see, *e.g.*, Ref. 111) is to evaporate a droplet of the nanoparticle dispersion deposited on the substrate, which causes the formation of a spatially ordered arrangement due to the capillary effects. The pioneering experiments involved fabrication of two-dimensional colloid nanocrystals by evaporating a droplet of a dispersion containing lyophobic particles, which was deposited on the substrate. This procedure was used to form the f.c.c. crystals from CdSe nanoparticles (see Ref. 111) and microscopic polystyrene particles (see Ref. 112).

The formation of a colloid crystal involves two stages.[113] First, seed crystals are formed from spheres under the action of capillary forces. Then, the solvent and spheres are supplied to the nuclei of the new phase in the course of evaporation of the liquid from the film at the peripheral area of the droplet. The formation of the colloid crystal is affected by the tilt angle of the substrate and the rate of solvent evaporation. The substrate must be tilted for nucleation to begin at the top of the droplet and for the crystal to grow on the substrate downward. Deformation of the droplet determines the limiting tilt angle for the substrate; it is related to the wetting angle hysteresis, while the capillary forces compensate the gravitational force. By changing the tilt angle it is possible to vary the parameters of the crystals grown.

Yet another important parameter is the rate of evaporation of the dispersion medium. Generally, the lower the rate of evaporation, the larger the colloid crystals that can be formed. The effect of the rate of evaporation was studied in detail.[114] Using video microscopy technique, it was shown that the particle attached to the edge of the crystal can be treated as mobile for some time, so

the freshly formed 'microcrystals' undergo rearrangements and experience reorientations on incorporating into the larger crystal. Rapid evaporation reduces the rearrangement time, thus resulting in the formation of polycrystals. The nature of the substrate also plays a significant role. For instance, the presence of hydroxyl groups on the surface of a glass substrate favours growth of larger crystals comprised of negatively charged colloid particles, because repulsion from the surface enhances their mobilities. In this case, growth of the crystals comprised of positively charged particles is strongly suppressed. Finally, an important role is played by the concentration of the dispersion medium. Knowing the droplet size, it is possible to estimate the concentration corresponding to the formation of a monolayer of particles on the substrate surface. However, in all model experiments we deal with the formation of multilayered crystals along the perimeter of the droplet. This is due to the fact that it is the peripheral area of the droplet where evaporation occurs more intensely; convective flows of the dispersion medium favour transfer of particles to that area. Therefore, fabrication of a monolayer requires that the actual particle concentration be higher than the corresponding calculated value.

Because of its simplicity, the droplet evaporation method remains quite attractive as yet.[115, 116] The technique was employed to grow colloid crystals comprised of the oxide,[117] sulfide,[118] noble metal [115, 116, 119, 120] and polymer [121] nanoparticles. Two-dimensional colloid crystals of nearly micrometre size were grown.[116] The methods developed to form ordered arrangements of the metal and semiconductor particles are also applicable to magnetic nanoparticles.[111, 122–125] In contrast to micrometre-size spheres, self-assembly of nanoparticles is governed by not only the entropy factor.[119, 126] Here, an important role is played by the particle–particle and particle–substrate interactions and by the nature of the stabiliser and binding agent molecules.[127]

The droplet evaporation method also involves self-assembly of particles on the mesoscopic level, namely, evaporation of large droplets leads to the formation of ring structures,[128, 129] which can be explained with ease [129] by analysing the hydrodynamics of the process. It should be noted that the use of more complex methods for the formation of ordered layers of nanoparticles sometimes causes [130, 131] complication of structural organisation on the mesoscopic level.

On the nanometre level, the degree of local order of the deposited nanoparticles is strongly dependent on the average particle size, because the larger particles are usually characterised by lower polydispersity [132] and are therefore more suitable for the formation of ordered structures. Such structures comprised of particles of size less than 2 nm are rare. Two-dimensional arrays of 'large' particles are characterised by orientation of the atomic lattices of nanoparticles relative to one another;[133] however, 3D-systems are usually disordered. At the same time, high-quality colloid crystals can be formed under particular conditions from particles of different size even using the classical scheme of fabrication of ordered ensembles *via* evaporation of a dispersion droplet. This was demonstrated taking alkylamine-stabilised gold nanoparticles as an example (see Ref. 134; the particle size varied from 1.8 to 8 nm). Using electron microscopy, a high degree of order of the nanoparticles in the colloid crystals was revealed, the atomic lattices of nanoparticles also being oriented in some way. Ordered structures were observed for both large and small particles organised into two- and three-dimensional arrays.

These results point out that the laws of self-assembly of particles to give ordered structures are still to be clarified. Therefore, the influence of various factors on the properties of the crystals formed from nanoparticles is studied. In particular, the effects of the temperature and initial particle concentration on the nucleation and growth of 3D-structures comprised of dodecanethiol-stabilised 5 nm silver nanoparticles were investigated.[135] Different methods of deposition of particle dispersions on the substrate were employed. In all experiments, 3D crystal structures were formed with good reproducibility. The average distance between the monolayers of spherical particles corresponded to the f.c.c. lattice or to hexagonal dense packing. Similarly to the case of monolayers, the size of the domains with ordered structure reduced as the temperature increased. This can be explained by the fact that faster evaporation of the solvent at elevated temperatures leads to shortening of the crystal growth time and the particles have no time to form ordered arrangements on large surface areas. As a consequence, fine-grained polycrystals are formed, which, by and large, corresponds to the situation with conventional crystalline substances.

However, the droplet evaporation technique has some drawbacks. There are (sometimes) irreproducible results and impossibility of fabrication of large ordered structures that are necessary in designing biosensors, biomaterials and catalysts. Large-area nanostructures are also necessary in creating functional bioactive surfaces. The nanoscale morphology of the surface strongly affects the interaction between the surface and cells and should be taken into account in the design of implants.[136]

Various methods are employed to control the nanoparticle–substrate interaction.[137–142] First of all, these are the ability of surfactant molecules to self-assemble on the substrate [143] and modification of substrates [140] by surfactant monolayers of different density to affect the structural organisation of the deposited nanoparticle layers. In some cases, substrates are covered [141, 142] with monolayers of the molecules (including dendrimer ones) containing the NH_2, CN and SH terminal groups, which are characterised by high affinity to metal particles.[141]

Particles are coated with bifunctional molecules [137–139] to bind them to the surface, which permits self-organisation of particles on the substrate surface [138] similarly to surfactant molecules. Using this method, it is possible to form rather stable structures comprised of nanoparticles. However, the procedure is of limiting use because the molecules used must form strong bonds with both the particle and the substrate.

In the early stage of studies on the self-organisation the formation of 3D colloid crystals faced some problems,[110, 144] though sometimes such objects were also formed by simply evaporating the dispersion droplets.[135] To enhance self-assembly of nanoparticles into three-dimensional crystals, electrochemical deposition of particles [145] and modification of their surfaces are employed.[144, 146, 147] Recently, it has been understood that this requires the use of special procedures that are determined by the nature of nanoparticles. For instance, two main methods employed to form ordered ensembles of gold nanoparticles are as follows. The first method involves the binding of gold nanoparticles *via* dithiol molecules, which form chemical bonds with two different particles through the terminal SH groups. By changing the alkyl chain length of dithiols, one can vary the constant of the nanoparticles' lattice.[148–153] According to the second method, ordered ensembles of nanoparticles are obtained from identically functionalised gold nanoparticles using a binding agent. Here, self-assembly of particles proceeds by the antigen–antibody reaction mechanism [154] or by the DNA binding,[155] hydrogen bonding [156] and complexation [157] mechanisms. The last-named technique is very often used to form hybrid inorgano-organic composites.[158] A comparative study of these two methods was reported.[159] Self-assembly of gold nanoparticles was performed using alkanedithiols and mercaptoaniline. In the latter case, succinyl chloride was added to the solution to control the bonds between NH_2 groups. Experiments with dithiols showed that nanoparticles on the substrate form a hexagonal lattice with a lesser degree of perfection than in the case of mercaptoaniline. This can be explained by faster aggregation of nanoparticles in the case of dithiols.

At present, a number of methods of fabrication of three-dimensional lattices have been developed. The next step is to perform targeted control of the structures of three-dimensional crystals to impart particular electrophysical and other characteristics to these objects.[160, 161] Recently, studies on the laws of formation of ordered structures in three-dimensional arrangements of polydisperse particles have begun.

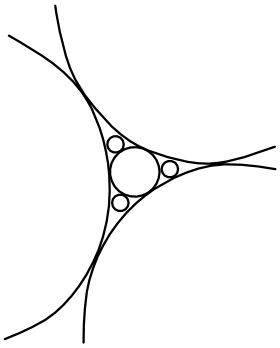

Figure 2. Ordered ensemble of polydisperse particles that form an Apollo figure.

The formation of cubic lattices in monodisperse systems of nanoparticles has been repeatedly pointed out. A bimodal ensemble of particles on the substrate can either undergo a separation into the components or form an ordered binary 'alloy'.[162, 163] Ordered structures in binary mixtures were also observed for two-dimensional systems.[164] Usually, the formation of ordered ensembles in polydisperse systems is thought to be impossible. However, numerical experiments[165] showed that the so-called Apollo figures (small particles fill the voids that form upon contact of large particles, see Fig. 2) can be formed in the systems characterised by 'hierarchical' polydispersity. Even more complex structures comprising polydisperse nanoparticles were observed in the experiments,[166] namely, the particles self-assembled into ordered structures in compliance with their sizes and the transition regions between the areas covered with particles of different sizes were smooth and defect-free. The formation of structures in ensembles of colloid spheres with controllable polydispersity was studied. The particle sizes varied between 5 and 50 nm. The ensemble of nanoparticles was prepared to provide a Gaussian particle size distribution with a polydispersity index of 30%. Particles were dispersed in an organic solvent and then a droplet of the dispersion was transferred on a solid substrate. Visual observations showed that after evaporation of the solvent the substrate surface is covered with large aggregates containing large particles in the central region and small particles in the peripheral regions. Within the aggregates, particles also form ordered arrangements (Fig. 3). The formation of such structures, which were called the 'Zenon clusters', was explained by the strength of the van der Waals interparticle interaction and by peculiarities of the fluid flow in the evaporating droplet.

A few theoretical studies on self-organisation of nanoparticles on substrates are available. Simulation[167] of particle deposition on solid substrates was carried out to study salient features of the structural organisation of nanoparticles that form upon electrochemical deposition on substrates.[29] Numerical experiments reproduced the situation corresponding to the binding of particles to the surface through bifunctional molecules and allowed the effect of polydispersity on the ordering of the particle monolayer to be studied.[168, 169] It was shown that the length of the binding agent molecule governs the particle layer morphology, which can correspond to the liquid, the hexatic phase or to two-dimensional crystal. Theoretically, the liquid–solid phase transition in two-dimensional system of hard disks has long been reported.[170] Recently, considerable attention has been given to the existence of the hexatic phase as intermediate between the liquid and crystalline phases[171] (for more detailed discussion, see below). Investigations on the effect of polydispersity on the two-dimensional phase transitions showed[169, 172, 173] that in polydisperse systems the liquid–crystal phase transition is shifted towards larger coverages and there is a limiting polydispersity value, starting from which no phase transition occurs. No hexatic phase is formed if the polydispersity index is rather high.[169]

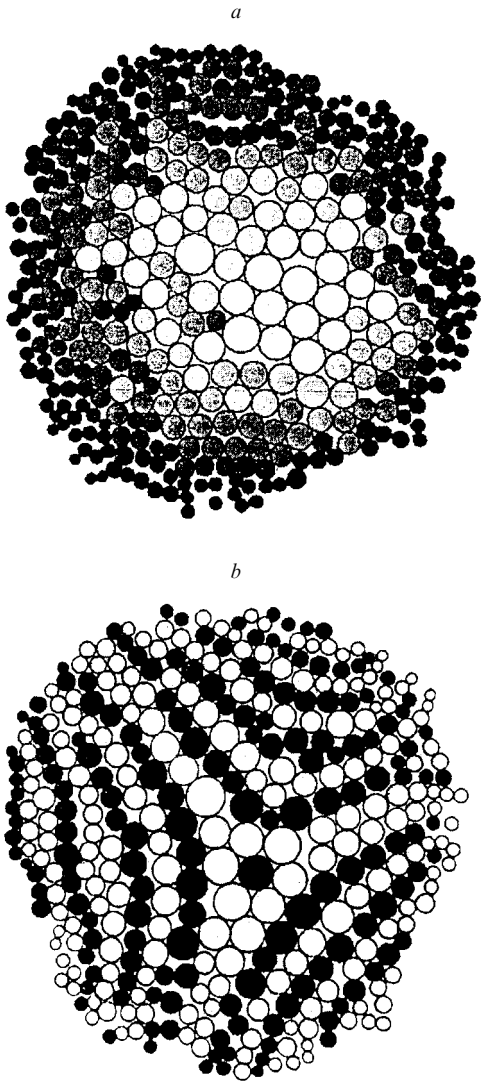

Figure 3. Ordered arrangement of polydisperse particles.[166] Experiment (*a*) and model (*b*).

Numerical experiments were also carried out to study peculiarities of the deposition of polydisperse nanoparticles on substrates in the case of random successive adsorption[174] and various packing types of particles in the monolayer at a given volume fraction of the particles.[175]

2. Non-spherical particles

The structural organisation of non-spherical particles on substrates corresponds to the cases reported in the literature[88, 176] and observed in bulk systems.[177–179] In the case of two dimensions, the phase behaviour is also governed by the maximum entropy condition. Various methods of formation of two-dimensional ordered structures comprised of non-spherical nanoparticles are developed. For instance, melt growth of silicon nanocrystals in the gap between two SiO_2 plates permits fabrication of ordered ensembles of such crystals with mutually oriented atomic lattices.[180]

It is possible to deposit rod-like cadmium selenide nanoparticles in such a way that their principal axis will be directed along the normal to the surface while the particles will be hexagonally packed in the plane of the substrate.[181] This way of packing nanoparticles imparts unusual optical properties to the crystal. Ordered ensembles of rod-like particles can also be fabricated by the droplet evaporation technique, which was demonstrated taking gold particles of length 55 nm and diameter

12 nm as an example.[182] The particle layers exhibited not only translational but also orientational symmetry. According to X-ray diffraction data, nanorods have a nearly identical crystallographic orientation at a length scale of the order of 500 nm. Namely, a total of 200 rod-like particles have the same crystallographic orientation (either [110] or [100]). This can be explained by the fact that nanorods on the {110} and {100} faces can be involved in the intercrystalline contacts.

The formation of ordered structures was attributed to the effect of capillary forces. If rod-like particles are oriented normal to the surface, the forces acting along the principal axis of the particles are greater than those acting in the transverse direction (for spherical particles, lateral capillary forces are proportional to the square of the particle radius).[183] This reason and the pressure applied to the particle monolayer [184] determined the packing of nanorods.

3. Effects of external fields

Self-assembly of particles (first of all, magnetic particles) can be favoured by the external fields. Most studies carried out in this field are concerned with the single-domain particles and their ensembles; however, data on the magnetic properties of ensembles of nanoparticles are strongly different. A possible reason for such discrepancies is the inhomogeneity of the ensembles studied. Because of this, increasing interest in the synthesis of ordered ensembles of magnetic particles has been expressed recently.[122, 123] Note that fabrication of ordered ensembles comprised of the nanoparticles that can be involved in strong interaction with external fields involves the formation of structures whose properties change under the action of external factors (the structures are usually similar to those formed by the 'inert' particles).

In contrast to the gold, silver and sulfide particles, no self-assembled three-dimensional ordered crystals comprised of magnetic cobalt particles are available as yet.[185] Usually, experiments resulted in structureless multilayered ensembles, which can be explained by magnetic interaction between nanoparticles. However, application of a magnetic field along the normal to the substrate led to the formation of two-dimensional structures [186] with hexagonally packed magnetic cobalt nanoparticles, which exhibited co-operative magnetic properties. Search for optimum methods of formation of ordered ensembles of magnetic particles is currently in progress.[187–189] The magnetic field can be used for both preliminary fractionation of nanoparticles and control of their self-assembly. For instance, evaporation of a droplet of a dispersion containing nanocrystallites of ferromagnetic or superparamagnetic cobalt on various substrates in a field of strength less than 1 T gave two-dimensional colloid crystals. An increase in the field strength up to 6 T led to the formation of three-dimensional crystals. The character of the structures obtained was independent of the size of the cobalt nanoparticles but changed with the change in the direction of the magnetic field. In some cases application of the magnetic field caused partial ordering of nanoparticles, which formed ensembles of isolated aggregates (points) or labyrinth structures.[185] The magnetic properties of the nanoparticle films differ from those of dispersions or bulk materials. This opens prospects for practical applications of the structures fabricated.

Deposition of 8 nm cobalt nanoparticles from a droplet of dispersion on the substrate (highly oriented pyrolytic graphite) at different orientations of the external magnetic field was studied.[190] If the field was directed normal to the substrate, evaporation of the dispersion medium led to the formation of a hexagonal arrangement of nanoparticles. If the field was directed along the substrate surface, aligned nanoparticle 'filaments' with nearly equidistant separation were formed. The lattice constant and the filament width depended on the magnetic field strength and decreased as the field strength increased. The 'filaments' were nearly 2 μm thick. This is close to the size of the 'points' at the sites of the hexagonal lattice formed upon deposition of nanoparticles in the field directed normal to the substrate.

A way to fabricate ordered colloid structures is to expose a colloid system to the standing electromagnetic waves created by interfering laser beams.[191] Colloid particles placed in the field of the standing electromagnetic wave can be considered as being in the potential

$$V_e(r) = -\frac{1}{2}\chi_p E^2(r),$$

where χ_p is the particle polarisability and $E(r)$ is the electromagnetic field strength at a given point. By varying the fringe pattern it is possible to change the structure formed from colloid particles. A number of nonlinear effects were observed at rather strong external electromagnetic fields. For instance, a colloid liquid compressed by an electromagnetic wave experienced a phase transition (crystallisation).[192] Often, the structures created using laser radiation are used to study the dynamics of colloid particles, *viz*., the diffraction characteristics of the probe beam are used to determine the spreading velocity of the structures, which allows the dynamic characteristics of the colloid dispersions to be determined.

Two- and three-dimensional colloid structures were also formed using the field of external mechanical forces.[193] On the glassy substrate covered with a thin layer of poly(methyl methacrylate), a system of grooves was created, which had the shape of stripes or rectangles. The plate was dipped in the colloid solution of poly(methyl methacrylate) spheres stabilised by 12-hydroxystearic acid. Then, a non-adsorbable polymer was introduced into the system. The polymer produced a pressure (by the depleted layer mechanism) to press the particles against the surface of the 'puckered' substrate. This resulted in the formation of ordered structures on the substrate. The particle size was either smaller or larger than the intergroove separation. Depending on the particle size, the structures had different symmetry (from linear to hexagonal). In the latter case, successive multilayered deposition of particles gave a f.c.c. crystal.

4. Gas–liquid interface

In the text above, we considered the main methods of fabrication of ordered arrangements of nanoparticles, namely, the droplet evaporation method and self-assembly due to modification of nanoparticles by bifunctional molecules. Both of them have some drawbacks. The first method gives poorly reproducible results, while practical implementation of the second procedure requires that particles be rather strongly bound to the substrate. In both cases, ordered structures are obtained only from the particles with specific ligand shells. The reactivity of particles, electron transfer between them, the ability of particles to participate in various physicochemical processes depend on the nature of the ligand shell. For instance the electrical conductivity of thiolate-stabilised gold nanoparticles can be substantially enhanced upon replacement of the alkanethiol ligands by bifunctional molecules (*e.g*., molecular wires). Electron transfer also depends on the character of the chemical bonds between the ligand shell and the metal core (the Au–S bond in thiolate molecules). It was established [194] that some thiolate ligands used to obtain metal nanoparticles can be replaced by other ligands, which opens up great prospects for variation of the functional properties of nanoparticles and their ensembles (surprisingly, ligands exhibit some mobility on the particle surfaces). In this connection we can say that a new research avenue, *viz*., the 'tuning' chemistry, is now in the early stage of its development. Research in this field requires the elaboration of such methods for fabrication of ordered nanoparticle layers that are almost independent of the nature of the ligand shell. The Langmuir–Blodgett method meets this condition.

Probably, it was Nagayama *et al*.[195, 196] who first employed the Langmuir–Blodgett method to this end. To form self-organised layers of polymer nanoparticles, they proposed to use the capillary forces, which are due to the meniscus between particles,

belong to attractive forces and can therefore favour self-assembly of crystals from nanoparticles.

Owing to the capillary forces, the Langmuir – Blodgett method also permits the formation of ordered particle monolayers on vertical surfaces; removal of the plate from the colloid solution and subsequent evaporation of the solvent causes the formation of ordered arrangements of particles. This method works well for the particles of size less than 400 nm, because larger particles precipitate under the action of the gravitational force faster than the solvent evaporates. However, sedimentation can be suppressed by, *e.g.*, applying a temperature gradient to the meniscus (such a gradient causes a convective motion of the fluid, which hampers sedimentation of particles).[197]

Hydrophobised nanoparticles can also be organised at the air – water interface and assembled in multilayered structures using the conventional Langmuir – Blodgett technique. Self-assembly of such particles at the interface is also possible in the absence of the ordering effect of the Langmuir surfactant monolayers, while hydrophobisation as such can be achieved in the course of particle formation in the organic medium.[198] This technique was employed in the fabrication of ordered arrangements of various metal and oxide nanoparticles [199–208] and bimetallic particles.[209] Bimetallic nanoparticles were obtained [209] immediately in the subphase and then, after special treatment, came to the surface. The Langmuir – Blodgett method can also be used for the formation of heterocolloid layers.[210, 211]

The Langmuir – Blodgett technique allows the particle size to be varied from several to several tens and even hundreds of nanometres. Nanoparticles can be stabilised using various compounds [212] and form a variety of structures on the surface of the liquid phase.[213] The hexagonal structure, which is usually formed at high monolayer pressures, remains after transfer of the monolayers to solid substrates. The degree of local order in the particles strongly depends on the stabiliser type. In the case of charged particles, the character of their packing is affected by the pH value of the solution. Under particular conditions, wire structures are formed.[214, 215] Usually, the compression isotherms of nanoparticle monolayers do not reflect structural peculiarities (see, *e.g.*, Refs 216 and 217, where both the particle size and the parameters of the stabiliser molecules were varied). At the same time, they exhibit hysteresis, the width of the hysteresis loop being dependent on the compression – expansion rate.

Practical implementation of the Langmuir – Blodgett method is complicated by the problem of fabrication of extended ordered structures. Similarly to compression of surfactant monolayers, compression of a monolayer of nanoparticles causes the formation of a domain structure, the particles being ordered only within domains. To some extent this problem can be considered solved.[218] Rather large ordered structures were fabricated due to particle aggregation caused by an increase in the system's temperature. On raising the temperature, convective flows are induced on the surface of the liquid phase and displace particles towards the growing two-dimensional crystal. Intense convection and capillary waves favour a rapid escape of defects from the growing crystal, which results in extension of the ordered structure.

Ordered structures can be transferred from the surface of the liquid phase to the solid substrate without significant distortion of two-dimensional crystal order (see above). However, the growing ensembles of nanoparticles are unstable, especially if monolayers are transferred at rather low surface pressures. This is due to weak particle – particle and particle – substrate interactions. Therefore, methods for improving the stability of nanoparticle monolayers are required. One of them is to modify the existing layers.[219] However, more efficient is the procedure for fabrication of stable monolayers from nanoparticles bound through bifunctional molecules,[220, 221] *e.g.*, dithiols (remember that these compounds are used [147] to form three-dimensional ordered structures) using the Langmuir – Blodgett method. By chemically binding nanoparticles it is possible to obtain rather stable ensembles. For instance, nanoparticles stabilised by alkanethiols (C_6 – C_{12}) can be strongly bound by arenedithiols at rather high monolayer pressures.[220, 221] To form two-dimensional structures, nanoparticles and the solid dithiol were simply placed in contact on the surface of the aqueous phase. Nanoparticle binding occurred due to the exchange reaction between dithiol and thiol that forms a protective layer on the particle surface. Transmission electron microscopy (TEM) studies showed that particles form two-dimensional layers with hexagonal packing. The interparticle distance was determined by the length of the binding agent molecule (dithiol), being virtually independent of the length of the stabiliser molecules.

If ordered arrangement of particles in the monolayer is not required, the Langmuir – Blodgett procedure is significantly simplified. At the same time, it permits fabrication of layered structures from nanoparticles [222] with the interlayer spacing, which is determined by the thickness of the ligand shell. According to data of X-ray diffraction studies, such layered structures exhibit a rather high degree of perfection.

Practical implementation of the Langmuir – Blodgett method in the case of magnetic particles faces some problems. Attempts at using this technique in experiments with iron oxide particles protected by fatty acid layers led to the formation of inhomogeneous films [223, 224] (multilayered ferroparticle films were also formed).‡ A procedure for fabrication of two-dimensional ensembles of magnetite (Fe_3O_4) and cobalt ferrite ($CoFe_2O_4$) particles stabilised by oleic acid was reported.[225] The particles were characterised by a broad size distribution. They were fractionated and fractions with narrow size distributions (particle size range 2 to 10 nm with a scatter of 10% to 20%) were isolated. Dispersions of the particles in octane or heptane were placed on the surface of water and the solvent was evaporated at 80 °C. The degree of order of the structures formed was particle size dependent, namely, larger particles (6 nm) formed ordered 'crystals' while small particles (2 nm) formed disordered structures. The size of the ordered areas reached several micrometres.

The Langmuir – Blodgett method can also be applied to non-spherical particles, which form a greater variety of ordered arrangements. The self-assembly technique was employed to obtain three-dimensional structures comprised of anisotropic $BaCrO_4$,[226] FeOOH [227] and CdSe [181] particles stabilised by oleic acid, as well as gold [182] and silver [228] nanorods. The formation of structures from rod-like $BaCrO_4$ particles of length 20 nm and diameter 5 nm was TEM monitored to follow the effect of the monolayer pressure on the organisation of particles.[229] At low pressures, 'raft'-shaped isotropic particle aggregates were observed. As the pressure increased, the 'rafts' formed the two-dimensional nematic phase, then the smectic phase and, finally, the three-dimensional nematic phase (Fig. 4). These changes in the structural organisation correspond to the Onsager scheme, according to which the ordering processes are responsible for an increase in entropy due to a decrease in the volume per particle.

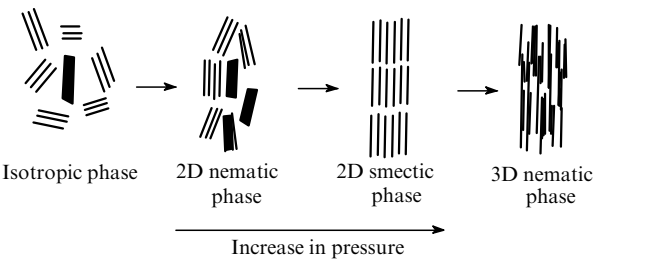

Figure 4. Structural rearrangement of the monolayer of rod-like particles upon an increase in the surface pressure.[229]

‡ Taking into account successful experiments with gold particles, these results seem to be quite unexpected.

5. Liquid – liquid interface

Self-assembly of particles can also occur at the liquid – liquid interface. It was shown that liquid-like colloid silver films can be obtained at the interface between the organic (dichloromethane) and aqueous phases.[230] However, these films are insulators.[231] More recently,[232] similar films were formed from both electrostatically and surfactant-stabilised gold nanoparticles. The formation of ordered structures nanoparticles at the liquid – liquid interface was also reported.[233]

Gold nanoparticles at the interface between the organic and aqueous phases can be immobilised by introducing aromatic molecules (*e.g.*, benzene or anthracene, which are strongly bound to the particle surfaces) into the organic phase.[232] In the case of anthracene the nanoparticle film formed at the liquid – liquid interface is a highly elastic membrane. Films can be transferred to the solid substrate by simply evaporating the contacting solvents. A detailed study on the mechanism of formation of such films showed [234] that the benzene and anthracene molecules are strongly bound to the gold particles due to the π-interaction with the gold cations present on the surface of nanoparticles and that ordered structures cover rather large surface areas.

Ordered layers of nanoparticles at an interface between two immiscible liquids can also be formed by chemical reduction immediately at the interface. For instance, interfacial reaction between an aqueous solution of cadmium carbonate and a solution of carbon disulfide in carbon tetrafluoride resulted in the formation of multilayered films comprised of cadmium sulfide nanoparticles of size from 1.8 to 3.9 nm.[235]

The thermodynamic properties of the particle monolayers were studied taking the monolayers of 2.6 μm polystyrene latex particles at the octane – aqueous surfactant solution interface.[236] In this system under particular conditions it is possible to form ordered interfacial structures, which represent hexagonally packed monolayers of particles with a polycrystalline structure. The monolayer compression isotherm exhibited no features. It was found that the pressure necessary to destroy the monolayer coincided with the interfacial tension at the interface between the above-mentioned liquids in the absence of particles. Destruction of the monolayer occurred by bending rather than transfer of particles to a certain phase. A similar phenomenon was observed [237] for the Langmuir monolayers of negatively charged latex particles of size 0.2 to 2.6 μm at the air – water and octane – water interfaces. The structure of the monolayer at the surface of water is sensitive to the electrolyte concentration. At low electrolyte concentrations, an ordered ensemble of hexagonally packed nanoparticles was formed; an increase in the concentration led to particle aggregation and the formation of disordered structures. At the octane – water interface, a hexagonal packing was formed at low surface pressures and a rhombohedral arrangement was formed at elevated pressures; the electrolyte concentration had little effect on the degree of local order of the monolayer.

6. Layer-by-layer deposition of nanoparticles

The method of layer-by-layer deposition developed [238] as an alternative to the Langmuir – Blodgett method involves successive immersion of a substrate into a dispersion of particles and into a solution of oppositely charged polymer or surfactant. To form polylayers of nanoparticles, this technique was first employed [239] in order to obtain stable ultrathin films comprised of alternating layers of the polyelectrolyte and semiconductor particles. The films appeared to be more stable than those formed using the Langmuir – Blodgett method. Yet another important advantage of the layer-by-layer deposition technique is that films can be deposited on substrates of any size and shape. However, similarly to the Langmuir – Blodgett method, the interparticle interaction is hard to control.

The layer-by-layer deposition method can be applied to obtain various structures.[240, 241] The absorption of the perfect films formed by this method increases linearly with their thickness in the visible and UV spectral regions, which means that all particle layers are characterised by the same packing density. High quality (constant period) of the films prepared by the layer-by-layer deposition is illustrated in Fig. 5, where the SAXS intensity is plotted *vs.* the angle of incidence. If nanoparticles are involved in strong electrostatic and dispersion interactions, the deposition of the polymer layer only slightly disturbs the structure of the ensemble. Immobilisation of particles makes it possible to create strongly inhomogeneous films by deposition of different polymer – particle bilayers in a specified order. By changing the order in which layers are deposited it is possible to impart particular functional properties to the films. Yet another advantage of the layer-by-layer deposition method is the possibility of formation of structures that are inhomogeneous in different directions. For instance, the preparation of gradient composite films of CdTe nanoparticles was reported.[242] The size of the films increased with their thickness. Such films are thought to be promising as elements of photodetectors, bipolar transistors and other high-speed electronic devices. They behave in an unusual manner upon injection and charge transport and can be used as light traps. Fabrication of these films using conventional methods based on molecular beam epitaxy or plasma-enhanced chemical vapour deposition requires various tricks (see, *e.g.*, Refs 243 and 244). The gradient films mentioned above [242] were prepared using four types of particles of size from 2 to 6 nm, which exhibit the luminescence bands in the 495 – 505, 530 – 545, 570 – 585 and 605 – 620 nm regions (from the red to green spectral region), thus providing a broadband luminescence spectrum. Note that the layer-by-layer deposition technique also permits fabrication of ordered layers of nanoparticles with a prescribed particle concentration gradient in the plane of the monolayer.[245]

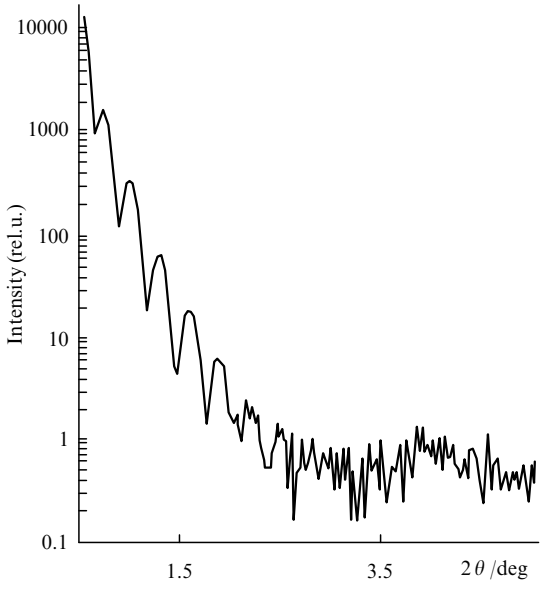

Figure 5. SAXS intensity by the polylayers of particles fabricated by layer-by-layer deposition plotted *vs.* angle of incidence.[241]

7. Biosystems and polymers

One way of development of methods for fabrication of colloid nanocrystals involves stabilisation of nanoparticles using some molecules that have binding sites. Such sites serve as specific 'pointers' of the positions to which other nanoparticles must be attached. On mixing, nanoparticles of one dispersion are linked to particles of the other dispersion through these sites. This permits the formation of a desired architecture of the colloid crystal. In this connection considerable attention is paid to aggregation of nanoparticles that are involved in biospecific interaction.[153, 154, 246 – 251] Interest in the studies of such objects is also

due to great prospects for their application in both microelectronics and biology.

The strategy of using biomolecules is based on their ability to interact with nanocrystals that have various active sites. As biomolecules are introduced into the system, the sites are recognised and a particular arrangement of nanocrystals is formed. Even replication of ensembles of nanoparticles is possible. To this end, it was proposed to use gold nanoparticles covered with adlayer of biotin (more exactly, a sulfur-containing analogue of biotin).[252] As streptavidine (this compound binds biotin) is introduced into the solution, aggregation of gold nanoparticles occurs (Fig. 6). The particles within aggregates are separated from one another by the distance equal to the bond length of the biotin and streptavidine molecules. The diffraction pattern exhibits several maxima, thus revealing some ordered arrangement of particles within aggregates.

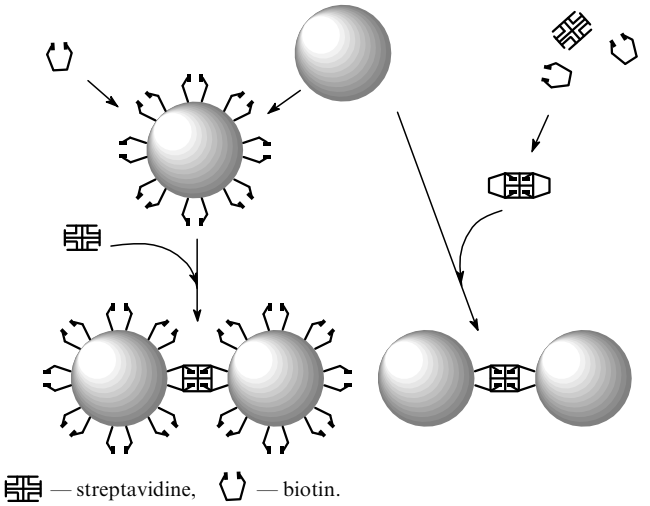

Figure 6. A scheme of aggregation of nanoparticles involving streptavidine molecules.[252]

A procedure for fabrication of gold nanoparticles stabilised by a chemisorbed monolayer of a dodecanethiol derivative and dibenzo-24-crown-8 was reported.[253] Such nanoparticles can recognise dibenzylammonium cations in solution and add them to form a pseudorotaxane shell. Therefore, introduction of bis(dibenzylammonium) into the dispersion of stabilised gold particles causes aggregation due to the assembly of the pseudorotaxane molecules. This approach was employed to study the laws of aggregation of gold and silver nanoparticles.[254]

An analogous procedure was used to obtain ordered (i) monolayers and multilayered structures on substrates and (ii) aggregates in the bulk of solution using proteins,[255] organic molecules [256–259] and polyelectrolytes.[260] Of particular interest is to use DNA molecules for binding particles, because this permits the interparticle distance, period of the particle arrangement and the aggregate compositions to be programmed by choosing a particular amino acid sequence in the DNA molecule.[246, 261–263] In this case, it is also possible to affect the optical characteristics and the melting temperatures of the particle aggregates. Studies on these effects will allow nanoparticle aggregates to be widely used as elements of biosensors. This can be exemplified by the development of a new method of DNA detection using oligonucleotide-functionalised nanoparticle probes.[246, 261, 264, 265] The method is based on the use of two different DNA-complementary oligonucleotides. As the probe meets the DNA molecule and aggregation occurs, the red dispersion turns purple. The change in the colour is due to the interaction between plasmons in the aggregated particles.[262, 266, 267]

This approach differs from other DNA hybridisation methods by enhanced selectivity, which is due to the well-defined melting point of the material fabricated from the oligonucleotide-functionalised gold nanoparticles linked through DNA molecules. The melting transitions in colloid crystals of different sizes formed on silica substrates were studied.[268] Crystals were obtained from 13 nm gold nanoparticles functionalised by various nucleotides. Structures containing different number of layers were formed. Raising the temperature caused breakdown of the adlayer structures due to the melting of nucleotides; the melting temperature depended on the number of the deposited particle layers. The temperature-dependent structure breakdown was found to be reversible; the sharpness of the transition was governed by the number of the layers deposited, while the transition region was nearly three times narrower than in the case of melting of nucleotides in the absence of particles. This narrowing is probably due to the co-operative effect.

It was proposed [269, 270] to use biosystems as substrates for fabrication of ordered colloid ensembles. For instance, latex particles were physically or chemically deposited on a giant lipid vesicle.[269] A single deposited particle deformed the surface of the vesicle and occupied the position corresponding to the highest curvature of the surface. This behaviour can be predicted with ease taking into account the energy expenditure for the deformation of the vesicle. If many particles are deposited, the interparticle interaction is determined by the attractive forces that are also related to the deformation of the vesicle. They cause particle aggregation and the formation of a quasi-two-dimensional hexagonal structure.

A procedure for fabrication of ordered structures, which involves the use of natural two-dimensional crystal order of bacteriorhodopsin molecules, was proposed.[270] This protein forms both *in vivo* and *in vitro* self-organised ordered structures that are called 'purple membranes'. Crystals of bacteriorhodopsin are used as specific templates for fabrication of ordered structures from nanoparticles.

IV. Template methods

1. Template techniques

Recently, methods of increasing the length scale of structural organisation of inorganic materials have been intensively developed. There are several ways of increasing the length scale to which the structural organisation of the assemblies fabricated is extended. One of them involves preliminary formation of 'building blocks'. This approach to fabrication of organised materials was called 'nanotectonics'.[271] Various schemes of practical implementation of the nanotectonics strategy involving biomaterials have been considered.[217] Design of such structures is to a great extent based on the principles of biomimetism (Biomimetic Materials Chemistry). Fabrication of hierarchically ordered structures is of interest for catalysis, materials science and development of resolution methods. Based on the biomimetic principles, some advances were made in creating inorganic materials with prescribed shape, molecular orientation and polymorphous crystal structure.[272] A number of methods for the synthesis of structures of a rather complex shape [273] and highly ordered hybrid ensembles [274, 275] that resemble natural hierarchical structures [276] were also developed. However, these structures are mainly of theoretical interest. More convenient for practical purposes are the 'classical' templates and first of all those based on micro- and nanospheres.

Nanosphere-based templates are used in lithography (see below) and for preparation of composite materials with ordered structure or porous metals with an ordered pore system. Porous metals are necessary for many practical purposes, *e.g.*, production of filters, catalysts, various carriers, heat transfer agents, fuel cells, electrochemical cells, thermal screens and vibration dampers. Often, porous metals with very large specific surface areas are required. Such metals can hardly be obtained by conventional

methods (sintering of powders, production of wires, foaming, *etc*.). This problem can be solved using the method of colloid templates,[277–286] which involves the formation of an ordered structure from spherical particles followed by filling of the interparticle space with the desired material (in particular, metal). The fact that usually the spherical particles contact one another allows them to be completely etched; as a result, a system of ordered spherical voids (the so-called inverted opals) is formed. This permits fabrication of materials with large specific surface areas, three-dimensional ordered pore systems and the pore sizes of several hundreds of nanometres. The pore system is an open system and possesses unique transport properties; these materials are also of considerable interest for photonics [287] (see below).

The technological procedures for fabrication of such materials are based on various methods. For instance, porous structures from Ni, Cu, Ag, Au and Pt were obtained [280] using chemical reduction, colloid crystals (silica) as templates and metal nanocrystals as catalysts. To form 'inverted' colloid crystals from gold the space between large particles was filled with gold nanoparticles.[277] Electrochemical reduction of metals was also employed. Three-dimensional porous crystals were fabricated *via* thermal decomposition of metal (Ni, Co, Fe) salts.[279] Templates are removed using various methods; the properties of the material obtained are strongly dependent on the procedure for template synthesis.

This approach was also used to form ordered structures of metal particles.[288] To this end, a non-metal (*e.g*., oxide) porous matrix was fabricated, which was filled with metal and then etched. This scheme can be used for preparation of ordered structures from not only metals and alloys but also semiconductor materials (see, *e.g*., Refs 289 and 290).

Porous membranes and ensembles of carbon nanotubes are also widely used as templates. In this case, either particles of irregular shape distributed within narrow channels or nanorods are formed.[291–293] It is also possible to obtain ensembles of rather complex composition and morphology. This approach was employed for the synthesis of polymer–cadmium sulfide composite nanowires [294] and various nanotubes [295–297] including those filled with metals [297, 298] (recently, considerable attention has been given to such objects, see review [299]).

Nanorods are most often formed using anodised porous alumina layers as templates. The pore diameter in these templates varies over a wide range (from 5 to 300 nm), the pore length exceeds 100 μm and the pores themselves are characterised by good linearity. Methods of fabrication of alumina templates have been well developed.[300, 301] Using these templates, it is possible to obtain composite materials with various nanowires [302–308] and fill almost all pores up to a depth of 100 μm (usually, only 10% to 20% of the pore space volume is filled) by employing specific procedures.[308] X-Ray studies showed that nanowires formed within the matrices have a crystal structure while their diameter is governed by the pore size. Ensembles of metal nanowires were also obtained using mesoporous silica SBA-15.[309]

Ordered ensembles of metal nanoparticles can be fabricated [310] with mesoporous silicas with an ordered pore structure, *viz*., MCM-41 (hexagonal structure) and MCM-48 (cubic structure). Silica is washed with the solution of a salt of the corresponding metal and then heat treated to form metal nanoparticles within the pore space. At elevated temperatures, the metal nanoparticles go to the outer surface of silica, thus forming an ordered lattice whose structure reproduces the two-dimensional pore structure of the silica template.

Ordered ensembles of nanoparticles can also be obtained by metal reduction in the 'micelles' of block copolymers, which can have a well-organised spatial structure. A procedure for fabrication of gold nanoparticles in laser irradiated copolymer of styrene and 4-vinylpyridine was considered.[311] The results of an experimental and theoretical study of the chemical method of preparation of lead sulfide nanoparticles in films of the same microseparated block copolymer were also reported.[312] The studies on the synthesis and properties of nanoparticles of different nature in polymer matrices were reviewed.[313]

Gel matrices of mixtures of a polyelectrolyte, surfactant [314] and organosilicon polymer [315, 316] are similar to the block copolymer matrices. They were used to obtain ordered ensembles of gold and platinum nanoparticles *via* chemical reduction. By varying the parameters of the microscopic gel network the particle size and the spatial distribution of the particles can be changed with ease.

2. Nanolithography methods

Not only the formation of colloid crystals but also fabrication of large ordered patterns from colloid ensembles is of considerable interest. Such patterns are prepared using a variety of methods, *viz*., lithography,[317] microcontact printing,[318] self-assembly involving polymers,[319] bidentate molecules,[320, 321] evaporation [322–324] or selective wetting.[325, 326] Various lithographic techniques allow one to obtain structures with prescribed geometric distribution, size and shape of the primary elements. The methods employed in the field include electron beam lithography,[327] X-ray lithography,[328] ion-beam lithography [329] and photolithography. The last-named technique is most widely used but, unfortunately, is unsuitable for the formation of structures whose elements are smaller than half the wavelength in the visible region. The region with $\lambda < 300$ nm is accessible to UV lasers [330] and holographic interferometry [331] only. The electron, ion-beam and X-ray lithographies cover the nanometre region; however, wide use of these methods is impossible as yet. The formation of ordered structures using heteroepitaxy of metals [332] and semiconductors [333] also faces some difficulties.

It was proposed [334] to use ordered arrangements of colloid particles as lithographic mask. This method was employed by many researchers. The possibilities of the technique were significantly extended.[335–338] It was shown that the use of two layers of spherical colloid nanoparticles allows the method of fabrication of nanostructures to be significantly simplified and the patterns formed to be diversified. The modified method permits fabrication of nanostructures comprised of different materials on various substrates. According to the data of atomic force microscopy studies, the type of the structure formed can be predicted with ease based on geometric considerations. This method allows the particle size to be varied with ease, thus changing the optical properties of the particles.[339]

A combined technique was also proposed.[340, 341] Patterns comprised of ordered gold nanocrystals were created with an electron beam. First, an ordered arrangement of gold particles was formed on the silicon nitride substrate by the droplet evaporation method. Then, the monolayer was exposed to an electron beam to destroy the protective ligand shell. This led to stronger binding between the particles and the substrate on the electron-beam patterned area of the substrate. The unbound particles were removed from the substrate with a solvent; as a result, the substrate was patterned in the desired manner.

Recently, the method of microcontact printing has been intensively developed. The technique involves fabrication of a pre-patterned stamp followed by transfer of the pattern (nanoparticles) to the substrate [325, 342] and permits the use of substrates of any nature.

Scanning tunnelling and atomic force microscopies are also used to obtain ordered structures. For instance, patterning was done by etching an organosilane monolayer from the substrate using a scanning tunnelling microscope (STM).[343] This was followed by nanoparticle deposition on the etched areas. A similar procedure was employed [320] to obtain ordered arrangements of gold nanoparticles with an atomic force microscope (AFM), which was used for detection of the STM-etched area and subsequent particle transfer to this area. An AFM was used to fabricate two-dimensional and three-dimensional ordered structures.[344] The technique was improved,[345] namely, deposition of 3 nm gold particles on a pre-treated surface area was followed by the formation of ordered structures using an AFM and then by

post-growth of the particles *via* immersion of the substrate in a $HAuCl_4$ solution.

Particular emphasis should be placed on the so-called dip-pen nanolitography technique,[346–349] which allows one to deposit films comprised of both organic molecules containing thiolate groups and nanoparticles on the surface of gold substrates. The method involves the spontaneous condensation of molecules or particles in the gap between the AFM tip and the substrate (Fig. 7); by scanning the surface it is possible to create the desired pattern. In the dip-pen nanolithography scheme, the microscope tip, organic molecules and substrate play the roles of 'pen,' 'ink' and 'paper,' respectively.

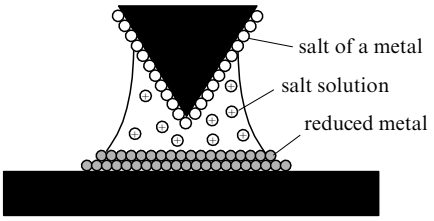

Figure 7. A scheme of dip-pen nanolithography.[349]

A method of preparation of gold 'ink' was proposed.[348, 349] This can be done using both electrochemical reduction of gold and a procedure which does not require a voltage to be applied to the microscope tip. According to the method, the microscope tip is preliminarily covered with a salt of gold and then a nanodroplet of water is placed within the gap between the salt and the silicon substrate. Dissolution of the salt as well as the metal reduction and deposition on the substrate proceed in the absence of special treatment of the system. The gold layer formed in the course of reduction was 0.4 – 1 nm thick. Details of the mechanism of gold reduction are still to be clarified; however, it was pointed out that no reduction of gold proceeds on the silica substrates. By appropriately choosing the salt – substrate pair it is possible to obtain structures from various materials.

3. Nanosphere lithography

Ordered arrangements of metal and semiconductor nanoparticles are usually fabricated by lithography techniques using planar substrates. Recently, a new trend has been towards deposition of ordered arrangements of nanoparticles on the surfaces of organised larger spherical particles. Such systems are of interest in studies on the Raman scattering and photoelectrochemical catalysis and as working elements of optical sensors. A uniform packing of nanoparticles on spherical particles can also be used for further fabrication of hollow spheres (the case where the core is somehow etched) [350] that have found application in pharmacology, catalysis, photonics and materials science.[351]

Metal particles are deposited on the surface of larger dielectric particles using various methods, *e.g.*, chemical reduction on the surface (to cover polystyrene latex particles with platinum [352] and silica particles with silver [353]), reactions with free radicals (to form silver nanoparticles on the surface of microspheres [354]) and sonochemical deposition of platinum,[355] zinc sulfide,[356] nickel [357] and cobalt.[358] An alternative approach involves activation of the surface of large particles with metal 'seeds' obtained by, *e.g.*, reduction of the corresponding precursor.[359, 360] It was employed to fabricate gold shells on silica spheres [359] and silver shells on polystyrene spheres.[360] Both these methods permit a uniform distribution of metals over the surface of spheres, though sometimes it is impossible to provide a dense packing of nanoparticles on large spheres.

The layer-by-layer deposition of nanoparticles and polymers (see, *e.g.*, Refs 361 – 363) is also employed in nanosphere lithography. Using this method, one can obtain composite films of different compositions, containing both the polymer and nanoparticles. The formation of dense layers of gold nanoparticles covered with thin silica layers on the surface of polystyrene spheres was reported.[364] To this end, layers of gold particles and poly(dialkyldimethylammonium chloride) were successively deposited on the surface of polystyrene spheres.

Ordered arrangements of 1 μm silica spheres 'capped' with gold or titanium were fabricated.[365] To this end, an ordered layer of silica particles was formed on the substrate and then covered with a photoresist layer. Then, photoresist was etched from the upper segments of the spheres, metal was deposited on the system and the remaining photoresist layer was completely etched. This led to the formation of ordered layers of metal 'capped' silica particles. The 'cap' size was varied by etching the deposited metal.

4. Functionalisation of substrates

Yet another efficient method of fabrication of ordered layers of nanoparticles involves pre-structurisation of the substrate.[366–368] Particles can be deposited using various procedures including a combination of the self-assembly on functionalised substrates with the droplet evaporation method. Other procedures include flow-induced packing of particles in the cavities with prescribed size and shape (Fig. 8); adsorption of particles on self-assembled monolayers characterised by different surface charge of different surface regions [370] and assembling of particles on the surface regions created by microcontact printing [371] or lithography.[372] A promising approach was also proposed,[373] which involves self-assembly of the charged particles on structured polyelectrolyte polylayers. In contrast to conventional self-assembly methods, this technique permits fabrication of ordered layers not only on the metal and oxide but also on the polymer surfaces. Layer-by-layer deposition of polyelectrolytes and particles allows films with unique properties to be designed.[374] In such films, the polyelec-

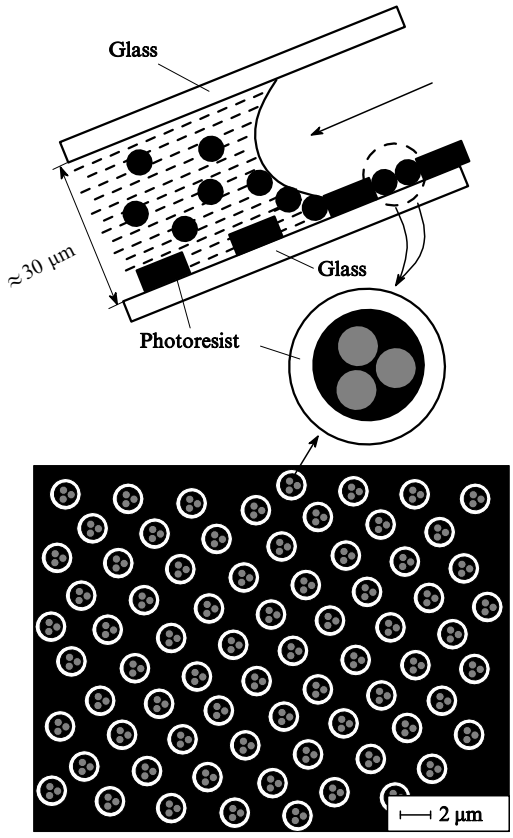

Figure 8. Deposition of nanoparticles on an ordered system of voids on substrate.[369]

trolyte polylayers can contain various functional groups [375] that provide the necessary electro-optic [376] and electroluminescent [377] properties, as well as the conducting [378] or dielectric layers and functional organic [379] and inorganic [380] particles. Polyelectrolytes permit enhancement of the adhesive binding between particles and the substrate. Patterns for polyelectrolyte deposition can be created using the microcontact printing technique;[381] therefore, the structures deposited can have arbitrary geometries.

Yet another widely used method is based on the creation of alternating hydrophilic and hydrophobic zones on the solid surface. It was employed to form ensembles of CdS nanoparticles on gold and silver substrates covered with self-assembled monolayers.[382] The methods necessary to prepare surface regions with different properties are based on the scanning probe nanolithography [383] or electron-beam patterning.[384] They are rather complicated; therefore, search for simpler procedures is currently in progress. Recently,[385] it was proposed to obtain ordered ensembles of nanoparticles as follows. First, a regular structure is formed on a silicon plate covered with the natural oxide layer from a self-assembled monolayer of siloxane containing a terminal CH_3 group by microcontact printing (see, *e.g.*, the procedure for fabrication of polydimethylsiloxane punches [386]). Then, the plate is dipped in a solution of the corresponding metal nitrate. After the plate is taken out from the solution, the droplets cover only the hydrophilic areas. The plate is then tilted so that the droplets are accumulated at the boundaries of the hydrophilic zones. After evaporation of the droplets the samples were heat treated, which resulted in the formation of nanoparticles. This method was used to fabricate ordered arrangements of cobalt, nickel and ferrite (MFe_2O_3; M = Mg, Ni) nanoparticles. The particle size and the interparticle distance were controlled by varying the solution concentration and by changing the structure of the monolayer (template), respectively.

An interesting effect, which can found practical applications, was reported.[387] The Si (100) surface covered with a natural 2 nm thick silica layer was coated with a patterned photoresist layer and the unpatterned photoresist was etched. Then, the a droplet of organic dispersion of thiol-stabilised gold particles was transferred to the substrate. It was found that narrow 'stripes' of the dispersion leak beyond the droplet at the resist – substrate interface. The 'stripe' length is at most 600 μm. Evaporation of the solvent (toluene) resulted in the formation of cluster chains of width $\approx$120 nm. The chain width remains nearly constant along the whole chain length. An analogous effect of 'escape' of nanoparticles along the boundaries of different-nature regions involving the formation of nanowires was also observed.[388]

V. Physicochemical properties of ensembles of nanoparticles

1. Electronic properties

Ordered arrangements of nanoparticles are considered as candidates for elements of electronic devices; because of this, considerable attention has been given to their electronic and optical properties.

The authors of numerous studies (see, *e.g.*, references cited in Ref. 4) observed a nonlinear current – voltage curve (the so-called Coulomb stairs) on passing electric current through individual particles. The current – voltage curves obtained in analogous experiments with self-assembled arrays of nanoparticles also have the shape of the Coulomb stairs.[138, 389, 390] For nanoparticles in organic media it is possible to draw a nearly complete analogy between the Coulomb stairs exhibited by single particles and their monolayers. For aqueous media, the current – voltage curves measured [390] on applying positive and negative potentials to the monolayer (experiments were carried out with 2 nm gold particles stabilised with alkanethiols and self-assembled into a monolayer using dithiols) are significantly different. Namely, the Coulomb stairs were observed after application of the positive potential and were not observed after the negative potential was applied. No unambiguous explanation for this effect has been given as yet.

Currently, considerable attention has been given to the studies on the laws of electron transfer within the monolayer plane. Electron transfer in the monolayered nanoparticle films involves the motion of electrons between the metal nanoparticles and overcoming of the potential barrier in the region of the stabiliser molecules (surfactant). The electron energy diagram for a composite film comprised of nanoparticles and a dielectric matrix is schematically shown in Fig. 9. Electron transfer between particles separated by an insulator proceeds by two main mechanisms, namely, by tunnelling and *via* thermally induced overcoming of the energy barrier. In weak electric fields ($eU_p < kT$, where U_p is the potential difference between the neighbouring particles), the insulator conductivity for electron transfer by the thermoionic emission mechanism is given by:

$$\sigma_e = \alpha T^2 \frac{e}{kT} \exp\left(-\frac{\phi_e}{kT}\right),$$

where α is a constant and ϕ_e is the height of the energy barrier. The barrier height is close to the work done by an electron to go from the metal particles to the matrix and includes the contribution of the image forces, which become significant in the case of small particles.

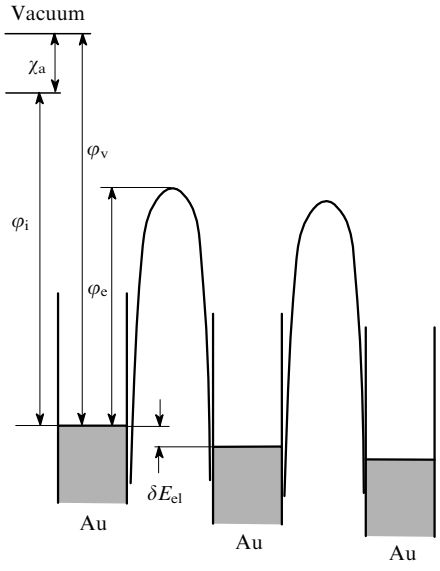

Figure 9. Electron energy diagram for a composite material of the 'nanoparticles – dielectric matrix' type;[390]
χ_a is the electron affinity towards the dielectric matrix, φ_v is the ionisation potential of the metal and φ_i is the ionisation potential of the metal in the dielectric medium.

The image forces reduce the work function by a value of the order of

$$\delta\phi = \frac{2e^2}{\varepsilon_\infty \varepsilon_0 h},$$

where ε_∞ is the high-frequency dielectric permeability of the medium and h is the interparticle distance. For gold particles, the work done to go vacuum is $\approx$5 eV and the decrease in the barrier due to the image forces at an interparticle distance of $\approx$1 nm is $\approx$2 eV. For dielectric media, the work done to go from gold decreases by up to 1 eV. Usually, the height of the energy barrier in the nanoparticle films is $\approx$2.5 eV.

The tunnelling current flowing between two metal particles is given by

$$J \propto \left(\frac{8me}{\pi^2\hbar^3 B}\right)\mathrm{sh}\left(\frac{eU_\mathrm{p}}{kT}\right)\exp(-A\phi_\mathrm{av}^{0.5})\exp\left\{-\left(\frac{\delta E_\mathrm{el}}{kT}\right)\right.$$
$$\left.\times\,[1-\exp(-B\delta E_\mathrm{el})]\right\},$$

$$B=\frac{A}{2\phi_\mathrm{av}^{0.5}},$$

$$A=\frac{4h(2m)^{0.5}}{\hbar},$$

$$\phi_\mathrm{av}=h^{-1}\int_0^h \phi_\mathrm{e}(x)x\mathrm{d}x.$$

Here, m is the mass of an electron and δE_el is the energy required to transfer an electron from one neutral particle to another,

$$\delta E_\mathrm{el}=\frac{0.5\,e^2h}{(4\pi\varepsilon\varepsilon_0 R)(R+h)}, \qquad (14)$$

where R is the particle radius.

Temperature dependences of the conductivity of two-dimensional ordered films fabricated using the Langmuir–Blodgett method from silver nanoparticles were reported.[391] Let us take them as examples. The 8 nm silver particles were stabilised by thiols with different chain length. The films were formed at different monolayer pressures. The temperature dependences of the film resistances are shown in Fig. 10. As can be seen, initially the resistance exponentially decreases with temperature. These dependences are well described by the relationship

$$R \propto \exp\frac{E_0}{kT},$$

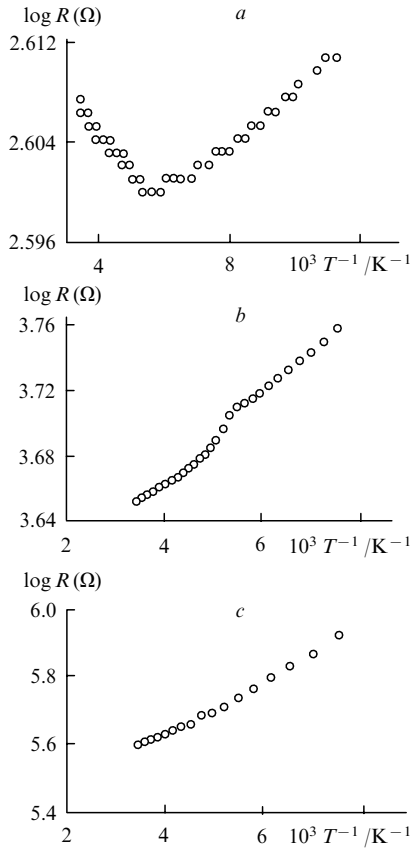

Figure 10. Temperature dependences of the resistance of the films formed by silver nanoparticles stabilised by ethanethiol (*a*), pentanethiol (*b*) and octanethiol (*c*).[391]

where E_0 is the activation energy for all the films under study. At $T \approx 200$ K, the resistance reaches its minimum value, which corresponds to the transition from the activation mechanism to the metal mechanism of conductivity. These dependences are indicative of the metal–dielectric transition in the two-dimensional monolayer. An analogous transition was detected using the tunnelling [392] and impedance spectroscopies.[393] The experimental E_0 values correspond to those calculated assuming that the energy barrier is due to Coulombic interaction between electrons and nanoparticles.

Somewhat different results were obtained in a study [394] on the electrical conductivity, photoconductivity and photoelectrochemical properties of the films comprised of dithiol-stabilised gold nanoparticles. Ordered layers were fabricated by particle deposition on substrates dipped in a colloid dispersion. At nearly the same size (6–8 nm) of particles covered with thiols of different chain lengths, the activation energy was found to lie between 5 and 25 meV, which is two or three orders of magnitude lower than the estimate (see above). Similar activation energies were obtained earlier.[147, 395] This probably indicates that the conductivity in these systems occurs by direct particle–particle contacts. Indeed, Fig. 10 shows that in the case of, *e.g.*, ethanethiol the temperature dependence of the conductivity has a complex shape and the resistance increases with raising the temperature in a certain interval. This is most probably due to the breakdown of interparticle contacts in the conductivity channels. Prolonged heating (100 °C) of the layer of particles was accompanied by a dramatic decrease in the resistance, which can be explained by thermally induced removal of the 'binding agent' from the interparticle space. The dependences of the photocurrent yield on the photon energy (Fig. 11) show that the work done to transfer electrons to the matrix is ~1 eV. Analysis of the dependences presented [the (yield)$^{0.5}$–energy dependence obeys the Fowler law for photoemission] suggested that the conductivity is of mixed character and is due to both the particle–particle contacts and the hopping mechanism. It should be noted that the mixed mechanism of

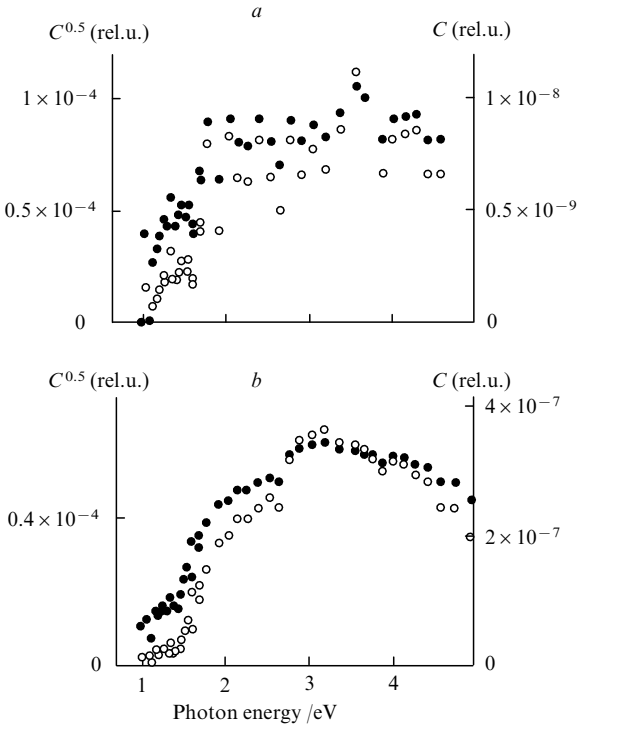

Figure 11. Photocurrent yield (C) for films comprised of silver nanoparticles stabilised by pentanethiol (*a*) and octanethiol (*b*).[391]
The right and left ordinate axes are for the open and full circles, respectively.

conductivity is typical of conventional composite materials.[396–398] The reversible metal–dielectric transition also occurs as the thickness of the ligand shell [213, 399] of nanoparticles changes.

A large number of experimental studies on various characteristics of ensembles of nanoparticles are available. At the same time, theoretical studies in this field are scarce. This is a consequence of the complexity of the systems under study (relevant solvable models can hardly be chosen). Yet another problem is that, strictly speaking, ordered ensembles are inhomogeneous structures. Structural inhomogeneity is due to the following reasons. First, nanoparticles are characterised by some size distribution. Second, it is virtually impossible to obtain a perfect structure comprised of nanoparticles. Third, different nanoparticles have different compositions because their ligand shells are also characterised by some degree of inhomogeneity. Fourth, nanoparticles execute thermal motion, thus introducing distortions in the lattice structure of the colloid crystal. Finally, electron transfer between particles can be accompanied by the electron scattering by structural inhomogeneities of the organic layer (this process can occur in different manner). In spite of this, serious efforts were made to take into account many salient features of the ensembles of nanoparticles. For instance, the following Hamiltonian was proposed to describe the electronic properties of ordered ensembles [400]

$$H_0 = \sum_{i,j}^{n} h_{ij} \sum_{\mu}^{2} \alpha_{i\mu}^{+} \alpha_{j\mu} + \frac{1}{2} I \sum (n_i - 1)^2 + \frac{1}{2} \gamma \sum_{i,j} n_i n_j, \qquad (15)$$

$$h_{ij} = \begin{cases} \alpha_i & i = j \\ \beta_{ij} & i \neq j, \end{cases}$$

where α_i is the energy level of an electron of particle i; β_{ij} is the 'transfer integral,' which is determined by the overlap of the electron orbitals of the neighbouring nanoparticles; $\alpha_{i\mu}^{+}$, $\alpha_{j\mu}$ are respectively the production and annihilation operators of electrons with the spin μ at the particle i; and n_i is the operator of the number of electrons at the particle of the type i,

$$n_i = \sum_{\mu}^{2} \alpha_{i\mu}^{+} \alpha_{i\mu} .$$

In expression (15), the second term describes the effect of Coulombic blockage and is determined by the energy required to charge a single particle

$$I = \frac{e^2}{4\pi\varepsilon_0 \varepsilon R},$$

while the last term describes the mutual polarisation of the neighbouring particles

$$\gamma = e^2 \left[2R \left(\frac{H}{2R} + \frac{e^2}{2IR} + a \right) \right]^{-1},$$

where H is the distance between the centres of the particles and a is a constant.

Calculations were carried out assuming that the constants α_i and β_{ij} fluctuate near their average values with the fluctuation amplitudes $\Delta\alpha$ and $\Delta\beta$, respectively. It was pointed out [400] that all the parameters introduced can be determined experimentally. Calculations of the electronic states of the system revealed the possibility for two types of the metal–dielectric transition (according to Anderson [401] and to Mott [402]) to occur in the system due to the fluctuations of different parameters. The Anderson transition occurs if the interaction between the neighbouring particles is rather weak and does not compensate the energy difference between the levels, which is due to fluctuations of the particles' characteristics. The Mott transition is observed when compression of the lattice of a colloid crystal causes suppression of the mutual repulsion between the electrons bearing oppositely directed spins and belonging to the same particle owing to the cooperative effects (screening), merging of the lowest occupied and upper unoccupied bands and the insulator–conductor transition. Disorder in the system also affects the Mott transition; however, this transition can be masked if the energy fluctuations due to structural inhomogeneities exceed the Coulombic interelectron repulsion energy. At small amplitudes of the energy level fluctuations, the Anderson transition occurs at much shorter interparticle distances compared to the Mott transition. These results were confirmed by the experimental data,[403] according to which at a rather long interparticle distance the ensembles behave as dielectrics due to the Anderson-type electron localisation even in the absence of the Coulombic gap.

The conducting properties of ensembles of nanoparticles can be changed by varying the layer compositions and using those particles whose state can be changed with ease under the action of external factors. In this connection mention may be made that it is possible to control the photoinduced electron transfer between the monolayers of the donor [a polypyridyl complex of Ru(II)] and acceptor [an acetylacetonate complex of Ru(III)] complexes by separating them by insulator layers [404] and that the probability of electron tunnelling in the superlattice of magnetic cobalt particles depends on the external field applied to the system, *i.e.*, on the orientation of the electron spins.[405]

2. Optical properties

Recently, increasing interest in the optical properties of nanoscale systems has been expressed.[406] This is mainly due to some prospects for the use of the near-field effects in creating devices for ultrahigh information recording density and ultrafast reading devices. In the case of three-dimensional ordered structures, of particular interest are the so-called photonic crystals (see below).

We will first consider the optical properties of two-dimensional aggregates and single-layered films comprised of metal nanoparticles. Single spherical particles are characterised by the resonance absorption band at the frequency ω_0 corresponding to the excitation of surface plasmons.[4, 406] Ellipsoidal particles are characterised by two maxima corresponding to the polarisation along and perpendicular to the principal axis. The absorption spectrum is usually calculated based on the Maxwell equations at a given dielectric constant of the external medium. The dependences of the optical and relaxation characteristics of nanoparticles on their size and shape were recently reviewed,[407] so we leave them out of our consideration.

The absorption spectra of aggregates should be calculated with inclusion of the interparticle interaction (*i.e.*, the size and shape of the aggregate formed). Pileni [408] reported the results of a detailed study of the optical and electronic properties of ordered films comprised of silver nanoparticles. Figure 12 presents the absorption spectrum of an aggregate comprising a total of nineteen hexagonally arranged nanoparticles. The characteristic feature of the spectrum is the appearance of maxima at certain ω^- and ω^+ values that meet the condition $\omega^- < \omega_0 < \omega^+$. For the s-polarised wave, there is only one maximum at $\omega = \omega^-$, while for the p-polarised wave there are two such maxima and the amplitude of the high-energy maximum increases as the angle of incidence increases. This is a consequence of the optical anisotropy of the system, namely, its polarisability is different along the normal and parallel to the surface of the substrate. This anisotropy manifests itself for the p-polarised wave, because it has components both in the surface plane and along the normal to this plane (the s-wave has only the component parallel to the surface). Experimental data obtained for silver nanoparticles [408] are in good agreement with the results of calculations.

The optical properties and electronic characteristics of the ordered films comprised of nanoparticles are determined by the classical (dipolar) and quantum (exchange) interactions between nanoparticles. The quantum interaction occurs only at distances shorter than 1 nm.[213] Because of this, the optical properties of composite materials are most often described using the Maxwell–Garnett theory as a first approximation, according to which

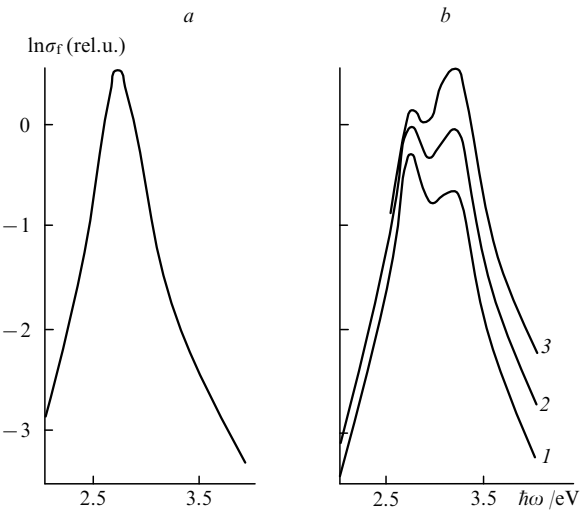

Figure 12. Absorption section by an aggregate comprised of nineteen silver nanoparticles for the s- (*a*) and p-polarised (*b*) waves.[408]
Angle of incidence /deg: 45 (*1*), 51 (*2*) and 60 (*3*).

the dielectric susceptibility of the medium is determined *via* the dielectric susceptibility of individual particles. This theory works well for dilute colloid systems. Various methods have been developed to calculate the dielectric susceptibility at a large volume fraction of particles. Here, we will present the main results of the most consistent approach.[409, 410] The frequency dependence of the nanoparticle polarisability can be obtained using the data on the dielectric response of bulk silver, on the electron relaxation time in nanoparticles and the Clausius–Mossotti formula. The dielectric susceptibility of bulk silver is given by the Drude relationship

$$\varepsilon_{\rm p} = 1 - \frac{\omega_0^2}{\omega^2 + v^2} + \frac{i\omega_0^2 v}{\omega(\omega^2 + v^2)},$$

where ω_0 is the plasmon frequency for the bulk metal and v is the collision frequency of electrons with impurities in the bulk of the metal and with the surface of nanoparticles (the width of the plasmon band),

$$v = \left(\frac{1}{l} + \frac{1}{R}\right) v_{\rm F},$$

where l is the free path length of electrons in the bulk metal, R is the particle radius and $v_{\rm F}$ is the Fermi velocity of electrons.

The Clausius–Mossotti formula for the polarisability of a metal sphere dipped in a dielectric medium with permeability $\varepsilon_{\rm m}$ has the form

$$\chi_{\rm p} = \frac{\varepsilon_{\rm p} - \varepsilon_{\rm m}}{\varepsilon_{\rm p} + 2\varepsilon_{\rm m}}.$$

The effective dielectric permeability of a two-dimensional composite medium comprised of spherical particles that are uniformly distributed over the volume of the matrix is given by

$$\varepsilon_{\rm ef} = \frac{1 + \chi_{\rm p}\varphi - (1-\varphi)^2\chi_{\rm p}^2\zeta}{1 - \chi_{\rm p}\varphi - (1-\varphi)^2\chi_{\rm p}^2\zeta}\varepsilon_{\rm m},$$

where φ is the packing density of the particles and ζ is the structure parameter, which includes three-particle correlations in the arrangement of spheres (calculated in Ref. 409). The parameter ζ depends on φ and changes from 0 (for dilute systems) to 1 (for close-packed systems). It also depends on the character of the packing of spherical particles, being much larger for random packing compared to regular one. In the former case, the parameter ζ has virtually the same value for both two-dimensional and three-dimensional systems.

Having found the dielectric permeability, it is an easy matter to calculate various optical characteristics of films, *e.g.*, the reflection coefficient $|R_{\rm s}|^2$, where

$$R_{\rm s} = \frac{r_1 + r_2 e^{-2i\delta}}{1 + r_1 r_2 e^{-2i\delta}}.$$

Here r_1 and r_2 are the Fresnel coefficients for the air–film and film–substrate interfaces,

$$\delta = \frac{2\pi}{\lambda} d n \cos\theta,$$

λ is the radiation wavelength, d is the film thickness, n is the refractive index of the films, θ is the angle of incidence of radiation.

The dependence of the reflection coefficient on the interparticle distance is shown in Fig. 13. As can be seen, the calculated and experimental data are in good agreement at rather long interparticle distances, being substantially different at short distances. Good correspondence between the theory and experiment holds up to $H/2R \approx 1.25$. This is due to the fact that the dielectric–metal transition occurs in the monolayer at $H/2R \approx 1.15$, which is not included in the model considered above. As the system approaches the transition point, rather large clusters are formed, which are characterised by the metal conductivity. For this reason, the differences between the theory and experiment increase. The metal–dielectric transition is also

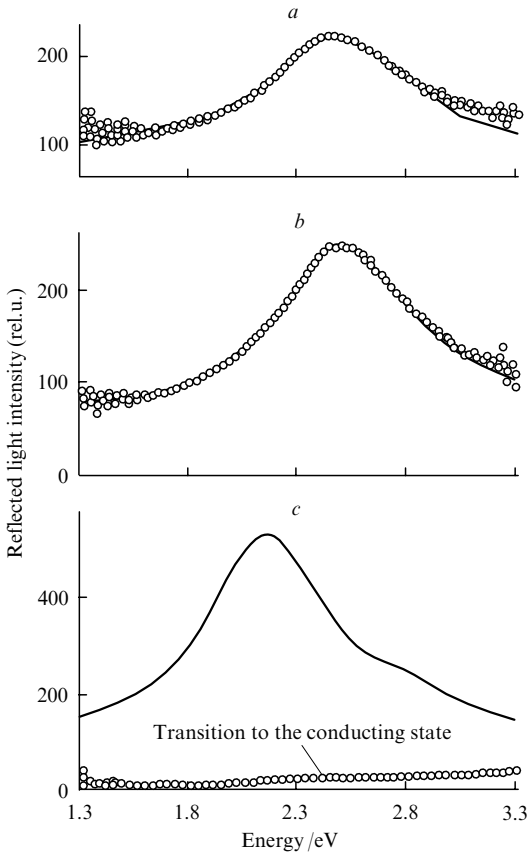

Figure 13. Reflected light intensity plotted *vs.* photon energy for different interparticle distances.[399]
Experimental data (open circles) and results of calculations (solid lines). The 'interparticle distance-to-particle-size' ratio ($H/2R$) is 1.60 (*a*), 1.38 (*b*) and 1.17 (*c*).

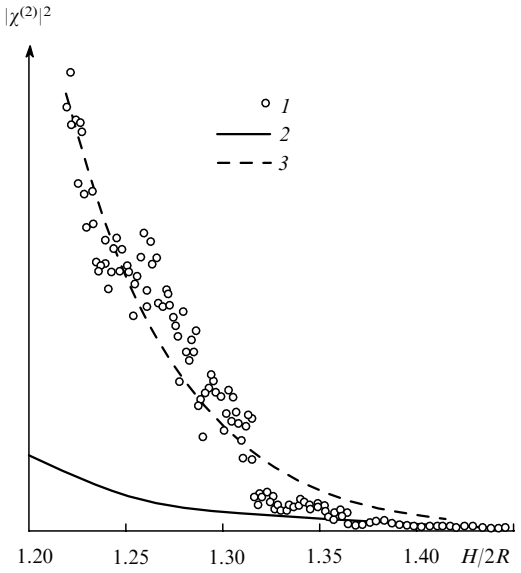

Figure 14. Second optical harmonic intensity as a function of the relative interparticle distance.[399]
Experiment (*1*) and results of calculations using the classical model (*2*) and exponential approximation (*3*).

clearly detected in measuring the intensity of the second optical harmonic (Fig. 14), namely, marked deviations of the calculated values from the experimental data are observed on approaching the point of the metal–dielectric transition.

A study on photon emission from a monolayer of particles under the action of a voltage applied to the tip of an STM also led to quite unexpected results.[408] Experiments were carried out with ordered layers of 4 nm silver nanoparticles separated by a distance of 2 nm on the Au(111) surface. First, the motion of particles across the surface was observed. Second, surprisingly, photon emission from the monolayer was inhomogeneous, that is, dark zones were observed near certain particles (the darkest zones corresponded to the vertices of the particles). The intensity of emission from the particle vertices was ten times lower than from the other sites. Experiments showed that highly mobile particles are bad photons emitters (*i.e.*, quenching of the emission is due to the motion of particles). The measurements were carried out in the d.c. regime, which is manily due to the resonant tunnelling of electrons. Non-resonant electron transfer and, correspondingly, photon emission are of the fluctuation nature. The photon emission is related to the relaxation of plasmons that are excited in the case of non-resonant electron transfer (non-resonant tunnelling).[411] Therefore, photon emission is affected by many factors. Electron relaxation can occur *via* the excitation of a plasmon, production of a photon or interaction with the surface phonons. For small particles, electron transfer to the particle occurs in the ballistic regime.[412] Because of this, electron relaxation is possible only *via* the electron–plasmon or electron–phonon interaction. The latter interaction is known to play an important role in the relaxation processes in the particles whose size is less than the free path length of an electron. It is assumed that the phonon excitation of highly mobile particles is facilitated as compared to the immobilised particles. Probably, the excitation of collective phonons also occurs. This effect, along with the well-known effect[4,413] of change in the transmission and reflection of light upon electrochemical injection of charges into the film, opens up new possibilities in controlling the electronic properties of nanofilms. In the latter case, changes in the electronic properties of the films can be explained by the change in the electron density in certain particles for which the relative changes in the electron density much exceed the corresponding value for the bulk material.

It should be noted that the interaction of electromagnetic waves with two-dimensional arrangements of particles are still poorly studied. At the same time, their understanding is necessary for not only the description of the optical properties of films but also creation of a new generation of memory devices. At the nanometre scale and femtosecond times, the electromagnetic energy is transferred by plasmons. For this reason, revealing the localisation effects of electromagnetic waves is of great practical interest. Delocalised modes govern energy transfer in the whole system, while the localised modes allow the energy to be concentrated within small regions of the system. A study[414] was reported on the properties of the eigenmodes in a two-dimensional composite containing randomly distributed metal inclusions that covered half the surface area. According to calculations, localisation of the surface plasmons in the whole spectral region is impossible. The localisation radius is distributed over the whole admissible range of sizes, from the smallest size to the size of the entire system. A typical eigenmode is simultaneously localised and delocalised, that is, there are small areas with intense field, which are distributed over a large surface area and are coherent. This propertiy of the surface plasmons makes them a promising object for data storage and transmission applications for ultrafast computations. The localisation areas can serve as energy reservoirs, while their long-range coherence allows information to be rapidly transmitted over long distances.

Currently, a new research avenue in the optics of nanofilms deposited on substrates is in prospect. It was shown[415] that the $Au@SiO_2$ particles (gold particles covered with silica layer) are suitable for fabrication of plasmon waveguides whose size is of the order of the particle size. Numerical experiments[416] showed that nanoparticles organised in linear chains are capable of transferring the energy localised in the regions with the characteristic size much smaller than the optical diffraction limit. The most important requirement is that the particles be separated by a layer, which must be sufficiently thin for the interaction between the plasmon modes in nanoparticles to occur in the near field.[417] According to numerical simulation, the signal propagation velocity in this plasmon waveguide is one tenth of the speed of light. The waveguide geometry admits the presence of acute angles.

From the aforesaid it follows that the optical properties of nanoparticle films are still far from being completely studied; therefore, they have been the subject of intensive research. The dependences of the optical characteristics of films on the properties of the substrate[418] and the dispersion medium were studied in detail.[419] Ellipsometry can also be used to study the properties of films.[420] Enhancement of the plasmon resonance upon reflection of light from bilayered films (from the substrate side)[421] and the luminescent characteristics of quantum dots upon their self-assembly into ordered structures were reported;[422–424] self-organised structures do possess not only the electroluminescence properties[425] but also enhance the laser effect.[426,427]

The surface plasmon resonance is used to study the interaction between various materials and thin metal films.[428] This method has found its main application in biochemical systems, especially in studies of proteins and DNA molecules. It involves studies on the shift of the plasmon resonance caused by the change in the refractive index of the medium contacting the metal. Such a change is observed upon variation of the interaction between macromolecules and solvents; it also manifests itself as a change in the angular dependence of the coefficient of reflection of electromagnetic radiation from metal films. The well-known effect of change in the scattering coefficient in the case of interaction between biomolecules and nanoparticles[265,266] can be considerably enhanced[429] by depositing nanoparticles on the surface of metal films. Experiments showed that the coefficient of reflection of laser radiation from a gold film significantly changes after deposition of gold nanoparticles of size 30–60 nm on the surface of the film (Fig. 15). The magnitude of the change depends on the particle size and is nearly proportional to the particle concentration on the surface. This effect permits significant improvement

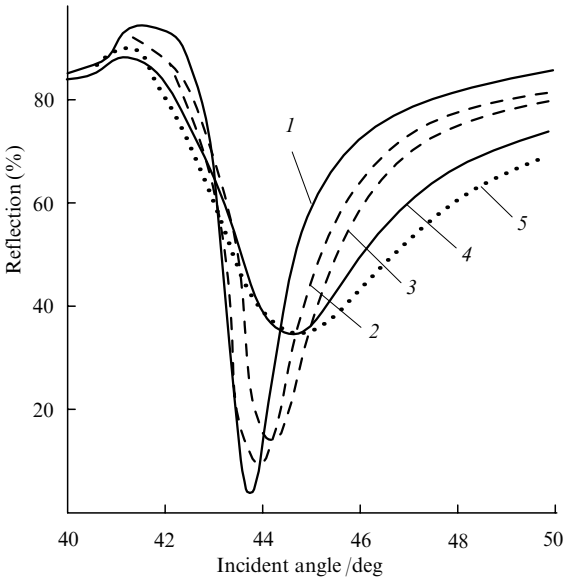

Figure 15. Reflected intensity *vs.* incident angle in the presence of gold particles of different size on the substrate.[429]
Pure gold plate (*1*); particle size /nm: 30 (*2*), 35 (*3*), 45 (*4*), 59 (*5*); particles 1.3×10^9 cm^{-2}.

of the sensitivity of detection of biomolecules using gold nanoparticles. The nature of the effect of the particles deposited on the surface is obvious: these particles make the surface rough, which causes broadening of the resonance peak.

Yet another biochemical application of single-layered films comprised of metal nanoparticles involves the use of the effect of surface enhanced Raman scattering (SERS), which is intrinsic in some metal nanoparticles. In the case of SERS, the section of scattering by the molecules adsorbed on rough metal surfaces increases by several orders of magnitude.[430] It is assumed that the nature of the SERS effect is related to both localisation of the surface plasmons and to the charge-transfer induced increase in the molecular polarisability near the metal surface.[431] In most cases, the former effect predominates; therefore, considerable attention has been given to the formation of various rough surfaces (in most cases, using colloid particles). The shape of the particle strongly influences the magnitude of the effect,[432] while the particles on the substrate should not be necessarily ordered.[433]

Numerous studies on the molecule – photon – surface interaction have been carried out since the discovery of the SERS effect; however, the mechanism of this effect is still to be clarified. It was established [434–436] that only a small fraction of particles is SERS active and that the active particles enhance the Raman scattering by 14 – 15 orders of magnitude. It was also found that the nanoparticle size is related to the exciting radiation wavelength corresponding to the SERS maximum.[434] For instance, 90 nm (140 nm) silver particles are most efficiently excited at 514 nm (570 nm). For 63 nm gold particles, the maximum enhancement is observed at an exciting radiation wavelength of 647 nm. This indicates that by sizing nanoparticles it is possible to obtain nanostructured materials with enhanced optical characteristics. Indeed, pre-fractionation of particles permits significant enhancement of the SERS effect.[437] To this end, films comprised of fractionated nanoparticles (particle size ranged from 30 to 100 nm) were obtained. Experiments confirmed that the use of certain fractions causes enhancement of the SERS effect by several orders of magnitude. The magnitude of the effect is also strongly influenced by the interaction between nanoparticles within the film.

Figure 16 presents the dependence of the SERS intensity on the degree of coverage of the substrate surface by nanoparticles for rhodamine 6G. As can be seen, the SERS intensity remains

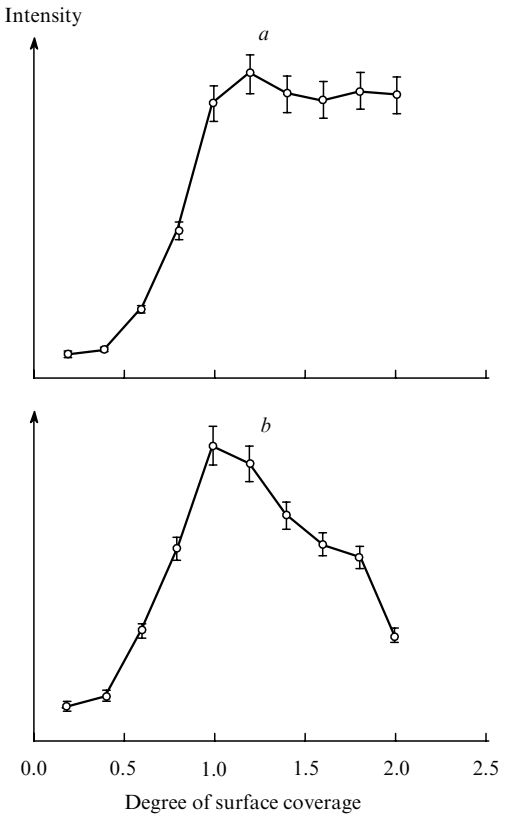

Figure 16. Absolute (*a*) and normalised (*b*) SARS intensities plotted *vs.* the degree of coverage of the substrate surface by nanoparticles.[437]

virtually unchanged as the coverage increases from 0 to 0.5, then markedly increases as the coverage approaches a unity and then remains constant. The presence of a plateau indicates that the three-dimensional ensemble of particles behaves as a two-dimensional film. Introduction of salt into the system causes a twofold increase in the intensity of the SERS signal.[437] The laws established permit the use of nanogranulated metal films as sensors in detecting biomolecules.

Consider now the optical characteristics of three-dimensional ordered colloid structures. Such structures are characterised by unusual colour gamma, being in many cases responsible for the unique protective colour of animals due to the formation of microstructures comprised of colloid particles on the surface of their bodies. Diffraction of light by such structures provides the appearance of a colour gamma which is different from that formed in the case of light absorption by dyes. Recently, studies on the optical properties of three-dimensional colloid structures have become of great importance, because colloid crystals are used as sensors,[438] tunable diffraction gratings,[439] narrow-band filters [440] and photonic crystals.[441–445] Photonic crystals serve as the basis for design of pigments and creation of a new generation of optical devices.[446–449]

The use of three-dimensional colloid crystals opens up new prospects for nanophotonics (because of this, such crystals are called photonic crystals). Nanophotonics is a new branch of optics, which describes the propagation, scattering and interaction of electromagnetic waves on the nanometre length scale. Research in this field is concerned with the interaction between the electromagnetic waves and matter at the length scales shorter than the wavelength of electromagnetic radiation, and, in particular, localised photochemical reactions. At present, nanophotonics has stimulated the elaboration of a number of novel technologies. Namely, a new type of laser and a number of optical systems and physicochemical methods were developed.[450] Colloid crystals allowed localisation of light to be performed experimentally and

have found application in laser physics and laser chemistry.[446, 447, 451–454] Recently, it has been shown that photonic crystals with band-shaped optical structure and thoroughly chosen parameters permit localisation of light, which is multiply scattered by nanoparticles.

Photonic crystals are three-dimensional structures with a periodic arrangement of particles (different phases). The refractive index of such a system is a periodic function with a period of the order of the optical wavelength. The propagation of light in photonic crystals is similar to the motion of electrons in a conventional crystal lattice. The refractive index difference between the particles and the matrix and the ordered arrangement of particles cause a strong scattering of electromagnetic waves with particular wavelengths. The Bragg diffraction occurs, which is characterised by forbiddenness for waves with particular wavelengths to propagate through the photonic crystal. Figure 17 presents the dependence of the transmission of a 12 μm-thick colloid crystal formed by polystyrene latex particles of diameter 0.23 μm on the wavelength for different angles of incidence. As can be seen, the transmission maximum (λ_{max}) is shifted from 574 to 538 nm as the angle changes from 0 to 40°. In Fig. 17 *d* we present the dependence of transmission on the wavelength for 0.36-μm latex particles at the same crystal thickness. The relation between λ_{max}, the angle of incidence and distance d_{111} between the (111) planes of a colloid crystal is given by the Bragg equation

$$\lambda_{max} = 2d_{111}(n_a - \sin^2\theta)^{1/2},$$

where n_a is the refractive index (1.489 for the ensemble of polystyrene spheres characterised by a packing density of 0.74%). Figure 18 presents the experimental and calculated λ_{max} values for colloid crystal comprised of polystyrene spheres.

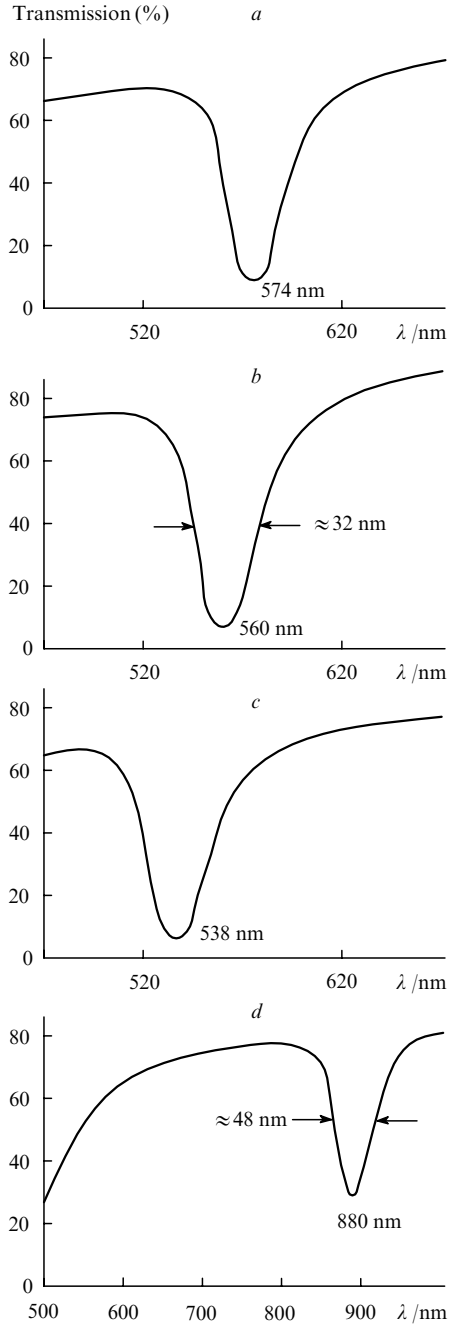

Figure 17. Transmission of a colloid crystal comprised of polystyrene particles of size 0.23 μm (*a*–*c*) and 0.36 μm (*d*) as a function of the wavelength.[455]
Angle of incidence /deg: 0 (*a*, *d*), 20 (*b*) and 40 (*c*).

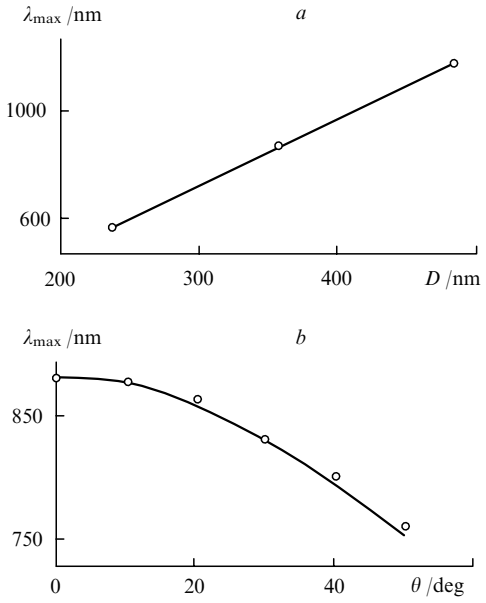

Figure 18. Absorption maximum wavelength plotted *vs.* particle size at zero angle of incidence (*a*) and *vs.* angle of incidence for 0.36 μm polystyrene particles (*b*).[455]
Experimental data (open circles) and results of calculations (solid lines).

It is possible to draw an analogy between the electron energy bands in semiconductors and in photonic crystals; however, in the latter case some features are observed. It should be noted that in photonic crystals it is possible to implement the lasing mechanism and superradiation associated with the boson nature of light, according to which a large number of photons can be in the same state. Recently, photonic crystals were fabricated,[456–458] which are characterised by localisation of electromagnetic waves in the spectral region extending from near IR to UV. Laser physics applications require that photonic crystals be tunable in the whole visible region.

A feature of photonic crystals is the change in the type of the interaction between the atoms and electromagnetic radiation. In particular, only radiation with particular wavelengths can propagate without losses through the band-type photonic crystals; therefore, atoms or molecules for which transitions between the energy levels correspond to the forbidden wavelengths, are not affected by the fluctuating vacuum field responsible for spontaneous quenching of excited states. As a result, a bound state atom–photon is created. A photon can travel a distance of several lattice constants from the atom by tunnelling before being trapped by another atom. As a consequence, relaxation of the excited

states of atoms in a photonic crystal obeys somewhat different laws compared to the case of free atoms and molecules.

Most often, photonic crystals are fabricated from silica spheres that are usually packed into the f.c.c. lattice.[459–461] By varying the size of the spheres it is possible to tune the band gap to the desired spectral region. Thermally induced tuning of the band gap is also possible.[462, 463] Fabrication of photonic crystals whose optical properties can be changed by applying the magnetic field was reported.[464, 465] By applying an external magnetic and electric field one can change the structure of the colloid crystals formed from particles of complex structure.[465] For instance, a martensite transition of the tetragonal b.c.c. lattice to the b.c.c. lattice followed by changes in the dielectric characteristics of the crystal was observed in crossed electric and magnetic fields. Recently, fabrication of inverted photonic crystals formed by the voids in the dielectric medium (usually, titania) was reported.[460, 461] Experiments showed that this structure is optimum for photonic crystals. To date, methods of fabrication of photonic crystals from various materials have been developed [466–472] and preparation of photonic crystals with the record characteristics seems not to be impossible. In this case, the interparticle distance is of great importance. Recently, methods of formation of nanoparticles coated with a thin silica shell were developed.[461, 473–476] This opens new possibilities of control of the optical properties of nanoparticles because permits variation of the core size and the thickness and composition of the shell. Spherical particles obtained following the above-mentioned routes are characterised by a narrow size distribution, being convenient building blocks for fabrication of photonic crystals. Ordered crystals obtained from such nanoparticles can be formed using various methods; however, the main procedure is based on the use of capillary forces. In particular, ordered structures from 50 nm gold nanoparticles covered with silica layers of different thickness were obtained.[415] Some examples illustrating the changes in the optical properties of photonic crystals fabricated from these particles covered with the SiO_2 shell of different thickness are shown in Fig. 19.

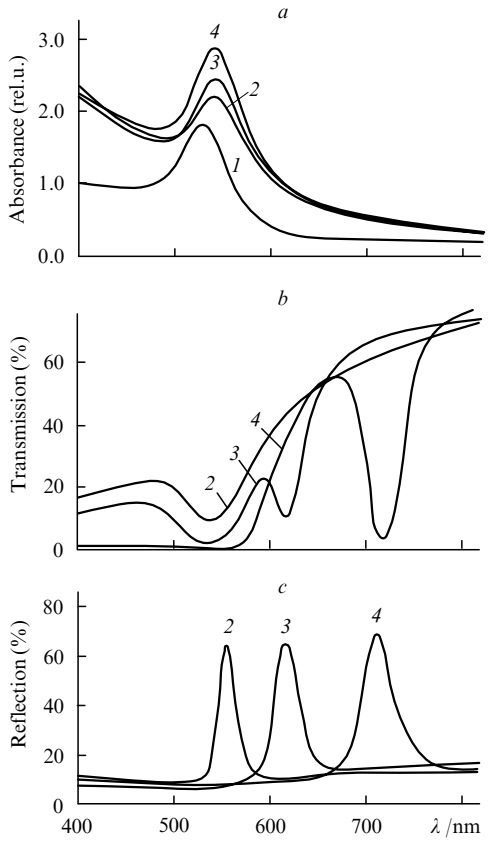

Figure 19. Optical characteristics of photonic crystals as functions of the thickness of the silica layer covering 50-nm gold nanoparticles.[415] Coverage thickness /nm: 0 (*1*), 70 (*2*), 80 (*3*) and 100 (*4*).

3. Magnetic properties

The monodomain structure of magnetic nanoparticles makes them of considerable interest, especially for fabrication of magnetic memory devices. The magnetic properties of nanoparticles differ from those of bulk magnets,[1, 6] because a decrease in the particle size is accompanied by an increase in the fraction of surface atoms. The electronic and magnetic structures of such atoms are affected by the smaller number of atoms in the particle compared to the bulk material; however, they are influenced by a large number of atoms of the dispersion medium (matrix). The surface effects can reduce the magnetic moment of particles;[477] however, for 'free' iron, cobalt and nickel particles the magnetic moment per atom increases [478] with the decrease in the particle size and tends to the limiting value characteristic of the single atom. Besides, the magnetic anisotropy of particles exceeds the corresponding bulk value.[479] The difference between these values is related to the increase in the magnetic orbital momentum of peripheral atoms.[480]

Magnetic nanoparticles are convenient objects for studying the quantum effects that manifest themselves on the mesoscopic length scale (between the quantum microscopic and classical macroscopic length scales).[481] However, real systems represent ensembles of particles, which are characterised by different size and shape. This hampers measurements of the quantum effects. The magnetic properties of such systems are determined by the properties of both the particles and the entire ensemble and these contributions are hard to be discriminated. Because of this, search for the systems suitable for wide-range variation of the average particle size, the particle size distribution and the spatial arrangement of the particles is topical. The properties of monolayers comprised of magnetic particles also depend on the procedure employed to form these objects.

A detailed study [482] on the magnetic properties of ensembles of nanoparticles involved the preparation of composites with different structural organisation of nanoparticles by layer-by-layer deposition [483] of magnetic cobalt particles on the Al_2O_3 matrix. Both ordered layers with controllable interparticle distance and random distributions of particles in the matrix (the particle size was 1 to 7 nm) were formed. Particles were formed by layer-by-layer deposition of cobalt and alumina. The results of electron microscopy study showed that the system contains isolated spherical nanoparticles whose size depends on the cobalt deposition time. This technique was used to form the films containing up to three hundred Co/Al_2O_3 bilayers. Measurements of the static and dynamic magnetic susceptibilities of these systems revealed the magnetic moment blockage effect, which is due to the magnetic anisotropy of particles. The reorientation time of the magnetic moment varies as follows

$$\tau = \tau_0 \exp\left(\frac{U_b}{kT}\right),$$

where $\tau_0 \approx 10^{-10}-10^{-13}$ s and U_b is the height of the energy barrier and is governed by the interaction between the magnetic moment of the particle and the phonon and magnon thermostats. The U_b value depends on the magnetic anisotropy constant K_{ef} and the particle volume V

$$U_b = K_{ef} V.$$

The magnetic anisotropy constant varies with the average particle size as

$$K_{ef} = K_\infty + \frac{6K_s}{\langle d \rangle},$$

where K_∞ is the magnetic anisotropy constant for the bulk material (5×10^4 J m^{-3}) and $K_s = 3.3 \times 10^{-1}$ mJ m^{-2}. An analogous increase in the magnetic anisotropy of nanoparticles was reported by many authors.[6, 479, 484]

The effect of the dipole–dipole interaction on the relaxation time of the magnetic moments of particles has been the subject of extensive literature. It was shown that the magnetic anisotropy constant increases as the number of the nearest neighbours increases.[485, 486] However, a model was proposed,[487] according to which the interaction between the magnetic moments causes a decrease in the parameter U_b. Experimental evaluation of these models faces some problems because the packing density of the particles can hardly be varied without changing the particle size. This can be done[482] by fabricating structures with different number of layers at the same cobalt sputtering tine. Experiments were carried out with the samples containing 1 and 30 monolayers of cobalt particles. The fact that both samples exhibited identical magnetisation curves confirmed coincidence of the particle sizes. The Curie–Weiss temperatures of the single-layered and thirty-layered films differed by nearly a factor of 2, which indicated a marked change in the average interparticle interaction. Measurements showed that the interaction between particles of the neighbouring layers (4.5 nm interlayer spacing) causes a substantial increase in the activation energy ($\sim$200 K for the systems under study). This value is nearly equal to the energy of the interaction between six nearest neighbours in the monolayer.

The magneto-optical properties of nanoparticles were studied.[225] Ordered ensembles of magnetite (Fe_3O_4) and cobalt ferrite ($CoFe_2O_4$) nanoparticles were first formed on the surface of the aqueous phase from the corresponding dispersions in organic solvents and then transferred on solid substrates. Particles stabilised by oleic acid were characterised by a broad size distribution; they were fractionated to obtain fractions with narrow size distributions in the range 2–10 nm and a scatter of 10% to 20%). It was established that the degree of local order of the structures under study depends on the particle size, namely, larger particles (6 nm) form ordered 'crystals', while small particles (2 nm) do not form ordered arrangements. The size of the ordered area can reach several micrometres. Figure 20 illustrates the effect of the strength of external magnetic field on the magnetic circular dichroism in the case of reflection of laser radiation by single-layered films. Measurements were carried out at different temperatures. The magnetisation curve of the two-dimensional ensemble of particles can be plotted using the results of measurements of the absorption difference between the waves with different circular polarisation as a function of the field strength. As can be seen, at room temperature the films behave as superparamagnetics. They exhibit no pronounced magnetisation hysteresis. As should be expected, the cobalt ferrite particles are first to possess hysteresis on lowering the temperature. The blocking temperature of cobalt ferrite is 200 K, while that of magnetite is 100 K. It should also be noted that cobalt ferrite is characterised by greater coercive force compared to magnetite. No significant changes in the magnetisation behaviour were observed after deposition of several layers. This indicates that in the systems under study the energy barrier associated with the crystal anisotropy is higher than the energy of the dipole–dipole interaction.

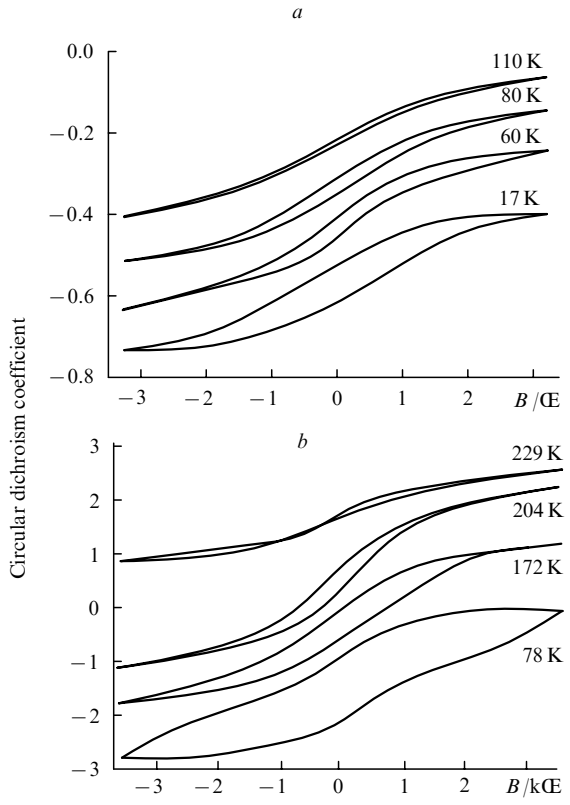

Figure 20. 'Circular dichroism–magnetic field strength (B)' dependences measured at different temperatures for a monolayer of magnetic particles;[225]
6 nm Fe_3O_4 particles (*a*) and 6 nm $CoFe_2O_4$ particles (*b*).

4. Thermal and mechanical properties

Colloid crystals are convenient for studying the phase transitions. Of particular interest are two-dimensional colloid crystals. It was established[488] that the melting transition in two-dimensional systems differs from the melting transition in three-dimensional crystals and occurs continuously involving dissociation of pair dislocations. More recently,[489, 490] it was shown that the newly formed phase is not an isotropic liquid and a second phase transition, which is due to the formation of disclinations, is necessary for the system to go from the so-called hexatic phase to the isotropic liquid. Such a two-step melting model is called the Kosterlitz–Thouless–Galperin–Nelson–Yang (KTGNY) theory. This theory predicts the temperatures at which the system becomes unstable and the topological defects (dislocations and disclinations) are formed. To test the theory, which was not necessarily confirmed in numerical experiments, the phase transition in a two-dimensional colloid crystal with well-defined magnetic interparticle interaction was studied.[491] Experiments with 4.7 μm iron oxide particles dispersed on the surface of water showed that melting of the crystal follows the KTGNY scenario. The shape of the pair distribution function was determined at different temperatures using a video camera. On melting of the two-dimensional crystal, the density correlation function first decreased following a power law with the exponent determined from the KTGNY theory and then decreased exponentially. Direct visual observations revealed the presence of a phase that was intermediate between the crystalline and liquid phases.

Two-step melting of two-dimensional ordered dusty plasma clusters was reported.[130] Numerical simulation showed that different cluster areas are disordered at different temperatures. However, this two-step mechanism can also be due to the finite size of the two-dimensional clusters under study.

The following should be pointed out. In spite of a large number of studies concerned with the formation of ordered monolayers comprised of nanoparticles, methods of structural characterisation of monolayers are still poorly developed. For instance, films formed at the gas–liquid interface are often characterised visually or by the packing density of the particles, which is determined from the compression isotherms. The only structural parameter used for the characterisation of monolayers is the regular lattice constant. Therefore, the general scheme[492] of analysis of the structure of nanoparticle monolayers is of great value. Two complementary methods were employed to derive this scheme. The properties of a monolayer were characterised using the pair distribution function while the presence of defects in the

monolayer was described by the Delaunay triangulation. A combination of the latter procedure and analysis of the Voronoi polyhedra can be applied to both two-dimensional and three-dimensional colloid structures.[493] The method was evaluated taking films comprised of silica particles formed on the surface of the liquid phase as an example. The particles were stabilised by alkylsilanes with different length of the hydrocarbon radical, which permitted variation of the force of the interparticle interaction. The properties of the films were also changed by varying the subphase composition and the degree of coverage of the particles with the alkylsilane adlayer. The energy of the particle–particle interaction on the surface of the subphase was calculated with inclusion of the van der Waals interaction and capillary forces. Figure 21 presents the dependence of the packing density of the particles in the monolayer on the surface of the liquid on the energy of the particle–particle interaction (at the minimum of the potential curve). In performing triangulation the triangles with vertices at the centres of spheres were plotted in such a way that no particles could pass through them. Figure 22 demonstrates some examples of the description of pores (defects) by different numbers of triangles (n_t). The pore size distribution was found to be lognormal. The pore size distribution for the monolayers of silica particles on the surfaces of various liquids is shown in Fig. 23.

These results were complemented with the data of a study on the structure and energy of defects in two-dimensional colloid crystal comprised of 0.36 μm polystyrene spheres.[494] Defects were formed using optical 'tweezers'. A colloid crystal with a lattice constant of 1.1 μm was formed by compression of the concentrated dispersion between two molten-quartz plates separated by a 2 μm gap. The motion of defects was studied using a video camera. General trends of the behaviour of dislocations were revealed. In particular, no single dislocations with the coordination number other than 6 (distorted coordination) were detected.

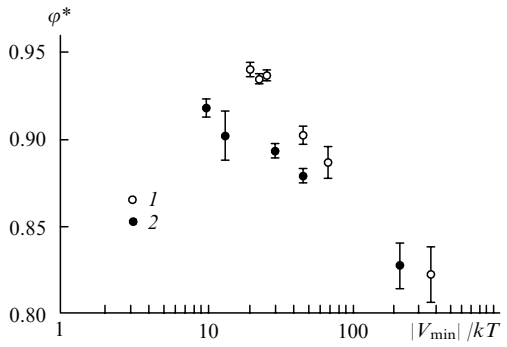

Figure 21. Packing degree of the monolayer of nanoparticles covered with octyltrichlorosilane (*1*) and octadecyltrichlorosilane (*2*) as function of the energy of the interparticle interaction at the potential well minimum.[492]

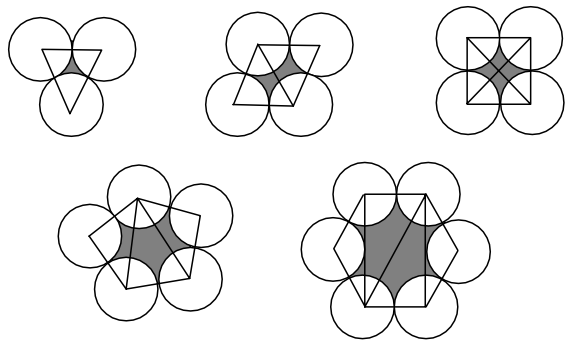

Figure 22. Triangulation schemes for various defects.[492]
For details, see text.

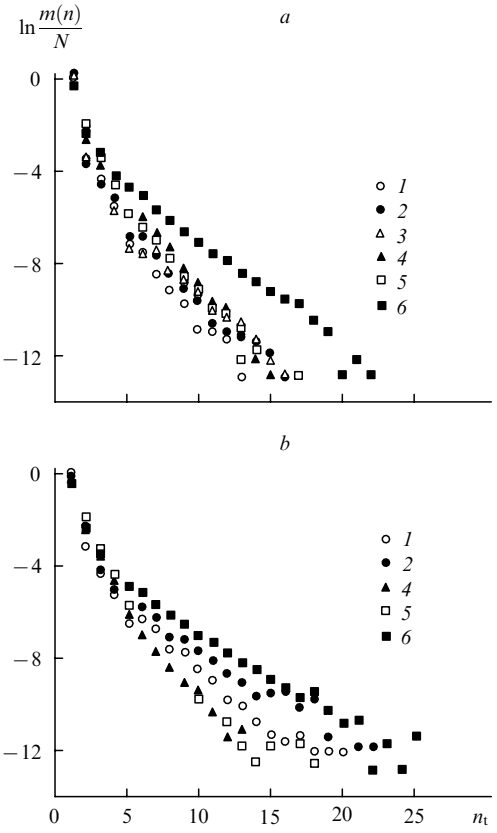

Figure 23. Pore size distribution in the monolayer of silica nanoparticles stabilised by octyltrichlorosilane (*a*) and octadecyltrichlorosilane (*b*) on the benzene (*1*), toluene (*2*), dichlorobenzene (*3*), dioxane (*4*), methoxyethanol (*5*) and water (*6*) surfaces.[492]

Only the pair, triplet, *etc*. dislocations with an average coordination number of 6 were observed. The sum of all vectors that emanate from the particles with a coordination number smaller than 6 and end at the neighbouring particles with a coordination number exceeding 6 equals nearly zero. This allows dislocations to be considered as multipoles with a zero summary Burgers vector.

The thermal and mechanical stability of the self-assembled ensembles of particles and their components play a significant role, because they can be at high temperature and pressure in the case of, *e.g*., catalytic applications. A particular role is played by the composition of the gaseous atmosphere. For instance, recrystallisation or even decomposition of platinum nanoparticles was observed at elevated temperature in an oxygen atmosphere in contrast to the hydrogen or noble-gas atmospheres,[495] whereas melting of the platinum particles of size from 5 to 20 nm on carbon substrate proceeds at 900 K.[496] The behaviour of single 20 nm platinum nanoparticles and their ensembles in oxygen atmosphere was studied.[497] An increase in the degree of crystallinity of the particles was observed at 700 K. The mechanism responsible for this process is still to be clarified, whereas the increase in the degree of crystallinity in the hydrogen atmosphere and *in vacuo* is due to diffusion of atoms in nanoparticles. According to atomic force microscopy data, the adhesive binding energy of the starting particles to the substrate was ≈ 0.8 mJ m^{-2} (the force measured was ≈ 10 nN). After treatment in hydrogen atmosphere at 700 K the adhesive binding energy became so high that it was impossible to measure its value. The observed changes in the degree of crystallinity and in the shape of the particles cannot be explained by their melting, because the particles of diameter 20 nm must melt at 2020 K even with inclusion of the dependence of the melting temperature on the particle size.

Recently, the properties of not only the metal 'core' of nanoparticles but also the single-layered organic shells have been the subject of investigations. The diversity of self-assembled ensembles of particles that can form on two-dimensional substrates [498] is also an intrinsic property of the molecular monolayers covering nanoparticles. These monolayers have a strong effect on the properties of the self-assembled ensembles of nanoparticles. A study on the ensembles of 4 nm silver and 3 nm gold nanoparticles stabilised by octadecanethiol, octanethiol, pentanethiol and butanethiol was reported.[499] The dried dispersions were mixtures of individual particles and colloid crystals. Analysis of the results of a differential scanning calorimetry study revealed two phase transitions corresponding to the melting of alkanethiol crystals (monolayers) and to the melting of the colloid crystal. The endothermic peak corresponding to the melting of the superlattice of gold particles is less pronounced than in the case of silver nanoparticles, thus indicating a lesser degree of crystallinity of the gold colloid crystal. The melting temperatures of the alkanethiol monolayers on the surface of silver nanoparticles also were found to be higher than on the surface of gold nanoparticles. This was explained by higher fraction of the organic phase in the case of gold particles.

The effect of thermal fluctuations in the ligand shell on the temperature dependence and on the topology of the order–disorder phase transition in the superlattice of nanoparticles was also studied [500] taking silver nanocrystals stabilised by alkanethiols (C_8, C_{12} and C_{16}) as examples. Measurements of the angular dependence of the X-ray scattering intensity at different temperatures showed that for all the samples under study the first diffraction peak disappeared in a rather narrow temperature range, thus indicating the topological disorder in the system. Near this temperature the peak markedly broadened due to enhancement of vibrations in the superlattice. This was similar to the situation observed for bulk crystals. However, above the melting temperature the superlattice behaved in another manner compared to conventional, 'atomic', crystals. All the samples under study were characterised by the appearance of a new peak at smaller values of the scattering vector q compared to those for the (111) diffraction peak. The new peak corresponds to the scattering region of size

$$\xi = \frac{2\pi}{q}.$$

As the temperature increases, the peak intensity increases and the peak is shifted towards small q values. This indicates the formation of a bicontinuous phase with spatially correlated regions whose sizes exceed both the thickness of the ligand shell and the size of nanocrystals. At a certain critical temperature T_c, the correlation region becomes infinitely large and the parameter ξ increases by a power law (Fig. 24):

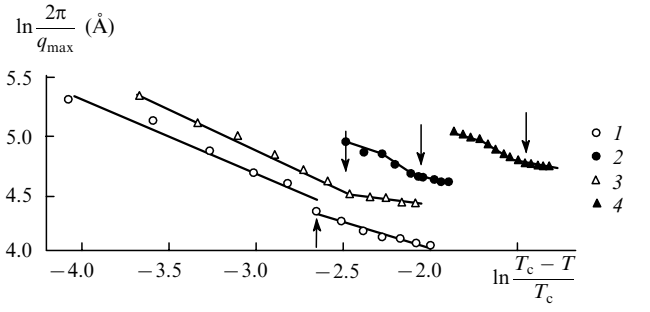

Figure 24. 'Characteristic size–temperature' plot for ensemble of sterically stabilised nanoparticles.[499]
The transition temperatures are shown by arrows. Particles were stabilised by alkanethiols containing a total of 8 (*1*), 12 (*2*, *3*) and 16 (*4*) carbon atoms in the alkyl chain. Chain length is 41 Å for (*2*) and 35 Å for (*3*).

$$\xi \propto \xi_0 \left(1 - \frac{T}{T_c}\right)^{-v}.$$

At a certain temperature T_x, the exponent v increases, becomes independent of the type of the ligand shell and corresponds to the critical index in the Ising model.

The supercrystal behaves similarly to the sponge phase of the surfactant, namely, its stabilisation is due to the long-range entropy forces related to fluctuations of the ligand 'membrane.' At high temperature (above the melting temperature of the superlattice), silver nanoparticles contacting one another bring closer together and form aggregates surrounded by the hydrocarbon chains attached to the surface of particles. The behaviour of such systems is governed by a complex combination of the van der Waals forces that act between the particles and hydrocarbon chains.

In conclusion, we will consider unusual self-assembled structures obtained upon binding of alkanethiol molecules functionalised by the COOH groups (*e.g.*, 11-mercaptoundecanoic or 1-mercaptohexadecanoic acids) and adsorbed on the surface of gold particles. Such structures are formed due to hydrogen bonds of the terminal carboxyl groups. They exhibit the ability to selectively transmit particular ions. The selectivity can be tuned by varying the pH value of the solution.[501] Changes in the morphology of ensembles of hydrogen bond stabilised nanoparticles upon variation of the pH value of the solution were studied.[502] To this end, gold nanoparticles stabilised by functionalised alkanethiols were obtained and alternating regions (of size nearly 2×2 μm) of monolayers of octadecanethiols containing the COOH and CH_3 terminal groups were formed by microcontact printing on a gold plate. The plate was dipped in a colloid solution containing gold nanoparticles. As a result, several layers of functionalised particles were deposited on the monolayer regions bearing the COOH groups, whereas no particle deposition occurred on the other regions. Atomic force microscopy studies revealed that variation of the pH value of the medium from 2 to 11 caused a twofold change in the height of the particle clusters (Fig. 25) due to the fact that the Debye length for the systems under study was several times longer than the interparticle distance and, hence, the charges of the particles were only partially screened. Such systems serve as the basis for fabrication of (i) membranes with tunable permeability towards different ions and (ii) recognition systems.

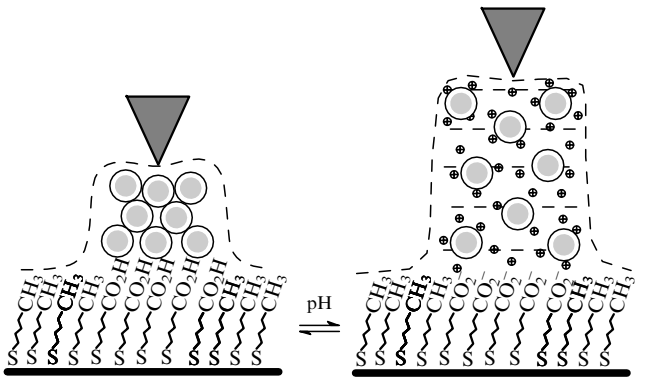

Figure 25. Changes in the size of a gold nanocluster depending on the pH of the solution.
For details, see text.

VI. Conclusion

Analysis of the available data (see above) shows that recently considerable advances in design of ordered ensembles of nano-

particles and in the studies of their properties have been achieved. The results obtained point to great prospects for the use of nanomaterials in the design of new-generation devices which can find various applications from medicine to microelectronics.

At the same time, many problems that arose in studies of ensembles of nanoparticles are still far from being solved. No efficient methods of fabrication of ensembles of monodisperse particles have been developed. Control of the interfacial behaviour of nanoparticles faces some problems (only preliminary results were obtained in this field). Realistic and reliable description of the physicochemical properties of ordered ensembles of nanoparticles with inclusion of co-operative effects is impossible, because most theories are still based on the single-particle approximation. Nevertheless, we hope that intensive research in the field will lead to new advances towards understanding of the physicochemical properties of ensembles of nanoparticles in the nearest future.

The author expresses his gratitude to V M Rudoy for help in the preparation of the review.

The review has been written with financial support from the Russian Foundation for Basic Research (Project No. 03-03-32513) and the Presidium of the Russian Academy of Sciences (Programme 'Fundamental Problems of Physics and Chemistry of Nanosystems and Nanomaterials').

References

1. Yu I Petrov *Klastery i Malye Chastitsy* (Clusters and Small Particles) (Moscow: Nauka, 1986)
2. S A Nepiiko *Fizicheskie Svoistva Malykh Metallicheskikh Chastits* (Physical Properties of Small Metallic Particles) (Kiev: Naukova Dumka, 1985)
3. A D Pomogailo, A S Rozenberg, I E Uflyand *Nanochastitsy Metallov v Polimerakh* (Metal Nanoparticles in Polymers) (Moscow: Khimiya, 2000)
4. V I Roldughin *Usp. Khim.* **69** 899 (2000) [*Russ. Chem. Rev.* **69** 821 (2000)]
5. B D Summ, N I Ivanova *Usp. Khim.* **69** 995 (2000) [*Russ. Chem. Rev.* **69** 911 (2000)]
6. I P Suzdalev, P I Suzdalev *Usp. Khim.* **70** 203 (2001) [*Russ. Chem. Rev.* **70** 177 (2001)]
7. G B Sergeev *Usp. Khim.* **70** 915 (2001) [*Russ. Chem. Rev.* **70** 809 (2001)]
8. R A Andrievskii *Usp. Khim.* **71** 967 (2002) [*Russ. Chem. Rev.* **71** 853 (2002)]
9. A I Gusev, A A Rempel' *Nanokristallicheskie Materialy* (Nanocrystalline Materials) (Fizmatlit: Moscow, 2001)
10. P Jensen *Rev. Mod. Phys.* **71** 1695 (1999)
11. S V Karpov, V V Slabko *Opticheskie i Fotofizicheskie Svoistva Fraktal'no-Strukturirovannykh Zolei Metallov* (Optical and Photophysical Properties of Fractal Structured Sols of Metals) (Novosibirsk: Siberian Branch of Russian Academy of Sciences, 2003)
12. A Globus, C W Bauschlicher, J Han, R L Jaffe, C Levit, D Srivastava *Nanotechnology* **9** 192 (1998)
13. A Martino, S A Yamanaka, J S Kawola, D A Loy *Chem. Mater.* **9** 423 (1997)
14. S Bharathi, N Fishelson, O Lev *Langmuir* **15** 1929 (1999)
15. T K Kundu, D Chakravorty *Appl. Organomet. Chem.* **13** 363 (1999)
16. N Sanz, A-C Gaillot, Y Usson, P I Baldeck, A Ibanez *J. Mater. Chem.* **10** 2723 (2000)
17. G De, G Mattei, C Sada, G Battaglin, A Quaranta *Chem. Mater.* **12** 2157 (2000)
18. A P Rao, G M Pajohk, A V Rao *J. Mater. Synth. Proc.* **9** 11 (2001)
19. M L Anderson, C A Morris, R M Strud, C I Merzbacher, D R Rolison *Langmuir* **15** 674 (1999)
20. D Schmeißer, O Böhme, A Yfantis, T Heller, D R Batchelor, I Lundstrom, A L Spetz *Phys. Rev. Lett.* **83** 380 (1999)
21. T Kawasaki, Y Takai, R Shimizu *Appl. Phys. Lett.* **79** 3509 (2001)
22. C P Collier, T Vossmeyer, J R Heath *Annu. Rev. Phys. Chem.* **49** 371 (1998)
23. C Wang, Y Li, X Bu, N Zheng, O Zivkovic, C-S Yang, P Feng *J. Am. Chem. Soc.* **123** 11506 (2001)
24. H Wu, N Bowden, G M Whitesides *Appl. Phys. Lett.* **75** 3222 (1999)
25. S R J Olover, T D Clark, N Bowden, G M Whitesides *J. Am. Chem. Soc.* **123** 8119 (2001)
26. I F Efremov *Periodicheskie Kolloidnye Struktury* (Periodical Colloid Structures) (Leningrad: Khimiya, 1971)
27. Y Xia, B Gates, Y Yin, Y Lu *Adv. Mater.* **12** 693 (2000)
28. S Matsushita, T Miwa, A Fujishima *Langmuir* **13** 2582 (1997)
29. J L Fransaer, R M Penner *J. Phys. Chem.* **103** 7643 (1999)
30. M Alejandro-Arellano, T Ung, A Blanco, P Mulvaney, L M Liz-Marzan *Pure Appl. Chem.* **72** 257 (2000)
31. B V Deryagin, N V Churaev, V M Muller *Poverkhnostnye Sily* (Surface Forces) (Moscow: Nauka, 1985)
32. P de Gennes *Adv. Colloid Interface Sci.* **27** 189 (1987)
33. S Ramakrishnan, C F Zukoski *J. Chem. Phys.* **113** 1237 (2000)
34. B A Korgel, D Fitzmaurice *Phys. Rev. B* **59** 14191 (1999)
35. S Hachisu, K Takano *Adv. Colloid Interface Sci.* **16** 233 (1982)
36. R Williams, R S Crandall *Phys. Lett. A* **48** 225 (1974)
37. W Y Shih, I A Aksay, R Kikuchi *J. Chem. Phys.* **86** 5127 (1987)
38. C G de Kruif, P W Row, J W Jansen, A Vrij *J. Phys. C* **46** 295 (1985)
39. P N Pusey, W van Megen *Nature (London)* **320** 340 (1986)
40. A R Denton, H Lowen *Phys. Rev. Lett.*, **81** 469 (1998)
41. L Beloni *J. Chem. Phys.* **85** 519 (1986)
42. S Kahn, T L Morton, D Ronis *Phys. Rev. A* **35** 4295 (1987)
43. G F Wang, S K Lai *Phys. Rev. Lett.* **82** 3645 (1999)
44. S K Lai, W P Peng, G F Wang *Phys. Rev. E* **63** 041511 (2001)
45. J Groenewold, W K Kegel *J. Phys. Chem. B* **105** 11702 (2001)
46. W van Mengen, S M Underwood *Nature (London)* **362** 616 (1993)
47. R J Speedy *J. Chem. Phys.* **100** 6684 (1994)
48. M D Rintoul, S Torquato *Phys. Rev. Lett.* **77** 4198 (1996)
49. W K Kegel *Langmuir* **16** 939 (2000)
50. B J Alder, W G Hoover, D A Yung *J. Chem. Phys.* **49** 3688 (1968)
51. Y Monovoukas, A P Gast *J. Colloid Interface Sci.* **128** 533 (1989)
52. G A McConnell, A P Gast *Phys. Rev. E* **54** 5447 (1996)
53. H M Lindsay, P M Chaikin *J. Chem. Phys.* **76** 3774 (1982)
54. E Liniger, R Raj *J. Am. Chem. Soc.* **70** 843 (1987)
55. S Hachisu, S Yoshimura *Nature (London)* **283** 188 (1980)
56. S Yoshimura, S Hachisu *J. Phys. Colloq., C3* **46** 115 (1987)
57. W Y Shih, W-H Shih, I A Aksay *J. Chem. Phys.* **90** 4506 (1989)
58. L D Landau, E M Lifshits *Statisticheskaya Fizika* (Statistical Physics) (Moscow: Nauka, 1976)
59. S Ichimaru *Rev. Mod. Phys.* **54** 1017 (1982)
60. J H Chu, I Lin *Phys. Rev. Lett.* **72** 4009 (1994)
61. V E Fortov, A P Nefedov, O F Petrov, A A Samarian, A V Chernyshov, A M Lipaev *Pis'ma Zh. Eksp. Teor. Fiz.* **63** 176 (1996) [a]
62. V E Fortov, A P Nefedov, O F Petrov, A A Samaryan, A V Chernyshev *Zh. Eksp. Teor. Fiz.* **111** 467 (1997) [b]
63. V N Tsitovich *Usp. Fiz. Nauk* **167** 57 (1997) [*Physics-Uspekhi* **40** 53 (1997)]
64. S P Bakanov, B V Deryagin, V I Roldughin *Usp. Fiz. Nauk* **129** 256 (1979) [c]
65. V I Roldughin, V M Zhdanov *Adv. Colloid Interface Sci.* **98** 121 (2002)
66. V V Balabanov, L M Vasilyak, S P Vetchinin, A P Nefedov, D N Polyakov, V E Fortov *Zh. Eksp. Teor. Fiz.* **119** 99 (2001) [b]
67. V E Fortov, A P Nefedov, O F Petrov, A A Samaryan, Ya K Khodataev, A V Chernyshev *Zh. Eksp. Teor. Fiz.* **116** 1601 (1999) [b]
68. D N Gerasimov, O A Sinkevich *Teplofiz. Vys. Temp.* **37** 853 (1999)
69. G E Astrakharchik, A I Belousov, Yu E Lozovik *Zh. Eksp. Teor. Fiz.* **116** 1300 (1999) [b]
70. M Dijkstra, R van Roij, R Evans *Phys. Rev. Lett.* **81** 2268 (1998)
71. A Vrij *Pure Appl. Chem.* **48** 471 (1976)
72. G A Vliegenthart, H N W Lekkerkerker *J. Chem. Phys.* **111** 4153 (1999)
73. S M Ilett, A Orrock, W C K Poon, P Pusey *Phys. Rev. E* **51** 1344 (1995)

74. H N W Lekkerkerker, W C K Poon, P N Pusey, A Stroobants, P Warren *Europhys. Lett.* **20** 559 (1992)
75. N A M Verhaegh, D Ashnagi, H N W Lekkerkerker, M Gigho, L Cipelletti *Physica A* **242** 104 (1997)
76. Y Mao, M E Cates, H N W Lekkerkerker *Physica A* **222** 10 (1995)
77. G A Vliegenthart, A van Blaaderen, H N W Lekkerkerker *Faraday Discuss.* **112** 173 (1999)
78. E K Hobbie *Phys. Rev. Lett.* **81** 3996 (1998)
79. M Adams, S Dogic, S L Keller, S Fraden *Nature (London)* **393** 349 (1998)
80. K Yaman, C Jeppesen, C M Marques *Europhys. Lett.* **42** 221 (1998)
81. P Bolhuis, D Frenkel *J. Chem. Phys.* **101** 9869 (1994)
82. M Schmidt *Phys. Rev. E* **63** 050201 (2001)
83. L Onsager *Anal. N.Y. Acad. Sci.* **51** 627 (1949)
84. I Langmuir *J. Chem. Phys.* **6** 873 (1938)
85. M P B van Bruggen, J K G Dhont, H N W Lekkerkerker *Macromolecules* **32** 2256 (1999)
86. X M Dong, T Kimura, J F Revol, D G Gray *Langmuir* **12** 2076 (1996)
87. T Folda, H Hoffmann, H Chanzy, P Smith *Nature (London)* **333** 55 (1988)
88. A V Kaznacheev, A Yu Kovalevskii, I A Ronova, A S Sonin *Kolloid. Zh.* **62** 606 (2000) [d]
89. F M van der Kooij, H N W Lekkerkerker *J. Phys. Chem. B* **102** 7829 (1998)
90. F M van der Kooij, D van der Beek, H N W Lekkerkerker *J. Phys. Chem. B* **105** 1696 (2001)
91. M A Bates, D Frenkel *J. Chem. Phys.* **110** 6553 (1999)
92. J-C Loudet, P Barois, P Poulin *Nature (London)* **407** 611 (2000)
93. P Fabre, C Casagrande, M Veyssie, V Cabuil, R Massart *Phys. Rev. Lett.* **64** 539 (1990)
94. C Quilliet, V Ponsinet, V Cabuil *J. Phys. Chem.* **98** 3566 (1994)
95. C Menager, L Belloni, V Cabuil, M Dubois, T Gulik-Krzywicki, Th Zemb *Langmuir* **12** 3516 (1996)
96. W Wang, S Efrima, O Regev *J. Phys. Chem. B* **103** 5613 (1999)
97. C Smits, J S van Duijneveldt, J K G Dhont, H N W Lekkerkerker, W J Briels *Phase Transitions* **21** 157 (1990)
98. T Palberg, M Würth, J Schwarz, P Leiderer *Prog. Colloid Polym. Sci.* **98** 6 (1995)
99. M Würth, J Schwarz, F Culis, P Leiderer, T Palberg *Phys. Rev. E* **52** 6415 (1995)
100. M S Ripoll, C F Tejero, M Baus *Physica A* **234** 311 (1996)
101. E J Meijer, D Frenkel *J. Chem. Phys.* **94** 2269 (1991)
102. J M A Hofman, H J H Clercx, P P J M Schram *Phys. Rev. E* **62** 8212 (2000)
103. I V Melikhov, E N Kitova, A N Kamenskaya, E D Kozlovskaya, N B Mikheev, S A Kulyukhin *Kolloid. Zh.* **59** 780 (1997) [d]
104. G Schmid (Ed.) *Clusters and Colloids. From Theory to Applications* (Weinheim: VCH, 1994)
105. J H Fendler (Ed.) *Nanoparticles and Nanostructured Films/ Preparation Characterization and Applications* (Weinheim: Wiley-VCH, 1998)
106. P M Tessier, O D Velev, A T Kalambur, A M Lenhoff, J F Rabolt, E W Kaler *Adv. Mater.* **13** 396 (2001)
107. B Gates, Y Xia *Adv. Mater.* **12** 1329 (2000)
108. H Andersson, W van der Wijngaart, G Stemme *Electrophoresis* **22** 249 (2001)
109. H Weller *Angew. Chem., Int. Ed. Engl.* **35** 1079 (1996)
110. C B Murray, C R Kagan, M G Bawendi *Science* **270** 1335 (1995)
111. S Sun, C B Murray, D Weller, L Folks, A Moser *Science* **287** 1989 (2000)
112. R Micheletto, H Fukuda, M Ohtsu *Langmuir* **11** 3333 (1995)
113. N D Denkov, O D Velev, P A Kralchevsky, I B Ivanov, H Yoshimura, K Nagayama *Langmuir* **8** 3183 (1992)
114. S Rakers, L F Chi, H Fuchs *Langmuir* **13** 7121 (1997)
115. T Yonezava, S Onoue, N Kimizuka *Langmuir* **17** 2291 (2001)
116. S He, J Yao, P Jiang, D Shi, H Zhang, S Xie, S Pang, H Gao *Langmuir* **17** 1571 (2001)
117. J S Yin, Z L Wang *Phys. Rev. Lett.* **79** 2570 (1997)
118. L Motte, F Billoudet, E Lacaze, M P Pileni *Adv. Mater.* **8** 1018 (1996)
119. B A Korgel, D Fitzmaurice *Phys. Rev. Lett.* **80** 3531 (1998)
120. W Wang, S Efrima, O Regev *Langmuir* **14** 602 (1998)
121. N Dingenouts, M Ballauff *Langmuir* **15** 3283 (1999)
122. V Russier, C Petit, J Legrand, M P Pileni *Phys. Rev. B* **62** 3910 (2000)
123. A J Rondinone, A S C Samia, Z J Zhang *J. Phys. Chem. B* **104** 7919 (2000)
124. S H Sun, C B Murray *J. Appl. Phys.* **85** 4325 (1999)
125. J Legrand, C Petit, D Bazin, M P Pileni *Appl. Surf. Sci.* **164** 186 (2000)
126. P C Ohara, D V Leff, J R Heath, W M Gelbart *Phys. Rev. Lett.* **75** 3466 (1995)
127. R P Andres, J D Bielefeld, J I Henderson, D B James, V R Lolagunta, C P Kubiak, W J Mahoney, R G Osifchin *Science* **273** 1690 (1996)
128. P C Ohara, J R Heath, W M Gelbart *Angew. Chem., Int. Ed. Engl.* **36** 1077 (1997)
129. P C Ohara, W M Gelbart *Langmuir* **14** 3418 (1998)
130. P Moriarty, M D R Taylor, M Brust *Phys. Rev. Lett.* **89** 248 303 (2002)
131. M Green, S Norager, P Moriarty, M Motevalli, P O'Brien *J. Mater. Chem.* **10** 1939 (2000)
132. Z L Wang, S A Harfenist, I Vezmar, R L Whetten, J Bentley, N D Evans, K B Alexander *Adv. Mater.* **10** 808 (1998)
133. S A Harfenist, Z L Wang, M M Alvarez, I Vezmar, R L Wetten *J. Phys. Chem.* **100** 13 904 (1996)
134. L O Brown, J E Hutchison *J. Phys. Chem. B* **105** 8911 (2001)
135. A Courty, O Araspin, C Fermon, M P Pileni *Langmuir* **17** 1372 (2001)
136. P Hanarp, D S Sutherland, J Gold, B Kasemo *Colloids Surf., A* **214** 23 (2003)
137. G Schmid *J. Chem. Soc., Dalton Trans.* 1077 (1998)
138. S Chen *J. Phys. Chem. B* **104** 663 (2000)
139. V L Colvin, A N Goldstein, A P Alivisatos *J. Am. Chem. Soc.* **114** 5221 (1992)
140. H Haidara, K Mougin, J Schultz *Langmuir* **17** 1432 (2001)
141. G Bar, S Rubin, R W Cutts, T N Taylor, T A Zawodzinski *Langmuir* **12** 1172 (1996)
142. R H Therill, T A Postlethwaite, C H Chen, C D Poon, A Terzis, A Chen, J E Hutchison, M R Clark, G Wignall, J D Londono, R Superfine, M Falvo, C S Johnoson, E T Samulski, R W Murray *J. Am. Chem. Soc.* **117** 12537 (1995)
143. L H Dubois, R G Nuzzo *Annu. Rev. Phys. Chem.* **43** 437 (1992)
144. L Cusack, R Rizza, A Gorelov, D Fitzmaurice *Angew. Chem., Int. Ed. Engl.* **36** 848 (1997)
145. S Bharathi, M Nogami, O Lev *Langmuir* **17** 2602 (2001)
146. X M Lin, C M Sorensen, K J Klabunde *Chem. Mater.* **11** 198 (1999)
147. X M Lin, G M Wang, C M Sorensen, K J Klabunde *J. Phys. Chem. B* **103** 5488 (1999)
148. M Brust, D Bethel, D J Schiffrin, J K Kiely *Adv. Mater.* **7** 795 (1995)
149. T Prozorov, R Prozorov, A Gedanken *Adv. Mater.* **10** 1529 (1998)
150. D I Gittings, D Bethell, R J Nichols, D J Schiffrin *Adv. Mater.* **11** 737 (1999)
151. J P Novak, D L Feldheim *J. Am. Chem. Soc.* **122** 3979 (2000)
152. R P Andres, D J Bielefeld, J I Henderson, D B Janes, V R Kolagunta, C P Kubiak, W J Mahoney, R C Osifchin *Science* **273** 1690 (1999)
153. K S Mayya, V Patil, M Sastry *Bull. Chem. Soc. Jpn.* **73** 1757 (2000)
154. W Shenton, S A Devis, S Mann *Adv. Mater.* **11** 449 (1999)
155. C J Loweth, W B Caldwell, X Peng, A P Alivisatos, P G Schultz *Angew. Chem., Int. Ed.* **38** 1808 (1999)
156. A K Bodal, V M Rotello *Langmuir* **16** 9527 (2000)
157. Y Kim, R C Johnson, J T Hupp *Nano Lett.* **1** 165 (2001)
158. C Sanchez, G Soler-Illia, F Ribot, T Lalot, C R Mayer, V Cabuil *Chem. Mater.* **13** 3061 (2001)
159. C R Mayer, S Neveu, V Cabuil *Adv. Mater.* **14** 595 (2002)
160. J E Martin, J P Wilcoon, J Odinek, P Provencio *J. Phys. Chem. B* **104** 9475 (2000)

161. J Fink, J Kiely, D Bethel, D J Schiffrin *J. Chem. Mater.* **10** 922 (1998)
162. P Bartlett, R H Ottewill, P N Pusey *Phys. Rev. Lett.* **68** 3801 (1992)
163. M D Eldridge, P A Madden, D Frenkel *Nature (London)* **365** 35 (1993)
164. C J Kiely, J Fink, M Brust, D Bethel, D J Schiffrin *Nature (London)* **396** 444 (1998)
165. S V Anishchik, N N Medvedev *Phys. Rev. Lett.* **75** 4314 (1995)
166. M Antonietti, J Hartmann, M Neese, U Seifert *Langmuir* **16** 7634 (2000)
167. J J Gray, R T Bonnecaze *J. Chem. Phys.* **14** 1366 (2001)
168. J J Gray, D H Klein, R T Bonnecaze, B A Korgel *Phys. Rev. Lett.* **85** 4430 (2000)
169. J J Gray, D H Klein, B A Korgel, R T Bonnecaze *Langmuir* **17** 2317 (2001)
170. B J Alder, T E Wainwright *Phys. Rev.* **127** 359 (1962)
171. A Jaster *Phys. Rev. E* **59** 2594 (1999)
172. W Vermöhlen, N Ito *Phys. Rev. E* **51** 14 636 (1995)
173. M R Sadr-Lahijany, P Ray, H E Stanley *Phys. Rev. Lett.* **79** 3206 (1997)
174. J Talbot, P Schaaf *Phys. Rev. A* **40** 422 (1989)
175. J van de Lagemaat, K D Benkstein, A J Frank *J. Phys. Chem. B* **105** 12433 (2001)
176. M Hosino, H Nakano, H Kimura *J. Phys. Soc. Jpn.* **46** 1709 (1979)
177. P A Forsyth, S Marcelja, D J Mitchell, B W Ninham *Adv. Colloid Interface Sci.* **9** 37 (1978)
178. J Tang, S Fraden *Liq. Cryst.* **19** 459 (1995)
179. Z Dogic, S Fraden *Phys. Rev. Lett.* **78** 2417 (1997)
180. G F Grom, D J Lockwood, J P McCaffrey, H J Labbe, P M Fauchet, B White, J Diener, D Kovalev, F Koch, L Tsybeskov *Nature (London)* **407** 358 (2000)
181. X Peng, L Manna, Y Yang, J Wickham, E Scher, A Kadavanich, A P Alivisatos *Nature (London)* **404** 59 (2000)
182. B Nikoobakht, Z L Wang, M A El-Sayed *J. Phys. Chem. B* **104** 8635 (2000)
183. P A Kralchevsky, K Nagayama *Langmuir* **10** 23 (1994)
184. P A Kralchevsky, N D Denkov, V N Paunov, O D Velev, I B Ivanov, H Yoshimura, K Nagayama *J. Phys. C* **6** A395 (1994)
185. J Legrand, A Ngo, C Petit, M P Pileni *Adv. Mater.* **13** 58 (2001)
186. C Petit, A Taleb, M P Pileni *J. Phys. Chem. B* **103** 1805 (1999)
187. M Giersig, M Hilgendorff *J. Phys. D* **32** L111 (1999)
188. M Hilgendorff, B Tesche, M Giersig *Aust. J. Chem.* **54** 497 (2001)
189. M A Hayes, N A Polson, A A Garcia *Langmuir* **17** 2866 (2001)
190. J Legrand, C Petit, M P Pileni *J. Phys. Chem. B* **105** 5643 (2001)
191. K Loudiyi, B J Ackerson *Physica A* **184** 26 (1992)
192. H R Krishnamurthy *J. Indian Inst. Sci.* **76** 465 (1996)
193. K Lin, J C Crocker, V Prasad, A Schofield, D A Weitz, T C Lubensky, A Yodh *Phys. Rev. Lett.* **85** 1770 (2000)
194. A C Templeton, W P Wuelfing, R W Murray *Acc. Chem. Res.* **33** 27 (2000)
195. N D Denkov, O D Velev, P A Kralchevsky, I B Ivanov, H Yoshimura, K Nagayama *Nature (London)* **361** 26 (1993)
196. A S Dimitrov, K Nagayama *Langmuir* **13** 1303 (1993)
197. D J Norris, Y A Vlasov *Adv. Mater.* **13** 371 (2001)
198. C Damle, A Gole, M Sastry *J. Mater. Chem.* **10** 1389 (2000)
199. Y C Tian, J H Fendler *Chem. Mater.* **8** 969 (1996)
200. B O Dabbousi, C B Murray, M F Rubner, M G Bawendi *Chem. Mater.* **6** 216 (1994)
201. Gy Tolnai, F Csempesz, M Kabai-Faix, E Kalman, Zs Keresztes, A L Kovacs, J J Ramsden, Z Horvolgyi *Langmuir* **17** 2683 (2001)
202. J R Heath, C M Knobler, D V Leff *J. Phys. Chem. B* **101** 189 (1997)
203. K Abe, T Hanada, T Yamaguchi, H Takiguchi, H Nagasawa, M Nakamoto, K Yase *Mol. Cryst. Liq. Cryst.* **322** 173 (1998)
204. X Zhou, J Li, C Liu *J.Sci. China, Ser. B* **45** 358 (2002)
205. B Kim, S L Tripp, A Wei *J. Am. Chem. Soc.* **123** 7955 (2001)
206. L Maya, G Muralidharan, T G Thundat, E A Kenik *Langmuir* **16** 9151 (2000)
207. Z L Wang *Aust. J. Chem.* **54** 153 (2001)
208. K Muramatsu, M Takahashi, K Tajima, K Kobayashi *J. Colloid Interface Sci.* **242** 127 (2001)
209. Y Jin, S Dong *Angew. Chem., Int. Ed.* **41** 1040 (2002)
210. K V Sarathy, J P Thomas, J P Kulkarni, C N R Rao *J. Phys. Chem. B* **103** 399 (1999)
211. A Kumar, A B Mandale, M Sastry *Langmuir* **16** 6921 (2000)
212. M Brust, N Stuhr-Hansen, K Nugaard, J B Christensen, L K Nielsen, T Bjurnholm *Nano Lett.* **1** 189 (2001)
213. C P Collier, R J Saykally, J J Shiang, S E Henrichs, J R Heath *Science* **277** 1978 (1997)
214. T Hassenkam, K Nurgaard, L Iversen, C J Kelly, M Brust, T Bjurnholm *Adv. Mater.* **14** 1126 (2002)
215. S -W Chung, G Markovich, J R Heath *J. Phys. Chem. B* **102** 6685 (1998)
216. F C Meldrum, N A Kotov, J H Fendler *Mater. Sci. Eng., C* **3** 149 (1995)
217. W Wang, X Chen, S Efrima *J. Phys. Chem. B* **103** 7238 (1999)
218. S H Im, Y T Lim, D J Suh, O O Park *Adv. Mater.* **14** 1367 (2002)
219. K Nakahama, H Kawaguchi, K Fujimoto *Langmuir* **16** 7882 (2000)
220. S Chen *Adv. Mater.* **12** 186 (2000)
221. S Chen *Langmuir* **17** 2878 (2001)
222. W Li, R Xu, L Wang, H Cui, S Xi *Mol. Cryst. Liq. Cryst.* **337** 185 (1999)
223. F C Meldrum, N A Kotov, J H Fendler *J. Phys. Chem.* **98** 4506 (1994)
224. S Lefebuer, C Menager, V Cabuil, M Assenheimer, F Gallet, C Flament *J. Phys. Chem. B* **102** 2733 (1998)
225. T Fried, G Shemer, G Markovich *Adv. Mater.* **13** 1158 (2001)
226. S Chang, C Shin, C Chen, C Lai, C R C Wang *Langmuir* **15** 701 (1999)
227. H Maeda, Y Maeda *Langmuir* **12** 1446 (1996)
228. B A Korgel, D Fitzmaurice *Adv. Mater.* **10** 661 (1998)
229. F Kim, S Kwan, J Akana, P Yang *J. Am. Chem. Soc.* **123** 4360 (2001)
230. D Yogev, S Efrima *J. Phys. Chem.* **92** 5754 (1988)
231. H Schwartz, Y Harel, S Efrima *Langmuir* **17** 3884 (2001)
232. K S Mayya, M Sastry *Langmuir* **15** 1902 (1999)
233. D Wyrwa, N Beyer, N Schmid *Nano Lett.* **2** 419 (2002)
234. A Kumar, S Mandal, S P Mathew, P R Selvakannan, A B Mandale, R V Chaudhair, M Sastry *Langmuir* **18** 6478 (2002)
235. S D Sathaye, K R Patil, D V Paranjape, A Mitra, S V Awate, A B Mandale *Langmuir* **16** 3487 (2000)
236. R Aveyard, J H Clint, D Nees, N Quirke *Langmuir* **16** 8820 (2000)
237. R Aveyard, J H Clint, D Nees, V N Paunov *Langmuir* **16** 1696 (2000)
238. R K Iler *J. Colloid Interface Sci.* **21** 569 (1966)
239. N A Kotov, I Dekany, H J Fendler. *J. Phys. Chem.* **99** 13065 (1995)
240. E Hao, T Lian *Langmuir* **16** 7879 (2000)
241. T Ung, L M Liz-Marzan, P Mulvaney. *J. Phys. Chem. B* **105** 3441 (2001)
242. A A Mamedov, A Belov, M Giersig, N N Mamedova, N A Kotov *J. Am. Chem. Soc.* **123** 7738 (2001)
243. A K Newman, J M Liu *J. Appl. Phys.* **82** 4637 (1997)
244. M R Geller *Phys. Rev. Lett.* **78** 110 (1997)
245. R R Bhat, D A Fischer, J Genzer *Langmuir* **18** 5640 (2002)
246. C A Mirkin, R L Letsibger, R C Mucic, J J Storhoff *Nature (London)* **382** 607 (1996)
247. J J Storhoff, C A Mirkin *Chem. Rev.* **99** 1849 (1998)
248. A P Alivisatos, K P Johnsson, X Peng, T E Wilson, C J Loweth, M P Bruchez, P G Schultz *Nature (London)* **382** 609 (1996)
249. E T Kisak, M T Kennedy, D Trommeshauser, J A Zasadzinski *Langmuir* **16** 2825 (2000)
250. S Mann, W Shenton, M Li, S Connolly, D Fitzmaurice *Adv. Mater.* **12** 147 (2000)
251. S Connolly, S Cobbe, D Fitzmaurice *J. Phys. Chem. B* **105** 2222 (2001)
252. S Connolly, D Fitzmaurice *Adv. Mater.* **11** 1202 (1999)
253. D Fitzmaurice, S N Rao, J A Prece, J F Stoddart, S Wenger, N Zaccheroni *Angew. Chem., Int. Ed.* **38** 1147 (1999)

254. D Ryan, S N Rao, H Rensmo, D Fitzmaurice, J A Prece, S Wenger, J F Stoddart, N Zaccheroni *J. Am. Chem. Soc.* **122** 6252 (2000)
255. S Brown *Nano Lett.* **1** 391 (2001)
256. J Zhang, A Alsayed, K H Lin, S Sanyal, W-J Pao, V S K Balagurusamy, P A Heiney, A G Yodh *Appl. Phys. Lett.* **81** 3176 (2002)
257. R M Bright, M D Musick, M J Natan *Langmuir* **14** 5695 (1998)
258. G Schmid, M Baumle, N Beyer *Angew. Chem., Int. Ed.* **39** 181 (2000)
259. S M Marinakos, L C Brousseau, A Jones, D L Feldheim *Chem. Mater.* **10** 1214 (1998)
260. J Schmitt, G Decher, W J Dressik, S L Brandow, R E Geer, R Shaahidhar, J M Calvert *Adv. Mater.* **9** 61 (1997)
261. P Alivisatos *Pure Appl. Chem.* **72** 3 (2000)
262. A D Lazardies, G C Schatz *J. Phys. Chem. B* **104** 460 (2000)
263. M L Sauthier, R L Carroll, C B Gormn, S Franzen *Langmuir* **18** 1825 (2002)
264. J J Storhoff, R Elghanian, R C Mucic, C A Mirkin, R L Letsinger *J. Am. Chem. Soc.* **120** 1959 (1998)
265. O D Velev, E W Kaler *Langmuir* **15** 3693 (1999)
266. N G Khlebtsov, V A Bogatyrev, L A Dykman, Ya M Krasnov, A G Melnikov *Izv. Vyssh. Uchebn. Zaved. AND* **10** 172 (2002)
267. A V Bogatyrev, L A Dykman, Ya M Krasnov, V K Plotnikov, N G Khlebtsov *Kolloid. Zh.* **64** 671 (2002) [d]
268. T A Taton, R C Mucic, C A Mirkin, R Letsinger *J. Am. Chem. Soc.* **122** 6305 (2000)
269. B Koltover, J O Ridler, C R Safinya *Phys. Rev. Lett.* **82** 1991 (1999)
270. S Nomura, N Kajimura, K Matoba, T Miyata, R Ortenberg, M Mevarech, H Kamikubo, M Kataoka, Y Harada *Langmuir* **15** 214 (1999)
271. S A Davis, M Dreulmann, K H Rhodes, B Zhang, S Mann *Chem. Mater.* **13** 3218 (2001)
272. S Mann *J. Mater. Chem.* **5** 935 (1995)
273. S Mann *J. Chem. Soc., Dalton Trans.* 3953 (1997)
274. M Antonietti, C Glltner *Angew. Chem., Int. Ed.* **36** 910 (1997)
275. N Combs, D Khushalani, S Oliver, G A Ozin, G S Shen, I Sokolov, H Yang *J. Chem. Soc. Dalton Trans.* 3941 (1997)
276. E Dujardin, S Mann *Adv. Mater.* **14** 775 (2002)
277. O D Velev, P M Tesier, A M Lenhoff, E W Kaler *Nature (London)* **401** 548 (1999)
278. G L Egan, J S Yu, C H Kim, S J Lee, R E Schaak, T E Mallouk *Adv. Mater.* **12** 1040 (2000)
279. H Yan, C F Blanford, J C Lytle, C B Carter, W H Smyrl, A Stein *Chem. Mater.* **13** 4314 (2001)
280. P Jiang, J Cizeron, J F Bertone, V L Colvin *J. Am. Chem. Soc.* **121** 7957 (1999)
281. H Yan, C F Blandford, B T Holland, M Parent, W H Smyrl, A Stein *Adv. Mater.* **11** 1003 (1999)
282. B T Holland, L Abrams, A Stein *J. Am. Chem. Soc.* **121** 4308 (1999)
283. H Miguez, F Meseguer, C Lopez, M Holdago, G Andreasen, A Mifsud, V Fornes *Langmuir* **16** 4405 (2000)
284. B T Holland, C F Blandford, A Stein *Science* **281** 538 (1998)
285. Z L Xiao, C Y Han, U Welp, H H Wang, V K Vlasko-Vlasov, W K Kwok, D J Muller, J M Hiller, R E Cook, G A Willing, G W Grabtree *Appl. Phys. Lett.* **81** 2869 (2002)
286. L Xu, W Zhou, M E Kozlov, I I Khayrullin, I Udod, A A Zakhidov, R H Baughman, J B Wiley *J. Am. Chem. Soc.* **123** 763 (2001)
287. D F Sievenpiper, M E Sickmiller, E Yablonovitch *Phys. Rev. Lett.* **76** 2480 (1996)
288. C Lellig, W Härtl, J Wagner, R Hempelmann *Angew. Chem., Int. Ed.* **41** 102 (2002)
289. P V Braun, P Wiltzius *Nature (London)* **402** 603 (1999)
290. A Y Vlasov, N Yao, D J Norris *Adv. Mater.* **11** 165 (1999)
291. C R Martin *Science* **266** 1961 (1994)
292. C R Martin *Chem. Mater.* **8** 1739 (1996)
293. A Huczko *Appl. Phys. A* **70** 365 (2000)
294. M Chen, Y Xie, H Chen, Z Qiao, Y Zhu, Y Qian *J. Colloid Interface Sci.* **229** 217 (2000)
295. G L Che, B B Lakshmi, C R Martin, E R Fisher, R S Ruoff *Chem. Mater.* **10** 260 (1998)
296. T Kyotani, L-F Tsai, A Tomita *Chem. Commun.* 701 (1997)
297. G L Che, B B Lakshmi, C R Martin, E R Fisher *Langmuir* **15** 750 (1999)
298. B K Pradhan, T Toba, T Kyotani, A Tomita *Chem. Mater.* **10** 2510 (1998)
299. M Freemantle *Chem. Eng. News* **74** 62 (1996)
300. H Masuda, F Hasegawa, S Ono *J. Electrochem. Soc.* **144** L127 (1997)
301. O Jessensky, F Müller, U Gösele *Appl. Phys. Lett.* **72** 1173 (1998)
302. D S Xu, Y J Hu, D P Chen, G L Guo, L L Gui, Y Q Tang *Chem. Phys. Lett.* **325** 340 (2000)
303. D S Xu, Y J Hu, D P Chen, G L Guo, L L Gui, Y Q Tang *Adv. Mater.* **12** 520 (2000)
304. Y Li, D S Xu, Q M Zhang, D P Chen, F Z Huang, Y J Xu, G L Guo, Z N Gu *Chem. Mater.* **11** 3433 (1999)
305. X Y Zhang, L D Zhang, W Chen, G W Meng, M J Zheng, L X Zhao *Chem. Mater.* **13** 2511 (2001)
306. M J Zheng, L D Zhang, G H Li, X Y Zhang, X F Wang *Appl. Phys. Lett.* **79** 839 (2001)
307. H Masuda, M Yotsuya, M Ishida. *Jpn J. Appl. Phys.* **37** L1090 (1998)
308. M S Sander, A L Prieto, R Gronsky, T Sands, A M Stacy *Adv. Mater.* **14** 665 (2002)
309. Y-J Han, J M Kim, G D Stucky *Chem. Mater.* **12** 2068 (2000)
310. L-Z Wang, J-L Shi, W- H Zhang, M-L Ruan, J Yu, D-S Yan *Chem. Mater.* **11** 3015 (1999)
311. L Bronstein, D Chernyshov, P Valetsky, N Tkachenko, H Lemmetyinen, J Hartmann, S Förster *Langmuir* **15** 83 (1999)
312. R S Kane, R E Cohen, R Silbey *Langmuir* **15** 39 (1999)
313. L I Trakhtenberg, G N Gerasimov, E I Grigor'ev *Zh. Fiz. Khim.* **73** 264 (1999) [e]
314. D I Svergun, E V Shtykova, A T Dembo, L M Bronstein, O A Platonova, A N Yakunin, P M Valetsky, A R Khokhlov *J. Chem. Phys.* **109** 11109 (1998)
315. F Baumann, B Deubzer, M Geck, J Dauth, S Sheiko, M Schmidt *Adv. Mater.* **9** 955 (1997)
316. C Roos, M Schmidt, J Ebenhoch, F Baumann, B Deubzer, J Weis *Adv. Mater.* **11** 761 (1999)
317. S H Choi, K L Wang, M S Leung, G W Stupian, N Presser, S W Chung, G Markovich, S H Kim, J R Heath *J. Vac. Sci. Technol., A* **17** 1425 (1999)
318. A Kumar, G M Whitesides *Appl. Phys. Lett.* **63** 2002 (1993)
319. T Sato, D G Hasko, H Ahmed *J. Vac. Sci. Technol., B* **15** 45 (1997)
320. J Zheng, Z Zhu, H Chen, Z Liu *Langmuir* **16** 4409 (2000)
321. M Winzer, M Kleiber, N Dix, R Wiesendanger *Appl. Phys. A: Mater. Sci. Process.* **63** 617 (1996)
322. F Burmeister, C Schäfle, B Keilhofer, C Bechinger, J Boneberg, P Leiderer *Adv. Mater.* **10** 495 (1998)
323. T L Morkved, P Wiltzius, H M Jaeger, D G Grier, T A Witten *Appl. Phys. Lett.* **64** 422 (1994)
324. R W Zehner, W A Lopes, T L Morkved, H Jaeger, L Sita *Langmuir* **14** 241 (1998)
325. P C Hidber, W Heldbig, E Kim, G M Whitesides *Langmuir* **12** 1375 (1996)
326. S Palacin, P C Hidber, J Bourgoin, C Miramond, C Fermon, G M Whitesides *Chem. Mater.* **8** 1316 (1996)
327. M A McCord *J. Vac. Sci. Technol., B* **15** 2125 (1997)
328. J P Silverman *J. Vac. Sci. Technol., B* **15** 2117 (1997)
329. J Melngailis, A A Mondelli, I L Berri, R Mohondro *J .Vac. Sci. Technol., B* **16** 927 (1998)
330. T M Bloomstein, M W Horn, M Rothschild, R R Kunz, S T Palmacci, R B Goodman *J. Vac. Sci. Technol., B* **15** 2112 (1997)
331. S C Kitson, W L Barnes, J R Sambles *IEEE Photonics Technol. Lett.* **8** 1662 (1996)
332. K Bromann, C Felix, H Brune, W Harbich, R Monot, J Buttet, K Kern *Science* **274** 956 (1996)
333. G Springholz, V Holy, M Pinczolits, G Bauer *Science* **282** 734 (1998)
334. H W Deckman, J H Dunsmuir, S Garoff, J A McHenry, D J Peiffer *J. Vac. Sci. Technol., B* **6** 333 (1988)
335. J C Hulteen, R P Van Duyne *J. Vac. Sci. Technol., A* **13** 2117 (1995)

336. J C Hulteen, D A Treichel, M T Smith, M L Duval, T R Jensen, R P Van Duyne *J. Phys. Chem. B* **103** 3854 (1999)
337. J C Hulteen, R P Van Duyne *J. Vac. Sci. Technol., A* **13** 1553 (1995)
338. F Burmeister W Badowsky, T Braun, S Wieprich, J Boneberg, P Leidere *Appl. Surf. Sci.* **144 – 145** 461 (1999)
339. T J Jensen, M L Duval, K L Kelly, A A Lazarides, G C Schatz, R P Van Duyne *J. Phys. Chem. B* **103** 9846 (1999)
340. X M Lin, R Parthasarathy, H M Jaeger *Appl. Phys. Lett.* **78** 1915 (2001)
341. M H V Werts, M Lambert, J-P Bourgon, M Brust *Nano Lett.* **2** 43 (2002)
342. J Y Chen, J F Klemic, M Elimelech *Nano Lett.* **2** 393 (2002)
343. H Sugimura, N Takgiri *J. Am. Chem. Soc.* **119** 9226 (1997)
344. R Resch, C Baur, A Bugacov, B E Koel, A Madhukar, A A G Requicha, P Will *Langmuir* **14** 6613 (1998)
345. S Meltzer, R Resch, B E Koel, M E Thompson, A Madhukar, A A G Requicha, P Will *Langmuir* **17** 1713 (2001)
346. R D Piner, J Zhu, F Xu, S H Hong, C A Mirkin *Science* **283** 661 (1999)
347. S H Hong, C A Mirkin *Science* **288** 1808 (2000)
348. Y Li, B B Maynor, J Liu *J. Am. Chem. Soc.* **123** 2105 (2001)
349. B W Maynor, Y Li J Liu *Langmuir* **17** 2575 (2001)
350. F Caruso, R A Caruso, H Möhwald *Science* **282** 1111 (1998)
351. F Caruso *Chem. Eur. J.* **6** 413 (2000)
352. C W Chen, T Serizawa, M Akashi *Chem. Mater.* **11** 1381 (1999)
353. Y Kobayashi, V Salgueirino-Maceira, L M Liz-Marzan *Chem. Mater.* **13** 1630 (2001)
354. C W Chen, M Q Chen, T Serizawa, M Akashi *Chem. Mater.* **10** 122 (1998)
355. A Dokuchaev, J T James, S C Koene, S Pathak, G K S Prakash, M E Tompson *Chem. Mater.* **11** 2389 (1999)
356. N Arul Dhas, A Zaban, A Gedanken *Chem. Mater.* **11** 806 (1999)
357. Z Zong, Y Mastay, Y Koltypin, Y Zhao, A Gedanken *Chem. Mater.* **11** 2350 (1999)
358. S Ramesh, Y Kohen, R Prosorov, K V P M Shafi, D Aurbach, A Gedanken *J. Phys. Chem. B* **102** 10234 (1998)
359. S L Westcott, S J Oldenburg, T Randall Lee, N J Halas *Langmuir* **14** 5396 (1999)
360. A B R Mayer, W Grebner, W Wannenmacher *J. Phys. Chem. B* **104** 7278 (2000)
361. C Caruso *Adv. Mater.* **13** 11 (2001)
362. G Decher, J D Hong *Ber. Bunsen-Ges. Phys. Chem.* **95** 1430 (1995)
363. G Decher *Science* **277** 1232 (1997)
364. F Caruso, M Spasova, V Salgueirino-Maceira, L M Liz-Marzan *Adv. Mater.* **13** 1090 (2001)
365. Z Bao, L Chen, M Weldon, E Chandross, O Cherniavskaya, Y Dai, J B-H Tok *Chem. Mater.* **14** 24 (2002)
366. K C Grabar, P C Smith, M D Musick, J A Davis, D G Water, M A Jackson, A P Guthrie, M J Nata *J. Am. Chem. Soc.* **118** 1148 (1996)
367. T Sato, D Brown, B F G Johnson *Chem. Commun.* 1007 (1997)
368. S Liu, T Zhu, R Hu, Z Liu *Phys. Chem. Chem. Phys.* **4** 6059 (2002)
369. Y Yin, Y Xia *Adv. Mater.* **13** 267 (2001)
370. J Aizenberg, P V Braun, P Wiltzius *Phys. Rev. Lett.* **27** 2997 (2000)
371. A Kumar, H A Beibuyck, G M Whiteside *Langmuir* **13** 5349 (1994)
372. A J Parker, P A Childs, R E Palmer, M Brust *Appl. Phys. Lett.* **74** 2833 (1999)
373. K M Chen, X Jiang, L C Kimerling, P T Hammond *Langmuir* **16** 7825 (2000)
374. G Decher, M Eckle, J Schmitt, B Struth *Curr. Opin. Colloid Interface Sci.* **3** 32 (1998)
375. P T Hammond *Curr. Opin. Colloid Interface Sci.* **4** 430 (2000)
376. J A He, L Li, J Kumar, S K Tripathy *J. Phys. Chem. B* **102** 7067 (1998)
377. A Wu, D Yoo J-K Lee, M F Rubner *J. Am. Chem. Soc.* **121** 4883 (1999)
378. J H Cheung, A F Fou, M F Rubner *Thin Solid Films* **244** 985 (1994)
379. Y M Lvov, G N Kamau, D L Zhou, J F Rusling *J. Colloid Interface Sci.* **212** 570 (1999)
380. A Mamedov, J W Ostrander, F Aliev, N A Kotov *Langmuir* **16** 3941 (2000)
381. I Lee, H Zheng, M F Rubner, P T Hammond *Adv. Mater.* **14** 572 (2002)
382. D Qin, Y Xia, B Xu, H Yang, H Zhu, G M Whitesides *Adv. Mater.* **11** 1433 (1999)
383. A D Kent, T M Show, S von Molnar, D D Awschalom *Science* **262** 1249 (1992)
384. K L Lee, M Hatzakis *J. Vac. Sci. Technol., B* **7** 1941 (1989)
385. Z Zhong, B Gates, Y Xia, D Qin *Langmuir* **16** 10369 (2000)
386. A Kumar, H Biebuyck, G M Whitesides *Langmuir* **8** 2672 (1994)
387. A J Parker, P A Childs, R E Palmer, M Brust *Nanotechnology* **12** 6 (2001)
388. T O Hutchinson, Y-P Liu, C Kiely, M Brust *Adv. Mater.* **13** 1800 (2001)
389. S Chen, R S Ingram, M J Hostetler, J J Pietron, R W Murray, T G Schaaff, J T Khoury, M M Alvarez, R L Whetten *Science* **280** 2098 (1998)
390. S Chen *J. Am. Chem. Soc.* **122** 7420 (2000)
391. J F Sampaio, K C Beverly, J R Heath *J. Phys. Chem. B* **105** 8797 (2001)
392. S Henrichs, C P Collier, R J Saykally, Y R Shen, J R Heath *J. Am. Chem. Soc.* **122** 4077 (2000)
393. G Markovich, C P Collier, J R Heath *Phys. Rev. Lett.* **80** 3807 (1998)
394. N Fishelson, I Shkrob, O Lev, J Gun, A D Modestov *Langmuir* **17** 403 (2001)
395. M Brust, D Bethel, C J Kiely, D J Schiffrin *Langmuir* **14** 5425 (1998)
396. V V Vysotskii, V I Roldughin *Kolloid. Zh.* **60**729 (1998) [d]
397. V V Vysotskii, V I Roldughin *Kolloid. Zh.* **61** 190 (1999) [d]
398. V I Roldughin, V V Vysotskii *Prog. Org. Coat.* **39** 81 (2000)
399. J J Shiang, J R Heath, C P Collier, R J Saykally *J. Phys. Chem. B* **102** 3425 (1998)
400. F Remacle *J. Phys. Chem. A* **104** 4739 (2000)
401. Y Imry *Introduction to Mesoscopic Physics* (2nd Ed.) (Oxford: Oxford University Press, 2002)
402. J M Ziman *Principles of the Theory of Solids* (2nd Ed.) (Cambride: Cambride University Press, 1972)
403. S-H Kim, G Meideiros-Ribeiro, D A A Ohlberg, R S Williams, J R Heath *J. Phys. Chem. B* **103** 10 341 (1999)
404. K Inukai, Y Hotta, S Tomura, M Takahashi, A Yamagishi *Langmuir* **16** 7679 (2000)
405. C T Blank, C B Murray, R L Sandstrom, S Sun *Science* **290** 1131 (2000)
406. U Kreibig, M Vollmer *Optical Properties of Metal Clusters* (Berlin: Springer, 1995)
407. S Link, M A El-Sayed *J. Phys. Chem. B* **103** 8410 (1999)
408. M P Pileni *Pure Appl. Chem.* **72** 53 (2000)
409. S Torquato, F Lado *Phys. Rev. B* **33** 6428 (1986)
410. I Farbman, O Levi, S Efrima *J. Chem. Phys.* **96** 6477 (1992)
411. R Berndt, J K Gimzewski, P Johansson *Phys. Rev. Lett.* **67** 3769 (1991)
412. C Girardin *J. Phys. III* **6** 661 (1996)
413. T Baum, D Bethell, M Brust, D J Schiffrin *Langmuir* **15** 866 (1999)
414. M I Stockman, S V Faleev, D J Bergman *Phys. Rev. Lett.* **87** 167401 (2001)
415. Y Lu, Y Yin, Z-Y Li, Y Xia *Nano Lett.* **2** 785 (2002)
416. M Quinten, A Leitner, J R Krenn, F R Aussenegg *Opt. Lett.* **23** 1331 (1998)
417. J R Krenn, A Dereux, J C Weeber, E Bourliott, Y Lacrout, J P Goudonnet, G Schider, W Gotschy, A Leitner, F R Aussenegg, C Giarad *Phys. Rev. Lett.* **82** 2590 (1999)
418. M D Malinsky, K L Kelly, G C Schatz, R P Van Duyne *J. Phys. Chem. B* **105** 2343 (2001)
419. M Yamada, T Tadera, K Kubo, H Nishihara *Langmuir* **17** 2363 (2001)
420. E S Kooij, H Wormeester, E A M Brouwer, E von Vroonhover, A von Silfhout, B Poelsema *Langmuir* **18** 4410 (2002)
421. E Hutter, J H Fendler, D Roy *J. Phys. Chem. B* **105** 11 159 (2001)

422. H Yanagi, N Matsuoka, M Kondo, M Nagawa, Y Taniguchi *Chem. Mater.* **13** 4800 (2001)
423. H Yanagi, N Matsuoka, M Kondo, M Nagawa, Y Taniguchi *Langmuir* **17** 5491 (2001)
424. M Sirota, E Minkin, E Lifshitz, V Hensel, M Lahav *J. Phys. Chem. B* **105** 6792 (2001)
425. J R Sheats, H Antoniadis, M Hueschen, W Leonard, J Miller, R Moon, R Roitman, A Stocking *Science* **273** 884 (1996)
426. N Tessler *Adv. Mater.* **11** 363 (1999)
427. J H Shön, Ch Kloc, A Dodabalapur, B Batlogg *Science* **289** 599 (2000)
428. P Schuck *Annu. Rev. Biophys. Biomol. Struct.* **26** 541 (1997)
429. L A Lyon D J Pena, M J Natan *J. Phys. Chem. B* **103** 5826 (1999)
430. R K Chang, T E Furtak (Eds) *Surface-Enhanced Raman Scattering* (New York: Plenum, 1981)
431. M Moskovits *Rev. Mod. Phys.* **57** 783 (1985)
432. R G Freeman, M B Hommer, K C Grabar, M A Jackson, M J Natan *J. Phys. Chem.* **100** 718 (1996)
433. J Hu, B Zhao, W Xu, Y Fan, B Li, Y Ozaki *Langmuir* **18** 6839 (2002)
434. S Nie, S R Emory *Science* **275** 1102 (1997)
435. H Xu, E J Bjerneld, M Käll, L Borjesson *Phys. Rev. Lett.* **83** 4357 (1999)
436. T L Haslett, L Tay, M Moskovits *J. Chem. Phys.* **113** 1641 (2000)
437. D J Maxwell, S R Emory, S Nie *Chem. Mater.* **13** 1082 (2001)
438. J H Holtz, S A Asher *Nature (London)* **389** 829 (1997)
439. J M Weissman, H B Sunkara, A S Tse, S A Asher *Science* **274** 959 (1996)
440. R J Spry, D J Kosan *Appl. Spectrosc.* **40** 782 (1986)
441. J D Joannopoulos, R D Meade, J N Winn *Photonic Crystals: Molding the Flow of Light* (Prinston: Prinston University Press, 1995)
442. I I Trahan, G H Watson *Phys. Rev. Lett.* **76** 315 (1996)
443. A R Parker, R C McPhedran, D R Mckenzie, L C Botten, N A P Nicorovici *Nature (London)* **409** 36 (2001)
444. K M Ho, C T Chan, C M Soukoulis *Phys. Rev. Lett.* **65** 3152 (1990)
445. A Moroz *Phys. Rev. Lett.* **83** 5274 (1999)
446. S John *Phys. Rev. Lett.* **58** 2486 (1987)
447. E Yablonovitch *Phys. Rev. Lett.* **58** 2059 (1987)
448. E Yablonovitch *Nature (London)* **401** 539 (1999)
449. A Blanco, E Chomski, S Grabtchak, M Ibisate, S John, S W Leonard, C Lopez, F Meseguer, H Miguez, J P Mondia, G A Ozin, O Toader, H M van Driel *Nature (London)* **405** 437 (2000)
450. Y Shen, C S Friend, Y Jiang, D Jakubczyk, J Swiatkiewicz, P Prasad *J. Phys. Chem. B* **104** 7577 (2000)
451. Y Yamamoto, R E Slusher *Phys. Today* **46** 66 (1993)
452. U Grüning, V Lehmann, S Ottow, K Busch *Appl. Phys. Lett.* **68** 747 (1996)
453. S Kawakami *Electron. Lett.* **33** 1260 (1997)
454. T Baba, T Matsuzaki *Jpn. J. Appl. Phys.* **35** 1348 (1996)
455. S H Park, Y Xia *Langmuir* **15** 266 (1999)
456. Y N Xia, B Gate, S H Park *J. Lightwave Technol.* **17** 1956 (1999)
457. Z-Z Gu, S Kubo, W Oian, Y Einaga, A Fujishima, O Sato *Langmuir* **17** 6751 (2001)
458. A A Zakhidov, R H Baughman, Z Iqbal, C X Cui, I Khayrullin, S O Dantas, I Marti, V G Ralchenko *Science* **282** 897 (1998)
459. Y Fink, A M Urbas, M G Bawendi, J D Joannopoulas, E L Thomas *J. Lightwave Technol.* **17** 1963 (1999)
460. J E G J Wijhoven, L V Vos *Science* **281** 802 (1998)
461. G Subramania, K Constant, R Biswas, M M Sigalas, K M Ho *Appl. Phys. Lett.* **74** 3933 (1999)
462. G Pan, R Kesavamoorthy, S A Asher *J. Am. Chem. Soc.* **120** 6525 (1998)
463. J Ballato, A Jame *J. Am. Ceram. Soc.* **82** 2273 (1999)
464. Y Lu, Y Yin, B T Mayers, Y Xia *Nano Lett.* **2** 183 (2002)
465. P Sheng, W Wen, N Wang, H Ma, Z Lin, W Y Zhang, X Y Lei, Z L Wang, D G Zheng, W Y Tam *Pure Appl. Chem.* **72** 309 (2000)
466. J Song, H Sun, Y Xu, Y Fu, S Matsuo, H Misawa, G Du *Opt. Quantum Electron.* **32** 1295 (2000)
467. Y D Yin, Y Lu, Y N Xia *J. Am. Chem. Soc.* **123** 771 (2001)
468. Y D Yin, Y Lu, B Gates, Y N Xia *J. Am. Chem. Soc.* **123** 8718 (2001)
469. R C Hayward, D A Saville, I A Aksay *Nature (London)* **404** 56 (2000)
470. O D Velev, A M Lenhoff, E W Kaler *Science* **287** 2240 (2000)
471. B A Ozin, S M Yang *Adv. Funct. Mater.* **11** 95 (2001)
472. Z-Z Gu, A Fujishima, O Sato *Angew. Chem., Int. Ed.* **41** 2068 (2002)
473. L M Liz-Marzan, P Mulvaney *New J. Chem.* **22** 1285 (1998)
474. G Wang, A Harrison *J. Colloid Interface Sci.* **217** 203 (1999)
475. L M Liz-Marzan, M Giersig, P Mulvaney *Chem. Commun.* 731 (1996)
476. V V Hardikar, E Matijevic *J. Colloid Interface Sci.* **221** 133 (2000)
477. R H Kodama, A E Berkovitz, E J McNiff, S Foner. *Phys. Rev. Lett.* **77** 394 (1996)
478. M L Billas, A Chatelain, W A de Heer *Science* **265** 1682 (1994)
479. J P Chen, C M Sorensen, K J Klabunde, G C Hadjipanayis *Phys. Rev. B* **51** 11527 (1995)
480. K W Edmons, C Binns, S H Baker, S C Thornton, C Norri, J B Goedkoop, F U Hillbrecht *Phys. Rev. B* **59** R701 (1999)
481. Y E Volokitin, Doctoral Thesis, University Leiden, Leiden, 1997
482. F Luis, J M Torres, L M Garcia, J Bartolome, J Stankiewicz, F Petroff, F Fettar, J-L Maurice, A Vaures *Phys. Rev. B* **65** 094 409 (2002)
483. D Babonneau, F Petroff, J-L Maurice, F Fettar, A Vaures *Appl. Phys. Lett.* **76** 2892 (2000)
484. M Respaud, J M Broto, H Rakoto, A R Fert, L Thomas, B Barbara, M Verelst, E Snoeck, P Lecante, A Mosset, J Osuna, T Ould Ely, C Amiens, B Chaudret *Phys. Rev. B* **57** 2925 (1998)
485. S Shtrikman, E P Wholfarth *Phys. Lett. A* **85** 467 (1981)
486. J L Dorman, L Bessais, D Fiorani *J. Phys. C* **21** 2015 (1988)
487. S Mørup, E Tronc *Phys. Rev. Lett.* **72** 3278 (1994)
488. J M Kosterlitz, D J Thouless *J. Phys. C* **6** 1181 (1973)
489. A P Young *Phys. Rev. B* **19** 1855 (1979)
490. D R Nelson, B I Halperin *Phys. Rev. B* **19** 2457 (1979)
491. K Zahn, R Lenke, G Maret *Phys. Rev. Lett.* **82** 2721 (1999)
492. P H F Hansen, S Rödner, L Bergtröm *Langmuir* **17** 4867 (2001)
493. S Sastry, D S Corti, P G Debenedetti, F H Stillinger *Phys. Rev. E* **56** 5524 (1997)
494. A Pertsinidis, X C Ling *Phys. Rev. Lett.* **87** 098 303 (2001)
495. S Johansson, K Wong, V P Zhdanov, B Kasemo *J. Vac. Sci. Technol., A* **17** 297 (1999)
496. Z L Wang, J L Petroski, T C Green, M A El-Sayed *J. Phys. Chem. B* **102** 6145 (1998)
497. A S Eppler, G Rupprechter, E A Anderson, G A Samorjai *J. Phys. Chem.* **104** 7286 (2000)
498. A Ulman *Chem. Rev.* **96** 1533 (1996)
499. N Sandhyarani, M R Resmi, R Unnikrishnan, R Vidyasagar, S Ma, M P Antony, G P Selvam, V Visalakshi, N Chandrakumar, K Pandian, Y T Tao, T Pradeep *Chem. Mater.* **12** 104 (2000)
500. B A Korgel *Phys. Rev. Lett.* **86** 127 (2001)
501. W X Zheng, M M Maye, F L Leibowitz, C J Zhong *Anal. Chem.* **72** 2190 (2000)
502. M M Maye, J Luo, L Han, C-J Zhong *Nano Lett.* **1** 575 (2001)

[a] — *J. Exp. Theor. Phys. Lett. (Engl. Transl.)*
[b] — *J. Exp. Theor. Phys. (Engl. Transl.)*
[c] — *Physics-Uspekhi (Engl. Transl.)*
[d] — *Colloid. J. (Engl. Transl.)*
[e] — *Russ. J. Phys. Chem. (Engl. Transl.)*

Russian Chemical Reviews **73** (2) 147 – 159 (2004) © 2004 Russian Academy of Sciences and Turpion Ltd

DOI 10.1070/RC2004v073n02ABEH000837

Self-propagating high-temperature synthesis of nanomaterials

A E Sytschev, A G Merzhanov

Contents

I.	Introduction	147
II.	Formation of nanostructures in the processes of self-propagating high-temperature synthesis	147
III.	Traditional processes of the self-propagating high-temperature synthesis	148
IV.	Gas-phase self-propagating high-temperature synthesis	151
V.	Stimulated self-propagating high-temperature synthesis	152
VI.	Conclusion	157

Abstract. The results of recent studies in the field of self-propagating high-temperature synthesis of nanosized materials are surveyed. The possibilities of the synthesis of nanomaterials in the combustion mode are demonstrated. Examples of applications of the self-propagating high-temperature synthesis for the preparation of nanopowders, films and compact materials are given. The bibliography includes 116 references.

I. Introduction

The self-propagating high-temperature synthesis (SHS) is an autowave process analogous to the propagation of a combustion wave.[1] In this process, a chemical reaction is localised in the combustion zone that spontaneously propagates over a chemically active medium. This process is actively exploited in the technology of inorganic materials: this makes it possible to produce powders, compact materials and workpieces as well as make coatings and weld component parts.[2]

The self-propagating high-temperature synthesis is effectively applied not only in technology but in a solution of various problems of modern materials science as well. Among such problems, the following may be mentioned: design of functionally graded materials,[3] single crystal growth,[4] development of gravity-sensitive processes,[5] realisation of chemical reactions under conditions of micro-gravity and zero gravity,[6, 7] mechanochemical treatment of reactants and reaction products,[8] thermochemical generation of electric and magnetic fields,[9] *etc*. As in the powder metallurgy, the particle size of reactants and reaction products plays a crucial role in the self-propagating high-temperature synthesis. In this respect, the SHS is closely interrelated with nanotechnology. Further reduction in the particle size is an urgent task since the size effects have a decisive influence on both the SHS process itself and properties of the resultant materials.

In the present review, the results of recent investigations in the field of SHS of nanosized materials are surveyed. Possibilities of its applications aimed at the preparation of nanopowders and films, compact materials with nanosized grains and pores are considered. Distinctive features of the SHS involving nanosized components (reactants, functional additives) are discussed.

A E Sytschev, A G Merzhanov Institute of Structural Macrokinetics and Materials Science, Russian Academy of Sciences, 142432 Chernogolovka, Moscow Region. Fax (7-095) 962 80 40. Tel. (7-095) 962 80 36.
E-mail: sytschev@ism.ac.ru (A E Sytschev). Tel. (7-095) 962 80 00.
E-mail: merzh@ism.ac.ru (A G Merzhanov)

Received 21 March 2003
Uspekhi Khimii **73** (2) 157 – 170 (2004); translated by Ya V Zubavichus

II. Formation of nanostructures in the processes of self-propagating high-temperature synthesis

The possibility of direct preparation of nanosized structures by SHS is not self-evident. Some specialists in materials science believe that SHS products are always large-grain structures due to high temperatures developed during combustion. In fact, conversion of initial reactants into final products as a result of SHS is a complicated multi-parameter process. Therefore, there are several ways to control it. Provided that the ways to adjust the required conditions are established, one may hope to succeed in the synthesis of nanostructured materials.

About one hundred papers devoted to the self-propagating high-temperature synthesis have been published over last few years. Most interesting of them are discussed below.

I P Borovinskaya suggested a concept[10] of further developments of investigations in the field of the SHS of nanomaterials, in which the formation of nanostructures is related to the combustion mechanism. The major types of such processes were considered including: solid flame combustion 'solid + solid' systems (including one of its modifications, *viz*., combustion with an interstitial molten layer); gas-phase SHS (*e.g*., chain flames, combustion of condensed systems with a gaseous interstitial zone); combustion of 'solid + gas' systems (*e.g*., filtration combustion, combustion of gaseous suspensions).

Let us analyse the potentials of these methods.[10]

In the case of a solid flame SHS process, the combustion reaction proceeds in the diffusion mode. As a result of a chemical reaction between two solid reactants, a continuous layer of solid products starts to grow on grains of one of the reactants, which separates the reactants. Thus, the total rate of the process is limited by the diffusion of the second component through the product layer. Since the change in the specific volume of grains of the starting reactants due to the formation of the product layer atop them is rather small, the size of the particles formed is similar to that of particles of the starting reactants. Owing to the high diffusion resistance of contacting areas of the particles, recrystallisation processes are virtually completely suppressed in such systems.

Thus, nanosized reactants have to be used in order to produce nanosized products by solid flame combustion processes.

In solid-state systems with an interstitial molten layer, the possibility of formation of nanocrystallites depends on the crystallisation and recrystallisation processes and thermal regimes of combustion and cooling of the product after the completion of the reaction.

Among synthetic methods allowing production of nanoparticles, the gas-phase SHS, *i.e.*, combustion of gases giving rise to a condensed product, is of particular importance. The reaction proceeds on nuclei that are formed by an agglomeration of primary particles of the product. The particles grow until the reactants are consumed. If the reaction mixture is allowed to rapidly expand, the process stops due to the fast artificial cooling (quenching) of the mixture. Using this technique, one may stop the particle growth at any required stage. A continuous combustion process with a continuous quenching of the mixture at a certain conversion level, which allows a control over the size of the particles formed, is readily realisable for gaseous mixtures.

Sedimentation of particles from a gaseous suspension gives rise to nanopowders that can be further used in various technological steps involving powder mixtures. The flame-cladding of powders (*i.e.*, their coating with a metal layer) is of particular interest. In particular, nanosized powders of titanium carbide coated with a nickel–molybdenum film, which can be used for production of hard alloys, have been prepared in this way.

Synthesis in the chain flames is one of the modifications of the gas flame SHS.[11] It involves the same processes as described above for the generic gas flame SHS but at a lower temperature. This allows preparation of thermally unstable products. Synthesis in the chain flames is most frequently applied to the preparation of nanosized oxides.[12, 13]

It has to be noted that heterogeneous condensation can also be carried out in flames. In order to make a coating (or deposit a film) on a workpiece, it is introduced into the suitable flame.

The chemical condensation combustion of condensed mixtures is of great interest. In this case, the reactants are brought to the gaseous state prior to the initiation of the reaction. If condensed products are formed exclusively or predominantly in the reaction, the gas-phase stage can even elude detection by researchers. This process is insufficiently explored to date. In the SHS processes that include a gas-phase stage of the chemical conversion, the formation of nanosized products is largely determined by conditions of the chemical condensation, which can be deliberately adjusted.

Unusual mechanisms of formation of nanoparticles are often observed for 'solid + gas' systems. In particular, the filtration combustion of porous solids (*e.g.*, powder bitstones or compacted blanks) or gaseous suspensions is worth mentioning.

The above qualitative analysis taken from the conceptual work [10] demonstrates that diverse physicochemical transformations are realised within the SHS processes, such as: chemical reactions, reaction diffusion, melting, dissolution, crystallisation, recrystallisation, evaporation, sublimation, dissociation, chemical condensation, *etc*. All these processes affect the crystal structure of the product formed. Generation and growth of nuclei are most important for the formation of nanoparticles. Therefore, if the problem of preparation of nanosized products by means of SHS is posed, special attention has to be paid to crystallisation, recrystallisation and chemical condensation.

III. Traditional processes of the self-propagating high-temperature synthesis

Let us first consider traditional SHS processes, which allow preparation of nanomaterials. They include the combustion processes in mixtures of powders and in solid + gas systems. Formally, the combustion involving nanosized powder reactants may also be classified as a traditional SHS process but studies in this field have begun only recently. Unfortunately, most authors report only the synthesis of nanomaterials by means of the SHS and do not analyse the mechanisms and kinetic features of their formation.

1. Preparation of nanomaterials based on powder mixtures

SHS processes involving powder mixtures are predominantly applied to the preparation of nanosized metal oxides and silicon carbide. For instance, nanocrystalline α-Al_2O_3 has been synthesised [14] from a mixture of powdered aluminium nitrate and urea. Heating followed by self-ignition of the mixture resulted in a melt from which a foamed α-Al_2O_3 structure was formed. After grinding the product, α-Al_2O_3 powder with the particle size of $\sim$ 100 nm was obtained.

An Al_2O_3–ZrO_2 solid solution has been synthesised [15] from a mixture of aluminium and zirconium nitrates (oxidants) with urea (combustible material). The process was conducted in the thermal explosion mode in the following sequence: heating of the mixture to 450–600 °C, melting, ignition and combustion. The resultant product composed of agglomerates with a size not exceeding 100 nm was ground, coated with BN, compacted and sintered at 1200 °C. The final product manifested high quality as regards its physicomechanical characteristics: relative density, 99%, the Vickers hardness, 4.45 GPa, crack resistance coefficient K_{1c}, 8.38 MPa $m^{1/2}$, the size of Al_2O_3 and ZrO_2 grains, less than 50 nm.

A technology of self-propagating high-temperature synthesis of β-SiC based on the direct heating of the green mixture has been developed.[16] The authors used an original means of heating, *viz*., the burner (flare) was moved along the sample with a velocity equal to that of the combustion front propagation. The size of the β-SiC grains produced was close to the nanorange (< 200 nm) and virtually independent of the particle size of the parent silicon.

Preparation of nanosized silicon carbide attracts a lot of attention. A direct synthesis of SiC has been accomplished [17] in the thermal explosion mode with microwave heating. The initial Si and C particles were of equal size ($\sim$ 43 μm). The silicon carbide powder produced was composed of needle-shaped particles with a diameter of 36–76 nm and length of 360–1500 nm.

In those cases where smaller Si and C particles were used, small fibres were produced. Note that in this process the combustion is initiated in the bulk of the sample and then propagates towards its surface in the SHS mode. This model is supported by conclusions of a theoretical investigation [18] into post-induction phenomena occurring in the course of a thermal explosion in 'porous reagent–reactive gas–solid product' systems.

A procedure for the preparation of an engineering ceramic according to the reaction:

$$TiO_2 + Al + C + ZrO_2 \xrightarrow[Ar]{SHS} Al_2O_3 + TiC + ZrO_2$$

has been described.[19] The reaction product was a mixture of crystalline TiC and ZrO_2 with amorphous Al_2O_3. The size of the TiC and ZrO_2 crystallites was *ca*. 20 nm. Crystallisation of Al_2O_3 from the amorphous phase occurs after completion of the chemical reaction. Note that although ZrO_2 is not involved in the reaction it undergoes structural transitions resulting in a decrease in its particle size from 10 μm to 20 nm.

The problem of what the chemical reactions or phase or structural transitions are that occur in the combustion wave during the SHS processes is of primary importance. Many phase and structural transformations of substances occur far beyond the combustion front when the chemical processes are already completed. This can lead to substantial changes in the microstructures of the combustion products. Figure 1 shows some typical examples of the dependence of the product grain size on the distance from the combustion front. The data presented suggest [20] that the recrystallisation processes leading to an increase in the grain size (by a factor of 10) [20] proceed actively in the system after completion of the chemical reactions in the combustion wave. Definitely, monitoring of the evolution of the microstructure is a

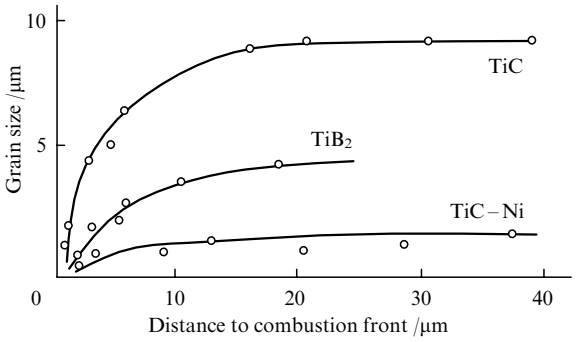

Figure 1. The dependence of sizes of TiC, TiB_2 and TiC – Ti grains on the distance from the combustion front.[20]

complicated task. Its solution requires dedicated techniques and high-resolution instruments.

2. Preparation of nanomaterials based on 'powder + gas' systems

An interesting two-stage synthesis of nanosized silicon carbide has been reported.[21] Its first stage involved combustion of a mixture of powdered Si and C (with an excess of Si) in a nitrogen atmosphere, which gives rise to Si_3N_4 and SiC. The second stage included a reburdening of the mixture produced with carbon (soot) followed by the carbothermal reduction of Si_3N_4 to Si and subsequent interaction of the latter with carbon. As a result of this two-stage process, the initial Si + C mixture is converted into nanosized SiC. Direct interaction of Si with C results in the formation of coarser particles. The chemical reaction may be represented as follows:

$$\mathrm{Si} + m\,\mathrm{C} \xrightarrow{\mathrm{N_2}} \frac{1-m}{3}\,\mathrm{Si_3N_4} + m\,\mathrm{SiC} + Q_1,$$

$$\frac{1-m}{3}\,\mathrm{Si_3N_4} + m\,\mathrm{SiC} + (1-m)\mathrm{C} + Q_2 \longrightarrow \mathrm{SiC} + \mathrm{N_2}\uparrow.$$

The scheme of structural changes occurring with the starting materials and intermediate products during the SHS is shown in Fig. 2.

A method of preparation of SiC – AlN powders (solid solutions) by means of combustion of mixtures of micrometer-sized powders of Al, C and AlN and a submicrometer powder of Si in a nitrogen atmosphere at a pressure of 4 atm has been suggested.[22] The authors used two routes, *viz*., synthesis in the thermal explosion mode and the propagating combustion wave mode. The SiC – AlN solid solutions prepared using both the filtration combustion and thermal explosion represented powders with the particle size smaller than 200 nm. The crystal structure of the SiC – AlN powder synthesised using the SHS showed disorder at the atomic level. In order to produce ceramics, the powdered SiC – AlN solid solutions were sintered. Such a thermal treatment led to the ordering of their crystal structures. The obtained engineering material possessed high mechanical properties, thermal and chemical stability.

Synthesis of filamentous silicon nitride with a particle diameter of 60 – 400 nm has been reported.[23] A silicon powder with the particle size of 0.5 – 2.0 μm doped with NH_4F and Al powder mixed with a β-Si_3N_4 powder (acting as a thinner) was used as the starting material. The reactants were mixed in the following proportions: $Si : Si_3N_4 : NH_4F : Al = 87 : 10 : 2 : 1$ (mass %). The combustion was conducted in a nitrogen atmosphere at a pressure of 100 atm. The authors emphasise the key role of NH_4F (it favours a decrease in the adiabatic combustion temperature and in the heat conductivity and accelerates the crystal growth) in the formation of β-Si_3N_4 nanofibres. The morphology of the silicon nitride microstructure is shown in Fig. 3. It is clearly seen that the crystals are either straight, stranded or wavy in shape.

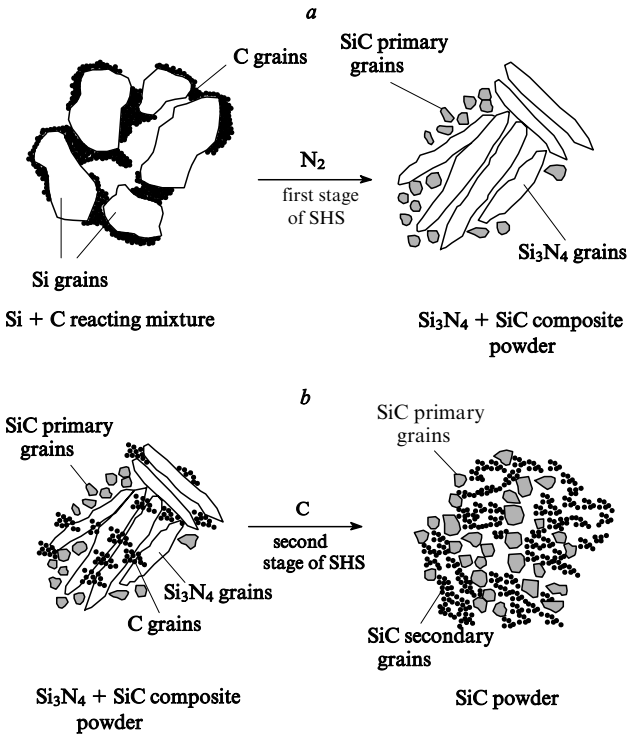

Figure 2. Morphological changes occurring in the course of the SHS of silicon carbide from powdered Si and C in a nitrogen atmosphere; (*a*) the stage of formation of the SHS products, Si_3N_4 + SiC; (*b*) the stage of SiC formation.

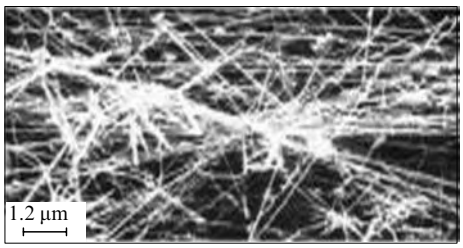

Figure 3. The morphology of silicon nitride microstructure.[23]

Two schemes for the preparation of nanosized β-Si_3N_4 – β-SiC materials by means of the solid-state chemical synthesis (*a*) and in the SHS mode (*b*) [24] are shown in Fig. 4.

Self-propagating high-temperature synthesis of various hydrogen-containing substances [25, 26] including nanosized hydride powders has been accomplished as a part of a systematic investigation into the combustion processes of metals and alloys in a hydrogen atmosphere. Unfortunately, the mechanism of formation of the nanopowders was not discussed.

The preparation of nanosized boron nitride powders in the SHS mode can be carried out in three ways according to the following reactions:[27]

(1) synthesis from elements

$$\mathrm{B} \xrightarrow{\mathrm{N_2}} \mathrm{BN},$$

(2) synthesis involving boron oxide

$$\mathrm{B} + \alpha\text{-}\mathrm{B_2O_3} \xrightarrow{\mathrm{N_2}} m\,\mathrm{BN} + n\,\mathrm{B_2O_3} + \mathrm{O_2}\uparrow,$$

(3) synthesis from B_2O_3 including a stage of magnesiothermic reduction

$$\mathrm{B_2O_3} + 3\,\mathrm{Mg} \xrightarrow{\mathrm{N_2}} 2\,\mathrm{BN} + 3\,\mathrm{MgO}$$

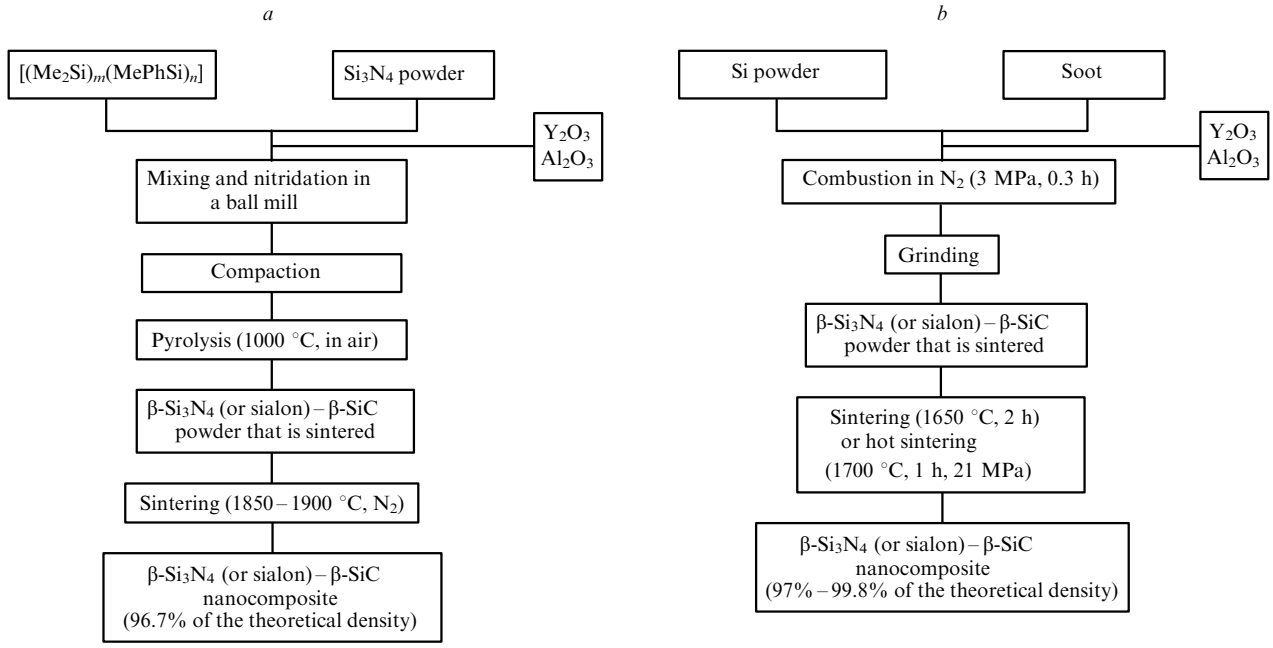

Figure 4. Two schemes of the preparation of Si_3N_4 – SiC nanocomposites from powders;[24] (*a*) chemical pathway, (*b*) in the SHS mode.

In all the cases, the products represented BN crystallites with a size of 100 – 200 nm combined in larger agglomerates.

In order to produce nanosized particles, it was necessary that the combustion product (semi-finished material) underwent further mechanical and thermochemical processing using acids and alkalies under drastic (for the dissolution of MgO) or mild (for the preparation of nanocrystalline samples through the chemical dispersion) conditions. The shape and size of BN particles were determined and the specific surface areas of both semi-finished material and the final product were calculated. Table 1 summarises the major characteristics of BN prepared by different methods.

The mechanical processing of the semi-finished material did not result in complete disintegration of the crystallites and thus the final product represented a powder containing agglomerated particles with different specific surface areas. Subsequent thermochemical treatment (chemical dispersion †) resulted in further disintegration of crystallites and in an increase in the specific surface area of the product. Fully disintegrated powders were obtained only from semi-products prepared by magnesiothermic reduction of B_2O_3. Such powders were composed of pure crystallites with a size of 100 – 200 nm. The specific surface area of the final product amounted to ~ 60 m^2 g^{-1}. The effectiveness of the above approach to the preparation of nanosized particles depends on whether crystallite formation process during the SHS can be controlled.

The microstructures of a boron nitride powder produced in the SHS mode before and after the chemical dispersion are shown in Fig. 5.[27]

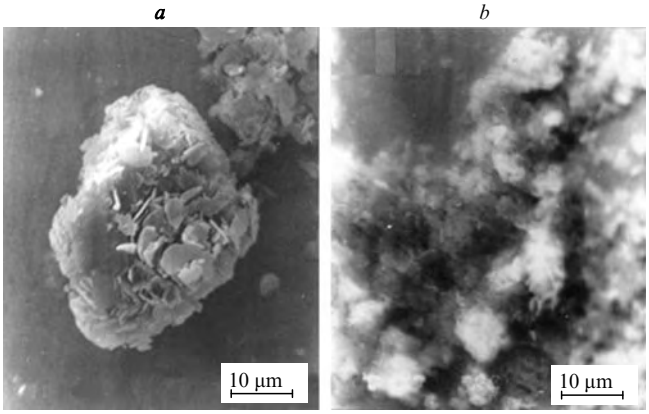

Figure 5. The microstructure of a BN powder;[27] (*a*) agglomerated hollow particles of powdered boron nitride taken from the SHS product, (*b*) single-crystalline BN formed as a result of the chemical dispersion.

† The chemical dispersion is one of the modifications of the thermochemical treatment of a product,[28] which leads to dissolution of boundary (typically, defective) layers of crystallites and to removal of contaminations, whereupon the crystallites themselves are not dissolved. As a result of such a treatment, a polycrystalline product is disintegrated into single-crystalline particles.

Table 1. Self-propagating high-temperature synthesis of fine BN powders.[24]

Powdered reactants	Intermediate product	Method for the isolation of the final product	Specific surface area /m^2 g^{-1}	
			of intermediate product	of target product
B	Polycrystalline BN cake	chemical dispersion	~6	10 – 12
$B + B_2O_3$	BN + B_2O_3 cake	treatment with water, chemical dispersion	4.5 – 5.5	8.5 – 12.0
$B_2O_3 + 3$ Mg	BN + MgO cake	chemical enrichment, chemical dispersion	3.0 – 10.5	9.5 – 60.0

IV. Gas-phase self-propagating high-temperature synthesis

Despite the fact that the combustion of gases is fairly well investigated (in contrast to the combustion of condensed systems), the gas-phase SHS has not been sufficiently explored to date. This is because there are only a few known gaseous systems that can undergo combustion to form condensed products. In particular, three processes have been studied:

(1) sodiothermic reduction of chlorides in the gas phase giving rise to chemical elements or compounds;

(2) gas-phase oxidation of combustible gases (hydrocarbons, silanes, boranes, *etc.*) with the formation of respective oxides;

(3) chemical reactions in independently generated flames that played a role of gas-phase 'chemical furnaces'.

1. Self-propagating high-temperature synthesis including a stage of sodiothermic reduction of chlorides

A remarkable feature of the sodiothermic reduction of chlorides is the formation of water-soluble NaCl as a by-product of the SHS. Therefore, the isolation of the target product from the reaction mixture faces no problems in contrast to that in the cases of magneso- or aluminothermy.

For the first time, the process of the sodiothermic reduction of chlorides by means of the gas flame combustion has been applied to the preparation of powders of reduced silicon and silicon and titanium nitrides [29, 30] using gaseous silicon and titanium chlorides as reactants and sodium or sodium–potassium vapour as the reducing agent. Other examples of syntheses of nanosized products through the SHS including a stage of sodiothermic reduction may be found elsewhere.[31–33] In particular, a gas-phase combustion of $TiCl_4$ and BCl_3 in sodium vapour yielded a titanium diboride powder, which represented agglomerates with a size of 20–100 nm composed of spherical TiB_2 particles with the diameter of less than 15 nm (after vacuum sublimation and annealing at 1000 °C) (Fig. 6).[31]

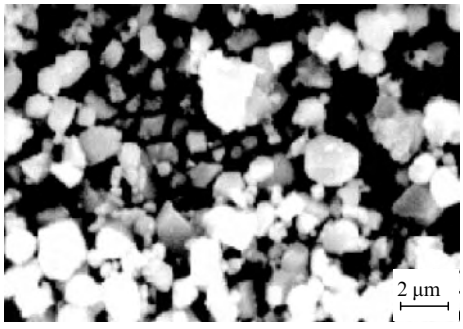

Figure 6. Nanoparticles of titanium diboride.[31]

An interesting example of preparation of a nanosized TiAl powder (~ 6 nm) under conditions of zero gravity, which favoured the formation of a stable air suspension has been reported.[34] Different condensation modes and their influence on the morphology of the particles formed were considered.

2. Gas-phase oxidation of combustible gases

Self-propagating high-temperature synthesis of particles and films of Si, Ge, SiO_2, GeO_2, Si_3N_4 by means of oxidation and pyrolysis of silane or germane [11, 35, 36] as well as gas-phase synthesis of ultradispersed amorphous powders of SiC, Si_3N_4, SiN_xC_y and of crystalline BN in the combustion mode [37] have been reported. The main advantage of this method for the production of insulating, protective and semiconductive films or nanosized powders is the possibility of performing the synthesis at relatively low temperatures and pressures, which allows one to avoid high charge densities on surfaces of the films, which greatly enhances the quality of the semiconducting products.

The chain character of the SHS processes makes it possible to apply a variety of well-established techniques developed for chain processes for their control without recourse to plasmochemistry or photochemistry. In particular, small amounts of suitable additives can be used to promote (*e.g.*, hydrazine) or, *vice versa,* inhibit (*e.g.*, olefins) the SHS. In most cases, the application of plasmochemistry is undesirable since the charged species formed in the plasma increase the surface charge density and thus deteriorate the product quality. Additionally, surface defects are developed under the action of flame or light.

Unfortunately, it is information on the products obtained that is normally given in publications devoted to the gas-phase SHS, whereas a discussion of relations of the combustion mechanism with the condensation processes and the effects of hydrodynamic factors on the combustion and the structure formation is lacking. A dependence of the morphology of the particles formed on the gas flow regime (laminar *vs.* turbulent) and its change upon a flow crisis have also eluded exploration.

To date, the gas-phase SHS has been studied only on a few case systems since gas mixtures forming solid products and having a relatively large thermal effect upon combustion are scarce. Further progress of this method can be connected with the utilisation of additional heating sources (*e.g.*, recuperative heating of reactants, plasma-induced heating, electrogas heating, *etc.*).

Realisation of the SHS using gaseous suspensions as reactants is highly problematic due to low heat evolution and poor heat exchange between particles. In this case, preliminary partial or complete gasification of reacting particles followed by a condensation of the combustion product is typically applied. The particles formed in such processes are usually substantially smaller than those of the starting reactants.

An original version of gaseous suspension SHS has been suggested.[38] In order to initiate the SHS, it is necessary to generate a cloud of metal particles in an atmosphere of a gas (oxygen, nitrogen, ammonia or another gas), which is subsequently ignited by a spark discharge. After completion of the reaction, the products are collected on a filter. Powders of Al_2O_3, MgO, SiO_2, TiO_2, ZrO_2, FeO, TiN and ZrN with the particle size of 10–100 μm were synthesised by this method.

Similar results concerning the preparation of nearly monodisperse spherical particles of γ-Al_2O_3, Fe_2O_3, Fe_3O_4, ZrO_2 with the size of ~40 nm have been reported.[39, 40] Fine metal particles with the size not exceeding 10 μm dispersed in a gas phase were taken as the starting reactants. The combustion process was induced by a diffusion or homogeneous flare.

3. Syntheses in flames

Pyrolysis of substances in flames may also be regarded as a modification of the gas-phase SHS. In this case, both the substances that are introduced into the flame and the chemical components of the flame itself can be involved in the synthesis, the reactions involving the flame components may differ from those involving the external components introduced to the flame (the formation of the target product). In those cases where the flame is chemically inert, it may be considered as a gas-phase 'chemical furnace' that only provides high temperature. Using this approach, it was possible to synthesise the following nanosized substances: TiAl,[41] Ti-W,[42] SiO_2,[42, 43] Si_3N_4,[44] TiB_2,[31] GaN,[45] Y_2O_3–Eu [46] and AlN.[47] For instance, SiO_2 nanopowders were prepared from an SiH_4–H_2–O_2–Ar gas mixture using a hybrid gas burner.[42] Adjustments of combustion conditions (*e.g.*, the stoichiometric composition of the fuel gas for the burner) made it possible to produce particles with the sizes ranging from 6–8 nm (at high oxygen concentration) to 18–20 nm (at low oxygen concentration).

V. Stimulated self-propagating high-temperature synthesis

It is well known that the SHS process can easily be subjected to external stimulation. The simplest and most common means is thermal action. Owing to a thermal energy transfer to the original mixture or the combustion zone, the temperature and combustion rate can be deliberately increased and thus the composition and characteristics of the combustion products can be affected.

Joule heating by passing electric current through the burden is one the simplest ways of such an energy input. Typically, two types of Joule heating are used in experiments, *viz*., the contact heating, which results in bulk self-heating of the whole sample turning into the thermal explosion (the so-called electrothermal explosion, ETE), and local heating leading to a local ignition and formation of a combustion wave.

The former method was first suggested by Knyazik *et al*.[48] in the mid 1980's. It was further developed and applied to the study of heat liberation kinetics of high-temperature (> 3000 °C) and fast reactions in heterogeneous condensed systems (*e.g*., Ti – C, Ti – B, Ta – C, Ni – Al, *etc*.).[49 – 51]

The latter method referred to as field-activated SHS was elaborated by Munir in the late 1990's.[52] It is used to enhance the completeness of the combustion in the solid flame SHS processes.

Several attempts to produce nanostructured materials making use of the thermal action on the combustion products have been undertaken.[20, 53, 54] In particular, quenching of a burning Ti + 2B mixture allowed production of TiB_2 grains with different sizes depending on the combustion front position.[53] The grain growth proceeded very fast resulting in a size change by one order of magnitude (see Fig. 1).

1. Mechanochemical self-propagating high-temperature synthesis

The SHS of nanosized materials can most efficiently be influenced by mechanical actions. These include mechanical treatment of a burden, mechanical action on a burning sample and mechanical treatment of products. All three methods give interesting results.

Mechanical activation of reactants before the initiation of the SHS process is a very important stage. This increases the reactivities of the particles that are treated due to an increase in the defect concentration and/or the reaction area (due to a decrease in the particle size). Therefore, the mechanical activation prepares the particles for the active involvement in the reaction. Its maximum effect is observed in the case of 'ideal' [55] solid flame SHS processes. For the liquid-phase SHS, such an effect can be either weak or even totally absent.

The mechanical activation can influence the velocity and conditions of the combustion front propagation (macrokinetic effect) as well as the shape and size of the crystallites and porosity of the structure (structural effect).

A control over processes of the wave propagation and of the structure formation in the product is a challenging task. To date, only the problems of the initiation of the SHS in weakly exothermic systems and of a decrease in the size of crystallites of the combustion products have been resolved.

Several examples of the influence of the mechanical activation on the course of the SHS are given below.

Preparation of titanium carbide with the composition $Ti_{44}C_{56}$ from a mixture of powdered Ti and C has been described.[56] Prior to the initiation of the SHS process, Ti and C powders were mechanically activated in a ball mill. The titanium carbide particles produced represented polycrystals with the size of ~ 0.5 μm composed of crystallites with the size of ~ 3 nm. It is very likely that subsequent mechanical or thermochemical processing of the product can result in a powder containing true nanosized particles. Note that the product can be formulated as $TiC_{1.27}$ or $Ti_{0.79}C$, which corresponds to carbon overstoichiometry. Therefore, the Ti sublattice of the product should have numerous defects (vacancies). This result is new in principle, which requires, in our opinion, a careful verification.

A mechanochemical synthesis of β-SiC starting from powdered Si and C has been accomplished.[57] It was shown that mixing of the starting reactants in a ball mill resulted in the full conversion of Si and C to β-SiC (100% degree of conversion). The product formed had a homogeneous structure with the grain size of ~ 7 nm.

A titanium carbide powder with the particle size of 30 nm has been produced by pressure-assisted sintering.[58] The deformation temperature of the resulted nanosized powder is 500 °C lower than the conventional temperature. The same authors reported a synthesis of nanostructured TiB_2.[59] The microstructure of the product and the particle size distribution therein are shown in Figs 7 and 8, respectively.

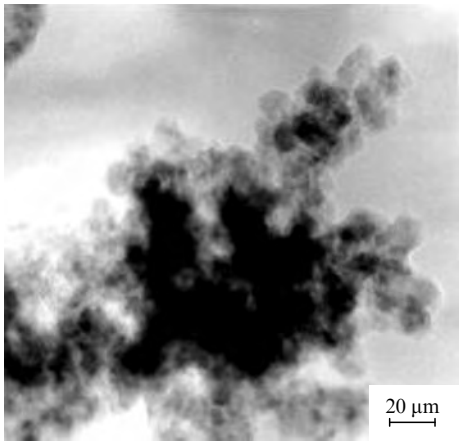

Figure 7. The microstructure of TiB_2.[59]

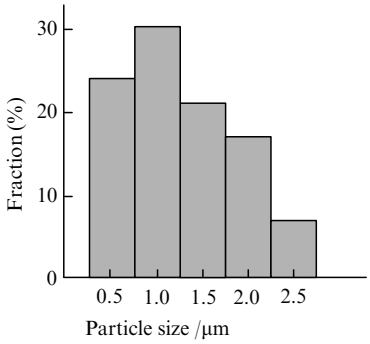

Figure 8. Size distribution of TiB_2 particles.[59]

Grinding of combustion products is an efficient way to produce nanosized particles. For instance, mixing and ball milling of powdered silicon and titanium with the particle sizes of 25 – 30 μm and 44 μm, respectively, yielded a series of silicides $TiSi_x$ (where x is defined by the ratio of the reactants) with a particle size less than 100 nm.[60] In cases of high Si content in the reaction mixture (34 at.% – 60 at.%), the reaction proceeds in the thermal explosion mode. During the mechanical activation, disintegration of the reactants occurs, which is accompanied by formation of grains of products with the following compositions: $Ti_{33.4}Si_{66.6}$, $Ti_{62.5}Si_{37.5}$,$Ti_{50}Si_{50}$ and $Ti_{55.6}Si_{44.4}$. For lower silicon contents, the components interact slowly giving an amorphous product. This process is especially interesting since it provides an example of a control over the final structure of the target powders.

Syntheses of various compounds (*e.g*., TiN) and alloys (*e.g*., Fe – Al – Cr) using mechanical activation have been described.[61 – 63] Unfortunately, the thermal patterns of the proc-

esses (*i.e.*, emergence of heating centres, thermal explosion, flame propagation, *etc.*) were not analysed.

The mechanical activation was shown[64] to have a great potential for the self-propagating high-temperature synthesis of metal alloys (*e.g.*, Ni–Al, Ni–Si, Ni–Ge, Ti–Ni) and oxides [*e.g.*, Ba–Zr(Ti, Hf, Mo, W, Al)–O, Ca–Mo–O, Sr–Mo–O, Pb–Mo–O, *etc.*]. The influence of the mechanical activation of both the reactants and the products was carefully studied and the industrial applicability of the technique was convincingly demonstrated. It was noted that even brief mechanical activation allows production of homogeneous monophasic nanosized powders of complex oxides, nitrides, borides, carbides, and so on with a particle size of ~ 10 nm. It was concluded that metastable phases normally formed as a result of the mechanical activation can be produced from equilibrium intermetallide products of the SHS as well.

A dedicated study aimed at the preparation of nanosized composite powders in the system TiB_2-TiAl_3 starting from powdered Ti, Al and TiB_2 has been conducted.[65] Prior to the SHS, the powder mixtures containing Al–50 at.% Ti and Al–25 at.% Ti–10 vol.% TiB_2 were first activated mechanically in a ball mill and then heated at the rate of 0.33 K s^{-1} and maintained *in vacuo* at various temperatures. After that, flashing and compaction of the mechanical mixtures *in vacuo* were followed by their heating to the sintering temperature. The microstructures of the final products TiB_2-TiAl_3 are shown in Fig. 9. Nanosized grains of TiB_2 (25 nm) are well-resolved in the microphotography (see Fig. 9 *b*).

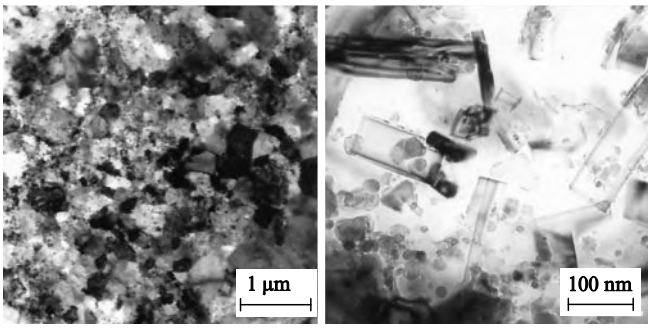

Figure 9. The microstructure of TiB_2-TiAl_3 nanocomposites;[65] (*a*) $TiAl_3$ grain, (*b*) TiB_2 grain.

The dependence of the size of the product grains on the duration of the mechanical treatment is plotted in Fig. 10 for the two systems, *viz.*, Al–50 at.% Ti (*a*) and Al–25 at.% Ti–10 vol.% TiB_2 (*b*). It is clearly seen that in the case of the Ti–Al system (see Fig. 10 *a*), prolonged mechanical treatment leads only to an insignificant increase in the grain size apparently approaching saturation, whereas in the Ti–Al–TiB_2 system (see Fig. 10 *b*), the grains become noticeably smaller after longer treatments under conditions of the isothermal storage at 973 K. Therefore, the effect of the addition of TiB_2 on the growth of $TiAl_3-TiB_2$ grains is revealed.

2. Gravity and shock-wave actions on the SHS products

In order to control the grain structure of materials, one can take advantage of gravity, which can lead to both the increase and decrease in the grain size of the combustion products.

The influence of the load factors on the microstructure has recently been demonstrated[66] for a $TiC-Cr_3C_2-Ni-Mo$ composite material (*i.e.*, a complex titanium–chromium oxide with a nickel–molybdenum binder) prepared by SHS from a powdered mixture of titanium, chromium, nickel and molybdenum oxides with aluminium and carbon (as soot or graphite). The grain size of

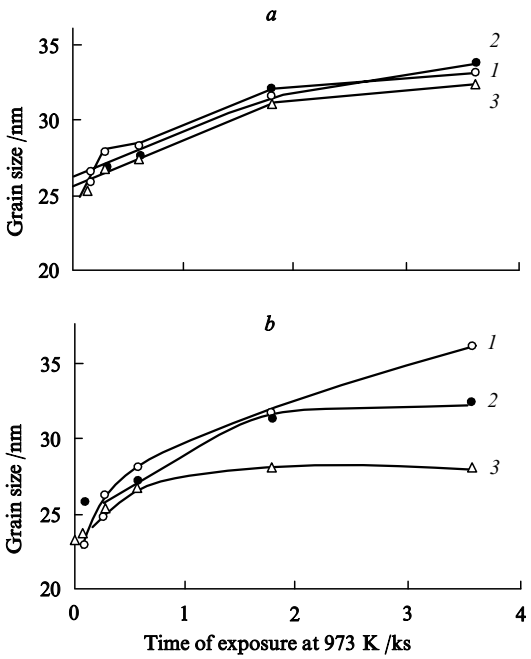

Figure 10. Grain size *vs.* duration of the mechanochemical treatment dependences for two systems: Al–50 at.% (Ti) (*a*) and Al–50 at.% Ti–TiB_2 (*b*).[65]
Duration of mechanical activation /ks: (*1*) 180, (*2*) 360, (*3*) 2880.

the solid product formed is plotted in Fig. 11 as a function of the load factor applied. It was established that this affects not only the microstructure but also the combustion rate and temperature along with the phase and chemical composition of the product. For instance, on going from the load factor of 10 g to 500 g, the content of bound carbon in the material was either increased 1.5-fold (if soot was taken as a reactant) or, *vice versa*, decreased more than two-fold (if coarse-grain graphite was used). This is explained by the gravity-assisted segregation of the reactants in the combustion wave under the action of the load factor.

The formation of unusual structures upon combustion of a NiO–Ni–Al system has been reported.[67] This experiment was conducted aboard the space station 'Mir' under microgravity conditions. As a result of the zero gravity, the molten intermetallide combustion product NiAl was deposited as large drops onto the surface of the oxide phase Al_2O_3 giving rise to mushroom-shaped crystallites (Fig. 12).

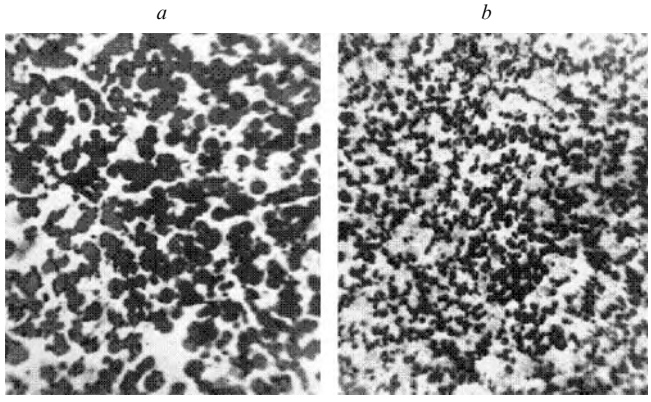

Figure 11. Effects of the load factor on the microstructure of the $TiC-Cr_3C_2$ + Ni–Mo system.[66]
(*a*) load factor of 100 g, (*b*) load factor of 1000 g.

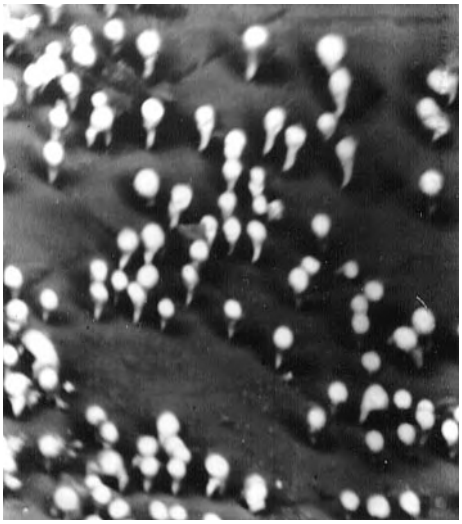

Figure 12. The formation of the NiAl intermetallide phase on the surface of the Al_2O_3 oxide phase under conditions of the zero gravity.[67]

A shock wave can be applied to reactants in the course of the SHS or to reaction products after its completion as an alternative means of the mechanical activation. The effects of shock waves on reactants at a certain stage of the process are different depending on the shock wave amplitude, loading diagram and characteristics of heat dissipation. All other parameters being the same, an increase in the pressure first leads to compaction and deformation of reactants (no chemical reactions are yet initiated). Upon further increase in the pressure, the concentration of structural defects is increased and an intense intermixing and heating of the reactants occurs, which leads to the initiation of the chemical reaction. Shear strains present in the shock wave front disintegrate the product so that only very fine particles are formed. A control over the heavily strained state of the matter that develops upon the shock-wave action would make it possible to deliberately change the chemical composition thus producing materials with preset characteristics at lower energy consumption.

Shock-wave compaction of titanium carbide prepared by the SHS has been reported.[68]

An attempt has been undertaken [69] to combine the SHS with the shock-wave load in the synthesis of titanium carbide. The size of the product grains produced in this experiment did not exceed 1 μm. The authors asserted that titanium carbide prepared in this way manifested improved mechanical properties. Such an approach has also been applied to syntheses of other carbides,[68–71] intermetallides [72, 73] and silicides.[74–79] However, according to the data reported, no nanostructures could be obtained upon the direct shock wave action on a sample during the SHS. Therefore, grinding of the final product remains the most suitable solution of the problem.

3. Self-propagating high-temperature synthesis in electric and magnetic fields

The effects of the electric and magnetic fields on the course of the SHS have been studied. In particular, in the SHS of tantalum carbide, the starting powders of Ta and C were mechanically activated and simultaneously subjected to the electric field.[80]

$$\text{Ta (45 μm)} + \text{C (13 nm)} \longrightarrow \text{TaC (30–50 nm)}.$$

This solid-phase system (neither solid reactants nor the products melt during the SHS) is characterised by a linear increase in the combustion rate and temperature with an increase in the electric field strength. The degree of conversion can be increased (*i.e.*, the underburning degree can be reduced) using Joule heating. It was found that two types of particles (*viz.*, rounded and

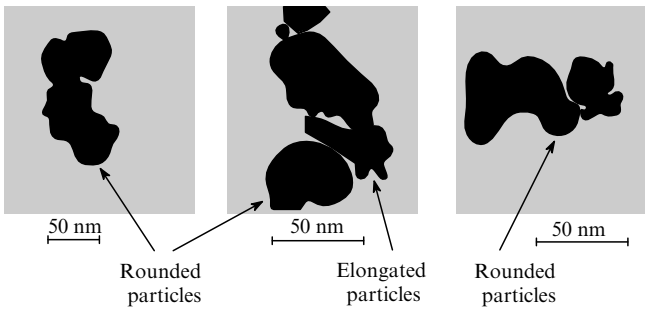

Figure 13. The microstructure of nanosized TaC particles as a function of the electric field strength.[80]
E /V cm^{-1}: 6.92 (*a*), 14.61 (*b*), 30.33 (*c*).

elongated, Fig. 13 *a*, *b*) are formed as a result of the SHS. Presumably, the particles tend to acquire a rounded shape at stronger electric fields. The composition of the product is also affected by the electric field strength. Indeed, the final product is composed of Ta_2C and TaC particles when the synthesis is performed at weak electric fields whereas only TaC particles are found at strong fields.

A procedure for the preparation of nanosized $MoSi_2$ by SHS combined with the mechanical activation and the electric field action has been described.[81] For the synthesis of molybdenum disilicide, a mixture of Mo and Si powders was used:

$$\text{Mo (150 μm)} + \text{Si (45 μm)} \longrightarrow \text{MoSi}_2\text{ (68–75 nm)}.$$

First, the Mo and Si powders were mechanically activated, then compacted, subjected to the electric field and ignited. The mechanical mixtures (Mo + Si) represented agglomerates with the sizes ranging from 0.2 to 200 μm composed of nanosized crystallites of molybdenum and silicon. According to powder X-ray diffraction data, the molybdenum and silicon particles had the sizes of 54 nm and 34 nm, respectively (note that the size of Mo crystallites varies in the range from 5 to 100 nm). The authors compared structures of the $MoSi_2$ products prepared by two routes, *viz.*, by combining the SHS with the mechanical activation (MASHS) and a complex approach involving mechanical activation, SHS and action of the electric current of up to 1500 A (MAFAPAS, Fig. 14). In the former case, the size of $MoSi_2$ grains reached 45 nm whilst in the latter case, 73 nm.

Yet another $MoSi_2$ synthesis has been reported.[82] In this work, the influence of the mechanical and electric activation on the formation of a dense $MoSi_2$ ceramics was elucidated. Finer Mo powders (3–7 μm) were taken for the synthesis. Prior to the SHS initiation, the reactants were mechanically activated in a

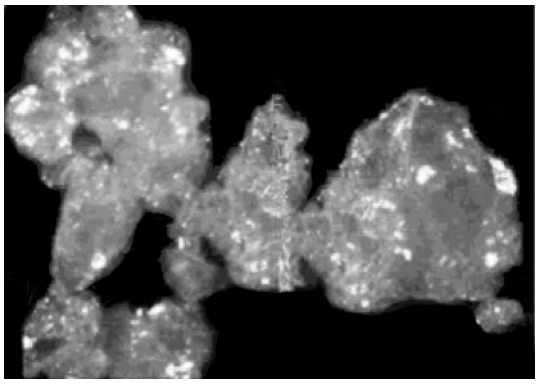

Figure 14. Nanocrystalline $MoSi_2$ produced from Mo and Si powders using the mechanical activation and electric field action.

planetary ball mill, compacted and then subjected to the electric field. The size of crystallites in the dense ceramics produced was ~ 20 nm.

The method applied to the preparation of the starting powders for this SHS process is worth a special note. The Mo and Si powders were ground in separate planetary ball mills. The size of the molybdenum particles decreased from 3–7 μm down to 20–110 nm depending on the milling conditions. With an increase in the duration of the mechanical treatment and in the electric field strength, the grain size decreased. This technique is of potential use in the technology of nanopowders.

The SHS method combined with mechanical activation of reactants has been utilised for the preparation of a composite based on $TiAl_3$ with Al_2O_3 inclusions.[83] Sintering of Ti and Al powders was conducted on a support, through which electric current passed. The growth of grains during sintering was decelerated by the presence of Al_2O_3 particles. The composite material produced had the grain size of ~ 10 nm. The authors noted that a decrease in the particle size resulted in the enhancement of the composite mechanical properties.

Synthesis of an AlN–SiC composite from powdered α-Si_3N_4, Al and C has been described.[84]

$$\alpha\text{-}Si_3N_4\,(0.5\ \mu m) + Al\,(7\ \mu m) + C\,(10\ \mu m) \longrightarrow$$

$$\longrightarrow AlN - SiC\ (< 100\ nm).$$

The synthesis included the following steps (Fig. 15): compaction of the starting Si_3N_4, Al and C powders, formation of blanks for the SHS process, induction heating followed by the thermal explosion turning into the SHS. As a result, a solid solution of AlN–SiC in Si_3N_4–Al–C was produced.

The authors analysed the mechanism of the formation of the AlN–SiC solid solution as a function of the electric field strength. They found that dissolution of silicon nitride in molten aluminium occurs in the first stage and only after that nitridation of aluminium starts. The reaction proceeds in the temperature range from 600 °C (melting point of aluminium) to 1400 °C.

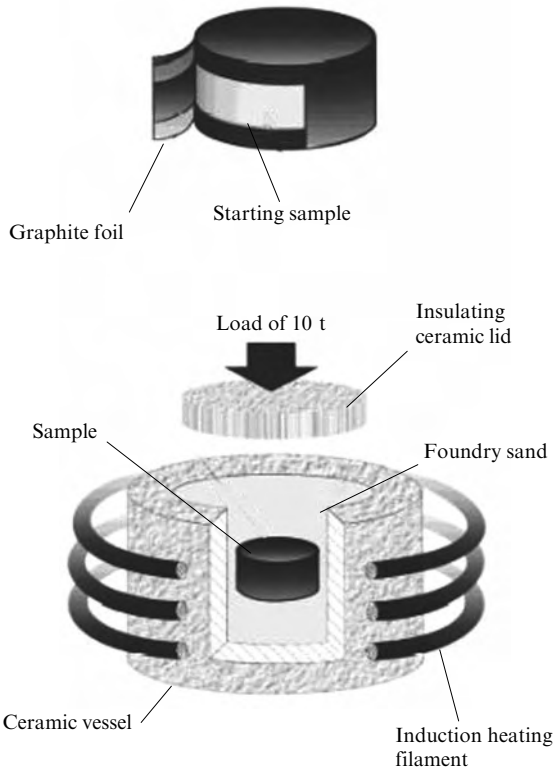

Figure 15. Experimental setup for the SHS of a solid solution of AlN – SiC in Si_3N_4–Al–C.[84]

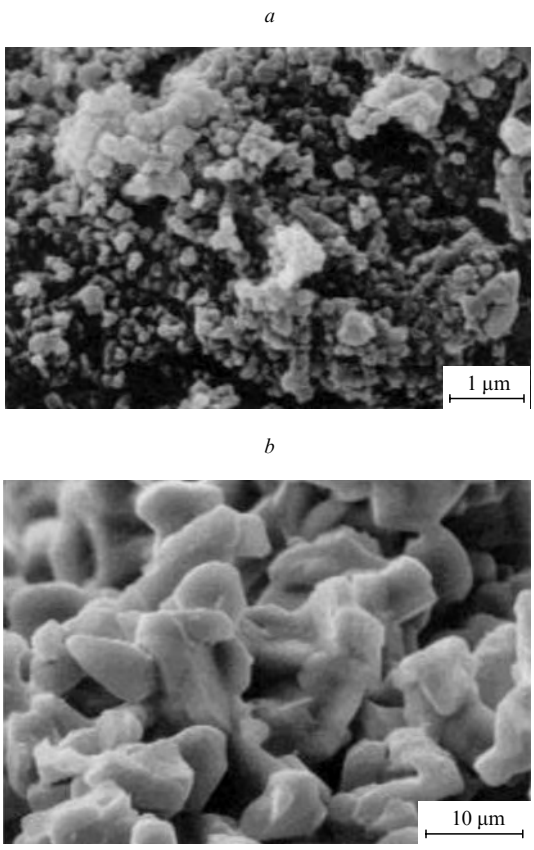

Figure 16. The microstructures of two solid solutions of AlN–SiC in Si_3N_4–Al–C produced at 1750 °C (*a*) and heated to 1850 °C (*b*).[84]

It is noteworthy that the microstructure of the product varies substantially depending on the annealing temperature of the product. The microstructures of solid solutions produced at temperatures of 1750 °C and 1850 °C are shown in Figs 16 *a* and 16 *b*, respectively. The authors did not perform a precise determination of the particle size, but, in their opinion, particles smaller than 100 nm were present in the solid solution.

The efficiency of the mechanical activation in the synthesis of nanosized powders by the SHS has recently been demonstrated [85] in the preparation of nanocrystalline $NbAl_3$ powders. The process was implemented in two steps: the mechanical activation of the starting Nb and Al powders was followed by the SHS. The powders were ground in a mill, compacted and then the SHS was initiated *in vacuo*. It is of note that agglomerates as large as 100 μm were present in the burden after the mechanical activation, which however disappeared after the completion of the SHS. The combustion product contained $NbAl_3$ particles with a size of ~ 60 nm.

Studies devoted to the preparation and compaction of iron powders have recently been reviewed.[86] The authors discuss features of the microwave-induced ‡ syntheses of iron powders and classify diverse methods of the preparation of nanocrystalline iron powders and of ceramic nanopowders (Table 2). They note that all the preparative techniques (except for that based on the microwave technique) are characterised by low performance. Additionally, not all of the techniques allow preparation of powders with the uniform size distribution. The authors conclude

‡ The microwave-induced synthesis can be considered as a modification of the SHS since it involves a stage of a self-propagating reaction that is initiated after ignition of the burden.

Table 2. The methods for the synthesis of ceramic nanopowders.[86]

Method of synthesis	Products
Mechanical activation in ball mills	Fe, Co, Ni, NiAl, TiAl, FeSn
Synthesis under laser irradiation	AlN, MnO_2, TiO_2, Ti
Condensation from a gas-phase	Fe, MgO, Cu, TiO_2
Sputtering deposition	Al, Cu, Mn
Chemical deposition	SiC, $BaTiO_3$, W–Cu, Mo–Cu
Plasma induction	Fe, AlN, Cu, metal borides, nitrides and carbides
Microwave plasma	Fe, Co, Mo, Ni, TiO_2, ZrO_2,Al_2O_3

that the microwave-induced synthesis of powders is the most cost-efficient method for the preparation of powders with the particle size of 10–15 nm.

Methods for the preparation of nanosized niobium aluminide using SHS preceded by the mechanical activation of the burden have been surveyed recently.[87] Different modes of the mechanical activation as applied to the synthesis of iron aluminides by the SHS have been considered.[88] The following scheme of the technological process was suggested: preparation of a mixture in a ball mill, formation of cylindrical blanks for the SHS, combustion of the blanks with the online monitoring by means of synchrotron radiation. The results of this monitoring are summarised in Table 3. It was found that the mechanical treatment of the initial mixture reduces the ignition temperature by more than 100 °C.

Table 3. Powder X-ray diffraction data on the phase composition of different cross-sections of an iron aluminide sample prepared by the SHS.[88]

Probing depth /mm	Phases revealed	Crystallite size /nm
0 (surface of the sample)	FeAl, Fe_2O_3, Fe_2Al_5	–
0.5	FeAl, Fe_2O_3	25
1.5	FeAl	40
2.5	FeAl	35
3.5	FeAl	25
4.5	FeAl	35
5.0 (back side of the sample)	FeAl, Fe_2O_3, Fe_2Al_5	–

The SHS of titanium nitride upon grinding of titanium in a ball mill in a nitrogen atmosphere has been investigated.[63] During the process, the system ignited, *i.e.*, a local thermal explosion occurred, which gave rise to a propagating combustion wave. The authors assume that there is a critical size of titanium particles (80 Å), just below which the system is ignited. Selected results of this study are given in Fig. 17 and Table 4.

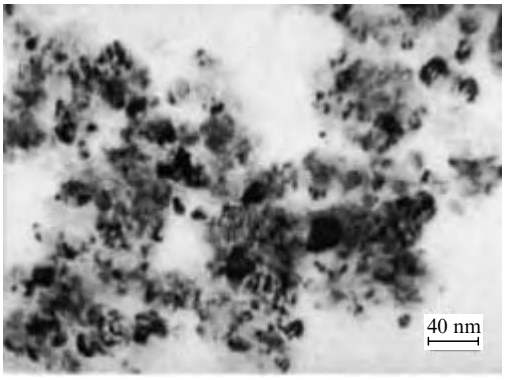

Figure 17. The microstructure of a titanium powder mechanically activated for 492 min.[63]

Table 4. The influence of the duration of mechanical activation on the nitrogen content and on the titanium and titanium nitride crystallite sizes in the sample.[63]

Duration of the mechanical activation /min	c_N (at.%)	d_{101} Ti /Å	d_{200} TiN /Å
Pressure of 11 Bar			
0	–	810	–
31	5.9	166	–
60	9.4	113	76
77	13.5	87	76
85	16.1	84	76
94	43.5	–	155
129	43.7	–	96
240	48.5	–	88
Pressure of 1.5 Bar			
0	–	810	–
60	5.8	134	–
91	9.9	89	76
131	24.0	80	75
152	40.3	–	78
185	42.2	–	84
256	43.9	–	77
492	50	–	76

Therefore, the mechanical activation is one of the most important processes in the technology of nanoparticles. The majority of numerous studies performed in this field confirm the great potential of various methods of activating the SHS aimed at the preparation of nanomaterials (as regards both powdered and compact products).[88–92]

4. Self-propagating high-temperature synthesis in thin films and in systems with nanosized reactants

The self-propagating high-temperature synthesis in thin films and in systems with nanosized reactants is a very new direction within the SHS.[93–97] Multilayer nanofilms built up of hundreds or thousands of alternating layers (each having a thickness of 1–100 nm) are very promising for the design of novel materials and coatings. They often exhibit unique properties. In particular, the hardness of a multilayer film can substantially exceed that of a single layer approaching the hardness of diamond. As has been established quite recently, autowave processes analogous to the gas-free combustion can be initiated in some multilayer films.[98] The velocity of the wave propagation can in such cases reach a few meters per second. To date, self-sustained reaction waves have been observed for several films composed of hundreds of alternating nanolayers, such as Al/Monel 400 (see Ref. 98) and Nb/Si.[99]

Previously, the gas-free combustion has been detected in layered systems built up of alternating Ni and Al foils with the thicknesses of 50 μm.[94] Combustion waves have also been observed in two-layer films prepared by electrochemical deposition [100] or vacuum deposition of a metal vapour.[97] In those films, the layer thickness was in the range from 0.1 to 200 μm.

The gas-free combustion in multilayer Ti/Al films has been studied [95] with the emphasis put on the elucidation of the structure formation in the reaction products (Fig. 18). A previously unknown effect of an inheritance of the preferable crystallographic orientation of the reactants by the gas-free combustion products was revealed.

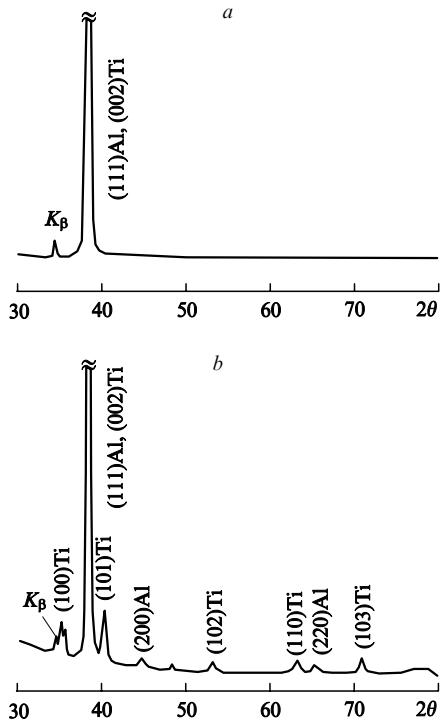

Figure 18. Powder diffraction patterns of the initial multilayer foil (*a*) and of the synthesis product (*b*).
Planes of the close packings of atoms in the initial foil and in the product are parallel to the sample surface.[95]

Combustion of films composed of 150 layers of titanium and aluminium (with the thickness of a single layer of 100 nm and the total thickness of 15 μm) in the SHS mode results in the formation of nanosized two-phase product containing TiAl and Ti_3Al.

First attempts to apply the SHS in thin films with a gradient composition have been undertaken [101] to solve the problem of hardening of composite armors (which is of military significance) (Fig. 19).

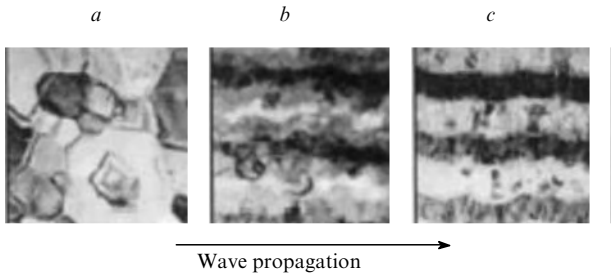

Figure 19. Microphotographs of the evolution of multilayer nanofoils during the SHS
Foils after the reaction (*a*), at the moment of the reaction (*b*), before the reaction (*c*).

The current status of investigations in the field of preparation of multi-component nanostructured thin (~1 nm) films has recently been reviewed.[102]

Nevertheless, it is the SHS using nanosized reactants that found most widespread applications in the synthesis of nanosized products. Primarily, this is due to the simplicity of the approach. Essentially, this implies that the reactants, on the one hand, serve as crystallisation centres and, on the other hand, suppress growth of the product grains.

The influence of the electric field on the morphology of products has been discussed [80] for a case reaction of Ta with C giving rise to TaC particles.[80] The use of a nanosized carbon powder (13 nm) allowed the authors to obtain tantalum carbide with the particle size of 30–50 nm.

Similar results have been reported for syntheses of Al_2O_3–TiAl–Ti_3Al composites [103] as well as of other inorganic powders doped with nanosized particles (ZrO_2, Al_2O_3, W, WC, NbC, *etc.*).[104,105]

The formation of nanosized particles as combustion products have also been confirmed in a series of SHS processes [19, 26, 80, 103, 105, 106] utilising nanosized reactants (*e.g.*, Y_2O_3, ZrO_2, TiO_2, C, *etc.*) (Table 5).

Table 5. Examples of nanosized materials produced by the SHS using nanosized reagents.

Product	Particle size /nm	Ref.
ZrO_2	8–12	106
Ti–H, Zr–H, Ti–N–H, Zr–N–H, Ti–Zr–N–H	<50	26
Al_2O_3–TiC–ZrO_2	10–20	19
(Ti, Cr)C–Ni	500–1500	105
Al_2O_3–TiAl–Ti_3Al	<100	103
TaC	30–50	80

Sol–gel processes and precipitation from solutions are further examples of the use of nanosized reactants for the synthesis of nanomaterials. Essentially, these processes imply conversion of a liquid into a gel (as a result of hydrolysis coupled with polycondensation) and further to a glass, monolithic composite, powder or thin coating (as a result of heating or combustion at relatively low temperatures). The sol–gel technology has several drawbacks related to the high costs of starting materials and to the large shrinkage of gels upon drying and sintering.

Synthesis of a widespread dielectric, $BaTiO_3$, from different precursors, such as BaO_2, $Ba(NO_3)_2$ and $Ba(OAc)_2$, using carbohydrazide, glycine or citric acid as a combustible material has been described in a recent review.[107] The combustion reaction was conducted in the presence of titanyl nitrate. Yet another review [108] lists nanocrystalline oxides (with the particle size of 10–35 nm) prepared by combustion of aqueous solutions containing metal and ammonium nitrates and redox mixtures.

Among chemical processes exploited for the preparation of nanomaterials, the self-propagating low-temperature synthesis is worth a special note. It is realised most easily in gas-releasing systems. For instance, titanyl hydrazinecarboxylate $TiO(N_2H_3COO)_2 \cdot 2H_2O$ undergoes an autocatalytic exothermic decomposition upon heating in air up to 300 °C, which proceeds in the combustion mode and is accompanied by liberation of large amounts of gases, *i.e.*, N_2, CO_2, H_2O. As a result of the reaction, a nanosized TiO_2 powder (8 nm) is formed, which is characterised by high free surface area (110 $m^2\ g^{-1}$). The formation of TiO_2 is described by the following equation:

$$TiO(N_2H_3COO)_2 \cdot 2H_2O \longrightarrow TiO_2 + 2N_2 + 2CO_2 + 5H_2O.$$

The SHS can also be realised in stages of condensation, coagulation and drying of the final product. Different modifications of these techniques are considered elsewhere.[109, 110]

VI. Conclusion

The self-propagating high-temperature synthesis of nanosized materials is a relatively new research field. Its active development was stimulated by a common enthusiasm regarding nanomaterials. Summarising the results discussed in this review, we conclude that the SHS is indeed an efficient route giving rise to nanosized

materials despite high temperatures of the process that typically favour growth of crystallites. Among factors beneficial for the formation of nanosized particles in combustion products, the following are of primary importance: utilisation of nanosized reactants; multitude of nuclei actuating the crystallisation (or condensation) of reaction products; control over the rate of cooling of combustion products; the action of crystallisation, recrystallisation and chemical condensation processes on the SHS; self-limitation of the crystallite growth in multiphase combustion products.

Potential applications of various types of the SHS aimed at the preparation of nanomaterials have not been equally explored. The area most studied is the mechanochemical SHS whereas the gas-phase SHS is the least investigated.

It is the experimental conditions leading to the formation of nanomaterials that attracted major attention of researchers. At the same time, specific properties of SHS-materials and advantages of their practical use are insufficiently represented in the scientific literature (though it is also true for nanomaterials produced by other methods).[111,112] Enhancements of properties of nanomaterials synthesised by the SHS (first of all, as regards their high inclination to sintering and compaction) has been documented by only a few researchers.[113–116] The mechanism and kinetic characteristics of the formation of nanomaterials by the SHS remain virtually unexplored. A quest for the most efficient ways to control the structure formation in combustion products along with investigations into the structure–property relations for the substances produced are promising directions of prospective studies.

References

1. A G Merzhanov, I P Borovinskaya *Dokl. Akad. Nauk SSSR* **204** 366 (1972) [a]
2. A G Merzhanov, in *Fizicheskaya Khimiya: Sovremennye Problemy* (Physical Chemistry: Modern Problems) (Ed. Ya M Kolotyrkin) (Moscow: Khimiya, 1983) p. 8
3. A N Pityulin, Yu V Bogatov, A S Rogachev *Int. J. Self-Propag. High-Temp. Synth.* **1** 111 (1992)
4. A S Shteinberg, M A Ponomarev, V A Raduchev, O V Uchakovskii, Yu A Sapronov *Int. J. Self-Propag. High-Temp. Synth.* **4** 149 (1995)
5. V I Yukhvid *Pure Appl. Chem.* **64** 977 (1992)
6. A G Merzhanov, A S Rogachev, E N Rumanov, V N Sanin, A E Sytschev, V A Shcherbakov, V I Yukhvid *Kosm. Issled.* **39** 226 (2001)
7. A G Merzhanov, A S Rogachev, A E Sytschev *Dokl. Akad. Nauk* **362** 217 (1998) [a]
8. F Bernard, E Gaffet *Int. J. Self-Propag. High-Temp. Synth.* **10** 109 (2001)
9. Yu G Morozov, M V Kuznetsov, A G Merzhanov *Int. J. Self-Propag. High-Temp. Synth.* **6** 1 (1997)
10. I P Borovinskaya, in *Kontseptsiya Razvitiya Samorasprostranyayushchegosya Vysokotemperaturnogo Sinteza kak Oblasti Nauchno-Tekhnicheskogo Progressa* (The Concept of Development of Self-Propagating High-Temperature Synthesis as a Field of Scientific and Technological Progress) (Chernogolovka: Territoriya, 2003) p. 178
11. R G Aivazyan, V V Azatyan, V I Kalachev, V I Rubtsov *Fiz. Goren. Vzryva* (4) 85 (1994) [b]
12. V V Azatyan, A G Merzhanov, in *Khimicheskaya Fizika na Poroge XXI Veka* (Chemical Physics on the Threshold of the XXIth Century) Vol. 2 (Moscow: Nauka, 1996) p. 13
13. V V Azatyan *Usp. Khim.* **68** 1122 (1999) [*Russ. Chem. Rev.* **68** 1021 (1999)]
14. E Zhou, S Bhaduri, I R Griffiths *Int. J. Self-Propag. High-Temp. Synth.* **7** 317 (1998)
15. S Bhaduri, S B Bhaduri, E Zhou *J. Mater. Res.* **13** 156 (1998)
16. C C Chen, C L Li, K Y Liao *Mater. Chem. Phys.* **73** 198 (2002)
17. J Peng, J Binner, S Bradshaw *J. Mater. Synth. Process.* **9** 363 (2001)
18. K G Shkadinskii, N I Ozerkovskaya, A G Merzhanov *Dokl. Akad. Nauk* **381** 763 (2001) [a]
19. Q Dong, Q Tang, W C Li, R Y Wu *J. Mater. Res.* **16** 2494 (2001)
20. A G Merzhanov, A S Rogachev *Pure Appl. Chem.* **64** 941 (1992)
21. D Kata, J Lis, R Pampuch, L Stobierski *Int. J. Self-Propag. High-Temp. Synth.* **7** 475 (1998)
22. L Stobierski, Z Wegrzyn, J Lis, M Bucko *Int. J. Self-Propag. High-Temp. Synth.* **10** 217 (2001)
23. H Chen, Y Cao, X Xiang, J Li, C Ge *J. Alloys Compd.* **325** L1–L3 (2001)
24. R Pampuch *J. Eur. Ceram. Soc.* **19** 2395 (1999)
25. H G Hakobyan, S K Dolukhanyan *Int. J. Self-Propag. High-Temp. Synth.* **3** 299 (1994)
26. V Sh Shekhtman, S K Dolukhanyan, G E Abrosimova, K A Abrahamyan, A G Aleksanyan, N N Aghajanyan, O P Ter-Galstyan *Int. J. Hydrogen Energy* **26** 435 (2001)
27. I P Borovinskaya, T I Ignat'eva, V I Vershinnikov, G G Khurtina, N V Sachkova *Neorg. Mater.* **39** 698 (2003) [c]
28. I P Borovinskaya, G A Vishnyakova, L P Savenkova *Int. J. Self-Propag. High-Temp. Synth.* **1** 560 (1992)
29. N F Calcott, W A Felder, in *Book of Abstracts of the First International Symposium on SHS, Alma-Ata, 1991* p. 38
30. K A Devis, K Brezinsky, I Glassman *Combust. Sci. Technol.* **77** 171 (1991)
31. R L Axelbaum, D P DuFaux, C A Frey, K F Kelton, S A Lawton, L J Rosen, S M L Sastry *J. Mater. Res.*, **11** 948 (1996)
32. D P DuFaux, R L Axelbaum *Combust. Flame* **100** 350 (1995)
33. R L Axelbaum, J I Huertas, C R Lottes, S Hariprasad, S M L Sastry *Mater. Manufact. Process.* **11** 1043 (1996)
34. R L Axelbaum, B H Chao, in *Proceedings of the Fourth International Workshop on Microgravity Combustion, Cleveland, 1997* p. 37
35. V V Azatyan, R G Aivazyan, A G Merzhanov *Mendeleev Commun.* 188 (1994)
36. V V Azatyan, R G Aivazyan, V I Rubtsov, A G Merzhanov *Kinet. Katal.* **35** 30 (1994) [d]
37. Yu M Grigor'ev, A G Merzhanov *Int. J. Self-Propag. High-Temp. Synth.* **1** 600 (1992)
38. Appl. 01 514 900 Europe (1985)
39. N D Ageev, Ya I Vovchuk, S V Goroshin *Fiz. Goren. Vzryva* (6) 54 (1990) [b]
40. A N Zolotko, Yu I Vovchuk, N I Poletaev, A V Florko, I S Al'tman *Fiz. Goren. Vzryva* (3) 24 (1996) [b]
41. R L Axelbaum, J I Huertas, C R Lottes, S Hariprasad, S M L Sastry *Mater. Manufact. Process.* 1997
42. M S Wooldridge, S A Danczyk, J F Wu *Nanostruct. Mater.* **11** 955 (1999)
43. I S Altman, D Lee, J D Chung, J Song, M Choi *Phys. Rev. B* **63** 161402 (2001)
44. Y L Li, Y Liang, F Zheng, X-F Ma, S-J Cui *J. Mater. Res.* **15** 988 (2000)
45. Y G Cao, X L Chen, Y C Lan, Y P Xu, T Xu, J K Liang *J. Mater. Res.* **15** 267 (2000)
46. Y C Kang, D J Seo, S B Park, H D Park *Jpn. J. Appl. Phys., Part 1* **40** 4083 (2001)
47. C C Hwang, C Y Weng, W C Lee, S L Chung *Int. J. Self-Propag. High-Temp. Synth.* **6** 419 (1997)
48. V A Knyazik, A G Merzhanov, V B Solomonov, A S Shteinberg *Fiz. Goren. Vzryva* (3) 69 (1985) [b]
49. V A Knyazik, A G Merzhanov, A S Shteinberg *Dokl. Akad. Nauk SSSR* **309** 899 (1988) [a]
50. V A Knyazik, A G Merzhanov, A S Shteinberg, in *Termanal'88. XI CSI Konf. oTermickej Analyze, Vysoke Tatry, 1988* Sekcia A-14, p. 64
51. V A Knyazik, A S Shteinberg, in *Proceedings of the Joint Meeting of the Soviet and Italian Sections of Combustion Institute* (Napoli: Combustion Institute Publ., 1990) p. 4
52. Z A Munir *Z. Phys. Chem.* **207** 39 (1998)
53. A S Rogachev, A S Mukas'yan, A G Merzhanov *Dokl. Akad. Nauk SSSR* **297** 1425 (1987) [a]
54. A S Rogachev, V M Shkiro, I D Chausskaya, M V Shvetsov *Fiz. Goren. Vzryva* (6) 86 (1988) [b]
55. A G Merzhanov *Combust. Sci. Technol.* **98** 307 (1994)

56. M Sherif El-Eskandarany *Metall. Mater. Trans. A* **27** 2374 (1996)
57. M Sherif El-Eskandarany, K Sumiyama, K Suzuki *J. Mater. Res.* **10** 659 (1995)
58. W Weimin, F Zhengyi, Y Runshang *J. Ceram.* **2** 73 (1998)
59. W Weimin, F Zhengyi, Y Runshang, in *Bilateral Symposium on SHS, Wuhan, China, 2002*
60. S Doppiu, M Monagheddu, G Cocco, F Maglia, U Anselmi-Tamburini, Z A Munir *J. Mater. Res.* **16** 1266 (2001)
61. P Nandi, P P Chattopadhyay, S K Pabi, I Manna *Mater. Phys. Mech.* **4** 116 (2001)
62. L He, E Ma *J. Mater. Res.* **11** 72 (1996)
63. F J Gotor, M D Alcalá, C Real, J M Criado. *J. Mater. Res.* **17** 1655 (2002)
64. T Grigorieva, M Korchagin, N Lyakhov *KONA* **20** 144 (2002)
65. K Uenishi, T Matsubara, M Kambara, K F Kobayashi *Scr. Mater.* **44** 2093 (2001)
66. A G Merzhanov, V I Yukhvid, in *Proceedings of the First US-Japanese Workshop on Combustion Synthesis* (Tokyo: Japan National Research Institute Metals Publ. 1990) p. 1
67. A G Merzhanov, V N Sanin, V I Yukhvid *Dokl. Akad. Nauk* **371** 38 (2000) [a]
68. E P Carton, M Stuivinga, A Boluijt *AIP Conf. Proc.* **620** 1127 (2002)
69. J C LaSalvia, L W Meyer, M A Meyers *J. Am. Ceram. Soc.* **75** 592 (1992)
70. Yu A Gordopolov, in *Proceedings of the International Conference AMPT'93, Dublin, 1993* Vol. 1, p. 533
71. Yu A Gordopolov, A G Merzhanov, in *Shock Waves in Materials Science* (Ed. A B Sawaoka) (Tokyo: Springer, 1993) p. 177
72. F D S Marquis, J A Puszynski *Environ. Res. Forum* **1**–**2** 369 (1996)
73. G R Shaik, W W McMilligan *Metall. Mater. Trans. A* **28** 859 (1997)
74. B R Krueger, A H Mutz, T Vreeland *Metall. Trans. A* **23** 55 (1992)
75. K S Vecchio, L H Yu, M A Meyers *Acta Metall. Mater.* **42** 701 (1994)
76. B K Yen, T Aizawa, J Kihara, N Sakakibara *Mater. Sci. Eng., A* **239**–**240** 515 (1997)
77. S-W Jo, G-W Lee, J-T Moon, Y-S Kim *Acta Mater.* **44** 4317 (1996)
78. B K Yen *J. Appl. Phys.* **81** 7061 (1997)
79. B K Yen, T Aizawa, J Kihara *J. Am. Ceram. Soc.* **81** 1953 (1998)
80. O A Graeve, Z A Munir *J. Mater. Res.* **17** 609 (2002)
81. C Gras, F Bernard, F Charlot, E Gaffer, Z A Munir *J. Mater. Res.* **17** 542 (2002)
82. R Orru, G Cao, Z A Munir *J. Mater. Res.* **16** 1439 (2001)
83. K Uenishi, T Matsubara, T Shibutani, K F Kobayashi *Intermetallics* **10** 105 (2002)
84. D Kata, M Ohyanagi, Z A Munir *J. Mater. Res.* **15** 2514 (2000)
85. F Bernard, V Gauthier, E Gaffet, J P Larpin *Int. J. Self-Propag. High-Temp. Synth.* **9** 281 (2000)
86. R Kalyanaraman, S Yoo, M S Krushankara, T S Sudarshan, R J Dowding *Nanostruct. Mater.* **10** 1379 (1998)
87. V Gauthier, F Bernard, E Gaffet, C Josse, J P Larpin *Mater. Sci. Eng., A* **272** 334 (1999)
88. F Bernard, F Charlot, E Gaffet, J C Niepce *Int. J. Self-Propag. High-Temp. Synth.* **7** 233 (1998)
89. S Paris, C Valot, L Gosmain, E Gaffet, F Bernard, Z Munir *J. Mater. Res.* **18** 2331 (2003)
90. V Gauthier, F Bernard, E Gaffet, Z Munir, J P Larpin *Intermetallics* **9** 571 (2001)
91. F Charlot, E Gaffet, F Bernard, Z A Munir *J. Am. Ceram. Soc.* **84** 910 (2001)
92. US P. 6 200 515 (2001)
93. T Weihs, in *Handbook of Thin Film Process Technology* (Delaware: University of Delaware, 1997) Vol. 7, Pt. B, Sect. F
94. V A Shcherbakov, A S Shteinberg, Z A Munir *Dokl. Akad. Nauk* **364** 647 (1999) [a]
95. A E Grigoryan, N G Elistratov, D Yu Kovalev, A G Merzhanov, A N Nosyrev, V I Ponomarev, V I Khvesyuk, P A Tsygankov *Dokl. Akad. Nauk* **381** 1 (2001) [a]
96. V G Myagkov, L E Bykova, G N Bondarenko, F B Myagkov *Tekhn. Fiz.* **47** 1049 (2002) [e]
97. V G Myagkov, L E Bykova *Dokl. Akad. Nauk* **354** 777 (1997) [a]
98. US P. 5 538 795 (1996)
99. M E Reiss, C M Esber, D Van Heerden, A J Gavens, M E Williams, T P Weihs *Mater. Sci. Eng., A* **261** 217 (1999)
100. S G Vadchenko, A M Bulaev, Yu A Gal'chenko, A G Merzhanov *Fiz. Goren. Vzryva* (6) 46 (1987) [b]
101. E S C Chin *Mater. Sci. Eng., A* **259** 155 (1999)
102. D V Shtanskii, E A Levashov *Tsvet. Metallurg.* (3) 52 (2001)
103. D Horvitz, I Gotman, E Y Gutmanas, N Claussen *J. Eur. Ceram. Soc.* **22** 947 (2002)
104. E A Levashov, A E Kudryashov, O V Malochkin *Tsvet. Metallurg.* (5) 68 (2000)
105. E A Levashov, A E Kudryashov, O V Malochkin, T A Sviridova, S A Glukhov, F Gammel, R Zukhentrung *Tsvet. Metallurg.* (3) 44 (2001)
106. K R Venkatachari, D Huang, S P Ostrander, W A Schulze, G C Stangle. *J. Mater. Res.* **10** 748 (1995)
107. T V Anuradha, S Ranganathan, T Mimani, K C Patil *Scr. Mater.* **44** 2237 (2001)
108. K C Patil, S T Aruna, S Ekambaram *Curr. Opin. Solid State Mater. Sci.,* **2** 158 (1997)
109. T Minami, K C Patil *Mater. Phys. Mech.* **4** 134 (2001)
110. R E Juares, D G Lamas, G E Lascalea, N E Walsöe de Reca *J. Eur. Ceram. Soc.* **20** 133 (2000)
111. M C Roco, R S Williams, P Alivisatos (Eds) *Nanotechnology Research Directions: IWGN Workshop Report. Vision for Nanotechnology in the Next Decade* (Dordrecht: Kluwer Academic, 2000)
112. R A Andrievskii *Perspektiv. Mater.* **6** 5 (2001)
113. L Wang, W M Sigmund, S Roy, F Aldinger *J. Mater. Res.* **14** 4562 (1999)
114. L W Wang, S Roy, W Sigmund, F Aldinger *J. Eur. Ceram. Soc.* **19** 61 (1999)
115. F Aldinger, S Prinnz, N Janakiraman, R Kumar, M Christ, M Wienmann, A Zimmermann. *Int. J. Self- Prop. High-Temp. Synth.* **10** 249 (2001)
116. R Pampuch *Int. J. Self- Prop. High-Temp. Synth.* **6** 187 (1997)

[a] — *Dokl. Chem. (Engl. Transl.)*
[b] — *Combust. Explos. Shock Waves (Engl. Transl.)*
[c] — *Inorg. Mater. (Engl. Transl.)*
[d] — *Kinet. Catal. (Engl. Transl.)*
[e] — *Techn. Phys. (Engl. Transl.)*

Russian Chemical Reviews **73** (2) 161 – 184 (2004) © 2004 Russian Academy of Sciences and Turpion Ltd

DOI 10.1070/RC2004v073n02ABEH000788

Acetylenic derivatives of quinones

M S Shvartsberg, I I Barabanov, L G Fedenok

Contents

I.	Introduction	161
II.	Synthesis methods	161
III.	Chemical properties	166
IV.	Conclusion	183

Abstract. Methods for the preparation and various transformations of acetylenic derivatives of quinones, which are key intermediates in the synthesis of fused heterocyclic quinoid structures and some highly unsaturated compounds, are surveyed in detail. The bibliography includes 114 references.

I. Introduction

Quinones belong to a unique class of organic compounds, which have a broad spectrum of practical applications.[1–3] Quinone derivatives are traditionally used as dyes, pigments, photomaterials and pharmaceuticals. In recent years, these compounds have found application also as luminophores, laser media, catalysts for chemical processes, *etc*. The latter half of the 20th century has witnessed a rapidly growing interest in biologically active quinones and quinoid compounds. This interest is associated with the fact that both natural quinones (anthracycline, mitomycin and anthrapyran antibiotics) and a series of structurally simple synthetic derivatives were found to exhibit antitumour activity. Some of these compounds were integrated into medical practice. Later on, it was revealed that quinoid compounds possess other physiological activities, including antibacterial, antiviral and fungicidal activities, and exhibit radiosensitising properties. New classes of antibiotics and biologically active pigments were found. An extensive search for new pharmacophore structures, elucidation of the structure – biological activity relationship for quinoid compounds and the synthesis of complex natural products and their analogues called for an extension and upgrade of the traditional synthetic base for investigation of this class of compounds. The problems to be solved included not only the development and application of new synthetic approaches but also the possible uses of new starting compounds, key intermediates and new reagents.

Systematic studies of acetylenic derivatives of the simplest quinones (benzo-, naphtho- and anthraquinones) were started in the late 1970s and the early 1980s.[4–10] Due to the simultaneous presence of two highly reactive fragments, *viz*., the quinoid moiety and the acetylenic group, influencing each other, these compounds were considered as intermediates in the synthesis of more complex quinoid structures. It was also expected that some acetylenic derivatives could be used as precursors of highly reactive unsaturated compounds of other classes. Besides, the possibility that these compounds, particularly, functionally substituted derivatives, could exhibit targeted biological action was not ruled out.

Extensive experimental data on the chemistry of alkynylquinones are presently available. Procedures were developed for the synthesis of these compounds, their chemical characteristic features were revealed and new chemical reactions were discovered and studied. However, the available data on the chemistry of alkynylquinones were not generalised. The aim of the present review is to close this gap, survey, as exhaustively as possible, the results of these investigations published in the literature and to call the attention of chemists to this promising group of polyfunctional compounds for the purpose of extending the scope of application of these derivatives in fine organic synthesis.

II. Synthesis methods

1. Cross-coupling of haloquinones with terminal acetylenes

Presently, cross-coupling of haloquinones with terminal acetylenes is recognised as the most versatile method for the synthesis of acetylenic derivatives of quinones. This method is based on the replacement of halogen atoms in carbo- and heteroaromatic rings as well as in vinyl halides by acetylenic groups.[11,12] Two main versions of this reaction, the catalytic and so-called acetylide, are generally used. In the catalytic version, aryl halides are condensed with terminal acetylenes in the presence of Pd(II) or Pd(0) triphenylphosphine complexes, cuprous iodide and a base (generally, amine). In the acetylide version, either condensation is performed directly with Cu(I) acetylide or the latter is prepared *in situ* from terminal acetylene in the presence of CuI and potassium carbonate. In both versions, the reactions are carried out under an inert atmosphere to prevent oxidative dimerisation of terminal acetylenes. In all cases, the reactivity of aryl halides decreases in the series ArI > ArBr > ArCl.

a. Catalytic method

Efficient cross-coupling in the presence of a combined Pd – Cu catalyst is used to introduce acetylenic substituents into the benzene rings of halogen derivatives of 9,10-anthra- and 1,4-naphthoquinones. The reactions are usually performed in an excess of amine (Et_3N or Et_2NH), which serves as a solvent and base, in the presence of $Pd(PPh_3)_2Cl_2$ and CuI at high temperature.[13–15] In some cases, amine is used in combination with an inert solvent[16] or, alternatively, an inorganic base (for example,

M S Shvartsberg, I I Barabanov, L G Fedenok Institute of Chemical Kinetics and Combustion, Siberian Branch of the Russian Academy of Sciences, ul. Institutskaya 3, 630090 Novosibirsk, Russian Federation. Fax (7-383) 234 23 50. Tel. (7-383) 233 33 49.
E-mail: shvarts@kinetics.nsc.ru (M S Shvartsberg), fedenok@kinetics.nsc.ru (L G Fedenok)

Received 23 October 2002
Uspekhi Khimii **73** (2) 171 – 196 (2004); translated by T N Safonova

K_2CO_3) in pyridine, DMF or dioxane is employed.[10, 17, 18] Iodine-containing quinones are reagents of choice. However, cheaper bromides were also successfully used in the synthesis of long-chain acetylenic derivatives of functionalised anthraquinones (components of coloured liquid-crystalline composites).[16] The chlorine atoms in the benzene rings of quinones are inactive.[10, 15]

In such catalytic systems, a series of acetylenic derivatives **1** were synthesised from mono- and polyiodo(bromo)anthraquinones **2**. The products were usually prepared in 70% – 90% yields, and the reaction time was 0.5 – 3 h.

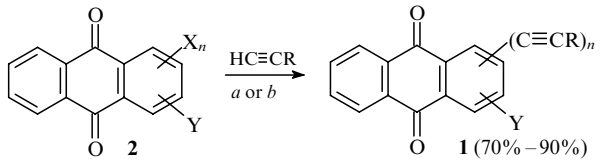

X = I, Br; n = 1, 2; Y = H, NH_2, NHMe, Cl, OCOPh;

R = C_5H_{11}, C_7H_{15}, CMe_2OH, CH_2N O, Ph;

(*a*) $Pd(PPh_3)_2Cl_2$ – CuI, Et_3N or Bu_3N; 50 – 90 °C;

(*b*) $Pd(PPh_3)_2Cl_2$ – CuI, K_2CO_3; Py, DMF or dioxane; 50 – 90 °C.

In both systems (*a* and *b*), the reactivity of 2-iodo-substituted isomers is comparable with that of 1-iodoanthraquinones.[10, 14] However, the presence of a bulky substituent at position 2 of the latter slows down the reaction due, apparently, to steric factors,[19] which hinder the formation of organopalladium complexes. For example, the reactions of methyl 1-iodoanthraquinone-2-carboxylate with terminal acetylenes, unlike those of 1-iodoanthraquinone, proceed slowly and ambiguously and are accompanied by substantial resinification.

These cross-coupling reactions of haloanthraquinones with acetylenes have virtually no limitations on the nature and arrangement of functional substituents in the starting compound. However, if the quinone moiety of the starting compound contains the hydroxy group adjacent to the halogen atom, the reaction results in intramolecular cyclisation of the primary condensation product, *viz*., hydroxyacetylene (see Section III.3.a). A standard procedure for the protection of the hydroxy group was used in the study.[17] Benzoyloxy derivative **2** (X = 2-I, Y = 1-OCOPh) in the presence of a weak nucleophilic base (K_2CO_3) in pyridine produced alkynyl(benzoyloxy)quinones,[17] whose subsequent alkaline hydrolysis afforded compounds **3**.

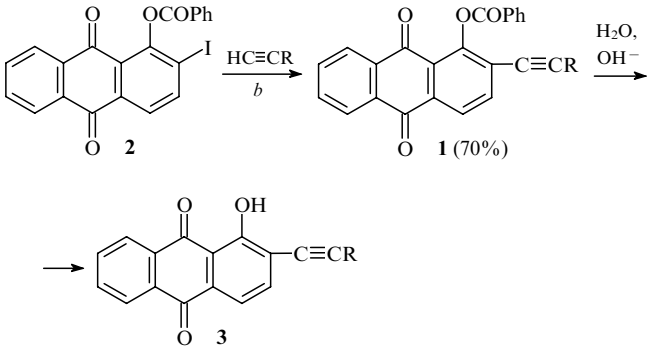

R = CMe_2OH, Ph;

(*b*) $Pd(PPh_3)_2Cl_2$ – CuI, K_2CO_3, Py; 50 – 90 °C.

Cross-coupling of halogen derivatives of 1,4-naphthoquinone with acetylenes is complicated by high electrophilicity of the quinoid ring. This ring can be blocked by introducing a strong electron-donating substituent. The efficiency of this protection was exemplified by the synthesis of compounds **4** from 3-diethylamino-5-iodo-1,4-naphthoquinone **5**.[13]

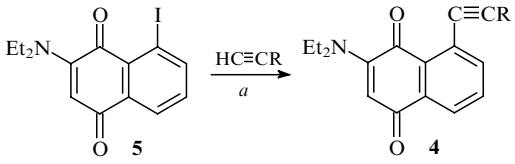

R = CMe_2OH, Ph;

(*a*) $Pd(PPh_3)_2Cl_2$ – CuI, Et_3N or Et_2NH; 50 – 90 °C.

Catalytic cross-coupling is used also for the introduction of acetylenic substituents into the quinoid ring of 1,4-naphthoquinone derivatives **6** to prepare compounds **7**.[20] In these reactions, the molecule is stabilised by the functional group, which is present in the quinoid ring and possesses a strong positive mesomeric effect.

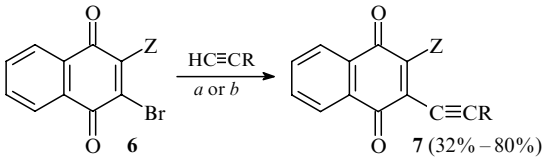

Z = NMe_2, N , N , OEt;

R = C_8H_{17}, CH_2OH, CH_2OMe, CH_2OAc, CH_2OPh, CMe_2OH, CMe_2OMe, CH_2N O, Ph;

(*a*) $Pd(PPh_3)_2Cl_2$ – CuI, Et_3N or Et_2NH; 50 – 90 °C;

(*b*) $Pd(PPh_3)_2Cl_2$ – CuI, K_2CO_3; Py or DMF; 50 – 90 °C.

Cross-coupling of acetylenes with quinones containing halogen atoms in the benzene rings is substantially intensified in an aqueous – organic medium (water – dioxane or water – pyridine mixtures) in the presence of the same Pd and Cu catalysts and an inorganic base (Na_2CO_3, K_2CO_3, $NaHCO_3$ or AcONa).[14 – 18, 21 – 31] The reaction time is an order of magnitude shorter than that in anhydrous media and is, as a rule, 5 – 30 min at 70 – 90 °C. This procedure was used in the synthesis of numerous acetylenic derivatives of quinones **8** – **10** (yields were 48% – 98%). It allows one to perform cross-coupling of haloquinones with labile acetylenes, for example, with ethyl propiolate.[25, 26] It should be noted that attempts to carry out condensation of the latter with aryl iodides in anhydrous media under standard conditions failed.[32]

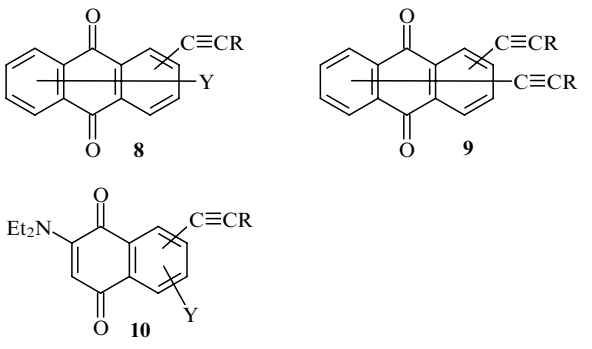

R = , CH_2OH, CH(OH)Pr, CMe_2OH, , , CH(OH)Ph, CH_2OPh, CO_2Et, CH_2N , Ph;

Y = NH_2, NHMe, NO_2, Cl.

Due to a high rate of the reaction in an aqueous – organic system, labile alkynylquinones can be prepared in rather high yields.

b. Acetylide method

Cross-coupling of quinones with cuprous acetylides in the absence of palladium complexes is used for the introduction of acetylenic substituents exclusively into the benzene rings of quinones. Due to the influence of electron-withdrawing groups conjugated with the benzene ring, the halogen atoms in the latter possess rather high nucleofugicity and can be replaced by acetylenic groups under relatively mild conditions (moderate temperature, moderate nucleophilicity of the medium and the absence of a strong base). For comparison, 1-iodonaphthalene reacts with Cu(I) phenylacetylide in pyridine at 115 °C for 10 h.[33] By contrast, the reaction of 1-iodoanthraquinone **2** (X = 1-I, Y = H) with phenylacetylide is completed in 1.5 h at 90 °C [10] and the reaction with butylacetylide is completed in 40 min at 60 °C to give the corresponding alkynylanthraquinones **11**.[23]

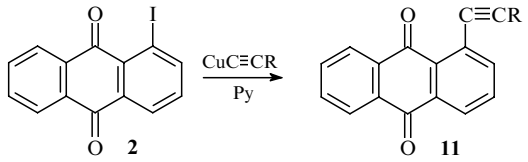

R = Bu, Ph.

Under these conditions, halonaphthoquinones with unsubstituted quinoid rings can also be introduced into reactions with cuprous acetylides. For example, 5-iodo-1,4-naphthoquinone **12** reacts with Cu(I) aryl- and hetarylacetylides in pyridine at 50 – 80 °C for 5 – 25 min to form the corresponding products **13**.[34]

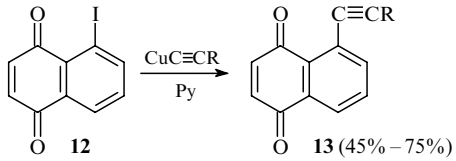

R = Ph, *p*-$MeOC_6H_4$, *p*-$Me_2NC_6H_4$, *p*-$O_2NC_6H_4$,

2-naphthyl, 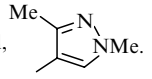

The iodine atom at the β position of the benzene ring of quinone is less easily replaced under the action of Cu(I) acetylides compared to that at the α position.[10] The reaction of 2-iodoanthraquinone with Cu(I) phenylacetylide proceeds ~20 times more slowly than that of 1-iodoanthraquinone.

Functionalised iodoquinones are, as a rule, readily condensed with acetylides, electron-withdrawing substituents noticeably accelerating the reaction.[10, 17 – 19, 23, 24, 35 – 37] 1-Iodoanthraquinones **14** bearing bulky substituents at position 2, which hinder Pd-catalysed condensation, react without complications with both Cu(I) acetylides and terminal acetylenes in the presence of Cu(I) salts and K_2CO_3.[19, 23, 30, 35, 37] The catalytic method can be applied to terminal acetylenes, which do not form acetylides stable in the solid state.

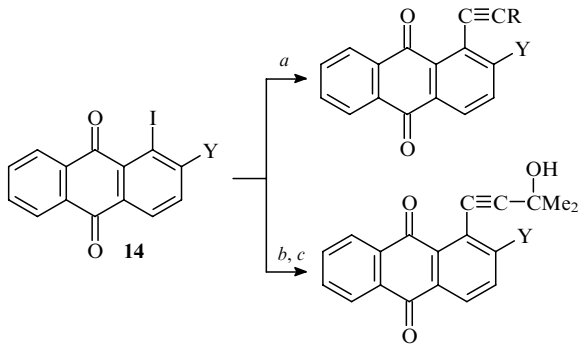

Y = CO_2Me, $CH(OEt)_2$, CHO; R = Bu, CH_2OPh, Ph;
(*a*) CuC≡CR, Py; (*b*) HC≡$CCMe_2OCH(OEt)Me$, K_2CO_3, CuI, Py;
(*c*) H_3O^+.

Under various conditions, copper-mediated condensation of vicinal hydroxy(halo)quinones results in intramolecular cyclisation to form the furan ring (see Section III.3.a).[38, 39] Unlike this reaction, condensation of *vic*-amino(iodo)anthraquinones with Cu(I) acetylide can be terminated in the step of formation of an acetylenic derivative of aminoanthraquinone. Under more drastic conditions, the latter undergoes cyclisation in the presence of an excess of acetylide to give the corresponding naphthoindoledione (see Section III.2.a).[18] For example, the reaction of 2-amino-3-chloro-1-iodoanthraquinone (**15**) with Cu(I) phenylacetylide in pyridine at 20 °C for 30 min affords 2-amino-3-chloro-1-phenylethynylanthraquinone (**16**).

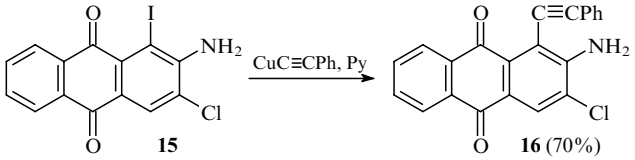

The *vic*-amino group facilitates the replacement of the halogen atom under the action of Cu(I) acetylides. For instance, the reaction of 1-amino-2-iodoanthraquinone with Cu(I) phenylacetylide in pyridine at 80 °C is completed in 2.5 h [18] (for 2-iodoanthraquinone, the reaction time is 26 h at 90 °C).[10]

The reactions of quinones containing halogen atoms in the quinoid ring with Cu(I) acetylides under rather mild conditions proceed only in the presence of the Pd catalyst.[40] The reactions are carried out in a mixture of DMSO and $CHCl_3$ at 20 – 50 °C. Condensation can be performed with both Cu(I) acetylides as such and acetylides prepared *in situ* from terminal acetylene, CuI and Et_3N. The second approach is used only if it is impossible to isolate stable acetylides in the solid state. The yields of alkynylquinones **17** and **18** vary from 35% to 84%.

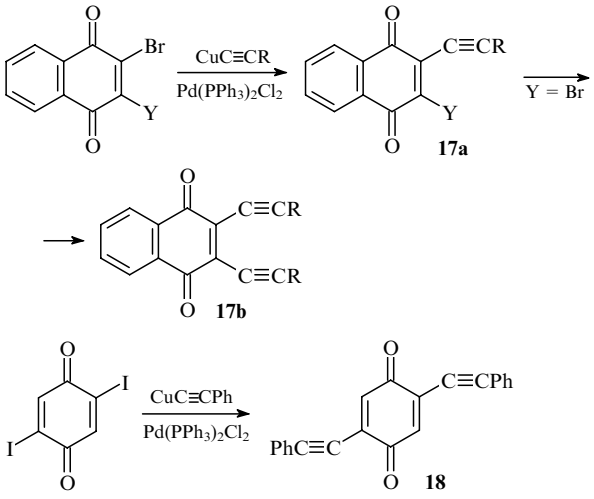

R = CMe_2OH, CMe_2OMe,

, Ph, *p*-$MeOC_6H_4$, *p*-$O_2NC_6H_4$;

Y = H, Br, NHAc, N(Ac)Ph, OEt.

2. Oxidation of alkynylarenes

Oxidation of aromatic compounds is one of the most general methods for the synthesis of quinones.[1 – 3, 41] Owing to the stability of the triple bond with respect to certain reagents, which can oxidise arenes to quinones, alkynylarenes can be used for the preparation of alkynylquinones.

Anthracenes **19** containing acetylenic substituents in the flank rings are readily oxidised with CrO_3 in 80% AcOH with retention of the triple bonds.[5, 7, 29] This procedure allows one to prepare 9,10-anthraquinones with various sets of acetylenic substituents.

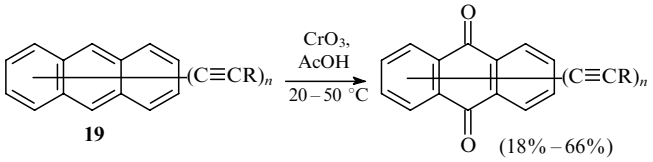

R = H, CH_2N O, COPh, *p*-$MeOC_6H_4$, *p*-$O_2NC_6H_4$, Ph; $n = 1, 2$.

The time of oxidation depends on the concentration of the substrate and the reaction temperature and varies over a wide range (5 – 240 min). Under these conditions, oxidation of 1,8-dialkynylanthracenes is sensitive to the nature of a substituent at the triple bond. For example, an attempt to oxidise 1,8-diethynylanthracene failed, whereas 1,8-bis(phenylethynyl)anthracene was oxidised at 60 °C for 6 min to form the corresponding anthraquinone in 31.5% yield.[7]

2-Phenylethynylnaphthalene (**20**), which contains no other substituents in the aromatic nucleus, is oxidised also with CrO_3 in 80% AcOH, the substituted ring being subjected to oxidation to give 2-phenylethynyl-1,4-naphthoquinone (**21**).[5]

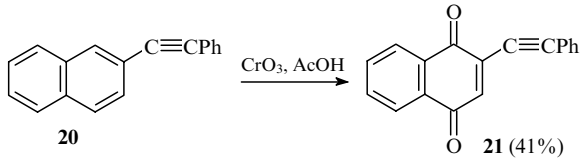

Aromatic compounds bearing two OR groups (R = H and/or Me) at the *para* positions are readily oxidised with Ce(IV) salts to give quinones.[1] These oxidising agents leave the triple bond intact and are used in the synthesis of various (mono- and polycyclic) quinones with acetylenic substituents in the benzene or quinoid ring.[5,8] For example, acetylenic derivatives of 1,4-dimethoxy- and 1-hydroxy-4-methoxybenzenes **22** – **24** were oxidised to the corresponding 1,4-benzoquinones with ammonium cerium nitrate (CAN) in aqueous MeCN or THF at room temperature.[5,8,42]

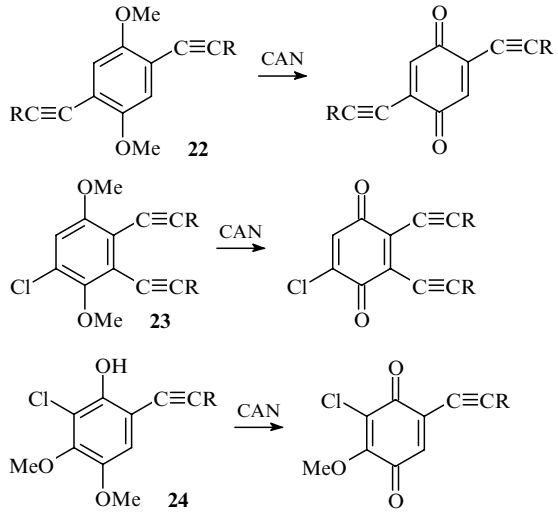

R = Bu, CMe_2OH, CH_2OCH_2Ph, Ph, *p*-$MeOC_6H_4$.

This reaction has a number of limitations. Oxidation proceeds satisfactorily in the presence of electron-donating or weak electron-withdrawing groups at the triple bond (yields are 40% – 89%). Strong electron-withdrawing groups, such as *p*-$O_2NC_6H_4$ or PhCO, hinder the reaction.[8] The substrate also remains non-oxidised if it forms an insoluble complex salt with the oxidising reagent [an example is 2,5-bis(2-pyridylethynyl)-1,4-dimethoxybenzene]. If the side chain of the substrate contains functional groups readily oxidised with cerium(IV), the reaction can afford other oxidation products. For instance, oxidation of 2,5-bis(3-morpholinoprop-1-ynyl)-1,4-dimethoxybenzene (**25**) with CAN gave rise to unsaturated dialdehyde **26** (in 46.5% yield) rather than quinone.

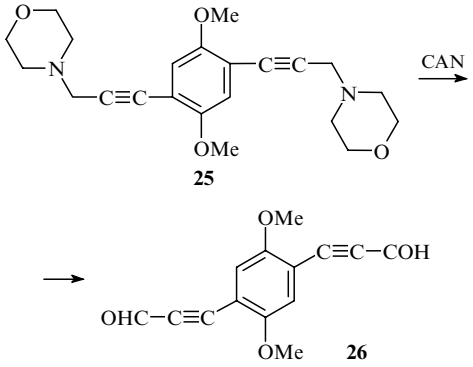

Unsuccessful attempts to prepare some alkynylquinones may also be associated with their lability. For example, an attempt to synthesise 2,5-diethynyl-1,4-benzoquinone from 2,5-diethynyl-1,4-dimethoxybenzene ended in failure.[8]

Depending on the structure of the starting compound, oxidation of acetylenic derivatives of 1,4-dimethoxynaphthalene **27** with ammonium cerium nitrate affords 1,4-naphthoquinones containing the substituent with the triple bond in either the quinoid or benzene ring. This procedure was used for the synthesis of 2-, 5- and 6-alkynyl-1,4-naphthoquinones.[5,8,13,43]

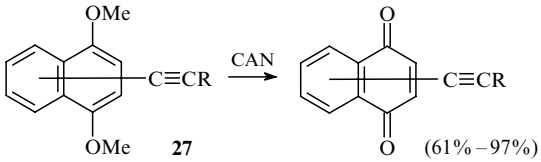

R = H, Ph.

In some cases, hydroquinones and their ethers are oxidised to quinones with Ag salts. For example, 2-hydroxymethyl-3-(3-methylbut-3-en-1-ynyl)hydroquinone, which is a metabolite of the natural antibiotic frustulosin, was oxidised with silver carbonate on celite in benzene.[44]

Potassium nitrosodisulfonate (fremy's salt) is a specific oxidising reagent, which allows one to transform aromatic amines and phenols into quinones under mild conditions.[45] This salt was used for oxidation of 1-naphthols **28** containing acetylenic substituents at position 6.[43] The reaction was carried out at 20 °C in an aqueous – methanolic solution of KH_2PO_4.

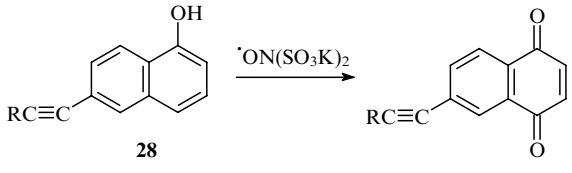

R = H, CMe_2OH, Ph.

On the whole, oxidation of aromatic acetylenic derivatives as a method for the synthesis of alkynylquinones has not been adequately investigated. However, there is no doubt that the scope of this method can be substantially extended.

3. Synthesis of acetylenic derivatives of *para*- and *ortho*-benzoquinones from dialkoxybenzoquinones

Moore and co-workers[4,6,9,42] developed an original procedure for the preparation of alkynylbenzoquinones from dialkoxy derivatives **29**. The synthesis involves the addition of lithium acetylides at the carbonyl groups of the starting quinone followed by acid hydrolysis of vinyl ether fragments of the resulting glycol **30** accompanied by dehydration. In some cases, the second step is

carried out with the use of $(CF_3CO)_2O$ in the presence of concentrated H_2SO_4. As a result of these transformations, the quinoid structure of the ring, which is initially destroyed due to the introduction of acetylenic substituents, is restored. This approach can be exemplified by the synthesis of 2,5-dialkynyl-1,4-benzoquinones **31** from 2,5-dialkoxy-1,4-benzoquinones **29**.[4,6]

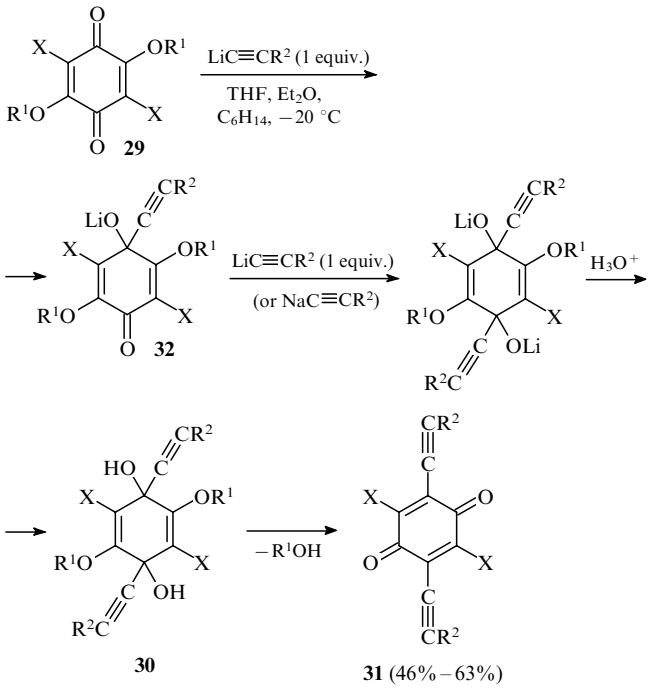

X = H, Cl; R^1 = Me, Et; R^2 = CH_2OMe, CH_2OBn, CH_2OTHP (THP is tetrahydropyranyl), CH_2Bn, Ph, *o*-MeC_6H_4, $MeC{=}CH_2$, $SiMe_3$.

Alkynylation of compounds **29** with some lithium acetylides bearing rather bulky substituents stops at monoadduct **32** or proceeds further very slowly.[42,46] In the latter case, the second step of alkynylation is carried out with the use of sodium acetylides instead of lithium acetylides because the former are less self-associated and, hence, more reactive.[42]

The reaction can be terminated in the step of formation of monoadduct **32** and the latter can be transformed into an unsymmetrical diadduct upon the addition of one equivalent of alkyl- or aryllithium. Hydrolysis and dehydration of the latter afford monoacetylenic *p*-benzoquinones **33**.

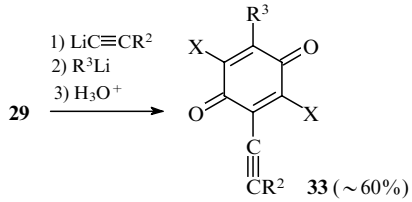

R^2 = CH_2OBn, CH_2OTHP, $(CH_2)_3OTHP$, Ph; R^3 = Me, Ph.

Monoadducts **32** can also serve as precursors of acetylenic derivatives of *ortho*-benzoquinone **34**.[42] In these reactions, a $(CF_3CO)_2O - H_2SO_4$ mixture is used in the second step.

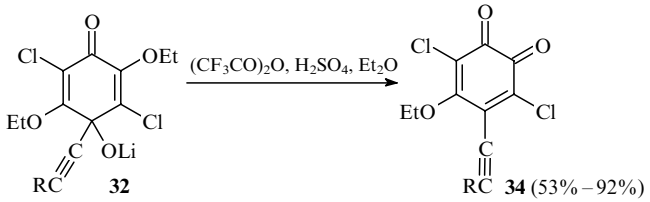

R = H, Bu, CH_2OTHP, $(CH_2)_4C{\equiv}CH$, $(CH_2)_2Ph$, $MeC{=}CH_2$, $CH{=}CHPh$, CO_2Et, Ph, *o*-$MeOC_6H_4$, α-$C_{10}H_7$, $SiMe_3$.

Under more drastic conditions, some 4-alkoxy-5-alkynyl-1,2-benzoquinones **34** can be hydrolysed to 5-alkynyl-2-hydroxy-1,4-benzoquinones **35**.[42]

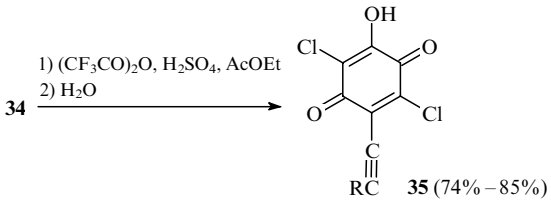

R = H, Bu, $(CH_2)_4C{\equiv}CH$, $MeC{=}CH_2$, CO_2Et.

The method developed by Moore and co-workers allows one to prepare 2-alkoxy-5-alkynyl-1,4-benzoquinones **37** and 4,5-dialkynyl-1,2-benzoquinones **38** (in 41% – 90% yields) from 4,5-dialkoxy-1,2-benzoquinones **36** through mono- (**39**) and diadducts **40**, respectively.[9,42]

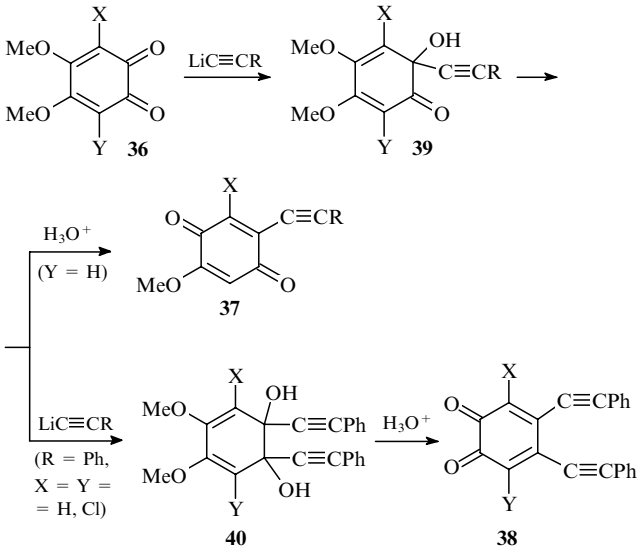

X = H, Cl, Br; Y = H, Cl; R = H, Pr, Bu, CH_2NEt_2, CH_2OCH_2Ph, $MeC{=}CH_2$, $(CH_2)_4C{\equiv}CH$, CO_2Et, Ph, OEt.

Interestingly, monoadducts **39** (X = Y = H) and diadduct **41** are readily transformed into the corresponding acetylenic derivatives of alkoxy-substituted chlorobenzenes under the action of $SOCl_2$ in THF in the presence of pyridine.[42] These reaction products, in turn, can serve as precursors of mono- or dialkynyl-1,4-benzoquinones (see Section II.2).

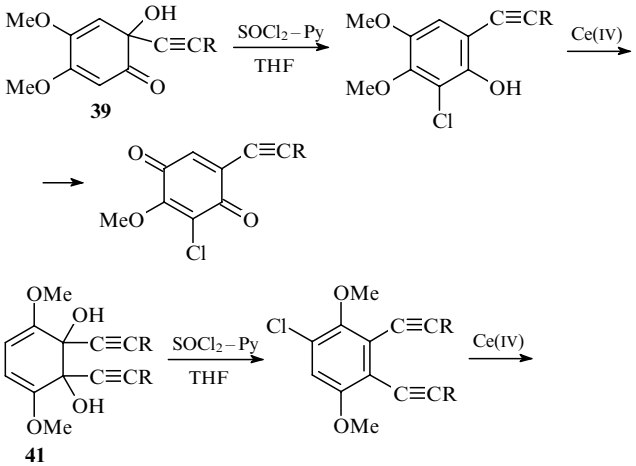

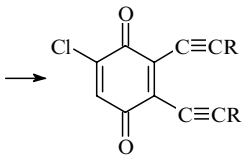

R = Bu, CH_2OBn, Ph.

In the reaction of 4,6-dibromo-3,5-dimethoxy-1,2-benzoquinone **42** with lithium phenylacetylide, the latter attacks the carbonyl group at position 2[42] to give monoadduct **43**, which is unstable and readily hydrolysed on treatment. This reaction leaves the methoxy groups intact and gives rise to 2-bromo-3,5-dimethoxy-6-phenylethynyl-1,4-benzoquinone **44**.

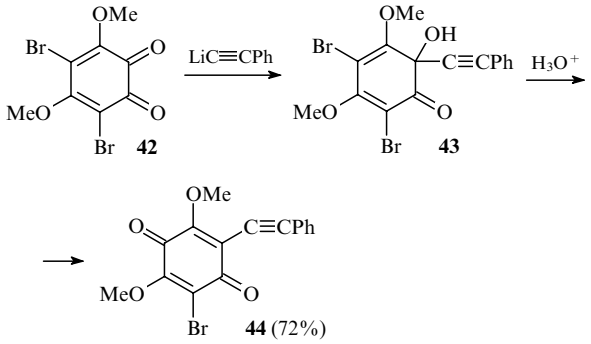

Apparently, it is impossible to extend the above-considered procedure for the synthesis of acetylenic derivatives of *p*- and *o*-benzoquinones to naphthoquinone derivatives. Hanhela and Paul[47] attempted to synthesise 1,4-dihydro-2,3-dimethoxy-1,4-di(phenylethynyl)naphthalene-1,4-diol by adding two moles of lithium phenylacetylide to 2,3-dimethoxy-1,4-naphthoquinone followed by reductive aromatisation of the diadduct; however, the reaction afforded a mixture of other products.

4. Other methods

Before the above-described general methods for the synthesis of acetylenic derivatives of quinones were developed, compounds of this class had been prepared according to procedures applicable only to particular cases. For example, bis(anthraquinon-2-yl)acetylene was prepared by reductive cross-coupling of 2-tribromomethylanthraquinone either under the action of copper metal in refluxing nitrobenzene[48] or by thermal condensation of 2-dibromomethylanthraquinone followed by dehalogenation of the resulting substituted dibromoethylene in refluxing diethylaniline or phenol in the presence of K_2CO_3.[49] The addition of chlorine to 1-(anthraquinon-2-yl)-2-(2,4-dinitrophenyl)ethylene followed by dehydrohalogenation of the adduct was used for the synthesis of 2-(2,4-dinitrophenylethynyl)anthraquinone.[50] Dehydrochlorination of a series of functionalised (2-chloro-2-propen-1-yl)anthraquinones was studied.[51,52] Depending on the structure of the starting compound, the chloropropenyl substituent can be transformed into the prop-1-ynyl, propanedienyl or 2-oxopropyl group. If there are two chloropropenyl substituents in the substrate, at least one of them is transformed into the propynyl group. A series of 2-(arylethynyl)anthraquinones were synthesised by the Wittig reaction.[53] Acid-catalysed dehydration of 3-alkynyl-1,2,3,4-tetrahydro-1,3,5,8-tetrahydroxyanthraquinones, in which the acetylenic group is not directly bound to either the quinoid or aromatic ring, afforded 6-alkynyl-1,4-dihydroxyanthraquinones.[54,55]

III. Chemical properties

1. Reactions with amines

In acetylenic derivatives of quinones, the triple bond is highly electrophilic due to conjugation with carbonyl groups located in the plane of the cyclic moiety of the molecule. These compounds, like other compounds bearing the activated triple bond, can add *N*-nucleophiles, for example, amines.

a. Quinones containing acetylenic substituents in the quinoid ring

Quinones containing acetylenic substituents in the quinoid ring are vinylogs of acetylenic ketones.

The reactions of 2-alkynyl-1,4-naphthoquinones with amines can follow two competitive pathways: addition at the triple bond and oxidative replacement of the hydrogen atom at position 3. The latter reaction involves the Michael-type 1,4-addition of amine to the ketovinyl group of quinone to form 1,4-dihydroxynaphthalene followed by oxidation of the latter.[1]

However, of the above two possible pathways, only oxidative amination takes place.[56] For example, 2-phenylethynyl-1,4-naphthoquinone **21** reacts with primary and secondary amines as well as with NH_3 at room temperature to give 2-amino-3-phenylethynyl-1,4-naphthoquinones **45**. Generally, dioxane, aqueous dioxane, diethyl ether or an excess of amine is used as the solvent. An additive of $Cu(OAc)_2$ catalyses oxidation of the hydroquinone intermediate.

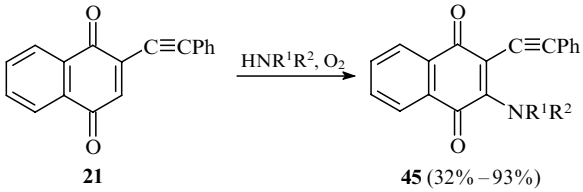

$R^1 = R^2 =$ H, Me, Et; $R^1 =$ H: $R^2 =$ Me, Et, cyclo-C_6H_{11}, $(CH_2)_2OH$, CH_2Ph, CH_2CO_2Me, $CH_2CO_2^-$, Ph; $R^1-R^2 = -(CH_2)_5-$, $-(CH_2)_2O(CH_2)_2-$.

In the reaction with 2-alkynyl-1,4-naphthoquinone containing an electron-withdrawing substituent at position 3 of the quinoid ring, amine adds at the triple bond. The introduction of an electron-donating group (for example, of the amino group) leads to deactivation of the adjacent triple bond. However, acylation of the latter restores the ability of the acetylenic substituent to add amines.[56]

Unlike monosubstituted 2-phenylethynyl-1,4-naphthoquinone, 2,3-bis(phenylethynyl)-1,4-naphthoquinone (**46**) readily adds one equivalent of morpholine (20 °C, 15 min)[56] to give monoadduct **47**. Due to low electrophilicity of the triple bond in the latter compound, the addition of the second amine molecule does not occur.

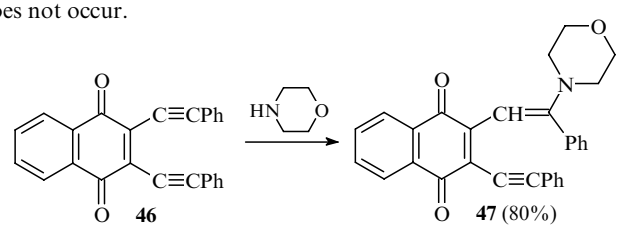

b. Quinones with an acetylenic substituent in the benzene ring

Anthraquinones and naphthoquinones **48** containing an acetylenic substituent in the benzene ring add secondary amines at the triple bond at 20–105 °C in dioxane or in an excess of amine to form adducts **49** in 50%–95% yields.[13,15,19,22,29,57]

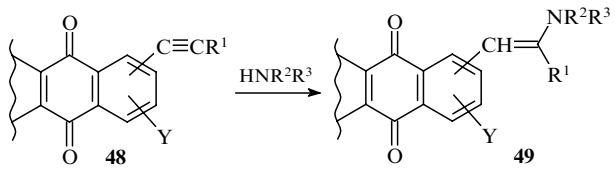

Y = H, Cl, NH_2, NO_2, CO_2Me; R^1 = H, CMe_2OH, CH_2N⟨O⟩, Ph, CH_2OPh; $R^2 = R^3$ = Et, Bu; R^2-R^3 = $-(CH_2)_4-$, $-(CH_2)_5-$, $-(CH_2)_2O(CH_2)_2-$.

Studies by ^1H NMR spectroscopy demonstrated that these reactions always afford only one geometric isomer. For ethynylquinones (R^1 = H), this isomer has a *trans* configuration.

Naphthoquinones devoid of substituents in the quinoid ring are subjected to oxidative amination at one of its positions. For example, the reaction of 5-phenylethynyl-1,4-naphthoquinone **50** with an excess of amine in the presence of $Cu(OAc)_2$ as the catalyst by bubbling air at 20 °C afforded a mixture of 3- (**51a**) and 2-amino derivatives (**52**) in a ratio of ~2 : 1 in 54.5% yield.[13] In isomer **51a**, the triple bond retains the ability to add amines. However, isomer **51a** forms adduct **53** with piperidine under more drastic conditions (at 80 °C for 10 h).

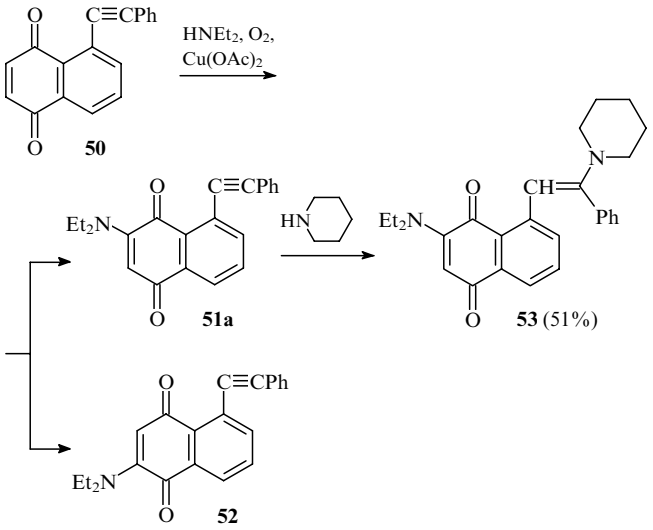

The reactivity of quinones containing an acetylenic substituent in the benzene ring depends on the nature of this substituent, its position and the presence of other functional groups. The acetylenic substituent at the α position of the benzene ring is more active than the substituent at the β position. In both cases, ethynyl derivatives are most reactive. For instance, the reactions of 1-ethynyl- (**54a**) and 2-ethynylanthraquinones (**55a**) with pyrrolidine at 20 °C were completed in 15 min and 12 h, respectively.[15] The reactions of 3-diethylamino-5-ethynyl- (**51b**) and 3-diethylamino-5-phenylethynyl-1,4-naphthoquinone **51a** with piperidine were completed in 1 h at 20 °C and in 10 h at 80 °C, respectively,[13] whereas the reaction time of the addition of piperidine to 2-phenylethynylanthraquinone **55b** at 80 °C was as long as 48 h.[15] The acetylenic substituent and the halogen atom present in the same ring activate each other. In going from 1-phenylethynylanthraquinone (**54b**) to its 2- and 3-chloro-substituted derivatives (compounds **54c**,**d**), the time of the reaction with piperidine decreases from 4 h to 8 and 20 min, respectively (80 °C).[15] The time of the competitive reaction, *viz*., the replacement of the halogen atom in 1-chloroanthraquinone **2** (X = 1-Cl, Y = H) by the piperidine group, decreases in the presence of the phenylethynyl substituent at positions 2 and 4 from 1.5 h to 12 and 20 min, respectively (80 °C). In 3-chloro-2-phenylethynylanthraquinone (**55c**), the addition of piperidine and the replacement of the chlorine atom with piperidine proceed at similar rates. The replacement and addition products (4 : 3 ratio; 79% total yield) do not react with the amine.

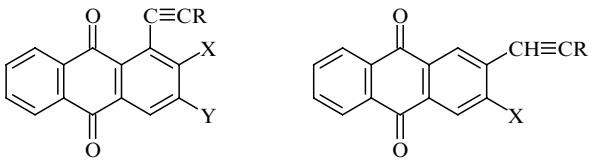

54	R	X	Y
a	H	H	H
b	Ph	H	H
c	Ph	Cl	H
d	Ph	H	Cl

55	R	X
a	H	H
b	Ph	H
c	Ph	Cl

In acylethynylanthraquinones, the triple bond is activated both by the carbonyl group of the substituent and the quinone ring. In *vic*-amino(acylethynyl)anthraquinones **56**, the influence of the carbonyl group prevails and the addition of amine occurs at the β position with respect to the carbonyl group[36, 39, 58] to give adducts **57** in 69% – 75% yields.

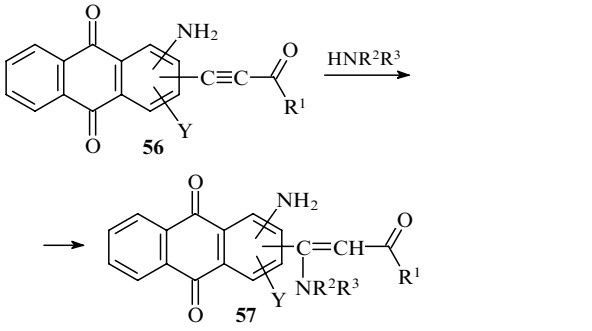

Y = H, Cl, NO_2; R^1 = Ph, Bu^t; R^2 = H: R^3 = Bu, C_8H_{17}; $R^2 = R^3$ = Et; R^2-R^3 = $-(CH_2)_4-$, $-(CH_2)_5-$, $-(CH_2)_2O(CH_2)_2-$.

Unlike ketones **56**, ethyl (1-aminoanthraquinon-2-yl)propiolate (**58**) adds amines to form two products, *viz*., the corresponding β-amino acrylate **59** (in 60% – 66% yields) and 1*H*-3-aminonaphtho[2,3-*h*]quinoline-2,7,12-trione **60** (in 12% – 18% yields).[25, 26] Evidently, the latter products are generated through rapid cyclisation under the conditions of the reaction of regioisomeric α-amino acrylates **61** (Scheme 1).

Apparently, the ease of intramolecular cyclisation of α-amino acrylates of type **61** as well as of the resulting β-amino acrylates (see Section III.4) indicates that the adducts of both types have an *E* configuration. Taking into account the regioselectivity of the addition of amines to acylethynylanthraquinones and the ratio between the yields of linear and cyclic products of addition to aminoanthraquinonyl propiolate **58**, the groups activating the triple bond can be arranged in the following series: CO > CO_2Et > 1-aminoanthraquinon-2-yl.

Secondary acetylenic alcohol, *viz*., 1-amino-2-(3-hydroxy-3-phenylpropynyl)anthraquinone (**62**), exhibits an unusual behaviour in reactions with amines.[27] The reactions of alcohol **62** with primary amines lead predominantly to its dehydrogenation. The reactions of alcohol **62** with secondary amines also afford dehydro adducts **64**, which are identical to products of addition of amines to 2-benzoylethynyl derivative **65** (in yields of up to 76%), rather than the expected enamino alcohols **63**. On heating with tertiary amine (Et_3N), alcohol **62** undergoes competitive dehydration to form acetylenic ketone **65** and isomerisation to vinyl ketone **66**. The mechanism of formal oxidation of the alcoholic group in compound **62** remains unclear (see Ref. 27) (Scheme 2).

Scheme 1

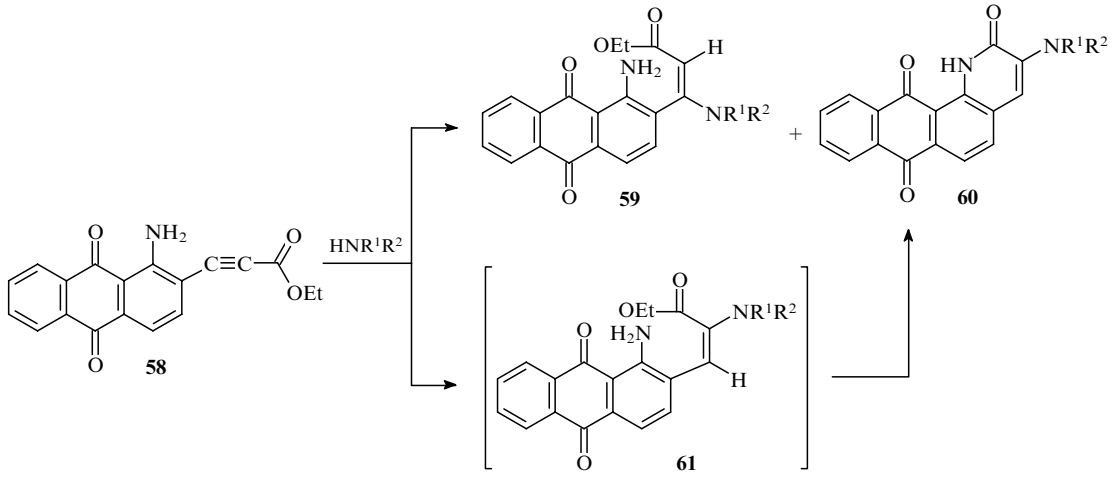

R^1 = H, R^2 = Bu; R^1 = R^2 = Et; R^1–R^2 = –$(CH_2)_5$–.

Scheme 2

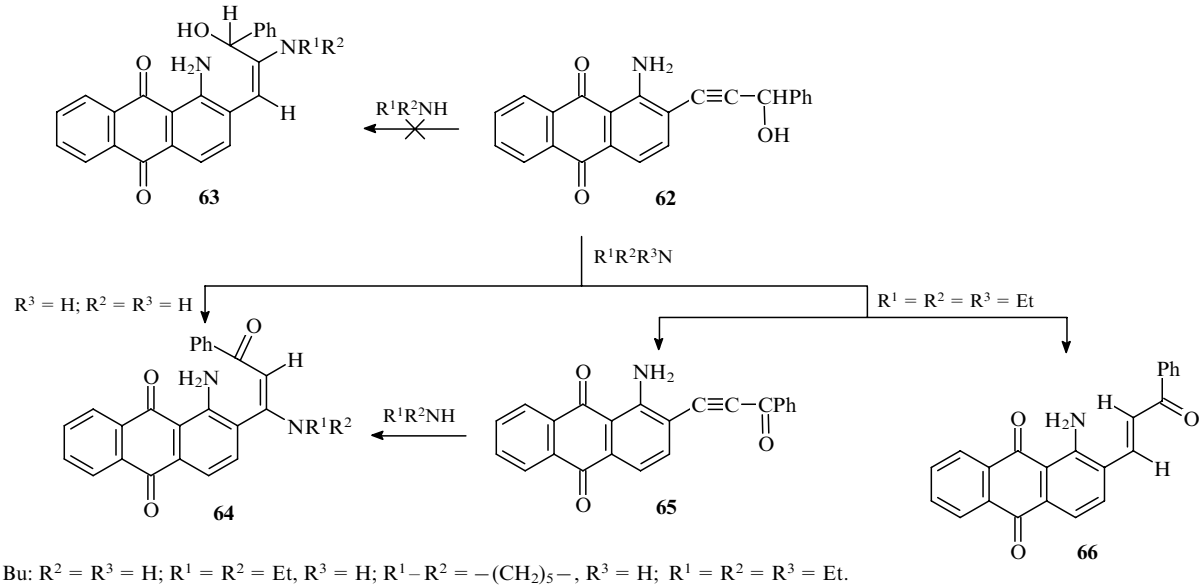

R^1 = Bu: R^2 = R^3 = H; R^1 = R^2 = Et, R^3 = H; R^1–R^2 = –$(CH_2)_5$–, R^3 = H; R^1 = R^2 = R^3 = Et.

The reactivity of amines in nucleophilic addition to alkynylanthraquinones is to a large extent determined by their spatial structure. For sterically similar amines, the reactivity increases as their basicity increases.[15]

Adducts of alkynylquinones with amines are intermediates for the synthesis of various fused heterocyclic quinoid structures.

2. Pyrrole-ring closure reactions of *vic*-amino(alkynyl)quinones

It is known that in the presence of Cu(I) compounds, Pd(II) and other transition metal salts, bases or, in some cases, mineral acids, aryl- and hetarylacetylenes containing a primary or secondary amino group in the *ortho* position with respect to the acetylenic substituent undergo cyclisation to form the pyrrole ring.[59–65] This reaction was extended to vicinal acetylenic derivatives of aminoquinones.[18,21,22,29,57,66,67]

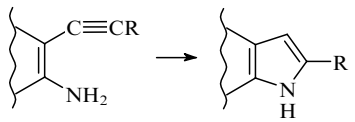

a. Catalytic cyclisation

Originally, intramolecular cyclisation of *vic*-amino(alkynyl)quinones seemed hardly possible due to low nucleophilicity of the amino group. However, it appeared that these compounds undergo intramolecular cyclisation in the presence of cuprous acetylide or powdered copper [but not Cu(I) halides] in pyridine or DMF at 80–153 °C to form the corresponding naphthoindoledione **67**–**69** with the differently fused pyrrole and anthraquinone rings (in 21%–85% yields; the reaction time is 0.5–7 h).[18,21,67]

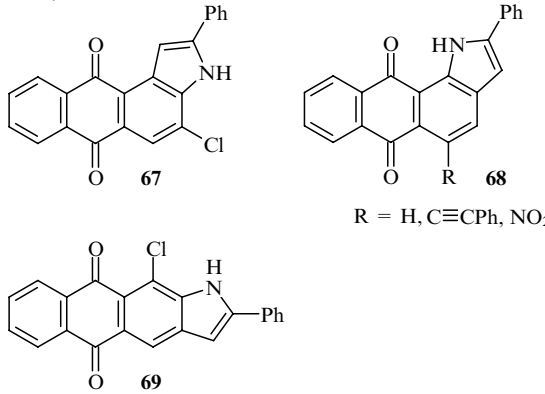

R = H, C≡CPh, NO_2

Naphthoindole **67** was prepared also in one step from *vic*-amino(iodo)anthraquinone **15** by cyclocondensation with CuC≡CPh under analogous conditions.

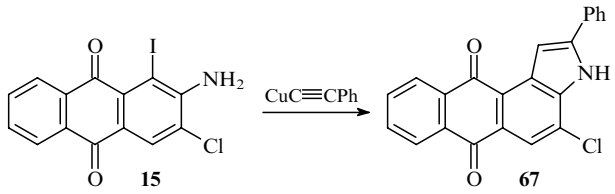

In this catalytic intramolecular reaction, like in the intermolecular addition of amines to alkynylanthraquinones, 1-alkynyl derivatives are more active. For example, 2-amino-3-chloro-1-phenylethynylanthraquinone **16** undergoes cyclisation to 2-phenylnaphtho[2,3-*e*]indole-4,9-dione (**67**) in 82% yield in pyridine in the presence of CuC≡CPh at 80 °C during 1 h, whereas isomeric 2-amino-1-chloro-3-phenylethynylanthraquinone gives 2-phenylnaphtho[2,3-*f*]indole-5,10-dione (**69**) in a yield of only 25% at 115 °C after 2 h. Under analogous conditions (80 °C, 20 min), cyclisation of 2-amino-1,3-di(phenylethynyl)anthraquinone (**70**) proceeds only involving the acetylenic substituent at position 1. In spite of the lower activity of the acetylenic group at position 3 and low nucleophilicity of the NH unit of the pyrrole ring, product **71** can undergo further cyclisation to produce 2,3-diphenylnaphtho[2,3-*e*]pyrrolo[3,2,1-*hi*]indole-6,11-dione (**72**) under more drastic conditions (115 °C, 45 h).

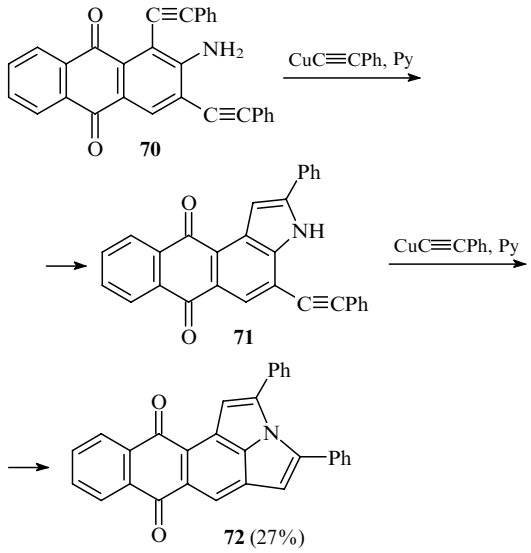

It is also of interest to compare the rates of cyclisation of 1-amino-2-phenylethynylanthraquinone derivatives giving rise to products **68**. Cyclisation of unsubstituted anthraquinone (R = H) was completed in 4.5 h at 115 °C (CuC≡CPh, pyridine), whereas the reaction of its nitro derivative (R = NO_2) was completed in less than 1 h at 80 °C (in spite of the fact that the nitro group should decrease the nucleophilicity of the amine thus slowing down the reaction).

It was proposed that *vic*-amino(alkynyl)anthraquinones, unlike *ortho*-alkynylanilines, can undergo cyclisation with preliminary deprotonation of the amino group under the action of bases. Solid KOH is a catalyst of choice for cyclisation of amino(alkynyl)anthraquinones **73**.[18,29]

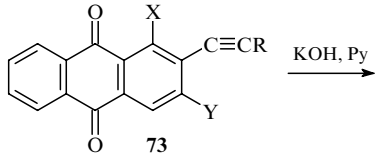

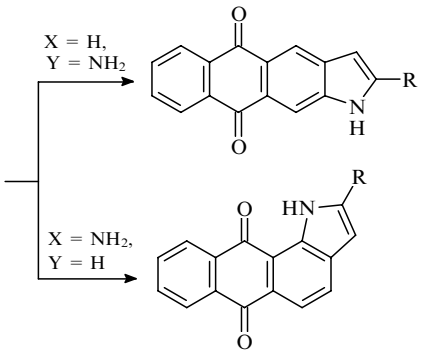

R = H, Ph; X = H, Y = NH_2; X = NH_2, Y = H.

Under these conditions, cyclisation of 1-amino-2-phenylethynylanthraquinone (**73**; R = Ph, X = NH_2, Y = H) in refluxing pyridine was completed in 15 min to give the product in 88% yield (for comparison, cyclisation of the same compound in the presence of CuC≡CPh was completed in 4.5 h, and the yield of the product was 57%). Other naphthoindolediones were prepared in 40% – 88% yields, and the reaction time was 8 – 90 min. To preclude alkaline hydrolysis, *vic*-amino(acylethynyl)anthraquinones are subjected to cyclisation with the use of K_2CO_3 in DMSO (65 – 70 °C, 10 – 20 min).[39]

Cyclisation of amino(alkynyl)-1,4-naphthoquinones **74** containing an acetylenic substituent and a secondary amino group in the quinoid ring proceeded analogously.[66] The reaction was carried out at 100 – 140 °C in pyridine, its mixture with dioxane, DMSO or mesitylene to prepare benzo[*f*]indole-4,9-diones (**75**) in 20% – 82% yields.

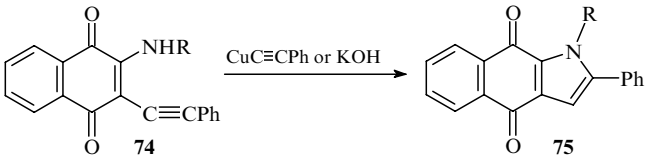

R = Me, $CH_2CH=CH_2$, $(CH_2)_2OH$, $(CH_2)_2OAc$, CH_2Ph, Ac, Ph.

Evidently, the characteristic features of cyclisation of amino(alkynyl)quinones cannot be explained only on the hypothesis that the process involves preliminary deprotonation of the amino group. It is hardly probable that the appearance of a charge on the nucleophilic centre could provide its interaction with the spatially remote β-carbon atom of the triple bond.

In the general case, the mechanism of intramolecular addition of the amino group at the triple bond catalysed by metal compounds involves the formation of a metal acetylenic π-complex and its cyclisation to a mixed organometallic compound (3-indolyl derivative), which is readily hydrolysed to the corresponding indole. Covalently bound copper from acetylide (or oxides on a copper powder surface) can be involved in stronger (compared to copper salts) dative interactions in π-complexes with a triple bond, and these interactions are additionally strengthened due to high electrophilicity of the triple bond in quinones, due to which the π-complex becomes rather stable. As a result of a change in the geometry of the triple bond in the complex, the reaction centres (the amino group and the β-carbon atom of the acetylenic substituent) are brought into proximity and the interaction between them becomes possible. Upon deprotonation of the amino group, the electrophilicity of the triple bond conjugated with this amino group decreases and the formation of a π-complex even with a proton becomes possible (for example, when KOH is used as a catalyst). This π-complex formation accompanied by a change in the geometry of the acetylenic substituent is, apparently, the necessary condition for the closure of the heterocycle.

Some acetylenic derivatives of aminoanthraquinones can undergo cyclisation to naphthoindolediones under acid cataly-

sis.[18,29] The possibility of this reaction is determined by regioselectivity of hydration of the triple bond. Actually, 1-amino-2-phenylethynylanthraquinone (**76a**) undergoes cyclisation in concentrated H_2SO_4 to form substituted naphthoindoledione **68** at 40 °C for 3 min, whereas 1-amino-2-ethynylanthraquinone **76b** gives only the hydration product, *viz*., 2-acetyl-1-aminoanthraquinone (**77**).

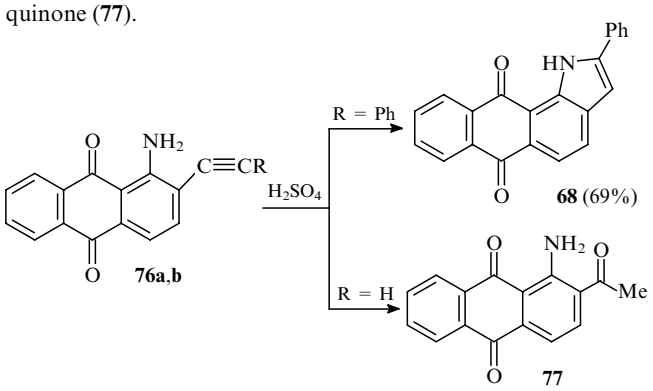

R = Ph (**a**), H (**b**).

b. Cyclisation through adducts with amines

Quinones **78** containing a vicinal primary amino group and an acetylenic substituent in the benzene ring can add secondary amines at the triple bond to form β-dialkylaminovinyl adducts **79**. Due to a change in the geometry of the unsaturated substituent (it is brought into proximity with the adjacent amino group), these adducts are easily subjected to intramolecular cyclisation in the presence of mineral acids or on SiO_2.

Some *vic*-amino(alkynyl)anthraquinones [for example, 1-amino-2-(3-hydroxyalk-1-ynyl)anthraquinones] are transformed into naphthoindolediones already on heating (80–105 °C) in an excess of secondary amine for several hours. The addition of amine to such acetylenes is hindered, and the resulting adducts are unstable and undergo rapid cyclisation with elimination of amine. This sequence of reactions provides the basis for a simple preparative procedure for annelation of quinones with the pyrrole ring.[18,22,27,29] This procedure was used for the synthesis of a series of naphtho[2,3-*g*]indole-6,11-diones **80**.

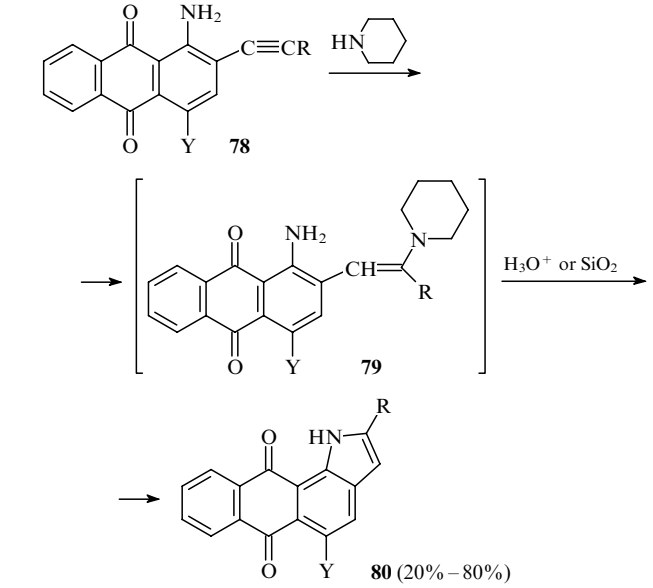

R = H, CH_2OH, CH(OH)Pr, CMe_2OH, CH_2OPh, CH_2N⟨O⟩;
Y = H, NO_2.

One of the possible pathways of transformations of dialkylaminovinyl derivatives of 1-aminoanthraquinone **81** into tetracyclic products involves their cyclisation to 2-dialkylamino-2,3-dihydronaphtho[2,3-*g*]indole-6,11-diones **82**, which are labile and readily undergo aromatisation with elimination of amine on silica gel or under the action of an acid.[57] The diethylaminopyrroline intermediate (R = Et) is particularly unstable: it eliminates diethylamine already under the synthesis conditions and is transformed into unsubstituted naphthoindoledione.

However, pyrroline intermediates **82** can undergo aromatisation not only through elimination of amine but also upon dehydrogenation. It appeared that these compounds underwent aromatisation with retention of the amino group at 20 °C in pyridine in the presence of KOH and atmospheric oxygen (yields were ~60%). 2-Diethylaminonaphtho[2,3-*g*]indole-6,11-dione **83** was also prepared in low yield (22%) by cyclisation of 1-amino-2-diethylaminovinylanthraquinone **81** under the same conditions. This reaction afforded unsubstituted naphthoindoledione **84** as the major product.

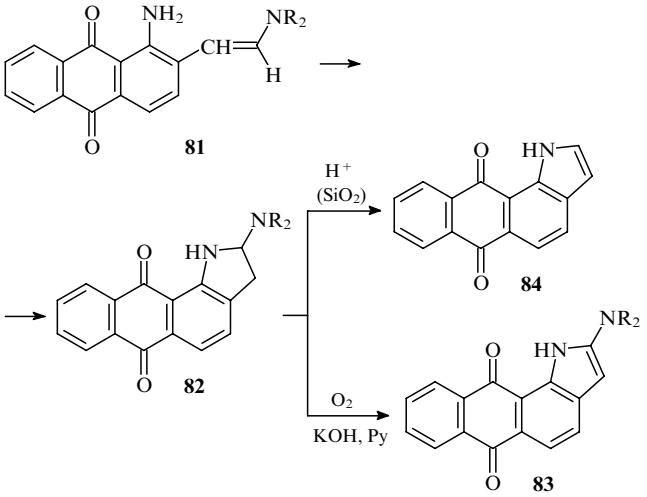

R–R = $-(CH_2)_5-$, $-(CH_2)_2O(CH_2)_2-$; R = Et.

Another pathway of cyclisation of adducts which involves hydrolysis of the dialkylaminovinyl substituent followed by the pyrrole-ring closure, is also not ruled out.

c. Photoinduced heterocyclisation

Another method for the construction of a system of fused pyrrole and quinoid rings is based on photochemical cyclisation of 3-alkynyl-2-dialkylamino-1,4-naphtho- or -1,4-benzoquinone.[68,69] This reaction involves two steps, as was exemplified by the reactions of 2-diethylamino-3-phenylethynyl- (**85a**) and 2-dimethylamino-3-(3-phenoxyprop-1-ynyl)-1,4-naphthoquinones (**85b**).[68] The first step is initiated with visible light (λ = 546 nm) and leads to the closure of the dihydrooxazole ring with the participation of the dialkylamino and vicinal carbonyl groups giving rise to intermediates **86**. On irradiation with light

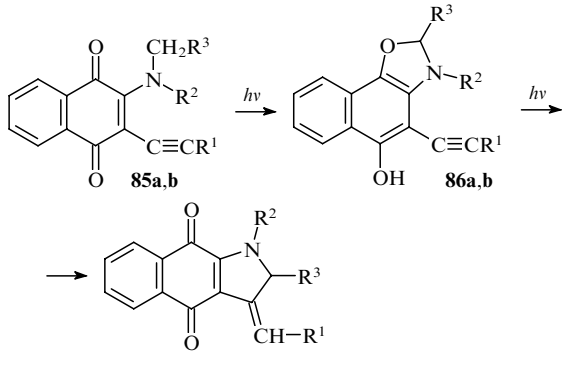

R^1 = Ph, R^2 = Et, R^3 = Me (**a**); R^1 = CH_2OPh, R^2 = Me, R^3 = H (**b**).

(λ = 436 nm), the latter undergo recyclisation to the corresponding 3-alkylidene-2,3-dihydronaphtho[2,3-*b*]pyrrole-4,9-diones **87**.

In the presence of catalytic amounts of mineral acids, photocyclisation products (compounds **87**) are isomerised into substituted naphtho[2,3-*b*]pyrrole-4,9-diones **88**.[69] The latter can be synthesised from alkynylquinones without isolation of intermediate dihydroindolequinones.

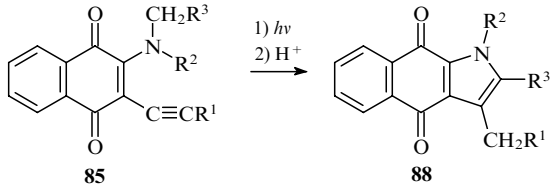

85 **88**

R^1 = H, CH_2OPh, Ph; R^2 = Me, Et; R^3 = H, Me.

If the dialkylamino group in the starting alkynylquinone **89** is a residue of cyclic amine, photocyclisation affords tetracyclic heterocyclic quinones **90**.[69]

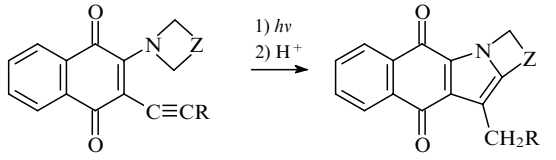

89 **90** (16% – 60%)

Z = $-(CH_2)_2-$, $-(CH_2)_3-$, $-CH_2OCH_2-$; R = Ph, CH_2OPh.

Analogously, tricyclic compounds **92** are derived from 3-alkynyl-2-amino-1,4-benzoquinones **91**.

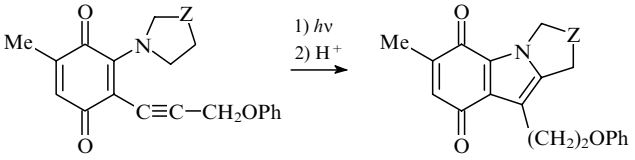

91 **92**

Z = $-CH_2-$, $-(CH_2)_2-$.

Quinones bearing a nitrogen atom at the fusion of two rings are structurally similar to natural antitumour antibiotics of the mitomycin family.

3. Furan-ring closure reaction

a. Reactions of *vic*-hydroxy(alkynyl)quinones

vic-Acetylenic derivatives of hydroxyanthraquinones (like *ortho*-hydroxyarylacetylenes[60,70–72]) undergo cyclisation in the presence of copper or palladium catalysts or bases to form the furan ring. Generally, the reactions proceed under mild conditions and give products in good yields.

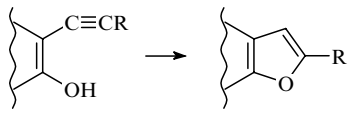

For example, 1-hydroxy-2-benzoylethynylanthraquinone (**93**) undergoes cyclisation under the action of CuC≡CPh in pyridine already at 20 °C during 30 min. Although the presence of the carbonyl group in the acetylenic substituent of quinone should hinder the attack of the nucleophile at the adjacent carbon atom, the yield of 2-benzoylanthra[1,2-*b*]furan-6,11-dione (**94**) amounts to 68%.[39]

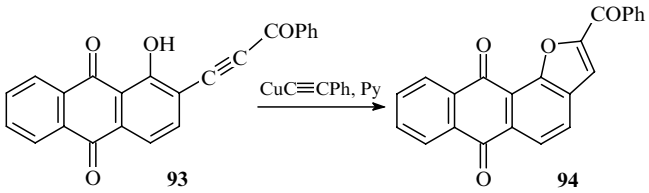

93 **94**

In the presence of solid K_2CO_3, 2-hydroxy-3-phenylethynylanthraquinone **95** undergoes cyclisation in refluxing pyridine to give 2-phenylanthra[2,3-*b*]furan-5,10-dione **96** during 3 min.[69]

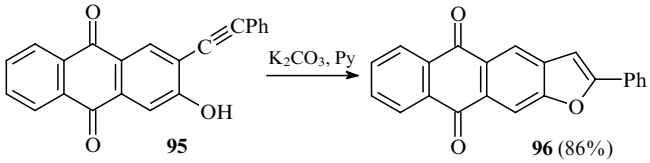

95 **96** (86%)

Cyclisation of 1,4-dihydroxy-2,3-di(prop-1-ynyl)anthraquinone (**97**) in a refluxing 1.5% KOH solution in MeOH proceed much more slowly; the conversion is approximately 90% after 24 h.[52]

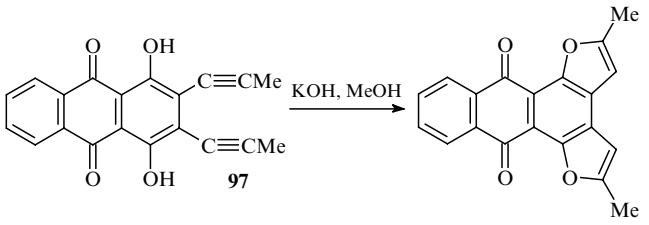

97

The mechanism of this heterocyclisation under various conditions was not studied in detail. However, this mechanism is, apparently, similar to that of the pyrrole-ring closure (see Section III.2.a).

Cross-coupling of *vic*-hydroxy(iodo)anthraquinones (**98**, Hal = I) both with cuprous acetylides[38,69] and terminal acetylenes catalysed by palladium complexes[17,69] affords directly anthrafurandiones. Unlike condensation of *vic*-amino iodides, the replacement of the halogen atom in this reaction is the rate-determining step and the expected acetylenic intermediates of the reaction (compounds of type **99**) are not detected. Stable cuprous acetylides (for example, CuC≡CPh) have proved themselves in the synthesis of anthrafurandiones. For instance, the reaction time of cyclocondensation at 20–115 °C is only 5–10 min.[38,69] This method was used for the synthesis of all three isomeric anthrafurandiones (**100**).

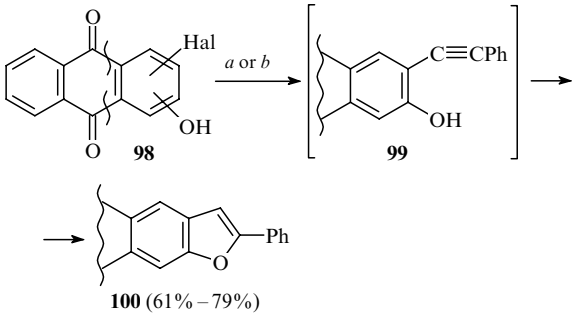

98 **99**

100 (61% – 79%)

Hal = I, Br;
(*a*) CuC≡CPh; (*b*) HC≡CPh, $Pd(PPh_3)_2Cl_2$, CuI, K_2CO_3, Py.

2-Hydroxy-1-iodoanthraquinone is most reactive in this reaction. In this case, cross-coupling is completed in the above-mentioned time at room temperature. The reactivity of the corresponding bromide is also high. For example, its condensation with CuC≡CPh is completed in 5 min at 115 °C. The reaction of 1-chloro-2-hydroxyanthraquinone virtually does not proceed.

Catalytic cross-coupling of *vic*-hydroxy(iodo)anthraquinones with terminal acetylenes has some advantages over acetylide condensation, because it allows one to use alkynes, which do not form stable acetylides (aminopropynes, acetylenic alcohols, *etc*.). Catalytic cyclocondensation was carried out for different isomers of *vic*-hydroxy(iodo)anthraquinones (the yields were 34% – 80%).[17, 69]

1,4-Naphthoquinones **101** containing the hydroxy and acetylenic groups in the quinoid ring undergo intramolecular cyclisation in the presence of CuC≡CPh under very mild conditions (pyridine – dioxane, 20 °C, 3 – 5 min) [69] to give the expected linear heterocyclic *para*-quinones **102** along with their isomers, *viz*., angularly fused *ortho*-quinones **103**.

2-Alkynyl-3-hydroxy-1,4-naphthoquinones can undergo cyclisation with the closure of the furan ring in the absence of catalysts as well.[69] At 110 °C, compounds **101** in toluene also give mixtures of heterocyclic *para*- and *ortho*-quinones, but in another ratio.

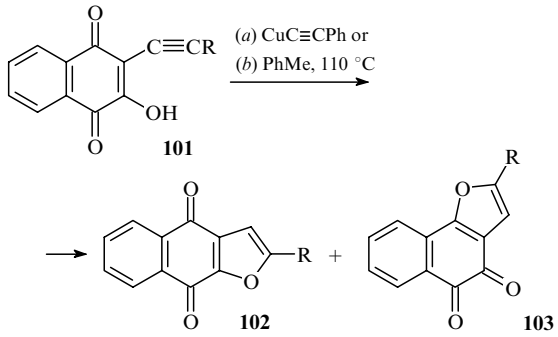

R	Reaction conditions	Yield (%)	
		102	**103**
Ph	*a*	59	16
	b	10	84
C_8H_{17}	*a*	23	6
	b	24	74

However, cyclocondensation of 2-halogeno-3-hydroxy-1,4-naphthoquinones **104** with Cu(I) acetylides at 100 °C proceeds regioselectively to form linear naphtho[2,3-*b*]furan-4,9-diones **102**.

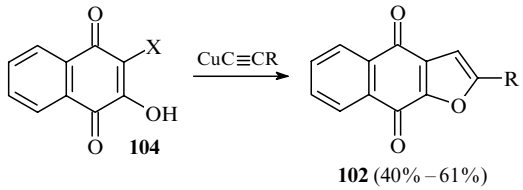

X = I, Br; R = Bu, C_8H_{17}, CH_2OMe, Ph.

b. Other reactions of the furan-ring closure

Angular annelation of the quinoid moiety with the furan ring occurred upon thermal cyclisation of 3-acetylamino-2-alkynyl-1,4-naphthoquinones **105**.[66]

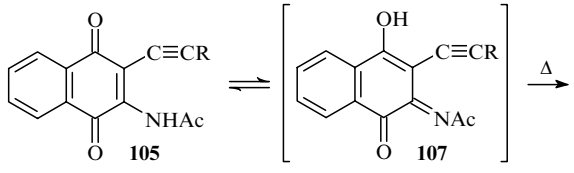

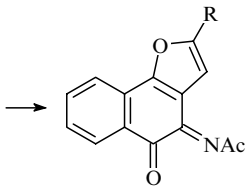

R = CMe_2OH, Ph.

The formation of products **106** can be attributed to the transformation of tautomer **107**. Actually, this cyclisation becomes impossible upon the replacement of the *N*-acetyl group by the *N*-alkyl group. Angular heterocyclisation is, apparently, associated with the acidic properties of the acetylamino group and, hence, structurally similar CH acids are also able to undergo this cyclisation. For example, malonic acid derivative **108** was transformed into naphthofuran **109** by heating in toluene in the presence of small amounts of CuC≡CPh and pyridine.[69]

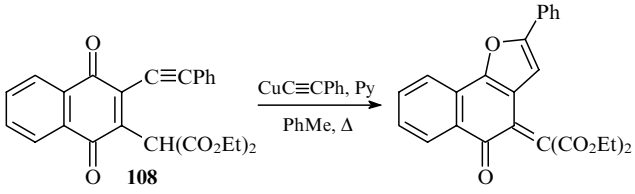

4. Pyridine-ring closure reactions

Intramolecular cyclisation of quinones bearing an acetylenic substituent and a nitrogen-containing group in the adjacent positions of the aromatic ring can be used for their annelation with the pyridine ring. Depending on the structures of the substituents involved in the formation of the heterocycle, the products contain either the quinoline or isoquinoline fragment.

a. Cyclisation of *vic*-alkynylanthraquinone aldoximes

1-Alkynylanthraquinone-2-aldoximes **110** are transformed into 2-substituted naphtho[2,3-*f*]isoquinoline-7,12-dione *N*-oxides **111** by refluxing in 90% aqueous EtOH in the presence of K_2CO_3 for 15 min. Compounds **111** can be reduced to the corresponding naphthoisoquinolinediones **112**.[35]

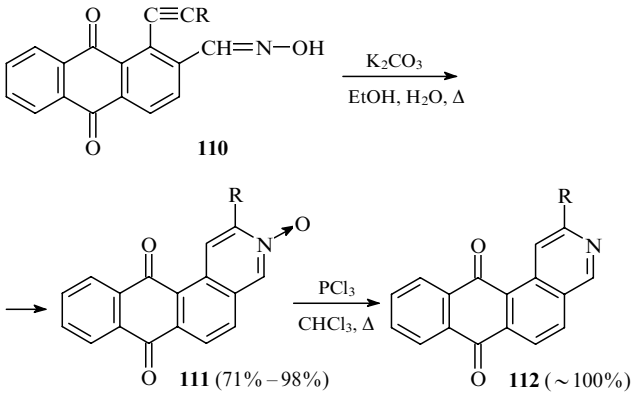

R = Bu, CH_2OPh, Ph.

This cyclisation was carried out also for analogous derivatives of indole,[73] benzene [64, 74] and pyridine.[64, 75]

b. Cyclisation of *vic*-amino(acylethynyl)- and *vic*-amino(ethoxycarbonylethynyl)anthraquinones

Another method for the construction of the anthrapyridine structure is based on the use of *vic*-acylethynyl derivatives of aminoanthraquinones **113**. This method involves the nucleophilic addition of amines (secondary or primary) at the activated triple

bond of the starting compound followed by intramolecular cyclisation of the adduct with the participation of the carbonyl group of the side chain and the aromatic amino group.[36, 58] The role of the amine addend consists, primarily, of changing the geometry of the unsaturated substituent resulting in a close arrangement of the reacting fragments, which is necessary for the closure of the heterocycle. In this case, the *Z* configuration of the adduct is reactive. The amino group introduced is retained in the newly formed pyridine ring.

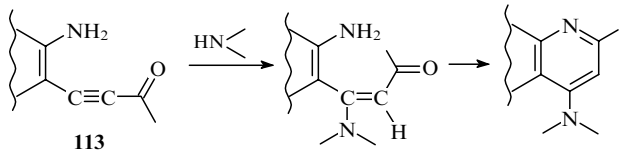

113

Substituted naphtho[2,3-*h*]quinoline-7,12-diones (**114**), naphtho[2,3-*f*]quinoline-7,12-dione (**115**) and naphtho[2,3-*g*]quinoline-6,11-dione (**116**) were synthesised by cyclisation of 2-acylethynyl-1-amino-, 1-acylethynyl-2-amino- and 3-acylethynyl-2-aminoanthraquinones, respectively.

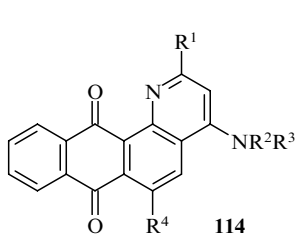

114

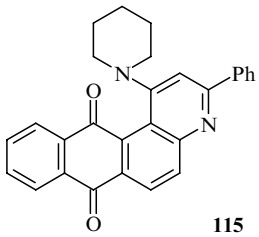

115

R^1 = Bu^t, Ph; R^2 = H, Et, R^3 = Et, Bu, C_8H_{17}; R^2-R^3 = $-(CH_2)_4-$, $-(CH_2)_5-$, $-(CH_2)_2O(CH_2)_2-$; R^4 = H, Cl, NO_2.

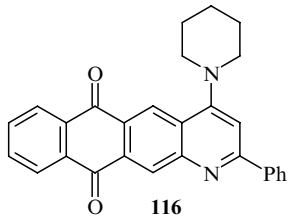

116

Cyclisation of adducts is carried out at room temperature (by shaking benzene solutions with dilute HCl over a short period of time or stirring with KOH in pyridine) or at 80 °C in the presence of $POCl_3$. In some cases, cyclisation proceeds already under the conditions of the preparation of the adduct (heating of acetylenic ketone **113** in an excess of amine). The rate of cyclisation depends on the structure of the adducts. Under alkaline conditions, the time of cyclisation of amino adducts of 1-amino-2-benzoylethynylanthraquinone is 5–15 min, whereas the time of cyclisation of the adduct of 2-amino-1-benzoylethynyl-3-chloroanthraquinone with piperidine is as large as 2 h due, apparently, to steric hindrance. Cyclisation of (monoalkylamino)vinyl ketones under the action of acids is more difficult to perform compared to that of analogous (dialkylamino)vinyl ketones. The yields of mono- and dialkylaminonaphthoquinolinediones in both acidic and basic media are in the range of 54%–100%.

Modified version of this method was used for the preparation of 4-aminonaphtho[2,3-*h*]quinoline-7,12-diones containing functional substituents at position 2.[25, 26] In this case, esters **117** rather than aminovinyl ketones are subjected to cyclisation (Scheme 3).

These compounds are transformed into 2-chloro-substituted 4-aminonaphthoquinolinediones **118** (in 41%–67% yields) under the action of $POCl_3$ in dioxane at 80 °C. The nucleophilic substitution of the labile halogen atom in the pyridine ring allows one to perform further modifications of the molecule.

The same 4-amino-2-chloronaphtho[2,3-*h*]quinoline-7,12-diones **118** can be prepared from esters **117** in two steps through δ-lactams (naphthoquinolinetriones **119**). The closure of the lactam ring in adducts **117** proceeds readily in the presence of solid KOH and dibenzo-18-crown-6 in benzene at 20 °C (the yields are 92%–97%). Under conditions of acid catalysis (H_2SO_4, benzene, 20 °C), adducts **117** give mixtures of lactams **119** and 4-amino-2-ethoxynaphthoquinolinediones **120** in a ratio of ~2 : 1. Naphthoquinolinetriones **119** are transformed into compounds **118** (in 67%–98% yields) by heating with $POCl_3$ in dioxane.

It should be noted that catalytic hydrogenation of secondary (1-aminoanthraquinon-2-yl)alk-1-yn-3-ols giving rise to *cis*-ethylenic alcohols and subsequent oxidation of the latter with MnO_2 or $CrO_3 \cdot 2\,Py$ can be used for the synthesis of naphtho[2,3-*h*]quinoline-7,12-diones, which are structurally analogous to compounds **114** but are devoid of the alkynylated amino group in the pyridine ring.[27] Naphthoquinolinediones **114** form chelate complexes with metal halides (Cr, Mn, Co, Cu, Ga, Zn, Pd, In or Ni) in which the nitrogen atoms of the heterocycle and the oxygen atom of the carbonyl group at position 12 are involved in coordination.[76] 4-Monoalkylamino derivatives **114** (R^3 = H) are involved in complexes as amino tautomers. Some aminonaphthoquinolinediones exhibit high cytotoxic activity with respect to malignant cells.[39, 77]

Scheme 3

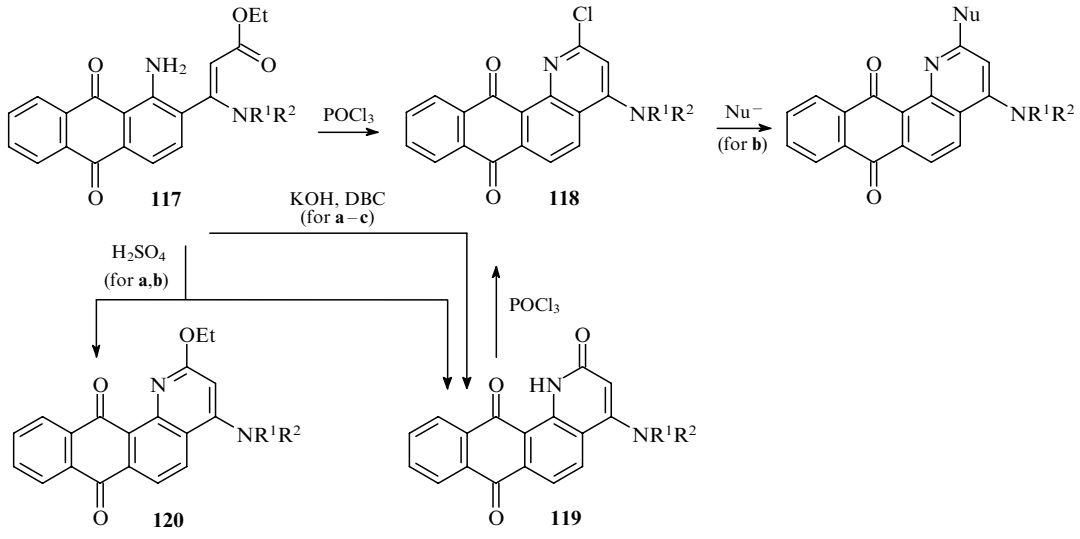

R^1 = R^2 = Et (**a**), R^1-R^2 = $-(CH_2)_5-$ (**b**); R^1 = H, R^2 = Bu (**c**); Nu = pip, SBu, $CH(CO_2Et)_2$; DBC is dibenzo-18-crown-6.

The above-considered method for heterocyclisation of acetylenic ketones through amino adducts is not specific only for anthraquinone derivatives.[36]

Under conditions of hydration of the triple bond, *vic*-amino(acylethynyl)anthraquinones **121** are subjected to cycloisomerisation to naphthoquinolinetriones **122**.[39,78,79] The reaction proceeds according to a scheme analogous to that of the formation of the aminonaphthoquinoline system under acidic conditions. Initially, water adds at the triple bond and then it is eliminated upon the closure of the heterocycle. Heterocyclisation is carried out either in concentrated H_2SO_4 at 75–85 °C or in the presence of $HgSO_4$ and a small amount of 50% H_2SO_4 by refluxing in dioxane.

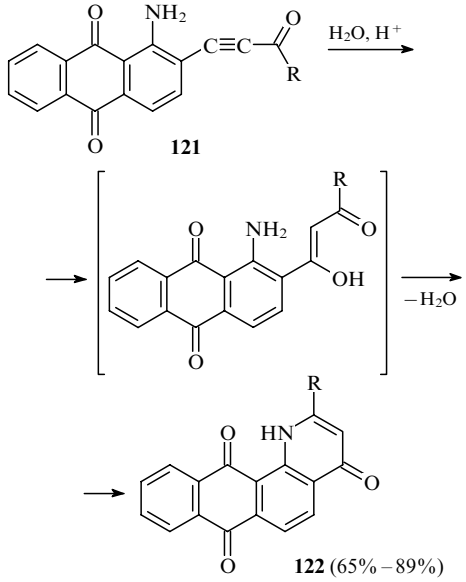

R = Bu^t, Ph.

Spectroscopic and quantum-chemical study of the structure of 1*H*-2-phenylnaphtho[2,3-*h*]quinoline-4,7,12-trione (**122**, R = Ph) demonstrated that this compound exists in the polarised quinolone form stabilised by an intramolecular hydrogen bond in both the crystalline state and solutions.[79]

Naphthoquinolinetriones **122** form labile complexes with Lewis acids ($GaCl_3$, $CoCl_2$, $MnCl_2$ or $CuCl_2$) in which the ligand is coordinated to the metal atom through the oxygen atom of pyridone.[80] Protonation of triones **122** also proceeds at this atom.[79]

5. Cyclisation with the pyrimidine-ring closure

N-(2-Phenylethynylanthraquinon-1-yl)-*N*′-phenylurea (**123**), which was prepared by the reaction of the corresponding amino(alkynyl)anthraquinone **76b** with PhNCO, underwent cyclisation to 1*H*-4-benzylidene-3-phenylnaphtho[2,3-*h*]quinazoline-2,7,12-trione (**124**) in the presence of KOH in aqueous DMSO.[81]

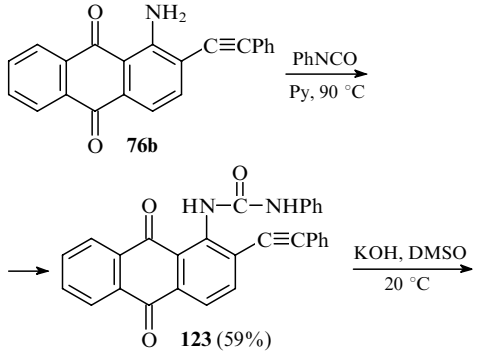

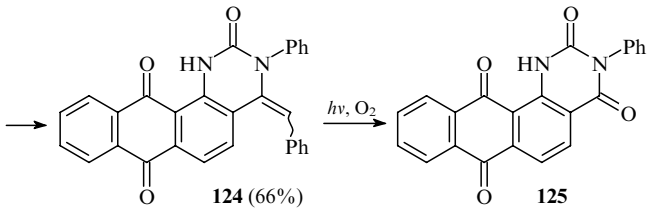

Product **124** was prepared as a mixture of *E* and *Z* isomers (in a ratio of 7 : 2). Upon photolysis (on SiO_2 or in solutions), the isomers are oxidised with atmospheric oxygen to 1*H*-3-phenylnaphtho[2,3-*h*]quinazoline-2,4,7,12-tetrone (**125**).

6. Pyrone-ring closure reactions

a. Reactions of *vic*-alkynylanthraquinonecarboxylic acids

In the presence of Cu(I) compounds, *vic*-acetylenic derivatives of anthraquinonecarboxylic acids (like those of other aromatic carboxylic acids) undergo cyclisation to give lactones. In these reactions, the closure of the γ- or δ-lactone rings (5-*exo*-dig or 6-*endo*-dig addition, respectively) can take place. 1-Alkynylanthraquinone-2-carboxylic acids form lactones in the presence of CuC≡CPh (pyridine, 20 °C, 77%–91% yields).[19] However, Cu-catalysed cyclisations of anthraquinonecarboxylic and parent benzoic acids follow different pathways. Thus anthraquinonecarboxylic acids have a tendency for 6-*endo*-dig addition (to form δ-lactones), whereas 5-*exo*-dig addition (giving rise to γ-lactones) is more typical of benzoic acids.[60,82]

1-Phenylethynyl- (**126a**) and hex-1-ynylanthraquinone-2-carboxylic acids (**126b**) give exclusively δ-lactones **127**, and only 1-(3-phenoxyprop-1-ynyl)-substituted acid (**126c**) forms a mixture of γ- and δ-lactones (**127** and **128**) in a ratio of 4 : 3.

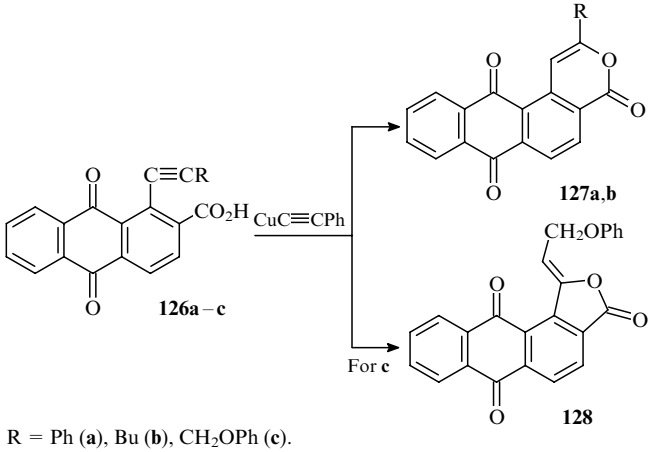

R = Ph (**a**), Bu (**b**), CH_2OPh (**c**).

b. Reactions of *vic*-acylethynyl(hydroxy)anthraquinones

The synthesis of anthra[1,2-*b*]pyran-4,7,12-triones attracts interest because this fused system represents a cyclic moiety of natural antitumour antibiotics of the kidamycin group[83–85] and their biologically active analogues prepared by biochemical methods.[86–88] 2-Acylethynyl-1-hydroxyanthraquinones (**129**, R^1 = H) serve as convenient precursors for the synthesis of these compounds. The simplest pathway of transformations of these compounds into target products **130** involves cyclisation under conditions of hydration of the triple bond.[39] The reaction proceeds readily in concentrated H_2SO_4 at 70–80 °C and is completed in 0.5–1.5 h. *O*-Acyl-substituted derivatives **129** (R^1 = COPh) can also be used in the synthesis.

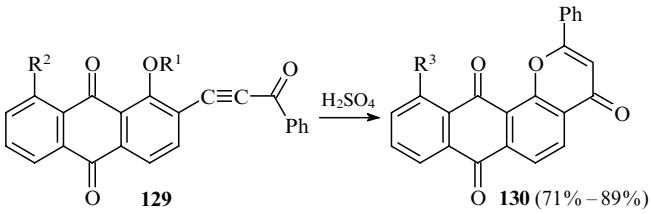

129 **130** (71% – 89%)

R^1 = H, PhCO; R^2 = H, OH, OAc; R^3 = H, OH.

Unfortunately, this procedure for the closure of the γ-pyrone ring is unsuitable for compounds containing acid-sensitive groups. Besides, kidamycin antibiotics contain unsaturated or epoxide fragments at position 2 of the anthrapyran moiety, which precludes the use of strongly acidic media in the synthesis of the starting compounds. However, under other conditions, the starting acetylenic ketones are more prone to cyclisation giving rise to a five-membered rather than a six-membered heterocycle.

It was expected that the use of alkynyl anthraquinonyl ketones **131a** as the starting compounds would facilitate the formation of the γ-pyrone ring and make it possible to perform cyclisation under rather mild conditions. In this connection, let us mention an attempt to prepare ketone **131a** by isomerisation of ketone **129a**.[39, 89, 90] Unfortunately, this isomerisation is accompanied by partial cyclisation of compound **131a** to isomeric furanone **132a**, which is also generated from **131a** by heating with CuC≡CPh in toluene at 90 °C.[39]

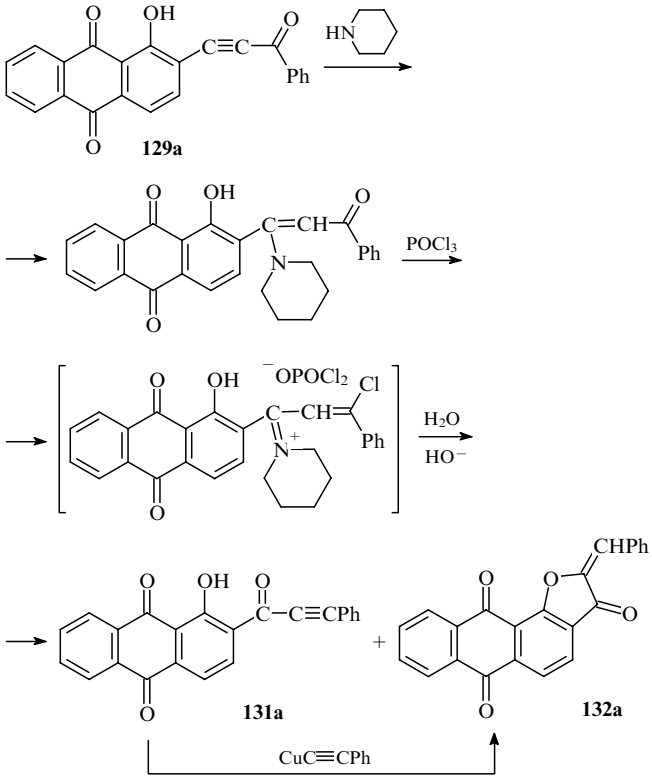

An alternative method for the synthesis of alkynyl hydroxyanthraquinonyl ketones **131** involves catalytic acylation of terminal acetylenes with 1-methoxyanthraquinone-2-carboxylic acid chloride (**133**) in the presence of $Pd(PPh_3)_2Cl_2$, CuI and Et_3N followed by removal of the methyl protective group.[91] Due to the presence of the carbonyl group in the *ortho* position, methoxy ketones **134**[92] are demethylated with Lewis acids under exceptionally mild conditions (dichloroethane, from −15 to −5 °C).

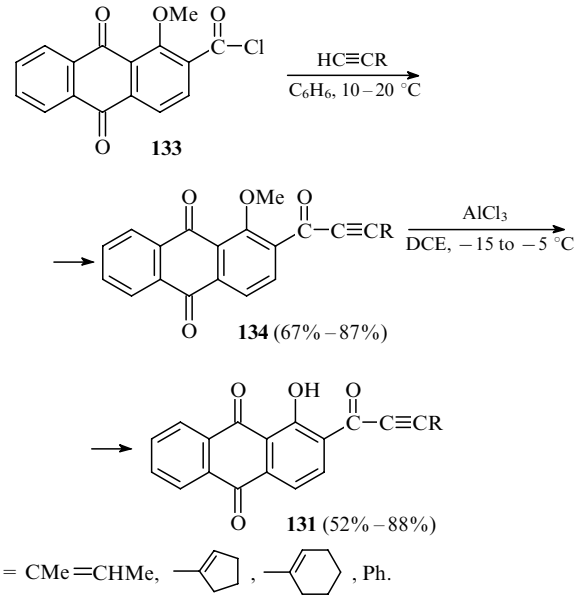

R = CMe=CHMe, , , Ph.

To develop a general procedure for cyclisation applicable to labile highly unsaturated hydroxy ketones, the transformation of 1-hydroxy-2-(1-oxo-3-phenylpropynyl)anthraquinone **131a** into phenylanthrapyrantrione **130a** was studied under various conditions.[39]

Evidently, in order for the desired six-membered ring to be formed, the oxygen atom of the hydroxy group and the γ-carbon atom of the acetylenic substituent must be brought into proximity, which is achieved by the attachment of secondary amine (for example, of piperidine) at the triple bond of the starting ketone. The resulting adduct **135** undergoes cyclisation with the closure of the γ-pyrone ring both under conditions of acid hydrolysis and base-catalysed intramolecular nucleophilic substitution of a secondary amino group. However, cyclisation of adduct **135** on SiO_2 as an adsorbent (82% yield) provides the formation of 2-phenylanthra[1,2-*b*]pyran-4,7,12-trione (**130a**) under the most mild conditions.

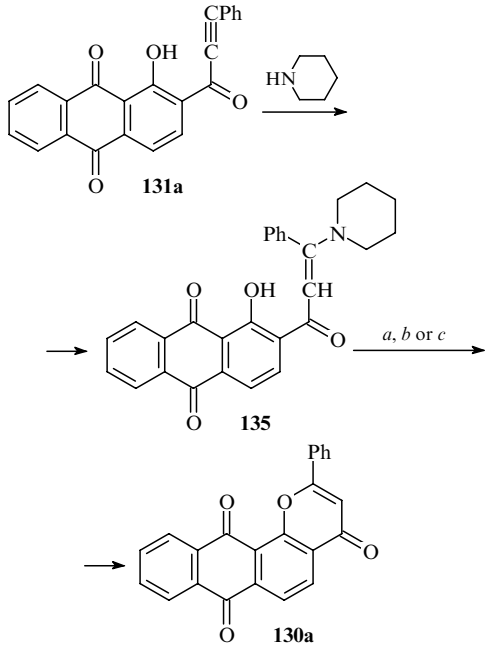

(*a*) H_2SO_4, $CHCl_3$ – dioxane – H_2O, 80 °C; (*b*) pip, C_6H_6, 80 °C; (*c*) SiO_2, $CHCl_3$.

This procedure was successfully extended to hydroxyanthraquinonyl vinylethynyl ketones[91] and opened the way to the synthesis of anthra[1,2-*b*]pyran-4,7,12-trione derivatives **136** containing unsaturated substituents at position 2.

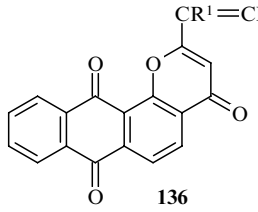

136

$R^1 = R^2 = Me$; $R^1 - R^2 = -(CH_2)_3-$, $-(CH_2)_4$.

7. Reactions with hydrazine

a. Cyclocondensation of *peri*-acetylenic derivatives of anthraquinone and naphthoquinone

1-Alkynylanthraquinones **11** react with hydrazine or hydrazine hydrate to form mixtures of substituted 4*H*-anthra[9,1-*cd*]-1,2-diazepin-8-one (diazepineanthrone **137**) and 7*H*-dibenzo[*de*,*h*]-quinolin-7-one (pyridineanthrone **138**), which are easily separated by chromatography (Scheme 4).[23, 93, 94]

Prolonged heating of diazepineanthrones **137** in pyridine in the presence of NH_2NH_2 leads to reductive elimination of one nitrogen atom from the seven-membered heterocycle giving rise to pyridineanthrones **138**. For example, the reaction of the compound with R = Ph is completed in 9 h at 115 °C (78% yield). This transformation occurs already under the conditions of cyclocondensation, and, hence, an increase in the reaction time leads to an increase in the percentage of pyridineanthrones **138** in a mixture of reaction products.

It is assumed that the mechanism of the seven-membered ring contraction involves hydration, ring opening and recyclisation to a six-membered ring followed by reduction with an excess of NH_2NH_2. The reduction step, unlike other steps, is irreversible.

Bulky substituents at position 2 of the starting alkynylanthraquinones hinder the formation of a seven-membered heterocycle. For example, fused pyridine derivative **140** is the only product generated from 1-(hex-1-ynyl)-2-diethoxymethylanthraquinone (**139a**).

In the presence of an alkoxycarbonyl substituent at position 2 (compounds **139b**–**e**), the reaction with hydrazine affords a mixture of substituted pyridineanthrone **141** and *N*-aminolactam **142**.[37, 93, 94] Apparently, the electron-withdrawing alkoxycarbonyl group enhances the reactivity of the acetylenic fragment and the reaction in refluxing EtOH is completed in 2–90 min (total yields are 72%–87%).

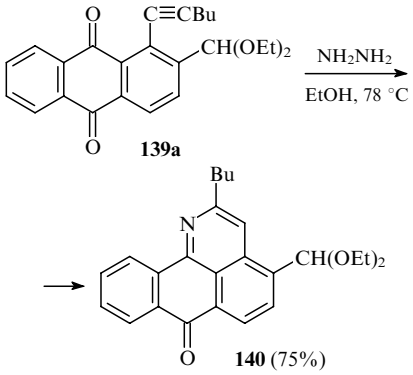

139a → **140** (75%)

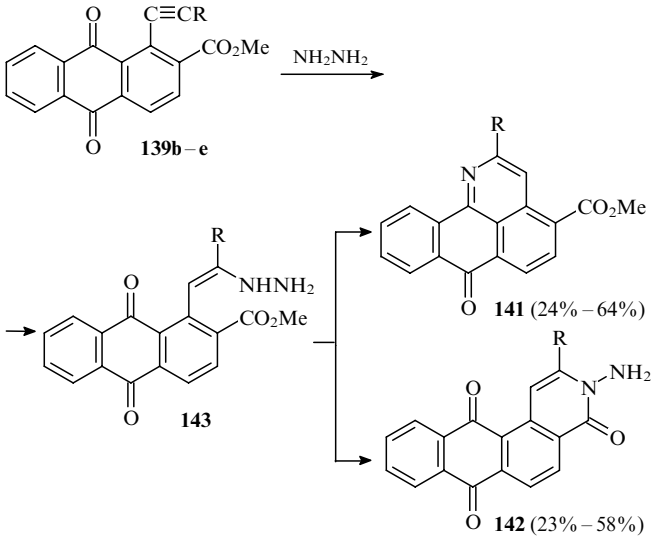

139b–**e** → **141** (24%–64%) + **142** (23%–58%) via **143**

R = H (**b**), Bu (**c**), CH_2OPh (**d**), Ph (**e**).

Investigation of the mechanism of formation of *N*-aminolactams **142** demonstrated that the reaction proceeds through adduct **143** as the intermediate. A comparison of the times of condensation of various acetylenic esters as well as the ratios between the reaction products showed that the formation of lactams through this adduct is the major pathway. It should be noted that cyclisation of *ortho*-alkynylbenzoic acid hydrazides proceeds with the closure of the γ-lactam ring.[95] Apparently, this difference is additional evidence for the fact that adducts **143**

Scheme 4

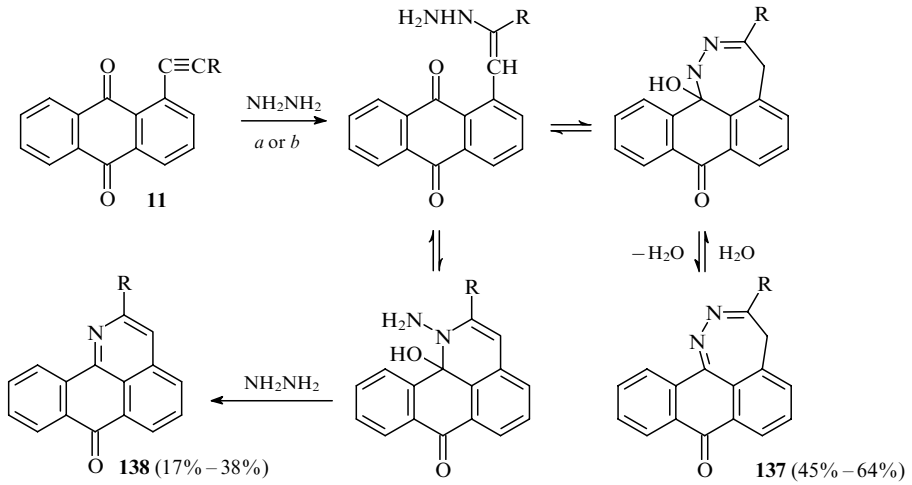

11 → **138** (17%–38%) + **137** (45%–64%)

R = Bu, Ph, CMe_2OH, CH_2OPh. (*a*) Py, 90–115 °C, 20–90 min; (*b*) EtOH, 78 °C, 10 h.

rather than acid hydrazides are initially generated in the course of cyclocondensation of compounds **139**.

N-Aminolactams **142** can also be prepared by hydrazinolysis of the corresponding lactones **127**.[37] The reaction involves the opening of the lactone ring to form labile 1-(2-oxoalkyl)anthraquinone-2-carboxylic acid hydrazides **144**, which undergo subsequent cyclisation. Deamination of aminolactams **142** under the action of oxygen in the presence of CuCl affords δ-lactams **145**.

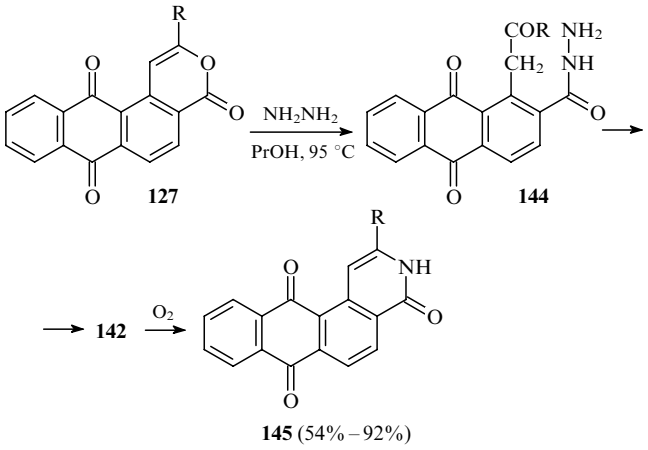

R = Bu, Ph.

Condensation of *peri*-acetylenic derivatives of 1,4-naphthoquinone with NH_2NH_2 follows a pathway which differs from that of *peri*-alkynylanthraquinones. For example, the reaction of 3-diethylamino-5-phenylethynyl-1,4-naphthoquinone (**146**, Ar = Ph) with an excess of $NH_2NH_2 \cdot H_2O$ in pyridine is accompanied by the closure of the pyridazine rather than the diazepine ring to form 3-benzyl-9-diethylaminobenzo[*de*]cinnolin-7-one (**147**) in 67% yield.[28,96]

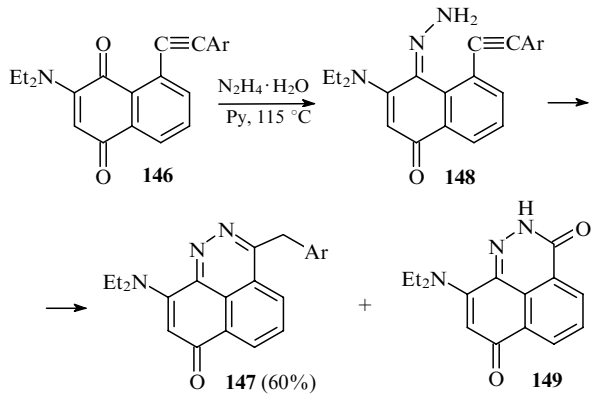

Ar = Ph, 4-$MeOC_6H_4$, 4-$NO_2C_6H_4$.

This pathway of cyclocondensation of *peri*-arylethynyl-1,4-naphthoquinones is attributable to the initial formation of hydrazone **148**, which undergoes subsequent cyclisation. This reaction is sensitive to the structure of the starting compound. For example, the introduction of the electron-donating methoxy group at the *para* position of the benzene ring of the acetylenic substituent (Ar = 4-$MeOC_6H_4$) leads to a substantial increase in the reaction time (from 8 to 35 h). In this case, the reaction mixture undergoes substantial resinification and the yield of the product sharply decreases. By contrast, the reaction with a compound containing the electron-withdrawing nitro group (Ar = 4-$O_2NC_6H_4$) proceeds vigorously and is completed in 1 – 3 min. In addition, the nitro group in the starting acetylene serves as an internal oxidiser, as a result of which compound **149**, which was generated due to oxidative elimination of the benzyl fragment, rather than the expected benzocinnolinone **147** (Ar = 4-$NO_2C_6H_4$) was obtained as the major product (the yields were 34% and 19%, respectively).

The replacement of the arylethynyl substituent in *peri*-alkynyl-1,4-naphthoquinones by a γ-hydroxyalkynyl group changes the regioselectivity of condensation.[28,97] Under the same conditions, the reactions of 3-diethylamino-5-(3-hydroxyalkyn-1-yl)-1,4-naphthoquinones **150** with $NH_2NH_2 \cdot H_2O$, unlike those of 5-arylethynyl derivatives **146**, lead to the closure of the seven-membered diazepine ring (analogously to the reactions of *peri*-alkynylanthraquinones).

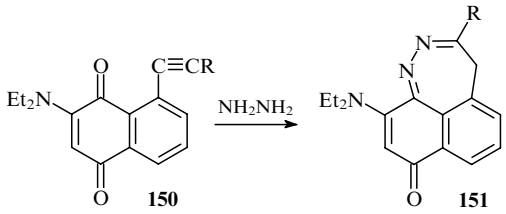

R = CMe_2OH, 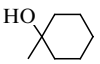 , 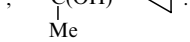

The reactions are completed in 5 – 6 h and are accompanied by noticeable resinification. Nevertheless, the preparative yields of substituted 4*H*-naphtho[1,8-*cd*]-1,2-diazepin-8-ones **151** are as high as 53% – 56%.

It is assumed that the direction of cyclisation changes due to association of the hydroxy group of the substrate with hydrazine *via* hydrogen bonds. As a result, the first step of condensation involves the addition of NH_2NH_2 at the triple bond rather than at the carbonyl group.

It should be noted that the nature of substituents in the quinoid ring of *peri*-alkynyl-1,4-naphthoquinones can also substantially influence the direction of their reactions with NH_2NH_2. For instance, the reaction of 2,3-dimethyl-5-phenylethynyl-1,4-naphthoquinone (**152**) involves reduction to the corresponding hydroquinone **153**, which undergoes subsequent cyclisation to give naphthopyran derivative **154**.[96]

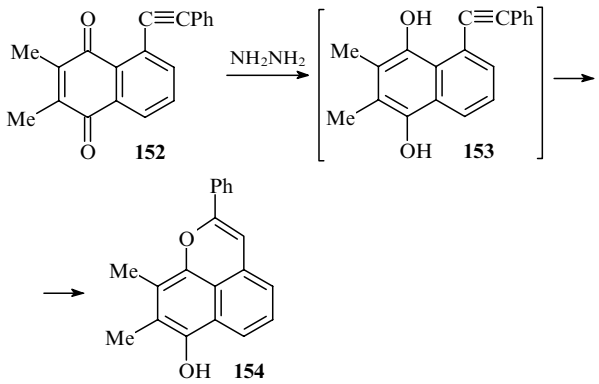

b. Cyclocondensation of 2-alkynyl-1-chloroanthraquinones

Several studies were devoted to cyclocondensation of aryl- and hetarylacetylenes containing the labile chlorine atom in the *ortho* position with hydrazine and its derivatives.[98 – 101] The reaction starts, apparently, with the replacement of the halogen atom[99] and always gives rise to a five-membered heterocyclic compound, *viz*., a derivative of pyrazole or *N*-substituted pyrrole.

2-Alkynyl-1-chloroanthraquinones **155**, in which the halogen atom has high nucleofugic lability, are readily condensed with NH_2NH_2 on heating in pyridine.[94,97] Under these conditions, the reactions of quinones bearing hydrocarbon (Alk or Ar) acetylenic substituents can follow two pathways with the pyrazole-ring closure involving either the carbonyl group of the quinoid ring (compound **156**) or the triple bond (compound **157**). The regioselectivity of the reaction depends on the nature of the substituent in the starting alkynylquinone.

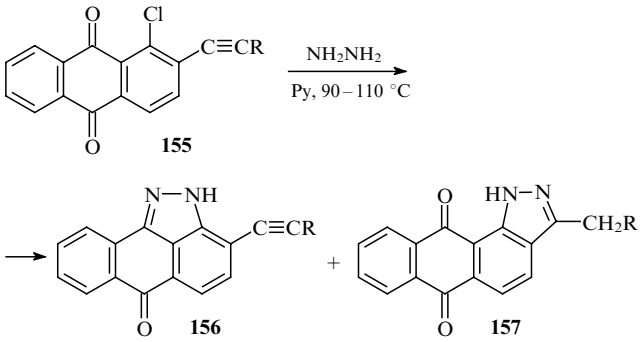

R	Yield (%)	
	156	**157**
Ph	44	22
C_5H_{11}	45	–

The introduction of the hydroxy or methoxy group at the γ position of the acetylenic substituent changes the regioselectivity of cyclocondensation. In this case, the reaction affords a compound containing the six-membered dihydropyridazine ring, *viz*., substituted 1,2-dihydronaphtho[2,3-*h*]cinnoline-7,12-dione (**158**), as the only product, which is readily oxidised with oxygen to give 1*H*-naphtho[2,3-*h*]cinnoline-4,7,12-trione (**159**).

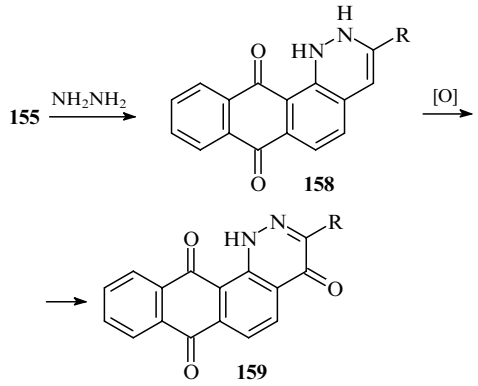

R = CH_2OH, $CH(OH)Pr^i$, CMe_2OH, $C(OMe)Me_2$.

A preparative one-pot procedure was developed for the synthesis of naphthocinnolinetriones **159** from alkynylquinones **155** with the use of 25% – 30% H_2O_2 as an oxidising agent, which is added to the reaction mixture after completion of cyclocondensation (20 – 40 °C, yields are 40% – 85%). This change in the direction of cyclocondensation is, apparently, attributable to association of hydrazine or the hydrazino group with the heterofunctional group *via* hydrogen bonds (see also Section III.7.a).

c. Reductive heterocyclisation of 2,3-dialkynyl-1,4-naphthoquinones

The enediyne system, which is partially involved in the quinoid ring, imparts particular chemical specificity to 2,3-dialkynyl-1,4-naphthoquinones **160**. Upon treatment with hydrazine in dioxane at 50 – 60 °C, these compounds undergo unusual heterocyclisation to give 1,3-disubstituted 2*H*-*N*-aminobenzo[*f*]isoindole-4,9-diones **161**.[94, 102] Apparently, the initial step of this reaction consists in reduction of the enediyne system to the tetraene one. The resulting bis-allenylidene intermediate **162** adds NH_2NH_2 at the double bonds activated by the carbonyl groups and undergoes isomerisation. Therefore, hydrazine serves as both a reducing and heterocyclising agent.

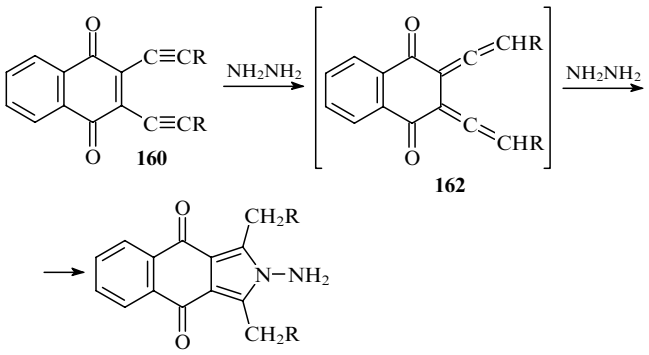

161 (53% – 80%)

R = $C(OH)Me_2$, 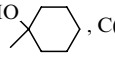 , $C(OMe)Me_2$, Ph.

According to the results of X-ray diffraction analysis, 2*H*-benzo[*f*]isoindole-4,9-dione is a planar polycyclic system. The distinguishing feature of this compound is that the quinoid and pyrrole rings share the aromatic C – C bond, which has a lower bond order. This bond length in the 2-amino-1,3-dibenzyl derivative is 1.434 Å (the other C – C bond lengths in the pyrrole ring are 1.370 Å).

Interestingly, a short time before the discovery of this heterocyclisation, the reaction of 2,3-diethynyl-5,6-dimethylhydroquinone (**163**) with primary amines was described.[103] The latter reaction gives rise to 2-substituted 1,3,5,6,-tetramethylisoindole-4,7-diones **164** and proceeds, in essence, by an analogous mechanism.

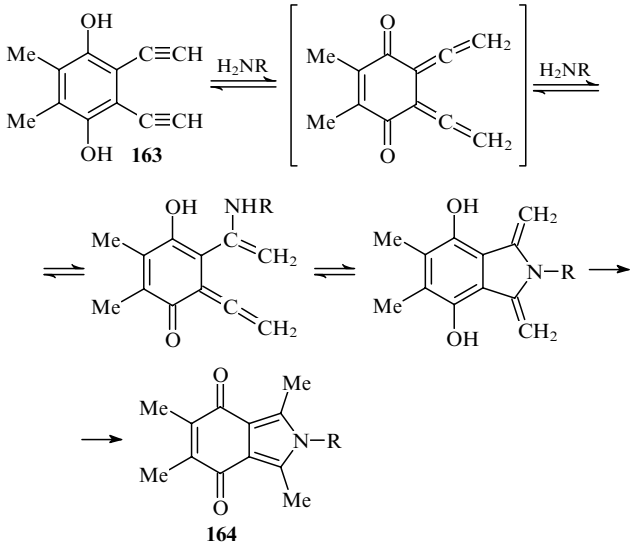

R = H, Me, Et, Pr, Bu, Ph.

A compound which bears the phenylethynyl substituents and is related to hydroquinone **163**, is not involved in analogous condensation with amines. Apparently, this may imply that cyclisation of bis-alkynyl-1,4-naphthoquinones does not afford bis-alkynylhydroquinones and the enediyne system of the substrate is reduced with hydrazine to the 1,2,4,5-tetraene system through another mechanism.

Taken together, these data provide a better insight into the essence of the chemical process responsible for both condensation reactions and give promise that a general procedure for the synthesis of this class of heterocyclic quinones will be developed.

8. Heterocyclisation of *vic*-acetylenic derivatives of anthraquinonediazonium salts

Intramolecular cyclisation of *ortho*-alkynylarenediazonium salts (Richter reaction) provides the basis for a general method for the synthesis of 4-hydroxy- and 4-halocinnolines.[104, 105] In attempting to extend this reaction to quinone derivatives, it was found that 2-alkynylanthraquinone-1-diazonium chlorides **165a**, which were prepared by diazotisation of the corresponding amines **166** ($NaNO_2$ in a mixture of dioxane and dilute HCl at 20 °C), underwent cyclisation to form the pyrazole rather than the pyridazine ring giving rise to 1*H*-3-(1,1-dichloroalkyl)- or 1*H*-3-acylnaphtho[2,3-*g*]indazole-6,11-diones of the general formula **167**.[24, 106, 107]

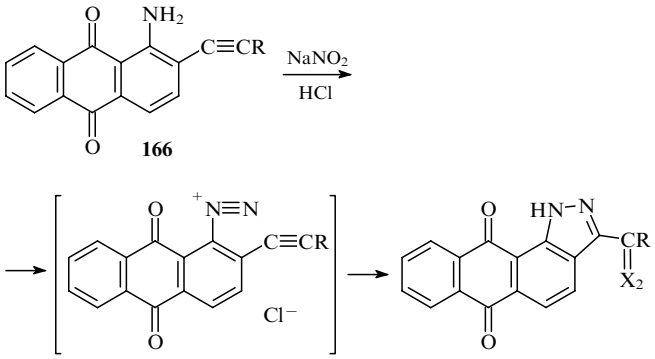

166 → **165a** → **167a**,**b** (62% – 83%)

R = H, Bu, CH_2OPh, , COPr, $COBu^t$, COPh, Ph;

X_2 = O (**167a**), Cl_2 (**167b**).

If the triple bond in the acetylenic substituent of the starting compound is conjugated with the carbonyl or aryl group, the reaction affords acyl derivatives of naphthoindazoledione **167a**,[107] otherwise it gives α,α-dichloroalkyl derivatives **167b**.[24] Cyclisation of the former proceeds more slowly.

Dichlorides **167b** can be transformed into the corresponding ketones by treatment with MeONa in MeOH followed by acid hydrolysis of the resulting acetals.[24]

In reactions with MeONa, 1*H*-3-[(1-hydroxycyclohexyl)dichloromethyl]naphtho[2,3-*g*]indazole-6,11-dione (**167b**, R = 1-HOC_6H_{10}), unlike other dichlorides, is subjected to dehydrochlorination accompanied by migration of the oxygen atom to give cyclohexenyl ketone **168**.[107] Apparently, the reaction proceeds through the intermediate formation of epoxide **169**.

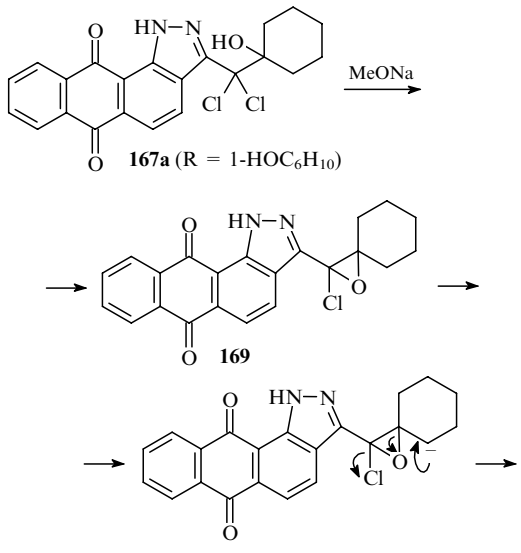

167a (R = 1-HOC_6H_{10}) → **169** → **168** (73%)

Cyclisation of diazo compounds **165b** was carried out under conditions which differ from those used for cyclisation of diazonium chlorides **165a**.[108] The steps of diazotisation of amines **166** and cyclisation of diazo compounds **165b** were separated. For this purpose, diazotisation of amines **166** was carried out in a mixture of acetone and dilute H_2SO_4 at 20 °C with the use of a 3 – 4 fold excess of $NaNO_2$, which made it possible to decrease the reaction time to 1 – 2 min. After completion of diazotisation, the solution of the diazonium salt was diluted with water or dilute H_2SO_4, thus providing the desired acidity of the medium in the step of cyclisation. The reaction was carried out at 65 °C. The exclusion of chloride anions from the reaction sphere changes its direction and the reaction affords naphthoindazolediones **167a** along with 1*H*-naphtho[2,3-*h*]cinnoline-4,7,12-triones **159**. The percentage of compounds **159** increases with increasing concentration of H_2SO_4 and they become virtually the only reaction products (yields are 71% – 91%) as the concentration of H_2SO_4 reaches 38%.

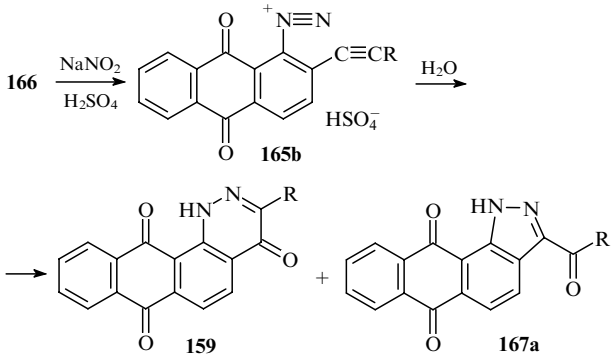

166 → **165b** → **159** + **167a**

R = H, Bu, $CH(OH)Pr^n$, $CH(OH)Pr^i$, CMe_2OH.

The reason for the influence of the counterions (Cl^- or HSO_4^-) on the course of cyclisation of salts **165** can be understood taking into account the data obtained in the in-depth study of the cyclisation mechanism of acetylenic derivatives of 1,4-naphthoquinone diazonium salts (see below).[109] In the case of highly nucleophilic chloride ions, 1-chloroalkylidene derivative **170** is generated as the key intermediate, which gives product **167a** or **167b** containing the five-membered ring. In the case of non-nucleophilic bisulfate ions, the nucleophilic addition of water giving rise to intermediate enol **171** takes place. The latter can undergo tautomerisation to ketone **167a** or rearrangement to pyridazine derivative **159**. This rearrangement becomes the major process as the concentration of the acid increases (Scheme 5). Therefore, cyclisation of diazonium salts prepared from 2-alkynyl-1-aminoanthraquinones enables one to synthesise derivatives of either 1*H*-naphtho[2,3-*g*]indazole-6,11-dione **167** or 1*H*-naphtho[2,3-*h*]cinnoline-4,7,12-trione **159** depending on the reaction conditions.

Cyclisation of naphthoquinonediazonium chloride **172** was carried out analogously to cyclisation of compounds **165b**.[109] The starting amine was diazotised with an excess of $NaNO_2$ in a mixture of dilute HCl and acetone and diluted with water, 18% HCl or a NaCl solution. It was found that the reaction proceeds through the formation of pyrazole intermediate **173**, which is subsequently transformed with either ring expansion or retention of the size of the heterocycle to give the final reaction products **174** – **176**. The compositions of the products depend on the cyclisation conditions.

In hydrochloric acid medium, intermediate **173** is generated at a high rate and a large portion of the diazo salt is transformed into

Scheme 5

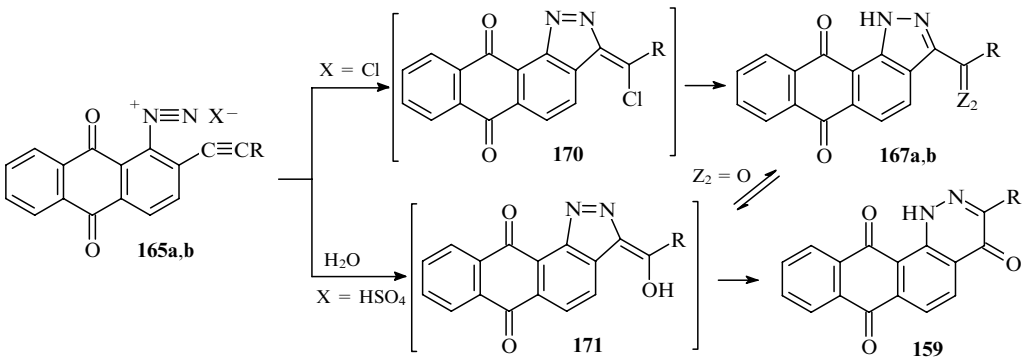

X = Cl (**a**), HSO_4 (**b**); Z_2 = O (**167a**), Cl_2 (**167b**).

this intermediate already within a few minutes. At that instant, the intermediate can be extracted from the reaction mixture with an organic solvent. Actually, it was isolated in this way in 79% yield. Intermediate **173** is chemically labile and can be transformed either with retention of the size of the heterocycle or its expansion not only in aqueous reaction systems but also on an adsorbent in an organic solvent. The mechanism of its transformation into the final products remains to be elucidated.

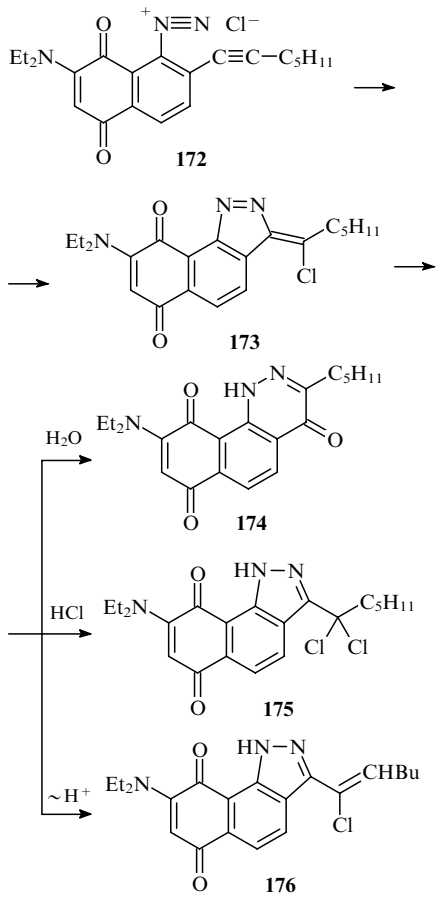

Reaction conditions	Yield (%)		
	174	**175**	**176**
H_2O, 20 °C, 5–6 h	80	–	–
HCl–$CHCl_3$, 7 h	25	60	16

Studies of cyclisation of alkynylquinonediazonium salts demonstrated that this process involves several steps. The reaction is, apparently, initiated by the attack of a nucleophile on the positively charged β-carbon atom of the acetylenic substituent resulting in the appearance of a negative charge on the α-carbon atom and a change in the geometry of this substituent. This leads to the closure of the heterocycle involving the α-C atom to give an intermediate of type **173**. It should be noted that the multistep mechanism of cyclisation of alkynylquinonediazonium salts is in contradiction with the mechanism of the Richter reaction represented as a concerted process of the direct formation of a six-membered heterocycle.[110]

9. Thermolysis of acetylenic derivatives of azidobenzoquinones

At temperatures above 75 °C, 3,6-dialkynyl-2,5-diazido-1,4-benzoquinones (**177**) are subjected to thermolysis to form alkynylcyanoketenes **178**.[111, 112] These compounds possessing the triple bond conjugated with the ketene group are unstable but can be fixed as rather stable adducts, for example, as azetidinones **179**, by performing the process in the presence of dicyclohexylcarbodiimide (DCC).[112]

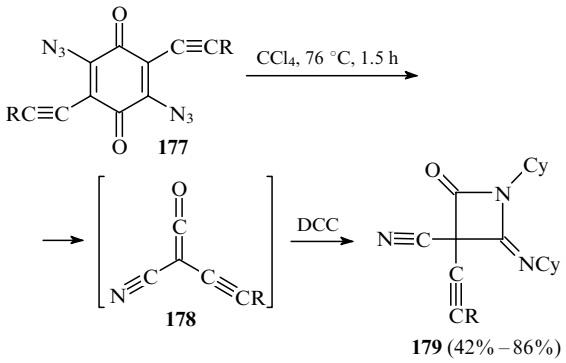

R = Bu (**a**), CMe=CH_2, CH_2OTHP, $(CH_2)_2Ph$, Ph, *o*-MeC_6H_4, *o*-$MeOC_6H_4$; Cy is cyclohexyl.

Schiff bases can also be used as trapping agents. For example, *N*-benzylideneaniline and *N*-(δ-phenylcinnamylidene)aniline react with ketene **178** to form β-lactams, whereas *N*-cinnamylideneaniline gives δ-lactams according to the [2+2]- and [2+4]-cycloaddition reactions, respectively.[111]

Alkynylcyanoketenes **178** are very reactive and, like most ketenes, are readily involved in cycloaddition to alkenes.[112] Hexynylcyanoketene **178a** reacts with substituted alkenes to form the corresponding substituted 2-(hex-1-ynyl)-2-cyanobutanones **180**. Cycloaddition of the ketene proceeds with retention of the configuration of alkenes.

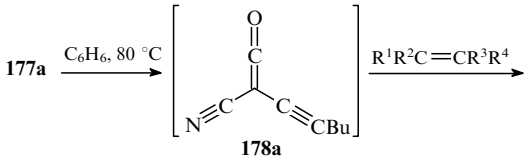

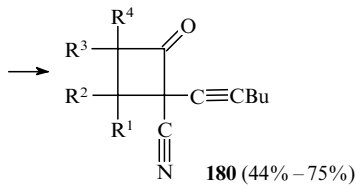

180 (44% – 75%)

$R^1 = R^3 = H$: $R^2 = R^4 = Et$, $R^2 – R^4 = –(CH_2)_4–$;
$R^1 = R^2 = R^3 = Me$: $R^4 = H$, Me.

The reactions of alkynylcyanoketenes **178** with alcohols are more complicated than those of simple ketenes.[111, 112] The initial nucleophilic attack of alcohol on the carbonyl group of ketene **178a** results in 1,4-addition to the enyne fragment to form 2-cyanoalka-2,3-dienoic acid ester (**181**). Then this allenic intermediate adds the second alcohol molecule to give 3-alkoxy-2-cyanoalk-2-enoic acid ester (**182**) as a mixture of *Z* and *E* isomers.

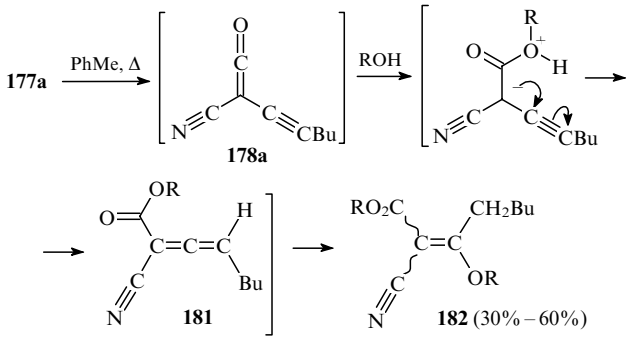

177a; **178a**; **181**; **182** (30% – 60%)

R = Pr^n, Pr^i, Bu^t, CH_2Ph.

The reaction is carried out by gradually adding a solution of 3,6-dialkynyl-2,5-diazido-1,4-benzoquinone **177** in toluene to refluxing alcohol.

4-Acetylenic derivatives of 3-azido-6-chloro-5-ethoxy-*o*-benzoquinone are also subjected to thermolysis giving rise to ketenes. For instance, refluxing of compound **183a** in cyclohexane affords (2-cyano-1-ethoxy-4-phenylbut-1-en-3-ynyl)chloroketene (**184**), which is easily trapped with dicyclohexylcarbodiimide as the corresponding azetidinone **185**.[113, 114]

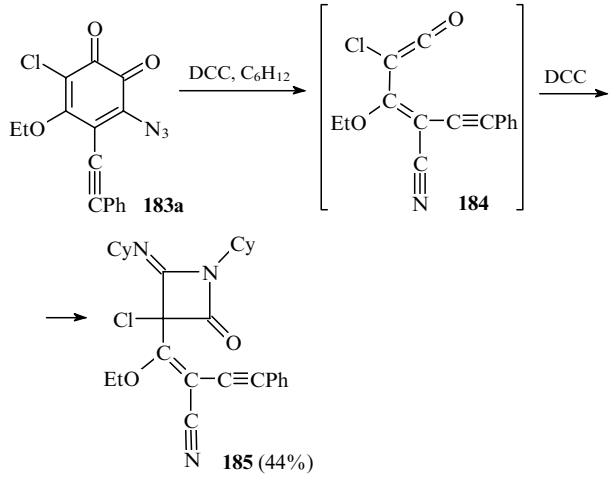

183a; **184**; **185** (44%)

Investigation of the reactions of ketenes generated from *o*-quinones **183** provided evidence that in the absence of trapping agents, these compounds undergo cyclisation to zwitterionic (or, probably, biradical) intermediate **186**, which is transformed into substituted phenol in reactions with external nucleophilic reagents or nucleophilic centres present in the molecule.[113] A solvent can also serve as a nucleophile when decomposition of the starting quinone is carried out by refluxing in benzene, *para*-xylene or thiophene.[113, 114] For example, products **187** – **191** are generated from azidoquinone **183a**.

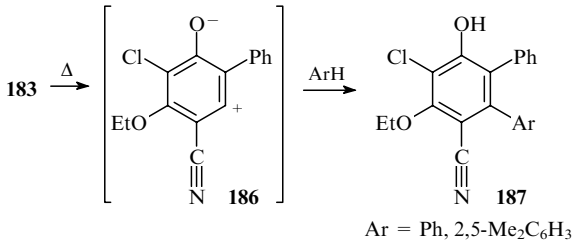

183; **186**; **187**

Ar = Ph, 2,5-$Me_2C_6H_3$

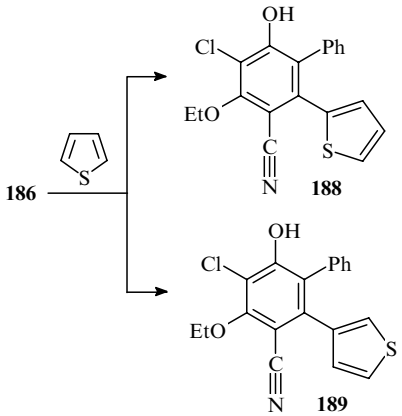

186; **188**; **189**

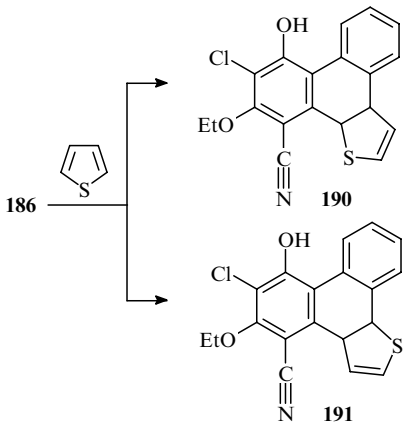

186; **190**; **191**

Thermolysis of compound **183a** in the presence of alkenes, in which the double bond is conjugated with the π electrons of the aromatic ring or the lone electron pair of the heteroatom, affords substituted dihydrophenanthrenes **192** (analogously to the reaction with thiophene, which gives rise to product **191**).

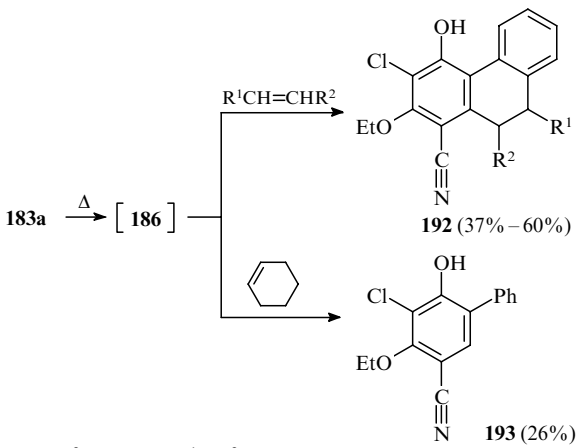

183a; **186**; **192** (37% – 60%); **193** (26%)

R^1 = Ph: R^2 = H, Ph; $R^1 – R^2 = –(CH_2)_3O–$.

Under these conditions, such alkenes as cyclohexene or tetramethylethylene do not form adducts of type **192** with quinone, but they can serve as hydrogen donors. For instance, thermolysis of phenylethynylquinone **183a** in the presence of cyclohexene afforded a complex mixture of compounds, from which only 2-chloro-4-cyano-3-ethoxy-6-phenylphenol (**193**) was isolated.[114]

Cyclic and acyclic ethers react with zwitterionic intermediate **186** in the presence of Me_3SiCl.[114]

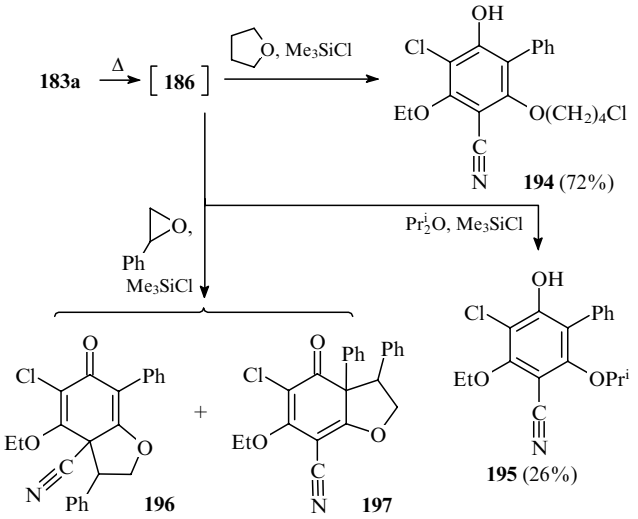

The reactions with tetrahydrofuran and diisopropyl ether give rise to alkoxy-substituted cyanophenols **194** and **195**. Under these conditions, styrene oxide produces two isomeric cyclohexadienones **196** and **197** in a ratio of ~1 : 1 in a total yield of 22%.

Thermal decomposition of compound **183a** in a mixture of ethyl acetate and cyclohexane in the presence of Me_3SiCl involves hydroxylation and partial acetoxylation of the zwitterionic intermediate to give resorcinol derivatives **198** and **199**.

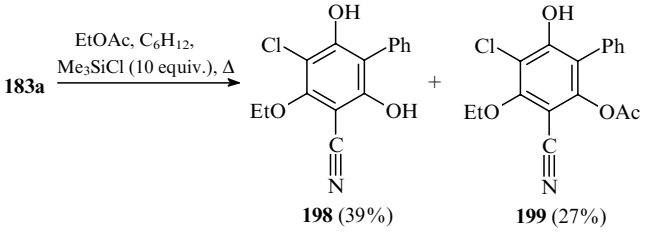

Intermediates generated upon thermolysis of other *ortho*-benzoquinones **183** can be stabilised intramolecularly with the involvement of a group of the acetylenic substituent to form polycyclic compounds (in 16% – 76% yields), which are difficult to prepare by other methods. In some cases, it is necessary to perform decomposition of the quinone in the presence of Me_3SiCl.

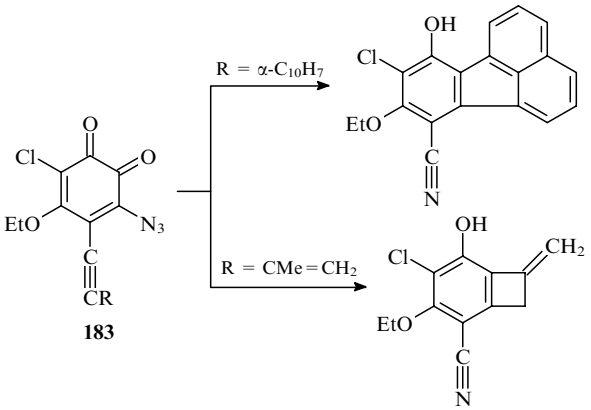

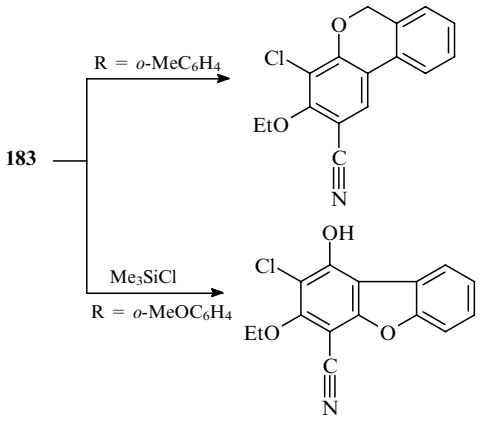

Thermal decomposition of the trimethylsilyl derivative of azido(ethynyl)-*o*-benzoquinone **183b** in benzene affords 2-chloro-4-cyano-5,8-etheno-3-ethoxy-5,8-dihydro-1-hydroxynaphthalene (**200**).[46] The authors believed that the reaction proceeds through biradical intermediate **201**, which is rearranged to substituted dehydrobenzene **202** through migration of $SiMe_3$ to the oxygen atom, and then compound **202** adds to benzene at positions 1,4.

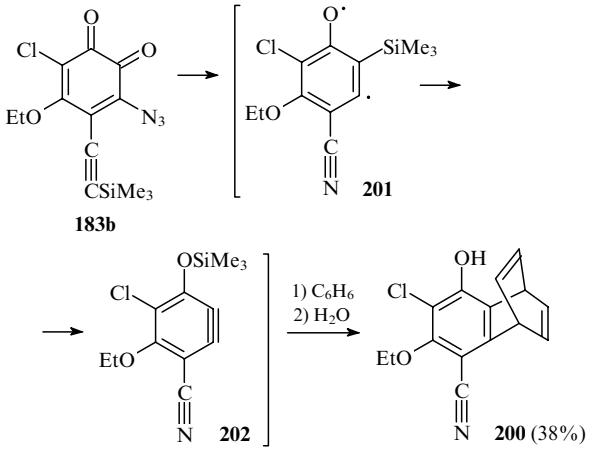

10. Other reactions

Alkynylquinones are involved in the addition reactions at the triple bond (for example, such as hydration or hydrogenation) which are typical of acetylenes of various classes. It was found that 1- and 2-acetylenic derivatives of anthraquinone add water in concentrated H_2SO_4 on heating to 40 – 80 °C for 1 – 5 min or in dioxane in the presence of catalytic amounts of $HgSO_4$ and dilute H_2SO_4 (80 °C). Ethynyl and phenylethynyl derivatives give the corresponding acetylquinones and phenacylquinones, respectively.[18, 19, 29, 30] Hydrogenation of the triple bond to the double bond in alkynylquinones on a deactivated palladium catalyst is generally accompanied by reduction of the carbonyl groups to give hydroquinones, which are readily oxidised with aqueous $FeCl_3$ or atmospheric oxygen in the course of isolation.[6, 31]

Ethynyl derivatives of quinones are also involved in usual reactions proceeding with the replacement of terminal hydrogen. Thus, *vic*-amino(ethynyl)anthraquinones are easily acylated by carboxylic acid chlorides in the presence of Et_3N and $Pd(PPh_3)_2Cl_2$ or the same palladium complex in combination with CuI in benzene. This method procedure was used for the synthesis of benzoylethynyl- and pivaloylethynylanthraquinones in 67% – 95% yields from 1-amino-2-ethynyl-, 1-amino-3-chloro-2-ethynyl- and 2-amino-3-ethynylanthraquinones.[36, 58, 78, 79] Cadiot – Chodkiewicz coupling of 3-diethylamino-5-ethynyl-1,4-naphthoquinone with 1-bromo-3-methylbut-1-yn-3-ol and Mannich aminomethylation of the former provide examples of the Cu-

catalysed replacement of the hydrogen atom of the ethynyl group in the quinone series.[69]

The alkaline cleavage of tertiary acetylenic alcohols (retro-Favorskii reaction), which is used for the synthesis of ethynyl-, diethynyl- and butadiynylquinones, belongs to a class of cleavage reactions in which the triple bond remains intact.[13, 14, 37, 69] Decomposition of alcohols is generally carried out in the presence of KOH (sometimes with an addition of dibenzo-18-crown-6 or a mixture of CaO and Na_2SO_4) in benzene or toluene at 60 – 110 °C (yields are 20% – 89%).

$$\mathrm{Quin[(C{\equiv}C)_{\mathit{n}}CMe_2OH]_{\mathit{m}}} \xrightarrow{\mathrm{KOH}} \mathrm{Quin[(C{\equiv}C)_{\mathit{n}}H]_{\mathit{m}}}$$

For the preparation of compounds containing the ethynyl group in the quinoid ring, this method is, apparently, applicable only in exceptional cases.[69]

IV. Conclusion

Acetylenic derivatives of quinones belong to a new group of polyfunctional compounds containing the activated triple bond. Their chemical properties are determined also by the presence of a mono- or polycyclic quinoid moiety containing a specific labile π-electron system and several reaction centres. Each reaction centre possesses particular inherent physicochemical properties, which influence each other and change the properties of the molecule as a whole. For instance, the triple bond in alkynylquinones possesses high electrophilicity due to the influence of the electron-withdrawing quinoid moiety regardless of the position of the acetylenic substituent, and this fact has a substantial effect on the reactivity of these compounds. For example, the nucleophilic addition of hydrazine at the triple bond of 1-alkynylanthraquinones, which proceeds readily and regiospecifically, leads to the closure of the sterically hindered diazepine ring involving the carbonyl group in the *peri* position. Under the reaction conditions, this ring can unexpectedly be transformed into the pyridine ring with a 'loss' of the nitrogen atom (see Section III.7.a). The ability to add N-nucleophiles in the absence of a catalyst also provides the basis for an original procedure for the closure of the pyrrole ring in *vic*-amino(alkynyl)anthraquinones (see Section III.2.b). Reductive cyclocondensation of 2,3-bis-alkynyl-1,4-naphthoquinones with NH_2NH_2 is used for the synthesis of isoindolequinones (see Section III.7.c), which are difficult to prepare by other methods. This reaction is *a priori* unpredictable and is, apparently, typical only of compounds containing two vicinal acetylenic substituents in the quinoid ring. Of other specific reactions of alkynylquinones, let us mention the non-trivial thermal cleavage of azidobenzoquinone derivatives, which serve as precursors of very reactive highly unsaturated ketenes (see Section III.9).

These and the above-considered data on the chemistry of acetylenic derivatives of quinones show that these compounds possess a high synthetic potential. It is evident that these compounds hold promise as key intermediates in the synthesis of fused heterocyclic quinoid structures with the aim of searching for new pharmaceuticals and industrial materials. These compounds are, apparently, applicable also for preparing immobilised biologically active quinones, film sensitisers, immobilised redox systems, components of liquid-crystalline composites, *etc*. However, some aspects of the chemistry of alkynylquinones remain unknown. Data on transformations of alkynyl-*ortho*-quinones and quinones containing acetylenic substituents in the quinoid ring are scarce. Efficient general methods for the synthesis of such compounds remain to be developed. The biological activities of alkynylquinones have been poorly studied.

This review will hopefully be found interesting and useful by chemists and contribute to the progress in the chemistry of acetylenic derivatives of quinones, their use in the practice of fine organic chemistry and pharmacological investigations.

References

1. *Methoden der Organischen Chemie (Houben-Weyl)* (4-te Aufl) (Stuttgart: Thieme, 1977) Bd. 7/3a, Tl. 1
2. *Methoden der Organischen Chemie (Houben-Weyl)* (4-te Aufl) (Stuttgart: Thieme, 1979) Bd. 7/3c, Tl. 1
3. M V Gorelik *Khimiya Antrakhinonov i Ikh Proizvodnykh* (The Chemistry of Anthraquinones and Their Derivatives) (Moscow: Khimiya, 1983)
4. H W Moore, Y-L Sing, R S Sidhu *J. Org. Chem.* **42** 3320 (1977)
5. M S Shvartsberg, A A Moroz, O D Kiseleva, A V Piskunov *Izv. Akad. Nauk SSSR, Ser. Khim.* 2154 (1979) [a]
6. H W Moore, Y-L Sing, R S Sidhu *J. Org. Chem.* **45** 5057 (1980)
7. A A Moroz, A V Piskunov, M S Shvartsberg *Izv. Akad. Nauk SSSR, Ser. Khim.* 386 (1981) [a]
8. M S Shvartsberg, A A Moroz, O D Kiseleva *Izv. Akad. Nauk SSSR, Ser. Khim.* 827 (1981) [a]
9. K F West, H W Moore *J. Org. Chem.* **47** 3591 (1982)
10. A A Moroz, I A Budzinskaya, T Z Mamedov, T P Galevskaya *Zh. Org. Khim.* **18** 1472 (1982) [b]
11. M S Shvartsberg *Izv. Sib. Otd. Akad. Nauk SSSR, Ser. Khim. Nauk* 875 (1983)
12. R Rossi, A Carpita, F Bellina *Org. Prep. Proced. Int.* **27** 127 (1995)
13. M S Shvartsberg, A A Moroz, N V Ivashkina, S B Cherepanov *Izv. Akad. Nauk SSSR, Ser. Khim.* 2485 (1986) [a]
14. A V Piskunov, A A Moroz, M S Shvartsberg *Izv. Akad. Nauk SSSR, Ser. Khim.* 828 (1987) [a]
15. A V Piskunov, A A Moroz, M S Shvartsberg *Izv. Akad. Nauk SSSR, Ser. Khim.* 864 (1986) [a]
16. Jpn. P. 61-17 533; *Ref. Zh. Khim.* 7 N 439P (1987)
17. A A Moroz, T P Galevskaya, M S Shvartsberg *Zh. Vsesoyuz. Khim. O-va im. D I Mendeleeva* **32** 711 (1987) [c]
18. M S Shvartsberg, A A Moroz, A V Piskunov, I A Budzinskaya *Izv. Akad. Nauk SSSR, Ser. Khim.* 2517 (1987) [a]
19. I D Ivanchikova, G E Usubalieva, P V Schastnev, A A Moroz, M S Shvartsberg *Izv. Akad. Nauk, Ser. Khim.* 2138 (1992) [a]
20. V S Romanov, A A Moroz, M S Shvartsberg *Izv. Akad. Nauk SSSR, Ser. Khim.* 851 (1985) [a]
21. M S Shvartsberg, A V Piskunov, A A Moroz *Izv. Akad. Nauk SSSR, Ser. Khim.* 1101 (1990) [a]
22. A V Piskunov, M S Shvartsberg *Izv. Akad. Nauk SSSR, Ser. Khim.* 1444 (1990) [a]
23. M S Shvartsberg, I D Ivanchikova, S F Vasilevskii *Izv. Akad. Nauk, Ser. Khim.* 2027 (1998) [a]
24. M S Shvartsberg, I D Ivanchikova, L G Fedenok *Izv. Akad. Nauk, Ser. Khim.* 1803 (1996) [a]
25. M S Shvartsberg, I I Barabanov, L G Fedenok *Mendeleev Commun.* 98 (1997)
26. I I Barabanov, L G Fedenok, M S Shvartsberg *Izv. Akad. Nauk, Ser. Khim.* 2327 (1998) [a]
27. I I Barabanov, L G Fedenok, N E Polyakov, M S Shvartsberg *Izv. Akad. Nauk, Ser. Khim.* 1585 (2001) [a]
28. I D Ivanchikova, R N Myasnikova, M S Shvartsberg *Izv. Akad. Nauk, Ser. Khim.* 1590 (2001) [a]
29. A V Piskunov, Candidate Thesis in Chemical Sciences, Novosibirsk Institute of Organic Chemistry, Siberian Branch of the Academy of Sciences of the USSR, Novosibirsk, 1986
30. I D Ivanchikova, Candidate Thesis in Chemical Sciences, Novosibirsk Institute of Organic Chemistry, Siberian Branch of the Russian Academy of Sciences, Novosibirsk, 1996
31. I I Barabanov, Candidate Thesis in Chemical Sciences, Novosibirsk Institute of Organic Chemistry, Siberian Branch of the Russian Academy of Sciences, Novosibirsk, 2002
32. T Sakamoto, F Shiga, A Yasuhara, D Uchiyama, Y Kondo, H Yamanaka *Synthesis* 746 (1992)
33. R E Dessy, S A Kandil *J. Org. Chem.* **30** 3857 (1965)
34. N V Ivashkina, V S Romanov, A A Moroz, M S Shvartsberg *Izv. Akad. Nauk SSSR, Ser. Khim.* 2561 (1984) [a]
35. I D Ivanchikova, A A Moroz, M S Shvartsberg *Izv. Akad. Nauk SSSR, Ser. Khim.* 1447 (1991) [a]
36. M S Shvartsberg, A V Piskunov, M A Mzhel'skaya, A A Moroz *Izv. Akad. Nauk, Ser. Khim.* 1423 (1993) [a]

37. I D Ivanchikova, R N Myasnikova, M S Shvartsberg *Izv. Akad. Nauk, Ser. Khim.* 2031 (1998) [a]
38. USSR P. 1 323 559; *Byull. Izobret.* (26) 119 (1987)
39. M A Mzhel'skaya, Candidate Thesis in Chemical Sciences, Novosibirsk Institute of Organic Chemistry, Siberian Branch of the Russian Academy of Sciences, Novosibirsk, 1996
40. USSR P. 1 019 789; *Byull. Izobret.* (47) (1983)
41. M Anastasia, P Allevi, C Bettini, A Fiecchi, A M Sanvito *Synthesis* 1083 (1990)
42. H W Moore, K F West, U Wriede, K Chow, M Fernandez, N V Nguyen *J. Org. Chem.* **52** 2537 (1987)
43. M S Shvartsberg, N V Ivashkina, A A Moroz, R N Myasnikova *Izv. Akad. Nauk SSSR, Ser. Khim.* 485 (1988) [a]
44. M S R Nair, M Anchel *Phytochemistry* **16** 390 (1977)
45. H Zimmer, D C Lankin, S W Horgan *Chem. Rev.* **71** 229 (1971)
46. K Chow, H W Moore *J. Org. Chem.* **55** 370 (1990)
47. P J Hanhela, D B Paul *Aust. J. Chem.* **34** 1687 (1981)
48. A Eckert *Monatsh. Chem.* **35** 289 (1914)
49. F Ullman, K L Klingenberg *Ber. Dtsch. Chem. Ges.* 46 712 (1913)
50. *Beilsteins Handbuch der Organischen Chemie* (4-te Aufl) (2-te Erg.) (Berlin, Göttingen, Heidelberg: Springer, 1948) Bd. 7, S. 778
51. R C Cambie, P S Rutledge, P D Woodgate *Aust. J. Chem.* **45** 483 (1992)
52. P J Boniface, R C Cambie, K S Higgs, P S Rutledge, P D Woodgate *Aust. J. Chem.* **48** 1089 (1995)
53. A P Stasyuk, V N Listvan, in *Tez. Dokl. 15 Ukr. Resp. Konf. po Organicheskoi Khimii, Uzhgorod, 1986* (Abstracts of Reports of the 15th Ukrainian Republic Conference on Organic Chemistry, Uzhgorod, 1986) p. 372
54. K Krohn, K Tolkiehn *Tetrahedron Lett.* 4023 (1978)
55. K Krohn, K Tolkiehn *Chem. Ber.* **113** 2976 (1980)
56. M S Shvartsberg, V S Romanov, O I Bel'chenko, P V Schastnev, A A Moroz *Izv. Akad. Nauk SSSR, Ser. Khim.* 842 (1985) [a]
57. A V Piskunov, M S Shvartsberg *Mendeleev Commun.* 155 (1995)
58. USSR P. 1 574 598; *Byull. Izobret.* (24) 89 (1990)
59. D E Ames, M I Brohi *J. Chem. Soc. Perkin Trans. 1* 1384 (1980)
60. C E Castro, E J Gaughan, D C Owsley *J. Org. Chem.* **31** 4071 (1966)
61. E C Taylor, A H Katz, H Salgado-Zamora, A McKillop *Tetrahedron Lett.* 5963 (1985)
62. D E Rudisill, J K Stille *J. Org. Chem.* **54** 5856 (1989)
63. R C Larock, L W Harrison *J. Am. Chem. Soc.* **106** 4218 (1984)
64. T Sakamoto, Y Kondo, H Yamanaka *Heterocycles* **27** 2225 (1988)
65. D Villemin, D Goussn *Heterocycles* **29** 1255 (1989)
66. V S Romanov, A A Moroz, M S Shvartsberg *Izv. Akad. Nauk SSSR, Ser. Khim.* 1090 (1985) [a]
67. I A Budzinskaya, Candidate Thesis in Chemical Sciences, Novosibirsk Institute of Organic Chemistry, Siberian Branch of the Academy of Sciences of the USSR, Novosibirsk, 1983
68. N P Gritsan, V M Shvartsberg, V S Romanov, M S Shvartsberg *Izv. Akad. Nauk SSSR, Ser. Khim.* 469 (1984) [a]
69. A A Moroz, Doctoral Thesis in Chemical Sciences, Novosibirsk Institute of Organic Chemistry, Siberian Branch of the Academy of Sciences of the USSR, Novosibirsk, 1988
70. N G Kundu, M Pal, J S Mahanty, S K Dasgupto *J. Chem. Soc., Chem. Commun.* 41 (1992)
71. S Torii, L H Xu, H Okumoto *Synlett* 515 (1992)
72. F Toda, M Nakagawa *Bull. Chem. Soc. Jpn.* **33** 1287 (1960)
73. T A Prikhod'ko, S F Vasilevskii, M S Shvartsberg *Izv. Akad. Nauk SSSR, Ser. Khim.* 2602 (1984) [a]
74. T Sakamoto, Y Kondo, N Miura, K Hayashi, H Yamanaka *Heterocycles* **24** 2311 (1986)
75. A Numata, Y Kondo, T Sakamoto *Synthesis* 306 (1999)
76. V V Davydov, M G Sarabia, A I Ezhov, G V Sheban, S L Kuznetsov, M A Mzhel'skaya, A V Piskunov, M S Shvartsberg, B E Zaitsev *Koord. Khim.* **20** 144 (1994) [d]
77. S I Dikalov, G V Rumyantseva, A V Piskunov, L M Weiner *Biochemistry* **31** 8947 (1992)
78. USSR P. 1 574 597; *Byull. Izobret.* (24) 88 (1990)
79. B E Zaitsev, V V Davydov, M G Sarabia, M S Shvartsberg, M A Mzhel'skaya, G V Sheban *Zh. Obshch. Khim.* **63** 389 (1993) [e]
80. V V Davydov, B E Zaitsev, M G Sarabia, M S Shvartsberg, M A Mzhel'skaya, G V Sheban, A I Ezhov *Zh. Obshch. Khim.* **63** 398 (1993) [e]
81. V A Savel'ev, V A Loskutov *Khim. Geterotsikl. Soedin.* 791 (1991) [f]
82. T Sakamoto, M Annaka, Y Kondo, H Yamanaka *Chem. Pharm. Bull.* **34** 2754 (1986)
83. I Hoyakawa, M Furukawa, G Ohta *Tetrahedron* **31** 2989 (1975)
84. G M Brill, J B McAlpine, D N Whittern, A M Buko *J. Antibiot.* **43** 229 (1990)
85. U Sequin *Tetrahedron* **34** 761 (1978)
86. Jpn. P. 61/189 280; *Chem. Abstr.* **106** 65 844 (1987)
87. Eur. P. 326 173; *Chem. Abstr.* **113** 22 200 (1990)
88. Jpn. P. 61/224 992; *Chem. Abstr.* **106** 137 013 (1987)
89. M S Shvartsberg, L G Fedenok *Izv. Akad. Nauk SSSR, Ser. Khim.* 2094 (1990) [a]
90. USSR P. 1 616 896; *Byull. Izobret.* (48) 80 (1990)
91. M A Mzhel'skaya, A A Moroz, M S Shvartsberg *Izv. Akad. Nauk SSSR, Ser. Khim.* 1656 (1991) [a]
92. L G Fedenok, R N Myasnikova, M S Shvartsberg *Izv. Akad. Nauk SSSR, Ser. Khim.* 1836 (1985) [a]
93. M S Shvartsberg, I D Ivanchikova, S F Vasilevsky *Tetrahedron Lett.* **35** 2077 (1994)
94. M S Shvartsberg, I D Ivanchikova, I I Barabanov, in *Azotistye Geterotsikly i Alkaloidy (Tez. Dokl. 1 Mezhdunarod. Konf. 'Khimiya i Biologicheskaya Aktivnost' Azotistykh Geterotsiklov i Alkaloidov')* [Nitrogenous Heterocycles and Alkaloids (Abstracts of Reports of the First International Conference 'The Chemistry and Biological Activity of Nitrogenous Heterocycles and Alkaloids')] (Moscow: Iridium-press, 2001) Vol. 1, p. 582
95. S F Vasilevskii, A V Pozdnyakov, M S Shvartsberg *Izv. Akad. Nauk SSSR, Ser. Khim.* 1367 (1985) [a]
96. M S Shvartsberg, I D Ivanchikova *Tetrahedron Lett.* **41** 771 (2000)
97. I I Barabanov, I D Ivanchikova, M S Shvartsberg *Mendeleev Commun.* 188 (2000)
98. D E Ames, D Bull *Tetrahedron* **38** 383 (1982)
99. S F Vasilevsky, T A Prikhod'ko *Mendeleev Commun.* 98 (1996)
100. T A Prikhod'ko, S F Vasilevsky *Mendeleev Commun.* 149 (1998)
101. T A Prikhod'ko, S F Vasilevsky *Izv. Akad. Nauk, Ser. Khim.* 1210 (2001) [a]
102. M S Shvartsberg, I D Ivanchikova, N I Lebedeva *Tetrahedron Lett.* **41** 5757 (2000)
103. M Chakraborty, D B McConville, G F Koser, C A Tessier, T Saito, P L Rinaldi, W J Youngs *J. Org. Chem.* **62** 8193 (1997)
104. A E A Porter in *Comprehensive Organic Chemistry* Vol. 4 (Oxford: Pergamon Press, 1979)
105. S F Vasilevsky, E V Tretyakov, H D Verkruijsse *Synth. Commun.* **24** 1733 (1994)
106. M S Shvartsberg, I D Ivanchikova, L G Fedenok *Tetrahedron Lett.* **35** 6749 (1994)
107. I D Ivanchikova, L G Fedenok, M S Shvartsberg *Izv. Akad. Nauk, Ser. Khim.* 110 (1997) [a]
108. L G Fedenok, I I Barabanov, I D Ivanchikova *Tetrahedron* **57** 1331 (2001)
109. L G Fedenok, I I Barabanov, I D Ivanchikova *Tetrahedron Lett.* **40** 805 (1999)
110. K Schofield, T Swain *J. Chem. Soc.* 2393 (1949)
111. N V Nguyen, H W Moore *J. Chem. Soc., Chem. Commun.* 1066 (1984)
112. N V Nguyen, K Chow, H W Moore *J. Org. Chem.* **52** 1315 (1987)
113. N V Nguyen, K Chow, J O Karlsson, R Doedens, H W Moore *J. Org. Chem.* **51** 419 (1986)
114. H W Moore, K Chow, N V Nguyen *J. Org. Chem.* **52** 2530 (1987)

[a] — *Russ. Chem. Bull., Int. Ed. (Engl. Transl.)*
[b] — *Russ. J. Org. Chem. (Engl. Transl.)*
[c] — *Mendeleev Chem. J. (Engl. Transl.)*
[d] — *Russ. J. Coord. Chem. (Engl. Transl.)*
[e] — *Russ. J. Gen. Chem. (Engl. Transl.)*
[f] — *Chem. Heterocycl. Compd. (Engl. Transl.)*

Russian Chemical Reviews **73** (2) 185 – 194 (2004) © 2004 Russian Academy of Sciences and Turpion Ltd

DOI 10.1070/RC2004v073n02ABEH000773

Chemical transformations of chlorophyll and its application in the design of a new generation of environmentally safe dyes

B D Berezin, S V Rumyantseva, A P Moryganov, M B Berezin

Contents

I.	Introduction	185
II.	Structure and chemical transformations of chlorophyll	185
III.	Chromophore systems of chlorophyll, its derivatives and analogues	188
IV.	Photochemical stability of chlorophyll and its derivatives	189
V.	Properties of chlorophyll and its derivatives in solutions. Solubility of porphyrins and energetics of solvation	190
VI.	Use of porphyrins and chlorins for dyeing textiles	192

Abstract. Chemical transformations of chlorophyll and physicochemical properties of its derivatives are considered. These compounds can be used in the design of a new generation of chlorophyll- and porphyrin-based dyes environmentally more safe than currently used arene dyes and possessing renewable sources of raw materials. The first results on the use of chlorophyll derivatives for dyeing wool, acetate fibres and cotton are reported. The bibliography includes 91 references.

I. Introduction

Chlorophyll as one of the main representatives of the plant world has been a subject of keen interest for investigators for many years.[1–8] An important characteristic feature of chlorophyll is its ability to absorb solar energy and to transform it into chemical energy in a photochemical reaction of water with carbon dioxide occurring in plant cells:

$$6\,H_2O + 6\,CO_2 \xrightarrow{h\nu} C_6H_{12}O_6 + 6\,O_2. \qquad (1)$$

This process represents a key reaction of photosynthesis of carbohydrates and ATP in the green leaf. The energy liberated in the decomposition of ATP is utilised for the synthesis of all the other classes of biomolecules.[9–16]

The specific chemical, photochemical and photophysical properties of chlorophyll attract attention with regard to the practical application of its derivatives in phototransformation of solar energy,[17] semiconductor engineering,[18] photochemical and electrochemical catalysis,[19] generation of singlet molecular oxygen,[20] thermo- and photostabilisation of fats and polymers,[21] *etc.*

Numerous vitally important applied problems (*e.g.*, purification of waste and heat-carrier gases, design of gas- and ion-sensitive electrodes, production of pure oxygen from atmospheric air, photodynamic therapy of cancerous diseases, *etc.*) that can be solved using chlorophyll derivatives and its structural analogues have been repeatedly discussed in the literature.[4, 22, 23]

One of the main challenges for investigators is the design of up-to-date high-quality dyes manifesting high chemical, thermal and photo stability, spectral colour purity and environmental safety as regards their manufacture and application in the textile, paint-and-varnish, printing, food and light industries. Complexes of Cu, Zn, Fe, Co, Ni and other metals with porphyrins and chlorins derived from chlorophyll meet all these requirements.

II. Structure and chemical transformations of chlorophyll

Specific chemical, spectral, chromophore and photochemical properties of chlorophyll **1** and pheophytin **2**, which determine their biological functions and natural coloristic characteristics, are due to the presence of a macrocyclic aromatic nucleus and functional groups in their molecules. These include a vinyl group, a cyclopentenone ring and two ester groups, *viz.*, a propionyl residue esterified by phytol in position 7 and a methoxycarbonyl group in position 10. Besides, the active reaction centre of chlorophyll **1** is represented by a Mg^{2+} ion coordinated to four pyrrole nitrogen atoms, while the active centre of pheophytin **2** contains two proton-donor (−NH−) and two basic (=N−) groups. The C(10)−H bond is strongly polarised due to the presence of three electronegative fragments (C=O, CO_2Me and the π-system of the macroring) and is therefore chemically active.

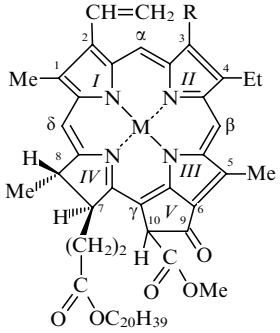

1, **2**

1: M = Mg, R = Me (**a**), CHO (**b**);
2: M = 2H, R = Me (**a**), CHO (**b**).

B D Berezin, S V Rumyantseva, A P Moryganov, M B Berezin
Institute of Solution Chemistry, Russian Academy of Sciences,
Akademicheskaya ul. 1, 153045 Ivanovo, Russian Federation.
Fax (7-093) 233 62 59. Tel. (7-093) 233 62 59.
E-mail: nvc@isc-ras.ru (B D Berezin).
Tel. (7-093) 233 62 90 (S V Rumyantseva). Tel. (7-093) 233 62 61.
E-mail: npp@isc-ras.ru (A P Moryganov). Tel. (7-093) 233 62 72.
E-mail: eva@isc-ras.ru (M B Berezin)

Received 14 January 2003
Uspekhi Khimii **73** (2) 197 – 207 (2004); translated by R L Birnova

It is impossible to consider the whole range of essential characteristics of chlorophyll and pheophytin in one review; therefore, we thought it expedient to highlight only chemical transformations of chlorophyll into its derivatives possessing all the properties of industrial dyes.

One of the main chemical features of chlorophyll is its ability to eliminate Mg^{2+} in acidic media to be converted into pheophytin:

$$MgChl + 2H_3O^+ \rightleftharpoons Mg^{2+}\cdot(H_2O)_2 + H_2Chl, \qquad (2)$$

where MgChl is chlorophyll and H_2Chl is pheophytin.

The dissociation of chlorophyll in various organic solvents has been studied in detail. The activation parameters and the mechanism of reaction (2) depending on the specific characteristics of the medium were established.[4] Pheophytin formed upon dissociation of chlorophyll reacts with metal salts in organic solvents (at high rates in carboxylic acids and alcohols and at low rates in pyridine and DMSO)[4] to give metallopheophytinates MChl.

$$MX_2(Solv)_{n-2} + H_2Chl \rightleftharpoons MChl + 2HX + (n-2)Solv, \qquad (3)$$

where MX_2 is the metal salt and Solv are the coordinated solvent molecules.

Pheophytin complexes with d-metals are much more stable than chlorophyll with the exception of Cd^{2+} and Hg^{2+} pheophytinates which, in contrast to MgChl, dissociate in carboxylic acids virtually instantaneously. Stable pheophytin metal complexes, like those of chlorophyll, can find application as dyes.

Yet another important feature of chlorophyll and pheophytin is their ability to undergo opening of the cyclopentenone ring. In contrast to four pyrrole rings (*I*–*IV*), the cyclopentenone ring (*V*) polarised by a keto group is insufficiently stable and contains a mobile hydrogen atom in position 10. The ring *V* causes significant distortions in the geometrical parameters of the planar chlorin macrocycle. The opening of the cyclopentenone ring occurs under the action of various reagents (*e.g.*, OH^-, O_2, amines, *etc.*). The oxidative destruction and opening of the cyclopentenone ring result in the formation of chlorin e_6 (**3**) from chlorophyll *a* (**1a**), and of rhodin g_7 (**4**) from chlorophyll *b* (**1b**).

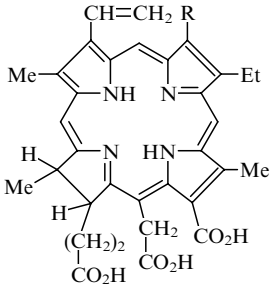

3, 4

R = Me (**3**), CHO (**4**).

This reaction is most often preceded by keto–enol tautomerism:

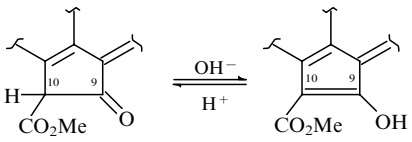

(4)

The reaction of a ketone with the OH^- ion may follow two different routes: one of them leads to ionisation of the C(10)–H bond, while the other one entails nucleophilic addition of OH^- to the C(9) atom with subsequent elimination of the H_2O molecule. The enol thus formed is unstable and is rapidly and irreversibly decomposed in alkaline solutions with the opening of the cyclopentenone ring.

The kinetics of cleavage of the cyclopentenone ring was studied under various conditions.[24,25] The addition of 0.1 M CsOH causes changes in the electronic absorption spectrum of pheophytin *a* manifested in the appearance of strong absorption in the region of 460–520 nm and a decrease in the intensity of the first absorption band [λ_I = 667 nm in an ethyl acetate–methanol mixture (12 : 1)]. In this reaction, known in chlorophyll biochemistry as the Molisch 'phase test', an unstable yellow-coloured enol form of chlorophyll or pheophytin (**5**) is initially formed. The electronic spectrum recorded 135 min after the onset of the reaction resembles that of the original pheophytin owing to the formation of a tricaesium salt of chlorin e_6 (**6**):

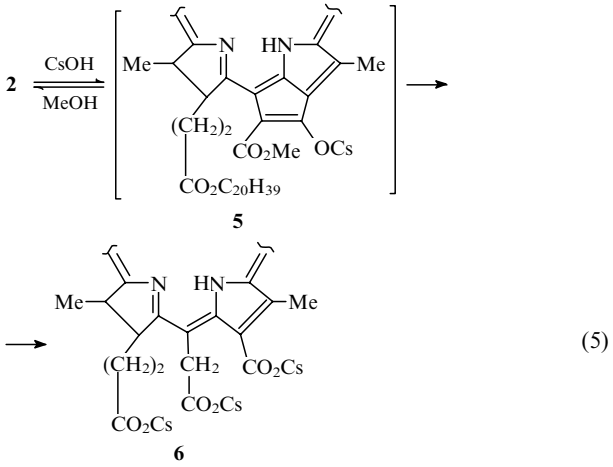

(5)

The keto–enol equilibrium constants (K_{KE}) have been determined:[24,25]

$$\underset{\text{Ketone form}}{H_2Chl} + Cs^+MeO^- \rightleftharpoons \underset{\text{Enol form}}{HChl^-Cs^+} + MeOH, \qquad (6)$$

$$K_{KE} = \frac{[HChl^-Cs^+][MeOH]}{[H_2Chl][Cs^+MeO^-]}. \qquad (7)$$

The K_{KE} values for ethyl acetate–methanol–CsOH and ethyl acetate–ethanol–CsOH mixtures measured at 298 K are equal to $(3.2 \pm 0.3) \times 10^{-3}$ and $(8.2 \pm 1.2) \times 10^{-3}$, respectively. Obviously, the equilibrium (6) is strongly shifted towards the keto form H_2Chl, the enol form being stabilised by ethanol more effectively than by methanol. In this respect, it is of note that glycerol shifts the keto–enol equilibrium to the right more strongly than other alcohols as a result of additional stabilisation of the enol form of pheophytin by intermolecular hydrogen bonds.[26]

The effective rate constants for the opening of the cyclopentenone ring of pheophytin in the presence of alkali in some organic solvents were measured using spectrophotometry from the decrement in the intensity of the absorption band at 460 nm (Table 1).[24,25] The rate of the second step of reaction (5) is independent of the concentration of alkali, since it affects only the reaction equilibrium (6) (which is shifted to the right) and is not directly involved in the cleavage of the exocycle. The double bond C(10)=C(9) of the exocycle is oxidised by atmospheric oxygen present in the solution. The putative mechanism of reaction (5) has been discussed.[25]

The effective rate constant k_{eff} for the second step of reaction (5) is determined by the equation:

$$-\frac{dc_i}{dt} = k_{eff}c_i, \qquad (8)$$

where c_i is the concentration of the intermediate **5**.

Table 1. Effective rate constants for oxidative degradation (k_{eff}) of pheophytin *a* in mixed organic solvents in the presence of an alkali (298 K) (the operating wavelength $\lambda = 460$ nm, $c^0_{H_2Chl} = 2 \times 10^{-5}$ mol litre^{-1}, $c^0_{O_2} \approx 0.2$ ml cm^{-3}).[24, 25]

Solvent (volume ratio)	c_{CsOH} /mol litre^{-1}	k_{eff} /s^{-1}
$MeCO_2Et$ – MeOH (12 : 1)	$(1.5-80) \times 10^{-3}$	$(2.5 \pm 0.1) \times 10^{-4}$
$MeCO_2Et$ – EtOH (12 : 1)	4×10^{-2}	2.05×10^{-3}
$MeCO_2Et$ – n-$C_5H_{11}OH$ (12 : 1)	3.7×10^{-2}	1.3×10^{-3}
Et_2O – MeOH (12 : 1)	1.1×10^{-2}	6.9×10^{-4}
CCl_4 – MeOH (12 : 1)	1.1×10^{-2}	3.0×10^{-4}
MeOH [a]	0.4 – 0.9	5.4×10^{-4}
EtOH [b]	0.1 – 0.8	6.3×10^{-5}
n-C_3H_7OH [a]	0.4	8.0×10^{-5}
n-$C_5H_{11}OH$ [a]	0.01 – 0.4	9.5×10^{-5}

[a] $c^0_{H_2Chl} = 2.0 \times 10^{-4}$ mol litre^{-1}; [b] $c^0_{H_2Chl} = 2.2 \times 10^{-4}$ mol litre^{-1}.

At the same time,

$$k_{eff} = k_v c_{O_2},$$

where k_v is the rate constant for the bimolecular reaction (5). With the molar concentration of O_2 in a saturated solution equal to 7×10^{-3} mol litre^{-1}, the rate constant for reaction (5) can be calculated by the formula:[24, 25]

$$k_v = \frac{k_{eff}}{c_{O_2}} = 1.4 \times 10^2 k_{eff}. \quad (9)$$

The opening of the cyclopentenone ring of methylpheophorbide *a* (**7**) under the action of amines has been studied.[27] These reactions result in the preferential amidation of one of the carboxy groups formed upon the opening of the exocycle to yield 6-monoamides of 7,γ-dimethyl ester of chlorin e_6.

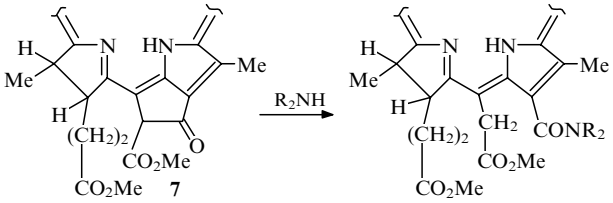

R = Me, Et.

Analogously, the reaction of methylpheophorbide *a* with yet another nucleophilic reagent, *viz*., morpholine, results in the opening of the cyclopentenone ring. The amide groups of the chlorin derivatives manifest higher affinity for natural and synthetic polyamide fibres.

The aminolysis of methylpheophorbide (**7**) by ethylenediamine and ethanolamine is of considerable interest for the synthesis of chlorophyll dyes. In dilute aqueous solutions of carboxylic acids, monoamides of dimethyl ester of chlorin e_6 and their complexes with d-metals are converted into cationic dyes containing an active NH_3^+ group able to bind tightly to amide-type fibres containing terminal COOH groups.

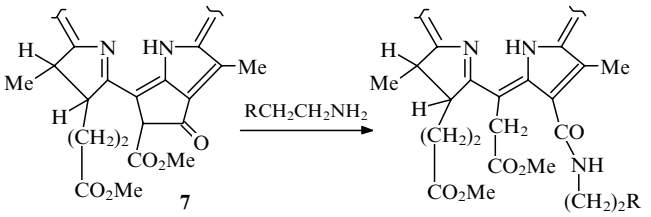

R = NH_2, OH.

Reactions involving alkoxycarbonyl groups, *viz*., the phytyl propionate group in the pyrrole ring *IV* and the methoxycarbonyl group in the ring *V*, are extremely important for chlorophyll and pheophytin. Mild alkaline hydrolysis results in the splitting of phytol $C_{20}H_{39}OH$ and methanol, while the central metal ion is preserved; under these conditions, chlorophyll is transformed into chlorophyllin **8**. Acid hydrolysis leads to the loss of Mg^{2+} and the phytol residue resulting in the formation of pheophorbide **9**.

The extended size of the phytyl residue favours its incorporation into the solvation shell of chlorophyll and pheophytin and creates steric hindrance for the reagents; removal of phytol increases the rates of many chemical reactions.

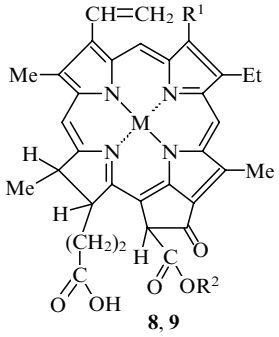

8, **9**

R^1 = Me, CHO; R^2 = H, M = Mg (**8**), R^2 = Me, M = 2 H (**9**).

Free carboxy groups favour not only the solvation of pigment molecules in highly polar solvents, but also their association in weakly polar media. Therefore, prior to their chemical modification compounds **8** and **9** are methylated (5% methanolic H_2SO_4), resulting in their conversion into methylchlorophyllin and methylpheophorbide, commonly used in the synthesis of diverse chlorophyll derivatives.

The vinyl group of pheophytin, pheophorbide and other chlorophyll derivatives reacts easily with HBr in organic solvents.[28]

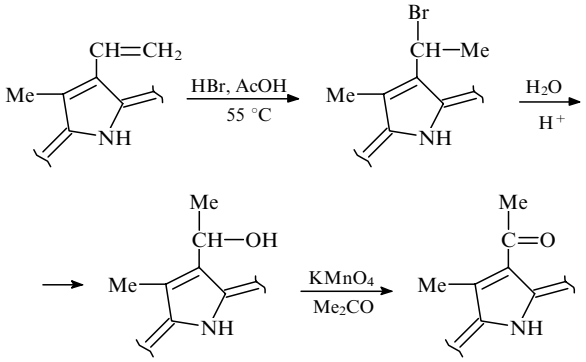

Bromine can be replaced by treatment with nucleophilic reagents,[29] which enables the preparation of chlorophyll derivatives with functional groups in position 2. For example, acid hydrolysis yields derivatives with an alcohol group which can be oxidised to the keto group by potassium permanganate.[30]

The reaction of chlorophyll with methylidenedimethylammonium iodide and subsequent treatment with acetic acid afford a cationic amino derivative [31] which is of interest in the chemistry of chlorophyll-based dyes due to its higher affinity for polyamide fibres. Quaternisation of tertiary amines affords chromophores that are readily soluble in water.

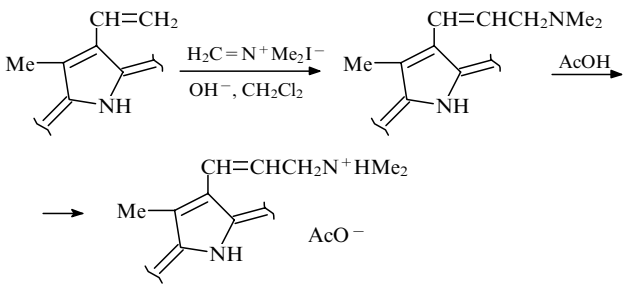

The oxidation of the vinyl group is an interesting approach to the modification of chlorophyll molecules. Treatment of chlorophyll *a* with $KMnO_4$ and then with $NaIO_4$ results in the incorporation of the aldehyde group into position 2 of the macrocycle which is not accompanied by the oxidation of the cyclopentenone ring. The formyl group can further be converted into a carboxy group.[32, 33]

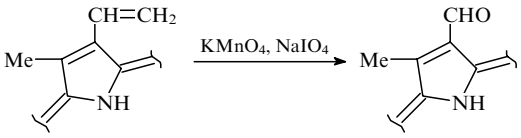

Chlorophyll and its derivatives contain a chlorin macrocycle with a partially hydrogenated pyrrole ring. Chlorophyll derivatives can successfully be converted into porphyrins among which phylloporphyrin (**10**), pyrroporphyrin (**11**) and rhodoporphyrin (**12**) are of considerable practical interest by virtue of their peculiar structures, and high thermal and chemical stabilities. These compounds represent final products of chlorin conversions under the most drastic redox conditions. The preparation of pyrroporphyrin methyl ester from a mixture of pheophytins *a* and *b* by heating it in an autoclave with 30% KOH in methanol in the presence of a silver catalyst (8 h, 185 °C) has been described.[30, 34] Rhodoporphyrin dimethyl ester is synthesised from pheophytins *a* and *b* under similar conditions but at 145 °C. Phylloporphyrin is prepared from a mixture of pheophorbides *a* and *b* by heating it in pyridine in the presence of 30% methanolic KOH (138 – 140 °C).[34, 35] The reduction of the vinyl group is accompanied by simultaneous dehydrogenation of the C—C bond in the pyrrole ring *IV* of chlorin. It is noteworthy that the preparation of these porphyrins does not require any preliminary separation of a mixture of chlorophylls *a* and *b*.

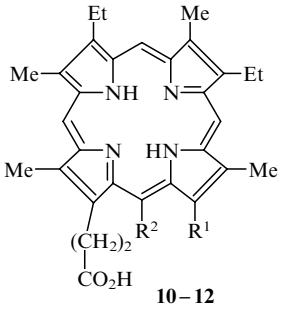

10 – 12

R^1 = H: R^2 = Me (**10**), H (**11**); R^1 = CO_2H, R^2 = H (**12**).

Chemical modification of peripheral substituents of chlorophyll is possible owing to the extremely high stability of the aromatic porphyrin macroring in acidic, alkaline and various redox media.

III. Chromophore systems of chlorophyll, its derivatives and analogues

Electronic absorption spectra (EAS) provide valuable information about chromophore properties of molecules and the possibility of their use, in principle, as dyes. The electronic absorption spectra of tetrapyrrole aromatic macrocyclic compounds are considered comprehensively in monographs,[4, 18, 36] so there is no need to discuss them in detail. Suffice it to say that EAS of porphyrins, phthalocyanines and chlorophylls differ considerably.[36]

The electronic absorption spectra of porphyrins (Fig. 1) are characterised by low molar extinction coefficients (ε) in the visible region, high intensity of the Soret band at the boundary of visible and near-ultraviolet regions ($\lambda \approx 400$ nm), low sensitivity to the character of inert organic solvents and very high sensitivity to protonating and complex-forming reagents (acids, salts, *etc.*).[4, 36] The positions and intensities of bands in the EAS of porphyrins

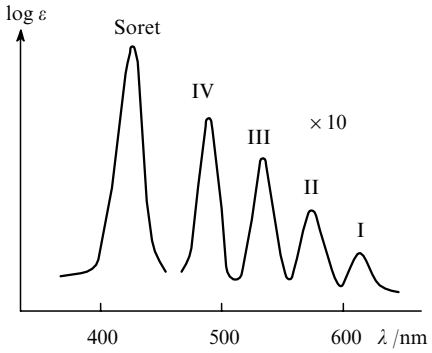

Figure 1. Electronic absorption spectrum of 1,3,5,7-tetramethyl-2,4,6,8-tetraethylporphin.

vary depending on the structures of the side substituents and their positions in the molecules.

In contrast to porphyrins, chlorins are characterised by a long-wave shift and high intensity of the first absorption band (Fig. 2), which enhances the chromophore properties of dyes.

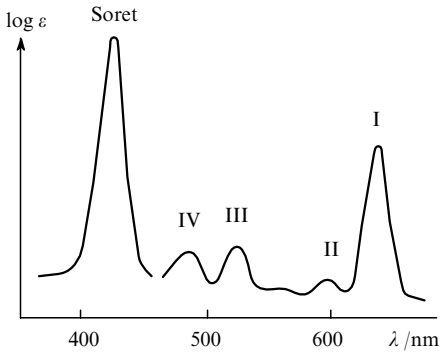

Figure 2. Electronic absorption spectrum of octaalkyl-7,8-dihydroporphin.

The intensities of the first absorption band of pheophytin (Table 2) and chlorophyll (Table 3) depend weakly on the nature of the solvent. In this case, its weak solvatochromic effect is determined by the symmetry of the macrocyclic chlorin chromophore, its atomic-electronic environment and, possibly, minor differences in the solvation of the ground and excited states of chlorophyll and pheophytin.

Special mention should be made of the relatively small dependence of the EAS of chlorins on the presence of substituents in the pyrrole fragments.

Incorporation of a metal atom into the centre of the chlorin molecule does not change the symmetry of the π-electron cloud of the chromophore. This is why EAS of metallochlorins do not differ significantly from that of pheophytin. In particular, the incorporation of Mg^{2+} or any other metal has little effect on the intensity of 'red' absorption bands of chlorins (see Tables 2, 3), since electron transitions in this band are permitted for both the ligand and the complexes.[36] However, the colour tones of crystalline chlorins, their complexes and solutions may vary widely, which is especially important for the chemistry of dyes.

In contrast, in the case of porphyrins the effects of metal cations on the electronic absorption spectra are very pronounced.[4] The complexation of metal ions with porphyrins results in degeneration of the energy levels for the electronic $\pi \rightarrow \pi^*$ transitions polarised along the coordination axes *x* and *y* in the plane of the macrocycle. The absorption bands I and III of free porphyrin corresponding to these transitions merge into one band (I) with an increase in the symmetry of metalloporphyrin mole-

Table 2. Wavelengths (λ /nm) and intensities ($\log \varepsilon$) of the absorption bands in the EAS of pheophytin *a* in organic solvents at 298 K.[36]

Solvent	λ ($\log \varepsilon$)				
	I	II	III	IV	Soret
Methanol	668 (4.417)	614 (3.688)	535 (3.702)	502 (3.876)	401 (4.852)
Ethanol	668 (4.504)	610 (3.834)	537 (3.852)	507 (3.901)	409 (4.814)
Pentanol	670 (4.583)	612 (3.884)	540 (3.933)	508 (3.951)	412 (4.888)
Acetone	666 (4.506)	608 (3.799)	535 (3.861)	505 (3.887)	410 (4.874)
DMF	669 (4.554)	610 (3.827)	535 (3.908)	506 (3.980)	411 (4.900)
Dioxane	670 (4.562)	611 (3.809)	537 (3.881)	507 (3.967)	412 (4.910)
Acetic acid	669 (4.547)	611 (3.882)	537 (3.872)	508 (3.902)	412 (4.922)
Pyridine	672 (4.516)	613 (3.785)	539 (3.861)	509 (3.920)	415 (4.870)
Quinoline	675 (4.570)	617 (3.839)	542 (3.928)	510 (3.945)	421 (4.911)
Glycerol – ethanol	695 (4.562)	640 (3.813)	—	518 (3.940)	415 (4.577)

Table 3. Positions (λ_1) and values of molar extinction coefficients (ε_1) of the first absorption band in the EAS of chlorophyll *a* in various organic solvents.[36]

Solvent	λ_1 /nm	$10^{-4}\varepsilon_1$	Solvent	λ_1 /nm	$10^{-4}\varepsilon_1$	Solvent	λ_1 /nm	$10^{-4}\varepsilon_1$
Methanol	666	6.66	Benzyl alcohol	672	6.66	Aniline	675	6.24
Ethanol	665	6.94	Isoamyl alcohol	667	7.33	Nitromethane	663	6.60
n-Pentanol	667	7.67	Acetonitrile	662	6.88	Carbon disulfide	672	6.80
Acetone	662	7.66	Acetophenone	668	7.65	α-Chloronaphthalene	670	6.94
DMF	664	7.39	Diethyl ether	661	8.51	Chloroform	665	7.15
DMSO	666	7.01	THF	664	8.18	Nitrobenzene	670	6.70
Dioxane	662	8.20	Ethyl acetate	662	7.94	Triethylamine	662	8.52
Pyridine	671	7.69	Benzene	666	7.82	Chlorobenzene	666	7.49
Quinoline	671	7.42						

cules. The intensity of this band increases, which is formally due to the fact that the corresponding electron transition becomes permitted, whereas the transitions I and III of free porphyrins are quasi-forbidden. The true reason for the increase in intensities of the absorption band I in the spectra of metalloporphyrins is that metalloporphyrins are more potent chromophores than the free porphyrins due to the rearrangements in their electronic and electronic-vibrational levels. The essence of these rearrangements is discussed in monographs.[36–38].

Coloured compounds are attributed to strong or weak chromophores based on the intensities of the absorption bands in the visible region of the spectrum. Of two coloured compounds with similar positions of the absorption bands, the one with a larger value of ε possesses more potent chromophore properties. The intensity of the absorption band I in the EAS of porphyrins increases 3–4-fold as a result of complexation, and a short-wave shift of this band by 40–60 nm occurs. In this respect, metalloporphyrins exhibit much more potent chromophore properties than the corresponding metal-free compounds (Tables 4 and 5).

IV. Photochemical stability of chlorophyll and its derivatives

Photochemical stability is a central problem in the design of novel dyes based on chlorophyll and related porphyrins. Chlorophyll and porphyrins are involved in diverse complex photochemical transformations; the theoretical aspects of these transformations are considered in detail in a monograph.[38] In this section, we shall discuss various problems connected with photochemical stabilities of chlorophyll and its derivatives in relation to their synthesis and application as dyes. Upon intense illumination, chlorophyll and porphyrins pass easily into singlet and triplet excited states characterised by high chemical activity and ability to generate singlet oxygen. Under these conditions, the macrocyclic chromophore passes into radical-cationic or radical-anionic forms in the presence of oxidants or reducing agents; their further conversions may lead to the cleavage of the macrocycle.[39] The cationic forms are generated in the presence of weak electron acceptors (O_2, quinones, Fe^{3+}, *etc.*), while stronger oxidants (H_2O_2, HNO_3, NO,

Table 4. Wavelengths (λ /nm) and intensities ($\log \varepsilon$) of the absorption bands in the EAS of pheophytin *a* and its complexes with metals.[36]

Compound	Solvent	λ ($\log \varepsilon$)				
		I	II	III	IV	Soret
H_2Chl *a*	EtOH	668 (4.50)	610 (3.83)	537 (3.85)	507 (3.90)	409 (4.814)
ZnChl *a*	EtOH	655 (4.68)	610 (4.01)	565 (3.74)	522 (3.51)	418 (4.94)
	AcOH	660 (4.71)	615 (4.04)	570 (3.77)	520 (3.59)	427 (4.84)
CuChl *a*	EtOH	650 (4.58)	610 (3.95)	548 (3.55)	501 (3.53)	411 (4.76)
	AcOH	651 (4.54)	610 (3.90)	550 (3.55)	502 (3.54)	411 (4.78)
CoChl *a*	EtOH	644 (4.50)	605 (3.95)	555 (3.66)	500 (3.39)	420 (4.65)
AgChl *a*	EtOH	650 (4.52)	605 (3.92)	555 (3.62)	510 (3.46)	422 (4.61)
MgChl *a*	EtOH	666 (4.73)	618 (4.10)	580 (3.84)	535 (3.54)	431 (4.78)
CdChl *a*	EtOH	665 (4.71)	618 (4.08)	582 (3.80)	532 (3.62)	434 (4.80)
NiChl *a*	AcOH	649 (4.50)	605 (4.00)	548 (3.55)	495 (3.46)	409 (4.67)
PdChl *a*	AcOH	638 (4.72)	595 (4.32)	536 (3.71)	493 (3.61)	393 (4.68)

Table 5. Positions (λ_1 /nm) and intensities ($\log \varepsilon_1$) of the absorption band I in the EAS of proto-, meso-, deutero- and hematoporphyrin and their complexes.[36]

Solvent	λ_1 ($\log \varepsilon_1$) in the spectrum of		
	porphyrin	copper complex	zinc complex
Protoporphyrin			
C_6H_6	634 (3.78)	571 (4.40)	579 (4.42)
Py	631 (3.77)	574 (4.30)	589 (4.26)
DMF	630 (3.75)	570 (4.38)	584 (4.33)
DMSO	630 (3.75)	570 (4.36)	586 (4.30)
EtOH	629 (3.76)	569 (4.32)	584 (4.33)
CCl_4	633 (3.81)	571 (4.41)	579 (4.32)
$CHCl_3$	630 (3.77)	570 (4.39)	561 (4.88)
AcOH	629 (3.44)	569 (4.38)	579 (4.18)
Mesoporphyrin			
C_6H_6	624 (3.79)	562 (4.47)	570 (4.43)
Py	622 (3.75)	564 (4.36)	579 (4.19)
DMF	621 (3.72)	560 (4.44)	579 (4.27)
DMSO	619 (3.73)	561 (4.41)	577 (4.24)
EtOH	619 (3.73)	561 (4.41)	575 (4.26)
CCl_4	626 (3.82)	564 (4.48)	570 (4.37)
$CHCl_3$	621 (3.75)	562 (4.42)	570 (4.34)
AcOH	593 (3.74)	560 (4.44)	569 (4.07)
Deuteroporphyrin			
C_6H_6	623 (3.71)	559 (4.41)	567 (4.34)
DMSO	620 (3.66)	557 (4.38)	571 (4.15)
$CHCl_3$	620 (3.70)	560 (4.38)	568 (4.25)
Hematoporphyrin			
C_6H_6	626 (3.75)	563 (4.41)	571 (4.38)
DMSO	621 (3.72)	562 (4.36)	577 (4.22)
$CHCl_3$	623 (3.74)	564 (4.38)	570 (4.34)

NO_2, $H_2S_2O_8$, *etc*.) result in the loss of chromophore properties. Abstraction of only two electrons from the binding π-orbitals of the porphyrin chromophore results in the disappearance of the absorption bands in the visible region of the spectrum. Thus, the absorption band I in the EAS of the radical cation of the magnesium octaethylporphyrin complex is characterised by lower intensity and has a bathochromic shift by 100 nm in comparison with its position in the spectrum of neutral porphyrin, whereas the corresponding dication is colourless. Pheophytin and its complexes manifest a similar behaviour. The alkyl groups, which represent σ-electron donors, favour the oxidation including photochemical oxidation. In contrast, protonation of porphyrins and chlorins prevents their oxidation. On the whole, chlorins are oxidised more easily than porphyrins. It should be remembered that the factors responsible for chemical and electrochemical oxidation can also influence photooxidation.[4,39]

Effects of metals on the oxidisability of complexes are of special interest. These metals can be divided into two groups that are different in principle. The metals of the first group (Mg, Cu, Zn, Cd, Ti) preserve their oxidation state in the transition of metalloporphyrins into radical-cationic and cationic forms. In this case, the electrons are abstracted from HOMO of the ligand, and the oxidation potential of the complex is lower than that of free porphyrin.[39]

The second group includes the metals (Mn, Fe, Co, Ni, Ag) the oxidation state of which changes upon transition into radical-cationic forms. As a result, the oxidation potentials of the complexes increase considerably.

The rate constants for photochemical destruction of metal analogues of chlorophyll are given in Table 6.[4]

Table 6. Rate constants (k_v) for the photochemical destruction of chlorophyll *a* and its metal complexes at different temperatures.[4]

Compound	Solvent	k_v /h^{-1}		
		20 °C	40 °C	60 °C
H_2Chl *a*	EtOH	very slow	very slow	very slow
	AcOH	0.019	0.039	0.081
MgChl *a*	EtOH	0.400	0.453	0.588
	AcOH	0.297	0.402	0.563
ZnChl *a*	EtOH	0.035	0.053	0.082
	AcOH	0.205	0.304	0.395
CdChl *a*	EtOH	0.460	0.466	0.493
HgChl *a*	EtOH	0.039	0.048	0.065
CoChl *a*	EtOH	–	–	0.025
	AcOH	–	–	0.006
CuChl *a*	AcOH	0.0101	0.015	0.024
PdChl *a*	AcOH	–	–	0.013
NiChl *a*	AcOH	–	–	0.0045
Fe(AcO)Chl *a*	AcOH	–	–	0.004

Ionic complexes with Cd and Mg and weakly covalent (Zn) complexes undergo photodestruction faster than pheophytin. The rate of photochemical oxidation of the covalent complexes with the metal ions (Cu, Co, Ni, Fe, Pd) that deactivate the triplet state and suppress the photogeneration of singlet oxygen is very low. This prompts an important practical conclusion that covalent metal-containing chlorin- and porphyrin-based dyes are much more resistant to photooxidation than free porphyrins.

V. Properties of chlorophyll and its derivatives in solutions. Solubility of porphyrins and energetics of solvation

Many natural porphyrins pass into a solution with difficulty. This is due to relatively high energies of their crystal lattices, low solvation energies of relatively non-polar chemical bonds and strong interactions of the π-systems of the neighbouring molecules. The solubility of porphyrins in organic solvents strongly depends on their structures.[40]

The structural and thermodynamic aspects of the solubilisation and solvation of the main types of porphyrins (chlorophyll, protoporphyrin and their derivatives, tetraphenylporphin, tetrabenzoporphin), their complexes and non-classical porphyrins (tetraazaporphyrins, phthalocyanines, chemical porphyrin dimers, *etc*.) have been investigated.[41–64] The main regularities of the thermodynamics of the solubilisation and solvation of porphyrins by various organic solvents and their binary mixtures have been established. The dependence of these processes on the conformational component of the free energy of solubilisation (ΔG_s), enthalpy (ΔH_s) and entropy (ΔS_s) of solubilisation caused by elimination of conformational strains in porphyrin molecules on phase transitions from the solid state to the solution has been established for the first time.

The energies of molecular lattices (ΔG_{lat}) for the majority of porphyrins are not determined. The contribution of the conformational component ΔG_{conf} for structurally similar porphyrins can be assessed only qualitatively. Therefore, a comparative analysis of experimental data on the solvation of porphyrins and their complexes is usually carried out based on the relative enthalpies of solubilisation of these compounds in a series of solvents with the least solvating one used as a standard.

Chlorins are much more soluble in organic solvents than porphyrins. The enthalpies of the transfer from benzene to another organic solvent (Table 7) are negative and vary from -2.3 (for chlorin e_6 in pyridine) to -71 kJ mol^{-1} (for pheophorbide *a* in piperidine).

Table 7. Standard changes in the enthalpies of solubilisation (ΔH_s°) (±2%) and the transfer (ΔH_t°) of chlorins.[64]

Chlorin	Solvent	ΔH_s° /kJ mol^{-1}	ΔH_t° /kJ mol^{-1}
H_2Chl *a*	C_6H_6	30.6	0
	CCl_4	22.5	−8.1
	$C_6H_5NO_2$	20.3	−10.3
	$CHCl_3$	1.3	−29.3
	DMF	23.6	−7.0
	pyridine	16.4	−14.2
	piperidine	−35.9	−66.5
Pheophorbide *a*	C_6H_6	16.9	0
	CCl_4	11.9	−5.0
	$C_6H_5NO_2$	5.7	−11.2
	$CHCl_3$	−9.2	−26.1
	DMF	8.0	−8.9
	pyridine	8.6	−8.3
	piperidine	−53.8	−70.7
Chlorin e_6	C_6H_6	14.2	0
	$CHCl_3$	−2.2	−16.4
	DMF	−10.3	−24.5
	pyridine	11.9	−2.3
	piperidine	−25.8	−40.0
Pheophorbide *b*	C_6H_6	14.4	0
	$C_6H_5NO_2$	4.8	−9.6
	$CHCl_3$	−9.8	−24.2
	DMF	4.4	−10.0
	pyridine	3.8	−10.0

The data listed in Table 7 suggest that benzene is the worst solvent, especially for H_2Chl *a* the phytol residue in which prevents its solubilisation in all organic solvents studied. The difference in the ΔH_s° values for phytol-free and phytol-containing molecules in all solvents constitutes, on average, −15 kJ mol^{-1} (see Table 7). This suggests that the phytol residue creates conformational hindrances for the solubilisation (but not the solvation). Thus the ΔH_t° values for pheophytin *a* and pheophorbide *a* are virtually identical for each of the solvents chosen.

The energy characteristics of the solubilisation and solvation of methyl esters of porphyrins of the chlorophyll group, *viz.*, pyrroporphyrin (**11**), rhodoporphyrin (**12**) and mesoporphyrin (**13**), are given in Table 8.

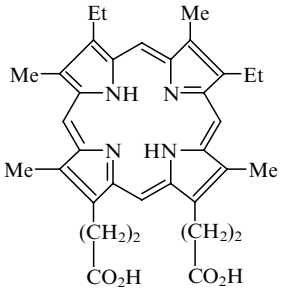

13

The endothermic character of solubilisation of porphyrin methyl esters in benzene increases considerably in the following order: **11** < **12** < **13**. Presumably, the appearance of a second methoxycarbonyl group in the porphyrin molecule creates steric hindrance (the absolute value of ΔG_{conf} for compound **13** is also increased) and hinders the solvation (ΔG_{solv}) in benzene. This order of changes in ΔH_s is preserved in CCl_4. The ΔH_t values of porphyrins with alkoxycarbonyl groups become highly negative in $CHCl_3$. The latter, being a weak acid, forms solvates with these compounds through hydrogen bonds. The solvation of porphyrins dissolved in DMF, pyridine or piperidine is determined by a weak acid – base interaction of porphyrins with solvent molecules of the type N−H···Solv.

Table 8. Standard changes in the enthalpies of solubilisation (ΔH_s°) (± 5%) and transfer (ΔH_t°) of porphyrins of the chlorophyll group.[64]

Porphyrin	Solvent	ΔH_s° /kJ mol^{-1}	ΔH_t° /kJ mol^{-1}
Pyrroporphyrin	C_6H_6	22.5	0
	CCl_4	15.1	−7.4
	$CHCl_3$	8.1	−14.4
	DMF	12.8	−9.7
	pyridine	15.3	−7.2
	piperidine	10.3	−12.2
Rhodoporphyrin	C_6H_6	42.8	0
	CCl_4	29.4	−13.4
	$CHCl_3$	21.0	−21.8
	DMF	35.3	−7.5
	pyridine	40.2	−2.6
	piperidine	24.1	−18.7
Mesoporphyrin	C_6H_6	53.2	0
	CCl_4	40.4	−12.8
	$CHCl_3$	16.5	−36.7
	DMF	20.9	−32.3
	pyridine	31.5	−21.7

Metal ions coordinated to chlorins and porphyrins change strongly their abilities for solvation in organic solvents. Such ions as Zn^{2+}, Cd^{2+} and Co^{2+} in metalloporphyrins take part in the coordination of molecules of electron-donor solvents (alcohols, pyridine, piperidine, DMF, DMSO, *etc.*),[4,39,65] which strongly increases the solubility of metalloporphyrins and favours their solvation. In contrast, virtually no solvation of copper and nickel complexes through axial coordination takes place (Table 9).

Table 9. Enthalpies of axial coordination (ΔH_{ec}°) of the solvent molecules by porphyrin complexes at 298 K.[41–46,62]

Complex	ΔH_{ec}° /kJ mol^{-1}		
	DMF	Py	Pip[a]
MgChl	−17.5	−33.6	–
CdPhe *a* (see[b])	−17.2	−55	−38.7
ZnChl	−17.6	−30.3	–
ZnPhe	−13.0	−29.2	−15.5
ZnPir[c]	−12.2	−36.1	−33.8
ZnGp[d]	−23.0	−42.9	−51.8
CoChl	−25.6	−84.1	−172.2
CoPhe	−23.4	−29.5	−57.6
CoRp[e]	−25.1	−38.5	–
CuChl	1.8	−5.6	–
NiChl	−1.7	−27.7	−7.0
NiPir	−2.8	−6.3	–

[a] Pip, piperidine; [b] Phe, pheophorbide; [c] Pir, pyrroporphyrin; [d] Gp, haematoporphyrin; [e] Rp, rhodoporphyrin.

The copper complex of tetraphenylporphin **14** is characterised by extremely low solubility in ethanol (Table 10).

Table 10. Solubilities of tetraphenylporphyrin and its complexes in ethanol at 298 K.[41–46, 62]

Compound	$10^3 S^{298}$ /mol litre^{-1}
H_2TPP [a]	0.018
	5.90 [b]
CoTPP	0.084
CuTPP	0.012
ZnTPP	0.682
CdTPP	0.802

[a] Tetraphenylporphyrin **14**; [b] in benzene.

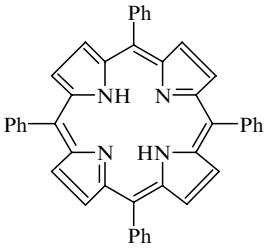

14

At the same time, the solubility of Co, Zn and Cd complexes is increased 7–60-fold due to the axial coordination of the solvent molecules to the fifth and sixth coordination positions along the *z* axis orthogonal to the porphyrin ring as a result of which the solvation energy decreases (on average, by 20–40 kJ mol^{-1}) depending on the electron-donor properties of the solvent.

Thermodynamic, thermochemical and spectral methods have been developed for the study of solvation of metalloporphyrins through axial coordination of solvent molecules.[39, 41, 63]

VI. Use of porphyrins and chlorins for dyeing textiles

The textile and light industries utilise an immense variety of synthetic dyes [66–72] many of which are toxic, irritate the skin and mucosa and cause otitis, laryngitis and various gastrointestinal disorders. Aniline dyes are especially hazardous in production and, possibly, application.[71, 72] Unfortunately, preventive measures are taken mostly during the production of synthetic dyes and, to a lesser degree, during colouration and utilisation of textiles. The effects of dyes on human skin in the course of wearing and laundering of dyed fabrics and their hazardous impact on living beings through waste waters have been little studied. One should not rule out the possibility that synthetic dyes of the arene series provoke cancerous and other severe diseases even in homeopathic doses. Therefore, in recent years the attention of investigators has been mainly focussed on natural dyes of plant origin.[73–76] A large body of literature data on this problem has been analysed.[75]

Chlorophyll, the most important natural dye, has a tetrapyrrole and not arene structure and is a component of foods consumed by warm-blooded animals. Therefore, chlorophyll itself, its derivatives and many porphyrins can be regarded as environmentally safe compounds. Dyes based on chlorophyll came into use as colouring matter for foodstuffs as early as the beginning of the 20th century and are currently widely used in medicine, perfumery and other areas.[34, 35] However, until recently the use of chlorophyll derivatives in the textile and light industries has been restrained due to the rapid progress in the chemistry of synthetic dyes and their ubiquitous application.

The necessity to find vast agricultural areas for growing plants as natural sources of dyes (*e.g.*, indigo) at the sacrifice of agricultural plants used as food for humans is the main obstacle to the transition to safe natural dyes.[73] No such problem exists for chlorophyll-based dyes, since chlorophyll is extracted from naturally abundant green plants (*e.g.*, nettle, conifers, algae, *etc.*). The annually renewable chlorophyll reserves on our planet constitute no less than 10^{12} tons.[11]

Several promising environmentally safe porphyrin dyes have been proposed,[77–81] and a simple, economic one-step procedure for the isolation of metallochlorophyll analogues from green plants has been developed.[82] Ni, Fe, Co, Cu, Mn complexes and complexes of other metals prepared by this method possess the entire set of characteristics required for them to be employed as dyes.

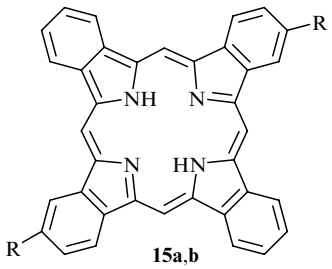

15a,**b**

R = CH_2N^+⟨pyridine⟩ Cl^- (**a**), $CH_2S^+{=}C(NMe_2)_2$ (**b**).

Pyridinium and thiouronium salts of tetrabenzoporphin **15a**,**b** were prepared in 98% yield by chloromethylation of tetrabenzoporphin [83–85] followed by heating of the reaction product with pyridine or tetramethylthiourea. These compounds are easily soluble in water and stable in weakly acidic solutions (1%–3% acetic acid). The derivatives **15a**,**b** impart an intensive bright green colouring to Nitron fibres in 40 min. Dyeing of cotton fibres with these salts also gave good results. Of substantial interest are active disperse porphyrin dyes for polyamide fibres based on tetra(*p*-chloromethylphenyl)porphin.[86, 87] The starting compounds for the synthesis of the latter are pyrrole, benzaldehyde and formaldehyde. The aforementioned porphyrin dyes can easily be converted into the corresponding metal complexes possessing enhanced chromophore properties.

Unique phthalocyanine pigments and dyes with a tetrabenzotetraazaporphin structure have been known for a very long time.[4, 88, 89] These compounds are prepared from phthalic acid derivatives and metal salts and are characterised by complete environmental safety owing to their extremely high chemical and photochemical stability which is not inherent in other classes of dyes.

The aforementioned properties of chlorophyll and the principles of its processing into chlorins and porphyrins enable its application as a potential source of environmentally safe dyes. Chlorophyll is isolated from green plant cells by extraction. In Russia, it is economically more effective to extract chlorophyll from nettle leaves.[4, 90] In the USA and European countries, food pigments have been prepared from chlorophyll extracted from finely ground alfalfa leaves since the early 1920's.[35] Acetone and light petroleum are used as extractants. Pheophytin is isolated by extraction with 96% ethanol and subsequent treatment with 6 M HCl. Treatment of plant tissues with acetone and 34% aqueous HCl yields a mixture of pheophorbides *a* and *b*.

Pheophorbide, chlorin e_6 and chlorin e_6 6-*N*-(2-aminoethyl)-amide dimethyl ester were tested as dyes for wool, cotton and acetate fibres in our laboratory.[91]

A wool specimen dyed with pheophorbide acquired a light green-brown colouring, while that dyed with chlorin e_6 was coloured bright green-brown. Dyeing with chlorin e_6 6-*N*-(2-aminoethyl)amide dimethyl ester gave the third specimen a khaki colour. Boiling of specimens dyed with chlorin e_6 and chlorin e_6 6-*N*-(2-aminoethyl)amide dimethyl ester with an aqueous solution of copper acetate resulted in complexation. In the former case, the colour of the specimen was bright blue-green, while in the latter it was green.

Chlorin e_6 6-*N*-(2-aminoethyl)amide dimethyl ester was used as a dye for conferring a khaki colour on acetate fibres. Subsequent boiling of the specimens with aqueous solutions of copper and nickel acetates gave the former an intensive light-green (lettuce) colour. After dyeing with chlorin e_6 and chlorin e_6 6-*N*-(2-aminoethyl)amide dimethyl ester by a pad-dry technique, which includes thermal treatment and steaming, the cotton specimens acquired green-yellow and khaki colouring, respectively. Subsequent boiling of the specimens with solutions of copper and nickel acetate gave dark-green and green colouring, respectively.

Chlorin e_6 was used for dyeing cotton fabrics by the colour-printing method which includes starch and cellulose thickening. The green-yellow coloured specimens appeared to be more sensitive to solar light than dyed wool specimens.

* * *

The state-of-the-art in chlorophyll chemistry allows gradual replacement of some environmentally unsafe classes of synthetic arene dyes by porphyrins and chlorophyll derivatives.

Chlorophyll and its derivatives, their cationic forms and metal complexes are potent chromophores characterised by purity of colour and photochemical stability. They can be used as direct, disperse, cationic and active dyes for regenerated protein (*e.g.*, wool, silk, *etc.*) and synthetic fibres giving stable and bright green tones. Chlorophyll-based porphyrins impart pink-red colouring to fabrics. The authors are currently engaged in the development of effective methods for extracting chlorophyll from natural raw materials (*e.g.*, nettle leaves, alfalfa powder, conifers, algae, *etc.*) and its modification into chemically stable and photostable derivatives possessing an ideal chromophore system and an affinity for textile fibres. The main practical results from their application give every reason to consider this class of chlorophyll dyes as promising industrially and operationally safe agents; their commercial production can be realised in the very near future.

References

1. K A Timiryazev *Nature (London)* **32** 342 (1885)
2. M S Tsvet *Khromatograficheskii Analiz* (Chromatographic Analysis) (Moscow: Academy of Sciences of the USSR, 1946)
3. T N Godnev *Khlorofill. Ego Stroenie i Obrazovanie v Rastenii* (Chlorophyll. Its Structure and Formation in a Plant) (Minsk: Academy of Sciences of the Bel.SSR, 1963)
4. B D Berezin *Koordinatsionnye Soedineniya Porfirinov i Ftalotsianina* (Coordinating Compounds of Porphyrins and Phthalocyanine) (Moscow: Nauka, 1978)
5. V M Kutyurin *Khlorofill* (Chlorophyll) (Minsk: Nauka i Tekhnika, 1974)
6. A A Krasnovskii *Usp. Khim.*, **29** 736 (1960) [*Russ. Chem. Rev.* **29** 344 (1960)]
7. V B Evstigneev *Zh. Fiz. Khim.* **32** 969 (1958)
8. B D Berezin *Koord. Khim.* **22** 285 (1996) [a]
9. L A Tumerman (Ed.) *The Photochemical Apparatus its Structure and Function* (New York: Academic Press, 1959)
10. A N Terenin *Fotokhimiya Khlorofilla i Fotosintez* (Photochemistry of Chlorophyll and Photosynthesis) (Moscow: Academy of Sciences of the USSR, 1951)
11. E Rabinovich *Photosynthesis* Vol. 1 (New York: Academic Press, 1948)
12. A N Terenin *Problemy Fotosinteza* (The Problems of Photosynthesis) (Moscow: Academy of Sciences of the USSR, 1959)
13. *Sovremennye Problemy Fotosinteza* (Modern Problems of Photosynthesis) (Moscow: Moscow State University, 1973)
14. R K Clayton *Photosynthesis. Physical Mechanisms and Chemical Patterns* (Cambridge: Cambridge University Press, 1980)
15. Yu G Chirkov *Fotosintez: Dva Veka Spustya* (Photosynthesis: Two Centuries Later) (Moscow: Znanie, 1981)
16. Gouvindgy (Ed.) *Photosynthesis* Vol. 1 (New York: Academic Press, 1982)
17. G Steinberg-Yfrach, P A Liddell, S-C Hung, A L Moore, D Gust, T A Moore *Nature (London)* **385** 239 (1997)
18. O A Golubchikov, O I Koifman, G V Ponomarev, in *Porfiriny: Spektroskopiya. Elektrokhimiya. Primenenie* (Porphyrins: Spectroscopy. Electrochemistry. Applications) (Moscow: Nauka, 1987) p. 214
19. O A Golubchikov, B D Berezin *Usp. Khim.* **55** 1361 (1986) [*Russ. Chem. Rev.* **55** 768 (1986)]
20. A A Krasnovskii, S Yu Egorov, N V Nazarova, E I Yartsev, G V Ponomarev *Biofizika* **32** 982 (1987) [b]
21. E A Venediktov, V V Mozhzhukhin, B D Berezin *Dokl. Akad. Nauk SSSR* **290** 1137 (1986) [c]
22. B D Berezin *Zh. Neorg. Khim.* **37** 1260 (1992) [d]
23. O A Golubchikov (Ed.) *Uspekhi Khimii Porfirinov* (Progress in the Chemistry of Porphyrins) Vol. 3 (St Petersburg: Research Institute of Chemistry, 2001)
24. B D Berezin, O B Lapshina *Zh. Fiz. Khim.* **48** 303 (1974) [e]
25. B D Berezin, O B Lapshina *Zh. Fiz. Khim.* **50** 2007 (1976) [e]
26. G I Smirnova, B D Berezin *Zh. Fiz. Khim.* **43** 659 (1969) [e]
27. D V Belykh, L P Karmanova, L P Spirikhin, A V Kutchin *Mendeleev Commun.* 77 (2002)
28. H Fischer, A Stern *Die Chemie des Pyrrols* Bd. II (Leipzig: Academische Verlagsgesellschaft, 1940)
29. B D Berezin, D B Berezin *Kurs Sovremennoi Organicheskoi Khimii* (Course of Modern Organic Chemistry) (Moscow: Vysshaya Shkola, 1999)
30. P H Hynnenen, in *Chlorophylls* (Ed. H Scheer) (Boca Raton, FL: CRC Press, 1991) p. 145
31. R K Pandey, F-Y Shiau, N W Smith, T J Dougherty, K M Smith *Tetrahedron* **48** 7591 (1992)
32. R K Pandey, F-Y Shiau, A B Sumlin, T J Dougherty, K M Smith *Bioorg. Med. Chem. Lett.* **4** 1263 (1994)
33. A S Holt, H V Morley *Can. J. Chem.* **37** 507 (1959)
34. O I Koifman, K A Askarov, B D Berezin, N S Enikolopyan, in *Porfiriny: Struktura, Svoistva, Sintez* (Porphyrins: Structure, Properties, Synthesis) (Moscow: Nauka, 1985) p. 175
35. A Humphrey *Food Chem.* **5** 57 (1980)
36. G P Gurinovich, A N Sevchenko, K N Solov'ev *Spektroskopiya Khlorofilla i Rodstvennykh Soedinenii* (Spectroscopy of Chlorophyll and Related Compounds) (Minsk: Nauka i Tekhnika, 1968)
37. K N Solov'ev, L L Gladkov, A S Starukhin, S F Shkirman *Spektroskopiya Porfirinov: Kolebatel'nye Sostoyaniya* (Spectroscopy of Porphyrins: Vibrational States (Minsk: Nauka i Tekhnika, 1985)
38. A N Terenin *Fotonika Molekul Krasitelei* (Photonics of Dye Molecules) (Leningrad: Nauka, 1967)
39. B D Berezin, N S Enikolopyan *Metalloporfiriny* (Metalloporphyrins) (Moscow: Nauka, 1988)
40. G M Mamardashvili, B D Berezin, in *Uspekhi Khimii Porfirinov* (Progress in the Chemistry of Porphyrins) (Ed. O A Golubchikov) (St Petersburg: Research Institute of Chemistry, 2001) Vol. 3, p. 130
41. B D Berezin, O I Koifman, V V Zelov, G E Nikitina *Zh. Fiz. Khim.* **52** 2214 (1978) [e]
42. O I Koifman, B D Berezin, V V Zelov, G E Nikitina *Zh. Fiz. Khim.* **52** 1782 (1978) [e]
43. B D Berezin, O I Koifman, G E Nikitina *Zh. Fiz. Khim.* **54** 2481 (1980) [e]
44. O I Koifman, G E Nikitina, B D Berezin *Zh. Fiz. Khim.* **56** 737 (1982) [e]
45. O I Koifman, G E Nikitina, B D Berezin *Zh. Fiz. Khim.* **57** 590 (1983) [e]
46. A S Semeikin, O I Koifman, G E Nikitina, B D Berezin *Zh. Obshch. Khim.* **57** 1599 (1984) [f]
47. B D Berezin, A S Semeikin, G E Nikitina, Z Ts Koifman, O I Koifman *Zh. Fiz. Khim.* **59** 2226 (1985) [e]
48. B D Berezin, S V Kharitonov, T I Potapova, R A Petrova *Zh. Fiz. Khim.* **59** 2425 (1985) [e]
49. O G Khelevina, G M Trofimenko, B D Berezin *Izv. Vyssh. Uchebn. Zaved., Khim. Khim. Tekhnol.* **32** (6) 57 (1989)
50. B D Berezin, O G Khelevina, G M Trofimenko *Zh. Fiz. Khim.* **65** 2055 (1991) [e]
51. G M Trofimenko, O G Khelevina, B D Berezin *Koord. Khim.* **17** 941 (1991) [a]

52. B D Berezin, G M Trofimenko, M B Berezin *Zh. Fiz. Khim.* **66** 546 (1992) [c]
53. G M Trofimenko, B D Berezin *Zh. Neorg. Khim.* **38** 1049 (1993) [d]
54. G M Trofimenko, N V Chizhova, B D Berezin *Zh. Obshch. Khim.* **63** 920 (1993) [e]
55. B D Berezin, G M Trofimenko, M B Berezin *Zh. Fiz. Khim.* **68** 1102 (1994) [e]
56. G M Trofimenko, A S Semeikin, M B Berezin, B D Berezin *Koord. Khim.* **22** 505 (1996) [a]
57. G M Trofimenko, N Zh Mamardashvili, O A Golubchikov, B D Berezin *Zh. Fiz. Khim.* **71** 298 (1997) [e]
58. G M Trofimenko, B D Berezin *Koord. Khim.* **23** 234 (1997) [a]
59. G M Mamardashvili, N Zh Mamardashvili, O A Golubchikov, B D Berezin *Koord. Khim.* **24** 648 (1998) [a]
60. G M Mamardashvili, N Zh Mamardashvili, O A Golubchikov, B D Berezin *Zh. Fiz. Khim.* **73** 1036 (1999) [e]
61. M B Berezin, G A Krestov, in *Problemy Khimii Rastvorov* (The Problems in Solution Chemistry) (Ed. G A Krestov) (Moscow: Nauka, 1989) p. 190
62. B D Berezin, M B Berezin, in *Problemy Khimii Rastvorov* (The Problems in Solution Chemistry) (Ed. A M Kutepov) (Moscow: Nauka, 2001) p. 254
63. A I V'yugin, M B Berezin, E V Antina, in *Problemy Khimii Rastvorov* (The Problems in Solution Chemistry) (Ed. A M Kutepov) (Moscow: Nauka, 2001) p. 298
64. A I V'yugin, E V Antina, M B Berezin, in *Problemy Khimii Rastvorov* (The Problems in Solution Chemistry) (Ed. A M Kutepov) (Moscow: Nauka, 1998) p. 208
65. B D Berezin, O I Koifman *Usp. Khim.* **49** 2389 (1980) [*Russ. Chem. Rev.* **49** 1188 (1980)]
66. B I Stepanov *Vvedenie v Khimiyu i Tekhnologiyu Organicheskikh Krasitelei* (Introduction in the Chemistry and Technology of Organic Dyes) (Moscow: Khimiya, 1984)
67. B N Mel'nikov, M N Kirilova, A P Moryganov *Sovremennoe Sostoyanie i Perspektivy Razvitiya Tekhnologii Krasheniya Tekstil'nykh Materialov* (Current State and Perspectives of Development of the Technology of Dyeing of Textile Materials) (Moscow: Legkaya i Pishchevaya Promyshlennost', 1983)
68. B N Mel'nikov, I B Blinicheva *Teoreticheskie Osnovy Tekhnologii Krasheniya Voloknistykh Materialov* (Theoretical Foundations of Dyeing of Fibrous Materials) (Moscow: Legkaya Industriya, 1978)
69. B N Mel'nikov, A P Moryganov, Yu A Kalinnikov *Teoriya i Praktika Vysokoskorostnoi Fiksatsii Krasitelei na Tekstil'nykh Materialakh* (The Theory and Practice of High-Speed Fixation of Dyes on Textile Materials) (Moscow: Legprombytizdat, 1987)
70. O M Lifentsev, B N Mel'nikov *Krashenie i Pechatanie Tkanei Putem Sinteza Pigmentov na Volokne* (Dyeing and Textile Printing by Synthesis of Pigments on Fibre) (Moscow: Legkaya Industriya, 1973)
71. B N Mel'nikov, G I Vinogradova *Primenenie Krasitelei* (Applications of Dyes) (Moscow: Khimiya, 1986)
72. A M Kiselev *Zh. Ross. Khim. O-va im. D I Mendeleeva* **46** (1) 20 (2002) [g]
73. *Dye Plants and Dyeing* (London: Henpert Press, 1994)
74. G A Krichevskii *Khimicheskaya Tekhnologiya Tekstil'nykh Materialov* Vol. 3 (Chemical Technology of Textile Materials) (Moscow: Izd. Ross. Zaoch. In-ta Tekst. Legk. Prom-sti, 2001)
75. Yu A Kalinnikov, I Yu Vashurina *Zh. Ross. Khim. O-va im. D I Mendeleeva* **46** (1) 77 (2002) [g]
76. B D Berezin, M B Berezin, D B Berezin, in *XVI Mendeleevskii S'ezd po Obshchei i Prikladnoi Khimii (Tez. Dokl.), Sankt-Peterburg, 1998* [The XVIth Mendeleev Congress on General and Applied Chemistry (Abstract of Reports), St Petersburg, 1998] p. 46
77. USSR P. 990 777; *Byull. Izobret.* (3) 111 (1983)
78. USSR P. 1 028 672; *Byull. Izobret.* (26) 75 (1983)
79. USSR P. 1 260 377; *Byull. Izobret.* (36) 88 (1986)
80. USSR P. 1 578 161; *Byull. Izobret.* (26) 95 (1990)
81. R A Petrova, N V Chizhova, T I Potapova, B D Berezin *Izv. Vyssh. Uchebn. Zaved., Khim. Khim. Tekhnol.* **30** (6) 79 (1987)
82. USSR P. 1 028 671; *Byull. Izobret.* (26) 75 (1983)
83. USSR P. 898 739; *Byull. Izobret.* (22) 487 (1981)
84. B D Berezin, S V Kharitonov, T I Potapova, R A Petrova *Organicheskie Poluprovodnikovye Materialy* (Organic Semiconductor Materials) (Perm': Perm' State University, 1982) p. 53
85. R A Petrova, T I Potapova, B D Berezin, S V Kharitonov, Z V Kharitonova *Izv. Vyssh. Uchebn. Zaved., Khim. Khim. Tekhnol.* **27** 1304 (1984)
86. R A Petrova, B D Berezin, T I Potapova, E L Toropova *Izv. Vyssh. Uchebn. Zaved., Khim. Khim. Tekhnol.* **29** (9) 55 (1986)
87. USSR P. 740 765; *Byull. Izobret.* (22) 144 (1980)
88. F Mozep *Phthalocyanine Compound* (New York: Renhold, 1934)
89. A Lever *Adv. Inorg. Chem. Radiochem.* **7** 27 (1965)
90. N S Enikolopyan (Ed.) *Porfiriny: Struktura, Svoistva, Sintez* (Porphyrins: Structure, Properties, Synthesis) (Moscow: Nauka, 1985)
91. B D Berezin, M B Berezin, A P Moryganov, S V Rumyantseva, N S Dymnikova *Zh. Prikl. Khim.* **76** 2008 (2003) [h]

[a] — *Russ. J. Coord. Chem. (Engl. Transl.)*
[b] — *Biophysics (Engl. Transl.)*
[c] — *Dokl. Chem. (Engl. Transl.)*
[d] — *Russ. J. Inorg. Chem. (Engl. Transl.)*
[e] — *Russ. J. Phys. Chem. (Engl. Transl.)*
[f] — *Russ. J. Gen. Chem. (Engl. Transl.)*
[g] — *Mendeleev Chem. J. (Engl. Transl.)*
[h] — *Russ. J. Appl. Chem. (Engl. Transl.)*

Russian Chemical Reviews **73** (2) 195 – 204 (2004) © 2004 Russian Academy of Sciences and Turpion Ltd

DOI 10.1070/RC2004v073n02ABEH000830

Quantitative estimation of the reactivity of the surface of solids on the basis of inductive constants

Yu K Ezhovskii

Contents

I.	Introduction	195
II.	Macromolecular concept of surface chemical reactions and quantitative estimation of the reactivity of the solid surface from the inductive constants	196
III.	Inductive effect of a silica matrix and regularities of its variation during dehydration	197
IV.	Estimation of the inductive effect of the core of some dispersed oxides	199
V.	Quantitative estimation of the reactivity of hydroxylated surfaces of single-crystal matrices	200
VI.	Effect of the thickness of the oxide layer on the activity of silanol groups on the silicon surface	201
VII.	Conclusion	203

Abstract. Attempts at using correlation analysis and the inductive constants for quantitative estimation of the reactivity of the solid surface and for predicting the character of surface reactions are discussed on the basis of the macromolecular concept of the structure of solids. The results of experimental studies of the reactivity of some solid oxides and single-crystal matrices, which confirm the good prospects of this approach, are presented. The bibliography includes 33 references.

I. Introduction

The active development of the chemistry and technology of a solid surface is associated with the prospects for using small-size surface structures in various fields of engineering, first of all, in micro- and nanoelectronics, heterogeneous catalysis and sorption techniques. Progress in the development of chemical methods for the synthesis of nanostructures is largely related to the possibility of predicting the pattern of surface reactions on the basis of a quantitative theory. An approach to quantitative estimation of the reactivity of the surface of solids is the use of correlation analysis, which underlies the quantitative theory of organic reactions [1, 2] based on the linear free energy (LFE) principle proposed by I Brønsted and M Polanyi. According to this principle, the reactivity of the members of a series of isostructural compounds having a reaction centre of the same type can be predicted using either empirical or experimentally determined constants. The numerical values of the constants can be used to compare and predict the equilibrium and kinetics of chemical processes involving these compounds. For example, compounds incorporating functional groups Y of the same type are combined into the reaction series

$$X_1-Y,\ X_2-Y,\ \ldots,\ X_n-Y;$$

Yu K Ezhovskii St Petersburg State Institute of Technology (Technical University), Moskovskii prosp. 26, 190013 St Petersburg, Russian Federation. Fax (7-812) 112 77 91. Tel. (7-812) 259 48 59.
E-mail: office@tu.spb.ru

Received 27 February 2003
Uspekhi Khimii **73** (2) 208 – 218 (2004); translated by Z P Bobkova

for any member of this series, the rate constant of the reaction

$$X_i-Y + Z \longrightarrow X_i-Z + Y$$

depends unambiguously on the nature of X_i. The influence of X_i can be described by a set of dimensionless constants. This allows one to predict the behaviour of various compounds in chemical processes.

Qualitatively, the reactivity of X_i-Y molecules can be described by revealing the mechanism of interaction between the substituent X_i and the reaction centre Y. The major contributions to this interaction are made by inductive, steric, resonance, and some other effects. When a particular chemical reaction is considered, various types of interaction are postulated to be independent of each other and additive.[1, 2] The ability of a substituent to be involved in a particular type of interaction is described quantitatively by a constant which is expressed as a relative value, *i.e.*, describes the effect of a given substituent with respect to a reference one. For example, the effective electronegativity of the substituent is usually characterised by the constant σ_I, which reflects the inductive effect of this substituent. The qualitative views on the inductive interaction represent an integral part of the classical electronic theory of organic reactions. However, this does not mean that the nature of the inductive effect is now completely clear. The most widely used concept is intramolecular polarisation transmitted along the chain of bonds. This polarisation, induced by some charged or electronegative group, decreases with distance.

Quantitatively, the inductive effect of substituents as a formal type of interaction has been considered by Hammett and Taft.[2, 3] They proposed one-parameter correlation equations for various reaction series

$$\log K_i = \log K_0 + \rho\sigma_I, \qquad (1)$$

where K_i and K_0 are the equilibrium (or rate) constants for the reactions for substituted and unsubstituted members of the series, respectively; ρ is the proportionality coefficient reflecting the sensitivity of the reaction centre to the effect of the substituent in this reaction. The first term represents the part of the reaction free energy that does not depend on the nature of the substituent X.

In Taft's opinion, strict correlations between the inductive constants and the electronegativities can be established only for

monoatomic substituents. However, while developing a quantitative theory of organic reactions, Palm[1] made the inductive constants universal and assumed that any influence of the inductive effect can be described by the equation

$$A = A_{XY} + \rho_Y \sigma_X, \quad (2)$$

where A is any correlated value (for example, log$K$). According to Palm, this equation is valid for a variable substituent X_i of any complexity.

The experience of using structure–property relationships accumulated in organic and organoelement chemistry,[3–5] can be successfully applied to surface processes. This was promoted by the appearance of the core model of the structure of solids and development of the chemistry of supramolecular compounds.[6–8] An approach based on the use of the LFE principle and correlation analysis in the chemistry of the surface of solids can provide the basis for the development of a quantitative theory of surface reactions.

This review considers some results that demonstrate good prospects of using correlation analysis in the chemical investigations of solid surfaces, in particular, for quantitative estimation of the reactivity of functional groups on the surfaces of dispersed and single-crystal matrices on the basis of their inductive constants. This approach was verified in relation to dispersed silica, beryllia, titania and alumina and single-crystal silicon.

II. Macromolecular concept of surface chemical reactions and quantitative estimation of the reactivity of the solid surface from the inductive constants

In conformity with the main concept of the structure of solids,[6] any solid can be represented as a combination of a chemically inert core and reactive functional groups located on the surface (*e.g.*, OH groups). All surface reactions involving these groups and not affecting the core structure are considered as polymer analogous transformations.[7] Within the framework of a formal approach, this allows one to apply the LFE principle to solids containing similar functional groups and to use linear correlations of type (1) and (2). Usually, experimental results are represented as more or less complicated correlation equations. When the results deviate from dependences of types (1) and (2), the factors responsible for these deviations (steric, resonance, π-conjugation or hyperconjugation, *etc.*) should be taken into account using the stage-by-stage 'from simple to complex' procedures.

In a quantitative description of the inductive effect, a reaction series of solid matrices is not necessarily considered resorting to the X–Y system. If X is any substituent, in the X–Y series, one can distinguish the X–G–Y subseries where G is any divalent structural unit. If the inductive interaction has at least limited universality within a particular set of substituents X, the values for the considered characteristic A, present in Eqn (2), for the X–Y and X–G–Y series with the same range of substituents X should follow a linear correlation with each other. This means that the correlation equation (2) for the X–G–Y series can be written in two ways

$$A_{X-G-Y} = A_{X_0-G-Y} + \rho_{GY}\sigma_X$$

and

$$A_{X-G-Y} = A_{X_0-G-Y} + \rho_Y\sigma_{GX},$$

which implies inclusion of the fragment G in the reaction centre and in the substituent, respectively. For solids with hydroxylated surfaces that present a separate reaction series (for example, metal oxides), the electrophilic and nucleophilic substitution reactions can be presented in the following way:

$$X-OH + B \longrightarrow X-OB,$$

$$X-OH + B \longrightarrow X-B.$$

The type and the rate of the reaction are dictated by the effective electronegativity of the surface group (X or X–O). The reactivity of the hydroxyl groups is affected by all atoms that form the core; however, the effect of the nearest atoms that form the surface group is the most significant. The effective electronegativity of this group as a substituent in a surface compound can be evaluated from the inductive effect using one-parameter correlations. The value for the inductive effect (inductive constant) can be derived from any physicochemical process or phenomenon in which it is manifested to a sufficient extent. High sensitivity to electronic effects is typical of nuclear magnetic resonance; this is one of the best methods for determining the inductive constants.[1] However, strict requirements to investigation objects restrict the scope of its applicability. The bond force constants (and, hence, the stretching frequencies) depend on the electronic state of the system; therefore, with allowance for the LFE principle, one can use the relationships between the parameters σ_I and the spectral characteristics of the compounds of interest (for example, data of IR spectroscopy). These relationships have been used, for example, in a study of organosilicon compounds.[4,5]

Study of the influence of substituents on the spectroscopic characteristics of the Si–Cl, Si–F, Si–O–Si, and Si–H bonds in organosilicon compounds has shown that the shifts of the stretching frequencies of these bonds depend on the electronic state of the substituents present in the surroundings of the functional group and obey an equation of the form

$$\nu_i = \nu_0 + \alpha\sum \sigma^*, \quad (3)$$

where ν_i, ν_0 are the stretching frequencies of the bonds in this compound and in the methyl-substituted silane (or siloxane), respectively, α is a coefficient, $\sum\sigma^*$ is the sum of the Taft inductive constants of all substituents in this compound.

Relation (3) reflects a general feature of these compounds — the dependence of spectral characteristics on the electronic effects of substituents. The steric factors are insignificant in this case, and the inductive effect predominates.[4] This allows one to separate quantitatively the effects of different substituents by juxtaposing the data on chemical transformations of particular compounds with their spectral characteristics.

The linear dependence (3) was first established by Thompson,[4] who analysed the spectral characteristics of a small series of silanes R_3SiH with different substituents R. For compounds $R_{3-n}X_nSiH$, where X is halogen, a deviation from linear dependence (3) was observed and suggested [5] to be due to conjugation. The deviation can be quantitatively described by the difference between the calculated (ν_{cal}) and experimental (ν_{exp}) vibration frequencies of the Si–H group

$$\Delta\nu = \nu_{calc} - \nu_{exp}.$$

The ν_{calc} value was found using Eqn (3) taking into account the inductive constants for the corresponding substituents X [σ^*(X)] and R [σ^*(R)] and the relation

$$\sum\sigma^* = n\sigma^*(X) + (3-n)\sigma^*(R).$$

However, for a particular substituent X, the $\Delta\nu$ value was constant and did not change upon the variation of R. This allowed the researchers to separate quantitatively the effects of substituents.[5]

An IR-spectroscopic study of the ≡Si–Cl, ≡Si–F and ≡Si–H groups on the silica surface showed a shift of the characteristic absorption bands of these groups.[9] The authors interpreted these shifts as being due only to the effect of the surface. Meanwhile, the quantitative analysis of the changes in the spectral characteristics of chemisorbed (and, hence, substituted) silanes provides information on the electronic structure and the influence of all substituents that belong to the environment of silicon, including the surface group. To study the surface proper-

ties, it is most convenient to follow the characteristic absorption frequencies of the silicon hydride bond. First of all, this is due to the values of the Si—H stretching frequencies, which occur in the range of 2100–2300 cm^{-1}. Here, the absorption of the IR emission by the core of most solids is insignificant and the observed changes in $\Delta\nu$(Si—H) for various substituted silanes are fairly great, being equal to 100 to 150 cm^{-1} (see Refs 5, 9). This increases the accuracy and reliability of the results.

The surface compounds containing Si—H bonds are formed on hydroxylated surfaces of solid oxides when they are treated with chloro- or alkoxysilane vapours. By analysis of the changes in the chemical reactivity and spectroscopic characteristics, one can estimate quantitatively the influence of the surface groups or the whole core of the solid on the reaction centre.

The real surfaces of most metals and semiconductors contain oxide layers; therefore, the reactivity of such surfaces will be dictated, first of all, by the oxide microstructure and the type of hydroxyl groups. Studies of the hydroxyl cover of silicas and other oxides (for example, Al_2O_3, $xAl_2O_3 \cdot ySiO_2$, TiO_2, ZnO) which exhibit catalytic properties have shown [10] that, in terms of the number of coordination bonds formed by oxygen, three types of OH bonds can be distinguished, those attached to the metal of the oxide core by one (I), two (II) and three (III) bonds (all the M—O bonds are considered to be equivalent). The ratio of the concentrations of hydroxyl groups of each type to their total concentration is determined by both the oxide composition and the surface temperature. The formation of an additional coordination bond results in a lower stretching frequency of the OH groups. This underlies the identification of the type of hydroxy group based on its spectral characteristics.[10–12] For a particular oxide, the relation

$$\Delta\nu(\text{OH})\ (\text{III}) > \Delta\nu(\text{OH})\ (\text{II}) > \Delta\nu(\text{OH})\ (\text{I})$$

usually holds, which is due to a decrease in the electron density on the O—H bond and an increase in the positive charge on the hydrogen atom following an increase in the coordination number of oxygen in the corresponding OH groups. The involvement in surface reactions is determined by both the proton-donor capacity and the steric arrangement (steric factor) of the hydroxyl group. Also, for quantitative estimation of the reactivity of the surface hydroxyl groups, one can use the inductive effect of the matrix and calculate its inductive constant σ_s from the shift of the adsorption maximum for the Si—H stretching vibrations of the surface compounds formed upon the chemisorption of silanes.[12–15] As noted above, this bond is highly sensitive to the electronic effects of substituents. In this case, relation (3) has the form

$$\nu_I = \nu_0 + \alpha(\sum\sigma_I + \sigma_s). \quad (4)$$

When the Taft constants are used as σ_I, the σ_s value can be determined from the scale of these constants.

The fact that the spectral characteristics [ν(Si—H)] of chemisorbed silanes depend only on the electronic effects of substituents allows one to distinguish the influence of each of them; therefore, this method should be considered as legitimate. Evidently, the substituent effect of the core of a solid follows a complex pattern; therefore, experimental results can either obey or depart from Eqn (4), which will provide additional information on the object in question. The availability of Taft inductive constants for a large number of low-molecular-mass substituents [16] markedly simplifies the computational part of the procedure and makes this approach versatile.

III. Inductive effect of a silica matrix and regularities of its variation during dehydration

We tested the above approach in relation to silica samples (Aerosil A-175). The coefficients present in correlation equation (4) were determined for a reaction series of oxides. The concentration of the hydroxyl groups was determined by a reported procedure [17] and compared with the data of IR spectroscopy [18] obtained in the experiments described below.

The characteristic stretching frequencies of the Si—H bond of chemisorbed silanes were determined from the IR spectra recorded on UR-20 and Bruker spectrometers. The deviations of individual measurements from the statistical average values in the region of 2100–3800 cm^{-1} were smaller than 2 cm^{-1}.

For calculation of the coefficients for correlation equation (4), experimental ν_i values for a series of chemisorbed silanes are needed. The frequencies of the maxima of the stretching bands of the Si—H bonds incorporated in different functional groups of compounds synthesised on the Aerosil surface pretreated at 673 K *in vacuo* are listed in Table 1. On chemisorption of methyldichlorosilane and phenyldichlorosilane, surface compounds with different compositions can be obtained. This is due to the fact that these silanes mainly react with the Aerosil surface as monofunctional reagents (compound No. 3 or No. 8), which was confirmed by Tertykh *et al.*[19] During the subsequent treatment of these samples with water or alcohol vapour, the Si—Cl groups remaining intact were hydrolysed or alkoxylated. These processes were accompanied by the corresponding changes in the IR spectra (Fig. 1), namely, partial restoration of the absorption band due to the Si—OH groups (ν = 3750 cm^{-1}, spectrum *2*) in the case of hydrolysis or the change in the shape and intensity of the C—H bands (spectrum *5*) upon alkoxylation. In both cases, the introduction of a new substituent (OH, OCH_3 or OC_2H_5) in the environment of the silicon hydride bond was accompanied by displacement of the ν(Si—H) mode (see Table 1, compounds Nos. 3, 5, 6, 7 and 8, 10, 11, 12; Fig. 1). The subsequent maintenance of these samples at T = 673 K for 1 h resulted in some decrease in the intensity of the ν(Si—H) absorption bands and the appearance of new bands (2260 and 2270 cm^{-1}). This was accompanied by the

Table 1. Influence of the nature of the substituent on the stretching frequency of the silicon hydride bond.[14]

No.	Chemisorbed chlorosilane	Surface compound	ν(Si—H) /cm^{-1}	$\sum\sigma^*$ (see [14])	$\sigma^* + \sum\sigma_s^*$
1	$ClMe_2SiH$	≡Si—O—$SiMe_2H$	2161	0	5.05
2	$ClPh_2SiH$	≡Si—O—$SiPh_2H$	2182	1.104	6.14
3	Cl_2MeSiH	≡Si—O—SiMeClH	2215	2.880	7.91
4	Cl_2MeSiH	$(\equiv Si-O)_2SiMeH$	2260	0	10.15
5	$Cl_2MeSiH + H_2O$	≡Si—O—SiMe(OH)H	2190	1.550	6.61
6	Cl_2MeSiH + MeOH	≡Si—O—SiMe(OMe)H	2189	1.450	6.50
7	Cl_2MeSiH + EtOH	≡Si—O—SiMe(OEt)H	2187	1.366	6.40
8	Cl_2PhSiH	≡Si—O—SiPhClH	2225	3.480	8.49
9	Cl_2PhSiH	$(\equiv Si-O-)_2SiPhH$	2270	0.552	10.67
10	$Cl_2PhSiH + H_2O$	≡Si—O—SiPh(OH)H	2203	2.147	7.23
11	Cl_2PhSiH + MeOH	≡Si—O—SiPh(OMe)H	2200	2.050	7.07
12	Cl_2PhSiH + EtOH	≡Si—O—SiPh(OEt)H	2199	1.966	7.03
13	Cl_3SiH	≡Si—O—$SiCl_2H$	2272	5.760	10.77

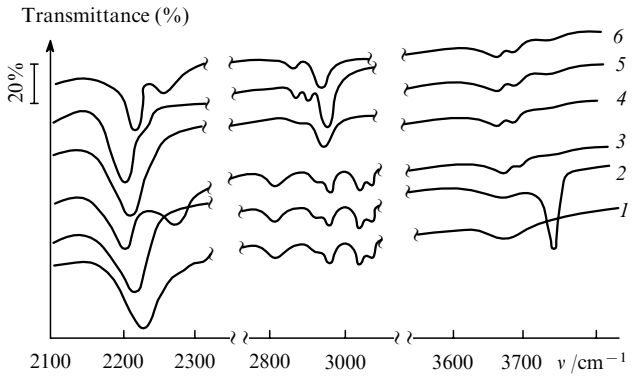

Figure 1. IR spectra of Aerosil treated with phenyldichlorosilane vapour at 473 K (*1*) with subsequent rehydration (*2*) and maintenance at 673 K for 60 min (*3*); and Aerosil treated with methyldichlorosilane vapour at 473 K (*4*) and then with ethanol vapour (*5*) and maintained at 673 K for 60 min (*6*).

disappearance of the absorption bands due to the OH groups (3750 cm^{-1}) and the C–H bonds of the alkoxy groups (2850, 3070 cm^{-1}, Fig. 1, spectra *3* and *6*).

On the basis of these results, it was concluded that the reactions

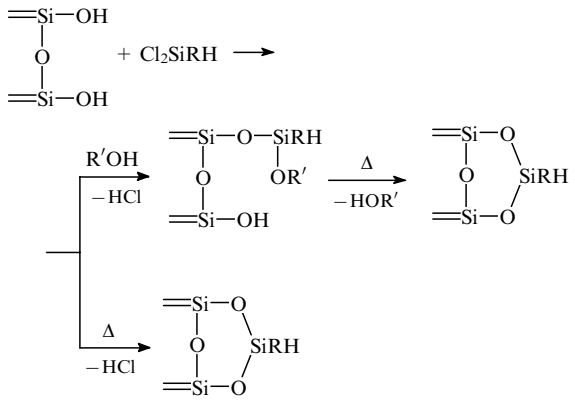

R = Me, Ph; R′ = H, Me, Et

yield silicon hydride groups linked to the surface by two siloxane bonds. It is noteworthy that the characteristic vibration frequencies of the Si–H bonds of the $(\equiv Si-O)_2-SiRH$ groups do not depend on the way they were prepared and are determined only by the structure of the groups.

By mathematical processing of the experimental data given in Table 1 using the Taft inductive constants ($\sum\sigma^*$) for known substituents,[16] the coefficients of relation (4) were determined and the following expression was derived:

$$\nu_i = 2064 + 19.21(\sum\sigma^* + \sigma_s^*). \quad (5)$$

The value $\sigma_s^* = 5.05$, which was also obtained using these experimental data, serves as a measure of the inductive effect of the silicon–oxygen group on the reaction centre.

It can be seen from Table 1 that the surface functional groups can contain various substituents (for example, Cl, Ph); however, this does not cause a significant departure of the ν_i values from linear dependence (5). The presence of a linear correlation between ν_i and σ^* shows that the electronic effects are transmitted through the silicon atom by the inductive mechanism, while the conjugation effects do not play a significant role. The value $\sigma_s^* = 5.05$ serves as a quantitative measure of the electronic state of the silica surface under the experimental conditions.

Table 2. Influence of thermal treatment on the concentration of hydroxyl groups and the inductive constant of silica.[18]

Parameter	Temperature of the thermal treatment /K						
	473	573	673	773	873	973	1073
Concentration of the OH groups /μmol m^{-2}	7.8	5.6	3.4	3.0	2.6	2.3	1.5
ν (Si–H) /cm^{-1}	2152	2155	2161	2163	2165	2168	2170
σ_s^*	4.57	4.73	5.05	5.15	5.25	5.41	5.52

The data of spectroscopic investigations [20, 21] and quantum-chemical data [22, 23] showed that the reactivity of the surface silanol groups depends on their concentration, which, in turn, is a function of the temperature of dehydroxylation of the silica surface. This is due to an increase in the electronegativity of some surface silicon atoms caused by the removal of hydroxyl groups and/or water molecules from their coordination sphere and to electron density redistribution in the Si–O bonds. Thus, for samples with different degrees of hydration, the numerical σ_s^* values should be different. This was confirmed by experimental results. The experimental ν(Si–H) values for a series of Aerosil A-175 samples pre-evacuated at 473–1073 K were used to calculate, from Eqn (5), the σ_s^* values (Table 2) for samples with different concentrations of hydroxyl groups. Analysis of these results taking into account the high sensitivity of the Si–H bond to electronic effects of substituents showed that the relative shift of ν(Si–H) upon dehydration is rather small, namely, it does not exceed 20 cm^{-1} ($\sim$10% of the absolute value). This is due to the fact that the surface silicon atoms responsible for the change in the electronegativity of the [SiO_4] substituent are linked to the Si–H centre by a siloxane bond, which can suppress the inductive effect. The suppression coefficient (the transmission factor of the bond) Z can be derived from the ratio of the inductive constants for compounds with a chain of bonds

$$\sigma_{\equiv Si-(OSi\equiv)n} = \sigma_{(\equiv Si-)}Z^n. \quad (6)$$

The numerical value of Z was found from the values of σ_s^* for the following surface groups: (*1*) $\equiv$Si–H ($n = 0$); (*2*) $\equiv Si-O-Si(CH_3)_2H$ ($n = 1$) (see Table 2); and (*3*) $\equiv Si-O-Si(CH_3)_2-O-Si(CH_3)_2H$ ($n = 2$).

Compounds with type *1* and *3* fragments were synthesised by the reactions

$$\equiv Si-OH + CH_3OH \xrightarrow[-H_2O]{} \equiv Si-OCH_3 \xrightarrow{1023\ K} \equiv Si-H + CH_2O,$$

$$\equiv Si-OH + Cl_2Si(CH_3)_2 \xrightarrow[-HCl]{} \equiv Si-O-SiCl(CH_3)_2 \xrightarrow[-HCl]{H_2O} \equiv Si-O-Si(CH_3)_2-OH \xrightarrow[-HCl]{ClSi(CH_3)_2H} \equiv Si-O-Si(CH_3)_2-O-Si(CH_3)_2H.$$

These reactions were monitored by IR spectroscopy directly in the IR cell serving as the reaction vessel, by following the disappearance of the absorption band for isolated Si–OH groups (3750 cm^{-1}) and the appearance of bands for the methoxy group [ν(C–H) = 2930 and 2970 cm^{-1}]. During high-temperature treatment, the methoxy groups were detached as formaldehyde to give silica hydride [24] with ν(Si–H) = 2280 cm^{-1}. The last reaction was accompanied by the appearance of absorption bands for the methyl groups with ν(C–H) = 2920 cm^{-1}. Using the ν(Si–H) values for the $\equiv Si-O-$, $\equiv Si-O-Si(CH_3)-O-$ and $\equiv Si-O-Si(CH_3)_2-O-Si(CH_3)_2-$ substituents, which were 2280, 2161 and 2120 cm^{-1}, respectively, the inductive

constants σ_s^* were calculated from Eqn (5) ($\sigma_{0s}^* = 11.24$ for $n = 0$; $\sigma_{1s}^* = 5.05$ for $n = 1$; $\sigma_{2s}^* = 2.91$ for $n = 2$). The Z value was determined as the average of the three values obtained by substitution of pairs of values into Eqn (6):

$$Z_1 = \frac{\sigma_{1s}^*}{\sigma_{0s}^*} = 0.449,$$

$$Z_2 = \frac{\sigma_{2s}^*}{\sigma_{1s}^*} = 0.576,$$

$$Z_3 = \left(\frac{\sigma_{2s}^*}{\sigma_{0s}^*}\right)^{0.5} = 0.509.$$

The resulting value, $Z = 0.51 \pm 0.04$, implies that the transmission ability of the siloxane bond in the synthesised surface compounds is rather great and does not differ much from that for linear siloxanes ($Z = 0.48$).[25] It can serve as a quantitative measure of the long-range effect of the silicon–oxygen core in the cases outlined below.

1. Variation of the reactivity of the functional group Y separated from the core by a chain of siloxane bonds, for example, $\equiv Si-(O-SiR_2-O)_n-Y$.

2. Variation of the reactivity of the functional group Y or X toward the reaction

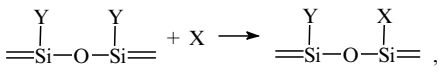

for example, in the synthesis of silicas with functional groups of different types.

The parameters of the $\equiv Si-O-Si\equiv$ bond for silicas (the Si–O distance is 0.160–0.167 nm, the SiOSi angle is 150–170°) vary in the same range as those for linear or cyclic siloxanes.[25] This suggests that the transmission ability of siloxane bonds located on the silica surface should not differ much from that for silanes synthesised on the silica surface; this was confirmed by experimental data.

The relatively small shifts of ν(Si–H) during dehydration can also be attributed to the fact that dehydroxylation of the surface is usually accompanied by the formation of new aqua complexes

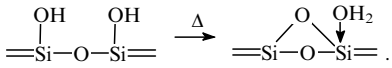

Therefore, the decrease in the coordination number of surface silicon atoms is partially compensated. The high sensitivity of the Si–H bond to the nature of the substituent allowed the researchers to detect the deviation of the dependence $\sigma_s^* = f(T)$ from the general linear dependence at $T < 600$ K ($c_{OH} > 5$ μmol m^{-2}) (Fig. 2). A substantial increase in the concentration of aqua complexes under these conditions and an increase in the coordination number of surface silicon atoms resulted in a decrease in their effective electronegativity, which told on the dependence $\sigma_s^* = f(T)$. The activation energy for dehydroxylation estimated based on the temperature dependence of the total concentration of the hydroxyl groups was ~160 kJ mol^{-1}; this value falls within the range reported by Gorlov *et al.*[26]

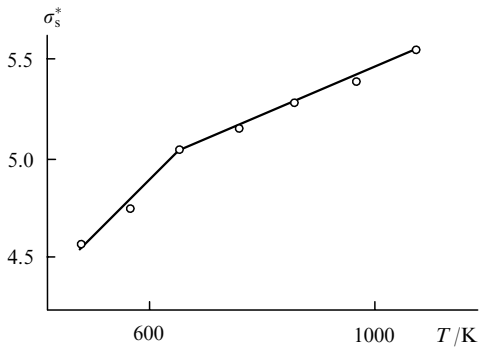

Figure 2. Influence of thermal treatment on the Taft inductive constant of silica.

IV. Estimation of the inductive effect of the core of some dispersed oxides

The good prospects of using correlation analysis for establishing the pattern of the electronic influence of a solid core were demonstrated for zinc, magnesium, beryllium, titanium and aluminium oxides, whose acidity constants vary over a rather broad range. Pelleted samples of these oxides were hydroxylated by water vapour and then treated with dimethylchlorosilane (DMCS) vapour at temperatures recommended for each oxide.[11,12]

For surface groups of the $MO-SiR_2H$ type, the ν(Si–H) values should depend not only on the metal of the surface but also on the type of OH groups involved in the formation of the silicon hydride group. In other words, the ν(Si–H) values should reflect the electron-withdrawing properties of the metal oxide surface fragment and, hence, the reactivity of the hydroxyl groups attached to it.

The IR spectra of these oxides treated with a DMCS vapour showed a number of specific features.[15] Figure 3 presents the IR spectra of the initial and DMCS-vapour treated samples of beryllia, titania and alumina. As a result of chemisorption, thermally stable compounds $MOSi(CH_3)_2H$ were formed on the

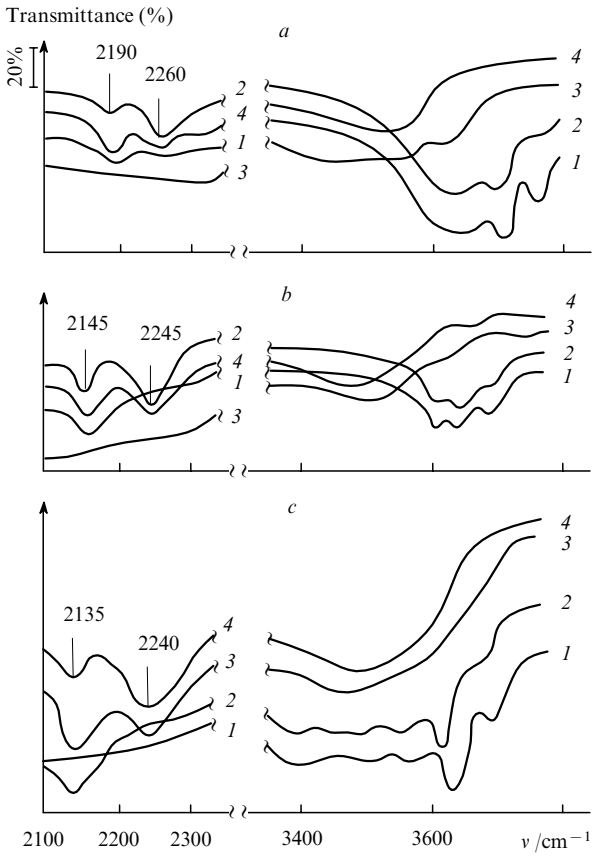

Figure 3. IR spectra of alumina (*a*), titania (*b*) and beryllia (*c*).[15] Samples: (*1*) initial; (*2*) treated with traces of DMCS at 473 K, $P = 1$ Pa, $\tau = 30$ min; (*3*) treated with traces of DMCS at 473 K, $P = 50$ Pa, $\tau = 30$ min; (*4*) evacuated while maintained at a constant temperature (523 K), $\tau = 60$ min.

oxide surface. For low pressures of DMCS vapour (~ 1 Pa), the spectrum of beryllia showed a decreased intensity of the band for the OH groups of type I (3720 cm^{-1}) and a new absorption band for the Si–H bond (2135 cm^{-1}, see Fig. 3 *c*; curves *1*, *2*). When the DMCS vapour pressure was increased to 50 Pa, the OH groups of type II (3630 cm^{-1}) entered into the reaction to give new silicon hydride groups [ν(Si–H) = 2240 cm^{-1}, see Fig. 3 *c*; curve *3*]. Similar changes were noted for TiO_2 (anatase) (see Fig. 3 *b*) and γ-Al_2O_3 samples (see Fig. 3 *a*).

It was found that the hydroxyl groups of type I were the first to react on the surfaces of all of the oxides. However, judging by the intensity of the Si–H absorption band and the thermal stability of the groups formed, type I hydroxyl groups are expected to be least reactive in electrophilic substitution. This contradiction can be explained by the influence of steric factors in heterogeneous chemical processes. The low concentration and the spatial positions of the 'sunk' OH groups of types II or III are unfavourable for surface reactions.

Treatment of the surfaces of zinc and magnesium oxides with DMCS vapour did not give thermally stable surface compounds of the $MOSiR_2H$ type. In this case, the absorption bands for type I and II hydroxyl groups were found to shift due to the presence of chlorosilane on the surface. The subsequent thermal treatment resulted in complete desorption, indicating the absence of chemical bonds with the surface. A possible reason is low electrophilicity of DMCS in surface reactions with the relatively inert hydroxyl groups of these matrices.

By comparison of the σ_s^* values calculated using the experimental ν(Si–H) frequencies for the $\equiv$SiH groups synthesised on reaction centres of the same type (Table 3), the oxides studied can be arranged in the following sequence according to increasing effective electronegativity of the core:

$$MgO \approx ZnO \ll BeO < TiO_2 < SiO_2 < \gamma\text{-}Al_2O_3.$$

No hydroxyl groups of type III were revealed in these experiments, probably, because they are present in a very low concentration if at all.

Table 3. Vibration frequencies of the OH and SiH groups and the Taft inductive constants of the oxide core ($T = 473$ K).[15]

Oxide	Type of OH groups	ν(OH) /cm^{-1}	ν(Si–H) /cm^{-1}	σ^*
BeO	I	3720	2135	3.70
	II	3630	2240	8.93
TiO_2	I	3700	2145	4.21
	II	3640	2245	9.42
γ-Al_2O_3	I	3780	2190	6.55
	II	3720	2260	10.20
SiO_2	I	3750	2152	4.57

The inductive effect is polarisation of σ bonds transferred along the chain of atoms; therefore, the inductive effect of the core would affect the electron density distribution in a hydroxyl group connected to this core. The above sequence reflects not only the effective electronegativity of the solid core; the particular value of σ_s^* of each member of the sequence can be used to estimate the reactivity of the surface hydroxyl groups. The data obtained using this approach are in good agreement with the results obtained by other procedures, for example, based on acidity constants.[10–12]

V. Quantitative estimation of the reactivity of hydroxylated surfaces of single-crystal matrices

The possibility of using the inductive effect to describe the surface phenomena demonstrated for dispersed oxide matrices opens up prospects for quantitative estimation of the reactivity of the surface hydroxyl groups on single-crystal, in particular semiconductor, matrices. Solution of this problem would allow one to predict the processes of template synthesis of nanostructures and promote the chemical nanotechnology for elaboration of the submicrometer component base for electronic engineering. As an example, one can consider the results obtained for silicon samples with (111) and (100) orientations by multiple attenuated total internal reflection (ATIR) IR spectroscopy.[27,28] In experiments, the angle of incidence of the beam θ was 45° and the number of reflections n was 28. The ATIR spectra were recorded directly in the cell-reaction vessel, which ensured treatment of the sample surfaces either in a vacuum (down to 10^{-3} Pa) or in a controlled medium in the temperature range of 20–600 °C.

Study of the hydroxylation of freshly etched silicon and the subsequent sorption of DMCS has shown[27,28] that the spectral pattern in the frequency region 3700–3750 cm^{-1} is similar to that observed for a dehydrated surface of narrow-pore silica gels.[29] The adsorption of DMCS resulted in the formation of tetramethyldisiloxane as a result of hydrolysis of the sorbed compound by the water molecules present on the surface as thermally stable aqua complexes. The tetramethyldisiloxane formed was not chemically bonded to the silicon surface and was completely desorbed upon temperature rise.[27,28]

On the basis of these data, it was concluded that silanol groups present on the silicon surface, like the hydroxyl groups of zinc and magnesium oxides, do not react with DMCS, whereas the OH groups on the silica surface are chemically reactive under similar conditions and form thermally stable surface compounds, $\equiv Si-O-Si(CH_3)_2H$ [ν(Si–H) = 2152 cm^{-1}]. This fact can be attributed either to low electrophilicity of DMCS or to different electronic structures of silicon and silica surface atoms. A surface of even freshly etched silicon contains an ultrafine (1.0–1.5 nm) oxide film;[30] therefore, on treatment with water vapour, in addition to silanol groups, one can also expect the formation of a hydration cover linked by coordination bonds. Presumably, the energy of the coordination bonds of aqua complexes is somewhat higher in this case, because the ultrafine oxide film on the surface of a single crystal is depleted in oxygen. In the depleted surface film, the probability of electron density displacement from silanol groups is much lower; therefore, they do not exhibit sufficient proton-donor capacity and do not react with DMCS.

The activation energy for the electrophilic replacement of the proton of silanol groups is known[31] to depend on the proton-acceptor properties of the attacking reagent; therefore, one can choose a substituted silane capable of reacting with relatively inert hydroxyl groups on the silicon surface. Triethoxysilane (TES) was chosen for this purpose. Its reaction with the silicon surface was studied at different temperatures ranging from room temperature

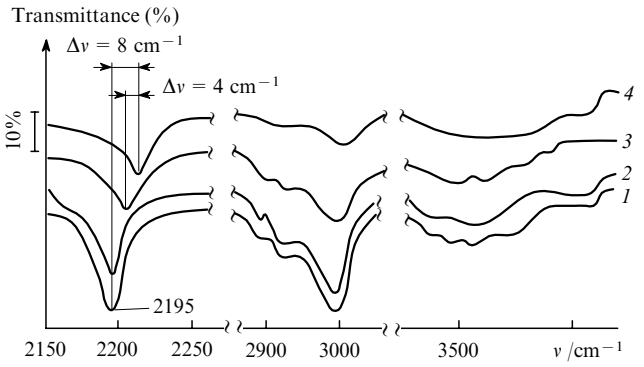

Figure 4. ATIR infrared spectra of a silicon surface;[28] (*1*) after hydration at 473 K and subsequent treatment with TES vapour at 300 K; (*2*, *3*) after evacuation at constant temperatures of 373 K and 473 K, respectively, for 30 min; (*4*) after rehydration in water vapour at 473 K.

to 673 K. Figure 4 shows the ATIR spectra of samples subjected to different types of thermochemical pretreatment. Stable surface compounds containing Si—H bonds were synthesised, and not only the inductive effect of the matrix but also the stoichiometry of the surface reaction was determined.

When samples evacuated for 1 h at 473 K are treated with water vapour at the same temperature, then cooled and treated with TES vapour at room temperature, the spectrum (see Fig. 4, spectrum *1*) exhibits an absorption band for the Si—H bond and a characteristic set of bands for the C—H bonds of the ethoxy groups. The ν(Si—H) frequency in this spectrum coincides with the Si—H stretching frequency for triethoxysilane (2195 cm^{-1}). This points to the absence of any chemical reactions in the system. After maintaining the sample for 30 min at 373 K, the spectrum (spectrum *2*) shows deformation of the low-frequency region of the Si—H band caused by the appearance on the silicon surface of adsorbed alkoxy-substituted disiloxane having formed in a reaction similar to the reaction with DMCS. Only after maintenance at 473 K for 1 h do the intensities of the Si—H and C—H absorption bands decrease. As this takes place, the band of the Si—H vibrations becomes symmetrical and its maximum shifts by 8 cm^{-1} to shorter wavelengths relative to the position of this band in the spectrum of sample *1* not kept at a constant temperature. The decrease in the intensity of the Si—H and C—H absorption bands is due to the thermal desorption of excess reagent and the disiloxane formed, while the observed shift of the ν(Si—H) absorption maximum is caused by the replacement of one or several alkoxy groups by more electronegative substituents. The above-listed changes in the spectral characteristics and the thermal stability of the product obtained at 473 K attest to its chemical bonding to the surface, which could result only from the reaction between the silanol groups and the ethoxy groups of the sorbed silane,

$$(\equiv Si-OH)_m + (C_2H_5O)_3SiH \longrightarrow$$
$$\longrightarrow (\equiv Si-O-)_mSi(OC_2H_5)_{3-m}H + m\,C_2H_5OH.$$

The alkoxy groups not involved in the reaction can be replaced by hydroxyl groups by treating the sample surface with water vapour. Indeed, when comparing spectra *2* and *3* (see Fig. 4), one can see that hydration entails an increase in the intensity of the C—H absorption band and substantial enhancement of the absorption in the OH stretching region (3600–3700 cm^{-1}). The ν(Si—H) mode shifts by 4 cm^{-1} to shorter wavelengths. The changes observed in spectra *3* and *4* are due to the reaction

$$(\equiv Si-O)_mSi(OC_2H_5)_{3-m}H + (3-m)\,H_2O \longrightarrow$$
$$\longrightarrow (\equiv Si-O)_mSi(OH)_{3-m}H + (3-m)\,C_2H_5OH.$$

The stoichiometry of the surface reactions, *i.e.*, the numerical value of the coefficient m, can be determined using correlation equation (5). By transforming this relation and replacing $(3-m)$ alkoxy groups with $\sigma^*(OC_2H_5) = 1.366$ (see Ref. 16) by an equivalent number of OH groups with $\sigma^*(OH) = 1.550$ (see Ref. 16), one can determine the shift of the stretching frequency of the Si—H bond

$$\Delta\nu(Si-H) = a(3-m)[\sigma^*(OH) - \sigma^*(OC_2H_5)];$$

hence,

$$m = 3 - \frac{\Delta\nu(SiH)}{a[\sigma^*(OH) - \sigma^*(OC_2H_5)]} =$$
$$= 3 - \frac{4}{19.21(1.550 - 1.366)} = 1.86 \approx 2.$$

Thus, the structure of the surface compounds formed in the reaction with TES can be represented as $(\equiv Si-O)_2Si(OC_2H_5)H$. By using Eqn (5) and substituting the value ν(Si—H) = 2203 cm^{-1} (see Fig. 4, spectrum *4*) for this compound into the equation, one can estimate the inductive effect of the silicon–oxygen groups present on the surface of single-crystal silicon against the scale of the Taft inductive constants

$$\sigma_s^* = \left[\frac{\nu_i - \nu_0}{a - \sigma^*(OC_2H_5)}\right]m^{-1} =$$
$$= \frac{(2203 - 2064)/19.21 - 1.366}{2} = 2.90.$$

For silica, this parameter is much higher. Thus for Aerosil dehydrated at the same temperature, $\sigma_s^* = 4.57$ (see Table 2). Comparison of the numerical values of these parameters showed that the silanol groups on the silicon surface are much weaker proton donors than the same groups on the silica surface. Most probably, this is due to the inhibitory inductive effect of the silicon core.

In addition, the hydration cover formed upon heating of the silicon surface in water vapour, was found to contain, apart from silanol groups, the OH groups of water molecules attached to the surface silicon atoms by coordination bonds. The results shown in Fig. 2 may suggest that quantitative dehydration of the surface of the oxidised single crystal would take place during evacuation only at $T > 600$ K. It is noteworthy that the observed changes in the spectral characteristics of silicon cells did not depend on the crystallographic orientation of the samples to within the sensitivity of the method. The lack of this dependence is due to the fact that the influence of the surface oxide layer is more significant than that of the single-crystal silicon core.

The inductive effect of the core of the GaAs binary semiconductor with orientation (100) was estimated for ATIR cells having $\theta = 30^\circ$ and $n = 28$. At temperatures of 423–523 K, active chemisorption of DMCS was observed on the GaAs surface containing a natural oxide layer [ν(Si—H) = 2165 cm^{-1}]; the calculated value is $\sigma^* = 5.25$. After etching of the surface of this semiconductor with a $CH_3OH : Br_2$ (100 : 1) mixture with subsequent washing with methanol and double-distilled water, the σ^* value decreased to 5.1 [ν(Si—H) = 2162 cm^{-1}], which is due to a decrease in the oxide layer thickness. However, in any case, the σ^* value is greater for the GaAs surface than for silicon or silica surfaces. The higher inductive effect of this matrix is caused by the fact that it incorporates a more electronegative component (arsenic) and its oxides. Therefore, there are grounds for believing that the hydroxyl groups on a real GaAs surface should exhibit rather high proton-donor capacity and hence, they can be used in surface chemical reactions with relatively weak electrophilic reagents. This fact is of certain interest for the production of surface nanostructures on this matrix.

VI. Effect of the thickness of the oxide layer on the activity of silanol groups on the silicon surface

On the basis of analysis of the experimental data concerning the inductive effect of silica, silicon and gallium arsenide cores, one can suggest that the reactivity of the hydroxyl groups occurring on the real surface of a semiconductor crystal would be determined by sample prehistory, namely, the thickness of the oxide layer formed during the pretreatment. From the inductive effect, this influence can be derived and the pattern of variation of the reactivity of the silanol groups present on the silicon surface with different degrees of oxidation can be elucidated. To this end, one merely has to analyse the spectral characteristics of chemisorbed silanes on matrices with different known thicknesses of the oxide. These experiments were carried out for silicon samples (ATIR cells) on which a specified oxide layer was synthesised by molecular layering,[27, 28, 31] *i.e.*, by alternating treatment of the surface with silicon tetrachloride and water vapours. The layer thickness was determined by ellipsometric measurements and calculated in the Drude–Tronston one-layer model approximation.[32] The measurements were carried out using an ellipsometer with a

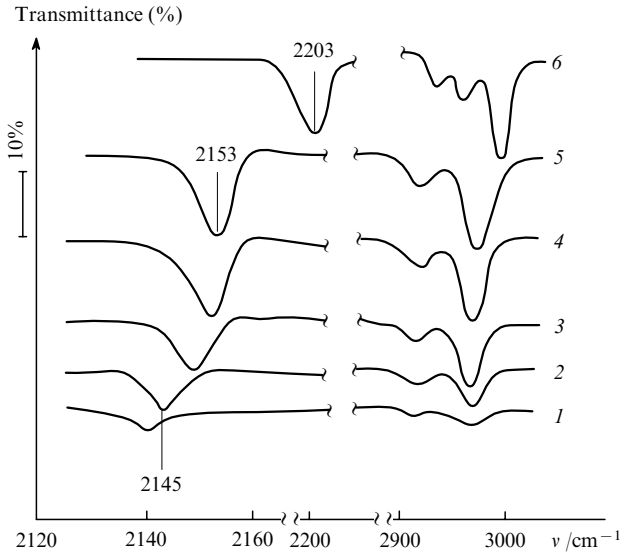

Figure 5. ATIR infrared spectra of the (111) silicon surface subjected to cyclic treatment with silicon tetrachloride and water vapours at 473 K with subsequent treatment with DMCS at the same temperature.[27,31]
The number of cycles is 4 (*1*), 10 (*2*), 20 (*3*), 30 (*4*), 40 (*5*); spectrum of the sample after etching and treatment with triethoxysilane (*6*).

fixed compensator and magnetic modulation of the light beam. The error of determination of these parameters did not exceed $\pm 0.01'$.

Figure 5 shows the IR spectra of ATIR silicon samples with a synthesised SiO_2 layer pretreated with DMCS vapour at 473 K, and Fig. 6 shows the dependence of the thickness of this layer (d) and the relative Si—H absorption intensity on the number of molecular layering cycles (N). Comparison of spectra *1–4* (see Fig. 5) showed that an increase in the thickness of the synthesised oxide layer entails a substantial increase in the absorption intensity in the region of the Si—H (2135–2150 cm^{-1}) and C—H (2900–3000 cm^{-1}) stretching frequencies and a noticeable shift of the ν(Si—H) bond to shorter wavelengths. This pointed unambiguously to an increase in the concentration of silanol groups capable of reacting with DMCS; moreover, up to $N \approx 15$ ($d \approx 3$ nm), the number of reactive centres increased in proportion to N and subsequently it changed only slightly (see Fig. 6).

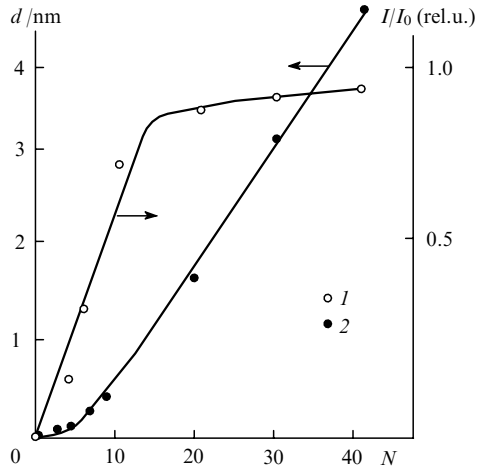

Figure 6. Relative intensity of the absorption bands for the Si—H bond (*1*) and thickness of the oxide layer (*2*) *vs.* the number of molecular layering cycles (N).[31]

As shown above, the silanol groups on a freshly etched silicon surface did not react with DMCS at all, but they did react with more active TES to give surface compounds. For comparison, Fig. 5 shows a fragment of the spectrum (curve *6*) of a freshly etched ATIR silicon cell pretreated with TES vapour. With an increase in the oxide thickness, the influence of the silicon core becomes less pronounced, while the role of the oxide with a large σ_s^* value is enhanced and, hence, the reactivity of the silanol groups increases. This appears to be also the reason for the retardation of the formation of the oxide layer upon chemisorption of $SiCl_4$, which is observed in the initial stages of the synthesis ($N < 10$) (see Fig. 6).

These results allowed the researchers to establish the quantitative relationship between the thickness of the oxide layer on the silicon matrix and its inductive effect and, hence, the activity of the hydroxyl groups (Fig. 7). As noted above, the most pronounced changes in σ_s^* were observed up to an oxide layer thickness of $\sim$3 nm. The inductive effect of the silicon core with thick oxide layers was almost the same as the effect of silica. In this case, as expected, active chemisorption of DMCS took place. It should be borne in mind that even a silicon surface freshly etched in aqueous solutions has a thin oxide layer ($\sim$1 nm, according to our estimates) and the σ_s^* value calculated from experimental ν(Si—H) to be 2.9, refers to such a surface.

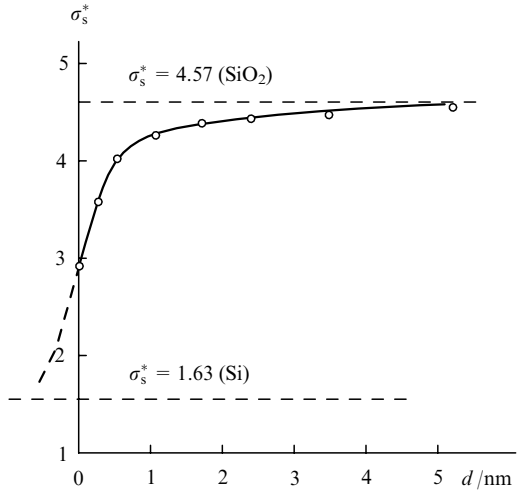

Figure 7. Influence of the thickness of the synthesised oxide layer on the inductive constant of silicon.[28]

The inductive constant estimated from the stretching frequency of the Si—H groups formed during etching of silicon with hydrofluoric acid [ν(Si—H) = 2096 cm^{-1}] amounts to 1.63. This value refers to a silicon surface almost deprived of the oxide layer and is indicative of a low reactivity of the silanol groups linked directly to the silicon core. If the surface contains a SiF group, the σ_s^* value can only increase; however extrapolation of the $\sigma_s^* = f(d)$ curve to $\sigma_s^* = 1.63$ (see Fig. 7) gives a real thickness of the residual oxide that coincides with ellipsometric estimates.

Thus, all real silicon matrices can be represented as a number of chemical compounds with the general formula $Si_m(SiO)_x.(SiO_2)_yOH$ where each particular composition (x and y values) is matched by a particular σ_s^*; at great y, this corresponds to the final member of the series, silica $(SiO_2)_yOH$.

The σ_s^* values obtained were indicative of relatively weak proton-donor properties of silanol groups both for a pure silicon surface and for a surface coated by a thin (< 3.0 nm) oxide layer. This means that for complete involvement of these groups in surface reactions, conditions should be provided for additional protonisation of hydroxyl groups. These conditions can be attained by raising the temperature (or by another activating

treatment) or by using proton-acceptor chemical reagents. For example, the use of triethylamine [27] as an exchange catalyst eliminates the latent period in the formation of silicon oxide layers (see Fig. 6) and allows the synthesis of silicon oxide nanostructures on hydroxylated surfaces of metals [33] in which the inductive effect of the core is relatively low for the same reasons as for silicon.

It should be noted that, judging by the transmission effect of the silicon–oxygen bond ($Z_{Si-O-Si} = 0.51$), the changes in $\Delta\sigma_s^*$ and, hence, the shift of ν(Si—H) should be much smaller for $N < 10$. If one oxide monolayer is synthesised per cycle of molecular layering, for N cycles, this should be

$$\Delta\sigma_s^* \sim Z^N = 0.51^N.$$

However, this relationship was not observed. Probably, in the initial stages of the molecular layering synthesis ($N < 10$), surface reactions involve only a part of hydroxyl groups and give rise to two-dimensional islet structures whose area increases upon further treatment. This is also indicated by the increase in the intensity of the bands for both Si—H and C—H bonds caused by the increase in the area occupied by the oxide.

An attempt to establish the general relationship between the inductive constants and the energetic characteristics of the studied matrices has revealed a linear correlation with the energy of the crystal core. For a gallium arsenide surface whose composition can be represented as a mixture of gallium and arsenic oxides, the experimental σ_s^* values fit well into the general linear dependence. The estimation of the presumptive σ_s^* values for MgO and ZnO using this dependence gave 2.8 and 2.2, respectively. These values could not be determined experimentally due to the low electrophilicity of DMCS.

VII. Conclusion

The material considered in this review shows good prospects for the use of the inductive effects and correlation analysis to study chemical transformations on the surface of solids. By comparison of inductive constants, it becomes possible not only to estimate quantitatively the influence of the core and the state of the surface for various solids on the processes taking place during thermal treatment but also to predict the pattern of surface reactions with various reagents. For this purpose, one should compare the σ_s^* and σ^* values for a substituent in a low-molecular-weight reagent. The reaction would proceed toward the replacement of the given substituent by a substituent with a greater inductive constant.

In a study of surface reactions on objects with small surface areas, for example, on single crystals, an important feature is the possibility of determining their stoichiometry when the use of direct chemical or analytical methods is difficult. The cited example of solving this problem for the silicon matrix convincingly demonstrates the utility of the parametric constants of the correlation equations.

Further development of the quantitative approach based on the use of inductive constants would involve selection of a standard surface reaction and determination of its characteristics (rate and equilibrium constants). This would enable quantitative prediction of the pathways and yields of surface reactions merely based on one-parameter correlation equations taking into account only the inductive effect. As a standard reaction, one can use the rearrangement [33] between chemisorbed chloro- and alkoxysilanes whose equilibrium constant can be found experimentally without much difficulty.

At the current stage of research, the inductive effect of substituents (including the core of a solid) can be estimated only as a certain approximation. Therefore, any task of exact determination of the inductive component in nonuniform surface phenomena is arbitrary and the result will depend on the choice of the standard process which underlies the scale of inductive constants used. However, this approach, which provides a quantitative description of surface processes, may prove useful for development of the routes of deliberate synthesis of surface nanostructures and development of chemical nanotechnology.

* * *

I am grateful to my colleagues who participated in joint studies and to the founder of the scientific school for the chemistry of highly organised substances, Corresponding Member of the RAS V B Aleskovsky for fruitful discussion of the results.

This review was partially supported by the grant of President of Russian Federation 'Leading Scientific Schools of Russia' (NSh 2336.2003.3 'Chemistry of Highly Organised Substances').

References

1. V A Palm *Osnovy Kolichestvennoi Teorii Organicheskikh Reaktsii* (The Foundations of the Quantitative Theory of Organic Reactions) (Leningrad: Khimiya, 1977)
2. L Hammett *Physical Organic Chemistry* (2nd Ed.) (New York: McGraw-Hill, 1970)
3. W Robert, J Taft *J. Am. Chem. Soc.* **74** 3120 (1952)
4. H W Thompson *Spectrochim. Acta* **16** 238 (1960)
5. V P Mileshkevich, N F Novikova *Usp. Khim.* **50** 85 (1981) [*Russ. Chem. Rev.* **50** 49 (1981)]
6. V B Aleskovskii *Zh. Prikl. Khim.* **55** 725 (1982) [a]
7. V B Aleskovskii *Khimiya Nadmolekulyarnykh Soedinenii* (The Chemistry of Supramolecular Compounds) (St Petersburg: St Petersburg State University, 1996)
8. V B Aleskovskii *Zh. Obshch. Khim.* **65** 1928 (1995) [b]
9. A V Kiselev, V I Lygin *Infrakrasnye Spektry Poverkhnostnykh Soedinenii* (Infra-Red Spectra of Surface Compounds) (Moscow: Nauka, 1972)
10. V F Kiselev *Poverkhnostnye Yavleniya v Poluprovodnikakh i Dielektrikakh* (Surface Effects in Semiconductors and Dielectrics) (Moscow: Nauka, 1970)
11. A A Tsyganenko, V N Filimonov *Dokl. Akad. Nauk SSSR* **203** 636 (1972) [c]
12. A A Tsyganenko, A V Khomenya, V N Filimonov *Adsorbtsiya Adsorbenty* **4** 86 (1976)
13. Yu K Ezhovskii, P M Vainshtein, I P Gavrilina *Khim. Fiz.* **15** 104 (1996) [d]
14. P M Vainshtein, Yu K Ezhovskii, S I Kol'tsov *Zh. Fiz. Khim.* **55** 394 (1981) [e]
15. Yu K Ezhovskii, A I Klyuikov *Zh. Fiz. Khim.* **72** 908 (1998) [e]
16. *Spravochnik Khimika* (Handbook for Chemist) (Moscow, Leningrad: Khimiya, 1971) Vol. 3
17. N G Roslyakova, V B Aleskovskii *Zh. Prikl. Khim.* **39** 795 (1966) [a]
18. Yu K Ezhovskii, P M Vainshtein *Izv. Akad. Nauk, Ser. Khim.* **10** 1757 (1997) [f]
19. V A Tertykh, V V Pavlov, K I Tkachenko, A A Chuiko *Teor. Eksp. Khim.* **11** 174 (1975) [g]
20. V N Pak, Yu P Kostikov *Zh. Prikl. Spektrosk.* **26** 755 (1977)
21. K B Yatsimirskii, V V Nemoshkalenko, A A Chuiko *Metallofizika* **60** 60 (1975)
22. V N Pak *Zh. Fiz. Khim.* **48** 1631 (1974) [e]
23. V I Lygin, Z M Muldakhemtov, I T Tusidbekov *Kinet. Katal.* **20** 780 (1979) [h]
24. C Morterra, M I Low *J. Chem. Phys.* **73** 321 (1969)
25. M G Voronkov, V P Mileshkevich, Yu L Yuzhelevskii *Siloksanovaya Svyaz'* (Siloxane Bond) (Novosibirsk: Nauka, 1976)
26. Yu G Gorlov, V G Golovatyi, N M Konoplya, A A Chuiko *Teor. Eksp. Khim.* **16** 202 (1980) [g]
27. Yu K Ezhovskii *Zh. Fiz. Khim.* **61** 1598 (1987) [e]
28. Yu K Ezhovskii, P M Vainshtein *Zh. Prikl. Khim.* **71** 227 (1998) [a]
29. M R Basila *J. Chem. Phys.* **35** 1151 (1961)
30. V G Litovchenko, in *Poluprovodnikovaya Tekhnika i Mikroelektronika* (Semiconductor Engineering and Microelectronics) (Kiev: Naukova Dumka, 1973) Vol. 12, p. 3
31. Yu K Ezhovskii, P M Vainshtein, S I Kol'tsov *Zh. Fiz. Khim.* **60** 701 (1986) [e]
32. R Azzam, N Bashara *Ellipsometry and Polarized Light* (Amsterdam: Narth-Holland, 1977)

33. P M Vainshtein, Yu K Ezhovskii, S I Kol'tsov *Zh. Prikl. Khim.* **58** 740 (1985) [a]

[a] — *Russ. J. Appl. Chem. (Engl. Transl.)*
[b] — *Russ. J. Gen. Chem. (Engl. Transl.)*
[c] — *Dokl. Chem. (Engl. Transl.)*
[d] — *Chem. Phys. Rep. (Engl. Transl.)*
[e] — *Russ. J. Phys. Chem. (Engl. Transl.)*
[f] — *Russ. Chem. Bull., Int. Ed. (Engl. Transl.)*
[g] — *Theor. Exp. Chem. (Engl. Transl.)*
[h] — *Kinet. Catal. (Engl. Transl.)*

Russian Chemical Reviews **73** (3) 205 – 223 (2004) © 2004 Russian Academy of Sciences and Turpion Ltd

DOI 10.1070/RC2004v073n03ABEH000825

Crystal chemistry, properties and synthesis of microporous silicates containing transition elements

N V Chukanov, I V Pekov, R K Rastsvetaeva

Contents

I.	Introduction	205
II.	Synthesis of microporous amphoterosilicates	205
III.	Crystal-chemical features of amphoterosilicates with zeolite properties	206
IV.	Properties of microporous silicates containing transition elements	219

Abstract. The review surveys and generalises recent data on synthesis methods, physicochemical properties and crystal chemistry of silicate microporous materials containing transition elements (amphoterosilicates). The frameworks of these materials, unlike those of usual aluminosilicate zeolites, are built from tetrahedrally coordinated atoms along with atoms of various elements (Ti, Nb, Zr, Ta, Sn, W, Fe, Mn, Zn, *etc*.) with coordination numbers of 6 or 5. Many amphoterosilicates possess ion-exchange properties and can serve as catalysts for redox reactions, sorbents, *etc*. The structural diversity of synthetic and natural amphoterosilicates provides the basis for the preparation of microporous materials with different properties. The bibliography includes 195 references.

I. Introduction

Zeolites are finding increasing applications in industry and agriculture due primarily to their sorption, ion-exchange and catalytic properties.

Framework structures of traditional zeolites and zeolite materials, such as aluminosilicates, aluminophosphates, silicoaluminophosphates and silicas, are formed by four-coordinate elements (Si, Al, P, B, Be, Zn, *etc*.). However, studies performed in the last two – three decades demonstrated that many titano-, niobo- and zirconosilicates, tantalates, niobates, uranylphosphates, *etc*. are also able to be involved in ion exchange with solutions, supercritical fluids and electrolyte melts without destruction of the crystal structure. The classification (although incomplete) of the active exchange sites based on the differences in the character of charged polyanionic matrices was given by Chelishchev *et al*.[1] In the cited study, it was also noted that a number of solids which have non-aluminosilicate frameworks and do not exhibit ion-exchange properties at room temperature, begin to take on these properties under supercritical conditions.

Beginning in the 1990s, the synthesis of zeolite-like materials of a new type, primarily, of silicates whose frameworks contain five- and six-coordinate Ti, Nb, Zr, Al, V, Ga, *etc*. atoms along with tetrahedral fragments, has attracted growing interest. The first review devoted to such investigations (43 original studies were surveyed) was published in 1996.[2] Zeolite materials of this type whose frameworks generally contain transition elements are characterised by a considerable structural diversity, which allows one to prepare microporous materials with a broad spectrum of physical and chemical properties.

Data on the synthesis and ion-exchange properties of microporous titano-, zircono- and niobosilicates are scarce because of laborious and time-consuming procedures for the synthesis of these materials, the lack of reliable methods for predicting the structures and properties of the products and problems associated with studies of these compounds, which are prepared as fine powders and are often structurally disordered and inhomogeneous. Available abundant data on the structures, properties and conditions of formation of natural aqueous alkali silicates containing amphoteric transition elements (Ti, Nb, Zr, Fe, Mn, Zn, *etc*.), the so-called amphoterosilicates (the term was proposed by Khomyakov[3]), can be of great help in designing experiments on the synthesis of aqueous titano-, niobo- and zirconosilicates. Amphoterosilicates are rather diverse and often form large single crystals suitable for X-ray diffraction analysis. Unfortunately, investigations on synthetic titano-, niobo- and zirconosilicates and studies of their natural analogues (minerals) are not generalised. In this connection, one of the aims of the present review is to bridge the gap between these fields of investigations. Hence, considerable attention is given to the crystal-chemical features of amphoterosilicates of natural origin along with those of synthetic non-aluminosilicate zeolites.

II. Synthesis of microporous amphoterosilicates

Until recently, studies on the synthesis of alkali silicates containing transition elements were aimed primarily at modelling processes of mineral formation. In particular, analogues of a number of zeolite-type minerals were synthesised. For example, one of the most structurally complex zirconosilicates, *viz*., eudialyte, was synthesised[4] in a weakly alkaline aqueous medium from a $6\,SiO_2 + ZrO_2 + 6\,Na_2CO_3 + CaCO_3 + FeCl_2 + 4\,H_2O$ mixture in the presence of Na_2SiF_6 or K_2SiF_6 as catalysts (the temperature range was 450 – 550 °C, the water vapour pressure was 85 – 700 atm). In the presence of aluminium, eudialyte is unstable. Khibinskite $K_2ZrSi_2O_7$ was synthesised by fusing a mixture of

N V Chukanov Institute of Problems of Chemical Physics, Russian Academy of Sciences, 142432 Chernogolovka, Moscow Region, Russian Federation. Fax (7-096) 515 54 20. Tel. (7-095) 720 49 59. E-mail: chukanov@icp.ac.ru
I V Pekov Department of Geology, M V Lomonosov Moscow State University, Leninskie Gory, 119992 Moscow. Fax (7-095) 932 88 94. Tel. (7-095) 939 49 59. E-mail: mineral@geol.msu.ru
R K Rastsvetaeva A V Shubnikov Institute of Crystallography, Russian Academy of Sciences, Leninsky prosp. 59, 119333 Moscow, Russian Federation. Fax (7-095) 135 52 10. Tel. (7-095) 135 03 30. E-mail: rast@ns.cryst.ras.ru

Received 21 February 2003
Uspekhi Khimii **73** (3) 227 – 246 (2004); translated by T N Safonova

KOH, K_2CO_3, SiO_2 and $ZrSiO_4$ at 1250 °C followed by gradual cooling at a rate of 10 K h^{-1}.[5] A sodium analogue of khibinskite, *viz*., parakeldyshite, was synthesised[6] under hydrothermal conditions in the $ZrO_2-SiO_2-Na_2O-H_2O$ system. Even these examples demonstrate that zeolite-like amphoterosilicates, like aluminosilicate zeolites, crystallise in a wide temperature range.

The titanium-doped aluminium-free silicate called the material TS-1[7] is one of the first synthetic microporous titanosilicates which has no mineral analogues. In the structure of this material, the Ti^{4+} ions occupy tetrahedral positions. This material proved to be an active catalyst for oxidation reactions.

The microporous titanosilicate ETS-10 belongs to materials which hold most promise for practical applications (ion exchange, catalysis). In its structure, alternating corner-sharing SiO_4 tetrahedra and TiO_6 octahedra form a three-dimensional framework with broad channels.[8,9] In one of the two polymorphs of ETS-10, these channels are helical. In ETS-10, silicon is readily replaced by aluminium and gallium.[2,10] The material ETS-10 is most often prepared under hydrothermal conditions at 200–220 °C and pH ~10.5 from a mixture of $TiCl_3$ and/or $TiCl_4$ (and/or rutile or anatase, TiO_2) with silica in a molar ratio Si : Ti = 5–6.[11] In some cases, the synthesis is carried out in the presence of tetramethylammonium.[12] The synthesis can also be performed with the use of more stable TiF_4, including in the presence of tetramethylammonium.[13] Yet another procedure is based on the preparation of ETS-10 directly from titanosilicate gels with additives of another titanosilicate zeolite, *viz*., ETS-4, or organic matrices or without additives.[14] A Co-substituted analogue of ETS-10 containing cobalt in octahedral coordination was synthesised.[15] The presence of cobalt atoms in octahedral coordination leads to an increase in the unit cell parameters. In the study,[16] a 23-factor method of optimisation of the total composition of the reaction mixture was used for the rapid synthesis of ETS-10 and ETS-4, and a procedure was developed for the preparation of high-crystallinity ETS-10 in the presence of a large excess of water and moderate alkalinity of a solution for 18 h. In the cited study, the kinetics of crystallisation of ETS-10 was investigated (for the composition which was optimum from the viewpoint of the yield of the final product) and the activation energy of the process was evaluated at 66.8 kJ mol^{-1}. The enthalpies of formation of ETS-10 with composition $K_{0.61}Na_{1.09}Ti_{1.10}Si_{4.98}O_{13}\cdot 2.89\,H_2O$ from oxides or elements, which were determined from the heats of dissolution in lead borate at 974 K, are -262.2 ± 3.1 and -6995.2 ± 6.1 kJ mol^{-1}, respectively.[17]

In 1996, an analogue of minerals of the labuntsovite group was synthesised for the first time under hydrothermal conditions.[18,19] This synthesis afforded a series of specimens which have the nenadkevichite structure and Ti : Nb ratios from 0.8 to 12.3. A niobium-free phase corresponding to korobitsynite was also prepared. In physical properties and chemical composition (sodium as an extraframework cation) as well as based on powder X-ray diffraction patterns, these materials are analogous to natural minerals of the nenadkevichite subgroup (space group *Pbam*, $a = 7.41$, $b = 14.20$, $c = 7.15$ Å).

The titanosilicate material ETS-4 was also synthesised in 1996. This material was considered alternatively either as a thin intergrowth of zorite with nenadkevichite[20] or as an analogue of zorite and an intermediate for the synthesis of nenadkevichite[18] (by nenadkevichite was meant its titanium analogue, *viz*., korobitsynite). Subsequent studies[21,22] confirmed that ETS-4 is identical to zorite. Hence, it became apparent that korobitsynite is formed as a by-product in the synthesis of ETS-4.

The ease of isomorphous replacement of titanium by niobium in most silicates and in many oxides allows one to smoothly control the characteristics of microporous materials based on these elements. The replacement of titanium by zirconium provides even greater scope for these purposes. The synthesis under hydrothermal conditions afforded[23] a broad spectrum of mesoporous titano- and zirconosilicates Ti-MCM-41 and Zr-MCM-41 with Si : Ti and Si : Zr ratios varying from 11 to 96 as well as a series of zirconotitanosilicate zeolites with composition $(H,K)_2(Zr,Ti)Si_3O_9\cdot n\,H_2O$ containing a three-dimensional system of channels, whose sizes are smoothly varied in the course of the isomorphous replacement of titanium by zirconium.[24] The hydrothermal synthesis of a microporous material possessing ion-exchange properties, which is a structural analogue of penkvilksite-1*M*, was carried out[25] in the $SiO_2-TiO_2-Na_2O-H_2O-$ trimellitic anhydride system. The discovery of the natural mineral tumchaite,[26] which is a tin-containing zirconium analogue of penkvilksite, gives promise that the completely isomorphous system $Na_2(Zr,Ti,Sn)Si_4O_{11}\cdot 2\,H_2O$ with smoothly variable properties will be prepared for this structure type.

In addition to the commonly accepted hydrothermal method, the dry-gel conversion method is also used for the synthesis of microporous titanosilicates. In particular, based on spectroscopic data, it was suggested that the application of this method to the Ti-Nu-1 gel gives rise to microporous materials containing titanium in tetrahedral coordination.[27] In some cases, titanium-containing microporous materials were prepared by modifications of boro- or aluminosilicate zeolites.[28,29] The problems of the synthesis and modifications of microporous titano-, niobo- and zirconosilicates were also considered in the studies.[30–47] Noteworthy is the hydrothermal synthesis in the homogeneous $NbCl_5-SiO_2-NaOH$ (KOH) $-H_2O_2-H_2O$ systems giving rise to framework potassium and sodium niobosilicates, which possess ion-exchange activity with respect to a broad spectrum of cations in acidic media.[34] Methods for the synthesis of microporous silicates of rare-earth elements were described in the studies.[48,49]

The M : Si ratio (where M is a framework-forming transition element) in synthetic micro- and mesoporous materials can be varied over a very wide range. Silicon-free microporous niobates, tantalates, zirconates, stannates and titanates can be considered as limiting cases of zeolites with a purely octahedral framework. In particular, syntheses of materials which have structures of pyrochlore and some other niobates and possess various ion-exchange, transport and electromagnetic properties, were described in many publications.[50–55]

III. Crystal-chemical features of amphoterosilicates with zeolite properties

1. Crystal structures of synthetic microporous titanium, niobium and zirconium silicates

The zeolite properties of many alkali silicates containing Ti, Nb or Zr are determined by the difference in the force characteristics of their constituent cations. Having high force characteristics, transition elements play (along with silicon) the key role in structures of most of these compounds by forming three-dimensional frameworks, whereas elements possessing low force characteristics occupy cavities of the framework (along with water molecules). Hereinafter, the T atoms which are involved in complex anions and form covalent bonds with oxygen, are called (which is common practice in crystal chemistry) cations.

Unlike aluminosilicate zeolites containing cations of only two types, *viz*., tetrahedrally coordinated (Si, Al) and extraframework, zeolite-like materials with mixed-type frameworks involve a series of framework cations, which can be arranged in order of decreasing force characteristics (this decrease is manifested, in particular, in a decrease in the frequencies of the characteristic bands in IR spectra; see Table 1).[56] Various groups of cations play different roles in structure formation. The T, M and, generally, D cations are involved in the framework formation. The A cations are usually weakly bound to the framework and can be involved in ion-exchange processes in the absence of steric hindrance.

By analogy with zeolites, the framework density (FD) of non-aluminosilicate microporous materials can be calculated as the number of framework sites, *i.e*., the number of T, M and D cations, per 1000 $Å^3$. In zeolites, this value for aluminosilicate frameworks generally varies from 14 to 21. For example, FD = 14.5 for the large-pore zeolite shabazite, FD = 17 for

Table 1. Properties of cations in amphoterosilicates.

Type of position	Coordination number	Ionic radius /Å	Examples of cations [a]	Tendency to isomorphous substitution	Tendency to formation of vacant positions	Tendency to formation of split positions	Frequency range in IR spectra /cm^{-1} (see [b])
T	4	< 0.6	Si, Al, Zn, P [c]	–	–	–	900 – 1100
M	6	0.6 – 0.7	Ti, Nb, Zr, Fe^{3+}, Y, Mn^{3+}, Sn^{4+}	+	–	–	660 – 700
D	6	0.7 – 1.0	Mn^{2+}, Fe^{2+}, Mg, Zn, Ca	+	+	–	440 – 470
A	> 6	1.1 – 1.5	Na, K, Ca, Sr, Ba, Pb^{2+}, H_3O^+	+	+	+	< 400

[a] Charges are given only if elements can exist in different oxidation states; [b] the cation – oxygen stretching vibrations; [c] in microporous silicate materials devoid of transition elements, B and Be atoms also often serve as T cations.

clinoptilolite, which is widely used in practice, FD = 18.6 for the small-pore zeolite analcime, *etc*. For the framework aluminosilicate nepheline, which does not possess zeolite properties under normal conditions, FD = 22.1. For α-quartz, FD = 26.8. Apparently, the limiting framework densities, above which the zeolite properties are not observed, are in the range of FD = 21 – 22. This criterion can be used also (with minor reservations) for estimating zeolite properties of various amphoterosilicates (see below). Evidently, one should take into account that the ion-exchange and other properties characteristic of zeolites depend on the width and configuration of the channels and, consequently, are determined not only by the framework density but also by the sizes of the framework-forming polyhedra and their mutual arrangement, including the non-uniform distribution in the space.

As mentioned above, studies of the crystal structures of synthetic microporous materials present difficulties due to crystal imperfection and contamination by by-products of the synthesis. As a consequence, direct single-crystal X-ray methods are generally inapplicable for these purposes. In most cases, the structures of synthetic amphoterosilicates were studied either by analysing powder X-ray diffraction patterns (the Rietveld method) or indirectly based on the results of studies of local structures by IR, Raman, UV, ESR, NMR spectroscopy, *etc*.

The microporous titanosilicate ETS-10 has received the most study. The crystal structure of this material was established by both the Rietveld method [8,9] and single-crystal X-ray diffraction analysis.[57] It was found [8,9] that there are at least two polymorphs of ETS-10 and numerous types of this material, which differ in the degree of ordering. Both polymorphs (A, space group $P4_1$; B, space group $C2/c$) are characterised by large pores formed by twelve-membered rings of silicon – oxygen tetrahedra. The rings are linked in a mixed-type three-dimensional framework by sharing corners with Ti octahedra. In the structure of the modification A, the channels adopt a helical configuration. Generally, the synthesis of ETS-10 produces a mixture of the polymorphs A and B. The spatial distribution of extraframework cations in ETS-10 was determined.[58,59] In the studies,[60,61] the nature of the active sites and the configuration of the Ti octahedra were investigated by spectroscopic methods (ESR and X-ray spectral analysis).

The crystal structure of the titanosilicate AM-4 with composition $Na_3(Na,H)Ti_2O_2(Si_2O_6)\cdot 2.2\,H_2O$ can be described [62] as a quasilayered motif composed of chains of edge-sharing titanium – oxygen octahedra.

The relative amounts of T, M and D cations in amphoterosilicates can be varied virtually without limit. As mentioned above, microporous niobates and other complex oxides can be considered as the limiting case of zeolite-like materials whose frameworks are formed exclusively by MO_6 octahedra. However, these structures are beyond the scope of the present review. The mobility of cations in such materials and, as a consequence, their ability to be involved in ion exchange and exhibit ion conductivity are associated with structural disorder (see, for example, Refs 63 – 66).

2. Crystal structures of natural amphoterosilicates

In the last decade, considerable advances have been made in the crystal chemistry of minerals. This is associated with both an extension of instrumental capabilities (the use of synchrotron radiation and highly sensitive CCD detectors as well as an improvement of software) and a great interest in minerals as prototypes of materials with various technologically important properties. These materials are formed under conditions varying over a wide range (pressure, temperature, composition and viscosity of a medium, pH) and have different characteristic crystallisation times. It is often difficult or even impossible to use a combination of these conditions in laboratory practice. Suffice it to say that mineral formation in nature takes place over a geological period numbering in the millions of years.

Of the four thousand presently known mineral species, several hundred have zeolite-like structures, *i.e*., possess rigid three-dimensional frameworks. The cavities and channels in the frameworks are occupied by mobile cations, which are weakly bound to the framework (more rarely, additional anions are also involved), and water molecules. As mentioned above, only a minority of such minerals belong to zeolites in a classical sense of this term (*i.e*., framework aluminosilicates with a low framework density). Zeolite-like amphoterosilicates are most numerous and structurally and chemically diverse. Many such minerals occur in nature only in extremely hyperalkaline (the so-called hyperagpaitic) rocks characterised by an extremely high sodium and/or potassium content at a rather low activity of aluminium. These rocks are relatively rare in occurrence, but are characterised by a unique diversity of the mineral composition. Their mineralogy has been extensively studied in the last two decades, when many zeolite-like amphoterosilicates were discovered in such rocks and thoroughly studied. Most minerals of this type were discovered in the following four massifs of hyperalkaline rocks: the Lovozero and Khibiny massifs (the Kola Peninsula, Russia), Saint-Hilaire mountain (Quebec, Canada) and Ilimaussaq (Greenland, Denmark). The crystal-chemical features of natural microporous amphoterosilicates are briefly summarised in Table 2,[26,67 – 125] where these minerals are arranged in order of increasing framework density. As can be seen from this table, traskite, seidite-(Ce) and zorite have the most loose frameworks (*i.e*., are characterised by the lowest framework density) among natural amphoterosilicates. In this respect, traskite containing twelve-membered rings of silicon – oxygen tetrahedra, which are unique the structures of minerals, is analogous to ETS-10. Zorite is an analogue of synthetic titanosilicate ETS-4, which is also considered as a promising microporous material. The ion-exchange properties of the large-pore rare-earth titanosilicate seidite-(Ce) with the framework density of 14.05 were studied.[67] It was demonstrated that most sodium ions in the latter mineral can be readily replaced by Tl, K, Rb, Cs and Ba in the reactions with aqueous solutions of these metal salts and these replacements are accompanied by changes in the unit cell parameters and optical properties. For steenstrupine (FD = 14.6), leaching of sodium was studied experimentally.[68]

Table 2. Brief crystal-chemical characterisation of zeolite-like amphoterosilicate minerals.

Name	Formula [a]	Space group	a /Å b /Å c /Å	α /deg β /deg γ /deg	FD [b]	Ref.	Brief description of the framework
Traskite	$Ba_{24}(Ca,Sr)(\mathbf{Ti,Fe,Mn})_{16}(\mathbf{Si}_{12}O_{36})$ $(\mathbf{Si}_2O_7)_6(O,OH)_{30}Cl_6 \cdot 14\,H_2O$	*P6m*2	17.88 17.88 12.30	 120	11.75	73	The $Si_{12}O_{36}$ rings are linked by clusters consisting of closely packed Si_2O_7 diortho groups and TiO_6 octahedra.
Seidite-(Ce)	$Na_4SrCe\mathbf{Ti}(\mathbf{Si}_8O_{22})F \cdot 5\,H_2O$	*C*2/*c*	24.74 7.19 14.47	 95.2	14.05	67	Tubular chains consisting of eight-membered silicon – oxygen rings, which are linked in layers by additional Si tetrahedra. The layers are linked by isolated TiO_6 octahedra to form a loose framework.
Zorite	$Na_6\mathbf{Ti}_5(\mathbf{Si}_6O_{17})_2O(OH)_4 \cdot 11\,H_2O$	*Cmmm*	23.24 7.24 6.95		14.5	74	Xonotlite bands consisting of eight-membered silicon – oxygen rings are linked by Ti half-octahedra and chains of Ti,Nb octahedra.
Steenstrupine-(Ce)	$Na_{14}Ce_6\mathbf{Mn}_2\mathbf{Fe}^{\mathbf{III}}_2\mathbf{Zr}(PO_4)_6$. $.(\mathbf{Si}_6O_{18})_2(OH)_2 \cdot 3\,H_2O$	*R*3*m*	10.46 10.46 45.48	 120	14.6	75	Twelve layers consisting of six-membered silicon – oxygen rings, which are linked by alternating Zr and Mn octahedra, pass through each unit cell. The Mn octahedra form clusters with Fe^{III} octahedra. The latter share corners with the PO_4 tetrahedra. The layers are linked through shared corners of the SiO_4 and MnO_6 polyhedra. The structure of thorosteenstrupine is unknown.
Thorosteenstrupine [c]	$Na_{0-5}Ca_{1-3}(Th,Y,Ln)_6(\mathbf{Mn,Fe,Ti})_{4-5}$. $.(\mathbf{Si}_6O_{18})_2[(\mathbf{Si,P})O_4]_6(OH,O)_x \cdot n\,H_2O$					76	
Komarovite group							
Na-komarovite	$(Na,K)(Na,Ca)_{6-x}Ln_x(\mathbf{Nb,Ti})_6$. $.\mathbf{Si}_4O_{26}F_2 \cdot 4\,H_2O$	*Cmmm*	7.31 24.59 7.40		15.0	77	Octahedral layers with a pyrochlore-like structure are linked by four-membered silicon – oxygen rings through shared corners of the polyhedra. The structure is unknown.
Komarovite [c]	$Ca_{2-x}(\mathbf{Nb,Ti})_6\mathbf{Si}_4O_{26}(OH)_2 \cdot n\,H_2O$? [d]	? (orthorhombic structure)	21.30 14.00 17.19		15.6	77	
Hilairite group						69	Infinite helical (Si_3O_9) chains extended along the main axis are linked to M octahedra through their pendant vertices to form the mixed {$M(Si_3O_9)$} framework, where Zr, Ti or (Y + Ln) are present as the dominant M cations in different structures. The repeat unit of the (Si_3O_9) chain along the *c* axis consists of three Si tetrahedra. The M octahedra are repeated in the same period. Each M octahedron is linked to three silicon – oxygen chains. In the crystal structures, there are two non-equivalent octahedral positions *M*. In the structures of hilairite, calciohilairite and komkovite, Zr prevail in both *M* positions. In the structure of sazykinaite-(Y), one of these positions (*M*1) is selectively occupied by the Y and Ln atoms (accompanied by the corresponding increase in the M – O distance), whereas the second *M* position (*M*2), like that in the above-mentioned structures, is occupied by zirconium. Pyatenkoite-(Y) is an isostructural analogue of sazykinaite-(Y), in which Zr is replaced by Ti. The structures contain large cavities and channels.
Sazykinaite-(Y)	$Na_5\mathbf{YZrSi}_6O_{18} \cdot 6\,H_2O$	*R*32	10.82 10.82 15.81	 120	15.0	78	
Pyatenkoite-(Y)	$Na_5\mathbf{YTiSi}_6O_{18} \cdot 6\,H_2O$	*R*32	10.70 10.70 15.73	 120	15.4	79	
Hilairite	$Na_2\mathbf{ZrSi}_3O_9 \cdot 3\,H_2O$	*R*32	10.56 10.56 15.85	 120	15.7	80	

Table 2 (continued).

Name	Formula [a]	Space group	*a* /Å *b* /Å *c* /Å	*α* /deg *β* /deg *γ* /deg	FD [b]	Ref.	Brief description of the framework
Hilairite group							Infinite helical (Si_3O_9) chains extended along the main axis are linked to M octahedra through their pendant vertices to form the mixed {M(Si_3O_9)} framework, where Zr, Ti or (Y + Ln) are present as the dominant M cations in different structures. The repeat unit of the (Si_3O_9) chain along the *c* axis consists of three Si tetrahedra. The M octahedra are repeated in the same period. Each M octahedron is linked to three silicon – oxygen chains. In the crystal structures, there are two non-equivalent octahedral positions *M*. In the structures of hilairite, calciohilairite and komkovite, Zr prevail in both *M* positions. In the structure of sazykinaite-(Y), one of these positions (*M*1) is selectively occupied by the Y and Ln atoms (accompanied by the corresponding increase in the M – O distance), whereas the second *M* position (*M*2), like that in the above-mentioned structures, is occupied by zirconium. Pyatenkoite-(Y) is an isostructural analogue of sazykinaite-(Y), in which Zr is replaced by Ti. The structures contain large cavities and channels.
Calciohilairite	Ca**ZrSi**$_3$O$_9$ · 3 H$_2$O	*R*32	10.50 10.50 7.97	 12	15.8	69, 81	
Komkovite	Ba**ZrSi**$_3$O$_9$ · 3 H$_2$O	*R*32	10.53 10.53 15.74	 120	15.9	82	
Gaidonnayite group							Zigzag chains consisting of alternating six-membered groups of silicon – oxygen tetrahedra are linked by isolated TiO_6 octahedra to form a framework.
Gaidonnayite	Na$_2$**ZrSi**$_3$O$_9$ · 2 H$_2$O	*P*2$_1$*nb*	11.74 12.97 6.73		15.6	80	
Georgechaoite	NaK**ZrSi**$_3$O$_9$ · 2 H$_2$O	*P*2$_1$*nb*	11.84 12.94 6.73		15.5	80	
Labuntsovite group							A mixed framework consists of infinite chains extended along the *a* axis. The chains are formed by corner-sharing octahedra occupied by titanium or niobium atoms, which are linked to one another in two other directions by the [Si_4O_{12}] rings. In structures of some monoclinic representatives of the labuntsovite group, the chains are linked by additional Mg, Fe, Mn, Zn or Ca octahedra. The SiO_4 tetrahedra are linked to the Ti(Nb)O_6 octahedra only by sharing corners; the Ti(Nb)O_6 octahedra are linked to additional octahedra through shared edges. The O atoms involved in the octahedral environment about Ti (or Nb) are partially replaced by the hydroxy groups. In the structures of orthorhombic members, the octahedral chains are almost linear. In the structures of monoclinic members, the chains are strongly bent in a wave-like fashion.
Nenadkevichite subgroup	Na$_{4-x}$(**Nb**,**Ti**)$_2$**Si**$_4$O$_{12}$(O,OH)$_2$ · · 4 H$_2$O [d]	*Pbam*	≈7.4 ≈14.2 ≈7.1		16.0 – 16.2	83 – 85	
Vuoriyarvite subgroup	(K,Na,Ca,Ba,Sr,H$_3$O)$_{3-x}$(**Ti**,**Nb**)$_2$. .**Si**$_4$O$_{12}$(OH,O)$_2$ · *n* H$_2$O [d]	*Cm*	≈14.7 ≈14.2 ≈7.9	 ≈118	16.3 – 17.8	84, 86 – 88	
Lemmleinite subgroup	NaK(K,Ba)$_{1-x}$**Ti**$_2$**Si**$_4$O$_{12}$(OH,O)$_2$ · · 2 H$_2$O [d]	*C*2/*m*	≈14.3 ≈13.8 ≈7.75	 ≈117	17.3 – 18.4	84, 89 – 92	
Karupmöllerite-Ca	Na$_2$(**Ca**,□)(**Nb**,**Ti**)$_4$[**Si**$_4$O$_{12}$]$_2$. .(OH,O)$_4$ · 7 H$_2$O	*C*2/*m*	14.64 14.21 7.915	 117.4	17.5	93, 94	
Organovaite subgroup	K$_2$(**Mn**,**Zn**,**Fe**)(**Nb**,**Ti**)$_4$(**Si**$_4$O$_{12}$)$_2$. .(O,OH)$_4$ · *n* H$_2$O	*C*2/*m*	≈14.5 ≈14.0 ≈15.7	 ≈118	18.3 – 18.8	84, 95 – 97	
Kuzmenkoite subgroup	K$_2$(**Mn**,**Zn**,**Fe**)(**Ti**,**Nb**)$_4$(**Si**$_4$O$_{12}$)$_2$. .(O,OH)$_4$ · *n* H$_2$O	*C*2/*m* or *Cm*	≈14.4 ≈13.85 ≈7.8	 ≈117	18.5	98 – 100	

Table 2 (continued).

Name	Formula [a]	Space group	*a* /Å *b* /Å *c* /Å	α /deg β /deg γ /deg	FD [b]	Ref.	Brief description of the framework
Labuntsovite group							
Gutkovaite subgroup	$Na_{1-x}(Ca,Sr,K)(K,Ba)_2(\mathbf{Mn},\mathbf{Zn},\mathbf{Fe})$. $.(\mathbf{Ti},\mathbf{Nb})_4(\mathbf{Si}_4O_{12})_2(O,OH)_4 \cdot n\,H_2O$ [d]	*Cm*	≈14.45 ≈13.9 ≈7.8	 117.5 	18.5	101 – 105	A mixed framework consists of infinite chains extended along the *a* axis. The chains are formed by corner-sharing octahedra occupied by titanium or niobium atoms, which are linked to one another in two other directions by the $[Si_4O_{12}]$ rings. In structures of some monoclinic representatives of the labuntsovite group, the chains are linked by additional Mg, Fe, Mn, Zn or Ca octahedra. The SiO_4 tetrahedra are linked to the $Ti(Nb)O_6$ octahedra only by sharing corners; the $Ti(Nb)O_6$ octahedra are linked to additional octahedra through shared edges. The O atoms involved in the octahedral environment about Ti (or Nb) are partially replaced by the hydroxy groups. In the structures of orthorhombic members, the octahedral chains are almost linear. In the structures of monoclinic members, the chains are strongly bent in a wave-like fashion.
Labuntsovite subgroup	$Na_2K_2(\mathbf{Mn},\mathbf{Mg},\mathbf{Fe})_{1-x}\mathbf{Ti}_4(\mathbf{Si}_4O_{12})_2$. $.(O,OH)_4 \cdot (5-6)\,H_2O$ [d]	*C*2/*m*	≈14.3 ≈13.8 ≈7.75	 ≈117 	18.4 – 18.9	84, 106, 107	
Altisite	$Na_3K_6\mathbf{Ti}_2(\mathbf{Si}_8\mathbf{Al}_2O_{26})Cl_3$	*C*2/*m*	10.36 16.31 9.13	 105.3 	16.1	108	Adjacent layers composed of alternating six- and ten-membered tetrahedral rings are linked by isolated TiO_6 octahedra to form a framework.
Lemoynite	$(Na,K)_2Ca\mathbf{Zr}_2\mathbf{Si}_{10}O_{26} \cdot (5-6)\,H_2O$	*C*2/*c*	10.37 15.92 18.60	 104.6 	16.15	80	Three-sheet layers composed of alternating six- and ten-membered tetrahedral rings are linked by isolated ZrO_6 octahedra.
Jagoite	$(Pb,Na)_{11}(\mathbf{Fe^{II}},\mathbf{Mg})_4(\mathbf{Si},\mathbf{Al})_{13}$. $.(O,OH)_{41}Cl_3$	*P*62*c*	8.53 8.53 33.33	 120	16.2	73	A pseudolayered structure. Alternating double (consisting of six-membered tetrahedral rings) and single (with broken five-membered rings) layers are linked by (Fe^{II},Mg) octahedra through shared corners to form a framework. Channels along the plane of double rings are formed by 14-membered rings of silicon – oxygen tetrahedra.
Sitinakite	$Na_2K\mathbf{Ti}_4(\mathbf{SiO}_4)_2O_5OH \cdot 4\,H_2O$	$P4_2/mcm$	7.82 7.82 12.02	 	16.3	109	The $Ti_4O_{12}(O,OH)_4$ clusters of edge-sharing octahedra are linked in chains through common (O,OH) corners. The chains are linked in a framework by isolated SiO_4 tetrahedra.
Kostylevite	$K_4\mathbf{Zr}_2\mathbf{Si}_6O_{18} \cdot 2\,H_2O$	$P2_1/a$	13.17 11.73 6.56	 105.3 	16.4	80	A framework with broad channels is formed by six-membered rings of silicon – oxygen tetrahedra linked by ZrO_6 octahedra.
Umbite	$K_2\mathbf{ZrSi}_3O_9 \cdot H_2O$	$P2_12_12_1$	10.21 13.24 7.17	 	16.5	80	Wollastonite chains of Si_3O_9 are cross-linked by individual ZrO_6 octahedra.
Catapleite group							
Catapleite	$Na_2\mathbf{ZrSi}_3O_9 \cdot 2\,H_2O$	$P6_2/mmc$, $B2/b$	7.40 7.40 10.07	 120	16.75	80	In the structure of catapleite, three-membered rings of silicon – oxygen tetrahedra are linked by TiO_6 octahedra. The structure of calciocatapleite is unknown.

Table 2 (continued).

Name	Formula [a]	Space group	a /Å b /Å c /Å	α /deg β /deg γ /deg	FD [b]	Ref.	Brief description of the framework
Catapleite group							
Calciocatapleite [c]	$CaZrSi_3O_9 \cdot 2\,H_2O$	hexagonal ?	7.32 7.32 10.15	 120	17.0	80	In the structure of catapleite, three-membered rings of silicon – oxygen tetrahedra are linked by TiO_6 octahedra. The structure of calciocatapleite is unknown.
Lovozerite group							
Petarasite	$Na_5Zr_2Si_6O_{18}(Cl,OH) \cdot 2\,H_2O$	$C2/m$	10.80 14.49 6.62	 113.2	16.8	80	
Lovozerite	$Na_{2-x}Ca(Zr,Ti)Si_6(O,OH)_{18}$ [d]	$C2$	10.48 10.20 7.33	 92.5	17.9	110	
Litvinskite	$Na_{3-x}(\square,Na,Mn^{II})ZrSi_6O_{12}.$ $.(OH,O)_6 \cdot n\,H_2O$ [d]	Cm	10.59 10.22 7.35	 92.9	18.5	111	Six-membered tetrahedral $[Si_6O_{12}(OH)_3(OH,O)_3]$-type rings are linked to each other by isolated M octahedra (M = Zr, Ti, Fe^{III}) through shared oxygen corners. Free vertices of the Si tetrahedra are occupied by the OH^- groups. The C octahedra, which are randomly and, generally, incompletely occupied by Na^+, Mn^{2+}, Ca^{2+} and Fe^{2+} cations, are also involved in the framework.
Imandrite	$Na_{12}Ca_3Fe_2(Si_6O_{18})_2$	$Pnnm$	10.33 10.55 7.43	 	19.5	112	
Zirsinalite	$Na_6(Ca,Mn,Fe^{II})ZrSi_6O_{18}$	$R3m$	10.29 10.29 26.31	 120	19.9	112	
Koashvite	$Na_6(Ca,Mn)(Ti,Fe)Si_6O_{18} \cdot H_2O$	$Pbam$	7.32 21.08 10.26	 	20.2	112	
Kazakovite	$Na_6MnTiSi_6O_{18}$	$R3m$	10.19 10.19 13.07	 120	20.4	112	
Tisinalite	$Na_3MnTiSi_6O_{15}(OH)_3$	$R3m$	10.02 10.02 12.88	 120	21.4	113	
Gaultite	$Na_4Zn_2Si_7O_{18} \cdot 5\,H_2O$	$F2dd$	10.21 39.88 10.30	 	17.2	114, 115	Layers consisting of four- and eight-membered rings of silicon – oxygen tetrahedra are linked by isolated ZnO_4 tetrahedra.
Keldyshite group							
Khibinskite	$K_2ZrSi_2O_7$	$C2/m$	19.22 11.10 14.10	 116.5 	17.8	80	A framework is formed by Zr octahedra and diortho groups (Si_2O_7), all non-bridging oxygen atoms of the diortho groups occupy the vertices of Zr octahedra.
Keldyshite	$(Na,H)_2ZrSi_2O_7 \cdot n\,H_2O$	$P\bar{1}$	9.0 5.34 6.96	92 116 88	20.0	80	

Table 2 (continued).

Name	Formula [a]	Space group	*a* /Å *b* /Å *c* /Å	α /deg β /deg γ /deg	FD [b]	Ref.	Brief description of the framework
Keldyshite group							
Parakeldyshite	Na_2**ZrSi**$_2O_7$	$P\bar{1}$	9.31 5.42 6.66	94.9 115.3 89.6	20.1	80	A framework is formed by Zr octahedra and diortho groups (Si_2O_7), all non-bridging oxygen atoms of the diortho groups occupy the vertices of Zr octahedra.
Penkvilksite group							
Tumchaite	Na_2(**Zr**,**Sn**)**Si**$_4O_{11} \cdot 2\,H_2O$	$P2_1/c$	9.14 8.82 7.54	 113.2	17.9	26	Layers with composition Si_4O_{11} formed by helical chains of Si_6O_{18} of two types (twisted clockwise and counter-clockwise) are linked by distorted (Ti,Zr,Sn) octahedra.
Penkvilksite-1*M*	Na_4**Ti**$_2$**Si**$_8O_{22} \cdot 5\,H_2O$	$P2_1/c$	8.96 8.73 7.39	 112.7	18.8	116	
Penkvilksite-2*O*	Na_4**Ti**$_2$**Si**$_8O_{22} \cdot 5\,H_2O$	*Pnca*	16.37 8.75 7.40		18.9	116	
Terskite	Na_4**ZrSi**$_6O_{16} \cdot 2\,H_2O$	*Pnc*2	14.12 14.69 7.51		18.0	117	Branched $[H_2Si_3O_6]_\infty$ chains (in each unit of the chains, two silicon atoms belong to the main chain and one silicon atom belongs to the side SiO_4 tetrahedron) are linked by ZrO_6 octahedra. Each octahedron is linked to four chains and shares two corners with the tetrahedra of the main chain and two corners with the side tetrahedra.
Elpidite	Na_2**ZrSi**$_6O_{15} \cdot 3\,H_2O$	*Pbcm*	7.14 14.68 14.65		18.2	80	Double chains (bands) composed of alternating four-membered silicon – oxygen rings and Si_2O_7 diortho groups are linked by ZrO_6 octahedra.
Strakhovite	$NaBa_3$**Mn**$_4$[(**Si**$_4O_{10}(OH)_2$]. .(**Si**$_2O_7$)$O_2(OH) \cdot H_2O$	*Pmna*	23.42 12.27 7.18		19.4	118	Alternating four-membered rings of silicon – oxygen tetrahedra and Si_2O_7 diortho groups are linked by manganese octahedra and half-octahedra.
Eakerite	Ca_2**Sn**(**Al**$_2$**Si**$_6O_{18}$)$(OH)_2 \cdot 2\,H_2O$	$P2_1/a$	15.89 7.72 7.44	 101.3	20.1	73	Corrugated networks consisting of four- and twelve-membered rings of silicon – oxygen tetrahedra are linked by SnO_6 octahedra by sharing edges.
Vinogradovite group							
Kukisvumite	Na_6**ZnTi**$_4$(**Si**$_2O_6)_4O_4 \cdot 4\,H_2O$	*Pccn*	28.89 8.60 5.22		20.1	119	The vinogradovite structure consists of alternating pyroxene chains, columns of edge-sharing TiO_6 octahedra and dimeta Si_4O_{10} chains. Columns of edge-sharing Li octahedra in the lintisite structure impart additional rigidity to the framework.
Vinogradovite	Na_4**Ti**$_4$**AlSi**$_6O_{23}(OH) \cdot 2\,H_2O$	*C*2/*c*	5.35 8.56 24.22	 101	20.2	120	
Lintisite	Na_3**LiTi**$_2$(**Si**$_2O_6)_2O_2 \cdot 2\,H_2O$	C2/*c*	28.58 8.60 5.22	 91.0	21.8	121	

Table 2 (continued).

Name	Formula [a]	Space group	*a* /Å *b* /Å *c* /Å	α /deg β /deg γ /deg	FD [b]	Ref.	Brief description of the framework
Dalyite group							
Dalyite	$K_2\mathbf{ZrSi_6}O_{15}$	$P\bar{1}$	7.37 7.73 6.91	106.2 111.5 100.0	20.2	80	Corrugated layers consisting of four-, six- and eight-membered rings of silicon – oxygen tetrahedra are linked by $(Zr,Ti)O_6$ octahedra through shared corners.
Davanite [c]	$K_2\mathbf{TiSi_6}O_{15}$	$P\bar{1}$	7.14 7.53 6.93	103.0 114.5 93.9	21.2	73	
Baotite	$Ba_4(\mathbf{Ti},\mathbf{Nb})_8\mathbf{Si_4}O_{28}Cl$	$I4_1/a$	19.99 19.99 5.91		20.3	80	Four-membered rings of corner-sharing (Ti,Nb) octahedra form infinite columns. The columns are linked by four-membered rings of silicon – oxygen tetrahedra to form a framework.
Eudialyte	$Na_{15}\mathbf{Ca_6Fe}^{\mathrm{II}}_{3-x}\mathbf{Zr_3Si_{26}}O_{73}(O,OH)_3Cl_2$ [d]	$R3m$	14.26 14.26 30.0	 120	20.6	122	A framework is formed by rings of silicon – oxygen tetrahedra Si_3O_9 and Si_9O_{27}, six-membered rings of edge-sharing Ca octahedra, ZrO_6 octahedra and additional cations with coordination numbers from 4 to 6.
Vlasovite	$Na_2\mathbf{ZrSi_4}O_{11}$	C2/c	11.11 10.11 8.61	 100.7	21.1	80	Chains formed by rings of silicon – oxygen tetrahedra are linked by ZrO_6 octahedra. Each octahedron shares corners with four chains.
Verplanckite	$Ba_4(\mathbf{Mn},\mathbf{Ti},\mathbf{Fe})_2\mathbf{Si_4}O_{12}(OH,H_2O)_3Cl_3$	$P6/mmm$	16.40 16.40 7.20	 120	21.5	123	Four-membered rings of silicon – oxygen tetrahedra are linked by three-membered groups of (Mn,Ti,Fe) octahedra; the effective diameter of the cavities in the framework is 7.2 Å.
Muirite	$Ba_{10}(\mathbf{Ca},\mathbf{Mn},\mathbf{Ti})_4\mathbf{Si_8}O_{24}(OH,Cl,O)_{12}\cdot$ $\cdot 4\,H_2O$	$P4/mmm$	14.03 14.03 5.64		$\leqslant 21.8$	124	Eight-membered rings of silicon – oxygen tetrahedra are linked by double trigonal prisms $(Ca,Mn,Ti)O_6$. The density of the framework sites depends on the amount of vacancies in (Ca,Mn,Ti) positions.
Naujakasite group							
Naujakasite	$Na_4\mathbf{Fe}^{\mathrm{II}}(\mathbf{Al_4Si_8}O_{26})$	$C2/m$	15.04 7.99 10.49	113.7	22.5	73	Two-layer packets formed by four- and six-membered rings of silicon – oxygen tetrahedra are linked by sharing edges with Fe and Mn octahedra to form a framework.
Manganonaujakasite	$Na_4\mathbf{Mn}^{\mathrm{II}}(\mathbf{Al_4Si_8}O_{26})$	$C2/m$	15.03 8.00 10.48	113.5	22.5	125	

[a] Framework cations are printed in bold type; [b] the framework density; [c] minerals with unknown structures are tentatively assigned to particular mineral groups by analogy with related minerals; [d] in these cases, the notation $(n-x)$ signifies that the position can be vacant ($0 \leqslant x < n$).

Minerals of the hilairite group [69] (FD varies from 15.0 to 15.9) are characterised by a constant T : M ratio of a mixed octahedral–tetrahedral framework, whereas the contents and ratio of extraframework cations (including oxonium) and the amount of molecular water can vary over wide ranges. There is evidence that ion exchange and decationation readily proceed in hilairite-like phases. The results of thermal analysis also provide unambiguous evidence for the zeolite character of hilairite-like minerals. For example, dehydration of hilairite on heating is completed already at 220 °C, after which the dehydrated material retains basically the hilairite structure up to at least 855 °C. The dehydration process is reversible. Thus, rehydration begins after cooling to 220 °C. At room temperature, the mineral absorbs about 95% of the initial amount of water during 15 h.[70] The major portion of water is eliminated from sazykinaite-(Y) at a temperature below 250 °C (more than 80% of the total mass loss as judged from the published thermogravimetric curve). After heating to 500 °C, the crystals, which turned white and lost transparency, gave a Debye powder pattern of sazykinaite with weak diffuse lines.[71] The zeolite nature of minerals of the hilairite group is also evidenced by the fact that additional Na^+ cations (compared to minerals of this group devoid of rare-earth elements) are easily incorporated into the channels of the frameworks of the sazykinaite and pyatenkoite structures. These additional cations are necessary for compensation of an excessive negative charge appearing upon heterovalent substitution

$$(Zr,Ti)^{4+} \longrightarrow Y^{3+}.$$

The idealised general scheme of isomorphism giving rise to cation-deficient calciohilairite can be represented as follows:

$$2\,Na^+ + H_2O \longrightarrow 0.5\,Ca^{2+} + 1.5\square + H_3O^+,$$

□ is a vacancy.

Taking into account the character of spatial inhomogeneity of the composition of calciohilairite crystals, it was suggested [69] that this scheme of isomorphism represents simultaneously the reaction scheme of the natural ion-exchange process responsible for the transformation of hilairite, which crystallised from highly alkaline solutions, into calciohilairite in the late-hydrothermal evolution stage.

Natural leaching of cations and ion-exchange processes, which occur without destruction of the crystal structure, were observed in many other amphoterosilicates: in minerals of the lovozerite group (elimination of sodium accompanied by the replacement of oxygen by OH groups), elpidite, gaidonnayite, eudialyte (substitution of Na for K, Ca, H_3O^+), *etc*.

In conclusion of this section, let us note that natural amphoterosilicates can not only serve as prototypes for the design of new microporous materials but are also of industrial interest in the case of their large deposits. For example, the Takhtarvumchorr deposit of keldyshite, which serves as a raw material for the production of zirconosilicate sorbents and ion-exchange materials, was included in the Cadaster of deposits of the Khibiny massif.[72] In the Lovozero and Ilimaussaq massifs, eudialyte serves as a rock-forming mineral and forms rich deposits with reserves of millions of tons. Economically important deposits in massifs of alkaline rocks were found for elpidite (Western Mongolia), steenstrupine (Greenland) and lovozerite (the Kola Peninsula). Deposits of microporous niobate pyrochlore and related minerals were discovered in many regions throughout the world.

3. Structures of labuntsovite and its analogues

Labuntsovite and its analogues belong to zeolite-like titano- and niobosilicates, which have been studied in depth.[126] These minerals are convenient to use for illustrating the general features concerning the composition, structure and properties of microporous amphoterosilicates.

All labuntsovite-like structures are based on a mixed framework, which involves infinite chains of corner-sharing M octahedra extended along the *a* axis. The M octahedra are occupied by titanium or niobium atoms. In two other directions, the chains are linked by the $[Si_4O_{12}]$ rings. In structures of some monoclinic representatives of the labuntsovite group, the chains are linked also by additional D octahedra. The SiO_4 tetrahedra share corners (O) with the M octahedra. The M octahedra are also linked to each other by sharing corners (O,OH). The M octahedra share edges (O–O) with the additional D octahedra.

The framework contains cavities and channels occupied by large alkali and alkaline-earth metal cations and water molecules. The extraframework positions are characterised by the presence of vacancies. These characteristic features of labuntsovite and related minerals make them similar to zeolite-type minerals (Figs 1 and 2).

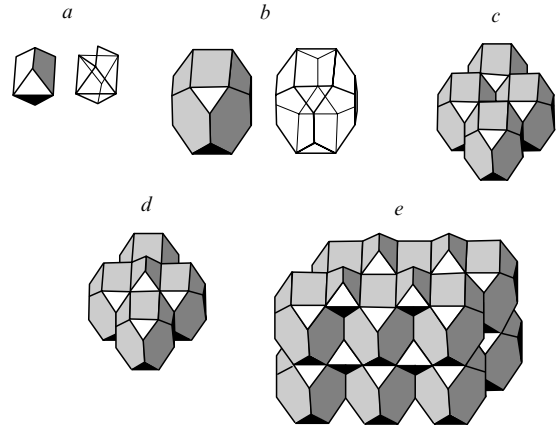

Figure 1. Zeolite polyhedra (*a*, *b*) and schemes of their arrangement (*c*, *d*, *e*) in the structures of minerals of the organovaite subgroup.[126]
The corners of the polyhedra are occupied by framework cations, and the oxygen atoms are located at the midpoint of the edges.

The minerals of the labuntsovite group can be divided into the following subgroups according to the symmetry and unit cell parameters:

— minerals with orthorhombic structures (the nenadkevichite subgroup), the space group *Pbam*;

— minerals with monoclinic structures and the unit cell parameter $c \approx 7$ Å (the labuntsovite, lemmleinite, kuzmenkoite, vuoriyarvite and gutkovaite subgroups), the space groups $C2/m$ or Cm;

— minerals with orthorhombic structures $c \approx 15$ Å (the paralabuntsovite and organovaite subgroups), the space group $C2/m$.

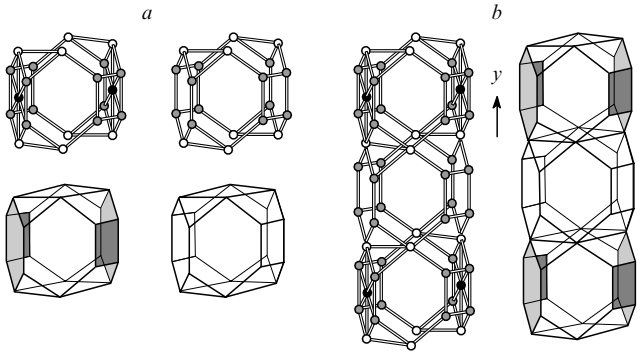

Figure 2. Zeolite polyhedra (*a*) and channels (*b*) in the structures of monoclinic minerals of the labuntsovite groups.[126] The D-octahedral, M-octahedral and tetrahedral sites are represented by solid, shaded and empty circles, respectively.

Minerals of the labuntsovite group are represented only by two topological types of the frameworks (*D*-occupied and *D*-vacant) as opposed to aluminosilicate zeolites characterised by several tens of topological types, which cannot be derived from one another by smooth transformations without cleavage of the chemical bonds. Each topological type of the labuntsovite group can be divided into two subtypes. In one of them, the adjacent octahedral layers are translationally equivalent, whereas in another one these layers are translationally non-equivalent. Nevertheless, minerals of the labuntsovite group are rather structurally diverse (10 structural types are known for this mineral group).

The crystal structures of nenadkevichite and its titanium analogue (korobitsynite) differ radically from those of all other (monoclinic) representatives of the labuntsovite group.[83–85] Both orthorhombic minerals belong to the space group *Pbam* and have similar unit cell parameters. This structural type is based on zigzag planar chains of corner-sharing Ti(Nb) octahedra extended along the *a* axis. The planes of the chains are parallel to the (001) plane. In labuntsovite and other monoclinic minerals of this group, the zigzag chains are parallel to the (010) plane and are strongly bent in the (001) plane in a wave-like fashion. In two other directions, the chains are linked by four-membered rings of Si tetrahedra to form a negatively charged framework with composition $[(Nb,Ti)_4(O,OH)_4(Si_4O_{12})_2]$ ($Z = 1$). The large cavities in the framework are occupied by Na^+ cations and crystallographically non-equivalent water molecules of three types. The possibility of the involvement of cations bulkier than Na^+ (such as K^+, Ba^{2+}, *etc*.) in these phases is limited due to steric hindrance.

In the structures of monoclinic minerals of the labuntsovite group, there are several non-equivalent positions occupied by extraframework cations (the most ordered structures have three such positions, *A*, *B* and *C*). The *D* position can be either vacant or occupied by divalent cations Q^{2+} (Q = Fe, Mn, Mg, Zn or, more rarely, Ca), which are involved in the D octahedron as the $[Q(H_2O)_2]^{2+}$ complex. The water molecules of this complex occupy the adjacent extraframework *C* positions. This is possible only if the latter positions are not occupied by cations. The simultaneous incorporation of K(Ba) into the *C* position and Q^{2+} into the *D* position would lead to a too short K(Ba)–Q^{2+} distance (~2.1 Å), which is unrealistic because of Coulombic repulsion. Hence, an interesting type of alternative isomorphism is observed in the labuntsovite structure:

$$\underset{C}{2(K,Ba)} + \underset{D}{\square} \longleftrightarrow \underset{C}{2H_2O} + \underset{D}{(Mn,Fe,Mg,Zn)}$$

In labuntsovites, continuous isomorphism according to this scheme occurs throughout the range of occupancies of the *C* and *D* positions by cations. This fact as well as the possibility of various mutual substitutions of cations in the *C* and *D* positions is responsible for a substantial compositional variability of labuntsovites. The general crystal-chemical formula for minerals of this group is as follows ($Z = 1$):

$$A_4B_4C_{4-2x}[D_x(H_2O)_{2x}][M_8(O,OH)_8][Si_4O_{12}]_4 \cdot n\,H_2O,$$

where $n \approx 8$; $x = 0–2$; A = Na, (Ca), □; B = K, Na, (H_3O), □; C = K, Ba, (H_3O), □; D = Mn^{2+}, Fe^{2+}, Mg, Zn, □; M = Ti, Nb, (Fe^{3+}); □ is vacancy.

Among monoclinic minerals of the labuntsovite group, representatives of the vuoriyarvite subgroup are characterised by the most disordered and loose structures.[86–88, 127–129] Some structural features of the framework of vuoriyarvite-K (Fig. 3) make it similar to nenadkevichite. In particular, both structures have no additional cross-linking D octahedra and are characterised by substantial displacements of the Nb and Ti atoms from the centres of octahedra toward one of the bridging corners. Distortions of the octahedral chains are manifested also in the fact that all (Nb,Ti)–O bonds in each tetrahedron have different lengths. In

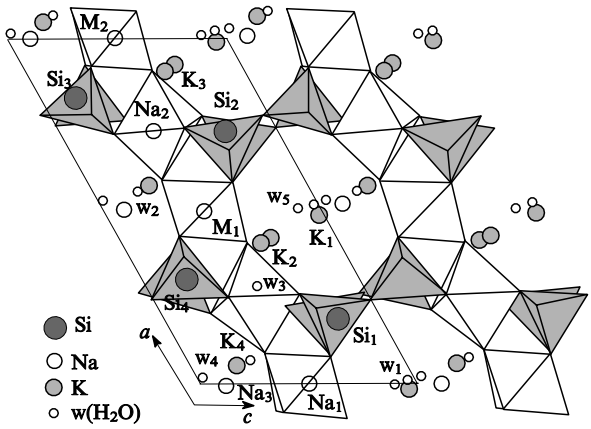

Figure 3. Crystal structure of vuoriyarvite-K, which is the *D*-vacant mineral of the labuntsovite group.[86]

the vuoriyarvite structure (unlike the nenadkevichite structure), the adjacent (Nb,Ti) octahedra are twisted about the axis of the chain (an analogous arrangement is observed in the labuntsovite structure) to form large cavities, which can be occupied by bulky potassium, barium and, probably, oxonium ions. Since the presence of these cations is very typical of monoclinic minerals of the labuntsovite group, this fact can be considered as an indication of a monoclinic symmetry.

The characteristic feature of the vuoriyarvite structure which distinguishes it from most other representatives of the labuntsovite group, is a large number of extraframework positions occupied by cations and water molecules, many of which are located at distances too close to be simultaneously occupied. As a result, most extraframework positions are predominantly vacant.

Vuoriyarvite-K is structurally similar to its analogues, *viz*., tsepinite-Na [128] and tsepinite-K, in which Na and Ti or K and Ti ions, respectively, prevail.[129]

The mixed framework in the kuzmenkoite structure [98–100] $K_4[(H_2O)_4(Mn,Zn)_2][(Ti,Nb)_8(O,OH)_8][Si_4O_{12}]_8 \cdot 8\,H_2O$ ($Z = 1$) is similar to the frameworks of minerals with labuntsovite-type structures. The only differences are the rotation and tilt angles of the adjacent polyhedra. The main distinguishing feature of the kuzmenkoite structure is that the *A* position is vacant due to a low sodium content. In addition to kuzmenkoites, this structural type includes their Fe,Nb-dominant analogue gjerdingenite-Fe.[130]

The organovaite subgroup,[95–97] which includes organovaite-Mn $K_2Mn(Nb,Ti)_4(Si_4O_{12})_2(O,OH)_4 \cdot 6\,H_2O$, organovaite-Zn $K_2Zn(Nb,Ti)_4(Si_4O_{12})_2(O,OH)_4 \cdot 6\,H_2O$ and parakuzmenkoite-Fe $(K,Ba)_2Fe(Ti,Nb)_4(Si_4O_{12})_2(O,OH)_4 \cdot 7\,H_2O$, is characterised by the space group $C2/m$ and the double (compared to labuntsovites) parameter *c* due to translational non-equivalence of the adjacent octahedral chains. Organovaites and parakuzmenkoite-Fe are isostructural to their *D*-deficient analogue paratsepinite-Ba,[129] in which extraframework positions are occupied predominantly by barium (Fig. 4).

In the structures of kuzmenkoites, organovaites and parakuzmenkoite, the *D* positions are completely or almost completely occupied by small divalent cations (Mn, Zn, Fe). Both extraframework positions are occupied primarily by large K and Ba cations. The sodium position is vacant. The excessive (with respect to the idealised formula of organovaite) Zn atoms can be incorporated into the potassium positions as the $[Zn(H_2O)_2]^{2+}$ complex.

The crystal structure of karupmøllerite-Ca,[94] which is a representative of the labuntsovite group characterised by the predominance of Ca and Nb [Ca > (Na, K, Ba, Sr), Nb > Ti], was studied by the Rietveld method.[93] In this structure, the D octahedra are occupied (by 70%) predominantly by Ca. Another distinguishing feature of karupmøllerite-Ca is that the *C* position is occupied by Ca and Na cations, unlike all other minerals of the

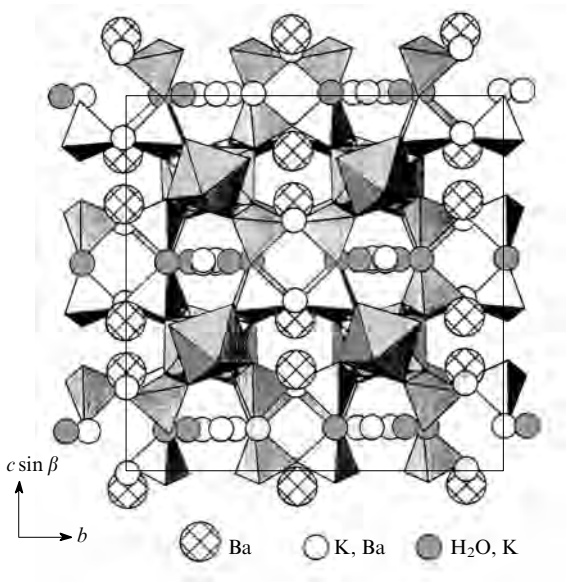

Figure 4. Crystal structure of paratsepinite-Ba, which is the *D*-vacant mineral of the labuntsovite group with the double unit cell parameter *c*.[126]

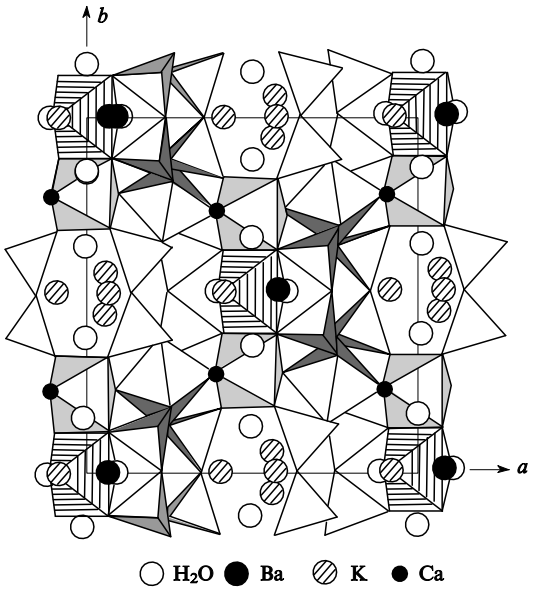

Figure 5. Crystal structure of gutkovaite-Mn, which is the *D*-occupied mineral of the labuntsovite group.[101]

labuntsovite group in which these positions are occupied by Ba and K. Therefore, calcium in the karupmøllerite-Ca structure serves both as a framework-forming cation (in the *D* position) and an extraframework cation (in the *C* position).

A radically different distribution of extraframework cations is observed in the gutkovaite structural type.[101–103] The structure of gutkovaite differs from that of labuntsovite primarily by splitting of the *A* position into two non-equivalent subpositions and a lowering of the symmetry to *Cm*. In addition to gutkovaite-Mn (Fig. 5), the gutkovaite structural type includes alsakharovite-Zn and neskevaaraite-Fe (Table 3).

It is noteworthy that all structurally studied crystals of minerals of the gutkovaite subgroup appeared to be microtwinned along the (001) and ($\bar{4}$01) planes of the true monoclinic lattice, which leads to a spurious increase in the symmetry to orthorhombic accompanied by an increase in the parameter *c* by a factor of four (c_{orthor} = 28.17 Å). An analogous twinning was revealed earlier in vuoriyarvite-K [86] and tsepinite-Na.[87]

The structural type of gutkovaite is of particular interest because it serves as a 'superefficient separator' of cations. The alsakharovite-Zn structure is the most prominent example. In this structure, Na + Ca, Sr, K, Ba and Zn ions occupy their own positions with good selectivity. The lemmleinite-Ba structure possesses a similar property. In this structure, the sodium, potassium, barium and manganese positions are strictly separated.

Due to non-rigid corner-sharing of octahedra in minerals of the labuntsovite group, the degree of deformation of the chains can vary depending on the type of the cations occupying the key *D* positions at the sites, where the chains approach each other. This is accompanied by a change in the parameter *a* along the axis of the chain and a smaller change in the parameter *b*. These changes are exemplified by several structurally studied representatives of the labuntsovite group.[87] In particular, the average distances in the D octahedron and the parameter *a* in labuntsovites are in the ranges of 2.0–2.1 and 14.2–14.3 Å, respectively. The corresponding characteristics for kuzmenkoite-Mn and vuoriyarvite-K (containing four-coordinate Na cations instead of D cations) are 2.2, 14.4 Å and 2.3, 14.7 Å, respectively, In monoclinic nenadkevichite (containing Ca in the 'cross-linking' position [107]) and tsepinite-Na (containing Sr and vacancies in the mixed *D* position), these parameters are 2.3, 14.75 Å and 2.35 (for Sr), 14.6 Å, respectively.

Among monoclinic minerals of the labuntsovite group, labuntsovites and lemmleinites (which are *D*-vacant analogues of labuntsovites) have the simplest and most ordered structures. Other structural types of this group can be derived from these simplest structures by shifting, splitting and varying the degree of occupancy of extraframework positions. For example, the gutkovaite structural type is derived by splitting the *A* position into two non-equivalent positions occupied by different cations, which leads to the disappearance of the centre of symmetry. The kuzmenkoite structure is characterised by the absence of A cations and the occupied *D* position. In this structure, the centre of symmetry is absent due to an unsymmetrical splitting of the *B* and *C* positions. The structures of organovaites and their titanium

Table 3. Comparative characteristics of minerals of the gutkovaite subgroup (the space group *Cm*).

Characteristics	Mineral		
	Gutkovaite-Mn	Neskevaaraite-Fe	Alsakharovite-Zn
Simplified formula	$CaK_2Mn(Ti,Nb)_4(Si_4O_{12})_2(O,OH)_4 \cdot 5H_2O$	$NaK_2Fe(Ti,Nb)_4(Si_4O_{12})_2(O,OH)_4 \cdot 6H_2O$	$NaSrKZn(Ti,Nb)_4(Si_4O_{12})_2(O,OH)_4 \cdot 7H_2O$
Composition of *A*(1) position	$Ca_{1.2}\square_{0.8}$	Na_2	$Na_{0.7}Ca_{0.7}\square_{0.6}$
Composition of *A*(2) position	$\square_2$	$K_{1.6}Na_{0.4}$	$\square_{1.0}Sr_{0.7}Na_{0.3}$
Composition of *B* position	$K_{3.0}\square_{1.0}$	$K_{2.2}\square_{1.0}(H_2O)_{0.8}$	$\square_{3.0}K_{1.0}$
Composition of *C* position	$(H_2O)_{3.6}K_{0.2}Ba_{0.2}$	$(H_2O)_{2.2}K_{0.72}Ba_{0.48}\square_{0.6}$	$(H_2O)_{3.6}Ba_{0.2}\square_{0.2}$
Composition of *D* position	$Mn_{1.7}Fe_{0.1}\square_{0.2}$	$Fe_{0.7}Mg_{0.4}\square_{0.9}$	$Zn_{1.6}Mn_{0.2}\square_{0.2}$
Composition of *M* position	$Ti_{7.8}Nb_{0.2}$	$Ti_{4.8}Nb_{3.2}$	$Ti_{5.7}Nb_{2.3}$

analogue parakuzmenkoite-Fe have the double (compared to kuzmenkoite) parameter *c*, which is associated with translational non-equivalence of the adjacent octahedral layers rather than with the ordered arrangement of the D cations, which takes place in paralabuntsovites with the space group $I2/m$.[84]

As mentioned above, minerals of the labuntsovite group can be divided into subgroups belonging to different structural types. These subgroups can be arranged according to changes in the physical properties of minerals (IR spectra, optical characteristics, behaviour on heating) and interplanar distances in powder X-ray diffraction patterns as follows: the labuntsovite, paralabuntsovite and lemmleinite subgroups → the gutkovaite subgroup → the kuzmenkoite and organovaite subgroups → the vuoriyarvite and paratsepinite subgroups → orthorhombic minerals (the nenadkevichite subgroup).

In most cases, this series correlates with the order of formation. Thus, the closer are the minerals to the end of the series, the later they crystallise, which is clearly manifested in intergrowths of different minerals of the labuntsovite group. Late minerals are characterised by weaker (according to IR spectroscopic data) hydrogen bonds formed by water molecules and lower dehydration temperatures, which is also indirect evidence for lower temperatures of formation.

It should be noted that in the structures of the first members of this series, the *D* positions are generally occupied, whereas the structures of the last members are characterised by the presence of *D*-deficient positions or do not have *D* positions at all (the vuoriyarvite, paratsepinite and nenadkevichite subgroups). The exceptions are lemmleinites, which, unlike other monoclinic *D*-deficient representatives of this group, are characterised by a high degree of cation ordering, which makes them similar to labuntsovites. The similarity of lemmleinites to labuntsovites is manifested also in the existence of continuous isomorphous series including minerals of these subgroups.

By contrast, isomorphism between representatives of other subgroups is often limited. This is confirmed, in particular, by the presence of sharp interfaces between intergrowth crystals of minerals belonging to different subgroups as well as by an essentially non-uniform distribution of various components (Na, Ca, Sr, Nb, the sum of D cations, *etc*.), which was established by a statistical analysis of the compositions using large specimen selections. In other words, minerals of each subgroup (structural type) possess an individual structurally-determined affinity for particular framework and extraframework cations.

The above-given series correlates also with the changes in the chemical composition of the minerals. This is most clearly reflected by the Ti : Nb ratio. For the labuntsovite, paralabuntsovite, lemmleinite and gutkovaite subgroups, high-niobium representatives are unknown, whereas virtually pure titanium specimens are usual for these minerals (except for members of the gutkovaite subgroup). By contrast, high-niobium specimens are known for the vuoriyarvite and nenadkevichite subgroups. Evidently, this fact is ralated to the condition of charge balance. Minerals of the vuoriyarvite, paratsepinite and nenadkevichite subgroups are characterised by the absence or deficiency of D-type cations and partial occupancies of the *A* positions resulting in the deficiency of the positive charge, which is compensated by the replacement of Ti^{4+} with Nb^{5+}. It should be emphasised that the framework density of minerals of the labuntsovite group is to a large extent determined by the presence of vacancies in the *D* positions.

4. Structures of eudialyte and its analogues

Minerals of the eudialyte group attract considerable interest not only because of their structural diversity, which leads to a wide range of physical and chemical properties and allows for their practical application, but also due to the fact that these minerals form giant and rich deposits. Two main fields of practical application of eudialytes hold promise. First, zirconium, hafnium, heavy rare-earth elements and other useful components can be extracted from these minerals. Second, ecologically harmful elements, such as radioactive isotopes of strontium, caesium, *etc*., can be incorporated into their decationated forms. Until recently, researchers attempted (rather unsuccessfully) to solve the former problem by technological approaches using total decomposition of eudialytes by inorganic acids. In these approaches, silicon goes into solution as polysilicic acids, which form filterable gels, thus hindering isolation and purification of valuable components. Recently, a new solvometallurgical method was developed[131,132] for the selective extraction of rare-earth elements and zirconium from mechanically activated minerals without their complete destruction.

The latter problem is associated with the ability of eudialytes to be involved in ion-exchange processes. Under natural conditions, the participation of these minerals in ion-exchange reactions is often accompanied by their hydration.[133]

Minerals of the eudialyte group, which are trigonal ring silicates with a complex and variable composition, belong to zeolite-like compounds. Their framework density calculated as the number of Si + (Zr,Ti) + Ca + Nb + (Fe,Mn) atoms per 1000 $Å^3$ varies from 18 to 21 and is comparable to the corresponding values for some aluminosilicate zeolites.

The framework of eudialyte contains three- and nine-membered rings of SiO_4 tetrahedra, which are linked to each other by Zr(Ti) octahedra and six-membered rings of edge-sharing Ca octahedra. The rings of the octahedra are linked to each other by Fe, Na, Zr, Mn, Ti atoms (more rarely, by Ta, *etc*. atoms) with coordination numbers of 4 (square planar), 5 (pyramid) or, more rarely, 6 (octahedron), which correspond to the *M*(2,1), *M*(2,2) and *M*(2,3) positions, respectively (see below). Sometimes, cations possessing high force characteristics are lacking in this microregion resulting in a decrease in the framework density. Based on abundant X-ray diffraction data,[122,134–159] the crystal-chemical formula of eudialytes in a typical unit cell ($c \approx 30$ Å) can be represented in the general form ($Z = 3$):

$$N_{12}A_3[M(1,1)M(1,2)]_3[M(2,1)M(2,2)M(2,3)]_{3-6}[M(3)M(4)].$$

$$.Z_3[Si_{24}O_{72}]\cdot OH_{2-6}X_{2-4},$$

where *N* are predominantly sodium ions occupying four types of extraframework positions (these positions can also involve substantial amounts of H_3O^+ ions and small amounts of other alkali and alkaline-earth metal ions); *A* = Na, K, Sr, Ln, Y, Ba, Mn, Ca, H_3O; *M*(1,1), *M*(1,2) = Ca, Mn, Y, Ln, Na, Sr, Fe; *M*(2,1) = Fe, Na, Zr, Ta; *M*(2,2), *M*(2,3) = Fe, Mn, Zr, Ti, Na, K, Ba, H_3O; *M*(3), *M*(4) = Si, Nb, Ti, W, Na; *Z* = Zr, Ti, Nb; *X* = Cl, F, H_2O, OH, CO_3, SO_4.

Therefore, the eudialyte structure incorporates almost all chemical elements present in a mineral-forming medium. The impurity cations in zeolite cavities can 'choose on their own' energetically favourable positions to compensate charges in the case of heterovalent substitutions. These cations are self-organised and occupy optimum positions in each particular case. Either additional SiO_4 tetrahedra or octahedra, which are most often occupied by Nb atoms (but in some cases, are occupied by W, Zr, Mn or Ti atoms), are located in the centres of the $[Si_9O_{27}]$ rings. Large cations (primarily, Na), additional *X* anions and water molecules are located in large cavities between these structural elements. Isomorphous substitutions in zeolite cavities are most often random. Relatively low-ordered minerals are most typical of the eudialyte group. The structures of these minerals are described by the hexagonal unit cell with the parameters $a \approx 14$ Å, $c \approx 30$ Å and the space group $R3m$ [eudialyte[122] $Na_{15}Ca_6Fe_3Zr_3.Si_{26}O_{72}(O,OH)_2Cl_2$ provides an example]. In some minerals, impurity cations are ordered. This ordering can occur both in the horizontal plane (in layers perpendicular to the threefold axis) and in the vertical direction (along the threefold axis). In the latter case, structures have the multiply larger period *c*.

Isomorphous substitutions, which are often accompanied by changes in the valence state and coordination number, can occur

in virtually all positions, both extraframework and framework (except for positions of the Si atoms in the silicon – oxygen rings). These processes most often lead to the disappearance of the centre of symmetry in the structure as a whole and give rise to cluster fragments composed of an octahedron located on a symmetry axis and three octahedra (or half-octahedra), which are arranged about the symmetry axis and share corners with the central octahedron. The structures of kentbrooksite [148] $(Na,Y,Ln)_{15}.Ca_6Mn_3Zr_3NbSi_{25}O_{73}(O,OH,H_2O)_3$ containing the $NbMn_3$ cluster and its analogue containing the $NbFe_3$ cluster [139] serve as such examples.

The octahedral positions in the six-membered rings are, as a rule, occupied predominantly by Ca atoms [for example, in feklichevite [134, 156] $Na_{11}Ca_9Fe_2Zr_3NbSi_{25}O_{73}(OH,H_2O,O,Cl)_5$]. In low-calcium minerals, other elements are also incorporated into these positions. In the case of their ordering, octahedrally coordinated sites of the six-membered ring break down into two groups consisting of three octahedra each, which are non-equivalent in both composition and size resulting in a lowering of the symmetry to $R3$. For example, Ca octahedra alternate with Mn octahedra in the oneillite structure [137, 143] (Fig. 6). Representatives containing ordered Ca and Fe [142] as well as ordered Mn and Na [146] were found.

An ordering along the main axis gives rise to superstructures, which are observed in a series of minerals of the eudialyte group. For example, half of Zr atoms in the octahedra of the framework in a high-titanium specimen [138] are replaced by Ti atoms in an ordered fashion. As a result, the octahedra containing predominantly either Zr or Ti atoms alternate along the threefold axis in the doubled unit cell.

The symmetry of structures with a doubled unit cell ($a \approx 14$ Å, $c \approx 60$ Å) can be either $R\bar{3}m$ (alluaivite [136]), $R3m$ or $R3$. In the lower-symmetry structures, an ordering along the threefold axis is accompanied by a horizontal ordering, including the positions in the six-membered rings.

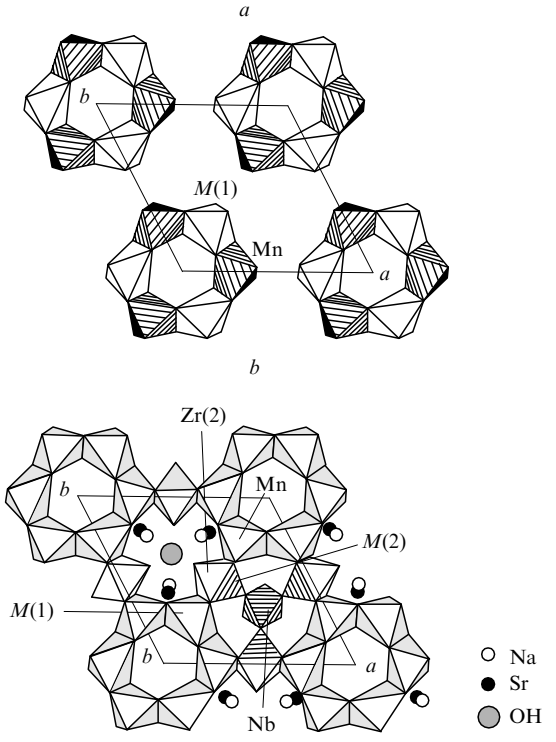

Figure 6. Ordering of the Mn and (Ca,Ce) ions in the rings of edge-sharing octahedra (*a*) and these rings linked by octahedra of *O*-coordinated transition metals (*b*) in oneillite, which is an analogue of eudialyte with the symmetry $R3$.[137]

The above examples do not exhaust the diversity of the structural features and chemical compositions of minerals of the eudialyte group. However, even these examples show that an analogous diversity is impossible for aluminosilicate zeolites, at least within the framework of one structural motif.

Decationation and cation substitution in eudialytes characterised by different degrees of hydration were studied [157] taking into account such structural features as occupancies of the framework positions, changes in the coordination numbers of the cations, the character of the complete and partial isomorphous substitution, the formation of vacancies, changes in the charges of the cations in particular positions, the lowering of the symmetry and/or doubling of the unit cell parameter c caused by ordering of the components over structural positions, *etc*.

Eudialytes, which were formed in hyperalkaline rocks in early evolution stages, contain large amounts of sodium ions, which can be involved in virtually all positions, except for silicon – oxygen rings and Zr octahedra. In the N and A positions, sodium ions can be replaced by equal-sized or larger cations. In the M positions, sodium ions are replaced by smaller cations. The exceptions are the $M(2,2)$ and $M(2,3)$ positions, which can be occupied by both smaller (compared to Na) and larger cations. In late stages of mineral formation involving a decrease in the temperature, the conditions are changed from hyperalkaline to less alkaline followed by the acid-leaching stage, where eudialytes sometimes almost completely lose sodium and are subjected to hydration.

The IR spectroscopic data provide evidence that the oxonium ions H_3O^+ can be incorporated into the cavities of the framework (Fig. 7) [the presence of larger single-charged groups, such as $(H_5O_2)^+$, is excluded for steric reasons].

The degree of hydration (*i.e*., the ratio of the number of oxonium groups and water molecules to the number of other extraframework cations) in structurally studied specimens varies from 0 (unaltered eudialyte) to ~ 2.2 (Na,Fe-decationated eudialyte [158]). Intermediate values for structurally studied specimens are 0.15, 0.6 and 1.4 (see Refs 157, 141 and 152, respectively).

A comparative analysis of the structures of six eudialytes, which differ in the degree of hydration,[157] revealed the following features.

1. Ion exchange in eudialytes occurs through the replacement of Na atoms by larger cations in all extraframework positions and, partially, in the $M(2,2)$ and $M(2,3)$ positions. Such substitutions in other M positions cannot take place.

2. The replacement of N and A cations by H_2O and H_3O^+ more often occurs in Zr- and Si-containing layers and, to a lesser degree, in layers containing Ca octahedra.

3. An increase in the degree of hydration is accompanied by an increase in the percentage of K, Sr, Ba, Ca and rare-earth cations, which stabilise the structure. Layers enriched in H_2O molecules

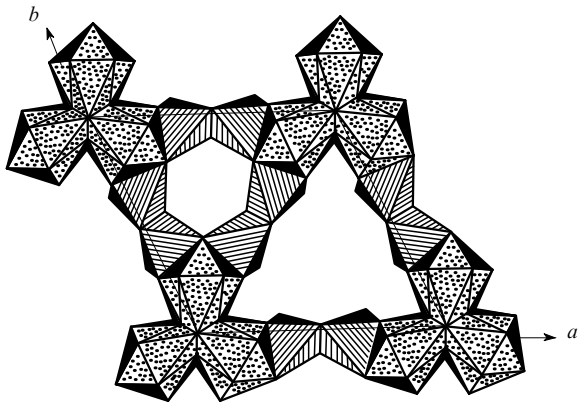

Figure 7. Fragment of the framework of the Fe,Sr-analogue of kentbrooksite.[140]
The rings of Ca octahedra are dashed and the $M(3)$ polyhedra are dotted.

and H_3O^+ ions are characterised by weaker bonds both within the layer and between the adjacent layers giving rise to cleavage perpendicular to the threefold axis. Apparently, the complete replacement of extraframework cations by H_3O^+ cannot occur because it would lead to destabilisation of the structure up to the transformation into the amorphous state. Under natural conditions, eudialyte is often replaced by amorphous aqueous zirconium silicate or an aggregate of water-containing zirconosilicates at low temperatures.

4. Because of the high mobility of H_3O^+ cations, their hydrogen atoms are not localised and the O atoms are characterised by high temperature parameters, random disorder, splitting and partial occupancies. A high content of oxonium groups generally leads to a symmetry lowering to *R*3. The limiting saturation can cause deformation of the unit cell accompanied by an increase in the parameter *c* by almost 1 Å and a decrease in the parameter *a* by 0.25 Å.

5. Isomorphous replacement of extraframework cations by H_3O^+ groups takes place either randomly in layers perpendicular to the threefold axis or in an ordered fashion along the threefold axis. In the latter case, modular structures with the double parameter *c* are formed. These structures are less stable (and the degree of their hydration is lower) compared to typical eudialytes (the parameter $c \approx 30$ Å).

Additional data on the crystal chemistry of natural amphoterosilicates were surveyed in the monographs by Pyatenko and co-workers.[80,160]

IV. Properties of microporous silicates containing transition elements

1. Ion-exchange and sorption properties

Studies of the ion-exchange properties of synthetic titanosilicates are rather scarce. It was demonstrated[34] that zeolite-like K and Na titanosilicates prepared by the hydrothermal synthesis efficiently adsorb Cs^+, Rb^+, Pb^{2+} and Hg^{2+} ions from solutions. In the patent,[161] nenadkevichite and the microporous aqueous titanosilicates ETS-10 and ETS-4 were described as sorbents of cations of radioactive isotopes of a number of metals (Cs, Sr, Co). It was also found that various cationic forms of synthetic titanosilicate having the pharmacosiderite structure remove trace amounts of ^{137}Cs and ^{89}Sr from aqueous solutions in a wide acidity range.[162] Complex oxides which contain Ti, Nb, Sb or W and have the pyrochlore structure, can also remove the above-mentioned isotopes from aqueous solutions.[52] A synthetic stibiosilicate and penkvilksite were used for extraction of ^{60}Co from aqueous solutions.[163]

In the microporous titanosilicate $K_2TiSi_3O_9 \cdot H_2O$, potassium ions can be replaced either completely by ammonium atoms or partially by other alkali metal cations through ion exchange with aqueous solutions. Due to high 'flexibility' of the framework, this cation substitution leads to a substantial change in the physicochemical properties of the material.[164]

Natural minerals of the labuntsovite group belong to zeolite-like titanosilicates. As mentioned above, these minerals are very structurally and compositionally diverse. The cation exchange was studied[165] under normal conditions for single-crystal grains of seven minerals of the labuntsovite group (korobitsynite, labuntsovite-Mn, lemmleinite-K, kuzmenkoite-Mn, organovaite-Mn, vuoriyarvite-K and tsepinite-Na) belonging to six structural types, which differ in the symmetry, the occupancies of the *D* positions and the character of ordering of extraframework A cations in the channels. In experiments, solutions of NaCl, Na_2CO_3, K_2CO_3, $CaCl_2$, $SrCl_2$, $BaCl_2$ and CsCl were used.

The cation exchange in aqueous solutions depends on the structural features and proceeds differently for various representatives of the labuntsovite group. Orthorhombic phases and minerals of the labuntsovite and lemmleinite subgroups, which are characterised by the maximum ordering of extraframework cations and high occupancies of their positions, do not exhibit cation-exchange properties under mild conditions. Representatives of the kuzmenkoite, organovaite and vuoriyarvite subgroups, which are characterised by relatively low occupancies of the cation positions in zeolite cavities and the low-ordered arrangement of cations in these cavities, possess pronounced cation-exchange properties. Minerals of the vuoriyarvite subgroup exhibit the strongest cation-exchange properties due to a combination of several factors: low saturation with extraframework (zeolite) cations, the maximum disordered distribution of these cations, the almost complete absence of D cations, which 'cut-off' some zeolite channels, weak hydrogen bonds involving water molecules in the channels and a high concentration of extended structural defects associated with microtwinning.

In each grain, the process occurs throughout the bulk, the intensity of saturation being dependent on local inhomogeneities of the crystal rather than on the distances of particular regions from the solution interface. In other words, the energy barrier which ions overcome at the crystal – solution interface, rather than diffusion in the crystal bulk is the rate-determining step. This suggests that the ion-exchange process can be accelerated by subjecting the solid particle surface to the corresponding modification.

The microporous silicates[24,166] $M_2TiSi_3O_9 \cdot 2.5\,H_2O$, where M are extraframework cations, and $K_2(Zr,Ti)Si_3O_9 \cdot H_2O$ as well as some perovskite-type[167] and pyrochlore-type[52] complex oxides exhibit pronounced ion-exchange properties.

Many amphoterosilicates serve not only as ion-exchange materials but also as sorbents due to their ability to absorb small molecules from gases and solutions. For example, ETS-10 efficiently adsorbs H_2, CO, N_2 and NO, Cu-modified ETS-10 adsorbs NO, CO, C_2H_4 and NH_3, and Mg-modified ETS-10 can adsorb CO and N_2. Sorption processes as well as the surface properties of modified ETS-10 and the states of adsorbed molecules were studied by IR spectroscopy and calorimetry.[168–170] It was demonstrated[171] that titanosilicate molecular sieves can adsorb various molecules with high selectivity.

2. Catalytic properties

In recent years, micro- and mesoporous silicates of transition elements as well as some niobates have found ever increasing application as catalysts and catalyst supports in various processes, primarily, in selective oxidation reactions. Titanosilicates are most commonly used for these purposes. For instance, ETS-10 was used to advantage as a catalyst for gas-phase oxidative dehydrogenation of cyclohexanol,[172] dehydration of n-butanol, isomerisation of *m*-xylene and 1,3,5-trimethylbenzene,[14] dehydration of *tert*-butanol,[173] acylation of alcohols[174] and polymerisation of alkynes.[175] By contrast, ETS-10 and ETS-4 do not generally exhibit catalytic activity in selective oxidation reactions with H_2O_2 because these materials are not prone to the formation of titanium hyperoxide complexes.[176] Modified forms of microporous titanosilicates containing various extraframework cations, *viz*., M-ETS-10 (M = Na + K, H, Li, Na, K, Ni^{II}, Cu^{II}, Co^{II}) and M-ETS-4 (M = Na, K), promote photoinduced charge transfer in methylphenothiazine at room temperature.[177] The catalysts Pt-ETS-10 and Pt-ETAS-10 appeared to be efficient in reforming of n-hexane.[178] The catalytic properties of ETS-10 containing various isomorphous impurities were also described in the study.[143] In the investigation,[179] the authors hypothesised that the catalytic properties of ETS-10 are associated with high basicity of this material.

In addition to ETS-10, the titanosilicates ETAS-10 and AM-6 also exhibit catalytic activity in dehydration of *tert*-butanol and show high selectivity for isobutene. Stability of these catalysts increases as the temperature increases from 200 to 300 °C.[173] In the above reaction, the catalytic activity of ETS-10, ETAS-10 and AM-6 is also determined by basic sites.

Epoxidation of *cis*-cyclooctene was carried out with a quantitative yield on the modified zeolite SSZ-33 containing extraframework tetrahedrally coordinated titanium atoms and on the Ti-beta

zeolite containing only framework titanium atoms.[28] Selective epoxidation of *cis*-cyclooctene was performed also on the titanium-containing zeolite TS-1.[28] Besides, TS-1 and, particularly, Ti-beta efficiently catalyse oxidation of dibutyl sulfoxide with dilute solutions of H_2O_2 in *tert*-butanol to form the corresponding sulfone.[180] In the latter study, the reaction kinetics was investigated and compared with that of catalytic oxidation of organic sulfides under analogous conditions.

The high catalytic activity of TS-1 and Ti-MCM-41 in selective oxidation reactions is associated with the formation of hydroperoxide complexes with titanium sites on the surface of the catalyst particles. In the presence of platinum, a mixture of hydrogen and oxygen can be used instead of H_2O_2 for the preparation of such complexes.[176] The catalytic sites in TS-1, Ti-MCM-41, ETS-10 and ETS-4 can also be modified in dry hydrogen at temperatures higher than 400 °C. Study by ESR spectroscopy [176] demonstrated that Ti^{3+} occurs in tetrahedral (in TS-1 and Ti-MCM-41) or octahedral (in ETS-10 and ETS-4) coordination, whereas reduction of TS-1 and Ti-MCM-4 at temperatures higher than 600 °C affords two types of non-equivalent Ti^{3+} positions.

Oxidation of various organic substrates with hydrogen peroxide in a three-phase system in the presence of TS-1 as the catalyst was described in the study.[181] In hydroxylation reactions of a series of aromatic compounds (benzene, toluene, anisole, benzyl chloride), the reaction rate increases by a factor of 3–10, the regioselectivity being also increased. The oxidative rearrangements of cyclohexanone and acetophenone (the Baeyer–Villiger reaction) afforded caprolactone and phenyl acetate, respectively; the selectivity was 70%–90%. Oxidation of benzyl chloride in this three-phase catalytic system gave rise to *p*- and *o*-hydroxybenzyl chlorides in a ratio of 85 : 15. In all such reactions, the activity and regioselectivity of catalysis are determined by the relative hydrophobicity and the pore size of titanosilicates used as catalysts as well as by their Brönsted acidity in the presence of H_2O and H_2O_2.

A broad spectrum of titanosilicate molecular sieves (TS-1, TS-2, Ti-beta, Ti-MCM-41, Ti-HMS, amorphous SiO_2–TiO_2) was examined in oxidation of propylamine with 30 mass % H_2O_2 to prepare a mixture of *syn*- and *anti*-propionaldoximes. Only TS-1, TS-2 and Ti-beta exhibit substantial catalytic activity. For these three catalysts, the influence of the conditions of oxidation on the reaction rate and selectivity was studied.[182] A series of studies devoted to the use of titanosilicates (primarily, TS-1) as catalysts for oxidation reactions were surveyed in the review;[36] in addition, different approaches to an increase in selectivity of oxidation reactions, mechanisms of these reactions and procedures for the synthesis of large-pore titanosilicate catalysts were considered.

The reactions of cyclohexanone and *m*-, *o*- and *p*-hydroxyacetophenones with NH_3 and H_2O_2 are catalysed by TS-1 and the Ti-modified zeolites Al-beta and ZSM-48.[183] In particular, *p*-hydroxyacetophenone is transformed in the presence of TS-1 into the corresponding oxime; the selectivity is 100% and the conversion is 50%. For other systems, high selectivity can also be achieved with the use of methanol as the solvent and in the presence of a large excess of NH_3.

Titanosilicate which was synthesised by the reaction of dealuminated ZSM-5 with $TiCl_4$ vapour, catalyses photochemical decomposition of NO.[29]

Soluble titanium complexes are widely used as homogeneous catalysts for redox reactions.[184] Apparently, the successful use of microporous titanosilicates as catalysts for selective oxidation of organic substrates is associated with the fact that these zeolite-like materials contain titanium catalytic sites directly in a microporous matrix.

Zirconosilicates are rarely used as catalysts in organic syntheses. In particular, in the study [23] the mesoporous molecular sieves Ti-MCM-41 and Zr-MCM-41 were demonstrated to catalyse hydroxylation of naphth-1-ol with an aqueous solution of H_2O_2 as well as epoxidation of norbornene.

Data on the use of niobosilicate catalysts are also relatively scarce.[44, 185, 186] The microporous niobosilicate AM-11, whose structure remains unknown, catalyses the synthesis of dimethyl ether from methanol in a flow reactor.[185] Under these conditions, the reaction proceeds primarily at the external active sites of the catalyst possessing high Brønsted acidity. In a closed reactor, the reaction of methanol in the presence of AM-1 affords primarily a mixture of hydrocarbons (from C_1 to C_5). In the latter case, catalysis occurs at the internal active sites. The compound AM-1 also catalyses the synthesis of methyl *tert*-butyl ether by the gas-phase reaction of methanol with *tert*-butanol in a flow reactor at 50–100 °C under atmospheric pressure.[186] In this reaction, high selectivity is achieved; the selectivity remains unchanged in the case of repeated use of the catalyst and only slightly decreases with increasing temperature.

The studies [187–193] were also concerned with the physicochemical properties of amphoterosilicates and the nature of their active sites.

In addition to titano- and niobosilicates, some microporous complex oxides, whose frameworks contain exclusively octahedrally coordinated atoms, also exhibit catalytic activity. For example, a ruthenium lead analogue of pyrochlore with composition $Pb_{2.25}Ru_{1.75}O_{7-y}$ catalyses electrochemical oxidation of formaldehyde and glucose.[194] Stannates with the pyrochlore structure $Ln_2Sn_2O_7$ (Ln = Y, La, Nd, Sm, Gd) catalyse decomposition of NO.[54] Catalysis of photochemical decomposition of water with caesium-doped potassium niobate was described in the study.[195]

* * *

To summarise, zeolite-like materials with mixed frameworks differ from aluminosilicate zeolites by having a wider diversity of chemical compositions, crystal structures and physicochemical properties. The fact that the configuration of the framework smoothly varies with composition makes it possible to synthesise zeolite materials possessing desired (ion-exchange, sorption, catalytic, *etc*.) properties. Additional advantages of zeolite materials containing transition elements are associated with the presence of various active sites. The available data on the crystal chemistry and mineralogy of natural microporous amphoterosilicates containing transition elements will, undoubtedly, be useful in preparing analogous synthetic materials.

References

1. N F Chelishchev, B G Berenshtein, V F Volodin *Tseolity — Novyi Tip Mineral'nogo Syr'ya* (Zeolites as a New Type of Mineral Raw Material) (Moscow: Nedra, 1987)
2. J Rocha, V Felix, M W Anderson *Rev. Port. Quim.* **3** 35 (1996)
3. A P Khomyakov, in *Materialy Vseros. Seminara 'Shchelochnoi Magmatizm Zemli', Moskva, 2002* (Proceedings of All-Russian Seminar 'Alkaline Magmatism of the Earth', Moscow, 2002) p. 96
4. M Christophe-Michel-Levy *Bull. Soc. Fr. Mineral. Cristallogr.* **84** 265 (1961)
5. A N Chernov, V G Chukhlantsev, A A Voronkov, B A Maksimov, V V Ilyukhin *Izv. Akad. Nauk SSSR, Ser. Neorg. Mater.* **7** 180 (1971) [a]
6. G Baussy, R Garuba, A Baumer, G Turco *Bull. Soc. Fr. Mineral. Cristallogr.* **97** 433 (1974)
7. US P. 4 410 501; *Chem. Abstr.* **95** 206 272 (1981)
8. M W Anderson, O Terasaki, T Ohsuna, A Philippou, S P MacKay, A Ferreira, J Rocha, S Lidin *Nature (London)* **367** 347 (1994)
9. M W Anderson, O Terasaki, T Ohsuna, P J O'Malley, A Philippou, S P MacKay, A Ferreira, J Rocha, S Lidin *Philos. Mag. B* **71** 813 (1995)
10. P Brandão, P Ferreira, J Rocha, A Philippou, M W Anderson, in *The IVth Meeting of the Inorganic Chemistry Division of the Portuguese Chemical Society, Aveiro, 1999* p. 189

11. J Rocha, A Ferreira, Z Lin, M W Anderson *Microporous Mesoporous Mater*. **23** 253 (1998)
12. V Valtchev, S Mintova *Zeolites* **14** 697 (1994)
13. X Yang, J-L Paillaud, H F W J van Breukelen, H Kessler, E Duprey *Microporous Mesoporous Mater*. **46** 1 (2001)
14. T K Das, A J Chandwadkar, S Sivasanker *J. Mol. Catal. A: Chem*. **107** 199 (1996)
15. A Eldewik, R F Howe *Microporous Mesoporous Mater*. **48** 65 (2001)
16. W J Kim, M C Lee, J C Yoo, D T Hayhurst *Microporous Mesoporous Mater*. **41** 79 (2000)
17. H Xu, Y Zhang, A Navrotsky *Microporous Mesoporous Mater*. **47** 285 (2001)
18. J Rocha, P Brandão, Z Lin, A P Esculcas, A Ferreira, M W Anderson *J. Phys. Chem*. **100** 14 978 (1996)
19. J Rocha, P Brandão, Z Lin, A Kharlamov, M W Anderson *Chem. Commun*. 669 (1996)
20. A Philippou, M W Anderson *Zeolites* **16** 98 (1996)
21. G Cruciani, P De Luca, A Nastro, P Pattison *Microporous Mesoporous Mater*. **21** 143 (1998)
22. C Braunbarth, H W Hillhouse, M Tsapatsis, A Burton, R F Lobo, R M Jacubinos, S M Kuznicki *Chem. Mater*. **12** 1857 (2000)
23. K Chaudhari, R Bal, D Srinivas, A J Chandwadkar, S Sivasanker *Microporous Mesoporous Mater*. **50** 209 (2001)
24. A Clearfield, A I Bortun, L N Bortun, D M Poojary, S A Khainakov *J. Mol. Struct*. **470** 207 (1998)
25. Y Liu, H Du, Y Xu, H Ding, W Pang, Y Yue *Microporous Mesoporous Mater*. **28** 511 (1999)
26. V V Subbotin, S Merlino, D Yu Pushcharovsky, Ya A Pakhomovsky, O Ferro, A N Bogdanova, A V Voloshin, N V Sorokhtina, N V Zubkova *Am. Mineral*. **85** 1516 (2000)
27. A Bhaumik, T Tatsumi *Microporous Mesoporous Mater*. **34** 1 (2000)
28. C B Dartt, M E Davis *Appl. Catal. A* **143** 53 (1996)
29. S Zhang, T Kobayashi, Y Nosaka, N Fujii *J. Mol. Catal. A: Chem*. **106** 119 (1996)
30. P Ferreira, A Ferreira, J Rocha, M R Soares *Chem. Mater*. **13** 355 (2001)
31. S Mintova, B Stein, J M Reder, T Bein *Stud. Surf. Sci. Catal*. **135** 1702 (2001)
32. Z Lin, J Rocha, P Brandão, A Ferreira, A P Exculcas, J D Pedrosa de Jesus, A Philippou, M W Anderson *J. Phys. Chem. B* **101** 7114 (1997)
33. J Rocha, L D Carlos, J P Rainho, Z Lin, P Ferreira, R M Almeida *J. Mater. Chem*. **10** 1371 (2000)
34. A I Bortun, L N Bortun, S A Khainakov, A Clearfield, C Trobajo, J R Garcia *Solvent Extr. Ion Exch*. **17** 649 (1999)
35. C M Braunbarth, L C Boudreau, M Tsapatsis *J. Membr. Sci*. **174** 31 (2000)
36. R J Saxton *Top. Catal*. **9** 43 (1999)
37. M W Anderson, A Philippou, Z Lin, A Ferreira, J Rocha *Angew. Chem., Int. Ed. Engl*. **34** 1003 (1995)
38. J Rocha, M W Anderson *Eur. J. Inorg. Chem*. 801 (2000)
39. P Brandão, P Ferreira, J Rocha, A Philippou, M W Anderson, in *The IVth Meeting of the Inorganic Chemistry Division of the Portuguese Chemical Society, Aveiro, 1999* p. 15
40. D Medoukali, P H Mutin, A Vioux *J. Mater. Chem*. **9** 2553 (1999)
41. J Rocha, P Brandão, J D Pedrosa de Jesus, A Philippou, M W Anderson *Chem. Commun*. 471 (1999)
42. Z Lin, J Rocha, P Ferreira, A Thursfield, J R Agger, M W Anderson *J. Phys. Chem. B* **103** 957 (1999)
43. P Brandão, P Ferreira, J Rocha, A Philippou, M W Anderson, in *The IVth Meeting of the Catalysis Division of the Portuguese Chemical Society, Aveiro, 1999* p. 14
44. P Brandão, P Ferreira, J Rocha, A Philippou, M W Anderson, in *The IVth Meeting of the Catalysis Division of the Portuguese Chemical Society, Aveiro, 1999* p. 207
45. A Eldewik, V Luca, N K Singh, R F Howe, in *Proceedings of the 12th International Zeolite Conference, Warrendale, 1999* Vol. 3, p. 1507
46. J P Rainho, L D Carlos, J Rocha *J. Lumin*. **87–89** 1083 (2000)
47. J Rocha *J. Phys. Chem. B* **103** 9801 (1999)
48. J Rocha, P Ferreira, L D Carlos, A Ferreira *Angew. Chem., Int. Ed*. **39** 3276 (2000)
49. J Rocha, P Ferreira, Z Lin, P Brandão *J. Phys. Chem. B* **102** 4739 (1998)
50. G Chen, H Takenoshita, M Kasuya, H Satoh, N Kamegashira *J. Alloys Compd*. **228** 127 (1995)
51. B Balzer, H Langbein *J. Alloys Compd*. **244** 1 (1996)
52. T Möller, A Clearfield, R Harjula *Microporous Mesoporous Mater*. **54** 187 (2002)
53. Y Mao, G Li, W Xu, S Feng *J. Mater. Chem*. **10** 479 (2000)
54. Y Teraoka, K-I Torigoshi, H Yamaguchi, T Ikeda, S Kagawa *J. Mol. Catal. A: Chem*. **155** 73 (2000)
55. H Zhao, S Feng, W Xu, Y Shi, Y Mao, X Zhu *J. Mater. Chem*. **10** 965 (2000)
56. R K Rastsvetaeva, N V Chukanov *Kristallografiya* **47** 1009 (2002) [b]
57. X Wang, A J Jacobson *Chem. Commun*. 973 (1999)
58. M E Grillo, J Carrazza *J. Phys. Chem*. **100** 12261 (1996)
59. M W Anderson, J R Agger, D-P Luigi, A K Baggaley, J Rocha *Phys. Chem. Chem. Phys*. **1** 2287 (1999)
60. A M Prakash, L Kevan, in *Science and Technology in Catalysis* (Eds H Hattori, K Otsuka) (Tokyo: Kodansha, 1999) p. 233
61. G Sankar, R G Bell, J M Thomas, M W Anderson, P A Wright, J Rocha *J. Phys. Chem*. **100** 2 449 (1996)
62. M S Dadachov, J Rocha, A Ferreira, Z Lin, M W Anderson *Chem. Commun*. 2371 (1997)
63. P J Wilde, C R A Catlow *Solid State Ionics* **112** 173 (1998)
64. P J Wilde, C R A Catlow *Solid State Ionics* **112** 185 (1998)
65. K W Eberman, B J Wuensch, J D Jorgensen *Solid State Ionics* **148** 521 (2002)
66. B J Kennedy *Physica B: Condens. Matter* **241–243** 303 (1998)
67. A P Khomyakov, G Ferraris, E Belluzo, S N Britvin, G N Nechelyustov, S V Soboleva *Zap. Vseross. Mineral. O-va* **127** (4) 94 (1998)
68. J Konnerup-Madsen, P M Holm, J Rose-Hansen *Rapp. Grunland Geol. Unders*. **103** 113 (1981)
69. I V Pekov, N V Chukanov, N N Kononkova, D Yu Pushcharovskii *Tr. Mineral. Muzeya Ross. Akad. Nauk* **38** 20 (2003)
70. F V Chukhrov (Ed.) *Mineraly. Spravochnik* (Minerals. Handbook) (Moscow: Nauka, 1981) Vol. III, No. 2
71. A P Khomyakov, G N Nechelyustov, R K Rastsvetaeva *Zap. Vseross. Mineral. O-va* **122** (5) 76 (1993)
72. A P Khomyakov *Mineralogiya Ul'traagpaitovykh Shcheloch-nykh Porod* (Mineralogy of Ultraagpaite Alkaline Rocks) (Moscow: Nauka, 1990)
73. G B Bokiy (Ed.) *Mineraly. Spravochnik* (Minerals. Handbook) (Moscow: Nauka, 1992) Vol. IV, No. 2
74. P A Sandomirskii, N V Belov *Kristallografiya* **24** 1198 (1979) [b]
75. P B Moore, J Shen *Tschermaks Mineral. Petrogr. Mitt*. **31** 47 (1983)
76. I V Pekov, I A Ekimenkova, N N Kononkova *Zap. Vseross. Mineral. O-va* **126** (6) 35 (1997)
77. T Balic-Zunic, O V Petersen, H-J Bernhardt, H I Micheelsen *Neues Jb. Miner. Monat*. 497 (2002)
78. R K Rastsvetaeva, A P Khomyakov *Kristallografiya* **37** 1561 (1992) [b]
79. R K Rastsvetaeva, A P Khomyakov *Dokl. Akad. Nauk* **351** 74 (1996) [c]
80. Yu A Pyatenko, T A Kurova, N M Chernitsova, Z V Pudovkina, V A Blinov, N V Maksimova *Niobii, Tantal i Tsirkonii v Mineralakh* (Niobium, Tantalum and Zirconium in Minerals) (Moscow: Institute of Mineralogy, Geochemistry and Crystal Chemistry of Rare Elements, 1999)
81. D Yu Pushcharovskii, I V Pekov, M Pazero, E R Gobechiya, S Merlino, N V Zubkova *Kristallografiya* **47** 814 (2002) [b]
82. E V Sokolova, A V Arakcheeva, A V Voloshin *Dokl. Akad. Nauk SSSR* **320** 1384 (1991) [c]
83. R K Rastsvetaeva, N V Chukanov, I V Pekov *Dokl. Akad. Nauk* **357** 364 (1997) [c]
84. N V Chukanov, I V Pekov, A P Khomyakov *Eur. J. Mineral*. **14** 165 (2002)

85. I V Pekov, N V Chukanov, A P Khomyakov, R K Rastsvetaeva, Ya V Kucherinenko, V V Nedel'ko *Zap. Vseross. Mineral. O-va* **128** (3) 72 (1999)
86. R K Rastsvetaeva, R A Tamazyan, D Yu Pushcharovsky, T N Nadezhina *Eur. J. Mineral.* **6** 503 (1994)
87. R K Rastsvetaeva, N I Organova, I V Rozhdestvenskaya, Z V Shlyukova, N V Chukanov *Dokl. Akad. Nauk* **371** 336 (2000) [c]
88. K A Rozenberg, R K Rastsvetaeva, N V Chukanov, I V Pekov *Dokl. Akad. Nauk* **386** 345 (2002) [c]
89. R K Rastsvetaeva, A V Arakcheeva, A P Khomyakov *Dokl. Akad. Nauk* **351** 207 (1996) [c]
90. R K Rastsvetaeva, N V Chukanov, I V Pekov *Dokl. Akad. Nauk* **357** 64 (1997) [c]
91. A P Khomyakov, G N Nechelyustov, R K Rastsvetaeva, G I Dorokhova *Zap. Vseross. Mineral. O-va* **128** (5) 54 (1999)
92. N V Chukanov, I V Pekov, R K Rastsvetaeva, A E Zadov, V V Nedel'ko *Zap. Vseross. Mineral. O-va* **130** (3) 36 (2001)
93. N A Yamnova, I V Pekov, Yu K Kabalov, Yu Shnaider, N V Chukanov *Dokl. Akad. Nauk* **375** 487 (2000) [c]
94. I V Pekov, N V Chukanov, O V Petersen, A E Zadov, N A Yamnova, Yu K Kabalov, J Schneider *Neues Jb. Miner. Monat.* 433 (2002)
95. N V Chukanov, I V Pekov, A E Zadov, S V Krivovichev, P K Berns, Yu Shnaider *Zap. Vseross. Mineral. O-va* **130** (2) 46 (2001)
96. N V Chukanov, I V Pekov, E I Semenov, A E Zadov, S V Krivovichev, P K Berns *Zap. Vseross. Mineral. O-va* **130** (6) 63 (2001)
97. I V Pekov, N V Chukanov, A E Zadov, S V Krivovichev, Yu V Azarova, P K Berns, Yu Shnaider *Zap. Vseross. Mineral. O-va* **131** (1) 28 (2002)
98. R K Rastsvetaeva, N V Chukanov, I V Pekov *Kristallografiya* **45** 830 (2000) [b]
99. N V Chukanov, I V Pekov, N I Golovina, A E Zadov, V V Nedel'ko *Zap. Vseross. Mineral. O-va* **128** (4) 42 (1999)
100. N V Chukanov, I V Pekov, A E Zadov, Yu V Azarova, E I Semenov *Zap. Vseross. Mineral. O-va* **131** (2) 45 (2002)
101. R K Rastsvetaeva, I V Pekov, Yu V Nekrasov *Kristallografiya* **46** 415 (2001) [b]
102. K A Rozenberg, R K Rastsvetaeva, I V Pekov, N V Chukanov *Dokl. Akad. Nauk* **383** 657 (2002) [c]
103. K A Rozenberg, R K Rastsvetaeva, N V Chukanov, V V Subbotin *Kristallografiya* **47** 453 (2002) [b]
104. I V Pekov, N V Chukanov, R K Rastsvetaeva, A E Zadov, N N Kononkova *Zap. Vseross. Mineral. O-va* **131** (2) 51 (2002)
105. I V Pekov, N V Chukanov, A E Zadov, K A Rozenberg, R K Rastsvetaeva *Zap. Vseross. Mineral. O-va* **132** (1) 52 (2003)
106. A P Khomyakov, G N Nechelyustov, G Ferraris, A Gula, G Ivaldi *Zap. Vseross. Mineral. O-va* **130** (4) 36 (2001)
107. N I Organova, Z V Shlyukova, N I Zabavnikova, A N Platonov, E S Rudnitskaya *Izv. Akad. Nauk, Ser. Geol.* 98 (1976)
108. G Ferraris, G Ivaldi, A P Khomyakov *Eur. J. Mineral.* **7** 537 (1995)
109. E V Sokolova, R K Rastsvetaeva, V I Andrianov, Yu K Egorov-Tismenko, Yu P Men'shikov *Dokl. Akad. Nauk SSSR* **307** 114 (1989) [c]
110. N A Yamnova, Yu K Egorov-Tismenko, I V Pekov *Kristallografiya* **46** 1019 (2001) [b]
111. N A Yamnova, Yu K Egorov-Tismenko, I V Pekov, I A Ekimenkova *Kristallografiya* **46** 230 (2001) [b]
112. R A Tamazyan, Yu A Malinovskii *Kristallografiya* **35** 398 (1990) [b]
113. N A Yamnova, Yu K Egorov-Tismenko, I V Pekov, L V Shchegol'kova *Kristallografiya* **48** 602 (2003) [b]
114. D S Coombs, A Alberti, T Armbruster, G Artioli, C Colella, E Galli, J D Grice, F Liebau, J A Mandarino, H Minato, E H Nickel, E Passaglia, D R Peacor, S Quartieri, R Rinaldi, M Ross, R A Sheppard, E Tillmanns, G Vezzalini *Can. Mineral.* **35** 1571 (1997)
115. T S Ercit, J Van Velthuizen *Can. Mineral.* **32** 855 (1994)
116. S Merlino, M Pasero, G Artioli, A P Khomyakov *Am. Mineral.* **79** 1185 (1994)
117. Z V Pudovkina, N M Chernitsova *Dokl. Akad. Nauk SSSR* **317** 645 (1991) [c]
118. V V Kalinin, D Yu Pushcharovskii, N A Yamnova, Yu P Dikov, S E Borisovskii *Zap. Vseross. Mineral. O-va* **123** (4) 94 (1994)
119. S Merlino, M Pasero, O Ferro *Z. Kristallogr.* **215** 352 (2000)
120. R K Rastsvetaeva, V I Simonov, N V Belov *Dokl. Akad. Nauk SSSR* **177** 832 (1967) [c]
121. S Merlino, M Pasero, A P Khomyakov *Z. Kristallogr.* **193** 137 (1990)
122. R K Rastsvetaeva, V I Andrianov *Dokl. Akad. Nauk SSSR* **293** 1122 (1987) [c]
123. A R Kampf, A A Khan, W H Bauer *Acta Crystallogr., Sect. B* **29** 2019 (1973)
124. Yu A Malinovskii, E A Pobedimskaya, N V Belov *Dokl. Akad. Nauk SSSR* **221** 343 (1975) [c]
125. A P Khomyakov, G N Nechelyustov, G Ferraris, G Ivaldi *Zap. Vseross. Mineral. O-va* **129** (4) 48 (2000)
126. N V Chukanov, I V Pekov, A E Zadov, A V Voloshin, V V Subbotin, R K Rastsvetaeva, N V Sorokhtina, S V Krivovichev *Mineraly Gruppy Labuntsovita (Kkristallokhimiya, Sistematika, Svoistva i Genezis)* [Minerals of the Labunzovite Group (Crystal Chemistry, Systematics, Properties and Genesis)] (Moscow: Nauka, 2003)
127. V V Subbotin, A V Voloshin, Ya A Pakhomovskii, A Yu Bakhchisaraitsev, D Yu Pushcharovskii, R K Rastsvetaeva, T N Nadezhina *Dokl. Akad. Nauk* **358** 517 (1998) [c]
128. Z V Shlyukova, N V Chukanov, I V Pekov, R K Rastsvetaeva, N I Organova, A E Zadov *Zap. Vseross. Mineral. O-va* **130** (3) 43 (2001)
129. N V Chukanov, I V Pekov, A E Zadov, K A Rozenberg, R K Rastsvetaeva, S V Krivovichev, L A Levitskaya *Zap. Vseross. Mineral. O-va* **132** (1) 38 (2003)
130. G Raade, G Ferraris, A Gula, G Ivaldi *Can. Mineral.* **40** 1629 (2002)
131. S V Chizhevskaya, A M Chekmarev, M Cox, in *Proceedings of the International Solvent Extraction Conference, Cape Town, 2002* Vol. 2, p. 1076
132. A M Chekmarev, S V Chizhevskaya, E P Buchikhin *Khim. Tekhnol.* (10) 2 (2000)
133. E E Kostyleva-Labuntsova, B E Borutskii, M N Sokolova, Z V Shlyukova, M D Dorfman, O B Dudkin, L V Kozyreva *Mineralogiya Khibinskogo Massiva* (Mineralogy of Khibiny Massif) (Moscow: Nauka, 1978)
134. R K Rastsvetaeva, I A Ekimenkova, I V Pekov *Dokl. Akad. Nauk* **368** 636 (1999) [c]
135. R K Rastsvetaeva, A P Khomyakov *Dokl. Akad. Nauk* **362** 784 (1998) [c]
136. R K Rastsvetaeva, A P Khomyakov, V I Andrianov, A I Gusev *Dokl. Akad. Nauk SSSR* **312** 1379 (1990) [c]
137. R K Rastsvetaeva, A P Khomyakov, Yu V Nekrasov *Kristallografiya* **44** 824 (1999) [b]
138. R K Rastsvetaeva, A P Khomyakov, G Chapuis *Z. Kristallogr.* **214** 271 (1999)
139. I A Ekimenkova, R K Rastsvetaeva, A P Khomyakov *Dokl. Akad. Nauk* **370** 477 (2000) [c]
140. I A Ekimenkova, R K Rastsvetaeva, A P Khomyakov *Kristallografiya* **45** 1010 (2000) [b]
141. I A Ekimenkova, R K Rastsvetaeva, N V Chukanov *Dokl. Akad. Nauk* **371** 625 (2000) [c]
142. I A Ekimenkova, R K Rastsvetaeva, N V Chukanov *Dokl. Akad. Nauk* **374** 352 (2000) [c]
143. O Johnsen, J D Grice, R A Gault *Can. Mineral.*, **37** 1295 (1999)
144. O Johnsen, J D Grice *Can. Mineral.* **37** 865 (1999)
145. R K Rastsvetaeva, A P Khomyakov *Kristallografiya* **45** 251 (2000) [b]
146. R K Rastsvetaeva, A P Khomyakov *Kristallografiya* **45** 649 (2000) [b]
147. R K Rastsvetaeva, A P Khomyakov *Kristallografiya* **46** 827 (2001) [b]
148. O Johnsen, J D Grice, R A Gault *Eur. J. Mineral.* **10** 207 (1998)
149. O Johnsen, R A Gault, J D Grice, T S Ercit *Can. Mineral.* **37** 893 (1999)

150. E V Pol'shin, A N Platonov, B E Borutsky, M N Taran, R K Rastsvetaeva *Phys. Chem. Miner.* **18** 117 (1991)
151. R K Rastsvetaeva, Z P Razmanova, B E Borutskii, M D Dorfman *Zap. Vseross. Mineral. O-va* **119** (3) 65 (1990)
152. R K Rastsvetaeva, M N Sokolova, B E Borutskii *Kristallografiya* **35** 1381 (1990) [b]
153. R K Rastsvetaeva, B E Borutskii *Mineral. Zh.* **12** (4) 81 (1990)
154. R K Rastsvetaeva, B E Borutskii, A I Gusev *Kristallografiya* **33** 353 (1988) [b]
155. R K Rastsvetaeva, N V Chukanov, Sh Mekkel' *Kristallografiya* **48** 250 (2003) [b]
156. I V Pekov, I A Ekimenkova, N V Chukanov, R K Rastsvetaeva, N N Kononkova, N A Pekova, A E Zadov *Zap. Vseross. Mineral. O-va* **130** (3) 55 (2001)
157. R K Rastsvetaeva, A P Khomyakov, S V Chizhevskaya, T V Anoprienko, in *Trudy Mezhdunarodnogo Simpoziuma 'Fazovye Prevrashcheniya v Tverdykh Rastvorakh i Splavakh', Sochi, 2002* (Proceedings of International Symposium 'Phase Transformations in Solid Solutions and Alloys', Sochi, 2002) Pt 2, p. 59
158. R K Rastsvetaeva, A P Khomyakov *Kristallografiya* **47** 267 (2002) [b]
159. R K Rastsvetaeva, B E Borutskii *Mineral. Zh.* **10** (1) 48 (1988)
160. Yu A Pyatenko, A A Voronkov, Z V Pudovkina *Mineralogicheskaya Kristallokhimiya Titana* (Mineralogical Crystal Chemistry of Titanium) (Moscow: Nauka, 1976)
161. Br. P. 9 958 243; *Chem. Abstr.* **131** 355 540 (1999)
162. A Dyer, M Pillinger, S Amin *J. Mater. Chem.* **9** 2481 (1999)
163. Y Koudsi, A Dyer *J. Radioanal. Nucl. Chem.* **247** 209 (2001)
164. V Valtchev, J-L Paillaud, S Mintova, H Kessler *Microporous Mesoporous Mater.* **32** 287 (1999)
165. I V Pekov, A G Turchkova, N N Kononkova, N V Chukanov, in *Materialy Vserossiiskogo Seminara 'Shchelochnoi Magmatizm Zemli', Moskva, 2002* (Proceedings of All-Russian Seminar 'Alkaline Magmatism of the Earth', Moscow, 2002) p. 76
166. V Valtchev, J-L Paillaud, S Mintova, H Kessler, in *The International Conference on Inorganic Materials, Versailles, 1998* p. 32
167. K Toda, T Teranishi, M Takahashi, Z-G Ye, M Sato *Solid State Ionics* **113–115** 501 (1998)
168. A Zecchina, C O Areán, G T Palomino, F Geobaldo, C Lamberti, G Spoto, S Bordiga *Phys. Chem. Chem. Phys.* **1** 1649 (1999)
169. C O Areán, G T Palomino, A Zecchina, S Bordiga, F X L I Xamena, C Pazè *Catal. Lett.* **66** 231 (2000)
170. A Gervasini, C Picciau, A Auroux *Microporous Mesoporous Mater.* **35–36** 457 (2000)
171. S M Kuznicki, V A Bell, S Nair, H W Hillhouse, R M Jacubinas, C M Braunbarth, B Y Toby, M Tsapatsis *Nature (London)* **412** 720 (2001)
172. A Valente, Z Lin, P Brandão, I Portugal, M W Anderson, J Rocha *J. Catal.* **200** 99 (2001)
173. A Philippou, M Naderi, J Rocha, M W Anderson *Catal. Lett.* **53** 221 (1998)
174. S B Waghmode, V V Thakur, A Sudalai, S Sivasanker *Tetrahedron Lett.* **42** 3145 (2001)
175. A Zecchina, F X L I Xamena, C Pazzh, G T Palomino, S Bordiga, C O Areán *Phys. Chem. Chem. Phys.* **3** 1228 (2001)
176. R Bal, K Chaudhari, D Srinivas, S Sivasanker, P Ratnasamy *J. Mol. Catal. A: Chem.* **162** 199 (2000)
177. R M Krishna, A M Prakash, V Kurshev, L Kevan *Phys. Chem. Chem. Phys.* **1** 4119 (1999)
178. A Philippou, M Naderi, N Pervaiz, J Rocha, M W Anderson *J. Catal.* **178** 174 (1998)
179. A Philippou, J Rocha, M W Anderson *Catal. Lett.* **57** 151 (1999)
180. P Moreau, V Hulea, S Gomez, D Brunel, F Di Renzo *Appl. Catal., A* **155** 253 (1997)
181. R Kumar, A Bhaumik *Microporous Mesoporous Mater.* **21** 497 (1998)
182. J S Reddy, A Sayari *Appl. Catal., A* **128** 231 (1995)
183. J Le Bars, J Dakka, R A Sheldon *Appl. Catal., A* **136** 69 (1996)
184. M Fujiwara, Y Souma, Q Xu, T Kobayashi *J. Mol. Catal. A: Chem.* **142** 77 (1999)
185. A Philippou, P Brandão, A Ghanbari-Siahkali, J Dwyer, J Rocha, M W Anderson *Appl. Catal., A* **207** 229 (2001)
186. P Brandão, A Philippou, J Rocha, M W Anderson *Catal. Lett.* **73** 59 (2001)
187. W Y Ching, Y-N Xu, Z-Q Gu *Phys. Rev. B* **54** R15585 (1996)
188. B Mihailova, V Valtchev, S Mintova, L Konstantinov *Zeolites* **16** 22 (1996)
189. B Mihailova, V Valtchev, S Mintova, L Konstantinov *J. Mater. Sci. Lett.* **16** 1303 (1997)
190. S Nair, M Tsapatsis, B H Toby, S M Kuznicki *J. Am. Chem. Soc.* **123** 12 781 (2001)
191. V Valtchev, S Mintova, B Mihailova, L Konstantinov *Mater. Res. Bull.* **31** 163 (1996)
192. L Al-Attar, A Dyer, R Blackburn *J. Radioanal. Nucl. Chem.* **246** 451 (2000)
193. D Gleeson, G Sankar, C R A Catlow, J M Thomas, G Spanó, S Bordiga, A Zecchina, C Lamberti *Phys. Chem. Chem. Phys.* **2** 4812 (2000)
194. J-M Zen, A S Kumar, J-C Chen *J. Mol. Catal. A: Chem.* **165** 177 (2001)
195. K-H Chung, D-C Park *J. Mol. Catal. A: Chem.* **129** 53 (1998)

[a] — *Inorg. Mater. (Engl. Transl.)*
[b] — *Crystallogr. Rep. (Engl. Transl.)*
[c] — *Dokl. Chem. (Engl. Transl.)*

Russian Chemical Reviews **73** (3) 225 – 249 (2004) © 2004 Russian Academy of Sciences and Turpion Ltd

DOI 10.1070/RC2004v073n03ABEH000843

State-of-the-art in the study of three-dimensional radical copolymerisation

V P Roshchupkin, S V Kurmaz

Contents

I.	Introduction	225
II.	A microheterogeneous mechanism of three-dimensional radical copolymerisation and structures of copolymers	225
III.	Methods for *in situ* investigation of three-dimensional radical copolymerisation	232
IV.	Control of three-dimensional radical copolymerisation and design of network macromolecular structures	236
V.	Conclusion	246

Abstract. The state-of-the art in the study of three-dimensional radical copolymerisation of multifunctional vinyl compounds with various monomers has been analysed. The mechanisms of relationships between copolymerisation kinetics with structure-physical transformations of the reaction medium and structures of cross-linked polymers are discussed. The key role of spectroscopic monitoring methods in the *in situ* studies of structure – kinetics relationships in three-dimensional radical copolymerisation is demonstrated. New approaches to control over these processes based on the use of chain transfer catalysis and living radical polymerisation are considered. The bibliography includes 178 references.

I. Introduction

The use of three-dimensional radical copolymerisation (TRCP) of multifunctional compounds (M_1) containing several double bonds with monomers (M_2) significantly extends the capabilities of directed design of network polymeric structures by varying the structures of starting compounds and the compositions of oligomer – monomer mixtures. High-tech processes based on TRCP are currently employed in the production of polymeric sorbents, membranes, laser videodisks, contact lenses,[1] gradient optical materials,[2] elements of computer optics,[3] microelectronics [4] and a variety of composite materials for special technique.[5] Commercial production or, in essence, synthesis of such articles demands high level of integration of such diverse processes as chemical reactions involved in TRCP, formation of a copolymer structure, microsyneresis of reaction components, vitrification of the reaction medium and diffusion-controlled exchange of monomers in gel polymer systems. Therefore, studies of TRCP as an integral complex of interrelated chemical and structure-physical transformations is a topical problem.

The majority of papers published thus far are devoted to determination of copolymerisation constants for the comonomers M_1 and M_2, analysis of mechanisms of gel formation, elucidation of structures and properties of copolymers formed, theoretical description and computer simulation of various TRCP processes. Some of them are considered in reviews,[1,4,6] but structure – kinetics relationships, which play a key role in the control over TRCP processes have not been taken into consideration. The increasing number of publications on this problem suggests the advent of a qualitatively new stage of research which is characterised by *in situ* analysis of structure – kinetics relationships in TRCP using spectroscopic monitoring in a real-time mode and development of novel efficient methods for the control over these processes using chain transfer catalysts and reagents for living radical polymerisation.

This review is devoted to the analysis of the most recent trends in the study of mechanisms of TRCP and encompasses a broad range of reaction systems $M_1 + M_2$ with oligomers and monomers differing significantly in the structures and properties.These systems allowed an analysis of effects of chemical (*e.g.*, relative reactivities of the C = C bonds in M_1 and M_2) and physical factors (*e.g.*, the lengths of oligomeric fragments and alkyl substituents, the presence of sites of strong intermolecular interactions in M_1 and M_2, *etc.*) on the kinetics of TRCP and structures and properties of the network copolymers formed.

A comprehensive analysis of TRCP reactions in $M_1 + M_2$ systems demands knowledge of homopolymerisation of the corresponding multifunctional compounds M_1. The expediency of studies into both copolymerisation and homopolymerisation of compounds M_1 is dictated by the similarity of their topologies and formation of pendant double bonds which differ from the double bonds in the starting oligomers M_1 in effective reactivities.† A detailed description of the state-of-the-art in the study of three-dimensional radical homopolymerisation is given in a review. [7]

II. A microheterogeneous mechanism of three-dimensional radical copolymerisation and structures of copolymers

1. Topological features of three-dimensional radical copolymerisation

It is known [8] that radical copolymerisation of monomers M_1 and M_2 yields linear macromolecules. With the exception of special cases of distortions in the uniform distribution of reactants,[9–11]

V P Roshchupkin, S V Kurmaz Institute of Problems of Chemical Physics, Russian Academy of Sciences, 142432 Chernogolovka, Moscow Region, Russian Federation. Fax (7-096) 515 54 20. Tel. (7-096) 517 10 89. E-mail: vrosh@icp.ac.ru (V P Roshchupkin), skurmaz@icp.ac.ru (S V Kurmaz)

Received 16 April 2003
Uspekhi Khimii **73** (3) 247 – 274 (2004); translated by R L Birnova

† Effective (as opposite to true) reactivities of monomer – polymer systems depend on external factors (*e.g.*, diffusional characteristics of the reaction medium, conformational mobility of the polymer network, cage effect, *etc.*) rather than on the electronic structures of the reacting bonds.

their compositions and alternation of the monomeric units in the polymer chain are determined by the composition of the initial monomer mixture and values of reactivity ratios of the monomers (r_1 and r_2, respectively). A totally different situation is observed on the transition to TRCP, where one of the components contains two (or more) reactive C=C bonds. In this case, the copolymerisation of a cross-linking reagent M_1 and a monomer M_2 is branched into different topological channels:[6]

1. Growth of linear chains carrying pendant double bonds and terminal radicals:

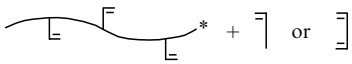

(1)

2. Primary intramolecular cyclisation:

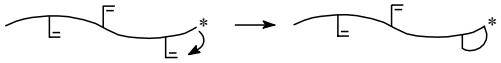

(2a)

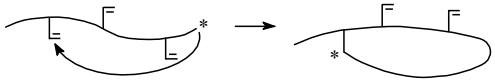

(2b)

3. Intermolecular chain cross-linking:

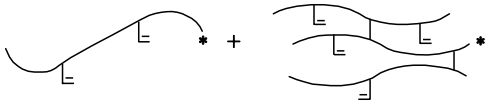

(3)

4. Secondary cyclisation in branched macromolecules, microgel particles and macrogel:

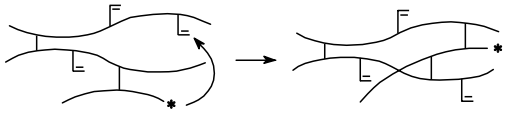

(4)

Primary intramolecular cyclisation (2a,b) is fairly inefficient as regards the formation of a network. This reaction results in a shift of the experimental gel point from a theoretical value calculated on the basis of the Flory–Stockmayer theory towards higher degrees of conversion.[6] Under these conditions, the formation of a microheterogeneous copolymer structure occurs at the topological level. Therefore, numerous papers deal with the analysis of factors determining the probability of this reaction.

The contribution of reactions (2a,b) is especially pronounced in early steps of TRCP where the probability of the bimolecular reaction (3) is very low because of a small concentration of the polymeric chains and growing macroradicals. In this step, effective reactivities of pendant C=C bonds in the vicinity of the terminal radical may exceed those of the C=C bonds of the oligomer M_1. Effective reactivities of the pendant double bonds also depend on the length and rigidity of the oligomeric fragment (spacer) which connects them with the main chain as well as on the flexibility of the main chain and the number of the rings formed.[1] The role of these factors is determined by the number and structure of the comonomer M_2 units which significantly influence the flexibility and conformation of chains in the growing macroradicals.[12, 13]

The feasibility of cyclisation during copolymerisation of ethylene glycol dimethacrylate (**1**) with styrene (**2**) has been established.[14] However, a completely soluble polymer devoid of double bonds and with rings in the main chain could be obtained only at low concentrations of the cross-linking reagent. Copolymerisation of dimethacrylate **1** and triethyleneglycol dimethacrylate (**3**) in highly dilute solutions resulted in cyclolinear polymers with M_w of $\sim$ 20 000.[15] An analysis of a hydrolysate of a polymer obtained from the dimethacrylate **3** revealed that the overwhelming majority of pendant double bonds are involved in intrachain cyclisation and the probability of formation of a ladder-type chain polymer is very low.

The dependence of the probability (DP) of intramolecular cyclisation on the length of the polymer chain of dimethacrylate **3** has been established.[16] The degree of polymerisation was controlled using a catalytic chain transfer agent and the number of double bonds was established by IR spectroscopy. It was found that only the products with DP < 9 had pendant methacrylate groups in each monomeric unit. With an increase in the DP to 15, the residual unsaturation of the products decreased to the level characteristic of the bulk polymer. This suggests that cyclisation in growing polymeric chains during polymerisation of dimethacrylate **3** occurs by route (2b).

The majority of papers devoted to cyclisation in TRCP consider only the reaction of the terminal radical and the pendant double bond. However, mathematical simulation of radical polymerisation reactions of oligomeric dimethacrylates on a cubic lattice[17] revealed that recombination of terminal and pendant radicals also contributes to cyclisation.

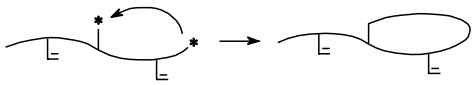

(5)

It was noted that at high initiator concentrations the intramolecular quadratic termination of radicals (5) is the main reason for cyclisation.

The probability of bimolecular intermolecular cross-linking (3) in the initial steps of (co)polymerisation is negligibly small, but increases rapidly with an increase in the concentration of primary polymeric chains. The interactions of growing macroradicals with the pendant double bonds of the polymeric chains result in the formation of branched macromolecules. The Monte Carlo simulation of topological structures of branched polymers in the pre-gelation step revealed[18] that the branching parameters strongly depend on the initiation rate of radical polymerisation of multifunctional monomers. Low initiation rates favour the formation of long-chain slightly branched polymers, whereas high initiation rates favour the formation of short-chain polymers with higher degrees of branching. The results of the simulation correlate qualitatively with the branching parameters of macromolecules isolated in the pre-gelation step of diallylic oligomers.[19, 20]

Favourable conditions for the reaction (4) between the radicals and pendant C=C bonds of different branching chains appear in branched macromolecules containing a large number of pendant double bonds. This process commonly referred to as secondary cyclisation[21] or intramolecular cross-linking[6] results in the formation of microgel particles, which consist of a dense nucleus and a loose shell.

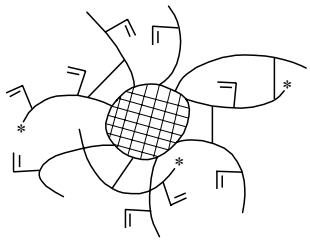

The consumption of double bonds in the cross-linking and primary and secondary cyclisation during polymerisation reactions of multifunctional compounds can be calculated on the basis of a kinetic model of network formation.[21] These calculations showed (Fig. 1) that primary cyclisation prevails in the initial steps due to enhanced reactivities of pendant C=C bonds in the vicinity of growing radicals, which stimulates the formation of microgel particles. The contribution of intermolecular cross-linking and secondary cyclisation increases with an increase in the degree of conversion and polymer concentration, as a result of

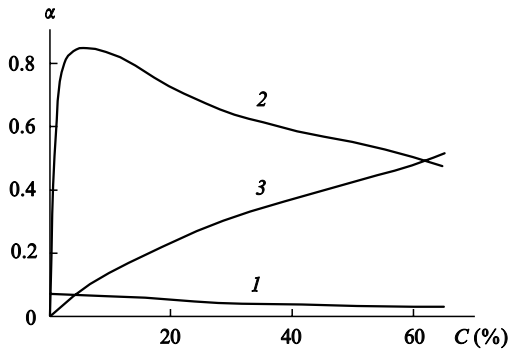

Figure 1. Dependence of the conversion of pendant double bonds (α) in cross-linking (*1*) and primary (*2*) and secondary cyclisation (*3*) on the overall conversion of the double bonds (C).[21]

which the macrogel is formed. Correspondingly, the homogeneity of the network increases with an increase in the contribution of secondary cyclisation and a simultaneous decrease in primary cyclisation.

2. Structural and kinetic heterogeneity of the reaction medium in three-dimensional radical copolymerisation

The true mechanism of three-dimensional (co)polymerisation is much more complicated than a model mechanism,[21] which takes into account only the topological peculiarities of network formation.[6,21] A crucial role in the formation of structures and properties of densely cross-linked polymers is assigned to microheterogeneous three-dimensional radical copolymerisation and structure-physical transformations, such as microsyneresis and vitrification of the reaction medium.[22–24]

From the moment of formation of microgel particles, the reaction medium becomes structurally and kinetically microheterogeneous due to lower mobility of the particles and a concomitant sharp decrease in the radical termination constant. As a result, the reaction is switched over to an autoacceleration mode (the gel effect).

Microgel particles can be regarded as microreactors consisting of two reaction zones, *viz*., an inner zone and a peripheral (near-surface) zone, which differ essentially in the effective reactivities and polymerisation rates of double bonds of a multifunctional oligomer.[23] The peripheral zone is characterised by higher rates of addition of double bonds of an oligomer to radicals localised on the surface of gel particles and thus unable to undergo recombination with analogous radicals of other particles. Slow polymerisation involving pendant double bonds occurs inside the microgel, its rate is limited by low mobility of the double bonds and steric hindrances, which prevents their addition to the radicals immobilised inside the microgel particles. Evidence for the existence of such limitations can be derived from the mode of attachment ('tail-to-tail'[25] or 'head-to-head'[26]) of the monomeric units, which is not typical of linear radical polymerisation. Steric constraints are important factors which control the stereoregularity of addition of the methacrylate groups and the topology of the netwok in the course of polymerisation of dimethacrylates.[27,28] They also determine the conformational state of network junctions, conformational dynamics and relaxation properties of the network itself.[27,29]

Pendant double bonds formed in a fast reaction of the radicals localised on the surface of microgel particles with one of the double bonds of the multifunctional oligomer M_1 are involved in a slow polymerisation inside the microgel particles. Consumption of the free oligomer and an increase in the size of a microgel particle result in a decrease in the effective size of the 'fast' reactor and an increase in the size of the 'slow' reactor to the size of a macrogel. As a result, the kinetics of three-dimensional polymerisation and copolymerisation of dimethacrylates switches over from an autoacceleration mode to an autoretardation mode.[23,30]

The structure–kinetic peculiarities of microheterogeneous three-dimensional radical polymerisation confer on it features of informal similarity with phase transition reactions, particularly crystallisation of polymers.[31] Based on this analogy, it was proposed to analyse the kinetic polymerisation curves conversion–time [$C(t)$] in the Avrami coordinates:[23]

$$C = 1 - \exp\left(-\sum_i k_i t^{n_i}\right), \qquad (6)$$

where k_i is the specific rate of polymerisation in the ith structural zone (*e.g*., in solution, on the surface or inside the microgel particle, *etc*.), which is proportional to the ratio of the rate constants for chain growth and chain termination (k_b) in this zone and n_i is the parameter which characterises the effect of the structure of the reaction medium on the rate of polymerisation in the ith zone.

Within the framework of this model, the value $n = 1$ corresponds to polymerisation under homogeneous conditions.[32,33] The value $n = 3$ entails total analogy to the polymerisation and phase transition where all the growing radicals are localised on the surface of polymer particles dispersed in the oligomer solution. In this case, $k_b = 0$ and the reaction proceeds in an autoacceleration regime. With an increase in the particle size, the particles merge and the contribution of the near-surface fast chain growth reaction diminishes and autoretardation of the polymerisation occurs. This structure–kinetic transition from near-surface to bulk polymerisation is manifested in a reduction of the parameter n due to diffusion-controlled constraints of the chain growth.

Studies into three-dimensional polymerisation of dimethacrylates have shown that, prior to autoretardation, the kinetic dependences plotted in the Avrami coordinates have one or two linear segments; their slopes yield the values of the parameter n in the range $1 \leqslant n \leqslant 3$ (see Refs 23 and 34). The autoretardation step is characterised by a gradual decrease of n to zero, which corresponds to termination of the reaction. The changes in the values of n are due to structural evolution of the reaction medium from a homogeneous solution of a polymer in an oligomer to the dispersion of microgel particles and the formation of a macrogel, which is accompanied by changes in the contributions of reactions occurring in different morphological zones to the overall reaction rate. The correctness of this statement was confirmed by *in situ* structural analysis of the reaction medium using light scattering techniques, NMR spectroscopy and dielectrometry.[22,35,36] The parameter n is highly sensitivite to changes in the structure-phase state of the reaction medium induced by solvents, precipitants, temperature, growth-limiting agents, *etc*.[23,34] Electron microscopic studies revealed a direct correlation between the numeric values of the parameter n and morphological characteristics of the polymers formed.[37] The validity of the use of the Avrami equation in the analysis of structure–kinetics relationships was confirmed by the fact that a similar equation was obtained with the help of an analytical method based on a kinetic scheme of three-dimensional radical polymerisation.[21]

In addition to topological and kinetic reasons, the microheterogeneous mechanism of three-dimensional radical polymerisation and copolymerisation has a thermodynamic reason which is related to the violation of the Flory–Rener[38] condition, *viz*., compatibility of a microgel with low-molecular-weight components of the reaction medium in the course of polymerisation. When the extent of the cross-linking inside microgel particles reaches a certain critical level, these components are displaced towards less densely cross-linked regions on the periphery of the microgel (syneresis). Because of diffusion-controlled limitations in macrogel formation, this process is not developed into separation of the system into two macroscopic phases, but is stopped in the microscopic level.[39] This process commonly referred to as microsyneresis results in structural and kinetic microheterogeneity of the reaction medium due to local vitrification in the central region

of microgel particles and violation of the homogeneous distribution of the reactants in the bulk of the reaction medium.

The redistribution of extrinsic molecular probes between zones with different network densities in the polymerisation of dimethacrylate **3** was established by the appearance of additional bands in the electronic absorption spectra of anthracene molecules localised in different zones of the polymeric matrix with different network densities.[27,28] The values of network densities calculated from absorption band frequencies of extrinsic anthracene molecules were equal to 1, 1.155 and 1.262 rel.u. The heterogeneity of molecular packing of the polymer of dimethacrylate **3**[28] was confirmed[40] by transmission electron microscopy, which revealed a bimodal distribution of heterogeneities according to their size (their diameters were 10 and 50–100 nm). These heterogeneities were related to the appearance of microgel particles preceding the macrogel formation.

Kinetic microheterogeneity of the initiation reaction can be due to involvement of initiator molecules in microsyneresis process[41] and increasing local concentrations of the initiator in less densely cross-linked areas. In this case kinetic heterogeneity can be further enhanced, since decomposition rates of radical polymerisation initiators increase with a decrease in the coefficient of molecular packing of the polymeric matrix.[42–44] Higher initiation rates of a monomer and pendant double bonds in areas with loose networks may result in homogenisation of network density over the bulk of the polymer. A significant improvement of the properties of network polymers after annealing and a relatively small increment in the conversion of the double bonds also suggest that in later polymerisation steps the reaction is predominantly localised in microzones with loosely cross-linked networks.[30]

In the case of three-dimensional copolymerisation, local relative concentrations of the comonomers M_1 and M_2 in the vicinity of growing radicals differ from their bulk-average concentrations due to microsyneresis.[12] This effect is manifested at higher effective reactivities of double bonds of the cross-linking reagent M_1 in comparison with the monomer M_2. It was shown[12,45] that microsyneresis observed in the copolymerisation of dimethacrylate **3** and butanediol dimethacrylate (**4**) with 2-methyl-5-vinyltetrazole (**5**) is accompanied by elimination of a less reactive compound **5** from the reaction zone of the microgel and a selective gel effect owing to consumption of double bonds of dimethacrylates **3** and **4** and pendant methacrylate groups. Specific heterogeneity of compositions of network copolymers formed is a natural consequence of microsyneresis and concomitant disturbances in the uniform distribution of comonomers.

The phenomenon of microphase separation of reaction components in the course of three-dimensional radical polymerisation and copolymerisation has found practical application in the production of liquid-crystal displays and synthesis of interpenetrating polymeric networks (IPN). One of the approaches to the production of such displays consists of polymerisation of diacrylates in solutions containing liquid-crystalline components.[46] The formation of a network induces phase separation and appearance of microdrops of a liquid-crystalline phase. By varying polymerisation conditions, one can control the degree of microphase separation and dispersity of liquid-crystalline inclusions into the network polymer matrix. Controlled microphase separation underlies the formation of structure and properties of interpenetrating polymeric networks one of which being formed by a three-dimensional radical (co)polymerisation mechanism, while the mechanism for the other is polycondensation (*e.g.*, urethane formation). Variation of relative rates of formation of these networks allows control over the degree of microphase separation of the reaction system components, phase morphology of IPN and their properties.[47,48]

3. Structures of network (co)polymers

In the context of this review, which is devoted to the analysis of structural and kinetic correlations in TRCP and their significance for the establishment of structure and properties of network copolymers, it seems expedient to highlight the role of reactivity ratios. If linear copolymerisation is carried out under homophasic conditions, the consumption of the monomers, the instantaneous composition of the copolymer formed and the distribution patterns of the monomeric units in the polymer chain are characterised by copolymerisation constants of the monomers r_1 and r_2.[49] Therefore, much attention is given to determination and refinement of these values for different comonomer pairs. The r_1 and r_2 values for many monomers are collected in reference books and are used in the design of experiments and simulation of copolymerisation processes.

In contrast to linear copolymerisation, three-dimensional copolymerisation cannot properly be described in terms of reactivity ratios of double bonds of a cross-linking reagent M_1 and a monomer M_2 because of the microheterogeneous mechanism of the three-dimensional copolymerisation, formation of pendant double bonds, microsyneresis of reaction components and vitrification of the reaction medium. These factors altogether largely determine effective reactivities of the double bonds in the starting oligomers M_1 and comonomers M_2 and pendant double bonds of the (co)polymer formed. The extent to which various factors affect the copolymerisation kinetics of individual reagents is different and depends on the composition of the original oligomer–monomer mixture and degree of conversion.[12,13,50]

Therefore, in order to minimise the specific effects of TRCP on r_1 and r_2 it is necessary that the values of the reactivity ratios of M_1 and M_2 were determined at low degrees of conversion ($< 1\%$) and at small concentrations of the cross-linking reagent ($< 1\%–3\%$). However, in this case, too, the differences in the reactivity ratios obtained by different authors are rather significant. Thus[51] the corresponding values for the copolymerisation of dimethacrylate **1** with methyl methacrylate (MMA, **6**) are as follows: $r_1 = 1.34$, $r_2 = 0.67$ (Ref. 51) or $r_1 = r_2 = 1$ (Ref. 52). Such discrepancies are due to the difficulty in isolation of the copolymer from the reaction mixture and different methods used for the determination of its composition and the content of pendant double bonds.

The ambiguity of the term 'monomer reactivity ratios', when speaking of the preparation of network copolymers, is spectacular as regards the differences in the values of r_1 and r_2 determined *in situ* in different steps of copolymerisation of *N*,*N*′-methylenebis(acrylamide) (**7**) and acrylamide (**8**) in D_2O using high-resolution ^{1}H NMR.[53] At a nearly zero conversion, $r_1 = 3.36$, $r_2 = 0.57$, whereas the corresponding values for the gel formation step ($C = 0.35$) are $r_1 = 1.77$ and $r_2 = 0.64$. It was suggested[53] that high reactivity of the double bonds in compound **7** at $C \approx 0$ favours the formation of microblocks of units **7** containing pendant double bonds as well as nonuniform distribution of the cross-links. The decrease in r_1 in the gelation step is attributed to microsyneresis and a decrease in effective reactivities of the double bonds.

It was suggested[12] that the ratio of copolymerisation rates of the cross-linking reagent and the monomer (w_1/w_2) was used as a parameter which takes into account all the structure-physical factors and characterises relative reactivities of double bonds. *In situ* determination of time dependences $w_1(t)$ and $w_2(t)$ throughout the whole polymerisation allows quantitative estimation of changes in the relative reactivities of the double bonds in the course of structural evolution of the reaction medium.

A comparison of experimental values of w_1/w_2 for different oligomer–monomer systems ($M_1 + M_2$) with those calculated from the Mayo–Lewis model (using experimental values of r_1 and r_2 for linear copolymerisation of the corresponding analogues) revealed their close fitting only for the very first reaction steps.[12,13,45] With an increase in the degree of conversion, both the experimental and calculated values diverge considerably. Thus in the copolymerisation of dimethacrylates **3** and **4** with deuterated methyl methacrylate (D-MMA) ($r_1 = r_2 = 1$ for linear copolymerisation of unlabelled and deuterated methyl methacrylate) this divergence amounts to 50% at high concentrations of the

cross-linking reagent. Obviously, in the three-dimensional copolymerisation the true reactivities of reagents determine the distribution of monomeric units in linear and branched macromolecules with pendant double bonds only in the initial steps of the reaction.[12] In turn, effective reactivities of M_1, M_2 and pendant double bonds begin to depend on the structure-physical state of the reaction medium with an increase in the degree of conversion, the appearance of microgel particles and the formation of a bulk polymer.

The topological, kinetic and thermodynamic factors altogether determine the microheterogeneous mechanism of three-dimensional copolymerisation and the structural heterogeneity of the network copolymer formed. It was found that the heterogeneity of moderately and strongly cross-linked networks increases with an increase in the density of the chemical cross-links.[54, 55] However, a specific type of non-homogeneity in a loosely cross-linked copolymer of methacrylate **6** with dimethacrylate **1** as a cross-linking reagent (0.1% – 0.5%) was observed.[56] Data from scanning near-field fluorescent microscopy suggest that local densities of segments within the copolymers under study exceed manyfold their average densities over the whole ensemble of chains. The segments vicinal to the cross-links form clusters ($\sim$ 10 nm) which merge to form heterogeneous structures the size of which amounts to several hundred nanometres. Presumably, the cross-links in such loose networks function as sites favouring supramolecular stacking of linear segments of polymer chains.

Convincing evidence in favour of microheterogeneity of network polymers was obtained by various methods which characterise different aspects of heterogeneity and differ in their resolution capacity. For example, microscopic methods allow revealing the microheterogeneity of polymer networks at the supramolecular level, whereas NMR and IR spectroscopy, at the molecular level.

High-resolution ^{1}H NMR provides direct information on the distribution of cross-links in model network copolymers prepared with involvement of a deuterated monomer M_2.[13] This method is based on the dependence of the width of the NMR line on the energy of magnetic dipole interactions between neighbouring H-containing units of the cross-linking reagent M_1. Since the units of deuterated M_2 function as non-magnetic diluents, the interaction of H-containing M_1 units and the width of the NMR line both depend on the distribution of the cross-links within the network. The efficiency of the method increases when network or linear copolymer analogues are analysed (Fig. 2).

The NMR line in linear copolymers prepared by copolymerisation of methyl methacrylate with a deuterated monomer (D-MMA) and containing up to 20% of H-MMA units remains narrow, which points to their statistical distribution among D-MMA units of the polymer chain. This is consistent with the values of their copolymerisation constants: $r_1 = r_2 = 1$. A further increase in the percentage of MMA units is accompanied by gradual broadening of the NMR line due to an increase in the number of MMA units constituting diads, triads and more lengthy sequences and the enhancement of their magnetic dipole interactions. In the case of network copolymers of triethylene glycol dimethacrylate with D-MMA, the broadening of the NMR line begins at dimethacrylate concentrations as low as < 5 mol.%. This points to a spatially heterogeneous distribution of cross-links in the bulk of the network copolymer. Apparently, such a heterogeneity can be accounted for by intramolecular cyclisation and microsyneresis, which results in the expulsion of D-MMA from microgel particles and a concomitant increase in the local concentration of the cross-links.

By virtue of their structural heterogeneity, network polymers and copolymers contain microzones which differ in local free volumes and mobilities of individual network elements. Using the polymer of dimethacrylate **3** as an example, it was shown [57, 58] that dynamic heterogeneity of network polymers causes the broadening of the time spectra of dielectric and mechanical α-relaxation. The microheterogeneity and the loss tangent a network increase

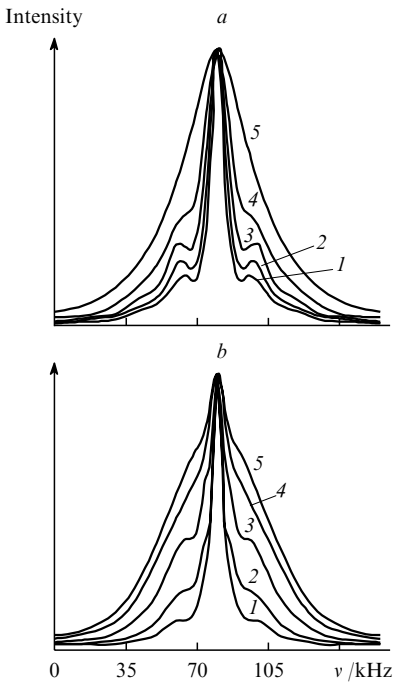

Figure 2. Dependence of linewidths in the NMR spectra of copolymers D-MMA with MMA (*a*) and with triethylene glycol dimethacrylate (*b*) on the concentrations of MMA and dimethacrylate.[13]
Concentrations of MMA (*a*) and dimethacrylate (*b*) /mol.%: (*1*) 1, (*2*) 5, (*3*) 20, (*4*) 50, (*5*) 100.

with an increase in its density.[58, 59] The width of the loss angle peak of a copolymer of **2** with divinylbenzene (**9**) prepared at 95 °C increases significantly with an increase in the concentration of compound **9** (from 5 mass % to 12 mass %). The glass-transition temperature of the copolymer (T_g) increases from 115 to 130 °C. The degree of deviation of T_g from the polymerisation temperature depends primarily on microheterogeneity of network polymers.[58] Synthesis of a microheterogeneous network polymer with T_g = 135 °C by polymerisation of diethylene glycol dimethacrylate (**10**) at room temperature supports this statement.

IR spectroscopy provides direct information about molecular structures of network polymers and copolymers. Studies of IR spectra of densely cross-linked polymers based on dimethacrylates

$$CH_2=C(CH_3)C(O)O-X-OC(O)C(CH_3)=CH_2$$

revealed that these spectra cannot be represented as a sum of the corresponding spectra of the linear poly(methyl methacrylate) (PMMA, **11**) and the oligomeric block X.[27, 28] The peculiarities of the IR spectra of poly(dimethacrylates) could be interpreted in terms of their cellular structure, which determines the conformation of atomic groups and stereoregularity of addition of methacrylate units.[27, 28] It was shown that syndiotactic addition of methacrylate units, which is thermodynamically more favourable than isotactic, is a more preferable route in linear radical polymerisation of the monomer **6** under ordinary conditions.[60] However, three-dimensional polymerisation of dimethacrylates shows a strong tendency of the probabilities of syndio- and isotactic addition of methacrylate groups to level off,[27, 28] which points to a greater contribution of thermodynamic factors responsible for the formation of the network structure in comparison with factors determining the stereospecificity of chain growth reactions in the linear polymer of **11**. In the case of three-dimensional polymerisation, the stereoregularity of the reaction of R* with C=C is controlled by steric factors and shrinkage stresses in the vicinity of the growing macroradicals.[16] When these stresses reach a certain critical level, the syndiotactic addition of methacrylate groups becomes thermodynamically less favourable and is replaced by

isotactic addition. The resulting changes in the packing conditions of atomic groups lead to alleviation of local stresses and a switchover of the chain growth reaction to a thermodynamically more favourable, *viz*., syndiotactic, route. Such a feedback between local stresses in network polymers and thermodynamics of a chemical reaction may bring about periodic switching of the chain growth reaction from one route of the addition of methacrylate groups to another. The microblock structure of polymethacrylate chains formed in this reaction seems to be the least significant (from the standpoint of structural hierarchy of network polymers) manifestation of the microheterogeneity of these processes.

The effects of steric hindrance and internal stresses on the stereoregularity of the addition of acrylate groups during the formation of network metallopolymers by radical polymerisation of zinc diacrylate have been established.[61]

The conformational state of methacrylate groups occupies a special place among characteristics of molecular structures of network (co)polymers based on oligodimethacrylates. These groups are localised in network nodes and their conformational dynamics determines largely the relaxation and physical-mechanical characteristics of poly(dimethacrylates).[29] The conformational states of methacrylate groups in network and linear polymers differ significantly [27, 28, 62] as can be evidenced from the differences in their IR spectra at the region of absorption bands of the C(O)O – R groups (1100 – 1300 cm^{-1}). Their frequencies depend on the values of the internal rotation angles φ_1 and φ_2.

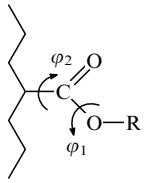

The bands at 1197 and 1172 cm^{-1} in the absorption spectrum of the polymer **11** (Fig. 3) correspond to the vibrations of *cis*- and *gauche*-isomers which differ in the angle φ_1, whereas the bands at 1246 and 1275 cm^{-1} correspond to the oscillations of the ester group in conformations differing by the rotation angle φ_2 relative to the main chain.[62, 63, 64] Similar absorption bands are present in the IR spectrum of poly(dodecyl methacrylate) (**12**). However, in contrast to the polymer **11**, the intensity of the band corresponding to its *gauche*-isomer exceeds markedly that of the *trans*-isomer. This suggests that stabilities of ester-group isomers in linear polymers are determined by intermolecular interactions of alkyl substituents.

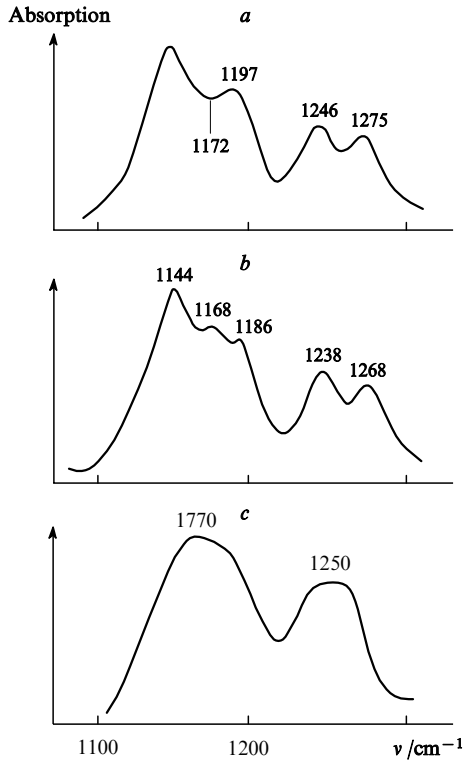

Figure 3. IR spectra of polymers of MMA (*a*), dodecyl methacrylate (*b*), butanediol dimethacrylate (*c*).[62]

In contrast to linear polymers **11** and **12,** the IR spectrum of a network polymer of dimethacrylate **4** (Fig. 3 *c*) contains only one broad absorption band around 1200 – 1140 cm^{-1} instead of several bands corresponding to individual isomers. This suggests a broad distribution of ester group conformations in network nodes over all possible values of the angle φ_1. The change in relative intensities of a pair of bands corresponding to ester groups with different rotation angles φ_2 relative to the main chain is also noted. This situation is typical of many densely cross-linked polymers, although some of its manifestations depend on the length and flexibility of the oligomeric block X.[29] It may thus be concluded that the conformational state of ester groups in network polymers is determined by the packing of several adjacent nodes and the spatial architecture of the network cells rather than by local energy minimum of intermolecular interactions, as in linear polymers.

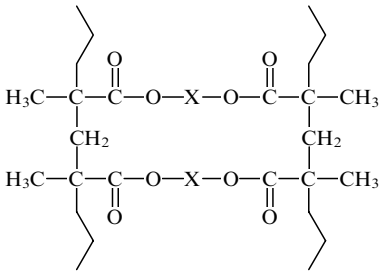

Obviously, such packing is provided by cooperative conformational dynamics and is limited by local free volume. The global energy minimum of the network cells is reached through variation of conformation energies of all of its constituent ester groups and the oligomeric blocks X.

The differences in the stereoregularity of the addition of methacrylate units and the conformation energies of ester groups in linear PMMA and in network polymers can be the reason for differences in specific heats of polymerisation of MMA and methacrylate groups in dimethacrylates.[16, 45, 62]

In some cases, chemical cross-links and the cellular structure of the network prevent approach of atomic groups to each other and intermolecular interactions in a rigid glassy matrix. This phenomenon commonly known as the loosening effect of chemical crosslinks [65] is manifested in a decrease in the molecular packing coefficient (MPC) for copolymers of **1** with MMA with an increase in the concentration of the cross-linking reagent.[66]

Concentration of **1** (mass %)	3	10	20
MPC	0.689	0.671	0.648

The copolymer with a maximum content of **1** manifests the highest compressibility in the glassy state due to the loosening of chemical cross-links. At the same time, a copolymer with a lower content of **1** manifests higher compressibility in a high-elasticity state.[66]

In densely cross-linked polymers of dimethacrylate, the loosening effect is manifested as higher amplitudes of torsional vibrations of atomic groups [65] and the dependence of the mechanism of water absorption on the network density.[67] It has been shown [30] that the loosening effect makes a significant contribution to physical-mechanical and sorption characteristics of a polymer of dimethacrylate **1** and copolymers of **1** with styrene.

Chemical shrinkage of the reaction medium has a strong impact on the structure and properties of network (co)polymers prepared by radical polymerisation of vinyl compounds.[4, 68–71] The reason should be sought in the fact that the distances between monomer molecules are determined by the sum of the van der Waals radii of outer atoms (~3.4 Å), while the distance between the monomeric units in the polymer chain depends on the length of the C–C bond (~ 1.5 Å). In turn, shrinkage depends on the size of the monomer molecule and decreases on going from MMA to butyl methacrylate (**13**) from 21.01 vol.% to 15.33 vol.%.[70]

In the linear polymerisation, shrinkage and polymerisation occur simultaneously, while in the case of three-dimensional polymerisation, shrinkage can lag behind as a result of which excess free volume can form in the polymer gel.[4, 69] In this case, the lag is caused by a virtually instantaneous addition of the double bond to the radical, while the relaxation of the excess free volume is limited by the low rate of cooperative rearrangements of the network. It was found that the higher the rate of photopolymerisation the greater the lag in shrinkage.[69] The maximum conversion of double bonds increases owing to the appearance of excess free volume and an increase in molecular mobilities of reaction components.

If three-dimensional polymerisation is accompanied by vitrification of the network polymer formed, the relaxation of the volume of the reaction medium to the equilibrium state is freezed virtually completely resulting in the appearance of internal stresses within the system.[16] These significantly deteriorate the quality of the articles prepared by TRCP and considerable attention is given to their analysis.[71, 72] It was found[72] that photopolymerisation of multifunctional (meth)acrylates is accompanied by the appearance of internal stresses following onset of vitrification, which increase monotonically and progressively throughout the reaction. The rates of stress appearance increase with an increase in the functionality of the monomer, a decrease in the length of the oligomeric chain and a decrease in the concentration of the plasticiser. These trends are much more pronounced for methacrylates than for acrylates. It was thus suggested that the level of internal stresses increases with an increase in the elasticity modulus of the polymer formed.[72]

The total level of shrinkage stresses can be estimated as the energy of formation of an excess free volume ΔV in a network polymer with a bulk modulus K (see Ref. 16).

$$U \approx K\Delta V.$$

However, this expression is valid only for a model of a homogeneous network. In practice, the distribution of stresses in the bulk of a polymer is non-homogeneous due to the microheterogeneity of the three-dimensional polymerisation mechanism. Shrinkage stresses are usually concentrated in network zones at the junction of microgel particles. These particles can be regarded as microreactors where the chemical shrinkage occurs in a direction opposite to the propagation of the polymerisation front.[27] Therefore, the superposition of polymerisation fronts of several microreactors can bring about tensile stresses in the passing chains connecting different zones of the polymer formed in different microreactors. Quite probably, these stresses stimulate the cleavage of polymer chains and initiate the formation of microcracks in attempted synthesis of supercross-linked polymers of dimethacrylate.[68]

The heterogeneous distribution of stresses in the bulk of a polymer is the reason for specific features of thermal degradation of MMA copolymers with ethylene glycol, butanediol and hexanediol dimethacrylates where the content of the latter varies from 0.5 mol.% to 27 mol.%.[73] The degradation of copolymers occurs in two steps. In the first step, the degradation rate decreases progressively as the degree of cross-linking increases irrespective of the length of the cross-linking reagent, which is characteristic of moderately dense networks. In the second step, the degradation rate changes abnormally: it increases progressively with an increase in the degree of cross-linking and a decrease in the length of the spacer. Such a two-step degradation mechanism can be attributed to the presence of alternating loosely and densely cross-linked zones in the copolymer; cleavage of chemical bonds in the latter zones is induced by internal stresses.[73]

Considerable internal stresses can be developed in network polymers prepared by radical polymerisation of multifunctional metal-containing monomers of the type C=C–M–C=C, where M is an atom of a metal or a complex.[61, 74] Because of a small distance between the double bonds of organic ligands and their strict spatial fixation by a bridging atom M, the target polymer has a rigid small-meshed structure

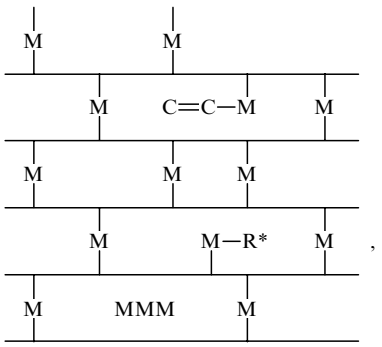

which prevents chemical shrinkage and volume relaxation. As a result, growth of the polymer chains occurs under conditions of strong steric limitations and at higher internal stresses.

Direct evidence for the presence of internal stresses in a network polymer prepared from zinc diacrylate was obtained in the analysis of low-frequency IR spectra in the region of oscillations of the central fragment –O–M–O– (see Ref. 61). Instead of two narrow bands at 300 and 410 cm^{-1} characteristic of the monomer, the spectrum of this polymer contained one broad band at 340 cm^{-1}, which suggests distortions in the geometry of the bridging group induced by internal stresses. It was found[74] that internal stresses developed upon radical polymerisation of the $PdCl_2Y_2$ complex (Y is 2-methyl-5-vinyltetrazole) induce the cleavage of the metal–ligand bond and evolution of the inorganic microphase (MMM). An X-ray diffraction analysis of this complex has shown that the high level of internal stresses that appear upon polymerisation is due to strong steric shielding of the C=C bonds.[75] The inorganic microphase evolved in network polymers by virtue of internal stresses represents special manifestation of mechanochemical syneresis.

Since the reason for internal stresses in three-dimensional (co)polymerisation is incomplete shrinkage, total shrinkage can be reduced through the use of oligomers with a greater length of the spacer and plasticisers.[72] The total level of shrinkage and internal stresses can successfully be decreased using two-step synthesis of network (co)polymers. Its first step includes the synthesis of oligo(methacrylates) containing a large number of reactive double bonds from dimethacrylates.[28, 76] The use of such precursors in paint-and-varnish compositions employed as polymeric coatings improves their quality due to elimination of shrinkage stresses.[77] Slightly cross-linked gels based on dimethacrylates are used for the preparation of gradient light-focusing optical materials.[2] To do this, cylindrical gels are placed into a vessel filled with a solution of a monomer with a lower refraction index. A parabolic gradient of the monomer concentration is developed due to diffusion and is fixed by photopolymerisation. Non-shrinking spiroorthoester vinyl compounds proved to be valuable materials in the production of high-precision optics.[78] Radical polymerisation of these compounds at the double bonds is accompanied by the ring opening and the formation of a carbonyl group, which has larger size than that of the original ester ortho group. As a result, this reaction occurs without shrinking or is accompanied by a small increase in the volume. Non-shrinking compositions are prepared by copolymerisation of spiroorthoesters with ordinary vinyl monomers.[78]

Three-dimensional radical (co)polymerisation is widely employed for compression moulding of miscellaneous articles; therefore, much attention is given to the study of relationships between physical-mechanical properties of network copolymers and the structure of the starting oligomers and polymerisation conditions. An attempt has been made [24] to estimate the contribution of the structure of the starting oligoester methacrylates, intermolecular interactions and MPC into physical-mechanical characteristics of network polymers. The lack of a correlation between MPC and physical-mechanical characteristics of the polymers formed suggests that it is the distribution function of free volume rather than its absolute value that determines the properties of densely cross-linked polymers. Evidence for this assumption can be derived from the bimodal distribution of free volume in a polymer of triethylene glycol dimethacrylate as established by IR spectroscopy of adsorbed water.[67] It was found that the relative fractions of microvoids adsorbing small clusters $(H_2O)_n$ and of large pores absorbing water condensate depend on the polymerisation temperature.

Studies on physical-mechanical properties of network polymers based on oligocarbonate (meth)acrylates have shown [79] that the elasticity moduli determined from the initial portion of the deformation–stress diagram decrease with an increase in the spacer length and lowering of the energy barrier to internal rotation around the C–C bond. The elasticity modulus on compression is smaller than on stretching, which may be due to a greater contribution of the high-elasticity deformation component on compression. The differences in the chemical nature and lengths of oligomers and, correspondingly, molecular structures of polymer networks are especially apparent at initial portions of these diagrams. In regions of nonlinear dependence of stress *vs.* deformation, the differences in morphological characteristics of polymers predominate. A close relationship was found between the deformation-strength and relaxation characteristics of the polymers studied.[79] A similar correlation exists between thermomechanical and relaxation characteristics of network polymers based on oligomeric dimethacrylates.[57]

Studies of opticomechanical properties of model polymers based of diallyl and divinyl compounds of homologous series:

$$CH_2=CHCH_2OC(O)-(CH_2)_n-C(O)OCH_2CH=CH_2$$

$n = 2-8$, **14**

$$CH_2=CHC(O)O-(CH_2)_n-OC(O)CH=CH_2$$

$n = 2-6$, **15**

$$CH_2=C(CH_3)C(O)O-(CH_2)_n-OC(O)C(CH_3)=CH_2$$

$n = 2-6$, **16**

have been undertaken aimed at elucidation of the role of topological and morphological structures in the establishment of physical-mechanical characteristics of network polymers.[80]

Isochronic temperature dependences of the elasticity moduli $E = f(T)$ and optical sensitivity with respect to stress $D = f(T)$ have been determined [80] rather than deformation–tension dependences.[24, 79] Such a comprehensive approach has demonstrated non-additive changes in isothermic values of functions $E = f(n)_T$ and $D = f(n)_T$ on the number of the CH_2 groups in the homologous series of the polymers under study. There was no strict correlation between elastic and photoelastic characteristics and the length of the starting oligomers **14** and **15**.

The dependence of opticomechanical characteristics of densely cross-linked polymers on the structure of the starting oligomers is indirect rather than direct and is manifested as the peculiarities of topological structures of networks formed in three-dimensional polymerisation.[80] The differences in the properties of the polymers prepared from diallyl (**14**) and divinyl (**15**, **16**) oligomers are due to the fact that the former are prepared by cross-linking branched macromolecules, while the latter are synthesised by cross-linking primary microgel particles having colloidal sizes. A cage model of a network polymer was proposed [80] based on the established contributions of energy and entropic elasticities of deformed network polymers. According to this model, some interjunction chains have a rigid conformation, while the other undergo rotational-isomeric transitions and are responsible for the entropic elasticity of polymeric networks. This model has been rationalised taking into account the microtactic characteristics of polymeric chains and conformational structures of densely cross-linked polymers based on oligomeric dimethacrylates.[27, 28]

It was found [24, 79, 80] that the control of physicomechanical properties of network polymers by variation of the structures of the starting oligomers is inefficient due to microheterogeneity of the three-dimensional polymerisation mechanism, which determines topological and morphological structures of the final polymer. This stimulates a search for novel approaches to a control over topological and morphological structures of network polymers in the stage of their synthesis, *e.g.*, through the control over intramolecular cyclisation and intermolecular cross-linking reactions.[30]

III. Methods for *in situ* investigation of three-dimensional radical copolymerisation

Structural and kinetic studies of TRCP demand separate determination of the kinetics of consumption of double bonds of the cross-linking reagent M_1 and the monomer M_2 over the whole process. The sampling method and the analysis of the compositions of the copolymer and the monomer mixture in the course of the reaction applicable in linear copolymerisation cannot be used in this case, since insoluble network copolymers are formed in the earliest steps of TRCP. As for the calorimetric method widely used in the kinetic studies of three-dimensional homopolymerisation,[7] its application in TRCP is limited, since it allows one to measure the overall heat of the copolymerisation reaction and concomitant structural and physical transformations of the reaction medium.

The calorimetric method was used [81] for the study of copolymerisation of dimethacrylate **1** with styrene. By analogy with linear copolymerisation of styrene with MMA, the authors assumed that this reaction is azeotropic and used averaged values of molar heats to calculate the conversion:

$$Q = 0.5(Q_1 + Q_2),$$

where Q_1 and Q_2 are the known molar heats of homopolymerisation of styrene and MMA. However, these calculations did not take into account the fact that the heats of bond formation in the diads M_1M_2 in the copolymerisation of these monomers differ from those in the diads M_1M_1 and M_2M_2.[60, 82] One should also keep in mind that, apart from chemical reactions of the opening of C=C bonds, differences in the conformation energies of network polymers and its linear analogue and shrinkage stresses make significant contributions to the overall heat of three-dimensional copolymerisation.[83] The contribution of these structure-physical components to the heats of formation of network copolymers can apparently be ignored only in comparative studies of kinetics of copolymerisation of the same type of systems at the qualitative level.

Thus, the experimental base for the study of TRCP could not be formed by simple borrowing methods for investigations into linear copolymerisation, on the one hand, and the performance of three-dimensional homopolymerisation, on the other hand. Therefore, special methods of spectroscopic monitoring for *in situ* structure-and-kinetic investigation of TRCP have been developed to solve this problem.

1. IR spectroscopic monitoring

IR spectroscopic monitoring of TRCP is based on the construction of curves of double bonds consumption in the oligomer $[C_1(t)]$ and the monomer $[C_2(t)]$ from the decreage in the intensities of

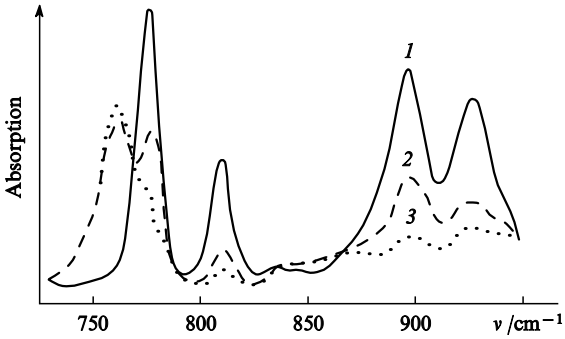

Figure 4. IR spectra of the original mixture (ethylene glycol dimethacrylate–styrene) (molar ratio, 1:2) (*1*), after 8 h polymerisation at 30 °C ([CPC] = 5 mass %) (*2*) and after 8 h annealing at 60 °C (*3*).[83]

absorption bands of the corresponding $C=CH_2$ groups. The main criterion in the choice of analytical bands is their minimum overlapping in the spectrum. In many oligomer–monomer systems, this criterion is met by the bands of deformation vibrations of hydrogen atoms in the region of 750–950 cm^{-1}. In the copolymerisation of ethylene glycol dimethacrylate with styrene and dicyclohexyl peroxydicarbonate (CPC) as an initiator, the intensities of all absorption bands related to deformation vibrations of $C=CH_2$ bonds of methacrylate groups (945, 812 cm^{-1}) and styrene (907, 780 cm^{-1}) shows a tendency to decrease reaching a constant level characteristic of residual unsaturation of the copolymer at a given temperature (Fig. 4).[83] Subsequent increase in the temperature results in 'thawing' of the mobilities of styrene, ethylene glycol dimethacrylate and pendant methacrylate groups, as a result of which copolymerisation continues up to the moment when the copolymer formed passes again into a glassy state (Fig. 4, curves *2* and *3*). Similar changes in the IR spectra are observed in the copolymerisation of triethylene glycol dimethacrylate with styrene.

The conversion curves of the methacrylate groups and styrene[83] are shown in Fig. 5. A decrease in the content of residual methacrylate groups on going from ethylene glycol dimethacrylate to triethylene glycol dimethacrylate suggests that the short oligomeric block significantly hinders the mobilities and decreases the effective reactivities of pendant methacrylate groups in comparison with a more lengthy oligomeric block.

Studies of TRCP of model systems based on monomers and multifunctional oligomers and carrying similar reactive groups (MMA with dimethacrylates, styrene with divinylbenzene) present considerable interest. However, the analytical bands of

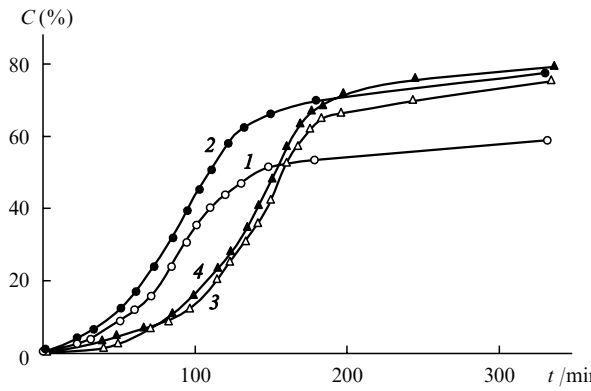

Figure 5. Copolymerisation kinetics of ethylene glycol dimethacrylate (*1*) with styrene (*2*) and triethylene glycol dimethacrylate (*3*) with styrene (*4*).[83]
Dimethacrylate : styrene ratio 2:1, T = 30 °C, [CPC] = 5 mass % (*1*, *2*) and 3 mass % (*3*, *4*).

the monomer and oligomer overlap completely. In this case, separate investigation of the copolymerisation kinetics can be carried out by replacing one of the comonomers by its deuterated analogue. Thus on going from MMA to D-MMA, the vibrational frequency of the C=C bond decreases from 1638 to 1592 cm^{-1}, which allows separate registration of copolymerisation rates of the double bonds of D-MMA and dimethacrylate.[13]

Monitoring of consumption of reactive groups using absorption bands of vibration overtones in the near IR region of the spectrum significantly expands the potential of the studies of (co)polymerisation in multicomponent systems. As the overtone frequences ν_{0-2} are associated with the main vibrational frequency ν_{0-1} by the ratio:

$$\nu_{0-2} \approx 2\,\nu_{0-1},$$

the absorption bands of the overtones are characterised by a better resolution than the neighbouring main vibration bands. Near-IR monitoring was used[48] in a study of two interpenetrating polymer networks one of which was prepared by radical copolymerisation of bisphenol A diglycidyl ether dimethacrylate (**17**) with styrene, while the other, by a reaction of diglycidyl ether of bisphenol A (**18**) with 4,4′-diaminodiphenylmethane (**19**). The kinetics of formation of each interpenetrating network could be studied by analysing overtones of vibration bands of the epoxy group, styrene and methacrylate groups at 6073, 6135 and 6166 cm^{-1}, respectively.

The achievements in the production of equipment for IR spectroscopy are so significant that they can meet virtually any demands of investigators in the field of three-dimensional (co)polymerisation. Modern Fourier spectrometers allow the registration of rates of superfast three-dimensional photopolymerisation reactions of acrylic and methacrylic compounds in microsecond time spans with time resolution of 10^{-3} s (see Ref. 84). Layer-by-layer scanning of polymeric coatings can be performed and the degree of conversion can be judged using real-time attenuated total reflectance-Fourier transform IR spectroscopy.[85] The use of optofibre connections permits one to conduct kinetic monitoring in polymerisation reactors located at a distance of up to 100 m from the spectrophotometer.[86]

An analysis of the kinetic data by spectroscopic monitoring is often confined to a discussion of the conversion *vs.* time dependences.[5,48,85] The presentation of experimental data in the copolymerisation rate–time coordinates makes it possible to increase the amount of information obtained by this method.[11–13] The ratio of copolymerisation rates in the oligomer M_1 and the monomer M_2 (υ_1/υ_2) is yet another important structure–kinetic feature of TRCP reactions which reflects the instantaneous composition of a copolymer. Valuable information about the state of a reaction system can be obtained from a comparison of experimental dependences of the rates *vs.* reaction time $(w_1/w_2)_{exp}$ with the dependences calculated on the basis of the Mayo–Lewis model according to the equation:

$$\left(\frac{w_1}{w_2}\right)_{cal} = \frac{r_1[M_1] + [M_2]}{r_2[M_2] + [M_1]}, \qquad (7)$$

where $[M_1]$ and $[M_2]$ are the current concentrations of the C=C bonds calculated on the basis of the experimental dependences $C(t)$.

IR spectroscopic monitoring allows one to follow the disturbances in the uniform distribution of reactants in TRCP. Such disturbances can be due to microsyneresis of the components from microgel particles (microreactors) and low molecular mobility of the medium in the vitrification step, as a result of which diffusional flows of the reactants to the active sites cannot compensate for the consumption of a more reactive monomer. Deviation of the experimental ratio of the reduced copolymerisation rates $(w_1/w_2)_{exp}$ from the values of $(w_1/w_2)_{cal}$ calculated by the Mayo–Lewis model is a criterion for the estimation of such disturbances.[12,45]

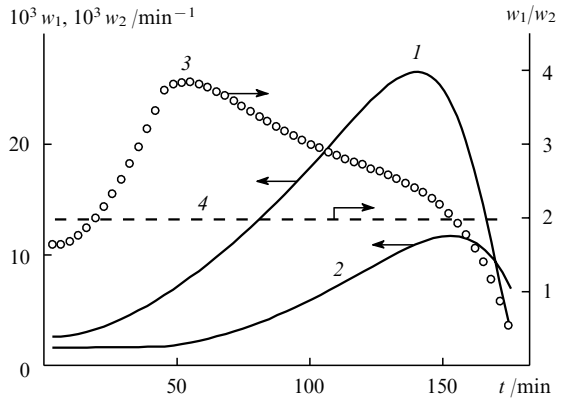

Figure 6. Copolymerisation kinetics of butanediol dimethacrylate (14.5 mass %) with 2-methyl-5-vinyltetrazole.[12]
(*1*, *2*) Copolymerisation rates (w_1 and w_2, respectively), (*3*) experimental values of w_1/w_2, (*4*) values of w_1/w_2 calculated from Eqn (7).

The TRCP of dimethacrylates with 2-methyl-5-vinyltetrazole is a special case of disturbances in the concentration homogeneity of the reaction medium.[12,45] Prerequisites for the appearance of concentration heterogeneities in such systems are significant differences in the reactivities of methacrylate groups of oligomers and vinyltetrazole (for linear copolymerisation of MMA with 2-methyl-5-vinyltetrazole $r_1 = 1.47$, $r_2 = 0.51$, respectively) and low content of the cross-linking reagent.

Figure 6 shows the experimental dependences of the reduced copolymerisation rates of butanediol dimethacrylate (**4**) and the monomer **5** as well as the experimental and calculated dependences of the ratios (w_1/w_2) *vs*. time. A comparison of curves *1* and *2* demonstrates that copolymerisation of methacrylate groups occurs as an autoaccelerating reaction from the very beginning, while the monomer **5** is polymerised initially at a constant rate. A possible reason for the selective gel effect in the polymerisation is disturbances in the initially uniform distribution of reagents in the vicinity of the growing macroradical due to the enrichment of the polymer chain with monomer units carrying pendant methacrylate groups due to low copolymerisation constant of vinyltetrazole.

As a result, the local concentration of methacrylate groups in the vicinity of the growing macroradical $[M_l]$ increases in comparison with their average concentration in a reactor $[M_m]$, the latter being determined by spectroscopic methods and used for the calculation of the reaction rates.

$$w = \frac{\upsilon}{[M_m]}.$$

This results in the overestimation of w values perceived as a selective gel effect. No such effect is observed at high concentrations of butanediol dimethacrylate. It was therefore concluded that high flexibility of the growing macroradical containing a large number of units of the monomer **5** is a prerequisite for its manifestation. Evidently, at high content of these units the macroradicals have a coil conformation, which favours intramolecular cyclisation. Selective gel effect can lead to the formation of a specific microheterogeneous network structure consisting of regions with higher concentration of the cross-links incorporated into a loosely cross-linked matrix enriched with units derived from 2-methyl-5-vinyltetrazole.[12]

The experimental values of w_1/w_2 significantly exceed the calculated values (see curves *3* and *4*, Fig. 6) over a broad range of conversions. This difference cannot be explained only by the increase in the local concentration of pendant methacrylate groups.[12] The exit of the monomer **5** from the reaction zone as a result of microsyneresis also seems to play a role in the concentration heterogeneity of the medium. Contrariwise, in the terminal step the experimental values of w_1/w_2, are much lower than the calculated ones.This can be due to higher mobility of the monomer **5** in comparison with dimethacrylate **4** and pendant methacrylate groups under conditions of vitrification of the reaction medium, as a result of which $[M_l]$ in the vicinity of the macroradicals becomes lower than $[M_m]$.

It was shown [12,13,45] that TRCP and the concomitant structure-physical transformations of the reaction medium may induce non-uniform distribution of the reactants in the vicinity of growing macroradicals and, as a consequence, compositional heterogeneity of copolymers. Thus topological peculiarities of TRCP play a role in the formation of compositional heterogeneity of network copolymers. These include cyclisation and selective gel effect in the initial steps of the process, microsyneresis of reactants, differences in the rates of diffusional transport of reactants to macroradicals in the step of vitrification of the reaction medium.

IR spectroscopic monitoring is a promising method for the *in situ* studies of structure–kinetic relationships in TRCP which consists of recording kinetic curves for the decomposition of initiators of the radical polymerisation $C_i(t)$.[50] The vibration bands of the C=O bonds of benzoyl peroxide and dicyclohexyl peroxydicarbonate lie in a convenient region for measurements (1770–1820 cm^{-1}) depending on the type of intermolecular interactions and do not overlap with the absorption bands of C=O in the decomposition products.[87] Their intensities are sufficiently high for registration of the dependences $C_1(t)$, $C_2(t)$ and $C_i(t)$ in one experiment. Combined analysis of these dependences enables the estimation of the contribution of a decrease in the decomposition rates of the initiator to inhibition of TRCP in the vitrification step.[50]

2. NMR studies of formation of network polymers

NMR spectroscopy is widely used for the *in situ* studies of copolymerisation kinetics and the structures of the copolymers formed. The conversion of the double bonds of comonomers is determined from the decrease in the intensities of signals for vinyl protons using high resolution ^{1}H NMR spectrometers.[88,89] Studies of ternary copolymerisation of hydroxyethyl methacrylate (**20**) with *N*-vinyl-2-pyrrolidone (**21**) and *tert*-butyl-2-hydroxycyclohexyl methacrylate (**22**) using this method made it possible to obtain conversion curves for each individual comonomer and to determine the instantaneous composition of the ternary copolymer at various degrees of conversion.[88]

The copolymerisation of acrylamide with bisacrylamide in D_2O has been studied in especially great detail.[26,53] This study revealed a nearly twofold decrease in effective reactivities of the double bonds of bisacrylamide with an increase in the depth of conversion due to accumulation of a great number of less mobile pendant acrylamide groups.[53] A large number of 'head-to-head' additions of the monomeric units testifies to the microheterogeneity of the copolymer structures at the molecular level.[26]

Pulse NMR was used [35,90,91] for the study of formation of network polymers during polymerisation of dimethacrylates. NMR data confirm the validity of the microheterogeneous mechanism of three-dimensional radical polymerisation [23,92] and enable more detailed investigations into formation of network polymers.

3. Dielectric relaxation spectroscopy

The effect of structure-physical transformations of the reaction medium on the kinetics of three-dimensional radical polymerisation is largely realised through changes in the molecular mobilities of the reactants.[36] On-line monitoring of three-dimensional polymerisation by dielectric relaxation spectroscopy in a broad frequency range (as a rule, from 1 to 10^5 Hz) provides comprehensive information about the evolution of structural and dynamic characteristics of the reaction medium. This allows one to follow *in situ* changes in the rotational mobilities of polar groups by changes in the dielectric conductivities ε and transla-

tional mobilities of impurity ions by changes in the electric conductivity σ and to observe microphase separation from the appearance of Maxwell–Wagner interlayer polarisation.[36, 57, 93–95] The informativity of this method increases appreciably when kinetic polymerisation studies are supplemented by calorimetry [36] and IR spectroscopy.[96]

The correlations between the features of molecular motion at different depths of polymerisation and kinetic characteristics of this process were established using a specially designed measuring cell [36] for simultaneous *in situ* registration of dielectric permittivity, conductivity of the reaction medium and heat evolution. It was found that a sharp decrease in the rate of linear polymerisation of MMA, which is due to the vitrification of the reaction medium, correlates with a sharp decrease in dielectric permittivity. This suggests that the freezing of the forward-rotational motion of MMA molecules over the whole bulk of the polymerisate is the main reason for autoretardation of the reaction.[36]

Three-dimensional polymerisation of oligomeric dimethacrylates, in contrast with polymerisation of MMA, is characterised by a broad range of autoretardation and an even broader (as regards conversion) zone of reduced dielectric permittivity.[36, 57] A broad range of dispersion of the dielectric permittivity testifies to the structural and dynamic heterogeneities of the polymerisates formed. Initial manifestations of a decrease in dielectric permittivity are due to the formation of fragments of a network with interjoint distances lower than the size of the kinetic segment (local vitrification). Further gradual decrease in dielectric permittivity down to maximum conversions suggests that fragments with a loose cross-linking where segmental mobility of the network components still remain in the polymer. This molecular mobility resource is used for enhancing the conversion in three-dimensional polymerisation and (co)polymerisation by increasing the temperature in the final step.[83]

The initial steps of three-dimensional polymerisation of dimethacrylates are often accompanied by abnormal increase in dielectric permittivity.[36, 57] The appearance of a positive increment $\Delta\varepsilon$ against the background of a general tendency of the dielectric permittivity to decrease owing to a decrease in the mobility of polar methacrylate groups included into the network is attributed to the formation of a microheterogeneous structure of the polymerisate, which restricts the mobilities of ionic impurities. An analysis of different models of microheterogeneous polymerisates revealed that these abnormalities can be explained by the 'reversal' of the matrix for the mechanism of interlayer polarisation and by using the theory of polarisation of the diffusion zone of the double electric layer.[97, 98]

A promising approach to the study of three-dimensional radical copolymerisation entails the use of complex techniques which include simultaneous monitoring of the reaction by dielectric relaxation and IR spectroscopy. The use of model oligomer–monomer systems allowing selective monitoring of molecular mobility of a polar cross-linking reagent (dimethacrylate) in a non-polar medium of the second monomer (styrene) seems to be a very informative approach.

4. Fluorescent probes

The use of fluorescent molecular probes for the study of polymerisation processes is based on high sensitivity of emission spectra parameters to intermolecular interactions and structure-physical state of the medium. The changes in the state of the nearest environment of luminophore molecules may bring about shifts in the maximum of the emission band, enhancement of the fluorescence intensity and changes in the anisotropy and fluorescence lifetime.[99] On-line measurements of these parameters in the course of polymerisation provide direct information about the structural evolution of the reaction medium.[100]

The fluorescence method was used for the study of the sol–gel transition in the copolymerisation of MMA with compound **1** [101–103] using pyrenemethyl pivalate as a probe. It was found that the intensity of fluorescence (I) at the moment of sol–gel transition (t_c) was sharply increased due to freezing of molecular mobility and an increase in the quantum yield of the fluorescence. A comparison of the experimental dependence t_c on the concentration of ethylene glycol dimethacrylate c_0 (see Ref. 101) with a calculated dependence obtained on the basis of a kinetic model of gel formation [104]

$$t_c = (kc_0)^{-1}, \tag{8}$$

where k is the combination of rate constants for all steps of the reaction, revealed that at the dimethacrylate concentrations above 0.5% the experimental values of t_c exceed manyfold the calculated values and are little dependent on the concentration of dimethacrylate in the reaction mixture (Fig. 7). These discrepancies are due to a decrease in the overall rate constant k caused by a decrease in the probability of involvement of pendant methacrylate groups in the molecular cross-linking.[101, 105]

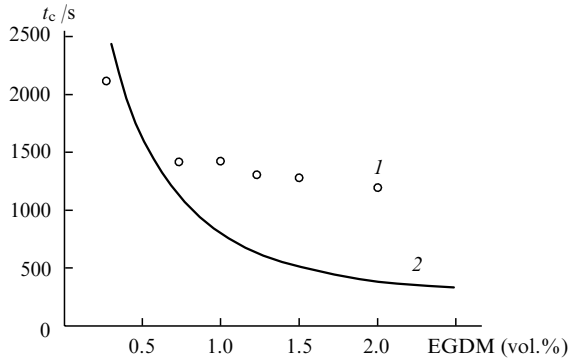

Figure 7. Dependence of the onset of gel formation in copolymerisation of MMA with ethylene glycol dimethacrylate (EGDM) at 75 °C on the concentration of dimethacrylate.[101]
(*1*) Experimental data, (*2*) curve calculated from Eqn (8).

The experimental dependences $I(t)$ were used [101–103] for determining the numerical value of a critical parameter β in the expression for the sol–gel transition in the framework of a percolation gel formation model:[106]

$$G = B(p - p_c)^{\beta}, \tag{9}$$

where G is the share of the gel fraction, B is the critical amplitude and p is the probability of formation of a bond between the adjacent junctions of the network. If $p = p_c$, this corresponds to the onset of formation of an infinite cluster, *viz*., the gel point. Assuming [101] that the reaction time t is proportional to the probability p, the time t_c corresponds to the gel point, and the fluorescence intensity corresponds to the amount of the gel formed, Eqn (9) can be converted into Eqn (10):

$$I = A(t - t_c)^{\beta}, \tag{10}$$

where A is a new critical amplitude. The values of β determined from the slope of the dependences:

$$\log I = \log A + \beta \log(t - t_c)$$

appeared to be the same for systems with different content of dimethacrylate; the average value of $\beta = 0.40 \pm 0.03$ was similar to that calculated on the basis of the percolation model.[106]

Copolymerisation of acrylamide with bisacrylamide in an aqueous solution was studied using 1-anilinonaphthalene-8-sulfonate (**23**) as a fluorescent probe.[99] The polymerisation was accompanied by a 20-fold increase in the fluorescence intensity with an increase in the volume fraction of the polymer in the hydrogel due to a decrease in the diffusion coefficient of the water molecules which play the role of fluorescence quenchers. There is a good correlation between the kinetic curves for the increment of I and the curves obtained using the dilatometric method. Both

methods gave similar values of rate constants for polymerisation and the reaction order with respect to the initiator.

An equipment for simultaneous *in situ* monitoring of conversion of double bonds and recording fluorescence spectra has been described.[100] In this equipment the differential scanning calorimeter and a spectrofluorimeter have a common measuring cell. 7-Nitro-2,1,3-oxadiazole dialkylamino derivatives (**24**, **25**) were used as fluorescent probes. That containing an acrylate group was incorporated into the network as a fluorescent label. Studies of photopolymerisation of dimethacrylates and other multifunctional oligomers revealed a good correlation between the increase in the fluorescence intensity and conversion of C=C bonds.

Both inert and reactive fluorescent probes (**26a**–**e**) based on 4-amino-4′-nitrostilbene were used for the study of microheterogeneity of the reaction medium in photopolymerisation of ethylene glycol, triethylene glycol, butanediol and hexanediol dimethacrylates.[107]

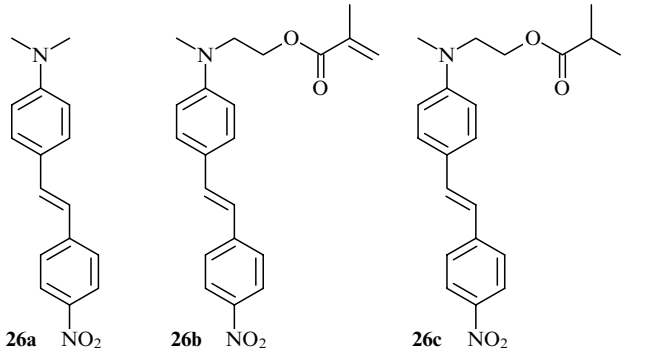

The inert probes **26a**, **26c** and **26e** simulated free oligomer molecules and participated in microsyneresis throughout the polymerisation; these concentrated in areas with a loose network and were surrounded by the oligomer molecules. The probes **26b** and **26d** containing methacrylate groups were incorporated into the network polymers formed and were distributed in the reaction medium more uniformly.[107]

The polymerisation of all dimethacrylates studied was accompanied by a shift of the maximum towards a short-wavelength region with a simultaneous broadening of the fluorescence band (λ_{max}); however, on reaching a $\sim 60\%$ conversion, the spectrum was slightly narrowed. In the authors' opinion,[107] the polymerisation results in the formation of a heterogeneous reaction medium in which the probe molecules are distributed between different microregions. As a consequence, the fluorescence spectrum represents a sum of spectra of probe molecules in different environments which vary from highly mobile regions enriched with the oligomer ($\lambda_{max} = 700-650$ nm) to regions consisting exclusively of rigid densely cross-linked polymer ($\lambda_{max} = 560-590$ nm). The changes in the spectral parameters of fluorescence are observed as a result of accumulation of a network polymer and the redistribution of probe molecules between different microregions. The probes **26a**, **26c** and **26e** are displaced from the areas with a high density of the network to more mobile loosely cross-linked areas. This can be evidenced from a smaller shift of λ_{max} in comparison with the shifts of λ_{max} in the case of probes **26b** and **26d**, which are immobilised in the network as a result of copolymerisation with dimethacrylates. A decrease in the width of the fluorescence band on reaching a $\sim 60\%$ conversion testifies to the tendency of the network density to equalise at greater depths of polymerisation. This tendency is consistent with the results of modelling and high-temperature annealing of network polymers.

IV. Control of three-dimensional radical copolymerisation and design of network macromolecular structures

Process control of three-dimensional radical copolymerisation and the formation of network copolymer structures entails control over growth, cyclisation and chain cross-linking reactions (1)–(5). Some authors (for bibliography, see Ref. 1) consider the intermolecular cross-linking reaction (3), responsible for the formation of macrogel, and secondary cyclisation (or intramolecular cross-linking) reaction (4), which results in the formation of microgel particles and a molecular network structure, as key objects for the control. However, the conventionality of such separation can be illustrated by the fact that the contribution of reactions (3) and (4) depends, in turn, on the lengths of the primary polymer chains formed in reaction (1).[6] Therefore, studies on three-dimensional radical (co)polymerisation are currently characterised by an intensive search for ways of control over the whole complex of reactions (1)–(5).

A characteristic feature of TRCP is the existence of tight structure–kinetic relationships realised at both topological and morphological levels of formation of the structure of the network polymer. Therefore, the studies devoted to the problem of control over TRCP processes can arbitrarily be divided into two groups depending on the factors (structure-physical or kinetic) used for this analysis. The conventionality of such division is determined by the fact that any changes in the structures of the starting monomers M_1 and M_2 and in the properties of the reaction medium (*e.g.*, type of solvent, nature of intermolecular interactions, *etc.*) determine the kinetics of the process. In turn, varying of the rates of initiation, growth and chain termination reactions is accompanied by changes in the structural and diffusional characteristics of the reaction medium, which influences the kinetics of the reaction in accordance with the feedback principle.

1. Structure-physical methods of control over three-dimensional radical copolymerisation

The structure-physical approach to the control over TRCP processes is based on variations of the types and intensities of intermolecular interactions in the reaction mixture. In practice, this approach is realised in several ways. Monomer units with bulky alkyl substituents, which create steric hindrance for the interaction of the growing radicals with pendant double bonds, are introduced into a copolymer chain in order to suppress cyclisation and intermolecular cross-linking. Monomers containing sites for strong intermolecular interactions resulting in the formation of a physical interaction network in the reaction medium are employed to stimulate intermolecular cross-linking and gel formation. And, finally, the contributions of cyclisation and intermolecular cross-linking can be controlled by varying the excluded volume factor through the use of solvents possessing different thermodynamic affinities for the copolymer formed.

Steric effects of alkyl substituents of methacrylate monomers on gel formation during their copolymerisation with multifunctional methacrylates have been studied.[108] It was shown that in copolymerisation of ethylene glycol dimethacrylate with dodecyl methacrylate (**27**) the intermolecular cross-linking can be completely suppressed due to steric hindrance created by the alkyl group of $C_{12}H_{25}$. This represents a new route to the preparation of reactive prepolymers carrying pendant methacrylate groups.

The effects of steric hindrance on the critical conversion (gel point) in the copolymerisation of allyl methacrylate (**28**) with MMA, dodecyl methacrylate, butyl methacrylate and hexadecyl methacrylate (**29**) have been studied.[109] The degree of polymerisation of the primary chains was maintained at the same level using a chain transfer agent, *viz*., dodecanethiol (**30**). A characteristic feature of the polymerisation of allyl methacrylate in comparison with dimethacrylates is that in the early steps of polymerisation a polymer is formed carrying only allyl pendant groups due to low reactivities of the allylic double bonds.[110, 111] Therefore, gel formation in the homopolymerisation of allyl methacrylate occurs later than in the polymerisation of dimethacrylates. In the copolymerisation of allyl methacrylate with MMA and butyl methacrylate, the experimental critical conversion corresponding to the gel point (C_c = 24.1%) coincided with that calculated with the use of the Stockmayer theory, whereas in the copolymerisation with methacrylates **27** and **29**, the gel point was shifted towards the critical conversion of 34.3% and 43.0%, respectively. It was shown [109] that as in copolymerisation of higher methacrylates with dimethacrylates, this shift is due to steric hindrance exerted by long-chain alkyl substituents, which prevents interaction of growing methacrylate radicals with pendant allyl groups.

The topology of the TRCP reaction strongly depends on the rigidity of the main chain of the copolymer macromolecule that is being formed.[6] This was established in comparative studies of gel formation during copolymerisation of dimethacrylates with MMA, on the one hand, and with *tert*-butyl methacrylate (**31**) and bornyl methacrylate (**32**), on the other hand. It was found that in copolymers prepared with involvement of the methacrylate units **31** and **32** cyclisation and inter- and intramolecular cross-linking are suppressed due to a decrease in the flexibility of the main chain and steric hindrance created by bulky substituents.

The effects of the physical network of the hydrogen bonds on intermolecular cross-linking and gel formation in three-dimensional copolymerisation have been studied.[112, 113] The copolymerisation of benzyl methacrylate (**33**) with 2 mol.% of hexanediol dimethacrylate was carried out in a solution of *tert*-butylbenzene in the absence and in the presence of 5 mol.% of (2-methacryloyloxyethyl) succinate (**34**).[112] The onset of gel formation occurred at conversions of 38.2% and 30.0%, respectively. The displacement of the gel point towards lower conversion values in the presence of the succinate **34** is due to the formation of hydrogen bonds between the carboxy groups of the succinate units **34** incorporated into the prepolymer and the growing macroradical. The presence of these bonds reduces the excluded volume effect thus favouring intermolecular cross-linking of the polymeric radicals with the pendant methacrylate groups of the prepolymer and the formation of macrogel.[112] A displacement of the gel point towards lower conversions under the influence of hydrogen binding of carboxy groups was also observed in ternary copolymerisation of hexanediol dimethacrylate with butyl methacrylate and the succinate **34**.

A combination of chemical and physical cross-linking makes it possible to realise the conditions of formation of network polymers which are consonant with the Flory–Stockmayer theory and to synthesise the networks close to ideal.[112] Copolymerisation of methacrylate **33** with 0.05 mol.% of poly(ethylene glycol) $(CH_2CH_2O)_{23}$ dimethacrylate (**35**) in *tert*-butylbenzene supplemented with 5 mol.% of the succinate **34** is an example. In the absence of the succinate **34**, no gel is formed even at maximum conversions of ~94%; however, in its presence, the network of hydrogen bonds favours the formation of a chemically cross-linked macrogel even at 58.4% conversion. The ratio of the experimental value of conversion, which corresponds to the gel point to the theoretical value is 1.9, which allows this network to be considered [112] as virtually ideal. The formation of such a network is favoured by the formation of a diphilic copolymer with a rigid non-polar primary chain built of units of methacrylate **33** and flexible polar pendant chains of dimethacrylate **35** in the pre-gel step.

Considerable attention is given to the study of three-dimensional copolymerisation of dimethacrylates with hydrophilic monomers containing hydroxy groups. The resulting hydrogels manifest good swelling properties in the presence of water. By virtue of their hydrophilic nature and good biocompatibility, such hydrogels find use in medicine and biology.[114]

Hydrogels based on hydroxyethyl methacrylate (**20**) are widely used in medicine. Large amounts of such hydrogels are used in the production of contact lenses,[115] while copolymers based on methacrylate **20** and dimethacrylates of ethylene glycol and diethylene glycol dimethacrylates are used as blood substitutes and drug depots.[116] Therefore, the regulation of processes of formation of the structure and properties of hydrogels based on methacrylate **20** should meet the most rigid criteria. Special attention is given to primary cyclisation, since it causes a significant deviation of mechanical properties, swelling index and diffusion characteristics of the copolymer from the corresponding parameters of an ideal network along with lower density of chain cross-linking. The effect of the composition of the monomeric mixture on primary cyclisation in photoinduced copolymerisation of methacrylate **20** with diethylene glycol dimethacrylate and poly[ethylene glycol(600) dimethacrylate] (**36**) has been studied.[114] A comparison of experimental results with the results of computer simulation of the reaction kinetics using a method developed by Elliot and Bowman [117] showed that the dependence of reactivities of pendant methacrylate groups on their spatial localisation, moment of 'generation' and length of the spacer as well as the differences in the local and averaged concentrations of polymeric radicals should be taken into consideration to fit the experimental data on the extent of cyclisation with the calculated values. The addition of a solvent increases the probability of cyclisation due to a decrease in the rate of the reaction of polymeric radicals with the monomer and an increase in the time of contact of the radical with the pendant methacrylate groups.[114]

The effects of the solvent on the formation of a network copolymer in the ternary copolymerisation of methacrylate **33**, ethylene glycol dimethacrylate and methoxytricosaethylene glycol methacrylate (**37**) have been studied.[6] The copolymer formed had a diphilic nature owing to a combination of a non-polar main chain and polar side chains of the comonomer **37**. As a result, the conformation of the copolymer depended on the nature of the solvent, which, in its turn, affected the cross-linking process. Thus the compression of the main chain and straightening of the side chain in a methanolic solution resulted in the formation of microgel particles.

Emulsion copolymerisation of styrene and MMA with divinylbenzene is used in the synthesis of reactive microgel particles having submicron sizes and carrying pendant C=C bonds.[118, 119] The microgels thus obtained are used in the production of polymeric coatings.

Three-dimensional radical copolymerisation in the presence of diluents is widely employed for the preparation of heterogeneous porous materials used as sorbents, membranes and materials for chromatography. Phase separation is the main driving force in the formation of a porous structure, while the morphology of the network polymer formed is determined by the microheterogeneous mechanism of copolymerisation.[1] Two-component mixtures consisting of a good solvent and a precipitant are often used for controlling the parameters of the porous structure of a copolymer in suspension copolymerisation.[120–122]

Hydrogen binding sites, which represent hydroxy groups localised in the oligomeric chain of dimethacrylate, have a pronounced effect on the TRCP processes and the structure and properties of the copolymers formed.[5] Studies of copolymerisation kinetics of such dimethacrylates by real-time IR spectroscopy revealed [5] that effective reactivities of methacrylate groups depend critically on the curing temperature. Thus in the initial steps, the rate of copolymerisation of methacrylate groups at 30 °C significantly exceeds that of styrene, whereas at 90 °C the difference is levelled off. A considerable effect of temperature on the relative

reactivities of the double bonds of comonomers can be explained [34] by the fact that low temperatures favour the formation of oligodimethacrylate associates stabilised by intermolecular hydrogen bonds and with methacrylate groups arranged favourably for the chain growth. An increase in temperature results in the dissociation of such associates and a decrease in effective reactivities of methacrylate groups.

Studies into mechanical properties of copolymers prepared at 30 and 90 °C and further cured to a state with identical conversion of the double bonds revealed that the strength and impact elasticity of the destruction of a low-temperature copolymer significantly exceed those of a high-temperature one. These differences correlate with the peculiarities of the microstructures of the copolymers as revealed in the analysis of the failure surface by atomic-force microscopy. Both copolymers have granular structures with the grain sizes of about 100 nm, the grain size in the low-temperature sample being larger. It was concluded [5] that the granular morphology of copolymers is due to the fact that TRCP occurs with the formation of microgel particles which then merge to form clusters. It was found also that microphase separation the early stages of which are temperature-dependent plays an important role in the formation of granular morphology.

Introduction of hydrogen-binding sites into network polymers based on dimethacrylates offers additional opportunities for modification of their properties owing to a combination of chemical physical networks. However, the problem of steric effects exerted by the rigid network of chemical bonds on the feasibility of realisation of an interpenetrating network of labile hydrogen bonds is still topical. Model hybrid networks based on triethylene glycol dimethylacrylate and containing COOH groups as potential junctions of a physical network were tested.[123] The carboxy groups were introduced in three different ways, *viz*., by copolymerisation of triethylene glycol dimethylacrylate with methacrylic acid, by polymerisation of dimethacrylate containing a solubilised copolymer of MMA with methacrylic acid and by thermal oxidation of residual double bonds in a homopolymer of triethylene glycol dimethacrylate. IR spectroscopic studies have shown that hydrogen bonds are formed both between the carboxy groups (dimers) and between the carboxy and ester groups; hydrogen bonds depleted by steric hindrance and a certain amount of free COOH groups are also present. The relative contents of different hydrogen bonds and free carboxy groups that cannot form H-bonds due to steric hindrance depend on the mode of introduction of these groups into the polymeric matrix.[123]

A significant effect on TRCP is produced by additives of various polymers introduced into the reaction medium in order to reduce shrinkage and modify the structure and properties of the network copolymers. A great number of papers are devoted to the effects of polymeric additives on curing of polyester resins which represent mixtures of unsaturated polyesters with styrene.[124–126] A characteristic feature of such processes is phase separation of the reaction mixture in the very early steps of the reaction and the formation of a biphasic structure where the components represent inclusions of the polymeric additives and the matrix represents a cured polyester resin.[126, 127] A polymeric additive can influence the topology and kinetics of network formation. The scope of this influence is determined by the concentration of the additive and its compatibility with the original reaction mixture and the network copolymer formed.[128]

A comprehensive structure–kinetic study of TRCP of a polyester and styrene in the presence of additives, *viz*., PMMA (**11**) and poly(vinyl acetate) (**38**) having a higher thermodynamic compatibility with the reaction medium has been carried out.[128] The reaction rate was recorded using differential scanning calorimetry; changes in the sizes of the microgel particles in the step preceding the formation of the macrogel were monitored by gel-permeating chromatography. It was found that the rate of copolymerisation decreases with an increase in the concentration of the additive, this effect being more pronounced for the polymer of **11**. The same factors determine the extent of reduction of microgel particles in early steps of the reaction. It was concluded [128] that poor compatibility of polymeric additives with the polyester results in compression of coils of polyester molecules in a mixture of styrene with the additive, which favours intramolecular cyclisation, reduction of the sizes of microgel particles and a shift of the onset of macrogel formation towards higher conversions.

2. Kinetic methods for the control over three-dimensional radical copolymerisation

The existence of a relationship between the kinetics of three-dimensional radical (co)polymerisation and structure formation of network (co)polymers has stimulated a search for efficient methods for the control over this process at different rates of initiation, growth and termination of polymeric chains.

The effect of the initiator concentration on the formation of microgel particles was studied for bulk polymerisation of ethylene glycol dimethacrylate.[129] This study included isolation and analysis of gel particles at different stages of the polymerisation process. The overall conversion of the double bonds was estimated using differential scannining calorimetry; the number of pendant methacrylate groups in gel particles was determined by IR spectroscopy. Dynamic light scattering studies have shown that a bimodal distribution of gel particles according to their size takes part in the reaction system in the very earliest steps of the reaction. It is of note that larger particles are formed upon aggregation of smaller particles.

The conversion of pendant double bonds in microgel particles increases in the course of polymerisation from 20% (at the overall conversion of double bonds of $\sim 1\%$) to 65% at the moment of formation of the macrogel (at the overall conversion of double bonds of 14%). An increase in the initiator concentration results in considerable broadening of the range of size distribution of macrogel particles: at the initiator concentration of 1%, the size of smaller particles ranges from 19 to 30 nm, whereas that of large particles is in the range 83–134 nm. If the initiator concentration increases to 5%, the ranges of the particle size increase to 11–32 and 44–154 nm, respectively, but the average size of larger particles diminishes from 105 to 80 nm, presumably at the expense of an increasing contribution of the quadratic radical termination reaction at invariably high rates of initiation and shortening of primary polymer chains involved in the formation of larger particles. The data obtained [129] suggest that the morphological structures of the polymers formed depend critically on the concentration of the initiator.

However, the experimental results reported by Chiu and Lee [129] do not correlate with the results obtained within the framework of a model of three-dimensional radical polymerisation.[24] According to this model, the reaction system contains, from the very beginning of polymerisation, only two components, *viz*., the starting oligomer and grains of a network polymer with the maximum possible degree of conversion. In the course of polymerisation, which occurs on the grain surface, the size of the grains increases and the latter begin to aggregate. Contrary to model concepts,[24] the degree of polymerisation of microgel particles increases gradually with time; the reaction of pendant methacrylate groups inside gel particles makes a significant contribution to the total conversion of the double bonds.[129]

It has been shown [130] that the experimental results obtained in the study cited [129] do not fit in kinetic and statistical network formation models, since they ignore the changes in structure–kinetic relations in polymerisation. However, it was found that these results can qualitatively be rationalised in the framework of a percolation model, which takes account of translational diffusion of monomeric and polymeric molecules, segmental diffusion of polymeric chains, excluded volume effect, formation of microgel particles and differences in effective reactivities of double bonds in the starting oligomer and pendant methacrylate groups. Presumably,[130] a more precise description of microheterogeneous

three-dimensional polymerisation should rely on a model which combines the advantages of the percolation model with those of the average field model.

The multimodal distribution of microgel particles according to their size [129] seems to be the most characteristic feature of three-dimensional radical polymerisation and copolymerisation. This was confirmed by the results of investigation of microgel particles obtained by copolymerisation of ethylene glycol dimethacrylate with MMA in toluene in which the cross-linking reagent was used at the concentrations of 9 mol.% and 15 mol.% (see Ref. 131). Data from exclusion chromatography suggest that in both cases the distribution of microgel particles according to their size changed gradually in the course of copolymerisation from monomodal to bimodal due to increasing fraction of larger particles. It was emphasised [131] that bimodal distribution of particles near the gel point provides conclusive evidence in favour of a coagulation macrogel-forming mechanism according to which small-sized (primary) particles aggregate to form larger particles. In earlier studies,[1] the formation of a macrogel in the course of TRCP was considered as a special manifestation of chemical aggregation of colloidal particles. The correlation between cross-linking and chain termination rate constants, on the one hand, and changes in the structures and sizes of reaction components, on the other hand, should be taken into consideration in describing the kinetics of gel formation as the interaction of microgel particles.[131]

IR spectroscopic monitoring was used [45] to study the effect of the initiator concentration on the copolymerisation kinetics of butanediol dimethacrylate with 2-methyl-5-vinyltetrazole (monomer **5**) over the whole range of conversion. It was found that the reduced copolymerisation rate of the methacrylate groups (w_1) in the initial steps of the reaction increases with the concentration of the initiator (dicyclohexyl peroxydicarbonate) (1 mass % – 3 mass %), this increase being more pronounced than that of the monomer **5** (w_2). This can be due to the fact that at high rates of initiation shrinkage lags behind copolymerisation in time, which leads to appearance of excess free volume in the vicinity of growing macroradicals. The mobilities and effective reactivities of pendant methacrylate groups increase correspondingly. The local concentration of the monomer **5** in the reaction zone may additionally decrease with an increase in the degree of cross-linking inside the microgel particles as a result of microsyneresis and a concomitant increase in the w_1/w_2 ratio. The differences in the effects of initiation rates on the copolymerisation kinetics of reaction components result in a significant effect of the initiator concentrations on the compositional and structural heterogeneities of network copolymers even if the compositions of original oligomer – monomer mixtures are identical.

An important role in the control over three-dimensional radical polymerisation is played by inhibitors and the polymer chain transfer agents. Their mechanisms of action are based on suppression of the intramolecular cyclisation reaction (2) by reduction of the lengths of primary polymeric chains. Trinitrotoluene (**39**) was found to be an effective regulator of structure formation in three-dimensional polymerisation of dimethacrylates.[23, 132] The addition of the polymerisation inhibitor **39** results in drastic changes in the kinetic and rheological characteristics of polymerisation of triethylene glycol dimethacrylate.[23] This is manifested in a shift in the onset of the gelation effect from the degree of conversion $\sim$ 1% to $\sim$ 15% with retention of fluidity of the polymerisate in this conversion range. In the Avrami coordinates, the polymerisation kinetics is characterised by the coefficient $n = 0.9$, which suggests homogeneity of polymerisation and the formation of short comb-like polymer chains with pendant methacrylate groups. Then, the system loses its fluidity, as a result of which the Avrami coefficient increases to 1.3 due to a decrease in the rate constant for quadratic termination of the macroradicals. The lack of the autoretardation step up to maximum conversions of $\sim$ 70% is a characteristic feature of the reaction carried out in the presence of 10 mol.% of the inhibitor **39.** Conventional microheterogeneous polymerisation of triethylene glycol dimethacrylate is described by a constant value of the Avrami index (1.6) even in the early steps up to a transition to the autoretardation mode at $\sim$ 40% conversion. The differences in the kinetics of ordinary and suppressed polymerisation of triethylene glycol dimethacrylate suggest that after addition of the inhibitor **39** the microheterogeneous formation of a network polymer can be replaced by a quasi-homogeneous one.

The effects of the inhibitor **39** on the copolymerisation kinetics of ethylene glycol and triethylene glycol dimethacrylates and oligocarbonate dimethacrylate as well as on the structures and properties of the polymers formed have been studied.[132] In this study, compound **39** suppressed the microheterogeneity of the reaction medium and favours the formation of polymers with more homogeneous structures. Compound **39** has an advantage over other, more rapidly consumed inhibitors in that it controls gel formation throughout the polymerisation time, since the value of the rate constant for the inhibition is $\sim$ 20 times lower than for chain growth.[132]

Chain transfer agents (alkanethiols and alkyl halides) are used to control three-dimensional (co)polymerisation much more frequently than inhibitors. Using chain transfer reactions, one can control successfully the degree of polymerisation of primary chains, prevent cyclisation and displace the gel point towards higher conversion values. Very often, this results in elimination of the gel effect. The main approaches to the use of chain transfer reactions for the control over three-dimensional thermally induced (co)polymerisation are discussed in a review.[6]

Considerable attention has recently been given to the role of the chain transfer reaction in three-dimensional photoinduced copolymerisation.[133, 134] The effect of initiation and chain transfer rates on the copolymerisation kinetics of hydroxyethyl methacrylate with 1 mass % of diethylene glycol dimethacrylate on the structure of the polymer chain was studied.[134] It was found that the lengths of the kinetic chains and the polymerisation rate decrease, while the rates of quadratic radical termination reactions increase in the presence of dodecane-1-thiol as the chain transfer agent. An increase in the initiation rate and a concomitant increase in the photoirradiation rate result in high concentration of short radicals, which also increases the probability of the chain termination reaction. Large number of short polymeric chains and the formation of a sol fraction significantly deteriorate the properties of network polymers of biomedical applications. Optimisation of conditions for their preparation demands selection of photoinitiation rates with account of the dependence of the chain termination reaction on the chain length.[134]

3. Chain transfer catalysts as regulators of three-dimensional radical (co)polymerisation and (co)polymer structures

The discovery of a catalytic chain transfer on a monomer in the linear polymerisation of MMA [135] has stimulated a search for possible applications of chain transfer catalysts in the control over three-dimensional polymerisation of oligodimethacrylates and the synthesis of soluble reactive polymers based on them.[28, 76, 136, 137] These and subsequent studies have demonstrated that the structure-forming role of chain transfer catalysts in linear and three-dimensional radical polymerisation differ substantially despite identical chemical mechanisms.

Low-spin cobalt(II) complexes with various macroligands proved to be highly efficient chain transfer catalysts in the polymerisation of methacrylates.[138] The type of ligand environment has a crucial effect on the rate constants of the catalytic chain transfer reaction, for the series of cobalt glyoximates these vary from 50 to 100 000. The steric factor, which determines the possibility of the interaction of cobalt with a growing polymeric radical, plays an important role. These data were taken into consideration in the design of catalysts that are efficient in the chain transfer from the methacrylate radicals, but completely inert with respect to styrene radicals.[138]

The pioneering study [135] was devoted to polymerisation of MMA in the presence of a cobalt – hematoporphyrin complex

[Co(II)P]. A two-step catalytic mechanism was proposed for the chain transfer from the growing radical R_n^* to the monomer M:

$$R_n^* + Co(II)P \longrightarrow Z_n + HCo(III)P, \quad (11)$$

$$HCo(III)P + M \longrightarrow Co(II)P + R_1^*. \quad (12)$$

According to IR spectroscopic data,[139] abstraction of the hydrogen atom from the terminal methyl group of the C-tertiary radical R_n^* in reaction (11) results in the formation of the unsaturated macromonomers Z_n:

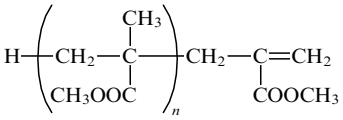

40

Because of the high value of the rate constant for the catalytic chain transfer (2.4×10^3), the Co(II)P added to the reaction medium in as low concentration as 6.6×10^{-4} mol litre^{-1} favours the formation of an oligomer P_n with a degree of polymerisation $n = 9$.[135] Preparation of an oligomer of the same degree of polymerisation in the presence of ordinary chain transfer agents of the thiol type demands $\sim$ 10 mass % of the latter, which is incorporated in the oligomer and thus presents serious technological problems.[140] The use of catalytic chain transfer agents not only eliminates these problems, but also enables access to reactive macromonomers of variable degrees of polymerisation which can be regulated by varying the concentration of the transfer agent.[138, 140]

Catalytic chain transfer reactions are widely used in the synthesis of macromonomers of the type **40** from various methacrylates.[141] Their reactivities differ significantly from those of ordinary unsubstituted methacrylates, since the radicals formed as a result of an attack on the vinyl group of the oligomers **40** have low growth rates due to steric shielding.[142] Therefore, the adducts formed in the reaction of the radicals R_n^* with macromonomers of the type **40** are prone to undergo reversible β-fragmentation, *i.e.,* elimination of the terminal fragment.[140, 143]

$$R_n^* + Z_k \rightleftharpoons Z_{n+1} + R_{k-1}^*. \quad (13)$$

Study of this reaction in a macromonomer **40**–butyl methacrylate mixture has led to suggestion [143] that macromonomers of the type **40** are involved neither in the copolymerisation with ordinary methacrylates nor in chain transfer catalysis through Co(II), but are themselves active participants of a catalytic chain transfer. A competition between catalytic chain transfer reactions through intermediacy of Co(II) and β-fragmentation is a characteristic feature of all reactions involving Co(II) complexes. Its role increases with an increase in the degree of conversion. Reaction (13) significantly extends the potential of radical polymerisation and allows one to perform synthesis of block and graft copolymers with acrylates, styrene and other monomers, which cannot normally be accomplished.[140, 143]

For the first time, the catalytic chain transfer reaction was used for the control over three-dimensional radical polymerisation of dimethacrylates.[28, 76] It was found that the polymerisation of triethylene glycol dimethacrylate in the presence of Co(II)P yields soluble linear oligo-*n*-methacrylates

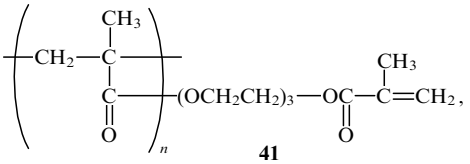

41

carrying a pendant methacryloyl group in each repeating unit. The degree of polymerisation of the oligomers **41** depends on the concentration of the chain transfer catalyst.

The oligomers **41** with degrees of polymerisation $n = 5-15$ manifest high reactivities. Substitution of oligomers **41** for dimethacrylates makes it possible to diminish chemical shrinkage and internal stresses within the polymer and to obtain networks with segmental structures made up of long and short polymethacrylate chains cross-linked with oligomeric chains. The polymers prepared from oligomers differ from ordinary triethylene glycol dimethacrylate-based polymers in syndiotactic attachment of their methacrylate groups and higher values of elastic moduli.[28] This testifies to gradual elimination of steric hindrances preventing the growth of polymethacrylate chains and alleviation of internal stresses associated with the two-step synthesis of the polymer. Possible applications of compounds **41** for improving the quality of paintwork materials based on oligoester acrylates are discussed.[77]

The addition of Co(II)P to triethylene glycol dimethacrylate in its bulk polymerisation strongly attenuates the gel effect which is shifted towards higher conversion values.[76] However, with an increase in the concentration of the catalyst up to the maximum limiting solubility values (5×10^{-3} mol litre^{-1}) the gel effect cannot totally be eliminated and insoluble network polymers are formed. Preparation of soluble products **41** and elimination of the gel effect can be achieved by polymerisation in DMF, which prevents aggregation of polymeric chains and the formation of a macrogel. In this context, degeneration of the gel effect can be regarded as a reliable test for the formation of multifunctional compounds **41**.[76]

The effect of the catalytic chain transfer reaction on polymerisation of ethylene glycol and diethylene glycol dimethacrylate with AIBN as the initiator has been studied.[29, 144] The addition of Co(II)P sharply decreases the polymerisation rate, diminishes the gel effect and changes the shapes of the kinetic curves (Figs 8 and 9). This suggests that Co(II)P significantly restricts the development of microheterogeneity of the reaction medium and the effect of the latter on the rates of chain growth and chain termination due to formation of multifunctional oligomers with pendant methacrylate groups.

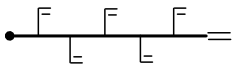

42

The probability of intramolecular cyclisation decreases sharply after the formation of low-molecular-weight intermedi-

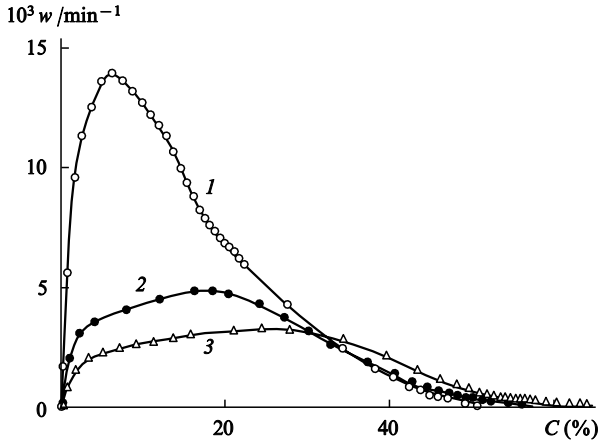

Figure 8. Kinetics of polymerisation of ethylene glycol dimethacrylate under ordinary conditions (*1*) and in the presence of 6×10^{-4} (*2*) and 3×10^{-3} mol litre^{-1} (*3*) Co(II)P.[30]
[AIBN] = 6.4×10^{-3} mol litre^{-1}, $T = 60$ °C.

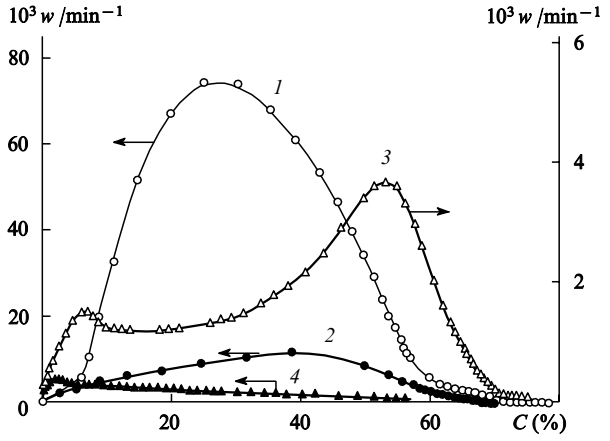

Figure 9. Kinetics of polymerisation of diethylene glycol dimethacrylate under ordinary conditions (*1*) and in the presence of 6.5×10^{-4} (*2*), 3.3×10^{-3} (*3*) and 13×10^{-3} mol litre^{-1} (*4*) Co(II)P.[144]
[AIBN] = 6.4×10^{-3} mol litre^{-1}, $T = 60$ °C.

ates **42** and prerequisites appear for the formation of more homogeneous polymers.

The extent to which the chain transfer catalyst influences the rate of polymerisation of ethylene glycol and diethylene glycol dimethacrylates and the shapes of kinetic curves vary significantly (see Figs 8 and 9). As a consequence, the effective rate constant for the catalytic chain transfer and the structure–kinetic relationships in three-dimensional radical polymerisation strongly depend on the structures of the starting oligomer and the polymer and physical characteristics of the reaction medium.

It is known that this rate constant decreases in linear polymerisation of methacrylates with an increase in the length of the alkyl substituent.[145] However, in the polymerisation of dimethacrylates, similar doses of Co(II)P more strongly inhibit the polymerisation rate of diethylene glycol dimethacrylate, an oligomer with a greater chain length (see Figs. 8 and 9). Higher efficiency of the chain transfer catalyst in the polymerisation of diethylene glycol dimethylacrylate can be ascribed to structural peculiarities of the growing polymeric radical, *viz*., the probability of intramolecular transfer of chains to the pendant double bonds of diethylene glycol dimethacrylate is higher than in the case of ethyleneglycol dimethacrylate due to the greater length of the spacer.[144]

Obviously, the role of a catalytic chain transfer in the formation of a more homogeneous network structure is not confined to the inhibition of intramolecular cyclisation (*1*):

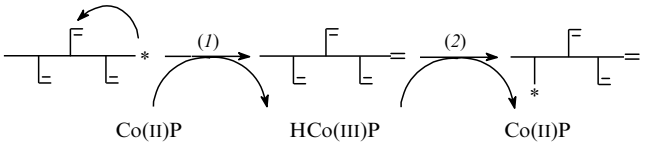

An important role is ascribed to the probability of intermolecular cross-linking of the intermediates **42**, which involve pendant radicals formed in the intramolecular chain transfer reaction (*2*).

Polymerisation of diethylene glycol dimethacrylate in the presence of high concentrations of Co(II)P is accompanied by an appearance of two maxima on the kinetic rate curve $w(C)$ which correspond to 6% and 53% conversion of the double bonds. The first maximum is unrelated to a classical gel effect and appears as a result of formation of multiple terminal C=C bonds in a fast catalytic chain transfer reaction. The formation of such bonds is accompanied by a reduction of the thermal effect of polymerisation (Q) depending on the number-averaged degree of polymerisation ($\bar{P}$) (see Ref. 141)

$$Q = \frac{Q_\infty (\bar{P} - 1)}{\bar{P}}, \qquad (14)$$

where Q_∞ is the specific heat of polymerisation in the absence of a chain transfer catalyst.

Thus, the first maximum (Fig. 9, curve *3*) corresponds to the apparent gel effect and is manifested if Q_∞ is used instead of Q in the processing of calorimetric data. A true gel effect is observed at the conversion $C > 30\%$ and develops in response to enhancement of diffusional control over the catalytic chain transfer reaction. This, in turn, is due to a decrease in the molecular mobilities of bulky Co(II)P complexes resulted from an increase in the concentration of the network polymer and vitrification of the reaction medium.

The effect of diffusion on the catalytic chain transfer reaction in the linear polymerisation of methacrylates were studied.[145] It was found that the structure–kinetic relationships can be expressed by an empirical equation:

$$C_k k \eta^\alpha \approx \text{const}, \qquad (15)$$

where C_k is the catalytic chain transfer constant, k is the rate constant for the chain growth and η is the viscosity of the reaction medium ($\alpha = 0.5-1$). From the expression (15), it follows that the efficiency of the chain transfer catalyst decreases with an increase in the viscosity of the reaction system. However in the case of three-dimensional bulk polymerisation of dimethacrylates the structure–kinetic relationships are more complicated, because the reaction occurs in a microheterogeneous medium.[29, 144]

When polymerisation of ethylene glycol and diethylene glycol dimethacrylates is carried out in DMF in the presence of high concentrations of Co(II)P, the gel effect is abolished completely, which points to elimination of the topological factors responsible for the microheterogeneity of the reaction medium.[144] The multimodal molecular-mass distribution of polymerisation products suggests the presence of dimeric and trimeric forms of the starting dimethacrylates and of the major high-molecular-weight fraction (Fig. 10). The average molecular masses of the polymerisation products depend substantially on the structure of the starting dimethacrylate, the concentrations of Co(II)P and the content of DMF. According to IR spectroscopic data, the products contain large amount of pendant methacrylate groups and can be related to compounds of the type **42**. High reactivities of these compounds were confirmed by separate determination of copolymerisation kinetics of pendant methacrylate groups with D-MMA (Fig. 11).[146]

In contrast to dimethacrylates, which are used exclusively in the synthesis of statistical polymers, the multifunctional compounds **42** can be used as starting reagents in the design of a new generation of polymeric materials having the structures of graft copolymers. Three-dimensional nanosized copolymers with controlled levels of microheterogeneities possessing entirely novel properties can be prepared by varying structural parameters of the precursors **42** and comonomers.[146]

The use of catalytic chain transfer agents for the control over three-dimensional copolymerisation was first proposed by the

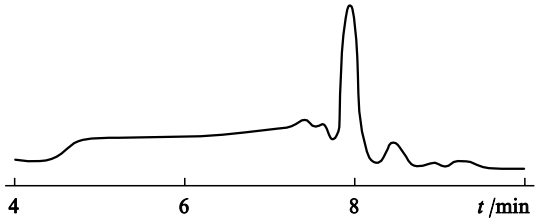

Figure 10. A gel-permeation chromatogram of polymerisation products of ethylene glycol dimethacrylate in the presence of 1×10^{-2} mol litre^{-1} Co(II)P and 40 mass % of DMF.[144]

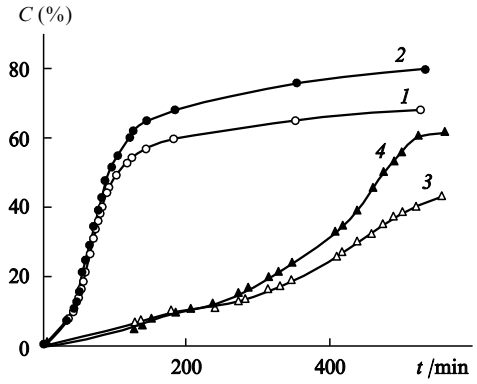

Figure 11. Copolymerisation kinetics of oligo-*n*-methacrylates based on ethylene glycol dimethacrylate (*1*, *3*) with D-MMA (*2*, *4*).[146]
Compositions of mixtures (mass %): (*1*, *2*) 64 : 36, (*3*, *4*) 74 : 26, T = 30 °C, [CPC] = 5 mass %.

present authors.[45] The use of oligomer – monomer systems, which differ considerably in the mechanisms of reactions of terminal radicals with chain transfer catalysts, seems to be especially promising in this respect. These systems include mixtures of dimethacrylates with styrene and acrylates, since reactions of catalytic transmitters with C-secondary styrene- and acrylate-derived radicals differ substantially from their reactions with tertiary methacrylate-derived radicals.[147–150]

It has been shown [147] that the coefficient of the chain transfer from the polymeric radical to the monomer in the polymerisation of styrene in the presence of Co(II)P is an order of magnitude lower than that in the polymerisation of MMA. In the authors' opinion, this is due to the involvement of the chain transmitter in the competing reactions of catalytic inhibition

$$HCo(III)P + R_m^* \longrightarrow P_m + Co(II)P \qquad (16)$$

and reversible inhibition due to the formation of a labile cobalt – carbon bond:

$$R_n^* + Co(II)P \longrightarrow R_n - Co(III)P. \qquad (17)$$

Reversible dissociation of the Co – C bond can lead to regeneration and further growth of the polystyrene radical, which corresponds to the passage of the reaction into a 'living' radical polymerisation mode.[148]

It has been shown [30, 151] that the addition of Co(II)P decreases drastically the rate of copolymerisation of ethylene glycol dimethacrylate with styrene in parallel with a shift of w_{max} towards higher degrees of conversion and an increase in the limiting conversion of the double bonds. An analysis of experimental results revealed that the formation of a network in the presence of Co(II)P is less subject to diffusion-controlled limitations in comparison with ordinary copolymerisation. As in the case of homopolymerisation of dimethacrylates,[29] the kinetic effects of Co(II)P are caused by a decrease in the microheterogeneity of the reaction medium due to the formation of intermediates of the type **42**. The sorption and physical-mechanical characteristics of the copolymers formed undergo significant modifications under the action of the chain transfer catalyst, which influences both the kinetics of copolymerisation and the formation of the network structure.[30]

In the bulk copolymerisation of dimethacrylate with styrene, the gel effect cannot completely be suppressed even by high concentrations of Co(II)P, which points to incomplete homogenisation of the reaction medium. The lack of the gel effect in the copolymerisation carried out in DMF suggests that the topological factors responsible for the microheterogeneity in the reaction of Co(II)P with macroradicals are eliminated virtually completely, as a result of which intramolecular cyclisation and cross-linking reactions are suppressed. The structures of reaction products obtained upon copolymerisation of an ethylene glycol dimethylacrylate – styrene mixture (1 : 1) in the presence of 20% of DMF provide supporting evidence. These reaction products represent multifunctional oligomers of the type **42** with M_n = 2270 and M_w = 14 350 (see Ref. 151).

The feasibility of preparation of soluble branched copolymers of MMA with tripropylene glycol diacrylate (**43**) in the presence of an ordinary (dodecanethiol) and a catalytic (cobalt difluoroboro dimethylglyoximate) chain transfer agents has been demonstrated.[152] This reaction was carried out in toluene (0.33 mol) with 0.15 mol of MMA and 5×10^{-3} mol of diacrylate (80 °C). The changes in the compositions and architectures of copolymers were recorded by NMR spectroscopy and chromatographic methods. It was found that linear copolymers with pendant acrylate groups are formed in the initial steps of the reaction. These groups react with the growing radicals to form branchings and loops. In turn, branched macromolecules can further be cross-linked through quadratic termination and recombination, which increases the molecular masses and polydispersities of the copolymers formed. Because of the differences in the reactivities of MMA ($r_1 \approx 2.0$) and diacrylate **43** ($r_2 \approx 0.5$), the concentration of the latter in branched copolymers increases with an increase in the degree of conversion, which favours further branching. The differences in the chain transfer constants for the reactions carried out in the presence of dodecanethiol for the methacrylate (~ 0.6) and acrylate (~ 1.7) radicals increase the probability of quadratic termination in the final period of the reaction due to consumption of the chain transfer agents and increasing concentrations of the growing acrylate radicals.

Although the persistent concentration of the catalytic chain transfer agents throughout the polymerisation reaction was noted [152] as its salient advantage, the problems of peculiarities of its interactions with acrylate and methacrylate were not touched upon. These include the possibility of formation of a cobalt – carbon bond between the terminal acrylate-derived radical of the copolymer and the transfer agents and the passage of the reaction into a living radical polymerisation mode upon reversible dissociation of this bond.[149, 150] The contribution of the aforementioned reaction should increase at higher conversions due to involvement of an increasing number of acrylate groups in copolymerisation. The β-fragmentation (13) resulting from the interaction of terminal C=C bonds in methacrylate branches of copolymers of the type **40** with various polymeric radicals [143] can also play a role in the character of the molecular-mass distribution and composition of branched copolymers.

The synthesis of superbranched polymers based on ethylene glycol dimethacrylate in the presence of cobalt glyoximate with a chain transfer constant of $\sim 10^3$ has been carried out.[153] By varying the concentration of the chain transfer catalyst, the author has succeeded in directing the polymerisation towards the formation of trimers of ethylene glycol dimethacrylate.

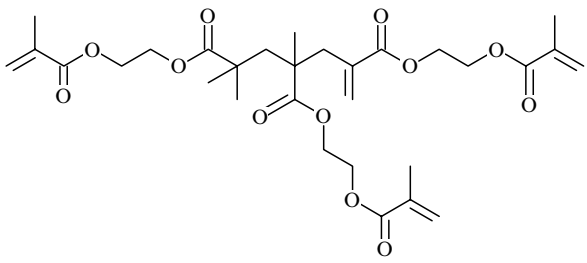

The reinitiation of terminal methacrylate groups of these trimers by a hydride transfer from the Co – H bond is accompanied by trimerisation and formation of new branching points. Cascade branching yields a soluble superbranched polymer with an average molecular mass ranging from several thousand to 40 000 Da. Soluble superbranched polymers are prepared by both bulk and solution polymerisation at dimethacrylate conversions

up to 70%. Special mention should be made of such remarkable characteristics of such superbranched polymers as high surface functionality and low viscosity, which is much lower than that of a linear poly(methyl methacrylate) of the same molecular mass.[153] Cascade radical polymerisation of dimethacrylates in the presence of a chain transfer catalyst can occupy a prominent place among more complex multistep procedures used in the synthesis of superbranched polymers and dendrimers.[154, 155]

Chain transfer catalysts based on triethylene glycol dimethacrylate can be used in the synthesis of linear polyesters.[156] However, the mechanism of their formation is still widely debated in the literature.[141] Note that linear polyesters can be prepared by catalytic chain transfer reactions (11) and (12) using hydride transfer to the pendant C=C bond of the terminal radical and the process occurs as alternating copolymerisation of these bonds with dimethacrylate molecules.

Studies on kinetics of three-dimensional radical (co)polymerisation of dimethacrylates in the presence of chain transfer catalysts [29, 30] have shown that the low-molecular-mass multifunctional intermediates **42** formed change dramatically the process of structure formation of network polymers in comparison with ordinary polymerisation where the role of transient species is played by microgel particles (Fig. 12 *a*). The formation of microgel particles in ordinary polymerisation of dimethacrylates and copolymerisation with styrene is the main reason for early manifestations of the gel effect, spatial heterogeneity of the network and formation of the microheterogeneous structure of the polymer. Using atomic-force microscopy, it was shown [157] that the degree of microheterogeneity of dimethacrylate–styrene copolymers increases with the concentration of the cross-linking reagent. This is accompanied by broadening of time relaxation spectra and an increase in fragility of the cross-linked copolymers.

The catalytic chain transfer reaction prevents the formation of microgel particles and development of the gel effect. In this case, the reaction medium represents a quasi-homogeneous solution of the intermediates **42** in the starting oligomer (Fig. 12 *b*).[151] The inhibition of intramolecular cyclisation sharply increases the probability of intermolecular cross-linking of the intermediates and favours the formation of a more uniform structure of the network (Fig. 12 *c*). It should be noted that not only the catalytic chain transfer reaction controls the morphology of the polymer by preventing the formation of large heterogeneous areas from microgel particles, but also stimulates the formation of a new in principle type of molecular networks consisting of short chains of the copolymer *1* cross-linked by the oligomeric chains *2*. By varying the concentration of a chain transfer catalyst, one can obtain chains *1* of any length and concentration and thus control the contribution of components *1* and *2* to the properties of the (co)polymers.

Comparative structure-physical studies of network polymers and copolymers prepared by conventional methods and in the presence of Co(II)P have shown that the structures and properties of the (co)polymers undergo significant modifications as a result of catalytic chain transfer reactions.[30, 151] The differences in the absorption kinetics of benzene and water induced by ethylene glycol dimethacrylate–styrene (4 : 1) copolymers synthesised by conventional methods and in the presence of Co(II)P provide an example (Fig. 13). The addition of Co(II)P also causes a ~ 10%

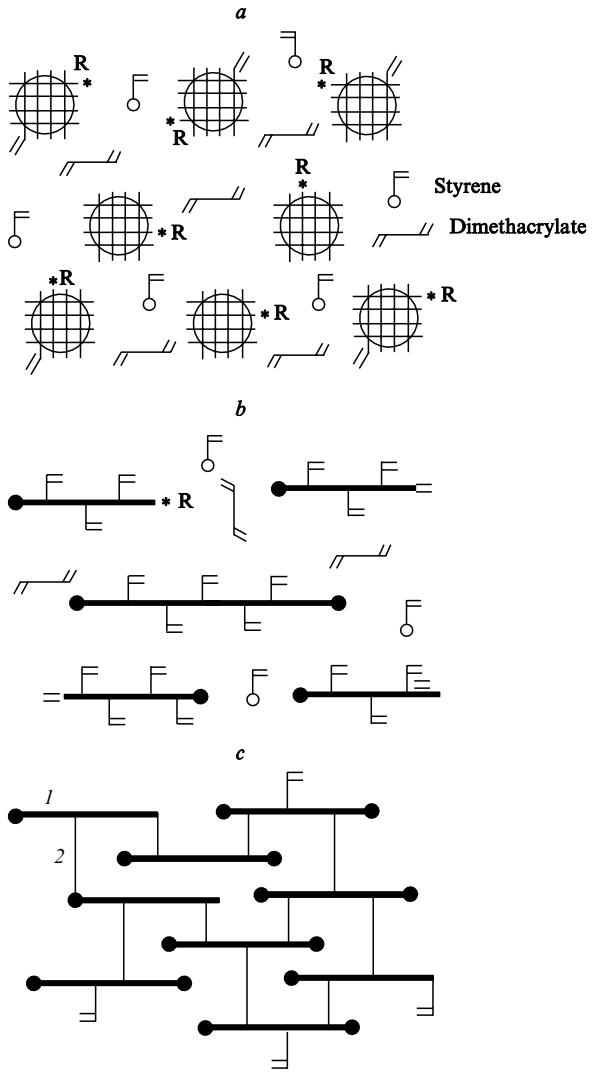

Figure 12. A scheme of synthesis of a network copolymer by conventional three-dimensional copolymerisation (*a*) and in the presence of a chain transfer catalyst (*b*, *c*).
For (*1*, *2*) see text.

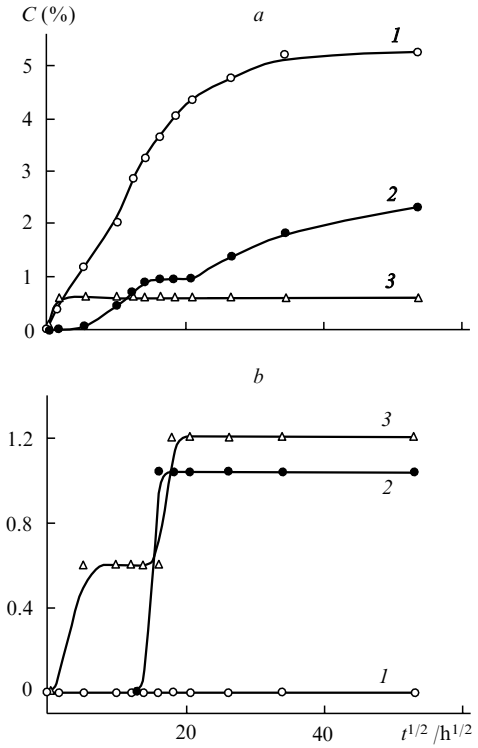

Figure 13. Kinetics of sorption of benzene (*a*) and water vapours (*b*) by copolymers of ethylene glycol dimethacrylate with styrene (4 : 1) prepared by ordinary copolymerisation (*1*) and in the presence of 3.4×10^{-4} (*2*) and 3.8×10^{-3} mol litre^{-1} Co(II)P (*3*).[30]

decrease in the elasticity modulus and a ~ 10% decrease in the forced elasticity modulus of copolymers. Homopolymerisation of ethylene glycol dimethacrylate in the presence of a chain transfer catalyst is accompanied by a ~ 30% decrease in the elasticity and forced elasticity moduli of the polymer. These data are at variance with the hypothesis [24] that a decrease in microheterogeneity of network polydimethacrylates will result in an increase in the elasticity modulus. Rather, they corroborate the hypothesis [158] that the microheterogeneities ('grains') play the role of reinforcing fillers in these polymers.

4. Three-dimensional radical (co)polymerisation in a 'living' chain growth mode

Significant achievements in the study of 'living' linear radical polymerisation in the past decade have paved the way to the synthesis of polymers with controllable structure and properties [159, 160] and stimulated attempts to use the 'living' polymerisation mode as a means of control over the formation of network (co)polymers. The agents of 'living' radical polymerisation influence substantially three-dimensional (co)polymerisation.[158] However, their efficiencies strongly depend on the structure-physical transformations of the reaction medium and can be brought to minimum through a decrease in the molecular mobilities of the reactants.[161]

The mechanism of 'living' radical (co)polymerisation is based on a reversible addition of growing polymeric radicals R* to low-molecular-mass radicals X* (see Refs 159 and 160).

$$R^* + X^* \rightleftharpoons R-X. \qquad (18)$$

Transition metal complexes, iminoxyl radicals and stable free radicals formed upon decomposition of the so-called iniferters (from Initiator Transfer Terminator Agent) can be used as polymerisation regulators X*.[159, 160] Owing to the high mobilities of the radicals X*, reaction (18) inhibits quadratic termination of polymeric radicals. Reiteration of decomposition and regeneration of a labile R–X bond induce the change in the fast chain growth mechanism into a slow step-by-step mechanism. The larger the number of steps in the chain growth mechanism the more completely the process meets the criteria of a true 'living' radical polymerisation, *i.e.*, the linear growth of the molecular mass of the polymer formed in parallel with the conversion of the monomer and narrow molecular mass distribution.[160]

There are hundreds of papers devoted to 'living' linear polymerisation of monofunctional compounds. The most recent advances are highlighted in several reviews [159, 160, 162, 163] which provide a detailed description of various types of compounds X and their applications as reagents for 'living' radical polymerisation and of mathematical models for predicting various parameters of the polymerisation reaction and the structures and properties of the reaction products. The use of polymers synthesised by ionic mechanisms, metathesis or polycondensation in 'living' radical polymerisation makes it possible to broaden the topology of the products (*e.g.*, linear, comb-like, superbranched, *etc.*, polymers) and compositions of copolymers (*e.g.*, statistical, regular, bulk, graft, *etc.*) and to ensure their controlled functionalisation.

However, the publications devoted to three-dimensional radical (co)polymerisation in a 'living' chain mode are not numerous due to the difficulties in conducting polymerisation in highly structured media. The main obstacle is that, in contrast to linear polymerisation, the mechanism of chain growth in three-dimensional polymerisation cannot be tested directly on the basis of such characteristics as molecular mass distribution, dependence of molecular masses of polymeric products on conversion, *etc.* Therefore, the contribution of the 'living' chain growth reaction to three-dimensional (co)polymerisation can be judged on the basis of indirect features, such as a critical conversion (gel point) shift,[164] suppression of autoacceleration of the reaction,[165] reduction of microheterogeneity of (co)polymerisation products and changes in their properties.[166] Some authors believe that these characteristics reflect the inhibition of intramolecular cyclisation due to a stepwise growth of the 'living' chains.[159] This hypothesis was corroborated in copolymerisation of styrene with 4,4′-divinylbiphenyl in the presence of an alkoxyamine, a 'living' radical polymerisation agent based on styrene and an iminoxyl radical 2,2,6,6-tetramethylpiperidin-1-oxyl (TEMPO).[167, 168] The calculated experimental copolymerisation constants suggest that the cyclisation involving the pendant double bonds, which usually proceeds at high rates in ordinary polymerisation, is fully suppressed on going to the living polymerisation mode. The final product, *viz.*, cross-linked polystyrene, is virtually devoid of topological defects, such as small rings.

Significant differences were found [168] in the characteristics of polystyrenes cross-linked by 4,4′-divinylbiphenyl prepared upon conventional radical copolymerisation and in the presence of 'living' radical polymerisation agents. The copolymers synthesised in the 'living' chain mode were characterised by higher elasticity and swelling moduli than the former. These differences were interpreted within the framework of a microheterogeneous mechanism. The copolymers obtained by 'living' polymerisation possessed a nearly statistical distribution of network junctions and were characterised as homogeneous, whereas copolymers prepared by conventional three-dimensional polymerisation were made up of densely crosslinked microgel particles connected by a loose network typical of microheterogeneous polymerisation.

The efficacy of alkoxyamines for performing 'living' radical copolymerisation of dimethacrylates with styrene has been found.[166, 169] Three-dimensional radical copolymerisation of styrene with dimethacrylates in the presence of alkoxyamines based on TEMPO, benzoyl peroxide (dicyclohexyl peroxydicarbonate) and styrene was studied by high-precision isothermic calorimetry, EPR and rheokinetics.[169] A shift in the gel point towards higher conversion values (> 10%) and high concentrations of the iminoxyl radical throughout the polymerisation with sufficiently high rates of the reaction provide conclusive evidence in favour of a 'living' copolymerisation process. Detailed structure-physical studies using mechanical, thermomechanical and diffusion-sorption methods have shown [166] that copolymers obtained in 'living' polymerisation possess higher elasticities and lower effective densities of the macromolecular network in comparison with copolymers prepared by conventional polymerisation. These differences were attributed [166] to the decrease in the microheterogeneity of the reaction medium and granularity of the cross-linked copolymers on going from the chain growth to the stepwise growth mechanism.

The use of alkoxyamines and iminoxyl radicals as agents for 'living' radical polymerisation is limited to styrene-containing systems; in addition, polymerisation should be conducted at high temperatures (~ 120 °C).[159, 160] Therefore, controlled radical polymerisation of acrylates and methacrylates in a 'living' chain growth mode usually includes transfer of a halogen atom (the so-called Atom Transfer Radical Polymerisation, ATRP).[160] The possibility to perform polymerisation at lower temperatures (~ 70 °C) is an obvious advantage of this method. ATRP has found extensive application in linear (co)polymerisation and proved to be an efficient tool for the synthesis of polymers with controlled molecular masses, low polydispersities and diverse architectures.[159, 162, 170, 171] However, only a few examples are known where ATRP has been used for the control of three-dimensional radical (co)polymerisation reactions.[161, 172, 173]

The ATRP of diethylene glycol dimethacrylate induced by methyl α-bromophenyl acetate using a Cu(I)Br – 1,1,4,7,10,10-hexamethyltriethylenetetramine (HMTETA) complex as a catalyst has been studied.[161] This study included investigation of the time dependence of the conversion of double bonds by differential scanning calorimetry, *in situ* EPR spectroscopy and gel-permeation chromatography of the sol fraction isolated in different steps of polymerisation. An analysis of experimental results led the authors to the conclusion that this polymerisation proceeds in a 'living' mode and at persistent (low) concentrations of the growing

radicals only to conversions below 40%. Subsequent structurisation of the reaction medium and limitation of the diffusional mobility of the catalyst–ligand complexes disturb the equilibrium

$$R-M_n-Br + Cu(I)Br-HMTETA \rightleftharpoons$$
$$\rightleftharpoons R-M_n^* + Cu(II)Br_2-HMTETA$$

between growing and 'dormant' polymeric chains and direct the reaction to a conventional radical polymerisation route.[161]

The possibility of controlling three-dimensional radical bulk polymerisation of dimethacrylates by ATRP catalysts is limited due to a sharp decrease in their efficiencies with an increase in the viscosity of the reaction medium.[161] The use of solvents eliminates these limitations and opens up new opportunities for the design of network macromolecular structures in a 'living' radical copolymerisation mode. These possibilities were realised in the synthesis of star-shaped polymers with a functional microgel core.[172, 173] This approach [172] entails the addition of a bifunctional (cross-linking) reagent to a solution containing 'living' chains of a linear polymer. In the initial step, the molecules of the cross-linking reagent are attached to 'living' linear polymers; subsequent three-dimensional polymerisation yields microgel particles with chains of a linear polymer branching radially from its surface.

Star-shaped polymers with a microgel core were synthesised [172] by adding bis(acrylamides) containing spacers of different lengths and structures to a solution of 'living' PMMA chains prepared in the presence of an ATRP catalyst $RuCl_2(PPh_3)$. By varying the lengths of PMMA molecules and content of the divinyl compound, it was possible to obtain star-shaped polymers with molecular masses of 10^5-10^7 and macromolecular sizes ranging from 5 to 42 nm. This novel approach to the synthesis of star-shaped polymers enables incorporation of diverse functional groups (amide, ester, hydroxy, *etc*.) into the microgel core employing a cross-linking reagent with a spacer containing appropriate groups. This opens up new ways to the synthesis of star-shaped polymers attenuated to selective interactions of the 'guest–host' type. It was found [173] that biphilic star-shaped polymers with a diacrylamide core carrying ~ 70 radially branching PMMA chains with a degree of polymerisation of 100 can extract hydrophilic compounds, such as benzoic acid, benzyl alcohol and benzylamine from an aqueous solution to an organic phase. These polymers selectively interact with benzoic acid in the presence of ethyl benzoate (an equimolar mixture) by virtue of hydrogen bonding of the carboxy group to the $-NH-CO-$ groups.

Iniferters, which decompose upon UV irradiation or thermal treatment into two radicals, *viz*., an active R*, which initiates polymerisation of a monomer, and a passive radical X*, which is an active participant in linear termination of the macroradicals P_n^*, are widely used as initiators of 'living' radical polymerisation of vinyl monomers. The growth of 'living' chains is maintained owing to the fact that the rate of linear termination by a small mobile radical X* significantly exceeds that of diffusion-controlled quadratic termination of the macroradicals P_n^*, while the labile terminal bond in the adduct P_n-X dissociates with regeneration of the radical P_n^*, which ensures further chain growth up to the next chain termination.[160] Different types of iniferters and numerous examples of a macromolecular design based on them and their applications in linear radical polymerisation have been reviewed.[162]

The attempts to use iniferters to control three-dimensional radical copolymerisation are not numerous and confined to photopolymerisation of dimethacrylates.[58, 165, 174–176] *p*-Xylylenebis(*N*,*N*-diethyl dithiocarbamate), which dissociates irreversibly upon UV irradiation into an initiating C-radical and a carbamate-type S-radical terminating the growth of the polymeric chain, was used as an iniferter. The dependence of kinetics of 'living' three-dimensional (co)polymerisation of dimethacrylates on iniferter concentration, intensity of UV irradiation, temperature and spacer length has been studied.[165] It was found that the reaction is not autoaccelerated in the presence of the iniferter, and the polymerisation rate decreases 100-fold in comparison with ordinary photopolymerisation of dimethacrylates performed under identical conditions. A significant feature of this approach, which makes it different from conventional polymerisation, is that the polymerisation rate and the maximum conversion do not increase but rather decrease with an increase in the spacer length. This phenomenon is attributed [165] to the fact that the density of the cross-links increases in the presence of the iniferter much more slowly than in conventional polymerisation. Besides, the polymerisation rate is so low that the localisation of the methacrylate groups in the vicinity of the growing radical enhances their effective reactivities to a greater extent than the increase in their mobilities due to elongation of the spacer.

Poor reproducibility of the kinetic data obtained in the polymerisation reactions initiated by a photoiniferter ordinary photopolymerisation has been stressed.[165] This is attributed to the reversible chain termination in the presence of sulfo radicals; however, the contribution of this reaction to the overall heat of the process has not been taken into consideration in the calculation of conversions of double bonds on the basis of calorimetric data. It is therefore not surprising that the polymerisation kinetics of dimethacrylates measured by a spectroscopic method in the presence of the same iniferter [58] differs substantially from those results of calorimetric studies.[165] Studies of polymerisation kinetics of diethylene glycol and triethylene glycol dimethacrylates and of copolymerisation kinetics of divinylbenzene with styrene by the decrease in intensities of the absorption bands in the overtone vibrations of C–H bonds in the near IR revealed that the polymerisation rate decreases in the presence of a photoiniferter, although it does not eliminate the autoacceleration effect due to the diffusion control of quadratic termination of polymeric radicals.[58] Thus, the data available on the effects of iniferters on the kinetics of three-dimensional photopolymerisation of dimethacrylates are controversial. The mechanism whereby iniferters influence the kinetics of thermally induced three-dimensional polymerisation also needs to be further elucidated. The use of tetramethylthiuram disulfide as a free radical source imparts non-trivial kinetic features to the polymerisation of triethylene glycol dimethacrylate, which are manifested in particular in the appearance of two additional maxima on the polymerisation rate *vs*. time curve.[158]

Polymers synthesised in the presence of photoinifertes are convenient models for the study of dependences of their structures and properties on the degree of conversion, since they do not contain immobilised radicals able to initiate the polymerisation process at higher temperatures.[174–176] The heterogeneities of copolymers of poly[ethylene glycol(200) dimethacrylate] and poly[ethyleneglycol(200) acrylate] were established from the widths of the maxima on the temperature dependence curve of mechanical loss tangent.[165] The equality of this parameter in the copolymers prepared under ordinary conditions and in the presence of an iniferter prompted a conclusion that 'living' radical polymerisation of densely cross-linked networks neither influences the reactivities of pendant double bonds nor diminishes the microheterogeneity of the copolymer formed.[165]

Studies of temperature dependences of mechanical loss tangents revealed a high level of structural microheterogeneity of network polymers based on triethylene glycol dimethacrylate synthesised in the presence of a photoiniferter.[58] It is of note that the microheterogeneity of the polymer formed was not considered [58] as a structural defect,[24] but rather as a beneficial factor which enables the preparation of a polymeric material with the vitrification temperature exceeding the polymerisation temperature by ~ 100 °C. The feasibility of this synthesis is due to the coexistence of densely cross-linked microgel clusters with highly mobile loosely cross-linked network areas where further interactions of free radicals with pendant double bonds and oligomer molecules occur. As a consequence, at low curing temperatures a

heterogeneous system can produce a polymer with higher vitrification temperature than a homogeneous system.

It was found [160] that irreversible chain termination in linear radical polymerisation can be prevented through the use of both 'living' radical polymerisation agents and a structure-physical approach where 'living' chain mode is provided by restriction of translational mobilities of macroradicals. This approach was first realised in low-temperature polymerisation of butyl methacrylate in a glassy state induced by γ-irradiation.[177, 178] In this case, the mobilities of growing radicals appeared to be completely suppressed due to high viscosity of the reaction medium. When analysing the effects of chemical agents of 'living' radical polymerisation on three-dimensional polymerisation of multifunctional methacrylates, one should take into consideration the fact that this process has an intrinsic 'living' component of its own due to uninterrupted chain growth on radicals localised on the surface of microgel particles and immobilised in the network. This component, being an integral element of a microheterogeneous three-dimensional polymerisation mechanism, enhances the microheterogeneity of the polymer formed. 'Living' radical polymerisation agents suppress microgeterogeneity only in the step of growth of linear chains containing pendant methacrylate groups. With a decrease in the mobility and efficiency of these compounds (due to increased viscosity of the medium), the network formation goes under control of an ordinary microheterogeneity mechanism which retains some elements of 'living' polymerisation induced by structure-physical factors.

V. Conclusion

An analysis of literature data demonstrates significant achievements in the studies of kinetics and mechanisms of TRCP and the development of methods for the control over the structure and properties of network polymers. Progress in this area has been made owing to the use of IR spectroscopy and NMR monitoring based on separate registration of conversion curves of C=C bonds of the monomer and the cross-linking reagent. The use of *in situ* spectral monitoring allows one to measure instantaneous compositions of the copolymers formed in the course of copolymerisation, to follow changes in effective reactivity ratios induced by structure-physical transformations of the reaction medium and to detect violations in the homogeneous distribution of reaction components in the vicinity of macroradicals caused by microsyneresis and limitations in the molecular mobilities of the reaction components. Direct information about the redistribution of reactants due to microsyneresis and formation of a microheterogeneous structure of network copolymers can be obtained through the use of fluorescent probes and labels. The use of these tools has made it possible to establish the correlations between different parameters of the microheterogenous structure and characteristics of network copolymers.

The formation of structures of network copolymers occurs under conditions of superposition of chain growth, intermolecular cross-linking, cyclisation and intramolecular cross-linking involving pendant double bonds. Considerable attention has been given to experimental and theoretical studies of factors which influence the contribution of these reactions to the overall conversion of double bonds and, as a consequence, to the topological structure and microheterogeneity of the copolymer formed. It was found that the copolymerisation process can be controlled by varying the character of intermolecular interactions of growing polymeric radicals and macromolecules. Thus, the use of comonomers carrying carboxy groups favours intermolecular cross-linking due to the forward formation of hydrogen bonds in the reaction medium. Cross-linking and cyclisation can be suppressed by addition of comonomers containing bulky alkyl substituents, which create steric hindrance for the interaction of macroradicals with pendant double bonds. The control over the lengths of primary polymeric chains by chain transfer agents (thiols and alkyl halides) also limits the cyclisation and enables formation of a more homogeneous structure of a network polymer. However, these approaches have significant limitations: the range of copolymers obtainable is rather small in the former case and environmental safety requirements have not been met, in the latter case.

The discovery of catalytic chain transfer reactions and living' radical polymerisation reactions has revolutionised the situation in linear polymerisation and paved the way to the synthesis of copolymers of any architecture, which in turn gave a strong impetus to the development of versatile and environmentally safe methods for control over TRCP. Pioneering studies have shown that chain transfer catalysts inhibit cyclisation and the gel effect in bulk (co)polymerisation of multifunctional compounds and favour the formation of more homogeneous polymeric networks than upon conventional polymerisation. Data on the effects of the agents of 'living' radical polymerisation on microheterogeneity of the networks formed are scarce and controversial. The potential of these methods in the control over three-dimensional bulk polymerisation is limited, since at more advanced stages of the reaction the activities of chain transfer catalysts and agents of 'living' radical polymerisation decrease with a decrease in their mobilities on going to media with a higher degree of structurisation.

Diffusion-controlled restrictions in reactions of chain transfer catalysts and agents of 'living' radical polymerisation with polymeric radicals are eliminated when these reactions are carried out in solutions. This opens up broad prospects for the design of network macromolecular nanosized structures possessing complex architectures. The data cited in this review clearly demonstrate that these potentialities have partly been realised in the synthesis of a vast variety of superbranched reactive macromolecules and microgels, dendrimers and star-shaped copolymers with a functional microgel core.

References

1. K Dusek *Collect. Czech. Chem. Commun.* **58** 2245 (1993)
2. L D Budovskaya, V N Ivanova, V I Kosyakov, L N Oskar, L Yu Tikhonova, V V Shamanin *Vysokomol. Soedin., Ser. A* **30** 1528 (1988) [a]
3. V S Solov'ev, Yu B Boiko *Komp. Optika* **8** 74 (1990)
4. J G Kloosterboer *Adv. Polym. Sci.* **84** 1 (1988)
5. S Ziaee, G R Palmese *J. Polym. Sci., Part B* **37** 725 (1999)
6. A Matsumoto *Adv. Polym. Sci.* **123** 41 (1995)
7. G V Korolev *Usp. Khim.* **72** 222 (2003) [*Russ. Chem. Rev.* **72** 197 (2003)]
8. G Odian *Principles of Polymerization* (New York: McGraw-Hill, 1970)
9. H J Harwood *Makromol. Chem., Macromol. Symp.* **10–11** 331 (1987)
10. Yu D Semchikov, L A Smirnova *Vysokomol. Soedin., Ser. B* **41** 734 (1999) [a]
11. Yu M Mikhailov, L V Ganina, S V Kurmaz, V S Smirnov, V P Roshchupkin *J. Polym. Sci., Part B* **40** 1383 (2002)
12. S V Kurmaz, V P Roshchupkin *Vysokomol. Soedin., Ser. B* **39** 1557 (1997) [a]
13. S V Kurmaz, V P Tarasov, M P Berezin, V P Roshchupkin *Vysokomol. Soedin., Ser. A* **46** 1637 (2000) [a]
14. H Galina, M J Ilavsky *Polym. Bull.* **3** 473 (1980)
15. N M Bol'bit, A L Izyumnikov E D Rogozhkina, N Kh Faizi, Yu A Chikin *Vysokomol. Soedin., Ser. A* **27** 1621 (1985) [a]
16. V P Roshchupkin, S V Kurmaz, in *Network Structure Formation (Radical Polymerization) in Polymeric Materials Encyclopedia* Vol. 7 (Ed. C Salamone) (Boca Raton, FL: CRC Press, 1996) p. 30
17. I I Romantsova, O V Pavlova, S M Kireeva, Yu M Sivergin *Vysokomol. Soedin., Ser. A* **29** 2353 (1987) [a]
18. I I Romantsova, O V Pavlova, S M Kireeva, Yu M Sivergin *Vysokomol. Soedin., Ser. A* **30** 2502 (1988) [a]
19. O V Pavlova, S M Kireeva, Yu M Sivergin, I I Romantsova, *Vysokomol. Soedin., Ser. A* **29** 1777 (1987) [a]

20. A Matsumoto, S Yokoyama, T Khono *J. Polym. Sci., Part B* **15** 127 (1977)
21. J Jakubiak, J F Rabek *Polimery* **46** 10 (2001)
22. V P Roshchupkin, B V Ozerkovskii, Yu B Kalmykov, G V Korolev *Vysokomol. Soedin., Ser. A* **19** 699 (1977) [a]
23. V P Roshchupkin, B V Ozerkovskii, Z A Karapetyan *Vysokomol. Soedin., Ser. A* **19** 2239 (1977) [a]
24. A A Berlin, G V Korolev, T Ya Kefeli, Yu M Sivergin *Akrilovye Oligomery i Materialy na ikh Osnove* (Acrylic Oligomers and Materials Based on Them) (Moscow: Khimiya, 1983)
25. I L Tyuleneva, A G Boldyrev, I A Shefer, E N Rostovskii, E V Kuvshinskii *Vysokomol. Soedin., Ser. B* **19** 789 (1977) [a]
26. J L Nieto, J Baselga, I Hernandes-Fuentes, M A Llorente, I F Pierola *Eur. Polym. J.* **23** 551 (1987)
27. V P Roshchupkin, B V Ozerovskii, in *Karbotsepnye Polimery* (Carbon-Chain Polymers) (Moscow: Nauka, 1977) p. 132
28. B V Ozerovskii, V D Plotnikov, V P Roshchupkin *Vysokomol. Soedin., Ser. A* **25** 1816 (1983) [a]
29. S V Kurmaz, E O Perepelitsina, M L Bubnova, V P Roshchupkin, in *Struktura i Dinamika Molekulyarnykh Sistem* (Structure and Dynamics of Molecular Systems) (Ufa: Institute of Physics of Molecules and Crystals, Urals Research Centre, Russian Academy of Sciences, 2002) Vol. 1, p. 309
30. S V Kurmaz, E O Perepelitsina, M L Bubnova, V P Roshchupkin *Vysokomol. Soedin., Ser. A* **45** 373 (2003) [a]
31. L Mandelkern *Crystallization of Polymers* (New York: McGeaw-Hill, 1964)
32. T E Lipatova, S A Zubko *Vysokomol. Soedin., Ser. A* **12** 1555 (1970) [a]
33. V PRoshchupkin, V V Kochervinskii, Z A Karapetyan, G V Korolev *Vysokomol. Soedin., Ser. B* **13** 317 (1971) [a]
34. S M Mezhikovskii *Fizikokhimiya Reaktsionnosposobnykh Oligomerov* (Physical Chemistry of Reactive Oligomers) (Moscow: Nauka, 1998)
35. A V Kotova, V M Lantsov, L A Abdrakhmanova, S M Mezhikovskii *Vysokomol. Soedin., Ser. A* **29** 1761 (1987) [a]
36. V V Kochervinskii, Z A Karapetyan, V P Roshchupkin, B R Smirnov, G V Korolev *Vysokomol. Soedin., Ser. A* **17** 2425 (1975) [a]
37. T D Muravleva *Vysokomol. Soedin., Ser.* **24B** 163 (1982)
38. P Flory, J Rener *J. Chem. Phys.* **11** 521 (1943)
39. K Dusek, in *Polymer Networks* (New York, London: Plenum, 1971) p. 245
40. K S Anseth, C N Bowman *J. Polym. Sci., Part B* **33** 1769 (1995)
41. V M Lagunov, M P Berezin, I V Golikov, G V Korolev *Vysokomol. Soedin., Ser. A* **27** 2056 (1985) [a]
42. H S Haas *J. Polym. Sci.* **39** 493 (1959)
43. V P Roshchupkin, B V Ozerkovskii, O S Roshchupkina, G V Korolev *Dokl. Akad. Nauk SSSR* **229** 145 (1976) [b]
44. V P Roshchupkin, U G Gafurov *Dokl. Akad. Nauk SSSR* **235** 869 (1977) [b]
45. S V Kurmaz, V P Roshchupkin *Strukturno-Kineticheskie Aspekty Trekhmernoi Radikal'noi Sopolimerizatsii Oligodimetakrilatov (Preprint)* [Structure-Kinetic Aspects in Three-Dimensional Radical Copolymerisation of Oligodimethacrylates (Preprint)] (Chernogolovka: Institute of Problems of Chemical Physics, Russian Academy of Sciences, 1997) p. 23
46. H Kloosterboer, F Towslager, in *Programme Booklet of 12th Polymer Networks Group Conference, Prague, 1994* p. 33
47. L H Sperling, V Mishra *Polym. Adv. Technol.* **7** 197 (1995)
48. K Dean, W D Cook, L Rey, J Galy, H Sautereau *Macromolecules* **34** 6623 (2001)
49. V A Myagchenkov, S Ya Frenkel' *Kompozitsionnaya Neodnorodnost' Sopolimerov* (Composition Heterogeneity of Copolymers) (Leningrad: Khimiya, 1987)
50. V P Roshchupkin, S V Kurmaz *Novye Podkhody k Issledovaniyu Trekhmernoi Radikal'noi Sopolimerizatsii Oligodimetakrilatov. Materialy VIII Mezhdunarodnoi Konferentsii 'Oligomery-2002' (Preprint)* [New Approaches to Investigation of Three-Dimensional Radical Copolymerisation of Oligodimethacrylates. Proceedings of the VIIIth International Conference 'Oligomers-2002' (Preprint)] (Chernogolovka: Institute of Problems of Chemical Physics, Russian Academy of Sciences, 2002)
51. R Mao, Y Liu, M B Haglin, P A Holmes *Macromolecules* **28** 6739 (1995)
52. D T Landin, C W Macosko *Macromolecules* **21** 846 (1988)
53. J Baselga, M A Llorente, J L Nieto, I Hernandes-Fuentes, I F Pierola *Eur. Polym. J.* **24** 161 (1988)
54. S Mallam, F Horkey, A M Hecht, E Ggeissler *Macromolecules* **22** 3356 (1989)
55. M Shibayama, T Norisuye, S Nomura *Macromolecules* **29** 8746 (1996)
56. H Aoki, S Tanaka, S Ito, M Yamamoto *Macromolecules* **33** 9650 (2000)
57. V P Roshchupkin, V V Kochervinskii, O G Sel'skaya, G V Korolev *Vysokomol. Soedin., Ser. B* **13** 497 (1971) [a]
58. H Lu, L G Lovell, C N Bowman *Macromolecules* **34** 8021 (2001)
59. J K Glatz-Reichenbach, L J Sorriero, J J Fitzgerald *Macromolecules* **27** 1338 (1994)
60. H Sawada *Thermodynamics of Polymerization* (New York: Marcel Dekker, 1976)
61. B S Selenova, G I Dzhardimalieva, M V Tsikalova, S V Kurmaz, V P Roshchupkin, I Ya Litvin, A D Pomogailo, M E Vol'pin *Izv. Akad. Nauk, Ser. Khim.* 500 (1993) [c]
62. V P Roshchupkin, S V Kurmaz, in *Struktura i Dinamika Molekulyarnykh Sistem* (Structure and Dynamics of Molecular Systems) (Kazan': Izd. Unipress, 1999) p. 38
63. T V Belopol'skaya *Vysokomol. Soedin., Ser. A* **14** 640 (1972) [a]
64. P Scmidt, D Schneider, S Dirlikov, M Mihailov *Eur. Polym. J.* **11** 229 (1975)
65. B V Ozerovskii, V P Roshchupkin *Dokl. Akad. Nauk SSSR* **248** 657 (1979) [b]
66. B P Shtarkman, N Yu Averbakh, I M Monich, S A Arzhakov *Vysokomol. Soedin., Ser. A* **19** 545 (1977) [a]
67. G M Chplakhyan, A Zh Barsegyan, V P Roshchupkin *Uch. Zap. Erevansk. Gosuniv.* 85 (1980)
68. J Kloosterboer, G Lijten, H Boots *Macromol. Chem., Makromol. Symp.* **24** 223 (1989)
69. K S Anseth, C N Bowman, N A Peppas *J. Polym. Sci., Part A* **32** 139 (1994)
70. J Jakubiak, L A Linden *Polimery* **46** 522 (2001)
71. L A Linden, J Jakubiak *Polimery* **46** 590 (2001)
72. M Wen, L E Scriven, A V McCormick *Macromolecules* **35** 112 (2002)
73. T G Chmykhova, I I Nikiforova, E F Samarina, B I Shtarkman, E G Pomerantseva, L M Terman *Vysokomol. Soedin., Ser. A* **23** 2444 (1981) [a]
74. S V Kurmaz, V P Grachev, V P Roshchupkin, in *Programme and Abstracts of Conference Networks 91 on Polymer Networks: Synthesis, Structure and Properties, Moscow, 1991* p. 13
75. Z G Aliev, T K Goncharov, V P Grachev, S V Kurmaz, V P Roshchupkin *Koord. Khim.* **17** 1101 (1991) [d]
76. I V Golikov, V A Semyannikov, M M Mogilevich *Vysokomol. Soedin., Ser. B* **27** 304 (1985) [a]
77. V A Semyannikov, O V Fufareva, I V Golikov, in *Tezisy Dokladov I Vsesoyuznogo Soveshchaniya po Problemam Khimii i Tekhnologii Progressivnykh Lakokrasochnykh Materialov, Yaroslavl', 1985* (Abstracts of Reports of the Ist All-Union Meeting on Problems of Chemistry and Technology of Advanced Paintwork Material, Yaroslavl', 1985) p. 78.
78. M Y Bailey, P Y Chen, W B Chiao, T Endo, in *Contemporary Topics in Polymer Science* Vol. 3 (New York: Plenum, 1979) p. 29
79. Yu M Sivergin, R Ya Pernikis, S M Kireeva *Polikarbonat-(met)akrilaty* [Polycarbonate(meth)acrylates] (Riga: Zinatne, 1988)
80. B M Zuev, O S Arkhireev, F P Filippova, E F Gubanov *Vysokomol. Soedin., Ser. A* **35** 669 (1993) [a]
81. G V Korolev, I S Kochneva, G M Bakova, M P Berezin *Vysokomol. Soedin., Ser. A* **43** 784 (2001) [a]
82. S I Kuchanov, M Y Gelfer *JMS-Pure Appl. Chem.* **30A** 571 (1993)
83. S V Kurmaz, V P Roshchupkin, I C Kochneva *Plastmassy* (3) 34 (2002)
84. C Decker *Polym. Int.* **45** 133 (1998)

85. J E Dietz, B J Elliot, N A Peppas *Macromolecules* **28** 5163 (1995)
86. T E Long, H Y Liu, B A Schell, D M Teegarden, D S Uerz *Macromolecules* **26** 6237 (1993)
87. V P Roshchupkin, S V Kurmaz, in *Struktura i Dinamika Molekulyarnykh Sistem* (Structure and Dynamics of Molecular Systems) (Ufa: Institute of Physics of Molecules and Crystals, Urals Research Centre, Russian Academy of Sciences, 2002) Vol. 2, p. 110
88. S J Martin, V J McBrierty, D C Douglass *Macromolecules* **34** 8934 (2001)
89. M R Aguilar, A Gallardo, M Fernandez, J Roman *Macromolecules* **35** 2036 (2002)
90. N N Volkova, A I Sosikov, M P Berezin, G V Korolev, L N Erofeev, L P Smirnov *Vysokomol. Soedin., Ser. A* **30** 2133 (1988) [a]
91. S M Usmanov, Yu M Sivergin, Yu B Monakov *Vysokomol. Soedin., Ser. A* **41** 474 (1999) [a]
92. G V Korolev, M M Mogilevich, I V Golikov *Setchatye Poliakrilaty. Mikrogeterogennye Struktury, Fizicheskie Setki, Deformatsionno-Prochnostnye Svoistva* (Cross-Linked Polyacrylates. Microheterogeneous Structures, Physical Networks, Deformation and Mechanical Properties) (Moscow: Khimiya, 1995)
93. G Williams, I K Smith, G A Aldrige *Macromolecules* **34** 7197 (2001)
94. G Williams, I K Smith, P A Holmes, S J Varma *J. Phys.: Condens. Matter* **11** A57 (1999)
95. I K Partridge, G M Maiatros *High Perform. Polym.* **8** 1 (1996)
96. S Andjelic, J Mijovic *Macromolecules* **31** 2872 (1998)
97. V V Kochervinskii, Yu V Zelenev *Vysokomol. Soedin., Ser. A* **17** 2475 (1975) [a]
98. B V Ozerovskii, G M Chplakhyan, V P Roshchupkin *Uch. Zap. Erevansk. Gosuniv.* 82 (1974)
99. T L Thomas, A K Mishra *Eur. Polym. J.* **38** 1805 (2002)
100. C Peinado, A Alonso, E F Salvador, J Baselga, F C Catalina *Polymer* **43** 5355 (2002)
101. O Pekcan, Y Yilmaz, O Okay *J. Appl. Polym. Sci.* **61** 2279 (1996)
102. O Pekcan, Y Yilmaz, O Okay *Polymer* **37** 2049 (1996)
103. O Pekcan, Y Yilmaz, O Okay *Chem. Phys. Lett.* **229** 537 (1994)
104. O Okay *Polymer* **35** 796 (1994)
105. O Okay, H J Naghash *Polym. Bull.* **33** 665 (1995)
106. D Stauffer, A Coniglio, M Adam *Adv. Polym. Sci.* **44** 103 (1982)
107. W F Jager, B Norder *Macromolecules* **33** 8576 (2000)
108. A Matsumoto, E Nishi, M Oiwa, J Ikeda *Eur. Polym. J.* **27** 1417 (1991)
109. A Matsumoto, S Asai, S Shimizu, H Aota *Eur. Polym. J.* **38** 863 (2002)
110. A Matsumoto, S Asai, H Aota Macromol *Chem. Phys.* **201** 2735 (2000)
111. A Matsumoto, H Ishido, K Urushido, M Oiwa *J. Polym. Sci., Part A* **20** 3207 (1982)
112. A Matsumoto, A Ueda, H Aota, J Ikeda *Eur. Polym. J.* **38** 1777 (2002)
113. A Matsumoto, A Ueda, H Aota, J Ikeda *J. Macromol. Rapid Commun.* **21** 701 (2000)
114. J E Elliot, J W Anseth, C N Bowman *Chem. Eng. Sci.* **56** 3173 (2001)
115. M Refojo, in *Contact Lenses. Concise Polymeric Materials Encyclopedia* (Ed. J Salomon) (Boca Raton, FL: CRC Press, 1999) p. 303
116. B D Ratner, A S Hoffman, S R Hansen *J. Polym. Sci., Part C* **66** 363 (1979)
117. J E Elliot, C N Bowman *Macromolecules* **32** 8621 (1999)
118. W E Funke *Br. Polym. J.* **21** 107 (1989)
119. H Chen, K Ishuzi, T Fukutomi, T Kakurai *J. Polym. Sci. Part A* **22** 2123 (1984)
120. B Gawdzik, M Maciejewska *J. Polym. Sci., Part A* **40** 3079 (2002)
121. D Rabelo, F M Coutinho *Polym. Bull.* **31** 585 (1993)
122. C Jegat, A Bois, M Camps *J. Polym. Sci., Part B* **39** 201 (2001)
123. M P Berezin, V P Roshchupkin, G V Korolev, in *Programme and Abstracts of Conference Networks 91 on Polymer Networks: Synthesis, Structure and Properties, Moscow, 1991* p. 12
124. C B Bucknall, P Davies, I K Partridge *Polymer* **26** 109 (1985)
125. C P Hsu, M Kinkelaar, P Hu, L J Lee *Polym. Eng. Sci.* **31** 1450 (1991)
126. L Suspene, D Forquier, Y S Yang *Polymer* **32** 1593 (1991)
127. C B Bucknall, I K Partridge, M J Phillips *Polymer* **32** 786 (1991)
128. B Sun, T L Yu *J. Appl. Polym. Sci.* **57** 57 (1996)
129. Y Chiu, L J Lee *J. Polym. Sci., Part A* **33** 257 (1995)
130. Y Chiu, L J Lee *J. Polym. Sci., Part A* **33** 269 (1995)
131. H J Naghash, O Okay *Polym. Bull.* **37** 207 (1996)
132. G V Korolev, M P Berezin, I S Kochneva, L I Makhonina, in *Struktura i Dinamika Molekulyarnykh Sistem* (Structure and Dynamics of Molecular Systems) (Ufa: Institute of Physics of Molecules and Crystals, Urals Research Centre, Russian Academy of Sciences, 2002) Vol. 1, p. 256
133. K A Berchtold, J Nie, B Hacioglu, C N Bowman *Macromolecules* **34** 5103 (2001)
134. B Hacioglu, K A Berchtold, L,G Lovell, J Nie, C N Bowman *Biomaterials* **23** 4057 (2001)
135. B R Smirnov, A P Marchenko, N S Enikolopov *Dokl. Akad. Nauk SSSR* **254** 130 (1980) [b]
136. V P Roshchupkin, B R Smirnov, in *IV Vsesoyuznaya Konferentsiya po Khimii i Primeneniyu Porfirinov (Tez. Dokl.), Erevan, 1984* [The IVth All-Union Conference on the Chemistry and Application of Porphyrins (Abstracts of Reports), Erevan, 1984] p. 163
137. I V Golikov, V A Semyannikov, M M Mogilevich, B R Smirnov, in *IV Vsesoyuznaya Konferentsiya po Khimii i Primeneniyu Porfirinov (Tez. Dokl.), Erevan, 1984* [The IVth All-Union Conference on the Chemistry and Application of Porphyrins (Abstracts of Reports), Erevan, 1984] p. 110
138. A Gridnev *J. Polym. Sci., Part A* **38** 1753 (2000)
139. B V Ozerovskii, V P Roshchupkin *Dokl. Akad. Nauk SSSR* **254** 157 (1980) [b]
140. D M Haddleton, D R Morsley, J P O Donnel, S N Richards *J. Polym. Sci., Part A* **37** 3549 (1999)
141. A Gridnev, S D Ittel *Chem. Rev.* **101** 3611 (2001)
142. C L Moad, G Moad, E Rizzardo, S H Thang *Macromolecules* **29** 7717 (1996)
143. D M Haddleton, D R Maloney, K G Saddaby *Macromolecules* **29** 481 (1996)
144. S V Kurmaz, V P Roshchupkin, M L Bubnova, E O Perepelitsina *Vysokomol. Soedin., Ser. A* **46** 5 (2004) [a]
145. J P A Heuts, D J Forster, T P Davis *Macromolecules* **32** 3907 (1999)
146. S V Kurmaz, V P Roshchupkin, in *Struktura i Dinamika Molekulyarnykh Sistem* (Structure and Dynamics of Molecular Systems) (Ioshkar-Ola: Moscow State Technological University, 2001) Vol. 2, p. 168
147. B R Smirnov, V D Plotnikov, B V Ozerkovskii, V P Roshchupkin, N S Enikolopov *Vysokomol. Soedin., Ser. A* **23** 2588 (1981) [a]
148. J P A Heuts, D J Forster, T P Davis, B Yamada, H Yamazoe, M Azukizava *Macromolecules* **32** 2511 (1999)
149. B B Wayland, L Basiskes, S Mukerjee, M Wai, M Fryd *Macromolecules* **30** 8109 (1997)
150. G E Roberts, J P A Heuts, T P Davis *Macromolecules* **33** 7765 (2000)
151. S V Kurmaz, E O Perepelitsina, M L Bubnova, G A Estrina, V P Roshchupkin *Mendeleev Commun.* 21 (2002)
152. P A Costello, I K Martin, A T Slark, D C Sherrington, A Titterton *Polymer* **43** 245 (2002)
153. Z Guan *J. Am. Chem. Soc.* **124** 5616 (2002)
154. J Freche, D Tomalia *Dendrimers and Other Dendritic Polymers* (Weinheim: Wiley-VCH, 2001)
155. Yu D Semchikov, M N Bochkarev *Vysokomol. Soedin., Ser. C* **44** 2293 (2002) [a]
156. US P. 4 608 423; *Chem. Abstr.* **105** 228 619 (1986)
157. L Rey, J Duchet, J Galy, H Sautereuau, D Vouagner, L Carrion *Polymer* **43** 4375 (2002)

158. G V Korolev, G M Bakova, M P Berezin, A P Marchenko, L I Makhonina *Vysokomol. Soedin., Ser. A* **45** 33 (2003) [a]
159. G V Korolev, A P Marchenko *Usp. Khim.* **69** 447 (2000) [*Russ. Chem. Rev.* **69** 409 (2000)]
160. M Yu Zaremskii, V B Golubev *Vysokomol. Soedin., Ser. C* **43**1689 (2001) [a]
161. Q Yu, F Zeng, S Zhu *Macromolecules* **34** 1612 (2001)
162. T Otsu, A Matsumoto *Adv. Polym. Sci.* **136** 75 (1998)
163. H Fischer *Chem. Rev.* **101** 3581 (2001)
164. G V Korolev, T F Irzhak, V I Irzhak *Vysokomol. Soedin., Ser. A* **43** 970 (2001) [a]
165. J H Ward, A Shahar, N A Peppas *Polymer* **43** 1745 (2002)
166. G V Korolev, I S Kochneva, G M Bakova, M P Berezin, L I Makhonina *Vysokomol. Soedin., Ser. A* **44** 1484 (2002) [a]
167. N Ide, T Fukuda *Macromolecules* **30** 4268 (1997)
168. N Ide, T Fukuda *Macromolecules* **32** 95 (1999)
169. G V Korolev, I S Kochneva, G M Bakova, M P Berezin *Vysokomol. Soedin., Ser. A* **43** 784 (2001) [a]
170. K Matyaszewski *Curr. Opin. Solid State Mater. Sci.* **1** 769 (1996)
171. S Sivaram *J. Sci. Ind. Res.* **56** 1 (1997)
172. K-Y Baek, M Kamigaito, M Sawamoto *Macromolecules* **34** 7629 (2001)
173. K-Y Baek, M Kamigaito, M Sawamoto *Macromolecules* **35** 1493 (2002)
174. A R Kannurpatti, K J Anderson, J W Anseth, C N Bowman *J. Polym. Sci., Part B* **35** 2297 (1997)
175. A R Kannurpatti, C N Bowman *Macromolecules* **31** 3311 (1998)
176. A R Kannurpatti, J W Anseth, C N Bowman *Polymer* **39** 2507 (1998)
177. G S Georgiev, A M Kaplan, V P Zubov, V B Golubev, I M Barkalov, V I Gol'danskii, V A Kabanov *Vysokomol. Soedin., Ser. A* **14** 177 (1972) [a]
178. G S Georgiev, A M Kaplan, V P Zubov, V B Golubev, I M Barkalov, V I Gol'danskii, V A Kabanov *Vysokomol. Soedin., Ser. A* **41** 1950 (1999) [a]

[a] — *Polym. Sci. (Engl. Transl.)*
[b] — *Dokl. Chem. (Engl. Transl.)*
[c] — *Russ. Chem. Bull., Int. Ed. (Engl. Transl.)*
[d] — *Russ. J. Coord. Chem. (Engl. Transl.)*

Russian Chemical Reviews **73** (3) 251 – 265 (2004) © 2004 Russian Academy of Sciences and Turpion Ltd

DOI 10.1070/RC2004v073n03ABEH000881

Methods of calculation of the critical conversion in the formation of network polymers

V I Irzhak

Contents

I.	Introduction	251
II.	Methods for the description of the kinetics of formation of cross-linked polymers	252
III.	Statistical methods	253
IV.	The bond block concept as a method to solve problems involving the substitution effect	254
V.	Three-dimensional polymerisation	258
VI.	Conclusion	264

Abstract. Mathematical methods of calculation of the critical conversion (gel point) in the formation of cross-linked polymers by polycondensation, cross-linking of macromolecules and three-dimensional polymerisation are considered. The results obtained using the statistical approach ('ideal' polycondensation), the concept of bond blocks (the 'non-ideal' or 'non-statistical' polycondensation) and kinetic calculations that allowed the determination of the gel point in three-dimensional polymerisation processes are discussed. The bibliography includes 105 references.

I. Introduction

The value of critical conversion in the formation of cross-linked polymers, the so-called gel point, characterises the transition of a system from a fluid state to a state with an equilibrium elastic modulus. It is a parameter of great importance both in applied and theoretical studies. At conversions smaller than the critical conversion, a polymer is characterised by a finite molecular mass. At higher conversions, the molecular mass becomes formally infinite, or, in mathematical terms, higher moments of molecular-mass distribution, starting from the second one, become infinite. The formation of an insoluble gel can result in complications in technological processes of polymer synthesis and, *vice versa*, finding the relationship between the critical conversion, on the one hand, and the structural and kinetic parameters of the process, on the other hand, makes it possible to state the conditions for forming a cross-linked polymer with required physico-mechanical characteristics.

The gel point determines the flow threshold in a polymeric system being formed, and finding the dependence of this value on kinetic and structural parameters is an important problem. For example, polymer properties in the critical point have recently become a subject of scientists' attention.[1] The relaxation properties of polymeric systems on transition from a sol to a gel have a distinctive feature due to the fact that macromolecules in this point are characterised by a specific structure shaped as fractal trees with an extraordinarily broad size distribution. The relaxation modulus has a power-law rather than exponential time dependence;[1–4] this is characteristic of pre-gel rather than post-gel regions. It follows that the real and imaginary components of the relaxation modulus are congruent and that the loss tangent is independent of frequency. Obviously, correct assessment of the critical conversion region in the formation of a three-dimensional polymeric system occurring by any mechanism can make it possible to determine conditions required to obtain a material with predefined properties.

The problem of determining the critical conversion for the polycondensation of *f*-functional monomers was solved by Flory [5] and Stockmayer [6] by statistical methods using combinatory analysis. The formulas they obtained were confirmed by kinetic calculations [7,8] and by experimental data.[5,8] They are applicable provided that intramolecular reactions (reactions between groups belonging to a single macromolecule) do not occur. It was later shown that probabilistic approaches are applicable only to those systems where the so-called substitution effect is absent, *i.e.*, where kinetic constants do not change during the process.[7,9,10] Otherwise, a strict kinetic calculation is required.

Three-dimensional polymerisation is usually described according to Flory [5] and Stockmayer [11] using the probabilistic approach,[12] which is of quite limited use for polymerisation processes. Monte Carlo computer simulation, which is also based on the probabilistic approach, was found to be more efficient.[13–15] Other approaches were also proposed, based on the analysis of infinite systems of differential equations describing different kinetic schemes of the polymerisation process: a method based on the calculation of the instantaneous value of molecular mass distribution;[11,16–20] approximation of a system of ordinary differential-difference equations by a continuous system of partial differential equations;[21–28] the method of moments;[29–35] the method of generating functions;[7,36,37] numeric inversion of *z*-[38] and Fourier transformations;[39] methods of discrete weighed residues;[40–42] numeric fractionation [43–45] and discrete population balance.[46,47] These methods were mainly used to evaluate the molecular mass distribution parameters in the formation of linear and branched polymers, and it is only in restricted cases (see, *e.g.*, Refs 7 and 48) that they were used to find critical conversion values.

The formulas obtained by any of these methods were not confirmed by experimental data. However, their validity was not disputed, because it is well known that intramolecular cyclisation occurs rather intensely under ordinary three-dimensional polymerisation conditions due to the fast chain growth in the case of

V I Irzhak Institute of Problems of Chemical Physics, Russian Academy of Sciences, 142432 Chernogolovka, Moscow Region, Russian Federation. Fax (7-095) 514 32 44. Tel. (7-096) 522 21 63. E-mail: irzhak@icp.ac.ru

Received 4 November 2003
Uspekhi Khimii **73** (3) 275 – 291 (2004); translated by S S Veselyi

the radical mechanism and the low concentration of chains at early process stages.[8] Repeated cross-linking between a single pair of chains (formation of multiplet nodes and 'staircase' macromolecular structures) is also believed to be a factor that decreases the effective concentration of inter-chain cross-links and thus increases the critical conversion.[49] Because of this, radical polymerisation is a typical microheterogeneous process.[50] The combination of all these reasons makes it difficult to expect that any theoretical dependencies would be obeyed.

In this review, we intend to determine the applicability ranges of the statistic and kinetic approaches. Based on this, well-founded results on the calculation of critical conversion values with different mechanisms of formation of cross-linked polymers will be presented. The author has previously developed the bond blocks (BB) concept.[9, 51] This approach, which combines kinetic and probabilistic methods, makes it possible to simplify considerably the solution of problems that cannot be solved using the purely statistical method. In this review we consider the results of critical conversion calculations obtained by this method.

Thus, the review consists of three parts. The first part presents the results of statistical calculations ('ideal' polycondensation); the second part, the results obtained using the BB concept ('non-ideal' or 'nonstatistical' polycondensation); the third part, the kinetic calculations that allowed the determination of the gel point in three-dimensional polymerisation processes to be carried out.

II. Methods for the description of the kinetics of formation of cross-linked polymers

Unlike low-molecular compounds (not bodies!) that are defined almost unambiguously by their chemical formulas, the structures of polymers, and hence their properties, are not exhausted by their chemistry. Polymer structure is a multilevel characteristic, and the topological level is the most important.[8] In fact, the properties of linear polymers cannot be described if their molecular mass distribution is neglected. For cross-linked polymers, the concentration of nodes and the length distribution of internode chains are the most important structural parameters. Branched and star polymers and dendrimers differ principally both from each other and from linear polymers due to differences in their topological structures. Therefore, consideration of the polymer formation kinetics should not be limited to chemical reactions; it is also necessary to analyse how the polymeric chain is formed.

Taking the above considerations into account, we should discriminate at least two reaction types: polymerisation type and, tentatively speaking, polycondensation type (called 'Addition Polymerisation' and 'Stepwise Polymerisation' in English-language literature). Turning aside from chemistry, the reagents involved in these reactions can be described by vectors; in the former case, as R(m,n,p), where R is a macromolecule comprising m units, n functional groups (for vinyl polymers, n is the number of double bonds) and p active centres; m, n, p = 0, 1, 2, 3, ... *etc*., to infinity; in the latter case, as R(m,n).

This is certainly the easiest description method, which does not take certain details of the topological structure into account, but these characteristics suffice for the solution of the problem of interest, *viz*., determination of the gel point.

The former reaction type is described by the following scheme:

$$\mathrm{I} \xrightarrow{k_\mathrm{i}} f\mathrm{R}(0,0,1)$$

$$\mathrm{R}(i,j,l) + \mathrm{R}(m,n,p) \longrightarrow \begin{cases} \xrightarrow{k_\mathrm{p}} \mathrm{R}(i+m, j+n-l, l+p) \\ \xrightarrow{k_\mathrm{tr}} \mathrm{R}(i+m, j+n, l+p-2), \\ \xrightarrow{k_\mathrm{td}} \mathrm{R}(i,j,l-1) + \mathrm{R}(m,n,p-1) \end{cases} \quad (1)$$

$$\mathrm{R}(i,j,l) + \mathrm{X} \xrightarrow{k_\mathrm{X}} \mathrm{R}(i,j,l-1) + \mathrm{R}(0,0,1),$$

$$\mathrm{R}(i,j,l) + \mathrm{Y} \xrightarrow{k_\mathrm{Y}} \mathrm{R}(i,j,l-1).$$

where I is the initiator; f is the initiation efficiency (number of active centres formed in one initiation act); R(0,0,1) is a primary active centre; k_i, k_p, k_tr, k_td, k_X and k_Y are the rate constants of initiation, growth, square-law termination by recombination and disproportionation, chain transfer on transfer agent X and linear inhibition-type termination on agent Y.

For simplicity, it was assumed when developing this scheme that initiation occurs by monomolecular decomposition of initiator I and that the reactivity of functional groups does not depend on the complexity and size of the macromolecule that carries them (Flory's principle [5]). The reactivity of active centres in the chain growth, transfer and termination is also independent of this factor.

The second reaction type is described by the scheme (also with the use of Flory's principle)

$$\mathrm{R}(i,j) + \mathrm{R}(m,n) \xrightarrow{k} \mathrm{R}(i+m, j+n-2). \quad (2)$$

This is a simplified version where it is assumed that the reacting functional groups belong to a single type.

Schemes (1) and (2) result in infinite systems of differential equations. For scheme (1):

$$\frac{\mathrm{d}\mathrm{I}}{\mathrm{d}t} = -k_\mathrm{i}\mathrm{I},$$

$$\frac{\mathrm{d}\mathrm{R}(0,0,1)}{\mathrm{d}t} = fk_\mathrm{i}\mathrm{I} - \mathrm{R}(0,0,1)\,(k_\mathrm{p}\mathrm{F} + k_\mathrm{X}\mathrm{X} + k_\mathrm{t}\mathrm{R} + k_\mathrm{Y}\mathrm{Y}) + k_\mathrm{X}\mathrm{X}\mathrm{R},$$

$$\frac{\mathrm{d}\mathrm{R}(i,j,l)}{\mathrm{d}t} = -\mathrm{R}(i,j,l)\,[k_\mathrm{p}(l\mathrm{F} + j\mathrm{R}) + l(k_\mathrm{X}\mathrm{X} + k_\mathrm{t}\mathrm{R})] + \mathrm{R}(i,j,l+1) \times$$

$$\times (k_\mathrm{Y}\mathrm{Y} + k_\mathrm{X}\mathrm{X} + k_\mathrm{td}\mathrm{R}) + k_\mathrm{p} \sum_{m,n,p}^{i,j,l} \{[n(k-p)\mathrm{R}(i-m, j-n+1, l-p) +$$

$$+ p(j-n+1)\,\mathrm{R}(i-m, j-n+1, l-p)]\mathrm{R}(m,n,p)\} + \quad (3)$$

$$+ \frac{1}{2}k_\mathrm{tr} \sum_{m,n,p}^{i,j,l} [(l-p+1)\mathrm{R}(i-m, j-n+1, l-p+1)\,(p+1) \times$$

$$\times \mathrm{R}(m,n,p+1)].$$

In the above equations, I is the initiator concentration, $\mathrm{R} = \sum_{i,j,l}^{\infty} l\,\mathrm{R}(i,j,l)$ is the total concentration of active centres, X is the concentration of the chain transfer agent, Y is the concentration of the linear termination agent, F is the total concentration of reactive functional groups, and $k_\mathrm{t} = k_\mathrm{tr} + k_\mathrm{td}$ is the overall square-law termination constant.

For scheme (2)

$$\frac{\mathrm{d}\mathrm{R}(i,j)}{\mathrm{d}t} = -kj\mathrm{R}(i,j) \sum_{m,n=1}^{\infty} n\mathrm{R}(m,n) +$$

$$+ \frac{1}{2}k \sum_{m,n=1}^{i-1,j-1} (j-n)\mathrm{R}(i-m, j-n)\, n\mathrm{R}(m,n). \quad (4)$$

Infinite systems of differential equations can be solved only in convolute form. The simplest method involves the use of generating functions [7, 36, 37]

$$\Phi(q_1, q_2, q_3) = \sum_{i,j,l}^{\infty} q_1^i q_2^j q_3^l R(i,j,l), \quad (5)$$

where q_1, q_2, q_3 are arbitrary variables.

This procedure results in relatively simple partial equations that are principally soluble (in simplest cases, they can even be solved analytically).[52]

In generating function terms, system (3) gives a partial equation (its development can be found, *e.g*., in Refs 7 and 52) of the form:

$$\frac{\partial\Phi(\boldsymbol{q})}{\partial t} = fk_{\mathrm{i}}q_3\mathrm{I} + k_{\mathrm{p}}\left[q_3\frac{\partial\Phi(\boldsymbol{q})}{\partial q_2}\frac{\partial\Phi(\boldsymbol{q})}{\partial q_3} - q_3F\frac{\partial\Phi(\boldsymbol{q})}{\partial q_3} - q_2\mathrm{R}\frac{\partial\Phi(\boldsymbol{q})}{\partial q_2}\right] + (k_{\mathrm{Y}}\mathrm{Y} + k_{\mathrm{X}}\mathrm{X})(1-q_3)\frac{\partial\Phi(\boldsymbol{q})}{\partial q_3} + \frac{1}{2}k_{\mathrm{tr}}\left[\frac{\partial\Phi(\boldsymbol{q})}{\partial q_3}\right]^2 + (k_{\mathrm{td}} - q_3k_{\mathrm{t}})\frac{\partial\Phi(\boldsymbol{q})}{\partial q_3}\mathrm{R}, \quad (6)$$

where $\boldsymbol{q} \equiv (q_1,q_2,q_3)$.

A similar equation describing polycondensation has the form

$$\frac{\partial\Phi(\boldsymbol{q})}{\partial t} = -kq_2\frac{\partial\Phi(\boldsymbol{q})}{\partial q_2}\mathrm{F} + \frac{1}{2}k\left[\frac{\partial\Phi(\boldsymbol{q})}{\partial q_2}\right]^2, \quad (7)$$

where

$$\mathrm{F} = \sum_{i,j,l}^{\infty} j\,\mathrm{R}(i,j).$$

Equation (6) cannot be solved analytically even in its simplest version. Numeric solution encounters the problem of finding a general expression for critical conversion (for arbitrary values of kinetic constants). We shall try to answer this question below.

In the version presented above, Eqn (7) is much more simple than Eqn (6) and has an analytical solution. In any case, as shown in Ref. 53, the solution of Eqns (6) and (7) branches in some instant of time t_{c}, which corresponds to the gel point, and finding this point solves the problem. However, it is not possible to obtain such a simple analytical or even numerical solution in more complex cases, for example, if the reaction involves several types of functional group with different reactivity. Therefore, a method to solve the problem based on a statistical approach was suggested.[5,6]

III. Statistical methods

Flory was probably the first to suggest the use of the statistical approach to describe the polycondensation kinetics and the structure of polymers obtained by this method.[5,54] The molecular-mass distribution upon *f*-functional polycondensation was calculated using combinatorial analysis and the critical conversion condition was obtained. Later calculations were based on the use of a formalised and therefore simpler and more elegant method,[55,56] which is based on the theory of branching processes.[57]

Assuming that cyclisation reactions are excluded, the structure of a macromolecule is represented [8] as a branching tree; any chain unit or a whole fragment can be considered as the root. Reagent molecules are chosen as such fragments in order to link the macromolecule structure with the process of its formation. After that, the probabilities of transitions from generation to generation are considered (the root is taken as the zeroth generation). Probabilities are analysed in terms of generating functions. The kinetic parameters of the process, the depth of conversion by functional groups and their concentrations determine the probabilities of transitions.

The key point of the theory of branching processes [57] is that the generating functions for probabilities of transitions from generation to generation do not depend on the generation number (except the zeroth one), and their calculation requires that algebraic rather than differential (!) equations be solved.

Let us consider the principle of finding the critical conversion in a simple example, *viz*., *f*-functional polycondensation.

In each generation except the zeroth generation, an *f*-functional unit can derive a maximum of $f-1$ units; the probability of the event that each functional group reacts, *i.e*., derives a new unit, equals the conversion value (α). Thus, the generating function of probabilities is

$$Z(q) = \sum_{i=0}^{f-1} q^i\frac{(f-1)!}{i!(f-i-1)}\alpha^i(1-\alpha)^{f-i-1} = (1-\alpha+\alpha q)^{f-1}. \quad (8)$$

The gel formation condition is determined from the solution of the equation

$$u(q) = qZ[u(q)] = q[1-\alpha+\alpha u(q)]^{f-1}. \quad (9)$$

The generating function $u(q)$ characterises the molecular mass distribution of a polymer. The moments of this function correspond to distribution moments. For example, $u(1)$ is the first moment of distribution, and the first derivative on q at $q = 1$ is the second moment of molecular mass distribution.

The critical conversion equals the value α where the derivative $\partial u(1)/\partial q$ turns to infinity

$$\frac{\partial u(q)}{\partial q} = [1-\alpha+\alpha u(q)]^{f-1} + q(f-1)[1-\alpha+\alpha u(q)]^{f-2}\frac{\partial u(q)}{\partial q}. \quad (10)$$

At $q = 1$, we have $u(1) = 1$ and

$$\frac{\partial u(1)}{\partial q} = \frac{1}{1-\alpha(f-1)}. \quad (11)$$

Hence we obtain the gel formation condition (critical conversion):

$$\alpha_{\mathrm{c}}(f-1) = 1. \quad (12)$$

The equation for the first distribution moment $u(1)$ has only one root $u(1) = 1$ below the gel point. Starting from the time instant corresponding to critical conversion, the second root $u(1) < 1$ appears, which characterises the fraction of the soluble polymer (the sol fraction),

$$u(1) = \{1-\alpha[1-u(1)]\}^{f-1}, \quad (13)$$

$$1-u(1) = \alpha(f-1)[1-u(1)]\{1 - \frac{f-2}{2!}\alpha[1-u(1)] + \frac{(f-2)(f-3)}{3!}\alpha^2[1-u(1)]^2 - \ldots\}. \quad (13a)$$

Dividing both parts of this equation by $[1-u(1)]$ and equating the equation root to unity (gel point), we obtain the same expression (12) for critical conversion.

The conversion value is found by solving the differential equation for functional groups

$$\frac{\mathrm{dF}}{\mathrm{d}t} = -k\mathrm{F}^2,$$

$$\alpha = 1 - \frac{\mathrm{F}}{\mathrm{F}(0)}. \quad (14)$$

We present below formulas for determining the critical conversion for different cases of polycondensation.

1. Monomers with different functionality and single-type functional groups with equal reactivity (reactions between any groups are possible):

$$\alpha_{\mathrm{c}}(\langle f\rangle_{\mathrm{w}} - 1) = 1, \quad (15)$$

$$\langle f\rangle_{\mathrm{w}} = \sum_i in_i,$$

$$n_i = \frac{im_i}{\sum_j jm_j},$$

where m_i is the molar concentration of a monomer containing i functional groups. Thus, $\langle f\rangle_{\mathrm{w}}$ is the weight-average functionality.

2. Monomers with different functionality and different-type functional groups (A and B), in which single-type groups cannot

react with each other and the rate constant of the reaction between different-type groups is the same.

$$\alpha_{c\,A}\alpha_{c\,B}(\langle f_A\rangle_w - 1)(\langle f_B\rangle_w - 1) = 1. \quad (16)$$

Since

$$F_{A0} - F_A = F_{B0} - F_B,$$

hence

$$\alpha_A = \frac{F_{B0}}{F_{A0}}\alpha_B,$$

where F_{A0} and F_{B0} are the initial concentrations of the corresponding functional groups.

If the reactivities of functional groups are initially different, it is acceptable to use the statistical approach. For example, the secondary and primary hydroxy groups are non-equal in reactivity in the reaction of glycerol (B) with diisocyanate (A). Therefore, the formula for critical conversion will have the form

$$\frac{2}{3}\alpha_{c\,A}(2\alpha_{c\,B1} + \alpha_{c\,B2}) = 1, \quad (16a)$$

where the indices 1 and 2 correspond to the primary and secondary hydroxy groups of glycerol, respectively. The conversions of functional groups α_{B1} and α_{B2} are determined by solving the corresponding kinetic equations. If the reactivities are equal, *i.e.*, $\alpha_{c\,B1} = \alpha_{c\,B2}$, we obtain the formula (16).

In the case that the functional groups of reagents differ in reactivity, it is also necessary to modify formula (16). Assume that in the reaction

$$A_f + \sum_i B_i \rightarrow \text{products}$$

(the subscript indicates the number of reactive functional groups in a monomer molecule), the functional groups of each monomer B_i have different rate constants of the reaction with A. Therefore, each of them will have its own value of conversion α_i at any given instant in time. Hence, one can write:

$$(f-1)\alpha_{c\,A}\sum_i (i-1)n_i\alpha_{c\,i} = 1. \quad (16b)$$

It is obvious that we obtain Eqn (16) at $\alpha_i = \alpha$.

3. Cross-linking of polymeric chains with a bifunctional reagent. If each polymeric chain unit carries a functional group, then this is essentially the case described above, with the difference that the weight-average functionality of the polymeric reagent equals the weight-average degree of polymerisation ($\langle P\rangle_w$), which is generally much greater than unity. Furthermore, the concentration of the cross-linking agent m_A is usually much lower than the concentration of polymer functional groups. It hence follows that $\alpha_{c\,A} \approx 1$; therefore, Eqn (16) is transformed to the form

$$\alpha_{c\,B}\langle P\rangle_w = 1. \quad (16c)$$

Equations (16c) and (15) coincide formally.

If reactive functional groups are not contained in each unit and their molar fraction is $\rho < 1$, then $\langle f\rangle_w = \rho\langle P\rangle_w$, and, accordingly,

$$\alpha_{c\,B}\rho\langle P\rangle_w = 1. \quad (16d)$$

Simple relationships obtained by the statistical method are widely used in the analysis of various polycondensation processes. However, the so-called substitution effect is usual for polyfunctional reagents: the reactivity of functional groups changes after one group has reacted. In fact, the reaction rate constants for the primary (k_1) and secondary amino group (k_2), which appears as a result of the first reaction, are different in the reaction of epoxy compounds with an amine (Table 1).

The results of calculating the molecular mass distribution in linear polycondensation with the substitution effect depend on the calculation method.[7] Hence, the statistical approach is not suitable in this case. It has been shown[48,59] that a statistical calculation gives wrong results for critical conversion if the formation of a cross-linked polymer involves the substitution effect.

Table 1. Relative rate constants (k_2/k_1) of addition of the second epoxy group to the amine.[58]

T/°C	DDS [a]	MDA [b]	MDEA [c]	MCDA [d]
80	0.46	0.65	–	0.67
135	0.42	–	0.66	0.64
160	0.51	–	–	0.70

[a] DDS is 4,4′-diaminodiphenylsulfone, [b] MDA is 4,4′-methylenediamine, [c] MDEA is 4,4′-methylenebis(2,6-diethylaniline), [d] MCDA is 4,4′-methylenebis(3-chloro-2,6-diethylaniline).

It was found equally fruitless to use the statistical approach for solving the cyclisation problem.[60] It was shown[61] that, as in the previous case, only a kinetic solution can give correct results.

Later, a hypothesis on the applicability limits of the statistical calculation method was proposed.[62] Its applicability limits were fully established using the BBs concept.[9,63] However, attempts to use this method to describe the kinetics of polymer formation in the presence of the substitution effect were made previously[64] and were continuing until recently.[65,66]

IV. The bond block concept as a method to solve problems involving the substitution effect

The bond block concept[9,51,63,67] assumes a combination of kinetic and statistical methods. It is this concept that made it possible to develop a general approach for determining the gel point; the formulas resulting from statistical calculations are obtained as a special case if certain conditions are met. The 'bond block' concept is not yet widespread, therefore let us consider it in more detail.

A bond block is understood as a structure that can belong to any macromolecule or cross-linked polymer.[63] It is represented as a connected graph G, whose verges and nodes are bonds and atoms (units) connected by these bonds. The total set of concentrations of all bond blocks in a system characterises unambiguously its composition and structure. In this sense, the concentration $y(G)$ is analogous to the polymer molecular mass distribution function in terms of the information it contains. On the other hand, it is richer, as it not only describes the length distribution of chains but also characterises the molecular and topologic structure of a polymeric system.

When we speak of bonds, we mean those which result from the reaction under consideration. Hence, the BB concept is closely related to the process chemistry. Each bond is determined by the groups (units) connected by that bond: an a – a bond connects A units, an a – b bond connects A and B units, *etc*. In other words, identification of different units is meaningful only as an attribute (characteristics) of a bond. The total set of BBs unambiguously characterises the chain size and structure.

In the case of a linear homopolymer, BBs only differ in the number of bonds but not in their type, as in the example presented above. Therefore, the relationship between the concentrations of BBs and chains has a simple form in this case:

$$y_n = \sum_{i=n}^{\infty}(i-n)x_i, \quad (17)$$

where y_n and x_i are the concentrations of BBs and chains, respectively; their sizes are shown by the indices. The $(i-n)$ factor equals the number of ways to arrange a BB of n bonds in a chain containing i units.

The reverse relationship follows from Eqn (17)

$$x_i = y_{i-1} - 2y_i + y_{i+1}. \quad (18)$$

The condition (18) can be generalised for chains and BBs with any configuration if the terminal block (TB) concept is introduced. A TB is understood as a BB in which one of the units bordering the block is also a terminal unit of the chain (polymeric structure).

The TB concentration (z_i) is expressed through the BB concentration:

$$z_i = y_{i-1} - y_i = y_{i-1}(1 - y_1). \quad (19)$$

(For simplicity, here we used symbolic multiplication as addition of indices.)

If the number of terminal groups z_i^k (the superscript identifies the terminal member type) in a selected polymeric structure is more than unity, then

$$z_i^{k,m} = z_i^k(1 - y_1^m) = y_{i-1}(1 - y_1^k)(1 - y_1^m). \quad (20)$$

If there are several terminal groups (branched polymer), the numbers of multiplicands and superscripts in formula (20) increase accordingly.

A polymeric chain with any topology (excluding rings!) can be defined as a TB where the number of terminal groups equals the number of terminal groups of a macromolecule (all the block's bonds are broken). This number equals two for a linear chain. In this case, we come to the relationship (17). For an arbitrary number and type of terminal groups, we obtain

$$x_i = y_{i-1}\prod_{j=1}^{n}(1 - y_1^j). \quad (21)$$

Thus,

$$x_i = \begin{cases} y_{i-1} - y_i & \text{for terminal block} \\ y_{i-1} - y_i^1 - y_i^2 + y_{i+1}^{1,2} & \text{for linear chain with terminal groups of types 1 and 2} \\ y_{i-1} - \sum_{j=1}^{3} y_i^j + y_i^{1,2,3} & \text{for branched chain with three terminal groups} \end{cases} \quad (22)$$

and so on.

An example of the use of formulas similar to those presented above [(17)–(22)] was considered by Hsieh and Randall.[68] To calculate the number of sequences in ethylene and butene copolymers, they used NMR data that allowed the concentrations of short TBs (containing one, two, and three units) to be found.

The system of kinetic equations for BBs was obtained from a usual scheme of chain formation and a (17)-type relationship. Let us develop equations for linear polycondensation

$$\begin{aligned} &X_1 + X_1 \xrightarrow{k_1} X_2, \\ &X_1 + X_i \xrightarrow{k_2} X_{i+1},\ i = 2, 3, \ldots \\ &X_i + X_j \xrightarrow{k_3} X_{i+j},\ i, j = 2, 3, \ldots, \end{aligned} \quad (23)$$

where X_1, X_2, X_i, and X_j are reagents.

The corresponding system of differential equations has the form

$$\begin{aligned} \frac{dx_1}{dt} &= -2k_1x_1^2 - k_2x_1\sum_{j=2}^{\infty}x_j, \\ \frac{dx_2}{dt} &= k_1x_1^2 - k_2x_1x_2 - k_3x_2\sum_{j=2}^{\infty}x_j, \\ \frac{dx_3}{dt} &= k_2x_1(x_2 - x_3) - k_3x_3\sum_{j=2}^{\infty}x_j, \\ \frac{dx_i}{dt} &= k_2x_1(x_{i-1} - x_i) - k_3x_i\sum_{j=2}^{\infty}x_j + \frac{1}{2}k_3\sum_{j=2}^{i-2}x_jx_{i-j},\ i = 4, 5, \ldots, \end{aligned} \quad (24)$$

where x_1, x_2, x_3, x_i, x_j are the chain concentrations.

After substituting (17) into (24) we obtain

$$\begin{aligned} \frac{dy_0}{dt} &= 0, \\ \frac{dy_1}{dt} &= k_1(y_0 - y_1)^2 + (y_1 - y_2)[(k_2 - k_1)(y_0 - y_1) + \\ &\quad + \frac{1}{2}(k_1 - 2k_2 + k_3)(y_1 - y_2)], \\ \frac{dy_2}{dt} &= (k_2 - k_3)(y_1 - y_2)(y_0 - 2y_1 + y_2) + \\ &\quad + \frac{1}{2}k_3\sum_{j=0}^{2}(y_j - y_{j+1})(y_{2-j-1} - y_{2-j}), \\ \frac{dy_i}{dt} &= (k_2 - k_3)(y_{i-1} - y_i)(y_0 - 2y_1 + y_2) + \\ &\quad + \frac{1}{2}k_3\sum_{j=0}^{i}(y_j - y_{j+1})(y_{i-j-1} - y_{i-j}),\ i = 3, 4, \ldots \end{aligned} \quad (25)$$

where the concentration of bond blocks y_0 equals the total number of units in the system and is therefore a constant; y_1 is the total number of bonds; the y_1/y_0 ratio is the conversion depth.

System (25) is as infinite as system (24). However, the distinctive feature is that it is a closed system starting from the second term of the series (y_2), and can therefore be solved numerically by a sequential method: y_i can be calculated if all the preceding values, *viz.*, y_j, $j < i$, are known. The truncation of the system occurs naturally: there is no sense in calculating the variables whose concentrations cannot be measured. For example, if an experiment allows the determination of sequences consisting of a maximum of five units, why should the concentration of a six-unit sequence be determined? Thus, in this case the system to be solved will consist of five equations. A similar statement corresponds to chain concentrations obtained from (25) by substitution of y_i into Eqn (18).

Analysis of the structure of kinetic equations for BBs showed that a simple rule is observed: all the possible ways of formation of a given block are totalled. This simplifies considerably the formulation of kinetic equations for BBs. In this case, the TB concept becomes of key importance: in essence, the TB concept is a generalisation of the 'functional group' concept. In fact, a reaction between functional groups results in one bond, or a single BB (y_1). A terminal block is a functional group with units (one, two or more) bound to it. The formation of a TB results from reactions of simpler TBs with starting reagents; the structures of all the reaction participants are simpler than the structure of the starting block. Thus, the system of equations for any arbitrary complex structure appears to be closed, and the requirements of an experiment determine the blocks for which the kinetic problem should be solved.

Analysis of the system of differential equations for BBs showed [9, 51, 67] that it can be broken into groups of equations in such a way that the concentrations of BBs described by these equations can be calculated directly by solving that group of equations. The concentrations of larger BBs can be found using probabilistic methods. If such a group consists of a single block, *i.e.*, a block involving only one bond, the probabilistic approach is applicable to calculations of a polymeric structure of any complexity. In almost all cases it is possible to separate such structures of minimum size from which structures of arbitrary complexity and size can be combined. It was found [9, 51, 67] that the criterion of 'simplicity' consists of the absence of substitution effects on the reactivity of functional groups. Such effects can exist within a 'simple' block.

Thus, the use of the BB concept makes it possible to simplify the solution of kinetic problems, because it becomes unnecessary to formulate differential equations for all sizes of blocks. It is sufficient to solve these problems for elementary blocks and to use probabilistic calculations for larger blocks. In other words, the method based on the BB concept combines the advantages of both kinetic and probabilistic approaches.

Let us illustrate the application of the BB concept to the solution of the problem of critical conversion for a particular system, *viz*., epoxide bifunctional oligomer–pentafunctional amine.[69] The presence of primary and secondary hydrogen atoms in the latter creates prerequisites for the substitution effect. If BB concentrations are used, then, as in the statistical calculation, not molar concentrations of reagents are used but functional fractions of reactive groups (n_i) and probabilities of reactions of the corresponding groups, *i.e*., conversion degree (α_i).

The functional fractions of the corresponding groups n_i that are capable of reacting with the amine (the functional fraction of which equals n_A) can be represented as

$$n_i = \frac{N_i}{\sum_j N_j},$$

where N_i is the molar concentration of the corresponding groups at a given instant in time (at a given conversion); moreover,

$$N_i = i m_i,$$

where m is the molar concentration of a reagent containing i reactive functional groups. The balance condition is

$$\sum_i N_i \alpha_i = A\alpha_A,$$

where the i index corresponds to the epoxide reagents and the A index corresponds to the amine. The values of α_i and n_i are found by solving the corresponding systems of kinetic equations.

The structure of the network is determined by the concentration of nodes with different functionality; in this case, fragments of the amine-type hardening agent play the role of nodes. It is these structural elements that are bond blocks, whose concentration in this case should be calculated by the kinetic method, *i.e*., by solving the appropriate kinetic equations. The functionality of a node is determined by the number of oligomeric fragments bound to it.

In the case of the 'bifunctional epoxide oligomer–pentafunctional amine' system [*e.g*., diethylenetriamine (DETA) contains one secondary and two primary amino groups], it is necessary to distinguish primary and secondary amino groups from the very start of the reaction. If we designate the numbers of primary and secondary hydrogen atoms by digits (the first and second digit, respectively), the following groups are involved in the building of the network:

A(41) — original amine, node of zero functionality;

A(40) — amine with reacted secondary amino group; its functionality is 1, and it is a terminal fragment in the network;

A(22) — reaction product of a primary amino group; its functionality is 1, and it is a terminal fragment;

A(21) — functionality 2, intermediate fragment;

A(03) — functionality 2, intermediate fragment;

A(20) — trifunctional node;

A(02) — trifunctional node;

A(01) — tetrafunctional node;

A(00) — pentafunctional node.

If the ratio of reaction rate constants of secondary and primary amino groups is designated as

$$\beta = \frac{k_2}{k_1},$$

then the system of equations for all amino groups can be represented as follows:

$$\begin{aligned}
\frac{dB}{dt} &= -B\{4A(41) + 4A(40) + 2A(22) + 2A(21) + 2A(20) + \\
&\quad + \beta[A(41) + 2A(22) + A(21) + 3A(03) + \\
&\quad + 2A(02) + A(01)]\},\\
\frac{dA(41)}{dt} &= -(4+\beta)BA(41),\\
\frac{dA(40)}{dt} &= [\beta A(41) - 4A(40)]B,\\
\frac{dA(22)}{dt} &= [4A(41) - 2(1+\beta)A(22)]B,\\
\frac{dA(21)}{dt} &= [4A(40) + 2\beta A(22) - (2+\beta)A(21)]B,\\
\frac{dA(03)}{dt} &= [2A(22) - 3\beta A(03)]B,\\
\frac{dA(02)}{dt} &= [3\beta A(03) + 2A(21) - 2\beta A(02)]B,\\
\frac{dA(20)}{dt} &= [\beta A(21) - 2A(20)]B,\\
\frac{dA(01)}{dt} &= [2\beta A(02) + 2A(20) - \beta A(01)]B,\\
\frac{dA(00)}{dt} &= \beta A(01)B.
\end{aligned} \tag{26}$$

The concentrations of nodes with different functionality change in the course of a reaction (Fig. 1). Characteristically, the concentration–conversion curves for different β values are similar in appearance: the maximum concentration of nodes with a given functionality corresponds to a single value of conversion depth, irrespective of the relative rate constant of the reaction involving the secondary amino group. On the other hand, the maximum value varies as a function of the kinetic parameters of polycondensation.

Since it is assumed that the reactivity of epoxy groups is unchanged during the reaction, the network structure can be calculated using a statistical approach based on calculated node concentrations.

According to the theory of branching processes,

$$u(q) = x\left[1 - \alpha + \alpha\sum n_{Ai} u^{i-1}(q)\right], \tag{27}$$

where α is the conversion degree of epoxy groups; n_{Ai} is the functional fraction of i-functional nodes.

Differentiation of the equation results in an expression for the gel formation condition

$$\alpha\sum_i (i-1)n_{Ai} = 1. \tag{28}$$

Formally, Eqn (28) coincides with the critical condition for f-functional polycondensation (15); however, the difference is that the weight-average functionality $\langle f\rangle_w$ changes during the process, *i.e*., it is a function of the conversion α.

The plots

$$y(\alpha) = 1 - \alpha\sum_i (i-1)n_{Ai}$$

are presented in Fig. 2 for different β values. The α_c value is determined by the condition $y(\alpha) = 0$. The critical conversion values for the diepoxide–DETA system for different β values are presented below.

β	1.0	0.7	0.5	0.3	0.1	0.01
α_c	0.5	0.507	0.514	0.524	0.535	0.535

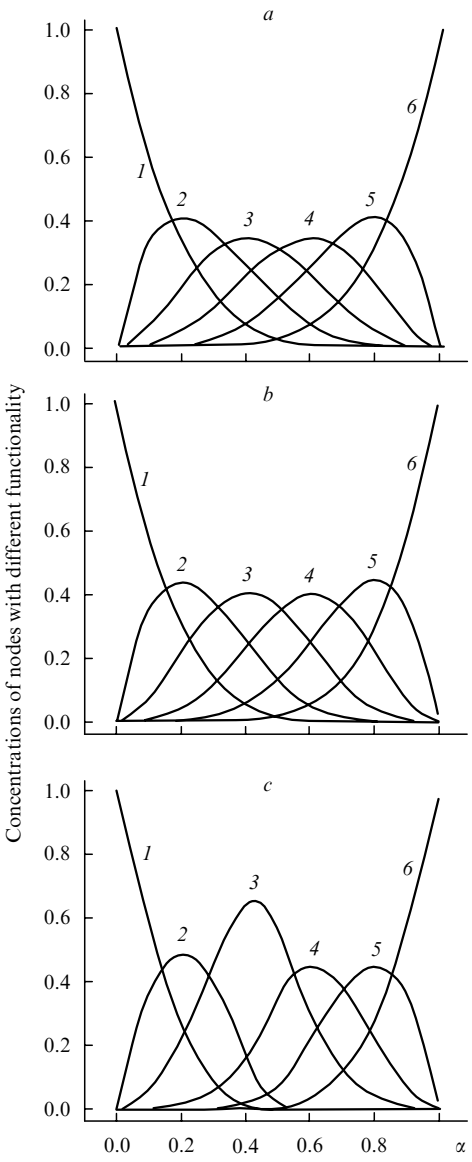

Figure 1. Dependencies of the concentrations of network nodes with different functionality on conversion for $\beta = 1$ (*a*), 0.5 (*b*), 0.1 (*c*).[69]
Node functionality: (*1*) 0, (*2*) 1, (*3*) 2, (*4*) 3, (*5*) 4, (*6*) 5.

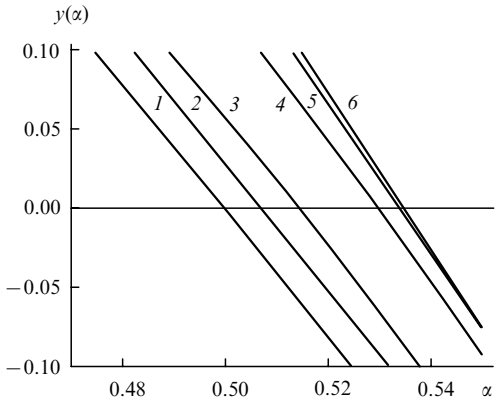

Figure 2. Graphical solution of the equation for finding the critical conversion at $\beta = 1$ (*1*), 0.7 (*2*), 0.5 (*3*), 0.2 (*4*), 0.1 (*5*), 0.01 (*6*).[69]

Thus, the solution result depends on the β value; this does not follow from the statistical theory at all. However, it can be shown easily that the known formula for the dependence of n_{Ai} on conversion is obtained if the applicability conditions of the statistical approach are met. In fact, according to statistics,

$$A_i = A\frac{f!}{i!(f-i)!}\alpha_A^i(1-\alpha_A)^{f-i}, \qquad (29)$$

where A_i is the concentration of the i-functional node and f is its maximum possible functionality ($f = 5$ for DETA).

Since

$$n_{Ai} = \frac{iA_i}{\sum_i iA_i},$$

substituting (29) into (28) we obtain

$$\alpha(f-1)\alpha_A = 1,$$

which coincides with Eqn (16) for a system of a bifunctional and an f-functional reagent.

The ratio of β constants affects considerably the gel point if the reagents are present in a non-equivalent ratio (Fig. 3).

When the scheme of a branching process is constructed (the statistical stage of solving the problem), the functionality of nodes that are formed should be taken into account. The presence of monofunctional reagents in the reaction mixture shifts the gel point towards higher conversions.[69] In this case, the gel formation condition has the form of Eqn (28); however, the presence of a monofunctional 'terminator' should be taken into account in the i index (as above, it means the node functionality). Here the functionality equals the number of added bifunctional oligomers rather than the number of hydrogen atoms that have reacted.

The strong dependence of the critical conversion on the concentration of the monofunctional modifier results from the decrease in the functionality of nodes (Table 2, Fig. 4). In comparison with the plots of changes in the concentrations of nodes with different functionality presented in Fig. 1, similar curves in Fig. 4 are shifted to the right along the x axis, the stronger the higher the content of the monofunctional modifier. While the final state of the system did not depend on the values of kinetic constants in the former case, in the latter case the presence of a monofunctional modifier strongly affects the structure of the

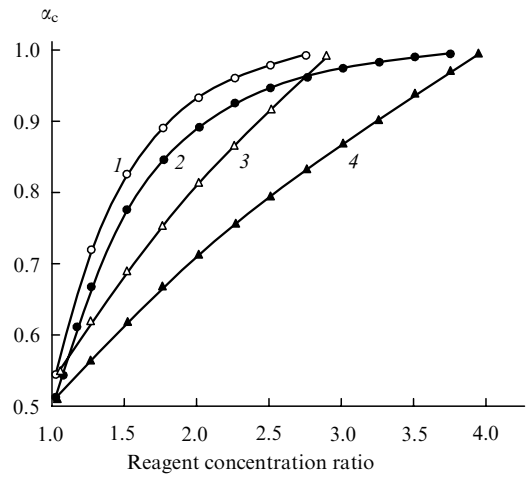

Figure 3. Dependence of the critical conversion on the ratios of the concentrations of amine (A) and epoxide oligomer (B) at different β values.[69]
A/B at $\beta = 0.1$ (*1*), 1 (*2*); B/A at $\beta = 0.1$ (*3*) and 1 (*4*).

Table 2. Critical conversion values at different monofunctional component concentrations (n_1) and different relative reaction rate constants of the modifier with primary (k_1) and secondary (β_2) amino groups (β_1 is the relative reaction rate constant of the secondary amino group with the epoxy group of the main oligomer).[69]

n_1	$k_1=1$, $\beta_1=\beta_2=1$	$k_1=5$, $\beta_1=\beta_2=1$	$k_1=1$, $\beta_1=\beta_2=0.5$	$k_1=0.5$, $\beta_1=\beta_2=1$	$k_1=0.5$, $\beta_1=\beta_2=0.5$
0	0.500	0.500	0.514	0.500	0.514
0.1	0.527	0.527	–	0.527	0.542
0.2	0.559	–	0.572	–	0.574
0.3	0.597	–	–	0.597	0.613
0.4	0.645	0.645	0.655	–	0.661
0.5	0.707	–	–	0.707	0.722
0.6	0.790	–	0.794	–	0.804
0.65	0.845	0.845	–	–	0.857
0.7	0.913	–	0.912	0.913	0.923
0.74	0.981	0.981	0.980	–	0.987

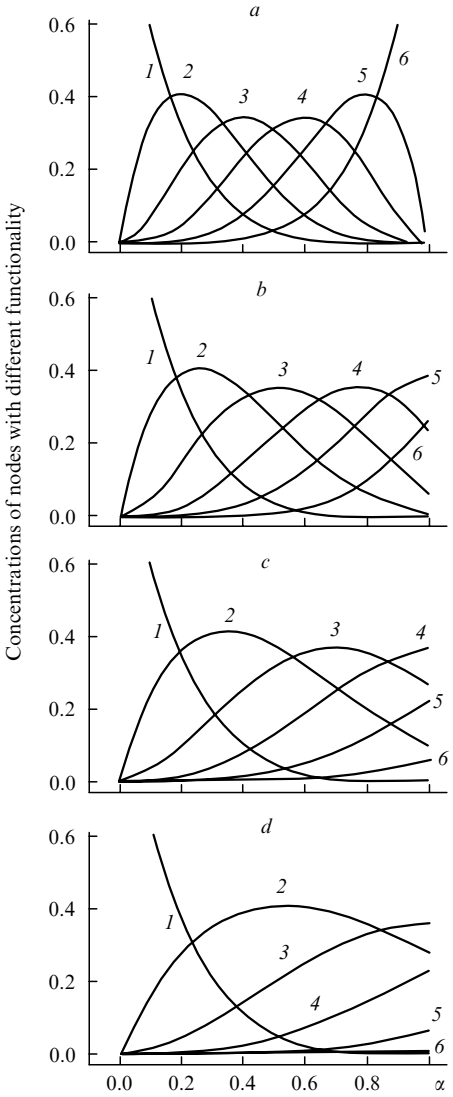

Figure 4. Dependencies of the concentrations of network nodes with different functionality on conversion for $\beta = 1$ at $n_1 = 0$ (*a*), 0.2 (*b*), 0.4 (*c*), 0.6 (*d*).
Node functionality: (*1*) 0, (*2*) 1, (*3*) 2, (*4*) 3, (*5*) 4, (*6*) 5.[69]

network formed, hence the gel point becomes unreachable at some concentration of the modifier.

Unlike a monofunctional modifier, a bifunctional modifier does not affect the critical conversion since neither of the components breaks network chains, hence the functionality of nodes does not depend on which of them is bound to an amine fragment. In this case, critical conversion is determined by the equation

$$(\alpha_b n_b + \alpha_2 n_2) \sum_i (i-1) n_{Ai} = 1, \tag{28a}$$

where the 'b' index corresponds to the main oligomer and the '2' index corresponds to the modifying one,

$$\alpha_b n_b + \alpha_2 n_2 \equiv \alpha_{ef}.$$

Both the difference of reaction rate constants of epoxy groups corresponding to different oligomers and the relative concentrations of oligomers affect the α_{ef} value but do not affect the gel point.

The use of the approach considered above for the solution of the problem of critical conversion values for other systems was considered by Deberdeev *et al.*[69,70].

V. Three-dimensional polymerisation

Polymerisation can be regarded as a process with a pronounced substitution effect. In fact, interaction of an active centre with a functional group recovers the active centre, *i.e.*, its reactivity changes. If there is no reagent with unchanged reactivity, the statistical approach to the description of such reactions is not applicable in any form (neither directly nor with the use of the BB concept). However, the statistical approach proposed long ago by Stockmayer [11,71] and improved by Gordon [72] is widely used even now.[18–20,73–76]

In essence, based on the statements of the statistical theory, the gel point condition for three-dimensional polymerisation consists of the requirement

$$\alpha_c = \frac{1}{\rho(\bar{P}_w - 1)}, \tag{16e}$$

i.e., this is considered as a cross-linking process. In this formula, α_c is the critical branching, a value introduced by Flory and Stockmayer;[5,71] ρ is the molar fraction of the bifunctional monomer if (as often happens) a mixture of mono- and bifunctional monomers is considered. The relationship between α_c and conversion was determined by solving kinetic equations describing the consumption of functional groups of monomers.[72]

Attempts were made to solve the problem kinetically. However, either the conditions used were not quite correct in some cases[77–79] or approximate and particular solutions were obtained.[7]

It should be noted that the question of experimental validation of theoretical calculations was non-topical for a long time, since it is well known that their feasibility conditions are not realised in three-dimensional polymerisation:[7,8,50] the fast chain growth by the radical mechanism and the low chain concentration at early stages of the process result in rather intense intramolecular cyclisation.[8,80–82] In this case, multiple cross-linking between a single pair of chains (formation of multiplet nodes and 'staircase'-type macromolecular structures) is also regarded as a factor decreasing the effective concentration of interchain cross-links and thus increasing the critical conversion. Because of that, microheterogeneous behaviour is typical of radical polymerisation.[8,50,83,84]

However, recent studies on living radical three-dimensional polymerisation (see, *e.g.*, Ref. 85) showed that the relationship (16e) is not fulfilled either,[86] though cyclisation does not play a significant role,[87] and the microheterogeneous character of the process does not manifest itself.[86,88]

It is convenient to solve Eqn (6) not in general form but by transforming it to a system of moments of the generating function.

Differentiation of Eqn (6) by all the q_i followed by equating them to 1 results in a system of differential equations for generating function moments and hence, moments of macromolecule distribution by length, chain functionality, and number of active centres. Obviously, all of these values are functions of time: $N = \Phi(\mathbf{1})$ is the total concentration of chains (zero moment);

first moments:

$$M = \frac{\partial \Phi(\mathbf{1})}{\partial q_1} = \sum_{i,j,l} i R(i,j,l)$$

is the total concentration of monomeric units in the system;

$$F = \frac{\partial \Phi(\mathbf{1})}{\partial q_2} = \sum_{i,j,l} j R(i,j,l)$$

is the total concentration of functional groups,

$$R = \frac{\partial \Phi(\mathbf{1})}{\partial q_3} = \sum_{i,j,l} l R(i,j,l)$$

is the total concentration of active centres;

second moments:

$$\Phi_{ij} \equiv \Phi_{ij}(\mathbf{1}) = \frac{\partial^2 \Phi(\bar{q})}{\partial q_i \partial q_j} \text{ at } \boldsymbol{q} = \mathbf{1}:$$

$$\Phi_{11} = \sum i(i-1)R(i,j,l),$$

$$\Phi_{12} = \sum ij R(i,j,l),$$

$$\Phi_{13} = \sum il R(i,j,l),$$

$$\Phi_{22} = \sum j(j-1)R(i,j,l),$$

$$F_{23} = \sum jl R(i,j,l),$$

$$\Phi_{33} = \sum l(l-1)R(i,j,l).$$

The system of differential equations for generating function moments has the form

$$\frac{dI}{dt} = -k_i I,$$

$$\frac{dN}{dt} = f k_i I - k_p FR - \frac{1}{2} k_t R^2 - k_Y Y,$$

$$\frac{dM}{dt} = 0,$$

$$\frac{dF}{dt} = -k_p FR,$$

$$\frac{dR}{dt} = f k_i I - k_t R^2 - k_Y Y,$$

$$\frac{dX}{dt} = -k_X XR,$$

$$\frac{d\Phi_{11}}{dt} = 2k_p \Phi_{12}\Phi_{13} + k_t(\Phi_{13})^2, \qquad (30)$$

$$\frac{d\Phi_{12}}{dt} = k_p(\Phi_{13}\Phi_{22} + \Phi_{12}\Phi_{23} - R\Phi_{12}) + k_t \Phi_{13}\Phi_{23},$$

$$\frac{d\Phi_{13}}{dt} = k_p(\Phi_{13}\Phi_{23} + \Phi_{12}\Phi_{33} + R\Phi_{12}) - (k_X X + k_Y Y)\Phi_{13} + k_t(\Phi_{33} - R)\Phi_{13},$$

$$\frac{d\Phi_{22}}{dt} = 2k_p(\Phi_{22}\Phi_{23} - R\Phi_{22}) + k_t(\Phi_{23})^2,$$

$$\frac{d\Phi_{23}}{dt} = k_p[(\Phi_{23})^2 + \Phi_{22}\Phi_{33} - R\Phi_{23} + R\Phi_{22}] - (k_Y Y + k_X X)\Phi_{23} + k_t(\Phi_{33} - R)\Phi_{23},$$

$$\frac{d\Phi_{33}}{dt} = 2k_p \Phi_{23}(\Phi_{33} + R) - 2(k_Y Y + k_X X)\Phi_{33} + k_t(\Phi_{33} - 2R)\Phi_{33}.$$

The solution of the system makes it possible to obtain comprehensive information about the course of polymerisation, including the value of critical conversion.

As noted above, the mathematical criterion of the formation of a cross-linked polymer is that the second moment of molecular mass distribution turns to infinity. However, it is the number of functional groups (as well as the number of active centres) that determines the chain growth rate during gel formation. Hence, distribution of macromolecules by functionality is the determining factor. In terms of generating function moments, it is the value of the second moment of the generating function by functionality

$$\Phi_{22}(t) = \sum_{i,j,l} j(j-1)R(i,j,l,t).$$

In a series of studies, Irzhak *et al.*[49,89–92] used the method considered above to study three-dimensional polymerisation processes involving different mechanisms: living polymerisation with instant and slow initiation, without and with chain transfer; polymerisation with square-law and linear termination. The main results of these studies are presented below.

The plots of $\Phi_{22}(t)$ during living polymerisation in the absence of chain transfer reactions under instant initiation conditions are presented in Fig. 5. One can see that $\Phi_{22}(t)$ increases by orders of magnitude (tends to infinity) in a very narrow range of conversions. Therefore, the critical conversion can be determined, without a considerable inaccuracy, as the x-axis intercept of the asymptote to the $\Phi_{22}(t)-\alpha$ curve. As calculations showed,[89] the critical conversion α_c obtained by this method is an unambiguous function of the starting $\Phi_{22}(0)$ value at a given concentration of active centres I_0 and does not depend on the starting concentration of functional groups, F(0).

The dependence of α_c on $\Phi_{22}(0)$ for living polymerisation with instantaneous initiation is presented in Fig. 6. It is evident that the square-root law is obeyed with good accuracy in this case; the

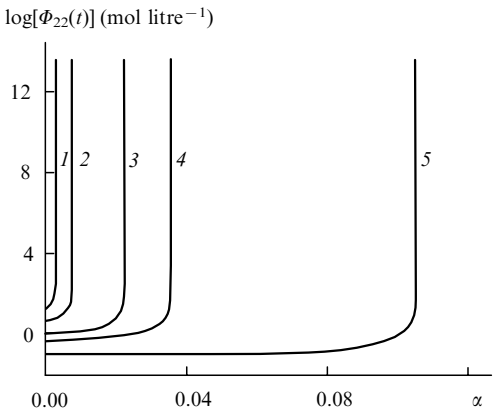

Figure 5. Kinetic curves of changes in the second moment of functionality distribution $\Phi_{22}(t)$ on instant initiation.
$I_0 = 10^{-3}$ mol litre^{-1}; $\Phi_{22}(0) = 20$ (*1*), 5 (*2*), 1 (*3*), 0.5 (*4*), 0.1 (*5*).[89]

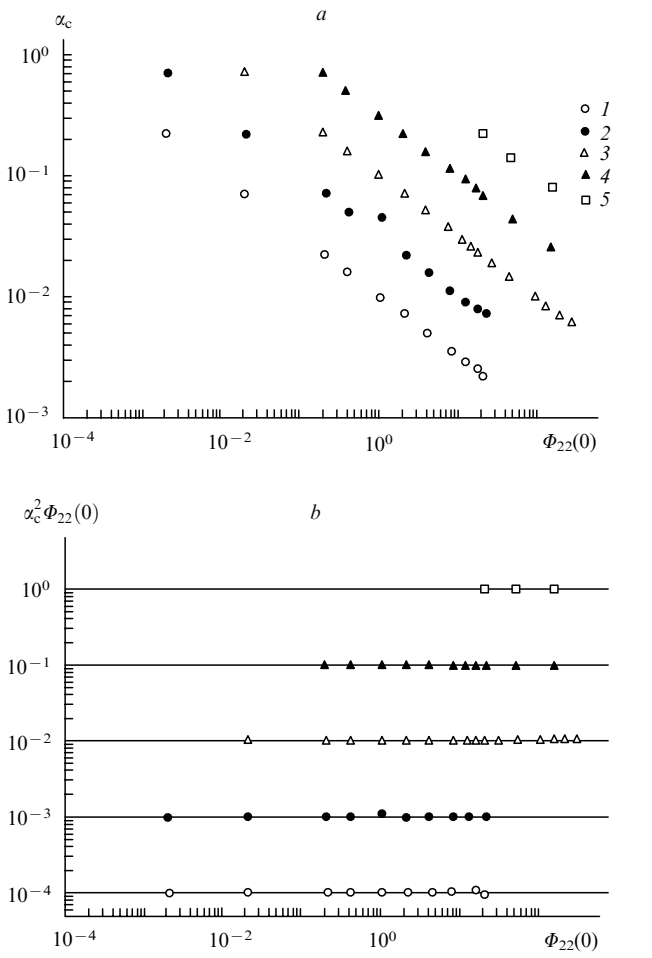

Figure 6. Dependencies of α_c on $\Phi_{22}(0)$ in the case of instant initiation. $I_0 = 10^{-4}$ (*1*), 10^{-3} (*2*), 10^{-2} (*3*), 10^{-1} (*4*), 1 mol litre^{-1} (*5*).[89]

straight lines corresponding to different concentrations of active centres are parallel to each other. Analysis showed that the critical conversion value is described by the formula

$$\frac{\alpha_c^2\Phi_{22}(0)}{I_0} = 1. \qquad (31)$$

The forms of the formulas (31) and (16) are similar. It fact, taking into account that

$$\frac{\Phi_{22}(0)}{F(0)} = \langle f\rangle_w - 1,$$

formula (31) can be converted to

$$\alpha_c^2 r(\bar{f_w} - 1) = 1. \qquad (31a)$$

However, this is just an outward similarity, since the r value, which is the ratio of concentrations of functional groups and active centres is much more than unity, whereas the F_{B0}/F_{A0} in formula (16) is close to unity. Furthermore, there is no multiplier characterising the distribution of the second reagent (active centres) by functionality. Anyway, it could not be present here because of the facts noted above, *i.e.*, that the starting molecules of active centres are monofunctional [R(0,0,1)/I_0 = 1] and that they are not consumed in polymerisation. Probably, the presence of the second power of α_c in formula (31) originates from the fact that the achievement of the critical point requires the reaction of at least two (per one chain) groups belonging to polyfunctional (branching) monomers, rather than the simultaneous reaction of two different functional groups, as is the case in Eqn (16).

Solution of the problem of radical copolymerisation of mono- and bifunctional monomers by the Monte Carlo method[93] resulted in an empirical relationship, whose form is similar to Eqn (31). The dependence of the critical conversion p_c on the inhibitor concentration C_I, the fraction of vacant lattice points C_V, and the molar fraction of bifunctional monomers f_{bif} was determined using the formula

$$p_c = \frac{C_I^{0.45}}{f_{bif}^{0.47}(1 - C_V)}.$$

As one can see, there are some differences, *viz.*, the index of power differs somewhat from 2 and the relative concentration of branching (bifunctional) comonomer appears in place of the second moment by functionality. The first difference is explained by the fact that cyclisation can be taken into account in the simulation of polymerisation. Therefore, the gel point should shift towards higher conversions in comparison with that calculated analytically. As regards the molar fraction of the branching comonomer, its use is not substantiated by any considerations.

Bansil *et al.*[93] reached the conclusion that the relationship obtained agreed with the ideas of Flory and Stockmayer. However, on the contrary, the calculation presented in that study suggests that there was no agreement.

Analysis of polymerisation processes with more complex mechanisms confirms the latter conclusion. Results for living polymerisation under slow initiation conditions are presented in Fig. 7. One can see that the α_c *vs.* $\Phi_{22}(0)$ plots in logarithmic

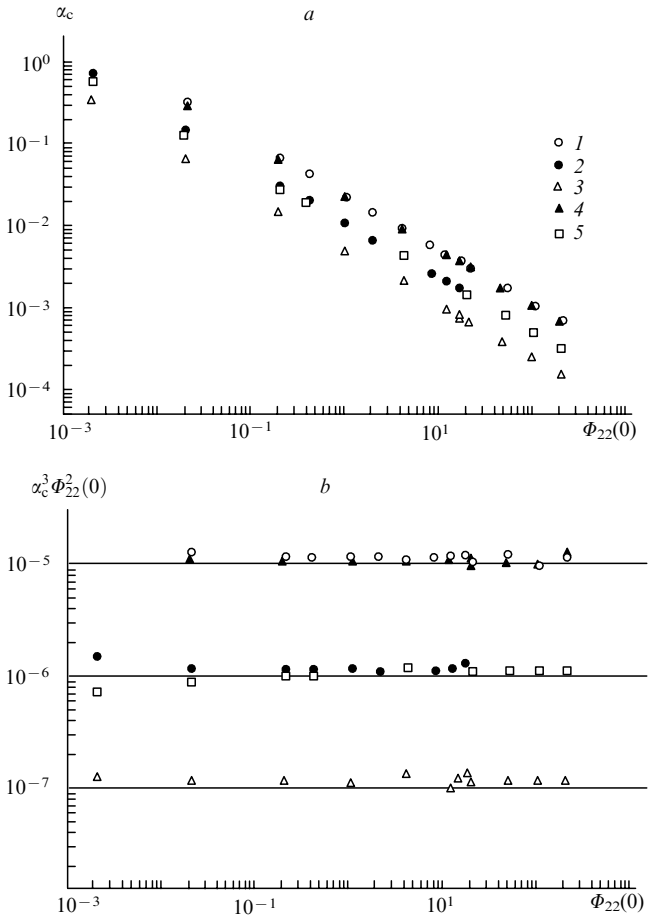

Figure 7. Dependencies of α_c on $\Phi_{22}(0)$ in the case of slow initiation. I_0 = 1 (*1*), 10^{-1} (*2*), 10^{-2} (*3*, *4*), 10^{-3} mol litre^{-1} (*5*); $k_i/k_p = 10^{-5}$ (*1–3*) and 10^{-3} (*4*, *5*).[89]

coordinates have the form of parallel straight lines demonstrating the relationship

$$\alpha_c \sim [\Phi_{22}(0)]^{-0.67},$$

shifted along the y-axis depending on the initiation rate. All the results are described with high accuracy by the following relationship:

$$\alpha_c^3 \frac{k_p \Phi_{22}^2(0)}{k_i I_0} = 1. \quad (32)$$

However, it is obvious that this result does not at all correlate with formulas provided by the statistical theory. On the other hand, both Eqns (31) and (32) relate the critical conversion value with the weight-average functionality of the starting monomer mixture referred to the concentration of chains [Eqn (31)] or to the rate of their accumulation [Eqn (32)].

It should be noted that the formulas (31) and (32) are some limiting cases that are obtained from a more general expression at $W_i \to \infty$ (instant initiation) or $W_i \to 0$ (slow initiation). The following formula can be an example:

$$\frac{\alpha_c^2 \Phi_{22}(0)}{I_0} = 1 - \exp\left[- \frac{k_i}{k_p \alpha_c \Phi_{22}(0)} \right] \longrightarrow$$

$$\longrightarrow \begin{cases} 1 & \text{at} \quad k_i \to \infty \\ \dfrac{k_i}{k_p \alpha_c \Phi_{22}(0)} & \text{at} \quad k_i \to 0 \end{cases}.$$

However, this result cannot be obtained in explicit form because the system (30) does not have an analytical solution. On the other hand, numeric calculation (Fig. 8) showed that the formula (31) is correct under the condition

$$\frac{k_i}{k_p \alpha_c \Phi_{22}(0)} \geqslant 6.$$

If

$$\frac{k_i}{k_p \alpha_c \Phi_{22}(0)} < 1,$$

then the critical conversion value is determined by the expression (32). The term 'instant initiation' should be used in the case $k_i/k_p > 0.1$ mol litre^{-1}.

Dusek and Somvarsky [94] gave a kinetic solution of the problem for living polymerisation with slow initiation. It was shown that the results given by the suggested approach differed from those of statistical calculations. Calculations carried out using the system (30) (taking into account that initiation occurs when an initiator reacts with a functional group) also give a somewhat different result (Table 3).

The difference between the critical conversion values is not high at a low inhibitor concentration and a low initiation constant, but it increases with an increase in these parameters.

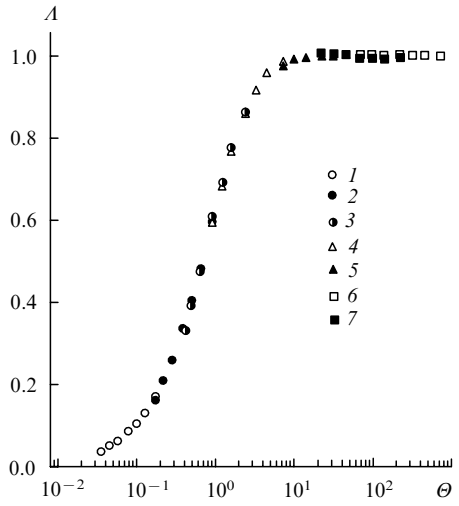

Figure 8. Dependence of α_c on the initiation rate in generalised coordinates $\Lambda - \Theta$.[49]
The curve shows the regions where the relationships (31) and (32) are obeyed.
$\Lambda = \alpha_c^2 \Phi_{22}(0)/I_0$, $\Theta = k_i/k_p \alpha_c \Phi_{22}(0)$; $\log(k_i/k_p) = -5$ (*1*), -4 (*2*), -3 (*3*), -2 (*4*), -1 (*5*), 0 (*6*), 1 (*7*).

Probably, the results of kinetic calculations differ because Dusek and Somvarsky [94] did not use the kinetic approach quite consistently: in order to take into account the interaction of active centres with 'dangling' functional groups, they derived a branching process and obtained the $G_1(z_a)$ probability generating function [see Eqns (14)–(16) in Ref. 94]. However, both variants give critical conversion values that differ considerably from those obtained using the statistical approach.

The significant dissimilarity between the results obtained and the statistical conclusions is also obtained if the concentration of chains is determined by a more complex mechanism, *viz*., chain transfer or chain termination.[89,90]

The relationships between the α_c, $\Phi_{22}(0)$ values and the chain transfer rate for instant and slow initiation are demonstrated in Fig. 9. In both cases, invariants characteristic of processes in the absence of chain transfer are plotted along the y axis. By selecting appropriate coordinates for the y axis it becomes possible to 'plot' the entire set of 'experimental' data on consolidated curves. The left branches of such curves correspond to the relationship

$$\alpha_c \approx \frac{1}{2} \frac{k_X X_0}{k_p \Phi_{22}(0)}, \quad (33)$$

i.e., critical conversion is determined by the ratio of the chain transfer rate to the growth rate on functional groups belonging to polyfunctional (branching) monomers.

The right branches of the curves for instant and slow initiation obey the relationships (31) and (32), respectively. The crossover points are described by the following relationships:

Table 3. Critical conversion calculation results: kinetic methods (I, II); statistical methods (III).

I_0/m_0	$k_i/k_p = 0.01$			$k_i/k_p = 0.1$			$k_i/k_p = 1.0$			$k_i/k_p = 10$		
	I	II	III	I	II	III	I	II	III	I	II	III
0.001	0.020	0.020	0.015	0.030	0.031	0.022	0.032	0.033	0.023	0.032	0.033	0.023
0.01	0.046	0.048	0.036	0.083	0.089	0.063	0.100	0.108	0.075	0.105	0.109	0.076
0.1	0.102	0.112	0.081	0.204	0.236	0.168	0.316	0.367	0.257	0.332	0.385	0.279
0.5	0.177	0.204	0.146	0.375	0.448	0.324	0.707	0.758	0.643	0.864	0.855	0.809

Note. I, III are data from Ref. 94, II is calculation using system (30); $F(0) = 10$, $\Phi_{22}(0) = 20$, monomer concentration $m_0 = 5$ mol litre^{-1}.

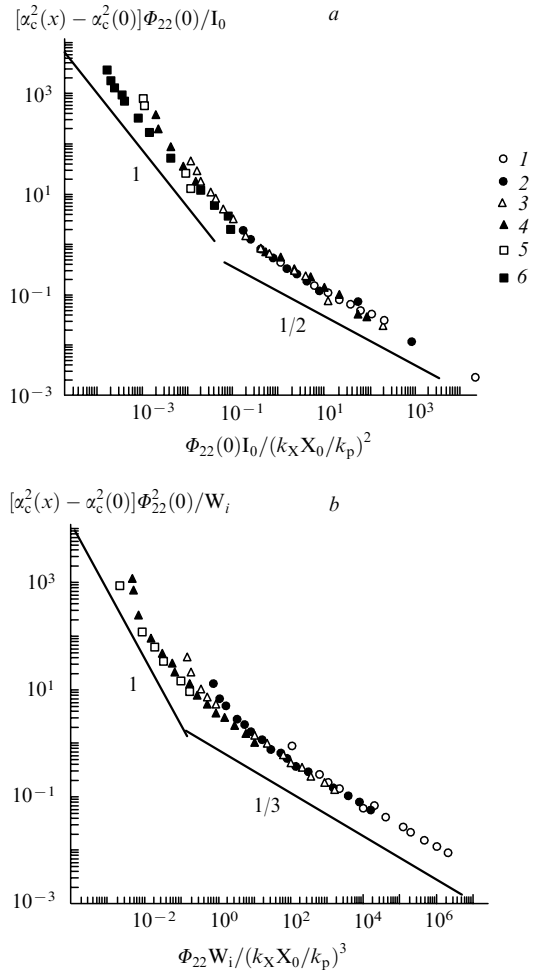

Figure 9. Dependencies of α_c on $\Phi_{22}(0)$ in the case of instant (*a*) and slow (*b*) initiation and chain transfer.[83]
$I_0 = 10^{-4}$ mol litre^{-1}: (*a*): $X_0 = 0$ (*1*), 1 (*2–4*, *6*); 10^{-1} mol litre^{-1} (*5*); $k_X/k_p = 10^{-3}$ (*1*, *2*), 10^{-2} (*3*), 10^{-1} (*4–6*); (*b*): $W_i = 10^{-4}$ (mol litre^{-1})^2 (see †). $X_0 = 0$ (*1*), 1 (*2–4*), 10^{-1} (*5*); $k_X/k_p = 10^{-3}$ (*1*, *2*), 10^{-2} (*3*), 10^{-1} (*4*, *5*). The numbers at the plots show the slopes of the straight lines.

$$\frac{k_p\Phi_{22}(0)}{k_X X_0} \approx \begin{cases} \dfrac{k_X X_0}{k_p I_0} & \text{(instant initiation)} \\ \dfrac{(k_X X_0)^2}{k_p k_i I_0} & \text{(slow initiation)} \end{cases} \qquad (34)$$

Therefore, if $k_X/k_p \approx 1$ and $X_0 \approx I_0$, one should use the formula (33) at $\Phi_{22}(0) < X_0$ and the relationships (31) and (32) at $\Phi_{22}(0) > X_0$. However, it is obvious that if $\Phi_{22}(0) < X_0$, then α_c exceeds 1, *i.e.*, the gel point cannot be reached. This means that it is the formulas (31) and (32) that make sense for practically important polymerisation conditions, *i.e.*, the chain transfer reaction and hence the actual length of the polymeric chain are not of importance in determining the critical conversion. In other words, the concentration of active centres in the former case and the initiation rate in the latter case are of importance not as factors determining the chain length but as those setting the concentration of the second reagent that participates in the formation of a macromolecule, which is an active centre.

Similar conclusions are obtained from analysis of polymerisation reactions with chain termination.[90, 92] The corresponding formulas are presented in Table 4.

† The initiation rate was attributed to the chain growth constant, therefore the (mol litre^{-1})^2 measurement units were obtained.

Table 4. Critical conversion calculation formulas.[89–92]

Process	small Φ_{22}	high Φ_{22}	Criterial conditions
Living polymerisation, instant initiation	$\frac{\alpha_c^2\Phi_{22}}{I_0} \approx 1$	$\frac{\alpha_c^2\Phi_{22}}{I_0} \approx 1$	$\frac{k_i}{k_p} > \sqrt{I_0\Phi_{22}}$
The same + chain transfer	$\alpha_c \approx \frac{1}{2}\frac{k_X X_0}{k_p\Phi_{22}}$	$\frac{\alpha_c^2\Phi_{22}}{I_0} \approx 1$	$\Phi_{22} >< \frac{(k_X X_0)^2}{k_p^2 I_0}$
Living polymerisation, slow initiation	$\frac{\alpha_c^3\Phi_{22}^2}{W_i} \approx 1$	$\frac{\alpha_c^3\Phi_{22}^2}{W_i} \approx 1$	$\frac{k_i}{k_p} < \sqrt{I_0\Phi_{22}}$
The same + chain transfer	$\alpha_c \approx \frac{1}{2}\frac{k_X X_0}{k_p\Phi_{22}}$	$\frac{\alpha_c^3\Phi_{22}^2}{W_i} \approx 1$	$\Phi_{22} >< \frac{(k_X X_0)^3}{k_p k_i^2 I_0}$
Slow initiation, termination by recombination	$\alpha_c \approx 0.33\frac{k_t R}{k_p\Phi_{22}}$	$\frac{\alpha_c^3\Phi_{22}^2}{W_i} \approx 1$	$\Phi_{22} >< \frac{\sqrt{k_1^3 W_i}}{k_p^2}$
Slow initiation, linear termination	$\alpha_c \approx \frac{1}{2}\frac{k_{tY} Y}{k_p\Phi_{22}(0)}$	–	–
'Substitution' effect, termination by disproportionation	$\alpha_c \approx \frac{1}{2}\frac{\sqrt{k_t W_i}}{k_{p2} Z_{22}}$	–	$\frac{k_{p1} Z_{22}}{\sqrt{k_t W_i}} < \frac{k_t}{k_{p2}}$

It is usual for three-dimensional radical polymerisation that a dilute solution of primary macromolecules in their own monomer is formed at early stages. Chain units carry functional ('dangling') groups; subsequent conversion of such groups is determined by two factors. On the one hand, the local concentration of these groups in the vicinity of a reactive end of a macroradical can be considerably higher than the mean bulk value, which results in their higher consumption with formation of intrachain rather than interchain cross-links. Because of that, both the apparent reactivity of 'dangling' groups and the critical conversion increase.[8] On the other hand, shielding of 'dangling' groups by the polymeric chain itself decreases the reactivity due to the steric factor, particularly if aggregation occurs. Finally, the substitution effect can manifest itself, *i.e.*, a change in the double bond reactivity, depending on whether it belongs to a monomer molecule or to a monomeric unit of a macromolecule. The combined effects of all these factors complicate the determination of the actual mechanism of the formation of cross-links in three-dimensional radical polymerisation.

In fact, conversion of double bonds (α_1) and 'dangling' groups (α_p) was observed separately in a number of studies [88, 95–97] on the kinetics of three-dimensional radical polymerisation. It was found that α_p reaches 0.2–0.4 at initial reaction stages where α_1 is close to zero. In terms of relative reactivity ε ($\varepsilon = k_{p2}/k_{p1}$, where k_{p1} and k_{p2} are reaction rate constants of chain growth on original and 'dangling' double bonds), this gives $\varepsilon \gg 1$.

The following copolymerisation systems were used: mixtures of styrene with 0.2 mol.%–2 mol.% of divinylbisphenol [88, 98–100] and mixtures of MMA with 1%–2% of ethylene glycol dimethacrylate.[98] In both cases, there are no reasons to believe that the reactivity of vinyl groups can increase when they are 'hung' on a polymeric chain. Probably, the increase in the local concentration of 'dangling' groups in the vicinity of the reactive macroradical end is the determining factor in both cases.

When three-dimensional radical polymerisation is carried out in the living chain mode,[86, 88] $k_{p2}/k_{p1} \approx 0.3$. This means that at the very start of the reaction, the concentration of macromolecules is high and the chain lengths are small, therefore the effect of local concentration of 'dangling' groups ceases and their decreased

reactivity in comparison with the original monomer is observed. It is likely that steric restrictions play a decisive role in this system.

On the other hand, it is obvious that the substitution effect can manifest itself in the three-dimensional radical polymerisation of diene monomers. This should primarily affect the structure of the cross-linked polymer:[101] a decrease in the reactivity of dangling groups in comparison with the original functional groups results in the formation of 'loose' interpenetrating clusters, while its increase results in compact, closely packed 'grains'.

Changes in the reactivity of functional groups within the suggested calculation scheme were taken into account by Korolev *et al.*[91] It was shown that it is necessary to separate original (monomeric) reagents from all polymeric chains and to introduce an own generating function for such chains

$$Z(\boldsymbol{q}) = \sum_i q_1 q_2^i m_i$$

(m_i is the concentration of the *i*-functional monomer). For example, in the case of bifunctional oligomers (*e.g.*, dimethacrylates)

$$Z(\boldsymbol{q}) = q_1 q_2^2 m_2.$$

The kinetic scheme of m_i consumption expressed by the equation

$$\frac{\mathrm{d}m_i}{\mathrm{d}t} = -k_{\mathrm{p}1} i m_i \mathrm{R}$$

($k_{\mathrm{p}1}$ is the growth rate constant on functional groups belonging to monomers) gives an ordinary differential partial equation for the generating function

$$\frac{\partial Z(\boldsymbol{q})}{\partial t} = -k_{\mathrm{p}1} q_2 \frac{\partial Z(\boldsymbol{q})}{\partial q_2} \mathrm{R}, \tag{35}$$

solution of which by the characteristics method gives

$$Z(\boldsymbol{q}) = \sum_i q_1 (q_2 \mathrm{e}^{-k_{\mathrm{p}1}\tau})^i m_i(0), \tag{36}$$

where

$$\tau = \int_0^t \mathrm{R}(\xi)\mathrm{d}\xi$$

(ξ is the variable of integration); $m_i(0)$ is the starting concentration of the *i*-functional monomer.

Equation (35) can be represented as a system for moments taking the distribution by functional groups (the '2' index) into account

$$\begin{aligned}
\frac{\mathrm{d}Z}{\mathrm{d}t} &= -k_{\mathrm{p}1}\mathrm{R}Z_2, \\
\frac{\mathrm{d}Z_2}{\mathrm{d}t} &= -k_{\mathrm{p}1}\mathrm{R}(Z_2 + Z_{22}), \\
\frac{\mathrm{d}Z_{22}}{\mathrm{d}t} &= -k_{\mathrm{p}1}\mathrm{R}(2Z_{22} + Z_{222}), \\
\frac{\mathrm{d}Z_{222}}{\mathrm{d}t} &= -k_{\mathrm{p}1}\mathrm{R}(3Z_{222} + Z_{2222}), \\
&\textit{etc.}
\end{aligned} \tag{37}$$

This system is not closed.

However, it should be taken into account that the initial reaction mixture consists of monomeric molecules with limited functionality. This fact makes it possible to truncate the system of equations. In fact, since

$$\begin{aligned}
Z_2(\boldsymbol{q}) &= q_1 \sum_{i=1}^n i q_2^{i-1} m_i, \\
Z_{22}(\boldsymbol{q}) &= q_1 \sum_{i=1}^n i(i-1) q_2^{i-2} m_i, \\
Z_{222}(\boldsymbol{q}) &= q_1 \sum_{i=1}^n i(i-1)(i-2) q_2^{i-3} m_i \\
&\textit{etc.},
\end{aligned} \tag{38}$$

$Z_{22}(1) = 0$ for linear polymerisation; $Z_{222}(1) = 0$ if the functionality does not exceed two ($n \leqslant 2$); $Z_{2222} = 0$ if n is no greater than three.

Naturally, the scheme describing radical polymerisation is more complex than Scheme (1). The system of differential equations for macromolecule concentrations and generating function moments changes accordingly. The initial conditions change as well: at $t = 0$ $m(1,i,0) = m_i(0)$, all $\mathrm{R}(i,j,l) = 0$.

Calculations showed[91] that the result obtained above is true with rather high precision, *viz.*, the critical conversion value depends only on the second distribution moment by functionality for initial molecules, $Z_{22}(0)$. Therefore, (31)- and (32)-type formulas are valid for living polymerisation. Results of calculations for radical polymerisation (with chain termination) are presented in Table 4.

As noted above, comparison of theoretical conclusions with experimental data for polymerisation processes is very difficult. Owing to the high distribution nonhomogeneity of reactive macromolecules in the reaction volume at early stages, intrachain cyclisation and aggregation of polymeric coils are highly probable at early stages. Therefore, assessment of the validity of particular formulas requires that the distribution nonhomogeneity of macromolecules be minimised. This can be achieved by minimising the degree of polymerisation by increasing the rates of chain transfer or chain termination reactions. When polymerisation occurs in the living chain mode, the steady-state concentration of active centres decreases by several orders in comparison with a similar value for polymerisation under ordinary conditions.[85,102] As a result, the concentration of chains is rather high even at small conversion levels. Therefore, the cyclisation probability decreases considerably in this case, too.[87] It can also be expected that cyclisation would contribute insignificantly to polymerisation if the content of the branching comonomer in the reaction mixture is decreased.

These approaches were used in a number of studies[75,86,87,90,98,103] on the determination of the critical conversion value in three-dimensional polymerisation processes.

Ide and Fukuda[86] carried out radical copolymerisation of styrene with certain bifunctional monomers in the presence of 2,2,6,6-tetramethylpiperidinyl 1-oxide, a stable radical that ensured the living polymerisation mode. The content of the bifunctional reagent

$$f_2 = \frac{m_2}{m_2 + m_1}$$

in the original mixture did not exceed two molar percent. As noted above, both factors (the living polymerisation mode and the small f_2 value) contribute to the insignificance of intrachain cyclisation. Some of the results obtained are presented in Table 5.

The fact that the calculation result obtained using formula (16e) exceeds the experimental critical conversion value suggests that this calculation is faulty; on the other hand, the overestimated values obtained using formula (31) can be due to the inaccuracy of determination of the number of chains, which may easily be smaller than I_0. Thus, experimental results can be regarded as evidence of the validity of the formula (31).

The use of dodecanethiol as the chain transfer agent in the polymerisation of neopentyl dimethacrylate[98] decreased the weight-average degree of polymerisation. As this value decreases from 142 to 49, the critical conversion value increases but remains higher than that calculated using formula (16e). Since formula (33) gives even lower values, it is not possible to assess the validity of the suggested approach. The cyclisation probability remains considerable even at such relatively low chain lengths.

Table 5. Critical conversion in living three-dimensional copolymerisation.[86]

f_2	I_0/m_1	$\langle P\rangle_w$	α_c		
			experiment	calculation using the formula	
				(16e)	(31) [a]
0.01	1/200	132	0.55	0.76	0.70
0.016	1/170	101	0.50	0.62	0.60
0.02	1/200	96	0.40	0.52	0.495

[a] In this case, formula (31) has the form

$$\alpha_c = \sqrt{\frac{I_0(1-f_2)}{f_2}}.$$

The effect of the number of branching links in a chain on the critical conversion value is demonstrated by data in Table 6.

Table 6. Critical conversion in three-dimensional copolymerisation of styrene with *m*-divinylbenzene (DVB).[75]

[DVN] (mol.%)	$10^{-3}\langle P\rangle_w$	$\Phi_{22}(0)$	α_c		
			experiment	calculation using the formula	
				(16e)	(see [a])
1	1.19	0.154	0.215	0.0425	0.032
0.5	0.79	0.077	0.333	0.133	0.065
0.25	0.74	0.039	0.488	0.271	0.128
0.17	0.67	0.026	0.549	0.435	0.192

[a] Calculation using the formula presented in Table 4.

Calculation gives lower critical conversion values in both versions. This suggests that cyclisation occurs at such a low content of the divinyl monomer. In fact, the molar fraction of the monomer was lower by an order of magnitude in the living polymerisation experiments described above; it is this factor that predefines the absence of cyclisation.

It is of note that statistical calculation gives overestimated gel point values. This may misguide researchers who assess the contributions of cyclisation to the polymerisation process. For example, the experimental gel point value in the polymerisation of triethylene glycol dimethacrylate in the presence of benzoquinone (0.05 mol litre^{-1}) as the inhibitor was found to be 0.19.[90] Statistical calculations gave a much higher value, *viz*., 0.72, which is physically unreasonable. Calculation with the use of formulas shown in Table 4 gave 0.18, which is very close to the experimental value. The corresponding values at the inhibitor concentration of 0.01 mol litre^{-1} are as follows: 0.135; 0.14; 0.036. In other words, cyclisation does not occur, judging by statistical calculation results. However, accurate calculation using the formulas in Table 4 indicates the opposite situation.

Thus, the statistical approach cannot be used to analyse three-dimensional polymerisation.

VI. Conclusion

In conclusion, it should be emphasised that calculation of critical conversion values in the case of the formation of network polymers can be regarded as a particular solution of a more general problem, *viz*., determination of molecular mass distribution parameters or, more exactly, distribution of macromolecules by functionality. Quite a few approaches have been proposed for this purpose; however, their physical substantiation is provided only in some cases. In this review we made an attempt to determine the applicability conditions of different solution methods, depending on the polymer formation mechanism. Calculation of molecular mass distributions is a problem of current interest for polymer technology, so the criteria formulated here appear to be quite significant.

In the review we summarise the achievements in the calculation methods for the critical sol–gel transition point during polymer formation. One can state with certainty that the principles underlying these methods are also applicable to the formation of physical gels.[104] In particular, the relationship between the temperature and the gel transition concentration of biopolymers discussed by Matveev[105] is determined, in essence, by general regularities of network structure formation, though in this case the nature of nodes is rather specific: the latter are formed due to phase separation rather than chemical reactions.

References

1. L Z Rogovina, G L Slonimskoi *Vysokomol. Soedin., Ser. B* **39** 1543 (1997) [a]
2. F Chambon, H H Winter *Polym. Bull. (Berlin)* **13** 499 (1985)
3. M Baumgaertel, H H Winter *Rheol. Acta* **28** 511 (1989)
4. A B Rodd, J Cooper-White, D E Dustan, D V Boger *Polymer* **42** 185 (2001)
5. P J Flory *Principles of Polymer Chemistry* (Ithaka: Cornell University Press, 1953)
6. W H Stockmayer *J. Chem. Phys.* **11** 45 (1943)
7. S I Kuchanov *Metody Kineticheskikh Raschetov v Khimii Polimerov* (Methods of Kinetic Calculations in the Chemistry of Polymers) (Moscow: Khimiya, 1978)
8. V I Irzhak, B A Rozenberg, N S Enikolopyan *Setchatye Polimery. Sintez, Struktura, Svoistva* (Cross-Linked Polymers. Synthesis, Structure, Properties) (Moscow: Nauka, 1979)
9. M L Tai, V I Irzhak *Vysokomol. Soedin., Ser. A* **25** 2305 (1983) [a]
10. H Galina *Europhys. Lett.* **3** 1155 (1987)
11. W H Stockmayer *J. Chem. Phys.* **13** 199 (1945)
12. H Tobita *J. Polym. Sci., Part B* **36** 2423 (1998)
13. H Tobita *Macromolecules* **26** 836 (1993)
14. H Tobita *Macromolecules* **29** 693 (1996)
15. H Tobita *Macromol. Theory Simul.* **7** 225 (1998)
16. A E Hamielec, J W Hodgins, K Tebbens *AIChE J.* **13** 1087 (1967)
17. A E Hamielec, J F MacGregor, A Penlidis *Macromol. Symp.* **10–11** 521 (1987)
18. H Tobita, A E Hamielec *Macromolecules* **22** 3098 (1989)
19. T Xie, A E Hamielec *Macromol. Theory Simul.* **2** 455 (1993)
20. S Fiorentino, A Ghielmi, G Storti, M Morbidelli *Ind. Eng. Chem. Res.* **36** 1283 (1997)
21. C H Bamford, A D Jenkins *Trans. Faraday Soc.* **56** 907 (1960)
22. R Zeman, N R Amundson *Chem. Eng. Sci.* **20** 331 (1965)
23. R Zeman, N R Amundson *Chem. Eng. Sci.* **20** 637 (1965)
24. D J Coyle, T J Tulig, M Tirell *Ind. Eng. Chem. Fundam.* **24** 343 (1985)
25. M F Ellis, T W Taylor, V Gonzalez, K F Jensen *AIChE J.* **34** 1341 (1988)
26. P E Bailagou, D S Soong *Chem. Eng. Sci.* **40** 87 (1985)
27. V M Gonzalez-Romero, B E Rodriguez *Chem. Eng. Commun.* **59** 185 (1987)
28. M Chaimberg, Y Cohen *Ind. Eng. Chem. Res.* **29** 1152 (1990)
29. K Nagasubramanian, W W Graessley *Chem. Eng. Sci.* **25** 1549 (1970)
30. L Blavier, J Villermeaux *Chem. Eng. Sci.* **39** 101 (1984)
31. H Tobita, K Ito *Polym. React. Eng.* **1** 407 (1992/1993)
32. T J Crowley, K Y Choi *Ind. Eng. Chem. Res.* **36** 1419 (1997)
33. P Pladis, C Kiparissides *Chem. Eng. Sci.* **53** 3315 (1998)
34. W J Yoon, J H Ryu, C Cheong, K Y Choi *Macromol. Theory Simul.* **7** 327 (1998)
35. P D Iedema, H C J Hoefsloot *Macromol. Theory Simul.* **11** 410 (2002)
36. W H Ray *Macromolecules* **4** 162 (1971)
37. W H Ray, T L Douglas, E W Godsalve *Macromolecules* **4** 166 (1971)
38. P L Mills *Comput. Chem. Eng.* **10** 399(1986)

39. H Nordhus, O Moen, P Singstad *J. Macromol. Sci., Pure Appl. Chem.* **34A** 1017 (1997)
40. U Budde, M Wulkow *Chem. Eng. Sci.* **46** 497 (1991)
41. P Canu, W H Ray *Comput. Chem. Eng.* **15** 549 (1991)
42. M Wulkow *Macromol. Theory Simul.* **5** 393 (1996)
43. F Teymour, J D Campbell *Macromolecules* **27** 2460 (1994)
44. A Batte, A Ghielmi, G Storti, M Morbidelli *Macromol. Theory Simul.* **8** 498 (1999)
45. G Papavasiliou, I Birol, F Teymour *Macromol. Theory Simul.* **11** 533 (2002)
46. S Kumar, D Ramkrishna *Chem. Eng. Sci.* **52** 4659 (1997)
47. A Batte, G Storti, M Morbidelli *Macromol. Theory Simul.* **11** 37 (2002)
48. S I Kuchanov, E S Pavolotskaya *Vysokomol. Soedin., Ser. A* **24** 2190 (1982) [a]
49. T F Irzhak, G V Korolev, V I Irzhak *Khim. Fiz.* **21** 58 (2002) [b]
50. G V Korolev, M M Mogilevich, I V Golikov *Setchatye Poliakrilaty. Strukturnaya Mikrogeterogennost', Fizicheskie Setki, Deformatsionnye i Prochnostnye Svoistva* (Cross-Linked Polyacrylates. Structural Microheterogeneity, Physical Networks, Deformation and Mechanical Properties) (Moscow: Khimiya, 1995)
51. V I Irzhak *Usp. Khim.* **66** 598 (1997) [*Russ. Chem. Rev.* **66** 541 (1997)]
52. S I Kuchanov *Adv. Polym. Sci.* **152** 157 (2000)
53. K Dusek *Polym. Bull. (Berlin)* **1** 523 (1979)
54. P J Flory *J. Am. Chem. Soc.* **63** 3083 (1941)
55. I J Good *Proc. Camb. Philos. Soc.* **56** 367 (1960)
56. M Gordon *Proc. R. Soc. London, Ser. A* **268** 240 (1962)
57. A T Bharucha-Reid *Elements of the Theory of Markov Processes and their Applications* (New York: McGraw-Hill, 1960)
58. E Girard-Reydet, C C Riccardi, H Sautereau, J-P Pascault *Macromolecules* **28** 7599 (1995)
59. H Galina, K Kaczmarski, B Sanecka *Macromol. Theory Simul.* **1** 37 (1992)
60. M Gordon, G R Scantlebury *Proc. R. Soc. London, Ser. A* **292** 380 (1966)
61. H Galina, J Lechowicz, B Paka, B Sanecka *Polimery-tworz. Wielcoszasteczk.*, **39** 429 (1994)
62. S I Kuchanov *Dokl. Akad. Nauk SSSR* **249** 899 (1979) [c]
63. M L Tai, V I Irzhak *Dokl. Akad. Nauk SSSR* **259** 856 (1981) [c]
64. M Gordon, G R Scantlebury *Trans. Faraday Soc.* **60** 604 (1964)
65. H Tobita *J. Polym. Sci., Polym. Phys.* **36** 2423 (1998)
66. T Nakao, F Tanaka, S Kohjiya *Macromolecules* **35** 5649 (2002)
67. V I Irzhak, M L Tai, N I Peregudov, T F Irzhak *Colloid Polym. Sci.* **272** 523 (1994)
68. E T Hsieh, J C Randall *Macromolecules* **15** 353 (1982)
69. T R Deberdeev, R M Garipov, R Ya Deberdeev, T F Irzhak, V I Irzhak *Vysokomol. Soedin., Ser. A* **46** 412 (2004) [a]
70. T R Deberdeev, R M Garipov, R Ya Deberdeev, T F Irzhak, V I Irzhak *Dokl. Akad. Nauk* **393** 209 (2003) [c]
71. W Stockmayer *J. Chem. Phys.* **12** 125 (1944)
72. M Gordon *J. Chem. Phys.* **22** 610 (1954)
73. C W Macosco, D R Miller *Macromolecules* **9** 199 (1976)
74. D Durand, C M Bruneau *Makromol. Chem.* **183** 1007 (1982)
75. A Matsumoto, Y Kitaguchi *Macromolecules* **32** 8336 (1999)
76. A Matsumoto, S Asai, S Shimizu, H Aota *Eur. Polym. J.* **38** 863 (2002)
77. H H Tvorogov *Vysokomol. Soedin., Ser. A* **18** 1919 (1976) [a]
78. H H Tvorogov, A A Berlin *Vysokomol. Soedin., Ser. A* **19** 1274 (1977) [a]
79. N N Tvorogov, A G Kondrat'eva *Vysokomol. Soedin., Ser. A* **20** 1550 (1978) [a]
80. H Galina, K Dusek *Polymer* **17** 185 (1980)
81. K S Anseth, Ch N Bowman *J. Polym. Sci., Polym. Phys.* **33** 1769 (1995)
82. J E Elliott, C N Bowman *Macromolecules* **32** 8621 (1999)
83. O Okay, M Kurz, K Lutz, W Funke *Macromolecules* **28** 2728 (1995)
84. X Sun, Y Y Chiu, J Lee *Ind. Eng. Chem.* **36** 1343 (1997)
85. G V Korolev, A P Marchenko *Usp. Khim.* **69** 447 (2000) [*Russ. Chem. Rev.* **69** 409 (2000)]
86. N Ide, T Fukuda *Macromolecules* **32** 95 (1999)
87. J H Ward, N A Peppas *Macromolecules* **33** 5137 (2000)
88. N Ide, T Fukuda *Macromolecules* **30** 4268 (1997)
89. G V Korolev, T F Irzhak, V I Irzhak *Vysokomol. Soedin., Ser. A* **43** 970 (2001) [a]
90. G V Korolev, T F Irzhak, V I Irzhak *Vysokomol. Soedin., Ser. A* **43** 2106 (2001) [a]
91. G V Korolev, T F Irzhak, V I Irzhak *Vysokomol. Soedin., Ser. A* **44** 5 (2002) [a]
92. V I Irzhak, T F Irzhak, G V Korolev *Macromol. Symp.* **171** 11 (2001)
93. R Bansil, H J Herrmann, D Stauffer *J. Polym. Sci., Polym. Symp.* **73** 175 (1985)
94. K Dusek, J Somvarsky *Polym. Bull. (Berlin)* **13** 313 (1985)
95. J Holdway, R N Haward, W Parsons *Makromol. Chem.* **179** 1939 (1978)
96. L Mrkvichkova, P Kratochvil *J. Polym. Sci., Polym. Phys. Ed.* **19** 1675 (1981)
97. D T Landlin, C W Macosco *Macromolecules* **21** 846 (1988)
98. D Mitomi, A Matsumoto, H Aota, J Ikeda *Polymer* **41** 1321 (2000)
99. A Matsumoto, Y Yamashita, M Oiwa. *Netsukokasci Yushi (J. Thermoset. Plast. Jpn.)* **14** 139 (1993)
100. B Soper, R N Haward, E F T White *J. Polym. Sci., Polym. Chem. Ed.* **10** 2545 (1972)
101. V A Sal'nikov, N M Bol'bit *Vysokomol. Soedin., Ser. A* **30** 2551 (1985) [a]
102. T F Irzhak, V I Irzhak *Vysokomol. Soedin., Ser. A* **42** 2137 (2000) [a]
103. A Matsumoto, S Okuno, H Aota *Angew. Makromol. Chem.* **240** 275 (1996)
104. K Te Nijenhuis *Adv. Polym. Sci.* **130** 1 (1997)
105. Yu I Matveev *Vysokomol. Soedin., Ser. B* **45** 841 (2003) [a]

[a] — *Polym. Sci. (Engl. Transl.)*
[b] — *Chem. Phys. Rep. (Engl. Transl.)*
[c] — *Dokl. Chem. (Engl. Transl.)*

Russian Chemical Reviews **73** (3) 267 – 291 (2004) © 2004 Russian Academy of Sciences and Turpion Ltd

DOI 10.1070/RC2004v073n03ABEH000840

Polyketones as alternating copolymers of carbon monoxide

G P Belov, E V Novikova

Contents

I.	Introduction	267
II.	Copolymers of carbon monoxide with olefins, dienes and other monomers	267
III.	The mechanism of alternating copolymerisation of carbon monoxide	278
IV.	Structure and properties of polyketones	279
V.	Modification of polyketones	287
VI.	Applications	287

Abstract. Characteristic features of the catalytic synthesis of alternating copolymers of carbon monoxide with various olefins, dienes, styrene and its derivatives are considered. The diversity of catalyst systems used for the copolymerisation of carbon monoxide is demonstrated and their influence on the structure and the molecular mass of the resulting copolymers is analysed. The data on the structure and physicochemical and mechanical properties of this new generation of functional copolymers are generalised and described systematically for the first time. The bibliography includes 296 references.

I. Introduction

Alternating copolymers of carbon monoxide with acyclic and cyclic alkenes, dienes, styrene and its derivatives represent a new generation of functional low- and high-molecular-weight compounds.

$$n\,RCH{=}CH_2 + n\,CO \longrightarrow -(CH(R)-CH_2-C(=O))_n-$$

Systematic data on the synthesis, structure, and properties of these unusual copolymers have been appearing in the literature since the mid-1980s. Some of them (for example, copolymers of alkenes with carbon monoxide) have already found practical application.

The considerable interest of researchers in the problem of alternating copolymerisation of carbon monoxide with various monomers is indicated by the annual increase in the number of relevant publications. About 60% of these papers are devoted to the synthesis of alternating copolymers of carbon monoxide with alkenes, dienes, styrene and its derivatives. The European patent authority has now granted more than 300 patents for catalyst systems and methods for the preparation of alternating copolymers from carbon monoxide and alkene or diene monomers and for compositions of these copolymers with other polymers. A number of reviews have been devoted to the copolymerisation of carbon monoxide with olefins.[1–8]

The ready availability and low cost of carbon monoxide are important factors in the preparation of carbon monoxide copolymers.[9] The possibility of controlling the structure of copolymers by changing the order of connection of the CO groups to other monomer units allows one to prepare polymers with a set of new properties (high adhesion, high stability against photo- and biodestruction and so on).[2, 10, 11]

The purpose of this review is to analyse the key results obtained during the last decade in the field of catalytic alternating copolymerisation of carbon monoxide not only with olefins but also with dienes and functionalised olefins. Taking carbon monoxide copolymerisation with ethylene (the best studied pair of comonomers) as an example, the stepwise mechanism of copolymerisation is considered. The data on the structure and physicochemical and mechanical properties of a new generation of polyketones are described systematically for the first time.

II. Copolymers of carbon monoxide with olefins, dienes and other monomers

1. Carbon monoxide – ethylene

The alternating copolymers of carbon monoxide with ethylene were first synthesised under the action of $Ni(CN)_2$ in 1941.[12] Subsequently, $Pd(CN)_2$ [13] and its hydride form [14] have been used as the catalysts. The resulting ethylene – carbon monoxide copolymers have high molecular masses and melting points. The yield and the intrinsic viscosity ($[\eta]$) of the copolymers are markedly influenced by the nature of the solvent used as the reaction medium. In particular, the yield and the intrinsic viscosity increase in the sequence of solvents water < acetonitrile < *m*-cresol < chloroform < methyl ethyl ketone < ethyl acetate.

The data on the preparation of ethylene copolymers with carbon monoxide published in the patent literature before 1980 indicated that the synthesis had to be carried out at high temperature (100 – 200 °C) and that the product yields were low (see, for example, patents [12–14]). The activity of the catalysts (various Ni and Pd complexes) described in these publications was very low.

The possibility of copolymerisation of these monomers at room temperature was first reported in 1982.[15] As the catalyst, the researchers used the complex $[Pd(MeCN)(PPh_3)_3](BF_4)_2$. Copolymerisation was carried out in chloroform at a pressure of an equimolar monomer mixture of 5 MPa. The average copolymerisation rate did not exceed 10 $g\,g_{Pd}^{-1}\,h^{-1}$. Later, it has been shown [16–18] that the rate of alternating copolymerisation of

G P Belov, E V Novikova Institute of Problems of Chemical Physics, Russian Academy of Sciences, 142432 Chernogolovka, Moscow Region, Russian Federation. Fax (7-096) 515 54 20. Tel. (7-096) 522 26 42. E-mail: gbelov@cat.icp.ac.ru (G P Belov), novik@cat.icp.ac.ru (E N Novikova)

Received 10 April 2003
Uspekhi Khimii **73** (3) 292 – 319 (2004); translated by Z P Bobkova

carbon monoxide and ethylene can reach 1000 g g_{Pd}^{-1} h^{-1} when the process is carried out in acetic acid in the presence of monodentate organophosphorus ligands. Ethylene copolymerisation with carbon monoxide in an acid medium has been considered.[19]

The use of bidentate organophosphorus ligands and acids with $pK_a \leqslant 2$ as components of Pd catalysts has initiated new vigorous research in this field.[20] A detailed study[21,22] of the kinetics of carbon monoxide copolymerisation with ethylene in the presence of $Pd(OAc)_2$–diphosphine–acid systems has shown that the reaction rate depends on the natures of the phosphine and the acid, the presence of an oxidant (for example, 1,4-benzoquinone), and also the amounts of these components with respect to palladium acetate.† These results have been supported by studies of Chinese researchers.[25]

As a rule, ethylene copolymerisation with carbon monoxide under the action of $Pd(OAc)_2$ and other Pd complexes is carried out in a rather polar medium (methanol is the best choice).[26,27] For increasing the catalytic activity of the Pd catalyst, the solvent must contain trace amounts (in some cases, several percent) of methanol or water.[27–29] The long induction period and low copolymerisation rate are due to the disregard of this requirement.[28]

Copolymerisation of ethylene with carbon monoxide in the presence of the palladium complexes $[(L)Pd(MeCN)_2](BF_4)_2$, $[(L)Pd(H_2O)(TsO)](TsO)$ [L = $Ph_2P(CH_2)_3PPh_2$ (**1**)] and *trans*-$[(PCy_3)_2Pd(H)(H_2O)](BF_4)$ (Cy is cyclohexyl)[27–30] proceeds at a somewhat lower rate than that in the presence of the $Pd(OAc)_2$–diphosphine–acid system.

Usually, CF_3COOH or TsOH are employed as the acids in the $Pd(OAc)_2$–$Ph_2P(CH_2)_3PPh_2$–acid catalyst system (the copper salts of these acids can also be used).[16,31,32] Data on the activating effect of perchloric[33] and phosphoric[34] acids and nickel, copper, iron, zirconium or vanadium sulfates or perchlorates have been reported. It was shown[31,35] that the rate of ethylene copolymerisation with carbon monoxide depends on the type of the acid and decreases in the sequence CF_3SO_3H > *p*-$MeC_6H_4SO_3H$ > CF_3COOH > PhCOOH ≈ HBF_4 > CCl_3COOH > $C_6H_3Cl_2$.COOH > HCl. However, to establish a quantitative correlation between the copolymerisation rate and the acid pK_a, systematic studies are required.

The rate of ethylene–carbon monoxide copolymerisation in the presence of the $Pd(OAc)_2$–diphosphine–acid catalyst system depends also on the nature of the diphosphine. Patent data on the synthesis of ethylene–carbon monoxide copolymers indicate that $Pd(OAc)_2$–CF_3COOH–$(2\text{-}MeOC_6H_4)_2P(CH_2)_3P(C_6H_4OMe\text{-}2)$ (**2**) is the most active catalyst system.[36] In this case, copolymerisation rate can reach 33 000 g g_{Pd}^{-1} h^{-1} (with an overall pressure of 9 MPa). When the copolymerisation is performed at a low pressure and temperature, its rate and the yield of the copolymer decrease. For ethylene copolymerisation with CO in methanol in the presence of CF_3COOH used as the acid component, the reaction rate increases in the following sequence of diphosphines: bis(diphenylphosphino)methane (**3**) < 1,6-bis(diphenylphosphino)hexane (**4**) < 1,5-bis(diphenylphosphino)pentane < 1,4-bis(dibutylphosphino)butane (**5**) < 1,4-bis(butylphenylphosphino)butane (**6**) < 1,2-bis(diphenylphosphino)ethane (dppe) (**7**) < 2,3-bis(diphenylphosphino)butane (*meso*, *rac*) (**8**) < 2,4-bis(diphenylphosphino)pentane (*meso*, *rac*) (**9**) < 1,3-bis(di-n-butylphosphino)propane (dbpp) (**10**) < 1,4-bis(diphenylphosphino)butane (**11**) < 1,3-bis(diphenylphosphino)propane (**1**) < 1,3-bis[di(2-methoxyphenyl)phosphino]propane (**2**).[21,31,34,37–39] Comparison of the activities of various diphosphines with the activity of 1,3-bis(diphenylphosphino)propane used most often has shown that the introduction of alkyl substituents into the 2-position of propane barely influences the catalyst activity, whereas the introduction of alkyl groups into the 1,3-positions changes the activity of the palladium catalyst. This attests to the influence of the electronic and steric factors on the catalyst activity. It has been shown[40–43] that for copolymerisation of carbon monoxide with ethylene in the presence of the $[Pd(Me).(MeCN)(P\text{-}P)](PF_6)$ complexes (P-P are ligands **1** and **9** or **7** and **8**) in an aprotic solvent (CH_2Cl_2), the molecular mass of the copolymer increases in the sequences **1** > *meso*-**9** > *rac*-**9** and *meso*-**8** > *rac*-**8** > **7**. The presence of traces of water in the reaction medium results in the formation of μ-hydroxo complexes $[Pd(\mu\text{-}OH)(P\text{-}P)_2](PF_6)_2$ and in a higher yield of the copolymer, which increases in the sequence *rac*-**9** < *meso*-**9** < **1**. In the case of bischelate complexes, $[Pd(P\text{-}P)_2]^{2+}$, a different activity series is observed, namely, $[Pd(rac\text{-}\mathbf{9})_2]^{2+} < [Pd(\mathbf{1})_2]^{2+} < [Pd(meso\text{-}\mathbf{9})_2]^{2+}$. When bischelate palladium complexes are used and carbon monoxide–ethylene copolymerisation is carried out in methanol, the yield of the copolymer increases in the sequence **1** ≪ *rac*-**9** < *meso*-**9**.

Despite the fact that no quantitative data on the relationship between the copolymerisation rate and structural (or other) characteristics of diphosphines are currently available, presumably, the essential factors that determine the catalytic activity of palladium diphosphine complexes include the ligand conformation, the length of the methylene chain (*n*) between the P atoms and the rigidity of the complex. The P–Pd–P angle increases with an increase in *n* from 74° (for *n* = 1) to 175° (for *n* = 5). The palladium diphosphine complexes considered above have a planar square structure of the coordination unit with *cis*-arrangement of the phosphorus atoms for *n* = 1–4. As the methylene chain grows longer ($n \geqslant 5$), the formation of a dimer with *trans*-arrangement of the ligands becomes more favourable. The increase in the structural rigidity of the Pd complex resulting in a higher catalyst activity (by about an order of magnitude) in the copolymerisation of carbon monoxide with ethylene was shown for the 1,2,3,4-tetrakis(diphenylphosphino)cyclobutane complex of Pd(II).[44]

Worthy of note is the publication[45] concerning the possibility of alternating copolymerisation of carbon monoxide with ethylene induced by a zwitter-ionic palladium complex,

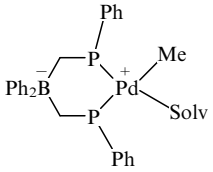

whose activity proved to be comparable with the activity of Pd complexes with 1,3-bis(diphenylphosphino)propane.

Some recent publications describe the use of palladium complexes with P-N and N-N bidentate ligands as catalysts of carbon monoxide copolymerisation with ethylene and the use of some aryl- and fluorine-containing arylboranes or their salts (Na, K or Li)[46–51] and alumoxanes,[52–55] instead of acids (CF_3COOH, *p*-$MeC_6H_5SO_3H$, *etc.*). Thus with the $Pd(OAc)_2$–$Ph_2P(CH_2)_3PPh_2$–$(Bu^t_2Al)_2O$ catalyst system, copolymerisation of ethylene with carbon monoxide in toluene proceeds at a rate of up to 2900 g g_{Pd}^{-1} h^{-1}.

It has been shown[56] that dicationic Pd complexes containing N-heterocyclic carbene ligands with the formula [*cis*-$CH_2\{N(H)C{=}C(H)N(R)C\}_2Pd(NCMe)_2](BF_4)_2$ (R = Me, 2,4,6-$Me_3C_6H_2$)‡ are active catalysts for ethylene copolymerisation with carbon monoxide. The reaction occurs at a rate of up to 810 g g_{Pd}^{-1} h^{-1}. Recently, a new family of P-N and P-P ligands based on 2-methyl-2-(2-pyridyl)-1,3-bis(diphenylphosphino)propane[57] and C_2-, C_3- and C_4-bridging bisphospholyl[58] ligands have been synthesised; their Pd complexes were shown to be active catalysts of the alternating copolymerisation of carbon monoxide

† The replacement of palladium acetate by nickel, cobalt, copper or silver acetate decreases the copolymerisation rate by a factor of several tens.[20,23,24]

‡ These complexes proved to be inactive in carbon monoxide copolymerisation with propylene or styrene.

with ethylene. Palladium phosphineimine complexes [Pd(P-N)(Me)(MeCN)](BF$_4$) induce living copolymerisation and block copolymerisation of carbon monoxide with ethylene.[59]

The ruthenium(II) phosphine complexes, *cis*-[Ru(PPh$_2$CH$_2$CH$_2$PPh$_2$)$_2$](OTs)$_2$ and [Ru{PPh(CH$_2$CH$_2$CH$_2$.PPh$_2$)$_2$}$_2$](OTs)$_2$], exhibit a very low activity in the copolymerisation of carbon monoxide with ethylene. However, the addition of trifluoroacetic acid and 1,4-benzoquinone increases substantially the catalytic activity.[60] In this case, besides the high-molecular-mass copolymer, the reaction gives a low-molecular product soluble in methanol. A similar type of behaviour was found for 1,1′-palladium(II) bis(diphenylphosphino)ferrocene complexes, [Pd(H$_2$O)$_2${Fe(C$_5$R$_4$PPh$_2$)$_2$}](OTf)$_2$ (R = H, Me). The copolymerisation of carbon monoxide with ethylene in the presence of these complexes gives rise to oligoketone and methyl propionate (resulting from methoxycarbonylation of ethylene).[61] The following palladium complexes with diphosphine monoxide ligands have been synyhesised:[62] [(MeCN)(Me)Pd(κ^2-P,O-Ar$_2$P(CH$_2$)$_n$.P(O)Ar$_2$)]X (Ar = Ph, *p*-MeC$_6$H$_4$, n = 1–3, X = BF$_4$, SbF$_6$), [(η^3-C$_3$H$_5$)Pd{κ^2-P,O-Ar$_2$P(CH$_2$)$_n$P(O)Ar$_2$}]X (Ar = Ph: n = 2, 3, X = OTs, OTf; n = 1, X = SbF$_6$; Ar = *p*-MeC$_6$H$_4$: n = 1, X = SbF$_6$). Unfortunately, the catalytic activities of these complexes are lower than those of the catalyst systems described above.[20,36]

Due to the high cost of palladium, repeated attempts have been made at replacing it by cheaper nickel or copper. Nickel(II) phosphine complexes, [Ni{Ph$_2$PCH=C(Ph)O}(PEt$_3$)Ph], have been used[63] for copolymerisation of carbon monoxide with ethylene. A more recent study[62,64] reports the synthesis of nickel(II) complexes with N-O-bidentate ligands, [Ni(N-O).(*o*-MeC$_6$H$_4$)PPh$_3$] (N-O is 4-nitropyridine-2-carboxylate, pyrazine-2-carboxylate, 4-methoxypyridine-2-carboxylate) and with diphosphine monoxide ligands, [(η^3-CH$_2$C(Me)CH$_2$)Ni{κ^2-P,O-Ph$_2$PXP(O)Ph$_2$}]SbF$_6$ (X = *o*-C$_6$H$_4$, NH).

Recently, a series of [(L)Ni(*o*-MeC$_6$H$_4$)(PPh$_3$)] nickel complexes with bidentate N-N- and N-O-chelate ligands (L),

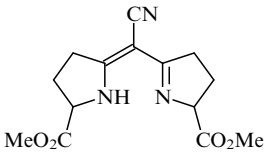

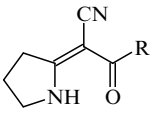

R = Me, OMe, Ph, CF$_3$, C$_3$F$_7$, C$_7$H$_{15}$.

have been prepared. These complexes catalyse carbon monoxide–ethylene copolymerisation at a rate of up to 2300 g g_{Ni}^{-1} h^{-1}.[65] In 1998, it was reported that Ni(*o*-MeC$_6$H$_4$)(PPh$_3$)(Tp^{Ph}) [Tp^{Ph} is a tripodal tris(pyrazolyl)borate ligand] performs copolymerisation of carbon monoxide with ethylene giving rise to a high-molecular-weight product (T_m = 260 °C, M_w = 5770).[66] However, the rate of copolymerisation at 50 °C was low, 1.2 g g_{Ni}^{-1} h^{-1}.

The conduction of carbon monoxide–ethylene copolymerisation in methanol or in another polar solvent poses some difficulties associated with the process safety, environmental impact, the necessity of regenerating the solvent and so on. These aspects play a crucial role in the design of the industrial process. Therefore, in recent years, vigorous search for catalysts that would perform the copolymerisation in aqueous media has been carried out. This possibility was first mentioned in the 1990s.[67–69] Palladium complexes with sulfonated bidentate ligands have been used as the catalysts.

It was shown[68,69] that in the presence of a water-soluble diphosphine ligand, dppp-(SO$_3$Na)$_4$, and the palladium complex, Pd(TsO)$_2$(MeCN), copolymerisation of carbon monoxide with ethylene can be carried out in an aqueous medium at 90 °C to give copolymers with the molecular mass (6–8) × 10^3; the reaction rate reaches 4000 g g_{Pd}^{-1} h^{-1}.

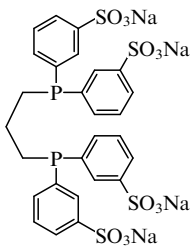

dppp-(SO$_3$Na)$_4$

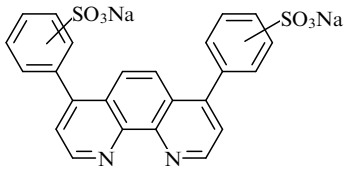

phen-(SO$_3$Na)$_2$

In the same years, data on conduction of the carbon monoxide–ethylene copolymerisation in the gas phase, appeared in the patent literature.[70–76] In this case, the Pd(OAc)$_2$–diphosphine–HBF$_4$ catalyst is applied onto a support (for example, the CO/C$_2$H$_4$ copolymer) impregnated with a nonpolymerising organic diluent. The gas phase should contain traces of methanol. The rate of this reaction is comparable with the rate of a similar process carried out in methanol.[35,77–79] Other polymers have also been used as catalyst supports, for example, porous polypropylene[79] or silica.[80] Although the first industrial process for the production of the alternating copolymer of carbon monoxide with ethylene was based on the reaction in solution,[81] subsequently, a pilot plant for gas-phase synthesis of polyketone has also been designed.[68] Copolymerisation of CO and C$_2$H$_4$ carried out in the gas phase would be noticeably more economic.

2. Carbon monoxide copolymers with propylene and higher olefins

When conducting copolymerisation of carbon monoxide with propylene and higher α-olefins (or with styrene or its derivatives), one should take into account a number of factors that influence the structure of the copolymer formed.[5] In addition to the major product with the 1,4-diketone structure [CHR–CH$_2$C(O)]$_n$, copolymerisation of carbon monoxide with α-olefins, styrene or its derivatives gives a copolymer with a spiroketal structure.[69,82]

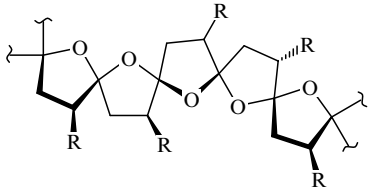

In the case of propylene, this copolymer is formed when the reaction is carried out at low temperature. In the copolymerisation of higher α-olefins (for example, hept-1-ene) with carbon monoxide, the spiroketal copolymer is formed at 50 °C.[83]

The activity of propylene in the reaction with carbon monoxide is about an order of magnitude lower than that of ethylene. The rates of copolymerisation of carbon monoxide with ethylene, propylene and but-1-ene under comparable conditions catalysed by the Pd(OAc)$_2$–CF$_3$COOH–Ph$_2$P(CH$_2$)$_3$PPh$_2$ system are 6000, 400 and 250 g g_{Pd}^{-1} h^{-1} (see Ref. 84). A similar dependence is observed with other catalyst systems, for example, heterogeneous and most of homogeneous Ziegler–Natta catalysts and the [(Ph$_2$P(CH$_2$)$_3$PPh$_2$)Pd(MeCN)$_2$](BF$_4$)$_2$ complex in a nitromethane–methanol medium.

The catalyst of choice for propylene–carbon monoxide copolymerisation is the [L$_2$PdX$_2$]$^{n+}$ complex (X is a weakly coordinating or non-coordinating anionic or neutral ligand, L is diphosphine) and an MeOH-containing solvent mixture is the best reaction medium.

Until recently, the resulting copolymers of CO and propylene had low molecular masses. A detailed study[85] of carbon monoxide copolymerisation with propylene has revealed the reasons for the formation of low-molecular-weight polymers. The main reason is the lack of control of the contents of MeOH and H$_2$O in the reaction medium. Later, CO/MeCH=CH$_2$ copolymers with M_w = 43.2 × 10^4 have been obtained.[5,86,87] As in the case of

ethylene – carbon monoxide copolymerisation, the highest rate of carbon monoxide copolymerisation with olefins is observed in the presence of 1,ω-bis(diphenylphosphino)alkanes, $Ph_2P(CH_2)_nPPh_2$, with $n = 3$ and 4. The activity of the $Pd(OAc)_2$ – diphosphine – p-$MeC_6H_4SO_3H$ catalyst system in the copolymerisation of propylene and CO increases in the following series of diphosphines:[38] $Ph_2P(CH_2)_3PPh_2 < Bu_2P(CH_2)_3PBu_2 < Bu_2P(CH_2)_4PBu_2$. The copolymers of propylene and carbon monoxide obtained using bis(diphenylphosphino)alkanes are characterised by poor stereoregularity. It was shown[85] that by varying the nature of the diphosphine ligand, one can obtain fully iso- or atactic carbon monoxide – propylene copolymers. For example, *P*,*P*-(6,6′-dimethoxybiphenyl-2,2′-diyl)bis(2,5-dimethylphospholane) (**12**) has been used to prepare completely atactic copolymer, while using *P*,*P*-*o*-phenylenebis(2,5-dimethylphospholane) (Me-DUPHOS, **13**), a completely isotactic polymer was obtained. The use of enantiopure C_2-symmetrical diphosphine (**12**, **13**) and phosphine – phosphite (**14**) ligands gives copolymers with a higher stereoregularity.

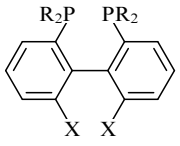

12

$PR_2 = PPh_2$: X = Me, OMe;
$PR_2 = PCy_2$: X = H, OMe;

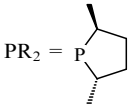

, X = OMe.

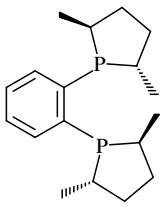

13 (Me-DUPHOS)

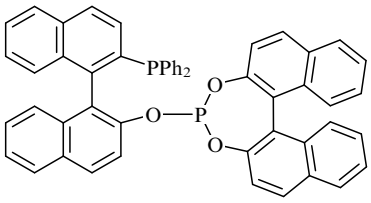

14 (BINAPHOS)

It is possible to prepare both dextro- and levorotatory stereoisomers.[88] The use of higher α-olefins (but-1-ene, hept-1-ene and oct-1-ene) in the copolymerisation with carbon monoxide in the presence of a Pd complex with diphosphine ligand **15** results in the formation of optically active copolymers.[89, 90]

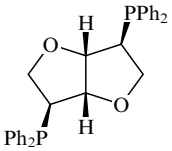

15 (DDPPI)

The alternating copolymerisation of α-olefins or styrene and its derivatives, dienes and some other monomers with carbon monoxide catalysed by chiral palladium complexes is a promising method for the preparation of optically active copolymers, mainly for two reasons: (i) the chirality of the backbone can be provided by using prochiral monomers; (ii) the presence of ketone groups in the backbone enables easy functionalisation of these polymers.

Olefins with internal double bonds can also be introduced in the copolymerisation with carbon monoxide. Thus it was shown[28] that in the presence of the $[Pd(Me\text{-}DUPHOS)(MeCN)_2](BF_4)_2$ catalyst, *cis*-but-2-ene copolymerises with CO to give an isotactic optically active oligomer with $M_n = 600$. The activity of *cis*-but-2-ene in this reaction is an order of magnitude lower than that of but-1-ene, which reacts with CO to give copolymer with $M_n = 4.0 \times 10^4$ and with both 1,4-ketone and the spiroketal structures in the backbone. The authors suggested that *cis*-but-2-ene isomerises into but-1-ene during copolymerisation. *trans*-But-2-ene does not copolymerise with carbon monoxide.

The synthesis of $C_2H_4/CO/MeCH=CH_2$ terpolymers with different contents of the CO/C_2H_4 and CO/C_3H_6 blocks in the polymer chain has been carried out in a hydrocarbon medium and the properties of the resulting copolymers have been studied.[85] Similar copolymers have been obtained in an aqueous medium[67] using water-soluble palladium complexes with dppp-$(SO_3Na)_4$ and phen-$(SO_3Na)_2$ as the catalysts. It is noteworthy that the rate of copolymerisation of propylene, ethylene and carbon monoxide in water was 4 – 22 g g_{Pd}^{-1} h^{-1}. These values are very low compared to those attained for the process carried out in methanol.[3] It was found that the rate of carbon monoxide copolymerisation with propylene in water is about 10 times as low as the rate of $CO/CH_2=CH_2$ copolymerisation under similar conditions. This is the main reason for the formation of a low-molecular-weight oily co-oligomer in the case of propylene. Co- and ter-polymerisation of ethylene, propylene and carbon monoxide in water catalysed by the $(NaO_3SC_6H_4CH_2)_2C(CH_2PPh_2)_2Pd(CF_3COO)_2 - TsOH - C_6H_4O_2$ system or by water-soluble palladium complexes with the $P(C_6H_4SO_3Na\text{-}m)_3$ and $(C_6H_4SO_3Na\text{-}m)_2P(CH_2)_3.P(C_6H_4SO_3Na\text{-}m)_2$ ligands have been reported.[91, 92] In the latter case, the product yield was $(2.6 - 7.2) \times 10^3$ g g_{Pd}^{-1} h^{-1}. Analysis of the structure of the resulting copolymers (at the terminal groups) by NMR shows that they have a diketone structure. When copolymerisation is carried out in methanol, the resulting copolymers have three types of terminal groups, namely, ketone, ketoester and ester groups.[92] Only low-molecular-weight terpolymers have been obtained in the aqueous medium.[92, 93] The possibility of copolymerisation in an aqueous emulsion in the presence of water-insoluble Pd complexes has been reported.[94]

3. Carbon monoxide – cyclic olefins

Copolymerisation of cyclopentene and carbon monoxide proceeds as 1,2- and 1,3-insertion of cyclopentene in the polymer chain.

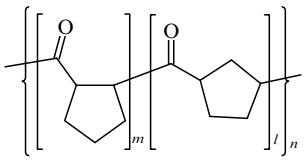

Study of the influence of the natures of the solvent and the ligand, the temperature and carbon monoxide pressure on the rate of carbon monoxide – cyclopentene copolymerisation and on the molecular mass of the resulting copolymers revealed the optimal conditions (a temperature of 40 °C, a 4 MPa pressure of CO, Pd complexes with P-P- and N-N-bidentate ligands) for the synthesis of a high-molecular-weight isotactic copolymer (the ratio $l:m > 9$).[5, 95] It should be noted that irrespective of the reaction conditions, groups of types **A** – **D** are the major terminal groups of the copolymers.

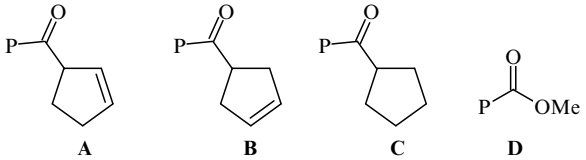

A **B** **C** **D**

P is polymer.

The synthesis of a carbon monoxide – cyclohexene copolymer under the action of the $[Pd(MeCN)_4](BF_4)_2 - PPh_3$ complex has been reported.[96]

Of cyclic olefins used in copolymerisation with carbon monoxide, norbornene (**16**) is mentioned most often in the literature. Carbon monoxide copolymers with norbornene have been prepared in the presence of various Pd complexes, in particular,

$Pd(PPh_3)_4$, $PdCl_2-PPh_3-HCl$, and $[(bipy)Pd(MeCN)_2](BF_4)_2$, *etc.*[5,37,97–105]

It is known that norbornene can polymerise either with C—C bond cleavage, or with C—C bond cleavage and transfer of the reaction centre, or with ring opening. Depending on the catalyst used, copolymerisation can furnish polymers with a ketone (**A**) or lactone (**B**, **C**) structure.

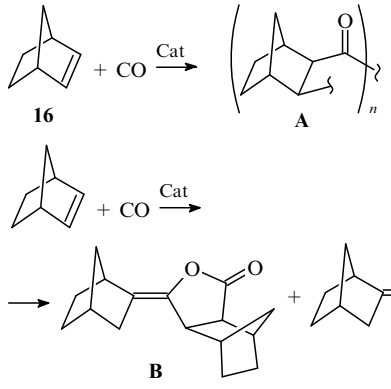

The data on the influence of the nature of the ligands in the palladium complex on the copolymerisation rate and the glass transition temperature of the carbon monoxide copolymer with norbornene are summarised in Table 1.[106]

Copolymerisation of norbornene and carbon monoxide carried out with the $Pd(OAc)_2-Ph_2P(CH_2)_3PPh_2-p\text{-}MeC_6H_5SO_3H$ catalyst system in methanol in the presence of an oxidant (1,4-naphthoquinone or 1,4-benzoquinone) has been reported.[107] The researchers note that an increase in the *p*-toluenesulfonic acid to $Pd(OAc)_2$ molar ratio from 10 to 30 decreases the molecular mass of the co-oligomer with 8000 to 5000, while the replacement of 1,4-naphthoquinone by 1,4-benzoquinone decreases the copolymer yield and solubility in common organic solvents.

Table 1. Influence of the ligand nature on the rate of copolymerisation and glass transition temperature (T_g) of the CO – norbornene copolymer.

Ligand	Copolymerisation rate /g g_{Pd}^{-1} h^{-1}	T_g/°C
bipy	334	111
phen	371	113
5-NO_2-1,10-phen	282	112
$Ph_2P(CH_2)_3PPh_2$	58	126
PPh_3	31	120
$AsPh_3$	28	100
NPh_3	23	105

Note. Reaction conditions: $[Pd(OAc)_2] = 0.01$ mol litre^{-1}, [norbornene] = 10 mol litre^{-1}, temperature 90 °C.

Scheme 1 shows a reaction mechanism proposed on the basis of the data from ^{13}C and ^1H NMR and IR spectroscopy and the molecular-mass characteristics of the products of carbon monoxide co-oligomerisation with norbornene (**16**) under various

Scheme 1

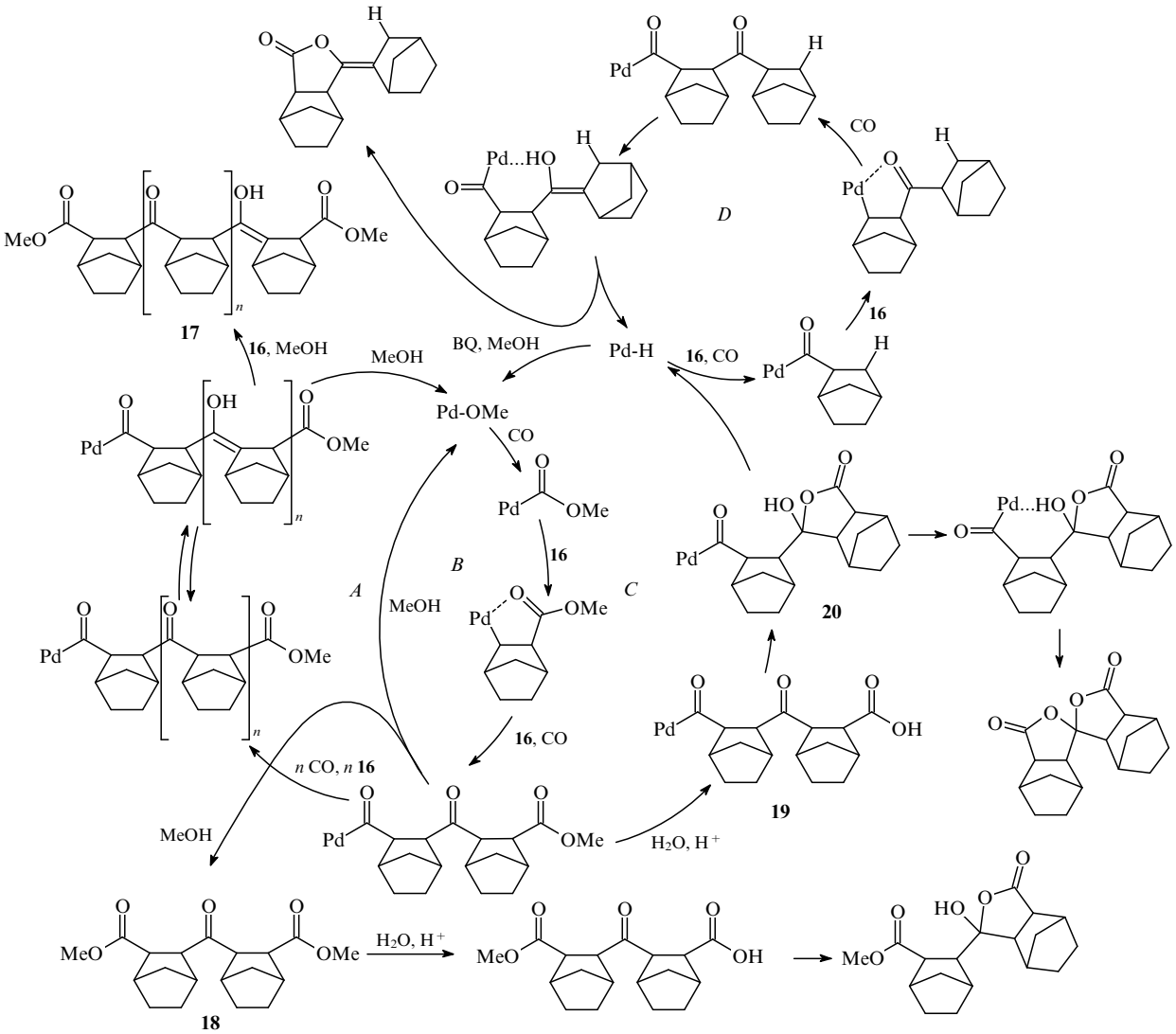

BQ is 1,4-benzoquinone.

conditions.[107] The mechanism explains the formation of co-oligomers with different structures. Catalytic cycle *A* (the major cycle) affords high-molecular-weight and oligomeric structures (both ketone and spiroketal structures may appear). Chain termination (*via* methanolysis) results mainly in diester co-oligomers **17**.

Cycle *B* is analogous to cycle *A* but chain termination occurs after the formation of di- (**18**) and trimeric structures. The presence of trace amounts of water in the reaction medium (as a rule, methanol is used without dehydration and *p*-toluenesulfonic acid, often present as a component of the catalyst, contains water of crystallisation) initiates one more catalytic cycle *C*. In this cycle, hydrolysis affords monocarboxylic acid **19** and lactol **20** (due to tautometric transformations). When nitrogen-containing ligands are used (instead of phosphines), the reaction mixture must contain an oxidant, which facilitates the formation of catalytically active Pd-OMe sites. In this case, apart from catalytic cycles *A*, *B*, and *C*, one more cycle *D* is realised in which the Pd-H centres are the active sites.

The synthesis of block copolymers of norbornene with the $(CO/CH_2=CH_2)_n$ oligomer has been described.[108] The reaction was catalysed by time-stable complex *trans*-$Pd(PPh_3)_2.(Cl)(COC_6H_4Me\text{-}p)$ and carried out in an aprotic medium. This gave block copolymers containing long $(CO/C_2H_4)_n$ blocks alternating with norbornene.

Alternating copolymers of carbon monoxide with norbornene derivatives containing ester groups RC(O)O with different lengths of the hydrocarbon chain (acetate, pentanoate, octanoate, decanoate, dodecanoate) have been synthesised.[109] The reaction was carried out at 60 °C and at a carbon monoxide pressure of 3.4 MPa for 24 h in a $MeNO_2$–MeOH (5 : 1) mixture in the presence of the $[(bipy)Pd(MeCN)_2)](BF_4)_2$ catalyst. Table 2 presents some properties of the resulting copolymers. These copolymers were better soluble than those formed by carbon monoxide and norbornene (the former were soluble in DMSO, DMF, *N*,*N*-dimethylacetamide, pyridine and acetone but insoluble in benzene, toluene, chloroform, chlorobenzene or ether). An increase in the length of the hydrocarbon chain entailed a lower degree of crystallinity of the resulting copolymers and a higher solubility in organic solvents.

Table 2 Physicochemical properties of carbon monoxide copolymers with the ester derivatives of norbornene.

R	M_n	T_g /°C	T_m /°C	T^1_{dec} /°C	T^2_{dec} /°C
Me	3800	117	–	310	424
n-C_4H_9	4500	84	–	210	401
n-C_7H_{15}	5000	54	–	205	240
n-C_9H_{19}	4900	26	125	195	230
n-$C_{11}H_{23}$	5300	−32	99	180	230
Ph	4600	93	–	341	406

Note. T_g and T_m were determined by differential scanning calorimetry (DSC) at a heating rate of 20 °C min^{-1}. T^1_{dec} and T^2_{dec} are the temperatures of 10% loss of the polymer mass and the maximum decomposition, respectively determined by thermogravimetric analysis (TGA) at a heating rate of 10 °C min^{-1}.

The data on the structure and properties of such copolymers are scarce. Photolysis of carbon monoxide copolymers with *exo*-norbornene having $M_n = 3200–4900$ and $M_w : M_n = 1.75–2.0$ has been studied by time-resolved EPR spectroscopy.[110] The EPR spectra of the copolymers exhibited weak signals for the *endo*-2-substituted norbornyl§ radicals, which attested to incomplete stereoregularity of this copolymer.

§ These radicals are produced by the Norrish-I mechanism on rupture of the polymer chain.

Copolymerisation of carbon monoxide with norbornene, cyclopentadiene or bicyclo[2.2.2]oct-2-ene in the presence of $[Pd(MeCN)_2(PPh_3)_2](BF_4)_2$ at 100 °C in acetonitrile yields low-molecular-weight polymers (M = 600–1000) containing lactone (**B** and **C**) and ketone (**A**) groups.[111] Copolymerisation of strained olefins with CO has been considered in detail in a review.[7]

4. Carbon monoxide – functional α-olefins and other monomers

Of obvious scientific and practical interest are the products of alternating copolymerisation of carbon monoxide with various functionally substituted monomers. It has been reported [112] that carbon monoxide undergoes alternating copolymerisation with unsaturated alcohols $CH_2=CH(CH_2)_nOH$ (n = 2, 3, 5, 9) and acids $CH_2=CH(CH_2)_nCOOH$ (n = 1, 2, 4, 8) in the presence of $[Pd(Me\text{-}DUPHOS)(MeCN)_2](BF_4)_2$. The copolymers thus formed had molecular masses of $(10–45)\times10^3$ and $(12–100)\times10^4$, polydispersities of 1.5–2 and 2.9–5.8 for the alcohols and the acids, respectively. They exist as poly(1,4-ketone) and/or polyspiroketal structures and are optically active. Exceptions are provided by the copolymers based on but-3-en-1-ol (copolymer **21**) and pent-4-en-1-ol (copolymer **22**), which have an unusual polycyclic spiroketal structure. They are formed upon the interaction of the hydroxy group in the side chain with the nearest carbonyl group of the polymer chain (intramolecular cyclisation).

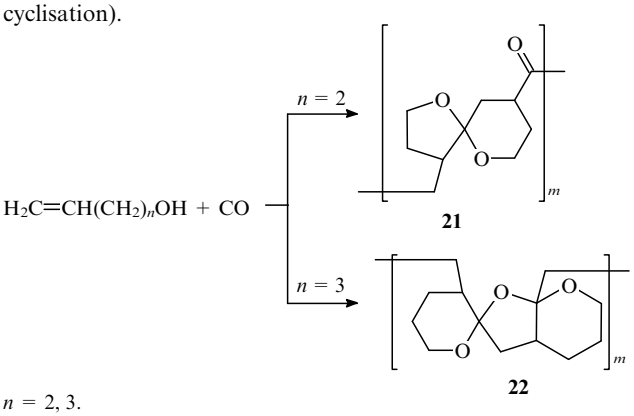

n = 2, 3.

The synthesis of the carbon monoxide copolymer with hepta-1,6-dien-4-ol ($M_w = 16\times10^3$ and T_g = 7 °C) has been reported.[113]

In the terpolymerisation of carbon monoxide with various α-olefins (C_3, C_6, C_{12} and C_{18}), a benzo-15-crown-5-functionalised α-olefin, undec-10-enyl[(benzo-15-crown-5)-4′-carboxylate], can be used as a comonomer.[114] It was found that an increase in the molecular mass of the α-olefin results in a decrease in the molecular mass of copolymer **23** from 12 800 (with C_6 α-olefin) to

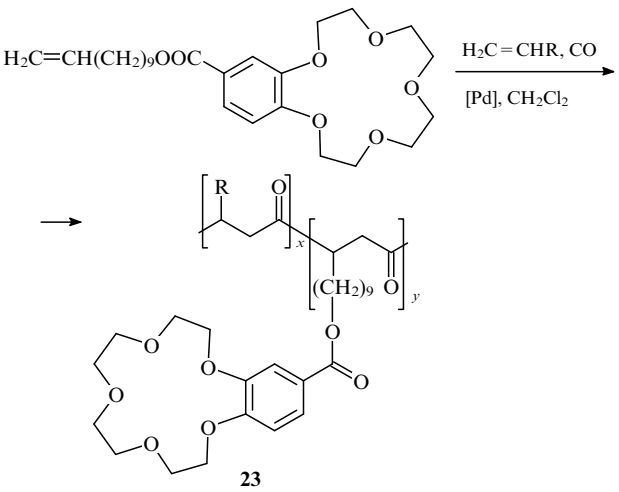

R = Me, Bu^n, n-$C_{10}H_{21}$, n-$C_{16}H_{33}$.

5 300 (for C_{18} α-olefin) and a decrease in T_g from 20 °C (for C_3) and −18 °C (for C_6) to −76 °C (for C_{12}). The polydispersities of the resulting terpolymers were 1.5–2.0. Despite the relatively low molecular mass of copolymers **23**, they were used to produce thin films suitable as ion selective membranes.

The synthesis of alternating copolymers of carbon monoxide with fluorinated alkenes $(C_nF_{2n+1})(CH_2)_mCH=CH_2$ ($m \geqslant 2$) has been described.[115] (see ¶). The resulting copolymers mainly had the spiroketal (rather than ketone) structure of the backbone.

Copolymerisation of carbon monoxide with epoxides occurs with opening of the epoxide ring. The possibility of alternating copolymerisation of epoxides with carbon monoxide was first demonstrated in 1965.[117] Copolymerisation was carried out in the presence of the $Co(acac)_3$ – $AlEt_3$ catalyst system (acac is acetylacetonate). The alternating copolymerisation of carbon monoxide with epoxides induced by the $Co_2(CO)_8$ – pyridine catalyst system and resulting in polyesters **24** with a regular structure has been described.[118, 119]

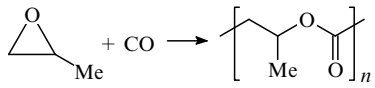

24

The $Co_2(CO)_8$ – $Ru_3(CO)_{12}$ system has also been used to catalyse this reaction.[120] The researchers showed that the Ru : Co ratio affects the yield, the molecular mass and the structure of the product.

Polyketones containing epoxide groups in the side chain were obtained by copolymerisation of carbon monoxide with vinyl epoxides (for example, 1,2-epoxyhex-5-ene, 1,2-epoxyoct-7-ene, 1,2-epoxydec-9-ene) in the presence of the [Pd{(*R*,*R*)-Me-DUPHOS}$(MeCN)_2$]$(BF_4)_2$ – $C_{10}H_6O_2$ – HCOOH catalyst system (Table 3).[121]

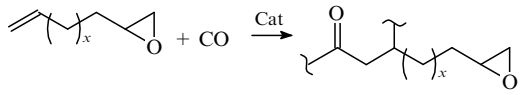

The copolymers formed have $M = (1-3) \times 10^4$ and a narrow molecular-mass distribution. They are soluble in CH_2Cl_2, THF, DMSO.

Table 3. Copolymerisation of CO with epoxides in the presence of the [Pd{(*R*,*R*)-Me-DUPHOS}$(MeCN)_2$]$(BF_4)_2$ – $C_{10}H_6O_2$ – HCOOH catalyst system.[121]

Epoxide	Time /h	Copolymer yield (%)	M_w	$M_w : M_n$
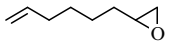	40	3.58	30 500	1.97
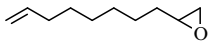	40	4.52	33 600	1.41
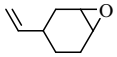	18	5.41	28 500	3.40
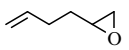	18	6.3	12 300	1.72
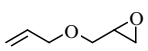	48	6.77	3 350	1.28
	24	–	–	–

¶ The synthesis and study of the properties of alternating copolymers of carbon monoxide with fluorinated allylbenzenes have been considered in the literature.[116]

In 1998, it was shown that carbon monoxide copolymerisation with imines gives polypeptides, which can be of interest as biomimetic materials.[122, 123]

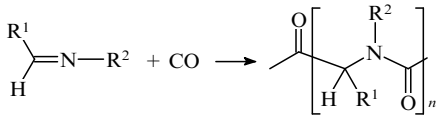

R^1, R^2 = H, Alk, Ar.

Later,[124] a crystalline polymer soluble in hot water, poly-β-alanine ($M = 14.1 \times 10^3$), has been prepared by copolymerisation of aziridine with carbon monoxide in the presence of the $CR_3C(O)Co(CO)_3PPh_3$ (R = H, D) and $HCo(CO)_3PPh_3$ complexes

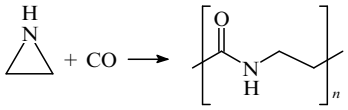

It was found that, when the catalyst concentration is low, the polymer formed contains ethyleneimine units apart from β-alanine units.

The synthesis of carbon monoxide copolymers with functionalised alkene monomers containing a carbamate or amide group has been described.[125] The [Pd(Me-DUPHOS)$(MeCN)_2$]$(BF_4)_2$ complex was used as the catalyst.

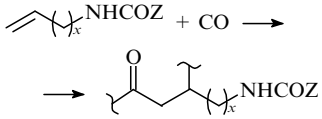

Z = OMe, OPh, Me, Ph; x = 1, 2.

This reaction carried out in CH_2Cl_2 or in a $MeNO_2$ – MeOH (2 : 1) solvent mixture gave copolymers with M_w ranging from 1×10^4 to 3×10^4, while in the absence of a solvent, $M_w = 6 \times 10^4$. Copolymerisation of carbon monoxide with *N*-(but-3-enyl)benzamide in CH_2Cl_2 or a $MeNO_2$ – MeOH (2 : 1) mixture gave two chiral copolymers, characterised by opposite signs of optical rotation.

The synthesis of alternating copolymers of carbon monoxide with cyclopropane derivatives has been described.[126–128] It has been proposed [127, 128] to carry out copolymerisation of 2-aryl-1-methylenecyclopropanes with CO in the presence of palladium diimine complexes such as [PdCl(R)(bipy)], [PdCl(R).(ArN=CHCH=NAr)] and [Pd(η^3-R′CHCHCH$_2$).(ArN=CHCH=NAr)] (R = Cl, Me; R′ = H, Ph; Ar = 4-MeC_6H_4, 4-$MeOC_6H_4$, 2,6-$Pr^i_2C_6H_3$).

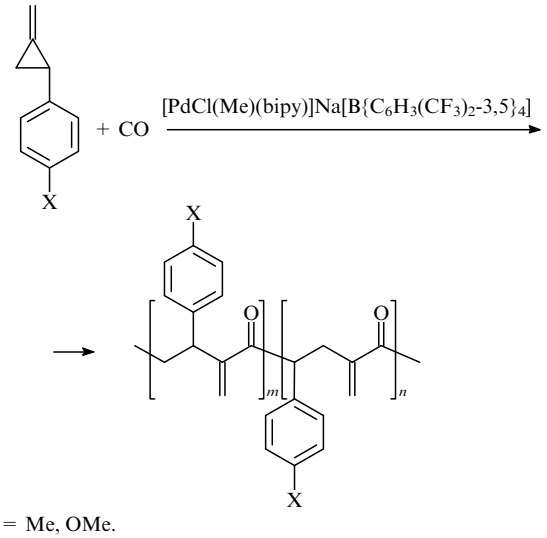

X = Me, OMe.

The yields of copolymers obtained in the presence of π-allyl palladium complex are lower than the yields of copolymers synthesised using the [PdCl(R)(ArN=CHCH=NAr)] and [PdCl(R)(bipy)] complexes; however, in the presence of the π-allyl complex, regular copolymers are formed.

Recently, using copolymerisation of carbon monoxide, propylene and polyalcohol (polyethylene glycol, polyvinyl alcohol or monomethyl ether of ethylene glycol), the possibility of obtaining linear and branched poly(1,4-ketone)–polyalcohol block copolymers was demonstrated.[129]

Some vinyl monomers that cannot copolymerise with carbon monoxide can nevertheless be inserted as single units into the polymeric chain during terpolymerisation with ethylene and carbon monoxide. The content of these units in the product depends on the monomer concentration, the type of the catalyst used, temperature, *etc*. In particular, terpolymerisation proceeds rather vigorously when isobutylene,[130] methyl acrylate,[130,131] chlorohex-1-ene,[131] undec-10-enoic acid and its methyl ester, undec-10-enyl alcohol,[108] maleic acid anhydride,[132,133] allyl acetate[131,134] and vinyl acetate[131,135] are used as the third components.

Polymeric materials that possess anisotropic properties are valuable for practical purposes. One way of creating anisotropy in polymers during the synthesis is incorporation of mesogenic groups in the side chain. At present, copolymers and terpolymers (with hex-1-ene as the third component) of carbon monoxide with α-olefins containing methoxybiphenyl mesogenic groups have been prepared. These copolymers exist as smectic E-mesophases with a periodicity corresponding to S_A. Their thermal stability is comparable to that of the CO/MeCH=CH_2 alternating copolymer whose thermal decomposition starts at 270 °C. The isotropiosation temperature of copolymers decreases with an increase in the length of the spacer,† while that for terpolymers decreases with an increase in the content of hex-1-ene.[136]

The aliphatic α-alkenes containing mesogenic substituents enter into copolymerisation with carbon monoxide in the presence of Pd(II) complexes. Depending on the type of the ligand (L), products with different stereo- and regioregularities are formed in the palladium complex (Scheme 2).

Scheme 2

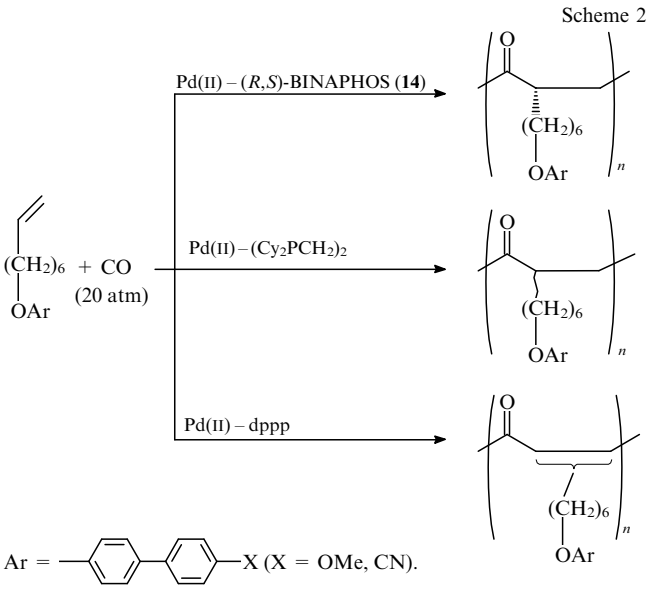

The properties of the resulting liquid-crystal polyketones[137] were studied by DSC and by polarisation optical microscopy.

† The length of the methylene chain that connects the polymer chain to the mesogenic group.

5. Carbon monoxide – linear dienes

Copolymerisation of carbon monoxide with butadiene in the presence of the $Pd(OAc)_2-Ph_2P(CH_2)_3PPh_2$ (or bipy)–CF_3COOH (or TsOH) catalyst system gives rise to low-molecular-mass copolymers in low yields.[5,138–140] On the basis of hexa-1,5-diene,[5,141,142] hepta-1,6-diene or octa-1,7-diene[5,113,142] and carbon monoxide, binary alternating copolyketones and terpolymers with ethylene have been synthesised. Hexa-1,5-diene[5,141,142] and hepta-1,6-diene react with carbon monoxide to give cyclic copolymers, whereas octa-1,7-diene copolymerises with CO to yield a linear alternating copolymer containing $CH_2CH=CH_2$ side groups.[5,113,141]

Data on the synthesis of the following terpolymers have been reported: hepta-1,6-dien-4-ol–carbon monoxide–propylene (T_g = 19 °C), propylene–carbon monoxide–methylenecyclopropane, propylene–carbon monoxide–octa-1,7-diene, hexa-1,5-diene–carbon monoxide–propylene,[113] ethylene–carbon monoxide–butadiene,[138–140] and ethylene–carbon monoxide–hexadiene.[141,142]

6. Carbon monoxide – cyclic dienes

The possibility of synthesis of an alternating copolymer of dicyclopentadiene (DCPD) with carbon monoxide was first mentioned in a patent.[98] Dicyclopentadiene is formed as a side product in the pyrolysis of petroleum products and represents a tricyclic hydrocarbon with two inequivalent C=C bonds, one highly reactive bond in the norbornene ring and one less reactive bond in the substituted cyclopentene ring. In the synthesis of DCPD/CO copolymers, the $Pd(OAc)_2$–bipy–TsOH–$C_6H_4O_2$ catalyst system was used. The copolymer is formed in a good yield even at room temperature, the presence of air in the reaction mixture being favourable for higher copolymer yield. When the $Pd(OAc)_2-Ph_2P(CH_2)_3PPh_2-CF_3COOH$ catalyst system is used, copolymerisation should be carried out at a temperature above 80–90 °C.[143] The synthesis of the CO copolymer with DCPD catalysed by $[Pd(MeCN)_2(PPh_3)_2](BF_4)_2$ (100 °C, carbon monoxide pressure of 1.0 MPa, 5 h) furnishes a solid white-coloured product, which is a mixture of CO/DCPD di- (**A**) and trimers (**B**).

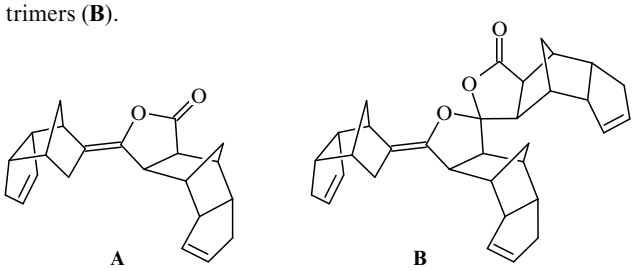

The copolymers of DCPD and carbon monoxide have, most often, a spiroketal structure, which is not tansformed into the ketone structure even on long-term heating.

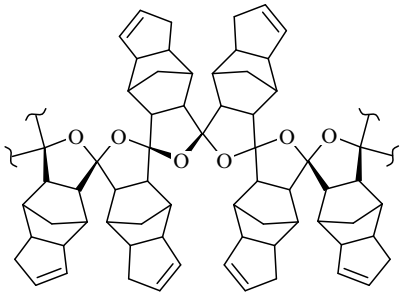

Copolymerisation of carbon monoxide and cyclopentadiene in the presence of $[Pd(MeCN)_4](BF_4)_2$ (60 °C, pressure 5.6 MPa, 24 h) and various monodentate ligands [PPh_3, $AsPh_3$, NPh_3, $PMePh_2$, $P(OPh)_3$] has been described.[96] The process gives a partially crystalline copolymer with T_m > 180 °C, soluble in

THF. The M_n values of the copolymer increase from 570 to 2750 following an increase in the carbon monoxide pressure from 2.1 to 5.6 MPa. The highest yield of the copolymer is attained when PPh_3 is used as the ligand and MeOH is used as the reaction medium. According to ^1H NMR, the resulting copolymer consists of macromolecules having 1,2- and 1,4-structures,

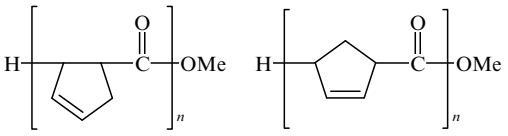

1,2-structure 1,4-structure

the content of 1,2-structures markedly increasing for copolymerisation carried out in polar solvents (MeOH, MeCN). The resulting copolymer is thermally unstable: a partial mass loss is observed at 120 °C. The activity of cyclohexadiene in this reaction is about 60 times lower.

Using the $PdCl_2$ – 1,4:3,6-dianhydro-2,5-dideoxy-2,5-bis(diphenylphosphino)-L-idite – $CuCl_2$ – 2,6-$Me_2C_6H_2O_2$ – TsOH catalyst system (45 °C, 24 h, carbon monoxide pressure 6 MPa), alternating copolymers of carbon monoxide with DCPD and methylcyclopentadiene with an isotactic (1,4-ketone) structure and molecular masses of 1300 ($M_w : M_n = 1.7$ for DCPD) and 944 ($M_w : M_n = 2.88$ for methylcyclopentadiene) have been obtained.[144]

A study[145] of the influence of the solvent on the yield of carbon monoxide copolymer with 4-vinylcyclohexene obtained in the presence of the $[Pd(MeCN)_4](BF_4)_2$ – L catalyst system (L = PPh_3, bipy, phen or 5-NO_2-phen) (60 °C, carbon monoxide pressure 5.5 MPa, 12 h) has shown that copolymerisation rate is higher (1.45 and 0.82 g g_{Pd}^{-1} h^{-1}) in polar solvents (MeOH and $MeNO_2$) than in $CHCl_3$ (0.53 g g_{Pd}^{-1} h^{-1}). The copolymer thus formed had a relatively low molecular mass (1070 – 6910) and contained both ketone and cyclic (cyclohexyl and norbornane) structures in the chain. The copolymer was soluble in DMSO, *N*,*N*-dimethylacetamide, DMF, pyridine, acetonitrile, THF, nitromethane, acetone, chloroform and 1-methyl-2-pyrrolidone but insoluble in benzene, toluene, 1,2-dichloroethane, chlorobenzene, methanol, ether, 1,4-dioxane or ethyl acetate. According to DTG analysis, the loss of copolymer mass starts at 190 °C. Treatment of the copolymer with a solution of $LiAlH_4$ in THF results in polyalcohol, which is soluble in chloroform, THF, DMSO and methanol but insoluble in benzene, n-hexane or ether.

The first mention of the synthesis of the alternating copolymer of carbon monoxide and norbornadiene appeared more than 30 years ago.[146, 147] Palladium chloride was used as the catalyst. The copolymer formed had $M_n = 2900$, $T_m < 300$ °C; it was soluble in benzene, chloroform and THF. However, on storage in air, the solubility of the copolymer decreased, apparently, due to oxidation processes. The use of palladium complexes with bidentate P-P and N-N ligands as catalysts resulted in a higher yield of the copolymer.[98, 148] Copolymerisation carried out in the presence of $[Pd(MeCN)(PPh_3)_3](BF_4)_2$ at a temperature of 60 °C and a carbon monoxide pressure of 5.6 MPa gave a carbon monoxide – norbornadiene copolymer with $M_n = 3380$ soluble in $CHCl_3$ and C_6H_6,[97] while at 100 °C, a copolymer with $M_n = 800 – 1200$ was formed.[111] The IR spectra of the polymer exhibit characteristic bands at 1778, 1722 and 1702 cm^{-1}, indicating the presence of γ-lactone, ester, vinyl, and ketone groups in the polymer chain.

The influence of the nature of the catalyst, the temperature, the nature of the solvent and the concentrations of carbon monoxide, *p*-toluenesulfonic acid and 1,4-benzoquinone on the yield and the molecular mass of carbon monoxide – norbornadiene copolymer has been studied.[148] The highest catalytic activity in this reaction was found for $[Pd(MeCN)_4](BF_4)_2$ in the presence of bidentate N-N-ligands such as bipy or phen (in this case, copolymerisation rate reached 60 g g_{Pd}^{-1} h^{-1}). The presence of diphosphine $PPh_2(CH_2)_3PPh_2$ in the reaction medium decreases the catalyst activity about 1.5-fold and in the presence of monodentate ligands PPh_3, $AsPh_3$, NPh_3, or $P(OPh)_3$, the activity decreases 5 – 20 fold; simultaneously, the copolymer molecular mass decreases from 9000 to 1250. The replacement of polar protic solvents (for example, MeOH) by less polar solvents (THF or benzene) results, on the one hand, in a decrease in the catalyst activity and, on the other hand, in an increase in the copolymer molecular mass to 16 000, indicating the participation of the solvent in a chain termination reaction. An increase in the concentrations of carbon monoxide, TsOH or 1,4-benzoquinone results in a higher yield of the copolymer. Upon the increase in the carbon monoxide concentration, the molecular mass of the copolymer also increases (upon an increase in the TsOH or 1,4-benzoquinone concentration, the molecular mass decreases). The DTG data show that the copolymer starts to lose mass at 167 °C (at 356 °C, the mass loss is 24.5%). Hydrogenation of this copolymer affords polyalcohol, which is completely soluble in chloroform, THF, DMSO and *m*-cresol, partially soluble in acetone and methanol and insoluble in benzene, n-hexane or water.

The characteristic features of synthesis and the structure of alternating co-oligomers of carbon monoxide with norbornadiene and the mechanism of formation of various structural units in the polymer chain in the presence of the $Pd(MeC_6H_4PPh_3)(Tp^{Ph})$ catalyst in an aprotic medium and methanol have been considered.[149]

The copolymerisation of carbon monoxide with *endo*-tricyclo[6.2.2.$0^{2,7}$]dodeca-3,9-diene gives rise to oil-like dimers (mainly, dimer **25**) and that with dibenzobicyclo[2.2.2]octatriene affords solid dimer **26**.[111]

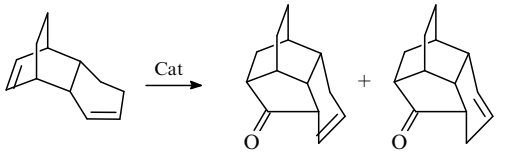

25

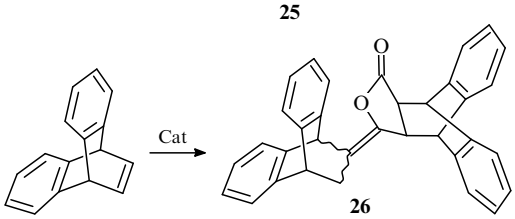

26

In the presence of Pd(II) complexes with σ,π-alkenyl ligands and a stabilising pyridine or triphenylphosphine ligand, alternating copolymers of carbon monoxide with diethylbicyclo-[2.2.1]hepta-2,5-diene-2,3-dicarboxylate (**27**) and diethyl 7-oxabicyclo[2.2.1]hepta-2,5-diene-2,3-dicarboxylate (**28**) have been obtained according to the living polymerisation mechanism.[150]

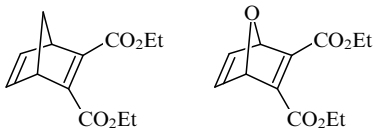

27 **28**

In the former case, dimeric palladium chloride complex was used as the catalyst (**29**), while in the latter case, this was triphenylphosphine complex **30**.

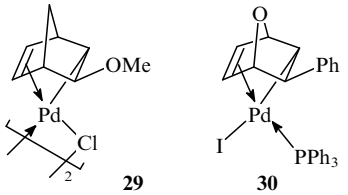

29 **30**

In the copolymerisation of carbon monoxide with diene **27**, the yield of the copolymer is nearly 100%, while in the copolymerisation with diene **28**, the yield was 60% – 65%. In the latter case, diethyl furan-3,4-dicarboxylate is formed as a side product. This side product can be isolated from the copolymer by heating at 70 °C. Diethyl furan-3,4-dicarboxylate is converted, in turn, into a polyconjugated polymer, polyketovinylene (**31**).

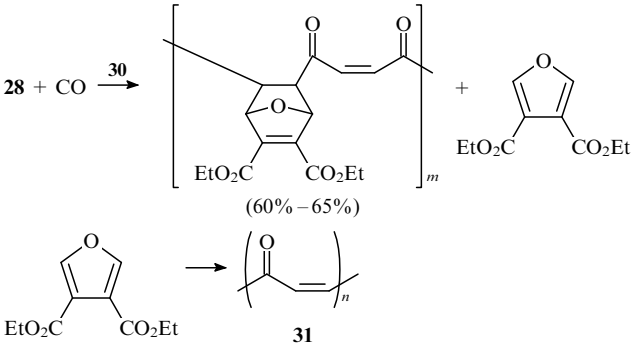

Study of the effect of the monomer and Pd complex concentrations on the kinetics of carbon monoxide copolymerisation with diene **27** has shown that the reaction is first order ($k = 8.2 \times 10^{-3}$ litre mol^{-1} s^{-1}) with respect to CO and Pd and a zero order with respect to diene. In all cases, the concentration of diene **27** was approximately two orders of magnitude higher than the carbon monoxide concentration. If monomer **28** is added to the CO/**27** copolymer, alternating block copolymer (CO/**27**)/(CO/**28**) can be obtained.

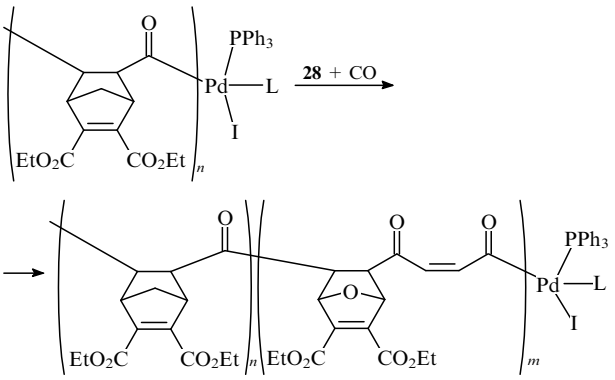

7. Carbon monoxide – allene derivatives

Although insertion of carbon mono- and dioxide and sulfur dioxide into the palladium – allyl bond has been mentioned in the literature,[151 – 155] no data on the synthesis of a binary copolymer of carbon monoxide with unsubstituted allene has been reported. Copolymers of carbon monoxide with 1,1-dimethylallene (1,2- and 2,3-isomers), 1,1,3,3-tetramethylallene [5, 156] and a large number of arylallenes *p*-$XC_6H_4CH=C=CH_2$ (X = H, Me, MeO, Cl, F, Bu^n, Bu^t) have now been prepared. The reaction with arylallenes was carried out at 25 °C, a CO pressure of 0.1 MPa (21 h) in the presence of a Rh complex, $Rh[\eta^3\text{-}CH(Ar)C\{C(=CHAr)CH_2C(=CHAr)CH_2CH_2CH=CHAr\}CH_2](PPh_3)_2$ (Ar = C_6H_4OMe-*p*).[5, 157] The reaction follows the living polymerisation mechanism. The alternating copolymers thus formed have $M = 10^4 – 10^5$, $M_w : M_n = 1.06 – 1.16$. Copolymerisation of phenylallene and carbon monoxide with subsequent addition of 4-methoxyphenylallene to the reaction mixture gives the block copolyketone $[CO-C(=CHPh)CH_2]_m/[CO-C(=CHC_6H_4OMe\text{-}p)CH_2]_n$; meanwhile, terpolymerisation of carbon monoxide with an equimolar mixture of phenylallene and 4-methoxyphenylallene yields a statistical copolymer. The same rhodium complex was used for terpolymerisation of carbon monoxide with 4-hexylphenylallene and 4-dodecylphenylallene. The T_m and T_g values of the $[CO/C(=CHC_6H_4Alk\text{-}p)CH_2]_n$ polyketones were found to increase in the series of alkyl radicals $C_{12}H_{25} < C_6H_{13} < Bu^n < Me < H$ from 65 to 170 °C and from 30 to 125 °C, respectively. By terpolymerisation of carbon monoxide with a mixture of phenylallene and 4-alkylphenylallene (Alk ≠ Me), statistical and block terpolymers were obtained, whereas the use of a mixture of 4-methylphenylallene and bisallenylbenzene results in cross-linked polyketones.[158, 159] The copolymerisation rate decreases in the sequence of comonomers: 1,1-dimethylallene > phenylallene > cyclohexylallene. Terpolymerisation of carbon monoxide with a mixture of 4-(allenyloxy)-azobenzene and 4-(methoxyphenyl)allene [or 4-(*tert*-butyl)-phenyloxyallene] resulted in statistical polyketones.[160]

The synthesis of new functional polyketones soluble in dichloromethane, THF and toluene was accomplished by terpolymerisation of propylene and carbon monoxide with 2-allylphenol, 2-allylmethoxybenzene, 4-allylmethoxybenzene and 4-allyl-2-methoxyphenol in the presence of the $[Pd(dppp)(MeCN)_2](BF_4)_2$ complex as the catalyst [160] and by carbon monoxide copolymerisation with 4-allylanisole catalysed by $[Pd\{(R,R)\text{-Me-DUPHOS}\}(MeCN)_2](BF_4)_2$.[5, 112]

Analysis of the state-of-the-art studies dealing with the synthesis of alternating copolymers of carbon monoxide with dienes shows that the search for effective catalysts is only at an early stage, unlike that for the synthesis of copolymers of carbon monoxide with alkenes. The obtained copolymers have a relatively low molecular mass ($10^3 – 10^4$) and only the use of some Pd complexes enables living copolymerisation mechanism; in this case, it is possible to obtain alternating copolymers with a molecular mass of $\sim 10^5$. Undoubtedly, effective catalysts for the synthesis of carbon monoxide copolymers with dienes would be found in the near future and these polymers would find extensive use.

8. Copolymers of carbon monoxide with styrene and its derivatives

Copolymerisation of carbon monoxide with styrene and its derivatives takes place only in the presence of nitrogen N-N- or hybrid P-X-ligands (X = N, O). In the presence of the $[(MeCO)Pd(MeCN)\{(R,S)\text{-BINAPHOS}\}][B\{3,5\text{-}(CF_3)_2C_6H_3\}_4]$ complex,[161] the chain initiation and propagation involved in the copolymerisation of carbon monoxide with *tert*-butylstyrene take place by the 1,2-inclusion mechanism.

Milani *et al.* [162] have studied the influence of the nature of the solvent [methanol or 2,2,2-trifluoroethanol (TFE)], the temperature, the carbon monoxide pressure and the concentration of 1,4-benzoquinone on the CO – styrene copolymerisation rate and on the molecular mass of the resulting copolymer. It was found that in TFE, the copolymerisation catalysed by the $[Pd(bipy)_2](PF_6)_2$ system is a quasi-steady-state process, whereas in methanol, the rate decreases with time. As the temperature is raised from 60 to 80 °C, the rate of copolymerisation increases from 271 to 1134 g g_{Pd}^{-1} h^{-1}, and the $[\eta]$ value decreases from 0.27 to 0.14 dl g^{-1}. The reaction time (7 – 48 h) and the carbon monoxide pressure have a little influence on the molecular mass of the resulting copolymer but influence the copolymerisation rate. Thus an increase in the carbon monoxide pressure from 1 to 4 MPa results in a sharp decrease in the reaction rate from 1081 to 290 g g_{Pd}^{-1} h^{-1}.

Interesting results have been obtained by Milani *et al.*,[163] who attained a rate of carbon monoxide – styrene copolymerisation equal to $\sim 17\,000$ g g_{Pd}^{-1} h^{-1} by using the $[Pd(bipy)_2](PF_6)_2 – C_6H_4O_2$ catalyst system, the reaction being conducted in TFE. The researchers noted that the catalyst system did not lose activity for at least 48 h. The presence of 1,4-benzoquinone influences not only the catalyst activity but also the molecular mass of the copolymer. With the molar ratio $C_6H_4O_2 : Pd = 5 : 1$, a copolymer with $M_w = 71\,710$ was obtained ($M_w : M_n = 2$), and in the absence of 1,4-benzoquinone, with $M_w = 84\,860$ ($M_w : M_n = 1.8$). It is noteworthy that this is the first example of synthesis of a carbon

monoxide copolymer with styrene with such a high molecular mass.

By varying the styrene : ethylene monomer ratio, one can prepare $C_2H_4/CO/H_2C=CHPh$ terpolymers in a high yield and with different contents of styrene. Recently, it has been shown [164] that the use of the palladium complex with the (*S*)-3-(1,2,2-$Me_3C_3H_4$)-1,10-phen ligand allows one to carry out carbon monoxide copolymerisation with styrene (or 4-methylstyrene) in TFE for 80 h almost without a decrease in the reaction rate and to obtain copolymers with a molecular mass of 20×10^4 (or 30×10^4). An increase in the styrene : Pd molar ratio (from 48 000 to 96 000) increases the yield and the molecular mass of product approximately twofold. The terminal groups present in the copolymers synthesised in TFE are PhCH=CH, Me(Ph)CH or CF_3CH_2O.[165] It has been shown [166] that the content of TFE should not exceed 3 mass % – 5 mass %.

The catalytic activity of the $[Pd(\eta^1,\eta^2\text{-}C_8H_{12}OMe).(bipy)]^+X^-$ complex [where $X = BPh_4$, CF_3SO_3, BF_4, PF_6, SbF_6, $B\{3,5\text{-}(CF_3)_2C_6H_3\}_4$] in the carbon monoxide copolymerisation with styrene in dichloromethane has been studied as a function of the activity of the counter-ion used.[167] The following activity series was elucidated: $BPh_4 \ll CF_3SO_3 < BF_4 < PF_6 < SbF_6 < B\{3,5\text{-}(CF_3)_2C_6H_3\}_4$. With an excess of the bipyridine ligand, the activity series changes to give $BPh_4 \ll CF_3SO_3 < BF_4 \approx B\{3,5\text{-}(CF_3)_2C_6H_3\}_4 \approx PF_6 \approx SbF_6$.

A new class of catalysts based on the Pd(II) bipyridyl complex containing $[B\{3,5\text{-}(CF_3)_2C_6H_3\}_4]^-$ as the counter-ion have been prepared. These catalysts were found to be more active in the carbon monoxide copolymerisation with styrene or *tert*-butylstyrene than catalysts with the PF_6 counter-ion.

A study [168, 169] of terpolymerisation in the $C_2H_4/CO/CH_2=CHPh$ system at high carbon monoxide pressures in the presence of various P-N-ligands as parts of the [Pd(COMe).(P-N)(solv)]O_3SCF_3 palladium complex [P-N is phosphino(dihydrooxazole) ligand, solv is solvent] has shown that a decrease in the carbon monoxide pressure from 29 to 14 MPa entails a decrease in the reaction rate from 27 to 12.9 mmol g_{Pd}^{-1} h^{-1}; simultaneously, the $(-C_2H_4-CO-):(-CH_2CHPh-CO-)$ ratio of copolymer units changes from 80 : 20 to 90 : 10. For $C_2H_4/CO/CH_2=CHPh$ terpolymers, the dependence of T_g on the composition $(C_2H_4/CO)/(CH_2=CHPh/CO)$ was determined. The copolymer containing 27 mol.% of the $-CH_2CHPhCO-$ units has $T_g = 37$ °C, a rupture resistance (σ_p) of 62 MPa, and a relative elongation at rupture (ε) of 270%.[170]

It was found that by varying the nature of the aryl substituent at the phosphorus atom in (*S*)-2-[2-(diarylphosphino)phenyl]-4-benzyl-4,5-dihydrooxazole (Ar = Ph, *p*-$MeOC_6H_4$, *o*-$MeOC_6H_4$, *o*-MeC_6H_4), one can affect the copolymerisation rate and the tacticity of the $CO/CH_2=CHPh$ copolymer.[171]

Ar	w /mmol g_{Pd}^{-1} h^{-1}	T_m /°C
Ph	81	228
p-$MeOC_6H_4$	28	175
o-$MeOC_6H_4$	71	127
o-MeC_6H_4	11.7	80

New homogeneous bismethoxycarbonyl complexes [Pd(L-L).$(MeOCO)_2$] (L-L are substituted phenanthroline ligands) have been used to synthesise the syndiotactic $CO/CH_2=CHPh$ copolymer.[172] In the $[Pd(L\text{-}L)(MeOCO)_2](X)_2$ – oxidant catalyst system, PF_6^- acts as the weakly coordinated counter-ion and 1,4-naphthoquinone acts as the oxidant. The rate of copolymerisation of carbon monoxide with styrene at 65 °C and at a carbon monoxide pressure of 4 MPa is ~194 g g_{Pd}^{-1} h^{-1}. The rate depends on the pK_a of the phenanthroline ligand. With an increase in the pK_a (caused by the introduction of substituents in the phenanthroline ring), the copolymerisation rate and the copolymer molecular mass decrease 2 – 6-fold with simultaneous decrease in the copolymer tacticity. A decrease in the copolymerisation rate following an increase in the pK_a of the N-N-ligand from 4.44 (bipy) to 6.31 (tetramethylphenanthroline) has also been reported in the study [46] describing styrene – carbon monoxide copolymerisation catalysed by the $[Pd(N\text{-}N)(MeCO_2)_2]$ and $[Pd(N\text{-}N)(CF_3CO_2)_2]$ complexes (N-N is bipy, 1,10-phenanthroline or their derivatives). The degree of polymerisation of the copolymer increases with time and after 6 h, it reaches 160. The copolymer thus obtained has $T_g = 99$ °C and $T_m = 273$ °C. On short-term (5 min) heating of the copolymer at temperatures of 200 °C and 220 °C, the number of terminal vinyl groups substantially increases, while the number of methoxycarbonyl groups decreases (their ratio in the initial copolymer is 1 : 1).

The syntheses of carbon monoxide – styrene and carbon monoxide – *p*-methylstyrene copolymers as well as styrene – carbon monoxide – ethylene, styrene – carbon monoxide – propylene, styrene – carbon monoxide – ω-undecyl alcohol and styrene – carbon monoxide – ω-methyl undecenecarboxylate terpolymers have been carried out using the $[Pd(5\text{-}Me\text{-}1,10\text{-}phen).(MeCN)_2](BF_4)_2 - C_6H_4O_2$ catalyst system.[173] The $CO/CH_2=CHPh$ copolymer is poorly soluble in 2-chlorophenol and in hexafluoroisopropyl alcohol and has $T_g = 94$ °C and $T_m = 290$ °C. The crystallinity of the copolymer sharply decreases after it has been dissolved and reprecipitated. For example, reprecipitation of the $CO/CH_2=CHC_6H_4Me\text{-}p$ copolymer from a solution in 2-chlorophenol by methanol gave an amorphous polymer, which was soluble in chloroform and dichloromethane.

The solubility of the $C_2H_4/CO/CH_2=CHPh$ and $CH_2=CHMe/CO/CH_2=CHPh$ terpolymers depends on the styrene : olefin ratio. For example, a terpolymer containing 11 mol.% – 12 mol.% of the $-C_2H_4CO-$ units is soluble in chloroform and dichloromethane but insoluble in acetone, whereas the material containing 80 mol.% of the $-C_2H_4CO-$ units is insoluble in common organic solvents but is soluble in 2-chlorophenol and hexafluoroisopropyl alcohol.

Japanese researchers ‡ have studied the asymmetric terpolymerisation of propylene and hex-1-ene with 4-(*tert*-butyl)styrene and carbon monoxide in the presence of the Pd complex with the phosphine phosphite ligand BINAPHOS (**14**). It was shown that the glass transition temperature of the copolymers depends on the olefin content in the copolymer.

In the copolymerisation of carbon monoxide and styrene in the presence of the $Pd(OAc)_2$ – bipy – TsOH catalyst system, the maximum copolymerisation rate (68 g g_{Pd}^{-1} h^{-1}) is observed at a bipy : Pd molar ratio of 15 : 1. The replacement of methanol used as the reaction medium by acetone, THF, DMSO, aniline or DMF results in a sharp decrease in the copolymerisation rate and the reduction of Pd(II) to Pd(0). When copolymerisation is carried out in petroleum ether, cyclohexane, nitrobenzene, ethyl acetate or phenyl ethyl ether, the rate decreases 3 – 4-fold compared to the copolymerisation rate in methanol.[174]

The effect of the nature of the bidentate N-N ligand on the structure of the resulting copolymer of carbon monoxide with styrene was demonstrated using two ligands: diazabutadiene and bioxazoline. It was found that in the former case, an isotactic copolymer is formed, while in the latter case, the product is a syndiotactic polymer.[175] When the Pd(II) acetonitrile complex with 2,2-bis[4-(*S*)-methyl-1,3-oxazolin-2-yl]propane [176] and (4*S*,4′*S*)-(−)-4,4′,5,5′-tetrahydro-4,4′-diisopropyl-2,2′-bioxazole,[177] which are ligands with C_2-symmetry, was used as the catalyst, the isotactic $CO/CH_2=CHPh$ copolymer and partially isotactic $CO/CH_2=CHC_6H_4Me\text{-}p$ copolymer with high optical activity were obtained. Using C_2-symmetric Pd complexes, (*R*,*R*/*S*,*S*)-*trans*-1,2-$[C_6H_{10}\{N=CH\text{-}2\text{-}C_5H_4N(PdMe(NCMe)_2)\}_2][B\{3,5\text{-}(CF_3)_2.C_6H_3\}_4]_2$ and $[C_2H_4\{N=CH\text{-}2\text{-}C_5H_4N(PdMe(NCMe)_2)\}_2].[B\{3,5\text{-}(CF_3)_2C_6H_3\}_4]_2$, syndiotactic copolymers of carbon monoxide with styrene and 4-methylstyrene were obtained.[178] Palladium complexes with C_s-symmetry with asymmetric chelating ligands on the basis of 2-(pyrazol-1-yl)pyridine, 2-(pyrazol-1-

‡ Y Kawashima, K Nozaki, T Hiyama *Inorg. Chim. Acta* **350** 577 (2003).

yl)pyrimidine and 2-[(3,5-dimethyl)pyrazol-1-yl]pyrimidine have been used for copolymerisation of carbon monoxide with 4-(*tert*-butyl)styrene. This gave syndiotactic copolymers.[179] The use of C_1-symmetric pyridinylimidazole ligands with different hydrocarbon substituents provides carbon monoxide–4-(*tert*-butyl)-styrene copolymers with different tacticities depending on the substituent.[180]

The synthesis of a stereoregular carbon monoxide–4-(*tert*-butyl)styrene block copolymer using the 2,2′-bipyridyl–bioxazoline Pd(II) complex catalyst system has been reported.[176] Bipyridyl is added to the palladium complex during the synthesis; as a result, fast ligand exchange takes place. The produced copolymer contains macromolecules of both isotactic and syndiotactic structures. Depending on the symmetry of the phosphino(dihydrooxazole) ligand used, both isotactic and atactic polymers were obtained.[181, 182] The synthesis of alternating copolymers of carbon monoxide with hydroxystyrene and its formate and acetate has been described.[183] It is noteworthy that $Pd(OAc)_2$ can be replaced by rare earth metal (Y, La, Nd, Sm, Dy) acetates or their mixtures with $Cu(OAc)_2$. For example, copolymerisation of carbon monoxide with styrene in the presence of rare earth metal acetates has been reported.[184]

III. The mechanism of alternating copolymerisation of carbon monoxide

In a study of the alternating copolymerisation of carbon monoxide with olefins, the ethylene–carbon monoxide system studied most comprehensively was chosen as the model system and the $Pd(OAc)_2$–diphosphine–acid system used most often was chosen as the catalyst.

When the catalyst is formed *in situ* under homogeneous conditions, depending on the nature of the solvent (alcohol, water or a less polar solvent), reactions (1)–(8) can take place between the catalyst components and the medium. If copolymerisation is carried out in methanol, L_2PdOMe^+ would act as the catalytically active species [reaction (2)].[185]

In water and in moist solvents, Pd hydride complexes may form [reactions (4), (8)]. In addition, palladium hydride species can be formed by reactions (3), (5) and (6).

$$Pd^{2+} + L_2 \longrightarrow L_2Pd^{2+} \text{ } (L_2 \text{ is a bidentate phosphine ligand}) \quad (1),$$

$$L_2Pd^{2+} + MeOH \longrightarrow L_2PdOMe^+ + H^+, \quad (2)$$

$$L_2PdOMe^+ \longrightarrow L_2PdH^+ + CH_2O, \quad (3)$$

$$L_2Pd^{2+} + CO + H_2O \longrightarrow L_2PdH^+ + CO_2 + H^+, \quad (4)$$

$$L_2Pd^{2+} + C_2H_4 + MeOH \longrightarrow L_2PdH^+ + CH_2{=}CHOMe + H^+, \quad (5)$$

$$L_2Pd^{2+} + H_2 \longrightarrow L_2PdH^+ + H^+. \quad (6)$$

In an aqueous medium, apart from L_2PdH^+, the L_2PdOH^+ species are also present; they react with CO by reactions (7) and (8).

$$L_2PdOH^+ + CO \longrightarrow L_2PdCOOH^+, \quad (7)$$

$$L_2PdCOOH^+ \longrightarrow L_2PdH^+ + CO_2. \quad (8)$$

Initiation and propagation of the polymer chain. The chain initiation in a solution (*i.e.*, primary insertion of a CO or C_2H_4 molecule into a Pd–alkyl or Pd–acyl complex) has been studied rather comprehensively by various physicochemical and theoretical methods.[25, 185–202] In a number of studies,[25, 186, 187, 200–202] the structure of the catalytically active species that run the copolymerisation process has been proposed on the basis of data from EXAFS, UV, IR and ^1H and ^{31}P NMR spectroscopy and mass spectrometry. In particular, it was found that the monochelate complex of diphosphine and palladium acetate is the active site of the copolymerisation. As the diphosphine : palladium molar ratio increases to 2 or more, the monochelate complex is transformed into an inert bischelate complex, which is unable to participate in copolymerisation. When the inert palladium complex is exposed to atmospheric oxygen, the equilibrium shifts toward the formation of the catalytically active monochelate palladium complex. The relationship between the contents of these complexes in the catalyst system and the rate and the induction period of copolymerisation has been established.[185] On the basis of ^1H NMR data, it was shown that the $CO-C_2H_4$ copolymerisation in protic (alcohols) and aprotic solvents is initiated by the insertion of the CO and C_2H_4 molecules into the Pd–OMe and Pd–H bonds, respectively. It should be noted that protic solvents not only serve as the reaction medium; they are also involved in chain initiation and termination reactions and also stabilise the Pd^{2+} cation. It was found [25] that in addition to the catalytically active 16-electron four-coordinate square planar $Pd(d^8)$ species (**A**), a five-coordinate 18-electron pyramidal $Pd(d^8)$ species is also present in the reaction area (**B**).

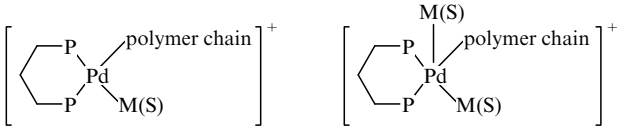

A **B**

M is monomer (CO or C_2H_4), S is solvent.

Studies of the initiation and propagation of the polymer chain have been carried out using a heterogeneous single-centre Pd complex, $[\{Ph_2P(CH_2)_3PPh_2\}Pd(Me)(OSO_2CF_3)]$. The polarisation-modulated absorption IR spectroscopy technique has been used [186] to observe the changes taking place in the IR spectra on the successive insertion of the CO and C_2H_4 molecules into the Pd–OMe bond in the active catalytic species [reactions (9), (10)]. It was found that the hydride species L_2PdH^+, formed during the formation of the catalyst and in the subsequent chain termination and transfer steps, can be transformed again into catalytically active species by reaction (14).

$$L_2PdOMe^+ + CO \longrightarrow L_2PdCOOMe^+, \quad (9)$$

$$L_2PdOMe^+ + C_2H_4 \longrightarrow L_2PdCH_2CH_2OMe^+, \quad (10)$$

$$L_2PdH^+ + C_2H_4 \longrightarrow L_2PdC_2H_5^+, \quad (11)$$

$$L_2PdH^+ + CO + MeOH + \text{ 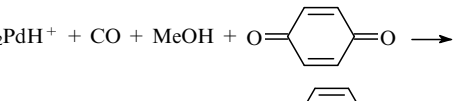 } \longrightarrow \quad (12)$$

$$\longrightarrow L_2PdCOOMe^+ + \text{ 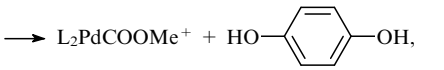 }$$

$$L_2Pd^{2+} + CO \longrightarrow L_2PdCO^{2+}, \quad (13)$$

$$L_2PdCO^{2+} + MeOH \longrightarrow L_2PdCOOMe^+ + H^+, \quad (13')$$

$$L_2PdH^+ + MeOH + \text{ 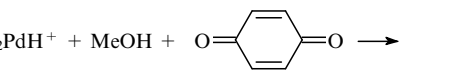 } \longrightarrow \quad (14)$$

$$\longrightarrow L_2PdOMe^+ + \text{ 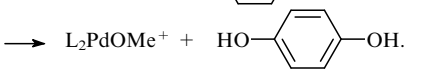 }$$

It should be noted that, depending on the nature of the initiating species (L_2PdOMe^+ or L_2PdH^+), the growing polymer chain would have a methoxyl or ethyl group at one end [reactions (15)–(17)].

$$L_2PdCOOMe^+ + C_2H_4 \longrightarrow L_2PdCH_2CH_2COOMe^+, \quad (15)$$

$$L_2PdCH_2CH_2OMe^+ + CO \longrightarrow L_2PdCOCH_2CH_2OMe^+, \quad (16)$$

$$L_2PdC_2H_5^+ + CO \longrightarrow L_2PdCOC_2H_5^+. \quad (17)$$

Chain restriction (termination and transfer). When the chain is transferred to the alcohol (by a protolysis or alcoholosis reaction), either methoxy or ethyl group is located at the end of the chain. In these cases, diester [reaction (18)], ketoester [reaction (19)] or diketone [reaction (20)] type copolymers are formed. Recently, it has been shown [203] that in a homogeneous medium (when the

length of the growing polymer chain does not exceed 500), chain termination and transfer occur mainly *via* protolysis of the active site, whereas in a heterogeneous medium (when the polymer chain is long and the polymer precipitates), both protolysis and alcoholysis reactions take place. (For determining the rates of these reactions depending on the type of catalyst and conditions of copolymerisation, further systematic research is required.)

$$L_2PdCO(CH_2CH_2CO)_nOMe^+ + MeOH \longrightarrow \quad (18)$$

$$\longrightarrow L_2PdH^+ + \underset{\text{diester}}{MeOCO(CH_2CH_2CO)_nOMe}$$

$$L_2PdCO(CH_2CH_2CO)_nOMe^+ + MeOH \longrightarrow \quad (19)$$

$$\longrightarrow L_2PdOMe^+ + \underset{\text{ketoester}}{HCO(CH_2CH_2CO)_nOMe}$$

$$L_2PdCO(CH_2CH_2CO)_nC_2H_5^+ + MeOH \longrightarrow \quad (20)$$

$$\longrightarrow L_2PdOMe^+ + \underset{\text{diketone}}{HCO(CH_2CH_2CO)_nC_2H_5}$$

During copolymerisation of CO and C_2H_4 in water or in water-containing solvents, the following reaction can take place:

$$L_2PdCO(CH_2CH_2CO)_nC_2H_5^+ + HOH \longrightarrow \quad (21)$$

$$\longrightarrow L_2PdOH^+ + \underset{\text{diketone}}{HCO(CH_2CH_2CO)_nC_2H_5}$$

Spontaneous chain termination. When copolymerisation is carried out in aprotic solvents, spontaneous chain termination takes place by β-elimination mechanism [reactions (22), (23)]. In this case, one end of the polymer chain would bear the vinyl group.

$$L_2Pd(CH_2CH_2CO)_nOMe^+ \longrightarrow$$

$$\longrightarrow L_2PdH^+ + CH_2{=}CHCO(CH_2CH_2CO)_{n-1}OMe, \quad (22)$$

$$L_2Pd(CH_2CH_2CO)_nC_2H_5^+ \longrightarrow$$

$$\longrightarrow L_2PdH^+ + CH_2{=}CHCO(CH_2CH_2CO)_{n-1}C_2H_5. \quad (23)$$

Irreversible destruction of the potential L_2PdH^+ active sites. The kinetic studies[21,22] show that, despite the steady-state copolymerisation character, the reaction rate decreases with time, due to the decrease in the concentration of catalytically active sites. Scheme 3 presents the most probable ways of destruction of the potentially active L_2PdH^+ sites.[7]

Scheme 3

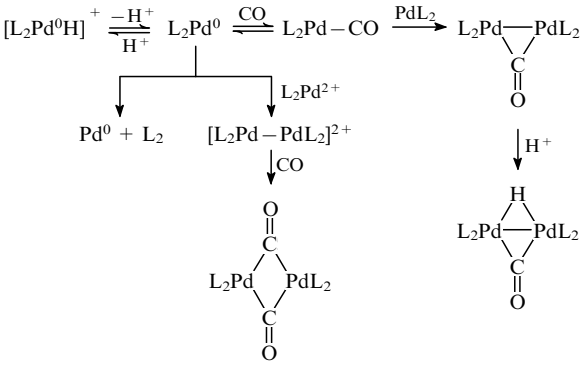

In terms of the above kinetic scheme, the inverse kinetic problem was solved and the rate constants for individual copolymerisation steps were estimated. This model describes quantitatively the dependence of the initial process rate on the comonomer pressure, the kinetic curves for the consumption of comonomers and the molecular-mass characteristics of the copolymers at different pressures of the $CO/CH_2{=}CH_2$ monomer mixture.[203]

* * *

It is worth noting that although the Pd complexes used in the alternating copolymerisation of carbon monoxide with various monomers seem to differ from the known Ziegler–Natta catalysts (including metallocene type catalysts) used in the synthesis of polyolefins, they still have much in common with these catalysts (Table 4). Both the palladium complexes and the Ziegler–Natta catalysts contain an electrophilic metal cation and a weakly coordinated anion. In both types of catalyst, the metal cations have a coordination number equal to four. However, the metal cations in the Ziegler–Natta catalyst are most often tetravalent and contain four anionic ligands [two strongly coordinated (for example, Cp ligands) and two weakly coordinated Z^- anions], whereas in Pd complexes, the Pd cation is divalent and contains two neutral (L) and two weakly coordinated (Z^-) anionic ligand. The active sites in both types of catalyst have a *cis*-structure during the growth of the polymer chain and monomer coordination. In the d^0-metallocene complex, the *cis*-structure involves the pseudotetragonal coordination environment of the metal, while in the square planar Pd(d^8) complex, the *cis*-structure is ensured by the presence of neutral ligands.

Table 4. Comparison of the catalysts used in the synthesis of polyolefins (**A**) and polyketones (**B**).[3]

Catalyst structure	**A**	**B**
Metal ion	Ti^{IV}, Zr^{IV}, Hf^{IV}	Pd^{II}
Ligands	2 Cp^-, 2 Z^-	2 L, 2 Z^-
Anions	non-coordinated	weakly coordinated or non-coordinated
Geometry	tetrahedral	square planar
Active site structure	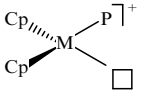	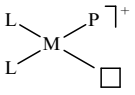

Note. Cp is cyclopentadienyl.

IV. Structure and properties of polyketones

1. Study of the structure and properties of polyketones

Copolymers of ethylene with carbon monoxide were described by NMR and IR spectroscopy. The IR spectra of low-molecular-weight aliphatic polyketones exhibit an intense characteristic absorption band in the region of 1715–1720 cm^{-1} due to the CO group.[204] The IR spectra of random ethylene–carbon monoxide copolymers containing ~1 mol.% of carbon monoxide[205] also contain an absorption band in this region. However, in the IR spectrum of the alternating C_2H_4/CO copolymer, this band is shifted to 1695 cm^{-1}. The vibration frequencies of some functional groups of the CO/C_2H_4 copolymer at room temperature are lower than those observed for low-molecular-weight model analogues.

A study of the IR spectra of solid samples of model ketoesters $MeO(COCH_2CH_2)_nH$ ($n = 1-5$) has shown that the absorption band due to CO shifts from 1720 to 1700 cm^{-1} with an increase in n (see Ref. 206). The IR absorption bands of the alternating copolymer of carbon monoxide with ethylene are listed in Table 5.[207]

Table 5. Absorption bands in the IR spectra of the $CO/CH_2=CH_2$ copolymer (25 °C, KBr pellet).[207]

ν /cm^{-1}	Type of vibration [a]
3250 – 3680	traces of H_2O
3392 w	$2\nu(C=O)$
2912 s	$\nu_{as}(CH_2)$
1692 vs	$\nu_{as}(C=O)$
1408 s	$\delta_s(CH_2)$
1334 s	δ_w, $\delta_{tw}(CH_2)$
1260 m	δ_w, $\delta_{tw}(CH_2)$
1057 s	$\nu(CH_2-CO-CH_2)$
810 m	skeletal vibrations
594 m	skeletal vibrations

[a] ν_{as} are asymmetric, δ_w are rocking; δ_{tw} are twisting, and δ_s are scissoring vibrations.

A study of the temperature variation of the IR spectra of the carbon monoxide – ethylene copolymer has shown that in the temperature range of 20 – 260 °C, the CO vibration frequency shifts from 1692 to 1709 cm^{-1} (Fig. 1 *a*), and the band for the CH_2COCH_2 groups shifts from 1055 to 1062 cm^{-1} (Fig. 1 *b*). The vibrational spectra of thin films (60 μm) of the ethylene – carbon monoxide copolymer deposited on gold-coated silicon substrates have been reported.[208, 209]

Investigations of 5 – 12-nm thick films from CO/C_2H_4-based polyketones deposited on the surface of gold by Raman (120 – 3300 cm^{-1}), IR (10 – 3300 cm^{-1}), reflection absorption IR (500 – 3300 cm^{-1}) and surface electromagnetic wave absorption (1000 – 1450 cm^{-1}) spectra have shown that 8 – 12 nm thick films are predominantly lamellar crystals with a complex conformation of chains, while in the 5-nm thick films, crystals with stretched chains predominate.[210]

By using ^1H and ^{13}C NMR spectroscopy, not only the composition of the random CO/C_2H_4 copolymer but also the distribution of the monomer units along the chain, the terminal groups, branchings and conformational transitions have been determined.[211]

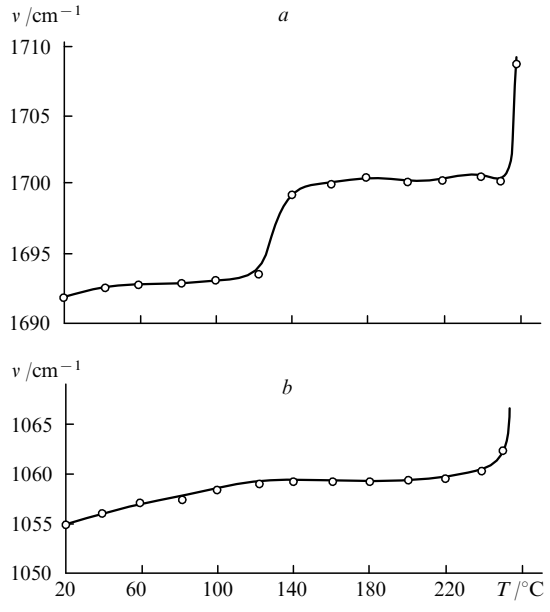

Figure 1. Effect of temperature on the shift of the absorption bands of the CO (*a*) and CH_2COCH_2 (*b*) groups in the IR spectra of the carbon monoxide – ethylene copolymer.

Belov *et al*.[212] reported the results of a ^1H and ^{13}C NMR study of the microsctructure of CO/C_2H_4 copolymers. The molecular-mass characteristics of the copolymers were determined by osmometry and gel permeation chromatography (GPC); in addition, the constants K and α of the Mark – Kuhn – Howink equation in the range of molecular mass from 10^3 to 10^6 were found.

The crystal structure of the ethylene – carbon monoxide copolymer with different ratios of the monomer units in the polymer chain has been studied.[213 – 215] In 1961, the crystal structure parameters of an alternating copolymer of ethylene and carbon monoxide (T_m = 175 – 185 °C), obtained by radiation copolymerisation were determined for the first time while studying the properties of oriented films.[213] More recently it has been shown [215] that this alternating copolymer has a β-structure, the *ab* projection of the orthorhombic cell of this structure being similar to that of polyethylene (PE). The alternating copolymer of ethylene and carbon monoxide obtained in a catalytic process has T_m = 250 – 260 °C and has the so-called α-structure. The conformations of the polymer backbone in these two structures are identical; however, the chain packings are different. This difference can be attributed to different orientations of the carbonyl groups relative to the chains arranged in the unit cell corners. The angles between the plane of the macromolecule and the *bc* plane are 26° and 40° in the α- and β-structures, respectively.

In the α-structure, the symmetry transformation that relates the corner and the central chains is $1/2-x$, $1/2+y$, z; while in the β-structure, this transformation is given by $1/2+x$, $1/2-y$, z. Thus, the difference between the two structures is described by rotation of the central chain through an angle of ~180° around the axis of this chain or by a translation of the central chain by half the unit cell dimension along the axis of the macromolecule. In the α-structure, the dipoles of all the carbonyl groups are oriented toward the same direction, whereas in the β-structure, the dipoles of the carbonyl groups of the corner and central chains point to different directions. As a consequence, the chain packing in the α-structure is less dense than that in the β-structure (the calculated densities are 1.383 and 1.297 g cm^{-3}, respectively). The cross section of the unit cell is perpendicular to the fiber axis and has an area of 35.2 Å^2, which is somewhat smaller than the area of the PE unit cell (36.2 Å^2). Table 6 presents data on the CO and CH_2 vibration frequencies for three forms [α, β and the amorphous form (or a melt)] of the co-polyketone based on $CH_2=CH_2$ and CO.

Table 6. Vibration frequencies of the main groups of the $CO/CH_2=CH_2$ copolymer in the IR spectrum.[208]

Type of vibration	ν /cm^{-1}		
	α-form	β-form	amorphous form or melt
$\nu_{as}(CH_2)$	2910 – 2912	2917	2911
$\nu(C=O)$	1692 – 1694	1697 – 1700	1708
$\delta_s(CH_2)$	1408	1415	1410
δ_w, $\delta_{tw}(CH_2)$	1334	1336	1358
$\nu(CH_2-CO)$	1056	1059	1079
Skeletal	811	804	835, 811, 794 [a]
Skeletal	591 – 594	603	616, 580, 558 [a]

[a] Vibration frequencies caused by the possible destructive processes in the polymer.

Table 7 contains the experimental densities of the alternating copolymer of ethylene and carbon monoxide (polyketone, POK), the unit cell parameters and T_m; the same characteristics for other polymers are given for comparison.

The α-form of POK has a greater density and a shorter $CH_2\cdots C=O$ distance (3 Å) than the β-form (3.41 Å). This is due

Table 7. Melting point, density and unit cell parameters for various polymers.[216]

Polymer	T_m /°C	d /g cm^{-3}	Sructure	a /Å	b /Å	c /Å
α-Form of POK	see [a]	1.38	ortho-rhombic	6.91	5.12	7.60 [b]
β-Form of POK	550	1.30		7.97	4.76	7.57 [b]
Polyalcohol prepared from POK	410	1.08	–	8.78	5.47	7.47 [b]
PVA [c]	540	1.35	monoclinic (β = 91.7°)	7.81	2.52	5.51
PE	414	1.00	ortho-rhombic	7.40	4.93	2.54 [b]

[a] The α-structure passes to the β-structure prior to the onset of melting of polyketone (at 110 – 130 °C). [b] Along the fibre axis. [c] PVA is poly(vinyl alcohol).

to the formation of intermolecular bonds between the CO and CH_2 groups. At room temperature, the α-form is more stable, whereas at a temperature of > 140 °C, only the β-form exists. The α→β temperature transition lies at about 113 °C (for the fibre) and 120 – 140 °C (for the film). The β→α transition takes place only upon drawing of POK samples. Thus, it can be concluded that the α- and β-forms of the copolymer are characterised by different strength of intermolecular cohesion caused by the presence of hydrogen bonds and dipole – dipole interactions.

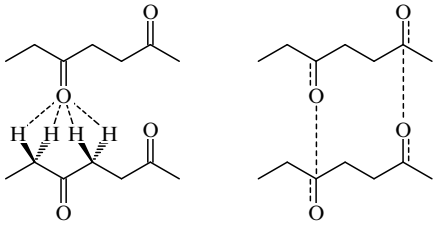

A 3D computer model of polyketone was constructed using the molecular dynamics method. The calculated values for density and crystal lattice parameters coincided almost entirely with experimental data over a broad temperature range. Using the 3D model, it was shown that the crystal structure of the α- and β-phases is largely determined by the Coulomb interaction between the polar carbonyl groups.[217]

The ethylene – carbon monoxide – α-olefin terpolymers (α-olefin is propylene,[218, 219] but-1-ene or hex-1-ene [218]) were studied by

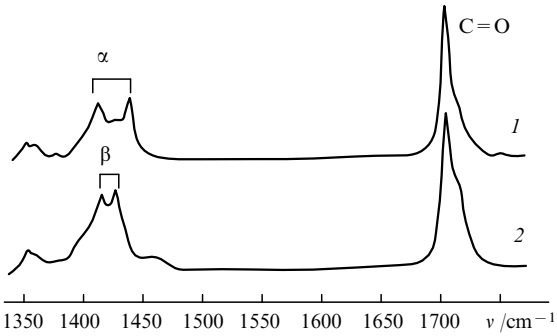

Figure 2. Raman spectra of the alternating ethylene – carbon monoxide – propylene terpolymers containing macromolecules of the α- (curve *1*) and β-form (curve *2*).

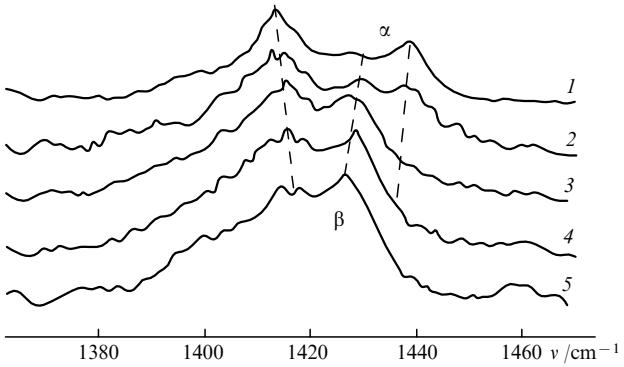

Figure 3. Raman spectra of the alternating ethylene – carbon monoxide – propylene terpolymers with different contents of propylene. [C_3H_6] (mol %): 0 (*1*), 1.2 (*2*), 2.9 (*3*), 4.6 (*4*), 7.2 (*5*).

wide-angle and small-angle X-ray diffraction, DSC and Raman spectroscopy. Copolymers containing hex-1-ene have a higher crystallinity than copolymers containing propylene and but-1-ene. The relative content of the α-form macromolecules in the terpolymers decreases in the sequence hex-1-ene > but-1-ene > propylene.[218] Figures 2 and 3 show the Raman spectra of the ethylene – carbon monoxide – propylene terpolymers which contain both α- and β-forms. It can be seen from Fig. 3 that the content of α-form macromolecules in the copolymer decreases with an increase in the propylene content.

The crystal structure of the CO/C_2H_4 copolymer and the $C_2H_4/CO/C_3H_6$ terpolymer (1.2 mol.%, 2.9 mol.%, 4.6 mol.% and 7.2 mol.% of propylene) was studied by DSC, Raman spectroscopy and wide-angle X-ray diffraction and the contents of α- and β-forms were determined.[220] The influence of the stereo- and regio-regularity of the propylene – carbon monoxide copolymer on its crystal structure and macroscopic properties was studied.[§]

Using X-ray examination and optical and electronic microscopy, the structure and morphology of the ethylene – carbon monoxide copolymer crystals prepared by crystallisation of the polymer from a mixture of hexafluoroisopropyl alcohol and hydroquinone have been studied.[221]

The crystal structure of iso- and syndiotactic copolymers of CO with styrene and some its derivatives has been studied.[222 – 224] The key crystallographic characteristics of these copolymers are listed in Table 8.

Table 8. Crystallographic parameters of copolymers of carbon monoxide with styrene or its derivatives.

Parameter	Copolymer $CO/CH_2=CHPh$		Copolymer $CO/CH_2=CHC_6H_4R$ (see [222])		
	isotactic [224]	syndiotactic [222]	R = *p*-F	R = *m*-Me	R = *p*-Me
a /Å	8.367	15.20	15.59	16.14	35.54
b /Å	7.574	6.166	6.168	6.816	6.262
c /Å	5.47	7.590	7.551	7.580	7.536
β /deg	100.0	102.5	98.8	100.3	96.0
d_{calc} /g cm^{-3}	1.347	1.262	1.388	–	–

The syndiotactic carbon monoxide copolymer with styrene (or *tert*-butylstyrene) can be converted into the atactic copolymer by heating in an organic base (for example, in a tertiary amine,

§ D V Anokhin, V M Neverov, S N Chvalun, N P Bessonova, Yu K Godovsky, F Hollmann, U Merer, B Rieger *Vysokomol. Soedin., Ser. A* **46** 69 (2004); [*Polym. Sci. (Engl. Transl.)*].

N-alkylamide or alkali metal phenoxide) at 40–200 °C [225] or by treatment of the copolymer in the NaOH–MeOH–THF medium.[226]

The IR spectra of carbon monoxide–DCPD copolymers exhibit high-intensity absorption bands in the regions of 1790 and 1721 cm^{-1} (for dimers **A**), indicating the presence of an enol lactone structure, and 1775, 1710–1735 cm^{-1} (for trimers **B**), indicating the presence of γ-lactone and ester vinyl groups.[111] The ^{13}C NMR spectra of these copolymers show signals at about 178–179 ppm (the carbonyl-group carbon atom in the lactone structure **A**), 147–149 (the carbon atoms of the ester vinyl group in structure **B**), 130–136 ppm (the C_{sp}^2 atoms of the cyclopentene ring) and 116–120 ppm (the carbon atom of the spiroketal structure **B**). The formation of terminal lactone groups can be regarded as intramolecular chain termination due to the reaction with methanol (methanolysis), usually resulting in the formation of terminal ester groups.

2. Thermal and thermodynamic properties

In a study of melting of ethylene–carbon monoxide copolymers, it was suggested that the increase in T_m for random carbon monoxide–ethylene copolymers with respect to PE is due to restriction of the rotation caused by the presence of carbonyl groups.[213] Determination of the heats of melting for random copolymers of ethylene and carbon monoxide has shown that the alternating copolymer has $T_m = 244$ °C and a low melting entropy.[227] Study of the melting of low- and high-molecular-weight alternating carbon monoxide–ethylene copolymers showed that their maximum melting points are 278 °C, the heats of melting are 4 and 6.2 kJ mol^{-1}, and the melting entropies are 7.3 and 11.3 J mol^{-1} K^{-1}, respectively.[214] In the case of $MeCH=CH_2/CO$ or $EtCH=CH_2/CO$ copolymers, the presence of side substituents in the position neighbouring to the carbonyl group promotes the formation of macromolecules with less regular structures. These copolymers have lower T_m values and lower solubilities in common solvents. The inclusion of propylene in the polymer chain on passing to the terpolymerisation of ethylene, propylene and carbon monoxide results in a noticeable decrease in T_m values of the terpolymer formed, which has a beneficial effect on the processing conditions. Figure 4 presents the dependences of the heat of melting (Fig. 4 *a*), the degree of crystallinity (Fig. 4 *b*) and T_m (Fig. 4 *c*) for the ethylene–carbon monoxide–α-olefin terpolymers (the α-olefin is propylene, but-1-ene, hex-1-ene) on the α-olefin concentration.[228]

As noted above, copolymerisation of propylene and α-olefins with carbon monoxide may yield macromolecules with the polyspiroketal structure. In the case of the propylene–carbon monoxide copolymer, the polyspiroketal structure is transformed into the usual ketone structure when the copolymer has been dissolved in hexafluoroiopropyl alcohol or heated to 70 °C (the process enthalpy is −11.8 to −10.5 kJ mol^{-1}). This value is close to the calculated enthalpy for the polymerisation of acetone (−10.0 kJ mol^{-1}).[229] The polyspiroketal structures of the but-1-ene–carbon monoxide and hept-1-ene–carbon monoxide copolymers are more stable than the polyspiroketal structure of the propylene–CO copolymer. The polyspiroketal structure of the hept-1-ene–carbon monoxide copolymer does not pass to the ketone structure even upon dissolution in chloroform. It is noteworthy that copolymers containing the spiroketal structure differ in physicochemical properties from copolymers with the ketone structure. For example, copolymers of carbon monoxide with but-1-ene and hept-1-ene having the ketone structure are completely soluble in acetone, while the same copolymers containing both spiroketal and ketone macromolecules are insoluble in acetone.[83]

The crystallisation kinetics of two samples of the ethylene–propylene–carbon monoxide terpolymer containing 3 mol.% and 6 mol.% of propylene has been studied.[230] In the epitaxial crystallisation of the ethylene–carbon monoxide copolymer carried out by the hypoeutectic growth technique on hydroquinone crystals, the axes of the polymeric chains are arranged parallel to the hydroquinone surface.[221] Tunnelling electron microscopy (TEM) has been used to study epitaxial crystallisation (at temperatures of 150–190 °C) of the carbon monoxide–ethylene copolymer on NaCl and KI crystals from a nitrobenzene solution. It was shown that the shape and orientation of macromolecular chains on the substrate surface depend on its nature.[231–233] The copolymer crystals grown under isothermal conditions (at 139 °C for 24 h) from a 0.01 mass % solution in nitrobenzene contained only macromolecules of the α-form (they were characterised by TEM and small-angle X-ray diffraction), whereas the copolymer crystals grown on the surface of alkali metals contained macromolecules of both (α and β) forms.[234]

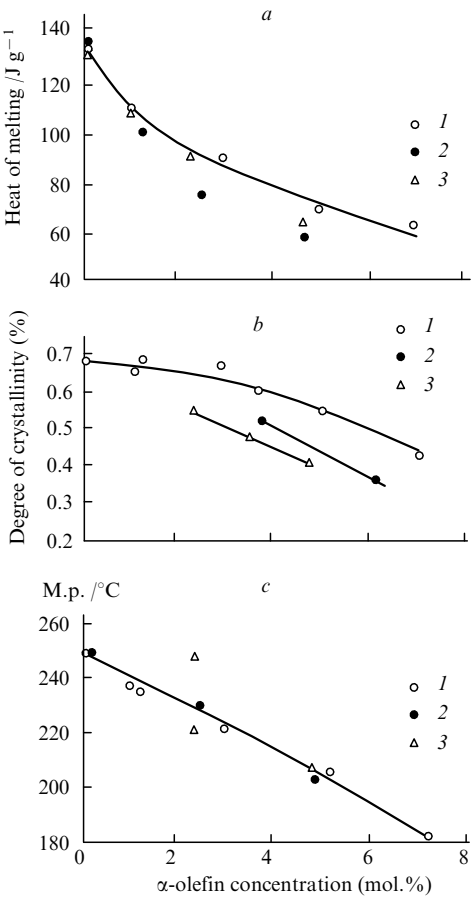

Figure 4. Effect of the α-olefin concentration on the heat of melting (*a*), degree of crystallinity (*b*) and T_m (*c*) of ethylene–CO–propylene (*1*), ethylene–CO–but-1-ene (*2*), ethylene–CO–hex-1-ene (*3*) terpolymers.[228]

Detailed study of the characteristic features of the crystallisation and melting of three samples of the ethylene–carbon monoxide–propylene terpolymer (I–III) by DSC, wide-angle and small-angle X-ray and optical spectroscopies has been reported.[235]

Sample	$[C_3H_6]$ /mol.%	M_w	$M_w : M_n$
I	0	4×10^4	3.09
II	6	8×10^4	2.99
III	6	4×10^4	2.32

It was noted that T_m decreases by about 1 °C, the heats of melting decrease by 2 J g^{-1} and the sample crystallinity also decreases after every heating to T_m, which is due to cross-linking reactions. The heats of melting for the crystalline (100%) C_2H_4/CO copolymer (β-form) and $C_2H_4/CO/C_3H_6$ terpolymer (β-form) were determined to be 239±11 and 226±16 J g^{-1}, respectively. The thickness of the lamellae increases linearly with an increase in the

crystallisation temperature. The isothermal crystallisation of the copolymer proceeds faster than that for the terpolymer. On the basis of comprehensive analysis, it was concluded that the equilibrium T_m for the high-molecular mass copolymer and terpolymer and that for the low-molecular-mass copolymer are 278, 252 and 249.5 °C, respectively.

The high T_m values of ethylene–carbon monoxide copolymers bring about difficulties in the material processing into articles. This is due to the fact that at elevated temperatures, in addition to thermal destruction, condensation may take place, giving rise to furan structures in the polymer chain according to the following scheme:

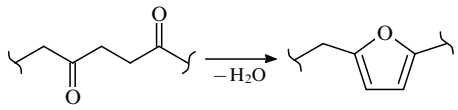

The thermal destruction of the carbon monoxide–ethylene copolymer at 500 °C to give linear polyketones, diketones and low-molecular-mass products has been studied.[236] A study of the thermal destruction of this polymer *in vacuo* at temperatures above T_m by flash pyrolysis–gas chromatography–mass spectrometry (FP-GCMS) has identified the formation of vinyl ketones with different molecular masses.[237]

The destruction of samples of the carbon monoxide–ethylene copolymers containing 70 ($[\eta] = 0.41$ dl g^{-1}) and 15 ppm Pd ($[\eta] = 2.5$ dl g^{-1}) has been studied by DTG, mass spectrometry, and UV and IR spectroscopy. The copolymer starts to lose mass at approximately 290 °C; the maximum mass loss is observed at 370–410 °C. The main decomposition products at temperatures of up to 215 °C are polyfuran structures and water. The residue obtained after the pyrolysis in an inert atmosphere and *in vacuo* amounts to 30 mass % and 10 mass %, respectively. After the pyrolysis, the polymer completely loses its solubility in hexafluoroisopropyl alcohol and crystallinity estimated based on the absorption bands in the region of 1082–1056 cm^{-1}. Cross-linking of polymer chains starts at 230 °C and is accompanied by the formation of ethylene, carbon monoxide and low-molecular-mass ketones. The rupture of polymer chains at this relatively low temperature affords macroradicals, which can be destroyed both upon intermolecular chain transfer and in bimolecular processes.

The pyrolysis products obtained at 500 °C were found to include CO, CO_2, water, linear low-molecular-mass polyketones, cyclopentanone derivatives, aromatic compounds (phenols, aromatic ketones and hydrocarbons having bi- and polycyclic structures). Pyrolysis of preliminarily 'aged' copolymer gives large amounts of water and CO_2 as well as furan, phenolic and aromatic derivatives, and linear polyketones. The thermal decomposition of the copolymer can be described as aldol condensation and/or dehydration to give furan structures at temperatures below 260 °C. On the basis of the DSC data, it was suggested that destruction starts in the amorphous regions of the copolymer.[238, 239]

The pyrolysis at 550 °C and thermal decomposition of the ethylene–carbon monoxide copolymer at 350 and 400 °C have been studied.[239] The volatile products of thermal decomposition were studied by GC and mass spectrometry, while the structural changes in the copolymer were examined by IR, UV and visible spectroscopy. It was found that all the volatile products are formed from **A**–**C** type radicals

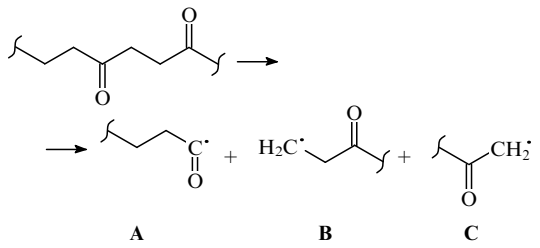

Depending on the temperature and duration of maintenance, the copolymer colour changes from while to pale yellow and dark brown; simultaneously, the polymer loses, either completely or partially, the solubility in hexafluoroisopropyl alcohol (due to cross-linking of polymer chains). Analysis of the IR spectra of thermally aged copolymers of carbon monoxide with ethylene shows that ageing is accompanied by the formation of new functional groups (Scheme 4).

Scheme 4

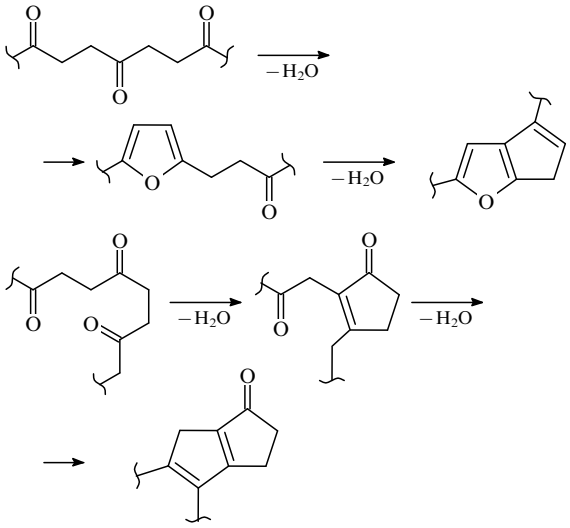

In addition, due to cross-linking of the polymer chains, copolymer loses crystallinity and becomes amorphous. The cross-linking of copolymer macromolecules can proceed according to Scheme 5.

Scheme 5

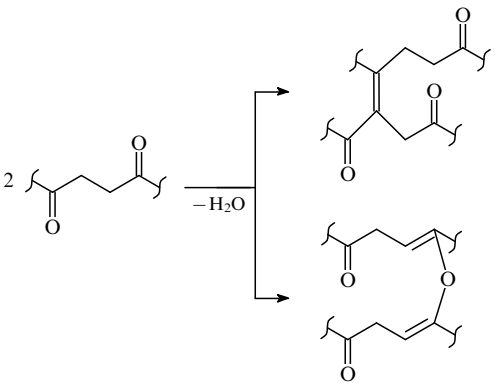

The influence of the remains of the Pd catalyst on the mass loss from the ethylene–carbon monoxide–propylene terpolymer in an inert atmosphere and in the presence of oxygen has been studied by TGA.[240, 241] On the basis of the DTG data, it was shown that under inert atmosphere, the maximum loss of mass (10%–30%) occurs at a Pd content of [Pd] ≈ 300 ppm (Fig. 5 *a*), while for the thermal destruction in air it barely depends on the Pd content up to 600–800 ppm and starts to decrease only at Pd > 800 ppm (Fig. 5 *b*). Thus, it was suggested that traces of palladium do not influence the temperature of the onset of thermal decomposition in the presence of oxygen, which is apparently related to the formation of stable palladium complexes with dioxygen, which subsequently react with the copolymer according to the following scheme:

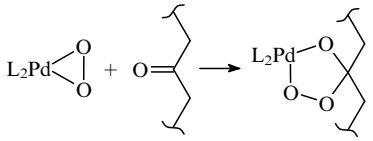

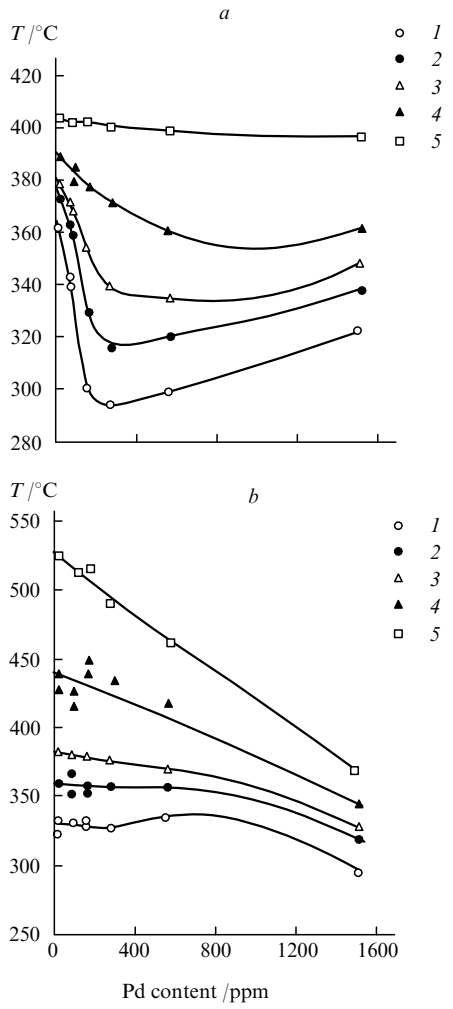

Figure 5. Effect of the palladium content in the ethylene–carbon monoxide–propylene terpolymer on the loss of its mass in an inert atmosphere (*a*) and in air (*b*).
Mass loss (%): 10 (*1*), 20 (*2*), 30 (*3*), 50 (*4*), 75 (*5*).

It was found that the oxidation state of palladium [Pd(II) or Pd(0)] has an influence on the destruction of copolymer. In the former case, destruction starts at a temperature lower by 60 °C than in the latter case.

Under an inert atmosphere, thermal decomposition is retarded with an increase in the palladium content (> 300 ppm). The higher the palladium content ¶ in the copolymer, the higher the degree of cross-linking.[240]

When the palladium content is less than 6 ppm, the ethylene–carbon monoxide–propylene terpolymer can be moulded to give transparent specimens which do not change their colour.[242]

A study of the uninhibited oxidation of the $CH_2=CH_2/CO$ copolymer (at 170–200 °C) and the $MeCH=CH_2/CO$ copolymer (at 80–180 °C) has shown that the patterns of oxidation of these copolymers are complex and differ considerably from each other.[243, 244] The kinetics of oxygen absorption during oxidation of the former copolymer shows two clear-cut steady-state sections with activation energies of 203 and 133 kJ mol^{-1}. For the second copolymer, the oxidation rate decreases with an increase in the temperature (> 140 °C) (negative temperature coefficient), the apparent activation energy being −59 kJ mol^{-1}. The mechanism of this phenomenon is related to switching from the standard oxidation mechanism [reactions (24), (25)] to a mechanism in which a significant role is played by decomposition of the $RO_2^{\bullet}$ radical [reaction (26)].

$$R^{\bullet} + O_2 \longrightarrow RO_2^{\bullet}, \quad (24)$$

$$RO_2^{\bullet} + RH \longrightarrow ROOH + R^{\bullet}, \quad (25)$$

$$RO_2^{\bullet} \longrightarrow R_1^{\bullet} + \text{products}. \quad (26)$$

In the search for compounds that could stabilise polyketones during processing to manufacture articles, the best results were obtained for aromatic carbodiimides, mono- and polyepoxy compounds, β-diketones and cellulose ethers in combination with hydroxyapatite. The key criteria used to estimate the efficiency of stabilisers in the processing of polyketones included the degree of crystallinity (DC), the shift of the crystallisation temperature in the second heating–cooling cycle (ΔT), the heat of crystallisation (C_2) in the second cycle and the ratio of the peak height in the second crystallisation cycle to the peak width at the half-height ($C_{h/w}$) (Table 9).

Table 9. Efficiency of various stabilisers (according to DSC).[245]

Stabiliser [a]	Degree of crystallinity	ΔT /°C	C_2 /J g^{-1}	$C_{h/w}$
Stabaxol P (1%)	0.73	12.1	−77	3.2
Stabaxol P (2%) + CaHA (2%)	0.88	5.1	−95	5.7
Stabaxol P (1%) + CaHA (1%) + R50 (1%)	0.85	2.7	−98	5.6
R50 (2%) + CaHA (2%)	0.81	1.3	−92	7.7
R83 (2%) + CaHA (2%)	0.77	−1.2	−81	3.0
ERL 4221 (2%)	0.70	10.7	−72	1.8
ERL 4221 (1%) + CaHA (1%) + R50 (1%)	0.77	3.3	−86	6.7
ERL 4221 (1%) + CaHA (1%) + R83 (1%)	0.75	5.7	−84	4.1
ERL 4221 (1%) + Naugard 445 (1%)	0.71	14.0	−68	1.0
DEN 444 (2%)	0.71	13.2	−79	2.2
Limonene monoxide (2%)	0.68	14.0	−74	1.0
Ethylcellulose (1%)	0.62	19.0	−68	2.1
Hydroxypropylcellulose (1%)	0.62	21.0	−65	1.8
Irganox 1425 (2%)	0.57	25.2	−62.8	–
Naugard 445 (2%)	0.48	41.2	−47.9	–
Stabaxol P (2%)	0.38	53.0	−37.3	–

[a] **Notation**: Stabaxol P is 2,2′,6,6′-tetraisopropyldiphenylcarbodiimide, CaHA is hydroxyapatite, R50, R83 are β-diketones, ERL 4221, DEN 444 are epoxides, Naugard 445 is alkylated diphenylamine, Irganox 1425 is calcium bis[monoethyl(3,5-di-*tert*-butyl-4-hydroxybenzyl)]phosphonate.

The photodestruction of the $CH_2=CH_2/CO$ and $MeCH=CH_2/CO$ copolymers has been studied under anaerobic conditions. The rate of photooxidation at room temperature does not depend on the palladium content in the copolymer. The photostability of the $CO/MeCH=CH_2$ copolymer was found to be lower than that of the $CO/CH_2=CH_2$ copolymer due to oxidation reactions proceeding by the Norrish-I and Norrish-II mechanisms.[246] ($CO/CH_2=CH_2$ is oxidised only according to the Norrish-I mechanism.[247])

The photolysis and γ-radiolysis of the $CO/CH_2=CH_2$ copolymers and the subsequent thermal and chemical transformations of samples following an increase in the irradiation temperature (from

¶ Traces of transition metal ions are often used as catalysts for the destruction of polymeric materials both in the presence and in the absence of oxygen.[241]

−196 to 27 °C) have been studied.[248, 249] The main reaction in the photolysis is the rupture of the polymer chain to give alkyl and acyl radicals with the quantum yields $\varphi_R = 2 \times 10^{-4}$ at −196 °C and $\varphi_R = 2 \times 10^{-3}$ at 27 °C. The major products formed in the copolymer photolysis at 27 °C include ethane, ethylene and carbon monoxide. Radiolysis of the copolymer at −196 °C affords the same alkyl and acyl radicals as the photolysis. At a dose of $\leqslant 50$ kGy, these radicals account for ~50% of all paramagnetic centres.

The biodegradation of the $CO/CH_2=CH_2$ copolymer has been studied and the results have been compared with the data on biodegradation of PE and cellophane.[250] In terms of the susceptibility to biodestruction, the copolymer in question occupies an intermediate position between PE and cellophane.

The systematic research into the thermodynamic characteristics of alternating copolymers has been started. Using adiabatic vacuum and dynamic calorimetry, the temperature dependence of the heat capacity was determined and the temperatures and enthalpies of the physical transformations of carbon monoxide copolymers with ethylene,[251] propylene,[252] styrene,[253] *endo*-dicyclopentadiene[254] and norbornadiene† were found.

Of high practical value is the study of blends of polyketones with various polymers (as compatibilisers). It was found that the propylene–carbon monoxide copolymer forms homogeneous transparent blends with the styrene–acrylonitrile (SAN) copolymer containing 37 mass % of acrylonitrile.[86] As the content of SAN increases from 20 mass % to 90 mass %, the glass transition temperature increases from ~30 to 100 °C, which is in good agreement with the dependence of T_g on the composition of the polymer blend described by the Fox equation. However, blending of the propylene–carbon monoxide copolymer with polystyrene or the styrene–maleic anhydride copolymer gives brittle heterogeneous blends. The physicomechanical properties of the initial and glass fibre reinforced (30 mass %) ethylene–carbon monoxide–propylene terpolymer (with a propylene content of 5 mass %–6 mass %) obtained by injection moulding with controlled drawing have been compared.[255]

A TGA study of the thermal decomposition of syndiotactic carbon monoxide–styrene copolymer has shown that the process occurs in three stages. The activation energy of the fastest second stage of thermal decomposition, equal to 31 kcal mol^{-1}, is lower than the activation energy of the thermal decomposition of polystyrene (PS) (55 kcal mol^{-1}), which is indicative of a lower stability of $CO/CH_2=CHPh$. Photolysis of the copolymer entails a decrease in its molecular mass and loss of the sample mass. The macroradicals formed in the photolysis of the copolymer initiate polymerisation of methyl methacrylate (MMA) to give the CO–styrene block copolymer and poly(methyl methacrylate).[177] Photolysis of samples of the carbon monoxide–4-(*tert*-butyl)styrene copolymer (M_n = 44 000–53 000, $M_w : M_n$ = 1.2–1.4), in particular, a sample containing ^{13}CO, has been studied by time-resolved EPR spectroscopy at two frequencies, in the X (9.5 GHz) and Q (35.1 GHz) ranges.[97]

3. Mechanical and other properties of copolyketones

At present, the properties of terpolymers ($CH_2=CH_2/CO/MeCH=CH_2$) have been studied most comprehensively; the properties of alternating copolymers ($CH_2=CH_2/CO$) traded under the name Carilon (Shell Chemical Co) or Ketoneks (British Polymer Co) have been less studied.

Films of the $CH_2=CH_2/CO/MeCH=CH_2$ terpolymer containing 0 mol.%–14.6 mol.% of propylene before and after 3–6-fold drawing have been studied by X-ray diffraction and DSC. Drawing was found to promote the formation of units of the copolymer α-form; the lower the drawing velocity, the greater the number of the α-form units.[256] As the content of propylene in the copolymer increases from 0 to 14.6%, the temperature of the α → β transition decreases from 91 to 60 °C and simultaneously, the melting peak is broadened.

The effect of the temperature (0–80 °C) on the mechanical strength (tensile strength and the fracture pattern in uniaxial and biaxial tests) of solid and hollow cylindrical specimens of the $CH_2=CH_2/CO/MeCH=CH_2$ terpolymer containing 6 mol.% of propylene was studied. The data obtained in this study were compared with the results of calculations for a model anisotropic material.[257, 258]

Karttunen and Lesser[259] have studied the effect of extrusion conditions (shear rate, cooling rate) during moulding of hollow cylindrical specimens on the mechanical properties of the ethylene–carbon monoxide–propylene terpolymer containing 6 mol.% of propylene (T_m = 225 °C, T_g = 12 °C, molecular mass 1×10^5, degree of crystallinity 33%–35%, density 1.24 g cm^{-3}). The methods used included DSC, dynamic mechanical analysis (DMTA), IR spectroscopy, wide-angle X-ray diffraction and electron microscopy. The crystal structure and the morphology of this copolymer were studied by X-ray diffraction, DSC and TEM. It was found that T_m of the copolymer linearly decreases with an increase in the propylene content from 6 to 10 mol.%. Further increase in the content of propylene in the copolymer (10%–16%) barely influences its T_m.[260] The obtained results are in line with the data of other publications.[261, 262]

High-strength (1.1 GPa) and high-modulus (13 GPa) fibres of four specimens (I–IV) of the $CH_2=CH_2/CO/MeCH=CH_2$ terpolymer were produced by extrusion at temperatures of 250, 255 and 266 °C.

Specimen	$[C_3H_6]$ /mol.%	M_w	$M_w : M_n$
I	6.0	4×10^4	2.84
II	6.0	6×10^4	3.00
III	3.5	6×10^4	3.10
IV	0	4×10^4	3.10

The structure and morphology of the resulting fibres were studied by DSC, wide- and small-angle X-ray diffraction and scanning electron microscopy. It was found that in the $CH_2=CH_2/CO/MeCH=CH_2$ terpolymers, the crystalline phase is always represented by the β-form. In the $CH_2=CH_2/CO$ copolymer, depending on the cooling rate, α-form is also present in addition to the major β-form.[263] The dependences of the physicomechanical properties, the degree of crystallinity and T_m of the ethylene–CO–propylene terpolymers on the amount of propylene in specimens I–IV are shown in Figs 6, 7.

The morphological features and the mechanisms of crack formation in specimens of the $CH_2=CH_2/CO/MeCH=CH_2$ terpolymer (Carilon DP P1000) with a degree of crystallinity of

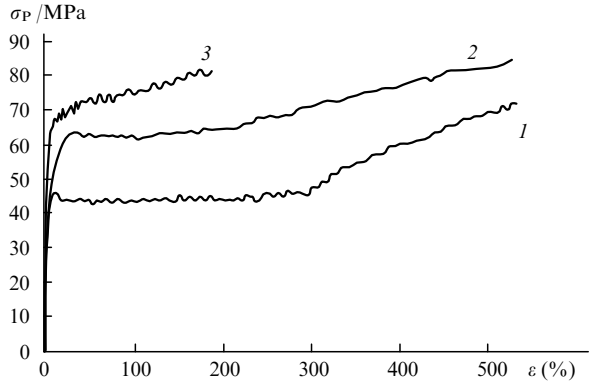

Figure 6. Load–elongation curve for specimens I (curve *1*), III (curve *2*) and IV (curve *3*).

† N N Smirnova, T A Bykova, T G Kulagina, L V Nikishchenkova, G P Belov, E V Novikova *Izv. Akad. Nauk, Ser. Khim.* (2004) (in the press) [*Russ. Chem. Bull., Int. Ed. (Engl. Transl.)*].

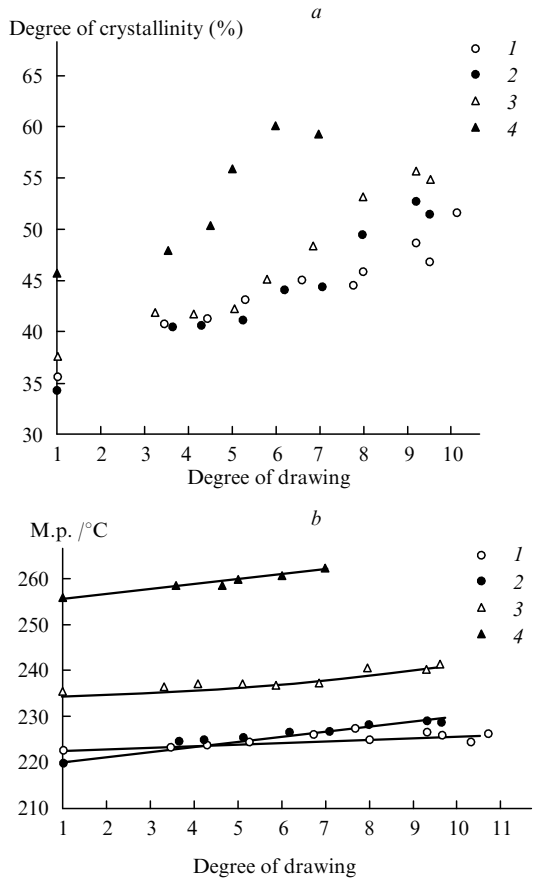

Figure 7. Degree of crystallinity (*a*) and T_m (*b*) of samples I–IV (points *1–4*, respectively) *vs.* degree of drawing.

38% obtained by injection moulding and mould pressing were studied by DSC, DMTA and optical microscopy.[264]

Studies of such copolymers carried out by thermoelastometry in the temperature range of 13–54 °C at pressures of 30–100 MPa have shown[265] that thermodynamic parameters of the terpolymers (specific volumes, thermal expansion and compression coefficients) are deteriorated with an increase in the content of the $(-C_2H_4CO-)_n$ blocks, whereas the thermal characteristics (heat and temperature conductivity, specific heat capacity) virtually do not depend on the polymer composition. The bell-shaped dependences of the Newton viscosity[266] and diamagnetic susceptibility[267] on the content of the $(-C_2H_4CO-)_n$ blocks in the ethylene–carbon monoxide–propylene terpolymer was described within the bounds of the classical copolymerisation theory taking the strictly alternating $CH_2=CH_2/CO$ and $MeCH=CH_2/CO$ copolymers as 'virtual homopolymers' and the strictly alternating $CH_2=CH_2/CO/MeCH=CH_2$ terpolymer, as a 'virtual copolymer.'

According to X-ray diffraction data,[266–268] the ethylene–CO–propylene terpolymers are amorphous to X-rays at room temperature; however, in the temperature range above the glass transition temperature ($T_g \approx 17$ °C), the heat capacity curves contain sections corresponding to slight endothermic effects. In the same temperature range, the intensity of the dielectric relaxation does not decrease with temperature but, conversely, increases. Moreover, hysteresis effects were found for the viscoelastic characteristics of the terpolymers in the melt on heating the specimens to 227 °C with subsequent cooling to 127 °C.[268] This set of data indicates that long-term storage of the terpolymers at room temperature promotes the formation of a network of $CH_2=CH_2/CO$ nanocrystallines with runs through the continuous phase of the noncrystalline $MeCH=CH_2/CO$ blocks. The low values of the shape parameter from the Kolmogorov–Avrami equation in combination with exceptionally long half-periods of nanocrystallisation[269] are consistent with the views stating that nanocrystallites are formed through lateral aggregation of the $CH_2=CH_2/CO$ blocks, which is retarded by the continuous $MeCH=CH_2/CO$ phase.

It was found that the activation energy of the relaxation processes at low temperatures equals 14 kcal mol^{-1}, while at elevated temperatures, this value is 38–61 kcal mol^{-1}. Young's modulus for the $CH_2=CH_2/CO/MeCH=CH_2$ terpolymer containing ~50% of the $-C_2H_4CO-$ units is three orders of magnitude lower than that of the $CH_2=CH_2/CO$ copolymer (1.6 GPa). As the content of the $-C_2H_4CO-$ units in the terpolymer increases, its melting heat increases, while T_g decreases from 22 °C (for the $MeCH=CH_2/CO$ copolymer) to 3 °C (for the terpolymer containing 80 mass % of the $-C_2H_4CO-$ units).[269]

Hollmann *et al.*[270] studied the dielectric (in the frequency range of 10^{-1}–10^6 Hz) and mechanical properties of terpolymers (with a content of the $-C_2H_4CO-$ units ranging from 0 mass % to 80 mass % and a molecular mass of 12×10^4–22.8×10^4) and determined their glass transition and melting temperatures. The structural changes taking place in the $CH_2=CH_2/CO/MeCH=CH_2$ specimens containing 47% and 69% of $-C_2H_4CO-$ units upon deformation were investigated by X-ray diffraction and DSC. It was shown that great reversible deformations are mainly due to the amorphous component of the terpolymer.[271]

The effect of the polyketone molecular mass and the conditions of surface formation (for example, during press moulding) on the energy characteristics of the surface has been studied.‡

Good adhesion of the alternating ethylene–CO copolymer to organic and inorganic materials allows the use of this copolymer in the production of composite materials without special adhesives. The properties of unfilled and glass fibre reinforced $CH_2=CH_2/CO$ copolymer are presented in Table 10. The influence of various types of surface treatment of glass fibre on the mechanical properties of the composites has been studied.§

Table 10. Properties of alternating $CO/CH_2=CH_2$ copolymer.[11]

Property	Unfilled copolymer	Glass fibre filled copolymer (30 mass %)
Density /g cm^{-3}	1.24	1.45
Melt index (240 °C, 2.16 kg) /g (10 min)$^{-1}$	6	5
Tensile strength /MPa	55	120
Elongation at rupture (%)	350	3
Vika softening temperature (5 kg) /°C	205	215
Shrinkage (%)	2	0.3–0.7

Owing to the specific structure of the polymer chain and the crystallinity (30%–50%), polyketones are not hydrolysed. Unlike other polymers such as PA, PC and polyesters, they are stable against aqueous solutions of weak acids and inorganic salts (Table 11).[272]

‡ S A Bogdanova, O R Shashkina, G P Belov, O N Golodkov, V P Barabanov, I A Starostina *Vysokomol. Soedin.* (2004) (in the press) [*Polym. Sci. (Engl. Transl.)*].

§ Yu N Smirnov, G P Belov, V V Barelko, O N Golodkov, E V Novikova, A D Pomogailo, K E Danilov *Plast. Massy*, (2004) (in the press).

Table 11. Effect of different media on the tensile strength of the alternating $CO/CH_2=CH_2$ copolymer [for comparison, data for polyamide (PA) are given].[272]

Medium	σ_p /MPa	
	polyketone	PA
Control run at 50% moisture content	57.7	57.2
Water	59.2	33.1
Sea water	60.0	33.1
Aqueous solutions		
MeCOOH (5 mass %)	57.9	33.8
$CaCl_2$ (5 mass %)	60.0	33.8
Antifreeze	59.2	35.8
H_2SO_4 (30 mass %)	59.3	dissolves
$ZnCl_2$ (50 mass %)	46.2	dissolves
HCl (10 mass %)	64.7	dissolves
NaOH (1 mass %)	58.6	28.2
NaOH (10 mass %)	60.0	28.9

Long-term keeping of polyketone in alcohols, ethyl acetate, benzene and methyl ethyl ketone has no effect on its properties, while keeping in chlorine-containing (trichloroethylene, dichloromethane, chloroform) and polar aprotic solvents (DMSO, *N*-methylpyrrolidone) results in swelling of the polymer (the gain in the mass is 8% to 35%) and a decrease in its strength (by up to 30%). The high hydrolytic and chemical stability of polyketone is combined with good barrier properties against hydrocarbons, oxygen and carbon dioxide (Table 12). Data on the permeability, diffusion coefficients and solubility of three gases (helium, oxygen and carbon dioxide) in the ethylene–propylene–carbon monoxide terpolymer (0.93 : 0.07 : 1) have been reported.[273]

The high crystallisation rate of polyketone ensures a short duration of the moulding cycle for articles based on this polymer (see Table 12) and eliminates the necessity for further conditioning, which substantially reduces the production costs.

V. Modification of polyketones

The chemical modification of polyketones at the carbonyl group allows one to create new classes of chiral and achiral polymers, which can serve themselves as the starting materials for the development of new low- and high-molecular-mass compounds *via* reactions in polymer chains.

The achiral $CH_2=CH_2/CO$ copolymer and atactic $MeCH=CH_2/CO$ copolymer can be converted into polyfurans,[275] polythiophenes,[275] polyoximes,[276–278] polycyanohydrins[1,276] and polyalcohols.[1,216,275–283] The reduction of isotactic $MeCH=CH_2/CO$ copolymer with lithium aluminium hydride gave polyalcohol whose stereochemistry has not been determined at that moment.[83] Later,[161] using tetrabutylammonium tetrahydroborate, the isotactic $MeCH=CH_2/CO$ copolymer was quantitatively reduced into the polyalcohol and the enantiomers present were identified by ^{13}C NMR spectroscopy ($S:R = 70:30$).

Other derivatives obtained include polyacetylenes,[284,285] polyamines,[1,286,287] poly(α-hydroxyphosphonic acids),[1,288] polythiols,[1,289] polyamides,[1,290] polyoximes,[1,290] polyketoesters,[291] polyketoximes,[278] dioxolane-containing derivatives,[292] nitrogen- and sulfur-containing heterocyclic derivatives of polyketone[293,294] and polymeric 1,2-diketones.[295] The molecular-topological structure of a polyketone modified by amines was studied.¶

VI. Applications

The alternating copolymers of olefins and CO can be used to manufacture high-strength fibres with a maximum strength of 3.8–3.9 GPa, which retain 85%–90% of their strength even at 140 °C. Due to the high polarity, these fibres possess a lower creep† than PE or PETF fibres. Highly oriented fibres have an elongation at rupture of 4%–5% and an initial modulus of 50–55 GPa.[216]

High-molecular-weight copolymers ($CO/MeCH=CH_2$) and terpolymers ($CH_2=CH_2/CO/MeCH=CH_2$) with the composition $(C_2H_4/CO):(C_3H_6/CO) = 1:1$ possess high elasticity and resemble poly(vinyl chloride) (PVC) in mechanical properties. As regards their barrier properties (N_2, O_2 and CO_2 permeability), they occupy an intermediate position between high-density polyethylene and PVC and in terms of water permeability, they are similar to polyurethane. Recently, the preparation of low-molecular-weight $CH_2=CH_2/CO/MeCH=CH_2$ terpolymers with $M_n = (1.5–5.0)\times10^3$ traded under the name Carilite Oligomer has been reported. These terpolymers can be cross-linked under the action of polyfunctional amines or converted into polyaminopyrroles by the reaction with asymmetrical diamines.[93]

As the chain length in the α-olefin increases, the glass transition temperature of α-olefin–carbon monoxide copolymers decreases from 25 °C (for $CO/MeCH=CH_2$) to −60 °C (for dodec-1-ene–carbon monoxide) and the contact angle increases from 65° (for $CO/MeCH=CH_2$) to 110° (for oct-1-ene–carbon monoxide); on further increase in the chain length in the α-olefin ($>C_6$), the contact angle almost does not change. In propylene–carbon monoxide–higher α-olefin terpolymerisation, a decrease

¶ Yu A Olkhov, Yu N Smirnov, O N Golodkov, G P Belov *Plast. Massy* (2004) (in the press).

† Creep is building-up of the deformation in the course of time under a constant load.

Table 12. Permeability with respect to O_2, CO_2 and moisture and other characteristics of the polymers used for packing foodstuffs.[274]

Polymer[a]	Permeability			Extrudability	Crystallisation rate	Duration of moulding
	O_2	CO_2	90% moisture (38 °C)			
PA (amorphous)	4–19	39	59–79	poor	see[b]	medium
PA (crystalline)	–	–	98	–	–	–
PETP (amorphous)	31–97	78–295	20–28	medium	see[b]	high
PETP (crystalline)	8.9–19	39–58	4.7–4.9	good	low	very high
PP	1170	3100	2.08	"	high	low
PC	777–970	1170	1239	medium	see[b]	medium
$CH_2=CH_2/CO/MeCH=CH_2$	8–19	93	12–47	very good	high	very low
$CH_2=CH_2/CO$	8–19	93	44–67	the same	"	the same

[a] Abbreviations: PA is polyamide, PETP is poly(ethylene terephthalate), PP is polypropylene, PC is polycarbonate. [b] Amorphous polymer.

in T_g can be attained by increasing the content of the higher α-olefin.

The ever-growing demand for thermally stable and easily processable polymers having specific gas permeability properties is due to the increased requirements for packaging of foodstuffs. The alternating copolymers of olefins and carbon monoxide are especially attractive in this respect because they are thermally and chemically stable. They are distinguished by good barrier characteristics (with respect to gases) not inferior to nylon or PETP; good compatibility with other polymeric packaging materials (*e.g.*, nylon, PC, PVC). The combination of high chemical stability and low permeability makes polyketones attractive also for the use as protective coatings and chemical containers especially in those cases where it is necessary to prevent the escape of organic compounds into the environment. Polyketones can be used for the manufacture of pipes and hoses meant for transfer of chemicals. In this case, in addition to chemical stability and low permeability, the polymers should possess high mechanical and abrasive strengths.

Due to the high adhesion to organic and inorganic materials, alternating copolymers can be used to design structural materials with high mechanical strength. Due to the low friction coefficient, high strength and relatively low specific gravity, these polymers can be advised for the use in mechanical engineering (gear units and other similar structures).

Low-molecular-mass polyketones are of interest for preparative small-tonnage chemistry. For example, ethyl vinyl ketone and 1,4-diketones can be used for the production of substituted cyclopentanones, which are structural elements of natural aromatic compounds possessing the jasmine odour.[296]

* * *

This review is an attempt to survey and analyse the key aspects of a new line of research promising for both scientific and practical purposes, namely, the synthesis of alternating copolymers and terpolymers of carbon monoxide with various monomers. The attention is focussed on the search of new Pd(II), Ni(II), Cu(II) and Ru(II) catalysts and new ligands and modification of known catalysts used in the synthesis of alternating copolymers based on carbon monoxide and olefins, dienes, styrene and their derivatives. Some properties and applications of the copolymers are considered.

The alternating terpolymers based on carbon monoxide, ethylene and propylene (so-called aliphatic polyketones) manufactured in industry refer to a new class of structural polymers that combine high melting points (220–260 °C), good adhesion to organic and inorganic materials, high strength, high chemical stability and so on.

It is clear that the research and industrial projects executed during the last 10–15 years (after the beginning of studies of the effective copolymerisation of carbon monoxide with ethylene) represent only an early stage of the comprehensive investigation of the alternating copolymerisation of CO with various monomers.

The review was written with the financial support of the Russian Foundation for Basic Research (Project Nos 01-03-33248, 01-03-07004) and the INTAS (grant 00-00677).

References

1. A Sen *Adv. Polym. Sci.* **73/74** 125 (1986)
2. A Sen *Acc. Chem. Res.* **26** 303 (1993)
3. E Drent, P H M Budzelaar *Chem. Rev.* **96** 663 (1996)
4. G P Belov *Vysokomol. Soedin., Ser. B* **40** 503 (1998) [a]
5. G P Belov *Vysokomol. Soedin., Ser. C* **43** 1651 (2001) [a]
6. G P Belov *Kinet. Katal.* **42** 336 (2001) [b]
7. C Bianchini, A Meli *Coord. Chem. Rev.* **225** 35 (2002)
8. R A M Robertson, D J Cole-Hamilton *Coord. Chem. Rev.* **225** 67 (2002)
9. *Neftegaz. Tekhnol.* (1) 80 (1997)
10. G P Belov, O N Golodkov, K Z Gumargalieva, I G Kalinina, A S Semenov *Int. Polym. Sci. Technol.* **25** (5) T/72 (1998)
11. P Mapleston *Mod. Plast.* (3) 23 (1995)
12. US P. 2 577 208; *Chem. Abstr.* **46** 6143c (1952)
13. US P. 4 076 911; *Ref. Zh. Khim.* 19 S 366 (1978)
14. US P. 3 835 123; *Chem. Abstr.* **83** 132 273q (1977)
15. A Sen, T W Lai *J. Am. Chem. Soc.* **104** 3520 (1982)
16. Russ. P. 1 636 417; *Byull. Izobret.* (11) 76 (1991)
17. E G Chepaikin, A P Bezruchenko, G P Belov *Izv. Akad. Nauk SSSR, Ser. Khim.* 2181 (1990) [c]
18. G P Belov, E G Chepaikin, A P Bezruchenko, V I Smirnov *Vysokomol. Soedin., Ser. B* **35** A1585 (1993) [a]
19. E G Chepaikin, A P Bezruchenko, A A Leshcheva *Kinet. Katal.* **40** 348 (1999) [b]
20. Eur. P. 0 121 965; *Chem. Abstr.* **102** 46 423t (1985)
21. G P Belov, O N Golodkov, E V Novikova *Vysokomol. Soedin., Ser. A* **40** 419 (1998) [a]
22. O N Golodkov, E V Novikova, V I Smirnov, M S Gabutdinov, G P Belov *Zh. Prikl. Khim.* **70** 2000 (1997) [d]
23. Eur. P. 0 560 455; *Chem. Abstr.* **120** 165 225m (1994)
24. J Kiji, A Yamada, F Bertini, G Audisio *Macromol. Rapid Commun.* **22** 598 (2001)
25. H-K Luo, Y Kou, X-W Wang, D-G Li *J. Mol. Catal. A: Chem.* **151** 91 (2000)
26. Eur. P. 0 301 664 (1988)
27. A X Zhao, J C W Chien *J. Polym. Sci., Part A: Polym. Chem.* **30** 2735 (1992)
28. Z Jiang, G M Dahlen, K Houseknecht, A Sen *Macromolecules* **25** 2999 (1992)
29. F Benetollo, R Bertani, G Bombieri, L Toniolo *Inorg. Chim. Acta* **233** 5 (1995)
30. V L K Valli, H Alper *J. Polym. Sci., Part A: Polym. Chem.* **33** 1715 (1995)
31. E Drent, J A M VanBroekhoven, M J Doyle *J. Organomet. Chem.* **417** 235 (1991)
32. Eur. P. 0 272 728; *Chem. Abstr.* **109** 191 059c (1988)
33. Eur. P. 0 319 083 (1988)
34. Eur. P. 0 263 564; *Chem. Abstr.* **109** 111 084w (1988)
35. Eur. P. 0 508 502 (1992)
36. Eur. P. 0 361 584 (1989)
37. A Vavasori, L Toniolo, G Cavinato, F Vistentin *J. Mol. Catal. A: Chem.* **204** 295 (2003)
38. Eur. P. 0 489 473; *Chem. Abstr.* **117** 192 551j (1992)
39. Eur. P. 0 443 687; *Chem. Abstr.* **115** 233 131b (1991)
40. C Bianchini, A Meli, G Muller, W Oberhauser, E Passaglia *Organometallics* **21** 4965 (2002)
41. C Bianchini, H M Lee, A Meli, S Moneti, F Vizza, M Fontani, P Zanello *Macromolecules* **32** 4183 (1999)
42. C Bianchini, H M Lee, P Barbaro, A Meli, S Moneti, F Vizza *New J. Chem.* **23** 929 (1999)
43. C Bianchini, H M Lee, A Meli, W Oberhauser, M Peruzzini, F Vizza *Organometallics,* **21** 16 (2002)
44. C Bianchini, H M Lee, A Meli, W Oberhauser, F Vizza, P Brüggeller, H B Rainer, C Langes *Chem. Commun.* 777 (2000)
45. C C Lu, J C Peters *J. Am. Chem. Soc.* **124** 5272 (2002)
46. B Milani, E Alessio, G Mestroni, A Sommazzi, F Garbassi, E Zangrando, N Bresciani-Pahor, L Randaccio *J. Chem. Soc., Dalton Trans.* 1903 (1994)
47. B Milani, E Alessio, G Mestroni, E Zangrando, L Randaccio, G Consiglio *J. Chem. Soc., Dalton Trans.* 1021 (1996)
48. B Milani, L Vicentini, A Sommazzi, F Garbassi, E Chiarparin, E Zangrando, G Mestroni *J. Chem. Soc., Dalton Trans.* 3139 (1996)
49. Eur. P. 0 759 453; *Chem. Abstr.* **126** 238 813n (1997)
50. J Schwarz, E Herdtweck, W A Herrmann, M G Gardiner *Organometallics* **19** 3154 (2000)
51. Russ. P. 2 160 745; *Byull. Izobret.* (35) 23 (2000)
52. Eur. P. 0 590 942; *Chem. Abstr.* **121** 109 887n (1994)
53. Eur. P. 0 707 025; *Chem. Abstr.* **125** 34 348 (1996)
54. Y Koide, A R Barron *Macromolecules* **29** 1110 (1996)
55. Y Koide, S G Bott, A R Barron *Organometallics* **15** 2213 (1996)
56. M G Gardiner, W A Herrmann, C P Reisinger, J Schwarz, M Spiegler *J. Organomet. Chem.* **572** 239 (1999)

57. S Doherty, G R Eastham, R P Tooze, T H Scanlan, D Williams, M R J Elsegood, W Clegg *Organometallics* **18** 3558 (1999)
58. S Doherty, E G Robins, M Nieuwenhuyzen, P A Champkin, W Clegg *Organometallics* **21** 4147 (2002)
59. Y C Chen, C L Chen, J T Chen, S T Liu *Organometallics* **20** 1285 (2001)
60. O V Gusev, A M Kal'sin, T A Peganova, P V Petrovskii, G P Belov, E V Novikova *Izv. Akad. Nauk, Ser. Khim.* 1119 (2000) [c]
61. O V Gusev, A M Kalsin, M G Peterleitner, P V Petrovskii, K A Lyssenko, N G Akhmedov, C Bianchini, A Meli, W Oberhauser *Organometallics* **21** 3637 (2002)
62. I Brassat, W Keim, S Killat, M Mothrath, P Mastrorilli, C F Nobile, G Suranna *J. Mol. Catal. A: Chem.* **157** 41 (2000)
63. U Klabunde, T H Tulip, D C Roe, S D Ittel *J. Organomet. Chem.* **334** 141 (1987)
64. S Y Desjardins, K J Cavell, J L Hoare, B W Skelton, A N Sobolev, A H White, W Keim *J. Organomet. Chem.* **544** 163 (1997)
65. W Klaui, J Bongards, G Reiβ *Angew. Chem., Int. Ed.* **39** 3894 (2000)
66. B Domhöver, W Kliui, A Kremer-Aach, R Bell, D Mootz *Angew. Chem., Int. Ed.* **37** 3050 (1998)
67. G Verspui, G Papadogianakis, R A Sheldon *Chem. Commun.* 401 (1998)
68. *Polym. News* **24** 313 (1999)
69. A Batistini, G Consiglio *Organometallics* **11** 1766 (1992)
70. US P. 5 245 123 (1992)
71. US P. 5 227 464 (1992)
72. US P. 5 237 047 (1992)
73. Eur. P. 0 702 045 (1995)
74. US P. 5 243 026 (1992)
75. US P. 5 331 083 (1993)
76. US P. 5 567 801 (1993)
77. Eur. P. 0 534 570 (1992)
78. Eur. P. 0 520 584; *Chem. Abstr.* **118** 169 797f (1993)
79. Eur. P. 0 572 087; *Chem. Abstr.* **121** 10 209f (1994)
80. Eur. P. 0 559 288; *Chem. Abstr.* **120** 192 571c (1994)
81. J A Grande *Mod. Plast.* (1) 28 (1997)
82. P K Wong, J A VanDoorn, E Drent, O Sudmeijer, H A Stil *Ind. Eng. Chem. Res.* **2** 986 (1993)
83. Z Jiang, A Sen *J. Am. Chem. Soc.* **117** 4455 (1995)
84. Eur. P. 0 181 014 (1985)
85. A S Abu-Surah, B Rieger *Top. Catal.* **7** 165 (1999)
86. S C de Vos, W Huhn, B Rieger, M Moller *Polym. Bull.* **42** 611 (1999)
87. Z Jiang, A Sen *Macromolecules* **27** 7215 (1994)
88. A Bronco, G Consiglio *Macromol. Chem. Phys.,* **197** 355 (1996)
89. J C Yuan, S J Lu *Tetrahedron Lett.* **42** 4069 (2001)
90. J C Yuan, S J Lu *Organometallics* **20** 2697 (2001)
91. G Verspui, J Feiken, G Papadogianakis, R A Sheldon *J. Mol. Catal. A: Chem.* **146** 299 (1999)
92. C Bianchini, H Lee, A Meli, S Moneti, V Patinec, G Petrucci, F Vizza *Macromolecules* **32** 3859 (1999)
93. W P Mul, H Dirkzwager, A A Broekhuis, H J Heeres, A J van der Linden, A G Orpen *Inorg. Chim. Acta* **327** 147 (2002)
94. A Held, L Kolb, M A Zuideveld, R Thomann, S Mecking, M Schmid, R Pietruschka, E Lindner, M Khanfar, M Sunjuk *Macromolecules* **35** 3342 (2002)
95. E Amevor, R Bürli, G Consiglio *J. Organomet. Chem.* **497** 81 (1995)
96. D J Liaw *J. Polym. Sci., Part A: Polym. Chem.* **31** 309 (1993)
97. A S Abu-Surrah, K Lappalainen, M Kettunen, T Repo, M Leskela, H A Hodali, B Rieger *Macromol. Chem. Phys.* **202** 599 (2001)
98. Eur. P. 0 229 408 (1986)
99. Eur. P. 0 399 617 (1990)
100. US P. 5 106 952 (1990)
101. US P. 5 177 184 (1992)
102. D Roberto, M Catellanni, G P Chusohi *Tetrahedron Lett.* **29** 2115 (1988)
103. G A Korneeva, I I Kerov, Z Kh Ibragimova, V I Kurkin, K L Makovetskii, E V Slivinskii *Izv. Akad. Nauk, Ser. Khim.* 368 (1998) [c]
104. P H P Brinkmann, G A Luinstra *J. Organomet. Chem.* **572** 193 (1999)
105. B A Markies, K A N Verkerk, M H P Rietveld, Y Boersma, H Kooijman, A Z Spek, G VanKoten *J. Chem. Soc., Chem. Commun.* 1317 (1993)
106. D J Liaw, B-F Lay *Polym. J.* **28** 266 (1996)
107. E V Novikova, G P Belov *Vysokomol. Soedin., Ser. A* **44** 1878 (2002) [a]
108. S Kacker, A Sen *J. Am. Chem. Soc.* **117** 10591 (1995)
109. D-J Liaw, J-Sh Tsai, H-Ch H Sang *J. Polym. Sci., Part A: Polym. Chem.* **36** 1785 (1998)
110. M D E Forbes, J C Barborak, K E Dukes, Sh R Ruberu *Macromolecules* **27** 1020 (1994)
111. T Kawaguchi, M Kanno, T Yanagihara, Y Inoue *J. Mol. Catal. A: Chem.* **143** 253 (1999)
112. S Kacker, Z Jiang, A Sen *Macromolecules* **29** 5852 (1996)
113. M Kettunen, A S Abu-Surrah, T Repo, M Leskela *Polym. Int.* **50** 1223 (2001)
114. H-A Klok, P Eibeck, M Schmid, A S Abu-Surah, M Moller, B Rieger *Macromol. Chem. Phys.* **198** 2759 (1997)
115. K Nozaki, F Shibahara, S Elzner, T Hiyama *Can. J. Chem.* **79** 593 (2001)
116. S Murtuza, S B Harkins, A Sen *Macromolecules* **32** 8697 (1999)
117. J Furukawa, Y Isida, T Saegusa, H Fujii *Makromol. Chem.* **89** 263 (1965)
118. J T Lee, P J Thomas, H Alper *J. Org. Chem.* **66** 5424 (2001)
119. M Allmendinger, R Eberhardt, G Luinstra, B Rieger *J. Am. Chem. Soc.* **124** 5646 (2002)
120. D Takeuchi, Y Sakaguchi, K Osakada *J. Polym. Sci., Part A: Polym. Chem.* **40** 4530 (2002)
121. J T Lee, H Alper *Chem. Commun.* 2189 (2000)
122. S Kacker, S J Kim, A Sen *Angew. Chem., Int. Ed.* **37** 1251 (1998)
123. R D Dghaym, K J Yaccato, B A Arndtsen *Organometallics* **17** 4 (1998)
124. L Jia, E Ding, W R Anderson *Chem. Commun.* 1436 (2001)
125. C Moineau, G Mele, H Alper *Can. J. Chem.* **79** 587 (2001)
126. S Kim, D Takeuchi, S Osakada *Macromol. Chem. Phys.* **204** 666 (2003)
127. D Takeuchi, S Kim, K Osakada *Angew. Chem., Int. Ed.* **40** 2685 (2001)
128. S Kim, D Takeuchi, K Osakada *J. Am. Chem. Soc.* **124** 762 (2002)
129. A Mücke, B Rieger *Macromolecules* **35** 2865 (2002)
130. Eur. P. 0 264 159 (1987)
131. Eur. P. 0 272 727 ; *Chem. Abstr.* **109** 191 089n (1988)
132. Eur. P. 0 315 279 (1988)
133. Eur. P. 0 351 023 (1989)
134. Eur. P. 0 345 847 (1989)
135. Eur. P. 0 251 373 (1987)
136. R P Nieuwhof, A T M Marcelis, R Wursche, B Rieger *Macromol. Chem. Phys.* **201** 2484 (2000)
137. K Nozaki, Y Kawashima, T Oda, T Hiyama, K Kanie, T Kato *Macromolecules* **35** 140 (2002)
138. G P Belov *Plast. Massy* (2) 37 (2001)
139. Eur. P. 0 315 266 (1988)
140. Eur. P. 0 357 101 (1989)
141. Eur. P. 0 504 985 (1992)
142. S L Borkowsky, R M Waymouth *Macromolecules* **29** 6377 (1996)
143. Eur. P. 0 429 105 (1990)
144. J-C Yuan, S-J Lu *J. Polym. Sci., Part A: Polym. Chem.* **38** 2919 (2000)
145. D-J Liaw, J-Sh Tsai *J. Polym. Sci., Part A: Polym. Chem.* **35** 2759 (1997)
146. J Tsuji, Sh Hosaka *J. Polym. Sci., Part C: Polym. Lett.* **3** 703 (1965)
147. M Grazini, G Carturan, U Belluco *Chim. Ind. (Milan)* **53** 939 (1971)
148. D-J Liaw, J-Sh Tsai *J. Polym. Sci., Part A: Polym. Chem.* **35** 1157 (1997)

149. E V Novikova, G P Belov, W Klaui, A A Solotnov *Vysokomol. Soedin., Ser. A* **45** 1605 (2003) [a]
150. A L Safir, B M Novak *J. Am. Chem. Soc.* **120** 643 (1998)
151. R P Hughes, J Powell *J. Organomet. Chem.* **60** 409 (1973)
152. T Hung, P W Jolly, G Wilke *J. Organomet. Chem.* **190** C5 (1980)
153. R Santi, M Marchi *J. Organomet. Chem.* **182** 117 (1979)
154. A Behr, K-D Juszak *J. Organomet. Chem.* **255** 263 (1983)
155. J H Groen, C J Elsevier, K Vrieze *Organometallics* **15** 3445 (1996)
156. S Kacker, A Sen *J. Am. Chem. Soc.* **119** 10028 (1997)
157. J-Ch Choi, I Yamaguchi, K Osakada, T Yamamoto *Macromolecules* **31** 8731 (1998)
158. K Osakada, Y Takenaka, J-C Choi, I Yamaguchi, T Yamamoto *J. Polym. Sci., Part A: Polym. Chem.* **38** 1505 (2000)
159. Y Takenaka, K Osakada *Macromol. Chem. Phys.* **202** 3571 (2001)
160. R Wursche, B Rieger, in *Proceedings of the 5th International Symposium on Polymers for Advances Technologies, Leipzig, 1997* Part 1, p. 22
161. K Nozaki, H Komaki, Y Kawashima, T Hiyama, T Matsubara *J. Am. Chem. Soc.* **123** 5340 (2001)
162. B Milani, A Anzilutti, L Vicentini, S A Santi, E Zagrando, S Geremia, G Mestroni *Organometallics* **16** 5064 (1997)
163. B Milani, G Corso, G Mestroni, C Carfagna, M Formica, A Musco, in *Proceedings of the 11th International Symposium on Homogeneous Catalysis, England, 1998* p. C.10
164. B Milani, A Scarel, G Mestroni, S Gladiali, R Taras, C Carfagna, L Mosca *Organometallics* **21** 1323 (2002)
165. B Milani, G Corso, G Mestroni, C Carfagna, M Formica, R Seraglia *Organometallics* **19** 3435 (2000)
166. A Macchioni, G Bellachioma, G Cardaci, M Travaglia, C Zuccaccia, B Milani, G Corco, E Zangrando, G Mestroni, C Carfagna, M Formica *Organometallics* **18** 3061 (1999)
167. S Stoccoro, G Alesso, M A Cinellu, G Minghetti, A Zucca, A Bastero, C Claver, M Manassero *J. Organomet. Chem.* **664** 77 (2002)
168. A Aeby, G Consiglio *Helv. Chim. Acta* **81** 35 (1998)
169. A Aeby, G Consiglio *J. Chem. Soc., Dalton Trans.* 655 (1999)
170. S Kacker, J A Sissano, D N Schulz *J. Polym. Sci., Part A: Polym. Chem.* **38** 752 (2000)
171. A Aeby, A Gsponer, G Consiglio *J. Am Chem. Soc.* **120** 11 000 (1998)
172. R Santi, A M Romano, R Garrone, I Abbondanza, M Scalabrini, G Bacchilega *Macromol. Chem. Phys.* **200** 25 (1999)
173. A Sen, Z Jiang *Macromolecules* **26** 911 (1993)
174. Y Feng, J Sun, Y Zhu, W Chen *J. Polym. Sci., Part A: Polym. Chem.* **35** 1283 (1997)
175. C Carfagna, G Gatti, D Martini, C Pettinari *Organometallics* **20** 2175 (2001)
176. M Brookhart, M I Wagner *J. Am. Chem. Soc.* **118** 7219 (1996)
177. S Bartolini, C Carfagna, A Musco *Macromol. Rapid Commun.* **16** 9 (1995)
178. C R Baar, M C Jennings, R J Puddephatt *Organometallics* **20** 3459 (2001)
179. A Bastero, A Ruiz, J A Reina, C Claver, A M Guerrero, F A Jalón, B R Manzano *J. Organomet. Chem.* **619** 287 (2001)
180. A Bastero, A Ruiz, C Claver, B Milani, E Zagrando *Organometallics* **21** 5820 (2002)
181. M Sperrle, A Aeby, G Consiglio, A Pfaltz *Helv. Chim. Acta* **79** 1387 (1996)
182. M Brookhart, M I Wagner, G G A Balavoine, H A Haddou *J. Am. Chem. Soc.* **116** 3641 (1994)
183. Y Feng, J Sun, Y Fanglian, Y Yingbo *J. Appl. Polym. Sci.* **68** 855 (1998)
184. F Yao, C Xu, L Deng, Y Bai, J Zhang, J Sun *J. Polym. Sci., Part A: Polym. Chem.* **40** 642 (2002)
185. A P Pivovarov, E V Novikova, G P Belov *Koord. Khim.* **26** 41 (2000) [e]
186. W P Mul, H Oosterbeek, G A Beitel, G-J Kramer, E Drent *Angew. Chem., Int. Ed.* **39** 1848 (2000)
187. D Fatutto, L Toniolo, R V Chaudhari *Catal. Today* **48** 49 (1999)
188. I Toth, C J Elsevier *J. Am. Chem. Soc.* **115** 10388 (1993)
189. P Margl, T Ziegler *J. Am. Chem. Soc.* **118** 7337 (1996)
190. P Margl, T Ziegler *Organometallics* **15** 5519 (1996)
191. M Svensson, T Matsubara, K Morokuma *Organometallics* **15** 5568 (1996)
192. F C Rix, M Brookhart, P S White *J. Am. Chem. Soc.* **118** 4746 (1996)
193. C S Shultz, J Ledford, J M DeSimone, M Brookhart *J. Am. Chem. Soc.* **122** 6351 (2000)
194. C S Shultz, J M DeSimone, M Brookhart *Organometallics* **20** 16 (2001)
195. K R Reddy, K Surekha, G-H Lee, S-M Peng, J-T Chen, S-T Liu *Organometallics* **20** 1292 (2001)
196. H von Schenk, S Strömberg, K Zetterberg, M Ludwig, B Akermark, M Svensson *Organometallics* **21** 2813 (2001)
197. Y Kayaki, H Tsukamoto, M Kaneko, I Shimizu, A Yamamoto, M Tachikawa, T Nakajima *J. Organomet. Chem.* **622** 199 (2001)
198. J Ledford, C S Shultz, D P Gates, P S White, J M DeSimone, M Brookhart *Organometallics* **20** 5266 (2001)
199. F De Angelis, A Sgamellotti, N Re *Organometallics* **21** 2036 (2002)
200. Z M Dzhabieva, Yu M Shul'ga, G P Belov *Zh. Fiz. Khim.* **69** 1580 (1995) [f]
201. Z M Dzhabieva, V P Kozlovskii, Yu M Shul'ga, A F Dodonov, G P Belov *Izv. Akad. Nauk, Ser. Khim.* 494 (1996) [c]
202. W P Mul, E Drent, P J Jansens, A N Kramer, M H W Sonnemans *J. Am. Chem. Soc.* **123** 5350 (2001)
203. G P Belov, B L Psikha *Vysokomol. Soedin., Ser. A* **45** 1272 (2003) [a]
204. R M Silverstein, G C Bassler, T C Morril *Spectrometric Identification of Organic Compounds* (5th Ed.) (Singapore: Wiley, 1983)
205. S K L Li, J E Guillet *J. Polym. Sci., Part A: Polym. Chem.* **18** 2221 (1980)
206. S DeVito, F Ciardelli, E Benedetti, E Bramanti *Polym. Adv. Technol.* **8** 53 (1997)
207. T W Lai, A Sen *Organometallics* **3** 866 (1984)
208. D M Shkrabo, G N Zhizhin, L A Kuzik, I A Garbuzova *Vib. Spectrosc.* **17** 155 (1998)
209. D M Shkrabo, G N Zhizhin, in *Khimiya i Fizika Polimerov v Nachale XXI Veka (Tez. Dokl. II Vseros. Karginskogo Simpoziuma), Chernogolovka, 2000* [The Chemistry and Physics of Polymers in the Beginning of the XXIst Century (Abstracts of Reports of the IInd All-Russian Kargin Symposium), Chernogolovka, 2000] S4-89
210. D M Shkrabo, G N Zhizhin, S A Klimits, G Beitel *Vysokomol. Soedin., Ser. A* **43** 1182 (2001) [a]
211. T K Wu, D W Ovenal, H H Hoehn, in *Application of Polymer Spectroscopy* (Ed. E G Brame) (New York: Academic Press, 1978)
212. G P Belov, T N Prudskova, Ya D Urman, O M Karan'yan, O N Golodkov *Vysokomol. Soedin., Ser. A* **40** 571 (1998) [a]
213. Y Chatani, T Takizawa, S Murahasi, Y Sakata, Y Nishimura *J. Polym. Sci.* **55** 811 (1962)
214. Y Chatani, T Takizawa, S Murahasi *J. Polym. Sci.* **62** S27 (1962)
215. B J Lommerts, E A Klop, J Aerts *J. Polym. Sci., Part B: Polym. Phys.* **31** 1319 (1993)
216. B J Lommerts, Ph.D. Thesis University Groningen, 1994
217. N B Shenogina, S V Shenogin, I A Karmilov, E F Oleinik, N K Balabaev, in *Polimery 2000. Khimicheskaya Fizika Polimerov i Kompozitnykh Materialov* (Polymers 2000. Chemical Physics of Polymers and Composite Materials) (Moscow: Institute of Chemical Physics, Russian Academy of Sciences, 2000) Vol. II, p. 112
218. J M Lagaron, M E Vickers, A K Powell, J G Bonner *Polymer* **43** 1877 (2002)
219. J M Lagaron, A K Powell, N S Davidson *Macromolecules* **33** 1030 (2000)

220. J M Lagaron, M E Vickers, A K Powell, N S Davidson *Polymer* **41** 3011 (2000)
221. V Grayer, B J Lommerts, P Smith, B Lotz, J C Wittmann *Polym. Commun.* **36** 1915 (1995)
222. M Trifuoggi, C De Rosa, F Auriemma, P Corradini, S Brückner *Macromolecules* **27** 3553 (1994)
223. C De Rosa, P Corradini *Eur. Polym. J.* **29** 163 (1993)
224. S Brückner, C De Rosa, P Corradini, W Porzio, A Musco *Macromolecules* **29** 1535 (1996)
225. US P. 5 122 579 (1990)
226. M Brookhart, F C Rix, J M DeSimone, J C Barborak *J. Am. Chem. Soc.* **114** 5894 (1992)
227. H W Starkweather *J. Polym. Sci., Part B: Polym. Phys.* **15** 247 (1977)
228. H Wittwer, P Pino, U W Suter *Macromolecules* **21** 1262 (1988)
229. D R Waywell *J. Polym. Sci.* **8** 327 (1970)
230. M Stadlbauer, G Eder, H Janeschitz-Kriegl *Polymer* **42,** 3809 (2001)
231. M Fujita, N Hamada, M Tosaca, M Tsuji, S Kohjiya *J. Macromol. Sci. Phys.* **B32** 681 (1997)
232. M Fujita, M Tsuji, S Kohjiya, J C Wittmann *Macromolecules* **32** 4383 (1999)
233. M Fujita, M Tsuji, S Kohjiya *Macromolecules* **34** 7724 (2001)
234. M Fujita, M Tsuji, S Murakami, S Kohjiya, J C Wittmann *Macromolecules* **34** 6147 (2001)
235. G A Holt, J E Spruiell *J. Appl. Polym. Sci.* **83** 2124 (2002)
236. J C W Chien, A X Zhao *Polym. Degrad. Stab.* **40** 257 (1993)
237. G Conti, A Sommazzi, in *Proceedings of EUCOMOS XXI, Vienna, 1992* Vol. 8, p. 23
238. S De Vito, F Ciardelli, G Ruggeri, O Chiantore, A Moro *Polym. Int.* **45** 353 (1998)
239. O Chiantore, M Lazzari, F Ciardelli, S De Vito *Macromolecules* **30** 2589 (1997)
240. S De Vito, S Bronco *Polym. Degrad. Stab.* **63** 399 (1999)
241. M Lazar, J Rychly *Adv. Polym. Sci.* **102** 189 (1982)
242. B J Lommerts *Polymer* **42** 6283 (2001)
243. I G Kalinina, G P Belov, K Z Gumargalieva, E V Novikova, O N Golodkov, Yu A Shlyapnikov *Vysokomol. Soedin., Ser. B* **41** 1351 (1999) [a]
244. I G Kalinina, G P Belov, Yu A Shlyapnikov *Polym. Degrad. Stab.* **65** 355 (1999)
245. S Shkolnik, E D Weil *J. Appl. Polym. Sci.* **69** 1691 (1998)
246. F Y Xu, J C W Chien *Macromolecules* **26** 3485 (1993)
247. A M Trozzolo, F H Winslow *Macromolecules* **1** 98 (1968)
248. S I Kuzina, A P Pivovarov, G P Belov, A I Mikhailov *Khim. Vys. Energ.* **31** 422 (1997) [g]
249. S I Kuzina, A P Pivovarov, A I Mikhailov, G P Belov *Eur. Polym. J.* **36** 975 (2000)
250. G P Belov, O N Golodkov, L Z Gumargalieva, I G Kalinina, A S Semenov *Plast. Massy* (9) 40 (1997)
251. B V Lebedev, K B Zhogova, Ya V Denisova, G P Belov, O N Golodkov *Izv. Akad. Nauk, Ser. Khim.* 284 (1997) [c]
252. B V Lebedev, A V Tsvetkova, N N Smirnova, G P Belov, O N Golodkov, Yu A Kurskii *Izv. Akad. Nauk, Ser. Khim.* 1527 (1999) [c]
253. A V Arapova, B V Lebedev, N N Smirnova, T G Kulagina, G P Belov, O N Golodkov *Izv. Akad. Nauk, Ser. Khim.* 2264 (2001) [c]
254. T A Bykova, N N Smirnova, G P Belov, E V Novikova *Vysokomol. Soedin., Ser. B* **46** 374 (2004) [a]
255. G Kalay, M J Bevis *J. Polym. Sci., Part B: Polym. Phys.* **35** 415 (1997)
256. A J Waddon, N R Karttunen *Polymer* **42** 2039 (2001)
257. N R Karttunen, A J Lesser *J. Mater. Sci.* **35** 2507 (2000)
258. N R Karttunen, A J Lesser *Polym. Eng. Sci.* **40** 2317 (2000)
259. N R Karttunen, A J Lesser *J. Appl. Polym. Sci.* **84** 318 (2002)
260. A J Waddon, N R Karttunen, A J Lesser *Macromolecules,* **32,** 423 (1999)
261. E F Klop, B J Lommerts, J Veurink, J Aerts, R R van Puijenbrock *J. Polym. Sci., Part B: Polym. Phys.* **33** 315 (1995)
262. F Garbassi, A Sommazzi, L Meda, G Merstroni, A Sciutto *Polymer* **39** 1503 (1998)
263. P Gupta, J T Schulte, J E Flood, J E Spruiell *J. Appl. Polym. Sci.* **82** 1794 (2001)
264. J Lu, K-Y Li, G-X Wei, H-J Sue *J. Mater. Sci.* **35** 271 (2000)
265. V P Privalko, V V Korskanov, E G Privalko, V I Dolgoshey, W Huhn, B Rieger *J. Macromol. Sci. Phys.* **B40** 83 (2001)
266. V P Privalko, V I Dolgoshey, E G Privalko, V F Shumsky, F Hollmann, B Rieger *J. Macromol. Sci. Phys.* **B42** 293 (2003)
267. V P Privalko, R V Dinzhos, N A Rekhteta, F J B Calleja *J. Macromol. Sci. Phys.* **B42** 929 (2003)
268. V P Privalko, P Pissis, G Polizos, V V Korskanov, E G Privalko, V I Dolgoshey, V Yu Kramarenko, W Huhn, F Hollmann, B Rieger *J. Macromol. Sci. Phys.* **B41** 99 (2002)
269. V P Privalko, V I Dolgoshey, E G Privalko, A Sikora *J. Macromol. Sci. Phys.* **B42** 953 (2003)
270. F Hollmann, A A Mansour, B Rieger *Polymer* **42** 93 (2001)
271. Yu K Godovsky, E V Konyukhova, S N Chvalun, V M Neverov, A S Abu-Surrah, B Rieger *Makromol. Chem. Phys.* **200** 2636 (1999)
272. *Carilon. Thermoplastic Polymers* (Amsterdam: Booklet of Shell Chem. Co., 1998)
273. M A DelNobile, G Mensitier, L Nocolais, A Sommazzi, F Gorbassi *J. Appl. Polym. Sci.* **50** 1261 (1993)
274. Eur. P. 0 306 115 (1988)
275. Z Jiang, S Sanganeria, A Sen *J. Polym. Sci., Part A: Polym. Chem.* **32** 841 (1994)
276. M M Brubaker, D D Coffman, H H Hoehn *J. Am. Chem. Soc.* **74** 1509 (1952)
277. S Lu, R M Paton, M J Green, A R Lucy *Eur. Polym. J.* **32** 1285 (1996)
278. P Khansawai, R M Paton, D Reed *Chem. Commun.* 1297 (1999)
279. Eur. P. 0 332 976; *Chem. Abstr.* **111** 195 667p (1989)
280. Eur. P. 0 372 602; *Chem. Abstr.* **113** 17 346q (1990)
281. US P. 2 495 292; *Chem. Abstr.* **46** 3294c (1952)
282. Jpn. P. 01 149 828; *Chem. Abstr.* **112** 57 079t (1990)
283. Jpn. P. 01 149 828; *Chem. Abstr.* **120** 299 571e (1994)
284. M J Green, A R Lucy, S Lu, R M Paton *J. Chem. Soc., Chem. Commun.* 2063 (1994)
285. US P. 5 091 486 (1990)
286. US P. 5 081 207 (1990)
287. D D Coffman, H H Hoehn, J T Maynard *J. Am. Chem. Soc.* **76** 6394 (1954)
288. US P. 2 599 501; *Chem. Abstr.* **46** 8416f (1952)
289. US P. 2 495 293; *Chem. Abstr.* **44** 3299i (1950)
290. R H Michel, W A Murphey *J. Polym. Sci.* **55** 741 (1961)
291. US P. 5 140 080 (1991)
292. US P. 4 826 932 (1987)
293. A Sen, Z Jiang, J-T Chen *Macromolecules* **22** 2012 (1989)
294. Ross. P. 1 742 280; *Byull. Izobret.* (23) (1992)
295. E A Krasnokutskaya, A S D'yakova, V D Filimonov, O N Golodkov, G P Belov *Izv. Vyssh. Uchebn. Zaved., Ser. Khim. Khim. Tekhnol.* **45** 51 (2002)
296. H Stetler, H Kuhlman *Org. React.* **40** 407 (1991)

[a] — *Polym. Sci. (Engl. Transl.)*
[b] — *Kinet. Catal. (Engl. Transl.)*
[c] — *Russ. Chem. Bull., Int. Ed. (Engl. Transl.)*
[d] — *Russ. J. Appl. Chem. (Engl. Transl.)*
[e] — *Russ. J. Coord. Chem. (Engl. Transl.)*
[f] — *Russ. J. Phys. Chem. (Engl. Transl.)*
[g] — *High Energy Chem. (Engl. Transl.)*

Russian Chemical Reviews **73** (3) 293 – 307 (2004) © 2004 Russian Academy of Sciences and Turpion Ltd

DOI 10.1070/RC2004v073n03ABEH000802

The mechanism of thermal decomposition of secondary nitramines

Yu Shu, B L Korsounskii, G M Nazin

Contents

I.	Introduction	293
II.	The mechanism of thermal decomposition of dimethylnitramine	294
III.	The mechanism of decomposition of hexogen and octogen	296
IV.	Structures and stabilities of secondary nitramines. Kinetic data	301
V.	Conclusion	306

Abstract. A critical review of the published data on the mechanism of decomposition of secondary nitramines is presented. Based on the data available, it is concluded that the first step of decomposition always includes cleavage of the $N-NO_2$ bond, which is followed by various secondary reactions and sometimes by chain processes. The effects of structures of nitramines on their stabilities are considered. The bibliography includes 113 references.

I. Introduction

Thermal decomposition of secondary nitramines including potent explosives, such as tetryl (*N*-methyl-*N*,2,4,6-tetranitroaniline), hexogen (1,3,5-trinitro-1,3,5-triazacyclohexane), octogen (1,3,5,7-tetranitro-1,3,5,7-tetraazacyclooctane), cyclotetramethylenetetranitramine, hexanitrohexaazaisowurtzitan (CL-20), *etc*.,[1] has been the subject of intensive studies over many decades. In addition to numerous original papers, this topic has been considered in several reviews.[2–8]. Elucidation of the mechanism of decomposition of secondary nitramines is one of the most complicated problems. The diversity of the decomposition products which depends on the reaction conditions suggests the existence of several competing channels of decomposition of secondary nitramines. More than 10 putative mechanisms for the first step of decomposition of hexogen and octogen have been proposed. These include abstraction of the oxygen atom from the nitro group, nitro – nitrite rearrangement, ring expansion and contraction, elimination of HNO_2 and heterolytic and homolytic dissociation of the $N-NO_2$ bond. All these mechanisms, with the exception of the latter, were rejected as being inconsistent with the thermochemical values of the thermal effects of the reactions or contradictory to the theoretical interpretation of the deuterium kinetic isotope effect (DKIE) or based on unreliable experimental data. The use of high-precision methods for kinetic measurements and analysis of the primary reaction products and calculation of the dissociation energy of the $N-NO_2$ bond have made it possible to establish a reliable reaction mechanism. By the late 1980's a definite conclusion could be drawn that the homolytic cleavage of the $N-NO_2$ bond is the only reaction characteristic of the first step of decomposition of secondary nitramines in both the melt and the solid state. This assumption was repetitively put forward in previous studies (see, *e.g.,* Refs 4 and 5). However, some of the results obtained in the study of secondary nitramines in solutions were at variance with a simple homolysis of the $N-NO_2$ bond. Thus the decomposition of hexogen in benzene is characterised by a DKIE of the solvent and in tetrahydrofuran this reaction has a negative activation volume, *i.e*., its rate does not decrease with an increase in the external pressure, which is typical of the bond cleavage, but shows a tendency to increase. It was not until the late 1990's that the decomposition of hexogen in certain solvents was shown to follow the chain mechanism; however, the first step of decomposition always includes the cleavage of the $N-NO_2$ bond.

The main attention in the study of the decomposition mechanism of secondary nitramines is given to three compounds, *viz*., *N*-nitrodimethylamine (dimethylnitramine, DMNA), the first member in the series of aliphatic nitramines and its typical representative, which is especially suitable for the study of the decomposition products; hexogen, a cyclic nitramine with pyramidal nitramine groups; and octogen, a hexogen analogue with planar nitramine groups. The nature of the decomposition products and the isotope effects have been established for these compounds and theoretical calculations of the rates of individual decomposition steps have been carried out. The kinetic parameters (the activation energies and preexponential factors) of decomposition reactions for several dozens of nitramines have been determined.

Analysis of the mechanism of thermal decomposition of nitramines (in the examples of the three aforementioned key compounds) is mainly based on the studies which contain information relevant to elucidation of the mechanism. The kinetic characteristics of initial decomposition steps of all nitramines studied are discussed and the correlation between the reaction rates, the structure of the starting compound and the specific decomposition mechanism is analysed.

We started our consideration of decomposition mechanism with the description of non-catalytic processes reflecting the thermal stabilities of concrete compounds. Other aspects of the decomposition of secondary nitramines, *e.g*., reactions on their combustion, are considered in detail in the review.[8]

Yu Shu, G M Nazin Institute of Problems of Chemical Physics, Russian Academy of Sciences, 142432 Chernogolovka, Moscow Region, Russian Federation. Fax (7-096) 576 40 09. Tel. (7-096) 524 50 48.
E-mail: nazin@icp.ac.ru (G M Nazin)
B L Korsounskii N N Semenov Institute of Chemical Physics, Russian Academy of Sciences, ul. Kosygina 4, 119991 Moscow, Russian Federation. Fax (7-095) 938 21 56. Tel. (7-095) 939 71 10.
E-mail: kors@polymer.chph.ras.ru

Received 18 December 2002
Uspekhi Khimii **73** (3) 320 – 335 (2004); translated by R L Birnova

II. The mechanism of thermal decomposition of dimethylnitramine

The first study devoted to the decomposition of DMNA was carried out by Flournoy[9] in 1962. It was found that the decomposition of this compound in vapour at pressures of 0.25–1.0 atm is first order, the reaction rate being independent of the addition of NO. The decomposition products include Me_2NNO (80%), $MeNO_2$, CO_2, CO, H_2O, N_2O, NO and N_2, the extent of decomposition at 165 °C being 1.6%. A comparison of the experimental value of the activation energy E_a (222 ± 21 kJ mol^{-1}) with the energy of the N–N bond cleavage [D(N–N)] calculated on the basis of approximate thermochemical data (230 kJ mol^{-1}) (see Ref. 10) prompted a conclusion that the decomposition of DMNA begins with the cleavage of the N–N bond and proceeds in accordance with the reactions (1)–(3).

$$Me_2NNO_2 \longrightarrow Me_2N^{\bullet} + NO_2, \quad (1)$$

$$NO_2 + Me_2NNO_2 \longrightarrow NO + \text{oxidation products}, \quad (2)$$

$$Me_2N^{\bullet} + NO \longrightarrow Me_2NNO. \quad (3)$$

It is noteworthy that the cited paper[9] does not provide any evidence for a direct reaction of NO_2 with DMNA. In all probability, the reaction (2) is an overall process of formation of light gases upon decomposition of DMNA. A more detailed description of the reaction (2) can be found in Refs 11 and 12. Using a manometric method, Korsounskii *et al.*[11,12] have demonstrated that at initial vapour pressures $p_0 = 0.08-0.5$ atm the reaction proceeds with acceleration by a two-step consecutive pathway. The rate constant for the initial step k_1 does not depend on p_0, while the rate constant for the second step k_2 increases with the increase in p_0. The Arrhenius parameters for k_1 [$E_a = 170.8$ kJ mol^{-1} and $\log A = 14.1$ (s^{-1})] were ascribed to the reaction (1). It was found that the decomposition rate of DMNA increases upon addition of NO_2, however, an increase in the decomposition rate was also observed after addition of formaldehyde which binds NO_2. In the presence of an excess of CH_2O, the decomposition of DMNA is described by a first-order equation; further addition of NO_2 does not influence the reaction rate. Thus, the increase in the reaction rate is limited by a factor of three.

To account for these facts, it was suggested that NO_2 plays a dual role in the decomposition of DMNA, namely, it reacts with nitramine by the reaction (2) and recombines with the radical $Me_2N^{\bullet}$ with regeneration of DMNA, *i.e.,* the reaction (–1) occurs, which is the reverse of the reaction (1).

$$Me_2N^{\bullet} + NO_2 \longrightarrow Me_2NNO_2. \quad (-1)$$

At NO_2 concentrations existing during decomposition of DMNA, the reaction (–1) prevails over the reaction (2). In the presence of CH_2O, the activation energy E_a is equal to 162.8 kJ mol^{-1} and $\log A = 13.7$ (s^{-1}). Probably, in this case the activation energy was determined not very accurately. Thus, the increase in the decomposition rate of DMNA in the presence of CH_2O should be due to an increase in the preexponential factor rather than to a decrease of the activation energy. In addition, it should be kept in mind that the values of $A < 10^{14}$ s^{-1} are not typical of the cleavage of the N–NO_2 bond. A more reliable value of E_a was obtained for pure DMNA, and this was identified with D(N–N).[11]

The decomposition rates and activation energies of other aliphatic and cyclic nitramines (*e.g.*, diethylnitramine, di-n-propylnitramine, nitromorpholine) and dinitropiperazine are similar to those for DMNA. Thermochemical calculations[2] give D(N–N) equal to 193.4 kJ mol^{-1}, which is inconsistent with that determined by a kinetic method; nevertheless, this is used in subsequent studies (see, *e.g.*, Ref. 13). Shaw and Walker[2] estimated D(N–N) in DMNA using the enthalpy of formation of the radical $Me_2N^{\bullet}$ (159 kJ mol^{-1}) calculated for the reaction:

$$Me_2NH \longrightarrow Me_2N^{\bullet} + H^{\bullet}$$

taking D(N–H) equal to 393.5 kJ mol^{-1}.

The last value was obtained in the study of high-vacuum pyrolysis (VLPP) of dimethylamine[14] and appeared to be erroneous. The use of a more precise value of D(N–H) (360 kJ mol^{-1}) and of $\Delta H_f^{\circ}(Me_2N)$ (123.4 kJ mol^{-1}) taken from the reference book[15] yields the magnitude of D(N–NO_2) in DMNA close to 167.5 kJ mol^{-1}.

In more recent studies,[16] the decomposition of DMNA was studied under static conditions at 193–251 °C and in a shock tube at 527–727 °C, the concentration of DMNA being determined by a spectral method. Over the whole temperature range, E_a was equal to 92 kJ mol^{-1}, which can most probably be explained by imperfection in the experimental procedure. Presumably,[16] the formation of Me_2NNO occurred in the reaction (3), whereas NO was formed in the reactions (4) and (5).

$$Me_2N^{\bullet} + NO_2 \longrightarrow 2\,MeNO, \quad (4)$$

$$MeNO \longrightarrow Me^{\bullet} + NO. \quad (5)$$

In 1989, Golden *et al.*,[17,18] who studied the pyrolysis of DMNA by the VLPP method, found the iminoxyl radical Me_2NO and NO among the reaction products. Assuming that these radicals are generated in the primary reaction, the authors proposed a decomposition mechanism for DMNA which involved the nitro–nitrite rearrangement, *i.e.*, an elementary reaction which proceeds *via* the formation of transition state **A**.

$$Me_2NNO_2 \longrightarrow \underset{\mathbf{A}}{(Me_2NONO)^{\neq}} \longrightarrow Me_2NO + NO.$$

However, the next year this conclusion was refuted. The decomposition of DMNA was studied by the multiphoton laser excitation method[13] at 1.3×10^{-7} atm using a CO_2-laser with $\nu = 971.9$ cm^{-1} close to the internal rotation frequency of the CH_3 group in DMNA (987 cm^{-1}). Mass spectrometric studies revealed Me_2NNO, $CH_2{=}NMe$, $CH_2{=}NOH$, NO, NO_2 and Me_2NNMe_2 to be the pyrolysis products. The effect of free radical scavengers, such as Cl_2, NOCl, NO and NO_2, on the composition of the reaction products was studied and the concentration ratios $Me_2NNO : Me_2NNO_2$, $Me_2NCl : Me_2NNO_2$, $CH_2{=}NOH : Me_2NNO_2$ and $NO_2 : Me_2NNO_2$ were determined quantitatively. The addition of Cl_2 and NOCl resulted in the formation of Me_2NCl; the yield of NO_2 increased and the yield of tetramethylhydrazine decreased. The yields of Me_2NNO, $CH_2{=}NOH$, Me_2NNMe_2 and NO_2 increased in the presence of NO. The addition of NO_2 had no effect on the yield of Me_2NNO, but increased the yield of $CH_2{=}NOH$. The addition of DMNA-d_6, which does not absorb the energy of the laser irradiation due to the lack of the resonance frequency and, correspondingly, does not dissociate, resulted in the formation of $(CD_3)_2NNO$ but not $(CD_3)_2NN(CD_3)_2$ or $Me_2NN(CD_3)_2$. The results obtained were rationalised[13] on the basis of occurrence of the following reactions:

$$Me_2NNO_2 \longrightarrow Me_2N^{\bullet} + NO_2, \quad (1)$$

$$Me_2N^{\bullet} + Cl_2 \longrightarrow Me_2NCl + Cl^{\bullet},$$

$$Me_2N^{\bullet} + Me_2NNO_2 \longrightarrow Me_2NO + Me_2NNO, \quad (6)$$

$$Me_2N^{\bullet} + Me_2N^{\bullet} \longrightarrow Me_2NNMe_2, \quad (7)$$

$$Me_2NO \longrightarrow MeNO + Me^{\bullet},$$

$$MeNO \longrightarrow CH_2{=}NOH,$$

$$Me_2N^{\bullet} + NO \longrightarrow Me_2NNO, \quad (3)$$

$$Me_2N^{\bullet} + NO_2 \longrightarrow Me_2NO + NO, \quad (8)$$

$$Me_2N^{\bullet} + NO_2 \longrightarrow Me_2NNO_2. \quad (-1)$$

Thus, it was concluded that the cleavage of the N–N bond is the primary step in the decomposition of DMNA. The reaction of

Table 1. Vibration frequencies of models of transition states for the reactions (1), (9) and (10).[13]

Bond or group	ν (ground state) /cm^{-1}	ν (transition state) /cm^{-1}		
		cleavage of N–N bond	elimination of HONO	rearrangement
C–H	2940(6)		2000	
N–O	1560			
H–C–H	1430(4)		1000	
N–O	1300		1200	1500
N–N	1250	see [a]	690	690
C–N–C	1200	840		
H–C–N	1150(6)	800(6)	800	
C–N	1100(2)		1430	
C–N–N	800(2)	560(2)		600
N–N–O	640(3)	450(3)	830	450
C–N	230(2)	160(2)	460	
N–N	150	50	see [a]	see [a]

[a] Free rotation.

the radical $Me_2N^{\bullet}$ with the starting DMNA (6) was introduced into the scheme of secondary reactions.

The Reiss–Ramsperger–Kassel–Marcus (RRKM) theory was used [13] to calculate the rate constants for the reactions (1), (9) and (10) depending on the internal excitation energy (E^*) of the DMNA molecule in the range of 188–335 kJ mol^{-1}. The vibration frequencies of the models of transition states of these reactions are given in Table 1, the energy characteristics are listed in Table 2.

$$Me_2NNO_2 \xrightarrow{k_{N-N}} Me_2N^{\bullet} + NO_2, \quad (1)$$

$$Me_2NNO_2 \xrightarrow{k_{iso}} Me_2NONO, \quad (9)$$

$$Me_2NNO_2 \xrightarrow{k_{elim}} CH_2{=}NMe + HONO. \quad (10)$$

It was found that $k_{N-N}/k_{iso} = 10^{2.2}\exp(-6.5/RT)$. Hence, at 877 °C where the nitro–nitrite rearrangement was supposed to take place,[18] the contribution of this route does not exceed 10%, which is below the threshold sensitivity of the experiment. The rate constant for the elimination of HONO at $E^* = 188.4$ kJ mol^{-1} was nearly 100 times lower than k_{N-N}.

It was also found [13] that Me_2NH, which is formed in the disproportionation reaction of the radical $Me_2N^{\bullet}$

$$Me_2N^{\bullet} + Me_2N^{\bullet} \longrightarrow Me_2NH + MeN{=}CH_2,$$

undergoes decay on the wall upon interaction with NO_2.

Table 2. Energy characteristics of transition states and kinetic parameters of the reactions (1), (9) and (10).[13]

Parameter	Ground state	Reactions		
		(1)	(9)	(10)
E_z /kJ mol^{-1}	249	220.6	241	245.3
E_0 /kJ mol^{-1}	–	194.6	178	167.4
I^*/I	1	6	1	1.5
ΔH_0 /kJ mol^{-1}	–	194.6	11.7	119.3
log$A$ (s^{-1})	–	15.5	12.7	13.3

Note. E_z is the zero energy of a molecule; E_0 is the critical energy of the reaction; I^*/I is the ratio of the moments of inertia of a molecule in the transition and ground states.

The energy profiles for the cleavage of the N–N bond and other reactions were calculated using the MNDO and MNDO/3 methods. [19] It was shown that the radical $Me_2N^{\bullet}$ readily reacts with NO_2. A mechanism of decomposition of DMNA including the reactions (3)–(5) and (8) *inter alia* has been substantiated.

$$Me_2NNO_2 \longrightarrow Me_2N^{\bullet} + NO_2, \quad (1)$$

$$Me_2N^{\bullet} + NO_2 \longrightarrow Me_2NO + NO, \quad (8)$$

$$Me_2N^{\bullet} + NO_2 \longrightarrow (MeNO)_2 \longrightarrow 2\,MeNO, \quad (4)$$

$$MeNO \longrightarrow Me^{\bullet} + NO, \quad (5)$$

$$Me_2N^{\bullet} + NO \longrightarrow Me_2NNO, \quad (3)$$

$$Me^{\bullet} + NO_2 \longrightarrow MeO^{\bullet} + NO,$$

$$Me^{\bullet} + NO_2 \longrightarrow MeNO_2.$$

Summation of the reactions that have been proved in the experimental and theoretical studies cited above together with well-established oxidation reactions of the radical $Me^{\bullet}$ and methyl nitrite by nitrogen dioxide [20] yields a detailed scheme of decomposition of DMNA in vapour (Scheme 1).

Scheme 1

$$Me_2NNO_2 \longrightarrow Me_2N^{\bullet} + NO_2, \quad (1)$$

$$Me_2N^{\bullet} + NO_2 \longrightarrow Me_2NNO_2, \quad (-1)$$

$$Me_2N^{\bullet} \longrightarrow CH_2{=}NMe + H^{\bullet}, \quad (11)$$

$$Me_2N^{\bullet} + NO_2 \longrightarrow Me_2NO + NO, \quad (8)$$

$$Me_2N^{\bullet} + NO \longrightarrow Me_2NNO, \quad (3)$$

$$Me_2N^{\bullet} + Me_2NNO_2 \longrightarrow Me_2NO + Me_2NNO, \quad (6)$$

$$2\,Me_2N^{\bullet} \longrightarrow Me_2NNMe_2, \quad (7)$$

$$Me_2NO \longrightarrow MeNO + Me^{\bullet},$$

$$MeNO + NO_2 \longrightarrow MeNO_2 + NO,$$

$$MeNO \longrightarrow Me^{\bullet} + NO,$$

$$MeNO \longrightarrow CH_2{=}NOH,$$

$$MeNO + 2\,NO \longrightarrow MeO^{\bullet} + N_2 + NO_2,$$

$$Me^{\bullet} + NO_2 \longrightarrow CH_2O + HNO_2,$$

$$2\,HNO_2 \longrightarrow H_2O + NO + NO_2,$$

$$MeO^{\bullet} + NO_2 \longrightarrow CH_2O + NO,$$

$$CH_2O + NO_2 \longrightarrow CO + CO_2 + H_2O + NO.$$

In Scheme 1, the reaction (11) is characterised by a relatively high activation energy and may compete with the reactions (3) and (8) at very low pressures. Under normal conditions, the reaction (6) does not occur (otherwise, the inhibiting effect of NO would be apparent); the recombination reaction (7) is also related to secondary processes. Undoubtedly, the oxidation of DMNA by nitrogen dioxide occurs at high pressures of NO_2, the relative ease of oxidation seems to be due to the presence of a trivalent nitrogen atom in the DMNA molecule.

The kinetics of decomposition of DMNA at 240 °C in various solvents was studied at DMNA concentrations ranging from 0.01 mass % to 0.5 mass %. The first-order rate constants $10^4 k$ s^{-1} were determined using a chromatographic method [21] and were found to be equal to 11 (in cyclopentane), 9.3 (in cyclohexane), 9 (in isooctane), 3.2 (in n-butanol), 1.73 (in benzene) and 0.71 [in glycerol triacetate (triacetin)].

The effect of the solvent on the decomposition of DMNA was interpreted [21] in terms of the cage effect, which should have been manifested due to the reversibility of the initial step of dissociation of the N–N bond. Presumably, cleavage of the N–N bond is accompanied by an alternative decomposition route, *viz*., elimination of HONO.

The DKIE value equal to 1.56 observed in the decomposition of DMNA-d_6 in benzene at 240 °C is an argument in favour of a mechanism which involves elimination of HNO_2. However, as follows from the general theory of the kinetic isotope effect,[22] this value is too small for the primary isotope effect, but is rather consistent with the secondary isotope effect due to a decrease in the rocking vibration frequencies of the CH_3 groups in the radical $Me_2N^{\bullet}$ formed upon cleavage of the N–N bond. This conclusion was totally confirmed by calculations of the isotope effects carried out in 1997.[23]

There is additional evidence in favour of the above-mentioned mechanism.[21] The volume of activation ($\Delta V^{\neq}$) of DMNA decomposition in isooctane (227 °C, 2% solution, 10^3-10^4 atm) was equal to 30 $cm^3\ mol^{-1}$. Should elimination of $HONO^{\bullet}$ occurred, the value of $\Delta V^{\neq}$ would be negative. The decomposition of a 1 : 1 $Me_2{}^{14}N{}^{14}NO_2 - Me_2{}^{15}N{}^{15}NO_2$ mixture resulted in total redistribution of the label in the reaction products, such as Me_2NNO, NO and N_2. The decomposition of $Me_2N^{15}NO_2$ in the presence of $^{14}NO_2$ resulted in total redistribution of the label in Me_2NNO as well. It was also found[21] that the $^{15}NO_2$ group in $Me_2N^{15}NO_2$ is partly exchanged for free nitrogen dioxide $^{14}NO_2$. These data altogether clearly demonstrate that Scheme 1 involves the reactions (−1) and (3).

The formation of N_2 upon decomposition of DMNA was rationalised[21] by insertion of oxygen of the nitro group into the C–H bond

$$\begin{array}{l} MeN(CH_2OH)-N=O \longrightarrow MeN(CH_2OH)-N=O \longrightarrow MeN=NOH + CH_2O, \\ MeN=NOH \longrightarrow N_2 + MeOH, \end{array} \qquad (12)$$

or by elimination of HNO_2 with subsequent nitrosation of $MeN=CH_2$.

$$Me_2NNO_2 \longrightarrow MeN=CH_2 + HNO_2 \longrightarrow MeN=NOH + CH_2O.$$

Since neither CH_2O nor MeOH was detected among DMNA decomposition products, the formation of N_2 can be explained by occurrence of the reaction (13), which proceeds with extremely high efficiency despite its trimolecular character.[24]

$$MeNO + 2\,NO \longrightarrow Me^{\bullet} + N_2 + NO_3. \qquad (13)$$

It was assumed[21] that the formation of N_2 and acetone upon decomposition of diisopropylnitramine results from insertion or elimination reactions:

$$2\,(Me_2CH)_2NNO_2 \longrightarrow (Me_2CH)_2NNO + 2\,Me_2CO + N_2 + H_2O.$$

However, in this case, too, these products can be formed in ordinary reactions, since it is known that radicals $Me_2\dot{C}H$ and $Me_2CHO^{\bullet}$ yield acetone in oxidising media.[25]

$$(Me_2CH)_2NNO_2 \longrightarrow (Me_2CH)_2N^{\bullet} + NO_2,$$

$$(Me_2CH)_2N^{\bullet} + NO_2 \longrightarrow Me_2CHNO + Me_2\dot{C}H + NO,$$

$$(Me_2CH)_2N^{\bullet} + NO \longrightarrow (Me_2CH)_2NNO,$$

$$Me_2CHNO + 2\,NO \longrightarrow Me_2\dot{C}H + N_2 + NO_3,$$

$$Me_2\dot{C}H + NO_2 \longrightarrow Me_2CHO^{\bullet} + NO,$$

$$Me_2CHO^{\bullet} + NO_2 \longrightarrow Me_2C=O + HNO_2.$$

Thus, the data available on the secondary decomposition products do not contradict the cleavage of the N–N bond in the first step. It may thus be expected that the decomposition of other aliphatic secondary nitramines will also proceed in a similar fashion ($E_a \approx 170$ kJ mol^{-1}, $A \approx 10^{14.5}\ s^{-1}$) and will yield *N*-nitroso compounds, aldehydes, N_2 and H_2O as the main products.

III. The mechanism of decomposition of hexogen and octogen

Decomposition of hexogen and octogen follows the same regularities; therefore, these reactions are often studied simultaneously. The differences in the spatial structures of the nitramine groups[26] of these compounds affect only the initial rates, but not the reaction mechanism.

The first study of thermolysis of hexogen melts was carried out in 1944 (for a review, see Ref. 8). The presence of nitrogen dioxide in the decomposition products suggested that the initial step involved the cleavage of the $N-NO_2$ bond.

More detailed studies on the decomposition kinetics of hexogen and octogen were carried out in 1948–1949.[27,28] The decomposition rates of hexogen were measured in the gas phase, melts and solutions in dicyclohexyl phthalate and 2,4,6-trinitrotoluene. The decomposition of octogen was studied both in vapour and in the solid state. The decomposition products contained large amounts of CH_2O and H_2O as well as N_2, N_2O, NO, CO and H_2. Tables 3 and 4 illustrate quantitative data on the

Table 3. Yields of hexogen decomposition products (mol).[4]

Products	Product yields at different temperatures (°C)										
	195 (5)[a]	195 (9)[a]	195 (92)[a]	206	212 (19)[a]	212 (93)[a]	225	267	300	600	800
N_2	0.83	0.65	1.26	1.00	1.08	0.99	1.16	1.03	0.72	0.66	0.60
N_2O	1.4	0.92	1.08	0.95	1.22	1.36	0.98	0.76	0.66	0.60	0.57
NO	0.86	1.30	0.509	0.98	0.23	0.45	0.54	0.75	2.27	2.70	–
H_2CO	1.1	1.2	1.04	traces	traces	0.97	traces	traces	0.33	–	–
CO	0.20	0.16	0.359	0.76	0.41	0.52	0.40	0.29	0.18	0.93	0.90
CO_2	0.50	0.30	0.698	0.89	0.54	0.61	0.48	0.44	0.12	0.18	0.15
HCN	traces	traces	traces	–	0.23	0.03	–	–	0.18	1.32	1.38
NO_2	–	–	–	–	traces	traces	–	–	–	–	–
NH_3	0.83	0.69	0.342	–	–	–	–	–	–	–	–
HCO_2H	0.93	0.60	0.367	–	–	–	–	–	–	–	–
NO_3^-	traces	0.29	0.095	–	–	–	–	–	–	–	–
NO_2^-	traces	traces	0.023	–	–	–	–	–	–	–	–
H_2O	traces	traces	traces	traces	traces	0.97	traces	traces	–	–	–
H_2	–	–	–	–	–	–	0.09	0.06	–	–	–
$HOCH_2NHCHO$	traces	traces	traces	–	–	–	–	–	–	–	–

[a] The extent of decomposition of hexogen is given in parentheses (%).

decomposition products of hexogen and octogen [27–32] which are summarised in the review.[4] Later, minor decomposition products (H_2NCHO, $MeNHCHO$, Me_2NCHO, Me_2NNO, Me_2NNO_2) were identified.[33] The reliability of the results obtained [33] is doubtful due to ambiguity of the interpretation of mass-spectrometric data. Therefore, it is the products formed in high molar yields (CH_2O, N_2O, N_2, NO, CO, CO_2, HCN and H_2O) that can serve as the basis for an analysis of the decomposition mechanism. The non-volatile residue † of the polyamide type was also taken into consideration; its yield depended on the experimental conditions and could reach 10%.[33]

Table 4. Yields of octogen decomposition products (mol).[4]

Products	Yields at different temperatures (°C)							
	226	226	258	280	285	300	600	800
N_2	0.19	0.47	0.47	1.16	0.93	0.80	1.00	0.88
N_2O	1.56	2.52	2.57	1.51	1.60	1.72	1.00	0.68
NO	0.24	0.42	0.55	0.95	1.20	2.40	2.80	–
CH_2O	2.71	1.26	0.47	traces	0.86	1.44	0.16	–
CO	0.19	0.40	0.47	0.57	0.42	0.24	1.44	1.28
CO_2	0.30	0.56	0.54	0.64	0.30	0.16	0.24	0.20
HCN	0.02	0.02	0.07	–	0.52	0.48	1.60	1.84
NO_2	–	–	–	–	–	–	–	–
NH_3	–	–	–	–	–	–	0.12	–
H_2O	–	–	–	traces	–	–	–	–
H_2	traces	traces	traces	–	–	–	–	–
$(CN)_2$	traces	traces	traces	–	–	–	–	–

According to Robertson,[28] the major reaction products, *viz*., CH_2O and N_2O, are formed due to transfer of an oxygen atom from the nitro group of hexogen (**1**) to the neighbouring CH_2 group. The ring expansion product, *viz*., compound **2**, undergoes decomposition to give CH_2O and N_2O.

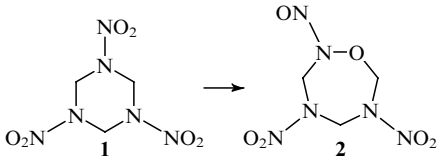

A typical methodological error has been made in the study [28] where the products of secondary reactions were ascribed to the first reaction step.[29]

Studies of the solid-phase and solution (*m*-dinitrobenzene) decomposition of hexogen and octogen revealed a weak concentration dependence of the reaction rate.[34] The experimental values of activation energies coincided with those obtained by Robertson.[28] Cleavage of the N–NO_2 bond was postulated as the initial step of the reaction on the basis of approximate thermochemical estimates of D(N–N) in hydrazine derivatives.[35]

Valuable information for the interpretation of the mechanism was obtained using a tracer method.[30] Studies of the decomposition of octogen with a ^{15}N-labelled nitro group and a ^{14}N-labelled amino group revealed formation of $^{14}N^{15}NO$, $^{14}N^{15}N$, ^{15}NO and $HC^{14}N$ exclusively. The formation of products with such distribution of the label may occur by various routes, but cleavage of the C–N bond (rather than of the N–N bond) was thought to be predominant and a fragmentation mechanism with simultaneous cleavage of four C–N bonds was postulated.[30]

† The term 'non-volatile residue' was introduced [33] for the description of condensation products of the polyamide type which are always formed in small amounts upon decomposition of hexogen and octogen.

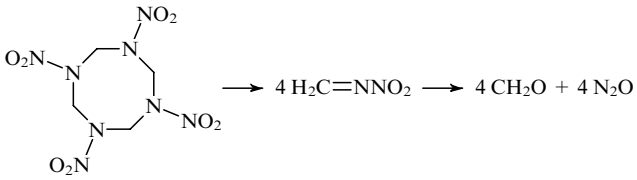

An X-ray diffraction analysis carried out in 1971 revealed [36] the existence of a very tight contact (smaller than the sum of the van der Waals radii of O and H atoms) between a nitro group of one hexogen molecule and a hydrogen atom of the other molecule. Based on these data, a bimolecular reaction was proposed which included direct interaction of two hexogen molecules. However, this hypothesis is untenable due to high endothermicity of this process.

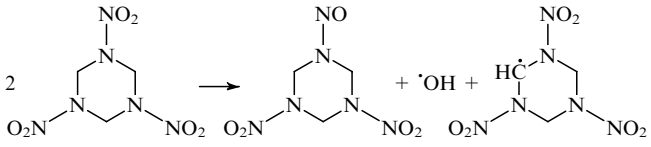

The decomposition of hexogen and octogen was studied using mass spectrometric methods. Thus the decomposition of hexogen vapour in a flow reactor at 240–290 °C resulted in the appearance of species with m/z 128. This has made it possible to propose a mechanism for fast cleavage of two HONO molecules (for a review, see Ref. 8).

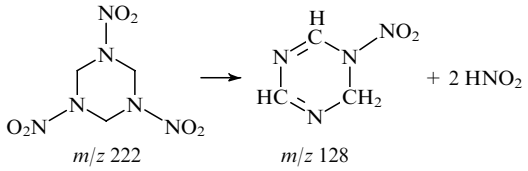

The decomposition of hexogen and octogen in vacuum (10^{-3}–10^{-5} atm) afforded species with m/z 148.[37,38] It was thus assumed that the decomposition of octogen involves opening and contraction of the ring and elimination of HNO_2.[38]

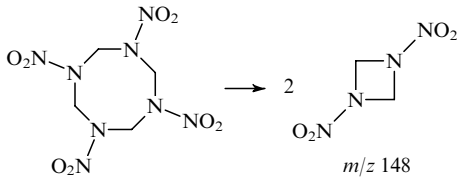

However, in these studies the vapours of the starting compounds and their decomposition products were not separated and their inlet into the chamber of the mass spectrometer occurred simultaneously. As a result, the ions generated upon fragmentation of the hexogen or octogen molecules under the electron impact might be mistaken for thermolysis products.

A significant contribution to the study of decomposition mechanisms of octogen was made in 1977 [2] when all the mechanisms postulated so far (with the exception of the cleavage of NO_2 and elimination of HNO_2 *via* a five-membered transition state) were abandoned based on the results of thermochemical estimates of thermal effects for different reactions. The equation for the calculation of the cleavage rate of the N–N bond appears as:

$$\log k_{N-N} = 16.4 - \frac{46\,200}{2.3\,RT}\ s^{-1},$$

and that for the elimination of HNO_2 as:

$$\log k_{elim} = 10.8 - \frac{38\,000}{2.3\,RT}\ s^{-1}.$$

It was found that a change in the decomposition mechanism occurred at 333 K.

A remarkably detailed analysis of the decomposition mechanism of hexogen and octogen was made by Schroeder [3,4] who has explained the formation of the major products by secondary reactions following cleavage of the $N-NO_2$ bond.[4]

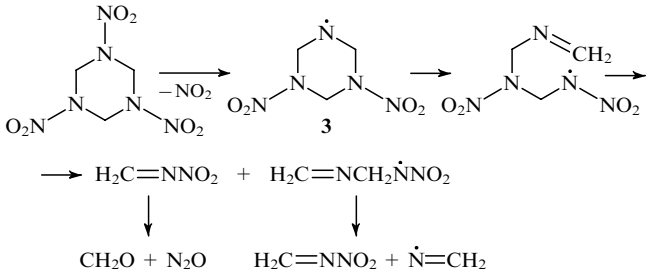

This scheme was supplemented by an entrapment of the radical **3** by nitrogen oxide and dissociation of the $N-NO_2$ bond in nitroso derivative of RDX **4** formed.

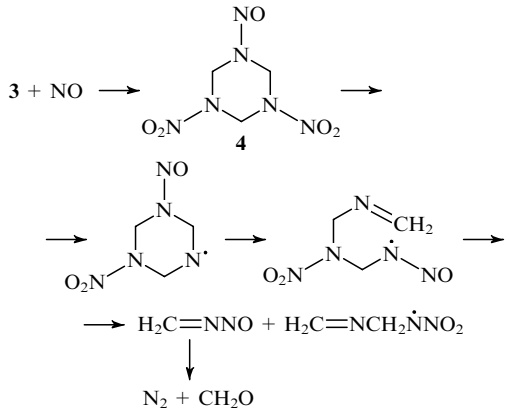

EPR studies have shown [39] that pyrolysis products of hexogen at 260 °C contain large amounts of NO_2 and $H_2C=N^{\bullet}$ radicals, which is a direct proof of the Schroeder scheme.[4]

However, Schroeder noted that it is the elimination of HNO_2, rather than the abstraction of NO_2 that prevails in the gas phase at low temperatures. This statement was made on the basis of the rather low activation energy obtained for the decomposition of hexogen vapour ($\sim$ 125 kJ mol^{-1}). In our opinion, the data available are contradictory and the use of the activation energy measured with a large error is unreliable for an adequate explanation of the mechanism.

The kinetic isotope effect in the decomposition of HMX-d_8 in the solid phase was measured.[40] It was found that the ratio of the rate constants for normal and labelled HMX (k_H/k_d) was equal to 2 in the induction period and to 0.8 and 1.0 in the acceleration and deceleration steps, respectively. These measurements were performed using differential thermal analysis; therefore, it was correctly noted that the data obtained were more relevant to the overall process rather than to its first elementary step, particularly to heat liberation reactions.[23] For example, the products of oxidation of formaldehyde by nitrogen dioxide were often found in early decomposition steps of octogen.[5,7,8]

The formal kinetic regularities of decomposition of hexogen and octogen in the solid phase and the effects of gaseous decomposition products on the reaction rates have been studied.[36,41–44] It was found that the solid-phase reaction is complicated by several factors, *e.g.*, evaporation of the sample and fast reaction occurring in the gas phase, melting of the sample on the decomposition products, autocatalysis and a cage effect. Thus, the decomposition rate depends on the degree of filling of the reaction vessel with the substance, pressure of extraneous gases, mass and even the shape of the sample. Some products, *e.g.*, N_2, CO and CO_2, inhibit the decomposition by preventing the evaporation of the substance and, as a consequence, the course of the gas-phase process. The addition of NO_2 and O_2 produces an even stronger effect, most probably due to reversibility of the first step of decomposition.

The rate and activation energy measured in the decomposition of solid samples do not fit into the mechanism of monomolecular radical cleavage of the N–N bond, since this reaction is superimposed by numerous secondary processes. All these side factors were taken into consideration and the lowest values of the rate constant were obtained in the solid phase (k_{solid}).[26]

Significant progress has been made in the past decade in the development of highly sensitive dynamic methods for monitoring the decomposition of hexogen and octogen. One of them, *viz.*, FT-IR spectroscopy, was used for monitoring the decomposition of solid hexogen and octogen in a nitrogen atmosphere at heating rates up to 200 K s^{-1} (see Refs 45 and 46). The main reaction products are NO_2, N_2O, CH_2O and HCN. The concentrations of NO_2 and CH_2O decrease with time, while that of NO increases, which suggests that formaldehyde is oxidised by nitrogen dioxide. These results fit well into the Schroeder scheme.[4]

A procedure for studying the primary step in the decomposition of hexogen in the solid phase has been developed.[47,48] A thin film of the sample is placed onto a massive support and irradiated *in vacuo* by short (35 μs) pulses of a CO_2 laser at 77 K. This leads to instantaneous heating of the support to 1200 K and cooling to 400 K within 3×10^{-3} s. The decomposition products were analysed by IR spectroscopy directly in the solid phase which remained after partial evaporation of the sample. The dimer N_2O_4 was identified as the only primary decomposition product. Further analysis based on the use of the tracer method revealed that NO_2 molecules forming the dimer originate from different hexogen molecules, *i.e.*, one hexogen molecule always yields only one NO_2 species. This can be regarded as a direct proof that the cleavage of the $N-NO_2$ bond is the only initial step in the decomposition of solid hexogen.

A more complicated situation was observed when the decomposition of hexogen was studied in solutions. An analysis of hexogen and its decomposition products in benzene and benzene-d_6 by liquid chromatography quite unexpectedly revealed [49] that the rate of this reaction is higher in solutions than in the melts. A kinetic isotope effect of the solvent was observed at 180 °C (k_H/k_d = 1.6). This was accounted for by a direct reaction of hexogen with a solvent:

$$>NNO_2 + RH \longrightarrow ROH + >NNO.$$

Actually, this reaction is hardly possible, since its endothermic thermal effect is no less than 250 kJ mol^{-1}, while the activation energy of hexogen decomposition does not exceed 170 kJ mol^{-1}. Besides, these data were not confirmed experimentally in further studies.[50] However, the possibility of the interaction of hexogen with solvents first postulated in 1985 [49] was corroborated by an analysis of their effects on the decomposition rate constant. The results of early studies suggest that such solvents as dicyclohexyl phthalate and *m*-dinitrobenzene are inert in the decomposition of hexogen.[28,34] However, subsequent studies have shown that the reaction rates strongly depend on the nature of the solvent in dilute solutions (Table 5).

It was found [52] that the decomposition of hexogen in THF has a negative activation volume ($\Delta V^{\neq} = -11$ cm^3 mol^{-1}). Thus, it was suggested that it is the elimination of HNO_2, rather than the homolytic cleavage of the N–N bond that is predominant in polar solvents. In this case, the transition state is polar and stabilised by the solvent. No additional evidence was given in favour of this pathway that was rejected earlier in the studies of DMNA decomposition in polar solvents and decomposition of hexogen in the melts and the solid state. As for elimination of HNO_2, it does not provide any adequate explanation for the fact that some hexogen analogues including octogen are characterised

Table 5. Effect of the solvent on the decomposition rate of hexogen at 180 °C.

Solvent	$10^4 k$ /s^{-1}	Ref.
Melt	0.43	28
Benzene	0.40	50
m-Dinitrobenzene	0.17	34
Dicyclohexyl phthalate	0.25	28
Trotyl	0.56	28
	1.32	51
Acetone	0.92	50
Benzophenone	1.95	51

by positive values of activation volumes in the decomposition in more polar solvents, *e.g.,* acetonitrile.[52]

The decomposition of 0.05% solutions of hexogen in benzene, acetone and isooctane was studied using a chromatographic method.[50] In this study, mononitrosohexogen, the yield of which in solution exceeded severalfold that in the melt, was identified as an intermediate product. This fact did not receive any adequate interpretation either, although it is evident that the solvent does influence the yields of nitroso derivative of RDX in one way or another. Unfortunately, the range of solvents used for the study of hexogen decomposition by chromatographic methods could not be expanded.

Clues to the problems related to decomposition of hexogen in solutions were obtained through the use of a highly efficient manometric technique which permits one to measure pressures up to 100 atm directly in glass reaction vessels.[53–55] The rate constants for the decomposition of hexogen at 180 °C were measured systematically in various solvents differing in their structures and properties. These studies included the measurements of DKIE of the solvents and an analysis of the effects of chain reaction inhibitors on the decomposition rate. The main results of these studies are summarised in Table 6.

The solvents from 1,2,4-trichlorobenzene to acetonitrile (Table 6) are inert with respect to hexogen, at least they do not cause any appreciable increase in the decomposition rate in comparison with the melt. This group includes structurally diverse compounds, *e.g.*, aliphatic and aromatic hydrocarbons, fluorinated alkanes, chloro- and nitro-derivatives of benzene. In benzene, naphthalene, isooctane and acetonitrile, the decomposition rates are similar within the limits of the experimental error and exceed only slightly that in the melt. However, in other solvents of this group they are lower than in the melt, which can be attributed to the cage effect characteristic of viscous media. A similar effect was observed for DMNA,[21] the first decomposition step for which, *viz*., the cleavage of the N—N bond, is reversible.

Acetonitrile and nitrobenzene manifest the highest values of dielectric permeability in comparison with other solvents, naphthalene being the most potent π-donor. However, all these compounds are inert with respect to hexogen. As a consequence, such

Table 6. Decomposition rate constants (k_1) of 1% solutions of hexogen in different solvents at 180 °C.[55]

Solvent	$10^4 k$ /s^{-1}	$k_1/k_{\text{isooctane}}$	Solvent	$10^4 k$ /s^{-1}	$k_1/k_{\text{isooctane}}$
Melt	0.43	0.86	Toluene	1.25	2.50
1,2,4-Trichlorobenzene	0.13	0.26	Toluene + NO (∼4 atm)	0.19	0.38
m-Dinitrobenzene	0.17	0.34	Toluene-d_3	0.33	0.66
$C_{12}F_{26}$	0.21	0.42	Toluene + NO_2	0.45	0.90
Nitrobenzene	0.23	0.46	Toluene + 1.54% DNB	0.76	1.52
Dicyclohexyl phthalate	0.25	0.50	Toluene + 0.6% $(CH_2O)_3$	1.31	2.62
Ph_3CH	0.26	0.52	Toluene + 1.44% I_2	2.55	5.10
Triacetin	0.32	0.64	Ionol	1.27	2.54
Biphenyl	0.38	0.76	Cyclohexanol	1.95	3.90
Naphthalene	0.48	0.96	Ethyl acetate	2.03	4.06
Isooctane	0.50	1.00	Phenol	2.03	4.06
Benzene	0.55	1.10	Phenol-d_6	1.60	3.20
	0.39	0.78	$CHCl_3$	2.04	4.08
	0.54 [a]	1.08	$CDCl_3$	1.41	2.82
	0.53 [b]	1.06	*m*-Xylene	2.67	5.34
Benzene + 4.4% I_2	0.54	1.08	*m*-Xylene + NO_2 (∼ 4 atm)	0.27	0.54
Benzene + 1.3% DNB [c]	0.55	1.10	*m*-Xylene-d_{10}	0.48	0.96
Benzene-d_6	0.58	1.16	THF	2.93	5.86
Benzene + 1% $(CH_2O)_3$	0.65	1.30	*p*-Xylene	2.96	6.92
Benzene + NO (4 atm)	0.69	1.38	*p*-Xylene + NO (∼ 4 atm)	1.52	3.04
Acetonitrile	0.63	1.26	*p*-Xylene + 0.78% DNB	1.96	3.92
Acetonitrile-d_3	0.73	1.46	*p*-Xylene + 1.5% I_2	2.57	5.14
Acetone	0.72	1.44	Butane-1,4-diol	3.59	7.18
	0.93	1.86		3.40 [d]	6.80
Acetone-d_6	0.28	0.56		3.48 [e]	6.96
Acetone + THF (1 : 1)	2.46	4.92	MeCH(OH)Me	4.32	8.64
Trinitrobenzene	0.74	1.48	$CD_3CD(OD)CD_3$	1.18	2.36
Diphenylmethane	0.79	1.58	Triethylene glycol	4.81	9.62
o-Dinitrobenzene	0.82	1.64	PhCHO	5.07	10.14
Trinitrotoluene	0.86	1.72	Glycerol	5.55	11.10
tert-Butylbenzene	0.95	1.90	Glycerol + NO_2	1.20	2.40
$PhCH_2OH$	0.96	1.92	Glycerol + NO	3.61	7.22
Cumene	1.18	2.36	Glycerol + 0.6% $(CH_2O)_3$	5.67	11.34

[a] Concentration of hexogen, 0.8 mass %. [b] Concentration of hexogen, 0.44 mass %. [c] DNB, 1,4-dinitrosobenzene. [d] Concentration of hexogen, 3 mass %. [e] Concentration of hexogen, 0.3 mass %.

factors as polarity or tendency of a solvent to form charge-transfer complexes do not influence the decomposition rate of hexogen.

The second group includes solvents where decomposition occurs at higher rates in comparison with the melt. This group includes alkylaromatic hydrocarbons, alcohols, ketones, aldehydes, chloroform and some other compounds. Their common property is the presence of labile hydrogen atoms, *i.e.*, unstable C–H bonds (in the case of non-polar compounds, *e.g.*, toluene) or relatively stable, but polarised and therefore highly reactive C–H bonds as, *e.g.*, chloroform and alcohols. These solvents always manifest DKIE, which suggests involvement of the cleavage of the C–H bond.

The curve for the dependence of the decomposition rate constant of hexogen (k_1) on the bond dissociation energy D(C–H) of the solvent has a maximum. The data on D(C–H) are scarce; therefore, a regularity can be established only approximately using the D(C–H) values (in kJ mol^{-1}) as reference points for the following solvents: aliphatic hydrocarbons, toluene (356), *m*-xylene (325), *p*-xylene (322), diphenylmethane (262) and triphenylmethane ($\sim$ 255).[15] The rate constants measured in aliphatic hydrocarbons, *e.g.*, isooctane, are nearly the same as in the melt. In toluene, this increases threefold, whereas in *m*- and *p*-xylene the difference between k_1 values in the melt and in solution is as high as five- to sevenfold. For diphenylmethane, the k_1 value is higher than for benzene, but lower than for xylenes and even for toluene. Triphenylmethane inhibits the decomposition. The solvents containing polar C–H bonds ($CHCl_3$, alcohols) strongly affect reaction rates at D(C–H) > 360 kJ mol^{-1}.

At 180 °C, the maximum increment in k_1 (11-fold when compared with the melt) is observed for glycerol. With a decrease in temperature, the difference between k_1 values in the melt and in solution is expected to increase due to lower activation energy in solutions. The activation energy E_a in inert benzene is equal to 169 and in toluene and butane-1,4-diol it is equal to 158 and 135 kJ mol^{-1}, respectively.

The decomposition products of hexogen in the gas phase contain N_2, N_2O, CO, CO_2, trace amounts of NO and small amounts of formaldehyde and water. Lower molar yields of gaseous products with a decrease in the concentration of hexogen is characteristic of decomposition in solutions. In the melt, the total yield of gaseous products is about 5 mol per mol of hexogen, whereas in 0.5% solution in benzene it is as low as 0.5 mol. It was found that the decomposition of 1% hexogen in toluene affords benzaldehyde, benzonitrile and benzyl alcohol in 0.43, 0.32 and 0.43 mol yields per mol of hexogen, respectively. Phenylnitromethane and benzoic acid are also present in small amounts. These findings provide supporting evidence for the involvement of the solvent in the reaction.

The DKIE was observed in all solvents that accelerate the decomposition, and typical inhibitors of chain reactions (*e.g.*, NO, NO_2, *p*-dinitrosobenzene) bring the rate constant down to a level characteristic of inert solvents. These data altogether led to a hypothesis [53] on a chain decomposition mechanism of hexogen in solvents containing reactive C–H bonds and a monomolecular mechanism for this decomposition in inert media. Detailed kinetic schemes for both mechanisms were developed and rationalised; it was shown that they are consistent with the experimental data.[53, 55]

An example of a non-chain decomposition mechanism of hexogen in solutions is given in Scheme 2.

Scheme 2

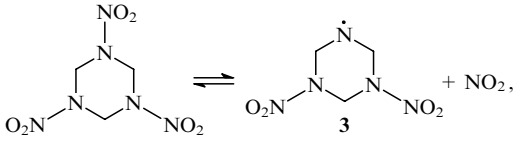

(14)

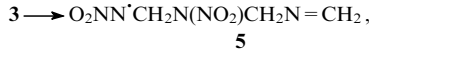

(15)

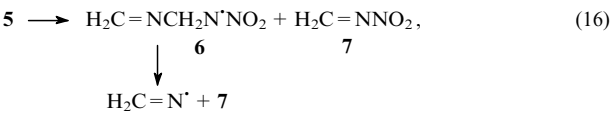

(16)

(17)

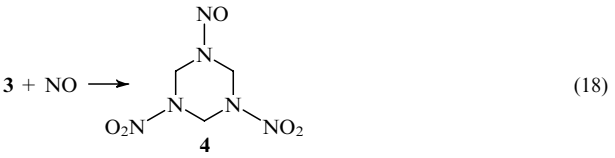

(18)

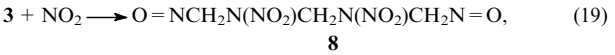

(19)

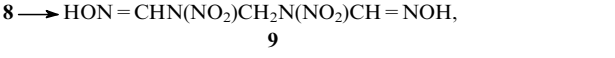

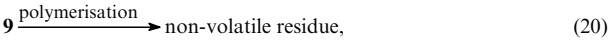

(20)

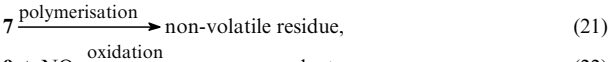

(21)

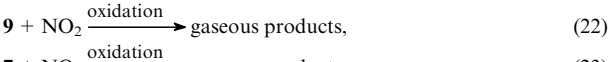

(22)

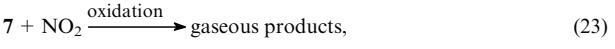

(23)

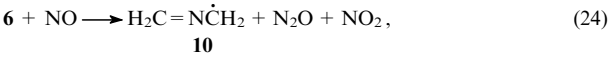

(24)

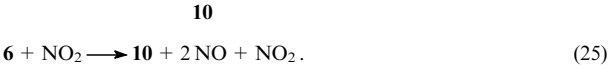

(25)

The reactions (14)–(18) reproduce the basic decomposition mechanism proposed by Schroeder.[4] Other reactions are common to the reactions of NO and NO_2 with free radicals of the C- and N-types as well as for polymerisation and oxidation of unsaturated compounds, isomerisation of nitroso compounds and some other reactions.

The decomposition begins with the dissociation of the N–N bond [reaction (14)]. Like any other dissociation of a molecule into radicals, this reaction is reversible and a cage effect can be observed in viscous media. The radical **3** undergoes isomerisation into the radical **5** which is then decomposed by the reaction (16) to yield an inactive radical $CH_2=N^{\cdot}$. The radical **3** reacts also with NO and NO_2. The reversible formation of mononitroso derivative of RDX **4** proceeds *via* the reaction (18). In contrast to unsubstituted aliphatic *N*-nitroso compounds, which are more stable than the corresponding secondary nitramines,[56, 57] nitroso compounds containing electronegative substituents (including diazacyclohexane derivatives) are less stable [58, 59] than their nitramine analogues. Compound **4** is formed as an intermediate product; its decomposition occurs 10 times faster than that of hexogen.[52] According to a theoretically rationalised mechanism of the reaction of aminyl radicals with NO_2 (see Ref. 60), the reaction (19) of the radical **3** with NO_2 should result in ring opening and the formation of a highly reactive dinitroso compound **8** and then of dioxime **9**. Polymerisation with the formation of a non-volatile residue [reaction (20)] is the most probable route to the conversion of the oxime **9**. Polymerisation of the unsaturated compound **7** [reaction (21)], which competes with its decomposition [reaction (17)], is yet another source of a non-volatile residue. Like nitroethylene, compound **7** is stable but prone to polymerisation. In the presence of NO_2, the unsaturated compounds **9** and **7** are easily oxidised to form gaseous products. It is noteworthy that the reactions (14) and (15) occur only with the radicals **3** and **5** containing a labile (75 kJ mol^{-1}) H_2C-NNO_2 bond in the β-position relative to the free valence.[61] The radical **6** contains no such bond.

The yield of N_2O is 1–1.5 molecules per molecule of hexogen rather than 2 as should follow from Scheme 2.[3] It is possible that the dissociation of the radical **6** into $CH_2=N^{\cdot}$ and compound **7** does not take place at all (the probability of such reaction in the

gas phase was first put in doubt [33]). Instead, the nitraminyl radical **6** is converted into the radical **10** in the presence of nitrogen oxides in the reactions (24) and (25).[62] The latter radical is easily oxidised to yield $HOCH_2NHCHO$, one of the decomposition products of hexogen,[3] and gaseous compounds.

The concentration of nitrogen dioxide in a solution depends on the partial pressure in the gas phase much more strongly than the concentration of NO. Therefore, the ratio of the rates of the reactions (19) and (18) will decrease with hexogen concentration, all other conditions being the same. The yield of the intermediate nitroso derivative **4** will increase correspondingly (*cf.* Refs 49 and 50). Similarly, the polymerisation reactions (20) and (21) will occur faster than the oxidation reactions (22) and (23) due to a sharp decrease in NO_2 concentration in very dilute solutions. This accounts for a significant decrease in the yields of gaseous products and an increase in the yield of the non-volatile residue at hexogen concentrations < 5%. Chain decomposition of hexogen in solution (RH is the solvent) is presented in Scheme 3.[55]

Scheme 3

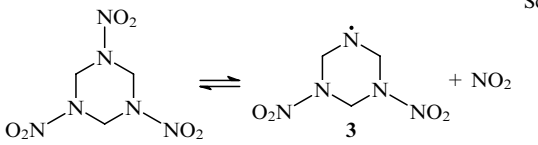

(14)

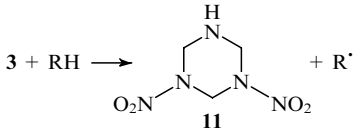

(26)

$$NO_2 + RH \longrightarrow HNO_2 + R^{\bullet}, \quad (27)$$

$$R^{\bullet} + \mathbf{1} \longrightarrow \mathbf{4} + RO^{\bullet}, \quad (28)$$

$$RO^{\bullet} + RH \longrightarrow ROH + R^{\bullet},$$

$$\mathbf{4} \longrightarrow \mathbf{3} + NO,$$

$$R^{\bullet} + NO_2 \longrightarrow RO^{\bullet} + NO,$$

$$RO^{\bullet} + NO_2 \longrightarrow R'CHO + HNO_2,$$

$$R^{\bullet} + NO_2 \longrightarrow RNO_2,$$

$$R^{\bullet} + NO \longrightarrow RNO \longrightarrow R'CH{=}NOH \longrightarrow R'CN + H_2O,$$

$$RNO + 2\,NO \longrightarrow RO^{\bullet} + N_2 + NO_2.$$

R′ is R containing one CH_2 unit less.

The chain reaction begins with the reactions of the free radical **3** and NO_2, which are generated in the first step of decomposition, with the solvent [reactions (26) and (27)]. The reaction (26) is preferable, since it is more exothermic than the reaction (27) by nearly 40 kJ mol^{-1}. As a source of free radicals, the latter reaction can be neglected, since the addition of NO_2 decelerates rather than accelerates the process.

By virtue of the reaction (26) free radicals are not extinguished, and N-centred radicals inactive with respect to the nitro group are converted into C-centred radicals of the solvent. The isotope effect of the solvent is manifested in this step. The maximum rate of the reaction of the radical **3** with the solvent [reaction (26)] is reached at those $D(C-H)$ values which enable the competition of the reaction with the rearrangement of the radical **3** [reaction (15)]. For non-polar solvents, this value is equal to 360 kJ mol^{-1}. In solvents containing polar C–H bonds adjacent to heteroatoms (chloroform, alcohols), the reaction (26) proceeds at a sufficiently high rate even at $D(C-H) >$ 360 kJ mol^{-1}. The reaction (28) occurs only in the solvents in which the radical $R^{\bullet}$ retains its activity and the chain propagates. A combination of the reactions (26) and (28) results in the appearance of an extremum on the experimental curve for the dependence of k_1 on $D(C-H)$.

Extinction of the radicals $R^{\bullet}$ occurs in their reactions with NO_2 and NO, these are consumed in the reaction (28) with hexogen. The reaction of the radical $R^{\bullet}$ with hexogen occurs only where the concentration of the inhibitor (NO, NO_2, *etc.*) is four orders of magnitude lower than that of hexogen. This condition is usually fulfilled, since NO is poorly soluble in the liquid phase where other non-volatile inhibitors are virtually absent.

The rates of bimolecular reactions of the chain generation and propagation [reactions (26) and (28)] increase with pressure; therefore, the stability of hexogen in non-inert solvents will decrease at high pressures used for the determination of the activation volume. Hence, the negative activation volume of decomposition of hexogen in THF, one of the most active solvents,[52] can easily be explained. Many structural analogues of hexogen, *e.g.*, trinitrosohexogen and 1,3,3,5,5-pentanitropiperazine, are also characterised by negative activation volumes in THF.[52] Other hexogen analogues, including octogen, that were studied in acetonitrile (but not in THF), which was inert in this concrete case,[55] have positive activation volumes.

Despite their obvious incompleteness, the schemes of monomolecular (see Scheme 2) and chain decomposition of hexogen (see Scheme 3) in solutions [53, 55] provide an explanation for the principal experimental results, *e.g.*, the dependence of the yields of gaseous products on the concentration of hexogen, high yields of mononitrosohexogen in very dilute solutions of inert solvents, cage effects and, what is even more important, enhancing effects of some solvents and the negative activation volumes in the decomposition of hexogen in THF.

Further chain propagation is provided by the reaction of the radicals **3** with the solvent. This is favoured by low concentrations of gaseous inhibitors (NO and NO_2) in solutions and the absence of non-volatile free radical scavengers which cannot be formed from the methylene groups of hexogen. Apparently, this factor is the most important. Thus the final decomposition products of DMNA contain stable dimethylnitrosamine, while the intermediate products contain nitrosomethane and formaldoxime,[13] both of which are efficient free radical acceptors. Therefore, no chain reactions occur in the case of DMNA. All the solvents including alcohols are inert with respect to DMNA. The solvents listed in Table 6 appeared to be inert with respect to hexanitrohexaazaisowurtzitan (CL-20) as well.[54] Although the nitramine groups of this compound are structurally similar to those of hexogen, CL-20 cannot be regarded as its complete analogue. Owing to the presence in CL-20 of a stable carbon backbone, its decomposition affords numerous reactive products which remain in the condensed phase and prevent the onset of the chain reaction.[63, 64]

In contrast, the chain decomposition of octogen is very well-expressed.[54] As in hexogen, the nitramine groups are separated only by methylene groups, therefore, the formation of condensed products possessing inhibitory properties is prevented.

The chain mechanism described above eliminates all contradictions in the interpretation of decomposition reactions of hexogen and octogen. In solutions as well as in the melt and in the solid state, homolysis of the N–NO_2 bond is the first decomposition step.

IV. Structures and stabilities of secondary nitramines. Kinetic data

Unlike studies on DMNA, hexogen and octogen that have been the subjects of comprehensive examination (both theoretical and experimental), studies on the thermal decomposition of other secondary nitramines were largely confined to measurements of reaction rates and determination of kinetic parameters under various experimental conditions. Since the kinetic parameters of decomposition reflect its mechanism, it is appropriate to consider the correspondence of the kinetic data with the mechanism involving dissociation of the N–NO_2 bond. The known formal

kinetic characteristics of the decomposition of secondary nitramines are given in Table 7.

The maximum difference in the decomposition rates of nitramines is three orders of magnitude, data on decomposition of nitramines in the solid phase being set aside, since the rates here are determined not only by their structures, but also by their physical properties. This difference is only partly due to the errors in the determination of activation energies used for extrapolation of rate constants to reference temperature. In general terms, the differences in the decomposition rates are determined by the dependence of the energy of the N—N bond on the structure of the nitramine. It has been shown for the first time [26] that stability of a nitramine depends critically on the spatial structure of its nitramine groups. The activation energies for the decomposition

Table 7. Kinetic characteristics of decomposition reactions of secondary nitramines.

Compound	Formula	Medium	Method [a]	T /°C	E_a /kJ mol^{-1}	log$A$ (s^{-1})	$10^5 k$ /s^{-1} (200 °C)	Ref.
Dimethylnitramine	Me_2NNO_2	gas	GLC	165–200	221.8	20	3.5	9
		"	see [b]	–	193.4	15.8	0.3	2
		"	MM	180–260	170.8	14.1	1.8	11
		gas + CH_2O	MM	180–240	162.8	13.7	0.6	12
		solution in isooctane	LC	200–300	195.5	17.8	17.9	50
		melt	LC	200–280	159.1	13.2	4.8	50
Diethylnitramine	Et_2NNO_2	gas	MM	180–240	174.1	15.1	1.3	65
		solution in isooctane	LC	200–300	188.8	16.6	2.6	50
Dipropylnitramine	$Pr^n_2NNO_2$	gas	MM	200–240	176.2	14.8	2.2	65
		solution in isooctane	LC	220–260	200.9	17.6	2.9	50
Diisopropylnitramine	$Pr^i_2NNO_2$	the same	LC	200–300	178.3	15.9	18.4	50
		solution in acetone	LC	220–250	183.8	161	9.2	50
N-Nitromorpholine	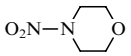	the same	MM	210–245	162.8	13.6	4.2	66
N-Nitropiperidine	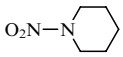	gas	MM	210–240	176.2	14.8	2.5	65
		solution in benzene	LC	220–300	201.8	16.6	0.2	50
		solution in acetone	LC	240–290	198.8	16.3	0.3	50
N-Nitropyrrolidine	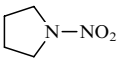	the same	LC	240–290	215.6	18.4	0.4	50
N,*N*′-Dinitropiperazine	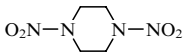	gas	MM	200–240	159.9	13.6	8.9	26
		gas + NO	MM	220–250	151.1	12.0	0.2	26
		solution in nitrobenzene	MM	225–245	155.3	12.0	0.8	66
		solution in trinitrobenzene	MM	230–245	191.7	15.7	0.4	67
		solution in acetone	LC	240–290	220.2	19.1	0.6	50
		melt	MM	216–250	198.4	17.3	2.5	66
N,*N*′-Dinitroimidazolidine	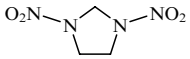	gas	MM	170–200	146.5	13.5	213	26
		gas + NO	MM	170–200	169.1	15.6	87	26
		solution in *m*-dinitrobenzene	MM	170–210	155.7	13.6	26	66
		solution in acetone	LC	200–240	200.1	19.1	132	50
		solution in trinitrobenzene	MM	120–210	158.6	14.0	29	67
		melt	MM	135–200	155.3	13.9	57	66
		"	LC	200–250	197.6	18.7	77	50
1,3-Dinitro-1,3-diazacyclohexane	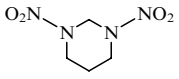	solution in acetone	LC	200–280	205.5	18.0	2.0	50
		solution in ethanol	LC	200–300	167.4	14.6	13	50
		melt	LC	240–260	175.4	15.4	11	50
1,3,3-Trinitroazetidine	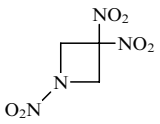	solution in acetone	LC	189–263	182.5	16.4	20	50
		melt	LC	220–250	182.9	16.3	12	50
		"	LC	160–250	195.9	17.5	10	68
		solution in benzene	LC	160–260	168.7	14.7	100	68
		solution in acetone	LC	189–280	182.5	16.5	44	68
		solution in methanol	LC	180–240	128.5	11.4	1600	68
trans-1,4,5,8-Tetranitrodecahydropyrazino[2,3-*b*]pyrazine	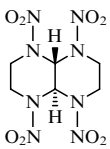	solid phase	DSC	204–234	209.7	18.9	6	69

Table 7 (continued).

Compound	Formula	Medium	Method [a]	T /°C	E_a /kJ mol^{-1}	log$A$ (s^{-1})	$10^5 k$ /s^{-1} (200 °C)	Ref.
Hexogen	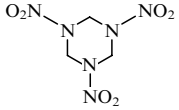	gas	DSC	208–256	145.2	13.5	550	70
		"	MM	170–190	125.6	11.7	688	71
		"	MM	170–200	146.5	13.5	213	26
		"	–	165–247	125.6	11.8	908	3
		"	MM	175–202	169.1	16.0	220	72
		gas + NO	MM	170–200	169.1	15.6	85	26
		solution in trotyl	MM	195–280	171.6	15.5	40	28
		solution in dicyclohexyl phthalate	MM	201–280	173.7	15.4	33	28
		solution in *m*-dinitro-benzene	MM	160–200	166.2	14.3	9	34
		solution in trotyl	MM	166–184	154.5	13.9	71	51
		solution in benzophenone	MM	–	158.2	14.5	110	51
		solution in polyphenyl ether	DSC	–	200.9	–	–	73
		solution in acetone	LC	200–240	190.0	17.9	83.4	50
		solution in benzene	LC	206–256	161.1	14.1	23	5
		melt	LC	200–250	158.2	14.3	68	50
		"	MM	232–247	197.2	18.3	34	70
		"	MM	213–299	198.8	18.5	35.5	28
		"	GLC	–	203.8	19.2	53	29
		"	DSC	210–261	189.2	–	–	74
		"	DSC	–	180.4	16.4	31	75
		"	Ic	204–225	171.6	–	–	76
		"	DSC	204–240	209.7	19.6	28	77
		"	TGA	205–220	200.1	18.7	41	78
		"	DTA	197–267	207.2	20.8	914	79
		solid phase	MM	150–197	213.1	18.6	12	80
		the same	MM	150–197	217.7	19.1	1.2	34
		"	MM	140–190	166.6	11.2	0.01	81
		"	MM	178–200	190.4	17.7	48	82
		"	MM	170–198	180–264	–	–	83
		solid phase + CH_2O	MM	170–197	184.2	–	–	84
		the same	MM	–	173.7	14.5	2.1	3
		"	MM	130–180	165.3	11.7	0.03	71
Octogen	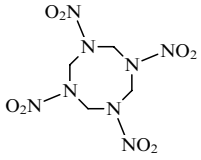	gas	MM	171–215	221.4	20.2	2630	51
		"	MM	230–250	133.9	13.2	6	28
		"	MM	205–280	165.3	14.2	9	26
		"	MM	245–275	159.1	12.5	0.9	72
		"	–	–	193.4	16.4	1.2	2
		solution in *m*-dinitro-benzene	MM	171–215	187.9	16.0	1.5	73
		solution in acetone	LC	189–289	210.1	18.9	5.7	50
		melt	MM	271–314	220.6	19.7	2.3	28
		"	DSC	271–285	214.7	18.8	1.2	82
		solid phase	MM	176–230	158.6	11.2	0.05	34
		the same	MM	150–170	150.7	10.8	0.15	85
		"	MM	180–210	171.6	12.8	0.1	71
		"	DTA	185–280	172.5	14.3	2.0	86
		"	DTA	160–250	113.0	10.0	170	86
		"	DSC	251–263	175.8	–	–	75
		"	MM	261–276	205.1	17.8	0.55	87
		"	MM	130–180	158.6	9.2	10^{-3}	88
		"	LC	230–270	221.4	18.4	9.0	50
		"	DTA	229–269	187.1	15.9	1.9	43
		"	IRS	166–194	204.3	19.8	192	87
		solid phase + N_2 (35 atm)	DTA	229–269	108.4	8.5	35.5	43
		solid phase + N_2 (1 atm)	TGA	229–269	146.9	11.5	2.0	43
		solid phase + air (1 atm)	TGA	229–269	205.1	17.0	0.25	43
		solid phase + O_2 (1 atm)	TGA	229–269	208.0	17.1	0.15	43

Table 7 (continued).

Compound	Formula	Medium	Method [a]	T /°C	E_a /kJ mol^{-1}	log$A$ (s^{-1})	$10^5 k$ /s^{-1} (200 °C)	Ref.
1,4-Dinitrotetrahydroimidazo-[4,5-*d*]imidazolidine-2,5-dione	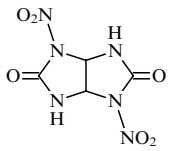	solid phase	DSC	225 – 245	217.7	20.9	27	59
1,5-Diacetyl-3,7-dinitro-1,3,5,7-tetraazacyclooctane	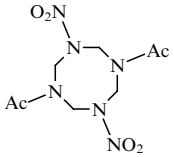	solid phase	DSC	250 – 270	175.8	15.3	4.0	59
3,7-Dinitro-1,3,5,7-tetraazabicyclo-[3.3.1]nonane	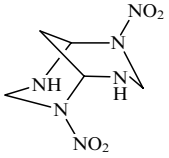	solid phase	–	–	192.1	16.6	4.0	59
Aliphatic nitramines	$R^1N(NO_2)R^2$							
	R^1 = Me, R^2 = $(CH_2)_2CO_2Me$	solution in di-butyl phthalate	MM	200 – 230	169.1	13.7	1.3	89
	R^1 = Me, R^2 = $(CH_2)_2CN$	the same	MM	190 – 230	175.4	14.4	1.2	90
	R^1 = Me, R^2 = CH_2OMe	"	MM	190 – 230	171.2	13.9	1.0	89
	R^1 = Me, R^2 = $(CH_2)_2CO_2H$	"	MM	200 – 230	170.8	14.0	1.5	89
	R^1 = Me, R^2 = $(CH_2)_2CO_2H$	"	MM	180 – 220	167.8	14.7	16	91
	R^1 = $(CH_2)_2CN$, R^2 = CH_2Fc (see [c])	"	MM	160 – 180	179.6	17.3	2.7	90
	R^1 = $(CH_2)_2$. .$C(NO_2)_2Me$, R^2 = CH_2Fc	"	MM	180 – 200	154.0	12.9	0.01	89
	R^1 = R^2 = $(CH_2)_2CN$	"	MM	210 – 250	172.9	13.9	0.1	89
	R^1 = R^2 = $(CH_2)_2CO_2H$	"	MM	200 – 240	170.8	14.1	1.6	89
	R^1 = R^2 = CH_2Fc	"	MM	190 – 200	161.2	13.5	0.05	90
	R^1 = R^2 = $(CH_2)_2CO_2Me$	"	MM	210 – 250	170.4	13.7	0.8	90
	R^1 = R^2 = $CH_2C(NO_2)_2Me$	solution in *m*-dinitrobenzene	MM	145 – 170	166.2	15.7	230	92
N-Methyl-*N*,2,4,6-tetranitroaniline (tetryl)	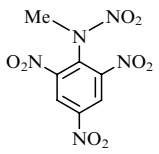	melt	MM	211 – 260	160.7	15.4	460	27
		"	TGA	132 – 164	146.1	12.9	59	93
		"	IC	131 – 155	150.7	13.8	148	94
		"	MM	140 – 165	167.4	16.0	330	95
		"	MM	150 – 175	150.3	13.5	166	90
		"	MM	130 – 139	254.9	27.3	10^3	96
		"	MM	140 – 150	232.3	14.5	10^3	97
		"	MM	150 – 175	146.5	–	–	98
		"	DSC	170 – 174	242.8	–	–	99
		solution in poly-phenyl ether	DSC	–	140.2	–	–	73
		solid phase	DSC	–	217.7	12.5	10^3	96
		the same	DSC	–	153.2	12.7	62	96
		"	DSC	–	229.8	–	–	73

Table 7 (continued).

Compound	Formula	Medium	Method [a]	T /°C	E_a /kJ mol^{-1}	log$A$ (s^{-1})	$10^5 k$ /s^{-1} (200 °C)	Ref.
Other aromatic nitramines	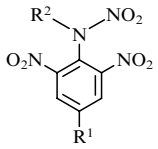							
	R^1 = OMe, R^2 = Me	solution in *m*-dinitrobenzene	MM	145–165	134.4	12.4	323	89
	$R^1 = R^2$ = Me	the same	MM	150–170	143.2	13.4	416	89
	R^1 = Cl, R^2 = Me	"	MM	145–165	141.1	13.1	346	89
	R^1 = Br, R^2 = Me	"	MM	155–175	141.5	13.4	638	89
	$R^1 = NO_2$, R^2 = Et	"	MM	144–165	139.4	13.9	3432	89
	$R^1 = NO_2$, $R^2 = Pr^n$	"	MM	135–155	136.9	13.3	1630	89
	$R^1 = NO_2$, $R^2 = Pr^n$	"	MM	130–150	140.2	14.2	5537	89
Hexanitrohexaaza-isowurtzitan (CL-20)	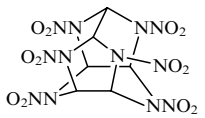	solution in acetone	LC	146–226	177.5	17.6	1088	50
		solution in *m*-dinitrobenzene	MM, TG	150–195	189.6	18.6	450	100
		solid phase	TGA	190–204	151.9	13.6	71	101
		the same	TGA, DSC	160–180	172.0	13.8	0.8	100
		solid phase + air (1 atm)	MM, TG	183–211	223.5	20.5	7.3	102
4,10-Dinitro-2,6,8,12-tetraoxa-4,10-diaza-tetracyclo[5.5.0.0^{5,9}0^{3,11}]-dodecane	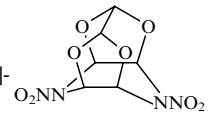	gas	MM	240–250	163.3	14.1	1.2	101
		solution in dibutyl phthalate	MM	210–250	167.5	13.5	1.0	101
		solid phase	MM	210–225	196.8	15.4	0.05	101

[a] Designations: GLC, gas-liquid chromatography; MM, manometric method; LC, liquid chromatography; DSC, differential scanning calorimetry; Ic, isothermic calorimetry; TGA, thermogravimetric analysis; DTA, differential thermal analysis; TG, thermogravimetry; IRS, IR spectroscopy. [b] Thermochemical calculation. [c] Fc, ferrocenyl.

of planar nitramine groups are, on average, 172 kJ mol^{-1}, whereas that for the pyramidal group does not exceed 160 kJ mol^{-1}. In the case of hexogen, two of three nitramine groups are pyramidal, and it is 100 times less stable than octogen with all of the four groups planar. Low stability is also characteristic of 1,3-dinitro-1,3-diazacyclopentane (see Table 7) with pyramidal nitramine groups. At the same time, all the nitramines containing planar groups are decomposed at approximately the same rates. The frequencies of anti-symmetrical oscillations of the nitro groups (ν_{as}) are determined by the extent of the deviation of the nitramine groups from the planar structure.[103] The dependence of ν_{as} on the length of the N–N bond is linear. In its turn, the elongation of the bond is accompanied by a decrease in its strength. The maximum values of ν_{as} around 1600 cm^{-1} are observed for the nitramine groups attached to a five-membered ring or to even more strained rings as, *e.g.,* in CL-20 (see Table 7) or in compounds **12** and **13**.[103]

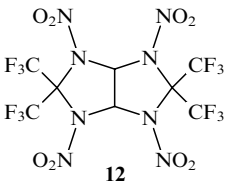

12

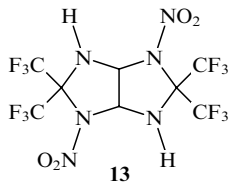

13

The frequency of anti-symmetrical oscillations of the nitro group ν_{as} of hexogen is 1570 (see Ref. 103) (*cf.* 1605 cm^{-1} for CL-20) (see Ref. 100). Therefore, CL-20 is 10 times less stable than hexogen.

There is a correlation between ^{13}C and ^{15}N chemical shifts in the NMR spectra and the kinetic parameters of the decomposition reactions.[104, 105] This correlation provides additional support in favour of a decomposition mechanism of secondary nitramines which involves cleavage of the N–NO_2 bond. This can also be used for predicting the stabilities of novel nitramines.

Resonance conjugation of the nitramine group with a phenyl substituent or another system of π-bonds is yet another factor which determines the stabilities of nitramines. For example, the activation energy for the decomposition of tetryl is 21 kJ mol^{-1} lower than that of dimethylnitramine and the reaction rate is 200 times higher. Nevertheless, the effect of conjugation on the D(N–NO_2) is rather weak. Similar structural changes, *i.e.*, passage from MeX to $PhCH_2X$, decrease the energies of the C–X bonds (X = H, NO_2, Hal) by 60 kJ mol^{-1} (see Ref. 15). The induction effects of substituents in the α- or β-positions on D(N–NO_2) and the decomposition rates of nitramines are very small.[90] This explains why virtually all secondary nitramines manifest high thermal stabilities and are widely used as explosives. The reduction of stabilities of secondary nitramines to a level which makes impossible their practical application requires a combination of two adverse factors, *viz*., the presence of two substituents that can manifest resonance conjugation (*e.g*., heterocycles) or a combined effect of the pyramidal structure of the nitramine group and one such substituent.

Thus, the formal kinetic parameters and the dependence of the decomposition rates on nitramine structures can be explained within the framework of an integral mechanism which postulates the cleavage of the N–NO_2 bond. It may be expected that other nitramines will manifest a decomposition mechanism similar to that of DMNA, hexogen or octogen and the decomposition rates will obey the regularities described above. For example, the decomposition rate in the liquid phase of a popular novel high-energy compound CL-20, which contains four pyramidal nitramine groups, is higher than that of hexogen or 1,3-dinitro-1,3-diazacyclopentane each containing two groups of the same structure.[54, 63, 64, 100–102, 106–108] This prognosis is fully corroborated by experimental results (see Table 7). Extrapolation of a detailed scheme of the non-chain decomposition of hexogen to CL-20 prompts an unambiguous conclusion about the formation of low-volatile nitroso compounds, aldehydes, unsaturated com-

pounds, and stable iminoxyl radicals. Determination of the functional groups in condensed products corroborates this conclusion.[63,64] The chain decomposition of CL-20 in solutions is impossible due to the formation of products able to scavenge free radicals. Indeed, all the solvents studied are inert with respect to CL-20.[54] Yet another novel promising explosive reagent, *viz.*, 1,3,3-trinitroazetidine (see Table 7), contains two functional groups that can undergo decomposition, *viz.*, a nitramine group and a dinitromethylene group. A comparison of parameters of decomposition of compounds containing such groups [109] suggests that the cleavage of the $N-NO_2$ bond at temperatures below 200 °C occurs several times faster than that of the $C-NO_2$ bond, whereas at 240 °C the rates of these reactions become similar. A conclusion about the existence of two parallel channels for decomposition of 1,3,3-trinitroazetidine with approximately the same rates was drawn on the basis of direct kinetic measurements and identification of the decomposition products.[68]

V. Conclusion

Significant progress has been achieved in the study of the mechanism of the first step of thermal decomposition of nitramines. Thus it has become possible to predict the rate of this step, which determines the thermal stability of a compound. Contrariwise, secondary reactions including those of the starting compound have been rather poorly studied. Reactions of nitramines with nitrogen dioxide have not been investigated; as yet, little is known about the autocatalysis of decomposition of nitramines in liquid and solid phases and the mechanism of autocatalysis also remains to be elucidated. Studies along these lines will be continued in the near future. A quantitative description of detailed decomposition schemes for the simplest molecules [110,111] can be used for the calculation of combustion rates.

The problem of decomposition of nitramines in the solid phase is closely related to the general problem of chemical kinetics, *viz.*, the development of a physical model of solid-phase monomolecular reactions. Analysis of effects of various factors, such as defects of a crystal lattice and phase transitions,[112] on the decomposition of hexogen and octogen have given a strong impetus to the further progress of these studies.[82,83,88] A search for nitramines that decompose in a non-localised manner, *i.e.*, uniformly over the whole crystal, presents special interest for investigators. Verification of semi-empirical models [113] allowing estimation of decomposition rate constants in the solid phase k_{solid}, requires comprehensive investigations which will include determination of the main characteristics of a crystal and study of a relationship between k_{solid} and melting temperature, structure and specific properties of a crystal, *e.g.*, compressibility, free volume, density and their temperature dependences. The immense diversity of secondary nitramines which differ in both decomposition rates and physical properties, leaves hope that compounds for such investigations will be found.

This review has been written with the financial support of the International Science and Technology Centre (Project No. 2324p).

References

1. Y P Agrawal *Prog. Energy Combust. Sci.* **24** 1 (1998)
2. R Shaw, F E Walker *J. Phys. Chem.* **81** 2572 (1977)
3. M A Schroeder, in *The 16th JANNAF Combustion Meeting, CPIA Pub. 308, 1979* Vol. 2, p. 17
4. M A Schroeder, in *The 18th JANNAF Combustion Meeting, CPIA Pub. 347, 1981* Vol. 2, p. 395
5. F I Dubovitskii, B L Korsunskii *Usp. Khim.* **50** 1828 (1981) [*Russ. Chem. Rev.* **50** 958 (1981)
6. T L Boggs *Prog. Astronaut. Aeronaut.* **90** 121 (1984)
7. R Fifer *Prog. Astronaut. Aeronaut.* **90** 177 (1984)
8. N E Ermolin, V E Zarko *Fiz. Goren. Vzryva* **33** 10 (1997) [a]
9. J M Flournoy *J. Chem. Phys.* **36** 1106 (1962)
10. R C Cass, S E Fletcher, C T Mortimer, P G Quincey, H D Springall *J. Chem. Soc.* 958 (1958)
11. B L Korsunskii, F I Dubovitskii *Dokl. Akad. Nauk SSSR* **155** 402 (1964) [b]
12. B L Korsunskii, F I Dubovitskii, G V Sitonina *Dokl. Akad. Nauk SSSR* **174** 1126 (1967) [b]
13. Y G Lazarou, P Papagiannakopoulos *J. Phys. Chem.* **94** 7114 (1990)
14. D M Golden, R K Soly, N A Gac, S W Benson *J. Am. Chem. Soc.* **94** 363 (1972)
15. V I Vedeneev, L V Gurvich, G K Karachevtsev, V N Kondrat'ev, V A Medvedev, E L Frankevich *Energii Razryva Khimicheskikh Svyazei. Potentsialy Ionizatsii i Srodstvo k Elektronu* (Energies of Rupture of Chemical Bonds. Ionisation Potentials and Electron Affinity) (Moscow: Nauka, 1974)
16. S A Lloyd, M E Umstead, M C Lin *J. Energ. Mater.* **3** 187 (1985)
17. S E Nigenda, D F McMillen, D M Golden *J. Phys. Chem.* **93** 1124 (1989)
18. P M Stewart, J B Jeffries, J M Zellweger, D M Golden, D F McMillen *J. Phys. Chem.* **93** 3557 (1989)
19. Y Ling, Z-H Tang, H-M Xiao, in *The 17th Proceedings of International Pyrotechnic Seminar Combined with the 2nd Beijing International Symposium on Pyrotechnics and Explosives* Vol. 1 (Beijing: Beijing Institute of Technology Press, 1991) p. 466
20. L Philips, R Shaw, in *The 10th Symposium on Combustion, Cambridge, 1964* p. 453
21. J C Oxley, M Hiskey, D Naud, R Szekeres *J. Phys. Chem.* **96** 2505 (1992)
22. R W Hoffmann *Aufklarung von Reaktionsmechanismer* (Stuttgart: Georg Thieme, 1976)
23. N J Harris, K Lammertsma *J. Phys. Chem. A* **101** 1370 (1997)
24. O P Strausz, H E Grunning *Can. J. Chem.* **41** 1217 (1963)
25. J M Ferguson, L Phillips *J. Chem. Soc.* 4416 (1965)
26. Yu M Burov, G M Nazin *Kinet. Katal.* **23** 12 (1982) [c]
27. A I B Robertson, A Yoffe *Nature (London)* **161** 806 (1948)
28. A I B Robertson *Trans. Faraday Soc.* **45** 85 (1949)
29. F C Rauch, A J Fanelli *J. Phys. Chem.* **73** 1604 (1969)
30. B Suryanarayana, R J Graybush, I R Autera *Chem. Ind.* 2177 (1968)
31. J D Cosgrove, A J Owen *Combust. Flame* **22** 13 (1974)
32. A E Axworthy, J E Flanagan, D O Woolery, in *The 15th JANNAF Combustion Meeting, CPIA Pub. 297, 1978* p. 253
33. R Behrens Jr *J. Phys. Chem.* **94** 6706 (1990)
34. Yu Ya Maksimov, in *Teoriya Vzryvchatykh Veshchestv (Trudy MKhTI)* [The Theory of Explosives (Proceedings of Moscow Chemical Technological Institute)] (Moscow: Vysshaya Shkola, 1967) Vol. 53, p. 73
35. G Coats, L Sutton *J. Chem. Soc.* 1187 (1948)
36. J J Batten *Aust. J. Chem.* **24** 945 (1971)
37. M Farber, R D Srivastava *Chem. Phys. Lett.* **64** 307 (1979)
38. M Farber, R D Srivastava *Chem. Phys. Lett.* **80** 345 (1981)
39. C V Morgan, R A Bayer *Combust. Flame* **2** 59 (1979)
40. S A Shackelford, M B Coolidge, B B Goshgarian *J. Phys. Chem.* **89** 3118 (1985)
41. J J Batten *Aust. J. Chem.* **23** 737 (1970)
42. K J Kraeutle, in *The 17th JANNAF Combustion Meeting, CPIA Pub. 329, 1980* Vol. 2, p. 509
43. K J Kraeutle, in *The 18th JANNAF Combustion Meeting, CPIA Pub. 347, 1981* Vol 2, p. 383
44. K J Kraeutle, in *The 19th JANNAF Combustion Meeting, CPIA Pub. 366, 1982* Vol. 1, p. 331
45. Y Oyumi, T B Brill *Combust. Flame* **62** 213 (1985)
46. T B Brill *Prog. Energy Combust. Sci.* **18** 91 (1992)
47. T R Botcher, C A Wight *J. Phys. Chem.* **97** 9149 (1993)
48. T R Botcher, C A Wight *J. Phys. Chem.* **98** 5441 (1994)
49. J C Hoffsommer, D J Glover *Combust. Flame* **59** 303 (1985)
50. J C Oxley, A B Koob, R Szekeres, W Zheng *J. Phys. Chem.* **98** 7004 (1994)
51. J Wilby, in *Symposium on Chemical Problems Connected with the Stability of Explosives, Stockholm, 1967* p. 51
52. J Wang, K R Brower, D L Naud *J. Org. Chem.* **62** 9055 (1997)
53. Yu Shu, V V Dubikhin, G M Nazin, G B Manelis *Dokl. Akad. Nauk* **368** 357 (1999) [b]

54. Yu Shu, V V Dubikhin, G M Nazin, G B Manelis, in *The 31st International Annual Conference of ICT, Karlsruhe, 2000* p. 7/1
55. Yu Shu, V V Dubikhin, G M Nazin, G B Manelis *Izv Akad. Nauk, Ser. Khim.* 1323 (2002) [d]
56. B L Korsunskii, V I Pepekin, Yu A Lebedev *Izv. Akad. Nauk SSSR, Ser. Khim.* 525 (1967) [d]
57. O F Golovanova, G V Sitonina, V I Pepekin, B L Korsunskii, F I Dubovitskii *Izv. Akad. Nauk SSSR, Ser. Khim.* 1012 (1988) [d]
58. B L Korsunskii, L Ya Kiseleva, R G Gafurov, E M Sogomonyan, L T Eremenko, F I Dubovitskii *Izv. Akad. Nauk SSSR, Ser. Khim.* 1781 (1974) [d]
59. S Zeman, M Dimun *Propel. Expl. Pyrotechn.* **15** 217 (1990)
60. Y Ling, Z-H Tang, H-M Xiao *Propel. Expl. Pyrotechn.* **17** 116 (1992)
61. C F Melius, J S Binkley, in *The 23rd JANNAF Combustion Meeting, CPIA Pub. 457, 1986* Vol. 1, p. 241
62. V V Charskii, A N Pavlov, G M Nazin, B L Korsunskii, B S Fedorov *Izv. Akad. Nauk, Ser. Khim.* 794 (1989) [d]
63. D G Patil, T B Brill *Combust. Flame* **92** 456 (1993)
64. M D Pace *Mol. Cryst. Liq. Cryst.* **219** 139 (1992)
65. B L Korsunskii, F I Dubovitskii, E A Shurygin *Izv. Akad. Nauk SSSR, Ser. Khim.* 1452 (1967) [d]
66. G V Sitonina, B L Korsunskii, N F Pyatakov, V G Shvaiko, I Sh Abdrakhmanov, F I Dubovitskii *Izv. Akad. Nauk SSSR, Ser. Khim.* 311 (1979) [d]
67. B A Lur'e, V N Ivakhov, in *Khimicheskaya Fizika Kondensirovannykh Vzryvchatykh Sistem (Trudy MKhTI)* [Chemical Physics of Condensed Explosive Systems (Proceedings of Moscow Chemical Technological Institute)] (Moscow: Vysshaya Shkola, 1979) Vol. 104, p. 12
68. J Oxley, J Smith, W Zheng, E Rogers, M Coburn *J. Phis. Chem. A* **101** 4375 (1997)
69. H Rongzu, Y Zhengnan, L Yanjun *Thermochim. Acta* **123** 135 (1988)
70. R N Rogers, G W Daub *J. Anal. Chem.* **45** 596 (1973)
71. M S Belyaeva, G K Klimenko, L T Babaitseva, P N Stolyarov, in *Khimicheskaya Fizika Protsessov Goreniya i Vzryva. Kinetika Khimicheskikh Reaktsii* (Chemical Physics of Combustion and Explosion. Kinetics of Chemical Reactions) (Chernogolovka: The Branch of Institute of Chemical Physics, Academy of Sciences of the USSR, 1977) p. 47
72. Yu Ya Maksimov, V N Apalkova, O V Broverman, A I Solov'ev *Zh. Fiz. Khim.* **59** 342 (1985) [e]
73. R N Rogers, E D Morris *J. Anal. Chem.* **38** 412 (1966)
74. P G Hall *Trans. Faraday Soc.* **67** 556 (1971)
75. K Kishore *Anal. Chem.* **50** 1079 (1978)
76. J L Janney, R N Rogers, in *Proceedings of the 7th International Conference on Thermic Analysis, Kingston, 1982* Vol. 2, p. 1426
77. R N Rogers, L S Smith *Thermochim. Acta* **1** 1 (1970)
78. Y Oyumi *Prop. Explos. Pyrotechn.* **13** 42 (1988)
79. K K Miles, M.S.Thesis, Navy Postgraduate School, Monterey, CA, 1972
80. K K Andreev *Termicheskoe Razlozhenie i Gorenie Vzryvchatykh Veshchestv* (Thermal Decomposition and Combustion of Explosives) (Moscow: Nauka, 1966) p. 67
81. Yu M Burov, G B Manelis, G M Nazin *Khim. Fiz.* **3** 1126 (1984) [f]
82. S Bon *Chemistry of Solid State* (Ed. W E Garner) (London: Butterworth, 1955)
83. J J Batten *Aust. J. Chem.* **23** 749 (1970)
84. J J Batten *Aust. J. Chem.* **24** 2025 (1971)
85. G K Klimenko, in *Gorenie i Vzryv* (Combustion and Explosion) (Moscow: Nauka, 1972) p. 785
86. A I Medvedev, G V Sakovich, V V Kostantinov, in *Soveshchanie po Kinetike i Mekhanizmu Khimicheskikh Reaktsii v Tverdom Tele (Tez. Dokl.)* [Meeting on Kinetics and Mechanism of Chemical Reactions in Solids (Abstracts of Reports)] (Novosibirsk: Institute of Physical Chemistry of Foundation of Processing of Mineral, Siberian Branch of Academy of Sciences of the USSR, 1977) Vol. 1, p. 163
87. T B Brill, R J Karpowicz *J. Phys. Chem.* **86** 4260 (1982)
88. Yu M Burov, G B Manelis, G M Nazin *Khim. Fiz.* **4** 956 (1985) [f]
89. R S Stepanov, V N Shan'ko, I P Medvetskaya, V M Gorodetskaya, in *Khimicheskaya Fizika Protsessov Goreniya i Vzryva. Kinetika Khimicheskikh Reaktsii* (Chemical Physics of Combustion and Explosion. The Kinetics of Chemical Reactions) (Chernogolovka: The Branch of Institute of Chemical Physics, Academy of Sciences of the USSR, 1977) p. 56
90. M A Stepanova, V P Tverdokhlebova, R S Stepanov *Zh. Org. Khim.* **13** 1364 (1977) [g]
91. V N Shan'ko, R S Stepanov, in *Fizicheskaya Khimiya* (Physical Chemistry) (Krasnoyarsk: Siberian Chemical Technological Institute, 1974) Vol. 1. p. 190
92. B L Korsunskii, L Ya Kiseleva, V I Ramushev, F I Dubovitskii *Izv. Aka. Nauk SSSR, Ser. Khim.* 1778 (1974) [d]
93. M A Cook, M T Abegg *Ind. Eng. Chem.* **48** 1090 (1956)
94. F I Dubovitskii, Yu I Rubtsov, G B Manelis *Izv. Akad. Nauk SSSR, Otd. Khim. Nauk* 1763 (1960) [d]
95. F I Dubovitskii, G B Manelis, L P Smirnov *Zh. Fiz. Khim.* **35** 521 (1961) [e]
96. R C J Farmer *J. Chem. Soc.* **117** 1603 (1920)
97. C V Hinshelwood *J. Chem. Soc.* **119**/**120** 721 (1921)
98. M A Cook *The Science of High Explosives* (Ed. L Reinhold) (New York: Chapman and Hall, 1958)
99. R N Rogers, L S Smith *Anal. Chem.* **39** 1024 (1967)
100. B Korsounskii, V Nedelko, N Chukanov, T Larikova, F Volk, in *The 30th International Annual Conference of ICT, Karlsruhe, 1999* p. 64/1
101. D G Patil, T B Brill *Combust. Flame* **87** 145 (1991)
102. S Lobbecke, M A Bohn, A Pfeil, H Krause, in *The 29th International Annual Conference of ICT, Karlsruhe, 1998* p. 145/1
103. T B Brill, Y Oyumi *J. Phys. Chem.* **90** 2679 (1986)
104. S Zeman *Thermochim. Acta* **202** 191 (1992)
105. S Zeman *Thermochim. Acta* **333** 121 (1999)
106. A Porollo, T Petuhova, V Ivshin, T Pivina, B Korsounskii, O Golovanov, in *The 32nd International Annual Conference of ICT, Karlsruhe, 2001* p. 87/1
107. X Zhao, L Li *Energetic Mater.* **3** 31 (1995)
108. J-H Kim, Y-J Yim *J. Chem. Eng. Jpn.* **32** 237 (1999)
109. G M Nazin, V V Prokudin, G B Manelis *Izv. Akad. Nauk, Ser. Khim.* 231 (2000) [d]
110. Y-X Zhang, S H Bauer *Int. J. Chem. Kinet.* **31** 655 (1999)
111. Y-X Zhang, S H Bauer *Int. J. Chem. Kinet.* **33** 70 (2001)
112. L N Erofeev, V P Tarasov, Yu B Kalmykov, Yu Shu, V V Dubikhin, G M Nazin *Izv. Akad. Nauk, Ser. Khim.* 958 (2001) [d]
113. Yu M Burov, G M Nazin, G B Manelis *Izv. Akad. Nauk, Ser. Khim.* 1261 (1999) [d]

[a] — *Combust. Explos. Shock Waves (Engl. Transl.)*
[b] — *Dokl. Chem. (Engl. Transl.)*
[c] — *Kinet. Catal. (Engl. Transl.)*
[d] — *Russ. Chem. Bull., Int. Ed. (Engl. Transl.)*
[e] — *Russ. J. Phys. Chem. (Engl. Transl.)*
[f] — *Chem. Phys. Rep. (Engl. Transl.)*
[g] — *Russ. J. Org. Chem. (Engl. Transl.)*

Russian Chemical Reviews **73** (4) 309 – 350 (2004) © 2004 Russian Academy of Sciences and Turpion Ltd

DOI 10.1070/RC2004v073n04ABEH000839

Phosphapalladacycles: preparation routes †

V V Dunina, O N Gorunova

Contents

I.	Introduction	309
II.	Direct intramolecular cyclopalladation	310
III.	Synthesis of phosphapalladacycles by oxidative addition	328
IV.	Transmetallation	330
V.	P,C-Chelation of phosphine-substituted phosphorus ylides	331
VI.	Other routes to phosphapalladacycles	332
VII.	Supplement	336
VIII.	Conclusion	345

Abstract. The review considers methods of synthesis of cyclopalladated compounds of the PC- and PCP-type including intramolecular activation of the C–H bonds in the P-donor ligands, oxidative addition of preliminarily functionalised substrates to palladium(0), transmetallation of lithiated compounds, chelation of phosphine-substituted phosphorus ylides, and some non-standard processes resulting in a new ligand formation on a metal template. Particular attention has been given to the structural factors and experimental conditions that determine the feasibility of direct cyclopalladation of mono- and bidentate phosphines, phosphites and phosphinites. The bibliography includes 384 references.

I. Introduction

A driving force for writing of this review was the impressive progress achieved in the modern homogeneous metal complex catalysis due to the use of metallacycles as catalysts or precatalysts.[1–5] A pronounced increase in the catalytic activity due to *ortho*-metallation (for phosphites) was first detected by Lewis in 1986.[6,7] The unique role of phosphine complexes of palladium in classical homogeneous catalysis is known; therefore, it is not surprising that phosphapalladacycles occupy a central place in the new branch of catalysis.[1,5,8–12]

Some data concerning the chemistry of mono- and bicyclic compounds of this class, including their dendrimeric forms,[13] can be found in recent reviews dealing with cyclometallation (involving all metals [14–20] or only palladium [21]) and organopalladium compounds.[22] Among the survey papers devoted to cyclometallated structures each with one particular heterodonor atom,[19,23–28] only one publication [19] is known dealing with complexes of various metals with P-donor ligands (up to mid-1979). The monograph by Omae,[18] which summarises his earlier reviews is largely a compilation (as noted in a book review [29]).

V V Dunina, O N Gorunova Department of Chemistry, M V Lomonosov Moscow State University, Leninskie Gory, 119992 Moscow, Russian Federation. Fax (7-095) 932 88 46. Tel. (7-095) 939 53 76.
E-mail: dunina@org.chem.msu.ru (V V Dunina), o.gorunova@org.chem.msu.ru (O N Gorunova)

Received 2 April 2003
Uspekhi Khimii **73** (4) 339 – 382 (2004); translated by Z P Bobkova

The intensive development of this field seen in recent years calls for a deliberate consideration of the existing routes to phosphapalladacycles known to date (up to the end of 2002) and elucidation of the specific features of the process of their formation.

The purpose of this review is to analyse the methods of synthesis of cyclopalladated complexes with P-donor atoms with the emphasis on the factors that determine the feasibility of this process. The reactions of phosphapalladacycles will be considered elsewhere. Compounds in which the metal is linked directly to one or two phosphorus(III) atoms and to one carbanionic centre incorporated in an anionic bi- or tridentate chelating ligand (mono- or bicyclic structures of kind **A** or **B**) were chosen as the objects. Optically active compounds of this type constitute the subject of a special review. Type **C** structures for palladium have not been obtained as yet, although for other transition metals (for example, Rh, Ir and Pt), not only CPC- [30,31] but also PCPC- [32] and PCCP-type complexes are known.[33]

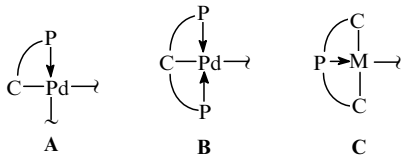

A **B** **C**

Compounds of structural types **D** – **G** are beyond the scope of this review, because their properties differ appreciably from those typical of classical mono- or dianionic phosphapalladacyclic systems. These include compounds with phosphines chelated to the metal due to additional π-coordination through their double bonds (**D**);[34–39] metallacycles of other types, for example, CN- (**E**) [40,41] or CC-types (**F**),[41–45] containing a non-donor phosphorus atom; and bicyclic structures with the Pd–C and Pd←P bonds located in two different metallacycles (*e.g.*, those of **G** type).[46,47]

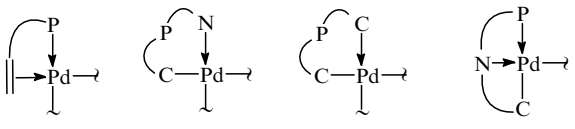

D **E** **F** **G**

† The first review in a series of publications devoted to the chemistry and stereochemistry of phosphapalladacycles.

Conversely, PC-chelated phosphine-substituted phosphorus ylides are covered in the review, despite the formally neutral character of these ligands (actually, they are zwitter-ionic), because their C-donor atom shows carbanionic properties. Dendrimers containing phosphapalladacycles[13] are not discussed, but their precursors[48–50] are included in Tables 1–4 (see Supplement).

The basic difference between metallacyclic systems with P-heterodonor atoms and their CN- or NCN-analogues is that the phosphorus atom can act not only as a σ-donor but also as a π-acceptor.[51–54] Many other properties of phosphapalladacyclic systems account for the fact that they are considered separately. These include the higher atomic radius of phosphorus, the lower basicity and greater 'softness' of this atom (the latter is especially important for the complexation with the 'soft' palladium atom) and much higher strength of the P → Pd bonds compared to the N → Pd bonds. Since the possibility of structural modification aimed at the optimisation of electronic and steric characteristics of the metal and its environment is extremely important for almost any field of application of cyclopalladated complexes, the demand for information on the synthetic routes to these compounds is evident.

An idea of the diversity of known phosphapalladacyclic compounds can be gained from Tables 1–4 given in the Supplement, which summarise methods for the synthesis of complexes classified in terms of structural features. Monochelate compounds of the PC-type (**A**) and their bicyclic or 'pincer' PCP analogues (**B**) are included in Tables 1 and 4, respectively; the bis(chelate) spiro complexes and derivatives of PC-coordinated phosphine-substituted phosphorus ylides are considered in Tables 2 and 3, respectively. The Tables give only the structures of primary cyclometallation products arranged according to the type of hybridisation of the metal-bound carbon atom (sp^3 or sp^2) and to the size of the chelate ring formed (six-, five- or four-membered). The reaction conditions, the types of intermediates (for multistage processes), the yields in the stage of cyclometallation itself and the total yield (for multistage routes) are also presented.

In the text and in the Tables, the ordinal number of the complex corresponds to the superscript in the designation of the cyclopalladated ligand HL^n, while letters designate all compounds derived from this ligand; the numbers of similar complexes of other metals are primed.

While Tables 1–4 can be useful for the synthesis of known complexes, the main goal of the discussion of published data is to elucidate the regular trends which could be useful for the design of new phosphapalladacycles and in the search for methods for their synthesis.

The routes to cyclopalladated complexes with P-donor atoms are diverse, the most important being direct activation of C–H bonds (Section II) and oxidative addition of a C–H or C–Hal bond of the ligand to a low-valence metal (Section III). Other possible approaches include complexation of Pd(II) with a prelithiated ligand (transmetallation, Section IV) or its simple chelation by formally neutral phosphine-substituted phosphorus ylide ligands (Section V). Some exotic transformations resulting in closure of phosphapalladacycles are considered in Section VI.

II. Direct intramolecular cyclopalladation

Direct intramolecular activation of C–H bonds in P-donor ligands seems to be the most attractive route to phosphapalladacycles.

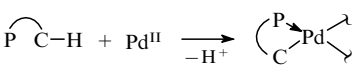

The efficiency of this method is determined, first of all, by the ligand structure; if necessary, it can be increased by optimisation of the reaction conditions. This Section is devoted to consideration of these factors.

1. Structural factors

The ease of cyclopalladation of a P-donor ligand depends, first of all, on its structural features including the position of the C–H bond to be activated (this dictates the size of the phosphapalladacycle formed) and hybridisation of the carbon atom involved, the steric conditions near the P-donor atom and near the metallation site, the basicity of phosphorus atom, *etc*.

a. Localisation of the C–H bond to be activated

The position of the C–H bond being activated with respect to the P-donor atom largely determines the ease of cyclopalladation: the tendency for the formation of five-membered PC-palladacycles is as pronounced as in the case of ligands with other donor atoms.[21]

For example, phosphine HL^1 forms only a five-membered metallacycle in complex **1** due to the activation of the C–H bond of the methylene group in the *o*-Et substituent,[55] despite the presence of aliphatic C–H bonds in sterically less hindered methyl groups of the *o*-Et and PBu^t substituents and an aromatic C–H bond whose activation could have resulted in six- or four-membered metallacycles. The reactions with other aryl-, benzyl- and alkyl-phosphines with PBu^t substituents also always lead to the closure of five-membered palladacycles (see Table 1).

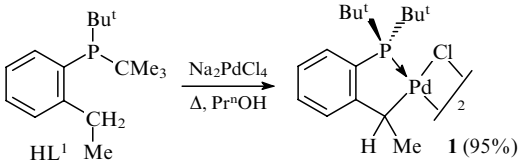

The same trend becomes apparent in Pd(II) reactions with phosphites. Cyclopalladation of tri(*o*-tolyl) phosphite (HL^2) both *via* the standard coordination precursor, $[Pd(\kappa^1\text{-}HL^2)_2Cl_2]$,[56] and *via* the organometallic compound, $[PdCl(\eta^5\text{-}Cp)(HL^2)]$,[57] affords only the five-membered palladacycle **2** due to the attack by palladium on the benzene ring, although the formation of a six-membered metal ring is also possible in principle through activation of the *o*-Me group of the tolyl substituent.

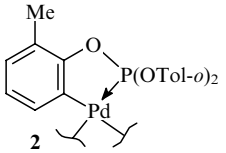

The six-membered metallacycles are rather uncommon; their formation is hampered and becomes possible only when there are no alternatives. For instance, all attempts to close six-membered PC-palladacycles upon activation of the $C(sp^3)$–H bond in the *o*-AlkO group of the phosphines HL^3–HL^9 failed, even in the case of sterically hindered HL^4, HL^6 and HL^8 ligands. It is noteworthy that the corresponding platinacycles **3′**–**9′** are formed upon metallation of not only the methyl group (ligands HL^3–HL^8) but also the methylene group of the *o*-alkoxy substituent (ligand HL^9).[58, 59]

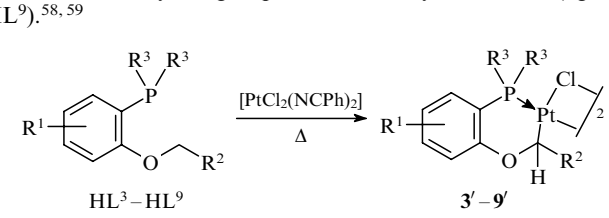

$R^1 = R^2 = H$: $R^3 = Ph$ (HL^3, **3′**), Bu^t (HL^4, **4′**);
$R^1 = 3\text{-MeO}$, $R^2 = H$: $R^3 = Ph$ (HL^5, **5′**), Bu^t (HL^6, **6′**);
$R^1 = 6\text{-MeO}$, $R^2 = H$: $R^3 = Ph$ (HL^7, **7′**), Bu^t (HL^8, **8′**);
$R^1 = H$, $R^2 = Me$, $R^3 = Ph$ (HL^9, **9′**).

As rare examples of six-membered phosphapalladacycles, one can mention bicyclic PCP structures **10a**, **11** and **12**, prepared from

2,2′-bis(diphenylphosphino)stilbene (HL^{10})[60,61] and 1,3-bis-(phosphinomethyl)-2,4,6-trimethylbenzenes (HL^{11} and HL^{12}).[62] In the case of complex **10a** and related derivatives of diphosphines with the dibenzyl skeleton (see Table 4), the unfavourableness of the formation of a six-membered chelate ring is partially compensated by the simultaneous closure of the optimal five-membered phosphapalladacycle.

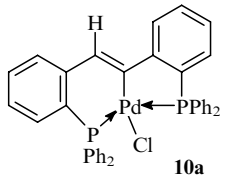

10a

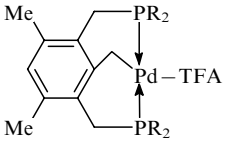

11 (R = Pr^i), **12** (R = Bu^t)

TFA is trifluoroacetate.

The only example of formation of a six-membered PC-palladacycle by a monodentate ligand is *ortho*-palladation of 4-(di-*tert*-butylphosphino)-3-(4-methoxyphenyl)sydnone (HL^{13}). The structure of dimer **13** was confirmed by X-ray diffraction.[63]

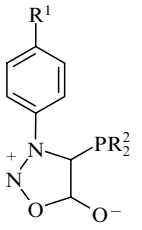

HL^{13}–HL^{16}

Ligand	R^1	R^2
HL^{13}	MeO	Bu^t
HL^{14}	H	Bu^t
HL^{15}	MeO	Ph
HL^{16}	H	Ph

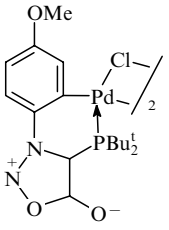

13

The *ortho*-palladation of sydnonylphosphine HL^{13} is possible only under simultaneous assistance of steric and electronic factors. Studies of other ligands of this class have shown that in the absence of the electron-donating 4-MeO group in the aromatic ring but with retention of the bulky substituents at phosphorus (HL^{14})[64] and, especially, upon replacement of the bulky PBu^t_2 group by the less bulky PPh_2 fragment in ligands HL^{15} (see Ref. 65) and HL^{16} (see Ref. 64), the reaction under the same conditions ($PdCl_2$–HCl, EtOH–H_2O, 80 °C, 4 h) gives simple coordination complexes of the type *trans*-[$PdCl_2(HL)_2$], instead of *ortho*-palladated compounds.

It is equally obvious that the formation of five-membered metallacycles in the case of PCP-complexes is facilitated. Unlike *m*-xylylene-α,α′-diphosphine (HL^{17}, $n = 1$), which is easily cyclopalladated under mild conditions (CH_2Cl_2, 20 °C) to give bicyclic structure **17a** with five-membered metallacycles,[66] its homologue with longer diatomic ($n = 2$) bridges between the PPh_2 groups and the phenylene skeleton cannot be involved in this process. Under the same and even under more rigorous conditions, it affords only a coordination complex of the *trans*-[$PdCl_2(HL)$] type with P,P-chelated diphosphine.[67]

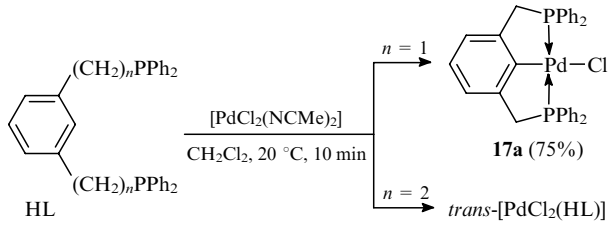

HL

$n = 1$ (HL^{17}), 2.

A forcible argument in favour of the preferred formation of five-membered phosphapalladacycles may be derived from the results of palladation of diphosphine HL^{18}. Despite the potential possibility of closure of two six-membered metal rings with participation of the C(sp^2)–H vinyl bond, a PCP-structure **19** with five- and seven-membered palladacycles is formed upon the formal 1,2-migration of the double bond in the ligand (as confirmed by X-ray diffraction).[68]

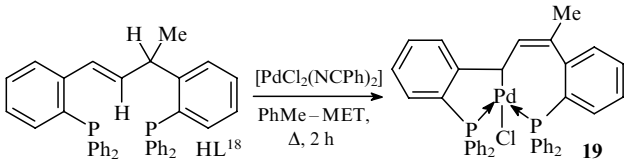

MET is 2-methoxyethanol.

Presumably, the reaction includes the formation of cationic η^3-allylic intermediate **A** upon deprotonation of the tertiary carbon atom of the ArC(Me)H fragment whose C–H bond is most 'acidified', due to its simultaneously benzylic and allylic positions.

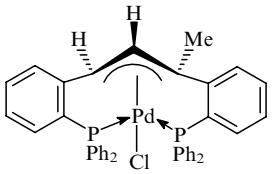

A

The formation of intermediate **A** was confirmed by isolation of its tetrafluoroborate upon dehalogenation of complex **19** under the action of $AgBF_4$. The driving force of subsequent rearrangement of intermediate **A** to the η^1-allylic structure **19** is minimisation of steric strain in the tetracyclic system consisting of two metallacycles and two aromatic rings.[68] This factor appears to be even more important in view of the fact that in the case of diphosphine ligands, the activation of the C(sp^2)–H bonds is usually preferred over the activation of the C(sp^3)–H bond and occurs much more easily (see below).

The closure of the four-membered metallacycle upon cyclopalladation of tri-*tert*-butylphosphine (HL^{20}) is also forced, as this ligand does not contain any C–H bonds suitable for the formation of five-membered rings.[69–74]

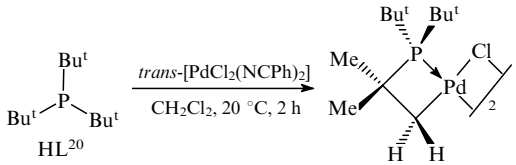

20a (70%)

Probably, the formation of these sterically 'inconvenient' metallacycles is facilitated by the rather large bulk of the phosphorus atom; to some extent, this is also stimulated by steric effects of P-substituents[75] (see below). It should be noted that, in spite of the smaller atomic radius of nitrogen, compounds with four-membered CN-palladacycles are also encountered, although rather seldom;[40,76–78] they are mainly formed with dianionic ligands[77,78] and are prone to ring expansion.[79]

b. Hybridisation of the metallated carbon

The hybridisation of the carbon atom in the C–H bond being metallated undoubtedly influences the ease of cyclometallation. Formal considerations concerning different strengths of aromatic and aliphatic C–H bonds (with an energy of ~110 and ~100 kcal mol^{-1}, respectively[80]) are of little utility due to the complex combination of various factors determining the course of this process (thermodynamics and kinetics, mechanistic features, steric effects, and so on). However, analysis of the available experimental results indicates that the hybridisation of carbon in the C–H bond that is metallated plays different roles in PC- and PCP-systems.

Comparison of the formation conditions of five-membered PC-palladacycles **21a** and **22a** from di-*tert*-butyl-substituted phosphines P(Tol-*o*)Bu^t_2 (HL^{21}) (Na_2PdCl_4, MeOH – PrOH, ~60 °C, 5 min, 90%) and $PBnBu^t_2$ (HL^{22}) (Na_2PdCl_4, MET, 125 °C, 5 days, 64%) shows that the C(sp^3) – H bond in the former ligand [81] is activated more readily than the C(sp^2) – H bond in the latter ligand,[82] as in the first case the reaction requires much less time and occurs at a lower temperature, the dimer being formed in a higher yield.

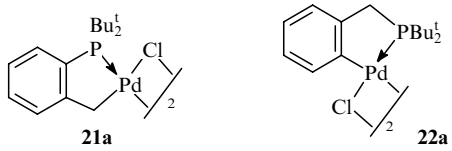

21a **22a**

This regularity is also retained in systems with four-membered metallacycles. Indeed, the bond to be activated during the cyclopalladation of the phosphine $PPhBu^t_2$ (HL^{23}) is the aliphatic C – H bond of the *tert*-butyl group [83,84] rather than the aromatic *o*-C – H bond of the P-phenyl substituent. The lower steric promotion required the use of silver acetate for halide abstraction in this process.

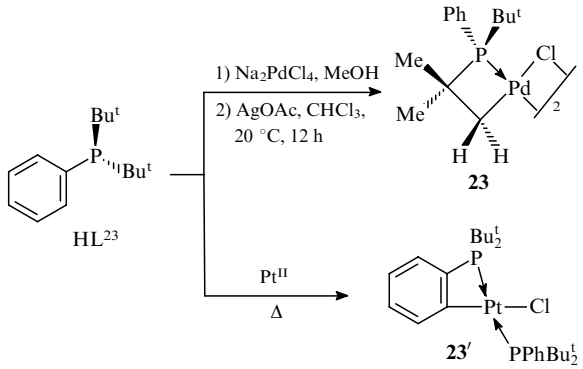

It should be noted that cycloplatination of the HL^{23} ligand and related phosphines follows an opposite trend, *i.e.*, the aromatic C – H bond is attacked preferably to give *ortho*-metallated platinum complex **23′**.[85–87] Moreover, measurements of the H/D exchange kinetics showed that in the presence of platinum(II), the exchange rate of *ortho*-protons in the PPh substituent of phosphine HL^{23} is 50 times as high as the exchange rate of protons in the PBu^t groups.[88] Palladium(II) compounds with four-membered phosphametallacycles, like complex **23′**, have been prepared by a different method (see Section III).

The opposite trend is observed in the formation of two related PCP-complexes, **24a** (260 °C, sublimation, 64%) [89] and **25a** (MET, 125 °C, 25 min, 75%),[90] in the reaction of diphosphines with the same reagent, [$PdCl_2(NCPh)_2$]. Namely, the activation of the aliphatic C – H bond requires higher temperature [or the use of a more efficient reagent, palladium(II) trifluoroacetate [91]] than the palladation involving the aromatic C – H bond.

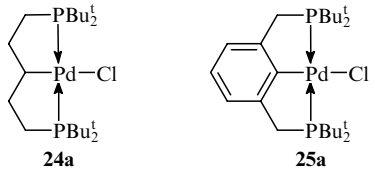

24a **25a**

This difference is even more pronounced in similar, but sterically non-crowded systems with PPh_2 donor groups. Of two diphosphines, one with a *m*-xylylene (HL^{17}) [66] and one with a fully hydrogenated *cis*-cyclohexane-1,3-dimethylene skeleton (HL^{26}),[92] only the former can be effectively palladated at the C(sp^2) – H bond under very mild conditions under the action of a mild reagent, [$PdCl_2(NCMe)_2$], whereas the latter forms only the coordination complex **26** even when treated with the more electrophilic palladium(II) trifluoroacetate.

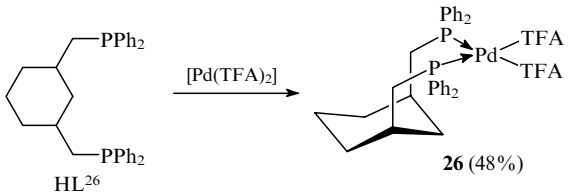

A similar, although less pronounced trend is found in cyclopalladation of the pair of diphosphines with dibenzyl (HL^{27}) or stilbene (HL^{10}) bridges: the activation of the C – H aliphatic bond in the former one requires longer-term refluxing in a more basic solvent (MET) than metallation of the latter HL^{10} ligand at the C(sp^2) – H bond.[60,61]

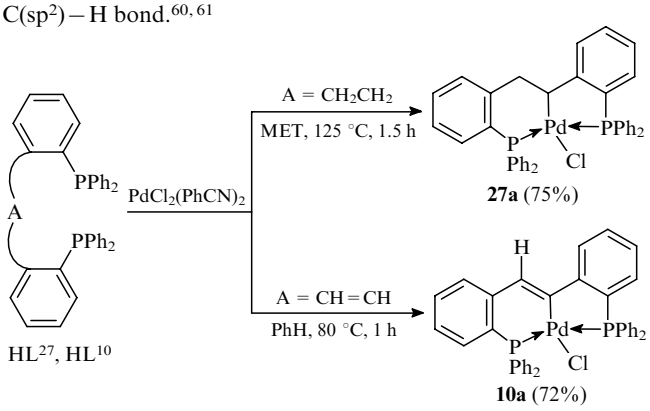

A = CH_2CH_2 (HL^{27}), *trans*-CH=CH (HL^{10}).

In support of the structure of the complex **10a**, X-ray data for the platinum analogue can be mentioned.[60,93] The mechanism of cyclometallation of two related ligands, HL^{27} and HL^{10}, has not been studied; however, it was suggested that activation of the C(sp^2) – H bond in diphosphine HL^{10} can be facilitated due to the formation of an ionic intermediate with a π-coordinated double bond.[61]

Cyclopalladation involving the C(sp^3) – H bond does not take place for diphosphine (2-$Ph_2PC_6H_4)_2CH_2$ (HL^{28}) with the diphenylmethane skeleton containing PPh_2 donor groups. Refluxing of the HL^{28} ligand with [$PdCl_2(NCPh)_2$] furnishes only the coordination complex *cis*-[$PdCl_2(HL^{28})$], despite the potential possibility of the closure of two optimal five-membered phosphapalladacycles.[94]

Thus, for mono- and diphosphine ligands, the ease of cyclopalladation follows opposite patterns of dependence on the type of hybridisation of the carbon atom in the C – H bond that is activated. This suggests that the reaction routes, resulting in the PC- and PCP-structures may be different.

c. The basicity of the phosphorus donor atom

Theoretically, the process rate can also be influenced by the basicity and the coordination ability of the donor atom of phosphorus [51–53] due to the change in the electron density on the metal atom in the coordination precursors. However, comparison of the results of cyclopalladation with palladium(II) acetate of two pairs of *o*-tolylphosphines (HL^{29}, HL^{30} and HL^{31}, HL^{32}) differing in the nature of two other substituents at the phosphorus atoms shows that these factors are relatively insignificant.

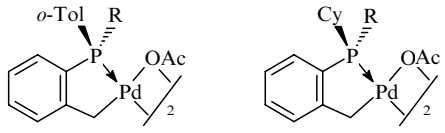

29a, **30a** **31**, **32**

Compound	R	θ /deg	Reaction conditions	Yield (%)
29a	*o*-Tol	194	50 °C, 3 min	93
30a	Bu^t	190	60 °C, 5 min	94
31	*o*-Tol	186	20 °C, 6 h	42
32	Cy	178	20 °C, 12 h	41

Indeed, when the aromatic *o*-tolyl group at the phosphorus atom is replaced by an aliphatic group [Bu^t or cyclohexyl (Cy)], the ligand basicity should substantially increase; this follows from the fact that aliphatic phosphines PBu^t_3 and PCy_3 are much more basic (pK_a 11.4 and 9.70, respectively) than the analogous aromatic phosphine P(Tol-*o*)$_3$ (pK_a 3.08).[52,53] Nevertheless, the activation of the C–H bond is hampered only slightly within any of the above pairs with similar steric characteristics, and the yields of complexes remain almost the same.[10] A decrease in the yield of the cyclopalladated complex on passing from the first pair of complexes to the second one (~90% and ~40%) may be related to both the lower temperatures used in the synthesis and, to some extent, to steric effects, which are measured in terms of the Tolman cone angles (θ) ‡ of the starting phosphines.[95]

d. Steric promotion

It is in phosphine substrates that the steric promotion of the activation of C–H bonds was first observed by Shaw and coworkers.[85,96,97] This phenomenon has developed into a potent tool in cyclometallation chemistry, which is actively applied to ligands with other heteroatoms, for example, to N-donors.[98–101] Since a phosphorus atom is larger than a nitrogen atom, the steric promotion of reactions of P-donor substrates requires the introduction of more bulky substituents: for example, *tert*-butyl or *o*-tolyl groups are desirable for phosphines, whereas for cyclometallation of benzylamines, it is sufficient to introduce *N*-methyl groups.[21,102] This effect has acquired the name of the *gem*-di-*tert*-butyl effect,[97] by analogy with the Thorpe–Ingold *gem*-dimethyl effect, known from the organic chemistry of small carbocycles.[103–105]

The nature of the steric promotion of cyclometallation processes is rather complex (see Section II.3) and the result is not always predictable. The steric crowding of the P-donor ligands ensures acceleration of the process only for some types of substrate and only for a definite location of bulky substituents.

Most often, bulky substituents at phosphorus markedly facilitate the activation of aromatic and aliphatic C–H bonds in monodentate phosphines, these effects being usually correlated with the Tolman angles of the ligands.[95,106,107] A classical example is the extremely easy closure of a strained four-membered metallacycle in complex **20a** in the reaction of bulky tri(*tert*-butyl)phosphine (HL^{20}) with weak palladating reagents, K_2PdCl_4 or *trans*-[$PdCl_2(NCPh)_2$], at room temperature.[69–71]

The accumulation of *tert*-butyl groups at phosphorus facilitates also the closure of five-membered PC-palladacycles. Spectroscopic (^{1}H NMR) monitoring of formation of cyclopalladated complexes **21a** and **30b** from the corresponding coordination compounds *trans*-[$PdCl_2(HL)_2$] with *o*-tolylphosphines HL^{21} and HL^{30} has shown that in the case of the di-*tert*-butyl-substituted ligand HL^{21}, the reaction is complete in 85 min (yield 100%), whereas with the mono-*tert*-butyl-substituted ligand HL^{30}, one-third of the intermediate coordination complex **A** remain intact even after 5 h.[81]

‡ Here and below, the θ values were taken from Ref. 95.

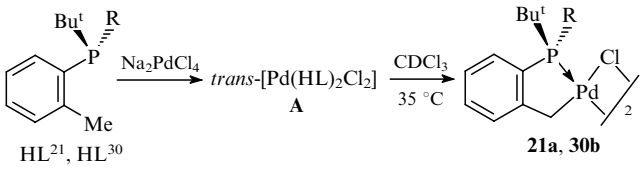

HL^{21}, HL^{30} **A** **21a**, **30b**

R = Bu^t (HL^{21}, **21a**), *o*-Tol (HL^{30}, **30b**).

Ligands of the $PRBu^t_2$ type incorporated in coordination precursors such as [$PdCl_2(HL)_2$] often undergo spontaneous cyclometallation even when the latter are kept at room temperature in solution (R = Bu^t)[70] or on attempted recrystallisation (R = 2-EtC_6H_4).[55] Thus, it is quite clear why all attempts at cyclopalladation of the *o*-tolylphosphines HL^{33} and HL^{34} with small substituents at the phosphorus atom have failed.[108]

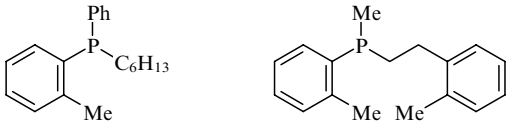

HL^{33} ($\theta \approx 157°$) HL^{34} ($\theta \approx 148°$)

Neither the use of Li_2PdCl_4 and $Pd(OAc)_2$ as palladating agents in the presence of bases (AcONa or K_2CO_3) or without any bases, nor thermolysis (up to 160 °C) of the intermediate coordination complexes [$Pd(HL^{33})_2Hal_2$] or [{$Pd(HL^{34})Hal(\mu$-Hal)}$_2$], nor even generation of a vacant coordination site in the latter complex on treatment with $AgBF_4$ (see Ref. 108) have led to the desired palladacycles.

Perhaps, steric effects are the most pronounced in the cyclometallation of trimesitylphosphine (HL^{35}).[10,109–111] X-Ray diffraction studies of this bulky ligand (θ = 212 °) have shown that repulsion of the three encumbered mesityl groups results in substantial flattening of the pyramidal configuration at phosphorus, in particular, the angles between the P–C bonds are increased to 108–111 ° compared to the typical values for acyclic phosphines being equal to 90–104 °.[112] Cyclopalladation of this phosphine proceeds under mild conditions, the contribution of the steric promotion being so high that variation of reaction conditions including the solvent (CH_2Cl_2, PhH, $CHCl_3$ or EtOH) and the metal : ligand ratio (1 : 2 or 1 : 1) has virtually no influence on the yields of dimer **35a**, which remain nearly quantitative (87%–98%) in reactions carried out at ~20 °C.[110] The ^{1}H NMR monitoring of the reaction presented below has shown that the process is really over after as soon as 5 min.[109]

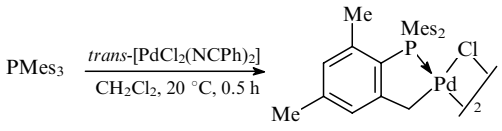

35a (98%)

A similar dependence on the bulk of the P-substituents is also observed in activation of the C(sp^2)–H bonds in benzylphosphines.[82,113,114] The HL^{36} ligand could be cyclometallated with moderate success only using highly electrophilic $Pd(OAc)_2$ (the yield of the dimer was 19%).[114] The intramolecular metallation with a weak electrophile such as Na_2PdCl_4 (AcONa, MET, 130 °C) becomes possible with appearance of the first Bu^t group and is essentially facilitated after the introduction of the second Bu^t group. Thus, the *ortho*-palladated derivatives of the phosphines HL^{37} and HL^{22} are formed in 12% and 75% yields over periods of 24 and 0.5 h, respectively.[82]

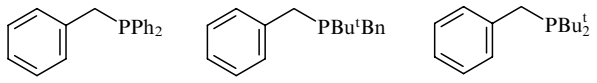

HL^{36} (θ = 151°) HL^{37} (θ = 161°) HL^{22} (θ = 177°)

Apparently, it is due to the lack of bulky P-substituents that the attempts to prepare phosphapalladacycles from dimethylnaphthalen-1-ylphosphine (HL^{38}) have not met with success. Neither pyrolysis of the intermediate coordination complexes of the *cis*-$[Pd(HL^{38})_2X_2]$ type (X = Cl, Br) nor long-term refluxing of their solutions in the presence of bases resulted in activation of the $C(sp^2)-H$ bond.[115]

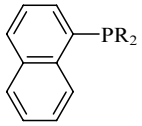

R = Me (HL^{38}), 1-Np (HL^{39});
Np is naphthyl.

HL^{38}, HL^{39}

However, a similar but more bulky tri(naphthalen-2-yl)phosphine (HL^{39}) is cyclometallated on treatment with a more electrophilic reagent, $Pd(OAc)_2$.[116] A certain contribution to increasing the reactivity may also be made by the lower basicity of the P-donor centre in HL^{39} compared to that in HL^{38}.

In substrates with P-donor atoms of other types, *ortho*-palladation also proceeds more readily when steric stimulation is involved. For instance, monodentate phosphaalkenes with an extremely bulky 'supermesityl' substituent (Mes* = 2,4,6-$Bu^t_3C_6H_2$) form phosphapalladocycles at room temperature on treatment with a moderately electrophilic palladating agent:[117]

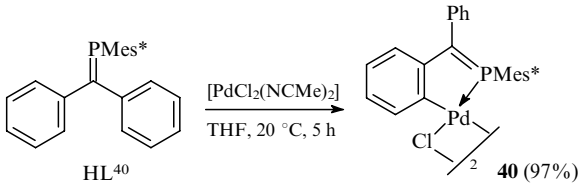

HL^{40} **40** (97%)

Thus, it is clear that cyclopalladation of monodentate phosphines is stimulated by the increase in the size of the P-substituents (*e.g.*, in the series Me < Ph < Bu^t).

It is likely that the activation of the aliphatic C–H bonds can be promoted by an increase in the number of substituents at the carbon atom adjacent to the metallation site. Using platinum analogues as examples, it was found that cyclometallation is markedly accelerated with an increase in the number of β-methyl groups in the $CH_2CR^1R^2Me$ alkyl substituent at phosphorus. Indeed, n-propylphosphine HL^{41} does not form a phosphametallacycle; cycloplatination of isobutylphosphine HL^{42} proceeds only on heating; and neopentylphosphine HL^{43} forms dimer **43′** over a period of several minutes at room temperature.[118, 119] The cyclopalladated derivative **42** is known only for phosphine HL^{42} (see Ref. 119).

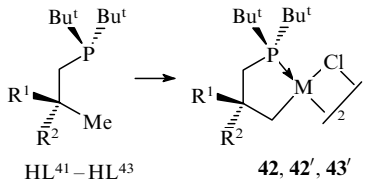

HL^{41}–HL^{43} **42**, **42′**, **43′**

M = Pt: $R^1 = R^2 = H$ (HL^{41}); R^1 = Me, R^2 = H (HL^{42}, **42′**);
$R^1 = R^2$ = Me (HL^{43}, **43′**); M = Pd: R^1 = Me, R^2 = H (**42**).

It is assumed that easier cyclometallation of sterically overcrowded ligands is determined by both the entropy and conformation effects [118, 119] (see Section II.3.a).

It may seem unexpected at first glance that steric stimulation of cyclopalladation of diphosphine ligands by bulky P-substituents is not always observed, the effect being appreciably dependent on the hybridisation of carbon in the C–H bond subject to metallation and perhaps also on the conformational features of the ligand.

As an example of normal steric promotion, one can mention successful cyclopalladation at the $C(sp^3)-H$ bond of diphosphine HL^{44}, containing PBu^t_2 donor groups. When $Pd(TFA)_2$ is used as the metallating agent, the reaction is completed over a short period and gives the product in a nearly quantitative yield.[91]

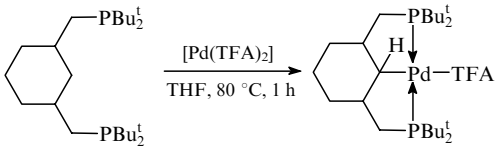

HL^{44} **44** (91%)

Recall that a similar ligand, HL^{26}, with PPh_2 donor groups forms only the *cis*-$[Pd(\kappa^2\text{-}HL^{26})(TFA)_2]$ (**26**) coordination complex under the same conditions.[92]

Conversely, in the activation of $C(sp^2)-H$ bonds, an increase in the steric demands of the P-substituents not only does not promote, but hampers this process. For example, cyclopalladation is substantially retarded when the Ph_2P groups in diphosphine HL^{10} are replaced by more bulky $(o\text{-Tol})_2P$ groups to form the HL^{45} ligand [for PPh_3 and $PPh(o\text{-Tol})_2$, the θ values are 145 and 178°, respectively]. The conversion of HL^{10} and HL^{45} into cyclopalladated complexes **10a** and **45a** in comparable yields required heating for 1 and 16 h, respectively.[60, 61]

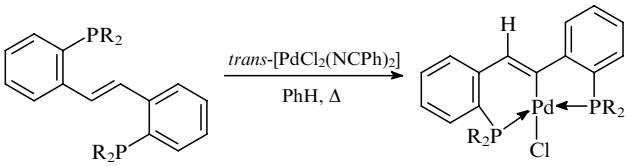

HL^{10}, HL^{45} **10a** (72%), **45a** (62%)

R = Ph (HL^{10}, **10a**), *o*-Tol (HL^{45}, **45a**).

The transformation of steric stimulation into steric impediment is even more obvious from comparison of the metallation conditions of two *m*-xylylene-α,α′-diphosphines HL^{17} and HL^{25}. The HL^{25} ligand with PBu^t_2 groups reacts at much higher temperature and in a more basic solvent (MET, 130 °C, 25 min)[90] than the PPh_2-analogue HL^{17} (CH_2Cl_2, 20 °C, 10 min),[66] despite the much greater cone angles of the P-donor fragments in the former compound (for the monophosphines $BnPBu^t_2$ and $BnPPh_2$, the θ values are 176 and 152°, respectively). The reasons why Milstein and coworkers[120] used much more rigorous conditions (MET, 150 °C) to prepare complex **17a** remain obscure (the yield of the complex is not documented). Presumably, the ease of cyclometallation in these systems is mainly determined by the geometry of the coordination precursors of the *trans*-$[PdCl_2(\kappa^2\text{-}HL)]$ type, in particular, by the degree of proximity of the C–H bond to be activated to the metal.[66]

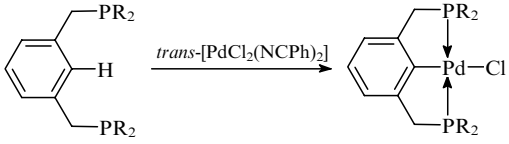

HL^{17}, HL^{25} **17a** (75%), **25a** (75%)

R = Ph (HL^{17}, **17a**), Bu^t (HL^{25}, **25a**).

The activation of the C–H bond in bis(phosphinites) HL^{46} and HL^{47} based on resorcinols containing the PPh_2 donor groups does not require steric stimulation either: on treatment with palladium(II) trifluoroacetate at 20 °C, PCP-complexes **46** and **47** are formed rather fast (2 h) and in high yields (78%–85%).[121]

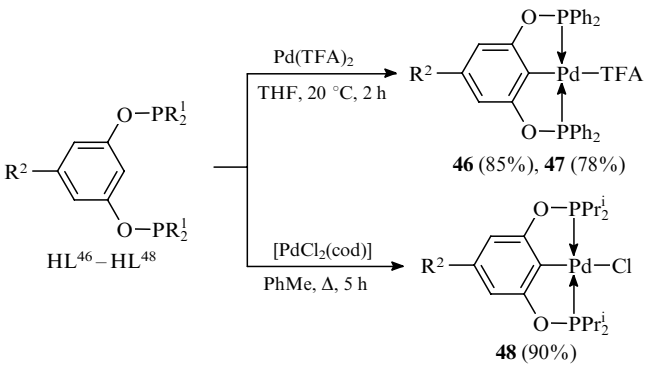

R^1 = Ph: R^2 = H (HL[46], **46**), Me (HL[47], **47**);

R^1 = Pr^i, R^2 = H (HL[48], **48**); cod is cycloocta-1,5-diene.

Conversely, cyclopalladation of sterically more hindered bis(phosphinite) ligand HL[48] with Pr^i_2P donor groups (for the phosphinites $PhOPPh_2$ and $PhOPPr^i_2$, the θ angles are 139 and 149 °, respectively) is obviously hampered and requires more drastic conditions: high yields in the reaction of HL[48] with $[PdCl_2(cod)]$ were attained after refluxing in toluene for 5 h.[122] This difference in the behaviours of bidentate ligands with PPh_2 and Pr^i_2P donor groups becomes even more significant if one takes into account the fact that the palladating agents used should tend[123] (or do tend[124]) to form mononuclear coordination intermediates (see Section II.3.a).

Apparently, the optimal structure of the coordination precursor makes a certain contribution (apart from the steric assistance from bulky supermesityl P-substituents) to the easy cyclopalladation of bis-*m*-diphosphaethene ligand HL[49] (see Ref. 117) and a number of related substrates.[125–127]

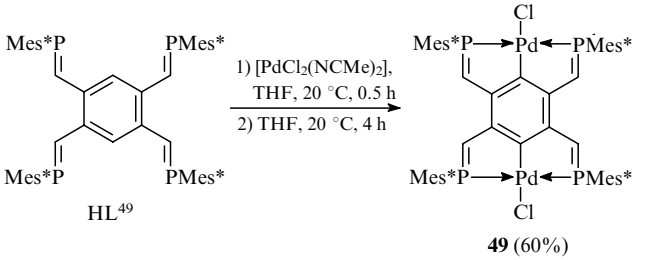

Whereas bulky substituents at the phosphorus atom or in the side chain promote activation of the C–H bonds in monophosphines, the substituents at the carbon atom subjected to metallation appreciably hamper this process.[55,81] This can be illustrated by the conditions of synthesis of PC-palladacycles from (*o*-alkylphenyl)di(*tert*-butyl)phosphines on treatment with Na_2PdCl_4 in alcohols.

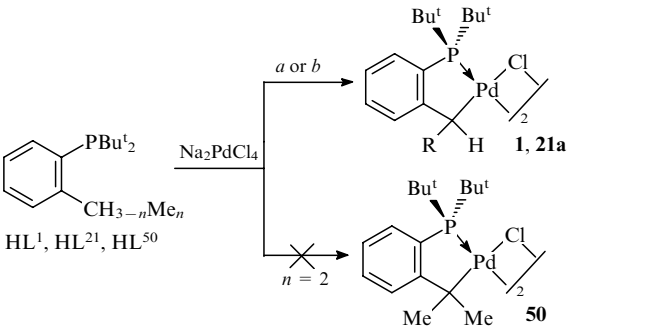

n = 0, R = H (HL[21], **21a**, 90%); n = 1, R = Me (HL[1], **1**, 95%);

n = 2 (HL[50], **50**);

(*a*) ~65 °C, 5 min; (*b*) ~97 °C, 20 min.

The metallation of the secondary C–H bond in the phosphine HL[1] requires a higher temperature and longer time than the metallation of the primary C–H bond in HL[21] analogue, while attempts at activation of the tertiary C–H bond in the phosphine HL[50] have failed at all.[55]

Similar results have also been obtained for reactions of aliphatic diphosphines. For instance, cyclometallation involving the secondary C–H bond in the HL[24] ligand was accomplished in a low yield (12%) by long-term thermolysis of the macrocyclic coordination precursor $[\{PdCl_2(\mu\text{-HL}^{24})\}_2]$ (**24b**) in alcohol;[128] by sublimation of intermediate **24b** *in vacuo* (10^{-2} mm Hg), the yield of the PCP-complex **24a** can be increased to 64%.[89] However, the tertiary C–H bond in the diphosphine HL[51] cannot be metallated under the same conditions.[129]

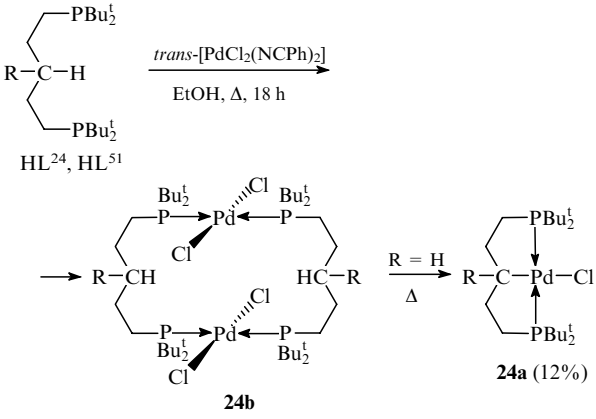

R = H (HL[24], **24a**,**b**); Me (HL[51]).

It is known from the chemistry of benzylaminate CN-systems that the introduction of any α-substituent (even a small Me group[98,130] and, especially, a bulky group[99–101]) into the side chain near the heterodonor atom promotes appreciably the activation of the aromatic C–H bond. Unfortunately, the possibility of estimating the influence of this factor on the activity of P-donor ligands is limited and the available data are rather contradictory.

On the one hand, comparison of the reaction conditions and the yields of the products of cyclopalladation of α-ferrocenylalkylphosphines HL[52] and HL[53] with palladium(II) acetate prompts the conclusion that the activation of the aromatic $C(sp^2)$–H bond is accelerated upon the introduction of a substituent into the side chain.[131,132] The reaction with the α-Me-substituted HL[53] ligand proceeds much faster and gives complex **53** in a higher yield (93% in 1 h) than that with the α-unsubstituted analogue **52** (70% in 8 h). Actually, this effect is even stronger, as it is manifested against the background of an additional steric stimulation by the bulky PBu^t_2 donor groups.

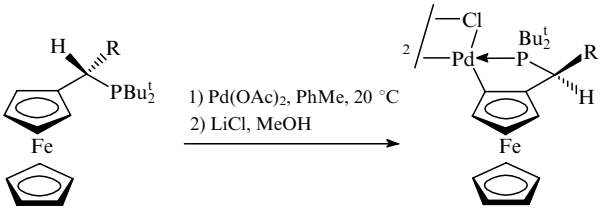

R = H (HL[52], **52**), Me (HL[53], **53**).

Signs of same assistance to the activation of the aliphatic $C(sp^3)$–H bond as a result of similar modification of the ligand structure can be found by comparing the cyclopalladation conditions for two aliphatic diphosphines, $Bu^t_2PCH_2CH(R).(CH_2)_3PBu^t_2$ with R = H (HL[24]) and R = Me (HL[54]), on treatment with *trans*-$[PdCl_2(NCPh)_2]$. The PCP-complex derived from the former ligand, **24a**, was isolated in a very low yield (12%) after long-term (18 h) refluxing in ethanol,[128] whereas the synthesis of

2-methyl-substituted analogue **54** in a moderate yield (36%) required only a 15-minute heating in MET.[133]

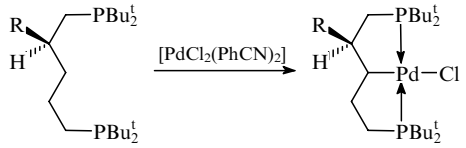

HL[24], HL[54] **24a** (12%), **54** (36%)

R = H (HL[24], **24a**), Me (HL[54], **54**).

On the other hand, an adverse influence of α-substituents can be inferred from comparison of reaction durations of *trans*-[$PdCl_2(NCPh)_2$] with the diphosphines HL[17] and HL[55] possessing aromatic core, under identical conditions (CH_2Cl_2, 20 °C) resulting in two related PCP-complexes **17a**[66,134] and **55a**[135]. The palladation of the HL[17] ligand unsubstituted in the benzylic positions required only 10 min, whereas for the cyclopalladation of its α,α′-dimethyl-substituted analogue HL[55], a 24 h period was required.

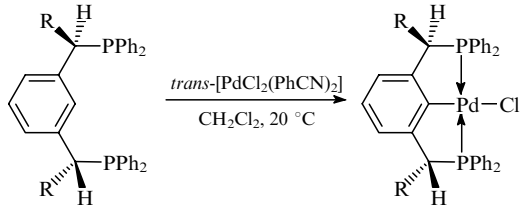

HL[17], HL[55] **17a** (75%), **55a** (85%)

R = H (HL[17], **17a**), Me (HL[55], **55a**).

This anomaly in the behaviour of diphosphine ligands can be due either to the entropy effects [which account for the fact that bulky substituents at phosphorus do not 'work' in these systems (see above)] or to the change in the ligand conformation in the stage of the formation of coordination intermediates. However, it cannot be ruled out that the mechanism of activation of the C—H bonds changes on passing from N- to P-donor ligands, from monodentate to bidentate phosphines, and from $C(sp^3)$—H to $C(sp^2)$—H bonds.

In conclusion, one more parameter important for the cyclopalladation of diphosphines should be mentioned, namely, the P,P-chelate bite angle essential for the formation of the coordination precursor. This parameter is mainly governed by the geometry of the bridging fragment between two P-donor atoms. Apparently, the too large funnel between the side chains in the HL[56] ligand with 1,3-ferrocenedimethylene skeleton (caused by the geometric demands of the five-membered Cp ring) precluded its cyclopalladation to give complex **56** (MX_n = PdCl),[136] whereas analogous 'pincer' complexes of type **A** (for example, **17a**, **25a**, *etc*., see Table 4) with the six-membered *m*-xylylene skeleton are quite accessible.

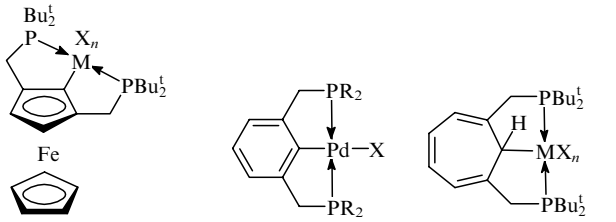

56′ (MX_n = RhHCl) **A** **57′** (MX_n = IrH(CO)Cl)

However, in this case, some mechanistic restrictions cannot be ruled out, because the formation of the hydride PCP-complex **56′** (MX_n = RhHCl) proved to be possible *via* oxidative addition of the HL[56] ligand to the [{Rh(η²-C_2H_4)$_2$(μ-Cl)}$_2$] dimer.[136] A PCP-complex with a bridge incorporating a seven-membered cycloheptatrienyl ring is unknown for palladium(II), although a similar iridium complex **57′** [MX_n = IrH(CO)Cl] has been obtained by the reaction of HL[57] with iridium(I).[137]

Apparently, the true role of the geometric requirements of five-, six- and seven-membered rings in the bridge connecting two donor phosphorus atoms in diphosphines in the intramolecular palladation giving PCP-structures of types **56**, **A** and **57** would be properly evaluated only after the synthesis (or attempts at the synthesis) of the last representative of this series, complex **57** (M = Pd) using this method.

2. Conditions of direct intramolecular cyclopalladation

From the previous section, it is evident that the ease of activation of the C—H bonds in P-donor ligands largely depends on their structural features. With a specified ligand structure, the success of cyclopalladation is determined to a large extent by the conditions chosen, including the type of the palladating agent and the base, the reactant ratio, the nature of the solvent and the temperature regime. Therefore, two equally important problems are to be solved: ensuring the ligand coordination to palladium through the phosphorus atom(s) and creating conditions for the subsequent intramolecular activation of the C—H bond in the resulting coordination precursor.

a. Standard routes and classical reagents

The set of palladating reagents suitable for the direct activation of the C—H bonds in phosphines, phosphites and phosphinites is rather broad (see Tables 1, 4). It includes simple salts ($PdCl_2$), carboxylates [$Pd(OAc)_2$ and $Pd(TFA)_2$] and palladium(II) complexes: anionic ($[PdHal_4]^{2-}$), neutral {$[PdCl_2(Q)_2]$, where Q = MeCN, PhCN or (Q_2) = cod} and cationic ($[Pd(NCMe)_4]^{2+}$) ones. However, the relative efficiency of the reagents is often not correlated with the efficiency characteristic of the reactions of substrates with more rigid donor atoms.[21]

The activity of the palladating agent depends on the nature of the anionic and neutral ligands bound to the metal and on the charge on the metal atom.

1. The electron density on the metal centre determines its electrophilic or nucleophilic behaviour.

2. The dissociative lability of the ligands bound to the metal is important for the creation of the coordination vacancy.

3. The nature of the ligands bound to Pd controls the steric effects in the coordination sphere.

Depending on the reagent used, both the structure of the coordination precursor formed in the first stage and the reaction route as a whole may vary (see Section II.3.a).

The solubility of the palladating agent in organic media is also important for practical use.

The simplest and the most readily available reagent, the insoluble $\{PdCl_2\}_n$ polymer, is applied rather rarely but in some cases, this reagent works quite satisfactorily. Thus in the *ortho*-palladation of the phosphinites HL[58] and HL[59], the yields of dimers **58** and **59** are 50%—52%, irrespective of the electronic properties of the substituents at the phosphorus atoms (aromatic or aliphatic ones),[138] and an increase in the substituent bulk (for example, for R = 2,4-Bu$^t_2$$C_6H_3O$) results in a nearly quantitative yield of the PC-complex **60**.[139]

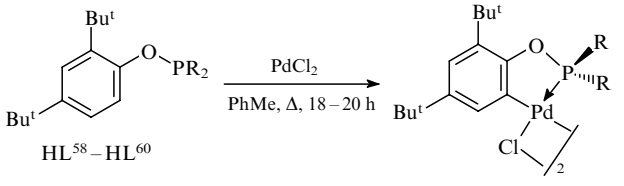

HL[58]—HL[60] **58** (52%), **59** (50%), **60** (96%)

R = Ph (HL[58], **58**), Pr^i (HL[59], **59**), 2,4-Bu$^t_2$$C_6H_3O$ (HL[60], **60**).

The $\{PdCl_2\}_n$ reagent is also able to activate the aliphatic C—H bonds provided that an additional steric stimulation is

involved. In the cyclopalladation of trimesitylphosphine HL^{35} on treatment with $PdCl_2$, good yields (70% – 80%) are attained even at 20 °C, although the process is much slower (8 – 10 h) than that with the soluble $[PdCl_2(NCPh)_2]$ complex (0.5 h).[110] Most likely, the lower activity of palladium chloride is due to retardation of the preliminary P-coordination of the ligand under heterogeneous conditions. Nevertheless, the excellent P-donor properties of the ligands (*e.g.*, HL^{58} – HL^{60}) ensure cleavage of the chloride bridges in the polymeric palladating reagent, while their rich hydrocarbon framing allows performing the reactions in nonpolar solvents (toluene, dichloromethane).

It should be noted that palladium(II) chloride is sometimes used to convert mononuclear bis(phosphine) intermediates into more reactive binuclear complexes in experiments carried out in three stages.[56, 140 – 142]

$$HL \longrightarrow [PdCl_2(\kappa^1\text{-}HL)_2] \longrightarrow \textit{trans}\text{-}[\{PdCl(\kappa^1\text{-}HL)(\mu\text{-}Cl)\}_2] \longrightarrow [\{Pd(\eta^2\text{-}L)(\mu\text{-}Cl)\}_2].$$

The differences caused by the nature of the donor atom are illustrated by the fact that tetrachloropalladates, which are relatively inert in cyclopalladation of N-donor ligands,[21] often ensure almost quantitative yields of the cyclopalladated complexes of the PC-type (mainly, when steric stimulation is involved). Most often, Na_2PdCl_4 is used, and the reaction is carried out in alcohols (MeOH, EtOH, Pr^nOH or MET). In some cases, the stages of monodentate P-coordination and C – H bond activation are carried out separately. Under these conditions, cyclopalladation involving the Me groups of bulky *o*-tolylphosphines ensures good yields of five-membered PC-palladacycles (76% – 97%,[55, 81] see Table 1); they decrease to 60% when the reagent is generated *in situ*.[57] The efficiency of Na_2PdCl_4 is lower in reactions with less bulky ligands ($Bu^iPBu^t_2$,[119] $PhPBu^t_2$,[84] the yields are 40% – 43%) and in the case of activation of aromatic C – H bonds both in phosphines (for $BnPBu^t_2$, the yield is 49%,[82] while for less bulky Bn_2PBu^t, the yield is 13%[82]) and in triaryl phosphites $P(OAr)_3$ (yields 40% – 64%).[143, 144] The decrease in the yields might be partly due to the use of the metal : ligand ratio of 1 : 2; in this case, thermolysis of the coordination precursor in high-boiling solvents is required (MET or decalin).

The drawbacks of sodium tetrachloropalladate include its amorphous structure, which brings about some problems in its purification, while the satisfactory solubility in alcohols is an advantage of this reagent. Strange as it may seem, the lithium salt Li_2PdCl_4, readily soluble in alcohols, which is the most popular reagent (despite its hygroscopicity) in the cyclopalladation of N-donor ligands,[21] has not yet been used for the synthesis of PC-palladacycles.

The crystalline potassium tetrachloropalladate is free from this drawback, however, it is virtually insoluble in alcohols, which has markedly restricted, until recently, the use of this reagent in cyclopalladation. Only one example of the use of K_2PdCl_4 is its reaction with PBu^t_3, which had to be performed in DMF (yield 72%).[69, 70] However, this problem can be solved successfully by passing to a two-phase system at the stage of formation of the coordination intermediate, because potassium tetrachloropalladate is perfectly soluble in water. This approach is illustrated by cyclopalladation of the phosphine $PBu^t(Tol\text{-}o)_2$ (HL^{30}), which includes *in situ* generation of the binuclear coordination precursor **30c** in the $CH_2Cl_2 - H_2O$ two-phase system.[145]

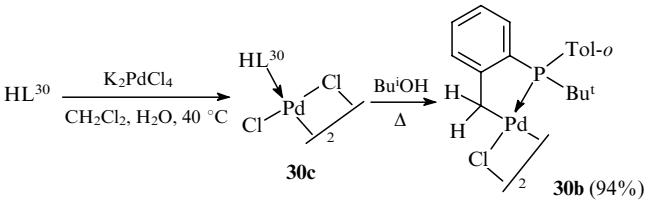

Note for comparison that cyclopalladation of *tert*-butyldi(*o*-tolyl)phosphine by Na_2PdCl_4 in alcohols (see Table 1) afforded dimer **30b** in 84% – 97% yields.[81]

For the formation of PCP-structures, tetrachloropalladates are not used at all and the examples of using the corresponding bromides (K_2PdBr_4) and iodides (Na_2PdI_4) are very scarce (see below).[60, 61]

The activation of the $C(sp^3) - H$ bonds in monodentate P-donor substrates is often performed by palladium(II) acetate, which has a macrocyclic trinuclear structure.[146] However, in this case, too, the outcome depends appreciably on the steric demands of the ligand. With thermal promotion of the process (50 – 60 °C), excellent yields of cyclopalladated complexes (> 90%) can be obtained in the reactions of bulky di-*o*-tolylphosphines $(o\text{-}Tol)_2PR$ with R = *o*-Tol, Bu^t (θ = 194 and 190°, respectively) proceeding in 3 – 5 min.[10, 147, 148] Moreover, the reaction can also be carried out at 20 °C; in this case, its duration has to be increased to 6 – 12 h. The yields are correlated with the steric demands of P-substituents, varying from ~40% in the reactions with $P(Tol\text{-}o)Cy_2$ or $P(Tol\text{-}o)_2Cy$ (θ = 178 and 186°, respectively) to 80% – 90% for $P(Tol\text{-}o)Bu^t_2$ or $PMes_3$ (θ = 186 and 212°, respectively).[10]

The cyclopalladation involving aliphatic fragments proceeds more easily when the chloride ligands in the intermediate coordination complexes are replaced by acetate anions on treatment with silver acetate. This method was used to obtain dimeric PC-complexes **20a** and **23** with strained four-membered phosphapalladacycles from the phosphines PBu^t_2R under mild conditions (20 °C). The yields of cyclopalladated complexes increased with increasing steric stimulation of the process from 55% for R = Ph (θ = 170°) to 100% for R = Bu^t (θ = 182°).[84]

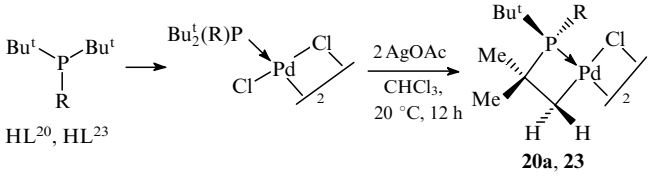

R = Bu^t (HL^{20}, **20a**), Ph (HL^{23}, **23**).

However, in the reactions with monodentate phosphines, palladium(II) acetate does not always show noticeable advantages over halides. Reagents of both classes are equally suitable for sterically hindered substrates, for example, for the *o*-tolylphosphines HL^{21} and HL^{30} (see Refs 10 and 81).

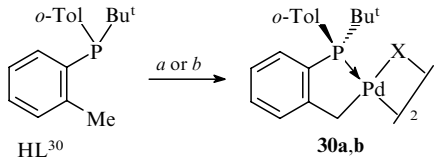

X = OAc (**a**), Cl (**b**); (*a*) $Pd(OAc)_2$, PhMe, 60 °C, 5 min, 90%; (*b*) Na_2PdCl_4, Pr^nOH – MeOH, 3 min, Δ, 96%.

Strange as it may seem, until recently, the electrophilic palladium(II) acetate has been seldom used to activate the aromatic $C(sp^2) - H$ bonds in monodentate phosphines. The rare examples of successful use of this reagent refer to cyclopalladation of the bulky α-ferrocenylalkylphosphines HL^{52} and HL^{53} (in yields ranging from 70% to 93%).[132, 149] In the absence of steric promotion, this reagent is of low utility: *ortho*-palladation of the benzylphosphine $PBnPh_2$ (HL^{36}, θ = 152°) in MeOH with heating (60 °C, 3 h) gave the PC-dimer $[\{Pd(\eta^2\text{-}L^{36})(\mu\text{-}OAc)\}_2]$ (**36b**) in a yield of only 19%.[114] A higher yield (85%) was attained in the reaction with more bulky PBn_2Ph ligand (θ = 158°), but this required longer heating (50 °C, 16 h).[150]

Palladium(II) acetate has not yet been used in reactions with diphosphines, although the more electrophilic trifluoroacetate is often used to create PCP-structures. The latter reagent activates

fairly efficiently both aliphatic [62, 91] and aromatic [151, 152] C–H bonds, thus ensuring the yields of cyclopalladated compounds ranging from 75% to 100%; however, in this case, thermal activation is required (70–130 °C). An exception is provided by the bis(phosphinites) HL[46] and HL[47], which react with $Pd(TFA)_2$ at 20 °C without steric promotion giving rise to PCP-complexes in 78%–85% yields over a period of 2 h.[121]

The next group of reagents is comprised by neutral mononuclear palladium(II) complexes with auxiliary ligands. The coordination compounds like *trans*-$[PdCl_2(NCR)_2]$ (R = Ph, Me) are most popular; the benzonitrile complex is known as the Karash reagent.[153] Reagents of this type are convenient from the practical standpoint, as they are readily soluble in organic solvents, both in alcohols or tetrahydrofuran and hydrocarbons (benzene, toluene, dichloromethane). It is more important that nitriles incorporated in these complexes are classified as weakly bound [154] ligands; therefore, they are replaced by P-donor substrates without any difficulty.

Despite the relatively low electrophilicity of the metal centre in the nitrile reagents, they are traditionally used for the synthesis of PCP-complexes (see Table 4); in the activation of the aromatic C–H bonds, they ensure yields of 60%–90% (with rare exceptions [155]). Their efficiency may be illustrated by the fact that some diphosphine and bis(phosphaalkene) ligands can be introduced in the reaction even at 20 °C;[66, 117, 125–127, 134, 135] nearly quantitative yields (75%–90%) of cyclopalladated compounds can be attained in 10–30 min.[66, 126] Nevertheless, in most cases, the activation of the $C(sp^2)$–H bonds is thermally stimulated (80–150 °C).[90, 120, 155, 156] The high efficiency of nitrile reagents with respect to bifunctional substrates with a rigid, aromatic skeleton is due, most likely, to the forced character of cyclometallation caused by the proximity of the C–H bond (subject to activation) to the metal in the coordination precursor if it has the *trans*-P,P-geometry.[66]

Perhaps, this accounts for the lower efficiency of *trans*-$[PdCl_2(NCPh)_2]$ in the activation of aliphatic $C(sp^3)$–H bonds in conformationally flexible diphosphines with a polymethylene bridge.[89, 128, 133, 157] Even upon high-temperature thermolysis (>260 °C) [128] or sublimation *in vacuo*,[89, 157] the yields of cyclopalladated compounds obtained from the pentamethylene-1,5-diphosphines HL[24] and HL[54] do not exceed 40%. However, in the cyclopalladation of the diphosphine HL[27] with the more rigid dibenzyl skeleton by treatment with the same reagent, a high yield of the PCP-complex **27a** (75%) is attained under milder conditions.[60, 61]

Nitrile palladating agents are used somewhat more rarely to prepare monocyclic PC-complexes, although they are rather effective (with rare exceptions [140]) towards the activation of the $C(sp^2)$–H and $C(sp^3)$–H bonds (see Table 1). To attain high yields in the *ortho*-palladation of monodentate benzylphosphines (83%–85%) [113] and phosphites (70%–90%),[56, 138, 141, 142] heating is usually required; however, cyclopalladation of the phosphaalkene HL[40] with the supermesityl substituent proceeds even at 20 °C (the yield of **40** is 97%).[117]

Under equally mild conditions (20 °C, 0.5–2 h), the aliphatic C–H bonds in the bulky phosphines PBu^t_3 and $PMes_3$ are usually activated (the yields are >80% [70, 71] and 98%,[109, 110] respectively). The (benzonitrile)chloride complex competes quite successfully with a powerful metallating agent such as $Pd(OAc)_2$: trimesitylphosphine HL[35] is cyclopalladated by this complex faster and with a higher yield [109] than by $Pd(OAc)_2$ (see Ref. 10).

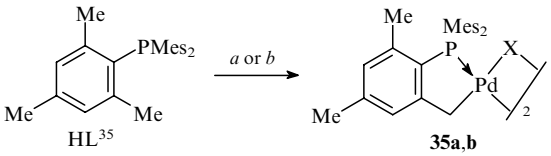

X = OAc (**35a**, 81%), Cl (**35b**, 98%); (*a*) $Pd(OAc)_2$, PhMe, 60 °C, 12 h; (*b*) *trans*-$[PdCl_2(NCPh)_2]$, 20 °C, 30 min.

The efficiency of reagents such as *trans*-$[PdCl_2(NCR)_2]$ is determined, first of all, by the easy replacement of the weakly coordinated nitrile by P- or P,P-donor ligand. Actually, these nitrile complexes can be regarded as solvation-stabilised forms of mononuclear palladium(II) chloride. When the nitrile in these complexes is replaced by a $\eta^2{:}\eta^2$-bound diene in the $[PdCl_2(cod)]$ reagent, restrictions apparently arise already in the stage of ligand coordination to the metal through phosphorus atoms due to both stronger binding of the diene to the metal and steric factors.

For example, all attempts at the intramolecular activation of the $C(sp^3)$–H bond of the trimesitylphosphine HL[35] (θ = 212°) [95] by the diene reagent even under conditions of long-term thermolysis in high-boiling solvents (toluene, xylene) failed, although the use of the benzonitrile reagent furnishes cyclopalladated complex **35a** in a quantitative yield at 20 °C.

The reason for the lack of success is the fact that the sterically crowded phosphine is unable to displace the diene from the starting $[PdCl_2(cod)]$ complex.[110] The diene reagent is markedly inferior to the benzonitrile analogue also in the reaction with the bulky phosphine PBu^t_3, whose cyclopalladation required 8 days (the yield was not reported),[69] whereas with the use of *trans*-$[PdCl_2(NCPh)_2]$, 70% yield was attained in 2 h.[71]

The activation of aromatic C–H bonds in the bidentate P,P-donor ligands by $[PdCl_2(cod)]$ is somewhat more efficient. Although cyclopalladation of diphosphinite HL[48] with the *meta*-phenylene skeleton [122, 158] and *m*-xylylene-α,α'-diphosphine HL[61] (see Ref. 159) gives PCP-complexes **48** and **61a** in almost quantitative yields (90%–98%), this still requires long-term (5 h) heating in toluene.

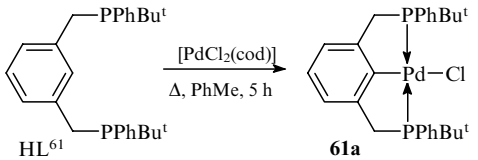

Note for comparison that the use of other reagents [the acetonitrile complex [66] or palladium(II) [121] trifluoroacetate] in reactions with related P,P-ligands allows one to attain rather high yields (75%–85%) at 20 °C over short periods of time (10 min to 2 h, see Table 4).

Assuming that the efficiency of nitrile reagents is mainly determined by the ease of replacement of the auxiliary neutral ligand, one should expect that the appearance of phosphines (that are held more tightly by the metal centre) in the palladating reagent would complicate the stage of formation of the coordination intermediate. From this standpoint, the results of cyclopalladation of the HL[62] ligand with a phosphine reagent, *trans*-$[PdBr_2(PPh_3)_2]$, appear rather unexpected: the PCP-complex **62a** has been obtained in a quite satisfactory yield.[155]

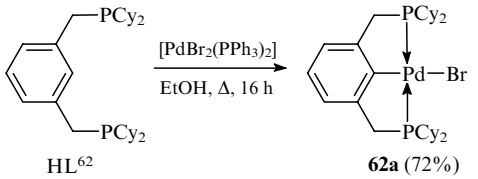

Conversely, the reaction of the same HL[62] ligand with the nitrile reagent $[PdCl_2(NCPh)_2]$ gave polymeric coordination complex *trans*,*trans*-$[\{PdCl_2(\mu\text{-HL}^{62})\}_n]$ as the major product; the C–H bond in this complex was activated with moderate success only upon long-term thermolysis (MET, 48 h, yield 31%).[155]

It could be suggested that in the above example, a positive role is played by the replacement of the chloride in the nitrile metallating agent by the bromide in the phosphine analogue. However, this appears unlikely in view of the behaviour of diphosphines with dibenzyl (HL[27]) and stilbene skeletons (HL[10] and HL[45]) with respect to various palladating reagents (see Table 4). For instance, the activation of the aliphatic C–H bond in the diphosphine HL[27]

is obviously hampered upon the replacement of the chloride reagent $[PdCl_2(NCPh)_2]$ by the bromide $K_2[PdBr_4]$ and, the more so, by the iodide $Na_2[PdI_4]$. Under similar conditions, the yield of the PCP-complexes **27** either sharply decreases (X = Cl, 75%; X = Br, 26%), or remains comparable (X = I, 86%) provided that the reaction duration is increased five- to seven-fold.[60,61]

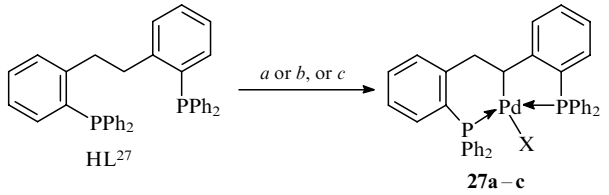

X = Cl (**a**), Br (**b**), I (**c**); (*a*) $[PdCl_2(NCPh)_2]$, MET, Δ, 1.5 h, 75%; (*b*) K_2PdBr_4, MET, Δ, 2 h, 26%; (*c*) $[PdI_2(PPh_3)_2]$, MET, Δ, 10 h, 86%.

Similar effects are also observed in the cyclopalladation of the vinyl fragment in the diphosphines HL[10] and HL[45] with the stilbene skeleton. On passing from $[PdCl_2(NCPh)_2]$ to K_2PdBr_4 and then to $[PdI_2(PPh_3)_2]$, the temperature regime become more drastic and the reaction duration increases; simultaneously, the yield of the cyclopalladated compound decreases (see Table 4).[60,61]

A similar halide-induced effect has been found in a study of *ortho*-metallation of phosphites of the $P(OAr)_3$ type (Ar = Ph, *o*-, *m*-, *p*-Tol, *p*-ClC_6H_4).[143,144] The thermal activation of the $C(sp^2)-H$ bond in the coordination complexes $[Pd(HL)_2Hal_2]$ is substantially hampered upon the variation of the halide in the series Cl < Br < I: under the same conditions (decalin, Δ, 3 h), the yield at this stage decreases 2.5-fold on the replacement of Cl^- by Br^-, and in the case of the iodide analogue, only traces of the PC-palladacycle are formed.

Unfortunately, such comparison has not been carried out for monodentate phosphines, although a process acceleration could be expected upon the replacement of Cl^- by Br^- and then by I^-. This assumption follows from several considerations, which are outlined below.

1. Cycloplatination of phosphines in the $[Pt(HL)_2Hal_2]$ type coordination complexes[86,160] is accelerated in the series Cl < Br < I, whereas for phosphites, the opposite order was found.[144]

2. In the complexation of the phosphine $PPhBu^t_2$ (HL^{23}) with palladium(II), this sequence (Cl < Br < I) reflects the increase in the tendency to form binuclear complexes in which the subsequent cyclopalladation proceeds more easily due to appearance of a coordination vacancy through cleavage of halide bridges. For example, the $[Pd(HL^{23})_2Cl_2]$ complex reacts with LiI being converted into the binuclear intermediate $[\{Pd(HL^{23})I(\mu\text{-}I)\}_2]$.[83]

3. The same dependence on the nature of the halide (Cl < Br < I) was observed in the case of intermolecular activation of C–H bonds by $[Pd(PPh_3)_2Hal_2]$ type complexes.[161,162]

Unfortunately, systematic investigations of the role of the anions in the palladating reagents of the similar structure or in the coordination intermediates of the same type are scarce. The true reasons for the halide effects remain obscure; in all probability, the final outcome depends on a complex combination of the electronegativity and the size of the halide atoms, their leaving-group properties and the tendency to accomplish the bridging function. All this is superimposed onto the steric effects stemming from the ligand subjected to metallation. A significant contribution to the slowing of cyclopalladation following the change in the nature of the halide (Cl < Br ≪ I) can be made by the increase in the strength of their binding to the metal (Lewis acid of class *b*).[154]

At first glance, cationic reagents of the $[Pd(NCR)_4]^{2+}$ type[163] free from halides and containing easily dissociating nitrile ligands appear especially attractive. The positive charge of the metal centre should ensure its high electrophilicity in the activation of the aromatic C–H bonds. However, analysis of the available published data shows that the situation is not that unambiguous.

The use of reagents of this class has been limited so far to cyclopalladation of only bidentate substrates with an aromatic skeleton, mainly *m*-xylylene-α,α′-diphosphines and their dendrimer analogues.[48–50,164,165] Most often, the preliminarily obtained $[Pd(NCMe)_4](BF_4)_2$ complex is used;[163,166,167] however, it can be generated *in situ*, for example, by treatment of a suspension of palladium chloride in acetonitrile with a stoichiometric amount of $AgBF_4$ with heating.[49]

The advantages of this approach include the possibility of isolation of the intermediate acetonitrile solvate **17b**, which is especially useful for the subsequent introduction of weakly coordinated ligands. However, most often, this solvate is converted without isolation into standard chloride PCP-complex, for example, **17a**.

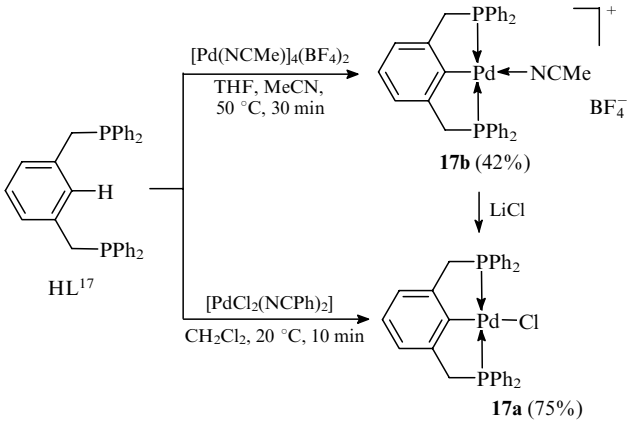

Unfortunately, the efficiency of this highly electrophilic cationic reagent is evidently lower than expected (see Table 4). In most cases, the PCP-complexes are isolated in moderate (42%–67%)[48,49,164] or even in low yields (15%–20%);[50,165] in some cases, the reaction does not proceed at 20 °C[48,127,165] and requires refluxing in acetonitrile.[49,50,164] The best results were obtained with generation of the solvated $[Pd(NCMe)_4](BF_4)_2$ reagent *in situ*. In this case, the acetonitrile derivative **17b** was isolated in 90% yield.[49]

The cationic complex $[Pd(NCMe)_4](BF_4)_2$ is far inferior in activity to the neutral chloride analogue, $[PdCl_2(NCPh)_2]$. The yield of the PCP-complex **17a** is lower with the former reagent[164] than with the latter,[66] despite a longer reaction time and a higher temperature. The same conclusion follows from comparison of the outcome of cyclopalladation of bis(phosphaalkenes) HL[63] (Ref. 125) and H_2L[64] (Ref. 126) (see Table 4). The reason for the lower efficiency of the cationic reagent is not clear, although a possible main reason is reduction of the reagent (extensive isolation of palladium black during the reaction has been noted[165]).

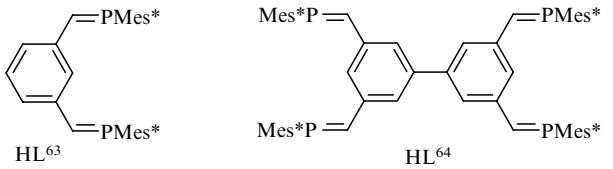

The role of the bases in cyclopalladation of P-donor substrates also differs from that observed for the N-analogues.[21] Phosphines and phosphites have lower basicities than N-donor ligands with a similar structure, but it varies over a fairly broad range depending on the nature of the substituents at the phosphorus atom. According to the pK_a values for the corresponding conjugate acids $[HPR_3]^+$ (see Refs 52–54), the basicity of aliphatic tertiary phosphines $PAlk_3$ is rather high (pK_a 8.0–11.4); but it markedly decreases on passing to triarylphosphines (pK_a 2.7–5.3) and sharply decreases for phosphites (pK_a from −1.8 to −2.0).

Nevertheless, P-donor substrates can often be cyclopalladated without introduction of an additional base. This function can be performed by phosphine ligands themselves; thus the isolation of the corresponding phosphonium salts as the chloride, $[HPBu^t_3]^+Cl^-$,[70] the tetrafluoroborate, $[HPBu^t_2(C_6H_4Et\text{-}2)]^+BPh^-_4$,[55] and the tetrachloropalladate, $[HPBu^t_3]^+_2[PdCl_4]^{2-}$,[69] from the reaction mixture (after cyclopalladation) has been reported.

The necessity of adding a base arises in the case of low-reactivity ligands. Usually, sodium acetate is used as the base; triethylamine[82] or potassium carbonate[140] are less effective and are used less often. Examples of substantial acceleration of the process following the introduction of a proton acceptor are few and mainly refer to reactions of benzylphosphines. Thus the metallation of PBu^t_2Bn (HL^{22}) on treatment with $[PdCl_4]^{2-}$ in boiling MET in the presence of AcONa proceeds much faster (0.5 h, 75%) than without a base (5 days, 64%).[82] *ortho*-Palladation of a less bulky substrate, PBu^tBn_2 (HL^{37}), was accomplished (in a yield of only 12%) only upon the addition of AcONa.[82] The base effect is most pronounced in the case of dialkoxy-substituted benzylphosphines; the C–H-bond activation in the HL^{65} and HL^{66} ligands under the action of *trans*-$[PdCl_2(NCPh)_2]$ is totally impossible without a base, and that in the case of HL^{67} occurs only by 10%. The same reactions carried out in the presence of AcONa in boiling MET ensure high yields of *ortho*-palladated dimers **65** and **66** (81%–84%), the reaction time (2 and 0.5 h) being dependent on the degree of steric assistance from the P-substituents (θ = 152 and 176°, respectively).[113]

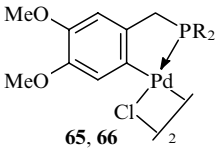

65, **66**

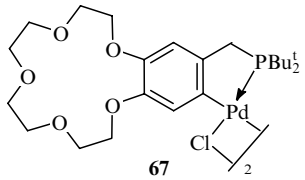

67

R = Ph (**65**), Bu^t (**66**).

In the cyclopalladation of the diphosphine HL^{68} with the lutidine skeleton, the pyridine ring of the ligand serves itself as the acceptor of liberated protons; hence, the reaction yields first the ionic PCP-complex **68a**, which is converted into neutral compound **68b** under the action of a base.[168]

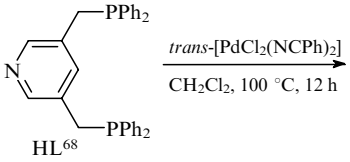

HL^{68}

trans-$[PdCl_2(NCPh)_2]$

CH_2Cl_2, 100 °C, 12 h

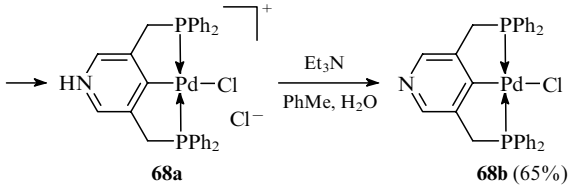

68a **68b** (65%)

However, under certain conditions, a base does not facilitate cyclometallation and, moreover, it can even inhibit the process. In addition to the known acid-catalysed cyclopalladation of $HPMes_2$ (see Section II.2.b),[169] noteworthy is the activation of the C(sp^2)–H bond in (3-arylsydnonyl)phosphine HL^{13}, which takes place in acid medium (EtOH, conc. HCl), to give the unfavourable six-membered PC-metallacycle in dimer **13**.[63]

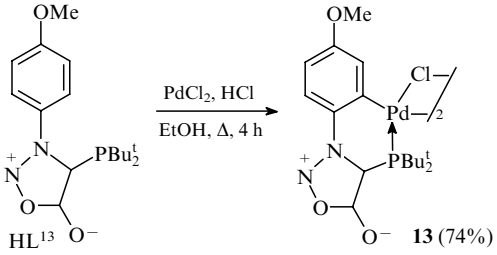

HL^{13} **13** (74%)

The possibility of stimulating the cyclopalladation by changing the nature of the solvent has not been studied in systematic mode; the choice of the medium was dictated first of all by the structure of the palladating reagent and the desire to conduct the reaction under homogeneous conditions. It can be suggested from general considerations that highly solvating polar and protic solvents should be favourable for the creation of a coordination vacancy. Perhaps, it is for this reason that alcohols (a MeOH–EtOH mixture,[81] Pr^nOH,[55] Bu^iOH,[145] MET[82,119]) are used for the transformation of chloride coordination precursors into cyclopalladated complexes using alcohols .

When choosing the solvent, one should take into account its ability to compete with the substrate for the site at the metallic centre. Thus cyclopalladation of the secondary phosphine $HPMes_2$ proceeds faster in THF or CH_2Cl_2 than in acetone and becomes impossible in a readily coordinating solvent, acetonitrile.[169] Apparently, for the same reason, cyclopalladation of tri(*tert*-butyl)phosphine under the action of potassium tetrachloropalladate in DMF requires 12 h, whereas the reaction of the same phosphine with $[PdCl_2(NCPh)_2]$ in CH_2Cl_2 is over after 2 h under the same conditions (20 °C, reactant ratio 2 : 1).[70]

The reactant ratio in cyclopalladation is among the most important factors determining the reaction rate, most of all, in 'halide' routes. The metal-to-ligand ratio influences the efficiency of vacation of the coordination site needed for the activation of the C–H bond. This goal is difficult to attain for Pd : HL = 1 : 2 due to the strong binding to the metal of all ligands in the bis(phosphine) intermediate of the $[Pd(HL)_2Hal_2]$ type. Therefore, it comes as no surprise that reactions with this stoichiometry often require rather drastic conditions (up to refluxing in decalin),[143,144] while the yields of cyclopalladated compounds leave much to be desired[82,143,144] (see Table 1). In addition, under these conditions, the reactions often do not give the dimeric complex, but instead, result in its adduct with the starting P-donor ligand.[69,143,144,170]

When equimolar amounts of reactants are used, the problem of generation of a coordination vacancy can be easily solved due to the cleavage of the halide bridges in the binuclear intermediate of the $[\{PdHal(HL)(\mu\text{-}Hal)\}_2]$ type, which allows this reaction to be carried out under milder conditions with good product yields.[57,81]

The reactant ratio becomes almost insignificant only when the process is efficiently sterically stimulated, for example, in reactions of phosphines such as PBu^t_3,[70,71] $PMes_3$,[109,110] and $P(Tol\text{-}o)_2Bu^t$.[81]

b. Organometallic reagents in cyclopalladation

A special group of cyclometallation processes is comprised by reactions involving organometallic or hydride reagents or intermediates. As a rule, these synthetic protocols show clear advantages over the classical methods considered above, possibly, due to different in kind mechanisms of transformations.

The C–H bonds of monodentate phosphines can be activated within hydride intermediates, $[PdH(X)(HL)_2]$. This approach has been mainly developed using di- and tri(*tert*-butyl)phosphine ligands as substrates.[71,171] The standard route to these hydrides[71,172,173] includes oxidative addition of the acid HX to a palladium(0) complex with the corresponding phosphine, $[Pd^0(HL)_2]$;[174] the existing alternative ways are based on the reduction of Pd(II) bis(phosphine) complexes, for example, by sodium borohydride.[175] The method including a short-term (0.5 h) heating of $PdCl_2$ with PBu^t_3 in DMF at 115 °C is more efficient and practically convenient (the yield of the hydride complex is 90%).[73]

Although hydride complexes of this type are rather stable in the solid state, in solutions, their phosphine ligands are cyclometallated rather easily (at 20 °C).[73] This process depends appreciably on the solvent and on the nature of the anion. In

dichloromethane, the reaction proceeds more rapidly than in benzene and it is markedly accelerated upon the addition of alcohol.[71, 171] The effect of the anion nature is clear-cut and differs from that observed for classical reagents (see Section II.2.a). For example, the hydrido chloride complex **20b** is converted into the phosphine adduct **20c** six times as fast (0.5 h) as the trifluoroacetate analogue **20d** (2 – 3 h), and the hydrido bromide precursor provides instantaneously the phosphapalladacycle, which is formed as the dimer **20a** (apparently, for steric reasons) rather than its mononuclear phosphine derivative.[71, 171]

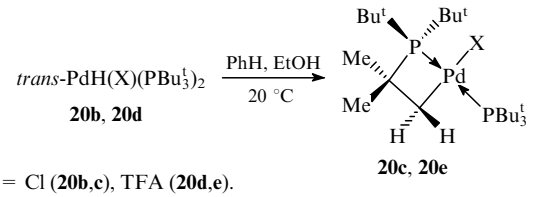

X = Cl (**20b**,**c**), TFA (**20d**,**e**).

Cyclometallation of mono- and dihydride platinum phosphine complexes proceeds equally easily and obeys the same type of dependence on the nature of the anion.[176] The [PdH(Cl)(AsBu$^t_3$)$_2$] hydride with bulky arsine ligands also readily forms a palladacycle (as an unusual dimeric compound with two hydride bridges),[177] whereas the standard coordination complexes cannot be involved in this process.[178]

The high efficiency of hydride complexes can be illustrated by closure of an additional four-membered palladacycle due to intramolecular activation of the C – H bonds of the PBu^t group in the iridium(III) PCP-complex [(η^3-HL′)IrH(Cl)] (H_2L' is the 4-MeO-substituted analogue of the HL[25] ligand), resulting in the formation of the [5.5.4]-tricyclic PCPC-complex, [(η^4-L′)Ir(Cl)].[32] No transformations of this type have been described in the chemistry of pincer palladium complexes, although their hydride derivatives are known.

The electronic state of the metal in the coordination precursors changes crucially following the appearance of C-bound ligands, which can serve as efficient acceptors for the proton liberated during cyclometallation or participate in the reductive elimination together with the hydride ligand formed upon the oxidative addition of the phosphine C – H bond. An alternative interpretation of the role of these ligands is easy generation of a vacant coordination position due to protolysis of the Pd – C bond.

The high activity of intermediates with M – Me bonds is well known. One can mention *ortho*-metallation of triphenylphosphine in the [MeRh(PPh$_3$)$_3$] complex, resulting in a strained four-membered PC-metallacycle and liberation of methane,[179] and double *ortho*-metallation of the simple phosphite P(OPh)$_3$ (H_2L^{69}) through the coordination intermediate [MeIr(cod)(H_2L^{69})], which furnishes bicyclic CPC-structure **69′**.[31]

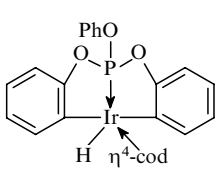

69′

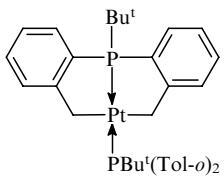

30′

The efficiency of replacement of halides by Me groups in the coordination intermediates of the [M(HL)$_2$X$_2$] type (X = Cl, Me) has been demonstrated with platinum(II) compounds.[115] The activity of organometallic intermediates can be illustrated by the formation of the [Pt(η^2-L)$_2$] bis(chelate) complexes from phosphine adducts of the [MePt(η^2-L)(κ^1-HL)] type [HL = PBu^t_n.(Tol-*o*)$_{3-n}$, where *n* = 1, 2] due to the activation of the C – H bond in the monodentatate phosphine ligand [30, 180] and by double cyclometallation of PBu^t(Tol-*o*)$_2$ at both *o*-tolyl fragments, giving rise to the CPC-structure **30′**.[30] Unfortunately, transformations of this type have not been studied for palladium analogues; palladium spiro complexes are available only through *ortho*-lithiated ligands (see Section IV), while the palladium(II) CPC-complexes are still unknown. This difference between the reactivities of compounds of the two d^8 metals might serve as indirect evidence pointing to different mechanisms of C – H bond activation.

The passage from classical to organometallic reagents can result in switching to another metallation site due to the modification of the reaction mechanism. Two different platinacycles obtained from the same HL[18] ligand can serve as examples.[68]

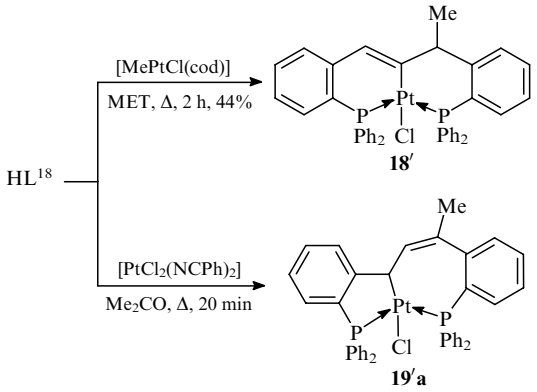

Although no comparison of the behaviours of the two types of reagent in the cyclopalladation of the HL[18] ligand has been carried out, it can still be suggested that this approach can be useful not only for facilitating the process but also for modification of the reaction pathways in systems that contain several alternative reaction sites.

One can only regret that organometallic reagents are seldom used for cyclopalladation. One of the few examples is easy activation of the C(sp^2) – H bond in the phosphite HL[2] in the [Pd(η^5-Cp){P(OTol-*o*)$_3$}Cl] complex, which takes place under unusual conditions — during chromatography of this compound on neutral alumina.[57] The regularities typical of classical systems (see Section II.2.a) are retained; these include the 'halide' effect (the iodide analogue of **2b** is inactive)[57] and the preferred formation of the five-membered PC-metallacycle {a four-membered ring is not formed from the [Pd(η^5-Cp)(PBu$^t_2$Ph)Cl] complex}.[84]

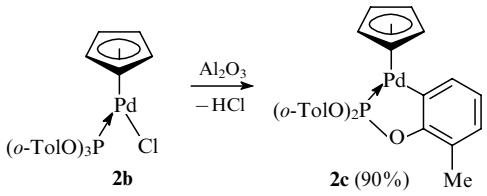

As yet another example of C – H bond activation with participation of a support, one can mention the quantitative formation of the cyclopalladated compound [{(η^2-L[70])Pd(μ-Cl)}$_2$] (**70**) on passage of the [{(κ^1-HL[70])PdCl(μ-Cl)}$_2$] coordination complex with the AsMes$_3$ ligand (HL[70]) through silica gel. The effect appears even more impressive in view of the fact that cyclopalladation of the HL[70] ligand could not be accomplished by the reaction with [PdCl$_2$(NCPh)$_2$] even in boiling benzene.[109]

An absolutely different role is played by the aryl or alkyl groups (Ph, Me) attached to palladium in the cyclometallation of the secondary dimesitylphosphine HPMes$_2$ (H_2L^{71}). The monodentate P-coordination of this bulky ligand giving cationic intermediates of the [(dppe)PdR(κ^1-H_2L^{71})]OTf (**71a**) type [dppe is 1,2-bis(diphenylphosphino)ethane, OTf is trifluoromethanesulfonate] is possible only after the removal of the halide ion from the reagent. A C(sp^3) – H bond of one of the *o*-Me groups of the mesityl substituent is activated on long-term keeping of solutions of these coordination precursors in CH_2Cl_2 or THF at 20 °C to give cationic complex **71b**.[169]

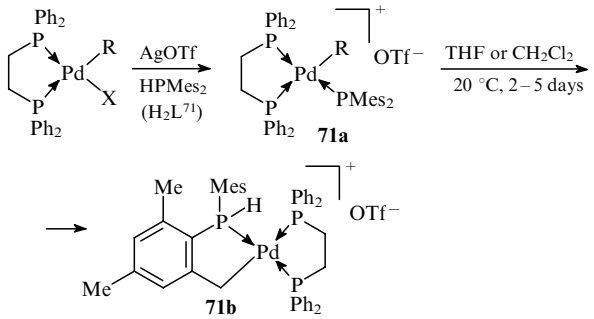

R = Me, Ph.

High activity of the intermediates containing alkyl or aryl groups bound to the metal is indicated by the fact that cyclopalladation of the secondary phosphine H_2L^{71} could not be accomplished using Pd(II) acetate. Detailed studies of the reactions of $HPMes_2$ with palladium(II) showed that cyclopalladation is catalysed by acids (presumably present as impurities in the solvents or reactants used) and inhibited by bases. Protolysis of the Pd–R bond needed for generation of the coordinatively unsaturated 14-electron species $\{(dppe)Pd^{II}(H_2L^{71})\}$ was confirmed by identification of the corresponding hydrocarbons RH (by spectroscopy and using ^{13}C-labelled model compounds). However, the researchers cited do not rule out the possibility of alternative pathways including oxidative addition of the P–H bond or benzyl C–H bond to palladium(II) followed by the reductive elimination of the hydrocarbon RH.[169]

Cases of acid catalysis (through organometallic intermediates) are also known in cycloplatination chemistry. Thus only in the presence of catalytic amounts of HCl, does the phosphine PPr^i_3 (HL^{72}) in the intermediate $[MePt(\kappa^1\text{-}HL^{72})_2(OTf)]$ complex form a four-membered metallacycle.[181]

The selectivity of the $PHMes_2$ (H_2L^{71}) → **71a** → **71b** transformation is remarkable due to the presence of two other potential reaction sites in the ligand molecule: activation can involve both the P–H bond of the secondary dimesitylphosphine H_2L^{71} (*via* deprotonation or oxidative addition) and the P–C(Mes) bond (processes of the latter type are known in the chemistry of arylphosphine complexes of transition metals [182]). It is noteworthy that both reaction directions are realised for the phosphine H_2L^{71} on the platinum(0) centre, giving rise to the phosphide complexes, [(dppe)PtH($PMes_2$)] and [(dppe)Pt(Mes)(PHMes)], respectively.[183]

Interesting possibilities appear when palladium(II) bis(β-diketonate) complexes are used as palladating agents. The synthetic routes to reagents of this class are simple and well-known,[184] and their complexation with N-[185–189] and P-donor ligands [185–187,190–194] have been the subject of detailed research for many years. The set of transformations of β-diketonates on palladium centres caused by the introduction of the additional ligand is fairly diverse.[195] On the basis of kinetic studies,[188,192] it was suggested that the reaction gives first five-coordinate species **A** with O,O′-chelated β-dicarbonyl ligands, one of which then partly undergoes dechelation (**B**). With excess Lewis base (HL), the β-diketonate ligand can be displaced from the metal coordination sphere (**C**) and returns there again after the rerarrangement

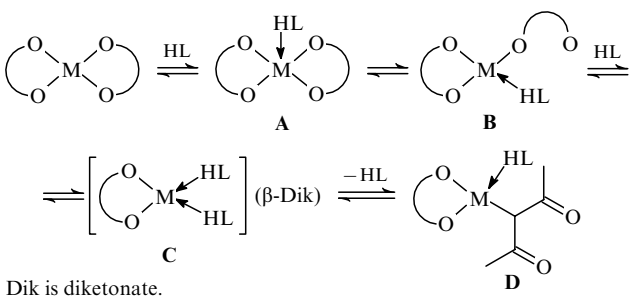

Dik is diketonate.

into the γ-C-bound state (**D**). The structures of the species involved in these multistage processes have been convincingly confirmed by both spectroscopic methods (*in situ* or after isolation) and X-ray diffraction, for example, for five-coordinate adducts of the $[Pd(hfac)_2(PR_3)]$ type ($hfac^-$ is hexafluoroacetylacetonate; R = *o*-Tol [191,196] or Ph [197]).

As regards the use of β-diketonate complexes for cyclometallation, species of type **A** and **D** seem to be the most valuable. In the former type of species, the monodentate O-coordinated β-diketonate with the hard donor atom is weakly bound to the metal and can easily depart, thus leaving a free coordination site needed for the activation of the C–H bond. In organometallic species of type **D**, the γ-C-bound diacylmethyl group $(RCO)_2CH^-$ can not only serve as a good acceptor for the protons being liberated but should also decrease substantially the electron density at the metallic centre due to conjugation and thus enhance its electrophilic properties. In this respect, the hexafluoroacetylacetonate reagent should be more reactive than the acetylacetonate analogue.

The efficiency of the β-diketonate reagents in the cyclometallation was first demonstrated for the *ortho*-palladation of primary benzylamine,[189,198] which had long been considered to be absolutely impossible.[21] Unfortunately, the use of this approach for the cyclopalladation of phosphines is limited to two examples,[116,196] and only one of these studies gives quantitative data.[196] The activation of the C–H bond in tri(*o*-tolyl)phosphine on treatment with palladium(II) bis(hexafluoroacetylacetonate) occurs with moderate success (the yield is 47%), but the reaction proceeds under mild conditions (20 °C), the transformation of the intermediate five-coordinate $[Pd(hfac)_2P(o\text{-}Tol)_3]$ (**29b**) adduct into the cyclopalladated compound **29c** being possible even in the solid phase during long-term storage of the sample.[196]

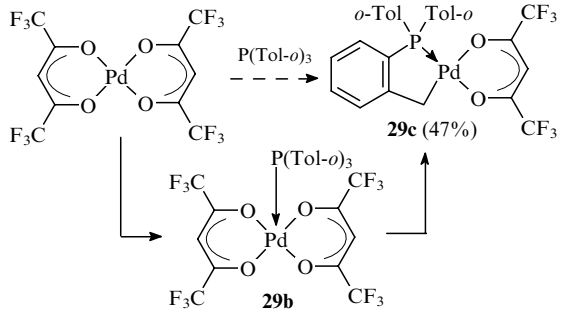

A certain role in this process may be performed by steric promotion: the large bulk of the phosphine ligand (θ = 194°)[95] hinders the rotation about the P→Pd bond in the five-coordinate precursor **29b**, which is manifested as non-equivalence of the three *o*-methyl groups in the ^1H NMR spectra recorded at −55 °C (δ 1.72, 2.10 and 2.94 ppm).[196] The substantial dispersion of these signals ($\Delta\delta$ > 2.2 ppm) may be related to the effect of the paramagnetic anisotropy of the metal on the protons of one of these groups located in the apical position near palladium. Thus, the stereochemistry of the coordination intermediate is favourable for the activation of the phosphine C–H bond.

Mention should be made of the synthetic pathway provided by the use of more readily available cyclopalladated complexes as metallating agents. This is the exchange of cyclopalladated ligands (ECL).[199,200] Recently,[201,202] the term 'transcyclometallation' has been proposed for these reactions.§ Detailed investigations of this process for N-donor ligands [99,200,203,204] have shown that it is

§ Although this concise term may seem attractive, it is not quite adequate to the process in question, because a similar term, 'transmetallation' is used to describe the processes based on replacement of one metal by another (rather than one ligand by another). Perhaps, it would be more appropriate to introduce the term 'transligandation' of palladacycles, which would describe the exchange of ligands at the same metallic centre.

fairly efficient with respect to 'difficult' N-donor substrates and can be useful for the preparation of palladacycles that are inaccessible or accessible with difficulty by other, simpler methods. In the simplified form, the ECL can be represented as follows:

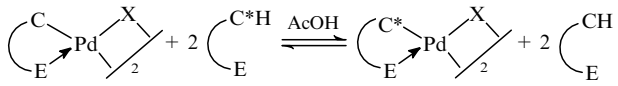

E is the heterodonor atom.

The views on the mechanism of the exchange of cyclopalladated ligands are rather contradictory. Both a dissociative route, which implies the destruction of the initial palladacycle as far as to the closure of a new ring,[199,200] and an associative route with a bis(chelate) intermediate containing both the initial and the new palladacycles have been considered.[203] Irrespective of the views on the mechanism, reactions of this type are carried out in protic media, most often, in acetic acid or its mixtures with aprotic organic solvents.

One can only regret that the use of this approach to phosphapalladacycles is limited to single examples. The use of the simplest CN-palladacycle (**A**) based on *N,N*-dimethylbenzylamine for the activation of the aromatic C–H bond of diphenylbenzylphosphine (HL^{36}) has been reported.[205] However, the cyclopalladated CN-complex proved to be inefficient in this process, like simpler but highly electrophilic $Pd(OAc)_2$. The dimer **36a** has been obtained in a yield of only 21%,[205] while its μ-acetate analogue (**36b**), in 19% yield.[114]

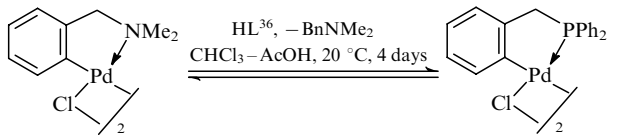

A **36a** (21%)

Some progress along this line has been attained due to the structural modification of the CN-reagent. When the cyclopalladated derivative of primary benzylamine (**B**) was introduced in the reaction with the phosphine $P(o\text{-Tol})_2Bu^t$ (HL^{30}) in the presence of acetic acid with heating, the dimer **30b** was obtained in 71% yield.[206,207]

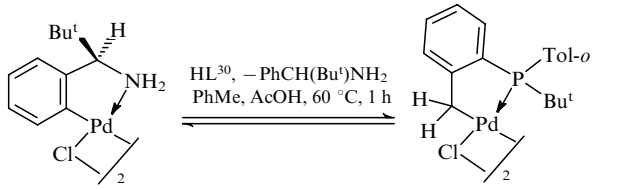

B (R_P,S_P)-**30b** (71%)

Formally, cyclopalladation of the tri-*tert*-butylphosphine HL^{20} under the action of the organometallic dimer **C** should be attributed to the same type of processes.[74] This reagent can be regarded as a specific analogue of a cyclopalladated complex in which the double bond of the alkene fragment replaces the heterodonor centre.

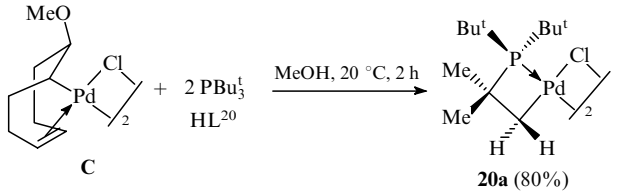

C **20a** (80%)

Unfortunately, this reaction is not discussed by the authors, but the data presented in the Experimental clearly indicate that it smoothly proceeds under mild conditions to give dimer **20a** in a high yield. The type **C** reagents are quite accessible through methoxypalladation[208] of the metal-bound cycloocta-1,5-diene in the commercially available $[PdCl_2(cod)]$ complex, which can also be generated *in situ*.[209,210]

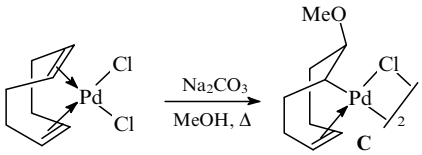

C

The data considered in this Section demonstrate that organometallic reagents possess high (and in some cases, unusual) activities in cyclopalladation. Although this field has not been adequately explored as yet, further progress along this line can provide valuable results.

3. Mechanistic aspects of the direct intramolecular cyclopalladation of P-donor ligands

Two features distinguish the cyclopalladation processes of P-donor ligands from those of substrates with harder donor atoms: first, the pronounced steric effects and, second, high stability of the intermediate coordination compounds. The latter feature is exceptionally convenient from a practical standpoint, because the problem of oxidative instability of phosphine ligands is eliminated when they are coordinated through heteroatom(s). In addition, even this preliminary stage largely determines the possibility (and ease) of the subsequent activation of the C–H bond. Therefore, analysis of the structural peculiarities of coordination precursors deserves attention, first of all, as a way of estimating the true causes of steric promotion of cyclopalladation processes.

a. Coordination intermediates

Usually, three factors are considered as underlying the steric effects involved in cyclopalladation: the entropy (a substantial portion of the inner rotation entropy is lost even in coordination precursors), enthalpy (the number of unfavourable interactions decreases upon cyclisation) and conformational factors (the conformational mobility of the ligand coordinated through the heteroatom decreases or the ligand is fixed in a rotamer that ensures proximity of the C–H bond suitable for activation with the metallic centre).[68,96,97,118,119] With fairly high steric crowding of the phosphine ligands, the barriers to rotation around the P→Pd and P–C bonds in the coordination complexes may increase, so that the rotamers can be detected by spectroscopy,[55,81,180,211–214] in some cases, even at 20 °C.

For the coordination intermediate to be perfectly prepared for the subsequent proper cyclometallation step, its structure should ensure not only the proximate positions of the C–H bond to be activated and the metal, but also the possibility of formation of a free coordination site in the equatorial plane. Presumably, effective solution of the last-mentioned problem in sterically overcrowded systems makes a substantial contribution to the steric assistance to the C–H bond activation.

The reactions of monodentate P-donor ligands with halide-containing palladating agents are often (especially in early publications) carried out in two or even in three stages with isolation of intermediate mono- or binuclear complexes of the $[Pd(\kappa^1\text{-}HL)_2Hal_2]$ or $[\{Pd(\kappa^1\text{-}HL)Hal(\mu\text{-}Hal)\}_2]$ type depending on the reactant ratio. The problem of formation of a coordination vacancy in these precursors can be solved in several ways. In complexes with bulky P-donor ligands, the P→Pd bonds are weakened,[215] which have to facilitate the phosphine dissociation. Indeed, a partial dissociation of *tert*-butyldi(*o*-tolyl)phosphine (HL^{30}) from the intermediate coordination complex, $[Pd(\kappa^1\text{-}HL^{30})_2Cl_2]$, was confirmed by molecular mass measurements (508 against the calculated value of 718).[81] In palladium(0) phosphine complexes, the coordination number of the metal decreases from four to two following an increase in the steric requirements of the ligands,[174,215–218] irrespective of their basicities.[216]

It is also assumed [97] that bulky ligands can stabilise coordinatively unsaturated species resulting from elimination of one of the ligands through steric shielding of the vacant site. A certain stabilising role can also be played by secondary interactions with the metal.[174, 217] Under these conditions, the structure of the initial intermediate (mono- or binuclear) is virtually insignificant. Apparently, this is why cyclometallation of sterically crowded ligands depends only slightly on the reaction conditions (see Section II.1).

In addition, due to the large number of unfavourable interactions between bulky substituents of the phosphine and *cis*-arranged ligands (usually halides) in bis(phosphine) complexes, they tend to be transformed into binuclear halide-bridged compounds [55, 219] (they are formed even at a metal : ligand ratio of 1 : 2 [55]). These binuclear complexes readily dissociate owing to cleavage of the halide bridges to give coordinatively unsaturated species. The tendency for the monomer → dimer transformation is known to increase with an increase in the size of the halide ion or its ability to perform the bridging function in the sequence $Cl^- < Br^- < I^-$. Thus upon the replacement of the chloride in *trans*-$[Pd(PPhBu^t_2)_2Cl_2]$ by iodide, the binuclear $[\{PdI(PPhBu^t_2)(\mu\text{-}I)\}_2]$ complex is formed instead of the expected mononuclear analogue, *trans*-$[Pd(PPhBu^t_2)_2I_2]$.[83] However, the dependence of the ease of cyclometallation on the nature of the halide follows the opposite order, indicating the predominant role of other factors at subsequent stages.

In the absence of steric promotion, the advantage of binuclear coordination precursors for the subsequent cyclopalladation becomes more pronounced. This can be confirmed by the results of a study of the H/D-exchange in mono- and binuclear complexes, $[Pd(HL)_2Cl_2]$ and $[\{Pd(HL)Cl(\mu\text{-}Cl)\}_2]$ [HL = (*o*-Tol)P(Ph)Hex (HL[33]) and (*o*-Tol)P(Me)CH_2CH_2Tol-*o* (HL[34])].[108] Only for binuclear compounds, was the H/D-exchange detected for the *o*-methyl group of the P-tolyl substituent upon prolonged storage of the compounds as solutions in d_4-methanol at 20 °C, which was indicative of reversible C–H bond activation. Although the corresponding phosphapalladacycles have not been synthesised (due to insufficient steric stimulation), their formation was detected in mass spectroscopic studies of the same binuclear coordination precursors. However, in the case of mononuclear bis(phosphine) intermediates, no activation of the C–H bond was observed.[108]

The structure of the coordination intermediates is also important for the cyclopalladation of diphosphine ligands. Unfortunately, purposeful studies of such intermediate complexes are scanty. The types of coordination of diphosphines are diverse and include both mononuclear structures with a P,P-chelating ligand with either *trans*- (**A**) or *cis*-geometry (**B**) and binuclear complexes with a bridging P,P-ligand linking two metal centres in either *trans*- (**C**) or *cis*-configuration (**D**).[123] The formation of coordination polymers cannot be ruled out either.

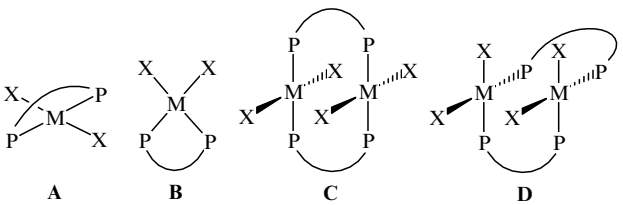

A **B** **C** **D**

It is reasonable to suggest that the optimal geometry of the coordination precursor should be largely determined by the structure of the fragment connecting two P-donor atoms. In the general case, *trans*-P,P-chelation is preferred for the subsequent cyclopalladation. This geometry ensures the closest proximity of the metal and the C–H bond to be activated, which is located in the middle of the bridging fragment in the vast majority of known ligands. However, the structure of such coordination intermediates has been convincingly confirmed only in a few cases.

In the coordination of a diphosphine having a rigid anthracene-1,8-diyl skeleton (HL[73]), the central C–H bond and Pd are forced to approach each other. The interaction of the ligand with the metal cannot be limited to only *trans*-P,P-chelation (despite the quite acceptable distance between the two phosphorus donor atoms equal to 5 Å) due to steric hindrance created by the C(9)–H bond of the anthracene skeleton; therefore, the formal insertion of the metal into this bond to give PCP-complex **73** becomes inevitable.[156]

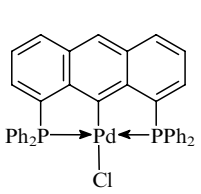

73

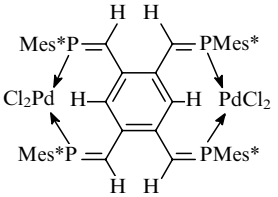

49b

The forced character of proximity of the metal atom and the C–H bond to be activated in the coordination precursor **49b** (detected by spectroscopy) was suggested for cyclopalladation of the H_2L[49] ligand.[117] This spatial proximity can be partly responsible (together with steric assistance of bulky supermesityl P-substituents) for the subsequent exceptionally easy cyclometallation of this and other similar ligands [125–127] (see Table 4).

The necessity of a mononuclear *trans*-chelate structure for the coordination intermediate of type **A** has also been assumed for cyclopalladation of diphosphines with relatively rigid *m*-xylylene skeletons.[66, 67, 155] However, no data on the isolation or reliable spectroscopic identification of such complexes have been reported as yet.

The possibility of controlling the types of ligand pre-coordination appears fairly attractive; however, studies of this type are scarce.[123, 155] For example, a study of cyclopalladation of *m*-xylylene-α,α′-diphosphine HL[62] by $[PdCl_2(PhCN)_2]$ has revealed predominant formation of an inactive polymeric coordination complex, *trans*,*trans*-$[\{PdCl_2(\mu\text{-}HL^{62})\}_n]$, whereas with the use of the phosphine-containing reagent $[PdBr_2(PPh_3)_2]$, cyclopalladation proceeds rather smoothly. While discussing the role of the phosphine ligand in the $[PdBr_2(PPh_3)_2]$ reagent, the researchers suggest that it can catalyse the rearrangement of the polymeric coordination intermediate into a mononuclear species with the *trans*-P,P-geometry, needed to bring together the C–H bond to be activated and the metal.[155]

A more detailed study [123] of the influence of neutral ligands in palladating agents on the structure of the coordination intermediates has been carried out using complexation with the diphosphine HL[74] as the example.

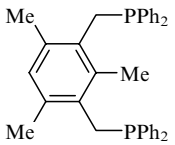

HL[74]

The cyclopalladated derivative of this diphosphine is unknown; however, the synthesis of its analogues **11** and **12** with two six-membered metal rings has been reported.[62]

The requirements of the structure of an optimal coordination precursor can vary depending on the position of the C–H bond subject to activation relative to the metal. This is the case on passing from *m*-xylylenediphosphine HL[17] to its homologue HL[74]. In the researchers' opinion,[123] of the three possible structural types of coordination complexes **B**–**D** (mononuclear *trans*-structures of type **A** are not considered in this work), the closest position of the specified $C(sp^3)$–H bond to the metal can be ensured only in the mononuclear species **B** having the *cis*-P,P-geometry.

An important result of this study is the established relationship between the type of coordination and the nature of the palladating reagent. Thus the reaction of the HL[74] ligand with

the nitrile reagents $[MCl_2(NCR)_2]$ (M = Pd, Pt; R = Ph, Me) at 20 °C gives selectively and quantitatively only binuclear macrocyclic compounds of the *trans*, *trans*-configuration with a bridging diphosphine (type **C**). The structure of the complex *trans*,*trans*-$[\{PdCl_2(\mu\text{-}HL^{74})\}_2]$ was confirmed by X-ray diffraction. However, the complexation of HL^{74} with the diene reagent $[PtCl_2(cod)]$ gives, equally selectively, the mononuclear complex *cis*-$[PtCl_2(\kappa^2\text{-}HL^{74})]$ with P,P-chelating diphosphine of type **B** with an eight-membered ring.[123] Although the reasons for these differences remained unknown, the possibility of controlling the process at the stage of coordination precursors is undoubtedly useful. For the subsequent cyclometallation, which is often carried out at elevated temperatures, it is also important that the binuclear platinum(II) complex of type **C** is converted into thermally more stable mononuclear compound of type **B** under relatively drastic conditions (CH_2Cl_2, 140 °C, autoclave).[123]

Possibly, type **A** or **B** mononuclear complexes are also formed intermediately in the reactions with palladium(II) trifluoroacetate. First, using this reagent, cyclopalladated derivatives of the PCP-type (complexes **11** and **12**) have been prepared from diphosphines similar to the ligand HL^{74} but containing PBu^t_2 and PPr^i_2 donor groups.[62] Second, mononuclear complex **75a** with the *cis*-P,P-configuration (type **B**) was the major product (72%) in the reaction of $Pd(TFA)_2$ with bis(phosphinite) HL^{75}, whereas the binuclear macrocyclic compound **75b** with the *trans*,*trans*-geometry is only a minor product under these conditions (8%). The structures of both coordination complexes isolated as iodides **75c** and **75d** were confirmed by X-ray diffraction.[124]

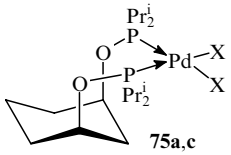

75a,c

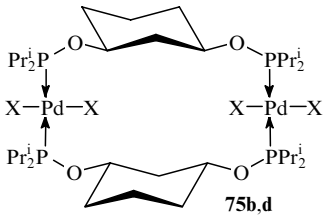

75b,d

X = TFA (**75a**,**b**), I (**75c**,**d**).

Probably, the efficiency of palladium(II) trifluoroacetate in the cyclopalladation of P,P-donor ligands is due, among other factors, to its tendency towards the formation of mononuclear (rather than binuclear or polymeric) coordination intermediates. An unsuccessful attempt at cyclopalladation of the bis(phosphinite) HL^{75} through the precursor **75a** with the *cis*-P,P-geometry [124] suggests that the activation of the C(sp^3)—H bond in ligands of this type should be preceded by a rearrangement of the mononuclear coordination intermediate from the *cis*-P,P- into the *trans*-P,P-configuration, which is hampered due to conformational features of the cyclohexane fragment. Indeed, the structural parameters of the complex **75a** clearly show that the *endo*-hydrogen of the central methylene group is removed away from the metal by a distance (CH···Pd = 3.725 Å),¶ longer than the sum of the van der Waals radii of these atoms (3.1 Å [220,221]). The activation of this C—H bond would require an essential structural reorganisation.

However, even when the structure of the coordination precursor appears optimal, this still does not guarantee the success of the subsequent activation of the C—H bond. The unsuccessful attempt to cyclopalladate the diphosphine HL^{28} can serve as an example of such restrictions. Even long-term (3 h) refluxing of this diphosphine with $[PdCl_2(NCPh)_2]$ gives only the coordination complex *cis*-$[PdCl_2(\kappa^2\text{-}HL^{28})]$ (**28**), despite the potential possibility of the formation of two optimal five-membered phosphapalladacycles.[94]

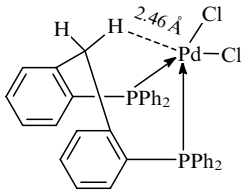

28

This seems even more surprising in view of the fact that an X-ray diffraction study of the coordination precursor **28** showed the occurrence of a close contact between the *endo*-hydrogen atom of the methylene group of the diphosphine and the metal (the distance is 2.46 Å). The substantial downfield shift of the ^{1}H NMR signal of this proton with respect to the signal of the *exo*-proton ($\Delta\delta$ = 2.7 ppm) confirms that the boat conformation is retained in solutions. Thus, the close geometric proximity of the metal and the C—H bond potentially suitable for activation is a necessary but not a sufficient condition.

The formation of mononuclear complexes with a *trans*-P,P-chelated ligand (type **A**) seems to be more realistic in the case of diphosphines with a flexible and rather long polymethylene bridge. The structure of these complexes has been the subject of keen attention at an early stage of research into their cyclometallation.[222–224]

It is believed that the preferableness of *trans*-P,P-chelation for long-chain diphosphines at the stage of coordination intermediates is determined by the presence of bulky PBu^t_2 groups (as opposed to the PPh_2 analogues, which usually form linear polynuclear species at this stage). The bulky donor groups restrict the freedom of rotation not only about the P→Pd and P—C bonds but also about the C(α)—C(β) and C(β)—C(γ) bonds of the polymethylene bridge, thus predetermining its conformation.[96,128,222–224] This type of pre-coordination should result in localisation of one of the central methylene groups in the axial position above the metal, thus ensuring the necessary proximity of one C—H bond with the metal. However, the coordination complex of type **A** — *trans*-P,P-$[Pd(HL^{76})Cl_2]$ — was isolated only upon the reaction with the decamethylenediphosphine $Bu^t_2P(CH_2)_{10}PBu^t_2$ (HL^{76}), whereas in the case of its pentamethylene analogue, HL^{24}, no signs of formation of mononuclear species were detected.[224] The most typical coordination complexes formed by these ligands are bimetallic macrocycles with the bridging diphosphine (type **C**).[128,129,222,224] The structures of *trans*, *trans*-$[\{Pd(\mu\text{-}HL)Cl_2\}_2]$ complexes with pentamethylenediphosphines HL^{24} (see Ref. 128) and HL^{44} (see Ref. 129) were confirmed by X-ray diffraction.

To conclude this Section, we can make some assumptions concerning the causes for the difference between the behaviours of mono- and diphosphines in cyclopalladation (see Section II.1). Most likely, the difference between them is due to entropy effects. Whereas the formation of a PC-palladacycle from the coordination intermediate with a monodentate phosphine is usually accompanied by a substantial decrease in the system entropy, in the case of diphosphines, the entropy has markedly decreased already upon their bridging P,P-coordination and, even more so, in the case of P,P-chelation.

b. The stage of activation of the C—H bonds

The importance of the processes of the C—H bond activation involving transition metal complexes (especially, in the catalytic regime [225–227]) dictates the permanent interest in experimental [80,162,228] and theoretical [229–234] studies in this field. However, most of the known relevant reviews consider intermolecular processes.[80,226,235,236] Only a few studies deal with analysis of the specific features of the intramolecular activation of C—H bonds by various transition metals,[14,237–241] and only some of these studies touch upon the mechanisms of reactions involving palladium.[238–240] Some general views on the mechanisms of

¶ Data from the Cambridge Structural Database; code MEXRID.

intramolecular activation of C—H bonds can be found in reviews on cyclometallation.[15, 17, 19]

It is generally believed that the activation of aromatic C—H bonds occurs *via* preliminary η^2-coordination of the arene fragment to the metal, which allows the reaction to follow a lower-energy pathway.[14, 80, 240] This accounts for the apparent anomaly: many metals are capable of even intermolecular activation of strong aromatic C—H bonds ($\sim$110 kcal mol^{-1}), but for weaker aliphatic C—H bonds (96– 102 kcal mol^{-1}), this process is impossible or substantially hampered.[80] A similar mechanism has been assumed for cyclopalladation.[240]

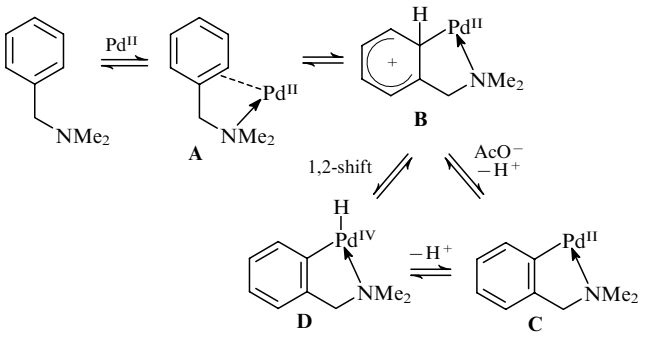

The intramolecular activation of the C(sp^2)—H bond in dimethylbenzylamine includes the preliminary η^2-coordination of the metal to the aromatic ring of the N-bound ligand and subsequent transformation of intermediate **A** into arenonium species **B**. In the classical versions of electrophilic cyclometallation,[14, 238] the process of formation of metallacycle **C** from **B** ends with proton elimination under the action of a base. However, the possibility of a 1,2-shift of hydrogen from the *ipso*-carbon atom of the arenonium species **B** to the metal with the intermediate formation of a Pd(IV)-containing hydride derivative of metallacycle **D** also cannot be ruled out.[240]

This version of the reaction seems even more likely if one recalls that Pd(IV) complexes[242–245] have ceased to be exotic compounds during the last decade. An extensive series of organometallic Pd(IV) derivatives has been prepared, including compounds with phosphine ligands[246, 247] and structures with CC-[248] and CN-palladacycles.[249] In the presence of stabilising ligands, Pd(IV) compounds become rather stable and can be isolated;[248–252] some of these are stable in solutions even at elevated temperatures.[240] The structures of most of these complexes were confirmed by X-ray diffraction.[248, 249, 251, 252]

η^2-Arene complexes which model intermediate **A** are also known, many of them have been studied not only by spectroscopy but also by X-ray diffraction.[253–257] Detailed analysis of their structural parameters[256] resulted in the suggestion that the mode of coordination of the arene fragment to palladium should rather be interpreted as being intermediate between η^2- and η^1-modes,[258] because the *ipso*-carbon of the arene ring is the main donor of π-electron density. In addition, in a recent study, direct transformation of such complexes into CC-palladacycles has been observed.[259, 260]

In most of the generally accepted mechanistic schemes proposed for cyclopalladation, an essential role is assigned to agostic interactions between the metal and the C—H bonds to be activated, both aliphatic[261, 262] and aromatic[263, 264] ones. It is believed that the oxidative addition of alkanes is preceded by η^1-, η^2- or η^3-coordination of the CH_n fragments to the metal.[235] The ease of this process depends on the degree of substitution of the carbon atom to be metallated both from purely statistical considerations ($CH_3 > CH_2 \gg CH$) and for steric reasons, because the access of the metal to the C—H bond becomes more complicated with an increase in the number of substituents in its surroundings.[241] An argument in favour of the possibility of subsequent oxidative addition of the aliphatic C—H bond to the palladium centre is provided by spectral identification of the hydrido(alkyl) [PdH(Cy)Br$_2$(PPh$_3$)$_2$] species in the intermolecular activation of cyclohexane by the [PdBr$_2$(PPh$_3$)$_2$] complex.[162]

Contacts of the Pd$\cdots$H type were detected by crystallography in many palladium compounds with bulky phosphines.[174, 217, 265, 266] For instance, in the structure of *trans*-[PdI$_2$(PMe$_2$Ph)$_2$], the Pd$\cdots$H distance between the Pd atom and the *o*-hydrogen atom of the benzene ring (in the axial position) is shortened to $\sim$2.8 Å (see Ref. 265). The substantial downfield shift of the ^{1}H NMR signal for the *o*-protons ($\delta > 9$ ppm) indicates that these axial contacts are also retained in solution.[174, 217] However, the direction of this shift is opposite to that expected of true agostic interactions, which impart a hydride nature to the hydrogen atom.

It has been assumed that the interaction of Pd with the C—H bond located in the axial position (even at distances shortened to 2.1 Å) is destabilising, but it can become attractive when the bond shifts to the coordination plane.[237] Therefore, bringing the Pd atom closer to the axial hydrogen atom can be a useful step in the overall process of C—H bond activation. This can be considered as a desirable condition but it does not ensure the success of cyclometallation. For example, the *trans*-[PdI$_2$(PMe$_2$Ph)$_2$] complex mentioned above[265] does not form a four-membered phosphapalladacycle, although the corresponding platinum analogues are known.[85]

Although agostic complexes with a two-electron three-centre C—H$\rightarrow$M bond are regarded as intermediates or transition states in the metallation of aromatic substrates,[267] cases where they have been isolated are rare. Recently,[264] such complexes have been synthesised by the reaction of a cationic Rh(I) reagent with the diphosphine HL^{25} and its 4,5,6-trimethoxy-substituted analogue. The structure of the former product, [Rh(HL^{25})CO]$^+$, was confirmed by X-ray diffraction. Moreover, an increase in the acidity of the aromatic proton involved in the agostic interaction was noted: its ^{1}H NMR signal is shifted to δ 4.13 ppm. The deprotonation of the agostic precursor giving rise to the PCP-complex [Rh(η^3-L^{25})(CO)] is easily induced by the action of weak bases (triethylamine or collidine). This process models the last stage of the electrophilic cyclometallation of diphosphines at the arene fragment. It has been suggested[264] that in this case, the contribution of the pathway involving the classical arenonium intermediate is small, if present at all.

These results are of interest as an illustration of the extensive potential for changing individual steps of the overall mechanism of C—H bond activation by varying not only the structures of the process participants but also the reaction conditions. For example, a decrease in the electron density on the metallic centre of the reagent proved to be sufficient to make Rh(I), known for its nucleophilic properties,[238, 239] react with the highly basic diphosphine HL^{25} by an electrophilic mechanism. Presumably, this pathway could also be realised in intramolecular activation of C—H aromatic bonds by palladium(II), which is more prone to electrophilic behaviour.

Comparative analysis of the available experimental data on the cyclopalladation of P-donor ligands with participation of both aromatic and aliphatic fragments (see Section II.1) has shown that mono- and bidentate ligands behave differently: the activation of aromatic C(sp^2)—H bonds is facilitated only for diphosphines and diphosphites (see Table 4), whereas for monodentate phosphines, it is rather hampered. If the role of the η^2-arene or agostic intermediate is assumed to reduce to bringing the metal closer to the C—H bond being activated, then the difference between mono- and diphosphines can be related to the fact that in the latter case, the tight contact is attained automatically even upon *trans*-P,P-coordination of the ligand, whereas in the case of monodentate ligands, conformational reorganisation is required.

The information on the mechanisms of direct intramolecular activation of C—H bonds in P-donor ligands by palladium is extremely sparse. It can only be suggested from general considerations that the reaction pathway should depend on a number of factors: the nature of the central metal atom and the donor atom

of the ligand [14, 15] (in particular, the ratio of its σ-donor to π-acceptor properties);[51, 53] hybridisation of and the electron density on the carbon atom in the C−H bond being metallated and the steric factors in its surroundings; the possibility of agostic or other secondary interactions between this bond and the metal, or η^2-coordination of the metal to the double bond of the aromatic ring.[14]

Apparently, the electron density on the metallic centre in the intermediate coordination complexes is one of the most important factors, because it determines the metal susceptibility to oxidative addition or to electrophilic attack. The former pathway is typical of electron-enriched metals; for Pd(II), electrophilic behaviour is assumed most often, whereas Pt(II) occupies an intermediate position.[15, 237, 238]

In the absence of experimental data, assumptions concerning the cyclometallation mechanism are often made on the basis of the influence of the nature of the metal on the ease of the process. This criterion is justified by the easier oxidative addition to Pt(II) compared to that to Pd(II) and by the lower stability of Pd(IV) complexes. Indeed, direct activation of the C−H bonds in phosphines and phosphites under the action of Pt(II) compounds often occurs much more easily than that with Pd(II)-containing reagents.[15, 59, 69, 81, 82, 86, 129, 143] However, numerous exceptions to this rule can be found. For example, cycloplatination of bulky ligands such as trimesitylphosphine [110] and *tert*-butyldi(*o*-tolyl)-phosphine [81] proceeds at higher temperatures than cyclopalladation. This points indirectly to the possibility of changing of the process mechanism. Similar anomalies can also be found among reactions of diphosphines. For example, attempts at cycloplatination of *m*-xylylene-α,α′-diphosphine HL[62] have not met with success, while it can be cyclopalladated quite readily by the action of *trans*-[$PdBr_2(PPh_3)_2$].[155] These contradictions can be due to the change in the mechanism of the proper C−H bond activation stage. However, difficulties in the stage of the coordination through heterodonor atoms caused by steric factors [268] or by kinetic intertness of Pt(II), which is several orders of magnitude higher than that of Pd(II), also cannot be ruled out.

The electron density on the metallic centre is largely determined by the nature of the attached organic ligands, in particular, the nucleophilic behaviour becomes more probable on passing from N- to P-donor substrates.[14] This assumption is supported by the increase in the activity of Ni(0) complexes with respect to the oxidative addition following the introduction of phosphines into the Ni(0) coordination sphere and the subsequent increase in the phosphine basicity [241] (for PPh_3 and PEt_3, the pK_a values are 2.73 and 8.69, respectively [53]).

$$[Ni(cod)(bipy)] < [Ni(PPh_3)_4] < [Ni(PEt_3)_4]$$

bipy is 2,2′-bipyridyl.

The increase in the electron density on the metal atom with an increase in the basicity of the coordinated phosphines was convincingly confirmed by calorimetric measurements of the protonation enthalpies of complexes ($-\Delta H_{HM}$). For example, upon replacement of PPh_3 by PMe_3 (pK_a 2.73 and 8.65, respectively), the basicity of complexes increases by 3−7 kcal mol^{-1} (see Ref. 269).

However, in view of the predominant influence of steric effects in the cyclopalladation of P-donor ligands, this criterion should be treated with caution. Indeed, from the standpoint of electronic effects and with the assumption of the electrophilic mechanism, one cannot interpret the failure [82] or the difficulty [114, 205] of the *ortho*-palladation of the benzylphosphine $PhCH_2PPh_2$ against the background of the brilliant results attained in the *ortho*-palladation of more bulky $PhCH_2PBu^t_2$.[82] An idea of the relative basicities of these two ligands can be gained from comparison of this parameter for phosphines PPh_3 and PBu^t_3 (pK_a 2.73 and 11.4, respectively).[53] If we assume that the considerable increase in the basicity of the metallic centre caused by the coordination of trialkylphosphine is responsible for the success of the reaction, this prompts the idea that the reaction has a nucleophilic mechanism. However, this conclusion is faulty, as indicated by the pronounced acceleration of the reaction upon the introduction of MeO substituents into the aromatic ring,[113] which attests in favour of an electrophilic pathway.

The attempts to predict the reaction mechanism on the basis of the effect of substituents in the triarylphosphine cannot be considered legitimate: in addition to the expected influence of substituents in the aromatic ring on the C−H bond being metallated, the electronic effects can be transferred to the metal through the donor phosphorus atom. The introduction of electron-donating substituents increases the electron density in the aromatic ring (and thus increases its susceptibility for the electrophilic attack), but the electron density on the metal also increases and this enhances its tendency for the oxidative addition.[14, 86] For example, the protonation enthalpy of [$Fe(CO)_3(PAr_3)_2$] type complexes (Ar = Ph, *p*-$MeOC_6H_4$) increases from 14.1 to 16.2 kcal mol^{-1} upon the introduction of *p*-MeO substituents into the triphenylphosphine ligand (the pK_a values for these ligands are 2.73 and 4.59, respectively).[269] This transfer of electronic effects makes problematic the choice between alternative mechanisms on the basis of this criterion and for the given class of ligands.

The formal charge of the metal is considerably affected by the anions linked directly to the metal. The measured protonation enthalpies of the complexes with different halides [269] provided a paradoxical outcome: their basicity increases along the sequence $I^- < Br^- < Cl^-$, opposite to that expected on the basis of electronegativities (but consistent with the proton affinity of these anions in the gas phase). A similar conclusion was drawn from detailed X-ray diffraction and ^{13}C, ^{19}F and ^{31}P NMR studies of organometallic complexes of the *trans*-[$(PPh_3)_2Pd(Ph)Hal$] type: the affinity of halides to palladium(II) in nonpolar media increases in the series $I^- < Br^- < Cl^- < F^-$ (see Ref. 270). This 'halide anomaly' is at variance with the standard views on the greater affinity of soft bases (here, I^-) for soft acids such as Pd(II). Presumably, for complexes of the type mentioned above and for other compounds of d^8 metals, this anomaly can be interpreted in terms of the concept of repulsion of filled orbitals (two-orbital four-electron destabilisation).[270] A certain contribution might be made by the change in the ratio of the σ- to π-donor properties of the anions.[269]

From the studies of cycloplatination of the P-donor ligands through the coordination precursors [$Pt(HL)_2X_2$], it is known that in the case of phosphines, the reaction rate decreases depending on the nature of the halide in the series I > Br > Cl,[85, 86] whereas on passing to phosphites, the order of reactivity is reversed (Cl > Br > I).[143, 144] On the basis of these data, it is usually assumed that reactions with phosphines proceed by a nucleophilic mechanism, while those with phosphites follow an electrophilic mechanism.[17]

For coordination complexes of palladium(II) with phosphites [143, 144] and phosphines, similar patterns of dependence of the reaction rate on the nature of the anions are obeyed, namely, Cl > Br > I (see Section II.2.a).

Examples of a similar dependence of the ease of cyclopalladation on the nature of the halide (Cl > Br > I) can also be found in the processes of formation of PCP-structures from diphosphines (see Table 4 and Section II.2.a). For instance, metallation of the aliphatic (in the HL[27] ligand) and vinylic fragments (in the diphosphines HL[10] and HL[45]) is markedly hampered as the chloride-containing palladating reagent is replaced by bromide- and then by iodide-containing analogues.[60, 61]

The observed halide effects may suggest a similar electrophilic mechanism for cyclopalladation of both phosphites and phosphines. However, assuming that the overall reaction rate is determined by the stage of C−H bond activation in the coordination precursors with similar structures and taking into account the increase in the basicity of the metallic centre in the series $I^- < Br^- < Cl^-$,[269] one can conclude that the halide effect

observed experimentally attests to the nucleophilic rather than electrophilic behaviour of the metal. An alternative interpretation of the halide effect is the increase in the *trans* influence of halides in the sequence $Br^- < Cl^-$;[270] as a result, the coordination site becomes vacant more readily due to weakening of the bond with the *trans*-ligand.

This criterion cannot be accepted as being perfect either, because the electronic and steric factors can influence the reaction mechanism in different ways, depending on the nature of P-donor ligands. With lower steric requirements of the ligands (phosphites are usually characterised by smaller Tolman cone angles[95, 107, 271]), electronic effects acquire primary importance, whereas for bulky phosphines, steric effects are more significant. In this case, the size and the leaving-group properties of the halide ion become more important and dissociation of one of the ligands with the formation of a coordination vacancy may become the rate-determining step.[272]

From determination of the protonation enthalpy for metal complexes, it is known that the appearance of the hydride ligand in the coordination sphere results in a sharp increase in the metal basicity: it can be 20 kcal mol^{-1} higher than that for analogous halide complexes.[269] During cyclopalladation through hydride intermediates, the opposite pattern of dependence of the reaction rate on the nature of the anions is observed: the formation of palladacycles from the $[PdH(X)(PBu^t_3)_2]$ precursors (X = Cl, Br, CF_3COO) is substantially accelerated in the sequence $CF_3COO^- < Cl^- < Br^-$.[71, 171] This type of dependence can be interpreted as indicating a nucleophilic pathway. It is assumed that in these reactions, direct intramolecular elimination of a hydrogen molecule (rather than an HX molecule) formed from the hydride ligand and one of the phosphine hydrogen atoms (forcibly located close to the metal) can take place.[71]

A similar dependence on the nature of the halides has been observed in the intermolecular activation of aliphatic C–H bonds of cyclohexane by the $[Pd(PPh_3)_2Hal_2]$ complexes.[161, 162] The hydride species $[CyPd^{IV}(H)(PPh_3)_2Hal_2]$ formed upon the oxidative addition were identified by spectroscopy; upon the subsequent reductive elimination of HHal, they were transformed into more stable $[CyPd^{II}(PPh_3)_2Hal]$ complexes.[162] The feasibility of this pathway in intermolecular processes has been confirmed by calculations.[229, 234]

The probability of the nucleophilic pathway should also increase in the cyclometallation with organoelement reagents containing Pd–R bonds[14] (see Section II.2.b). The fact that the hydride intermediate containing Pd(IV) (the product of oxidative addition of the C–H bond) has not been detected does not eliminate the possibility of such pathway, because these compounds are highly reactive and should easily undergo the reductive elimination of the hydrocarbon.

A convenient criterion for elucidation of the mechanism is the regiochemistry of reactions of substrates containing several alternative sites.[238] The only study of this kind known in the chemistry of cyclopalladation of P-donor ligands is the analysis of the isomeric composition of the phosphametallacycles formed by *m*-fluorobenzylphosphine HL^{77} (see Ref. 272). Upon the introduction of an electron-withdrawing substituent (in this particular case, fluorine) into the aromatic ring, the electron density in the ring markedly decreases, especially in the *ortho*-positions, one of which is to be attacked predominantly by a nucleophilic metal ion (for example, Ir^I, Rh^I). Conversely, in the case of an electrophilic mechanism, the C–H bond located in the *para*-position to the electronegative substituent should be attacked predominantly; exactly this outcome (the formation of only the *para*-isomer **77a**) was obtained in the reaction of the phosphine HL^{77} with Na tetrachloropalladate. When phosphines are metallated by compounds of electron-enriched monovalent iridium and rhodium, mixtures of *ortho*- and *para*-isomers (*o*-**77′b** and *p*-**77′a**) are formed in a 4 : 1 ratio.[272]

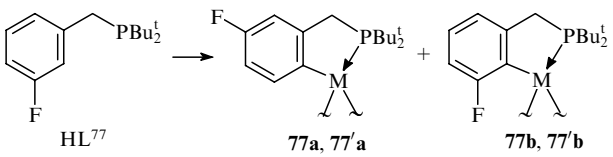

M = Pd (**77a**, 100%; **77b**, 0%); M = Ir (**77′a**, 20%; **77′b**, 80%)

Indirect evidence for the electrophilic mechanism of *ortho*-palladation of other benzylphosphines is provided by acceleration of the process upon the introduction of electron-donating substituents into the aromatic ring of the ligand.[14] For example, the formation of a phosphapalladacycle from benzyldi(*tert*-butyl)-phosphine (HL^{22}), with the unsubstituted aromatic ring, without assistance by a base requires long-term (5 days) refluxing of the intermediate chloride coordination complex in MET.[82] If the aromatic ring is modified by a crown-ether fragment (with electron-donating alkoxy groups in positions 3 and 4), the reaction becomes possible even at 20 °C.[113] The introduction of electron-donating substituents into the aromatic ring is especially efficient in the case of sterically non-crowded phosphines. For example, attempts to accomplish *ortho*-palladation of the phosphine $PhCH_2PPh_2$ (HL^{36}) failed during a long period,[82] whereas the 3,4-dimethoxy-substituted analogue HL^{65} reacts with an almost quantitative yield (91% in the step of C–H bond activation).[113]

It has been assumed[272] that substituents in the aromatic ring of benzylphosphines can also influence the charge and, hence, the reactivity of the metal; however, the transfer of electronic effects through the methylene group appears rather problematic. It can be considered that their influence is mainly limited to the aromatic C–H bond subjected to activation.

As opposed to cyclopalladation of benzylphosphines, *ortho*-palladation of phosphites of the type $4\text{-}RC_6H_4OP(OEt)_2$ (R = MeO, Me, NO_2) virtually does not depend on the electronic properties of the *para*-substituent in the aromatic ring: the product yields in the activation step of the C–H bond under comparable conditions remain unchanged (90% – 97%)[56] (see Table 1).

It can be suggested that this lack of sensitivity to the nature of the substituent in the aromatic ring can be related to the π-acceptor properties of the phosphites,[51, 53] whose P-coordination results in a sharp decrease in the electron density on the metal centre, thus facilitating the electrophilic attack. Indeed, the phosphites $P(OPh)_3$ and $P(OTol\text{-}o)_3$ have very low basicities (pK_a values are −2.00 and −1.83, respectively[53]). No data for $P(CH_2Ph)_3$ are available, but it follows from the pK_a values for $P(OPr^i)_3$ and $P(CH_2Pr^i)_3$ (4.08 and 7.97, respectively[53]) that the basicity decreases by four orders of magnitude upon the replacement of the methylene group present in the phosphine by the oxygen atom (in the phosphite ligand). Recall that the electrophilic mechanism is also assumed for the cycloplatination of phosphites.[17, 237]

In conclusion, it should be noted that the mechanisms of cyclopalladation of P-donor ligands have not been adequately studied and further research along this line can provide a lot of interesting results.

III. Synthesis of phosphapalladacycles by oxidative addition

An alternative way for the construction of phosphapalladacycles is oxidative addition of the C–Hal bonds of preliminarily functionalised substrates to zerovalent palladium. This method is less attractive due to the necessity of preparing these substrates; therefore, the number of relevant publications is moderate.

A classical example of this approach is the reaction of the $Pd(dba)_2$ complex (dba is dibenzylideneacetone) with *o*-bromobenzylphosphines $(o\text{-}BrC_6H_4CH_2)PR^1R^2$, resulting in the cyclopalladated complexes as μ-bromide dimers.[273, 274] In this case (unlike direct intramolecular activation of the C–H bonds), the

enhancement of the steric requirements of the P-donor fragment of the $L^{78}Br$, $L^{36}Br$ and $L^{22}Br$ ligands in the series PMePh ($\theta' = 96°$)† < PPh_2 ($\theta' = 97°$) < PBu^t_2 ($\theta' = 121°$) entails a decrease in the yields of cyclopalladated complexes from nearly quantitative to moderate.[273]

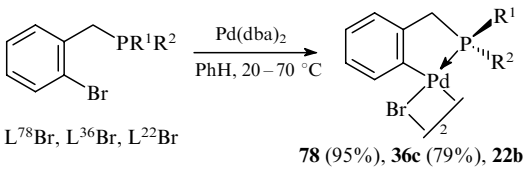

$L^{78}Br$, $L^{36}Br$, $L^{22}Br$ **78** (95%), **36c** (79%), **22b** (68%)

$R^1 = Me$, $R^2 = Ph$ ($L^{78}Br$, **78**); $R^1 = R^2 = Ph$ ($L^{36}Br$, **36c**); $R^1 = R^2 = Bu^t$ ($L^{22}Br$, **22b**).

This route to PC-palladacycles can be considered justified if the synthesis by direct activation of the C–H bond is either difficult (the μ-AcO analogue of the complex **36c** was obtained in ~20% yield) or impossible (for example, in the case of compound **78**).[114, 205]

The efficiency of the method based on oxidative addition for the creation of PCP-structures is difficult to estimate as the available information is sparse but, most likely, it is rather low. For example, in the synthesis of bis(phosphite) complex **79** by treatment of the 2-iodinated $L^{79}I$ ligand with $Pd_2(dba)_3 \cdot CHCl_3$, the overall yield over several steps (including generation of the ligand *in situ* from 2-iodoresorcinol) was only 26%.[275]

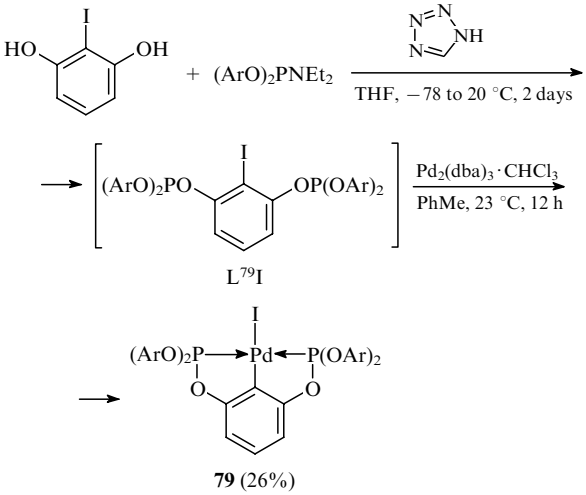

79 (26%)

Ar = 4-$MeOC_6H_4$.

This approach was even less efficient as applied to the synthesis of the bromide analogue of the PCP-complex **61a** from the diphosphine $L^{61}Br$: the yield in the proper oxidative addition step was only 19%.[165]

A rare example of direct activation of the C–H bond in triphenylphosphine with the assistance by fluoride ions in the cycloplatination has been reported.[276] A similar formation of a four-membered PC-palladacycle has been proposed earlier [170] for the reactions catalysed by the Pd(0)–PPh_3 system. However, the cyclopalladated structure of the resulting complex can hardly be considered established for the following reasons: (i) its alternative synthesis by direct activation of the *o*-C–H-bond in the coordination complex $[PdCl_2(PPh_3)_2]$ has been carried out under too mild conditions (AcOLi, DMF, 20 °C); (ii) the isolated compound was characterised only by elemental analysis and IR spectra.

A four-membered PC-palladacycle sterically strained due to annelation to a benzene ring has been prepared only by using the oxidative addition of the *o*-bromo-substituted phosphine $L^{80}Br$ to Pd(0); the product structure was confirmed by X-ray diffraction analysis of the adduct *trans*-(P,P)-**80a**.[277]

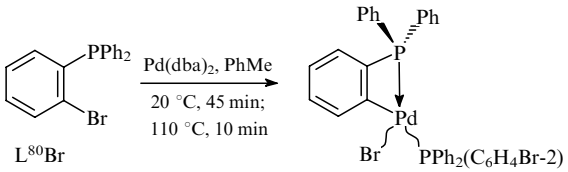

$L^{80}Br$ *cis*,*trans*-**80a** (53%)

The strained character of the metallacycle in **80a** is evident from the fact that in the absence of excess $L^{80}Br$ ligand, the reaction gives a macrocyclic tetranuclear compound with bridging (rather than chelating) PC-ligands — $[\{Pd(\mu\text{-}L^{80})(\mu\text{-}Br)\}_4]$, whose structure was confirmed by X-ray diffraction. Species of two types, those with μ- and η^2-bound ligand $(L^{80})^-$, exist in solutions in an equilibrium, whose position can be controlled by varying the auxiliary monodentate phosphines, in particular, bulky ligands stabilise the phosphapalladacycle, whereas in the presence of small-size phosphines (PMe_3, PMe_2Ph), the PC-palladacycle is cleaved giving rise to bi- or tetranuclear species.[277, 278] An attempt to elucidate the reaction mechanism by spectroscopic monitoring has shown only the intermediate formation of the coordination complex $[Pd(dba)(\kappa^1\text{-}L^{80}Br)_2]$.[277]

The scope of the method considered in this Section is not limited to reactions of aromatic $C(sp^2)$–Hal bonds. At least one example is known where the aliphatic PC-palladacycle is formed through oxidative addition of the $C(sp^3)$–Cl bond of the γ-chloropropylphosphine $L^{81}Cl$ to Pd(0) stabilised by 1,2-bis(diisopropylphosphino)ethane (dippe).[279]

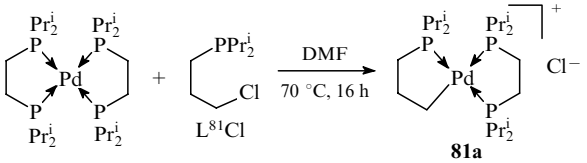

Initially, compound **81a** was detected as a side product in attempted preparation of the $[Pd^0(dippp)_2]$ catalyst [280] from 1,3-bis(diisopropylphosphino)propane (dippp) contaminated by γ-chloropropylphosphine $L^{81}Cl$. The structure of the isolated binuclear complex **81b** with a bridging diphosphine was confirmed by X-ray diffraction.

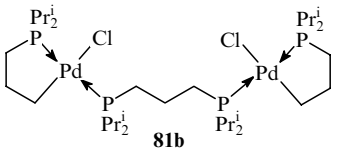

The researchers cited reasonably believe [279] that activation of the aliphatic C–Cl bond is promoted by the preliminary P-coordination of the substrate to the metal, because the rate of the intermolecular oxidative addition of butyl chloride to the same Pd(0) complex is lower by several orders of magnitude (even with excess alkyl halide and when the reaction is conducted under more drastic conditions, at 100 °C). This process may be additionally stimulated by the bulky diphosphines (dippp and dippe).

Thus, the method for the synthesis of PC (but not PCP) complexes by activation of the C–Hal bonds by palladium(0) is rather efficient, but the necessity of preliminary functionalisation of the phosphorus-containing substrate should be regarded as its drawback. The complication of the synthetic protocols could be avoided in the case of direct activation of the C–H bond by Pd(0) compounds.[281]

However, to the best of our knowledge, only one example of reaction of this type is known in the chemistry of complexes of zerovalent palladium, namely, the oxidative addition to Pd(0)

† From here on, the θ' value designates the contribution from the PR^1R^2 fragment to the Tolman θ angle.

complexes of the α-stabilised phosphino-P-ylide HL^{82} or its synthetic precursor, the phosphonium salt $[H_2L^{82}]^+$ (see Ref. 282).

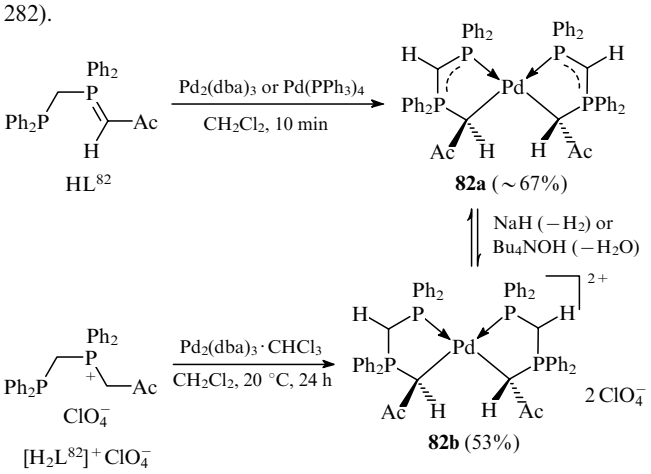

In both processes, *cis*-bis(chelate) complexes are formed and molecular hydrogen is evolved, which was confirmed by gas chromatography. A significant distinctive feature of the former reaction is additional deprotonation of the phosphino-P-ylide ligand in complex **82a** compared to its formally neutral state in the analogue **82b** formed according to the latter pathway. The structural characteristics of the spiro complex **82a** obtained by X-ray diffraction analysis confirm both the methanide nature of the $\{PC(H)P\}^-$ fragment with the central sp^2-hybridised carbon atom and the substantial delocalisation of the electron density in this fragment. The transoid arrangement of two acetyl groups at the ylide carbon atoms (in the axial positions on opposite sides of the coordinate plane) points to a high diastereoselectivity of the formation of C* stereocentres, which are fixed in identical (*S*,*S*)- or (*R*,*R*)-configurations.

The true mechanism of these transformations is unknown, but a rough estimation of the reactivities of the two forms of the ligand used on the basis of the yields and reaction durations shows that the free phosphino-P-ylide HL^{82} is much more reactive in the oxidative addition than the phosphonium salt $[H_2L^{82}]^+ClO_4^-$. Note for comparison that direct activation of the C−H bond in the latter ligand under the action of $Pd(OAc)_2$ to give complex **82b** is more efficient (yield 73%).[282]

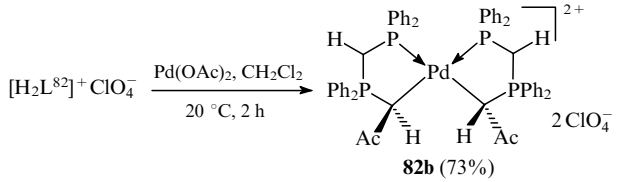

IV. Transmetallation

The transmetallation of lithiated phosphines on treatment with palladium(II) coordination complexes is a unique method for the synthesis of phosphapalladacycles as bis(chelate) compounds of the spiro structure.[16,283,284] Recall that direct intramolecular activation of the C−H bonds results in PC-palladacycles as μ-halide or μ-carboxylate dimers or their mononuclear derivatives (see Section II and Table 1).

The $[PdCl_2(SEt_2)_2]$ coordination complex serves usually as the source of palladium(II) in the stage of metal exchange; for example, it is used in the synthesis of spiro complex **22c** from the *ortho*-lithiated ligand HL^{22} (see Refs 283, 285).

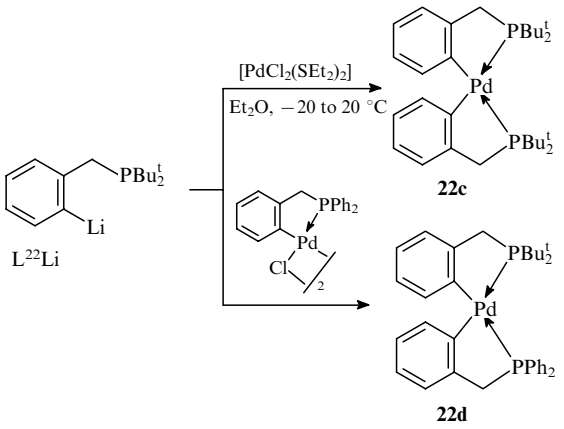

The introduction of standard μ-chloride dimeric cyclopalladated complexes into the reactions with lithiated phosphines opens up the way to asymmetrical spiro structures both with identical (*e.g.*, complex **22d**) and with different donor atoms (P and N; see Table 2).[284,286,287] It has been assumed that mixed-ligand bis(chelate) compounds containing both soft and hard donor atoms at the same metallic centre can be of interest for catalysis.[287] However, as far as we know, their potential as (pre)catalysts has not been evaluated as yet.

Usually, reactions of this type proceed under mild conditions with rather high yields (60%−90%) and do not require steric stimulation.[283,284] For instance, this method was used to prepare complex **83** with the smallest donor groups, PMe_2,[283] whereas, attempts at direct activation of the aromatic C−H bond in dimethylbenzylphosphine (HL^{83}, $\theta = 134°$) have been unsuccessful.[288]

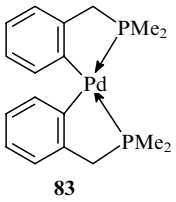

83

The practical value of these bis(chelate) PC-complexes increases due to the fact that they can be easily converted in high yields into standard dimeric cyclopalladated compounds with halide or acetate bridges.

In this version, transmetallation has been applied only to tertiary benzylphosphines, the preparation of *ortho*-lithiated ligands being the key problem. As opposed to tertiary benzylamines where (provided that no steric contraindications are involved)[289,290] direct activation of the $C(sp^2)-H$ bond in the benzene ring is possible and is widely used,[291−295] in the case of phosphorus analogues, direct *ortho*-lithiation proved to be impossible.[296,297] Therefore, a standard method for the synthesis of *ortho*-lithiated benzylphosphines is replacement of bromine by lithium,[298,299] which requires preliminary *ortho*-functionalisation of phosphine. However, in this case, too, the reactions of *ortho*-halogenated benzylphosphines with organolithium reagents can be complicated by at least two side reactions, namely, α-metallation and nucleophilic substitution at phosphorus (depending on the nature of the P-substituents, the nature of the halide, and the reaction conditions).[298,300] For example, *o*-chlorobenzylphosphines are metallated predominantly at the α-benzyl position, while the bromine atom in the *ortho*-position of the aromatic ring can be replaced by lithium almost quantitatively under appropriate conditions.[300−302] The susceptibility for α-lithiation can be illustrated by the replacement of the α-benzyl protons of all three

benzyl groups of the phosphonium salt $[PhP(CH_2Ph)_3]Cl$ in the reaction with BuLi.[303]

Detailed investigation of the behaviour of two *ortho*-lithiated benzylphosphines, $R_2PCH_2C_6H_4Li$-2 (R = Me, Ph), has shown that in donor-type solvents and in the presence of *N*,*N*,*N*′,*N*′-tetramethylethane-1,2-diamine (TMEDA), they are easily isomerised into the corresponding thermodynamically more stable α-lithiated derivatives *via* 1,3 proton migration. The structures of two isomeric products of lithiation of dimethylbenzylphosphine, **83′a** and **83′b**, were confirmed by X-ray diffraction.[299]

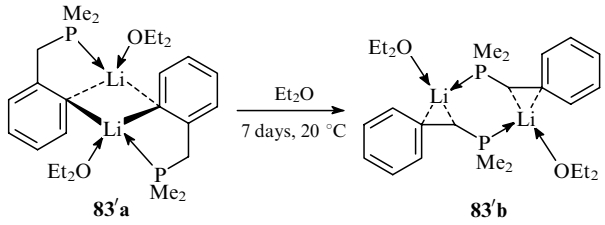

83′a **83′b**

For the synthesis of spiro complexes with the $C(sp^3)-Pd$ bond from *o*-tolylphosphines, an alternative approach involving the potassium salt of the ligand (for example, HL[84]) has been proposed.[304, 305] Among obvious advantages of this method, one should mention the possibility of direct metallation of the *o*-methyl group of the tolyl substituent. Butyllithium in the presence of TMEDA and an approximately equimolar amount of potassium *tert*-butoxide was used as the reagent.

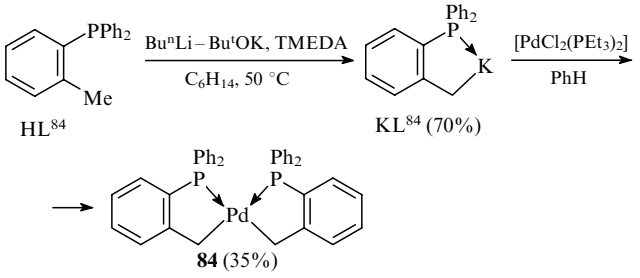

HL[84] KL[84] (70%)

84 (35%)

Presumably,[305] the success of metallation is determined by the exchange between two reagents, Bu^tOK and Bu^nLi, resulting in the formation of butylpotassium species. When Bu^tONa is used, the yields decrease to 40%, and in the presence of Bu^tOLi, metallation does not proceed at all.[305] For the synthesis of PC-palladacycles, the coordination complexes *trans*-$[PdQ_2Cl_2]$ are used (Q = PEt_3, SEt_2). This choice is determined by good solubility of these reagents, the volatility of the auxiliary ligands Q, and their indifference with respect to metallated KL ligands. Unfortunately, the yield of complex **84** obtained in this way did not exceed 35%.

All the above examples refer to the preparation of five-membered PC-palladacycles. In a recent study,[306] this method was used to prepare platinum(II) *cis*-spiro-complex **80′b** with two four-membered PC-metallacycles on the basis of the *ortho*-brominated triphenylphosphine $L^{80}Br$.

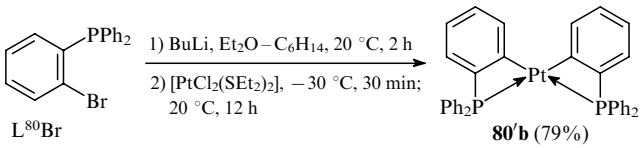

$L^{80}Br$ **80′b** (79%)

It is noteworthy that most of bis(chelate) spiro complexes of both PC- and NC-type[307] are formed as *cis*-isomers, which is explained by the 'antisymbiosis' effect,[308] namely, in transition metal complexes, the *trans*-arrangement of two 'soft' donor atoms markedly destabilises the system. However, in the case of mixed-ligand complexes with different donor atoms in two metallacycles (for example, of the PC and NC types), the formation of the *trans*-isomer is also possible, the isomer ratio being dependent on the order in which the metallacycles are closed.[284]

V. P,C-Chelation of phosphine-substituted phosphorus ylides

In the coordination chemistry of α-stabilised P-ylides, C-binding to soft metals, in particular, palladium and platinum, is usually preferred.[309] The functionalisation of these P-ylides by an additional phosphine fragment opens up the new route to the closure of phosphapalladacycles by simple chelation. A fundamental feature that distinguishes phosphino-P-ylides from other classes of ligands considered in this review is their zwitter-ionic structure, which imparts quasi-carbanionic properties to the ylide carbon atom (structure **B**) even before the reaction with the metal.[309, 310]

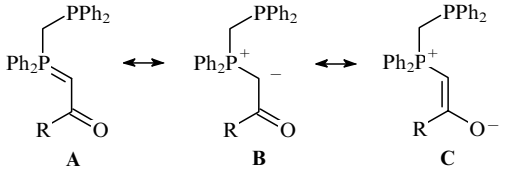

A **B** **C**

The presence of electron-withdrawing substituents (in particular, the carbonyl group) in the P-ylide molecule provides partial delocalisation of the negative charge of the ylide carbon with participation of the carbonyl oxygen (structure **C**), which makes ligands of this class rather stable in the free state and convenient to work with. An adverse consequence of this α-stabilisation is the somewhat reduced nucleophilicity of the ylide carbon; however, it remains sufficiently quasi-anionic to enable direct efficient binding to soft transition metals. Due to the presence of an additional phosphine group, the process of formation of PC-palladacycles is reduced to mere chelation of the zwitter-ionic ligand with Pd(II) compounds involving no activation of the C–H bond or deprotonation. The X-ray diffraction data available for complexes of this class[282, 311–314] clearly demonstrate that the greatest contribution to the electronic structure of the PC-bound phosphino-P-ylides is made by the bipolar canonical form **B**, whereas for free ligands, form **C** prevails.

Phosphino-P-ylide ligands are readily available; they are prepared by condensation of a diphosphine, namely, 1,1-bis(diphenylphosphino)methane (dppm) or dppe, with the corresponding α-halogen-substituted carbonyl compound of the $HalCH_2C(O)R$ type and subsequent deprotonation of the intermediate phosphino-phosphonium salt.[310, 315]

Cyclopalladated derivatives of phosphino-P-ylides are prepared using both preliminarily isolated ylide ligands and their precursors, phosphonium salts (see Table 3). The former version can be illustrated by the synthesis of the simplest monochelate dichloride complex **85a** by the reaction of phosphino-P-ylide L[85] with the benzonitrile reagent.

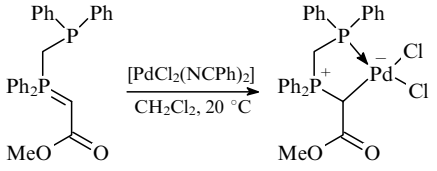

L[85] **85a** (80%)

The reaction is carried out under mild conditions and with high yields[315–317] almost irrespective of the size of the metallacycle to be formed (five- or six-membered) or the nature of the substituent R in the carbonyl fragment (R = Ph, Me, MeO, EtO). The monochelate P-ylide complexes of this type are thermally and oxidatively stable; compounds with five-membered PC-rings are more stable than those with six-membered rings; and the stability depends on the nature of the substituent R in the carbonyl fragment (Ph > Me > MeO).[317]

The same principle of simple chelation of phosphino-P-ylides is applicable to the synthesis of mono- and diaryl complexes **86a** and **86b**.[318] The corresponding binuclear complexes, [{ArPd.(μ-Hal)(THT)}$_2$] (THT is tetrahydrothiophene) or [Bu_4N]$_2$.[{Ar_2Pd(μ-Hal)}$_2$], are used as the reagents. In this case, too, reactions proceed under mild conditions and give products in satisfactory yields (60% – 80%).

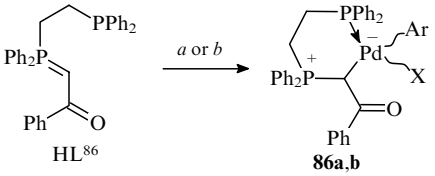

X = Cl, Ar = C_6Cl_5 (**86a**); X = Ar = C_6F_5 (**86b**);

(*a*) [{Pd(μ-Cl)(C_6Cl_5)(THT)}$_2$], PhH, 20 °C, 20 min, 69%;

(*b*) (Bu_4N)$_2$[{Pd(μ-Cl)(C_6F_5)$_2$}$_2$], Me_2CO, 20 °C, 30 min, 57%.

Asymmetrical monoarylated compounds such as **86a** are formed as mixtures of *trans*-C,C-/*cis*-C,C-isomers in 10 : 1 to 2 : 1 ratios.[318]

The synthesis of cyclopalladated derivatives of phosphino-P-ylides from the corresponding phosphonium salts [HL]$^+$X$^-$ is also reduced to direct chelation, as it implies generation of the P-ylide ligand *in situ* by deprotonation of the phosphonium precursor by a base. Since phosphonium bromides are normally used and an additional amount of bromide ions is introduced, phosphapalladacycles are formed as dibromide complexes (for example, **87a**).[313]

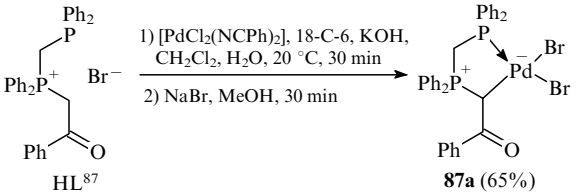

18-C-6 is 18-crown-6 ether.

The problem of solubility is solved by conducting the reaction in a two-phase system with the addition of 18-crown-6 ether (0.2 equiv.) as a phase transfer catalyst. The possibility of using less expensive reagents, for example, Na_2PdCl_4 can also be considered as an advantage. However, under any conditions (including experiments with a crown ether), the yields of the dibromide complex **87a** remained moderate (60% – 65%).

The phase transfer strategy has also been applied to prepare peculiar spiro complexes in which the metal is incorporated simultaneously into a five- or six-membered P-ylide phosphapalladacycle and a four-membered C,C-metallacycle formed by dianionic bis-S-ylides.[313] In this case, the PC-palladacycle (for example, that in the complex **87c**) is formed in a two-stage process through the intermediate monodentate P-coordination of the cationic [HL^{87}]$^+$ ligand to the S-ylide reagent and subsequent deprotonation under the action of a base in the presence of crown ether.

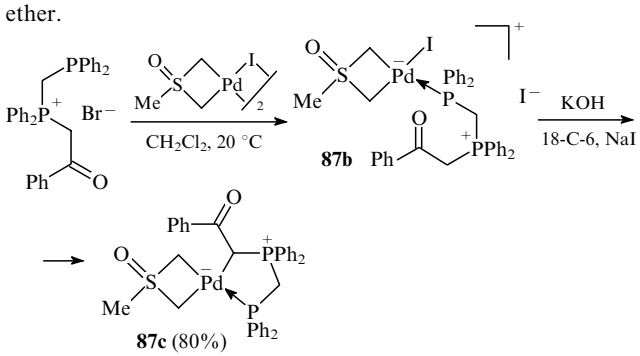

Although the yields of spiro complexes such as **87c** are, most often, relatively high (60% – 80%), the effect of the crown ether is still insignificant. Indeed, five-membered PC-palladacycles can be closed not only in the absence of a phase transfer catalyst but even without a base — due to the activation of the C – H bond with palladium. The structure of the complex **87c** was confirmed by X-ray diffraction data.[313]

VI. Other routes to phosphapalladacycles

This Section describes a number of unusual transformations, giving rise to PC- or PCP-palladacycles due to activation of the C – C, C = P, C – F or C – O bonds; in these processes, the new ligand is formed on a metallic template.

The key step in the transformation of the cyclopropylmethylphosphine HL^{88} into the dimer **89** is the activation of the C – C bond in the strained cyclopropane ring in the coordination complex *trans*-[$PdCl_2(HL^{88})_2$] (**88**) during its thermolysis in glacial acetic acid.[319]

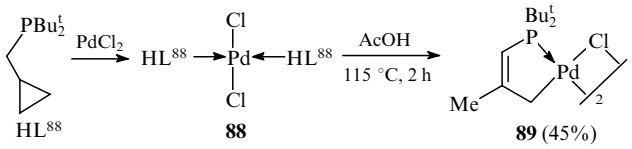

It is assumed [319] that the HL^{88} ligand is converted into dimer **89** by a route usual for the chemistry of cyclopropane.

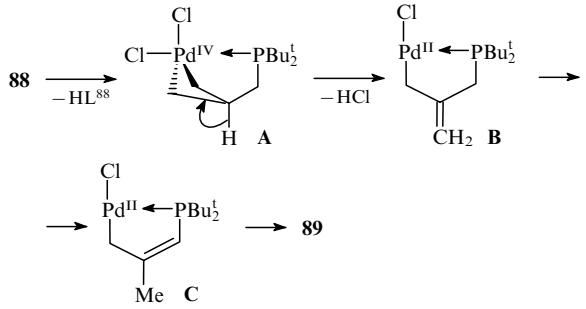

The elimination of one of the phosphine ligands from precursor **88** is followed by activation of the C – C bond in the three-membered ring in the coordinatively unsaturated [$PdCl_2(HL^{88})$] species. The β-elimination of the proton from intermediate **A** yields phosphapalladacycle **B** with an *exo*-double bond; this product is then isomerised through a 1,3-hydride shift to form the PC-palladacycle **C** with an *endo*-double bond. The last-mentioned species further dimerises to give complex **89**.[319]

A similar process takes place at a platinum(II) centre;[320] meanwhile, in the reactions of the phosphine HL^{88} with iridium(I) [321] and di-*tert*-butyl(cyclobutylmethyl)phosphine with platinum(II),[321] the C – H bond of the small ring (retained in the final product) is subjected to activation.

Unusual results have been obtained in a study of the reactions between the HL^{90} and HL^{91} phosphaalkene ligands and the organometallic reagent, [MePd(cod)Cl].[322] Although cyclometallated derivatives of phosphaalkenes of both PC- [117, 323] and PCP-types [117, 125, 127] are known (see Tables 1 and 4), these reactions were found to give three-membered PC-palladacycles under very mild conditions, instead of the expected cyclopalladated products of PC- or PCN-type with the optimal five-membered metallacycles or coordination complexes with P-mono- or P,N-bidentate ligands. One can see that the phosphaalkenes HL^{90} and HL^{91} with N-donor substituents R are converted into macrocyclic binuclear complexes **92** and **93** in high yields.

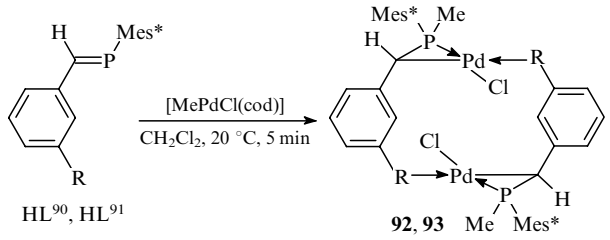

R = 2-Py (HL^{90}, **92**, 90%); R = CH=NPh (HL^{91}, **93**, 71%).

It has been suggested [322] that this process includes carbopalladation of the C=P bond in the starting ligand, *i.e.*, the formal addition of the Pd–Me fragment to the C=P double bond. The regiochemistry of the reaction complies with the polarisation of this bond ($C^{\delta-}=P^{\delta+}$) caused by the higher electronegativity of the carbon atom (2.5) compared to phosphorus (2.1):[324] the quasi-carbanionic methyl group attacks the phosphorus atom, while the metal goes to the carbon atom. Although the researchers do not discuss the stereochemistry of this process in which two stereocentres arise (C* and P*), the presence of only one signal in the ^{31}P NMR spectrum and only one set of ^{1}H NMR signals suggest that the reaction is highly diastereoselective. In the case of dimer **92**, this was confirmed by X-ray diffraction data: the crystal contains only enantiomeric three-membered PC-palladacycles of the (S_CR_P)- and (R_CS_P)-configurations.[322] It should be noted that despite the strained character of such structures, three-membered palladacycles with other heteroatoms, for example, CS- [325, 326] and CO-types are also known.[327]

Non-symmetrical bicyclic PCP-structures (for example, **95**) with annelated three- and six-membered PC-palladacycles and two chemically different P-donor centres (phosphaalkene and phosphinite ones) are formed in the reaction of the coordination complex **94** with alcohols. The regiochemistry of this process is also dictated by the inverted polarity of the $C^{\delta-}=P^{\delta+}$ bond (with respect to the polarity of the C=N bond): the nucleophilic attack by ROH occurs regioselectively involving only the $P^{\delta+}$ atom. This reaction is also diastereoselective; the formal *syn*-addition of the alcohol gives rise to two stereocentres with the same configuration, either (S_CS_P) or (R_CR_P).[328]

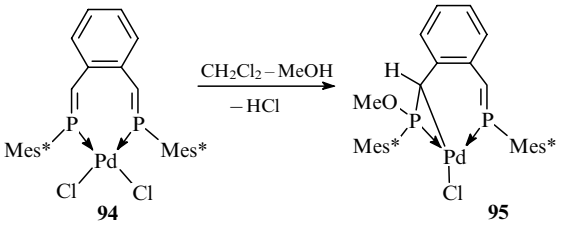

It should be noted that strained three-membered PC-metallacycles are also found in structures with other metals: Ru,[329, 330] Os,[331, 332] W,[333] and Ta [334] and so on.

The formation of a PC-palladacycle upon the reaction of iodobenzene and the Pd(0) complex with the (2-vinylphenyl)diphenylphosphine ligand HL^{96} is based on a complex sequence of transformations, resulting finally in the modification of the starting ligand (the structure of adduct **97a** was confirmed by X-ray diffraction [335]).

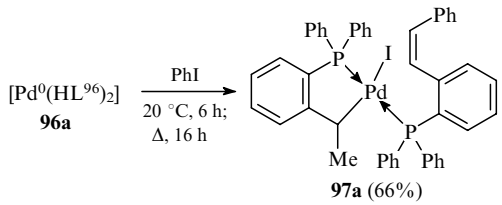

The process is assumed to start with the oxidative addition of PhI to the initial complex **96a** to give adduct **96b**, which appears quite reasonable in view of the coordinative unsaturation of the 16-electron particles. The migration of the metal-bound Ph group to the vinyl fragment of the monodentate P-coordinated HL^{96} ligand in intermediate **96b** gives rise to a new phenylated phosphine HL^{97} (*via* a transformation similar to the Heck reaction). Further, the HL^{97} ligand is closed to give a five-membered PC-palladacycle as adduct **A** with the starting phosphine HL^{96}.

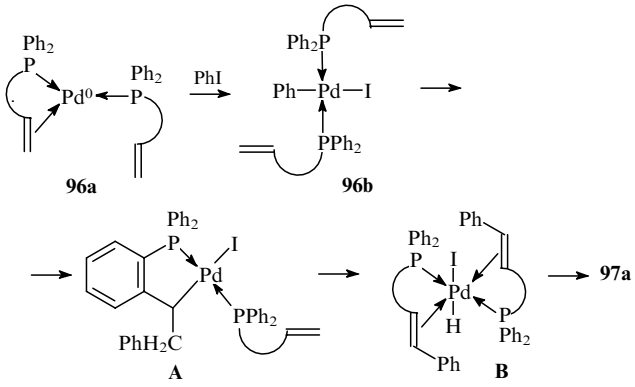

The subsequent steps include β-elimination of hydrogen from the σ-bound alkyl group in the intermediate **A** to afford Pd(IV) hydride derivative **B** and, as the final step, the addition of the hydride to the olefinic fragment, which is either linked to the metal (or merely located close to the metal in space).[335]

A similar cyclopalladated compound is also formed in the reaction of the complex **96a** with bromobenzene, whereas chlorobenzene is inactive in this process. The decrease in the reactivity of aryl halides in the sequence PhI ⩾ PhBr ≫ PhCl is typical of palladium-catalysed cross-coupling [336] and implies the crucial role of the oxidative addition of aryl halide.

An X-ray diffraction study of the starting complex **96a** has shown a shortened contact between Pd(0) and the α-hydrogen of the non-coordinated vinyl group of the phosphine HL^{96} (the Pd···H distance is 2.46 Å,[34] which is much shorter than the sum of the van der Waals radii of these atoms, equal to 3.1 Å, see Ref. 220). The attractive nature of this interaction seems obvious in view of both the displacement of the palladium atom toward the α-vinyl hydrogen by 0.22 Å and the existing way for a monodentately linked phosphine to avoid these contacts through rotation about the P–C bonds. Interactions of this type are usually considered as an intermediate step in the activation of the C–H bonds.[261, 262] Moreover, study of the temperature dependence of the ^{31}P NMR spectra of complex **96a** has shown that this complex exists in solutions in equilibrium with two-coordinate [Pd(κ^1-HL^{96})$_2$] species, the latter being the predominant form. Hence, the real state of the complex **96a** is nearly 14-electron, and this coordinative unsaturation should stimulate efficiently the oxidative addition. Indeed, treatment of the complex **96a** with an equimolar amount of aqueous HBF_4 under low-temperature conditions gives cationic cyclopalladated compound **97b** stabilised by η^2:κ^1-coordination of the non-metallated HL^{96} ligand.[34]

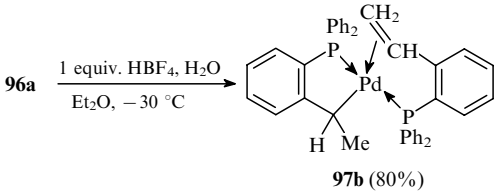

Yet another unusual route to the PC-palladacycle has been discovered in a study of reactions of polynuclear μ-imidoyl complex **98** with phosphides.[337] In this case, a new phosphine ligand is formed due to activation of the C–F bond in the C_6F_5 aryl group. The *ortho*-direction of the attack by the nucleophile (Ph_2P^-) is presumably caused by assistance by the metallic centre.

The product of this reaction, dimeric complex **99a**, differs from the analogues considered previously in that the bridging function is performed by the N-donor atoms of the C-metallated aldimine $(L^{99})^-$ rather than by the halide anions. The dimer **99a** is easily converted into mononuclear adducts (for example, complex **99b**) upon the reaction with auxiliary ligands. The initial compound **98** results from insertion of MeNC into the Pd–Ar bond of the organometallic reagent $[Pd(C_6F_5)_2(CNMe)_2]$ upon its interaction with $[PdCl_2(NCPh)_2]$.[338]

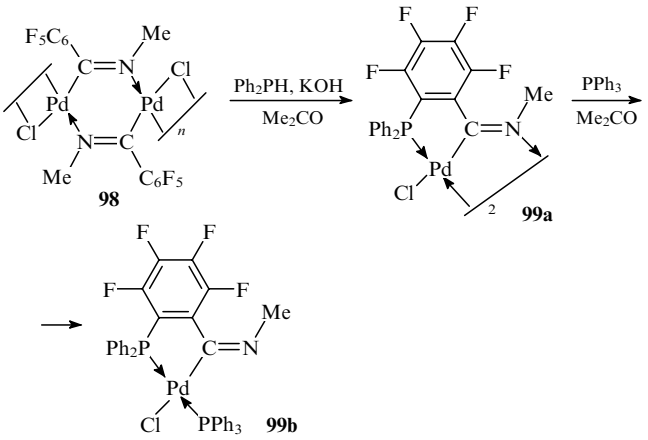

The formation of the P–C bond underlies an unusual pathway of the transformation of methylenediphosphine (dppm) into alkenyl phosphorus ylide ligands on a palladium(II) template.[339] The coordination complex **100**[340] with P,P-chelated diphosphine serves as the starting substrate. Long-term thermolysis of this compound in the presence of excess terminal alkyne yields complexes **101a–c** with zwitter-ionic phosphonium-alkenyl-P-ylide ligands, which possess high stability (thermal, oxidative and hydrolytic).

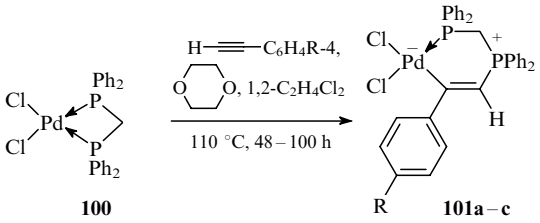

R = NMe_2 (**101a**, 31%), Ph (**101b**, 49%), NO_2 (**101c**, 73%).

Reactions of this type are regiospecific: the Pd–C bond is formed only with the terminal carbon atom of the monosubstituted alkyne. This regiochemistry may be due to the substantial steric crowding of the reacting P-donor atom of the diphosphine and relatively slight shielding of the metallic centre (disubstituted alkynes cannot be introduced in this process). Although this reaction looks formally to be the insertion of the alkyne into the Pd←P bond, the researchers proposed a more realistic mechanism including (i) solvolytic dechelation of diphosphine in complex **100** to give coordinatively unsaturated species **A**; (ii) η^2-binding of alkyne to the metal at the newly formed coordination vacancy;

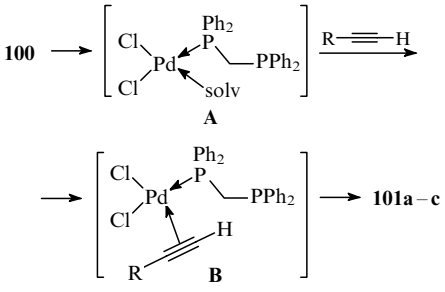

(iii) nucleophilic attack of the free PPh_2 group of the monodentate phosphine in intermediate **B** on the π-coordinated alkyne.

A number of experimental observations are consistent with this scheme. First, the reaction occurs only in the complex with dppm, which forms a strained (and, hence, unstable) four-membered chelate ring.[341] Transformation of this type proved impossible for the similar $[PdCl_2(dppe)]$ complex with diphosphine which forms a stable five-membered chelate ring. Second, the success of this transformation depends appreciably on the coordination capacity of the solvents used, which is important for dechelation of diphosphine: the reaction proceeds only in the presence of dioxane. Third, the coordination of alkynes to the metal should make them more susceptible to the nucleophilic attack. This is consistent with the regular increase in the reactivity of alkynes of the $4\text{-}RC_6H_4C{\equiv}CH$ type following the introduction of electron-withdrawing substituents R (Me_2N < H < NO_2) in the aromatic ring (the yields of complexes **101a–c** increase in this series).[339] A similar process proved possible for platinum(II) complexes with dppm.[342]

Alkenyl phosphametallacycles can be constructed from anionic β-phosphino enolates P,O-chelated to palladium through the formation of a new C–C bond.[343–345] The specific reactivity of ligands of the $R^1_2PCH{=}C(R^2)O^-$ type is due to high nucleophilicity of the carbon atom adjacent to phosphorus. Experiments were carried out with two spiro complexes of phosphino enolates, namely, the symmetrical bis(chelate) coordination compound **102a** and mixed-ligand analogue **102b** containing a CN-metallacycle.[346] Bis(chelate) **102a** reacts with dimethyl acetylenedicarboxylate to give spiro complex *cis*-**103a** of the alkenyl type containing a $C(sp^2)$–Pd bond.[343, 344]

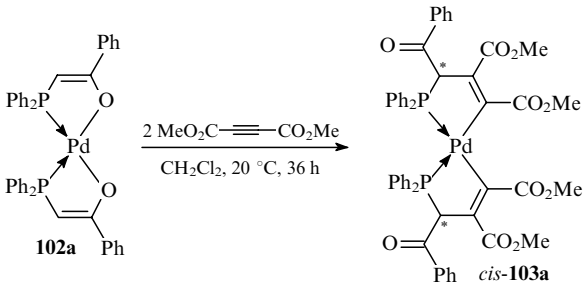

The stereoselectivity of this process, which gives rise to a C*-stereocentre in each of the metallacycles, is relatively low: complex **103a** is formed as a mixture of two diastereomers (3 : 1) with the same geometric *cis*-P,P-configuration. The predominant *meso*-form was isolated from the mixture by fractional crystallisation and characterised by X-ray diffraction.[343]

The same phosphapalladacycle as a part of a mixed-ligand spiro complex **103b** is formed in the reaction of alkyne with a phosphino enolate P,O-chelated to the benzylaminate CN-palladacycle (**102b**).[344, 345]

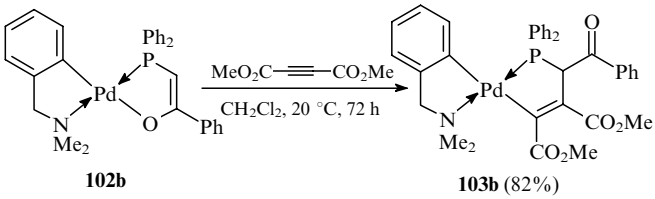

The mechanism of C–C-coupling of the enolate fragment of the P,O-bound ligand with the alkyne triple bond has not been studied. The activating role of the metallic centre is evident from the dependence of the reactivity of complexes on the nature of the metal (Ni > Pd > Pt). β-Phosphino enolates may be activated towards nucleophilic attack upon dechelation and tautomerisation to the keto form $M^+ \leftarrow PPh_2CH^-C(=O)Ph$, in which the α-carbon atom at phosphorus has a more pronounced carbanionic nature.[343–345]

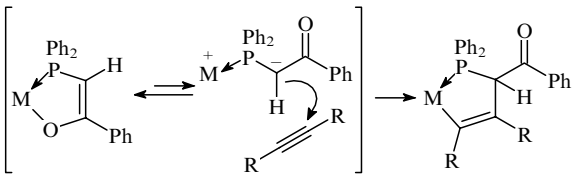

This suggestion seems quite reasonable from general considerations: the Pd—O bond between the 'soft' metal and the 'hard' oxygen donor atom cannot be strong. The dissociative mechanism is supported indirectly by a sharp acceleration of the process when carried out in an efficiently coordinating solvent. Thus complex **104** with a modified P,O-ligand reacts instantaneously with dimethyl acetylenedicarboxylate in THF to give spiro complex **105**,[345] whereas a similar reaction involving complex **102b** in dichloromethane proceeds to completion in 72 h.[344]

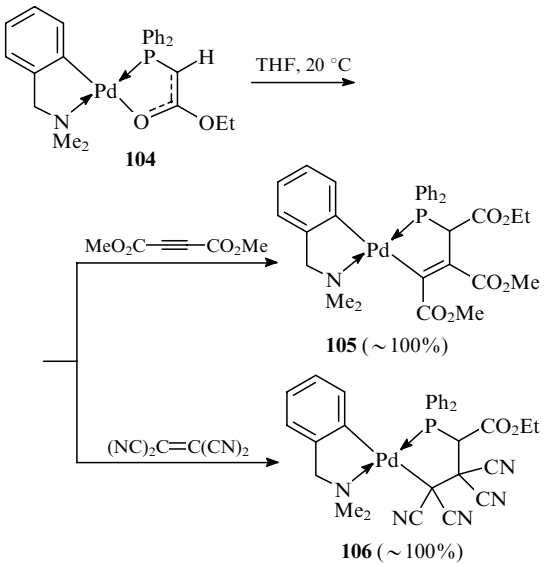

The reaction of complex **104** with an electron-deficient alkene (tetracyanoethylene) gives a phosphapalladacycle **106** of the alkyl type with the C(sp^3)—Pd bond whose structure was confirmed by X-ray diffraction.[345]

By contrast with homoleptic spiro complexes of type **103a**, which are formed as *cis*-C,C-isomers (but are completely isomerised into thermodynamically more stable *trans*-isomers on long-term heating),[344] their mixed-ligand analogues **103b**, **105** and **106** have initially the *trans*-C,C-geometry, which is at variance with the 'antisymbiosis' concept,[308] according to which the *trans*-arrangement of two soft donor atoms at a soft metallic centre destabilises the system.

The method for the synthesis of PCP-structures from derivatives of 2,6-bis(phosphinomethyl)phenols developed by Milstein [151, 347] seems fairly unusual, if one takes into account the high strength of the Ar—O bonds. Although this transformation can be easily performed on rhodium(I) centres, in the case of Pd(II), an attack on the weaker ArO—Alk bond to give phenoxy complexes is preferred under similar conditions (the structure of one of such complex has been confirmed by X-ray diffraction).[151] Also surprising is the effect of the minor modification of the alkyl group in the phenol ether on the direction of reaction with palladium(II) trifluoroacetate. Whereas in the case of the methyl ether L^{107}OMe, no cyclopalladation signs were found, in the case of ethyl-substituted analogue L^{107}OEt, $Pd(TFA)_2$ reacts along two competing pathways to give products of the formal insertion of the metal into the ArO—Alk (**107**) and Ar—OAlk (**25b**) bonds in the kinetically controlled 9 : 1 ratio, *i.e.*, the former pathway remains preferred.[151]

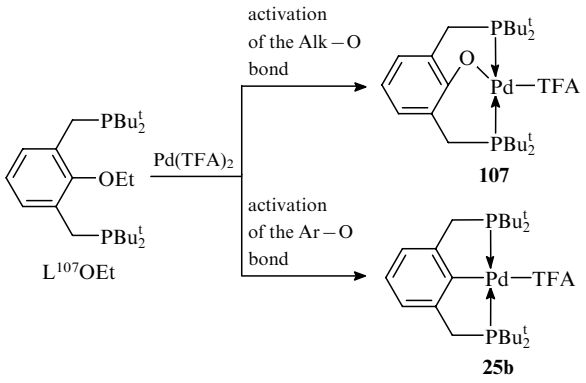

The differences in the behaviour of analogous substrates, L^{107}OMe and L^{107}OEt, have been attributed [151] to steric effects. Since the mechanism of the formation of phenoxy complex **107** postulated by these researchers includes an S_N2 attack by the anion (here, the $CF_3CO_2^-$ group) on the alkyl group of the ether, the replacement of the MeO group by the EtO group makes the nucleophilic attack on the α-carbon atom sterically more hindered, which opens up the way for competing cyclopalladation.

The POP-phenolate complexes **107** and **108** predominating in these processes can be converted into cyclometallated PCP-structures **25b** and **109** by long-term thermolysis in a hydrogen atmosphere, resulting in activation of the Ar—O bond.[151]

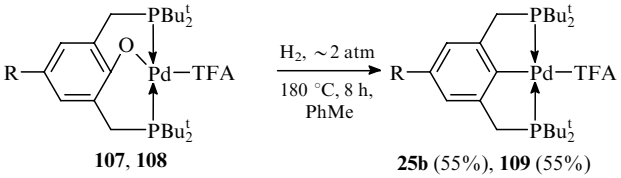

R = H (**107**, **25b**), Me (**108**, **109**).

Presumably, the mechanism of this process includes opening of the ArO—Pd σ-bond under the action of excess hydrogen, and the phenol ArOH thus formed participates further in two competing reactions, namely, reversible activation of the O—H bond and irreversible activation of the Ar—O bond, the latter being responsible for the closure of the phosphapalladacycles. Unusual as it may seem, this hydrodeoxygenation process is of no preparative value, because these products are available *via* direct activation of C—H bonds under mild conditions (see Table 4).

VII. Supplement

Table 1. Phosphapalladacycles of the PC-type.

Complex [a]	Designation of the compound	X	R^1	R^2	Reagents and reaction conditions	Yield [b] (%)	Ref.
PC-Complexes with the C(sp^3)—Pd bond							
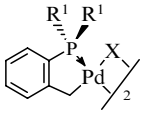	**29a** [c]	AcO	*o*-Tol		1) $Pd(OAc)_2$ – P(Tol-*o*)$_3$ (1 : 1.3), PhMe, 50 °C, 3 min 2) $Pd(OAc)_2$ – P(Tol-*o*)$_3$ (1 : 1), Me_2CO, Δ, 1 h	93 79	8 [c], 10 148
	29d	TFA	*o*-Tol		$Pd(TFA)_2$ – P(Tol-*o*)$_3$, PhMe, 20 °C, 6 h	–	348
	29e [c]	I	*o*-Tol		$Pd(OAc)_2$ – P(Tol-*o*)$_3$, Et_3N, ArI, diene	–	349, 350 [c]
	21a	Cl	Bu^t		(*a*) Na_2PdCl_4 – P(Tol-*o*)Bu^t_2 (1 : 2), MeOH, −6 °C, 45 min; (*b*) Na_2PdCl_4 (1 equiv.), EtOH – MeOH, Δ, 5 min	76 [d] (90)	81
	21b	AcO	Bu^t		$Pd(OAc)_2$ – P(Tol-*o*)Bu^t_2 (1 : 1), PhMe, 20 °C, 6 h	90	10
	32	AcO	Cy		$Pd(OAc)_2$ – P(Tol-*o*)Cy_2 (1 : 1), PhMe, 20 °C, 12 h	41	10
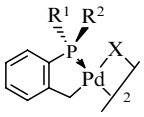	**30a** [c]	AcO	*o*-Tol	Bu^t	$Pd(OAc)_2$ – P(Tol-*o*)$_2Bu^t$ (1 : 1), PhMe, 60 °C, 5 min	94	10, 147 [c]
	30b	Cl	*o*-Tol	Bu^t	1) Na_2PdCl_4 – P(Tol-*o*)$_2Bu^t$ (1 : 1), PrOH – MeOH, Δ, 3 min; 2) (*a*) Na_2PdCl_4 – P(Tol-*o*)$_2Bu^t$ (1 : 2), EtOH – MeOH, 20 °C, 30 min; (*b*) Pr^nOH, Δ, 3 min 3) (*a*) Na_2PdCl_4 – P(Tol-*o*)$_2Bu^t$ (1 : 2), EtOH – MeOH, 20 °C, 30 min; (*b*) Na_2PdCl_4 (1.2 equiv.), MeOH, 50 °C, 2 min; Pr^nOH, Δ, 5 min 4) (*a*) K_2PdCl_4 – P(Tol-*o*)$_2Bu^t$ (1 : 1), CH_2Cl_2 – H_2O, 40 °C, 5 min; (*b*) Bu^iOH, Δ, 7 min 5) [{Pd(η^2-$C_6H_4CH(Bu^t)NH_2$-2)(μ-Cl)}$_2$] – P(Tol-*o*)$_2Bu^t$ (1 : 2), PhMe – AcOH, 60 °C, 1 h	97 84 [d] (96) 85 [e] (97) 94 [f] 71	81 81 81 145 206, 207
	31	AcO	*o*-Tol	Cy	$Pd(OAc)_2$ – P(Tol-*o*)$_2$Cy (1 : 1), PhMe, 20 °C, 6 h	42	10
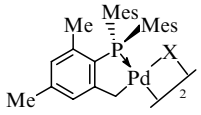	**35a** [c]	Cl			1) $[PdCl_2(NCPh)_2]$ – $PMes_3$ (1 : 2), CH_2Cl_2, 20 °C, 30 min 2) $[PdCl_2(NCPh)_2]$ – $PMes_3$ (1 : 1), CH_2Cl_2, 20 °C, 30 min 3) $PdCl_2$ – $PMes_3$ (1 : 2), CH_2Cl_2, 20 °C, 8 – 10 h	98 94 ~75	109, 110, 351 [c] 110 110
	35b	AcO			$Pd(OAc)_2$ – $PMes_3$ (1 : 1), PhMe, 20 °C, ~12 h	81	10
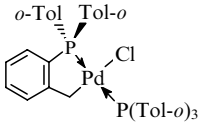	**29f**				$[PdCl_2\{P(Tol\text{-}o)_3\}_2]$, AcOLi, AcOH, H_2, Δ, 2 h	–	170
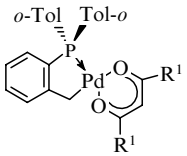	**29b**		CF_3		1) (*a*) $[Pd(hfac)_2]$ – P(Tol-*o*)$_3$ (1 : 1), hexane, Δ; (*b*) CH_2Cl_2, 20 °C, 10 days 2) $[Pd(hfac)_2]$ – P(Tol-*o*)$_3$, PhH, Δ	40 [g] (47) –	196 116
	29g		Me		$Pd(acac)_2$ – P(Tol-*o*)$_3$, PhH, Δ	–	116
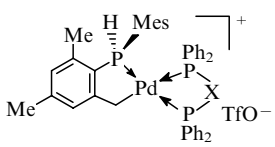	**71b** [c]	CH_2CH_2			(*a*) [Pd(dppe)(Me)Cl] – $PHMes_2$ (H_2L^{71}) – AgOTf (1 : 1 : 1), MeCN – THF, 1 h; (*b*) Me_2CO, HOTf (1 equiv.), 60 °C, 3 days	68 [h] (85)	169
	71c	CH=CH			(*a*) [Pd(dppen)(Me)Cl] – $PHMes_2$ (H_2L^{71}) – AgOTf (1 : 1 : 1), MeCN – THF, 15 min; (*b*) THF, 60 – 65 °C, 3 days	59 [h] (63)	352
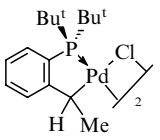	**1**				(*a*) Na_2PdCl_4 – HL^1 (1 : 2), MeOH – EtOH, 20 °C, 1 h; (*b*) Pr^nOH, Δ, 20 min	83 [d] (~100)	55
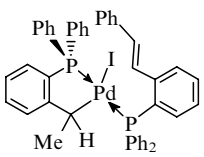	**97a** [c]				(*a*) [Pd(η^5-Cp)(η^3-All)] – HL^{96} (1 : 2); (*b*) PhI (excess), PhH, 20 °C, 6 h; 80 °C, 16 h	see [i] (66)	335

Table 1 (continued).

Complex [a]	Designation of the compound	X	R^1	R^2	Reagents and reaction conditions	Yield [b] (%)	Ref.
PC-Complexes with the $C(sp^3)-Pd$ bond							
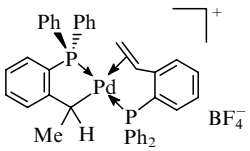	**97b**				(*a*) [Pd(η⁵-Cp)(η³-All)] – HL^{96} (1 : 2), PhMe, 20 °C, > 3 h; (*b*) $HBF_4 - H_2O$ (1 equiv.), Et_2O, −30→20 °C	52 [i] (80)	34
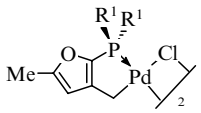	**110**		3,5-Me_2-2-furyl		$[PdCl_4]^{2-}$ – HL^{110}, MeOH $HL^{110} = PR^1_3$	–	353
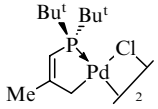	**89** [c]				(*a*) $PdCl_2$ – HL^{88} (1 : 2), EtOH – H_2O, 20 °C, 3 days; (*b*) AcOH, Δ, 2 h	43 [d] (45)	319
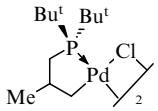	**42**				(*a*) Na_2PdCl_4 – $PBu^t_2Bu^i$ (1 : 1), EtOH, Δ, 0.5 h; (*b*) MET, Δ, 23 h	40 [f] (48)	119
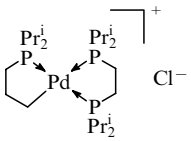	**81a**				$[Pd^0(dippe)_2]$ – $Pr^i_2P(CH_2)_3Cl$ (1 : 1), DMF, 70 °C, 16 h (in a sealed tube)	–	279
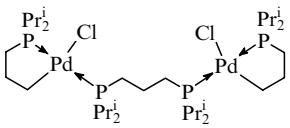	**81b** [c]				[{Pd(η³-CH_2=$CMeCH_2$)(μ-Cl)}₂] – dippp – $L^{81}Cl$ (1 : 1 : 2), MeO^-, MeOH – PhMe	< 50 [j]	279
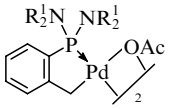	**111**		Me_2		$Pd(OAc)_2$ – (Tol-*o*)$P(NMe_2)_2$, PhMe, Δ, 2 h	~90	354
	112		$(CH_2)_4$		$Pd(OAc)_2$ – (Tol-*o*)$P\{N(CH_2)_4\}_2$, PhMe, Δ, 2 h	~90	354
	113		$(CH_2)_5$		$Pd(OAc)_2$ – (Tol-*o*)$P\{N(CH_2)_5\}_2$, PhMe, Δ, 2 h	~90	354
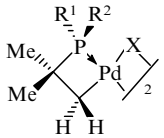	**20a** [c]	Cl	Bu^t	Bu^t	1) K_2PdCl_4 – PBu^t_3 (1 : 2), DMF, 20 °C, 12 h	72	69, 70, 149 [c], 355 [c]
					2) Na_2PdCl_4 – PBu^t_3 (1 : 3), DMF, 20 °C, 48 h	75	73
					3) $[PdCl_2(NCPh)_2]$ – PBu^t_3 (1 : 2), CH_2Cl_2, 20 °C, 2 h	70	70
					4) $[PdCl_2(NCPh)_2]$ – PBu^t_3 (1 : 1), CH_2Cl_2, 20 °C, 2 h	> 80	71
					5) [{$Pd(PBu^t_3)Cl(\mu\text{-}Cl)$}₂] – AgOAc (1 : 2), $CHCl_3$, 20 °C, 12 h	~100	83, 84
					6) [{(η² : η¹-Z)Pd(μ-Cl)}₂] – PBu^t_3 (1 : 2), MeOH, 20 °C, 2 h; Z^- = 2-MeO-cycloocten-5-yl	80	74
	20f [c]	Br	Bu^t	Bu^t	$[Pd^I_2(PBu^t_3)_2(\mu\text{-}Br)_2]$ – O_2, PhH, 20 °C	traces	356
	23	Cl	Bu^t	Ph	(*a*) Na_2PdCl_4 – PBu^t_2Ph (1 : 2), MeOH, 20 °C, 1 h; (*b*) Na_2PdCl_4 (1 equiv.), EtOH – Et_2O, Δ, 1 h; (*c*) AgOAc (2 equiv.), $CHCl_3$, 20 °C, 12 h	43 [k] (55)	83, 84
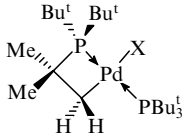	**20c**	Cl			1) $[PdCl_2(cod)]$ – PBu^t_3 (1 : 2), PhH, 20 °C, 8 days	–	69
					2) (*a*) $[Pd^0(PBu^t_3)_2]$, HCl – Et_2O, 20 °C; (*b*) PhH – EtOH, 0.5 h	> 80 [l]	71, 171
	20e	TFA			(*a*) $[Pd^0(PBu^t_3)_2]$, TFAH, Et_2O, 20 °C; (*b*) PhH – EtOH, 3 h	> 80 [l]	71, 171
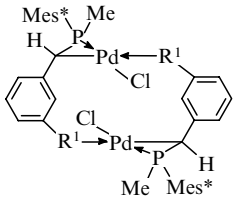	**92** [c]		2-Py		$[MePdCl(cod)]$ – 3-$R^1C_6H_4CH$=PMes* (1 : 1), CH_2Cl_2, 20 °C, 5 min	90	322
	93		CHN=Ph		$[MePdCl(cod)]$ – 3-$R^1C_6H_4CH$=PMes* (1 : 1), CH_2Cl_2, 20 °C, 5 min	71	322

Table 1 (continued).

Complex [a]	Designation of the compound	X	R^1	R^2	Reagents and reaction conditions	Yield [b] (%)	Ref.
PC-Complexes with the $C(sp^2)-Pd$ bond							
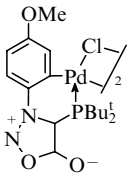	**13** [c]				$PdCl_2$ – HL^{13} (1 : 1), HCl(conc.) – EtOH (1 : 1), 80 °C, 4 h	74	63
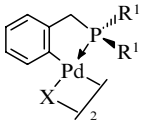	**22a**	Cl	Bu^t		1) (*a*) Na_2PdCl_4 – PBu^t_2Bn (1 : 2), MeOH, 20 °C, 3 h; (*b*) MET, Δ, 5 days	49 [d] (68)	82
					2) (*a*) Na_2PdCl_4 – PBu^t_2Bn (1 : 2), MeOH, 20 °C, 3 h; (*b*) AcONa (excess), MET, Δ, 0.5 h	72 [d] (100)	82
					3) (*a*) Na_2PdCl_4 – PBu^t_2Bn (1 : 2), MeOH, 20 °C, 3 h; (*b*) Et_3N, decalin, Δ, 17 h	46 [d] (64)	82
	22b	Br	Bu^t		1) $[Pd(dba)_2]$ – $L^{22}Br$ (1 : 1), PhH, 20 °C, 1 h; 40 °C, 1 h; 70 °C, 0.5 h	68	273
					2) $[Pd_2(dba)_3]$ – $L^{22}Br$, 1,2-$Me_2C_6H_4$	–	274
	114	Br	Et		$[Pd_2(dba)_3]$ – $L^{114}Br$, 1,2-$Me_2C_6H_4$	–	274
	36a	Cl	Ph		$[\{Pd(\eta^2\text{-}2\text{-}Me_2NCH_2C_6H_4)(\mu\text{-}Cl)\}_2]$ [m] – $PBnPh_2$, $CHCl_3$ – AcOH, 20 °C, 4 days	21	205, 358
	36b	AcO	Ph		$Pd(OAc)_2$ – $PBnPh_2$, MeOH, 60 °C, 3 h	19	114, 358
	36c	Br	Ph		1) $[Pd(dba)_2]$ – $L^{36}Br$ (1 : 1), PhH, 20 °C, 1 h; 40 °C, 1 h; 70 °C, 0.5 h	79	273
					2) $[Pd_2(dba)_3]$ – $L^{36}Br$, 1,2-$Me_2C_6H_4$	–	274
	115a	AcO	Bn		–	–	358
	115b	Cl	Bn		–	–	358
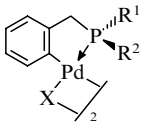	**37**	Cl	Bu^t	Bn	1) (*a*) Na_2PdCl_4 – PBu^tBn_2 (1 : 2), MeOH – PhH, 20 °C, 1 h; (*b*) AcONa (excess), MET, Δ, 24 h	30 [d] (35)	82
					2) (*a*) Na_2PdCl_4 – PBu^tBn_2 (1 : 2), MeOH – PhH, 20 °C,1 h; (*b*) Na_2PdCl_4 (1 equiv.), MET, Δ, 16 h; (*c*) AcONa (excess), MET, Δ, 25 h	13 [k] (15)	82
	78	Br	Ph	Me	$[Pd(dba)_2]$ – $L^{78}Br$ (1 : 1), PhH, 20 °C, 1 h; 40 °C, 1 h; 70 °C, 0.5 h	95	273
	116	AcO	Ph	Bn	$Pd(OAc)_2$ – HL^{116} (1 : 1.3), PhMe, 50 °C, 16 h	85	150, 358
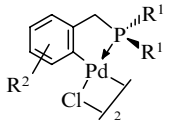	**65**		Ph	4,5-$(MeO)_2$	(*a*) $[PdCl_2(NCPh)_2]$ – HL^{65} (1 : 2), MeOH, 20 °C, 24 h; (*b*) AcONa (excess), MET, Δ, 2 h	83 [d] (91)	113
	66		Bu^t	4,5-$(MeO)_2$	(*a*) $[PdCl_2(NCPh)_2]$ – HL^{66} (1 : 2.1), EtOH, 20 °C, 15 h; (*b*) AcONa (excess), MET, Δ, 0.5 h	85 [d]	113
	77		Bu^t	4-F	Na_2PdCl_4 – HL^{77}	–	272
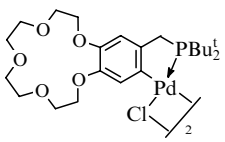	**67**				$[PdCl_2(NCPh)_2]$ – HL^{67} (1 : 2.1), EtOH, 20 °C, 24 h, $CHCl_3$ – EtOH, 20 °C, > 42 days	10 [n]	113
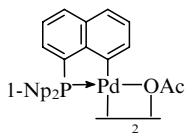	**39a**				$Pd(OAc)_2$ – P(1-Np)$_3$, PhMe, Δ	–	116
	39b		Me		$[Pd(acac)_2]$ – P(1-Np)$_3$, PhH, Δ	–	116
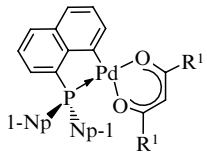	**39c**		CF_3		$[Pd(hfac)_2]$ – P(1-Np)$_3$, PhH, Δ	–	116

Table 1 (continued).

Complex [a]	Designation of the compound	X	R^1	R^2	Reagents and reaction conditions	Yield [b] (%)	Ref.
PC-Complexes with the $C(sp^2)-Pd$ bond							
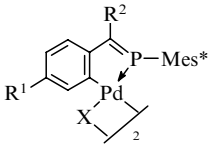	**40**	Cl	H	Ph	$[PdCl_2(NCMe)_2]$ [o] – HL^{40}, ÇHF, 20 °C, 5 h	97	117
	117 [c]	Cl	Bu[t]	Ph	$[PdCl_2(NCMe)_2]$ – HL^{117}, THF, 20 C, 5h	–	117
	118 [c]	Br	H	H	(*a*) $[Pd(dba)_2]$ – $L^{118}Br$, C_5H_{12}; (*b*) PhH, Δ, 1 h	–	323
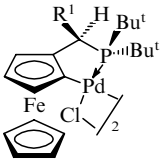	**52** [c]		H		(*a*) $Pd(OAc)_2$ – HL^{52} (1 : 1), PhMe, 20 °C, 8 h; (*b*) LiCl (2 equiv.), 20 °C, 2 h	70	132
	53		Me		(*a*) $Pd(OAc)_2$ – HL^{53} (1 : 1), PhMe, 20 °C, 1 h; (*b*) LiCl (5 equiv.), 20 °C, 20 min	93	131
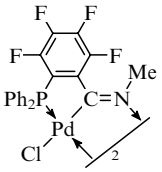	**99a** [c]				$[\{Pd(\mu\text{-}Cl)_2Pd(\mu\text{-}C(C_6F_5)=NMe)_2\}_n]$ – Ph_2PH, KOH (1 equiv.), Me_2CO	45	337
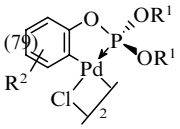 (79)	**69a** 56		Ph	H	(*a*) $[PdCl_2(NCPh)_2]$ – $P(OPh)_3$ (1 : 2), CH_2Cl_2, 20 °C; (*b*) $PdCl_2$ (1 equiv.), PhMe, Δ, 5 h, N_2		76 [p, q]
	119a		*p*-Tol	5-Me	(*a*) $[PdCl_2(NCPh)_2]$ – $P(OTol\text{-}p)_3$ (1 : 2), CH_2Cl_2, 20 °C; (*b*) $PdCl_2$ (1 equiv.), PhMe, Δ, 5 h, N_2	80 [p, q] (100)	56
	120a		*m*-Tol	4-Me	(*a*) $[PdCl_2(NCPh)_2]$ – $P(OTol\text{-}m)_3$ (1 : 2), CH_2Cl_2, 20 °C; (*b*) $PdCl_2$ (1 equiv.), 1,4-$Me_2C_6H_4$, Δ, 1 h, N_2	71 [p, q] (79)	56
	60 [c]		2,4-$Bu^t_2C_6H_3$	3,5-Bu^t_2	$PdCl_2$ – HL^{60}	96	139
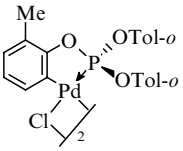	**2a**				1) (*a*) $[PdCl_2(NCPh)_2]$ – $P(OTol\text{-}o)_3$ (1 : 2), CH_2Cl_2, 20 °C; (*b*) $PdCl_2$ (1 equiv.), PhMe, Δ, 5 h, N_2	70 [p, q] (80)	56
					2) (*a*) $PdCl_2$ – NaCl – $P(OTol\text{-}o)_3$ (1 : 2 : 2), EtOH, 20 °C, 2 h; (*b*) $PdCl_2$ – NaCl (1 : 1 : 2), EtOH, Δ, 1.5 h	see. [p] (60)	57
					3) (*a*) $[(\eta^5\text{-Cp})Pd(\eta^3\text{-}CH_2C(Cl)=CH_2)]$ – $P(OTol\text{-}o)_3$ (1 : 1), C_5H_{12}, 20 °C; (*b*) 80 °C, vacuum; (*c*) Al_2O_3, CH_2Cl_2 – C_5H_{12}; (*d*) CH_2Cl_2, HCl (gas)	14 [r] (90)	57
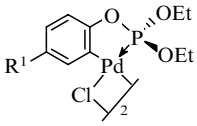	**121**		MeO		(*a*) $[PdCl_2(NCPh)_2]$ – HL^{121} (1 : 2), CH_2Cl_2, 20 °C; (*b*) $PdCl_2$ (1 equiv.), 1,4-$Me_2C_6H_4$, Δ, 1 h, N_2	77 [p] (90)	56
	122		Me		(*a*) $[PdCl_2(NCPh)_2]$ – HL^{122} (1 : 2), CH_2Cl_2, 20 °C; (*b*) $PdCl_2$ (1 equiv.), 1,4-$Me_2C_6H_4$ Δ, 1 h, N_2	88 [p] (96)	56
	123		NO_2		(*a*) $[PdCl_2(NCPh)_2]$ – HL^{123} (1 : 2), CH_2Cl_2, 20 °C; (*b*) $PdCl_2$(1 equiv.), PhMe, Δ, 3 h, N_2	89 [p] (97)	56
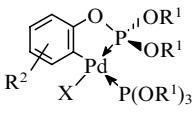	**69c**	Cl	Ph	H	(*a*) Na_2PdCl_4 – HL^{69} (1 : 2), EtOH, Δ, 0.5 min; 20 °C, 10 min; (*b*) decalin, Δ, 3 h	43 [p, q] (50)	143, 144
	119b	Cl	*p*-Tol	5-Me	(*a*) Na_2PdCl_4 – HL^{119} (1 : 2), EtOH, Δ, 0.5 min; 20 °C, 10 min; (*b*) decalin, Δ, 3 h	40 [p, q] (50)	143, 144
	120b	Cl	*m*-Tol	4-Me	(*a*) Na_2PdCl_4 – HL^{120} (1 : 2), EtOH, Δ, 0.5 min; 20 °C, 10 min; (*b*) decalin, Δ, 3 h	40 [p, q] (50)	143, 144
	124	Cl	4-ClC_6H_4	5-Cl	(*a*) $[PdCl_2(cod)]$ – HL^{124} (1 : 2), PhH, Δ, 0.5 min; 20 °C, 10 min; (*b*) decalin, Δ, 3 h	64 [p, q] (80)	143, 144
	2d	Cl	*o*-Tol	3-Me	(*a*) Na_2PdCl_4 – $P(OTol\text{-}o)_3$ (1 : 2), EtOH, Δ, 0.5 min; 20 °C, 10 min; (*b*) decalin, Δ, 3 h	40 [p, q] (50)	143, 144
	2e	Br	*o*-Tol	3-Me	(*a*) Na_2PdBr_4 – $P(OTol\text{-}o)_3$ (1 : 2), EtOH, Δ, 0.5 min; 20 °C, 10 min; (*b*) decalin, Δ, 3 h	15 [p, q] (20)	143, 144

Table 1 (continued).

Complex [a]	Designation of the compound	X	R^1	R^2	Reagents and reaction conditions	Yield [b] (%)	Ref.
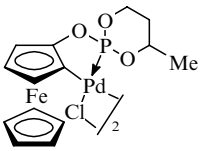	**125**				(*a*) $[PdCl_2(NCPh)_2]$ – HL^{125}, CH_2Cl_2, 20 °C, 15 min; (*b*) $PdCl_2$, K_2CO_3, PhMe (or PhH), Δ, 3 h	< 35 [p, s] (< 41)	140
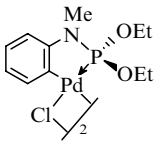	**126**				(*a*) $[PdCl_2(NCPh)_2]$ – HL^{126} (1 : 2), CH_2Cl_2, 20 °C; (*b*) $PdCl_2$ (1 equiv.), PhMe, Δ, 3 h, N_2	see [p]	56
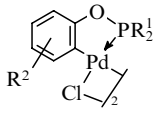	**58**		Ph	3,5-Bu^t_2	$PdCl_2$ – HL^{58}, PhMe, Δ, 18 – 20 h	52	138
	59		Pr^i	3,5-Bu^t_2	$PdCl_2$ – HL^{59}, PhMe, Δ, 18 – 20 h	50	138
	127		Ph	H	$[PdCl_2(NCPh)_2]$ – HL^{127}, THF, Δ, 20 h	65	138
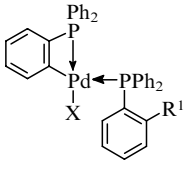	**80a** [c, t]	Br	Br		$[Pd(dba)_2]$ – 2-$BrC_6H_4PPh_2$ (1 : 2), PhMe, 20 °C, 45 min; Δ, 10 min	53	277, 278 [c]
	80b	Cl	H		$[PdCl_2(PPh_3)_2]$, DMF – H_2O, AcOLi	–	170
	80c [t]	Br	Cl		(*a*) $[Pd(dba)_2]$ – 2-$BrC_6H_4PPh_2$ (1 : 1), PhMe, 20 °C, 45 min; Δ, 10 min; (*b*) $PPh_2(C_6H_4Cl$-*o*) (4 equiv.), CH_2Cl_2, 20 °C, 15 days	44 [u] (60)	278
	80d [t]	Br	MeO		(*a*) $[Pd(dba)_2]$ – 2-$BrC_6H_4PPh_2$ (1 : 1), PhMe, 20 °C, 45 min; Δ, 10 min; (*b*) $PPh_2(C_6H_4OMe$-*o*) (4 equiv.), CH_2Cl_2, 20 °C, 48 h	63 [u] (86)	278
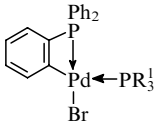	**80e** [t]		Ph		(*a*) $[Pd(dba)_2]$ – 2-$BrC_6H_4PPh_2$ (1 : 1), PhMe, 20 °C, 45 min; Δ, min; (*b*) PPh_3 (4 equiv.), CH_2Cl_2, 20 °C, 30 min	62 [u] (85)	277
	80f [t]		Cy		(*a*) $[Pd(dba)_2]$ – 2-$BrC_6H_4PPh_2$ (1 : 1), PhMe, 20 °C, 45 min; Δ, 10 min; (*b*) PCy_3 (4 equiv.), CH_2Cl_2, 20 °C, 30 min	58 [u] (79)	277
	80g [t]		*p*-Tol		(*a*) $[Pd(dba)_2]$ – 2-$BrC_6H_4PPh_2$ (1 : 1), PhMe, 20 °C, 45 min; Δ, 10 min; (*b*) P(Tol-*p*)$_3$ (4 equiv.), CH_2Cl_2, 20 °C, 1 h	55 [u] (75)	278
	80h [t]		*m*-Tol		(*a*) $[Pd(dba)_2]$ – 2-$BrC_6H_4PPh_2$ (1 : 1), PhMe, 20 °C, 45 min; Δ, 10 min; (*b*) P(Tol-*m*)$_3$ (4 equiv.), CH_2Cl_2, 20 °C, 1 h	47 [u] (65)	278
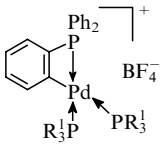	**80i**		Ph		(*a*) $[Pd(dba)_2]$ – 2-$BrC_6H_4PPh_2$ (1 : 1), PhMe, 20 °C, 45 min; Δ, 10 min; (*b*) $AgBF_4$ (4 equiv.), CH_2Cl_2 – THF, 20 °C, 5 h; *c*) PPh_3 (8 equiv.), 20 °C, 15 min	63 [u] (86)	278
	80j		*p*-Tol		(*a*) $[Pd(dba)_2]$ – 2-$BrC_6H_4PPh_2$ (1 : 1), PhMe, 20 °C, 45 min; Δ, 10 min; (*b*) $AgBF_4$ (4 equiv.), CH_2Cl_2 – THF, 20 °C, 5 h; (*c*) P(Tol-*p*)$_3$ (8 equiv.), 20 °C, 15 min	68 [u] (93)	278
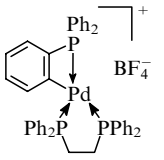	**80k**				(*a*) $[Pd(dba)_2]$ – 2-$BrC_6H_4PPh_2$ (1 : 1), PhMe, 20 °C, 45 min; Δ, 10 min; (*b*) $AgBF_4$ (4 equiv.), CH_2Cl_2 – THF, 20 °C, 5 h; (*c*) dppe (4 equiv.), 20 °C, 15 min	66 [u] (91)	278

[a] The structure of the primary cyclopalladation product is shown. [b] In the case of two- and three-stage syntheses, the overall yield is given, and the value in parentheses is the yield in the stage of closure of the PC-palladacycle. [c] The structure of the complex was confirmed by X-ray diffraction analysis. [d] Prepared by a two-stage route *via* a coordination intermediate of the *trans*-$[PdCl_2(HL^n)_2]$ type. [e] Prepared by a two-stage route *via* coordination intermediates of the *trans*-$[PdCl_2(HL^n)_2]$ and $[\{Pd(HL)Cl(\mu\text{-}Cl)\}_2]$ types without isolation of the latter. [f] Obtained by a two-stage route *via* binuclear coordination complex of the $[\{Pd(HL)Cl(\mu\text{-}Cl)\}_2]$ type. [g] Prepared *via* the intermediate complex $[Pd(hfac)_2(P(o\text{-}Tol)_3)]$ characterised by X-ray diffraction analysis.[196] [h] Two-stage synthesis through the intermediate [Pd(P⁀P)(Me)(H_2L^{71})]OTf complex, where P⁀P is ditertiary diphosphine. [i] Obtained by a two-stage route *via* the $[Pd^0(HL')_2]$ complex (HL′ = 2-$Ph_2PC_6H_4CH=CH_2$), whose structure was confirmed by X-ray diffraction.[34] [j] Binuclear complex **81b** is formed as a mixture with the mononuclear derivative of the same palladacycle with κ^1-bound diphosphine dippp. [k] Obtained by a three-stage route *via* two coordination intermediates, *trans*-$[PdCl_2(HL^n)_2]$ and $[\{Pd(HL)Cl(\mu\text{-}Cl)\}_2]$. [l] The reaction proceeds through a hydride intermediate, $[Pd(H)(X)(HL^{20})_2]$. [m] The starting complex was prepared by a known method.[357] [n] Isolated from a mixture with *trans*-$[PdCl_2(HL^{67})_2]$ by manual separation of the crystals. [o] The complex was characterised by X-ray diffraction analysis.[359] [p] Prepared by a two-stage route *via* the coordination intermediate *cis*-$[PdCl_2(HL^n)_2]$. [q] The synthesis of the intermediate coordination complex has been reported.[360] [r] Prepared by four-stage route *via* intermediate complexes, [η^5-CpPd(HL^2)(η^1-All′)], where All′ is $CH_2C(Cl)=CH_2$, [η^5-CpPdCl(HL^2)] and [η^5-CpPd(η^2-L^2)]. [s] A mixture of diastereomers. [t] A mixture of *cis* – *trans* isomers. [u] Prepared *via* the intermediate $[\{Pd(\mu\text{-}L^{80})_2Pd(\mu\text{-}Br)_2\}_2]$ complex whose synthesis has been reported.[277]

Table 2. Bis(chelate) spiro PC-complexes.

Complex [a]	Designation of the compound	R	Reagents and reaction conditions	Yield (%)	Ref.
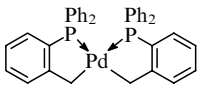	**84**		1) *trans*-$[Pd(PEt_3)_2Cl_2]$ – KL^{84} (~1 : 2), PhH, 20 °C, 1 h 2) *trans*-$[Pd(SEt_2)_2Cl_2]$ – KL^{84} (~1 : 2), PhH, 20 °C, 1 h	35 –	304, 305 304, 305
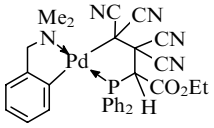	**106b**		$[\{Pd(\eta^2\text{-}2\text{-}Me_2NCH_2C_6H_4)(\kappa^2\text{-}L')\}]$ [c] – $(NC)_2C{=}C(CN)_2$, THF, 20 °C; $(L')^-$ = $Ph_2PCH{=}C(OEt)O^-$	~100	345
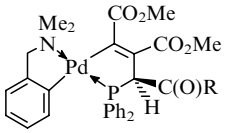	**103b**	Ph	$[Pd\{\eta^2\text{-}2\text{-}Me_2NCH_2C_6H_4)(\kappa^2\text{-}L')\}]$ [c] – $MeO_2CC{\equiv}CCO_2Me$ (1 : 1), CH_2Cl_2, 20 °C, 72 h; $(L')^-$ = $Ph_2PCH{=}C(Ph)O^-$	82	344
	105	OEt	$[Pd\{\eta^2\text{-}2\text{-}Me_2NCH_2C_6H_4)(\kappa^2\text{-}L')\}]$ [c] – $MeO_2CC{\equiv}CCO_2Me$ (1 : 1), THF, 20 °C; $(L')^-$ = $Ph_2PCH{=}C(OEt)O^-$	~100	345
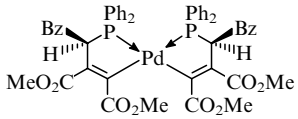	**103a** [b, d]		(*a*) *cis*-$[Pd(\kappa^2\text{-}L')_2]$ [c] – $MeO_2CC{\equiv}CCO_2Me$ (1 : 2), CH_2Cl_2, 20 °C, 36 h; (*b*) fractional crystallisation of a 3 : 1 mixture of diastereomers; $(L')^-$ = $Ph_2PCH{=}C(Ph)O^-$	66	343 [b], 344
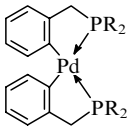	**36d** [e]	Ph	1) *trans*-$[PdCl_2(SEt_2)_2]$ – LiL^{36} (1 : 2), Et_2O, −20 to 20 °C, 2 h 2) *trans*-$[PdCl_2(SEt_2)_2]$ – LiL^{36} (1 : 2), PhH, 20 °C, 2 h	90 76	283 285
	83	Me	*trans*-$[PdCl_2(SEt_2)_2]$ – LiL^{83} (1 : 2), Et_2O, −20 to 20 °C, 2 h	70	283
	22c	Bu^t	*trans*-$[PdCl_2(SEt_2)_2]$ – LiL^{22} (1 : 2), Et_2O, −20 to 20 °C, 2 h	86	283
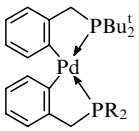	**36e**	Ph	1) $[\{Pd(\eta^2\text{-}C_6H_4CH_2PBu^t_2\text{-}2)(\mu\text{-}Cl)\}_2]$ [f] – LiL^{36} [g] (1 : 2), PhH, 20 °C, 2 h 2) $[\{Pd(\eta^2\text{-}C_6H_4CH_2PBu^t_2\text{-}2)(\mu\text{-}Cl)\}_2]$ [f] – LiL^{36} [g] (1 : 2), Et_2O, −20 to 20 °C, 2 h	87 –	285, 301 283, 298
	83b	Me	$[\{Pd(\eta^2\text{-}C_6H_4CH_2PBu^t_2\text{-}2)(\mu\text{-}Cl)\}_2]$ [f] – LiL^{83} (1 : 2), Et_2O, −20 to 20 °C, 2 h	61	283, 298
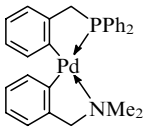	**36f** [b, e]		$[\{Pd(\eta^2\text{-}2\text{-}Me_2NCH_2C_6H_4)(\mu\text{-}Cl)\}_2]$ [h] – LiL^{36} (1 : 2), Et_2O, −20 to 20 °C, 2–3 h	89	284, 287, 361 [b]

[a] The structure of the primary cyclopalladation product is shown. [b] The complex was characterised by X-ray diffraction. [c] The synthesis of the starting complex has been reported.[346] [d] Complex *cis*-**103a** quantitatively isomerises into the *trans*-form upon thermolysis (THF, Δ, 12 h).[344] [e] A *cis*–*trans*-isomer mixture. [f] The starting complex was prepared by a known method.[82] [g] The synthesis of the LiL ligand has been reported.[301] [h] The synthesis of the starting complex has been reported.[357]

Table 3. PC-Chelating phosphine-substituted phosphorus ylides.

Complex [a]	Designation of the compound	X	R^1	R^2	Reagents and reaction conditions	Yield [b] (%)	Ref.
PC-Complexes with the $C(sp^3)-Pd$ bond							
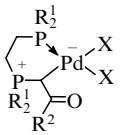	**86c** [c]	Cl	Ph	Ph	$PdCl_2(NCPh)_2$ – L^{86} (1 : 1), CH_2Cl_2, 20 °C	82	311 [c], 312 [c] 316, 317
	86d	Br	Ph	Ph	(*a*) $PdCl_2(NCPh)_2$ – $[HL^{86}]Br$ [d] (1 : 1), KOH, 18-C-6 (0.2 equiv.), CH_2Cl_2 – H_2O, 20 °C, 30 min; (*b*) NaBr, MeOH, 20 °C, 30 min	–	313
	128a	Cl	Ph	Me	$PdCl_2(NCPh)_2$ – L^{128} (1 : 1), CH_2Cl_2, 20 °C	56	315, 317
	129	Cl	Ph	MeO	$PdCl_2(NCPh)_2$ – L^{129} (1 : 1), CH_2Cl_2, 20 °C	85	315, 317
	130	Cl	Ph	EtO	$PdCl_2(NCPh)_2$ – L^{130} (1 : 1), CH_2Cl_2, 20 °C	85	315
	131	Cl	Bn	Ph	$PdCl_2(NCPh)_2$ – L^{131}	–	362

Table 3 (continued).

Complex [a]	Designation of the compound	X	R^1	R^2	Reagents and reaction conditions	Yield [b] (%)	Ref.
PC-Complexes with the $C(sp^3)-Pd$ bond							
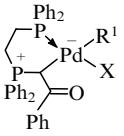	**86a** [e]	Cl	C_6Cl_5		$[\{R^1(THT)Pd(\mu\text{-}Cl)\}_2]-L^{86}$ (1 : 2), PhH, 20 °C, 30 min	69	318
	86b [e]	C_6F_5	C_6F_5		$[\{R^1_2Pd(\mu\text{-}Cl)\}_2]-L^{86}$ (1 : 2), Me_2CO, 20 °C, 30 min	57	318
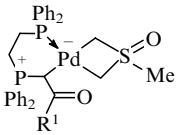	**86e**		Ph		(*a*) $[\{Pd(\eta^2(C,C)\text{-}(CH_2)_2S(O)Me)(\mu\text{-}I)\}_2]-[HL^{86}]Br$ (1 : 2), CH_2Cl_2, 20 °C; (*b*) 18-C-6 (0.2 equiv.), KOH, NaI, $CH_2Cl_2-H_2O$, 20 °C, 30 min	60	313
	128b		Me		(*a*) $[\{(\eta^2(C,C)\text{-}(CH_2)_2S(O)Me)Pd(\mu\text{-}I)\}_2]-[HL^{128}]Br$ (1 : 2), CH_2Cl_2, 20 °C; (*b*) 18-C-6 (0.2 equiv.), KOH, NaI, $CH_2Cl_2-H_2O$, 20 °C, 30 min	–	313
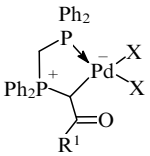	**87a**	Br	Ph		1) (*a*) $[PdCl_2(NCPh)_2]-[HL^{87}]Br$ [d] (1 : 1), KOH, 18-C-6 (0.2 equiv.), $CH_2Cl_2-H_2O$, 20 °C, 30 min; (*b*) NaBr, MeOH, 20 °C, 30 min	65	313
					2) $Na_2PdCl_4-[HL^{87}]Br$ [d] (1 : 1), KOH, 18-C-6 (0.2 equiv.), $CH_2Cl_2-H_2O$, 20 °C	60	313
	87d	Cl	Ph		$[PdCl_2(NCPh)_2]-L^{87}$ (1 : 1), CH_2Cl_2, 20 °C	78	315, 317
	82c	Cl	Me		$[PdCl_2(NCPh)_2]-L^{82}$ (1 : 1), CH_2Cl_2, 20 °C	85	317
	82d	Br	Me		(*a*) $[PdCl_2(NCPh)_2]-[HL^{82}]Br$ [d] (1 : 1), KOH, 18-C-6 (0.2 equiv.), $CH_2Cl_2-H_2O$, 20 °C, 30 min; (*b*) NaBr, MeOH, 20 °C, 30 min	–	313
	85	Cl	MeO		$[PdCl_2(NCPh)_2]-L^{85}$ (1 : 1), CH_2Cl_2, 20 °C	80	317
	132a	Br	EtO		(*a*) $[PdCl_2(NCPh)_2]-[HL^{132}]Br$ [d] (1 : 1), KOH, 18-C-6 (0.2 equiv.), $CH_2Cl_2-H_2O$, 20 °C, 30 min; (*b*) NaBr, MeOH, 20 °C, 30 min	–	313
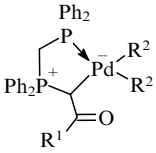	**87e**		Ph	C_6F_5	$[Bu_4N]_2[\{R^2_2Pd(\mu\text{-}Cl)\}_2]-L^{87}$ (1 : 2), Me_2CO, 20 °C, 30 min	67	318
	82e		Me	C_6F_5	$[Bu_4N]_2[\{R^2_2Pd(\mu\text{-}Cl)\}_2]-L^{82}$ (1 : 2), Me_2CO, 20 °C, 30 min	70	318
	87f		Ph	C_6Cl_5	$[Bu_4N]_2[\{R^2_2Pd(\mu\text{-}Br)\}_2]-L^{87}$ (1 : 2), Me_2CO, 20 °C, 30 min	69	318
	82f		Me	C_6Cl_5	$[Bu_4N]_2[\{R^2_2Pd(\mu\text{-}Br)\}_2]-L^{82}$ (1 : 2), Me_2CO, 20 °C, 30 min	65	318
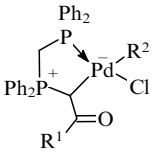	**87g** [e]		Ph	C_6F_5	$[\{R^2(THT)Pd(\mu\text{-}Cl)\}_2]-L^{87}$ (1 : 2), PhH, 20 °C, 30 min	78	318
	82g [e]		Me	C_6F_5	$[\{R^2(THT)Pd(\mu\text{-}Cl)\}_2]-L^{82}$ (1 : 2), PhH, 20 °C, 30 min	76	318
	87h [e]		Ph	C_6Cl_5	$[\{R^2(THT)Pd(\mu\text{-}Cl)\}_2]-L^{87}$ (1 : 2), PhH, 20 °C, 30 min	81	318
	82h [e]		Me	C_6Cl_5	$[\{R^2(THT)Pd(\mu\text{-}Cl)\}_2]-L^{82}$ (1 : 2), PhH, 20 °C, 30 min	72	318
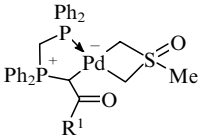	**87c** [c]		Ph		(*a*) $[\{Pd(\eta^2(C,C)\text{-}(CH_2)_2S(O)Me)(\mu\text{-}I)\}_2]-[HL^{87}]Br$ (1 : 2), CH_2Cl_2, 20 °C; (*b*) 18-C-6 (0.2 equiv.), KOH, NaI, $CH_2Cl_2-H_2O$, 20 °C, 30 min	80	313
	82i		Me		(*a*) $[\{Pd(\eta^2(C,C)\text{-}(CH_2)_2S(O)Me)(\mu\text{-}I)\}_2]-[HL^{82}]Br$ (1 : 2), CH_2Cl_2, 20 °C; (*b*) 18-C-6 (0.2 equiv.), KOH, NaI, $CH_2Cl_2-H_2O$, 20 °C, 30 min	63	313
	132b		Et		(*a*) $[\{Pd(\eta^2(C,C)\text{-}(CH_2)_2S(O)Me)(\mu\text{-}I)\}_2]-[HL^{132}]Br$ (1 : 2), CH_2Cl_2, 20 °C; (*b*) 18-C-6 (0.2 equiv.), KOH, NaI, $CH_2Cl_2-H_2O$, 20 °C, 30 min	70	313
PC-Complexes with the $C(sp^2)-Pd$ bond							
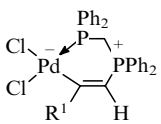	**101a** [c]		4-Me_2N-C_6H_4		$[Pd(dppm)Cl_2]$ [f] – 4-$Me_2NC_6H_4C\equiv CH$ (2 : 3), 1.4-dioxane – EDC, 105 °C, 72 h	31	339
	101b		Ph		$[Pd(dppm)Cl_2]$ [f] – $PhC\equiv CH$ (2 : 3), 1.4-dioxane – EDC, 110 °C, 90 h	49	339
	101c		4-NO_2-C_6H_4		$[Pd(dppm)Cl_2]$ [f] – 4-$NO_2C_6H_4C\equiv CH$ (1 : 1.1), 1.4-dioxane – EDC, 105 °C, 48 h	73	339
	101d		C_9H_{19}		$[Pd(dppm)Cl_2]$ [f] – $C_9H_{19}C\equiv CH$ (1 : 4), 1.4-dioxane – EDC, 110 °C, 100 h	48	339

Table 3 (continued).

Complex [a]	Designation of the compound	X	R^1	R^2	Reagents and reaction conditions	Yield [b] (%)	Ref.
Spiro PC-complexes with phosphino-phosphorus ylides							
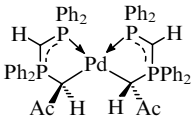	**82a** [c]				1) $Pd_2(dba)_3 \cdot CHCl_3 - HL^{82}$ (1 : 4), CH_2Cl_2, 20 °C, 10 min 2) $Pd(PPh_3)_4 - HL^{82}$ (1 : 2), CH_2Cl_2, 20 °C, 10 min 3) (*a*) $Pd(OAc)_2 - [H_2L^{82}]^+ ClO_4^-$ (1 : 2), CH_2Cl_2, 20 °C, 2 h; (*b*) NaH (excess), THF, 20 °C, 2 h $[H_2L^{82}]^+ = [Ph_2PCH_2P(Ph_2)CH_2Ac]^+$	66 67 –	282 282 282
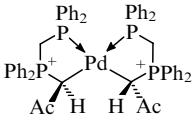	**82b**	ClO_4			1) $Pd_2(dba)_3 \cdot CHCl_3 - [H_2L^{82}]^+ ClO_4^-$ (1 : 8), CH_2Cl_2, 20 °C, 24 h 2) $Pd(OAc)_2 - [H_2L^{82}]^+ ClO_4^-$ (1 : 2), CH_2Cl_2, 20 °C, 2 h 3) (*a*) $Pd(PPh_3)_4 - HL^{82}$ (1 : 2), CH_2Cl_2, 20 °C, 10 min; (*b*) $HClO_4$(aq) (1 : 2), CH_2Cl_2, 20 °C, 1 h	53 73 43 (29)	282 282 282

[a] The structures of the primary products of closure of the phosphapalladacycle are shown. [b] In the case of two- and three-step syntheses, the total yield is given, while the yield in the stage of phosphapalladacycle closure is given in parentheses. [c] The structure of the complex was confirmed by X-ray diffraction analysis. [d] The synthesis of phosphonium salt has been reported.[315] [e] A mixture of *cis*–*trans* -isomers. [f] The synthesis of the starting complex has been reported.[340]

Table 4. Bicyclic PCP-structures.

Complex [a]	Designation of the compound	X/Y	R^1	R^2 (*n*)	Reagents and reaction conditions	Yield [b] (%)	Ref.
PCP-Complexes with the $C(sp^3) - Pd$ bond							
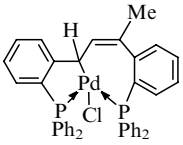	**19** [c]				$[PdCl_2(NCPh)_2] - HL^{18}$ (1 : 1), PhMe, MET, Δ, 2 h	70	68
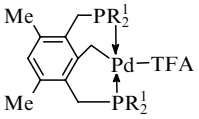	**11**			Pr^i	$Pd(TFA)_2 - HL^{11}$, THF, 80 °C	–	62
	12 [c]			Bu^t	$Pd(TFA)_2 - HL^{12}$, THF, 80 °C	–	62
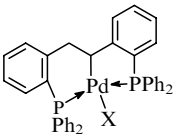	**27a**	Cl			$[PdCl_2(NCPh)_2] - HL^{27}$ (1 : 1), MET, Δ, 1.5 h	75	60, 61
	27b	Br			$K_2PdBr_4 - HL^{27}$ (1 : 1), MET, Δ, 2 h	26	60, 61
	27c	I			$[PdI_2(PPh_3)_2] - HL^{27}$ (1 : 1), MET, Δ, 10 h	86	60, 61
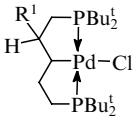	**24a**	Cl	H		1) $[PdCl_2(NCPh)_2] - HL^{24}$ (1 : 1), EtOH, Δ, 18 h 2) (*a*) $[PdCl_2(NCPh)_2] - HL^{24}$ (1 : 1), EtOH, Δ, 18 h; (*b*) Δ, > 260 °C 3) (*a*) $[PdCl_2(NCPh)_2] - HL^{24}$ (1 : 1), EtOH, Δ, 18 h; (*b*) sublimation (260 °C, 0.01 atm)	12 [d] see [e] 40 [e] (64)	128 128 89, 157
	54 [c]	Cl	Me		$[PdCl_2(NCPh)_2] - HL^{54}$ (1 : 1), MET, Δ, 15 min	36	133
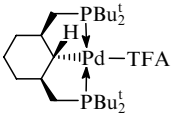	**44**				$Pd(TFA)_2 - HL^{44}$ (1 : 1), THF, 80 °C, 1 h	91	91
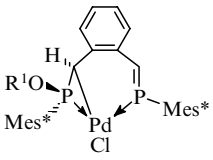	(*R*$_C$*R*$_P$)*-**95**	Me			(*a*) $[PdCl_2(NCPh)_2] - HL^{94}$ (1 : 1), CH_2Cl_2, 20 °C; (*b*) MeOH (excess), CH_2Cl_2, Δ, 24 h	~100 [f]	328
	(*R*$_C$*R*$_P$)*-**133** [c]	Et			(*a*) $[PdCl_2(NCPh)_2] - HL^{94}$ (1 : 1), CH_2Cl_2, 20 °C; (*b*) EtOH (excess), CH_2Cl_2, Δ, 5 days	~100 [f]	328

Table 4 (continued).

Complex [a]	Designation of the compound	X/Y	R^1	R^2 (*n*)	Reagents and reaction conditions	Yield [b] (%)	Ref.
PCP-Complexes with the C(sp^2)—Pd bond							
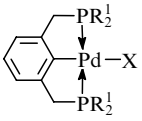	**25a** [c]	Cl	Bu^t		$[PdCl_2(NCPh)_2]-HL^{25}$ (1 : 1) , MET, Δ, 25 min	75	90, 363 [c]
	25b	TFA	Bu^t		1) $Pd(TFA)_2-HL^{25}$ (1 : 1), PhMe, 130 °C, 1 h (in a sealed tube)	~ 100	151
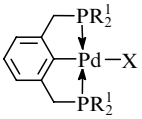	**25b**	TFA	Bu^t		2) $Pd(TFA)_2-L^{25}OEt$ (1 : 1), PhMe, 130 °C, 3 h (in a sealed tube)	< 10 [g]	151
					3) (*a*) $Pd(TFA)_2-L^{25}OMe$ (1 : 1), C_6D_6, 85 °C, 3 h (in a sealed tube); (*b*) PhMe, 30 atm of H_2, 180 °C, 8 h	~ 55 [h] (~ 55)	151
	17a [c]	Cl	Ph		1) $[PdCl_2(NCMe)_2]-HL^{17}$ (1 : 1), CH_2Cl_2, 20 °C, 10 min	75	66, 364 [c]
					2) $[PdCl_2(NCMe)_2]-HL^{17}$, MET, 150 °C	—	120
	62a [c]	Br	Cy		*trans*-$[PdBr_2(PPh_3)_2]-HL^{62}$ (1 : 2), EtOH, Δ, 16 h	72	155
	62b [c]	Cl	Cy		1) $[PdCl_2(NCPh)_2]-HL^{62}$ (1 : 1.3), MET, Δ, 25 min	17 [i]	155
					2) (*a*) $[PdCl_2(NCPh)_2]-HL^{62}$ (1 : 1.3), MET, Δ, 25 min; (*b*) MET, Δ, 48 h	31 [j] (43)	155
	134	Cl	4-Me_2N-C_6H_4		$[PdCl_2(NCPh)_2]-HL^{134}$ (1 : 1.1), CH_2Cl_2, 120 °C, 12 h (autoclave)	63	120
	135	TFA	Pr^i		$Pd(TFA)_2-HL^{135}$, THF, 80 °C	—	62
	136	TFA	cyclo-C_5H_9		(*a*) $HL^{136}\cdot 2\,BH_3$, morpholine, 120 °C, 2 h; (*b*) $Pd(TFA)_2$, THF, 70 °C	75 [k]	152
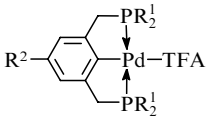	**109**		Bu^t	Me	(*a*) $Pd(TFA)_2-L^{109}OH$ (1 : 1), PhMe, 20 °C, 12 h; (*b*) PhMe, 30 atm of H_2, 180 °C, 8 h	~ 55 [l] (~ 55)	151
	137		cyclo-C_5H_9	BnO	(*a*) $HL^{137}\cdot 2\,BH_3$, morpholine, 120 °C, 2 h; (*b*) $Pd(TFA)_2$, THF, 70 °C	55 [k]	152
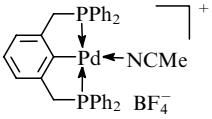	**17b**				$[Pd(NCMe)_4](BF_4)_2-HL^{17}$ (1 : 1), THF–MeCN, 50 °C, 30 min	42	164
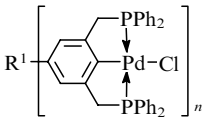	**138a**		C≡C	(2)	(*a*) $[Pd(NCMe)_4](BF_4)_2-H_2L^{138}$ (2 : 1), MeCN, Δ, 2 h; (*b*) NaCl (excess), $CH_2Cl_2-H_2O$, 20 °C, 12 h	50 (51)	50
	139a		$(C\equiv C)_2$	(2)	(*a*) $[Pd(NCMe)_4](BF_4)_2-H_2L^{139}$ (2 : 1), MeCN, Δ, 1 h; (*b*) NaCl (excess), $CH_2Cl_2-H_2O$, 20 °C, 12 h	20 (21)	50
	140a		1,3,5-$(C\equiv C)_3$. .C_6H_3	(3)	(*a*) $PdCl_2-AgBF_4$ (1 : 2), MeCN, Δ, 5 min (*in situ*); (*b*) H_3L^{140} (0.33 equiv.), CH_2Cl_2, Δ, 1 h; (*c*) NaCl (excess), $CH_2Cl_2-H_2O$, 20 °C, 3 h	88 (90)	49
	141		1,3,5-$(OCH_2)_3C_6H_3$	(3)	(*a*) $[Pd(NCMe)_4](BF_4)_2-H_3L^{141}$ (3 : 1) , MeCN, 20 °C, 15 min; (*b*) NaCl (excess), $CH_2Cl_2-H_2O$, 20 °C,12 h	67	48
	142		1,3-$(OCH_2)_2$. .$C_6H_3CH_2CN$-5	(2)	(*a*) $[Pd(NCMe)_4](BF_4)_2-H_2L^{142}$ (2 : 1), MeCN, 20 °C, 15 min; (*b*) NaCl (excess), $CH_2Cl_2-H_2O$, 20 °C, 12 h	55	48
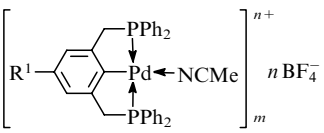	**138b** [c]		C≡C	(2)	$[Pd(NCMe)_4](BF_4)_2-H_2L^{138}$ (2 : 1) , MeCN, Δ, 2 h	51	50
	139b		$(C\equiv C)_2$	(2)	$[Pd(NCMe)_4](BF_4)_2-H_2L^{139}$ (2 : 1), MeCN, Δ, 1 h	21	50
	140b		1,3,5-$(C\equiv C)_3C_6H_3$	(3)	(*a*) $PdCl_2-AgBF_4$ (1 : 2), MeCN, Δ, 5 min (*in situ*); (*b*) H_3L^{140} (0.33 equiv.), CH_2Cl_2, Δ, 1 h	90	49
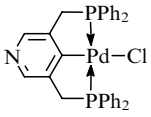	**68b**				(*a*) $[PdCl_2(NCPh)_2]-HL^{68}$ (1 : 1), CH_2Cl_2, 100 °C, 12 h (autoclave); (*b*) Et_3N, PhMe–H_2O	(63) [m]	168

Table 4 (continued).

Complex [a]	Designation of the compound	X/Y	R^1	R^2 (*n*)	Reagents and reaction conditions	Yield [b] (%)	Ref.
PCP-Complexes with the C(sp^2) – Pd bond							
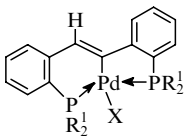	**10a**	Cl	Ph		$[PdCl_2(NCPh)_2]$ – HL^{10} (1 : 1), PhH, Δ, 1 h	72	60, 61
	10b	Br	Ph		K_2PdBr_4 – HL^{10} (1 : 1), MET, Δ, 2 h	79	60, 61
	45a	Cl	*o*-Tol		$[PdCl_2(NCPh)_2]$ – HL^{45} (1 : 1), PhH, Δ, 16 h	62	60, 61
	45b	Br	*o*-Tol		K_2PdBr_4 – HL^{45} (1 : 1), 1,3,5-$Me_3C_6H_3$, Δ, 24 h	67	60, 61
	45c	I	*o*-Tol		$PdCl_2$ – NaI – HL^{45} (1 : 13 : 1), MET, Δ, 96 h	50	60, 61
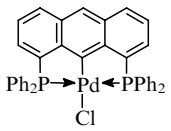	**73** [c]				$[PdCl_2(NCPh)_2]$ – HL^{73} (1 : 1), MET, Δ, 2h	73	156
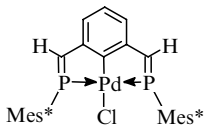	**63a** [c]				$[PdCl_2(NCPh)_2]$ – HL^{63} (1 : 1), CH_2Cl_2, 20 °C, 2 h	–	125, [c] 127
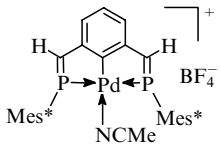	**63b**				$[Pd(NCMe)_4](BF_4)_2$ – HL^{63} (see [n]) (1 : 1), CH_2Cl_2, 20 °C, 2 h	–	127
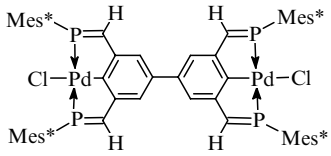	**64** [c]				$[PdCl_2(NCPh)_2]$ – H_2L^{64} (1 : 1), CH_2Cl_2 , 20 °C, 0.5 h	90	126
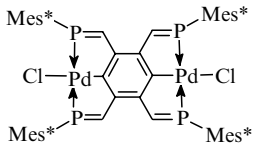	**49**				(*a*) $[PdCl_2(NCMe)_2]$ – H_2L^{49} (2 : 1), THF, 20 °C, 0.5 h; (*b*) THF, 20° C, 4 h	(60) [o]	117
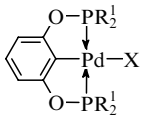	**79** [c]	I	4-$MeOC_6H_4O$		(*a*) 2,6-$(HO)_2C_6H_3I$ – $(4\text{-}MeOC_6H_4O)_2PNEt_2$ – tetrazole (1 : 3 : 6), THF, −78 to 20 °C, 2 days (*b*) $Pd_2(dba)_3 \cdot CHCl_3$ (0.5 equiv.), PhMe, 23 °C, 12h	(26)	275
	48 [c]	Cl	Pr^i		$PdCl_2(cod)$ – HL^{48} (1 : 1), PhMe, Δ, 5 h	90 – 95	122, [c] 158
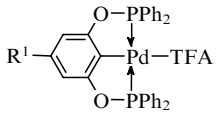	**46** [c]		H		$Pd(TFA)_2$ – HL^{46} (1 : 1), THF, 20 °C, 2 h	85	121
	47		Me		$Pd(TFA)_2$ – HL^{47} (1 : 1), THF, 20 °C, 2 h	78	121

[a] The structure of the primary cyclopalladation product is shown. [b] In the case of two- and three-step syntheses, the total yield is given, while the yield in the stage of phosphapalladacycle closure is given in parentheses. [c] The structure of the complex was confirmed by X-ray diffraction analysis. [d] The major reaction product (62%) is the macrocyclic coordination complex, $[Cl_2Pd(\mu{:}\kappa^2\text{-}HL^{24})_2PdCl_2]$. [e] Prepared *via* the $[Cl_2Pd(\mu\text{-}HL^{24})_2PdCl_2]$ coordination complex whose synthesis has been reported.[128] [f] Prepared *via* the intermediate $[Pd(\kappa^2\text{-}L^{94})Cl_2]$ complex, where $L^{94} = C_6H_4(CH{=}PMes^*)_2$-1,2, whose structure has been confirmed by X-ray diffraction analysis.[328] [g] The product is formed as a mixture with $[(\kappa^3\text{-}L^{25}O)Pd(TFA)]$ (1 : 9 ratio), which was characterised by X-ray diffraction.[151] [h] Prepared through the intermediate $[(\kappa^3\text{-}L^{25}O)Pd(TFA)]$ complex, whose synthesis has been reported.[347] [i] The major reaction product (71%) is the dimeric $[Cl_2Pd(\mu{:}\kappa^2\text{-}HL^{62})_2PdCl_2]$ complex. [j] Prepared in two stages *via* the intermediate $[\{Cl_2Pd(\mu\text{-}HL)\}_2]$ coordination complex. [k] The yield is given over two stages including the removal of ligand protection. [l] Prepared in two stages *via* the intermediate $[(\kappa^3\text{-}L^{109}O)Pd(TFA)]$ complex. [m] The complex was obtained *via* the PCP-intermediate $[(\eta^3\text{-}L^{68}H)PdCl]^+Cl^-$. [n] The ligand structure was confirmed by X-ray diffraction analysis. [o] The complex was obtained through the $[(PdCl_2)_2(\mu{:}\ \kappa^2,\kappa^2\text{-}H_2L^{49})]$ intermediate.

VIII. Conclusion

Despite the diversity of the known structural types of phosphapalladacycles and routes for their synthesis, the topicality of further development of the chemistry of this highly interesting and practically valuable class of organometallic compounds is beyond doubt.

Among the preparative aspects of this field of chemistry, development of the processes based on the use of highly reactive organometallic reagents for direct intramolecular activation of the C – H bonds of P-donor ligands seems to be most fruitful. For

example, η^3-allylic palladium complexes have been barely used for this purpose as yet, and examples of using other metallating agents with the Pd—C bond are sparse. From the structural standpoint, of interest are the synthesis and evaluation of properties and reactivity of CPC-, CPP- and CPN-type bicyclic complexes and diverse tricyclic compounds with phosphapalladacyclic fragments.

Apparently, further development of the chemistry of phosphapalladacycles would not be limited to the extention of the collection of mono- and bicyclic complexes of this class. Highly topical is detailed investigation into the mechanisms of direct intramolecular activation of the C—H-bonds in P-donor ligands, which would enable more purposeful construction of new structures of this class.

* * *

As the manuscript was being prepared for publication, a number of studies appeared that cover to some extent the 'blank spots' mentioned above. A significant contribution to the development of this domain of chemistry has been made by the synthesis of a number of cyclopalladated derivatives of P-donor ligands of new structural types. The first PCP-complex with two fused six-membered metallacycles with a palladated sp^2-hybridised carbon atom has been prepared by oxidative addition of the bromo-substituted diphosphine 2,6-$(Ph_2PCH_2CH_2)_2C_6H_3Br$ to $Pd(dba)_2$.[365] The earlier attempts to produce such a structure by direct activation of the C—H bond failed.[67] Methods of synthesis of new non-symmetrical tricyclic PCP-[366,367] and PCN-type structures,[368,369] differing in the sizes of two metallacycles (five- and six-membered [366–369]) and/or the nature of two heterodonor centres (with a phosphino [367] or amino group [368,369] in combination with a phosphinite branch) from mono- and bis(phosphinites) have been developed. Previously, only three asymmetrical PCP-complexes with phosphine donor groups were known.[60,61,68]

In addition to the known PC-complexes with a six-membered metallacycle (based on the exotic sydnonylphosphine ligand [63]), two other representatives of this class have been synthesised from (2-diphenylphosphinophenyl)ferrocene [370] and 2-(dicyclohexylphosphino)biphenyl.[371] Double cyclopalladation of the same aromatic ring of 2-methylresorcinolbis(phosphinite) was implemented for the first time.[372] The collection of monocyclic cyclopalladated phosphite [373–375] and phosphinite [376] derivatives with five-membered PC-palladacycles has been substantially extended. Most of the new PC- and PCP-complexes have been obtained by direct activation of the C—H bonds in the corresponding ligands on treatment with $PdCl_2$,[374–376] $[PdCl_2(cod)]$,[366,367] $[PdCl_2(NCR)_2]$,[373,376] $Pd(OAc)_2$ [370,371] or $Pd(TFA)_2$,[372] the product yields ranging from moderate (43%–48% [367,375]) to nearly quantitative (92%–94% [370,371]). A new approach based on chloropalladation of alkynes bearing heterodonor substituents has been developed for the preparation of asymmetrical pincer PCN-structures.[368,369] An interesting way of generating PCC-complexes from bis(phosphonium) salts (precursors of P-ylides) has been developed only for platinum(II): the process formally includes the activation of three C—H and one C—P bond.[377]

The vast majority of new complexes have been synthesised with the aim of being tested as (pre)catalysts. The presence of persisting interest in this line of practical use of phosphapalladacycles is indicated by the multitude of new reviews [378–383] devoted to this topic. For solving the problem of regeneration of cyclopalladated catalysts, methods of fixing of one of the PCP-complexes on silica gel have been developed, in particular, by direct activation of the C—H bond of the pre-immobilised diphosphine ligand under the action of $Pd(TFA)_2$.[384]

The authors are sincerely grateful to Prof. I P Smolyakova (USA, The University of North Dakota) and to Dr. M Yu Rubina (USA, The University of Illinois at Chicago) for valuable aid in the work on the manuscript. The work was done with partial financial support of the NATO (Grant PST.CLG.979757), the Russian Foundation for Basic Research (Project No. 04-03-3298a), and the Foundation for the Support of Russian Science.

References

1. W A Herrmann, V P W Böhm, C-P Reisinger *J. Organomet. Chem.* **576** 23 (1999)
2. V Sridharan *Annu. Rep. Prog. Chem., Sect. B* **96** 85 (2000)
3. I P Beletskaya, A V Cheprakov *Chem. Rev.* **100** 3009 (2000)
4. J Dupont, M Pfeffer, J Spencer *Eur. J. Inorg. Chem.* 1917 (2001)
5. N J Whitcombe, K K Hii, S E Gibson, *Tetrahedron* **57** 7449 (2001)
6. L N Lewis *J. Am. Chem. Soc.* **108** 743 (1986)
7. L N Lewis, J F Smith *J. Am. Chem. Soc.* **108** 2728 (1986)
8. M Beller, H Fischer, W A Herrmann, C Brossmer, K Öfele, T Priermeier, H Fischer *Angew. Chem., Int. Ed. Engl.* **34** 1844 (1995)
9. M Beller, H Fischer, W A Herrmann, K Öfele, C Brossmer *Angew. Chem., Int. Ed. Engl.* **34** 1848 (1995)
10. W A Herrmann, C Brossmer, C-P Reisinger, T H Riermeier, K Öfele, M Beller *Chem. Eur. J.* **3** 1357 (1997)
11. K Krogh-Jerpersen, M Czerw, A S Goldman *J. Mol. Catal. A: Chem.* **189** 95 (2002)
12. X-Q Gu, W Chen, D Morales-Morales, C M Jensen *J. Mol. Catal. A: Chem.* **189** 119 (2002)
13. I P Beletskaya, A V Chuchurjukin *Usp. Khim.* **69** 699 (2000) [*Russ. Chem. Rev.* **69** 639 (2000)]
14. G W Parshall *Acc. Chem. Res.* **3** 139 (1970)
15. J Dehand, M Pfeffer *Coord. Chem. Rev.* **18** 327 (1976)
16. H P Abicht, K Jssleib *Z. Chem.* 1 (1977)
17. M J Bruce *Angew. Chem.* **89** 75 (1977)
18. I Omae, in *Organometallic Intramolecular-Coordination Compounds* (Amsterdam, New York: Elsevier, 1986)
19. J Omae *Coord. Chem. Rev.* **32** 235 (1980)
20. J Omae *Coord. Chem. Rev.* **83** 137 (1988)
21. V V Dunina, O A Zalevskaya, V M Potapov *Usp. Khim.* **57** 434 (1988) [*Russ. Chem. Rev.* **57** 250 (1988)]
22. R Uson, J Fornies *Adv. Organomet. Chem.* **28** 219 (1988)
23. I Omae *Coord. Chem. Rev.* **28** 97 (1979)
24. I Omae *Chem. Rev.* **79** 287 (1979)
25. I Omae *Coord. Chem. Rev.* **42** 245 (1982)
26. I Omae *Coord. Chem. Rev.* **53** 261 (1984)
27. E C Constable *Polyhedron* **3** 1037 (1984)
28. G R Newkome, W E Puckert, V K Gupta, G E Kiefer *Chem. Rev.* **86** 451 (1986)
29. L Weber *Angew. Chem.* **99** 378 (1987)
30. A J Cheney, W S McDonald, K O'Flynn, B L Shaw, B L Turtle *J. Chem. Soc., Chem. Commun.* 128 (1973)
31. R B Bedford, S Castillon, P A Chaloner, C Claver, E Fernandez, P B Hitchcock, A Ruiz *Organometallics* **15** 3990 (1996)
32. H A Y Mohammad, J C Grimm, K Eichele, H-G Mack, B Speiser, F Novak, M G Quintanilla, W C Kaska, H A Mayer *Organometallics* **21** 5775 (2002)
33. W Winter *Angew. Chem., Int. Ed. Engl.* **15** 241 (1976)
34. M A Bennett, C Chiraratvatana, G B Robertson, U Tooptakong *Organometallics* **7** 1403 (1988)
35. M A Bennett, K J Cavell, K Y Chan *Inorg. Chim. Acta* **163** 153 (1989)
36. H Hagelin, M Svensson, B Akermark, P-O Norrby *Organometallics* **18** 4574 (1999)
37. M Herberhold, Th Schmalz, W Milius, B Wrackmeyer *Inorg. Chim. Acta* **334** 10 (2002)
38. M Herberhold, Th Schmalz, W Milius, B Wrackmeyer *Z. Anorg. Allg. Chem.* **628** 437 (2002)
39. M Herberhold, Th Schmalz, W Milius, B Wrackmeyer *Z. Anorg. Allg. Chem.* **628** 979 (2002)
40. M W Avis, M E van der Boom, C E Elsevier, W J J Smeets, A L Spek *J. Organomet. Chem.* **527** 263 (1997)
41. J Vicente, A Arcas, D Bautista, M C R de Arellano *Organometallics* **17** 4544 (1998)
42. M L Illingsworth, J A Teagle, J L Burmeister, W C Fultz, A L Rheingold *Organometallics* **2** 1364 (1983)
43. J A Teagle, J L Burmeister *Inorg. Chim. Acta* **118** 65 (1986)

44. J A Albanese, A L Rheingold, J L Burmeister *Inorg. Chim. Acta* **150** 213 (1988)
45. J Vicente, M T Chicote, J Fernandez-Baeza *J. Organomet. Chem.* **364** 407 (1989)
46. Ch Lee, Y Kang, S O Kang, J Ko, J W Yoo, M H Cho *J. Organomet. Chem.* **587** 165 (1999)
47. A D Getty, K I Goldberg *Organometallics* **20** 2545 (2001)
48. W T S Huck, B Snellink-Ruël, F C J M van Veggel, D N Reinhoudt *Organometallics* **16** 4287 (1997)
49. I P Beletskaya, A V Chuchurjukin, H P Dijkstra, G P M van Klink, G van Koten *Tetrahedron Lett.* **41** 1081 (2000)
50. I P Beletskaya, A V Chuchurjukin, H P Dijkstra, G P M van Klink, G van Koten *Tetrahedron Lett.* **41** 1075 (2000)
51. G Pacchioni, P S Bagus *Inorg. Chem.* **31** 4391 (1992)
52. R Romeo, G Arena, L M Scolaro *Inorg. Chem.* **31** 4879 (1992)
53. M M Rahman, H-Y Liu, K Eriks, A Prock, W P Giering *Organometallics* **8** 1 (1989)
54. K Abdur-Rashid, T P Fong, B Greaves, D G Gusev, J G Hinman, Sh E Landau, A J Lough, R H Morris *J. Am. Chem. Soc.* **122** 9155 (2000)
55. D F Gill, B E Mann, B L Shaw *J. Chem. Soc., Dalton Trans.* 270 (1973)
56. A Albinati, S Affolter, P S Pregosin *Organometallics* **9** 379 (1990)
57. D J Tune, H Werner *Helv. Chim. Acta* **58** 2240 (1975)
58. Ch E Jones, B L Shaw, B L Turtle *J. Chem. Soc., Dalton Trans.* 992 (1974)
59. H D Empsall, P N Heys, B L Shaw *J. Chem. Soc., Dalton Trans.* 257 (1978)
60. M A Bennett, P W Clark, G B Robertson, I B Tomkins, P O Whimp *J. Organomet. Chem.* **63** C15 (1973)
61. M A Bennett, P W Clark *J. Organomet. Chem.* **110** 367 (1976)
62. M Ohff, A Ohff, E van der Boom, D Milstein *J. Am. Chem. Soc.* **119** 11687 (1997)
63. S T Lin, H-S Cheo, L-S Liu, J-C Wang *Organometallics* **16** 1803 (1997)
64. S T Lin, H-S Choe, L-S Liu, J-C Wang *J. Organomet. Chem.* **610** 1 (2000)
65. S T Lin, K J Peng, T M Barclay, A W Cordes *Inorg. Chim. Acta* **321** 89 (2001)
66. H Rimml, L M Venanzi *J. Organomet. Chem.* **259** C6 (1983)
67. H Rimml, M Venanzi *Phosphorus Sulfur Relat. Elem.* **30** 297 (1987)
68. M A Bennet, G B Robertson, I B Tomkins, P O Whimp *J. Am. Chem. Soc.* **98** 3514 (1976)
69. R G Goel, R G Montemayor *Inorg. Chem.* **16** 2183 (1977)
70. H C Clark, A B Goel, R G Goel, S Goel, W O Ogini *Inorg. Chim. Acta* **31** L441 (1978)
71. H C Clark, A B Goel, S Goel *Inorg. Chem.* **18** 2803 (1979)
72. H C Clark, A B Goel, R G Goel, S Goel, W O Ogini *Transition Met. Chem.* **5** 378 (1980)
73. R G Goel, W O Ogini *Organometallics* **1** 654 (1982)
74. A B Goel, S Goel, W O Ogini *Inorg. Chim. Acta* **98** 67 (1985)
75. W A Herrmann, V P W Böhm *J. Organomet. Chem.* **572** 141 (1999)
76. R Arnek, K Zetterberg *Organometallics* **6** 1230 (1987)
77. Y Agnus, M Gross, M Labarelle, R Louis, B Metz *J. Chem. Soc., Chem. Commun.* 939 (1994)
78. W Henderson, A G Oliver, C E F Rickard, L J Baker *Inorg. Chim. Acta* **292** 260 (1999)
79. L Zhang, K Zetterberg *Organometallics* **10** 3806 (1991)
80. W D Jones, F J Feher *Acc. Chem. Res.* **22** 91 (1989)
81. A J Cheney, B L Shaw *J. Chem. Soc., Dalton Trans.* 860 (1972)
82. B L Shaw, M Truelock *J. Organomet. Chem.* **102** 517 (1975)
83. B E Mann, B L Shaw, R M Slade *J. Chem. Soc., Dalton Trans.* 2976 (1971)
84. H Werner, H J Kraus *J. Organomet. Chem.* **204** 415 (1981)
85. A J Cheney, B E Mann, B L Shaw, R M Slade *J. Chem. Soc., Chem. Commun.* 1176 (1970)
86. A J Cheney, B E Mann, B L Shaw, R M Slade *J. Chem. Soc., Dalton Trans.* 3833 (1971)
87. M A Bennett, M Contel, D C R Hockless, L L Welling, A C Willis *Inorg. Chem.* **41** 844 (2002)
88. A A Kiffen, Ch Masters, L Raynand *J. Chem. Soc., Dalton Trans.* 853 (1975)
89. A L Seligson, W C Trogler *Organometallics* **12** 738 (1993)
90. C J Moulton, B L Shaw *J. Chem. Soc., Dalton. Trans.* 1020 (1976)
91. S Sjövall, O F Wendt, C Andersson *J. Chem. Soc., Dalton Trans.* 1396 (2002)
92. S Sjövall, M H Johansson, C Andersson *Eur. J. Inorg. Chem.* 2907 (2001)
93. G B Robertson, P O Whimp *Inorg. Chem.* **13** 2082 (1974)
94. W Lesueur, E Solari, C Floriani, A Chiesi-Villa, C Rizzoli *Inorg. Chem.* **36** 3354 (1997)
95. C A Tolman *Chem. Rev.* **77** 313 (1977)
96. B L Shaw *J. Am. Chem. Soc.* **97** 3856 (1975)
97. B L Shaw *J. Organomet. Chem.* **200** 307 (1980)
98. B N Cockburn, D V Hove, T Keating, B F G Johnson, J Lewis *J. Chem. Soc., Dalton Trans.* 404 (1973)
99. V V Dunina, N S Gulyukina, E B Golovan', I Yu Nalimova, A A Koksharova, I P Beletskaya *Metalloorg. Khim.* **6** 36 (1993) [a]
100. V V Dunina, M Yu Kazakova, Yu K Grishin, O R Malyshev, E I Kazakova *Izv. Akad. Nauk, Ser. Khim.* 1375 (1997) [b]
101. V V Dunina, L G Kuz'mina, M Yu Kazakova, O N Gorunova, Yu K Grishin, E I Kazakova *Eur. J. Inorg. Chem.* 1029 (1999)
102. A C Cope, E C Friedrich *J. Am. Chem. Soc.* **90** 909 (1968)
103. C K Ingold *J. Chem. Soc.* 305 (1921)
104. C K Ingold *J. Chem. Soc.* 951 (1921)
105. N L Allinger, V Zalkov *J. Org. Chem.* **25** 701 (1960)
106. Ch A Tolman *J. Am. Chem. Soc.* **92** 2956 (1970)
107. T K Woo, T Ziegler *Inorg. Chem.* **33** 1857 (1994)
108. M Beller, T H Riermeier, S Haber, H-J Kleiner, A W Herrmann *Chem. Ber.* **129** 1259 (1996)
109. S A Dias, E C Alyea *Transition Met. Chem.* **4** 205 (1979)
110. E C Alyea, J Malito *J. Organomet. Chem.* **340** 119 (1988)
111. E C Alyea, G Malito *Gazz. Chim. Ital.* **123** 709 (1993)
112. J F Blount, C A Maryanoff K Mislow *Tetrahedron Lett.* 913 (1975)
113. E M Hyde, B L Shaw, I Shepherd *J. Chem. Soc., Dalton Trans.* 1696 (1978)
114. K Hiraki, Y Fuchita, T Uchiyama *Inorg. Chim. Acta* **69** 187 (1983)
115. J M Duff, B E Mann, B L Shaw, B Turtle *J. Chem. Soc., Dalton Trans.* 139 (1974)
116. B L Shaw, S D Perera, E A Staley *Chem. Commun.* 1361 (1998)
117. H Kawanami, K Toyota, M Yoshifuji *Chem. Lett.* 533 (1996)
118. R Mason, M Textor *J. Chem. Soc., Chem. Commun.* 292 (1976)
119. A R H Bottomley, C Grocker, B L Shaw *J. Organomet. Chem.* **250** 617 (1983)
120. H-B Kraatz, D Milstein *J. Organomet. Chem.* **488** 223 (1995)
121. R B Bedford, S M Draper, P N Scully, S L Welch *New J. Chem.* **24** 745 (2000)
122. D Morales-Morales, C Grause, K Kasaoka, R Redon, R E Cramer, C M Jensen *Inorg. Chim. Acta* **300**–**302** 958 (2000)
123. M E van der Boom, M Gozin, Y Ben-David, L J W Shimon, F Frolow, H-B Kraatz, D Milstein *Inorg. Chem.* **35** 7068 (1996)
124. S Sjövall, C Andersson, O F Wendt *Inorg. Chim. Acta* **325** 182 (2001)
125. A Jouaiti, M Geofforoy, G Terron, G Bernardinelli *J. Chem. Soc., Chem. Commun.* 155 (1992)
126. A Jouaiti, M Geoffroy, G Bernardinelli *Tetrahedron Lett.* **34** 3413 (1993)
127. A Jouaiti, M Geofforoy, G Terron, G Bernardinelli *J. Am. Chem. Soc.* **117** 2251 (1995)
128. N A Al-Salem, H D Empsall, R Markham, B L Shaw *J. Chem. Soc., Dalton Trans.* 1972 (1979)
129. N A Al-Salem, W S McDonald, R Markham, M C Norton, B L Shaw *J. Chem. Soc., Dalton. Trans.* 59 (1980)
130. V V Dunina, O A Zalevskaya, V M Potapov *Zh. Obshch. Khim.* **54** 389 (1984) [c]
131. V V Dunina, O N Gorunova, M V Livantsov, Yu K Grishin, L G Kuz'mina, N A Kataeva, A V Churakov *Inorg. Chem. Commun.* **3** 354 (2000)
132. V V Dunina, O N Gorunova, M V Livantsov, Yu K Grishin, L G Kuz'mina, N A Kataeva, A V Churakov *Tetrahedron: Asymmetry* **11** 3967 (2000)

133. R J Errington, W S McDonald, B L Shaw *J. Chem. Soc., Dalton Trans*. 1829 (1982)
134. H Rimml, L M Venanzi *J. Organomet. Chem*. **260** C52 (1984)
135. J M Longmire, X Zhang, M Shang *Organometallics* **17** 4374 (1998)
136. E J Farrington, E M Viviente, B S Williams, G Van Koten, J M Brown *Chem. Commun*. 308 (2002)
137. S Nemeh, R J Flesher, K Gierling, C Maichle-Mossmer, H A Mayer, W C Kaska *Organometallics* **17** 2003 (1998)
138. R B Bedford, S L Welch *Chem. Commun*. 129 (2001)
139. D A Albisson, R B Bedford, S E Lawrence, P N Scully *Chem. Commun*. 2095 (1998)
140. L L Troitskaya, S T Ovseenko, Yu L Slovokhotov, I S Neretin, V I Sokolov *J. Organomet. Chem*. **642** 191 (2002)
141. V I Sokolov, L A Bulygina *Izv. Akad. Nauk, Ser. Khim*. 1268 (1998)
142. V I Sokolov, L A Bulygina, O Ya Borbulevych, O V Shishkin *J. Organomet. Chem*. **582** 246 (1999)
143. E W Ainscough, S D Robinson *J. Chem. Soc., Chem. Commun*. 130 (1971)
144. N Ahmad, E W Ainscough, T A James, S D Robinson *J. Chem. Soc., Dalton Trans*. 1151 (1973)
145. V V Dunina, O N Gorunova, L G Kuz'mina, M V Livantsov, Yu K Grishin *Tetrahedron: Asymmetry* **10** 3951 (1999)
146. N N Lyalina, S V Dargina, A N Sobolev, T M Buslaeva, I P Romm *Koord. Khim*. **19** 57 (1993) [d]
147. G J Gainsford, R Mason *J. Organomet. Chem*. **80** 395 (1974)
148. L R Falvello, J Fornies, A Martin, V Sicilia, P Villarroya *Inorg. Chem*. **36** 6166 (1997)
149. J D Oliver, D F Mullica, W O Milligan *Inorg. Chem*. **21** 3284 (1982)
150. M Castella, F Calahorra, D Sainz, D Velasco *Org. Lett*. **3** 541 (2001)
151. M E Van der Boom, S-Y Liou, Y Ben-David, L J W Shimon, D Milstein *J. Am. Chem. Soc*. **120** 6531 (1998)
152. K Kiewel, Y S Liu, D E Bergbreiter *Tetrahedron Lett*. **40** 8945 (1999)
153. M S Karash, R C Seyler, F R Mayo *J. Am. Chem. Soc*. **60** 882 (1938)
154. J A Davies, F R Hartley *Chem. Rev*. **81** 79 (1981)
155. R J Cross, A R Kennedy, K W Muir *J. Organomet. Chem*. **487** 227 (1995)
156. M W Haenel, D Jakubik, C Krüger, P Betz *Chem. Ber*. **124** 333 (1991)
157. A L Seligson, W C Trogler *J. Am. Chem. Soc*. **114** 7085 (1992)
158. D Morales-Morales, R Redon, C Yung, C M Jensen *Chem. Commun*. 1619 (2000)
159. D Morales-Morales, R E Cramer, C M Jensen *J. Organomet. Chem*. **654** 44 (2002)
160. F-T Luo, A Jeevanandam, M K Basu *Tetrahedron Lett*. **39** 7939 (1998)
161. A N Vedernikov, A I Kuramshin, B N Solomonov *Zh. Org. Khim*. **29** 2129 (1993) [e]
162. A N Vedernikov, A I Kuramshin, B N Solomonov *J. Chem. Soc., Chem. Commun*. 121 (1994)
163. O F Wendt, N-F K Kaiser, L I Elding *J. Chem. Soc., Dalton Trans*. 4733 (1997)
164. B D Steffey, A Miedaner, M L Maciejewski-Farmer, P R Bernatis, A M Herring, V S Allured, V Carperos, D L DuBois *Organometallics* **13** 4844 (1994)
165. B S Williams, P Dani, M Lutz, A L Spek, G Van Koten *Helv. Chim. Acta* **84** 3519 (2001)
166. B J Hathaway, D G Holah, A E Underhill *J. Chem. Soc*. 2444 (1962)
167. A Sen, L Ta-Wang *J. Am. Chem. Soc*. **103** 4627 (1981)
168. A Weisman, M Gozin, H-B Kraatz, D Milstein *Inorg. Chem*. **35** 1792 (1996)
169. M A Zhuravel, N S Greval, D S Gluecl *Organometallics* **19** 2882 (2000)
170. D M Fenton *J. Org. Chem*. **38** 3192 (1973)
171. H C Clark, A B Goel, S Goel *J. Organomet. Chem*. **166** C29 (1979)
172. T Yoshida, S Otsuka *J. Am. Chem. Soc*. **99** 2134 (1977)
173. V V Grushin *Chem. Rev*. **96** 2011 (1996)
174. S Otsuka, T Yoshida, M Matsumoto, K Nakatsu *J. Am. Chem. Soc*. **98** 5850 (1976)
175. H Imoto, H Moriyama, T Saito, Y Sasaki *J. Organomet. Chem*. **120** 453 (1976)
176. H C Clark, A B Goel, R G Goel, W O Ogini *J. Organomet. Chem*. **157** C16 (1978)
177. R G Goel, W O Ogini *Inorg. Chim. Acta* **44** L165 (1980)
178. R G Goel, W O Ogini, R C Srivastava *Inorg. Chem*. **20** 3611 (1981)
179. W Keim *J. Organomet. Chem*. **14** 179 (1968)
180. A J Cheney, B L Shaw *J. Chem. Soc., Dalton Trans*. 754 (1972)
181. D L Thorn *Organometallics* **17** 348 (1998)
182. Ph E Garrou *Chem. Rev*. **85** 171 (1985)
183. I V Kourkine, M D Sargent, D S Glueck *Organometallics* **17** 125 (1998)
184. S Okeya, Sh-i Ooi, K Matsumoto, Y Nakamura, S Kawaguchi *Bull. Chem. Soc. Jpn*. **54** 1085 (1981)
185. S Baba, T Ogura, Sh Kawaguchi *Inorg. Nucl. Chem. Lett*. **7** 1195 (1971)
186. M Horike, Y Kay, N Yasuoka, N Kasai *J. Organomet. Chem*. **72** 441 (1974)
187. S Baba, T Ogura, S Kawaguchi *Bull. Chem. Soc. Jpn*. **47** 665 (1974)
188. S Matsumoto, S Kawaguchi *Bull. Chem. Soc. Jpn*. **53** 1577 (1980)
189. S Okeya, H Sazaki, M Ogita, T Takemoto, Y Onuki, Y Nakamura, B K Mohapatra, S Kawaguchi *Bull. Chem. Soc. Jpn*. **54** 1978 (1981)
190. T Ito, T Kiriyama, A Yamamoto *Bull. Chem. Soc. Jpn*. **49** 3250 (1976)
191. S Okeya, T Miyamoto, S Ooi, Y Nakamura, S Kawaguchi *Inorg. Chim. Acta* **45** L135 (1980)
192. S Matsumoto, S Kawaguchi *Bull. Chem. Soc. Jpn*. **54** 1704 (1981)
193. S Okeya, Y Nakamura, S Kawaguchi *Bull. Chem. Soc. Jpn*. **54** 3396 (1981)
194. S R Childress, R A Holwerda *Synth. React. Inorg. Met.-Org. Chem*. **22** 57 (1992)
195. S Kawaguchi *Coord. Chem. Rev*. **70** 51 (1986)
196. S Okeya, T Miyamoto, S Ooi, Y Nakamura, S Kawaguchi *Bull. Chem. Soc. Jpn*. **57** 395 (1984)
197. A R Siedle, R A Newmark, L H Pignolet *J. Am. Chem. Soc*. **104** 6584 (1982)
198. S Baba, S Kawaguchi *Inorg. Nucl. Chem. Lett*. **11** 415 (1975)
199. A D Ryabov *Zh. Obshch. Khim*. **57** 249 (1987) [c]
200. A D Ryabov, in *Synthetic and Mechanistic Aspects of Exchange of Cyclometallated Ligands in Pd(II) and Pt(II) Complexes. Perspective in Coordination Chemistry* (Eds A F Williams, C Floriani, A Merbach) (Weinheim: VCH, 1994) p. 271
201. P Dani, M Albrecht, G P M van Klink, G Van Koten *Organometallics* **19** 4468 (2000)
202. M Albrecht, P Dani, M Lutz, A L Spek, G Van Koten *J. Am. Chem. Soc*. **122** 11822 (2000)
203. J Granell, D Sainz, J Sales *J. Chem. Soc., Dalton Trans*. 1785 (1986)
204. R M Ceder, M Gomez, J Sales *J. Organomet. Chem*. **361** 391 (1989)
205. A D Ryabov, A V Usatov, V N Kalinin, L I Zakharkin *Izv. Akad. Nauk, Ser. Khim*. 2790 (1986) [b]
206. V V Dunina, O N Gorunova, E D Razmyslova, M V Livantsov, Yu K Grishin, in *Novel Routes to Optically Active Palladacycles. Book of Abstracts of the International Symposium on Chirality 'Chirality-2000' (ISCD 12), Chamonix Mont-Blanc, France, 2000* p. A8
207. O N Gorunova, Candidate Thesis in Chemical Sciences, M V Lomonosov Moscow State University, Moscow, 2001
208. J Chatt, L M Vallarino, L M Venanzi *J. Chem. Soc*. 3413 (1957)
209. D A White *J. Chem. Soc., A* 145 (1971)
210. J K Stille, D E James *J. Organomet. Chem*. **108** 401 (1976)
211. J H Nelson, D A Redfield *Inorg. Nucl. Chem. Lett*. **9** 807 (1973)
212. H D Empsall, E M Hyde, E Mentzer, B L Shaw *J. Chem. Soc., Dalton Trans*. 2285 (1977)
213. C Bartolomé, P Espinet, F Villafane, S Giesa, A Martin, A G Orpen *Organometallics* **15** 2019 (1996)

214. A Bright, B E Mann, C Masters, B L Shaw, R M Slade, R E Stainbank *J. Chem. Soc., A* 1826 (1971)
215. S Otsuka *J. Organomet. Chem.* **200** 191 (1980)
216. A Musco, W Kuran, A Silvani, M W Anker *J. Chem. Soc., Chem. Commun.* 938 (1973)
217. M Matsumoto, H Yoshioka, K Nakatsu, T Yoshida, S Otsuka *J. Am. Chem. Soc.* **96** 3322 (1974)
218. T Matsumoto, T Kasai, K Tatsumi *Chem. Lett.* 346 (2002)
219. V V Grushin, H Alper *Organometallics* **15** 5242 (1996)
220. A Bondi *J. Phys. Chem.* **68** 441 (1964)
221. T W Hambley *Inorg. Chem.* **37** 3767 (1998)
222. A J Pryde, B L Shaw, B Weeks *J. Chem. Soc., Chem. Commun.* 947 (1973)
223. F C March, R Mason, K M Thomas *J. Chem. Soc., Chem. Commun.* 584 (1975)
224. A J Pryde, B L Shaw, B Weeks *J. Chem. Soc., Dalton Trans.* 322 (1976)
225. G W Parshall *Acc. Chem. Res.* **8** 113 (1975)
226. A E Shilov, G B Shul'pin *Usp. Khim.* **56** 754 (1987) [*Russ. Chem. Rev.* **56** 442 (1987)]
227. A N Vedernikov, A I Kuramshin, M D Sayakhov, A A Sobanov, B N Solomonov *Zh. Org. Khim.* **33** 39 (1997) [c]
228. J A M Simkhes, J L Beauchamp *Chem. Rev.* **90** 629 (1990)
229. G A Shamov, A N Vedernikov, B N Solomonov *Zh. Obshch. Khim.* **67** 1061 (1997) [c]
230. A N Vedernikov, G A Shamov, B N Solomonov *Zh. Obshch. Khim.* **67** 1237 (1997) [c]
231. A N Vedernikov, G A Shamov, B N Solomonov *Zh. Obshch. Khim.* **68** 709 (1998) [c]
232. A N Vedernikov, G A Shamov, B N Solomonov *Zh. Obshch. Khim.* **68** 718 (1998) [c]
233. A N Vedernikov, G A Shamov, B N Solomonov *Zh. Obshch. Khim.* **69** 1144 (1999) [c]
234. A N Vedernikov, G A Shamov, B N Solomonov *Zh. Obshch. Khim.* **70** 1263 (2000) [c]
235. B A Arndtsen, R G Bergman, T A Mobley, T H Peterson *Acc. Chem. Res.* **28** 154 (1995)
236. A E Shilov, G B Shul'pin *Chem. Rev.* **97** 2879 (1997)
237. A J Deeming, I P Rothwell *Pure Appl. Chem.* **52** 649 (1980)
238. A D Ryabov *Metalloorg. Khim.* **1** 994 (1988) [a]
239. A D Ryabov *Chem. Rev.* **90** 403 (1990)
240. A J Canty, G Van Koten *Acc. Chem. Res.* **28** 406 (1995)
241. B Rybtchinski, D Milstein *Angew. Chem., Int Ed.* **38** 870 (1999)
242. A J Canty *Acc. Chem. Res.* **25** 83 (1992)
243. A J Canty *Platinum Met. Rev.* **37** 2 (1993)
244. C J Elsevier *Coord. Chem. Rev.* **185–186** 809 (1999)
245. A J Canty, J Patel, M Pfeffer, B W Skelton, A H White *Inorg. Chim. Acta* **327** 20 (2002)
246. A Bayler, A J Canty, B W Skelton, A H White *J. Organomet. Chem.* **595** 296 (2000)
247. A Bayler, A J Canty, P G Edwards, B W Skelton, A H White *J. Chem. Soc., Dalton Trans.* 3325 (2000)
248. A J Canty, H Jin, A S Roberts, B W Skelton, P R Traill, A H White *Organometallics* **14** 199 (1995)
249. A J Canty, J L Hoare, J Patel, M Pfeffer, B W Skelton, A H White *Organometallics* **18** 2660 (1999)
250. D G Brown, P K Byers, A J Canty *Organometallics* **9** 1231 (1990)
251. P K Byers, A J Canty, B W Skelton, P R Traill, A A Watson, A H White *Organometallics* **11** 3085 (1992)
252. A J Canty, A Dedieu, H Jin, A Milet, B W Skelton, S Trofimenko, A H White *Inorg. Chim. Acta* **287** 27 (1999)
253. H Ossor, M Pfeffer, J T B H Jastrzebski, C H Stam *Inorg. Chem.* **26** 1169 (1987)
254. C-S Li, C-H Cheng, F-L Liao, S L Wang *J. Chem. Soc., Chem. Commun.* 710 (1991)
255. L R Falvello, J Fornies, R Navarro, V Silicia, M Tomas *J. Chem. Soc., Dalton Trans.* 3143 (1994)
256. M Catellani, C Mealli, E Motti, P Paoli, E Perez-Carreno, P S Pregosin *J. Am. Chem. Soc.* **124** 4336 (2002)
257. N Feiken, P S Pregosin, G Trabesinger, A Albinati, G L Evoli *Organometallics* **16** 5756 (1997)
258. J Cámpora, J A López, P Palma, P Valeria, E Spillner, E Carmona *Angew. Chem., Int. Ed.* **38** 147 (1999)
259. Ch-H Liu, D-Ch Jou, Ch-H Cheng *Organometallics* **12** 3945 (1993)
260. Ch-H Liu, Ch-Sh Li, Ch-H Cheng *Organometallics* **13** 18 (1994)
261. R R Crabtree *Chem. Rev.* **85** 245 (1985)
262. Ch Hall, R N Perutz *Chem. Rev.* **96** 3125 (1996)
263. M Lavin, E M Holt, R H Crabtree *Organometallics* **8** 99 (1989)
264. A Vigalok, O Uzan, L J W Shimon, Y Ben-David, J M L Martin, D Milstein *J. Am. Chem. Soc.* **120** 12 539 (1998)
265. N A Bailey, J M Jenkins, R Mason, B L Shaw *J. Chem. Soc., Chem. Commun.* 237 (1965)
266. N A Bailey, R Mason *J. Chem. Soc., A* 2594 (1968)
267. M Brookhart, M L H Green *J. Organomet. Chem.* **250** 395 (1983)
268. G K Andersson, H C Clark, J A Davies *Inorg. Chem.* **20** 3607 (1981)
269. R J Angelici *Acc. Chem. Res.* **28** 51 (1995)
270. J P Flemming, M C Pilon, O Ya Borbulevitch, M Yu Antipin, V V Grushin *Inorg. Chim. Acta* **280** 87 (1998)
271. J M Smith, N J Coville, L M Cook, J C A Boeyens *Organometallics* **19** 5273 (2000)
272. S Hietkamp, D J Stufkens, K Vrieze *J. Organomet. Chem.* **168** 351 (1979)
273. H-P Abicht *J. Organomet. Chem.* **311** 57 (1986)
274. S Gibson, D F Foster, G R Eastham, R P Tooze, D J Cole-Hamilton *Chem. Commun.* 779 (2001)
275. F Miyazaki, K Yamaguchi, M Shibasaki *Tetrahedron Lett.* **40** 7379 (1999)
276. H C S Clark, J Fawcett, J H Holloway, E G Hope, L A Peck, D R Russel *J. Chem. Soc., Dalton Trans.* 1249 (1998)
277. A M Aarif, F Estevan, A Garsia-Bernabe, P Lahuerta, M Sanau, M A Ubeda *Inorg. Chem.* **36** 6472 (1997)
278. F Estevan, A Garsia-Bernabe, P Lahuerta, M Sanau, M A Ubeda, R M C de Arellano *Inorg. Chem.* **39** 5964 (2000)
279. M Portnoy, Y Ben-David, D Milstein *J. Organomet. Chem.* **503** 149 (1995)
280. M Portnoy, D Milstein *Organometallics* **12** 1655 (1993)
281. A Ohtaka, N Kato, H Kurosawa *Organometallics* **21** 5464 (2002)
282. L R Falvello, S Fernandes, R Navarro, E P Urriolabeitia *Inorg. Chem.* **39** 2957 (2000)
283. H-P Abicht, K Issleib *J. Organomet. Chem.* **185** 265 (1980)
284. H-P Abicht, K Issleib *J. Organomet. Chem.* **289** 201 (1985)
285. H-P Abicht, K Issleib *J. Organomet. Chem.* **149** 209 (1978)
286. K Schmiedeknecht, M Rudolph, H-P Abicht *Z. Anorg. Allg. Chem.* **462** 106 (1980)
287. H-P Abicht *Z. Chem.* **24** 387 (1984)
288. R L Bennett, M I Bruce, G A Stone *J. Organomet. Chem.* **38** 325 (1972)
289. G van Koten, T B H Jastrzebski *Tetrahedron* **45** 569 (1989)
290. K Schwarzkopf, J O Metzger, W Saak, S Pohl *Chem. Ber.* **130** 1539 (1997)
291. F N Jones, M F Zinn, C R Hauser *J. Org. Chem.* **28** 663 (1963)
292. F N Jones, M F Zinn, C R Hauser *J. Org. Chem.* **28** 3461 (1963)
293. A C Cope, R N Gourley *J. Organomet. Chem.* **8** 527 (1967)
294. K P Klein, C R Hauser *J. Org. Chem.* **32** 1479 (1967)
295. J T B H Jastrzebski, G Van Koten *Inorg. Synth.* **26** 150 (1989)
296. A M Aguiar, J Giacin, A Mills *J. Org. Chem.* **27** 674 (1962)
297. A M Aguiar, J Giacin, A Mills *J. Org. Chem.* **27** 1001 (1962)
298. H-P Abicht, K Issleib *Z. Chem.* **21** 341 (1981)
299. G Müller, H-P Abicht, M Waldkircher, J Lachmann, M Lutz, M Winkler *J. Organomet. Chem.* **622** 121 (2001)
300. H-P Abicht, U Baumeister, H Hartung, K Issleib, R A Jacobson, J Richardson, S M Socol, J G Verkade *Z. Anorg. Allg. Chem.* **494** 55 (1982)
301. H-P Abicht, K Issleib *Z. Anorg. Allg. Chem.* **422** 237 (1976)
302. H-P Abicht, K Issleib *Z. Anorg. Allg. Chem.* **447** 53 (1978)
303. Ph J Bailey, T Barrett, S Parsons *J. Organomet. Chem.* **625** 236 (2001)
304. G Longoni, P Chini, F Canziani, P Fantucci *J. Chem. Soc., Chem. Commun.* 470 (1971)
305. G Longoni, P Chini, F Canziani, P Fantucci *Gazz. Chim. Ital.* **104** 249 (1974)
306. M A Bennett, S K Bhargava, M Ke, A C Willis *J. Chem. Soc., Dalton Trans.* 3537 (2000)
307. G Longoni, P Fantucci, P Chini, F Canziani *J. Organomet. Chem.* **39** 413 (1972)

308. R G Pearson *Inorg. Chem.* **12** 712 (1973)
309. U Belluco, R A Michelin, M Mozzon, R Bertani, G Facchin, L Zanotto, L Pandolfo *J. Organomet. Chem.* **557** 37 (1998)
310. R Navarro, E P Urriolabeitia *J. Chem. Soc., Dalton Trans.* 4111 (1999)
311. H Takahashi, Y Oosawa, A Kobayashi *Inorg. Nucl. Chem. Lett.* **9** 15 (1976)
312. H Takahashi, Y Oosawa, A Kobayashi, T Saito, Y Sasaki *Bull. Chem. Soc. Jpn.* **50** 1771 (1977)
313. I J B Lin, H C Shy, C W Liu, L-K Liu, Sh-K Yeh *J. Chem. Soc., Dalton Trans.* 2509 (1990)
314. L R Falvello, S Fernandes, R Navarro, E P Urriolabeitia *New. J. Chem.* **21** 909 (1997)
315. Y Oosawa, T Saito, Y Sasaki *Chem. Lett.* 1259 (1975)
316. Y Oosawa, T Miyamoto, T Saito, Y Sasaki *Chem. Lett.* 33 (1975)
317. Yo Oosawa, H Urabe, T Saito, Yu Sasaki *J. Organomet. Chem.* **122** 113 (1976)
318. R Usun, J Forniis, R Navarro, A M Ortega *J. Organomet. Chem.* **334** 389 (1987)
319. W J Youngs, J Mahood, B L Simms, P N Swepston, J A Ibers *Organometallics* **2** 917 (1983)
320. W J Youngs, J A Ibers *Organometallics* **2** 979 (1983)
321. W J Youngs, J A Ibers *J. Am. Chem. Soc.* **105** 639 (1983)
322. M Van der Sluis, V Beverwijk, A Termaten, F Bickelhaupt, H Kooijman, A L Spek *Organometallics* **18** 1402 (1999)
323. M Chentit, M Geoffroy, G Bernardinelli *Acta Crystallogr., Sect. C* **53** 866 (1997)
324. M van der Sluis, V Bewerwijk, A Termaten, E Gavrilova, Fr Bickelhaupt, H Kooijman, N Veldman, A L Spek *Organometallics* **16** 1144 (1997)
325. M Basato, B Sesto, M Zecca, G Valle, S Antonello, F Maran *J. Organomet. Chem.* **601** 201 (2000)
326. J Vicente, J-A Abad, Fr S Hernandez-Mata, P G Jones *J. Am. Chem. Soc.* **124** 3848 (2002)
327. M Sakamoto, I Shimizu, A Yamamoto *Organometallics* **13** 407 (1994)
328. A Jouaiti, M Geofforoy, G Bernardinelli *J. Chem. Soc., Chem. Commun.* 437 (1996)
329. J Chatt, J M Davidson *J. Chem. Soc., A* 843 (1965)
330. H Werner, R Werner *J. Organomet. Chem.* **209** C60 (1981)
331. J Götzig, R Werner, H Werner *J. Organomet. Chem.* **290** 99 (1985)
332. R S Shinomoto, P J Desrosiers, T G P Harper, Th C Flood *J. Am. Chem. Soc.* **112** 704 (1990)
333. D Rabinovich, G Parkin *J. Am. Chem. Soc.* **112** 5381 (1990)
334. V C Gibson, P D Grebenik, M L H Green *J. Chem. Soc., Chem. Commun.* 1101 (1983)
335. M A Bennett, P N Kapoor *J. Organomet. Chem.* **336** 257 (1987)
336. J P Collman, L S Hegedus, J R Norton, R G Finke *Principles and Applications of Organotransition Metal Chemistry* (2nd Ed.) (Mill Valley: University Science Books, 1987)
337. R Uson, J Fornies, P Espinet, A Garcia, M Tomas *J. Organomet. Chem.* **282** C35 (1985)
338. R Uson, J Fornies, P Espinet, E Labinde, P G Jones, G M Sheldrick *J. Chem. Soc., Dalton Trans.* 2389 (1982)
339. A Allen, W Lin *Organometallics* **18** 2922 (1999)
340. W L Steffen, G J Palenik *Inorg. Chem.* **15** 2432 (1976)
341. R J Puddephatt *Chem. Soc. Rev.* **12** 99 (1983)
342. V W-W Yam, K-L Yu, B W-K Chu, K-K Cheung *Organometallics* **20** 3632 (2001)
343. F Balegroune, P Braunstein, T M G Catneiro, D Grandjean, D Matt *J. Chem. Soc., Chem. Commun.* 582 (1989)
344. P Braunstein, T M G Catneiro, D Matt *Organometallics* **8** 1737 (1989)
345. F Balegroune, D Grandjean, D Lakkis, D Matt *J. Chem. Soc., Chem. Commun.* 1084 (1992)
346. S-E Bouaoud, P Braunstein, D Grandjean, D Matt, D Nobel *Inorg. Chem.* **25** 3765 (1986)
347. M E van der Boom, Sh-Y Liou, Y Ben-David, A Vigalok, D Milstein *Angew. Chem., Int. Ed. Engl.* **36** 625 (1997)
348. N Shezad, R Sc Oakes, A A Clifford, Ch M Rayner *Tetrahedron Lett.* **40** 2221 (1999)
349. T-a Mitsudo, W Fischetti, R F Heck *J. Org. Chem.* **49** 1640 (1984)
350. A L Rheingold, W C Fultz *Organometallics* **3** 1414 (1984)
351. E C Alyea, G Ferguson, J Malito, B L Ruhl *Organometallics* **8** 1188 (1989)
352. M A Zhuravel, D S Glueck, L N Zakharov, A L Rheingold *Organometallics* **21** 3208 (2002)
353. M Nouroozian, V Kaiser, D E Kaufmann, in *Tris-2-(3,5-dimethyl-furyl)phosphine. A Novel Ligand in Transition Metal Catalysed Reactions: Cyclometallation and Mechanistic Studies. OMCOS-9, Göttingen, 1997* p. 175
354. J M Brunel, A Heumann, G Buone *Angew. Chem. Int. Ed.* **39** 1946 (2000)
355. A B Goel, S Goel, D Vanderveer *Inorg. Chim. Acta* **54** L267 (1981)
356. V Dura-Vila, D M P Mingos, R Vilar, A J P White, D J Williams *Chem. Commun.* 1525 (2000)
357. M Pfeffer *Inorg. Synthesis* **26** 211 (1989)
358. Y El Bakkali, G Muller, D Panyella, D Sainz, L A Martinez-Cruz, in *The XIIth FECHEM, Prague, 1997* p. B20
359. M Yoshifuji, K Toyota, I Matsuda, T Niitsu, N Inamoto, K Hirotsu, T Higuchi *Tetrahedron* **44** 1363 (1988)
360. N Ahmad, E W Ainscough, T A James *J. Chem. Soc., Dalton Trans.* 1148 (1973)
361. K Peters, E-M Peters, H G von Schnering, H-P Abicht *Z. Kristallogr.* **171** 313 (1985)
362. N Sugita, T Miyamoto, Y Sasaki *Chem. Lett.* 659 (1976)
363. B F M Kimmich, W J Marshall, P J Fagan, E Hauptman, R M Bullock *Inorg. Chim. Acta* **330** 52 (2002)
364. F Gorla, L M Venanzi, A Albinati *Organometallics* **13** 43 (1994)
365. Q-N Lu, S Chaloupka, L M Venanzi *Wuji Huaxue Xuebao* **17** 227 (2001); *Chem. Abstr.* **135** 5682 (2001)
366. Z Wang, M R Eberhard, C M Jensen, Sh Matsukawa, Y Yamamoto *J. Organomet. Chem.* **681** 189 (2003)
367. M R Eberhard, S Matsukawa, Y Yamamoto, C M Jensen *J. Organomet. Chem.* **687** 185 (2003)
368. G Ebeling, M R Meneghetti, Fr Rominger, J Dupont *Organometallics* **21** 3221 (2002)
369. G R Rosa, G Ebeling, J Dupont, A L Monteiro *Synthesis* 2894 (2003)
370. F X Roca, C J Richards *Chem. Commun.* 3002 (2003)
371. D Zim, S L Buchwald *Org. Lett.* **5** 2413 (2003)
372. R D Bedford, M E Blake, S J Coles, M B Hursthouse, P N Scully *J. Chem. Soc., Dalton Trans.* 2805 (2003)
373. R B Bedford, S L Hazelwod (née Welch), M E Limmert *Chem. Commun.* 2610 (2002)
374. R D Bedford, S L Hazelwood (née Welch), M E Limmert, J M Brown, S Ramdeehul, A R Cowley, S J Coles, M B Hursthouse *Organometallics* **22** 1364 (2003)
375. R D Bedford, S L Hazelwood (née Welch), M E Limmert, D A Albisson, S M Draper, P N Scully, S J Coles, M B Hursthouse *Chem. Eur. J.* **9** 3216 (2003)
376. R D Bedford, S L Hazelwood (née Welch), P N Norton, M B Hursthouse *J. Chem. Soc., Dalton Trans.* 4164 (2003)
377. C Gracia, G Marco, R Navarro, P Romero, T Soler, E P Urriolabeitia *Organometallics* **22** 4910 (2003)
378. R B Bedford *Chem. Commun.* 1787 (2003)
379. W A Herrmann, K Ofele, D V Preysing, S K Schneider *J. Organomet. Chem.* **687** 229 (2003)
380. J T Singleton *Tetrahedron* **59** 1837 (2003)
381. M E van der Boom, D Milstein *Chem. Rev.* **103** 1759 (2003)
382. D Milstein *Pure Appl. Chem.* **75** 445 (2003)
383. M Albrecht, G Van Koten *Angew. Chem., Int. Ed.* **40** 3750 (2001)
384. R Chanthateyanonth, H Alper *J. Mol. Catal. A: Chem.* **201** 23 (2003)

[a] — *Russ. J. Organomet. Chem. (Engl. Transl.)*
[b] — *Russ. Chem. Bull., Int. Ed. (Engl. Transl.)*
[c] — *Russ. J. Gen. Chem. (Engl. Transl.)*
[d] — *Russ. J. Coord. Chem. (Engl. Transl.)*
[e] — *Russ. J. Org. Chem. (Engl. Transl.)*

Russian Chemical Reviews **73** (4) 351 – 370 (2004) © 2004 Russian Academy of Sciences and Turpion Ltd

DOI 10.1070/RC2004v073n04ABEH000768

The theory of formation of surface complexes and its application to the description of multicomponent dynamic sorption systems

W H Höll, A I Kalinitchev

Contents

I.	Introduction	351
II.	Uptake of ions due to protonation/dissociation reactions of surface groups	352
III.	Uptake of ions due to Lewis acid/Lewis base interactions	355
IV.	Evaluation of the SCT model parameters from experimental data	356
V.	Calculations of multicomponent equilibria using the SCT model	360
VI.	Application of the SCT model to nonlinear theory of multicomponent sorption dynamics and chromatography	362
VII.	Steady-state binary concentration distributions	364
VIII.	Computerised description of ion exchange dynamics in multicomponent systems using the SCT model	364
IX.	Modelling of the dynamics of ion exchange due to Lewis acid/Lewis base interactions, as applied to multicomponent systems	365
X.	Dynamics of ion exchange in multicomponent systems with allowance for ion complexation in the mobile liquid phase	366
XI.	Conclusion	368

Abstract. The fundamentals of the theory of formation of surface complexes (or the surface complexation theory, SCT), which is used in processing the results of studies on the equilibria in multicomponent ion exchange sorption systems, are outlined. The advantage of the theory is the use of the sorption characteristics of binary ion exchange systems for the description and calculation of multicomponent equilibria with allowance for the medium pH value. The solutions to some problems of nonlinear sorption dynamics theory obtained using the description of multicomponent equilibria in the framework of the SCT model are considered. Experimental data on the concentration distributions of components in frontal and displacement chromatograms are compared with the results of corresponding numerical calculations using various sets of parameters of the SCT model (including versions with allowance for the effect of complexation reactions in the mobile phase). The bibliography includes 88 references.

I. Introduction

The aim of this review is to highlight a recently developed model for the description of multicomponent ion exchange equilibria and its applications to nonlinear sorption dynamics theory. The model is called the theory of formation of surface complexes (or the surface complexation theory, SCT), because it assumes that near the surface of a sorbent (ion exchanger) each kind of counterion is located in the form of a surface complex within an individual Stern layer. Application of the SCT approach to nonlinear theory of multicomponent sorption dynamics and chromatography is a specific, complicated theoretical problem, which is solved by the authors of this review.

In the text below we will briefly outline a number of earlier models for the description of sorption phenomena (in some cases, with consideration of surface ion complexation).

Inorganic and organic ion exchange sorbents consist of either a crystalline or a polymeric matrix and various functional groups. Depending on the pH value of the solution contacting the ion exchanger, functional groups can be protonated or dissociated. Therefore, such sorbents can interact with ions in the liquid phase. As a result, sorption of ions at the surface of the ion exchanger becomes possible.[1] The surface charges produce an electric field directed normal to the surface. Consideration of the resulting electrostatic interactions led to development of various models for the description of sorption equilibria.[2–5]

Helmholtz postulated [1] that the surface charges are compensated by counterions which are located within an ordered (outer Helmholtz) layer some distance from the sorbent surface. The distribution of counterions is governed by the degree of hydration of the solute molecules. Gouy and Chapman [3,4] treated counterions as mass points randomly distributed over a diffusion layer. In this model, the corresponding electrostatic potential and charge density are described by the Poisson equation.

Later, Stern [5] used a combination of the two approaches mentioned above. He assumed that a fraction of counterions is located within an ordered layer near the sorbent surface, while the rest of the counterions are distributed over the neighbouring diffusion layer. The Stern model included finite sizes and thermal motion of hydrated ions.

Modern models consider not only electrostatic interactions but also chemical interactions (solvation of metal ions,[6–8] protonation of ligands,[9] adsorption) and a specific interaction between protons and hydroxyl ions.[10]

Yet another theoretical approach treats the adsorption of counterions as a result of (mainly) chemical interactions between functional groups located on the sorbent surface and dissolved species. Sorption of protons (or other ions) is considered as a local equilibrium established as a result of corresponding reactions. Specific (in the case of protons and hydroxyl ions) and nonspecific (for other ions) interactions cause the formation of ion

W H Höll Institute for Technical Chemistry, Karlsruhe Research Centre, PO Box 3640, D-76021 Karlsruhe, Helmholtz-Platz, Germany.
Fax (49-724) 782 23 77. E-mail: wolfgang.hoell@itc.frk.de
A I Kalinitchev Institute of Physical Chemistry, Russian Academy of Sciences, Leninsky prosp. 31, 119991 Moscow, Russian Federation.
Fax (7-095) 952 53 08. Tel. (7-095) 955 44 05.
E-mail: kalina@phyche.ac.ru

Received 23 September 2002
Uspekhi Khimii **73** (4) 383 – 403 (2004); translated by A M Raevsky

pairs at the sorbent surface, which can be treated as various types [1,2] of surface complexes.[11]

In this case, to include the additional contribution of electrostatic interactions to the adsorption,[7,8,12–16] one should know the electric capacitance of the sorbent. This parameter is usually unknown; therefore, a constant ion exchanger capacity model [15,17,18] is employed. Detailed consideration of this model can be found in the literature.[12,19,20]

Spectroscopic studies of the surfaces of ion exchangers revealed [21] that correct description of the adsorption of counterions requires a sorption model with more than one near-surface ion layer to be used. This led to the development [12,22,23] of a triple-layer model with the sorbent surface, β-plane and the diffusion layer as the first, second and third layers, respectively. In the framework of this model counterions can be adsorbed on both the outer layer (β-plane) and the inner layer (sorbent surface).

The surface adsorption of counterions on ion exchange resins was studied [24] using the Gouy–Chapman model [3,4] taking a weakly functionalised Amberlite XAD-2 resin as an example. Applicability of the SCT approach to the description of individual properties of different types of sorption sites was first appreciated by Horst [25] who used the triple-layer model to describe the ion exchange equilibrium on commercially available weakly acid resins.

Initially, the SCT model was developed only for weakly acid polymeric ion exchangers.[25] Further stages of its development and application to the quantitative description of ion equilibria in various organic ion exchange materials have been well documented.[26–36] In this model individual sorption layers are credited to each kind of counterion. Then, the model was extended to other ion exchange systems and currently it permits the description of pure cation or anion exchange equilibria [26,29,36] on various resins [27,28,35] and activated alumina and carbons,[30–32,36] as well as of the adsorption of heavy metal salts.[33,34]

The basic SCT model assumptions and the results obtained by applying the model to the description of equilibria in various multicomponent ion exchange systems including different types of ion exchangers [25–36] are presented in Sections II–V.

The use of the SCT approach appeared to be rather fruitful for solving a number of problems of nonlinear dynamics of multicomponent ion exchange sorption.[37–53] Methods for solution of these theoretical problems with consideration of equilibria using the SCT model as well as the results obtained are described in Sections VI–X.

II. Uptake of ions due to protonation/dissociation reactions of surface groups

1. Simplified description of reactions on charged surfaces of amphoteric ion exchange resins

In deriving mathematical relationships of the surface complexation theory we will consider an idealised planar sorbent surface containing OH groups as sorption sites. We also assume that the sorption sites are uniformly distributed over the sorbent surface.[26,27] In liquid-phase systems the surface OH groups can be protonated in two ways.

In acid media the sorbent surface (S) containing the OH functional groups can be protonated following the reaction

$$S-OH + H^+ \rightleftharpoons S-OH_2^+. \quad (1)$$

To meet the condition for electroneutrality, the positive charge of the surface must be balanced by the negative charge of an anion (*e.g.*, Cl^- ion)

$$S-OH_2^+ + Cl^- \rightleftharpoons S-OH_2Cl. \quad (2)$$

From Eqns (1) and (2) it follows that sorption of acids can occur in sufficiently acid media similarly to the uptake of acids with weakly basic ion exchangers.

In alkaline solutions the surface hydroxy groups can dissociate and release protons to the liquid phase

$$S-OH \rightleftharpoons S-O^- + H^+. \quad (3)$$

The negative surface charges must be compensated by the positive charges of, *e.g.*, Na^+ cations

$$S-O^- + Na^+ \rightleftharpoons S-ONa. \quad (4)$$

Taken together, Eqns (3) and (4) describe a cation exchange on an arbitrary cation exchanger.[30,31,36]

Each protolysis model mentioned above holds for the description of the uptake of acids or the exchange of protons for other monovalent cations in arbitrary pure anion or cation exchange processes. If the equilibrium state is considered for amphoteric ion exchangers and a liquid phase containing various cations and anions, the uptake of anions will decrease with an increase in the pH value until sorption is completely suppressed. The exchange of protons for cations increases in the same way. The pH regions of almost exclusive sorption of cations (or anions) are separated by the region corresponding to the maximum possible concentration of neutral surface groups. In this transient region, sorption of both cations and anions occurs, resulting in coverage of the surface with equal amounts of chemical equivalents of positively and negatively charged counterions.[30,31,36]

2. Basic SCT model assumptions

During the protonation or dissociation of the surface OH groups either a positive or negative electrostatic potential is generated, which depends on the pH value and on the ionic strength of the liquid phase. Due to the sorption of counterions at functional groups this potential is decreased. The SCT model assumes that each kind of counterion (i) is located at a characteristic distance from the surface. Therefore, ordered electrical double layers of Stern layers (1, ..., i, ... , N) are formed near the surface. The layer sequence begins at the sorbent surface: $S|1|...|i|...|j|...|N|D$, where D is the most distant diffusion layer. The excess surface charge is balanced by the charges of counterions in the diffusion layer, which also contains co-ions (Fig. 1 *a*).[26–36]

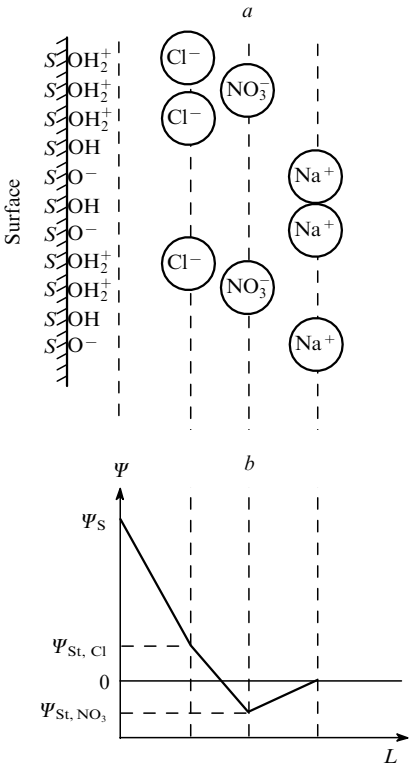

Figure 1. Stern layers (St) near an amphoteric surface (*a*) and the plot of electrostatic potential Ψ *vs.* distance, L, from the surface of sorbent (*b*).[30]

As a consequence, the electrostatic potential Ψ continuously decreases along the normal to the surface. The arrangement of counterions and the potential distribution within the Stern layers and within the diffusion layer for different types of ion exchangers have been well documented (see, *e.g.*, Refs 26–28, 30, 31, 34, 36). The arrangement of counterions and co-ions within the Stern layers is schematically depicted in Fig. 1 *a* and the corresponding electrostatic potential distribution for a solution containing Cl^-, NO_3^- and Na^+ ions is shown in Fig. 1 *b*. The $\Psi(L)$ dependence between the layers $i|(i+1)$ is linear, because each electrical double layer is an electric capacitor of capacitance $C(i, i+1)$. The ions sorbed within the layers $1|...|j|...|N$ form a system of capacitors connected in series. The potential distribution in the diffusion layer D (this layer is not shown in Fig. 1) is described by the Poisson – Boltzmann equation [26–31, 36] and the potential reaches a zero value in the liquid phase (see Fig. 1 *b*).

The equilibrium between the solid and liquid phases is mainly governed by protolytic reactions (1)–(4). Therefore, it is protons (H^+) sorbed at the surface that are responsible for the electrostatic potential. It is assumed that the anion rather than the cation layers are located closer to the surface (see Fig. 1 *a*).

3. Sorption equilibrium relationships in the SCT model

a. General assumptions

The equilibrium relationships in the SCT model were derived assuming that

— functional groups are uniformly distributed across a planar surface;

— activity coefficients in the ion exchanger phase equal unity;

— any ion exchange is treated as replacement of a surface complex by a new one [as a consequence, the charge of the surface sorption sites (z_R) is defined as the least common multiple of the charges of the counterions involved in the exchange process].

b. Surface reactions

Let us consider the derivation of the equilibrium relationships taking a simple system containing Cl^- and Na^+ ions as an example (for the arrangement of the Stern sorption layers, see Fig. 1 *a* except for the NO_3^- ions). The protolytic reactions (1) and (3) at the surface can be described using the mass action law (the corresponding expressions contain the local equilibrium constants). For instance, the protonation and dissociation/neutralisation reactions are characterised by the following constants:[30, 31, 36]

protonation [reaction (1)]

$$K_H^+ = \frac{c(S{-}OH_2^+)}{c(H^+)_{St}\, c(S{-}OH)}, \tag{5}$$

dissociation/neutralisation [reaction (3)]

$$K_H^- = \frac{c(S{-}OH)}{c(S{-}O^-)\, c(H^+)_{St}}. \tag{6}$$

The sorption of counterions (Cl^- and Na^+) is considered in a similar way:[30, 31, 36]

sorption of anions [reaction (2)]

$$K_{Cl}^- = \frac{c(S{-}OH_2Cl)}{c(S{-}OH_2^+)\, c(Cl^-)_{St}}, \tag{7}$$

sorption of cations [reaction (4)]

$$K_{Na}^+ = \frac{c(S{-}ONa)}{c(S{-}O^-)\, c(Na^+)_{St}}. \tag{8}$$

The subscript St denotes the corresponding Stern sorption layer. The unknown concentrations, $c(i)_x$, of the component i at a point x of the electric field within the sorption layers are excluded from consideration. They are expressed *via* the experimentally determined liquid-phase concentrations [$c(i)$, mol litre^{-1}] using the Poisson – Boltzmann relationship [26–28, 30, 31, 36]

$$c(i)_x = c(i)\exp\left[-\frac{z(i)F}{RT}\Psi_x\right], \tag{9}$$

where F is the Faraday constant (in C kmol^{-1}) and Ψ_x is the electrostatic potential at the distance x from the sorbent surface (in volts).

The sorption of anions (in this case, chloride ions) includes the sorption of protons [see Eqn (1)] followed by the sorption of chloride ions [see Eqn (2)]. Since we have a sequence of reactions (1) and (2), the equilibrium constant for this process in the $S{-}OH_2^+$ portions (see Fig. 1 *a*) is given by [30, 31, 36]

$$K_{Cl}^H = K_H^+ K_{Cl}^-. \tag{10}$$

The uptake of cations (in this case, Na^+) develops as the competitive sorption of protons and sodium ions. As a consequence, the equilibrium constant for cation exchange equals the ratio of the corresponding individual equilibrium constants given by expressions (6) and (8) (see Refs 30, 31, 36)

$$K_{Na}^H = \frac{K_H^-}{K_{Na}^+}. \tag{11}$$

Using Eqns (5)–(11), we get [30, 31]

$$K_{Cl}^H = \frac{c(S{-}OH_2Cl)}{c(S{-}OH)c(Cl^-)c(H^+)}\exp\left[\frac{F}{RT}(\Psi_S - \Psi_{Cl})\right], \tag{12}$$

$$K_{Na}^H = \frac{c(S{-}OH)c(Na^+)}{c(S{-}ONa)c(H^+)}\exp\left[\frac{F}{RT}(\Psi_S - \Psi_{Na})\right], \tag{13}$$

where Ψ_S is the electrostatic potential of the sorbent surface (in Volts).

It was shown [30, 31, 36] that the concentrations of the surface complexes, $c(S{-}Oi)$, are converted into solid-phase loadings $q(i)$ (in mg-equiv g^{-1}) of the sorbent, namely, q(OH), $q(Cl^-)$ and $q(Na^+)$ [q(OH) denotes the surface groups which remain undissociated and unprotonated].

Therefore, the pre-exponents in relationships (12) and (13) contain exclusively those quantities which can be determined experimentally. In the SCT model both expressions are called the generalised separation factors (Q_j^i) (see Refs 26–36). After introducing dimensionless sorbent loadings

$$y(i) = \frac{q(i)}{q_{max}}, \tag{14}$$

where q_{max} is the maximum loading, the coefficients Q_j^i are given by:[30, 31, 36]

$$Q_{Cl}^H = \frac{q(Cl^-)}{q(HO^-)c(H^+)c(Cl^-)} = \frac{y(Cl)}{y(HO^-)c(H^+)c(Cl^-)},$$
$$Q_{Na}^H = \frac{q(HO^-)c(Na^+)}{q(Na^+)c(H^+)} = \frac{y(HO^-)c(Na^+)}{y(Na^+)c(H^+)}. \tag{15}$$

Similar relationships can be derived for any monovalent counterions.

c. Binary parameters

The electrostatic potential differences in Eqns (12) and (13) can be expressed *via* the surface charge densities in the series of electric capacitors formed by the Stern layers, *via* the charge densities in the diffusion layer [26–28] and *via* the loadings, $y(i)$, of the amphoteric sorbent surface with Cl^- and Na^+ ions.[30, 31, 36] Mathematical treatment of the corresponding equations in the framework of

the SCT approach gives the following expressions for the generalised separation factors:[30,31,36]

$$\log Q^{H}_{Cl} = \log K^{H}_{Cl} + m(H,Cl)[-y(Cl) + y(Na)], \quad (16)$$

$$\log Q^{H}_{Na} = \log K^{H}_{Na} + m(H,Cl)y(Cl) + m(H,Na)y(Na). \quad (17)$$

The parameters $m(H,i)$ in Eqns (16) and (17) depend on the electric capacitance [$C(S,i)$, in F m^{-2}] of the capacitor formed by the sorbent surface and the corresponding Stern layer (i). They are defined as follows[26–31,36]

$$m(H,i) = \frac{1}{\ln 10}\frac{z_R q_{max} F^2}{A_0 C(S,i) RT}, \quad (18)$$

where A_0 (in m^2 g^{-1}) is the specific surface area of the sorbent, $z_R < 0$ for cation exchangers and $z_R > 0$ for anion exchangers. For binary exchange the numerical value of the parameter z_R equals the least common multiple of the charges of two counterions.[30,31,36]

The general relationship of the SCT model for a system containing an arbitrary number of monovalent counterions can be deduced from similar considerations. For the component i it has the form[30,31,36]

$$\log Q^{H}_{i} = \log K^{H}_{i} + \sum_{j=2}^{i-1}[m(H,j)V(j)y(j)] + m(H,i)\sum_{i}^{n} V(i)y(i). \quad (19)$$

Here i and j are the indices of counterions ($i = 2, 3, ..., n$; $j = 2, 3, ..., i-1$); $i = 1$ corresponds to hydrogen ions; and $V(j)$ and $V(i)$ are the signs of the charges of the counterions, namely, $V(i) = -1$ for anions and $V(j) = +1$ for cations.

For a given component i the second term in expression (19) describes summation of the parameters for those counterions j, which in these Stern layers are located closer to the surface than the species i. The third term comprises the parameters for the counterions located at longer distances from the surface than the ions i. For an ion exchange system containing n counterions there are $n-1$ equations of the type (19).

It is of great importance that all binary parameters of the SCT model $\{\log K^{H}_{i}; m(H,i)\}$ from $i = 2$ on can be successively evaluated from the experimental data for binary exchanges. Since in the framework of the SCT approach all equilibria are calculated using these pairs of binary parameters, the equilibrium constants for multicomponent ion exchange systems can be determined in a similar way. Some examples of calculations of multicomponent equilibria using the SCT model are given below.

d. Extension to systems containing mixtures of monovalent and multivalent counterions

During the exchange of a divalent counterion for two monovalent counterions the divalent species replaces two adjacent ions at the surface. If the liquid phase contains one kind of divalent ions to be exchanged for the monovalent ions initially present in the sorbent, it is necessary that the sorbent have divalent sorption sites. They can be formed by two monovalent sites. As a consequence, two types of surface complexes, namely, two monovalent counterions (*e.g.*, Cl^-) — two monovalent sites (type a) and divalent counterion (*e.g.*, SO_4^{2-}) — two monovalent sites (type b) exist and exchange near the surface.

For a system containing H^+, Na^+, Cl^- and SO_4^{2-} counterions the generalised separation factors are given by the following expressions:[30,31,36]

for exchange of SO_4^{2-} anions involving protonation [see Eqns (1) and (2)] and the formation of a complex of the type b

$$Q^{H}_{II\,SO_4} = \frac{c[(S{-}OH_2^+)_2{=}SO_4^{2-}]}{c(S{-}OH, S{-}OH)[c(H^+)]^2 c(SO_4^{2-})}; \quad (20)$$

for exchange of Cl^- anions involving protonation [see Eqns (1) and (2)] and the formation of a complex of the type a

$$Q^{H}_{II\,Cl} = \frac{c(S{-}OH_2Cl, S{-}OH_2Cl)}{c(S{-}OH, S{-}OH)[c(H^+)]^2[c(Cl^-)]^2}; \quad (21)$$

for Na^+/H^+ exchange and the formation of a complex of the type a

$$Q^{H}_{II\,Na} = \frac{c(S{-}OH, S{-}OH)}{c(S{-}ONa, S{-}ONa)[c(H^+)]^2}. \quad (22)$$

The subscript 'II' means that expressions (20)–(22) were derived assuming the presence of divalent sorption sites.

The probability, $p(i,i)$, for two adjacent monovalent counterions i,i to be found on the surface is given by[31,32]

$$p(i,i) = \left[\frac{y(j)}{\sum y(j)}\right]^2 \sum y(j), \quad (23)$$

where $\sum y(j)$ is the sum of the dimensionless loadings of the sorbent with all monovalent counterions. Using the dimensionless loadings $y(i)$, the separation factors (20)–(22) can be expressed as follows:[30,31,36]

$$Q^{H}_{II\,SO_4} = \frac{y(SO_4)[y(H) + y(Cl) + y(Na)]}{[y(HO)]^2[c(H^+)]^2 c(SO_4^{2-})}, \quad (24)$$

$$Q^{H}_{II\,Cl} = \frac{[y(Cl)]^2}{[y(HO)]^2[c(H^+)]^2[c(Cl^-)]^2} \equiv (Q^{H}_{I\,Cl})^2, \quad (25)$$

$$Q^{H}_{II\,Na} = \frac{[y(HO)]^2[c(Na^+)]^2}{[y(Na)]^2[c(H^+)]^2} \equiv (Q^{H}_{I\,Na})^2. \quad (26)$$

Analogous relationships can be derived for those relatively rare cases where trivalent cations (*e.g.*, Al^{3+}) are involved in ion exchange processes.

e. Equilibrium parameters for differently charged counterions

If an ion exchange system contains exclusively monovalent counterions and a sorbent contains divalent sorption sites, the equilibrium parameters $\log K^{H}_{II\,i}$ and $m_{II}(H,i)$ should be transformed to the parameters for monovalent sorption sites $\log K^{H}_{I\,i}$ and $m_I(H,i)$ using the following relationships[30,31,36]

$$\log K^{H}_{I\,i} = \frac{\log K^{H}_{II\,i}}{2}, \quad (27)$$

$$m_I(H,i) = \frac{m_{II}(H,i)}{2}. \quad (28)$$

If an ion exchange system contains a mixture of monovalent and divalent counterions, calculations should be carried out assuming divalent sorption sites. The equilibrium parameters $\log K^{H}_{I\,i}$ and $m_I(H,i)$ derived for systems with monovalent counterions should be replaced by the parameters $\log K^{H}_{II\,i}$ and $m_{II}(H,i)$ converted using relationships (27) and (28).

4. Pure cation (anion) exchange on weak electrolyte resins

a. Weakly acid ion exchangers

The equilibrium of the uptake of, *e.g.*, Na^+ cations on weakly acid ion exchangers can be schematically described as follows:

$$\overline{R-COOH} + Na^+ \rightleftharpoons \overline{R-COO^- - Na^+} + H^+, \quad (29)$$

where $\overline{R}$ is the polymeric matrix of the ion exchanger (according to commonly accepted designations, the species under the horizontal line refer to the ion exchanger phase). Normally, weakly

acid ion exchangers cannot adsorb anions. Hence, the terms for anions in the general Eqn (19) of the SCT model vanish. Correspondingly, the equation of the SCT model is simplified [30, 31, 36]

$$\log Q^{H}_{Na} = \log K^{H}_{Na} + m(H, Na)y(Na). \quad (30)$$

b. Weakly basic ion exchangers

The uptake of a mixture of cations and anions (*e.g.*, H^+ and Cl^-) by weakly basic polymeric ion exchangers can be written as

$$\overline{R-NH_2} + H^+ + Cl^- \rightleftharpoons \overline{R-NH_3^+-Cl^-}. \quad (31)$$

Because weakly basic ion exchangers do not sorb alkali metal and alkaline-earth metal cations, Eqn (16) is simplified [30, 31, 36]

$$\log Q^{H}_{Cl} = \log K^{H}_{Cl} - m(H, Cl)y(Cl). \quad (32)$$

The uptake of chloride ions by the protonated functional groups of the ion exchanger is also described as the exchange of Cl^- ions for hydroxy groups [34]

$$\overline{(R-NH_2)\cdot H_2O} + Cl^- \rightleftharpoons \overline{R-NH_3^+-Cl^-} + OH^-. \quad (33)$$

In this case consideration of the ion equilibrium in the framework of the SCT model is performed analogously to that given in Section II.3 and leads to the following relationship

$$\log Q^{OH}_{Cl} = \log K^{OH}_{Cl} + m(OH, Cl)y(Cl). \quad (34)$$

5. Strongly acid and strongly basic ion exchangers

The SCT model also allows the relationships for the description of equilibria for sorption of ions by strongly acid and strongly basic resins to be derived from Eqn (19). However, one should keep in mind that in the case of cation exchangers the hydrogen ions cannot be assumed to be adsorbed on the surface, because of complete dissociation of the ion exchanger. Besides, protons are surrounded by the hydration shell and therefore cannot closely approach the surface. Similar considerations also hold for another sorbent–sorbate pair, namely, a strongly basic anion exchanger and OH^- ions. For both strongly acid and strongly basic ion exchangers the sequence of the Stern layers begins with the layer corresponding to that kind of counterions which is located in the closest proximity to the surface.[30, 31, 36]

6. Liquid-phase equilibrium relationships

The liquid-phase ion equilibria are calculated using the following equations: relationships for the dissociation of water, mass balances for each component and the condition for electroneutrality. The activity coefficients in the liquid phase can be calculated from the ionic strength of the solution using the Debye–Hückel relationship.[54]

Note that in systems containing water, hydrolysis of trivalent (*e.g.*, Al^{3+}) cations should be taken into account. The formation constants of the charged and neutral molecules can be found in the literature (see, *e.g.*, Refs 54–57).

III. Uptake of ions due to Lewis acid/Lewis base interactions

1. Reactions on the sorbent surface

The sorption of chloride ions by weakly basic anion exchangers can be treated as adsorption of the acid by free amino groups [see Eqn (31)]. A similar character of the uptake of cations and an equivalent amount of anions is due to the Lewis-base properties of amino groups, which can be coordinatively bound to Lewis acids (metals, M). Taking chloride and copper ions as examples, the equation for this kind of sorption can be written as follows:[33, 34, 38, 55]

$$\overline{R-NH_2} + Cu^{2+} + 2Cl^- \rightleftharpoons \overline{R-NH_2[Cu^{2+}(Cl^-)_2]}. \quad (35)$$

Metal coordination can occur in a variety of fashions. Figure 2 shows a schematic (in the framework of the SCT model) diagram of the Stern layers for an ion exchange system containing protons, two kinds of divalent metal cation M_A^{2+} and M_B^{2+} and monovalent and divalent anions X_A^- and X_B^{2-}.

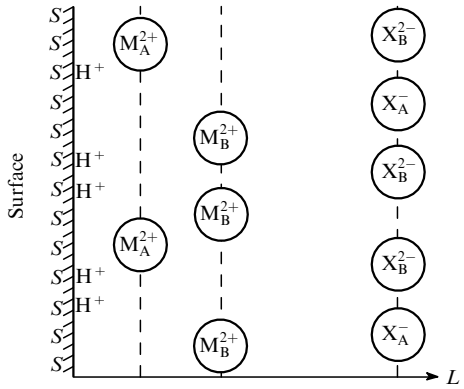

Figure 2. Ion layers near the surface of a weakly basic ion exchanger during the uptake of metal salts (L is the distance from the surface).[34]

We will assume that metals are present in the liquid phase exclusively as divalent cations. To derive the equilibrium relationships, let us consider the competitive uptake of metal salts and the corresponding strong acids.[33, 34] First, we will analyse a simple ion exchange system containing one kind of metal and one kind of anion species, namely, protons (H^+), metal cations (M^{2+}) and monovalent anions (X^-). As mentioned above, the surface charge of the ion exchanger equals the least common multiple of the charges of the ions sorbed. In the case under study (divalent metals M^{2+}), for the parameter z_R we have $z_R = 2$ (see Ref. 34). The surface reactions can be written as follows:[33, 34]

sorption of strong acids $(HX)_2$ or H_2X_2

$$\overline{R-(NH_2)_2} + 2H^+ \rightleftharpoons \overline{R-(NH_3^+)_2}, \quad (36)$$

$$\overline{R-(NH_3^+)_2} + 2X^- \rightleftharpoons \overline{R-(NH_3^+-X^-)_2}, \quad (37)$$

overall

$$\overline{R-(NH_2)_2} + 2H^+ + 2X^- \rightleftharpoons \overline{R-(NH_3^+-X^-)_2}; \quad (38)$$

sorption of metal salts

$$\overline{R-(NH_2)_2} + M^{2+} \rightleftharpoons \overline{R-(NH_2)_2-M^{2+}}, \quad (39)$$

$$\overline{R-(NH_2)_2-M^{2+}} + 2X^- \rightleftharpoons \overline{R-(NH_2)_2-[M^{2+}, (X^-)_2]}, \quad (40)$$

overall

$$\overline{R-(NH_2)_2} + M^{2+} + 2X^- \rightleftharpoons \overline{R-(NH_2)_2-[M^{2+}, (X^-)_2]}. \quad (41)$$

The concentrations of surface complexes $\overline{R-(NH_3^+-X^-)_2}$ and $\overline{R-(NH_2)_2-[M^{2+}, (X^-)_2]}$ (in mg-equiv g^{-1}) in the reactions (38) and (41) characterise the loadings of the resin with the acid and metal salt, respectively. Applying the mass action law to processes (38) and (41) and taking into account relationship (14), we get the following relationships for calculations of the formation constants of the complexes

$$K_{H_2X_2} = \frac{y(H)}{y(\overline{R-NH_2})c_{St}(M^{2+})[c_{St}(X^-)]^2}, \quad (42)$$

$$K_{MX_2} = \frac{y(M)}{y(\overline{R-NH_2})c_{St}(M^{2+})[c_{St}(X^-)]^2}, \quad (43)$$

where $y(H)$, $y(M)$ and $y(\overline{R-NH_2})$ are the loadings of the resin with the acid and metal salt and the concentration of neutral functional groups, respectively.

By applying the Boltzmann relationship and using the description of the sequence of electrical double layers as electric capacitors connected in series near the surface in the framework of the SCT model it is possible to derive the expressions relating the generalised separation factors to the loadings of the resin with the metal salt and acid [33, 34]

$$\log Q_{MX_2} = \log K_{MX_2} - \frac{2}{\ln 10}\frac{F^2 q_{max}}{RTA_0C_2}y(X), \quad (44)$$

$$\log Q_{H_2X_2} = \log K_{H_2X_2} - \frac{2}{\ln 10}\frac{F^2 q_{max}}{RTA_0C_1}y(H) - \frac{2}{\ln 10}\frac{F^2 q_{max}}{RTA_0C_2}y(X). \quad (45)$$

Using designation

$$B = \frac{2}{\ln 10}\frac{F^2 q_{max}}{RTA_0},$$

Eqns (44) and (45) can be written in a more compact form

$$\log Q_{MX_2} = \log K_{MX_2} + m_2 y(X), \quad (46)$$

$$\log Q_{H_2X_2} = \log K_{H_2X_2} + m_1 y(H) + m_2 y(X), \quad (47)$$

where

$$m_1 = -\frac{B}{C_1(H,M)}, m_2 = -\frac{B}{C_2(H,M)}. \quad (48)$$

From Eqns (46) and (47) it follows that four parameters (m_1, m_2 and the formation constants of the complexes K_{MX_2}, $K_{H_2X_2}$) are required for the description of equilibria in the system under study.

2. Ion exchange systems containing two different metals

Competitive sorption in a system with higher dimension compared to that of the system considered above can be treated in a similar way. For instance, for a ternary system containing two different metal cations, M_A and M_B, and one kind of anion, $X^{z(X)}$, we get the system of three equilibrium relationships [33, 34]

$$\log Q_{M_BX_n} = \log K_{M_BX_n} - \frac{B}{C_3}y(X), \quad (49)$$

$$\log Q_{M_AX_n} = \log K_{M_AX_n} + \frac{B}{C_2}\left[y(M_B) - y(X)\right] - \frac{B}{C_3}y(X), \quad (50)$$

$$\log Q_{H_2X_n} = \log K_{H_2X_n} - \frac{B}{C_1}y(H) + \frac{B}{C_2}\left[y(M_B) - y(X)\right] - \frac{B}{C_3}y(X), \quad (51)$$

where

$$m_1 = -\frac{B}{C_1(H,M_A)}, \quad (52a)$$

$$m_2 = \frac{B}{C_2(M_A,M_B)}, \quad (52b)$$

$$m_3 = -\frac{B}{C_3(M_B,X)}. \quad (52c)$$

As a consequence, six equilibrium parameters of the SCT model are needed for the ternary ion exchange system containing two kinds of metal ion, M_A^{2+} and M_B^{2+}, and the acid H^+X^-. The geometric interpretation of Eqns (44)–(47) is straightforward and evaluation of the binary parameters $\{\log K, m\}$ of the SCT model is simple.[26–31, 33–36] In the text below we will give some illustrative examples.

Note that numerical values of the parameters $\{\log K, m\}$ of the SCT model for the binary (bin) systems remain unchanged for ternary (tern) systems, namely [33, 34]

$$\log K_{tern} = \log K_{bin}, \quad (53)$$

$$m_{1,tern} = m_{1,bin}. \quad (54)$$

The quantity m_3 of the ternary system corresponds to m_2 in the binary case [33, 34]

$$m_{3,tern} = m_{2,bin}; \quad (55)$$

the parameter m_2 of the ternary system $H/M_A/M_B$ is calculated as the difference between the respective m_1 values of the binary subsystems H/M_A and H/M_B

$$m_{2,tern} = m_{1,bin}(M_A) - m_{1,bin}(M_B). \quad (56)$$

This treatment of the ternary ion exchange system can be extended to multicomponent systems containing N different metal cations (M_i, $i = A, \ldots i, \ldots, N$) and one type of anion, $X^{z(X)}$.

IV. Evaluation of the SCT model parameters from experimental data

Experimental studies of ion exchange equilibria were carried out taking systems containing either cation or anion exchangers [26, 29, 36] as well as systems containing amphoteric ion exchangers (in particular, activated alumina and activated carbon) [30–32, 36] as examples. Adsorption equilibria were studied for the sorption of heavy metal salts by commercially available ion exchangers and by weakly basic anion exchangers.[33, 34] Methods of pre-treatment of these materials and the experimental conditions necessary for obtaining the corresponding equilibrium data have been well documented.[26–36] In particular, experimental studies of equilibria in amphoteric systems were carried out at constant concentrations of counterions in the liquid phase and at constant amounts of alumina or activated carbon in each sample. The sample volume-to-mass ratios were adjusted in such a way that the degree of sorption and the equilibrium concentration were sufficiently high to be measured reliably. The equilibrium state is mainly governed by the pH value of the liquid phase; therefore, this parameter was varied in each series of samples. The experimental conditions have been reported in detail.[29–31]

To investigate the adsorption of heavy metal salts, the ion exchange resin samples were equilibrated with acid–metal salt mixtures of different composition. Systems containing hydrochloric and sulfuric acids were studied.[33, 34] Numerous experimental data for ion exchange systems were processed using the SCT model in order to evaluate the binary parameters $\{\log K_j^i; m(i,j)\}$ (see Refs 26–32, 34–36).

1. Calculations of the SCT model parameters using experimental data

a. Pure cation or anion exchange

In evaluating the equilibrium parameters of the SCT model the generalised separation factors Q_i^j can be determined using the experimental data (the equilibrium concentrations of counterions and resin loadings). Then, a linear dependence of $\log Q_i^j$ on y_i must be plotted. For binary cation or anion exchange systems the corresponding plots allow sets of binary equilibrium parameters $\{\log K_j^i, m(i,j)\}$ of the SCT model to be determined from the Y-intercept and the slope of the straight line, respectively.

Figures 3–8 show a number of examples for different types of polymeric ion exchangers.[26–31, 33–36] In Fig. 3 we present linear dependences for two weakly acid resins. Systematic deviations from linearity were found only at small loadings. This is due to the

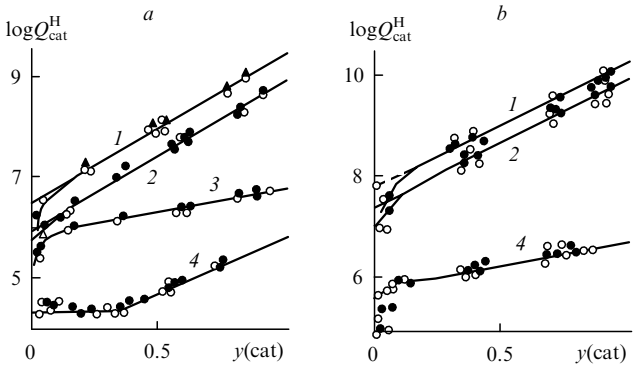

Figure 3. Generalised separation factors Q_{cat}^{H} plotted *vs.* loading of sorbent with cations (cat) for the exchange of various divalent cations for protons with two weakly acid ion exchange resins, Lewatit CNP 80 (*a*) and Amberlite IRC 50 (*b*).[31]
Cation: Mg^{2+} (*1*), Ca^{2+} (*2*), Zn^{2+} (*3*) and Cu^{2+} (*4*). Experimental data (full and open circles and full and open triangles) were obtained at different metal salt concentrations in the liquid phase.

fact that basic relationships (19) of the SCT model were derived neglecting low concentrations of counterions in the diffusion layer *D*. They can be included for simple systems (see above), which leads to good agreement between the results of calculations and experimental data for the dependence of $\log Q_i^j$ on y_i.[27] Two kinds of sorption sites were discriminated for the sorption of Cu^{2+} counterions by acrylic resin Lewatit CNP 80 (see Fig. 3 *a*): the amount of copper ions adsorbed directly on the surface reaches up to one third of the maximum resin loading, while other Cu^{2+} ions are located far from the resin surface. This is in agreement with the published data on the character of the bonding of Cu^{2+} ions to an acrylic matrix.[57]

Experimental data and the results of SCT calculations of exchange of several anions on a weakly basic ion exchanger are shown in Fig. 4. The visual appearance of the straight lines in the plots indicates that sulfate ions are sorbed at a longer distance from the sorbent surface (larger slope of the corresponding line) compared to chloride and nitrate ions in spite of preferred uptake of the SO_4^{2-} ions by the ion exchanger.

Figure 5 presents the results obtained in evaluating the equilibria with two strongly acid ion exchangers. Exchange of magnesium and sodium counterions and protons for the same

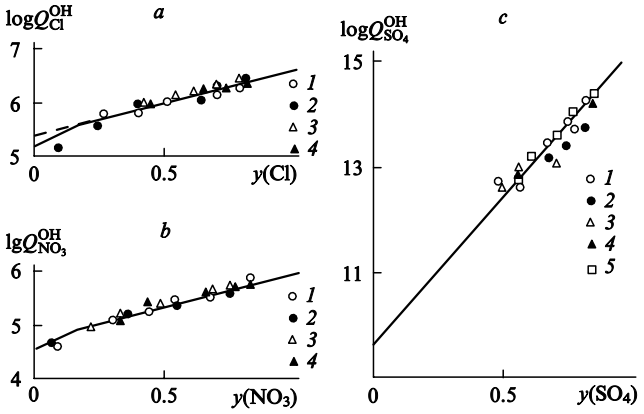

Figure 4. Development of generalised separation factors Q_j^{OH} for the exchange of chloride (*a*), nitrate (*b*) and sulfate (*c*) ions (*j*) for hydroxyl ions with the weakly basic ion exchange resin Amberlite IRA 93.[31]
(*a*) *c*(NaCl) /mmol litre^{-1}: 0 (*1*), 5 (*2*), 10 (*3*) and 20 (*4*); (*b*) *c*($NaNO_3$) /mmol litre^{-1}: 0 (*1*), 5 (*2*), 10 (*3*) and 20 (*4*); (*c*) *c*(Na_2SO_4) /mmol litre^{-1}: 0 (*1*), 5 (*2*), 10 (*3*), 20 (*4*) and 50 (*5*); c_0(NaOH) = 10 mmol litre^{-1}.

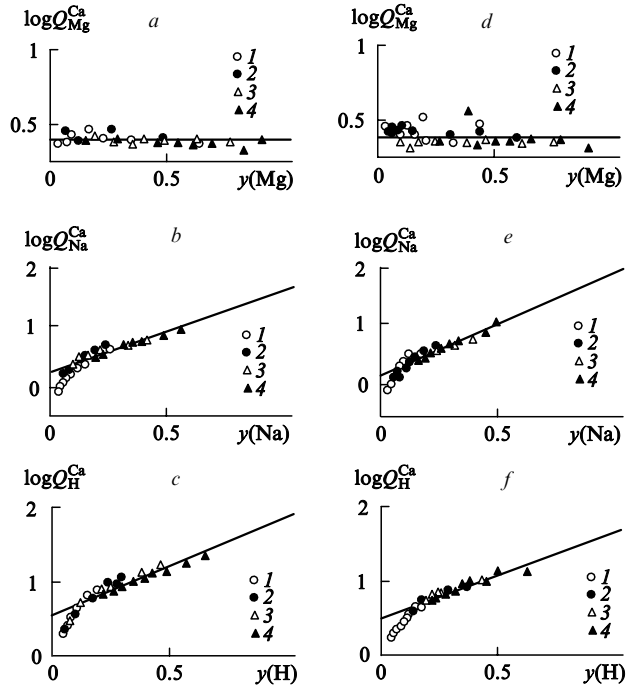

Figure 5. Plots of generalised separation factors Q_{cat}^{Ca} for the exchange of magnesium and sodium cations and protons for calcium ions with the strongly acid ion exchange resins Dowex HCRS (*a*–*c*) and Lewatit S 100 (*d*–*f*).[26, 31]
(*a*, *d*) *c*($MgCl_2$) /mmol litre^{-1}: 2.5 (*1*), 5 (*2*), 10 (*3*) and 25 (*4*); (*b*, *e*) *c*(NaCl) /mmol litre^{-1}: 10 (*1*), 25 (*2*), 50 (*3*) and 100 (*4*);
(*c*, *f*) *c*(HCl) /mmol litre^{-1}: 25 (*1*), 50 (*2*), 100 (*3*) and 200 (*4*).

calcium ion used as a reference in the calculations of binary equilibria with other counterions was studied. Similarly to Figs 3

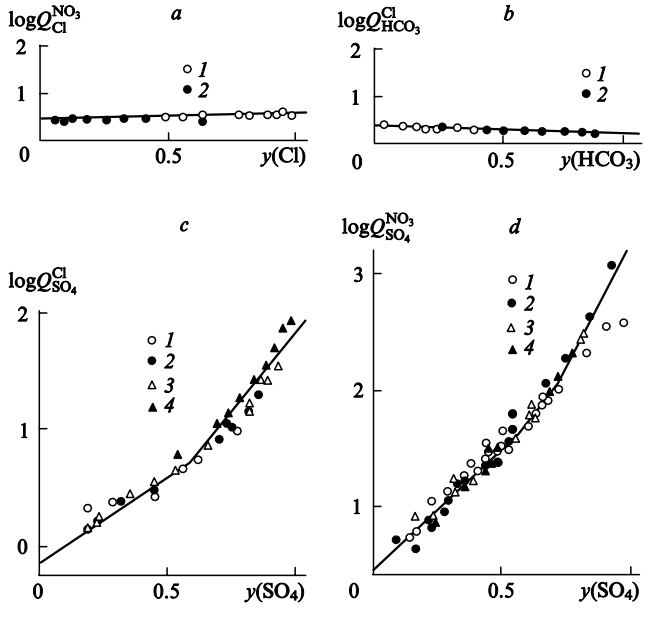

Figure 6. Plots of generalised separation factors for different binary exchange equilibria with the strongly basic ion exchange resin Amberlite IRA 410.[26, 31]
(*a*, *b*) *c*($NaNO_3$) /mmol litre^{-1}: 5 (*1*) and 50 (*2*); (*c*) *c*(Na_2SO_4) /mmol litre^{-1}: 25 (*1*), 5 (*2*), 10 (*3*) and 50 (*4*); (*d*) *c*($NaNO_3$) /mmol litre^{-1}: 5 (*1*), 10 (*2*), 20 (*3*) and 50 (*4*); and *c*(Na_2SO_4) /mmol litre^{-1}: 2.5 (*1*), 5 (*2*), 10 (*3*) and 25 (*4*).

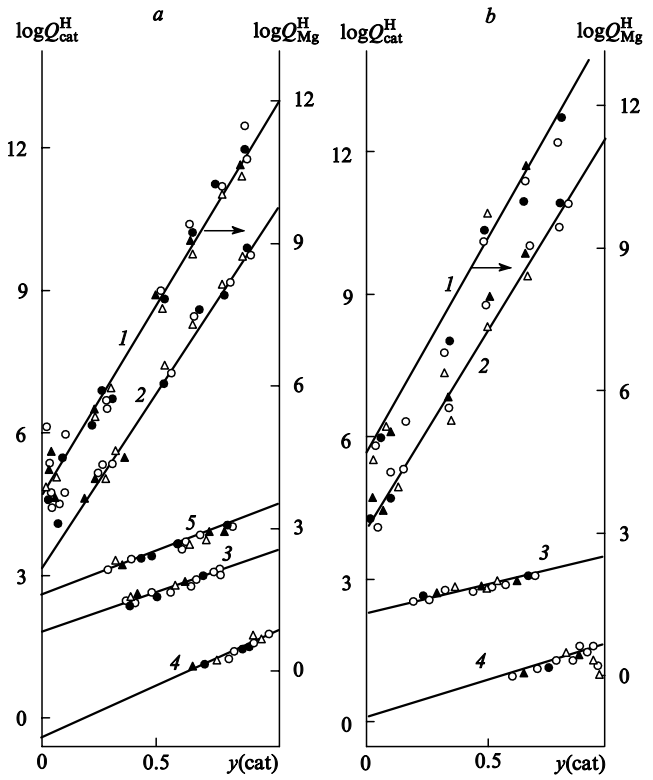

Figure 7. Plots of generalised separation factors for $H^+ - Mg^{2+}$ (*1*), $H^+ - Ca^{2+}$ (*2*), $H^+ - Ni^{2+}$ (*3*), $H^+ - Cu^{2+}$ (*4*) and $H^+ - Zn^{2+}$ (*5*) cation exchange with the Lewatit TP 207 (*a*) and Amberlite IRC 718 (*b*) ion exchangers.[26] Experimental data (full and open circles and full and open triangles) were obtained at different metal salt concentrations in the liquid phase.

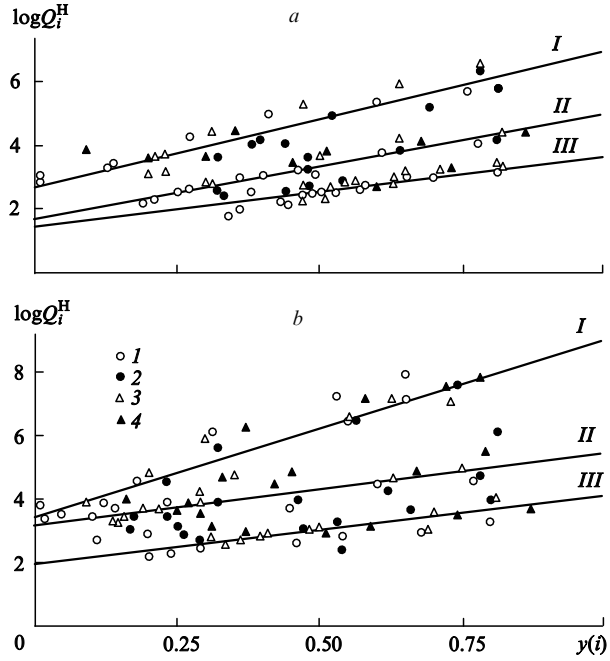

Figure 8. Development of generalised separation factors for the exchange of Ni^{2+} (*I*), Cd^{2+} (*II*) and Cu^{2+} (*III*) (*a*) and Ca^{2+} (*I*), Co^{2+} (*II*) and Zn^{2+} (*III*) (*b*) for protons with the Purolite S 940 ion exchanger containing aminophosphonate functional groups (Purolite S 940).[35] $c_0(HCl) = 10$ mmol litre^{-1}; $c(MCl_2)$ /mmol litre^{-1}: 0 (*1*), 5 (*2*), 10 (*3*) and 25 (*4*); the straight lines were plotted using the linear regression technique.

and 4, the dependences of $\log Q^j_i$ on y_i are approximated by straight lines. However, the regions of deviations from linearity are somewhat larger, which can be due to higher mobility of the counterions in such resins.

Data for anion exchange equilibria on a strongly basic ion exchanger are shown in Fig. 6. As can be seen, the exchange of monovalent anions (Cl^-/NO_3^-, Cl^-/HCO_3^-) is described by horizontal straight lines. A slightly negative slope was found for the Cl^-/HCO_3^- exchange (see Fig. 6 *b*). The SCT approach treats this as an artifact, which is due to the fact that the ternary ion exchange system contains not only HCO_3^- ions but also CO_3^{2-} species ignored in the binary calculations. The exchange of sulfate ions is characterised by an increase in the slopes of the $\log Q^j_i - y_i$ dependences with an increase in $y(SO_4)$ (kink of the lines in Figs 6 *c*, *d*). Obviously, in this case different near-surface Stern layers are formed, which are successively filled with sulfate ions. This is consistent with the fact that strongly basic anion exchangers contain a variety of functional groups. Again, we can state that divalent sulfate ions are sorbed at longer distances from the surface compared to monovalent counterions (see Figs 6 *c*, *d*).

Evaluation of ion exchange equilibria using the SCT model were successfully extended to the systems containing organic counterions, *e.g.*, oxalate, malate and EDTA species. It was found that the corresponding separation factors $\log Q^j_i$ are linear functions of y_i and the binary parameters $\{\log K^i_j; m(i,j)\}$ of the SCT model were determined (Table 1).

Figure 7 presents the results of calculations of equilibria on two chelating selective resins Lewatit TP 207 and Amberlite IRC 718 containing iminodiacetate groups for the exchange of protons for divalent (calcium, magnesium, copper, zinc and nickel) cations. Analogous dependences obtained in calculations of equilibria on resins containing aminophosphonate functional groups are shown in Fig. 8. In both cases linear dependences of $\log Q^j_i$ on y_i can be deduced. The equilibrium constants $\{\log K^A_B; m(A,B)\}$ calculated using the experimental data for equilibria on different resins are listed in Table 1.

b. Amphoteric surfaces

In the framework of the SCT model evaluation of equilibria on amphoteric surfaces requires a more sophisticated procedure compared to those considered above. The first step (prior to calculations) is the assumption of a certain sequence of the Stern layers. Calculations begin with the evaluation of the equilibrium for the exchange of protons at the surface and counterions in the adjacent (first) layer. Calculations of the sorption of ions in the next Stern layer require the corresponding parameters for the first layer. Determination of the SCT model parameters for the third Stern layer requires both sets of binary parameters $\{\log K^A_B; m(A,B)\}$ of the two inner (first and second) layers. The procedure should be continued until all sets of binary parameters for all the Stern layers are calculated. The sequence of the Stern layers is treated as determined correctly if both calculated sets of binary parameters $\{\log K^A_B; m(H,i)\}$ of the SCT model show a monotonic increase in the parameter values with the distance from the surface. If this condition is not met, the computational procedure must be repeated using a modified sequence of Stern layers.

Let us consider a system of Stern layers for H^+, Cl^-, NO_3^- and Na^+ on activated alumina (see Fig. 1) as a simple example. The equilibrium parameters are calculated using the following relationships of the SCT model:[30, 31, 36]

$$\log Q^H_{Cl} = \log K^H_{Cl} + m(H,Cl)[y(Na) - y(Cl) - y(NO_3)], \quad (57)$$

Table 1. Parameters of the surface complexation theory for strongly basic resins.[26, 32, 33–35]

Resin	A/B	z_R	$\log K_B^A$	m(A, B)	Resin	A/B	z_R	$\log K_B^A$	m(A, B)
Amberlite IRA 410	Cl^-/HCO_3^-	1	0.45	-0.26	Amberlite IRC 50	H^+/Cu^{2+}	−2	5.72	0.84
	NO_3^-/HCO_3^-	1	0.83	0.10	Amberlite IRA 93	OH^-/Cl^-	−1	5.35	1.32
	NO_3^-/Cl^-	1	0.46	0.06		OH^-/NO_3^-	−1	4.65	1.32
	NO_3^-/SO_4^{2-}	2	0.47	2.62		OH^-/SO_4^{2-}	−2	9.65	5.65
			−1.03 [a]	4.45 [a]	Amberlite IRA 68	OH^-/NO_3^-	−1	3.88	0.67
Amberlite IRA 458	NO_3^-/Cl^-	1	0.42	0.00	Dowex MWA-1	OH^-/Cl^-	−1	5.85	0.17
	Cl^-/SO_4^{2-}	2	−0.4	1.54		OH^-/NO_3^-	−1	5.40	0.17
Amberlite IRA 996	NO_3^-/Cl^-	2	0.91	-0.08		OH^-/SO_4^{2-}	−2	15.85	3.95
	NO_3^-/SO_4^{2-}	2	2.6	2.98	Lewatit S 100	Ca^{2+}/H^+	−2	0.55	1.35
Amberlite IRA 958	Cl^-/CuX^{2-} (see [b])	2	−1.66	1.46		Ca^{2+}/Na^+	−2	0.23	1.47
	Cl^-/NiX^{2-} (see [b])	2	−1.82	1.53		Ca^{2+}/Mg^{2+}	−2	0.40	0
Imac HP 555	Cl^-/NO_3^-	2	0.61	2.24	Dowex HCRS	Ca^{2+}/H^+	−2	0.60	1.49
	Cl^-/NO_2^-	2	−0.76	1.86		Ca^{2+}/Na^+	−2	0.20	1.77
	Cl^-/SO_4^{2-}	2	0.33	1.57		Ca^{2+}/Mg^{2+}	−2	0.42	0
	$Cl^-/H_2PO_4^-$	2	−0.85	1.85	Lewatit TP 207	H^+/Mg^{2+}	−2	3.80	8.20
	Cl^-/Y (see [c])	2	1.08	1.27	(iminodiacetate	H^+/Ca^{2+}	−2	3.15	5.55
	Cl^-/Z (see [d])	2	0.79	1.48	groups)	H^+/Cu^{2+}	−2	−0.30	2.05
Wofatit SN 36L	Cl^-/NO_3^-	2	0.40	2.51		H^+/Ni^{2+}	−2	1.80	1.80
	Cl^-/NO_2^-	2	−0.71	2.58		H^+/Zn^{2+}	−2	2.60	1.90
	Cl^-/SO_4^{2-}	2	0.48	1.43	Amberlite IRC 718	H^+/Mg^{2+}	−2	4.70	9.65
	$Cl^-/H_2PO_4^-$	2	−0.27	1.56	(iminodiacetate	H^+/Ca^{2+}	−2	4.12	8.23
	Cl^-/Y (see [c])	2	1.08	1.44	groups)	H^+/Cu^{2+}	−2	0.20	1.40
	Cl^-/Z (see [d])	2	0.79	1.37		H^+/Ni^{2+}	−2	2.30	1.25
Sybron Ionac SR-6	Cl^-/NO_3^-	2	1.10	2.33	Purolite S 940	H^+/Cu^{2+}	−2	1.44	2.15
	Cl^-/NO_2^-	2	−0.31	2.33	(aminophosphonate	H^+/Ni^{2+}	−2	2.63	4.22
	Cl^-/SO_4^{2-}	2	0.45	1.40	groups)	H^+/Zn^{2+}	−2	1.96	2.02
	$Cl^-/H_2PO_4^-$	2	−0.10	1.58		H^+/Cd^{2+}	−2	1.65	3.28
	Cl^-/Y (see [c])	2	0.97	1.44		H^+/Co^{2+}	−2	3.11	2.22
	Cl^-/Z (see [d])	2	0.88	1.33		H^+/Ca^{2+}	−2	3.37	5.62
Lewatit CNP 80	H^+/Na^+	−1	3.65	2.78		H^+/Na^+	−1	1.34	3.71
	H^+/Mg^{2+}	−2	6.49	2.88	Purolite S 950	H^+/Cu^{2+}	−2	1.66	1.56
	H^+/Ca^{2+}	−2	5.95	2.88	(aminophosphonate	H^+/Ni^{2+}	−2	3.03	3.31
	H^+/Zn^{2+}	−2	5.80	0.89	groups)	H^+/Zn^{2+}	−2	2.30	1.18
	H^+/Cu^{2+}	−2	4.35 [e]	0		H^+/Cd^{2+}	−2	2.44	1.66
	H^+/Cu^{2+}	−2	5.00	2.13		H^+/Co^{2+}	−2	2.96	2.11
	H^+/Al^{3+}	−6	11.32	3.95		H^+/Ca^{2+}	−2	2.81	4.81
Amberlite IRC 50	H^+/Na^+	−1	4.38	2.38		H^+/Na^+	−1	1.95	3.71
	H^+/Mg^{2+}	−2	7.73	2.32		H^+/NH_4^+	−1	1.29	5.11
	H^+/Ca^{2+}	−2	7.40	2.32					

[a] $y(SO_4) > 0.6$. [b] X = EDTA. [c] Y is oxalate ion. [d] Z is malate ion. [e] $y(Cu) > 0.33$.

$$\log Q^H_{NO_3} - m(H, Cl)[-y(Cl)] = \log K^H_{NO_3} + \\ + m(H, NO_3)[y(Na) - y(NO_3)], \quad (58)$$

$$\log Q^H_{Na} - m(H, Cl)[-y(Cl)] - m(H, NO_3)[-y(NO_3)] = \\ = \log K^H_K + m(H, K)y(Na). \quad (59)$$

Evaluation of the equilibrium data on the sorption of Cl^-, NO_3^- and SO_4^{2-} ions on the Compalox AN7V 800 alumina and on the uptake of carbonate and sulfate ions and Na^+ cations by activated carbon using relationships (57)–(59) has been reported.[26, 30, 31, 36] Although the experimental data obtained for the sorption of sodium ions were not satisfactory, calculations led to linear dependences of $\log Q_i^j$ on y_i.

2. Sorption of metal salts

The binary SCT parameters $\{\log K_B^A; m(A,B)\}$ characterising the sorption equilibria for metals (M) are calculated using Eqns (46) and (47). The SCT parameters for the sorption of metal salts (m_1, m_2 and the formation constants of complexes, K_{MX_2} and $K_{H_2X_2}$) can be evaluated from experimental data as follows. The first step involves plotting $\log Q_{MX_2}$ *vs.* the dimensionless loading of the resin with the anions X^-, y_X. Linear regression (lines in Fig. 9 *a*) gives the parameters $\log K_{MX_2}$ as the *Y*-intercept and m_2 as the slope of the regression line. Then, the quantity $(\log Q_{MX_2} - m_2 y_X)$ is plotted *vs.* $y(H^+)$ using the experimental data and the m_2 value obtained (full and open circles and full and open triangles in Fig. 9 *b*). Linear regression using Eqn (47) again gives the parameters $K_{H_2X_2}$ and m_1 (see the corresponding line in Fig. 9 *b*).[34] The results of calculations for a number of systems for exchange of various metal cations and Cl^- anions with a weakly basic ion exchanger are illustrated in Fig. 9. The binary SCT parameters $\{\log K_B^A; m(A, B)\}$ for the $H^+/M^{2+}/Cl^-$ systems on the Purolite A 109 anion exchanger were calculated [34] using relationships (46) and (47) with consideration of the sorption (see Fig. 2) of two kinds of anions (Cl^- or SO_4^{2-}).

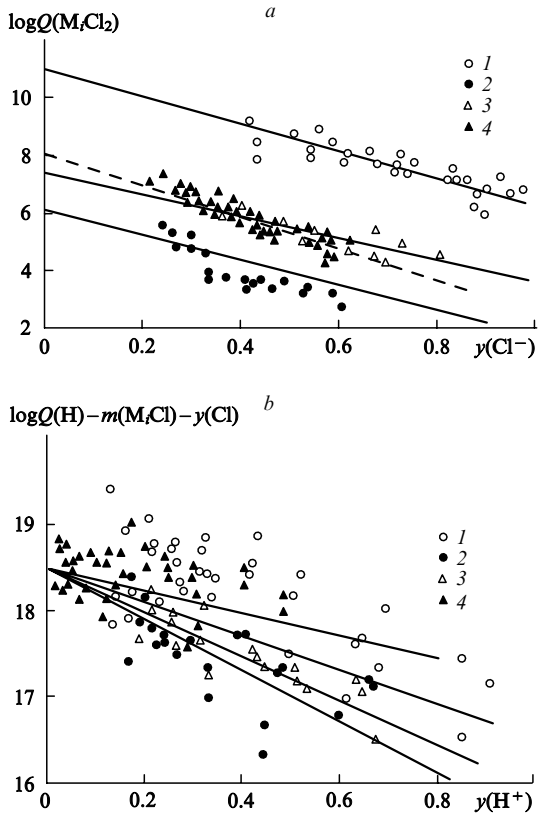

Figure 9. Plots of generalised separation factors for the sorption of hydrochloric acid and different metal chlorides (M_i) onto the weakly basic ion exchanger Purolite A 109.[34]
The parameter m_2 was calculated using Eqn (46) (*a*); the parameter m_1 was calculated using Eqn (47). M_i: Cu (*1*), Ni (*2*), Cd (*3*) and Zn (*4*).

V. Calculations of multicomponent equilibria using the SCT model

Calculations of multicomponent ion exchange equilibria in an arbitrary system require a system of conditions to be fulfilled. These are conservation of masses of the components, electroneutrality in the liquid phase and in the ion exchanger phase and chemical equilibria (for, *e.g.*, dissociation or complexation) in the liquid phase.[26–36]

The conditions for electroneutrality (stoichiometry) of exchange describe the constancy of chemical equivalents of components in the liquid phase (X_s) and in the resin phase (y_s), respectively

$$\sum_{s=\mathrm{A}} X_s = 1, \sum_{s=A} y_s = 1, s = \mathrm{A, B, C, E...}, \tag{60}$$

$$X_s = \frac{z_s c_s}{c_0}, y_s = \frac{a_s}{a_0},$$

where c_0 and a_0 are the coefficients for conversion of the corresponding concentrations c_s and a_s into dimensionless form.

The major advantage of the SCT approach is that the equilibria in multicomponent ion exchange systems {1, ..., *i*, ..., *j*, ...} can be predicted with ease provided that the binary parameters $\{\log K_j^i;\ m(i,j)\}$ for a number of binary exchanges, *i*/*j*, of the components of the system under study are known. It is particularly convenient if the binary parameters for the exchange of different counterions for the same (reference) counterion are obtained. Consideration of equilibria in a ternary system containing three ions, namely, A (reference), B and C leads to the following relationships:[26]

$$\log Q_{\mathrm{B}}^{\mathrm{A}} = \log K_{\mathrm{B}}^{\mathrm{A}} + m(\mathrm{A,B})[y(\mathrm{B}) + y(\mathrm{C})], \tag{61}$$

$$\log Q_{\mathrm{C}}^{\mathrm{B}} = \log K_{\mathrm{C}}^{\mathrm{B}} + m(\mathrm{B,C})y(\mathrm{C}). \tag{62}$$

As shown above, the equilibrium parameters of the SCT model for the binary exchange A/B in the ternary system A/B/C are the same as in the pure binary case. This also holds for the binary parameters of the A/C exchange. Therefore, only the B/C exchange parameters should be determined, which can be done with ease. The $\log K_{\mathrm{C}}^{\mathrm{B}}$ values are calculated using the relationship[26]

$$\log K_{\mathrm{C}}^{\mathrm{B}} = \log K_{\mathrm{C}}^{\mathrm{A}} - \log K_{\mathrm{B}}^{\mathrm{A}}, \tag{63}$$

while the unknown slope m(B,C) in Eqn (62) can be determined using representation of the sequence of Stern layers by electric capacitors connected in series (for substantiation, see above).[26–31] Since the parameter $m(i,j)$ is defined in relationships (18) or (48) *via* the electric capacitance, $C(i,j)$, of the capacitor formed by two Stern layers (i,j), one can make use of the well-known expression for the capacitance (C) of two capacitors connected in series (AB and BC)

$$\frac{1}{C(\mathrm{A,C})} = \frac{1}{C(\mathrm{A,B})} + \frac{1}{C(\mathrm{B,C})}. \tag{64}$$

Thus, we get[26, 31, 32, 36]

$$m(\mathrm{B,C}) = m(\mathrm{A,C}) - m(\mathrm{A,B}). \tag{65}$$

Similar relationships were also derived for multicomponent ion exchange systems containing more than three types of counterions.

In Figs 10–12 we present a number of examples of the experimental data and the results of calculations of multicomponent equilibria using the SCT model and corresponding data on binary ion exchange.

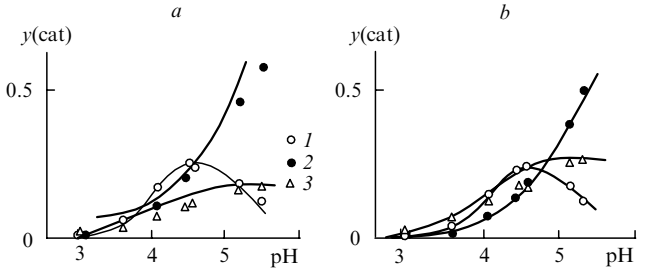

Figure 10. Experimental data (full and open circles and open triangles) and the calculated curves of ion exchange equilibria in the quaternary system $Mg^{2+}/Ca^{2+}/Zn^{2+}/H^+$ on the Lewatit CNP 80 weakly acid ion exchanger (originally in the Ca^{2+} form) obtained using the SCT model at $MgCl_2$ concentrations of 25 (*a*) and 50 mol litre^{-1} (*b*), $ZnCl_2$ concentration of 5 mol litre^{-1} and HCl concentration of 10 mol litre^{-1} (see Ref. 26)
Zn^{2+} (*1*), Ca^{2+} (*2*) and Mg^{2+} (*3*).

Figure 10 shows the results obtained for the sorption of different counterions by a weakly acid resin, which originally was in the Ca^{2+} form, in a quaternary ion exchange system. The equilibria are represented as the dimensionless loadings of different cations plotted *vs.* the pH value. As can be seen, the experimental data and the SCT predictions are in good agreement. Similar results were also obtained for strongly acid and strongly basic ion exchangers.[26, 31, 32, 36] In both cases the results of calculations exhibit reasonable agreement with the experimental data.

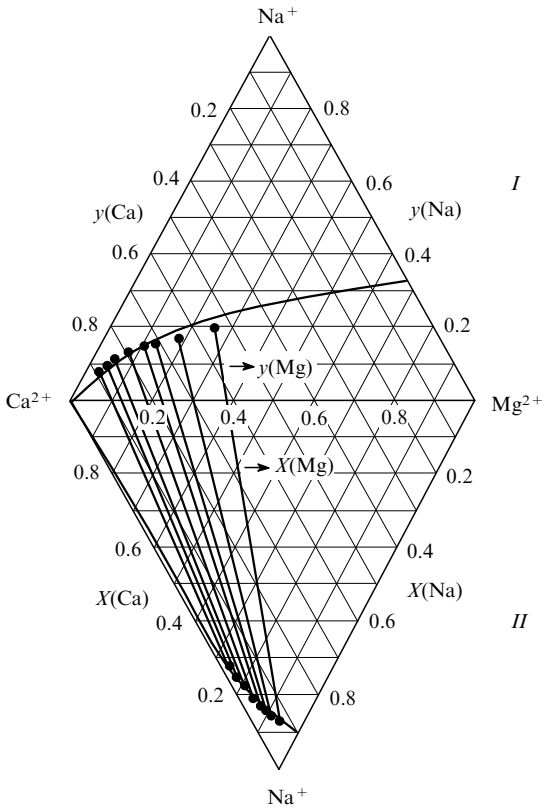

Figure 11. Experimental data (full circles) and the calculated curves of ion exchange equilibria in the ternary system $Na^+/Mg^{2+}/Ca^{2+}$ on the Lewatit S 100 strongly acid ion exchanger for the resin phase (*I*) and liquid phase (*II*) obtained using the SCT model.[26]
$y(Na) + y(Ca) + y(Mg) = 1$; $X(Na) + X(Ca) + X(Mg) = 1$; $c_0(Mg) = 2.5$, $c_0(Na) = 50$ mmol litre^{-1}.

The exchange of three ions with a strongly acid ion exchanger (Lewatit S 100), which exhibits no preferred affinity towards a particular ion, is illustrated by Fig. 11. Here, we deal with similar concentrations of all components; therefore, the ternary equilibrium can be represented using the triangular diagram. Some differences between the experimental and calculated values for the resin phase can be explained by neglect of the concentration of the counterions in the diffusion layer *D* adjacent to the most distant Stern layer: *N*|*D* (see above).

Figure 12 presents a comparison of the experimental data (full and open circles) with the loadings $y(i)$ calculated using the SCT model for the $NiCl_2/NiSO_4/HCl/H_3BO_3$ and $Ni(SO_3NH_2)_2/HCl/H_3BO_3$ systems on the Purolite S 950 resin containing aminophosphonate functional groups.

The individual equilibrium parameters of amphoteric sorbents were determined above. In Fig. 13 we compare the experimental data on the adsorption equilibria for various counterions (protons, carbonate and chloride ions and calcium cations) on activated carbon. As can be seen, an increase in the pH value of the solution causes the relative loading with chloride ions to decrease and the loadings with calcium, hydrogen and carbonate ions to increase. Nevertheless, the uptake of calcium is small (*i.e.*, the sorbent capacity towards the sorption of these cations is low). Comparison of the results of calculations and experimental data also demonstrates a high predictive power of the SCT model.

The results of an experimental study on the adsorption of $CuCl_2$ and $NiCl_2$ on the Purolite A 109 weakly basic anion exchanger are presented in Fig. 14 as functions of the pH value. These data are in reasonable agreement with the results of calculations using the sets of binary parameters $\{\log K_B^A; m(A,B)\}$ of the SCT model.[26–36]

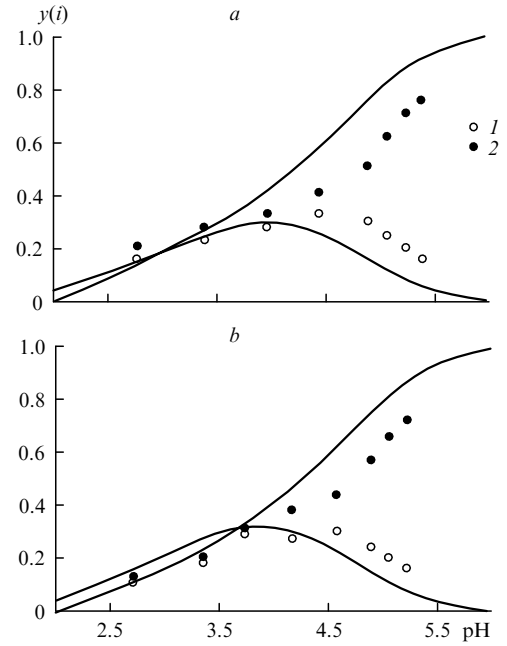

Figure 12. Experimental data (full and open circles) and the calculated curves of ion exchange equilibria in the systems $NiCl_2/NiSO_4/HCl/H_3BO_3$ (*a*) and $Ni(SO_3NH_2)_2/HCl/H_3BO_3$ (*b*) on the Purolite S 950 aminophosphonate resin (originally in the Ca^{2+} form) obtained using the SCT model.[35]
(*a*): $c_0(NiCl_2) = 4$, $c_0(NiSO_4) = 6$, $c_0(HCl) = 10$, $c_0(H_3BO_3) = 5$ mmol litre;
(*b*): $c_0(Ni(SO_3NH_2)_2) = 10$, $c_0(HCl) = 10$, $c_0(H_3BO_3) = 5$ mmol litre^{-1}; Ni (*1*) and Ca (*2*).

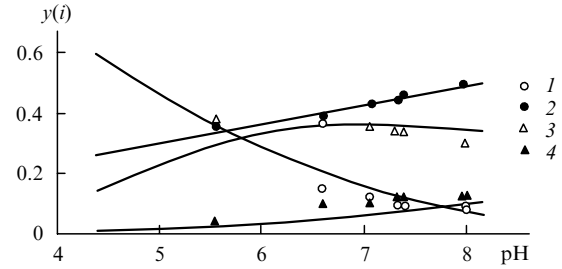

Figure 13. Experimental data (full and open circles and full and open triangles) and the predicted loadings of activated carbon (Chemivron F 100) with various species calculated using the SCT model (curves) .[32]
Species: SOH_2Cl (*1*), SOH (*2*), $(SOH_2) = CO_3$ (*3*) and $(SO_2) = Ca$ (*4*).

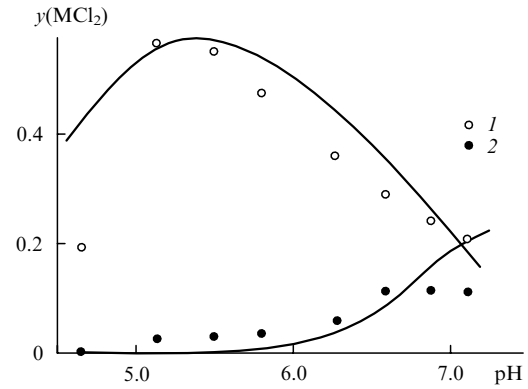

Figure 14. Experimental data (full and open circles) and the predicted loadings of the Purolite A 109 anion exchanger with copper chloride (*1*) and nickel chloride (*2*) calculated using the SCT model (curves).[34]
$c_0(CuCl_2) = c_0(HCl) = 5$, $c_0(NiCl_2) = 25$ mmol litre^{-1}.

VI. Application of the SCT model to nonlinear theory of multicomponent sorption dynamics and chromatography

The sorption equilibria characterise the fundamental thermodynamic properties of an ion exchange system.[58–68] The first step in solving problems of multicomponent sorption dynamics is to choose a model for multicomponent equilibria. Until recently the main difficulty consisted in the lack of models suitable for correct description of multicomponent equilibria in real sorption systems. However, in spite of the development of such models, the model of competitive multicomponent sorption proposed by Langmuir remains the most popular as yet. It should be considered as an idealised model, because the separation coefficients, α_{ij}, of components in such a nonlinear system of multicomponent equilibria are assumed to be constant and independent of the concentrations $\{X_1,..., X_n\}$ in the mixture of n ions (components).[58–66] In this case the exchange of equally charged ions is described by the following analytical relationships:[58–66]

$$X_i^{eq} = \frac{\alpha_{1i} y_i}{U} = y_i / \sum_{s=1}^{n} \alpha_{is} y_s \,,$$

$$U = \sum_{s=1}^{n} \alpha_{1s} y_s = \alpha_{1n} + \sum_{s=1}^{n-1} (\alpha_{1s} - \alpha_{1n}) y_s,$$

or

$$y_i^{eq} = \frac{\alpha_{i1} X_i}{V} = X_i / \sum_{s=1}^{n} \alpha_{si} X_s \,,$$

$$V = \sum_{s=1}^{n} \alpha_{s1} X_s = \alpha_{n1} + \sum_{s=1}^{n-1} (\alpha_{s1} - \alpha_{n1}) X_s, \qquad (66)$$

$$V = \frac{1}{U}.$$

Here α are the binary separation coefficients, (s,i) or (i,s), of the components in the n-component mixture

$$\alpha_{is} = \frac{y_i / X_i}{y_s / X_s},$$

$$\alpha_{is} = \frac{1}{\alpha_{si}}, \; i,s = 1, 2, ..., n, \qquad (67)$$

and y and X are the dimensionless concentrations of ions (i or s) in the sorbent phase and in solution, respectively.

The Langmuir model[67] of an idealised localised monolayer was proposed for a one-component system. This simple model is inapplicable to multicomponent mixtures; however, it was formally extended to multicomponent systems.[58–66, 68] Studies on the multicomponent Langmuir model and a number of related phenomenological models were thoroughly reviewed.[58–62, 65, 66] In particular, it was shown[58] that application of the mass action law relationships to the exchange of equally charged ions in a mixture [with consideration of the condition for electroneutrality (60)] allows the sorption equilibria to be formally described by Eqns (66). Analytical relationships (66) and (67) for the description of competitive multicomponent sorption equilibria have long been known.[58–66, 68] The symmetric and simple form of these relationships permits their use in not only numerical solution to problems of the sorption and ion exchange dynamics (for analysis, see Refs 58–66, 69–71) but also electrophoresis theory.[72]

In his review[64] Tondeur analysed theoretical concepts and problems of multicomponent sorption dynamics and chromatography. He pointed out three properties of the Langmuir model which have a significant impact on the modern view of competitive multicomponent sorption dynamics. These are the kinetic approach to the description of equilibria, the symmetric form of relationships (66) and (67) for the Langmuir isotherms and the implications beyond the scope of adsorption theory (see, *e.g.*, Ref. 72).

The basics of the kinetic approach leading to relationships (66) are as follows:[64] (1) an adsorption equilibrium is treated as equality of the sorption–desorption rates simultaneously for all components; (2) the desorption rate of each component is proportional to the relative coverage of the sorbent surface with the corresponding component; and (3) the adsorption rate is proportional to the product of two factors, *viz*., the concentration of a given component in the liquid phase and the fraction of uncovered sorbent surface.

Using relationships (19) and (60), it was shown[26] that the Langmuir competitive model (66) and (67) is naturally described as a particular case for the SCT model provided that two conditions are simultaneously met, namely, all exchanging counterions have equal charges and all SCT parameters $m(i,j)$ are equal to zero. The latter condition means that all the electrical double layers $|i\,j|$ have infinitely large electric capacities [see Eqn (18)]. Therefore, in the framework of the SCT model the Langmuir multicomponent sorption corresponds to the formation of surface complexes of various ions on the same Stern layer (at the surface near the reactive sites).[26] In this case, the generalised separation factors Q_j^i of the SCT model [see Eqn (19)] are transformed into the constants α_{is} [see Eqn (67)] of multicomponent Langmuir isotherms [see Eqn (66)].

The separation factors α_{ij} characterise the relative selectivity of the sorbent in binary exchange i/j. Namely, if $\alpha_{ij} > 1$, the component i has a higher affinity than the component j. The ith concentration distribution ratio

$$\gamma_i = \frac{y_i}{X_i}$$

characterises the affinity towards sorbent of each ith component of an n-component mixture. Using the concentration distribution ratios, an 'affinity sequence' of the species $(1 > 2 > ... > i > ... > j > ... > n)$ is determined, which is widely used in studies of the dynamics of multicomponent sorption systems. In the 'affinity sequence' the species are arranged in order of decreasing γ ($\gamma_i > \gamma_j$). Therefore, the species i (with smaller number in the affinity sequence) possesses a higher affinity towards the sorbent compared to the species j, because $\gamma_i > \gamma_j$ (or $\gamma_i/\gamma_j > 1$).

When the mixture composition $\{X_1, ..., X_n\}$ is varied, the position of the components in the 'affinity sequence' may remain unchanged (the so-called 'invariant affinity sequence') or it may vary (this is called 'inversion' or 'selectivity reversal').[51–53, 58, 60, 65] For the Langmuir isotherms (66) inversion is impossible because the separation factors are constants and the affinities of the mixture components remain unchanged. Using Eqns (49)–(51) of the SCT model, the effect of affinity inversion on the shape of multicomponent frontal and displacement chromatograms in the case of ion exchange in the $H^+/M_A^{2+}/M_B^{2+}/An^-$ (An^- is an anion) systems was studied.[51–53]

From the general theory of chromatography it follows that the behaviour of multicomponent concentration waves propagating in a sorption column is mainly governed by the set of adsorption properties of the mixture components which form the corresponding 'affinity sequence'.[51–53, 58–66] Multicomponent sorption equilibria are mainly responsible for the order, shape and velocities of propagation of such waves (examples can be found in the literature[46, 47, 51–53, 58–66]).

The sorption dynamics is described using, *e.g.*, the term 'effect of interference of mixture components' (see a monograph[58] and reviews[63–65]). Generally, the interference of species can arise as a consequence of various forms of their interaction. There are the equilibrium interference effects (mutual influence of species on the equilibrium interphase distributions) and the kinetic interference effects (mutual influence of species on the time taken to establish the equilibrium between the concentrations of a given component in the disperse and continuous phases in the presence of other components). The equilibrium and kinetic interference effects can arise simultaneously upon changes in the state of components

(molecules or ions) due to chemical reactions (*e.g.*, complexation).[58]

Successful solution to a number of problems of sorption dynamics and chromatography related to interference of species and propagation of multicomponent concentration waves became possible after introducing the fundamental coherence concept.[58, 73–76]

The multicomponent model of liquid chromatography is described by a system of nonlinear mass balance equations for each *i*th component of a mixture containing *n* components [58–66, 77]

$$\delta\frac{\alpha_0}{c_0}\frac{\partial y_i}{\partial t}+\frac{\partial X_i}{\partial t}+u\frac{\partial X_i}{\partial Z}=0, \tag{68}$$

$$\frac{\alpha_0}{c_0}\frac{\partial y_i}{\partial t}=\zeta_i[X_i-X_i^{eq}(y_i)], \tag{69a}$$

or

$$\frac{\partial y_i}{\partial t}=\beta_i[y_i^{eq}(X_i)-y_i]. \tag{69b}$$

Here $\delta\equiv(1-\varepsilon)/\varepsilon$ (ε is the layer porosity); t is time (in s); u is the flow rate of the mobile phase (in m s^{-1}); Z is the distance along the sorption layer (in m); and ζ_i and β_i are the kinetic coefficients (in s^{-1}) for the film diffusion kinetics and intraparticle diffusion kinetics of limiting stages, respectively.

The mass balance equations (68) and (69) make use of the dimensionless concentrations of the components in the liquid phase (X_i) and in the sorbent phase (y_i). The equations (69a) or (69b) represent phenomenological model equations of sorption kinetics for mixtures. They are based on the concept of linear driving forces,[78–82] according to which the rate of a kinetic process in the sorbent phase for a given component i is proportional to the corresponding kinetic coefficient ζ_i or β_i. In the case under study the effects of longitudinal dispersion are considered insignificant; therefore, the mass balance equation (68) ignores the longitudinal dispersion in the sorption layer of the column.

The system of equations (68) and (69a) [or (69b)] should be augmented with the system of equations for multicomponent sorption isotherms $y_i^{eq}(X)$ [or the system of reverse relationships $X_i^{eq}(y)$], which determines the equilibria between the concentrations of the mixture components in the mobile liquid phase (X_i) and in the sorbent phase (y_i^{eq}):

$$\begin{aligned} &y_i^{eq}(X)=[X_i^{eq}(y)]^{-1},\\ &y_i^{eq}(X)=y_i^{eq}(X_1, X_2, ..., X_n),\\ &X_i^{eq}(y)=X_i^{eq}(y, y_2, ..., y_n). \end{aligned} \tag{70}$$

To include the relationships of the SCT model of the type (19) for multicomponent ion exchange equilibria in these considerations, one should elaborate relevant computational methods, as well as procedures for solving the dynamic equations (68) and (69). Here, the condition for stoichiometry (equivalence of exchange) [see Eqns (60)] should be taken into account.

The SCT model was employed to describe the dynamics of simple (A/B) binary ion exchange systems in which the concentration fronts of the A/B exchange in the column are considered.[37–39, 43] The shape of the concentration profile, $X_A(Z,t)$, is governed by the shape of the binary isotherm $y^{eq}(X_A)$, which depends on the binary parameters $\{K_B^A; m(A,B)\}$ of the SCT model and on the counterion charge ratio, z_A/z_B (see Refs 26, 36–39, 50). The corresponding relationships of the SCT model for the (A/B) binary ion exchange systems have the form

$$\frac{y_A^{eq}(X_B^{eq}/z_B)^{2/z_B}}{y_B^{eq}(X_A^{eq}/z_A)^{2/z_A}}=K_B^A\exp[\ln 10(m_{AB}y_B^{eq})], \tag{71}$$

where $y_B^{eq}=1-y_A^{eq}$; $X_B^{eq}=1-X_A^{eq}$.

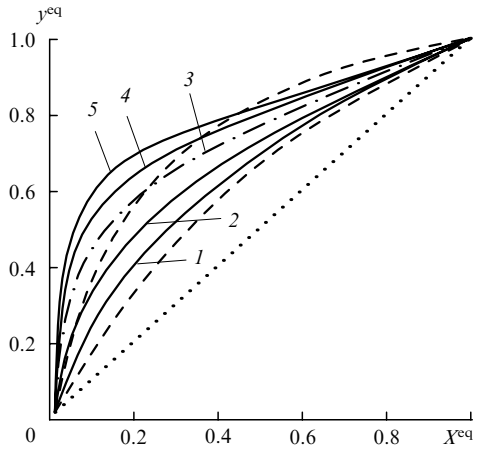

Figure 15. Binary A/B ion exchange isotherms at $z_A/z_B = 1$ and $K_B^A = 2$; $m(A,B) = 0.2$ (*1*), 0.5 (*2*), 1.0 (*3*), 1.5 (*4*) and 2 (*5*).[50]
Two Langmuir isotherms [$m(A,B) = 0$; $K_B^A = 2$ and 5] are shown by the dashed lines and the diagonal of the 'concentrational rectangle' is shown by the dotted line.

The binary exchange isotherms calculated at different values of the parameters $\{K_B^A; m(A,B)\}$ and different z_A/z_B ratios are shown in Figs 15 and 16 (see also Ref. 26). As can be seen, their curvatures and asymmetries depend on the joint effects of the two SCT parameters. The curvatures of the isotherms monotonically increase with an increase in the parameters $m(A,B)$ (see Fig. 15) and K_B^A (see Fig. 16). A comparison of the plots for the same values of the SCT parameters at different z_A/z_B ratios (dash-and-dotted curves in Figs 15 and 16) shows that the larger the z_A/z_B ratio, the higher the curvature of the isotherm.

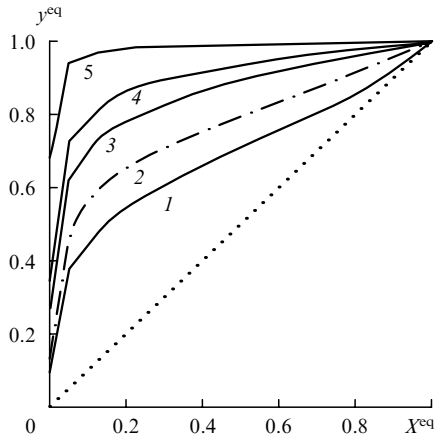

Figure 16. Binary A/B ion exchange isotherms at $z_A/z_B = 3/2$ and $m(A,B) = 1$; $K_B^A = 1$ (*1*), 2 (*2*), 5 (*3*), 10 (*4*) and 100 (*5*).[50]
The diagonal of the 'concentrational rectangle' is shown by the dotted line.

The SCT isotherms for equally charged counterions at $m = 0$ (dashed lines in Fig. 15) are reduced to the Langmuir isotherms. In the region of normalised concentrations ($0 < y^{eq}, X^{eq} < 1$), the binary Langmuir isotherms are symmetrical with respect to the back diagonal.[26] At the same time, the binary SCT isotherms for exchange of differently charged counterions ($z_A \neq z_B$) are essentially asymmetric (see, *e.g.*, inflection points in the plots in Fig. 16).

VII. Steady-state binary concentration distributions

The results of computer simulation were compared with the theoretical results obtained using analytical solutions of the mass balance equations (68) and (69) for binary (A/B) ion exchange and a steady-state concentration front X_A using relationship (71) at different values of the binary parameters $\{K_B^A; m(A,B)\}$.[37–39, 42, 43] This was done (for analytical solutions, including differently charged ions z_A, z_B and the case $m = 0$, see Refs 37 and 38) using an original code written for calculations of the dynamics of ion exchange in multicomponent systems. To test the code and evaluate the accuracy of the results obtained, the breakthrough binary output curves were calculated for both intraparticle (see Ref. 38) and film diffusion kinetics [37, 43] in various nonlinear ion exchange systems.

The mass balance equation (69a) for binary exchange of equally charged ions ($z_A = z_B$) was found to be integrable at $0 < m(A,B) < 1$ assuming film diffusion kinetics. The corresponding analytical solutions which describe steady-state concentration waves for A/B binary exchange were first reported recently.[42] In Fig. 17 we compare the results of numerical simulation and the theoretical results obtained using analytical solutions.[42,50] Shown are the output concentration distribution curves for a binary ion exchange system at different HETP values. The parameter HETP characterises the efficiency of the sorption layer in the column. It is related to the kinetic coefficient ζ (or β) by a simple algebraic relationship,[82] which in the case of film diffusion kinetics has the form

$$\mathrm{HETP} = \frac{2u(a_0/c_0)^2}{\zeta(1 + \delta a_0/c_0)^2}.$$

From the general theory of chromatography it follows that the higher the curvature of the SCT isotherms the greater the slope of the calculated profiles of the corresponding concentration fronts.[39, 42, 50] Clearly, the smaller the HETP value for the same isotherm the narrower the concentration front (*cf.* curves *1–3* in Fig. 17).

Agreement between the results obtained using analytical solutions and numerical calculations for steady-state concentration fronts in A/B binary exchange systems points, first, to high accuracy of the iterative numerical procedure employed for both ion exchange equilibria and component concentrations in a dynamic sorption process and, second, to successful implementation of the SCT model in computer simulation of the ion exchange dynamics in nonlinear multicomponent systems.

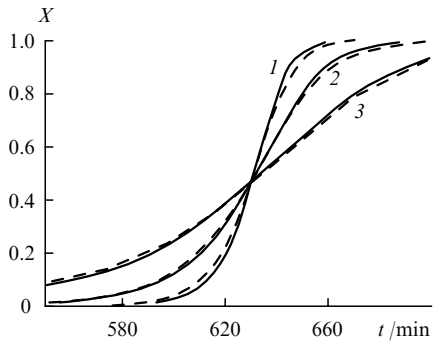

Figure 17. Steady-state breakthrough concentration distributions for binary exchange at the SCT model parameters $K_B^A = 2$, $m = 0.12$ and different heights of equivalent theoretical plate (HETP). HETP = 0.5 (*1*), 1 (*2*) and 2 cm (*3*).[42] Solid lines correspond to analytical solutions and dashed lines correspond to the results of numerical calculations; column length is $L = 30$ cm; film diffusion kinetics.

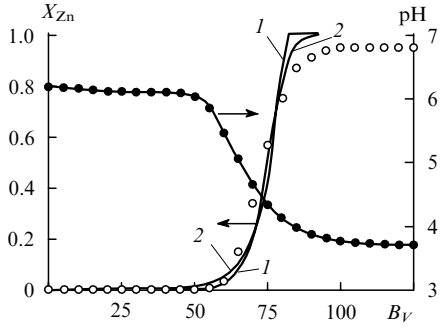

Figure 18. Breakthrough concentration dependences for the Zn^{2+}/Ca^{2+} exchange on the Purolite S 940 ion exchanger.[83]
Film diffusion kinetics (*1*) and intraparticle diffusion kinetics (*2*). Full and open circles stand for experimental data while the results of calculations are shown as solid curves; B_V is the number of column volumes.

Summing up, note that Kiefer [83] studied a number of binary systems containing metal ions (Cu^{2+}/Ca^{2+}, Ni^{2+}/Ca^{2+}, Zn^{2+}/Ca^{2+}, Cd^{2+}/Ca^{2+}) and compared the calculated and experimental output concentration curves obtained with columns filled with various Purolite resins (S 950, S 940, D 3342, D 3343). As an example in Fig. 18 we present the curves for the Zn^{2+}/Ca^{2+} ion exchange system on the Purolite S 940 resin. As can be seen, the results of numerical calculations are in agreement with experimental data.

VIII. Computerised description of ion exchange dynamics in multicomponent systems using the SCT model

Nonlinear mass balance equations for multicomponent systems are solved using the method of finite differences and an appropriate explicit numerical computational scheme (predictor–corrector).[84] To calculate various types of multicomponent equilibria based on the SCT model, iterative procedures have been developed.[37–40, 43, 44, 46–53]

Test calculations of multicomponent frontal and displacement chromatograms using an original code have been reported.[37–39, 50] As an example, in Figs 19 and 20 we present such chromatograms for Langmuir-type ion exchange systems [see Eqns (66)] containing equally charged ions (A, B, C, E) that form the 'affinity sequence' A > B > C > E in order of decreasing affinity towards sorbent. The chromatograms in Figs 19 and 20 were obtained for the ternary (A/B/C) and quaternary (A/B/C/E) exchange systems, respectively.

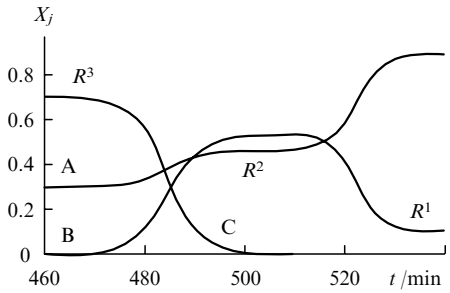

Figure 19. Steady-state concentration profiles in the output chromatogram for a ternary exchange system of equally charged ions A/B/C; column length $L = 100$ cm.[38, 39]
Concentration plateau: R^1 {0.9; 0.1; 0}, R^2 {0.466; 0.533; 0}, R^3 {0.3; 0.7; 0}.

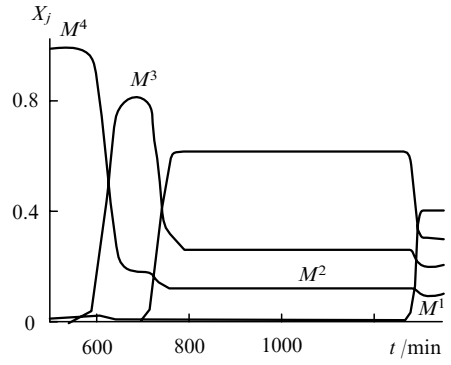

Figure 20. Steady-state concentration profiles in the output chromatogram for a quaternary exchange system of equally charged ions A/B/C/E; column length $L = 30$ cm.[38,39]
Concentration plateau: M^1 {0.4; 0.3; 0.2; 0.1}, M^2 {0; 0.616; 0.264; 0.118}, M^3 {0; 0; 0.885; 0.115}, M^4 {0; 0; 0; 1}.

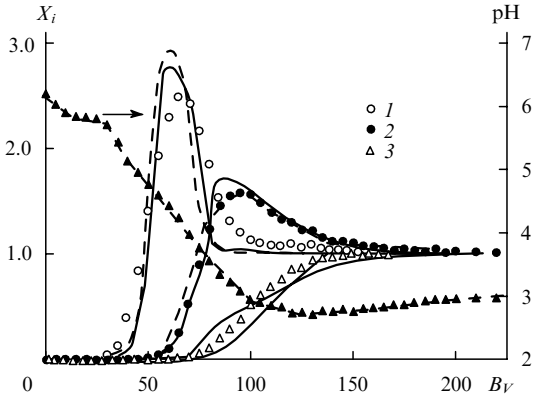

Figure 21. Experimental (full and open circles and open triangles) and calculated (curves) chromatograms for the $Cu^{2+}/Ni^{2+}/Zn^{2+}$ exchange on a column with the Purolite S 940 ion exchanger (originally in the Ca^{2+} form).[50,83]
The dashed lines correspond to film diffusion kinetics and the solid lines correspond to intraparticle diffusion kinetics; Ni (*1*), Zn (*2*) and Cu (*3*).

For multicomponent Langmuir systems the concentrations at the plateau R^s (see Fig. 19) or M^s (see Fig. 20) separating the concentration s-waves (s is the wave number; $s = 1, 2,...$) were calculated[37–41] analytically using the relations derived for the idealised equilibrium dynamic model (see Refs 58 and 74). In the steady-state regime the concentrations at the plateau on the left (R^s or M^s) and on the right (R^{s+1} or M^{s+1}) of a concentration s-wave depend exclusively on the equilibrium properties of the ion exchange systems and are determined by the parameters of multicomponent Langmuir isotherms [separation factors α_{ij}, see Eqn (67)].[58] Both analytical solutions and computer simulation of the dynamic process gave the same values of the concentrations $X_i^{(s)}$ at the multicomponent concentration plateau.

The results of numerical calculations of the concentration profiles shown in Figs 19 and 20 were compared with the results obtained using a number of analytical solutions[63,69–71] for multicomponent Langmuir systems assuming that all components of the mixture are characterised by the same dispersion parameters ($\beta_1 = \beta_2 = ... = \beta_m$ or $\zeta_1 = \zeta_2 = ... = \zeta_m$). Here, it is convenient to use a simple criterion derived from analytical solutions for the Langmuir isotherms.[63,69–71] At equal kinetic dispersion factors of the steady-state waves of the mixture components, relationships between the dimensionless and normalised concentration distributions (N_i^s) for each ith component of the multicomponent mixture are linear

$$N^s = N_i^s = \frac{X_i - X_i^s}{X_i^{s+1} - X_i^s} = N_j^s = \frac{X_j - X_j^s}{X_j^{s+1} - X_j^s}, \qquad (72)$$

$1 < i, ..., j < m$.

From this it follows that the variable concentration N^s in the multicomponent concentration s-wave is the same for all components. Similar linear relationships were obtained[37–39] in computer simulation of the R^sR^{s+1} and M^sM^{s+1} concentration waves (see Figs 19 and 20) in the Langmuir systems, which indicates a high accuracy of numerical calculations.

Column experiments[83] with a number of ternary and quaternary ion exchange systems showed that the corresponding equilibria are well described by the SCT model.[25–36] Multicomponent frontal and displacement chromatograms for the exchange of various metal ions (Cu^{2+}, Ni^{2+}, Zn^{2+}, Cd^{2+}, Ca^{2+}) were obtained. Experimental studies[83] and numerical calculations[37–39] were carried out for both film diffusion and intraparticle diffusion kinetics. As an example, Fig. 21 shows the experimental chromatographic data obtained for a quaternary exchange system and the corresponding results of numerical calculations. A comparison revealed reasonable agreement between the theory and experiment, especially taking into account the difficulties in obtaining such multicomponent chromatograms and their relative accuracy.

Thus, the above-mentioned method of numerical calculations of the ion exchange dynamics in multicomponent systems and the iterative procedure for calculations of multicomponent equilibria allows the SCT model to be successfully employed in studies of the dynamic behaviour of nonlinear multicomponent ion exchange systems.

IX. Modelling of the dynamics of ion exchange due to Lewis acid/Lewis base interactions, as applied to multicomponent systems

The approach to modelling of multicomponent ion exchange systems based on the SCT model (see Section VIII) was extended[49,51–53] to calculations of the dynamics of the sorption of metal salts involving coordination bonding due to the Lewis-base properties of amino groups of weak-electrolyte ion exchangers (see Section III). In this case, anions of these metal salts are also sorbed in solution near the surface of the weak-electrolyte ion exchanger. According to the SCT model, the distribution of counterions (M^{2+}) and co-ions (X^-) near the resin surface is shown in Fig. 2.[33,34]

To model this mechanism of sorption, the system of dynamic equations (68) and (69) must be augmented with the SCT equilibria (49)–(52). The corresponding SCT equilibria are calculated iteratively and the equilibrium ion concentrations (y_i^{eq}; X_i^{eq}) thus obtained are included in the computational scheme for the concentration distributions in the concentration wave moving through the column.[49,51–53]

Two examples illustrating the results of computer simulation of frontal and displacement chromatograms for the $H^+/M_A^{2+}/M_B^{2+}/An^-$ ($An^- = Cl^-$, SO_4^{2-}) ion exchange systems[43,49,51–53] are shown in Fig. 22. Since in this system the $H^+/M_A^{2+}/M_B^{2+}/An^-$ ion exchange due to the Lewis acid/Lewis base interaction is accompanied by sorption of metal salt anions, the conditions for electroneutrality in solution and in the sorbent phase have the form:[49,51–53]

$$X_{An^-} = X_A + X_B + X_H, \qquad (73a)$$

$$y_{An^-} = y_A + y_B + y_H. \qquad (73b)$$

Ion exchange systems for exchange of various metals (Cu^{2+}, Ni^{2+}, Zn^{2+}, Cd^{2+}) accompanied by sorption of various anions,

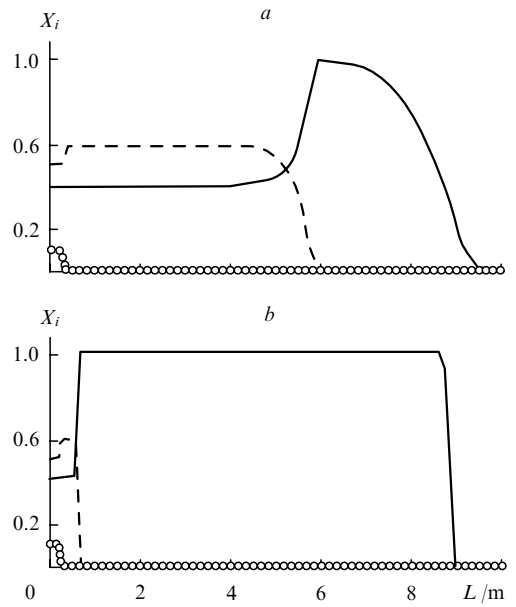

Figure 22. Calculated concentration (X_i) distributions along a chromatographic column filled with the Purolite A 109 weakly basic anion exchanger for the $H^+/Cu^{2+}/Ni^{2+}/An^{-1}$ exchange accompanied by sorption of Cl^- (*a*) and SO_4^{2-} anions (*b*).[51]
H^+ (open circles), Cu^{2+} (dashed lines) and Ni^{2+} (solid lines);
$c_0 = 0.3$ mol litre^{-1}, $X^0_H = 0.1$, $X^0_{Cu} = 0.5$, $X^0_{Ni} = 0.4$; $B_V = 7.4\,(a), 2\,(b)$.

namely, chloride ions (Cl^-, see Fig. 22 *a*) or sulfate ions (SO_4^{2-}, see Fig. 22 *b*) were studied.[49, 51–53] The anion distribution was calculated using Eqn (73a). Dynamic calculations were carried out using the experimental[33, 34] values of the binary SCT parameters $\{K^A_B; m(A,B)\}$.

The total concentration c_0 (in mol litre^{-1}) of the components, metal salt ions and protons at the column input was kept constant

$$z_A c^0_A + z_B c^0_B + z_H c^0_H = c_0$$

or in the dimensionless form

$$X^0_A + X^0_B + X^0_H = 1.$$

A dimensionless parameter commonly accepted in chromatography (see Fig. 22)

$$B_V = \frac{V_t}{V_0} = \frac{ut}{L}$$

denotes the number of the column volumes, V_0, which passed through the cross section of the column of length L, and characterises the elapsed time t from the start of the process. The B_V values (see Fig. 22) indicate that the dynamic displacement of metal ions accompanied by the sorption of Cl^- anion is more than three times slower than an analogous process accompanied by the sorption of SO_4^{2-} anions. Indeed, Figs 22 *a* and 22 *b* show that displacement of metal ions (both Ni^{2+} and Cu^{2+}) is much more efficient in the presence of divalent SO_4^{2-} anions compared to monovalent Cl^- anions. The influence of the inversion effects on the dynamic behaviour of various related systems for two types of weakly basic anion exchangers has been considered.[51–53]

X. Dynamics of ion exchange in multicomponent systems with allowance for ion complexation in the mobile liquid phase

Using the SCT model, relationships describing chemical reactions in the liquid phase can be included in calculations of multicomponent equilibria in a relatively simple way.[26, 32] However, in this case the theory of chromatography requires that the nonlinear multicomponent system of dynamic mass balance equations be transformed and represented in the form:[44, 46, 47, 50]

$$\delta \frac{\alpha_0}{c_0} \frac{\partial y_i}{\partial t} + \frac{\partial X_{\text{sum}\,i}}{\partial t} + u \frac{\partial X_{\text{sum}\,i}}{\partial Z} = 0,\ i = 1, 2, \ldots . \tag{74}$$

Now the total concentration of each component, $X_{\text{sum}\,i}$, includes not only the concentration of the ion i in the liquid phase but also the corresponding fractions of this component in various compounds formed as a result of chemical reactions. This approach to simulation of the dynamics of various ion exchange systems with allowance for chemical reactions was employed[44–50] in calculations of the dynamics of the $H^+/M^{2+}_A/M^{2+}_B$ ion exchange with inclusion of complexation reactions.

Let us calculate various ion concentrations taking the $H^+/M^{2+}_A/M^{2+}_B$ exchange with inclusion of complexation reactions in the mobile (liquid) phase of a chromatographic column as an example. Multicomponent equilibria in these systems are described by the SCT model (see Section II) while the accompanying complexation reactions in the mobile (liquid) phase of the column are described by relationships related to the mass action law.

For instance, the ion exchange $H^+/Ni^{2+}/Co^{2+}$ ('affinity sequence' H > Ni > Co) in the presence of citrate ion (Cit^{3-}) as a complex-forming agent can be calculated using the following system of relationships:[44, 46, 47, 50]

$$\begin{aligned}
&K_1 = X_1X_4, && K_2 = X_1X_7/X_6,\\
&K_3 = X_1X_8/X_7, && K_4 = X_1X_5/X_8,\\
&K_5 = X_3X_5/X_{14}, && K_6 = X_2X_5/X_9,\\
&K_7 = X_2X_5^2/X_{10}, && K_8 = X_2X_8/X_{11},\\
&K_9 = X_2X_7/X_{12}, && K_{10} = X_5X_{11}/X_{13},\\
&K_{11} = X_3X_8/X_{15}, && K_{12} = X_3X_7/X_{16}.
\end{aligned} \tag{75}$$

Here the constant parameters are $K_1 = 10^{-14}$ [the dissociation constant of water, in (mol litre^{-1})^2] and the reaction constants $K_2 - K_{12}$ listed in Table 2; X_i are the dimensionless concentrations of the ions ($i = 1-3$) and the components formed as a result of chemical reactions ($i = 6-16$):

i	Species	i	Species
1	H^+	9	$NiCit^-$
2	Ni^{2+}	10	$NiCit_2^{4-}$
3	Co^{2+}	11	$NiHCit$
4	OH^-	12	NiH_2Cit^+
5	Cit^{3-}	13	$NiHCit_2^{3-}$
6	H_3Cit	14	$CoCit^-$
7	H_2Cit^-	15	$CoHCit$
8	$HCit^{2-}$	16	CoH_2Cit^+

In accordance with the mass conservation law we have

$$X_0(\text{Cit}) = X_5 + X_6 + X_7 + X_8 + X_9 + 2X_{10} + X_{11} + X_{12} + 2X_{13} + X_{14} + X_{15} + X_{16}. \tag{76}$$

This equality describes the constancy of the total amount of the complex-forming agent (Cit^{3-}) in solution.

As usual, in describing the ion exchange we have to take into account the relations of equivalence for the concentrations of free ions ($H^+/Ni^{2+}/Co^{2+}$) in the ion exchanger and in solution:

$$y_1 + y_2 + y_3 = 1, \tag{77a}$$

$$X_1 + X_2 + X_3 = 1. \tag{77b}$$

Table 2. Parameters for calculations of ion exchange dynamics in multicomponent systems with inclusion of exchange equilibria described in the framework of the SCT model and complexation reactions.[46, 47, 50]

System No.	Purolite resin	Ion exchange	Complex-forming agents	Reaction constants [a]	Binary SCT parameters	
					$\log K_j^H$	$m(H,j)$
1	S 950	$H^+/Ni^{2+}/Ca^{2+}$	$H_2BO_3^-$, $SO_3NH_2^-$, Cl^-	K_1-K_{12}	3.03	3.31
					2.81	4.81
2	S 950	$H^+/Ni^{2+}/Ca^{2+}$	$H_2BO_3^-$, SO_4^{2-}, Cl^-	K_1-K_{12}	3.03	3.31
					2.81	4.81
3	S 940	$H^+/Cu^{2+}/Ca^{2+}$	SO_4^{2-}	K_1-K_4	1.44	2.15
					3.37	5.62
4	S 940	$H^+/Cd^{2+}/Ca^{2+}$	NH_3, NO_3^-	K_1-K_{12}	1.65	3.28
					3.37	5.62
5	S 940	$H^+/Zn^{2+}/Ca^{2+}$	NH_3, Cl^-	K_1-K_{12}	1.96	2.02
					3.37	5.62
6	S 950	$H^+/Ni^{2+}/Zn^{2+}$	Cit^{3-}	K_1-K_{12}	3.03	3.31
					2.3	1.18
7	S 950	$H^+/Ni^{2+}/Na^+$	Cit^{3-}	K_1-K_{10}	3.03	3.31
					1.95	1.82
8	S 940	$H^+/Co^{2+}/Na^+$	Cit^{3-}	K_1-K_8	3.11	2.22
					1.34	3.71
9	S 940	$H^+/Zn^{2+}/Co^{2+}$	Cit^{3-}	K_1-K_{11}	1.96	2.02
					3.11	2.22
10	S 950	$H^+/Ni^{2+}/Co^{2+}$	Cit^{3-}	K_1-K_{12}	3.03	3.31
					2.96	2.11

[a] $K_2 = 102$, $K_3 = 4.4$, $K_4 = 6.3 \times 10^6$, $K_5 = 6.2$, $K_6 = 1.26$, $K_7 = 1.66$, $K_8 = 50.1$, $K_9 = 4 \times 10^{-3}$, $K_{10} = 0.008$, $K_{11} = 831$.

In this case the number of the differential mass balance equations (74) for the concentrations $X_{sum\,1}(H^+)$, $X_{sum\,2}(Ni^{2+})$ and $X_{sum\,3}(Co^{2+})$ equals three ($n = 3$):

$$X_{sum\,1}(H^+) = X_1 - X_4 + 3X_6 + 2X_7 + X_8 + X_{11} + 2X_{12} + X_{13} + X_{15} + 2X_{16}, \quad (78a)$$

$$X_{sum\,2}(Ni^{2+}) = X_2 + X_9 + X_{10} + X_{11} + X_{12} + X_{13}, \quad (78b)$$

$$X_{sum\,3}(Co^{2+}) = X_3 + X_{14} + X_{15} + X_{16}. \quad (78c)$$

Numerical simulation of the dynamics of such ion exchange systems was carried out using the experimental[83] values of the binary SCT parameters $\{K_B^A; m(A,B)\}$ obtained for various Purolite resins. The corresponding parameters of the Purolite S 940 and S 950 resins are listed in Table 2. The complexation constants K_i included in relationships (75) can be found in the literature (see, *e.g.*, Ref. 54). To illustrate the large differences between the values of these constants (orders of magnitude), the corresponding data are listed in Table 2.

The nonlinear multicomponent system of dynamic mass balance equations (74)–(78) was numerically solved by the method of finite differences. In this case, in addition to the numerical schemes based on the SCT equilibria (19), iterative procedures for solving the Eqns (75) and (76) describing the complexation reactions with allowance for the relations of equivalence (77) must be included. A software package for calculations of the dynamics of various multicomponent ion exchange systems including quinary systems has been created.[44–48, 50] Some examples are given in Table 2.

Based on the models elaborated, the propagation of n-component concentration waves formed in the sorption field of the column was calculated. A number of calculated output frontal-displacement curves for the ion exchange sorption and regeneration in two ion exchange systems are presented in Figs 23 and 24 as examples. Here, shown are the distributions for the exchange of metal ions (A^{2+}/B^{2+}); the concentration of the third exchanging ion (H^+) is low and the corresponding curves are therefore omitted.

The multicomponent output frontal and displacement chromatograms presented in Fig. 23 in the pseudo-3D space $\{X_i, t, s\}$ are the same as those given in two dimensions in Fig. 24 *c*. The distributions in Fig. 23 clearly illustrate the relative positions of the output concentration curves during the sorption and regeneration processes, obtained for columns of different length L_s. The s values ($s = 1, 2, 3, 4$) for columns of different length $L_{1,2,3,4}$ (L_s/HETP = 30 or 60) are plotted on the y axis directed 'perpendicular' to the plane of Fig. 23.

In Fig. 24 *a*, *b* we present the calculated output concentration curves obtained for the ion exchange systems Nos 1 and 8 (see Table 2) with allowance for the effect of chemical reactions.[44–48, 50] To compare the dynamic behaviour of different

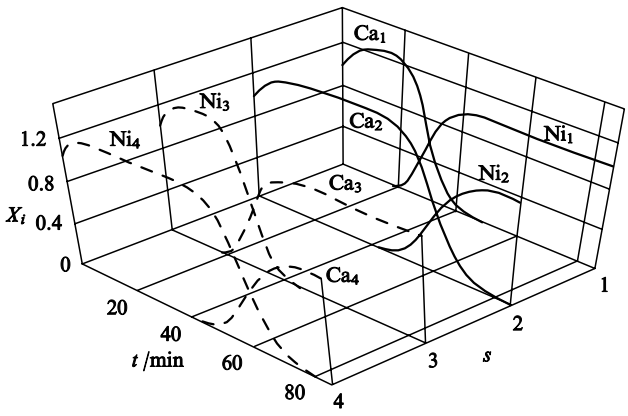

Figure 23. Output concentration distributions $X_i(t)$ shown in the $\{X_i, t, s\}$ space for $H^+/Ni^{2+}/Ca^{2+}$ exchange; column lengths are $L_{1,3} = 30$ HETP and $L_{2,4} = 60$ HETP.[46, 50]
$Ni_{1,2}/Ca_{1,2}$ sorption (solid lines), $L_{1,2}$; $Ca_{3,4}/Ni_{3,4}$ regeneration (dashed lines), $L_{3,4}$.

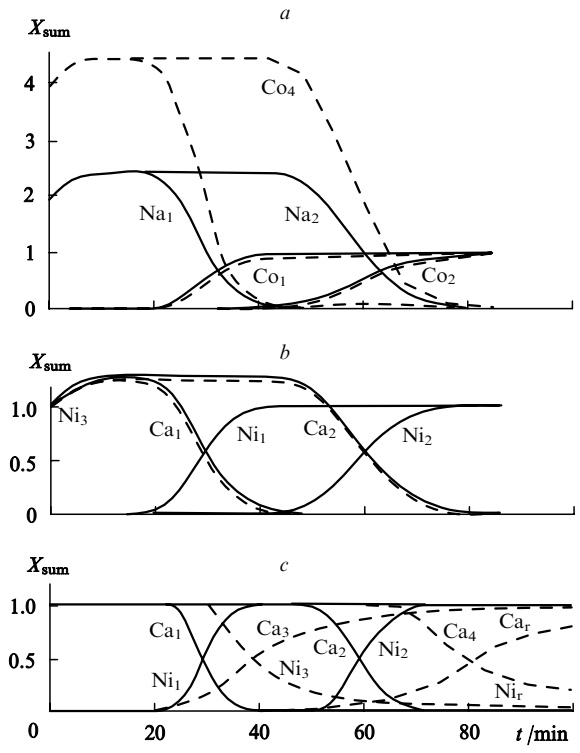

Figure 24. Calculated concentration distributions for $H^+/A^{2+}/B^{2+}$ ion exchange on columns of different length L_s.[46,47]
$H^+/Co^{2+}/Na^+$ exchange with inclusion of chemical reactions (*a*); $H^+/Ni^{2+}/Ca^{2+}$ exchange with inclusion of chemical reactions (*b*); and $H^+/Ni^{2+}/Ca^{2+}$ exchange ignoring chemical reactions (*c*); solid lines describe the ion exchange (B/A) sorption of the mixture, $X_i(t)$; dashed lines describe the ion exchange regeneration (A/B) of the column, $X_{ir}(t)$ (Ca_r, Ni_r).

ion exchange systems, Fig. 24 *c* also shows the calculated output curves obtained for the former system in the absence of complexation reactions.

A comparison reveals essential changes in the character of the output concentration curves for the same system caused by the effect of complexation reaction. The output curves of both sorption and regeneration processes obtained with inclusion of complexation exhibit no long 'tails' (see Fig. 24 *a*, *b*); the shapes of the output curves in Fig. 24 *b* obey an identical pattern and the corresponding solid and dashed lines nearly match one another.

In the case of conventional ion exchange the regeneration processes are characterised by the output concentration curves with very long 'tails' (see Fig. 24 *c*), which significantly slow down the regeneration. Besides, both sorption and regeneration accompanied by complexation proceed at higher rates and the output concentrations of the displaced ions are much higher. Therefore, the allowance for chemical reactions permits a more efficient regeneration of ion exchange columns.

XI. Conclusion

The surface complexation theory used for calculations of multicomponent equilibria has been developed during the last decade.[25–36] It is based on a relatively simple model for the arrangement of ions, which are assumed to be located in ordered Stern layers extended parallel to the planar sorbent surface.

The description of arbitrary equilibria in the framework of the SCT model is based on the concept of generalised separation factors, which can be determined using experimental data on binary exchange. The dependence of these coefficients on the sorbent composition provides valuable information on the binary equilibria. An individual sorption equilibrium can be characterised by two constant parameters of the SCT model, $\{K_{i+1}, m(i,i+1)\}$, which are independent of the pH value or the ionic strength of the solution (liquid phase).[26,30,31,36] These parameters also remain constant in arbitrary multicomponent systems for which simple (binary) equilibria can be calculated for a wide range of experimental conditions.[26–36] The SCT model treats multicomponent equilibria as a kind of superposition of several simple equilibria and allows them to be calculated using the parameters of binary subsystems.[26–36] Arbitrary chemical equilibria in the liquid phase with inclusion of dissociation, association or complexation phenomena can be taken into account in a relatively simple manner for both multicomponent equilibria [30,31,36] and dynamic systems.[44–48,50]

One field of application of the SCT model is the prediction of multicomponent ion exchange kinetics. The potentialities of the approach were demonstrated in calculations of the film diffusion kinetics where this method for the description of equilibria was implemented in solving the Nernst–Planck equations.[85,86]

Sorption equilibria in ternary and quaternary systems with strong- and weak-electrolyte ion exchangers can be predicted very accurately even with inclusion of chemical reactions. The method was incorporated into commercially available software for the design of demineralisers in ultrapure water production.[87]

The theory of formation of surface complexes (or the surface complexation theory, SCT model) can be applied with ease to calculations of the performance of sorption filters. It has been implemented in simple approximate equilibrium calculations using an idealised model in which the filter is represented by a series of stirred tanks (layer-by-layer calculation technique). This approach was shown [88] to be suitable for quite correct prediction of, *e.g.*, combined softening and dealkalisation of water with weakly acid ion exchangers.

The SCT model has also been incorporated into more sophisticated procedures for calculations of dynamic systems based on the theory of multicomponent sorption dynamics and chromatography. This field of application of the SCT approach seems to be quite promising because no appropriate models for multicomponent equilibria suitable for the description of the properties of real sorbents (ion exchangers) were proposed until recently.[37–53]

In a particular case where the SCT parameters $m(i,i+1)$ of all binary exchanges equal zero, the SCT equilibrium relationships are reduced to the well-known multicomponent Langmuir isotherms. This allows the accuracy and correctness of the methods elaborated for solving problems of multicomponent sorption dynamics to be evaluated.[37–42]

Currently, evaluation of the dynamic behaviour of nonlinear multicomponent ion exchange systems is based on the results of calculations of the output column concentration distributions for various ion exchangers.[37–53] Newly developed iterative procedures for calculations of multicomponent equilibria and new software permit successful implementation of the SCT model in the computational schemes for calculations of the dynamic behaviour of nonlinear multicomponent ion exchange systems.

In spite of obvious simplifications of the SCT model, the results obtained demonstrate the efficiency of this method in the calculations of multispecies equilibria and the kinetics and dynamics of sorption in multicomponent systems. The SCT approach can be used in both basic research and applied (in particular, engineering) studies.

Calculations of the propagation of multicomponent concentration waves in the sorption fields of ion exchange columns involve computer simulation. To facilitate perception of the complex dynamics of ion exchange, a kind of computer visualisation is used, namely, animation of the dynamic processes occurring in the chromatographic column.[48–53]

The results presented in this review have been obtained with financial support from the Deutsche Forschungsgemeinschaft (DFG, joint German–Russian Project Nos 463 RUS 113/596/0-1 (R) and 436 RUS 113/83), Deutsche Akademische Aus-

TauschDienst (DAAD, Project No. 325 sm) and the NATO Foundation (Project No. SA 12-2-02, CRG.971709).

References

1. W Stumm *Chemistry of the Solid— Water Interface* (New York: Wiley, 1992)
2. H V Helmholtz *Wiss. Abh. Phys. Techn.* **1** 925 (1879)
3. C Gouy *J. Phys.* **9** 457 (1910)
4. D I Chapman *Philos. Mag.* **25** 45 (1913)
5. O Stern *Z. Elektrochem.* **30** 508 (1924)
6. R O James, T W Healy *J. Colloid Interface Sci.* **40** 42 (1972)
7. R O James, T W Healy *J. Colloid Interface Sci.* **40** 53 (1972)
8. R O James, T W Healy *J. Colloid Interface Sci.* **40** 65 (1972)
9. J W Bowden, M D Bolland, A M Posner J P Quirk *Nature Phys. Sci.* **245** 81 (1973)
10. M A Anderson, J F Ferguson, J Gavis *J. Colloid Interface Sci.* **54** 391 (1976)
11. D E Yates, S Levine, T W Healy *J. Chem. Soc., Faraday Trans. 1* 1807 (1974)
12. J A Davis, R O James, J O Leckie *J. Colloid Interface Sci.* **63** 480 (1978)
13. W Stumm, H Hohl, F Dalang *Croat. Chem. Acta* **48** 491 (1972)
14. R Kummert, W Stumm *J. Colloid Interface Sci.* **7** 373 (1980)
15. W Stumm, R Kummert, L Sigg *Croat. Chem. Acta* **53** 291 (1980)
16. J A Davis, J O Leckie *J. Colloid Interface Sci.* **67** 90 (1978)
17. P W Schindler, B Furst, R Dick, P Wolf *J. Colloid Interface Sci.* **55** 281 (1976)
18. P R Anderson, M M Benjamin, in *Chemical Modelling of Aqueous Systems* (Eds D C Melchior, R I Basset) (Washington, DC: American Chemical Society, 1990) p. 272
19. L Sigg, Ph.D. Thesis, Swiss National Technical University, Zürich, 1979
20. L S Balistrieri, T T Chao *Geochim. Cosmochim. Acta* **54** 739 (1990)
21. K F Hayes, A L Roe, G E Brown *Science* **23** 783 (1987)
22. D E Yates, Ph.D. Thesis, University of Melbourne, Melbourne, 1973
23. K F Hayes, J O Leckie *J. Colloid Interface Sci.* **115** 563 (1987)
24. F F Kantwell *Ion Exch. Solvent Extr.* **9** 339 (1985)
25. J Horst, Ph.D. Thesis, University and Research Centre of Karlsruhe, Karlsruhe, 1988
26. W H Höll, J Horst, M Franzreb, S H Eberle, in *Ion Exchange and Solvent Extraction, a Series of Advances* Vol. 11 (Eds J Marinsky, Y Marcus) (New York, Basel, Hong Kong: Marcel Dekker, 1993) p. 151
27. J Horst, W H Höll , S H Eberle *React. Polym.* **13** 209 (1990)
28. W H Höll, J Horst, M Wernet *React. Polym.* **14** 251 (1991)
29. W H Höll, J Horst, M Franzreb *React. Polym.* **19** 123 (1993)
30. J Horst, W H Höll *J. Colloid Interface Sci.* **195** 250 (1997)
31. W H Höll, J Horst, in *Encyclopedia of Separation Science* Vol. 2 (London: Academic Press, 2001) p. 1640
32. W H Höll *Water Sci. Technol.* **35** 287 (1997)
33. C Stöhr, Ph.D. Thesis, Karlsruhe University and Research Centre, Karlsruhe, 2001
34. W H Höll, C Stöhr *React. Funct. Polym.* **49** 117 (2001)
35. W H Höll, R Kiefer *Ind. Eng. Chem. Res.* **40** 4570 (2001)
36. W H Höll, J Horst, in *Sorbtsionnye i Khromatograficheskie Protsessy* (Sorptional and Chromatographic Processes) Vol. 1, No. 2 (Voronezh: Voronezh State University, 2001) p. 145
37. A I Kalinitchev, W H Höll, R Kifer *Zh. Fiz. Khim.* **73** 1627 (1999) [a]
38. A I Kalinitchev, W H Höll *Teor. Prak. Sorb.Prots.* (25) 44 (1999)
39. A I Kalinitchev, W H Höll *Zh. Fiz. Khim.* **74** 466 (2000) [a]
40. A I Kalinitchev, in *Problemy Khimii i Khimicheskoi Tekhnologii. Trudy VI Regional'noi Konferentsii, Voronezh 1998* (The Problems of Chemistry and Chemical Technology. Proceedings of the VIth Regional Conference, Voronezh 1998) p. T1–98
41. A I Kalinitchev, W H Höll, in *Ion Exchange at the Millennium. Proceedings of IEX 2000* (Ed. J Greig) (London: Imperial College Press, 2000) p. 201
42. A I Kalinitchev *Zh. Fiz. Khim.* **74** 1673 (2000) [a]
43. A I Kalinitchev, W H Höll, in *Trudy IX Mezhdunarodnoi Konferentsii 'Sovremennoe Sostoyanie i Perspektivy Razvitiya Teorii Adsorbtsii' (K 100-letiyu Akademika M M Dubinina)* [Proceedings of the IXth International Conference 'Modern State and Prospects for Development of Adsorption Theory (Academician M M Dubinin 100 Year Anniversary)] (Moscow: Institute of Physical Chemistry, Russian Academy of Sciences, 2001) p. 270
44. A I Kalinitchev, W H Höll, in *Sorbtsionnye i Khromatograficheskie Protsessy* (Sorptional and Chromatographic Processes) (Voronezh: Voronezh State University, 2001) Vol. 1, No. 2, p. 157
45. W H Höll, A I Kalinitchev, in *Materialy Konferentsii 'FaGran-2002' Voronezh, 2002* (Proceedings of Conference 'FaGran-2002',Voronezh, 2002) p. 26
46. A I Kalinitchev, W H Höll *Zh. Fiz. Khim.* **77** 70 (2003) [a]
47. A I Kalinitchev, W H Höll *Teor. Osnovy Khim. Tekhnol.* **37** 278 (2003)
48. A I Kalinitchev, W H Höll, in *The XYIth European Chemistry at Interfaces Conference. Book of Abstracts, Vladimir, 2003* p. 21
49. A I Kalinitchev, W H Höll, in *ICIE'03 Proceedings of International Ion Exchange Conference* (Kanazawa: Kanazawa University, 2003)
50. A I Kalinitchev, in *100 Let Khromatografii* (100 Years of Chromatography) (Ed. B A Rudenko) (Moscow: Nauka, 2003) p. 337
51. A I Kalinitchev, W H Höll *Teor. Osnovy Khim. Tekhnol.* **38** 304 (2004) [b]
52. A I Kalinitchev, W H Höll *Zh. Fiz. Khim.* **78** 1118 (2004) [a]
53. A I Kalinitchev, W H Höll, in *Ion Exchange Technology for Today and Tomorrow. Proceedings of IEX 2004* (London: Imperial College Press, 2004) p. 349
54. R M Smith, A E Martell *Critical Stability Constants* (New York: Plenum, 1976)
55. S H Eberle *Report KfK 3930UF* (Karlsruhe: Karlsruhe Nuclear Research Centre, 1986)
56. W H Höll, in *Ion Exchange Developments and Applications (Proceedings of IEX 96)* (Ed. J Greig) (Cambridge: Royal Society of Chemistry, 1996) p. 404
57. J A Marinsky *J. Chem. Phys.* **86** 3318 (1982)
58. G Klein, F Helfferich *Multicomponent Chromatography. Theory of Interference* (New York: Marcel Dekker, 1970)
59. G Klein, D Tondeur, T Vermeulen *Ind. Eng. Chem. Fund.* **6** 339 (1967)
60. A E Rodrigues, D Tondeur (Eds) *Percolation Process: Theory and Applications* (The Hague, Sijthoff and Noordhoff, 1981)
61. D M Ruthven *Principles of Adsorptions and Adsorption Processes* (New York: Wiley, 1984)
62. H Sontheimer, J C Crittenden, R S Summers *Activated Carbon for Water Treatment* (Karlsruhe: Druckerei G Braun, 1988)
63. A Kalinitchev *Ind. Eng. Chem. Res.* **34** 2625 (1995)
64. D Tondeur *Ind. Eng. Chem. Res.* **34** 2782 (1995)
65. A I Kalinitchev *Usp. Khim.* **65** 103 (1996) [*Russ. Chem. Rev.* **65** 95 (1996)
66. C Tien *Adsorption Calculations and Modelling* (Boston, London, Oxford, Singapore, Sydney, Toronto, Wellington: Butterworth-Heineman, 1998)
67. I Langmiur *J. Am. Chem. Soc.* **40** 1361 (1918)
68. M M Dubinin *Fiziko-Khimicheskie Osnovy Sorbtsionnoi Tekhniki* (Physicochemical Foundations of Sorption Equipment) (Moscow: ONTI, 1935)
69. A I Kalinitchev *Zh. Fiz. Khim.* **59** 2000 (1985) [a]
70. A I Kalinitchev *Teor. Osnovy Khim. Tekhnol.* **20** 532 (1986) [b]
71. A I Kalinitchev *Zh. Fiz. Khim.* **68** 1658 (1994) [a]
72. V G Babskii, M Yu Zhukov, V I Yudovich *Matematicheskaya Teoriya Elektroforeza* (Mathematical Theory of Electrophoresis) (Kiev: Naukova Dumka, 1983)
73. F G Helfferich, in *Migration and Fate of Pollutants in Soils and Subsoils* (Eds D Petruzzelli, F G Helfferich) (Berlin, Heidelberg: Springer, 1993)
74. F Helfferich *New Directions in Sorption Technology* (Eds G Keller, R Yang) (Boston: Butterworth, 1989)

75. F G Helfferich *AIChE Symp. Ser.* **80** 1 (1984)
76. F G Helfferich *Chem. Eng. Commun.* **44** 275 (1986)
77. V V Rachinskii *Vvedenie v Obshchuyu Teoriyu Dinamiki Sorbtsii i Khromatografii* (Introduction to General Theory of Dynamics of Sorption and Chromatography) (Moscow: Nauka, 1964)
78. E Glueckauf, in *Ion Exchange and its Application* (London: Society of Chemical Industry, 1954) p. 34
79. E Glueckauf, J I Coates *J. Chem. Soc.* **149** 1315 (1947)
80. E Glueckauf *Trans. Faraday Soc.* **51** 1540 (1955)
81. T Vermeulen, G Klein, N K Hiester, in *Perry's Chemical Engineering Handbook* (Eds R H Perry, C H Chilton) (New York: McGraw-Hill, 1973) p. 11
82. F G Helfferich *Ion Exchange* (New York: McGraw-Hill, 1962)
83. R Kiefer, Ph.D. Thesis, University and Research Centre of Karlsruhe, Karlsruhe, 1999
84. A A Samarskii, A V Gulin *Chislennye Metody* (Numerical Methods) (Moscow: Nauka, 1989)
85. M Franzreb, W H Höll, H Sontheimer *React. Polym.* **21** 117 (1993)
86. M Franzreb, W H Höll, S H Eberle *Ind. Eng. Chem. Res.* **34** 2670 (1995)
87. V Chowdiah, G Foutch, in *Ion Exchange Developments and Applications (Proceedings IEX 96)* (Ed. J Greig) (Cambridge: Royal Society of Chemistry, 1996) p. 10
88. W H Höll, J Horst, M Franzreb, in *New Developments in Ion Exchange. Proceedings of the International Conference on Ion Exchange ICIE 91* (Eds M Abe, T Kataoka, T Suzuki) (Tokyo: Kodansha, 1991) p. 279

[a] — *Russ. J. Phys. Chem. (Engl. Transl.)*
[b] — *Theor. Found. Chem. Eng. (Engl. Transl.)*

Russian Chemical Reviews **73** (4) 371 – 400 (2004) © 2004 Russian Academy of Sciences and Turpion Ltd

DOI 10.1070/RC2004v073n04ABEH000811

Lead difluoride and related systems

I I Buchinskaya, P P Fedorov

Contents

I.	Introduction	371
II.	Properties of lead difluoride	372
III.	Systems $PbF_2 - MF$	373
IV.	Systems $PbF_2 - MF_2$	375
V.	Systems $PbF_2 - MF_3$	378
VI.	Systems $PbF_2 - MF_4$	382
VII.	Systems $PbF_2 - MF_5$	383
VIII.	Ternary systems involving PbF_2	384
IX.	Other compounds involving fluorine and divalent lead	388
X.	Characteristic features of phase diagrams involving PbF_2	388
XI.	Conclusion	396

Abstract. Properties of lead difluoride are considered. Phase equilibria in $PbF_2 - MF_n$ systems ($n = 1 - 5$) and data on compounds and solid solutions formed in these systems are analysed. The characteristic features of phase diagrams of systems involving lead difluoride are discussed. Composites of PbF_2 with other inorganic compounds hold promise as a basis for the design of new functional materials. The bibliography includes 331 references.

I. Introduction

In 1834, M Faraday discovered [1] that PbF_2 has high electrical conductivity when heated. This was the second (after silver sulfide) example of a solid electrolyte and the first example of anion (fluoride ion) conductors. Later on, both lead difluoride and fluoride ion conductors, *viz*., solid solutions, composite materials and glasses based on lead difluoride, were the subjects of extensive studies (see, for example, Refs 2 – 12). Of known chemical compounds, $PbSnF_4$ (see Refs 10 and 12) and non-stoichiometric phases in the $PbF_2 - KF$ system have the highest fluoride ion conductivity.

The high-temperature cubic modification of lead difluoride crystallises in one of the simplest structure types, the so-called fluorite structure type.[2] The phase transition discovered by Faraday appeared to be an inherent characteristic of all compounds with the fluorite structure (this transition is also known as the Faraday transition). This transition involves mass displacements of anions from their crystallographic positions, *viz*., disordering of the anion sublattice, without a change in symmetry (sometimes, this phenomenon is referred to as sublattice melting) resulting in the appearance of high ionic conductivity. This phenomenon attracts considerable attention and is studied both experimentally and theoretically.[13 – 32] Apparently, this disorder is responsible for the formation of wide regions of heterovalent solid solutions based on the fluorite modification of lead fluoride.

Lead difluoride has a relatively low melting point, due to which it is used as a component of fluxes for growing single crystals using the flux technique.[33 – 36] Examples are $PbF_2 - PbO$, $PbF_2 - V_2O_5$, $PbF_2 - Bi_2O_3$, $PbF_2 - B_2O_3$ and more complex systems.

Certain eutectic composites involving lead difluoride hold promise as operating materials for nuclear reactors (breeders), because they are characterised by good fusibility and high density.[37] Due to low affinity for fluorine, lead difluoride can be used as a fluorinating agent. Single crystals of refractory fluorides (CaF_2, LaF_3, *etc*.) are grown in the presence of small additives (2 mass % – 5 mass %) of PbF_2 as scavengers to purify melts from oxygen contamination.[38, 39] In this case, the following reactions proceed

$$CaO + PbF_2 \longrightarrow CaF_2 + PbO.$$

Melts are purified from PbF_2 and PbO due to high volatility of these components. Lead difluoride is used in fluorination of organic compounds.[40, 41]

Single-crystalline lead difluoride, PbF_2, is known as an optical functional material, which has transparency in a wide region from UV to mid-IR.[42, 43] Lead difluoride can form films with a high index of refraction and is involved in the composition of various optical antireflection coatings.[44 – 48]

A new generation of elementary particle accelerators (AAC in Protvino, Moscow region; LEP and LHC at the CERN Accelerator Complex, Switzerland) † imposes more stringent requirements on materials for high-energy particle detectors, which gave impetus to a search for new materials.[39, 49] High-speed combined systems of detectors involving scintillation and Cherenkov color-

I I Buchinskaya A V Shubnikov Institute of Crystallography, Russian Academy of Sciences, Leninsky prosp. 59, 119333 Moscow, Russian Federation. Fax (7-095) 135 10 11.
E-mail: buchinskaya@rambler.ru
P P Fedorov Laser Materials and Technologies Research Centre at the A M Prokhorov General Physics Institute, Russian Academy of Sciences, ul. Vavilova 38/D, 119991 Moscow, Russian Federation.
Fax (7-095) 135 02 70. E-mail: ppf@newmail.ru

Received 13 January 2003
Uspekhi Khimii **73** (4) 404 – 434 (2004); translated by T N Safonova

† AAC is the Accelerator Accumulator Complex; LEP is the Large Electron Positron Collider (electron-positron ring); LHC is the Large Hadron Collider.

imeters (total absorption spectrometers) are used in experiments performed on accelerators. Requirements on working substances of such colorimeters are as follows: a radiation resistance of no lower than 10^7 rads per year; a high density ($> 5.5-6.5$ g cm^{-3}); a luminescence decay time, which determines the detector time resolution, shorter than 3–30 ns and at least a moderate specific light yield ($\sim 1\%$ of the specific light yield of NaI : Tl) for scintillators; good mechanical characteristics and the absence of hygroscopicity; low price of raw materials and high manufacturability of optical elements several tens of centimetres in length. The cubic modification of PbF_2, which meets most of these requirements, can be considered as a promising material for electromagnetic colorimetry.[39,49–54] The study [55] was devoted to a search for improved PbF_2-based materials, which could be prepared as homogeneous bulk single crystals.

Scintillation efficiency of dopant ions is enhanced as the matrix density increases. Hence, lead difluoride as well as PbF_2-based crystals and glasses are investigated taking into account this dependence. However, it appeared that divalent lead ions very efficiently quench luminescence, in particular, from trivalent cerium, in fluorides.[56–59]

Lead difluoride forms numerous compounds, in which it generally acts as a Lewis base. This compound is a constituent of many fluoride and oxofluoride glasses serving as one of the most important modifying agents.[60,61] The introduction of PbF_2 into a glass causes network depolymerisation, thus stabilising the glass. Binary composites of lead fluoride with all main glass-forming materials, such as fluorides of aluminium, indium, gallium, zinc, zirconium, *etc*., are parent compounds of families (parent compositions) of fluoride glasses containing large amounts (tens of percent) of PbF_2.[59–67] Examples are provided by the so-called 'transition metal fluoride glasses' in $PbF_2-M'F_2-M''F_3$ systems (M' and M'' are transition metals)[66] and CLAP glasses ($CdF_2-LiF-AlF_3-PbF_2$).[68,69] In the pure form, a lead difluoride melt does not undergo a glass transition even at very high cooling rates (10^6 K s^{-1}). However, glasses can be prepared in the presence of oxygen-containing dopants.[63,70–72] Stable lead fluoride oxide glasses are formed in the PbF_2-GeO_2, $PbF_2-PbO-SiO_2$, and $PbF_2-AlF_3-PbO-B_2O_3$ [71,72] systems. Additives of PbF_2 make it possible to vary the physical properties of fluoride glasses, for example, to increase the density[60] and the index of refraction.[61,73,74] This fact is used in the design of optical fibres, whose cladding should possess a higher index of refraction than their core, all other properties being similar. In particular, the ZBLAN ($ZrF_4-BaF_2-LaF_3-AlF_3-NaF$) glasses with various PbF_2 contents were studied for this purpose.[75–77]

The foregoing demonstrates that lead difluoride and PbF_2-based materials are of practical importance. Data on the properties of PbF_2 are often contradictory and disembodied. In the present review, data on the phase diagrams of PbF_2-based systems with inorganic fluorides are analysed and chemical compounds involving PbF_2 are briefly characterised. Taking into account that, according to N S Kurnakov,[78] phase diagrams provide a special language for the description of chemical properties, data on phase diagrams of systems including PbF_2 form the basis of our review.

II. Properties of lead difluoride

Lead difluoride can easily be prepared by the reaction of hydrofluoric acid with lead hydroxide (or carbonate) or by precipitation of lead salts from aqueous solutions with ammonium fluoride.[79,80] At 25 °C, the solubility of PbF_2 in water is 0.66 g litre^{-1}.

Crystals of lead difluoride are colourless. They are stable in dry air at ambient temperature. At high temperature, PbF_2 is subject to pyrohydrolysis in a wet atmosphere. This process occurs at a noticeable rate starting at 400 °C. The reaction affords oxyfluoride Pb_2OF_2 as an intermediate. Lead difluoride is hydrolysed more readily than alkaline-earth (Mg–Ba) fluorides, is more resistant to water vapour than Cd, Zn, Co, Ni, Fe, Cr and Ag fluorides and is comparable in stability to MnF_2.[81]

Unlike other metal difluorides with the fluorite structure, lead fluoride has two structural modifications under normal pressure. The Pb^{2+} ion has a lone electron pair,[31] which is responsible for such properties of lead difluoride as high deformability of the electron shell of the cation, high polarisability, high refraction and index of refraction as well as high dielectric permeability [2,32] and a low melting point.

There are two structural modifications of PbF_2, *viz*., orthorhombic (low-temperature) and cubic (high-temperature).‡ The melting point of the latter modification is 822 ± 3 °C.

The low-temperature modification of PbF_2 crystallises in the structure type of the mineral cotunnite $PbCl_2$, space group *Pnma*, $Z = 4$. The structure consists of lead nine-vertex polyhedra, which can be described as trigonal prisms with additional anions (caps) in the vicinity of each lateral face.[82] It should be noted that other (non-standard) settings of the orthorhombic unit cell (having the interchanged *a*, *b*, *c* axes and described by different symbols of the space group) are also possible. This problem was exemplified by isostructural $PbCl_2$.[83]

The high-temperature modification of PbF_2 crystallises in the fluorite (CaF_2) structure type [space group $Fm\bar{3}m$ (O_h^5), $Z(F) = 4$, the coordination polyhedron is a tetrahedron, $Z(Pb) = 8$, the coordination polyhedron is a cube].

In the cubic modification, the anion sublattice is disordered on heating (the Faraday transition), which was assumed to be a second-order phase transition. However, detailed experimental and theoretical investigations revealed only a strong symmetric anomaly of heat capacity with a maximum at 710 ± 10 K and a half-width of ~ 70 K. Therefore, sublattice disordering occurs gradually and, strictly speaking, this process does not belong to phase transitions. According to the nomenclature used in the study,[84] such a disordering process can be assigned to 'supercritical' phase transitions. In terms of the catastrophe theory,[85] this is a catastrophe flag. The term 'diffuse phase transition' is also used.[13] Its physical meaning is that cooperative interactions between anti-Frenkel anion point defects appear as their concentration increases with increasing temperature resulting in strong anharmonism of anion vibrations, mass displacements of anions from their crystallographic positions and the possible formation of cluster defects. The heat and entropy of melting of the fluorite modification of lead difluoride are abnormally small.[86]

Under standard conditions, both modifications have similar thermodynamic characteristics.[86,87] There is a strongly hindered first-order transition from the low-temperature modification to the high-temperature one, the transition being irreversible at normal pressure. The transition temperature determined in different studies [17,80,88–91] varies from 280 to 460 °C. The transition temperature of 447 °C was reported in the handbook.[86] Such a large difference is, apparently, associated with non-stoichiometry as well as with the fact that the reaction rate depends substantially on the particle size and the presence of stable-phase nuclei and impurities. The transition temperature and enthalpy are 330 ± 5 °C and 1.51 ± 0.13 kJ mol^{-1}, respectively.[92,93] After cooling to room temperature, the cubic modification remains in a metastable state for an indefinitely long time.§

Both modifications can be prepared from aqueous solutions. Single crystals of the orthorhombic modification are prepared by precipitation using cross diffusion of solutions,[88] crystallisation from perchlorate solutions [57] and the hydrothermal synthesis

‡ In the literature, there is a confusion about the notations of the modifications of PbF_2 by the Greek letters α and β; hence, we tried not to use these notations; where these notations are, however, used, α and β denote the high- and low-temperature modifications, respectively.

§ According to the results of the study by G Ren, D Qun, Z Li, D Shen *J. Crystal Growth* **247** 141 (2003), an oxygen impurity promotes the phase transition.

from KF solutions.[90] Single crystals of the cubic modification can be prepared by directed crystallisation using the flux techniques.[43, 50–55]

The orthorhombic modification is stabilised with increasing pressure. The density of the orthorhombic modification (8.47 g cm^{-3}) is higher than that of the cubic modification. The cubic → orthorhombic transition occurs at room temperature under a pressure of ~ 4 kbar (0.4 GPa). Even grinding of a sample in a mortar or mechanical treatment of single crystals can lead to a partial transformation.

The temperature of the orthorhombic → cubic transition increases with increasing pressure. At ~4 kbar, the transformation becomes reversible.[94, 95] Yet another first-order phase transition was observed at ~11 GPa (a Co_2Si-type phase, the orthorhombic system, the space group *Pnma*).[95, 96] The high-pressure phase retains the space group and the main structural motif of orthorhombic PbF_2 based on trigonal prisms with caps above the lateral faces.

The unit cell parameters of orthorhombic PbF_2 determined in the different studies are in good agreement with each other.[79, 80, 97] Typical values are as follows: $a = 3.89098 \pm 0.00003$, $b = 6.42689 \pm 0.00002$, $c = 7.63574 \pm 0.00018$ Å (see Ref. 88) and $a = 3.8999(7)$, $b = 7.6479(9)$, $c = 6.4436(9)$ Å.[96] A different situation is observed for the cubic modification. Abundant published data [79, 80, 97] give the following two groups of values: 5.940 ± 0.003 and 5.927 ± 0.003 Å. Generally, the smaller value corresponds to samples prepared from aqueous solutions (see, for example, Ref. 88), whereas the larger value corresponds to samples prepared by melting or high-temperature annealing. Intermediate values of the lattice parameter for PbF_2 were observed [98, 99] depending on the thermal prehistory of samples. It is highly probable that the larger lattice parameter is attributable to a frozen configuration of defects corresponding to a high-temperature disordered form of cubic PbF_2.

There are experimental data (A I Boltalin and N S Tkachenko, Moscow State University, 1990) providing evidence that the transformation of orthorhombic PbF_2 into the cubic modification is a complex process, which involves the formation of a liquid phase co-existing with the solid one on heating of the orthorhombic modification from 510 to 550 °C.

Polish researchers [100–102] revealed complex polymorphism of PbF_2 (five polymorphs) by differential thermal analysis (DTA). In the range of existence of the cubic phase, phase transitions at 560 and 720 °C were additionally observed. However, to our knowledge, these facts were not confirmed by other researchers and with the use of other methods.

The temperature dependences of the vapour pressure of PbF_2 and some other fluorides are shown in Fig. 1. The thermal expansion coefficients were documented.[88, 106] The results of NMR studies were published.[107] The electronic structure and selected properties were calculated.[108]

Phase equilibria involving PbF_2 are studied primarily by DTA and using the solid-phase synthesis followed by powder X-ray diffraction analysis of samples. Operations with PbF_2 and PbF_2-containing samples have a number of characteristic features, which can influence the validity of construction of phase diagrams. Because of a high vapour pressure of PbF_2, it is desirable to perform studies in closed systems under an inert atmosphere (N_2, Ar or He). Since lead difluoride is prone to hydrolysis (in particular, due to the presence of water adsorbed on the powder particle surface), it is essential that the starting compounds should be fluorinated. Due to high reactivity of PbF_2 and the ease of reduction of Pb^{2+}, one must use hermetically sealed gold or platinum crucibles (tubes); in some cases, copper or open graphite crucibles can be used.[55, 105] Open platinum crucibles are unusable, because partial reduction of lead fluoride gives rise to a low-melting Pb–Pt alloy and leads to destruction of crucibles. Crystallisation of the cubic modification of PbF_2 and solid solutions based on this modification occurs virtually without supercooling of the melt.

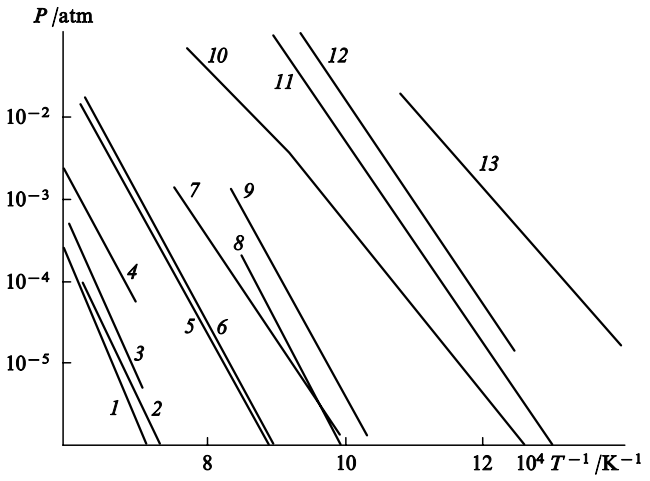

Figure 1. Temperature dependences of the vapour pressure for LaF_3 (*1*), BaF_2 (*2*), CeF_3 (*3*), YF_3 (*4*), InF_3 (*5*), ThF_4 (*6*), LiF(liq.) (*7*), UF_4 (*8*), AlF_3 (*9*), PbF_2 (*10*), HfF_4 (*11*), ZrF_4 (*12*) and BiF_3 (*13*).[103–105]

III. Systems PbF_2 – MF

PbF_2 – LiF. The phase diagram of this system (Fig. 2 *a*) was described in two studies [109, 110] (points *1* and *2*, respectively). The results of these studies are in good agreement with each other. The thermal effects in the solid state at 430 °C were assigned to the polymorphic transformation of PbF_2.[109] A narrow region of a LiF-based solid solution with the maximum PbF_2 content (3 ± 1 mol.%) was found to exist at the eutectic temperature.[110] The PbF_2-based solid solution region is very narrow. These data are in contradiction with the results of the study,[111] where single crystals of PbF_2 containing 6% of LiF (the percentage type was not reported) were prepared by melt crystallisation. The formation of a solid solution is evidenced by a substantial decrease in the lattice parameter from 5.94 to 5.83 Å. Apparently, this system has a retrograde solubility. The possibility of the existence of the $LiPbF_3$ compound with the inverse perovskite structure containing octahedrally coordinated Li^+ ions (analogous to the structure of the known $LiBaF_3$ compound) in the PbF_2–LiF system was examined.[112] However, attempts to synthesise this compound failed. Nevertheless, the existence of this compound was mentioned in the studies [113, 114] with a reference to the investigation.[112] The ionic conductivity of a eutectic composite was studied.[115]

PbF_2 – NaF. The system was examined in two studies [110, 116] (Fig. 2 *b*; points *1* and *2*, respectively). The results of these studies are in good agreement with each other. This system is of the eutectic type without the formation of compounds. Solid solution regions based on the components are very small.[110] However, high ionic conductivity of a eutectic composite in this system is indicative of the existence of the $Pb_{1-x}Na_xF_{2-x}$ solid solution.[117] The mechanism of the formation of the solid solution was confirmed by NMR spectroscopy.[118]

It should be noted that compounds are not formed in the condensed state. However, the $LiPbF_3$ and $NaPbF_3$ molecules were found in the vapour phases of the above-mentioned systems.[119]

Phase diagrams of systems involving potassium and rubidium fluorides are substantially more complicated and the results of different studies are in poorer agreement. These systems (and the PbF_2–CsF system to an even greater extent) are difficult to study due to high hygroscopicity of alkali metal fluorides.

PbF_2 – KF. Phase equilibria in this system (Fig. 2 *c*) were studied in detail.[116, 120–124] There is a consensus about the existence of the fluorite solid solution $Pb_{1-x}K_xF_{2-x}$, the limiting concentration being attained at $x = 0.10–0.12$. This solid solution is one of the best fluoride ion conductors.[118, 121, 123, 125–127]

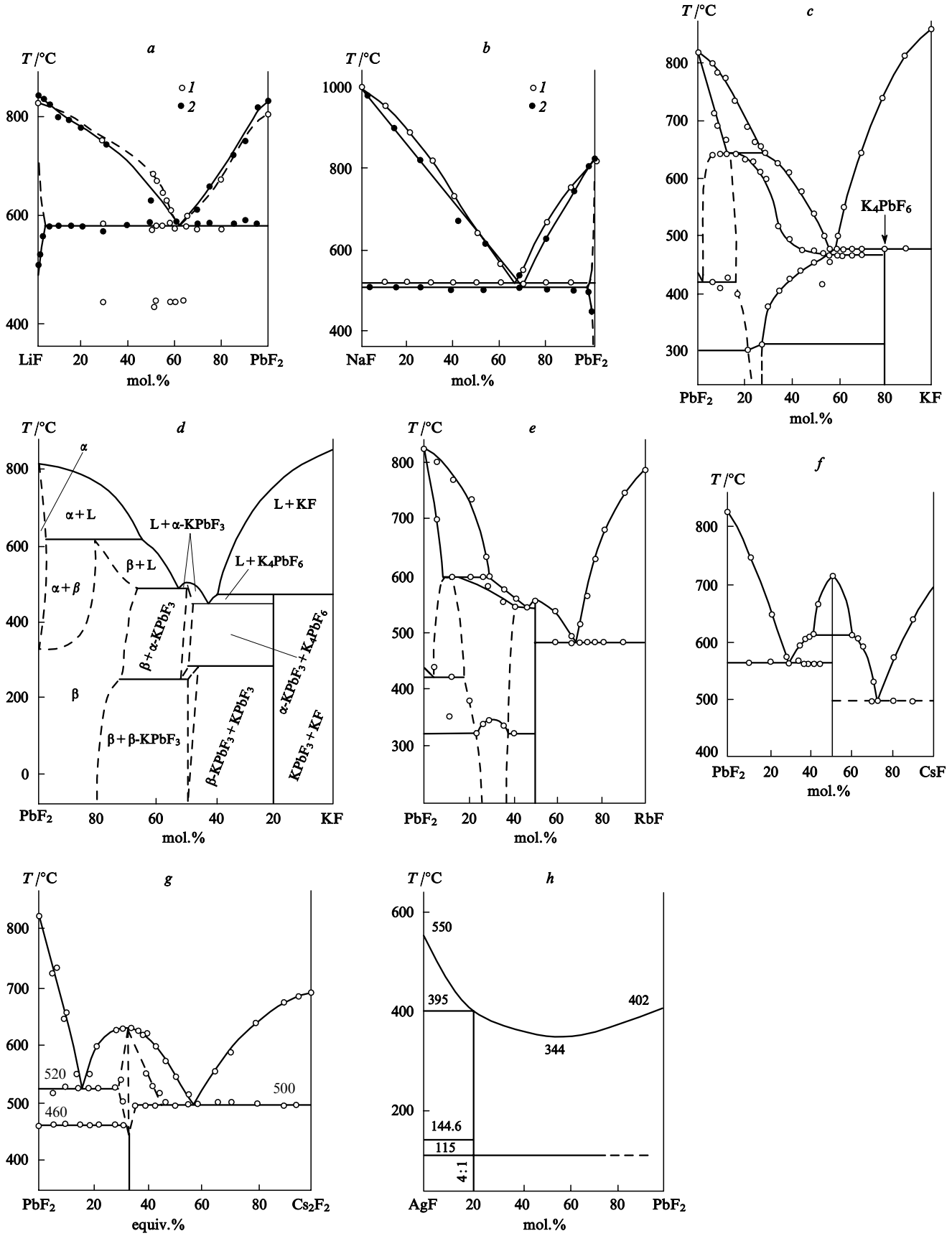

Figure 2. Phase diagrams of the PbF_2–LiF (*a*),[109,110] PbF_2–NaF (*b*),[110,116] PbF_2–KF (*c*),[116] PbF_2–KF (*d*),[122] PbF_2–RbF (*e*),[116] PbF_2–CsF (*f*),[116] PbF_2–CsF (*g*)[91] and PbF_2–AgF (*h*)[134] systems.
The numbers at the curves indicate the temperature in °C, (*1*) DTA data, (*2*) powder X-ray diffraction data.

According to the results of the study,[116] this system has an incongruently melting phase of the variable composition $K_nPb_{1-n}F_{2-n}$ ($\sim$15%–55% of KF), which undergoes a reversible polymorphic transition in the range of 300–315 °C, and the K_4PbF_6 compound, which melts according to a peritectic reaction. The high-temperature modification of the $K_nPb_{1-n}F_{2-n}$ phase has a body-centred cubic (BCC) structure of the defect anti-α-AgI type. Under a pressure of up to 40 kbar, the $KPbF_3$ compound, which undergoes a polymorphic transformation at 300 °C (the low-temperature low-symmetry modification of $KPbF_3$ II), was synthesised.[120] Attempts to synthesise $K_nPb_{1-n}F_{2-n}$ or K_4PbF_6 failed.[120] The $K_nPb_{1-n}F_{2-n}$ phase and a phase which is X-ray identical to $KPbF_3$ II (this metastable phase was observed on cooling of melts containing 25 mol.% of KF), were revealed in the investigation.[121]

A radically different interpretation of phase equilibria was proposed in the publication.[122] A solid solution based on the low-temperature orthorhombic modification of PbF_2, which is stabilised by the addition of potassium fluoride, was hypothesised to exist instead of an individual phase of variable composition (Fig. 2*d*). This solid solution melts according to a peritectic reaction. The $KPbF_3$ compound melts congruently at 500 °C, has a homogeneity region and undergoes a polymorphic transition. According to the results of high-temperature neutron diffraction measurements,[123, 124] the $2\,PbF_2 \cdot KF$ composite adopts a BCC structure of the defect anti-α-AgI type upon heating above 250 °C, which was confirmed by the results of the investigation.[116] This process is accompanied by a step increase in the ionic conductivity to $\sim 1\ \Omega^{-1}\ cm^{-1}$ (this value is higher than the conductivity of the fluorite phase), which corresponds to the superionic state. The X-ray diffraction pattern of this composite at room temperature is similar to that of orthorhombic PbF_2, but it was non interpreted. The homogeneity region of the BCC phase extends from 33 mol.% to 68 mol.% of KF.[124] It should be noted that the procedure for the preparation of samples used in the studies [123, 124] did not involve fluorination and, consequently, oxygen contamination of these samples cannot be ruled out. The $KPbF_3$ molecules were found in the vapour phase of the system.¶

PbF_2–RbF. A cubic non-stoichiometric phase of the anti-α-AgI type, which is analogous to that present in the potassium system, was found to exist in this system (Fig. 2*e*).[116, 124] The homogeneity region of the BCC phase extends from 33 mol.% to 50 mol.% of RbF, *i.e.*, includes the $RbPbF_3$ composite.[124] The authors of the study [116] believed that the $RbPbF_3$ compound exists in the individual state, melts congruently and is characterised by a complicated X-ray diffraction pattern. In the investigation,[128] this compound was mentioned as a cubic phase with the perovskite structure (a = 4.790 Å). According to the results of investigations,[129, 130] the transformation into the high-temperature cubic perovskite-type modification takes place at 206 °C. Data on the melting points of eutectics and $RbPbF_3$ obtained in the study [37] differ substantially from those published in the investigation.[116] It was noted [131] that non-stoichiometric phases in this system have high ionic conductivity. The $RbPbF_3$ molecules were found in the vapour phase of the system.¶

PbF_2–CsF. In this system, only the $CsPbF_3$ compound was revealed.[91, 116, 124, 129, 130, 132] According to the results of the study,[116] this compound melts congruently and undergoes the first-order polymorphic transition (Fig. 2*f*). At 145 K, this compound undergoes the second-order phase transition from the tetragonal modification to the perovskite cubic modification.[130, 132] In the study,[91] $CsPbF_3$-based solid solutions (up to 4 mol.% of PbF_2 at 520 °C and 10 mol.% of CsF at 495 °C) were found to exist, the polymorphism of $CsPbF_3$ being unobservable (Fig. 2*g*). The melting point (630 °C) is substantially lower than that reported in the study [116] and could correspond to metastable melting of the low-temperature modification of $CsPbF_3$.[116] An ordered perovskite structure was established for $CsPbF_3$ in the investigation.[124] The $CsPbF_3$ molecules were also found in the vapour phase (see¶ and Ref. 133).

PbF_2–AgF. The phase diagram of this system constructed in the study [134] (Fig. 2*h*) does not satisfy the phase rule. The $Pb_{1-x}Ag_xF_{2-x}$ solid solution is characterised by high ionic conductivity.[3]

PbF_2–TlF. The system was not studied, but the $TlPbF_3$ compound with the cubic perovskite structure was described (a = 4.62 Å).[129]

IV. Systems PbF_2–MF_2

PbF_2–BeF_2. This system (Fig. 3*a*) was examined in the study.[135] Two compounds with compositions Pb_3BeF_6 and $PbBeF_4$ and a wide region of a $PbBeF_4$-based solid solution were revealed. X-ray diffraction data for this system were not interpreted. According to the results of the study,[136] $PbBeF_4$ crystallises in the orthorhombic system. The $Pb_3Be_2F_{14}$ compound available in the JCPDS (Joint Committee on Powder Diffraction Standards) database under the entry number 37-1055 is erroneous, because the $Pb_3Ge_2F_{14}$ compound was described in the original publication.[137]

PbF_2–MgF_2. The system is characterised by the phase diagram (Fig. 3*b*) of the eutectic type.[55, 138] The Pb_2MgF_6 compound was found to exist in the solid state in this system. The exact temperature of its decomposition into components was not determined, but it was determined that it is in the range from 510 to 670 °C.

PbF_2–CaF_2. An outline of the phase diagram of the system is shown in Fig. 3*c*.[101, 139] This diagram was analysed in more detail in the investigations [55, 140, 141] (Fig. 3*d*). The phase diagram of the peritectic type containing solid solutions based on both components is presented in Fig. 3*c*. The peritectic temperature is 860 ± 5 °C. The limiting solubility of CaF_2 in PbF_2 increases from 6 mol.% to 15 mol.% as the temperature increases from 510 to 750 °C. According to the results of the studies,[101, 139] the solid solution regions based on both components cover ranges of approximately 18 mol.%–20 mol.%. The interpretation of numerous phase transitions presented in Fig. 3*c* is still an open question.

PbF_2–SrF_2 and PbF_2–BaF_2. Continuous fluorite solid solutions are formed in these systems (Fig. 3*e*, *f*).[55, 140–144]

Continuous solid solutions were prepared by co-precipitation from Pb and Sr nitrate solutions with HF followed by calcination of the precipitate at 500 °C.[143] By the third law of thermodynamics, continuous solid solutions should either decompose or undergo ordering with decreasing temperature. According to the results of two studies,[55, 144] the critical solid solution temperatures in the PbF_2–SrF_2 and PbF_2–BaF_2 systems are below 500 °C and at about 450 °C, respectively.

PbF_2–CdF_2. A continuous solid solution formed in this system has a minimum in the liquidus curve (Fig. 3*g*, *h*).[5, 55, 100, 141, 145–159] The coordinates of the minimum were evaluated at 60 mol.% of PbF_2 and 720 °C,[149] 60 mol.% of PbF_2 and 745 °C [150] and 67 ± 2 mol.% of PbF_2 and 745 ± 5 °C,[55, 141] *i.e.*, the composition corresponds to the stoichiometry Pb_2CdF_6. The addition of CdF_2 to lead difluoride stabilises the high-temperature cubic phase. The solid solution (particularly, in the vicinity of the minimum) is characterised by high fluoride ion conductivity.[5, 55, 151–157] The solid solution can undergo ordering at low temperature.[157, 158]

Systems of PbF_2 with Mn, Fe, Co, Ni, Cu and Zn difluorides were studied [145, 146] by DTA and powder X-ray diffraction analysis of samples synthesised in platinum tubes (Fig. 4). In all systems, the Pb_2MF_6 compounds were revealed. In the case of M = Mn, Fe, Co, Ni and Zn, these compounds have a tetragonal fluorite-like structure similar to the Ba_2MF_6 structure but with the doubled a parameter of the tetragonal unit cell. The Pb_2MnF_6 compound exhibits antiferromagnetic ($T_N = 30 \pm 1$ K) and

¶ See A I Boltalin, A N Rykov, Yu M Korenev *Zh. Neorg. Khim.* **34** 2617 (1989); **34** 2908 (1990) [*Russ. J. Inorg. Chem. (Engl. Transl.)*]

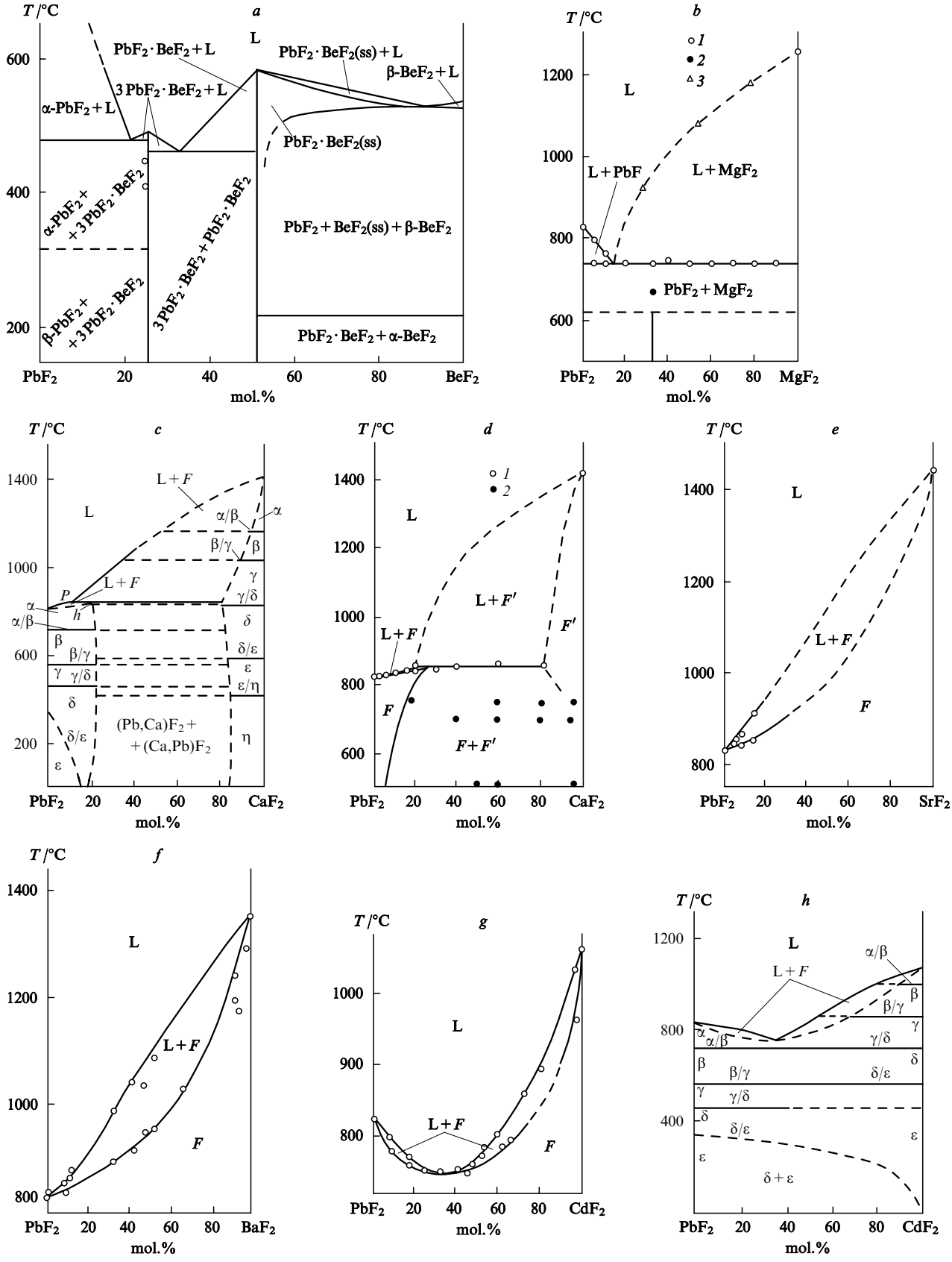

Figure 3. Phase diagrams of the PbF_2-BeF_2 (*a*),[135] PbF_2-MgF_2 (*b*),[55,138] PbF_2-CaF_2 (*c*),[101,139] PbF_2-CaF_2 (*d*),[55,140] PbF_2-SrF_2 (*e*),[55,140] PbF_2-BaF_2 (*f*),[55,144] PbF_2-CdF_2 (*g*)[55,141] and PbF_2-CdF_2 (*h*)[100] systems.
(*1*) DTA data, (*2*) powder X-ray diffraction data, (*3*) calculations using a model of an ideal liquid solution.

superionic (~500 K) properties.[147] Not only Pb_2MnF_6 but also $PbMnF_4$ was found in products of crystallisation of an amorphous phase prepared by rapid (10^6 K s^{-1}) quenching of a melt in the PbF_2-MnF_2 system.[63]

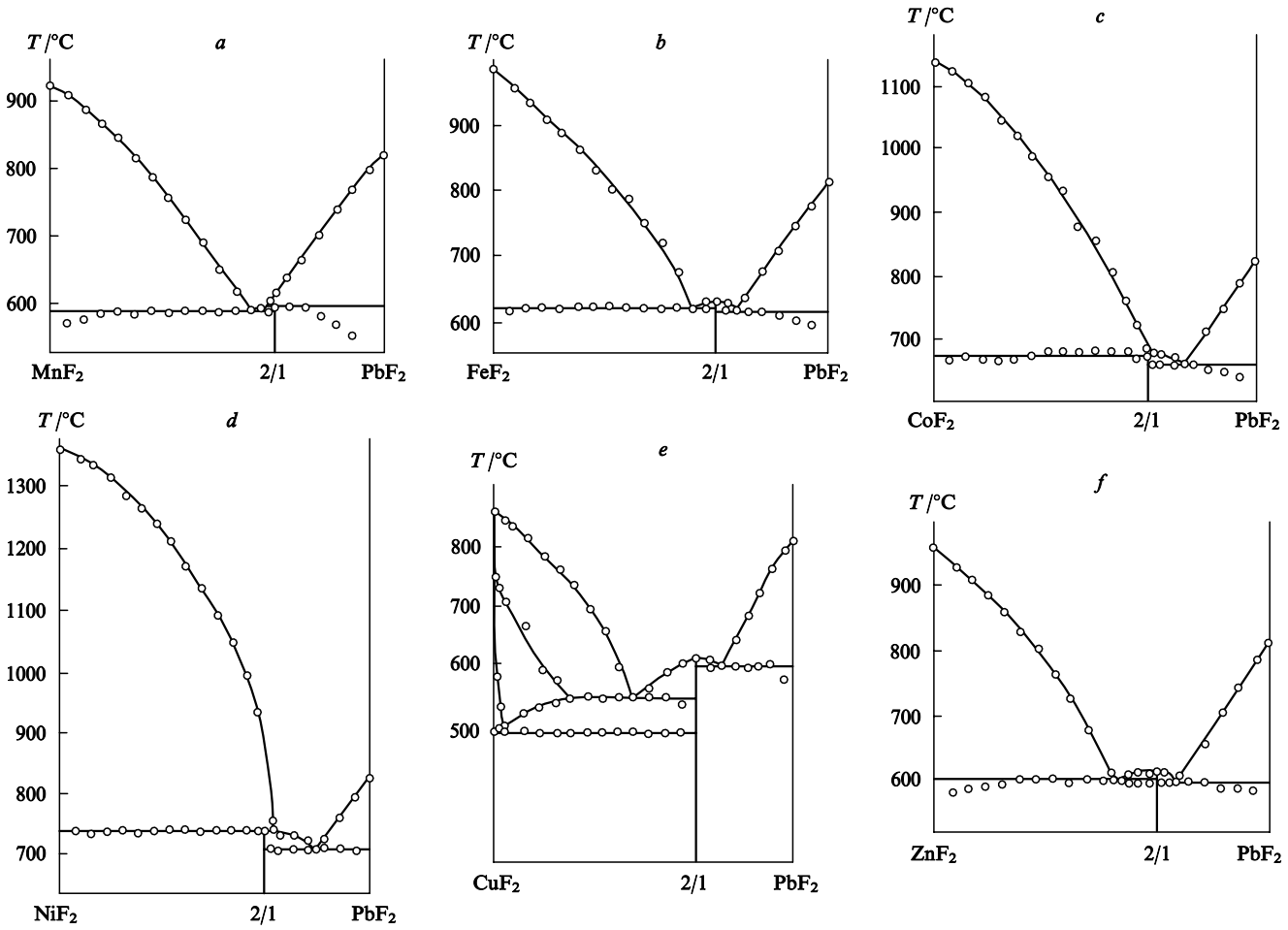

Figure 4. Phase diagrams of the PbF_2-MnF_2 (*a*), PbF_2-FeF_2 (*b*), PbF_2-CoF_2 (*c*), PbF_2-NiF_2 (*d*), PbF_2-CuF_2 (*e*) and PbF_2-ZnF_2 (*f*) [146] systems.

The Pb_2CuF_6 compound crystallises in the monoclinic system.[146, 148] Judging from the phase diagram reported in the study,[146] the starting CuF_2 compound presumably undergoes partial pyrohydrolysis (Fig. 4 *e*).

PbF_2-SnF_2. The $PbSnF_4$ compound is formed in this system (Fig. 5).[10, 12, 160–176] The superionic conductivity revealed in this compound [10] gave impetus to extensive experimental studies. The $PbSnF_4$ compound is characterised by complex polymorphism. The following scheme of polymorphism was proposed:[165, 166]

$$\left.\begin{matrix}\alpha\text{-}PbSnF_4\\ \alpha'\text{-}PbSnF_4\end{matrix}\right\} \xrightarrow{80\ ^\circ C} \beta\text{-}PbSnF_4 \xrightarrow{350\ ^\circ C} \beta'\text{-}PbSnF_4 \xrightarrow{380\ ^\circ C}$$

$$\longrightarrow \gamma\text{-}PbSnF_4 \xrightarrow{390\ ^\circ C} \text{melt.}$$

The high-temperature γ modification has a cubic fluorite structure; the β and β′ modifications have tetragonal structures, the α and α′ modifications belong to the monoclinic system. A somewhat different scheme was published in the study [163] (without monoclinic phases). A monoclinic distortion of the tetragonal lattice was observed below room temperature.[173] The crystal structure of $PbSnF_4$ was solved in several studies.[170, 171, 173, 174] The investigation [169] provided evidence for the existence of a $PbSnF_4$-based homogeneity region.[169] The influence of the synthesis condition on the character of distortions of the fluorite lattice in samples of $PbSnF_4$ was examined.[175]

A PbF_2-based cubic solid solution containing ~20 mol.% of SnF_2 exists in the PbF_2-SnF_2 system. In addition, a series of fluorite-like phases were revealed in the solid state in the region of 30 mol.% – 50 mol.% of SnF_2.[169]

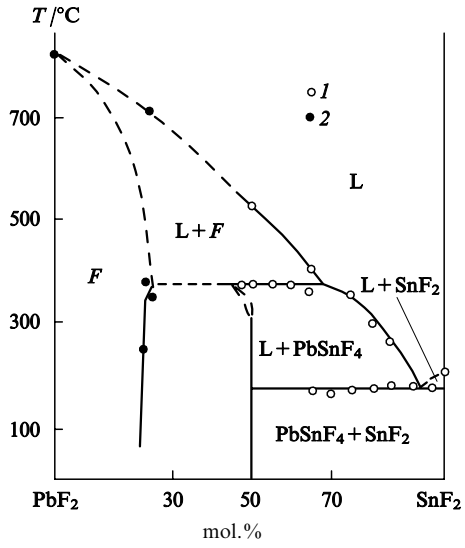

Figure 5. Phase diagram of the PbF_2-SnF_2 system.
(*1*) unpublished data of T Yu Glazunova, A I Boltalin (Moscow State University) and P P Fedorov, (*2*) according to the results of the studies.[10, 164, 169, 174]

The $PbSnF_4$ compound melts incongruently at 370 °C. The liquidus temperature for this composition is 520 °C. The compounds which were reported in the study [160] based on the DTA data, are apparently artefacts. A phase with the fluorite structure was prepared [175] by quenching a melt with composition $PbSn_4F_{10}$. This phase rapidly decomposes at room temperature. The thermogram of this sample shows reversible effects at 190 (non-variant) and 280 °C (monovariant), which agrees well with the phase diagram shown in Fig. 5.

$PbF_2 - PdF_2$. The $PbPdF_4$ compound (the tetragonal system, the $K[BrF_4]$ structure type) was synthesised at 820 °C by the reaction of PbF_2 with PdF_2 in a gold bomb.[177]

V. Systems $PbF_2 - MF_3$

The common characteristic feature of the $PbF_2 - MF_3$ systems is the formation of the heterovalent solid solutions $Pb_{1-x}M_xF_{2+x}$ and ordered fluorite-like compounds.

$PbF_2 - BF_3$. Two compounds, *viz*., $Pb_2(BF_4)F_3$ and $Pb_4(BF_4)F_7$, exist in this system. These compounds were prepared by the reaction of BF_3 with PbF_2.[178, 179] Two allotropic modifications of $Pb_4(BF_4)F_3$ are formed by the reaction of BF_3 with orthorhombic and cubic PbF_2.

$PbF_2 - AlF_3$. The system was studied in detail.[62, 180–197] The cubic solid solution $Pb_{1-x}Al_xF_{2+x}$ with a limiting concentration of ~10 mol.% – 12 mol.% of AlF_3 was revealed in this system by several research groups.[180, 181, 183, 184, 191] This solid solution is characterised by high fluoride ion conductivity. In addition to the solid solution, the $PbAlF_5$ (the tetragonal system, the $SrAlF_5$/$BaFeF_5$ structure type), $PbAl_2F_8$ and $Pb_9Al_2F_{24}$ compounds were found to exist in the solid state at 550 °C.[181, 182] However, examination of the phase diagram (Fig. 6 *a*) revealed only one incongruently melting intermediate compound with composition $Pb_3Al_2F_{12}$,[180] whose powder X-ray diffraction pattern is similar to that of $PbAlF_5$.[181] A careful reinvestigation of the phase diagram [184] (Fig. 6 *b*) confirmed the $Pb_3Al_2F_{12}$ composition of this compound. In addition, the $Pb_9Al_2F_{24}$ compound, which was described in earlier publications,[181, 182] was revealed. In the solid state, the latter compound decomposes according to a peritectoid reaction, whose temperature is close to the eutectic temperature. The $PbAl_2F_8$ compound was not observed.

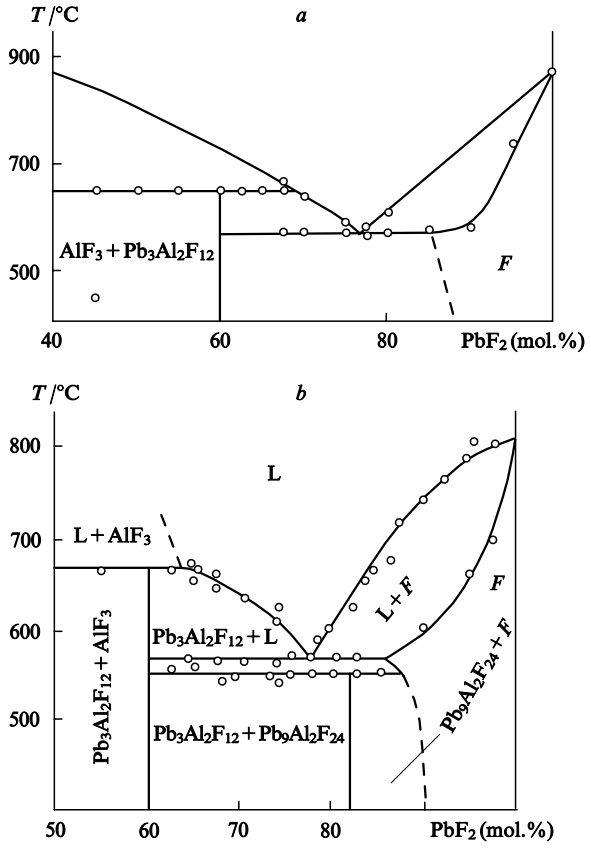

Figure 6. Fragments of the phase diagram of the $PbF_2 - AlF_3$ system. (*a*) according to the results of the study,[180] (*b*) according to the results of the study.[184]

The tetragonal phase in the $PbF_2 - AlF_3$ system and its analogues in the $M'F_2 - MF_3$ systems (M′ = Pb, Sr, Ba; M = Ti, V, Cr, Fe, Ga) attract interest because of detection of ferroelectric phase transitions.[185, 192] This transition was observed in $PbAlF_5$ at 312 °C.[192] The composition of the tetragonal phase was refined in the study.[185] The existence of the $Pb_5Al_3F_{19}$ compound was postulated by analogy with the chromium analogue, whose crystal structure was established. The $Pb_5Al_3F_{19}$ compound was prepared (along with analogues for Ti, V, Cr, Fe and Ga) by solid-phase synthesis. The parameters of the tetragonal unit cell of $Pb_5Al_3F_{19}$ determined in the study [185] are similar to those reported for $PbAlF_5$.[181] For this compound, a ferroelectric phase transition was revealed at close to room temperature. It should be noted that the phase transition temperature determined for $Pb_5Al_3F_{19}$ differs substantially (by 300 °C) from that of $PbAlF_5$.[185, 192] This indicates that either different compounds were studied or the researchers dealt with non-stoichiometry of the same phase.

Later on, the coordinates of the peritectic and eutectic equilibria in this system were reproduced with a good accuracy (±3 mol.%, ±10 °C).[186] Single crystals of an incongruently melting compound were grown from a flux containing an excess of PbF_2. It was determined that this compound has the composition $Pb_5Al_3F_{19}$. An investigation of these single crystals revealed a monoclinic distortion of the tetragonal unit cell. Further studies of the crystal structure of $Pb_5Al_3F_{19}$ did not clarify this problem. For example, different space groups were reported for these crystals.[188–190] Investigations of other compounds of the ferroelectric family $Pb_5M_3F_{19}$ showed that doubling of the *a* parameter is typical of high-temperature paraelectric phases.[185]

The compound with composition $Pb_3Al_2F_{12}$ was prepared by hydrothermal synthesis. However, this phase differs in the packing of octahedra.[186]

$PbF_2 - GaF_3$. The system (Fig. 7) has the fluorite-type solid solution $Pb_{1-x}Ga_xF_{2+x}$ ($0 < x \leqslant 0.11$) and three intermediate phases,[182, 198] *viz*., the congruently melting $Pb_3(GaF_6)_2$ phase and the incongruently melting $PbGaF_5$ and $Pb_9Ga_2F_{24}$ phases (in the study,[182] the latter phase was denoted as the β phase with the

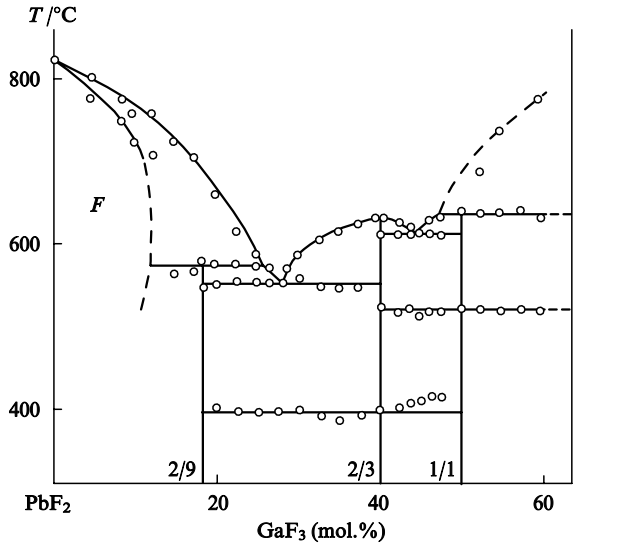

Figure 7. Fragment of the phase diagram of the $PbF_2 - GaF_3$ system.[198]

range of existence of ~20 mol.% of GaF_3). The $Pb_9Ga_2F_{24}$ phase has a distorted fluorite-like lattice. The structural model for this phase was proposed in the study.[199] The $Pb_3(GaF_6)_2$ compound is transformed into the ferroelectric state at 347 °C.[200]

The $PbGaF_5$ compound was found[192] to undergo a ferroelectric phase transition at 312 °C. The formula $Pb_5Ga_3F_{19}$ was proposed[185] for the tetragonal phase by analogy with other ferroelectric compounds. This composition is intermediate between $Pb_3(GaF_6)_2$ and $PbGaF_5$.[182] According to the results of two studies,[185,200] $Pb_5Ga_3F_{19}$ and $Pb_3(GaF_6)_2$ have the same phase transition temperature. Apparently, the authors studied the same sample, to which different compositions were assigned. The same statement is true for other $Pb_3(MF_6)_2$ compounds, where M = Ti, Fe, V or Cr (for M = V, the difference in the temperature is 4 K; for M = Cr, the difference is 5 K). This problem requires additional investigation. The position of the maximum in the liquidus curve for $Pb_3(GaF_6)_2$ (see Ref. 198) corresponds to the composition containing 40 mol.% of PbF_2. The phase equilibria in the PbF_2-GaF_3 system unambiguously indicate that there are at least two compounds. The difference in the phase transition temperature determined for $Pb_3(GaF_6)_2$ in two studies[198,200] is substantially larger than the experimental error.

PbF_2-InF_3. The system was studied by several research groups.[182,201–203] A fragment of the phase diagram of this system is shown in Fig. 8 *a*. The fluorite-type $Pb_{1-x}In_xF_{2+x}$ solid solution and the Pb_2InF_7 and $Pb_7In_5F_{29}$ compounds were observed in this system. In the study,[201] the composition $Pb_5In_4F_{22}$ was reported instead of $Pb_7In_5F_{29}$.[182] The limiting concentration of the solid solution is $x = 0.25$; $a = 5.82$ Å.[201] After quenching, a tetragonal distortion with metastable ordering was observed at $x = 0.25$. The $Pb_7In_5F_{29}$ compound melts according to a peritectic reaction at 525 °C. The phase diagram shown in Fig. 8 *b* agrees satisfactorily with the results of the study.[201] The difference is that a small homogeneity region was revealed for the $Pb_7In_5F_{29}$ compound in the study[201] and thermal effects were interpreted differently: the temperature of 525 °C corresponds to a eutectic rather than to decomposition of the $Pb_7In_5F_{29}$ compound, which melts according to a peritectic reaction at 535 ± 5 °C. The ionic conductivity of phases in this system was studied.[202] The structure of the solid solution was investigated by NMR spectroscopy.[204,205]

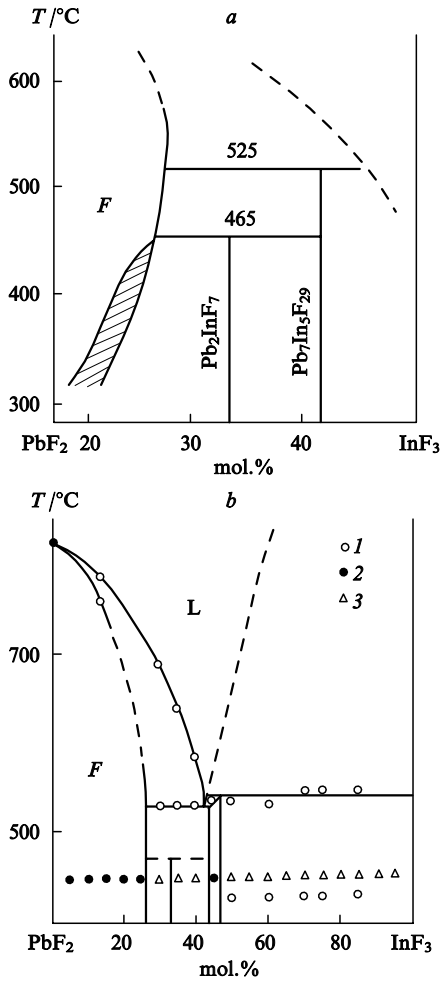

Figure 8. Phase diagram of the PbF_2-InF_3 system;
(*a*) according to the results of the study,[201] (*b*) according to the results of the study;[203] (*1*) DTA data, (*2*) single-phase samples, (*3*) two-phase samples (according to the results of the solid-phase synthesis and powder X-ray diffraction analysis); the numbers at the curves indicate the temperature in °C.

PbF_2-ScF_3. The system is of the eutectic type (Fig. 9) without the formation of compounds.[9] The $Pb_{1-x}Sc_xF_{2+x}$ solid solution ($0 < x \leqslant 0.16$), which exhibits high fluoride ion conductivity, was described.[6,7,9,12]

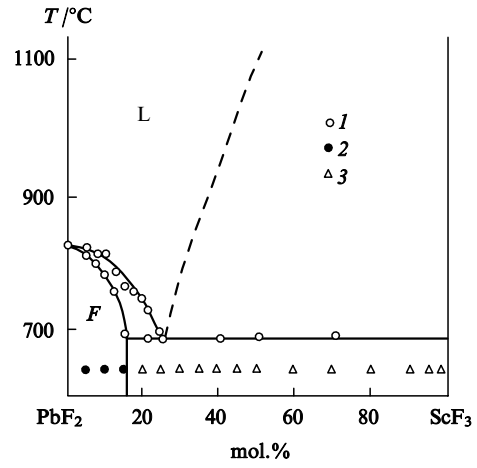

Figure 9. Phase diagram of the PbF_2-ScF_3 system.[9]
(*1*) DTA data, (*2*) single-phase samples, (*3*) two-phase samples (according to the results of the solid-phase synthesis and powder X-ray diffraction analysis).

PbF_2-RF_3 (R = Y, La–Lu). A series of PbF_2-containing systems with rare-earth fluorides were investigated[9,28,105,206–208] by DTA and powder X-ray diffraction analysis of annealed and quenched samples (Fig. 10). Similar results were obtained in studies of phase equilibria in the solid state.[209,210] The $Pb_{1-x}R_xF_{2+x}$ solid solutions with the fluorite structure exist in these systems. The character of melting of these solid solutions changes from peritectic (LaF_3-EuF_3) to eutectic with a maximum in the melting curve. The phase diagram of the PbF_2-GdF_3 system is very similar to that of the transition type. A change in the coordinates of non-variant transformations in the PbF_2-LnF_3 systems in a series of rare-earth elements is shown in Fig. 11. Trigonal fluorite-like $Pb_4R_3F_{17}$-based phases are formed in systems involving RF_3 (R = Sm–Lu, Y) (Fig. 12). Their stability increases with decreasing ionic radius of R^{3+}.[28,206,210,211] The regions of existence of the cubic solid solutions $Pb_{1-x}R_xF_{2+x}$ are limited by the $Pb_4R_3F_{17}$ compounds. The precision lattice parameters of $Pb_4R_3F_{17}$ were determined.[212] An investigation of the crystal structure of $Pb_4Y_3F_{17}$ revealed oxygen contamination of the samples corresponding to the formula $Pb_8Y_6F_{32}O$.[210] In addition, phases with a tetragonally distorted fluorite lattice were observed. A tetragonal distortion for the phase containing ~48 mol.% of YF_3 was observed.[207] A similar phase was demonstrated[209] to have the composition Pb_2YF_7. Dissolution

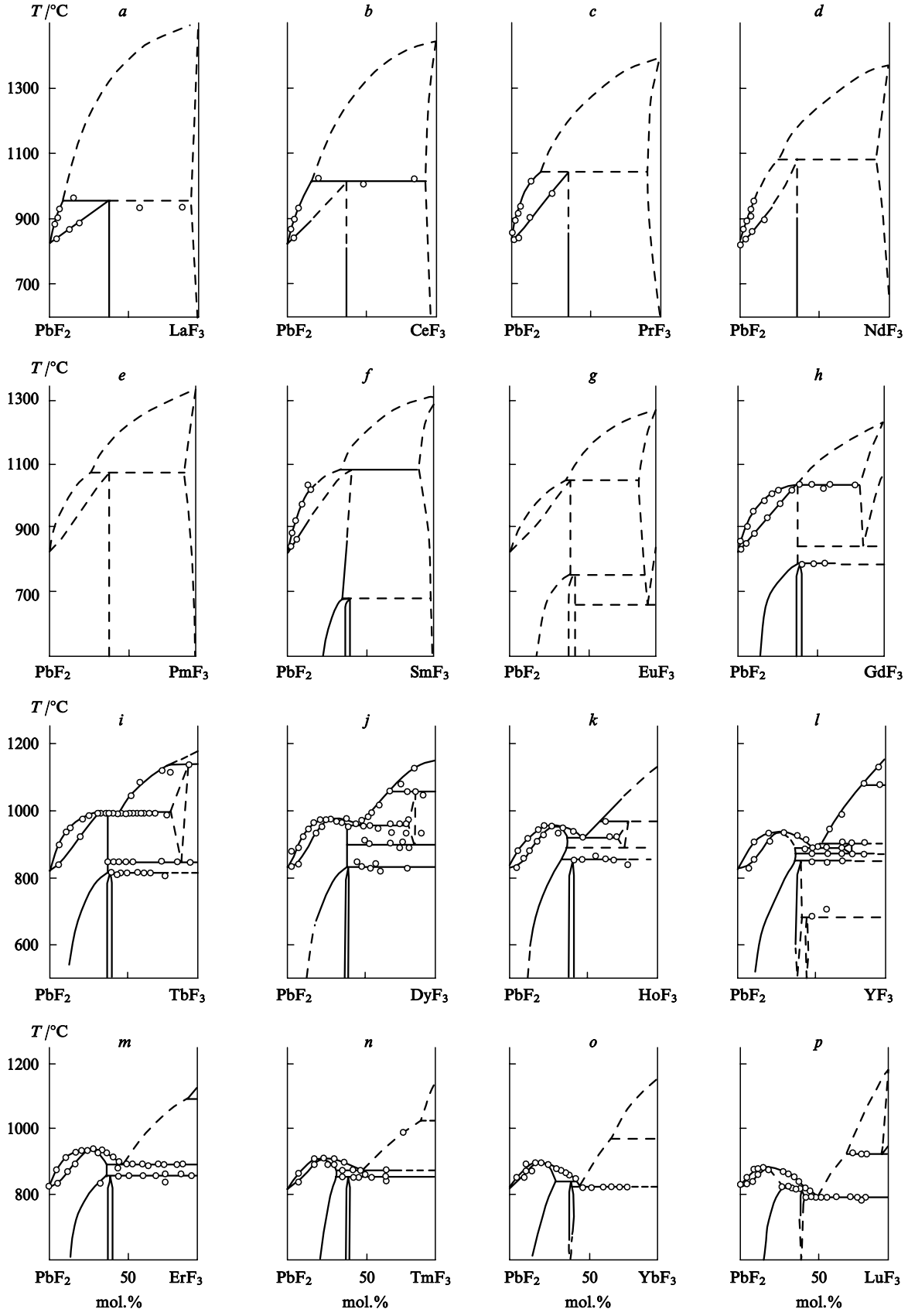

Figure 10. Phase diagrams of the $PbF_2 - RF_3$ systems, where R = La (*a*), Ce (*b*), Pr (*c*), Nd (*d*), Pm (*e*), Sm (*f*), Eu (*g*), Gd (*h*), Tb (*i*), Dy (*j*), Ho (*k*), Y (*l*), Er (*m*), Tm (*n*), Yb (*o*) and Lu (*p*).[105, 206] Powder X-ray diffraction data are lacking.

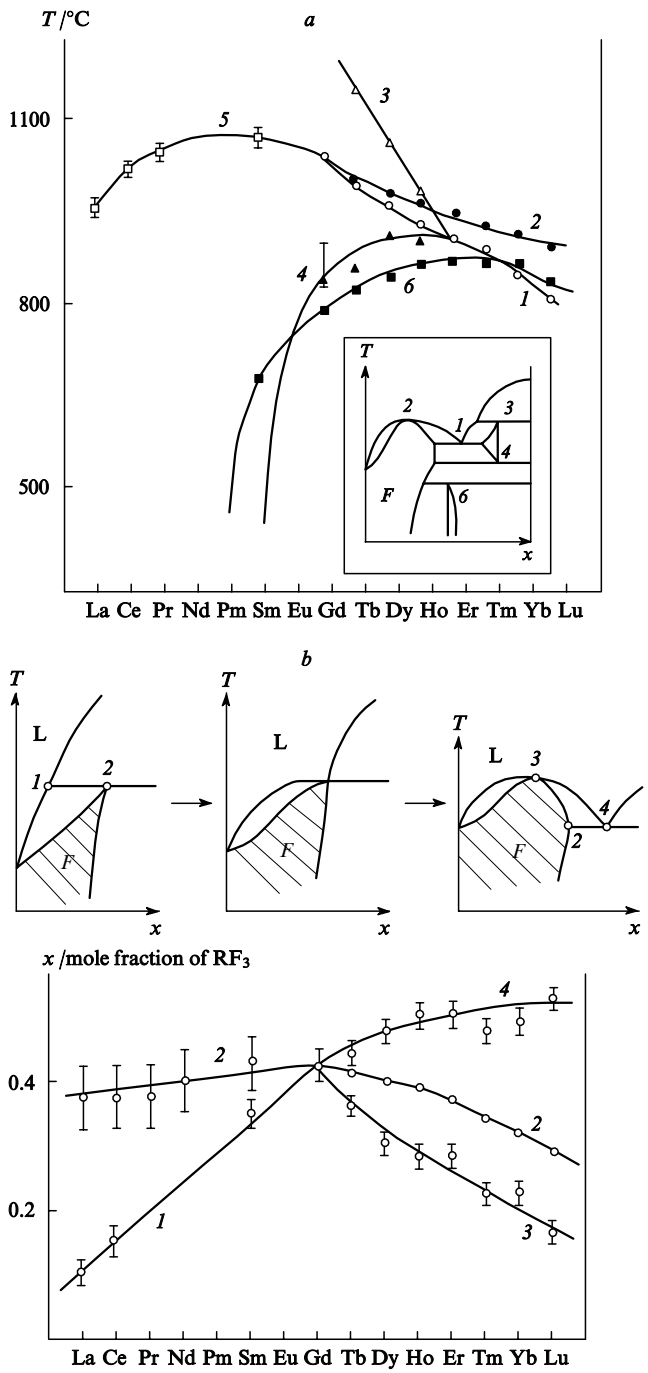

Figure 11. Changes in the temperatures of nonvariant equilibria (*a*) and compositions of the phases involved in these equilibria (*b*) in the PbF_2-RF_3 systems (R = La–Lu);[105]
(*a*): (*1*) a eutectic, (*2*) the maximum in the melting curves of the $Pb_{1-x}R_xF_{2+x}$ solid solution with the fluorite structure (phase *F*), (*3*) and (*4*) the upper and lower limits of stability of a phase of variable composition with the tysonite structure, (*5*) peritectic melting of the phase *F*, (*6*) the upper temperature limit of stability of the $Pb_4R_3F_{17}$ phase; (*b*): (*1*) the composition of the melt involved in the peritectic equilibrium, (*2*) the limiting concentration of the $Pb_{1-x}R_xF_{2+x}$ solid solution, (*3*) the composition corresponding to the maximum in the melting curve of the phase *F*, (*4*) the composition of the eutectic.

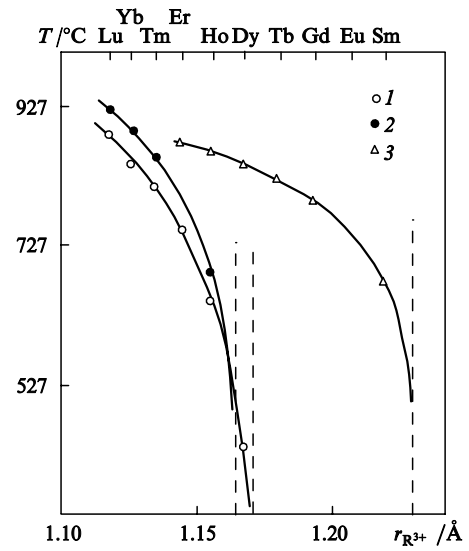

Figure 12. Decomposition temperature of the Ca_2RF_7 (*1*), $Ca_8R_5F_{31}$ (*2*) and $Pb_4R_3F_{17}$ (*3*) compounds *vs.* the ionic radius of R^{3+} (equation $T = 1430|r-1.23|^{[0.091]}$).[105, 211]

of PbF_2 in RF_3 (R = La–Gd) afforded trigonal solid solutions with the LaF_3-type (tysonite-type) structure. For R = Tb–Ho and Y, berthollide phases of variable composition with the tysonite structure occur. The regions of existence of these phases decrease with decreasing ionic radius of R^{3+}. The electrical conductivity and defect structures of the $Pb_{1-x}R_xF_{2+x}$ solid solutions were investigated in detail.[4, 6–9, 205, 213–216]

PbF_2-MF_3 (M = Ti, V, Cr, Fe). These systems are similar to the PbF_2-MF_3 systems with M = Al or Ga .[182, 185] In addition to the fluorite solid solutions, fluorite-like phases with an orthorhombically distorted structure derived from the fluorite structure were revealed for systems with M = Ga, Ti, V, Cr and Fe. For M = Ga and Cr, $x = 0.20$, the doubled unit cell of fluorite undergoes an orthorhombic distortion.[182] In the study,[199] it was hypothesised that excess anions in ordered anion-excess fluorite-like phases are located in the seven-vertex polyhedra $[MF_7]$, which form various parallel structures of zigzag chains incorporated into the fluorite lattice. One-dimensional clusters formed by chains of the $[MF_7]$ polyhedra can be considered as basic structural units for the homologous series $Pb_nM_2F_{2n+6}$ ($n \geqslant 2$). For titanium, $n = 3$; for vanadium, $n = 4$; and for gallium, $n = 5$. An analogous situation was observed also for ordered fluorite-like phases in the PbF_2-MF_4 system (see the next section).

PbF_2-TiF_3. Solid-phase equilibria were partially studied at 500 °C.[182, 217] The $Pb_{1-x}Ti_xF_{2+x}$ solid solution with the fluorite structure at $0 < x \leqslant 0.15$, an ordered β phase with an orthorhombically distorted fluorite structure at $0.25 \leqslant x \leqslant 0.26$ [199] and the $Pb_3(TiF_6)_2$ compound belonging to the tetragonal system were found to exist in this system. In the publication,[185] the composition $Pb_5Ti_3F_{19}$ rather than $Pb_3(TiF_6)_2$ was assigned to the ferroelectric phase.

PbF_2-VF_3. Phase equilibria in this system were investigated.[182, 218, 219] The phase diagram is shown in Fig. 13 *a*. The $Pb_{1-x}V_xF_{2+x}$ solid solution with the fluorite structure exists at $0 < x \leqslant 0.15$ (see Refs 182 and 218) or $0 < x \leqslant 0.22$ (see Ref. 219). An ordered fluorite-like phase characterised by an orthorhombic distortion of the cubic lattice exists in this system in the range of 27 mol.% – 28.5 mol.% of VF_3.[182, 218] In the study,[219] the composition Pb_4VF_{11} was assigned to this phase, the phase undergoing a polymorphic transformation. The high-temperature modification has a homogeneity region. The structural model for this phase was described in the study.[199] In addition, the system contains a tetragonal phase. The data on the composition of this phase (in spite of similar unit cell parameters) are contradictory (analogously to the system with aluminium trifluoride). For example, the composition $PbVF_5$ was assigned to this phase in the study, [218] where it was mentioned that this phase melts congruently at 566 ± 7 °C. By contrast, the composition $Pb_3(VF_6)_2$ was proposed for this phase in the

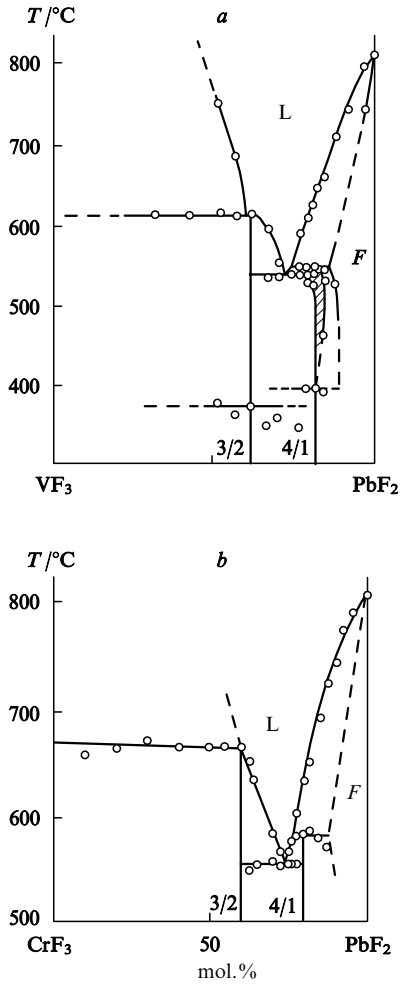

Figure 13. Phase diagrams of the PbF_2-VF_3 (*a*)[219] and PbF_2-CrF_3 (*b*) systems.[220]

studies,[182,219] the compound undergoing a polymorphic transformation and the character of melting being intermediate between congruent and incongruent (see Fig. 13 *a*). The same composition was reported in the investigation.[200] However, this composition was corrected to $Pb_5V_3F_{19}$ in the more recent study.[185]

PbF_2-CrF_3. The system was studied in-depth (Fig. 13 *b*).[182,185,193,220–222] The $Pb_{1-x}Cr_xF_{2+x}$ solid solution with the fluorite structure at $0 < x \leqslant 0.12$ and two compounds, Pb_4CrF_{11} and $Pb_3(CrF_6)_2$, were revealed in this system. The character of melting of $Pb_3(CrF_6)_2$ is intermediate between congruent and incongruent. The composition of the $Pb_3(CrF_6)_2$ compound was refined[185,193,222] based on results of X-ray diffraction analysis, and the compound was found to have the composition $Pb_5Cr_3F_{19}$ rather than $Pb_3(CrF_6)_2$.

PbF_2-FeF_3. The solid-phase equilibrium in the system was studied at 500 °C.[182,223] The $Pb_{1-x}Fe_xF_{2+x}$ solid solution with the fluorite structure at $0 < x \leqslant 0.17$, the new $Pb_{1-x}Fe_xF_{2+x}$ phase with an orthorhombically distorted fluorite structure at $0.26 \leqslant x \leqslant 0.27$ and the $Pb_3(FeF_6)_2$ compound belonging to the tetragonal system were found to exist in this system. In the study,[185] the composition $Pb_5Fe_3F_{19}$ instead of $Pb_3(FeF_6)_2$ was assigned to the ferroelectric phase. The $Pb_3(FeF_6)_2$ compound was prepared by hydrothermal synthesis,[224] but this was another phase, which belongs to the triclinic system and contains the ring-like $[Fe_4F_{20}]^{8-}$ tetramers consisting of the $(FeF_6)^{3-}$ octahedra.

PbF_2-SbF_3. Solid-phase equilibria in this system were studied at 250 °C.[225] The $Pb_{1-x}Sb_xF_{2+x}$ solid solution with the fluorite structure at $0 < x \leqslant 0.40$ and the $Pb_2Sb_3F_{13}$ compound were revealed. The structure of the latter compound was not established.

PbF_2-BiF_3. The system was studied by several research groups.[226–230] The phase diagram of the system is shown in Fig. 14. The following two phases of variable composition exist in this system: the fluorite solid solution $Pb_{1-x}Bi_xF_{2+x}$ based on high-temperature PbF_2 with a maximum in the melting curve at ~25 mol.% of BiF_3 and 890 °C and the berthollide phase $Bi_{1-y}Pb_yF_{3-y}$ with the tysonite structure. The homogeneity region of $Pb_{1-x}Bi_xF_{2+x}$ extends up to 50 mol.% of BiF_3.[226] However, the dependence of the lattice parameter on the composition (a linear decrease up to $x = 0.3$ followed by concentration independence) is abnormal. A careful X-ray diffraction study[227,228] showed ordering and the formation of the $PbBiF_5$ compound with a tetragonally distorted structure. The homogeneity region of the tysonite phase is $0.05 \leqslant y \leqslant 0.25$ (see Ref. 230) or $0.075 \leqslant y \leqslant 0.175$ (see Ref. 228). The polymorphic transition for BiF_3 described in the study[230] is indicative of possible oxygen contamination because no polymorphic transformations are observed in pure BiF_3.[231,232]

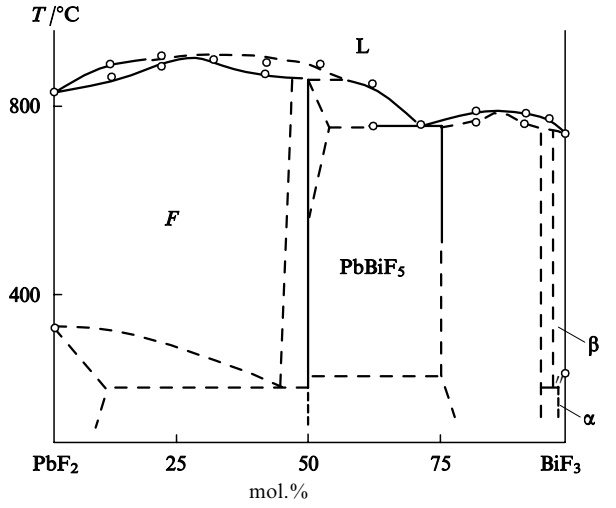

Figure 14. Phase diagram of the PbF_2-BiF_3 system.[230]

PbF_2-RhF_3. The system was not studied, but the Pb_2RhF_7 compound was synthesised.[233,234]

VI. Systems PbF_2-MF_4

PbF_2-UF_4. The phase diagram of the system (Fig. 15 *a*) has two maxima in the liquidus curve, which were assigned to the formation of compounds. The homogeneity regions are absent. The interpretation of compositions in the region of high PbF_2 concentrations was found to be erroneous.[236,237] The reinvestigation (Fig. 15 *b*) revealed the $Pb_{1-x}U_xF_{2+2x}$ solid solution (0 mol.% – 25 mol.% of UF_4), which has a maximum in the liquidus curve at 923 °C corresponding to the composition $Pb_{0.85}U_{0.15}F_{2.3}$.[238,239] In addition, a phase of variable composition with the tysonite structure (45 mol.% – 50 mol.% of UF_4) was observed. The maximum in the liquidus curve of the solid solution at 836 °C corresponds to the composition $Pb_{0.55}U_{0.45}F_{2.9}$. The phases formed in the system under consideration are characterised by high fluoride ion conductivity.[239,240] In the $Pb_{1-x}U_xF_{2+2x}$ solid solution, a decrease in the temperature and diffusion of the Faraday phase transition are observed with increasing concentration of uranium fluoride.

PbF_2-ThF_4. The system was studied with the aim of revealing ion transport. There is evidence for the existence of the $Pb_{1-x}Th_xF_{2+2x}$ solid solution ($0 < x \leqslant 0.2$) with the fluorite

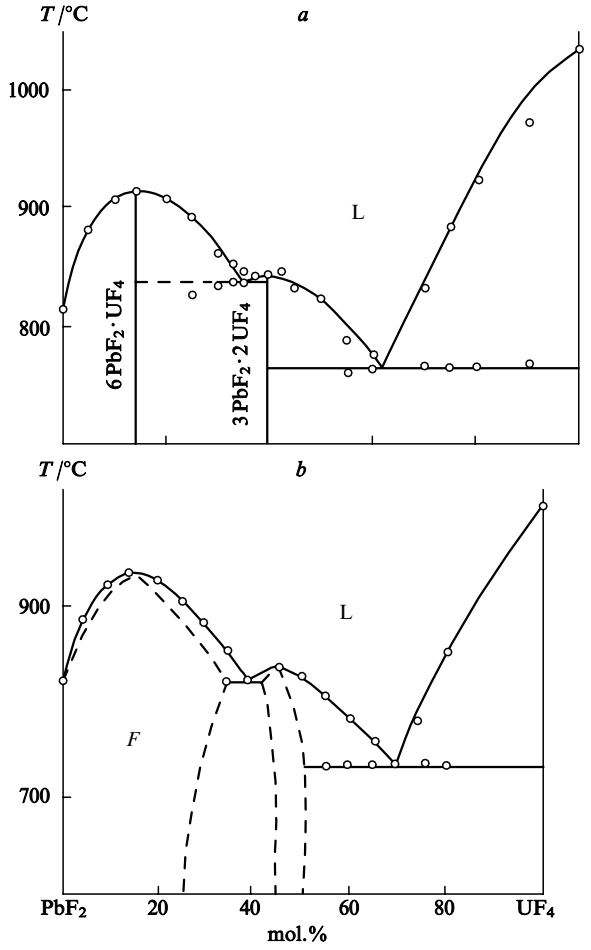

Figure 15. Phase diagram of the PbF_2-UF_4 system.
(*a*) according to the results of the study;[235] (*b*) according to the results of the study.[238]

structure.[241,242] The $PbThF_6$ compound with the tysonite structure was synthesised.[56,243] In this compound, a substantial amount of PbF_2 can be dissolved.[241] The mobility of fluoride ions in $PbThF_6$ was investigated.[244]

PbF_2-ZrF_4. The system was examined by several research teams.[199,245–251] The phase diagram of the system is shown in Fig. 16. The system contains the congruently melting $PbZrF_6$ compound, the incongruently melting Pb_3ZrF_{10} compound and the cubic solid solution $Pb_{1-x}Zr_xF_{2+2x}$ ($0 < x \leqslant 0.18$), whose structure undergoes ordering with decreasing temperature.[248] Like Pb_3ZrF_{10} ($n = 6$),[199] the monoclinic pseudotetragonal fluorite-like phase ($a \simeq a_F$, $b \simeq c \simeq 3a_F$) with approximate composition Pb_5ZrF_{14} is apparently a member of the homologous series $Pb_nR_2F_{2n+8}$ ($n = 10$). Ordering is based on formation of one-dimensional infinite clusters consisting of the ZrF_8 antiprisms.

A phase formed in the temperature range of $510 \leqslant T \leqslant 560$ °C at $0.34 \leqslant x \leqslant 0.35$ was interpreted[248] as a series of microphases, which can be described as orthorhombic superstructures with the unit cell parameters $a \simeq n \cdot 10$, $b \simeq 11.6$, $c \simeq 5.4$ Å. The case $n = 3$ corresponds to the Pb_2ZrF_8 compound.

According to the results of the study,[251] ZrF_4 is characterised by polymorphic transformations, which is apparently indicative of oxygen contamination.[252]

The $PbZrF_6$, Pb_5ZrF_{14} and Pb_2ZrF_8 compounds were synthesised by the reactions of solutions of ammonium fluorozirconates with lead nitrate.[253,254]

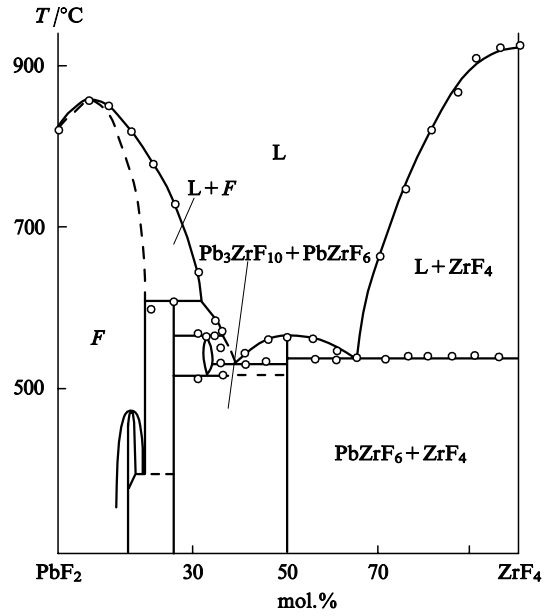

Figure 16. Phase diagram of the PbF_2-ZrF_4 system constructed based on the unpublished data of V K Goncharuk, G D Lukiyanchuk (Institute of Chemistry, Far-East Branch of the Russian Academy of Sciences) and P P Fedorov taking into account low-temperature equilibria published in the study.[248]

PbF_2-GeF_4. The system has[137] the $Pb_{1-x}Ge_xF_{2+2x}$ solid solution with the fluorite structure in the concentration range $0 < x \leqslant 0.08$ and the Pb_3GeF_{10}, $Pb_3Ge_2F_{14}$ and $PbGeF_6$ compounds. The liquidus of the system was not studied.

PbF_2-SnF_4. An analogous solid solution at $0 < x \leqslant 0.10$ and one $PbSnF_6$ compound exist in the system.[137] The liquidus of the system was not examined. The ionic conductivity of $Pb_{1-x}Sn_xF_{2+2x}$ was examined.[255]

PbF_2-TeF_4. The system was investigated[256] with the aim of revealing ionic conductivity in the solid state at 200 °C (TeF_4 decomposes above 193 °C). The PbF_2-based solid solution $Pb_{1-x}Te_xF_{2+2x}$ was found to exist at $0 \leqslant x \leqslant 0.2$. The lattice parameter sharply non-linearly increases as x increases to ~6.05 Å. The $Pb_7Te_4F_{30}$, $PbTeF_6$ and $PbTe_2F_{10}$ compounds were also mentioned, but their characteristics were not reported.

A series of compounds of lead difluoride with tetravalent metal fluorides were synthesised: $PbCeF_6$, $PbNpF_6$,[243] $PbPbF_6$ (PbF_3)[257] and $PbPtF_6$.[258]

VII. Systems PbF_2-MF_5

PbF_2-NbF_5. Interactions in this system were examined in detail[259,260] (Fig. 17). Five compounds formed at the NbF_5/PbF_2 ratios of 4/1, 5/2, 2/1, 1/1 and 1/3 were revealed.

PbF_2-TaF_5. The system was partially studied by DTA and X-ray diffraction analysis of annealed samples.[261] In the range $0 < x \leqslant 0.14$, the $Pb_{1-x}Ta_xF_{2+3x}$ solid solution with the fluorite structure exists. The lattice parameter of this solid solution changes from 5.940 ± 0.005 for $x = 0$ to 5.946 ± 0.005 Å for $x = 0.14$. Annealing of samples from $0.14 \leqslant x \leqslant 0.15$ at 400 °C demonstrated the presence of a low-temperature phase with the idealised composition Pb_6TaF_{17} ($x = 0.143$), which is transformed into the high-temperature modification at 460 °C. The ordered fluorite-like Pb_3TaF_{11} phase exists at $x = 0.25$.

The $PbAs_2F_{12}$ and $PbSb_2F_{12}$ compounds were synthesised.[262,263] The coordinates of eutectics in the PbF_2-MF_n binary systems and characteristics of the compounds formed in these systems are given in Tables 1 and 2, respectively.

Table 1. Coordinates of eutectics in PbF_2-MF_n systems.

MF_n	[PbF_2] (mol.%)	T /°C	Ref.	MF_n	[PbF_2] (mol.%)	T /°C	Ref.
LiF	60	580	109	AlF_3	78	560	186
	62 ± 2	583 ± 5	110	GaF_3	72.3, 55.5	550, 605	198
NaF	64	510	110	InF_3	58	525 ± 5	203
	66	520	116	ScF_3	74 ± 2	685 ± 5	9
KF	42	465	116	YF_3	49	885	105, 206, 207
RbF	55, 32	550, 485	116	GdF_3	58	1033	105, 206
	65, ~36	501, 457	37	TbF_3	56	991	105, 206
CsF	71, 28	565, 500	116	DyF_3	52.5	967	105, 206
	72, 28	520, 500	91	HoF_3	50	925	105, 206
BeF_2	79, ~68; ~8	477, 465, ~527	135	ErF_3	50	900	105, 206
MgF_2	11 ± 2	740 ± 5	138	TmF_3	52	880	105, 206
MnF_2	60	588	146	YbF_3	51	842	105, 206
FeF_2	72, 60	620, 623	146	LuF_3	47.5	807	105, 206
CoF_2	78	655	146	VF_3	70, 59	540, 620	219
NiF_2	82.5	708	146	CrF_3	74	561	220
ZnF_2	71.5, 54	600, 603	146		74	571	221
CuF_2	71.5, 54	600, 603	146	BiF_3	30	745	230
SnF_2	10	200	see [a]	UF_4	60, 30	820, 732	238
AlF_3	76.5	570	180	ZrF_4	62, 35	530, 538	see [b]
	77.5	565	184	NbF_5	~2	78	260

[a] See Fig. 5. [b] See Fig. 6.

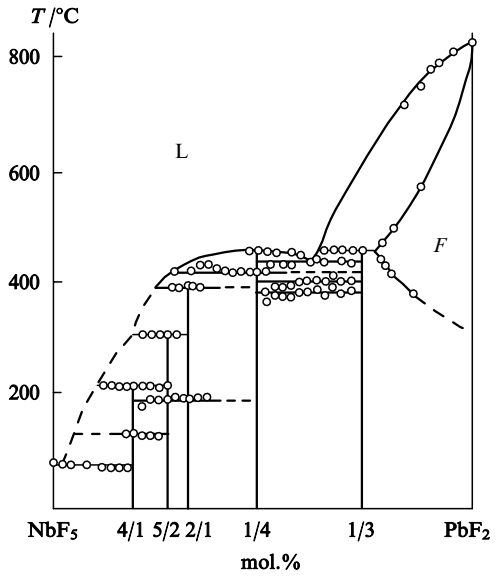

Figure 17. Phase diagram of the PbF_2-NbF_5 system.[260]

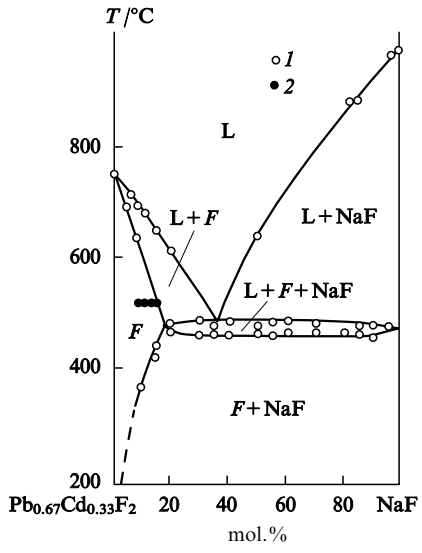

Figure 18. Polythermal section $NaF-Pb_{0.67}Cd_{0.33}F_2$ of the $NaF-PbF_2-CdF_2$ ternary system.[55,272]
(*1*) DTA data, (*2*) single-phase samples (powder X-ray diffraction data).

VIII. Ternary systems involving PbF_2

Numerous compounds involving PbF_2 were synthesised [264–271] (see Table 2). Data on phase equilibria in the corresponding systems are scarce.

$NaF-PbF_2-CdF_2$. The system was examined [55,272] using the $NaF-Pb_{0.67}Cd_{0.33}F_2$ section passing through a minimum in the melting curves of the phase diagram of the PbF_2-CdF_2 system (Fig. 18). Sodium fluoride was found to be readily dissolved in a fluorite matrix, the solubility being as much as 16 mol.%.

$NaF-PbF_2-BiF_3$. Phase equilibria in the system were studied at 400 °C (Fig. 19). The system has a band of a continuous solid solution F between a non-stoichiometric fluorite phase in the $NaF-BiF_3$ system and the $Pb_{1-x}Bi_xF_{2+x}$ solid solution based on cubic PbF_2 as well as the $NaBiF_4$ phase with the gagarinite structure ($NaNdF_4$) characterised by a narrow homogeneity region. A change in the lattice parameter of the ternary solid solution does not follow Vegard's law. Apparently, a melt was present in the concentration triangle formed by the $NaF-F-NaBiF_4$ phases at the experimental temperature (400 °C). Non-stoichiometry is typical of compounds with the gagarinite-type structure. Phases with the idealised composition $KPbRF_6$ (R = REM) belong to this family (see Table 2).

$RbF-PbF_2-BiF_3$. The melting points of a number of composites in the system were determined [37] (Fig. 20). These results provided evidence for the existence of the congruently melting $RbPbBiF_6$ compound.

Table 2. Selected characteristics of compounds involving lead difluoride.

Compound	Crystal system, structure type, space group	Unit cell parameters				Z	Density /g cm^{-3}		Transformation temperature /°C	Ref.
		a /Å	b /Å	c /Å	α, β, γ /deg		experiment	calculation		
$K_{0.33}Pb_{0.67}F_{1.67}$	cubic, *Im*3*m*	4.6655(1), at 673 K				2	–	–	–	123
$KPbF_3$	–	–	–	–	–	–	–	–	298.5 (p)	120
K_4PbF_6	trigonal, *R*3*c*	9.6		12.3		–	4.07	3.93	475 (i)	116
$Rb_{0.33}Pb_{0.67}F_{1.67}$	cubic, *Im*3*m*	–				2	–	–	–	124
$RbPbF_3$	–	–	–	–	–	–	–	–	560 (c)	116
	–	–	–	–	–	–	–	–	524 (c)	37
	cubic, *Pm*3*m*	4.790				1	–	–	–	128
α-$CsPbF_3$	the same	4.800				1	–	–	615 (p)	116
	–	–	–	–	–	–	–	–	725 (c), 630 (c)	91
$TlPbF_3$	cubic, *Pm3m*	4.62				1	–	–	–	129
$PbBeF_4$	orthorhombic, *Pnma*	8.310	5.350	6.370		–	–	6.853	585 ± 5 (c)	135, 136
Pb_2BeF_6	–	–	–	–	–	–	–	–	482 ± 5 (c)	135
Pb_2MgF_6	tetragonal, $P4_2/nbc$	7.93		16.15		8			< 670 (d)	138, 141
Pb_2MnF_6	the same	7.98		16.92		8	7.10	7.19	592 (i)	145, 146, 147
Pb_2FeF_6	"	7.97		16.66		8	7.25	7.33	628 (c)	143, 144
Pb_2CoF_6	"	7.92		16.46		8	7.50	7.56	670 (i)	143, 144
Pb_2NiF_6	"	7.88		16.22		8	7.67	7.74	738 (i)	143, 144
Pb_2ZnF_6	"	7.92		16.33		8	7.63	7.70	613 (c)	143, 144
Pb_2CuF_6	monoclinic, $I2/m$	4.04 ± 0.01	15.80 ± 0.02	4.04 ± 0.01	91.3 ± 0.1	2	7.55	–	618 (c)	145,146
$PbSnF_4$	tetragonal,	4.20 ± 0.02		11.36 ± 0.1		2	–	6.65	–	160
	*P*4/*nmm*	4.2196		311.415		2	6.60	–	–	163
	the same	4.215(3)		11.744(32)		2	–	–	–	172
	"	4.2262(3)		11.4407		2	–	–	–	173
β-$PbSnF_4$	tetragonal, *P*4/*n*, *P*4/*nmm*	4.193		22.83		4	–	–	–	165
β-$PbSnF_4$	tetragonal, $P4_2/n$, $P4_2/nnm$	5.969		51.50		18	–	–	–	165
$PbSnF_4$	tetragonal,	16.834		23.063		64	–	–	–	163
α-$PbSnF_4$	monoclinic, *P*2/*n*	4.204	4.205	11.414	91.34	2	–	–	–	165
	monoclinic, *P*2/*n* (at 20 K)	4.1860(8)	4.1849(8)	11.3806(10)	90.724(6)	2	–	–	–	173
α-$PbSnF_4$	monoclinic, $P2_1/n$	4.193		22.83	91.54	4	–	–	–	165
$PbSnF_4$	orthorhombic, *Aba*2	22.845(2)	5.850(2)	6.021(2)		8	–	6.63	–	170
$Pb_{0.7}Sn_{0.3}F_4$	tetragonal, $I4_1/acd$	5.923(4)		105.87(2)		72	–	–	–	169
$Pb_{0.6}Sn_{0.4}F_4$	the same	5.962(4)		80.54(2)		56	–	–	–	169
$PbPdF_4$	tetragonal, *I*4, $K[BrF_4]$ type	5.837		10.833		–	6.80	6.92	–	176
$PbAl_2F_8$	–	–	–	–	–	–	4.82 ± 5		614 ± 20 (i)	181
$PbAlF_5$	tetragonal, *I*4	14.25		7.230		–	5.91 ± 5	5.965	618 ± 20 (i)	181, 182
	–	–	–	–	–	–	–	–	312 ± 10 (p)	192
$Pb_9Al_2F_{24}$	–	–	–	–	–	–	7.30 ± 5		560 ± 12 (i)	181
	–	–	–	–	–	–	–	–	555 ± 10 (d)	184
$Pb_3Al_2F_{12}$	tetragonal, *I*4/*m*	14.23		7.20		6	6.47		649 (i)	180
		–	–	–	–	–	–	–	665 ± 10	184
$Pb_3Al_2F_{12}$	monoclinic, $P2_1/n$	9.435(6)	9.610(5)	10.100(9)	90.59(5)	4		6.55		187
$Pb_5Al_3F_{19}$	tetragonal, *I*4	20.174(15)		7.220(5)		–		6.720	12 (p)	185
	monoclinic	14.23	14.51	7.22	92	4	6.62	–	660 (p)	186
	tetragonal, *P*4/*n*	20.17		7.22		–	6.60	6.681	–	188
	tetragonal, *I*4/*m*	14.28		7.227		–	6.60	6.656	–	189
	tetragonal, *I*4*cm*	14.07		7.300		–	6.60	6.793	–	190
$PbGaF_5$	tetragonal, *I*4	14.42		7.30		16	–	6.45	630 (i), 510 (p)	198
	–	–	–	–	–	–	–	–	312 ± 10 (p)	192
	tetragonal, *I*4	14.485		7.324		16	–	–	–	182
$Pb_9Ga_2F_{24}$	orthorhombic	4.172	4.205	5.905		–	–	–	571 (i)	198
$Pb_3(GaF_6)_2$	tetragonal	14.26		7.39(5)		6		6.67	626 ± 5, 395 (p)	198
	the same	14.349		7.443		6	–	–	–	192, 200

Table 2 (continued).

Compound	Crystal system, structure type, space group	Unit cell parameters				Z	Density /g cm^{-3}		Transformation temperature /°C	Ref.
		a /Å	b /Å	c /Å	α, β, γ /deg		experiment	calculation		
$Pb_5Ga_3F_{19}$	tetragonal	14.361(10)		7.441(5)		–	–	6.952	372 (p)	185
Pb_2InF_7	monoclinic, $P2_1/c$	5.616(3)	12.452(6)	8.416(4)	90.25(5)	4	7.45	7.47	465 (d)	201, 202
$Pb_7In_5F_{29}$	monoclinic, $C2/c$	24.580(5)	37.917(6)	8.026(3)	90.74(5)	12	6.82	6.86	535 (i)	201 – 203
$Pb_4Sm_3F_{17}$	trigonal, $R3$	10.9551(3)		20.283(1)		42	–	7.58	–	209
	the same	10.9463(8)		20.326(2)		–	–	–	–	212
	"	–	–	–	–	–	–	–	680 ± 10 (d)	105, 211
$Pb_4Eu_3F_{17}$	"	10.9237(4)		20.227(1)		42	–	7.66	–	209
$Pb_4Gd_3F_{17}$	"	10.904(1)		20.173(4)		42	–	7.79	–	209
	"	10.9012(8)		20.187(3)		–	–	–	–	212
	"	–		–		–	–	–	785 ± 10 (d)	105, 211
$Pb_4Tb_3F_{17}$	"	10.856(2)		20.071(4)		42	–	7.92	–	209
	"	–		–		–	–	–	819 ± 10 (d)	105, 211
$Pb_4Dy_3F_{17}$	"	10.826(2)		20.094(6)		42	–	8.01	–	209
	"	–		–		–	–	–	835 ± 10 (d)	105, 211
$Pb_4Y_3F_{17}$	"	10.814		19.931		42	–	–	845 ± 10 (d)	105, 207,
	"	10.816(2)		19.942(5)		–	–	6.99	–	209
$Pb_4Ho_3F_{17}$	"	10.825(1)		19.967(3)		42		8.10	–	209
	"	–		–		–	–	–	860 ± 10 (d)	105, 211
$Pb_4Er_3F_{17}$	"	10.766(1)		19.891(4)		42	–	8.25	–	209
	"	10.8108(3)		19.963(1)		–	–	–	–	212
	"	–		–		–	–	–	865 ± 10 (d)	105, 211
$Pb_4Tm_3F_{17}$	"	10.724(2)		19.905(7)		42	–	8.34	–	209
	"	10.7928(6)		19.913(1)		–	–	–	–	212
	"	–		–		–	–	–	860 ± 10 (d)	105, 211
$Pb_4Cb_3F_{17}$	"	10.7459(8)		19.854(3)		42	–	8.38	–	209
	"	10.7691(5)		19.856(1)		–	–	–	–	212
	"	–		–		–	–	–	850 ± 10 (i)	105, 211
$Pb_4Lu_3F_{17}$	"	10.7037(8)		19.848(2)		42	–	8.48	–	209
	"	10.7524(6)		19.8794(2)		–	–	–	–	212
	"	–		–		–	–	–	825 ± 10 (i)	105, 211
Pb_2YF_7	tetragonal, $I4$, $I4/m$	4.0799(7)		17.392(4)		2	–	–	–	209
$Pb_3(TiF_6)_2$	tetragonal, $I4$, $I\bar{4}$, $I4/m$	14.576		7.424		6	5.98	5.969	575 ± 15 (c)	182, 217
	the same	–		–		6	–	–	557 ± 15, 422 (p)	200
$Pb_5Ti_3F_{19}$	–	14.560(10)		7.405(5)		4	–	6.442	422 (p)	185
$PbVF_5$	tetragonal, $I4$, $I\bar{4}$, $I4/m$	14.510		7.444		16	5.99	5.988	566 ± 7 (c)	218
Pb_4VF_{11}	–	–		–	–	–	–	–	552 (i), 400 (p)	219
$Pb_3(VF_6)_2$	tetragonal	14.26		7.414		6	6.12	–	620 (c), 370 (p)	219
	the same	14.510		7.444		–	–	–	602 ± 1, 361 (p)	182, 200
$Pb_5V_3F_{19}$	"	14.485(10)		7.420(5)		4	–	–	357 (p)	185
Pb_4CrF_{11}	–	–	–	–	–	–	–	–	592 (i)	220, 221
$Pb_3(CrF_6)_2$	tetragonal, $I4$, $I\bar{4}$, $I4/m$	14.38		7.41		6	–	–	672 (c)	220, 221
	–	–		–		6	–	–	683 ± 2, 277 (p)	200
	the same	14.424		7.417		6	–	–		182
$Pb_5Cr_3F_{19}$	tetragonal, $I4cm$	14.384(5)		7.408(2)		4	–	6.729	272 (p)	185, 193
	–	–				–	–	–	–	222
$Pb_3(FeF_6)_2$	tetragonal, $I4$, $I\bar{4}$, $I4/m$	14.449		7.441		6	6.18	6.167	569	182, 223
	–	–	–	–	–	–	–	–	583, 467 (p)	200
$Pb_5Fe_3F_{19}$	tetragonal, $I4cm$	14.420(10)		7.440(5)		4	–	6.717	467 (p)	185
$Pb_3Fe_2F_{12}$	triclinic, $P1$	7.403(2)	7.621(2)	9.890(3)	110.45(2), 107.98(1), 95.92(2)	2	–	6.607		224
Pb_2RhF_7	monoclinic, $C2/c$	5.51(9)	11.66(8)	8.63(5)	90.94	4	–	–	–	234
	monoclinic, $P2_1/c$	5.569	11.85	8.832	91.00	4	6.26	6.409	–	233
$PbCeF_6$	tysonite type	7.214(1)		7.287(1)		3	–	7.01	–	243
$PbUF_6$	the same	7.242		7.370		3	–	8.33	836 (c)	238
	"	7.245(5)		7.355(5)		–	–	8.33	–	243
$PbThF_6$	tysonite type	7.280(5)		7.404(5)		3	–	8.10	–	243
$PbNpF_6$	the same	7.212(5)		7.360(5)		3	–	8.38	–	243
Pb_3ZrF_{10}	orthorhombic, $Cmcm$, $Cmc2_1$	10.713(3)	12.817(4)	5.909(2)		4	–	–	604 ± 10 (i)	248

Table 2 (continued).

Compound	Crystal system, structure type, space group	Unit cell parameters				Z	Density /g cm^{-3}		Transformation temperature /°C	Ref.
		a /Å	b /Å	c /Å	α, β, γ /deg		experiment	calculation		
Pb_5ZrF_{14}	monoclinic	5.851(1)	17.685(3)	17.743(3)	90.86	–	–	–	–	248
$PbZrF_6$	orthorhombic, *Cmma*, *Abm*2	7.549(4)	11.123(6)	5.310(3)		4	5.90	6.14	620 (c)	245
	orthorhombic, *Cmma*	7.54(6)	11.11(8)	5.30(8)		–	–	–	–	246
	–	–	–	–	–	–	–	–	570 ± 10 (c)	248
$PbSnF_6$	–	–	–	–	–	–	–	–	–	237
$PbGeF_6$	$R\bar{3}m$	7.179(3)		6.941(3)		1	–	–	–	237
$Pb^{II}Pb^{IV}F_6$	tetragonal, $KNbF_6$ type, $P\bar{4}c2$	5.201		4.523		–	–	–	–	257
$PbPtF_6$	trigonal, $R\bar{3}m$	7.220		7.07		–	–	–	–	258
α-$Pb_2Nb_5F_{29}$	cubic	13.40				–	–	–	304 (i)	259, 260
β-$Pb_2Nb_5F_{29}$	tetragonal	16.12		8.10		–	–	–	190 (p)	259, 260
α-$PbNb_2F_{12}$	cubic	13.29				–	–	–	392 (i), 190 (p)	259, 260
$PbNbF_7$	–	–	–	–	–	–	–	–	452 (c), 416 (p)	259, 260
$PbNb_4F_{22}$	–	–	–	–	–	–	–	–	212 (i), 130 (p)	259, 260
Pb_3NbF_{11}	–	–	–	–	–	–	–	–	454 (i)	259, 260
α-Pb_6TaF_{17}	orthorhombic	4.284	4.110	41.15		2	–	–	460 ± 10 (p)	261
$Na_3Pb_2(BeF_4)_3F$	hexagonal, $P6_3/m$, apatite type	9.531		7.028		2	–	–	–	264
$K_2Pb(BeF_4)_2$	trigonal, $R\bar{3}m$	5.455		20.50		–	–	–	–	265
$Tl_2Pb(BeF_4)_2$	the same	5.577		21.89		–	–	6.639	–	265
$Rb_2Pb(BeF_4)_2$	"	5.558		21.35		–	–	–	–	265
$KPbLaF_6$	hexagonal, gagarinite type	6.549		3.804		1	–	–	–	266
$KPbCeF_6$	the same	6.530		3.772		1	–	–	–	266
$KPbPrF_6$	"	6.516		3.751		1	–	–	–	266
$KPbNdF_6$	hexagonal	6.506		3.731		1	–	–	–	266
$KPbSmF_6$	the same	6.487		3.697		–	–	–	–	266
$KPbEuF_6$	"	6.483		3.692		–	–	–	–	266
$LiPbVF_6$	hexagonal, $P\bar{3}1c$, $LiCaAlF_6$ type	5.23(9)		10.48(1)		2	–	–	–	82
$LiPbCrF_6$	the same	5.20(8)		10.44(2)		2	–	–	–	82
$LiPbFeF_6$	"	5.23(6)		10.45(2)		2	–	–	–	82
$LiPbGaF_6$	"	5.19(8)		10.42(3)		2	–	–	–	82
$NaPbFe_2F_9$	monoclinic, $C2/c$	7.308	12.55	7.640	93.06	–	4.865	–	–	267
$KPbCr_2F_9$	orthorhombic, *Pnma*	9.81(5)	5.412(3)	13.93(1)		4	4.680	4.679	–	268
$Pb_8Fe_3F_{24}$	triclinic, $C\bar{1}$	20.11	5.597	9.44	89.750, 105.790, 89.38	–	7.407	–	–	269
$Pb_8(MnFe_2F_{14})F_{10}$	$P2_1/a$	20.18	5.625	9.438	105.00	–	7.317	–	–	270
$Al_2Pb_9Sn_9F_{42}$	$P4/n$	9255		11.30		–	–	–	–	271

Note. The following notations are used: c is congruent melting, i is incongruent melting, p is a phase transition, d is decomposition in the solid state.

$NaF-PbF_2-UF_4$ and $KF-PbF_2-UF_4$. The liquidus surfaces for these systems are shown in Figs 21 and 22, respectively. In both cases, solid-phase equilibria were not reported.

$PbF_2-CdF_2-RF_3$. The systems were partially examined in the studies.[55,274,275] The PbF_2-CdF_2-based $(Pb_{1-y}Cd_y)_{1-x}Ce_xF_{2+x}$ solid solution with the fluorite structure and the CeF_3-based $(Pb_{1-y}Cd_y)_{1-x}Ce_xF_{3-x}$ solid solution with the tysonite structure were found to exist in the $PbF_2-CdF_2-CeF_3$ system in the temperature range of 600–760 °C (Fig. 23).

Regions of the $Pb_{0.67}Cd_{0.33}F_2-RF_3$ polythermal sections of the $PbF_2-CdF_2-RF_3$ ternary systems (R = Ce, Gd, Er, Lu, Sc, Y) were investigated.[55,275] These sections are similar to quasibinary sections (Fig. 24). The $(Pb_{0.67}Cd_{0.33})_{1-x}R_xF_{2+x}$ solid solutions (phases F) are observed in these sections. In the sections with R = Ce and Gd, the phases F melt according to peritectic reactions. In the section with Er, the phases F melt according to a eutectic reaction, the melting curves of the solid solution in this section having a maximum. This maximum is also observed in the section with Lu, where the fluorite-like phase R containing 40 mol.% of LuF_3 is involved in phase equilibria with the melt. This character of the sections is indicative of the existence of saddle points on liquidus surfaces of solid solutions in systems with rare-earth elements of the yttrium group.

The $PbF_2-Sn_2F_6$ section belonging to the $PbF_2-SnF_2-SnF_4$ ternary system was partially studied[255] and the boundary of the $Pb_{1-x}(Sn^{II}_{0.5}Sn^{IV}_{0.5})_xF_{2+x}$ solid solution ($x \leqslant 0.15$) with the fluorite structure was determined.

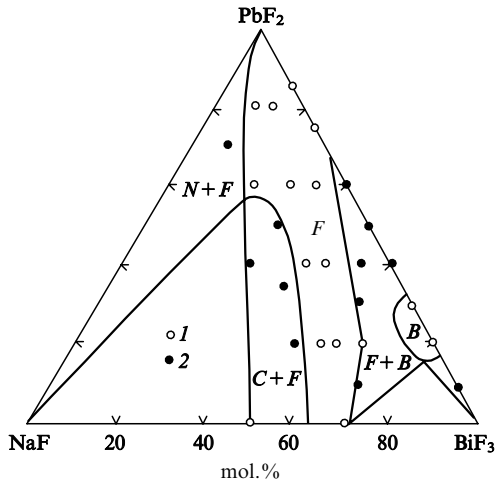

Figure 19. Isothermal section of the $NaF-PbF_2-BiF_3$ system at 400 °C.[273]
Samples: (*1*) single-phase, (*2*) two-phase.

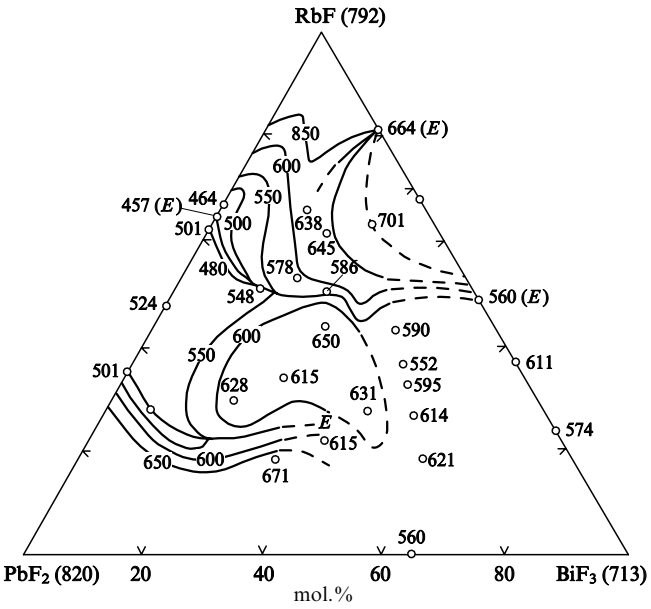

Figure 20. Liquidus surface of the $RbF-PbF_2-BiF_3$ system.[37]
Here and in Figs 21 and 22, the numbers in the diagrams indicate the temperature in °C.

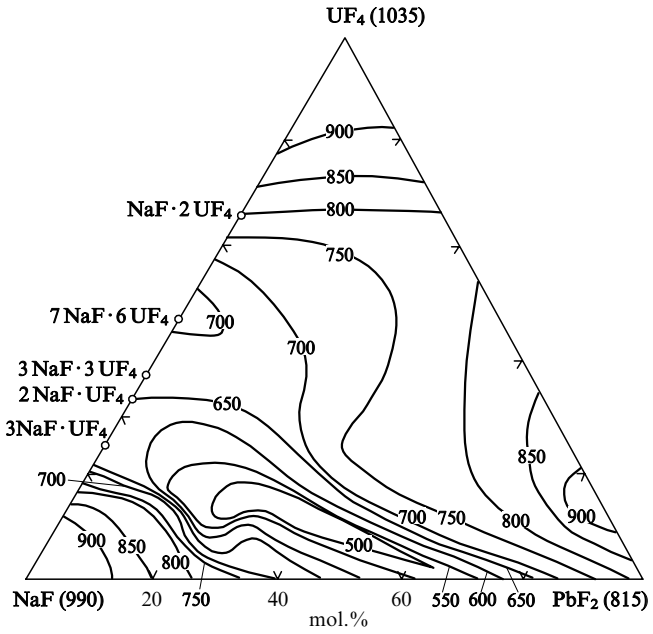

Figure 21. Liquidus surface of the $NaF-PbF_2-UF_4$ system.[235]

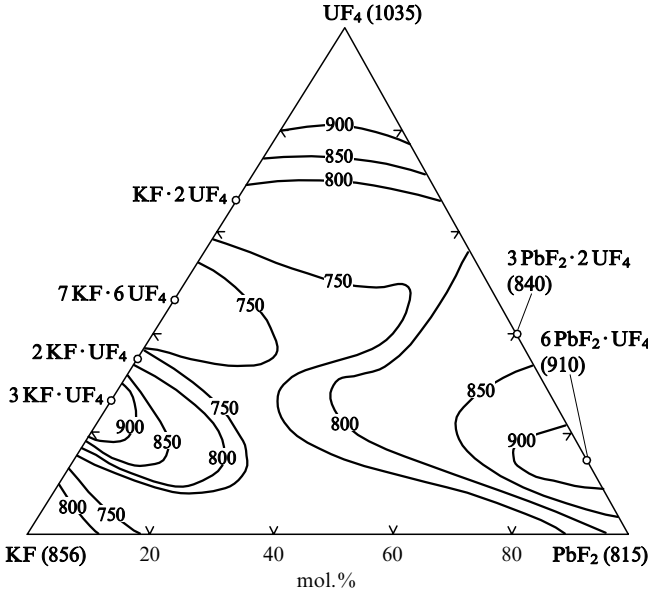

Figure 22. Liquidus surface of the $KF-PbF_2-UF_4$ system.[235]

IX. Other compounds involving fluorine and divalent lead

Lead compounds with mixed anions, including $Pb_2SO_4F_2$, $Pb_6SO_4F_{10}$, $Pb_2CO_3F_2$ and $Pb_5(PO_4)_3F$, were studied.[102] Lead fluoride halides PbXF (X = Cl, Br, I; the rare mineral matlockite PbClF occurs in nature) and other compounds with a more complex stoichiometry were synthesised.[276–283]

Lead oxofluoride Pb_2OF_2 is known.[79, 284] Oxofluoride phases involving lead fluoride hold promise as solid electrolytes and fluxes. Numerous compounds occur in the PbF_2-MO_x systems [for example, with M = V (see Ref. 36) or Te (see Ref. 285)]. Many studies were devoted to phases formed in the Pb,Bi//O,F system (see Refs 286–291) and in more complex systems.[292]

X. Characteristic features of phase diagrams involving PbF_2

1. Formation of compounds

As a rule, both solid solutions based on the cubic modification of PbF_2 and numerous compounds are formed in systems involving lead difluoride. Generally, the formation of chemical compounds (phases characterised by narrow homogeneity regions) leads to limitation of homogeneity regions of solid solutions according to the Hume-Rothery rule.[293]

To gain insight into the nature of compounds formed, let us consider the diagram presented in Fig. 25, where the representative points of cations are shown in the generalised

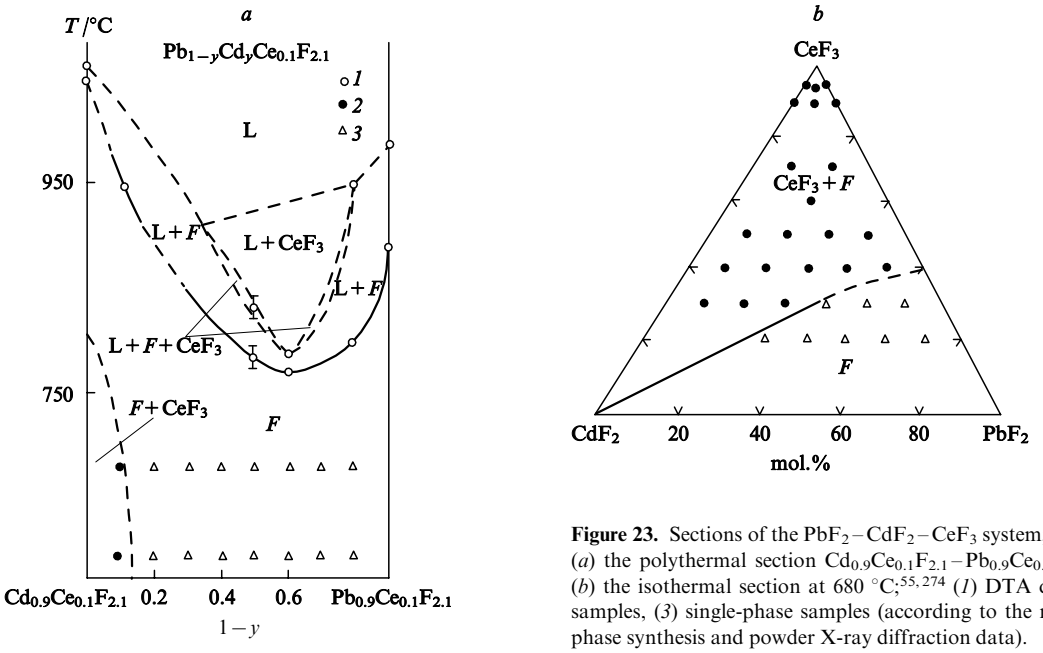

Figure 23. Sections of the $PbF_2-CdF_2-CeF_3$ system; (*a*) the polythermal section $Cd_{0.9}Ce_{0.1}F_{2.1}-Pb_{0.9}Ce_{0.1}F_{2.1}$ (see Ref. 55), (*b*) the isothermal section at 680 °C;[55,274] (*1*) DTA data, (*2*) two-phase samples, (*3*) single-phase samples (according to the results of the solid-phase synthesis and powder X-ray diffraction data).

moment† – electronegativity coordinates. This combination of variables, which was first proposed in the study,[294] is convenient for classification of binary salt systems according to the formation of compounds in systems containing one constant component.[295,296] Figure 25 was constructed with the use of the ionic radii of fluorine according to Schannon (the coordination number is 6)[297] and the electronegativities according to Batsanov.[298] Some required parameters (for example, characteristics of divalent tin) were estimated by us.

Two regions of existence of compounds are observed in the $M-x$ diagram (in Fig. 25, these regions are separated by a dark field), which is indicative of the amphoteric character of the basic compound PbF_2. Lead difluoride serves as Lewis acid and Lewis base in the lower left and upper right regions, respectively. Lead difluoride exhibits very weak acidic properties. This compound can be considered as a complex-forming agent only in combination with fluorides MF, where M is heavy alkali metal (K, Rb or Cs) or monovalent thallium. Compounds with francium and monovalent gold are predicted to exist. In the $MPbF_3$ compounds with the perovskite structure belonging to this group, lead has an octahedral coordination. Since the phase diagram of the PbF_2-AgF system[134] is incorrect, it is necessary to study this system in more detail.

In addition, PbF_2 acts as a base in numerous compounds. The structures of this type of compounds are determined by the structure of a complex-forming agent. Lead plays a passive role. The structures contain constructions of tetrahedra (compounds involving BeF_2), octahedra (compounds involving aluminium, iron, chromium, *etc.* trifluorides), eight- and nine-vertex polyhedra (compounds involving rare-earth or zirconium fluorides).

† The ratio of the oxidation state to the ionic radius.

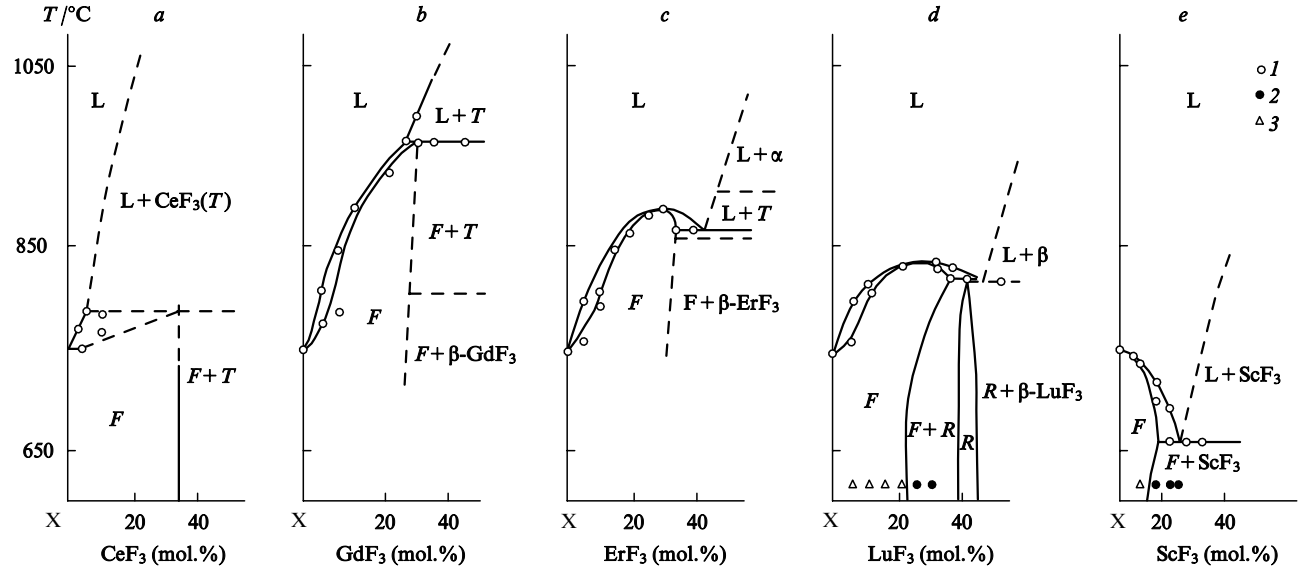

Figure 24. Polythermal sections $X-RF_3$ ($X = Pb_{0.67}Cd_{0.33}F_2$) of the $PbF_2-CdF_2-RF_3$ systems, where R = Ce (*a*), Gd (*b*), Er (*c*), Lu (*d*) and Sc (*e*). (*1*) DTA data, (*2*) two-phase samples, (*3*) single-phase samples (according to the results of the solid-phase synthesis and powder X-ray diffraction data).[55,275]

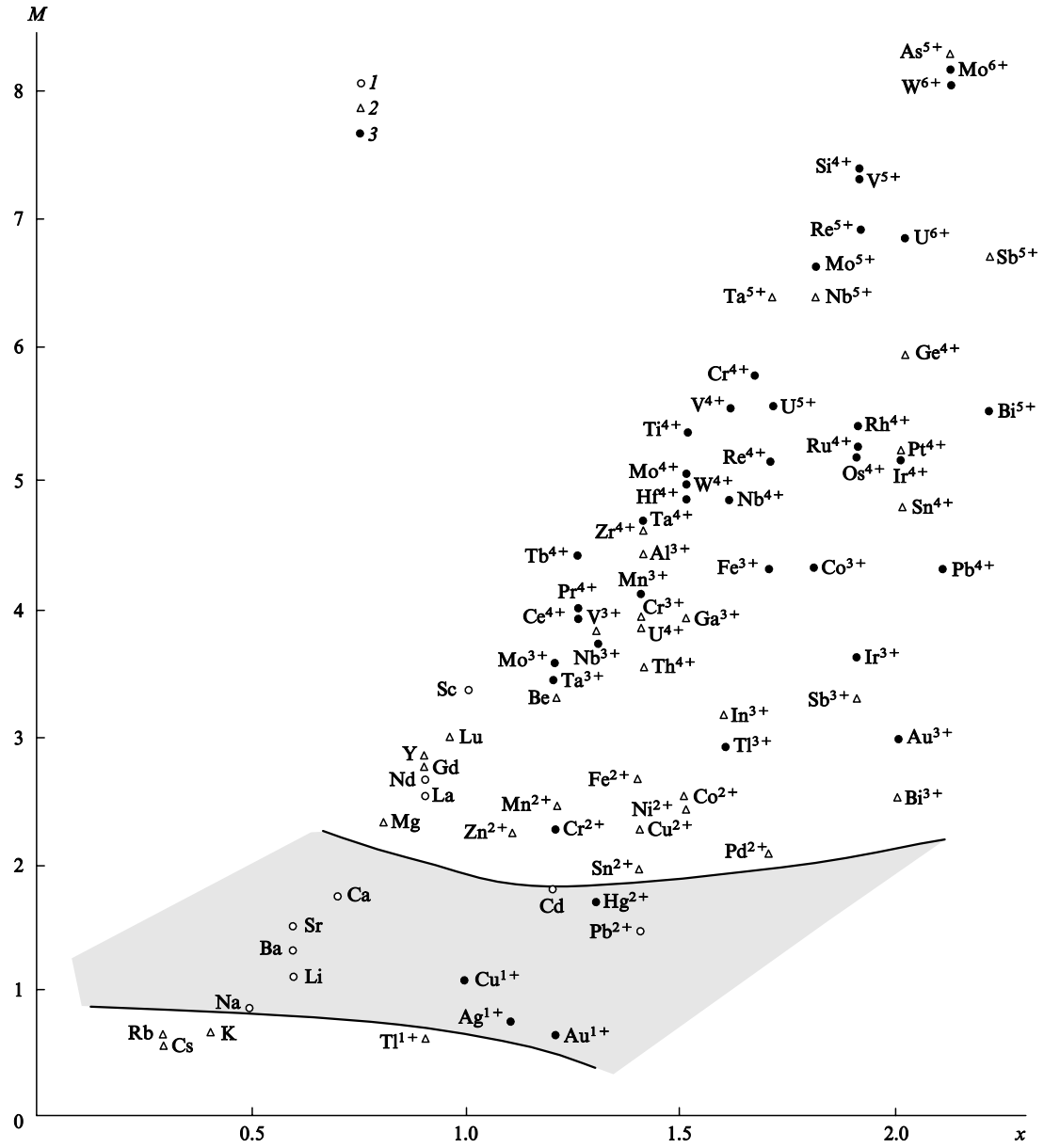

Figure 25. Generalised moment of a cation (M) – electronegativity (x) diagram for the $PbF_2 - MF_n$ systems.
(*1*) The corresponding fluoride does not form compounds with PbF_2, (*2*) the corresponding fluoride forms compounds with PbF_2, (*3*) the system was not studied.

An analysis of the diagram presented in Fig. 25 provides evidence for the existence of compounds which are as yet unknown. These are primarily compounds in systems with TiF_4, SiF_4 and molybdenum fluorides, $PbHfF_6$, Pb_3HfF_{10} and other phases analogous to lead fluorozirconates.[248] By analogy with the known $PbF_2 - NbF_5$ system,[259,260] a series of compounds are predicted to exist in a system with tantalum pentafluoride in addition to those isolated in the study.[261] It is worthwhile searching for compounds in the $PbF_2 - ScF_3$ system. Such compounds can be formed in the solid state at low temperatures. It should be taken into account that there are restrictions on the formation of compounds with fluorides of metals in high oxidation states due to the possibility of redox reactions (accompanied by transformations of lead into higher oxidation states), but there are no such restrictions on the formation of compounds containing metals in low oxidation states, even exotic (for example, divalent chromium and vanadium).

2. Phases of variable composition

According to the third law of thermodynamics, both iso- and heterovalent solid solutions undergo ordering and/or decomposition with decreasing temperature.

The $PbSnF_4$ and Pb_2MF_6 compounds (M = Mg, Mn, Fe, Co, Ni, Zn, Cu) can (should) be considered as ordered fluorite-like phases formed in the $PbF_2 - MF_2$ systems. The distribution of cations in their structures leads to lowering of the symmetry, the fluorite motif being retained.

Figures 26 and 27 present possible phase diagrams of the $PbF_2 - MF_2$ systems taking into account decomposition and ordering of solid solutions according to the mechanism of first-order phase transitions as well as possible transformations of phase diagrams caused by an increase in the temperature of the upper critical points. The critical temperatures of the domes of decomposition of continuous high-temperature solid solutions in the $PbF_2 - MF_2$ systems (M = Ba, Sr) are higher than the temperature of the polymorphic transformation between the orthorhombic and cubic modifications of PbF_2.[140,144] Hence, Fig. 26 *c*

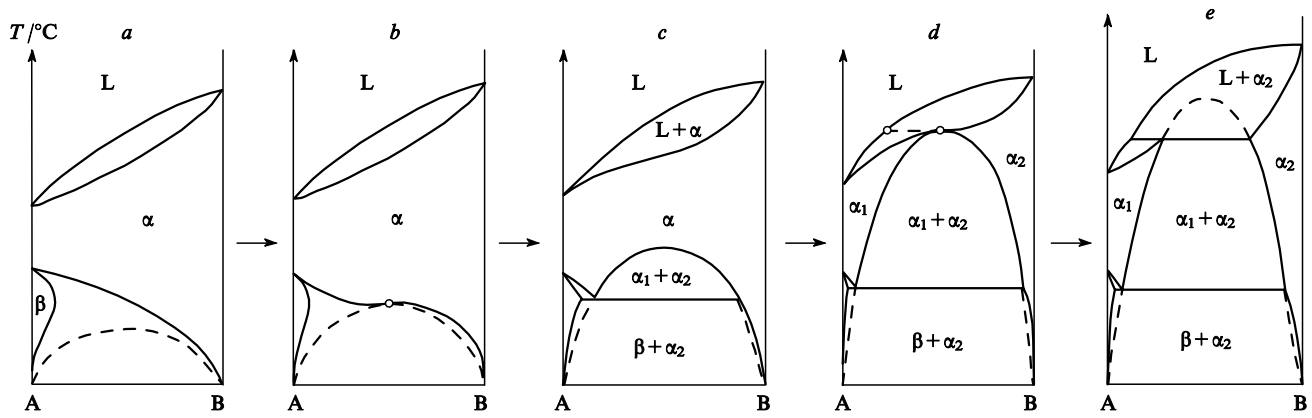

Figure 26. Transformation of the phase diagram of the binary system (A – B) with a high-temperature continuous solid solution α and polymorphism (α ⇌ β) of one of the components (*a*) with increasing temperature of the upper critical point of the dome of decomposition.
Metastable equilibria are indicated by dashed lines, bifurcations are shown by circles; (*b* – *e*) see comments in the text.

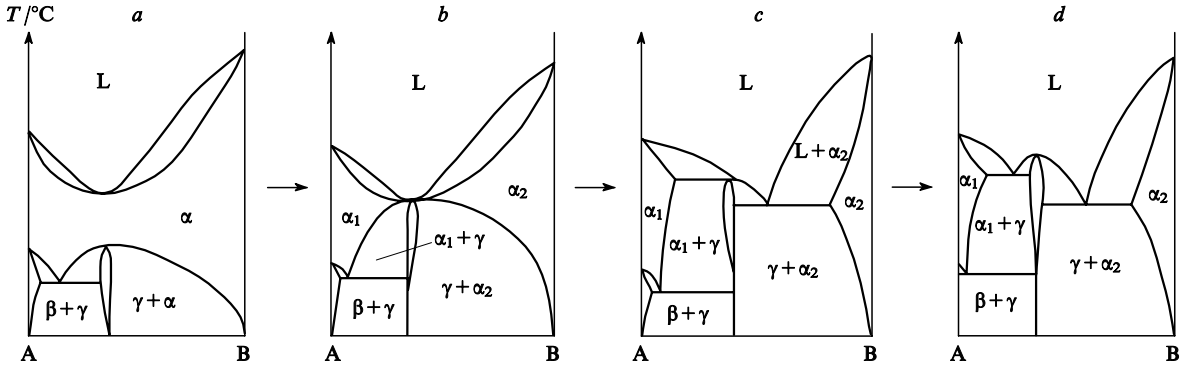

Figure 27. Transformation of the phase diagram of the binary A – B system with a high-temperature continuous solid solution, a minimum in the melting curve, polymorphism (α ⇌ β) of one of the components and the formation of a low-temperature compound γ with increasing temperature stability of the latter; (*a* – *d*) see comments in the text.

corresponds apparently to phase diagrams of these systems. The phase diagram with a discontinuity of miscibility shown in Fig. 26 *e* corresponds to the $PbF_2 - CaF_2$ system. Phase diagrams with transition points (Fig. 26 *b*, *d*) correspond to a change in the topology (bifurcations). According to the classification proposed in the studies,[105, 299, 300] these bifurcations belong to types B_1III and B_1VI, respectively.

The diagram presented in Fig. 27 *a* corresponds apparently to the $PbF_2 - CdF_2$ system. In this system, the composition corresponding to a minimum in the melting curves is characterised (within the experimental error) by the ratio $PbF_2 : CdF_2 = 1 : 2$ analogously to the Pb_2MF_6 compounds revealed in systems with difluorides of other metals with smaller ionic radii. The structure of single crystals of $Pb_{0.67}Cd_{0.33}F_2$ was studied by different methods.[157, 158] Analysis of these results suggests that single crystals contain domains with the corresponding structure.

Phase diagrams shown in Fig. 27 *b* – *d* correspond to a bifurcation point and incongruent and congruent melting of the γ phase, respectively. Figure 27 *c*, where incongruent melting of a compound is observed, corresponds to the $PbF_2 - MnF_2$ system taking into account a change in the crystal structure of MnF_2 as a result of a morphotropic transformation in the MF_2 series. Correspondingly, a noticeable region of a cubic PbF_2-based solid solution would be expected to exist in this system. Actually, the experimental data [145] provided evidence for the existence of this solid solution. However, these data were ignored in the construction of the phase diagram.

Experimental studies of compounds in low-temperature regions of phase diagrams present methodological difficulties. The time of solid-phase annealing required for the establishment of equilibrium increases exponentially with decreasing temperature. The dependence of the time required for sintering of samples in the $PbF_2 - RF_3$ systems on the annealing temperature was experimentally determined [105, 301] (Fig. 28). According to these results, ~100 and ~1000 h are required for the establishment of the equilibrium at 600 and 500 °C, respectively. At lower temperatures, the equilibrium cannot be attained with the use of this procedure. Data on solid-phase equilibria in the $PbF_2 - ZrF_4$ system in the range of 600 – 300 °C were reported.[248] According to these results, a sample of the Pb_5ZrF_{14} compound was synthesised at 450 °C over 8 days. The above difference is attributable to the lower melting point of ZrF_4 compared to those of rare-earth fluorides.

To accelerate chemical reactions and gain information on low-temperature states, it is worthwhile performing the synthesis with the use of a solvent [although this procedure can give rise to non-equilibrium compounds (modifications) as well]. One can perform precipitation from nitrate solutions, hydrothermal synthesis and synthesis by the flux techniques. It should be noted that water and nitrates can serve as a source of oxygen contamination. Hence, a search for appropriate low-temperature solvents is an important problem. For example, the former method was used for the preparation of compounds in the $PbF_2 - SrF_2$ (see Ref. 143) and $PbF_2 - ZrF_4$ systems (see Refs 253 and 254). The second method was used for the synthesis of $PbSnF_4$.[12, 170]

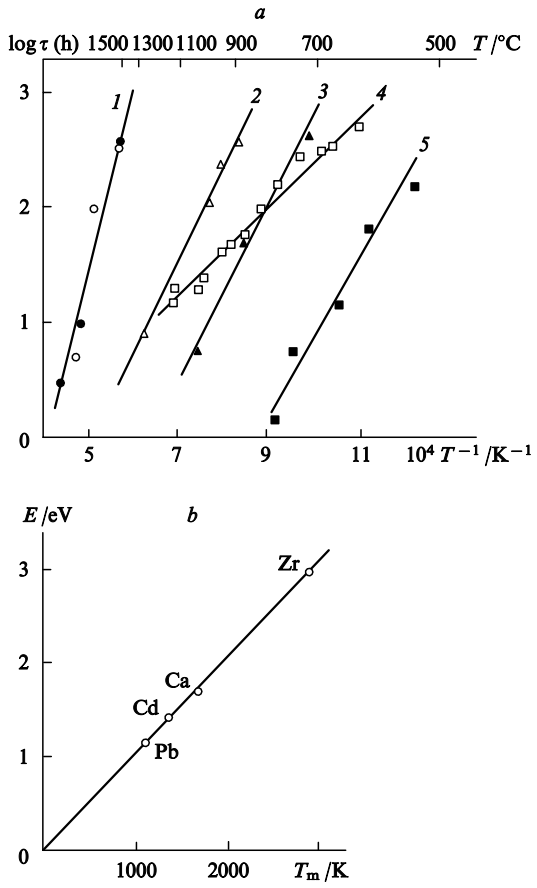

Figure 28. Required sintering time (τ) *vs.* the temperature (T) in fluoride and oxide systems (*a*), and the apparent activation energies (E) of formation of solid solutions with the fluorite structure *vs.* the melting point (T_m) of the basic component (*b*).[105, 301]
The system: (*1*) $ZrO_2-R_2O_3$, (*2*) CaF_2-RF_3, (*3*) CdF_2-RF_3, (*4*) MF_2-ZrF_4 (M = Ca, Sr, Ba), (*5*) PbF_2-RF_3.

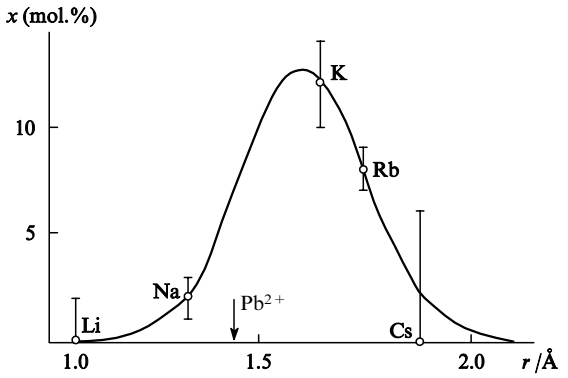

Figure 29. Dependence of the limiting concentrations of the $Pb_{1-x}M_xF_{2-x}$ solid solutions with the fluorite structure on the ionic radius of M.[91, 115, 116, 119]
The curve is constructed according to the equation $x = 12.6\exp[-23.4(r-1.605)^2]$; the ionic radii are given according to Schannon,[297] the coordination number is 8.

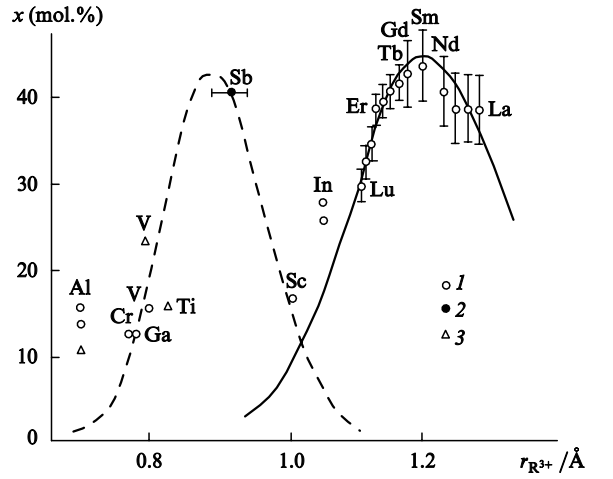

Figure 30. Dependence of the limiting concentrations of the $Pb_{1-x}R_xF_{2+x}$ solid solutions with the fluorite structure on the ionic radius of R^{3+}.
(*1*) Results of the studies,[105, 180, 184, 198, 201, 203, 208, 219, 221] (*2*) data obtained in the study[225] for 250 °C, (*3*) data obtained in the study[182] for 500–550 °C; the solid line corresponds to the equation $x = 44\exp[-36(r-1.22)^2]$; the dashed line corresponds to the equation $x = 42\exp[-90(r-0.9)^2]$.

3. Heterovalent solid solutions

The above-considered systems are characterised by the formation of heterovalent solid solutions based on the cubic modification of PbF_2. Anion-deficient (PbF_2-MF systems) and anion-excess (PbF_2-MF_n systems, $n = 3$, 4, 5) solid solutions are distinguished.

The characteristic features of heterovalent isomorphism with a variable number of ions in the unit cell were analysed.[206, 302] In the simplest case, the dependence of the limiting concentration of heterovalent solid solutions on the ionic radius of the replacing component can be described by the Gaussian. The maximum solubility corresponds to neither the equality of the ionic radii of isomorphous cations nor the constancy of the lattice parameter upon the formation of a solid solution. The dependence of this type satisfactorily describes the data on the PbF_2-MF systems (Fig. 29). In the case of the $Pb_{1-x}R_xF_{2+x}$ solid solutions in the PbF_2-RF_3 system, the situation is much more complicated (Figs 30 and 31).

In the first approximation, the mechanism of formation of solid solutions involves the replacement of lead ions with cations of different valence. The electrostatic compensation occurs through the formation of an equivalent number of anion vacancies (in the case of anion deficient solid solutions) according to the equation

$$Pb^{2+} + F^- \rightleftharpoons M^+ + V_F$$

or through the introduction of additional (interstitial) fluoride ions (in the case of anion excess solid solutions, $n > 2$) according to the equation

$$Pb^{2+} \rightleftharpoons M^{n+} + (n-2)F^-_{int}.$$

Association of point defects and cluster formation are natural processes at high concentrations of a solid solution. The cluster formation in heterovalent fluorite solid solutions is studied by different methods. The data on the fluorite solid solutions $M_{1-x}R_xF_{2+x}$ (M are alkaline-earth metals, cadmium or lead) were surveyed in publications.[2, 25, 304–310]

The first step of association involves the formation of dipoles, *viz.*, associates of oppositely charged defects of the $R^{3+}-F^-_{int}$ type. In the fluorite structure (Fig. 32 *a*), two types of dipoles can exist, the so-called *nn* (nearest neighbour) dipoles with tetragonal (C_{4v}) symmetry and *nnn* (next nearest neighbour) dipoles with trigonal (C_{3v}) symmetry. As the concentration of solid solutions increases,

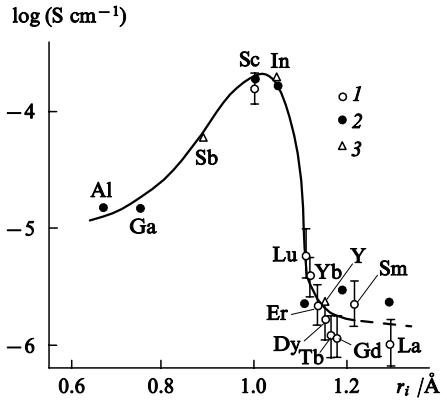

Figure 31. Dependence of the ionic conductivity of $Pb_{0.9}R_{0.1}F_{2.1}$ on the ionic radius.
(*1*) Results of the study,[8] (*2*) results of the study,[303] (*3*) results of the study.[207]

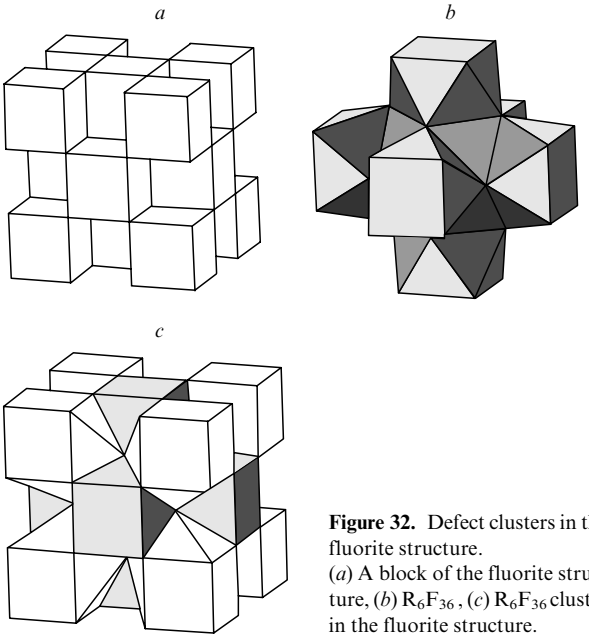

Figure 32. Defect clusters in the fluorite structure.
(*a*) A block of the fluorite structure, (*b*) R_6F_{36}, (*c*) R_6F_{36} cluster in the fluorite structure.

dipoles are transformed into more complex clusters, which coalesce into superclusters due to percolation. These processes are accompanied by the development of short-range order in the cation sublattice and substantial rearrangement of the anion sublattice of the solid solution. Hence, the corresponding solid solutions are nanocrystalline composites.[206, 306, 311] The formation of ordered phases proceeds as ordering of the cluster arrangement. The structure of ordered phases determines the structure of solid solutions (*i.e.*, the type of clusters present in these solutions).

In dilute solid solutions of rare-earth fluorides based on the fluorite modification of lead fluoride containing ~0.1 mol.% of RF_3, the type of major dipoles changes from *nn* to *nnn* on going from metals of the cerium group to metals of the yttrium group. This change is typical also of SrF_2-based and, in part, of BaF_2-based solid solutions, but is untypical of CaF_2-based solid solutions.[307] However, a very complicated pattern of defect association was revealed[213, 214] for dilute solid solutions (even at 0.1 mol.% – 0.01 mol.% of RF_3 in PbF_2) by laser spectroscopy and dielectric relaxation spectroscopy.

In concentrated solid solutions ($x > 0.05$) with rare-earth fluorides of the yttrium subgroup (R = Sm – Lu, Y), the presence of clusters of the R_6F_{36}/R_6F_{37} type is highly probable (Fig. 32 *b*). These clusters contain six trivalent cations. The coordination polyhedron about each cation is a Thompson cube (antiprism) formed by 8 fluoride ions. The cluster has a cuboctahedral cavity, which can be occupied by fluoride ions (or oxygen ions in the case of partial pyrohydrolysis). These clusters were observed in many ordered fluorite-like structures, including $Ba_4R_3F_{17}$, isostructural with lead compounds.[306, 312] Clusters containing oxygen ions in the cuboctahedral cavity were observed in single crystals of $Pb_4Y_3F_{18}O$.[210] Clusters of this type are readily incorporated into the fluorite structure.[313] The results of X-ray diffraction study of $Pb_{1-x}Y_xF_{2+x}$ (see Ref. 219) are consistent with the presence of Y_6Y_{37} in the solid solution, although the authors proposed another cluster model.

It should be noted that thermal stability of the $Pb_4R_3F_{17}$ compounds in the REM series passes through a maximum in a series R = Y – Er. This indicates that the cluster structure of solid solutions varies with the ionic radius of the cations. Since the coordination number of 8 is untypical of R = La – Nd, the $Pb_4R_3F_{17}$ phases with these rare-earth elements lose stability. In such solid solutions, the R_4F_{26}-type clusters, in which the cations have a coordination number of 10, can exist.[314] A decrease in the ionic radius of the rare-earth metal leads to a decrease in the coordination number. Seven-vertex polyhedra observed in the ordered fluorite-like phase Pb_2InF_7 (see Refs 201, 205, 234) should prevail for indium. It was hypothesised[199] that in ordered fluorite-like compounds observed in the $PbF_2 – MF_3$ systems (M = Ga, Ti, V), the seven-vertex polyhedra are linked to form infinite linear clusters. In fluorides (including the $Pb_3Al_2F_{12}$ compound[315]), the coordination number of 6 is typical of Al^{3+}, which has an even smaller radius. Hence, octahedral clusters would be expected to occur in the solid solution.[191]

The structure solution of the ordered fluorite-like Pb_3ZrF_{10} phase revealed yet another type of clusters, whose existence in heterovalent solid solutions is highly probable.[199] These clusters, like the R_6F_{36} clusters, contain also eight-vertex polyhedra, *viz.*, the ZrF_8 antiprisms. The antiprisms are linked to form infinite zigzag chains giving rise to a family of one-dimensional clusters. The existence of clusters of this type is assumed in solid solutions of lead fluoride with fluorides of both tetravalent and trivalent elements.

A comparison of the data on the defect structures of the $Pb_{1-x}R_xF_{2+x}$ solid solutions depending on their limiting solubility (Fig. 33) provides evidence that there are three dependences corresponding to different types of rearrangement of the anion sublattice upon the replacement of cations in their crystallo-

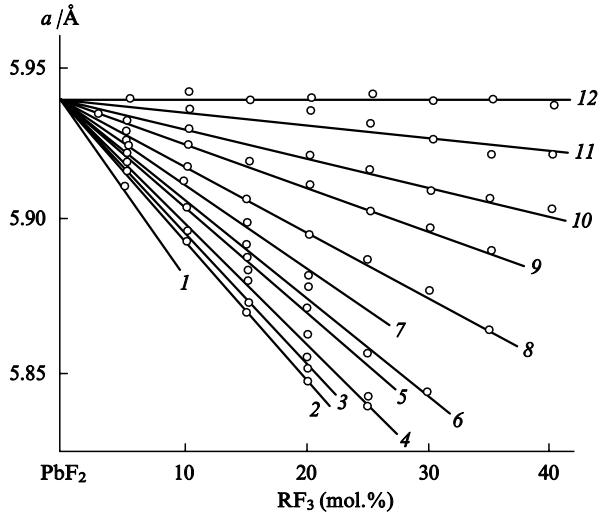

Figure 33. Dependence of the lattice parameters of the $Pb_{1-x}R_xF_{2+x}$ solid solutions on their composition.[105, 316]
R = Sc (*1*), Lu, Yb, Tm (*2*), Er (*3*), Ho, Y (*4*), Dy (*5*), Tb (*6*), Gd (*7*), Sm (*8*), Nd (*9*), Pr (*10*), Ce (*11*) and La (*12*).

graphic positions giving rise to eight- or ten-vertex, seven-vertex and six-vertex polyhedra RF_n linked in clusters. The ionic conductivity changes with a change in the defect structure (see Fig. 32).

The formation of heterovalent solid solutions is accompanied by a change in the lattice parameter depending on the concentration of RF_3.[105,316] In the first approximation, this change is linear, *i.e.*, Vegard's law is fulfilled (see Fig. 33). The results of accurate measurements (see, for example, Refs 201 and 248) and the data on the high-pressure synthesis of solid solutions, which extends the concentration range of their existence,[215,317] are indicative of deviations from linear dependences. We ignore these deviations in subsequent analysis.

The slopes α depend linearly on the ionic radius of rare-earth metals (Fig. 34). Hence, in the general form, the data on the PbF_2-RF_3 systems can be described [105,316] by the expression

$$\alpha = 5.490 + [2.48(r-r_0) + \varepsilon_1]x,$$

where r_0 is the ionic radius of Pb^{2+}, $\varepsilon_1 = 0.3694$ Å mol^{-1} is the contribution of excess fluoride ions with respect to the stoichiometry PbF_2 upon the formation of the $Pb_{1-x}R_xF_{2+x}$ solid solutions, x is the mole fraction of RF_3. In the studies, [105,316] r_0 was corrected compared to its value in the Schannon table [297] (for the coordination number of 8, $r_0 = 1.456$ instead of 1.43 Å).

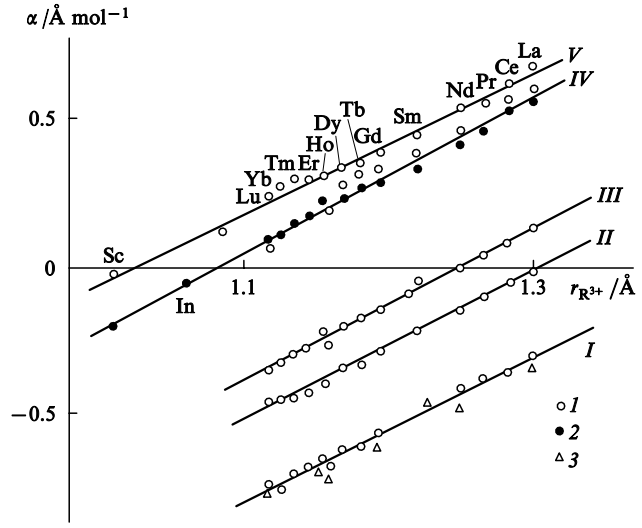

Figure 34. Slopes of the concentration dependences of the lattice parameters of the heterovalent solid solutions $M^{II}_{1-x}R_xF_{2+x}$ *vs.* the ionic radii of trivalent cations.[105,316]
(*1*) Samples quenched after solid-phase annealing, (*2*) slowly cooled samples, (*3*) sintered samples; M = Ba (*I*), Pb (*II*), Sr (*III*), Ca (*IV*), Cd (*V*).

Based on the published data,[238,242,248] we derived the following equation for solid solutions of tetravalent metal fluorides in lead fluoride:

$$\alpha_{cal} = 2.48(r-1.456) + 0.804. \quad (1)$$

Analogous dependences are observed for solid solutions of tetravalent metal fluorides in other fluorite matrices (Fig. 35). Taking into account that $\varepsilon_2 \simeq 2\varepsilon_1$ (this corresponds to insertion of two additional fluoride ions into the lattice in the case of heterovalent isomorphism), an approximate expression can be obtained for solid solutions of pentavalent element fluorides ($\varepsilon_3 \simeq 1.5\varepsilon_2 \simeq 3\varepsilon_1$).

The experimental and calculated slopes are given in Table 3. Discrepancies observed in some cases require a careful experimental verification.

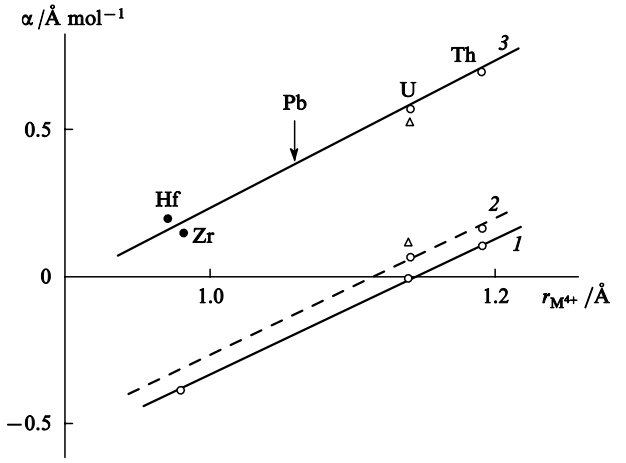

Figure 35. Slopes of the concentration dependences of the lattice parameters of the solid solutions $M^{II}_{1-x}M^{IV}_xF_{2+2x}$ *vs.* the ionic radii of tetravalent cations (according to the results of the studies [318–320]).
M^{II} = Pb (*1*), Sr (*2*), Ca (*3*). Circles correspond to data obtained in different studies.

Table 3. Coefficients of the concentration dependence of the unit cell parameters of heterovalent solid solutions $Pb_{1-x}R_xF_{2+x}$, $Pb_{1-x}M_xF_{2+2x}$, $Pb_{1-x}M'_xF_{2+3x}$.

R, M, M′	r /Å (see [297])	Slope		α_{cal} /Å mol^{-1}
		α_{exp} /Å mol^{-1}	Ref.	
RF_3, $\alpha_{cal} = 2.48(r-1.456) + 0.369$				
La	1.300	+0.003	105	−0.025
Ce	1.283	−0.043	105	−0.067
Pr	1.266	−0.095	105	−0.110
Nd	1.249	−0.141	105	−0.152
Sm	1.219	−0.218	105	
		−0.202	212	−0.226
Eu	1.206			−0.258
Gd	1.193	−0.303	105	
		−0.265	212	−0.291
Tb	1.180	−0.335	105	−0.323
Dy	1.167	−0.340	105	−0.355
Ho	1.155	−0.391	105	−0.385
Er	1.144	−0.424	105	
		−0.395	212	−0.412
Tm	1.134	−0.449	105	
		−0.437	212	−0.437
Yb	1.125	−0.446	105	
		−0.470	212	−0.459
Lu	1.117	−0.454	105	
		−0.491	212	−0.479
Y	1.159	−0.387	105	−0.375
In	1.06	−0.513	182	−0.62
Sc	1.01			−0.74
Al	0.66	−0.16	182	−1.61
Ga	0.76	−0.46	198	−1.36
MF_4, $\alpha_{cal} = 2.48(r-1.456) + 0.804$				
Th	1.19	+0.119	242	+0.144
U	1.14	+0.056	238	+0.020
Zr	0.98 [a]	−0.39	248	−0.376
Pb	1.08			−0.128
$M'F_5$, $\alpha_{cal} = 2.48(r-1.456) + 1.2$				
Nb	0.88	+0.227	259	−0.228

[a] The value was refined by us.

4. Non-stoichiometry of lead difluoride

Taking into account a possible change in the valence state of lead in fluorides (from two to four) and the ease of formation of heterovalent solid solutions of the cubic modification of PbF_2 with tetravalent metal fluorides, a region of the $Pb^{II}_{1-x}Pb^{IV}_{x}F_{2+2x}$ ($PbF_{2+\delta}$) solid solutions would be expected to occur. In the region of existence of lead difluoride, the PbF_2-PbF_4 system (Pb–F) (Fig. 36) should have features in common with the $EuCl_2-EuCl_3$ system (Eu–Cl). Europium dichloride $EuCl_2$ undergoes a polymorphic transformation, both modifications being isostructural with lead difluoride (the low-temperature orthorhombic cotunnite-type phase and the high-temperature cubic fluorite-type phase). A close examination of the experimental data [321] revealed the region of the $EuCl_{2+x}$ solid solution, which decomposes according to a eutectoid scheme.[322]

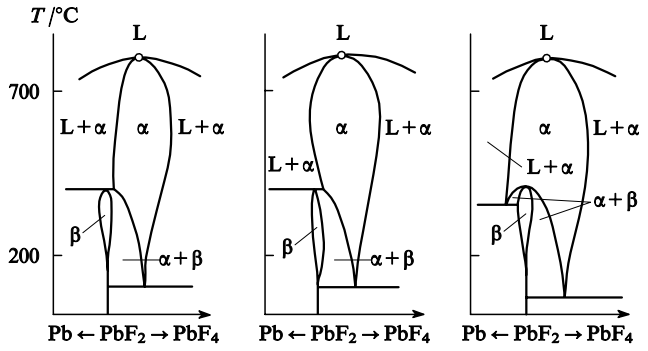

Figure 36. Schemes of possible phase equilibria in the Pb–F system.

The assumed non-stoichiometry is one of the possible reasons for the observed difference in the lattice parameter of cubic PbF_2 determined in different studies. The substitution of the ionic radius of Pb^{4+} [r = 1.08 Å (see Ref. 297)] into Eqn (1) gives $\alpha_{cal} = -0.14$ Å mol^{-1}. Therefore, if these estimates (including those for the ionic radius of Pb^{4+}) are correct, an additive of tetravalent lead should cause an insignificant decrease in the lattice parameter of PbF_2.

In addition, a consideration of the fluorite phase $PbF_{2\pm\delta}$ as non-stoichiometric provides an explanation for the data obtained by A I Boltalin (Moscow State University) on the polymorphism of PbF_2: a liquid phase, which appears upon heating of the low-temperature orthorhombic modification, is apparently a melt enriched in metallic lead (according to the medium phase diagram shown in Fig. 36). In the general case, the maximum in the melting curve for a non-stoichiometric phase does not correspond to stoichiometry (PbF_2). This phenomenon was observed for the fluorite solid solution EuF_{2+x}.[316] It is also worthwhile searching for low-temperature ordered intermediate phases of lead fluoride, for example, $Pb^{II}_3Pb^{IV}F_{10}$ (Pb_2F_5).

5. Partition coefficients of additives

For crystallisation of a PbF_2 melt, the partition coefficients of additives k can be estimated using phase diagrams of binary systems. For infinitely diluted solutions, the coefficients can be estimated using the modified cryoscopy method [323, 324] based on the Van't Hoff equation

$$\lim\left(\frac{dT_L}{dx}\right) = \frac{RT^2}{\Delta H}(k-1),$$

where T is the temperature, ΔH is the enthalpy of melting of the matrix. This method differs from conventional cryoscopy in that the limiting slope of the liquidus line dT_L/dx with $x \to 0$ is determined by differentiation of a polynomial approximating the experimental curve in a wide concentration range. The error of the calculation of k is, on average, 10%–15%.

Calculations were carried out using ΔH = 3000 cal mol^{-1}.[325] The results of calculations are presented in Table 4. The dependences of the partition coefficients on the ionic radius of the replacing cation are described by Gaussian-type distribution functions (Fig. 37).

Table 4. Partition coefficients k of additives for crystallisation of PbF_2.

Additive	k	Additive	k
LaF_3	5.10	AlF_3	0.27
CeF_3	5.17	GaF_3	0.71
PrF_3	4.45	InF_3	0.89
NdF_3	3.98	VF_3	0.13
SmF_3	3.79	CrF_3	0.34
GdF_3	3.08	MgF_2	0.11
TbF_3	2.62	CaF_2	1.0
DyF_3	2.67	BaF_2	1.35
HoF_3	2.69	SrF_2	1.77
ErF_3	2.26	CdF_2	0.65
TuF_3	2.25	KF	1.65
YbF_3	2.19	RbF	0.73
LuF_3	2.03	LiF	0.04
YF_3	2.14	NaF	0.04
ScF_3	1.10		

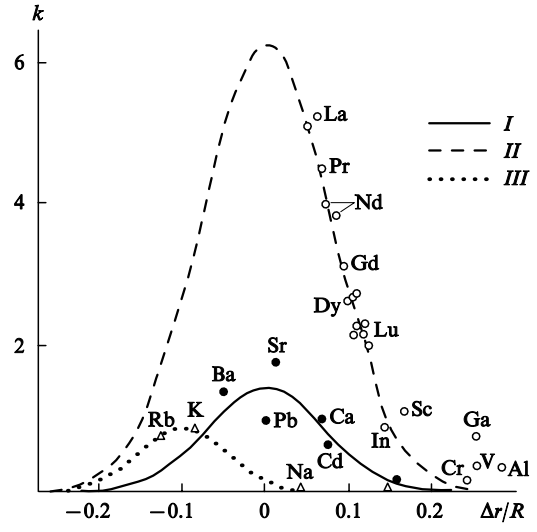

Figure 37. Partition coefficients of MF_n (k) for crystallisation of a PbF_2 melt as a function of the normalised difference in the ionic radii $\Delta r/R$.[206] $\Delta r = r_{Pb} - r_M$, $R = a\sqrt{3}/4$ is the cation–anion distance in the lattice of PbF_2, a is the lattice parameter, n = 2 (*1*), 3 (*2*), 1 (*3*); curves *I*–*III* were constructed according to the equations $k = 1.44\exp[-102(\Delta r/R)^2]$, $k = 6.25\exp[-82.2(\Delta r/R)^2]$ and $k = 0.89\exp[-174(\Delta r/R + 0.09)^2]$, respectively.

6. Saddle points

The $PbF_2-CdF_2-RF_3$ systems (R = Er, Lu, Y) are characterised [275] by the presence of specific stationary (corresponding to congruent melting) points, the so-called saddle points, on the liquidus surface (Fig. 38). The compositions of congruently melting solid solutions are favourable for growing homogeneous crystals. Hence, a search for such solutions is of importance.

Saddle points on equilibrium surfaces of two-phase multicomponent systems were theoretically predicted by Gibbs.[326] The corresponding phase diagrams were constructed,[327] but they were

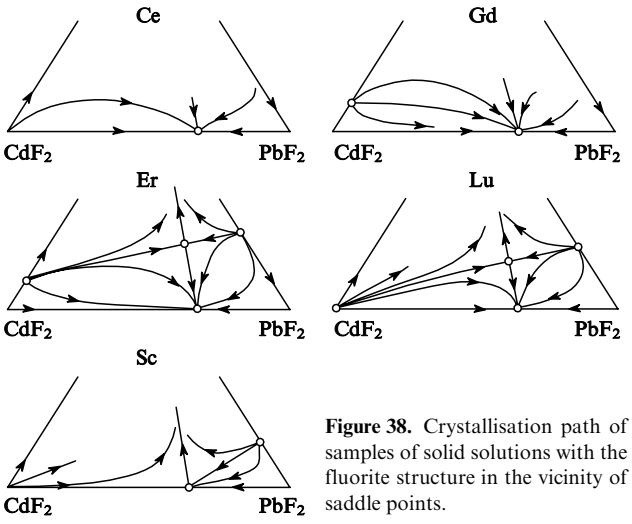

Figure 38. Crystallisation path of samples of solid solutions with the fluorite structure in the vicinity of saddle points.

not studied experimentally until 1996, when the first publication on this problem appeared.[275] According to the thermodynamic topological analysis,[328] saddle points can appear in ternary systems that have two maxima (minima) and one minimum (maximum) in the melting curves of binary systems, which form the ternary system. Therefore, about 40 congruently melting composites would be expected to occur in the $MF_2-M'F_2-RF_3$ systems. This prediction [329] was confirmed when we performed an experimental study of the $PbF_2-CdF_2-RF_3$ systems (R = Tb–Lu). Analysis of the polythermal sections revealed the positions of compositions corresponding to saddle points. For example, the coordinates of the saddle points in such systems with Er, Lu and Y are as follows:

Er: 30 ± 2 mol.% of ErF_3, 23 ± 2 mol.% of CdF_2, 890 ± 5 °C;

Lu: 25 ± 2 mol.% of LuF_3, 25 ± 2 mol.% of CdF_2, 835 ± 5 °C;

Y: 17.5 ± 2 mol.% of YF_3, 27 ± 2 mol.% of CdF_2, 885 ± 5 °C;

It appeared that these points lie virtually exactly in the section which links the minimum in the CdF_2-PbF_2 system to the point corresponding to RF_3.

7. Tetragonal phases in the PbF_2-MF_3 systems (M = Al, Ti, V, Cr, Fe, Ga)

As mentioned above, there is no consensus among experts as to stoichiometry and regions of stability for phases with a tetragonal structure formed in the PbF_2-MF_3 systems (M = Al, Ti, V, Cr, Fe, Ga) in the region of 50 mol.% – 62.5 mol.% of PbF_2. It was hypothesised that the $PbMF_5$, $Pb_3M_2F_{12}$ and $Pb_5M_3F_{19}$ compounds exist in these systems. In some cases, different compositions were assigned to the same samples. According to the results of different studies,[188–190, 192–196] $Pb_5M_3F_{19}$ (M = Al, Cr), $SrAlF_5/BaFeF_5$ and $Sr_3Fe_2F_{12}$ are characterised by rather similar structural motifs, which can be described as infinite chains of vertex-sharing octahedra oriented along the *c* axis of the tetragonal unit cell. A change in the composition from 1:1 to 2:3 is attained due to the presence of additional fluoride ions. In the PbF_2-AlF_3 system, like in other analogous systems consisting of di- and trivalent metal fluorides, several phases of similar composition and structure can exist in the region between 40 mol.% and 50 mol.% of AlF_3. Ravez *et al.*[185] believed that a solid solution exists in this region.

Apparently, this structural motif serves as a structural basis of fluoride aluminate glasses.[62, 64] A tetragonal phase systematically appears upon crystallisation of glasses of the Ba,In,Pb,Al//F system.[64, 197] In the study,[197] the composition $Pb_3Al_2F_{12}$ was assigned to the tetragonal phase in the PbF_2-AlF_3 system.

An analogous situation is observed in systems with $M'F_2-MF_3$ (M′ = Sr, Ba); Sc and In can be involved along with trivalent ions (see, for example, Refs 330 and 331).

Presumably, the compositions of compounds and the types of phase equilibria in the systems under consideration can be correctly determined on the assumption that these phases are characterised by high-temperature non-stoichiometry accompanied by the formation of ordered compounds with particular stoichiometry on cooling. Real samples prepared by high-temperature syntheses and cooled to room temperature could contain domains corresponding to various low-temperature compounds. Studies of samples by high-resolution electron microscopy and electron microdiffraction are desirable.

XI. Conclusion

The present review demonstrates that lead difluoride and its composites with other inorganic compounds hold promise as a basis for the construction of new functional materials, which will find use in such fields as photonics and solid-state ionics.

Analysis of the data on phase equilibria in PbF_2-containing systems revealed a number of problems, which call for further experimental studies. To solve these problems, it is necessary to:

— study a lead–fluorine system and construct the corresponding phase diagram; carry out experimental studies and determine the width of the homogeneity region of the $PbF_{2+\delta}$ phase, the concentration dependence of the lattice parameter, the position of the maximum in the melting curve and the presence of low-temperature ordered fluorite-like intermediate phases, *viz*., lead fluorides;

— elucidate the reasons for doubling of the lattice parameter for the cubic modification of PbF_2, find the relationship between this phenomenon and ordering of the anion sublattice, reveal the influence of the lattice parameter on the properties of PbF_2;

— synthesise a series of lead fluorides ($PbHfF_6$, Pb_3HfF_{10}, *etc*.), whose existence was predicted based on analysis of phase diagrams for systems involving PbF_2;

— reveal the effect of the lone electron pair of the Pb^{2+} ion on the properties of lead compounds;

— investigate polymorphism and non-stoichiometry in tetragonal phases of the $PbMF_5$, $Pb_5M_3F_{19}$ and $Pb_3M_2F_{12}$ types;

— reveal factors responsible for high fluoride ion mobility in materials based on lead difluoride and the relationship between the mobility and the characteristic features of the cluster structure of solid solutions with the fluorite structure.

References

1. M Faraday *Ann. Phys. (Leipzig)* **107** 247 (1834)
2. W Hayes *Crystals with the Fluorite Structure* (Oxford: Clarendon, 1974)
3. R W Bonne, J Schoonman *J. Electrochem. Soc.* **124** 28 (1977)
4. A Rhandour, J-M Reau, S F Matar, P Hagenmuller *J. Phys. Chem. Solids* **47** 587 (1986)
5. I V Murin, S V Chernov *Neorg. Mater.* **18** 168 (1982) [a]
6. S V Chernov, Candidate Thesis in Chemical Sciences, Leningrad State University, Leningrad, 1982
7. J Eicken, W Gunsser, S V Chernov, A V Glumov, I V Murin *Solid State Ionics* **53–56** 843 (1992)
8. N I Sorokin, P P Fedorov, B P Sobolev *Neorg. Mater.* **33** 5 (1997) [a]
9. P P Fedorov, V Trnovcová, V A Meleshina, V D Chugunov, B P Sobolev *Neorg. Mater.* **30** 406 (1994) [a]
10. J-M Reau, C Lucat, J Portier, P Hagenmuller, L Cot, S Vilminot *Mater. Res. Bull.* **13** 877 (1978)
11. V Trnovcová, P P Fedorov, M Ožvoldova, I I Buchinskaya, B A Zchurova *J. Optoelectron. Edv. Mater.* **5** 627 (2003)
12. N I Sorokin, P P Fedorov, O K Nikol'skaya, O A Nikeeva, E G Rakov, E I Ardashnikova *Neorg. Mater.* **37** 1378 (2001) [a]
13. M A Bredig *Colloq. Int. C.N.R.S.* **205** 183 (1972)

14. C E Derrington, A Navrotsky, M O'Keeffe *Solid State Commun.* **18** 47 (1976)
15. C R A Catlow, J D Comins, F A Germano, R T Harley, W Hayes *J. Phys. C: Solid State Phys.* **11** 3197 (1978)
16. R E Gordon, J H Strange *J. Phys. C: Solid State Phys.* **11** 3213 (1978)
17. D S Rimai, R J Sladek *Solid State Commun.* **31** 473 (1979)
18. W Schroter, J Nolting *J. Phys. Colloq.* **41** 20 (1980)
19. J Schoonman *Solid State Ionics* **1** 121 (1980)
20. J Oberschmidt *Phys. Rev. B* **23** 5038 (1981)
21. P R Findley, Z Wu, W C Walker *Solid State Ionics* **7** 49 (1982)
22. W Andreoni, M P Tosi *Solid State Ionics* **11** 49 (1983)
23. M T Hutchings, K Clausen, M H Dickens, W Hayes, J K Kjems, P G Schnabel, C Smith *J. Phys. C: Solid State Phys.* **17** 3903 (1984)
24. E Vlieg, H W den Hartog, M Winnik *J. Phys. Chem. Solids* **47** 521 (1986)
25. C R A Catlow, in *Superionic Solids and Solid Electrolytes* (Eds A L Lasker, S Chandra) (Boston: Academic Press, 1989) p. 339
26. J P Goff, W Hayes, S Hull, M T Hutchings *J. Phys.: Condens. Matter* **3** 3677 (1991)
27. Y Bouteiller *Phys. Rev. B* **45** 8734 (1992)
28. P P Fedorov *Zh. Fiz. Khim.* **70** 365 (1996) [b]
29. A G Dudorov, A Ya Kupryazhkin *Fiz. Tv. Tela* **40** 699 (1998) [c]
30. F Zimmer, P Ballone, M Pariinello *Solid State Ionics* **127** 277 (2000)
31. J Galy, R Enjalbert *J. Solid State Chem.* **44** 1 (1982)
32. M Makur, S Ghosh *Pramana J. Phys. (India)* **36** 393 (1991)
33. K-T Wilke *Kristallzüchtung* (Berlin: Vebditschir Verlag der Wissenschaften, 1973)
34. V A Timofeeva *Rost Kristallov iz Rastvorov-Rasplavov* (Growth of Crystals from Solutions-Melts) (Moscow: Nauka, 1978)
35. N S Andrushchenko, E A Bezrukova, E L Dukhovskaya, Yu L Sapozhnikov *Izv. Akad. Nauk SSSR, Neorg. Mater.* **7** 1005 (1971) [a]
36. D K Kunev, B I Lucheva *Zh. Neorg. Khim.* **35** 2382 (1990) [d]
37. K Furukawa, H Ohno, J Mochinaga, K Igarashi *J. Nucl. Sci. Technol.* **17** 562 (1980)
38. P C Stocbarger *J. Opt. Soc. Am.* **39** 731 (1949)
39. B P Sobolev (Ed.) *Multicomponent Crystals Based Heavy Metal Fluorides for Radiation Detectors* (Barcelona: Institut d'Estudis Catalans, 1994)
40. J Ichihara, Y Takai, T Hanafusa *J. Fluorine Chem.* **71** 131 (1995)
41. J Ichihara, M Takahashi, S Emura *J. Synchrotron Radiat.* **6** 602 (1999)
42. E M Voronkova, B N Grechushnikov, G I Distler, I P Petrov *Opticheskie Materialy dlya Infrakrasnoi Tekhniki* (Optical Materials for Infrared Equipment) (Moscow: Nauka, 1965)
43. V A Arkhangel'skaya, V I Baklanova, I A Ivanova, M I Kiseleva, E D Kaplan, V M Reiterov *Tr. Gos. Opt. In-ta im. S I Vavilova* **54** 129 (1983)
44. M Saito, S Nakamura, M Miyagi *Appl. Opt.* **28** 6139 (1992)
45. G A Teterin, R S Sokolova, K A Nadzhkharyan *Zh. Prikl. Khim.* **64** 1200 (1991) [e]
46. H J Kuhn, A Duparre, W Richter *Thin Solid Films* **2** 281 (1991)
47. E M Gavrishchuk, P L Krupkin, A A Pereskokov, V I Plekhanov, N D Savchenko, D I Tetel'baum, M L Trunov *Vysokochistye Veshch.* (3) 24 (1993)
48. J D T Kruschwitz, W T Pawlewicz *Appl. Opt.* **36** 2157 (1997)
49. M Ishii, M Kobayashi *Prog. Cryst. Growth* **23** 245 (1991)
50. D E Anderson, M Kobayashi, C L Woody, Y Yoshimura *Nucl. Instrum. Methods Phys. Res., Sect. A* **290** 385 (1990)
51. R D Appuhn, F Brasse, T Deckers *Nucl. Instrum. Methods Phys. Res., Sect. A* **350** 208 (1994)
52. R Y Zhu, G Gratta, H Newman *Nucl. Phys. B, Proc. Suppl.* **44** 88 (1995)
53. P Achenbach, I Altarev, K Grim *Nucl. Instrum. Methods Phys. Res., Sect. A* **416** 357 (1998)
54. D Z Chen, G H Ren, S H Wang *J. Inorg. Mater.* **14** 12 (1999)
55. I I Buchinskaya, Candidate Thesis in Chemical Sciences, Moscow State Academy of Fine Chemical Technology, Moscow, 1996
56. P Mesnard, A Garsia, J Grannec, C Fouassier, D Bouttet, C Pedrini *Chem. Phys. Lett.* **229** 139 (1994)
57. A B Kulakov, A A Zhokhov, G A Emel'chenko, N V Klassen *J. Cryst. Growth* **151** 107 (1995)
58. D L Alov, S I Rybchenko *J. Phys.: Condens. Matter* **7** 1475 (1995)
59. W Zhou, S W Martin, D Schwellenbach, J Hauptman *J. Non-Cryst. Solids* **184** 84 (1995)
60. P P Fedorov *Kristallografiya* **42** 1141 (1997) [f]
61. P P Fedorov, R M Zakalyukin, L N Ignat'eva, V M Bouznik *Usp. Khim.* **69** 767 (2000) [*Russ. Chem. Rev.* **69** 705 (2000)]
62. S Shibata, T Kanamory, S Mitachi, T Manabe *Mater. Res. Bull.* **15** 129 (1980)
63. G Demortain, A Tressaud, B Tanguy, J Portier, P Hagenmuller *Rev. Chim. Miner.* **24** 117 (1987)
64. N I Sorokin, R M Zakalyukin , T Yu Glazunova, A I Boltalin, P P Fedorov, B P Sobolev *Neorg. Mater.* **36** 1008 (2000) [a]
65. C Jacoboni, O Perrot, B Boulard *J. Non-Cryst. Solids* **184** 184 (1995)
66. C Jacoboni, A Le Ball, R de Pape *Glass Technol.* **24** 164 (1983)
67. J-P Miranday, C Jacoboni, R de Pape *J. Non-Cryst. Solids* **43** 393 (1981)
68. P A Tick *Mater. Sci. Forum* **5** 165 (1985)
69. C T Moynihan *J. Am. Ceram. Soc.* **76** 1081 (1993)
70. P Nachimuthu, R Jagannathan *Phys. Chem. Glasses* **36** 77 (1995)
71. V A Vopilov, E A Vopilov, V M Bouznik, V L Bogdanov, V D Khalilev *Issledovanie Kislorodnykh Ftorsoderzhashchikh Stekol Metodom Yadernogo Magnitnogo Rezonansa. Preprint No. 293 F* (Investigation of Oxygen Fluorine-Containing Glasses by Nuclear Magnetic Resonance. Preprint No. 293 F) (Krasnoyarsk: Institute of Physics, Siberian Branch of the Academy of Science of the USSR, 1984)
72. J E Shelby, E A Bolden *J. Non-Cryst. Solids* **142** 269 (1992)
73. J Coon, M Horton, J E Shelby *J. Non-Cryst. Solids* **102** 143 (1988)
74. N Rigout, J L Adam, J Lucas *Eur. J. Solids State Inorg. Chem.* **30** 997 (1993)
75. S F Carter, P W France, M W Moore, J M Parker, A G Clare *Phys. Chem. Glasses* **28** 188 (1987)
76. T Kogo, M Onishi, H Kanamory, H Yokota *J. Non-Cryst. Solids* **161** 169 (1993)
77. J S Javorniczky, P J Newman, D R MacFarlane *J. Non-Cryst. Solids* **184** 336 (1995)
78. N S Kurnakov *Izbrannye Trudy* (Selected Works) (Moscow: Academy of Sciences of the USSR, 1960)
79. *Gmelin Handbuch der Anorganischen Chemie. System-number 47* (Weinheim: Verlag Chemie, 1969)
80. I G Ryss *Khimiya Ftora i Ego Neorganicheskikh Soedinenii* (The Chemistry of Fluorine and Its Inorganic Compounds) (Moscow: Goskhimizdat, 1956)
81. L Domange *Ann. Chim.* **7** 225 (1937)
82. D Babel, A Tressaud, in *Inorganic Solid Fluorides* (Ed. P Hagenmuller) (New York: Academic Press, 1985) p. 77
83. J Hubler *Cryst. Res. Technol.* **23** 1127 (1988)
84. V K Semenchenko *Zh. Neorg. Khim.* **25** 272 (1980) [d]
85. L Gilmore *Catastrophere Theory for Scientists and Engineers* (New York: Wiley, 1981)
86. V P Glushko (Ed.) *Termicheskie Konstanty Veshchestv. Spravochnik* (Thermal Constants of Substances. Handbook) (Moscow: Izd. VINITI, 1970) No. 4
87. L T Ho, D P Dandekar, J C Ho *Phys. Rev. B* **27** 3881 (1983)
88. Ya Sauka *Zh. Fiz. Khim.* **25** 41 (1951) [b]
89. G A Samara *Phys. Rev. B* **13** 4529 (1976)
90. O K Nikol'skaya, L N Dem'yanets *Neorg. Mater.* **30** 1180 (1994) [a]
91. I N Belyaev, T G Lupeiko, T I Ivleva *Zh. Neorg. Khim.* **29** 202 (1984) [d]
92. L M Volodkovich, G S Petrov, R A Vecher, A A Vecher *Thermochim. Acta* **92** 535 (1985)
93. J P Auffredic, A Coupe, D Longer *J. Mater. Sci.* **20** 2119 (1985)
94. J Oberschmidt, D Lazarus *Phys. Rev. B* **21** 2952 (1980)
95. H E Lorenzana, J E Klepeis, M J Lipp, W J Evans, H B Radousky, M van Schilfgaarde *Phys. Rev. B* **56** 543 (1997)
96. J Haines, J M Leger, O Schulte *Phys. Rev. B* **57** 7551 (1998)
97. H E Swanson, E Tatge *NBS Circular* No. 539, Washington, 1953
98. Y Ito, K Koto *Solid State Ionics* **9** 527 (1983)

99. Y Ito, K Koto, S Yoshikada, T Ohachi *Solid State Ionics* **15** 253 (1985)
100. H Podsiadlo *Prace Naukowe Akad. Ekonom. Wroclawiu* **526** 259 (1990)
101. H Podsiadlo *J. Therm. Anal. Calorim.* **54** 863 (1998)
102. J Berak, H Dabrowiecka *Pol. J. Chem.* **10** 1223 (1982)
103. A N Nesmeyanov, B Z Iofa *Zh. Neorg. Khim.* **4** 486 (1959) [d]
104. H Wartenberg, O Bosse *Z. Electrochem.* **28** 384 (1922)
105. P P Fedorov, Doctoral Thesis in Chemical Sciences, Moscow Institute of Fine Chemical Technology, Moscow, 1991
106. W Hussain, D B Sirdeshmukh *Pramana J. Phys. (India)* **29** 583 (1987)
107. E A Vopilov, A A Sukhovoi, V M Bouznik *Zh. Strukt. Khim.* **23** 39 (1982) [g]
108. M Nizam, Y Bouteiller, B Silva, C Pisani, M Causa, R Dovesi *J. Phys. C: Solid State Phys.* **21** 5351 (1988)
109. N Saito, K Kawamura, H Tanaka, R Takagi *Denki Kagakoybi Kogyo Butsuri Kagaky* **54** 864 (1986)
110. P P Fedorov, G A Lovetskaya, G V Zimina, B P Sobolev *Zh. Neorg. Khim.* **31** 768 (1986) [d]
111. I Kosacki, K Hibner, F P Litvinchuk, M Ya Valakh *Phys. Status Solidi B* **134** 495 (1986)
112. R Roy *J. Am. Ceram. Soc.* **37** 581 (1954)
113. B V Beznosikov *Kristallografiya* **23** 113 (1978) [f]
114. K S Aleksandrov, A T Anistratov, B V Beznosikov, N V Fedoseeva *Fazovye Perekhody v Kristallakh Galoidnykh Soedinenii ABX_3* (Phase Transitions in the Crystals of ABX_3 Halides) (Novosibirsk: Nauka, 1981)
115. P P Fedorov, M Yu Trubitsyn, V Trnovtsova, B P Sobolev *Neorg. Mater.* **28** 2215 (1992) [a]
116. O Schmitz-Dumont, G Bergerhoff *Z. Anorg. Allg. Chem.* **283** 314 (1956)
117. V Trnovcova, P P Fedorov, I I Buchinskaya, B P Sobolev *Neorg. Mater.* **32** 1257 (1996) [a]
118. D I Vainshtein, V D Shchepkin, V A Safin, V M Vinokurov, A V Chadvik *Fiz. Tv. Tela* **24** 1904 (1982) [c]
119. A I Boltalin, A N Rykov, Yu M Korenev *Zh. Neorg. Khim.* **34** 2398 (1989) [d]
120. C Pistorius, J van Rensburg *Z. Anorg. Allg. Chem.* **383** 204 (1971)
121. N A Veleshko, V V Krokhina, Yu V Shirokov, N K Zhigareva, A B Ivanova, V E Prokopets *Izv. Akad. Nauk SSSR, Neorg. Mater.* **16** 342 (1980) [a]
122. A I Boltalin, Yu M Korenev *Zh. Neorg. Khim.* **41** 962 (1996) [d]
123. S Hull, P Berastegui, S G Eriksson, N J G Gadner *J. Phys.: Condens. Matter* **10** 8429 (1998)
124. S Hull, P Berastegui, *J. Phys.: Condens. Matter* **11** 5257 (1999)
125. C C Liang, A V Jouhi *J. Electrochem. Soc.* **122** 466 (1975)
126. R Ya Zakirov, V A Legasov, A S Marinin, in *VII Vsesoyuznyi Simpozium po Khimii Neorganicheskikh Ftoridov (Tez. Dokl.)* [The VIIth All-Union Symposium on the Chemistry of Inorganic Fluorides (Abstracts of Reports)] (Moscow: Nauka, 1984) p. 137
127. Y Ito, T Mukoyama, F Kanamaru, S Yoshikado *Solid State Ionics* **73** 283 (1994)
128. J Q Wu, R Hoppe *Z. Anorg. Allg. Chem.* **514** 92 (1984)
129. V A Vopilov, V N Voronov, V M Bouznik, in *YaMR i Vnutrennie Dvizheniya v Kristallakh* (Nuclear Magnetic Resonance and Internal Movements in the Crystals) (Krasnoyarsk: Institute of Physics, Siberian Branch of Academy of Sciences of the USSR, 1981) p. 149
130. V M Bouznik, Yu N Moskvich, V N Voronov *Chem. Phys. Lett.* **37** 464 (1976)
131. N A Veleshko, V V Krokhina, Yu V Shirokov, N K Zhigareva, A B Ivanova *Neorg. Mater.* **16** 1657 (1980) [a]
132. I N Flerov, I M Iskornev, V N Voronov, K S Aleksandrov *Fiz. Tv. Tela* **22** 912 (1980) [c]
133. V S Lyutsarev, V S Lobanov, V P Spiridonov *Zh. Fiz. Khim.* **67** 975 (1993) [b]
134. C Tubandt, S Eggert *Z. Anorg. Allg. Chem.* **110** 223 (1920)
135. D M Roy, R Roy, E F Osborn *J. Am. Ceram. Soc.* **37** 300 (1954)
136. J Krausse, J Rentsch *Silikattechnik* **19** 44 (1968)
137. W Granier, M Gengry, A El Mansouri, S Vilminot, L Cot *Z. Anorg. Allg. Chem.* **506** 59 (1983)
138. P P Fedorov, I I Buchinskaya, O S Bondareva, G A Lovetskaya, M D Val'kovskii *Zh. Neorg. Khim.* **40** 1380 (1995) [d]
139. H Podsiadlo *Prace Naukowe Akad. Ekonom. Wroclawiu* **526** 271 (1990)
140. I I Buchinskaya, P P Fedorov *Zh. Neorg. Khim.* **43** 1202 (1998) [d]
141. I I Buchinskaya, P P Fedorov, B P Sobolev, in *SPIE Proceedings, Solid State Crystals: Growth and Characterization, Zakopane, 1996* Vol. 3178, p. 59
142. V Trnovcova, P P Fedorov, I I Buchinskaya, V Smatko, F Hanic *Solid State Ionics* **119** 181 (1999)
143. I I Kozhina, G V Malinin, A A Murzin, N L Smirnov *Vestn. Leningr. Univ., Fiz., Khim.* **3** 100 (1984)
144. I I Buchinskaya, P P Fedorov, O L Evdokimova, B P Sobolev *Kristallografiya* **39** 539 (1994) [f]
145. M Samouel *C.R. Seances Acad. Sci., Ser. C* **268** 409 (1969)
146. M Samouel *Rev. Chem. Miner.* **8** 537 (1971)
147. R Dorshow, R D Hogg, V Jaccarino *Phys. Lett. A* **37** 250 (1979)
148. M Samouel, A de Kozak *C.R. Seances Acad. Sci., Ser. C* **268** 1789 (1969)
149. M P O'Horo, W B White *J. Am. Ceram. Soc.* **54** 588 (1971)
150. A de Kozak, M Samouel, A Chretien *Rev. Chem. Miner.* **8** 805 (1971)
151. N I Sorokin, I I Buchinskaya, B P Sobolev *Zh. Neorg. Khim.* **43** 1773 (1998) [d]
152. N I Sorokin, I I Buchinskaya, B P Sobolev *Zh. Neorg. Khim.* **37** 2653 (1992) [d]
153. V A Vopilov, E A Vopilov, V N Voronov, V M Bouznik, in *YaMR i Vnutrennie Dvizheniya v Kristallakh* (Nuclear Magnetic Resonance and Internal Movements in the Crystals) (Krasnoyarsk: Institute of Physics, Siberian Branch of Academy of Sciences of the USSR, 1984) p. 105
154. M Ya Valakh, I Kosatskii, A P Litvinchuk, G G Tarasov *Fiz. Tv. Tela* **27** 3667 (1985) [c]
155. I Kosacki *Solid State Ionics* **28–30** 449 (1988)
156. I Kosacki *J. Appl. Phys. A* **49** 413 (1989)
157. V M Bouznik, A A Sukhovskoi, V A Vopilov, V M Mastikhin, P P Fedorov, I I Buchinskaya, B P Sobolev *Zh. Neorg. Khim.* **42** 2092 (1997) [d]
158. A I Matsulev, Yu N Ivanov, A I Livshits, V M Bouznik, P P Fedorov, I I Buchinskaya, B P Sobolev *Zh. Neorg. Khim.* **45** 296 (2000) [d]
159. M A P Silva, Y Messaddeq, V Briois, M Poulain, F Villain, S J L Ribeiro *Solid State Ionics* **147** 135 (2002)
160. J D Donaldson, B J Senior *J. Chem. Soc. A* **11** 1821 (1967)
161. G Denes, J Pannetier, J Lucas *C.R. Seances Acad. Sci., Ser. C* **280** 831 (1975)
162. R Kanno *Mater. Res. Bull.* **26** 1111 (1991)
163. J Pannetier, G Denes, J Lucat *Mater. Res. Bull.* **14** 627 (1979)
164. C Lucat, A Rhandor, L Cot, J-M Reau *Solid State Commun.* **32** 167 (1979)
165. G Perez, S Vilminot, W Granier, L Cot, C Lucat, J-M Reau, J Portier, P Hagenmuller *Mater. Res. Bull.* **15** 587 (1980)
166. G Perez, W Granier, S Vilminot *C.R. Seances Acad. Sci., Ser. C* **290** 337 (1980)
167. M Durand, J Pannetier, G Denes *J. Physique* **41** 831 (1980)
168. S Vilminot, G Perez, W Granier, L Cot *Solid State Ionics* **2** 87 (1981)
169. S Vilminot, G Perez, W Granier, L Cot *Solid State Ionics* **2** 91 (1981)
170. S V Chernov, A L Moskvin, I V Murin *Solid State Ionics* **47** 71 (1991)
171. G Denes, Y H Yu, T Tyliszczak, A P Hitchcock *J. Solid State Chem.* **91** 1 (1991)
172. Y Ito, T Mukoyama, H Funatomi, S Yoshikado, T Tanaka *Solid State Ionics* **67** 301 (1994)
173. R Kanno, K Ohno, H Izumi, Y Kawamoto, T Kamiyama, H Asano, F Izumi *Solid State Ionics* **70/71** 253 (1994)
174. Y Ito, T Mukoyama, K Ashio, K Yamamoto, Y Suga, S Yoshikado, Ch Julien, T Tanaka *Solid State Ionics* **106** 291 (1998)

175. G Denes *J. Solid State Chem.* **74** 343 (1988)
176. A Collin, J Denes, D Le Roux, M C Madamba, J M Parris, A Salaun *Int. J. Inorg. Mater.* **1** 289 (1999)
177. H Muller, R Hoppe *Mater. Res. Bull.* **7** 1297 (1972)
178. J Ravez, R de Pape, P Hagenmuller *Bull. Soc. Chim. Fr.* (2) 1811 (1964)
179. J Ravez, R de Pape, P Hagenmuller *Bull. Soc. Chim. Fr.* (1) 240 (1966)
180. R G Shore, B M Wanklyn *J. Am. Ceram. Soc.* **5** 79 (1969)
181. J Ravez, D Dumora *C.R. Seances Acad. Sci., Ser. C* **269** 331 (1969)
182. J Ravez, M Darriet, R von der Muhll, P Hagenmuller *J. Solid State Chem.* **3** 234 (1971)
183. J Schoonman, K E D Wapenaar *J. Electrochem. Soc.* **126** 1385 (1979)
184. L V Multon, R S Feigelson *J. Mater. Res.* **6** 2188 (1991)
185. J Ravez, V Andriamampianina, A Simon, J Grannec, S C Abrahams *J. Appl. Phys.* **70** 1331 (1991)
186. V Andriamampianina, J Ravez, J P Chaminade, F Weill, P Hagenmuller, S C Abrahams *C.R. Seances Acad. Sci., Ser. 2* **314** 1319 (1992)
187. G Decap, R Retoux, Y Calage *Z. Anorg. Allg. Chem.* **620** 1449 (1994)
188. V Andriamampianina, P Gravereau, J Ravez *Acta Crystallogr., Sect. B* **50** 135 (1994)
189. S Sarraute, J Ravez *Acta Crystallogr., Sect. C* **51** 1731 (1995)
190. S Sarraute, J Ravez, R von der Mull, G Bravic, R S Feigelson, S C Abrahams *Acta Crystallogr., Sect. B* **52** 72 (1996)
191. M E Omari, J Senegas, J-M Reau *Solid State Ionics* **100** 233 (1997)
192. J Ravez, S C Abrahams, J P Chaminade, A Simon, J Grannec, P Hagenmuller *Ferroelectrics* **38** 773 (1981)
193. S G Abrahams, J Albertsson, C Svensson, J Raves *Acta Crystallogr., Sect. B* **46** 497 (1990)
194. R von der Mull, S Andersson, J Galy *Acta Crystallogr., Sect. B* **27** 2345 (1971)
195. J Albertsson, A K Larsson, S C Abrahams, J Ravez *Acta Crystallogr., Sect. A* **46** 342 (1990)
196. R M Zakalyukin, Candidate Thesis in Chemical Sciences, A V Shubnikov Institute of Crystallography, Russian Academy of Sciences, Moscow, 2002
197. R M Zakalyukin, T Yu Glazunova, A I Boltalin, P P Fedorov, B P Sobolev *Zh. Neorg. Khim.* **44** 10 (1999) [d]
198. J Chassaing, A Erb *C.R. Seances Acad. Sci., Ser. C* **270** 949 (1970)
199. B Frit, J P Laval *J. Solid State Chem.* **39** 85 (1981)
200. S C Abrahams, J Ravez, S Canouet, J Grannec, G M Lolacono *J. Appl. Phys.* **55** 3056 (1984)
201. S Kacim, J C Champarnaud-Mesjard, B Frit *Rev. Chim. Miner.* **19** 199 (1982)
202. J M Reau, S Matar, S Kacim, J C Champarnaud-Mesjard, B Frit *Solid State Ionics* **7** 165 (1982)
203. P P Fedorov, I P Zibrov, E V Tarasova, L V Medvedeva, B P Sobolev, I V Shishkin, P I Fedorov *Zh. Neorg. Khim.* **34** 3150 (1989) [d]
204. J M Reau, J Senegas, J P Laval, B Frit *Solid State Ionics* **31** 147 (1988)
205. J Senegas, A Mikou, J P Laval, B Frit *J. Fluorine Chem.* **37** 67 (1987)
206. P P Fedorov *Russ. J. Inorg. Chem.* **45** S268 (2000)
207. J M Reau, P P Fedorov, L Labardel, S F Matar, P Hagenmuller *Mater. Res. Bull.* **16** 1235 (1983)
208. P P Fedorov, I P Zibrov, E V Tarasova, S M Polunina, B P Sobolev, P I Fedorov *Zh. Neorg. Khim.* **33** 3222 (1988)
209. A Dib, S Aleonard, M Th Roux *J. Solid State Chem.* **52** 292 (1984)
210. A Dib, S Aleonard *J. Solid State Chem.* **64** 148 (1986)
211. P P Fedorov, L V Medvedeva, B P Sobolev *Zh. Neorg. Khim.* **67** 1073 (1993)
212. O Greis, B M Uwais, W Horne *Z. Kristallogr.* **186** 104 (1989)
213. M C Wintersgill, J J Fontanella, F P Pursel, A V Chadwick, A Azimi, V N Carr, C G Andeen *Radiat. Eff. Defects Solids* **75** 263 (1983)
214. S Mho, J C Wright *J. Chem. Phys.* **79** 3962 (1983)
215. L P Otroshchenko, V B Aleksandrov, N A Bendeliani, I A Verin, B P Sobolev *Kristallografiya* **35** 405 (1990) [f]
216. D R Figueroa, J J Fontanella, M C Wintersgill, J P Calame *Radiat. Eff. Defects Solids* **114** 263 (1990)
217. J Ravez, V Vassiliadis *C.R. Seances Acad. Sci., Ser. C* **270** 219 (1970)
218. J Ravez, D Dumora *C.R. Seances Acad. Sci., Ser. C* **269** 235 (1969)
219. J C Cretenet *Rev. Chim. Miner.* **10** 416 (1973)
220. A de Kozak *C.R. Seances Acad. Sci., Ser. C* **268** 2184 (1969)
221. A de Kozak *Rev. Chim. Miner.* **8** 329 (1971)
222. S Arquis-Canouet, J Raves, S C Abrahams *J. Appl. Crystallogr.* **19** 374 (1986)
223. J Ravez, M Duale *C.R. Seances Acad. Sci., Ser. C* **270** 56 (1970)
224. G Decap, R Retoux, Y Calage *Z. Anorg. Allg. Chem.* **619** 1850 (1993)
225. P Darbon, J M Reau, P Hagenmuller *Mater. Res. Bull.* **16** 273 (1981).
226. C Lucat, G Campet, J Claverie, J Portier, J M Reau, P Hagenmuller *Mater. Res. Bull.* **11** 167 (1976)
227. C Lucat, J Portier, J M Reau, P Hagenmuller *J. Solid State Chem.* **32** 279 (1980)
228. A Rhandor, J M Reau, S F Matar, S B Tian, P Hagenmuller *Mater. Res. Bull.* **20** 1309 (1985)
229. Y Ito, K Koto *Solid State Ionics* **19**/**20** 1202 (1986)
230. K J Kim, M Yoshimura, S Somiya *Solid State Ionics* **44** 281 (1991)
231. O Greis, M Martinez-Ripoll *Z. Anorg. Allg. Chem.* **436** 105 (1977)
232. F V Kalinchenko, M P Borzenkova, A V Novoselova *Zh. Neorg. Khim.* **28** 2351 (1983) [d]
233. R Domesle, R Hoppe *Z. Anorg. Allg. Chem.* **501** 1021 (1983)
234. J Shaffler, R Hoppe *J. Fluorine Chem.* **25** 27 (1984)
235. R E Thoma, in *Advances in Molten Salt Chemistry* Vol. 3 (Ed. J Braunstein) (New York, London: Plenum, 1975) p. 275
236. P P Fedorov, B P Sobolev *Zh. Neorg. Khim.* **24** 1038 (1979) [d]
237. P I Fedorov, P P Fedorov *Oshibki pri Postroenii Diagramm Sostoyaniya Dvoinykh Sistem* (Mistakes in the Construction of Phase Diagrams of Binary Systems) (Moscow: M V Lomonosov Moscow Institute of Fine Chemical Technology, 1992)
238. I V Murin, O V Glumov, A N Murin *Radiokhimiya* (1) 31 (1983) [h]
239. I V Murin, O V Glumov, I I Kozhina *Vestn. Leningr. Univ., Fiz. Khim.* (4) 87 (1980)
240. M Ouwerk, E M Kelder, J Schoonman *Solid State Ionics* **9**/**10** 531 (1983)
241. J M Reau, A Randor, C Lucat, J Portier, P Hagenmuller *Mater. Res. Bull.* **13** 827 (1978)
242. J L Soubeyreux, J M Reau, S Matar, P Hagenmuller, C Lucat *Solid State Ionics* **2** 215 (1981)
243. C Keller, M Salzer *J. Inorg. Nucl. Chem.* **29** 2925 (1967)
244. M G Izosimova, A I Livshits, V M Bouznik, Yu V Amelin, I V Murin, A N Murin *Neorg. Mater.* **23** 2056 (1987) [a]
245. J P Laval, D Mercurio-Lavaud, B Gaudreau *Rev. Chim. Miner.* **11** 742 (1974)
246. B Mehlhorn, R Hoppe *Z. Anorg. Allg. Chem.* **425** 180 (1976)
247. P Darbon, J M Reau, P Hagenmuller, C Depierrefixe, J P Laval, B Frit *Mater Res. Bull.* **16** 389 (1981)
248. C Depierrefixe, R M Awedallah, J P Laval, B Frit *Rev. Chim. Miner.* **20** 96 (1983)
249. J P Laval, C Depierrefixe, B Frit, G Roult *J. Solid State Chem.* **54** 260 (1984)
250. J Senegas, J P Laval, B Frit *J. Fluorine Chem.* **32** 197 (1986)
251. A A Babitsina, T A Emel'yanova, A P Chernov *Zh. Neorg. Khim.* **34** 3145 (1989) [d]
252. I D Ratnikova, Yu M Korenev, P P Fedorov, B P Sobolev *Zh. Neorg. Khim.* **42** 302 (1997) [d]
253. G F Krysenko, D G Epov, E I Mel'nichenko *Zh. Neorg. Khim.* **34** 2412 (1989) [d]
254. G F Krysenko, E I Mel'nichenko, D G Epov, S A Polishchuk *Zh. Neorg. Khim.* **36** 302 (1991) [d]
255. P Lagassie, J Grannec, J M Reau *Solid State Ionics* **21** 343 (1986)

256. A Ider, J P Laval, J Carre, J P Bastide, B Frit *J. Fluorine Chem.* **74** 141 (1995)
257. R Charpin *C.R. Seances Acad. Sci., Ser. C* **275** 1503 (1978)
258. V Wilhelm, R Hoppe *Z. Anorg. Allg. Chem.* **414** 130 (1975)
259. D Bizot *Rev. Chim. Miner.* **8** 797 (1971)
260. D Bizot *Rev. Chim. Miner.* **10** 519 (1973)
261. A Rhandor, J M Reau, P Hagenmuller *J. Solid State Chem.* **61** 197 (1986)
262. B Filec *J. Fluorine Chem.* **19** 485 (1982)
263. D Gantar *J. Chem. Soc., Dalton Trans.* **1987** 2379 (1987)
264. G Engel, U Fisher *J. Less-Common Met.* **158** 123 (1990)
265. Y Le Fur, S Aleonard *Bull. Soc. Fr. Mineral. Cristallogr.* **93** 260 (1970)
266. A Dib, M Roux, S Aleonard *J. Solid State Chem.* **66** 47 (1987)
267. A Le Bail JCPDS Card 42-0730
268. M Vlasse, J P Chaminade, J M Dance, M Saux, P Hagenmuller *J. Solid State Chem.* **41** 272 (1982)
269. A Pierrard *Z. Anorg. Allg. Chem.* **621** 1053 (1995)
270. A Le Bail, A M Mercier *Eur. J. Solid State Inorg. Chem.* **29** 183 (1992)
271. R Kanno, S Nakamoto, Y Kawamoto *Solid State Ionics* **51** 53 (1992)
272. I I Buchinskaya, P P Fedorov, N I Sorokin, M Sh Akchurin, B P Sobolev *Zh. Neorg. Khim.* **41** 172 (1996) [d]
273. P P Fedorov, A V Andreev, G V Zimina, B P Sobolev *Zh. Neorg. Khim.* **37** 1880 (1992) [d]
274. I I Buchinskaya, P P Fedorov, O S Bondareva, B P Sobolev *Neorg. Mater.* **28** 1202 (1992) [a]
275. P P Fedorov, I I Buchinskaya, V A Stasyuk, O S Bondareva *Zh. Neorg. Khim.* **41** 464 (1996) [d]
276. N K Voskresenskaya, N N Evseeva, S I Berul', I P Vereshchekina *Spravochnik po Plavkosti Solevykh Sistem* (Handbook on Fusibility of Salt Systems) (Moscow: Academy of Sciences of the USSR, 1961) Vol. 1
277. A F Corsmit, G J Dirksen *J. Cryst. Growth* **37** 104 (1977)
278. A F Halff *J. Solid State Chem.* **27** 201 (1979)
279. A F Halff, J Schoonman *Z. Phys. Chem., Neue Folge* **109** 161 (1978)
280. A F Halff, J Schoonman *J. Solid State Chem.* **27** 397 (1979)
281. B Aurivillius *Chem. Scr.* **10** 206 (1976)
282. B Aurivillius *Chem. Scr.* **15** 153 (1980)
283. M Sieskind, J P Lambour, Ch Steer, G Guigue *Phys. Status Solidi, A* **145** 89 (1994)
284. B Aurivillius *Chem Scr.* **10** 156 (1976)
285. D K Kunev, B I Lucheva *Zh. Neorg. Khim.* **35** 1619 (1990) [d]
286. S Matar, J M Reau, P Hagenmuller *J. Fluorine Chem.* **20** 529 (1982)
287. P Laborde, J M Reau, P Hagenmuller *Mater. Res. Bull.* **22** 723 (1987)
288. P Laborde, G Villeneuve, J M Reau *Phys. Status Solidi B* **141** 379 (1987)
289. C Follet-Houttemane, J Canonne, J C Boivin, J S Champarnaud-Mesjard, D Mercurio, B Frit, G Roult *Solid State Ionics* **28–30** 458 (1988)
290. J Senegas, J S Champarnaud-Mesjard, D Mercurio, B Frit *Mater. Res. Bull.* **23** 1019 (1988)
291. C Follet-Houttemane, J Canonne, J C Boivin, J S Champarnaud-Mesjard, D Mercurio, B Frit *Solid State Ionics* **66** 267 (1993)
292. F Desanglois, C Follet-Houttemane, J C Boivin *Solid State Ionics* **70/71** 229 (1994)
293. W Hume-Rothery, G V Reynor *The Structure of Metals and Alloys* (London: Institute of Metals, 1956)
294. P I Fedorov, P P Fedorov *Zh. Neorg. Khim.* **19** 215 (1974) [d]
295. P P Fedorov, P I Fedorov *Zh. Neorg. Khim.* **20** 1088 (1975) [d]
296. P P Fedorov, L A Ol'khovaya *Zh. Neorg. Khim.* **26** 218 (1981) [d]
297. R D Schannon *Acta Crystallogr., Sect. A* **32** 751 (1976)
298. S S Batsanov *Zh. Neorg. Khim.* **18** 205 (1973) [d]
299. P P Fedorov *Zh. Fiz. Khim.* **73** 1567 (1999) [b]
300. P P Fedorov *Zh. Neorg. Khim.* **46** 1724 (2001) [d]
301. P P Fedorov *Zh. Neorg. Khim.* **37** 1891 (1992) [d]
302. P P Fedorov, B P Sobolev, P I Fedorov *Kristallografiya* **26** 512 (1981) [f]
303. I V Murin *Izv. Sib. Otd. Akad. Nauk. SSSR, Ser. Khim. Nauk* (3) 53 (1984)
304. V V Osiko *Lazernye Kristally. Izbrannye Trudy* (Laser Crystals. Selected Works) (Moscow: Nauka, 2002)
305. P P Fedorov *Butll. Soc. Catalanes Fisica, Quim., Matem. Tecnol. (Barcelona)* **12** 349 (1991)
306. B P Sobolev *The Rare Earth Trifluorides. Introduction to Materials Science of Multicomponent Metal Fluoride Crystals* Pt. 2 (Barcelona: Institut d'Estudis Catalans, 2001)
307. I V Murin, W Gunsser *Solid State Ionics* **53–56** 837 (1992)
308. P J Bendall, C R A Catlow, J Corish, P W M Jacobs *J. Solid State Chem.* **51** 159 (1984)
309. S A Kazanskii, in *Spektroskopiya Kristallov* (Spectroscopy of Crystals) (Leningrad: Nauka, 1989) p. 110
310. J M Reau, P Hagenmuler *Appl. Phys. A: Solid Surf.* **49** 3 (1989)
311. P P Fedorov *Kondens. Sredy Mezhfaz. Gran.* **4** 346 (2002)
312. O Greis, J M Haschke, in *Handbook on the Physics and Chemistry of Rare Earth* Vol. 5, Ch. 45 (Eds K A Gscheidner, L Eyring) (Amsterdam, New York, Oxford: North-Holland, 1982) p. 387
313. D J M Bevan, O Greis, J Strahle *Acta Crystallogr., Sect. A* **36** 889 (1980)
314. B A Maksimov, L A Muradyan, V I Simonov *Koord. Khim.* **12** 1398 (1986) [i]
315. J Fernandez, M Sanz, A Mendioroz, R Balda, J P Chaminade, J Ravez, L M Lacha, M Voda, J Arriandiada *J. Alloys Compd.* **323–324** 267 (2001)
316. P P Fedorov, B P Sobolev *Kristallografiya* **37** 1210 (1992) [f]
317. N A Bendeliani, Doctoral Thesis in Chemical Sciences, Moscow State University, Moscow, 1982
318. A Mikoi, Ph.D.Thesis, Limoges, 1986
319. I D Ratnikova, Candidate Thesis in Chemical Sciences, Moscow State University, Moscow, 1978
320. E Catalano, E W Wrenn *J. Cryst. Growth* **30** 54 (1975)
321. H Oppermann, C Hennig *Z. Anorg. Allg. Chem.* **626** 450 (2000)
322. P P Fedorov *Z. Anorg. Allg. Chem.* **628** 29 (2002)
323. P P Fedorov, T M Turkina, O I Lyamina, E V Tarasova, I P Zibrov, B P Sobolev *Vysokoch. Veshch.* (6) 67 (1990)
324. P P Fedorov, I I Buchinskaya, in *X Simpozium po Khimii Neorganicheskikh Ftoridov. Ftoridnye Materialy. (Tez. Dokl.)* [The Xth Symposium on the Chemistry of Inorganic Fluorides. Fluoride Materials (Abstracts of Reports)] (Moscow: Dialog-MGU, 1998) p. 167
325. E I Banashek, N N Patsukova, I S Rassonskaya *Izv. Sektora FKhA* **27** 223 (1956)
326. J W Gibbs *The Collected Work. Vol. 1* (New York: Langmans Green, 1948)
327. F A N Schreinemakers *Z. Phys. Chem.* **52** 503 (1905)
328. V T Zharov, L A Serafimov *Fiziko-Khimicheskie Osnovy Distillyatsii i Rektifikatsii* (Physicochemical Foundations of Distillation and Rectification) (Leningrad: Khimiya, 1975)
329. P P Fedorov, in *Growth of Crystals* Vol. 20 (Eds E I Givargizov, A M Melnicova) (New York, London: Consultants Bureau, 1996) p. 103
330. A de Kozak, M Samouel, J Ranaudin, G Ferey *Z. Anorg. Allg. Chem.* **613** 98 (1992)
331. P Gerdin, A De Kozak, M Quarton *Z. Anorg. Allg. Chem.* **619** 1088 (1993)

[a] — *Inorg. Mater. (Engl. Transl.)*
[b] — *Russ. J. Phys. Chem. (Engl. Transl.)*
[c] — *Phys. Solid State (Engl. Transl.)*
[d] — *Russ. J. Inorg. Chem. (Engl. Transl.)*
[e] — *Russ. J. Appl. Chem. (Engl. Transl.)*
[f] — *Crystallogr. Rep. (Engl. Transl.)*
[g] — *J. Struct. Chem. (Engl. Transl.)*
[h] — *Radiochemistry (Engl. Transl.)*
[i] — *Russ. J. Coord. Chem. (Engl. Transl.)*

Russian Chemical Reviews **73** (4) 401 – 414 (2004) © 2004 Russian Academy of Sciences and Turpion Ltd

DOI 10.1070/RC2004v073n04ABEH000847

Disaccharide nucleosides

E V Efimtseva, S N Mikhailov

Contents

I. Introduction 401
II. Structures and properties of natural disaccharide nucleosides 401
III. General methods for the synthesis of disaccharide nucleosides 406

Abstract. Structural features and biological properties of natural disaccharide nucleosides and related compounds are considered. The main methods for the synthesis of these compounds are described and their advantages and disadvantages are discussed. These methods include condensations of a protected disaccharide with a heterocyclic base or of a protected nucleoside with an activated monosaccharide. The bibliography includes 172 references.

I. Introduction

Disaccharide nucleosides constitute an important group of natural compounds, but in contrast to ordinary nucleosides, it is their disaccharide rather than monosaccharide moiety that is linked to a heterocyclic base. Over one hundred such compounds and their derivatives have been isolated from various sources.[1] These compounds manifest a broad spectrum of biological (including antibacterial, fungicidal, herbicidal, antitumour and antiviral) activities. The review by Lerner[2] published in 1991 provides a detailed description of the structures of disaccharide nucleoside antibiotics and the approaches to the synthesis of some of them (the works cited therein were published up to 1988). Since that time, many new publications devoted to this problem have appeared in the current literature. Disaccharide nucleosides occur in nature not only in the free state, but also as components of biopolymers, such as poly(ADP-ribose) and tRNA which play an important role in the vital activities of living organisms. The first part of the present review is devoted to analysis of structural peculiarities and biological activities of natural disaccharide nucleosides and their analogues. The second part deals with the description of general methods for the synthesis of disaccharide nucleosides, *i.e.*, the formation of O- and N-glycosidic bonds.

II. Structures and properties of natural disaccharide nucleosides

1. Low-molecular-mass disaccharide nucleosides

A sufficiently large number of disaccharide nucleosides and related compounds are found among antibiotics, which has significantly stimulated the interest in their investigation. The structures and biological activities of nucleoside antibiotics were reviewed by Isono[3,4] in 1988 and 1991. The methods for their isolation and structural elucidation and some approaches to their synthesis are surveyed by Buchanan and Wightman.[5] Some of the published data on the synthesis of complex nucleoside antibiotics are summarised in the reviews by Garner[6] and Knapp.[7]

The structures of nucleoside antibiotics are extremely diverse[2–5] and their elucidation is rather a complicated task. In addition to a heterocyclic base and two monosaccharide residues, these compounds contain various functional substituents, such as acyl and alkyl groups as well as phosphate and sulfate residues, fatty acids, amino acids and peptides. Their degradation by acid and alkaline hydrolysis or methanolysis, periodate oxidation and subsequent reduction yields fragments the structures of which can be established by physicochemical methods. At present, the structures of many complex antibiotics are determined mainly by NMR spectroscopy and mass spectrometry supplemented by hydrolysis and oxidative degradation.

The first disaccharide nucleoside antibiotic amicetin (**1**) was isolated from *Streptomyces sp.* in the early 1950's; [8] however, its structure was established only in the 1960's.[9,10] Its structural analogues, *viz.*, the antibiotics bamicetin (**2**), plicacetin (**3**),[11]

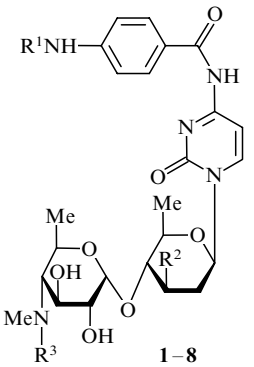

1–8

Compound	R^1	R^2	R^3
Amicetin (**1**)	$COCMe(NH_2)CH_2OH$	H	Me
Bamicetin (**2**)	$COCMe(NH_2)CH_2OH$	H	H
Plicacetin (**3**)	H	H	Me
Norplicacetin (**4**)	H	H	H
Oxamicetin (**5**)	$COCMe(NH_2)CH_2OH$	OH	Me
Oxyplicacetin (**6**)	H	OH	Me
SF2457 (**7**)	$COCHMeNH_2$	OH	H
Cytosaminomycin B (**8**)	Me	OH	Me

E V Efimtseva, S N Mikhailov V A Enhelhardt Institute of Molecular Biology, Russian Academy of Sciences, ul. Vavilova 32, 119991 Moscow, Russian Federation. Fax (7-095) 135 14 05. Tel. (7-095) 135 97 04. (E V Efimtseva). Tel. (7-095) 135 97 33. E-mail: smikh@eimb.ru (S N Mikhailov)

Received 18 April 2003
Uspekhi Khimii **73** (4) 435 – 448 (2004); translated by R L Birnova

norplicacetin (**4**),[12] oxamicetin (**5**),[13] oxyplicacetin (**6**),[14] SF2457 (**7**)[15] and cytosaminomycin (**8**)[16] were isolated and characterised starting from 1958. The presence of an α-(1→4)-glycoside bond between 4-methylamino- or 4-dimethylamino-4,6-dideoxy-D-glucose and 2,6-dideoxy- or 2,3,6-trideoxyhexose is the most characteristic feature of this group of antibiotics. The amino group of cytosine is acylated by *p*-aminobenzoic acid to which an (+)-α-methylserine or D-alanine residue is attached. The amicetin group antibiotics inhibit bacterial peptidyl transferase[17,18] and are active against gram-negative and gram-positive bacteria.

Oxyplicacetin **6** analogues, *viz*., cytosaminomycins A, C and D (**9a–c,** respectively) have been isolated recently.[16,19] In contrast to the antibiotics **1–8**, the amino group of cytosine in cytosaminomycins **9** is acylated by unsaturated acids.

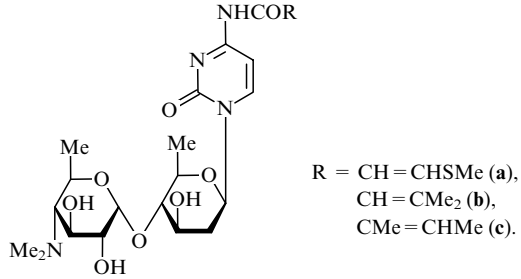

R = CH=CHSMe (**a**),
CH=CMe$_2$ (**b**),
CMe=CHMe (**c**).

Cytosaminomycins (**9a–c**)

Adenomycin (**10**)[20] produced by *Streptomyces griseoflavus* is not formally related to disaccharide nucleosides, since it is devoid of the disaccharide fragment. It contains adenosine, (−)-*chiro*-inositol and L-gulosamine as well as L-serine.[20] This antibiotic inhibits growth of gram-positive and gram-negative bacteria and is endowed with antitumour activities. Yet another structurally similar compound, *viz*., deseryladenomycin (**11**)[21] isolated from *Str*. *pseudogriseolus,* possesses insecticidal properties.

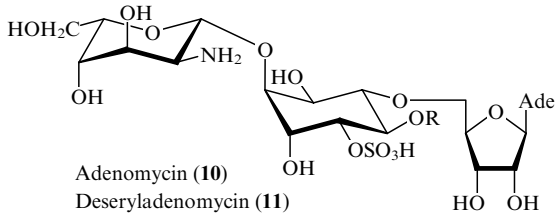

Adenomycin (**10**)
Deseryladenomycin (**11**)

R = COCH(NH$_2$)CH$_2$OH (**10**), H (**11**).

The antibiotic capuramycin (**12**)[22] isolated from *Str*. *griseus* contains uracil and a derivative of L-talofuranuronamide glycosylated by 4-deoxy-D-*erythro*-hex-4-enuronic acid; its carboxylic group is linked to 2(*S*)-aminocaprolactam through an amide bond. The antibiotic **12** is active against certain streptococci and mycobacteria. Capuramycin was the first natural product which was found to contain caprolactam as a substituent.

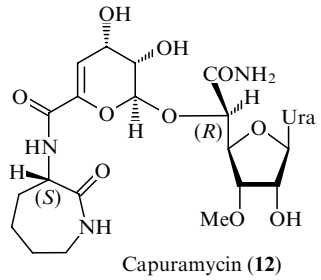

Capuramycin (**12**)

Dapiramicins (**13–15**) isolated from *Micromonospora sp*. contain 7-deazaguanine.[23,24] Its exocyclic amino group is involved in the formation of the N-glycosidic bond between the heterocyclic base and the disaccharide fragment (4′-*O*-methylcellobiose or 4′-*O*-methyl-6-deoxycellobiose). This bond is α in dapiramicin A (**13**) and β in the antibiotics **14** and **15**. It is believed that the configuration of the N-glycosidic bond determines the biological activities of dapiramicins. Dapiramicin A (**13**) exhibits strong fungicidal properties, while epidapiramicin A (**14**) and dapyramicin B (**15**) are less active.[24]

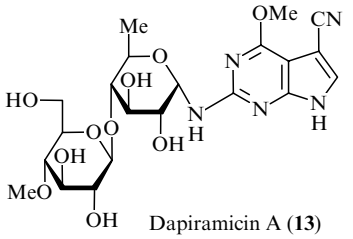

Dapiramicin A (**13**)

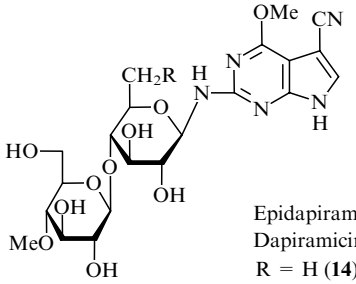

Epidapiramicin A (**14**)
Dapiramicin B (**15**)
R = H (**14**), OH (**15**).

Ezomycins (**16–21**) isolated from the cultural medium of *Streptomyces sp*. and possessing fungicidal activities[25] belong to the group of nucleoside antibiotics which includes higher monosaccharides; the β-anomers **16** and **17** are more active.

A characteristic structural feature of ezomycins **16–21** is the presence of N- or C-glycosides of 3,7-anhydrooctofuranuronic acid glycosylated by ezoaminuronic acid which is linked with L-cystathionine in the case of compounds **16–18**.[25–27] Ezomycins A$_2$, B$_2$ and C$_2$ (**19–21**) do not contain this amino acid.[26] Compounds **17**, **18** and **20**, **21** contain 5-substituted uracil and can therefore be regarded as pseudouridine derivatives. Under mild conditions, ezomycins B$_1$ and B$_2$ (**17**, **20**) are easily anomerised into thermodynamically more stable ezomycins C$_1$ and C$_2$ (**18**, **21**).[27] Similar interconversions in acidic media are typical of pseudouridine. The α-configuration of compounds **18** and **21** was established based on circular dichroism (CD) and NMR spectroscopic studies. The ease of anomerisation of pseudouridine derivatives accounts for the formation of ezomycins C$_1$ and C$_2$ (**18**, **21**) during the isolation of compounds B$_1$ and B$_2$ (**17**, **20**) from biological objects.

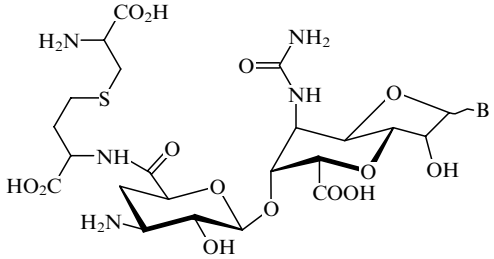

16–18

Compound	B
Ezomycin A$_1$ (**16**)	β-Cytosin-1-yl
Ezomycin B$_1$ (**17**)	β-Uracil-5-yl
Ezomycin C$_1$ (**18**)	α-Uracil-5-yl

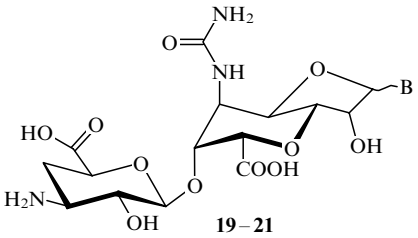

19–21

Compound	B
Ezomycin A_2 (**19**)	β-Cytosin-1-yl
Ezomycin B_2 (**20**)	β-Uracil -5-yl
Ezomycin C_2 (**21**)	α-Uracil -5-yl

Anthelmycin (or hikizimycin, **22**) was isolated from *Str. longissimus* and *Str. hikiziensis*.[28,29] Analysis of the degradation products of compound **22** revealed that the latter contains cytosine, 3-amino-3-deoxy-D-glucopyranose (canosamine) and 4-aminoundecose (hikosamine).[29,30] The β-configurations of O- and N-glycosidic bonds of both amino sugars were established by NMR spectroscopy. The antibiotic **22** manifests antiparasitic and fungicidal properties and inhibits prokaryotic and eukaryotic peptidyl transferase.[31]

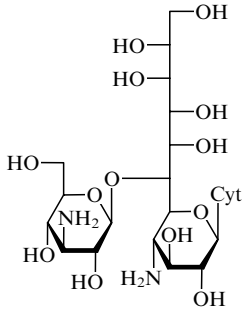

Anthelmycin or hikizimycin (**22**)

Many disaccharide nucleoside antibiotics contain fatty acid residues.

The microorganism *Str. lysosuperificus* is a producer of tunicamycins (**23**).[32] This group of antibiotics contains uracil, an undecose derivative (tunicamine) glycosylated by *N*-acetyl-D-glucosamine and a higher fatty acid residue.[33] At least ten tunicamycin derivatives **23** differing in acyl residues have been described.[33] α,β-Unsaturated acids are usually present as *trans*-isomers. Tunicamycins possess antibacterial and antiviral activities and effectively inhibit the biosynthesis of glycoproteins and peptidoglycans.[34,35]

The antibiotics streptovirudins (**24**) isolated from *Str. griseoflavus* are structurally similar to tunicamycins, they contain dihydrouracil along with uracil.[36]

Corynetoxins (**25**), which are structurally similar to tunicamycins, were isolated from the pasture crops-damaging bacterium *Corynebacterium rathay* by Australian scientists.[37,38]

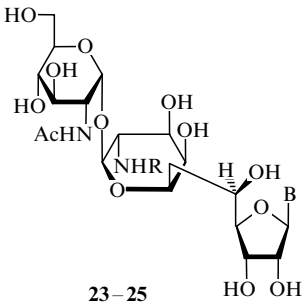

23–25

Compound	B	R
Tunicamycins I–X (**23**)	uracil-1-yl	$COCH=CH(CH_2)_nPr^i$, $n = 7–11$; $COCH=CH(CH_2)_nMe$, $n = 10–13$; $CO(CH_2)_{11}Pr^i$
Streptovirudins A_1, B_1, B_{1a}, C_1, D_1 (**24**)	uracil-1-yl	$COCH=CH(CH_2)_nPr^i$, $n = 6–8$; $COCH=CH(CH_2)_nBu^s$, $n = 6, 8$
Streptovirudins A_2, B_2, B_{2a}, C_2, D_2 (**24**)	dihydro-uracil-1-yl	$COCH=CH(CH_2)_nPr^i$, $n = 6–8$; $COCH=CH(CH_2)_nBu^s$, $n = 6, 8$
Corynetoxins (**25**)	uracil-1-yl	$COCH=CH(CH_2)_nBu^s$, $n = 10, 12$; $COCH_2CH(OH)(CH_2)_nBu^s$, $n = 10, 12$

The lipid-containing nucleoside antibiotics liposidomycins A I, B and C (**26a–c,** respectively) were isolated from *Str. griseosporeus*.[39,40] Liposidomycins **26** contain uridine glycosylated by 5-amino-5-deoxy-D-ribofuranose, 1,4-diazepane and β-hydroxy fatty acids acylated by 3-methylglutaric acid. The configuration of the double bonds of the lipid moiety of liposidomycin A I is *cis*.[40] It is of note that the absolute configuration of the chiral centres 5″ and 6″ has not been finally established yet. A series of papers devoted to the stereoselective synthesis of the disaccharide[41] and 1,4-diazepan-3-one[42–46] fragments and their comparison with the degradation products of liposidomycin have been published recently.[45,46] This enabled the determination of configurations of the other two chiral centres, *viz*., 5′(*S*) and 2″(*S*).[41,46]

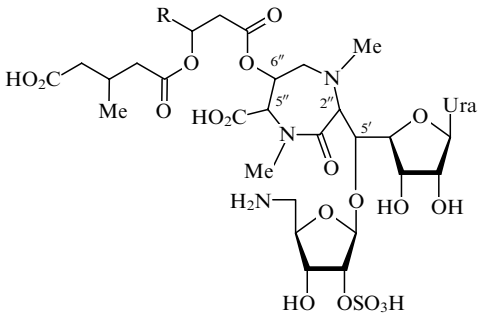

Liposidomycins (**26a–c**)

R = $(CH_2)_3CH=CHCH_2CH=CHC_5H_{11}$ (**a**), $(CH_2)_8Pr^i$ (**b**), $(CH_2)_{10}Me$ (**c**).

A series of liposidomycins produced by *Streptomyces sp*. SN-1061M have recently been discovered.[47] In contrast to liposidomycin A I, liposidomycin A II does not contain a sulfate group, while liposidomycin A III lacks the 3-methylglutaric acid residue and liposidomycin A IV is devoid of both substituents. Like tunicamycins, liposidomycins control the synthesis of glycoproteins and peptidoglycans[35,48] and inhibit bacterial translocase;[41,48] their cytotoxicities are significantly lower than those of tunicamycins.[48] Liposidomycins A II and A IV contain no sulfate groups and manifest high antimicrobial activities.[47]

A series of biologically active *O*-hexopyranosyl ribonucleosides (**27–29**), which are not related to antibiotics, have been isolated from various natural sources.

The adenosine derivatives adenophostins A and B (**27a**,**b**) are produced by the microorganism *Penicillum brevicompactum*.[49,50] Compounds **27** are the strongest agonists of receptors of inositol triphosphate which plays a crucial role in the release of Ca^{2+} ions (see Refs 51 and 52). The presence of an α-glycosidic bond between the glucopyranose and ribofuranose residues is a characteristic structural feature of adenophostins (**27**). A vast variety of analogues of compounds **27** have been synthesised and their structure–activity relationships have been studied.[53–55] The presence, in adenophostins (**27**), of an adenine residue is essential

for the manifestation of their biological activity. Adenophostin A derivatives where adenine is lacking or replaced by other heterocyclic bases are less active.[55]

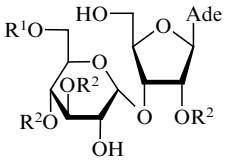

Adenophostins (**27a**,**b**)

R^1 = H (**a**), Ac (**b**);
R^2 = PO_3H_2.

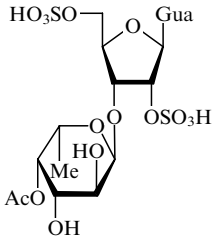

HF-7 (**28**)

A neuroactive compound HF-7 (**28**) was isolated from the venom of the spider *Hololena curta* and its chemical synthesis was carried out.[56] Compound **28** is an anionic nucleoside and, similar to adenophostins **27**, affects intracellular concentrations of Ca^{2+} ions in nervous tissues.

Sea algae, invertebrates (sponges, tunicata, molluscs) and symbiotic microorganisms (bacteria, fungi, microalgae, *etc*.) represent an abundant source of biologically active compounds as potential medicinal drugs.[57] Thus 9-(β-D-arabinofuranosyl)adenine, which possesses antiviral activity, was isolated from sea sponges as early as the 1950's. Several examples of disaccharide nucleosides from different marine organisms can be given.

Thus a group of Japanese investigators have isolated a series of disaccharide nucleosides, *viz*., shimofuridins A–G (**29a**–**g**, respectively), which differ in the geometries of the double bonds and the lengths of the hydrocarbon chains of the acyl residues.[58,59] The configuration of the chiral centre (*S*) was established only for shimofuridin A.[58] 2′-*O*-α-L-Fucopyranosylinosine is the main structural element of shimofuridins. Shimofuridin A is active against gram-positive bacteria and manifests antifungal activity.

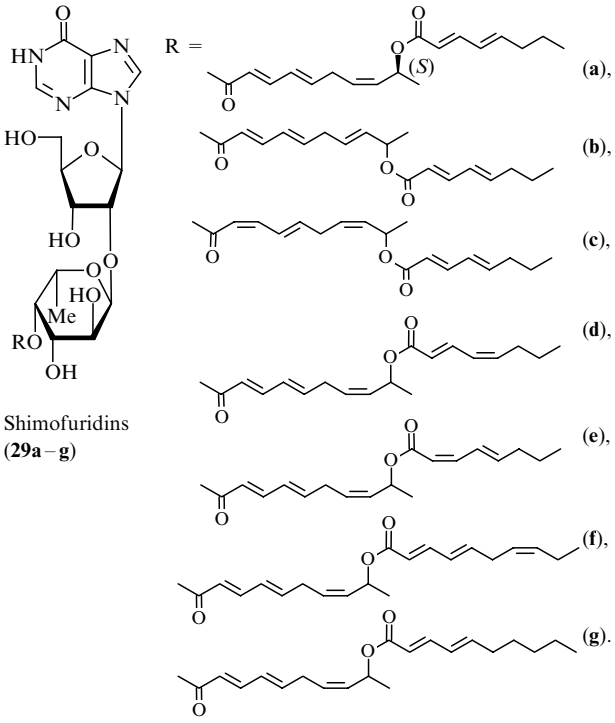

Shimofuridins (**29a**–**g**)

5′-*O*-α-D-Glucopyranosyl derivatives of tubercidin and toyocamycin, which contain 7-deazaadenosine and 7-cyano-7-deazaadenosine, respectively, were isolated from blue-green algae.[60] These compounds possess fungicidal properties and manifest cytotoxic activities. The crustacean *Ligia exotica* serve as a source of 3′-*O*-α-D-glucopyranosylinosine.[61] Disaccharide nucleosides were also isolated from plants. Thus an N^6-benzyl adenosine derivative glucosylated in the 3′-*O*-position is formed in petunia seedlings grown on an artifical medium in the presence of N^6-benzyladenine.[62]

Let us consider some structurally similar analogues of disaccharide nucleosides where the nucleoside fragment and the monosaccharide residue are linked through a non-O-glycosidic bond in more detail. Thuringiensin (or β-exotoxin, **30**) isolated from *Bacillus thuringiensis* simultaneously by two independent groups of investigators is an example.[63,64] This is built of adenosine linked to α-D-glucopyranose through an ether bond and a phosphorylated allaric acid.[65] The α-configuration of the O-glycosidic bond and the (*R*)-configuration of the C(2) atom of allaric acid have been established. Thuringiensin (**30**) possesses insecticidal properties and manifests pronounced cytotoxic activity. Compound **30** inhibits DNA-dependent RNA polymerase in prokaryotes and eukaryotes.[66]

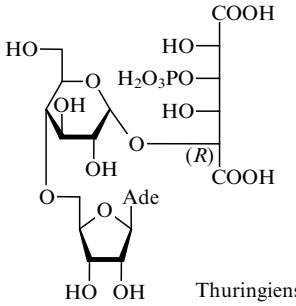

Thuringiensin (**30**)

The recently discovered antibiotics guanofosfocins (**31a**–**c**) have unusual structures.[67,68] Guanofosfocin A (**31a**) was isolated from *Streptomyces sp*. and guanofosfocins B (**31b**) and C (**31c**), from *Trichoderma sp*. They contain a hemiacetal bond between the monosaccharide residues. Guanofosfocins (**31**) inhibit chitin synthetase and are effective antifungal agents. However, these compounds are highly labile, which significantly complicates their synthesis and further studies.[68,69]

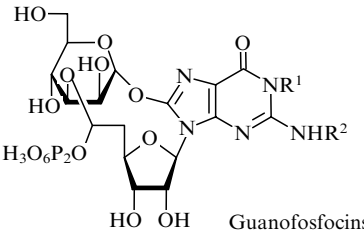

Guanofosfocins (**31a**–**c**)

R^1 = Me (**a**), H (**b**); R^2 = H;

R^1 = H, R^2 = 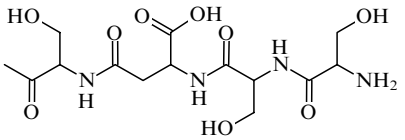 (**c**).

By way of illustration, the antibiotic EM 2487 (**32**) isolated from *Streptomyces sp*. represents a carbocyclic analogue of a disaccharide nucleoside.[70] Its cyclopentene fragment is linked to

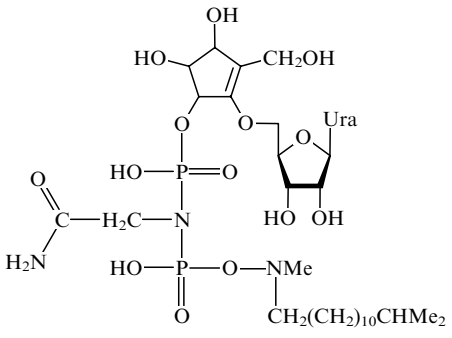

EM 2487 (**32**)

uridine through an ether bond. The antibiotic **32** manifests pronounced anti-HIV activity.[71]

Even a brief survey demonstrates the diversity of structural peculiarities and biological activities of disaccharide nucleosides. In conclusion, special mention should be made of the studies devoted to the chemical synthesis of some of the compounds mentioned above. Complete syntheses of plicacethin (**3**),[72] capuramycin (**12**),[73] hikizimycin (**22**),[74] tunicamycin V (**23**) [75–77] and thuringiensin (**30**) [78] have been performed and approaches to the synthesis of fragments of the most complex antibiotics ezomycin A_1 (**16**) [79,80] and liposidomycin C (**26**) have been developed.[41–46,81,82] The syntheses of adenophostin (**27**), HF-7 (**28**) and shimofuridin A (**29**) will be considered in detail in the second part of the review. The development of methods for the synthesis of guanofosfocins (**31**) and EM 2487 (**32**) still presents a problem for modern bioorganic chemistry.

2. Disaccharide nucleosides as structural elements of biopolymers

Purine disaccharide nucleosides with two O-glycosidically linked ribofuranose residues were identified as components of poly(ADP-ribose) and transfer RNA.

An enzyme responsible for the conversion of nicotinamide adenine dinucleotide (NAD^+) into a homopolymer, poly(ADP-ribose), with simultaneous release of nicotinamide was discovered in eukaryotic cell nuclei in the 1960's.[83–85] The polymer is covalently linked to histones and other nuclear proteins, as a rule, through glutamic acid and, less frequently, through aspartic acid.[84,85] Its multifaceted biological role is highlighted in a review.[84] Thus it is known that poly(ADP-ribose) is involved in structural modulation of chromatin, in replication, transcription and repair of DNA and in cell differentiation. In-depth studies on intracellular functions of poly(ADP-ribose) are currently underway.

Molecules of poly(ADP-ribose) both isolated from natural sources and synthesised *in vitro* using the corresponding poly(ADP-ribose) polymerase have a branched structure and contain over 200 monomeric units.[86,87] Their linear fragments contain 20–50 units and alternate with branched fragments, which probably confer stability on the conformation of the biopolymer.

The degradation of poly(ADP-ribose) is mediated by two enzymes, *viz*., ADP-ribosyl protein lyase and poly(ADP-ribose) glycohydrolase.[83,84] The former is involved in the hydrolysis of the bond between the protein and the ADP ribose fragment. Glycohydrolase, which is endowed with both exo- and endoglycosidase activities, cleaves the bonds between ribofuranose and adenosine resulting in ADP ribose.[84,88]

Accessibility of polymerase enables an easy synthesis of poly(ADP-ribose) *in vitro*. Enzymatic hydrolysis of poly(ADP-ribose) synthesised *in vitro* by snake venom phosphodiesterase yields compound **33**; its structure was established by NMR spectroscopy.[89–91] Treatment of compound **33** with alkaline phosphatase results in 2′-*O*-α-D-ribofuranosyl adenosine (**34**). The absence of a signal for the 2′-hydroxy group of the adenosine residue in the ^1H NMR spectrum of the latter in DMSO-d_6 suggests the presence of a 1″→2′-glycosidic bond between the ribofuranose and adenosine residues.[91] The configurations of the O-glycosidic bond were established by ^{13}C NMR spectroscopy of compound **33** and anomeric methyl D-ribofuranosides.[89] A comparison of the spin–spin coupling constants $J_{1',2'}$ in the diphosphate **33**, methyl-β- and -α-D-ribofuranosides ($J_{1',2'}$ = 4.2, 1.2 and 4.5 Hz, respectively) confirmed the α-configuration of the O-glycosidic bond.[91] The structure of the nucleoside **35** localised in the branching point was also established using physicochemical methods.[92]

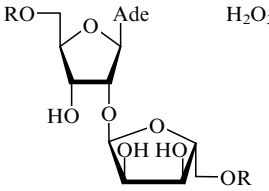

33: R = PO_3H_2;
34: R = H.

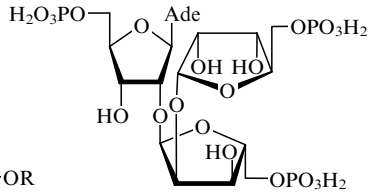

35

It is of note that compound **33** represents a fragment of the prosthetic group of compound **36** which is linked to the serine residue of bacterial citrate lyase [93,94] and malonate decarboxylase.[95] In contrast to poly(ADP-ribose), dephosphorylated coenzyme A is a precursor of compound **36**, while ATP is a contributor of an additional 5-phosphoribofuranose residue.[94,95]

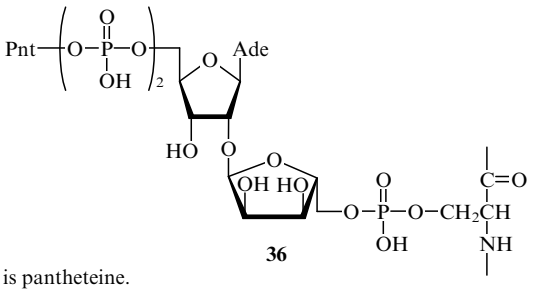

36

Pnt is pantheteine.

The purine disaccharide nucleosides **37** and **38** were isolated from lower eukaryotic initiator tRNAs ($tRNA_i^{Met}$) and several plant sources.[96,97] These minor nucleosides located in the steam of the T-loop of $tRNA_i^{Met}$ and occupy the 64th position in the primary structure of the molecule.[98–101] The 3′- and 5′-hydroxy groups of the nucleoside residue take part in the formation of internucleotide bonds. The site of the attachment of the ribofuranose residue to the nucleoside and the position of an additional phosphate group were established using periodate oxidation of mono- and dinucleotides containing fragments **37** and **38** with subsequent β-elimination under the action of cyclohexylamine.[99,100] In contrast to the monomeric unit of poly(ADP-ribose) (compound **33**), the additional ribofuranose residues in the disaccharide nucleosides **37** and **38** are linked to the nucleoside by a β-glycosidic bond.

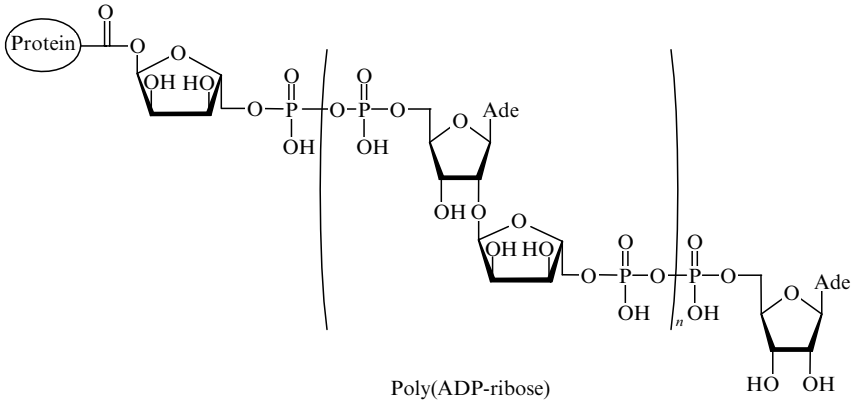

Poly(ADP-ribose)

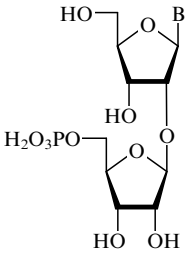

37: B = Ade;
38: B = Gua.

Total chemical synthesis of these minor nucleosides, *O*-β-D-ribofuranosyl-(1″→2′)-adenosine 5″-phosphate (**37**)[102] and *O*-β-D-ribofuranosyl-(1″→2′)-guanosine 5″-phosphate (**38**), has been carried out recently;[103] the synthesis of the α-anomer **33** has not been described so far.

The values of the spin–spin coupling constants of the natural disaccharide nucleoside **33** (see Ref. 91) and its synthetic isomer **37** as revealed by ^{1}H NMR spectroscopy are listed in Table 1.[102] These compounds possess similar coupling constants with the exception of $J_{1',2'}$ and $J_{3',4'}$ of the ribofuranose fragment.

Table 1. Experimental values of spin–spin coupling constants determined from the ^{1}H NMR spectra of compounds **33**[91] and **37**[102] (in D_2O).

Coupling protons	*J* /Hz			
	fragment **33**		fragment **37**	
	Ado	α-ribosyl	Ado	β-ribosyl
1′–2′	5.5	4.6	6.4	1.2
2′–3′	5.1	6.4	5.5	4.6
3′–4′	3.7	0.7	3.1	6.4
4′–5′a	2.8	4.4	2.7	4.3
4′–5′b	3.8	4.1	3.7	5.7
5′a–5′b	−11.6	−11.3	−12.8	−11.6
5′a–P	4.3	5.8		6.4
5′b–P	4.8	4.4		7.0

It is believed that the presence of the disaccharide nucleosides **37** and **38** in position 64 is the most characteristic feature of lower eukaryotic $tRNA_i^{Met}$. According to data from X-ray diffraction analysis, the bulky 5″-phosphoribofuranosyl residue of the nucleoside **37** occupies a strictly definite position in the minor groove in the tertiary structure of yeast $tRNA_i^{Met}$ (see Ref. 104). The additional phosphate group forms a hydrogen bond with the 2-amino group of the vicinal guanosine residue G_{63}. After selective removal of the 5″-phosphoribofuranose residue (oxidation, β-elimination), tRNA begins to act as an elongator one, however, with a lower efficiency in comparison with native $tRNA_i^{Met}$ (see Refs 105 and 106). This suggests that the modification of the purine nucleoside **64** in $tRNA_i^{Met}$ plays a role in the discrimination of the initiation–elongation process of protein synthesis and thus prevents the formation of a tRNA complex with the elongation factor EF-1α and guanosine triphosphate characteristic of the elongation reaction.

The mechanisms of biosynthesis of modified nucleosides **37** and **38** have not been finally elucidated yet. It is hypothesised that adenosine and guanosine undergo post-transcriptional ribosylation in the precursor $tRNA_i^{Met}$ with involvement of 5-phosphoribosyl-1-pyrophosphate.[99]

III. General methods for the synthesis of disaccharide nucleosides

Disaccharide nucleosides can be synthesised by one of two routes. These consist of coupling of a protected disaccharide with a heterocyclic base derivative or the formation of an O-glycosidic bond between a nucleoside carrying one free hydroxy group and an activated monosaccharide.

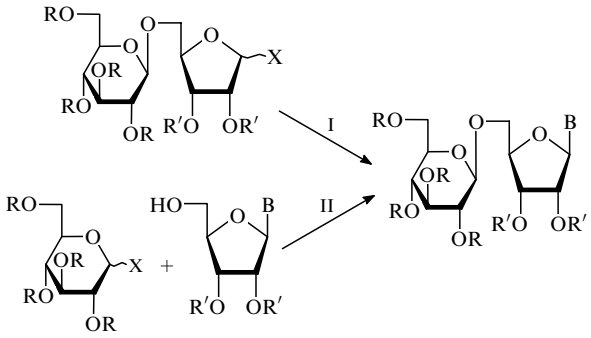

X = Hal, OAcyl, SAlk, SPh *etc.*; B is heterocyclic base.

The choice of the order of formation of O- and N-glycosidic bonds is essential in the design of methods for the synthesis of disaccharide nucleosides. In each concrete case, the reaction sequence is determined by the structure and stability of final and intermediate products as well as by availability of starting compounds. Obviously, the use of readily available natural carbohydrates and nucleosides can significantly shorten the synthetic procedure. Special attention should be given to the choice of protective groups, estimation of their stability under various coupling conditions and stereoselectivity of formation of glycosidic bonds. The strategy and tactics of the syntheses of capuramycin (**13**), ezomycin A_1 (**16**), hikizimycin (**22**), tunicamycin (**23**), liposidomycin C (**26**) and thuringiensin (**30**) are reviewed by Knapp.[7]

1. Coupling of disaccharides with nucleic bases (N-glycosylation)

The classical methods for the synthesis of nucleosides[107] include coupling of acylglycosyl halides with silver or mercury salts of purine bases or with 2,4-dialkoxypyrimidines. A detailed account of the use of these methods in the first syntheses of disaccharide nucleosides starting from heterocyclic bases and derivatives of accessible natural disaccharides (lactose, maltose, cellobiose, melibiose, *etc.*) is given in a review by Lerner.[2] The yields in the coupling step did not usually exceed 50%. The main drawback of these methods is the necessity to prepare rather unstable glycosyl halides. Besides, the synthesis of purine derivatives demands the use of toxic mercury salts.

Stereoselective formation of the N-glycosidic bond is the key step in the synthesis of nucleosides. This problem is considered in detail in several reviews.[107–111] The presence of a participating 2-*O*-acyl group in the monosaccharide ensures stereoselective formation of 1,2-*trans*-products; in other cases, mixtures of α- and β-anomers are formed. These regularities hold also for the reactions involving disaccharides.

A procedure proposed by Vorbruggen[108,110,111] has replaced virtually completely the previously employed methods for the synthesis of nucleosides and their analogues. This consists of the interactions of silyl derivatives of heterocyclic bases with peracylated sugars in aprotic solvents in the presence of Lewis acids ($SnCl_4$ or trimethylsilyl trifluoromethanesulfonate, TMSOTf). The use of this approach has significantly simplified the reaction procedure and increased the yields of the target products.

Thus the glycosylation of bis(trimethylsilyl)cytosine [$(TMS)_2$-Cyt] by octaacetyllactose (**39**), octaacetylcellobiose and octaacetylmaltose in the presence of $SnCl_4$ in boiling dichloroethane occurred at a sufficiently high rate (2 h) and afforded disaccharide nucleosides (*e.g.*, lactosylcytosine **40**) in high yields (60%–90%).[112] The use of acylglycosyl chlorides resulted in the formation of regioisomers.[112] The glycosylation of the silyl derivative of 5-fluorouracil $(TMS)_2$-5FUra by 1,6-anhydrolactose hexaacetate (**41**) required more drastic conditions (boiling in

acetonitrile, 10 h); the yield of the β-anomer **42** was 35%.[113] Peracylated tri- and tetrasaccharides can also be involved in the coupling.[112]

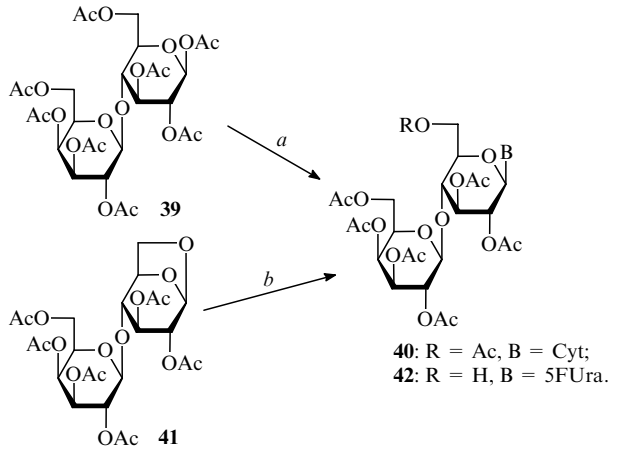

(*a*) $(TMS)_2$ – Cyt, $SnCl_4$, DCE (1,2-dichloroethane), Δ, 2 h;
(*b*) $(TMS)_2$ – 5FUra, $SnCl_4$, MeCN, Δ, 10 h.

The reaction of octaacetylcellobiose with a silyl derivative of theophylline was carried out under similar conditions ($SnCl_4$, acetonitrile, 75 °C, 16 h) and gave 7-(hepta-*O*-acetyl-β-cellobiosyl)theophylline in 90% yield.[114]

Preparation of 5′-*O*-glucuronides of the known antitumour nucleosides, 5-fluorouridine and 5-fluorocytidine, has been described.[115] The coupling of the glycosyl chloride **43** with a trimethylsilyl derivative of 5-fluorocytosine (boiling in acetonitrile, 24 h) resulted in the disaccharide nucleoside **44** in 49% yield. Under similar conditions (boiling in 1,2-dichloroethane, 35 min), the peracetylated disaccharide **45** reacted much faster; the products **46** were obtained in 90% yield. Removal of protective groups gave the free acid **47** or the amide **48**.

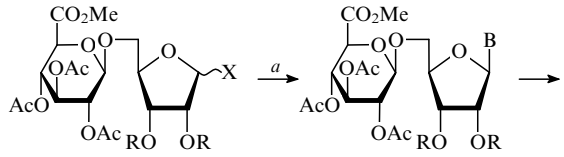

43: X = α- or β-Cl, R = Bz;
45: X = β-OAc, R = Ac.
44: R = Bz, B = 5FCyt;
46: R = Ac, B = 5FCyt, 5FUra.

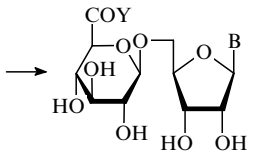

47: Y = OH; **48**: Y = NH_2;
B = 5FCyt, 5FUra.

(*a*) $(TMS)_2$ – 5FCyt or $(TMS)_2$ – 5FUra, $SnCl_4$, MeCN or DCE.

An alternative route to the synthesis of 5′-*O*-glycosylribonucleosides entailed the Koenigs – Knorr *O*-glycosylation of 2′,3′-*O*-isopropylidene-5-fluorouridine (**49**) by glucuronosyl bromide **50**; the yield of the disaccharide nucleoside **51** was 65%. However,

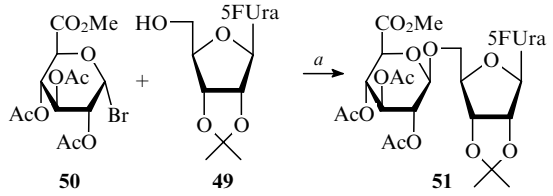

50 **49** **51**

(*a*) Ag_2O, C_6H_6 – MeCN, Δ, 16 h.

subsequent removal of the 2′,3′-*O*-isopropylidene group in an acidic medium (boiling in 80% AcOH, 30 min) was accompanied by a significant cleavage of the O-glycosidic bonds and the formation of the target product in a low yield.

A comparison of these approaches to the synthesis of 5′-*O*-glycosylribonucleosides has demonstrated a salient advantage of the Vorbruggen *N*-glycosylation by acetate **45** which is also employed in the synthesis of purine disaccharides. Thus the coupling of bis(trimethylsilyl)hypoxanthine with peracetylated 5-*O*-(β-D-glucopyranosyl)-β-D-ribofuranose and subsequent deacetylation gave 5′-*O*-(β-D-glucopyranosyl)inosine.[116]

At present, the synthesis of disaccharide nucleosides is usually performed by the Vorbruggen procedure. Thus the disaccharide fragment of the antibiotic liposidomycin (**26**)[41] and some of its derivatives have recently been synthesised using this method.[117] The reaction of fully protected 1-*O*-acetyl-5-*O*-(5-azido-5-deoxy-β-D-ribofuranosyl)-D-allofuranose or -L-talofuranose derivatives with bis(trimethylsilyl)uracil in the presence of TMSOTf in acetonitrile was carried out under mild conditions (room temperature, 3 h); the yields were up to 70%. Similar glycosylation was used[53,54,118] in the synthesis of numerous analogues of adenophostin (**27**).

In all cases studied, *N*-glycosylation by furanose derivatives occurs under milder conditions and at much faster rates than by pyranoses. The best results were obtained when 1-*O*-acetyl sugars were used.

Substitution of heterocyclic bases is an alternative route to the synthesis of disaccharide nucleosides.[111] A mixture of compounds **53** and **54** was prepared starting from a thymine disaccharide (compound **52**[119]) and a 1.5-fold excess of bis(trimethylsilyl)-N^6-benzoyladenine, the overall yield of the reaction products being 68%.[120] As expected, the β- and α-anomers **53** and **54** are formed in a 1 : 2 ratio in the absence of a participating group at the C(2′) atom.

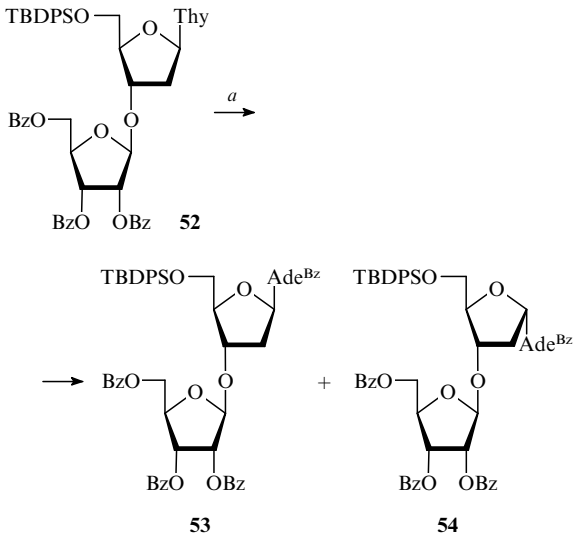

TBDPS is *tert*-butyldiphenylsilyl;
(*a*) $(TMS)_2$ – Ade^{Bz}, TMSOTf, MeCN, Δ, 2.5 h.

2. Coupling of monosaccharides with nucleosides (O-glycosylation)

The formation of the O-glycosidic bond is considered in detail in the reviews devoted to carbohydrate chemistry.[121–123] Early syntheses of disaccharide nucleosides were carried out using the Koenigs – Knorr method or its modifications, *i.e.*, coupling of glycosyl halides with alcohols in the presence of mercuric or silver salts. As in the case of N-glycoside synthesis, the presence of a participating acyl group at the O(2) atom of a monosaccharide favours stereoselective formation of 1,2-*trans*-substituted products, while in its absence a mixture of α- and β-anomers is usually

formed. Directed synthesis of 1,2-*cis*-substituted products is a more complicated process.

Studies by Lichtenthaler *et al.*[124–126] have shown that the yields in the Koenigs–Knorr glycosylation of 2′,3′-*O*-isopropylidene nucleosides by per-*O*-acetylglycopyranosyl bromides strongly depend on the nature of the solvent and the promoter. The reaction of 2′,3′-*O*-isopropylideneinosine (**55**) with tetra-*O*-acetyl-α-D-glucopyranosyl bromide (**56**) (Scheme 1) in the presence of silver carbonate in chloroform (24 h, 60 °C) gave predominantly the O^6-glycoside **57** (yield 66%); prolonged heating (3–4 days) gave the second product, *viz.*, N^9-glycoside **58**. The disaccharide nucleoside **59** was obtained in 41% yield when the reaction was carried out in the presence of a silver carbonate–silver perchlorate mixture in chloroform (24 h, 0 °C).[125]

Similar reactions of 2′,3′-*O*-isopropylideneadenosine and -guanosine afforded complex mixtures of products.[125] Thus the glycosylation of compound **55** in nitromethane in the presence of mercuric cyanide (2 days, 40 °C) yielded a mixture of all possible

Scheme 1

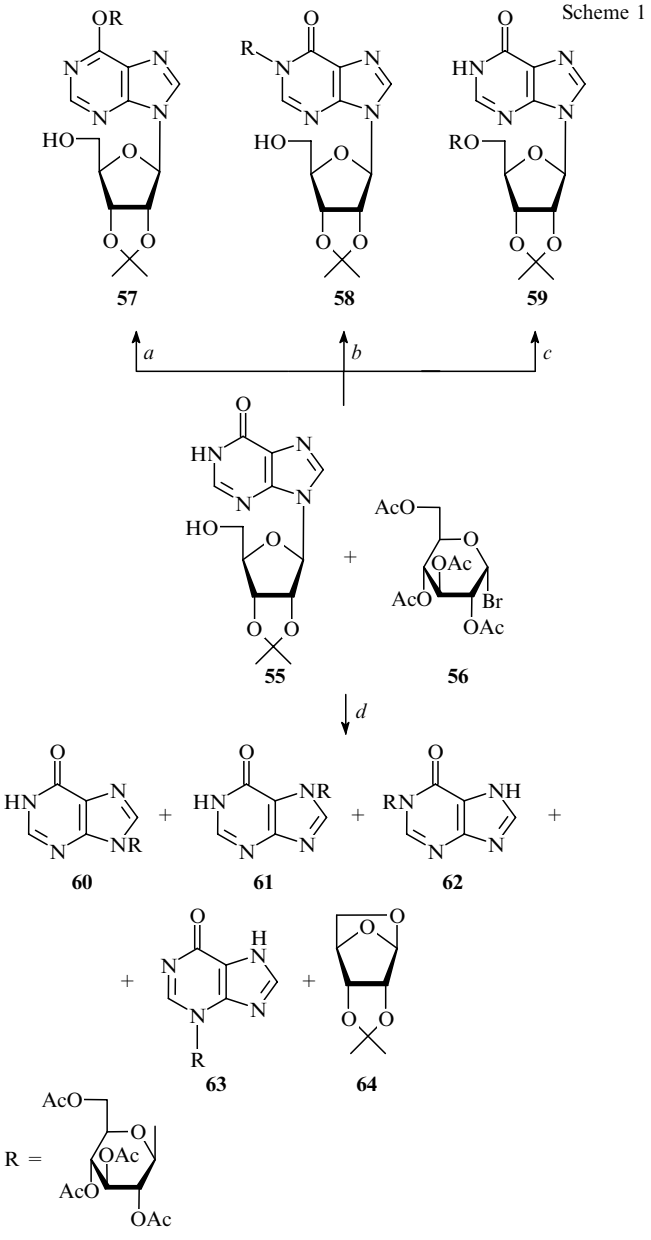

(*a*) Ag_2CO_3, $CHCl_3$, 60 °C, 24 h; (*b*) Ag_2CO_3, $CHCl_3$, 60 °C, 3–4 days; (*c*) Ag_2CO_3–$AgClO_4$, $CHCl_3$, 0 °C, 24 h; (*d*) $Hg(CN)_2$, $MeNO_2$.

N-glycopyranosylhypoxanthines **60**–**63** and 2,3-*O*-isopropylidene-1,5-anhydro-D-ribofuranose (**64**).[124]

More encouraging results were obtained when this method was used in the synthesis of pyrimidine nucleosides. Thus the reaction of 2′,3′-*O*-isopropylideneuridine with glycosyl bromide **56** under identical conditions occurred at much faster rates (3 h, 55 °C) and gave a protected 5′-*O*-glucopyranosyluridine derivative in 73% yield.[126] Good yields of disaccharide derivatives were achieved upon glycosylation of 2′,3′-*O*-isopropylideneuridine with tetra-*O*-acetyl-α-D-galactopyranosyl bromide in the presence of mercuric cyanide.[126, 127] A similar reaction of 2′,3′-*O*-isopropylideneuridine with 3,4,6-tri-*O*-acetyl-2-*O*-benzyl-α-D-glucopyranosyl bromide yielded a mixture of α- and β-anomers (2 : 1).[126]

As expected, the Koenigs–Knorr glycosylation of nucleosides by 3-deoxynon-2-ulosonic acid derivatives gave a mixture of α- and β-anomers; the overall yields of the derivatives **65** and **66** after deprotection were rather small.[128, 129]

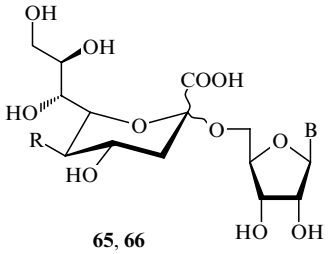

65: R = NHAc, B = Cyt, Hyp; **66**: R = OH, B = Ura, Cyt, 5FUra.

In some studies,[130–132] 5′-*O*-glucopyranosylnucleoside derivatives were synthesised using the Bredereck modification. The reactions of 5′-*O*-trityl-2′-deoxynucleosides (**67**) with glucosyl bromide **56** in nitromethane in the presence of silver perchlorate gave compounds **68** in 22% and 41% yields.[130] 5′-*O*-Glucuronides of 6-azauridine **69**[131] and 1-(β-D-arabinofuranosyl)cytosine **70**[132] were synthesised in a similar way; the yields in the coupling step were 38% and 20%, respectively.

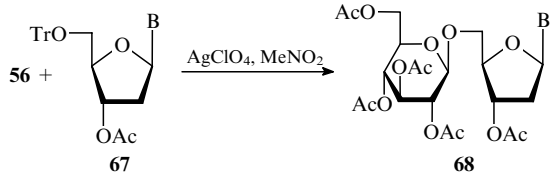

B = Cyt^{Ac}, Thy.

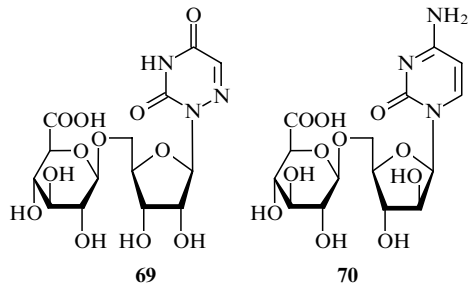

The glycosylation of ribavirin derivatives has been described.[133] The Koenigs–Knorr coupling of glucosyl bromide **56** with 2′,3′-*O*-isopropylideneribavirin (**71**) in the presence of silver carbonate and silver perchlorate gave a complex mixture; the orthoester **72** was isolated in 30% yield. At the same time, the Bredereck glycosylation of the trityl ether **73** afforded the disaccharide nucleoside **74** in 15% yield. Similar results were obtained in the glycosylation of compounds **71** and **73** by galactosyl bromide.[133] It is noteworthy that the formation of an orthoester derivative (27%) also took place upon Koenigs–Knorr coupling of tetra-*O*-acetyl-α-D-glucopyranosyl bromide

56 with 2′-deoxy-N^4-acetylcytidine in nitromethane in the presence of silver carbonate.[130]

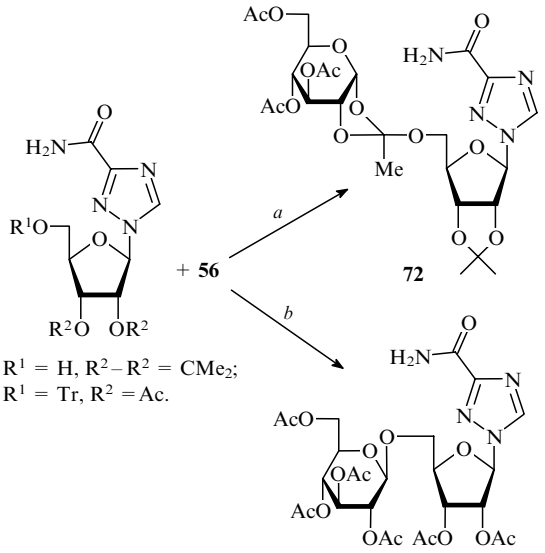

71: R^1 = H, R^2–R^2 = CMe_2;
73: R^1 = Tr, R^2 = Ac.

Tr is triphenylmethyl (trityl);
(*a*) Ag_2CO_3–$AgClO_4$, CH_2Cl_2; (*b*) $AgClO_4$, $MeNO_2$.

The aforementioned data clearly demonstrate that the Koenigs–Knorr method and its modifications have been often employed for the glycosylation of 5′-hydroxy groups of nucleosides by glycopyranosyl bromide derivatives. These reactions are usually accompanied by the formation of side products; the yields of target disaccharide nucleosides (with rare exceptions) are rather low. The glycosylation of the 5′-hydroxy group of uridine derivatives by acylglycofuranosyl halides was used in the synthesis of analogues of the disaccharide fragment of liposidomycin.[41, 134]

Later, alternative methods of *O*-glycosylation of nucleosides were developed. A simple and efficient synthesis of disaccharide nucleosides has been performed which includes coupling of a peracylated monosaccharide with a partly protected nucleoside in the presence of Lewis acids under conditions similar to those used in the synthesis of alkyl β-D-ribofuranosides.[135]

Coupling of *N*-protected 3′,5′-*O*-tetraisopropyldisiloxane-1,3-diyl ribonucleosides (**75**)[136] with a small excess of 1-*O*-acetyl-2,3,5-tri-*O*-benzoyl-β-D-ribofuranose (**76**) in the presence of $SnCl_4$ was stereospecific and afforded protected 2′-*O*-β-D-ribofuranosyl nucleosides (**77**).[137–140] This reaction was carried out

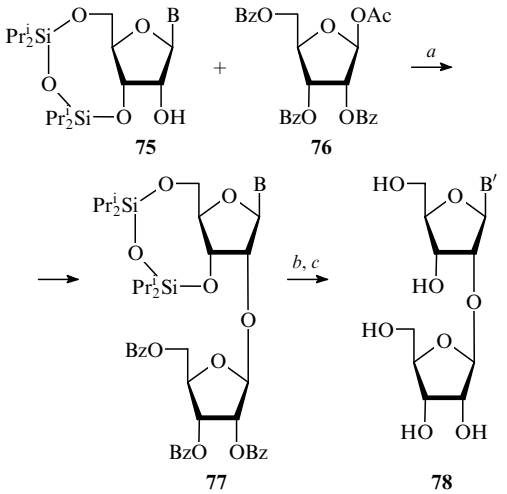

B = Ura, Thy, Cyt^{Bz}, Ade^{Bz}, Gua^{Bu^i}; B′ = Ura, Thy, Cyt, Ade, Gua;
(*a*) $SnCl_4$, DCE; (*b*) Bu_4NF, THF; (*c*) NH_3, MeOH.

under mild conditions (0 °C, 1,2-dichloroethane, 2 h for pyrimidine nucleosides, 7–16 h for purine derivatives); the yields of the target compounds **77** were 74%–82%.[138, 139] At room temperature, this reaction occurred faster (30 min), but the yields in the coupling steps were lower (40%–77%).[137, 140] After deprotection, the disaccharide nucleosides **78** were obtained in good overall yields.[137–140] The synthesis of the minor nucleosides **37** and **38** could be performed using this method.[102, 103]

The use of the above-described procedure ensures an easy and efficient synthesis of pyrimidine 3′-*O*-β-D-ribofuranosyl- [119] and 5′-*O*-β-D-ribofuranosyl-2′-deoxynucleosides [141, 142] as well as 5′-*O*-β-D-ribofuranosyl nucleosides.[143, 144] Other peracylated furanoses and pyranoses [145] (D- and L-arabinofuranose, D-erythrofuranose, 5-azido-5-deoxyribofuranose, D-ribopyranose) were successfully employed in the glycosylation of the nucleoside **75**.[145] The synthesis of numerous 2′-*O*-β-D-ribofuranosylnucleoside derivatives (**77**) containing various monosaccharide residues at O(2′) shows explicitly the versatility of the coupling based on the use of peracylated sugars as glycosyl donors in the presence of $SnCl_4$.

The stabilities of various protective groups in O-glycosylation have been studied.[141, 142] It was found that TMSOTf can be used as a Lewis acid. This glycosylation procedure was used in the synthesis of disaccharide fragments of liposidomycin (**26**).[134] It is of note that incorporation of 2′-*O*-β-D-ribofuranosylnucleosides and their analogues into synthetic oligonucleotides has found application in the studies of enzymes of nucleic acid metabolism.[146–150]

Despite good reproducibility of *O*-glycosylation in the presence of peracylated sugars, side reactions occur sometimes. For example, the synthesis of purine 5′-*O*-β-D-ribofuranosylnucleosides was sometimes accompanied by the formation of trisaccharide nucleosides.[144] Coupling of the nucleoside **79** with fully protected ribofuranose **76** in the presence of $SnCl_4$ yielded a mixture of mono-, di- and trisaccharide nucleosides (**80**–**82**) in 18%, 29% and 17% yields, respectively. The formation of compounds **80** and **82** is attributed to the instability of the N-glycosidic bond in the starting purine ribonucleoside **79** and/or in the disaccharide nucleoside **81** in the presence of $SnCl_4$.[144] The use of 2′,3′-*O*-isopropylidene derivatives **83** containing a more stable N-glycosidic bond has made it possible to avoid the formation of trisaccharide nucleosides and to obtain target purine 5′-*O*-ribofuranosylnucleosides (**84**) in 60%–65% yields.[144]

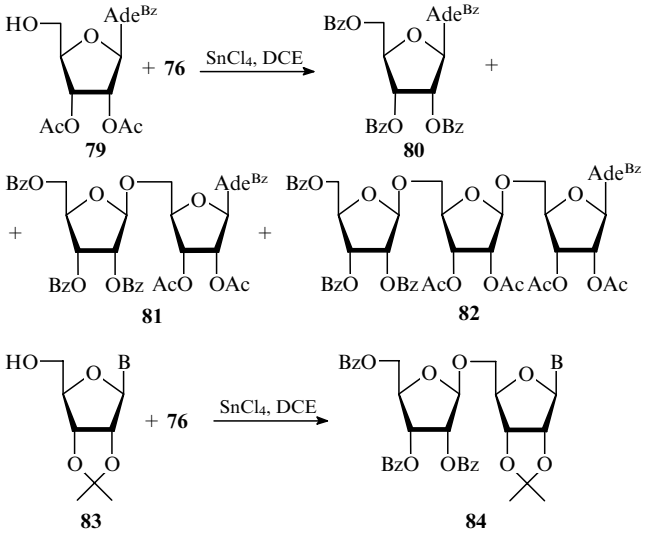

B = Ade^{Bz}, Gua^{Bu^i}.

Recently, sugar trichloroacetimidates have found application as glycosyl donors.[151] The coupling of nucleoside **75** (B = Ade^{Bz}) with trichloroacetimidate **85** in tetrahydrofuran was carried out under different conditions.[152]

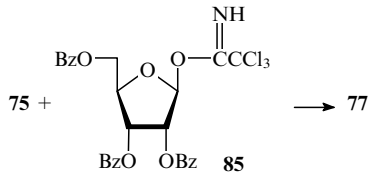

Conditions	TMSOTf, 0 °C	$BF_3 \cdot Et_2O$, 20 °C	TfOH, 0 °C
Yield (%)	64	57	93

It was found[153, 154] that the glycosylation of the primary hydroxy group of the pyrimidine nucleosides **86** by trichloroacetimidate **87** is far less efficient. After activation with $BF_3 \cdot Et_2O$ (conditions *a*), the yields of the products **88** did not exceed 24%, whereas the use of TfOAg in $CHCl_3$ (*b*) made it possible to increase the yields up to 35%–41%.[153, 154] The acetylation of the free 5′-hydroxy group in nucleosides **86** is the main side reaction. Low reactivity of the primary 5′-hydroxy group with respect to *O*-glycosylation was attributed to the presence of a hydrogen bond with a 2-carbonyl group of the pyrimidine heterocycle observable in the ^1H NMR spectra in aprotic solvents.[153]

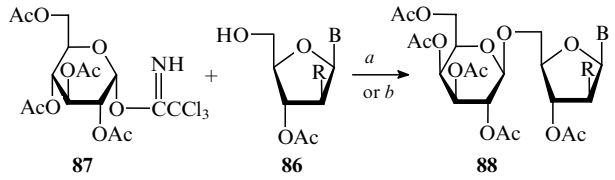

R = H: B = Cyt^{Ac}, Thy, 5FUra; R = OAc, B = Cyt^{Ac};
(*a*) $BF_3 \cdot Et_2O$, CH_2Cl_2; (*b*) TfOAg, $CHCl_3$.

A series of isomeric α-L-fucopyranosylguanosines have been synthesised in order to establish the structure of the disaccharide nucleoside HF-7 (**28**).[56] L-Fucopyranosyl 1-*O*-imidazolecarboxylate **89** containing a benzyloxy group at the C(2) atom, which ensures good stereoselectivity in the formation of the α-glycosidic bond, was used as a glycosyl donor. The coupling of the nucleoside **90** with the glycosyl donor **89** in the presence of $ZnBr_2$ in CH_2Cl_2 gave the disaccharide nucleoside **91** in 80% yield. A mixture of 2′- and 3′-isomers **93** and **94** was prepared starting from nucleoside **92** under identical conditions (yields 38% and 40%, respectively). Compound **28** identical to the natural product was obtained upon removal of the silyl protective group in compound **94** with subsequent sulfation and hydrogenolysis. Attempts to use the glycosyl donor **89** for the glycosylation of the guanosine derivative **92** containing an additional 2′-*O*-*tert*-butyldimethylsilyl group failed, apparently due to the steric hindrance of the 3′-hydroxy group.[56]

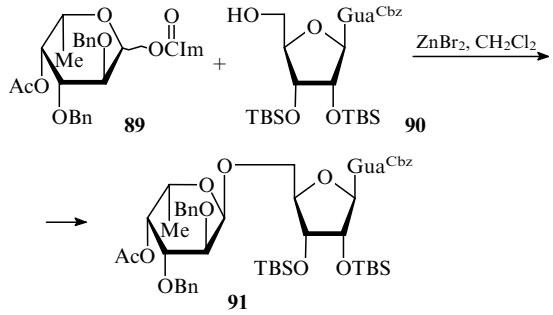

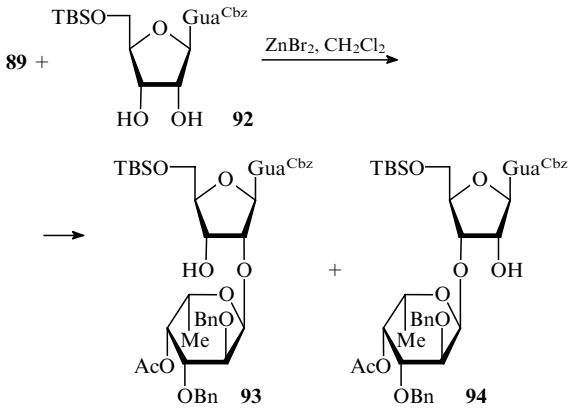

Im is imidazolyl; TBS is *tert*-butyldimethylsilyl.

The synthesis of the shimofuridin analogues **29** also included the formation of the O-glycosidic bond. The coupling of the phenyl 1-thioglycoside **95a** with a selectively protected inosine derivative **96a** in the presence of *N*-iodosuccinimide (NIS) and TfOH gave the product **97a** in a moderate yield of 37%.[155] If the heterocyclic base did not contain a protective group, no desired disaccharide nucleoside was formed. This can be attributed to the glycosylation at the O(6) of hypoxanthine, which was earlier observed by Lichtenthaler *et al.*[124, 126] The use of L-fucopyranose dibutyl phosphate **95b** as a glycosyl donor has been described; its reaction with the pivaloyl derivative **96b** in the presence of TMSOTf made it possible to increase the yield of the disaccharide **97b** to 53%.[156]

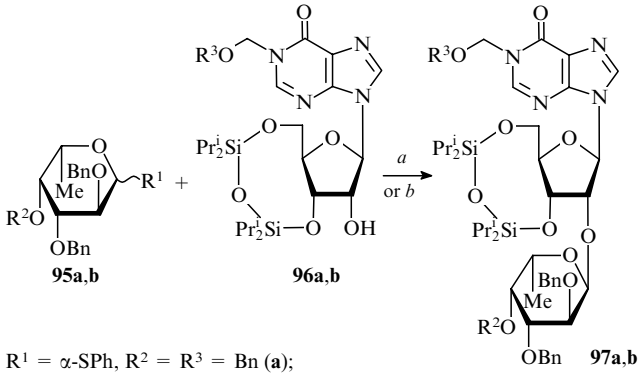

R^1 = α-SPh, R^2 = R^3 = Bn (**a**);
R^1 = α- or β-OP(O)$(OBu)_2$, R^2 = Ac, R^3 = Piv (**b**);
(*a*) NIS, TfOH, CH_2Cl_2; (*b*) TMSOTf, Et_2O, DCE.

The highest (90%) yields of α-L-fucopyranosylthymidine and -uridine **98** were achieved in the glycosylation of the pyrimidine nucleosides **99** by pyrimidin-2-yl 1-thiofucopyranoside **100** in the presence of trimethylsilyl triflate.[157, 158]

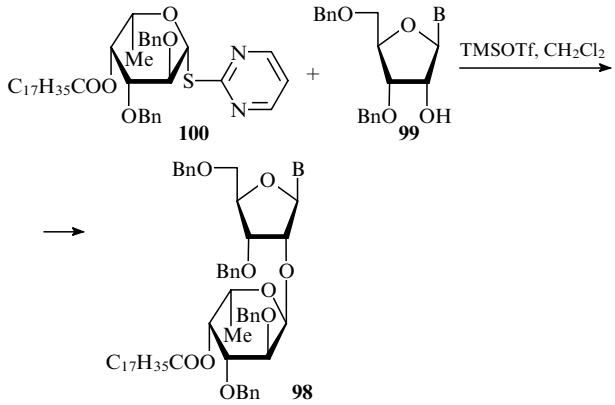

B = Thy, Ura.

O-Glycosylation of the sterically hindered secondary hydroxy group in the nucleoside **101** was a problem in the synthesis of the antibiotic hikizimycin (**22**).[74] It was suggested to use glycosyl sulfoxides as glycosyl donors in the glycosylation of non-reactive alcohols.[121, 159] Compound **103** was prepared from glycosyl sulfoxide **102** and the nucleoside **101** in a satisfactory yield (38%).[74] Deprotection and reduction of the azido groups afforded the target hikizimycin (**22**).

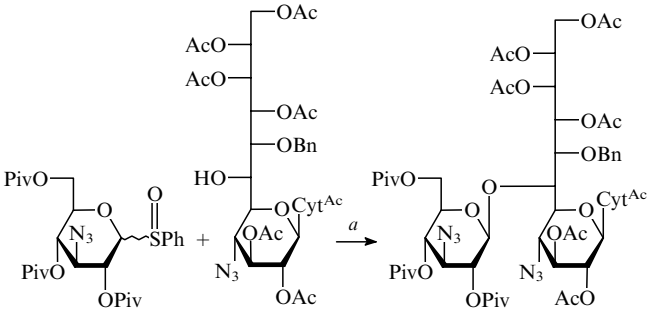

102 **101** **103**

(*a*) Tf_2O, PhMe.

Two different routes of the formation of disaccharide nucleosides were explored in the synthesis of the adenophostin derivatives (**27**).[160–163] The coupling of the selectively protected nucleoside **104** with the glycosyl bromide **105** in the presence of $AgClO_4$ and γ-collidine afforded the product **106** (yield 48%).[160] The use of Ag_2CO_3 as an *O*-glycosylation promoter as described earlier was ineffective.[126]

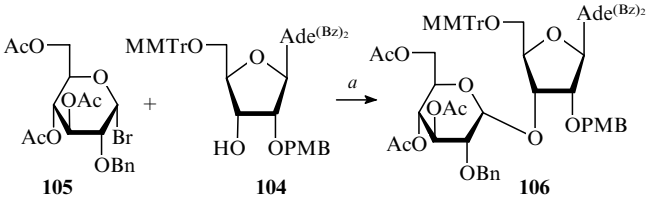

105 **104** **106**

MMTr is mono-*p*-methoxytrityl, PMB is *p*-methoxybenzyl;
(*a*) $AgClO_4$, γ-collidine, $CHCl_3$.

The synthesis of adenophostin A (**27**) starting from the disaccharide nucleoside **106** included the following steps: removal of the methoxybenzyl (oxidation by dichlorodicyanoquinone, DDQ), acid-labile monomethoxytrityl and acyl groups; *N*,*O*-monomethoxytritylation of the exocyclic amino group of adenine and primary hydroxy groups; phosphorylation, detritylation and hydrogenolysis in the presence of palladium black. The overall yield of adenophostin A was 22%.[160]

The Vorbruggen *N*-glycosylation of the bis(trimethylsilyl) derivative of N^6-benzoyladenine by the disaccharide glycosyl donor **107** (see Refs 161–163) is an alternative route to the synthesis of adenophostin **27**.[108–111] The yield of the disaccharide nucleoside **108** in the coupling step was significantly higher (71%) than in the former case; the overall yield of the product **27** was 28%.

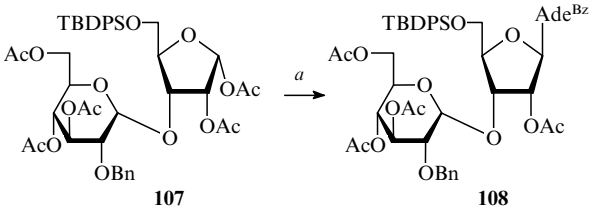

107 **108**

(*a*) $(TMS)_2$–Ade^{Bz}, TMSOTf, DCE.

* * *

While considering the methods for the synthesis of disaccharide nucleosides, special mention should be made of the possibility of microbiological and enzymatic *O*-glycosylation. Some papers are devoted to the synthesis of *O*-hexopyranosyl derivatives of purine nucleosides [164, 165] and 1-(β-D-arabinofuranosyl)cytosine [166] using various glycosidases. Thus the use of β-galactosidase and 4-nitrophenyl β-D-galactopyranoside as glycosyl donors has made it possible to synthesise *O*-galactosides of adenosine, guanosine, inosine, uridine, 2′-deoxyuridine and thymidine.[167–170] In these syntheses, the formation of 5′-O- and 3′-O-derivatives of galactopyranosyl nucleosides usually occurred. The glycosylation of thymidine and 1-(β-D-arabinofuranosyl)cytosine in the presence of glycosidases isolated from various sources using di- and polysaccharide donor substrates was studied.[171, 172] The yields of disaccharide nucleosides in enzymatic glycosylation rarely exceeded 10%.

An analysis of the published data prompts a conclusion that the majority of natural disaccharide nucleosides[2] were synthesised by coupling of a protected disaccharide with a heterocyclic base. This synthetic route is more common, since *O*-glycosylation of nucleosides is sometimes concomitant with *N*-glycosylation of the heterocyclic base and hydrolysis of the N-glycosidic bond of purine nucleosides. In some cases, protective groups cause a further decrease in the stability of the N-glycosidic bond under reaction conditions. It is noteworthy that acid hydrolysis of the O-glycosidic bond in purine disaccharide nucleosides occurs simultaneously with apurinisation, whereas the fragmentation of pyrimidine disaccharides occurs exclusively at the O-glycosidic bond and yields a nucleoside and a monosaccharide.[141] Despite the aforementioned difficulties, efficient procedures for *O*-glycosylation of nucleosides that have been developed significantly simplify and supplement the first approach to the synthesis of disaccharide nucleosides.

In conclusion, it may be noted that several reliable and reproducible *N*- and *O*-glycosylation procedures are known, which enable successful synthesis of natural disaccharide nucleosides and their analogues.

This review has been written with the financial support of the Russian Foundation for Basic Research (Project Nos 02-04-49125 and 02-04-48570) and the Programme 'Research and Development of Priority Trends in Science and Technology'.

References

1. Dictionary of Natural Products on CD-ROM Version 9:2 (Boca Raton, FL: Chapman and Hall–CRC Press, 2001)
2. L M Lerner, in *Chemistry of Nucleosides and Nucleotides* Vol. 2 (Ed. L B Townsend) (New York: Plenum, 1991) p. 27
3. K Isono *J. Antibiot.* **41** 1711 (1988)
4. K Isono *Pharmacol. Ther.* **52** 269 (1991)
5. J G Buchanan, R H Wightman, in *Topics in Antibiotic Chemistry* Vol. 6 (Ed. P G Sammes) (New York: Wiley, 1982) p. 229
6. P Garner, in *Studies in Natural Products Chemistry* Vol. 1, Pt. A (Ed. Atta-ur-Rahman) (Amsterdam: Elsevier, 1988) p. 397
7. S Knapp *Chem. Rev.* **95** 1859 (1995)
8. E H Flynn, J W Hinman, E L Caron, D O Woolf Jr *J. Am. Chem. Soc.* **75** 5867 (1953)
9. C L Stevens, K Nigarajan, T H Haskell *J. Org. Chem.* **27** 2991 (1962)
10. S Hanessian, T H Haskell *Tetrahedron Lett.* 2451 (1964)
11. T H Haskell *J. Am. Chem. Soc.* **80** 747 (1958)
12. R Evans, G Weare *J. Antibiot.* **30** 604 (1977)
13. M Konishi, M Naruishi, T Tsuno, H Tsukiura, H Kawaguchi *J. Antibiot.* **26** 757 (1973)
14. Y Chen, A Zeeck, Z Chen, H Zahner *Kangshengsu* **10** (5) 285 (1985); *Chem. Abstr.* **104** 65 478 (1986)
15. J Itoh, S Miyadoh *J. Antibiot.* **45** 846 (1992)

16. K Haneda, M Shinose, A Seino, N Tabata, H Tomoda, Y Iwai, S Omura *J. Antibiot.* **47** 774 (1994)
17. F W Lichtenthaler, J Cerna, I Rychlik *FEBS Lett.* **53** 184 (1975)
18. Z Gu, P S Lovett *J. Bacteriol.* **177** 3616 (1995)
19. K Shiomi, K Haneda, H Tomoda, Y Iwai, S Omura *J. Antibiot.* **47** 782 (1994)
20. T Ogita, N Otake, Y Miyazaki, H Yonehara, R D Macfarlane, C J McNeal *Tetrahedron Lett.* **21** 3203 (1980)
21. T Iwasa, S Harada, Y Sato *Takeda Kenkyushoho* **40** 12 (1981); *Chem. Abstr.* **95** 148 651 (1981)
22. H Seto, N Otake, S Sato, H Yamaguchi, K Takada, M Itoh, H S M Lu, J Clardy *Tetrahedron Lett.* **29** 2343 (1988)
23. T Shomura, N Nishizawa, M Iwata, J Yoshida, K Takada, M Ito, S Amano, M Koyama, M Kojima, S Unouye *J. Antibiot.* **36** 1300 (1983)
24. N Nishizawa, Y Kondo, M Koyama, S Omoto, M Iwata, T Tsuruoka, S Unouye *J. Antibiot.* **37** 1 (1984)
25. K Sakata, A Sakurai, S Tamura *Agric. Biol. Chem.* **40** 1993 (1976)
26. K Sakata, A Sakurai, S Tamura *Agric. Biol. Chem.* **41** 2033 (1977)
27. K Sakata, J Uzawa, A Sakurai *Org. Magn. Reson.* **10** 230 (1977)
28. S Ennifar, B C Das, S M Nash, R Nagarajan *J. Chem. Soc., Chem. Commun.* 41 (1977)
29. M Vuilhorgne, S Ennifar, B C Das, J W Paschal, R Nagarajan, E W Hagaman, E Wenkert *J. Org. Chem.* **42** 3289 (1977)
30. M Vuilhorgne, S Ennifar, B C Das *Carbohydr. Res.* **97** 19 (1981)
31. A Gonzalez, D Vazquez, A Jimenez *Biochim. Biophys. Acta* **561** 403 (1979)
32. A Takatsuki, K Arima, G Tamura *J. Antibiot.* **24** 215 (1971)
33. T Ito, A Takatsuki, K Kawamura, K Sato, G Tamura *Agric. Biol. Chem.* **44** 695 (1980)
34. W C Mahoney, D Duksin *J. Biol. Chem.* **254** 6572 (1979)
35. P E Brandish, K I Kimura, M Inukai, R Southgate, J T Lonsdale, T D Bugg *Antimicrob. Agents Chemother.* **40** 1640 (1996)
36. K Eckardt, W Ihn, D Tresselt, D Krebs *J. Antibiot.* **34** 1631 (1981)
37. J A Edgar, J L Frahn, P A Cockrum, N Anderton, M V Jago, C C J Culvenor, A J Jones, K Murray, K J Shaw *J. Chem. Soc., Chem. Commun.* 222 (1982)
38. K Eckardt *J. Nat. Prod.* **46** 544 (1983)
39. M Ubukata, K Isono, K Kimura, C C Nelson, J A McCloskey *J. Am. Chem. Soc.* **110** 4416 (1988)
40. M Ubukata, K Kimura, K Isono, C C Nelson, J M Gregson, J A McCloskey *J. Org. Chem.* **57** 6392 (1992)
41. C Dini, P Collette, N Drochon, J C Guillot, G Lemoine, P Mauvais, J Aszodi *Bioorg. Med. Chem. Lett.* **10** 1839 (2000)
42. M R Spada, M Ubukata, K Isono *Heterocycles* **34** 1147 (1992)
43. C Gravier-Pelletier, I Charvet, Y LeMerrer, J-C Depezay *J. Carbohydr. Chem.* **16** 129 (1997)
44. Y Le Merrer, C Gravier-Pelletier, M Gerrouache, J-C Depezay *Tetrahedron Lett.* **39** 385 (1998)
45. S Knapp, G J Morriello, S Nandan, T J Emge, G A Doss, R T Mosley, L Chen *J. Org. Chem.* **66** 5822 (2001)
46. S Knapp, G J Morriello, G A Doss *Org. Lett.* **4** 603 (2002)
47. K Kimura, Y Ikeda, S Kagami, M Yoshihama, M Ubukata, Y Esumi, H Osada, K Isono *J. Antibiot.* **51** 647 (1998)
48. K Kimura, Y Ikeda, S Kagami, M Yoshihama, K Suzuki, H Osada, K Isono *J. Antibiot.* **51** 1099 (1998)
49. M Takahashi, T Kagasaki, T Hosoya, S Takahashi *J. Antibiot.* **46** 1643 (1993)
50. S Takahashi, T Kinoshita, M Takahashi *J. Antibiot.* **47** 95 (1994)
51. M Takahashi, K Tanzawa, S Takahashi *J. Biol. Chem.* **269** 369 (1994)
52. S A Morris, E P Nerou, A M Riley, B V L Potter, C W Taylor *Biochem. J.* **367** 113 (2002)
53. R D Marwood, D J Jenkins, V Correa, C W Taylor, B V L Potter *J. Med. Chem.* **43** 4278 (2000)
54. S Shuto, G Horne, R D Marwood, B V L Potter *Chem. Eur. J.* **7** 4937 (2001)
55. V Correa, A M Riley, S Shuto, G Horne, E P Nerou, R D Marwood, B V L Potter, C W Taylor *Mol. Pharmacol.* **59** 1206 (2001)
56. J McCormick, Y B Li, K McCormick, H I Duynstee, A K van Engen, G A van der Marel, B Ganem, J H van Boom, J Meinwald *J. Am. Chem. Soc.* **121** 5661 (1999)
57. P Proksch, R A Edrada, R Ebel *Appl. Microbiol. Biotechnol.* **59** 125 (2002)
58. J Kobayasi, Y Doi, M Ishibashi *J. Org. Chem.* **59** 255 (1994)
59. Y Doi, M Ishibashi, J Kobayasi *Tetrahedron* **50** 8651 (1994)
60. J B Stewart, V Bornemann, J L Chen, R E Moore, F R Caplan, H Karuso, L K Larsen, G M Patterson *J. Antibiot.* **41** 1048 (1988)
61. S H Kim, S M Yoo, I S Park, Y H Kim *J. Nat. Prod.* **63** 1188 (2000)
62. C A Auer, J D Cohen *Plant Physiol.* **102** 541 (1993)
63. K Sebesta, K Horska, J Vancova *Collect. Czech. Chem. Commun.* **34** 891 (1969)
64. R P M Bond, C B C Boyce, S J French *Biochem. J.* **114** 477 (1969)
65. J Farkas, K Sebesta, K Horska, Z Samek, L Dolejs, F Sorm *Collect. Czech. Chem. Commun.* **42** 909 (1977)
66. K Sebesta, H Sternbach *FEBS Lett.* **8** 233 (1970)
67. H Katoh, M Yamada, K Lida, M Aoki, Y Itezono, N Nakayama, Y Suzuki, M Watanabe, H Shimada *Tennen Yuki Kagobutsu Toronkai Koen* **38** 115 (1996); *Chem. Abstr.* **125** 322 575 (1996)
68. H Sugimura, K Stansfield *Synlett* 985 (1998)
69. K Stansfield, H Kanamori, H Sugimura *New J. Chem.* **23** 9 (1999)
70. H Takeuchi, N Asai, K Tanabe, T Kozaki, M Fujita, T Sakai, A Okuda, N Naruse, S Yamamoto, T Sameshima, N Heida, K Dobashi, M Baba *J. Antibiot.* **52** 971 (1999)
71. M Baba, M Okamoto, H Takeuchi *Antimicrob. Agents Chemother.* **43** 2350 (1999)
72. C L Stevens, J Nemec, G H Ransford *J. Am. Chem. Soc.* **94** 3280 (1972)
73. S Knapp, S R Nandan *J. Org. Chem.* **59** 281 (1994)
74. N Ikemoto, S L Schreiber *J. Am. Chem. Soc.* **114** 2524 (1992)
75. T Suami, H Sasai, K Matsuno, N Suzuki *Carbohydr. Res.* **143** 85 (1985)
76. S Danishefsky, S L DeNinno, S Chen, L Boisvert, M Barbachyn *J. Am. Chem. Soc.* **111** 5810 (1989)
77. A G Myers, D Y Gin, D H Rogers *J. Am. Chem. Soc.* **116** 4697 (1994)
78. M Prystas, L Kalvoda, F Sorm *Collect. Czech. Chem. Commun.* **41** 1426 (1976)
79. S Knapp, W-C Shieh, C Jaramillo, R V Trilles, S R Nandan *J. Org. Chem.* **59** 946 (1994)
80. S Knapp,V K Gore *Org. Lett.* **2** 1391 (2000)
81. S Knapp, S Nandan, L Resnick *Tetrahedron Lett.* **33** 5485 (1992)
82. K S Kim, I H Cho, Y H Ahn, J I Park *J. Chem. Soc., Perkin Trans. 1* 1783 (1995)
83. T Sugimura, M Miwa *Mol. Cell. Biochem.* **138** 5 (1994)
84. D D'Amours, S Desnoyers, I D'Silva, G G Poirier *Biochem. J.* **342** 249 (1999)
85. M Ziegler *Eur. J. Biochem.* **267** 1550 (2000)
86. R Alvarez-Gonzalez, M K Jacobson *Biochemistry* **26** 3218 (1987)
87. G Keith, J Desgres, G de Murcia *Anal. Biochem.* **191** 309 (1990)
88. L Davidovic, M Vodenicharov, E B Affar, G G Poirier *Exp. Cell Res.* **268** 7 (2001)
89. M Miwa, H Saito, H Sakura, N Saikawa, F Watanabe, T Matsushima, T Sugimura *Nucl. Acids Res.* **4** 3997 (1977)
90. F Inagaki, T Miyazawa, M Miwa, H Saito, T Sugimura *Biochem. Biophys. Res. Commun.* **85** 415 (1978)
91. A M Ferro, N J Oppenheimer *Proc. Natl. Acad. Sci. USA* **75** 809 (1978)
92. M Miwa, M Ishihara, S Takishima, N Takasuka, M Maeda, Z Yamaizumi, T Sugimura, T Yokoyama, T Miyazawa *J. Biol. Chem.* **256** 2916 (1981)
93. N J Oppenheimer, M Sing, C C Sweeley, S J Sung, P A Srere *J. Biol. Chem.* **254** 1000 (1979)
94. K Schneider, P Dimroth, M Bott *FEBS Lett.* **483** 165 (2000)
95. S Hoenke, M R Wild, P Dimroth *Biochemistry* **39** 13223 (2000)
96. P A Limbach, P F Crain, J A McCloskey *Nucl. Acids Res.* **22** 2183 (1994)
97. The RNA Modification Database, University of Utah http://medlib.med.utah.edu/RNAmods/

98. J Desgres, G Keith, K C Kuo, C W Gehrke *Nucl. Acids Res.* **17** 865 (1989)
99. G Keith, A-L Glasser, J Desgres, K C Kuo, C W Gehrke *Nucl. Acids Res.* **18** 5989 (1990)
100. A-L Glasser, J Desgres, J Heitzler, C W Gehrke, G Keith *Nucl. Acids Res.* **19** 5199 (1991)
101. G Keith, J Heitzler, C Eladlouni, A-L Glasser, C Fix, J Desgres, G Dirheimer *Nucl. Acids Res.* **21** 2949 (1993)
102. A A Rodionov, E V Efimtseva, S N Mikhailov, J Rozenski, I Luyten, P Herdewijn *Nucleosides Nucleotides Nucl. Acids* **19** 1847 (2000)
103. E V Efimtseva, A A Shelkunova, S N Mikhailov, K Nauwelaerts, J Rozenski, E Lescrinier, P Herdewijn *Helv. Chim. Acta* **86** 504 (2003)
104. R Basavappa, P B Sigler *EMBO J.* **10** 3105 (1991)
105. S Kiesewetter, G Ott, M Sprinzl *Nucl. Acids Res.* **18** 4677 (1990)
106. C Forster, K Chakraburtty, M Sprinzl *Nucl. Acids Res.* **21** 5679 (1993)
107. K A Watanabe, D H Hollenberg, J J Fox *J. Carbohydr. Nucleosides Nucleotides* **1** 1 (1974)
108. H Vorbruggen *Acc. Chem. Res.* **28** 509 (1995)
109. L J Wilson, M W Hager, Y A El-Kattan, D C Liotta *Synthesis* 1465 (1995)
110. H Vorbruggen *Acta Biochim. Pol.* **43** 25 (1996)
111. H Vorbruggen, C Ruh-Pohlenz, in *Organic Reactions* Vol. 55 (Ed. L A Paquette) (New York: Wiley, 2000)
112. U Niedballa, H Vorbruggen *J. Org. Chem.* **39** 3664 (1974)
113. H Ogura, K Iwaki, K Furuhata, in *Nucleic Acid Chemistry* Pt. 4 (Eds L B Townsend, R S Tipson) (New York: Wiley, 1991) p. 109
114. T Halmos, J Filippi, J Bach, K Antonakis *Carbohydr. Res.* **99** 180 (1982)
115. K A Watanabe, A Matsuda, M J Halat, D H Hollenberg, D H Nisselbaum, J J Fox *J. Med. Chem.* **24** 893 (1981)
116. B Kraska, F W Lichtenthaler *Chem. Ber.* **114** 1636 (1981)
117. C Dini, S Didier-Laurent, N Drochon, S Feteanu, J C Guillot, F Monti, E Uridat, J Zhang, J Aszodi *Bioorg. Med. Chem. Lett.* **12** 1209 (2002)
118. R D Marwood, S Shuto, D J Jenkins, B V L Potter *Chem. Commun.* 219 (2000)
119. S N Mikhailov, E De Clercq, P Herdewijn *Nucleosides Nucleotides* **15** 1323 (1996)
120. I V Gulayeva, E V Efimtseva, S N Mikhailov *Nucleosides Nucleotides Nucl. Acids* (2004) (in the press)
121. K Toshima, K Tatsuta *Chem. Rev.* **93** 1503 (1993)
122. R R Schmidt, in *Comprehensive Organic Synthesis* Vol. 6 (Ed. B M Trost) (Oxford: Pergamon Press, 1991) p. 33
123. N K Kochetkov, in *Studies in Natural Products Chemistry* Vol. 14 (Ed. Atta-ur-Rahman) (Amsterdam: Elsevier, 1994) p. 201
124. K Kitahara, B Kraska, Y Sanemitsu, F W Lichtenthaler *Nucleic Acids Res., Special Publ.* (1) 21 (1975)
125. F W Lichtenthaler, K Kitahara, W Riess *Nucl. Acids Res., Special Publ.* (4) 115 (1978)
126. F W Lichtenthaler, Y Sanemitsu, T Nohara *Angew. Chem.* **90** 819 (1978)
127. R Wang, D H Steensma, Y Takaoka, J W Yun, T Kajimoto, C Wong *Bioorg. Med. Chem.* **5** 661 (1997)
128. S Sato, K Furuhata, M Itoh, Y Shitori, H Ogura *Chem. Pharm. Bull.* **36** 914 (1988)
129. M Nakamura, S Fujita, H Ogura *Chem. Pharm. Bull.* **41** 21 (1993)
130. N D Chkanikov, V N Tolkachev, M N Preobrazhenskaya *Bioorg. Khim.* **4** 1620 (1978) [a]
131. N D Chkanikov, M N Preobrazhenskaya *Bioorg. Khim.* **6** 67 (1980) [a]
132. N D Chkanikov, V N Tolkachev, M Z Kornveits, M N Preobrazhenskaya *Bioorg. Khim.* **8** 1143 (1982) [a]
133. N B Hanna, R K Robins, G R Revankar *Carbohydr. Res.* **165** 267 (1987)
134. C Dini, N Drochon, J C Guillot, P Mauvais, P Walter, J Aszodi *Bioorg. Med. Chem. Lett.* **11** 533 (2001)
135. S Hanessian, J Banoub, in *Methods in Carbohydrate Chemistry* (New York: Academic Press, 1980) p. 243
136. W T Markiewicz, M Wiewiorowski, in *Nucleic Acid Chemistry, Improved and New Synthetic Procedures and Techniques* Pt. 3 (Eds L B Townsend, R S Tipson) (New York: Wiley, 1986) p. 229
137. A Niewczyk, A Krzyzaniak, J Barciszewski, W T Markiewicz *Nucleosides Nucleotides* **10** 635 (1991)
138. S N Mikhailov, A DeBruyn, P Herdewijn *Nucleosides Nucleotides* **14** 481 (1995)
139. S N Mikhailov, E V Efimtseva, G V Gurskaya, M V Fomitcheva, S V Meshkov, V E Zavodnik, A DeBruyn, G Janssen, J Rozenski, P Herdewijn *J. Carbohydr. Chem.* **16** 75 (1997)
140. W T Markiewicz, A Niewczyk, Z Gdaniec, D A Adamiak, Z Dauter, W Rypniewski, M Chmielewski *Nucleosides Nucleotides* **17** 411 (1998)
141. S N Mikhailov, A A Rodionov, E V Efimtseva, M V Fomitcheva, N Sh Padyukova, P Herdewijn, M Oivanen *Carbohydr. Lett.* **2** 321 (1997)
142. A A Rodionov, E V Efimtseva, M V Fomicheva, N Sh Padyukova, S N Mikhailov *Bioorg. Khim.* **25** 203 (1999) [a]
143. S N Mikhailov, A A Rodionov, E V Efimtseva, B S Ermolinsky, M V Fomitcheva, N Sh Padyukova, K Rothenbacher, E Lescrinier, P Herdewijn *Nucleosides Nucleotides* **18** 691 (1999)
144. S N Mikhailov, A A Rodionov, E V Efimtseva, B S Ermolinsky, M V Fomitcheva, N Sh Padyukova, K Rothenbacher, E Lescrinier, P Herdewijn *Eur. J. Org. Chem.* 2193 (1998)
145. E V Efimtseva, G V Bobkov, S N Mikhailov, A Van Aerschot, G Schepers, R Busson, J Rozenski, P Herdewijn *Helv. Chim. Acta* **84** 2387 (2001)
146. V L Tunitskaya, E E Rusakova, L V Memelova, S N Kochetkov, A Van Aerschot, P Herdewijn, E V Efimtseva, B S Ermolinsky, S N Mikhailov *FEBS Lett.* **442** 20 (1999)
147. O M Gritsenko, S N Mikhailov, E V Efimtseva, A Van Aerschot, P Herdewijn, E S Gromova *Nucleosides Nucleotides Nucl. Acids* **19** 1805 (2000)
148. I Luyten, R M Esnouf, S N Mikhailov, E V Efimtseva, P Michiels, H A Heus, C W Hilbers, P Herdewijn *Helv. Chim. Acta* **83** 1278 (2000)
149. E V Efimtseva, S N Mikhailov *Biokhimiya* **67** 1374 (2002) [b]
150. E V Efimtseva, S N Mikhailov *Collection, Symp. Ser.* **5** 181 (2002)
151. R R Schmidt *Angew. Chem., Int. Ed. Engl.* **25** 212 (1986)
152. K Kamaike, H Takahashi, K Morohoshi, N Kataoka, T Kakinuma, Y Ishido *Acta Biochim. Pol.* **45** 949 (1998)
153. D M Whitfield, S P Douglas, T-H Tang, I G Csizmadia, H Y S Pang, F L Moolten, J J Krepinsky *Can. J. Chem.* **72** 2225 (1994)
154. J J Krepinsky, D M Whitfield, S P Douglas, N Lupescu, D Pulleyblank, F L Moolten *Methods Enzymol.* **247** 144 (1994)
155. S Knapp, V K Gore *J. Org. Chem.* **61** 6744 (1996)
156. H I Duynstee, E R Wijsman, G A van der Marel, J H van Boom *Synlett* 313 (1996)
157. J Ning, F Kong *Bioorg. Med. Chem. Lett.* **7** 2941 (1997)
158. J Ning, Y Xing, F Kong *Carbohydr. Res.* **338** 55 (2003)
159. D Kahne, S Walker, Y Cheng, D Van Engen *J. Am. Chem. Soc.* **111** 6881 (1989)
160. H Hotoda, M Takahashi, K Tanzawa, S Takahashi, M Kaneko *Tetrahedron Lett.* **36** 5037 (1995)
161. N C R van Straten, G A van der Marel, J H van Boom *Tetrahedron Lett.* **37** 3599 (1996)
162. N C R van Straten, G A van der Marel, J H van Boom *Tetrahedron* **53** 6509 (1997)
163. N C R van Straten, N M A J Kreik, Z A C Cziria, G A van der Marel, J H van Boom *Tetrahedron* **53** 6539 (1997)
164. Jpn. P. 74 117 689; *Chem. Abstr.* **78** 27 900 (1973)
165. Jpn. P. 7 223 599; *Chem. Absr.* **82** 153 800 (1975)
166. Y Suzuki, K Uchida *Biosci. Biotechnol. Biochem.* **58** 639 (1994)
167. Y Suzuki, K Uchida, S Fujimori *Nippon Nogei Kagaku Kaishi* **48** (11) 605 (1974); *Chem. Abstr.* **82** 134 727 (1975)
168. Y Suzuki, K Uchida *Nippon Nogei Kagaku Kaishi* **50** (5) 231 (1976); *Chem. Abstr.* **85** 74 157 (1976)
169. Y Suzuki, K Uchida *Nippon Nogei Kagaku Kaishi* **50** (5) 237 (1976); *Chem. Abstr.* **85** 74 158 (1976)

170. W H Binder H Kahlig, W Schmid *Tetrahedron: Asymmetry* **6** 1703 (1995)
171. N N Karasev, R N Grebeshova, N D Chkanikov, Yu V Stukalov, V N Gagloev, I V Yartseva, M N Preobrazhenskaya *Bioorg. Khim.* **9** 1254 (1983) [a]
172. H Fujimoto, T Takayanagi, K Ajisaka *J. Med. Chem.* **37** 3668 (1994)

[a] — *Russ. J. Bioorg. Chem. (Engl. Transl.)*
[b] — *Biochemistry (Engl. Transl.)*

Russian Chemical Reviews **73** (5) 415 – 416 (2004) © 2004 Russian Academy of Sciences and Turpion Ltd

DOI 10.1070/RC2004v073n05ABEH000927

A N Nesmeyanov Institute of Organoelement Compounds of the Russian Academy of Sciences

This issue of the Journal comprises reviews written by researchers of the A N Nesmeyanov Institute of Organoelement Compounds of the Russian Academy of Sciences (INEOS), one of the leading chemical research institutes of the Russian Academy of Sciences. This year INEOS is celebrating its 50th anniversary.

The Institute was founded in 1954 on the initiative of Academician A N Nesmeyanov on the basis of several laboratories of the N D Zelinsky Institute of Organic Chemistry concerned with organoelement (organometallic) and polymer chemistry.

Academician A N Nesmeyanov, who was President of the USSR Academy of Sciences in that period (1951 – 1961), became the first director of INEOS and remained in this post until 1980. In later periods, the Institute was directed by Academicians A V Fokin (1980 – 1988) and M E Vol'pin (1989 – 1996). Since 1996, INEOS has been headed by Academician Yu N Bubnov.

From the very beginning, research activities at INEOS were envisaged as a harmonious combination of synthetic and theoretical studies; therefore, investigations in many laboratories of the Institute were carried out at the junction of different branches of chemistry and physics. According to the figurative expression of Academician A N Nesmeyanov, this trend has charted the 'points of growth' in the development of modern science and technology. Following this principle, the chemistry of organic compounds of transition metals, π-complexes of metals and clusters has emerged at the interface between organic, organometallic and coordination chemistry. The unique properties of these compounds have enabled the preparation of novel organometallic catalysts and the development of processes for activating small molecules, such as nitrogen, carbon oxides, hydrocarbons, *etc*. A combination of organic and organoelement chemistry with modern experimental and theoretical methods in physical chemistry has fostered investigations into reactivities of organic and organoelement compounds which in turn has made it possible to obtain new in principle data on their structures and molecular dynamics.

At present, INEOS is one of the leading research centres in the area of organoelement and polymer chemistry. The main investigations carried out by the Institute are developing successfully along the following lines:

— development of novel methods for the synthesis of organoelement compounds and their application in organic synthesis and catalysis;

— fundamental studies in the field of organoelement and organic chemistry including investigations of novel structures, chemical activities and kinetics;

— development of novel methods of catalytic asymmetric synthesis;

— synthesis of biologically active compounds possessing a broad range of action for their possible use in medicine and agriculture;

— fundamental studies of the synthesis, structure and properties of polymers and composites, organoelement and organometallic polymers; development of methods for introducing organometallic and metallic fragments into polymeric matrices;

— development of novel experimental approaches to the analysis of organic and organoelement compounds.

Other remarkable achievements of the Institute researchers in the field of development of novel methods for the synthesis of organoelement compounds and their application in organic synthesis and catalysis over the past decade include synthesis of

multidecker sandwich-type metallocenes, of novel classes of σ-, π- and mixed metal complexes with alkene, acetylene and vinylidene ligands, of organoelement compounds with polyhedral substituents (carboranes and fullerenes) and of novel Hg-containing anticrowns binding complex anions, which significantly expands the range of practical applications of these unusual compounds. A new generation of rhodium, iridium and platinum chelate complexes based on metallocenes conjugated to tridentate P,C,P ligands synthesised in INEOS can find use in hydrogen production. Methods have been developed for the synthesis of methylcarbamoylmethylphosphinic acids and their derivatives as inexpensive and efficient bidentate extractants and sorbents of transuranium elements, from raw materials in the framework of a conversion programme. Flame suppressants based on phosphites, phosphates and phosphonates of lower primary alkanols and polyfluoroalkanols, which surpass currently used trifluorobromomethane banned by the Montreal Protocol in efficiency, have also been prepared.

The most impressive results in the field of chemistry of polymers and composites include synthesis of a novel class of polymers consisting of organoelement and inorganic chains, of polymers with remarkable thermal, catalytic, sorption and electrophysical properties; preparation of engineering plastics, thermostable composite materials and adhesives, membranes and polymers for electronic engineering and medicine; synthesis of novel aromatic and heterocyclic polymers including polyconjugated, super-rigid and network polymers. Special attention is given to the development of procedures for introducing organometallic and metallic fragments into a polymeric matrix; the use of polymeric systems for the synthesis of nanoparticles; preparation of liquid-crystalline polymers. Polymeric semiconductors possessing novel in principle structural properties and high electroconducting characteristics have been prepared by radiation-induced template gas-phase copolymerisation on extended polyamide films. Compounds that both manifest catalytic activity in polycyclotrimerisation of diisocyanates and behave as dyes have also been obtained. Other achievements include the development of an environmentally safe method for the synthesis and modification of polymers in supercritical media and synthesis of self-assembling hydrophobised ternary copolymers (terpolymers) by micellar polymerisation in aqueous solutions.

Many important discoveries made by researchers of INEOS have won international recognition. These include the first synthesis of carboranes and their numerous analogues, which represent a novel class of cage boron derivatives (L I Zakharkin, 1963); synthesis and analysis of carbyne, the third form of carbon (V V Korshak and A M Sladkov, 1971); theoretical prediction of fullerene C_{60}, the fourth form of carbon (D A Bochvar and E G Gal'pern, 1973) and discovery of a 1,2-rearrangement of polyhaloaliphatic radicals in the liquid phase (A N Nesmeyanov and R Kh Freidlina, 1973). Such important achievements as chemical fixation of molecular nitrogen and other small molecules under mild conditions (M E Vol'pin and V B Shur, 1967) and ionic hydrogenation (D N Kursanov, 1979) have acquired worldwide recognition. The discovery of an ability of achiral molecular structures to recognise enantiomers (V A Davankov and S V Rogozhin, 1992) has stimulated the development of ligand-exchange chromatography. And, last but not least, cyclic migration of unpaired electrons through polyvalent atoms of non-transition elements is yet another important discovery made in the mid-1990's (M I Kabachnik).

The priority in the development of 'synthetic food', of 'synthetic caviar' in particular also goes to INEOS. The idea of A N Nesmeyanov to introduce advanced chemical technology for the conversion of irrationally utilised natural proteins into a foodstuff has been realised in the production of synthetic caviar. Implementation of this process has been carried out by researchers of INEOS headed by S V Rogozhin and G L Slonimsky.

The staff of INEOS exceeds 550 researchers including 5 Full Members and Corresponding Members of the RAS, 78 Doctors of Science and 262 Ph.Ds. The Institute has in its structure 58 laboratories and research teams. About 2000 publications and 13 monographs summarise the achievements of INEOS over the past 5 years. The Institute collaborates with more than 150 universities, institutes and industrial centres both in Russia and abroad. It takes an active part in organization of diverse conferences, symposia and seminars, primarily those in the field of organometallic and organoelement chemistry. Among them are 'Chemistry of Organophosphorus Compounds' (1998), 'Horizons of Organic and Organometallic Chemistry' (1999), 'IMEBORON-XI' (2002), 'New Trends in Organometallic Chemistry and Catalysis' (to mark the 80th birthday of M E Vol'pin, 2003).

Some of the papers published in this issue reflect the main trends of research carried out at the Institute.

The review by A Z Kreindlin and M A Rybinskaya 'Cationic and neutral transition metal complexes with a tetramethylfulvene or trimethylallyldiene ligand' is devoted to systematisation of the published data on the synthesis, chemical properties and structures of transition metal complexes with tetramethylfulvene and trimethylallyldiene ligands formed from the respective precursor compounds (cyclopentadienyl complexes of these metals) upon thermolysis, photolysis, redox conversions and reactions with strong bases. A quantum-chemical description of the structures of these complexes has been given.

The review by V I Bregadze, S V Timofeev, I B Sivaev, I A Lobanova 'Substitution reactions at boron atoms in metallacarboranes' is a survey of the published data on substitution reactions in 10–12-apical metallacarboranes, which are being studied especially intensively. Special emphasis is laid on putative reaction mechanisms and effects of the metal fragment on the substitution site in the polyhedron.

The results of structural investigations of fullerene derivatives using diffraction methods are considered in the review by I S Neretin and Yu L Slovokhotov 'Crystal chemistry of fullerenes' which deals with an analysis of peculiarities of crystal structures of this type of compounds. This review presents the first generalisation of molecular and crystal structures of this group of compounds, which is one of the most difficult objects for investigation by diffraction methods.

The review by S V Vinogradova and V A Vasnev 'Trends in the development of polycondensation and condensation polymers' is an overview of progress in the polycondensation procedures. It provides a detailed description of the main principles of macromolecular design of condensation polymers and of some novel types of condensation polymers.

The review by L M Bronstein, S N Sidorov, P M Valetsky 'Nanostructured polymeric systems as nanoreactors for nanoparticle formation' gives a detailed description of the methods for the preparation of polymeric nanocomposites containing nanoparticles (block copolymers, dendrimers, nanoporous polymers, polyelectrolyte gel-surfactant complexes, multilayer films prepared by application of oppositely charged polyelectrolytes, *etc*.). Properties of nanostructurised polymeric nanocomposite materials are described.

The limited size of the issue prevents comprehensive presentation of the main research lines of the Institute.

All those who are interested in more detailed information about the Institute are invited to visit our web-site: http://www.ineos.ac.ru

Academician Yu N Bubnov,
Director of INEOS RAS

Russian Chemical Reviews **73** (5) 417 – 432 (2004) © 2004 Russian Academy of Sciences and Turpion Ltd

DOI 10.1070/RC2004v073n05ABEH000842

Cationic and neutral transition metal complexes with a tetramethylfulvene or trimethylallyldiene ligand

A Z Kreindlin, M A Rybinskaya (deceased)

Contents

I.	Introduction	417
II.	Metal complexes with tetramethylfulvene and trimethylallyldiene ligands	417
III.	The synthesis of complexes with tetramethylfulvene and trimethylallyldiene ligands	418
IV.	The reactivity of neutral and cationic complexes	423
V.	Structural characteristics of metal complexes with a fulvene or allyldiene ligand	425
VI.	Spectral characteristics of complexes	426
VII.	Quantum-chemical description of complexes	428
VIII.	Trimethylene complexes	429
IX.	Conclusion	430

Abstract. Published data on the synthesis and chemical properties of complexes of Group 4 – 10 transition metals (d elements) with η^6-tetramethylfulvene and η^7-trimethylallyldiene ligands, formed from the pentamethylcyclopentadienyl complexes of these metals, are described systematically. A description of the structures of these complexes in terms of a 'specific' resonance hybrid of fulvene and methylenecyclopentadienyl (or allyldiene and dimethylenecyclopentadienyl) structures is proposed. It is noted that similar properties or behaviours of the fulvene and allyldiene complexes can be followed both for compounds formed by metals of the same Group and for compounds of elements of the same transition row with identical electron configurations. The bibliography includes 102 references.

I. Introduction

The discovery of ferrocene in 1951 [1,2] and elucidation of its structure [3,4] and properties [5–7] triggered vigorous development of the chemistry of cyclopentadienyl organometallic complexes. Cyclopentadienyl derivatives have now been synthesised for the vast majority of chemical elements. More than 80% of known organometallic complexes contain either unsubstituted cyclopentadienyl ligand (Cp) or its derivatives (Cp′).[8] In the latter group, a special place is occupied by transition metal complexes with the pentamethylcyclopentadienyl ligand (Cp^*). The chemistry of these complexes started to develop intensively only in recent years, after facile methods for the synthesis of pentamethylcyclopentadiene and some of its derivatives had been proposed.[9] The key feature of metal complexes with pentamethylcyclopentadienyl ligands is the ability to split off one or two hydrogen atoms of methyl groups to be converted into cationic or neutral complexes with the $C_5Me_4CH_2$ or $C_5Me_3(CH_2)_2$ ligands, which are often referred to as tetramethylfulvene and trimethylallyldiene complexes, respectively. The chemistry of these complexes is of substantial interest not only because they have been prepared for many Group 4 – 10 transition metals but also due to the fact that the mode of metal coordination to these ligands depends essentially on the nature of the metal.

Vast experimental information concerning the chemistry of this class of compound has now been accumulated; however, to the best of our knowledge, the data have not been generalised. This stimulated us to compose this review, which covers the synthesis, the reactivity, and the structures of pentamethylcyclopentadienyl complexes of transition metals and quantum chemical calculations of their structures. As follows from the literature, the way of describing the structures of these complexes is debatable; this also calls for systematic consideration of the results of theoretical studies.

A Z Kreindlin, M A Rybinskaya A N Nesmeyanov Institute of Organoelement Compounds, Russian Academy of Sciences, ul. Vavilova 28, 119991 Moscow, Russian Federation. Fax (7-095) 135 50 85. Tel. (7-095) 135 93 19. E-mail: krekis@ineos.ac.ru (A Z Kreindlin)

Received 16 April 2003
Uspekhi Khimii **73** (5) 453 – 469 (2004); translated by Z P Bobkova

II. Metal complexes with tetramethylfulvene and trimethylallyldiene ligands

Metal complexes with the $C_5Me_4CH_2$ and $C_5Me_3(CH_2)_2$ ligands are formed in various transformations of compounds with the pentamethylcyclopentadienyl ligand. However, before we discuss properties of the coordinated η^5-Cp^* ligand, it is expedient to characterise briefly non-coordinated pentamethylcyclopentadiene. The properties of pentamethylcyclopentadiene (Cp^*H) differ from those of unsubstituted cyclopentadiene (CpH). It is a weaker acid ($pK_a = 26.1$) than CpH ($pK_a = 18.0$);[10] the non-aromatic 5π and 4π species, $C_5Me_5^{\bullet}$ ($Cp^{*\bullet}$) and $C_5Me_5^+$ (Cp^{*+}), it forms are more stable than their non-methylated analogues. The permethylated $Cp^{*\bullet}$ radical has been detected by EPR,[11] and the Cp^{*+} cation has been found as an intermediate [12] in the reactions of the metal Cp^* complexes with nucleophiles (alcohols, alkoxides, amines, organolithium compounds). The transformations of the η^5-Cp^* ligand in the coordination sphere of the metal atom proceed rather easily during a variety of processes.

Theoretically, the fulvene ligand $C_5H_4CH_2$ can be coordinated to a metal according to the η^2-, η^4-, and η^6 -modes. The same mode of coordination is typical of the tetramethylfulvene ligand. η^2-Coordination is encountered very rarely. Complexes with η^4-coordination of the $C_5Me_4CH_2$ and $C_5Me_3(CH_2)_2$ ligands are typical only of Groups 9 and 10 metals. Most abundant are neutral and cationic η^6-complexes formed by Group 4 – 8 metals.

When describing the structure of complexes with the $C_5Me_4CH_2$ ligand, researchers use either fulvene (**A**) or methylenecyclopentadienyl (**B**) structures; in some cases, they give preference to structure **A** without good reason. Complexes with the $C_5Me_3(CH_2)_2$ ligand are described by either an allyldiene (**C**) or dimethylenecyclopentadienyl (**D**) structure.

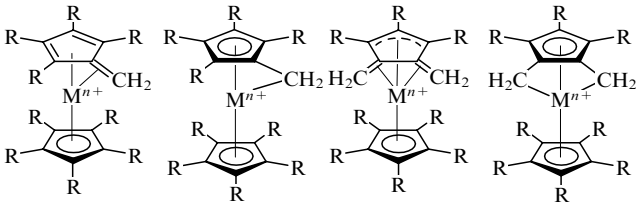

A (η^2,η^4) **B** (σ,η^5) **C** (η^4,η^3) **D** (σ,σ,η^5)

However, it is impossible to give preference to a particular structure without deciding beforehand which parameters characterise each of the structures. Apparently, it should be postulated that complexes with the fulvene structure contain a planar or nearly planar fulvene ligand, while complexes in which the tilt angle of the $C_{Cp}-C_{(\alpha)}H_2$ bond to the metal atom (α) equals 40° should be classified as methylenecyclopentadienyl complexes. It is evident that the deviation of the CH_2 group from the cyclopentadienyl plane by 40° virtually removes this group from conjugation with the ring; therefore, this ligand should not be termed as a fulvene ligand. A similar type of description should be applied to complexes with the $C_5Me_3(CH_2)_2$ ligand. Note that complexes with this extreme type of geometry are seldom encountered; those with an intermediate geometry are more common. The structure of complexes with the $C_5Me_4CH_2$ and $C_5Me_3(CH_2)_2$ ligands can be described using a 'specific' resonance hybrid, which takes into account the presence of both forms, $\mathbf{A} \leftrightarrow \mathbf{B}$ and $\mathbf{C} \leftrightarrow \mathbf{D}$, respectively. It should be taken into account that, unlike classical resonance, in this case, not only electrons are displaced but also the geometry changes. Note that in most of original publications, no clear or unambiguous assignment of the structures of transition metal complexes with the $C_5Me_4CH_2$ and $C_5Me_3(CH_2)_2$ ligands to forms **A** and **B** ($\eta^2,\eta^4 \leftrightarrow \sigma,\eta^5$) or **C** and **D** ($\eta^4,\eta^3 \leftrightarrow \sigma,\sigma,\eta^5$) has been carried out; therefore, in this review, we describe them as complexes with η^6- and η^7-modes of coordination, respectively.

In all studies considered below, the researchers discuss rather comprehensively the structure of each complex they prepare and give numerous facts obtained by chemical, structural, spectral, and quantum-chemical methods supporting one or another structure.

The description of the structures of these compounds in terms of a 'specific' resonance hybrid proposed in this review is underlain by earlier views. As will be shown below, these views were formulated on the basis of systematic research of cationic complexes, but they can also be applied to neutral analogues.

It is worth noting that similar properties or behaviours of complexes can be followed, first of all, for compounds of metals of the same Group. However, in some cases, analogies can also be traced for 16- and/or 18-electron compounds of elements of the same transition row. Therefore, when describing the chemical and spectroscopic properties of complexes, we will emphasise, as far as possible, the analogies found within the Groups or transition rows of elements.

III. The synthesis of complexes with tetramethylfulvene and trimethylallyldiene ligands

Metal complexes with the $C_5Me_4CH_2$ and $C_5Me_3(CH_2)_2$ ligands are often prepared by thermolysis of pentamethylcyclopentadienyl complexes Cp^*ML_n (L_n = Cp, Cp^*) of transition metals. Apparently, the reaction proceeds *via* radical intermediates. For example, heating of 16-electron $(\eta^5\text{-}Cp^*)_2MMe_2$ complexes (M = Ti, Zr) affords η^7-complexes, while the compounds $(\eta^5\text{-}Cp^*)_2MR_2$ (M = Zr, R = Ph; M = Hf, R = Bn) are converted into η^6-complexes.[13–15]

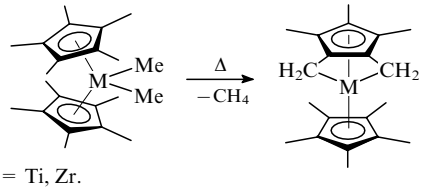

M = Ti, Zr.

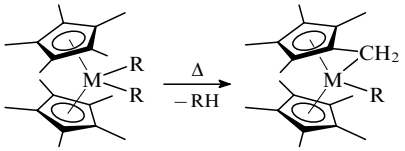

M = Zr, R = Ph; M = Hf, R = Bn.

Usually, $\eta^6\text{-}C_5Me_4CH_2$ complexes are synthesised starting from neutral and positively charged hydride complexes, $[(\eta^5\text{-}Cp^*)_2MH]^+An^-$, which are formed upon protonation of bis(pentamethylcyclopentadienyl) complexes of Group 8 metals or upon the reaction of Cp^*H with vapours of Group 6 and 7 transition metals. Ultraviolet photolysis of solutions of 18-electron metallocenes in acids (*in situ*) or the hydrides $[(\eta^5\text{-}Cp^*)_2MH_m]^{n+}An_n^-$ (M = Mo, W, Re,[16] Ru,[17] Os;[18] n = 0, 1; m = 0, 1, 2), isolated in a pure state, results in the complexes $[(\eta^5\text{-}Cp^*)MH_{m-1}(\eta^6\text{-}C_5Me_4CH_2)]^{n+}$. Thus UV irradiation of 18-electron neutral (**1a**,**b**) and cationic (**2**) η^5-complexes of Group 6 (Mo, W) and 7 (Re) metal hydrides yields successively η^6- (**3a**,**b**, **4**) and η^7-complexes (**5a**,**b**, **6**).[16] Apparently, in the case of Mo, W and Re, the final products are formed *via* 17-electron intermediates, $[\eta^5\text{-}Cp_2^*M^{\bullet}H]^{n+}$ (n = 0, 1), similar to complexes **3a**,**b**.

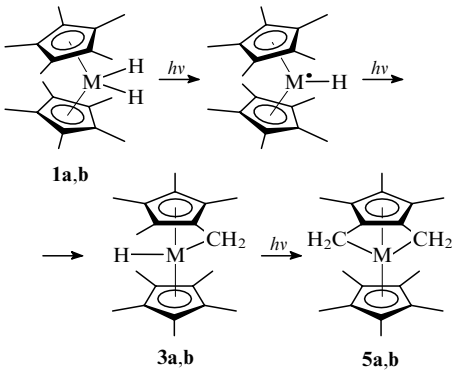

1a,**b** **3a**,**b** **5a**,**b**

M = Mo (**a**), W (**b**).

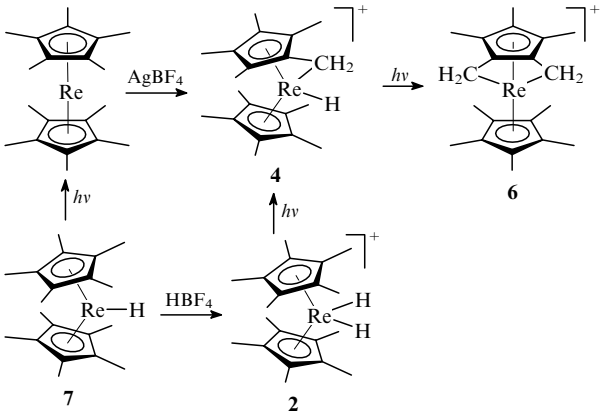

7 **4** **2** **6**

The 17-electron complex Cp_2^*Re (unlike the Mo and W analogues) is quite stable and has been isolated. Photolysis of Cp_2^*Re furnishes initially complex **4**, which is then transformed

into complex **6**.[16] The same products are formed from the cationic rhenium dihydrate **2**, resulting from protonation of $(\eta^5\text{-Cp}^*)_2\text{ReH}$ (**7**) (synthesised by co-condensation of Re vapour with Cp^*H)[16] on treatment with HBF_4 . Photolysis of cationic complexes of Group 8 metal hydrides, $[(\eta^5\text{-Cp}^*)_2\text{MH}]^+$ (**9a**,**b**) (M = Ru, Os), prepared from complexes $(\eta^5\text{-Cp}^*)_2\text{M}$ (**10a**,**b**) and a number of acids (CF_3CO_2H, HBF_4, HPF_6 and CF_3SO_3H), proceeds in a similar way (giving rise to η^5-complexes **8a**,**b**).[17,18] A ^{1}H NMR study showed the intermediate formation of the $[(\eta^5\text{-Cp}^*)_2\text{M}]^{+\bullet}$ radical cations (**11a**,**b**), which confirms the radical mechanism of the reaction.

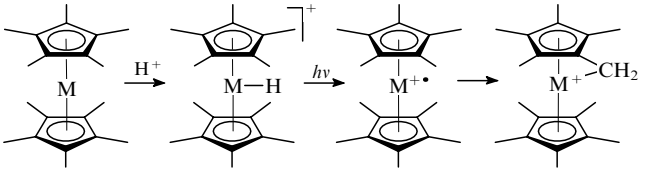

10a,**b** **9a**,**b** **11a**,**b** **8a**,**b**

M = Ru (**a**), Os (**b**).

The difference in the behaviours of neutral and cationic hydrides of Group 6–8 transition metals in the photolysis is manifested in the rate of formation of neutral and cationic products.

The 4d-metal $[(\eta^5\text{-Cp}^*)\text{MH}_x(\eta^6\text{-C}_5\text{Me}_4\text{CH}_2)]^{y+}$ complexes are formed faster than similar 5d-metal derivatives (Table 1).[16–18] However, for complexes formed by 3d metals, Cr, Mn and Fe, such transformations are unknown.

Table 1. Time (τ) of formation of $[(\eta^5\text{-Cp}^*)\text{MH}_x(\eta^6\text{-C}_5\text{Me}_4\text{CH}_2)]^{y+}$ from $[\text{Cp}_2^*\text{MH}_n]^{m+}$.

M	*n*	*m*	*x*	*y*	τ /h
Mo	2	0	1	0	3
W	2	0	1	0	24
Re	2	1	1	1	1
Ru	1	1	0	1	3
Os	1	1	0	1	15

These results are consistent with the data of theoretical calculations of diatomic cations $(\text{MH})^+$; the strength of the M—H bond for elements of the 4d row (Mo and Ru) is lower than that for 5d-row elements (W and Os).[19] Indeed, the $\text{Cp}'_n\text{ML}_m$ compounds (Cp′ = Cp, Cp*) formed by 5d elements tend to have higher basicities than their analogues formed by 4d elements; as a consequence, the dihydride $[(\eta^5\text{-Cp}^*)_2\text{MH}_2]^{n+}$ (M = Re, *n* = 1; M = Os, *n* = 2) or monohydride $[(\eta^5\text{-Cp}^*)\text{MH}.(\eta^6\text{-C}_5\text{Me}_4\text{CH}_2)]^{n+}$ (M = Re, *n* = 1; M = Os, *n* = 2) complexes with the η^6-fulvene ligand are formed in the first stage.[16,20] Note that doubly charged ruthenium complexes, $[(\eta^5\text{-Cp}^*)_2\text{RuH}_2]^{2+}$ and $[(\eta^5\text{-Cp}^*)\text{RuH}(\eta^6\text{-C}_5\text{Me}_4\text{CH}_2)]^{2+}$, are not formed under these conditions. (In original publications, doubly and triply charged cations are sometimes referred to as di- and trications, respectively.)

The formation of dimethylene neutral complexes **5a**,**b** and cationic complex **6** upon UV irradiation requires 48, 96 and 20 h, respectively, whereas monomethylene complexes are formed within 3, 24 and 1 h, respectively (see Table 1).[16] For preparing doubly charged Ru- and Os-containing complexes $[(\eta^5\text{-Cp}^*)\text{M}(\eta^7\text{-C}_5\text{Me}_3(\text{CH}_2)_2\text{-1,2})]^{2+}$ (**12a**,**b**) and $[\text{M}(\eta^6\text{-C}_5\text{Me}_4\text{CH}_2)_2]^{2+}$ (**13a**,**b**), a mere increase in the time of $[\text{Cp}_2^*\text{MH}]^+$ irradiation is insufficient (more than 3 and 15 h, respectively, see Table 1). The reaction medium must also contain an oxidant (Ox) or a substance that promotes oxidation. Indeed, mixtures of complexes **12a**, **13a** and **12b**, **13b** are formed in a high yield only upon UV photolysis in the presence of 20%–25% of oleum in the reaction mixture.[17,18,20–23]

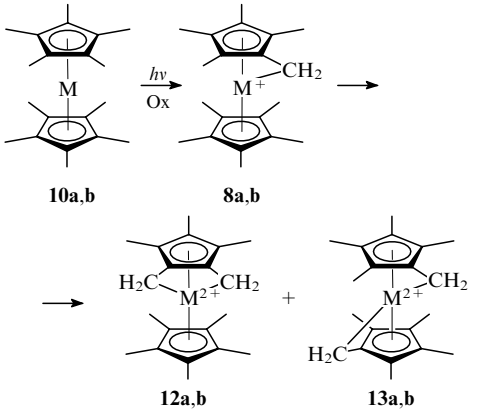

10a,**b** **8a**,**b** **12a**,**b** **13a**,**b**

The key stages in this process include (i) the formation of 16- and 17-electron intermediates of the $[\text{Cp}_2^*\text{Re}]^+$ or $[\text{Cp}_2^*\text{M}]^{+\bullet}$ type (M = Ru, Os) as a result of homolytic cleavage of the M—H bond followed by activation of the C—H bonds and (ii) the transformation of these intermediates into the $[(\eta^5\text{-Cp}^*)\text{ReH}(\eta^6\text{-C}_5\text{Me}_4\text{CH}_2)]^+$ and $[(\eta^5\text{-Cp}^*)\text{M}(\eta^6\text{-C}_5\text{Me}_4\text{CH}_2)]^+$ complexes (M = Ru, Os), respectively. These intermediates can also be prepared by oxidation of $(\eta^5\text{-Cp}^*)_2\text{M}$ (M = Re, Ru, Os) with one-electron oxidants, AgX (X = CO_2CF_3, BF_4). One-electron oxidation proved to be a versatile approach to the synthesis of a number of complexes of the $\text{LMC}_5\text{R}^1_4\text{CR}^2\text{R}^3$ type [M = Ru, Os; L = Cp, Cp*, η^5-C_9H_7 (indenyl); R^1, R^2, R^3 = H, Me]. Thus it was shown[21] that oxidation of LRuCp^* with $AgBF_4$ yields the complexes $[\text{LRu}(\eta^6\text{-C}_5\text{Me}_4\text{CH}_2)]^+\text{BF}_4^-$ (L = η^5-Cp, η^5-C_9H_7). A number of publications describe one-electron oxidation of methylated derivatives of ferrocene,[24] ruthenocene[25–27] and osmocene[28] and non-methylated ruthenocene[29,30] to give $[(\eta^5\text{-C}_5\text{R}^1_5)\text{M}(\eta^6\text{-C}_5\text{R}^1_4\text{CR}^2\text{R}^3)]^+\text{An}^-$ (M = Ru, Os; R^1 = H, Me; R^2, R^3 = Alk, Ar; An = BF_4, PF_6) from 17-electron metallocenium derivatives $[(\eta^5\text{-C}_5\text{R}^1_5)\text{M}(\eta^5\text{-C}_5\text{R}^1_4\text{CHR}^2\text{R}^3)]^{+\bullet}$

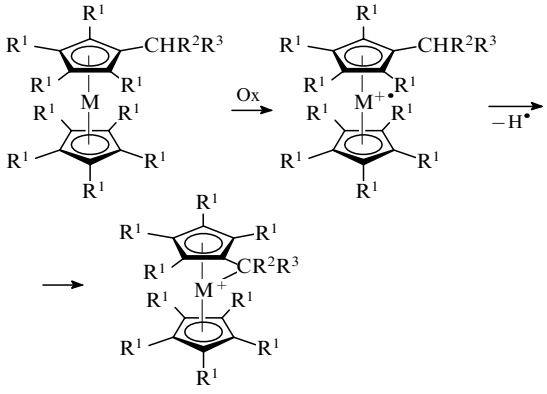

M = Ru, Os; R^1 = H, Me; R^2, R^3 = Alk, Ar.

For iron derivatives, this reaction does not occur and η^6-$C_5Me_4CH_2$ complexes are not formed.

Thus, any 17-electron radical cation, $[\text{LM}(\eta^5\text{-C}_5\text{R}^1_4.\text{CHR}^2\text{R}^3)]^{+\bullet}$ (M = Ru, Os; L = Cp, Cp*, η^5-C_9H_7; R^1 = H, Me; R^2, R^3 = Alk, Ar), having at least one α-C—H bond is capable of being converted into an 18-electron cationic complex,[21] $[\text{LM}(\eta^6\text{-C}_5\text{R}^1_4\text{CR}^2\text{R}^3)]^+$. It was shown that the radical cations add the nucleophile Nu^{n-} (n = 0, 1) giving rise to 19-electron radical cations (n = 0) or radicals (n = 1). The subsequent transformations of these 19-electron species furnish the reaction products. Detailed putative schemes of these reactions are documented.[31,32] It is noteworthy that 19-electron intermediates play a

fairly important role in the transformations of compounds of late transition metals (Groups 9 and 10, see below).

The photolysis, reduction and oxidation of half-sandwich complexes of Group 5–8 metals also occur *via* the formation of 16- and 17-electron intermediates. Thus the reduction of Cp^*TaCl_4 with trimethylphosphine yields two complexes,[33] one containing the η^7-$C_5Me_3(CH_2)_2$ ligand.

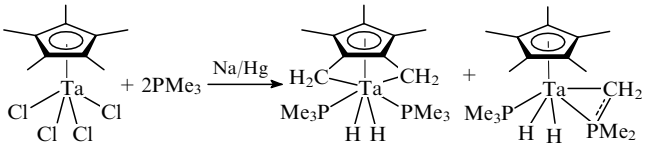

Rhenium complex **14** tends to undergo the following transformations:[34]

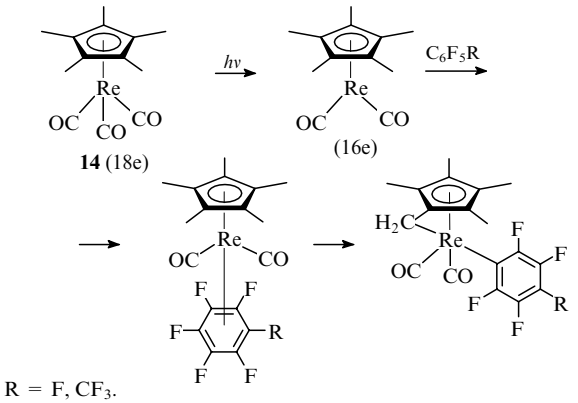

R = F, CF_3.

The formation of ruthenium complexes with the η^6-$C_5Me_4CH_2$ ligand is observed in various oxidation processes. For example, oxidation of binuclear halide complex **15** with oxygen involves the intermediate formation of oxide and affords dimeric complex **16**.[35]

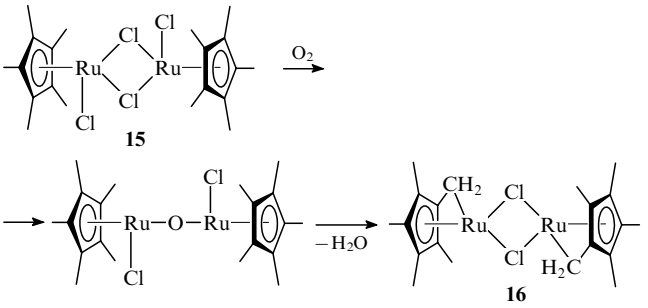

The cationic complex **17** is formed upon the oxidation of the binuclear ruthenium complex **18**.[36] In this case, intramolecular interligand transfer of a hydrogen atom takes place in the intermediate 17-electron radical cation.

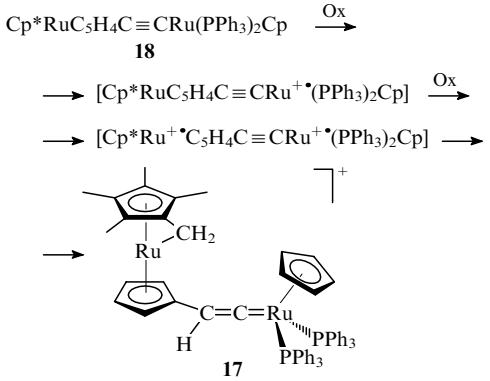

The oxidation of ruthenocene derivatives containing no Me or CHR^1R^2 substituents but having a multiple bond (C=C or C≡C) in the α-position affords compounds with the μ-η^6:η^6-ligand, which is an extensive polyconjugated system.[37]

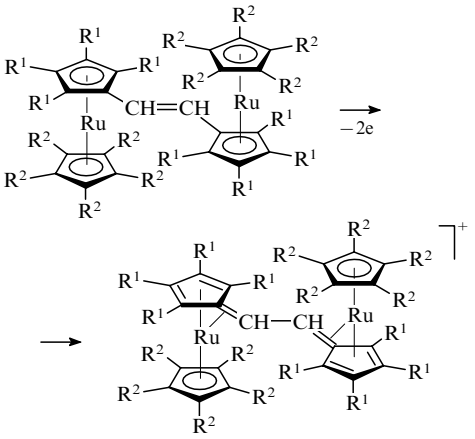

R^1, R^2 = H, Me.

The transformation of a ruthenium complex with the η^4-norbornadiene ligand into a complex with the η^6-$MeCHC_5H_4$ ligand (rather than η^6-$C_5Me_4CH_2$) *via* a 16-electron η^4-complex (activation or cleavage of the C–C bonds) has been reported.[38]

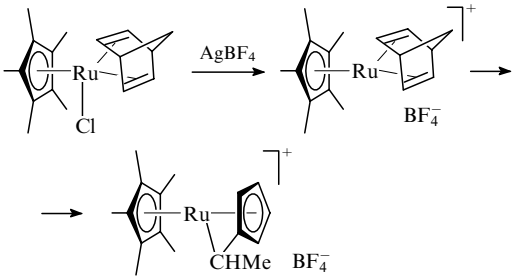

The oxidation of metallocenes Cp^*_2M (**10a**,**b**) in oleum or in the CF_3SO_3H – O_2 system, like photolysis, affords a mixture of η^5:η^7-(**12a**,**b**) and bis-η^6-complexes (**13a**,**b**). Note that the salts $[(\eta^5\text{-}Cp^*)M(\eta^6\text{-}C_5Me_4CH_2)]^+An^-$ (**8a**,**b**, An = BF_4 , PF_6) are preferred over metallocenes as the starting compounds for the preparation of the mixture of doubly charged cations; in this case, the product yield is higher and the reaction proceeds under milder conditions.[18,23]

The most interesting feature of the oxidation of metallocenes **10a**,**b** and cations **8a**,**b** on treatment with molecular oxygen in CF_3SO_3H is the fact that the reaction can proceed further and end in the formation of complexes containing three CH_2 groups, $[(\eta^6\text{-}C_5Me_4CH_2)M\{\eta^7\text{-}C_5Me_3(CH_2)_2\text{-}1,2\}]^{3+}$, which have no analogues among organometallic compounds. The properties and the possible structure of these compounds[20,39] are discussed below.

η^6-Fulvene complexes are also formed on treatment of the corresponding precursors with strong bases (for example, lithium alkoxides Pr^iOLi, Bu^tOLi or carbazolyl potassium).[40,41]

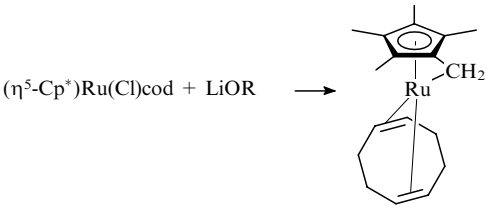

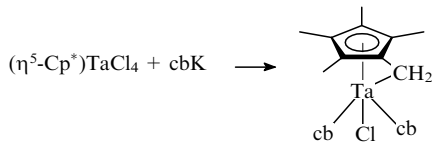

19

cod is 1,5-cyclooctadiene, cb is carbazolyl.

The reaction of chloride **19** with $LiCH_2SiMe_3$ or BnMgCl involves replacement of Cl by CH_2SiMe_3 or Bn without cleavage of the $Ta-CH_2$ bond.[41]

Deprotonation of cationic complexes under the action of strong bases is fairly typical of Group 9 metal derivatives. Generally, this gives rather labile complexes with the η^4-fulvene ligand with a non-coordinated exocyclic double bond. These complexes cannot be isolated due to high reactivity; their formation is indicated by the products of their reactions with various electrophiles. Thus deprotonation of iridium complex **20** followed by the reaction with electrophiles RX gives complexes with the ligands $C_5Me_4CH_2R$ (R = $SiMe_3$, All, Bn, CPh_2OH, CPh(Me)OH, CO_2Li).[42]

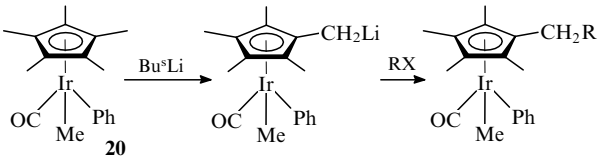

20

For penta- and decamethylrhodocenium and pentamethylcobaltocenium, deprotonation and the reaction with RX (X = Cl: R = Me_3Si, Bn; X = I: R = Me, Et) proceed by an elimination–addition mechanism *via* hypothetical intermediate η^4-fulvene complex **21**, the reaction involving all five (or ten) methyl groups. Treatment with alkyl iodides results in replacement of two hydrogen atoms at each Me group.[43, 44]

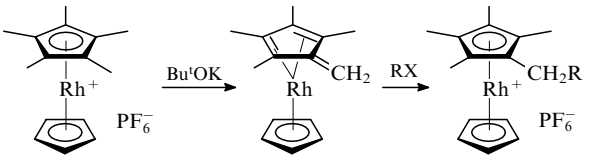

21

R = $SiMe_3$, Bn.

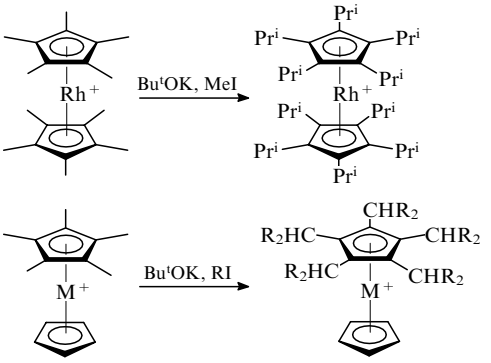

M = Rh, Co; R = Me, Et.

For compounds of Group 9 metals, η^4-fulvene complexes may also arise in oxidation and reduction processes. The reduction of the dimeric rhodium complex **22** and subsequent oxidation of the resulting compound **23** through intermediate complex **24** afford cationic η^4-complex **25**[45] rather than η^6-complexes, as in the case of Group 4–8 metals.

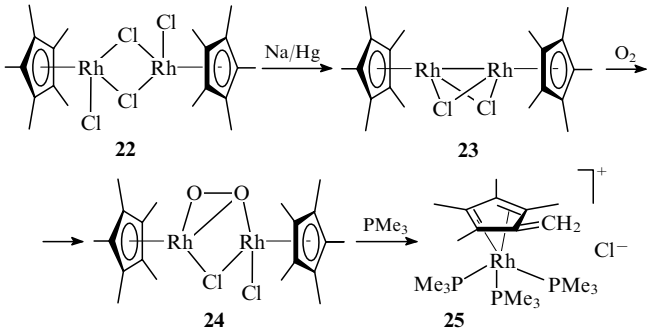

22 **23** **24** **25**

X-Ray diffraction analysis of complex **25** has shown that the CH_2 group and the carbon atom of the cyclopentadienyl ring attached to it are not involved in coordination with the Rh atom and that the methylene group is deflected from the metal atom by 23°.[45]

It is noteworthy that transformations of the η^5-cyclopentadienyl complexes of Group 9 metals (Co, Rh, Ir) do not often give mononuclear η^4-coordinated fulvene or cyclopentadiene complexes. For example, the reduction of 18-electron cationic complexes $[Cp^*_2M]^+X^-$ and $[Cp^*MCp]^+X^-$ (M = Rh, Ir, X is an anion) gives, in the first stage, extremely reactive 19-electron radicals, which either trap a hydrogen atom or react with the initial 18-electron cations to give bi- or polynuclear complexes with μ-η^4:η^4-ligands. Nevertheless, it is expedient to consider these transformations for obtaining the general picture of the reactivity of Cp^* compounds of Group 4–10 d-elements.

It is worth noting that the 19-electron intermediates resulting from reduction of complexes formed by Group 9 and 10 metals show more substantial differences between the behaviours of the derivatives of the second (4d) and third (5d) transition row metals than the 17-electron intermediates. Thus the reduction of $[Cp^*_2Rh]^+X^-$ gives rise to mononuclear η^5:η^4-complex, while that of its Ir analogue affords η^5 :η^4-dimer.[46, 47]

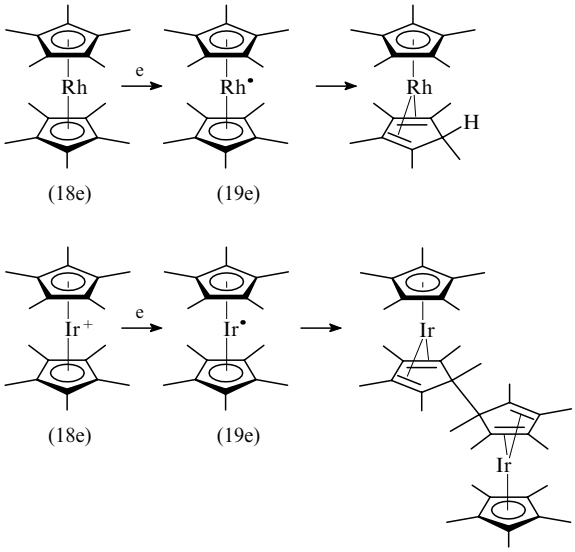

(18e) (19e)

The rhodium and iridium complexes having one pentamethyl-substituted and one unsubstituted Cp ligand are converted into dimers with different contents of spatial isomers. The formation of only one Rh-containing complex (**26a**) and predominance of one isomer for the Ir analogue (**26b**) (isomer ratio **26b** : **27b** = 2 : 1) with total absence of the third isomer **28b** (which is spatially the less hindered isomer with the μ-η^4:η^4-$C_5H_5C_5H_5$ ligand) attests to a reaction of the 19-electron radical with the initial 18-electron cation, because dimerisation of radicals would have yielded a random mixture (1 : 1 : 1) of all three spatial isomers.[47]

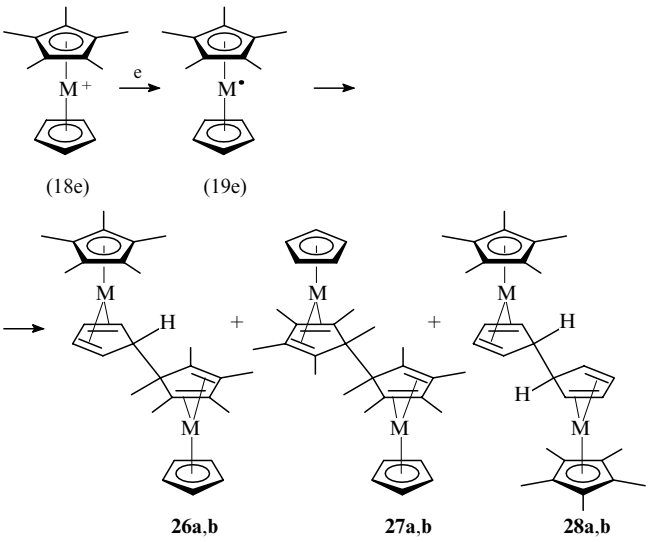

M = Rh (**a**), Ir (**b**).

Metal	Compound	Isomer content (%)
Rh	**26a**	100
	27a	0
	28a	0
Ir	**26b**	66
	27b	33
	28b	0

The reduction of Rh and Ir complexes containing η^5-Cp* and η^5-C_9H_7 ligands proceeds in a different way. For instance, electrochemical reduction of the 18-electron rhodium complex is a two-step process, each step being reversible.[46] The reaction gives mononuclear 19-electron radical **29a** and 20-electron anion (**30a**), respectively (or their 17- and 18-electron η^3-isomers **29b** and **30b**, respectively) (*i.e.*, a decrease in the hapticity of the indenyl ligand is involved).

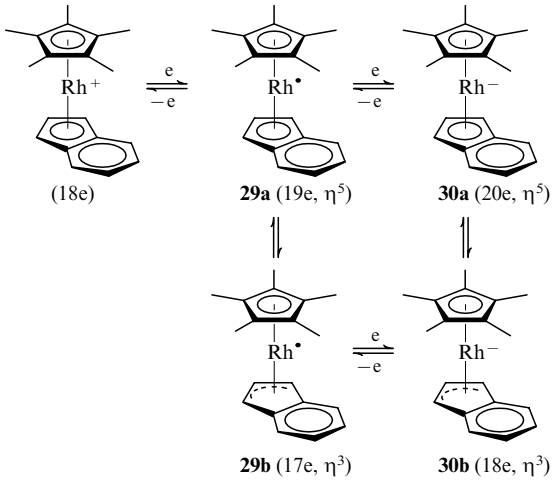

Chemical (1% Na amalgam in THF) or electrochemical reduction of $[(\eta^5\text{-Cp}^*)\text{Ir}(\eta^5\text{-C}_9\text{H}_7)]^+$ proceeds irreversibly, giving rise to a large tetranuclear splayed six-decked complex $[(\eta^5\text{-Cp}^*)\text{Ir}(\mu\text{-}\eta^5\text{-C}_9\text{H}_7)\text{Ir}(\mu\text{-}\eta^4\text{:}\eta^4\text{-C}_5\text{Me}_5\text{C}_5\text{Me}_5)\text{Ir}(\mu\text{-}\eta^5\text{-C}_9\text{H}_7)\text{Ir}.(\eta^5\text{-Cp}^*)]$.[47] Presumably, the reduction of the initial cation results in a 19-electron radical (analogous to the Rh-containing radical **29**), which splits off an indenyl ligand to give the solvate $[(\eta^5\text{-Cp*})\text{Ir}(\text{THF})_x]$. This complex then reacts with the initial cation yielding the cationic dimer $[(\eta^5\text{-Cp}^*)\text{Ir}(\mu\text{-}\eta^5\text{-C}_9\text{H}_7)\text{Ir}(\eta^5\text{-Cp}^*)]^+$. The reduction of this cation results in the final tetranuclear reaction product.

The electrochemical properties of some Cp* complexes of Group 10 metals (M = Pd, Pt) have been studied in detail.[48–51] For example, it was shown that oxidation of cationic 18-electron complexes $[(\eta^5\text{-Cp}^*)\text{M}(\eta^4\text{-Cp}^*\text{H})]^+$ (**31**) through 17-electron doubly charged radical cations (**32**) furnishes previously unknown 18-electron doubly charged pallado- and platinocenes **33**.[48,51] The electrochemically reversible reduction of platinocene *via* 19-electron radical cation **34** gives the initial complex **31**. Meanwhile, the successive reduction of the Pd analogue reversible in each one-electron stage gives no identifiable products. Further reduction of Pt complex **31** *via* 19-electron radical **35** or its reaction with a strong base (Bu^{t}OK) yields a mixture of η^3- (**36**) and σ:η^2-complexes (**37**).[51] It should be noted that in the intermediate 19-electron complex $(\eta^5\text{-Cp}^*)\text{Pt}(\eta^4\text{-Cp}^*\text{H})$, it is the C—H bond in the methyl group of the η^4-C_5Me_5H ligand that is cleaved rather than the C—H bond in the C(Me)H fragment of this ligand. No transformations of this type are known for Pd complexes.[48]

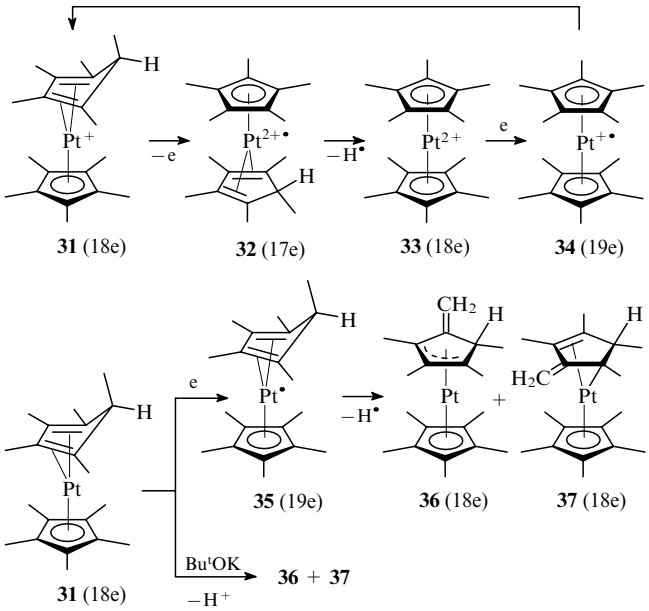

Deprotonation with potassium *tert*-butoxide or reduction with 19-electron $CpFeC_6Me_6$ of dienic Pt complexes containing simultaneously the C_5Me_5H and Cp ligands (**38a**,**b**) yields a mixture of compounds **39**, **40** and **41**, **42**, respectively.[48]

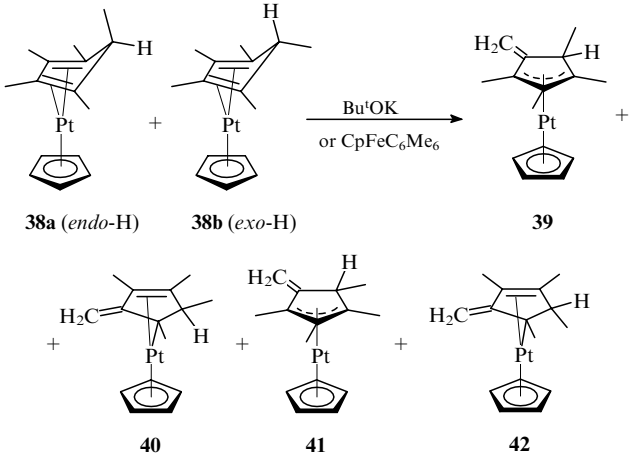

It should be noted that in the reactions listed above, the ligand hapticity decreases as follows: $\eta^5 \rightarrow \eta^4$ and $\eta^4 \rightarrow \eta^3$. Cases of $\eta^5 \rightarrow \eta^2$ transition are also known. For example, the reaction of $(\eta^3\text{-}C_3H_5)\text{Pd}(\eta^5\text{-Cp}^*)$ with PMe_3 affords $(Me_3P)_2\text{Pd}(\eta^2\text{-}$

$CH_2C_5Me_4$), in which the Pd atom is coordinated at the exocyclic double bond of the fulvene ligand.[52]

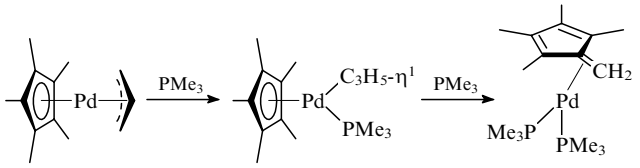

Apparently, the reaction of the Rh complex with isonitriles under UV radiation follows the same pattern to give 1,2,3,4-tetramethylfulvene *via* intermediate η^5-Cp*, η^3-Cp* and η^1-Cp* complexes.[53]

$$(\eta^5\text{-Cp}^*)\text{Rh(CNR)}_2 \xrightarrow{\text{RNC, } h\nu} (\eta^3\text{-Cp}^*)\text{Rh(CNR)}_3 \xrightarrow{\text{RNC, } h\nu}$$

$$\longrightarrow (\eta^1\text{-Cp}^*)\text{Rh(CNR)}_4 \longrightarrow C_5Me_4CH_2$$

R = CH_2Bu^t.

IV. The reactivity of neutral and cationic complexes

The reactivities of neutral and cationic fulvene complexes towards nucleophiles are fairly similar. Neutral complexes of Group 4–8 metals can also react with electrophilic reagents.[34] In some cases, the reactions of η^6-fulvene complexes with electrophiles (strong acids) proceed without rupture of the M–C_α bond to yield a singly or doubly charged cationic complex. For example, the neutral Re complex [16] and the cationic Os complex [23] react in this way.

$$\text{Cp*Re}(\eta^6\text{-}C_5Me_4CH_2) + HBF_4 \longrightarrow$$

$$\longrightarrow [\text{Cp*ReH}(\eta^6\text{-}C_5Me_4CH_2)]^+BF_4^-,$$

$$[\text{Cp*Os}(\eta^6\text{-}C_5Me_4CH_2)]^+BF_4^- + CF_3SO_3H \longrightarrow$$

$$\longrightarrow [\text{Cp*OsH}(\eta^6\text{-}C_5Me_4CH_2)]^{2+}An_2^-.$$

An = BF_4, CF_3SO_3.

For a 16-electron titanium complex containing two fulvene ligands,[54] reversible CO addition without rupture of the Ti– C_α bonds is also possible.

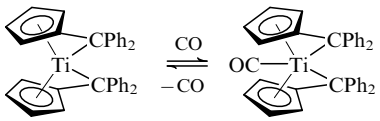

In addition, the 16-electron complexes of Group 4 metals (Ti, Zr, Hf) tend to undergo insertion into the M–CH_2 bonds with extension of the chelate ring and formation of a metal–hetero-atom bond.[55–57]

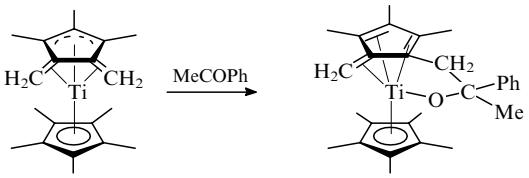

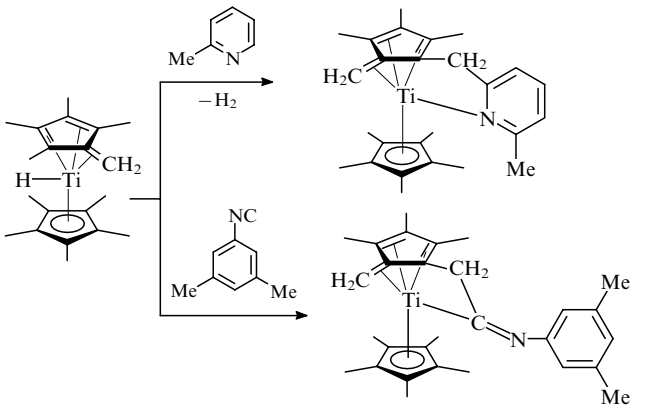

However, more often, reactions of cationic and neutral η^6-fulvene complexes with electrophiles are accompanied by rupture of the M–CH_2 bond, as for example, in the case of Re complexes.[34]

$$[(C_6F_5)(CO)_2\text{Re}(\eta^6\text{-}C_5Me_4CH_2)] + HHal \longrightarrow$$

$$\longrightarrow \textit{cis}\text{-}[(C_6F_5)(CO)_2\text{Re(Hal)}(\eta^5\text{-Cp}^*)] \longrightarrow$$

$$\longrightarrow \textit{trans}\text{-}[(C_6F_5)(CO)_2\text{Re(Hal)}(\eta^5\text{-Cp}^*)],$$

$$[(C_6F_5)(CO)_2\text{Re}(\eta^6\text{-}C_5Me_4CH_2)] + Hal_2 \longrightarrow$$

$$\longrightarrow \textit{cis}\text{-}[(C_6F_5)(CO)_2\text{Re(Hal)}(\eta^5\text{-}C_5Me_4CH_2Hal)] \longrightarrow$$

$$\longrightarrow \textit{trans}\text{-}[(C_6F_5)(CO)_2\text{Re(Hal)}(\eta^5\text{-}C_5Me_4CH_2Hal)].$$

Hal = Cl, Br, I.

In the reaction of neutral molybdenum complex **43** with HCl, the M–C_α bond is also cleaved to give binuclear complex **44** with halide bridges.[58]

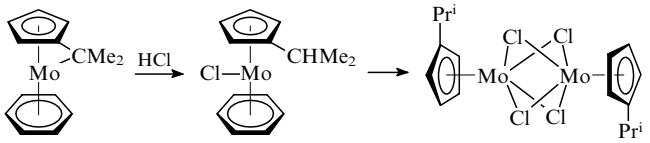

43 **44**

The rupture of two M–C_α bonds also takes place in the reaction of Ta complex with CO.[33]

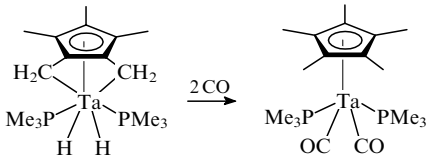

Rupture of the M–C_α bonds can also occur during the reduction of complexes.

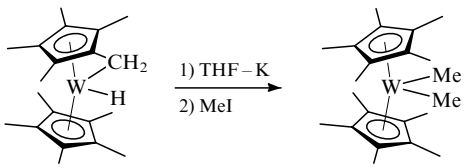

In some cases, the reactions of fulvene complexes involve not only the M–C_α bonds but also the bonds of the metal atom with other ligands;[15, 16, 59] in this case, rather unusual transformations, for example *ortho*-metallation, can occur in the metal coordination sphere.

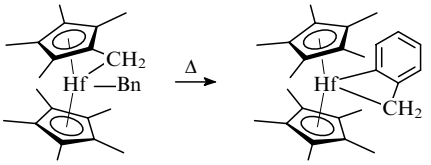

The neutral zirconium fulvene complex **45** reacts with ethylene and electrophilic boranes $XB(C_6F_5)_2$ (X = H, C_6F_5) with cleavage of the $M-C_\alpha$ bond. In the latter case, the reaction gives a zwitterionic complex, which has found use in homogeneous catalysis.[60, 61]

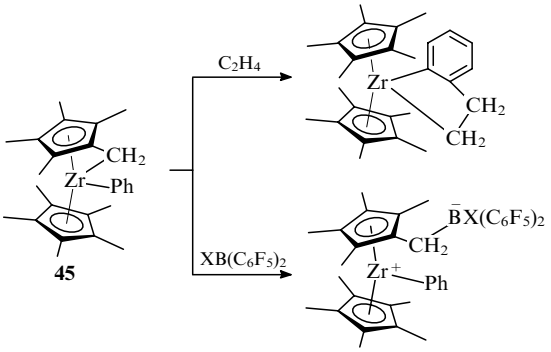

The reactivity of the non-methylated cationic fulvene complexes $[CpMC_5H_4CR^1R^2]^+X^-$ (M = Fe, Ru, Os) has been studied in detail (mainly in relation to ferrocene derivatives) in numerous studies by Russian and foreign researchers (see the reviews [62, 63] and references cited therein). Methylated derivatives are much less studied. Only a few papers dealing with the properties of cationic metal complexes containing the η^6-$C_5Me_4CH_2$ ligand have been published. The reactions of $[C_5HMe_4FeC_5Me_4CH_2]^+BF_4^-$ with a number of nucleophiles accompanied by rupture of the $Fe-CH_2$ bond have been studied.[64]

$[(\eta^5\text{-}C_5HMe_4)Fe(\eta^6\text{-}C_5Me_4CH_2)]^+BF_4^- \longrightarrow$

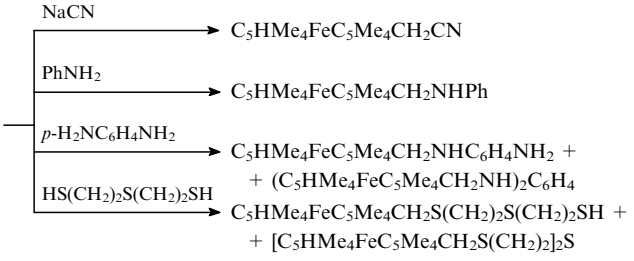

The reactions of salts of nonamethylruthenocenylmethyl cations with nucleophiles have been studied by Kölle *et al.*[25, 65] and Rybinskaya *et al.*[17]

$[Cp^*M(\eta^6\text{-}C_5Me_4CH_2)]^+An^- + KOH \longrightarrow Cp^*MC_5Me_4CH_2OH$

M = Fe, Ru; An = PF_6, CF_3SO_3.

$[Cp^*Ru(\eta^6\text{-}C_5Me_4CH_2)]^+PF_6^- \longrightarrow$

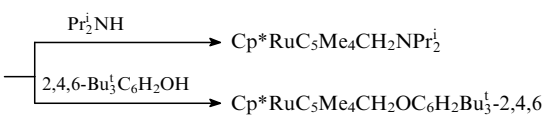

In cationic complexes, the M–CHR bond is easily cleaved under the action of $NaBH_4$, the complexes being reduced to metallocenes.

$[Cp^*M(\eta^6\text{-}C_5Me_4CHR)]^+An^- \xrightarrow{NaBH_4} Cp^*M(\eta^5\text{-}C_5Me_4CH_2R)$

M = Fe: R = H, Ph, Mes; M = Ru, Os: R = H; An = BH_4, PF_6.

The reactions of cationic complexes with the most typical nucleophiles have been studied.[27, 66]

$[Cp^*M(\eta^6\text{-}C_5Me_4CH_2)]^+An^- + MeONa \longrightarrow Cp^*MC_5Me_4CH_2OMe,$

M = Fe, Ru; An = BF_4, PF_6.

$[Cp^*Fe(\eta^6\text{-}C_5Me_4CH_2)]^+An^- + PhSH \longrightarrow Cp^*FeC_5Me_4CH_2SPh,$

An = BF_4, PF_6.

The C–O and C–S bonds in the resulting neutral ethers and thioethers are easily cleaved on treatment with acids yielding the initial cationic compounds.

The salts containing metallocenylmethyl (metallonium) cations readily react with amines and phosphines to give ammonium and phosphonium salts (onium exchange reactions).[67, 68]

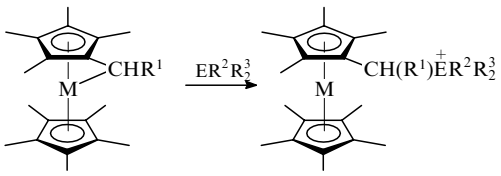

M = Os: R^1 = H, $ER^2R^3_2$ = $PPhMe_2$, PPh_3, NMe_3;
M = Ru: R^1 = H, $ER^2R^3_2$ = $PPhMe_2$; R^1 = Ph, $ER^2R^3_2$ = PPh_3.

Unlike neutral ethers and thioethers, in cationic metallocenylmethylammonium and -phosphonium cations, the C–N or C–P bonds are not cleaved in the reaction with CF_3SO_3H; instead, protonation at the metal atom to give dications takes place.[67]

$Cp^*MC_5Me_4CH_2P^+PhMe_2 \xrightarrow{CF_3SO_3H}$

$\longrightarrow Cp^*M^+H(C_5Me_4CH_2P^+PhMe_2)$

M = Ru, Os.

The reaction of $[Cp^*RuC_5H_4CHMe]^+$ with Bu^tOOLi [38] and the reaction of the cationic binuclear Ru complex with MeONa [36] have been studied.

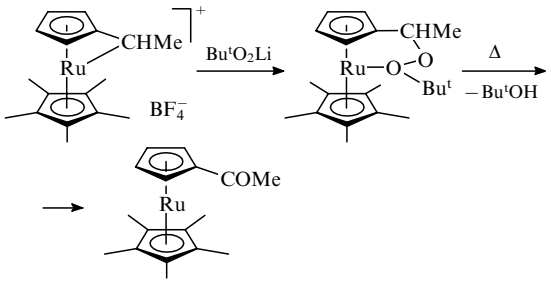

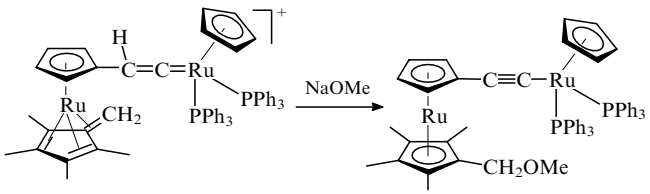

These reactions can be used to prepare functional derivatives of methylated metallocenes and their analogues.

V. Structural characteristics of metal complexes with a fulvene or allyldiene ligand

When discussing the structural characteristics of the complexes considered in this review, one should follow first of all the effect of the covalent radii of Group 4–10 transition metal atoms on the structure of compounds and, in particular, on the interatomic distances and bond angles. The covalent radii of Group 4–10 metals have been derived [69] from plenty of experimental data (Table 2). It can be seen from Table 2 that the radii of metal atoms of the 4th Period (3d metals) are much smaller, irrespective of the Group, than the radii of metal atoms of the 5th and 6th Periods (4d and 5d metals †). By following the variation of the radii over the Periods, one can see that the greatest values are found for Group 4 elements, then they smoothly decrease to reach the smallest values for Group 9 elements, and for Group 10 elements, they again somewhat increase.

Table 2. Covalent radii of transition metals (Å).[69]

Period	Group						
	4	5	6	7	8	9	10
4	Ti	V	Cr	Mn	Fe	Co	Ni
	1.56	1.49	1.46	1.38	1.34	1.29	1.35
5	Zr	Nb	Mo	Tc	Ru	Rh	Pd
	1.76	1.66	1.58	1.53	1.49	1.46	1.49
6	Hf	Ta	W	Re	Os	Ir	Pt
	1.77	1.66	1.59	1.51	1.50	1.47	1.43

When considering the structural characteristics of the neutral $L_nM(\eta^6\text{-}C_5R^1_4CR^2R^3)$ (M = Ti, Zr, Hf, Ta, Cr, Mo, W, Re, Ru; L = Cp, Cp*, Ar, CO; R^1 = H, Me; R^2, R^3 = H, Me, Ph) and cationic $[Cp'M(\eta^6\text{-}C_5R^1_4CR^2R^3)]^+$ An^- (Cp′ = Cp, Cp*; M = Fe, Ru, Os; R^1 = H, Me; R^2, R^3 = H, Ph) transition metal complexes with a fulvene ligand (metallocenylmethyl cations) studied to date (Tables 3, 4), one cannot but notice that they are closely similar. Only a few structurally characterised neutral allyldiene (or dimethylenecyclopentenyl) complexes with the $\eta^7\text{-}C_5Me_3(CH_2)_2$ ligand have been reported. Indeed, only one publication has been devoted to the X-ray diffraction study of the Ta complex — $(Me_3P)_2H_2Ta[\eta^7\text{-}C_5Me_3(CH_2)_2]$,[33] and one study [82] reports the structures of three related Ti complexes (see below).

Table 3 presents the X-ray diffraction characteristics of neutral and cationic η^6-fulvene metal complexes $[L_nMC_5R^1_4CR^2R^3]^{m+}An^-_m$ (M are Group 4–10 metals; L_n = Cp, Cp*, Ar, CO, PR^3_3, H; R^1 = H, Me; R^2, R^3 = H, Me, Ph; m = 0, 1, 2) studied to date.

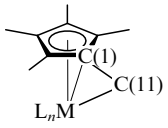

The data for Ti complexes have been collected in a separate Table (Table 4), as they require separate consideration. It can be seen from Table 3 that, despite the different ligand environments of the metal M (L_n ligands) and the substituents in the cyclopentadienyl ring, the M–C(11) and M–C(1) distances are usually commensurable. For compounds of elements of the third transition row (5d), they are somewhat smaller than the distances in complexes formed by metals of the second transition row (4d).

The shortest M–C(11) and M–C(1) distances were found for the 18-electron cationic complex $[Cp^*Os(C_5Me_4CH_2)]^+BPh^-_4$.

† The radii of 5d-metal atoms differ little from one another due to lanthanide contraction.

Table 3. X-Ray diffraction characteristics of transition metal complexes with the $\eta^6\text{-}C_5R^1_4CR^2R^3$ and $\eta^7\text{-}C_5R^1_3(CR^2R^3)_2$ ligands.

Compound	M–C(11) /Å	M–C(1) /Å	The angle α /deg [a]	Ref.
$[Cp^*Os(C_5Me_4CH_2)]^+$	2.224	2.069	41.8	68
$(Me_3SiCH_2)(cb)_2Ta(C_5Me_4CH_2)$	2.246	2.206	–	41
$(PhCH_2)(cb)_2Ta(C_5Me_4CH_2)$	2.254	2.203	–	41
$Cl(cb)_2Ta(C_5Me_4CH_2)$	2.258	2.207	–	41
$[CpRu(C_5£_4CH_2)]^+$	2.272	2.080	42.6	70
$[CpRu(C_5Me_4CH_2)]^+$	2.267	2.071	41.5	71
$[Cl(\mu\text{-}Cl)(C_5Me_4CH_2)Ru]_2$	2.268, 2.271	2.166, 2.172	– –	35
$[Cp^*Ru(C_5Me_4CH_2)]^+$	2.270	2.066	40.3	72
$(cyclo\text{-}C_8H_{12})ClRu(C_5Me_4CH_2)$	2.323	2.072	36	40
$Cp^*Hf(CH_2Ph)(C_5Me_4CH_2)$	2.320	2.258	37	59
$(CO)_2(C_6F_5)Re(C_5Me_4CH_2)$	2.36	2.14	39.6	34
$Cp^*ZrPh(C_5Me_4CH_2)$	2.388	2.282	37	15
$(Me_3P)_2H_2Ta\{C_5Me_3(CH_2)_2\}$	2.394	–	33.4	33
$[Cp^*Os\{C_5Me_4CH(C_6F_5)\}]^+$	2.401	2.094	–	73
$[CpOs(C_5H_4CPh_2)]^+$	2.387	2.088	–	74
$(C_6H_6)W(C_5H_4CPh_2)$	2.33	2.11	39	54
$(CO)_3Cr(C_5H_4CH_2)$	2.352	2.044	35	75
$[Cp^*Ru(C_5Me_4CHPh)]^+$	2.506	2.097	–	73
$[CpRu(C_5H_4CPh_2)]^+$	2.482	2.098	–	76
$(C_6H_5Me)Mo(C_5H_4CPh_2)$	2.374	2.125	38	54
$(CO)_3Cr(C_5H_4CPh_2)$	2.548	–	31	77
$[Cp^*Fe(C_5Me_4CH_2)]^+$	2.567	1.968	23.6	78
$[CpFe(C_5H_4CPh_2)]^+$	2.715	2.009	20.7	79

[a] Here and below, α is the tilt angle of the $C_{Cp}-CR^2R^3$ bond toward the metal.

Table 4. X-Ray diffraction parameters of the Ti complexes with the $\eta^6\text{-}C_5R^1_4CR^2_2$ and $\eta^7\text{-}C_5R^1_3(CR^2_2)_2$ ligands.

Compound	M–C(11) /Å	M–C(1) /Å	The angle α /deg	Ref.
$Cp^*Ti(C_5Me_4CH_2)$	2.281	2.093	35	80
ansa-$(C_5Me_4SiMe_2)Ti(C_5Me_3PhCH_2)$	2.328	2.156	–	81
$Cp^*Ti\{C_5Me_3(OCMePh)CH_2\}$	2.317	2.281	36.3	56
$(BnC_5Me_4)Ti\{C_5Me_3(CHPh)CH_2\}$	2.298,[a] 2.228	2.086, 2.072	44.0	82
$(BnC_5Me_4)Ti\{C_5Me_2Bn(CH_2)_2\}$	2.316, 2.252	2.117, 2.107	43.0	82
$Ti(C_5H_4CPh_2)_2$	2.347, 2.348	2.256, 2.264	36 (37)	54

[a] The Ti–CHPh bond length.

These distances are somewhat longer in 16-electron neutral 'primary' (η^6-6,6-H,H-fulvene) tantalum complexes. Attention is attracted by somewhat greater (and virtually equal to each other) Ru–C(11) distances in the $[Cp'Ru(C_5R_4CH_2)]^+An^-$ cationic complexes (Cp′ = Cp, Cp*; R = H, Me) and the neutral Ru complex, $[\{Cl(\mu\text{-}Cl)C_5Me_4CH_2\}Ru]_2$. In the $[(cyclo\text{-}C_8H_{12})ClRu(C_5Me_4CH_2)]$ complex, the Ru–C(11) distance is somewhat longer.

The data of Table 3 indicate that for 16-electron compounds of Group 4 metals, $[Cp^*ZrPh(C_5Me_4CH_2)]$ and $[Cp^*Hf(CH_2Ph)(C_5Me_4CH_2)]$, and for 18-electron compounds of Group 6 metals, $[(C_6H_5Me)Mo(C_5H_4CPh_2)]$ and $[(C_6H_6)W(C_5H_4CPh_2)]$, the M–C(11) distance tends to increase on going up along the group (5d → 4d). An increase in the M–C(11) and M–C(1) distances in the 18-electron complexes

of Group 8 metals is observed on passing from 4d (Ru) to 3d metals (Fe), despite the smaller covalent radius of the iron atom.

A similar pattern is observed for the 18-electron η^6-6,6-diphenylfulvene cationic complexes of Group 8 metals $[CpM(C_5H_4CPh_2)]^+$ (M = Os, Ru, Fe), neutral complexes of Group 6 metals, $(C_6H_6)W(C_5H_4CPh_2)$, (C_6H_5Me).$Mo(C_5H_4CPh_2)$, $(CO)_3Cr$-$(C_5H_4CPh_2)$, and for two η^6-6-H,6-Ph-fulvene cationic complexes, $[Cp^*M(C_5Me_4CHAr)]^+$ (M = Os, Ar = C_6F_5; M = Ru, Ar = Ph). Thus, most often, for 18-electron complexes of Group 6 and 8 metals and for 16-electron compounds of Group 4 metals, the M–C(11) distances tend to decrease in the sequences Cr > Mo > W; Fe > Ru > Os; and Zr > Hf (5d → 4d → 3d). These regularities clearly attest to the increase in the degree of interaction of the lone electron pair (LEP) of the metal atom with the carbocationic centre in cationic complexes or with the appropriate vacant orbital of the fulvene ligand in neutral complexes along these sequences. It can also be seen from the data of Table 3 that for compounds of Group 8 metals and for Cr-containing complexes, the M–C(11) distance tends to increase with enhancement of steric restrictions in the fulvene ligand (the bulk or the size of substituents), *i.e.*, on passing from primary $[Cp^*M(C_5Me_4CH_2)]^+An^-$ cations to tertiary $[CpM(C_5H_4CPh_2)]^+$ An^- cations (M = Fe, Ru, Os). The corresponding neutral complexes behave in a similar way: the M–C(11) distance increases on passing from $(CO)_3Cr(C_5H_4CH_2)$ to $(CO)_3Cr(C_5H_4CPh_2)$.

More detailed analysis of structural data, both presented in Table 3 and absent from the Table but contained in original publications shows that in all neutral and cationic η^6-$C_5R_4CH_2$ complexes of Group 4 (Zr, Hf), 6 (Mo, W) and 8 (Ru, Os) metals of the second and third transition rows, the M–C(11) bond length barely differs from the lengths of the bonds between the metal and other atoms of the cyclopentadienyl ring of the fulvene ligand. Quantum-chemical calculations (see below) indicate that in the cationic $[Cp^*M(C_5Me_4CH_2)]^+An^-$ complexes (M = Ru, Os), the positive charge is concentrated almost entirely on the metal atom. In any of these compounds, one LEP of the metal atom (Fe and, especially, Ru and Os) is involved in substantial donor–acceptor interaction with the carbocationic centre. In the doubly charged Group 8 metal complexes, donor–acceptor interaction takes place between two LEP of the metal atom (Ru and Os and, to a lesser extent, Fe) and two carbocationic centres. Cationic compounds of this type have been termed metallonium compounds.[83] Apparently, the term 'neutral metallonium complexes' is applicable to neutral fulvene or allyldiene complexes in which the M–C(11) bond length does not differ much from the bond lengths between the metal atom and the carbon atoms of the Cp or Cp^* ring and which are characterised by a substantial donor–acceptor interaction between one or two LEP of the metal atom (Ti, Zr, Hf, Ta, Mo, W, Ru and, to a lesser extent, Cr) and one or two vacant orbitals of the fulvene or allyldiene ligand (see below). Their formation from the starting cyclopentadienyl complexes is actually accompanied by an increase in the hapticity of the metal atom ($\eta^5 \rightarrow \eta^6 \rightarrow \eta^7$). The structure of these complexes is best described by resonance forms **B** (σ,η^5) and **D** (σ,σ,η^5), respectively. Recall that the formation of cationic onium complexes, ER_n^+ (E = N, P, As, O, S, I; R = H, Me), anionic ('inverted') onium complexes, ER_n^- (E = B, Al; R = H, F, Cl), or neutral 'onium' $Me_3N\cdot BH_3$ or $Et_3N\cdot BF_3$ complexes (these are also characterised by interaction of the donor LEP with an acceptor vacant orbital) of organic or organoelement compounds of non-transition elements from the corresponding precursors is also accompanied by an increase in the coordination number of the central atom by unity.

In the case of Ti complexes, it is possible to compare directly structures with the η^6-$C_5R_4^1CR_2^2$ and η^7-$C_5R_3^1(CR_2^2)_2$ ligands. The first characteristic feature that can be noted when comparing the data of Tables 3 and 4 is the shorter M–C(11) distances for Ti complexes compared to similar Zr and Hf complexes; apparently, this is a consequence of the smaller covalent radius of Ti. The Ti–CH_2 bond length in the 15-electron $Cp^*Ti(C_5Me_4CH_2)$ complex is virtually equal to or even somewhat greater than that in the 16-electron complexes with the η^7-$C_5Me_3(CH_2)_2$ and η^7-$C_5Me_3(CHPh)CH_2$ ligands. In the $Ti(C_5H_4CPh_2)_2$ complex, the Ti–CPh_2 bonds (as in the Cr, Fe, Ru and Os complexes) are longer than the Ti–CH_2 bonds in other compounds. An increase in the Ti–CH_2 distance in the *ansa*-$(C_5Me_4SiMe_2)Ti$.$(C_5Me_3PhCH_2)$ complex and the $Cp^*Ti\{C_5Me_3(OCMePh)CH_2\}$ complex containing a TiC(Me)(Ph)O fragment should also be noted.

VI. Spectral characteristics of complexes

1. Chemical shifts

The number of fulvene and allyldiene complexes studied by NMR spectroscopy is much greater, as this does not require growing the crystals. In view of the fact that preparation of suitable crystals for some compounds is either difficult or impossible, the significance of the NMR spectroscopy can hardly be overestimated. The NMR spectral data are complementary to X-ray diffraction data. These data allow one (subject to some restrictions) to elucidate the same features as X-ray diffraction data.

The degree of interaction between the metal atom and the carbocationic centre or a vacant orbital in all the cationic and neutral complexes studied can be estimated by analysing the ^{13}C NMR chemical shifts (δ) of the C(11) nuclei. Of course, certain regularities of the variations of chemical shifts can also be followed in the ^1H NMR spectra but they are usually much less vivid than the corresponding changes in the ^{13}C NMR spectra and are not considered in this review. Tables 5–7 present the chemical

Table 5. Chemical shifts $\delta(^{13}C)$ of the C(11) nuclei in the 'primary' neutral and cationic η^6-6,6-H_2-fulvene and η^7-allyldiene metal complexes.

Compound	δ (^{13}C) /ppm	Ref.
$[Cp^*Fe(C_5Me_4CH_2)]^+$	90.7	84, 85
$Cl(cb)_2Ta(C_5Me_4CH_2)$	90.7	41
$(PhCH_2)(cb)_2Ta(C_5Me_4CH_2)$	89.6	41
$[CpFe(C_5H_4CH_2)]^+$	88.6	86
$[Cp^*Ru\{C_5Me_3(CH_2)_2\}]^{2+}$	88.4	87
$(Me_3SiCH_2)(cb)_2Ta(C_5Me_4CH_2)$	88.4	41
$(BnC_5Me_4)Ti\{C_5Me_3(CHPh)CH_2\}$	81.0	82
$[Cp^*Ru(C_5Me_4CH_2)]^+$	74.6	72
$(C_5HMe_4)TiMe(C_5HMe_3CH_2)$	74.4	88
$[(\eta^5\text{-}C_9H_7)Ru(C_5Me_4CH_2)]^+$	73.9	89
$(PhC_5Me_4)Ti\{C_5Me_2Ph(CH_2)_2\}$	71.3; 73.2	82
$(4\text{-}FC_6H_4C_5Me_4)Ti\{C_5Me_2(C_6H_4F\text{-}4)(CH_2)_2\}$	71.3; 72.7	82
$Cp^*TiMe(C_5Me_4CH_2)$	73.9	55
$(CO)_3Cr(C_5H_4CH_2)$	73.4	73
$[Cp(PPh_3)_2Ru{=}C{=}CHC_5H_4Ru(C_5Me_4CH_2)]^+$	71.7	36
$Cp^*Hf(CH_2Ph)(C_5Me_4CH_2)$	71.2	59
$[Cp^*Os\{C_5Me_3(CH_2)_2\}]^{2+}$	71.1	87
$[CpRu(C_5Me_4CH_2)]^+$	69.4	89
$(BnC_5Me_4)Ti\{C_5Me_2Bn(CH_2)_2\}$	68.19; 68.29	82
$Cp^*Ti\{C_5Me_3(CH_2)_2\}$	67.7	55
$[Cp^*OsH(C_5Me_4CH_2)]^{2+}$	66.5	23
$Cp^*Zr(Ph)(C_5Me_4CH_2)$	63.5	15
$Cp^*Zr\{C_5Me_3(CH_2)_2\}$	56.5	55
$Cp^*Mo\{C_5Me_3(CH_2)_2\}$	56.2	16
$[Cp^*Os(C_5Me_4CH_2)]^+$	55.4	68
$[Cp^*Re\{C_5Me_3(CH_2)_2\}]^+$	53.8	16
$Cp^*WCl(C_5Me_4CH_2)$	51.1	90
$Cp^*W\{C_5Me_3(CH_2)_2\}$	45.9	16
$(Me_3P)_2H_2Ta\{C_5Me_3(CH_2)_2\}$	45.0	33
$[Cp^*ReH(C_5Me_4CH_2)]^+$	45.0	16
$Cp^*Re(C_5Me_4CH_2)$	36.9	16
$Cp^*WH(C_5Me_4CH_2)$	35.3	16

Table 6. Chemical shifts $\delta(^{13}C)$ of the C(11) nuclei in the 'secondary' neutral and cationic η^6-6-R-6-H-fulvene metal complexes.

Compound	$\delta(^{13}C)$ /ppm	Ref.
$[CpFe(C_5H_4CHMe)]^+$	119.5	86
$[Cp^*Ru(C_5H_4CHMe)]^+$	100.1	38
$[(CO)_3Mn(C_5H_4CHPh)]^+$	144.5	91
$[Cp^*Fe(C_5Me_4CHPh)]^+$	132.1	92, 93
$[CpFe(C_5H_4CHPh)]^+$	122.2	94
$[Cp^*Ru(C_5Me_4CHPh)]^+$	104.4	96
$[CpRu(C_5H_4CHPh)]^+$	101.2	94
$[Cp^*Os(C_5Me_4CHPh)]^+$	83.9	93
$[CpOs(C_5H_4CHPh)]^+$	79.0	94
$[Cp^*Fe(C_5Me_4CHMes)]^+$	137.5	92
$[Cp^*Ru(C_5Me_4CHMes)]^+$	134.5	93
$[Cp^*Os(C_5Me_4CHMes)]^+$	102.4	93
$[Cp^*Ru(C_5Me_4CHC_6F_5)]^+$	83.9	93
$(BnC_5Me_4)Ti\{C_5Me_3(CHPh)CH_2\}$	90.2	82
$[Cp^*Os(C_5Me_4CHC_6F_5)]^+$	55.4	93

shifts in neutral and cationic $[L_nM(\eta^6\text{-}C_5R^1_4CR^2R^3)]^{m+}$ and $[L_nM\{\eta^7\text{-}C_5Me_3(CH_2)_2\}]^{m+}$ complexes ($m = 0, 1$).

It can be seen from the data of Tables 5–7 that for most primary, secondary and tertiary cationic and neutral complexes, shielding of ^{13}C nuclei in the CR^1R^2 (CH_2, CHMe, CHPh, CHMes, CHC_6F_5, CMe_2 and CPh_2) groups increases (δ values decrease) from top to bottom along the Groups. Thus, the results obtained by NMR are correlated with X-ray diffraction data, which attest to a decrease in the M–C(11) distance and an increase in the angle α along the same sequences (*i.e.*, Ti–Zr–Hf, Cr–Mo–W and Fe–Ru–Os). Thus, both physical methods provide the same conclusion: the donor–acceptor interaction of the LEP of the metal atom with the carbocationic centre or with the vacant orbital increases on going from top to bottom along the Groups of elements.

The effect of the metal atom [an increase in the shielding (a decrease in the δ values) of the C(11) carbon nuclei from top to bottom along the Group] is often manifested in the fact that the δ values for elements of different Groups but of the same Period are fairly similar. The effect of the metal often counterbalances not only the influence of the charge (see below) but also the degree of substitution at C(11).

The similarity of the δ values for Ru and, especially, Os cationic complexes to those for neutral fulvene complexes with a similar structure (Ti, Zr, Mo, W, *etc.*), apparently, indirectly confirms the conclusion based on extended Hückel (EHT) calculations,[97] according to which the major positive charge in these complexes is concentrated on the metal atom rather than on the CR^1R^2 group. However, it should be noted that the comparison of the carbon δ values for the CR^1R^2 groups is more or less legitimate only in the case of isostructural compounds or compounds with similar structures, because in the general case, the influence of other ligands (ligand environment) cannot be neglected.

Table 7. Chemical shifts $\delta(^{13}C)$ of the C(11) nuclei in the 'tertiary' neutral and cationic η^6-6,6-R_2-fulvene metal complexes.

Compound	$\delta(^{13}C)$ /ppm	Ref.
$[CpFe(C_5H_4CMe_2)]^+$	158.6	86
$[(CO)_3Mn(C_5H_4CPh_2)]^+$	201.0	91
$[CpFe(C_5H_4CPh_2)]^+$	171.6	94
$[CpRu(C_5H_4CPh_2)]^+$	139.6	94
$(CO)Ti(C_5H_4CPh_2)_2$	132.1	54
$(CO)_3Cr(C_5H_4CPh_2)$	126.0	77
$(C_6H_6)Mo(C_5H_4CPh_2)$	103.0	54
$[CpOs(C_5H_4CPh_2)]^+$	95.7	94

Table 8. Chemical shifts $\delta(^{13}C)$ of the C(11) nuclei in the complexes $[(\eta^5\text{-}Cp^*)M\{\eta^7\text{-}C_5Me_3(CH_2)_2\}]^{n+}$ ($n = 0, 1, 2$).

M	$\delta(^{13}C)$ /ppm	Charge	Ref.
Mo	56.2	0	16
Ru	88.4	2+	87
W	45.9	0	16
Re	53.8	1+	16
Os	71.1	2+	87

It can be seen from Table 5 that in the case of 18-electron complexes of Group 6, 7 and 8 metals with η^7-dimethylenecyclopentadienyl ligands, the δ values decrease with a decrease in the overall charge of the complex, *i.e.*, in the series: doubly charged > singly charged > neutral. This can be seen in Table 8.

Therefore, for 18-electron complexes of Group 6, 7 and 8 metals (W, Re, Ru, Os), deshielding (an increase in the δ values) is typically observed on passing from η^6-monomethylene (neutral or singly charged) complexes to η^7-dimethylene compounds (singly or doubly charged). However, for neutral 16-electron Ti complexes, no regularities in the variation of chemical shifts on passing from η^6-monomethylene to η^7-dimethylene compounds, nor changes in the X-ray diffraction characteristics can be revealed.

It should be noted that for primary CH_2 derivatives, it is easier to elucidate regular features in the variation of the δ values depending on the nature of the metal atom, the charge or other electronic effects than for secondary CHR^1 and tertiary CR^1R^2 complexes due to the spatial and electronic effects of the substituents R^1 and R^2. The observed decrease in the δ values following the migration from top to bottom along the Groups appears to be quite natural, because the diffuseness of atomic orbitals of transition metals tends to increase from top to bottom along the Subgroups. On the basis of EHT calculations[95] for the cationic complexes of Group 8 metals, $[Cp^*M(C_5Me_4CH_2)]^+$ (M = Fe, Ru, Os), it was shown that the M–C(11) bond order increases ($0.01 < 0.16 < 0.22$) in the sequence Fe $\ll$ Ru < Os. It is common knowledge that the bond length increases following a decrease in the bond order. The shielding constant σ (or its paramagnetic component σ_p, which makes the greatest contribution to this constant), is a function of a charge density and the M–C(11) bond order. This clarifies the observed decrease in the δ values of the C(11) nuclei for the $[Cp^*M(C_5Me_4CH_2)]^+$ cations in the sequence Fe > Ru > Os. Apparently, similar regularities are also typical of cationic and neutral $\eta^6\text{-}C_5R^1_4CR^2R^3$ complexes formed by metals of other Groups.

2. The spin–spin coupling constants $^1J_{CH}$ for η^6 and η^7 neutral and cationic complexes

Apart from the data on chemical shifts, the spin–spin coupling constants ($^1J_{CH}$) of the carbon atom of the CHR groups are often used to determine the structures of cationic and neutral fulvene complexes. Unfortunately, no systematic research into the spin–spin coupling constants of isostructural cationic and neutral η^6-complexes of Group 4–8 metals has been carried out. A fairly large number of scattered $^1J_{CH}$ values have been reported in the literature. They are summarised in Table 9.

It can be seen that the spin–spin coupling constants ($^1J_{CH}$) for the CH_2 group in the series of the primary $[Cp^*M(C_5Me_4CH_2)]^+$ (M = Fe, Ru, Os) and for the CHR group in the series of the secondary $[Cp^*Os(C_5Me_4CHC_6F_5)]^+$ and $[CpM(C_5H_4CHPh)]^+$ (M = Ru, Os) cationic nonmethylated complexes of Group 8 metals and their neutral analogues barely depend on the nature of the metal.

Meanwhile, the coupling constants of the studied doubly charged dimethylene complexes, $[Cp^*M\{C_5Me_3(CH_2)_2\}]^{2+}$ (M = Ru, Os), and their neutral analogues (Table 10) show that these values increase somewhat on passing from neutral complexes to doubly charged ones. However, generally, the presented

Table 9. Spin–spin coupling constants ($^1J_{CH}$) for the C(11) atom.

Compound	$^1J_{CH}$ /Hz	Ref.
$C_6F_5(CO)_2Re(C_5Me_4CH_2)$	162.0	34
$Cp^*Re(C_5Me_4CH_2)$	157.7	16
$Cp^*WH(C_5Me_4CH_2)$	151.3	16
$Cp^*ZrPh(C_5Me_4CH_2)$	144.8	15
$Cp^*Hf(CH_2Ph)(C_5Me_4CH_2)$	142.0	59
$[Cp^*Fe(C_5Me_4CH_2)]^+$	164.7	84, 85
$[Cp^*Ru(C_5Me_4CH_2)]^+$	164.2	72
$[Cp^*Os(C_5Me_4CH_2)]^+$	166.0	68
$[(\eta^5\text{-}C_9H_7)Ru(C_5Me_4CH_2)]^+$	167.2	89
$[CpRu(C_5Me_4CH_2)]^+$	167.0	89
$[CpRu(C_5H_4CHPh)]^+$	163.2	94
$[CpOs(C_5H_4CHPh)]^+$	164.9	94
$[Cp^*Os(C_5Me_4CHC_6F_5)]^+$	167.9	93
$[Cp^*Ru(C_5Me_4CHMe)]^+$	163.6	93
$Cp^*ReH(C_5Me_4CH_2)$	162.4	16
$[CpFe(C_5H_4CH_2)]^+$	165	86
$[CpFe(C_5H_4CHMe)]^+$	165	86
$[CpFe(C_5H_4CHPr^i)]^+$	163	86
$[CpFe(C_5H_4CHBu^t)]^+$	158	86
$[CpFe(C_5H_4CHPh)]^+$	160	86

Table 10. Spin–spin coupling constants ($^1J_{CH}$) of the doubly charged complexes and their neutral analogues.

Compound	$^1J_{CH}$ /Hz	Ref.
$Cp^*Ti\{C_5Me_3(CH_2)_2\}$	160.0	55
$Cp^*Zr\{C_5Me_3(CH_2)_2\}$	148.0	55
$Cp^*Mo\{C_5Me_3(CH_2)_2\}$	154.0	16
$Cp^*W\{C_5Me_3(CH_2)_2\}$	152.0	16
$[Cp^*Ru\{C_5Me_3(CH_2)_2\}]^{2+}$	171.2	87
$[Cp^*Os\{C_5Me_3(CH_2)_2\}]^{2+}$	172.3	87

data indicate that the spin–spin coupling constants for cationic and neutral compounds, unlike the tilt angles of the $C_{Cp}-CHR$ bond relative to the metal (α), the $M-C_\alpha R$ distances, or the chemical shifts δ, are little dependent on the degree of interaction of the metal with the carbocationic centre or a vacant orbital.

VII. Quantum-chemical description of complexes

The electronic structure of the α-ferrocenylmethyl cation (the cationic fulvene complex), $[CpFe(C_5H_4CH_2)]^+$, was first calculated by the EHT method with charge self-consistence.[96] Gleiter and Seeger[96] have predicted the most typical feature of the structure of complexes of this type, namely, distortion of the planarity of the fulvene ligand, which is manifested as a deviation of the carbon atom of the CH_2 group toward the metal atom (the angle α) through 40°. The researchers also showed that the charge on the Fe atom in this monocation is 0.5, while the rest of the charge (0.5) is delocalised over all carbon atoms of the ligands. Subsequently, it has been shown that neutral and cationic complexes, $[L_nM(C_5H_4CR^1R^2)]^{m+}$ [$L_nM = (CO)_3Cr$, $m = 0$; L_nM = CpFe, $m = 1$] with a fulvene ligand have a similar structure.[97] In a more recent study,[95] EHT calculations for a number of monocations, $[Cp'M(C_5R_4CH_2)]^+$ (M = Fe, Ru, Os; Cp′ = Cp, Cp^*; R = H, Me), were used to calculate the angles α, the energy gaps ($\Delta E = E_{LUMO} - E_{HOMO}$), the charges on the metal atoms (Q) and the CH_2 groups (q), and Mulliken bond orders (Table 11).

It is of interest that the minimum total energy (*i.e.*, the most effective $Mo-CH_2$ interaction) in the neutral fulvene complex $(C_6H_6)Mo(\eta^6\text{-}C_5H_4CH_2)$ corresponds to the angle $\alpha = 35°$ (see Ref. 54), which is well correlated with the experimental values for the angle α (37–39°) found for $(C_6H_5R^1)M(\eta^6\text{-}C_5H_4CR^2_2)$ (M = Mo, W; R^1 = H, Me; R^2 = Me, Ph). Similar calculations for the neutral fulvene complex, $(CO)_3Cr(\eta^6\text{-}C_5H_4CH_2)$, give $\alpha = 21°$ (according to X-ray diffraction data, the angle α in this complex equals 35°).[75]

Table 11. Energy and charge characteristics of the $[(C_5R_5)M(C_5R_4CH_2)]^+$ cations according to EHT calculations.[95]

R	M	α /deg	ΔE /eV	Q(M)	q(CH_2)
H	Fe	5.0	1.28	0.25	0.36
H	Ru	41.5	1.68	1.48	0.04
H	Os	35.0	0.85	0.85	0.12
Me	Fe	26.0	1.33	0.10	0.31
Me	Ru	40.3	2.53	1.35	−0.13
Me	Os	41.8	3.32	0.84	−0.08

The molecular orbital energies for a number of neutral Ti complexes, $(\eta^5\text{-}Cp^*)TiMe(\eta^6\text{-}C_5Me_4CH_2)$, $(\eta^5\text{-}C_5HMe_4).TiMe(\eta^6\text{-}C_5HMe_3CH_2)$, $(\eta^5\text{-}Cp^*)Ti(\eta^6\text{-}C_5Me_4CH_2)$ and $(\eta^5\text{-}Cp^*)TiMe\{\eta^7\text{-}C_5Me_3(CH_2)_2\}$ have been calculated by the EHT method.[98] For the cationic complexes, $[(\eta^5\text{-}Cp)Os(\eta^6\text{-}C_5H_4CH_2)]^+$ and $[(\eta^5\text{-}Cp)Os\{C_5Me_3(CH_2)_2\text{-}\eta^7\}]^{2+}$, the angles α (40 and 35°, respectively) calculated by EHT[87] were compared with the values obtained experimentally for the $[(\eta^5\text{-}Cp^*)Os(\eta^6\text{-}C_5Me_4CH_2)]^+$ complex ($\alpha = 41.8°$).[95] The calculated $Os-CH_2$ bond length in the $[CpOs\{C_5Me_3(CH_2)_2\}]^{2+}$ complex is 2.33 Å.[99]

The M–C(11) and M–C(1) bond lengths and the tilt angles α in 18-electron singly and doubly charged cationic $\eta^6\text{-}C_5Me_4CH_2$ and $\eta^7\text{-}C_5Me_3(CH_2)_2$ complexes of Group 8 metals calculated using the density functional theory (DFT)[100] are listed in Table 12. It can be seen that the calculated M–C(11) bond lengths tend to increase on passing from η^6-complexes to η^7-complexes. This is indicative of some decrease in the metal–carbocation centre interaction in doubly charged complexes with respect to similar singly charged ones. Comparison of the data of Tables 3 (X-ray diffraction data) and 12 (DFT calculations) shows that the structures of the complexes in the crystal and in the gas phase are somewhat different. A more detailed consideration of the data published in original publications[100,101] permits the conclusion that transition from the gas phase to a condensed (crystalline) state induces the most pronounced change in the M–C(11) bond length, while the lengths of the metal bonds with other atoms of the ligand change insignificantly. Similar conclusions were drawn in another study[70] in which X-ray diffraction analysis and DFT calculations for the $[CpRu(C_5H_4CH_2)]^+$ cationic complex have been performed. Doubly and especially triply charged complexes (see below) also tend to undergo structural changes on passing from the gas phase into a condensed state (solution).

Table 12. Calculated geometric parameters in the cationic complexes of Group 8 metals with the $\eta^6\text{-}C_5Me_4CH_2$ and $\eta^7\text{-}C_5Me_3(CH_2)_2$ ligands.[23,100]

Compound	M–C(11) /Å	M–C(1) /Å	The angle α /deg
$[Cp^*Fe(C_5Me_4CH_2)]^+$	2.324	2.020	34.0
$[Cp^*Fe\{C_5Me_3(CH_2)_2\}]^{2+}$	2.504; 2.511	2.064; 2.063	25.03; 24.58
$[Cp^*Ru(C_5Me_4CH_2)]^+$	2.410	2.156	32.4
$[Cp^*Ru\{C_5Me_3(CH_2)_2\}]^{2+}$	2.456; 2.456	2.200; 2.192	24.62; 24.30
$[Ru(C_5Me_4CH_2)_2)]^{2+}$	2.586; 2.547	2.194; 2.187	25.91; 27.87
$[Cp^*Os(C_5Me_4CH_2)]^+$	2.341	2.158	36.9
$[Cp^*Os\{C_5Me_3(CH_2)_2\}]^{2+}$	2.401; 2.395	2.195; 2.182	31.24; 31.11
$[Os(C_5Me_4CH_2)_2]^{2+}$	2.441; 2.441	2.180; 2.180	32.5; 32.5

The angles α and other geometric parameters, charge characteristics and the rotation energies for the *syn*, *gauche*- and *anti*-conformers of the $[M(C_5Me_4CH_2)_2]^{2+}$ cationic complexes (M = Fe, Ru, Os) have been reported.[99, 100] The EHT calculations showed [99] that of the three possible conformers (*syn, gauche* and *anti*), *gauche*-conformers are thermodynamically most stable in the gas phase and in solutions.

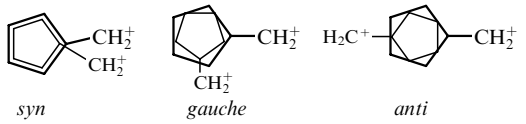

syn *gauche* *anti*

The calculated α values for the *gauche*-conformers of the Fe, Ru and Os complexes are 30, 40 and 40° (EHT data [99]), and the M–C(11) bond lengths are 2.43, 2.20 and 2.22 Å, respectively.

In the *gauche*-conformer, the overlap energy of the corresponding orbitals of the metal atom and the ligands exceeds the Coulomb repulsion energy (which is the lowest in the *anti*-conformer). This is not surprising, because, according to the same calculations, the CH_2 groups bear virtually no positive charge, the charge being concentrated almost entirely on the metal atom. The results of EHT calculations for the structures of doubly charged complexes (predominance of *gauche*-conformers) were confirmed by ^{1}H NMR spectra.[99]

The higher thermodynamic stability of the *gauche*-conformers for the ruthenium complexes was confirmed by subsequent calculations (DFT *ab initio*).[100] Meanwhile, for the osmium analogue, the energies of the *anti*- and *gauche*-conformers are equal.[23] Density functional theory calculations indicate higher thermodynamic stability of 1,2-dimethylene complexes compared to 1,1′-dimethylene complexes.[100] It follows from the results of the same calculations (see Table 12) that in the $[Cp^*Ru\{C_5Me_3(CH_2)_2\}]^{2+}$ and $[Os(C_5Me_4CH_2)_2]^{2+}$ complexes, the distances from the metal atom to both carbocation centres are identical, while in $[Cp^*Os\{C_5Me_3(CH_2)_2\}]^{2+}$ and $[Ru(C_5Me_4CH_2)_2]^{2+}$, these distances are different. In the condensed state (in solution), the interaction of the metal atom with both carbocation centres is the same in any of the four complexes, as indicated by the ^{13}C NMR data [the presence of only one signal from C(11) nuclei]. Thus, in this case, too, the structures of the cationic species in the gas phase and in solution are somewhat different.

VIII. Trimethylene complexes

The representation of η⁶-fulvene and η⁷-allyldiene complexes as a 'specific' resonance hybrid of structures **A** ↔ **B** or **C** ↔ **D** (see Section II) is especially significant for describing the structures of complexes containing three methylene groups in the molecule. It is noteworthy that the whole set of chemical, structural and calculated data available until recently did not allow one to distinguish clearly and unambiguously the structures of mono- and dimethylene complexes. Apparently, it should be stated that forms **B** (σ,η⁵) and **D** (σ,σ,η⁵) are characterised by more substantial donor–acceptor interaction between the metal LEP and the vacant orbitals of carbon atom(s) and, hence, by shorter M–C(11) bonds and greater tilt angles of the C(1)–C(11) bond toward the metal atom than forms **A** and **C**. These shorter bonds can be called metallonium.[101]

The complexes containing three methylene groups in the molecule have been prepared by oxidation of decamethylmetallocenes or monocations **8** (M = Ru, Os) with molecular oxygen in a CF_3SO_3H solution.[20, 39] Their structure has been described in the literature.[22, 101] The Group 8 metal atoms (Fe, Ru, Os) are known to contain three lone electron pairs in three non-bonding orbitals. The LEP are able to interact with three vacant orbitals of the carbon atoms of three carbocation centres or, in other words, they can stabilise the compounds containing three CH_2 groups. According to calculations, in these compounds, the major portion of the positive charge is concentrated on the metal atom.[22, 101] However, it should be noted that, as shown by DFT calculations, in the $[Cp^*M\{\eta^7\text{-}C_5Me_3(CH_2)_2\text{-}1,2\}]^{2+}$ and $[M(\eta^6\text{-}C_5Me_4CH_2)_2]^{2+}$ dimethylene complexes (M = Ru, Os), the lengths of both M–CH_2 bonds in the gas phase are either equal or do not differ much (see Table 12).[100] However, in trimethylene osmium complex **46**, the Os–C(1′)H_2 bond length is much longer (2.768 Å) than the other two lengths, Os–C(1)H_2 and Os–C(2)H_2 (2.431 and 2.435 Å , respectively) and the angles α are 27.2, 26.2 and 20.4°, respectively, *i.e.*, this complex can be described by structure **D**(σ,σ,η⁵),**A**(η²,η⁴). For the Ru analogue **47**, the Ru–C(1)H_2 bond is markedly shorter (2.442 Å) than the Ru–C(2)H_2 and Ru–C(1′)H_2 bonds (2.925 and 2.950 Å, respectively) and the angles α are 20.8, 13.4 and 11.7°, respectively, *i.e.*, the trication has structure **C**′(σ,η²,η⁴),**A**(η²,η⁴). In other words, osmium complex **46** is characterised by the presence of two metallonium bonds and one fulvene fragment, and the ruthenium analogue **47** has only one metallonium bond and two fulvene fragments. The spatial structure of both complexes is similar to that for the *gauche*-conformers of the corresponding complexes **13**.

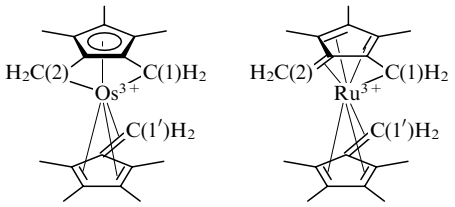

46 (**D**,**A**) **47** (**C**′,**A**)

Thus, according to DFT calculations, the trimethylene ruthenium and osmium complexes have different structures in the gas phase, the Os compound having two short bonds and the Ru analogue containing one short bond. This circumstance indicates that the interaction between the metal atom and the carbocation centres is enhanced from top to bottom along the Group. This trend has been noted above for mono- (**8**) and dimethylene (**12**) complexes; however, in the case of complexes **46** and **47**, it is most pronounced.

The presence of three methylene groups in the molecules of complexes **46** and **47** was proved unambiguously by ^{1}H and ^{13}C NMR spectroscopy (Table 13).[20, 22, 39, 101] According to NMR

Table 13. ^{1}H and ^{13}C NMR spectral data for mono-, di- and trimethylene complexes of ruthenium and osmium.

Compound	δ(^{1}H) /ppm	$^2J_{HH}$ /Hz	δ(^{13}C) /ppm	$^1J_{CH}$ /Hz
$[Cp^*Ru(\eta^6\text{-}C_5Me_4CH_2)]^+$ (**8a**)	4.75s		74.6t	164–167
$[Cp^*Os(\eta^6\text{-}C_5Me_4CH_2)]^+$ (**8b**)	4.42s		55.4	
$[Cp^*Ru\{\eta^7\text{-}C_5Me_3.$	4.82d	1.9	88.4t	170–172
$.(CH_2)_2\text{-}1,2\}]^{2+}$ (**12a**)	5.27d			
$[Cp^*Os\{\eta^7\text{-}C_5Me_3.$	4.90d	2.4	71.1	
$.(CH_2)_2\text{-}1,2\}]^{2+}$ (**12b**)	5.52d			
$[(\eta^6\text{-}C_5Me_4CH_2)Ru.$	5.03d	1.9	88.6t	170–172
$.\{\eta^7\text{-}C_5Me_3(CH_2)_2\text{-}1,2\}]^{3+}$ (**48a**)	(2H)		(2C)	
	5.51d	1.9	65.7t	157
	(2H)		(1C)	
	5.50s			
	(2H)			
$[(\eta^6\text{-}C_5Me_4CH_2)Os.$	5.04d	2.3	71.3	
$.\{\eta^7\text{-}C_5Me_3(CH_2)_2\text{-}1,2\}]^{3+}$ (**48b**)	(2H)		(2C)	
	5.66d	2.3	65.8	
	(2H)		(1C)	
	5.49s			
	(2H)			

Note. s is singlet, d is doublet, t is triplet.

spectral data, the structures of Ru- and Os-containing derivatives are similar. It should be noted that the DFT calculations also confirm the existence of three methylene groups in these compounds. The enthalpies of formation (ΔH) of complex **8a** from Cp^*_2Ru, complex **12a** from **8a** and complex **47** from **12a** in the gas phase are -232.2, -124.5 and -13.6 kcal mol^{-1}, respectively,[101] *i.e.*, complex **47** is thermodynamically stable, although its stability is an order of magnitude lower than that for complex **12a**. Thus, according to these calculations, there is a certain probability that trimethylene complexes would be formed in solutions. Indeed, upon the reaction of metallocenes or monomethylene complexes with oxygen in a solution of a strong acid (superacid), three methyl groups are oxidised to give three carbocation centres. However, the ways of stabilisation and, correspondingly, the forms of existence of these unusual species in solution may differ from those of the previously studied analogues **8** and **12**, which have a smaller charge. Thus the ^{1}H and ^{13}C NMR spectra of trimethylene compounds exhibit a number of specific features, which call for discussion. Table 13 presents the chemical shifts (δ) and the spin–spin coupling constants observed in the ^{1}H and ^{13}C NMR spectra of compounds $[Cp^*M(\eta^6\text{-}C_5Me_4CH_2)]^+$ (**8a**,**b**), $[Cp^*M\{\eta^7\text{-}C_5Me_3(CH_2)_2\text{-}1,2\}]^{2+}$ (**12a**,**b**) and $[(\eta^6\text{-}C_5Me_4CH_2)M\{\eta^7\text{-}C_5Me_3(CH_2)_2\text{-}1,2\}]^{3+}$ (**48a**,**b**) formed in solution.

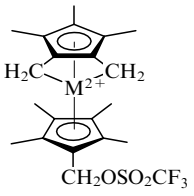

48a,**b**

M = Ru (**a**), Os (**b**).

The ^{1}H NMR spectra of trimethylene cations **48a**,**b** exhibit two doublets and one singlet (the ratio of integral intensities is 1 : 1 : 1). Thus, the species obtained in solution really have three methylene groups and a plane of symmetry[20,39] that passes through one of these groups half way between the other two. Presumably, the structure of molecules in solution is analogous, to an extent, to the structure in the gas phase. Meanwhile, the data of the ^{13}C NMR spectra clearly indicate that in Ru- and Os-containing molecules, the metal atom interacts differently with the three carbocation centres and that in both species, the interaction with two of these centres markedly differs from the interaction with the third one. Thus, the structure of the osmium complex in solution does not contradict its structure in the gas phase (according to DFT calculations), whereas the structures of the Ru analogue in solution and in the gas phase are different, *i.e.*, transition from the gas phase to a solution induces more pronounced structural changes in the case of less stable Ru species.

It follows from the data of Table 13 that on passing from compounds **8a**,**b** to **12a**,**b**, the resonance carbon signals substantially shift downfield and the spin–spin coupling constants slightly decrease. Conversely, in the ^{13}C NMR spectra of complexes **48a**,**b**, the δ values and spin–spin coupling constants of the signals for the CH_2 groups of the η^7-$C_5Me_3(CH_2)_2$-1,2 ligand virtually coincide with those for complexes **12a**,**b**. However, the signals for the CH_2 groups of the η^6-$C_5Me_4CH_2$ ligand are shifted upfield, this signal for ruthenium complex **48a** being located in even higher field than in compound **8a**. The coupling constants of the CH_2 group in the trimethylene complex also decrease somewhat with respect to those observed for the monomethylene complex. In addition, the δ values for the carbon nuclei of the CH_2 groups of the η^7-$C_5Me_3(CH_2)_2$-1,2 ligand in complexes **12** and **48** decrease substantially on passing from Ru to Os (higher shielding), whereas the signals for the CH_2 groups of η^6-$C_5Me_4CH_2$ in complexes **48a**,**b** almost coincide (*i.e.*, the chemical shift does not depend on the nature of the metal).

Of course, it cannot be stated with full confidence that on passing from dimethylene complexes to trimethylene complexes, the NMR spectra should show the same trends (a decrease in shielding) as those observed (as has been shown above for numerous examples) on passing from neutral fulvene complexes to singly and doubly charged ones. In the general case, there is no direct correlation between the charge on the carbon atom and the ^{13}C NMR chemical shift of this atom; however, for singly, doubly and triply charged compounds (almost isostructural or with similar structures), the regularities we found in the variation of spectral characteristics allow one to ascribe structures **46** and **47** to the trimethylene species in the gas phase.

The stabilisation of the trimethylene complexes formed in solutions differs from that for complexes **8a**,**b** and **12a**,**b**. Apparently, complexes **8** and **12** in solutions of acids tend to form solvent-separated ion pairs and the nature of the anion (counterion) virtually does not influence the structure of the cations. For the triply charged trimethylene complexes, the interion (cation–anion) interaction is so pronounced that it seems to result in contact ion pairs or, more likely, a covalent bond. According to X-ray diffraction data (see above), the monomethylene cations **8a**,**b** and the BPh_4^- anions[68,72] are arranged in the crystal lattice fairly far from each other. The mono- (**8a**,**b**) and dimethylene cations (**12a**,**b** and **13a**,**b**) occur in solutions of CF_3SO_3H as kinetically independent species with the $CF_3SO_3^-$ anion, and trimethylene species **46**, **47** are partially esterified (at one methylene group) under these conditions to give esters **48a**,**b**.[22] In the ^{13}C NMR spectra, the signals of the CH_2 groups linked covalently to the O_3SCF_3 group are manifested as triplets (δ 65.7 and 65.8, J 157 Hz), while the ^{1}H NMR signals (δ 5.50 and 5.49) are singlets. The observed spin–spin coupling constants and chemical shifts are typical of CH_2 groups linked to two electron-withdrawing substituents, $[Ru]^{2+}$ and $CF_3SO_3^-$, which implies structure **48a**,**b**.[102]

IX. Conclusion

The data presented in this review show that the chemistry of neutral and cationic tetramethylfulvene and trimethylallyldiene complexes of transition metals is of substantial interest. These complexes have been obtained for almost any of Group 4–10 transition metals; they contain a non-planar six- (η^6) or seven-electron (η^7) ligand with a substantial deviation of one or two carbon atoms from the plane of the Cp ring toward the metal atom. This is indicative of the interaction of the LEP of the metal atom with the carbocation centre in cationic complexes or with the corresponding vacant orbital of the fulvene ligand in neutral complexes. The degree of this interaction increases from top to bottom along the Subgroups of the Periodic Table. These structural features (relatively low symmetry) of tetramethylfulvene and trimethylallyldiene complexes determine their properties and distinguish them from η^6-arene or η^7-cycloheptatrienyl complexes with a higher symmetry. The tetramethylfulvene and trimethylallyldiene transition metal complexes are characterised by (i) general methods for the synthesis (mainly, from η^5-pentamethylcyclopentadienyl precursors); (ii) essential similarity in the chemical behaviour [many reactions involving these complexes occur *via* the formation of odd-electron (17- and 19-electron) intermediates]; (iii) rupture of the M–C(11) bond on treatment with nucleophiles (more rarely, electrophiles) to give η^5-derivatives with the C(11)–Nu bond; (iv) similarity of the structural and spectral characteristics, which often do not depend on whether or not the complex is charged. Apparently, these properties allow one to classify tetramethylfulvene and trimethylallyldiene complexes, to a certain approximation, as a separate class of chemical compounds.

References

1. T J Keally, P L Pauson *Nature (London)* **168** 1038 (1951)
2. A Miller, J A Tebboth, J F Tremaine *J. Chem. Soc.* 632 (1952)
3. E O Fisher, W Pfab *Z. Naturforsch., B: Anorg. Chem. Org. Chem. Biochem. Biophys. Biol.* **7** 377 (1952)
4. E Ruch, E O Fisher *Z. Naturforsch., B: Anorg. Chem. Org. Chem. Biochem. Biophys. Biol.* **7** 632 (1952)
5. G Wilkinson, M Rosenblum, M C Whiting, R B Woodward *J. Am. Chem. Soc.* **74** 2125 (1952)
6. R B Woodward, M Rosenblum, M C Whiting *J. Am. Chem. Soc.* **74** 3458 (1952)
7. J D Dunitz, L E Orgel *Nature (London)* **171** 121 (1953)
8. C Janiak, H Schumann *Adv. Organomet. Chem.* **31** 291 (1991)
9. R S Trelkel, J E Bercaw *J. Organomet. Chem.* **136** 1 (1977)
10. F G Bordwell, M J Bausch *J. Am. Chem. Soc.* **105** 6188 (1983)
11. A G Davis, J Lusztyk *J. Chem. Soc., Perkin Trans. 2* 692 (1981)
12. P Jutzi, A Mix *Chem. Ber.* **125** 951 (1992)
13. S Evans, M L H Green, B Jewitt, G H King, A F Orchard *J. Chem. Soc., Faraday Trans. 2* **70** 356 (1974)
14. G E Herberich, J Schwarzer *Chem. Ber.* **103** 2016 (1970)
15. L E Schock, C P Brock, T J Marks *Organometallics* **6** 232 (1987)
16. F G N Cloke, J P Day, J C Green, C P Morley, A C Swain *J. Chem. Soc., Dalton Trans.* 789 (1991)
17. A A Kamyshova, A Z Kreindlin, M I Rybinskaya, P V Petrovskii *Izv. Akad. Nauk, Ser Khim.* 587 (1999) [a]
18. A A Kamyshova, A Z Kreindlin, M I Rybinskaya, P V Petrovskii *Izv. Akad. Nauk, Ser Khim.* 517 (2000) [a]
19. G Ohanessian, W A Goddard III *Acc. Chem. Res.* **23** 386 (1990)
20. M I Rybinskaya, A A Kamyshova, A Z Kreindlin, P V Petrovskii *Mendeleev Commun.* 137 (2001)
21. A Z Kreindlin, P V Petrovskii, M I Rybinskaya *Metallorg. Khim.* **4** 63 (1991) [b]
22. M I Rybinskaya, A Z Kreindlin, A A Kamyshova *Izv. Akad. Nauk, Ser Khim.* 1485 (2002) [a]
23. A A Kamyshova, A Z Kreindlin, M I Rybinskaya, P V Petrovskii, N V Kruglova, Yu A Borisov *Izv. Akad. Nauk, Ser Khim.* 2293 (2003) [a]
24. R B Materikova, V N Babin, S P Solodovnikov, P V Petrovsky, E I Fedin *Z. Naturforsch., B: Anorg. Chem. Org. Chem.* **35** 1415 (1980)
25. U Kölle, J Grub *J. Organomet. Chem.* **289** 133 (1985)
26. L I Denisovich, M G Peterleitner, D N Kravtsov, A Z Kreindlin, S S Fadeeva, M I Rybinskaya *Metalloorg. Khim.* **1** 301 (1988) [b]
27. A Z Kreindlin, Doctoral Thesis in Chemical Sciences, Institute of Organoelement Compounds of the Russian Academy of Sciences, Moscow, 2002
28. D O'Hare, J C Green, T P Chadwick, J S Miller *Organometallics* **7** 1335 (1988)
29. M Watanabe, T Iwamoto, S Nakashima, H Sakai, I Motoyama, H Sano *J. Organomet. Chem.* **448** 167 (1993)
30. I A Mamedyarova, M N Nefedova, V I Sokolov *J. Organomet. Chem.* **524** 181 (1996)
31. S V Kukharenko, V V Strelets, L I Denisovich, M G Peterleitner, A Z Kreindlin, A R Kudinov, M I Rybinskaya *Izv. Akad. Nauk, Ser Khim.* 2394 (1995) [a]
32. S V Kukharenko, V V Strelets, A R Kudinov, A Z Kreindlin, M G Peterleitner, L I Denisovich, M I Rybinskaya *J. Organomet. Chem.* **519** 1 (1996)
33. S T Carter, W Clegg, V C Gibson, T P Kee, R D Sanner *Organometallics* **8** 253 (1989)
34. A H Klahn, B Oelckers, F Godoy, M T Garland, A Vega, R N Perutz, C L Higgitt *J. Chem. Soc., Dalton Trans.* 3079 (1998)
35. L Fan, M L Turner, M B Hursthouse, K M A Malik, O V Gusev, P M Maitlis *J. Am. Chem. Soc.* **116** 385 (1994)
36. M Sato, Y Kawata, H Shintate, Y Habata, S Akabori, K Unora *Organometallics* **16** 1693 (1997)
37. M Sato, Y Kawata, A Kudo, A Iwai, H Saitoh, S Ochino *J. Chem. Soc., Dalton Trans.* 2215 (1998)
38. H Suzuki, T Kakigano, H Fukui, M Tanaka, Y Moro-oka *J. Organomet. Chem.* **473** 295 (1994)
39. M I Rybinskaya, A A Kamyshova, A Z Kreindlin, P V Petrovskii *Mendeleev Commun.* 85 (2000)
40. U Kölle, B S Kang, U Thewalt *J. Organomet. Chem.* **386** 267 (1990)
41. P N Riley, J R Parker, P E Fanwick, I P Rothwell *Organometallics* **18** 3579 (1999)
42. J A Miguel-Garsia, P M Maitlis *J. Chem. Soc., Chem. Commun.* 1472 (1990)
43. B Gloaguen, D Astruc *J. Am. Chem. Soc.* **112** 4607 (1990)
44. D Buchholz, D Astruc *Angew. Chem., Int. Ed. Engl.* **33** 1637 (1994)
45. D W Hoard, P R Sharp *Inorg. Chem.* **32** 612 (1993)
46. O V Gusev, L I Denisovich, M G Peterleitner, A Z Rubezhov, N A Ustynyuk *J. Organomet. Chem.* **452** 219 (1993)
47. O V Gusev, M G Peterleitner, M A Ievlev, A M Kal'sin, P V Petrovskii, L I Denisovich, N A Ustynyuk *J. Organomet. Chem.* **531** 95 (1997)
48. O V Gusev, L N Morozova, M G Peterleitner, S M Peregudova, P V Petrovskii, N A Ustynyuk, P M Maitlis *J. Organomet. Chem.* **509** 95 (1996)
49. O V Gusev, L N Morozova, T A Peganova, P V Petrovskii, N A Ustynyuk *J. Organomet. Chem.* **472** 359 (1994)
50. O V Gusev, T A Peganova, M G Peterleitner, S M Peregudova, L I Denisovich, N A Ustynyuk, P M Maitlis *J. Organomet. Chem.* **480** C16 (1994)
51. O V Gusev, L N Morozova,T A Peganova, M G Peterleitner, S M Peregudova, L I Denisovich, P V Petrovskii, Y F Oprunenko, N A Ustynyuk *J. Organomet. Chem.* **493** 181 (1995)
52. H Werner, G T Grisp, P W Jolly, H J Kraus, C Krueger *Organometallics* **2** 1369 (1983)
53. W D Jones, F J Feher *Organometallics* **2** 686 (1983)
54. J A Bandy, V S B Mtetwa, K Prout, J C Green, C E Davis, M L H Green, N J Hasel, A Izquierdo, J J Martin-Polo *J. Chem. Soc., Dalton Trans.* 2037 (1985)
55. J W Pattiasina, C E Hissink, J L de Boer, A Meetsma, J H Teuben, A L Spek *J. Am. Chem. Soc.* **107** 7758 (1985)
56. J W Pattiasina, F van Bolhuis, J H Teuben *Angew. Chem., Int. Ed. Engl.* **26** 330 (1987)
57. R Fandos, A Meetsma, J H Teuben, *Organometallics* **10** 2665 (1991)
58. P D Grebenik, M L H Green, F Izquierdo, V S B Mtetwa, K Prout *J. Chem. Soc., Dalton Trans.* 9 (1987)
59. A R Bulls, W P Schaefer, M Serfas, J E Bercaw *Organometallics* **6** 1219 (1987)
60. Y Sun, W E Piers, G P A Yap *Organometallics* **16** 2509 (1997)
61. X Song, M Bochmann *J. Organomet. Chem.* **545-546** 597 (1997)
62. W E Watts *J. Organomet. Chem. Libr.* **7** 399 (1979)
63. A A Koridze *Usp. Khim.* **55** 277 (1986) [*Russ. Chem. Rev.* **55** 113 (1986)]
64. C Zou, M S Wrighton *J. Am. Chem. Soc.* **112** 7578 (1990)
65. U Kölle, A Salzer *J. Organomet. Chem.* **243** C27 (1983)
66. N V Kruglova, A Z Kreindlin, P V Petrovskii, M I Rybinskaya *Izv. Akad. Nauk, Ser Khim.* 2533 (1998) [a]
67. L N Kiseleva, A Z Kreindlin, P V Petrovskii, M I Rybinskaya, in *The Vth Finish-Russian Seminar. Chemistry and Ecology of Organoelement Compounds (Abstracts of Reports), St Petersburg, 2001* P15
68. M I Rybinskaya, A Z Kreindlin, Yu T Struchkov, A I Yanovsky *J. Organomet. Chem.* **359** 233 (1989)
69. V G Andrianov, B P Biryukov, Yu T Struchkov *Zh. Strukt. Khim.* **10** 1129 (1969) [c]
70. S Barlow, A Cowley, J C Green, T J Brunker, T Hascall *Organometallics* **20** 5351 (2001)
71. A Z Kreindlin, K Yu Suponitskii, F M Dolgushin, Z A Starikova, M I Rybinskaya *Izv. Akad. Nauk, Ser Khim.* 1539 (2001) [a]
72. A I Yanovsky, Yu T Struchkov, A Z Kreindlin, M I Rybinskaya *J. Organomet. Chem.* **369** 125 (1981)
73. K Yu Suponitsky, T V Timofeeva, A Z Kreindlin, M Yu Antipin, in *Modern Trends in Organometallic and Catalytic Chemistry (Abstracts of Reports), Moscow, 2003* p. 8
74. U Turpeinen, A Z Kreindlin, P V Petrovskii, M I Rybinskaya *J. Organomet. Chem.* **441** 109 (1992)
75. B Lubke, F Edelman, U Behrens *Chem. Ber.* **116** 11 (1983)

76. F M Dolgushin, A I Yanovsky, Yu T Struchkov, M I Rybinskaya, A Z Kreindlin, P V Petrovskii, L M Epshtein, E S Shubina, A N Krylov *Izv. Akad. Nauk, Ser Khim.* 1308 (1994) [a]
77. V G Andrianov, Yu T Struchkov *Zh. Strukt. Khim.* **18** 318 (1977) [c]
78. A Z Kreindlin, F M Dolgushin, A I Yanovsky, Z A Kerzina, P V Petrovskii, M I Rybinskaya *J. Organomet. Chem.* **616** 106 (2000)
79. U Behrens *J. Organomet. Chem.* **182** 89 (1979)
80. J M Fisher, W E Piers, V G Yong Jr *Organometallics* **15** 2410 (1996)
81. H Lee, J B Bonanno, T Hascall, J Cordaro, J M Hahn, G Parkin *J. Chem. Soc., Dalton Trans.* 1365 (1999)
82. V Kupfer, U Thewalt, I Tišlerova, P Štepnička, R Gyepes, J Kubišta, M Horaček, K Mach *J. Organomet. Chem.* **620** 39 (2001)
83. M I Rybinskaya, A Z Kreindlin, R Hoffmann, R M Minyaev *Izv. Akad. Nauk, Ser Khim.* 1701 (1994) [a]
84. A Z Kreindlin, S S Fadeeva, M I Rybinskaya *Izv. Akad. Nauk SSSR, Ser. Khim.* 403 (1984) [a]
85. E I Fedin, A L Blumenfeld, P V Petrovskii, A Z Kreindlin, S S Fadeeva, M I Rybinskaya *J. Organomet. Chem.* **292** 257 (1985)
86. S Braun, T S Abram, W E Watts *J. Organomet. Chem.* **97** 429 (1975)
87. A Z Kreindlin, E I Fedin, P V Petrovskii, M I Rybinskaya, R M Minyaev, R Hoffmann *Organometallics* **10** 1206 (1991)
88. K Mach, V Varga, V Hanu *J. Organomet. Chem.* **415** 87 (1991)
89. A Z Kreindlin, M I Rybinskaya, in *The 206th American Chemical Society National Meeting (Abstracts of Reports), Chicago, IL, 1993* p. 31
90. G Parkin, J E Bercaw *Polyhedron* **7** 2053 (1988)
91. N M Loim, P V Petrovskii, V I Robas, Z N Parnes, D N Kursanov *J. Organomet. Chem.* **117** 265 (1976)
92. A Z Kreindlin, S S Fadeeva, P V Petrovskii, M I Rybinskaya *Izv. Akad. Nauk SSSR, Ser. Khim.* 170 (1988) [a]
93. M I Rybinskaya, A Z Kreindlin, S S Fadeeva, P V Petrovskii *J. Organomet. Chem.* **345** 341 (1988)
94. A Z Kreindlin, L S Shilovtseva, P V Petrovskii, M I Rybinskaya *Metalloorg. Khim.* **5** 1047 (1992) [b]
95. E G Gal'pern, N P Gambaryan, A Z Kreindlin, M I Rybinskaya, I V Stankevich, A L Chistyakov *Metalloorg. Khim.* **5** 831 (1992) [b]
96. R Gleiter, R Seeger *Helv. Chim. Acta* **54** 1217 (1971)
97. W E Watts *J. Organomet. Chem.* **220** 165 (1981)
98. T Vondrák, K Mach, V Varga, A Tepstra *J. Organomet. Chem.* **425** 27 (1992)
99. M I Rybinskaya, A Z Kreindlin, P V Petrovskii, R M Minyaev, R Hoffmann *Organometallics* **13** 3903 (1994)
100. M I Rybinskaya, Yu S Nekrasov, Yu A Borisov, A I Belokon', A Z Kreindlin, A A Kamyshova, N V Kruglova *J. Organomet. Chem.* **631** 9 (2001)
101. Yu A Borisov, M I Rybinskaya, Yu S Nekrasov, A Z Kreindlin, A A Kamyshova *J. Organomet. Chem.* **645** 87 (2002)
102. G E Maciel, J W McIver, N S Ostlund, J A Pople *J. Am. Chem. Soc.* **92** 1 (1970)

[a] — *Russ. Chem. Bull., Int. Ed. (Engl. Transl.)*
[b] — *Russ. J. Organomet. Chem. (Engl. Transl.)*
[c] — *J. Struct. Chem. (Engl. Transl.)*

Russian Chemical Reviews **73** (5) 433 – 453 (2004) © 2004 Russian Academy of Sciences and Turpion Ltd

DOI 10.1070/RC2004v073n05ABEH000868

Substitution reactions at boron atoms in metallacarboranes

V I Bregadze, S V Timofeev, I B Sivaev, I A Lobanova

Contents

I.	Introduction	433
II.	Mechanisms of substitution in metallacarboranes	433
III.	Substitution in 12-vertex metallacarboranes	434
IV.	Substitution in non-icosahedral metallacarboranes	448
V.	Substitution in *exo-nido*-metallacarboranes	449

Abstract. Data on substitution reactions at boron atoms in 10 – 12-vertex metallacarboranes, which are of fundamental and applied significance, are generalised. The possible mechanisms of substitution reactions and the influence of the metal fragment on substitution positions in the polyhedron are discussed. The bibliography includes 161 references.

I. Introduction

For many years, metallacarboranes † were of only academic interest.[2 – 7] Most studies of this period were devoted primarily to the construction of unusual chemical structures and investigation of their structural features. Metallacarboranes, whose polyhedral cage contains both transition and main-group metals of all groups of the periodic table, have already been synthesised. In recent years, practical aspects of the use of metallacarboranes have attracted increasing interest [8] because some compounds of this class were found to possess useful properties. For example, particular metallacarboranes show promise as catalysts,[9 – 12] extractants for nuclear waste processing,[13 – 18] new materials for microelectronics [19 – 23] or drugs in nuclear medicine.[24 – 28]

The synthesis of new compounds and materials possessing desired properties is associated with the necessity of changing the structural parameters responsible for the qualitative and quantitative characteristics of compounds. In the case of metallacarboranes, such changes can be achieved by varying either components of the molecule (metal atoms and organic ligands involved in the metal coordination sphere) or the structure and electronic properties of the carborane fragment. The latter can be achieved by introducing various substituents, which are responsible for the final properties of the compounds synthesised, into the carborane fragment.

Therefore, the synthesis and investigation of substituted metallacarboranes are of both fundamental and applied importance.

V I Bregadze, S V Timofeev, I B Sivaev, I A Lobanova A N Nesmeyanov Institute of Organoelement Compounds, Russian Academy of Sciences, ul. Vavilova 28, 119991 Moscow, Russian Federation.
Fax (7-095) 135 50 85. Tel. (7-095) 135 74 05. E-mail: bre@ineos.ac.ru (V I Bregadze). Tel. (7-095) 135 92 42. E-mail: sivaev@ineos.ac.ru (I B Sivaev). Tel. (7-095) 135 92 37 (S V Timofeev, I A Lobanova)

Received 8 December 2003
Uspekhi Khimii **73** (5) 470 – 491 (2004); translated by T N Safonova

In this connection, studies of substitution reactions in metallacarborane systems and elucidation of the characteristic features of these processes are of particular interest.

There are two approaches to the synthesis of substituted metallacarboranes: (1) the synthesis from substituted carborane ligands and metal complexes (salts), (2) substitution in the already available metallacarborane molecule. The first approach is used primarily for the construction of metallacarboranes containing substituents at carbon atoms [5, 6, 29 – 32] and is virtually the only procedure for the synthesis of such derivatives. Examples of substitution at carbon atoms in metallacarboranes are scarce.[33, 34] Metallacarboranes containing substituents at boron atoms are synthesised primarily with the use of the second procedure.

The present review surveys data on substitution in metallacarboranes, which were published primarily in the last 15 years, some earlier investigations being also included.

The published data are classified according to the types of carborane ligands. Substitution reactions in small metallacarboranes, *viz*., *nido*-C_2B_4-carborane derivatives, are beyond the scope of our review because the chemistry of the latter has been covered in the excellent review by Grimes [35] (see also recent studies [36 – 40]).

II. Mechanisms of substitution in metallacarboranes

At pesent, polyhedral boron hydrides are commonly considered as three-dimensional aromatic systems.[41] In particular, halogenation and mercuration of carboranes are adequately described within the framework of the mechanism of electrophilic aromatic substitution. Since metallacarboranes are derivatives of polyhedral boron hydrides, it is reasonable to assume that this mechanism is one of the main mechanisms of substitution in metallacarboranes. Apparently, most substitution reactions considered below proceed according to this mechanism.

At the same time, taking into account the hydride character of hydrogen atoms in polyhedral boron hydrides, another possible mechanism may involve the attack of an electrophilic agent resulting in elimination of the hydride hydrogen atom to form a pseudoelectrophilic centre on the boron atom, which is then subjected to the attack of a nucleophilic species (Scheme 1). This mechanism is called Electrophile Induced Nucleophilic Substitution (EINS).[42, 43] The nature of the intermediate generated upon the attack of the electrophilic agent remains unclear. Probably, this is the arenium ion (Wheland intermediate), from which both

† First representatives of this class were synthesised in 1965.[1]

Scheme 1

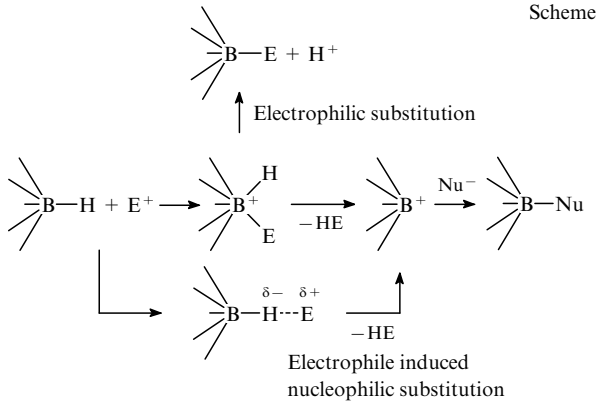

the electrophilic species and the hydride hydrogen atom are simultaneously eliminated. Another possible intermediate is an ion pair formed by the electrophilic species and the hydride hydrogen atom.

Electrophile induced nucleophilic substitution is the mechanism of numerous reactions of polyhedral boron hydrides with solvent molecules accompanied by the formation of numerous charge-compensated derivatives, in which the solvent molecule (tetrahydrofuran, 1,4-dioxane or tetrahydropyran) serves as a substituent bound to the boron atom.[44–47] Acid-catalysed nucleophilic substitution reactions, in particular, the formation of acetoxy and hydroxy derivatives, also proceed according to this mechanism.[48–50]

It should be noted that many substitution reactions can occur by two competitive mechanisms to form mixtures of products of both electrophilic and nucleophilic substitution. An example is acylation of the dodecahydro-*closo*-dodecaborate anion $[B_{12}H_{12}]^{2-}$ giving rise both to the acyl derivative $[B_{12}H_{11}COR]^{2-}$ (product of electrophilic substitution) and the hydroxy derivative $[B_{12}H_{11}OH]^{2-}$ (product of electrophile induced nucleophilic substitution).[51] The ratio between the products of electrophilic and nucleophilic substitution is determined by the strength of the attacking electrophilic agent.

In addition to substitution reactions typical of all polyhedral boron hydrides, substitution reactions involving the metal atom occur in metallacarboranes containing labile ligands in the metal coordination sphere.

It is of importance to determine the substitution position in metallacarboranes. Earlier studies of electrophilic substitution of hydrogen atoms in icosahedral *o*- and *m*-carboranes $C_2B_{10}H_{12}$ have demonstrated that the reactions proceed primarily at the boron atoms, which are most spatially remote from carbon atoms, *i.e.*, at the boron atoms in position 9.[52,53] The presence of the metal fragment has a substantial effect on the direction of substitution in the metallacarborane moiety.

III. Substitution in 12-vertex metallacarboranes

1. Derivatives based on the 7,8-dicarbollyl ligand $[7,8\text{-}C_2B_9H_{11}]^{2-}$

Since the 7,8-dicarbollyl ligand $[7,8\text{-}C_2B_9H_{11}]^{2-}$ is readily accessible, substitution in icosahedral metallacarboranes based on this ligand has been well studied. This ligand is prepared by partial destruction of the icosahedral carborane cage *o*-$C_2B_{10}H_{12}$ with bases.[52] Among numerous metallacarboranes, cobalta-, ferra- and nickelacarboranes $[3\text{-L-}3,1,2\text{-}MC_2B_9H_{11}]^{n-}$ based on the 7,8-dicarbollyl ligand (Fig. 1) were studied in most detail.[5,6]

Bromination of bis(1,2-dicarbollyl)cobalt [*commo*-3,3′-Co(1,2-$C_2B_9H_{11})_2]^-$ (**1**) (the atomic numbering scheme is shown in Fig. 1 *d*)[54] was the first example of substitution in metallacarboranes. Later on, halogenation of anion **1** was studied by different research groups of chemists. Substitution was demonstrated to proceed stepwise. Initially, the hydrogen atoms at

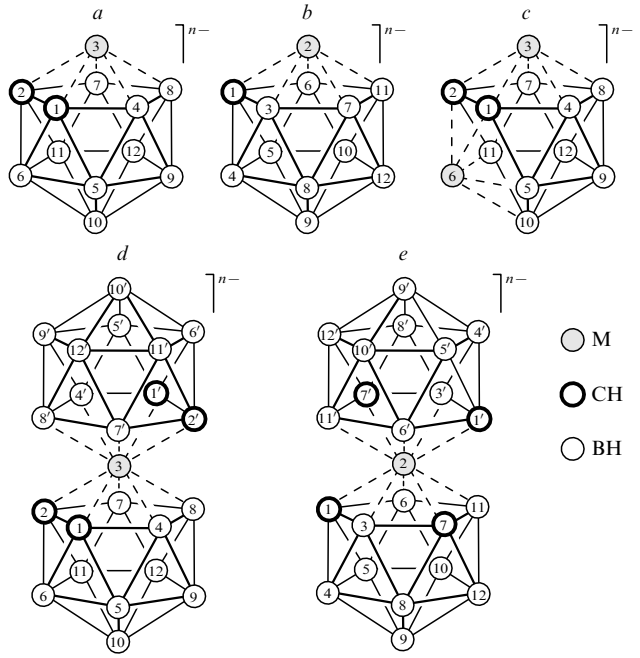

Figure 1. Atomic numbering schemes for different types of icosahedral metallacarboranes.
(*a*) 1,2-dicarba-3-metalla-*closo*-dodecaborane, (*b*) 1-carba-2-metalla-*closo*-dodecaborane, (*c*) 1,2-dicarba-3,6-dimetalla-*closo*-dodecaborane, (*d*) *commo*-3,3′-metallabis(1,2-dicarbollide), (*e*) *commo*-2,2′-metallabis(1,7-dicarbollide).

positions 8 and 8′ adjacent to the metal atom are replaced. In the next step, the hydrogen atoms at positions 9, 9′ and 12, 12′, which are most remote from the carbon atoms, are replaced. Examples are chlorination of *o*- and *m*-carboranes (Scheme 2). For instance, when passed through a solution of Cs[*commo*-3,3′-Co(1,2-$C_2B_9H_{11})_2$] (Cs[**1**]) in an EtOH – CCl_4 or $PhNO_2$ – CCl_4 mixture, chlorine successively replaces the hydrogen atoms at the B(8), B(8′), B(9), B(9′), B(12) and B(12′) atoms to form Cs[8-Cl-3,3′-Co(1,2-$C_2B_9H_{10}$)(1′,2′-$C_2B_9H_{11}$)] (Cs[**2a**]), Cs[8,8′-Cl_2-3,3′-Co(1,2-$C_2B_9H_{10})_2$] (Cs[**3a**]), Cs[8,8′,9-Cl_3-3,3′-Co(1,2-$C_2B_9H_9$)(1′,2′-$C_2B_9H_{10}$)] (Cs[**4**]), Cs[8,8′,9,9′-Cl_4-3,3′-Co(1,2-$C_2B_9H_9)_2$] (Cs[**5**]) and Cs[8,8′,9,9′,12,12′-Cl_6-3,3′-Co(1,2-$C_2B_9H_8)_2$] (Cs[**6a**]).[55]

The reaction of Cs[**1**] with bromine in methanol at room temperature affords either Cs[8-Br-3,3′-Co(1,2-$C_2B_9H_{10}$)(1′,2′-$C_2B_9H_{11}$)] (Cs[**2b**]) or Cs[8,8′-Br_2-3,3′-Co(1,2-$C_2B_9H_{10})_2$] (Cs[**3b**]) depending on the reagent ratio.[55] The reaction of [Me_3NH][**1**] with bromine in boiling tetrahydrofuran produces the dibromo derivative [Me_3NH][**3b**].[56] The reaction of Rb[**1**] with an excess of bromine in boiling acetic acid yields the hexabromo derivative Rb[8,8′,9,9′,12,12′-Br_6-3,3′-Co(1,2-$C_2B_9H_8)_2$] (Rb[**6b**]).[54]

The reaction of Cs[**1**] with iodine in methanol at room temperature produces the monoiodo derivative Cs[8-I-3,3′-Co(1,2-$C_2B_9H_{10}$)(1′,2′-$C_2B_9H_{11}$)] (Cs[**2c**]),[55] whereas the reaction with a small excess of iodine in ethanol[55] or in acetic acid (at 100 °C)[57] gives rise to the diiodo derivative Cs[8,8′-I_2-3,3′-Co(1,2-$C_2B_9H_{10})_2$] (Cs[**3c**]). The latter can also be prepared by refluxing Cs[**1**] with iodine chloride.[58] The cross-coupling reactions of the monoiodo-substituted derivative Cs[**2c**] with organomagnesium and -zinc compounds in the presence of a Pd catalyst afford the corresponding alkyl and aryl derivatives [8-R-3,3′-Co(1,2-$C_2B_9H_{10}$)(1′,2′-$C_2B_9H_{11}$)]$^-$ (R = Me, Et, Ph, CH_2CH_2Ph, C_6H_4Bu-4, C_6H_4OMe-4, C_6H_4Ph-4, 9-anthracenyl, 2-thienyl).[59,60] The reactions of Cs[**3c**] with RMgBr (R = Me or

Scheme 2

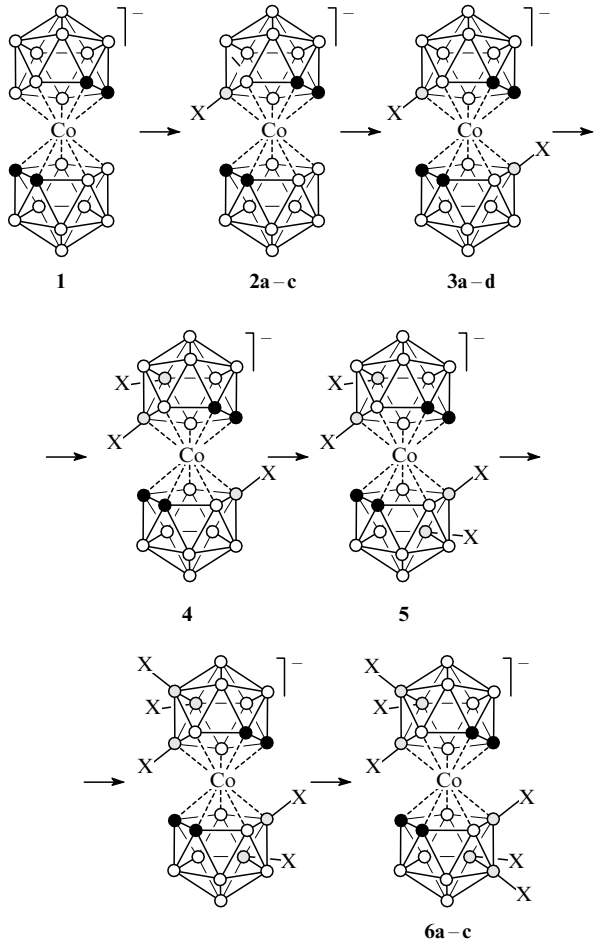

Here and below ● CH ○ BH ⊙ B;
X = Cl (**a**), Br (**b**), I (**c**), F (**d**).

Et) form Cs[8,8′-R_2-3,3′-Co(1,2-$C_2B_9H_{10})_2$] along with [8-R-8′-OH-3,3′-Co(1,2-$C_2B_9H_{10})_2$]$^-$ as a by-product.[58]

The reaction of Cs[**1**] with a high excess (more than sixfold) of iodine in the presence of $AlCl_3$ in benzene made it possible to prepare the hexaiodo derivative Cs[8,8′,9,9′,12,12′-I_6-3,3′-Co(1,2-$C_2B_9H_8)_2$] (Cs[**6c**]).[55] The compound Cs[**6c**] can also be synthesised with the use of iodine chloride.[61] The iodine atoms in Cs[**6c**] are readily replaced with methyl groups by the reaction with MeMgBr in the presence of $PdCl_2(PPh_3)_2$ and CuI in boiling THF. The corresponding hexamethyl derivative [8,8′,9,9′,12,12′-Me_6-3,3′-Co(1,2-$C_2B_9H_8)_2$]$^-$ was isolated as the triphenylmethylphosphonium salt.[61]

The difluoro derivative [Bu_4N][8,8′-F_2-3,3′-Co(1,2-$C_2B_9H_{10})_2$] ([Bu_4N][**3d**], the yield was 80%) was prepared by the reaction of [Bu_4N][**1**] with an excess of 4-chloromethyl-1-fluorobicyclo[2.2.2]octane-1,4-diazonium bis(tetrafluoroborate) in acetone at 50 °C.[62]

The structures of the compounds Cs[**2c**],[63] K[**3a**],[64] [$(Ph_3P)_2N$][**3a**],[56] Cs[**3c**],[65] [Bu_4N][**3d**],[62] [Me_4N][**6b**][66] and Cs[**6b**][67] were established by X-ray diffraction analysis. In the di- and hexahalogen-substituted derivatives, the dicarbollyl ligands adopt a transoid conformation.

It should be noted that the replacement at other positions of bis(dicarbollyl)cobalt (**1**) does not occur even under severe conditions. Such derivatives can be synthesised by the direct assembly of the metallacarborane fragment from $CoCl_2$ and the corresponding substituted carboranes. This procedure was used for the preparation of [9,9′-Cl_2-3,3′-Co(1,2-$C_2B_9H_{10})_2$]$^-$,[55] [9,9′,12,12′-Cl_4-3,3′-Co(1,2-$C_2B_9H_9)_2$]$^-$,[55] [9,9′-Br_2-3,3′-Co(1,2-$C_2B_9H_{10})_2$]$^-$,[68] [9,9′,12,12′-Br_4-3,3′-Co(1,2-$C_2B_9H_9)_2$]$^-$,[68] [4,4′,7,7′-Cl_4-3,3′-Co(1,2-$C_2B_9H_9)_2$]$^-$,[69] [4,4′,7,7′-Br_4-3,3′-Co(1,2-$C_2B_9H_9)_2$]$^-$ (see Ref. 69) and [9,9′-I_2-3,3′-Co(1,2-$C_2B_9H_{10})_2$]$^-$.[70]

Halogenation of unsymmetrical cobaltacarborane 3-Cp-3,1,2-$CoC_2B_9H_{11}$ (**7**) was studied in less detail. Depending on the reagent ratio, the reaction of compound **7** with bromine in dichloromethane in the presence of $AlCl_3$ affords mono-, di- and trisubstituted products. It is assumed that the first step of the reaction involves the replacement of the hydrogen atom at position 8 [like in the case of bis(dicarbollyl)cobalt] followed by the replacement of the hydrogen atoms at positions 9 and 12 of the dicarbollyl ligand. In the presence of an excess of bromine, the reaction yields the tribromo derivative 8,9,12-Br_3-3-Cp-3,1,2-$CoC_2B_9H_8$ (**8**).[71,72]

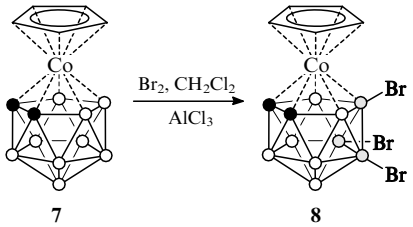

Refluxing of compound **7** in benzene with an excess of AlX_3 (X = Cl, Br, I) affords the corresponding monohalogen-substituted derivatives.[73] It is assumed that the substitution occurs at position 8. However, no evidence for this structure of the halogenation product was reported.

Due to the paramagnetic nature of Fe^{III}-based metallacarboranes, substitution in these compounds was studied in much less detail compared to substitution in Co^{III}-based metallacarboranes. Nevertheless, it can be assumed that these reactions proceed analogously. For example, chlorination of [*commo*-3,3′-Fe(1,2-$C_2B_9H_{11})_2$]$^-$ (**9**) affords the dichloro derivative [8,8′-Cl_2-3,3′-Fe(1,2-$C_2B_9H_{10})_2$]$^-$ (**10**). The structure of its potassium salt was established by X-ray diffraction analysis.[64]

Halogenation of ferracarborane 3-Cp-3,1,2-$FeC_2B_9H_{11}$ (**11**) was studied more thoroughly. Bromination of compound **11** in dichloromethane at room temperature in the absence of a catalyst gives rise to the monobromo derivative 8-Br-3-Cp-3,1,2-$FeC_2B_9H_{10}$ (**12**) (Scheme 3). In the presence of $AlCl_3$, the substitution occurs less selectively and affords monobromide **12** along with dibromo [8,9-Br_2-3-Cp-3,1,2-$FeC_2B_9H_9$ (**13**)] and tribromo [8,9,12-Br_3-3-Cp-3,1,2-$FeC_2B_9H_8$ (**14**)] derivatives. Bromination in acetic acid and nitromethane proceeds analogously. The dibromo derivative **13** can also be prepared by bromination of 9-Br-3-Cp-3,1,2-$FeC_2B_9H_{10}$ (**15**) and the tribromo derivative can be synthesised by bromination of 9,12-Br_2-3-Cp-3,1,2-$FeC_2B_9H_9$ (**16**), which was prepared by direct synthesis from the corresponding substituted *nido*-carborane (Scheme 3).[74]

Bromination of 4-Br-3-Cp-3,1,2-$FeC_2B_9H_{10}$ (**17**) derived from the corresponding *nido*-carborane produces 4,8-Br_2-3-Cp-3,1,2-$FeC_2B_9H_9$ (**18**).[74]

The published data on mercuration of anion **1** are contradictory. The reaction of the mercury salt Hg[**1**]$_2$ with mercury acetate in boiling acetic acid forms the disubstituted product Hg[9,9′-$(AcOHg)_2$-3,3′-Co(1,2-$C_2B_9H_{10})_2$]$_2$. It was hypothesised that the hydrogen atoms most remote from the carbon atoms, *viz.*, those at positions 9,9′, are replaced.[75]

By contrast, mercuration of K[**1**] in an aqueous–organic medium leads to the replacement of one dicarbollyl ligand at position 8 followed by the replacement of another ligand at position 9′ (Scheme 4).[76] However, it should be noted that the proposed structures of the reaction products were not supported by rigorous evidence.

Scheme 3

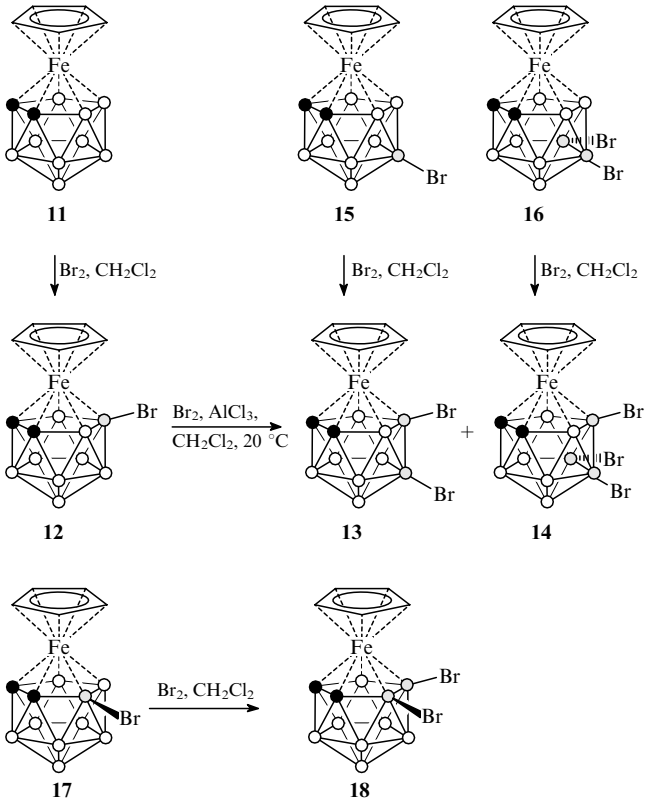

The reaction of bis(dicarbollyl)nickel(IV), *viz*., *commo*-3,3′-Ni(1,2-$C_2B_9H_{11})_2$ (**19**), with mercury oxide in boiling trifluoroacetic acid followed by the replacement of the trifluoroacetate group with the chlorine atom gave rise to the disubstituted derivative $(ClHg)_2$-3,3′-Ni(1,2-$C_2B_9H_{10})_2$ (substitution positions were not established).[77]

Scheme 4

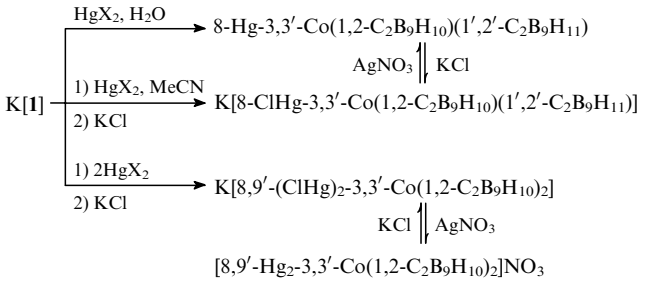

X = BF_4, AcO, CF_3CO_2.

Mercuration of compound **7** was examined in the studies.[75,78] It was noted that different products can be prepared by varying the reaction conditions. For example, mercuration under severe conditions, *i.e*., the reaction of cobaltacarborane **7** with mercury trifluoroacetate in trifluoroacetic acid followed by treatment with NaCl in a water–acetone system, afforded the disubstituted derivative 9,12-$(ClHg)_2$-3-Cp-3,1,2-$CoC_2B_9H_9$ (**20**) and polymercuration products (Scheme 5). The reaction with the use of a softer system (mercury trifluoroacetate in dichloromethane) yielded a mixture of two isomeric 8- (**21a**) and 9-substituted (**21b**) monomercury derivatives in a ratio of 1 : 5. The structure of the 9-substituted monomercury derivative was confirmed by X-ray diffraction analysis.[78] A diacetomercury-substituted derivative was prepared by the reaction of compound **7** with mercury acetate in acetic acid, whereas the reaction in the CH_2Cl_2–AcOH system gave rise to a disubstituted complex along with two isomeric 8- and 9-substituted monomercury derivatives.

The 9-chloromercury derivative 9-ClHg-3-Cp-3,1,2-$FeC_2B_9H_{10}$ (**22**) was synthesised by mercuration of ferracarborane **11** with mercury trifluoroacetate in a trifluoroacetic acid–

Scheme 5

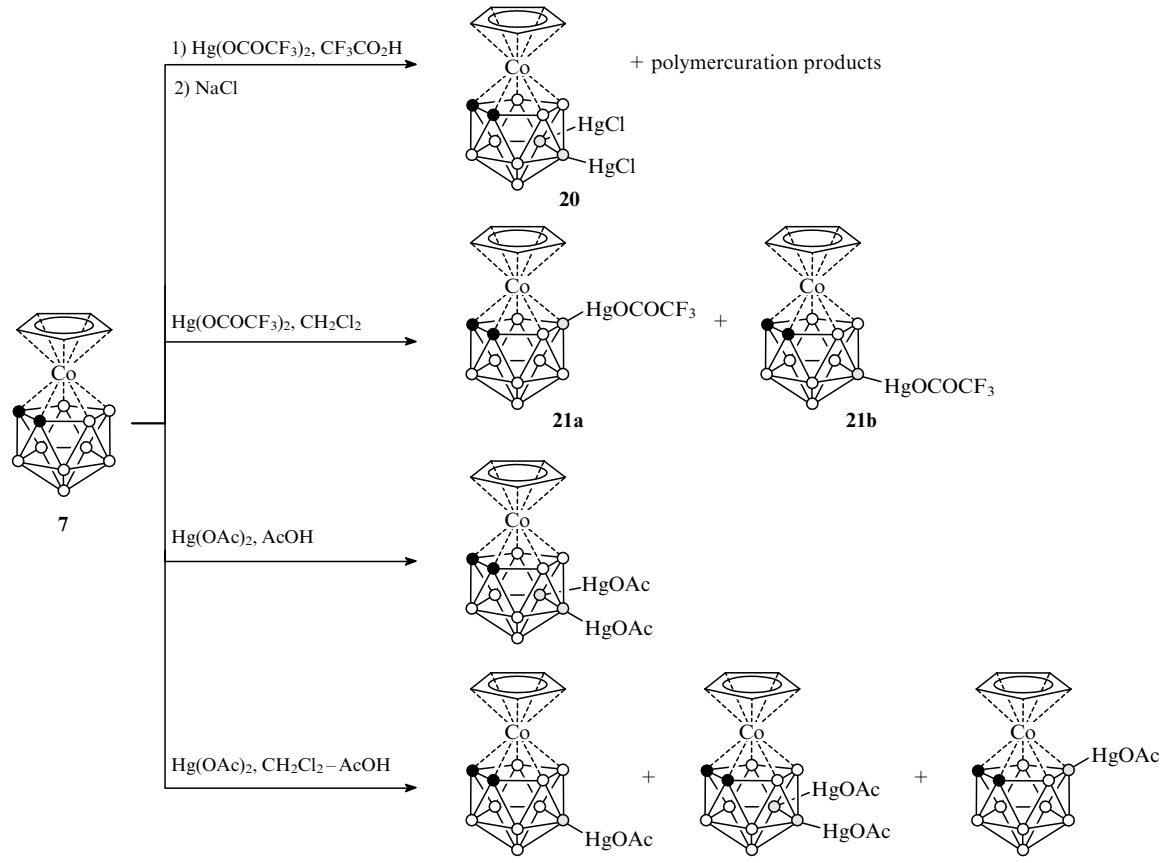

Scheme 6

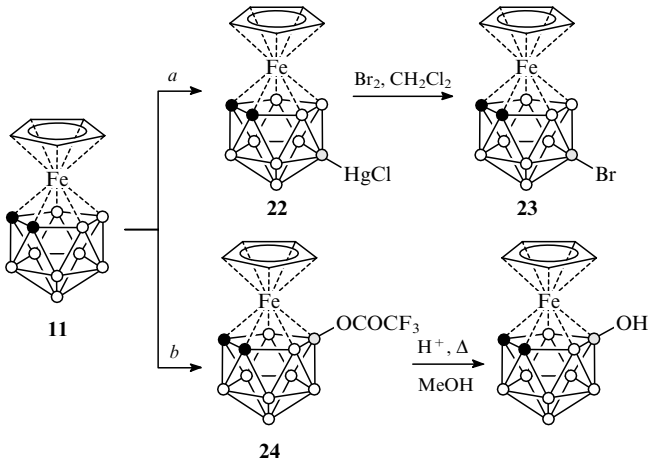

(*a*): 1) $Hg(OCOCF_3)_2$, $CF_3COOH - CH_2Cl_2$, 2) NaCl, H_2O;
(*b*): $Tl(OCOCF_3)_3$, Δ, CF_3COOH.

dichloromethane mixture followed by the replacement of the trifluoroacetoxy group with chlorine (Scheme 6). The reaction of compound **22** with bromine in dichloromethane afforded the corresponding bromide, *viz*., 9-Br-3-Cp-3,1,2-$FeC_2B_9H_{10}$ (**23**).[79]

In attempting to prepare a thallium derivative by heating ferracarborane **11** with thallium(III) trifluoroacetate in trifluoroacetic acid, the 8-trifluoroacetoxy derivative 8-CF_3COO-3-Cp-3,1,2-$FeC_2B_9H_{10}$ (**24**) was isolated instead of the expected thallation product. The structure of this reaction product was established by X-ray diffraction analysis.[80] The reaction with cobaltacarborane **7** proceeds analogously. However, this reaction afforded the 8-trifluoroacetoxy derivative 8-CF_3COO-3-Cp-3,1,2-$CoC_2B_9H_{10}$ along with a small amount of the 8-hydroxy derivative 8-OH-3-Cp-3,1,2-$CoC_2B_9H_{10}$.[80]

The mechanism of formation of trifluoroacetoxy derivative **24** remains unclear. Apparently, it may involve both the electrophilic substitution followed by elimination of thallium and the electrophile induced nucleophilic substitution with the initial attack of the thallium reagent followed by the attack of the trifluoroacetate anion (see below). The ricochet mechanism also cannot be ruled out.

Analysis of the above data shows that halogenation of metallacarboranes $[3\text{-L-}3,1,2\text{-}MC_2B_9H_{11}]^{n-}$ occurs first at position 8 and then at positions 9 and 12 of the metallacarborane moiety. Unlike halogenation, mercuration generally gives rise to a mixture of 8- and 9-substituted metallacarboranes with the 9-substituted isomer predominating. This anomaly is attributable to the fact that the first step of the process gives rise to an intermediate, in which the mercury atom coordinates the B(8)B(9)B(12) face of the metallacarborane moiety. The subsequent substitution can occur at both positions 8 and 9(12), and the product ratio depends on the electronic properties of the intermediate.

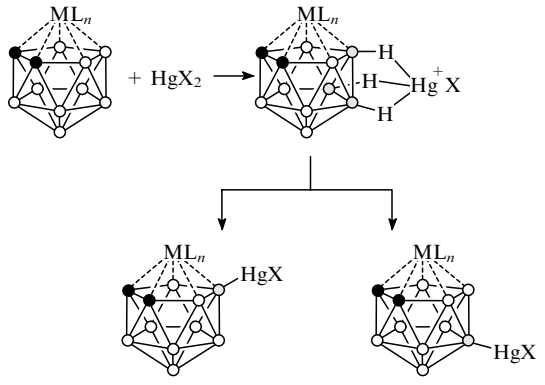

The formation of such boron hydride complexes with various transition metals is well known. The mercury complex $[Ph_4P][1,2,3\text{-}PhHg\text{-}1,2,3\text{-}(\mu\text{-}H)_3B_6H_3]$ was isolated and characterised by X-ray diffraction analysis.[81]

The influence of the *exo*-polyhedral substituents on the direction of substitution in metallacarborane systems is of interest. Let us consider the effect of the Me_2S^+ substituent in the carborane cage of diamagnetic ferracarborane 4-Me_2S-3-Cp-3,1,2-$FeC_2B_9H_{10}$ (**25**) on the mechanism of substitution. The reaction of compound **25** with 1 equiv. of bromine in dichloromethane affords the monobromo derivative 8-Br-4-Me_2S-3-Cp-3,1,2-$FeC_2B_9H_9$ (**26**), whereas the reaction with two or more equivalents of bromine gives rise to the disubstituted derivative 7,8-Br_2-4-Me_2S-3-Cp-3,1,2-$FeC_2B_9H_8$ (**27**). The use of $AlCl_3$ as the catalyst does not allow one to introduce more than two boron atoms into the ferracarborane moiety and the reaction forms dibromo derivative **27** as the final product. The structure of complex **27** was confirmed by X-ray diffraction analysis.[82]

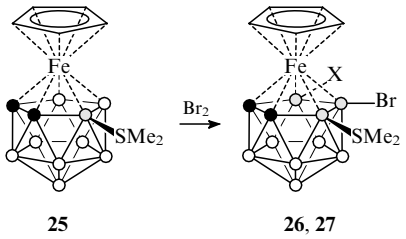

X = H (**26**), Br (**27**).

The reaction of compound **25** with mercury trifluoroacetate in a ratio of 1 : 1 in dichloromethane at room temperature yields 8-CF_3COOHg-4-Me_2S-3-Cp-3,1,2-$FeC_2B_9H_9$ (**28**) as the only product.[82]

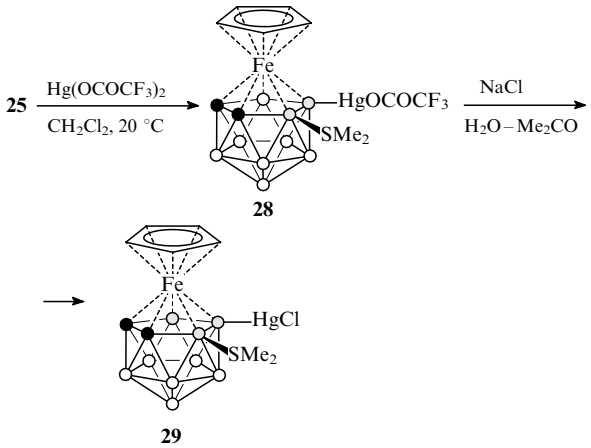

The position of the substituent in ferracarborane **28** was determined by ^{11}B and $^{11}B-^{11}B$ COSY NMR spectroscopy and confirmed by X-ray diffraction study of its chloro derivative **29**.

The reaction of ferracarborane **25** with a threefold excess of mercury trifluoroacetate gave a mixture of four products,[83] which were isolated as HgCl derivatives after treatment with sodium chloride in acetone.

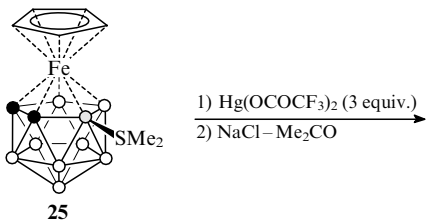

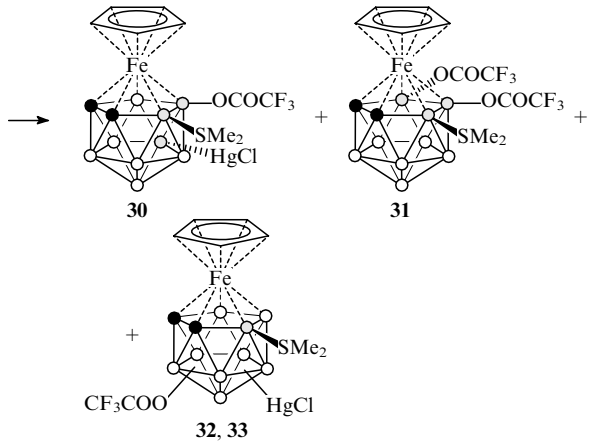

This reaction afforded 8-CF_3COO-12-HgCl-4-Me_2S-3-Cp-3,1,2-$FeC_2B_9H_8$ (**30**) as the major product in 52% yield. In addition, the reaction produced small amounts of 7,8-$(CF_3COO)_2$-4-Me_2S-3-Cp-3,1,2-$FeC_2B_9H_8$ (**31**) containing three substituents at the open face and two isomers **32** and **33** each bearing one HgCl group and one CF_3COO fragment, the positions of which were not unambiguously determined.

The reaction with a 12-fold excess of the mercurating agent followed by treatment of the reaction mixture with NaCl gave a mixture of complexes **34** and **35**. The structures of the reaction products were determined by spectroscopic methods. The structure of ferracarborane **35** was confirmed by X-ray diffraction analysis.[83]

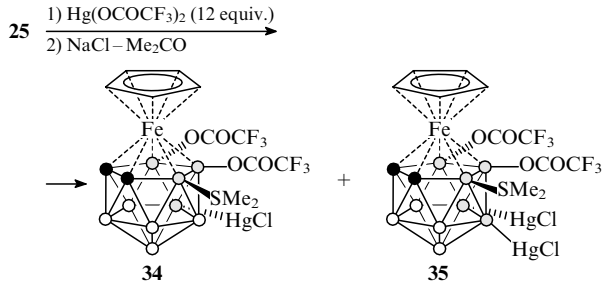

Therefore, from one to four substituents can be introduced into the carborane moiety depending on the ratio between the starting ferracarborane **25** and the mercurating agent (mercury trifluoroacetate).[82, 83]

It should be noted that further substitution in ferracarboranes depends on the nature of the substituents. For example, like in the case of unsubstituted derivative **11**, bromination of bromine-substituted ferracarboranes **15**, **16** and **17** leads to substitution at position 8. The introduction of the Me_2S^+ substituent has a much more substantial effect on the direction of substitution. Mercuration of unsubstituted ferracarborane **11** results in the replacement of the hydrogen atom at position 9(12), whereas mercuration of its 4-Me_2S^+-substituted derivative **25** leads to substitution of the hydrogen atom at position 8. Substitution at position 9 or 12 requires an excess of the mercurating agent, substitution at position 9 being attained only in the presence of a large excess of mercury trifluoroacetate due, apparently, to the deactivating effect of the Me_2S^+ group.

An analogous situation was observed earlier in the study of substitution in the *closo*-dodecaborate anion $[B_{12}H_{12}]^{2-}$. In this compound, the effect of *exo*-polyhedral substituents on the replacement of hydrogen atoms with electrophilic reagents is much less pronounced compared to carboranes and is manifested only in the presence of strong electron-withdrawing substituents (R_2O^+, R_2S^+ or R_3N^+).[84, 85] Unfortunately, data on the influence of the *exo*-polyhedral substituents on substitution in metallacarboranes are insufficient to give an unambiguous answer to this question. This problem requires additional investigation.

The reactions of metallacarboranes $[3\text{-L-}3,1,2\text{-}MC_2B_9H_{11}]^{n-}$ with arylsulfenyl chlorides provide yet another typical example of electrophilic substitution in this class of compounds. For instance, the reaction of 4-nitrophenylsulfenyl chloride with ferracarborane **11** in acetonitrile affords 8-(4-$NO_2C_6H_4S$)-3-Cp-3,1,2-$FeC_2B_9H_{10}$, whereas the analogous reaction with K[**1**] yields $[8,8'\text{-}(4\text{-}NO_2C_6H_4S)_2\text{-}3,3'\text{-}Co(1,2\text{-}C_2B_9H_{10})_2]^-$. Interestingly, the reactions of phenylsulfenyl and 2-nitrophenylsulfenyl chlorides with K[**1**] form the monosubstituted derivatives $[8\text{-ArS-}3,3'\text{-}Co(1,2\text{-}C_2B_9H_{10})(1',2'\text{-}C_2B_9H_{11})]^-$ (Ar = Ph or $C_6H_4NO_2$-2) as the final products even in the presence of an excess of ArSCl. This difference in the behaviour of sulfenyl halides was accounted for by the difference in the basicity of the sulfur atoms in the monosulfides that formed. In the case of phenylsulfenyl and 2-nitrophenylsulfenyl chlorides, protonation of sulfur with HCl that is eliminated affords the sulfonium salt, whose positive charge deactivates the molecule and hinders the replacement in the second dicarbollyl ligand.[86]

The use of other electrophilic reagents can give unexpected results. For instance, the reaction of cobaltacarborane **7** with acetyl chloride in carbon disulfide in the presence of $AlCl_3$ produced a complex mixture of acetyl (**36**), acetoxy (**37**), hydroxy (**38**) and chlorine derivatives (**39**).[73]

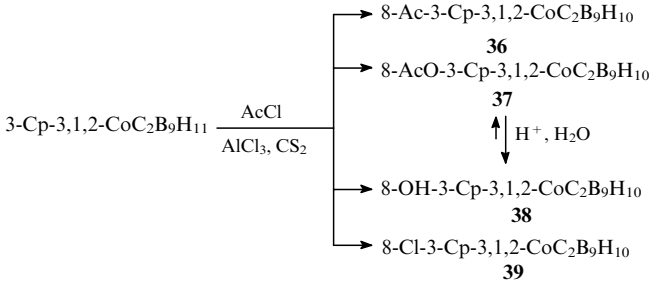

The substitution positions in 8-Ac-3-Cp-3,1,2-$CoC_2B_9H_{10}$ (**36**) and 8-AcO-3-Cp-3,1,2-$CoC_2B_9H_{10}$ (**37**) were determined by X-ray diffraction analysis.[73]

Acid hydrolysis of acetoxy derivative **37** gives the corresponding hydroxy derivative **38**. The reactions of the latter with acetic anhydride, acetyl chloride and benzoyl chloride afford the corresponding acyloxy derivatives.

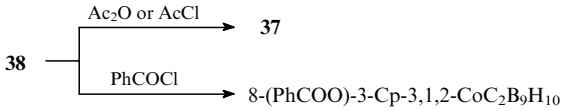

Reduction of acetyl derivative **36** with zinc in hydrochloric acid gives the corresponding ethyl derivative 8-Et-3-Cp-3,1,2-$CoC_2B_9H_{10}$.[73]

The reactions of cobaltacarborane **7** and its methyl- [1-Me-3-Cp-3,1,2-$CoC_2B_9H_{10}$ (**7a**)] and phenyl-substituted derivatives [1-Ph-3-Cp-3,1,2-$CoC_2B_9H_{10}$ (**7b**)] with acetyl chloride in dichloroethane in the presence of $AlCl_3$ form the corresponding hydroxy derivatives, *viz.*, 8-OH-3-Cp-3,1,2-$CoC_2B_9H_{10}$ (**38**), 1-Me-8-OH-3-Cp-3,1,2-$CoC_2B_9H_9$ (**38a**) and 1-Ph-8-OH-3-Cp-3,1,2-$CoC_2B_9H_9$ (**38b**).[29] Heating of compound **7** and CrO_3 in a mixture of acetic anhydride, acetic acid and sulfuric acids affords a mixture of hydroxy, acetoxy and diacetoxy derivatives.[29]

The above results provide evidence that the substitution in carbon disulfide occurs by competitive mechanisms of electrophilic and electrophile induced nucleophilic substitution, whereas substitution in dichloroethane occurs predominantly by the latter mechanism.

Analogously, the reactions of Cs[8,8′,9-Cl_3-3,3′-Co(1,2-$C_2B_9H_9$)(1′,2′-$C_2B_9H_{10}$)] (**4**) with alkyl halides in the presence of $AlCl_3$ afford complex mixtures of halogen- and alkyl-substituted derivatives.[87] In our opinion, this fact can also be attributable to competition between two substitution mechanisms.

We believe that the formation of nitrates 8-NO_3-3-Cp-3,1,2-$CoC_2B_9H_{10}$, 1-Ph-8-NO_3-3-Cp-3,1,2-$CoC_2B_9H_9$ and 8-NO_3-3-(η^5-$C_5H_4C_6H_4NO_2$)-3,1,2-$CoC_2B_9H_{10}$ by nitration of the compounds **7**, **7b** and 3-(η^5-C_5H_4Ph)-3,1,2-$CoC_2B_9H_{11}$ with a mixture of nitric and sulfuric acids in dichloromethane [87] also occurs by the mechanism of electrophile induced nucleophilic substitution. Reduction of these nitrates with tin in hydrochloric acid affords the corresponding hydroxy derivatives.[87]

The reaction of the [3-C_5Me_5-3,1,2-$RuC_2B_9H_{11}$]$^-$ complex with [CpFe(C_6H_6)]$^+$ in tetrahydrofuran under UV irradiation produces 8-$(CH_2)_4O$-3-C_5Me_5-3,1,2-$RuC_2B_9H_{10}$, which is a product of electrophile induced nucleophilic substitution.[88] An analogous result was obtained in the reaction of [1,2-(μ-CH_2OCH_2)-3-C_5Me_5-3,1,2-$RuC_2B_9H_9$]$^-$ (**39**) with [(C_5Me_5)RuCl]$_4$ in tetrahydrofuran.[88]

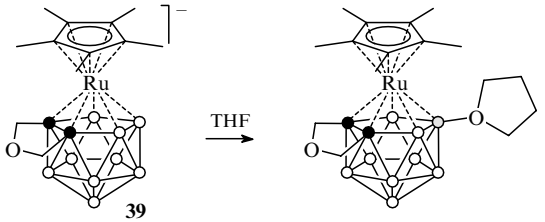

39

The reaction of acetic anhydride with K[**1**] in sulfuric acid or in acetic acid in the presence of $HClO_4$ proceeds in an unusual way.[89,90] Apparently, this reaction also occurs by the mechanism of electrophile induced nucleophilic substitution but gives 8,8′-(μ-AcO)-3,3′-Co(1,2-$C_2B_9H_{10}$)$_2$ (**40**) in which two dicarbollyl ligands are linked by the bridging acetate group through the B(8) and B(8′) atoms.[89,90] The structure of compound **40** was established by X-ray diffraction analysis.[90] Hydrolysis of the acetate derivative in boiling aqueous ethanol affords the corresponding diol [8,8′-(HO)$_2$-3,3′-Co(1,2-$C_2B_9H_{10}$)$_2$]$^-$ (**41**).[89,90]

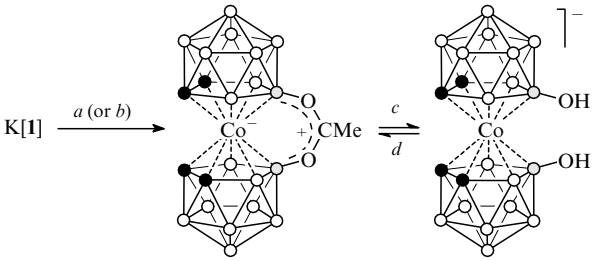

40 **41**

(*a*) Ac_2O, H_2SO_4, 80 °C; (*b*) Ac_2O, AcOH, $HClO_4$;
(*c*) H^+, 50% EtOH, 80 °C; (*d*) Ac_2O, H_2SO_4, 80 °C.

Dihydroxy derivative **41** can also be prepared by heating Cs[**1**] in 80% sulfuric acid to 140 °C. Heating of Cs[**1**] in 60% sulfuric acid at 120 °C affords the monohydroxy derivative [8-OH-3,3′-Co(1,2-$C_2B_9H_{10}$)(1′,2′-$C_2B_9H_{11}$)]$^-$ (**42**). The latter was prepared also by heating Cs[**1**] with acetic anhydride in a mixture of acetic and sulfuric acids.

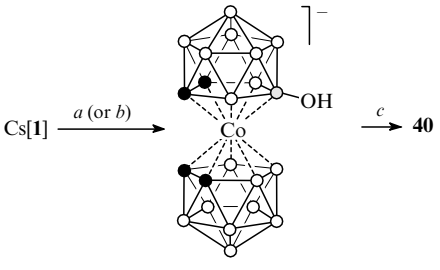

42

(*a*) 60% H_2SO_4, 120 °C; (*b*) Ac_2O, AcOH, $HClO_4$; (*c*) Ac_2O, H_2SO_4, 80 °C.

The reactions of both mono- and dihydroxy derivatives with acetic anhydride in sulfuric acid produce bridged acetate derivative **40**.[90]

The reaction of Cs[**41**] with $POCl_3$ in chloroform in the presence of triethylamine yields the bridged [Et_3NH][8,8′-(μ-OPO(Cl)O)-3,3′-Co(1,2-$C_2B_9H_{10}$)$_2$] derivative (**43**). Hydrolysis of the latter affords acid [8,8′-(μ-OPO(OH)O)-3,3′-Co(1,2-$C_2B_9H_{10}$)$_2$]$^-$.

The reaction of compound **43** with diethylamine produces the corresponding amide [Et_3NH][8,8′-(μ-OPO(NEt_2)O)-3,3′-Co(1,2-$C_2B_9H_{10}$)$_2$] (**43a**).[91] The structures of compounds **43** and **43a** were established by X-ray diffraction analysis.[90] The reactions of monohydroxy derivative **42** with $POCl_3$ and $PhPOCl_2$ followed by hydrolysis afford [8-PO_2(OH)$_2$-3,3′-Co(1,2-$C_2B_9H_{10}$)(1′,2′-$C_2B_9H_{11}$)]$^-$ and [8-HO_2P(Ph)O-3,3′-Co(1,2-$C_2B_9H_{10}$)(1′,2′-$C_2B_9H_{11}$)]$^-$, respectively.[91]

It should be noted that the formation of bridged derivatives is typical of the chemistry of cobalt and iron bis(dicarbollyl) complexes, although the latter complex was studied to a much lesser extent.

The reaction of Cs[**1**] with dimethyl sulfate in the presence of $AlCl_3$ at 80 °C forms the sulfate-bridged derivative [8,8′-(μ-OSO_2O)-3,3′-Co(1,2-$C_2B_9H_{10}$)$_2$]$^-$. The structure of its tetramethylammonium salt was determined by X-ray diffraction analysis.[92]

Heating of Cs[**1**] with dimethyl sulfate and sulfuric acid in 1,4-dioxane affords the oxonium derivative 8-O(CH_2CH_2)$_2$O-3,3′-Co(1,2-$C_2B_9H_{10}$)(1′,2′-$C_2B_9H_{11}$) (**44**).[92] This compound was also prepared by heating Cs[**1**] with $BF_3 \cdot OEt_2$ in 1,4-dioxane.[93] It should be noted that monosubstituted bis(dicarbollyl)cobalt derivatives are generated primarily by introducing onium substituents, whose involvement in the carborane ligand gives rise to neutral charge-compensated products. The presence of the positive charge on the onium substituent causes a substantial electron density redistribution in the metallacarborane moiety and deactivation of the second dicarbollyl ligand.

The reactions of compound **44** with various nucleophilic agents are accompanied by the dioxane-ring opening to form various functional derivatives with composition [8-X(CH_2CH_2O)$_2$-3,3′-Co(1,2-$C_2B_9H_{10}$)(1′,2′-$C_2B_9H_{11}$)]$^-$ [X = OH, OR, CN, NH_2, $CH(NH_2)COOH$, P(O)$(OBu)_2$, P(O)(OBu)OH, NEt_3, Py].[18,27,93,94]

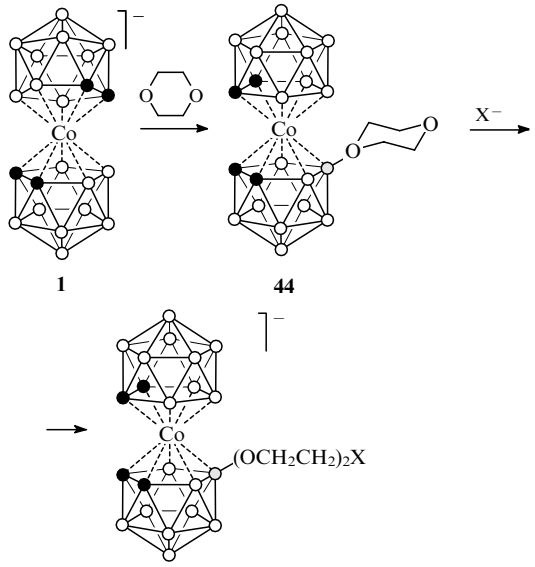

1 **44**

Analogously, the reaction of Cs[**1**] with dimethyl sulfate in the presence of sulfuric acid in tetrahydropyran yields 8-$C_5H_{10}O$-3,3′-Co(1,2-$C_2B_9H_{10}$)(1′,2′-$C_2B_9H_{11}$) (**45**). The tetrahydropyran-ring opening in the reactions of derivative **45** with nucleophiles made it possible to prepare a series of derivatives of the [8-X(CH_2)$_5$O-3,3′-

$Co(1,2\text{-}C_2B_9H_{10})(1',2'\text{-}C_2B_9H_{11})]^-$ type (X is 1-pyrrolyl, 1-indolyl or 9-carbazolyl).[95]

Thioformate-bridged bis(dicarbollyl) derivatives of cobalt and iron, 8,8′-(μ-HCS_2)-3,3′-M(1,2-$C_2B_9H_{10})_2$ (**46** and **47**), were prepared by the reactions of K[**1**] and K[**9**], respectively, with carbon disulfide in the presence of aluminium chloride.[89,96] The structure of compound **46** was determined by X-ray diffraction analysis.[96]

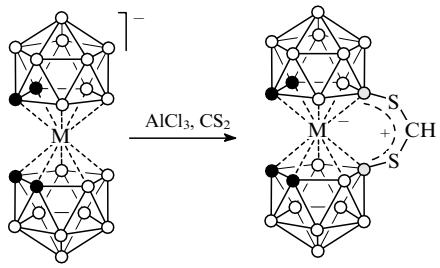

1, **9** **46**, **47**

M = Co (**1**, **46**), Fe (**9**, **47**).

Hydrolysis of compound **46** in boiling 50% ethanol affords the dimercapto derivative [8,8′-$(HS)_2$-3,3′-Co(1,2-$C_2B_9H_{10})_2]^-$ (**48**). Oxidation of the latter with hydrogen peroxide gives [8,8′-(μ-S_2)-3,3′-Co(1,2-$C_2B_9H_{10})_2]^-$ (**49**), in which the dicarbollyl fragments are linked by the disulfide bridge.[89,96] Derivative **49** was also prepared by heating Cs[**1**] with S_2Cl_2 in dichloromethane.[97]

Refluxing of $[(Me_2SO)_2H]^+$[**1**]$^-$ with acetic anhydride in benzene gives rise to the monosubstituted dimethylsulfonium derivative 8-Me_2S-3,3′-Co(1,2-$C_2B_9H_{10})(1',2'\text{-}C_2B_9H_{11})$ (**50**),[97] which can also be prepared by assembly from $CoCl_2$ and the corresponding dicarbollyl ligands.[98] The analogous diethylsulfonium derivative 8-Et_2S-3,3′-Co(1,2-$C_2B_9H_{10})(1',2'\text{-}C_2B_9H_{11})$ (**51**) was synthesised by the reaction of [Ph_3PMe][**1**] with diethyl sulfide in a strongly acidic medium.[99]

Treatment of a suspension of ferracarborane [Ph_3PMe][**9**] with gaseous HCl in diethyl sulfide yields a mixture of 8-Et_2S-3,3′-Fe^{III}(1,2-$C_2B_9H_{10})(1',2'\text{-}C_2B_9H_{11})$ (**52**) and 8,8′-$(Et_2S)_2$-3,3′-Fe(1,2-$C_2B_9H_{10})_2$ (**53**).[99] The charge-compensated complex **52** can also be synthesised by oxidation of the [8-Et_2S-3,3′-Fe^{II}(1,2-$C_2B_9H_{10})(1',2'\text{-}C_2B_9H_{11})]^-$ anion.[99]

The carborane derivative [8,8′-(μ-S)-3,3′-Co(1,2-$C_2B_9H_{10})_2]^-$ (**54**) containing a one-atom sulfide bridge was synthesised[100] by refluxing $[(Me_2SO)_2H]$[**1**] with S_2Cl_2 in dichloromethane followed by methanolysis and reprecipitation. Complex **54** can also be prepared by refluxing compound **1** with sulfur in benzene in the presence of $AlCl_3$.[97]

The reaction of complex **54** with dimethyl sulfate produces the neutral complex 8,8′-(μ-MeS)-3,3′-Co(1,2-$C_2B_9H_{10})_2$ (**55a**).[97,100] The latter can also be prepared by intramolecular cross-linking of compound **50** in boiling benzene in the presence of $AlCl_3$ [the reaction gives 8-Me_2S-8′-Cl-3,3′-Co(1,2-$C_2B_9H_{10})_2$ as the second product].[97]

The sulfonium derivatives 8,8′-(μ-RS)-3,3′-Co(1,2-$C_2B_9H_{10})_2$ [R = Et (**55b**), Bu (**55c**), Bn (**55d**), $CH_2CH{=}CH_2$ (**55e**), $CH_2C{\equiv}CH$ (**55f**) and CH_2COOH (**55g**)] were prepared by the reactions of compound **54** with the corresponding halides.[15,97] Protonation of derivative **54** with sulfuric acid in benzene affords very active acid 8,8′-(μ-HS)-3,3′-Co(1,2-$C_2B_9H_{10})_2$, which readily reacts with acrylonitrile and formaldehyde to form 8,8′-(μ-RS)-3,3′-Co(1,2-$C_2B_9H_{10})_2$ [R = CH_2CH_2CN (**55h**), CH_2OMe (**55i**)].[97,101] The reaction of complex **54** with bromine in acetic acid gives unstable bromide 8,8′-(μ-BrS)-3,3′-Co(1,2-$C_2B_9H_{10})_2$, which immediately reacts with benzene in the presence of $AlCl_3$ to form 8,8′-(μ-PhS)-3,3′-Co(1,2-$C_2B_9H_{10})_2$ (**55j**).[97]

Oxygen, selenium, tellurium and nitrogen atoms can also serve as bridges linking the dicarbollyl ligands (Scheme 7).[42]

Scheme 7

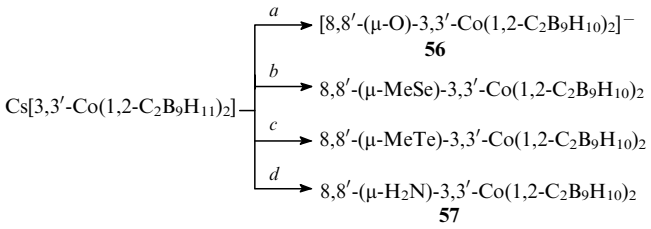

(*a*) HCHO, H_2SO_4, Ac_2O; (*b*) 1) SeO_2, H_2SO_4, Ac_2O, C_6H_6, 2) KOH – Me_2SO_4; (*c*) 1) Te, H_2SO_4, Ac_2O, 2) KOH – Me_2SO_4; (*d*) $NaNO_2$, H_2SO_4, C_6H_6.

Heating of cobaltacarborane Cs[**1**] with formaldehyde in acetic anhydride in the presence of sulfuric acid affords the [8,8′-(μ-O)-3,3′-Co(1,2-$C_2B_9H_{10})_2]^-$ complex (**56**)[42,102] [in the absence of formaldehyde, 8,8′-(μ-EtO)-3,3′-Co(1,2-$C_2B_9H_{10})_2$ was obtained[42]]. Derivative **56** was also prepared by refluxing [8-Me-8′-HO-3,3′-Co(1,2-$C_2B_9H_{10})_2]^-$ with iodine in ethanol.[58]

The reaction of ferracarborane **9** with formaldehyde in the presence of HCl produces 8,8′-(μ-MeO)-3,3′-Fe(1,2-$C_2B_9H_{10})_2$. Its structure was established by X-ray diffraction analysis.[103] By contrast, the reaction of nickelacarborane **19** with formaldehyde in a strongly acidic medium affords a mixture of the methoxy derivatives 8-MeO-3,3′-Ni(1,2-$C_2B_9H_{10})(1',2'\text{-}C_2B_9H_{11})$ and 8,8′-$(MeO)_2$-3,3′-Ni(1,2-$C_2B_9H_{10})_2$ (the structure of the disubstituted derivative was established by X-ray diffraction analysis[104]) rather than the bridged derivative.

The reaction of Cs[**1**] with H_2SeO_3 in a mixture of benzene, acetic anhydride and sulfuric acid followed by treatment of the intermediate with dimethyl sulfate yields 8,8′-(μ-MeSe)-3,3′-Co(1,2-$C_2B_9H_{10})_2$, whereas heating of Cs[**1**] with tellurium in a mixture of acetic anhydride and sulfuric acid followed by treatment of the intermediate with dimethyl sulfate gives 8,8′-(μ-MeSe)-3,3′-Co(1,2-$C_2B_9H_{10})_2$ (see Scheme 7).[42]

The reaction of Cs[**1**] with $NaNO_2$ in a $C_6H_6 - H_2SO_4$ mixture produces a mixture of 8,8′-(μ-H_2N)-3,3′-Co(1,2-$C_2B_9H_{10})_2$ (**57**) (47%), 4,8′-(μ-H_2N)-3,3′-Co(1,2-$C_2B_9H_{10})_2$ (6%) and 8,8′-(μ-NH_2O)-3,3′-Co(1,2-$C_2B_9H_{10})_2$ (21%).[42,105,106] Methylation of compound **57** with dimethyl sulfate in a benzene – water mixture in the presence of KOH gives rise to the *N*-methyl derivative 8,8′-(μ-MeNH)-3,3′-Co(1,2-$C_2B_9H_{10})_2$, whereas methylation in an aqueous solution affords the *N*,*N*-dimethyl derivative 8,8′-(μ-Me_2N)-3,3′-Co(1,2-$C_2B_9H_{10})_2$.[87] The reaction of compound **57** with chloroacetic acid in methanol in the presence of KOH yields 8,8′-(μ-$HOOCCH_2NH$)-3,3′-Co(1,2-$C_2B_9H_{10})_2$.[107]

Refluxing of Cs[**1**] with white phosphorus in benzene in the presence of $AlCl_3$ followed by alkylation with dimethyl sulfate in alkaline ethanol affords a mixture of 8,8′-(μ-Me_2P)-3,3′-Co(1,2-$C_2B_9H_{10})_2$ and 8-Me_3P-3,3′-Co(1,2-$C_2B_9H_{10})(1',2'\text{-}C_2B_9H_{11})$ in low yields.[107]

The iodonium-bridged derivative Cs[8,8′-(μ-I)-3,3′-Co(1,2-$C_2B_9H_{10})_2$] (**58**) was synthesised by refluxing Cs[**2c**] in benzene in the presence of $AlCl_3$.[108]

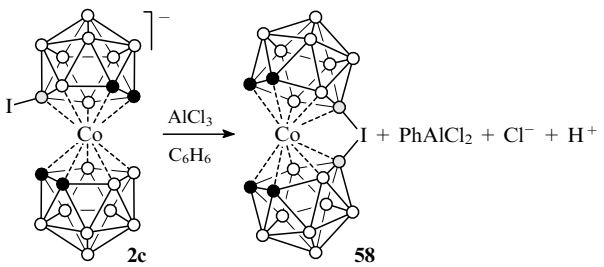

2c **58**

Compound **58** is highly reactive and is readily transformed into the corresponding bifunctional derivatives 8-I-8′-L-3,3′-$Co(1,2\text{-}C_2B_9H_{10})_2$ under the action of Lewis bases L, such as SMe_2, C_5H_5N, Me_3N and NH_3. An analogous bromonium-bridged derivative is very unstable due to which it was not isolated in the individual state. However, products of its reactions with dimethyl sulfide and dioxane with composition 8-Br-8′-L-3,3′-$Co(1,2\text{-}C_2B_9H_{10})_2$ (L = Me_2S and 1,4-$O_2C_4H_8$, respectively) were isolated.[109]

An interesting result was obtained when performing the reaction of an aqueous solution of K[**1**] with phenyldiazonium borofluoride. The reaction was accompanied by cation exchange to form the phenyldiazonium salt of bis(dicarbollyl)cobalt [PhN_2][**1**] instead of the expected arylation or coupling products.[110] At room temperature, this salt is virtually insoluble in benzene, but it completely dissolves on heating above 60 °C with elimination of N_2 to give biphenyl and the [8,8′-(μ-1,2-C_6H_4)-3,3′-$Co(1,2\text{-}C_2B_9H_{10})_2]^-$ complex (**59**).

Refluxing of the unstable phenyldiazonium salt of bis(dicarbollyl)iron [PhN_2][**9**] in benzene also affords the 1,2-phenylene-bridged [8,8′-(μ-1,2-C_6H_4)-3,3′-$Fe(1,2\text{-}C_2B_9H_{10})_2]^-$ compound.[111]

Decomposition of the phenyldiazonium salt in toluene and decomposition of the tolyldiazonium salt in benzene give rise to tolyl- and phenylene-bridged complexes, respectively, and methylbiphenyl (this is evidence that the aryl group of the diazonium cation is not involved in the reaction product).[110, 111]

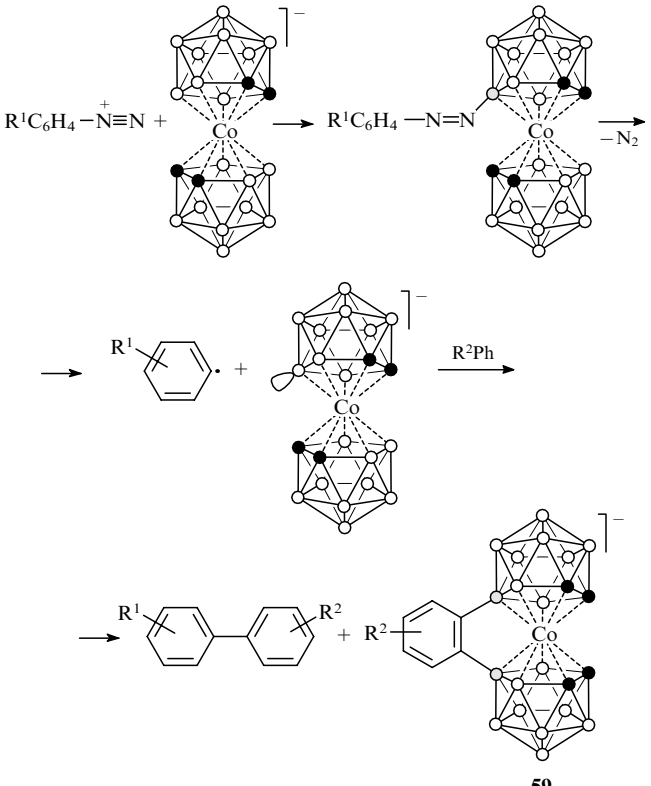

59

R^1, R^2 = H, Me.

The reaction of cobaltacarborane **1** with benzene in the presence of aluminium chloride produces bridged compound **59** (R^2 = H) and cobaltacarborane [4,8′-8,4′-(μ-1,2-C_6H_4)$_2$-3,3′-$Co(1,2\text{-}C_2B_9H_9)_2]^-$ containing two bridging 1,2-phenylene groups. The structures of these compounds were confirmed by X-ray diffraction analysis.[111, 112]

The reaction of compound **1** with naphthalene at 80 °C yields a 1-methyleneinden-2-yl-bridged derivative (which was proved by X-ray diffraction analysis).[113]

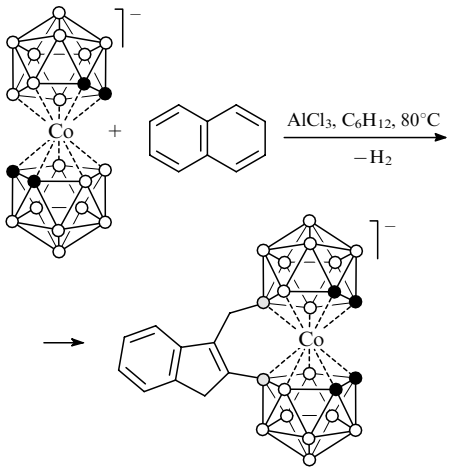

An interesting result was obtained in the reaction of $Me_3SiC{\equiv}CH$ with the complex Cs[**2c**] in the presence of a Pd catalyst (under conditions of the Sonogashira reaction). This reaction gives the ethene-bridged derivative [8,8′-(μ-CH = CH)-3,3′-$Co(1,2\text{-}C_2B_9H_{10})_2]^-$ instead of the expected addition product of acetylene with composition [8-$Me_3SiC{\equiv}$C-3,3′-$Co(1,2\text{-}C_2B_9H_{10})(1',2'\text{-}C_2B_9H_{11})]^-$. The structure of the caesium salt of the reaction product was established by X-ray diffraction analysis.[114] The synthesis of the alkyl and aryl derivatives [8-R-3,3′-$Co(1,2\text{-}C_2B_9H_{10})(1',2'\text{-}C_2B_9H_{11})]^-$ by Pd-catalysed cross-coupling of the complex [**2c**] with organomagnesium and -zinc reagents was mentioned above.[59, 60]

The phenyl derivative [8-Ph-3,3′-$Co(1,2\text{-}C_2B_9H_{10})(1',2'\text{-}C_2B_9H_{11})]^-$ was also prepared by the direct reaction of Cs[**1**] with dimethyl sulfate in benzene at 80 °C in the presence of concentrated sulfuric acid.[92] The diphenyl derivative [6,6′-Ph_2-3,3′-$Co(1,2\text{-}C_2B_9H_{10})_2]^-$ was synthesised by the reaction of Na_2[3-Ph-7,8-$C_2B_9H_{10}$] with $CoCl_2$ in tetrahydrofuran followed by precipitation as the tetramethylammonium salt.[115]

Metallacarborane complexes containing labile ligands in the metal coordination sphere are characterised by diverse chemistry because the presence of labile ligands increases the probability of substitution reactions involving the metal atom. In addition, such metallacarboranes can be involved in the above-mentioned electrophilic and electrophile induced nucleophilic substitution reactions.

For example, the reaction of [Et_4N][3-(η^3-C_3H_5)-3,3-$(CO)_2$-3,1,2-$MoC_2B_9H_{11}$] (**60**) with [Ph_3C][BF_4] and Et_2O in dichloromethane affords 8-Et_2O-3-(η^3-C_3H_5)-3,3-$(CO)_2$-3,1,2-$MoC_2B_9H_{10}$ (**61**), which is a typical product of electrophile induced nucleophilic substitution. The reactions of [Et_4N][1,2-Me_2-3-(η^3-C_3H_5)-3,3-$(CO)_2$-3,1,2-$MoC_2B_9H_9$] (**62**) with various donor molecules L proceed analogously. This procedure was used for the synthesis of various charge-compensated complexes 8-L-1,2-Me_2-3-(η^3-C_3H_5)-3,3-$(CO)_2$-3,1,2-$MoC_2B_9H_8$ (**63a**–**f**) (L = OEt_2, THF, SMe_2, PPh_3, Py, 4,4′-bipy). The reaction of [Et_4N][1,2-Me_2-3-(η^3-C_3H_5)-3,3-$(CO)_2$-3,1,2-$WC_2B_9H_9$] (**64**) with [Ph_3C][BF_3] and Et_2O also yields the 8-substituted derivative 8-Et_2O-1,2-Me_2-3-(η^3-C_3H_5)-3,3-$(CO)_2$-3,1,2-$WC_2B_9H_8$ (**65**).[116]

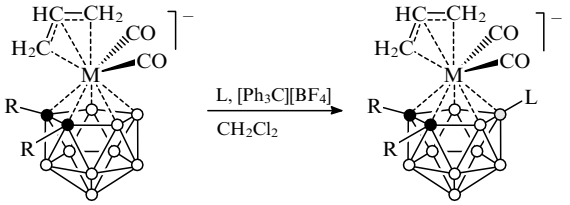

60, **62**, **64** **61**, **63a**–**f**, **65**

Compound	M	R	L	Compound	M	R	L
60	Mo	H	–	**63d**	Mo	Me	PPh_3
61	Mo	H	OEt_2	**63e**	Mo	Me	Py
62	Mo	Me	–	**63f**	Mo	Me	4,4′-bipy
63a	Mo	Me	OEt_2	**64**	W	Me	–
63b	Mo	Me	THF	**65**	W	Me	OEt_2
63c	Mo	Me	SMe_2				

Treatment of compounds **63a** and **65** with nucleophilic agents ($K[HBBu^s_3]$ and Et_4NX, where X = Cl or F) leads to elimination of one ethyl group to form $[Et_4N][8\text{-EtO-1,2-Me}_2\text{-3-}(\eta^3\text{-C}_3\text{H}_5)\text{-3,3-(CO)}_2\text{-3,1,2-MC}_2\text{B}_9\text{H}_8]$ (M = Mo, W), whereas treatment of the tetrahydrofuran derivative $8\text{-(CH}_2)_4\text{O-1,2-Me}_2\text{-3-}(\eta^3\text{-C}_3\text{H}_5)\text{-3,3-(CO)}_2\text{-3,1,2-MoC}_2\text{B}_9\text{H}_8$ (**63b**) with the R_4NF salt (R = Et, Bu) results in the tetrahydrofuran-ring opening to give $[R_4N][8\text{-F(CH}_2)_4\text{O-1,2-Me}_2\text{-3-}(\eta^3\text{-C}_3\text{H}_5)\text{-3,3-(CO)}_2\text{-3,1,2-MoC}_2\text{B}_9\text{H}_8]$.[116] By contrast, the reaction of complex **60** with $Me_3SiC{\equiv}CSiMe_3$ in the presence of $HBF_4\cdot Et_2O$ gives rise to a mixture of $3,3\text{-}(\eta^2\text{-Me}_3\text{SiC}{\equiv}\text{CSiMe}_3)_2\text{-3-CO-3,1,2-MoC}_2\text{B}_9\text{H}_{11}$ (**66**) and $8,3\text{-}(\sigma,\eta^2\text{-Me}_3\text{SiCH}{=}\text{CH})\text{-3,3,3-(CO)}_3\text{-3,1,2-MoC}_2\text{B}_9\text{H}_{10}$ (**67**).[117] It is assumed that the first step involves the replacement of the labile (allyl and carbonyl) ligands with the alkyne molecule $Me_3SiC{\equiv}CSiMe_3$. The second step involves, apparently, the formation of the vinylidene fragment $Mo{=}C{=}CHSiMe_3$ followed by its insertion into the B–H bond of the pentagonal face of the dicarbollyl ligand.

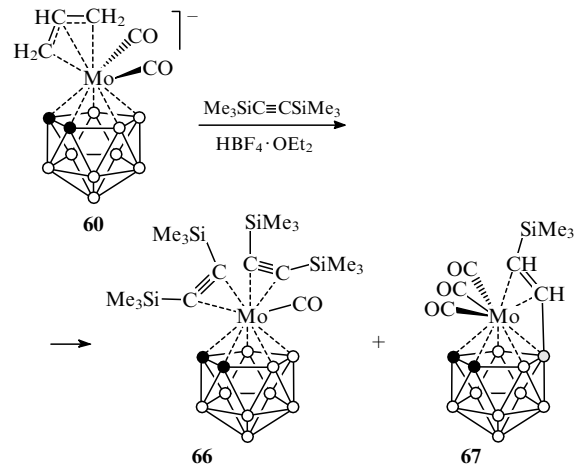

60 **66** **67**

An analogous complex with composition $8,3\text{-}(\sigma,\eta^2\text{-PhCH}{=}\text{CPh})\text{-1,2-Me}_2\text{-3,3-(CO)}_2\text{-3-Ph}_3\text{P-3,1,2-MoC}_2\text{B}_8\text{H}_8$ (**68**) was prepared by the rearrangement of $1,2\text{-Me}_2\text{-3-CO-3-Ph}_3\text{P-3-}(\eta^2\text{-PhC}{\equiv}\text{CPh})\text{-3,1,2-MoC}_2\text{B}_9\text{H}_9$ in dichloromethane at room temperature, which is evidence for the formation of the acetylene complex in the first step of the reaction of metallacarborane with acetylene.[117]

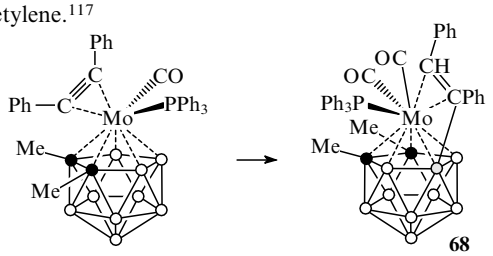

68

Ruthenacarborane $3,3\text{-(CO)}_2\text{-3-THF-3,1,2-RuC}_2\text{B}_9\text{H}_{11}$ (**69**) reacts with $Bu^tC{\equiv}CH$ to give a mixture of isomeric derivatives (Scheme 8), *viz.*, $4,3\text{-}(\sigma,\eta^2\text{-Bu}^t\text{CH}{=}\text{CH})\text{-3,3-(CO)}_2\text{-3,1,2-}$

Scheme 8

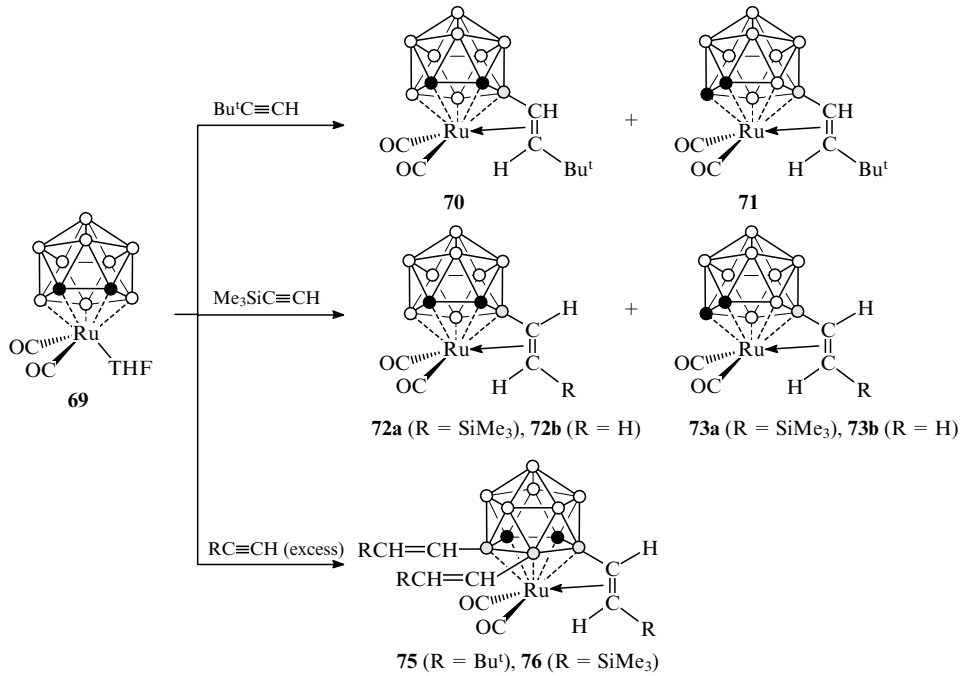

69

70 **71**

72a (R = $SiMe_3$), **72b** (R = H) **73a** (R = $SiMe_3$), **73b** (R = H)

75 (R = Bu^t), **76** (R = $SiMe_3$)

$RuC_2B_9H_{10}$ (**70**)‡ and 8,3-(σ,η^2-Bu^{t}CH = CH)-3,3-$(CO)_2$-3,1,2-$RuC_2B_9H_{10}$ (**71**).[118] The reaction of compound **69** with $Me_3SiC{\equiv}CH$ is accompanied by partial elimination of the $SiMe_3$ group to form a mixture of isomers 4,3-(σ,η^2-RCH = CH)-3,3-$(CO)_2$-3,1,2-$RuC_2B_9H_{10}$ (**72a**,**b**) and 8,3-(σ,η^2-RCH = CH)-3,3-$(CO)_2$-3,1,2-$RuC_2B_9H_{10}$ (**73a**,**b**) (R = $SiMe_3$, H), respectively, with the 4-isomer **72a** predominating.

Compound **73b** reacts with $PhMe_2P$ in heptane to give the ylide complex 8-[σ-$CH_2CH(PMe_2Ph)$]-3,3-$(CO)_2$-3,1,2-$RuC_2B_9H_{10}$ (**74**). Its structure was determined by X-ray diffraction analysis.[118]

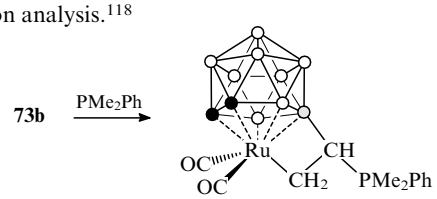

74

The reactions with an excess of alkyne RC≡CH (R = Bu^t, Me_3Si) produce the 4,3-(σ,η^2-RCH = CH)-7,8-(RCH = CH)$_2$-3,3-$(CO)_2$-3,1,2-$RuC_2B_9H_8$ complexes (**75**, R = Bu^t; **76**, R = $SiMe_3$) containing three alkene fragments in the open face of the dicarbollyl ligand. Treatment of complex **75** with trimethylphosphine leads to the replacement of the vinyl substituent from the metal coordination sphere to form 4,7,8-(Bu^{t}CH = CH)$_3$-3,3-$(CO)_2$-3-Me_3P-3,1,2-$RuC_2B_9H_8$ (**77**), whose structure was established by X-ray diffraction analysis. The reaction of PMe_3 with trimethylsilyl derivative **76** yields ylide 4-[σ-CH($SiMe_3$)CH(PMe_3)]-7,8-(Me_3SiCH = CH)$_2$-3,3-$(CO)_2$-3,1,2-$RuC_2B_9H_8$ (**78**).[118]

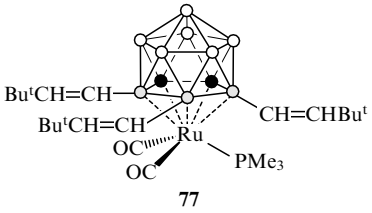

77

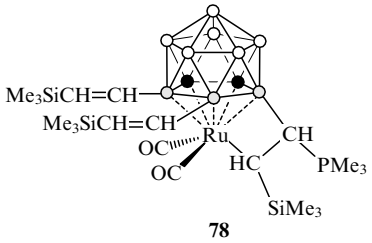

78

Interestingly, the reaction of ruthenacarborane 3-CO-3-Ph_3P-3-THF-3,1,2-$RuC_2B_9H_{11}$ (**79**) containing the triphenylphosphine ligand with a threefold excess of PhC≡CH is accompanied by the selective replacement of the hydrogen atom at position 4 nearest to the carbon atom of the dicarbollyl ligand to form the 4,3-(σ,η^2-PhCH = CH)-3-CO-3-Ph_3P-3,1,2-$RuC_2B_9H_{10}$ complex (**80**), whose structure was established by X-ray diffraction analysis.[119] By contrast, the reaction with a threefold excess of Bu^{t}C≡CH gives the disubstituted derivative 4,3-(σ,η^2-Bu^{t}CH = CH)-8-(Bu^{t}CH = CH)-3-CO-3-Ph_3P-3,1,2-$RuC_2B_9H_9$ (**81**) (Scheme 9). The reactions of the latter with PMe_3, CNBu^t and CO are accompanied by the displacement of the vinyl substituent from the metal coordination sphere to form 4,8-(Bu^{t}CH = CH)$_2$-3-CO-3-Ph_3P-3-L-3,1,2-$RuC_2B_9H_9$ (**82**) (L = PMe_3, CNBu^t and CO, respectively). The reaction of compound **79** with $Me_3SiC{\equiv}CH$ yields the 4,3-(σ,η^2-H_2C = CH)-3-CO-3-Ph_3P-3,1,2-$RuC_2B_9H_{10}$ isomer (**83**) as the only product. The latter reacts with CNBu^t and Me_3P to form 4-(H_2C = CH)-3-CO-3-Ph_3P-3-Bu^{t}NC-3,1,2-$RuC_2B_9H_{10}$ (**84**)§ and ylide 4-[σ-$CH_2CH(PMe_3)$]-3-CO-3-Ph_3P-3,1,2-$RuC_2B_9H_{10}$ (**85**), respectively.[119]

‡ The structure of complex **70** was established by X-ray diffraction.[118]

§ The structure of compound **84** was established by X-ray diffraction.

Scheme 9

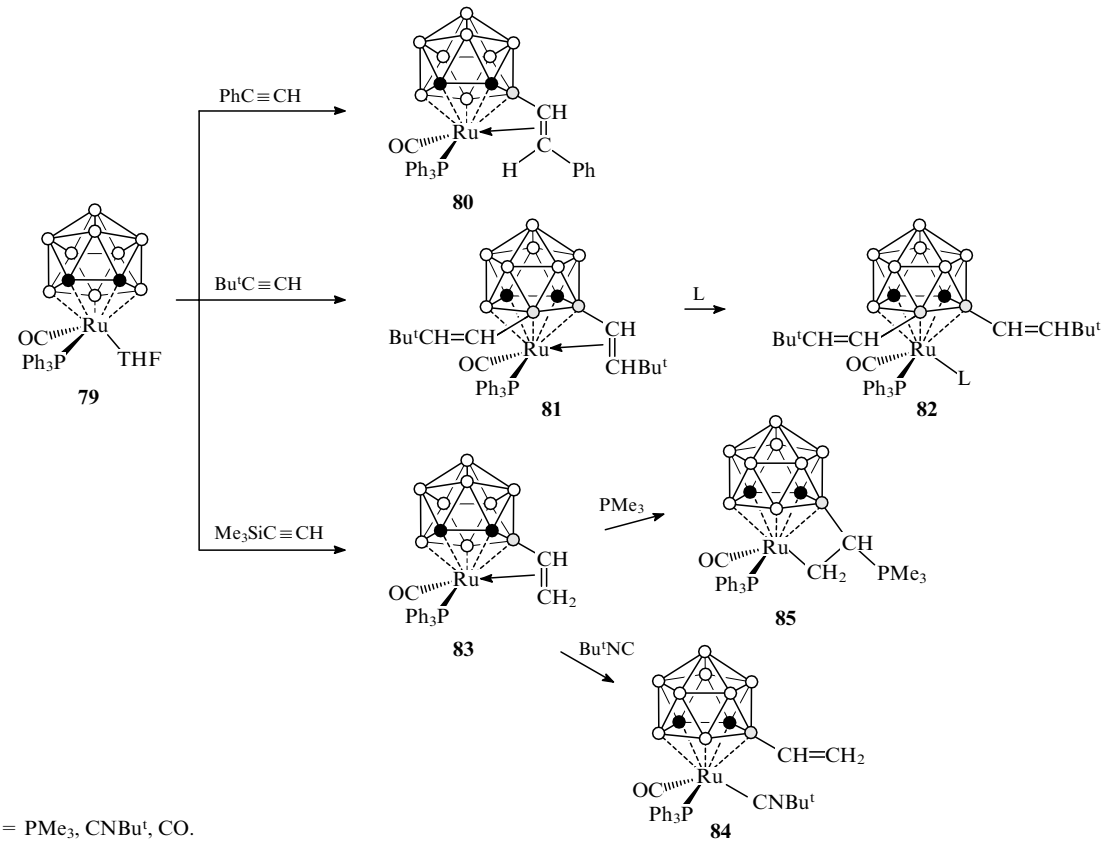

79 **80** **81** **82** **83** **85** **84**

L = PMe_3, CNBu^t, CO.

In most of the above-described examples, the reactions with the use of an excess of alkyne lead to the replacement of the H atoms in the band of the dicarbollyl ligand nearest to the metal atom; the degree of substitution may be as high as 3 (compounds **75** and **76**). The assumed mechanism of substitution involves the replacement of the labile ligand (for example, THF or CO) with the alkyne group η^2-RC≡CR, the rearrangement of the latter to form the vinylidene fragment Ru=C=CHR, its subsequent insertion into the B–H bond of the dicarbollyl ligand, and the displacement of the vinyl substituent from the metal coordination sphere with the next alkyne molecule. However, the degree of substitution in ruthenacarborane **79** containing the PPh_3 ligand in the presence of an excess of alkyne is no higher than 2, which is attributable to steric hindrance caused by the bulky triphenylphosphine substituent. However, the influence of the electronic properties of the ligands involved in the coordination environment about the metal atom on the depth of substitution cannot also be ruled out.

Recently, it has been demonstrated that metal-induced activation of the B–H bond can occur not only in metallacarboranes but also in metal complexes containing substituted *o*-carborane derivatives as a ligand. For example, the reaction of the Cp*Rh(1,2-S_2-1,2-$C_2B_{10}H_{10}$) complex with HC≡CCOOMe affords the substituted Cp*Rh(3,6-(μ-MeOOCCH=CH)$_2$-1,2-S_2-1,2-$C_2B_{10}H_8$) complex.[120, 121]

The rearrangement of the alkylidyne complexes belong to another type of reactions involving metal. The reaction of [Et_4N][1,2-Me_2-3-(≡CR)-3,3-$(CO)_2$-3,1,2-$WC_2B_9H_9$] [R = C_6H_4Me-4 (**86**), Me (**87**)] with $HBF_4 \cdot Et_2O$ in a saturated CO solution in dichloromethane is accompanied by the migration of the alkylidyne group to the carborane moiety to form the 8-RCH_2-1,2-Me_2-3,3,3,3-$(CO)_4$-3,1,2-$WC_2B_9H_8$ complexes (**88**, **89**).[122]

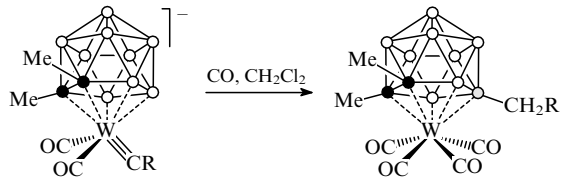

86, **87** **88**, **89**

R = C_6H_4Me-4 (**86**, **88**), Me (**87**, **89**).

The reactions of compound **87** with $HBF_4 \cdot Et_2O$ and $Ph_2PCH_2CH_2PPh_2$ (dppe) or $Me_2PCH_2CH_2PMe_2$ (dmpe) in dichloromethane produce 8-Et-1,2-Me_2-3,3-$(CO)_2$-3,3-(μ-L_2)-3,1,2-$WC_2B_9H_8$ [L_2 = dppe (**90**) or dmpe (**91**)].[123]

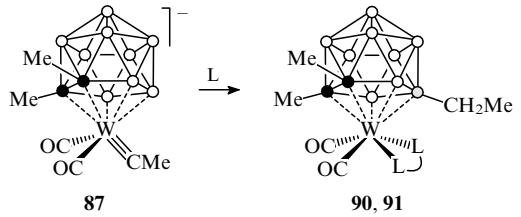

87 **90**, **91**

L–L = dppe (**90**), dmpe (**91**).

The reaction of [Et_4N][1,2-Me_2-3-(≡CC_6H_4Me-4)-3-CO-3-$P(OMe)_3$-3,1,2-$MoC_2B_9H_9$] (**92**) with $Fe_2(CO)_9$ proceeds through the intermediate formation of 8-[σ-CH(C_6H_4Me-4)]-1,2-Me_2-3,3,3-$(CO)_3$-3,1,2-$MoC_2B_9H_8$ (**93**), which was isolated in the individual state. Treatment of compound **93** with $HBF_4 \cdot Et_2O$ and PMe_3 afforded a mixture of 8-(4-$MeC_6H_4CH_2$)-1,2-Me_2-3,3,3,3-$(CO)_4$-3,1,2-$MoC_2B_9H_8$ (**94**) and 8-(4-$MeC_6H_4CH_2$)-1,2-Me_2-3,3,3-$(CO)_3$-3-Me_3P-3,1,2-$MoC_2B_9H_8$ (**95**).[124]

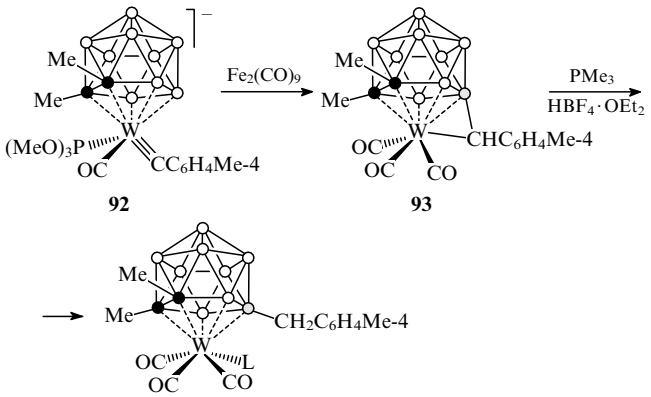

92 **93**

94 (L = CO), **95** (L = PMe_3)

The reaction of the complex Y[**86**] (Y = $(Ph_3P)_2N$ (PPN), Ph_4P or Et_4N) with 1 equiv. of HX (X = Cl or I) proceeds in a more complex way and is accompanied not only by migration of the alkylidyne group from metal to the boron atom but also by the skeletal rearrangement of the dicarbollyl ligand to form Y[11-(4-$MeC_6H_4CH_2$)-1,8-Me_2-2-X-2,2,2-$(CO)_3$-2,1,8-$WC_2B_9H_8$] [X = Cl (**96**) or I (**97**)]. The reaction of the complex [Et_4N][**87**] with HI proceeds analogously to give [Et_4N][11-Et-1,8-Me_2-2-I-2,2,2-$(CO)_3$-2,1,8-$WC_2B_9H_8$] (**98**).[124, 125]

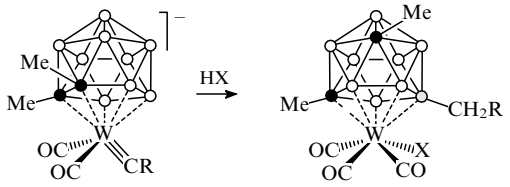

86, **87** **96**–**98**

R = C_6H_4Me-4 (**86**, **96**, **97**), Me (**87**, **98**); X = Cl (**96**), I (**97**, **98**).

The rearrangement of 3,3-$(Ph_3P)_2$-3,1,2-$NiC_2B_9H_{11}$ (**99**) into 3,8-$(Ph_3P)_2$-3-H-3,1,2-$NiC_2B_9H_{10}$ (**100**) in boiling benzene[126] provides another example of substitution caused by migration of a ligand from the metal atom to the carborane moiety. The reaction of nickelacarborane **99** with CO is accompanied by the replacement of one Ph_3P ligand with the carbonyl group to form complex **101**. Refluxing of the latter in benzene under CO pressure results not only in migration of the triphenylphosphine ligand to the carborane moiety but also in dimerisation to give *closo*-[3-(μ-CO)-8-Ph_3P-3,1,2-$NiC_2B_9H_{10}$]$_2$ (**102**) containing the Ni–Ni bond. The structure of complex **102** was established by X-ray diffraction analysis.[127, 128] Compound **102** can also be prepared by refluxing compound **100** in benzene under CO pressure.

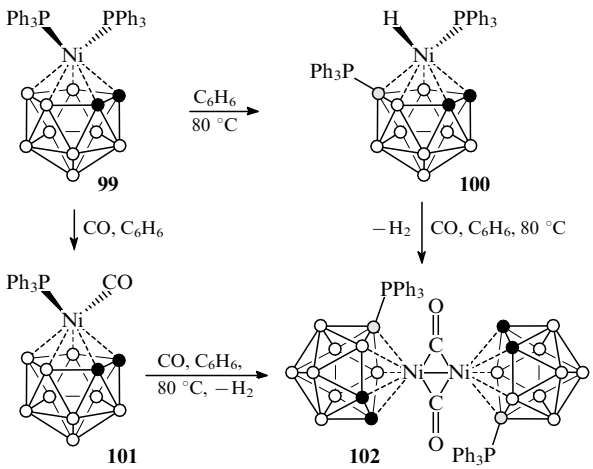

99 **100**

101 **102**

The reaction of tris(dimethylamino)-*closo*-tantalacarborane **103** with four equivalents of thiophenol producing the charge-compensated 8-Me_2HN-3,3,3,3-$(SPh)_4$-3,1,2-$TaC_2B_9H_{10}$ complex (**104**) is yet another example of migration of a ligand from the metal atom to the carborane cage. The structure of compound **104** was determined by X-ray diffraction analysis.[129]

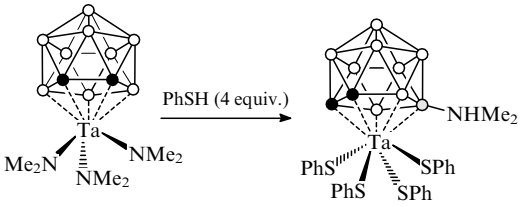

103 **104**

It should be noted that the primary substitution in all metallacarboranes containing the 7,8-dicarbollyl ligand (except for mercuration reactions) occurs at the position adjacent to the metal atom, *i.e.*, the hydrogen atoms at the boron atoms belonging to the open pentagonal face of the ligand are replaced. In the case of both electrophilic and electrophile induced nucleophilic substitution, the primary attack occurs at position 8 of metallacarborane, whereas the substitution with the direct involvement of the metal atom proceeds less selectively.

2. Derivatives based on the 7,9-dicarbollyl ligand $[7,9\text{-}C_2B_9H_{11}]^{2-}$

Substitution in metallacarboranes based on the 7,9-dicarbollyl ligand was exemplified by the only metallacarborane, *viz.*, bis(1,7-dicarbollyl)cobalt [*commo*-2,2′-$Co(1,7\text{-}C_2B_9H_{11})_2]^-$ (**105**) (the atomic numbering scheme is shown in Fig. 1 *e*). Substitution in complex **105** resembles that in analogous complex **1** (see p. 435) and is accompanied by the formation of compounds containing various bridges between two dicarbollyl ligands. For instance, the reaction of complex **105** with carbon disulfide in the presence of $AlCl_3$ and HCl affords (μ-HCS_2)-2,2′-$Co(1,7\text{-}C_2B_9H_{10})_2$ (**106**) with the three-atom SCS bridge.[89]

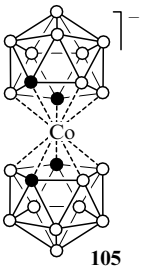

105

The reaction of complex **105** with formaldehyde in an HCl(conc.)–$CHCl_3$ mixture at 60 °C gives rise to the bridged 6,6′-(μ-MeO)-2,2′-$Co(1,7\text{-}C_2B_9H_{10})_2$ compound (**107**) in high yield. The latter is readily demethylated with Lewis bases in methanol to form [6,6′-(μ-O)-2,2′-$Co(1,7\text{-}C_2B_9H_{10})_2]^-$.[130]

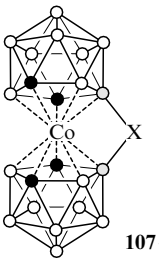

107–**119**

X = OMe (**107**), NH_2 (**108**), NMe_2 (**109**), NHMe (**110**), S (**111**), SEt (**112**), SPr^n (**113**), SPr^i (**114**), SBu^n (**115**), SC_6H_{13} (**116**), $SCH_2CH{=}CH_2$ (**117**), $SCH_2C(O)OMe$ (**118**), PMe_2 (**119**).

The reaction of compound **105** with $NaNO_2$ in benzene in the presence of sulfuric acid produces the corresponding derivative 6,6′-(μ-H_2N)-2,2′-$Co(1,7\text{-}C_2B_9H_{10})_2$ (**108**) with a one-atom nitrogen bridge. Treatment of the latter with dimethyl sulfate in 30% NaOH affords the *N*,*N*-dimethylation product 6,6′-(μ-Me_2N)-2,2′-$Co(1,7\text{-}C_2B_9H_{10})_2$ (**109**). The monoalkylated complex 6,6′-(μ-MeNH)-2,2′-$Co(1,7\text{-}C_2B_9H_{10})_2$ (**110**) was prepared by treatment of a benzene suspension of [Me_4N][6,6′-(μ-HN)-2,2′-$Co(1,7\text{-}C_2B_9H_{10})_2$] with diiodomethane in 10% aqueous alkali.[130]

The reaction of complex **105** with sulfur in benzene in the presence of $AlCl_3$ at 80 °C yields the [6,6′-(μ-S)-2,2′-$Co(1,7\text{-}C_2B_9H_{10})_2]^-$ complex (**111**),[131] whose alkylation with various alkyl halides in isopropyl alcohol affords the corresponding alkylsulfonium derivatives 6,6′-(μ-RS)-2,2′-$Co(1,7\text{-}C_2B_9H_{10})_2$ [R = Et (**112**), Pr^n (**113**), Pr^i (**114**), Bu^n (**115**), C_6H_{13} (**116**) or $CH_2CH{=}CH_2$ (**117**)].[130, 132] The reaction of complex **105** with chloroacetic acid in an aqueous Na_2CO_3 solution gives an acid, whose esterification in methanol in the presence of $SOCl_2$ affords 6,6′-(μ-$MeOC(O)CH_2S$)-2,2′-$Co(1,7\text{-}C_2B_9H_{10})_2$ (**118**).[130]

The reaction of compound **105** with phosphorus in benzene at 80 °C followed by reaction with dimethyl sulfate in the presence of sodium hydroxide in ethanol gives rise to a mixture of 6,6′-(μ-Me_2P)-2,2′-$Co(1,7\text{-}C_2B_9H_{10})_2$ (**119**) and 6-Me_3P-2,2′-$Co(1,7\text{-}C_2B_9H_{10})(1',7'\text{-}C_2B_9H_{11})$ (**120**).[108]

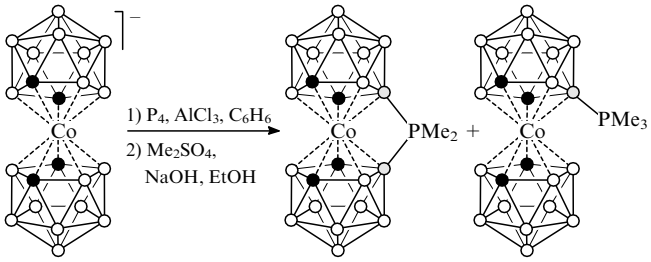

105 **119** **120**

It should be noted that in all the above-described reactions, substitution in metallacarboranes occurs at position 6 adjacent to the metal atom.

3. Derivatives based on the carbollyl ligand $[CB_{10}H_{11}]^{3-}$

There are abundant data on substitution in metallacarboranes based on the carbollyl ligand $[CB_{10}H_{11}]^{3-}$. As in the case of metallacarboranes based on the 7,8-dicarbollyl anion, substitution in metal complexes with carbollyl ligands can occur involving both the metal and boron atoms (by the mechanism of electrophilic or electrophile induced nucleophilic substitution).

The reactions of ferracarboranes [PPN][2,2-$(CO)_2$-2-L-2,1-$FeCB_{10}H_{11}$] [L = SMe_2 (**121**) or PPh_3 (**122**)] with sulfuric acid in dimethyl sulfide or tetrahydrofuran produce charge-compensated products of electrophile induced nucleophilic substitution with composition 7-L′-2,2-$(CO)_2$-2-L-2,1-$FeCB_{10}H_{10}$ [L = SMe_2: L′ = SMe_2 (**123**), $O(CH_2)_4$ (**124**); L = PPh_3: L′ = SMe_2 (**125**), $O(CH_2)_4$ (**126**)] containing the L′ substituent in the open face at position 7, which is one of the most remote from the carbon atom.[133]

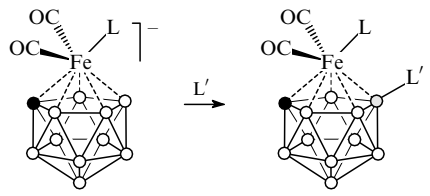

121, **122** **123**–**126**

L = SMe_2 (**121**, **123**, **124**), PPh_3 (**122**, **125**, **126**);
L′ = SMe_2 (**123**, **125**), $O(CH_2)_4$ (**124**, **126**).

The reactions with the [PPN][2,2,2-(CO)$_3$-2-L-2,1-MCB$_{10}$H$_{11}$] complexes [L = Ph$_3$P: M = Mo (**127**), W (**128**); L = Bu^{t}NC: M = Mo (**129**), W (**130**)] proceed analogously. For example, the reactions of compounds **127** – **130** with CF_3SO_3Me or sulfuric acid in the presence of the donors of L′ [L′ = SMe$_2$, OEt$_2$, O(CH$_2$)$_4$, S(CH$_2$)$_4$, cyclo-1,4,7-S$_3$(CH$_2$)$_6$, NCBu^t, CNBu^t, CNC$_6$H$_3$Me$_2$-2,6] give rise to the corresponding zwitterionic 7-L′-2,2,2-(CO)$_3$-2-L-2,1-MCB$_{10}$H$_{10}$ complexes (**131** – **134**).[134] The structure of molybdacarborane 7-CNBu^t-2,2,2-(CO)$_3$-2-Ph$_3$P-2,1-MoCB$_{10}$H$_{10}$ (**131g**) was confirmed by X-ray diffraction analysis.[134]

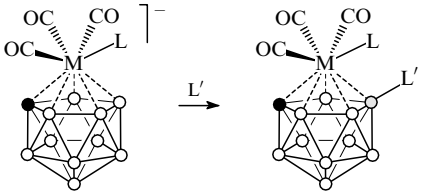

127 – **130** **131a** – **h**, **132a** – **h**, **133**, **134**

L = PPh$_3$: M = Mo (**127**, **131a** – **h**), W (**128**, **132a** – **h**); L′ = SMe$_2$ (**a**), OEt$_2$ (**b**), O(CH$_2$)$_4$ (**c**), S(CH$_2$)$_4$ (**d**), cyclo- 1,4,7-S$_3$(CH$_2$)$_6$ (**e**), NCBu^t (**f**), CNBu^t (**g**), CNC$_6$H$_3$Me$_2$-2,6 (**h**);
L = CNBu^t: M = Mo (**129**, **133**), W (**130**, **134**); L′ = OEt$_2$ (**133**, **134**).

Treatment of compounds **132b** and **132c** with trimethylamine oxide in the presence of Ph$_4$PBr in tetrahydrofuran affords the corresponding alkoxy derivatives [Ph$_4$P][7-RO-2,2,2-(CO)$_3$-2-Ph$_3$P-2,1-WCB$_{10}$H$_{10}$] (R = Et, (CH$_2$)$_3$CHO).[134]

The reaction of cobaltacarborane [PPN][2-Et$_3$P-2-NO-2,1-CoCB$_{10}$H$_{11}$] with methyl triflate in a mixture of CH_2Cl_2 and THF yields the corresponding charge-compensated derivative 7-(CH$_2$)$_4$O-2-Et$_3$P-2-NO-2,1-CoCB$_{10}$H$_{10}$,[133] whereas the reaction in a mixture of CH_2Cl_2 and acetonitrile affords 7-MeCN-2-Et$_3$P-2-NO-2,1-CoCB$_{10}$H$_{10}$ with an impurity of *closo*-7-(NMe=CHMe)-2-Et$_3$P-2-NO-2,1-CoCB$_{10}$H$_{11}$.[135]

The reactions of ferracarboranes [PPN][2,2-(CO)$_2$-2-L-2,1-FeCB$_{10}$H$_{11}$] [L = PPh$_3$ (**122**), CO (**135**), Bu^{t}NC (**136**)] with methyl triflate in acetonitrile produce 7-[(*E*)-MeCH=NMe]-2,2-(CO)$_2$-2-L-2,1-FeCB$_{10}$H$_{10}$ (**137** – **139**) [L = PPh$_3$ (**137**), CO (**138**), Bu^{t}NC (**139**)] (Scheme 10).[133] It is assumed that acetonitrile is initially methylated with methyl triflate to form the *N*-methylnitrilium cation [MeC≡NMe]$^+$,[136] which is involved in electrophile induced nucleophilic substitution (Scheme 10).

The *E* form of an imine is, apparently, more stable due to which only one isomer is formed. Complex **138** is readily hydrolysed in the presence of bases as catalysts to give 7-MeH$_2$N-2,2,2-(CO)$_3$-2,1-FeCB$_{10}$H$_{10}$ and is reduced to 7-Me(Et)HN-2,2,2-(CO)$_3$-2,1-FeCB$_{10}$H$_{10}$ in the presence of Na[BH$_3$CN].[133]

As in the case of analogous iron complexes, the reactions of compounds **127** and **128** with CF_3SO_3Me in acetonitrile produce the iminium derivatives 7-[(*E*)-MeCH=NMe]-2,2,2-(CO)$_3$-2-Ph$_3$P-2,1-MCB$_{10}$H$_{10}$ (M = Mo, W). The reaction with the use of Bu^{t}NC instead of acetonitrile gives rise to a mixture of *E* and *Z* isomers of 7-(MeCH=NBu^t)-2,2,2-(CO)$_3$-2-Ph$_3$P-2,1-MCB$_{10}$H$_{10}$.[134]

Substitution in *C*-substituted molybdacarborane [PPN][1,2-[μ-MeC(O)NH]-2,2,2-(CO)$_3$-2,1-MoCB$_{10}$H$_{10}$] (**140**) occurs analogously. The reaction of complex **140** with CF_3SO_3Me in a mixture of THF and dichloromethane yields the charge-compensated 7-(CH$_2$)$_4$O-1,2-[μ-MeC(O)NH]-2,2,2-(CO)$_3$-2,1-MoCB$_{10}$H$_9$ complex (**141**). The reaction of complex **140** with concentrated sulfuric acid in a CH_2Cl_2 – SMe$_2$ mixture affords the

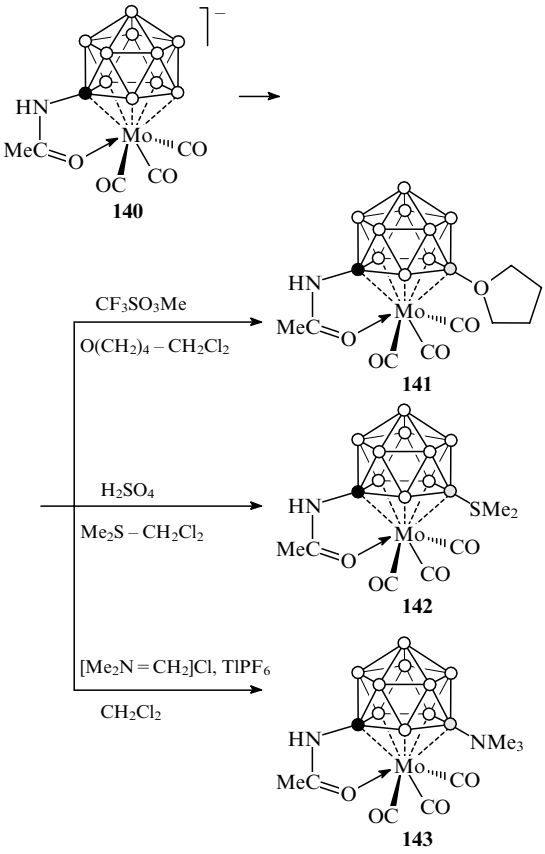

Scheme 10

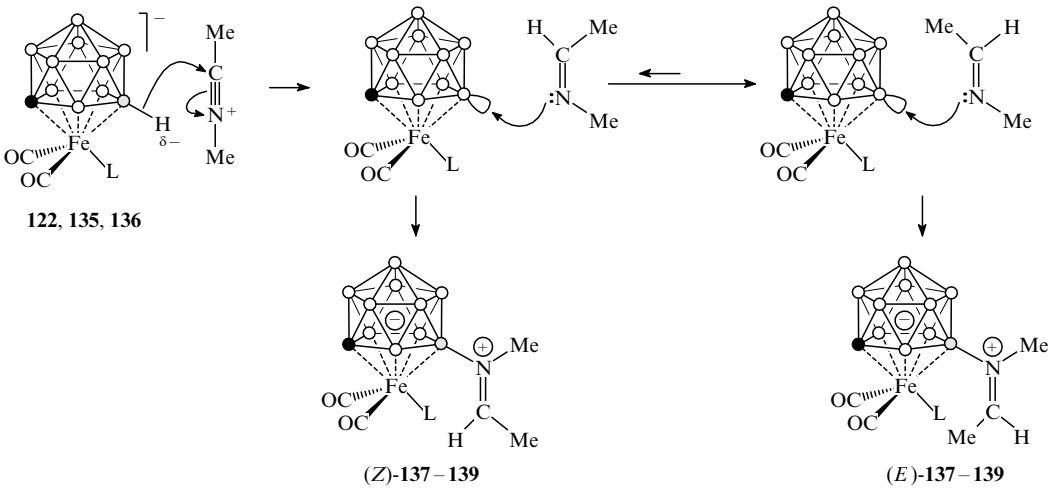

122, **135**, **136** (*Z*)-**137** – **139** (*E*)-**137** – **139**

L = PPh$_3$ (**122**, **137**), CO (**135**, **138**), Bu^{t}NC (**136**, **139**).

dimethylsulfonium derivative 7-Me_2S-1,2-[μ-MeC(O)NH]-2,2,2-$(CO)_3$-2,1-$MoCB_{10}H_9$ (**142**), whereas the reaction of this complex with $[Me_2N=CH_2]Cl$ and $TlPF_6$ in dichloromethane gives the corresponding trimethylammonium derivative 7-Me_3N-1-[μ-MeC(O)NH]-2,2,2-$(CO)_3$-2,1-$MoCB_{10}H_9$ (**143**).[137]

Interestingly, the reaction of [PPN][2,2-$(CO)_2$-2-(η^2-Bu^{t}C≡CH)-2,1-$MCB_{10}H_{11}$] (M = Mo, W) with CF_3SO_3Me in a $CH_2Cl_2-Et_2O$ mixture produces the corresponding charge-compensated derivatives 7-Et_2O-2,2-$(CO)_2$-2-(η^2-Bu^{t}C≡CH)-2,1-$MCB_{10}H_{10}$ rather than leads to the rearrangement of the Bu^{t}C≡CH ligand followed by the insertion of the alkene fragment at the B—H bond (which occurs in the reactions of alkyne dicarbollyl complexes).[134] By contrast, the reaction of ferracarborane **135** with *tert*-butylacetylene in THF in the presence of Me_3NO forms 3-[η^2-(*E*)-Bu^{t}CH = CH]-2,2,2-$(CO)_3$-2,1-$FeCB_{10}H_{10}$ (**144**), *i.e.*, substitution (as in the case of metallacarboranes based on the dicarbollyl ligand) occurs at the position adjacent to the carbon atom in the open face of the carborane ligand. The reaction of complex **144** with CF_3SO_3Me in acetonitrile affords 3-[η^2-(*E*)-Bu^{t}CH=CH]-7-(MeCH=NMe)-2,2,2-$(CO)_3$-2,1-$FeCB_{10}H_9$, in which the imine fragment is located in the open face of the carborane ligand occupying the position most remote from the carbon atom and the boron atom bearing the alkene substituent.[133]

Under similar conditions, the reactions of platinacarborane Na[2,2-$(Et_3P)_2$-2,1-$PtCB_{10}H_{11}$] (**145**) with PhSeCl and PhTeI in tetrahydrofuran proceed differently. The reaction with PhTeI proceeds according to the electrophilic mechanism to give (after chromatography with the use of CH_2Cl_2 as the eluent) the charge-compensated 7-$ClCH_2$(Ph)Te-2,2-$(Et_3P)_2$-2,1-$PtCB_{10}H_{10}$ complex (**146**), whose structure was established by X-ray diffraction analysis. By contrast, the reaction with PhSeCl proceeds with the participation of the metal atom to give a mixture of 7,2-$(PhSe)_2$-2-Et_3P-2,1-$PtCB_{10}H_{10}$ (**147**), 3,2-$(PhSe)_2$-2-Et_3P-2,1-$PtCB_{10}H_{10}$ (**148**) and 3-$Cl(CH_2)_4O$-2-PhSe-2-Et_3P-2,1-$PtCB_{10}H_{10}$ (**149**).¶ It is assumed that complex **149** is generated as a result of the tetrahydrofuran-ring opening in the oxonium derivative under the action of the chloride ion.[138]

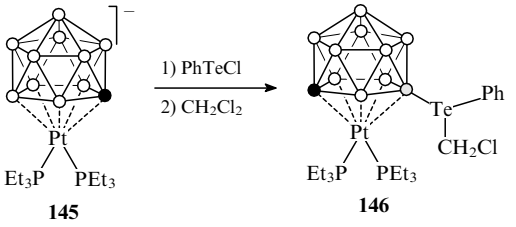

145 **146**

¶ The structure of complex **149** was established by X-ray diffraction.

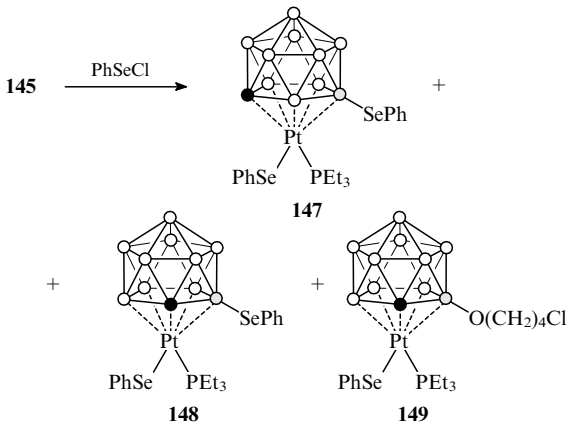

147 **148** **149**

The reactions of metallacarboranes, which contain labile ligands in the metal coordination sphere, with halides proceed in an unusual way. For example, treatment of the molybdenum complex [PPN][2,2,2,2-$(CO)_4$-2,1-$MoCB_{10}H_{11}$] (**150**) with iodine in tetrahydrofuran leads not only to the replacement of one of the carbonyl ligands with iodine but also to the replacement of the hydrogen atom at position 7 of the carborane moiety with tetrahydrofuran to form [PPN][7-$(CH_2)_4$O-2,2,2-$(CO)_3$-2-I-2,1-$MoCB_{10}H_{10}$] (**151**) (Scheme 11). The structure of complex **151** was determined by X-ray diffraction analysis. The reaction of a solution of compound **151** in tetrahydrothiophene with iodine is accompanied by the replacement of one more hydrogen atom in the open face of the carborane ligand with tetrahydrothiophene to give the neutral 3-$(CH_2)_4S$-11-$(CH_2)_4O$-2,2,2-$(CO)_3$-2-I-2,1-$MoCB_{10}H_9$ complex (**152**). The reaction of complex **150** with iodine in CH_2Cl_2 in the presence of cyclic thioesters (L) also affords two types of substituted molybdacarboranes. In both cases, the substitution involves the metal atom (one of the carbonyl groups at the Mo atom is replaced with the iodide ion). Derivatives of one type, *viz.*, 3,11-L_2-2,2,2-$(CO)_3$-2-I-2,1-$MoCB_{10}H_9$ (**153**), contain two sulfonium substituents in the open face of the monocarbollyl ligand, whereas derivatives of another type, *viz.*, 7-L-2,3-(μ-I)-2,2,2-$(CO)_3$-2,1-$MoCB_{10}H_9$ (**154**) and 11-L-2,3-(μ-I)-2,2,2-$(CO)_3$-2,1-$MoCB_{10}H_9$ (**155**), bear the sulfonium substituent along with the bridging iodine atom between Mo and the boron atom at the position nearest to the carbon atom.[139]

The reactions of the molybdenum complexes [PPN][3-Me_3N-2,2,2-$(CO)_3$-2-X-2,1-$MoCB_{10}H_{10}$] [X = I (**156**) or Br (**157**)] with 1,4-dithiane and iodine in dichloromethane afford the 3-Me_3N-6-$S(CH_2CH_2)_2S$-2,2,2-$(CO)_3$-2-I-2,1-$MoCB_{10}H_9$ complex containing substituents in the pentagonal face of the monocarbollyl ligand at the positions adjacent to the carbon atom. Interestingly,

Scheme 11

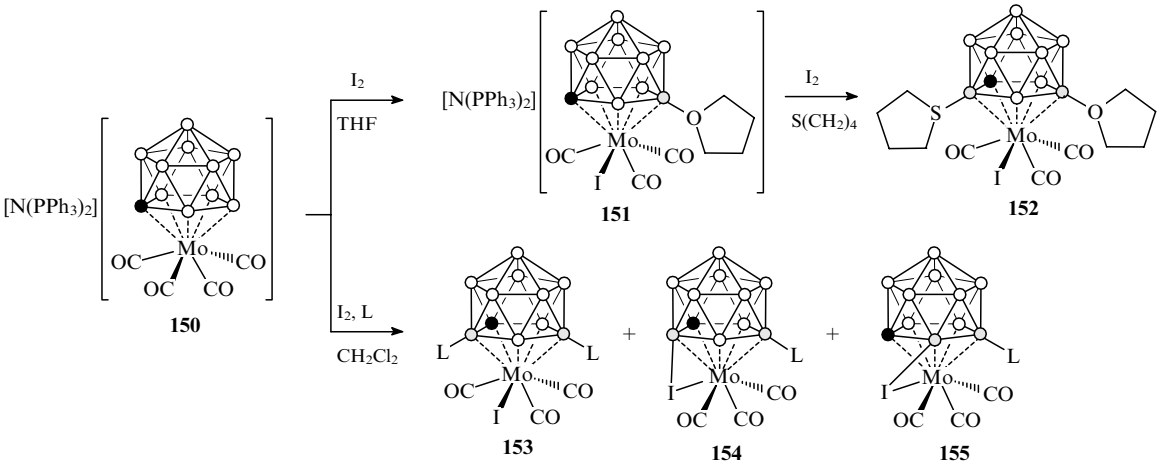

150 **151** **152** **153** **154** **155**

the reaction of [PPN][3-Me_3N-2,2,2-$(CO)_3$-2-Br-2,1-$MoCB_{10}H_{10}$] (**157**) with Bu^tNC and iodine (or bromine) in dichloromethane leads to the replacement of the trimethylamino group in the monocarbollyl ligand with the halogen atom to form 3-Y-2,2,2,2-$(Bu^tNC)_4$-2-Br-2,1-$MoCB_{10}H_{10}$ [Y = Br (**159**) or I (**160**)].[140]

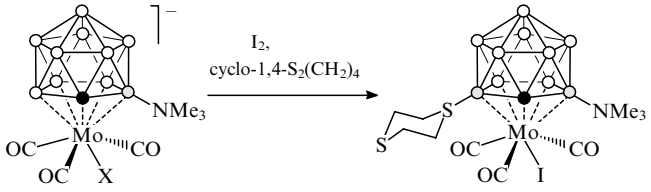

156 (X = I), **157** (X = Br) **158**

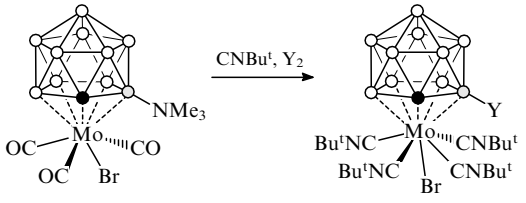

157 **159** (Y = Br), **160** (Y = I)

Y = Br, I.

It should be noted that in none of the above-considered reactions does the replacement of the hydrogen atom with halogen occur through the mechanism of electrophilic substitution.

4. Dicobaltacarborane derivatives

The reaction of dicobaltacarborane 3,6-Cp_2-3,6,1,2-$Co_2C_2B_8H_{10}$ (**161**) containing two CpCo fragments with mercury acetate in boiling dichloromethane (Scheme 12) followed by the replacement of the acetate group with chlorine gives rise to a mixture of 3,6-Cp_2-8-HgCl-3,6,1,2-$Co_2C_2B_8H_9$ (**162**)† and 3,6-Cp_2-9-HgCl-3,6,1,2-$Co_2C_2B_8H_9$ (**163**) in a ratio of 1 : 1.2.[141]

† The structure of 8-monomercury derivative **162** was confirmed by X-ray diffraction.[126]

The reaction with an excess of mercury acetate in acetic acid allows one to introduce up to four substituents into the carborane moiety to form the 3,6-Cp_2-8,10,9,12-$(HgCl)_4$-3,6,1,2-$Co_2C_2B_8H_6$ complex (**164**).

An attempt to prepare a thallium derivative by the reaction of complex **161** with thallium(III) trifluoroacetate in trifluoroacetic acid failed; instead, this reaction gave 8,9-bistrifluoroacetate derivative **165**.[141]

IV. Substitution in non-icosahedral metallacarboranes

Substitution in non-icosahedral metallacarboranes has received less study because these compounds are less readily accessible. Substitution in 10- and 11-vertex metallacarboranes was studied only for CpCo carboranes.

1. Substitution in 11-vertex cobaltacarboranes

Zakharkin *et al.*[142] studied bromination of 1-Cp-1,2,3-$CoC_2B_8H_{10}$ (**166**). The reaction of complex **166** with 1 equiv. of bromine in dichloromethane in the absence of a catalyst or in the presence of $AlCl_3$ produces a mixture of the isomeric bromine derivatives 10-Br-1-Cp-1,2,3-$CoC_2B_8H_9$ (**167**) and 4-Br-1-Cp-1,2,3-$CoC_2B_8H_9$ (**168**). The reaction with the use of glacial acetic acid as the solvent gives a mixture of the same monobromides with an impurity of dibromo derivatives. The ratio between the 10- and 4-isomers is (4.5 – 6) : 1. The structure of complex **166** was established by X-ray diffraction analysis.[142]

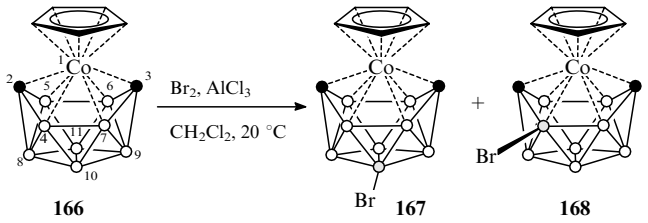

166 **167** **168**

The reactions of complex **166** with two, three or four equivalents of bromine in the presence of $AlCl_3$ yield a mixture of di-,

Scheme 12

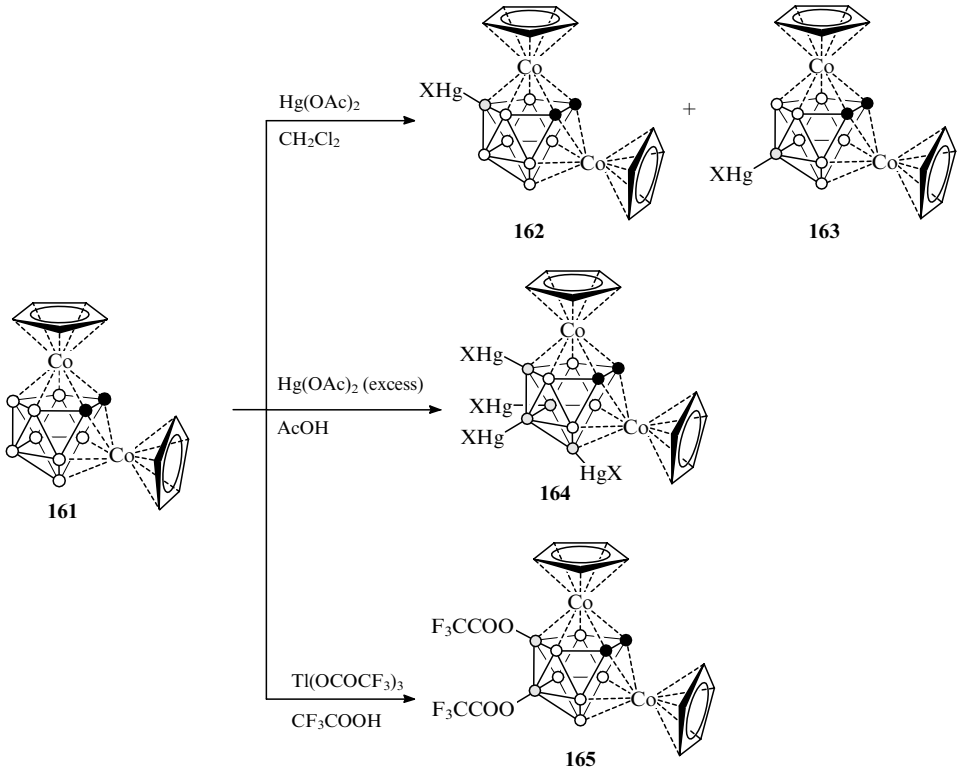

161 **162** **163** **164** **165**

tri- and tetrabromo derivatives. Attempts to separate these derivatives failed. The pentabromo derivative 4,5,6,10,11-Br_5-1-Cp-1,2,3-$CoC_2B_8H_5$ was synthesised by refluxing compound **166** with 8 equiv. of bromine in the presence of $AlCl_3$ in dichloromethane.[142]

Based on the above results, it was hypothesised that the electron density on the boron atoms of the π-carborane ligand decreases in the series B(10, 11) > B(4, 5, 6, 7) > B(8, 9).

The reaction of cobaltacarborane *isonido*-1-Cp-1,2,4-$CoC_2B_8H_{10}$ (**169**) (which is isomeric to compound **166**) with 1 equiv. of bromine in CCl_4 produces two isomeric monobromides, *viz*., 3-Br-1-Cp-1,2,4-$CoC_2B_8H_9$ (**170**) and 6-Br-1-Cp-1,2,4-$CoC_2B_8H_9$ (**171**), in a ratio of 1 : 10.[143]

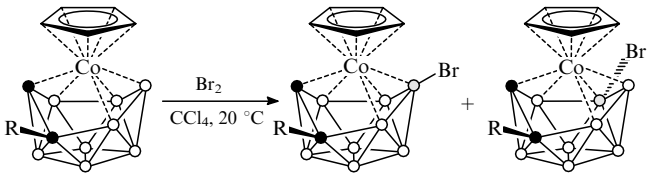

169, **172** **170**, **173** **171**, **174**

R = H (**169**, **170**, **171**), Me (**172**, **173**, **174**).

The reaction of complex **169** with *N*-bromosuccinimide also gives rise to a mixture of monobromides **170** and **171**, but in much lower yields.

At room temperature, each isomer in a benzene solution slowly (during two days) undergoes rearrangement to form an equilibrium mixture of monobromides **170** and **171** in a ratio of 1 : 1.3. This suggests that isomer **171** is a kinetic substitution product, whereas isomer **170** is a rearrangement product.

Only 6-Br-4-Me-1-Cp-1,2,4-$CoC_2B_8H_8$ (**174**) was isolated as a product of bromination of the *C*-methyl derivative *isonido*-4-Me-1-Cp-1,2,4-$CoC_2B_8H_9$ (**172**). This product underwent partial rearrangement into complex **173** (presumably) upon prolonged storage in a benzene solution. However, the percentage of **173** (according to the ^{11}B NMR spectroscopic data) was no higher than 10%.[143] Evidently, the introduction of the methyl substituent at the C(4) atom hinders the rearrangement of the substitution product.

It should be noted that chloro-substituted derivatives of isostructural metallacarboranes 3-Cl-1-(η^6-Ar)-1,2,4-$RuC_2B_8H_9$ and 6-Cl-1-(η^6-Ar)-1,2,4-$RuC_2B_8H_9$ (Ar = C_6H_6, PhMe, 1,4-$Me_2C_6H_4$, 1-Me-4-$Pr^iC_6H_4$, 1,2,4-$Me_3C_6H_3$, 1,3,6-$Me_3C_6H_3$, 1,2,4,5-$Me_4C_6H_2$, C_6Me_6) were prepared by the reactions of $RuCl_2(PPh_3)_3$ with *nido*-5,6-$C_2B_8H_{12}$ in benzene and other aromatic solvents.[144] The reaction of *nido*-7-Br-5,6-$C_2B_8H_{11}$ with $[(\eta^6\text{-}C_6Me_6)RuCl_2]_2$ also produces a mixture of isomers 5-Br-1-(η^6-C_6Me_6)-1,2,4-$RuC_2B_8H_9$ and 7-Br-1-(η^6-C_6Me_6)-1,2,4-$RuC_2B_8H_9$.[145] The formation of such pairs of halogen derivatives indicates that the rearrangements of various metallacarboranes with the 1,2,4-MC_2B_8 skeleton occur by a similar mechanism.

The reaction of compound **169** with a tenfold excess of bromine produces exclusively the dibromo derivative 6,9-Br_2-1-Cp-1,2,4-$CoC_2B_8H_8$ (**175**). Derivatives containing the bromine atom at position 3 of the cobaltacarborane moiety were not found.[143]

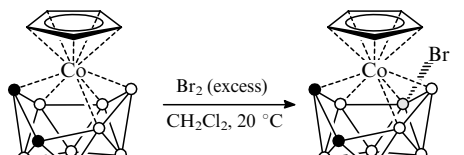

169 **175**

The chloromercury derivative 6-HgCl-1-Cp-1,2,4-$CoC_2B_8H_9$ (**176**) was synthesised by mercuration of complex **169** with mercury trifluoroacetate followed by treatment of the resulting complex with NaCl. The structure of compound **176** was established by X-ray diffraction analysis. The reaction of compound **176** with bromine in dichloromethane at room temperature affords monobromide **171**.[143]

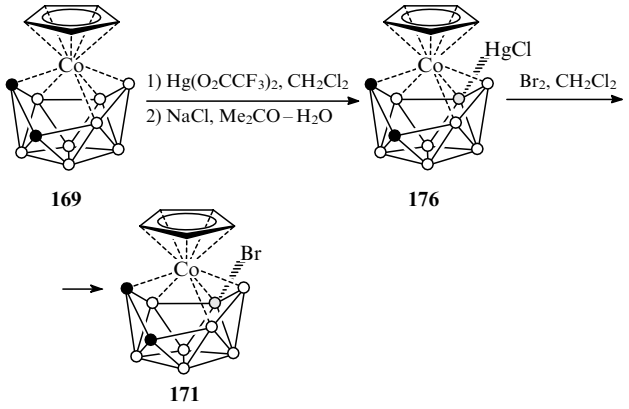

169 **176** **171**

2. Substitution in 10-vertex cobaltacarboranes

Hawthorne and co-workers [146] studied bromination and acylation of 2-Cp-2,1,6-$CoC_2B_7H_9$ (**177**). The reaction of compound **177** with an excess of bromine in CCl_4 produces dibromo derivative **178**, in which the bromine atoms occupy positions 8 and 10, with a small impurity of tribromide.

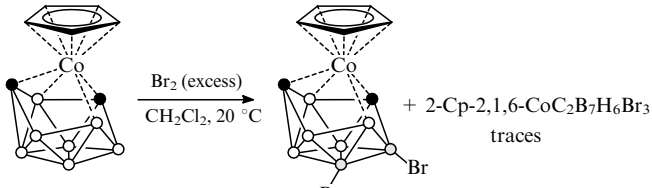

177 **178**

Acylation of complex **177** with acetyl chloride in the presence of $AlCl_3$ in dichloromethane gives the monoacetyl derivative 8-Ac-2-Cp-2,1,6-$CoC_2B_7H_8$.[146]

It should be noted that the above results agree well with the data on substitution in purely polyhedral boron hydrides devoid of the metal fragment. For example, electrophilic substitution in the ten-vertex polyhedra $[B_{10}H_{10}]^{2-}$ and $[1\text{-}CB_9H_{10}]^-$ occurs predominantly at the five-coordinate boron atoms.[147, 148] In the case of structurally flexible eleven-vertex polyhedral boron hydrides, which readily undergo rearrangement (for example, $[B_{11}H_{11}]^{2-}$), the substitution position is determined by the relative stability of intermediate and substitution products.[149–151]

V. Substitution in *exo-nido*-metallacarboranes

Interesting results were obtained in the study of substitution in ruthenacarboranes containing the hydride ligand in the metal coordination sphere. Metallacarboranes with the hydride ligand can exist as two isomers, *viz*., *closo*- and *exo-nido*-metallacarboranes. Stability of a particular form depends on the nature of the metal atom and substituents in the carborane ligand.[152] For example, ruthenacarborane *exo-nido*-5,6,10-[$Cl(Ph_3P)_2Ru$]-5,6,10-(μ-H)$_3$-10-H-7,8-$C_2B_9H_8$ (**179**) [153] undergoes isomerisation into *closo*-3,3-$(PPh_3)_2$-3-H-3-Cl-3,1,2-$RuC_2B_9H_{11}$ (**180**) [154] on heating in benzene at 80 °C

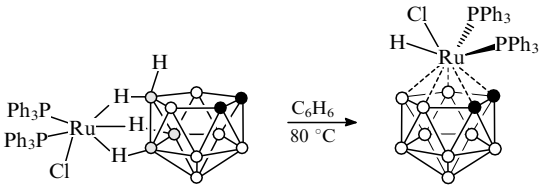

179 **180**

Isomers **179** and **180** differ in chemical behaviour. For example, isomer **180** does not react with $Hg(OAc)_2$ in CH_2Cl_2 or acetone and decomposes in acetic acid, whereas isomer **179** is involved in substitution reactions with various mercurating agents to form *exo-nido*-ruthenacarboranylmercury derivatives.[155]

It should be noted that ruthenacarborane **179** exists in solution as an equilibrium mixture of two geometric isomers (*cis* and *trans*) due to isomerism of the ligands at the six-coordinate ruthenium atom. The *cis* : *trans* isomer ratio is $\sim 1:1$.[156]

The reaction of complex **179** with mercury acetate or trifluoroacetate in dichloromethane at 20 °C affords the symmetrical mercury derivative 10,10′-Hg-[*exo-nido*-5,6,10-$(Cl(Ph_3P)_2Ru)$-5,6,10-$(\mu\text{-}H)_3$-7,8-$C_2B_9H_8]_2$ (**181**) in 46% yield. The latter was prepared as a mixture of geometric isomers, *viz*., *cis* (**A**) and *trans* (**B**). According to the ^{31}P NMR spectroscopic data, the **A** : **B** ratio was 5 : 1.[155]

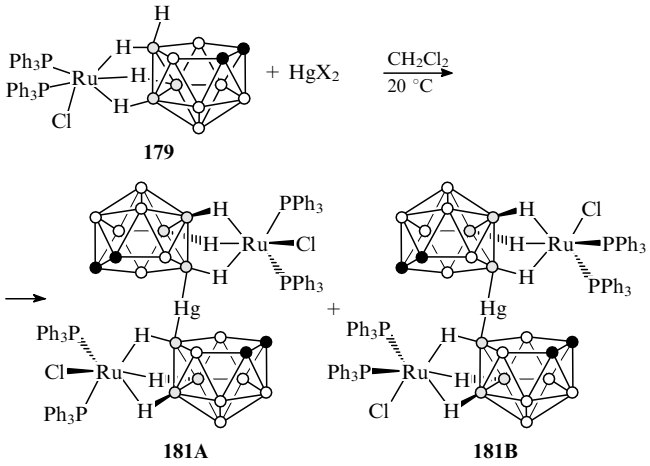

179

181A **181B**

X = AcO, CF_3COO.

In the isomers **A** and **B**, the hydrogen atom at B(10) in the open face of the *exo-nido*-carborane ligand and the chlorine atom at the ruthenium atom are in the *cis* and *trans* positions, respectively.

An analogous mixture of isomers was prepared by the reaction of $Ru(Ph_3P)_3Cl_2$ with the symmetrical mercury derivative of the *nido*-7,8-dicarbaundecaborate anion $Cs_2[10,10'\text{-}Hg\text{-}(7,8\text{-}C_2B_9H_{11})_2]$.[157] Here, as in the first case, the isomer **A** prevails.[155]

In the study,[155] it was proposed to use trifluoroacetoxy-*o*-carboranylmercury 9-$CF_3COOHgC_2B_{10}H_{11}$ (see Ref. 158) along with mercury salts. The reaction of complex **179** with this reagent affords mercurated ruthenacarborane *exo-nido*-5,6,10-$[Cl(Ph_3P)_2Ru]$-5,6,10-$(\mu\text{-}H)_3$-10-$(C_2B_{10}H_{11}Hg)$-7,8-$C_2B_9H_8$ (**182**) containing both the *closo*- and *nido*-carborane moieties.[155] It should be noted that, unlike complex **181**, compound **182** is generated predominantly as the *trans* isomer (**182B**). According to the ^{31}P NMR spectroscopic data, the *cis* : *trans* ratio is 1 : 2.

The independent synthesis of compound **182** by the reaction of $Ru(PPh_3)_3Cl_2$ with $Cs[10\text{-}(9\text{-}HgC_2B_{10}H_{11})(7,8\text{-}C_2B_9H_{11})]$ gave an analogous result.[159]

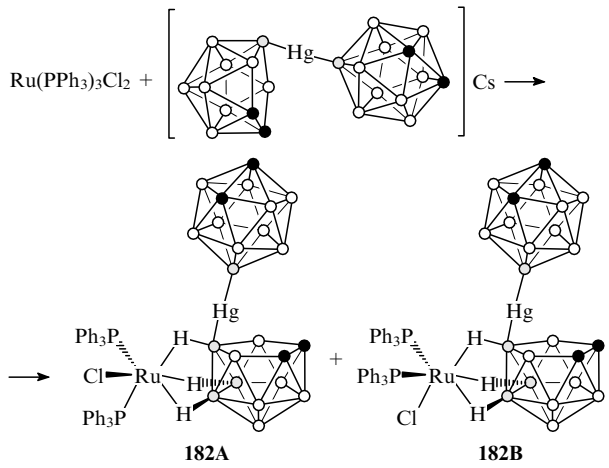

182A **182B**

Isomers **182A** and **182B** were isolated in the individual state. The structure of isomer **182B** was confirmed by X-ray diffraction analysis.

Refluxing of complexes **181** and **182** in benzene does not lead to their *exo-nido* → *closo* rearrangement. Carbon-substituted *exo-nido*-ruthenacarboranes behave analogously.[154] The B—Hg bond in compounds **181** and **182** is resistant to the action of HCl and $HgCl_2$ in acetone or THF at room temperature.

In the studies,[160, 161] mercurated ferracarborane **28** and cobaltacarborane **21** were used as mercurating agents for the first time.‡ The reaction of complex **179** with 1 equiv. of ferracarborane **28** affords the only product, *viz*., *exo-nido*-5,6,10-$[Cl(Ph_3P)_2Ru]$-5,6,10-$(\mu\text{-}H)_3$-10-$(3'\text{-}Cp\text{-}4'\text{-}SMe_2\text{-}8'\text{-}Hg\text{-}3',1',2'\text{-}FeC_2B_9H_9)$-7,8-$C_2B_9H_8$ (**183**), as a mixture of geometric isomers.

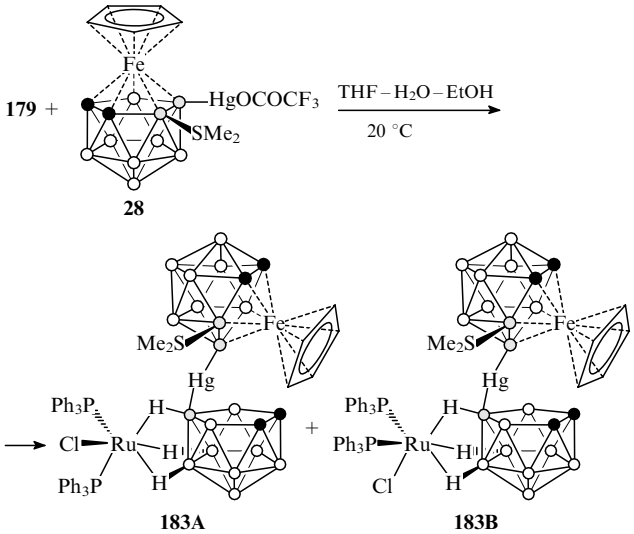

28

183A **183B**

Analogous results were obtained when performing mercuration of complex **179** with cobaltacarborane **21**. Like the above-described complexes **181**, **182** and **183**, complex **184** exists as a mixture of geometric (*cis* and *trans*) isomers (due to isomerism of the ligands with respect to the six-coordinate ruthenium atom). The structure of complex **183B** was confirmed by X-ray diffraction data.

‡ The synthesis of derivatives **21** and **28** was described in the studies.[78, 83]

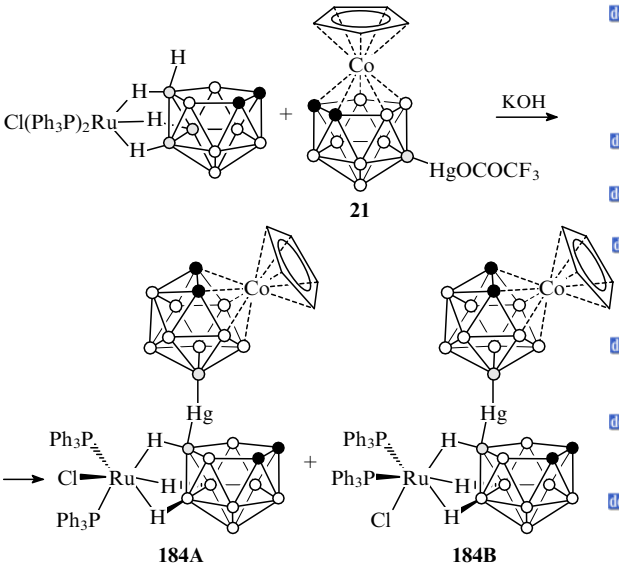

Analysis of the published data on substitution in metallacarboranes makes it possible to compare these reactions with analogous reactions of other polyhedral boron hydrides and draw a conclusion about the influence of the metal atom and the coordinated ligands as well as of the substituents in the polyhedral moiety on the direction of substitution and possible mechanisms of the process.

The above-considered data provide evidence in favour of three major mechanisms of substitution: electrophilic aromatic substitution, electrophile induced nucleophilic substitution and substitution with direct involvement of the metal atom. In some cases, the reactions proceed simultaneously through several competitive mechanisms to give a mixture of substitution products.

The direction of substitution in metallacarboranes often differs from that in carboranes. For example, electrophilic substitution in *o*- and *m*-carboranes occurs at the boron atoms most remote from carbon atoms, whereas the influence of the metal fragment in metallacarboranes is manifested in that the replacement of hydrogen atoms generally occurs at positions adjacent to the metal atoms.

This review has been written with the financial support of the Russian Foundation for Basic Research (Project No. 02-03-32192), the Chemistry and Materials Science Division of the Russian Academy of Sciences (Project No. 591-07, the Program of Basic Research) and the INTAS (Grant 99-00806).

References

1. M F Hawthorne, D C Young, P A Wegner *J. Am. Chem. Soc.* **87** 1818 (1965)
2. L I Zakharkin, V N Kalinin *Usp. Khim.* **43** 1207 (1974) [*Russ. Chem. Rev.* **43** 551 (1974)]
3. E V Leonova *Usp. Khim.* **49** 283 (1980) [*Russ. Chem. Rev.* **49** 147 (1980}
4. L I Zakharkin, V V Kobak, G G Zhigareva *Usp. Khim.* **55** 974 (1986) [*Russ. Chem. Rev.* **55** 531 (1986)]
5. I B Sivaev, V I Bregadze *Collect. Czech. Chem. Commun.* **64** 783 (1999)
6. I B Sivaev, V I Bregadze *J. Organomet. Chem.* **614-615** 27 (2000)
7. R N Grimes *Coord. Chem. Rev.* **200-202** 773 (2000)
8. J Plesek *Chem. Rev.* **92** 269 (1992)
9. J A Long, T B Marder, P E Behncken, M F Hawthorne *J. Am. Chem. Soc.* **106** 2979 (1984)
10. A Demonceau, M A Fontaine, R Messere, A F Noels, I T Chizhevsky, T V Zinevich, V I Bregadze *Rhodium Express* **12** 32 (1995)
11. A Felekidis, M Goblet-Stachow, J F Liégeois, B Pirotte, J Delarge, A Demonceau, M Fontaine, A F Noels, I T Chizhevsky, T V Zinevich, V I Bregadze, F M Dolgushin, A I Yanovsky, Yu T Struchkov *J. Organomet. Chem.* **536** 405 (1997)
12. F Teixidor, R Nuñez, M A Flores, A Demonceau, C Viñas *J. Organomet. Chem.* **614-615** 48 (2000)
13. E Makrlik, P Vanura *Talanta* **32** 423 (1985)
14. J Rais, P Selucky *Nucleon* **1** 17 (1992)
15. J Vohlidal, J Plešek, J Sedlacek, I Cisarova, P Matejka, S Heřmanek *Collect. Czech. Chem. Commun.* **61** 877 (1996)
16. C Viñas, S Gomez, J Bertran, F Teixidor, J-F Dozol, H Rouquette *Inorg. Chem.* **37** 3640 (1998)
17. C Viñas, J Bertran, S Gomez, F Teixidor, J-F Dozol, H Rouquette, R Kivekis, R Sillanpää *J. Chem. Soc., Dalton Trans.* 2849 (1998)
18. J Plešek, B Grüner, S Heřmánek, J Báča, V Mareček, J Jänchenová, A Lhotský, K Holub, P Selucký, J Rais, I Císařová, J Čáslavský *Polyhedron* **21** 975 (2002)
19. J M Forward, D M P Mingos, A V Powell *J. Organomet. Chem.* **465** 251 (1994)
20. Y-K Yan, D M P Mingos, M Kurmoo, W-S Li, I J Scowen, M McPartlin, A T Coomber, R H Friend *J. Chem. Soc., Dalton Trans.* 2851 (1995)
21. Y-K Yan, D M P Mingos, D J Williams, M Kurmoo *J. Chem. Soc., Dalton Trans.* 3221 (1995)
22. P A Chetcuti, W Hofherr, A Liegard, G Rihs, G Rist, H Keller, D Zech *Organometallics* **14** 666 (1995)
23. J D McKinney, F S McQuillan, H Chen, T A Hamor, C J Jones, M Slaski, G H Cross, C J Harding *J. Organomet. Chem.* **547** 253 (1997)
24. M F Hawthorne, A Varadarajan, C B Knobler, S Chakrabarti, R J Paxton, B G Beatty, F L Curtis *J. Am. Chem. Soc.* **112** 5365 (1990)
25. R J Paxton, B G Beatty, M F Hawthorne, A Varadarajan, L E Williams, F L Curtis, C B Knobler, J D Beatty, J Shively *Proc. Natl. Acad. Sci. USA* 3387 (1991)
26. B G Beatty, R J Paxton, M F Hawthorne, L E Williams, K J Rickard-Dickson, T Do, J E Shively, J D Beatty *J. Nucl. Med.* **34** 1294 (1993)
27. I B Sivaev, Z A Starikova, S Sjöberg, V I Bregadze *J. Organomet. Chem.* **649** 1 (2002)
28. J F Valliant, P Morel, P Schaffer, J H Kaldis *Inorg. Chem.* **41** 628 (2002)
29. L I Zakharkin, R Kh Bikkineev *Izv. Akad. Nauk SSSR, Ser. Khim.* 1338 (1976) [a]
30. R M Garrioch, G M Rosair, A J Welch *J. Organomet. Chem.* **614-615** 153 (2000)
31. A V Safronov, T V Zinevich, F M Dolgushin, E V Vorontsov, O L Tok, I T Chizhevsky *J. Organomet. Chem.* **680** 111 (2003)
32. S Robertson, D Ellis, G M Rosair, A J Welch *J. Organomet. Chem.* **680** 286 (2003)
33. R M Chamberlin, B L Scott, M M Melo, K D Abney *Inorg. Chem.* **36** 809 (1997)
34. S A Fino, K A Benwitz, K M Sullivan, D L LaMar, K M Stroup, S M Giles, G J Balaich, R M Chamberlin, K D Abney *Inorg. Chem.* **36** 4604 (1997)
35. R N Grimes *Collect. Czech. Chem. Commun.* **67** 728 (2002)
36. H Yao, M Sabat, R N Grimes *Organometallics* **21** 2833 (2002)
37. J M Russell, M Sabat, R N Grimes *Organometallics* **21** 4113 (2002)
38. J M Russell, M Sabat, R N Grimes *Organometallics* **21** 5613 (2002)
39. H Yao, R N Grimes *J. Organomet. Chem.* **680** 51 (2003)
40. H Yao, M Sabat, R N Grimes, P Zanello, F Fabrizi de Biani *Organometallics* **22** 2581 (2003)
41. R B King *Chem. Rev.* **101** 1119 (2001)
42. J Plešek, S Hermanek, K Base, L J Todd, W F Wright *Collect. Czech. Chem. Commun.* **41** 3509 (1976)
43. J Plešek, K Base, S Hermanek, in *Abstracts of Reports of the 2nd International Meeting on Boron Chemistry, Leeds, 1974* p. 46

44. I B Sivaev, A A Semioshkin, B Brellochs, S Sjöberg, V I Bregadze *Polyhedron* **19** 627 (2000)
45. V Mustyatsa, K Zhizhin, N Votinova, I Polyakova, N Kuznetsov in *Abstracts of Reports of the 11th International Conference on Boron Chemistry* (Moscow: INEOS, 2002) p. 133
46. B Gruner, I Cisarova, J Caslavsky, B Bonnetot, D Cornu *Collect. Czech. Chem. Commun.* **67** 953 (2002)
47. O Tutusaus, F Teixidor, R Nuñez, C Viñas, R Sillanpää, R Kivekäs *J. Organomet. Chem.* **657** 247 (2002)
48. U Krause, W Preetz *Z. Anorg. Allg. Chem.* **621** 516 (1995)
49. K Yu Zhizhin, O O Vovk, E A Malinina, V N Mustyatsa, L V Goeva, I N Polyakova, N T Kuznetsov *Koord. Khim.* **27** 613 (2001) [b]
50. T Peymann, C B Knobler, M F Hawthorne *Inorg. Chem.* **39** 1163 (2000)
51. A A Semioshkin, P V Petrovskii, D Gabel, B Brellochs, V I Bregadze *Izv. Akad. Nauk, Ser. Khim.* 980 (1998) [a]
52. R Grimes *Carboranes* (New York: Academic Press, 1970)
53. V V Grushin, V I Bregadze, V N Kalinin *J. Organomet. Chem. Libr.* **20** 1 (1988)
54. M F Hawthorne, D C Young, T D Andrews, D V Howe, R L Pilling, A D Pitts, M Reintjes, L F Warren, P A Wegner *J. Am. Chem. Soc.* **90** 879 (1968)
55. L Mátel, F Mácášek, P Rajec, S Heřmánek, J Plešek *Polyhedron* **1** 511 (1982)
56. P K Hurlburt, R L Miller, K D Abney, T M Foreman, R J Butcher, S A Kinkead *Inorg. Chem.* **34** 5215 (1995)
57. J Plešek, K Base, F Mares, F Hanousek, B Štibr, S Heřmánek *Collect. Czech. Chem. Commun.* **49** 2776 (1984)
58. I Rojo, F Teixidor, R Kivekäs, R Sillanpää, C Viñas *Organometallics* **22** 4642 (2003)
59. I Rojo, F Teixidor, C Viñas, R Kivekäs, R Sillanpää *Chem. Eur. J.* **9** 4311 (2003)
60. V I Bregadze, I P Beletskaya, V A Ivushkin, I B Sivaev, G G Zhigareva, S Sjöberg, in *Abstracts of Reports of the XVth FECHEM Conference on Organometallic Chemistry, Zurich, 2003* OP34, p. 39
61. M D Mortimer, C B Knobler, M F Hawthorne *Inorg. Chem.* **35** 5750 (1996)
62. A N Gashti, J C Huffman, A Edwards, G Szekeley, A R Siedle, J A Karty, J P Reilly, L J Todd *J. Organomet. Chem.* **614-615** 120 (2000)
63. P Sivy, A Preisinger, O Baumgartner, F Valach, B Koren, L Matel *Acta Crystallogr., Sect. C* **42** 30 (1986)
64. N I Kirilova, A S Zhdanov, A I Gusev, V N Kirin, S P Knyazev, T V Sokolova *Metalloorg. Khim.* **2** 859 (1989) [c]
65. P Sivy, A Preisinger, O Baumgartner, F Valach, B Koren, L Matel *Acta Crystallogr., Sect. C* **42** 28 (1986)
66. B G DeBoer, A Zalkin, D H Templeton *Inorg. Chem.* **7** 2288 (1968)
67. P Sivy, A Preisinger, O Baumgartner, F Valach, B Koren, L Matel *Acta Crystallogr., Sect. C* **42** 24 (1986)
68. A R Siedle, G M Bodner, A R Garber, D C Beer, L J Todd *Inorg. Chem.* **13** 2321 (1974)
69. E C Santos, A B Pinkerton, S A Kinkead, P K Hurlburt, S A Jasper, C W Sellers, J C Huffman, L J Todd *Polyhedron* **19** 1777 (2000)
70. L I Zakharkin, V A Ol'shevskaya, E V Balagurova, P V Petrovskii *Zh. Obshch. Khim.* **70** 590 (2000) [d]
71. L I Zakharkin, R Kh Bikkineev *Izv. Akad. Nauk SSSR, Ser. Khim.* 2377 (1974) [a]
72. W E Geiger, W L Bowden, N E Murr *Inorg. Chem.* **18** 2358 (1979)
73. T Totani, H Nakai, M Shiro, T Nakagawa *J. Chem. Soc., Dalton Trans.* 1938 (1975)
74. L I Zakharkin, V V Kobak, A I Kovredov, V A Antonovich *Izv. Akad. Nauk SSSR, Ser. Khim.* 2122 (1979) [a]
75. A Ya Usyatinskii, O B Zhidkova, P V Petrovskii, V I Bregadze *Izv. Akad. Nauk, Ser. Khim.* 719 (1994) [a]
76. S P Knyazev, V N Kirin, A V Kisin, E A Chernyshev *Dokl. Akad. Nauk* **336** 61 (1994) [e]
77. G A Kats, A Ya Usyatinskii, O B Zhidkova, V I Bregadze, L G Komarova *Metalloorg. Khim.* **3** 1199 (1990) [c]
78. V I Bregadze, A Ya Usyatinsky, O B Zhidkova, F M Dolgushin, A I Yanovsky, Yu T Struchkov *ARKIVOC* 81 (2001)
79. L I Zakharkin, V V Kobak, V A Antonovich *Zh. Obshch. Khim.* **53** 2153 (1983) [d]
80. L I Zakharkin, V V Kobak, A I Kovredov, N G Furmanova, Yu T Struchkov *Izv. Akad. Nauk SSSR, Ser. Khim.* 1097 (1979) [a]
81. T Schaper, W Preetz *Z. Naturforsch., B* **52** 57 (1997)
82. S V Timofeev, I A Lobanova, A R Kudinov, V I Meshcheryakov, O L Tok, P V Petrovskii, F M Dolgushin, Z A Starikova, V I Bregadze *Izv. Akad. Nauk, Ser. Khim.* 1609 (2000) [a]
83. V I Bregadze, I A Lobanova, S V Timofeev, A R Kudinov, V I Meshcheryakov, O L Tok, P V Petrovskii, Z A Starikova *J. Organomet. Chem.* **657** 171 (2002)
84. I B Sivaev, V I Bregadze, S Sjlberg *Collect. Czech. Chem. Commun.* **67** 679 (2002)
85. R G Kultyshev, S Liu, H T Leung, J Liu, S G Shore *Inorg. Chem.* **42** 3199 (2003)
86. S P Knyazev, V N Kirin, E A Chernyshev *Dokl. Akad. Nauk* **333** 732 (1993) [e]
87. L I Zakharkin, I V Pisareva, R Kh Bikkineev *Izv. Akad. Nauk SSSR, Ser. Khim.* 641 (1977) [a]
88. A R Kudinov, D S Perekalin, S S Rynin, K A Lyssenko, G V Grintselev-Knyazev, P V Petrovskii, in *Boron Chemistry at the Beginning of the 21st Century* (Moscow: INEOS, 2003) p. 239
89. M F Hawthorne, J N Francis *Inorg. Chem.* **10** 594 (1971)
90. J Plešek, B Grüner, J Báča, J Fusek, I Císařová *J. Organomet. Chem.* **649** 181 (2002)
91. J Plešek, B Grüner, I Císařová, J Báča, P Selucký, J Rais *J. Organomet. Chem.* **657** 59 (2002)
92. J Plešek, S Hermanek, A Franken, I Císařová, Ch Nachtigal *Collect. Czech. Chem. Commun.* **62** 47 (1997)
93. B Grüner, J Plešek, J Báča, I Císařová, J-F Dozol, H Rouquette, C Viñas, P Selucký, J Rais *New J. Chem.* **26** 1519 (2002)
94. J Llop, C Masalles, C Viñas, F Texidor, R Sillanpää, R Kivekäs *J. Chem. Soc., Dalton Trans.* 556 (2003)
95. F Teixidor, J Pedrajas, I Rojo, C Viñas, R Kivekäs, R Sillanpää, I Sivaev, V Bregadze, S Sjöberg *Organometallics* **22** 3414 (2003)
96. M R Churchill, K Gold, J N Francis, M F Hawthorne *J. Am. Chem. Soc.* **91** 1222 (1969)
97. Z Janoušek, J Plešek, S Heřmánek, K Baše, L J Todd, W F Wright *Collect. Czech. Chem. Commun.* **46** 2818 (1981)
98. J Plešek, Z Janoušek, S Heřmánek *Collect. Czech. Chem. Commun.* **43** 2862 (1978)
99. M F Hawthorne, L F Warren, K P Callahan, N F Travers *J. Am. Chem. Soc.* **93** 2407 (1971)
100. J Plešek, S Heřmánek, Z Janoušek *Chem. Ind. (London)* 108 (1974)
101. J Plešek, S Heřmánek *Collect. Czech. Chem. Commun.* **43** 1325 (1978)
102. A Petrina, V Petricek, K Maly, V Subrtova, A Linek, L Hummel *Z. Kristallogr.* **154** 217 (1981)
103. V Subrtova, K Maly, V Petricek, A Linek *Acta Crystallogr., Sect. B* **38** 2028 (1982)
104. V Petricek, K Maly, A Petrina, K Base, A Linek *Z. Kristallogr.* **166** 1 (1984)
105. J Plešek, B Grüner, S Heřmánek, J Fusek, H Votavova *Collect. Czech. Chem. Commun.* **59** 374 (1994)
106. J Plešek, F H Rajabi, V Vangani, J Fusek *Collect. Czech. Chem. Commun.* **59** 1326 (1994)
107. I Cisarova, K Maly, L Hummel *Acta Crystallogr., Sect. C* **50** 198 (1994)
108. A Franken, J Plešek, J Fusek, M Semrau *Collect. Czech. Chem. Commun.* **62** 1070 (1997)
109. J Plešek, B Stibr, S Heřmánek *Collect. Czech. Chem. Commun.* **49** 1492 (1984)
110. J N Francis, C J Jones, M F Hawthorne *J. Am. Chem. Soc.* **94** 4878 (1972)
111. K Shelly, C B Knobler, M F Hawthorne *New J. Chem.* **12** 317 (1988)
112. J Plešek, S Heřmánek *Collect. Czech. Chem. Commun.* **60** 1297 (1995)
113. A Franken, J Plešek, C Nachtigal *Collect. Czech. Chem. Commun.* **62** 746 (1997)

114. I Rojo, F Teixidor, R Kivekäs, R Sillanpää, C Viñas *J. Am. Chem. Soc.* **125** 14720 (2003)
115. M F Hawthorne, P A Wegner *J. Am. Chem. Soc.* **90** 896 (1968)
116. D F Mullica, E L Sappenfield, F G A Stone, S F Woolam *Organometallics* **13** 157 (1994)
117. S J Dossett, S Li, D F Mullica, E L Sappenfield, F G A Stone *J. Chem. Soc., Dalton Trans.* 3551 (1993)
118. S Anderson, D F Mullica, E L Sappenfield, F G A Stone *Organometallics* **15** 1676 (1996)
119. S Du, D D Ellis, P A Jelliss, J A Kautz, J M Malget, F G A Stone *Organometallics* **19** 1983 (2000)
120. M Herberhold, H Yan, W Milius, B Wrackmayer *Angew. Chem., Int. Ed.* **38** 3689 (1999)
121. M Herberhold, H Yan, W Milius, B Wrackmeyer *Chem. Eur. J.* **6** 3026 (2000)
122. S A Brew, D D Devore, P D Jenkins, M U Pilotti, F G A Stone *J. Chem. Soc., Dalton Trans.* 393 (1992)
123. S A Brew, P D Jenkins, J C Jeffery, F G A Stone *J. Chem. Soc. Dalton Trans.* 401 (1992)
124. D D Devore, C Emmerich, J A K Howard, F G A Stone *J. Chem. Soc., Dalton Trans.* 797 (1989)
125. S A Brew, J C Jeffry, M U Pilotti, F G A Stone *J. Am. Chem. Soc.* **112** 6148 (1990)
126. S A Brew, N Carr, J C Jeffry, M U Pilotti, F G A Stone *J. Am. Chem. Soc.* **114** 2203 (1992)
127. S B Miller, M F Hawthorne *J. Chem. Soc., Chem. Commun.* 786 (1976)
128. R E King III, S B Miller, C B Knobler, M F Hawthorne *Inorg. Chem.* **22** 3548 (1983)
129. C K Broder, A E Goeta, J A K Howard, A K Hughes, A L Johnson, J M Malget, K Wade *J. Chem. Soc., Dalton Trans.*, 3526 (2000)
130. J Plešek, B Grüner, J Holub *Collect. Czech. Chem. Commun.* **62** 884 (1997)
131. J Plešek, A Franken, R Fröhlich *Collect. Czech. Chem. Commun.* **62** 57 (1997)
132. J Plešek, B Grüner, J Fusek, H Votavova *Collect. Czech. Chem. Commun.* **58** 2936 (1993)
133. A Franken, S Du, P A Jelliss, J A Kautz, F G A Stone *Organometallics* **20** 1597 (2001)
134. S Du, A Franken, P A Jellis, J A Kautz, F G A Stone, P-Y Yu *J. Chem. Soc., Dalton Trans.* 1846 (2001)
135. J A Kautz, T D McGrath, F G A Stone *Polyhedron* **22** 109 (2003)
136. B L Booth, K O Jibodu, M F J R P Proenca *J. Chem. Soc., Perkin Trans. 1* 1216 (1983)
137. J A Kautz, D A Kissounko, N S Kissounko, F G A Stone *Organometallics* **21** 2547 (2002)
138. S A Batten, J C Jeffery, L H Rees, M D Rudd, F G A Stone *J. Chem. Soc., Dalton Trans.* 2839 (1998)
139. S Du, J A Kautz, T D McGrath, F G A Stone *J. Chem. Soc., Dalton Trans.* 2791 (2001)
140. S Du, J A Kautz, T D McGrath, F G A Stone *Inorg. Chem.* **41** 3202 (2002)
141. A Y Usiatinsky, O M Khitrova, P V Petrovskii, F M Dolgushin, A I Yanovsky, Y T Struchkov, V I Bregadze *Mendeleev Commun.* 169 (1994)
142. L I Zakharkin, L N Kanakhina, A I Yanovsky, V A Antonovich, Yu T Struchkov *Koord. Khim.* **7** 1692 (1981) [b]
143. S V Timofeev, I A Lobanova, P V Petrovskii, Z A Starikova, V I Bregadze *Izv. Akad. Nauk, Ser. Khim.* 1604 (2001) [a]
144. V E Konoplev, I V Pisareva, D A Lemenovskii, P V Petrovskii, O L Tok, F M Dolgushin, I T Chizhevskii *Collect. Czech. Chem. Commun.* **67** 936 (2002)
145. M Bown, B Grüner, B Štbr, X L R Fortaine, M Thornton-Pett, J D Kennedy, *J. Organomet. Chem.* **614-615** 269 (2000)
146. B M Graybill, M F Hawthorne *Inorg. Chem.* **8** 1799 (1969)
147. W Preetz, H-G Srebny, H C Marsmann *Z. Naturforsch., B* **39** 6 (1984)
148. S V Ivanov, J J Rockwell, S M Miller, O P Anderson, K A Solntsev, S H Strauss *Inorg. Chem.* **35** 7882 (1996)
149. E I Tolpin, W N Lipscomb *J. Am. Chem. Soc.* **95** 2384 (1973)
150. E H Wong, M G Gatter *Inorg. Chim. Acta* **61** 95 (1982)
151. E H Wong, M G Gatter, R M Kabbani *Inorg. Chem.* **21** 4022 (1982)
152. I T Chizhevskii *Metalloorg. Khim.* **5**183 (1992) [c]
153. I T Chizhevsky, I A Lobanova, V I Bregadze, P V Petrovskii, V A Antonovich, A V Poljakov, A I Yanovsky, Yu T Struchkov *Mendeleev. Commun.* 477 (1991)
154. I T Chizhevskii, I A Lobanova, V I Bregadze, P V Petrovskii, A V Polyakov, A I Yanovsky, Yu T Struchkov *Metalloorg. Khim.* **4** 957 (1991) [c]
155. I A Lobanova, V I Bregadze, S V Timofeev, P V Petrovskii, Z A Starikova, F M Dolgushin *J. Organomet. Chem.* **597** 48 (2000)
156. I T Chizhevskii, Doctoral Thesis in Chemical Sciences, Institute of Organoelement Compounds, Moscow, 1999
157. L I Zakharkin, V A Ol'shevskaya *Zh. Obshch. Khim.* **62** 138 (1992) [d]
158. V I Bregadze, V Ts Kampel, N N Godovikov *J. Organomet. Chem.* **112** 249 (1976)
159. L I Zakharkin, V A Ol'shevskaya, V N Lebedev, P V Petrovskii *Zh. Obshch. Khim.* **62** 132 (1992) [d]
160. I A Lobanova, S V Timofeev, A R Kudinov, V I Meshcheryakov, P V Petrovskii, Z A Starikova, V I Bregadze *Izv. Akad. Nauk, Ser. Khim.* 480 (2002) [a]
161. I A Lobanova, O M Khitrova, P V Petrovskii, V I Bregadze *Izv. Akad. Nauk, Ser. Khim.* 241 (2004) [a]

[a] — *Russ. Chem. Bull., Int Ed. (Engl. Transl.)*
[b] — *Russ. J. Coord. Chem. (Engl. Transl.)*
[c] — *Russ. J. Organomet. Chem. (Engl. Transl.)*
[d] — *Russ. J. Gen. Chem. (Engl. Transl.)*
[e] — *Dokl. Chem. (Engl. Transl.)*

Russian Chemical Reviews **73** (5) 455 – 486 (2004) © 2004 Russian Academy of Sciences and Turpion Ltd

DOI 10.1070/RC2004v073n05ABEH000891

Chemical crystallography of fullerenes

I S Neretin, Yu L Slovokhotov

Contents

I.	Introduction	455
II.	The molecular structures of fullerenes	456
III.	Crystal structures of individual fullerenes	458
IV.	Molecular complexes	458
V.	Metal fullerides	471
VI.	Fullerene-based oligo- and polymers	472
VII.	'Binary' compound	473
VIII.	σ-Derivatives	475
IX.	π-Derivatives	478
X.	Endohedral fullerenes	479
XI.	Conclusion	481

Abstract. The state-of-the-art in the structural investigations into fullerene derivatives is surveyed. The crystal structures of individual fullerenes and of their derivatives determined experimentally by single-crystal X-ray diffraction are systematised. The results of powder X-ray diffraction and EXAFS spectroscopy are overviewed for those classes of derivatives that have been insufficiently studied by single-crystal X-ray diffraction. Patterns of packing of the fullerene spheres encountered in crystal structures are described and representative examples of the most typical motifs are given. Reasons for the rotational disorder, which often hampers structure determination for fullerene derivatives, and its classification are considered. A model of the 'rubber cavity' is introduced, which allows prediction of typical mutual orientations of disordered molecules. The redistribution of bond lengths upon σ- and π-functionalisation of the carbon core is analysed based on the information retrieved from the Cambridge Structural Database. Factors affecting the molecular packing density in crystalline derivatives of fullerenes are discussed in relation to the quality of the diffraction data attainable for them. The bibliography includes 282 references.

I. Introduction

Fullerenes are a family of allotropic forms of carbon, the crystals of which are built up of hollow spheroidal molecules C_n united by van der Waals interactions. The C_{60} (also referred to as buckminsterfullerene) and C_{70} fullerenes and their derivatives are the most studied. To date, the C_n fullerenes, where $n = 60, 70, 76, 78, 80, 82, 84, 88$, and 92 (see Ref. 1) have been isolated as individual substances.

I S Neretin, Yu L Slovokhotov A N Nesmeyanov Institute of Organoelement Compounds, Russian Academy of Sciences, ul. Vavilova 28, 119991 Moscow, Russian Federation. Fax (7-095) 135 50 85. Tel. (7-095) 135 93 04. E-mail: ivan@neretin.ru (I S Neretin), slov@ineos.ac.ru (Yu L Slovokhotov)

Received 15 December 2003
Uspekhi Khimii **73** (5) 492 – 525 (2004); translated by Ya V Zubavichus

The overall number of publications on fullerenes by the end of 2001 exceeded 10 000, however, the fraction of those devoted to single-crystal X-ray diffraction studies remains relatively small (*i.e.*, < 400 structures by the end of 2003). A large concentration of defects and twinning are very common for single crystals of fullerenes and their derivatives. Furthermore, the quasi-spherical C_n molecules were found to be rotationally disordered in the crystal structures of many fullerene derivatives. The co-existence of different orientations of a fullerene molecule similar in energies in one crystal results in a deterioration of the experimental diffraction pattern. The problem of the rotational disorder is of special importance in the van der Waals complexes comprising chemically non-modified fullerene molecules. On the other hand, co-crystallisation of different difficult-to-separate addition isomers becomes a serious issue for the chemically modified fullerenes. For higher fullerenes, the overall structural disorder may be increased due to the presence of different geometrical isomers statistically occupying equivalent crystallographic positions of the crystal lattice. All these factors hamper diffraction studies and decrease the accuracy of structure elucidation. However, it is these methods and, primarily, single-crystal X-ray diffraction, that are the most important in the studies of fullerene derivatives because of their structural complexity.

Several reviews on the crystal structures of particular groups of fullerene derivatives have been published,[2–6] but the general regularities of molecular and crystal structures within the whole class of compounds are still lacking. In the present review, the results of single-crystal X-ray diffraction studies of fullerene derivatives are surveyed and distinctive features of their structures are analysed. Special attention is paid to the crystallographic data retrieved from the Cambridge Structural Database (CSD) and original journal papers. The available information still admits a comprehensive coverage within one review paper, thus making it possible to reveal the most general tendencies in the crystallography of fullerene derivatives. For certain compounds closely related to the subject of the present review, the results of other experimental techniques (such as gas electron diffraction, neutron diffraction, powder X-ray diffraction, and XAFS spectroscopy) are also considered.

II. The molecular structures of fullerenes

The stability of a C_{60} molecule having the symmetry of a truncated icosahedron was predicted in the early 1970s independently by Osawa [7] and by Bochvar and Gal'pern.[8] Experimentally, C_{60} has been registered for the first time as a molecular ion in a mass-spectral analysis of gaseous species produced by laser ablation of graphite.[9] The nonequilibrium cooling of carbon vapour gives rise to formation of various C_n clusters with C_{60} being the dominant. Clusters with even smaller n have been detected in mass spectra of graphite sublimation products, however, the respective individual substances have not been isolated so far.

Later, a method for production of fullerenes in macroscopic quantities has been elaborated based on graphite evaporation in an electrical arc plasma with graphite electrodes performed in an inert atmosphere (He or Ar at a pressure of 10–100 mbar).[10] The soot produced in this process contains up to 15%–20% of fullerenes that are further extracted and separated by column chromatography. C_{60} (85%) and C_{70} (14%) are the dominant products while the remaining 1% falls within higher fullerenes, such as C_{76}, C_{84}, C_{90}, and so on.

The molecules of fullerenes represent convex polyhedra with carbon atoms in their vertices, which have only penta- and hexagonal faces, *i.e.*, the carbocycles characterised by the minimum steric strain. According to the Euler theorem, such polyhedra have exactly twelve pentagonal and any number of hexagonal faces.† The simplest fullerene-like polyhedron is a pentagondodecahedron, which has no hexagonal faces. The respective saturated hydrocarbon (*i.e.*, dodecahedrane $C_{20}H_{20}$) was prepared in the 1980s by a complex multistage organic synthesis.[11] Non-modified fullerene C_{20} is, most likely, unstable due to the large steric strain in the unsaturated carbon core. Nevertheless, C_{20} clusters have been detected in the gas phase upon thermal decomposition of brominated dodecahedrane.[12] The isolation of the C_{36} fullerene has been reported [13] but its crystal structure has not been determined. Probably, this structure involves C_{36} units covalently bound to each other rather than independent molecules.

Virtually all fullerenes, for which molecular structures have been determined experimentally, obey the so called Isolated Pentagon Rule, or IPR:[14] the pentagonal rings in their molecules must not have shared vertices. Taking this rule as a requisite, the simplest fullerene is buckminsterfullerene C_{60} (Fig. 1 *a*) and the next one is C_{70}. Furthermore, any fullerenes with even numbers of carbon atoms are allowed. The isolated pentagon rule substantially reduces the number of allowed fullerene structures. For instance, theoretically, the IPR-forbidden C_{66} cluster will have 4478 geometrical isomers if this rule is not taken into account.[15] Note, however, that metallofullerenes such as $Sc_2@C_{66}$ and $Sc_3N@C_{68}$ (see Refs 15, 16) have been isolated. Apparently, this means that the IPR is not stringent and may be violated, at least, in the case of chemically modified carbon cages.

For every fullerene starting from C_{76}, there are several geometrical isomers complying with the IPR. Some of them are chiral and may occur as enantiomers. The number of the fullerene-type polyhedra (M) complying with the IPR as a function of the number of atoms in the carbon cage (n) is given below:

n	60	62–68	70	72	74	76	78	80	82	84	86	90	96
M	1	–	1	1	1	2	5	7	9	24	35	46	187

A topological nomenclature of fullerenes taking into account their probable chirality has been suggested.[17] The relative stabilities of different fullerenes have been thoroughly studied theoretically by methods of quantum chemistry.[18, 19] In particular, the calculations predicted instability of C_{72} and C_{74} fullerenes (complying with the IPR) as neutral molecules.[20] These 'quantum chemistry-forbidden' fullerenes should be highly reactive biradicals. However, they can be stabilised as dianions, in particular, in endohedral derivatives, in which such a stabilisation is achieved owing to charge transfer from the metal atom located inside the carbon cage.[21]

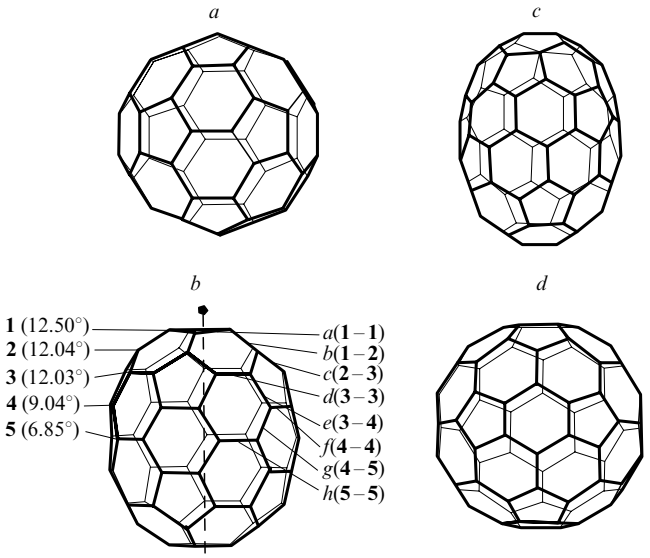

Figure 1. Molecular structures of C_{60} (*a*), C_{70} (*b*), C_{76} (*c*) and I_h isomer of C_{80} (*d*);
(*b*) (to the left): types of symmetrically nonequivalent carbon atoms and their spherical excesses; (to the right): types of bonds and atoms forming these bonds.

The molecular structures of best studied carbon cores are shown in Fig. 1. Buckminsterfullerene C_{60} having the icosahedral symmetry (I_h) is the most abundant fullerene. Its molecular structure has been first established based on the ^{13}C NMR data (the spectrum comprises only one singlet).[22] All carbon atoms in the C_{60} molecule are symmetrically equivalent (*i.e.*, they are transferred to each other by symmetry operation describing the molecule). Meanwhile, there are two nonequivalent types of bonds: those joining pentagons and hexagons and those joining two hexagons (referred to as 5/6 and 6/6 bonds, respectively). The latter bond is characterised by a larger π-contribution and thus is shorter. The CC distances in C_{60} are 1.40 Å (6/6) and 1.46 Å (5/6) according to the gas electron diffraction data.[23] The corresponding mean values for 52 ordered molecular complexes of C_{60} calculated by us based on the crystallographic data retrieved from the CSD are 1.39 Å (6/6) and 1.45 Å (5/6). The bond angles are 108° in pentagons and 120° in hexagons. The spherical excess φ, defined as a difference between 360° and the sum of the bond angles at a certain carbon atom, is, in the case of C_{60}, 12° for all carbon atoms.

After C_{60}, the non-centrosymmetrical C_{70} (see Fig. 1 *b*) having the D_{5h} symmetry is the next most studied fullerene. It differs from C_{60} by an additional equatorial belt of hexagons. In C_{70}, there are 5 symmetrically nonequivalent carbon atoms and 8 different bond types, which is consistent with the NMR data.[24] For the free molecule, the bond lengths have been determined using gas electron diffraction [25] coupled with the quantum chemistry optimisation of the molecular geometry within the density functional theory. The bond lengths in C_{70} from the electron diffraction data and from the single-crystal X-ray diffraction data for the molecular complex $C_{70} \cdot 6S_8$, which has been determined with the highest accuracy,[26] are listed in Table. 1. In C_{70}, the longest bond is the equatorial bond *h* (type 6/6) (see Fig. 1 *b*). All

† The Euler theorem states that for any convex polyhedron, $V - E + F = 2$, where V, E and F are the numbers of vertices, edges and faces of the polyhedron, respectively. Let a polyhedron be composed of n pentagonal and m hexagonal faces. Then, $F = n + m$, $E = (5n + 6m)/2$, since each edge is shared by two faces and $V = (5n + 6m)/3$, since each vertex resides in the intersection of three edges. After substitution of F, E and V in the above equation and simplification thereof, one gets $n = 12$.

Table 1. Bond lengths in the molecule of fullerene C_{70} (for notations, see Fig. 1 *b*).

Bond	Type	Number of bonds	Length (Å) determined using	
			gas electron diffraction [25]	single-crystal X-ray diffraction [26]
a	5/6	10	1.46	1.45
b	6/6	10	1.39	1.38
c	5/6	20	1.45	1.45
d	6/6	10	1.39	1.37
e	5/6	20	1.47	1.45
f	5/6	10	1.42	1.43
g	6/6	20	1.40	1.41
h	6/6	5	1.54	1.47

other 5/6 and 6/6 bonds are similar in length and character to the respective bonds in C_{60}. The spherical excess is the largest for the carbon atoms located at the pole positions of the molecule and the smallest for the equatorial atoms.

The molecular structures of higher fullerenes are less studied. The C_{76} fullerene, which has been isolated as a pure substance, represents a chiral isomer with D_2 symmetry (see Fig. 1 *c*) according to the single-crystal X-ray diffraction data of its molecular complex with sulfur $C_{76} \cdot 6\,S_8$.[27] The crystal contained a racemic mixture of enantiomers statistically occupying the same crystallographic positions.

The C_{78} fullerene is a mixture of two isomers with C_{2v} and D_3 symmetry in a ratio of 5 : 1, according to the NMR data.[28] The dominant isomer of the C_{80} fullerene has D_{2d} symmetry,[29] though an isomer with D_{5h} symmetry has also been isolated.[30] An isomer of C_{80} with icosahedral symmetry I_h (see Fig. 1 *d*), which is the least stable in the free form according to the quantum chemistry calculations, has been prepared and structurally characterised as an endohedral derivative. In these substances, the carbon cage is stabilised due to a charge transfer from the metal atoms to the carbon core. In contrast to C_{60}, which possesses regularly alternating 6/6 and 5/6 bonds in each hexagon, this I_h isomer of C_{80} comprises perylene fragments with five fused hexagons.

The structural study of higher C_{76} and C_{82} fullerenes as solvates with toluene using synchrotron radiation (SR) powder X-ray diffraction [31] has been conducted but not yielded reliable geometry of their carbon cores.

According to the quantum chemistry calculations,[19] the relative stabilities of isomeric fullerene cages C_n^{q-} change depending on the charge q (Fig. 2). The results of single-crystal X-ray diffraction studies of the endohedral derivatives $M_n@C_{82}$ and $M_n@C_{84}$ are discussed below (Section X).

According to the IR data,[32] pure C_{84} fullerene represents a mixture of two major isomers with D_{2d} and D_2 symmetry. Its π-complex with iridium, which has been isolated and structurally characterised,[33] contains a carbon cage having D_{2d} symmetry with a contribution of other unidentified isomers. The NMR data on the C_{88} fullerene have been interpreted [34] as a superposition of spectra attributable to three isomers. This spectral assignment has been made on the basis of the quantum chemistry calculations of all possible isomers complying with the IPR.

Among even larger fullerenes, C_{92} has been isolated and partially separated into fractions. One of them contained the only isomer with C_{2v} symmetry (according to the ^{13}C NMR data), whilst the other fraction represented a mixture of isomers.[35] Furthermore, there has been a report on a preparation of an individual cluster-'onion' (not studied structurally) with a C_{60} internal core and a C_{240} outer shell.[36]

Upon partial substitution of boron or nitrogen atoms for the carbon atoms, various heterofullerenes are produced. One of them with the stoichiometry $C_{59}N$ has been isolated and studied by means of powder X-ray diffraction using Rietveld refinement. This substance was identified as a molecular crystal containing dimeric molecules $(C_{59}N)_2$.[37] A cationic derivative of this heterofullerene, $[(C_{59}N^+CB_{11}H_6Cl_6)_2Ag] \cdot 3(o\text{-}C_6H_4Cl_2)$, has been studied by single-crystal X-ray diffraction.[38] In the crystal structure of this compound, the nitrogen atom is disordered over two positions in the $C_{59}N^+$ cluster, which is isolectronic and isostructural to buckminsterfullerene.

The energy diagram of the molecular π-orbitals for C_{60} has been calculated for the first time by the simple Hückel method.[8] The energy level diagrams for C_{60} and C_{70} are shown in Fig. 3. Due to the high symmetry of the buckminsterfullerene molecule, its lowest unoccupied molecular orbital (LUMO) is triply degenerate and its highest occupied orbital (HOMO) is quintuply

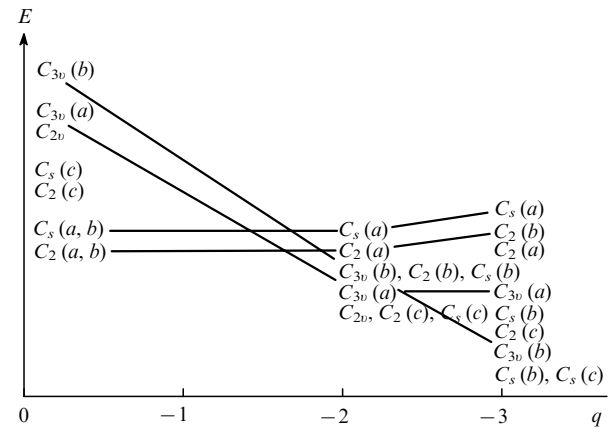

Figure 2. The relative stabilities of different geometrical isomers of C_{82}^{q-} (see Ref. 19).

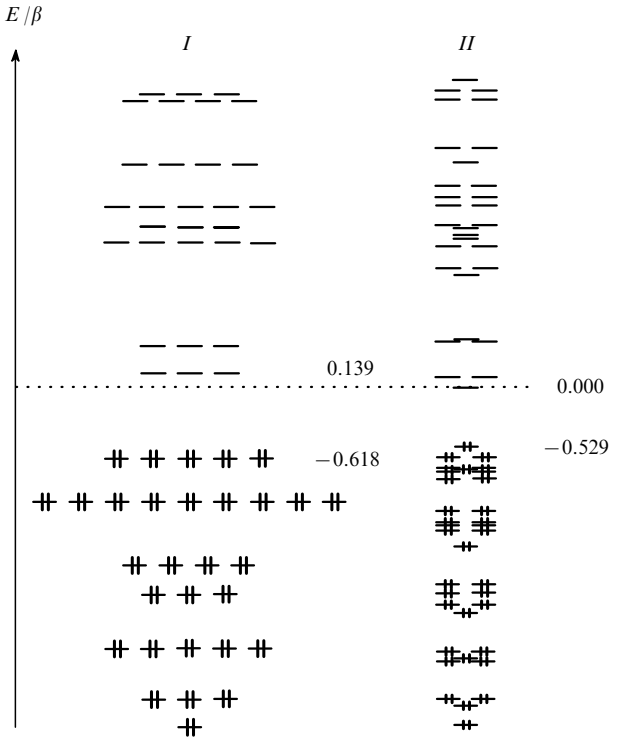

Figure 3. The energy diagram of π-orbitals in C_{60} (*I*) and C_{70} (*II*) in units of the resonance integral (β). The dotted line corresponds to the energy of 2p-AOs of an isolated carbon atom.

degenerate (see Fig. 3 *I*). The less symmetrical C_{70} molecule has only nondegenerate and doubly degenerate levels (see Fig. 3 *II*). On average, the energy difference (LUMO – HOMO) in stable C_n fullerenes, as determined by the quantum chemistry calculations, decreases with an increase in n approaching ultimately zero (as in graphite [39]).

Thus, polyhedral molecules of fullerenes retain important features of planar π-conjugated systems, such as low-energy π-bonding and stabilisation of alternant structures. As a result, energies of their frontier orbitals can be fairly reproduced using the simple Hückel method. Meanwhile, the C_n molecules themselves manifest many properties of unsaturated hydrocarbons, *e.g.*, addition reactions to 'double' 6/6 bonds and π-complexation to metals are typical of them. On the other hand, non-modified fullerenes do not contain fully delocalised π-systems, similar to those in aromatics, and their double bonds remain partially localised.

III. Crystal structures of individual fullerenes

The fullerene-containing substances, crystal structures of which have been deposited into CSD (2003 version) are listed in Table 2. The overall number of related CSD entries is 382 (including repeated studies). In several cases, no coordinates of carbon atoms have been deposited into the CSD. All the compounds are subdivided into classes according to the extent of the chemical modification of the corresponding fullerene molecule. Table 2 also contains single-crystal X-ray diffraction results published in scientific journals but not included in the CSD version of October, 2003, as well as some substances studied by powder X-ray diffraction.

Pure crystalline buckmisterfullerene C_{60} prepared by resublimation *in vacuo* possesses a face-centred cubic (fcc) lattice.[53] At room temperature, the fullerene molecules in this structure are rotationally disordered. Upon a decrease in the temperature down to 258 K, a phase transition occurs, which is accompanied by partial ordering of the molecules and lowering of the symmetry of the cubic lattice from $Fm3m$ to $Pa\bar{3}$. Upon further cooling, the dynamic disorder is gradually replaced by the static disorder.[54] At even lower temperatures (*e.g.*, at 5 K),[55] the crystal reveals a statistical mixture of only two molecular orientations (neutron diffraction data), however, no complete 'freezing' of this degree of freedom has been reached. The shortest interatomic C···C contacts between the neighbouring C_{60} molecules (3.00 Å) are almost 0.2 Å shorter than the interlayer C···C distances in graphite,[56] *i.e.*, they are likely to correspond to the van der Waals repulsion compensated by the mutual attraction of more distant atoms from the neighbouring molecules. Most probably, no local charge transfer within the carbon cage is involved, which would have given rise to the electrostatic attraction of the neighbouring molecules mutually oriented so as to expose oppositely charged sides (initially proposed as an explanation for the shortened C···C distances, see Ref. 57). Physical investigations into the dynamics of the disordered fullerene clusters in crystals will not be addressed in any detail here since this review is focused primarily on the structures of fullerene derivatives in their relation to chemical properties.

Under special conditions, it is possible to prepare polycrystalline powder of the metastable hexagonal modification of C_{60} in which the fullerene molecules make up a two-layer close packing of spheres.[58, 59] Earlier reports [60] on another hexagonal modification of buckminsterfullerene with the parameters $a = 33.54$ Å and $c = 10.11$ Å have not been confirmed. Probably, these parameters correspond to a fullerene-rich solvate rather than pure fullerene.

The C_{70} fullerene composed of molecules that may be approximated as ellipsoids has a more complex phase diagram. The high-temperature fcc phase, which is characterised by isotropic rotations of the molecules, converts, upon a decrease in the temperature down to 340 K, into a trigonal (rhombohedral) phase, in which the long axes of the ellipsoids are oriented along the crystallographic three-fold axis, and the rotational disorder appears only due to revolution around them (Fig. 4). At even lower temperature (*viz.*, 280 K), the molecules get completely ordered forming a monoclinic phase similar to the trigonal one as regards the lattice parameters ($a \approx c$, $\beta \approx 120$). As for C_{60}, a metastable modification of C_{70} with the hexagonal close packing (hcp) of isotropically disordered molecules is known. Upon a decrease in the temperature, this phase undergoes two phase transitions accompanied by an ordering of the molecular rotations, analogous to those described above. Apart from the two regular high-temperature modifications, *viz.*, fcc and hcp, there exists a series of intermediate phases characterised by irregular layer sequences.[61]

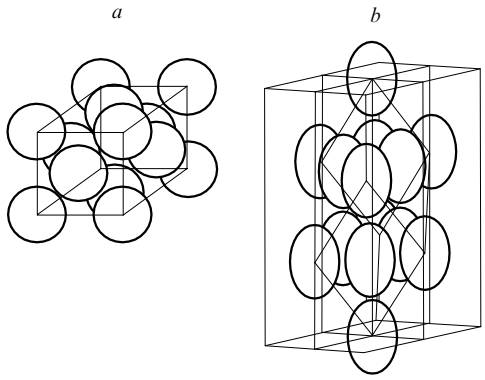

Figure 4. Schematic representation of the crystal structure of the fcc phase of C_{60} (*a*) and rhombohedral phase of C_{70} (*b*).

For some of the higher fullerenes with rather spheroidal molecules, only high-temperature fcc phases have been detected, while information on the phase transitions at low temperatures is lacking.[62] For the C_{84} fullerene, two phase transitions at 235 K and 181 K have been revealed by powder X-ray diffraction, although the structures of the low-temperature phases have not been determined.[63]

IV. Molecular complexes

Numerous derivatives of fullerenes may be classified as molecular complexes with non-polar molecules. Sometimes, they are also referred to as mixed or van der Waals crystals. As was first pointed out by A I Kitaygorodsky,[64] the most energetically favourable molecular packing in a crystal formed exclusively by van der Waals interactions normally coincides with the densest one. Any close packing of large spheroidal C_n molecules contains cavities of an appreciably large size. Therefore, fullerenes readily form molecular complexes (clathrates, inclusion compounds) with many 'guest' molecules. The structures and properties of such substances have been reviewed by several authors.[2, 3, 6] Many crystallographic regulations observed for this class of compounds may be extended to include fullerene derivatives.

The cavities in the parent close packing of fullerene 'spheres' can accomodate only single atoms, for instance, of alkali metals (see Section V). The majority of crystalline fullerene molecular complexes contain looser structural motifs of the C_n clusters formed as a result of incorporation of larger molecules or ions. It is convenient to characterise these motifs with the 'partial' molecular coordination number (MCN), which is the number of neighbouring fullerene clusters forming the van der Waals C···C contacts in the range 3.2 – 3.5 Å with the central cluster. For

Table 2. Structurally characterised fullerene derivatives (only one mention of each structure is given, repeated and independent studies are omitted).

CSD Refcode or (Ref.)	Formula [a]	*R*-factor	Motif	MCN (see [b])	*T*/K
SOCTOT01	C_{60}	0.100	fcc	12	110
SOCTOT02	C_{60}	0.059	"	12	295
QUQDOV	$(C_{70})_\infty$	0.066	distorted hcp	12	100
Solvates and molecular complexes					
MAPSUR	$C_{60} \cdot 1.5\,CS_2$	0.058	3*D* framework	10	90
POFKUQ	$C_{60} \cdot n\text{-}C_5H_{12}$	0.130	"	10	295
EDEWAL	$C_{60} \cdot C_2H_3Cl_3$	–	–	–	223
TEYCEF	$C_{60} \cdot 2\,(m\text{-}C_6H_4Me_2)$	0.147	3*D* framework	10	20
PIGWUX	$C_{60} \cdot 2\,CCl_4$	–	simple hexagonal	8	295
YOLTEY	$C_{60} \cdot 2\,CHBr_3$	–	the same	8	295
YOLTIC	$C_{60} \cdot 2\,CHCl_3$	–	"	8	295
YOLTOI	$C_{60} \cdot 2\,CH_2Cl_2$	–	–	–	295
HOSJAA	$C_{60} \cdot 2\,PhBr$	0.057	hexagonal layers	6	150
JUGCET	$C_{60} \cdot 4\,C_6H_6$	0.101	honeycomb	6	173
YOLTAU	$C_{60} \cdot 13\,CCl_4$	–	isolated	0	295
YOLSOH	$C_{60} \cdot 13\,C_6H_{12}$	–	"	0	295
JOCSOJ	$(C_{60}, C_{70}) \cdot x\,C_6H_{12}$	0.109	"	0	295
YOLSUN	$C_{70} \cdot 13\,C_6H_{12}$	–	"	0	295
NUDDOF	$C_{70} \cdot m\text{-}C_6H_4Me_2$	0.213	3*D* framework	10	295
ZOYSOV	$C_{76} \cdot PhMe$	0.048	simple hexagonal	8	295
ZOYSEL	$C_{82} \cdot PhMe$	–	the same	8	295
XIFMEE	$C_{60} \cdot 3\,TiCl_4$	0.038	diamond-like	4	180
XOBVIT	$C_{70} \cdot 2\,TiCl_4$	0.059	3*D* framework	7, 8	180
JUVYAA	$C_{60} \cdot CH_2I_2 \cdot C_6H_6$	0.055	simple hexagonal	8	122
LAVNIF	$C_{60} \cdot I_2 \cdot PhMe$	0.076	3*D* framework	8	143
MAQFIT	$4\,C_{60} \cdot 3\,TDZ$	0.046	"	9	100
YITCUZ	$C_{60} \cdot S_8 \cdot CS_2$	0.069	honeycomb	8	295
HEGPAK	$C_{60} \cdot 2\,S_8$	0.041	diamond-like	4	295
TONDUV	$C_{60} \cdot TMPD$	0.080	hexagonal layers	6	295
SOMGIK	$C_{60} \cdot 3\,[p\text{-}C_6H_4(OH)_2]$	0.198	simple cubic	6	295
MIMROP	$C_{60} \cdot PBMP$	0.131	3*D* framework	6	293
NIYBOM	$2\,C_{60} \cdot TPBP \cdot 4\,CS_2$	0.049	"	5	170
NIRLOP	$C_{60} \cdot Ph_3SiH$	0.156	honeycomb	6	213
YEKBOF	$3\,C_{60} \cdot 2\,CTV \cdot PhMe$	0.142	hexagonal layers	6	295
CEMPAL	$C_{60} \cdot AT$	0.086	honeycomb	6	150
ZUMCIT	$C_{60} \cdot BTX \cdot CS_2$	0.057	columns	2	295
TAWKEH	$C_{60} \cdot CCTV$	0.123	chains	2	183
PASQAB	$C_{60} \cdot DAN \cdot 3\,C_6H_6$	0.069	tetragonal layers	4	295
CEMNUD	$C_{60} \cdot 2\,Trip \cdot 2\,(o\text{-}C_6H_4Me_2)$	0.095	hexagonal layers	6	150
FOFKEQ	$C_{60} \cdot OPCTSil \cdot 0.5\,PhMe$	0.051	double chains	4	123
YOLVOK	$C_{60} \cdot 2\,HMTPH$	0.098	–	–	295
BACQAX	$C_{60} \cdot TBBCN \cdot 1.5\,PhMe$	0.114	columns	2	153
KUVNOE	$C_{60} \cdot 2\,Cp_2Fe$	0.060	hexagonal layers	6	143
NAGNAK	$C_{60} \cdot 3\,C_6H_6 \cdot 2\,Pd_6Cl_{12}$	0.093	chains	2	130
PIGPEA	$C_{60} \cdot Cp_4Fe_4(CO)_4 \cdot 3\,C_6H_6$	0.065	–	–	173
NUWYOT	$2\,C_{60} \cdot 4\,BEDT\text{-}TTF \cdot Cp_2Fe \cdot 0.5\,CS_2$	–	–	–	295
SADVUO	$C_{60} \cdot TBrCalix[3]$	0.105	diamond-like	4	295
SADWAV	$C_{60} \cdot TBuCalix[3]$	0.198	graphite-like	3	295
NIFYAC	$C_{60} \cdot TMCalix[5] \cdot 4\,H_2O$	0.085	island	1	295
NIFXUV	$C_{60} \cdot PMCalix[5] \cdot CH_3OH \cdot 3\,H_2O$	0.097	"	1	295
FAJFAX	$C_{60} \cdot TBTPCalix[4]$	0.117	columns	2	173
NOBLEV	$2\,C_{60} \cdot Calix[6] \cdot PhMe$	0.119	3*D* framework	5	173
PUJROB	$C_{60} \cdot TPCalix[4]R \cdot 4\,Pr^iOH \cdot o\text{-}C_6H_4Cl_2$	0.119	isolated	0	173
TUDCOK	$C_{60} \cdot 2\,DIDMCalix[5] \cdot 8\,H_2O$	0.168	"	0	295
JAYDIW	$C_{60} \cdot 2\,TBzCalix[3]$	0.136	"	0	273
BOXQOU	$C_{60} \cdot 2\,TBuCalix[3]N$	0.154	"	0	193
NIGPOI	$C_{60} \cdot 2\,TITBCalix[4]$	0.089	"	0	295
JAXYIQ	$C_{60} \cdot 2\,PBzCalix[5] \cdot 2\,PhMe$	0.124	"	0	173
ADACIR	$5\,C_{60} \cdot 4\,Calix[5] \cdot 2\,PhMe$	0.209	complex chains	4, 6	173
MEQGIY	$C_{60} \cdot biCalix[5] \cdot 2\,PhMe$	0.098	isolated	0	148
FIBVIV	$C_{60} \cdot TMTSeF \cdot 0.5\,C_6H_6$	0.061	3*D* framework	6	295
NIXPOZ	$C_{60} \cdot TMTSeF \cdot 2\,CS_2$	0.047	tetragonal layers	4	295
UCIKEW	$C_{60} \cdot DBTTF \cdot C_6H_6$	0.069	–	–	153
XOCJII	$C_{60} \cdot MDT\text{-}TTF \cdot 2\,CS_2$	0.070	hexagonal layers	6	293

Table 2 (continued).

CSD Refcode or (Ref.)	Formula [a]	*R*-factor	Motif	MCN (see [b])	*T*/K
Solvates and molecular complexes					
YOCFOL	$C_{60}\cdot$ BDMT-TTeF$\cdot CS_2$	0.038	–	–	295
LITPUZ	$C_{60}\cdot$ DTDSeF	0.050	tetragonal layers	4	295
FONPED	$C_{60}\cdot 1.33\,S_4N_4\cdot 0.67\,C_6H_6$	0.132	–	–	153
SUGBUR	$C_{60}\cdot$ BEDTB(EDT)$\cdot CS_2$	0.073	double chains	3	295
KUMMEK	$C_{60}\cdot 2$ BEDT-TTF	0.058	the same	4	150
TODZUH	$C_{60}\cdot 2$ DMTEDT-TTF	–	–	–	295
TOFBAR	$C_{60}\cdot 2$ TMTTF	–	–	–	295
DAGSUZ	$C_{60}\cdot 2$ TMDTDM-TTF$\cdot 3\,CS_2$	0.060	–	–	153
UBOJOK	$2\,C_{60}\cdot H_2TPP\cdot 4\,C_6H_6$	0.062	puckered graphite	3	120
UBOJUQ	$2\,C_{60}\cdot H_2TPP\cdot 3\,C_6H_6$	0.131	3*D* with channels	5	120
VEMNOQ	$C_{60}\cdot H_2TPP\cdot 3$ PhMe	0.087	chains	2	203
VEMQAF	$3\,C_{60}\cdot 2$ TDMPP$\cdot 4$ PhMe	0.092	isolated	0	203
VEMQEJ	$C_{60}\cdot$ TPivP	0.088	"	0	295
VEMPEI	$C_{60}\cdot H_2$TDBPP	0.091	"	0	203
ZAPNEJ	$C_{60}\cdot 2\,H_2$-ODAPz$\cdot$ PhMe	0.165	columns	2	295
BAQRUG	$C_{60}\cdot$ CuTMCTD	0.104	puckered layers	5	123
PIQHOM	$C_{60}\cdot$ NiTMCTD	0.052	the same	5	173
HIVKEC	$C_{60}\cdot$ NiOMCTD$\cdot 2\,CS_2$	0.088	chains	2	123
FOPZEP	$C_{60}\cdot$ NiODAPz	0.061	"	2	295
CELYOH	$C_{60}\cdot$ ClFeOEP$\cdot CHCl_3$	0.126	"	2	130
ABOSOZ	$C_{60}\cdot$ AgOEP$\cdot 2\,C_6H_6$	0.036	puckered graphite	3	83
QARPUU	$C_{60}\cdot$ PdOEP$\cdot 1.5\,C_6H_6$	0.079	graphite-like	3	83
QARQAB	$C_{60}\cdot$ CuOEP$\cdot 2\,C_6H_6$	0.037	"	3	83
QARQEF	$C_{60}\cdot$ Ru(CO)OEP$\cdot 2$ PhMe	0.095	chains	2	83
KEQKIA	$C_{60}\cdot 2\,Ph_3AsAuCl$	0.032	isolated	0	140
LOHSOQ	$C_{60}\cdot 2\,Ph_3PAuCl$	0.078	"	0	295
QUFLUY	$2\,C_{60}\cdot$ CoTAP$\cdot 3.3\,(o\text{-}C_6H_4Cl_2)\cdot 0.45\,C_6H_6$	0.083	island	1	146
FOPYEO	$C_{60}\cdot 2$ CuODAPz$\cdot 2\,C_6H_6$	0.054	isolated	0	295
CELTIW	$C_{60}\cdot 2$ CoOEP$\cdot CHCl_3$	0.082	"	0	154
CELVAQ	$C_{60}\cdot 2$ ZnOEP$\cdot CHCl_3$	0.069	"	0	156
CELVUK	$C_{60}O\cdot 2$ CoOEP$\cdot CHCl_3$	0.069	"	0	130
QARQIJ	$C_{60}\cdot 2$ ZnOEP$\cdot 2\,C_6H_6$	0.167	"	0	83
ABOSUF	$C_{60}\cdot 2$ NiOEP$\cdot 2$ PhCl	0.077	"	0	83
TIKHAW	$C_{60}\cdot$ CoTDBPP	0.032	"	0	83
UBOJIE	$C_{60}\cdot 2$ CuTPP	0.058	columns	2	110
XEYZAC	$C_{60}\cdot$ BPZnOEP	0.075	isolated	0	163
YIKVET	$C_{60}\cdot 6\,Ph_3Sb$	0.041	"	0	130
BEJLOR	$C_{70}\cdot 2\,Cp_2Fe$	0.077	hexagonal layers	7	130
NOBLIZ	$2\,C_{70}\cdot$ Calix[6]$\cdot$ PhMe	0.126	the same	7	173
DATQEU	$C_{70}\cdot$ BTX$\cdot 0.5\,CS_2$	0.080	tetragonal layers	4	295
HAZQAA	$C_{70}\cdot$ OMDBCTD	0.047	puckered layers	5	173
VEMQUZ	$2\,C_{70}\cdot$ NiTTolP$\cdot 2$ PhMe	0.071	double chains	3	198
HASWIH	$2\,C_{70}\cdot 9\,[p\text{-}C_6H_4(OH)_2]\cdot 2\,C_6H_6$	0.104	island	1	295
WITRAS	$3\,C_{70}\cdot 4$ BNDTY$\cdot 4\,C_6H_6$	0.090	distorted simple cubic	4	295
GOSYOC	$C_{70}\cdot C_2B_{10}H_{12}\cdot$ CTV$\cdot C_6H_4Cl_2$	0.094	chains	2	123
CELWAR	$C_{70}\cdot$ CoOEP$\cdot CHCl_3\cdot C_6H_6$	0.102	"	2	156
CELYEX	$C_{70}\cdot$ NiOEP$\cdot CHCl_3\cdot C_6H_6$	0.099	"	2	130
CELYIB	$C_{70}\cdot$ CuOEP$\cdot CHCl_3\cdot C_6H_6$	0.126	"	2	156
QEZFIK	$C_{60}\cdot$ PdBPPyP$\cdot 2\,C_6H_{14}\cdot 0.5$ PhMe	0.075	island	1	213
LAZMEE	$C_{70}\cdot 6\,S_8$	0.037	hexagonal layers	6	100
UBOJEA	$C_{70}\cdot$ CuTPP$\cdot 1.5$ PhMe$\cdot 0.5\,C_2HCl_3$	0.103	chains	2	110
VEMQOT	$C_{70}\cdot$ ZnTPP	0.102	"	2	203
VEMQIN	$C_{70}\cdot H_2$TDMPP$\cdot 4$ PhMe	0.143	isolated	0	295
RATCUK	$C_{76}\cdot 6\,S_8$	0.040	hexagonal layers	6	180
(40)	$C_{60}\cdot CHBr_3$	0.137	3*D* framework	10	150
(41)	$C_{60}\cdot 2$ PhI	0.030	hexagonal layers	6	110
(41)	$C_{60}\cdot 2\,(m\text{-}C_6H_4Br_2)$	0.029	cubic framework	6	110
(41)	$C_{60}\cdot 3\,(o\text{-}C_6H_4Br_2)$	0.144	diamond-like	4	110
(42)	$C_{60}\cdot 1,3,5\text{-}C_6H_3Ph_3$	0.078	graphite-like	3	110
(42)	$C_{60}\cdot 2\,(1,3,5\text{-}C_6H_3Ph_3)\cdot$ PhCl	0.090	columns	2	110
(43)	C_{60}^{-}TDAE$^{+}\cdot 2$ TBPD	0.100	isolated	0	110
(44)	$2\,C_{60}\cdot$ BNTTF$\cdot$ PhMe	0.099	3*D* framework	7	110

Table 2 (continued).

CSD Refcode or (Ref.)	Formula [a]	*R*-factor	Motif	MCN (see [b])	*T* /K
Solvates and molecular complexes					
(44)	$2\,C_{60}\cdot EDT(DET)TTF$	0.136	3*D* framework	7	110
(45)	$C_{60}\cdot 2\,PyZnTPP\cdot PhMe\cdot Cp_2Fe$	0.099	isolated	0	110
(45)	$C_{70}\cdot 2\,PyZnTPP\cdot PhMe\cdot 0.5\,C_2HCl_3$	0.116	"	0	110
(46)	$2\,C_{60}\cdot TPyP\cdot 4\,ZnTPP\cdot 1.75\,PhCN$	0.087	island	1	110
Ionic complexes with neutral fullerene					
PIBQOG	$C_{60}\cdot 4\,NaH$	0.086	–	–	295
HIFCOO	$C_{60}\cdot 5\,AgNO_3$	0.149	cubic framework	6	140
XAYXOK	$C_{60}\cdot BEDT\text{-}TTF^+\cdot I_3^-$	0.034	hexagonal layers	6	90
GUDZEK	$C_{60}\cdot FeTPP^+\cdot(C_6F_5)_4B^-\cdot 2.5\,(o\text{-}C_6H_4Cl_2)$	0.093	chains	2	203
Radical-ion salts and fullerides					
KUGGIC	$C_{60}^-\cdot TDAE^+$	0.086	cubic framework	6	295
GEXQUV	$C_{60}^-\cdot(PhMe)_2Cr^+\cdot CS_2$	0.138	honeycomb	6	150
MOBWUV	$C_{60}^-\cdot(PhMe)_2Cr^+$	0.077	distorted simple cubic	6	235
PUKHAE	$C_{60}^-\cdot Cp_2Co^+\cdot CS_2$	0.151	3*D* framework	8	123
ZESHIO	$C_{60}^-\cdot(Me_5Cp)_2Ni^+\cdot CS_2$	0.045	tetragonal layers	4	150
LAZPAD	$C_{60}^-\cdot 2\,Ph_4P^+\cdot I^-$	0.047	isolated	0	295
YEBDUE	$C_{60}^-\cdot 2\,Ph_4P^+\cdot Cl^-$	0.051	"	0	295
YUXCAV	$C_{60}^-\cdot 2\,Ph_4P^+\cdot Br^-$	0.083	"	0	295
YUXCEZ	$C_{60}^-\cdot 2\,Ph_4As^+\cdot Cl^-$	0.126	"	0	295
POFWEM	$C_{70}^-\cdot 2\,Ph_4P^+\cdot I^-$	0.210	"	0	295
FULLER	$C_{60}^-\cdot Cs^+$	0.043	bcc	8	295
YEXLIW	$C_{60}^-\cdot K^+$	–	–	–	295
HEJDEF	$C_{60}^{n-}\cdot n\,Na^+\cdot m\,THF$	–	–	–	295
HEJDIJ	$C_{60}^{n-}\cdot n\,K^+\cdot m\,THF$	–	–	–	295
PAVLAZ	$C_{60}^-\cdot(Ph_3P)_2N^+$	0.020	–	–	295
WEZYEF	$C_{60}^{2-}\cdot 2\,(Ph_3P)_2N^+$	0.042	isolated	0	108
NAPPOJ	$C_{60}^{2-}\cdot 2\,PhCH_2NMe_3^+\cdot 3\,NH_3$	0.052	tetragonal layers	4	113
TUQTAA	$C_{60}^{2-}\cdot 2\,CryptK^+\cdot 4\,PhMe$	0.109	isolated	0	113
PUHJIL	$C_{60}^{2-}\cdot Mn(NH_3)_6^{2+}\cdot 6\,NH_3$	0.035	tetragonal layers	4	113
RAJNIZ	$C_{60}^{2-}\cdot Co(NH_3)_6^{2+}\cdot 6\,NH_3$	0.053	the same	4	143
NUHJUV	$C_{60}^{2-}\cdot Ni(NH_3)_6^{2+}\cdot 6\,NH_3$	0.037	"	4	113
RAJNOF	$C_{60}^{2-}\cdot Zn(NH_3)_6^{2+}\cdot 6\,NH_3$	0.079	"	4	143
PUHJOR	$C_{60}^{2-}\cdot Cd(NH_3)_6^{2+}\cdot 6\,NH_3$	0.047	"	4	113
NUSVAY	$C_{60}^{2-}\cdot Ba(NH_3)_7^{2+}\cdot NH_3$	0.023	cubic framework	6	113
EBOYOJ	$C_{70}^{2-}\cdot Ba(NH_3)_9^{2+}\cdot 7\,NH_3$	0.119	diamond-like	4	143
TADQAQ	$C_{60}^{3-}\cdot 3\,K^+\cdot 14\,THF$	0.109	isolated	0	140
YAPRAI	$C_{60}^{3-}\cdot NH_3\cdot 3\,K^+$	0.031	distorted fcc	12	295
GORXUG	$C_{60}^{3-}\cdot 3\,CrownK^+\cdot 2\,PhMe$	0.082	isolated	0	110
WEHRUW	Na_2RbC_{60}	0.129	fcc	12	27
WESYEY	Na_2CsC_{60}	0.052	"	12	20
XASKUX	$RbCs_2C_{60}$	–	"	12	295
ICECEY	$Sm_{2.75}C_{60}$	–	"	12	200
QUHYOH	$K_3Ba_3C_{60}$	0.075	bcc	8	10
(47)	$C_{60}^-Cs^+\cdot CoTPP\cdot 1.64\,PhCN\cdot 0.36\,(o\text{-}C_6H_4Cl_2)\cdot CH_3CN$	0.121	island	1	110
(38)	$C_{59}N^+Ag(CB_{11}H_6Cl_6)_2^-\cdot 3\,(o\text{-}C_6H_4Cl_2)$	0.069	isolated	0	223
(48)	$Eu_{3-x}C_{70}$	see [c]	fcc	12	298
(48)	$Eu_{9-x}C_{70}$	see [c]	"	12	298
Binary compounds					
VUWFUO	$C_{60}O$	0.096	isolated	0	19
YOSHIX	$C_{60}O_2$	0.052	"	0	295
CELZAU	$(C_{60})_2O\cdot 2\,CoOEP\cdot 1.2\,CHCl_3\cdot 0.8\,C_6H_6$	0.151	"	0	130
EBUFAI	$C_{60}F_{48}\cdot 2\,(1,3,5\text{-}C_6H_3Me_3)$	0.051	"	0	108
JUHJIF	$C_{60}Br_{24}\cdot Br_2$	0.038	"	0	143
MEBBOK	$C_{60}F_{18}O\cdot PhMe$	0.052	see [d]	see [d]	173
SUDVIW	$C_{60}Br_8\cdot 2\,Br_2$	0.137	–	–	173
SUDVOC	$C_{60}Br_6\cdot Br_2$	0.092	–	–	173
XAFLIZ	$C_{60}F_{18}\cdot PhMe$	0.049	see [d]	see [d]	100
XAPSEM	$C_{60}F_{17}CF_3\cdot 2\,PhMe$	0.066	see [d]	see [d]	173
ACULUF	$C_{60}Me_4PhO_2(OH)$	0.045	honeycomb	7	173

Table 2 (continued).

CSD Refcode or (Ref.)	Formula [a]	*R*-factor	Motif	MCN (see [b])	*T*/K
Binary compounds					
ACUMAM	$C_{60}Me_6$	0.123	puckered hexagonal layers	7	173
(49)	$C_{70}Br_{10}$	0.055	3*D* framework	5	153
(49)	$C_{70}Br_{10} \cdot 3\,Br_2$	0.139	honeycomb	5	170
σ-Derivatives					
AFICAT	$C_{60}C_2(CN)_4O \cdot HMTTF$	–	–	–	295
BAVKUE	$C_{60}Mcbcd \cdot CHCl_3 \cdot 0.5\,C_6H_{14}$	0.049	puckered layers	5	120
BIFFUR	$C_{60}Ppo \cdot CS_2$	0.084	–	–	295
CODVOG	T_h-$C_{60}(Tmp)_6 \cdot 4\,H_2O$	0.071	isolated	0	100
COFCIJ	D_3-$C_{60}(Tmp)_6 \cdot 0.11\,C_3H_6O \cdot 4\,H_2O$	0.053	"	0	148
DEXSOO	$C_{60}DMalK^+PF_6^- \cdot CH_2Cl_2 \cdot 0.5\,C_6H_6$	0.078	double chains	3	243
DIPWEE	$C_{60}(Fl)_2 \cdot TBrCalix[3] \cdot 2\,PhMe$	0.081	isolated	0	295
FERYOQ	$C_{60}(CN)(Tmopp) \cdot PhMe$	0.046	honeycomb	6	123
GASFEL	$(C_{60}Mal_5CPy_2)_2[Pt(PPh_3)_2]_2^{4+} \cdot 4\,(CF_3SO_3^-)$	0.092	isolated	0	295
GASFIP	$C_{60}Mal_5CPy_2 \cdot C_6H_6 \cdot 1.2\,CH_3CO_2Et$	0.096	"	0	295
HATGOY	$C_{60}(Dmxy) \cdot 0.5\,C_6H_6$	0.038	3*D* framework	6	295
HELWEA	$C_{60}C(Ph)C_6H_3(MeO)_2 \cdot 2\,CHCl_3$	0.062	diamond-like	4	295
HERNAT	$C_{60}C(C_4SiMe_3)_2 \cdot 0.5\,CS_2$	0.053	honeycomb	5	100
HERNEX	$C_{60}C(C_4SiMe_3)_2 \cdot 2\,PhMe$	0.049	graphite-like	3	100
HUCNAU	$C_{60}PPZnTPP \cdot C_7H_{16}$	0.092	chains	2	218
JUTNAN	$C_{60}Dpbdm \cdot o$-$C_6H_4Cl_2$	0.098	layers	5	295
LIKGER	$C_{60}Mal \cdot CHCl_3$	0.045	3*D* framework	8	193
NACVIW	$C_{60}CHE \cdot 2\,(o$-$C_6H_4Cl_2)$	0.055	cubic framework	6	178
NACVIX	$C_{60}Ant$	–	–	–	295
NAFDAZ	$C_{60}[Si(SiMe_3)_3]_2 \cdot CS_2$	0.062	double chains	4	295
NAFKUA	$C_{60}(Pip)_2 \cdot 0.5\,CH_2Cl_2$	0.063	3*D* framework	6, 7	295
NAFLAH	$C_{60}(Pip)_2 \cdot 0.5\,Et_2O$	0.052	honeycomb	6, 8	130
NARZIP	$(C_{60})_2 \cdot 4\,(o$-$C_6H_4Cl_2)$	0.067	layers	5	295
NAWLAY	$C_{60}Mpc \cdot 0.5\,C_6H_6$	0.043	double layers	7, 8	120
NISNOS	$C_{60}C(C_6H_4Br)_2$	0.033	hexagonal layers	6	100
NITGAY	$C_{60}(Fl)_4 \cdot 3\,PhMe$	0.061	chains	2	203
PIPNIL	$C_{60}AIz \cdot CS_2$	0.060	3*D* framework	6	173
RERLAB	$C_{60}AIz \cdot PhMe$	0.040	separated hexagonal layers	6	253
QAJMET	$C_{60}(m$-$XMal)_3 \cdot 3.5\,CH_2Cl_2$	0.085	isolated	0	228
QAWRUB	$C_{60}(CH_2Ph)_4 \cdot CS_2 \cdot 0.5\,C_6H_{14}$	0.062	tetragonal layers	4	223
QAWSAI	$C_{60}(CH_2Ph)_4 \cdot 2\,CS_2$	0.063	puckered graphite	3	223
QICZIL	$(C_{60}O)_2[NMe(CH_2)_3NMe]_4 \cdot 2\,CHCl_3$	0.198	puckered layers	3–4	295
RAWQAH	$C_{60}Ph_5Tl \cdot 2.5\,THF$	0.079	chains	2	295
RAZZUN	$C_{60}Bqd \cdot C_6H_6$	0.025	–	–	295
REBLAL	$C_{60}SPPIz \cdot 2\,(o$-$C_6H_4Cl_2)$	0.056	puckered graphite	3	148
RECCIL	$C_{60}TPPPyr \cdot CHCl_3$	0.080	island	1	163
REDJEP	$C_{60}Epp$	0.062	3*D* framework	10	295
RERKUU	$C_{60}BCIz \cdot PhMe$	0.047	honeycomb	7	295
RUNQEW	$C_{60}(Mal)_4 \cdot 2\,CHCl_3$	0.041	columns	2	100
TEKRIK	$C_{60}Mpd \cdot CS_2$	0.045	honeycomb	7	295
TIMTIS	$[C_{60}C(C_2SiPr^i_3)]_2C_4 \cdot 2\,PhMe$	0.047	"	5	100
TIYGAJ	$C_{60}DmPhe \cdot CS_2$	0.046	–	–	295
TODBUJ	$C_{60}Trz$	0.091	3*D* framework	9	193
TOPROF	$C_{60}(o$-$XMal) \cdot CHCl_3$	0.064	puckered layers	5	295
TOWQOL	$C_{64}H_4Fe(CO)_3 \cdot 2.5\,CS_2$	0.060	cubic framework	6	156
TUJSIA	$C_{60}S_2Fe_2(CO)_6 \cdot 0.25\,PhMe \cdot 0.5\,C_5H_{12}$	0.057	3*D* framework	6	198
TUJXEB	$C_{60}(H)Fl \cdot 2\,C_6H_6$	0.049	puckered tetragonal layers	4	295
TUQJIY	$C_{60}Dtdm \cdot CS_2$	0.056	3*D* framework	7	295
VEHQII	$C_{60}C(COOH)Pcp$	0.167	puckered tetragonal layers	4	295
VUBBEZ	$C_{60}OsO_4(4$-$Bu^tPy)_2$	0.103	–	–	295
WECZAF	$C_{60}Me_5O_2(OH)$	0.075	honeycomb	8	173
YAPWIV	$C_{60}Hex \cdot 1.5\,PhCl$	0.116	double chains	4	295
YIRXEC	$C_{60}CCpdm \cdot 3\,C_6H_6$	0.063	graphite-like	3	295
ZAKMUT	$C_{60}(Mal)_3Mbde \cdot 2\,C_6H_6$	0.049	isolated	0	233
ZEDWEK	$C_{60}(Mal)_6 \cdot 2\,PhBr$	0.066	"	0	295
ZIHJOP	$C_{60}Pip \cdot 1.5\,CH_2Cl_2$	0.060	tetragonal layers	8	130
ZIHJUV	$C_{60}(Pip)_2 \cdot 0.7\,CH_2Cl_2 \cdot 0.3\,Et_2O$	0.098	the same	4	130
ZIJCOK	$C_{60}(CN)_2 \cdot 2\,(o$-$C_6H_4Cl_2)$	0.084	cubic framework	6	295
ZUHSEA	$C_{60}C(C_6H_4OMe)_2$	0.038	tetragonal layers	4	295

Table 2 (continued).

CSD Refcode or (Ref.)	Formula [a]	*R*-factor	Motif	MCN (see [b])	*T*/K
σ-Derivatives					
ZUSSUB	$C_{64}H_4CoCp \cdot PhMe$	0.076	puckered hexagonal layers	6	156
BUBQIY	$(C_{60})_2(Mal)_{10} \cdot 4\,PhCl$	0.075	island	1	103
NEPHAR	$C_{60}Phd \cdot 2\,CS_2$	0.087	diamond-like	4	91
UBIJAQ	$C_{60}(Ant)_2 \cdot 1.5\,CS_2 \cdot C_6H_{14}$	0.068	chains	2	218
UBIJEU	$C_{60}(Ant)_2 \cdot 1.5\,CS_2$	0.053	double chains	3	218
VODZIX	$C_{60}(MalBr)_3F_{15} \cdot PhMe$	0.049	island	1	173
VOKFOQ	$C_{60}(1\text{-}MeAnt) \cdot 2\,CHCl_3$	0.067	columns	2	223
XARVAN	$C_{70}(DMal) \cdot 6\,CHCl_3$	0.077	chains	2	233
SERDUO	$C_{70}Phe \cdot PhMe$	0.089	3*D* framework	8	295
REFTOL	$C_{70}TMOIz \cdot 0.5\,CS_2$	0.046	"	10	170
CELQUF	$C_{70}CCl_2 \cdot 0.45\,C_5H_{12} \cdot 0.05\,PhMe$	0.089	"	10, 11	110
GIZCIB	$C_{70}(C_6H_4CF_3)_3Tl \cdot o\text{-}C_6H_4Cl_2$	0.085	hexagonal layers	6	295
ZADQUQ	b-C_{70}Dmxy $\cdot 2\,CS_2$	0.045	3*D* framework	6	193
ZADRAX	d-C_{70}Dmxy $\cdot 2\,CS_2$	0.049	cubic framework	6	100
(50)	$C_{60}Me_5Ph_5O_3(OH)_2 \cdot PhCl$	0.145	puckered graphite	–	173
(51)	$C_{62}(p\text{-}C_6H_4Me)_2 \cdot CHCl_3 \cdot CS_2$	0.059	columns	2	100
π-Derivatives					
HADSIO	$C_{60}Pd(PPh_3)_2$	0.094	puckered layers	5	193
RACTUK	$C_{60}Pt(PPh_3)_2$	0.069	–	–	295
PECTAS	$C_{60}Pt(PPh_3)_2 \cdot THF$	0.059	–	–	203
BEJKUW	$C_{70}Pd(PPh_3)_2 \cdot CH_2Cl_2$	0.093	diamond-like	4	130
GUDNOI	$C_{60}Rh(PPh_2CH_2)_3CCH_3$	0.072	island	1	295
HAJYIA	$C_{60}Rh(CO)H(PPh_3)_2 \cdot 3.27\,CH_2Cl_2$	0.072	3*D* framework	2, 4	123
KOKXUD	$C_{60}Ir(CO)Cl(PPh_3)_2 \cdot 5\,C_6H_6$	0.067	island	1	130
WIHFUO	$C_{60}OIr(CO)Cl(PPh_3)_2 \cdot 0.53\,CHCl_3 \cdot 4.47\,C_6H_6$	0.057	isolated	0	123
ZEKXAO	$C_{60}O_2Ir(CO)Cl(PPh_3)_2 \cdot 4.8\,C_6H_6$	0.055	"	0	130
ZOQBUC	$C_{60}OIr(CO)Cl(AsPh_3)_2 \cdot 0.18\,CHCl_3 \cdot 4.82\,C_6H_6$	0.066	"	0	123
JOHGOC	$C_{70}Ir(CO)Cl(PPh_3)_2 \cdot 2.5\,C_6H_6$	0.068	graphite-like	3	120
TUFTIX	$C_{70}OIr(CO)Cl(PPh_3)_2 \cdot 5\,C_6H_6$	0.099	"	3	125
SUMZUV	$C_{84}Ir(CO)Cl(PPh_3)_2 \cdot 4\,C_6H_6$	0.036	diamond-like	4	295
KUFHEY	$C_{60}Ir(CO)Cl(podp)_2$	0.066	chains	2	130
LIXTUH	$C_{60}TiCp_2 \cdot PhMe$	0.076	3*D* with channels	6	120
MAZBIY	$C_{60}Mo(CO)_3(dppbz) \cdot 3\,THF$	0.051	graphite-like	3	295
MAZBOE	$C_{60}W(CO)_3(dppbz) \cdot 3\,THF$	0.068	"	3	295
NOWSOH	$C_{60}Mo(CO)_2(Phen)(bml) \cdot 2\,C_6H_6 \cdot C_5H_{12}$	0.125	chains	2	295
NOWSUN	$C_{60}W(CO)_2(Phen)(bml) \cdot 2\,C_6H_6 \cdot C_5H_{12}$	0.087	"	2	295
SUXGAT	$C_{70}Mo(CO)_2(Phen) \cdot 2\,Pr^iOH \cdot 2.5\,H_2O$	0.095	diamond-like	4	173
MINSAD	$(C_{60})_2W(CO)_2(BBPy) \cdot C_5H_{12} \cdot 3\,CS_2$	0.085	honeycomb	5, 6	123
MINSEH	$(C_{60})_2Mo(CO)_2(BBPy) \cdot C_5H_{12} \cdot 4\,CS_2 \cdot H_2O$	0.098	"	5, 6	123
POKMOR	$C_{60}Rh(DMPy)_2(acac) \cdot C_6H_6$	0.057	diamond-like	4	295
POQJOU	$C_{60}W(dppe)(CO)_3 \cdot 2\,(o\text{-}C_6H_4Cl_2) \cdot C_6H_{12}$	0.051	island	1	198
PUKWAT	$C_{60}Ru(NO)Cl(PPh_3)_2 \cdot 5\,C_6H_6$	0.061	isolated	0	295
PUNDOR	$C_{60}Mo(dppe)(CO)_3 \cdot CS_2$	0.041	chains	2	198
PUNDUX	$C_{70}Mo(dppe)(CO)_3 \cdot 3\,CHCl_3$	0.082	double chains	4	198
XAWHUY	$C_{60}Mn(CO)_4^-(PPh_3)_2N^+ \cdot THF$	0.136	puckered tetragonal layers	4	173
TIBJAP	$C_{60}Pt(dodppb) \cdot C_8H_{14}$	0.065	diamond-like	4	148
LADLAD	$C_{60}[Ir(CO)Cl(PPhMe_2)_2]_2 \cdot C_6H_6$	–	isolated	0	120
LADLEH	$C_{60}[Ir(CO)Cl(PPhMe_2)_2]_2 \cdot 2\,C_6H_6$	0.034	columns	2	123
XEHYOY	$(C_{60})_2Ir_2(CO)_2Cl_2(dpph)_2 \cdot 4\,C_6H_6 \cdot 2\,CH_2Cl_2$	0.053	chains	2	130
YEMVOB	$(\eta^2,\eta^2\text{-}C_{60})[Ir(CO)Cl(PMe_3)_2]_2 \cdot 2\,C_6H_6$	0.065	isolated	0	123
YEMVUH	$(\eta^2,\eta^2\text{-}C_{60})[Ir(CO)Cl(PEt_3)_2]_2 \cdot C_6H_6$	0.073	columns	2	123
PUHXUL	$(\eta^2,\eta^2\text{-}C_{60})Ir_2(MeO)(PhO)(C_8H_{12})_2 \cdot CH_2Cl_2$	0.110	tetragonal layers	4	295
PUKWEX	$(\eta^2,\eta^2\text{-}C_{60})Re_2(PMe_3)_4 \cdot 1.5\,C_6H_6$	0.034	graphite-like	3	295
VURTEH	$(\eta^2,\eta^2\text{-}C_{70})[Ir(CO)Cl(PPhMe_2)_2]_2 \cdot 3\,C_6H_6$	0.051	chains	2	130
ZISJOA	$(\eta^2,\eta^2\text{-}C_{60})Ru_2(Me_5Cp)_2(H)(Cl) \cdot PhMe$	0.040	graphite-like	3	295
ZISJUG	$(\eta^2,\eta^2\text{-}C_{60})Ru_2(Me_5Cp)_2(Cl)_2 \cdot 2\,PhMe$	0.045	"	3	295
TOPNER	$(\eta^2,\eta^2,\eta^2\text{-}C_{60})Ru_3(CO)_9 \cdot CS_2$	0.076	double hexagonal layers	7	295
NAXNIJ	$(b,b,d\text{-}\eta^2,\eta^2,\eta^2\text{-}C_{70})Ru_3(CO)_9 \cdot CS_2$	0.086	3*D* with channels	8	198
PUKBIG	$(\eta^2\text{-}C_{60})Os_3(CO)_{11} \cdot CH_2Cl_2$	0.064	diamond-like	4	295
OBINIW	$(\eta^2,\eta^2,\eta^2\text{-}C_{60})Os_3(CO)_8(BIC) \cdot 0.25\,CS_2$	0.069	puckered hexagonal layers	5, 6	293
OBINOC	$(\sigma,\eta^2,\sigma\text{-}C_{60})Os_3(CO)_8(BIC)_2 \cdot CS_2$	0.045	puckered graphite	3	293

Table 2 (continued).

CSD Refcode or (Ref.)	Formula [a]	*R*-factor	Motif	MCN (see [b])	*T* /K
π-Derivatives					
OBINUI	$(\sigma,\eta^2,\sigma\text{-}C_{60})Os_3(CO)_8(BIC)_2$	0.078	puckered graphite	3	293
HISVAG	$(\eta^2,\eta^2,\eta^2\text{-}C_{60})Os_3(PPh_3)(CO)_8 \cdot 1.5\,CS_2$	0.063	puckered tetragonal layers	4	295
MAZLUU	$(\eta^2,\eta^2,\eta^2\text{-}C_{60})Os_3(PMe_3)_2(CO)_7 \cdot CS_2$	0.065	hexagonal layers	6	295
MAZMAB	$(\eta^2,\eta^2,\eta^2\text{-}C_{60})Os_3(PMe_3)_3(CO)_6 \cdot 2\,CH_2Cl_2$	0.065	graphite-like	3	295
AFOXEY	$(\eta^2,\eta^2,\eta^2\text{-}C_{60})Os_3(BIC)_2(PPh_3)(CO)_7 \cdot o\text{-}C_6H_4Cl_2$	0.041	chains	2	298
AFOXIC	$(\eta^2,\eta^2\text{-}C_{60})Os_3(PPh_3)(PPh_2)(C_{12}H_{13}N_2)(CO)_6$	0.065	"	2	233
AFOXOI	$(\sigma,\eta^2,\sigma\text{-}C_{60})Os_3(BIC)_2(PMe_3)(CO)_7 \cdot CS_2$	0.076	tetragonal layers	4	233
MOCPID	$(\eta^2,\eta^2,\eta^2\text{-}C_{60})Re_3(BIC)(CO)_8 \cdot CS_2$	0.053	diamond-like	4	233
MOHYEN	$(\sigma,\eta^2,\sigma\text{-}C_{60})Os_3(BIC)(CO)_9 \cdot 0.5\,CS_2$	0.082	puckered layers	5, 6	233
YAPXOC	$C_{60}[Ir_2Cl_2(C_8H_{12})_2]_2 \cdot 2\,C_6H_6$	0.032	columns	2	295
ZOHVOH	$C_{70}[Pt(Ph_3P)_2]_4 \cdot 6.5\,C_6H_6 \cdot 0.5\,CH_3OH$	0.074	isolated	0	130
MEKXOP	$(\eta^2,\eta^2\text{-}C_{60})Os_5C(CO)_{12}PPh_3$	0.061	double chains	4	295
MEKYAC	$(\eta^2,\eta^2\text{-}C_{60})Os_5C(CO)_{11}PPh_3 \cdot CS_2 \cdot 0.5\,H_2O$	0.120	puckered layers	5	295
MEKXUV	$(\eta^2,\eta^2,\eta^2\text{-}C_{60})Os_5C(CO)_{11}(BIC)PPh_3 \cdot 0.5\,CS_2$	0.140	double chains	4	295
MEKYEG	$(\eta^2,\eta^2,\eta^2\text{-}C_{60})Os_5C(CO)_{11}(BIC)PPh_3$	0.074	the same	4	295
NOGNUS	$(\eta^2,\eta^2,\eta^2\text{-}C_{60})Ru_5C(CO)_{11}PPh_3 \cdot 1.5\,CS_2$	0.069	puckered layers	5	198
GAQCEG	$(\eta^2,\eta^2,\eta^2\text{-}C_{60})Ru_5C(CO)_{10}(dppm) \cdot CH_2Cl_2$	0.131	graphite-like	3	198
GAQCIK	$(\eta^2,\eta^2,\eta^2\text{-}C_{60})Ru_5C(CO)_{10}(dppfc) \cdot CH_2Cl_2$	0.102	chains	2	198
MIDMIV	$(\eta^2,\eta^2,\eta^2\text{-}C_{60})Ru_5C(CO)_{10}(PPh_3)(BIC) \cdot 2\,CS_2$	0.058	"	2	233
NOGPAA	$(\eta^2,\eta^2,\eta^2\text{-}C_{60})Ru_6(CO)_{12}(dppm) \cdot 3\,CS_2$	0.085	"	2	295
NAXNOP	$C_{70}[Ru_3(CO)_9]_2 \cdot 1.5\,CS_2$	0.085	puckered layers	5	198
GAQCUW	$(\eta^2,\eta^2,\eta^2\text{-}C_{60})\,PtRu_5C(CO)_{11}(dppm) \cdot 2\,CS_2$	0.044	island	1	198
XIJQEM	$(\eta^2,\eta^2,\eta^2\text{-}C_{60})Rh_6(dppm)_2(CO)_9$	0.104	"	1	293
XIJQIQ	$(\eta^2,\eta^2,\eta^2\text{-}C_{60})_2Rh_6(dppm)_2(BIC)(CO)_5 \cdot$ $\cdot 1.5\,(o\text{-}C_6H_4Cl_2) \cdot 2.75\,CS_2$	0.085	puckered layers	3	293
KOLSOT	$C_{60}[Pt(Ph_3P)_2]_6$	0.033	isolated	0	203
(52)	$\eta^2\text{-}C_{60}Ir(Cbpp)(Bu^tNC)_2 \cdot 4\,PhMe$	0.045	chains	2	190
(52)	$\sigma\text{-}C_{60}IrO_2(Cbpp)(Bu^tNC)_2 \cdot 3.67\,CHCl_3$	0.065	loose layers	3	100
Endohedral metallofullerenes and their derivatives					
BOJNIX	$Sc_3N@C_{80} \cdot CoOEP \cdot 1.5\,CHCl_3 \cdot 0.5\,C_6H_6$	0.224	chains	2	130
BEZCUE	$ErSc_2N@C_{80} \cdot CoOEP \cdot 0.3\,CHCl_3 \cdot 1.5\,C_6H_6$	0.087	"	2	90
QOFZIU	$Sc_3N@C_{78} \cdot CoOEP \cdot 0.3\,CHCl_3 \cdot 1.5\,C_6H_6$	0.111	"	2	110
XILSUG	$Sc_3N@C_{80}Dmxy \cdot 2\,C_6H_6$	0.064	puckered hexagonal layers	5	91
XIMKOT	$Er_2@C_{82} \cdot CoOEP \cdot 1.4\,C_6H_6 \cdot 0.3\,CHCl_3$	0.148	chains	2	113
(16)	$Sc_3N@C_{68} \cdot NiOEP \cdot 2\,C_6H_6$	0.094	isolated	0	91

[a] Abbreviated names of molecules and ligands are explained in Table 3. [b] Molecular coordination number. [c] According to powder X-ray diffraction. [d] Not applicable due to substantial nonsphericity of the carbon cage.

Table 3. Molecules and ligands as comonents of fullerene derivatives.

Abbreviation	Formula	Name
Neutral molecules and ligands		
acac	$C_5H_7O_2$	acetylacetonate
AT	$C_{19}H_{13}N$	azatriptycene
BBPy	$C_{20}H_{24}N_2O_4$	4,4′-bis(n-butoxycarbonyl)-2,2′-bipyridyl
BDMT-TTeF	$C_{14}H_{12}S_2Te_4$	bis(dimethylthieno)tetrathiafulvalene
BEDTB(EDT)	$C_{20}H_{16}S_{16}$	bis(ethylenedithio)bis(ethylenedithiotetrathiafulvalene)
BEDT-TTF	$C_{10}H_8S_8$	bis(ethylenedithio)tetrathiafulvalene
bml	$C_{12}H_{20}O_4$	di(n-butyl) maleate
BIC	C_8H_7N	benzyl isocyanide
BNDTY	$C_{22}H_{12}S_4$	bi(naphtho[1,8-*d*,*e*]-1,3-dithiin-2-ylidene)
BNTTF	$C_{22}H_{16}S_4$	binaphthotetrathiafulvalene
BPZnOEP	$C_{108}H_{124}N_8O_4Zn_2$	μ2-5,5′:15,15′-bis[1,6-bis(*m*-phenyleneoxy)hexane]bis(2,3,7,8,12,13,17,18-octaethyl-porphyrinato) zinc
BTX	$C_{26}H_{18}Te_2$	9,9′-*trans*-bitelluraxanthenyl
Calix[6]	$C_{42}H_{36}O_6$	calix[6]arene
Crown	$C_{12}H_{24}O_6$	18-crown-6
Crypt	$C_{18}H_{36}N_2O_6$	2,2,2-cryptand
CTV	$C_{27}H_{30}O_6$	cyclotriveratrylene

Table 3 (continued).

Abbreviation	Formula	Name
Neutral molecules and ligands		
DAN	$C_{28}H_{20}$	9,10-[9,10]anthracenoanthracene
DBTTF	$C_{14}H_8S_4$	dibenzotetrathiafulvalene
DIDMCalix[5]	$C_{38}H_{34}I_2O_5$	3,16-diiodo-10,22,28-trimethylcalix[5]arene
Diox	$C_4H_8O_2$	dioxane
DMPy	C_7H_9N	3,5-dimethylpyridine
DMTEDT-TTF	$C_{10}H_{10}S_8$	di(methylthio)ethylenedithiotetrathiafulvalene
dodppb	$C_{31}H_{32}O_2P_2$	*O*,*O*′-isopropylidene-2,3-dihydroxy-1,4-bis(diphenylphosphino)butane
dppbz	$C_{30}H_{24}P_2$	bis(diphenylphosphino)benzene
dppe	$C_{26}H_{24}P_2$	bis(diphenylphosphino)ethane
dppfc	$C_{34}H_{28}P_2Fe$	bis(diphenylphosphino)ferrocene
dpph	$C_{31}H_{34}P_2$	bis(diphenylphosphino)heptane
dppm	$C_{25}H_{22}P_2$	bis(diphenylphosphino)methane
DTDSeF	$C_8H_8S_3Se_2$	2-(4-thioxo-1,3-dithiolane-5-ylidene)-4,5-dimethyl-1,3-diselenol
EDT(DET)TTF	$C_{12}H_{14}S_8$	ethylenedithio(diethylthio)tetrathiafulvalene
HMTPH	$C_{24}H_{24}O_6$	hexamethoxytriphenylene
HMTTF	$C_{12}H_{12}S_4$	hexamethylenetetrathiafulvalene
MDT-TTF	$C_8H_4S_8$	methylenedithiotetrathiafulvalene
ODAPz	$C_{32}H_{48}N_{16}$	octakis(dimethylamino)porphyrazin
OEP	$C_{36}H_{40}N_4$	octaethylporphyrin
OMCTD	$C_{26}H_{30}N_4$	5,14-dihydro-2,3,6,8,11,12,15,17-octametyldibenzotetraaza(14)annulene
OMTTF	$C_6H_{16}S_4$	octametylenetetrathiafulvalene
OPCTSil	$C_{48}H_{40}O_4Si_4$	octaphenylcyclotetrasiloxane
PBMP	$C_{17}H_{14}N_2O_2$	4-benzoyl-3-methyl-1-phenylpyrazol-5-one
PBzCalix[5]	$C_{70}H_{60}O_5$	pentabenzylcalix[5]arene
biCalix[5]	$C_{70}H_{58}O_{10}$	bicalix[5]arene
PdBPPyP	$C_{134}H_{150}N_{10}Pd_3Cl_2$	bis[μ_2-5-(3-pyridyl)-10,15,20-tris(3,5-dibutylphenyl)porphyrin]dichlorotripalladium
Calix[5]	$C_{35}H_{30}O_5$	calix[5]arene
Phen	$C_{12}N_2H_8$	1,10-phenanthroline
PMCalix[5]	$C_{40}H_{40}O_5$	5,11,17,23,29-pentamethylcalix[5]arene
podp	$C_{26}H_{23}OP$	4-benzyloxybenzyldiphenylphosphine
Py	C_5H_5N	pyridine
TAP	$C_{92}H_{76}N_2$	tetrakis(2,3,6,7-tetramethyl-9,10-dihydro[9,10]anthracene)porphyrin
TBBCN	$C_{63}H_{42}O_{12}$	tris(4,5-dibenzoyloxybenzo)[*a*,*d*,*g*]cyclonona-1,4,7-triene
TBPD	$C_{34}H_{32}N_4$	*N,N,N',N'*-tetrabenzyl-*p*-phenylenediamine
TBrCalix[3]	$C_{24}H_{21}Br_3O_6$	tribromotris(oxadihomo)calix[3]arene
TBTPCalix[4]	$C_{40}H_{44}Br_4O_4$	5,11,17,23-tetrabromo-25,26,27,28-tetra-*O*-n-propylcalix[4]arene
TBuCalix[3]	$C_{36}H_{48}O_6$	tri-*tert*-butyltris(oxadihomo)calix[3]arene
TBuCalix[3]N	$C_{48}H_{54}O_6$	8,18,28-tributyltris(oxadihomo)calix[3]naphthalene
TBzCalix[3]	$C_{45}H_{42}O_6$	7,15,23-tribenzyltrioxadihomocalix[3]arene
TDAE	$C_{10}H_{24}N_4$	tetrakis(dimethylamino)ethylene
TDBPP	$C_{76}H_{94}N_4$	5,10,15,20-tetrakis(3,5-di-*tert*-butylphenyl)porphyrin
TDMPP	$C_{52}H_{44}N_4$	tetrakis(dimethylphenyl)porphyrin
TDZ	$C_4N_4S_6$	3,3′,4,4′-tetrathiabis(1,2,5-thidiazole)
THF	C_4H_8O	tetrahydrofuran
TITBCalix[4]	$C_{56}H_{44}I_4O_4$	5,11,17,23-tetraiodo-25,26,27,28-tetra-*O*-benzylcalix[4]arene
TMCalix[5]	$C_{38}H_{36}O_5$	5,17,23-trimethylcalix[5]arene
TMCTD	$C_{22}H_{22}N_4$	5,7,12,14-tetramethyldibenzotetraaza(14)annulene
TMDTDM-TTF	$C_{12}H_{14}S_6$	tetramethylenedithiodi(methylthio)tetrathiafulvalene
TMPD	$C_{10}H_{16}N_2$	*N*,*N*,*N*′,*N*′-tetramethyl-*p*-phenylenediamine
TMTSeF	$C_{10}H_{12}Se_4$	tetramethyltetraselenafulvalene
TMTTF	$C_{10}H_{12}S_8$	tetra(methylthio)tetrathiafulvalene
TPBP	$C_{34}H_{24}O_2$	2,2′,6,6′-tetraphenyldipyranylidene
TPivP	$C_{64}H_{66}N_8O_4$	tetrakis(*o*-pivalamido)phenylporphyrin
TPCalix[4]R	$C_{60}H_{56}O_8$	tetra(phenethyl)calix[4]resorcinarene
TPP	$C_{44}H_{28}N_4$	tetraphenylporphyrin
TPyP	$C_{40}H_{28}N_8$	tetrakis(4-pyridyl)porphyrin
Trip	$C_{20}H_{14}$	triptycene
TTF	$C_6H_4S_4$	tetrathiafulvalene
TTolP	$C_{48}H_{36}N_4$	tetra(*p*-tolyl)porphyrin

Table 3 (continued).

Abbreviation	Formula	Name
Substituents		
Ant	$C_{14}H_8$	anthracene-9,10-diyl
Bqd	$C_8H_6O_2$	1,4-benzoquinone-2,3-diyldimethylene
Cbpp	$C_{15}B_{10}H_{22}P$	(diphenylphosphinomethylene)carboranyl
CCpdm	$C_{35}H_{27}Co$	(1,2,3,4-tetraphenylcyclobutadiene)cobaltcyclopentadienyldimethylenediyl
CHE	C_6H_8	cyclohex-2-ene-1,4-diyl
DMal	$C_{32}H_{36}O_{14}$	dibenzo-18-crown-6-3,3′-diyl-bis[(ethoxycarbonyl)methoxycarboranylmethylene]
DmPhe	$C_8H_8O_2$	4,5-dimethoxyphenylene
Dmxy	$C_{10}H_{12}O_2$	dimethoxyxylylene
Dpbdm	$C_{22}H_{20}$	1,4-dimethyl-2,3-diphenylphenylenedimethyldiyl
Dtdm	$C_5H_4S_3$	1,3-dithiole-2-thione-4,5-dimethylenediyl
Epp	$C_6H_8O_2$	1-ethoxycarbonylpropene-1,2-diyl
Fl	$C_{13}H_9$	9-fluorenyl
Hex	$C_{32}H_{38}O_2$	dimethoxy-7,14-dimethyl-7,14-cyclo-6,15:8,13-dimethano-5,16-ethanohexahydro-hexacenediyl
Mal	$C_7H_{10}O_4$	(diethyl malonate)diyl
Mbde	$C_{19}H_{30}O_4$	bis[4-hexyl(diyl)benzyl]malonatediyl
Mcbcd	$C_{13}H_{18}O_2$	7-butyloxycarbonyl-3-methylbicyclo[4.1.0]heptane-2,5-diyl
Mpc	$C_9H_7NO_4$	(4-methoxycarbonylphenyl)carbamate-*N*,*N*-diyl
Mpd	C_9H_9NO	2-(5-methoxyphenyl)-2-azapropane-1,3-diyl
Pcp	$C_{20}H_{16}O_2P$	1-(triphenylphosphonio)acetylide
Phe	C_6H_4	*o*-phenylene
Phd	$C_{20}H_{19}N_5$	6-phenyl-1,4-bis(2-pyridyl)-2,3,5-triazahepta-1,4-diene-1,3-diyl
Ppo	$C_8H_{12}O_2$	8,8-dimethyl-6,10-dioxaspiro[4,5]decane-1,2-diyl
PPZnTPP	$C_{52}H_{38}N_6Zn$	1-(4-pyridyltetraphenylporphyrinatozinc)-2-methyl-2-azapropane-1,3-diyl
Pip	$C_4H_8N_2$	piperazine-1,4-diyl
Tmopp	$C_{12}H_{15}O_5$	(3,4,5-trimethoxyphenylpropionate)-3,3-diyl
XMal	$C_{18}H_{18}O_8$	*o*-phenylenebis[(ethoxycarbonyl)methoxycarbonylmethylene]
Annelated heterocycles		
C_{60}AIz	$C_{75}H_9NO$	3-(9-anthryl)-4,5-dihydroisoxazolofullerene
C_{60}BCIz	$C_{69}H_7NO_3$	3-benzyloxycarbonylizoxazolofullerene
C_{60}SPPIz	$C_{71}H_{13}NO_3S$	3-[*o*-(*tert*-butylsulfonyl)phenyl]isoxazolofullerene
C_{60}TMOIz	$C_{70}H_{11}NO_4$	3-(2,4,6-trimethoxyphenyl)isoxazolofullerene
$C_{60}(Tmp)_6$	$C_{96}H_{78}N_6$	hexakis(2,2,5,5-tetramethylpyrrolidino)fullerene
C_{60}TPPPyr	$C_{107}H_{35}N_5$	1-methyl-2-(tetraphenylporphyrin)-3,4-pyrrolidinofullerene
C_{60}Trz	$C_{64}H_9N_3O_2$	1-(2-methoxyethoxymethyl)triazolofullerene

derivatives of C_{60}, this is equivalent to distances of 9.9 – 10.3 Å between the centres of the adjacent molecules. As a semiquantitative measure of the density of the fullerene packing, it has been proposed [65] to use the dilution parameter defined as

$$\rho = \frac{V_{\text{cell}} - V_{\text{full}}}{V_{\text{full}}}, \qquad (1)$$

where V_{cell} is the unit cell volume and V_{full} is the volume occupied by fullerene molecules within the unit cell. The dilution parameter ρ ranging from 0.33 (for an fcc packing) to ∞ is linked to the commonly adopted partial packing coefficient of fullerene spheres in a crystal

$$\kappa = \frac{V_{\text{full}}}{V_{\text{cell}}}$$

through a simple relation

$$\frac{1}{\kappa} = \rho + 1.$$

An increase in ρ, which corresponds to progressive 'dilution' of fullerene clusters with other (non-fullerene) molecular components in the crystal, typically leads to a change in the packing motif of the carbon clusters $(C_n)_\infty$ at specific threshold values of ρ. For C_{60} derivatives, the typical ranges of various motifs can easily be estimated based on simple geometrical considerations.[65]

Since the overall structure in this type of compound is kept by non-specific van der Waals interactions, many 'guest' molecules that are similar in size and shape to the van der Waals surfaces form analogous structural motifs with similar values of ρ in the fullerene complexes. The crystal structures of the corresponding complexes may belong to different systems and differ significantly in the unit cell parameters. The packing motif $(C_n)_\infty$ in these structures plays the role of a flexible van der Waals matrix thus justifying the utilisation of MCN and ρ as classification criteria.

Solvent molecules often act as 'guests' in molecular complexes of C_n fullerenes. Crystal solvates are often formed upon growth of fullerene crystals from solutions. Some solvents form several solvates with different compositions. For instance, in the case of CCl_4, two solvates with C_{60} : solvent ratios of 1 : 2 (see Ref. 66) and 1 : 13 (see Ref. 67) have been isolated and characterised; $CBrCl_3$ behaves similarly (see Ref. 68).

Buckminsterfullerene is characterised by a relatively good solubility in aromatic hydrocarbons and their non-polar derivatives, but is virtually insoluble in polar solvents (alcohols, esters, *etc*.).[69] Aliphatic hydrocarbons are poor solvents for C_{60}, but nevertheless also form solvates. Solubility curves of fullerene in many solvents manifest a characteristic inflection, sometimes expressed as a distinct maximum. This phenomenon is known as the 'anomalous temperature dependence',[69] although a number of inorganic systems, *e.g*., $Na_2SO_4 - H_2O$, manifest similar changes in the solubility.[70] Initially, this peculiarity of C_{60} was suggestively

Table 4. Structural motifs of fullerene molecules in fullerene molecular complexes.

Type	MCN	Example	Ref.
'Almost dense' three-dimensional frameworks	9–11	$C_{60}\cdot 2/3\,C_8H_{10}$, $C_{60}\cdot C_5H_{12}$	76, 77
Double layers	7–10	$C_{60}Mpc\cdot 0.5\,C_6H_6$	78
Hexagonal layers with trigonal prismatic cavities in-between	6–8	$C_{60}\cdot 2\,P_4$	79
Loose three-dimensional frameworks (spatial honeycombs with channels or diamond-like frameworks)	4–6	$C_{60}\cdot 4\,C_6H_6$	80
Spatially separated closely packed layers	4–6	$C_{70}\cdot 6\,S_8$	26
Loose layers, including graphite-like	3–6	$C_{60}\cdot PdOEP\cdot 1.5\,C_6H_6$	81
Columnar motifs	2–4	$C_{70}\cdot CoOEP\cdot CHCl_3\cdot C_6H_6$	82
Island motifs	0–1	$C_n\cdot 13\,C_6H_{12}$ (n = 60, 70)	67

associated with a phase transition in pure fullerene[69] or with a formation of multi-molecule clusters in solution.[71] Nowadays, it is widely accepted that it is caused by formation of solvates.[72] At a specific temperature T^* (which, for aromatic solvents, typically lies below the boiling point of the solvent), the solvates incongruently melt, *i.e.*, decompose into fullerene and the solvent. According to the calorimetric studies on a number of fullerene–solvent systems, the enthalpy of the incongruent melting is normally 10–50 kJ per mole of fullerene.[73, 74] Properties of solutions of higher fullerenes are, in general, similar to those of C_{60}, but the solubility of, for example, C_{70} in organic media is usually slightly higher than that of buckminsterfullerene.[75]

The major motifs $(C_n)_\infty$ formed by chemically unbound fullerene spheres encountered in structurally characterised molecular complexes of fullerenes are listed in Table 4. For all the substances, the values of the MCN for fullerene molecules are given. The major motifs of the fullerene–'guest' packings are depicted schematically in Fig. 5.

Packing $(C_n)_\infty$, the least diluted by 'guest' molecules, is found in C_{60} solvates with *m*-xylene,[76] mesitylene,[83] and other small molecules of 1,3- and 1,3,5-substituted benzenes (A). These solvates have the stoichiometry $3\,C_{60}\cdot 2\,A$ and reveal an hcp motif of fullerene spheres with 'excised' columns (MCN = 9–10); the solvent molecules are located in the channels (see Fig. 5 *a*).

Among three-dimensional frameworks of fullerene spheres, the motif found in a series of 1:1 C_{60} solvates with pentane, hexane, dichloroethane, trichloroethane and trichloroethylene, is quite typical. In this structural motif, tetragonal dense layers $(C_{60})_\infty$ are stacked in such a way that the close and the closest stacking arrangements are regularly alternating; the solvent molecules occupy cavities (Fig. 6). The formation of characteristic polysynthetic twins with an approximate 10-fold symmetry axis has been reported for all of these solvates.[84] Higher fullerenes C_{82} and $M@C_{82}$ form toluene solvates of the same structural type.[31, 85] Furthermore, a 1:1 bromoform solvate of C_{60} with the closely packed framework structure is known, in which the disordered solvent molecules are located in cavities.[40]

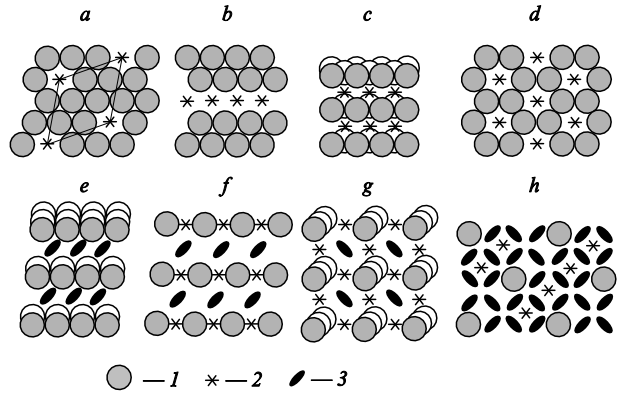

Figure 5. The main packing motifs in molecular complexes of C_{60}.
Motifs: (*a*) 'almost dense', (*b*) double layers, (*c*) closely packed layers, (*d*) framework, (*e*) separated closely packed layers, (*f*) loose layers, (*g*) columns, (*h*) islands (for examples of structures, see Table. 4); (*1*) fullerene, (*2*) solvent molecule, (*3*) 'guest' molecule.

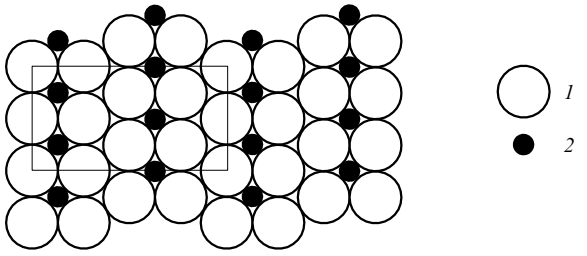

Figure 6. The molecular packing motif in the 1:1 pentane solvate of fullerene.[77]
(*1*) C_{60} molecule, (*2*) pentane molecule; projection of the unit cell is indicated by the rectangle.

Buckminsterfullerene forms an extended series of solvates and molecular complexes with the composition 1:2 [$C_{60}\cdot 2\,A$, where A = P_4,[79] CCl_4,[66] PhBr,[86] Cp_2Fe (see Ref. 87), *etc.*] built up of closely packed hexagonal layers of the fullerene molecules with the 'guest' molecules A in the interlayer space (see Fig. 5 *c*). Such a motif is characterised by the values of MCN = 6–8 and ρ = 0.7–0.8. It is encountered in crystal structures belonging to different systems from hexagonal (*e.g.*, $C_{60}\cdot 2\,P_4$) to triclinic (*e.g.*, $C_{60}\cdot 2\,Cp_2Fe$). In benzene solvates of the fullerene molecular complex with sulfur nitride with the variable composition $C_{60}\cdot 0.67\,S_4N_4\cdot 1.33\,C_6H_6$, half of the 'guest' positions is occupied by the ordered benzene molecules while the other half is statistically occupied by disordered C_6H_6 and S_4N_4 molecules.[88] It is noteworthy that in 1:2 fullerene solvates with bromobenzene and iodobenzene, which are characterised by similar packings but twice larger unit cells, the C_{60} molecules are rotationally disordered in the bromobenzene solvate and fully ordered in the iodobenzene solvate. The distances between the centres of the adjacent C_{60} molecules in the two solvates are 10.16 Å and 9.89 Å, respectively.[41]

A number of 'closely packed' molecular complexes can be prepared by direct intercalation of small molecules into solid fullerene at elevated pressure. In particular, the insertion of oxygen molecules into the octahedral cavities of the fcc packing of fullerene at room temperature and 1 kbar has been detected by NMR.[89] However, the main method of preparation of molecular complexes consists of co-crystallisation of the components from a suitable solvent. Co-crystallisation of buckminsterfullerene with tetrahedral molecules of white phosphorus P_4 from a solution yields the complex $C_{60}\cdot 2\,P_4$ (ρ = 0.82), which has closely packed hexagonal layers of C_{60} molecules. With larger sulfur molecules,

the complex $C_{60} \cdot 2\,S_8$ ($\rho = 1.08$) is formed,[90] which contains a three-dimensional framework of the fullerene molecules with channels. Meanwhile, C_{70} forms a molecular complex with sulfur with the composition 1 : 6 ($\rho = 2.13$)[26] in which layers of the C_{70} molecules are separated by layers of the sulfur molecules (see Fig. 5 *e*). The latter structural motif is also observed in $C_{76} \cdot 6\,S_8$ (see Ref. 27). All the molecular complexes with sulfur reveal short C···S contacts with lengths in the range of 3.20 – 3.50 Å, which apparently stabilise the crystal structures.

Loose layers $(C_{60})_\infty$ (which may be regarded as approximately tetragonal with the MCN = 4) are formed upon insertion of relatively small solvent molecules (C_6H_6, CS_2) from the 'guest' layers into the fullerene layers. For instance, this type of structure is observed for two buckminsterfullerene molecular complexes with tetramethyltetraselenafulvalene, $C_{60} \cdot TMTSeF \cdot 2\,(CS_2)$,[91] and with 9,10-[9,10]-anthracenoanthracene (DAN), $C_{60} \cdot DAN \cdot 3\,C_6H_6$.[92] The latter complex is remarkably stable thus making it possible to isolate buckminsterfullerene from a benzene solution of a mixture of C_{60} and C_{70}. Graphite-like layers with the MCN = 3 are revealed in two benzene solvates of molecular complexes $C_{60} \cdot PdOEP \cdot 1.5\,C_6H_6$[81] and $2\,C_{60} \cdot H_2TPP \cdot 3\,C_6H_6$.[93] Note that another fullerene – tetraphenylporphyrin molecular complex differing from the latter only in the benzene content, *viz*., $2\,C_{60} \cdot H_2TPP \cdot 4\,C_6H_6$ is characterised by a totally different molecular packing involving a three-dimensional framework of the C_{60} molecules with hexagonal channels.

As an example of the columnar motifs, the complex $C_{60} \cdot 2\,(CuTPP)$[93] may be taken, which contains linear chains $(C_{60})_\infty$ with the MCN = 2. In several compounds, more complex one-dimensional motifs are observed, in particular, zigzag chains (*e.g*., in $C_{60} \cdot CTV$, see Ref. 94) or double columns of the fullerene molecules with the MCN = 4 (*e.g*., in $C_{60} \cdot 2\,BEDT\text{-}TTF$, see Ref. 95).

The island packings are typical of complexes with predominating non-fullerene components that separate and isolate the fullerene molecules from each other. In the crystal structures of such complexes, the interaction between fullerene molecules is not a structure-forming factor. Fullerene solvates $C_{60} \cdot 13\,(Solv)$ with cyclohexane, CCl_4 (see Ref. 67) and $CBrCl_3$ (see Ref. 68) are typical examples of such substances. In several cases, the islands are formed by two fullerene cages ('the van der Waals dimers'), which corresponds to the MCN = 1 {*e.g*., in $2\,C_{70} \cdot 9\,[p\text{-}C_6H_4(OH)_2] \cdot 2\,C_6H_6$, see Ref. 96}.

Fullerene forms complexes with inorganic compounds. In the case of molecular inorganic 'guests', such complexes have a normal van der Waals character. As examples, two complexes $C_{60} \cdot 3\,TiCl_4$ and $C_{60} \cdot 3\,C_6H_6 \cdot 2\,Pd_6Cl_{12}$ can be mentioned. The former contains a diamond-like framework,[97] while the latter comprises columns built up of rotationally disordered C_{60} molecules.[98] In some substances, the 'guest' component is represented by charged species of ionic salts, as in $C_{60} \cdot 5\,(Ag^+NO_3^-)$, which reveal a distorted simple cubic packing of the fullerene spheres.[99]

The following large donor molecules forming molecular complexes with fullerenes are worth a special note: derivatives of tetrachalcogenafulvalenes, polyaryl and fused aromatic hydrocarbons, macrocyclic tetraaza-compounds and their complexes with metals, bulky cage molecules (*i.e*., calixarenes, cyclodextrins) with the cavities large enough to accomodate a fullerene sphere. A mismatch in the dimensions of the cavity and the 'guest' in the latter type of compounds results in a decrease in the density and an increase in the structural disorder, which additionally diminishes the accuracy of the structure determination.

Substituted tetrathiafulvalenes (TTF) are prototypical components of radical-ionic salts with aromatic molecules functionalised by strong electrophilic substituents as anions. Planar geometry of both the cation and anion favours their regularly alternating parallel arrangement formed due to the stacking interactions. Nevertheless, systematic single-crystal X-ray diffraction studies have shown that such stacking motifs are not typical

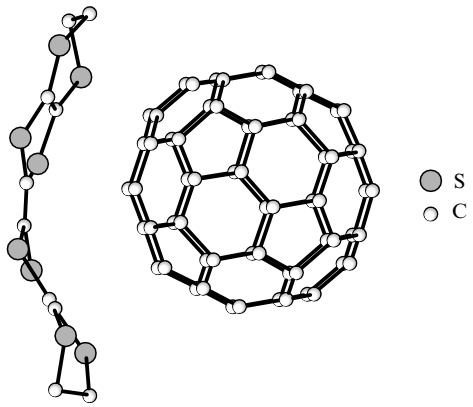

Figure 7. The mutual arrangement of bis(ethylenedithio)tetrathiafulvalene (BEDT-TTF) and fullerene molecule in the crystal structure of $C_{60} \cdot 2\,BEDT\text{-}TTF$.[95]

of fullerene molecular complexes with TTF derivatives. Vibrational spectroscopy data support a lack of significant charge transfer from the donor molecules to fullerene.[100] A distinctive feature of the molecular packing in such crystals is that the TTF derivatives forming the van der Waals contacts with adjacent fullerene molecules are non-planar (Fig. 7).

An analysis of structural data from the CSD regarding TTF-based molecular complexes (> 300 unique structures) shows that the molecules of TTF derivatives with bulky substituents or in the van der Waals crystals with large non-planar acceptors are often bent. Bending of the TTF moiety observed in almost all fullerene complexes with tetrachalcogenafulvalenes provides closer adjacency to a spheroidal C_n molecule and thus has purely van der Waals character (see Fig. 7). The complex $C_{60} \cdot (BEDT\text{-}TTF^+I_3^-)$ may be considered as an exception. It contains planar fulvalene as a radical cation.[101] Doping of the molecular complex $OMTTF \cdot C_{60} \cdot C_6H_6$ with alkali metals (K, Rb) gives rise to superconducting phases with relatively high temperatures of the transitions into the superconducting state T_c (17 K in the case of potassium and 23 K in the case of rubidium).[102]

Fused aromatic hydrocarbons and polyarenes, which are complementary to fullerenes in terms of the van der Waals shapes of their molecules, also form molecular complexes with fullerenes. Apart from the aforementioned buckminsterfullerene complex with 9,10-[9,10]anthracenoanthracene (DAN) $C_{60} \cdot DAN \cdot 3\,C_6H_6$,[92] the solvated complex with triptycene $C_{60} \cdot 2\,Trip \cdot 2\,(o\text{-}C_6H_4Me_2)$ may be taken as an example.[103] In many crystal structures, such polyarene derivatives adopt a conformation 'encompassing' the fullerene cage, thus increasing the number of energetically favourable van der Waals contacts.

The metal atoms in the coordination compounds with macrocyclic tetraazaligands (that form molecular complexes with fullerenes) have a square-planar coordination environment and thus are prone to additional coordination. In this class of compounds, zigzag chains of alternating fullerene and porphyrin molecules (Fig. 8) with shortened metal···fullerene contacts are frequently found. Such complexes are often regarded as supramolecular matrices capable of fixing a fullerene molecule in a specific orientation and therefore decreasing the rotational disorder of the crystal structure. In particular, the 'cage' molecule containing two zinc porphyrinate moieties linked in a way similar to that in paracyclophane strongly binds fullerene C_{60} in a complex with the composition 1 : 1, which is stable in solution. This complex has been isolated by chromatography[104] and studied by single-crystal X-ray diffraction.[105] Yet another complex, where one buckminsterfullerene molecule is embraced by two palladium porphyrinate units linked through a bridging group (Fig. 9), has also been characterised by single-crystal X-ray diffraction.[106] However,

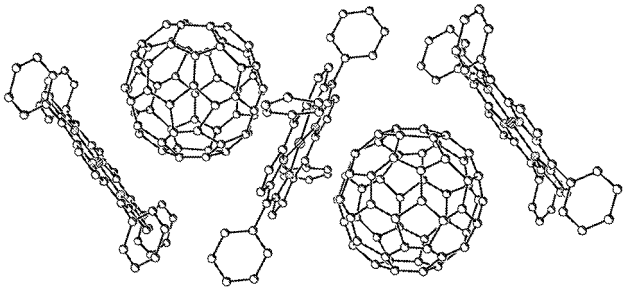

Figure 8. Zigzag chains in the crystal structures of fullerene complexes with metal porphyrinates.[47]

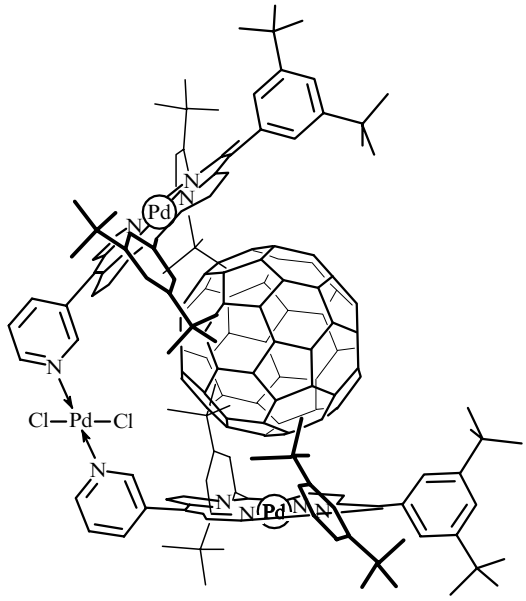

Figure 9. The molecular structure of a C_{60} complex with PdBPPyP containing two chemically bound Pd porphyrinate fragments.

both ordered and disordered fullerene molecules are revealed in the structurally characterised complexes with metal porphyrinates. Probably, the secondary metal···fullerene bonding is quite weak and does not exert decisive influence on the general molecular packing, though it can affect the degree of ordering of the fullerene molecules at specific favourable mutual arrangements of the porphyrin and fullerene molecules.[45]

The 'secondary' interactions of metalloporphyrins or related compounds with carbon cages, LM···C_n (L is a macrocyclic ligand), are characterised by the M···C distances intermediate between typical π-coordination (~2.0–2.3 Å) and van der Waals contacts (≥ 3.0 Å). For instance, the Fe···C distances are 2.70 Å in $C_{60}\cdot FeTPP^+\cdot(C_6F_5)_4B^-\cdot 2.5(o\text{-}C_6H_4Cl_2)$ complex.[107] In many cases, the secondary metal–fullerene interactions stabilise unique orientation of the fullerene cage preventing disorder. Nevertheless, in several substances of this class, for example, in the C_{60} complex with cobalt tetrakis(3,5-di-*tert*-butylphenyl)porphyrinate, both the short Co···C distances (2.59 Å) and disordering of the fullerene molecules are observed.[108]

Yet another class of fullerene molecular complexes includes cycloveratrylene and calixarenes. Some of these complexes contain molecules of water or alcohol in a crystal. This is quite nontypical for other classes of fullerene derivatives, which are most often hydrophobic. In the complexes with calixarenes, spheres of the fullerene molecules are laid on the bowl-shaped organic molecules. To date, sixteen different C_{60} complexes with substituted calixarenes starting from calix[3]- to calix[6]arenes have been characterised structurally (see Table 2). Water-soluble cyclodextrin also forms a complex with fullerene thus making it possible to transfer fullerene into an aqueous solution with a concentration of up to 10^{-5} mol litre^{-1}. The crystal structure of this complex has not been determined so far.[109]

Since the structural motifs $(C_n)_\infty$ in fullerene molecular complexes and chemically modified fullerenes are similar, it is convenient to analyse them in parallel. Figure 10 shows the numbers of all known crystalline fullerene derivatives as functions of the dilution parameter, MCN and the *R*-factor. The histogram of the dilution parameter distribution (see Fig. 10 *a*) manifests two maxima corresponding to $\rho = 0.8$ and 2.0. The former value is typical of layered hexagonal close packings and the latter, of loose framework structures. The values of $\rho \geqslant 3$, as a rule, correspond to chain or island motifs.

The distribution according to the MCN (see Fig. 10 *b*) of all fullerene structures deposited into the CSD indicates a large fraction of loose dilute structural motifs and a gradual decrease in the number of structures for the MCN ≥ 6. It is noteworthy that even molecular coordination numbers prevail over the odd ones, which may be explained by the frequent occurrence of the centrosymmetric motifs $(C_n)_\infty$.

The distribution according to the *R*-factor (see Fig. 10 *c*) is shifted to $R \geqslant 0.05$ and manifests a characteristic 'tail' at $R \geqslant 0.10$; the latter indicates a somewhat decreased accuracy of single-crystal X-ray diffraction for this specific class of crystalline compounds. Defects, stacking faults and very typical rotational disorder of spheroidal C_n clusters (dominated in the crystal structures with $R \geqslant 0.10$) are the reasons for the relatively low accuracy of the structure determination. For some fullerene

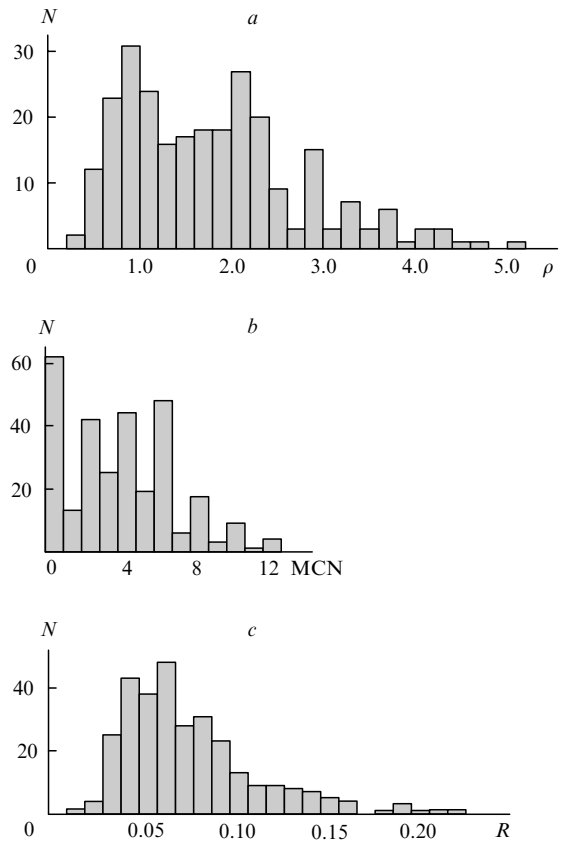

Figure 10. The number of fullerene structures from the CSD as a function of the dilution parameter (*a*), MCN (*b*) and *R*-factor (*c*).

molecular complexes, the 'guest' component is also disordered, which additionally reduces the quality of the crystallographic data.

In certain cases, it proves possible to approximate the rotational disorder of the fullerene molecules by superposition of C_n molecules in two orientations leading to coincidence of some of the atomic positions from the two orientations and partial occupancies of the remaining positions. In order to reduce correlations between fittable atomic positions in the least-squares refinement, a carbon cage with a fixed idealised geometry is often used. For C_{60}, two types of the rotational disorder occur most frequently (Fig. 11), *viz*., two orientations related to each other through a rotation by 90° around a molecular two-fold axis and two orientations related to each other through a rotation by 60° around a three-fold axis. In the former case, common positions determine 48 pairs of closely located carbon atoms from the two orientations, while the disordered part of the molecule (formed by spatially separated atomic positions with partial occupancies) forms characteristic 'crosses' at the vertices of an octahedron over the fullerene sphere. In the latter case, the disordered C_{60} molecule may be described as the ordered 'poles' and a disordered equatorial belt. For C_{70}, no similar regular superpositions of different molecular orientations have been revealed. Therefore, disordered structures are normally approximated by a superposition of two molecules with a fixed idealised geometry devoid of common atomic positions.

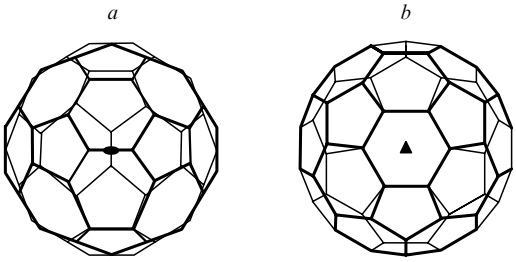

Figure 11. The major types of rotational disorder of the buckmisnterfullerene molecules in crystal structures (the two orientations are shown with bold and normal lines, respectively).
(*a*) rotation by 90° around the two-fold axis, (*b*) rotation by 60° around the three-fold axis.

To predict the preferred mutual orientations of rotationally disordered fullerene molecules, a model of the 'rubber cavity' has been proposed.[110] According to this model, all carbon atoms of the fullerene molecule residing in an equilibrium orientation occupy minima of the shallow van der Waals potential. To a first approximation, an increase in the interaction energy upon rotation of a molecule is proportional to the sum of squared radial stretches of the fullerene's van der Waals surface in the vicinity of atomic positions with respect to the initial equilibrium surface corresponding to the minimum interaction energy

$$\Delta U = k \sum \Delta r_i^2, \qquad (2)$$

where the summation is performed over radius-vectors of all carbon atoms. The most probable alternative orientations occurring in the case of a rotational disorder should correspond to the local minima of ΔU, *i.e*., to the least deformed van der Waals shape of molecule. A calculation based on the 'rubber cavity' model well reproduces both experimentally observed types of the rotational disorder for C_{60} as well as the lack of characteristic disorder types for C_{70}. Furthermore, this allows predictions of probable types of the rotational disorder for other highly symmetric spheroidal molecules (Fig. 12).

In some fullerene molecular complexes, as in pure fullerene, the second order phase transitions of the order–disorder type

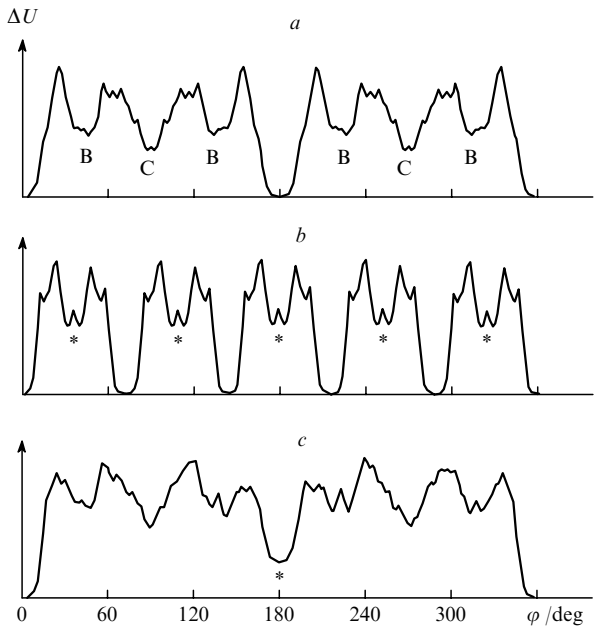

Figure 12. Profile of the interaction potential ΔU calculated within the model of the 'rubber cavity' for C_{60} (*a*), C_{80} (*b*) and $C_{60}F_{48}$ (*c*).
(*a*) Rotation by an angle φ around a two-fold axis; angles corresponding to the orientations giving rise to 'crosses' (C) and 'belt' (B) with partial occupancies of the atomic positions; (*b*) rotation by an angle φ around a five-fold axis; (*c*) rotation by an angle φ around a two-fold axis passing through the centres of two opposite 6/6 bonds; asterisks mark the second preferred orientations.

have been observed. For instance, such a phase transition takes place for the complex $C_{60} \cdot (C_6H_5)_2$ [111] where both the fullerene and biphenyl molecules are disordered. Upon a decrease in the temperature, two consecutive phase transitions occur resulting in the ordering of the two constituents: the biphenyl and fullerene molecules become ordered at 212 K and 147 K, respectively.

Fullerene-containing salts with bulky ions constitute a separate group, which is close to molecular complexes as regards their crystal chemistry. In such salts, fullerene may either be neutral [*e.g*., in $C_{60} \cdot$ BEDT-TTF$^+ \cdot I_3^-$ (see Ref. 110)] or charged [*e.g*., in $C_{60}^- \cdot 2\,Ph_4P^+ \cdot Cl^-$ (see Ref. 112)]. Both organic and metal-containing species can act as counterions. The latter can be exemplified by a series of isomorphous salts solvated by ammonia, *viz*., $C_{60}^{2-} \cdot M(NH_3)_6^{2+} \cdot 6\,NH_3$ [M = Mn, Cd (see Ref. 113), Co, Zn (see Ref. 114), Ni (see Ref. 115)]. These structures are built up of flat tetragonal layers of fulleride dianions and metal ammines with the octahedral coordination of the metals. Two other examples are the tetrahydrofuran solvate of potassium fulleride, $C_{60}^{3-} K_3^+ \cdot 14\,THF$ (see Ref. 116), and the toluene solvate of potassium 2,2,2-cryptand fulleride, $C_{60}^{2-} \cdot 2\,CryptK^+ \cdot 4\,PhMe$ (see Ref. 117) (both compounds are characterised by the island packing of the fullerene anions).

The properties of fulleride anions in the solid state and in solution have been recently reviewed.[118] As evidenced by cyclic voltammetry, buckminsterfullerene can undergo reversible reduction in solution yielding mono-, di- and trianions. Since the LUMO of fullerene is triply degenerate, the anions possess one, two and three unpaired electrons, respectively, and thus produce characteristic ESR spectra. Reduction of C_{60} to a diamagnetic hexaanion is possible in aprotic media.[119]

In this class of fullerene derivatives, as in molecular complexes, the structural motifs are determined primarily by van der Waals potential of the large C_n molecules. The packing of fulleride anions is somewhat denser than that in molecular complexes due to the electrostatic interactions with the cations. However, the

negative charge is evenly distributed over the fullerene molecule and does not prevent its rotation. Therefore, both ordered and disordered structures are found among anionic fullerene derivatives.

The low-temperature ferromagnetism has been observed for the fullerene radical-ionic salt with tetrakis(dimethylamino)ethylene, $C_{60}^{-} \cdot TDAE^{+}$, with the transition temperature of $T_c = 16$ K.[120] Some other analogous salts of buckminsterfullerene with donor amines (which have not been characterised structurally) also exhibit different types of ferromagnetic or antiferromagnetic ordering.[3] Attempts have been undertaken at the correlation of the magnetic properties of such compounds with rotation of the negatively charged fullerene cage.[121]

The fulleride anion carrying a negative charge from 1 – to 5 – is subject to Jahn – Teller distortions that result in deviations from the idealised I_h symmetry of the molecule. In the crystal structure of $C_{60}^{2-} \cdot 2(Ph_3P)_2N^{+}$, which has been determined with the highest accuracy, the completely ordered C_{60} molecule occupies the inversion centre.[122] The lengths of the 6/6 and 5/6 bonds lie in the ranges of 1.39 – 1.41 Å and 1.43 – 1.46 Å, respectively. The radial distortions of the carbon cage, calculated by us for this anion based on the atomic coordinates from the CSD, are shown in Fig. 13.

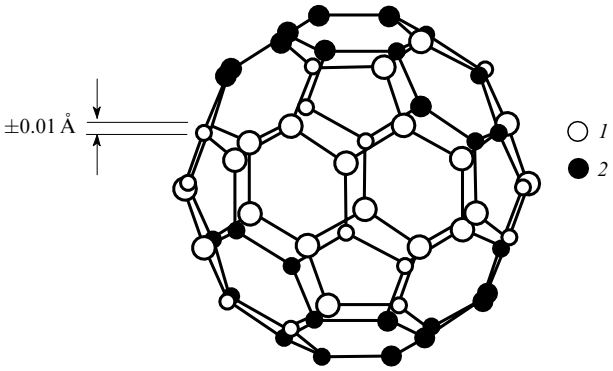

Figure 13. Radial Jahn – Teller distortions of the molecule C_{60} in the crystal structure of $C_{60}^{2-} \cdot 2(Ph_3P)_2N^{+}$ caclulated based on the atomic coordinates from the CSD.
(*1*) Atoms pushed out, (*2*) atoms pressed in. The magnitudes of the deviations from the idealised sphere are proportional to the radii of the circles (the scale is indicated).

Two ionic salts containing C_{60} dications, *viz*., $C_{60}(SbF_6)_2$ and $C_{60}(AsF_6)_2$, have been reported but not characterised structurally.[123] According to the ^{19}F NMR data, the hexafluoride anions therein freely rotate. Photoelectron spectra of the C_{60}^{+} ions in a molecular beam measured using SR have indicated dynamic Jahn – Teller disortions.[124]

V. Metal fullerides

The packing of carbon cages in ionic fullerene compounds with bulky inorganic or organic cations deviates from the close one and thus obeys the same regularities as in molecular complexes. In addition to these compounds, fullerene forms binary and ternary phases with metals that are similar to binary inorganic ionic salts. The majority of these phases have been characterised structurally using SR-based powder X-ray diffraction augmented with the Rietveld crystal structure refinement.

An interaction of solid buckminsterfullerene with alkali metals yields crystalline metal fullerides. A filling of, first, octahedral and then tetrahedral cavities in the fcc packing of the carbon spheres by alkali metal atoms gives rise to fullerides with stoichiometries MC_{60} and M_3C_{60}.[125, 126] Further doping results in substantial rearrangement of the whole structure. The final

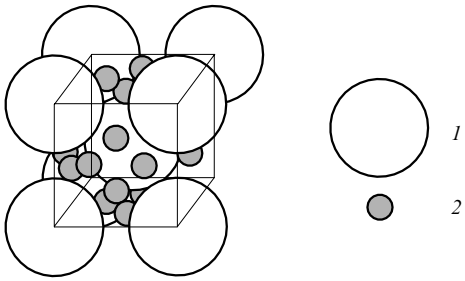

Figure 14. The crystal packing in metallofullerenes M_6C_{60}.
The unit cell is shown with thin lines; (*1*) C_{60}^{-}, (*2*) metal atom.

doping product is the M_6C_{60} phase[127] that is composed of the fullerene spheres forming a body-centred cubic packing and the squares of four metal cations situated in the centres of the faces of the cubic lattice (Fig. 14). An intermediate phase with the composition M_4C_{60} also exists. In its crystal structure, a part of the cavity is filled by 2 rather than 4 metal atoms so that the symmetry is lowered from cubic to orthorhombic.[128] Deeper doping is possible only in the case of lithium. It results in a product with the stoichiometry $C_{60}Li_{15}$, which is characterised by an fcc packing of the fullerene cages.[129]

Alkali metal fullerides containing buckminsterfullerene trianions (the LUMO of which is half-filled) are conductors at room temperature and transit into the superconducting state at low temperatures (18 K for K_3C_{60}).[130] As a result of systematic studies of phases with varied metallic component composition, a positive correltation between the critical temperature and the cubic lattice parameter has been established.[131] For the $Cs_xRb_{3-x}C_{60}$ salt, a value of $T_c = 33$ K has been obtained (see Ref. 132), while doping with a rubidium – thallium mixture has given rise to even higher temperature $T_c = 45$ K (see Ref. 133), which is the current record for fullerene derivatives. In a series of studies, Schön *et al.*[134] reported substantially higher critical temperatures achieved for the hole-doped fullerene and its solvates but these results were later disproved.[135] According to the calorimetric studies of M_3C_{60} salts, the orientational phase transition, typical of pure C_{60}, is also observed for them, but at higher temperatures (299 K for Na_2CsC_{60}, 313 K for Na_2RbC_{60} and 305 K for Na_2KC_{60}).[136]

The $KCsBaC_{60}$ and KBa_2C_{60} fullerides, which are characterised by similar structures but the higher charge of the fullerene anion, are relatively poor metallic-type conductors and do not manifest superconductivity.[137]

The fullerides containing the C_{60}^{6-} anions are dielectrics. A substitution of bications for a part of metal monocations resulting in an increase in the formal negative charge of the fullerene cage to nine (as in $K_3Ba_3C_{60}$), restores electroconductivity. A phase transition into the superconducting state has also been observed for the latter substance but at a lower temperature (5 K).[138] Fullerides of calcium Ca_5C_{60} (see Ref. 139) and barium Ba_6C_{60} (see Ref. 140) have crystal structures analogous to those of the M_6C_{60} salts (in the case of calcium derivative, one sixth of the metal atom sites remains vacant). They are conductors and show a supercondivity with the critical temperatures in the range of 4 – 8 K.

The crystal structure of ytterbium fulleride with the composition $Yb_{2.75}C_{60}$ can be described as an analogue of K_3C_{60}, in which 1/8 of all octahedral cavities is vacant, while the cations are shifted from the centres of the cavities. Due to ordering of the vacant sites, the lattice parameters of the original cubic cell are doubled and the lattice symmetry is lowered to orthorhombic.[141] Fullerides $M_{2.75}C_{60}$ similar to those discussed above and M_6C_{60} with a structure of K_6C_{60} have also been found in the systems C_{60} – Eu (see Ref. 142) and C_{60} – Sm (see Refs 143, 144). The orthorhombic phase $Sm_{2.75}C_{60}$ manifests an anomalous temperature dependence of the lattice constants (see Fig. 15): at $T < 32$ K, the thermal

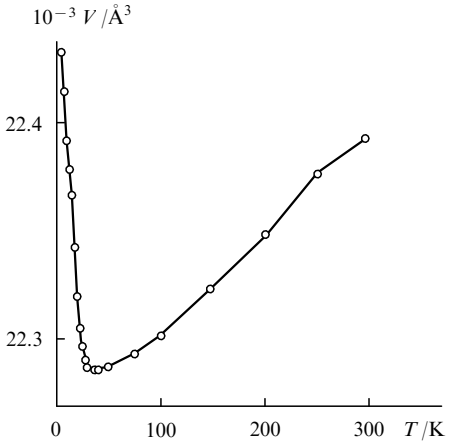

Figure 15. The temperature dependence of the unit cell volume for $Sm_{2.75}C_{60}$.[145]

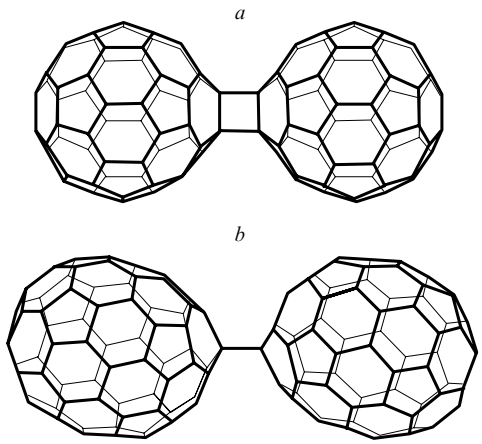

Figure 16. The molecular structures of the dimer $(C_{60})_2$ (*a*) [154] and dimeric anion $(C_{70}^-)_2$ (*b*).[155]

expansion coefficient becomes negative due to ordering of sites occupied by samarium di- and trications in the crystal lattice.[145]

With palladium and platinum, buckminsterfullerene forms crystalline compounds with the variable stoichiometry $C_{60}M_x$ ($1 \leqslant x \leqslant 7$) where formally zerovalent metal atoms are, probably, coordinated by double bonds of the fullerene molecules.[146, 147] This structural model has not been supported by diffraction techniques but it agrees well with the results of EXAFS on the palladium derivatives,[148] and gives a plausible explanation for the conversion of the palladium and platinum fullerides into the respective π-complexes with the η^2-C_{60} ligand upon action of organic phosphines PR_3.[6] The existing data on the structure of metallofullerenes have recently been surveyed by Ivanova.[149]

The C_{70} fullerene forms a series of fullerides with alkali metals characterised by stoichiometries MC_{70}, M_4C_{70} and M_6C_{70}.[150] The M_3C_{70} phase with an fcc lattice is stable only at elevated temperatures and readily converts upon cooling into the trigonal phase or disproportionates. Nevertheless, it can be stabilised by a proper selection of cations with suitable sizes (*e.g.*, sodium and caesium in Na_2CsC_{70}) so that the two smaller sodium cations occupy the tetrahedral cavities while the larger caesium cation is in the octahedral cavity.[151] An fcc phase with the composition Ba_3C_{70} has also been prepared.[152] Since the LUMO of the C_{70} molecule is nondegenerate and the next-in-energy orbital is doubly degenerate (see Fig. 3), the HOMO of the C_{70}^{4-} anion is half-filled. Respectively, salts M_4C_{70}, like M_3C_{60}, manifest superconductivity. A series of rare earth metal [70]-fullerides have also been described. In particular, two europium fullerides with stoichiometries $Eu_{3-x}C_{70}$ and $Eu_{9-x}C_{70}$ have been isolated.[48] According to powder X-ray diffraction, the former phase is antiferromagnetic and has a monoclinic structure, which is similar to $M_{2.75}C_{60}$ in the arrangement of the guest atoms. The latter phase is ferromagnetic and similar in structure to face-centred cubic M_6C_{60} fullerides. However, in the europium derivative, small metal clusters rather than single atoms occupy the octahedral cavities.[48]

Fullerides of higher fullerenes are less explored. The final product of doping of C_{84} with potassium is the salt $K_{8+x}C_{84}$, which is structurally similar to K_6C_{60} and contains fully ordered fullerene anions. Yet another fulleride, K_3C_{84}, is characterised by a rotational disorder of fullerene molecules and a lower metal content due to partial occupancies of potassium sites.[153]

VI. Fullerene-based oligo- and polymers

Due to the presence of double bonds, fullerenes form oligo- and polymers upon irradiation, under pressure, upon heating or action of chemical anionic or radical initiators. Transformations of fullerenes at elevated pressures have recently been reviewed.[5]

Pure buckminsterfullerene forms dimers under conditions of anionic catalysis.[154] According to the single-crystal X-ray diffraction studies of the dimer C_{120} solvate with *o*-dichlorobenzene, the dimerisation proceeds as a [2 + 2] cycloaddition at the 6/6 bond (Fig. 16 *a*). In the four-membered ring composed of the sp^3-hybridised carbon atoms (the corresponding spherical excesses are 26.2 – 26.7°), the C – C bond lengths are 1.581 Å and 1.575 Å for the 6/6 bonds within the fullerene core and exopolyhedral bonds, respectively. Synthesis of the C_{60} dimer from the molecular complex $(BEDT\text{-}TTF)_2C_{60}$ in which the 6/6 bonds of the adjacent fullerene molecules are mutually oriented to each other at a pressure of 5 GPa has been described.[156] Several isomeric C_{60} trimers have been produced as evidenced by mass spectrometry and high-resolution electron microscopy; however, these species have not been isolated as individual substances.[157]

A cross-dimer of C_{60} and C_{70} with an unknown structure has been prepared by means of mechanochemistry.[158] According to the quantum chemistry calculations, this may represent a [2 + 2] cycloaddition product to the C_{70} moiety at the *b*-type 6/6 bond (see Fig. 1 *b*).

Buckminsterfullerene forms several polymer phases at elevated pressures. Some of them have been obtained as single crystals and studied by single-crystal X-ray diffraction. At early stages of the modification, the phase contains linear polymeric chains of fullerene cores and is characterised by an orthorhombic lattice.[159] A deeper modification at a pressure of 2 – 5 GPa yields rhombohedral [160] and tetragonal [161] phases composed of hexagonal and tetragonal layers of covalently bound C_{60}, respectively. A detailed single-crystal X-ray diffraction study of the tetragonal phase [162] has revealed that it is rather orthorhombic with a tetragonal pseudosymmetry ($a \approx b$), though in another work, the lattice has been interpreted as being tetragonal.[163] The interfullerene C – C bond in the polymer is 1.60 Å. According to the powder X-ray diffraction, polymerisation at higher pressures (13 GPa) results in a quite irregular three-dimensional network of bound fullerenes.[164] Polymerisation of C_{60} and C_{70} at a pressure of 8 GPa and 800 – 900 °C is accompanied by partial destruction of the carbon clusters and formation of amorphous carbon materials. Densities of some of these materials were reported to approach that of diamond.[164, 165]

Polymerisation of fullerene anions occurs more easily. In particular, a linear polymer is formed from the cubic fulleride Na_2CsC_{60} at 0.7 GPa.[166] Alkali metal fullerides with the stoichiometry MC_{60}, in which fullerene anions are rotationally disordered at room temperature, form polymers with the C_{60} units joined into infinite chains by single C – C bonds upon lowering tempertures.[167] The radical-ionic salt $Cp'_2Cr \cdot C_{60} \cdot 2C_6H_4Cl_2$ ($Cp' = C_5Me_5$) at room temperature contains the $(C_{60})_2^{2-}$ dimers

linked by one C–C bond with a length of 1.60 Å.[168] Another radical-ionic salt, $(C_6H_5Me)_2Cr^+ \cdot C_{60}^- \cdot CS_2$, represents, according to single-crystal X-ray diffraction data, a linear polymer with unusually short non-bonding intermolecular C–C contacts of 2.24 Å.[169] In the $(C_6H_5Me)_2Cr-C_{60}$ system, a solvent-free molecular complex with the composition 1 : 1 has been found, in which C_{60} clusters exist as independent rotationally disordered anions at high temperatures (> 250 K) and as dimeric dianions bound by one σ-bond at low temperatures.[170]

The C_{70} fullerene also undergoes polymerisation both as a neutral molecule and an anion. The crystal structure of a polymer prepared from pure hexagonal C_{70} (a calculation within the atom–atom potential approach has shown that the mutual orientation of the molecules in cubic C_{70} is unfavourable for a formation of polymeric chains) has been determined.[171] In the polymer, the C_{70} molecules are joined in chains as a result of a [2 + 2] cycloaddition at the *b*-type 6/6 bonds (see Fig. 1 *b*). In the dimethylformamide–benzene solvate of a molecular complex of the radical-ion salt $Cs_2(C_{70})_2 \cdot CTV \cdot (DMF)_5 \cdot C_6H_6$ with cycloveratrylene (see Table 2), the fulleride anion exists as a dimer $(C_{70}^-)_2$. Two fullerene moieties are linked through one bond with the length of 1.56–1.58 Å (for different symmetrically independent dimers) involving the type **1** carbon atoms (see Fig. 1 *b*). The C_{70} core is non-symmetrically distorted so that the pentagonal 'pole' of the molecule acquires an envelope conformation with the C(sp^3) atom at the top point (Fig. 16 *b*).[155] In ammonia-solvated fullerides $MC_{70} \cdot n\,NH_3$ (M = Ca, Sr, Ba, Eu, Yb), the C_{70}^{2-} anions are bound into infinite chains by the exopolyhedral C–C bonds.[172]

VII. 'Binary' compound

In terms of chemical reactivity, fullerenes are similar to conjugated polyalkenes. The stable fullerene core may be considered as a large pseudoatom in reactions of addition and substitution involving exopolyhedral fragments. In this section, fullerene 'binary' compounds C_nX_m where X is an external atom or a stable substituent (CH_3, CF_3) covalently bound to the fullerene core C_n are discussed.

Structural studies of polyadduct mixtures C_nX_m are hindered by the multitude of addition isomers. For instance, a symmetrical addition of two functional groups to one of the 30 equivalent 6/6 bonds in buckminsterfullerene divides the remaining 6/6 bonds into nine nonequivalent classes. The number of theoretically possible isomers increases tremendously with an increase in the number of groups attached (*e.g.*, 6×10^{14} for $C_{60}H_{36}$, see Ref. 173), which makes impossible a comprehensive quantum chemistry analysis with a search for the global minimum.

Upon exposure of buckminsterfullerene to air, traces of C_{60} oxides are formed. For purposeful preparation of oxides, *m*-chloroperoxybenzoic acid is used, which is a standard reagent for the oxidation of alkenes into epoxides. Monoxide $C_{60}O$ (see Ref. 174) and dioxide $C_{60}O_2$ (see Ref. 175), which have been isolated and characterised structurally, form single crystals isomorphous to pure buckminsterfullerene. Exopolyhedral oxygen atoms occupying cavities of the fcc packing have not been revealed due to rotational disorder. For the $C_{60}O$ oxide, an orientational phase transition has been registered at 278 K. According to the single-crystal X-ray diffraction study of oxyfullerene π-complexes, the oxygen atom in $(\eta^2\text{-}C_{60}O)Ir(CO)Cl(PPh_3)_2$ is attached to the 6/6 bond of the fullerene cage while the iridium atom is coordinated to another 6/6 bond of the same hexagon.[176] In the $C_{60}O_2$ core of another complex, *viz*., $(\eta^2\text{-}C_{60}O_2)Ir(CO)Cl(PPh_3)_2$, two oxygen atoms are attached to neighbouring 6/6 bonds; the complex represents a mixture of isomers with metal atoms coordinated to different 6/6 bonds.[177] In the $C_{70}O$ core of the complex $(\eta^2\text{-}C_{70}O)Ir(CO)Cl(PPh_3)_2$,[178] the oxygen and iridium atoms are attached to adjacent *b*-type 6/6 bonds (see Fig. 1 *b*).

The properties of fullerene hydrides have been reviewed by Goldshleger and Moravsky.[4] The principal buckminsterfullerene hydrogenation product is $C_{60}H_{36}$, which was suggested to be a mixture of D_{3d} and S_6 isomers based on the data from IR and Raman spectroscopy.[179] Meanwhile, a fullerene hydride with the same composition was attributed[180] to a mixture of two other isomers with the C_3 and C_1 symmetry (isostructural to isomers of fullerene fluoride $C_{60}F_{36}$, see below) using the ^1H, ^{13}C and ^3He NMR data for the endohedral derivative $He@C_{60}H_{36}$. Another hydride, $C_{60}H_{18}$, was also suggested to be isostructural to the respective fluoride[181] based on the ^3He NMR data for $^3He@C_{60}X_{18}$ (X = H, F).[182] To our knowledge, no single-crystal X-ray difraction studies of fullerene hydrides have been conducted so far. In a study of $C_{60}H_{36}$ using powder X-ray diffraction, a bcc lattice with a lattice parameter of 11.75 Å was determined.[183]

Iodine forms no covalent compounds with C_{60} but rather a molecular complex $C_{60} \cdot 2I_2$ belonging to a structural type with closely packed hexagonal layers $(C_{60})_\infty$.[184] An iodine-containing solvate $C_{60} \cdot PhMe \cdot I_2$ falling into the same type of molecular packing has also been characterised.[185] All other halogens react with fullerenes to form addition products.

A series of fluorinated buckminsterfullerenes from $C_{60}F_2$ (see Ref. 186) to $C_{60}F_{48}$ (see Ref. 187), in which the polyhedral C_{60} core is retained, have been prepared and characterised. The methods of synthesis of fluorofullerenes and reported data on their structures have been recently reviewed by Taylor.[188] To date, single-crystal X-ray diffraction data are available for $C_{60}F_{18}$ (see Refs 189, 190), $C_{60}F_{18}O$ (see Ref. 191), $C_{60}F_{17}CF_3$ (see Ref. 192), $C_{60}F_{36}$ (three isomers)[193, 194] and $C_{60}F_{48}$ (see Refs 195, 196). The Schlegel diagrams for the structurally studied fullerene fluorides and bromides are given in Fig. 17. The molecular structures of three C_{60} fluorides are shown in Fig. 18, and their basic geometrical parameters are listed in Table 5.

In the molecule $C_{60}F_{18}$ with the C_{3v} symmetry studied as a toluene solvate[189] and individual fullerene fluoride,[190] all eighteen fluorine atoms are attached to one hemisphere of the fullerene core around a flattened hexagonal ring (the spherical excess is $\varphi_i \leqslant 0.1^\circ$) isolated from the π-system of the remaining part of the molecule (see Fig. 17 *a*). All the sp^3-hybridised carbon atoms are pyramidised ($26.4^\circ \leqslant \varphi_i \leqslant 29.9^\circ$) while the atoms adjacent to them are flattened ($\varphi_i = 3–6^\circ$) with respect to pristine C_{60}. Consequently, the carbon cage acquires the shape of a 'tortoise shell' (see Fig. 18 *a*).

Table 5. Parameters of the molecular geometry of structurally characterised fluorofullerenes.

Formula	Symmetry	C–C bonds /Å				k [a]	*R*-factor	Disorder	Ref.
		$sp^3–sp^3$	$sp^3–sp^2$	aromatic	C=C				
$C_{60}F_{18} \cdot PhMe$	C_{3v}	1.54–1.67	1.47–1.53	1.37	–	0.74	0.049	no	189
$C_{60}F_{36} \cdot 1.75\,PhMe$	T	1.55–1.66	1.48–1.49	1.36–1.38	–	0.70	0.090	yes	193
$C_{60}F_{36} \cdot 3.5\,PhMe$	C_1	1.54–1.68	1.46–1.54	1.37–1.38	1.32	0.70	0.059	no	194
$C_{60}F_{48} \cdot C_6H_3Me_3$-1,3,5	S_6	1.54–1.61	1.49–1.58	–	1.29–1.30	0.71	0.051	yes	195

[a] k is the Kitaygorodsky molecular packing coefficient.[64]

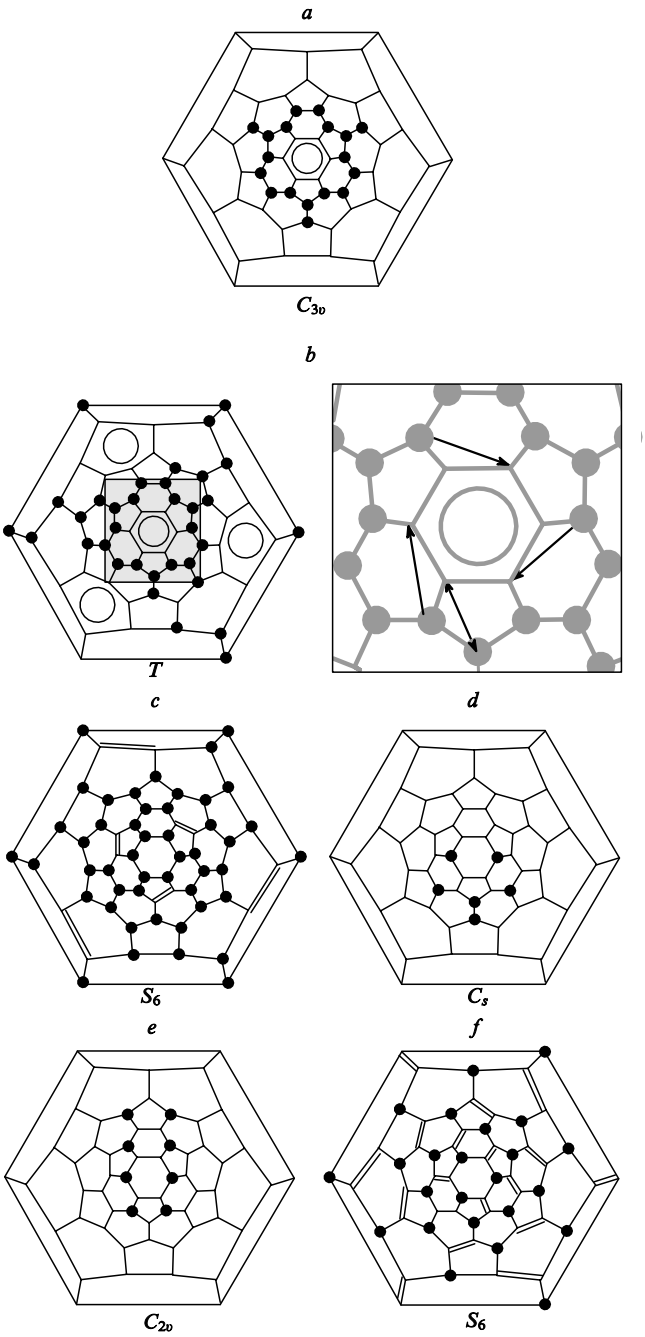

Figure 17. The Schlegel diagrams for $C_{60}F_{18}$ (*a*), $C_{60}F_{36}$ (*b*), $C_{60}F_{48}$ (*c*), $C_{60}Br_6$ (*d*), $C_{60}Br_8$ (*e*), $C_{60}Br_{24}$ (*f*); (*b*) (to the right): the arrows show the 1,3-shifts of fluorine atoms giving rise to the C_3 isomer, the double arrow shows the shift transforming the C_3 isomer further to the C_1 isomer; (*a*, *b*): aromatic rings are shown; (*c*, *f*): positions of double bonds are shown.

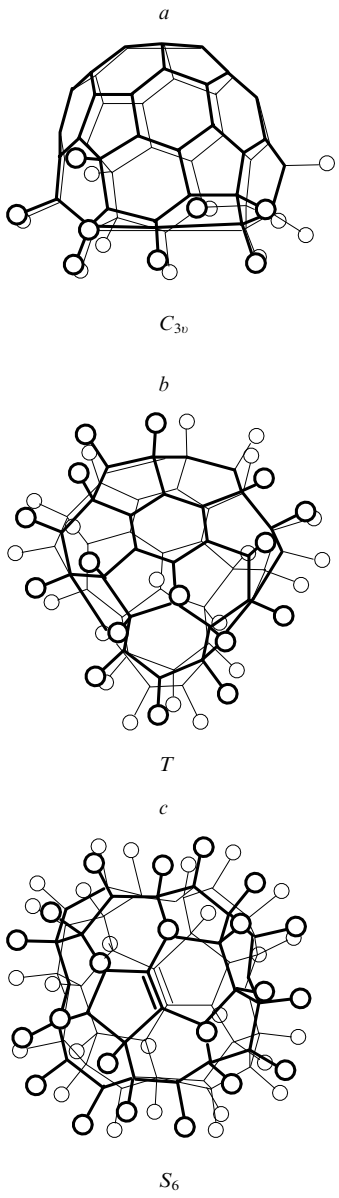

Figure 18. The molecular structures of $C_{60}F_{18}$ (*a*), $C_{60}F_{36}$ (*b*) and $C_{60}F_{48}$ (*c*).

Three symmetrically equivalent 5/6 $C(sp^3)-C(sp^3)$ single bonds in the molecule $C_{60}F_{18}$ are elongated to 1.67 Å. The addition of an oxygen atom at one of these bonds (to give $C_{60}F_{18}O$) results in its cleavage.[191] Three fluorine atoms the most remote from the isolated aromatic hexagon can be substituted by phenyl groups (using the Friedel – Crafts reaction) to give $C_{60}F_{15}Ph_3$ [197] and undergo nucleophilic substitution.[198] In the crystal structure of $C_{60}F_{17}CF_3$, the trifluoromethyl group occupies one of the peripheral fluorine sites; the crystal contains a mixture of two substitution isomers in different orientations.[192]

The molecular structure of the fluoride $C_{60}F_{20}$ (not studied by single-crystal X-ray diffraction) has been determined by NMR spectroscopy. According to Boltalina *et al.*,[199] all fluorine atoms in $C_{60}F_{20}$ are located at the equatorial belt of the molecule, *i.e.*, this fluoride does not include a fragment of the $C_{60}F_{18}$ structure. This suggests that, under the reaction conditions, the fluorine atoms migrate over the surface of C_{60}.

Several isomers of $C_{60}F_{36}$ are known. The major isomer with the exceptionally rare point symmetry *T* has been isolated and structurally characterised as a toluene solvate. This molecule contains four aromatic rings with equal bond lengths analogous to the single aromatic ring in $C_{60}F_{18}$. All other carbon atoms are sp^3-hybridised and bound to fluorine atoms. The strongly distorted carbon core acquires a shape resembling a tetrahedron with rounded edges and vertices (see Fig. 18 *b*). The crystal is statistically disordered and represents a racemic mixture of enantiomers.[194] The C_3 symmetry has been attributed to the isomer second in abundance based on the NMR data. The third isomer having the C_1 symmetry has been isolated and studied by single-crystal X-ray diffraction. Its molecular structure can be derived from that of the C_3 isomer by a 1,3-shift of one of the fluorine atoms in the five-membered ring [194] (see Fig. 17 *b*).

The fluorine-rich fullerene fluoride, $C_{60}F_{48}$, has been characterised by single-crystal X-ray diffraction as a solvate with mesitylene.[195, 196] The molecule occupies a special position of the $\bar{3}$ symmetry in a pseudocentred cubic lattice (space group $Pa\bar{3}$) and is rotationally disordered. It can be interpreted as a superposition of the D_{3d} and S_6 isomers in an overall ratio of 0.61 : 0.39.[195] In another study,[196] the unit cell was erroneously attributed to a bcc lattice and the molecule $C_{60}F_{48}$ was described as an S_6 isomer.

The $C(sp^3)-C(sp^3)$ bond lengths in $C_{60}F_{48}$ lie in the range 1.54 – 1.61 Å.[195] Six double carbon – carbon bonds (1.29 – 1.30 Å) situated at vertices of an octahedron (see Fig. 17 *c*), which belong to the 5/6 type (in contrast to respective bonds in the pristine fullerene), are noticeably pressed inside the molecule (the spherical excesses are from -2° to -9°).‡ This is consistent with the impossibility of further fluorination of C_{60} derivatives without disruption of the carbon cage.[200]

Due to the strong electrostatic dipole – dipole interactions (the dipole moment is 12 – 15 D, according to *ab initio* quantum chemistry calculations), both components of the $C_{60}F_{18}\cdot PhMe$ solvate are ordered. The Kitaygorodsky density coefficient[64] of the molecular packing for $C_{60}F_{18}\cdot PhMe$ is 0.74 (the packing of pure $C_{60}F_{18}$ is significantly looser since the lattice cavities cannot be filled with the solvent molecules). Meanwhile, solvates of the high-symmetry fluorides $C_{60}F_{36}$ and $C_{60}F_{48}$, which are characterised by zero dipole moments, are looser and more disordered ($k = 0.70 – 0.71$, see Table 5). The pattern of the rotational disorder of the molecules $C_{60}F_{48}$ observed in the crystal structure of $C_{60}F_{48}\cdot 2(1,3,5\text{-}C_6H_3Me_3)$[196] can be reproduced within the model of the 'rubber cavity'[110] (see Fig. 12).

Chlorination of fullerene yields a mixture of products $C_{60}Cl_n$, $n \leqslant 24$. These products have been studied by IR spectroscopy and mass spectrometry.[201] Using a mild chlorinating agent (ICl), the chloride $C_{60}Cl_6$ can be prepared. According to the NMR and IR data, its structure is similar to that of hexabromide (see Fig. 17 *d*).[202]

Six exopolyhedral fragments in hexamethylfullerene $C_{60}Me_6$ produced by methylation of $C_{60}Cl_6$ with methyllithium are arranged in the same mode as in hexachloride according to its single-crystal X-ray diffraction study.[203] Partial substitution of the methyl groups for the chlorine atoms to give $C_{60}Me_5Cl$ followed by a nucleophilic substitution of OH for Cl and epoxidation of the two C – C bonds in the isolated five-membered ring yields $C_{60}Me_5(OH)O_2$, the crystal structure of which has also been determined.[204] In this structure, the molecules are ordered and characterised by the C – C bond lengths of 1.52 – 1.57 Å for the $C(sp^3)-C(sp^3)$ bonds and 1.48 Å for the epoxy-rings. The C – O bond lengths lie in the range 1.44 – 1.46 Å. Five chlorine atoms around a five-membered ring in $C_{60}Cl_6$ can also be substituted by phenyl groups using the Friedel – Crafts reaction (in this reaction, $C_{60}Ph_4$ is produced as a by-product).[205] The electronic properties of the main product $C_{60}Ph_5Cl$ are similar to pentasubstituted cyclopentadiene. In particular, its two-electron electrochemical reduction gives rise to an aromatic anion,[206] and its chemical modification enables preparation of metal π-complexes of the η^5 type.

Nakamura *et al.*[50] isolated and studied structurally a fullerene derivative functionalised in a similar way at two opposite pentagonal faces. The equiatorial belt of such a fullerene cage is composed of sp^2-hybridised carbon atoms resembling a fragment of a [5,5]-nanotube (Fig. 19). Trifluoromethylation of C_{60} using silver trifluoroacetate on heating yields CF_3 addition products to the neighbouring 6/6 and 5/6 bonds, according to the NMR data.[207]

Single-crystal X-ray diffraction data for three buckminsterfullerene bromides $C_{60}Br_6$, $C_{60}Br_8$ and $C_{60}Br_{24}$ crystallised as solvates with liquid bromine have been published (the respective Schlegel diagrams are shown in Fig. 17 *b*). In the two latter molecules, the nearest bromine atoms occupy 1,3-positions to each other, which is, probably caused by steric reasons. In the molecule $C_{60}Br_{24}$, there are isolated double bonds belonging both to the 5/6 and 6/6 types. They are shortened to 1.33 – 1.34 Å, while the $C(sp^2)-C(sp^3)$ bonds are elongated to 1.46 – 1.51 Å. The packing of the molecules $C_{60}Br_{24}$ in the crystal lattice is close to fcc.

‡ Negative spherical excesses correspond to a pyramidal carbon atom with an apex directed towards the centre of the fullerene cage.

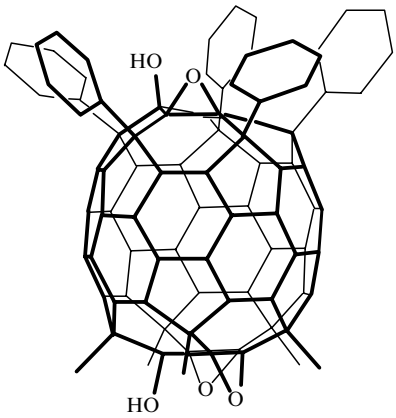

Figure 19. The molecular structure of $C_{60}Me_5Ph_5O_3(OH)_2$ with the fullerene core functionalised at two opposite pentagonal faces.[49]

Binary derivatives of C_{70} are less studied. The major hydrogenation products fall into the composition range $C_{70}H_{36} – C_{70}H_{44}$ (see Ref. 4). The fluorine-rich derivative is, likely, $C_{70}F_{56}$,[208] while chlorination stops at the $C_{70}Cl_{10}$ stage.[209] Substitution of methyl groups for chlorine atoms in this chloride is accompanied by partial reduction and yields $C_{70}Me_8$. The crystal structure of this substance has been determined.[210] The Me-fragments are attached to the type **4** carbon atoms (see Fig. 1 *b*) at both sides with respect to the equator of the molecule. In the bromide $C_{70}Br_{10}$, which has been also studied by single-crystal X-ray diffraction (Fig. 20), the bromine atoms are attached to the type **4** carbon atoms as well.[49] Synthesis of another bromide $C_{70}Br_{14}$ has been reported,[211] but its crystal structure has not been determined. Among binary derivatives of higher fullerenes, only one bromide $C_{78}Br_{18}$ has been studied, which contains statistically disordered molecules of two bromination isomers with the C_{2v} symmetry; no admixtures of probable bromination products of the D_3 isomer were detected.[212]

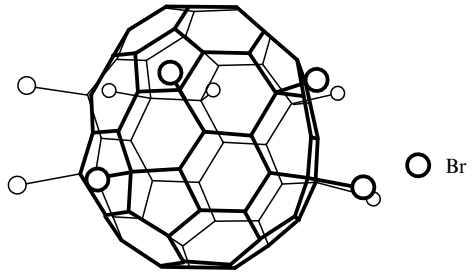

Figure 20. The molecular structure of $C_{70}Br_{10}$ from the single-crystal X-ray diffraction data.[49]

VIII. σ-Derivatives

Derivatisation of fullerene typically involves an addition to the 6/6 double C – C bond as the first stage. Thus, exocoordinated carbon atoms acquire the sp^3-character and protrude over the surface of the original C_{60} sphere due to an elongation of the C – C bond

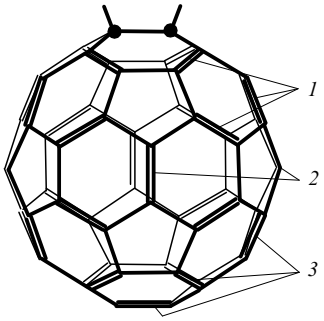

Figure 21. Symmetrically non-equivalent 6/6 bonds in the molecule C_{60} chemically modified at one of the 6/6 bonds.
Positions of bonds: (*1*) *cis*, (*2*) equatorial, (*3*) *trans*.

linking them and an increase in the spherical excesses φ_i from 12° to 16–32° ($\varphi = 31.7°$ for an unstrained sp^3-hybridised carbon atom). Such an addition to one of the 6/6 bonds divides the remaining 6/6 bonds in the fullerene molecule into 9 symmetrically nonequivalent types. Three of these types are conventionally referred to as *cis*-positions, four — *trans*-positions and two — equatorial positions (Fig. 21).

The main types of the σ-addition products to the molecule C_{60} are shown in Fig. 22. The binary products $C_{60}X_n$ produced by multiple σ-addition of one-electron fragments X to C_{60} were discussed in the previous section.

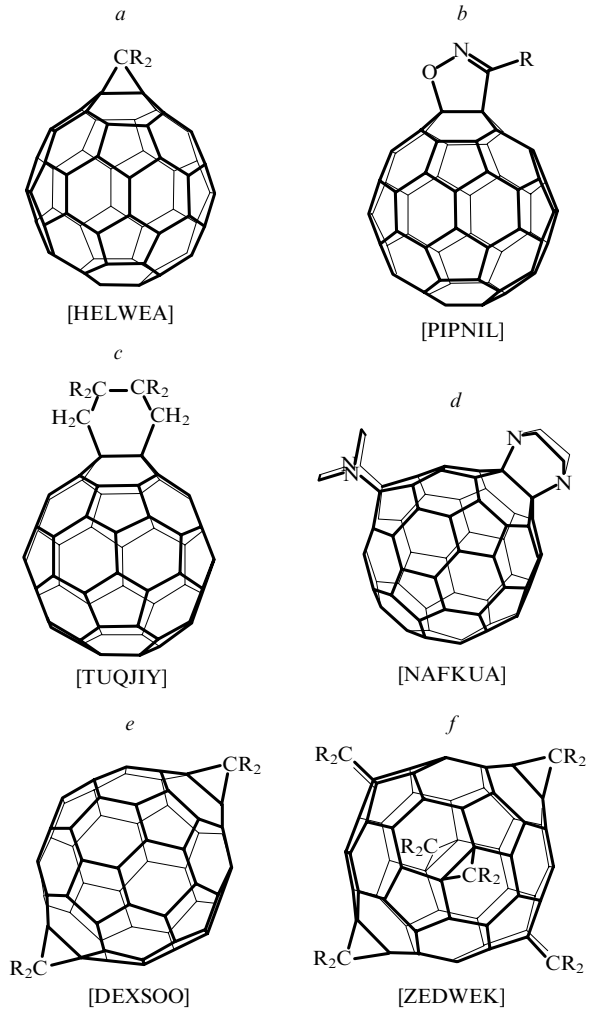

Figure 22. The possible types of σ-functionalisation of the fullerene molecule (CSD Refcodes are given).

The addition of carbene to a double carbon–carbon bond within the fullerene molecule yields a three-membered ring (see Fig. 22 *a*,*e*,*f*). On average, the key $C(sp^3)-C(sp^3)$ bond in these compounds is elongated to 1.59 Å, which is 0.04–0.05 Å longer than a typical single C–C bond. This clearly indicates substantial steric strains around the sp^3-hybridised carbon atoms in the fullerene core. Four-membered rings have been found only in derivatives of the dimeric molecule $(C_{60})_2$. Numerous derivatives with five- and six-membered rings (see Fig. 22 *b*–*d*) are formed in the reactions of [2 + 3] and [2 + 4] cycloaddition. As a result, the mean length of the C–C bond involved in the attachment increases to 1.60 Å and 1.61 Å, respectively.

Functionalisation of a double bond activates the five other 6/6 bonds, which form together an octahedron over the C_{60} core (see Fig. 22 *d*,*e*), towards further addition. Subsequent addition proceeds predominantly at these bonds giving rise ultimately to a hexaadduct with the T_h symmetry of the carbon cage (see Fig. 22 *f*). For instance, the crystal structure of the adduct containing six malonate groups $C_{60}[C(COOEt)_2]_6$ has been determined.[213] However, a hexaaduct violating this addition pattern is known, which is characterised by the composition $C_{60}(Tmp)_6 \cdot Solv$ and D_3 symmetry.[214]

Homofullerenes (*i.e.*, the addition products to the 5/6 bonds) are less abundant. Formally, this bond is single, and the attachment to it results in its cleavage and removal of the two carbon atoms to a distance ~2.1 Å from each other.[191,215]

The fullerene C_{70} possesses 8 non-eqivalent C–C bonds, which are characterised by different steric accessibilities. In the majority of structurally characterised derivatives, the addition occurs at the *b* type double bond (see Fig. 1 *b*), which is characterised by the largest sum of spherical excesses of its two carbon atoms among all the 6/6 bonds. Two exceptions to this rule are the adduct $C_{70}C_{10}H_{12}O_2$ [216] in which the *d* type bond is affected and a homofullerene produced by the addition of CCl_2 to the *f* type single bond, which results in its cleavage.[215]

Crystal packing of certain functionalised fullerenes is affected to a great extent by the external groups attached to the C_{60} or C_{70} core (which, for instance, link two fullerene cores or coordinate metal atoms). In particular, OsO_4, which is often used in organic synthesis for oxidation of alkenes to diols, reacts with buckminsterfullerene yielding an osmate ester of fulleren-1,2-ol. Note that the complex $C_{60}O_2OsO_2(4\text{-}BuPy)_2$ is the very first C_{60} derivative studied by single-crystal X-ray diffraction.[217] There are several other complexes, in which metal atoms are coordinated to exopolyhedral fragments attached to a fullerene core. As an example, a solvate of $C_{60}S_2Fe_2(CO)_6$ may be mentioned, in which two sulfur atoms attached to the fullerene core in 1,2-positions additionally coordinate the binuclear $Fe_2(CO)_6$ fragment.[218]

In addition to the aforementioned fullerene dimer, there are other molecules containing two fullerene cages bound to each other. Some typical examples are given in Fig. 23. Oxybifullerene $C_{120}O$ (its radical cation $C_{120}O^+$ is readily formed upon oxidation of solutions of C_{60} in air giving rise to a characteristic ESR signal, see Ref. 118) has been characterised by single-crystal X-ray diffraction as a molecular complex with octaethylporphyrin. Despite the positional disorder of the oxygen atoms, it was established that the molecule represents a dimer, in which one of the interfullerene C–C bonds is replaced by the C–O–C bridge.[82] In $C_{60}C(C{\equiv}CSiPr^i_3){-}C{\equiv}CC{\equiv}C(C{\equiv}CSiPr^i_3)CC_{60}$ (see Fig. 23 *a*), two 1,2-disubstituted fullerene cores are linked by a four-atomic butadiynediyl bridge.[219] A derivative of the dimer C_{60} where each of the fullerene cages is additionally functionalised at five bonds giving the addition pattern similar to C_{60} hexaadducts has been studied (see Fig. 23 *b*).[220] Yet another metallocomplex involving two fullerene fragments functionalised to hexaadducts and acting as bidentate σ-ligands has been synthesised and structurally characterised. The fullerene fragments in this complex

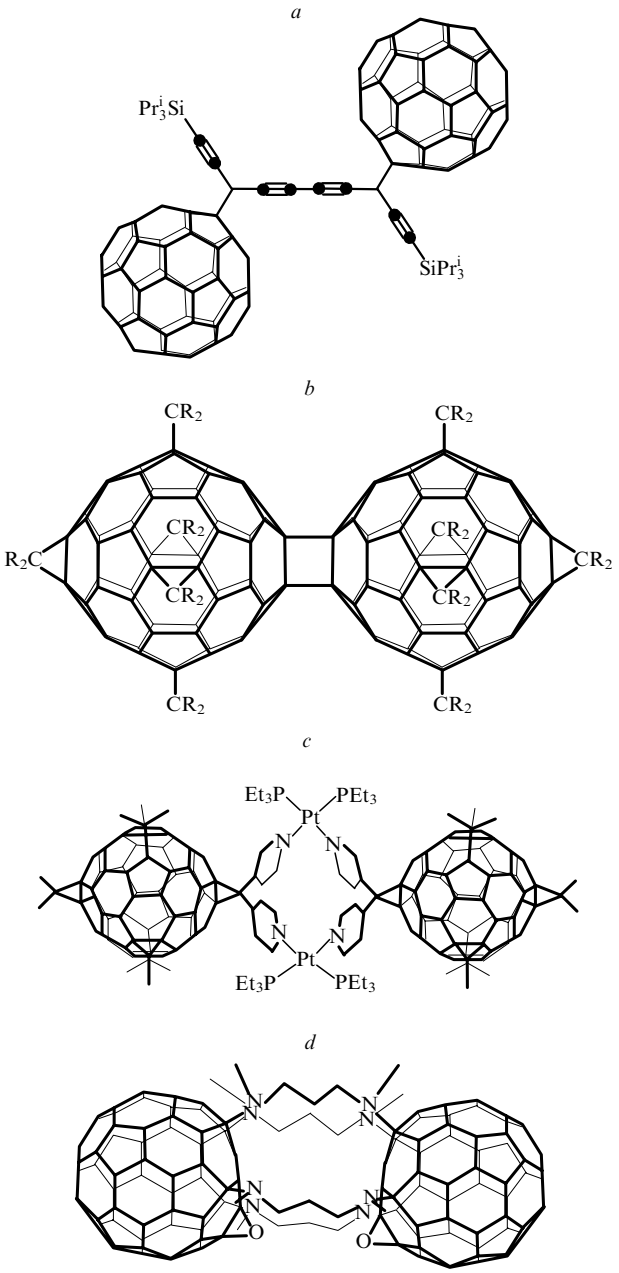

Figure 23. The structures of molecules containing two C_{60} moieties; (*a*) 1,4-bis{(1,2-dihydro-61-[(triisopropylsilyl)ethynyl]-1,2-methano-C_{60}-fullerene-61-yl}buta-1,3-diyne,[219] (*b*) bis[decakis(ethoxycarbonyl)pentacyclopropa(1,9 : 16,17 : 44,45 : 52,60)-C_{60}-fullerenediyl],[220] (*c*) bis{[μ^2-66,66-bis(4-pyridyl)-1,2 : 18,36 : 22,23 : 27,45 : 31,32 : 55,56-hexakis(methano)-C_{60}-fullerene-61,61,62,62,63,63,64,64,65,65-decakis(ethylcarbonate)-*N*,*N*′] bis(triphenylphosphino) platinum(II)},[221] (*d*) tetrakis(*N*,*N*′-dimethylpropanediamine-*N*,*N*′)bis(epoxy-C_{60}-fullerene).[222]

are linked by two bridging platinum atoms (see Fig. 23 *c*).[221] In 2000, the first fullerene-containing cryptand $(C_{60}O)_2 \cdot [NMe(CH_2)_3NMe]_4$ was synthesised, which may be regarded as a derivative of fullerene hexachloride, in which two chlorine atoms are substituted by an epoxy oxygen atom, while the other four atoms are substituted by propanediamine bridges joining two $C_{60}O$ moieties (see Fig. 23 *d*).[222]

The changes in the C–C bond lengths in the C_{60} core upon σ- and π-functionalisation are illustrated in Figs 24 and 25. It is clearly seen that the addition of any exopolyhedral fragment to a 6/6 bond results in its elongation and a specific redistribution of lengths of the neighbouring C–C bonds. The distortions of the

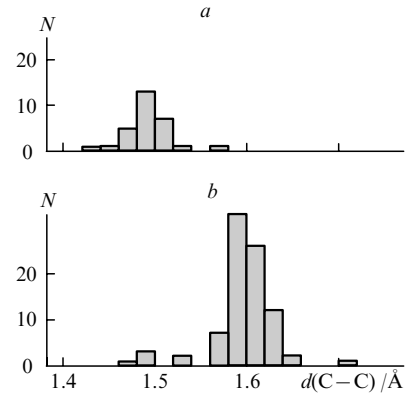

Figure 24. The distribution of lengths of the coordinated 6/6 C–C bonds in π- (*a*) and σ-derivatives of buckminsterfullerene (*b*).

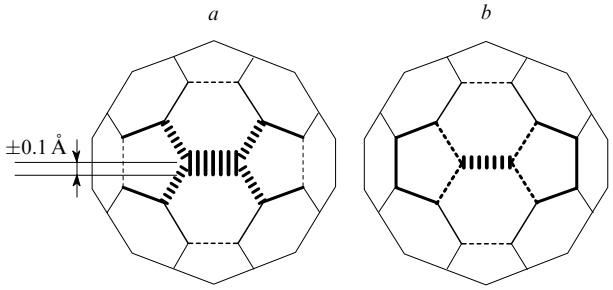

Figure 25. The elongation (dashed lines) and shortening (solid lines) of bonds in the fullerene molecule upon σ- (*a*) and π-addition (*b*). The magnitude of the bond length changes is proportional to the line width (the scale is shown).

C_{60} core due to coordination to a η^2-ML fragment (where M denotes a transition metal atom and L is its ligand shell) are substantially weaker as compared to those in σ-adducts, including $C_{60}CR_2$ derivatives. Note that the geometrical distortions of the cluster C_{60} are localised in the immediate proximity to the modified 6/6 bond both in σ- and π-derivatives, *i.e.*, the fullerene cage 'poorly transmits' the influence of attached fragments. As for chemically modified derivatives of C_{70}, structural data available for them are too sparse to derive reliable correlations.

A deeper chemical modification can result in opening and rearrangement of the carbon core. In particular, the molecule of a fullerene diketo derivative with an open 11-membered face admits penetration of small molecules, such as H_2, inside the fullerene core.[223] Another way to modify fullerene consists in 1,2-addition leading to the opening of the carbon cage and formation of a new fullerene with a four-membered carbocycle and two extra carbon atoms.[50] The cobalt complex σ,η^2,σ-$C_{64}H_4CoCp$, which contains an open fullerene core with a C_4H_4 fragment attached can be taken as an example.[224]

The crystal packings in chemically modified fullerenes obey the same regularities as molecular complexes. If a small externally attached fragment (*e.g.*, an oxygen atom) is present, a packing similar to the structure of pure C_{60} is formed. Covalently bound exopolyhedral fragments smaller than the van der Waals diameter of the fullerene sphere perform as 'diluents' in the standard structural motifs $(C_{60})_\infty$ (see Table 4). For instance, the crystal structure of the carbene monoadduct $C_{60}C(COOEt)_2 \cdot CHCl_3$ (ρ = 0.81)[225] may be classified as a three-dimensional framework with the MCN = 8 (here, the term MCN applies only to the fullerene subunit rather than to the whole molecule). At the same time, 3-benzyloxycarbonyl-(60)fullereno[1,2-*d*]isoxazole with the

bulkier five-membered isoxazole ring attached to the fullerene molecule, is composed of hexagonal layers of the C_{60} cores with the MCN = 6.[226] Bulkier exopolyhedral fragments together with solvate molecules result in looser packings down to motifs comprising isolated fullerene cores, such as the one encountered in the hexaadduct $C_{60}[C(COOEt)_2]_6$.[219] Note that fragments chemically attached to the fullerene core suppress rotational disorder, which typically leads to higher accuracy of the structure determination.

IX. π-Derivatives

The chemical properties of fullerenes as π-ligands are closer to polyalkenes rather than aromatic hydrocarbons. Chemically non-modified buckmisnterfullerene coordinates a few metal atoms by its 6/6 bonds acting exclusively as a η^2-ligand. As for σ-addition, η^2-coordination to one of the 6/6 bonds in buckminsterfullerene activates five analogous bonds forming together an octahedron over the fullerene cage (T_h symmetry, see Fig. 22 *f*). Upon π-coordination, the elongation of the affected 6/6 bond is not as significant as in the case of σ-addition (see Fig. 24). As a rule, the second group is π-coordinated at a *trans*-position with respect to the first one. The maximum number of metal-containing groups ML_n attached in this way is 6 (realised in the case of platinum), and the metal atoms are located in the vertices of an octahedron.[227]

Closely spaced double bonds enable fullerenes to act as polydentate η^2:η^2- and η^2:η^2:η^2-ligands in complexes with clusters of the platinum-group metals (Fig. 26). Such a coordination type is typical of arene ligands, *e.g.*, $C_6H_6Os_3(CO)_9$.[228] In a series of fullerene complexes with osmium and ruthenium, three metal atoms forming a triangular cluster are coordinated by three double bonds of one hexagonal face of the fullerene molecule.[229] A few complexes with buckminsterfullerene acting as a η^2-ligand for a triangular osmium carbonyl cluster have been reported.[230] In a series of closely related complexes described by Park *et al.*,[231] the osmium triangle coordinates fullerene as a η^2:η^2:η^2-, σ:η^2:σ- or η^2:η^2-ligand, depending on the non-fullerene ligand environment of the metal atoms.

In total, the CSD contains 30 entries, in which fullerene cages are π-coordinated to a single metal atom, 10 entries — to two metal atoms, 14 — to three, 2 — to four, 9 — to five and 6 — to six metal atoms. Furthermore, π-complexes containing two fullerene ligands coordinated to one cluster unit, such as Rh_6,[232] and even to one metal atom (Mo or W, see Fig. 26 *e*) [233] are known. For the π-complex $(\eta^2\text{-}C_{60})Ir(o\text{-}C_2B_{10}H_{10}CH_2PPh_2)(Bu^tNC)_2$, which contains the carborane and fullerene moieties coordinated to one iridium atom, insertion of an O_2 molecule at the metal–carbon bond upon oxidation in air has been confirmed by single-crystal X-ray diffraction. The resultant five-membered peroxide metallacycle has an Ir–C σ-bond with a length of 2.24 Å (Fig. 27).[52]

A η^2-coordination of an ML fragment to the fullerene core results in a redistribution of the C–C bond lengths, which is similar to that observed upon σ,σ-addition, but is less pronounced. Upon π-coordination, the 6/6 bond involved is elongated, on the average, to 1.48 Å (as compared to 1.60 Å in $C_{60}X_2$). The adjacent 5/6 bonds are elongated to 1.49 Å and a redistribution of the lengths of the adjacent bonds takes place (see Fig. 25). As in the case of σ-derivatives, the influence of the η^2-coordination on neighbouring bonds quickly attenuates with increasing distance from the coordinated bond and the 'rear' hemisphere of the fullerene core remains virtually unaffected.

In a series of structurally similar mononuclear fullerene complexes with iridium (fullerene)·$[Ir(CO)Cl(PPh_3)_2]_n$, n = 1, 2 (fullerene = C_{60}, $C_{60}O$, C_{70}, $C_{70}O$, C_{84}), the iridium atoms have approximately trigonal bipyramidal coordination environment. Essential geometrical parameters of these complexes are given in Table 6. Note that the volume occupied by the fullerene ligand in the coordination environment of iridium is larger than that of the triphenylphosphine ligand (the P–Ir–P bond angle is less than 120°, see Table 6).

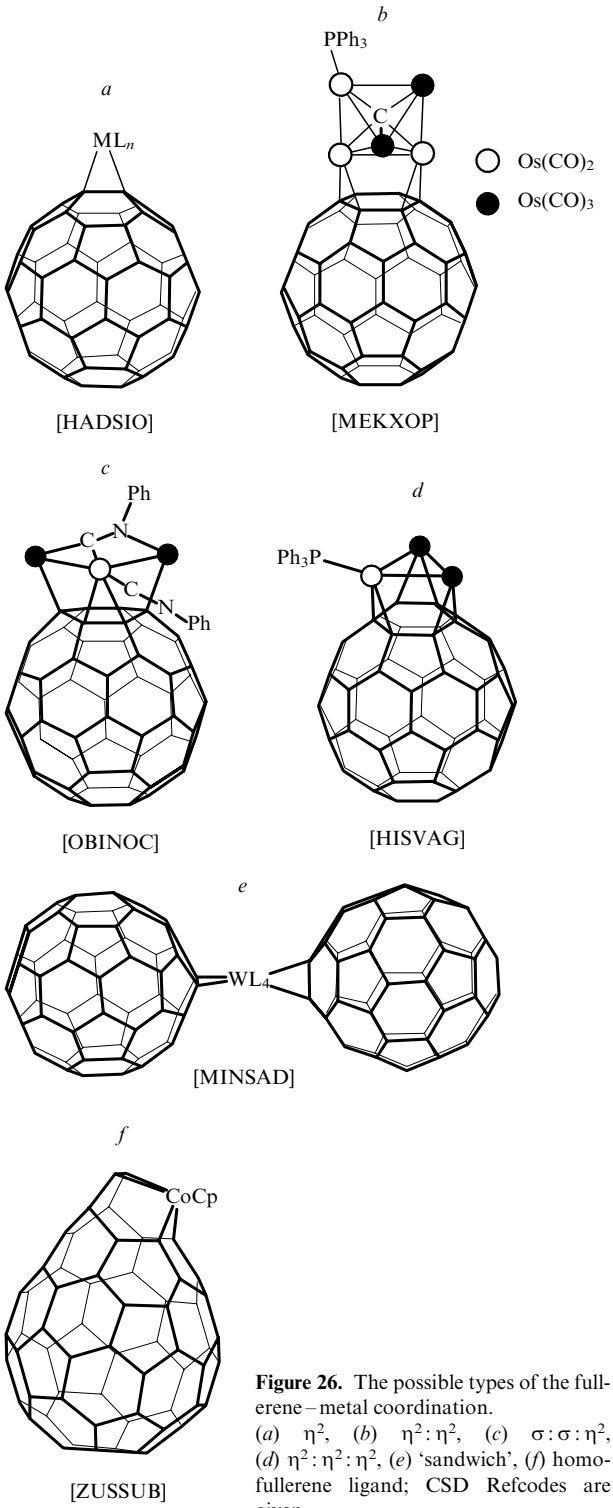

Figure 26. The possible types of the fullerene–metal coordination.
(*a*) η^2, (*b*) η^2:η^2, (*c*) σ:σ:η^2, (*d*) η^2:η^2:η^2, (*e*) 'sandwich', (*f*) homofullerene ligand; CSD Refcodes are given.

Penta-functionalised fullerene derivatives $C_{60}R_5$, in which the attached groups are located around a five-membered ring, are similar in terms of their electronic structure to pentasubstituted cyclopentadiene and thus can be involved into the η^5-coordination. In the structurally chracterised thallium salt $C_{60}Ph_5^-$,[238] which is analogous to cyclopentadienyl complexes of alkali metals with the essentially ionic metal–ligand bonding of the η^5-type, the

Table 6. The geometrical parameters of the coordination environment of iridium atoms in the (η^2-fullerene)·Ir(CO)Cl(PPh_3)$_2$ π-complexes.

Fullerene	Ir–C /Å	Ir–CO /Å	Ir–Cl /Å	Ir–P /Å	P–Ir–P /deg	Cl–Ir–CO /deg	Ref.
C_{60}	2.190	1.923	2.401	2.384	113.4	179.7	234
C_{60}/2	2.171	1.852	2.410	2.330	109.8	175.8	235
$C_{60}O$	2.172	1.840	2.396	2.386	113.5	179.0	176
C_{70}	2.182	1.834	2.362	2.384	114.9	178.8	236
C_{70}/2	2.176	1.838	2.366	2.356	104.2	176.1	237
$C_{70}O$	2.234	1.845	2.355	2.364	114.5	178.7	178
C_{84}	2.197	1.824	2.418	2.376	114.7	178.4	33

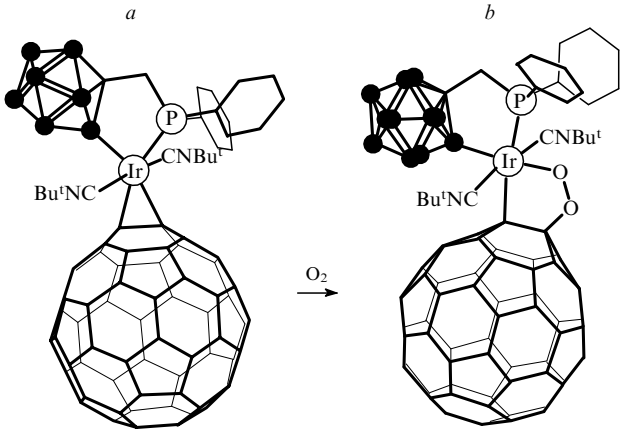

Figure 27. The molecular structures of the carborane–fullerene π-complex of iridium η^2-C_{60}Ir(*o*-$C_2B_{10}H_{10}CH_2PPh_2$)(Bu^{t}NC)$_2$·4 PhMe (*a*) and the product of its air oxidation (*b*) (single-crystal X-ray diffraction data).[52]

Tl–C lengths lie in the range 2.83–2.89 Å. The thallium atom is additionally coordinated to an oxygen atom of the THF solvate molecule at a distance of 3.16 Å. In another rhodium-based complex $C_{60}Me_5Rh(CO)_2$, the $C_{60}Me_5$ core acts as a real η^5-ligand coordinated to a metal atom[239] with the bonding Rh–C distances in the range of 2.12–2.27 Å.

As in the case of σ-addition, the fullerene C_{70} π-coordinates external metal atoms most typically by the *b* type bonds or, in complexes with metal clusters or several independent metal atoms, by *b* and *d* type bonds (see Fig. 1 *b*). In the thallim derivative $C_{70}(C_6H_4CF_3)_3Tl\cdot o$-$C_6H_4Cl_2$, the $C_{70}(C_6H_4CF_3)_3$ fragment acts as a cyclopentadienyl-like anion.[240] The molecular structures of the η^5-coordinated derivatives of C_{60} and C_{70} are depicted schematically in Fig. 28.

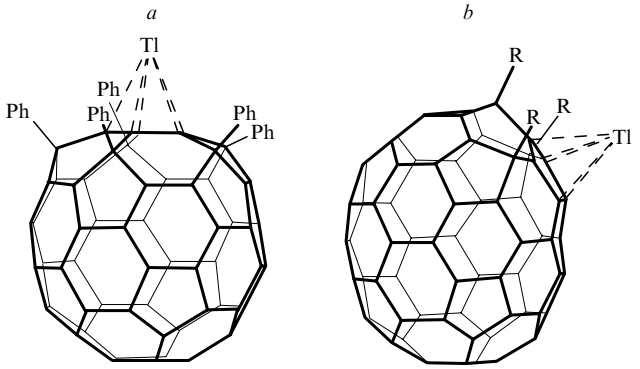

Figure 28. Examples of the η^5-coordination fullerene–metal. (*a*) $C_{60}Ph_5Tl\cdot 2.5\,THF$, Tl–C = 2.83–2.89 Å (see Ref. 238), (*b*) $C_{70}(C_6H_4CF_3)_3$ $Tl\cdot C_6H_4Cl_2$, Tl–C = 2.84–3.08 Å (R = *p*-$C_6H_4CF_3$).[240]

The D_{2d} isomer of C_{84} in the structurally investigated complex $C_{84}\cdot Ir(CO)Cl(PPh_3)_2$ is coordinated to iridium through the 6/6 bond located at the intersection of two symmetry planes. The coordinated bond is elongated to 1.45 Å, and the spherical excesses of its carbon atoms are increased to 21° and 18°.[33]

Of particular interest are the structures and chemical properties of fullerene metallocomplexes containing metal atoms bound to strongly modified 'open' carbon cages and involving attached exopolyhedral functional groups. For instance, the cobalt atom in the crystal structure of $C_{60}C_4H_4CoCp\cdot C_7H_8$ is coordinated to bishomofullerene acting as a (η^2,σ,σ)-ligand (see Fig. 26 *f*).[82] In this compound, the fullerene cage is open due to the formation of an 11-membered ring.

Bulky and sterically flexible molecules of fullerene π-complexes often form several different solvates with the same solvent. A typical example is two benzene solvates of the complex $C_{60}[Ir(CO)Cl(PPhMe_2)_2]_2$ (Fig. 29).[235] In one of the solvates with the composition $C_{60}[Ir(CO)Cl(PPhMe_2)_2]\cdot C_6H_6$ (ρ = 2.21), the fullerene cores are isolated from each other while in the second complex, which is characterised by the stoichiometry $C_{60}[Ir(CO)Cl(PPhMe_2)_2]\cdot 2\,C_6H_6$ (ρ = 2.45), the packing of fullerene fragments may be described as separated columns.

It is convenient to describe the crystal packings encountered in fullerene π-complexes (as well as in other derivatives) in terms of motifs formed by fullerene spheres. A distinctive feature of the π-complexes is an appreciable volume of the non-fullerene part. This often gives rise to loose and isolated motifs. Fullerene π-complexes with palladium and platinum having the composition $C_{60}M_n$ (attributed in the present review to fullerides) represent an exception from this tendency.

X. Endohedral fullerenes

Endohedral fullerenes, *i.e.*, compounds containing different 'guests', such as metal or nonmetal atoms (including atoms of inert gases) or small cllusters, inside the carbon cage, take a special place among diverse fullerene derivatives. The regularities of the formation of these compounds have been reviewed by Shinohara[241]. Endohedral metallofullerenes (EMFs) have been detected by mass spectrometry for the first time simultaneously with the 'empty' fullerenes,[242] and later were isolated in microgram quantities.[243] However, structural studies of these species are impeded to a great extent by their high reactivity and the multitude of isomers (see below).

A heating of 'empty' fullerenes C_n in the atmosphere of an inert gas A under pressure allows preparation of endohedral§ derivatives A@C_n in trace amounts.[244] In particular, endohedral compounds of C_{60} with ^{3}He (see Ref. 245) and ^{129}Xe (see Ref. 246) were prepared and studied by NMR. In the case of C_{70}, endohedral derivatives $A_2@C_{70}$ [A = He (see Ref. 247) and Ne (see Ref. 248)] with two inert gas atoms inside the fullerene cage were produced using this route. The ratio between the products A@C_{70} and $A_2@C_{70}$ suggests the 'classical' mechanism of the synthesis involving cleavage of a C–C bond with subsequent closure of the

§ In chemical formulas, the endohedral component is denoted with the sign @.

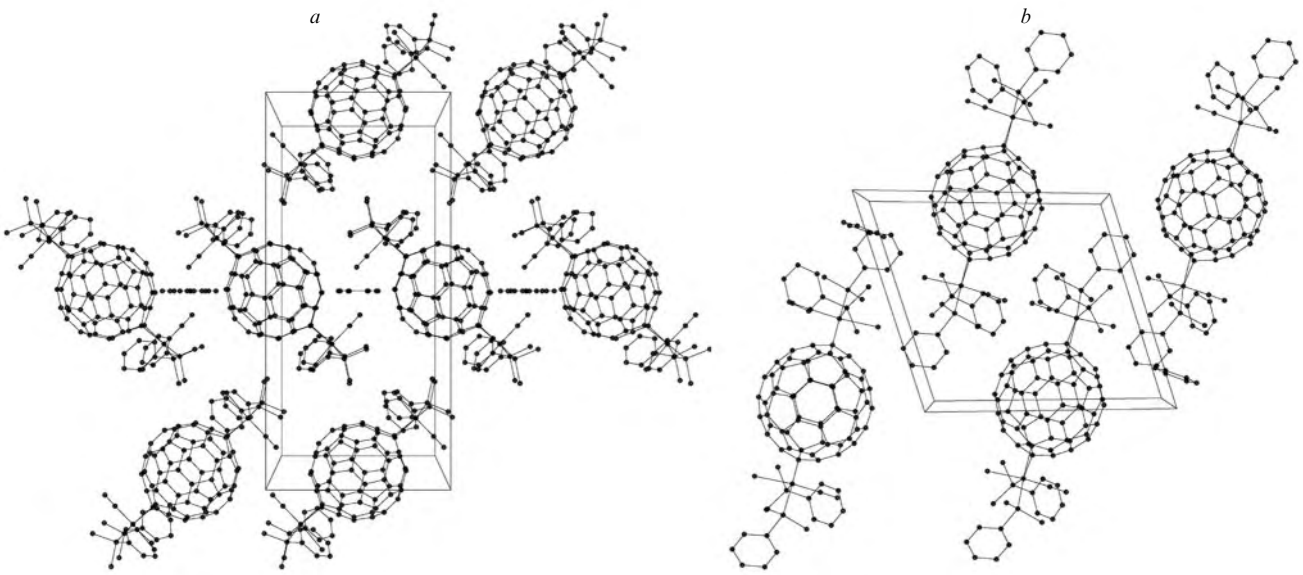

Figure 29. The molecular packings in the crystal structures of $C_{60}\cdot[Ir(CO)Cl(PPhMe_2)_2]\cdot C_6H_6$ (*a*) and $C_{60}\cdot[Ir(CO)Cl(PPhMe_2)_2]\cdot 2\,C_6H_6$ (*b*).[235]

cage. The single-crystal X-ray diffraction study of a solid solution of $Kr@C_{60}$ in crystalline $C_{60}\cdot NiOEP\cdot 2\,C_6H_6$ has shown that the krypton atom is located in the centre of the fullerene cage at distances of 3.54 Å from carbon atoms (which is 0.2 Å shorter than the sum of their van der Waals radii). The fraction of $Kr@C_{60}$ in the single crystal was estimated to be 9% based on the refinement of the Kr position occupancy.[249] A series of endohedral derivatives $X@C_{60}$ [where X = Li (see Ref. 250), N (see Ref. 251) and P (see Ref 252)] have been synthesised using an ion bombardment of C_{60} films *in vacuo* and studied with ESR. For the two latter cases, it was shown that the atoms of the fifth-group elements do not bind to the walls of the carbon cage and thus are in the quadruplet state, *i.e.*, have three unpaired electrons.

The standard method of the synthesis of endohedral metallofullerenes consists of a plasma-induced sublimation of graphite impregnated with the corresponding metal oxide (1 at.% – 2 at.%) in a helium atmosphere (10 – 100 Torr). Mass spectra of the products synthesised, in addition to C_{60}^+ and C_{70}^+, reveal peaks attributable to MC_n^+ ions ($n = 60-100$) with the predominance of MC_{60}^+ and MC_{82}^+.[241] Using extraction with polar organic solvents or CS_2 followed by chromatographic separation, the endohedral derivatives $M@C_{82}$, $M@C_{84}$ and $M_2@C_{80}$ moderately stable in air can be isolated while pure $M@C_{60}$ is very difficult to isolate due to its high reactivity. Individual EMFs of more than 20 metals (predominantly, lanthanides) have been synthesised to date in milligram quantities.[253 – 256]

One of the factors hampering the structural studies of EMFs (as well as of 'empty' higher fullerenes) is the isomerism of their carbon cores.[253] Quantum chemistry calculations on EMFs revealed a substantial charge transfer from the metal atoms to the carbon cage, which stabilises higher-symmetry isomers and can even result in a violation of the isolated pentagon rule.[257] Quantum chemistry optimisation of the geometry of mononuclear endohedral metallofullerenes $M@C_n$ predicts a shift of the metal atom from the centre of the cavity towards the walls giving rise to the bonding intrapolyhedral M···C contacts with lengths ~ 2.5 Å and a large molecular dipole moment (4 – 5 D). Furthermore, quantum chemistry calculations and spectroscopic data show the easiness of the metal atom migration inside the carbon cage, which poses additional difficulties for the structural studies.[19, 253, 257, 258]

The most studied mononuclear lanthane derivative $Ln@C_{82}$ represents, according to the spectral data,[256] a mixture of isomers with the C_{2v} (isomer I, content 70% – 80%) and C_{3v} symmetry (isomer II, content 20% – 30%) (Fig. 30). For derivatives of some other metals, the isomers III (Er, Dy, Tm, Ca) and IV (Ca) were

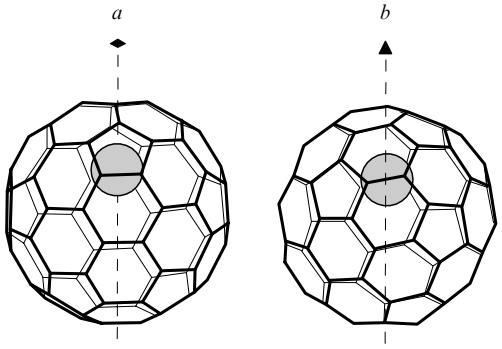

Figure 30. The molecular structures of endohedral metallofullerenes having the isomeric C_{82} cores with the C_{2v} symmetry (*a*) and the C_{3v} symmetry (*b*) (quantum-chemistry calculations).[253]

additionally found.[256, 259] Therefore, in order to avoid a thorough statistical disorder in single crystals, preparation of endohedral metallofullerenes for structural studies should always involve a time-consuming stage of the chromatographic separation of isomer mixtures.

For the majority of endohedral fullerenes, experimental data on their structures have been obtained by means of XAFS spectroscopy [260 – 264] and powder X-ray diffraction utilising synchrotron radiation. The position and overall shape of the X-ray Absorption Near-Edge Structure (XANES) spectra confirm the intramolecular charge transfer from the 'guest' metal atoms to the carbon cage. A shift of the metal atom from the centre of the fullerene cage and its coordination to carbon atoms have been established experimentally for the first time in the EXAFS studies of $Y@C_{82}$ (see Ref. 261) and $La@C_{82}$ (see Ref. 262). In mononuclear actinide-based (Th, U and so forth) endohedral derivatives of fullerenes $C_{82}-C_{84}$, the charge of the metal ions was estimated as 3+ according to the results of XANES.[265]

The most essential details of the molecular and crystalline structures for a series of polycrystalline EMFs were determined in an extended series of diffraction studies [85, 264 – 270] based on the maximum entropy method (MEM). For all the studied phases, the insertion of metal atoms into carbon cages was objectively revealed. Preparation of the binuclear derivative $Sc_2@C_{66}$ has been reported, in which the geometry of the carbon cage does not obey the IPR, in agreement with the quantum chemistry calcu-

lations.[15] In the strongly disordered crystal structure of $Sc_2C_2@C_{84}$ (see Ref. 271), a carbide cluster with two carbon atoms at a distance of 1.42(6) Å has been revealed inside the fullerene cage. The metal–metal distances in binuclear $La_2@C_{80}$ (3.90–3.94 Å)[271] and $Sc_2@C_{84}$ (3.91 Å)[268] derivatives imply that there is no direct metal–metal bonding. On the other hand, the Sc–Sc bonds with a length of 2.89 Å are revealed in $Sc_2@C_{66}$, which has a smaller carbon cage.[15] Furthermore, abnormally short Sc–Sc bonds with the length of 2.3(3) Å (see Ref. 270) (as compared to 3.20–3.30 Å in bulk scandium[272]) were found in the (1 : 1) toluene solvate of the three-nuclear derivative $Sc_3@C_{82}$. This result contradicts to the quantum chemistry calculations[257] and is probably caused by a rotational disorder of the EMF molecule. Estimates of charges of the endohedral fragments obtained by integrating the electron density distribution reconstructed from the powder X-ray diffraction data[15,85,270,272] are doubtful since they lie far beyond the standard accuracy of the technique. Notwithstanding, these studies report very important structural information concerning EMFs at a semiquantitative level.

A series of endohedral fullerenes, $M_3N@C_n$ (M = Sc, Er; n = 78, 80, 68), which have been synthesised and characterised by single-crystal X-ray diffraction,[16,273–275] contain triangular nitridometal clusters inside the respective carbon cages. They were produced through the plasma evaporation route in a dynamical N_2-containing atmosphere and crystallised as (1 : 1) molecular complexes with cobalt octaethylporphyrinate CoOEP also contaning solvent molecules. Despite the presence of short intermolecular Co···C (fullerene) contacts in the range of 2.71–2.78 Å, fullerene moieties and endohedral M_3N 'guest' fragments are strongly rotationally disordered. The molecular structures of two high-symmetry isomers of C_{78} (D_{3h}) and C_{80} (I_h) stabilised by a charge transfer from the metal atoms were established. The geomertry of the endohedral M_3N fragment (Fig. 31) was determined and a lability of the M···C (fullerene) bonding was pointed out. The same group of authors reported the preparation and crystal structure study of the dimethoxyxylylene derivative $Sc_3N@C_{80}$Dmxy.[276] In this structure, the fullerene cage is chemically modified from the outer side through a [4 + 2] cycloaddition to a 5/6 bond, which results in its elongation to 1.63 Å, but the endohedral group is nevertheless disordered. As has been determined, in the case of the C_{78} core, endohedral metal atoms are located above the 6/6 bonds of the pyracylene fragment, in agreement with the quantum-chemical predictions.[277] Meanwhile, in the case of the C_{80} core, which has no pyracylene fragments, the endohedral M_3N group is chracterised by a stronger rotational disorder. A smaller endohedral fullerene isolated and studied by single-crystal X-ray diffraction as a complex with the analogous composition, likely contains the C_{68} core that violates the isolated pentagon rule.[16] Both the fullerene cage and the endohedral fragment in this substance are strongly disordered, its stoichiometry was confirmed by mass spectrometry.[16]

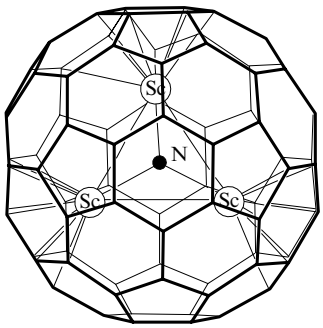

Figure 31. The molecular structure of $Sc_3N@C_{80}$ (single-crystal X-ray diffraction data).[273]
Interatomic distances: Sc–N 2.00–2.01 Å, Sc–C 2.15–2.73 Å, Sc–Sc 3.48 Å.

A single-crystal X-ray diffraction study of another endohedral metallofullerene molecular complex $Er_2@C_{82}\cdot CoOEP\cdot(C_6H_6)_{2-x}\cdot(CHCl_3)_x$ revealed[278] a carbon cage of the C_s symmetry and a strong disorder of the erbium atoms over numerous positions. The second isomer of this substance with the C_{3v} symmetry of the carbon core and the disordered endohedral fragment was also prepared and characterised.[279]

Solvent-free EMFs at room temperature are characterised by an fcc lattice[280] isomorphous to that of high-temperature modifications of C_{60} and C_{70}. Upon slow cooling, $La@C_{82}$ single crystal undergoes two phase transitions due to orientational ordering of the ellipsoid EMF molecules giving rise to the rhombohedral (180–150 K) and metastable triclinic (150–20 K) modifications. Rapid cooling of the rhombohedral polymorph yields a disordered simple cubic phase, which is stable below 132 K.[280] In strongly disordered EMF solvates $M@C_{82}\cdot 1.5\,CS_2$, the carbon disulfide molecules occupy cavities within a bcc lattice. This phase undergoes a magnetic phase transition at 150 K, which was suggestively attributed to the ordering of the metal-containing fullerene cores.[281] Endohedral fullerene derivatives, like pure fullerenes, are able to polymerise at elevated pressures.[282]

According to the powder X-ray diffraction data, monoclinic toluene solvates $M@C_{82}\cdot PhMe$ are isomorphous to the respective solvates of 'empty' higher fullerenes $C_{82}\cdot PhMe$ and $C_{76}\cdot x\,PhMe$.[31] The molecular packing motif in these structures conforms to that found earlier in the (1 : 1) solvates of buckminsterfullerene with n-pentane, dichloroethane and other solvents[84] (see Fig. 6) but the intermolecular electrostatic interactions favour the 'head-to-tail' arrangement of neighbouring molecules in the case of the endohedral derivatives.[267] The crystal structures of the $M_3N@C_{80}\cdot CoOEP\cdot Solv$ complexes discussed above contain zigzag chains of fullerene cages similar to those in molecular complexes of C_{60} and C_{70} with metalloporphyrins (see Fig. 8). The shortest distance between the centres of fullerene cores in the EMFs with known crystal structures lie in the range of 11.00–11.22 Å.

XI. Conclusion

The distinctive features of crystal chemistry of fullerenes summarised above are defined primarily by the involvement of bulky spherical-like carbon clusters and the predominance of non-bonding intermolecular interactions. The results of structural investigations into various derivatives of fullerenes including chemically modified and endohedral ones demonstrate the typical rotational disorder of carbon cores (which can be attenuated down to a complete ordering at low temperatures), high affinity of fullerenes towards formation of molecular complexes and diversity of their crystalline phases. Patterns of the rotational disorder typical of C_n molecules in crystals can be conveniently described within the model of the 'rubber cavity', which postulates occurrence of specific orientations corresponding to local minima of the shallow interaction potential. In all the considered classes of compounds, similar motifs of arangement of fullerene cores are observed, which are defined by the volume fraction occupied by the fullerene component in the total unit cell volume. Non-fullerene molecules and exopolyhedral fragments fill cavities of these motifs thus acting as a flexible van der Waals matrix.

Coulomb attraction (in ionic fullerides) and specific intermolecular interactions stabilise the crystal packing and increase the degree of ordering, which enables collection of more accurate crystallographic data for the corresponding substances. Some authors suggest weak Jahn–Teller distortions in mono- and dianions of buckminsterfullerene and proneness of anionic fullerenes to polymerisation. Chemical bonding between two or more fullerene molecules gives rise to dimers and trimers as well as to infinite motifs composed of chain, layer and framework polymeric structures.

The presence of 'guest' atoms inside the fullerene cages in the case of endohedral derivatives can, on the one hand, stabilise the crystal packing due to the polarisation of the carbon clusters and, on the other hand, increase structural disorder due to multiple positions of the endohedral atoms and/or dynamical transitions inside the carbon cage. According to the quantum chemistry calculations and experimental spectral data, endohedral metallofullerenes are characterised by a metal → carbon cage charge transfer stabilising the higher-symmetry isomers. Additional degrees of freedom in endohedral metallofullerenes, such as molecular dipole moment or magnetic moment of the 'guest' atoms, increase the number of possible ordering types and respective phase transitions.

The most typical way of a chemical modification of fullerenes (to form either σ- or π-derivatives) consists of an addition to one of the 6/6 bonds, which is accompanied by its elongation and a specific distortion of the carbon cage localised in the proximity to the exopolyhedral coordinated atoms. In the case of C_{70}, a functionalisation preferably occurs at the stereochemically strained and the most 'pyramidised' *b* type 6/6 bond. For several C_{60} and C_{70} derivatives, the addition occurs at a 5/6 bond and results in its cleavage and formation of 'open' homofullerene cages. As compared to crystals of non-modified fullerenes, functionalised derivatives are typically better ordered owing to the nonsphericity of their molecular shapes.

The multiple σ,σ- or η^2-addition of exopolyhedral fragments not interacting with each other proceeds at the most distant 6/6 bonds ultimately yielding (in the case of C_{60}) hexadducts with six exopolyhedral fragments octahedrally surrounding the fullerene core. If a metal cluster is taken as the exopolyhedral fragment, the fullerene molecule can act as a polydentate π-ligand coordinating the cluster through one of its hexagonal faces. In the case of σ-modified fullerenes, the η^5-coordination to single metal atoms is possible and even η^6-bonding can be realised in the future. Multiple σ-addition of small exopolyhedral fragment X leads to 'binary' fullerene derivatives C_nX_m (n = 60, 70; X = H, O, F, Cl, Br, Me, CF_3). When the number of attached fragments m is small (up to 5–6), they are typically localised in the same specific part of the carbon cage. Meanwhile, a more profound modification is accompanied by spreading of the attached groups X over the fullerene hemisphere (*e.g.*, in $C_{60}F_{18}$ and its analogues) or the entire sphere (*e.g.*, in $C_{60}Br_{24}$, $C_{60}F_{36}$ and $C_{60}F_{48}$). A deep chemical modification induces substantial distortions of the fullerene polyhedral cage and can even result in its opening.

The present structural data survey is in part a result of our own research activities, which have been conducted starting from the second half of the 1990s. We are grateful to all our colleagues who provided us with single crystals of new substances synthesised in their laboratories and shared with us the most recent structural results of their own (sometimes even prior to publication). We thank Corresponding Member of RAS M Yu Antipin (INEOS RAS, Moscow), Profs. G Saito (University of Kyoto, Japan), O Kashino and I Kubozono (Okayama University, Japan), R N Lyubovskaya (IPPC RAS, Chernogolovka), M V Korobov and O V Boltalina (Department of Chemistry, MSU, Moscow), J Howard (University of Durham, UK), R Taylor (University of Sussex, UK) and Dr. D V Konarev (IPCP RAS, Chernogolovka). Very interesting and useful information was collected owing to our participation in the series of the biannual international conferences IWFAC (International Workshop 'Fullerenes and Atomic Clusters') held in St Petersburg.

This review has been prepared and written with financial support of the Russian programme 'Fullerenes and Atomic Clusters' and the Russian Foundation for Basic Research (Project No. 02-03-33225).

References

1. K M Kadish, R S Ruoff (Eds) *Fullerenes: Chemistry, Physics, and Technology* (New York: Wiley, 2000)
2. O A Dyachenko, A Graja *Fullerene Sci. Technol.* **7** 317 (1999)
3. D V Konarev, R N Lyubovskaya *Usp. Khim.* **68** 23 (1999) [*Russ. Chem. Rev.* **68** 19 (1999)]
4. N F Goldshleger, A P Moravsky *Usp. Khim.* **66** 353 (1997) [*Russ. Chem. Rev.* **66** 323 (1997)]
5. B Sundqvist *Adv. Phys.* **48** (1) 1 (1999)
6. A L Balch, M M Olmstead *Chem. Rev.* **98** 2123 (1998)
7. E Osawa *Kagaku* (*Kyoto*) **25** 854 (1970)
8. D A Bochvar, E G Gal'pern *Dokl. Akad. Nauk SSSR* **209** 610 (1973) [a]
9. H W Kroto, J R Heath, S C O'Brien, R F Curl, R E Smalley *Nature (London)* **318** 162 (1985)
10. W Kraetschmer, L D Lamb, K Fostiropoulos, D R Huffman *Nature (London)* **347** 354 (1990)
11. J C Gallucci, C W Doecke, L A Paquette *J. Am. Chem. Soc.* **108** 1343 (1986)
12. H Prinzbach, A Weller, P Landenberger, F Wahl, J Worth, L T Scott, M Gelmont, D Olevano, B von Issendorff *Nature (London)* **407** 60 (2000)
13. C Piskotti, J Yarger, A Zettl *Nature (London)* **393** 771 (1998)
14. D Bakowies, W Thiel *J. Am. Chem. Soc.* **113** 3704 (1991)
15. C-R Wang, T Kai, T Tomiyama, T Yoshida, Y Kobayashi, E Nishibori, M Takata, M Sakata, H Shinohara *Nature (London)* **408** 426 (2000)
16. M M Olmstead, H M Lee, J C Duchamp, S Stevenson, D Marciu, H C Dorn, A L Balch *Angew. Chem., Int. Ed.* **42** 900 (2003)
17. A Rassat, I Laszlo, P W Fowler *Chem. Eur. J.* **9** 644 (2003)
18. P W Fowler, D E Manolopoulos *Nature (London)* **355** 428 (1992)
19. S Nagase, K Kobayashi, T Akasaka, T Wakahara, in *Fullerenes: Chemistry, Physics and Technology* (Eds K M Kadish, R S Ruoff) (New York: Wiley, 2000) p. 395
20. M D Diener, J M Alford *Nature (London)* **393** 668 (1998)
21. V I Kovalenko, A R Khamatgalimov *Chem. Phys. Lett.* **377** 263 (2003)
22. R D Johnson, G Meijer, D S Bethune *J. Am. Chem. Soc.* **112** 8983 (1990)
23. K Hedberg, L Hedberg, D S Bethune, C A Brown, H C Dorn, R D Johnson, M De Vries *Science* **254** 410 (1991)
24. R Tycko, R C Haddon, G Dabbagh, S H Glarum, D C Douglas, A M Mujsce *J. Phys. Chem. B* **95** 518 (1991)
25. K Hedberg, L Hedberg, M Buhl, D S Bethune, C A Brown, R D Johnson *J. Am. Chem. Soc.* **119** 5314 (1997)
26. H B Burgi, P Venugopalan, D Schwarzenbach, F Diederich, C Thilgen *Helv. Chim. Acta* **76** 2155 (1993)
27. R H Michel, M M Kappes, P Adelmann, G Roth *Angew. Chem., Int. Ed. Engl.* **33** 1651 (1994)
28. F Diederich, R L Whetten, C Thilgen, R Ettl, I Chao, M M Alvarez *Science* **254** 1768 (1991)
29. F H Hennrich, R H Michel, A Fischer, S R Schneider, S Gilb, M M Kappes, D Fuchs, M Burk, K Kobayashi, S Nagase *Angew. Chem., Int. Ed. Engl.* **35** 1732 (1996)
30. C-R Wang, T Sugai, T Kai, T Tomiyama, H Shinohara *Chem. Commun.* 557 (2000)
31. H Kawada, Y Fujii, H Nakao, Y Murakami, T Watanuki, H Suematsu, K Kikuchi, Y Achiba, I Ikemoto *Phys. Rev. B* **51** 8723 (1995)
32. T J S Dennis, M Hulman, H Kuzmany, H Shinohara *J. Phys. Chem. B* **104** 5411 (2000)
33. A L Balch, A S Ginwalla, J W Lee, B C Noll, M M Olmstead *J. Am. Chem. Soc.* **116** 2227 (1994)
34. G Y Sun *Chem. Phys. Lett.* **367** (1–2) 26 (2003)
35. N Tagmatarchis, D Arcon, M Prato, H Shinohara *Chem. Commun.* 2992 (2002)
36. V Mordkovich, Y Shiratori, H Hiraoka, Y Takeuchi *Phys. Solid State* **44** 581 (2002)

37. C Brown, L Cristofolini, K Kordatos, K Prassides, C Bellavia, R Gonzalez, M Keshavarz, F Wudl, A Cheetham, J Zhang, W Andreoni, A Curioni, A Fitch, P Pattison *Chem. Mater.* **8** 2548 (1996)
38. K-C Kim, F Hauke, A Hirsch, P D W Boyd, E Carter, R S Armstrong, P A Lay, C A Reed *J. Am. Chem. Soc.* **125** 4024 (2003)
39. P A Cox *The Electronic Structure and Chemistry of Solids* (Oxford: Oxford University Press, 1981)
40. M J Hardie, R Torrens, C L Raston *Chem. Commun.* 1854 (2003)
41. M V Korobov, E B Stukalin, A L Mirakyan, I S Neretin, Y L Slovokhotov, A V Dzyabchenko, A I Ancharov, B P Tolochko *Carbon* **41** (14) 2743 (2003)
42. A L Litvinov, D V Konarev, A Y Kovalevsky, I S Neretin, Y L Slovokhotov, P Coppens, R N Lyubovskaya *Cryst. Eng. Commun.* **4** 618 (2002)
43. D V Konarev, I S Neretin, G Saito, Y L Slovokhotov, A Otsuka, R N Lyubovskaya *J. Chem. Soc., Dalton Trans.* 3886 (2003)
44. D V Konarev, I S Neretin, Y L Slovokhotov, A L Litvinov, A Otsuka, R N Lyubovskaya, G Saito *Synth. Met.* **131** 87 (2002)
45. D V Konarev, A Y Kovalevsky, X Li, I S Neretin, A L Litvinov, N V Drichko, Y L Slovokhotov, P Coppens, R Lyubovskaya *Inorg. Chem.* **41** 3638 (2002)
46. D V Konarev, I S Neretin, Y L Slovokhotov, R N Lyubovskaya, D S Yufit, J A K Howard *Cryst. Growth Des.* (2004) http://pubs3.acs.org/acs/journals/doilookup?in_doi=10.1021/cg034259f
47. D V Konarev, I S Neretin, G Saito, Y L Slovokhotov, A Otsuka, R N Lyubovskaya *Eur. J. Inorg. Chem.* 1794 (2004)
48. T Takenobu, D H Chi, S Margadonna, K Prassides, Y Kubozono, A N Fitch, K Kato, Y Iwasa *J. Am. Chem. Soc.* **125** 1897 (2003)
49. S I Troyanov, A A Popov, N I Denisenko, O V Boltalina, L N Sidorov, E Kemnitz *Angew. Chem., Int. Ed.* **42** 2395 (2003)
50. E Nakamura, K Tahara, Y Matsuo, M Sawamura *J. Am. Chem. Soc.* **125** 2834 (2003)
51. W Qian, S-C Chuang, R B Amador, T Jarrosson, M Sander, S Pieniazek, S I Khan, Y Rubin *J. Am. Chem. Soc.* **125** 2066 (2003)
52. A V Usatov, E V Martynova, F M Dolgushin, A S Peregudov, M Y Antipin, Y N Novikov *Eur. J. Inorg. Chem.* **1** 29 (2003)
53. S Liu, Y-J Lu, M M Kappes, J A Ibers *Science* **254** 408 (1991)
54. W I F David, R M Ibberson, T J S Dennis, J P Hare, K Prassides *Europhys. Lett.* **18** 219 (1992)
55. W I F David, R M Ibberson, J C Matthewman, K Prassides, T J S Dennis, J P Hare, H W Kroto, R Taylor, D R M Walton *Nature (London)* **353** 147 (1991)
56. A F Wells *Structural Inorganic Chemistry* (Oxford: Oxford University Press, 1987)
57. H-B Burgi, E Blanc, D Schwarzenbach, S Liu, Y Lu, M M Kappes, J A Ibers *Angew. Chem., Int. Ed. Engl.* **31** 640 (1992)
58. J L de Boer, S Vansmaalen, V Petricek, M Dusek, M A Verheijen, G Meijer *Chem. Phys. Lett.* **219** 469 (1994)
59. E V Skokan, I V Arkhangelskii, N A Zhukova, Y A Velikodnyi, N B Tamm, N V Chelovskaya *Carbon* **41** 1387 (2003)
60. J M Hawkins, T A Lewis, S D Loren, A Meyer, J R Heath, R J Saykally, F J Hollander *J. Chem. Soc., Chem. Commun.* 775 (1991)
61. A P Isakina, A I Prokhvatilov, M A Strzhemechny, K A Yagotintsev *Low Temp. Phys.* **27** 1037 (2001)
62. J F Armbruster, H A Romberg, P Schweiss, P Adelmann, M Knupfer, J Fink, R H Michel, J Rockenberger, F Hennrich, H Schreiber, M M Kappes *Z. Phys. B* **95** 469 (1994)
63. R Almairac, D Tranqui, J P Lauriat, J Lapasset, J Moret *Solid State Commun.* **106** 437 (1998)
64. A I Kitaigorodsky *Molekulyarnye Kristally* (Molecular Crystals) (Moscow: Nauka, 1971)
65. Y L Slovokhotov, I V Moskaleva, V I Shilnikov, E F Valeev, Y N Novikov, A I Yanovsky, Y T Struchkov *Mol. Cryst. Liq. Cryst.* **8** 117 (1996)
66. R Ceolin, V Agafonov, D Andre, A Dworkin, H Szwarc, J Dugue, B Keita, L Nadjo, C Fabre, A Rassat *Chem. Phys. Lett.* **208** 259 (1993)
67. M Jansen, G Waidmann *Z. Anorg. Allg. Chem.* **621** 14 (1995)
68. M Barrio, D O Lopez, J L Tamarit, P Espeau, R Ceolin, H Allouchi *Chem. Mater.* **15** 288 (2003)
69. R S Ruoff, R Malhotra, D L Huestis, D S Tse, D C Lorents *Nature (London)* **362** 140 (1993)
70. B P Nikol'skii (Ed.) *Spravochnik Khimika* (Handbook for Chemist) Vol. 3 (Moscow, Leningrad: Khimiya, 1964)
71. V N Bezmelnitsin, A V Eletskii, E V Stepanov *J. Phys. Chem. B* **98** 6665 (1994)
72. M Korobov, A Mirak'yan, N Avramenko, R S Ruoff *Dokl. Akad. Nauk* **349** 346 (1996) [a]
73. A Smith, E Walter, M V Korobov, O L Gurvich *J. Phys. Chem. B* **100** 6775 (1996)
74. M Korobov, A L Mirakyan, N V Avramenko, G Olofsson, A L Smith, R S Ruoff *J. Phys. Chem. B* **103** 1339 (1999)
75. N Sivaraman, R Dhamodaran, I Kaliappan, T G Srinivasan, P R V Rao, C K Mathews *Fullerene Sci. Technol.* **2** 233 (1994)
76. M Ramm, P Luger, W Duczek, J C A Boyens *Cryst. Res. Technol.* **31** 43 (1996)
77. G Oszlanyi, G Bortel, G Faigel, S Pekker, M Tegze *Solid State Commun.* **89** 417 (1994)
78. M Ramm, P Luger, M Strumpel, G Beurskens, J Averdung, J Mattay *Z. Kristallogr.* **213** 69 (1998)
79. R E Douthwaite, M L H Green, S J Heyes, M J Rosseinsky, J F C Turner *J. Chem. Soc., Chem. Commun.* 1367 (1994)
80. M F Meidine, P B Hitchcock, H W Kroto, R Taylor, D R M Walton *J. Chem. Soc., Chem. Commun.* 1534 (1992)
81. T Ishii, N Aizawa, M Yamashita, H Matsuzaka, T Kodama, K Kikuchi, I Ikemoto, Y Iwasa *J. Chem. Soc., Dalton Trans.* 4407 (2000)
82. M M Olmstead, D A Costa, K Maitra, B C Noll, S L Phillips, P M V Calcar, A L Balch *J. Am. Chem. Soc.* **121** 7090 (1999)
83. N V Avramenko, A L Mirakyan, I S Neretin, Y L Slovokhotov, M V Korobov *Thermochim. Acta* **344** 23 (2000)
84. R M Fleming, A R Kortan, B Hessen, T Siegrist, F A Thiel, P Marsh, R C Haddon, R Tycko, G Dabbagh, M L Kaplan, A M Mujsce *Phys. Rev. B* **44** 888 (1991)
85. E Nishibori, M Takata, M Sakata, M Inakuma, H Shinohara *Chem. Phys. Lett.* **298** 79 (1998)
86. M V Korobov, A L Mirakian, N V Avramenko, E F Valeev, I S Neretin, Y L Slovokhotov, A L Smith, G Oloffson, R S Ruoff *J. Phys. Chem. B* **102** 3712 (1998)
87. J D Crane, P B Hitchcock, H W Kroto, R Taylor, D R M Walton *J. Chem. Soc., Chem. Commun.* 1764 (1992)
88. D V Konarev, E F Valeev, Y L Slovokhotov, R N Lyubovskaya *J. Phys. Chem. Solids* **58** 1865 (1997)
89. R A Assink, J E Schirber, D A Loy, B Morosin, G A Carlson *J. Mater. Res.* **7** 2136 (1992)
90. L I Buravov, O A D'yachenko, S V Konovalikhin, N D Kushch, I P Lavrent'ev, N G Spitsyna, G V Shilov, E B Yagubskii *Izv. Akad. Nauk, Ser. Khim.* 262 (1994) [b]
91. S V Konovalikhin, O A D'yachenko, G V Shilov, N G Spitsyna, K V Van, E B Yagubskii *Izv. Akad. Nauk, Ser. Khim.* 1480 (1997) [b]
92. D V Konarev, E F Valeev, Y L Slovokhotov, Y M Shul'ga, R N Lyubovskaya *J. Chem. Res.* **442** 2647 (1997)
93. D V Konarev, I S Neretin, Y L Slovokhotov, E I Yudanova, N V Drichko, Y M Shul'ga, B P Tarasov, L L Gumanov, A S Batsanov, J A K Howard, R N Lyubovskaya *Chem. Eur. J.* **7** 2605 (2001)
94. J L Atwood, M J Barnes, M G Gardiner, C L Raston *J. Chem. Soc., Chem. Commun.* 1449 (1996)
95. A Izuoka, T Tachikawa, T Sugawara, Y Suzuki, M Konno, Y Saito, H Shinohara *J. Chem. Soc., Chem. Commun.* 1472 (1992)
96. O Ermer, C Robke *J. Am. Chem. Soc.* **115** 10 077 (1993)
97. S I Troyanov, E Kemnits *Zh. Neorg. Khim.* **46** 1704 (2001) [c]
98. M M Olmstead, A S Ginwalla, B C Noll, D S Tinti, A L Balch *J. Am. Chem. Soc.* **118** 7737 (1996)
99. M M Olmstead, K Maitra, A L Balch *Angew. Chem., Int. Ed.* **38** 231 (1999)

100. D Konarev, V Semkin, R Lyubovskaya, A Graja *Synth. Met.* **88** 225 (1997)
101. D V Konarev, A Y Kovalevsky, P Coppens, R N Lyubovskaya *Chem. Commun.* 2357 (2000)
102. A Otsuka, G Saito, A A Zakhidov, K Yakushi *Synth. Met.* **85** 1459 (1997)
103. E M Veen, P M Postma, H T Jonkman, A L Spek, B L Feringa *Chem. Commun.* 1709 (1999)
104. K Tashiro, T Aida, J-Y Zheng, K Kinbara, K Saigo, S Sakamoto, K Yamaguchi *J. Am. Chem. Soc.* **121** 9477 (1999)
105. J-Y Zheng, K Tashiro, Y Hirabayashi, K Kinbara, K Saigo, T Aida, S Sakamoto, K Yamaguchi *Angew. Chem., Int. Ed.* **40** 1858 (2001)
106. D Sun, F S Tham, C A Reed, L Chaker, M Burgess, P D W Boyd *J. Am. Chem. Soc.* **122** 10 704 (2000)
107. D R Evans, N L P Fackler, Z Xie, C E F Rickard, P D W Boyd, C A Reed *J. Am. Chem. Soc.* **121** 8466 (1999)
108. T Ishii, R Kanehama, N Aizawa, M Yamashita, H Matsuzaka, K Sugiura, H Miyasaka, T Kodama, K Kikuchi, I Ikemoto, H Tanaka, K Marumoto, S Kuroda *J. Chem. Soc., Dalton Trans.* 2975 (2001)
109. T Andersson, K Nilsson, M Sundahl, G Westman, O Wennerstrom *J. Chem. Soc., Chem. Commun.* 604 (1992)
110. I S Neretin, Y L Slovokhotov, in *IWFAC-2003 (Abstracts of Reports), St Petersburg, 2003* p. 37
111. A Marucci, P Launois, R Moret, A Penicaud *Eur. Phys. J. B* **26** 29 (2002)
112. A Penicaud, A Perez-Benitez, R V Gleason, E P Munoz, R Escudero *J. Am. Chem. Soc.* **115** 10 392 (1993)
113. K Himmel, M Jansen *Eur. J. Inorg. Chem.* 1183 (1998)
114. H Brumm, M Jansen *Z. Anorg. Allg. Chem.* **627** 1433 (2001)
115. K Himmel, M Jansen *Chem. Commun.* 1205 (1998)
116. C Janiak, S Muhle, H Hemling, K Kohler *Polyhedron* **15** 1559 (1996)
117. T F Fassler, A Spiekermann, M E Spahr, R Nesper *Angew. Chem., Int. Ed.* **36** 486 (1997)
118. C A Reed, R D Bolskar *Chem. Rev.* **100** 1075 (2000)
119. L Echegoyen, L E Echegoyen *Acc. Chem. Res.* **31** 593 (1998)
120. P M Allemand, K C Khemani, A Koch, F Wudl, K Holczer, S Donovan, G Gruner, J D Thompson *Science* **253** 301 (1991)
121. V Buntar, H W Weber, M Ricco *Solid State Commun.* **98** 175 (1995)
122. P Paul, Z Xie, R Bau, P D W Boyd, C A Reed *J. Am. Chem. Soc.* **116** 4145 (1994)
123. A M Panich, H M Vieth, P K Ummat, W R Datars *Physica B* **327** 102 (2003)
124. S E Canton, A J Yencha, E Kukk, J D Bozek, M C A Lopes, G Snell, N Berrah *Phys. Rev. Lett.* **89** 045502 (2002)
125. Q Zhu, O Zhou, J E Fischer, A R McGhie, W J Romanow, R M Strongin, M A Cichy, A B Smith *Phys. Rev. B* **47** 13948 (1993)
126. P W Stephens, L Mihaly, P L Lee, R L Whetten, S M Huang, R Kaner, F Deiderich, K Holczer *Nature (London)* **351** 632 (1991)
127. O Zhou, J E Fischer, N Coustel, S Kycia, Q Zhu, A R McGhie, W J Romanow, J P M Junior, A B Smith, D E Cox *Nature (London)* **351** 462 (1991)
128. R M Fleming, M J Rosseinsky, A P Ramirez, D W Murphy, J C Tully, R C Haddon, T Siegrist, R Tycko, S H Glarum, P Marsh, G Dabbagh, S M Zahurak, A V Makhija, C Hampton *Nature (London)* **352** 701 (1991)
129. T Shiroka, M Ricco, F Barbieri, E Zannoni, M Tomaselli *Phys. Solid State* **44** 498 (2002)
130. A F Hebard, M J Rosseinsky, R C Haddon, D W Murphy, S H Glarum, T T M Palstra, A P Ramirez, A R Kortan *Nature (London)* **350** 600 (1991)
131. R M Fleming, A P Ramirez, M J Rosseinsky, D W Murphy, R C Haddon, S M Zahurak, A V Makhija *Nature (London)* **352** 787 (1991)
132. K Tanigaki, T W Ebbesen, S Saito, J Mizuki, J S Tsai, Y Kubo, S Kuroshima *Nature (London)* **352** 222 (1991)
133. Z Iqbal, R H Baughman, B L Ramakrishna, S Khare, N S Murthy, H J Bornemann, D E Morris *Science* **254** 826 (1991)
134. J H Schön, C Kloc, B Batlogg *Science* **293** 2432 (2001)
135. M Beasley, H Kroemer, H Kogelnik, D Monroe, S Datta *Report of the Investigation Committee on the Possibility of Scientific Misconduct in the Work of Hendrik Schön and coauthors*. Lucent Technologies http://www.lucent.com/press/0902/020925.bla.html
136. K Tanigaki, I Hirosawa, T Manako, J S Tsai, J Mizuki, T W Ebbesen *Phys. Rev. B* **49** 12307 (1994)
137. T Yildirim, L Barbedette, J E Fischer, G M Bendele, P W Stephens, C L Lin, C Goze, F Rachdi, J Robert, P Petit, T T M Palstra *Phys. Rev. B* **54** 11981 (1996)
138. S Margadonna, E Aslanis, W Z Li, K Prassides, A N Fitch, T C Hansen *Chem. Mater.* **12** 2736 (2000)
139. A R Kortan, N Kopylov, S Glarum, E M Gyorgy, A P Ramirez, R M Fleming, F A Thiel, R C Haddon *Nature (London)* **355** 529 (1992)
140. A R Kortan, N Kopylov, S Glarum, E M Gyorgy, A P Ramirez, R M Fleming, O Zhou, F A Thiel, P L Trevor, R C Haddon *Nature (London)* **360** 566 (1992)
141. E Ozdas, A R Kortan, N Kopylov, A P Ramirez, T Siegrist, K M Rabe, H E Bair, S Schuppler, P H Citrin *Nature (London)* **375** 126 (1995)
142. D Claves, Y Ksari-Habiles, G Chouteau, P Touzain *Solid State Commun.* **106** 431 (1998)
143. D Claves, A Hamwi *Solid State Commun.* **113** 357 (1999)
144. Z Sun, X H Chen, T Takenobu, Y Iwasa *J. Phys.: Condens. Matter* **12** 8919 (2000)
145. J Arvanitidis, K Papagelis, S Margadonna, K Prassides, A Fitch *Nature (London)* **425** 599 (2003)
146. H Nagashima, Y Kato, H Yamaguchi, E Kimura, T Kawanishi, M Kato, Y Saito, M Haga, K Itoh *Chem. Lett.* 1207 (1994)
147. H Nagashima, A Nakaoka, Y Saito, M Kato, T Kawanishi, K Itoh *J. Chem. Soc., Chem. Commun.* 377 (1992)
148. V A Chernov, V N Ivanova, A N Kozhevnikova, G A Mardezhova, S G Nikitenko, A A Nikiforov *Nucl. Instrum. Methods Phys. Res., Sect. A* **359** 250 (1995)
149. V N Ivanova *Zh. Strukt. Khim.* **41** 164 (2000) [d]
150. M Knupfer, D M Poirier, J H Weaver *Phys. Rev. B* **49** 8464 (1994)
151. M S Denning, I D Watts, S M Moussa, P Durand, M J Rosseinsky, K Tanigaki *J. Am. Chem. Soc.* **124** 5570 (2002)
152. X H Chen, D H Chi, Z Sun, T Takenobu, Z S Liu, Y Iwasa *J. Am. Chem. Soc.* **122** 5729 (2000)
153. M S Denning, T J S Dennis, M J Rosseinsky, H Shinohara *Chem. Mater.* **13** 4753 (2001)
154. G-W Wang, K Komatsu, Y Murata, M Shiro *Nature (London)* **387** 583 (1997)
155. D V Konarev, S S Khasanov, I I Vorontsov, G Saito, M Y Antipin, A Otsuka, R N Lyubovskaya *Chem. Commun.* 2548 (2002)
156. Y Iwasa, K Tanoue, T Mitani, A Izuoka, T Sugawara, T Yagi *Chem. Commun.* 1411 (1998)
157. M Kunitake, S Uemura, O Ito, K Fujiwara, Y Murata, K Komatsu *Angew. Chem., Int. Ed.* **41** 969 (2002)
158. K Komatsu, K Fujiwara, Y Murata *Chem. Commun.* 1583 (2000)
159. V A Davydov, L S Kashevarova, A V Rakhmanina, A V Dzyabchenko, V Agafonov, P.Dubois, R Ceolin, H Szwarc *JETP Lett.* **66** 120 (1997)
160. X Chen, S Yamanaka, K Sako, Y Inoue, M Yasukawa *Chem. Phys. Lett.* **356** 291 (2002)
161. V A Davydov, L S Kashevarova, A V Rakhmanina, V Agafonov, H Allouchi, R Ceolin, A V Dzyabchenko, V M Senyavin, H Szwarc *Phys. Rev. B* **58** 14786 (1998)
162. X A Chen, S Yamanaka *Chem. Phys. Lett.* **360** 501 (2002)
163. B Narymbetov, V Agafonov, V A Davydov, L S Kashevarova, A V Rakhmanina, A V Dzyabchenko, V I Kulakov, R Ceolin *Chem. Phys. Lett.* **367** 157 (2003)
164. L A Chernozatonskii, N R Serebryanaya, B N Mavrin *Chem. Phys. Lett.* **316** 199 (2000)

165. L Marques, J L Hodeau, M Nunez-Regueiro, M Perroux *Phys. Rev B* **54** 12633 (1996)
166. S Margadonna, C M Brown, A Lappas, K Prassides, K Tanigaki, K D Knudsen, T L Bihan, M Mezouar *J. Solid State Chem.* **145** 471 (1999)
167. P W Stephens, G Bortel, G Faigel, M Tegze, A Janossy, S Pekker, G Oszlanyi, L Forro *Nature (London)* **370** 636 (2001)
168. D V Konarev, S S Khasanov, A Otsuka, G Saito *J. Am. Chem. Soc.* **124** 8520 (2002)
169. W E Broderick, K W Choi, W C Wan *Proc.-Electrochem. Soc.* **97** 1102 (1997)
170. A Honnerscheid, R E Dinnebier, M Jansen *Acta Crystallogr., Sect. B* **58** 482 (2002)
171. A V Soldatov, G Roth, A Dzyabchenko, D Johnels, S Lebedkin, C Meingast, B Sundqvist, M Haluska, H Kuzmany *Science* **293** 680 (2001)
172. U Wedig, H Brumm, M Jansen *Chem. Eur. J.* **8** (12) 2769 (2002)
173. K Balasubramanian *Chem. Phys. Lett.* **182** 257 (1991)
174. G B M Vaughan, P A Heiney, D E Cox, A R McGhie, D R Jones, R M Strongin, M A Cichy, A B Smith *Chem. Phys.* **168** 185 (1992)
175. W Bensch, H Werner, H Bartl, R Schlogl *J. Chem. Soc., Faraday Trans.* **90** 2791 (1994)
176. A L Balch, D A Costa, J W Lee, B C Noll, M M Olmstead *Inorg. Chem.* **33** 2071 (1994)
177. A L Balch, D A Costa, B C Noll, M M Olmstead *J. Am. Chem. Soc.* **117** 8926 (1995)
178. A L Balch, D A Costa, M M Olmstead *J. Chem. Soc., Chem. Commun.* 2449 (1996)
179. R Bini, J Ebenhoch, M Fanti, P W Fowler, S Leach, G Orlandi, C Ruchardt, J P B Sandall, F Zerbetto *Chem. Phys.* **232** 75 (1998)
180. J Nossal, R K Saini, A K Sadana, H F Bettinger, L B Alemany, G E Scuseria, W E Billups, M Saunders, A Khong, R Weisemann *J. Am. Chem. Soc.* **123** 8482 (2002)
181. A D Darwish, A G Avent, R Taylor, D R M Walton *J. Chem. Soc., Perkin Trans. 2* 2051 (1996)
182. O V Boltalina, M Buhl, A Khong, M Saunders, J M Street, R Taylor *J. Chem. Soc., Perkin Trans. 2* 1475 (1999)
183. L E Hall, D R McKenzie, M I Attalla, A M Vassallo, R L Davis, J B Dunlop, D J H Cockayne *J. Phys. Chem. B* **97** 5741 (1993)
184. Q Zhu, D E Cox, J E Fischer, K Kniaz, A R McGhie, O Zhou *Nature (London)* **355** 712 (1992)
185. P R Birkett, C Christides, P B Hitchcock, H W Kroto, K Prassides, R Taylor, D R M Walton *J. Chem. Soc., Perkin Trans. 2* 1407 (1993)
186. O V Boltalina, A Y Lukonin, J M Street, R Taylor *Chem. Commun.* 1601 (2000)
187. H Selig, C Lifshitz, T Peres, J E Fischer, A R McGhie, W J Romanow, J P McCauley, A B Smith *J. Am. Chem. Soc.* **113** 5475 (1991)
188. R Taylor *J. Fluorine Chem.* **125** 359 (2004)
189. I S Neretin, K A Lyssenko, M Y Antipin, Y L Slovokhotov, O V Boltalina, P A Troshin, A Y Lukonin, L N Sidorov, R Taylor *Angew. Chem., Int. Ed.* **39** 3273 (2000)
190. I V Goldt, O V Boltalina, L N Sidorov, E Kemnitz, S I Troyanov *Solid State Sci.* **4** 1395 (2002)
191. O V Boltalina, B de La Vaissiere, P W Fowler, P B Hitchcock, J P B Sandall, P A Troshin, R Taylor *Chem. Commun.* 1325 (2000)
192. O V Boltalina, P B Hitchcock, P A Troshin, J M Street, R Taylor *J. Chem. Soc., Perkin Trans. 2* 2410 (2000)
193. P B Hitchcock, R Taylor *Chem. Commun.* 2078 (2002)
194. A G Avent, B W Clare, P B Hitchcock, D L Kepert, R Taylor *Chem. Commun.* 2370 (2002)
195. S I Troyanov, P A Troshin, O V Boltalina, I N Ioffe, L N Sidorov, E Kemnitz *Angew. Chem., Int. Ed.* **40** 2285 (2001)
196. I S Neretin, K A Lysenko, M Yu Antipin, Yu L Slovokhotov *Izv. Akad. Nauk, Ser. Khim.* 695 (2002) [b]
197. O V Boltalina, J M Street, R Taylor *Chem. Commun.* 1827 (1998)
198. X W Wei, A D Darwish, O V Boltalina, P B Hitchcock, J M Street, R Taylor *Angew. Chem., Int. Ed.* **40** 2989 (2001)
199. O V Boltalina, V Y Markov, P A Troshin, A D Darwish, J M Street, R Taylor *Angew. Chem., Int. Ed.* **40** 787 (2001)
200. A A Tuinman, A A Gakh, J L Adcock, R N Compton *J. Am. Chem. Soc.* **115** 5885 (1993)
201. G Olah, I Bucsi, C Lambert, R Aniszfield, N J Trivedi, D K Sensharma, G K S Prakash *J. Am. Chem. Soc.* **113** 9385 (1991)
202. P R Birkett, A G Avent, A D Darwish, H W Kroto, R Taylor, D R M Walton *J. Chem. Soc., Chem. Commun.* 1230 (1993)
203. H Al-Matar, A K Abdul-Sada, A G Avent, P W Fowler, P B Hitchcock, K M Rogers, R Taylor *J. Chem. Soc., Perkin Trans. 2* 53 (2002)
204. H Al-Matar, P B Hitchcock, A G Avent, R Taylor *Chem. Commun.* 1071 (2000)
205. P R Birkett, A G Avent, A D Darwish, H W Kroto, R Taylor, D R M Walton *J. Chem. Soc., Perkin Trans. 2* **3** 457 (1997)
206. P R Birkett, R Taylor, N K Wachter, M Carano, F Paolucci, S Roffia, F Zerbetto *J. Am. Chem. Soc.* **122** 4209 (2000)
207. A D Darwish, A G Avent, A K Abdul-Sada, R Taylor *Chem. Commun.* 1374 (2003)
208. A A Tuinman, P Mukherjee, J L Adcock, R L Hettich, R N Compton *J. Phys. Chem. B* **96** 7584 (1992)
209. P R Birkett, A G Avent, A D Darwish, H W Kroto, R Taylor, D R M Walton *J. Chem. Soc., Chem. Commun.* 683 (1995)
210. A D Darwish, P de Guio, R Taylor *Fullerenes, Nanotubes, Carbon Nanostruct.* **10** 261 (2002)
211. G Waidmann, M Jansen *Z. Anorg. Allg. Chem.* **623** 623 (1997)
212. S I Troyanov, E Kemnitz *Eur. J. Org. Chem.* 3916 (2003)
213. I Lamparth, C Maichle-Mossmer, A Hirsch *Angew. Chem., Int. Ed. Engl.* **34** 1607 (1995)
214. G Schick, M Levitus, L Kvetko, B A Johnson, I Lamparth, R Lunkwitz, B Ma, S I Khan, M A Garcia-Garibay, Y Rubin *J. Am. Chem. Soc.* **121** 3246 (1999)
215. A F Kiely, R C Haddon, M S Meier, J P Selegue, C P Brock, B O Patrick, G-W Wang, Y Chen *J. Am. Chem. Soc.* **121** 7971 (1999)
216. P Seiler, A Herrmann, F Diederich *Helv. Chim. Acta* **78** 344 (1995)
217. J M Hawkins, A Meyer, T A Lewis, S Loren, F J Hollander *Science* **252** 312 (1991)
218. M D Westmeyer, T B Rauchfuss, A K Verma *Inorg. Chem.* **35** 7140 (1996)
219. P Timmerman, H L Anderson, R Faust, J F Nierengarten, T Habicher, P Seiler, F Diederich *Tetrahedron* **52** 4925 (1996)
220. K Fujiwara, K Komatsu *Chem. Commun.* 1986 (2001)
221. T Habicher, J F Nierengarten, V Gramlich, F Diederich *Angew. Chem., Int. Ed.* **37** 1916 (1998)
222. H Isobe, A Ohbayashi, M Sawamura, E Nakamura *J. Am. Chem. Soc.* **122** 2669 (2000)
223. Y Rubin, T Jarrosson, G W Wang, M D Bartberger, K N Houk, G Schick, M Saunders, R J Cross *Angew. Chem., Int. Ed.* **40** 1543 (2001)
224. M J Arce, A L Viado, Y-Z An, S I Khan, Y Rubin *J. Am. Chem. Soc.* **118** 3775 (1996)
225. E F Paulus, C Bingel *Acta Crystallogr., Sect. C* **51** 143 (1995)
226. H Irngartinger, A Weber, T Escher *Liebigs Ann. Chem.* 1845 (1996)
227. P J Fagan, J C Calabrese, B Malone *J. Am. Chem. Soc.* **113** 9408 (1991)
228. M P Gomez-Sal, B F G Johnson, J Lewis, P R Raithby, A H Wright *J. Chem. Soc., Chem. Commun.* 1682 (1985)
229. H Song, K Lee, J T Park, M-G Choi *Organometallics* **17** 4477 (1998)
230. J T Park, H Song, J-J Cho, M-K Chung, J-H Lee, I-H Suh *Organometallics* **17** 227 (1998)
231. H Song, K Lee, M-G Choi, J T Park *Organometallics* **21** 1756 (2002)
232. K Lee, H Song, B Kim, J T Park, S Park, M-G Choi *J. Am. Chem. Soc.* **124** 2872 (2002)
233. X Jin, X Xie, K Tang *Chem. Commun.* 750 (2002)
234. A L Balch, V J Catalano, J W Lee *Inorg. Chem.* **30** 3980 (1991)
235. A L Balch, J W Lee, B C Noll, M M Olmstead *J. Am. Chem. Soc.* **114** 10984 (1992)

236. A L Balch, V J Catalano, J W Lee, M M Olmstead, S R Parkin *J. Am. Chem. Soc.* **113** 8953 (1991)
237. A L Balch, J W Lee, M M Olmstead *Angew. Chem., Int. Ed. Engl.* **31** 1356 (1992)
238. M Sawamura, H Iikura, E Nakamura *J. Am. Chem. Soc.* **118** 12 850 (1996)
239. M Sawamura, Y Kuninobu, E Nakamura *J. Am. Chem. Soc.* **122** 12 407 (2000)
240. M Sawamura, H Iikura, A Hirai, E Nakamura *J. Am. Chem. Soc.* **120** 8285 (1998)
241. H Shinohara *Rep. Prog. Phys.* **63** 843 (2000)
242. J Heath, S C O'Brien, Q Zhang, Y Liu, R F Curl, H W Kroto, F K Tittel, R E Smalley *J. Am. Chem. Soc.* **107** 7779 (1985)
243. Y Chai, T Guo, C Jin, R E Haufler, L P F Chibante, J Fure, L Wang, J M Alford, R E Smalley *J. Phys. Chem. B* **95** 7564 (1991)
244. M Saunders, R J Cross, H A Jimenez-Vazquez, R Shimshi, A Khong *Science* **271** 1693 (1996)
245. E Shabtai, A Weitz, R C Haddon, R E Hoffman, M Rabinovitz, A Khong, R J Cross, M Saunders, P C Cheng, L T Scott *J. Am. Chem. Soc.* **120** 6389 (1998)
246. M S Syamala, R J Cross, M Saunders *J. Am. Chem. Soc.* **124** 6216 (2002)
247. A Khong, H A Jimenez-Vazquez, M Saunders, R J Cross, J Laskin, T Peres, C Lifshitz, R Strongin, A B Smith *J. Am. Chem. Soc.* **120** 6380 (1998)
248. J Laskin, T Peres, C Lifshitz, M Saunders, R J Cross, A Khong *Chem. Phys. Lett.* **285** 7 (1998)
249. H M Lee, M M Olmstead, T Suetsuna, H Shimotani, N Dragoe, R J Cross, K Kitazawa, A L Balch *Chem. Commun.* 1352 (2002)
250. E E B Campbell, R Tellgmann, N Krawez, I V Hertel *J. Phys. Chem. Solids* **58** 1763 (1997)
251. A Weidinger, M Waiblinger, B Pietzak, T A Murphy *Appl. Phys. A* **66** 287 (1998)
252. C Knapp, N Weiden, K Kass, K P Dinse, B Pietzak, M Waiblinger, A Weidinger *Mol. Phys.* **95** 999 (1998)
253. H Shinohara, in *Fullerenes: Chemistry, Physics and Technology* (Eds K M Kadish, R S Ruoff) (New York: Wiley, 2000) p. 357
254. K Yamamoto, H Funasaka, T Takahashi, T Akasaka, T Suzuki, Y Maruyama *J. Phys. Chem. B* **98** 12831 (1994)
255. T Akasaka, S Okubo, M Kondo, Y Maeda, T Wakahara, T Kato, T Suzuki, K Yamamoto, K Kobayashi, S Nagase *Chem. Phys. Lett.* **319** 153 (2000)
256. K Kikuchi, K Akiyama, K Sakaguchi, T Kodama, H Nishikawa, I Ikemoto, T Ishigaki, Y Achiba, K Sueki, H Nakahara *Chem. Phys. Lett.* **319** 472 (2000)
257. K Kobayashi, S Nagase *Chem. Phys. Lett.* **313** 45 (1999)
258. K Kobayashi, S Nagase *Chem. Phys. Lett.* **282** 325 (1998)
259. T J S Dennis, H Shinohara *Appl. Phys. A* **66** 243 (1998)
260. S Iida, Y Kubozono, Y Slovokhotov, Y Takabayashi, T Kanbara, T Fukunaga, S Fujiki, S Emura, S Kashino *Chem. Phys. Lett.* **338** 21 (2001)
261. C H Park, B O Wells, J DiCarlo, Z X Shen, J R Salem, D S Bethune, C S Yannoni, R D Johnson, M S de Vries, C Booth, F Bridges, P Pianetta *Chem. Phys. Lett.* **213** 196 (1993)
262. M Nomura, Y Nakao, K Kikuchi, Y Achiba *Physica B* **208/209** 539 (1995)
263. H Giefers, F Nessel, S I Gyory, M Stecker, G Wortmann, Y S Grushko, E G Alekseev, V S Kozlov *Carbon* **37** 721 (1999)
264. Y Kubozono, T Inoue, Y Takabayashi, S Fujiki, S Kashino, T Akasaka, T Wakahara, M Inakuma, H Kato, T Sigai, H Shinohara, S Emura *J. Synchrotron Radiat.* **8** 551 (2001)
265. K Akiyama, K Sueki, H Haba, K Tsukada, M Asai, T Yaita, Y Nagame, K Kikuchi, M Katada, H Nakahara *J. Radioanal. Nucl. Chem.* **255** 155 (2003)
266. E Nishibori, M Takata, M Sakata, H Tanaka, M Hasegawa, H Shinohara *Chem. Phys. Lett.* **330** 497 (2000)
267. M Takata, B Umeda, E Nishibori, M Sakata, Y Saito, M Ohno, H Shinohara *Nature (London)* **377** 46 (1995)
268. M Takata, E Nishibori, B Umeda, M Sakata, E Yamamoto, H Shinohara *Phys. Rev. Lett.* **78** 3330 (1997)
269. E Nishibori, M Takata, M Sakata, A Taninaka, H Shinohara *Angew. Chem., Int. Ed.* **40** 2998 (2001)
270. M Takata, E Nishibori, M Sakata, M Inakuma, E Yamamoto, H Shinohara *Phys. Rev. Lett.* **83** 2214 (1999)
271. C R Wang, T Kai, T Tomiyama, T Yoshida, Y Kobayashi, E Nishibori, M Takata, M Sakata, H Shinohara *Angew. Chem., Int. Ed.* **40** 397 (2001)
272. B F Ormont, in *Struktury Neorganicheskikh Veshchestv* (Structures of Inorganic Compounds) (Moscow, Leningrad: GITTL, 1950) p. 278
273. S Stevenson, G Rice, T Glass, K Harich, F Cromer, M R Jordan, J Craft, E Hadju, R Bible, M M Olmstead, K Maitra, A J Fisher, A L Balch, H C Dorn *Nature (London)* **401** 55 (1999)
274. M M Olmstead, A de Bettencourt-Dias, J C Duchamp, S Stevenson, H C Dorn, A L Balch *J. Am. Chem. Soc.* **122** 12 220 (2000)
275. M M Olmstead, A de Bettencourt-Dias, J C Duchamp, S Stevenson, D Marciu, H C Dorn, A L Balch *Angew. Chem., Int. Ed.* **40** 1223 (2001)
276. H M Lee, M M Olmstead, E Iezzi, J C Duchamp, H C Dorn, A L Balch *J. Am. Chem. Soc.* **124** 3494 (2002)
277. J M Campanera, C Bo, M M Olmstead, A L Balch, J M Poblet *J. Phys. Chem. A* **106** 12356 (2002)
278. M M Olmstead, A de Bettencourt-Dias, S Stevenson, H C Dorn, A L Balch *J. Am. Chem. Soc.* **124** 4172 (2002)
279. M M Olmstead, H M Lee, S Stevenson, H C Dorn, A L Balch *Chem. Commun.* 2688 (2002)
280. T Watanuki, A Fujuwara, I Ishii, Y Mashuoka, H Suematsu, K Ohwada, H Nakao, Y Fujii, T Kodama, K Kikuchi, Y Achiba, in *Electronic Properties of Novel Materials — Science and Technology of Molecular Nanostructures (Proceedings of Conference)* (Eds H Kuzmany, J Fink, M Mehring, S Roth) (Melville, NY: American Institute of Physics, 1999) P. 124
281. C J Nuttall, Y Inada, K Nagai, Y Iwasa *Phys. Rev. B* **62** 8592 (2000)
282. S G Buga, V D Blank, B A Kulnitskiy, N R Serebryanaya, M Klaeser, G Liu, S Lebedkin *Synth. Met.* **121** 1093 (2001)

[a] — *Dokl. Chem. (Engl. Transl.)*
[b] — *Russ. Chem. Bull., Int. Ed. (Engl. Transl.)*
[c] — *Russ. J. Inorg. Chem. (Engl. Transl.)*
[d] — *J. Stryct. Chem. (Engl. Transl.)*

Russian Chemical Reviews **73** (5) 487 – 500 (2004) © 2004 Russian Academy of Sciences and Turpion Ltd

DOI 10.1070/RC2004v073n05ABEH000884

Trends in the development of polycondensation and condensation polymers

S V Vinogradova, V A Vasnev

Contents

I.	Introduction	487
II.	Novel types of polycondensation	487
III.	Macromolecular design of condensation polymers	491
IV.	Conclusion	497

Abstract. New trends in the development of polycondensation methods, elucidation of the main principles of macromolecular design of polymeric chains and preparation of novel promising condensation polymers are considered and analysed. The bibliography includes 152 references.

I. Introduction

Polycondensation is one of the most important methods for the synthesis of polymers. This is based on an elementary substitution reaction and opens up access to an immense variety of polymers — from linear aliphatic compounds to complex fused aromatic and heterocyclic systems including highly branched dendritic polymers.

Starting from 1833,[1] polycondensation has invariably attracted the keen attention of investigators. At present, this branch of polymer chemistry is being intensely developed owing to the discovery of hitherto unknown reactions leading to the formation of high-molecular-mass compounds. However, a search for alternative polycondensation routes and their intensification, elaboration of principles of macromolecular design, preparation of novel promising polymeric materials and detailed analysis of their properties still remain topical problems. These trends are considered in the present review.

II. Novel types of polycondensation

Studies aimed at the search for ways of involvement of less reactive starting compounds and new types of monomers in known polycondensation processes have been carried out since the 1980 – 1990's. These processes include carbonylation polycondensation,[2–12] polycondensation of monomers that undergo ring–chain isomerisation,[13–19] polynitrosubstitution,[20–22] radical-ion polycondensation in the presence of samarium iodide,[23–29] catalytic polycondensation of arylene halides, [30–43] *etc*. Some of these processes will be considered in the subsequent sections.

S V Vinogradova, V A Vasnev A N Nesmeyanov Institute of Organoelement Compounds, Russian Academy of Sciences, ul. Vavilova 28, 119991 Moscow, Russian Federation. Fax (7-095) 135 50 85. Tel. (7-095) 135 92 25 (S V Vinogradova), (7-095) 135 92 12. E-mail: vasnev@ineos.ac.ru (V A Vasnev)

Received 24 November 2003
Uspekhi Khimii **73** (5) 526 – 541 (2004); translated by R L Birnova

1. Carbonylation polycondensation

The recently discovered carbonylation polycondensation reaction [2–12] is based on the use of carbon monoxide and aromatic dihalogen derivatives instead of conventionally employed dicarboxylic acids or their activated derivatives (most commonly, dichlorides). These compounds react with dinucleophiles (*e.g.*, diamines, dihydrazides, diphenols, aminophenols, *etc*.) in the presence of palladium catalysts to yield the corresponding high-molecular-mass products, *viz*., polyamides, polyhydrazides, polyarylates, *etc*. This approach to the synthesis of polymers directly from CO and aryl halides is attractive, since the latter are readily available by direct halogenation of aromatic compounds and are rather stable, and carbon monoxide is very cheap. In contrast, aromatic dicarboxylic acid chlorides are hydrolytically unstable and the acids themselves are synthesised in many steps. This approach was used in the synthesis of, *e.g.*, polyamides (Scheme 1).

Scheme 1

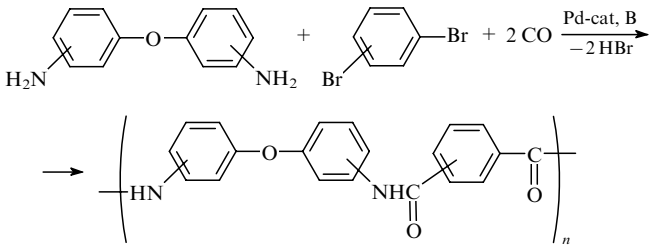

B is a base.

Carbonylation polycondensation was used in the synthesis of aromatic, aliphatic-aromatic and silicon-containing polyamides. Using polycondensation of *m*-dibromobenzene, 4,4′-diaminodiphenyl oxide and CO as an example, it was shown that the best results were obtained if the reaction was carried out in *N*,*N*-dimethylacetamide (DMA) (115 °C, 1.5 h) using the $[PdCl_2(Ph_3P)_2]-Ph_3P$ complex as a catalyst and 1,8-diazabicyclo[5.4.0]undec-7-ene (DBU) as a base.[4] The reaction rate and the length of the polymeric chain increase if diiodoarenes are used instead of dibromides.[5] Thus the polycondensation of *m*-diiodobenzene with 4,4′-diaminodiphenyl oxide at a CO pressure of 0.1 MPa yields a polyamide with a molecular mass (*M*) of 24 000 at 90 °C in 2 h, whereas the molecular mass of a polymer prepared from *m*-dibromobenzene does not exceed 14 000 after 6 h. Moreover, the molecular mass of the polymer formed is even higher (up to 91 000 kDa) if the reaction is carried out in the presence of a 5% excess of the diamine.

Carbonylation polycondensation was used in the synthesis of polyarylates and aliphatic-aromatic polyesters.[4–6] In the former case, the solutions of the polymers formed had a logarithmic viscosity of up to 0.69 dl g^{-1} in *o*-chlorophenol, in the latter case, the viscosity was 0.18–0.36 dl g^{-1} (see Refs 6 and 7). The polycondensation of 4,4′-dibromodiphenyl oxide with 2,2-bis(4-hydroxyphenyl)propane in an atmosphere of CO in chlorobenzene as a solvent was carried out at 115 °C using a DBU–K_2CO_3 mixture as a base and various palladium derivatives {*e.g.*, the $[PdCl_2(Ph_3P)_2]$–PPh_3 complex} as catalysts and was complete within 3 h. The M_n and M_w values for the polyacrylate were equal to 70 000 and 88 000, respectively; the logarithmic viscosity (η_{log}) in chlorobenzene was 0.51 dl g^{-1}.

The best results in the synthesis of polyhydrazides from dibromoarenes, dicarbohydrazides and CO were obtained when the polycondensation was performed in DMSO or DMF (T = 95 °C) in the presence of $Pd(Ph_3P)_4$ and DBU.[8] A polymer with η_{log} = 0.65 dl g^{-1} was prepared starting from 4,4′-dibromodiphenyl oxide, CO and terephthalohydrazide.[8]

High-molecular-mass polyether ketoamides were synthesised using Pd-catalysed polycondensation of dibromoarenes containing etheroxo groups with aromatic diamines and CO.[9] Reactions of diiodoarenes with bis(*o*-aminophenols) and CO yield polyhydroxyamides with molecular masses M_w = 34 000–49 000 and M_n = 13 000–31 000; their thermal polycyclisation (T = 250–300 °C) gave the corresponding polybenzooxazoles.[10]

Tetraiodobenzene, tetraiodo-*p*-xylene, 3,3′,4,4′-tetraiododiphenyl sulfone and 1,4-dibromo-2,5-diiodobenzene were used as the halogen derivatives in the synthesis of polyimides.[4, 11] Thus a polyimide with M_w = 28 000 and M_n = 17 000 was synthesised in 95% yield from 1,2,4,5-tetraiodobenzene and 5-amino-3-(4-aminophenyl)-1,1,3-trimethylindane under CO pressure of 0.78 MPa in the presence of DBU, 6 mol.% of the complex $[PdCl_2(Ph_3P)_2]$ and 12 mol.% of triphenylphosphine (DMA, 115 °C, 24 h).
High-molecular-mass polyamidoimides were prepared from 4-chloro-*N*-(4-iodophenyl)phthalide, bis(aminophenyl) oxide and carbon monoxide using carbonylation polycondensation in DMA or *N*-methylpyrrolidone (*N*-MP) (T = 100 °C) in the presence of a palladium catalyst.[12]

However, the attempts to replace expensive palladium catalysts by nickel catalysts [2] were unsuccessful. Obviously, the search for inexpensive efficient catalytic systems for the carbonylation polycondensation is a problem for future studies.

Thus, carbonylation polycondensation opens up new prospects for the synthesis of diverse polymers. It may be hoped that in the near future it will be used not only for preparation of novel polymers, but also for optimisation of synthetic procedures.

2. Polycondensation of monomers that undergo ring–chain isomerisation

Electrophilic substitution of monomers that undergo ring-chain isomerisation (or tautomerisation) is a new approach to the synthesis of aromatic polymers. Carboxylic acid pseudochlorides are examples of such non-traditional monomers.

According to the scheme:

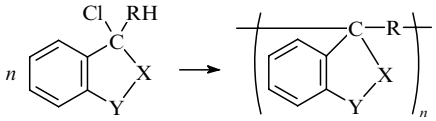

R is arylene; X = O, NAlk, NAr; Y = CO, SO_2

the growth of the polymeric chain results from the formation of a C–C bond between the carbon atoms of aromatic and heterocyclic (phthalide, phthalimidine and sulfophthalimide) nuclei. Such a polycondensation can be used for the preparation of polyarylenephthalides (X = O, Y = CO), polyarylenephthalimidines (X = NAr, Y = CO) and polyarylenesulfophthalides (X = O, Y = SO_2).

The synthesis of polyarylenephthalides from carboxylic acid pseudochlorides and their properties have been studied in much detail.[13–19]

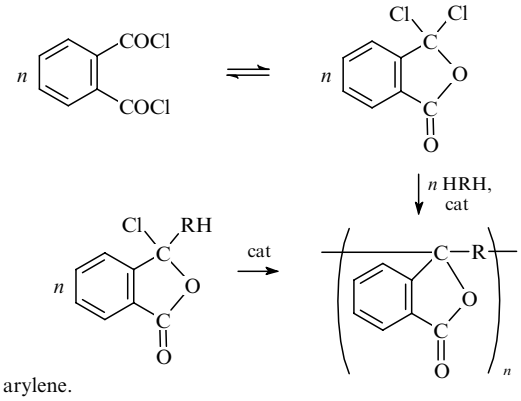

R is arylene.

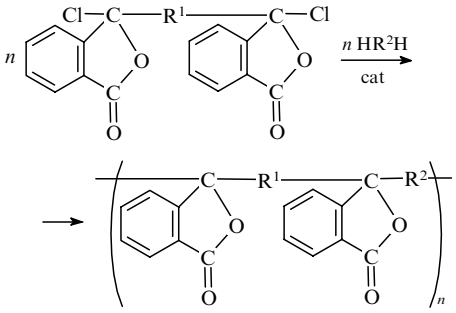

R^1,R^2 are arylenes.

Chlorinated hydrocarbons (dichloromethane, dichloroethane, *etc.*) or nitrobenzene were used as solvents; the latter proved to be the most versatile. The temperature was varied from 770 to 140 °C; metal halides (*e.g.*, $ZnCl_2$, $AlCl_3$, $AlBr_3$, $FeCl_3$, $InCl_3$, $SbCl_5$, *etc.*) (0.01–1.5 mol per chloride group) were used as catalysts.[13] For example, the reaction occurs selectively and yields a polymer with M = 46 000–60 000 under conditions that are optimum for the synthesis of poly-*p*-diphenylenephthalide from 4-(3-phthalyl-3-chloro)biphenyl (monomer concentrations, 2–3 mol $litre^{-1}$, $SbCl_5$ (7 mol.%–10 mol.%) or $InCl_3$ (3 mol.%–10 mol.%) as a catalyst, nitrobenzene, 100–110 °C. The same reaction was performed in the so-called 'precipitation system', *i.e.,* in the presence of $AlCl_3$ in dichloroethane (20 °C, 24 h).[15] In the early steps, this reaction occurs in a homogeneous medium and then the polymer formed is precipitated to give a product with a higher molecular mass.

The presence of reactive groups in polyarylenephthalides opens up broad prospects for further chemical modifications at the lactone ring. Thus reactions of these polymers with amines yield *N*-substituted polyarylenephthalimidines:[17, 18]

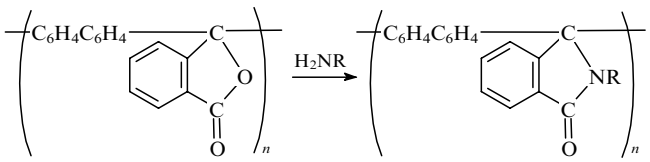

R = Me, Bu^n, C_8H_{17}, $C_{18}H_{37}$, Ph, C_2H_4OH, *etc.*

The properties of these compounds depend on the nature of the substituent at the nitrogen atom. With an increase in the length of the aliphatic substituent (from C_1 to C_{18}), the softening temperatures of the polymers decrease from 390 to 80 °C and the decomposition temperatures decrease from 360 to 260 °C. The possibility of thermal dehydration of polybiphenylene-*N*-(β-hydroxyethyl)phthalimidine, which yields an insoluble structurised polymer, has been demonstrated. A polymer which contains

phenyl substituents at the nitrogen atom manifests the best thermal characteristics: its softening temperature and the temperature of the onset of decomposition are equal to 450 and 475 °C, respectively. Thermolysis of polyterphenylenephthalide at 390–450 °C results not only in the cleavage of its polymeric chain but also in its structurisation.[16]

Polyarylenephthalimidines can also be synthesised by direct polycondensation of monomers of appropriate structures.

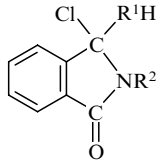

R^1 is arylene; R^2 = Alk, Ar.

It has been noted that, unlike the synthesis of polyarylenephthalides, the polycondensation in nitrobenzene cannot be realised with $SbCl_5$ and $InCl_3$ as catalysts. High-molecular-mass polyarylenephthalimidine could only be prepared in a reaction catalysed by $AlCl_3$ (2.5–3.5 equiv.).[18]

The synthesis of high-molecular-mass polyarylenesulfophthalides with phenylene fragments alternating with sulfophthalide groups in the main chains of the macromolecules has been carried out.[19] High reactivity of the sulfophthalide groups is a characteristic feature of these polymers. For example, the opening of the sulfophthalide ring under the action of aqueous solutions of alkalis results in quantitative formation of the corresponding polysulfonic acid salts. Such sulfonic acids can be regarded as a special type of polyelectrolyte, *viz*., aromatic polymers with side ionogenic sulfonate groups. In addition, the presence of triphenylmethane fragments determines the unusual optical properties of these compounds.[19]

Thus, the use of monomers of carboxylic acids of the pseudochloride type, which undergo ring-chain isomerisation, in the synthesis of polymers opens up attractive prospects for the development of novel polymers. The materials thus prepared combine high thermal and chemical stabilities with excellent solubilities in organic solvents, good physicomechanical characteristics and various unique properties.

Studies in this area were begun in the 1990's and are ongoing. They are aimed predominantly at the in-depth analysis of specific (thermal, electrical, optical, *etc*.) properties of these polymeric systems.

3. Radical-ion polycondensation in the presence of samarium iodide

The efficient syntheses of organic compounds using bivalent metal halides of the lanthanide family, which are known to be potent reductants, have been documented relatively recently.[23] The use of such compounds as reaction initiators and coreactants ensures highly selective reactions under mild conditions and at high rates. SmI_2, which possesses an unusually high redox potential (for compounds soluble in organic solvents) is the most reactive amongst bivalent lanthanide halides.

Thus α-diketones are synthesised from aromatic acid chlorides and SmI_2 within several minutes in THF at room temperature (yields 70%–80%).[24] The use of aromatic dicarboxylic chlorides in such reactions is a relatively simple route to the synthesis of poly-α-diketones.[25–27]

$$n\,\mathrm{ClOCArCOCl} + n\,\mathrm{SmI_2} \longrightarrow$$

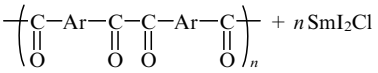

Ar = *m*-C_6H_4, *p*-C_6H_4, $C_6H_4OC_6H_4$, $C_6H_4C(CF_3)_2C_6H_4$, *etc*.

Based on the literature data of the mechanism of condensation of acid chlorides in the presence of SmI_2,[25] it may be supposed that it is radical ions generated under the action of compounds with high redox potentials that are the reactive species in the polycondensation. Their dissociation yields acyl radicals which are rapidly reduced into acyl anions; the latter react with the second acid chloride group to give α-diketone fragments:

$$\mathrm{a-A-a} + \mathrm{SmI_2} \longrightarrow [\mathrm{a-A-a}]^{\bullet -}\mathrm{SmI_2^+},$$

$$[\mathrm{a-A-a}]^{\bullet -}\mathrm{SmI_2^+} \longrightarrow [\mathrm{a-A-a}]^{\bullet -} + \mathrm{SmI_2^+},$$

$$[\mathrm{a-A-a}]^{\bullet -} \longrightarrow \mathrm{a-A^{\bullet}} + \mathrm{a^-},$$

$$\mathrm{a-A^{\bullet}} + \mathrm{a-A^{\bullet}} \longrightarrow \mathrm{a-A-A-a},$$

$$\mathrm{SmI_2^+} + \mathrm{a^-} \longrightarrow \mathrm{SmI_2a},$$

$$\mathrm{a-A^{\bullet}} + \mathrm{SmI_2} \longrightarrow \mathrm{a-A^-SmI_2^+},$$

$$\mathrm{a-A^-SmI_2^+} + \mathrm{a-A-a} \longrightarrow \mathrm{a-A-A-a} + \mathrm{SmI_2a}.$$

a = Cl, F; A = −C(O)ArC(O)−.

Thus, such a polycondensation can be termed as radical-ion polycondensation.

Studies of the pattern of this process have shown that the structures and yields of the polymers formed strongly depend on the reaction conditions, *viz*., the order of addition of the reagents, their ratios, concentrations and reaction time.[27] The units in these polymers often possess different structures; they contain hydroxymethylene groups along with α-diketone groups as a result of partial reduction of the carbonyl group by samarium iodide.

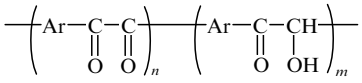

Polymers devoid of hydroxy ketone groups could be prepared only by adding a solution of SmI_2 in a THF–methyl iodide mixture to a solution of a dicarboxylic acid dichloride in THF (0.3–0.03 mol litre^{-1}, SmI_2 : substrate = 2.8 : 1.0, 30 °C, 20 min). The addition of a dicarboxylic acid dichloride to a solution of SmI_2 (4 : 1) yielded polymers with different-unit structures, the content of the diketone and hydroxyketone groups being the same.[27]

Radical-ion polycondensation in the presence of SmI_2 was also used in the synthesis of polypinacones from aromatic dialdehydes.[28]

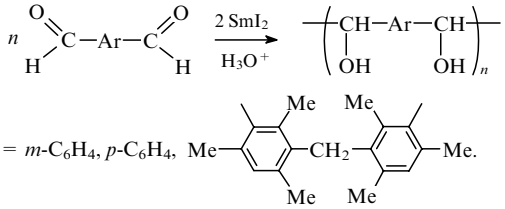

In this case, the polymers had relatively low molecular masses (12 000–15 000).

The presence of reactive functional groups, *viz*., keto and hydroxy groups, in poly-α-diketones and polypinacones, opens prospects for their further chemical modification. For example, zirconocene dichloride reacts with the hydroxy ketone groups of the polymer to form covalent bonds owing to the presence of the hydroxy groups and coordination compounds due to interaction with the keto groups. Such polymers hold promise as catalysts for certain organic reactions.[29]

4. Polycondensation with arylene halides catalysed by palladium and nickel complexes

Since the 1990's, the need for polymeric materials with specific properties, such as electroconductivity, photo- and electroluminescence, third-order nonlinear optical activity, *etc*., has stimu-

lated studies on polycondensation of aromatic dihalides with alkenes and alkynes, aromatic diboronic acids, aromatic organometallic compounds, *etc*. Dehydrohalogenation and dehalogenation reactions, which are catalysed by palladium and nickel complexes and result in the formation of the C–C bond, are usually referred to as cross-coupling reactions. They were used in the synthesis of polyaryleneethynylenes $(-Ar-C\equiv C-)_n$,[30–36,42] polyconjugated polyarylenevinylenes $(-Ar-CH=CH-)_n$[30,32,34,37–40] as well as carbo- and heterocyclic polyarylenes.[32,41]

The use of aromatic halides, which are much more accessible than the monomers used in conventional polycondensation processes, is the advantage of this method. As a rule, polyconjugated polymers are poorly soluble in organic solvents due to high rigidity of their macromolecules, which significantly restricts their practical applications. Pd- and Ni-catalysed polycondensation circumvents this limitation, since side substituents or bulky groups can easily be introduced into the starting aromatic halides or ethynyl derivatives, which favour their solubility.[30,33,34]

Thus relatively short-chain polyaryleneethynylenes (M = 5800–8000) readily soluble in amide solvents were prepared from dibromides and diiodides derived from branched aromatic heterocyclic compounds (hexa- and pentaphenylarylenes, compounds **1**), quinoxalines, compounds **2**, phenylimidazoles

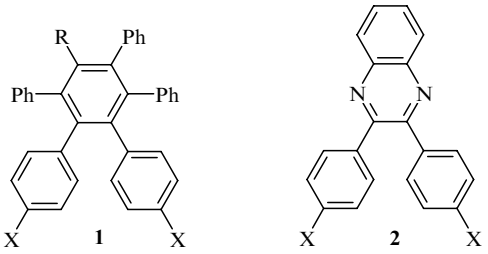

R = H, Ph (**1**); X = Br, I.

and diethynyl aromatic compounds in the presence of palladium catalysts (DMA, 90 °C, 6–8 h).[30,33]

Pd-Catalysed polycondensation was used in the synthesis of some novel regular polyaryleneethynylenes from dibromides and substituted diethynyloligothiophenes, -anthracenes and -benzenes. Such polymers (especially those containing anthracene fragments) are characterised by high quantum yields of luminescence.[31]

The synthesis of polyarylenevinylenes was carried out using ethylene and divinylbenzene as the starting monomers.[37,38]

The reaction of *p*-divinylbenzene with dialkoxy-substituted *p*-diiodobenzene derivatives gave polymers (M_w = 32 000–62 000) of the general formula

$$-\!\left(CH{=}CHC_6H_4CH{=}CHC_6H_2(OR)_2\right)_n-,$$

R = C_mH_{2m+1}, m = 4, 7, 8, 12, 16,

which are readily soluble in organic solvents and manifest liquid crystalline properties.[40]

Homopolycondensation of dibromotetraarylethylenes in the presence of a Ni(0) complex prepared *in situ* from anhydrous $NiCl_2$, Ph_3P, bipyridyl and Zn in a dipolar aprotic solvent (100 °C, 2 h) resulted in polyarylenevinylenes containing phenyl substituents in the vinylene group:[43]

$$-\!\left[C_6H_4C(Ar){=}C(Ar)C_6H_4\right]_n-,$$

Ar, phenyl; 2,4,6-triphenylphenyl; 2,4,6-tris(biphenylyl)phenyl.

Polymers that contain branched polyphenyl substituents usually possess fairly high quantum yields of luminescence (22%–23%).

A series of unsaturated polymers of the polycinnamide type

$$-\!\left(ArCH{=}CHCONHAr'NHCOCH{=}CH\right)_n-$$

have been synthesised[30] from aromatic *N*,*N*′-arylenediamides and arene dihalides in the presence of palladium catalysts. Thus a high-molecular-mass polymer with M_n = 93 000 and M_w = 488 000 has been synthesised from 4,4′-diiododiphenyl oxide and bisacrylamide with Ar′ = *p*-$C_6H_4OC_6H_4$-*m*.

Polycondensation cross-coupling with the use of transition metal complexes as catalysts allows preparation of various carbo- and heterochain polymers (*e.g*., substituted polyphenylenes, polyimides, polyether ketones, polythiophenes, *etc*.) (for review, see Ref. 41).

The above-described polycondensation, which occurs under relatively mild conditions, opens up new prospects for the synthesis of structurally diverse polymers. However, it demands further investigation, especially as regards the synthesis of polymers with high molecular masses, primarily of linear polyconjugated polymers possessing valuable electrical and optical properties. Systematic development of this approach aimed at the design of branched conjugated dendritic polymers and investigation of their optical properties is of special interest. And, of course, special attention should be given to the search for, and development of, novel efficient catalytic systems for cross-coupling reactions including catalytically active and selective metal–polymer composites.

5. Polycondensation in non-traditional media

It is known that many polycondensation processes demand large amounts of toxic or flammable organic solvents which are often nonrecoverable. In this context, a search for alternative reaction media is a topical ecological and economical problem. Therefore, supercritical carbon dioxide[44] and the so-called 'ionic liquids'[45,46] have attracted considerable attention in recent decades.

Supercritical carbon dioxide is interesting in that it manifests the properties of an inert solvent for numerous substances, on the one hand, and can be completely removed from the reaction mixture as a gas upon depressurisation, on the other hand.[44]

Ionic liquids usually represent organic salts or mixtures of organic and inorganic salts which exist in a liquid ionic state at, or close to, room temperature. Their main characteristic features include low vapour pressure, non-inflammability and the possibility to be repeatedly regenerated. Other advantages include high chemical and thermal stability; they are also good solvents for a broad range of compounds. Their melting points vary over a wide range — from −90 to 200 °C; in addition, these compounds manifest catalytic activity and other valuable properties.[45,46]

From the above, it follows that supercritical carbon dioxide and ionic liquids are promising media for polycondensation, however, their application is still poorly explored.[46,47] In contrast to polymerisation, there are very few examples of the use of supercritical carbon dioxide in polycondensation.[44] A recently published paper[47] is devoted to the use of this compound as a medium in the synthesis of polyimides based on a 4,4′-(hexafluoropropane-2,2-diyl)diphthalic dianhydride and 4,4′-(hexafluoropropane-2,2-diyl)aniline or diaminofluorene. This reaction was carried out at 130–180 °C for 3–6 h and under a CO_2 pressure of 32.5 MPa. It is noteworthy that polycondensation in CO_2 of a very high degree of purity [>99.997%, $c(H_2O)$ = 0.001%] yielded a polymer with a logarithmic viscosity as low as 0.14 dl g^{-1}, whereas polycondensation in the presence of small amounts of water gave higher-molecular-mass polymers. This suggests that in this case CO_2 plays a dual role of a solvent and a catalyst. Indubitably, polycondensation in supercritical CO_2 demands further investigation.

Some recently published papers describe polycondensation in ionic liquids.[48,49] These studies were the first to demonstrate the possibility in principle to perform the synthesis of condensation

polymers (polyimides and polyamides) in ionic solvents which are alternative to conventional organic solvents, and sometimes manifest catalytic activity, as in the synthesis of polyimides. 1,3-Dialkylimidazolium [bromide (**1**) and tetrafluoroborate], 1,3-dibutylimidazolium salts, *etc*., were used as the reaction media. The polycondensation of 1,4,5,8-naphthalenetetracarboxylic dianhydride with 5-amino-2-(4-aminophenyl)benzoimidazole in ionic liquid **1** at 180 °C with the concentrations of the starting compounds varying from 0.4 to 0.6 mol litre^{-1} afforded high-molecular-mass polynaphthoyleneimides (the logarithmic viscosity of a solution of the polymer in sulfuric acid was $\sim$ 0.6 dl g^{-1}). Polycondensation in an ionic liquid was successfully employed in the synthesis of high-molecular-mass aromatic polyamides. It is noteworthy that the rate of the polycondensation and the molecular mass of the polymer formed strongly depend on the nature of the ionic liquid cations. Using the synthesis of polyterephthalamide of 5-amino-2-(4-aminophenyl)benzoimidazole as an example, it was demonstrated that the ionic liquid used can be repeatedly regenerated.[48]

These data should be regarded as an initial step in the study of polycondensation in ionic liquids, which proved to be highly promising and deserving of further investigation.

* * *

On the whole, the novel types of polycondensation considered in this section significantly extend the range of its applications in the synthesis of high-molecular-mass compounds. Such methods open up new ways to the preparation of important special-purpose polymers needed in small amounts to suit the specific areas of their application.

III. Macromolecular design of condensation polymers

1. Construction of a polymeric chain in the course of polycondensation

A search for ways to a directed design of polymeric chains is the main challenge in polycondensation, since it is the only possibility to obtain materials with predetermined properties. This problem can be solved using different approaches. One of them is variation of the chemical structure of the monomers, which is widely employed at present (see Section III.3). The other consists of synthesis of copolymers or polymers from non-symmetrical monomers. This route is especially important, since it allows broad variations of specific characteristics of polymeric systems. However, this approach requires directed design of a polymeric chain, which is impossible without knowledge of the fundamental principles of formation of such chains in the course of polycondensation, *i.e*., the principles of macromolecular design.

Non-equilibrium acceptor-catalytic polyesterification was used as a model system. It is a detailed study of this type of polycondensation that has made it possible to establish the basic principles of macromolecular design, particularly with respect to different mechanisms of alternation of co-monomers and non-symmetrical monomers along the polymeric chain.[50–53] Copolycondensation of two co-monomers, *viz*., $y-M_2-y$ and $y-M_3-y$, *e.g*., 2,2-bis(4-hydroxyphenyl)propane, hexamethylene glycol, *etc*., with an intermonomer $x-M_1-x$ (*e.g*., terephthalic dichloride, *etc*.) entails different alternations of monomers along the polymeric chain in regularly alternating (RA), block (BL) and statistical (ST) modes.

$$2\,x-M_1-x + y-M_2-y + y-M_3-y \longrightarrow$$

$$\longrightarrow -(M_1-M_2-M_1-M_3)_n- \quad \text{RA}$$

$$\longrightarrow -(M_1-M_2-M_1-M_2-M_1-M_3-M_1-M_2-M_1-M_3)_n- \quad \text{ST}$$

$$\longrightarrow -(M_1-M_2)_n-(M_1-M_3)_m- \quad \text{BL}$$

x, y are terminal functional groups.

If polycondensation involves two monomers, one of which has a non-symmetrical 'head' and 'tail' structure (*e.g.,* β-hydroxyethyl ether of a diphenol), the limiting cases entail either regular alternation of the 'head-to-tail', 'head-to-tail' (HTHT) or 'head-to-head', 'tail-to-tail' (HHTT) types or statistic alternation.

$$x-M_1-x + y-M_2M_3-y \longrightarrow$$

$$\longrightarrow -M_1-M_2M_3-M_1-M_3M_2-M_1-M_2M_3-M_1-M_3M_2- \quad \text{HHTT}$$

$$\longrightarrow -M_1-M_2M_3-M_1-M_2M_3-M_1-M_2M_3- \quad \text{HTHT}$$

$$\longrightarrow -M_1-M_2M_3-M_1-M_2M_3-M_1-M_3M_2-M_1-M_2M_3- \quad \text{ST}$$

Prior to these studies, there was an erroneous concept that blocks built up of a more reactive monomer are formed in the initial steps of the reaction, provided the co-monomers possess different reactivities, which results in block-copolymers. If the reactivities of non-symmetrical monomers are different, it is the more reactive groups that react in the first step thus leading to the formation of 'head-to-head' or 'tail-to-tail' structures, which favours the formation of regular polymers consisting predominantly of these fragments.[54, 55] However, this hypothesis does not take into account the violation of the rule of non-equivalence of the functional groups, which is extremely important for polycondensation. This has led to formulation of improper rules.

The generalisation of numerous experimental results, which take into account kinetic theory,[50–53] has made it possible to formulate the basic principles of a macromolecular design for non-equilibrium polycondensation. The presence of all monomers (irrespective of their reactivities) in the initial steps of the reaction favours the formation of statistical polymers, and deviation from this type of structure is related to a change in the reactivities of the functional groups of the intermonomer (symmetrical monomer). Gradual introduction of co-monomers into the reaction zone is not sufficient for the synthesis of block-copolymers.

In the case of one-step reactions, gradual addition of a symmetrical intermonomer into the solution of co-monomers favours the formation of block-copolymers (*i.e*., regular polymers of the HHTT type); the lengths of the blocks (*i.e*., the ratios of the 'head-to-head', 'tail-to-tail' fragments) reflect the differences in the reactivities of the co-monomers used. The prerequisites for the formation of block-copolymers by one-step non-equilibrium copolycondensation in a homogeneous system include noticeably different reactivities of co-monomers and the introduction of the intermonomer into the reaction zone at a rate lower than its reaction with the more reactive co-monomer. The passage of a one-step polycondensation to two-step and multistep processes significantly extends the potential of macromolecular synthesis and allows preparation of block-copolymers made up of blocks of required lengths. Using this approach, one can control the microstructure of a polymeric chain and thus regulate the properties of the polymers formed.

Further progress in the development of novel types of polycondensation, of non-equilibrium matrix polycondensation in

particular, has established a number of characteristic features, *e.g.*, the effect of a heterogeneous matrix on the formation of copolymer microstructure and other properties of polymeric systems.[3, 56–60] In contrast to polymerisation in the presence of fillers, which has been studied in great detail,[61, 62] polycondensation and polyaddition in the presence of a dispersed solid phase were first described in the 1970's. The subjects of these studies were polysiloxanes,[63] polyurethanes [64] and epoxide oligomers.[65] It was not until the 1990's that systematic studies of non-equilibrium polycondensation in the presence of fillers, such as graphite and molybdenum disulfide, were begun.[3, 56, 57]

Studies of model esterification

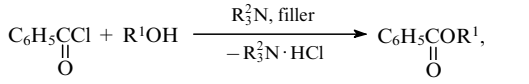

R^1 = Bu^n, Ph; R^2_3N = Et_3N, Py.

and copolyesterification

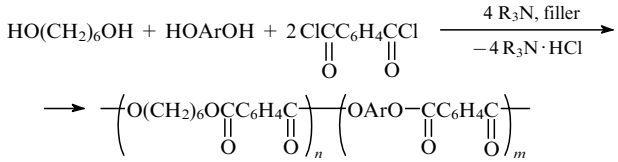

have shown that polyesters prepared in benzene in the presence of graphite had much higher molecular masses than polymers synthesised in the absence of graphite (Table 1), because the filler plays the role of a heterogeneous matrix. This influences the reactivities of functional groups and the ratios of chain propagation and termination rates.

Table 1. Effect of a matrix (graphite) on the molecular mass of a polyarylate prepared from 2,2-bis(4-hydroxy-3-chlorophenyl)propane and terephthalic dichloride.[56]

Matrix (mass %)	S [a] /m^2 g^{-1}	$[\eta]$ [b] /dl g^{-1}	$M \times 10^{-3}$
–	–	0.68	30
30	9.5	0.87	53
30	14.0	0.92	60
60	14.5	1.15	70

[a] Specific surface of the matrix. [b] The viscosity η was measured in THF at 25 °C.

In the absence of a filler in non-polar solvents (*e.g.*, benzene), the reactivity of phenol exceeds that of n-butanol 200-fold. The copolymers formed upon gradual introduction of terephthaloyl dichloride into the reaction zone have a block structure and are characterised by a microheterogeneity coefficient $K_m = 0.23$.†

In the presence of graphite (80 mass%), which has a specific surface of 14 m^2 g^{-1}, the activity of phenol in the acylation by aromatic acid chlorides is 3 times lower than in the absence of a filler, while that of butanol increases nearly 1.5-fold under similar conditions. As a result, the difference in the activities of phenolic and alcoholic groups decreases from 200- to 40-fold, *i.e.*, the difference in the reactivities of aromatic and aliphatic hydroxy groups is levelled off. As a result, the K_m value of copolymers of hexamethylene glycol and 2,2-bis(4-hydroxy-3-chlorophenyl)propane with terephthaloyl dichloride obtained in the presence of a filler is 0.53 rather than 0.23, *i.e.,* the structure of the copolymer becomes more statistical.

† The microheterogeneity coefficient K_m reflects the degree of orderliness of the copolymer units. At $K_m = 1$, the units of a macromolecular chain are distributed statistically, whereas at $K_m \neq 1$ the copolymer has a block structure, the size of its blocks increasing with a decrease in K_m.

The changes in the reactivities of these components are caused by sorption, by the filler, of the active complexes formed. Since the acylation mechanisms of phenol and butanol are different, *viz.*, general basic (phenol) and nucleophilic (butanol),[66] the effects of graphite on each of these catalytic pathways are oppositely directed. It is this factor that influences the microstructure of the copolymers formed. The polycondensation in the presence of graphite also has a beneficial effect on the properties of the filled compositions formed. Apparently, this is due to the fact that the growth of macromolecules in a non-polar solvent in the presence of the filler largely occurs on its surface, which ensures more uniform distribution of graphite within the polymer in comparison with an analogous mixture prepared by simple mechanical blending of the components.[56]

As can be seen from Table 2, the 'synthetic' composition of a copolyester surpasses the corresponding 'mechanical' mixture in softening temperature, thermal stability, specific impact strength and specific electroconductivity. In addition, it has lower values of friction and wear factors.[56]

Table 2. Properties of compositions based on 2,2-bis(4-hydroxy-3-chlorophenyl)propane polyterephthalate prepared using different methods.[56]

Characteristics	Mechanical blending	Synthesis in the presence of a filler (graphite, 30 mass %)
Softening temperature /°C	220	260
Thermolysis (350 °C, vacuum),		
[CO] /10^3 mol $unit^{-1}$	9	1
[CO_2] /10^3 mol $unit^{-1}$	63	2
Specific impact strength /kJ m^{-1}	45	118
Specific electroconductivity /10^{13} Ω^{-1} m^{-1}	1	500

Interesting results were obtained when non-equilibrium acceptor-catalytic copolyesterification was carried out in the presence of hetero- and carbochain polymeric matrices.[58–60] These included 'active matrices', *i.e.*, polymers containing oxygen or nitrogen atoms in the main chain which can form hydrogen bonds with hydroxyl-containing monomers, such as polyphenylquinoxaline (a polyether based on 2-phenylquinoxaline), polynaphthoyleneimidobenzoimidazole **3** [a polyimide based on naphthalene-1,4,5,8-tetracarboxylic dianhydride and 5-amino-2-(4-aminophenyl)benzoimidazole], polyethylene oxide

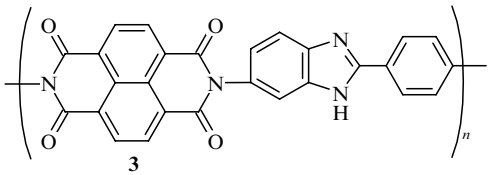

3

and 'inert matrices', which do not react with monomers (*e.g.*, hyper-cross-linked polystyrene). The latter had a well-developed internal surface of their granules and differed from one another in pore size and structure of the cross-linking reagent (the cross-linking bridges are $-CH_2-$ or $-CH_2C_6H_4CH_2-$ groups, the pore sizes vary from 10 to 850 Å).

The results obtained suggest that the microstructures of the copolyesters formed with polymeric matrices introduced into the reaction system depend on the following factors, *viz.*, the presence and accessibility of nucleophilic sites which influence the kinetic parameters of intermonomer–co-monomer interactions, the convergence of reactivities of bisphenol and glycol, the presence and

sizes of pores in matrices and the ratios of sizes of pores and co-monomer molecules.

If porous matrices are used, two processes may occur simultaneously, which have opposite effects on the formation of the copolymer microstructure, *viz*., gradual desorption from the surface of the matrix, which results in an increase in K_m, and selective desorption of monomers from matrix pores, which decreases K_m (the so-called 'sponge effect'). Depending on the ratios of pore sizes of polymeric matrices to the molecular sizes of the co-monomers, one of these processes will predominate, which is reflected on the degree of the block structure of the copolymer formed. The use of polymeric matrices differing in the physicochemical properties of their particles opens up new possibilities for the synthesis of copolymers, since this allows purposeful variation of the microstructure of the chain formed and, correspondingly, the properties of the target product.

Thus it was found that copolymers having different microstructures [*e.g*., block ($0.3 < K_m < 1$) or statistical ($K_m = 1$)] can be prepared by copolycondensation of terephthaloyl dichloride with 2,2-bis(4-hydroxy-3-chlorophenyl)propane and hexaethylene glycol in the presence of triethylamine (benzene, 40 °C) at different concentrations of polyphenylquinoxaline or hypercross-linked polystyrene.[58, 59] Some examples of microstructures of copolyterephthalates prepared with the use of polymeric matrices are given in Table 3.

Table 3. Microheterogeneity coefficients of copolyterephthalates obtained in the presence of polymeric matrices (62 mass % Et_3N, benzene, 40 °C).[59]

Co-monomers	Matrix	K_m
DCD – HMG	PPQO	1.11
DCD – HMG	PEO	0.50
DCD – HMG	PS 10	0.89
DCD – HMG	PS 75	0.25
DMD – HMG	PS 10	0.92
DMD – HMG	PS 850	0.26
PP – DCD	PS 10	0.89
PP – DCD	PS 850	0.72

Notes. Abbreviations: HMG, hexamethylene glycol; DCD, 2,2-bis(4-hydroxy-3-chlorophenyl)propane; DMD, 2,2-bis(4-hydroxy-3-methylphenyl)propane; PP, bis(4-hydroxyphenyl)fluorene; PPQO, polyphenylquinoxaline; PS 10, polystyrene (pore size 10 – 15 Å); PS 75, polystyrene (pore size 75 – 85 Å); PEO, polyethylene oxide; PS 850, polystyrene (pore size 850 – 950 Å).

It may thus be expected that the use of polymeric matrices in polycondensation can in principle result in the manifestation of such effects as changes in the local concentrations of functional groups of reactants and 'sponge effects', *i.e*., initial sorption of monomers by the matrix with subsequent gradual desorption over the course of the reaction. This accounts for the changes in the reactivities of functional groups and conformations of molecules and for enhanced interactions of the macromolecules formed with the matrix.

In predicting the further fate of matrix-assisted polyesterification, one may suppose that one of the trends will be directed towards increasing the conformational specificity of this reaction. This will enable improvement of the microstructure of the polymeric chain if conformationally regular polymers are synthesised.

Polymeric matrices were also used for polycyclocondensation of tetracarboxylic dianhydrides with diamines.[67] In this case, amorphous cardo polyimides prepared from pyromellitic dianhydride and 3,3-bis(4-aminophenyl)phthalide or diphenyl oxide-3,3′,4,4′-tetracarboxylic dianhydride and 9,9-bis(4-aminophenyl)-fluorene, which are readily soluble in organic solvents and in reaction media, were used as matrix polymers.

Polyimides based on diphenyl oxide-3,3′,4,4′-tetracarboxylic dianhydride and 4,4′-diaminodiphenyl oxide or 5-amino-2-(4-aminophenyl)benzoimidazole and a polyimide from pyromellitic dianhydride and 9,9-bis(4-aminophenyl)anthrone were the target polymers. Their processability into films from solutions or into moulded articles from melts is difficult (or virtually impossible) because of their insolubility and high softening temperatures.

Sequential polycyclisation of these monomers in fusible catalytic media containing *p*-nitrotoluene (or diphenyl sulfone) and benzoic acid together with matrix cardo polyimides synthesised in previous steps in the same medium yielded novel polymeric systems. The latter differ from the corresponding crystalline polyimides synthesised by standard methods both in structures and properties (solubility, thermal stability, strength, *etc*.), which extends the range of their processability and practical applications. The data obtained demonstrate a high degree of control over the properties of these polymer – polymeric systems. Copolymers having both block and statistical structures should be formed, although this suggestion needs further verification.

The widening of the scope of these investigations is of indubitable interest. First of all, one should pay attention to the formation of systems from other classes of polymers and soluble matrix polyimides and the use of other polymers as matrices. It can be expected that the rate of formation of such polymers, their molecular masses and structures will be controlled, which will enable the preparation of finely dispersed homogeneous products and, if necessary, molecular composites. This offers an opportunity to improve the properties and processabilities of incompatible or partly compatible polymers in comparison with mixtures obtained by simple mechanical blending of the corresponding components.[67]

2. Polycondensation – polymerisation systems

The good solubility of polyheteroarylenes containing cardo and fluorine-containing groups in both common organic solvents and some unsaturated monomers has prompted an interesting route to the synthesis of novel polycondensation – polymerisation systems. Radical polymerisation and copolymerisation of (meth)acrylates, fluoro(meth)acrylates, styrene, acrylonitrile and other monomers in the presence of variable amounts of polyheteroarylenes (cardo and fluorine-containing polyimides, polyarylates, *etc*.) were used for the synthesis of novel soluble high-molecular-mass products.[68 – 72]

Together, the results obtained suggest that the transfer of a growing chain to the benzene nuclei of polyheteroarylenes in the radical polymerisation of unsaturated monomers in the presence of soluble polyheteroarylenes is not the only way to the synthesis of copolymers.[71] The mechanism of formation of such condensation – polymerisation systems is not finally elucidated, although the very fact of their synthesis is extremely important. The copolymers formed differ significantly from the corresponding carbochain polymers in solubility and enhanced thermal, mechanical, thermofrictional, *etc*., characteristics even at low concentrations of a polyheteroarylene[69 – 71] (Table 4). Such polymeric systems are distinguished for better solubility, and, in some

Table 4. Some properties of polymeric systems prepared upon polymerisation of methyl methacrylate in the presence of a polyarylate from 4,4′-hexafluoropropane-2,2-diyldiphenol and terephthalic acid.[70]

Concentration of polyarylate (mass%)	η_{log} /dl g^{-1}	T_g /°C	Characteristics of films		
			σ /MPa	ε (%)	$10^3 E$ /mPa
0	3.85	110	40	20	1.08
4	5.80	130	60	4	2.20
100	0.60	215	55	75	1.83

Note. σ, breaking strength; ε, relative elongation at breaking point; E, elasticity modulus.

cases, enhanced strength properties in comparison with starting polyheteroarylenes.

The possibility in principle to perform anionic polymerisation of ε-caprolactam in the presence of aromatic polyimides as macromolecular activators has been demonstrated.[72] The involvement of five-membered imide rings of polyheteroarylenes in the reaction enables the synthesis of novel polycondensation–polymerisation systems, *e.g.*, partly cross-linked graft copolymers with enhanced thermal and tribological characteristics and high water resistance as compared with ordinary polycaprolactam.

The design of novel polymeric systems based on polyheteroarylenes and epoxide polymers can also be related to such 'symbiotic' polymer formation.[73,74] In particular, a combination of cardo polyheteroarylenes [*e.g.*, poly(phenolphthalein terephthalate)] with epoxide oligomers upon moderate heating is a promising approach to their reprocessing into monolithic articles. The chemical reaction of an epoxy oligomer with a polyarylate, which occurs by the insertion (and opening) of the oxirane ring into the ester bond, results in the formation of a network structure, which manifests a set of specific properties. Enhanced (in comparison with classical compositions based on oligoepoxides) thermal durability is the main advantage of such compositions. Reactions of cardo polyimides with oligoepoxides favour the synthesis of novel polymeric materials which manifest good thermal, strength and electroinsulating properties.[74]

It may be hoped that the above-described processes hold great promise in the directed control of the properties of carbo- and heterochain polymers.

The polymer formation described above should more correctly be referred to as a 'symbiotic' process, since the reactants eventually complement the useful properties of each other. There is no doubt that this trend requires further development and perfection.

3. Variations of chemical structures of monomers

Rapid progress in high-tech branches of modern industry and growing demands for novel materials pose the problem to the polymer chemist of design of high-molecular-mass compounds possessing enhanced specific properties, such as thermal stability, high working capacity under extreme operating conditions and excess loads, photochemical stability, optical conductivity, low permittivity, *etc*. The variability and versatility of polycondensation opens new ways to the synthesis of such polymeric materials. The use of monomers with appropriate chemical structures leading to directed variation of the structures of the polymeric chains of condensation polymers is a promising approach to the macromolecular design of the latter.

a. Ring–chain polyheteroarylenes

The structures of ring–chain polyheteroarylenes possessing a set of useful properties have been much attended to in the past decade. Preparation of modified polyheteroarylenes which, contrary to infusible and insoluble polymers, manifest better solubility in organic solvents, thus favouring their processing into finished articles, is a topical problem in this area.

Studies carried out in the 1980's have shown that introduction of cardo groups into various polyheteroarylenes using the corresponding monomers is an effective route to improve their solubility.[3,75] This can also be attained due to the presence of 'hinge' and side groups in the resulting macromolecules and the nonsymmetrical structure of the polymeric chain.[3,75,76] Of particular interest is construction of a polymeric chain structure which combines the enhanced solubility of a polymer with advanced thermal characteristics and, in some cases, new specific properties conferred on the polymer.

The introduction of phenyl substituents into the macromolecules of ring–chain polyheteroarylenes has proved a promising approach to increase their solubility, thermal plasticity and resistance against thermooxidation.[77] For example, polymers prepared from 5,6-diphenylbenzene-1,2,3,4-tetracarboxylic dianhydride and *p*- and *m*-phenylenediamines or 4,4′-diaminodiphenyl oxide soften at temperatures above 400 °C and lose 5% of their mass in air at 487, 523 and 591 °C, respectively. These polymers are soluble in a broad range of organic solvents, *e.g.*, *sym*-tetrachloroethane (TCE), *N*-MP, DMSO, DMA, DMF and *m*-cresol.

A series of novel soluble phenylated polyimides have been prepared starting from 4-(4-benzoylphenyl)-3,5,6-triphenylbenzenedicarboxylic dianhydride and various aromatic diamines. These polymers are amorphous, have glass transition temperatures (T_g) of 345–395 °C and lose 10% of their mass in air at 565–624 °C. The significant interval between their decomposition and glass transition temperatures enables their successful processing by pressing. Strong films prepared from polymer solutions are characterised by dielectric constants varying from 2.72 to 3.00.[78] Starting from 1,4-bis[2,3,4,5-tetraphenyl-6-(4,5-dicarboxy-1-naphthyl)phenyl]benzene dianhydride and benzidine or 3,3′,4,4′-tetraaminobiphenyl, soluble thermostable polynaphthylimide and the so-called polynaphthoylenebenzoimidazole, respectively, which manifest high luminescence efficiency due to the presence of aromatic groups, have been synthesised.[79] Methoxy- and phenoxy-substituted polyimides were synthesised based on 3,5-diaminoanisole,[80] 3-amino-5-(4-aminophenoxy)diphenyl ether,[81] 3,5-diaminodiphenyl oxide[82] and aromatic tetracarboxylic dianhydrides.

In the majority of cases, phenoxy-substituted polyimides manifest better solubilities in comparison with methoxy-substituted and unsubstituted analogues. A phenoxy-substituted polyimide containing hexafluoroisopropylidene groups manifests the best solubility.[82] Phenoxy-substituted polyimides based on tetracarboxylic dianhydrides containing 'hinge' groups are also easily soluble in common organic solvents. They are characterised by a large interval between the decomposition and glass transition temperatures and high thermal stabilities.[83] Polynaphthylimides and polyperylenimides possessing enhanced solubilities were synthesised from phenoxy-substituted diamines.[84]

The reaction of 2,6-diamino-4-hydroxytoluene and bis(3,5-diamino-4-hydroxyphenyl) oxide with tetracarboxylic dianhydrides gave a series of novel hydroxy-containing polyimides possessing good thermal characteristics. These polyimides are subject to further chemical modification. For example, the action of acryloyl chlorides yields photosensitive polymers.[85,86] Some soluble film-forming sulfur-containing polyimides[87–89] were synthesised from aromatic diamines containing phenylsulfonyl, phenylthio and benzothiazole-3-ylthio groups.

An interesting case of a chemical modification of polyimides has been described which includes incorporation of side phthalimide fragments into the polymer. These polymers were synthesised based on bis(phthalic anhydrides), bis(*o*-phenylenediamines) and chloral derivatives followed by reaction with phthalic anhydride.[90]

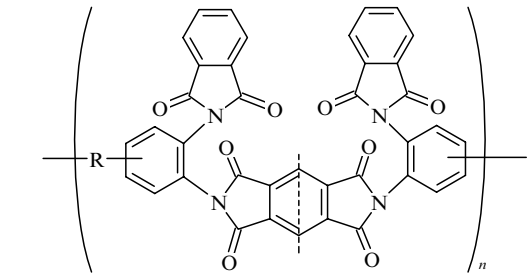

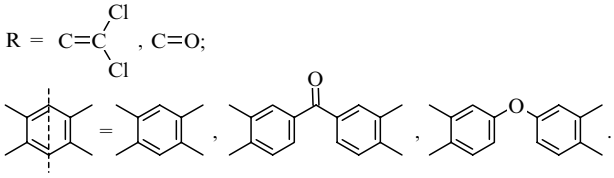

Polyimides with these structures are easily soluble in organic solvents, they manifest high thermal characteristics and fire-resistance. Polymers containing 1,1-dichloroethylene groups undergo structurisation upon thermal treatment, which renders them insoluble.

Polyimides containing phthalimide substituents were also prepared starting from 2,4-diamino-6-phthalimidotoluene and bisphthalic anhydrides[91] as well as from 2,4,6-triaminotoluene by sequential treatment with equimolar amounts of phthalic and bisphthalic anhydrides.[92] All the polymers thus modified are readily soluble in *N*-MP, DMF and a TCE–phenol mixture. Their softening temperatures are 270–360 °C; 10% mass loss temperatures are 400–450 °C.

The presence of side functional substituents has a beneficial effect on the properties of other polyheteroarylenes as well having ring–chain structures. For example, polyquinoxalines containing diarylether substituents[93,94] combine good processability with high thermal stability and low (in comparison with phenylquinoxaline) dielectric permittivity.[94]

The presence of fluorine-containing (*e.g.*, trifluoromethyl, hexafluoroisopropylidene, trifluoromethylphenoxide, *etc.*) groups is also beneficial as regards the properties of different polyheteroarylenes.[95–102] Thus polyimides based on 2,2-bis[4-(3,4-dicarboxyphenoxy)phenyl]hexafluoropropane and aromatic diamines[87] are easily soluble not only in *m*-cresol, but also in chloroform, dichloromethane, DMF, DMA and *N*-MP. Their softening temperatures are 200–220 °C, while their 5% mass loss temperatures in air are around 500 °C. These polyimides are readily processed into strong monolithic articles and films by moulding, extrusion and casting from solutions. Apart from high solubility, heat resistance, thermal stability and easy processability, phenyl-substituted polyimides of 4,4′-bis[tetraphenyl(4,5-dicarboxy-1-naphthyl)phenyl]benzophenone containing trifluoromethyl and hexafluoroisopropylidene groups have low dielectric constants (2.85 and 2.8, respectively).[96]

There is evidence that electric conductivities of these polymers change on going to fluorine-substituted polyimide derivatives. Thus substitution of fluorine for four hydrogen atoms in the benzene nuclei of polyimides decreases their dielectric permittivities, whereas substitution of one atom increases them.[100] Substitution of a methyl group for a trifluoromethyl group decreases the dielectric permittivity. Dielectric permittivities of fluorine-containing polyimides vary from 2.58 to 2.85, whereas those of ordinary polyimides are equal to 2.9–3.4.

A search for new routes to the synthesis of novel promising low-permittivity polymeric materials for microelectronics has been a challenge to polymer chemists in the past decade. The main approaches to the design of polymeric film materials manifesting low permittivities on the basis of various condensation polymers are considered in a recent review.[98] According to computer prognoses,[101] significant advances in this area can be achieved through the use of phenylated polyphenylenes devoid of polar groups. Different modifications of such polymers can result in materials with dielectric constants of 2.50–2.60.

Significant progress has been achieved in recent years in the synthesis of soluble polynaphthyl- and polyperylenimides containing six-membered imide rings. These polymeric systems possess enhanced thermal and chemical stabilities, optical conductivity, unusual electrographic properties and easy processability into articles by conventional methods.[103]

In addition to the broad potential of chemical modification of the known classes of ring–chain polyheteroarylenes by changing the framework of their polymeric chains, attempts are being made to modify the polymers through the formation of new heterocycles in the chain. For example, the use of bisnaphthalic anhydrides and bisanthranylamides in the synthesis of polymers has made it possible to prepare a novel class of thermostable polyheteroarylenes, *viz.*, polynaphthoylenequinazolones with six-membered heterocycles.[104]

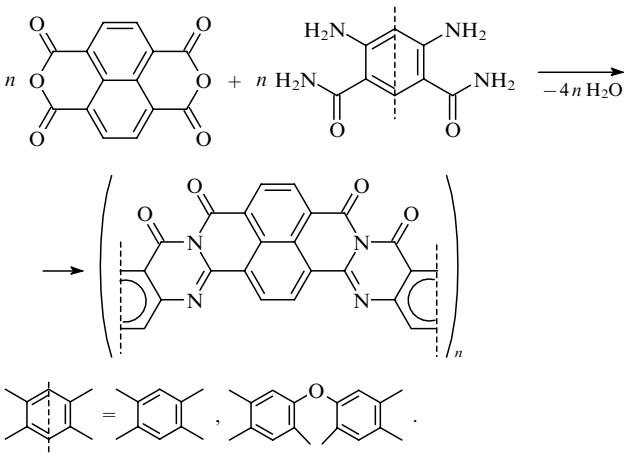

Properties of ring–chain polyheteroarylenes strongly depend on the composition of the basic polymeric chain, which determines its rigidity and flexibility.[105] The design of polymeric chains with high thermodynamic rigidity (*i.e.*, containing maximally straightened polymeric chains) is determined by the necessity to create thermostable, high-strength and high-modulus materials. Rigid-chain (the Kuhn segment is 320×10^{-8} cm) high-molecular-mass ($M = 1\,200\,000$) polynaphthoyleneimidobenzoimidazole **3** (see above) presents special interest in this respect.

Isotropic films of this polymer, which have been given the name 'iplon', are endowed with unique deformation characteristics: their breaking stress at specific elongation of $\varepsilon = 40\%$ and the elasticity modulus of $E = 46\,000$ kilogram-force cm^{-2} is $\sigma = 4700$ kilogram-force cm^{-2} (see Ref. 106). Their orientation (60%) gave anisotropic films with $\sigma = 9300$ kilogram-force cm^{-2}, $\varepsilon = 10\%$ and $E = 200\,000$ kilogram-force cm^{-2}.

With regard to these parameters, 'iplon' has no analogues among other heterocyclic non-composite polymeric materials. Approaches to further enhancing the strength characteristics of polynaphthoylenebenzoimidazole films have already been outlined. These include additional incorporation of rigid rod-like fragments into their polymeric chains. To meet this goal, a series of copolymers based on 1,4,5,8-naphthalenetetracarboxylic dianhydride, 5-amino-2-(4-aminophenyl)benzoimidazole and rod-like aromatic diamines have been synthesised.[107] The breaking strengths of oriented films of a copolymer based on 4,4′-diaminobiphenyl (30 mol.%) reaches 1.5×10^4 kilogram-force cm^{-2}, the elasticity modulus being 38×10^4 kilogram-force cm^{-2}.

Molecular composites, which represent mixtures of rigid-chain and flexible-chain polymers, are promising materials with enhanced physicomechanical characteristics. In such composites, rigid-chain components play the role of a reinforcing filler, which is dispersed at the molecular level in a flexible-chain polymer, which represents a permanent matrix. This allows fine attenuation of the microstructures of these polymeric systems (in comparison with mechanical mixtures) by synthesising block-type molecular composites with the corresponding structures. A series of block copolymers including those based on rigid-chain polynaphthoyleneimidobenzoimidazole with a Kuhn segment of 320×10^{-8} cm and flexible-chain polynaphthtoylenebenzoimidazole with a Kuhn segment of 50×10^{-8} cm have been synthesised specially for this purpose (Scheme 2).[108] These polymers manifest high physicomechanical characteristics ($\sigma = 4100$ kilogram-force cm^{-2}, $\varepsilon \approx 20\%$, $E = 82\,000$ kilogram-force cm^{-2}). Electron-microscopic studies have shown that at the molecular level the flexible matrix is reinforced by a rigid-chain block. The data on the molecular composites based on rigid-chain polybenzobisazoles have been generalised in a review.[109] It is reported that these composites are the most promising materials for those fields where low mass, high strength, thermal and chemical stability, and transparency with respect to radio waves are critical.

Scheme 2

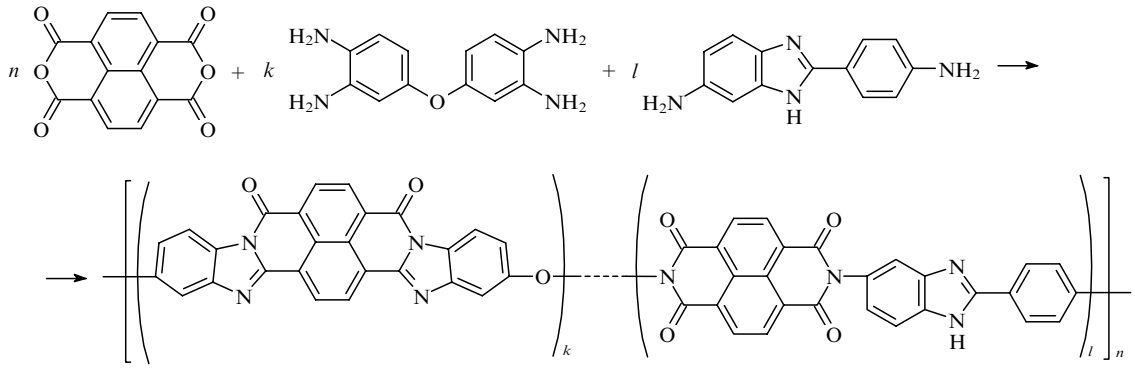

Publications of the past decade consider miscellaneous properties of ring–chain polyheteroarylenes and various aspects of their applications in diverse branches of modern engineering, such as antifriction and self-lubricating plastics, composite materials, films, membrane and foamed materials, fibres, wave guides, adhesives, photoresists, *etc*.[3, 77, 79, 98, 103, 104, 109–115]

b. Polyarylenes

Recent investigations into the synthesis and chemical modification of polyarylenes,[116–119] polyaryleneethynylenes and polyarylenevinylenes[30–32, 120–124] attract considerable attention. In particular, the Diels–Alder homocondensation of 2,5-diphenyl-3,4-bis[4-(phenylethynyl)phenyl]cyclopentadienone was used for the preparation of a highly branched thermostable polyphenylene with M_w 160 000 that was readily soluble in organic solvents.[116] Polycyclocondensation of 4,4′-bis(4-acetylphenoxy)diphenyl sulfone was used in the synthesis of polyphenylenes containing acenaphthyl groups. Their subsequent dehydrogenation to acenaphthylenyl fragments gave a structurised polymer. The polymers containing reactive acenaphthylene groups are promising for production of thermostable plastics.[113]

The Diels–Alder reaction was used in the synthesis of hexafluoroisopropylidene-containing phenyl-substituted polyphenylenes which combine high thermal stability with solubility in organic solvents and have low dielectric constants.[119] Diethynylarenes and tolanes containing phenylated cyclopentadiene substituents[120–122] and other similar starting reagents[123, 124] were used, as in the synthesis of a series of thermostable thermoset phenylated polyphenylenes containing acetylene fragments under similar conditions. Some representatives of this class are easily soluble in organic solvents, have low dielectric constants[120] and manifest strong fluorescence.[121]

Polyconjugated polyaryleneethynylenes were synthesised by reaction of the corresponding dibromoarylenes and diethynylarenes in the presence of palladium or nickel complexes.[30–32] The fluorescence maxima of the polymers formed lie in the yellow-to-blue region.

A series of investigations of various physical characteristics of phenyl-substituted polyphenylenes, such as electrical birefringence,[125] hydrodynamic, optical and conformational characteristics[126] and radiation-induced conductivity,[127] have been carried out. No doubt, further development of the synthesis of high-molecular-mass polymers and in-depth study of their specific properties are topical.

The progress in investigations aimed at the synthesis of condensation polymers considered above would be impossible without further achievements in the chemistry of monomers based on readily available raw materials, *e.g*., 2,4,6-trinitrotoluene and chloral. Thus a series of aromatic diamines have been synthesised from 2,4,6-trinitrotoluene in order to obtain the corresponding ring–chain polyheteroarylenes containing methoxy-, fluoromethoxy-, phenoxy-, hydroxy-, sulfur-containing and other side groups.[80, 82, 83, 87–89] Diverse polyarylenes are accessible from arylene dihalides that can be prepared from chloral.[33, 128, 129]

c. Polyarylene ethers

A series of recently published papers are devoted to the directed design of polymeric chains of polyarylene ethers. These polymers have attracted much attention since the 1960–1970's and are considered to be promising themoplastic materials owing to their high thermal stabilities and numerous valuable construction properties.[130] However, these compounds are not very heat-resistant, which inevitably poses the problem of their further modification. An analysis of the main regularities of their formation and effect of their molecular masses (*i.e*., the lengths of the polymeric chains) on their physicochemical properties is yet another central task.

Polyarylene ethers are usually synthesised by nucleophilic substitution of arylene dihalides with alkali metal phenolates or by electrophilic substitution (*e.g*., by reaction of aromatic dicarboxylic acid dichlorides with diaryl ethers in strongly acidic media). A recent study[131] aimed at the synthesis of polyarylene ether ketones from 4,4′-difluoro- or 4,4′-dichlorobenzophenone and cardo-type bisphenolates (phenolphthalein, phenolfluorene, phenolanthrone, phenolphthalein anilide) has significantly extended the knowledge of the pattern of this polycondensation process, enabled its optimisation and estimation of the effects of the chemical structures of the monomers on the properties of the polymers. In addition, it has enabled the synthesis of polymers with controllable molecular masses from 10 000 to 100 000 and above.[131]

The introduction of bulky cardo groups into macromolecules enhances considerably their thermal stabilities, so that glass transition temperatures of the above-mentioned polymers are 230–240 °C. They are amorphous, readily soluble and thermostable. The presence of the constituent cardo groups also favours the enhanced breaking stress and elasticity moduli of the films prepared from them.[132] The physicomechanical properties of polymers prepared from phenolphthalein and 4,4′-difluorobenzophenone were virtually unchanged starting from M = 40 000–60 000. In this range, poly(ether ketones) are easily molded from melts owing to their good fluidity. Such polymers were used for the preparation of unfilled monolithic materials as well as fiber glass and black-reinforced plastics possessing uniquely high specific impact strength. Thus the impact strength of an unfilled uncut specimen was 92 kJ m^{-2}.

Phthalide groups were also introduced into polyarylene ether ketones using an alternative procedure which employs a highly reactive difluoroderivative, *viz*., {3,3-bis[4-(4-fluorobenzoyl)phenyl]phthalide}.[133] This compound and various bisphenolates were used as starting materials in the synthesis of novel polyarylene ether ketones with softening temperatures up to 250 °C. It is noted that monolithic samples of cardo copolyarylene ether ketones containing 4,4′-propane-2,2-diyldiphenol fragments manifest uniquely high impact strength with incision (up to 44 kJ m^{-2}).[134]

Scheme 3

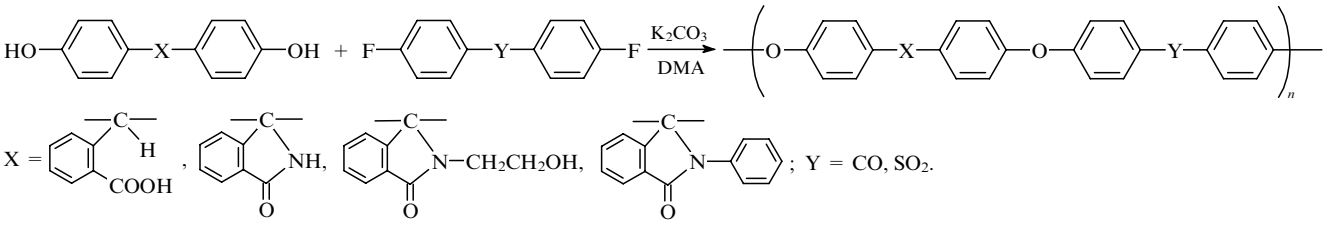

A series of crystallisable cardo copolyarylene ether ketones have been synthesised; their crystallisation is determined by the simultaneous presence of cardo bisphenols and hydroquinone (or 4,4′-dihydroxybiphenyl) fragments.[135,136] The glass transition temperatures of these compounds reach 250 °C, whereas the melting temperatures lie in the range of 300–350 °C.

Further developments in the field of chemistry of polymers will be directed at the incorporation of reactive groups into polymeric chains.[137–145] The development of methods for the synthesis of monomers containing functional groups (carboxy, alcoholic and phthalimide) is currently under way (Scheme 3).[137–139] Side groups in polyarylene ethers synthesised from these monomers allow their further chemical modification.

The polymers obtained have high softening temperatures (up to 260–290 °C); derivatives containing free carboxy groups are soluble in DMA, pyridine, cyclohexanone, THF and dioxane, and insoluble in chlorinated hydrocarbons. It is noted that the range of solvents for these polymers is wide and includes non-polar or low polarity solvents owing to the ability to form hydrogen bonds and to be involved in intra- and intermolecular interactions.[140] Polyarylene ethers containing free carboxy groups present interest as polyelectrolytes and polymeric composites.[139]

The use of difluoroarylenes containing α-diketone fragments as monomers has enabled the synthesis of the corresponding polyarylene ether ketones:[26,140–143]

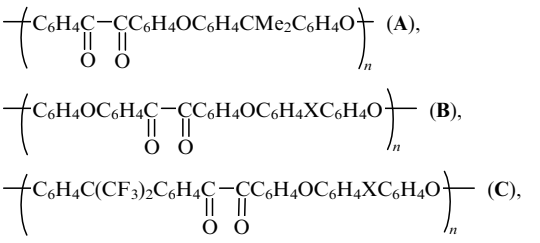

X = CMe_2, $C(CF_3)_2$, *etc.*

The glass transition temperatures of the polymers **B** and **C** vary in the range 165–245 °C, their 10% mass loss temperatures in air lie around 460–540 °C, and their dielectric constants vary from 2.90 to 3.25. These polymers are soluble in organic solvents.[142,143] The presence of α-diketone fragments in these macromolecules opens up new ways to their further conversion into, *e.g.*, linear polymers containing quinoxaline and triazine fragments or into cross-linked polymeric structures containing interchain quinoxaline fragments. It may be expected that the thermal and mechanical characteristics of these polymers will be enhanced in comparison with the original ones.

Chemical modification of polyarylene ethers can also be achieved through the introduction of double and triple bonds into their structures. The reaction of 1,1-dichloro-2,2-diphenylethylene with bisphenols was used in the synthesis of oligomers of the general formula:

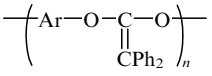

Ar = $C_6H_4CMe_2C_6H_4$, $C_6H_4C(O)C_6H_4$,

which are promising candidates for thermoset fire-resistant materials.[144] Polycondensation of various bisphenols with difluoroarylenes containing acetylene groups was used for the preparation of unsaturated polyarylene ether ketones.[145]

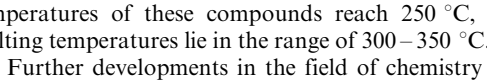

X = CO, COCO; Ar = $C_6H_4CMe_2C_6H_4$, $C_6H_4CMePhC_6H_4$, *etc.*

Their thermal treatment is accompanied by structurisation at the triple bonds and results in enhancement of their thermal characteristics.

Thus, the studies of polyarylene ethers are mainly directed at the perfection of their synthesis and the design of novel promising polymeric structures. A search for hitherto unknown activators of electrophilic monomers employed in the synthesis of polyarylene oxides is currently under way. Thus it was found that the acyclic and heterocyclic groups present in arylene dihalide molecules activate halogen atoms. This line of research, which holds much promise both for the optimisation of nucleophilic substitution and for the preparation of novel polymeric systems possessing valuable properties, has been considered in a special review.[146]

IV. Conclusion

Because of the limited size of the present review, we cannot dwell further on all recent achievements in polycondensation and encompass the whole range of novel polymers synthesised by this method, since such examples are too numerous. The advances in the study of carborane-[147] and sulfur-containing[148] condensation polymers and polyorganophosphazenes[149,150] have been adequately covered in recently published papers. Suffice it to mention yet another promising trend which has been successfully developed over the past decade, *viz.*, design and investigation into highly branched dendritic polymers which are considered in detail in special reviews.[151,152]

In conclusion, it should be noted that polycondensation is still a very diverse and intensively explored area of research which is being further developed, being aimed at a search for novel polymer-forming reactions, methods for macromolecular design in polycondensation processes and purposeful design of polymeric chains for the most promising classes of polymers with the ultimate goal of conferring novel useful properties to existing polymers and of preparing new polymer systems. There is every reason to believe that future studies will provide interesting new data in this field of polymer chemistry.

This review has been written with the financial support of the Russian Foundation for Basic Research (Project No. 03-03-07011).

References

1. J Gay-Lussak, J Pelouze *Annalen* **7** 40 (1833)
2. Y Imai, in *Polymer Science Contemporary Themes* Vol. 1 (New Delhi: McGraw-Hill, 1991) p. 3
3. S V Vinogradova, V A Vasnev *Chem. Rev. Harwood Acad. Publ., Pt. 2* **21** 1 (1995)

4. A L Rusanov, I A Khotina *Vysokomol. Soedin., Ser. B* **36** 1399 (1994) [a]
5. R J Perry, S R Turner, R W Blevins *Am. Chem. Soc. Polym. Prepr.* **33** 491 (1992)
6. Y Imai *Chem.-Tech. (Heidelberg)* **21** 560 (1991)
7. M Yoneyama, M Kakimoto, Y Imai *Macromolecules* **22** 2593 (1989)
8. M Yoneyama, M Kakimoto, Y Imai *Macromolecules* **22** 4152 (1989)
9. M Yoneyama, M Kakimoto, Y Imai *J. Polym. Sci., Part A: Polym. Chem.* **27** 1985 (1989)
10. R J Perry, S R Turner, R W Blevins, B D Wilson *Am. Chem. Soc. Polym. Prepr.* **35** 706 (1994)
11. R J Perry, S R Turner *Makromol. Chem., Macromol. Symp.* **54/55** 159 (1992)
12. R J Perry, S R Turner, R W Blevins *Macromolecules* **28** 2607 (1995)
13. S N Salazkin, S R Rafikov, G A Tolstikov, M G Zolotukhin *Dokl. Akad. Nauk SSSR* **262** 355 (1982) [b]
14. S N Salazkin, in *V Vserossiiskaya Konf. 'Kondensatsionnye Polimery: Sintez, Struktura, Svoistva', Moskva, 1999* (The Vth All-Russian Conference 'Condensation Polymers: Synthesis, Structure, Properties', Moscow, 1999) P-3
15. M G Zolotukhin, V A Kovardakov, S N Salazkin, S R Rafikov *Vysokomol. Soedin., Ser. B* **41** 1984 (1999) [a]
16. V A Kraikin, Z N Musina, E A Sedova, Yu I Puzin, S N Salazkin, Yu B Monakov *Dokl. Akad. Nauk* **373** 635 (2000) [b]
17. V A Kraikin, S K Belen'kaya, F G Valyamova, S N Salazkin *Vysokomol. Soedin., Ser. A* **41** 1655 (1999) [a]
18. S N Salazkin, S K Belen'kaya, Z G Zemskova, M E Shumanskii, Sh S Akhmetzyanov, V A Kraikin *Dokl. Akad. Nauk* **357** 68 (1997) [b]
19. V G Vasil'ev, G G Nikiforova, L Z Rogovina, L V Dubrovina, T P Bragina, L I Komarova, G I Timofeeva, M I Buzin, S N Salazkin, V V Shaposhnikova, V S Papkov *Dokl. Akad. Nauk* **382** 649 (2002) [b]
20. D M White, T Takekoshi, F J Williams , H M Relles, P E Donahul, H J Klopfer , G R Loucks, J S Manello, R O Matthews, R W Schluenz *J. Polym. Sci., Polym. Chem. Ed.* **19** 1635 (1981)
21. W Sederel *Kunststoffe* **76** 905 (1986)
22. I W Serfary, in *Engineering Thermoplastics: Properties and Applications* (Ed. J M Margolis) (New York: Marcel Dekker, 1985) p. 283
23. H B Kagan, in *Fundamental and Technological Aspects of Organo-f-element Chemistry* (Boston: Reidel, 1985) p. 49
24. P Girard, R Coffignal, H B Kagan *Tetrahedron Lett.* **22** 3959 (1981)
25. N E Brandukova, Ya S Vygodskii, S V Vinogradova *Usp. Khim.* **63** 361 (1994) [*Russ. Chem. Rev.* **63** 345 (1994)]
26. N E Brandukova, Ya S Vygodskii, S V Vinogradova, H Raubach *Acta Polym.* **42** 82 (1991)
27. N E Brandukova, Ya S Vygodskii, T V Strelkova *Vysokomol. Soedin., Ser. A* **38** 1803 (1996) [a]
28. N E Brandukova, Ya S Vygodskii, S V Vinogradova *Vysokomol. Soedin., Ser. A* **36** 10 (1994) [a]
29. O A Platonova, M V Seregina, L M Bronshtein, P M Valetskii, M G Ezernitskaya, I Ya Yanovskaya, Ya S Vygodskii, N E Brandukova *Vysokomol. Soedin., Ser. B* **38** 1619 (1996) [a]
30. A L Rusanov, I A Khotina, M M Begretov, M L Keshtov, A I Kovalev, G I Timofeeva *Vysokomol. Soedin., Ser. A* **40** 909 (1998) [a]
31. S Destri, W Porzio, I A Khotina, C Botta, R Consonni *Macromol. Chem. Phys.* **202** 2572 (2001)
32. I A Khotina, M L Keshtov, S Destri, W Porzio, A L Rusanov, in *V Vserossiiskaya Konf. 'Kondensatsionnye Polimery: Sintez, Struktura, Svoistva', Moskva, 1999* (The Vth All-Russian Conference 'Condensation Polymers: Synthesis, Structure, Properties', Moscow, 1999) P-6
33. A L Rusanov, M L Keshtov, M M Begretov, I A Khotina, A K Mikitaev *Izv. Akad. Nauk, Ser. Khim.* 1229 (1996) [c]
34. I A Khotina, M M Teplyakov, A L Rusanov *Izv. Akad. Nauk, Ser. Khim.* 447 (1994) [c]
35. J S Moore, Z Xu *Macromolecules* **24** 5893 (1991)
36. T Yamamoto, K Honada, N Ooba, S Tomaru *Macromolecules* **31** 7 (1998)
37. W-K Chan, L Yu *Macromolecules* **28** 6410 (1995)
38. A Helber, H-Y Brouwer, D-J Scheer *Macromolecules* **28** 4525 (1995)
39. M Jikei, Y Ishida, Y Seo, M Kakimoto, Y Imai *Macromolecules* **28** 7924 (1995)
40. Z Bao, Y Chen, R Cai, L Yu *Macromolecules* **26** 5281 (1993)
41. A L Rusanov, I A Khotina *Usp. Khim.* **65** 852 (1996) [*Russ. Chem. Rev.* **65** 785 (1996)]
42. K Kondo, M Okuda, T Fujitani *Macromolecules* **26** 7382 (1993)
43. I A Khotina, V A Izumrudov, N V Tchebotareva, A L Rusanov *Macromol. Chem. Phys.* **202** 2360 (2001)
44. J L Kendall, D A Canelas, J L Young, J M De Simone *Chem. Rev.* **99** 543 (1999)
45. T Welton *Chem. Rev.* **99** 2071 (1999)
46. Ya S Vygodskii, E I Lozinskaya, A S Shaplov *Vysokomol. Soedinen., Ser. C* **43** 2350 (2001) [a]
47. E E Said-Galiev, Ya S Vygodskii, L N Nikitin, R A Vinokur, M O Galyamov, A R Khokhlov *Vysokomol. Soedin., Ser. B* **43** 1434 (2001) [a]
48. Ya S Vygodskii, E I Lozinskaya, A S Shaplov *Dokl. Akad. Nauk* **381** 634 (2001) [b]
49. Ya S Vygodskii, E I Lozinskaya, A S Shaplov *Macromol. Rapid Commun.* **23** 676 (2002)
50. V A Vasnev, S I Kuchanov, in *Advances in Polymer Chemistry* (Ed. V V Korshak) (Moscow: Mir, 1986) p. 117
51. K R Papava, V A Vasnev, S V Vinogradova, G D Markova *Acta Polym.* **42** 91 (1991)
52. S V Vinogradova, V A Vasnev *Chem. Rev. Harwood Acad. Publ., Pt. 1* **21** 1 (1995)
53. V A Vasnev, S V Vinogradova, G D Markova, V Yu Voitekunas *Vysokomol. Soedin., Ser. A* **39** 412 (1997) [a]
54. E A Turska *Vysokomol. Soedin., Ser. A* **15** 313 (1973) [a]
55. J Preston, W Black, J Hofferbert *J. Macromol. Sci. Chem.* **7A** 119 (1973)
56. V N Ignatov, A I Kuznetsov, V A Vasnev, I A Gribova, S V Vinogradova, G I Gureeva, B D Lavrukhin, A P Krasnov *Macromolecules* **25** 1652 (1992)
57. A I Kuznetsov, V A Vasnev, I A Gribova, A P Krasnov, G I Gureeva, V N Ignatov *Polymer Yearbook* Vol. 14 (Ed. R A Pethrick) (London: Gordon and Breach, 1997) p. 33
58. V V Istratov, V A Vasnev, A I Tarasov, S V Vinogradova *Vysokomol. Soedin., Ser. B* **44** 357 (2002) [a]
59. V V Istratov, V A Vasnev, A I Tarasov, S V Vinogradova *Ros. Khim. Zh.* **45** 1628 (2001) [d]
60. V V Istratov, V A Vasnev, A I Tarasov, O S Kopysova *Vysokomol. Soedin., Ser. A* **43** 616 (2001) [a]
61. S S Ivanchev, A V Dmitrienko *Usp. Khim.* **51** 1178 (1982) [*Russ. Chem. Rev.* **51** 670 (1982)]
62. M T Bryk, A F Burban *Usp. Khim.* **58** 664 (1989) [*Russ. Chem. Rev.* **58** 394 (1989)]
63. M T Bryk, I A Varavko, O D Kurilenko *Ukr. Khim. Zh.* **41** 1080 (1975)
64. T E Lipatova *Kompozitsionnye Polimernye Materialy* (Composition Materials) (Ed. Yu S Lipatov) (Kiev: Naukova Dumka, 1975)
65. E B Trostyanskaya, A M Poimanov, E F Nosov *Vysokomol. Soedin., Ser. A* **15** 1080 (1973) [a]
66. V A Vasnev, S V Vinogradova *Usp. Khim.* **48** 30 (1979) [*Russ. Chem. Rev.* **48** 16 (1979)]
67. Ya S Vygodskii, N A Churochkina, S V Lavrov, B V Kotov *Vysokomol. Soedin., Ser. A* **41** 1557 (1999) [a]
68. Ya S Vygodskii, A P Krasnov, L S Fedorova, A A Sakharova, O V Afonicheva, I O Volkov *Vysokomol. Soedin., Ser. A* **41** 74 (1999) [a]
69. Ya S Vygodskii, A A Sakharova, A M Matieva *Vysokomol. Soedin., Ser. B* **42** 538 (2000) [a]
70. Ya S Vygodskii, T V Volkova, A A Sakharova, D A Sapozhnikov, A M Matieva *Vysokomol. Soedin., Ser. A* **44** 2096 (2002) [a]
71. Ya S Vygodskii, A M Matieva, A A Sakharova, D F Sapozhnikov, T V Volkova *High Perform. Polym.* **13** (Spec. Issue) 317 (2001)

72. Ya S Vygodskii, T V Volkova, T A Batalova, D A Sapozhnikov, I I Dubovik, L A Chekulaeva *Vysokomol. Soedin., Ser. A* **45** 188 (2003) [a]
73. L I Komarova, S N Salazkin, Ya S Vygodskii, S V Vinogradova *Vysokomol. Soedin., Ser. A* **32** 1571 (1990) [a]
74. Ya S Vygodskii, L I Komarova, Yu V Antipov *Vysokomol. Soedinen., Ser. A* **37** 197 (1995) [a]
75. S V Vinogradova, V A Vasnev, Ya S Vygodskii *Usp. Khim.* **65** 266 (1996) [*Russ. Chem. Rev.* **65** 249 (1996)]
76. A A Askadskii *Struktura i Svoistva Teplostoikikh Polimerov* (Structure and Properties of Heat-Resistant Polymers) (Moscow: Khimiya, 1981)
77. Z Y Wang, Y Qi *Macromolecules* **28** 4207 (1995)
78. M L Keshtov, A L Rusanov, A R Khokhlov, V V Kireev, A A Kirillov, S V Keshtova, F W Harris *Vysokomol. Soedinen., Ser. B* **43** 547 (2001) [a]
79. I A Khotina, S V Tolkachev, A L Rusanov, P M Valetskii *Dokl. Akad. Nauk* **389** 648 (2003) [b]
80. A L Rusanov, L G Komarova, A M Trushin, S A Shevelev, M D Dutov, O V Serushkina, A M Andrievskaya *Vysokomol. Soedin., Ser. B* **35** 883 (1993) [a]
81. A L Rusanov, L G Komarova, M P Prigozhina, T S Sheveleva, A A Askadskii, S A Shevelev, M D Dutov, I A Vatsadze *Vysokomol. Soedin., Ser. B* **38** 2060 (1996) [a]
82. A L Rusanov, L G Komarova, M P Prigozhina, T S Sheveleva, A A Askadskii, K A Bychko, S A Shevelev, M A Dutov, I A Vatsadze, O V Serushkina *Vysokomol. Soedin., Ser. A* **38** 1462 (1996) [a]
83. A L Rusanov, L G Komarova, M P Prigozhina, T S Sheveleva, A A Es'kov, S A Shevelev, M D Dutov, I A Vatsadze *Vysokomol. Soedin., Ser. B* **39** 1701 (1997) [a]
84. A L Rusanov, E G Bulycheva, L B Elshina, S A Shevelev, M D Dutov, I A Vatsadze *Vysokomol. Soedin., Ser. A* **42** 2082 (2000) [a]
85. A L Rusanov, L G Komarova, M P Prigozhina, S A Shevelev, A Kh Shakhnes, S S Vorob'ev *Vysokomol. Soedin., Ser. B* **43** 1430 (2001) [a]
86. V Yu Voitekunas, L G Komarova, M Abadie, A L Rusanov, M P Prigozhina *Vysokomol. Soedin., Ser. A* **44** 768 (2002) [a]
87. A L Rusanov, L G Komarova, M P Prigozhina, S A Shevelev, M D Dutov, O V Serushkina *Vysokomol. Soedin., Ser. B* **44** 2039 (2002) [a]
88. A L Rusanov, M P Prigozhina, L G Komarova, T S Sheveleva, S A Shevelev, M D Dutov, O V Serushkina *Vysokomol. Soedin., Ser. A* **41** 70 (1999) [a]
89. A L Rusanov, L G Komarova, M P Prigozhina, S A Shevelev, M D Dutov, O V Serushkina *Vysokomol. Soedin., Ser. B* **42** 705 (2000) [a]
90. M L Keshtov, Yu N Margalitadze, L Kh Plieva, Z B Shifrina, A L Rusanov, A K Mikitaev *Vysokomol. Soedin., Ser. B* **38** 1066 (1996) [a]
91. A L Rusanov, L G Komarova, M P Prigozhina, S A Shevelev, V I Gulevskaya, A Kh Shakhnes, E F Litvin, L M Kozlova, V Z Sharf *Vysokomol. Soedin., Ser. B* **44** 1276 (2002) [a]
92. A L Rusanov, L G Komarova, M P Prigozhina *Vysokomol. Soedin., Ser. B* **44** 2228 (2002) [a]
93. A L Rusanov, M L Keshtov, N M Belomoina, O N Budylina, A K Mikitaev, F Mercer *Vysokomol. Soedin., Ser. A* **38** 1797 (1996) [a]
94. A L Rusanov, M L Keshtov, N M Belomoina, P V Petrovskii *Vysokomol. Soedin., Ser. A* **41** 66 (1999) [a]
95. G S Matvelashvili, A L Rusanov, V M Vlasov, G V Kazakova, O Yu Rogozhnikova *Vysokomol. Soedin., Ser. B* **37** 1941 (1995) [a]
96. M L Keshtov, A L Rusanov, A A Askadskii, V V Kireev, A A Kirillov, S V Keshtova, F W Harris *Vysokomol. Soedin., Ser. A* **43** 399 (2001) [a]
97. G Maier, S Banerjee, R Hecht, J M Schneider *Am. Chem. Soc. Polym. Prepr.* **39** 798 (1998)
98. A L Rusanov, T A Stadnik, K Müllen *Usp. Khim.* **68** 760 (1999) [*Russ. Chem. Rev.* **68** 685 (1999)]
99. P E Cassidy *J. Macromol. Sci., Rev. Macromol. Chem. Phys.*, **34** 1 (1994)
100. G Hougham, G Tesoro, A Viehbeck, J D Chapple-Sekol *Macromolecules* **27** 5964 (1994)
101. A A Askadskii, A L Rusanov, in *Polyimides and Other Low K Dielectrics (Abstracts of Reports of the 6th International Conference), New York, 1997* p. 12
102. A L Rusanov, M L Keshtov, A A Kirillov, V V Kireev, S V Keshtova, P V Petrovskii *Vysokomol. Soedin., Ser. B* **42** 1947 (2000) [a]
103. A L Rusanov, L B Elshina, E G Bulycheva, K Müllen *Vysokomol. Soedin., Ser. A* **41** 7 (1999) [a]
104. I I Ponomarev, N A Skuratova, S V Lindenman, M K Sinichkin, S V Vinogradova, A L Rusanov *Vysokomol. Soedin., Ser. A* **36** 730 (1994) [a]
105. Z B Shifina, A L Rusanov *Usp. Khim.* **65** 648 (1996) [*Russ. Chem. Rev.* **65** 599 (1996)]
106. O G Nikol'skii, I I Ponomarev, A L Rusanov, S V Vinogradova, V Yu Levin *Vysokomol. Soedin., Ser. B* **32** 636 (1990) [a]
107. I I Ponomarev, O G Nikol'skii, Yu A Volkova, A V Zakharov *Vysokomol. Soedin., Ser. A* **36** 1429 (1994) [a]
108. I I Ponomarev, O G Nikol'skii, A L Rusanov, S V Vinogradova, E S Obolonkova, N G Metvelashvili, V Yu Levin *Vysokomol. Soedin., Ser. B* **32** 637 (1990) [a]
109. L G Komarova, A L Rusanov *Usp. Khim.* **70** 88 (2001) [*Russ. Chem. Rev.* **70** 81 (2001)]
110. *Mod. Plast. Int.* **72** 87 (1995); *Ref. Zh. Khim.* 18T215 (1995)
111. I A Gribova, A P Krasnov, A N Chumaevskaya, H M Timofeeva, N I Antonova *Polymer Yearbook* Vol. 14 (Ed. R A Pethrick) (London: Gordon and Breach, 1997) p. 69
112. V M Svetlichnyi, L A Myagkova, V V Nesterov, N G Bel'nikevich, I V Gofman, G N Gubanova, V E Yudin, T A Kostereva, Yu N Panov, A I Grigor'ev, T E Sukhanova, V V Kudryavtsev *Vysokomol. Soedin., Ser. A* **44** 373 (2002) [a]
113. I V Bulgarovskaya, V M Vozzhennikov, V M Shchechka, D V Pebalk *Vysokomol. Soedin., Ser. B* **39** 131 (1997) [a]
114. V V Kudryavtsev, V P Sklizkova, Yu G Baklagina, Yu N Sazanov, T A Kostereva, A Ya Volkov, N D Stepin, V V Klechkovskaya, V V Belyaev, A Z Kazak-Kazakevich, L A Feigin *Vysokomol. Soedin., Ser. A* **43** 1211 (2001) [a]
115. E I Mal'tsev, D A Lypenko, B I Shapiro, M A Brusentseva, E V Lunina, V I Berendyaev, B V Kotov, A V Vannikov *Vysokomol. Soedin., Ser. A* **41** 1480 (1999) [a]
116. A L Rusanov, M L Keshtov, A N Shchegolikhin, P V Petrovskii, N M Belomoina, S V Keshtova, G I Timofeeva, I A Ronova, K Myullen, F Torgenorot *Izv. Akad. Nauk, Ser. Khim.* 953 (1999) [c]
117. R A Dvorikova, A I Kovalev, Yu I Fedotova, P V Petrovskii, A A Rusanov *Vysokomol. Soedin., Ser. A* **41** 923 (1999) [a]
118. A I Kovalev, A L Rusanov, I A Khotina *Vysokomol. Soedin., Ser. B* **41** 1212 (1999) [a]
119. A L Rusanov, M L Keshtov, N M Belomoina, A N Shchegolikhin, P V Petrovskii, A R Khokhlov, I V Blagodatskikh, A A Askadskii *Vysokomol. Soedin., Ser. A* **42** 404 (2000) [a]
120. A L Rusanov, A L Keshtov, A R Khokhlov, S V Keshtova, A S Peregudov *Vysokomol. Soedin., Ser. A* **43** 581 (2001) [a]
121. M L Keshtov, A L Rusanov, V V Kireev, A A Kirillov, S V Keshtova, B M Uzhinov *Vysokomol. Soedin., Ser. A* **43** 957 (2001) [a]
122. M L Keshtov, A L Rusanov, S V Keshtova, P V Petrovskii, V M Men'shov *Vysokomol. Soedin., Ser. A* **44** 20 (2002) [a]
123. A L Rusanov, M L Keshtov, S V Keshtova, P V Petrovskii, Yu F Kundina *Vysokomol. Soedin., Ser. B* **42** 1931 (2000) [a]
124. A L Rusanov, M L Keshtov, N M Belomoina *Vysokomol. Soedin., Ser. B* **42** 399 (2000) [a]
125. N V Tsvetkov, I V Ksenofontov, V O Kurakina, M S Averina, M L Keshtov, Z B Shifrina, A L Rusanov *Vysokomol. Soedin., Ser. A* **44** 297 (2002) [a]
126. L M Andreeva, S V Bushin, E V Belyaeva, M A Bezrukova, M S Averina, M L Keshtov, Z B Shifrina, A L Rusanov *Vysokomol. Soedin., Ser. A* **44** 248 (2002) [a]
127. A P Tyutnev, M L Keshtov, V S Saenko, E D Pozhidaev, A L Rusanov, Yu I Sezonov *Vysokomol. Soedin., Ser. B* **43** 911 (2001) [a]

128. A L Rusanov, M L Keshtov, N M Belomoina, A N Shchegolikhin, P V Petrovskii, S V Keshtova, A K Blagodatskikh, A K Mikitaev *Vysokomol. Soedin., Ser. B* **40** 902 (1998) [a]
129. M L Keshtov, A L Rusanov, V V Kireev, S A Keshtova, P V Petrovskii, A A Karimov *Vysokomol. Soedin., Ser. A* **43** 963 (2001) [a]
130. P A Staniland, in *Comprehensive Polymers Sciences: The Synthesis, Characterisation, Reactions and Applications of Polymers* Vol. 5 (Oxford, New York: Pergamon Press, 1989) p. 473
131. V V Shaposhnikova, S N Salazkin, K I Donetskii, G V Gorshkov, A A Askadskii, K A Bychko, V V Kazantseva, A V Samoryadov, A P Krasnov, B S Lioznov, O V Afonicheva, N A Svetlova, A S Kogan, A S Tkachenko *Vysokomol. Soedin., Ser. A* **41** 217 (1999) [a]
132. V V Kazantseva, A A Askadskii, S N Salazkin, V V Shaposhnikova, T I Kiseleva, K I Donetskii *Vysokomol. Soedin., Ser. B* **43** 125 (2001) [a]
133. S N Salazkin, V V Shaposhnikova, K I Donetskii, G V Gorshkov, P V Petrovskii, L I Komarova, M M Genina, A S Tkachenko *Izv. Akad. Nauk, Ser. Khim.* 1099 (2000) [c]
134. V V Shaposhnikova, S N Salazkin, K I Donetskii, G V Gorshkov, D S Shirapov, I A Mamedova, P V Petrovskii, A A Askadskii, K A Bychko, V V Kazantseva, A P Krasnov, O V Afonicheva, A S Tkachenko, M M Genina *Vysokomol. Soedin., Ser. A* **44** 925 (2002) [a]
135. S N Salazkin, K I Donetskii, G V Gorshkov, V V Shaposhnikova, Ya V Genin, M M Genina *Vysokomol. Soedin., Ser. A* **39** 1431 (1997) [a]
136. V V Shaposhnikova, K I Donetskii, G V Gorshkov, S N Salazkin *Am. Chem. Soc. Polym. Prepr.* **38** 253 (1997)
137. S N Salazkin, K I Donetskii *Dokl. Akad. Nauk* **362** 789 (1998) [b]
138. S N Salazkin, K I Donetskii, G V Gorshkov, L I Komarova, in *V Vserossiiskaya Konf. 'Kondensatsionnye Polimery: Sintez, Struktura, Svoistva', Moskva, 1999* (The Vth All-Russian Conference 'Condensation Polymers: Synthesis, Structure, Properties', Moscow, 1999) p. 1-6
139. K I Donetskii, S N Salazkin, G V Gorshkov, V V Shaposhnikova *Dokl. Akad. Nauk* **350** 213 (1996) [b]
140. L V Dubrovina, S N Salazkin, G I Timofeeva, K I Donetskii, T P Bragina, L Z Rogovina *Vysokomol. Soedin., Ser. A* **43** 2170 (2001) [a]
141. A L Rusanov, M L Keshtov, S V Keshtova, N M Belomoina, A N Shchegolikhin, A K Mikitaev, A A Askadskii *Vysokomol. Soedin., Ser. B* **39** 1539 (1997) [a]
142. M L Keshtov, A L Rusanov, S V Keshtova, P V Petrovskii, G B Sarkisyan *Vysokomol. Soedin., Ser. A* **43** 2059 (2001) [a]
143. M L Keshtov, A L Rusanov, S V Keshtova, A N Shchegolikhin, P V Petrovskii *Vysokomol. Soedin., Ser. A* **43** 2071 (2001) [a]
144. R M Kumykov, E G Bulycheva, A A Beev, in *V Vserossiiskaya Konf. 'Kondensatsionnye Polimery: Sintez, Struktura, Svoistva', Moskva, 1999* (The Vth All-Russian Conference 'Condensation Polymers: Synthesis, Structure, Properties', Moscow, 1999) p. 1-12
145. A L Rusanov, M L Keshtov, S V Keshtova, N M Belomoina, A K Mikitaev, A N Shchegolikhin *Vysokomol. Soedin., Ser. A* **40** 397 (1998) [a]
146. A L Rusanov, G B Sarkisyan, M L Keshtov *Vysokomol. Soedin., Ser. A* **41** 27 (1999) [a]
147. S V Vinogradova, P M Valetskii, Yu A Kabachii *Usp. Khim.* **64** 390 (1995) [*Russ. Chem. Rev.* **64** 365 (1995)]
148. B A Zachernyuk, E D Savin, V I Nedel'kin *Vysokomol. Soedin., Ser. C* **44** 2322 (2002) [a]
149. S V Vinogradova, D R Tur, V A Vasnev *Chem. Rev. Harwood Acad. Publ., Pt. 1* **24** 1 (1998)
150. S V Vinogradova, D R Tur, V A Vasnev *Usp. Khim.* **67** 573 (1998) [*Russ. Chem. Rev.* **67** 515 (1998)]
151. Yu D Semchikov, M N Bochkarev *Vysokomol. Soedin., Ser. C* **44** 2293 (2002) [a]
152. S A Ponomarenko, N I Boiko, V P Shabaev *Vysokomol. Soedin., Ser. C* **43** 1601 (2001) [a]

[a] — *Polym. Sci. (Engl. Transl.)*
[b] — *Dokl. Chem. (Engl. Transl.)*
[c] — *Russ. Chem. Bull., Engl. Ed. (Engl. Transl.)*
[d] — *Mendeleev Chem. J. (Engl. Transl.)*

Russian Chemical Reviews **73** (5) 501 – 515 (2004) © 2004 Russian Academy of Sciences and Turpion Ltd

DOI 10.1070/RC2004v073n05ABEH000782

Nanostructured polymeric systems as nanoreactors for nanoparticle formation

L M Bronstein, S N Sidorov, P M Valetsky

Contents

I.	Introduction	501
II.	Nanoparticle formation in amphiphilic block copolymers	501
III.	Formation of metal nanoparticles in polyelectrolyte systems with regular morphologies	505
IV.	Synthesis of dendrimer-encapsulated metal nanoparticles	506
V.	Metal nanoparticle formation in cavities (pores) of a polymer matrix	507
VI.	Properties of nanostructured polymeric systems containing metal nanoparticles	510

Abstract. The review concerns the syntheses of polymeric nanocomposites containing encapsulated nanoparticles formed in nanostructured polymeric systems including block copolymers, dendrimers, nanoporous polymers, polyelectrolyte gel – surfactant complexes and multilayered films. Nanostructures in amphiphilic block copolymers can form spontaneously both in the bulk (block microsegregation) and in solution (block copolymer micelle). In polymeric systems, nanostructures play the role of nanoreactors for the growing nanoparticles. The nanoparticle size, shape and size distribution are controlled by the nanostructure characteristics and synthesis conditions. The catalytic, magnetic and optical properties of these nanostructured polymeric nanocomposites are discussed. The bibliography includes 131 references.

I. Introduction

At present, increasing interest in the synthesis of nanoparticles and nanosystems and in the studies on their properties has been expressed.[1–3] Various methods for the synthesis of nanoparticles and the properties of these systems have been thoroughly reviewed (see Refs 4, 5 and 6 – 8, respectively). However, no systematic review of nanoparticle formation in nanostructured polymeric systems has been reported so far.

Nanostructures in a polymeric composite are defined as regular nanosized heterogeneous domains (*i.e.*, certain regions of the polymeric material that are separated by some interface). Due to the presence of nanostructures one can control the growth of nanoparticles, the particle size distribution and interfacial interactions. These factors are to a great extent responsible for the unique catalytic, magnetic, semiconductor, nonlinear optical, *etc.* properties of nanocomposites and, finally, for the fields of their application. Nanostructured matrices are quite promising for being used for nanoparticle formation. This is indicated by the tremendous progress achieved during the decade that has passed since the first use of block copolymers (the first representatives of nanostructured polymeric systems) for the formation of metal nanoparticles. At present, it is possible to obtain nanoparticles of different shape and size (*e.g.*, nanotubes, nanowires and other nanoscale objects) in nanostructured polymeric environment using various polymeric systems and different approaches.

L M Bronstein, S N Sidorov, P M Valetsky A N Nesmeyanov Institute of Organoelement Comounds, Russian Academy of Sciences, ul. Vavilova 28, 119991 Moscow, Russian Federation. Fax (7-095) 135 50 85. Tel. (7-085) 135 93 00. E-mail: lybronst@indiana.edu (L M Bronstein), dist@ineos.ac.ru (S N Sidorov). Tel. (7-095) 135 93 07. E-mail: val@ineos.ac.ru (P M Valetsky)

Received 16 October 2002
Uspekhi Khimii **73** (5) 542 – 558 (2004); translated by A M Raevsky

II. Nanoparticle formation in amphiphilic block copolymers

A feature of amphiphilic block copolymers is the ability to undergo microsegregation in the bulk and to form micelles in dilute solutions in selective solvents.[9–11] To synthesise nanoparticles, one block of a diblock or triblock copolymer must contain functional groups that can be involved in reactions with metal compounds.

1. Nanoparticles in microsegregated blocks

Block copolymers containing incorporated complexes or encapsulated nanoparticles in a specified block can be prepared in several ways. These are, *e.g.*, copolymerisation of organometallic monomers followed by corresponding transformations of the system; reactions of metal complexes with functional groups of block copolymers in solutions followed by microsegregation of the organometallic block copolymers (either in the form of films or in the bulk); and sorption of organometallic compounds into microdomains of block copolymer films. The sorption of metal complexes into diblock and triblock copolymers causes significant changes in the properties of polymeric systems (first of all, in the Flory – Huggins interaction parameter χ_{AB}). One can expect the greatest changes in χ_{AB} for non-polar flexible blocks, *e.g.*, polyisoprene (PI) or polybutadiene (PB) due to the appearance of polar groups and to the change in the chain conformation.

A typical example is provided by the introduction of $Fe(CO)_3$ groups into the PB block of a polystyrene – PB – polystyrene triblock copolymer (Kraton) containing 30 mol.% of polystyrene (PS) *via* complexation.[12] Complexation leads to a considerable increase in the force of adhesive binding of the polymer film to polar surfaces (glass, metals) and in the rigidity of the PB block (the higher the iron concentration, the higher the glass transition temperature of the PB block) and causes reduction of the PB block mobility. At the same time, in spite of significant changes in the chemical structure, the material retains its morphology ('cylinders in matrix').

A similar mophological stability was also observed in highly assymetrical diblock ionomers in which the shorter polyacrylic

acid (PAA) block forms spherical microdomains encapsulated in the matrix of the major component (PS).[13] It was found that neither sorption of Cd^{2+} ions nor formation of CdS nanoparticles change the block copolymer morphology. Experiments with a diblock copolymer based on isoprene and 2-vinylpyridine (2VP) showed [14] that at low content of palladium nanoparticles the block copolymer retains its lamellar structure and that an increase in the palladium content causes distortion of the ordered (regular) structure. The growth of nanoparticles influences the block copolymer structure. The system is also characterised by feedback, namely, the interfaces between different domains and the free surfaces of the polymer films affect the formation of nanoparticles inside the block copolymer microphase. In particular, as was shown by transmission electron microscopy (TEM), the size of the growing silver,[15] palladium [14, 16] (Fig. 1) and other metal nanoparticles confined within microsegregated layers is limited to the corresponding layer thicknesses. Almost no penetration of the metal seeds and growing particles into adjacent non-polar layers was observed; *i.e.*, the block copolymer domain acts as a nanoreactor in the formation of metal nanoparticles. The synthesis of nanoparticles in thick homopolymer films led to uncontrolled growth of nanoparticles and resulted in large particles characterised by a broad size distribution.[15] As the thickness of the metal-containing homopolymer film decreased down to the characteristic lamella size in the block copolymer ($\sim$100 nm), the free surface of the thin film behaved as an interface.[15]

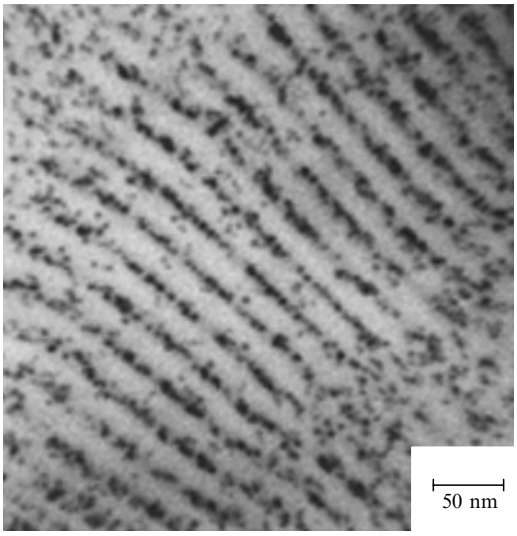

Figure 1. TEM image of a sample prepared by reduction of the system [polyisoprene-*block*-poly(2-vinylpyridine)] – $Pd(acac)_2$ – benzyl alcohol with a component ratio of 32.5 : 2.6 : 64.9 (mass %) after evaporation of the solvent.[16]

Metal nanoparticles encapsulated in multilayered thin films based on block copolymers were synthesised analogously.[17] The films were prepared by adsorption of symmetrical PS and poly(4-vinylpyridine) (P4VP), which form a lamellar structure, in the bulk, on a solid substrate. These films (they resemble multilayered films fabricated by adsorption of oppositely charged polyelectrolytes) were pre-loaded with a metal compound (*e.g.*, $HAuCl_4$) and then with the reducing agent. Nanoparticles were formed only within the P4VP block. It was shown that nanoparticles can affect the lamella size.[18] The best ordered arrangement of nanoparticles in multilayered block copolymer films was obtained for the films prepared under nonequilibrium conditions that provided the possibility for highly asymmetrical nanoparticles to be formed.[19, 20]

Sometimes, particle formation in the nanoreactor causes significant changes in the reaction conditions. For instance, cobalt ferrite ($CoFe_2O_4$) is usually obtained by high-temperature synthesis from corresponding hydroxides. If $CoFe_2O_4$ nanoparticles are formed inside the block copolymer domains,[21] the reaction can proceed at room temperature.

2. Metal nanoparticles in block copolymer micelles

a. Formation of metal nanoparticles in block copolymer micelle cores

Amphiphilic block copolymers dissolved in selective solvents (they dissolve only one block) form micelle. The size and shape of these objects depend on the nature of the blocks, the type of solvent (to a first approximation, a hydrophilic or hydrophobic one) and on the molecular mass of the blocks.[9, 11] If, in the case of diblock and triblock copolymers, the micelle core comprises a block containing certain groups capable of being involved in reactions with metal compounds to give metal complexes or salts, this core can be loaded with the corresponding metal constituent of the complex or salt and then used as a nanoreactor for metal nanoparticle formation. Appropriate block materials include, *e.g.*, poly(2-vinylpyridine) (P2VP) or P4VP, polymethacrylic acid (PMAA) or PAA, PB or PI and some other polymers. The micelle corona must be built of a block that contains no functional groups but provides the solubility and stability of micelles in corresponding solvents. Materials appropriate in this case include PS, poly(ethylene oxide) (PEO), polyisobutylene (PIB) and other polymers.

The synthesis of metal nanoparticles in block copolymer micelle cores was nearly simultaneously employed by several research groups.[13, 22–25] Studies on the formation of gold, palladium, platinum and other metal nanoparticles in PS-*block*-P4VP-based micelles revealed that the nanoparticle morphology strongly depends on the type of the reducing agent. With 'sluggish' reducing agents only one particle can be formed in the micelle core in the absence of inter-micellar exchange reactions. Using 'fast' reducing agents, the nucleation and growth of a large number of particles occur simultaneously; therefore, each micelle contains many small particles. This morphology is most preferable for catalysis (Fig. 2).[26] Both morphologies are schematically shown in Fig. 3. To prevent inter-micellar exchange, the micelle cores can be cross-linked. Then, variation of the reducing agent permits fine control of not only the particle morphology but also the particle size.[27] Using micelle cores as nanoreactors, both monometallic and bimetallic nanoparticles can be synthesised; their morphologies depend on the nature of the metal employed.[28] Adsorption of nanoparticle-containing micelles onto different substrates results

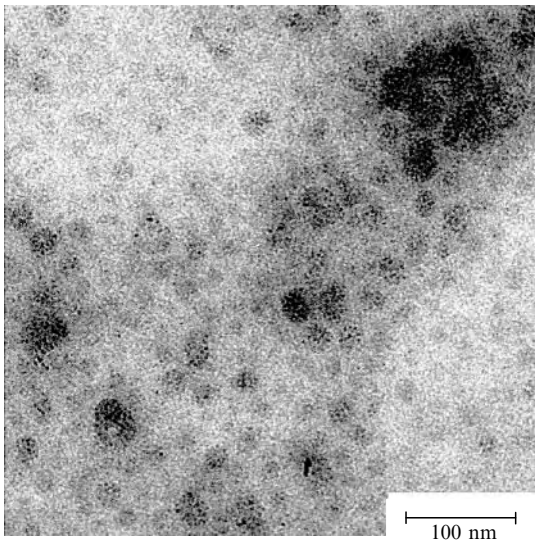

Figure 2. TEM image of bimetallic Pd – Pt nanoparticles formed in PS-*block*-P4VP-based micelles.[26]

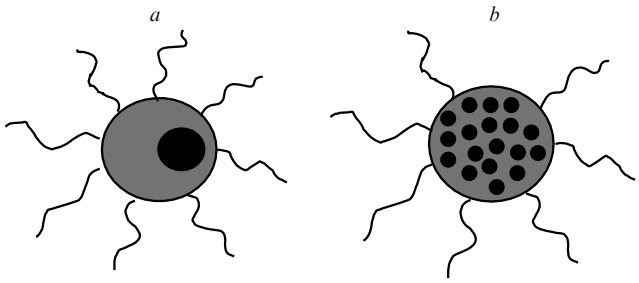

Figure 3. Schematic representation of nanoparticles with 'cherry' (*a*) and 'raspberry' (*b*) morphologies.

in the formation of monomolecular layers; this phenomenon is used in nanolithography.[29]

Nanoparticles confined within micelle cores can also be prepared using star-like block copolymers. For instance, block copolymer micelles based on star-like block copolymers with a P2VP core and PS shell were used [30] to form gold nanoparticles with a narrow size distribution. It is believed [30] that star-like polymer micelles are more stable, thus being responsible for the nanoreactor stability and improved control of particle growth.

When using a triblock copolymer in which only the middle block can be coordinated by metal compounds, and nanoparticles can be formed within the outer layer of the core rather than the entire core space when the middle block and one of the two terminal blocks are insoluble in the reaction medium. This can be exemplified by the synthesis of gold nanoparticles in PS-*block*-P2VP-*block*-PEO micelles in aqueous solutions.[31] Such systems can be of particular interest for catalysis, because nanoparticles present in the outer layer of the core are better accessible to substrates.

Analogously to the synthesis of nanoparticles in block copolymer micelle cores in organic media, metal nanoparticles can be produced in aqueous media; however, only a few block copolymers are available in this case, *e.g.*, PEO-*block*-P2VP and PEO-*block*-PB.[32, 33] In the former system, the situation is complicated by the fact that micellisation of the polymer depends on the pH value of the medium (at pH < 5, the PEO-*block*-P2VP micelles undergo disassembling). Nevertheless, in the presence of metal compounds or after formation of nanoparticles micelles are retained even in acid media; however, they become very loose. The reverse situation is observed in the case of PEO-*block*-PB. In water, this block copolymer forms very dense micelles that can act as both nanoreactors for the formation of palladium, platinum or rhodium nanoparticles and excellent templates for mesoporous silica formation.[33] Such systems are of great interest as promising heterogeneous catalysts of various reactions.

Not only micelle cores (see above) but also the inner micelle corona layer can be cross-linked to stabilise the nanoreactor. Triblock copolymers comprised of PEO, poly(glycerol monomethacrylate) (PGMA) and poly(diethylaminoethyl methacrylate) (PDEAEMA) blocks [poly(2-hydroxyethyl methacrylate), PHEMA, was also used as the middle block] completely dissolved in water at low pH values but formed multilayered onion-like micelles with PDEAEMA cores at pH > 7–8.[34] The middle block in the micelles was cross-linked by reaction with divinyl sulfone. These micelles were used as nanoreactors for the formation of gold nanoparticles. The authors [34] believe that the micelles cross-linked in the corona interior provide the stability of nanoparticles and prevent inter-micellar reactions. Yet another possible advantage of these micelles is a substantial increase in their loading without deterioration of sedimenting stability; however, this has not been confirmed so far.

Another approach was employed to form ferrous oxide nanoparticles in PI–poly(2-cinnamyl methacrylate)–poly(*tert*-butyl acrylate) (PI-*block*-PCM-*block*-PtBA) cross-linked triblock copolymer micelles in a THF–hexane mixture.[35] These micelles are comprised of a PI corona and two core layers with PCM as the outer layer and PtBA as the inner layer. The PCM layer was cross-linked by exposure to UV radiation, which resulted in the formation of stable nanospheres. Subsequent hydroxylation of the PI block to impart hydrophilic properties to the nanospheres was followed by removal of the *tert*-butyl groups to allow the nanosphere cores to react with metal compounds. The possibility of using such nanospheres as nanoreactors was demonstrated by taking the formation of magnetic ferrous oxide particles with a narrow size distribution as an example. However, this technique is very labour-consuming and seems to be of little promise.

We believe that targeted synthesis of block copolymer micelles opens up great prospects for the design of materials suitable for the fabrication of various devices. However, anionic polymerisation employed for the synthesis of most block copolymers is a quite expensive method. Besides, it is very sensitive to external factors, which hampers progress in this area of research. Another method, namely, charge transfer radical polymerisation, is thought to be a cheaper and more reproducible method of synthesis of block copolymers with a narrow molecular mass distribution.[36, 37]

b. Double hydrophilic block copolymers. Micellisation during complexation

In some cases, a metal compound incorporated into a polymer matrix can induce nanostructuring of the matrix. This is observed when using, *e.g.*, the so-called 'double hydrophilic' block copolymers comprised of blocks with similar hydrophilicities. One block must contain functional groups while the other block must be inert towards metal compounds. Dissolution of such a block copolymer in water results in a true solution, but the addition of some metal salts can induce micellisation due to coordination of the metal by one of the blocks (Fig. 4).[38] In this case micelles are formed and exist due to the coordination between the metal ions and functional groups of the polymer. Such block copolymers can be obtained by simply coupling two blocks after relevant functionalisation.[39] Another 'double hydrophilic' block copolymer, poly(ethylene oxide)-*block*-poly[(*N*-carboxymethyl)ethyleneimine] (PEO-*block*-PCMEI), was designed for controlled mineralisation (control of formation of $CaCO_3$ nanoparticles), because PCMEI can interact with calcium ions.[40]

Poly(ethylene oxide)-*block*-polyethyleneimine (PEO-*block*-PEI) was proposed for the synthesis of transition metal nanoparticles in aqueous media because the PEI block readily interacts with these metal ions affording coordination compounds.[38] The

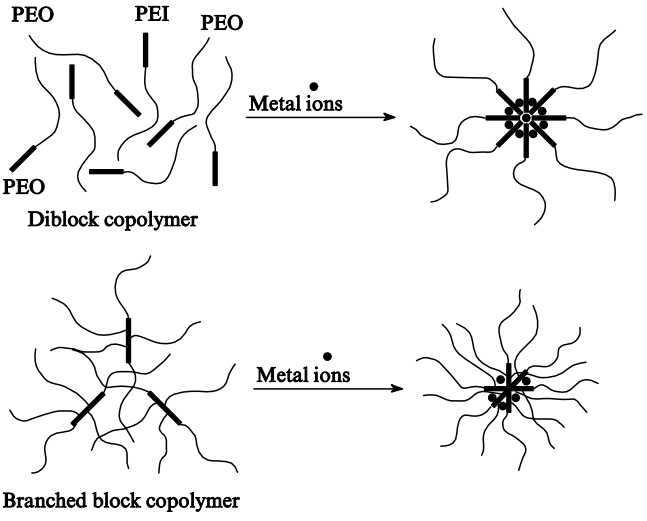

Figure 4. Scheme of micelle formation in PEO-*block*-PEI due to the interaction with metal ions in aqueous solution.[38]

PEI blocks undergo aggregation, thus formng the micelle core, while the PEO blocks form the micelle corona. These micellar systems can control the nucleation and growth of nanoparticles analogously to the amphiphilic block copolymer micelles described above. Moreover, a typical amphiphilic block copolymer, PEO-*block*-P2VP, also becomes soluble on the molecular level at pH < 5 and behaves like PEO-*block*-PEI in the reactions with metal compounds. Reduction of the metal ions is accompanied by the formation of nanoparticles, yet the PEO-*block*-PEI micelles do not decompose; only their hydrodynamic characteristics are changed (Table 1). This block copolymer was successfully used to form CdS nanoparticles [41] which exhibited oxidative stability for many months due to the polymeric environment. By varying the polymer concentration and the type of the solvent the nanoparticle size was varied from 2 to 4 nm.

Table 1. Hydrodynamic diameter (D_h) and its standard deviation (σ) for Pt-containing PEO-*block*-PEI micelles.[39]

Polymeric system	Molar ratio PEI : Pt	D_h /nm	σ (%)
PEO-*block*-PEI + H_2PtCl_6	8 : 1	138	32
	4 : 1	154	29
	2 : 1	176	32
	1 : 1	201	30
PEO-*block*-PEI + Na_2PtCl_6	8 : 1	210	29
PEO-*block*-PEI + K_2PtCl_4	8 : 1	578	115
PEO-*block*-PEI + H_2PtCl_6 reduced with $N_2H_4 \cdot H_2O$	4 : 1	110	24
PEO-*block*-PEI + H_2PtCl_6 reduced with H_2	4 : 1	149	27

To control the morphology of nanoparticles formed, one can use the relations described for amphiphilic block copolymer micelles. The nanoparticle morphology is affected by the nature of the reducing agent, the concentration of the metal compound and the pH value of the medium. Unlike amphiphilic block copolymer micelles, the micelles obtained *via* complexation are loose, which favours inter-micellar exchange of metal ions and prevents control of the growth of nanoparticles.

c. Nanoparticle formation in micelle coronas

Metal nanoparticles can be synthesised in coronas of amphiphilic block copolymer micelles. If the micelle corona contains no groups suitable to coordination by metal compounds, nanoparticles are stabilised only by the hydrophobic interactions with the core. This procedure was employed to synthesise palladium, platinum and gold nanoparticles stabilised in aqueous solutions of PS-*block*-PEO and PS-*block*-PMAA.[42, 43] It was shown that the reduction of metal compounds results in the formation of small nanoparticles and that stabilisation of the nanoparticles exclusively due to hydrophobic interactions with the PS micelle cores is insufficient for obtaining solutions with high sedimenting stability. At the same time, accessibility of the nanoparticles in the micelle corona can play an important role for applications of such systems in catalysis.

To make the nanoparticles located within coronas of amphiphilic micelles more stable, it was proposed to design hybrid systems comprising amphiphilic block copolymers and surfactants.[44–46] It was assumed that the hydrophobic surfactant 'tails' would penetrate hydrophobic PS-*block*-PEO micelle cores while the charged groups of the surfactant would be arranged at the core surface (Fig. 5). Exchange of the surfactant counterions by platinum, palladium or rhodium ions was assumed to enable the loading of the corona with metal ions.

Light scattering and ultracentrifugation experiments showed that hybrid systems PS-*block*-PEO–surfactant have a complex structure and comprise micelles, micellar clusters and supermicellar aggregates. The addition of positively or negatively charged

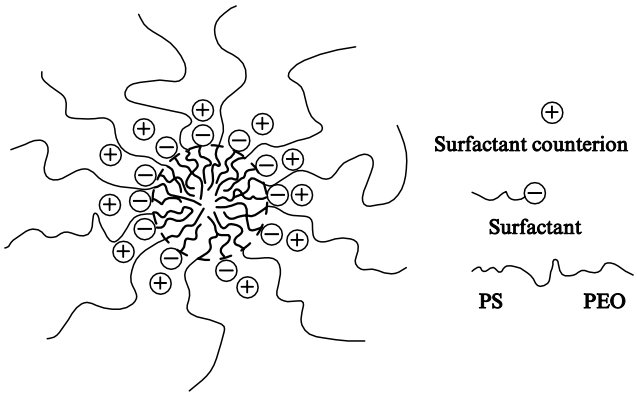

Figure 5. Schematic illustration of PS-*block*-PEO micelles containing anionic surfactant.[38]

surfactants to the PS-*block*-PEO micellar solutions causes an increase in the size and mass of micelles and micellar clusters. This holds until a certain surfactant concentration is reached, which depends on the type of the surfactant. An increase in the concentration [as a rule, above the critical micelle concentration (CMC)] causes a decrease in the size of micelles and micellar clusters. ^{1}H NMR studies revealed that the addition of surfactant significantly enhances the mobility in the PS core, which confirmes co-micellisation of the block copolymer and cationic (or anionic) surfactant molecules. Ion exchange of cetylpyridinium chloride (CPC) counterions by $PtCl_6^{2-}$ or $PdCl_4^{2-}$ ions in the system PS-*block*-PEO/CPC leads to saturation of the micellar structures with palladium or platinum ions. Subsequent reduction of the metal-containing systems thus obtained with sodium borohydride or dihydrogen is accompanied by the formation of (mostly) micelle-encapsulated metal nanoparticles. The morphology and stability of the palladium and platinum nanoparticles synthesised in these systems depend on the type of the reducing agent and on the metal salt concentration. Reduction with $NaBH_4$ results in breakdown of micellar clusters and formation of micelles containing encapsulated nanoparticles (Fig. 6). These systems exhibited very high stability for one year, provided that the metal salt concentration was at most 1.24×10^{-2} mol litre^{-1}. Reduction with dihydrogen results in the formation of metal nanoparticles both in micelles and in micellar clusters. In this case, colloid solutions were stable at the metal salt concentrations of at most 3.36×10^{-3} mol litre^{-1}. Platinum particles formed using the reducing agents

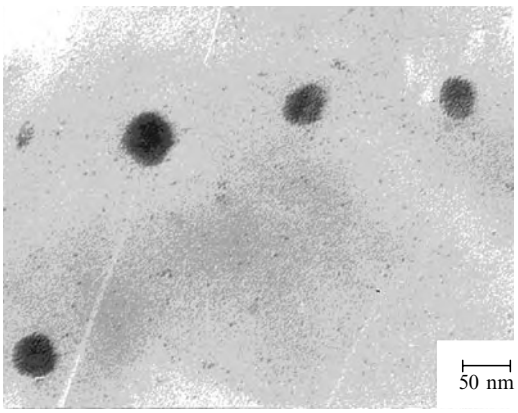

Figure 6. TEM micrograph of platinum nanoparticles obtained *via* reduction of $H_2PtCl_6 \cdot 6\,H_2O$ (1.24×10^{-2} mol litre^{-1}) with sodium borohydride and stabilised in the PS-*block*-PEO/CPC hybrid micelles in water.[44]

mentioned above were 2–4 nm in diameter, while palladium particles were somewhat larger (4 to 6 nm in diameter).

If the metal salt ions exist only in the form of cations, one can use hybrid systems containing an anionic surfactant, sodium dodecyl sulfate (SDS). For instance, the hybrid system PS-*block*-PEO/SDS allows sodium counterions to be exchanged with rhodium ions generated during dissociation of $[Rh(Py)_4Cl_2]Cl \cdot 6\,H_2O$. Reduction of the system thus obtained with sodium borohydride also leads to saturation of micelles with rhodium nanoparticles of sizes 2–3 nm. Thus, by adding surfactants to 'inert' (containing no functional groups) amphiphilic micelles, one can use them as a good stabilising system for the formation of metal nanoparticles of size 2 to 6 nm. The drawback of this approach is the absence of direct methods of varying the nanoparticle size.

An interesting method of transformation of core-embedded nanoparticles into corona-embedded ones has been reported.[47] When a solution of PS-*block*-P2VP–CdS micelles in an organic solvent was placed in an aqueous medium characterised by a low pH value, the PS block collapsed and a PS core was formed (in the organic medium, the core consisted of the P2VP block). Simultaneously, protonation-induced dissolution of the P2VP block occurred. Protonated (charged) P2VP formed the micelle corona and stabilised the CdS nanoparticles grown in the P2VP core in organic solvent. This permitted fine control of the growth of nanoparticles.

III. Formation of metal nanoparticles in polyelectrolyte systems with regular morphologies

1. Formation of nanoparticles in polystyrenesulfonate microgels

Microgels are spherical particles several nanometres in diameter.[48,49] Taking into account the structure-stabilising factors, *viz*., the size and cross-linked structure of microgels, they can be treated as nanoreactors, or molecular containers that allow the growth of nanoparticles to be controlled. Taking the reduction of gold compounds in these microgels as an example, the nanoparticle formation was studied.[50] The effects of the reduction rate and of the characteristics of the microgel on the nanoparticle parameters was studied. It was found that fast reduction of gold compounds with sodium borohydride in water results in the formation of small gold particles (4.5 nm in diameter according to X-ray diffraction data) in microgels. Slowing down the reduction using sodium borohydride in alkaline solution (0.1 M NaOH) changed the nanoparticle morphology, namely, long 'filaments' (according to X-ray diffraction and TEM data) were formed from the particles 7 nm in diameter. Very slow reduction with hydrazine hydrate led to the formation of large particles (25 nm), which were found only in 15% of the microgel (85% of the microgel contained no gold particles at all). Apparently, in the case of sluggish nucleation, small clusters and metal ions non-uniformly migrate towards disordered microgel domains and then easily undergo aggregation. Clearly, microgels with disordered morphologies cannot be used to control nanoparticle growth.

Yet another parameter, which strongly affects both the nanoparticle and the entire sample morphology, is the degree of cross-linking of the microgel. The larger this parameter, the higher the probability of formation of spherical metal nanoparticles encapsulated in microgels. A high resolution TEM study confirmed the fact that nanoparticles grew from the same core and that the exterior of the particles was governed by the microgel environment. In the experiments with $NaBH_4$, the particle growth was controlled by the elasticity of the surrounding gel matrix. This means that particles grow along a given direction until the surrounding polymer chains become completely aligned in this direction. Thus, the system ensures the 'cage' effect though the 'cage' itself is not rigid.

In addition to gold nanoparticles, this method was employed to synthesise palladium and platinum nanoparticles.[51] Microgel-grown nanoparticles and amphiphilic PS-*block*-PEO copolymers were used as templates for obtaining mesoporous silica. Hence, microgels can have two functions, namely, to act as nanoreactors for the formation of metal nanoparticles and to serve as pore-forming templates in the formation of mesoporous silica.

2. Polyelectrolyte gel–surfactant complexes as nanostructured media for the interaction with metal ions and formation of metal nanoparticles

Polyelectrolyte gel complexes with oppositely charged surfactants are highly ordered self-organised nanostructures. They have been the subject of intensive research in the last decade.[52–57] The SAXS spectra of the cationic gel–anionic surfactant and anionic gel–cationic surfactant complexes exhibit very sharp and intense peaks indicating the presence of large ordered surfactant domains in gel. Statistical disorder in gel has no effect on the regular ordered arrangement of surfactant aggregates. Moreover, at the same surfactant concentration the surfactant molecules in oppositely charged gels are better ordered compared to aqueous media.[57] Spatial ordering in the gel–surfactant complexes is of interest from the standpoint of preparation of a nanostructured medium for the formation of metal nanoparticles.

It was established that sorption of metal ions by hydrogel–surfactant complexes occurs when the charges of the ions and of the charged groups of the gel are opposite in sign.[58–60] The ions sorbed form metal compound clusters arranged between the charged groups of the polymer chain and the head groups of the surfactant molecules (Fig. 7). These clusters serve as the nucleation centres of metal nanoparticles. In the case of fast reduction, particles are formed in an ordered environment. Moreover, the surfactant molecules in the immediate vicinity of the growing particles are even more ordered (though generally the growth of nanoparticles makes the surfactant more disordered), thus providing an extra means for control of the particle growth, which results in a narrow particle size distribution (Fig. 8).[60] This effect is observed for various metal compounds and hydrogel–surfactant complexes. In the case of slow nucleation, small clusters and metal ions non-uniformly migrate towards the disordered region of hydrogel and then undergo aggregation into large particles characterised by a broad size distribution. Polyelectrolyte gels without nanostructured morphologies cannot be used to control the growth of metal nanoparticles.

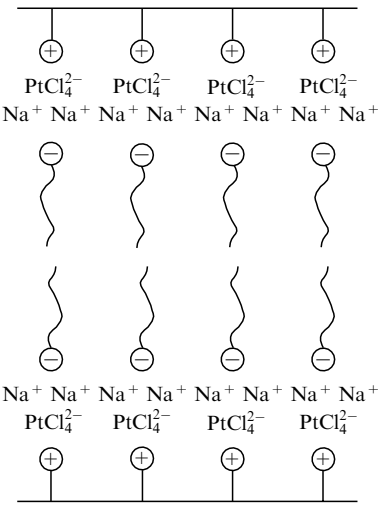

Figure 7. Schematic view of hydrogel–surfactant complexes with a sorbed metal salt.

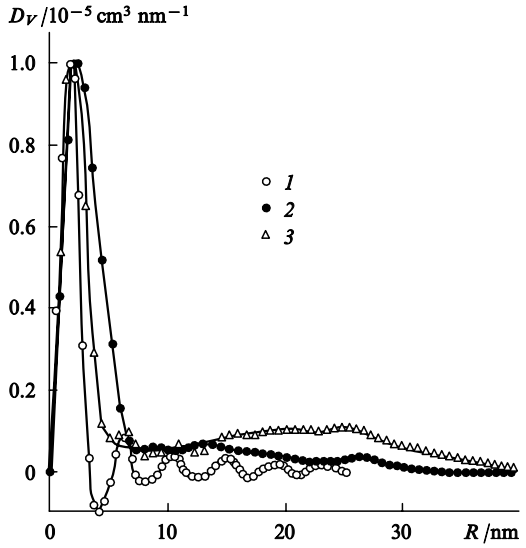

Figure 8. Volume distribution functions obtained for poly(diallyldimethylammonium chloride) hydrogel – sodium dodecylbenzosulfonate complex containing $H_2Pt(OH)_2Cl_4$ clusters (*1*) and encapsulated platinum nanoparticles reduced with $NaBH_4$ (*2*) and $N_2H_4 \cdot H_2O$ (*3*).[60]
R is the particle radius.

3. Nanoparticle formation in thin layers of supported polyelectrolytes

Thin polyelectrolyte layers are prepared by depositing a polyelectrolyte layer onto a charged substrate. This can be followed by layer-by-layer deposition of oppositely charged polyelectrolytes (Fig. 9).[61] Nanoparticles can also be used as 'substrates.' This permits preparation of various core – shell materials or hollow spheres.[62,63] These multilayered materials are treated as nanostructured systems in which each layer is a nanoreactor. For instance, cadmium sulfide nanoparticles were prepared[64] by sequential deposition of cadmium polystyrenesulfonate and polyvinylpyridine layers on PEI-modified silica or other substrates. Then, the multilayered film was exposed to H_2S for 30 min at room temperature, which resulted in a hybrid system containing CdS nanoparticles. Silver nanoparticles were produced in multilayered polyelectrolyte films based on PAA and protonated polyamine.[65] Repeated treatment with the silver salt (carboxyl groups are released after formation of nanoparticles on exposure to UV radiation) permitted an increase in the metal content in the film from 4% to 24%.

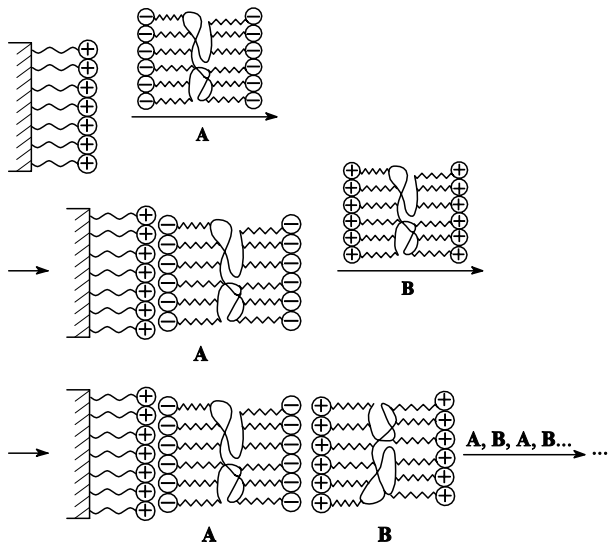

Figure 9. A scheme showing the formation of polyelectrolyte layers involving layer-by-layer adsorption of cationic and anionic polyelectrolytes (counterions are not shown).[61]

In order to provide better control of the particle growth, nanoparticles are sometimes prepared in surfactant micelles, which are then incorporated into polyelectrolytes to give multilayered films containing nanoparticles.[66] In this case, nanoparticles grow outside the polymeric system, which goes beyond the scope of this review. However, this approach is noteworthy. Indeed, recent studies revealed that, in contrast to amphiphilic block copolymers, multilayered composites are characterised by the presence of broad transient regions between each pair of electrolytes. As a consequence, the 'nanoreactor' size changes appreciably. In this case, it is difficult to synthesise particles with narrow size distribution, though their arrangement is governed by the particular polyelectrolyte layer.

Nanoparticles can also be formed using Langmuir – Blodgett polymer films, which resemble thin homopolymer films considered above. Only a few studies on the subject are available. Usually, nanoparticles were prepared separately and then mixed with an amphiphilic polymer before film formation.[67] Interesting results were reported in the article[68] concerned with the formation of CdS nanoparticles in the Langmuir – Blodgett film based on nonacosa-10,12-diyne acid after polymerisation of the acid on exposure to UV radiation. Exposure of the polymerised film containing cadmium ions to H_2S resulted in the formation of nanoparticles 10 nm in diameter. The photochemical and electrochemical properties of these films were described.[68] Another example of similar approach was also reported.[69] Here, cadmium sulfide nanoparticles of different size were prepared in Langmuir – Blodgett films formed by a polymer based on the octadecyl ester of polymaleic acid with different carboxyl group/hydrocarbon chain ratios. This permitted variation of the nanoparticle size and the photochemical properties of the films. Clearly, the systems developed cannot be used for fabrication of bulk materials or thick films, because ordered nanostructures in these amphiphilic homopolymers are formed under specific conditions (*e.g.*, at the air – water interface).

Controlled growth of nanoparticles can be performed in any thin homopolymer films. For instance, bimetallic Au/Cu nanoparticles of different composition were obtained by evaporation of metals in thin nylon-11 films.[70] The composition of bimetallic particles and their sizes were changed by varying the amount of metals evaporated. Experiments led to preparation of bimetallic nanoparticles of different composition with a narrow size distribution.

IV. Synthesis of dendrimer-encapsulated metal nanoparticles

The formation of dendrimer-encapsulated metal nanoparticles can be treated as a specific kind of nanoparticle synthesis in loose cores of block copolymer micelles. At the same time, there are significant differences between these processes (see below). In most cases researchers use commercially available poly(amidoamines) (PAMAM) dendrimers. By varying the dendrimer size (or dendrimer generation) and the metal compound loadings one can control the metal nanoparticle size. All publications on the subject are quite recent. It was Bar *et al.*[71] who pioneered the use of dendrimers as stabilisers in the formation of gold and silver nanoparticles. More recently,[72] it was shown that hydroxyl-terminated PAMAM dendrimers can be used as templates and stabilisers for the preparation of monodisperse transition metal nanoparticles possessing catalytic properties (Fig. 10). It is believed that the dendrimer macromolecule has an internal cavity, which is used for the formation (stabilisation) of a nanoparticle. However, broad nanoparticle size distribution when metal ions

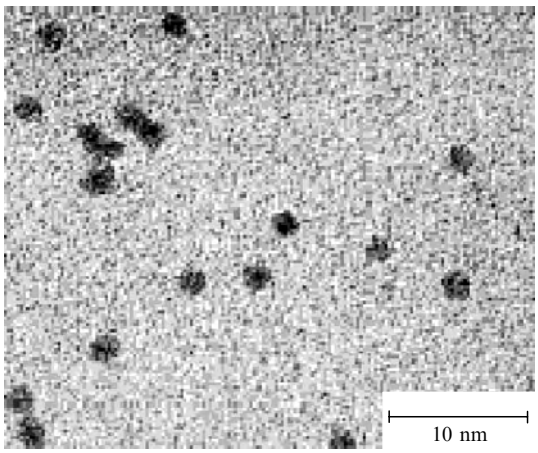

Figure 10. A HRTEM image of hydroxyl-terminated G4 dendrimer containing a total of 60 Pt atoms in each dendrimer.[72]
Platinum nanoparticles are monodisperse in size and shape.

exchange between dendrimer macromolecules (the metal compound migrates from one dendrimer to another) suggests that this cavity plays an insignificant role in the limitation of nanoparticle growth. These materials are prepared *via* sorption of metal ions into dendrimers followed by complexation with amino groups. Subsequent chemical reduction results in the formation of dendrimer-encapsulated metal nanoparticles comprising exactly the same number of atoms as that pre-'loaded' into the dendrimer. If no exchange of metal ions between dendrimer macromolecules occurs, the nanoparticle size distribution is narrow and fine control of the particle growth is possible. Nanocomposites thus obtained are water soluble and retain their stability for months. They exhibit a high catalytic activity towards alkene hydrogenation in water.[73] What is more, the catalytic activity can be controlled by varying the dendrimer size (generation), *i.e.*, the dendrimer acts as a nanofilter. Dendrimers are used as nanoreactors for the formation of not only monometallic but also bimetallic particles.[3]

When using PAMAM dendrimers containing amino groups at the surface, the size of the gold nanoparticles synthesised by exposing the dendrimer solutions to UV radiation was strongly dependent on the amino group/metal compound concentration ratio.[74,75] The particle size distribution was much broader than in the case of hydroxyl-terminated PAMAM dendrimers. Probably, the presence of the surface amino groups favours ion exchange between dendrimers during the formation of gold nanoparticles. By using penetration of hydroxyl-terminated PAMAM dendrimers into PHEMA followed by the formation of dendrimer-encapsulated nanoparticles one can prepare novel hybrid materials containing nanostructured polymer fragments and encapsulated nanoparticles.[76]

The effect of the dendrimer generation in systems with surface hydroxyl groups on the nanocomposite morphology has been studied in detail.[77] It was shown that low dendrimer generations undergo aggregation upon stabilisation of metal nanoparticles, whereas G6–G9 dendrimers can stabilise one nanoparticle per dendrimer and the particle size can be controlled with ease by varying the number of metal atoms. These results are consistent with the published data.[74] Experiments with G10 dendrimers revealed the formation of several small metal particles per dendrimer. To increase the stability of metal nanoparticles in various media, dendrimers can be modified by attaching PEO chains to the terminal amino groups of PAMAM macromolecules.[78] This has no effect on the ability of dendrimers to control the nanoparticle growth but provides better compatibility with a broad range of solvents and with a number of polymers. When using dendrimers with terminal glucose residues, the reduction of gold and silver ions and subsequent formation of nanoparticles from them is performed in an alkaline medium. Oxidation of hydroxyl groups does not require the use of additional amount of the reducing agent; however, nanoparticles thus obtained are characterised by a very broad size distribution.[79,80] Apparently, here we deal with facilitated exchange of metal ions between the dendrimer molecules because the terminal groups are involved in the reduction of metal ions.

Hydrophobically modified PAMAM dendrimers were used to form gold nanoparticles of size 2 to 4 nm in toluene and chloroform.[81] Recently, polypropyleneimine-based dendrimer modified by adamantyl groups have been reported.[82] The idea of these experiments was to involve hydrophobic groups in the interaction with amphiphilic block-cyclodextrin (the inner cavity of this molecule also possesses hydrophobic properties) and thus to prevent inter-dendrimers reactions during the sorption of metal ions and formation of nanoparticles. However, in spite of the complexity of this approach, the degree of control of nanoparticle growth was the same as that achieved using hydroxyl-terminated PAMAM dendrimers. Namely, no stabilisation of nanoparticles was observed with low-generation dendrimers, whereas higher-generation dendrimers permitted formation of nanoparticles with a narrow size distribution.

Another type of hydrophobic modification is to use polypropyleneimine-based dendrimers with stearyl terminal groups.[83] In toluene, they form inverse micelles with collapsed cores; however, sorption of metal salts causes the formation of cylindrical multi-dendrimer structures with swollen cores containing no metal salt. The action of the reducing agent leads to the formation of spherical gold nanoparticles and to the breakdown of cylindrical structures. These composite materials are thought to be of interest as catalysts and in the design of materials with specific optical properties (though these properties were not studied). Higher generation PAMAM dendrimers are commercially available but their synthesis is a multistage process. Because of this, the use of dendrimers seems to be no more promising compared to block copolymers.

Analogously to other nanostructured polymer matrices (*e.g.*, block copolymers or microgels), dendrimers containing encapsulated nanoparticles can be used as templates for the formation of mesoporous materials containing nanoparticles in pores. For instance, dendrimers containing Cu^{2+} ions were used[84] as templates for the formation of mesoporous silica. However, these templates provided no high SiO_2 porosity and ordered pore structure. Structural ordering is of great importance for the manifestation of optical properties while low porosity is inappropriate for catalytic applications (those materials containing encapsulated CuO nanoparticles were assumed to be efficient catalysts). We believe that only those templates that allow interpenetrating pores to be formed are promising for the fabrication of mesoporous materials containing encapsulated nanoparticles.

Introduction of metals and synthesis of nanoparticles can also be performed with carbosilane dendrimers[85] as well as nitrogen-containing and phosphorus-containing dendrimers[86,87] that offer the possibility of sorption of mixed transition metal clusters.

Thus, the use of dendrimers provides a means for fine control of nanoparticle growth under particular conditions. However, multistage synthesis of these macromolecules and the necessity of purification in each stage of the process complicate practical implementation of these systems as nanoreactors.

V. Metal nanoparticle formation in cavities (pores) of a polymer matrix

Controlled growth of metal nanoparticles in a polymer matrix is possible if it occurs in cavities or pores. In this case, the size of the growing particles can be limited to the cavity size. In the text below we consider two cases: (1) cavities contain no functional groups interacting with metal compounds and with the surface of nano-

particles and (2) cavities contain reactive groups favouring sorption of metal compounds into the polymer.

The first case can be illustrated taking the synthesis of metal nanoparticles in pores of crazed polymers [88] and in pores of hyper-cross-linked polystyrene (HPS) developed at the A N Nesmeyanov Institute of Organoelement Compounds, Russian Academy of Sciences.[89,90]

1. Nanoparticle growth in pores formed as a result of delocalised crazing of polymers

Delocalised crazing of polymers upon mechanical tension in adsorption active media (solvents) permits preparation of polymers containing reactant accessible open interpenetrating pores 3–6 nm in diameter. These pores can be used as templates for metal nanoparticle formation after introduction of corresponding reactants.[91,92] This procedure was employed to obtain nickel nanoparticles in porous polypropylene (PP) and poly(ethylene terephthalate) (PETP). A study of the reduction of nickel perchlorate with sodium borohydride in polymers with different morphologies and pore structures showed that the pore sizes govern the growth of nanoparticles. An interesting aspect of development of a crazed morphology is deformation of the polymer in a solution containing the corresponding metal complex. The synthesis of copper nanoparticles in high density polyethylene (HDPE) matrix was reported.[93] HDPE was crazed in monoethanolamine (MEA) solution containing complex copper salts and MEA. The formation of cavities in HDPE was accompanied by sorption of the copper compound into them. Subsequent heating of the composite material resulted in the formation of metal nanoparticles. However, this technique is inappropriate for preparation of nanoparticles with a narrow size distribution.

2. Metal nanoparticle formation in pores of hyper-cross-linked polystyrene

Hyper-cross-linked polystyrene is the first representative of a new class of cross-linked polymers characterised by unique topology and unusual properties. The internal morphology of HPS is schematically shown in Fig. 11.[94]

Hyper-cross-linked polystyrene has a rather large inner surface area (usually nearly 1000 $m^2\ g^{-1}$) and the ability to swell in any liquid medium including precipitating agents of the starting polymer. The HPS matrix used to form cobalt and platinum nanoparticles was characterised by a formal degree of cross-linking of 200%, an inner surface area of 833 $m^2\ g^{-1}$ and a narrow pore size distribution with a maximum at about 2 nm.

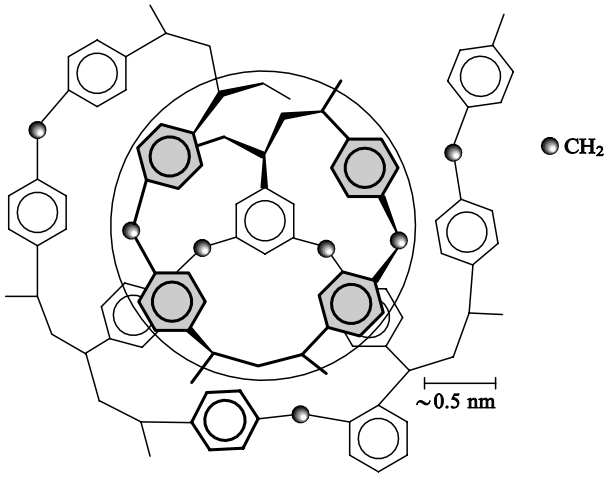

Figure 11. Schematic view of the HPS morphology.[94]
Shaded phenyl rings are in the foreground and bright phenyl rings are in the background. The circle denotes an individual pore of the hyper-cross-linked network.[94]

a. Cobalt nanoparticles in hyper-cross-linked polystyrene

The formation of metal nanoparticles in the HPS matrix was studied taking cobalt particles as examples, because the size and shape of cobalt nanoparticles are known to be related to their magnetic characteristics. Changes in the magnetic properties of the particles manifest themselves in changes in the spectral parameters of ferromagnetic resonance (FMR).[95] Particles of size less than 1 nm do not possess any magnetic properties. Particles 1 to 10 nm in diameter possess superparamagnetic properties. Larger particles are ferromagnetic. Moreover, the width of the signal of spherical particles in the FMR spectrum (ΔH) depends on the particle size while the position of the absorption maximum (H_0) is related to the shape of the cobalt nanoparticles.[95,96] Thus, information on the size and shape of cobalt nanoparticles can be extracted from their FMR spectra.

A cobalt compound, $Co_2(CO)_8$, was introduced into the HPS matrix from solutions in DMF and isopropyl alcohol. The reaction of $Co_2(CO)_8$ with DMF results in a relatively stable complex, $[Co(DMF)_6]^{2+}[Co(CO)_4]^{2-}$, while in isopropyl alcohol, a molecular solution is formed. Both materials were heat-treated at 200 °C. The H_0 and ΔH values for the HPS–Co samples prepared using the starting compound $Co_2(CO)_8$ in isopropyl alcohol and $[Co(DMF)_6]^{2+}[Co(CO)_4]^{2-}$ are listed in Table 2. As can be seen, an increase in the Co content to 8 mass % has little effect on the FMR spectral parameters and they are independent of the type of the starting Co-containing compound used in the experiments. The position of the absorption maximum, H_0, for all the samples under study indicated the formation of spherical cobalt nanoparticles.[95] According to TEM data, the average particle diameter was 2.1 ± 1.0 and 2.6 ± 1.6 nm for the samples with a cobalt content of 5.07 mass % and 10.08 mass %, respectively.[94]

Table 2. H_0 and ΔH values for HPS–Co samples prepared from different starting metal compounds.[94]

Co content (mass %)	H_0 /Œ	ΔH /Œ
Starting compound — $Co_2(CO)_8$ in isopropyl alcohol		
0.85	3100	125
2.58	3050	125
3.41	3100	200
5.69	3100	200
7.09	3125	200
Starting compound — $[Co(DMF)_6]^{2+}[Co(CO)_4]^{2-}$		
0.26	3100	125
1.85	3050	150
5.07	3075	160
8.22	3090	200
11.22	3105	350

Thus, it is the nanoscale voids in HPS that are responsible for controlled formation of Co nanoparticles in the relatively wide range of cobalt concentrations (from 0.9 mass % to 8.0 mass %). The most probable reason for controlled growth of Co particles in the HPS matrix is non-specific interaction between the phenyl rings and the metal surface, which must result in steric stabilisation of the cobalt nanoparticles. At cobalt concentrations exceeding a certain limiting value (> 8 mass %), growth of large nanoparticles begins. In this case, the particle size can reflect either the HPS pore size distribution statistics or the rearrangement of HPS morphology caused by the presence of the metal.

b. Formation of platinum nanoparticles in hyper-cross-linked polystyrene pores

Hyper-cross-linked polystyrene is an interesting object for the creation of novel catalytic systems. This compound can act as a

nanostructured matrix, which governs the particle growth, and as a carrier of catalytically active particles. Moreover, HPS can swell in almost all solvents. This can provide access to catalytic sites in virtually all reaction media.

A model study was carried out taking the formation of platinum nanoparticles in HPS pores as an example. Platinum was introduced into the polymer matrix by sorption of H_2PtCl_6 from solutions in THF or methanol. In contrast to the synthesis of cobalt nanoparticles, the formation of platinum nanoparticles involved the reduction of platinum compounds with hydrogen gas at moderate temperatures (the case of restricted migration of these compounds within the HPS matrix). In Fig. 12 we present a TEM micrograph of HPS containing encapsulated platinum nanoparticles (sorption of H_2PtCl_6 was conducted in THF) and a nanoparticle size distribution histogram. As can be seen, the average particle size is 1.3 ± 0.3 (*cf.* the average size of Co nanoparticles in HPS is ~ 2 nm). This difference can be explained by different mechanisms of formation of metal nanoparticles. At 200 °C, cobalt clusters can readily migrate into the HPS pores, thus forming particles that match the pore size. In the case of platinum, reduction with H_2 proceeds at room temperature (no migration of the platinum atoms or clusters or the molecules of the starting metal compound occurs); therefore, the nanoparticle size exactly matches the number of metal ions in the pores.[97] Thus, in the formation of cobalt nanoparticles the HPS matrix directly controls the metal nanoparticle size by physically limiting the particle size to the pore size (2 nm). In the case of platinum nanoparticles the pores impose restrictions on the amount of the starting metal compound that fills an individual pore; the reduction causes the volume of this compound to decrease (particle density increases) down to the volume of a single particle.

We believe that nanoporous polymers are promising as matrices for creation of efficient heterogeneous catalysts. However, they are inappropriate if the goal is to form thin films or homogeneous solutions.

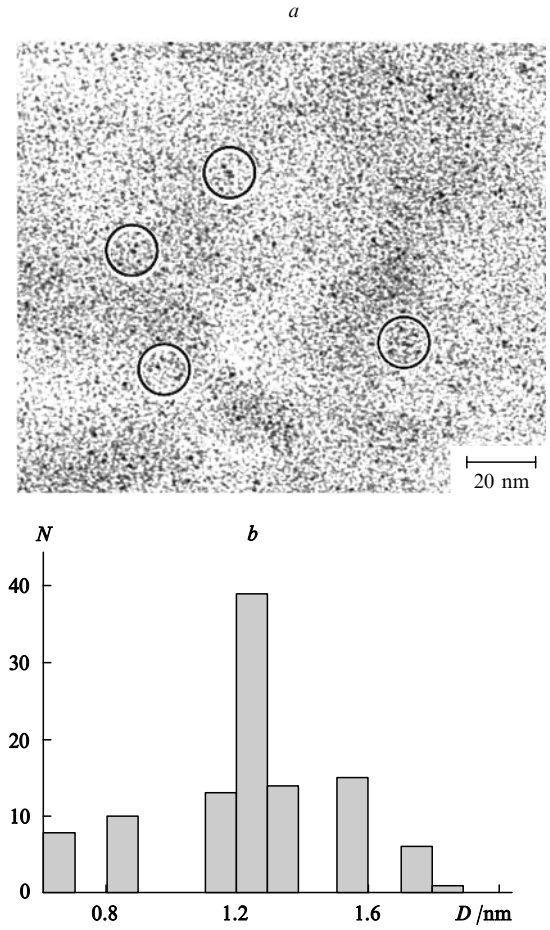

Figure 12. TEM micrograph of HPS containing encapsulated platinum nanoparticles (sorption of H_2PtCl_6 was conducted in THF) (*a*) and a histogram of nanoparticle size distribution (*b*).[97]
D is the particle diameter and *N* is the number of particles.

3. Formation of metal nanoparticles in cavities of nanostructured polyoctadecylsiloxane

Yet another example of control of the growth of metal particles confined in a cavity is provided by the formation of nanoparticles in the bisiloxane layers present in polyoctadecylsiloxane (PODS).[98, 99] This polymer is obtained by hydrolytic polycondensation of octadecyltrichlorosilane in water. The reaction results in a polymeric condensate comprising lamellar microcrystallites in which inorganic siloxane chains form periodically arranged layers separated by crystalline domains (alkyl chains). It was assumed that (i) placing the polymer in a metal salt solution would lead to the sorption of the salt into the hydrophilic layer of the polymer and (ii) subsequent reduction must result in the formation of metal nanoparticles regularly arranged within the material (see Fig. 13). However, it was found that sorption of metal compounds into this nanostructured polymer strongly depends on the type of the metal compound employed.[101] Ions with a planar structure (*e.g.*, $PtCl_4^{2-}$) easily penetrate into the interior of the thin layer (2–3 nm), while the penetration of octahedral ions $PtCl_6^{2-}$ is hindered. The penetration of metal ions is assumed to be entropy driven; namely, an increase in entropy results from the formation of hydrogen bonds between the Cl atoms of the salt anions and the silanol groups (each $PtCl_4^{2-}$ ion can replace up to four water molecules). The formation of nanoparticles in the siloxane double layer occurs upon the reduction of platinum and palladium compounds. The process is independent of the type of the reducing agent and the metal compound and on the concentration of the latter and is governed exclusively by the growth of the metal particles confined within the siloxy bilayer cavity. The particle size distribution for platinum particles obtained in this polymer is shown in Fig. 14. Figure 15 presents a TEM micrograph of a material containing palladium nanoparticles.[100] As can be seen, the metal particles are located exclusively within the siloxy bilayers.

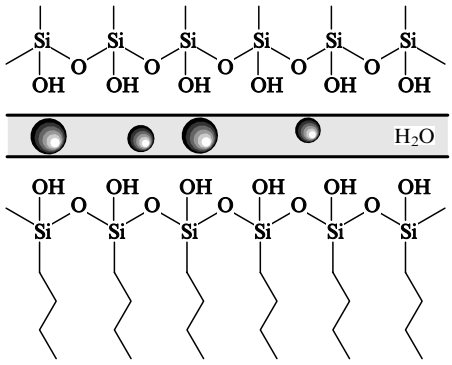

Figure 13. Scheme of nanoparticle formation in the siloxy bilayer of PODS.[100]

Thus, the presence of voids in nanostructured polymers permits control of the nanoparticle growth while the presence of functional groups ensures efficient and uniform sorption of metal compounds into the bulk material. At the same time, the metal content in these polymers is low because only the siloxy bilayers contain silanol groups.

The synthesis of novel highly functionalised colloidal polymer particles by hydrolytic condensation of *N*-(6-aminohexyl)aminopropyltrimethoxysilane was developed.[102] Polysilsesquioxane (PSSO) thus obtained is water soluble and has a structure

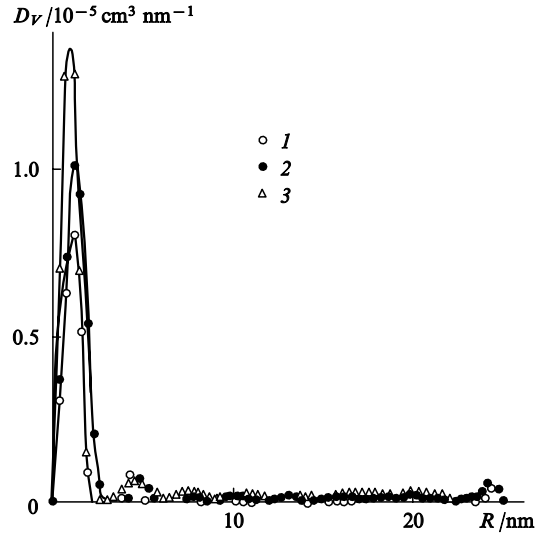

Figure 14. Volume distribution functions of platinum nanoparticles in PODS.[101]
Samples were prepared *via* sorption of K_2PtCl_4 after reduction with silanol groups of PODS (*1*) and *via* sorption of $H_2PtCl_6 \cdot 6\,H_2O$ after reduction with H_2 (*2*) and sodium borohydride (*3*).

Figure 15. TEM micrograph of palladium nanoparticles formed in PODS from Na_2PdCl_4 upon reduction with $NaBH_4$.[100]
Palladium nanoparticles were prepared in the siloxy bilayers of PODS with lamellar nanostructure. Palladium and silicon atoms provide a rather high contrast relative to the alkyl layers.

characterised by high degrees of cross-linking and functionalisation. Functionalised cavities in the PSSO structure act as nanoreactors for nanoparticle formation and provide a high metal loading (up to 35 mass %). The nanoparticles are 1–2 nm in diameter and do not undergo aggregation within the PSSO matrix. Colloidal PSSO particles filled with metals or metal compounds can form surface dendritic structures. We believe these systems are candidates for catalysts and chemical sensors.

VI. Properties of nanostructured polymeric systems containing metal nanoparticles

The unique properties of metal nanoparticles are mainly due to the large total surface area and to the considerable number of surface atoms. For instance, nearly 60% of the total number of atoms in a gold particle 2 nm in diameter are on the surface. In semiconductor and metal nanoparticles, this permits efficient charge transfer from the bulk of the material to the surface and *vice versa* (this manifests itself in, *e.g.*, changes in the optical absorption spectra). The surface of nanoparticles plays an important role in catalysis, being responsible for their selectivity and activity. Therefore, the characteristics of the stabilising polymer (its functionality and nanostructuring) and nanoparticles are of great importance, because they mainly determine the state of the surface of nanoparticles.[103]

1. Catalytic properties

Polymer-stabilised colloidal metal particles have been known to be hydrogenation catalysts for more than five decades. For instance, olefin hydrogenation catalysts based on palladium, platinum,[104,105] rhodium [106] and iridium [107] were prepared using poly(vinyl alcohol) and poly(vinyl acetate) as stabilisers. Most studies are concerned with the synthesis of nanoparticles inside homopolymer matrices that cannot provide a narrow particle size distribution (because of this, particles within the same sample can possess quite different catalytic properties). This reduces the selectivity and activity of a given catalyst.

Taking platinum nanoparticles stabilised by polymer surfactant micelles as an example, it was shown [108,109] that the state of the surface of metal nanoparticles plays an important role. These catalysts prepared within inverse micelles formed by cationic, anionic and non-ionic polymeric surfactants were employed in the isomerisation and hydrogenation of n-butene. The highest activity of the catalyst was achieved using a non-ionic surfactant; however, in all cases, the catalysts were an order of magnitude less active than conventional supported catalysts. Probably, the layer of the surfactant molecules adsorbed on the surface of a metal particle made the catalyst sites inaccessible to the substrate. At first glance, this negative conclusion is quite interesting from the standpoint of improvement of catalyst selectivlty. By choosing an appropriate stabiliser it is possible to achieve a great difference between the diffusion rates of different substrates towards the surface of the catalyst. The effect of surfactant micelles on the hydrogenation of long-chain unsaturated acids (*e.g.*, isomers of undecenoic acid and oleic acid) was studied taking platinum and palladium nanoparticles stabilised with a non-ionic surfactant poly(ethylene glycol monolaurate) as examples.[110] In these systems, the surface of the metal particle is protected by hydrophobic laurate chains while hydrophilic poly(ethylene glycol) chains form the micelle shell.

In this case, the position of the double bond in the substrate governs the hydrogenation rate because the substrate molecule is specifically arranged in the micelle wall. The ordered environment of the metal particle forces the acid molecule to be oriented in such a way that the polar carboxyl group is in the hydrophilic fragment of the micelle and the hydrophobic fragment of the molecule is surrounded by hydrophobic core-forming laurate chains. The acid hydrogenation rates obey the following pattern: undec-10-enoic acid > oleic acid > undec-2-enoic acid. This indicates that the terminal double bond is best accessible to the active sites of the catalyst, whereas the inner double bond has poorer access to the surface of the platinum particles. Platinum nanoparticles stabilised by poly(*N*-vinyl-2-pyrrolidone) (PVP) possessed no regioselectivity except in the cases where sodium salts of unsaturated acids were used. Here, the substrate behaved as a surfactant and the effect of PVP could be ignored.

Modification of the catalyst properties by forming a stabilising shell surrounding the particle is possible only in the case of metal nanoparticles. This is a great advantage of these particles over other catalysts of polyfunctional substrate hydrogenation. Thus, the use of nanostructured polymers permits not only control of nanoparticle growth but also further modification of the nanoparticle surface, which is of considerable value for catalytic applications.

A somewhat different approch was also developed.[42,43] As described above, corona-embedded metal nanoparticles were synthesised by the reduction of corresponding starting compounds of palladium and platinum in the presence of amphiphilic block copolymers (PS-*block*-PEO and PS-*block*-PMAA) in alcoholic and aqueous solutions. The catalytic activity of nanoparticles was assessed taking cyclohexene hydrogenation as a model

reaction. The particle activity was strongly dependent on the procedure for preparation and on the type of starting compounds. The formation of palladium and platinum nanoparticles in the presence of latex dispersions of different hydrophobicity was studied.[111, 112] In some cases, metal nanoparticles were adsorbed and immobilised on the latex surfaces, which was confirmed by TEM data. These dispersions exhibited catalytic activity in the model reaction of cyclohexene hydrogenation. Highly hydrophobic latexes caused such strong immobilisation of nanoparticles that they remained on the latex surface after performing catalytic cycles.

Silver and platinum nanoparticles synthesised in multilayered polyelectrolyte films[113] possessed electrocatalytic properties in methylene bromide reduction; however, these catalysts are less efficient than pure silver electrode because polymer films are insulators. These data are consistent with the results obtained by Zhao and Crooks[72] who used dendrimer-encapsulated platinum nanoparticles deposited on an electrode as a catalyst for an electrocatalytic reaction. Clearly, in spite of some catalytic activity these polymeric systems with encapsulated metal nanoparticles are of no promise as electrode coatings in electrocatalytic reactions, because the insulating properties of the polymer reduce the catalyst efficiency.

Hydrogenation of dehydrolinalool (DHL, oct-6-ene-1-yne-3-ol) is an industrially important reaction in fragrance chemistry. Using catalysts based on palladium nanoparticles synthesised in PS-*block*-P4VP micelles, a selectivity of 99.5% in hydrogenation of the triple bond in DHL to a double bond was achieved.[114] Probably, modification of the metal surface by pyridine units of the P4VP core also contributes to the reaction selectivity. The use of bimetallic nanoparticles Pd/Au, Pd/Pt and Pd/Zn causes a modification of the electronic structure and surface geometry of palladium, which additionally enhances the selectivity up to 99.8%.[28]

Palladium nanoparticles stabilised by PS-*block*-P4VP micelles were used as catalysts of cross-coupling reactions between aryl halides and alkenes (Heck reaction).[115] These hybrid systems exhibited nearly the same efficiency as low-molecular-mass palladium complexes (conventional catalysts of the Heck reaction), being at the same time much more stable.

Direct catalytic L-sorbose oxidation into 2-keto-L-gulonic acid is an intermediate stage of the synthesis of ascorbic acid (vitamin C). At present, direct sorbose oxidation is not used on industrial scale because of the low selectivity of the process. Another synthetic route involves transformation of sorbose into di-*O*-isopropylidenesorbose followed by oxidation of the latter to give di-*O*-isopropylidene-2-keto-L-gulonic acid and then 2-keto-L-gulonic acid. Direct L-sorbose oxidation into 2-keto-L-gulonic acid was performed using the HPS–Pt samples described above. They were obtained by sorption of H_2PtCl_6 from methanol and THF both before and after the reduction with H_2, and contained different amounts of platinum.[97] It was found that the yield of 2-keto-L-gulonic acid (*i.e.*, oxidation selectivity) is strongly dependent on the conditions for preparation of catalysts. In particular, the highest yield (nearly 98%) was achieved with the HPS–Pt(H_2PtCl_6 + THF) samples. Additional reduction of the samples with H_2 reduced the selectivity by 8%–10%. A study on the structure of HPS–Pt before the catalytic reaction, after the induction period and after the catalytic reaction revealed transformations of H_2PtCl_6 and THF in the HPS pores, which resulted in the formation of mixed clusters comprised of $Pt^0/Pt^{II}/Pt^{IV}$ and ligands. Reduction with H_2 increases the proportion of Pt^0 in the sample, which can upset the optimum composition of the complex.

The $\ln\tau_{0.1} - 1/T$ Arrhenius plot constructed using the experimental data obtained at different temperatures gave a value of 34 kJ mol^{-1} for the apparent activation energy, E_a. This is lower than the activation energy for the reaction conducted with the conventional catalyst Pt/SiO_2 ($\sim$45 kJ mol^{-1}).

Metal nanoparticles are widely used in the important catalytic reaction known as the Suzuki reaction. The effect of the stabiliser matrix on the catalytic properties and stability of transition metal nanoparticles in solution was studied.[116] Palladium nanoparticles were prepared *via* the reduction of metal salt in the presence of three different polymer stabilisers, namely, hydroxyl-terminated PAMAM dendrimers (Gn–OH, where Gn is the *n*th dendrimer generation), PS-*block*-PANa (PANa is sodium polyacrylate) and PVP. The nanostructured systems obtained were used to study the effect of the matrix type on their catalytic activity and stability in the catalytic cross-coupling reaction between phenylboronic acid (or 2-thienylboronic acid) and iodobenzene in aqueous medium. The stability of palladium nanoparticles was evaluated using the data on the formation of palladium black after catalytic cycles. The Suzuki reaction is a good test for the stability of nanoparticles, because it proceeds at 100 °C for 24 h. Palladium nanoparticles stabilised by PAMAM-G3 dendrimer and PVP were found to be efficient catalysts of the Suzuki reaction. The G4 dendrimer was found to be a very efficient stabiliser; however, strong encapsulation of palladium nanoparticles in the dendrimer led to reduction of the catalytic activity. The two properties were found to be interrelated, namely, the higher the stability, the lower the catalytic activity (due to inaccessibility of the nanoparticle surface to the substrate). Both palladium- and platinum-containing PAMAM exhibited catalytic activity in the electrochemical reduction of oxygen.[117]

2. Magnetic properties

If the critical distance responsible for a physical property becomes comparable with the nanoparticle size, the magnetic properties of the nanomaterials change significantly. Changes in the magnetisation of a material always require the overcoming of an energy barrier, while any physical mechanism proposed for the description of the corresponding energy barrier includes a relevant linear parameter (length or distance). The main linear parameters used to describe the magnetic properties are as follows: the linear crystalline anisotropy, l_k, the action range of the applied field, l_H, and the magnetostatic distance, l_s; they are defined by the respective equations[118]

$$l_k = \sqrt{\frac{J}{K}},$$

$$l_H = \sqrt{\frac{2J}{HM}},$$

$$l_s = \sqrt{\frac{J}{2\pi M^2}},$$

where J is the constant for intradomain exchange, K is the anisotropy constant, H is the magnetic field strength and M is the saturation magnetisation.

If there is more than one energy barrier, the magnetic properties are determined by the shortest characteristic distance. For the most widely used magnetic materials these values are of the order of 1 to 100 nm (*e.g.*, $l_H \approx 19$, $l_k \approx 45$ and $l_s \approx 8$ nm for nickel in a magnetic field of 1000 Œ at room temperature).

The most interesting magnetic properties of nanoparticles are manifested in the case of monodomain nanoparticles. (Remind that a domain is a group of aligned spins that act in a concerted way and are characterised by the total magnetic moment.) In bulk materials, domains are separated by domain walls characterised by their thickness and formation energy. The reversible magnetisation effect is due to the domain wall motion. The formation of domain walls in bulk metal is energetically favourable but a decrease in the particle size down to a certain critical value, R_c, makes the formation of domain walls energetically unfavourable. This is the case for monodomain particles.[119, 120] Here, the magnetisation changes are due to synchronous spin rotation

resulting in a large coercive force rather than domain wall motion. Further decrease in the particle size causes the spins to be more sensitive to the influence of thermally induced fluctuations. Finally, all spins become completely disordered as the external magnetic field is switched off. Such systems possess properties of superparamagnetics and are characterised by zero remanent magnetisation and zero coercive force.

If magnetic nanoparticles were formed inside a polymer matrix, the nanocomposites obtained possess unique magnetic properties and can be used for electromagnetic shileding and for creation of novel magnetic and magneto-optical devices.[118, 119]

Metallic cobalt is often used in the fabrication of various magnetic devices. Cobalt nanoparticles less than 60 nm in size are monodomain particles characterised by a nonzero total magnetic moment. If the particle size lies between 10 and 60 nm (these values are rough estimates and depend on the particle shape), the total magnetic moment dominates the thermal motion of particles and they form linear chains due to the dipole–dipole interaction. Such materials are the best candidates for production of permanent magnets, magnetic pigments, coatings for magnetic data storage devices, *etc*.[119, 120]

Nearly monodisperse cobalt nanoparticles with controlled morphology were synthesised [121] using PS-*block*-P4VP micelles in organic solvents. Metallic cobalt particles were produced in two ways, by the chemical reduction of $CoCl_2$ and by the thermal decomposition of $Co_2(CO)_8$. The amount of the block copolymer was kept constant but the concentration of the starting metal compound was varied. This permitted the preparation of non-magnetic, superparamagnetic or ferromagnetic materials. Experiments with the ferromagnetic samples allowed the conditions for obtaining very high specific coercive forces (with respect to the cobalt concentration in the sample) to be chosen. Apparently, this is mainly due to the very narrow size distribution of the cobalt nanoparticles. These particles are characterised by high magnetisation and extremely high stability in air, which can be explained by the high degree of adsorption of pyridine units on the particle surfaces.

The magnetic properties of γ-Fe_2O_3 nanoparticles formed inside microdomains of an optically transparent block copolymer based on $[NORCOOH]_{30}[MTD]_{300}$ (NORCOOH is 2-norbornene-5,6-dicarboxylic acid; MTD is methyltetracyclododecene) have been reported.[122, 123] The nanoparticle size was 5 nm. The magnetic properties of the material were strongly dependent on the quantum effects, *e.g*., co-operative magnetisation and superparamagnetic relaxation. It was shown that these nanocomposite films exhibit superparamagnetic properties and possess no remanent magnetisation and coercive force at room temperature. At low temperatures, the coercive force of these films was 530 Œ.

3. Optical properties

The synthesis of manganese- and terbium-doped ZnS nanoparticles in the microsegregated films of diblock copolymers containing carboxyl groups in one block has been reported.[124] The concentration of dopant ions in the microdomain containing the carboxyl groups was controlled by varying either the concentrations of aqueous solutions of the metal salt or the exposure time of the polymer film in solution. The doped ZnS nanoclusters were formed during subsequent treatment of the films with hydrogen sulfide. These films exhibit photoemission characteristic of the dopant ions (manganese and terbium). The synthetic procedure has no features and can be used for the preparation of doped semiconductor nanoparticles involving combinations of various metal salts.

Optically stable CdS nanoparticles were synthesised within a hydroxyl and amino group terminated G4 PAMAM dendrimer.[125] The UV spectra and luminescence spectra showed that the dendrimer stabilises nanoparticles whose optoelectronic properties differ from the corresponding properties of bulk CdS. Dendrimers are prone to aggregation, which depends on the temperature and particle concentration; however, the characteristics of the cadmium sulfide nanoparticles remained unchanged. Studies of the solutions stored at -10 °C revealed that the dendrimers did not undergo aggregation over a period of several months and that the solutions also possessed photoluminescent properties.

Another procedure for the formation of analogous nanocomposites involves PEI as the polymer stabiliser.[126] The optical properties of the particles thus obtained were similar to those of the particles described above (emission in the blue spectral region) but the quantum yield of luminescence was lower. The authors [126] believe that high local concentration of chelating nitrogen atoms (in the dendrimer or PEI) is the major factor affecting the formation of small nanoparticles with perfect morphology.

A XANES study of nanocomposites based on CdS nanoparticles and G4 PAMAM dendrimers was also reported.[127] Investigation of the structure of CdS nanoparticles revealed the presence of sulfates and oxides. A joint X-ray induced optical luminescence–XANES study also revealed correlations between the optical properties and the structure of CdS nanoparticles.

An interesting nanocomposite was obtained by incorporating CdTe nanoparticles into thin films prepared by layer-by-layer deposition of an anionic polyelectrolyte containing a poly(*para*-phenylenethynylene) (PFE) chain and poly(allylamine hydrochloride) (PAAHC) as the polycation.[128] The CdTe nanoparticles were stabilised by poly(ethylene glycol) (PEG)-containing reactive terminal groups. Nanoparticles were incorporated into the multilayered composite *via* chemical bonding to the stabiliser (PEG). The interaction between polyconjugated polymer and nanoparticles provided conjugation transfer, which manifested itself as changes in the optical properties. The luminescence spectrum exhibited a new peak at 600 nm due to the emission of CdTe nanoparticles. The excitation spectrum of CdTe–PEG-*block*-PFE recorded at 600 nm exhibited a new intense band at 400 nm corresponding to the absorption band of the multilayered composite. This is evidence of energy transfer between PFE and the nanoparticles. By varying certain structural parameters of the composite (*e.g*., the PEG chain length) one can change the optical properties. This system is expected to be suitable for fabrication of multilayered optical devices.

4. Electrical properties

A trend towards miniaturisation and high integration of elements of electric circuits has been a salient feature of modern microelectronics. As a rule, the shorter the distance between the elements of a device, the higher the performance of the device. Lithography techniques permit fabrication of working elements of size up to 100 nm, which has opened new prospects for their application using quantum effects. At present, using the Coulomb effect in electric circuits (including submicrometre-sized tunnelling junctions) allows one to control single charge carriers. Research in this field serves as the basis for fabrication of the so-called single-electron devices (SEDs).[129]

The Coulomb effect has long been known, however, studies on SEDs have been a particular avenue of scientific research only recently. Fifteen years have passed since the beginning of intensive studies into ultrasmall sandwich structures of the type metal–insulator–metal (tunnelling junctions).[130] It was shown that the electric charge discreteness becomes significant under particular conditions. Namely, quantum electron tunnelling in the system of tunnelling junctions is affected by the Coulomb inter-electron interaction, which can in turn be varied by applying an external voltage. This phenomenon is called single-electron tunnelling. It serves as the basis for the operation of any SED.

A practical implementation of the SED idea in systems with characteristic capacities of the order of 10^{-15} to 10^{-16} F (these values are typical of modern lithography techniques) requires that the samples be cooled down to a few thousandths of a Kelvin. Room-temperature operation of the SED dictates a reduction of the characteristic capacity by at least two orders of magnitude, which can be achieved using nanometre-sized metal nanoparticles.

Recent advances in lithography, made due to miniaturisation of electronic devices, cannot meet all the requirements from room-temperature operation of SEDs.[131] This problem can be solved by using ligand shell stabilised metal nanoparticles. These particles are thought to be promising as structural elements of novel nanoelectronic devices. A challenge is to develop novel methods for the fine adjustment of such elements in SED design at different scales of integration. Therefore, the use of the principles of self-organisation and controlled intermolecular interaction favours progress towards the design and fabrication of new electronic devices.

The use of dendrimers for the synthesis of metal nanoparticles can simplify some engineering aspects of SED fabrication. The dendrimer macromolecules are characterised by very narrow particle size distribution and an exact number of functional groups. This allows single nanoparticles to be synthesised within individual macromolecules. In contrast to low-molecular-mass ligands, dendrimers have particular chemical structures characterised by the absence of exchange and relaxation processes, provided that the surface functional groups are protected by hydrophobic groups. This permits fine control of the nanoparticle parameters and the thickness of the insulating layer, which is impossible in the case of conventional low-molecular-mass ligands. Dendrimer molecules can self-assemble in the course of, *e.g.*, adsorption from solutions onto appropriate surfaces. Block copolymer micelles with cross-linked cores or coronas can also be used for these purposes. In these systems, micelles are characterised by a very narrow size distribution, which allows a single nanoparticle per core to be generated under particular conditions.[27] A necessary condition for proper SED operation consists in self-organisation of such filled micelles on the surface (this is usually employed in nanolithography [29]). Because of this, we believe that the use of the unique properties of nanoparticles formed in nanostructured polymeric systems for fabrication of SEDs is a promising field of application.

* * *

There are a variety of nanostructured polymeric systems that can provide control of the formation of nanoparticles, stabilise nanoparticles and modify their surface due to the effect of the polymer chains. Among them, prospects for particular systems are determined by the possible fields of application. We believe that block copolymer micelles and dendrimers are the best candidates for use as nanostructured polymeric systems providing the possibility of nanoparticle formation in solutions. It should be noted that block copolymer micelles can form films and coatings, which is of particular importance for application in catalytic, magnetic and optical systems. Block copolymer micelles and dendrimers can adsorb on surfaces to form monolayers. Nanoporous materials are thought to be the most promising for the formation of nanocomposite catalysts of heterogeneous processes. These materials are simple and cheap, they permit control of particle growth, accessibility of reactive sites to substrates and do not require additional heterogenisation.

This review has been written with financial support from the Russian Foundation for Basic Research (Project No. 01-03-32937) and NATO SfP Programme (Colloidal Catalysts – 974173).

References

1. G P Schmid (Ed.) *Clusters and Colloids: From Theory to Applications* (Weinheim: VCH, 1994)
2. J H Fendler (Ed.) *Nanoparticles and Nanostructured Films: Preparation, Characterisation and Applications* (Weinheim: Wiley-VCH, 1998)
3. R M Crooks, B I Lemon, L Sun, L K Yeung, M Zhao *Top. Curr. Chem.* **212** 81 (2001)
4. V I Roldugin *Usp. Khim.* **69** 899 (2000) [*Russ. Chem. Rev* **69** 821 (2000)]
5. G B Sergeev *Usp. Khim.* **70** 915 (2001) [*Russ. Chem. Rev* **70** 809 (2001)]
6. V I Bukhtiyarov, M G Slin'ko *Usp. Khim.* **70** 167 (2001) [*Russ. Chem. Rev* **70** 147 (2001)]
7. I P Suzdalev, P I Suzdalev *Usp. Khim.* **70** 203 (2001) [*Russ. Chem. Rev* **70** 177 (2001]
8. R F Khairutdinov *Usp. Khim.* **67** 125 (1998) [*Russ. Chem. Rev* **67** 109 (1998)]
9. I U Hamley *The Physics of Block Copolymers* (Oxford: Oxford University Press, 1998)
10. F S Bates, G H Fredrickson *Phys. Today* **52** 32 (1999)
11. S Förster, M Antonietti *Adv. Mater.* **10** 195 (1998)
12. L M Bronstein, P M Valetsky *J. Inorg. Organomet. Polym.* **4** 415 (1994)
13. M Moffitt, L McMahon, V Pessel, A Eisenberg *Chem. Mater.* **7** 1185 (1995)
14. A E Ribbe, A Okumura, K Matsushige, T Hashimoto *Macromolecules* **34** 8239 (2001)
15. J F Ciebien, R T Clay, B H Sohn, R E Cohen *New J. Chem.* **22** 685 (1998)
16. T Hashimoto, M Harada, N Sakamoto *Macromolecules* **32** 6867 (1999)
17. B H Sohn, B H Seo *Chem. Mater.* **13** 1752 (2001)
18. B H Sohn, B W Seo, S I Yoo *J. Mater. Chem.* **12** 1730 (2002)
19. W A Lopes *Phys. Rev. E* **65** 031 606 (2002)
20. W A Lopes, H M Jaeger *Nature (London)* **414** (6865) 735 (2001)
21. S R Ahmed, P Kofinas *Macromolecules* **35** 3338 (2002)
22. M Antonietti, S Henz *Nachr. Chem: Technol. Lab.* **40** 308 (1992)
23. R Saito, S Okamura, K Ishizu *Polymer* **34** 1189 (1993)
24. M Antonietti, E Wenz, L Bronstein, M Seregina *Adv. Mater.* **7** 1000 (1995)
25. J P Spatz, A Roescher, M Müller *Adv. Mater.* **8** 337 (1996)
26. M V Seregina, L M Bronstein, O A Platonova, D M Chernyshov, P M Valetsky, J Hartmann, E Wenz, M Antonietti *Chem. Mater.* **9** 923 (1997)
27. L Bronstein, M Antonietti, P Valetsky, in *Nanoparticles and Nanostructured Films: Preparation, Characterisation and Applications* (Ed. J H Fendler) (Weinheim: Wiley-VCH, 1998) p. 145
28. L M Bronstein, D M Chernyshov, I O Volkov, M G Ezernitskaya, P M Valetsky, V G Matveeva, E M Sulman *J. Catal.* **196** 302 (2000)
29. J P Spatz, T Herzog, S Mössmer, P Ziemann, M Müller *Adv. Mater.* **11** 149 (1999)
30. J H Youk, M-K Park, J Locklin, R Advincula, J Yang, J Mays *Langmuir* **18** 2455 (2001)
31. T J Martin, K Prochazka, P Munk, S E Webber *Macromolecules* **29** 6071 (1996)
32. L M Bronstein, S N Sidorov, P M Valetsky, J Hartmann, H Coelfen, M Antonietti *Langmuir* **15** 6256 (1999)
33. L Bronstein, E Kraemer, B Berton, C Burger, S Foerster, M Antonietti *Chem. Mater.* **11** 1402 (1999)
34. S Liu, J V M Weaver, M Save, S P Armes *Langmuir* **18** 8350 (2002)
35. R S Underhill, G Liu *Chem. Mater.* **12** 2082 (2000)
36. P J Miller, K Matyjaszewski *Macromolecules* **32** 8760 (1999)
37. K A Davis, K Matyjaszewski *Macromolecules* **34** 2101 (2001)
38. S N Sidorov, L M Bronstein, P M Valetsky, J Hartmann, H Cllfen, H Schnablegger, M Antonietti *J. Colloid Interface Sci.* **212** 197 (1999)
39. L M Bronstein, S N Sidorov, A Y Gourkova, P M Valetsky, J Hartmann, M Breulmann, H Cölfen, M Antonietti *Inorg. Chim. Acta* **280** 348 (1998)
40. M Sedlak, M Antonietti, H Cölfen *Macromol. Chem. Phys.* **199** 247 (1998)
41. L Qi, H Cölfen, M Antonietti *Nano Lett.* **1** 61 (2001)
42. A B R Mayer, J E Mark, R E Morris *Polym. J.* **30** 197 (1998)
43. A B R Mayer, J E Mark *Colloid Polym. Sci.* **275** 333 (1997)

44. L M Bronstein, D M Chernyshov, G I Timofeeva, L V Dubrovina, P M Valetsky, E S Obolonkova, A R Khokhlov *Langmuir* **16** 3626 (2000)
45. L M Bronstein, D M Chernyshov, G I Timofeeva, L V Dubrovina, P M Valetsky, A R Khokhlov *J. Colloid Interface Sci.* **230** 140 (2000)
46. L M Bronstein, D M Chernyshov, E V Vorontsov, G I Timofeeva, L V Dubrovina, P M Valetsky, S Kazakov, A R Khokhlov *J. Phys. Chem. B* **105** 9077 (2001)
47. H Zhao, E P Douglas *Chem. Mater.* **14** 1418 (2002)
48. M Antonietti *Angew. Chem.* **100** 1813 (1988)
49. M Antonietti, W Bremser, M Schmidt *Macromolecules* **23** 3796 (1990)
50. M Antonietti, F Gröhn, J Hartmann, L Bronstein *Angew. Chem., Int. Ed.* **36** 2080 (1997)
51. N T Whilton, B Berton, L Bronstein, H-P Hentze, M Antonietti *Adv. Mater.* **11** 1014 (1999)
52. A R Khokhlov, S G Starodubtsev, V V Vasilevskaya *Adv. Polym. Sci.* **109** 123 (1993)
53. A R Khokhlov, E Y Kramarenko, E E Makhaeva, S G Starodubtsev *Macromol. Theory Simul.* **1** 105 (1992)
54. Yu V Khandurina, A T Dembo, V B Rogacheva, A B Zezin, V A Kabanov *Vysokomol. Soedin., Ser. A* **36** 235 (1994) [a]
55. H Okuzaki, Y Osada *Macromolecules* **28** 380 (1995)
56. F Yeh, E L Sokolov, A R Khokhlov, B Chu *J. Am. Chem. Soc.* **118** 6615 (1996)
57. A T Dembo, A N Yakunin, V S Zaitsev, A V Mironov, S G Starodubtsev, A R Khokhlov, B Chu *J. Polym. Sci., Part B* **34** 2893 (1996)
58. L M Bronstein, O A Platonova, A N Yakunin, I M Yanovskaya, P M Valetsky, A T Dembo, E E Makhaeva, A V Mironov, A R Khokhlov *Langmuir* **14** 252 (1998)
59. L M Bronstein, O A Platonova, A N Yakunin, I M Yanovskaya, P M Valetsky, A T Dembo, E S Obolonkova, E E Makhaeva, A V Mironov, A R Khokhlov *Colloids Surf., A* **147** 221 (1999)
60. D I Svergun, E V Shtykova, M B Kozin, V V Volkov, A T Dembo, E V J Shtykova, L M Bronstein, O A Platonova, A N Yakunin, P M Valetsky, A R Khokhlov *J. Phys. Chem. B* **104** 5242 (2000)
61. Y Lvov, G Decher, H Möhwald *Langmuir* **9** 481 (1993)
62. G B Sukhorukov, E Donath, H Lichtenfeld, E Knippel, M Knippel, A Budde, H Mohwald *Colloids Surf., A* **137** 253 (1998)
63. R A Caruso, A Susha, F Caruso *Chem. Mater.* **13** 400 (2001)
64. H Xiong, Z Zhou, Z Wang, Z Xi, J Shen *Supramol. Sci.* **5** 623 (1998)
65. T C Wang, M F Rubner, R E Cohen *Langmuir* **18** 3370 (2002)
66. N A Kotov, I Dekany, J H Fendler *J. Phys. Chem.* **99** 13 065 (1995)
67. D K Lee, Y S Kang, C S Lee, P Stroeve *J. Phys. Chem. B* **106** 7267 (2002)
68. H S Mansur, W L Vasconcelos, F Grieser, F Caruso *J. Mater. Sci.* **34** 5285 (1999)
69. J Jin, L S Li, Y Q Tian, Y J Zhang, Y Liu, Y Y Zhao, T S Shi, T J Li *Thin Solid Films* **327 – 329** 559 (1998)
70. S Deki, K Akamatsu, Y Hatakenaka, M Mizuhata, A Kajinami *Nanostruct. Mater.* **11** 59 (1999)
71. G Bar, S Rubin, R W Cutts, T N Taylor, T A Zawodzinski Jr *Langmuir* **12** 1172 (1996)
72. M Zhao, R M Crooks *Adv. Mater.* **11** 217 (1999)
73. M Zhao, R M Crooks *Angew. Chem., Int. Ed.* **38** 364 (1999)
74. K Esumi, A Suzuki, N Aihara, K Usui, K Torigoe *Langmuir* **14** 3157 (1998)
75. A Manna, T Imae, K Aoi, M Okada, T Yogo *Chem. Mater.* **13** 1674 (2001)
76. F Gröhn, J Kim, B J Bauer, E J Amis *Macromolecules* **34** 2179 (2001)
77. F Gröhn, B J Bauer, Y A Akpalu, C L Jackson, E J Amis *Macromolecules* **33** 6042 (2000)
78. R C Hedden, B J Bauer, A P Smith, F Gröhn, E Amis *Polymer* **43** 5473 (2002)
79. K Esumi, T Hosoya, A Suzuki, K Torigoe *Langmuir* **16** 2978 (2000)
80. K Esumi, T Hosoya, A Suzuki, K Torigoe *J. Colloid Interface Sci.* **226** 346 (2000)
81. K Esumi, T Hosoya, A Suzuki, K Torigoe *J. Colloid Interface Sci.* **229** 303 (2000)
82. J J Michels, J Huskens, D N Reinhoudt *J. Chem. Soc., Perkin Trans. 2* 102 (2002)
83. F Gröhn, B J Bauer, E J Amis *Macromolecules* **34** 6701 (2001)
84. R Velarde-Ortiz, G Larsen *Chem. Mater.* **14** 858 (2002)
85. M Benito, O Rossell, M Seco, G Segales *J. Organomet. Chem.* **619** 245 (2001)
86. M Benito, O Rossell, M Seco, G Segales, V Maraval, R Laurent, A-M Caminade, J-P Majoral *J. Organomet. Chem.* **622** 33 (2001)
87. O Rossell, M Seco, A-M Caminade, J-P Majoral *Gold Bulletin* **34** 88 (2001)
88. A L Volynskii, L M Yarysheva, O V Arzhakova, N F Bakeev, *Vysokomol. Soedin., Ser. A* **33** 418 (1991) [a]
89. V A Davankov, M P Tsyurupa *React. Polym.* **13** 27 (1990)
90. M P Tsyurupa, V A Davankov *J. Polym. Sci.: Polym. Chem. Ed.* **18** 1399 (1980)
91. N I Nikonorova, S V Stakhanova, A L Volynskii, N F Bakeev *Vysokomol. Soedin., Ser. A* **39** 1311 (1997) [a]
92. N I Nikonorova, E S Trofimchuk, P G Elkin, N E Belova, S S Fanchenko, A L Volynskii, N F Bakeev *Vysokomol. Soedin., Ser. A* **44** 1185 (2002) [a]
93. N I Nikonorova, E S Trofimchuk, E V Semenova, A L Volynskii, N F Bakeev *Vysokomol. Soedin., Ser. B* **42** 1298 (2000) [a]
94. S N Sidorov, L M Bronstein, V A Davankov, M P Tsyurupa, S P Solodovnikov, P M Valetsky, E A Wilder, R J Spontak *Chem. Mater.* **11** 3210 (1999)
95. S V Vonsovskii *Magnetizm* (Magnetism) (Moscow: Nauka, 1971)
96. C P Bean, J D Livingston, P S Rodbell *Acta Metall.* **5** 682 (1957)
97. S N Sidorov, I V Volkov, V A Davankov, M P Tsyurupa, P M Valetsky, L M Bronstein, R Karlinsey, J W Zwanziger, V G Matveeva, E M Sulman, N V Lakina, E A Wilder, R J Spontak *J. Am. Chem. Soc.* **123** 10 502 (2001)
98. A N Parikh, M A Schivley, E Koo, K Seshadri, D Aurentz, K Mueller, D L Allara *J. Am. Chem. Soc.* **119** 3135 (1997)
99. W R Thompson, J E Pemberton *Langmuir* **11** 1720 (1995)
100. L M Bronstein, D M Chernyshov, P M Valetsky, E A Wilder, R J Spontak *Langmuir* **16** 8221 (2000)
101. D I Svergun, M B Kozin, P V Konarev, E V Shtykova, V V Volkov, D M Chernyshov, P M Valetsky, L M Bronstein *Chem. Mater.* **12** 3552 (2000)
102. L M Bronstein, C Linton, R Karlinsey, B Stein, D I Svergun, J W Zwanziger, R J Spontak *Nano Lett.* **2** 873 (2002)
103. J H Fendler, Y Tian, in *Nanoparticles and Nanostructured Films: Preparation, Characterisation and Applications* (Ed. J H Fendler) (Weinheim: Wiley-VCH, 1998) p. 429
104. L D Rampino, F F Nord *J. Am. Chem. Soc.* **63** 2745 (1941)
105. K E Kavanagh, F F Nord *J. Am .Chem. Soc.* **65** 2121 (1943)
106. L Hernandez, F F Nord *J. Colloid Sci.* **3** 363 (1948)
107. W P Dunsworth, F F Nord *J. Am. Chem. Soc.* **72** 4197 (1950)
108. M Boutonnet, J Kizling, P Stenius, G Maire *Colloids Surf.* **5** 209 (1982)
109. M Boutonnet, J Kizling, R Touroude, G Maire, P Stenius *Appl. Catal.* **20** 163 (1986)
110. M Ohtaki, N Toshima, M Komiyama, H Hirai *Bull. Chem. Soc. Jpn.* **63** 1433 (1990)
111. A B R Mayer, J E Mark *J. Polym. Sci., Part B* **35** 1207 (1997)
112. A B R Mayer, J E Mark *Angew. Makromol. Chem.* **52** 268 (1999)
113. J Dai, M L Bruening *Nano Lett.* **2** 497 (2002)
114. E Sulman, Y Bodrova, V Matveeva, N Semagina, L Cerveny, V Kurtc, L Bronstein, O Platonova, P Valetsky *Appl. Catal., A* **176** 75 (1999)
115. S Klingelhöfer, W Heitz, A Greiner, S Oestreich, S Flrster, M Antonietti *J. Am. Chem. Soc.* **119** 10 116 (1997)
116. Y Li, M A El-Sayed *J. Phys. Chem. B* **105** 8938 (2001)
117. M Zhao, R M Crooks *Chem. Mater.* **11** 3379 (1999)

118. E P Wohlfarth, in *Magnetism* (Eds G T Rado, H Suhl) (New York: Academic Press, 1963) p. 351
119. L Gunther *Phys. World* **3** 28 (1990)
120. J R Thomas *J. Appl. Phys.* **37** 2914 (1966)
121. O A Platonova, L M Bronstein, S P Solodovnikov, I M Yanovskaya, E S Obolonkova, P M Valetsky, E Wenz, M Antonietti *Colloid Polym. Sci.* **275** 426 (1997)
122. B H Sohn, R E Cohen *Chem. Mater.* **9** 264 (1997)
123. B H Sohn, R E Cohen, G C Papaefthymiou *J. Magn. Magn. Mater.* **182** 216 (1998)
124. R S Kane, R E Cohen, R Silbey *Chem. Mater.* **11** 90 (1999)
125. L H Hanus, K Sooklal, C J Murphy, H J Ploehn *Langmuir* **16** 2621 (2000)
126. J Huang, K Sooklal, C J Murphy, H J Ploehn *Chem. Mater.* **11** 3595 (1999)
127. P Zhang, S J Naftel, T K Sham *J. Appl. Phys.* **90** 2755 (2001)
128. W Sebastian, N A Kotov *J. Am. Chem. Soc.* **124** 2448 (2002)
129. M H Devoret, H Grabert, in *Single Charge Tunnelling Coulomb Blockade Phenomena in Nanostructures* (New York: Plenum, 1992) p. 1
130. K K Likharev *IBM J. Res. Develop.* **32** 144 (1988)
131. G Schön, U Simon *Colloid Polym. Sci.* **273** 101 (1995)

[a] — *Polym. Sci. (Engl. Transl.)*

Russian Chemical Reviews **73** (6) 517 – 540 (2004) © 2004 Russian Academy of Sciences and Turpion Ltd

DOI 10.1070/RC2004v073n06ABEH000894

Metallacyclopentadienes: structural features and coordination in transition metal complexes †

F M Dolgushin, A I Yanovsky, M Yu Antipin

Contents

I.	Introduction	517
II.	Dinuclear complexes with the metallacyclopentadiene fragment	518
III.	Coordination of the metallaindene fragment	527
IV.	Trimetallic clusters with a pentagonal-bipyramidal geometry	529
V.	Coordination of the metallacyclopentadiene fragment to transition metal clusters	531
VI.	Conclusion	537

Abstract. Results of structural studies of polynuclear transition metal complexes containing the metallacyclopentadiene fragment are overviewed. The structural features of the complexes in relation to the nature of the substituents in the organic moiety of the metallacycles, the nature of the transition metals and their ligand environment are analysed. The main structural characteristics corresponding to different modes of coordination of metallacyclopentadienes to one or two additional metal centres are revealed. The bibliography includes 154 references.

I. Introduction

Metallacycles and their complexes occupy a special place in modern organometallic chemistry because of their higher stability compared to acyclic analogues (the so-called chelating effect) as well as the diverse applications of metallacyclic compounds in both fundamental and applied investigations. The formation of metallacyclic fragments is observed in many reactions of organic substrates with transition metal complexes, for example, in cycloaddition, insertion of metal atoms into C–H bonds, reactions accompanied by dimerisation of unsaturated molecules through C–C coupling or reactions involving carbonyl, nitrile and other ligands of the starting complex. Methods for the synthesis of compounds containing metallacyclic fragments and their chemical properties were described in general reviews [1,2] as well as in reviews devoted to special problems.[3–5] Transition metal complexes containing metallacyclic fragments play an important role in metal-catalysed chemical transformations, such as alkene and acetylene metathesis, isomerisation of strained rings, cycloaddition of alkenes, oligomerisation of dienes and polymerisation.

Coupling of alkenes or alkynes in the coordination sphere of metal atoms is widely used in the synthesis of metallacyclic compounds giving rise primarily to five-membered metallacycles.[1,2] Of particular interest are five-membered unsaturated metallacycles, the so-called metallacyclopentadienes (MCPs).

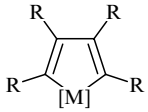

The MCP fragment is considered as an important intermediate in the synthesis of organic compounds from alkynes,[5–10] for example, in cyclotrimerisation of alkynes to form benzene derivatives and in the synthesis of quinones and tropones. Synthesis methods and studies of the chemical properties and structural features of transformation products of alkynes involved in transition metal complexes, including investigations of polynuclear complexes with the MCP fragment, were covered in the reviews.[11–14] In these complexes, the metallacycle generally serves as a π ligand with respect to transition metal atoms. Investigation of the coordination ability of the MCP fragment, particularly, taking into account its close analogy to the cyclopentadienyl ligand, is of interest not only for the development of the chemistry of certain systems but also for solution of more general problems of organometallic chemistry associated with a search for new 'non-classical' π ligands. Single-crystal X-ray diffraction is used as the main experimental method for studying the structures of MCP complexes.

Extensive experimental data on the structures of polynuclear transition metal complexes, in which the MCP fragment is involved in binding to one or several metal atoms, are available. According to the Cambridge Structural Database (CSD),[15] more than 350 structures of such compounds were characterised. For some series of related compounds, the results of structural studies were systematised (see, for example, the reviews [13,16,17]). However, abundant data on the structures of complexes with the MCP fragment have remained beyond the scope of these publications.

The present review covers the results of structural studies of polynuclear complexes containing the MCP fragment with special emphasis on comparative analysis of the structure of the MCP fragment and the modes of its coordination in transition metal complexes depending on the ligand environment, electronic state, the type and number of metal atoms, electronic and steric characteristics of substituents in the organic moiety of the metallacycle. We have restricted ourselves to complexes containing

F M Dolgushin, A I Yanovsky, M Yu Antipin A N Nesmeyanov Institute of Organoelement Compounds, Russian Academy of Sciences, ul. Vavilova 28, 119991 Moscow, Russian Federation. Fax (7-095) 135 50 85. Tel. (7-095) 135 92 14. E-mail: fedya@xray.ineos.ac.ru (F M Dolgushin)

Received 29 December 2003
Uspekhi Khimii **73** (6) 563 – 587 (2004); translated by T N Safonova

† The present review completes a series of publications covering main fields of research of the A N Nesmeyanov Institute of Organoelement Compounds of the Russian Academy of Sciences [see *Russian Chemical Reviews* **73** (5) (2004)].

more than three metal atoms. Prominence is given to bi- and trinuclear complexes of metals for which most representative data are available in the CSD (metals of the iron and cobalt subgroups). The structure of the uncoordinated MCP fragment has been discussed in detail earlier.[2,18] Hence, we do not consider mononuclear complexes. Complexes with metallacycles, in which one or several carbon atoms are replaced with heteroatoms (N, O, S, *etc.*), are also beyond the scope of our review.

II. Dinuclear complexes with the metallacyclopentadiene fragment

The first structure of an MCP-containing dinuclear complex with composition $Fe_2(CO)_6\{C(OH)C(Me)C(Me)C(OH)\}$ (**1**) was published in 1961.[19] The structure of complex **1** is shown in Fig. 1. The authors believed that the Fe(1) and Fe(2) atoms are in different oxidation states (0 and 2+, respectively); the diene fragment is coordinated to the Fe(2) and Fe(1) atoms through two σ-bonds and two π-bonds, respectively. Equalisation of the C–C bond lengths in the ring is indicative of strong conjugation. One of the six carbonyl groups, *viz.*, C(10)O(10), is apparently semibridging with the Fe(1)–C(10)–O(10) angle of 168°. However, in the authors' opinion, the Fe(2)···C(10) distance (2.48 Å) is too large to be indicative of interaction between these atoms.

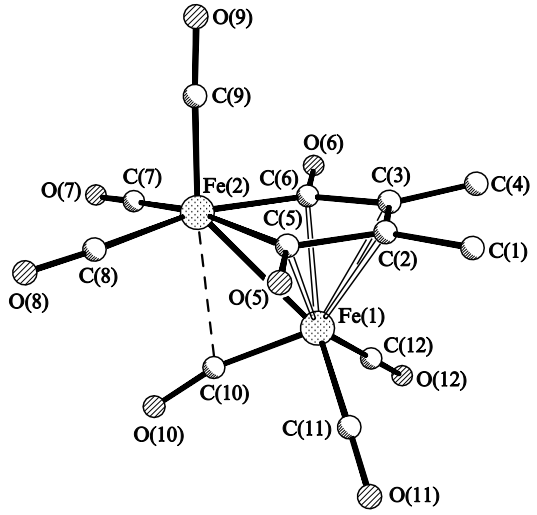

Figure 1. Structure of the $Fe_2(CO)_6\{C(OH)C(Me)C(Me)C(OH)\}$ complex (**1**).[19]
The hydrogen atoms are omitted, the atomic numbering scheme corresponds to that used in the original paper.

In the above-described compound, the structural motif, which proved to be typical of many bi- and polynuclear transition metal complexes, was found for the first time. Later on, the ferracyclopentadienyl fragment in complex **1** was given the short name ferrole. Nowadays all structurally similar dinuclear complexes are called complexes of the ferrole type regardless of the metal atoms involved in such complexes.

The structures of 158 dinuclear complexes of this type with different transition metals are included in the CSD. For convenience of comparison and discussion, typical compounds are shown in Fig. 2. The compounds are divided into five groups according to which subgroup of the Periodic Table the metal atom of the MCP fragment belongs. Each column in Fig. 2 begins with homometallic complexes with identical ligands (in most cases, these are carbonyl complexes) followed by heterometallic complexes (two different metal atoms, M^1 and M^2) and complexes with metal atoms in a non-equivalent ligand environment.

All compounds can formally be divided into two types according to the modes of distribution of electrons donated by an organic ligand between the metal atoms depending on the external ligand environment. In complexes of one type, the butadiene fragment forms two σ-bonds with one metal atom giving rise to a five-membered metallacycle, which is coordinated to the second metal atom through the metal–metal σ-bond and π-coordination of two alkene bonds of the diene fragment (η^1-η^4-coordination of the MCP fragment). For both metal atoms, the effective atomic number (EAN) rule is fulfilled, *i.e.*, the metal atoms have the filled 18-electron configuration (**A2**, **B1**, **B2**, **C4**, **D1** – **D3** in Fig. 2). In complexes of another type (**A1**, **C1** – **C3**, **D4**, **D5**, **E1**, **E2**), this description of coordination leads to non-equivalence of the electronic states of the metal atoms, which can be remedied by considering the metallacycle as a completely delocalised π-system (η^5-coordination of the MCP fragment). It should be emphasised that the use of these two limiting forms for the description of binding of the MCP fragments in dinuclear transition metal complexes of the ferrole type is based only on the formal application of the EAN rule. Nevertheless, as will be demonstrated below, the predominant contribution of one particular form was confirmed by the experimentally observed differences in the geometric parameters of ferrole complexes of different types.

1. Carbonyl complexes with metals of the iron subgroup

In crystals, dinuclear ferrole-type carbonyl complexes with metal atoms of the iron subgroup exist as one of two conformers, which differ in the orientation of the $M(CO)_3$ fragments with respect to the M–M bond. In most structures, like in complex **1**, the carbonyl groups have a staggered conformation giving rise to a shortened intramolecular contact between the endocyclic metal atom and one of the carbonyl groups at the exocyclic metal atom (this carbonyl group will be called semibridging). The second conformer is characterised by the eclipsed orientation of the carbonyl groups with the result that semibridging interaction is absent. In the general form, the structures of two conformers can be represented by the following scheme:

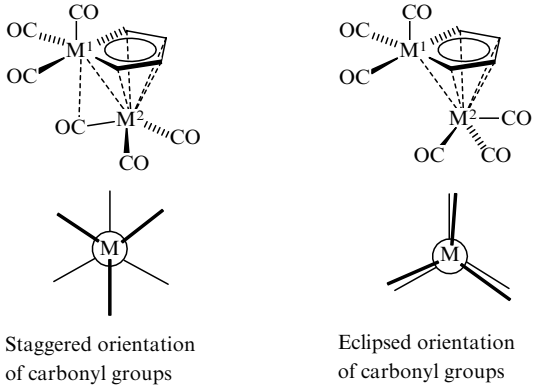

Dinuclear iron, ruthenium and osmium carbonyl complexes containing the MCP fragment are listed in Table 1 (structures available in the CSD and two compounds **31** and **32**, which were not deposited with CSD). Analogous complexes in which one or several carbonyl groups are replaced with other ligands (phosphine, alkene, *etc.*) are not considered. Polynuclear (containing more than two metal atoms) complexes bearing a ferrole-type fragment are also not included in Table 1. Selected compounds of this type are described below.

Analysis of the data from Table 1 shows that, first, isomers with a staggered conformation of carbonyl groups occur much more frequently than those with an eclipsed conformation of these groups (except for complexes of osmium for which only three structures of the type under consideration are known, and all these complexes have carbonyl groups in an eclipsed orientation). Second, for all compounds containing the semibridging carbonyl

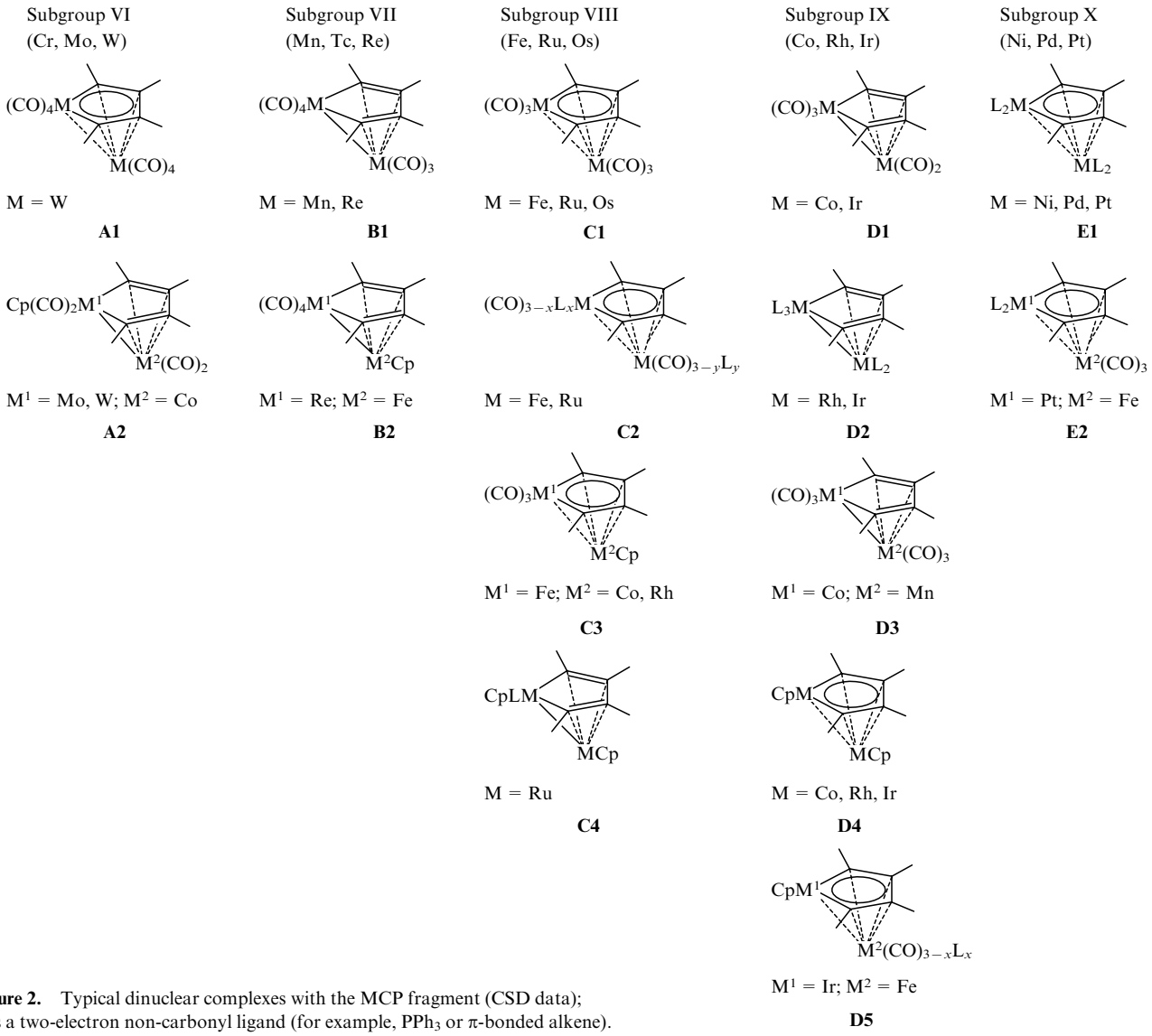

Figure 2. Typical dinuclear complexes with the MCP fragment (CSD data); L is a two-electron non-carbonyl ligand (for example, PPh_3 or π-bonded alkene).

group, there is a clear correlation between the $M^1\cdots CO(4)$ distance and the deviation of the metal carbonyl group $M^2-C-O(4)$ from linearity. These parameters vary over rather wide ranges, whereas the M^1-M^2 bond lengths are in a relatively narrow range. For example, the $M^1\cdots CO(4)$ distances in the iron complexes with a staggered conformation of carbonyl groups vary from 2.281 to 2.596 Å, whereas the M^1-M^2 distances are in the range of 2.463–2.533 Å, which is apparently indicative of high mobility of the carbonyl ligands at the M^2 atom relative to the relatively rigid metal–metal bond and a very weak interaction between the M^1 atom and the semibridging carbonyl group. It should be noted that the iron complexes with an eclipsed conformation of carbonyl ligands (compounds **21**, **22** and **23**) are characterised by somewhat larger metal–metal bond lengths (2.538, 2.544 and 2.568 Å, respectively). However, such a correlation is not observed for ruthenium complexes.

The nature of the metal–semibridging CO group interaction, its role in stabilisation of the molecule, the reasons for the existence of one of two possible conformers and other problems associated with this interesting characteristic feature of dinuclear ferrole-type carbonyl complexes with metals of the iron subgroup were discussed in numerous structural and theoretical studies. In particular, the following scheme of charge redistribution in complex **2** with unsubstituted ferrole was proposed [20] (the formal description assumes a negative charge on the metal atom involved in the metallacycle and a positive charge on the second metal atom): back donation from the occupied d orbitals of Fe^1 to the π* orbital of the semibridging CO group, which, in turn, leads to an increase in σ-donation from this carbonyl group to the electron-deficient Fe^2 atom.

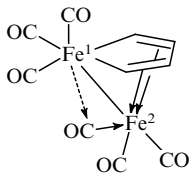

This scheme of charge density redistribution in transition metal complexes involving semibridging carbonyl ligands was proposed in the studies by Cotton (see, for example, Refs 50 and 51).

An alternative description was proposed in the publication,[46] where two ruthenium complexes (**31** and **32**) were considered. The authors of the cited study noted that the lengths of the $M^1-C(1)$ and $M^1-C(4)$ σ-bonds in these complexes and a number of other analogous compounds are close to the M=C double bond lengths in carbene complexes (the same fact was also mentioned in the study [20]). It is therefore concluded that there is a substantial additional π-contribution to binding of the metal atom M^1 in the ring. Hence, the charge redistribution in such complexes can occur as follows: $M^2 \rightarrow M^1 \rightarrow$ π electrons of the ring $\rightarrow M^2$. Therefore,

Table 1. Main geometric parameters for the dinuclear carbonyl complexes with general composition $(C_4R_4)M_2(CO)_6$ containing the MCP fragment (M^1, M^2 = Fe, Ru, Os; distances are given in Å, angles are given in degrees).

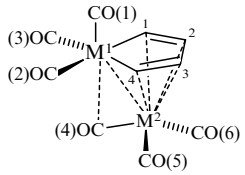

Compound [a]	MCP fragment	M^1-M^2	$M^1\cdots CO(4)$	$M^2-C-O(4)$ angle	$M^1-CO(1)$	$M^1-CO(2)$, $M^1-CO(3)$	$M^1-C(1)$, $M^1-C(4)$	C(1)–C(2), C(2)–C(3), C(3)–C(4)	ω [b]	τ [c]	Ref.
1	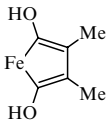	2.494	2.484	167.9	1.744	1.809 1.799	1.944 1.947	1.413 1.430 1.424	0.4	7.1	19
2		2.515	2.509	167.2	1.744	1.814 1.822	1.938 1.953	1.406 1.413 1.368	0.3	8.7	20
3	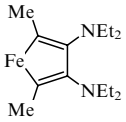	2.506	2.386	162.0	1.719	1.817 1.805	2.000 2.033	1.440 1.457 1.415	2.1	16.0	21
4	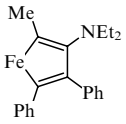	2.497	2.398	162.8	1.747	1.808 1.818	1.978 1.972	1.421 1.442 1.431	5.6	15.6	22
5	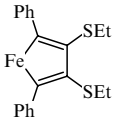	2.496	2.414	164.3	1.753	1.798 1.789	1.974 1.975	1.410 1.454 1.433	5.0	12.8	23
6	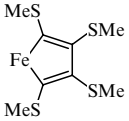	2.533	2.505	166.5	1.764	1.824 1.804	1.965 1.970	1.429 1.436 1.439	0.6	12.3	24
7	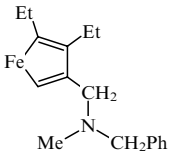	2.488	2.406	165.3	1.775	1.798 1.808	1.992 1.950	1.409 1.430 1.431	0.3	9.3	25
8	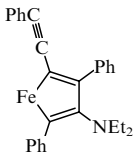	2.500	2.479	166.5	1.757	1.807 1.825	2.016 1.956	1.425 1.441 1.429	9.3	14.0	26
9	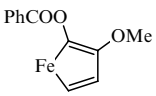	2.522	2.596	169.5	1.757	1.814 1.830	1.955 1.921	1.410 1.429 1.410	5.1	11.7	27
10	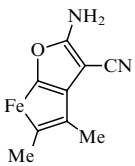	2.510	2.545	167.8	1.761	1.809 1.818	1.911 2.007	1.413 1.417 1.414	2.5	11.3	28

Table 1 (continued).

Compound [a]	MCP fragment	M^1-M^2	$M^1\cdots CO(4)$	$M^2-C-O(4)$ angle	$M^1-CO(1)$	$M^1-CO(2)$, $M^1-CO(3)$	$M^1-C(1)$, $M^1-C(4)$	$C(1)-C(2)$, $C(2)-C(3)$, $C(3)-C(4)$	ω [b]	τ [c]	Ref.
11	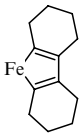	2.463	2.321	161.9	1.722	1.787 1.739	1.936 1.987	1.413 1.429 1.403	0.2	10.1	29
12	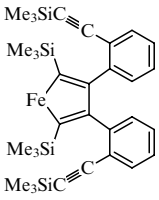	2.494	2.281	156.9	1.772	1.807 1.803	2.018 2.012	1.414 1.439 1.428	1.0	12.9	30
13	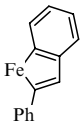	2.520	2.472	164.8	1.765	1.749 1.778	1.970 1.978	1.386 1.440 1.442	5.4	7.3	31
14	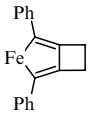	2.490	2.436	163.8	1.760	1.804 1.817	2.041 2.030	1.403 1.408 1.397	0.1	15.0	32
15	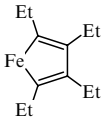	2.504	2.483	166.9	1.764	1.805 1.819	1.970 1.982	1.433 1.435 1.423	0.05	9.6	33
16	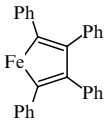	2.503	2.374	162.1	1.777	1.827 1.824	1.981 1.956	1.418 1.439 1.427	2.9	9.7	34
17	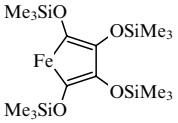	2.500	—	—	$\langle M^1-CO\rangle$ = 1.83		$\langle 1.92\rangle$	—	—	—	35
18	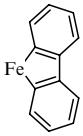	2.468	2.320	158.4	1.773	1.786 1.807	2.002 2.004	1.409 1.455 1.424	0.1	8.1	36
19	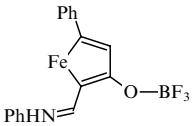	2.505	2.552	169.8	1.782	1.836 1.832	1.989 1.992	1.438 1.420 1.422	6.9	14.9	37
20	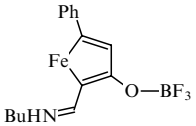	2.498	2.501	167.4	1.802	1.816 1.829	2.002 1.989	1.435 1.434 1.413	9.1	12.8	37
21	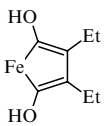	2.544	eclipsed orientation of carbonyl groups		1.734	1.795 1.809	1.930 1.935	1.419 1.436 1.411	0.7	−1.2	38
22	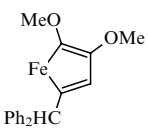	2.538	the same		1.745	1.786 1.749	1.885 1.953	1.414 1.392 1.392	5.4	5.9	39

Table 1 (continued).

Compound [a]	MCP fragment	M^1-M^2	$M^1\cdots CO(4)$	$M^2-C-O(4)$ angle	$M^1-CO(1)$	$M^1-CO(2)$, $M^1-CO(3)$	$M^1-C(1)$, $M^1-C(4)$	$C(1)-C(2)$, $C(2)-C(3)$, $C(3)-C(4)$	ω [b]	τ [c]	Ref.
23	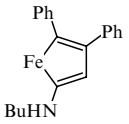	2.568	eclipsed orientation of carbonyl groups		1.773	1.816 1.792	1.956 1.988	1.416 1.436 1.414	16.9	−8.5	37
24	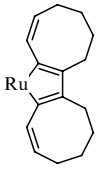	2.632	2.565	164.6	1.877	1.962 1.980	2.072 2.100	1.397 1.449 1.388	1.1	10.6	40
25	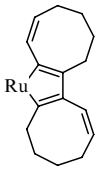	2.706	2.666	166.0	1.888	1.951 1.964	2.115 2.032	1.415 1.411 1.457	1.9	12.1	40
26	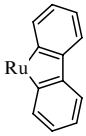	2.700	2.326	148.7	1.910	1.920 1.937	2.125 2.137	1.425 1.474 1.433	2.7	11.4	41
27	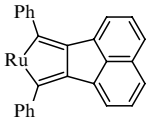	2.712	2.549	161.5	1.889	1.964 1.956	2.114 2.123	1.412 1.460 1.424	0.6	13.3	42
28 [d]	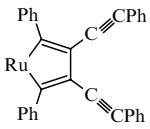	2.714 2.728	2.49 2.69	157 161	1.84 1.83	1.94 1.91 1.97 1.93	2.11 2.08 2.12 2.08	1.41 1.46 1.47 1.38 1.45 1.48	4.0 6.0	14.7 13.4	43
29 [d]	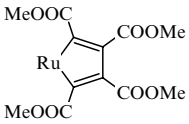	2.735 2.753	2.853 2.968	174.2 173.0	1.872 1.867	1.943 1.968 1.981 1.939	2.068 2.070 2.052 2.076	1.413 1.433 1.401 1.441 1.417 1.421	0.7 0.7	8.6 10.1	44
30	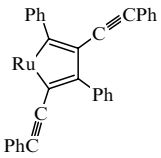	2.703	2.700	166.2	1.790	1.930 1.959	2.064 2.063	1.386 1.461 1.405	1.3	10.1	45
31 [e]	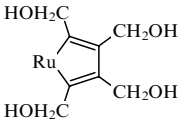	2.743	2.76	169	1.90	1.97 2.00	2.08 2.06	1.43 1.42 1.44	—	10.0	46
32 [e]	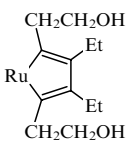	2.717	2.762	169.0	1.874	1.967 1.950	2.101 2.089	1.42 1.44 1.42	—	9.2	46

Table 1 (continued).

Compound [a]	MCP fragment	M^1-M^2	$M^1\cdots CO(4)$	$M^2-C-O(4)$ angle	$M^1-CO(1)$	$M^1-CO(2)$, $M^1-CO(3)$	$M^1-C(1)$, $M^1-C(4)$	$C(1)-C(2)$, $C(2)-C(3)$, $C(3)-C(4)$	ω [b]	τ [c]	Ref.
33	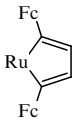	2.720	eclipsed orientation of carbonyl groups		1.892	1.949 1.949	2.074 2.074	1.410 1.397 1.410	0	−4.8	47
34	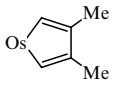	2.74	the same		–	–	–	–	–	–	48
35		2.754	"		1.891	1.902 1.958	2.054 2.116	1.404 1.415 1.455	5.7	4.6	49
36	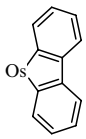	2.725	"		1.897	1.937 1.921	2.124 2.087	1.460 1.485 1.462	1.3	2.8	41

[a] M^2 = Fe (**1**–**24**), Ru (**25**–**33**), Os (**34**–**36**). [b] The C(1)−C(2)−C(3)−C(4) torsion angle. [c] The dihedral angle between the C(1)C(2)C(3)C(4) and C(1)M^1C(4) planes; the positive value corresponds to the deviation of the M^1 atom from the plane of the diene fragment in the direction opposite to the M^2 atom, the negative value corresponds to the deviation of the M^1 atom toward the M^2 atom. [d] Values are given for two independent molecules in the crystal. [e] The structures are unavailable in the CSD.

this process can take place without the involvement of a semibridging carbonyl group.

The contributions of Fe atoms and the diene fragment to the molecular orbitals of the ferrole complex $Fe_2(CO)_6(C_4H_4)$ were analysed in detail in the systematic study of the electronic structures of complexes containing the dinuclear fragment $M_2(CO)_6$, which is bound to various organic ligands.[52] It was demonstrated that there is an insignificant (0.2 eV) difference in the energy of two conformers of the complex with carbonyl ligands in eclipsed and staggered orientations. In the former case, there is a better overlap between the orbitals of the Fe^2 atom and the diene fragment. In the latter case, bonding interaction occurs between the Fe^1 atom and the semibridging carbonyl group.

It should be emphasised that the interaction between the M^1 atom and the semibridging carbonyl group is weak in both cases. The results of ^{13}C NMR and IR spectroscopic studies of dinuclear complexes of the ferrole type at low temperatures (below −125 °C)[53–55] provide evidence for free rotation of the $M^2(CO)_3$ fragment in solution.

An interesting observation was made in the study of ruthenium complex **29**.[44] There are two independent molecules in the crystal. These molecules have similar geometry, except for the orientation of the semibridging carbonyl group (CO_{sb}); the $Ru(1)\cdots CO_{sb}$ distances in two independent molecules are 2.852(9) and 2.968(8) Å. An even larger difference in the $Ru(1)\cdots CO_{sb}$ distances [2.49(3) and 2.69(3) Å] was observed in two crystallographically independent molecules of complex **28**,[43] although the molecules differ only in the angle of rotation of the phenyl substituents with respect to the plane of the MCP fragment. Such substantial differences in the length of the $Ru(1)\cdots CO_{sb}$ contact, which are caused only by the crystal packing effects, confirm the conclusion as to a fine balance between forces responsible for the existence of one of two possible conformers.

Consequently, the structures of dinuclear ferrole-type carbonyl complexes with metals of the iron subgroup should be described with consideration for the contribution of two possible limiting forms (**A** and **B**):

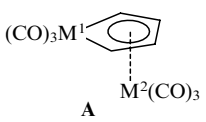

A

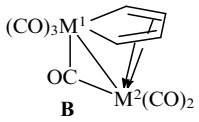

B

In the first case (**A**), it is presumed that the endocyclic metal atom M^1 is completely integrated into the common π system of the MCP fragment through which the charge redistribution between two metal atoms occurs. For another limiting form (**B**), the charge redistribution occurs through the bridging carbonyl group, and the M^1 atom is not involved in the interaction with the π system of the butadiene unit of the metallacycle. However, the fact that the interaction between the endocyclic metal atom and the semibridging carbonyl group is weak as well as the flattened structure of the MCP fragment are indicative of the predominant contribution of the form **A**.

It can be assumed that the semibridging interaction characterises the degree of involvement of the endocyclic metal atom in the common π system of the MCP fragment. This assumption is supported by analysis of the structure of the MCP fragment in complexes **1**–**36** (see Table 1). With rare exceptions, the butadiene fragment in the metallacycles retains a planar structure (see the ω torsion angles in Table 1), whereas the endocyclic metal atom generally deviates from the plane of the butadiene system in the direction opposite to the second metal atom (parameter τ in Table 1). An interesting exception is compound **33**, which provides the only example of ruthenium complexes with carbonyl ligands in an eclipsed orientation.[47] The structure of this complex is shown in Fig. 3.

In the crystal, the molecule occupies a special position on the symmetry plane passing through both ruthenium atoms and the midpoint of the C(6)−C(6A) bond. Four carbon atoms of the metallacycle are coplanar, whereas the endocyclic Ru(1) atom deviates from the plane of the butadiene fragment by 0.134(1) Å toward the second metal atom Ru(2), *i.e.*, there is 'negative' folding ($\tau = -4.8°$) of the metallacycle along the C(5)···C(5A) line. It should be noted that the presence of two bulky ferrocenyl substituents in the α positions of the metallacycle in complex **33** has apparently only a slight effect on the structure of the MCP fragment, as evidenced by the absence of shortened intramolecu-

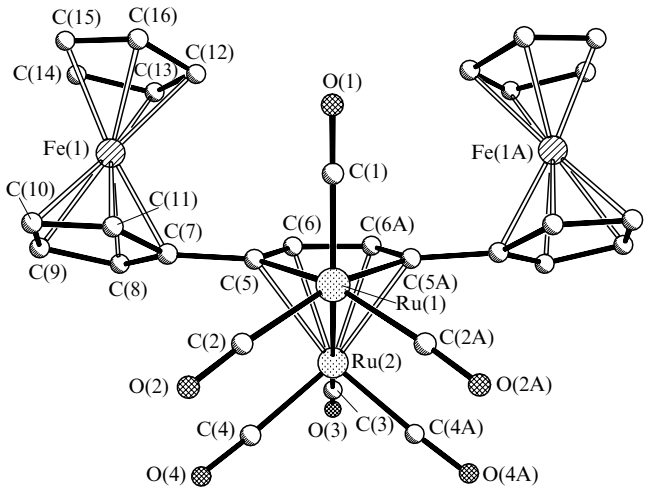

Figure 3. Structure of complex **33**.[47]

lar contacts. Besides, the negative value of the parameter τ is observed in two iron complexes (**21** and **23**), which also contain carbonyl ligands in an eclipsed orientation (see Table 1) and are devoid of sterically crowded substituents in the MCP fragment. In all other complexes with an eclipsed conformation of carbonyl ligands (**22**, **35** and **36**, see Table 1), the endocyclic metal atom deviates from the mean plane through four carbon atoms of the metallacycle in the direction opposite to the second metal atom. Nevertheless, in all complexes with eclipsed carbonyl ligands, folding of the MCP fragment is substantially smaller (the average angle $\tau = 4^\circ$) than that in complexes with staggered ligands and the semibridging carbonyl group (the average angle $\tau = 11^\circ$). Therefore, the MCP fragment is substantially flattened in complexes which contain carbonyl ligands in an eclipsed orientation and in which, correspondingly, additional interactions with the semibridging carbonyl group are absent.

The surprising thing is that the crystal structures of three dinuclear osmium complexes of the ferrole type (compounds **34**, **35** and **36**) are characterised by the eclipsed orientation of carbonyl ligands, whereas the staggered orientation (with the formation of the semibridging CO group) is typical of iron and ruthenium complexes. This fact was explained on the basis of *ab initio* calculations for $M_2(CO)_6(C_4H_4)$ (M = Fe, Ru, Os) complexes and comparison of these results with the data from UV photoelectron spectroscopy.[56] The authors proposed two mechanisms of charge redistribution in the dinuclear system: the direct metal–metal interaction and back donation from the d orbitals of the endocyclic metal atom to the π orbitals of the butadiene fragment and the semibridging carbonyl group. The absence of osmium complexes with staggered carbonyl ligands was accounted [56] for by substantial strengthening of the metal–metal interaction in the series Fe, Ru, Os, because the charge balance in such complexes can be established without the involvement of the semibridging carbonyl group.

It should be noted that derivatives containing only carbonyl ligands (**A1**, **B1**, **C1**, **D1**) were found for almost all dinuclear complexes with the MCP fragment (with the exception of Ni, Pd and Pt complexes; see Fig. 2). However, the existence of complexes as two conformers, *viz*., with the semibridging carbonyl group and without this group, is typical only of metals of the iron subgroup. In none of the complexes with other metals does a shortened contact between the endocyclic metal atom and one of the carbonyl groups coordinated to the second metal atom occur.

Yet another interesting characteristic feature of ferrole-type complexes is the rapid ferrole ring exchange **A** $\rightleftharpoons$ **C** characterised by the transition state **B** with the symmetry C_{2v}. This exchange was exemplified by optically active alkoxy- and hydroxy-substituted ferroles, which undergo racemisation at high temperatures.[57] The transformation from the hypothetical intermediate state **B** with the symmetry C_{2v} into ferrole was theoretically considered in the study.[52]

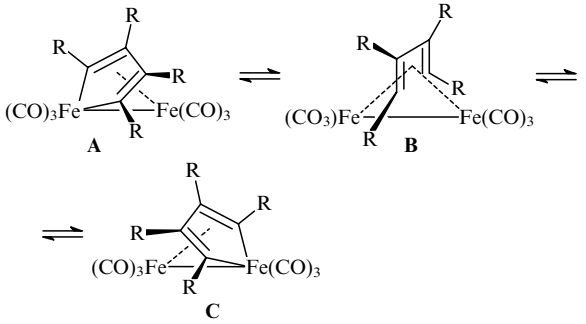

A remarkable example of the equilibrium transition between ferroles **A** and **C** was reported in the study,[58] where two isomers **37** and **38** (Fig. 4) were prepared in 18% and 57% yields, respectively, by thermolysis of the trimetallic cluster $Fe_3(CO)_9(N_2Et_2)$ with phenylacetylene. Heating of the pure isomers in solution afforded an equilibrium mixture of two complexes, which clearly confirms the occurrence of the dynamic transition **A** $\rightleftharpoons$ **C**. The enthalpy of isomerisation determined from the temperature dependence of the equilibrium constant is 90 ± 20 kJ mol^{-1} (low accuracy is related to slow decomposition of the compounds at high temperatures). The structures of both isomers were established by X-ray diffraction analysis.[59]

Both clusters contain the linear trimetallic core [the Fe(1)–Fe(2)–Fe(3) angle is 162° and 167° in isomers **37** and **38**, respectively]. The central iron atom is coordinated by both the

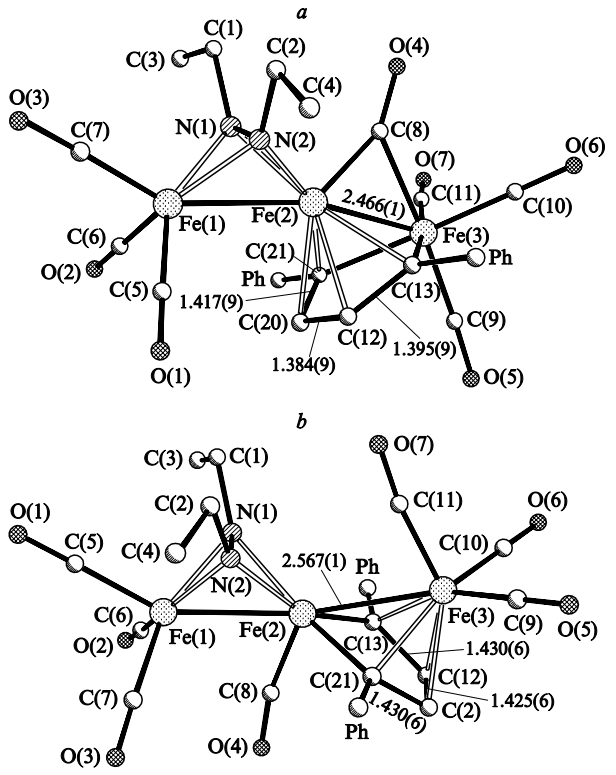

Figure 4. Structures of isomers **37** (*a*) and **38** (*b*) with composition $Fe_2(CO)_7(\mu\text{-}N_2Et_2)(\mu\text{-}HCCPh)_2$.[59]
Hereinafter, the bond lengths are given in Å. The phenyl substituents at the C(13) and C(21) atoms are omitted. The average Fe–C distances in the metallacycle are 2.02 and 1.93 Å, the Fe–C_{MCP} distances (π-coordination) are 2.09 and 2.11 Å in isomers **37** and **38**, respectively.

μ-azoalkane and μ-butadienyl ligands, which are located on opposite sides of the metal chain. The MCP fragments in both isomers are structurally similar to those in dinuclear ferrole complexes. The C—C bond lengths are equalised and the endocyclic metal atom deviates from the plane of the butadiene fragment in the direction opposite to the π-coordinated metal atom [the folding angle along the C(13)···C(21) line in the metallacycle is 15.2° and 12.9° for complexes **37** and **38**, respectively].

An analogous structure was described also for several homo- and heterometallic trinuclear complexes [60–65] containing an open metal chain and the MCP fragment. Only in one complex,[60] is the central metal atom involved in the metallacycle (like in isomer **38**). In other cases, the metallacycle is formed by the terminal metal atom (analogously to isomer **37**). In all compounds, the structure of the dinuclear fragment with the metallacycle is similar to that observed in dinuclear complexes of the ferrole type.

2. Phosphine derivatives

A characteristic feature of dinuclear carbonyl complexes of the ferrole type (see Table 1) is a shorter bond between the metal atom M^1 and the carbonyl group CO(1) located perpendicular to the plane of the metallacycle compared to two other bonds [M^1—CO(2) and M^1—CO(3)] involving the carbonyl groups in *trans* positions with respect to the M^1—C(1) and M^1—C(4) σ-bonds. For example, the average M^1—CO(1) and M^1—CO(2,3) bond lengths in the iron complexes are 1.76 and 1.81 Å, respectively.

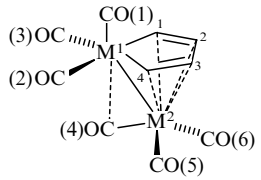

A noticeable shortening of the M^1—CO(1) bond can be explained by two alternative hypotheses:[17] (a) an increase in the electron density on the M^1 atom due to the $M^2 \rightarrow M^1$ dative bond, which, in turn, leads to an increase in back donation from the M^1 atom to the CO(1) group; (b) the electron deficiency on the metal atom M^1 is compensated by an increase in electron donation by the CO(1) group. The second hypothesis was confirmed by the fact that it is this carbonyl group that is replaced with a stronger σ-donor, for example, with the phosphine ligand.[54,66–68] For instance, prolonged refluxing of $(C_4Ph_4)Fe_2(CO)_6$ with triphenylphosphine in toluene afforded the only product $(C_4Ph_4)Fe_2(CO)_5PPh_3$ (**39**). Its structure was established by X-ray diffraction analysis [54] and is shown in Fig. 5 (prior to this study, it was believed that the phosphine ligand is coordinated to the exocyclic iron atom [69]).

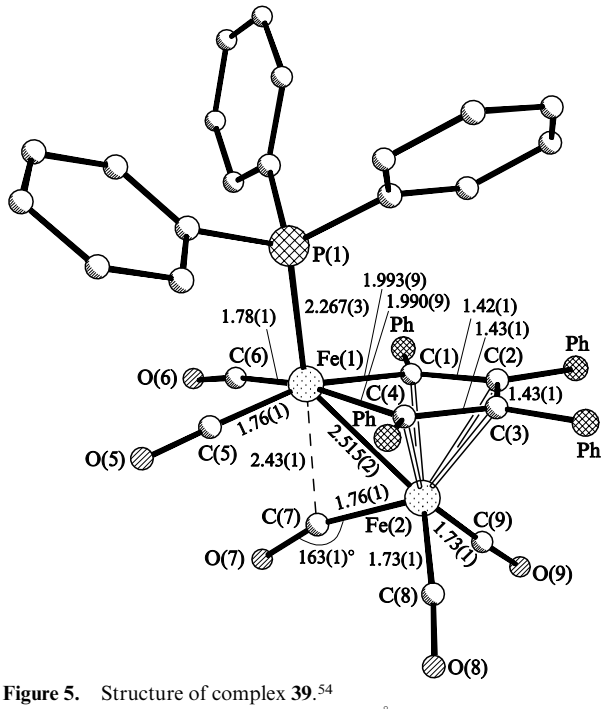

Figure 5. Structure of complex **39**.[54]
The average Fe(2)—C_{MCP} distance is 2.14 Å.

A comparison of the geometric parameters of complex **39** and its carbonyl analogue (compound **16**, Table 1) reveals no substantial differences in their structures. By contrast, the shortest $M^1 \cdots CO_{sb}$ distances [2.223(8) Å for Fe (see Ref. 66) and 2.236(3) Å for Ru (see Ref. 67)] in the series of ferrole-type carbonyl complexes (see Table 1) are observed in iron and ruthenium complexes with the trimethylphosphine ligand,[66,67] which is a stronger donor compared to the triphenylphosphine ligand.

It should be noted that in all monophosphine derivatives whose structures were established, the phosphine ligand is coordinated to the metal atom of the MCP fragment. Apparently, this isomer is thermodynamically more stable than the isomer in which this ligand is coordinated to the second metal atom (M^2). Coordination of the phosphine ligand to the M^2 atom was found only in diphosphine derivatives prepared by successive substitution of two CO groups in dinuclear hexacarbonyl complexes.[67,68]

3. Complexes with η^5- and η^1-η^4-coordination of the metallacyclopentadiene fragment

When describing complexes of the ferrole type, many authors (see, for example, Refs 61 and 63) invoked the analogy between the MCP fragment and the cyclopentadienyl ligand. This analogy is supported by the geometry of the metallacycle (a nearly planar structure, equalisation of the C—C bond lengths), the data from spectroscopic and electrochemical studies [70] and results of theoretical calculations.[18,52] A series of homo- and heteronuclear complexes of the ferrole type in which the exocyclic metal atom is coordinated simultaneously to the metallacycle and the cyclopentadienyl ligand (**B2**, **C3**, **C4**, **D4** in Fig. 2) belong to a peculiar type of metallametallocenes.[70–73] The structures of two ruthenium complexes **40** [74] and **41** [75] (see Fig. 6) are of interest.

Unlike homometallic dinuclear carbonyl complexes with metals of the iron subgroup characterised by η^5-coordination of the MCP fragment (**C1** and **C2** in Fig. 2), complexes **40** and **41** contain the η^1-η^4-coordinated metallacycle. This is related to the difference in the number of electrons donated to the metal atoms from the external ligand environment. In carbonyl complexes, each metal atom acquires six electrons, whereas the endocyclic ruthenium atom in complexes **40** and **41** has seven electrons and the exocyclic ruthenium atom has five electrons. Two different descriptions of the coordination modes of the MCP fragment in dinuclear complexes assume different electronic structures of the metallacycles. We proposed these descriptions based on the formal application of the EAN rule (see description of Fig. 2). The validity of this approach is supported also by the differences in the geometric structure of the complexes under consideration.

In complex **40**, the Ru(1)—Ru(2) bond is substantially elongated [2.831(1) Å)] compared to the Ru—Ru bonds in ruthenium carbonyl complexes **25**–**33** (the average bond length is 2.721 Å, see Table 1). In addition, the structure of the MCP fragment in complex **40** is non-planar, the folding angle of the metallacycle along the C(1)···C(4) line is 18.2°, which is also substantially larger than the average value (10.7°) for carbonyl complexes **25**–**33** (parameter τ in Table 1). It can be assumed that these changes in complex **40** are caused only by steric repulsions between the methyl groups of the pentamethylcyclopentadienyl ligands located in *cis* positions relative to the metal—metal bond. However, a comparison with complex **41**, in which the cyclopentadienyl ligands are in *trans* positions with respect to the metal—metal bond and steric hindrance is absent, provides

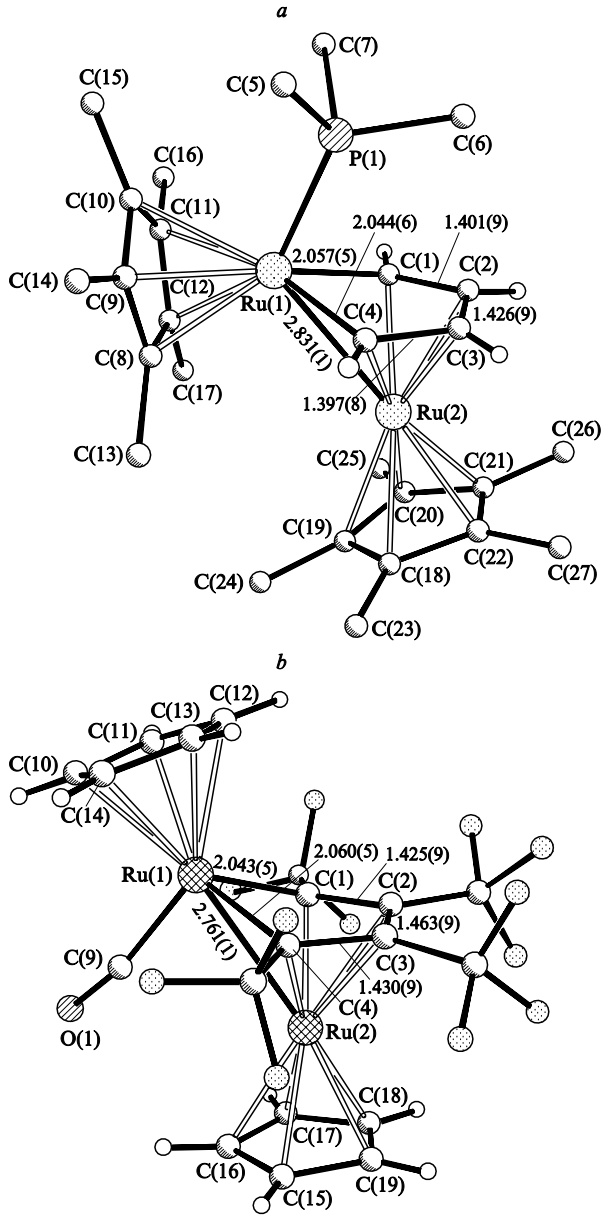

Figure 6. Structures of the complexes (η^5-C_5Me_5)Ru(PMe_3)(μ-η^4-C_4H_4)Ru(η^5-C_5Me_5) (**40**)[74] (*a*) and (η^5-C_5H_5)Ru(CO)(μ-η^4-$C_4(CF_3)_4$)Ru(η^5-C_5H_5) (**41**)[75] (*b*).

evidence for the predominant influence of the electronic properties of the ligand environment about the ruthenium atoms on the structure of the dinuclear fragment containing the metallacycle. The Ru(1)—Ru(2) bond length in complex **41** is smaller [2.761(1) Å] than that in complex **40** but it is noticeably larger than the average bond length in ruthenium carbonyl complexes **25**–**33**. The structure of the MCP fragment in complex **41**, where steric hindrance is absent, is analogous to that observed in complex **40**. The folding angle of the metallacycle is 23.1°. In both complexes, the C—C bonds are equalised. The Ru—C bond lengths in the metallacycles are close to the values typical of other ruthenacyclopentadienyl fragments.

In addition to complexes **40** and **41**, a number of analogous ruthenium compounds with cyclopentadienyl ligands and various ligands of another nature at the Ru(1) atom were also described.[76–78] In all complexes, the Ru—Ru bond is elongated and the MCP fragment shows greater deviations from planarity compared to those observed in ruthenium hexacarbonyl complexes of the ferrole type. In this connection, it is of interest to compare these compounds with the dinuclear cobalt carbonyl complexes $Co_2(CO)_5(C_4R_4)$ (**D1** in Fig. 2), whose formal consideration also reveals the η^1-η^4-coordination of the MCP fragment. The structures of all known dinuclear cobalt carbonyl complexes with the MCP fragment were described in the publication.[8] The authors noted that the structures of the complexes are independent of the nature of substituents in the organic moiety of the metallacycle and are characterised by equalisation of the C—C bond lengths in the diene fragment, a substantial deviation of the metallacycle from planarity (the average folding angle of the metallacycle is 16.5°) and a slight shortening of the Co—C bonds in the metallacycle (1.973 Å) compared to the values typical of the Co—C σ-bonds. Therefore, in the authors' opinion,[8] the use of the analogy between the MCP fragment and the cyclopentadienyl ligand in these complexes is not quite correct.

To compare complexes with different coordination modes of the MCP fragment (η^1-η^4- or η^5-coordination of the metallacycle) in more detail, we chose compounds with the same metal atoms and different ligand environments. In addition to the above-described ruthenium complexes, such pairs are known for cobalt and rhodium. The structures of these compounds are shown in Fig. 7 and their main geometric parameters are given in Table 2.

Table 2. Selected average geometric parameters for complexes with different coordination modes of the MCP fragment.

Metal	Coordination mode of the MCP fragment	M^1-M^2 /Å	$M^1-C(1,4)$ /Å	τ [a] /deg	Compounds
Ru	η^1-η^4	2.806	2.060	21.8	**40**–**44**
	η^5	2.725	2.073	9.3	**25**–**33**
Co	η^1-η^4	2.488	1.973	16.5	**45**–**49**
	η^5	2.451	1.889	5.7	**50**–**52**
Rh	η^1-η^4	2.708	2.048	16.5	**53**, **54**
	η^5	2.648	1.991	4.2	**55**–**58**

[a] The folding angle of the metallacycle along the C(1)···C(4) line.

The numbers of electrons donated by the external ligand environment to the metal atoms M^1 and M^2 are given in parentheses in Fig. 7. For complexes in which the numbers of electrons donated to the M^1 and M^2 atoms differ from each other (compounds at the left of Fig. 7), the fulfillment of the EAN rule assumes the formation of two σ-bonds between the organic ligand and the M^1 atom giving rise to the MCP fragment, which, in turn, is η^1-η^4-coordinated to the M^2 atom (the metal—metal σ-bond and π-coordination of the butadiene fragment). For complexes containing the M^1 and M^2 atoms in the same ligand environment (compounds at the right of Fig. 7), this consideration leads to non-equivalence of the metal atoms and, consequently, the electron density redistribution occurs apparently through the common π system of the metallacycle (η^5-coordination of the MCP fragment).

As can be seen from Table 2, the metal—metal bonds in the compounds with η^5-coordination of the MCP fragment are 0.03–0.08 Å shorter than those in the compounds with η^1-η^4-coordination. The structure of the MCP fragment also depends on its coordination mode. In the complexes with η^5-coordination, the metallacycle is more flattened than that in the complexes with η^1-η^4-coordination (parameter τ). In addition, the $M^1-C(1)$ and $M^1-C(4)$ bonds in the metallacycles are substantially shortened in the cobalt and rhodium complexes with η^5-coordination of the MCP fragment. This situation is not observed in ruthenium complexes.

Therefore, two coordination modes of the metallacycle occur in dinuclear complexes containing the MCP fragment depending on the number of electrons donated by the ligand environment

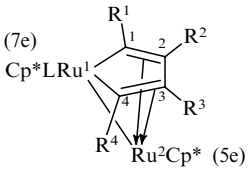

40–**44**

Compounds	L	Substituents	Ref.
40	PMe_3	R^1, R^2, R^3, R^4 = H	74
41	CO	R^1, R^2, R^3, R^4 = CF_3; Cp* = C_5H_5	75
42	C_2H_4	R^1, R^4 = Me; R^2, R^3 = H	76
43	2{Cl}	R^1, R^2, R^3, R^4 = H	77
44	2{Me}	R^1, R^3 = COOMe; R^2, R^4 = H	78

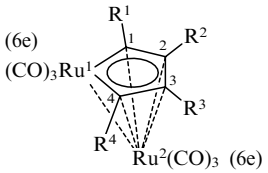

25–**33** (see Table 1)

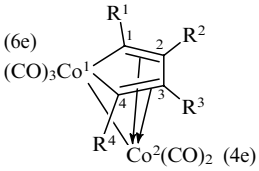

45–**49**

Compounds	Substituents	Ref.
45	$R^1-R^2=R^3-R^4=(CH_2)_6$	8
46	R^1, R^4 = SF_5; R^2, R^3 = H	8
47	R^1, R^4 = H; R^2-R^3 = $CMe_2N(Me)CMe_2$	8
48	R^1, R^4 = Ph; R^2, R^3 = H	8
49	R^1 = Ph; R^2 = H; R^3, R^4 = Me	8

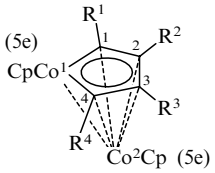

50–**52**

Compounds	Substituents	Ref.
50	R^1, R^2, R^3, R^4 = Cl	79
51	$R^1-R^2=R^3-R^4=C_4H_4$, Cp = C_5Me_5	80
52	$R^1-R^2=C_4H_4$, R^3 = Me, R^4 = H	81

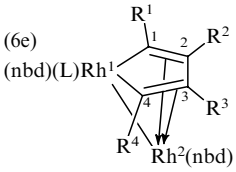

53, **54** (nbd is norbornadiene)

Compounds	L	Substituents	Ref.
53	PMe_3	R^1, R^4 = H; R^2, R^3 = Me	82
54	PPh_3	R^1 = C≡CPh; R^2, R^4 = Ph; R^3 = H	83

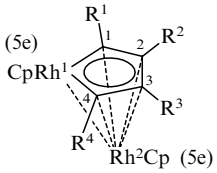

55–**58**

Compounds	Substituents	Ref.
55	R^1 = COOMe; R^2 = Me; R^3, R^4 = CF_3	84
56	$R^1-R^2=R^3-R^4=C_4H_4$; Cp = C_5Me_5	80
57	$R^1-R^2=C_4H_4$, R^3 = Ph, R^4 = H	85
58	$R^1-R^2=C_4H_4$, R^3 = Me, R^4 = H	85

Figure 7. Dinuclear complexes with the η^1-η^4- and η^5-coordinated MCP fragment.

about each metal atom. These coordination modes differ in the geometric parameters (see Tables 1 and 2). Complexes with η^1-η^4-coordination of the MCP fragment are characterised by a non-planar structure of the metallacycle with the endocyclic metal atom deviating from the plane of the butadiene unit in the direction opposite to the second metal atom (the folding angle of the metallacycle is close to 20°). Complexes with η^5-coordination of the MCP fragment are characterised by a more flattened structure of the metallacycle with an insignificant deviation of the endocyclic metal atom from the plane of the butadiene unit (the folding angle of the metallacycle is close to 5°). In this case, it is apparently more reasonable to assign the metallacycle to aromatic heterocycles. Shortening of the metal–metal bond is also typical of complexes with η^5-coordination. In some cases, shorter metal–carbon bonds were found in the metallacycle. In dinuclear carbonyl complexes with metals of the iron subgroup and carbonyl ligands in a staggered orientation, the structure of the MCP fragments is intermediate between the η^1-η^4 and η^5-coordination modes (the average folding angle of the metallacycles is 11°). This is attributable to an additional interaction between the metal atoms through the semibridging carbonyl group. Apparently, this additional interaction provides an alternative electron density redistribution between the metal atoms and results in a smaller contribution of the π system of the metallacycle to this process. The above analysis demonstrates that the folding angle of the metallacycle, which characterises the deviation of the endocyclic metal atom from the plane of the butadiene fragment, is most sensitive to a change in the coordination mode of the MCP fragment in dinuclear transition metal complexes.

III. Coordination of the metallaindene fragment

Among transition metal complexes involving the MCP fragment, many bi- and polynuclear compounds contain the five-membered metallacycle fused to the benzene ring to form the metallaindene system.

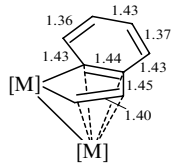

The above scheme gives the average C–C bond lengths (in Å) in dinuclear complexes with the metallaindene fragment.[31,49,67,80,81,85–89] We did not take into account polynuclear complexes (because the presence of additional metal atoms complicates the consideration) as well as complexes in which the six-membered ring is fused at the C–C single bond of the MCP fragment or the five-membered metallacycle is fused to two six-membered rings (as, for example, in complex **18** [36]).

The distribution of the bond lengths in the metallaindene system is indicative of a noticeable difference in the double and single C–C bonds and also of a decrease in the order of the double bond at which two rings are fused. It should be noted that a planar structure is typical of the metallaindene fragments (the average dihedral angle between the planes of the five- and six-membered rings is 6.4°; if the metal atom is ignored, this angle is 3.6°).

The fact that the common π system of the metallaindene fragment is divided into two butadiene units was clearly demonstrated in the study,[90] where the structure of trinuclear complex **59** was described (Fig. 8).

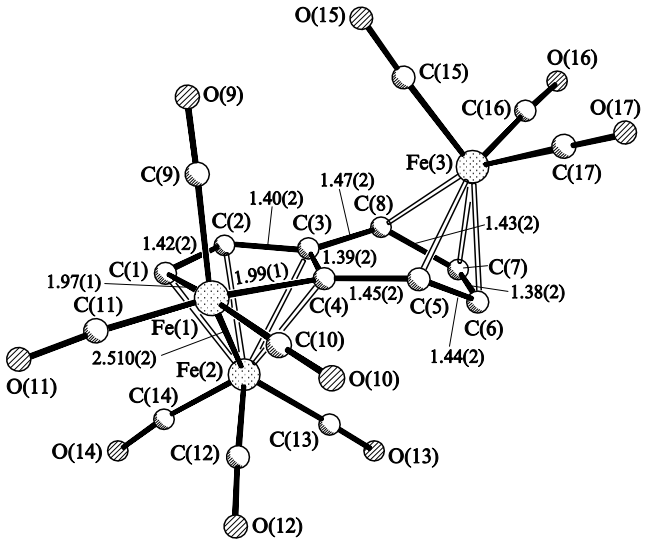

Figure 8. Structure of the ferraindene complex $Fe_3(CO)_9(C_8H_6)$ (**59**).[90]

As can be seen from Fig. 8, the Fe(2) and Fe(3) atoms are located on opposite sides of the bicyclic fragment, whose structure is essentially non-planar. There are two planar fragments, *viz*., C(1)C(2)C(3)C(4)C(5)C(8) and C(5)C(6)C(7)C(8). The dihedral angle between these planes is 32.5°. Hence, molecule **59** can be considered as consisting of two isolated fragments, *viz*., *cis*-butadienetricarbonyliron and the dinuclear ferrole complex. The latter has a structure typical of such complexes. The carbon–carbon bonds in the MCP fragment are equalised. The Fe(1) atom deviates from the plane through four carbon atoms by 0.16 Å in the direction opposite to the Fe(2) atom; the folding angle of the metallacycle along the C(1)···C(4) line is 8.0°. The carbonyl groups in the $Fe_2(CO)_6$ fragment are in a staggered orientation [the semibridging carbonyl group C(12)O(12) deviates from the linear coordination by 11°, the Fe(1)···C(12) distance is 2.53 Å]. The C(3)–C(8) and C(4)–C(5) bond lengths have values typical of the $C(sp^2)–C(sp^2)$ single bond within experimental error. Later on, an analogous complex containing the *p*-tolyl substituent at the C(2) atom and the methyl substituent at the C(7) atom was described.[91]

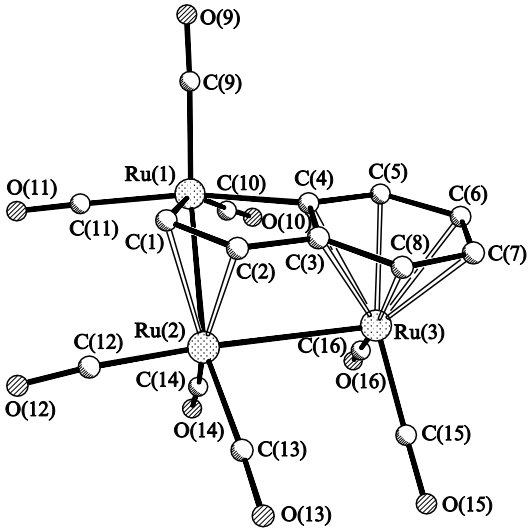

Figure 9. Structure of the ruthenaindene complex $Ru_3(CO)_8(C_8H_6)$ (**60**).[92]

Even more interesting results were obtained in the study,[92] where benzothiophene was subjected to desulfurisation in the reaction with $Ru_3(CO)_{12}$. The structure of trinuclear complex **60** (Fig. 9, Table 3) containing the metallaindene system was described. However, the coordination mode in this complex differs from that observed in compound **59**.

Table 3. Main geometric parameters for complexes **61**–**63** (bond lengths are given in Å, angles are given in degrees).

Parameter	Compound			
	60	**61**	**62**	**63**
Ru(1)–Ru(2)	2.781	2.774	2.781	2.783
Ru(2)–Ru(3)	2.946	2.951	2.951	2.958
Ru(1)–C(1)	2.058	2.042	2.052	2.057
Ru(1)–C(4)	2.088	2.093	2.106	2.096
Ru(2)–C(1)	2.237	2.246	2.252	2.233
Ru(2)–C(2)	2.257	2.266	2.280	2.249
Ru(3)–C(3)	2.351	2.374	2.342	2.352
Ru(3)–C(4)	2.322	2.335	2.316	2.356
Ru(3)–C(5–8)	2.248–2.295	2.244–2.305	2.261–2.299	2.275–2.280
C(1)–C(2)	1.400	1.394	1.394	1.394
C(2)–C(3)	1.458	1.445	1.478	1.453
C(3)–C(4)	1.454	1.450	1.449	1.440
C–C (in benzene ring)	1.399–1.430	1.384–1.432	1.400–1.438	1.392–1.438
Ru(1)–Ru(2)–Ru(3)	83.5	85.2	84.8	86.8

In complex **60**, both additional ruthenium atoms are located on the same side of the bicyclic system. The five-membered metallacycle coordinates the second ruthenium atom, Ru(2), through one C(1)=C(2) double bond, whereas two other carbon atoms of the metallacycle, *viz*., C(3) and C(4), are involved in η^6-coordination to the third ruthenium atom, Ru(3). Taking into account the planar structure of the metallaindene system (the dihedral angle between the mean planes of the five-membered metallacycle and the six-membered benzene ring is 7.6°), the

authors considered the $C_8H_6Ru(CO)_3$ fragment as the 8-electron ligand π-coordinated to the $Ru_2(CO)_5$ group.

Three structurally similar ruthenaindene complexes **61**–**63** were described in studies of the products obtained in reactions of $Ru_3(CO)_{12}$ with substituted benzenes.[93–95] Main geometric parameters of complexes **61**–**63** are given in Table 3.

The metallaindene system in complexes **61**–**63**, like that in complex **60**, is planar (the dihedral angle between the planes of the five-membered metallacycle and the six-membered ring is, on average, 4.5°).

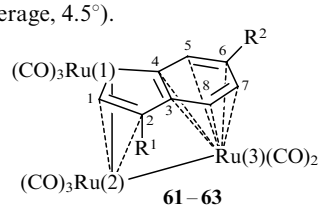

61–**63**

Compound	R^1	R^2	Ref.
61	Me	H	93
62	Me	$C(CH_2)Me$	94
63	H	Me	95

Evidently, the coordination mode of the MCP fragment in these four complexes differs radically from that observed in all the above-described compounds in which the metallacycle is symmetrically η^5-coordinated to one additional metal centre. In complexes **60**–**63**, the five-membered metallacycle is bound to two additional metal centres, one metal atom, Ru(2), being η^3-coordinated [the free C(1)=C(2) double bond and the Ru(1) atom are involved in coordination], whereas another metal atom, Ru(3), is η^2-coordinated [coordination by the C(3)=C(4) double bond involved in fusion to the six-membered ring]. The coordination is accompanied by localisation of the carbon–carbon bonds in the five-membered metallacycle. This is particularly clearly manifested in the C(2)–C(3) bond length. In all complexes, this bond corresponds to the length of the $C(sp^2)-C(sp^2)$ single bond. An interesting structural feature of the MCP fragment in complexes **60**–**63** is the deviation of the Ru(1) atom from the plane through four carbon atoms [C(1), C(2), C(3) and C(4)] toward two other metal atoms [Ru(2) and Ru(3)]. The mean folding angle of the metallacycle along the C(1)···C(4) line is 9.4°. The C(1)–C(2)–C(3)–C(4) torsion angle is 2.5°. It should also be noted that none of the complexes has an additional semibridging interaction between the ruthenium atoms involving carbonyl ligands, which is typical of ruthenium complexes of the ferrole type.

As is evident from the foregoing, the presence of the second additional metal centre in complexes containing the MCP fragment can lead to a substantial change in the coordination mode of the metallacycle. The main coordination modes of the MCP fragment in polynuclear transition metal complexes are described below.

IV. Trimetallic clusters with a pentagonal-bipyramidal geometry

In addition to the above-described dinuclear complexes with the MCP fragment, there is one more large class of related compounds with a pentagonal-bipyramidal geometry.

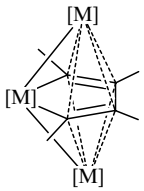

In these compounds, the MCP fragment is η^5-coordinated to two metal atoms located symmetrically on opposite sides of the plane of the metallacycle. Such complexes are often produced in reactions which also give dinuclear complexes of the ferrole type. This is particularly typical of reactions of metal carbonyls of the iron subgroup with alkynes.[12,13]

The first structure of the trinuclear iron complex $Fe_3(CO)_8(PhC_2Ph)_2$ characterised by pentagonal-bipyramidal geometry was described almost 40 years ago.[96] Later on, the structures of a series of analogous homonuclear iron and ruthenium clusters were studied. Their main geometric parameters are given in Table 4.

Table 4. Main geometric parameters (distances are given in Å, angles are given in degrees) of trinuclear iron and ruthenium complexes with a pentagonal-bipyramidal geometry.

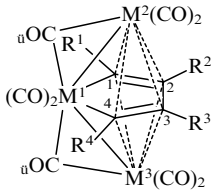

Compound [a]	Substituents	M^1-M^2, M^1-M^3	$M^2-M^1-M^3$ angle	$M^1-C(1)$, $M^1-C(4)$	C(1)–C(2), C(2)–C(3), C(3)–C(4)	τ [b]	M^1-CO_M	M^2-CO_M, M^3-CO_M	Ref.
64	$R^1=R^2=R^3=R^4=Ph$	2.428 2.435	87.6	2.062 2.031	1.457 1.458 1.434	1.3	1.991 1.988	1.841 1.770	96
65	$R^1=R^3=NEt_2$, $R^2=R^4=Me$	2.430 2.437	88.1	2.093 2.067	1.447 1.466 1.467	1.1	2.061 2.061	1.865 1.869	97
66	$R^1=R^4=F$, $R^2=R^3=H$	2.436 2.433	88.4	1.986 1.971	1.414 1.420 1.436	0.2	2.097 2.078	1.850 1.860	98
67	$R^1=R^2=F$, $R^3=R^4=H$	2.433 2.433	88.4	1.988 2.054	1.418 1.414 1.427	0	2.081 2.081	1.876 1.876	98

Table 4 (continued).

Compound [a]	Substituents	M^1-M^2, M^1-M^3	$M^2-M^1-M^3$ angle	$M^1-C(1)$, $M^1-C(4)$	$C(1)-C(2)$, $C(2)-C(3)$, $C(3)-C(4)$	τ [b]	M^1-CO_M	M^2-CO_M, M^3-CO_M	Ref.
68	$R^1 = R^4 = F$, $R^2 = Ph$, $R^3 = Me$	2.425 2.426	88.8	2.007 1.948	1.422 1.457 1.459	1.9	1.964 2.127	1.902 1.828	98
69	$R^1 = R^2 = Ph$, $R^3 = Me$, $R^4 = OEt$	2.440 2.440	87.8	2.061 2.053	1.441 1.438 1.444	1.7	2.046 2.072	1.861 1.849	99
70	$R^1 = R^2 = SiMe_3$, $R^3 = OEt$, $R^4 = Me$	2.426 2.439	87.2	2.118 2.012	1.465 1.465 1.425	3.4	2.087 2.003	1.846 1.884	99
71	$R^1 = R^3 = Ph$, $R^2 = NEt_2$, $R^4 = CCPh$	2.442 2.422	88.4	2.058 1.996	1.476 1.468 1.445	0.6	2.061 2.066	1.754 1.825	26
72	$R^1 = Ph$, $R^2 = R^3 = NEt_2$, $R^4 = CHCHMe$	2.429 2.420	88.7	2.076 2.075	1.431 1.477 1.440	1.2	2.085 2.005	1.841 1.854	100
73 [c]	$R^1 = R^4 = H$, $R^2-R^3 = =CMe_2NHCMe_2$	2.427 2.411	88.1	2.053 2.073	1.428 1.443 1.436	0.3	2.044 2.006	1.860 1.856	101
		2.419 2.406	88.7	2.062 2.064	1.431 1.439 1.423	0.6	2.056 2.001	1.865 1.859	
74	$R^1 = R^2 = Et$, $R^3 = H$, $R^4 = CH_2N(Me)CH_2Ph$	2.431 2.440	87.3	2.058 2.036	1.443 1.445 1.432	0.7	2.085 2.046	1.845 1.859	25
75	$R^1 = R^2 = R^3 = R^4 = Ph$	2.670 2.672	89.1	2.218 2.216	1.460 1.472 1.451	0.9	2.158 2.156	2.028 2.008	102
76	$R^1 = R^4 = Ph$, $R^2-R^3 = C_5H_4FeC_5H_4$	2.669 2.652	89.1	2.198 2.243	1.436 1.471 1.439	1.4	2.155 2.096	2.000 1.988	103
77	$R^1 = R^3 = Bu^t$, $R^2 = H$, $R^4 = CHCHBu^t$	2.661 2.669	88.8	2.172 2.226	1.425 1.450 1.419	0.6	2.117 2.142	2.008 1.976	104
78	$R^1 = R^2 = R^3 = R^4 = Me$	2.651 2.651	88.6	2.207 2.219	1.450 1.460 1.441	0	2.190 2.190	1.999 1.999	105
79	$R^1 = R^4 = Ph$, $R^2 = R^3 = H$	2.683 2.683	89.0	2.209 2.209	1.442 1.454 1.442	0.4	2.169 2.169	2.014 2.014	106
80	$R^1-R^2 = C_{10}H_{16}$, $R^3 = R^4 = Ph$	2.668 2.664	88.7	2.203 2.220	1.427 1.493 1.469	1.0	2.196 2.136	1.964 1.998	107

[a] M = Fe (**64**–**74**), Ru (**75**–**80**). [b] The folding angle of the metallacycle along the C(1)···C(4) line. [c] Two crystallographically independent molecules.

Complexes **64**–**80** contain an open trimetallic core with two nearly equal-length metal–metal bonds; the angle between these bonds is close to 90°. Each metal atom is coordinated by two terminal CO groups. Two other carbonyl groups form bridges between the central and peripheral metal atoms. The bridging CO groups are slightly shifted to the peripheral metal atoms (the M^1-CO_M distances are, on average, 0.2 Å longer than the M^2-CO_M and M^3-CO_M distances). The central metal atom is involved in two σ-bonds with the butadiene moiety to form the MCP fragment, which is, in turn, symmetrically π-coordinated to both peripheral metal atoms at the vertices of the bipyramid.

The metallacycle is planar (parameter τ in Table 4) and dissects the structure into two equivalent moieties, each moiety being structurally similar to dinuclear iron and ruthenium complexes of the ferrole type. The common symmetry of these complexes is particularly pronounced in the crystal structures of compounds **67**, **78** and **79**. Molecules of these compounds occupy special positions on the mirror symmetry plane passing through the plane of the metallacycle. The carbon–carbon bonds in the MCP fragments of complexes **64**–**80** are equalised, whereas the metal–metal distances (the average values are 2.429 and 2.666 Å for the iron and ruthenium complexes, respectively) are noticeably shortened compared to the corresponding bonds in dinuclear complexes of the ferrole type (see Table 1).

The structures of the trinuclear complexes listed in Table 4 are often described using polyhedral clusters (see, for example, the

studies [26, 100] and the review [13]), for which the number of skeletal electrons (*i.e.*, electrons involved in bonding in the polyhedron) is counted according to the so-called Wade's rule (or the '$2n+2$' rule).[108]

In complexes **64**–**80**, the M_3C_4 system can be considered as a *closo*-pentagonal-bipyramidal structure. According to Wade's rules, 16 skeletal electrons are required for a seven-vertex polyhedron. It is easy to demonstrate that this rule is fulfilled for all compounds listed in Table 4. After the removal of one vertex of the bipyramid occupied by the $Fe(CO)_2$ or $Ru(CO)_2$ group, which donates no skeletal electrons, the seven-vertex *closo* system is transformed into a six-vertex pyramidal cluster with a *nido* structure, the total number of skeletal electrons remaining unchanged. The six-vertex clusters thus obtained represent the above-described dinuclear carbonyl complexes of the ferrole type. It should be noted that all dinuclear complexes which are presented in Fig. 2 and contain different transition metal atoms with different ligand environments, can be described as *nido*-pentagonal-pyramidal systems bearing 16 skeletal electrons.

The possibility of the transformation of trinuclear complexes with composition $M_3(CO)_8(RC_2R)_2$ into the dinuclear complexes $M_2(CO)_6(RC_2R)_2$ has been demonstrated in the pioneering studies on the chemical behaviour of these clusters [109, 110] and was subsequently confirmed in many investigations (see, for example, Refs 98 and 111). This transformation occurs in the course of thermolysis under severe conditions, no other products being formed, which is indicative of high stability of ferrole complexes and the MCP fragment. Investigation of the electronic structures of ferracyclopentadiene derivatives (dinuclear and trinuclear complexes) by photoelectron spectroscopy and *ab initio* calculations [112] demonstrated a high degree of electron density delocalisation in these clusters as well as the strong Fe–C σ-interaction in the metallacycle, which accounts for the stability of the MCP fragment in chemical reaction. Substantial delocalisation of the electron density in trinuclear iron and ruthenium clusters with a pentagonal-bipyramidal geometry is also evidenced by the data from spectroscopic (^1H and ^{13}C NMR and IR) and electrochemical studies of a large number of compounds containing various substituents at the carbon atoms of the metallacycles.[111, 113]

In addition to the above-mentioned pentagonal-bipyramidal trinuclear iron and ruthenium carbonyl complexes **64**–**80**, six structurally similar compounds with other transition metal atoms and/or with another ligand environment were described. These are two heteronuclear complexes with composition $Re_2Fe(CO)_9(CH=CHC_6H_4)$ (**81**)[114] and $Cp^*WRe_2(CO)_7$.$(\mu\text{-}H)(CH=CHC_6H_8)$ (**82**),[115] the trinuclear iridium complex $Ir_3(2\eta^2\text{-cod})_3(\mu\text{-}H)(C_4H_4)$ (cod is cyclooctadiene) (**83**)[82] and the trinuclear ruthenium complexes $Ru_3(CO)_6(dppm)(C_4H_2Ph_2)$ [dppm is bis(diphenylphosphine)methane] (**84**),[116] $Cp^*_3Ru_3$.$(H)(C_4H_3Et)$ (**85a**)[117] and $Cp_2Ru_3(CO)_3\{C_2(CF_3)_2$.$C_2(CO_2Me)_2\}$ (**86b**),[118] the latter two complexes having an unusual triple-decker sandwich structure. All complexes satisfy the '$2n+2$' rule for the number of skeletal electrons in the *closo*-pentagonal-bipyramidal polyhedron. The structure of the MCP fragments in complexes **81**–**85** is analogous to that observed in trinuclear iron and ruthenium carbonyl complexes **64**–**80**.

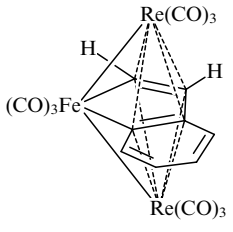

81

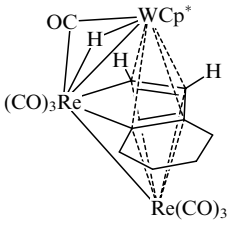

82

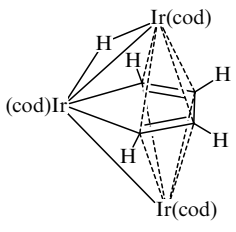

83

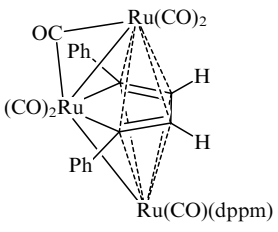

84

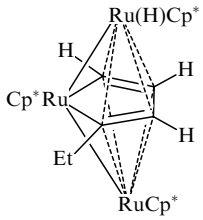

85a

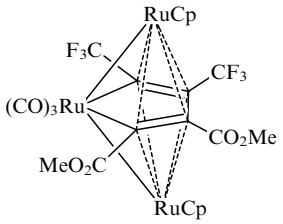

85b

V. Coordination of the metallacyclopentadiene fragment to transition metal clusters

Many trinuclear and polynuclear complexes with the MCP fragment include the structural motif presented in the following scheme:

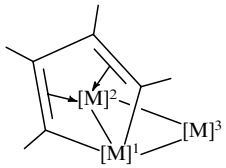

The lateral or $\mu_2\text{-}2\eta^1\text{-}\eta^4$-coordination of an organic ligand to the triangular metal core is typical of trimetallic iron, ruthenium and osmium clusters.[97, 119–137] The formation of such complexes was observed in the reactions of metal carbonyl clusters of the iron subgroup with alkynes and their functional derivatives. The complexes contain the dinuclear ferrole-type fragment and the third metal atom, which is not directly bound to the organic moiety of the metallacycle.

The structural formulae and selected geometric parameters of the triangular metal complexes of the iron subgroup with this coordination mode of the MCP fragment are given in Table 5. All complexes contain the MCP fragment, whose diene moiety is π-coordinated to the M^2 atom. Besides, in some complexes (**86**, **87**, **92**–**99** and **107**–**109**), the functional group at one of the α-carbon atoms of the metallacycle is coordinated to the third metal atom (M^3), which is not involved in a direct bond with the MCP fragment. This additional interaction results in inclination of the MCP fragment relative to the plane of the triangle formed by the metal atoms (the average angle between the planes is 63°). In complexes in which an additional coordination to the third metal atom is absent, the metallacycle is located almost perpendicular to the $M^1M^2M^3$ plane (the average angle between the planes is 83°).

In complexes listed in Table 5, the metal–metal bond lengths are non-equivalent. The M^1-M^2 bond lengths are close to the values observed in the dinuclear complexes of the ferrole type (see Table 1, complexes **1**–**36**). The M^2-M^3 bonds have similar or even somewhat larger lengths, whereas the M^1-M^3 bond between the endocyclic metal atom and the metal atom which is not directly bound to the MCP fragment, is noticeably elongated in most complexes. This tendency is most pronounced in complexes **91** and **100**–**103** bearing no bridging ligands, whose tightening effect may substantially influence the M–M bond lengths. For this reason, it is of interest to compare two related ruthenium complexes $Ru_3(CO)_8(PPh_3)\{C_4Ph_2(CH=CHPh)_2\}$ (**91**)[123] and $Ru_3(CO)_8\{C_4Ph_2(CH=CHPh)_2\}$ (**92**)[124] containing, along with the MCP fragment, only terminal two-electron ligands (CO or PPh_3). Complex **92** was prepared by the thermal reaction of enyne $PhCH=CHC\equiv CPh$ with $Ru_3(CO)_{12}$. The reaction of complex **92**

Table 5. Selected geometric parameters (bond lengths are given in Å, angles are given in degrees) for trinuclear iron, ruthenium and osmium clusters with the laterally coordinated MCP fragment.

Compound	Formula	M^1-M^2, M^2-M^3, M^1-M^3	$M^1-C(1)$, $M^1-C(4)$	C(1)–C(2), C(2)–C(3), C(3)–C(4)	ω [a]	τ [b]	θ [c]	Ref.
86	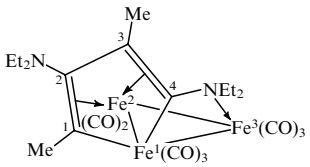	2.506 2.604 2.564	2.006 1.970	1.419 1.440 1.418	1.8	12.4	55.4	97
87	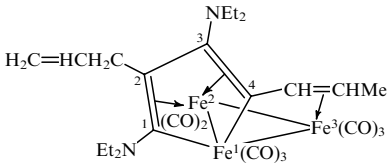	2.557 2.590 2.642	2.136 1.965	1.453 1.453 1.444	3.6	16.3	58.9	119
88	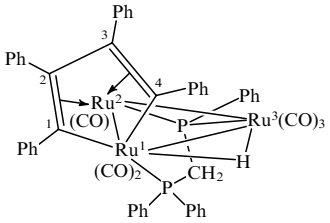	2.663 2.800 3.034	2.168 2.114	1.400 1.443 1.384	1.1	6.2	75.6	120
89	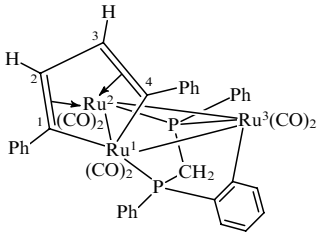	2.714 2.827 2.982	2.21 2.07	1.33 1.41 1.46	7.0	3.5	78.4	121
90	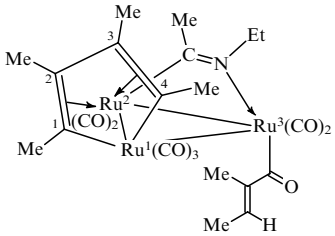	2.779 2.897 3.073	2.053 2.060	1.388 1.450 1.374	3.5	10.9	89.5	122
91	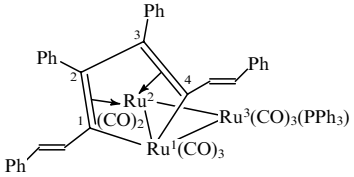	2.757 2.732 2.927	2.128 2.137	1.409 1.438 1.428	0.1	9.6	88.4	123
92	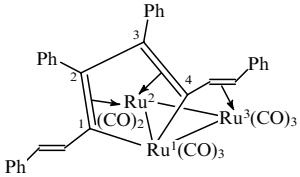	2.733 2.802 2.823	2.146 2.082	1.432 1.443 1.430	4.7	14.6	58.5	124
93	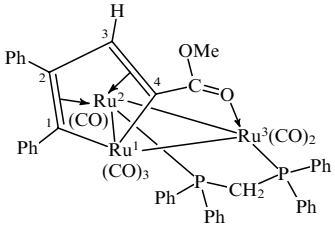	2.701 2.697 2.830	2.174 2.083	1.426 1.404 1.403	4.4	14.5	66.1	120

Table 5 (continued).

Compound	Formula	M^1-M^2, M^2-M^3, M^1-M^3	$M^1-C(1)$, $M^1-C(4)$	$C(1)-C(2)$, $C(2)-C(3)$, $C(3)-C(4)$	ω [a]	τ [b]	θ [c]	Ref.
94	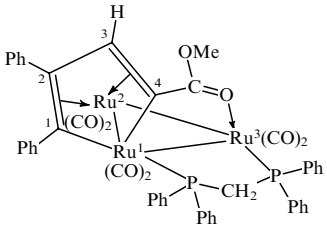	2.730 2.679 2.880	2.154 2.108	1.432 1.435 1.408	3.2	13.3	64.6	120
95	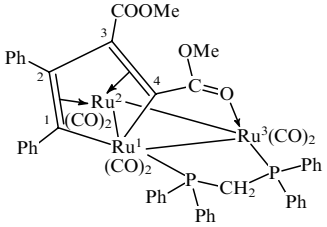	2.744 2.683 2.860	2.141 2.111	1.457 1.428 1.417	5.7	15.0	65.3	120
96	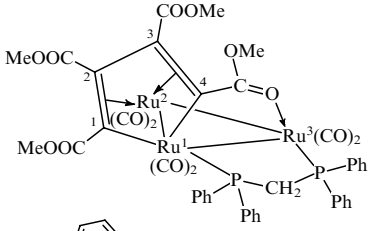	2.739 2.698 2.863	2.116 2.115	1.418 1.439 1.419	5.8	13.3	64.2	125
97	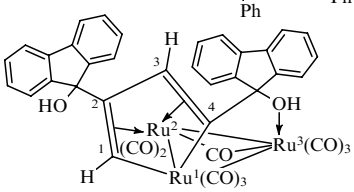	2.777 2.879 2.833	2.069 2.111	1.386 1.425 1.395	0.4	9.5	63.1	126
98	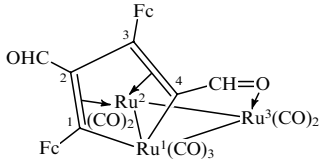	2.712 2.701 2.822	2.185 2.086	1.455 1.417 1.449	0.9	14.6	64.4	127
99 [d]	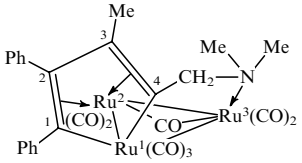	2.771 2.884 2.855 2.773 2.850 2.829	2.09 2.10 2.07 2.09	1.40 1.45 1.37 1.46 1.45 1.38	2.6 1.2	8.0 8.1	61.9 62.8	128
100 [e]	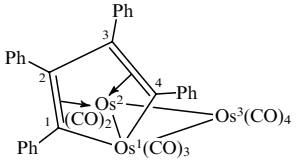	2.739 2.741 2.894 2.729 2.723 2.917	2.14 2.13 2.01 2.14	1.37 1.42 1.47 1.37 1.47 1.40	4.0 0.5	9.8 9.1	85.9 84.9	129
101	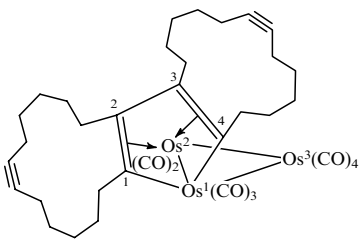	2.743 2.731 2.928	2.183 2.183	1.402 1.472 1.402	0	9.3	90.0	130

Table 5 (continued).

Compound	Formula	M^1-M^2, M^2-M^3, M^1-M^3	$M^1-C(1)$, $M^1-C(4)$	C(1)–C(2), C(2)–C(3), C(3)–C(4)	ω [a]	τ [b]	θ [c]	Ref.
102	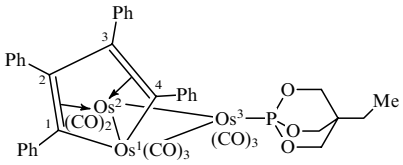	2.752 2.739 2.905	2.132 2.149	1.400 1.442 1.439	0.3	7.9	89.9	131
103	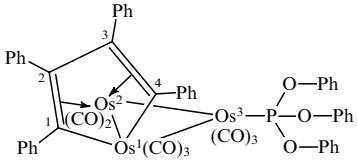	2.761 2.732 2.921	2.182 2.054	1.269 1.509 1.521	2.4	6.4	87.4	131
104	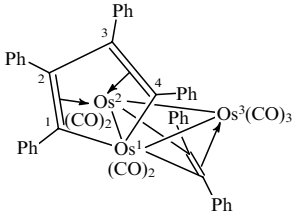	2.677 2.794 2.737	2.150 2.097	1.361 1.475 1.437	4.9	−9.0	80.4	132
105	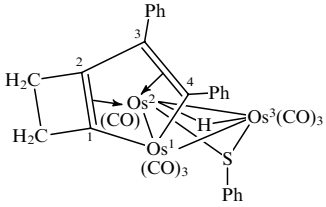	2.725 2.722 3.017	2.11 2.23	1.41 1.44 1.42	4.0	11.7	78.5	133
106	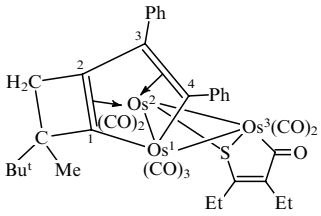	2.747 2.770 3.054	2.06 2.14	1.41 1.44 1.45	4.6	2.3	77.9	134
107	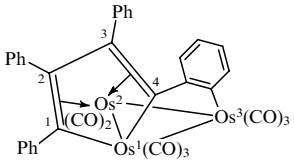	2.747 2.873 2.943	2.247 2.158	1.561 1.269 1.514	8.8	19.6	66.7	135
108	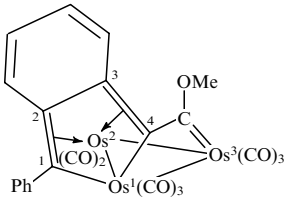	2.720 2.754 2.903	2.16 2.12	1.41 1.44 1.40	3.8	13.9	59.9	136
109	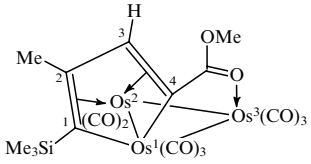	2.718 2.722 2.854	2.202 2.108	1.440 1.458 1.401	4.8	12.5	64.7	137

[a] The C(1)–C(2)–C(3)–C(4) torsion angle. [b] The dihedral angle between the C(1)C(2)C(3)C(4) and C(1)M^1C(4) planes. [c] The dihedral angle between the mean plane of the MCP fragment and the plane of the $M^1M^2M^3$ triangle. [d] Two crystallographically independent molecules. [e] Two crystal modifications: monoclinic $P2_1/c$ and orthorhombic *Iba*2.

with triphenylphosphine led to the displacement of the alkenyl ligand π-coordinated to the Ru(3) atom giving rise to complex **91**.[123] The triphenylphosphine ligand in complex **91** occupies an equatorial position at the Ru(3) atom in the *trans* position with respect to the Ru(1)–Ru(3) bond.

The Ru(1)–Ru(2) bond length in complexes **92** and **91** [2.733(1) and 2.757(1) Å, respectively] remains virtually unchanged and is typical of the Ru–Ru bonds in dinuclear ruthenium complexes of the ferrole type (2.703–2.753 Å, see Table 1). This fact is indicative of structural rigidity of the fragment regardless of the type of the complex, the ligand environment about the metal atoms and substituents at the carbon atoms of the metallacycle.

It is noteworthy that two other metal–metal bond lengths in complexes **92** and **91** are different. The Ru(1)–Ru(3) bond in complex **91** [2.927(1) Å] is substantially elongated compared to the analogous bond in complex **92** [2.823(1) Å]. Apparently, this is associated with the influence of the phosphine ligand in the *trans* position with respect to the Ru(1)–Ru(3) bond and can also be attributable to the lack of the tightening effect which occurs in the case of additional coordination by the alkenyl group of an organic ligand. The latter explanation seems to be more reasonable because an analogous change in the Ru(1)–Ru(3) bond length is observed in complexes **88**–**90** (2.982–3.073 Å) compared to complexes **93**–**99** (2.822–2.880 Å), in which an additional coordination to the Ru(3) atom is respectively absent and present (see Table 5).

The shortening of the Ru(2)–Ru(3) bond in complex **91** [2.732(1) Å] compared to that in complex **92** [2.802(1) Å] is less pronounced. A comparison of complexes **88**–**90** and **93**–**99** from Table 5 reveals no changes in the Ru(2)–Ru(3) bond length. Presumably, the mode of electron density redistribution in the cluster plays an important role in establishing electron balance on metal atoms. For example, the bridging ligands have a dominant role in complexes **88**–**90**, whereas the role of the direct metal–metal interaction increases significantly in complex **91** in which bridging interactions are absent (all carbonyl ligands are terminal). In this connection, it should be emphasised that the distribution of the bond lengths in the triangle formed by the metal atoms in analogous osmium complexes (**100**–**103**, Table 5), which also have no bridging ligands, is similar to that observed in complex **91**.

Reversible dissociation of the π-coordinated alkenyl group was exemplified by complexes **91** and **92**.[123] The transformation of one triruthenium cluster into another cluster is accompanied by migration of the MCP fragment relative to the plane of the Ru_3 triangle. In addition, the transformation is accompanied by the redistribution of the Ru(1)–Ru(3) and Ru(2)–Ru(3) bond lengths, which is indicative of high lability of the third metal centre bound to the dinuclear ferrole-type fragment. Apparently, it is this metal atom through which the electron density in the triangular clusters is redistributed to establish charge balance in a similar way to that observed in dinuclear ferrole-type complexes with staggered carbonyl ligands involving the semibridging carbonyl group. For example, the structure of complex **96** was described [125] as a result of the formal substitution of the semibridging carbonyl group in compound **29** (see Table 1) with the isolobal $Ru(CO)_3(PR_3)$ group. A comparison of complexes **96** and **29** demonstrates that there is a complete analogy in the structure of the dinuclear fragment with the metallacycle.

In addition to the triangular iron, ruthenium and osmium complexes with the laterally coordinated MCP fragment, there are also a number of heteronuclear complexes with more complicated structures (this is often associated with the presence of additional metal centres), which have a trimetallic core analogous to that of the metallacycle. The commonly used reactions of acetylide clusters with alkynes or alkyne complexes afford tri-, tetra- and polynuclear mixed complexes with the MCP fragment [WOs_3,[138–140] WRe_2,[115] Mo_2Re_2 (see Ref. 141)]. Since the structure of the metallacycle and its coordination are analogous to those described above for complexes **86**–**109**, we will not consider them in more detail.

An alternative mode of coordination of the MCP fragment to triangular transition metal clusters can be described as the μ_3-2η^1-2η^2 interaction between the organic ligand and the metal core. Symmetrical binding of the diene moiety to the triangle consisting of metal atoms is referred to as facial coordination, unlike the above-described lateral coordination. The assumption about the possibility of this coordination mode was made when studying the reactions between metal carbonyl complexes of the iron subgroup and an excess of alkynes giving rise to the $M_3(CO)_9(RC_2R)_2$ clusters, for which two structures (**A** and **B**) with the μ-2η^1-η^4- and μ_3-2η^1-2η^2-coordinated organic ligand were considered.[142, 143]

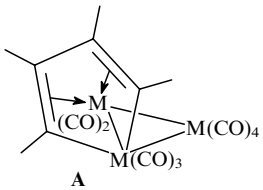

A

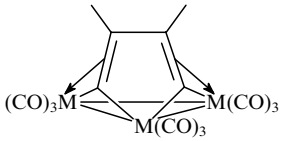

B

X-Ray diffraction study of one of the first $Os_3(PhC_2Ph)_2(CO)_9$ clusters demonstrated that it has the structure **A**.[129] Later on, analogous structures were assigned to all related compounds.[144, 145] Until recently, there was no convincing evidence for the existence of complexes with the structure **B**.

The experimental proof of the existence of isomers with the structure **B** was obtained for the first time in studies of the reactions of the alkyne cluster Os_3(μ-CO)$(CO)_9$(μ-2η^1-η^2-Me_3SiC_2Me) (**110**) with phenylacetylene [146, 147] as well as with other monosubstituted alkynes, *viz*., ferrocenylacetylene [148] and methyl propiolate.[137] The reactions involve alkyne–alkyne coupling and afford triosmium clusters with the facially coordinated osmacyclopentadiene fragment (complexes **112a**,**b**, **114** and **115** in Scheme 1). It should be noted that an analogous reaction with silyl-substituted alkyne $Me_3SiC{\equiv}CBu^n$ is accompanied by the acetylene–vinylidene rearrangement to give a cluster with the osmacyclobutadiene unit $Os_3(CO)_9\{\mu_3$-2η^1-2η^2-C$(SiMe_3)$=C.$(Me)C=C(SiMe_3)Bu^n\}$ (**111**).[149]

As can be seen from Scheme 1, thermolysis of the complexes with the facially coordinated MCP fragment gives rise to trinuclear complexes with the laterally coordinated MCP fragment. For example, complexes **112a**,**b** are transformed into hydride clusters with the *ortho*-metallated phenyl (**113a**) [146, 147] or ferrocenyl (**113b**) [148] fragment, respectively. The reaction of alkyne cluster **110** with methyl propiolate produces two isomeric complexes **114** and **115** with the facially coordinated MCP fragment, which differ in the mode of coupling of unsymmetrical alkynes.[137] Subsequent thermolysis of complex **115** containing the ester group in the α position of the osmacyclopentadiene ring affords complex **109**.[137]

Cluster **114** was studied by IR and NMR spectroscopy. In this cluster, the α position of the metallacycle contains no groups which are susceptible to *ortho*-metallation, or functional substituents capable of being coordinated to the metal atom. It was demonstrated that cluster **114** can undergo an intramolecular rearrangement and is a precursor of cluster **116**.[150] This previously unknown intramolecular rearrangement involves a change in the coordination mode of the dienediyl ligand (μ_3-2η^1-2η^2 → μ-2η^1-η^4) and the internuclear migration of one CO group. The trimetallic cluster with the facially coordinated MCP fragment, in which the hydrocarbon ligand forms η^2-bonds with two metal atoms, was demonstrated [150] to be thermodynamically less stable than the isomer in which the ligand forms the diene η^4-bond with one metal atom (lateral coordination of the MCP fragment).

The structures of three complexes (**112a**,[147] **112b** [148] and **114** [137]) with the facially coordinated MCP fragment were estab-

Scheme 1

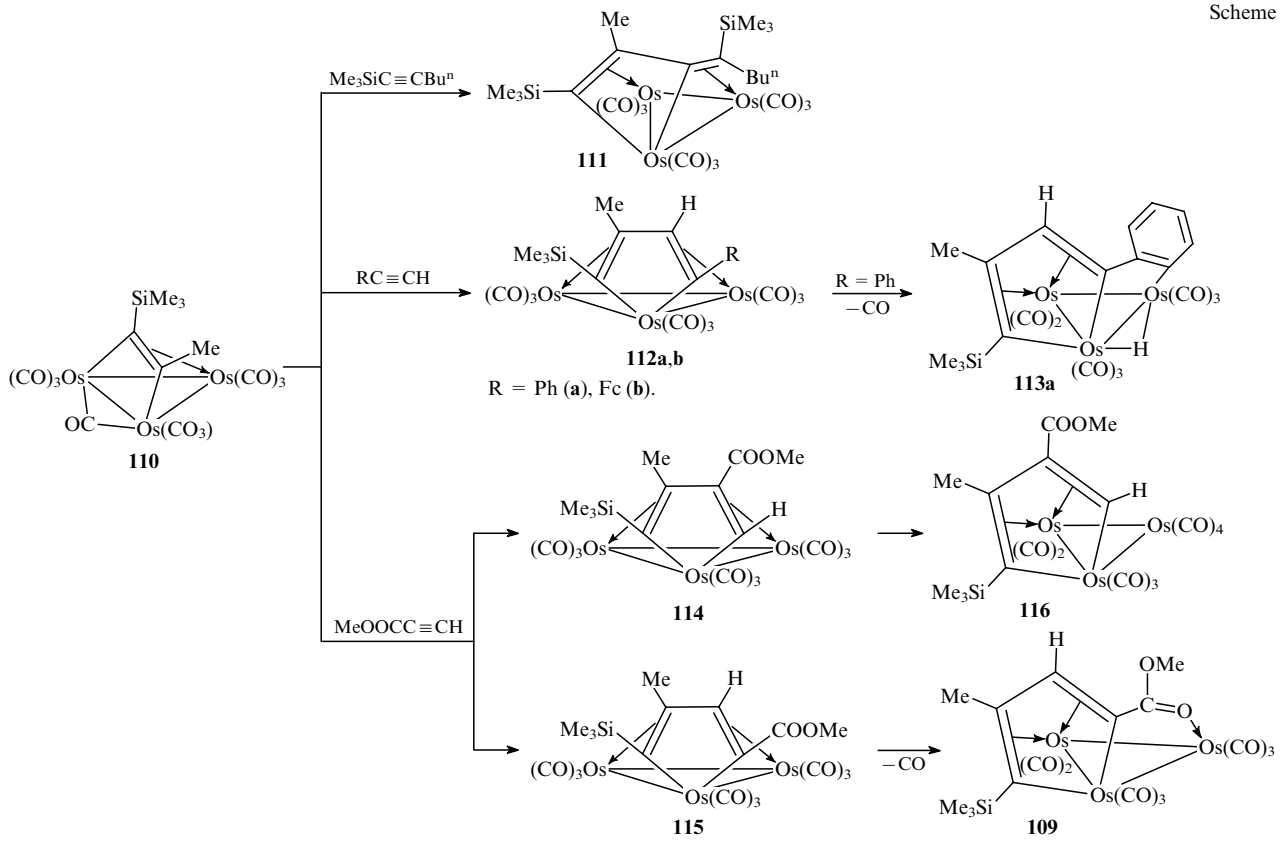

lished by X-ray diffraction analysis. The molecular structure of complex **112a** is shown in Fig. 10. Main geometric parameters for complexes **112a**,**b** and **114** are given in Table 6.

The formation of complexes **112a**,**b** involves coupling of monosubstituted alkyne (phenyl- or ferrocenylacetylene, respectively) with the already coordinated silyl-substituted alkyne, which proceeds in such a way that the hydrogen atom is bound to the β-carbon atom of the MCP fragment. In complex **114**, the hydrogen atom is bound to the α-carbon atom of the MCP fragment. Otherwise complexes **112a**,**b** and **114** are structurally similar and the presence of different substituents in the MCP fragments has no noticeable effect on the geometry of the coordination unit of the complexes.

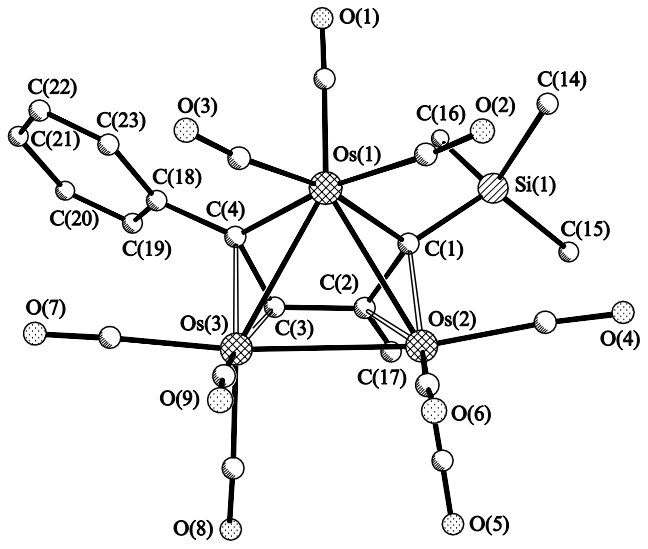

Figure 10. Molecular structure of the triangular osmium cluster $Os_3(CO)_9\{\mu_3\text{-}2\eta^1\text{-}2\eta_2\text{-}C(SiMe_3)C(Me)C(H)C(Ph)\}$ (**112a**) with the facially coordinated MCP fragment.[147]

In the complexes under consideration, the osmacyclopentadiene ring is substantially non-planar due to the deviation of the endocyclic osmium atom from the plane of the butadiene fragment toward two other metal atoms. The folding angle of the metallacycle along the C(1)···C(4) line is 30° (parameter τ in Table 6) and is substantially larger than the values typical of the MCP fragments coordinated to one metal atom (in dinuclear complexes of the ferrole type and trinuclear complexes with the laterally coordinated MCP fragment).

In complexes **112** and **114**, the C−C bond lengths in the butadiene moiety of the metallacycle are more differentiated than those in the complexes with the η^5-coordinated metallacycle. Although the differences in the bond lengths are only slightly larger than the experimental error, the tendency to an increase in the C(2)−C(3) bond length compared to the C(1)−C(2) and C(3)−C(4) alkene bond lengths is observed in all cases (the average values are 1.48, 1.41 and 1.42 Å, respectively). On the other hand, the lengths of the endocyclic σ-bonds involving the Os(1) atom are in the range typical of analogous bonds in complexes with the η^5-coordinated osmacyclopentadienyl fragment (2.01–2.25 Å; dinuclear complexes **35** and **36** listed in Table 1 and trinuclear complexes **100**–**109** presented in Table 5). However, it should be noted that the Os(1)−C(1) and Os(1)−C(4) bonds in complexes **112** and **114** are non-equivalent. In all cases, the distance to the C(1) atom bearing the trimethylsilyl substituent is somewhat larger than the Os(1)−C(4) bond length (the average values are 2.18 and 2.13 Å, respectively). The reasons for this non-equivalence are not quite clear. It can be assumed that an elongation of the Os(1)−C(1) distance eliminates unfavourable contacts between the trimethylsilyl group and the carbonyl groups at the Os(1) atom. It cannot also be excluded that some geometric distortions are related to the positive inductive effect of the trimethylsilyl group. Presumably, this is responsible for another structural feature of these complexes, *viz*., asymmetry of

Table 6. Selected geometric parameters for trinuclear osmium complexes with the facially coordinated MCP fragment (distances are given in Å, angles are given in degrees).[a]

Compound	Os(1)–Os(2), Os(1)–Os(3), Os(2)–Os(3)	Os(1)–C(1), Os(1)–C(4)	C(1)–C(2), C(2)–C(3), C(3)–C(4)	ω [b]	τ [c]	θ [d]	Os(2)–C(1), Os(2)–C(2)	Os(3)–C(4), Os(3)–C(3)
112a	2.811(1) 2.811(1) 2.825(1)	2.19(2) 2.12(1)	1.44(2) 1.46(2) 1.48(2)	4.3	28.8	32.9	2.18(1) 2.42(2)	2.22(1) 2.25(1)
112b (see [e])	2.819(1) 2.818(1) 2.804(1)	2.19(1) 2.15(1)	1.39(2) 1.49(2) 1.41(2)	5.1	27.5	34.0	2.17(1) 2.43(1)	2.25(1) 2.26(1)
	2.831(1) 2.825(1) 2.815(1)	2.18(1) 2.15(1)	1.41(2) 1.47(2) 1.41(2)	4.3	26.0	35.1	2.17(1) 2.48(1)	2.25(1) 2.27(1)
114	2.8248(7) 2.8254(7) 2.7932(7)	2.174(7) 2.099(8)	1.42(1) 1.49(1) 1.42(1)	3.2	23.8	36.4	2.167(9) 2.441(9)	2.178(8) 2.277(9)

[a] For the atomic numbering scheme, see Fig. 10. [b] The C(1)–C(2)–C(3)–C(4) torsion angle. [c] The folding angle of the metallacycle along the C(1)···C(4) line [the dihedral angle between the C(1)C(2)C(3)C(4) and C(1)Os(1)C(4) planes]. [d] The dihedral angle between the C(1)C(2)C(3)C(4) and Os(1)Os(2)Os(3) planes. [e] Two crystallographically independent molecules.

π-coordination of the Os(2) and Os(3) atoms to the corresponding alkene bonds in the metallacycle. One osmium atom [Os(3)] is located at virtually equal distances from the carbon atoms of the C(3)–C(4) alkene bond [the average Os(3)–C(3) and Os(3)–C(4) bond lengths are 2.27 and 2.23 Å, respectively], whereas another osmium atom [Os(2)] forms non-equivalent bonds with the carbon atoms of the C(1)–C(2) alkene bond [the average Os(2)–C(1) and Os(2)–C(2) bond lengths are 2.17 and 2.44 Å, respectively].

The osmacyclopentadiene ring in complexes **112** and **114**, unlike that in the trinuclear complexes with the laterally coordinated MCP fragment, is located above the plane of the triangular metal core (facial coordination of the MCP fragment). The averaged dihedral angle between the plane passing through four carbon atoms of the butadiene moiety of the metallacycle and the plane of the triangle formed by the osmium atoms (parameter θ in Table 6) is 34.5°.

The trinuclear complexes with the laterally coordinated MCP fragment differ from those with the facially coordinated MCP fragment also in that the metal–metal bond lengths in the latter are equalised. All Os–Os bond lengths in complexes **112** and **114** vary within a narrow range (2.793–2.834 Å).

In addition to the above-described compounds **112** and **114**, only one compound belonging to trimetallic clusters with the facially coordinated MCP fragment, *viz*., trinuclear molybdenum cyclopentadienyl complex **117**, was structurally characterised.[151] The structure of complex **117** is shown in Fig. 11.

The metal core in complex **117** is V-shaped. The bond between the Mo(1) and Mo(2) atoms is absent, although they are linked through the bridging chlorine atom. All Mo atoms are linked by the μ_3-bridging oxygen atom. In the study,[151] the μ_3-O, μ-Cl and $C_4(CF_3)_4$ groups in complex **117** were considered as four-, three- and six-electron ligands, respectively, and consequently, the complex as a whole has 46 valence electrons, which implies the presence of four metal–metal bonds (in this case, the molybdenum atoms have an 18-electron configuration). Based on this analysis and the results of theoretical calculations, the Mo(1)–Mo(3) and Mo(2)–Mo(3) bonds in complex **117** were assumed to be double and it was postulated that there is no direct interaction between the Mo(1) and Mo(2) atoms. The structure of the MCP fragment in complex **117** is analogous to that described for complexes **112** and **114** and differs substantially from that observed in complexes with η^5-coordination of the metallacycle. For example, the carbon–carbon distances in the metallacycle

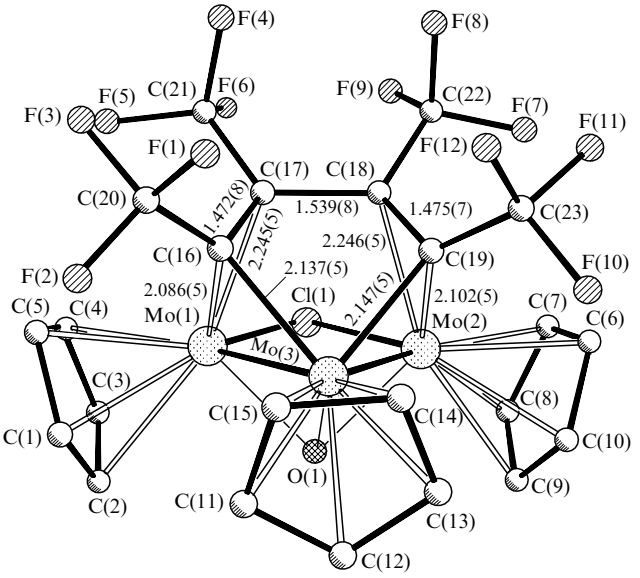

Figure 11. Structure of the $Mo_3(\mu\text{-Cl})(\mu_3\text{-O})(C_5H_5)_3\{C_4(CF_3)_4\}$ complex (**117**).[151]
The Mo(1)–Mo(3) and Mo(2)–Mo(3) bond lengths are 2.5723(7) and 2.5790(7) Å, respectively; the Mo(1)···Mo(2) distance is 2.8930(7) Å.

are noticeably differentiated (short–long–short) and the metallacycle is significantly folded (38.9°) along the C(16)···C(19) line.

VI. Conclusion

In conclusion of the description of complexes containing the MCP fragment, is should be emphasised once again that this metallacycle exhibits various coordination modes with transition metal atoms. The most commonly observed coordination mode is described as the symmetrical η^5-coordination to an additional metal centre (dinuclear complexes of the ferrole type and trimetallic clusters with the laterally coordinated MCP fragment). In these complexes, the MCP fragment is nearly planar. The equalisation of the carbon–carbon bond lengths in the diene moiety is indicative of strong conjugation in the carbon chain. The degree of deviation of the metallacycle from planarity can serve as a

criterion of the involvement of the endocyclic metal atom in the interaction with the π system of the diene moiety and, in the case of dinuclear complexes, corresponds to two different modes of coordination of the MCP fragment to an additional metal centre (η^1-η^4- or η^5-coordination). The symmetrical η^5-coordination of the MCP fragment to two additional metal centres is observed also in trimetallic clusters with a pentagonal-bipyramidal geometry. The presence of additional metal centres can substantially influence the coordination properties of the MCP fragment, as demonstrated for trimetallic complexes with the metallaindene system or clusters with the facially coordinated metallacycle. In the latter case, the MCP fragment is η^3-coordinated to two additional metal centres, which excludes the formation of the common π system. The structure of the MCP fragment is characterised by a substantial deviation from planarity and localisation of the carbon–carbon bonds in the diene moiety. However, it should be noted that complexes of this type are observed much more rarely than complexes with the η^5-coordinated MCP fragment.

Polynuclear complexes with the MCP fragment are most often formed in the reactions of metal derivatives with acyclic organic molecules, *i.e.*, the metallacyclic ligand is formed simultaneously with the complex as such. The analogy between the MCP fragment and the cyclopentadienyl ligand is invoked many times in discussions of the structures of particular compounds, *i.e.*, in the 'post-factum' analysis of the already formed MCP complexes. However, examples of the use of mononuclear complexes with the MCP fragment as ligands in reactions with other transition metal complexes are scarce (see, for instance, Ref. 152).

A growing number of publications devoted to investigations of metal-containing fragments as potential representatives of a new class of π ligands demonstrates that this problem has attracted increasing interest. Many aspects of these studies were covered in reviews on aromaticity of metallacycles [153] and investigations of the structures and chemical properties of six-membered metallabenzenes.[154]

Undoubtedly, the use of metallacyclic fragments, including metallacyclopentadienes, as non-classical ligands is a promising area of modern chemistry of transition metal π-complexes.

This review has been written with the financial support of the Russian Foundation for Basic Research (Project Nos 02-07-90322 and 04-03-32371) and Grant from the President of the Russian Federation (the Federal Program for the Support of Leading Scientific Schools, Projects NSh-1060.2003.03 and MK-60.2003.03).

References

1. S D Chappell, D J Cole-Hamilton *Polyhedron* **1** 739 (1982)
2. E Lindner *Adv. Heterocycl. Chem.* **39** 237 (1986)
3. E Müller *Synthesis* 761 (1974)
4. V V Dunina, O A Zalevskaya, V M Potapov *Usp. Khim.* **57** 434 (1988) [*Russ. Chem. Rev.* **57** 250 (1988)]
5. D B Grotjahn, in *Comprehensive Organometallic Chemistry II* Vol. 12 (Eds E W Abel, F G A Stone, G Wilkinson) (Oxford: Pergamon Press, 1995) p. 741
6. R Giordano, E Sappa, D Cauzzi, G Predieri, A Tiripicchio *J. Organomet. Chem.* **511** 263 (1996)
7. T Shimura, A Ohkubo, K Aramaki, H Uekusa, T Fujita, S Ohba, H Nishihara *Inorg. Chim. Acta* **230** 215 (1995)
8. R J Baxter, G R Knox, P L Pauson, M D Spicer *Organometallics* **18** 197 (1999)
9. R J Baxter, G R Knox, J H Moir, P L Pauson, M D Spicer *Organometallics* **18** 206 (1999)
10. R J Baxter, G R Knox, P L Pauson, M D Spicer *Organometallics* **18** 215 (1999)
11. A N Nesmeyanov, M I Rybinskaya, L V Rybin, V S Kaganovich *J. Organomet. Chem.* **47** 1 (1973)
12. E Sappa *J. Cluster Sci.* **5** 211 (1994)
13. E Sappa *J. Organomet. Chem.* **573** 139 (1999)
14. A A Koridze *Izv. Akad. Nauk, Ser. Khim.* 1 (2000) [a]
15. *Cambridge Structural Database* Version April, 2003
16. G Dettlaf, U Kruerke, N Kuhn, M Mirbach, in *Gmelin Handbuch der Anorganischen Chemie. Fe, Organoiron Compounds* Part C3 (Berlin: Springe, 1980) p. 24
17. W P Fehlhammer, H Stolzenberg, in *Comprehensive Organometallic Chemistry* Vol. 4 (Eds G Wilkinson, F G A Stone, E W Abel) (Oxford: Pergamon Press, 1982) p. 548
18. D L Thorn, R Hoffmann *Nouv. J. Chim.* **3** 39 (1979)
19. A A Hock, O S Mills *Acta Crystallogr.* **14** 139 (1961)
20. G Dettlaf, E Weiss *J. Organomet. Chem.* **108** 213 (1976)
21. J-C Daran, Y Jeannin *Organometallics* **3** 1158 (1984)
22. E Cabrera, J-C Daran, Y Jeannin *Organometallics* **7** 2010 (1988)
23. S Jeannin, Y Jeannin, F Robert, C Rosenberger *J. Organomet. Chem.* **480** 111 (1994)
24. H G Raubenheimer, G J Kruger, L Linford *Inorg. Chim. Acta* **150** 173 (1988)
25. R Calderon, H Vahrenkamp *J. Organomet. Chem.* **555** 113 (1998)
26. J-C Daran, E Gilbert, M Gouygou, S Halut, B Heim, Y Jeannin *J. Cluster Sci.* **5** 373 (1994)
27. D Seyferth, C M Archer, J C Dewan *Organometallics* **10** 3759 (1991)
28. G Dettlaf, U Behrens, T Eicher, E Weiss *J. Organomet. Chem.* **152** 203 (1978)
29. H B Chin, R Bau *J. Am. Chem. Soc.* **95** 5068 (1973)
30. A S Dreiding, J H Bieri, R Prewo, A Linden, E Gesing *Cambridge Structural Database* Private Communication Refcode HACKUR (1993)
31. Y Degreve, J Meunier-Piret, M van Meerssche, P Piret *Acta Crystallogr.* **23** 119 (1967)
32. G H Young, R R Willis, A Wojcicki, M Calligaris, P Faleschini *Organometallics* **11** 154 (1992)
33. A Marzotto, M B Cingi, A Ciccarese, D A Clemente *Acta Crystallogr., Sect. C* **47** 96 (1991)
34. P E Riley, R E Davis *Acta Crystallogr., Sect. B* **31** 2928 (1975)
35. M J Bennett, W A G Graham, R A Smith, R P Stewart *J. Am. Chem. Soc.* **95** 1684 (1973)
36. K Singh, W R McWhinnie, H L Chen, M Sun, T A Hamor *J. Chem. Soc., Dalton Trans.* 1545 (1996)
37. T E Snead, C A Mirkin, K-L Lu, S T Nguyen, W-C Feng, H L Beckman, G L Geoffroy, A L Rheingold, B S Haggerty *Organometallics* **11** 2613 (1992)
38. S Aime, L Milone, E Sappa, A Tiripicchio, A M Manotti Lanfredi *J. Chem. Soc., Dalton Trans.* 1664 (1979)
39. J A D Jeffreys, C M Willis *J. Chem. Soc., Dalton Trans.* 2169 (1972)
40. I Noda, H Yasuda, A Nakamura *J. Organomet. Chem.* **250** 447 (1983)
41. W-Y Yeh, S C N Hsu, S-M Peng, G-H Lee *Organometallics* **17** 2477 (1998)
42. R D Adams, W Fu, B Qu *J. Cluster Sci.* **11** 55 (2000)
43. S P Tunik, E V Grachova, V R Denisov, G L Starova, A B Nikol'skii, F M Dolgushin, A I Yanovsky, Yu T Struchkov *J. Organomet. Chem.* **536–537** 339 (1997)
44. M I Bruce, J G Matisons, B W Skelton, A H White *J. Organomet. Chem.* **251** 249 (1983)
45. M I Bruce, N N Zaitseva, B W Skelton, A H White *Inorg. Chim. Acta* **250** 129 (1996)
46. A Astier, J-C Daran, Y Jeannin, C Rigault *J. Organomet. Chem.* **241** 53 (1983)
47. A A Koridze, A I Yanovsky, Yu T Struchkov *J. Organomet. Chem.* **441** 277 (1992)
48. R P Dodge, O S Mills, V Schomaker *Proc. Chem. Soc., London* 380 (1963)
49. P J Harris, J A K Howard, S A R Knox, R P Phillips, F G A Stone, P Woodward *J. Chem. Soc., Dalton Trans.* 377 (1976)
50. F A Cotton, J M Troup *J. Am. Chem. Soc.* **96** 1233 (1974)
51. F A Cotton *Prog. Inorg. Chem.* **21** 1 (1976)
52. D L Thorn, R Hoffmann *Inorg. Chem.* **17** 126 (1978)
53. S Aime, L Milone, E Sappa *J. Chem. Soc., Dalton Trans.* 838 (1976)

54. L J Todd, J P Hickey, J R Wilkinson, J C Huffman, K Folting *J. Organomet. Chem.* **112** 167 (1976)
55. B V Lokshin, M G Ezernitskaya, V I Zdanovich, A A Koridze *J. Organomet. Chem.* **580** 36 (1999)
56. M Casarin, D Ajz, A Vittadini, D E Ellis, G Granozzi, R Bertoncello, D Osella *Inorg. Chem.* **26** 2041 (1987)
57. R Case, E R H Jones, N V Schwartz, M C Whiting *Proc. Chem. Soc., London* 256 (1962)
58. M Tasi, A K Powell, H Vahrenkamp *Angew. Chem., Int. Ed. Engl.* **28** 318 (1989)
59. M Tasi, A K Powell, H Vahrenkamp *Chem. Ber.* **124** 1549 (1991)
60. B F G Johnson, R Khattar, J Lewis, P R Raithby *J. Organomet. Chem.* **335** C17 (1987)
61. I D Scott, D O Smith, M J Went, L J Farrugia *J. Chem. Soc., Dalton Trans.* 1375 (1989)
62. M J Chetcuti, L A DeLiberato, P E Fanwick, B E Grant *Inorg. Chem.* **29** 1295 (1990)
63. H Bantel, A K Powell, H Vahrenkamp *Chem. Ber.* **123** 1607 (1990)
64. S Pasynkewicz, A Pietrzykowski, B Kryza-Niemiec, J Zachara *J. Organomet. Chem.* **566** 217 (1998)
65. M I Bruce, S M Pyke, N N Zaitseva, B W Skelton, A H White *Helv. Chim. Acta* **84** 3197 (2001)
66. T Sielisch, U Behrens *J. Organomet. Chem.* **327** 85 (1987)
67. W Ziegler, U Behrens *J. Organomet. Chem.* **427** 379 (1992)
68. V I Zdanovich, V Yu Lagunova, F M Dolgushin, A I Yanovsky, M G Ezernitskaya, P V Petrovskii, A A Koridze *Izv. Akad. Nauk, Ser. Khim.* 1836 (1998) [a]
69. E Weiss, W Hmbel, R Mergnyi *Chem. Ber.* **95** 1155 (1962)
70. S B Colbran, B H Robinson, J Simpson *Organometallics* **4** 1594 (1985)
71. E F Epstein, L F Dahl *J. Am. Chem. Soc.* **92** 502 (1970)
72. M King, E M Holt, P Radnia, J S McKennis *Organometallics* **1** 1718 (1982)
73. J Holton, M F Lappert, R Pearce, P I W Yarrow *Chem. Rev.* **83** 135 (1983)
74. H Omori, H Suzuki, Y Moro-oka *Organometallics* **8** 1576 (1989)
75. L A Brady, A F Dyke, S E Garner, S A R Knox, A Irving, S M Nicholls, A G Orpen *J. Chem. Soc., Dalton Trans.* 487 (1993)
76. H Suzuki, H Omori, D H Lee, Y Yoshida, M Fukushima, M Tanaka, Y Moro-oka *Organometallics* **13** 1129 (1994)
77. B K Campion, R H Heyn, T D Tilley *Organometallics* **9** 1106 (1990)
78. M Nishio, H Matsuzaka, Y Mizobe, T Tanase, M Hidai *Organometallics* **13** 4214 (1994)
79. K Sunkel *J. Organomet. Chem.* **391** 247 (1990)
80. C Perthuisot, B L Edelbach, D L Zubris, W D Jones *Organometallics* **16** 2016 (1997)
81. H Wadepohl, T Borchert, K Buchner, M Herrmann, F-J Paffen, H Pritzkow *Organometallics* **14** 3817 (1995)
82. J Muller, T Akhnoukh, J Pickardt, M Siewing, B Westphal *J. Organomet. Chem.* **459** 325 (1993)
83. Y Kishimoto, P Eckerle, T Miyatake, M Kainosho, A Ono, T Ikariya, R Noyori *J. Am. Chem. Soc.* **121** 12 035 (1999)
84. C W Baimbridge, R S Dickson, G D Fallon, I Grayson, R J Nesbit, J Weigold *Aust. J. Chem.* **39** 1187 (1986)
85. H Wadepohl, A Metz, H Pritzkow *Chem. Eur. J.* **8** 1591 (2002)
86. T Sielisch, U Behrens *J. Organomet. Chem.* **322** 203 (1987)
87. W D McGhee, R G Bergman *J. Am. Chem. Soc.* **110** 4246 (1988)
88. A A Koridze, V I Zdanovich, A S Batsanov, Yu T Struchkov *Mendeleev Commun.* 126 (1991)
89. T Shima, H Suzuki *Organometallics* **19** 2420 (2000)
90. F H Herbstein, M G Reisner *Acta Crystallogr., Sect. B* **33** 3304 (1977)
91. M Iyoda, T Yada, S Tashiro, H Maeda, M Yoshida, Y Kuwatani *Chem. Lett.* 39 (1997)
92. A J Arce, Y De Sanctis, A Karam, A J Deeming *Angew. Chem., Int. Ed. Engl.* **33** 1381 (1994)
93. A J Blake, P J Dyson, P E Gaede, B F G Johnson *Inorg. Chim. Acta* **241** 11 (1996)
94. P E Gaede, B F G Johnson, M McPartlin, M-A Pearsall *J. Chem. Soc., Dalton Trans.* 4621 (1996)
95. B F G Johnson, J M Matters, P E Gaede, S L Ingham, N Choi, M McPartlin, M-A Pearsall *J. Chem. Soc., Dalton Trans.* 3251 (1997)
96. R P Dodge, V Schomaker *J. Organomet. Chem.* **3** 274 (1965)
97. E Cabrera, J-C Daran, Y Jeannin, O Kristiansson *J. Organomet. Chem.* **310** 367 (1986)
98. D Lentz, H Michael-Schulz, M Reuter *Organometallics* **11** 2916 (1992)
99. D Nuel, F Dahan, R Mathieu *J. Am. Chem. Soc.* **107** 1658 (1985)
100. B Heim, J C Daran, Y Jeannin, B Eber, G Huttner, W Imhof *J. Organomet. Chem.* **441** 81 (1992)
101. G Gervasio, R Giordano, E Sappa, M Costa, G Predieri, A Tiripicchio *J. Cluster Sci.* **4** 33 (1993)
102. M V Capparelli, Y DeSanctis, A J Arce *Acta Crystallogr., Sect. C* **51** 1819 (1995)
103. K Onitsuka, K Miyaji, T Adachi, T Yoshida, K Sonogashira *Chem. Lett.* 2279 (1994)
104. E Sappa, A M Manotti Lanfredi, A Tiripicchio *Inorg. Chim. Acta* **42** 255 (1980)
105. V Ferrand, A Neels, H Stoeckli-Evans, G Suss-Fink *Inorg. Chem. Commun.* **2** 561 (1999)
106. J E Davies, B F G Johnson, C M Martin, R H H Pearson, P J Dyson *J. Organomet. Chem.* **550** 431 (1998)
107. M I Bruce, R J Surynt, B W Scelton, A H White *Aust. J. Chem.* **50** 701 (1997)
108. K Wade *Adv. Inorg. Chem. Radiochem.* **18** 1 (1976)
109. W Hübel, E H Braye *J. Inorg. Nucl. Chem.* **9** 204 (1959)
110. J F Blount, L F Dahl, C Hoogzand, W Hübel *J. Am. Chem. Soc.* **88** 292 (1966)
111. D Osella, G Arman, M Botta, R Gobetto, F Laschi, P Zanello *Organometallics* **8** 620 (1989)
112. M Casarin, D Ajo, G Granozzi, E Tondello *Inorg. Chem.* **24** 1241 (1985)
113. D Osella, G Arman, R Gobetto, F Laschi, P Zanello, S Ayrton, V Goodfellow, C F Housecroft, S M Owen *Organometallics* **8** 2689 (1989)
114. A D Shaposhnikova, G L Kamalov, R A Stadnichenko, A A Pasynskii, I L Eremenko, S E Nefedov, Yu T Struchkov, A I Yanovsky *J. Organomet. Chem.* **405** 111 (1991)
115. J-J Peng, K-M Horng, P-S Cheng, Y Chi, S-M Peng, G-H Lee *Organometallics* **13** 2365 (1994)
116. M I Bruce, N N Zaitseva, B W Skelton, A H White *J. Organomet. Chem.* **536** 93 (1997)
117. A Inagaki, T Takemori, M Tanaka, H Suzuki *Angew. Chem., Int. Ed.* **39** 404 (2000)
118. K J Adams, J J Barker, S A R Knox, A G Orpen *J. Chem. Soc., Dalton Trans.* 975 (1996)
119. E Cabrera, J-C Daran, Y Jeannin *Organometallics* **8** 1811 (1989)
120. M I Bruce, J R Hinchliffe, P A Humphrey, R J Surynt, B W Skelton, A H White *J. Organomet. Chem.* **552** 109 (1998)
121. M I Bruce, P A Humphrey, E Horn, E R T Tiekink, B W Skelton, A H White *J. Organomet. Chem.* **429** 207 (1992)
122. S E Kabir, E Rosenberg, L Milone, R Gobetto, D Osella, M Ravera, T McPhillips, M W D Carlot, S Hajela, E Wolf, K Hardcastle *Organometallics* **16** 2674 (1997)
123. A A Koridze, V I Zdanovich, V Yu Lagunova, M G Ezernitskaya, P V Petrovskii, F M Dolgushin, A I Yanovsky *Izv. Akad. Nauk, Ser. Khim.* 1017 (1998) [a]
124. A A Koridze, V I Zdanovich, N V Andrievskaya, Yu Siromakhova, P V Petrovskii, M G Ezernitskaya, F M Dolgushin, A I Yanovsky, Yu T Struchkov *Izv. Akad. Nauk, Ser. Khim.* 1261 (1996) [a]
125. M I Bruce, P A Humphrey, H Miyamae, B W Skelton, A H White *J. Organomet. Chem.* **429** 187 (1992)
126. C S-W Lau, W-T Wong *J. Chem. Soc., Dalton Trans.* 607 (1999)
127. C S-W Lau, W-T Wong *J. Organomet. Chem.* **588** 113 (1999)
128. D Osella, R Gobetto, L Milone, P Zanello, S Mangani *Organometallics* **9** 2167 (1990)
129. G Ferraris, G Gervasio *J. Chem. Soc., Dalton Trans.* 1813 (1974)
130. W-Y Yeh, M-A Hsu, S-M Peng, G-H Lee *Organometallics* **18** 880 (1999)
131. A J Poe, D H Farrar, R Ramachandran, C Moreno *Inorg. Chim. Acta* **274** 82 (1998)
132. G Ferraris, G Gervasio *J. Chem. Soc., Dalton Trans.* 1933 (1973)

133. R D Adams, G Chen, X Qu, W Wu *Organometallics* **12** 3426 (1993)
134. R D Adams, X Qu, W Wu *Organometallics* **14** 1377 (1995)
135. G Ferraris, G Gervasio *J. Chem. Soc., Dalton Trans*. 1057 (1972)
136. W-Y Yeh, J R Shapley, J W Ziller, M R Churchill *Organometallics* **6** 1 (1987)
137. A M Sheloumov, A A Koridze, M G Ezernitskaya, P V Petrovskii, O L Tok, Z A Starikova, F M Dolgushin, A I Yanovsky *Izv. Akad. Nauk, Ser. Khim*. 1789 (1999) [a]
138. Y Chi, C-H Wu, S-M Peng, G-H Lee *Organometallics* **9** 2305 (1990)
139. Y Chi, H-Y Hsu, S-M Peng, G-H Lee *J. Chem. Soc., Chem. Commun*. 1023 (1991)
140. Y Chi, R-C Lin, C-C Chen, S-M Peng, G-H Lee *J. Organomet. Chem*. **439** 347 (1992)
141. A D Shaposhnikova, G L Kamalov, R A Stadnichenko, A A Pasynskii, I L Eremenko, Yu T Struchkov, A I Yanovsky, P V Petrovskii *J. Organomet. Chem*. **378** 67 (1989)
142. O Gambino, G A Vaglio, R P Ferrari, G Cetini *J. Organomet. Chem*. **30** 381 (1971)
143. R Giordano, E Sappa *J. Organomet. Chem*. **448** 157 (1993)
144. A J Deeming, S Hasso, M Underhill *J. Chem. Soc., Dalton Trans*. 1614 (1975)
145. M Tachikawa, J R Shapley, C G Pierpont *J. Am. Chem. Soc*. **97** 7172 (1975)
146. A A Koridze, N M Astakhova, F M Dolgushin, A I Yanovsky, Yu T Struchkov, P V Petrovskii *Izv. Akad. Nauk, Ser. Khim*. 766 (1994) [a]
147. A A Koridze, N M Astakhova, F M Dolgushin, A I Yanovsky, Yu T Struchkov, P V Petrovskii *Organometallics* **14** 2167 (1995)
148. A A Koridze, A M Sheloumov, F M Dolgushin, A I Yanovsky, Yu T Struchkov, P V Petrovskii *Izv. Akad. Nauk, Ser. Khim*. 741 (1996) [a]
149. A A Koridze, A M Sheloumov, F M Dolgushin, A I Yanovsky, P V Petrovskii *Izv. Akad. Nauk, Ser. Khim*. 1024 (1998) [a]
150. A A Koridze, A M Sheloumov, P V Petrovskii, O L Tok *Izv. Akad. Nauk, Ser. Khim*. 1026 (1999) [a]
151. J L Davidson, K Davidson, W E Lindsell, N W Murrall, A J Welch *J. Chem. Soc., Dalton Trans*. 1677 (1986)
152. J Chen, V G Young, R J Angelici *Organometallics* **15** 1414 (1996)
153. H Masui *Coord. Chem. Rev*. **219–221** 957 (2001)
154. J R Bleeke *Chem. Rev*. **101** 1205 (2001)

[a] — *Russ. Chem. Bull., Int. Ed. (Engl. Transl.)*

 © 2004 Russian Academy of Sciences and Turpion Ltd

DOI 10.1070/RC2004v073n06ABEH000821

The structure of X-ray photoelectron spectra of light actinide compounds †

Yu A Teterin, A Yu Teterin

Contents

I. Introduction 541
II. Thorium compounds 542
III. Uranium compounds 547
IV. Neptunium compounds 560
V. Plutonium compounds 564
VI. General rules of the formation of fine structure in the XPS spectra of actinide compounds 568
VII. Conclusion 575

Abstract. The results of X-ray photoelectron spectroscopy (XPS) studies of the structures of the outer and inner electron shells of compounds of light actinides (Th, U, Np, Pu, Am, Cm, Bk, Cf) in the binding energy (E_b) range of 0 – 1250 eV are generalised. The regularities of formation of the fine structure in the X-ray photoelectron (XPS) spectra of these compounds are considered. The mechanisms of appearance of such structure are analysed, and the correlations between the fine structure parameters and actinide oxidation states and local environment, the magnetic properties of compounds, the nature of the chemical bond and secondary electronic processes that accompany photoemission of electrons are discussed. Experimental evidence for effective formation of the outer (E_b = 0 – 15 eV) and inner valence (E_b = 15 – 50 eV) molecular orbitals, in particular, from the fully occupied An6p and L*n*s orbitals of the neighbouring actinide (An) and ligand (L) atoms in the compounds in question is presented. The use of fine spectral structure parameters, together with the electron binding energies and line intensities extends significantly the scope of application of the XPS method in structural studies.
The bibliography includes 276 references.

I. Introduction

Actinides (An) are the An5f transition elements located after actinium in the Periodic Table with atomic numbers (Z) in the range $90 \leqslant Z \leqslant 103$. These elements can be conventionally subdivided into two groups, namely, light actinides (Th, Pa, U, Np, Pu, Am, Cm), which are readily accessible for X-ray spectral studies, and heavy actinides (Bk, Cf, Es, Fm, Md, No, Lr), less accessible for such studies, which is mainly due to the relatively short half lives of the longest-lived actinide isotopes (Table 1). The electronic configuration of actinide atoms can be expressed as $\{Rn\}5f^n6d^m7s^2$, where $\{Rn\}$ is the electronic configuration of radon, $0 \leqslant n \leqslant 14$, $m = 0, 1$. In the ground state, actinides, except for thorium, protactinium, uranium, neptunium, curium and, possibly, lawrencium have no An6d electrons ($m = 0$); however, transition of one or two An5f electrons to the An6d shell does not require much energy. In compounds, actinides can occur in various oxidation states.[1–4]

Currently, nuclear energy is widely used in science and engineering. The permanent growth of the demand for the raw materials stimulates the design of economical nuclear-chemical processes used in all stages of nuclear energy production ranging from ore mining to transmutation of the spent nuclear fuel [1–7] and for the solution of the concomitant environmental problems using X-ray spectral methods.[8–16] Despite the fact that a number of industrially important actinide (Th, U, Pu) compounds have been widely studied in the last decades, many aspects concerning the physicochemical properties of these compounds still remain unknown.[1–4] Therefore, study of the electronic structures of actinide compounds and elucidation of the relationship between

Table 1. Electronic configurations and half lives ($T_{1/2}$) of the longest-lived isotopes of actinides.[1–3]

Isotope	Electronic configuration	Z	$T_{1/2}$ (see [a])
^{227}Ac	$6d7s^2$	89	21.8
^{232}Th	$6d^27s^2$	90	1.41×10^{10}
^{231}Pa	$5f^26d7s^2$	91	3.28×10^4
^{238}U	$5f^36d7s^2$	92	4.47×10^9
^{237}Np	$5f^46d7s^2$	93	2.14×10^6
^{244}Pu	$5f^67s^2$	94	8.1×10^7
^{243}Am	$5f^77s^2$	95	7380
^{247}Cm	$5f^76d7s^2$	96	1.64×10^7
^{247}Bk	$5f^97s^2$	97	1380
^{249}Cf	$5f^{10}7s^2$	98	350
^{254}Es	$5f^{11}7s^2$	99	277 days
^{257}Fm	$5f^{12}7s^2$	100	100 days
^{258}Md	$(5f^{13}7s^2)$ [b]	101	54 days
^{259}No	$(5f^{14}7s^2)$ [b]	102	~1.5 h
^{260}Lr	$(5f^{14}6d7s^2$ or $5f^{14}7s^27p)$ [b]	103	~3 min

[a] When no units are given, the half lives are expressed in years. [b] Putative electronic configurations.

Yu A Teterin, A Yu Teterin Institute of General and Nuclear Physics, Russian Research Centre 'Kurchatov Institute', pl. Kurchatova 1, 123182 Moscow, Russian Federation. Fax (7-095) 196 05 31.
Tel. (7-095) 196 92 52. E-mail: teterin@ignph.kiae.ru (Yu A Teterin),
Tel. (7-095) 196 90 28. E-mail: ateterin@tochka.ru (A Yu Tetererin)

Received 10 February 2003
Uspekhi Khimii **73** (6) 588 – 631 (2004); translated by Z P Bobkova

† Dedicated to Academician Anatolii Petrovich Aleksandrov on the occasion of the 100th anniversary of his birthday.

its parameters and their properties is a fairly topical task. In addition, investigation routes for the electronic structures and properties of transactinide compounds with atomic numbers in the range of $104 \leqslant Z \leqslant 118$ have taken shape in recent years.[17,18]

In the last decades, the design of high-precision X-ray photoelectron spectrometers[19–23] and development of quick methods for the calculation of electronic structures such as X_α-methods[24–28] and spectral structure parameters[29–35] enabled X-ray photoelectron spectroscopy studies into the electronic structures of actinide compounds to be carried out at a qualitatively new level. The results show that not only the spectra of core electronic shells[29,36,37] or outer valence molecular orbitals (OVMO),[38–44] but also spectra of the inner valence molecular orbitals (IVMO)[38,45–48] provide information about the physical and chemical properties of these compounds. Not only the chemical shifts of electronic levels and line intensities can be used for analysis. Useful information concerning the physicochemical properties of compounds and secondary processes that accompany photoemission can also be drawn from fine structure parameters of the spectra of both the core and outer electrons.[20–23,49–56] This is especially important in those cases where reliable determination of electron binding energies and line intensities of some electronic levels is difficult. In the spectra of actinide compounds, a complex fine structure is observed for almost all electron shells in the binding energy (E_b) range of $\sim 0 \leqslant E_b \leqslant 1250$ eV. This energy range is normally used for XPS measurements. The fine structure provides information on the actinide oxidation states in compounds (Th,[23,57–64] U,[39,40,60–78] Np,[79–81] Pu,[29,64,79,81–86] Am,[29,79,87,88] Cm, Bk, Cf[79,81,87,88]), on the magnetic properties (Th,[44,58,89] U,[43,44,55,89–91] Np[44,55,89,90]), on the structures of compounds (Th,[55,58] U,[26,38,45,47,48,55,66,92–97] Np,[55,80] Pu,[29,55,82] Am,[29,79] Cm, Bk, Cf[79]), on the nature of the chemical bond (Th,[37,52,53,55,58,98–100] U,[26,40,47,48,52,53,55,66,92–94,98,101–112] Np,[41,51–53,55,80,81,87–90,113–115] Pu,[29,37,41,52,53,55,82,87–91,115,116] Am,[29,37,79,81,87–89,91] Cm, Bk, Cf[79,81,87,88]), on the secondary electronic processes that accompany the emission of photoelectrons (Th,[55,58,117–120] U,[47,55,56,103–105,117] Np,[55,56,79,80] Pu,[29,55,79,82,121] Am,[29,79] Cm, Bk, Cf[79]), and so on. Therefore, analysis of the reasons for the appearance of the fine spectral structure and identification of the correlation between its characteristics and the properties of the considered compounds, which represent key goals of this review, are fairly topical.

The XPS spectra of light actinide compounds clearly show the bands for the outer valence MO (Th,[39,58] U,[38,40,65,66,70,111,122] Np,[41,80,89] Pu,[41,82,83,89] Am,[79,88,89] Cm, Bk, Cf[79,88]); inner valence MO (Th,[53,58] U,[47,53,66,93,94,102,104,109,110,123] Np,[36,53,80,113] Pu,[36,53,82] Am,[29] Cm, Bk, Cf[53]); the multiplet line splitting due to the presence of unpaired An5f electrons in actinide ions (Th,[55,58] U,[55] Np,[80] Pu,[82] Am,[29] Cm, Bk, Cf[79]); a dynamic effect due to the giant Coster–Kronig transitions within the core and valence levels during the core electron photoemission (Th,[56,62,119,120,124] U,[47,56,66] Np,[55,56,80] Pu,[29,82] Am,[29] Cm, Bk, Cf[54,55]); many-body perturbation caused by simultaneous excitation of valence electrons during photoemission, which gives rise to satellites on the higher binding energy side from the basic XPS lines (so-called shake up satellites) (Th,[117,118,125] U,[52,66,105] Np,[79,80] Pu,[29,82,85,126] Am,[29,127,128] Cm, Bk, Cf[79]), and other effects.

Despite the fact that different mechanisms of the appearance of fine spectral structure occur simultaneously, for electrons of a particular shell, the probability of a particular mechanism is usually much higher than that of other mechanisms.[52,54,55] Therefore, to study particular mechanisms of the formation of fine spectral structure in actinide compounds, it is expedient to use compounds of those elements in the spectra of whose electronic shells this mechanism shows itself with the highest probability.

Most often, the fine structure of the XPS spectra of actinide compounds is interpreted based on the results of theoretical calculations (U,[24–26,31,32,42,55,93,129–137] Th,[124,125,129] Np,[33,36,136] Pu,[33,36,138] Am,[33,35,138] Cm, Bk, Cf[35,137,138]). However, such calculations are usually labour-consuming and are performed after the experimental spectra have already been measured. Therefore, in practice, spectra that have been thoroughly studied both theoretically and experimentally are often used as references to analyse the XPS spectra of new compounds.

X-Ray photoelectron spectroscopy is the most appropriate technique for the study of the physicochemical states of actinides. It is used to estimate the oxidation states of actinides, their electronic configurations, and the degree of participation of electrons in the chemical bond on the surface of solids (Th,[79] U,[139,140] Pu[141,142]), in alloys and other materials (Th,[143] U,[144–147] Pu,[82,146] Am, Cm, Bk, Cf[79]) and to determine radionuclides in the environment. This method is used in the quantitative elemental analysis of actinide materials;[148] in particular, it has been successfully used to determine the elemental and ionic composition of the reactor fuel melts from the Chernobyl nuclear power plant,[9,91,149,150] to study the nature and the structure of 'new-formed' materials grown on these melts,[10,150,151] to study the mechanisms of interaction of the uranyl group (UO_2^{2+}) with calcite and diabase,[12,152–157] humic acids,[11,157–160] apatite[161,162] and biosorbents,[91] to study the microbial reduction of the U^{6+} ions to U^{4+} (Refs 163, 164) and the effect of visible light on the decomposition of the uranyl citrate complex;[165] and to study the elemental and ionic composition of highly hazardous 'hot' particles[8] containing U, Cs,[15,166–169] Sr[15,170–172] and Ru,[13,14,173–175] which have been formed during the simulation of a nuclear power plant accident under laboratory conditions. Together with other X-ray spectral methods,[16] X-ray photoelectron spectroscopy[11,152,158,161] is efficiently used to solve problems related to radionuclide transfer in the environment.

For interpretation of XPS spectra, in particular, of actinide compounds, as has been shown previously for lanthanide compounds,[54] the binding energy range of the electrons (0–1250 eV) can be divided conventionally into three regions. The first one is from 0 to ~15 eV; this exhibits the spectral structure mainly caused by the An5f and OVMO electrons. The second region (~15 to ~50 eV) shows a structure that is largely related to the IVMO electrons and whose parameters correlate with the degree of participation of the An6p and L*n*s atomic orbitals (AO) in the chemical bond and with the structure of the local environment of the actinide ion. The third region (~50 to 1250 eV) reflects the fine spectral structure of the core electron levels; the mechanisms of its formation may be different.

This review mainly deals with the fine structure of the X-ray photoelectron spectra of compounds of light actinides (Th, U, Np, Pu, Am, Cm, Bk, Cf) observed in the binding energy range of 0–1250 eV, the mechanisms of formation of this structure and the dependence of its characteristics on the physicochemical properties of compounds and the nature of the chemical bond in them. We are going to answer the following questions.

1. What are the mechanisms and general regularities of the formation of fine XPS structure for actinide compounds?

2. How do the parameters of the fine structure in question correlate with the properties of actinide compounds and the nature of the chemical bond in them?

3. What new quantitative and qualitative information on the physicochemical properties of actinide compounds can be gained from the parameters of the fine XPS structure?

To simplify the discussion of the fine structure of XPS spectra in the region of valence electrons, we use atomic designations in addition to molecular ones.

II. Thorium compounds

Since the electronic configuration of thorium is $\{Rn\}6d^27s^2$ (see Table 1), the simplest structure of the XPS spectra should be expected of compounds formed by tetravalent thorium. This is due to the fact that Th^{4+} does not contain unpaired electrons (the electronic configuration is $\{Rn\}5f^0$). Filling of the An5f shell with

an increase in the atomic number of the actinide complicates the spectral structure due to the multiplet splitting, which is caused, as noted above, by the presence of unpaired valence electrons in the actinide ion; this results in a complex structure of the final state of this ion upon photoemission of an outer or an inner electron.

This Section presents the results of analysis of the XPS spectra of thorium [57, 120, 176, 177] and its compounds,[52, 55, 59–62, 64, 118, 119, 125, 177] in particular, ThO_2,[53, 58, 61, 98, 99, 117] ThF_4,[53, 58, 98, 99] $Th(NO_3)_4 \cdot 4H_2O$,[53, 58] $Th(SO_4)_2 \cdot nH_2O$, $Th(OH)_4$, $Th(CO_3)_2 \cdot nH_2O$,[55] $ThSiO_4 \cdot nH_2O$,[61, 63] mainly dealing with their fine structure and dependence of its characteristics on the oxidation state of thorium, the structure of compounds, and the nature of the chemical bond in them. This information is also necessary for interpretation of the XPS structure of heavier actinide compounds containing unpaired An5f electrons.

1. Spectral range of valence electrons

In the low binding energy range (around the Fermi level for metals), the XPS spectra of thorium compounds (Figs 1, 2) exhibit a poorly resolved band due to electrons of the OVMO. This band largely reflects the participation of the $Th6d^27s^2$ and L*n*p electrons of thorium and the surrounding ligands L in chemical bonds. The full widths at half maximum (FWHM) of these bands for ThO_2, $Th(NO_3)_4 \cdot 4H_2O$ and ThF_4 are 3.3, 2.5 and 3.7 eV, respectively [55, 58] (see Fig. 2).

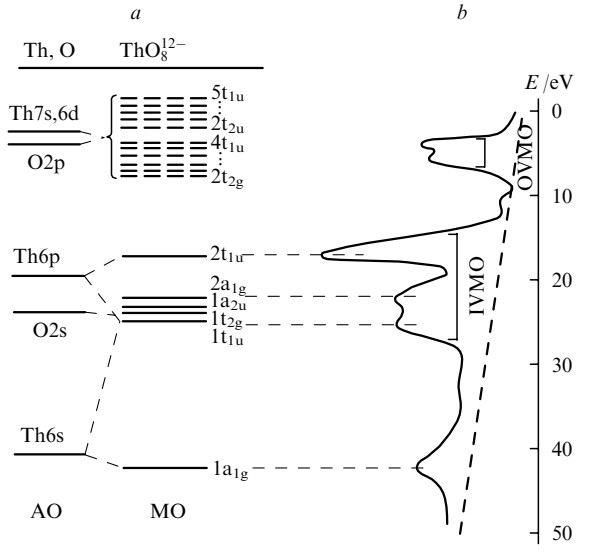

Figure 1. Scheme of MO formation in the ThO_8^{12-} cluster (O_h group of symmetry) (*a*) and X-ray photoelectron spectrum of the oxide ThO_2 (*b*).[58, 62] The dashed line in Fig. 1 *b* is the background.

In a binding energy range of ~10–50 eV, the spectra show a structure due to the Th6s, Th6p and L*n*s electrons. This structure is more complicated than that expected for the sum of the atomic spectra of the elements contained in the given compounds. Thus, the experimental spin–orbit splittings (ΔE_{sl}) for the Th6p electrons differ markedly for the oxide (9.0 eV), fluoride (7.2 eV), thorium metal (7.9 eV) and atomic thorium (9.2 eV) (Tables 2, 3).[55, 57, 58, 62, 178, 179] For ThO_2 and ThF_4, this binding energy difference between the $Th6p_{3/2}$ and $Th6p_{1/2}$ electrons cannot be attributed to the superposition of the Th6p line onto the neighbouring lines related to the ligands. In this case, the components of the thorium doublet would shift in the opposite direction, and apparent splitting of this level for ThO_2 would be lower than for ThF_4. It is known from numerous experimental data that in the low-energy range, the spin–orbit splitting of the core levels depends only slightly on the chemical environment.[21, 23]

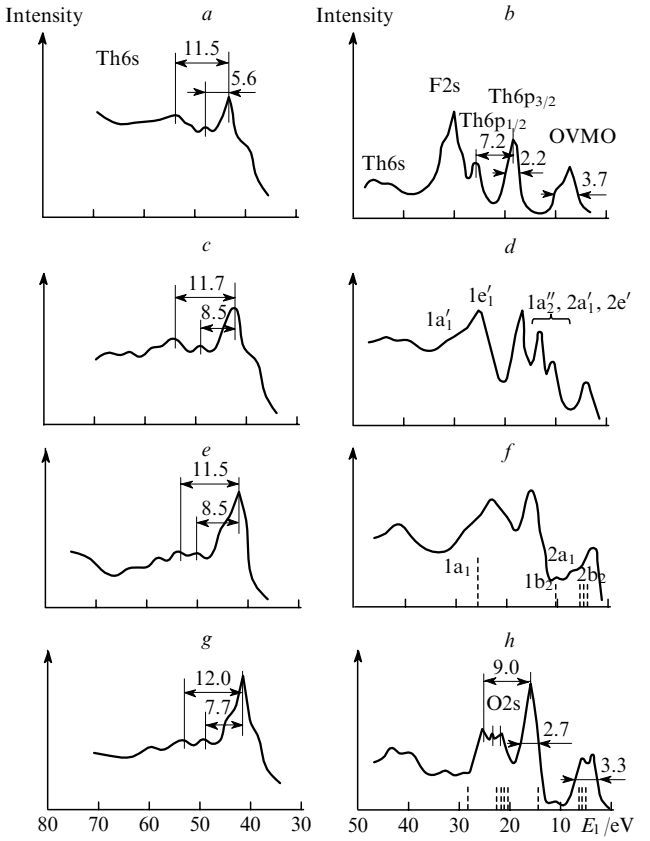

Figure 2. XPS spectra of thorium compounds in the range of weakly bound electrons
(*a*, *b*) ThF_4; (*c*, *d*) $Th(NO_3)_4 \cdot nH_2O$; (*e*, *f*) $Th(OH)_4$; (*g*, *h*) ThO_2. The Th6s spectra (*a*, *c*, *e*, *g*) show the dynamic effect with the formation of final states of the type $Th6s^16p^66d^0 \rightleftharpoons Th6s^26p^46d^1$; the vertical lines below the spectrum *h* show the MO energies for the ThO_8^{12-} cluster (O_h symmetry);[180] the vertical strokes below spectrum *f* show the experimental spectrum of H_2O;[19] the designations for the MO of the NO_3^- ligand (D_{3h} symmetry) are presented above spectrum *d*.

The extra structure present in the O2s and F2s binding energy range cannot be explained by the presence of ligand atoms in different oxidation states in ThO_2 and ThF_4. In this case, the corresponding structure would also be observed in the O1s and F1s spectra. This is due to the fact that the chemical shift does not depend significantly on the core electron binding energy in the E_b range up to ~1000 eV.[21, 23] The O1s and F1s spectra of ThO_2 and ThF_4 consist of single lines with FWHM of 1.4 and 1.7 eV, respectively.[58]

The most complicated fine structure is observed in the low-energy XPS range for thorium compounds containing organic ligands. In this case, the thorium spectrum is superimposed by a spectrum of the IVMO electrons of the ligands. (For some compounds, these MO are also shown in Fig. 2.)

On the basis of the XPS data, taking into account the results of theoretical calculations,[129, 137, 180, 181] it has been suggested [51, 55, 58, 59, 101, 102] that an important reason for the formation of the fine structure in the spectra of these thorium compounds is efficient (experimentally observed) formation of IVMO from the Th6p and L2s atomic shells.

The foregoing can be illustrated in relation to the spectrum of the low binding energy electrons of ThO_2. The local environment of thorium in this compound can be simulated by the ThO_8^{12-} cluster (O_h group of symmetry) in which the Th–O bond length (R_{Th-O}) equals 0.241 nm (Fig. 3, see Fig. 1).[54] The results of theoretical calculations performed for the ground state of this cluster in the non-relativistic spin-limited SCF X_α-DV approx-

Table 2. Binding energies (E_b) and photoionisation cross-sections (σ) for thorium and its compounds.[62]

Orbital Th, L (nl_j)	E_b /eV								σ(Th, L) [a]
	ThF_4	$Th(SO_4)_2 \cdot n H_2O$	$Th(NO_3)_4 \cdot n H_2O$	$Th(OH)_4$	$Th(CO_3)_2 \cdot n H_2O$	ThO_2	Th_{metal} (see [57])	Th_{theor} (see [178])	
OVMO	8.3	7.3	5.6	5.6	5.2	5.8			–
Th6$p_{3/2}$	18.4	18.8	18.4	17.5	17.2	16.5	16.6	24.8	0.37
Th6$p_{1/2}$	25.6	–	–	–	–	25.5	24.5	34.0	0.13
Th6s (see [b])	44.5	44.6, 50.8	43.7	42.6	41.9, 50.1	41.9	41.4	53.5	0.16
Th5$d_{5/2}$	88.5	88.2	87.8	86.8	86.7	86.3	85.4	95.6	3.15
Th5$d_{3/2}$	95.5	95.2	94.8	93.8	93.6	93.3	92.5	102.7	2.15
Th5$p_{3/2}$ (see [b])	177.8, 181.0, 197.9	177.3, 181.1, 198.6	176.7, 180.0, 198.9	– 179.2, 197.0	– 179.0, 198.8	175.1, 178.6 194.1	– 177.2	– 197.6	– 2.05
Th5$p_{1/2}$	236.7	–	237.0	234.8	236.6	233.4	233.8	244.1	0.66
Th5s	288.7	289.1	289.0	289.7	289.0	288.7	–	307.4	0.70
Th4$f_{7/2}$	336.6	336.3	335.8	335.0	334.8	334.3	333.1	343.6	23.94
Th4$f_{5/2}$	345.9	345.7	345.2	344.2	344.0	343.6	342.4	352.8	18.81
Th4$d_{5/2}$	678.4	677.9	677.1	676.4	676.1	675.6	675.2	678.0	16.31
Th4$d_{3/2}$	715.5	715.0	714.8	713.9	713.6	712.7	712.4	715.0	10.82
Th4$p_{3/2}$ (see [b])	967.5, 969.5	969.2	–	969.2	966.6	966.7	966.4	969.8	7.46
O2s		25.4	26.7	22.5	24.9	22.0			0.14
O1s		532.5	533.3	532.0	531.8	530.2			2.93
F2s	29.8								0.21
F1s	685.5								4.43
N1s			407.7						1.80
S2$p_{3/2}$		169.7							1.68
S2s		233.4							1.43
C1s					289.0				1.00

[a] The σ values are expressed in the units used in Ref. 62: 13.6 barn (b) per atom. [b] The E_b values corresponding to the line maxima in the corresponding binding energy ranges are given.

Table 3. Binding energy differences (ΔE_i) for various electron shells of thorium and ligands.[55]

Compound	$\Delta E_i = E_k - E_l$ /eV					
	6$p_{3/2}$ – 6$p_{1/2}$	6$p_{3/2}$ – 6$s_{1/2}$ (see [a])	6$p_{3/2}$ – 4$f_{7/2}$	6$s_{1/2}$ – 4$f_{7/2}$ (see [a])	5$d_{5/2}$ – 4$f_{7/2}$	L2s – L1s (see [b])
ThO_2	9.0	25.4	317.8	292.4	248.0	508.2, 506.2
$Th(CO_3)_2 \cdot \cdot n H_2O$	–	24.7	317.6	292.9	248.1	506.9
$Th(OH)_4$	–	25.1	317.5	292.4	248.2	509.5
$Th(NO_3)_4 \cdot \cdot n H_2O$	–	25.3	317.4	292.1	248.0	506.6
$Th(SO_4)_2 \cdot \cdot n H_2O$	–	25.8	317.5	291.7	248.1	507.1
ThF_4	7.2	26.1	318.2	292.1	248.1	655.7
Th_{metal} (see [57])	7.9	24.8	316.5	291.7	247.7	–
Th_{theor} (see [178])	9.2	28.7	318.8	290.1	248.0	–

[a] The binding energies corresponding to the most intense peaks in the Th6s spectra are used. [b] The ΔE_i differences for oxygen and fluorine are given.

imation[180] are presented in Fig. 3 for convenient qualitative comparison with the experimental data. It follows from Fig. 3 that the MO system can be conditionally subdivided into two groups, inner valence and outer valence MO.

The outer valence MO (OVMO) group consists of vacant $2t_{2u}-6t_{1u}$ orbitals and filled $2t_{2g}-4t_{1u}$ orbitals, which contain occupied Th5f states, whereas free thorium atoms contain no Th5f electrons. It has been shown experimentally [99, 100] that relatively high line intensity in the XPS spectra of ThO_2 and ThF_4 in the OVMO energy range is largely related to the presence of filled Th5f states in these compounds. This is consistent with the results of studies of $L_{\alpha 1,\beta 2,4}$(Th)-emission of thorium oxide and halides.[182]

The other group of molecular orbitals includes the $1a_{1g}$, $1t_{1u}$, $1t_{2g}$, $1a_{2u}$, $2a_{1g}$ and $2t_{1u}$ IVMO. Analysis shows that, whereas OVMO mainly consist of vacant valence Th5f, Th7s, Th6d, Th7p and O2p atomic orbitals, the IVMO are mainly composed of fully occupied inner valence Th6s, Th6p and O2s AO. For example, orbitals of the $1t_{1u}$ and $2t_{1u}$ IVMO pair, one of which can be considered as a bonding orbital ($1t_{1u}$) and the other, as an antibonding one ($2t_{1u}$), consist of 18% of Th6p plus 68% of O2s and 55% of Th6p plus 27% of O2s, respectively (see Fig. 3). Significant mixing of the Th6s and O2s AO takes place during formation of the $1a_{1g}$ and $2a_{1g}$ IVMO pair. However, for uranium oxides, it has been shown [123, 180] that inclusion of relativistic effects in the calculation leads to a lower degree of mixing. This is mainly due to splitting off of the Th6$p_{1/2}$ component from the Th6$p_{3/2}$ level (ΔE_{sl} = 7.9 eV), which allows the use of non-relativistic calculation results in interpretation of the low binding energy spectra of actinide compounds.

The energies of occupied OVMO electronic levels do not differ much (−11.21 to −9.39 eV) and fall within a range of 1.82 eV. The energies of the inner valence MO vary over a broader range and form an energy structure typical of this cluster. This makes it possible to construct qualitative structural schemes for the IVMO of various model clusters (see Figs 1, 3).

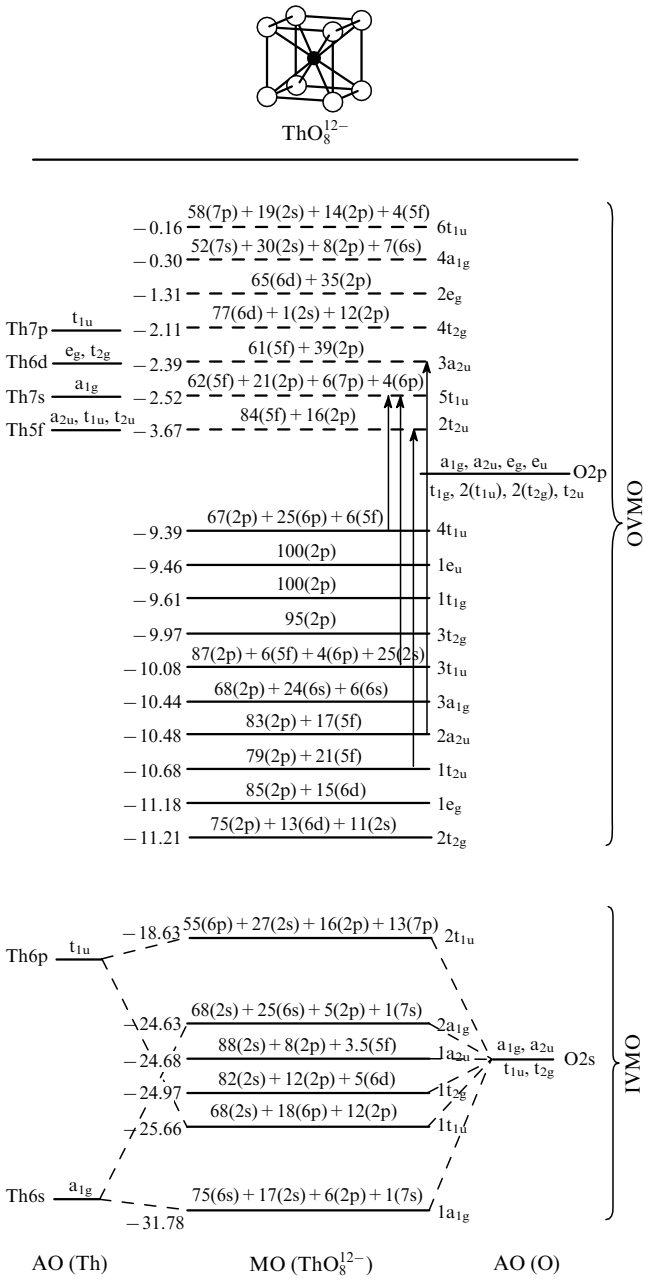

Figure 3. Composition (%) and the structure of MO of the ThO_8^{12-} cluster (O_h symmetry) for $R_{Th-O} = 0.241$ nm (X_α-DVM calculations).[180] The vacant MO are shown by horizontal dashed lines; here and below, AO and related IVMO are connected by dashed lines. The arrows show the most probable electronic shake up transitions which accompany the photoemission of a core electron (the energy scale is not maintained).

Experimental data for ThO_2 are presented in Fig. 4, which provides their qualitative comparison with the results of theoretical calculations and shows the binding energy differences between the valence and core electrons for separate atoms and the ThO_8^{12-} cluster, which can be determined experimentally.

It can be seen from Fig. 4 that the formation of molecular orbitals from the Th6p and O2s AO can induce a relative shift of the $2t_{1u}$ level toward lower binding energies compared to that of the Th6p electrons by a Δ_1' value. The formation of IVMO from the Th6s and O2s AO can entail a relative shift of the $1a_{1g}$ level toward higher binding energies compared to that of the Th6s electrons of the Th metal by a Δ_2 value. Note that MO formation can induce some other significant effects that influence the line shifts, for example, a change in the effective charge of the nucleus.

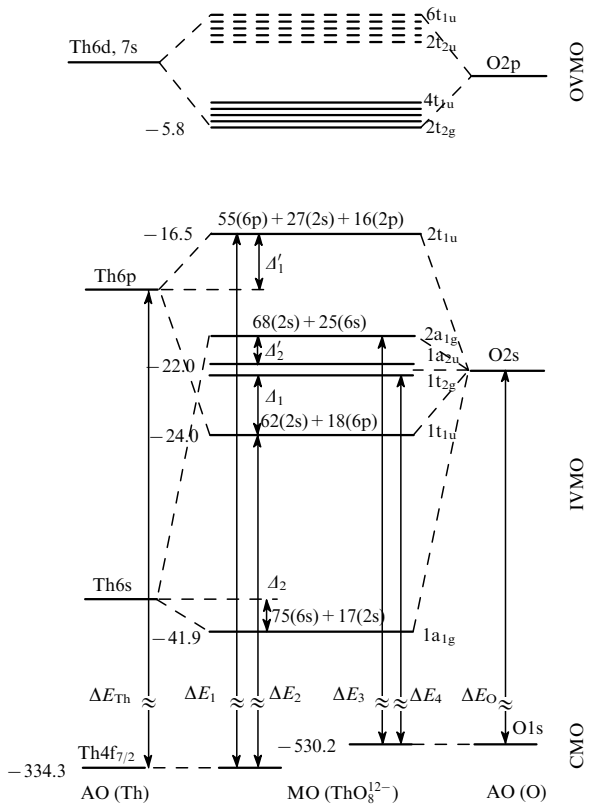

Figure 4. Diagram of MO of the ThO_8^{12-} cluster (O_h symmetry) reflect the structure of the nearest environment of the thorium atom in ThO_2. Chemical shifts induced by MO formation from AO are not reflected. The diagram is based on the XPS spectrum and calculation results.[180]

These shifts of the levels related to MO formation can be determined rather reliably by comparing the energy differences between various valence and core levels ΔE_i ($i = 1-4$), ΔE_{Th} and ΔE_O (see Fig. 4) found from the XPS spectra of thorium compounds (see Table 3).

It follows from the data of Table 3 that on passing from thorium metal to thorium compounds, the binding energy differences (ΔE_i) between the core $Th4f_{7/2}$ and $Th5d_{5/2}$ electrons change to the least extent. Substantial deviations in the ΔE_i energies are found for the formal $\Delta E_{sl}(Th6p_{3/2} - Th6p_{1/2})$ and $\Delta E_1(Th6p_{3/2} - Th4f_{7/2})$ values, which describe the energy shifts of valence electrons. These results are consistent with the assumption that at least the $Th6p_{3/2}$ and O2s atomic shells are involved in the $2t_{1u}$ IVMO, which is formally antibonding.

The formation of IVMO in the oxide ThO_2 and the fluoride ThF_4 is confirmed by X-ray $O_{4,5}$(Th) emission spectroscopy.[99,100,183–186] Additional information on the valence electron states of thorium dioxide and tetrafluoride can be gained from X-ray $O_{4,5}$(Th) [187–190] and $M_{3,4,5}$(Th) absorption spectra.[191]

2. Electronic structure of ligands

The low binding energy spectra of $Th(SO_4)_2 \cdot n\,H_2O$, $Th(NO_3)_4 \cdot n\,H_2O$, $Th(CO_3)_2 \cdot n\,H_2O$ and $Th(OH)_4$ [55] can be represented approximately as the summary spectra of clusters with a Th central atom surrounded by the ligands NO_3^-, SO_4^{2-}, CO_3^{2-}, OH^- and H_2O (see Fig. 2).

To estimate qualitatively the contribution of ligands to complication of the structure of the general low binding energy spectrum of thorium compounds, let us consider the spectral structure of the ligands taking the NO_3^- group as an example.

The low binding energy spectral range of $Th(NO_3)_4 \cdot n\,H_2O$ can be approximately regarded as a superposition of the spectra from thorium involved in the chemical binding with oxygen, the

NO_3^- ligand and H_2O (see Fig. 2 *c*,*d*). The experimental XPS spectrum of water (C_{2v} group of symmetry)[19,55] reflecting the system of its MO is shown in Fig. 2 *f* by vertical dashed lines. The spectral structure of the NO_3^- ligand (D_{3h} group of symmetry) with $R_{N-O} = 0.121$ nm is conveniently illustrated by the MO diagram (Fig. 5) constructed on the basis of results of semiempirical CNDO/2 calculations. These results are in satisfactory agreement with the data for $Ni(NO_3)_2 \cdot 6\,H_2O$ whose XPS spectrum exhibits, in the low binding energy range, only an OVMO band for nickel at low E_b values.[55] Except for the thorium line in the valence band, the spectral structures for nickel and thorium nitrates have much in common. The molecular orbitals of the NO_3^- ligand are shown in Fig. 2 *d* above the spectra of thorium nitrate. The contributions of the electrons from various MO to the covalent bonding in the NO_3^- ligand [58] were estimated based on the resonance energy value E^{α}_{N-O} (measured in au),[52,53] which characterises the fraction of covalent bonding in the chemical bond; the corresponding energy values are indicated in parentheses in Fig. 5.

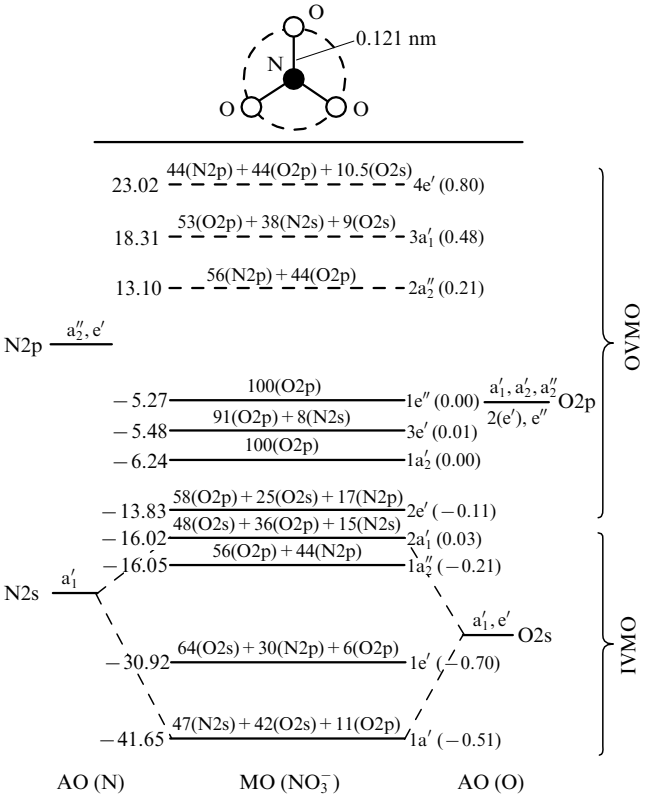

Figure 5. Composition (%) and structure of the MO of the NO_3^- ligand (D_{3h} symmetry) (CNDO/2 calculation).[58]
The values in parentheses are resonance energies (E^{α}_{N-O}, au; see Refs 52, 53). The vacant MO are shown by horizontal dashed lines (the energy scale is not maintained).

As can be seen from Fig. 5, the energies of occupied MO of the NO_3^- ligand are located within a 36.38 eV range, which almost overlaps the range of MO of the ThO_8^{12-} cluster; taking them into account provides a satisfactory description of the additional structure observed in the experimental XPS spectrum of thorium nitrate (see Fig. 2 *d*). This IVMO structure is expected to arise also in the spectra of compounds containing CO_3^{2-} and SO_4^{2-} groups (D_{3h} and T_d symmetry, respectively).[52]

The results indicate that the spectra of complex ligands of the thorium compounds studied have a characteristic structure caused by OVMO and IVMO electrons extended in a binding energy range of ~35 eV. This structure can be used to identify these substances. In addition, the low energy range of the spectra may display an additional structure caused by secondary electrons and other processes. Since these processes are also reflected in the core electron spectral structures, they can be studied more conveniently in the spectra of core levels.

3. Core electron spectra of thorium compounds

When performing quantitative elemental and ionic analysis using XPS spectra, the stoichiometric compositions of compounds and the oxidation states of ions are determined using the most intense single sharp lines for the core levels. The most suitable line for these studies of thorium compounds is a component of the doublet (caused by the spin–orbit splitting) of the $Th4f_{7/2}$ electrons.[58,60,117,121,125]

The core electron fine structure (shake up satellites) related to many-body perturbation reflects the composition and energy distribution of molecular orbitals. The many-body perturbation is due to the extra final states of thorium ion which arise upon the transition (excitation) of a valence electron to a vacant outer MO simultaneously with the photoemission of a core electron (shake up process[21–23,49]). This gives rise to shake up satellites on the higher binding energy side from the basic lines. Such satellites are observed in the spectra of all core and valence levels; however, as the electron binding energy decreases, their intensity diminishes (see, for example, the study[192] dealing with $LnNbO_4$). These satellites are more specific in the Th4f and Th5d spectra (Fig. 6). Since the excitation of ligand-related electrons from filled MO to vacant, mainly metallic AO can take place during the electron photoemission from a core metallic level (see Fig. 3), the corresponding satellites can be attributed to the charge transfer from the ligand L to the metal M: $Lnl \rightarrow Mn'l'$, where n (n') and l (l') are the principal and orbital quantum numbers, respectively.[23] These excitations, which satisfy the monopolistic selection rules, $\Delta l = \Delta s = 0$ (s is the spin quantum number) are shown for ThO_8^{12-} in Fig. 3 by arrows. A simple two-level theoretical model[22,23,118,193] makes it possible to calculate the satellite intensity, which is related to the change in the partial electron density on a filled AO of the metal caused by electron photoemission from a core level. On the basis of this model, it was shown that the satellite intensity diminishes as the metal electron density on a certain filled MO increases and the magnitude of its change upon the photoemission of the core electron decreases. The energy distance from a satellite to the basic line depends on the ionic–covalent nature of the chemical bond in the compound. In the case of 3d-metal compounds, this distance increases and the satellite intensity decreases with an increase in the ionic contribution to the bond.[193] The spectra containing shake up satellites are typical of a particular thorium compound and reflect the actinide oxidation

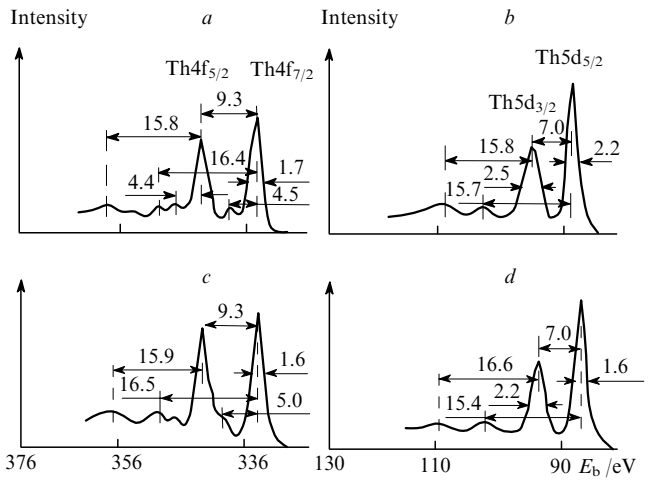

Figure 6. XPS spectra of thorium compounds in the Th4f (*a*, *c*) and Th5d (*b*, *d*) binding energy ranges.[55] (*a*, *b*) ThF_4; (*c*, *d*) ThO_2.

state and the stoichiometric composition. A similar satellite structure can also be followed in the Th5d spectra (see Fig. 6).

It is also noteworthy that, despite the complication of the Th4f and Th5d spectral structures due to many-body perturbation, the observed basic lines are relatively sharp. The intensity ratios of individual components of doublets are close to the theoretical values, while the spin–orbit splittings (ΔE_{sl}) are constant for different compounds, being equal to 9.3 and 7.0 eV for the Th4f and Th5d electrons, respectively. A similar spectral pattern for some shells of transition elements is usually observed when the multiplet splitting and dynamic effect are feebly manifested in the spectra of these electrons.[22, 23, 193]

The Th6s binding energies reported in several papers [20, 57, 58] are different. This discrepancy can be explained by the errors of measurements resulting from the relatively small Th6s photoionisation cross-section and unexpectedly wide energetic interval ($\sim$40 eV) in which the complex fine spectral structure arises. The most intense maximum in the Th6s spectrum from ThO_2 is observed at $E_b \approx 42$ eV (see Fig. 2 *g*).

On the basis of theoretical calculations, [129, 137, 180] it was suggested that the Th6s shell can markedly participate in the MO formation in thorium compounds. Therefore, for a number of thorium compounds, the low binding energy XPS spectra of Th6s electrons were recorded and analysed [55, 58] (see Fig. 2). In a range of $\sim$40 eV, the Th6s spectra show structure that cannot be attributed to the participation of Th6s in the chemical bond alone. This participation could result in the shift of the Th6s line or appearance of a fine structure with a width of several electron-volt. Since the compounds in question are diamagnetic and do not contain unpaired electrons, their XPS spectra are not expected to display multiplet splitting. The maxima observed at the same relative energies as the Th4f and Th5d spectra can probably be attributed to the shake up satellites in those cases where the corresponding line intensities do not exceed $\sim$10% of the basic lines.

Similar considerations are also valid for spectral structure of the Th5p electrons (Fig. 7). Instead of the expected doublet caused by the spin–orbit splitting, this spectrum exhibits a much more complicated fine structure. The spin–orbit splitting is given by ΔE_{sl}(Th5p) = 47 eV, while the binding energies (see Table 2) are as follows: $E_b(Th5p_{3/2}) = 182$ eV and $E_b(Th5p_{1/2}) = 229$ eV.[20] However, the spectra of thorium compounds exhibit a clear-cut additional line at $\sim$200 eV and the $Th5p_{1/2}$ lines are broadened (see Fig. 7). These structural changes in the spectra of relatively deep electron shells cannot be attributed to the crystal field splitting. Moreover, splittings of about several electron-volt are also observed in the $Th4p_{3/2}$ spectra.[55] These spectra are complicated due to the appearance of additional broad OKLL Auger bands. The most individual fine structure in the $Th4p_{3/2}$ spectra is found in the spectrum of thorium tetrafluoride containing no O atoms.[55]

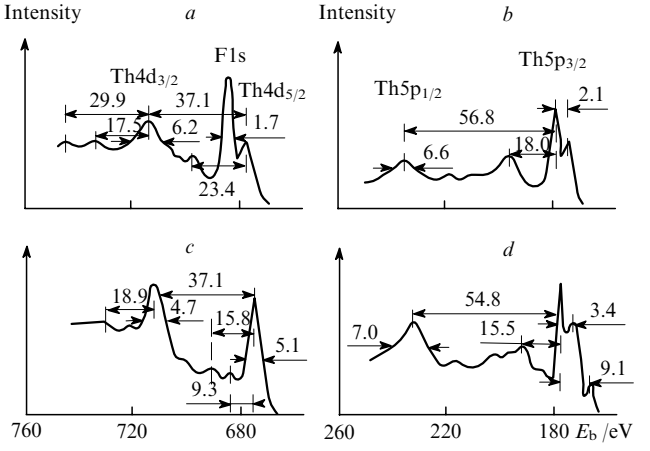

Figure 7. XPS spectra of thorium compounds in the Th4d (*a*, *c*) and Th5p (*b*, *d*) binding energy ranges.[58] (*a*, *b*) ThF_4; (*c*, *d*) ThO_2. The Th5p spectra for both compounds show the dynamic effect, resulting in the formation of final states of the type $Th5p^5 5d^{10}(6s^2 6p^6)5f^0 \rightleftharpoons Th5p^6 5d^8(6s^2 6p^6)5f^1$.

The XPS spectra of thorium and its compounds may clearly manifest the dynamic effect due to the giant Coster–Kronig transitions within the core and outer shells during the electron photoemission from an atom or an ion. This results in several final states of an ion and, as a consequence, a complicated fine structure is observed in the spectra instead of sharp single lines. For thorium compounds, the ratios of the binding energies of core and outer electronic levels are favourable for this effect to appear during the photoemission of core electrons from the Th atom. Indeed, since the binding energies of thorium levels obey the ratios $E_b(Th6s) \approx 2E_b(Th6p)$; $E_b(Th5d) \approx 2E_b(Th6s)$; $E_b(Th5p) \approx 2E_b(Th5d)$; $E_b(Th4f) \approx 2E_b(Th5p)$; $E_b(Th4d) \approx 2E_b(Th4f)$; $E_b(Th4p) \approx E_b(Th4d) + E_b(Th5s)$, and the dynamic effect has a resonance nature,[55] the probability of this effect for thorium compounds is rather high (see Table 2). The dynamic effect gives rise to an additional two-hole final state (apart from the ground one-hole state), due to the electron transition from an intermediate fully occupied level to a level with a hole that has appeared upon electron photoemission from the atom and to the nearest low-energy vacant level in the molecule under consideration. This two-hole state should have the same orbital quantum number L as the ground one-hole final state and a similar energy.[119, 120, 194] According to estimates,[119, 124] the following one-hole and two-hole final states are expected to appear with the highest probability for Th^{4+} compounds after photoemission of the core electron: $Th6s^1 6p^6 6d^0 \rightleftharpoons Th6s^2 6p^4 6d^1$ (see Fig. 2); $Th5p^5 5d^{10}(6s^2 6p^6)5f^0 \rightleftharpoons Th5p^6 5d^8(6s^2 6p^6)5f^1$ (see Fig. 7, Table 2); $Th5s^1 5p^6 5d^{10}(6s^2 6p^6) \rightleftharpoons Th5s^2 5p^5 5d^9(6s^2 6p^6)5f^1$. It is assumed [55, 58] that the dynamic effect can also be observed in the $Th4p_{3/2}$ spectra. This can be attributed, for example, to the formation of final states of the type $Th4p^5 4d^{10} 5s^2 . (5p^6 5d^{10} 6s^2 6p^6) \rightleftharpoons Th4p^6 4d^9 5s^1 (5p^6 5d^{10} 6s^2 6p^6) 7p^1$.

The structure of the Th5s spectra caused by the dynamic effect is difficult to observe, as it is superimposed by the C1s spectrum;[55, 58] however, it has been shown theoretically that this structure should occur in this binding energy range.[124, 194]

It follows from the above examples that, on the one hand, the fine spectral structure complicates gaining the traditional information concerning the binding energies and line intensities for the core electrons, but, on the other hand, this structure provides significant additional information on the electron structure, the nature of chemical bonds and the secondary electronic processes that accompany the electron photoemission from ions.

A number of industrially important thorium compounds have now been studied by XPS. Although thorium is formally tetravalent in each of the compounds studied, the binding energies imply that the thorium oxidation state increases in the following sequence: ThO_2, $Th(CO_3)_2 \cdot n H_2O$, $Th(OH)_4$, $Th(NO_3)_4 \cdot 4 H_2O$, $Th(SO_4)_2 \cdot n H_2O$, ThF_4.[55, 58] This results in an increase in the $Th4f_{7/2}$ binding energy by $\Delta E_b = 1.8$ eV. Thus, in the series of thorium compounds, the ionic nature of the chemical bond increases.

To conclude this Section, we would like to note that the understanding of the mechanism of fine structure formation in the XPS spectra of thorium compounds is highly favourable for gaining the most detailed and reliable information on the properties of these compounds and the nature of the chemical bond in them.

III. Uranium compounds

Solid-state uranium compounds have been studied by XPS in most detail.[45, 47, 53, 55, 57, 65, 66, 75, 78, 93, 94, 177, 195–198] The gaseous UF_6, $U(BH_4)_4$, $U(BH_3Me)_4$ and $U(C_8H_8)_2$ molecules have been

studied.[199–201] Photoelectron spectroscopy data for the UF_4, UCl_4 and ThF_4, $ThCl_4$ molecules in the gas phase have also been reported.[179, 202] Theoretical analysis of the electronic structures of these compounds has received much attention.[53, 55, 123, 129–132, 203–206] X-Ray photoelectron spectroscopy has proved to be the most adequate method for determining the oxidation states and ionic compositions of uranium in oxides and other compounds, in particular, in ores.[66] Knowledge of the uranium oxidation state in ores is especially important for underground leaching.[207, 208] In a number of studies,[47, 65, 66, 92–94] uranium compounds have been studied by XPS in order to develop a non-destructive method for determining the uranium oxidation states in compounds and minerals and the stoichiometric compositions of minerals on the basis of XPS fine structure parameters.

1. Uranium oxides

a. The U5f spectra

X-Ray photoelectron studies of uranium oxides have shown[38–40, 45, 53, 65–68, 76, 77, 93, 111, 190, 209, 210] that the fine structures of the low binding energy spectra ($E_b = 0-50$ eV) of UO_2 and UO_3 are substantially different (Fig. 8). Since the U^{6+} ion in the trioxide γ-UO_3 has the electronic configuration $\{Rn\}5f^0$, while the electronic configuration of U^{4+} in the dioxide UO_2 is $\{Rn\}5f^2$, the XPS spectrum of the latter,[40, 45, 65–68, 93, 209] unlike the spectrum of γ-UO_3, exhibits a rather narrow intense line at $E_b = 1.9$ eV, which belongs to the U5f electrons participating only slightly in the chemical bond. In addition, some differences in the structures of OVMO and IVMO bands for uranium dioxide and trioxide are also observed (see Fig. 8).

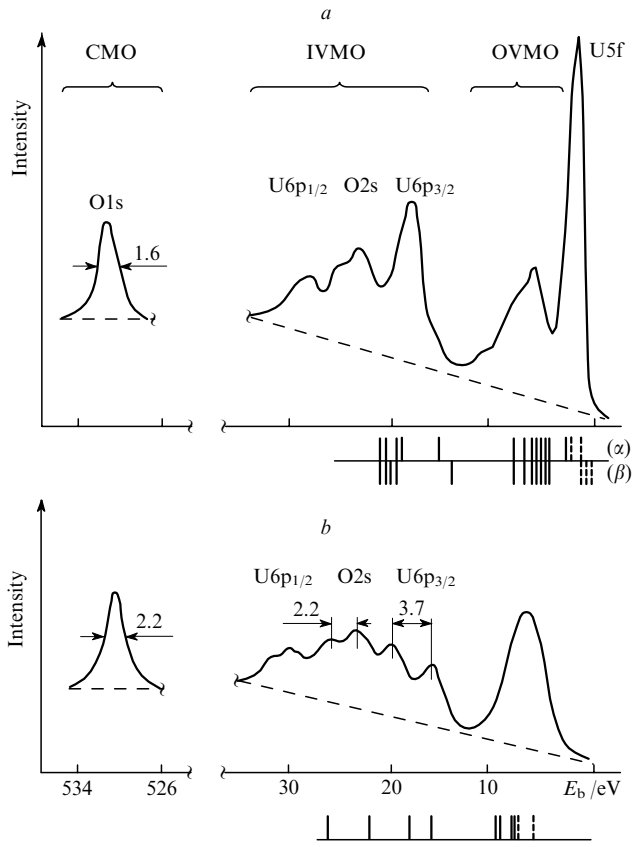

Figure 8. XPS spectra of uranium oxides UO_2 and γ-UO_3 in the low binding energy range and in the O1s range.[53, 93]
(*a*) UO_2, (*b*) γ-UO_3. The intensities of electrons from different shells are not normalised. The dashed lines show the background. The vertical lines under the spectra show the energy levels found by non-relativistic spin-unrestricted (*a*) and spin-restricted (*b*) SCF X_α-SW calculations.[93]

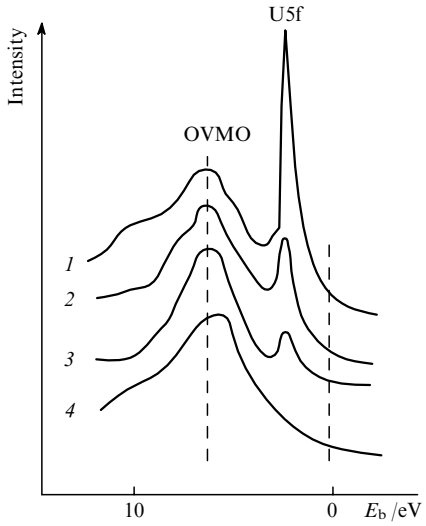

Figure 9. XPS spectra of synthetic uranium oxides in the U5f and OVMO binding energy ranges.[65]
(*1*) $UO_{2.06}$; (*2*) U_2O_5; (*3*) U_3O_8; (*4*) γ-UO_3.

X-Ray photoelectron spectra of low binding energy electrons (0 to $\sim$50 eV) which participate in the MO formation reflect the band structure and represent lines with a width of several electron-volt. The line around a zero binding energy observed in the spectrum of uranium dioxide containing unpaired U5f electrons has the FWHM $\Gamma \approx 1.4$ eV, which is typical of core electrons (see Fig. 8). In the spectra of the U_4O_9, U_2O_5 and U_3O_8 oxides, the intensity of the U5f line decreases (Fig. 9).

Since the ratio of photoionisation cross-sections $\sigma(U6d)/\sigma(U5f)$ is appreciably lower than unity,[203] the U6d line in the XPS spectra should be much less intense than the line for the unbound U5f electrons. For the U^{4+} ion with the electron configuration $\{Rn\}5f^2$, $\sigma(U5f_{5/2})/[3\sigma(U4f_{7/2})] = 0.0213$,[35] which is almost half the corresponding experimental relative intensity[65] $I = I(U5f)/I(U4f_{7/2})$ for UO_2, equal to 0.0383 (Fig. 10).

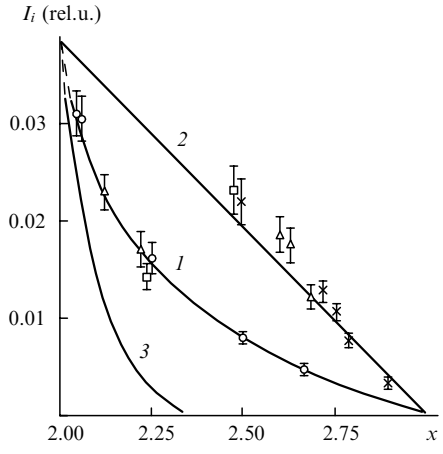

Figure 10. Relative intensity (I_i) of the U5f line in the XPS spectra of synthetic and natural uranium oxides UO_x *vs.* the oxygen coefficient x.[65, 66]
(*1*) I_1 calculated from Eqn (1); (*2*) I_2 calculated from Eqn (2), (*3*) I_3 calculated from Eqn (6); the dots correspond to experimental data: the circles show the data for synthetic oxides; triangles and squares, natural oxides; crosses, UO_2 and γ-UO_3 mixtures.

The energy difference between the U5f and OVMO lines is ~4.2 eV, which permits reliable determination of the intensity of the former. For elucidating the dependence of the intensity (I_1) of the U5f line on the number of oxygen atoms (oxygen coefficient x) in the UO_x oxides, found as the intensity ratio of the U5f lines to the $U4f_{7/2}$ lines without inclusion of the shake up satellites, a number of synthetic uranium oxides have been studied.[65,66] The dependence of the relative intensity I_1 of the line observed in the XPS spectra of the UO_x oxides around zero binding energy, which is caused presumably by the unbound U5f electrons, on the oxygen coefficient x for synthetic oxides can be described as follows (see Fig. 10):

$$I_1 = 5.4x^{-7.2}. \quad (1)$$

Extrapolation of the curve for the dependence of I_1 on x gave the relative intensity $I_1 = 0.0383$ for UO_2. This allows one to construct a similar dependence for mixtures of UO_2 and UO_3 obtained upon homogenisation. This dependence is given by[66]

$$I_2 = -0.0383x + 0.1148. \quad (2)$$

The values of the relative intensity I_2 of the U5f line for mechanical mixtures of the UO_2 and γ-UO_3 oxides fit satisfactorily into this straight line (see Fig. 10).

Since unpaired electrons are responsible for paramagnetism of molecules, it appeared pertinent to compare the dependences of the U5f line intensity in the XPS spectra and the magnetic susceptibility (χ) of the UO_x oxides on the oxygen coefficient x. An increase in x in the range $2 < x \leqslant 3$, entails a decrease in the magnetic susceptibility,[55,90,211] the corresponding dependence being described by the following relation (Fig. 11)

$$\chi = (55.8x^{-0.95} - 19.6) \times 10^{-6}\ g^{-1}. \quad (3)$$

Similar results as regards the magnetic properties have been obtained in another study.[212] It was concluded that $\{Rn\}5f^2$ or $\{Rn\}5f^16d^1$ is the most probable electronic configuration of uranium in the dioxide UO_2 ($\mu_{ef} = 3.2\ \mu_B$), while the trioxide UO_3 possesses a weak temperature-independent paramagnetism, which can be neglected.[212]

For synthetic oxides, the specific magnetic susceptibility χ correlates with the relative intensity I_1 in the following way[91] (Fig. 12):

$$\chi = 62.3 \times 10^{-6} I_1^{0.579}\ g^{-1}. \quad (4)$$

In this case, the I_1 grows faster than the magnetic susceptibility following a decrease in x (see Fig. 10–12).

It has been noted[212] that on a further decrease in the oxygen coefficient x from 2 to 1.835, the magnetic susceptibility of UO_x drops from 8.74×10^{-6} to $8.38 \times 10^{-6}\ g^{-1}$. Unfortunately, the change in the U5f line intensity upon the removal of an oxygen atom from the UO_2 surface, for example, by means of an argon gun, has not been studied quantitatively.

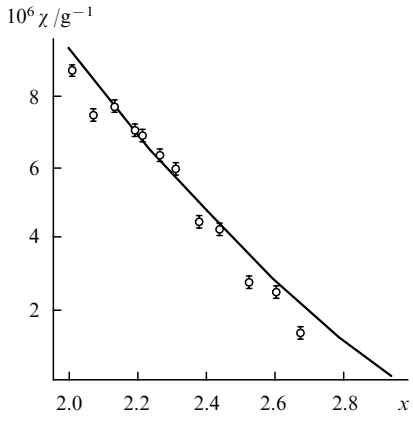

Figure 11. Specific magnetic susceptibility (χ) of synthetic oxides UO_x *vs.* the oxygen coefficient x [see Eqn (3)] plotted using the data of Ref. 211.

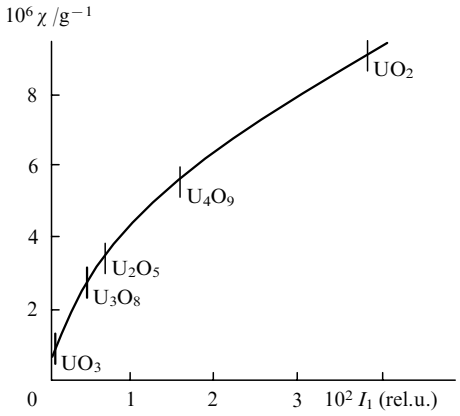

Figure 12. Specific magnetic susceptibility (χ) of synthetic oxides UO_x *vs.* relative intensity I_1 of the U5f line in the XPS spectrum [see Eqn (4)].[65,211] No correction for diamagnetism was done.

For oxide mixtures, the dependence of χ on the intensity I_2 is nearly linear[44,55] (Fig. 13):

$$\chi = 730 \times 10^{-6} I_2^{1.35}\ g^{-1}. \quad (5)$$

It is natural to expect that the magnetic susceptibility would grow proportionally to the intensity I_2 following an increase in the UO_2 concentration in the mixture provided that the intensity of the line under consideration is due to the unpaired unbound U5f electrons.

It follows from the above correlations that the line around the zero binding energy in the XPS spectra of UO_x can be assigned to the unpaired U5f electrons and the configuration of the U^{4+} ion in the dioxide UO_2 is given by $\{Rn\}5f^2$ (see Ref. 55). The relationship between the χ and I values is not as simple as would be expected if the magnetic properties of uranium oxides were governed only by the full spin of the U5f electrons. In addition, the results imply that synthetic oxides are not mere mixtures of UO_2 and UO_3. For example, the dependence of the intensity I_1 on the x value cannot be interpreted under the assumption that the oxides UO_x contain only U^{4+} and U^{6+} ions (see Fig. 10), but it can be explained with the assumption that these oxides contain also U^{5+} ions.[65,66] The presence of U^{5+} ions in complex oxides is consistent with the results of XPS studies[74] and the data of X-ray $L_{III}(U)$ near-edge absorption spectroscopy of the UO_{2+x} oxides.[182] In this case, the difference $\Delta I = I_2 - I_1$ describes the decrease in the content of U^{4+} ions and the formation of U^{5+} ions in UO_x following an increase in x. The approximate relation for the decrease in the

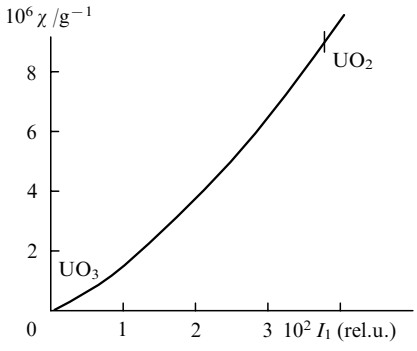

Figure 13. Specific magnetic susceptibility (χ) of synthetic oxides UO_x ($2 \leqslant x \leqslant 3$) *vs.* relative intensity I_2 of the U5f line in the XPS spectrum of oxide mixtures [see Eqn (5)].[55] No correction for diamagnetism was done.

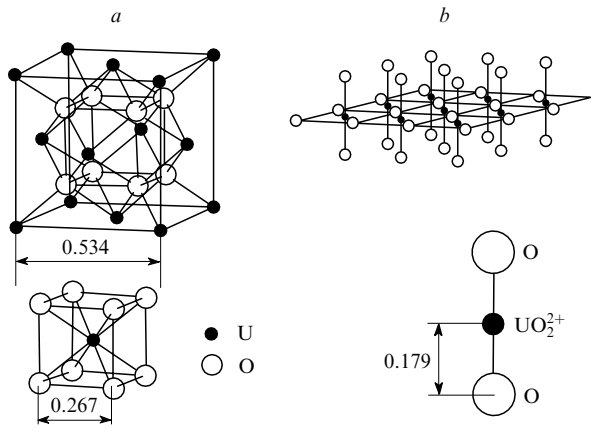

Figure 14. Crystal structure and the local environment of uranium ions in oxides.[5,7]
(*a*) UO_2, (*b*) γ-UO_3. The bond lengths are in nm.

relative intensity I_3 depending on the content of U^{4+} ions has the form

$$I_3 = I_2 - 2(I_2 - I_1) = 2I_1 - I_2. \quad (6)$$

It follows from Fig. 10 that upon an increase in x from 2 to 2.35, the U^{4+} ions disappear from UO_x. This is consistent with X-ray diffraction data indicating that synthetic uranium oxides with $x \to 2.38$, virtually do not contain a structure with the lattice parameters of UO_2 containing eight-coordinate uranium (Fig. 14).[213]

The above dependences (see Fig. 10) can be used to determine the relative contents of different uranium ions in oxides (Table 4). For example, it follows from the data of Table 4 that the oxides U_2O_5 and U_3O_8 mainly contain ions with spectral characteristics close to those of U^{5+} and U^{6+} in 1 : 1 and 1 : 2 ratios, respectively. This does not attest to any violation of the stoichiometric compositions of these oxides, as we are dealing with the formal ionic oxidation states determined from the spectral parameters that reflect the formal number of unbound U5f electrons. More information on the energy distribution of the uranium U5f electrons in oxides can be gained from $O_{4,5}(U)$,[187,189] $M_{III,IV,V}(U)$[191] and $L_{III}(U)$[214] near-edge X-ray absorption spectra. The U, UO and UO_2 species have been studied by high-temperature photoelectron spectroscopy in the gas phase;[215] the results of relativistic Hartree–Fock–Slater theoretical calculations of the electronic structures of these molecules were used to assign the spectral lines to the electrons of some shells.

Table 4. Binding energies (E_b / eV), binding energy differences (ΔE_i / eV) and relative contents of uranium [k (%)] in synthetic uranium oxides.[65,66]

Parameter	UO_2	U_4O_9	U_2O_5	U_3O_8	γ-UO_3
E_b(U5f)	1.9	2.1	2.0	2.1	–
E_b(OVMO)	6.1	6.2	6.0	6.0	6.2
E_b(U6p$_{3/2}$)	–	–	14.4,[b]	–	–
	–	15.7,	15.8,	16.0,	15.7,
	18.0	17.8,	18.0,	18.2,	–
		19.3	19.6	19.4	19.4
ΔE_i(U6p$_{3/2}$)[a]	–	3.6	3.8	3.4	3.7
E_b(U6p$_{1/2}$)	28.5	28.4,	28.9,	29.2,	28.9,
		31.1	31.2	31.1	30.4
E_b(O2s)	23.3,	23.5,	23.5,	23.2,	23.3,
	24.8	25.6	25.7	26.0	25.5
ΔE_i(O2s)	–	2.1	2.2	2.8	2.2
E_b(O1s)	530.5	530.8,	530.5,	530.5,	–
		532.0	531.5	531.5	531.4
ΔE_i(O1s)	–	1.2	1.0	1.0	–
k(U^{4+})	65	9	–	–	–
k(U^{5+})	29	66	50	33	–
k(U^{6+})	6	25	50	67	100

[a] Difference ΔE_i (U6p$_{3/2}$) for the U^{6+} state. [b] Energy corresponding to the additional peak.

b. Structure of the U6p–O2s spectra

In the U6p–O2s binding energy ranges (E_b = ~12–35 eV), a complex fine spectral structure is observed instead of the expected summary atomic spectrum due to the U6p doublet with the spin–orbit splitting ΔE_{sl}(U6p) = 10.0 eV and the O2s lines (see Fig. 8). This structure is more pronounced in the spectrum of γ-UO_3 than in the spectrum of uranium dioxide.[38,45,51,53,65,66,93] Unlike the spectrum of UO_2, the spectrum of γ-UO_3 in the U6p$_{3/2}$ binding energy range (~12–21 eV) displays two clear-cut components. In the U6p$_{1/2}$ spectral range (~27–~35 eV), two components are also observed for these oxides. For oxygen-containing U^{6+} compounds, the presence of two components in the U6p$_{3/2}$ spectrum was explained[45] by splitting of the U6p$_{3/2}$ level of the U^{6+} ion in the asymmetric electric crystal field of ligand ions present in the local environment, which arises on passing from the symmetric structure of the UO_2 dioxide to the asymmetric planar structure of γ-UO_3 (see Fig. 14 *b*).

A structure containing at least two peaks is also observed in the binding energy range of O2s electrons (~21–~27 eV). In the XPS spectrum of γ-UO_3, these peaks are separated by 2.2 eV. These have been attributed[45] to different oxygen ions located in the axial and equatorial positions with respect to the central atom in the uranyl compounds containing a U^{6+} ion. However, it has been noted[66,92,93,103,104] that this explanation does not work for the two peaks observed in this range in the case of UO_2 (see Table 4), because all the oxygen ions in this oxide are chemically equivalent (see Fig. 14 *a*). It should be expected[21,23] that the shifts of the O2s and O1s lines should be commensurable in magnitude. However, the spectrum of UO_2 exhibits a single relatively sharp O1s line, while in the spectrum of γ-UO_3, this line is broadened by 0.6 eV, due to the non-equivalence of two oxygen atoms (see Fig. 8). This single line is also present in the spectra of some uranium complexes.[216] This has led to the conclusion[66,92,93,103,104] that the two peaks observed in the spectrum of γ-UO_3 in the O2s binding energy range cannot be attributed to different types of oxygen ions present in this oxide, as was believed earlier.[45]

Comparison of the binding energy differences between the low-energy ($E_b \approx 12-35$ eV) and core electrons in uranium metal (which has a virtually atomic spectrum in this energy range) and uranium oxides shows that the formation of chemical bonds between uranium and oxygen atoms brings about significant differences between the XPS spectra of the metal and oxides (Table 5). Thus the energy level characteristic of the U6p$_{3/2}$ electrons in the UO_2 spectrum is shifted with respect to the U4f$_{7/2}$ level of uranium metal to lower binding energies by ΔE = 2.3 eV. In the case of γ-UO_3, the corresponding shift of the higher binding energy component equals 2.4 eV and that for the lower binding energy component is 6.1 eV. It is noteworthy that this allows one to observe the shifts of the low binding energy peaks not only for γ-UO_3 but also for UO_2 in which the environment of the uranium ion is symmetric.

Using the data on the causes and mechanisms of formation of the fine structure in the XPS spectra of actinides and other elements[38–40,45,52,65,79] and taking into account the results of theoretical calculations,[24,25,92,93,129–131,137,180,217] Teterin and coworkers[66,92,93,103,104,112] have suggested that the fine structure in the binding energy range $E_b \approx 12-35$ eV of the spectra of uranium oxides is due to IVMO electrons supplied mainly from the filled U6p and O2s AO of neighbouring atoms. This is consistent with the conversion electron spectroscopy data for uranium oxides in this energy range,[218–221] the

Table 5. Binding energy differences (ΔE_i) for various shells of uranium and ligands.[55]

Compound, element	$\Delta E_i = E_k - E_l$ /eV					
	$6p_{3/2} - 6p_{1/2}$	$6p_{3/2} - 6s_{1/2}$ (see [a])	$6p_{3/2} - 4f_{7/2}$	$6s_{1/2} - 4f_{7/2}$ (see [a])	$5d_{5/2} - 4f_{7/2}$	$L2s_{1/2} - L1s_{1/2}$ (see [b])
UO_2	10.5	27.6, 29.4	362.9	335.3, 333.5	283.6	507.2, 505.7
UO_2 (see [57])	10.6	27.8	362.5	334.7	283.8	507.9
UF_4	–	28.2	362.6	334.4	283.6	655.6
UF_4 (see [70])	11.7	–	362.8	–	–	655.4
γ-UO_3	–	–	363.0, 366.7	–	284.0	505.9, 508.1
U_{metal}	10.0	–	360.6	–	283.0	–
U (see [57])	10.0	27.1	360.6	333.5	283.2	–
U_{theor} (see [178])	10.4	31.0	360.9	329.9	283.0	–

[a] The E_i values corresponding to the most intense peaks in the U6s spectra were used. [b] The ΔE_i differences for oxygen and fluorine are given.

structure of the XPS spectra of uranium halides [26, 43, 44, 47, 53, 55, 69, 70, 82, 98, 101, 102, 105, 109, 200, 201] and the results of theoretical calculations.[31, 122, 123, 132–134, 202, 222–233] The formation of IVMO in uranium oxides is confirmed by the X-ray $O_{4,5}$(U) emission [185, 234] and $OL_IL_{II,III}L_{II,III}$-Auger spectroscopy data.[235, 236]

The energetic spectral structure in the U6s, U6p and O2s binding energy range can be illustrated by a diagram reflecting the formation of IVMO in γ-UO_3 in the non-relativistic approximation (Fig. 15). This Figure shows the changes that take place in the IVMO system on passing from the UO_2^{2+} cluster ($D_{\infty h}$ group of symmetry) to the $[UO_2O_4]^{6-}$ cluster (D_{4h} group of symmetry). The spectrum of γ-UO_3 in the same binding energy range is given for comparison. It follows from this diagram that the XPS spectra in this binding energy range reflect the electron distribution in oxides over quasi-atomic and molecular orbitals. The partial contributions of the U6p AO and the O2s AO into each MO characterise the substantial overlap of these uranium and oxygen AO. Although these results were obtained in the non-relativistic approximation, they allow one to identify the spectral lines in the U6$p_{3/2}$ and O2s binding energy ranges. However, complete description of the electronic structure of γ-UO_3 requires performing relativistic calculations (see Section VI).

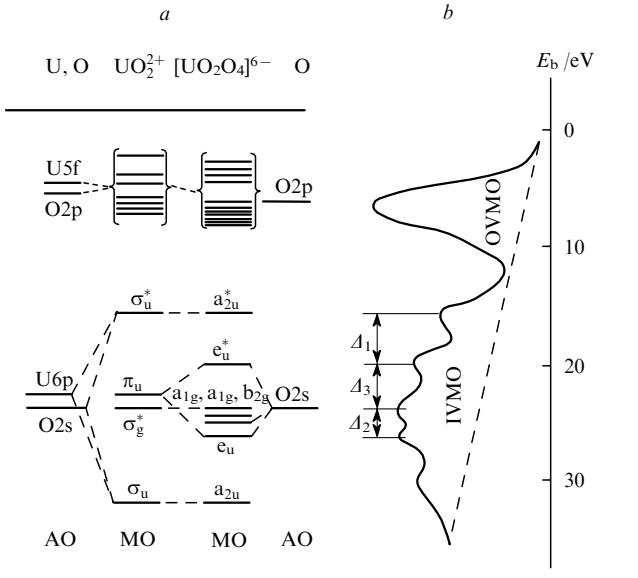

Figure 15. Diagram of MO formation in the UO_2^{2+} and $[UO_2O_4]^{6-}$ clusters ($D_{\infty h}$ and D_{4h} groups of symmetry, respectively) from the studies [25, 26, 102] (*a*) and X-ray photoelectron spectrum of the oxide γ-UO_3 (*b*).
The dashed line in Fig. 15 *b* corresponds to the background.

Analysis of the spectral structures of UO_2 and γ-UO_3 caused by MO electrons in the $\sim 0-35$ eV binding energy range suggests that the fine structure in the spectra of the U_4O_9, U_2O_5 and U_3O_8 oxides in this energy range can be considered to be a superposition of the spectra of simple oxides. It was shown [66] that the spectral structure in the U6$p_{3/2}$ energy range due to the UO_2^{2+} uranyl group becomes more pronounced as the oxygen coefficient x increases. Simultaneously, an additional line appears in the O2s energy range and the intensity of the U5f line diminishes.

c. XPS spectra of synthetic uranium oxides in the core electron binding energy range

The XPS spectra of UO_x oxides in the binding energy range of the core levels ($E_b \approx 40-1250$ eV), which exhibits the lines for U4p, U4d, U4f, U5s, U5p, U5d and U6s electrons, have been extensively studied.[47, 55, 66, 103, 105, 108, 109, 210, 215, 229]

The results are presented in Table 6 and in Figs 16–18. As the oxygen coefficient x for the synthetic oxides UO_x increases in the $2 < x \leqslant 3$ range, the core level binding energy grows by $\sim 0-1.5$ eV (see Table 6). This is due to the increase of uranium oxidation state on going from UO_2 to γ-UO_3. All of the spectra in this energy range show a complex fine structure; in some cases, this precludes precise determination of the binding energies and line intensities for some levels. Nevertheless, as has been mentioned above, the structure itself is characteristic of particular oxides and can be used for identification and for study of their properties.

Table 6. Binding energies (E_b /eV), line widths at half maximum (Γ /eV), spin–orbit splittings (ΔE_{sl} /eV), distances from the basic lines to satellites (ΔE_{Sat} /eV) and their relative intensities [I_{Sat}/I_0 (%)] for synthetic uranium oxides.[66]

Parameter	UO_2 (see [a])	U_4O_9	U_2O_5	U_3O_8	γ-UO_3
$E_b(U4f_{7/2})$	380.9	381.4	381.6	381.9	382.4
$\Gamma(U4f_{7/2})$	2.1	2.8	2.6	2.1	1.5
$E_b(U4f_{5/2})$	391.8	392.3	392.5	392.6	393.1
ΔE_{sl}(U4f)	10.9	10.9	10.9	10.7	10.7
ΔE_{Sat}	– 6.9	4.2, 6.7	– 7.8	3.8, 7.3	3.9, 9.5
I_{Sat}/I_0 (see [b])	25	10	10	10	29
$E_b(U4d_{5/2})$	739.3	740.4	740.6	740.4	741.0
$\Gamma(U4d_{5/2})$	5.9	9.8	5.9	5.1	5.1
$E_b(U4d_{3/2})$	781.6	782.2	782.7	782.4	783.3
ΔE_{sl}(U4d)	42.3	41.8	42.1	42.0	42.3
$E_b(U5d_{5/2})$	97.3	97.7	97.9	98.0	98.4
$\Gamma(U5d_{5/2})$	2.5	2.7	2.9	2.0	1.8
$E_bU5d_{3/2}$	105.5	106.4	105.9	106.6	107.1
ΔE_{sl}(U5d)	8.2	8.7	8.0	8.6	8.7
ΔE_{Sat}	– 7.1	4.6	3.0, 5.4	4.2	3.8, 7.8
$E_b(U5p_{3/2})$ (see [c])	197.4	–	197.5	198.2	199.1
$\Gamma(U5p_{3/2})$	7.8	–	7.0	6.8	7.4
$E_b(U4p_{3/2})$ (see [c])	1046.7	–	–	–	1048.0
$\Gamma(U4p_{3/2})$	7.4	–	–	–	6.6
E_b(U6s) (see [d])	46.5, – 75.0	–	–	–	47.5, 50.4, 74.4

[a] The binding energies are given for $UO_{2.06}$. [b] The ratio of the satellite intensity I_{Sat} to the basic line intensity I_0. [c] The binding energies were measured as the weight average of the complex line. [d] Binding energies for the most intense components.

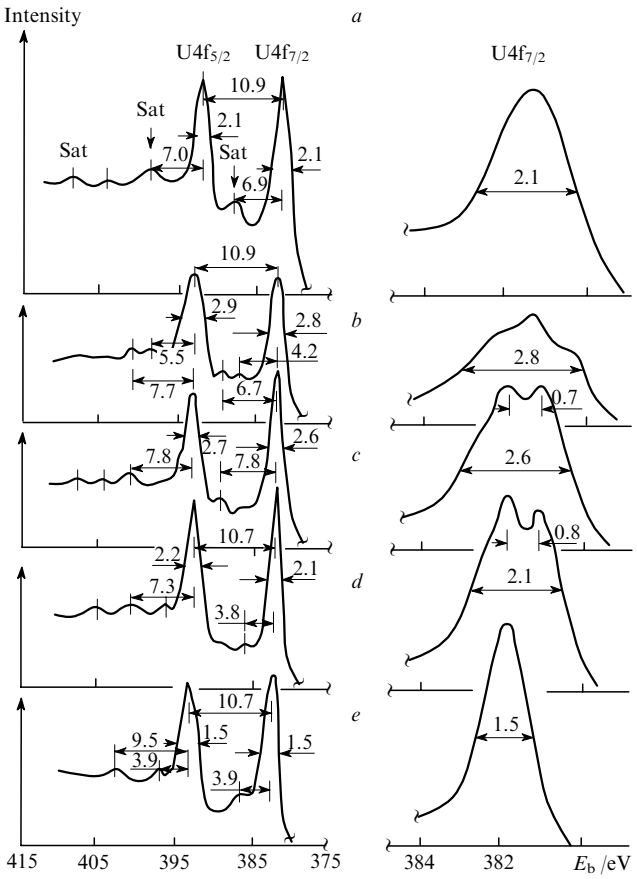

Figure 16. XPS spectra of synthetic uranium oxides in the U4f binding energy range.[66]
(*a*) UO_2, (*b*) U_4O_9, (*c*) U_2O_5, (*d*) U_3O_8, (*e*) γ-UO_3; Sat is satellite. The $U4f_{7/2}$ lines are shown separately for clarity.

d. The spectra of U4f electrons

The U4f XPS spectra of uranium oxides exhibit shake up satellites.[66, 105, 151, 237, 238] These spectra, like the spectra of U5f electrons, show that the U_2O_5 and U_3O_8 oxides contain two types of uranium ions.[66] However, these oxides are not mere mechanical mixtures of the simple oxides UO_2 and UO_3, they are complex phases whose lattices contain interrelated uranium and oxygen ions of two types.[55]

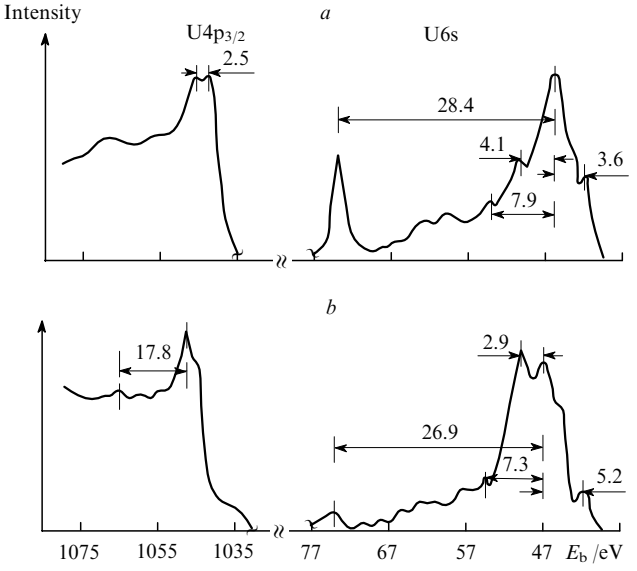

Figure 17. XPS spectra of uranium oxides in the U6s and U4p binding energy ranges.[56]
(*a*) UO_2, (*b*) γ-UO_3.

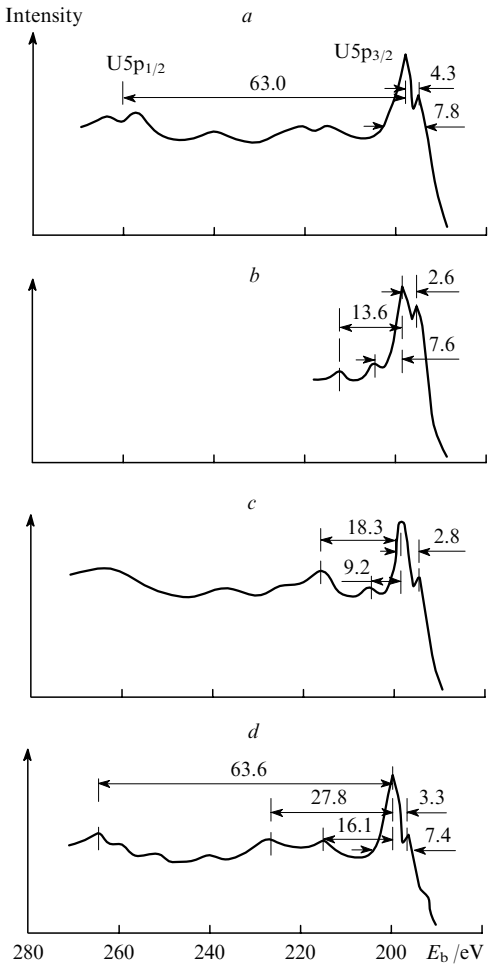

Figure 18. XPS spectra of uranium oxides in the U5p binding energy range.[56, 66]
(*a*) UO_2, (*b*) U_2O_5, (*c*) U_3O_8, (*d*) γ-UO_3; $\Delta E_{sl}(U5p) = 65$ eV.[20]

The spectral characteristics suggest that these complex oxides contain U^{5+} and U^{6+} ions. In this approximation, the $U4f_{7/2}$ lines of the given oxides were decomposed into two components (Fig. 16) and the contribution of each of the ions was quantitatively estimated.[55, 66] It was found that U_2O_5 and U_3O_8 contain U^{5+} and U^{6+} ions in 1 : 1 and 1 : 2 ratios, respectively, which agrees with the XPS spectra of the U5f electrons in these oxides. In addition, these conclusions are confirmed by the intensity ratio of the components of the $U4f_{7/2}$ lines and the corresponding $U4f_{7/2}$ binding energies found from decomposition of these lines (for U_2O_5, 381.5 and 382.3 eV; for U_3O_8, 381.5 and 382.4 eV).

The data on the contents of the two types of uranium ion in these oxides[55, 66] are in line with XPS data,[38, 60, 105] magnetic measurements,[211] and, in the case of U_3O_8, also with X-ray diffraction data.[5] The UO_2 and γ-UO_3 oxides contain U^{4+} and U^{6+} ions, respectively,[55, 66] which is also consistent with X-ray diffraction data.[5]

The binding energy distances between the satellites and the basic U4f lines in the XPS spectra reflect the MO structure and are characteristic of particular oxides (see Fig. 16). Thus in the spectrum of UO_2, the distance from the low energy satellite to the basic $U4f_{7/2}$ line is 6.9 eV, while the spectrum of γ-UO_3 exhibits two satellites spaced by 3.9 eV and 9.5 eV from the basic

$U4f_{5/2}$ component of the doublet. The spectra of other oxides exhibit more complicated satellite structures, which can be correlated to a certain approximation with the satellite structures in the spectra of UO_2 and γ-UO_3.

e. The spectra of the U5d and U4d electrons

The U5d binding energy range of the spectra of the oxides under study [55, 66, 103, 104] exhibits, instead of the expected doublet caused by the spin – orbit splitting, a more complicated fine structure. The $U5d_{3/2}$ component is broadened compared to the $U5d_{5/2}$ line, the binding energy difference between these electrons increasing on passing from UO_2 to UO_3. This is not related to the change in the spin – orbit splitting [(ΔE_{sl}(U5d) = 8.6 eV for U metal [57]] following the increase in the uranium oxidation number, but is due, first of all, to the multiplet splitting. Since the U^{6+} ion in γ-UO_3 does not contain unpaired electrons, this splitting should not be manifested in the XPS spectrum in the U5d binding energy range. Therefore, the value ΔE_{sl}(U5d) = 8.7 eV is closer to the true value of the spin – orbit splitting (see Table 6). Other reasons for broadening of the U5d doublet may include the superimposition of the shake up satellites onto the $U5d_{3/2}$ component and the dynamic effect.

In the spectra of deeper U4d electrons, the spin doublet lines are much broader than the U4f lines,[55, 238] which complicates decomposition of the U4d line of complex oxides into separate components. Nevertheless, the measured spin – orbit splittings for the U4d level for uranium dioxide and trioxide are equal and amount to 42.3 eV [ΔE_{sl}(U4d) = 42.3 eV for U metal [57]]. The observed change in the ΔE_{sl} value for complex oxides is attributable to the structure caused by the presence of uranium in different oxidation states.

f. The spectra of the U6s, U5p and U4p electrons

The XPS spectra of uranium and its compounds exhibit a complex structure in the U6s binding energy range.[55, 56, 106] Indeed, instead of the expected single relatively sharp line, the spectra of UO_2 and γ-UO_3 contain a complex fine structure in an energy range covering up to $\sim$40 eV (see Fig. 17).[56]

The spectral structure observed in the U6s range has much in common with the XPS structure observed for the Th6s electrons (see Fig. 2). Therefore, this structure has been suggested [55, 56] to be mostly due to the dynamic effect giving rise to the final states of the type $U6s^1 6p^6 5f^n 6d^m \rightleftharpoons U6s^2 6p^4 5f^n 6d^{m+1}$, because E_b(U6s) $\approx$ 2 E_b(U6p). This is in qualitative agreement with the results of calculation [32] of the U6s spectrum performed with the assumption that uranium occurs in the U^{6+} state.

A similar analysis of the reasons of formation of the fine spectral structure has also been carried out [56, 66] for the U5p and $U4p_{3/2}$ electrons (see Figs 17, 18). This structure in the spectra of uranium oxides in the U5p binding energy range induces splitting of the $U5p_{3/2}$ line and substantial smearing of the $U5p_{1/2}$ component of the doublet [(ΔE_{sl}(U5p) = 65 eV [20]. A similar situation is observed in the $U4p_{3/2}$ energy range [56] (see Fig. 17). Comparison of the magnitudes of splitting of the main components in the U6s, U5p and $U4p_{3/2}$ spectra has shown that these values change insignificantly as the electron binding energy increases from $\sim$50 to $\sim$1000 eV and, hence, the fine structure cannot be mainly due to the effect of the crystal field, as has been suggested [79] for the electrons of some shells.

Since the fine structure observed in the range of core levels for thorium dioxide containing no unpaired Th5f electrons has much in common with the corresponding spectral structure of UO_2, it has been suggested [56, 66] that this structure in the spectra of U5p and U4p electrons of UO_x cannot be related, to a large extent, to the multiplet splitting or many-body perturbation, but is mainly due to the dynamic effect, resulting in the final states of the types $U5p^5 5d^{10}(6s^2 6p^6)5f^n \rightleftharpoons U5p^6 5d^8(6s^2 6p^6)5f^{n+1}$ and $U4p^5 4d^{10}(4f^{14}).5s^2(5p^6 5d^{10} 6s^2 6p^6)5f^n np^0 \rightleftharpoons U4p^6 4d^9(4f^{14})5s^1(5p^6 5d^{10} 6s^2 6p^6).5f^n np^1$, respectively.[55, 56] This structure is superimposed by the satellites corresponding to many-body perturbation. This further complicates the spectral structure.

2. Uranyl compounds

Uranyl compounds contain the UO_2^{2+} group coordinated by four, five or six atoms of the ligand L (L = O, F, Cl, Br, *etc.*) in the equatorial plane.[239–241] The U – O bond length (R_{U-O}) in the UO_2^{2+} group of these compounds is usually smaller than the distances from the uranium atoms to the neighbouring ligand atoms located in the equatorial plane.[7, 53, 71–73, 240–243] In recent years, researchers' attention has been focused on the calculation of the electronic structures of uranyl derivatives (Refs 24, 26–28, 36, 42, 93, 102, 123, 130, 204, 233) which has been stimulated by the appearance of numerous publications devoted to X-ray photoelectron spectra of these compounds (Refs 26, 42–48, 55, 82, 94–97, 102, 109, 216, 244). It should be noted that only the actinyl group AnO_2^{n+} (An = U, Np, Pu, Am, *etc.*) has an almost linear structure, whereas a molecule of gaseous ThO_2 is bent at an angle of 122 $\pm$ 2° (see Ref. 245).

A number of uranyl compounds have been studied by XPS (Table 7) in order to establish the relationship of fine spectral structure parameters with the structure of these compounds and the nature of the chemical bond in them.[47, 55] To confirm the stoichiometric compositions and the structures of these compounds, the spectra of all elements contained in their molecules were analysed. For identification of XPS lines of uranyl compounds in the low binding energy range, the spectra of ligands based on $Ni(NO_3)_2$, NaOAc, Na_2CO_3 and CsCl have also been studied.

a. The spectra of uranyl compounds in the low binding energy range

As noted above, the XPS spectra of highly symmetric U^{4+} compounds (see Fig. 14), for example, UO_2 (see Fig. 8) and UF_4 (Fig. 19), containing U5f electrons not involved in the chemical bond, exhibit a sharp line at around a zero binding energy.

The spectra of uranyl compounds containing U^{6+}, for example, γ-UO_3 (see Fig. 8) and UO_2F_2 (see Fig. 19), do not exhibit this line. The absence of the U5f line in the XPS spectra of uranyl compounds directly confirms that the uranium oxidation state is

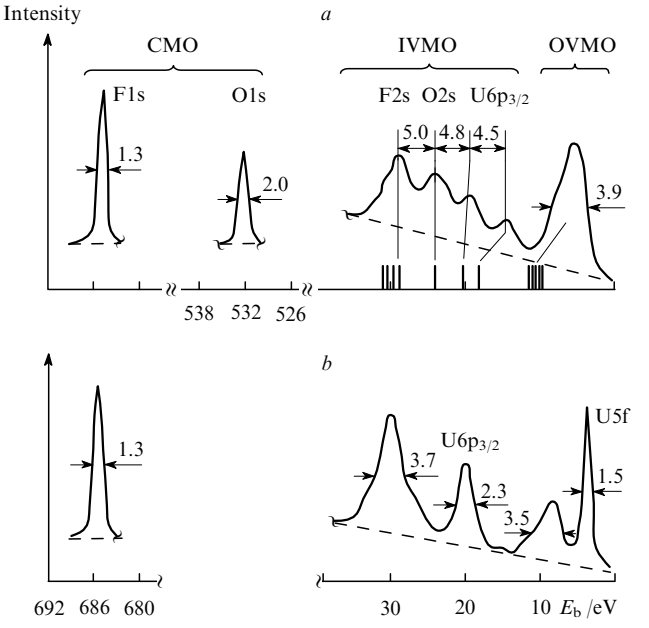

Figure 19. XPS spectra of uranium compounds.[98]
(*a*) UO_2F_2, (*b*) UF_4. Vertical lines below the spectrum: (*a*) results of non-relativistic calculation (X_α-DV [102]) of the electronic structure of the $[UO_2F_6]^{4-}$ cluster (D_{6h} group of symmetry) for R_{U-O} = 0.174 nm, R_{U-F} = 0.243 nm. The dashed lines show the background.

Table 7. Binding energies (E_b/ eV), binding energy differences (ΔE_i/ eV), bond lengths in the UO_2^{2+} groups (R_{U-O}/ nm), distances from the basic lines to the satellites (ΔE_{Sat}/ eV) and their relative intensities [I/I_0 (%)].[47]

Compound	E_b(OVMO) (see [a])	E_b(U6p$_{3/2}$)	ΔE_i(U6p$_{3/2}$)	R_{U-O} (see [b])	E_b(O2s)	ΔE_i(O2s)	E_b(U6p$_{1/2}$) (see [c])	E_b(U6s) (see [a])	E_b(O1s)	E_b(U5d$_{5/2}$)	E_b(U5d$_{3/2}$)	ΔE_{Sat} (see [d])	I/I_0	E_b(U5p$_{3/2}$) (see [c])
UF_4	9.0	20.1						48.3		99.1	107.1	7.0	10	195.9, 199.8, 203.0
UO_2F_2	6.7	15.6, 20.1	4.5	0.174	22.3, 24.9	2.6		49.3	532.4	99.2	107.9	4.1	5	200.2
$K_4UO_2(CO_3)_3$	5.1	14.6, 19.8	5.2	0.172	22.7, 24.4	1.7	28.8, 31.2	47.1	531.4	98.1	106.5	3.4	20	195.0, 198.5, 200.6
$UO_2(OAc)_2 \cdot 2H_2O$	6.0	15.6, 19.8	4.2	0.174	23.3, 25.3	2.0	28.4, 31.4	49.0	532.3	98.8	107.4	3.6	8	199.8, 205.4
$NaUO_2(OAc)_3$	5.8	15.1, 20.0	4.9	0.173	22.3, 25.1	3.0	28.6	48.2	532.2	98.5	107.3	3.8	19	199.5
$CsUO_2(OAc)_3$	5.6	15.2, 20.1	4.9	0.173				49.5	532.1	98.4	106.9	3.4	20	193.8, 199.8, 204.0
$UO_2(NO_3)_2 \cdot 2H_2O$	6.4	19.9	4.0	($\leqslant$0.175)	26.0, 27.5	1.5	29.0, 31.4	48.0	533.6	99.2	107.7	3.2	20	202.2, 204.1
$CsUO_2(NO_3)_3$	6.9	20.1	3.5	($\leqslant$0.176)	24.6, 27.2	2.6	29.9, 32.2	49.0	533.9	99.5	108.1	3.5	20	200.2, 203.0
$RbUO_2(NO_3)_3$	6.5	20.3	3.5	($\leqslant$0.176)	25.8, 27.3	1.5	29.7, 32.5	50.3	533.6	99.9	107.9			200.4
$UO_2(DMSO)_5(ClO_4)_2$	6.0	17.1, 20.9	3.8	0.176	25.6, 27.4	1.8	30.2, 32.5	46.7	532.4	98.8	107.6	2.5	20	190.8, 199.8, 204.9
$K_4UO_2(OO)_3 \cdot 5H_2O$	4.9	14.5, 19.5	5.0	0.172	24.9, 26.7	1.8	30.7		531.5	97.2	106.1	3.4	20	190.7, 198.4
$CaUO_2O_2$	5.2	15.7, 17.2	1.5	0.191	21.6		29.2, 30.0		530.2	97.6	106.3	4.0	10	195.3, 199.0
$K_3UO_2F_5$	6.7	15.5, 19.5	4.0	0.175	22.6, 24.5	1.9	30.0, 33.0	47.6	531.9	99.2	107.8	2.4	8	197.4, 200.3
$Cs_3UO_2F_5$	5.9	15.3, 19.3	4.0	0.175				50.7	531.6	98.9	107.4	2.8	5	191.8, 198.4
$Cs_2UO_2Cl_4$	5.6	15.4, 19.8	4.4	0.174	24.5, 26.5	2.0	30.9, 32.8	48.2	531.6	98.1	106.9	3.3	20	
$Cs_2UO_2Br_4$	4.6	15.2, 19.8	4.6	0.173			30.8, 32.9	49.9	532.4	97.8	106.9	3.7	20	199.4, 203.7

Compound	E_b(U5p$_{1/2}$) (see [a])	E_b(U4f$_{7/2}$)	ΔE_{Sat} (see [d])	E_b(U4f$_{5/2}$)	ΔE_{Sat} (see [d])	I/I_0	E_b(U4d$_{5/2}$)	E_b(U4d$_{3/2}$)	E_b(U4p$_{3/2}$) (see [c])	L (nl_j)	E_b[L (nl_j)]	L (nl_j)	E_b[L (nl_j)]
UF_4	264.5	382.7	7.3	393.5	6.9	20	741.2	783.6	1048.1				
UO_2F_2	264.1	383.4	3.5	394.1	3.5	10	741.5	784.0	1048.2			F2s,1s	29.9, 685.3
$K_4UO_2(CO_3)_3$	263.8	382.1	3.7	392.9	3.7	18	740.6	782.7	1047.1	K3p$_{3/2}$,3s,2s	16.9, 32.8, 377.4		
$UO_2(OAc)_2 \cdot 2H_2O$	261.4	382.7	3.7	393.6	3.8	12	741.3	783.9	1047.5				
$NaUO_2(OAc)_3$	264.6	382.6	3.6	393.5	3.5	20	740.1	783.1	1047.1	Na2p$_{3/2}$,2s,1s	30.5, 63.5, 1071.6		
$CsUO_2(OAc)_3$		382.4	3.5	393.3	3.5	18		782.8	1048.3	Cs5p$_{3/2}$,5s,4s	11.0, 23.9, 230.2		
$UO_2(NO_3)_2 \cdot 2H_2O$		383.1	3.3	394.0	3.3	18	741.9	784.8	1048.7			N1s	407.8
$CsUO_2(NO_3)_3$	264.7	383.3	3.5	394.1	3.6	16		783.6	1048.1	Cs5p$_{3/2}$,5s	10.8, 24.1	N1s	407.9
$RbUO_2(NO_3)_3$		383.0	3.4	393.8	3.4	18	742.0	784.0	1049.0	Rb4p$_{3/2}$,4s	14.2, 29.7	N1s	407.8
$UO_2(DMSO)_5(ClO_4)_2$		382.9	2.8	393.6	2.8	17	741.4	783.5	1051.8	S3p,2s	12.0, 230.8	Cl3s,2p$_{3/2}$	15.0, 208.1
$K_4UO_2(OO)_3 \cdot 5H_2O$	266.9	381.3	4.2	392.2	4.0	17	739.6	781.8	1055.7	K3p$_{3/2}$,3s,2s	17.2, 33.1, 377.5		
$CaUO_2O_2$	261.0	381.6	3.7	392.4	3.8	8	740.4	782.8	1047.3	Ca3p$_{3/2}$,3s	25.0, 44.2		
$K_3UO_2F_5$	262.8	383.2	2.4	394.1	2.4	7	741.8	784.0	1049.2	K3p$_{3/2}$,3s	17.1, 33.1	F2s,1s	28.5, 684.2
$Cs_3UO_2F_5$		382.8	2.8	393.6	2.8	5		783.1	1046.5	Cs5p$_{3/2}$,5s	10.3, 23.3	F2s,1s	28.1, 683.8
$Cs_2UO_2Cl_4$		382.1	3.7	393.0	3.8	15		783.1	1044.9	Cs5p$_{3/2}$,5s	10.2, 23.6	Cl3s,2p$_{3/2}$	15.8, 198.8
$Cs_2UO_2Br_4$		381.7	3.7	392.5	3.9	25		783.3	1047.6	Cs5p$_{3/2}$,5s	10.3, 23.7	Br4s,3d$_{5/2}$	26.4, 69.1

[a] Weight average binding energies. [b] Determined upon estimation of the bond lengths in the UO_2^{2+} groups on the basis of relation (8). The values in parentheses are given with an accuracy of $\pm$0.002 nm. [c] The E_b values for the peaks in the corresponding binding energy ranges. [d] ΔE_{Sat} for the most intense satellites.

Table 8. Symmetry of the environment of UO_2^{2+} in compounds, binding energy differences (ΔE_i, Δ_i /eV) for various electronic levels, $U-O_{ax}$ bond lengths (R_{U-O} /nm) in UO_2^{2+} and distances from uranium atoms to equatorial atoms of the ligands (R_{U-L} /nm).[94]

Compound	Cluster	Group of symmetry	n_O/n_L (see [a])	ΔE_1	ΔE_2	Δ'_1	Δ_1	Δ'_2	Δ_2	R_{U-O} (see [b,c])	R_{U-L} (see [b,c])	Symmetry of the environment of UO_2^{2+} (see [b,d])
γ-U (**1**)	UO_8^{12-}	O_h		360.6	–	–	–	–	–		0.297 [e]	
UO_2 (**2**)	$[UO_2O_6]^{10-}$	D_{6h}	2:6	362.9 [f]	–	2.3	2.9	–	–	0.237		
$Ca(UO_2)O_2$ (**3**)	$[UO_2O_6]^{10-}$	D_{6h}	2:6	365.9	364.4	5.3	6.1	3.8	–	0.191	0.229	S_6
$CsUO_2(NO_3)_3$ (**4**)	$[UO_2O_6]^{10-}$	D_{6h}	2:6	(367.0) [g]	363.2	(6.4)	7.4	2.6	4.1	0.180	0.250	D_{3h} (C_3)
$RbUO_2(NO_3)_3$ (**5**)	$[UO_2O_6]^{10-}$	D_{6h}	2:6	(367.2)	362.7	(6.6)	8.0	2.1		0.178(2)	0.248(1)	D_{3h} (C_3)
$UO_2(NO_3)_2(H_2O)_2$ (**6**)	$[UO_2O_6]^{10-}$	D_{6h}	2:6	(367.4)	363.2	(6.8)	7.4	2.6	3.5	0.176(7) [h]	0.248(5)	C_{2v}
$K_4UO_2(CO_3)_3$ (**7**)	$[UO_2O_6]^{10-}$	D_{6h}	2:6	367.5	362.3	6.9	7.6	1.7	3.0	(0.175)	(0.260)	
$UO_2(OAc)_2(H_2O)_2$ (**8**)	$[UO_2O_6]^{10-}$	D_{6h}	2:6	367.1	362.9	6.5	7.2	2.3	3.1	0.172	0.250	C_{2v} (C_2)
$NaUO_2(OAc)_3$ (**9**)	$[UO_2O_6]^{10-}$	D_{6h}	2:6	367.5	362.6	6.9	–	2.0	3.5	0.171	0.249	D_{3h} (C_3)
$CsUO_2(OAc)_3$ (**10**)	$[UO_2O_6]^{10-}$	D_{6h}	2:6	367.2	362.3	6.6	8.0	1.7	3.5	(0.178)	(0.261)	
$K_4UO_2(CO)_3 \cdot 5H_2O$ (**11**)	$[UO_2O_6]^{10-}$	D_{6h}	2:6	366.8	361.8	6.2	7.9	1.2	3.3	(0.182)	(0.270)	
$UO_2(DMSO)_5(ClO_4)_2$ (**12**)	$[UO_2O_5]^{8-}$	D_{5h}		365.8	362.0	5.2	5.9	1.4	3.1	(0.192)	(0.266)	
UO_2F_2 (**13**)	$[UO_2F_6]^{4-}$	D_{6h}	2:6	367.8	363.3	7.2	–	2.7	3.2	0.174(2)	0.243(2)	S_6
UF_4 (**14**)	UF_8^{4-}	D_{4d}		362.6 [f]	–	2.0	2.5	–	–		0.229(3)	
$K_3UO_2F_5$ (**15**)	$[UO_2F_5]^{3-}$	D_{5h}	2:5	367.7	363.7	7.1	–	3.1	3.5	0.176(3)	0.224(3)	D_{5h}
$Cs_3UO_2F_5$ (**16**)	$[UO_2F_5]^{3-}$	D_{5h}	2:5	367.5	363.5	6.9	–	2.9	3.5	(0.175)	(0.239)	D_{5h}
γ-UO_3 (**17**)	$[UO_2O_4]^{6-}$	D_{4h}	2:4	366.7	363.0	6.1	7.1	2.4	3.2	0.179(6)	0.230(5)	
$Cs_2UO_2Cl_4$ (**18**)	$[UO_2Cl_4]^{2-}$	D_{4h}	2:4	366.7	362.3	6.1	7.4	–	–	0.181	0.262	D_{4h} (D_{2h})
$Cs_2UO_2Br_4$ (**19**)	$[UO_2Br_4]^{2-}$	D_{4h}	2:4	366.5	361.9	5.9	7.6	–	–	0.169	0.281	D_{4h}

Note. The ΔE_1, ΔE_2, Δ'_1, Δ_1, Δ'_2, Δ_2 parameters are shown in Fig. 23. They have been found using the values ΔE_U [$\Delta E(U6p_{3/2}) = 360.6$ eV, $\Delta E(U6p_{1/2}) = 350.6$ eV], $\Delta E_O = 508.1$ eV, $\Delta E_F = 655.3$ eV, $\Delta E(U6p_{3/2} - O2s) = 2.1$ eV. The ΔE_1 and ΔE_2 values were measured to an accuracy of ±0.2 eV; the Δ'_1, Δ_1, Δ'_2, Δ_2 values, to an accuracy of ±0.3 eV. [a] Ratio of the number of oxygen atoms located in the axial position (O_{ax}) to the number of ligand atoms located in the equatorial plane. [b] Data of the studies [240–242] [c] The R_{U-O} values given in parentheses were measured to an accuracy of ±0.002 nm, the R_{U-L} values, to an accuracy of ±0.004 nm. [d] Experimental results. [e] Bond length between the closest uranium atoms in metallic γ-U.[243] [f] For UO_2 and UF_4, the ΔE_i and Δ_i differences are shown in Fig. 24. [g] The values in parentheses are ΔE_1 determined using relations (9) and (10). [h] The average R_{U-O} and R_{U-L} values are underlined.

six.[96,98] The presence of the UO_2^{2+} group may be indicated, in particular, by the structure of the XPS spectrum in the U6p and O2s ranges. Thus in the fluoride UF_4, the uranium ion occurs in a relatively symmetric environment formed by fluorine atoms (D_{4d} group of symmetry). In this case, as for UO_2, the XPS spectrum of the $U6p_{3/2}$ electrons exhibits a single line (see Fig. 19). The uranium environment in the UO_2F_2 molecule is less symmetric (D_{6h} group of symmetry), and the spectrum shows two components of the $U6p_{3/2}$ line. The spectra of UO_2F_2 and UF_4 exhibit fine structure over the whole U6p and O2s-, F2s binding energy ranges (see Fig. 19 [246–248]). The O2s and F2s lines in the XPS spectra of these compounds are much broader than the corresponding O1s and F1s lines and exhibit a fine structure. The binding energy difference $\Delta E_i(6p_{3/2} - 4f_{7/2}) = 362.6$ eV for UF_4 is much greater than the similar value $\Delta E_i = 360.6$ eV for uranium metal (Table 8, see also Table 5). This is consistent with the assumption that the $U6p_{3/2}$ line in the spectrum of UF_4 is not atomic, but is due to electrons of an antibonding MO. Therefore, it has been suggested [47,55,246–248] that the structure of low energy spectra of UF_4 and UO_2F_2 is mainly due to the effective formation of IVMO largely composed of U6p, O2s and F2s AO. In the case of UO_2F_2, this is in qualitative agreement with the results of calculation of the electronic structure of the $[UO_2F_6]^{4-}$ cluster (D_{6h} group of symmetry).[246–248]

The low binding energy region of the XPS spectrum of $Cs_2UO_2Cl_4$ shows a more complicated structure than the spectrum of UO_2F_2, due to the Cs5p and Cs5s lines present in this energy range (Fig. 20). The line for the Cl3s electrons that belong to chlorine atoms arranged in the equatorial plane occurs in the binding energy range of the U6p electrons, which implies a more essential involvement of the Cl3s AO, together with the $U6p_{3/2}$ AO, in the formation of IVMO than in the case of the F2s and $U6p_{3/2}$ fluorine and uranium AO.[26,47]

The results of non-relativistic SCF X_α-SW calculation [26] for the electronic structure of the $[UO_2Cl_4]^{2-}$ cluster (D_{4h} group of symmetry), which mimics the local environment of uranium in $Cs_2UO_2Cl_4$ molecules, provide a qualitative interpretation of the low binding energy spectrum of the compound under consideration (see Fig. 20). The energy range of OVMO, mainly consisting of the U5f, U6d, O2p and Cl3p AO, covers 3.9 eV, which is

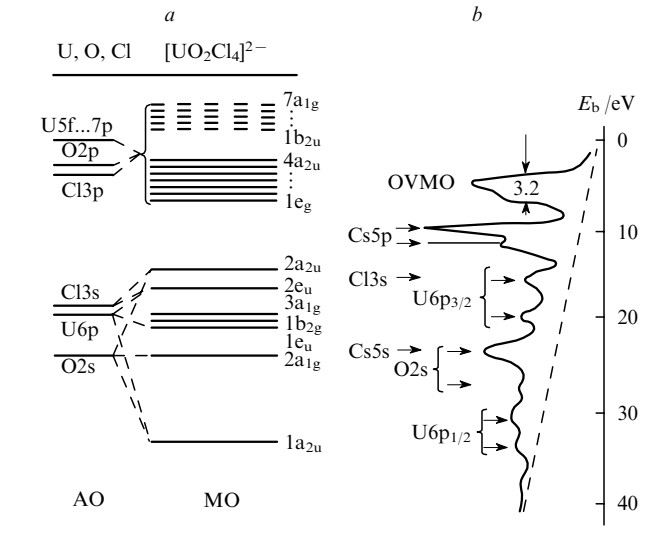

Figure 20. Diagram of MO in the $[UO_2Cl_4]^{2-}$ cluster (D_{4h} symmetry) based on the data of X_α-SW calculations (*a*) and XPS spectrum of $Cs_2UO_2Cl_4$ (*b*).[26,47] The dashed line in Fig. 20 *b* shows the background.

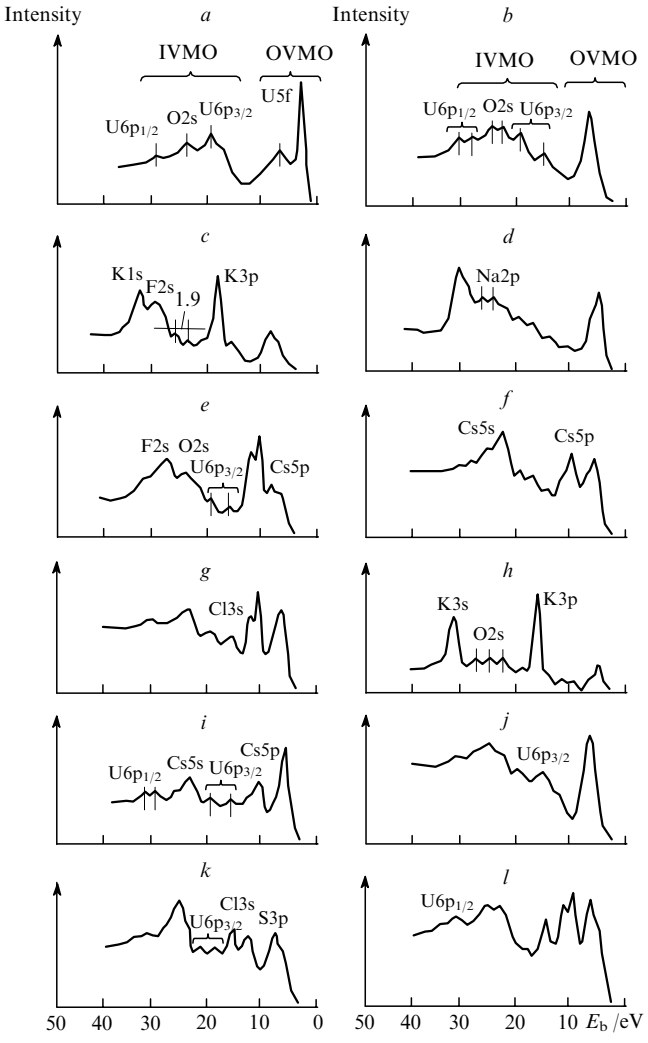

Figure 21. Low-energy range of the XPS spectrum of oxygen-containing uranium compounds.[26,47]
(*a*) UO_2, (*b*) $UO_2(OAc)_2 \cdot 2H_2O$, (*c*) $K_3UO_2F_5$, (*d*) $NaUO_2(OAc)_3$, (*e*) $Cs_3UO_2F_5$, (*f*) $CsUO_2(OAc)_3$, (*g*) $Cs_2UO_2Cl_4$, (*h*) $K_4UO_2(CO_3)_3$, (*i*) $Cs_2UO_2Br_4$, (*j*) $UO_2(NO_3)_2 \cdot 2H_2O$, (*k*) $UO_2(DMSO)_5(ClO_4)_2$, (*l*) $CsUO_2(NO_3)_3$.

comparable with the experimental width of these lines in the spectrum, which equals 3.2 eV. In this compound, IVMO are formed efficiently from U6p, O2s and Cl3s AO.

The fine structure caused by the IVMO electrons is observed also in the XPS spectra of other uranyl compounds (Fig. 21).[47] The line near the binding energy zero also corresponding to U5f electrons not involved in chemical bonds is not detected for these compounds. This is in qualitative agreement with the known fact that the oxidation number of uranium in these compounds is six.

The OVMO-related bands in the spectra of uranyl compounds are characterised by FWHM of $\sim 3-4$ eV and by poorly resolved structures (see Fig. 21). The binding energies of these electrons in oxygen-containing uranium compounds measured as weight average values of the components lie in the range of $\sim 5-6$ eV (see Table 7). If fluorine or the NO_3 group are present as ligands, these values are somewhat greater (~ 7 eV).

The XPS spectra of the compounds in question in the IVMO region may become more complicated due to the overlap with the lines due to alkali metal ions. However, these lines can be interpreted rather easily

b. The IVMO spectral structure and the structure of uranyl compounds

In an early stage of the XPS studies of uranyl compounds, it was found[45,47,55,65,66,92,93,104] that the line splitting in the $U6p_{3/2}$ binding energy range [$\Delta E(U6p_{3/2})$] depends on the bond length R_{U-O} in the UO_2 group (Fig. 22). It has been suggested[45] that this splitting is due to the crystal field.

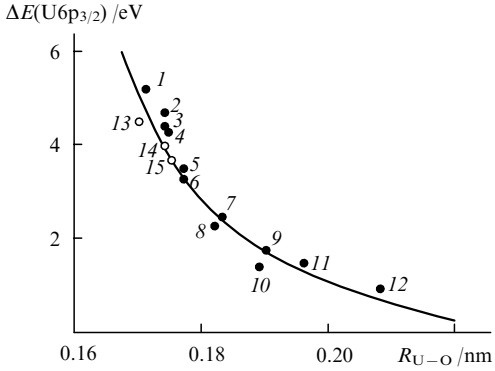

Figure 22. Dependence of splitting $\Delta E_b(U6p_{3/2})$ on the R_{U-O} bond length in the UO_2^{2+} group [see Eqn (7)] for a number of uranium compounds.
(*1*) UO_2CO_3, (*2*) $LiUO_2F_3 \cdot 2H_2O$, (*3*) $NaUO_2F_3 \cdot 2H_2O$, (*4*) $UO_2C_2O_4 \cdot 3H_2O$, (*5*) β-$UO_2(OH)_2$, (*6*) γ-$UO_2(OH)_2$, (*7*) $Li_2U_2O_7$, (*8*) LiU_3O_{10}, (*9*) Li_2UO_4, (*10*) α-Na_2UO_4, (*11*) $CaUO_4$, (*12*) Cr_2UO_6, (*13*) UO_2F_2, (*14*) $UO_2(NO_3)_2 \cdot 2H_2O$, (*15*) γ-UO_3; the light circles show the data from the study;[55] dark circles, from the study.[45]

The dependence of the $\Delta E(U6p_{3/2})$ value on R_{U-O} shown in Fig. 22 can be expressed as follows:

$$\Delta E(U6p_{3/2}) = -1.59 + 0.138(R_{U-O} - 0.149)^{-1}. \quad (7)$$

Hence, the expression for R_{U-O} has the form

$$R_{U-O} = 0.149 + 0.138[\Delta E(U6p_{3/2}) + 1.59]^{-1}. \quad (8)$$

Equation (8) can be used to estimate the R_{U-O} bond lengths in the UO_2^{2+} groups in these compounds (see Table 7).

A more profound understanding of the nature of the fine spectral structure in the low binding energy range of uranium compounds can be gained from theoretical and experimental results which allow one to consider the data on fine XPS spectral structure from a different standpoint.[94,96,97,107–109,245] Comparison of the E_b values for the outer electrons for various uranium compounds does not provide a vivid representation of the dependence of spectral characteristics on the properties and structures of these compounds. Indeed, the $U6p_{3/2}$ binding energies usually change little on passing from one compound to another (see Table 7). Therefore, for elucidating the regular features of the formation of IVMO structure, the binding energy differences between the valence and core electrons (ΔE_i) in these compounds have been considered (see Table 8). The data of Table 8 are illustrated by the MO diagram for the $[UO_2O_6]^{10-}$ cluster (D_{6h} group of symmetry), which reflect the local environment for a large number of oxygen-containing uranyl compounds (Fig. 23). The diagram shows the binding energy differences ΔE_U, $\Delta E_1 - \Delta E_6$, ΔE_O and ΔE_L. The ΔE_i values for uranium metal and its compounds can be measured experimentally. This provides the values Δ_1, Δ_2, Δ_3 and Δ'_1, Δ'_2, Δ'_3, which characterise quantitatively the type of MO (bonding, antibonding, non-bonding) and the degree of participation of the corresponding AO of the neighbouring atoms in the MO formation (see Fig. 23). Thus, the MO structure for uranium compounds can be determined experimentally.

The above results imply that, to a certain approximation, ligand atoms located in the axial positions and in the equatorial

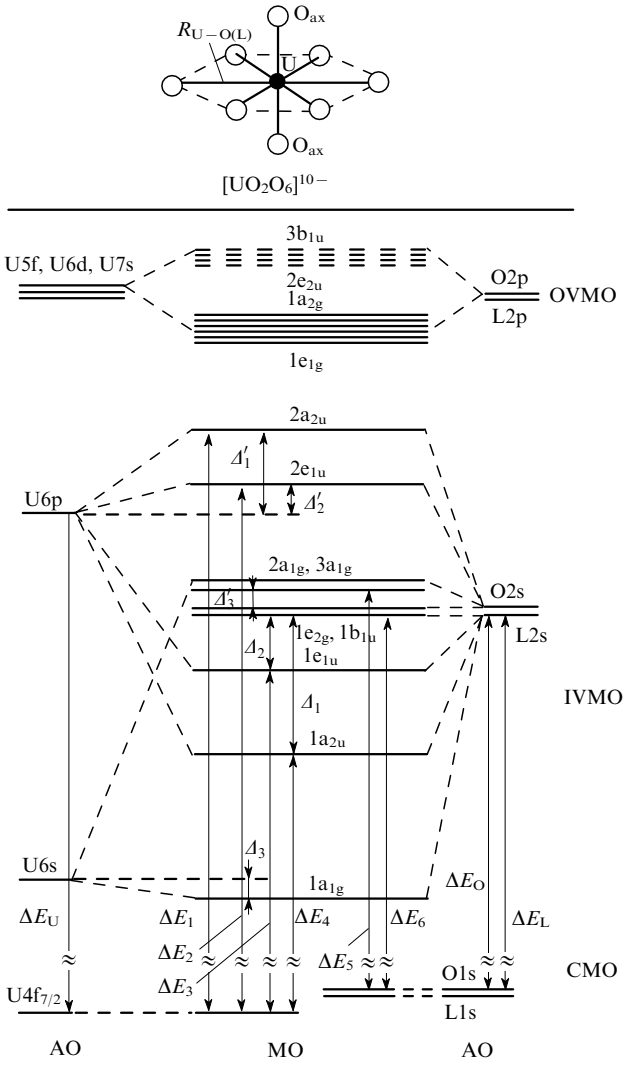

Figure 23. Diagram of MO energy levels in $[UO_2O_6]^{10-}$ (D_{6h} symmetry) constructed using experimental data and results of calculations.[26, 48]
The chemical shifts of the energy levels upon the formation of the cluster from single atoms are not shown. The arrows show the energy differences that can be derived from experimental spectra.

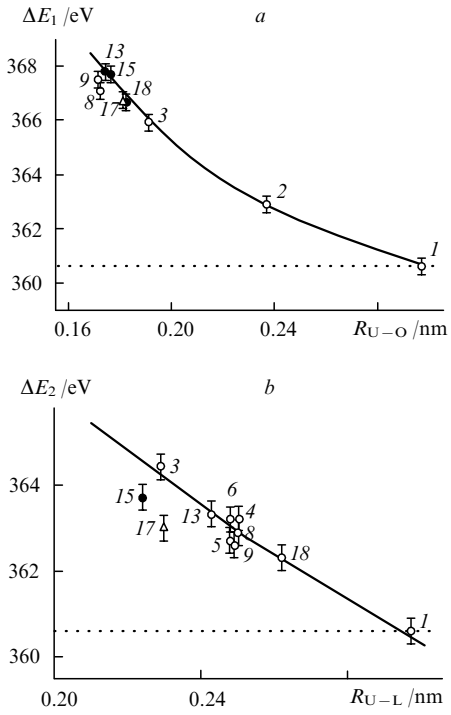

Figure 24. Dependences [see Eqns (9), (11)] of the relative binding energies ΔE_i ($U6p_{3/2} - U4f_{7/2}$) on the $R_{U-O_{ax}}$ bond lengths (*a*) and distances from the uranium atom to the ligand atom in the equatorial plane R_{U-L} (*b*) in the uranyl compounds (the dots are experimental data, the curves correspond to the calculation).[48, 94]
The theoretical curve in Fig. 24 *b* corresponds to oxygen-containing compounds (L = O) with D_{6h} symmetry. Here and in Fig. 25, the numbers of dots correspond to the numbers of compounds in Table 8; the light circles are oxygen-containing ligands; dark circles, F, Cl; triangle, γ-UO_3.

plane around a uranium ion influence in different ways the XPS spectral structure in the low binding energy range. Thus, it is possible to obtain experimental dependences of the spectral structure parameters in the given range on both the R_{U-O} bond length in the UO_2^{2+} group and the R_{U-L} distance between the uranium atom and the ligands L located in the equatorial plane (Fig. 24).

As an illustration of the efficiency of IVMO formation in uranium compounds, Fig. 24 shows also the ΔE_U and ΔE_1 values for the oxide UO_2. It can be seen that the formation of a chemical bond in uranium compounds is accompanied by a substantial relative shift of the upper $2a_{2u}$ IVMO towards lower binding energies (by more than 7.0 eV). This value is 1.5 orders of magnitude higher than the experimental error and can serve as a reliable and convincing proof for the effective formation of IVMO in uranium compounds. The dependence presented in Fig. 24 *a* has the form

$$\Delta E_1 = 356.07 + 0.55(R_{U-O})^{-1.75}, \quad (9)$$

hence,

$$R_{U-O} = \frac{0.55}{(\Delta E_1 - 356.07)^{0.571}}, \quad (10)$$

where ΔE_1 is expressed in eV, and R_{U-O}, in nm. Equations (9) and (10) have been used to determine the ΔE_1 values and bond lengths in the uranyl groups of some compounds (see Table 8).

When constructing the experimental dependence of the relative $U6p_{3/2}$ binding energy in the high energy spectral range on the R_{U-L} bond length for uranyl compounds, several points are to be borne in mind (see Fig. 24 *b*). First, the structure of the local environment of the uranium atom in these compounds should be described by the same cluster, specifically, $[UO_2L_6]^{10-}$ (D_{6h} group of symmetry). Second, the ligands should be identical. In this particular case, an oxygen atom acts as the ligand L and the influence of substituents is neglected.

For such compounds, the relative electron energy (ΔE_2) obeys the following dependence on the bond length R_{U-L}

$$\Delta E_2 = 343.84(R_{U-L})^{-0.039}; \quad (11)$$

this can be transformed into the expression

$$R_{U-L} = \left(\frac{383.84}{\Delta E_2}\right)^{25.71}, \quad (12)$$

which allows one to determine the average distance from the uranium atom to the equatorial oxygen atoms based on the ΔE_2 value. For comparison, Fig. 24 *b* shows the data for uranyl compounds with oxygen-free ligands in the equatorial plane (L = Cl, F). As was to be expected, some of the points markedly deviate from the basic curve (see Fig. 24 *b*). Figure 25 shows a more comprehensive dependence[96, 97, 109] of the ΔE_i values on R_{U-O} in the UO_2^{2+} group, which reflects the variation of the IVMO energies and agrees qualitatively with the results of theoretical calculations.[26, 102] Relations have been proposed[95] for determining the distances from the uranium ion to the nearest

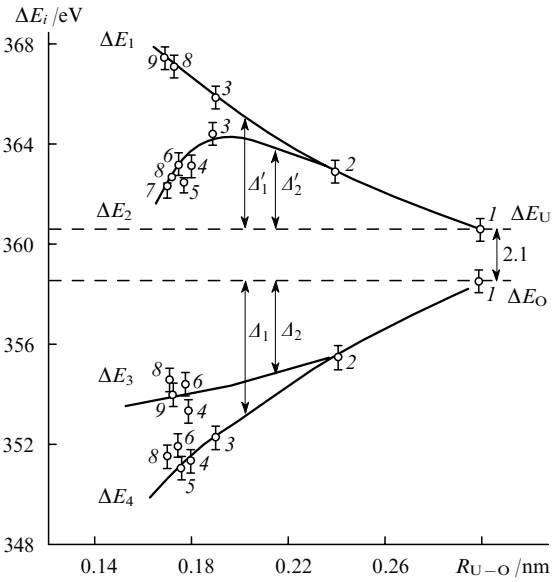

Figure 25. Experimental dependence of binding energy differences between the core and valence electrons corresponding to $\Delta E_1(2a_{2u})$, $\Delta E_2(2e_{1u})$, $\Delta E_3(1e_{1u})$ and $\Delta E_4(1a_{2u})$ for the $[UO_2O_6]^{10-}$ cluster (D_{6h} symmetry).[109] The designations of ΔE_i are given in Fig. 23.

ligand ion in the axial and equatorial positions in the uranyl compounds on the basis of U6p$_{3/2}$ line splitting ΔE:

$$R_{U-O} = b_1 \ln\left(\frac{a_1}{c_1 + \Delta E}\right), \quad (13)$$

$$R_{U-L} = b_2 \ln\left(\frac{a_2}{c_2 - \Delta E}\right), \quad (14)$$

where $a_1 = 157$ eV, $a_2 = 348$ eV, $b_1 = b_2 = 0.069$ nm, $c_1 = 8.57$ eV, $c_2 = 15.0$ eV.

Note that for uranyl difluoride (UO_2F_2), the formation of IVMO was confirmed by X-ray $O_{4,5}$(U) emission spectroscopy.[246–248]

c. XPS spectra of the core electrons

The XPS spectra of the core electrons of uranyl compounds resemble in many respects the corresponding spectra of uranium trioxide. The above considerations concerning the nature of the fine structure in the spectra of uranium oxides are largely valid for the spectral structure observed for uranyl compounds in the energy range of core electrons.

The U4f$_{7/2}$ line is used most often to determine the uranium oxidation state in compounds. The difference between the U4f$_{7/2}$ binding energies for the UO_2 and γ-UO_3 oxides equals 1.5 eV. Thus, the binding energies of the core electrons can, in principle, be used to draw conclusions about the oxidation state of uranium in a particular compound; however, this determination of the oxidation state is not always legitimate. For example, for $K_4UO_2(CO)_3 \cdot 5H_2O$ containing U^{6+}, the U4f$_{7/2}$ binding energy is lower than this value for the fluoride UF_4 in which the formal oxidation state of uranium is four (see Table 7). This indicates that for determining the oxidation state of uranium in compounds, one should resort to the whole set of data on the binding energies of the valence and core electrons and the relevant fine spectral structure.

As noted for oxides, the oxidation state of uranium can be derived from the structure of shake up satellites. The structure related to many-body perturbation is most pronounced in the U4f and U5d spectra.[47] It should be noted that in the spectra of uranyl compounds, the low-energy shake up satellites occur on the higher energy side (by $\sim$3–4 eV) of the basic lines of the U4f doublet and have a $\sim$20% intensity (see Table 7). The spin–orbit splitting of the U4f level is virtually constant for different uranyl compounds being equal on average to 10.9 eV [for uranium metal, ΔE_{sl}(U4f) = 10.8 eV].[57] The spectra of compounds containing U^{4+} ions display satellites at a distance of $\sim$7 eV from the basic lines.

Unlike the spectrum of UO_2, in the spectra of uranyl compounds, the U5d lines are sharp. This is probably due to the fact that the spectra of the UO_2 oxide, which contains U5f electrons, exhibit multiplet splitting in the U5d binding energy range. The average spin–orbit splitting of the U5d level found from the spectra of uranyl compounds [$\overline{\Delta E_{sl}}$(U5d) = 8.6 eV] is in good agreement with the corresponding value for uranium metal (8.6 eV).[57] The shake up satellites that arise in the U5d range complicate somewhat the spectra of these compounds but barely influence the spin–orbit splitting.

The U5p spectra exhibit a complex fine structure, which markedly suppresses the intensity of the U5p$_{1/2}$ component.[47] In the case of uranium oxides, the formation of this fine structure has been attributed[47,55,56] to the dynamic effect manifested in this range, which gives rise to final states of the type $U5p^55d^{10}(6s^26p^6)5f^0 \rightleftharpoons U5p^65d^8(6s^26p^6)5f^1$. The data obtained for uranyl compounds do not contradict this assumption.

The first detailed study of the U4p$_{3/2}$ spectra of uranyl compounds has been reported.[47] In all cases, the spectral structure was similar to the structure of the U5p spectra. These data are consistent with the assumption, based on the spectra of uranium oxides, stating that the structure in the U4p$_{3/2}$ spectra is due to the dynamic effect, resulting in the final states of the type $U4p^54d^{10}4f^{14}5s^2(5p^65d^{10}6s^26p^6)5f^0 \rightleftharpoons U4p^64d^94f^{14}5s^1(5p^65d^{10}.6s^26p^6)5f^0np^1$.

The U4d binding energy range also contains a fine structure, which is characteristic of particular compounds.[55] The doublet lines in the spectra are sharper than in the case of tetravalent uranium. The average spin–orbital splitting [$\overline{\Delta E_{sl}}$(U4d)] determined from the spectra of uranyl compounds is 42.4 eV, which is somewhat greater than the value of 42.1 eV found for uranium metal.[57]

On the basis of the U6s spectra of oxides, it was concluded that the final states described by the configurations $U6s^16p^65f^06d^0$ and $U6s^26p^45f^06d^1$ can arise with comparable probabilities upon photoemission of the U6s electrons from uranium compounds.[56] This gives rise to a spectral structure extending for $\sim$40 eV. The U6s spectral structure is characteristic of uranyl compounds and can be used for identification.

The experimental results on the binding energies of core and valence electrons and fine structure parameters of the XPS spectra altogether allow one to determine unambiguously the uranium oxidation states in compounds and to draw conclusions concerning the structure of the local environment of the central uranium atom and the nature of the chemical bond between this ion and the neighbouring ligand atoms. Procedure for quantitative elemental and ionic analysis of uranium compounds and for determination of the oxidation states of other ions involved on the basis of fine structure parameters of the XPS spectra of core and valence electrons has been elaborated.[47,53,55,94]

3. Natural uranium oxides

Determination of the relative contents of uranium ions in different oxidation states and the structural and phase compositions of natural uranium oxides (pichblendes) is very important for studying the conditions of formation of uranium deposits and for the exploration and development of the deposits.[208] Therefore, the possibility of using XPS studies for solving these problems has been evaluated.[65,66] The oxygen coefficients of the natural UO_x oxides were determined according to the standard procedure;[6] the specimens of minerals were taken from the collection of the researchers.[66]

The structure of the low binding energy XPS spectra of the natural oxides UO_x has much in common with the corresponding structure of complex synthetic oxides.[66] The spectra of all natural

oxide samples exhibit a relatively sharp line around a zero binding energy, which is assigned to the U5f electrons not involved directly in the chemical bond. The U6p and O2s spectral range exhibits a structure partially attributed to the IVMO electrons in natural uranium oxides. This spectral range can exhibit lines for the lead oxide PbO ($Pb5d_{5/2}$ and $Pb_{3/2}$ electrons, 19.5 and 21.8 eV, respectively; Pb6s electrons, 9.5 eV).[55] The possible occurrence of lead impurities in natural uranium oxides and complication of the structure caused by the Pb lines is taken into account in the identification of spectral peaks. The O2s energy range can also exhibit additional lines from oxygen atoms of the concomitant oxides and water molecules adsorbed on the oxide surface. Despite this possible complication of the spectra of natural uranium oxides, the most information-rich spectral ranges (0–4 and 10–20 eV) are almost free from impurity-related lines.

The line of the unbound U5f electrons in the spectra of natural uranium oxides is rather narrow and can be easily distinguished from the overall spectrum. The relative intensity of this line changes with an increase in the oxygen coefficient x in the range of $2.13 \leqslant x \leqslant 2.24$, as in the case of synthetic oxides (see Fig. 10). Then the intensity jumps up, and in the $2.47 \leqslant x \leqslant 2.68$ range, it decreases according to the same law as observed for UO_2 and γ-UO_3 mixtures (see Fig. 10).

The dependences of the lines for the U5f electrons not involved in the chemical bond on the x value established for synthetic oxides allow one to determine the ionic composition of the pitchblende studied (Table 9). This is done assuming that the natural oxides can contain three types of ions, U^{4+}, U^{5+} and U^{6+}. The results obtained in this approximation lead to the conclusion that an increase in the oxygen coefficient x in the range $2.13 \leqslant x \leqslant 2.24$ entails a sharp decrease in the U^{4+} content in the pitchblende. On further increase in x in the range $2.47 \leqslant x \leqslant 2.68$, the concentration of U^{4+} ions increases and the concentration of the U^{6+} ions decreases. No U^{5+} ions are present in the natural oxides in this x range.

The IVMO spectral range corresponding to the U6p and O2s AO (binding energy range 10–20 eV) exhibits a series of peaks. On the basis of binding energy differences between the core and inner valence electrons, one can distinguish lines corresponding to the IVMO of the U^{4+}, U^{5+} and U^{6+} ions. With allowance for relations (9) and (10), these data permit one to estimate the R_{U-O} bond lengths in natural oxides (see Table 9).

Analysis of the spectral structure of natural uranium oxides in the U6p–O2s binding energy range and the intensity of the line for the U5f unbound electrons shows that natural uranium oxides are composed of several structural phases containing U^{4+}, U^{5+} and U^{6+} ions (see Table 9). The same conclusion can be drawn on the basis of the data on the core electron spectra.[66] For example, it follows from the U4f spectral structure that natural uranium oxides contain uranium ions in different oxidation states. This can be seen from both the shapes of the U4f lines and the structure of shake up satellites, which cannot be described as a superposition of individual U4f satellites due to U^{4+} and U^{6+}, but is more complicated.

The decomposition of the $U4f_{7/2}$ line into components has made it possible to determine the relative concentrations of uranium ions in different oxidation states. The results were similar to those derived from the line intensities of unbound U5f electrons (see Fig. 10, Table 9). The $U4f_{7/2}$ binding energies presented in this Table were found as weight-average values for the electrons of the components, which characterise the uranium ions in different oxidation states. As expected, these values grow upon an increase in the U^{6+} concentration in the samples. The substantial broadening of the $U4f_{7/2}$ line compared to the narrower lines observed for individual UO_2 and γ-UO_3 oxides is itself an important

Table 9. Binding energies (E_b / eV), binding energy differences (ΔE_i / eV), line widths at half maximum (Γ / eV), relative contents of uranium ions [k (%)] and bond lengths [R_{U-O}, $R_{U-O(L)}$ / nm] in natural uranium oxides.[66]

Parameter	$UO_{2.13}$	$UO_{2.23}$	$UO_{2.24}$	$UO_{2.47}$ (see [a])	$UO_{2.47}$ (see [a])	$UO_{2.60}$	$UO_{2.63}$	$UO_{2.68}$
E_b(U5f)	2.0	2.0	2.0	1.9	2.0	2.0	2.0	1.9
E_b(OVMO)	6.2	6.3	6.2	6.1	6.2	6.1	6.2	6.1
$E_b(U6p_{3/2})$	–	–	–	14.0,	14.0,	–	14.1,	14.0,
	15.4,	15.5,	14.4,	15.7,	16.0,	14.7,	16.0,	16.1,
	17.3,	17.5,	18.0,	18.2,	18.2,	17.7,	18.0,	17.9,
	19.0	19.5	19.6	20.5	20.6	19.8	19.5	19.9
$\Delta E_i(U6p_{3/2})$	3.6	4.0	5.2	4.8	4.6	5.1	3.5	3.8
$E_b(U6p_{1/2})$	28.6,	28.7,	28.7,	28.3,	28.5,	28.8,	28.9,	28.7,
	30.1	31.2	30.7	30.5	30.2	30.6	30.9	30.1
E_b(O2s)	22.8,	22.8,	22.9,	23.0,	23.5,	22.9,	23.0,	23.0,
	25.4	25.1	25.6	25.0	26.0	25.9	25.6	25.5
ΔE_i(O2s)	2.6	2.3	2.7	2.0	2.5	3.0	2.6	2.5
E_b(O1s)	530.5,	530.8,	–	–	530.5,	530.5,	–	–
	531.7	532.1	532.0	531.7	532.0	532.0	532.1	531.3
ΔE_i(O1s)	1.2	1.3	–	–	1.5	1.5	–	–
$E_b(U4f_{7/2})$	381.4	381.6	381.7	381.9	381.5	381.9	381.7	381.8
$\Gamma(U4f_{7/2})$	2.9	2.7	2.6	2.7	2.0	2.7	2.5	2.9
$k(U^{4+})$ [b]	33	12	2	60	60	49	37	32
$k(U^{5+})$ [b]	54	65	74	–	–	–	–	–
$k(U^{6+})$ [b]	13	23	24	40	40	51	63	68
$R_{U-O}(U^{6+})$ [c]	–	–	–	0.168,	0.168,	–	0.169,	0.170,
	0.180	0.181	0.172	0.183	0.186	0.174	0.186	0.187
$R_{U-O}(U^{4+})$ [c]	0.223	0.227	0.236	0.240	0.240	0.230	0.236	0.234
$R_{U-O(L)}(U^{6+})$ [c]	0.241	0.250	0.252	0.268	0.270	0.255	0.250	0.257

[a] The samples were obtained from different deposits. [b] The error of measurement of k is ±10%. [c] The error of measurement of $R_{U-O}(U^{n+})$ ($n = 4, 6$) is ±0.002 nm, that for $R_{U-O(L)}(U^{6+})$ is ±0.004 nm.

indication of the fact that pitchblende contains uranium ions in different oxidation states.

The lines of the U5d and U4d doublets of natural oxides are broader than the corresponding lines in the spectra of synthetic uranium oxides. As the content of U^{6+} ions in the samples increases, the U5d and U4d binding energies measured as the weight average values for different states of ions increase by about 1.0 eV. A more complicated structure than that observed in the spectra of synthetic uranium oxides is also found in the $U4p_{3/2}$, U5p and U6s spectra of natural oxides. These data confirm that natural uranium oxides do not show complete similarity to either complex synthetic oxides or mixtures of simple uranium oxides but represent complex structural phases. It follows from the obtained results that at $2.13 \leqslant x \leqslant 2.24$, the natural oxides UO_x are closer in properties to berthollides, while at $2.47 \leqslant x \leqslant 2.68$, they are closer to daltonides.[5]

The XPS data obtained for a broad range of technologically important uranium compounds show that the fine structure parameters of their spectra reflect the properties of these compounds, the nature of the chemical bond in them and the secondary electronic processes which accompany the electron photoemission.

IV. Neptunium compounds

In recent years, studies of physicochemical properties of neptunium compounds have attracted considerable attention.[1, 3, 239, 249, 250] Neptunium dioxide NpO_2,[41, 79] single crystals of $Cs_3NpO_2Cl_4$ and $Cs_2NpO_2Cl_4$,[51, 53, 80] the compounds $Cs_2NpO_2(OAc)_3$, $NaNpO_2(OAc)_3$ and $RbNpO_2(NO_3)_2 \cdot 2\,H_2O$ [55] have been studied by XPS. A number of studies have been devoted to elucidation of correlations between the fine structure parameters of the XPS spectra of outer and core electrons and the neptunium oxidation states in compounds,[44, 80, 81] magnetic properties,[44, 89, 90] the nature of the chemical bond (Refs 36, 41, 51 – 53, 55, 81, 87 – 90, 115) and the secondary electronic processes.[55, 56] Non-relativistic X_α-SW calculations have been carried out for the electronic structure of the NpO_2^{2+} cluster ($D_{\infty h}$ group of symmetry) with $R_{Np-O} = 0.171$ nm,[115] while calculations for the $[NpO_2Cl_4]^{2-}$ cluster (D_{4h} group of symmetry) with $R_{Np-O} = 0.171$ nm and $R_{Np-L} = 0.262$ nm were carried out in the relativistic X_α-DV approximation.[36]

In a number of studies,[51, 53, 55, 56, 80, 114, 115] the XPS spectra of several neptunyl compounds (Table 10) have been analysed in order to establish the relationships of the spectral structure with the properties and structures of the compounds and the nature of the chemical bond in them. A key goal was to confirm the assumed formation of IVMO in neptunium compounds, which has been established for thorium and uranium compounds on the basis of the XPS spectral structure.

1. The low binding energy range of the spectra

The structure of the low binding energy XPS spectra of neptunyl compounds is fairly similar to that of the corresponding spectra of uranyl compounds. Since these compounds contain other elements apart from neptunium, the low binding energy range of the spectra exhibits an additional structure caused by electrons of these elements, which markedly complicates interpretation of the fine structure of the spectra of neptunium compounds. Thus the neptunium lines in this binding energy range in the spectra of the $Cs_3NpO_2Cl_4$ and $Cs_2NpO_2Cl_4$ single crystals are overlapped by caesium and chlorine lines and their satellites, which occur on the higher-energy side of the basic lines (Fig. 26). The spectra of other neptunium compounds also exhibit additional lines (Fig. 27). For comparison, Fig. 27 shows the spectra of NaOAc and $Ni(NO_3)_2$.

a. The spectra of the Np5f electrons

The spectra of the studied neptunium compounds exhibit a sharp line near a zero binding energy (the Fermi level for metals), like the spectra of U^{4+} (see Figs 26, 27). As the oxidation number of

Table 10. Binding energies (E_b) [55] and photoionisation cross-sections (σ) of neptunium compounds.[203]

Orbital Np, L (nl_j)	E_b /eV							σ (see [d, e])
	$NaNpO_2(OAc)_3$ (see [a])	$Cs_2NpO_2Cl_4$ (see [a])	$RbNpO_2(NO_3)_2$ (see [b])	$Cs_2NpO_2(OAc)_3$ (see [b])	$Cs_3NpO_2Cl_4$ (see [b])	NpO_2 (see [c]) [79]	Np_{theor} (see [d]) [178]	
Np5f	3.4	3.3	2.9	2.3	2.5	–	7.4	0.52
OVMO (see [f])	5.9	5.3	5.4	4.3	4.9	–		–
$Np6p_{3/2}$	15.7,	15.5,	–	–	15.7,	–	–	–
	20.2	20.0	19.3	18.9	18.6	17.5	24.6	0.39
$Np6p_{1/2}$	–	30.6	–	30.4	30.0	29.3	36.2	0.14
Np6s	50.5	50.2	49.8	49.7	48.7	–	57.2	0.17
$Np5d_{5/2}$	102.7	102.4	101.5	100.8	101.1	100.9	107.1	3.62
$Np5d_{3/2}$	112.2	112.1	–	109.9	110.0	–	120.4	2.46
$Np5p_{3/2}$ (see [f])	207.6	208.7	205.5	206.9	207.3	206.3	220.8	2.31
$Np5p_{1/2}$	–	–	–	–	–	–	280.7	0.68
Np5s (see [g])	–	338.7	335.4, 344.1	335.1, 344.2	335.2, 343.9	–	349.3	0.75
$Np4f_{7/2}$	405.2	404.6	403.6	403.0	403.4	402.5	408.4	29.18
$Np4f_{5/2}$	417.0	416.4	415.3	414.6	415.2	414.3	420.9	22.91
$Np4d_{5/2}$	771.8	771.4	770.7	769.6	770.3	771.2	779.6	17.44
$Np4d_{3/2}$	816.7	816.0	815.8	814.8	815.4	816.1	824.9	11.44
$Np4p_{3/2}$	1087.5	1087.4	1086.9	1086.0	1086.1	–	1096.6	7.83
O2s	24.2,	–	–	–	–	23.8		0.14
	26.0	25.8	27.0	27.2	26.2			
O1s	532.0	531.9	531.5, 533.1	531.5	532.3	529.7		2.93
C1s	288.8			288.3		284.5		1.00
N1s			407.1					1.80

[a] The state of neptunium is described as Np^{6+}. [b] The state of neptunium is described as Np^{5+}. [c] Np^{4+}. [d] For atomic neptunium. [e] The s values were obtained at 1487 eV and are expressed in 13.6 b per atom shell. [f] Weight average E_b values for fine structure components. [g] The E_b values corresponding to the most intense peaks in the fine structure of the corresponding binding energy range.

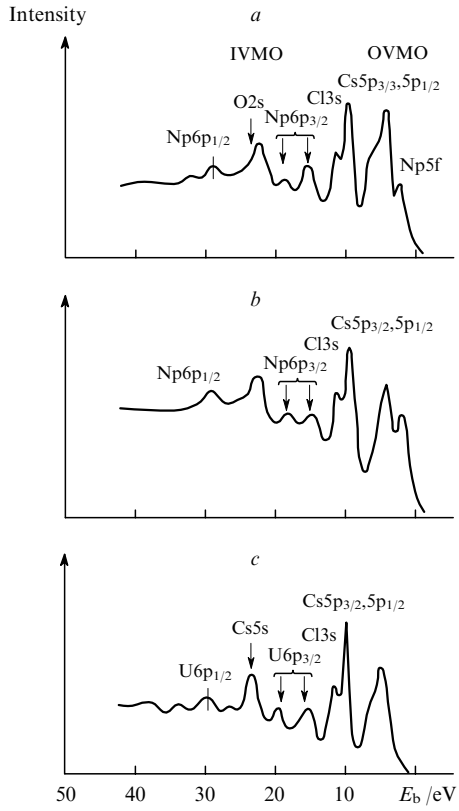

Figure 26. XPS spectra of the single crystals of $Cs_2NpO_2Cl_4$ (*a*), $Cs_3NpO_2Cl_4$ (*b*), $Cs_2UO_2Cl_4$ (*c*), containing the NpO_2^{2+}, NpO_2^{+} and UO_2^{2+} groups, respectively, in the low binding energy range.[53, 80]

Table 11. Relative intensity of the Np5f line [$I_{5f}^{exp} = I(Np5f)/I(Np4f_{7/2}) \times 10^2$] in the spectra of Np^{n+} compounds, effective magnetic moment (μ_{eff}/μ_B) and Weiss temperatures (θ / K).[55]

Compound	Np^{n+}	I_{5f}^{exp}	μ_{eff} (see [251])	θ (see [251])
NpO_2	Np^{4+}	5.9 ± 0.6	3.3 ± 0.2	181
$Cs_3NpO_2Cl_4$	Np^{5+}	4.6 ± 0.5	3.2 ± 0.2	249
$Cs_2NpO_2Cl_4$	Np^{6+}	2.6 ± 0.3	2.3 ± 0.1	216
$NaNpO_2(OAc)_3$	Np^{6+}	1.8 ± 0.2	2.2 ± 0.1	51.5

neptunium increases, the intensity of this line diminishes (Table 11). Hence, it has been suggested that this relatively narrow line near a zero binding energy is due to the Np5f electrons not involved in the chemical bond.[55, 80] As the neptunium oxidation state increases, the number of unbound Np5f electrons decreases, so does the effective magnetic moment μ_{eff} (see Table 11).

It follows from the XPS spectra [55, 79] and calculation results [137] that on passing from uranium compounds to neptunium compounds, the binding energy difference between the OVMO and An5f electrons decreases. This imposes some limitations on the accuracy of determination of the relative intensity of the Np5f line in neptunium compounds containing unbound Np5f electrons. Nevertheless, the intensity of this line can serve as not only a qualitative but also a quantitative measure of the neptunium oxidation state in compounds.

b. The spectra of the Np6p and O2s electrons

As noted above, the low binding energy range of the XPS spectra of the neptunium compounds studied contains, in addition to the

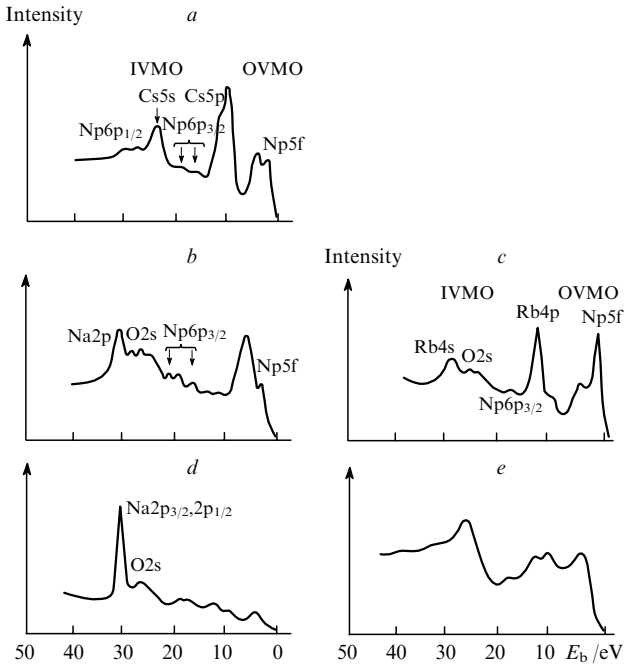

Figure 27. XPS spectra of neptunium compounds in the low binding energy range (for comparison, XPS spectra of sodium acetate and nickel nitrate are given).[55]
(*a*) $Cs_2NpO_2(OAc)_3$, (*b*) $NaNpO_2(OAc)_3$, (*c*) $RbNpO_2(NO_3)_2 \cdot 2H_2O$, (*d*) NaOAc, (*e*) $Ni(NO_3)_2$.

Np6p and O2s lines, some lines due to ligand electrons (Table 12, see Figs 26, 27), which complicate the spectrum. For example, the OVMO and IVMO spectra of the NO_3^- and AcO^- ligands exhibit a complex structure covering a range of approximately 35 eV. This structure [55] has been studied both experimentally and theoretically (for NO_3^-, it is shown in Figs 5 and 27 *e*).

Despite the complexity of the low binding energy XPS spectra of neptunium compounds containing an NpO_2^{n+} group, the structure of the $Np6p_{3/2}$ spectrum is similar to that observed in the $U6p_{3/2}$ spectra of uranyl compounds (see Fig. 26). In all cases, two components appear instead of the single $An6p_{3/2}$ line. The lower binding energy component is partially superimposed onto the Cl3s line.

The R_{An-O} bond lengths in the AnO_2^{n+} groups have been estimated using relation (8) with the assumption that the effect of the difference between the charges of the Np and U nuclei can be neglected.[80] This gave the following values: $R_{U-O} = 0.174$ nm, $R_{Np-O} = 0.180$ nm and $R_{Np-O} = 0.174$ nm for the UO_2^{2+}, NpO_2^{+} and NpO_2^{2+} groups in the compounds $Cs_2UO_2Cl_4$, $Cs_3NpO_2Cl_4$ and $Cs_2NpO_2Cl_4$, respectively. The appearance of two components in the $Np6p_{3/2}$ spectral range for neptunium compounds confirms the assumption that the XPS spectra of compounds containing AnO_2^{n+} groups should exhibit the structure typical of the IVMO.

The participation of low-energy occupied Np6p and L*n*s AO in the IVMO formation can be established on the basis of the binding energy difference between the core AO and valence MO. The researchers cited [80] could not carry out this comparison due to the lack of data for neptunium metal. However, comparison of these values for neptunium compounds shows that they are different. A reason for this discrepancy may be dissimilar participation of the Np6p and L*n*s AO in the IVMO formation in different compounds (Table 13).

Table 12. Binding energies (E_b /eV) of electrons of the ligands contained in neptunium compounds.[55]

Orbital	NaL^1	Na_2CO_3	NiL_2^2	Orbital	CsCl	Orbital	$RbYL_2^2 \cdot 2H_2O$	Orbital	$Cs_2YL_3^1$	Cs_3YCl_4	Cs_2YCl_4	Orbital	$NaYL_3^1$
MO	4.6,	3.1,	4.3,	MO	4.4	Rb4p	14.3	Cs5p	10.8	10.5	10.4,	Na2p	30.5
	9.8,	5.3,	11.8,	$Cs5p_{3/2}$	10.1	Rb4s	29.9				11.9	Na2s	63.3
	12.1,	9.6,	14.5,	$Cs5p_{1/2}$	11.7	Rb3d	110.9	Cl3s		15.8	16.0	Na1s	1071.5
	13.8,	11.7	18.2	Cl3s	15.0 (30.6,	Rb3p	238.4	Cs5s	23.4	23.7	23.6		
	17.8,				34.5, 38.4) [a]	Rb3s	321.8	$Cs4d_{5/2}$	75.5	75.5	75.4		
	19.5			Cs4d	75.3 (87.1,			$Cs4d_{3/2}$	77.6	77.7	77.7		
O2s	25.2,	23.2,	26.9,		98.9, 122.1) [a]			Cs4s	229.9	229.9	229.8		
	26.9	24.7	32.4	Cs4p	158.8			$Cs3p_{3/2}$	1065.2	1065.0	1065.2		
Na2p	30.2	30.2		Cs4s	229.5			Cl2p		198.9	199.0		
Na2s	63.0	62.8		$Cs3d_{5/2}$	724.5 (733.8) [a]								
C1s	285.0,	–		$Cs3d_{3/2}$	728.5 (747.9,								
	288.5	289.3			761.9)								
O1s	531.5	531.3	533.1	Cl2p	197.6, 199.3								
					(208.5, 216.6) [a]								

Note. The following designations are used: Y = NpO_2, L^1 = OAc, L^2 = NO_3. [a] The binding energies for the electrons responsible for the appearance of satellites are given in parentheses.

Table 13. Binding energy differences (ΔE_i) between various neptunium and oxygen shells.[55]

Compound, element	$\Delta E_i = E_k - E_l$ /eV				
	$6p_{3/2} - 6p_{1/2}$	$6p_{3/2} - 4f_{7/2}$	$5d_{5/2} - 4f_{7/2}$	$4f_{7/2} - 4d_{5/2}$	O2s – O1s
$NaNpO_2(OAc)_3$	–	389.5, 385.0	302.5	366.6	506.0, 507.8
$Cs_2NpO_2Cl_4$	–	389.1, 384.6	302.2	366.8	506.1, 508.3
$Cs_3NpO_2Cl_4$	–	387.7, 384.8	302.3	366.9	505.4, 508.1
$RbNpO_2(NO_3)_2 \cdot 2H_2O$	–	384.3	302.1	367.1	504.5
$Cs_2NpO_2(OAc)_3$		384.1	302.2	366.7	504.3
NpO_2 (see [79])	11.8	385.0	301.6	368.7	505.9
Np_{theor} (see [178])	11.6	383.8	301.3	371.2	

2. The spectra of the core electrons

In the binding energy range of core electrons, XPS spectra of neptunium compounds exhibit a complex fine structure (Figs 28 – 31).[55, 56, 79, 80] The binding energies for the most intense lines are listed in Table 10. The most intense lines correspond to the Np4f electrons (see Fig. 28). The basic lines of these spectra are least distorted due to the additional structure; therefore, the Np4f spectrum is most suitable for quantitative elemental and ionic analyses and determination of the neptunium oxidation state. For compounds containing neptunium ions in only one formal oxidation state, the Np4f binding energy varies within a range of 0.6 eV (see Table 10).[55] The greatest change in the $Np4f_{7/2}$ binding energy on passing from compounds with formally pentavalent neptunium to hexavalent neptunium compounds equals 2.2 eV, while the smallest change is 1.0 eV. Hence, the chemical shifts can be used to draw conclusions concerning the formal oxidation state of neptunium and the relative ionic – covalent natures of the bond in compounds.

In caesium- and chlorine-containing neptunium compounds, the binding energies formed by these elements are somewhat greater than the corresponding binding energies in CsCl (see Table 12). This is due to the increase in the caesium and chlorine oxidation states upon their incorporation in the compounds considered. Thus, it can be concluded that the bonds between Cl and the AnO_2^{n+} group are more covalent than the Cs–Cl bond, while the bond between the caesium and chlorine atoms in a neptunium compound is more ionic than that in CsCl.

a. The spectra of Np4f electrons

The basic lines of the Np4f doublet related to the spin – orbit splitting [ΔE_{sl}(Np4f) = 11.8 eV [80]] are relatively narrow (see Fig. 28). In this binding energy range, satellites caused by many-body perturbation appear with the highest probability. The maxima corresponding to these satellites can also be seen in the spectra of other core electron levels. However, the Np4f range exhibits most characteristic shake up satellites. For example, for Np^{4+} (NpO_2),[79] Np^{5+} ($Cs_3NpO_2Cl_4$) and Np^{6+} ($Cs_2NpO_2Cl_4$), the ΔE_{Sat} values equal ~7.0, 9.4 and 3.5 eV, and the intensities of low-energy satellites are ~17%, 12% and 20%, respectively.[80] These values are correlated satisfactorily with corresponding values for U^{4+} (UO_2) and U^{6+} ($Cs_2UO_2Cl_4$): 6.9 and 3.8 eV, 25% and 20%, respectively. This indicates that the electronic structures of isostructural neptunium and uranium compounds have much in common, which also agrees with the results of theoretical calculations.[115, 137] It is noteworthy that the structure of the Np4f spectrum related to many-body perturbation can serve as a reliable characteristic of the neptunium formal oxidation state.

b. Spectra of the Np5d and Np4d electrons

In the Np5d binding energy range, the intensity of the $Np5d_{3/2}$ line is essentially suppressed and the line is broadened (see Fig. 29). This results in a seeming substantial change in the spin – orbit splitting. Thus the average value is given by $\Delta\bar{E}_{sl}$(Np5d) = 9.2 eV and the difference between these values for the studied neptunium compounds does not exceed 0.8 eV.

The change in the spin – orbit splitting is due to the formation of the complex structure of the Np5d spectral lines. This structure may arise due to the multiplet splitting caused by the presence of unpaired Np5f electrons. In addition, the Np5d spectra may exhibit a structure related to the dynamic effect, which gives rise to the final electronic states like $Np5d^96s^26p^65f^n np^0 \rightleftharpoons Np5d^{10}6s^06p^65f^n np^1$, because the relation E_b(Np5d) ≈ $2E_b$(Np6s) holds. However, this process is relatively unlikely ($\Delta n = 1$, $\Delta l = 2$). The value ΔE_{sl}(Np5d) = 9.7 eV should be considered to be most realistic.

The Np4d spectral structure is also complicated due to superposition of lines related to the many-body effects involving ligand atoms (see Fig. 29). The other observed maxima cannot be explained in this way. Presumably,[55] this structure is a consequence of the dynamic effect, resulting in final states like $Np4d^94f^{14}(5s^25p^65d^{10}6s^26p^6)5f^n \rightleftharpoons Np4d^{10}4f^{12}(5s^25p^65d^{10}6s^2.6p^6)5f^n6d^1$. This is one of the possible mechanisms for the formation of the fine structure in the Np4d spectra.

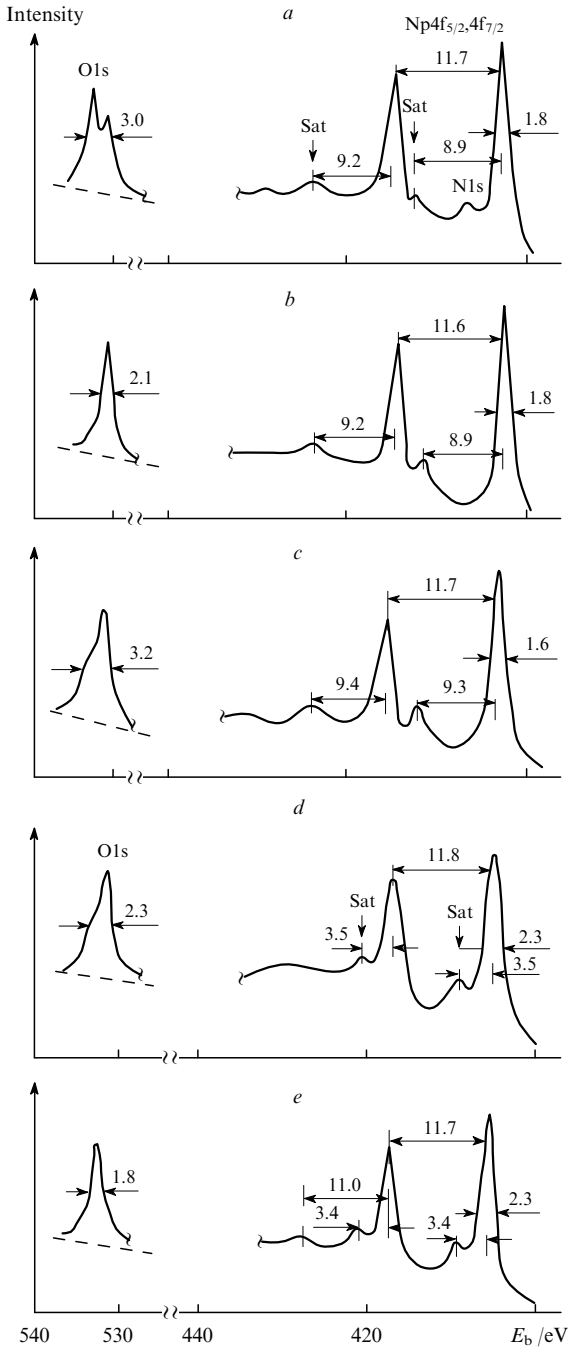

Figure 28. XPS spectra of neptunium compounds containing the NpO_2^+ (*a*–*c*) and NpO_2^{2+} (*d*, *e*) groups in the Np4f and O1s binding energy ranges.[55]
(*a*) $RbNpO_2(NO_3)_2 \cdot 2H_2O$, (*b*) $Cs_2NpO_2(OAc)_3$, (*c*) $Cs_3NpO_2Cl_4$, (*d*) $Cs_2NpO_2Cl_4$, (*e*) $NaNpO_2(OAc)_3$. The dashed lines show the background.

The appearance of the complicated fine structure in the Np4d spectra leads to a seeming change in the spin–orbit splitting on passing from one compound to another. The average value $\Delta\bar{E}_{sl}$(Np4d) is equal to 45.0 eV. This does not allow any accurate measurements of the binding energies on the basis of the Np4d spectra.

c. Spectra of the Np5p and Np4p$_{3/2}$ electrons

The Np5p binding energy range of the XPS spectra of neptunium compounds exhibits lines for the core electrons of the ligand atoms (see Fig. 30).[56] The structure of the Np5p$_{1/2}$ spectra cannot be observed, as the ΔE_{sl}(Np5p) value equals 77 eV; the binding

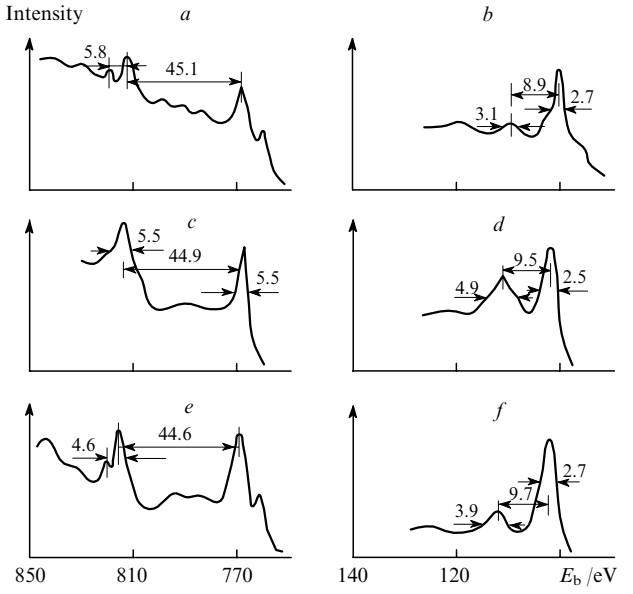

Figure 29. XPS spectra of neptunium compounds in the Np4d (*a*, *c*, *e*) and Np5d (*b*, *d*, *f*) binding energy ranges.[55, 80]
(*a*, *b*) $Cs_3NpO_2Cl_4$; (*c*, *d*) $NaNpO_2(OAc)_3$; (*e*, *f*) $Cs_2NpO_2Cl_4$.

energy of these electrons [E_b(Np5p$_{1/2}$] is approximately 283.0 eV,[20] their spectrum being superimposed onto the intense C1s lines of the AcO groups or the residual oil vapour molecules adsorbed on the sample surface. However, for some compounds, individual spectra of the Np5p$_{3/2}$ electrons can be observed (see Fig. 30).[56]

The reported[20] values for the neptunium binding energy E_b(Np5p$_{3/2}$) = 206 eV and E_b(Np5d$_{5/2}$) = 101 eV roughly satisfy the condition E_b(Np5p$_{3/2}$) $\approx 2\,E_b$(Np5d$_{5/2}$). This suggests[56] that the structure observed in the Np5p$_{3/2}$ spectra is largely caused by the dynamic effect, resulting in final states of the type $Np5p^5 5d^{10}(6s^2 6p^6)5f^n \rightleftharpoons Np5p^6 5d^8(6s^2 6p^6)5f^{n+1}$. Apparently, additional broadening of these lines can be due to multiplet

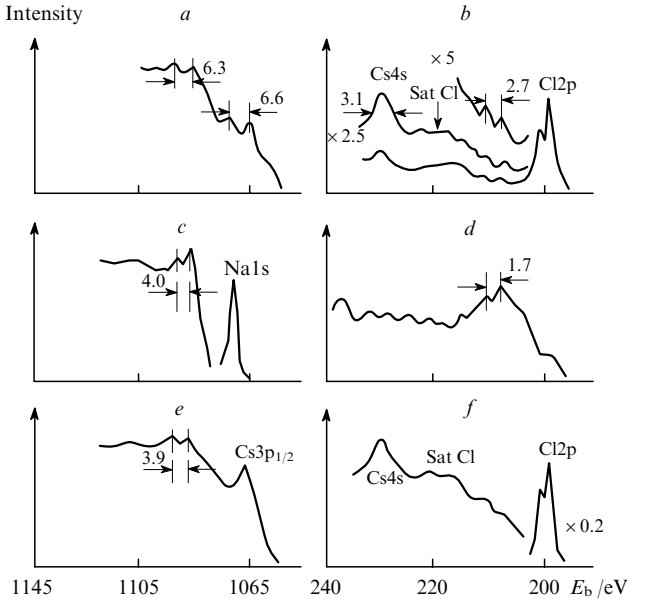

Figure 30. XPS spectra of neptunium compounds in the Np4p$_{3/2}$ (*a*, *c*, *e*) and Np5p (*b*, *d*, *f*) binding energy ranges.[56] (*a*, *b*) $Cs_3NpO_2Cl_4$; (*c*, *d*) $NaNpO_2(OAc)_3$; (*e*, *f*) $Cs_2NpO_2Cl_4$.

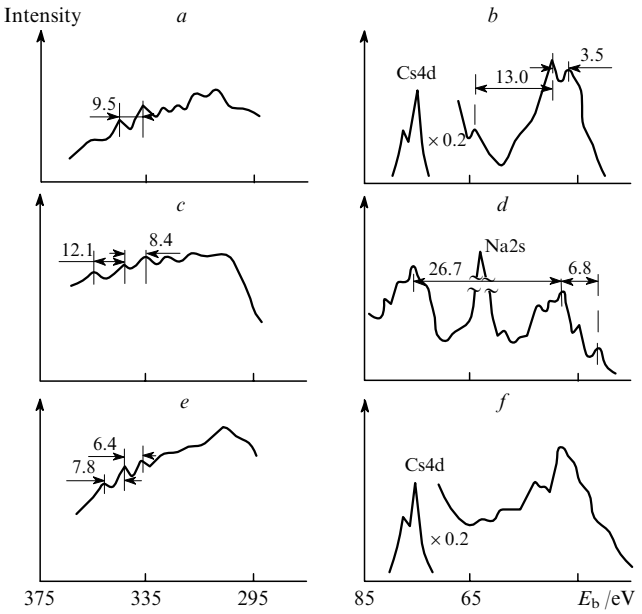

Figure 31. XPS spectra of neptunium compounds in the Np5s (*a*, *c*, *e*) and Np6s (*b*, *d*, *f*) binding energy ranges.[56] (*a*, *b*) $Cs_3NpO_2Cl_4$; (*c*, *d*) $NaNpO_2(OAc)_3$; (*e*, *f*) $Cs_2NpO_2Cl_4$.

splitting, because all the neptunium compounds considered contain unbound Np5f electrons. Some of the peaks can be attributed to shake up satellites (see Fig. 30).

The spectra of the $Np4p_{3/2}$ electrons of caesium-containing neptunium compounds are overlapped by satellites of the $Cs3p_{1/2}$ structure (see Fig. 30). The spectrum of the $Np4p_{3/2}$ electrons of $RbNpO_2(NO_3)_2 \cdot 2\,H_2O$ contains no ligand-related lines over a broad binding energy range; nevertheless, this range also displays fine structure. The binding energies of neptunium electrons reported in a study,[20] $E_b(Np4p_{3/2}) = 1087$ eV, $E_b(Np4d_{3/2}) = 773$ eV and $E_b(Np5s) = 338$ eV, roughly satisfy the relation $E_b(Np4p_{3/2}) \approx E_b(Np4d_{5/2}) + E_b(Np5s)$. Hence, one may suggest that the $Np4p_{3/2}$ spectral structure is due to the dynamic effect, resulting in final states of the type $Np4p^54d^{10}4f^{14}5s^26p^65f^n np^m \rightleftharpoons Np4p^64d^94f^{14}5s^16p^65f^n np^{m+1}$.

d. Structure of the Np6s and Np5s spectra

It is known that the Np6s electrons have a relatively small photoionisation cross-section [203] and their spectra exhibit a relatively complex fine structure. Nevertheless, the sample preparation and experimental procedures allowed researchers [55, 56] to measure the spectra of these electrons (see Fig. 31).[56] The fine structure of the Np6s spectrum extends over a binding energy range of ~40 eV. The electron binding energies found as the weight average values for electrons around the most intense band are listed in Table 10. The spectra of $RbNpO_2(NO_3)_2 \cdot 2\,H_2O$ and $NaNpO_2(OAc)_3$ exhibit a rather intense spectral structure in addition to the relatively broad bands at ~50 and ~75 eV. The spectra of these compounds reflect most fully the Np6s spectral structure over the whole binding energy range considered (see Fig. 31).

Presumably, the formation of the Np6s fine structure over this broad binding energy range may be due to the dynamic effect, resulting in final electronic states like: $Np6s^16p^65f^n6d^0 \rightleftharpoons Np6s^26p^45f^n6d^1$. The presence of unbound Np5f electrons in all of the studied neptunium compounds may give rise to an additional structure caused by multiplet splitting. Finally, shake up satellites should also be manifested in these spectra.[55, 56]

It should be noted that, without thorough theoretical analysis of the spectral structure in the Np6s binding energy range and without identification of individual lines, it is difficult to draw any qualitative conclusions concerning the involvement of the Np6s shell in the IVMO formation in neptunium compounds.

Attempted study of the Np5 spectral structure has been reported.[55, 56] In this energy range, against the relatively intense background of the broad C1s satellite band due to the OAc group or the residual vacuum oil, the spectrum exhibits an additional structure missing from the C1s spectrum of graphite (see Fig. 31). This structure always consists of two lines that cannot result from the multiplet splitting, because the corresponding binding energy difference does not exceed 2–3 eV. Therefore, it is assumed that the structure manifested in the Np5s spectra is due to the dynamic effect, which results in final states of the type $Np5s^15p^65d^{10}6s^26p^65f^n np^m \rightleftharpoons Np5s^25p^55d^{10}6s^16p^65f^n np^{m+1}$.

Thus, it can be concluded that parameters of the fine structure manifested in the spectra of neptunium compounds provide information on their magnetic properties, neptunium oxidation states and the degree of participation of the Np6p and L*n*s AO in the formation of the IVMO whose structure is determined by the local environment of the neptunium ion. The fine structure observed in the spectra of core electrons, which arises due to different mechanisms, is characteristic of particular neptunium compounds and can be used for identification.

V. Plutonium compounds

Plutonium oxides on the metal surface,[41, 64, 79, 83–86, 116, 121, 126] $Pu(NO_3)_4 \cdot n\,H_2O$,[29, 55] and the single crystal of $Cs_2PuO_2Cl_4$ [55, 82] have been studied by XPS. The correlations of fine structure parameters of the spectra of inner and outer electrons with plutonium oxidation states in compounds,[29, 64, 79, 81–86] the structures of compounds,[29, 55, 82] the types of chemical bond,[29, 37, 41, 44, 51–53, 55, 81, 82, 87–91, 115, 116] and secondary electronic processes that accompany photoemission of electrons [29, 55, 79, 82, 121] have been studied. The relativistic electronic structure parameters of plutonium were evaluated;[33, 35] nonrelativistic X_α-SW calculations were carried out for the electronic structure of the PuO_2^{2+} cluster ($D_{\infty h}$ group of symmetry) with $R_{Pu-O} = 0.171$ nm [115] and relativistic X_α-DV calculations were performed for the $PuO_2Cl_4^{2-}$ cluster (D_{4h} group of symmetry) with $R_{Pu-O} = 0.171$ nm and $R_{Pu-L} = 0.262$ nm.[36] On the basis of the XPS spectrum of outer valence electrons, the mechanism of formation of a PuO_2 film on the surface has been studied;[64] the dependence of valence and core level spectral parameters for metallic plutonium on the number of monolayers on the substrate has been analysed.[85]

For the single crystal of $Cs_2PuO_2Cl_4$ containing the PuO_2^{2+} group, the XPS spectra of various electron shells in the binding energy range from 0 to ~1250 eV have been studied [82] in order to determine the relationship between the fine spectral structure parameters and the structure of the local environment of the plutonium ion, plutonium oxidation state and the nature of the chemical bond in the compound. The spectral lines were identified using the spectra of plutonium metal [83, 116, 127] and plutonium dioxide,[41, 79, 84] the results of calculations for individual atoms [178] and model clusters,[36, 115] photoionisation cross-sections [203] and the XPS spectra of thorium, uranium and neptunium compounds and CsCl.[55] The procedure used for sample preparation and for recording made it possible to obtain the first spectra of the core and valence electrons for a bulky sample, which was a $Cs_2PuO_2Cl_4$ single crystal. This double salt contains a plutonium ion formally as Pu^{6+} with the electronic configuration $\{Rn\}5f^2$. Therefore, the fine spectral structure of the core and valence levels can be discussed conveniently using this compound as an example.

1. The spectra of valence electrons

The low binding energy XPS spectrum of $Cs_2PuO_2Cl_4$ largely resembles the spectra of isostructural uranium and neptunium compounds (see Figs 26, 31).

a. The spectrum of the Pu5f electrons

Comparison of the An5f spectra of uranium,[47] neptunium,[80] plutonium,[82] the oxides NpO_2 (see Refs 41 and 79) and PuO_2 (see Refs 41, 79 and 84) shows that on passing from uranium to plutonium, the difference between the weight-average An5f binding energy and the OVMO binding energy substantially decreases. This results in a significant overlap of the corresponding lines in the spectra of plutonium compounds (Fig. 32); this increases the error of determination of the relative intensity of the Pu5f lines.

It follows from the spectra of PuO_2 [41, 79, 84] and $Cs_2PuO_2Cl_4$ [82] that an increase in the plutonium oxidation state in compounds entails a decrease in the intensity of the Pu5f line. The magnetic properties of plutonium compounds have not been adequately studied, hence, they cannot be quantitatively correlated with the intensity of the Pu5f lines in the spectra; nevertheless, there exists some qualitative correlation. Thus on passing from the tetravalent plutonium in PuO_2 to hexavalent plutonium in the fluoride PuF_6, the specific molar susceptibility (χ) decreases from 536×10^{-6} to 170×10^{-6} mol^{-1} (see Ref. 251). This is in line with the fact that a decrease in the number of the unbound Pu5f electrons in the molecule induces both a decrease in the intensity of the Pu5f lines and a decrease in the paramagnetic term in the specific magnetic susceptibility of the compound. However, as follows from the data on the An5f line intensity and the published data on the magnetic behaviour of actinide compounds, no direct correlation can be followed between the magnetic moment and the number of unpaired An5f electrons for $n_f > 2$.[252–254]

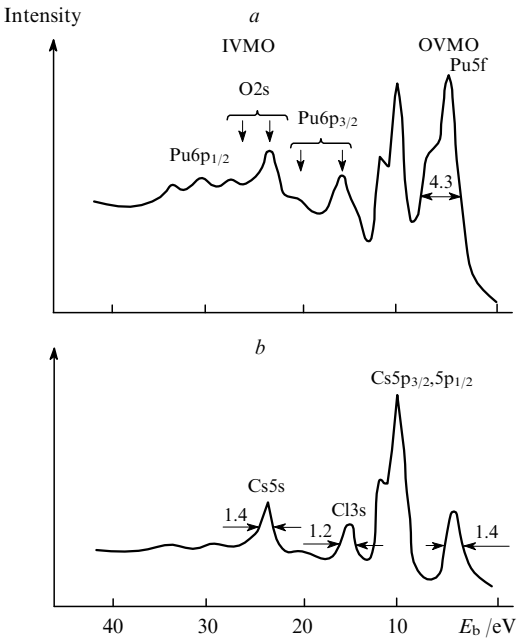

Figure 32. Low energy range of the XPS spectrum of the single crystal of $Cs_2PuO_2Cl_4$ (*a*).[82] For comparison, the XPS spectrum of caesium chloride is given (*b*).

b. The spectra of the Pu6p and O2s electrons

The $Pu6p_{3/2}$ spectrum of $Cs_2PuO_2Cl_4$, like the $An6p_{3/2}$ spectra of $Cs_2AnO_2Cl_4$ (An = U, Np), consists of two lines (see Figs 26, 32). The line characterised by the lower binding energy partially overlaps with the Cl3s line. In the spectrum of the O2s and $Pu6p_{1/2}$ binding energy range, a complex fine structure typical of compounds containing the actinyl group AnO_2^{n+} can be observed, in addition to the Cs5s peak.

Table 14. Binding energy differences (ΔE_i) between various plutonium and oxygen shells.

Compound, element	$E_i = E_k - E_l$ /eV				
	$6p_{3/2} - 6p_{1/2}$	$6p_{3/2} - 4f_{7/2}$	$5d_{5/2} - 4f_{7/2}$	$4f_{7/2} - 4d_{5/2}$	O2s – O1s
$Cs_2PuO_2Cl_4$ (see [82])	–	412.5, 408.2	321.1	374.8	506.5, 508.8
PuO_2 (see [79])	12.2	408.2	321.6	375.2	507.5
Pu_{metal} (see [83])	12.0	403.9	319.8	377.0	
Pu_{theor} (see [178])	11.9	403.8	319.3	379.8	

Comparison of the binding energy differences between the valence and core levels ΔE_i ($Pu6p_{3/2} - Pu4f_{7/2}$) for plutonium and its compounds (Table 14) shows that IVMO are formed effectively from the Pu6p and O2s AO not only in the case of $Cs_2PuO_2Cl_4$, containing the PuO_2^{2+} group, but also for the oxide PuO_2, which has a more symmetric structure. Indeed, the difference between the $Pu4f_{7/2}$ and $Pu6p_{3/2}$ binding energies for plutonium metal equals 403.9 eV. For PuO_2, this value is greater by 4.3 eV, and for the $Cs_2PuO_2Cl_4$ single crystals, these values are greater by 8.6 and 4.3 eV for the two components arising due to IVMO formation in these compounds (see, for example, Figs 4, 23).

These data also provide the conclusion concerning the nature (either bonding or antibonding) of some IVMO. The contribution of the IVMO electrons in the PuO_2^{2+} cluster to the covalent component of chemical bonding estimated on the basis of determination of the orbital forces (f^{α}_{Pu-O} /au) [53] amounts to 22% of the total contribution of the electrons of all MO.[115]

2. The spectra of core electrons of plutonium

The XPS spectra of $Cs_2PuO_2Cl_4$ for all core electron levels in the energy range from ~40 to ~1250 eV exhibit fine structure which is also typical of other plutonium compounds (Figs 33–37). The corresponding binding energies are given in Table 15. In those cases where a complex fine structure is present, instead of the expected single lines, the Table gives the weight average values for the binding energies corresponding to the most intense lines.

On passing from plutonium metal to PuO_2 or $Cs_2PuO_2Cl_4$, the core electron binding energies regularly increase (see Table 15). It can be seen that the core electron energies are correlated with the Pu oxidation states in the compound.

a. The spectrum of Pu4f electrons

The Pu4f spectrum consists of a spin doublet of sharp intense peaks accompanied by satellites on the higher binding energy side (see Fig. 33).

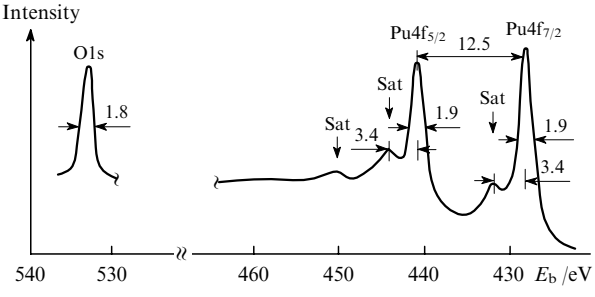

Figure 33. XPS spectra of the single crystal of $Cs_2PuO_2Cl_4$ containing the PuO_2^{2+} group in the Pu4f and O1s binding energy range.[82]

Table 15. Binding energies (E_b) and photoionisation cross-sections (σ) for plutonium compounds.

Orbital Pu, L (nl_j)	E_b /eV					σ [a]
	$Cs_2PuO_2Cl_4$ (see [82])	PuO_2 (see [79])	$Pu(NO_3)_4 \cdot n H_2O$ (see [29])	Pu_{metal} (see [83])	Pu_{theor} (see [178])	
Pu5f	5.0	–	4.1	–	4.7	0.81
OVMO	6.0	–	–			–
$Pu6p_{3/2}$	16.2, 20.5	– 18.4	19.5, 21.3	– 17.2	– 22.7	– 0.38
$Pu6p_{1/2}$	30.4, 33.3	30.6	31.4, 33.9	29.2, 32.0	34.6	0.13
Pu6s	49.0, 54.5	–	–	45.2, 52.7	55.8	0.17
$Pu5d_{5/2}$	107.6	105.0	106.0,	101.3	107.2	3.76
$Pu5d_{3/2}$	117.7	–	112.0, 118.3	113.7	123.0	2.56
$Pu5p_{3/2}$	218.0	216.2	217.4	211.1,	224.6,	2.38,
$Pu5p_{1/2}$	–	–	–	284.2	289.5	0.68
Pu5s	359.2	–	–	353.1, 365.1	359.7	0.76
$Pu4f_{7/2}$	428.7	426.6	427.1	422.1	426.5	31.03
$Pu4f_{5/2}$	441.2	439.8	439.3	435.1	440.3	24.36
$Pu4d_{5/2}$	803.5	801.8	803.9	798.1	806.3	17.81
$Pu4d_{3/2}$	851.7	849.8	852.2	844.8	854.4	11.60
$Pu4p_{3/2}$	1128.9	–	–	1122.6	1131.8	7.95
O2s	24.0, 26.3	22.8	25.8, 27.1			0.14
O1s	532.8	530.3	533.0			2.93
$Cs5p_{3/2}$	10.4 (10.1) [b]					0.33
Cs5s	23.7 (23.4) [b]					0.18
Cl3s	16.1 (15.0) [b]					0.19

[a] Obtained at 1487 eV and expressed in 13.6 b per atomic shell.[203] [b] The electron binding energies for CsCl are given in parentheses.

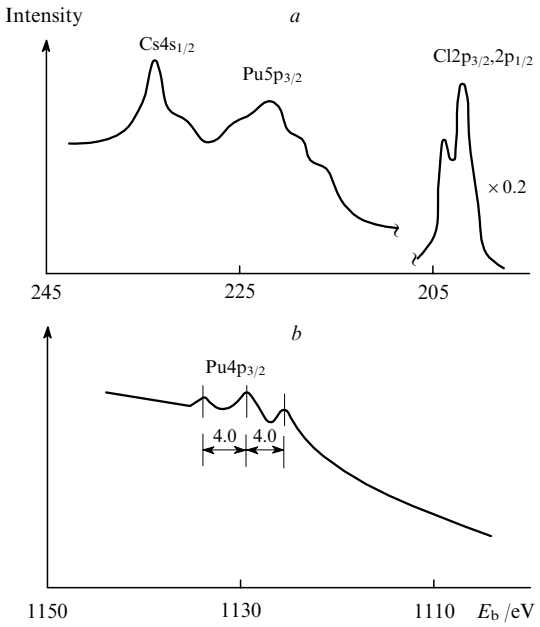

Figure 35. XPS spectra of $Cs_2PuO_2Cl_4$ in the $Pu5p_{3/2}$ (*a*) and $Pu4p_{3/2}$ (*b*) binding energy ranges.[55]

Comparison of the Pu4f lines in the spectra of $Cs_2PuO_2Cl_4$,[82] containing Pu^{6+}, and the dioxide PuO_2,[79] containing Pu^{4+}, shows that the binding energy distance from the basic lines of the doublet to the satellites (ΔE_{Sat}) can characterise, as in the case of uranium and neptunium compounds, the plutonium oxidation state. In the spectra of $Cs_2AnO_2Cl_4$ with An = Pu^{6+}, Np^{6+} and U^{6+}, the ΔE_{Sat} values equal 3.4, 3.5 and 3.8 eV, and the intensities I_{Sat} are 20, 20 and 20%, respectively. In the spectra of AnO_2 for An = Pu^{4+}, Np^{4+} and U^{4+}, the ΔE_{Sat} values amount to ~7,

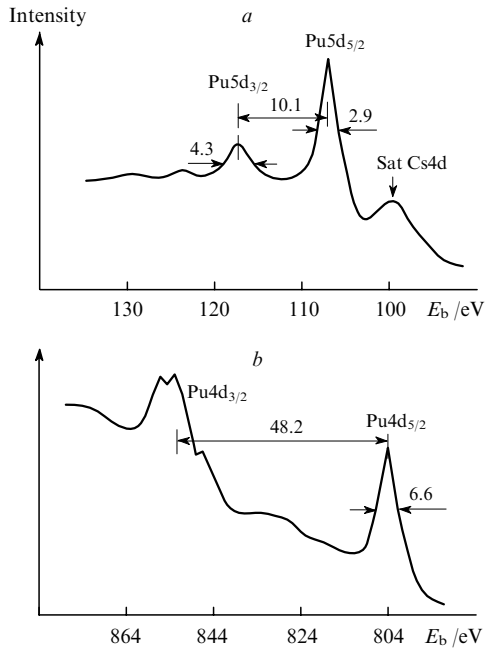

Figure 34. XPS spectra of $Cs_2PuO_2Cl_4$ in the Pu5d (*a*) and Pu4d (*b*) binding energy ranges.[82] A satellite arising on the higher binding energy side of the basic Cs4d line is shown.

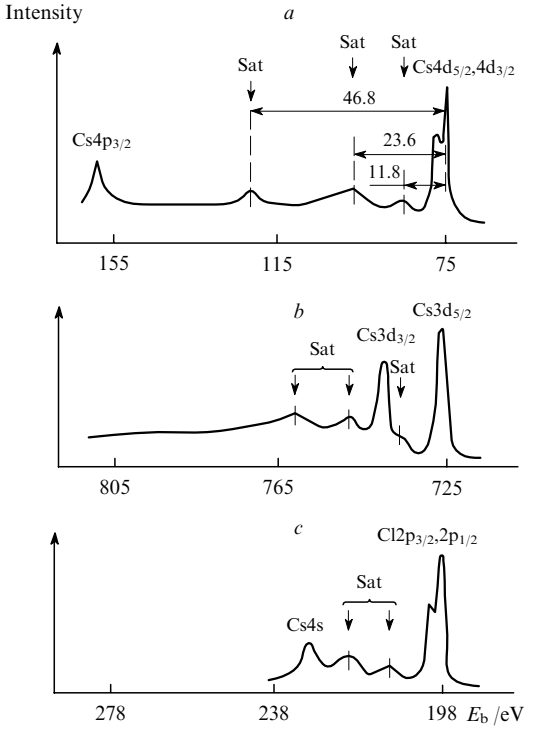

Figure 36. XPS spectra of caesium chloride in the binding energy range of core electrons.[55]
(*a*) $Cs4p_{3/2}$ and Cs4d electrons; (*b*) Cs3d-electrons, (*c*) Cs4s electrons.

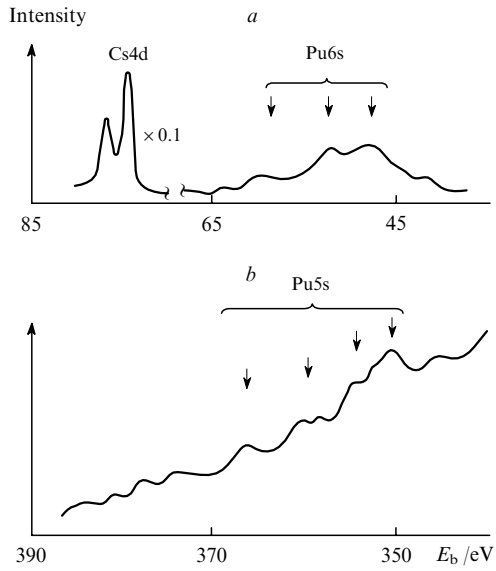

Figure 37. XPS spectra of $Cs_2PuO_2Cl_4$ in the Pu6s (*a*) and Pu5s binding energy ranges (*b*).[55]

~7 and 6.9 eV, while I_{Sat} are ~20, ~17 and 25%, respectively. The spin–orbit splitting ΔE_{sl}(Pu4f) values found by different researchers are 13.0, 12.7 and 12.5 eV for plutonium metal,[83] PuO_2 oxide[79] and $Cs_2PuO_2Cl_4$,[82] respectively. The observed differences in the ΔE_{sl}(Pu4f) values are related to the error of determination (see Table 15).

b. The spectra of Pu5d and Pu4d electrons

In the Pu5d binding energy range (see Fig. 34), an intense band with $E_b \approx 100$ eV due to the satellite of the Cs4d line is observed on the lower binding energy side of the basic $Pu5d_{5/2}$ line. The intensity of the $Pu5d_{3/2}$ component is largely suppressed, and it is broad compared to the basic $Pu5d_{5/2}$ line.

Despite the complicated spectral structure, the $Pu5d_{5/2}$ line can be used to determine the Pu oxidation state in compounds. Thus on passing from plutonium metal to the Pu^{6+} ion, the binding energy of these electrons decreases by $\Delta E_b(Pu5d_{5/2}) = 6.3$ eV (see Table 15). When the plutonium oxidation state changes from Pu^{4+} to Pu^{6+}, the corresponding energy difference is 2.6 eV. For individual compounds, these differences can be easily measured experimentally. The fine structure of the Pu5d spectra can also characterise the plutonium oxidation states in compounds. However, the exact energy of the spin–orbit splitting of the Pu5d line [ΔE_{sl}(Pu5d) = 11 eV][20] is difficult to determine due to the complex shape of this line (see Table 15).

The $Pu4d_{5/2}$ line for $Cs_2PuO_2Cl_4$ (see Fig. 34) is relatively broad ($\Gamma = 6.6$ eV) and symmetric. In the $Pu4d_{3/2}$ binding energy range, fine structure is observed. A structured band, possibly associated with Auger transition electrons, occurs at these energies. Against the background of this structure, a peak attributable to the $Pu4d_{3/2}$ electrons is observed. The spin–orbit splitting ΔE_{sl}(Pu4d) found from this spectrum is 48.2 eV. This coincides with the value $\Delta E'_{sl}$(Pu4d) = 48.2 eV obtained from the PuO_2 spectra,[79] but differs from the value $\Delta E''_{sl}$(Pu4d) = 46.7 eV, found from the spectrum of plutonium metal in the Pu4d binding energy range, by 1.5 eV.[83]

c. The spectra of $Pu5p_{3/2}$ and $Pu4p_{3/2}$ electrons

The Pu5p binding energy range of the XPS spectrum of $Cs_2PuO_2Cl_4$ contains several rather intensive peaks attributed to ligands and carbon atoms of the residual organic substances adsorbed on the surface in vacuum (see Fig. 35). For example, the $Pu5p_{1/2}$ line is superimposed by the C1s spectrum, which precludes drawing conclusions concerning its structure.

The spectra of various ligands have been analysed.[55] In particular, the spectrum of CsCl has been thoroughly studied (see Table 12, Fig. 36). This allowed researchers to identify the structure due to the $Pu5p_{3/2}$ electrons upon comparison of the spectra of $Cs_2PuO_2Cl_4$ and CsCl in the Cl2p and Cs4s binding energy ranges (see Fig. 35).

Comparison of the $Pu5p_{3/2}$ spectral structure for the studied compounds with the An5p spectra of other actinides shows that this structure can be attributed to the dynamic effect resulting in final states of the type $Pu5p^5 5d^{10}(6s^2 6p^6)5f^n \rightleftharpoons Pu5p^6 5d^8.(6s^2 6p^6)5f^{n+1}$. Indeed, the ratio of the Pu5p and Pu5d binding energies does not contradict this assumption. Thus for $Cs_2PuO_2Cl_4$, $E_b(Pu5p_{3/2}) = 218$ eV and $E_b(Pu5d_{5/2}) = 107.6$ eV (see Table 15), which approximately satisfies the condition $E_b(Pu5p_{3/2}) \approx 2\,E_b(Pu5d_{5/2})$.

The structure observed in the $Pu4p_{3/2}$ spectrum largely resembles that observed in the $Pu5p_{3/2}$ spectrum. The binding energies $E_b(Pu4p_{3/2}) = 1128.9$ eV, $E_b(Pu4d_{3/2}) = 851.7$ eV and $E_b(Pu5s) = 359.2$ eV approximately satisfy the condition $E_b(Pu4p) \approx E_b(Pu4d) + E_b(Pu5s)$. This suggests that, as for thorium, uranium and neptunium compounds, in this case, too, the structure observed in the spectrum of $Cs_2PuO_2Cl_4$ in the $Pu4p_{3/2}$ binding energy range may be due to a large extent to the dynamic effect, resulting in the formation of final states of the type $Pu4p^5 4d^{10}(4f^{14})5s^2(5p^6 5d^{10}6s^2 6p^6)5f^n np^m \rightleftharpoons Pu4p^6 4d^9(4f^{14})5s^1.(5p^6 5d^{10}6s^2 6p^6)5f^n np^{m+1}$.

d. The spectra of Pu6s and Pu5s electrons

Instead of the expected single peak for Pu6s electrons, the spectrum exhibits a complicated fine structure in an energy span covering ~30 eV.[55] A number of averaged peaks at 49.0, 54.5, 59.5 and 67.3 eV can be noted. The weight-average binding energy for these electrons E_b – (Pu6s) amounts to 51.2 eV (see Fig. 37).

Probably, the structure of the Pu6s spectrum is mainly due to the dynamic effect giving final states like $Pu6s^1 6p^6 5f^n 6d^m \rightleftharpoons 6s^2 6p^4 5f^n 6d^{m+1}$. Indeed, the values $\overline{E}_b$ (Pu6s) = 51.2 eV, $E_b(Pu6p_{3/2}) = 20.5$ eV and $E_b(Pu6p_{1/2}) = 30.4$ eV obey satisfactorily the condition $\overline{E}_b$ (Pu6s) $\approx 2\,E_b$(Pu6p), which is not at variance with the assumption concerning the dynamic effect. The spectral structure parameters can hardly allow a conclusion about the possible participation of the Pu6s shell in the OVMO and IVMO formation.

The Pu5s spectrum is expected to exhibit a fine structure in the region where the intensity of the C1s satellite corresponding to the carbon atoms of the adsorbed oil declines (see Fig. 37). Indeed, this range in the spectrum of $Cs_2PuO_2Cl_4$ contains peaks at 351.2, 354.9, 358.2 and 365.8 eV (see Fig. 37) for which the weight average binding energy is given by $\overline{E}_b$ (Pu5s) = 359.2 eV (see Table 15).

In the Pu5s binding energy range equal to ~35 eV, the XPS spectrum of Pu metal exhibits two peaks with the width $\Gamma \approx 10$ eV having a fine structure.[83] Hence, it can be suggested that the structure at 351.2 and 354.9 eV ($\Delta E_b = 3.7$ eV) (see Fig. 37) is partially due to the multiplet splitting. It is evident that the pronounced broadening (to ~35 eV) of the Pu5s binding energy range containing fine structure in the spectrum of $Cs_2PuO_2Cl_4$ cannot be attributed to the multiplet splitting alone.

For $Cs_2PuO_2Cl_4$, the binding energies $\overline{E}_b$ (Pu5s) = 359.2 eV, $E_b(Pu5p_{3/2}) = 218.0$ eV and $E_b(Pu5d_{5/2}) = 107.6$ eV satisfy the condition $\overline{E}_b$ (Pu5s) $\approx E_b$(Pu5p) + E_b(Pu5d). Thus, it can be suggested that the structure observed in the Pu5s binding energy range can also be attributed to the dynamic effect with the final states like $Pu5s^1 5p^6 5d^{10}(6s^2 6p^6)5f^n \rightleftharpoons Pu5s^2 5p^5 5d^9(6s^2 6p^6)5f^{n+1}$. The same conclusions have been drawn by other researchers,[83] who analysed the XPS spectral structure for plutonium metal.

It should be noted that, as for compounds of other actinides, this XPS spectral structure can be used to identify particular plutonium compounds.

VI. General rules of the formation of fine structure in the XPS spectra of actinide compounds

The fine structures of the XPS spectra of light actinide compounds have much in common. As noted above, this is due to the fact that actinides form a row of transition elements in which the An5f shell is gradually occupied by electrons with the increase in the atomic number. A complex fine structure is manifested to one or another extent in the XPS spectra of all electronic levels in the binding energy range of 0 – 1250 eV. On the one hand, the reasons for fine structure formation in the spectra of various electron shells of actinide compounds are largely similar, but on the other hand, parameters of the fine spectral structure are characteristic of particular compounds. Thus, the XPS spectral structure of the core and outer electron shells can be used to elucidate the physicochemical properties of actinide compounds. A typical feature of the An6p$_{3/2}$ and An5f valence electrons of actinides is relatively weak dependence of the binding energies (E_b) on the atomic number (Z) compared to analogous dependences for core electrons (Fig. 38). In the series of actinide dioxides, the binding energy for the valence An5f electrons increases by 3.1 eV, that of the An6p$_{3/2}$ electron, by 2.7 eV, and the core An5d$_{5/2}$ binding energy increases by 38.0 eV as the atomic number increases in the range of $90 \leqslant Z \leqslant 98$. The substantial increase in the An6p$_{1/2}$ binding energy is due to enhancement of the spin – orbit splitting ΔE_{sl}(An6p). Indeed, as noted above, the peaks in the An6p$_{3/2}$ and An6p$_{1/2}$ binding energy ranges observed in the spectra of actinide dioxides reflect the inner valence molecular orbitals rather than atomic levels. As a result, the An6p electrons are delocalised and shielded from the core charge, their energy depending only slightly on the atomic number Z. As was to be expected, the An5d, An4f and An4d binding energies of the core levels of actinides (Th, U, Np, Pu, Am, Cm, Bk, Cf), for example, in oxides,[79] increase appreciably with an increase in the atomic number (Table 16).

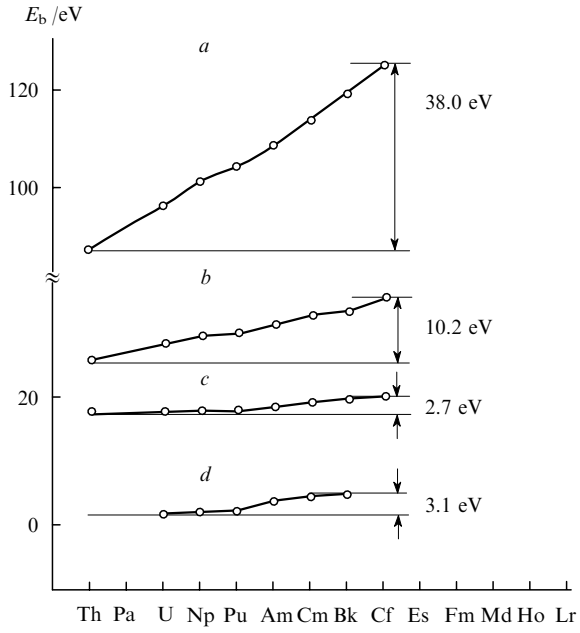

Figure 38. Variation in the binding energies (E_b) of valence and inner electrons in actinide dioxides in the series Th – Lr.[79]
(*a*) An5d$_{5/2}$ electrons; (*b*) An6p$_{1/2}$ electrons; (*c*) An6p$_{3/2}$ electrons; (*d*) An5f electrons.

1. Spectra of the An5f electrons

The An5f electrons not involved in the chemical bond largely determine the magnetic properties of actinide compounds.[143, 255–257] The XPS spectra of compounds containing the An5f electrons exhibit a relatively narrow line around a zero binding energy (Fig. 39). The assumption that this line is due to free An5f electrons based on experimental data [38–40, 67, 68, 87, 127, 197, 252, 253] is consistent with the results of theoretical calculations.[93, 129, 137, 180] In particular, the correlation between the core An4f binding energy and the An5f line intensity observed for uranium and neptunium compounds confirms the assignment of the lines near a zero binding energy in the XPS spectra to the An5f electrons.[81, 88] Indeed, a decrease in the intensity of the line for the An5f electrons not involved in the chemical bond (*i.e.*, a decrease in the relative density of the An5f electrons on the actinide ions) brings about an increase in the actinide oxidation state and, hence, an increase in the core electron binding energies (Fig. 40).

It follows from the above results that the An5f electrons not involved in the chemical bond are largely accumulated on the actinide ions in compounds, and the corresponding orbitals are quasi-atomic (see Fig. 39).

Figure 41 shows that the slopes of the straight lines that reflect the dependence of the relative intensity of the An5f lines on the actinide oxidation state (Table 17) are equal to within the experimental error.[55] This allowed a group of researchers [81, 88–90] to find a general mathematical expression for the dependence of the relative intensity I_{5f}^{exp} on the number n_{5f} of free An5f electrons (Fig. 42).

It can be seen from Figs 41 and 42 that the An5f line intensity in the XPS spectra of the studied actinide compounds in the range of $0 \leqslant n_f \leqslant 7$ is proportional to the number of electrons not involved in the chemical bond. Within the framework of the approximations used, it can be inferred that the oxidation state of actinides changes discretely and that the An^{n+} ions have the electron configuration $\{Rn\}5f^n$.

Table 16. Binding energies (E_b) for core electrons in actinide oxides.[79]

Oxide	E_b /eV										
	6p$_{3/2}$	6p$_{1/2}$	5d$_{5/2}$	5p$_{3/2}$ (see [a])	4f$_{7/2}$	4f$_{5/2}$	4d$_{5/2}$	4d$_{3/2}$	O2s	O1s	C1s
ThO_2	17.2	25.2	87.0	178.9	334.6	343.9	675.7	713.0	22.9	530.5	285.4
UO_2	17.2	28.1	96.0	197.2	379.6	390.5	737.7	780.1	22.5	529.7	284.6
NpO_2	17.5	29.3	100.9	206.3	402.5	414.3	771.2	816.1	23.8	529.7	284.5
PuO_2	18.4	30.6	105.0	216.2	426.6	439.3	801.8	849.8	22.8	530.3	285.3
AmO_2	18.1	31.1	108.4	–	448.2	462.5	832.0	883.1	23.1	529.0	284.4
CmO_2	18.4	32.1	113.2	231.7	472.7	487.4	865.2	918.7	22.7	530.1	284.0
BkO_2	18.3	34.0	120.1	245.8	498.5	514.4	901.4	957.7	23.4	529.5	285.3
Cf_2O_3	19.4	34.9	124.5 [b]	–	523.3	541.1	933.1	993.7	24.7	530.3	283.9
AnO_x									23.2 [c]	529.9 [c]	284.7 [c]

[a] High energy component of the doublet. [b] The highest peak. [c] Average values.

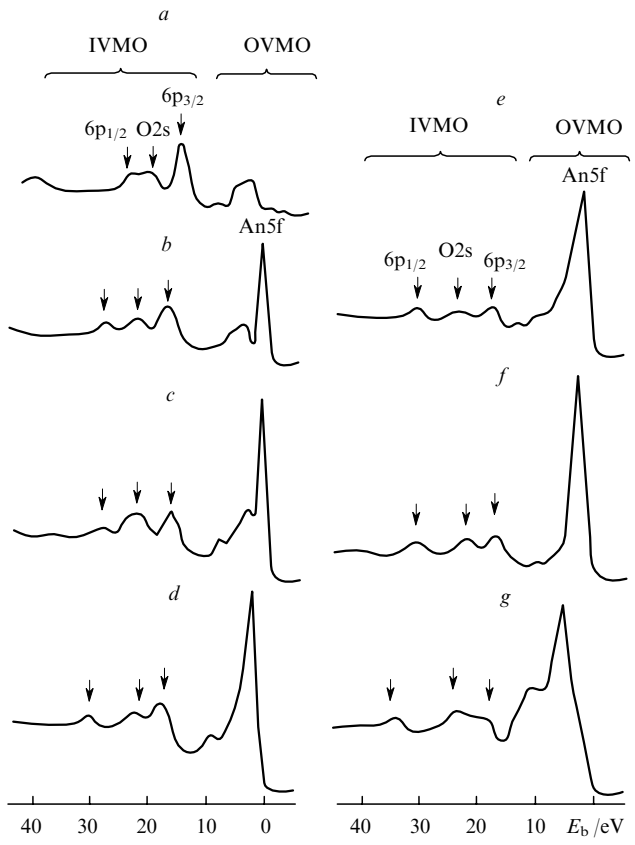

Figure 39. XPS spectra of actinide dioxides (AnO_2) in the low binding energy range.[79]
(*a*) ThO_2, (*b*) UO_2, (*c*) NpO_2, (*d*) PuO_2, (*e*) AmO_2, (*f*) CmO_2, (*g*) BkO_2.

The relative intensity of the An5f line was measured as the ratio of the area confined by the An5f line to the area confined by the $An4f_{7/2}$ line, $I_{5f}^{exp} = I(An5f)/I(An4f_{7/2})$. The satellite lines caused by the shake up process which accompanies the photo-

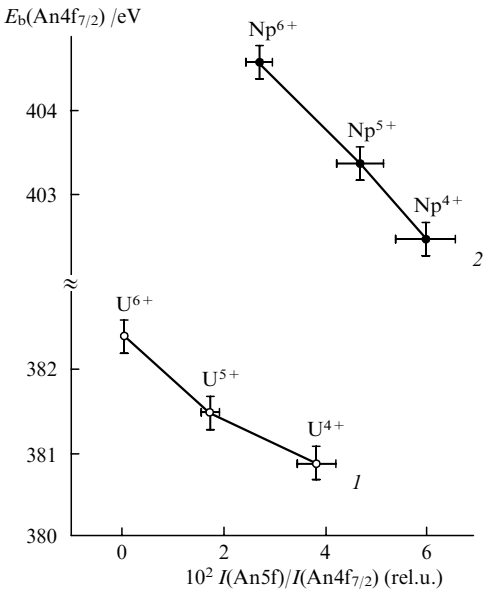

Figure 40. Correlation of the $An4f_{7/2}$ binding energy [$E_b(An4f_{7/2})$] with the relative intensity of the An5f lines [$I(An5f)/I(An4f_{7/2})$] in the XPS spectrum of uranium (*1*) and neptunium compounds (*2*).[81, 88] The dots are experimental data.

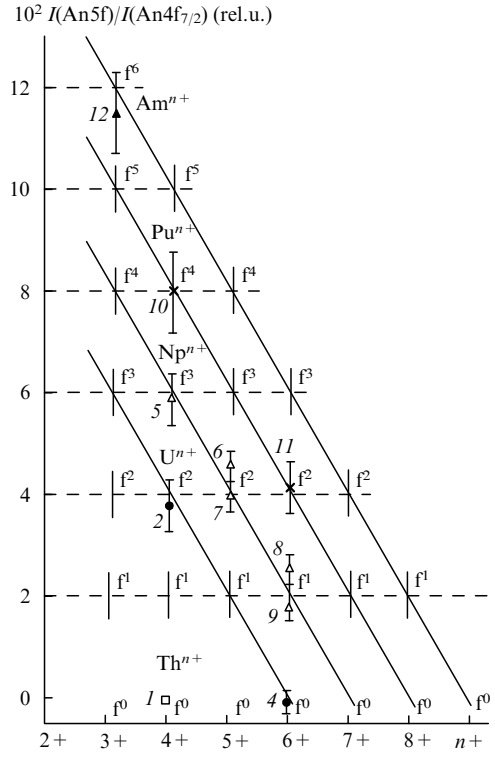

Figure 41. Relative intensity of the An5f lines [$I(An5f)/I(An4f_{7/2})$] in the XPS spectra of actinides (An = Th, U, Np, Pu, Am) *vs*. their oxidation state (n^+) in oxygen-containing compounds of thorium (square), uranium (dark circles), neptunium (light triangles), plutonium (crosses), and americium (dark triangle).[90, 253]
The dots show the experimental data; their numerals correspond to the numbers of compounds in Table 17.

Table 17. Binding energy differences between the An5f levels and OVMO (ΔE_i), relative intensities (I_{5f}^{exp}) of the lines for the An5f electrons not involved in the chemical bond for actinide ions in various oxidation states (An^{n+}).[81]

Compound	ΔE_i[a] /eV	$10^2\, I_{5f}^{exp}$ (red.u.)			n_{5f} (see [b])
		An^{4+}	An^{5+}	An^{6+}	
ThO_2 (**1**)	–	0			0
UO_2 (**2**)	4.2	3.8			2
UO_2 (**3**)[c]	–	3.8			2
γ-UO_3 (**4**)	–			0	0
NpO_2 (**5**)[c]	2.0	5.9			3
$Cs_3NpO_2Cl_4$ (**6**)	2.4		4.6		2
$RbNpO_2(NO_3)_2 \cdot 2H_2O$ (**7**)	2.5		4.0		2
$Cs_2NpO_2Cl_4$ (**8**)	2.0			2.6	1
$NaNpO_2(OAc)_3$ (**9**)	2.5			1.8	1
PuO_2 (**10**)[c]	1.0	8.0			4
$Cs_2PuO_2Cl_4$ (**11**)	1.0			4.2	2
$Am(NO_3)_3 \cdot n\,H_2O$ (**12**)[d]	–				6
AmO_2 (**13**)[c]	0.5	11.6			5
CmO_2 (**14**)[c]	–	12.2			6
BkO_2 (**15**)[c]	–	13.9			7
$Pu(NO_3)_4 \cdot n\,H_2O$ (**16**)	–	8.3			4

[a] Binding energy differences found from the maxima of the An5f lines and OVMO (energy gap). [b] The number of weakly bound An5f electrons. [c] The I_{5f}^{exp} values were found by renormalisation of published data[41, 79] with allowance for the I_{5f}^{exp} value for UO_2 and are expressed in units used in Ref. 81. [d] For An^{3+}, the I_{5f}^{exp} value is 11.5×10^{-2} red.u.

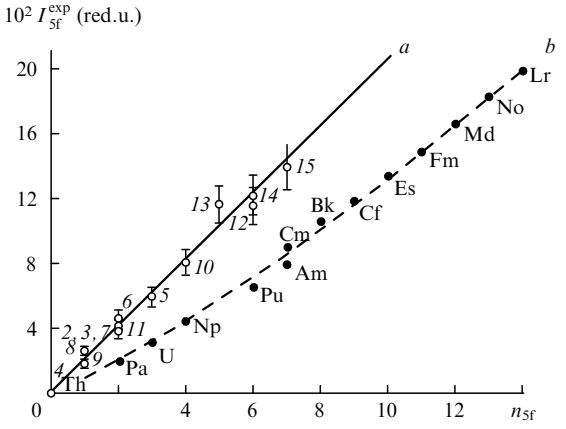

Figure 42. Relative intensity of the An5f lines [$I_{5f}^{exp} = I(An5f)/I(An4f_{7/2})$] in the XPS spectra of actinides and their compounds *vs*. the number of 5f electrons (n_{5f}).[88]
(*a*) Experimental values for actinide compounds (the numerals correspond to the numbers of compounds in Table 17); (*b*) calculated values for actinide atoms.

emission of the An4f electron were not taken into account.[81, 88–90] The area confined by the lines for such satellites can reach 20% of the area corresponding to the basic lines.[90] For example, the OVMO band in the spectra of actinide oxides located in the binding energy range from 0 to ~15 eV is mainly formed by the An5f, An6d and An7s electrons of the actinide and the O2p electrons of oxygen. For the X-ray excitation energy normally used in XPS studies (1486.6 eV), the photoionisation cross-sections (σ) for the O2s and $O2p_{3/2}$ electrons are equal to 0.00191 and 0.000263 Mb, respectively,[258] which is substantially lower than the value $\sigma \approx 0.02$ Mb for the An5f electrons. In addition, the photoionisation cross-sections for the An5f electrons of all actinides are much greater than the corresponding σ value for the $An6d_{3/2}$ (~0.0020 Mb) and An7s electrons (~0.00018 Mb).[258] Therefore, the intensity of the low binding energy XPS spectrum is mainly due to the An5f electrons.

The experimental data for the dependence of the relative intensity of the An5f line on the number of weakly bound electrons reported in several publications [81, 88–90] (see Table 17, Fig. 42) are described satisfactorily by the following equation:[90]

$$I_{5f}^{exp} = 0.0217\, n_{5f}. \qquad (15)$$

Equation (15) was derived with the assumption that the oxidation states of actinides in compounds are integers and the photoionisation cross-section barely depends on the atomic number (Z). This approximation is most adequate for light actinides since the energy gap between the E_b values for weakly bound An5f electrons and OVMO electrons determined from the XPS spectra of these actinides is rather narrow (see Table 17). Physically, this means that the An5f electron involved in chemical bonding passes from the localised state corresponding to a relatively narrow low binding energy XPS line to the delocalised state corresponding to the OVMO band. Despite the roughness of this approximation, the experimental dependence considered (see Fig. 42) can be effectively used for determination of actinide oxidation states in compounds.[90] For example, for AmO_2 (see Table 17, Fig. 42), this dependence suggests that either the oxide Am_2O_3 or another Am^{3+} compound is formed on the sample surface.

In the MO LCAO approximation, during the MO formation in actinide compounds, the An5f electrons can either directly participate in a chemical bond with retention of their nature ($l = 3$, where l is the orbital quantum number) [137] or be first excited, for example, to the An6d level, and participate in the chemical bond having the new d nature ($l = 2$). The relative intensity of the X-ray photoelectron lines of the OVMO electrons (I_{OVMO}^{theor}) in actinide oxides,[81] equal to the ratio of the intensities of the lines due to the OVMO (including An5f) and IVMO (including An6p and O2s orbitals) electrons, was estimated theoretically taking into account the corresponding photoionisation cross-sections [258] according to the equation

$$I_{OVMO}^{theor} = \frac{n_{5f}\sigma_{5f} + n_{6d}\sigma_{6d} + n_{7s}\sigma_{7s} + \nu n_{O2p}\sigma_{O2p}}{n_{6p}\sigma_{6p} + \nu n_{O2s}\sigma_{O2s}}, \qquad (16)$$

where n_{nl} and σ_{nl} are the numbers of electrons and the corresponding photoionisation cross-sections, and ν is the number of oxygen atoms ($\nu = 2$ for AnO_2 and 3 for AnO_3). Since all the considered lines fall in a binding energy range of ~35 eV, no corrections taking into account the binding energy differences between the electrons of different levels were introduced in relation (16).

The I_{OVMO}^{theor} values obtained in this approximation can be compared with the corresponding experimental data for actinide oxides (Table 18). The experimental values of I_{OVMO}^{exp} are presented in Table 18 for the electronic configurations acquired by the actinide ions in those cases where the An5f electrons involved in the chemical bond lose their f nature upon the formation of the bond. Although the error in the measurement of I_{OVMO}^{exp} can reach 20% and An5f and other valence electrons become delocalised upon chemical bonding and their photoionisation cross-sections should decrease, a number of qualitative conclusions have been reported.[81, 87, 88] Indeed, the fact that the I_{OVMO}^{exp} values (0.35 for ThO_2 and 0.72 for γ-UO_3) are substantially greater than the I_{OVMO}^{theor} values (0.20 and 0.30, respectively) can be related to the involvement of the An5f AO in the OVMO formation. As a result, An5f states occupied by electrons are present in the valence band of the oxides, ThO_2 and γ-UO_3; these states are missing, for example, for the thorium atom. This experimental result, although qualitative, is very important and agrees with the data of calculations of the electronic structures of these oxides.[137] It follows from the foregoing that upon the formation of chemical bond in actinide oxides, the An5f electrons can lose the f nature only partially.

In order to evaluate the validity of the assumption of localisation of weakly bound An5f electrons in actinide compounds made on the basis of experimental data, [35, 81, 87, 88] the experimental intensities of the An5f lines were compared with the corre-

Table 18. Theoretical [I_{OVMO}^{theor} (rel.u.)] and experimental [I_{OVMO}^{exp} (rel.u.)] relative intensities of the OVMO line in the XPS spectra for various occupancies of the shells (n_{nl}).[81]

Oxide	n_{5f}	n_{6d}	n_{7s}	I_{OVMO}^{theor}	I_{OVMO}^{exp}
ThO_2	0	2	2	0.20	0.35
UO_2	3	1	2	1.15	–
	2	2	2	0.87	1.03
γ-UO_3	3	1	2	1.01	–
	2	2	2	0.77	–
	1	3	2	0.52	–
	0	4	2	0.30	0.72
NpO_2	4	1	2	1.63	–
	3	2	2	1.30	1.38
	2	3	2	0.99	–
PuO_2	6	0	2	2.39	–
	5	1	2	2.06	–
	4	2	2	1.73	1.73
AmO_2	7	0	2	3.05	–
	6	1	2	2.71	–
	5	2	2	2.33	2.34
CmO_2	7	1	2	3.41	–
	6	2	2	3.03	2.45
BkO_2	9	0	2	4.57	–
	8	1	2	4.14	–
	7	2	2	3.72	2.75

sponding theoretical values determined from the photoionisation cross-sections of these electrons with allowance for the influence of spectroscopic and other factors on the An5f line intensity (see Fig. 42). The question of why the experimental dependence [see Fig. 42, Eqn (15)] is approximately linear was considered.

The dependences of the photoionisation cross-section $\sigma(An4f_{7/2})$ and $\sigma(An5f)$ on the number of An5f electrons n_{5f} (see Refs 53, 81) are shown in Fig. 43. It can be seen that these dependences are not linear. However, the variation of the $\sigma(An5f)/\sigma(An4f_{7/2})$ ratio as a function of n_{5f} is described by a smoother curve and, to a certain approximation, it can be regarded as linear. This explains qualitatively the course of the corresponding experimental dependence (see Fig. 42). However, the calculated $\sigma(An5f)/\sigma(An4f_{7/2})$ values are much smaller than the experimental values derived from the intensities of spectral lines.

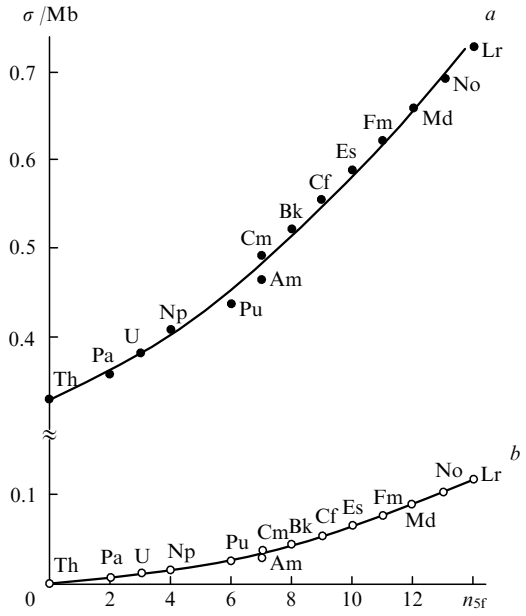

Figure 43. Photoionisation cross-sections (σ) for $An4f_{7/2}$ (*a*) and An5f shells (*b*) of actinide atoms *vs.* the number of An5f electrons (n_{5f}). The calculations were carried out in the Dirac – Fock approximation with precise calculation of the exchange integral.[35,81]

The theoretical values of the relative intensity I_{5f}^{theor} calculated using full photoionisation cross-sections and spectroscopic and other factors[81,88] for the basic configurations of actinide atoms are given in Fig. 42 in comparison with the corresponding experimental data. This comparison is qualitative, because the theoretical dependence was constructed without taking into account the participation of actinide atoms in the chemical bond. Nevertheless, it follows from Fig. 42 that the overall pattern of the theoretical curve following the increase in the number of An5f electrons is in qualitative agreement with experimental data.

The experimental relative intensity $I_{5f}^{exp} = I(An5f)/I(An4f_{7/2})$ of the An5f line was used[35] to estimate the non-formal number of these electrons (n_{5f}) in actinide ions. This was done according to the equation

$$n_{5f} = I_{5f}^{exp}\frac{f_{4f}n_{4f}\sigma'_{4f}\lambda_{4f}[1-\beta_{4f}(0.75\cos^2\theta-0.25)]F_{4f}}{f_{5f}\sigma'_{5f}\lambda_{5f}[1-\beta_{5f}(0.75\cos^2\theta-0.25)]F_{5f}}, \qquad (17)$$

where f is the spectroscopic factor, σ'_{nf} is the photoionisation cross-section per electron, λ is the electron free path, β is the asymmetry parameter, θ is the angle between the non-polarised radiation and the photoelectron escape (in this case, $\theta = 90°$), F is the transmittance of the analyser. Only the $An4f_{7/2}$ shell was considered, therefore the subscript 7/2 is omitted. The spectroscopic factor (the fraction of the basic peak without inclusion of satellites) has been calculated.[35]

It was shown[35] that for a neptunium oxidation state of 4+ the number of the Np5f electrons, equal to 4.25, differs little from the number of these electrons for the free atom. For pentavalent neptunium, the number of Np5f electrons is approximately 3, while for hexavalent neptunium, it is between 1 and 2. For UO_2, these data are consistent with the results presented in Table 18. Indeed, the value $I_{OVMO}^{exp} = 1.03$ for UO_2 corresponds to an n_{5f} value ranging from 2 to 3 (see Table 18). The data for other oxides indicate that the An5f orbitals take a significant part in chemical bonding.

Thus, for analysis of the electronic structure and quantitative ionic composition of actinides and for determination of actinide oxidation states in compounds, important information can be gained from the XPS spectral parameters for the An5f binding range. The quantitative correlation found between the relative intensity of the line for the weakly bound An5f electrons and the actinide oxidation state (U, Np, Pu, Am, Cm, Bk) in compounds is used to determine the ionic composition of actinides. The fact that the An5f electrons can directly participate in chemical bond formation is in line with the data of resonance X-ray $O_{4,5}$(U) emission spectra of uranium oxides measured using synchrotron radiation.[259–261] On the basis of chemical shifts of the X-ray $L_{\alpha1}$, $L_{\beta2,4}$, $L_{\beta1,5}$ and $L_{\gamma1}$ emission spectra, the conclusion about the existence of bound Th5f states in thorium oxide and halides has also been drawn.[262]

Despite the scantiness of the information on the magnetic behaviour of actinide compounds, a number of conclusions have been reached[44,89,90] from comparison of the data on their magnetic moments and magnetic susceptibilities with XPS data. During filling of the An5f shell in uranium and neptunium compounds, no direct proportionality between the effective magnetic moment (μ_{eff}) and the An5f line intensity can be followed (Fig. 44). The curve shown in the Figure is in good agreement with the dependence of molar magnetic susceptibility on the number of the Np5f electrons obtained previously.[254] The magnetic susceptibility data for the Pu^{4+} and Pu^{3+} ions also indicate that further filling of the An5f shell ($n_{5f} = 4, 5$) should entail a decrease in the

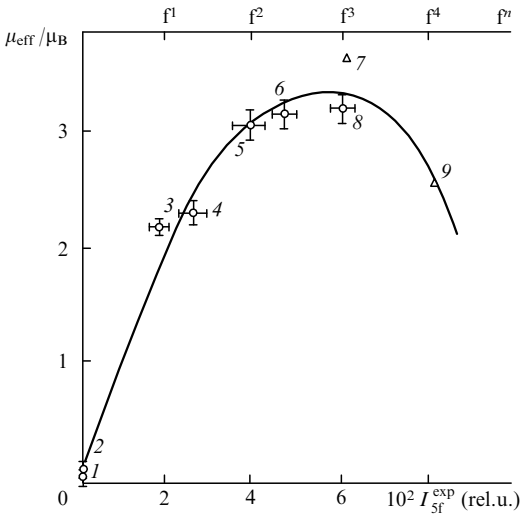

Figure 44. Relationship between the effective magnetic moments (μ_{eff}) of actinide compounds and relative intensity (I_{5f}^{exp}) of the XPS line for unbound An5f electrons.[89,90,253]
The μ_{eff} values were taken from Refs 211 and 251 (light circles) and from Ref. 263 (triangles). (*1*) ThO_2, (*2*) γ-UO_3, (*3*) $NaNpO_2(OAc)_3$, (*4*) $Cs_2NpO_2Cl_4$, (*5*) UO_2, (*6*) $Cs_3NpO_2Cl_4$, (*7*) $U(HCO_2)_3$, (*8*) NpO_2, (*9*) $Np(HCO_2)_3$. For $U(HCO_2)_3$ and $Np(HCO_2)_3$, the I_{5f}^{exp} values were not measured.

magnetic moment.[98, 254, 263] These results attest to a complex pattern of the influence of unbound An5f electrons on the magnetic properties of actinide compounds. Many problems are still to be solved in this field.

2. The spectra of the An6p and O2s, L*n*s electrons

Th comparison of binding energy differences between the core and valence electron levels of metals and compounds used in a number of studies [53–55] allowed the researchers to elucidate legitimately the MO structure, to construct the MO diagrams and to estimate the degree of participation of the low-energy occupied An6p and O2s L*n*s AO of the neighbouring atoms in the formation of the IVMO in actinide compounds. This approach provides the possibility of estimating the effect of IVMO formation not only in asymmetric actinide compounds containing AnO_2^{n+} actinyl groups, but also in highly symmetric compounds like AnO_2 (AnO_8^{12-}, O_h group of symmetry), whose XPS spectra exhibit less pronounced IVMO structure in the low energy XPS range. For example, the splitting between bonding and antibonding IVMO in uranium compounds can reach 15 eV,[109] which is comparable with the energy difference between IVMO in the nitrogen molecule (18.7 eV).[19] The method of 'differences' can also be used to evaluate the nature (bonding, antibonding or non-bonding) of individual IVMO, which is important for comparison with the results of calculations of the contribution of IVMO electrons to chemical binding. The use of this method, with allowance for the data of theoretical calculations of the electron structure, allows one to identify the IVMO structure based on the low binding energy XPS spectra and to correlate the parameters of this structure with the structure of the local environment of the actinide ion in the compound. The distances from the actinide to the nearest ligand atoms can often be estimated experimentally. For amorphous compounds, these data can hardly be obtained by X-ray diffraction.

Theoretical estimates have shown [52, 102, 115, 226] that the contribution of the IVMO electrons to the energy of chemical bonds in the AnO_2^{2+} clusters (An = U, Np, Pu) is approximately 25% of the contribution of the electrons from all MO. The experimental data on the natures of various IVMO do not contradict qualitatively these results. The XPS data on the OVMO and IVMO structures in actinide compounds are qualitatively in line with the results of non-relativistic X_α-DV calculation of the electronic structure of the $[UO_2F_5]^{3-}$ cluster (D_{5h} group of symmetry) [264] and relativistic X_α-DV calculation for the UF_6, NpF_6, PuF_6,[265] UF_6 [266–268] and $UO_2(NO_3)_2 \cdot 2H_2O$ [204, 269] molecules as well as with the data of X-ray emission,[100, 182, 185, 186, 188, 234, 246, 247, 259] Auger,[235, 236] X-ray absorption,[189, 191, 270] conversion electron spectroscopy,[218–221] *etc*.

3. The role of the An6p and An5f electrons in the formation of chemical bond

Since the XPS spectra of actinide compounds together with the ionisation cross-sections reflect the total valence electron density in a binding energy range of 0–50 eV, additional information for determination of the partial density, for example, of the An6p and An5f states, can be derived from other X-ray spectral methods.

While examining the XPS spectra of actinides, it has been noted [53, 55, 103, 104] that the lines observed in the low binding energy range (E_b = 0–50 eV) are usually several electron-volt wide, being often wider than the lines for deeper core electrons.[53, 55] For example, in the case of UO_2, the FWHM (Γ) of the O1s line (E_b = 531.4 eV) amounts to 1.6 eV, whereas the width of the O2s line ($E_b \sim 23.3$ eV) exceeds 4 eV, and this line is structured.[66] In conformity with the uncertainty principle $\Delta E \Delta\tau \sim h/2\pi$ (h is Planck's constant), the natural width (ΔE) of the level from which the photoelectron has been removed is inversely proportional to the hole lifetime ($\Delta\tau$) of the ion formed. Since the hole lifetime decreases as the absolute binding energy increases, the width of the XPS lines for some atoms is expected to decrease rather than increase, as is really the case in experiments (see, for example, Figs 8, 19). This served as the main reason for the thorough investigation of the spectral structure for actinide compounds in this energy range.[53, 55, 103, 104] It was found that, among other reasons, line broadening in the low energy range (0–50 eV) of the XPS spectra is due to the formation of OVMO and IVMO in actinide compounds (see, for example, the studies [51–55]). These spectra reflect the band structure and are observed as several electron-volt wide lines. In particular, in uranium compounds, the IVMO arise due to the significant overlap of the U6p and L(O,F,Cl)*n*s shells of neighbouring atoms and ligands.

Yet another important aspect vigorously studied in recent years is efficient participation of the An5f shell in the OVMO formation. Previously, it has been traditionally assumed that prior to chemical bonding, the An5f electrons are excited to, for example, the An6d AO. However, the calculation results show that the An5f shells can be directly involved in the formation of MO in actinide compounds.[129, 228] This basically important fact requires experimental corroboration.[81, 88] The commensurability of experimental and theoretical values for the partial density of the An5f and An6p electrons of actinide compounds can serve as a criterion for the consistency of calculations.

As an example of the information on the An6p and An5f electronic states of actinides that can be gained from X-ray spectral and theoretical data, we shall consider the results obtained for uranium trioxide. In particular, the fine structure of the low binding energy range of the XPS spectrum of uranium trioxide has been analysed taking into account the results of calculations of the electronic structure of the $[UO_2O_4]^{6-}$ cluster (D_{4h} group of symmetry) reflecting the local environment of the uranium atom in γ-UO_3 (first carried out in the relativistic X_α-DV approximation).[110, 123, 271] The fine structure of the X-ray $O_{4,5}$(U) emission spectrum of γ-UO_3, reflecting the partial densities of the U6p and U5f electronic states in the valence band, has been studied for the first time.[185, 234]

As noted above, the low energy range (0–40 eV) of the XPS spectrum of uranium trioxide can be divided conventionally into two parts (Fig. 45). The first part (0–13 eV) exhibits a structure caused by the OVMO, which are mainly formed from partially occupied outer valence U5f, U6d, U7s and O2p AO of neighbouring atoms. The fine structure observed in the second part of the spectrum (13–40 eV) is due to the IVMO, which mainly arise due to the substantial interaction of the electrons from completely occupied valence U6p and O2s AO of the neighbouring atoms. The OVMO spectral structure has three characteristic features and can be divided into three components. Eight clear-cut peaks can be observed in the IVMO range, and eight components can be distnguished (see Fig. 45). Despite the formalism of such subdivision, it allows one to perform qualitative and quantitative comparison of parameters of the XPS spectrum with the corresponding parameters of the X-ray O4,5(U) emission, Auger and other spectra and with the results of relativistic calculations for the electronic structure of the $[UO_2O4]^{6-}$ cluster (D_{4h} symmetry group).

The intensity of the OVMO band was found to contain a contribution of the outer valence U5f, U6d and O2p AO and a substantial contribution of the inner valence U6p AO of neighbouring atoms. Experimental evidence for the direct participation of the U5f electrons in the chemical bonding with partial loss of their f nature has been obtained. Indeed, the experimental intensity ratio of the OVMO and IVMO bands is 0.70,[81] which is comparable with the theoretical value (0.93).[123] Since the U5f AO almost does not participate in the formation of the IVMO, the difference between these values may be due to the decrease in the photoionisation cross-section of the U5f electrons involved in chemical bonding. However, if the intensity of the OVMO band in uranium trioxide is assumed to be formed only by the $U6d^47s^2$ and $3O^2p^4$ electrons, and the IVMO intensity, by $U6p^6$ and $3O2s^2$ electrons, the corresponding theoretical value would have been 0.30 (see Table 18), which is significantly smaller than the

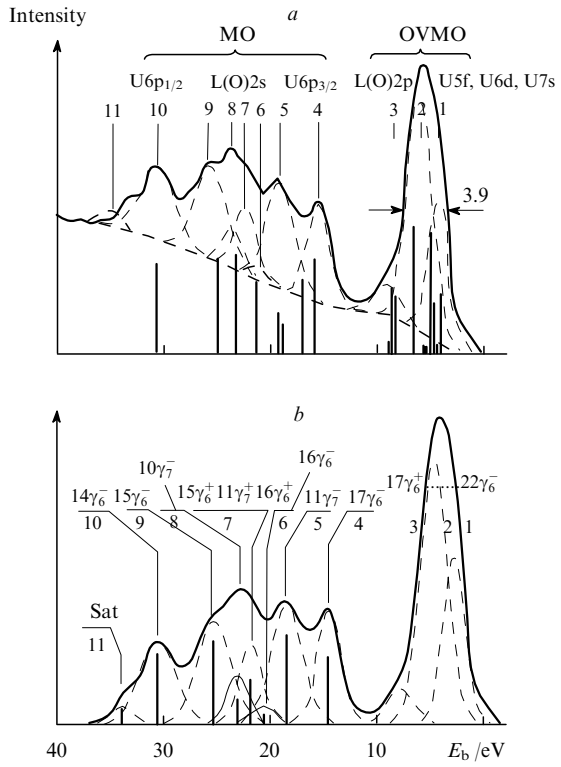

Figure 45. X-Ray photoelectron spectrum of γ-UO_3 with (*a*) and without (*b*) the background. The dashed lines show the spectral pattern of the subtracted background and thin lines show the conventional decomposition of the spectrum into components. The vertical segments in Fig. 45 *a* are the results of relativistic X_α-DV calculation for the $[UO_2O_4]^{6-}$ cluster (D_{4h} symmetry);[123] the vertical segments in Fig. 45 *b* show the expected correct spectrum simulated with allowance for calculations and experimental data;[110] $n\gamma_i^+$ and $n\gamma_i^-$ are designations of molecular orbitals; the digits are the numbers of peaks.

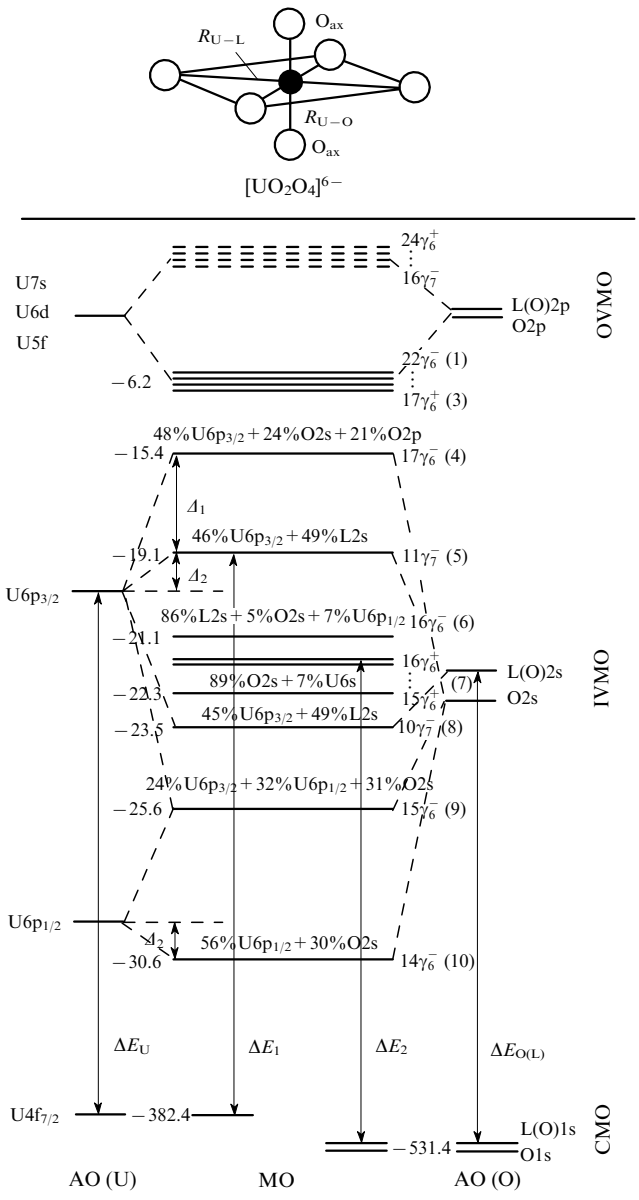

Figure 46. Diagram of MO energy levels in the $[UO_2O_4]^{6-}$ cluster (D_{4h} symmetry) constructed with allowance for calculations and experimental data.[271]
The chemical shifts of the energy levels upon the formation of the cluster from single atoms are not shown. The arrows show the energy differences that can be measured experimentally. The digits on the left are experimental E_b values, eV (the energy scale is not maintained).

experimental value.[81] This contradicts the traditional view that, before being involved in chemical bonding, the U5f electrons are excited to the U6d shell. Thus, the results of the relativistic calculation reflect rather reliably the partial electron density of the U5f states (see Fig. 45). This means that about two U5f electrons participate directly in the chemical bond, while the vacant U5f states are located in an energy range of 6 eV near the absorption edge.[123] This is in qualitative agreement with the X-ray $O_{4,5}$(U) emission spectroscopy [185] and X-ray near-edge $O_{4,5}$(U) absorption spectroscopy data for uranium trioxide.[189, 270]

In the IVMO binding energy range, the best agreement has been obtained for the $17\gamma_6^-$, $15\gamma_6^-$ and $14\gamma_6^-$ orbitals characterising the width of the spectrum of these electrons. Since the theoretical and experimental total relative intensities are comparable, the calculated energies of the $11\gamma_7^-$ – $10\gamma_7^-$ IVMO (see Fig. 45) may differ appreciably from the corresponding experimental values.

Using the data of relativistic calculations for the $[UO_2O_4]^{6-}$ cluster (D_{4h} group of symmetry) and experimental binding energy differences between the core and outer electron levels of uranium [57] and for uranium trioxide (see, for example, the studies [55, 109]), an MO diagram has been constructed in the MO LCAO approximation (Fig. 46).[123] This diagram provides understanding of the real XPS structure of uranium trioxide. In this approximation, one can distinguish conventionally the $17\gamma_6^-$ (4), $15\gamma_6^-$ (9) and $14\gamma_6^-$ (10) IVMO, which characterise the U – O bond length in the UO_2^{2+}; the $11\gamma_7^-$ (5) and $10\gamma_7^-$ (8) IVMO which characterise the U – L bond and its length in the equatorial plane of the cluster and the quasiatomic $16\gamma_6^-$ (6), $16\gamma_6^+$ (7), $11\gamma_7^+$ (7) and $15\gamma_6^+$ (7) orbitals formed from the O(L)2s AO of two types of oxygen atoms (O and L). Note that this separation of the IVMO has been experimentally substantiated.[55, 109] It follows from the experimental data that the energies of the quasi-atomic $16\gamma_6^-$ (6) – $15\gamma_6^+$ (7) IVMO should be similar to each other. Indeed, it follows from the parameters of the XPS spectrum of γ-UO_3 in the O1s binding energy range that the difference between the E_b values for these orbitals should not exceed 0.9 eV, as this line is asymmetric and its FWHM (Γ) equals 2.2 eV. The binding energy should be approximately 23.4 eV, because $\Delta E_{L,O}$ = 508 eV and the O1s binding energy for γ-UO_3 is 531.4 eV (see Fig. 46). In view of the fact that ΔE_U = 360.6 eV and ΔE_1 = 363.0 eV, one can find Δ_2 = 2.4 eV and Δ_1 = 3.7 eV.[55] Since the binding energy difference between the $14\gamma_6^-$ (10) and $17\gamma_6^-$ (4) IVMO equals 15.2 eV and the U6p spin – orbit splitting in the atom is given by ΔE_{sl}(U6p) = 10.0 eV,[57] it is possible to estimate the perturbation Δ_3 = 2.6 eV (*i.e.*, it is comparable with the value Δ_2 = 2.4 eV). These data led to the conclusion [123] that the contribution of U6p to the $11\gamma_7^-$ (5) and

$14\gamma_6^-$ (10) IVMO should be markedly higher, while that to the $10\gamma_7^-$(8) IVMO should be much lower than its contribution to the$17\gamma_6^-$ (4) IVMO. As expected, the width of lines corresponding to quasi-atomic orbitals, $16\gamma_6^-$ (6) – $15\gamma_6^+$ (7) is smaller than the corresponding values for other IVMO. The observed relative reduction of the $17\gamma_6^-$ (4) IVMO line width can be attributed to the partial loss of the antibonding nature of this MO resulting from a significant admixture of O2p AO (21%).[53]

It is noteworthy that a stricter comparison of the theoretical and experimental electron binding energies requires resorting to values calculated [272] for the transition state.

For qualitative and quantitative comparative analysis of the experimental and theoretical intensities of spectral lines, the spectra were decomposed into components with allowance for the data given in Fig. 46. The electron binding energies were derived from experiments, while the theoretical intensities were calculated. The results of identification of the XPS spectral structure are shown in Fig. 45. However, experimental IVMO intensities often differ significantly from the corresponding theoretical values. The closest agreement is observed for the electrons of the $17\gamma_6^-$ (4), $16\gamma_6^-$ (6) and $14\gamma_6^-$ (10) IVMO. It has been found[123] that $\sim$1.3 U6p electrons (mainly, the U6p$_{3/2}$ electrons) are involved in the formation of the OVMO. This is comparable with the theoretical value, equal to 1.0 e. Similar agreement is observed in some cases for the IVMO energy range. For example, the antibonding $17\gamma_6^-$ (4) IVMO contains 0.8 U6p$_{3/2}$ electrons, which does not differ much from the calculated value equal to 0.98 e. Similar agreement is observed for the bonding $14\gamma_6^-$ (10) IVMO. For the antibonding $11\gamma_7^-$ (5) and the corresponding bonding $10\gamma_7^-$ (8) IVMO, the calculated overlap of the U6p and O2s AO is approximately twice as great as the experimental value.

Since the pattern of variation of line intensities in the XPS spectra upon the change in the MO energy levels is known from quantum mechanics, it is possible to discuss whether the experimental and theoretical results agree with each other. As has been shown previously,[53, 55] the greater the participation (bonding or antibonding) of AO in the MO formation, the wider the MO lines. The sharpest lines are those corresponding to non-bonding or quasi-atomic MO. Therefore, the relatively small width of the $17\gamma_6^-$ (4) IVMO line can be attributed, as noted above, to the substantial content of the O2p AO in this MO, which also results in a significant decrease in its intensity and the loss of the antibonding nature (see Fig. 46). The observed discrepancy in the intensities of the $11\gamma_7^-$ (5) IVMO lines confirms the assumption that the degree of participation of the U6p AO in this MO is about twice as high as that in the $17\gamma_6^-$ (4) IVMO. The degree of participation of the U6p state in the corresponding bonding $10\gamma_7^-$ (8) IVMO is approximately the same. Unfortunately, it is difficult to determine reliably the line width corresponding to the $10\gamma_7^-$ (8) IVMO electrons.

The energy region of the $16\gamma_6^-$ (6) – $10\gamma_7^-$ (8) IVMO is most ambiguous for interpretation. As can be seen, the structure of this spectral range is mainly due to the O(L)2s electrons, which agrees with the results of calculations. However, the overlap of the uranium U6p AO with the oxygen L2s MO, which occurs in the equatorial plane upon the formation of the $11\gamma_7^-$ (5) and $10\gamma_7^-$ (8) IVMO, was apparently overestimated in the calculations; this resulted in a wrong order of the $16\gamma_6^-$ (6) – $10\gamma_7^-$ (8) IVMO. This may be due to the fact that the distances between the uranium and oxygen atoms in the equatorial plane used in the calculation of the $[UO_2O_4]^{6-}$ cluster were understated compared to the real values. In view of the foregoing, this spectral range has been decomposed.[123] The correct order of the IVMO is especially important for elucidation of their contribution to the covalent component of the chemical bond in uranium trioxide. The peak (11) observed in the spectrum (see Fig. 45) is apparently due to the shake up process which accompanies the emission of electrons from the sample. The expected theoretical spectrum is shown in Fig. 45 *b* by vertical segments.

In conclusion, we would like to note that, despite a number of approximations used in the calculation of the electronic structure of the $[UO_2O_4]^{6-}$ cluster, which models the nearest environment of uranium in γ-UO_3, the results obtained agree qualitatively with experimental data. This allowed the first reliable identification of a series of lines, at least, the upper and lower IVMO lines. These data can be used, in particular, to determine the structures and bond lengths in uranyl compounds [55, 109] and to interpret the structures of other X-ray spectra of uranium compounds. Since the electronic structures of actinide compounds are fairly similar, the results can be used for qualitative discussions of the electronic structures of compounds of not only uranium but also other actinides.

4. Parameters of the fine spectral structure of core electrons

Analysis of the fine XPS structure of the core electron shells of actinide compounds ($\sim$40 – 1250 eV) has shown that there exist general regularities of the formation of such structure and that its parameters depend on the physicochemical properties of compounds. For some actinide compounds, the fine structure parameters are characteristic and can be used for identification. For example, within the error of measurement, the spin – orbit splitting (ΔE_{sl}) of lines corresponding to the core electron levels of actinides does not change on passing from one compound to another. The observed apparent differences between the ΔE_{sl} values for actinides contained in various compounds are related, most often, to multiplet splitting and dynamic effect.

It was found that shake up satellites arise in the spectra of all electronic levels accessible for measurements, their intensity decreasing with a decrease in the electron binding energy. The parameters of these satellites were found to be correlated with the actinide oxidation state and the ionic – covalent nature of the bond.

For all actinide compounds studied, the structure of the An4f spectra is very sensitive to changes in the stoichiometric composition, the structure parameters being correlated with the oxidation state of the central actinide ion. Thus, the distance (along the energy scale) from the basic lines of the An4f doublet to the satellites related to many-body perturbation (ΔE_{Sat}) for An^{6+} lies in the range of 3 – 4 eV, while that for An^{4+} is 7 eV.

The An5d spectra of actinide compounds containing unpaired An5f electrons exhibit multiplet splitting, resulting in a substantial broadening of the An5d$_{3/2}$ line relative to the An5d$_{5/2}$ component of the doublet.

The XPS fine structure caused by the dynamic effect is most clear-cut for electrons whose binding energies are in a certain ratio to the binding energies of electrons less involved in the bonding, so that the energy conservation law and the selection rules hold. In particular, the dynamic effect results in substantial spreading of the An5s and An6s spectral lines; as a consequence, the An6s spectral structure covers a range of $\sim$40 eV. The intensity of the high binding energy component related to the An5p$_{1/2}$ electrons is strongly suppressed, and the An5p$_{3/2}$ component exhibits a complex fine structure. In all cases, fine structure is present in the An4p$_{3/2}$ spectra. It was shown experimentally that the structure in the XPS spectra of actinide compounds in the An4p, An5s, An5p and An6s binding energy range is mainly due to interaction of final state configurations of the type $An4p^54d^{10}(4f^{14})5s^2(5p^65d^{10}6s^26p^6)\ 5f^np^m \rightleftharpoons An4p^64d^9(4f^{14})5s^1.(5p^65d^{10}6s^26p^6)5f^np^{m+1}$; $An5s^15p^65d^{10}(6s^26p^6)5f^n \rightleftharpoons An5s^25p^5.5d^9(6s^26p^6)5f^{n+1}$; $An5p^55d^{10}(6s^26p^6)5f^n \rightleftharpoons An5p^65d^8(6s^26p^6).5f^{n+1}$; and $An6s^16p^65f^n \rightleftharpoons An6s^26p^45f^n6d^1$, respectively.

X-Ray photoelectron studies of the properties of actinide compounds and the nature of the chemical bond in them have provided a number of interesting results. It should also be noted that in recent years, X-ray photoelectron spectroscopy has been used more and more extensively for ecological studies to determine the physical and chemical state of radionuclides in the environment (see, for example, a series of studies [262, 273 – 276]).

VII. Conclusion

Thus, we have shown that knowledge of the parameters of fine XPS structure, together with the traditional information (line intensities and chemical shifts) significantly extends the potential of the XPS method for diverse studies in solid state physics and theoretical and physical chemistry, in particular, studies of the electronic structure and properties of actinide compounds and the nature of the chemical bond in them. The mechanisms of formation of this fine structure have been analysed using compounds with well-known properties. The understanding of the nature of the fine structure provides new information on the physicochemical properties of actinide compounds and the ions they contain. The three questions stated in the Introduction can be answered in the following way.

1. The XPS spectra of compounds of light actinides (Th, U, Np, Pu, Am, Cm, Bk, Cf) exhibit a complex fine structure for almost all electron shells in the energy range of 0 – 1250 eV. This structure may be due to many reasons, in particular, the formation of inner and outer valence molecular orbitals; multiplet splitting; spin – orbit splitting; splitting due to the induced charge; dynamic effect; many-body perturbation; overlap with the Auger spectral lines; the presence of actinide ions in different oxidation states and so on. General regularities of the formation of the fine spectral structure can be followed for particular electron shells.

2. It was found experimentally that particular mechanisms of fine structure formation are manifested in the spectra of different electron shells with different probabilities. This made it possible to establish qualitative and quantitative correlations of structure parameters with the physical and chemical properties of actinide compounds. For example, the line intensity around a zero binding energy is proportional to the number of An5f electrons not involved in the chemical bond. The structure of the low binding energy spectral range (0 – 50 eV) reflects the degree of participation of the An6p and An5f shells in the formation of outer and inner valence molecular orbitals, the nature and the sequence of these orbitals and the structure of the local environment of the actinide ion. The multiplet splitting of the core levels characterises the number of unpaired electrons in the compound. The spectral structures caused by the dynamic effect and many-body perturbation reflect the secondary many-body processes that accompany electron photoemission and the configuration of the final states of the electronic system.

3. The fine structure parameters of the spectra of actinide compounds can be used to determine the degree of delocalisation of the An5f electrons; the degree of their participation in the chemical bond; the electron configuration and oxidation state of the metal atom in these compounds; the density of unpaired electrons on paramagnetic ions; the degree of participation of the low-energy occupied An6p and L*n*s shells of neighbouring actinide atoms and ligand atoms in the formation of outer and inner valence molecular orbitals; the structure and the nature of these orbitals; and the structure of the local environment, in particular, uranium ions in amorphous substances. These data cannot be obtained directly by other methods.

Despite the substantial advances in the understanding of the electronic and crystal structures of actinide compounds and extension and deepening of the knowledge on the nature of the chemical bond in them, some points still remain obscure. For example, the structures of the IVMO spectra for compounds of most actinides still cannot be completely interpreted, due to the lack of results of proper relativistic calculations. The role of the IVMO electrons in the formation of the chemical bonds in compounds has not been ultimately clarified, because procedures for experimental and theoretical estimation of the contributions of particular orbitals to the binding energy have not been adequately developed.

The greatest success in solving the problems mentioned above can be attained by performing X-ray photoelectron spectral studies for diatomic gaseous molecules such as thorium and uranium monoxides using synchrotron radiation for excitation. In this case, relativistic calculations of the electronic structures can be done most easily as, for example, for the UF_6 molecule. No ultimate opinion on the role of IVMO in the formation and structures of actinide compounds has been formed as yet. However, there already exist a number of examples that imply that the concept of efficient IVMO formation allows one to interpret some experimental results, for example, the formation of the complex fine structure in the XPS spectra of actinide compounds in the $\sim 15-50$ eV binding energy range; the relationship between fine XPS structure characteristics in this region and the structure of the nearest environment and distances from the metal atoms to the closest ligand atoms in the compounds; the appearance of peaks and fine structure in the binding energy range of $\sim 15-50$ eV in the emission spectra of thorium oxide and fluoride and uranium oxides, Auger spectra of uranium oxide and conversion spectra of uranium oxides and fluorides. The formation of IVMO might also be a reason for the appearance of stable actinyl groups AnO_2^{n+}. In conclusion, it should be noted that the experimental and theoretical studies of the electronic structure of compounds and solids and the nature of the chemical bond carried out in recent years deal, most often, with the binding energy range of 0 – 50 eV rather than 0 – 15 eV studied traditionally. This is a recent and important achievement in chemistry, biology and solid-state physics.

This review was written with the financial support of the International Science and Engineering Centre (Grant No. 1358), the Russian Foundation for Basic Research (Project Nos 02-03-32693 and 04-03-32892), and the State Program for the Support of Leading Scientific Schools (Project No. 1763).

References

1. J J Katz, G T Seaborg, L R Morss *The Chemistry of the Actinide Elements* Vols 1-3 (London, New York: Chapman and Hall, 1986)
2. D Brown *Halides of the Transition Elements. Halides of the Lanthanides and Actinides* (London, New York, Sydney: Wiley-Interscience, 1968)
3. M P Mefod'eva, N N Krot *Soedineniya Transuranovykh Elementov* (Compounds of Transuranium Elements) (Moscow: Nauka, 1987)
4. G I Ionova, V G Pershina, V I Spitsyn *Elektronnoe Stroenie Aktinidov* (Electronic Structure of Actinides) (Moscow: Nauka, 1986)
5. Yu M Dymkov *Priroda Uranovoi Smolyanoi Rudy* (The Nature of Pitchblende) (Moscow: Atomizdat, 1973)
6. A K Lisitsin *Gidrogeokhimiya Rudoobrazovaniya* (Hydrogeochemistry of Ore Formation) (Moscow: Nauka, 1975)
7. G A Sidorenko *Kristallokhimiya Mineralov Urana* (Crystal Chemistry of Uranium Minerals) (Moscow: Atomizdat, 1978)
8. A S Baev, A S Bogatov, E I Bykhovskaya, E I Lebedeva, E A Obukhova, Yu A Teterin *Preprint IAE-5484/14* (Moscow: I V Kurchatov Institute of Nuclear Energy, 1992)
9. A S Baev, Yu A Teterin, S K Lisin, in *Voprosy Atomnoi Nauki i Tekhniki (Ser. Obshchaya i Yadernaya Fizika)* [Problems of Nuclear Science and Engineering (General and Nuclear Chemistry Series)] (Moscow: Russian Research Centre 'Kurchatov Institute' 1992) Vol. 3, p. 55
10. Yu A Teterin, A S Baev, S A Bogatov *J. Electron Spectrosc. Relat. Phenom.* **68** 685 (1994)
11. V I Nefedov, Yu A Teterin, A M Lebedev, A Yu Teterin, A P Dementiev, M Bubner, T Reich, S Pompe, K Heise, H Nitsche *Inorg. Chim. Acta* **273** 234 (1998)
12. Yu A Teterin, K E Ivanov, A S Baev, V I Nefedov, G Gaipel, T Reich, H Nische *Surf. Inv.* **13** 613 (1998)
13. Yu A Teterin, C Ronneau, R M Polevoi, V F Shikalov, P Froment, J Cara, I O Utkin, A S Nikitin, K E Ivanov *Poverkhnost'* **3** 54 (2001)
14. Yu A Teterin, V I Nefedov, C Ronneau, A S Nikitin, P Froment, J Cara, I O Utkin, A P Dementiev, A Yu Teterin, K E Ivanov *Radiokhimiya* **43** 537 (2001) [a]

15. Yu A Teterin, V I Nefedov, A S Nikitin, C Ronneau, J Vanbegin, J Cara, A P Dementiev, I O Utkin, A Yu Teterin, K E Ivanov, V G Yarjemsky *J. Nucl. Sci. Technol.* (Suppl. 3) 477 (2002)
16. R J Silva, H Nitshe *Radiochim. Acta* **70**/**71** 377 (1995)
17. V G Pershina *Chem. Rev.* **96** 1977 (1996)
18. G V Ionova *Usp. Khim.* **71** 461 (2002) [*Russ. Chem. Rev.* **71** 401 (2002)]
19. K Siegbahn, C Nordling, G Johansson, J Hedman, P F Heden, K Hamrin, U Gelius, T Bergmark, L O Weme, Y Baer *ESCA Applied to Free Molecules* (Amsterdam: North-Holland, 1969)
20. K Siegbahn, C Nordling, A Fahlman, R Nordberg, K Hamrin, J Hedman, C Johansson, T Bergmark, S E Karlsson, I Lindgren, B Lindberg *ESCA: Atomic, Molecular, and Solid State Structure Studied by Means of Electron Spectroscopy* (Uppsala: Almqvist and Wiksells, 1967)
21. V I Nefedov, in *Stroenie Molekul i Khimicheskaya Svyaz' (Itogi Nauki i Tekhniki)* [The Structure of Molecules and Chemical Bond (Advances in Science and Engineering Series)] (Moscow: Izd-vo VINITI, 1973) Vol. 1, p. 1
22. V V Nemoshkalenko, V G Aleshin *Elektronnaya Spektroskopiya Kristallov* (Electronic Spectroscopy of Crystals) (Kiev: Naukova Dumka, 1978)
23. V I Nefedov *Rentgenoelektronnaya Spektroskopiya Khimicheskikh Soedinenii* (X-Ray Photoelectron Spectroscopy of Chemical Compounds) (Moscow: Khimiya, 1984)
24. D E Ellis, A Rosen, P F Walch *J. Quant. Chem. Symp.* **9** 351 (1975)
25. P F Walch, D E Ellis *J. Chem. Phys.* **65** 2387 (1976)
26. A L Gubskii, A P Kovtun, Yu A Teterin, A S Baev *Preprint IAE-4053/12* (Moscow: I V Kurchatov Institute of Nuclear Energy, 1984)
27. V A Gubanov, E Z Kurmaev, A L Ivanovskii *Kvantovaya Khimiya Tverdogo Tela* (Quantum Chemistry of Solid) (Moscow: Nauka, 1984)
28. V A Gubanov, A L Ivanovskii, M V Ryzhkov *Kvantovaya Khimiya v Materialovedenii* (Quantum Chemistry in Material Science) (Moscow: Nauka, 1987)
29. Yu A Teterin, A S Baev, N G Yakovlev, in *Voprosy Atomnoi Nauki i Tekhniki (Ser. Yaderno-Fizicheskie Issledovaniya)* [Problems of Nuclear Science and Engineering (Nuclear Physical Investigations Series)] (Moscow: TsNIIatominform, 1992) Vol. 3, p. 58
30. M Ya Amus'ya *Atomnyi Fotoeffekt* (Nuclear Photoeffect) (Moscow: Nauka, 1987)
31. P Pyykko, L L Lohr *Inorg. Chem.* **20** 1950 (1981)
32. V L Sukhorukov, S A Yavna, V F Demekhin *Fiz. Tv. Tela* **24** 1856 (1982) [b]
33. P Pyykko, L Laaksonen *J. Phys. Chem.* **88** 4892 (1984)
34. V I Nefedov, V G Yarjemsky, M M Gofman, in *Khimicheskaya Svyaz' i Stroenie Molekul* (The Chemical Bond and Molecular Structure) (Moscow: Nauka, 1984) p. 108
35. V G Yarjemsky, V I Nefedov, N M Band, M B Trzhaskovskaya, Yu A Teterin, A Yu Teterin *Dokl. Akad. Nauk* **364** 653 (1999) [c]
36. M V Ryzhkov, V A Gubanov, Yu A Teterin, A S Baev *Radiokhimiya* **34** 81 (1992) [a]
37. Yu A Teterin, in *Proceedings of the 9th Congress of Physicists of Yugoslavia, Petrovats na Moru* (Montenegro: Society of Mathematicists and Physicists, 1995) p. 793
38. J Verbist, J Riga, J J Pireaux, R Caudano *J. Electron Spectrosc. Relat. Phenom.* **5** 193 (1974)
39. B W Veal, D J Lam *Phys. Rev. B* **10** 4902 (1974)
40. B V Veal, D J Lam *Phys. Lett. A* **49** 466 (1974)
41. B W Veal, D J Lam, H Diamond *Physica B* **86**–**88** 1193 (1977)
42. M V Ryzhkov, V A Gubanov, Yu A Teterin, A S Baev *Radiokhimiya* **33** 22 (1991) [a]
43. Yu A Teterin, A S Baev, L G Mashirov, D N Suglobov, in *Voprosy Atomnoi Nauki i Tekhniki (Ser. Yaderno-Fizicheskie Issledovaniya)* [Problems of Nuclear Science and Engineering (Nuclear Physical Investigations Series)] (Moscow: TsNIIatominform, 1986) Vol. 3 (36), p. 60
44. Yu A Teterin, A S Baev, in *Voprosy Atomnoi Nauki i Tekhniki (Ser. Yaderno-Fizicheskie Issledovaniya)* [Problems of Nuclear Science and Engineering (Nuclear Physical Investigations Series)] (Moscow: TsNIIatominform, 1986) Vol. 3 (36), p. 63
45. B W Veal, D J Lam, W T Carnall, H R Hoekatra *Phys. Rev. B* **12** 5651 (1975)
46. Yu A Teterin, in *Voprosy Atomnoi Nauki i Tekhniki (Ser. Yaderno-Fizicheskie Issledovaniya)* [Problems of Nuclear Science and Engineering (Nuclear Physical Investigations Series)] (Moscow: TsNIIatominform, 1985) Vol. 4 (33), p. 54
47. A S Baev, Yu A Teterin, L G Mashirov, D N Suglobov *Radiokhimiya* **28** 460 (1986) [a]
48. A S Baev, Yu A Teterin, in *Voprosy Atomnoi Nauki i Tekhniki (Ser. Yaderno-Fizicheskie Issledovaniya)* [Problems of Nuclear Science and Engineering (Nuclear Physical Investigations Series)] (Moscow: TsNIIatominform, 1986) Vol. 3 (36), p. 61
49. V M Kulakov, Yu A Teterin *Priroda* **2** 78 (1977)
50. V I Nefedov, V I Vovna *Elektronnaya Struktura Khimicheskikh Soedinenii* (Electronic Structure of Chemical Compounds) (Moscow: Nauka, 1987)
51. Yu A Teterin, in *Rentgenovskie, Elektronnye Spektry i Khimicheskaya Svyaz'* (X-Ray and Electron Spectra and Chemical Bond) (Vladivostok: Far Eastern University, 1986) p. 165
52. Yu A Teterin, S G Gagarin *Vnutrennie Valentnye Molekulyarnye Orbitali i Vliyanie ikh Elektronov na Kharakter Khimicheskoi Svyazi Soedinenii* (Inner Valence Molecular Orbitals and The Effect of their Electrons on the Nature of Chemical Bond in Compounds) (Moscow: TsNIIatominform, 1985)
53. Yu A Teterin, S G Gagarin *Usp. Khim.* **65** 895 (1996) [*Russ. Chem. Rev.* **65** 825 (1996)]
54. Yu A Teterin, A Yu Teterin *Usp. Khim.* **71** 403 (2002) [*Russ. Chem. Rev.* **71** 347 (2002)]
55. Yu A Teterin, A S Baev *Rentgenovskaya Fotoelektronnaya Spektroskopiya Soedinenii Legkikh Aktinoidov* (X-Ray Photoelectron Spectroscopy of Light Actinide Compounds) (Moscow: TsNIIatominform, 1986)
56. Yu A Teterin, I O Utkin, A M Lebedev, A Yu Teterin, K E Ivanov, A S Nikitin, in *Proceedings of the Workshop on Speciation, Techniques, and Facilities for Radioactive Materials at Synchrotron Light Sources, Grenoble, France, 1998* (Paris: Nuclear Energy Agency, OECD, 1999) p. 297
57. J C Fuggle, A F Burr, W Lang, L M Watson, D Y Fabian *J. Phys. F: Met. Phys.* **4** 335 (1974)
58. Yu A Teterin, A S Baev, S G Gagarin, V D Klimov *Radiokhimiya* **27** 3 (1985) [a]
59. V D Klimov, V A Legasov, A V Lebedev, S S Khoroshev, Yu A Teterin, A S Baev, N S Tolmacheva *Radiokhimiya* **27** 415 (1985) [a]
60. E Thibant, J J Pireaux, J Riga, C Tenret-Nokl, R Caudano, E G Deronane, J Verbist, in *Proceedings of the 2nd International Conference on Electronic Strict. Actinides, Wroclaw, Poland, 1976* p. 139
61. A S Baev, Yu A Teterin, in *Voprosy Atomnoi Nauki i Tekhniki (Ser. Yaderno-Fizicheskie Issledovaniya)* [Problems of Nuclear Science and Engineering (Nuclear Physical Investigations Series)] (Moscow: TsNIIatominform, 1990) Vol. 5 (13), p. 82
62. Yu A Teterin, I O Utkin, I V Melnikov, A Yu Teterin, A M Lebedev, K E Ivanov, L Vuckchevich, A S Nikitin, in *Proceedings of the Workshop on Speciation, Techniques, and Facilities for Radioactive Materials at Synchrotron Light Sources, Grenoble, France, 1998* (Paris: Nuclear Energy Agency, OECD, 1999) p. 287
63. Yu A Teterin, I O Utkin, I V Mel'nikov, A M Lebedev, A Yu Teterin, K E Ivanov, A S Nikitin, L Vukchevich *Zh. Strukt. Khim.* **41** 1167 (2000) [d]
64. T Gouder, L Havela, F Miserque, F Wastin, J Rebizant, in *Extended Abstracts of 31emes Journees des Actinides, Saint-Malo, France, 2001* p. O29
65. Yu A Teterin, V M Kulakov, A S Baev, A G Zelenkov, N B Nevzorov, I V Mel'nikov, V A Strel'tsov, L G Mashirov, D N Suglobov *Dokl. Akad. Nauk SSSR* **255** 434 (1980) [c]
66. Yu A Teterin, V M Kulakov, A S Baev, N B Nevzorov, I V Melnikov, V A Streltsov, L G Mashirov, D N Suglobov, A G Zelenkov *Phys. Chem. Miner.* **7** 151 (1981)
67. S Evans *J. Chem. Soc., Faraday Trans. 2* **73** 1341 (1977)
68. N Beatham, A P Orchard, G Thornton *J. Electron Spectrosc. Relat. Phenom.* **19** 205 (1980)

69. E Thibaut, J-P Boutique, J J Verbist, J-C Level, H Nokl *J. Am. Chem. Soc.* **104** 5266 (1982)
70. J J Pireaux, N Martensson, R Didriksson, K Siegbahn, J Riga, J Verbist *Chem. Phys. Lett.* **46** 213 (1977)
71. G C Allen, A J Griffiths, B J Lee *Transition Met. Chem.* **3** 229 (1978)
72. A H Al Rayyes, C Ronneau *Radiochim. Acta* **54** 189 (1991)
73. P Benard, D Louer, N Dacheux, V Brandel, M Genet *Chem. Mater.* **6** 1049 (1994)
74. G C Allen, N R Holmes *Can. J. Appl. Spectrosc.* **38** 124 (1993)
75. C Miyake, M Kanamaru, S Imoto, K Taniguchi *Nuclear Mater.* **138** 36 (1986)
76. G S Allen, N R Holmes *J. Chem. Soc., Dalton Trans.* 3009 (1987)
77. T Gouder, C Colmenares, J R Naegele, J Verbist *Surf. Sci.* **235** 280 (1989)
78. E Talik, M Kulpa, W Suski, R Tros, in *Extended Abstracts of 32emes Journees des Actinides, Ein-Gedi, Israel, 2002* p. P3
79. B W Veal, D J Lam, H Diamond, H R Hoekstra *Phys. Rev. B* **15** 2929 (1977)
80. Yu A Teterin, A S Baev, L G Mashirov, D N Suglobov *Dokl. Akad. Nauk SSSR* **276** 154 (1984) [c]
81. Yu A Teterin *Kondens. Sredy i Mezhfaz. Granitsy* **2** 60 (2000)
82. Yu A Teterin, A S Baev, L G Mashirov, D N Suglobov *Dokl. Akad. Nauk SSSR* **277** 131 (1984) [c]
83. R Baptist, D Courteix, J Chayrouse, L Heintz *J. Phys. F: Met. Phys.* **12** 2103 (1982)
84. D Courteix, J Chayrouse, L Heintz, R Baptist *Solid State Commun.* **39** 209 (1981)
85. T Gouder, L Havela, F Wastin, J Rebizant, in *Extended Abstracts of 31emes Journees des Actinides, Saint-Malo, France, 2001* p. O36
86. A J Arko, J J Joyce, L Morales, J Wills, J Lashley, F Wastin, J Rebizant *Phys. Rev. B* **62** 1773 (2000)
87. Yu A Teterin, K E Ivanov, A Yu Teterin, I O Utkin, A S Nikitin, in *Proceedings of the 3rd International Yugoslav Nuclear Society Conference* (*YUNSC-2000*) (Belgrade: VINCA Institute of Nuclear Sciences, 2001) p. 396
88. Yu A Teterin, A Yu Teterin, K E Ivanov, I O Utkin *J. Nucl. Technol.* (Suppl. 3) 140 (2002)
89. Yu A Teterin, A S Baev, A Yu Teterin, K E Ivanov, L Vukchevich, in *Proceedings of Yugoslav Nuclear Society Conference (YUNSC'96)* (Belgrade: VINCA Institute of Nuclear Sciences, 1997) p. 453
90. Yu A Teterin, A S Baev, A Yu Teterin, K E Ivanov *Dokl. Akad. Nauk* **348** 213 (1996) [c]
91. Yu A Teterin, V M Kulakov, K E Ivanov, in *NATO ASI-Series. Microbial Degradation Processes in Radioactive Waste Repository and in Nuclear Fuel Storage Areas. Ser. 1. Disarmament Technologies* (Ed. J H Wolfram) (Dordrecht: Kluwer Academic, 1997) p. 233
92. Yu A Teterin, A S Baev, R V Vedrinskii, A L Gubskii, A G Zelenkov, A P Kovtun, V M Kulakov, V P Sachenko, in *Fizicheskie i Matematicheskie Metody v Koordinatsionnoi Khimii* (Physical and Mathematical Methods in Coordination Chemistry) (Kishinev: Shtiintsa, 1980) p. 73
93. Yu A Teterin, A S Baev, R V Vedrinskii, A L Gubskii, A G Zelenkov, A P Kovtun, V M Kulakov, V P Sachenko *Dokl. Akad. Nauk SSSR* **256** 381 (1981) [c]
94. Yu A Teterin, A S Baev, K E Ivanov, L G Mashirov, D N Suglobov *Radiokhimiya* **38** 395 (1996) [a]
95. V I Nefedov, Yu A Teterin, T Reich, H Nitshe *Dokl. Akad. Nauk* **348** 634 (1996) [c]
96. Yu A Teterin, K E Ivanov *Poverkhnost'* **4**–**5** 211 (1997)
97. Yu A Teterin, K E Ivanov, in *Proceedings of Yugoslav Nuclear Society Conference* (*YUNSC'96*) (Belgrade: VINCA Institute of Nuclear Sciences, 1997) p. 437
98. Yu A Teterin, A S Baev, in *Voprosy Atomnoi Nauki i Tekhniki (Ser. Yaderno-Fizicheskie Issledovaniya)* [Problems of Nuclear Science and Engineering (Nuclear Physical Investigations Series)] (Moscow: TsNIIatominform, 1985) Vol. 4, p. 53
99. Yu A Teterin, V A Terehov, M V Ryzhkov, A Yu Teterin, I O Utkin, K E Ivanov, A S Nikitin, L J Vukchevich, in *Workshop Proceedings on Speciation, Techniques, and Facilities for Radioactive Materials at Synchrotron Light Sources, Grenoble, France, 2000* (Paris:Nuclear Energy Agency, OECD, 2002) p. 325
100. Yu A Teterin, V A Terehov, M V Ryzhkov, A Yu Teterin, I O Utkin, K E Ivanov, L J Vukchevich, in *Extended Abstracts of 32emes Journees des Actinides, Ein-Gedi, Israel, 2002* p. C2
101. Yu A Teterin, M V Ryzhkov, V A Gubanov, S G Gagarin, in *Kvantovaya Khimiya Tverdogo Tela* (*Preprint UNTs Akad. Nauk SSSR*) [Quantum Chemistry of Solids (Preprint Urals Scientific Centre, Academy of Sciences of the USSR)] (Sverdlovsk: Institute of Chemistry, 1984) p. 62
102. Yu A Teterin, M V Ryzhkov, V A Gubanov, S G Gagarin *Dokl. Akad. Nauk SSSR* **264** 915 (1985) [a]
103. A S Baev, A G Zelenkov, V M Kulakov, L G Mashirov, V P Smilga, D N Suglobov, Yu A Teterin, in *Tez. Dokl. XII Vsesoyuz. Soveshchaniya po Rentgenovskoi Spektroskopii* (Abstracts of Reports of the XIIth All-Union Meeting on X-Ray Spectroscopy) (Leningrad: Leningrad State University, 1978) p. 118
104. Yu A Teterin, V M Kulakov, A S Baev, A G Zelenkov, I V Mel'nikov, N B Nevzorov, V A Strel'tsov, in *Tez. Dokl. Vsesoyuz. Soveshchaniya 'Rentgenovskie i Rentgenoelektronnye Spektry i Elektronnaya Struktura Metallov, Splavov i Khimicheskikh Soedinenii'* (Abstracts of Reports of the All-Union Meeting 'X-Ray and X-Ray Photoelectron Spectra and Electronic Structure of Metals, Alloys and Chemical Compounds) (Izhevsk: Physical and Technical Institute, 1979) p. 25
105. J J Pireaux, J Riga, E Thibaut, C Tenret-Nöl, R Caudano, J J Verbist *Chem. Phys.* **22** 113 (1977)
106. P R Norton, R L Tapping, D K Creber, W J L Buyers *Phys. Rev. B* **21** 2572 (1980)
107. A S Baev, Yu A Teterin, in *Proceedings of the 5th Seminar on Electron Spectroscopy of Socialist Countries* (Dresden: Technische Universität, 1984) p. 15
108. Yu A Teterin, A S Baev, in *X-84. International Conference on X-Ray and Inner Shell Processes in Atoms, Molecules and Solid (Abstracts of Reports), Leipzig, 1984* Pt. 2, p. 466
109. Yu A Teterin, K E Ivanov *Surf. Inv.* **13** 623 (1998)
110. Yu A Teterin, M V Ryzhkov, A Yu Teterin, A D Panov, A S Nikitin, K E Ivanov, I O Utkin *J. Nucl. Technol.* (Suppl. 3) 74 (2002)
111. L E Cox *J. Electron Spectrosc. Relat. Phenom.* **26** 167 (1982)
112. Yu A Teterin, in *Abstracts of Reports of the 5th Seminar on Electron Spectroscopy of Socialist Countries* (Dresden: Technische Universität, 1984) p. 145
113. A S Baev, V M Kulakov, Yu A Teterin, N G Gorshkov, L G Mashirov, D N Suglobov, in *Tez. Dokl. XII Mendeleevskogo S'ezda po Obshchei i Prikladnoi Khimii. Radiokhimiya* (Abstracts of Reports of the XIIth Mendeleev Congress on General and Applied Chemistry. Radiochemistry) (Moscow : Nauka, 1981) Vol. 1, p. 154
114. A S Baev, N G Gorshkov, V M Kulakov, L G Mashirov, D N Suglobov, Yu A Teterin *Radiokhimiya* **24** 576 (1982) [a]
115. Yu A Teterin, A S Baev, A D Sidorenko, S G Gagarin, in *Rentgenovskaya Spektroskopiya Tverdogo Tela* (*Preprint UNTs AN SSSR*) (X-Ray Spectroscopy of Solids (Preprint Urals Scientific Centre, Academy of Sciences of the USSR)] (Sverdlovsk: Institute of Chemistry, 1984) p. 23
116. L E Cox, J W Ward *Inorg. Nucl. Chem. Lett.* **17** 265 (1981)
117. R J Thorn *J. Phys. Chem. Solids* **43** 571 (1982)
118. G M Bancroft, T K Sham, J L Esquivel, S Larsson *Chem. Phys. Lett.* **51** 105 (1977)
119. G T Bancroft, T K Sham, S Larsson *Chem. Phys. Lett.* **46** 551 (1977)
120. T K Sham, G Wendin *Phys. Rev. Lett.* **44** 817 (1980)
121. T Novakov, J M Hollander *Phys. Rev. Lett.* **21** 1133 (1968)
122. R L Dekock, E J Baerends, P M Boerrigter, J G Snijders *Chem. Phys. Lett.* **105** 308 (1984)

123. Yu A Teterin, M V Ryzhkov, A Yu Teterin, A D Panov, A S Nikitin, K E Ivanov, I O Utkin *Radiokhimiya* **44** 206 (2002) [a]
124. M Ohno *Phys. Rev. B* **35** 5453 (1987)
125. O Gunnarson, K Schönhammer, D D Sarma, F U Hillebrecht, M Campagna *Phys. Rev. B* **32** 5499 (1985)
126. D T Larson *J. Vac. Sci. Technol.* **17** 55 (1980)
127. J R Naegele, L Manes, J C Spirlet, W Muller *Phys. Rev. Lett.* **52** 1834 (1984)
128. B Johansson *Phys. Rev. B* **30** 3533 (1984)
129. V A Gubanov, A Rosen, D E Ellis *Solid State Commun.* **22** 219 (1977)
130. M Boring, J H Wood, J M Moscowitz *J. Chem. Phys.* **63** 638 (1975)
131. D D Koelling, D E Ellis, R J Bartlett *J. Chem. Phys.* **65** 3331 (1976)
132. G L Gutsev, A A Levin *Dokl. Akad. Nauk SSSR* **246** 1366 (1979) [c]
133. S Shiokawa, H Adachi, S Imoto *J. Phys. Soc. Jpn.* **48** 327 (1980)
134. I A Topol', B I Zhilinskii *Teor. Eksp. Khim.* **20** 406 (1984) [e]
135. V I Nefedov, V G Yarjemsky, I S Nefedova, I M Band, M B Trzhaskovskaya, Yu A Teterin *Poverkhnost'* **6** 16 (2000)
136. N Kaltsoyannis, B E Bursten *Inorg. Chem.* **34** 2735 (1995)
137. V A Gubanov, A Rosen, D E Ellis *J. Phys. Chem. Solids* **40** 17 (1979)
138. F Gerken, J Schmidt-May *J. Phys. F: Met. Phys.* **13** 1571 (1983)
139. T H Gouder, C A Colmenares *Surf. Sci.* **341** 51 (1995)
140. T Gouder, J R Naegele, C A Colmenares. *Surf. Sci.* **342** 299 (1995)
141. T Gouder *J. Electron Spectrosc. Relat. Phenom.* **101 – 103** 419 (1999)
142. J W Allen, J M Peek, L E Cox *Physica B* **259 – 261** 1147 (1999)
143. B Reihl, N Martenson, D E Eastman *Phys. Rev. B* **24** 406 (1981)
144. L Black, T Gouder, F Wastin, J Rebizant, L Havela *Surf. Sci.* **504** 83 (2002)
145. Y Saito, S Suzuki, Y Onuki, N Sato, S-I Fujimori, T Komatsubara, S Sato, Y Haga, K-i Yamak *J. Electron Spectrosc. Relat. Phenom.* **88 – 91** 353 (1998)
146. J W Allen, Y-X Zhang, L H Tjeng, L E Cox, M B Maple, C-T Chen *J. Electron Spectrosc. Relat. Phenom.* **78** 57 (1996)
147. K Sato, Y Saito, S Suzuki, T Komatsubara, K Tamura, M Seki, T Okane, S-I Fujimori, N Sato, S Sato, A Tanaka, M Mizuta, Y Tezuka, S Shin, K-I Yamaki *J. Electron Spectrosc. Relat. Phenom.* **101 – 103** 439 (1999)
148. T Gouder, L Havela *Mikrochim. Acta* **138** 207 (2002)
149. A S Baev, Yu A Teterin, K E Ivanov, A Yu Teterin, S A Bogatov *Radiokhimiya* **39** 171 (1997) [a]
150. Yu A Teterin, in *Proceedings of Second International Yugoslav Nuclear Society Conference (YUNSC'98)* (Belgrade: VINCA Institute of Nuclear Sciences, 1999) p. 503
151. Yu A Teterin, A S Baev, A Yu Teterin, K E Ivanov, L G Mashirov, D N Suglobov *Radiokhimiya* **39** 177 (1997) [a]
152. Yu A Teterin, V I Nefedov, K E Ivanov, A S Baev, G Geipel, T Reich, H Nitshe *Dokl. Akad. Nauk* **344** 206 (1995) [c]
153. Yu A Teterin, V I Nefedov, K E Ivanov, A S Baev, G Geipel, T Reich, H Nitshe *Zh. Neorg. Khim.* **41** 1884 (1996) [f]
154. T Reich, G Geipel, Yu A Teterin, V I Nefedov, K E Ivanov, A S Baev, M A Denecke, G Bernhard, H Nitshe, P G Allen, J J Bucher, in *Extended Abstracts of the 4th International Conference on Nuclear and Radiochemistry (NRC4)* Vol. 1 (St Malo, France: Institute de Physique Nucleare, 1996) p. DP-11
155. Yu A Teterin, V I Nefedov, K E Ivanov, A S Baev, G Geipel, T Reich, H Nitshe *Dokl. Akad. Nauk* **350** 503 (1996) [c]
156. Yu A Teterin, K E Ivanov, A S Baev, V I Nefedov, G Geipel, T Reich, H Nitsche *Poverkhnost'* **4 – 5** 202 (1997)
157. Yu A Teterin, V I Nefedov, A Yu Teterin, A M Lebedev, K E Ivanov, A P Dementiev, G Geipel, M Bubner, T Reich, S Pompe, K-H Heise, H Nitshe, in *Sbornik Dokl. Natsional'noi Konf. po Primeneniyu Rentgenovskogo, Sinkhrotronnogo Izlucheniya Neitronov i Elektronov dlya Issledovaniya Materialov (RSNE'97)* [Collection of Reports of National Conference on Application of X-Ray and Synchroton Radiation of Neutrons and Electrons for Investigation of Materials (RSNE'97)] (Dubna: Joint Institute for Nuclear Research, 1997) Vol. 2, p. 436
158. Yu A Teterin, V I Nefedov, A Yu Teterin, A M Lebedev, A P Dementiev, I O Utkin, M Bubner, T Reich, S Pompe, K-H Heise, H Nitshe *Zh. Neorg. Khim.* **44** 593 (1999) [f]
159. Yu A Teterin, V I Nefedov, A Yu Teterin, A M Lebedev, K E Ivanov, A P Dementiev, I O Utkin, G Geipel, M Bubner, T Reich, S Pompe, K-H Heise, H Nitshe *Poverkhnost'* **2** 79 (1999)
160. Yu A Teterin, A Yu Teterin, A M Lebedev, A P Dementiev, I O Utkin, V I Nefedov, M Bubner, T Reich, S Pompe, K-H Heise, H Nitsche *J. Prakt. Chem.* **341** 773 (1999)
161. Yu A Teterin, V I Nefedov, A Yu Teterin, A M Lebedev, A P Dementiev, I O Utkin, I V Melihov, in *Proceedings of the Workshop on Speciation, Techniques, and Facilities for Radioactive Materials at Synchrotron Light Sources, Grenoble, France, 1998* (Paris: Nuclear Energy Agency, OECD, 1999) p. 307
162. Yu A Teterin, A Yu Teterin, A P Dementiev, A M Lebedev, I O Utkin, I V Melikhov, V I Nefedov, D G Berdonosova, Dj Bek-Uzarov, L Vukchevich *Zh. Strukt. Khim.* **41** 749 (2000) [d]
163. A F Francis *J. Alloys Compd.* **213/214** 226 (1994)
164. A F Francis, C J Dodje, F Lu, G P Halada, C R Clayton *Environ. Sci. Technol.* **28** 636 (1994)
165. C J Dodje, A F Francis *Environ. Sci. Technol.* **28** 1300 (1994)
166. Yu A Teterin, V I Nefedov, A S Nikitin, C Ronneau, J Vanbegin, J Cara, A P Dementiev, I O Utkin, A Yu Teterin, K E Ivanov, V G Yarzhemsky, in *Proceedings of the Workshop on Speciation, Techniques, and Facilities for Radioactive Materials at Synchrotron Light Sources, Grenoble, France, 2000* (Paris: Nuclear Energy Agency, OECD, 2002) p. 305
167. Yu A Teterin, I O Utkin, A Yu Teterin, A S Nikitin, K E Ivanov, A M Lebedev, V I Nefedov, C Ronneau, J Vanbegin, J Cara, L J Vukchevich, Dj Bek-Uzarov, in *Proceedings of the 3rd International Yugoslav Nuclear Society Conference* (*YUNSC-2000*) (Belgrade: VINCA Institute of Nuclear Sciences, 2001) p. 401
168. Yu A Teterin, V I Nefedov, C Ronneau, J Vanbegin, J Cara, I O Utkin, A Yu Teterin, A S Nikitin, K E Ivanov, L Vukchevich, Dj Bek-Uzarov *Radiokhimiya* **43** 531 (2001) [a]
169. Yu A Teterin, V I Nefedov, A S Nikitin, C Ronneau, J Vanbegin, J Cara, A P Dementiev, I O Utkin, A Yu Teterin, K E Ivanov, V G Yarjemsky *Radiokhimiya* **43** 544 (2001) [a]
170. Yu A Teterin, V I Nefedov, C Ronneau, J Vanbegin, J Cara, I O Utkin, A P Dementiev, A Yu Teterin *Kondens. Sredy Mezhfaz. Granitsy* **2** 67 (2000)
171. Yu A Teterin, V I Nefedov, C Ronneau, A S Nikitin, J Vanbegin, J Cara, I O Utkin, A P Dementiev, A Yu Teterin, K E Ivanov, L Vukchevich, Dj Bek-Uzarov *Radiokhimiya* **43** 524 (2001) [a]
172. Yu A Teterin, C Ronneau, R M Polevoi, V F Shikalov, P Froment, J Cara, I O Utkin, A S Nikitin, K E Ivanov, in *Proceedings of the Workshop on Speciation, Techniques, and Facilities for Radioactive Materials at Synchrotron Light Sources, Grenoble, France, 2000* (Paris: Nuclear Energy Agency, OECD, 2002) p. 337
173. Yu A Teterin, in *Proceedings of the 3rd International Yugoslav Nuclear Society Conference (YUNSC-2000)* (Belgrade: VINCA Institute of Nuclear Sciences, 2001) p. 391
174. Yu A Teterin, V I Nefedov, C Ronneau, J Vanbegin, J Cara, I O Utkin, A P Dementiev, A Yu Teterin, A S Nikitin, K E Ivanov *Kondens. Sredy Mezhfaz. Granitsy* **2** 75 (2000)
175. Yu A Teterin, V I Nefedov, C Ronneau, J Vanbegin, J Cara, I O Utkin, A P Dementiev, A Yu Teterin, A S Nikitin, K E Ivanov, L J Vukchevich, Dj Bek-Uzarov *Bulg. J. Phys.* **27** (2) 9 (2000)
176. Y Baer, J K Lang *Phys. Rev. B* **21** 2060 (1980)
177. S B Nornes, R G Meisenheimer *Surf. Sci.* **88** 191 (1979)
178. K N Huang, M Aouogi, M H Chen, B Grasemant, H Mark *At. Data Nucl. Data Tables* **18** 243 (1976)
179. J M Dyke, G D Josland, A Morris, P M Tucker, J W Tyler *J. Chem. Soc., Faraday Trans. 2* **77** 1273 (1981)
180. V A Gubanov, A Rosen, D E Ellia *J. Inorg. Nucl. Chem.* **41** 975 (1979)

181. V P Zhukov, V A Gubanov, V I Anisimov *Opt. Spektrosk.* **46** 85 (1979) [g]
182. Yu F Batrakov, R V Bogdanov, E V Puchkova, A S Surgeev *Radiokhimiya* **42** 112 (2000) [a]
183. Yu A Teterin, V A Terekhov, A Yu Teterin, I O Utkin, A M Lebedev, L Vukchevich *Dokl. Akad. Nauk* **358** 637 (1998) [c]
184. Yu A Teterin, V A Terekhov, A Yu Teterin, I O Utkin, A M Lebedev, L Vukchevich *Zh. Strukt. Khim.* **39** 1052 (1998) [d]
185. Yu A Teterin, V A Terekhov, A Yu Teterin, K E Ivanov, I O Utkin, A M Lebedev, L Vukchevich *J. Electron Spectrosc. Relat. Phenom.* **96** 229 (1998)
186. Yu A Teterin, V A Terekhov, A Yu Teterin, I O Utkin, A M Lebedev, L Vukchevich, in *Proceedings of Second International Yugoslav Nuclear Society Conference (YUNSC'98)* (Belgrade: VINCA Institute of Nuclear Sciences, 1999) p. 507
187. T M Zimkina, I I Lyakhovskaya, A S Shulakov *Opt. Spektrosk.* **62** 285 (1987) [g]
188. I I Lyakhovskaya, V M Ipatov, T M Zimkina *Zh. Strukt. Khim.* **18** 688 (1977) [d]
189. G Kalkowski, G Kaindl, W D Brewer, W Knore *Phys. Rev. B* **35** 2667 (1987)
190. L E Cox, W P Ellis, R D Covan, J W Allen, S-J Oh, I Lindau, B B Pate, A J Arko *Phys. Rev. B* **35** 5761 (1987)
191. J Petiau, G Calas, D Petitmaire, A Bianconi, M Benfatto, A Marcelli *Phys. Rev. B* **34** 7350 (1986)
192. Yu A Teterin, T N Bondarenko, A Yu Teterin, A M Lebedev, I O Utkin *Radiokhimiya* **40** 103 (1998) [a]
193. S A Prosandeev, Yu A Teterin, R V Vedrinskii, V M Kulakov *Preprint IAE-3206* (Moscow: I V Kurchatov Institute of Nuclear Energy, 1979)
194. M Boring, R D Cowan, R L Martin *Phys. Rev. B* **23** 445 (1981)
195. F U Hillebrecht, D D Sarma, N Martensson *Phys. Rev. B* **33** 4376 (1986)
196. J Brunner, M Erbudak, F Hulliger *Solid State Commun.* **38** 841 (1981)
197. F U Hillebrecht, D D Sarma, N Martensson *J. Magn. Magn. Mater.* **52** 129 (1985)
198. S Suga, M Yamamoto, K Soda, T Mori, S Takagi, N Nitsuma, T Suzuki, T Kasuya *J. Magn. Magn. Mater.* **52** 297 (1985)
199. D B Beach, K D Bomben, N M Edelstein, D C Eisenberg, W L Jolly, R Shinomoto, A Streitwieser *J. Inorg. Chem.* **25** 1735 (1986)
200. N Martensson, P-A Maisquiat, S Svensson, B Johansson *J. Chem. Phys.* **80** 5458 (1984)
201. N Martensson, P-A Malmquiat, S Svensson *Chem. Phys. Lett.* **100** 375 (1983)
202. J M Dyke, N K Fayad, A Morris, I R Trickle, G C Alien *J. Chem. Phys.* **72** 3822 (1980)
203. J H Scofield *J. Electron Spectrosc. Relat. Phenom.* **8** 129 (1976)
204. M Hirata, H Monjyushiro, R Sekine, J Onoe, H Nakamatsu, T Mukoyama, H Adachi, K Takeuchi *J. Electron Spectrosc. Relat. Phenom.* **83** 59 (1997)
205. T Mukoyama, H Nakamatsu, H Adachi *J. Electron Spectrosc. Relat. Phenom.* **63** 409 (1993)
206. C K Jurgensen *Chem. Phys. Lett.* **89** 455 (1982)
207. A S Vil'nyanskii, I S Glazunov *At. Tekhn. za Rubezhom* **7** 3 (1984)
208. B N Laskorin, V A Mamilov, Yu A Koreisho, D I Skorovarov, L I Vodolazov, I P Smirnov, O L Kedrovskii, V P Shchulika B V Nevskii, V N Mosinets *At. Energ.* **54** 286 (1983)
209. Y Baer, J Schoenes *Solid State Commun.* **33** 885 (1980)
210. G C Allen, J A Crofts, M T Curtis, P M Tucker, D Chadwick, P J Hampson *J. Chem. Soc., Dalton Trans.* 1296 (1974)
211. Y K Dawson, M W Lister *J. Chem. Soc.* 2181 (1950)
212. A Arrott, J E Goldman *Phys. Rev.* **108** 948 (1957)
213. R P Rafal'skii, V A Alekseev, L A Anan'eva *Geokhimiya* **11** 1601 (1979) [h]
214. S Bertram, G Kaindl, J Jove, M Pages, J Gal *Phys. Rev. Lett.* **63** 2680 (1989)
215. G C Allen, E J Baerends, P Vernooijs, J M Dyke, A M Ellis, M Feher, A Morris *J. Chem. Phys.* **89** 5363 (1988)
216. C Miyake, H Sakurai, S Imoto *Chem. Phys. Lett.* **36** 158 (1975)
217. M Boring, J H Wood, J V Moskowitz *J. Chem. Phys.* **61** 3800 (1974)
218. V I Zhudov, A G Zelenkov, V M Kulakov, B V Odinov, Yu A Teterin, in *Tez. Dokl. XXX Vsesoyuz. Soveshchaniya po Yadernoi Spektroskopii i Strukture Atomnogo Yadra* (Abstracts of Reports of the XXXth All-Union Meeting on Nuclear Spectroscopy and The Structure of Atomic Nucleus) (Leningrad: Nauka, 1980) p. 614
219. D P Grechukhin, V I Zhudov, A G Zelenkov, V M Kulakov, B V Odinov, A A Soldatov, Yu A Teterin *Pis'ma Zh. Eksp. Teor. Fiz.* **31** 627 (1980) [i]
220. A D Panov, V I Zhudov, Yu A Teterin *Zh. Strukt. Khim.* **39** 1047 (1998) [d]
221. Yu A Teterin *Zh. Strukt. Khim.* **39** 1037 (1998) [d]
222. M Boring, J H Wood *J. Chem. Phys.* **71** 32 (1979)
223. M Boring, J H Wood *J. Chem. Phys.* **71** 392 (1979)
224. P J Hay, W R Wadt, L R Kahn, R C Raffenetti, D H Phillips *J. Chem. Phys.* **71** 1767 (1979)
225. D A Case, C Y Yang *J. Chem. Phys.* **72** 3443 (1980)
226. V A Glebov *Elektronnoe Stroenie i Svoistva Uranilovykh Soedinenii* (Electronic Structure and Properties of Uranyl Compounds) (Moscow: Energoatomizdat, 1983)
227. J H Wood, M Boring, S B Woodruff *J. Chem. Phys.* **74** 5225 (1981)
228. D E Ellis, A Rosen, V A Gubanov *J. Chem. Phys.* **77** 4051 (1982)
229. G C Allen, P M Tucker, J W Tyier *J. Phys. Chem.* **86** 224 (1982)
230. N B Borkovskii, A B Kovrikov, D S Umreiko *Dokl. Akad. Nauk Bel. SSR* **27** 213 (1983)
231. V I Sergeenko, L I Ignat'eva, G L Gudev, A I Boldyrev *Zh. Strukt. Khim.* **26** 131 (1985) [d]
232. A A Soldatov *Zh. Strukt. Khim.* **26** 3 (1985) [d]
233. S G Gagarin, A A Soldatov, A D Sidorenko, Yu A Teterin, in *Tez. Dokl. XIV Vsesoyuz. Soveshch. po Rentgenovskoi i Elektronnoi Spektroskopii, Irkutsk, 1984* (Abstracts of Reports of the XIVth All-Union Meeting on X-Ray and Electronic Spectroscopy, Irkutsk, 1984) p. 91
234. Yu A Teterin, V A Terekhov, K E Ivanov *Dokl. Akad. Nauk* **345** 356 (1995) [c]
235. Yu A Teterin, K E Ivanov, A Yu Teterin, A M Lebedev, L Vukchevich, in *Proceedings of Yugoslav Nuclear Society Conference (YUNSC'96)* (Belgrade: VINCA Institute of Nuclear Sciences, 1997) p. 449
236. Yu A Teterin, K E Ivanov, A Yu Teterin, A M Lebedev, I O Utkin, L Vukchevich *J. Electron Spectrosc. Relat. Phenom.* **101–103** 401 (1999)
237. J Weber, V A Gubanov *J. Inorg. Nucl. Chem.* **41** 693 (1979)
238. L E Cox, W P Ellis, R D Cowan, J W Allen, S-J Oh *Phys. Rev. B* **31** 2467 (1985)
239. D L Clark, D E Hobart, M P Neu *Chem. Rev.* **95** 25 (1995)
240. Yu M Mikhailov *Khimiya Platinovykh i Tyazhelykh Elementov. Problemy Koordinatsionnoi Khimii* (The Chemistry of Platinum and Heavy Elements. The Problems of Coordination Chemistry) (Moscow: Nauka, 1975)
241. L V Volod'ko, A I Komyak, D S Umreiko *Uranilovye Soedineniya* (Uranyl Compounds) (Minsk: Byelorussian State University, 1981) Vol. 1
242. M E Dyatkina, Yu M Mikhailov *Kompleksnye Soedineniya Urana* (Complex Compounds of Uranium) (Ed. I I Chernyaev) (Moscow: Nauka, 1964)
243. B F Ormont *Struktura Neorganicheskikh Veshchestv* (The Structure of Inorganic Substances) (Moscow, Leningrad: Gos. Izd. Tekhn.-Teoret. Lit., 1950)
244. Yu A Teterin, A S Baev, V M Kulakov, A G Zelenkov, in *Voprosy Atomnoi Nauki i Tekhniki (Ser. Obshchaya i Yadernaya Fizika)* [Problems of Nuclear Science and Engineering (General and Nuclear Chemistry Series)] (Khar'kov: Khar'kov Physicotechnical Institute, 1982) Vol. 2 (20), p. 68
245. W R Wadt *J. Am. Chem. Soc.* **103** 6053 (1981)
246. Yu A Teterin, V A Terekhov, M V Ryzhkov, I O Utkin, A S Nikitin, E D Haritonova *Kondens. Sredy Mezhfaz. Granitsy* **2** 83 (2000)
247. Yu A Teterin, V A Terekhov, V M Ryzhkov, I O Utkin, A S Nikitin, E D Kharitonova *Poverkhnost'* **3** 44 (2001)

248. Yu A Teterin, V A Terehov, M V Ryzhkov, I O Utkin, K E Ivanov, A S Nikitin *J. Electron Spectrosc. Relat. Phenom.*, **114**–**116** 915 (2001)
249. N N Krot, D N Suglobov *Radiokhimiya* **6** 1 (1989) [a]
250. I A Lebedev, B F Myasoedov *Radiokhimiya* **6** 700 (1982) [a]
251. C Keller *The Chemistry of the Transuranium Elements* Vol. 3 (Ed. K H Lieser) (Weinhem: Verlag Chemie, 1971)
252. B C Frazer, G Shirane, D E Cox, C E Olsen *Phys. Rev. A.* **140** 1448 (1965)
253. Yu A Teterin, A S Baev, L G Mashirov, D N Suglobov, in *Tez. Dokl. III Vsesoyuz. Konf. po Khimii Urana* (Abstracts of Reports of the IIIth All-Union Conference on Uranium Chemistry) (Moscow: Nauka, 1985) p. 39
254. G T Seaborg, J J Kats (Eds) *The Actinide Elements* (New York: McGraw-Hill, 1954)
255. W Suski *Physica B* **86**–**88** 11 (1977)
256. K G Gurtovoi, R Z Levitin *Usp. Fiz. Nauk* **153** 193 (1987) [j]
257. J R Moore, S E Nave, R G Haire, P G Huray *J. Less-Common Met.*, **121** 187 (1986)
258. I M Band, Yu I Kharitonov, M B Trhaskovskaya *At. Data Nucl. Data Tables* **23** 443 (1979)
259. D K Shuh, K E Ivanov, S M Butorin, J Guo, M Magnuson, E J Nordgren, in *Abstracts of Reports of the International Conference Actinides-2001, Hayama, Japan, 2001* p. 55
260. K E Ivanov, D K Shuh, Yu A Teterin, A Yu Teterin, S M Butorin, J-H Guo, M Vagnusov, J Nordgren, in *Proceedings of the 4th International Yugoslav Nuclear Society Conference (YUNSC-2002)* (Belgrade: Yugoslav Nuclear Society, 2003) p. 31
261. Yu A Teterin, V A Terekhov, K E Ivanov, in *Proceedings of the 9th Congress of Physicists of Yugoslavia, Petrovats na Moru* (Montenegro: Society of Mathematicists and Physicists, 1995) p. 797
262. L L Makarov, R I Karaziya, Yu F Batrakov, N P Chibisov, A N Masevich, Yu M Zaitsev, A I Udris, L V Shishkunova *Radiokhimiya* **1** 116 (1978) [a]
263. J Drozdzynski, K Schwochan, H-J Schenk *J. Inorg. Nucl. Chem.* **43** 1845 (1981)
264. V I Sergeev, L I Ignat'eva, G L Gutsev, A I Boldyrev *Zh. Strukt. Khim.* **26** 131 (1985) [d]
265. D E Ellis, in *Proceedings of the Actinides-1981 Conference, Pacific Grove, CA, 1982* p. 123
266. J Onoe, K Takeuchi, H Nakamatsu, T Mukoyama, R Sekine, H Adachi *J. Electron Spectrosc. Relat. Phenom.* **60** 29 (1992)
267. J Onoe, K Takeuchi, H Nakamatsu, T Mukoyama, R Sekine, Bong-Il Kim, H Adachi *J. Chem. Phys.* **99** 6810 (1993)
268. J Onoe, H Nakamatsu, R Sekine, T Mukoyama, H Adachi, K Takeuchi *J. Electron Spectrosc. Relat. Phenom.* **70** 89 (1994)
269. M V Ryzhkov, V A Gubanov *J. Radioanal. Nucl. Chem.* **143** 85 (1990)
270. K E Ivanov, D K Shuh, A Yu Teterin, S M Butorin, J-H Guo, M Magnuson, J Nordgren, in *Proceedings of the 4th International Yugoslav Nuclear Society Conference (YUNSC-2002)* (Belgrade: Yugoslav Nuclear Society, 2003) p. 431
271. Yu A Teterin, M V Ryzhkov, A Yu Teterin, A D Panov, A S Nikitin, K E Ivanov, I O Utkin *J. Nucl. Technol. Radioact. Protect.* **1**–**2** 3 (2002)
272. J C Slater, K H Johanson *Phys. Rev. B* **5** 844 (1972)
273. Yu A Teterin, V I Nefedov, A S Nikitin, A Yu Teterin, K E Ivanov, K I Maslakov, I O Utkin, M Bubner, T Reich, S Pompe, K H Heise, H Nitsche, in *Workshop Proceedings on Speciation, Techniques, and Facilities for Radioactive Materials at Synchrotron Light Sources, Grenoble, France, 2002* (Paris: Nuclear Energy Agency, OECD, 2002) p. 317
274. Yu A Teterin, V I Nefedov, A S Nikitin, A Yu Teterin, K E Ivanov, K I Maslakov, I O Utkin, M Bubner, T Raikh, S Pompe, K-H Heise, H Nitshe *Inzh. Fiz.* **2** 28 (2001)
275. Yu A Teterin, V I Nefedov, A S Nikitin, A Yu Teterin, K E Ivanov, K I Maslakov, I O Utkin, M Bubner, T Raikh, S Pompe, K-H Heise, H Nitshe *Zh. Neorg. Khim.* **46** 990 (2001) [f]
276. Yu A Teterin, in *Biotechnology for Waste Management and Site Restoration. Technological, Educational, Business, Political Aspects. (NATO ASI Ser. 2, Environment)* Vol. 34 (Eds C Ronneau, O Bitchaeva) (Dordrecht: Kluwer Academic, 1997) p. 135

[a] — *Radiochemistry (Engl. Transl.)*
[b] — *Phys. Solis State (Engl. Transl.)*
[c] — *Dokl. Chem. (Engl. Transl.)*
[d] — *Russ. J. Struct. Chem. (Engl. Transl.)*
[e] — *J. Theor. Exp. Chem. (Engl. Transl.)*
[f] — *Russ. J. Inorg. Chem. (Engl. Transl.)*
[g] — *Opt. Spectrosc. (Engl. Transl.)*
[h] — *Geochem. Int. (Engl. Transl.)*
[i] — *J. Exp. Theor. Phys. Lett. (Engl. Transl.)*
[j] — *Physics-Uspekhi (Engl. Transl.)*

Russian Chemical Reviews **73** (6) 581 – 608 (2004) © 2004 Russian Academy of Sciences and Turpion Ltd

DOI 10.1070/RC2004v073n06ABEH000778

Chiral 1,3,2-oxazaborolidines in asymmetric synthesis: recent advances

V A Glushkov, A G Tolstikov

Contents

I.	Introduction	581
II.	1,3,2-Oxazaborolidines as catalysts of enantioselective reduction of ketones	581
III.	Reduction of oximes and imines	594
IV.	Use of 1,3,2-oxazaborolidines in miscellaneous reactions	596
V.	Reduction by immobilised 1,3,2-oxazaborolidines	601
VI.	1,3,2-Oxazaborolidine analogues	603

Abstract. The use of chiral 1,3,2-oxazaborolidines in asymmetric organic synthesis, particularly, in enantioselective reduction of ketones, imines and oxime ethers, asymmetric Diels – Alder reactions, aldol condensation and atroposelective reduction of lactones is reviewed. Reactions of immobilised 1,3,2-oxazaborolidines are also considered. The bibliography includes 266 references.

I. Introduction

Enantioselective reduction of ketones, imines and oximes by boranes in the presence of chiral catalysts, *viz*., 1,3,2-oxazaborolidines, is one of the most convenient methods for the preparation of enantiomerically enriched secondary alcohols and amines. This rapidly developing research area has been the subject of numerous reviews;[1–7] however, early papers [1–4] encompass the literature published before 1993, and the review of 1998 [5] and some selected chapters in monographs [6,7] are devoted exclusively to enantioselective reduction of ketones using Corey – Bakshi – Shibata catalysts (CBS catalysts).

A great number of papers concerned with this problem have been published recently. Some papers report on the possible use of chiral 1,3,2-oxazaborolidines as Lewis acids, which significantly expands the area of application of these derivatives in synthetic organic chemistry. We undertook an attempt to systematise the results of investigations carried out in this field in the past decade (references to earlier publications having fundamental significance are also given).

II. 1,3,2-Oxazaborolidines as catalysts of enantioselective reduction of ketones

This trend in asymmetric synthesis dates back to 1981 when Itsuno [6–10] reported the reduction of prochiral ketones by an (*S*)-valinol – $BH_3 \cdot THF$ mixture (1 : 2) to optically active secondary alcohols in up to 100% yields and with enantiomeric excess (*ee*) up to 73%.[8]

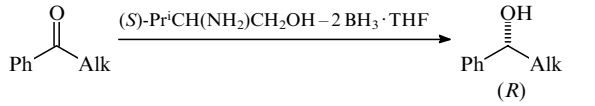

Alk = Me, Et, Pr, Bu. (*ee* 49% – 73%)

According to Itsuno, this reaction is catalysed by 1,3,2-oxazaborolidine (**1**) (form **A** or **B**).

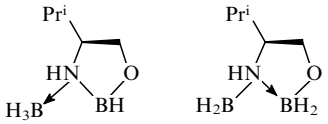

1A **1B**

Later, Corey showed [11] that hydrogen (2 equiv.) is released in the reaction of (*S*)-diphenylvalinol with 2 equiv. of borane in THF at 35 °C. On removal of residual amounts of borane and the solvent in vacuum and twofold distillation of the residue (105 – 130 °C, 0.05 Torr), a colourless crystalline compound with a molecular mass of 265.16365 (265.16379, according to the mass spectrometric data) was obtained. This compound was formulated as **2** · BH_3.

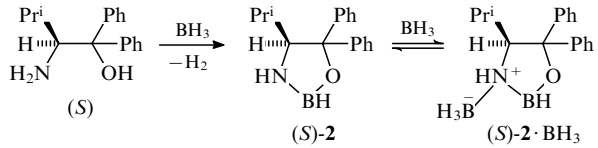

According to X-ray diffraction analysis data of this compound, this exists in the form **A**.

The same group of investigators have succeeded in obtaining 1,3,2-oxazaborolidine **3** · BH_3 and its *B*-methyl derivative.[12]

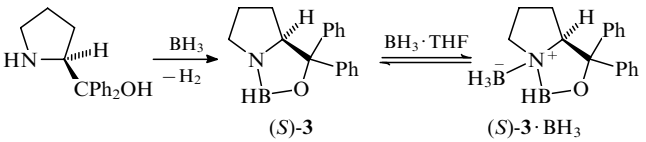

It was shown that (*S*)-perhydro-3,3-diphenylpyrrolo-[1,2-*c*][1,3,2]oxazaborolidine-borane [(*S*)-**3** · BH_3] and its

V A Glushkov, A G Tolstikov Institute of Technical Chemistry, Urals Branch of the Russian Academy of Sciences, ul. Lenina 13, 614990 Perm, Russian Federation. Fax (7-3422) 12 62 37. Tel. (7-3422) 39 63 10. E-mail: chemist@mpm.ru (V A Glushkov). Tel. (7-095) 420 21 43. E-mail: tagtolst@presidium.ras.ru (A G Tolstikov)

Received 27 February 2003
Uspekhi Khimii **73** (6) 632 – 661 (2004); translated by R L Birnova

B-methyl derivative catalyse enantioselective reduction of ketones even more efficiently than (*S*)-4-isopropyl-5,5-diphenyl-1,3,2-oxazaborolidine-borane [(*S*)-**2**·BH_3] and reduce acetophenone to (*R*)-1-phenylethanol in more than 99% yield and *ee* 97%.[12,13] The structure of the *B*-methyl derivative was studied by X-ray diffraction analysis.[14]

In the general case, synthesis of 1,3,2-oxazaborolidines containing a B–H bond is accompanied by the formation of various dimers (Scheme 1); this was confirmed by ^{11}B NMR spectroscopy (see Refs 15–17) and X-ray diffraction analysis.[16]

Scheme 1

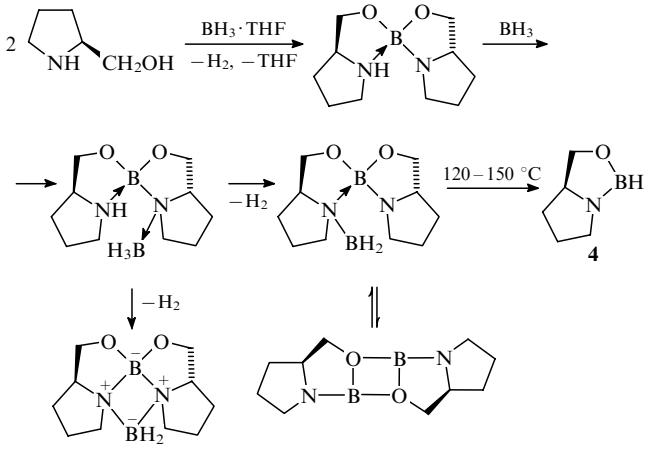

Whereas the ^{11}B NMR spectrum of compound **2** (THF, 23 °C)[11] contains a broad signal at δ 28.1 (relative to $Et_2O \cdot BF_3$, external standard), the ^{11}B NMR spectrum of compound **3** (0.17 M solution in THF, 23 °C) contains signals at δ 28.3 and 7.6, which were assigned to the monomer and the dimer, respectively. The dimers are converted into monomers (*e.g.*, **4**) upon heating; therefore, the procedure used for the synthesis of substituted 1,3,2-oxazaborolidine plays a crucial role in the catalytic reduction of carbonyl compounds (for temperature regime and the solvent see below).

Methyl-substituted 1,3,2-oxazaborolidine **5** was prepared using two approaches, *viz*., starting from methylboronic acid[13] and from trimethylboroxine.[18] The presence of additional signals in the ^{11}B NMR spectra in 1,3,2-oxazaborolidine (*S*)-**5** prepared from (*S*)-diphenylprolinol and trimethylboroxin is explained by the formation of side products of the type **6** and **7** (Scheme 2).[18]

Scheme 2

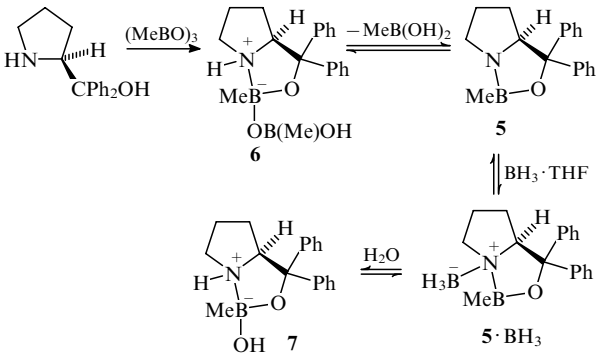

In contrast to compounds **2** and **3**, compound **5** is more resistant to the action of atmospheric oxygen,[13] but undergoes hydrolysis in the presence of moisture. It is of note that all 1,3,2-oxazaborolidines undergo hydrolysis, therefore, all manipulations with these compounds demand thorough dehydration of the solvents.

1. The reduction mechanism

The mechanism of reduction of acetophenone by the complex (*S*)-**2**·BH_3 is shown in Scheme 3.

Scheme 3

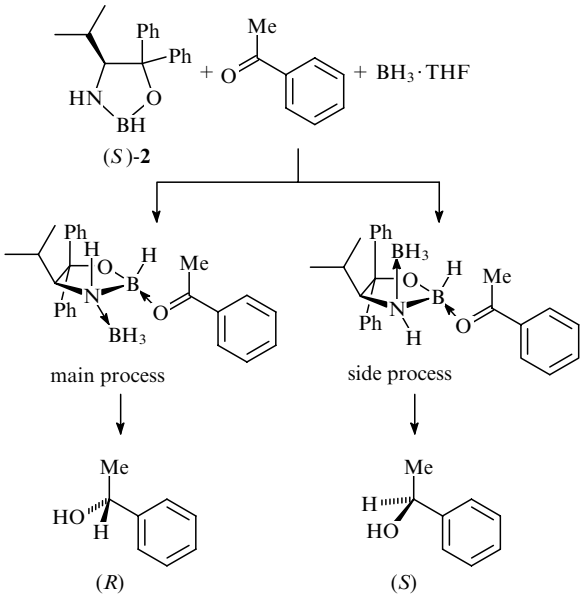

Of fundamental importance is the fact that 1,3,2-oxazaborolidine **2** itself does not reduce ketones and becomes active only after addition of the second equivalent of borane.[11] During the formation of a catalytic complex, borane coordinates the nitrogen atom of 1,3,2-oxazaborolidine in such a way that it itself comes to occupy the *trans*-position relative to the isopropyl group; the *cis*-position of borane results in a steric strain in the complex. Subsequent coordination of acetophenone and the hydride ion transfer also proceed in a stereospecific manner to afford (*R*)-1-phenylethanol with high *ee* (up to 99%). The stereospecificity of the CBS catalyst is comparable to that of enzymes; therefore, Corey termed it 'chemzyme' (a chemical catalytic system similar to an enzyme).[19] If a catalyst based on an (*R*)-amino acid is used, the reduction of a ketone results in an (*S*)-alcohol. The possibility of control over stereoselectivity is an attractive feature of reductions based on the use of the CBS catalysts.

A mechanistic model of the reaction of an active catalytic complex with a substrate has been developed in order to explain high stereospecificity of ketone reduction.[5–7] Let us consider the mechanism of ketone reduction in which (*S*)-diphenylprolinol is used as a catalyst in more detail (Scheme 4).

This model implies a multistep reduction mechanism of acetophenone. In the first step, a catalytically active complex of 1,3,2-oxazaborolidine with BH_3 is formed. The coordination of the nitrogen atom by borane strongly increases the Lewis acidity of the boron atom of the heterocycle[5] as a result of which it acquires the ability to coordinate the carbonyl group of acetophenone. This is followed by the hydride ion transfer from the boron atom of borane to the carbon atom of the carbonyl group (direct reduction).

It was suggested that coordination of a ketone affords a transition state (complex **8**) with a six-membered quasi-heterocycle *A* where the bulkier ketone substituent (the phenyl radical) occupies an equatorial position. In other words, the boron atom of the 1,3,2-oxazaborolidine ring coordinates the electron pair of the oxygen atom of the ketone occupying the *anti*-position relative to the phenyl group, which ensures high enantioselectivity of the reduction similar to that in enzyme systems.[5] This hypothesis was also confirmed by the results of quantum-chemical calculations.[20–25]

Scheme 4

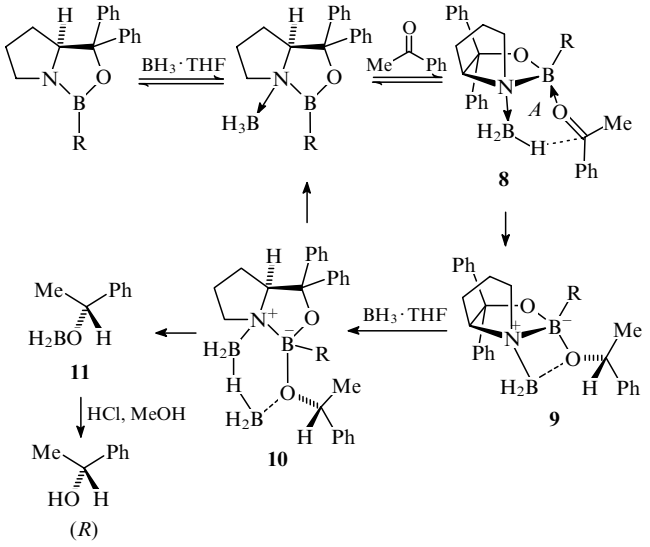

R = H, Me.

The last step includes the decomposition of the complex **9** (presumably, *via* the intermediate complex **10**) resulting in the original catalytically active complex and the ester **11**. The latter is converted into the final product, *viz*., (*R*)-1-phenylethanol.

The conformation of the transition state was also considered. According to semi-empirical MNDO calculations, the transition state **8** where the heterocycle *A* acquires a chair conformation possesses much lower energy than in the case of a boat conformation.[20] A detailed analysis of *ab initio* quantum-chemical calculations of various conformations of all the transient species **8**–**11** in the basis sets 3-12G, 4-13G, 6-31G, 4-31G* and 6-31G* has been carried out.[23–27] The transition state **8** has two stable conformations, *viz*., *twist-boat* and *twist-chair*.[24]

According to quantum-chemical calculations,[21] the potential energy of the formation of the transition state **8** (coordination of the ketone) was similar to that of the transition state **9** (the hydride ion transfer), and the kinetic isotope effect k_H/k_D = 1.8 (23 °C) calculated for the reduction of acetone by the complex (*S*)-**5**·BH_3 virtually coincided with the experimental value k_H/k_D = 1.7 for the reduction of acetophenone.[28] It was therefore supposed that the hydride ion transfer is the rate-determining step.[28] The kinetics of reduction of *para*-substituted acetophenones was studied in order to establish the limiting step of the overall catalytic process. The rate ratios for the reduction of *p*-nitro- and *p*-methoxy acetophenones to that of non-substituted acetophenone were 3.4 and 1.8, respectively.[28] This suggests that the hydride ion transfer step, like the ketone complex formation with the catalyst, controls the rate of the overall process.[5]

The formation of the transient species of the types **8, 9** and **10** was also confirmed by ^{11}B NMR spectroscopy.[29]

2. Structural types of 1,3,2-oxazaborolidines

Further perfection of structures of catalysts of enantioselective reduction of ketones (CBS catalysts) followed several routes. These involved modification of the rigid skeleton of a chiral amino alcohol and selection of substituents in the alcoholic group of the starting amino alcohol † and at the boron atom of the borane. Thus Bu-substituted 1,3,2-oxazaborolidine (**12**) was synthesised along with the Me-substituted catalyst **5**.[30]

The dependence of enantioselectivity of the reduction using CBS catalysts on the nature of the substituent at the HO-bearing carbon atom of the amino alcohol has been reviewed.[5–7] Bulky substituents provide stereochemical control over the reaction, but hinder the complexation of the ketone with 1,3,2-oxazaborolidine. Besides, they decrease the optical yields due to competitive non-catalytic reduction. In some cases, bulky substituents 'reverse' the selectivity so that *S*-enantiomers are formed instead of *R*-enantiomers.

The dependence of enantioselectivity on the nature of the substituent R at the boron atom has been studied. It should be noted that in terms of the mechanistic model of the transition state **8** (see Scheme 4) the steric strain between the substituent R at the boron atom and the substituents at the carbonyl group of the ketone is critical for the discrimination between different types of ketone coordination. Thus the presence of bulky aromatic substituents at the boron atom favours their steric interactions with more remote fragments of a coordinated ketone molecule,[5] as a result of which the enantioselectivity of reduction increases considerably. Thus, in each concrete case the choice of an optimum substituent R at the borane B atom should depend on the nature of the substrate (ketone). However, it is 1,3,2-oxazaborolidines carrying H-, Me- and Bu-substituents at the boron atom that are commonly used as catalysts because of the ease of their preparation.

A representative set of CBS catalysts based on various chiral amino alcohols is listed in Table 1. Natural amino acids or their analogues served as starting compounds in the synthesis of many of these catalysts.[27,35–38] The results presented in Table 1 were obtained for catalytic variants of the reaction, *viz*., the reduction of a ketone by 0.6–1.0 equiv. of $BH_3 \cdot THF$ or $BH_3 \cdot Me_2S$ in the presence of 0.05–0.10 equiv. of a catalyst (1,3,2-oxazaborolidine), although in some cases the catalyst, the reducing agent and the substrate were used in equal amounts in order to ensure higher enantioselectivity. The amount of the reducing agent (borane) is usually 0.6–0.7 equiv. per carbonyl group of the ketone, since 2 equiv. of the hydride ion are transferred.[5–7] The chemical yields of secondary alcohols are usually > 90%.

The majority of papers devoted to enantioselective reduction of ketones describe the reduction of acetophenone. As can be seen from Table 1, 1,3,2-oxazaborolidines **26** and **30** based on prolinol derivatives are the best catalysts for the acetophenone reduction.

The use of catalysts based on phenylalanine in the enantioselective hydrogenation of acetophenone also gives good results, the catalyst based on *o*-chlorophenylalanine **15** manifesting somewhat higher enantioselectivity in comparison with its unsubstituted analogue **14**. Presumably,[36] this is due to the formation of an additional coordination bond between the boron and chlorine atoms.

1,3,2-Oxazaborolidines **13** and **51** based on two diastereomers of 2-amino-1,2-diphenylethanol effectively catalyse the reduction of many carbonyl compounds (see, *e.g*., Refs 34 and 71), whereas the catalyst **48** based on 2-amino-1,1,2-triphenylethanol (R = Me) was found to be suitable for the reduction of alkyl methyl ketones[66] (*ee* of the product is 70%).

The catalysts based on diastereomeric 1-aminoindan-2-ols (compounds **27** and **39**)[47–49,59,61,71] and 1-amino-2-hydroxy-1,2,3,4-tetrahydronaphthalene **41**,[60] as well as on spiro derivatives (**28**–**31**, **55**) also appeared to be highly efficient.[50,51,68,69]

As can be seen from Table 1, the use of the catalyst **49** based on norephedrine for the reduction of tetralone gives good results,[27,67] while its analogue **50** prepared from pseudo-ephedrine is ineffective.[27] The catalyst **46** containing a 1-naphthyl group is less active in the reduction of butyrophenone than the catalyst **47** containing a 2-naphthyl group.[65] It was noted that the stereoselectivity of the reaction increases upon introduction of the 2-naphthyl group into the carbon atom of the C–O fragment of 1,3,2-oxazaborolidine.[19] The catalysts **18** and **38** with aziridine[39] and azetidine[58] rings, respectively, manifested higher activities than the catalyst **19** with the pyridine ring.[40] The enantioselectivity of the reduction in the case of the catalyst **23** is lower than that

† The starting (*S*)- and (*R*)-diphenylprolinols commonly used in the synthesis of 1,3,2-oxazaborolidines can be prepared by different methods (see, *e.g*., Refs 13, 31–33).

Table 1. Catalytic enantioselective reduction of carbonyl compounds (in THF).

Ketone	Catalyst	Amount of the catalyst [a]	Amount of the reducing agent [a]		T /°C	Configuration of the alcohol	*ee* (%)	Ref.
			$BH_3 \cdot THF$	$BH_3 \cdot Me_2S$				
PhC(O)Me	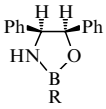 (**13**, R = Me)	0.1		0.7	25	*R*	92	34
	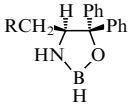 (**14**, R = Ph)	0.05		0.7	25	*R*	82	35
	(**15**, R = C_6H_4Cl-*o*)	0.1	excess		30	*R*	94.6	36
	(**16**, R = SPh)	0.1	1		50 – 65	*R*	74.5	37
	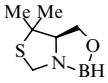 (**17**)	1	1		25	*S*	84	38
	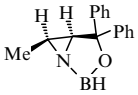 (**18**)	0.05		1 [b]	25	*R*	94	39
	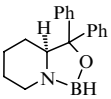 (**19**)	0.1	0.6		0	*R*	87	40
	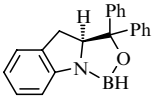 (**20**)	0.1	excess		30	*R*	91	41
	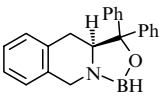 (**21**)	0.1	1.1		50	*R*	51	42
	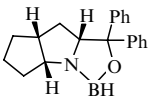 (**22**)	0.1	1		25	*S*	61	43
	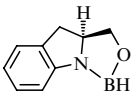 (**23**)	0.1		1.1	25	*R*	59	44
		0.1		1.1	25	*R*	8	41
		0.1		1.1	25	*R*	82	45
	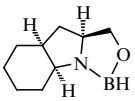 (**24**)	0.1	1		25	*S*	90	45
	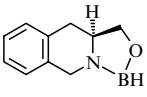 (**25**)	0.1	1.1		50	*R*	71	42
	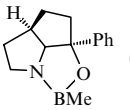 (**26**)	0.1	0.6		0	*R*	98	46
	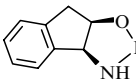 (**27**, R = H)	0.1		0.6	25	*S*	88	47
	(**27**, R = Me)	0.1	2		0	*S*	84	48, 49
	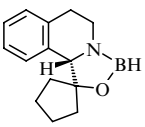 (**28**)	0.05	1		30	*R*	88	50

Table 1 (continued).

Ketone	Catalyst	Amount of the catalyst [a]	Amount of the reducing agent [a]		T /°C	Configuration of the alcohol	*ee* (%)	Ref.
			$BH_3 \cdot THF$	$BH_3 \cdot Me_2S$				
PhC(O)Me	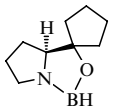 (**29**)	0.16	excess		0	*S*	67	51
	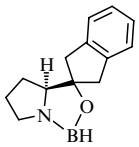 (**30**)	0.16	"		0	*S*	96	51
	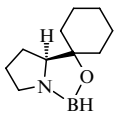 (**31**)	0.16	"		0	*S*	71	51
	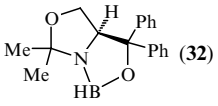 (**32**)	0.2	1.1 [c]		20	*R*	49	52
	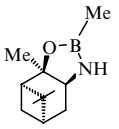 (**33**)	0.1		0.6	0–5	*R*	93	53, 54
	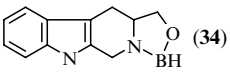 (**34**)	0.1	0.6		50	*R*	88	55
	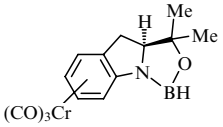 (**35**)	0.1	excess		25	*R*	20	56
	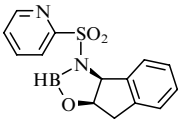 (**36**)	0.1		1	40	*R*	80	57
	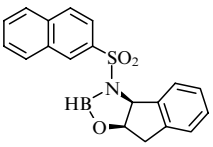 (**37**)	0.1		1	40	*R*	24	57
$PhC(O)CH_2Cl$	**5**	0.5	0.5		30	*S*	97	11
	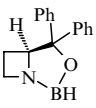 (**38**)	0.1	0.6		23	*S*	97	58
	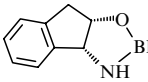 (**39**, R = H)	0.1		1	0–25	*S*	92	59
	(**39**, R = Me)	0.1	0.8		0	*S*	94	49
$PhC(O)CH_2Br$	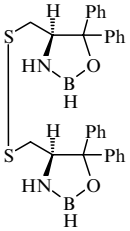 (**40**)	0.05	1		50–65	*S*	87	37

Table 1 (continued).

Ketone	Catalyst	Amount of the catalyst [a]	Amount of the reducing agent [a]		T /°C	Configuration of the alcohol	*ee* (%)	Ref.
			$BH_3 \cdot THF$	$BH_3 \cdot Me_2S$				
$PhC(O)CH_2Br$	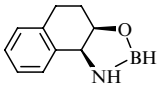 (**41**)	0.05		0.65	25	*S*	90	60
	27 (R = Me)	0.1	2		0	*R*	96	61
m-$ClC_6H_4C(O)CH_2Br$	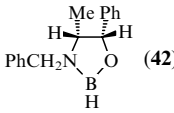 (**42**)	0.05	1		0	*R*	91	62–64
PhC(O)Et	**1**	1.25	1.25		30	*R*	61	9
	2	1.25	1.25		30	*R*	94	10
	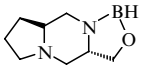 (**43**)	0.2	1.1 [c]		20	*S*	78	52
	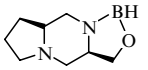 (**44**)	0.2	1.1 [c]		20	*S*	58	52
	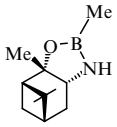 (**45**)	0.1		0.6	0–5	*S*	92	53, 54
$PhC(O)Pr^n$	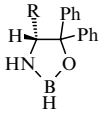 (**46**, R = 1-naphthyl)	0.05	1		39	*S*	58.6	65
	(**47**, R = 2-naphthyl)	0.05	1		39	*S*	100	65
$PhC(O)Pr^i$	**44**	0.2	1.1 [c]		20	*R*	29	52
$MeC(O)Bu^n$	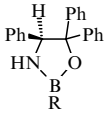 (**48**, R = Me)	0.1		1.2	0	*S*	70	66
	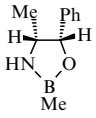 (**49**)	0.05		0.7	25	*S*	94	27, 67
	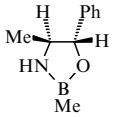 (**50**)	0.05		0.7	25	*S*	2	27
	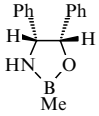 (**51**)	0.1		0.7	25	*R*	94	34
	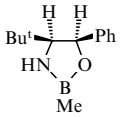 (**52**)	0.05		0.7	25	*R*	82	27
	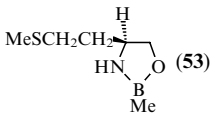 (**53**)	0.05		0.7	25	*R*	36	27
	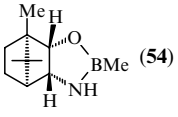 (**54**)	0.05		0.7	25	*R*	78	27

Table 1 (continued).

Ketone	Catalyst	Amount of the catalyst [a]	Amount of the reducing agent [a]		T /°C	Configuration of the alcohol	*ee* (%)	Ref.
			$BH_3 \cdot THF$	$BH_3 \cdot Me_2S$				
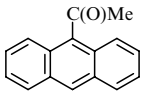	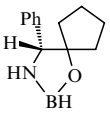 (**55**)	0.1	0.9		30	*S*	90	68
(1*R*,4*R*)	**55**	0.1	1		30	see [d]		69
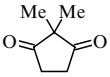	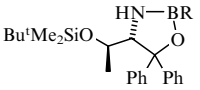 (**56**, R = Me) [e]	1	5		0–25	see [f]	>99	70
$PhC(O)CH_2OSiMe_2Bu^t$	**13** (R = H)	0.1	0.6		25	*S*	74	71
	48 (R = H)	0.1	0.6		25	*S*	52	71
	27 (R = H)	0.1	0.6		25	*S*	84	71

[a] The amount of the catalyst and the reducing agent is expressed in equiv. (equiv. of ketone)$^{-1}$; [b] The reaction is carried out in toluene; [c] The reaction is carried out in the presence of 0.2 equiv. of diethylaniline; [d] A mixture of (1*R*,2*R*,4*R*) and (1*R*,2*S*,4*R*) isomers (6 : 94) was obtained; [e] For other reactions with this catalyst, see Refs 72 and 73; [f] A mixture of *dl*- and *meso*-isomers with predominance of the *dl*-isomer (*dl* : *meso* > 99 : 1) was obtained.

with its diphenyl-substituted (**20**) and fully hydrogenated (**24**) analogues.

A search for cheap and renewable sources of raw materials for the commercial production of CBS catalysts has stimulated the synthesis of 1,3,2-oxazaborolidines **33**, **45** and **54** from chiral amino alcohols of the terpene series which gave encouraging results (*ee* 80%–93%).[27, 53, 54] An attempt to increase *ee* by replacing 1,3,2-oxazaborolidines by their chromotricarbonyl complexes [56] was unsuccessful (*cf*. *ee* obtained in the presence of the catalysts **35, 20** and **23**).

Considerable recent interest in sulfonylated 1,3,2-oxazaborolidines is explained by their higher stabilities and ease of purification and regeneration in comparison with the classical CBS catalysts. It is believed that these catalysts form more stable complexes owing to additional coordination of the hetero atom to the boron atom within the catalytic complex.[57] For example, *N*-arylsulfonylated (*S*)-diphenylprolinol is a good catalyst for the reduction of bromoacetophenone. When the reaction is carried out in boiling toluene, the yield of (*R*)-2-bromo-1-phenylethanol is 96% (*ee* is 91%).[74] This suggests that the amino alcohol reacts as the complex (**57**).

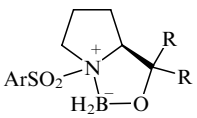

57

R = H: Ar = *p*-MeC_6H_4, 1-naphthyl, 2-naphthyl, 2,4,6-$Pr^i_3C_6H_2$;
R = Ph: Ar = *p*-MeC_6H_4.

It is believed that in the case of enantiomerically pure 2-hydroxymethylpiperazines (**58** and **59**) as catalysts, the formation of dimeric 1,3,2-oxazaborolidines takes place.[75]

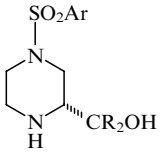

58

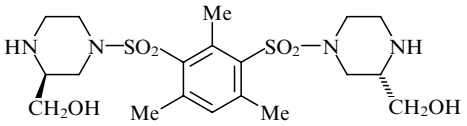

59

R = H, Ph; Ar = *p*-MeC_6H_4, 1-naphthyl, 2-naphthyl, 2,4,6-$Pr^i_3C_6H_2$.

1,3,2-Oxazaborolidine prepared from compound **59** catalyses the reduction of acetophenone to (*S*)-2-phenylethanol with *ee* 71%.

Dimeric 1,3,2-oxazaborolidines are presumably also formed in the reduction by (1*R*,4*R*,2*S*,3*S*)-1,4-diamino-1,4-dibenzylbutane-2,3-diol and BH_3.[76]

The formation of the original chelate 1,3,2-oxazaborolidine **60** has been reported:[66]

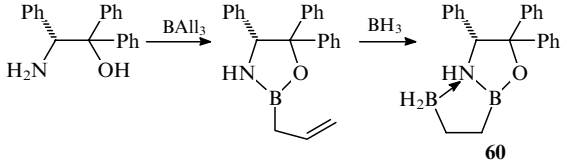

60

The reduction of acetophenone by borane in the presence of binary mixtures of homochiral amino alcohols (1*S*,2*R*)-1-amino-2-indanol, (*S*)-prolinol and (*S*)-phenylglycinol has been studied.[77]

On the whole, the analysis of literature data suggests that the relatively accessible catalysts for ketone reduction, 1,3,2-oxazaborolidines **3** and **5** based on (*S*)-diphenylprolinol recommended by Corey are the most efficient.[5, 11–13] The use of other boron-substituted (*S*)-diphenylprolinol-based 1,3,2-oxazaborolidine derivatives in the reduction of ketones has recently been reported. All these catalysts manifest high enantioselectivity in the reduction of various carbonyl compounds and are successfully used in asymmetric Diels–Alder reactions, aldol condensation, enantioselective cleavage of acetals, *etc*. (see below).

3. Effects of the catalyst preparation procedure, temperature, solvent and reducing agent on the enantioselectivity of the ketone reduction

The purity of a catalyst was shown [5, 7, 18, 33, 76] to be of crucial importance for obtaining high *ee* in the enantioselective catalytic reduction of carbonyl compounds. The presence of admixtures of starting amino alcohols and boronic acids decreases *ee*. Some CBS catalysts are available from Aldrich and Lancaster, but the catalysts do not always meet necessary requirements.[18, 78] Their application in laboratory practice gives irreproducible results due to high content of admixtures and poor storage stability.[78] Therefore, the preparation of a catalyst is a key step in the reduction. 1,3,2-Oxazaborolidines can be prepared using various approaches, *e.g.,* (a) by reactions of amino alcohols with 3 equiv. of $BH_3 \cdot THF$ or $BH_3 \cdot Me_2S$ in an argon atmosphere in boiling THF or toluene with a subsequent removal of the solvent *in vacuo* (the product formed is used without additional purification [7–10] or is purified by sublimation [11–13]); (b) boiling of an amino alcohol with the corresponding alkylboronic acid $RB(OH)_2$ in toluene with azeotropic distillation of water formed;[30] (c) boiling of an amino alcohol with boroxine $(RBO)_3$ [18, 27, 30] in toluene in the presence of molecular sieves 3–5 Å with azeotropic distillation of water formed.

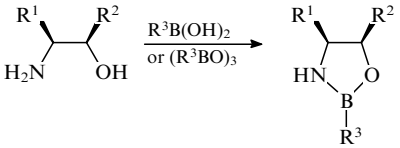

R^1, R^2 = Alk, Ar; R^3 = Me, Bu, Ar.

In many cases, the catalyst is prepared *in situ* by mixing an amino alcohol with $Me_2S \cdot BH_3$ or $BH_3 \cdot THF$ at room temperature, which is especially convenient for the synthesis of 1,3,2-oxazaborolidines non-substituted at the boron atom based on non-cyclic amino acid derivatives. An express method for the synthesis of 1,3,2-oxazaborolidines with a substituted boron atom (1 h) has been developed.[79] In this approach, the amino alcohol is mixed with bis(2,2,2-trifluoroethyl) alkylboronate in toluene. Subsequent vacuum evaporation of toluene, trifluoroethanol and the excess of $RB(OCH_2CF_3)_2$ and heating (110 °C, 0.07 Torr) give pure 1,3,2-oxazaborolidine.

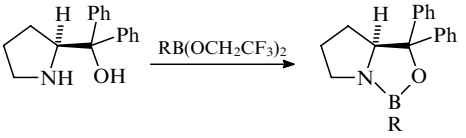

R = Alk, Ar. (*S*)

As mentioned above, special care should be taken over the removal of traces of moisture from the catalyst, reagents and solvents, since water decomposes the 1,3,2-oxazaborolidine ring.[33] It was found [61] that the addition of 2.5 mg of H_2O per g of bromoacetophenone decreases *ee* of the (*R*)-1-phenyl-2-bromoethanol formed from 96% to 85%, while the addition of 10 mg of H_2O per g of the substrate decreases it to 50%. The content of H_2O in the reaction mixture should not exceed 40 μg ml^{-1} at the ketone concentration of 70 mg ml^{-1} (see Ref. 78), while the maximum *ee* is reached at the H_2O content not exceeding 20 μg ml^{-1} (see Ref. 18). Contrariwise, the addition of propan-2-ol or any other aliphatic alcohol increases *ee*,[80, 81] which suggests its involvement in the decomposition of the intermediates **9** and **10** (see Scheme 4).

The effect of temperature on the enantioselectivity of the reduction has been considered in several publications.[76, 82, 83] The dependence of *ee* on temperature is usually described by a curve with a maximum at 30–50 °C, which is typical of catalysts prepared *in situ*. At temperatures below −30 °C, 1,3,2-oxazaborolidine is formed at a very slow rate, the reaction mixture contains many catalytically inactive components and non-selective reduction of the carbonyl compound by borane predominates.[5] The low values of *ee* observed at temperatures exceeding the optimum temperature corresponding to the maximum value of *ee* can be explained by thermal decomposition of the catalytic complex. Thus compound **5** is decomposed at 124–126 °C with liberation of B_2H_6.[18]

However, there is still no unambiguous answer to the question of the effect of temperature on the value of *ee*. In some cases, high values of *ee* were obtained when the reaction was carried out in toluene at temperatures below −10 °C with additional amounts of a freshly prepared catalyst $\mathbf{5} \cdot BH_3$ added to the reaction mixture in the course of the reduction.[18, 78] In others, the highest values were reached when the reaction was performed in boiling toluene.[15, 74] This suggests that the optimum temperature should be selected in each concrete case and for each concrete catalyst.

The value of *ee* also depends on the rate of addition of the ketone and the nature of the solvent. The lower the rate of ketone addition the higher the *ee*. In some solvents favouring coordination of borane (*e.g.*, THF) only 10% of the catalyst is involved in the complexation with BH_3. This factor should also be taken into consideration in the optimisation of reduction processes.[18]

As a rule, high enantioselectivity is attained in the presence of as little as 0.05–0.1 equiv. of the $BH_3 \cdot Cat$ complex (Cat is 1,3,2-oxazaborolidine) with respect to the substrate (ketone). However, in some cases the optical yield of the target product depends on the amount of the catalyst used. Thus the value of *ee* for (*R*)-1-phenylethanol in the reduction of acetophenone by the complex $BH_3 \cdot THF$ in the presence of the catalyst **4** increases from 63% and 89% to > 95% as the concentration of the catalyst is increased, correspondingly, from 2 mol.% and 4 mol.% to 10 mol.%.[15]

Other reducing agents, *e.g.*, the borane complex with 1,4-thioxane (**61**),[83] catecholborane (**62**) and the *N,N*-diethylaniline complex with borane (**63**), are used along with $BH_3 \cdot THF$ and $BH_3 \cdot SMe_2$ in the reduction of ketones. Compounds **61**–**63** are less reactive than $BH_3 \cdot THF$ and $BH_3 \cdot SMe_2$, however in some cases they give better results.

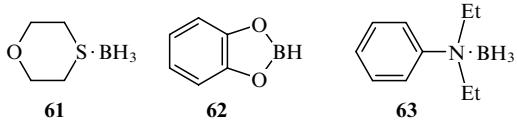

61 **62** **63**

Thus the use of catecholborane **62**, which does not require any additional ligands for its stabilisation, allows highly enantioselective reduction of ketones in non-coordinating solvents (*e.g.*, toluene, CH_2Cl_2).[5, 30] This reagent was used in the reduction of trihaloketones,[73, 84] α,β-enones [85] and oxophosphonates [86] as well as in the preparation of (3*S*)-2,3-epoxysqualene [87] and non-natural amino acids.[88] If the reaction is carried out at −78 °C and lower temperatures, the reduction of carbonyl compounds occurs without the involvement of other functional groups (C=C, C≡C) sensitive to hydroboration under ordinary conditions.[5]

In some cases, enantioselectivity can be increased if tertiary amines are added to the reaction mixture.[38, 52, 70] The catalytic reduction of aromatic ketones by oxazaborolidines prepared *in situ* from amino alcohols and borane complexes with tertiary amines has been studied.[89] Thus the reduction of acetophenone by the complex **63** in the presence of the catalyst **3** has made it possible to increase *ee* of (*R*)-1-phenylethanol to 99% (see Refs 90 and 91).

The *ee* of the product also depends on the presence of admixtures in commercial reducing agents. According to most recent reports,[92] the admixtures of $NaBH_4$ added to the commercial reagent $BH_3 \cdot THF$ for its stabilisation favour non-catalytic reduction and thus decrease *ee* of the reduction product. It is recommended to use the reverse order of addition of reagents to increase *ee*, *e.g.*, to add ketone to the catalyst and the reducing agent.[92] This should also be taken into consideration in those

cases where borane is synthesised *in situ* using the $I_2 - NaBH_4$ (see Ref. 89) or the $Me_3SiCl - NaBH_4$ system.

4. Examples of reduction of carbonyl compounds

Let us consider some characteristic features of enantioselective reduction of carbonyl compounds (particularly those not listed in Table 1) in more detail. The reduction of aromatic ketones by $BH_3 \cdot THF$ or catecholborane (**62**) in the presence of catalysts [(*S*)-**5** or (*S*)-**12** based on (*S*)-diphenylprolinol] has been studied in especially great detail.

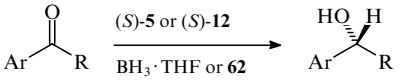

R = CH_2Cl,[82,90] CH_2Br,[90,93,94] CH_2OTHP (THP is tetrahydropyranyl),[95] CH_2N_3 (*ee* 91% – 100%),[96] $(CH_2)_nC(O)R$ (R = Me, Bu^t, Ph; *n* = 0 – 4, both carbonyl groups are reduced simultaneously),[97] CH_2SO_2Ar,[98] $(CH_2)_nP(O)(OPr^i)_2$ (*n* = 1, 2),[86,99] CF_3,[57,84] CCl_3;[28,84,88] Ar = Ph, *m*(*p*)-$R'C_6H_4$ (R′ = Alk, Hal),[100–103] α(β)-$C_{10}H_7$ *etc*.

A large body of experimental evidence has made it possible to formulate a general rule, *viz*., the greater the difference in the size (steric discrimination) between the Ar and R groups the higher the *ee* in enantioselective reduction of ketones.[5–7] The enantioselectivity of reduction of acetophenone, propiophenone and other alkyl aryl ketones by boranes is rather high (*ee* is 94% – 98%, see Table 1).

In the presence of the catalyst **12**, catecholborane reduces α-, β- and γ-oxophosphonates to α-, β- and γ-hydroxy phosphonates (*ee* 51% – 99%) depending on the nature of the substituents in the aromatic nucleus (it is of note that the phosphonate group is considered to be bulkier than the aromatic radical).[86] 1-Oxo-(2*S*)-phthalimidophosphonates are reduced by catecholborane exclusively to (1*R*)-hydroxy-(2*S*)-phthalimidophosphonates (yields 63% – 77%).[99]

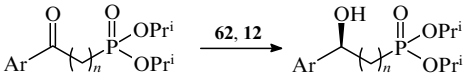

Ar = Ph, XC_6H_4 (X = Hal, Me, OMe); *n* = 0 – 2.

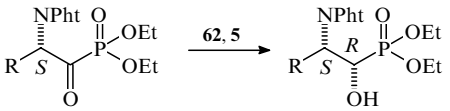

R = $PhCH_2$, Pr^iCH_2, Me, *p*-$BnOC_6H_4CH_2$; Pht is phthalimido.

In contrast to oxophosphonates, the arylsulfonyl group of β-oxosulfones is considered to be less bulky than the aromatic residue; such compounds are usually reduced by borane in the presence of the catalyst **3** to give (*S*)-enantiomers of β-hydroxy sulfones.[98]

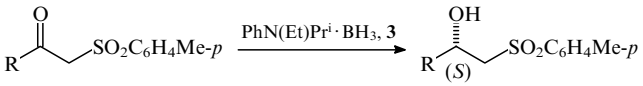

(*ee* 97% – 99%)

R = Ar, Alk.

$BH_3 \cdot THF$ (in the presence of the catalyst **5**)[100] and catecholborane **62** [in the presence of the catalyst **3** generated *in situ* from (*S*)-diphenylprolinol and $NaBH_4 - Me_3SiCl$] were used for the reduction of 2-acetylnaphthalene.[101] The *ee* of naphthylethanol formed was 96% – 98%. Efficient reduction of cyclic ketones, such as 1-tetralone (see Table 1), 1-indanone[18] and 1-suberone, also occurs under similar conditions.[18]

If the substrate to be reduced contains a nitro group[104] or other functional groups able to coordinate the boron atom,[105] the reducing agent should be used in larger amounts, an additional equivalent should be added. Chiral alcohols containing a heterocyclic substituent were prepared from 2-acylfurans,[16,106] 3-acetylpyridine[5] and 2-acylthiophenes.[96,106]

The reduction of substituted benzophenones[104] and 2-benzoylpyridinium triflates[107] yields optically active benzhydrols. It was found that the introduction of substituents into the *ortho*-position of the aromatic nucleus of alkyl aryl ketones (MeCOAr and EtCOAr) decreases the *ee* of the alcohols formed upon their reduction by the system $BH_3 \cdot Me_2S$ in the following order: Ph > *o*-Tol > Mes.[108]

Modest enantioselectivity was achieved in the reduction of aliphatic ketones: high values of *ee* were obtained only for sterically hindered ketones where the spatial difference between two alkyl substituents was high enough. Thus the reduction of isopropyl methyl ketone and *tert*-butyl methyl ketone gave the corresponding alcohols with *ee* 91% and 93% – 97.3%, respectively.[13,66,90] High values of *ee* (99%) were also obtained in the reduction of cyclohexyl methyl ketone by the complex **63**.[90]

It is of note that the reduction product of cyclopropyl isopropyl ketone has a configuration in which the cyclopropyl group plays the role of a bulky substituent (R_L) and the isosteric isopropyl group acts as a minor substituent (R_S).[5] This can be attributed to the fact that the cyclopropyl group is a more potent electron donor than the isopropyl group; therefore, the former increases the electron density of the free electron pair of the carbonyl group which is in the relative *anti*-position (the intermediate **8** in Scheme 4).[104]

The use of 1,3,2-oxazaborolidines for the enantioselective reduction of alkanones does not give good results;[109,110] only alkyl methyl ketones containing alkyl substituents C_nH_{2n+1} ($n \geqslant 4$) are reduced with satisfactory enantioselectivity [*ee* of the alcohol (*R*)-MeCH(OH)Bu^n is 47% (see Ref. 34) or 66%,[105] *ee* of (*R*)-MeCH(OH)C_6H_{13}-n is 70%[66]]. The reduction of phenylacetone proceeds with moderate stereoselectivity, *viz*., in the presence of $Me_2S \cdot BH_3$ and the catalyst **48**, (2*R*)-phenylpropan-2-ol is formed with *ee* 61%,[66] whereas in the presence of $BH_3 \cdot THF$ and the catalyst **4** *ee* is 81%.[15]

The reduction of ketones containing alkyl and 1,3-dithianyl substituents is a convenient method for the synthesis of optically active ketols **64**.[72,111] The bulky 1,3-dithianyl substituent possesses a high discriminative ability which increases *ee* of ketols **64**. This reaction proceeds *via* the alcohols **65**. The desulfurisation of the alcohols **65** by Raney nickel yields the secondary alcohols **66**.

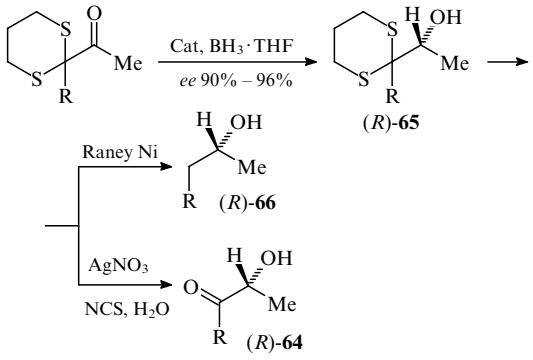

R = Alk, Ar; Cat = 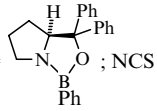 ; NCS is *N*-chlorosuccinimide.

It is known that the non-catalytic reduction of dicarbonyl compounds by borane yields diols in the *meso*-form.[97] In the catalytic reduction of diphenyl diketones **67** (R^1 = Ph) (10 mol.% of the catalyst **51**), the *meso* : *R*,*R* (or *S*,*S*) ratio varies from 48 : 52 (*n* = 1) to 21 : 79 (*n* = 2), 9 : 91 (*n* = 3) or 2 : 98 (*n* = 4).[112–114]

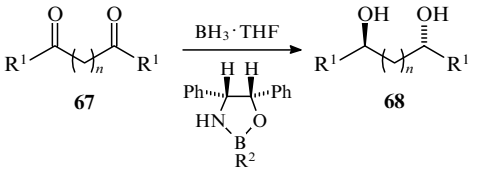

67 **68**

n = 1 – 4; R^1 = Me, Bu^t, Ph; R^2 = H, Me.

After crystallisation of the diol **68**, *ee* of the *S*,*S*-enantiomer was 99% (the content of the *meso*-form was < 1%). (For n = 1, the configuration of the diol formed was *R*,*R*).

α-Diketones RC(O)C(O)Ph (R is a heterocyclic substituent) are reduced to (*S*,*S*)-RCH(OH)CH(OH)Ph by $BH_3 \cdot SMe_2$ in the presence of the catalyst (*S*)-**3** with *ee* 99%.[113]

The reduction of 1,4-diphenylbutane-1,4-dione by the $BH_3 \cdot SMe_2$ complex in the presence of 1,3,2-oxazaborolidine (*S*)-**69** proceeds with high selectivity. The diol **68** formed (*ee* 99%) is easily converted into chiral 2,5-diphenylpyrrolidine with high *ee*.[114] The catalyst (*S*)-**69** was obtained *in situ* from (*S*)-diphenylprolinol and trimethyl borate.

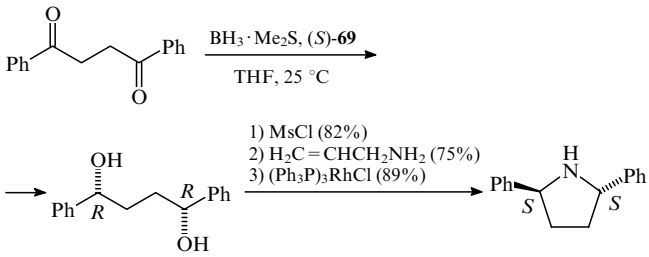

68 (96%, *ee* 99%) (55%, *ee* 99%)

(*S*)-**69** =

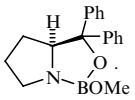

The reduction of hexane-2,5-dione under identical conditions yields the corresponding diol with *ee* 33%.[114]

The reduction of spiro[4.4]nonane-1,6-dione (1.5 equiv. of borane, 0.1 equiv. of the catalyst (*S*)-**12**) at 78 °C gives ketol **70** (60%) and *trans*,*trans*-spirodiol **71** (40%). With an increase in temperature to 22 °C and of borane concentration to 2 equiv., a mixture of *cis*,*trans*-spirodiol **72** (83%) and the *trans*,*trans*-isomer **71** (17%) is formed.[115]

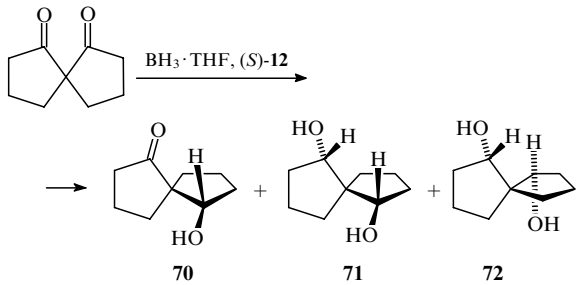

70 **71** **72**

A simple method for the synthesis of (1*S*,2*R*)-indenoxide with *ee* > 99% and (1*S*,2*S*)-*trans*-2-bromoindan-1-ol with *ee* 87% has recently been developed. The enantioselective reduction of 2-*p*-tolylsulfonyloxy-1-indanone was carried out using a borane complex with *N*-ethyl-*N*-isopropylaniline in the presence of the catalysts **5** and **39** (R = Me).[116]

A detailed description of enone reduction is given in the reviews.[5–7] To prevent the non-catalytic reduction of the double bond, enones are usually reduced by catecholborane **62** at low temperatures in the presence of the catalysts **5** and **12**. It is of note that the alkene residue of acyclic enones plays the role of the larger substituent (R_L).[5–7, 112, 117] In conformity with this rule, the catalytic reduction of enones in the presence of 1,3,2-oxazaborolidines (*S*)-**5** and (*S*)-**12** yields (*R*)-enantiomers of substituted allylic alcohols.[5, 30, 103, 118–123]

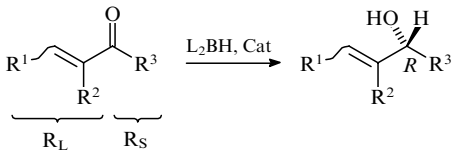

(*S*)-Enantiomers are formed exclusively in the presence of α-substituents in R^2 and R^3 groups (see Ref. 117).

The enantioselective catalytic reduction of alk-2-ene-1,4-diones is documented in the studies.[112, 124]

The catalytic reduction of cyclic enones containing an endocyclic double bond yields allylic alcohols with *ee* > 90%. In this case, the key role in the selectivity control is played by the nature of the substituent R at the α-carbon atom.[5]

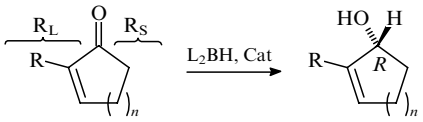

n = 1, 2.

The reduction of enones with R = Me,[30] Br,[13, 125–127] Bu^{t}Me$_2$SiOCH$_2$ [128] and (MeO)$_2$CHCH$_2$ [129] in the presence of the catalysts (*S*)-**5** and (*S*)-**12** gave exclusively (*R*)-enantiomers of allylic alcohols.

The alkene residue of cyclic enones containing an exocyclic double bond also plays the role of a bulky group R_L.[130]

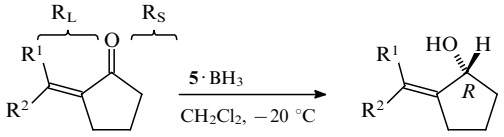

73 **74**

The yield of the alcohol **74** in the reduction of the ketone **73** (R^1 = H, R^2 = Ph) was 84% and its enantiomeric excess was 96%. To ensure high selectivity, the reduction was performed in dichloromethane at low temperature by slowly adding the enone solution to the reducing agent ($BH_3 \cdot SMe_2$) (the enone : reducing agent : catalyst ratio was 1 : 1 : 0.2).[130]

A method for the synthesis of chiral allenes from α-tributylstannylated allylic alcohols has been developed:[118]

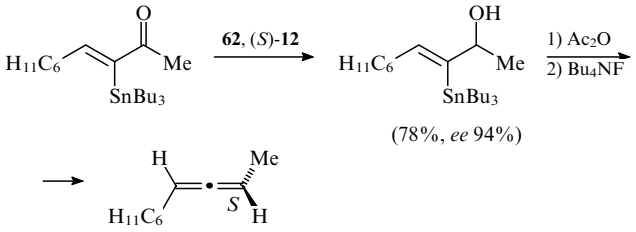

(78%, *ee* 94%)

(*ee* 94%)

The reduction of acetylenic ketones gave unexpected results. It was found that the acetylene residue plays the role of a minor substituent R_S irrespective of the size of the substituent R^1 as a result of which the reduction of acetylenic ketones yields (*S*)-enantiomers of acetylenic alcohols.[124, 131]

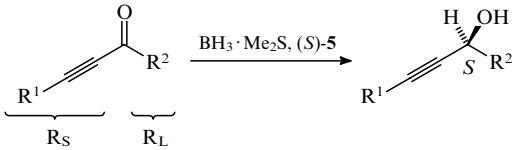

R^1 = H, Ph; R^2 = Me, Et, n-C_6H_{13}, Pr^i, cyclo-C_6H_{11}.

The introduction of a bulky $SiPr^i_3$ group into the acetylene residue converts it from R_S into R_L. Thus the reduction of the ketone **75** by catecholborane **62** in the presence of 1,3,2-oxazaborolidine based on (*S*)-diphenylprolinol having a trimethylsilyl substituent at the B atom results in the formation of the (*R*)-acetylenic alcohol **76**.[85]

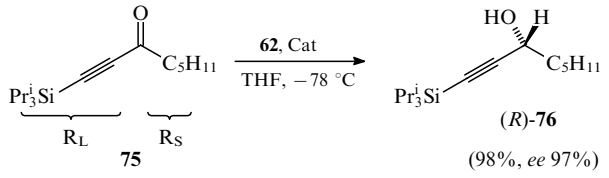

75

In order to make the acetylenic substituent play the role of a bulky R_L group, this can be converted into a π-complex with dicobalthexacarbonyl. Following the reduction, the complex is converted into an acetylenic alcohol by oxidative decomplexation.[104]

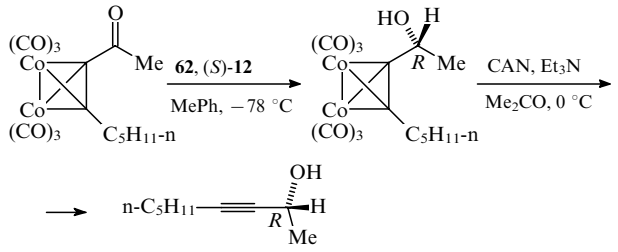

CAN = $(NH_4)_2Ce(NO_3)_6$.

The enantioselective reduction of acetylenic diketones and their π-complexes with dicobalthexacarbonyl has been described.[124]

The reduction of 4-(η^6-chromotricarbonylbenzoyl)chlorobenzene[104] was used in the synthesis of the second-generation histamine antagonist Cetirisine (**77**).[132]

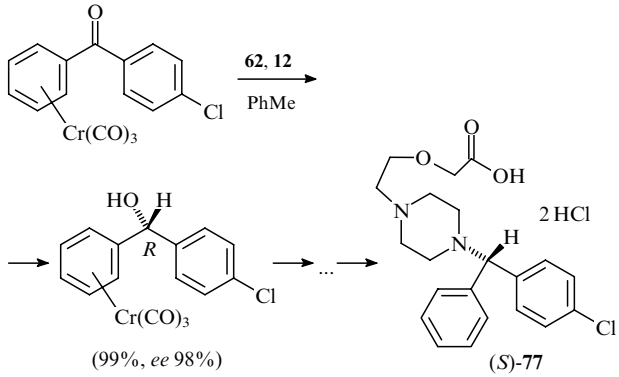

An attempt to perform the kinetic resolution of η^6-chromotricarbonyl complexes of 1-tetralone using CBS reduction failed.[133] It was expected that this reaction would result in the predominant formation of the *endo*-isomer **78** (which could correspond to the hydride ion transfer from the side opposite to the ligand $Cr(CO)_3$). However, under kinetic resolution conditions (*i.e.,* in the presence of 0.3 equiv. of the reducing agent) the reaction mixture contained the starting ketone (44% – 54%), the *endo*-isomer **78** (36% – 42%) and the *exo*-isomer **79** (10% – 14%); a mixture of the alcohols **78** and **79** (52 : 48) was formed in the presence of an excess of the reducing agent and after complete conversion of the original complex.

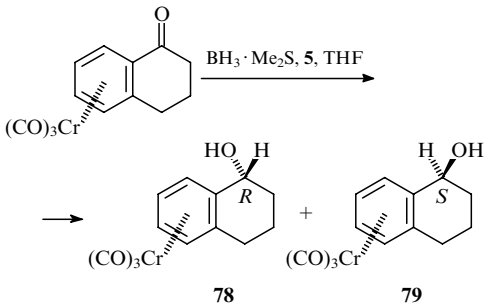

78 **79**

These results are rationalised as being due to the hydride ion transfer from the side of the $Cr(CO)_3$ group. An approach which includes primary catalytic reduction of the tetralone‡ and subsequent formation of the chromiumtricarbonyl complex **80** (the latter was used in the synthesis of (1*R*,4*R*)-7,8-dihydroxycalamenene **81**) appeared to be far more efficient.[134] The reduction of dimethoxytetralone by $Me_2S \cdot BH_3$ was carried out in THF in the presence of 0.2 equiv. of a catalyst based on (*R*)-proline which provided the (*S*)-configuration of the substituted tetralol. The stereospecific formation of the chromiumtricarbonyl *endo*-complex **80** is attributed to the regulatory effect of the hydroxy group which forms a complex with the chromium atom. Subsequent stereoselective alkylation of the complex **80** is well known in the chemistry of η^6-$Cr(CO)_3$ – arene complexes.

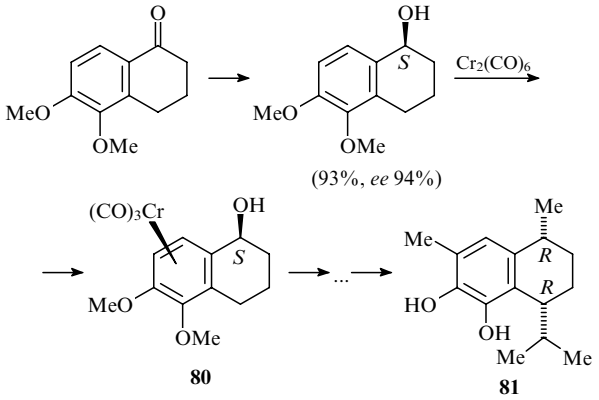

80 **81**

The catalytic reduction of the ferrocene derivatives[135–137] in the presence of 1,3,2-oxazaborolidines yields the chiral alcohols **82a**,**b** and **83** which were used in the synthesis of the chiral amines **84a,b** and **85**.§ The latter are used in enantioselective deprotonation and alkylation reactions.[136]

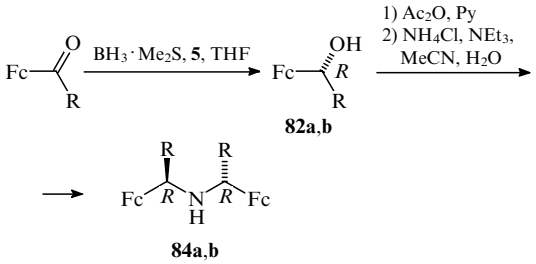

Compound	R	Yield (%)	*ee* (%)
82a	Me	97	98
82b	Ph	94	97
84a	Me	52	> 99
84b	Ph	90	> 99

‡ In this reaction, the enantiomeric excess of (*S*)-tetralol was 94%, while that after recrystallisation from EtOAc was 99%.

§ This reaction is similar to that involving the diols **68**.[114]

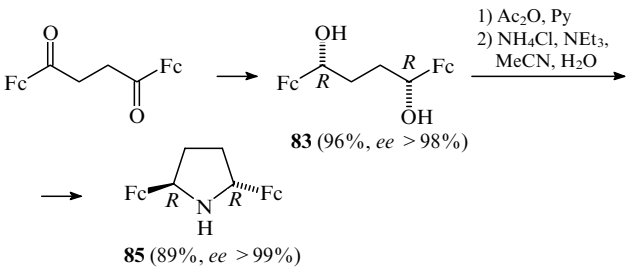

83 (96%, *ee* > 98%)

85 (89%, *ee* > 99%)

The reduction of cyclic *meso*-imides in the presence of the catalyst (*S*)-**3** yields a mixture of *cis*- and *trans*-5-hydroxypyrrolidones **86**; however, their rapid treatment with an EtOH – H_2SO_4 mixture yields predominantly *trans*-ethoxy lactam **87** in 73% yield (*ee* 75%).[138,139]

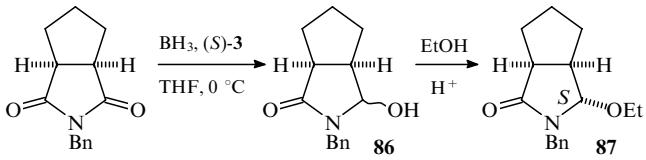

86 **87**

The reduction of imides in the presence of 1,3,2-oxazaborolidine **56** (R = H) was used in the synthesis of (+)-deoxybiotin **88**.[140]

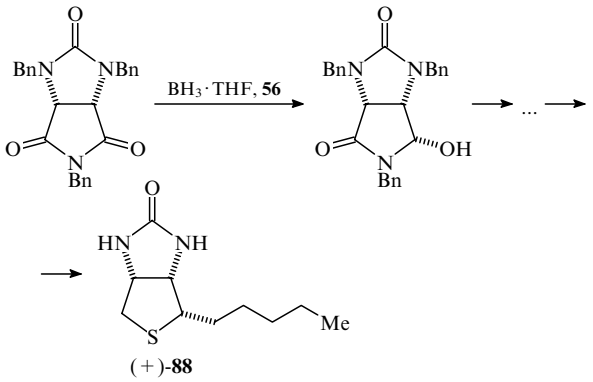

(+)-**88**

5. Synthesis of biologically active substances and natural compounds

The catalytic reduction of trichloromethyl ketones by catecholborane **62** in the presence of 0.1 equiv. of (*S*)-**12** can be used in the synthesis of both natural and non-natural (*S*)- or (*R*)-amino acids.[88]

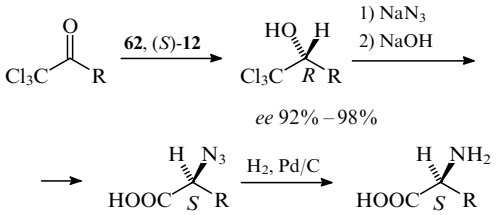

R = Alk, Ph.

A combination of enantioselective reduction with the Mitsunobu reaction opens up new routes to the synthesis of enantiomerically pure azides [141] and substituted 1-arylethylamines.[100]

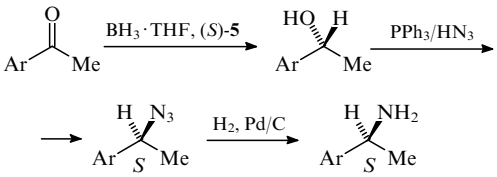

Ar = C_6H_4Br-*m*, C_6H_4OH-*m*, C_6H_4OMe-*m*.

The reduction of α-haloacetophenones catalysed by 1,3,2-oxazaborolidines is the most promising approach to secondary amino alcohols: (*R*,*R*)-formoterol (**89**),[61,94] (*R*)-denopamine (**90**)[142] and (*R*)-salmeterol (**91**),[93] which represent β-adrenoreceptor agonists [the biological activity is manifested predominantly by (*R*)-enantiomers].

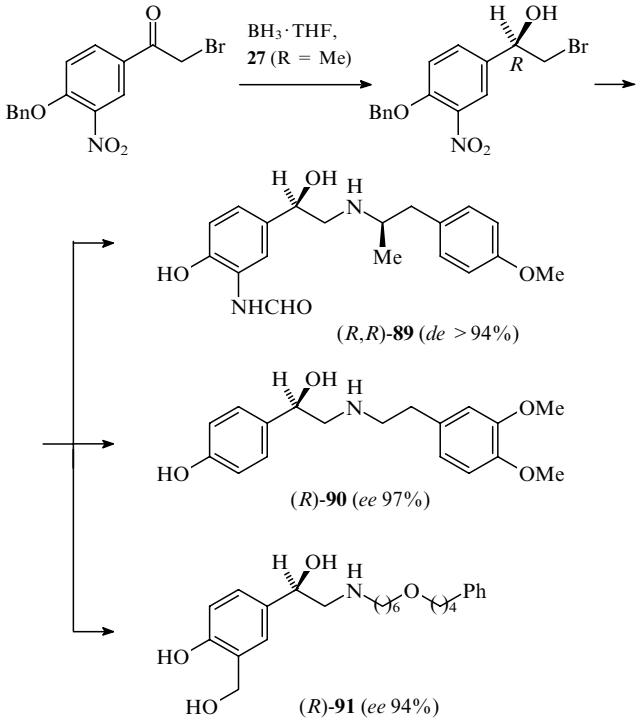

(*R*,*R*)-**89** (*de* > 94%)

(*R*)-**90** (*ee* 97%)

(*R*)-**91** (*ee* 94%)

The antidepressant fluoxetine (**92**) (Prozac©) is a potent selective serotonin uptake inhibitor and is widely used in medicine [143] (for the synthesis of fluoxetine and its metabolites see Ref. 144 and references cited therein). It was found that the (*R*)-enantiomer **92** possesses biological activity; the first step in its synthesis includes CBS reduction of β-chloropropiophenone.[143]

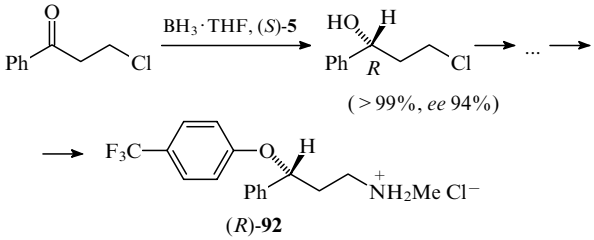

(> 99%, *ee* 94%)

(*R*)-**92**

An improved method for the synthesis of (*R*)-fluoxetine **92** and its main metabolite (*R*)-norfluoxetine **93** (isolated as D-tartrate) includes CBS reduction, Hoffmann rearrangement induced by diacetoxyiodobenzene and cleavage of the intermediate cyclic carbamate **94** (Scheme 5).[144]

Catalytic CBS reduction was used by Kaufman for the synthesis of chiral 1,2,3,4-tetrahydro- and 1,2-dihydroisoquinolines, *viz*., (*S*)-(−)-salsolidine (**95**) [145] and the intermediate (*R*)-**96** used in the synthesis of the β-adrenoreceptor antagonist MY336-a (Scheme 6).[102]

The stereoselective (*ee* 94%) synthesis of (3*R*,4*E*)-19-methyleicos-4-en-1-yn-3-ol (**97**) (a metabolite from the sea sponge *Cribrochalina vasculum*), which possesses immunosuppressive and antitumour properties, has been described.[146] This example is interesting in that the molecule of the starting compound **98** contains simultaneously the C=C and C≡C bonds. In this case, the role of the minor substituent R_S is played by the acetylenic fragment. The borane – dimethyl sulfide complex (THF, 0 °C) was

Scheme 5

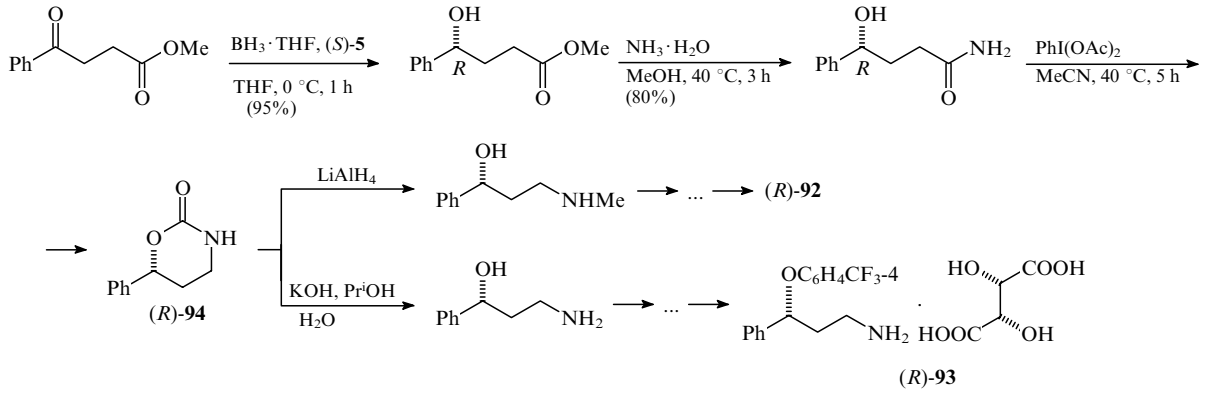

Scheme 6

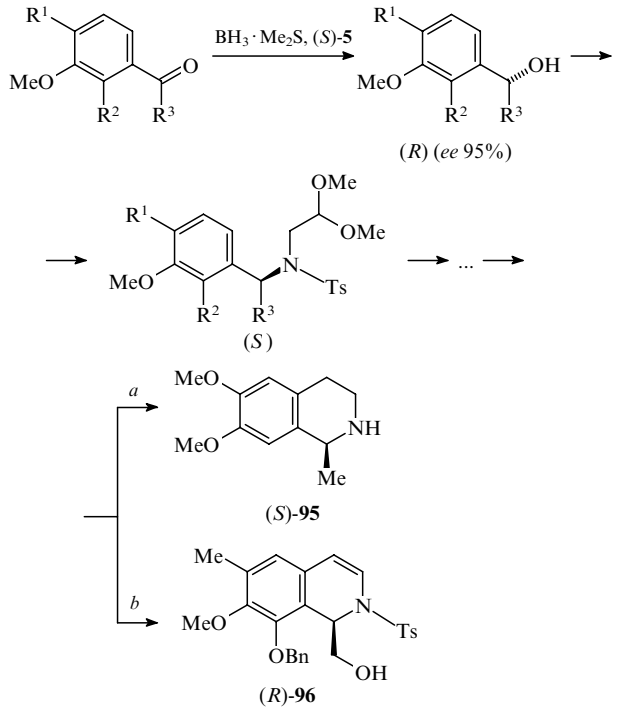

(*a*) R^1 = OMe, R^2 = H, R^3 = Me;
(*b*) R^1 = Me, R^2 = OBn, R^3 = CH_2OBn.

used as a reducing agent while (*R*)-**5** or (*R*)-**48** (R = Me) was used as a catalyst.

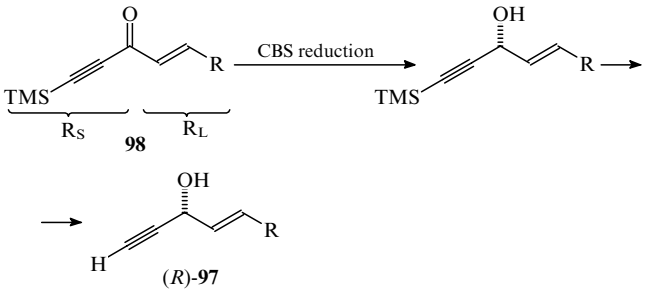

R = $(CH_2)_{13}Pr^i$, TMS = $SiMe_3$.

The key synthon (*R*)-**99** used in the synthesis of nicandrenones was prepared by CBS reduction of ketones **100** using (*S*)-**101** as a catalyst.[147]

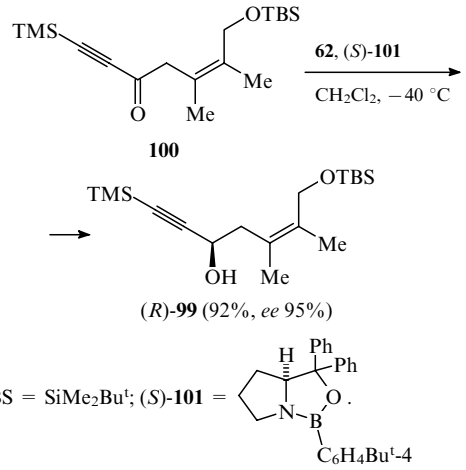

The mild conditions of CBS reduction have made possible its wide application in the chemistry of prostaglandins. Thus the enantioselective catalytic reduction of diynone **102** by catecholborane (**62**) was used in the synthesis of the ω-chain of the orally active cicaprost **103**, a metabolically stable analogue of prostaglandin I_2.[5]

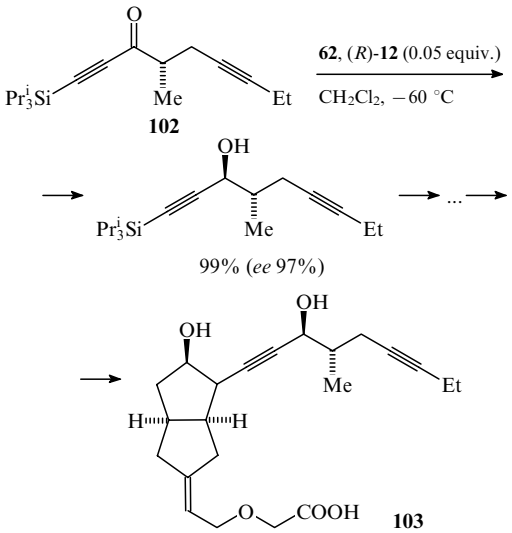

The stereoselective introduction of a hydroxy group into the C(15) atom in the synthesis of the protected prostaglandin PGE_2 **104** [(*S*) : (*R*) ≈ 10 : 1] is carried out in a similar way.[13]

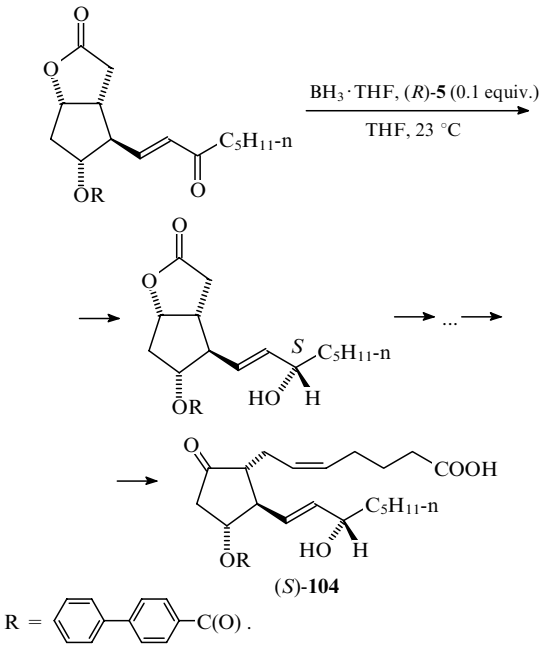

Other examples of the synthesis of biologically active and natural compounds by enantioselective reduction of carbonyl compounds can be found in the reviews.[5,6]

The above data suggest that CBS reduction of prochiral ketones has a number of advantages over other reduction procedures. These include versatility, *i.e.*, the possibility of reduction of different types of carbonyl compounds, predictable stereochemistry of the alcohol formed, relative availability of catalysts in any of their enantiomeric forms, easy regenerability of the catalyst precursor (an amino alcohol), low cost, high yields and relative simplicity of the experimental procedure.

III. Reduction of oximes and imines

The unflagging interest of investigators in optically active amines is due to the wide diversity of their practical applications, *e.g.*, in separation of enantiomers,[148] preparation of drugs[149] and as auxiliary reagents in asymmetric synthesis and catalysis.[150] It is therefore not surprising that the enantioselective reduction of ketones in the presence of chiral oxazaborolidines was extended to the synthesis of optically active amines. In this case, oxime ethers were used as the starting compounds.[10,151]

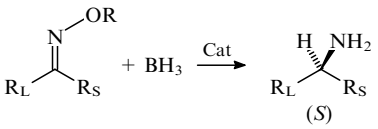

R = Me, Et, Bn, $SiMe_3$; R_L = Ph, 1(2)-naphthyl; R_S = Me, Alk.

On the whole, the product yields and the stereoselectivity of reduction of oxime ethers are lower than those of ketones.¶

Let us point out the differences in the conditions of preparation of optically active alcohols and amines.

First, the synthesis of amines requires that the reaction is carried out with only individual geometrical oxime isomers, since the stereochemistry of the final product (an amine) depends on the configuration of the precursor [*e.g.*, the (*S*)-enantiomer of the amine is usually formed from the *E*-isomer of the oxime containing small R_L and R_S fragments].[2,152] Second, high efficiency of the catalytic reaction (high values of *ee*) requires usually an increase in the reaction time up to 20–70 h and the use of equivalent amounts of 1,3,2-oxazaborolidine[153] (only a few examples of effective catalytic reactions are known[154,155]). Third, in the case of oxime ethers the *ee* value of the reaction product depends on the nature of the substituent R [the reduction of oximes non-substituted at the oxygen atom is non-selective (*ee* 0.6%), the best results are achieved for R = Me or CH_2Ph] and the catalyst type.[10,75]

As a rule, 2 equiv. of borane and 1 equiv. of the catalyst (**2**,[151–153] **3**[151,153] or 1,3,2-oxazaborolidine based on norephedrine[152]) are used per 0.8–1 equiv. of the oxime ether;† the reaction is carried out in THF at 30 °C for 24 h.

Let us consider the mechanism of reduction of oxime ethers in more detail (Scheme 7).[152]

Scheme 7

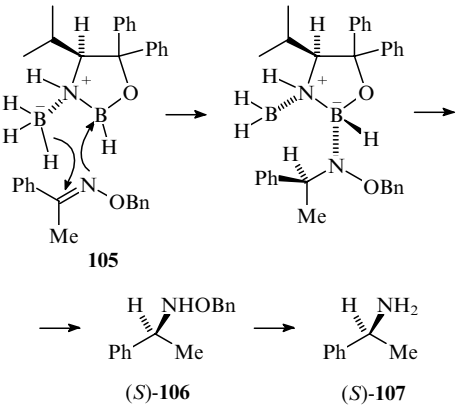

As was shown above in the example of the Corey model for ketones[5] (see Section II), the addition of borane to chiral 1,3,2-oxazaborolidine **2** occurs from the side opposite to the isopropyl group. The nitrogen atom of the *E*-isomer of the oxime ether coordinates the endocyclic boron atom by the free electron pair to form a six-membered transition state **105** where the bulkier phenyl radical of the oxime occupies an equatorial position. Subsequent stereoselective hydride ion transfer yields protected (*S*)-hydroxylamine **106** which is reduced to the (*S*)-enantiomer of the amine **107**. In some cases, hydroxylamines (*S*)-**106** were isolated together with the amines (*S*)-**107**.[152]

A somewhat different, but essentially similar interpretation for the formation of the (*S*)-enantiomer was given by Itsuno[156] who suggested that the steric interaction of the *O*-benzyl group with the *trans*-phenyl group is critical for the stereoselectivity (the solid-phase enantioselective reduction of ketoxime ethers[157–158] will be considered in Section V).

The reduction of imines occurs in a similar way.

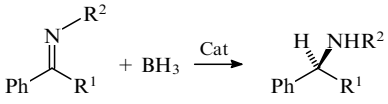

R^1 = Me, Et, Pr^i; R^2 = Ph, Bn, Alk.

The imines with R^2 = Ph are reduced best of all, the yields of the corresponding amines are 96%–98%, *ee* is 71%–88%.[153,159] The reduction of *N*-alkylketimines is less selective (*ee* 46%–52%), while the selectivity of reduction of dialkyl ketone imines is very low (*ee* 7.4%–24%).[153] The *ee* increases with an increase in the size of the radical R^1.

The structure of the catalyst is known to influence the course of the reduction of oxime ethers and imine.[75] It was found that the

¶ The early procedures[10,151] were further improved which enabled one to obtain semi-preparative amounts of substituted (*S*)-1-phenylethylamines with *ee* 90%–99%.[152] Hence, enantioselective reduction of oxime ethers and imines by boranes in the presence of chiral 1,3,2-oxazaborolidines is one of the most efficient methods for the synthesis of optically active amines.

† An experimental procedure for the regeneration of the catalyst **2** as a hydrochloride is reported.[152]

reduction of acetophenone *O*-methyloxime to 1-phenylethylamine by 1 equiv. of $BH_3 \cdot THF$ in the presence of *N*-arylsulfonylated 1,3,2-oxazaborolidine derived from **58** results in the formation of either an (*S*)- or an (*R*)-enantiomer depending on the nature of the substituents in compound **58**. Thus the (*S*)-enantiomer is formed with Ar = Tol-*p*, R = H (yield 61%, *ee* 84%), while (*R*)-2-phenylethylamine is formed with Ar = 1-naphthyl, R = H (yield 31%, *ee* 84%).[75] This is an illustrative example of a reversal of stereoselectivity due to replacement of a substituent in the arylsulfonyl group from tolyl to naphthyl. A similar dependence is observed in the reduction of prochiral ketones.[75]

The possibility of preparing chiral amino alcohols, which are valuable intermediates in asymmetric synthesis, by diastereoselective reduction of imino ketones and *O*-ethers of α-hydroxyimino ketones has also been studied.[154, 160–163] In the first experiments, the enantioselectivity and diastereoselectivity were rather low.[160] Thus the reduction of the imino ketone **108** (R = *p*-$MeOC_6H_4$, Ar = Ph) by the complex $BH_3 \cdot THF$ in the presence of 0.2 equiv. of the catalyst **56** (R = H) (see Table 1) gave a mixture of *syn*-(1*S*,2*S*)- and *anti*-(1*S*,2*R*)-isomers **109** (58 : 42) with the enantiomeric purity of the products < 14% (yield 88%).[162]

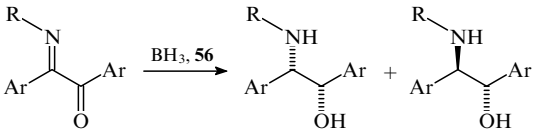

108 *syn*-(1*S*,2*S*)-**109** *anti*-(1*S*,2*R*)-**109**

R = *p*-$MeOC_6H_4$, BnO, *p*-$MeC_6H_4SO_2$;
Ar = Ph, *p*-$MeOC_6H_4$, *p*-MeC_6H_4, *p*-BrC_6H_4, 2-furyl.

The stereoselectivity increased on going from α-imino ketones (R = *p*-$MeOC_6H_4$) to ethers of α-hydroxyimino ketones (R = OBn): the enantiomeric purity of the target product reached 88%. In the presence of 1 equiv. of the catalyst **56** and $Al(OPr^i)_3$, the enantioselectivity increased to 90%, however, the diastereoselectivity was not changed (the *syn* : *anti* ratio was 47 : 53). It was thus concluded that under these conditions the catalytic reduction of the keto group was followed by non-selective reduction of the oxime group by borane.[162] This process was complicated by the formation of a side 1,3,2-oxazaborolidine from BH_3 and the amino alcohol formed, which catalysed the reduction in a non-selective manner.[160]

It was found experimentally that the keto group is reduced more easily than the oxime group.[154, 160] The stereoselectivity could be increased, if stepwise reduction was used under optimum conditions for each step.[162, 163] The reduction of the ether of hydroxyimino ketone **108** (R = OBn, Ar = Ph) in the presence of 1 equiv. of the catalyst **56** (R = H) at room temperature gave (*S*)-hydroxy oxime **110** (yield 78%, *ee* 98%).[162]

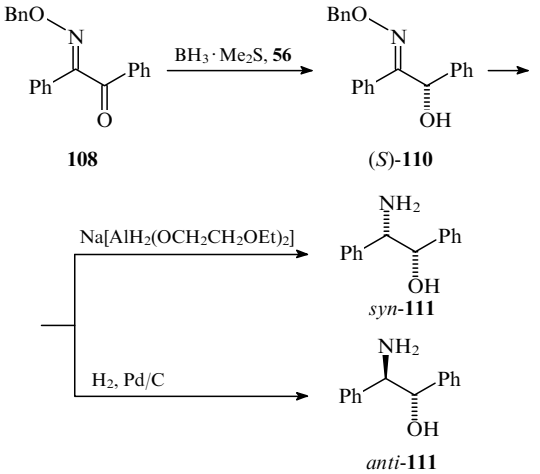

108 (*S*)-**110** *syn*-**111** *anti*-**111**

Subsequent reduction of the oxime function was carried out in the absence of 1,3,2-oxazaborolidine. The *syn*-isomer **111** was prepared by treatment of compound **110** with the complex hydride $Na[AlH_2(OCH_2CH_2OEt)_2]$, while the *anti*-isomer **111** was obtained by catalytic reduction of compound **110** with hydrogen in the presence of 10% Pd/C.[162, 163]

The reduction of ethers of α-hydroxyimino ketones **112** yields predominantly the *cis*-amino alcohols *cis*-(1*S*,2*R*)-**113**, *cis* : *trans* = 10 : 1 (for R = Bu^tPh_2Si, *ee* is 96%, after recrystallisation *ee* > 99%),[154] or 9 : 1 (for R = CPh_3, *ee* 90%).[160]

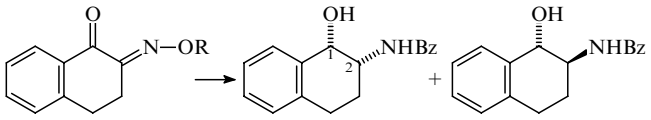

112 *cis*-(1*S*,2*R*)-**113** *trans*-(1*S*,2*S*)-**113**

R = Bu^tPh_2Si, Ph_3C.

The reduction of compounds **112** containing less bulky groups in the ether moiety proceeds with lower selectivity.

The reduction of ketoxime ethers by a borane–dimethyl sulfide complex in the presence of chiral 1,3,2-oxazaborolidines **69**, **114** and **115** prepared from trimethyl borate and the corresponding alcohols has been described.[160]

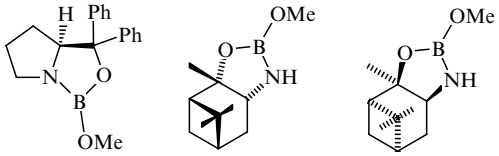

69 **114** **115**

The introduction of a bulky *O*-trityl (Tr) group into oximes is yet another approach to increase the selectivity of reduction of α-hydroxyimino ketones.[160, 161] This approach was used in the diastereoselective synthesis of sphinganine (dihydrosphingosine).[161]

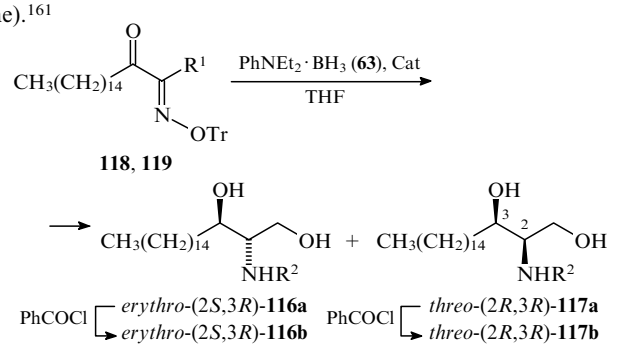

118, **119**

R^1 = CO_2Me (**118**), $CH_2OSiMe_2Bu^t$ (**119**); R^2 = H (**116a**, **117a**), PhCO (**116b**, **117b**); Cat = **69**, **114**, **115**.

Depending on the substrate, the catalyst and reduction conditions, one can obtain either the *erythro*-(2*S*,3*R*)-isomer **116** or the *threo*-(2*R*,3*R*)-isomer **117** [natural sphingosine has the *erythro*-(2*S*,3*R*)-configuration]. These conversions provide a typical example of so-called 'substrate control'.

Substrate	Catalyst	Reducing agent	*erythro* : *threo*	*ee* (%)
118	**69**	**63**	13 : 87	89 (*threo*)
119	**115**	**63** + $BH_3 \cdot SMe_2$	98 : 2	97 (*erythro*)

The catalytic reduction of diimines of the type **120** in the presence of 0.05 equiv. of the catalyst **56**, which yields substituted (*R*,*R*)-1,2-diphenylethylenediamines with *ee* 99% [the (*R*,*R*)-**121** : *meso*-**122** ratio is 95 : 5], has been described.[155]

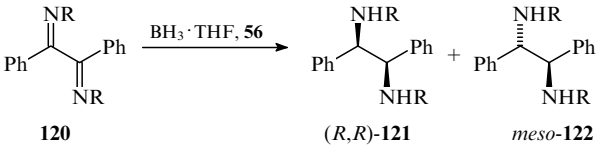

120 (*R*,*R*)-**121** *meso*-**122**

R = *p*-$MeOC_6H_4$.

An attempt to use this method for the reduction of 1,2-dioximes failed.[155]

The reduction of α-imino ketone **123** is the key step in the synthesis of the β-blocker (*S*)-albuterol (**124**).[164]

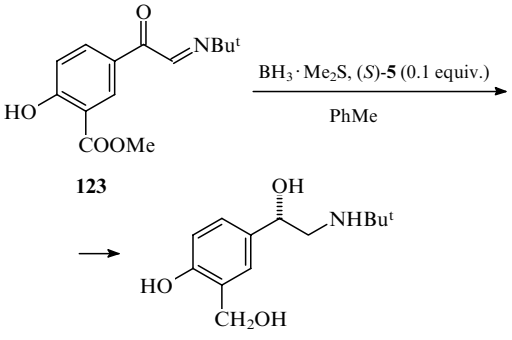

123

124 (90%, *ee* 93%–95%)

Despite the obvious success in the reduction of imines and oxime ethers, this reaction has a number of limitations. Thus no 1,3,2-oxazaborolidines able to catalyse effectively the reduction of 3,4-dihydroisoquinolines and carbolines have been found so far.[2] There are virtually no publications devoted to large-scale semi-industrial synthesis of chiral amines required for the synthesis of some medicinal drugs, *e.g.*, α- and β-adrenoblockers, antidepressants, *etc.*[149]

IV. Use of 1,3,2-oxazaborolidines in miscellaneous reactions

In addition to reduction of ketones, imines and oximes, chiral 1,3,2-oxazaborolidines find wide application in other branches of synthetic organic chemistry. Some applications of these catalysts in the Diels–Alder reaction, aldol condensation and some other reactions are considered in the review;[165] however, the articles cited therein were published before 1991. Therefore, we thought it expedient to systematise the literature data published in the past decade.

1. Aldol condensation

At the end of the 20th century, the efforts of many chemists were focused on the development of methods for enantioselective and diastereoselective aldol condensation [166–168] owing to the high versatility and wide applicability of this reaction in the synthesis of natural compounds, of macrolide antibiotics, in particular.

The aldol condensation of aldehydes with enol silyl ethers or ketone silyl acetals catalysed by Lewis acids (the Mukaiyama reaction) [169–171] can be implemented in an asymmetric version.[172]

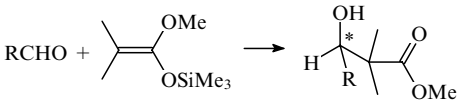

If an aldehyde introduced into the reaction contains a chiral α-carbon atom, the condensation product will contain two chiral centres.[172, 173]

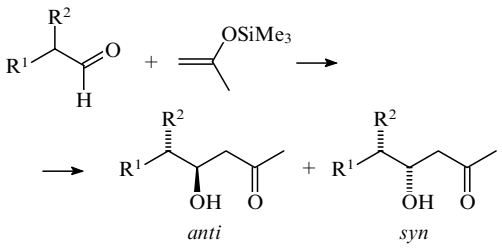

In the general case, this reaction yields a mixture of diastereomers. In a recent study,[174] the possibility of effective control over *syn*- and *anti*-selectivities by changing the spatial structure of the catalyst (the latter is used in amounts not exceeding 20 mol.%) has been demonstrated. It was found that high enantioselectivity (*syn* : *anti* > 98 : 2) can be achieved with a proper catalyst chosen with due regard to the nature of the substituents R^1 and R^2 in the starting aldehyde.[175, 176] This type of reaction can be referred to as a catalytically controlled process.[172] (Far from all reactions considered in this section can be carried out under conditions of catalytic control, often equimolar amounts of the catalyst are required.) The minor diastereomer formed is easily separated by chromatography.[172] Chiral *N*-acyl- and *N*-tosyl-1,3,2-oxazaborolidin-5-ones were found to be suitable catalysts for such conversions. The use of these compounds as catalysts was proposed simultaneously by Corey,[177, 178] Yamamoto,[179] Helmchen [180, 181] and Masamune.[182] Catalysts based on natural (*S*)-enantiomers of the amino acids **125a–e**,[172, 183] **126a–e** [184] and **127a–e** [185] are the most common.

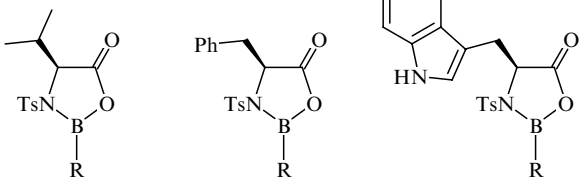

(*S*)-**125a–e** (*S*)-**126a–e** (*S*)-**127a–e**

R = H (**a**), Me (**b**), Bu (**c**), Ph (**d**), 3,5-$(CF_3)_2C_6H_3$ (**e**).

Compounds **125a, 126a** and **127a** were prepared by treatment of the corresponding *N*-tosylated amino acid with borane.[186] For example:

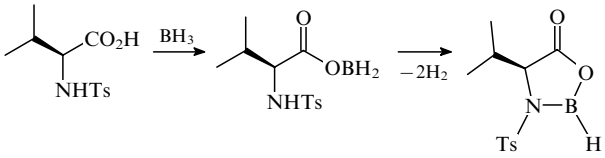

(*S*)-**125a**.

Esters of alkyl- or aryl-boronic acids were used instead of BH_3 in the synthesis of compounds **125b–e**, **126b–e** and **127b–e** containing B—Alk or B—Ar bonds.[184, 185]

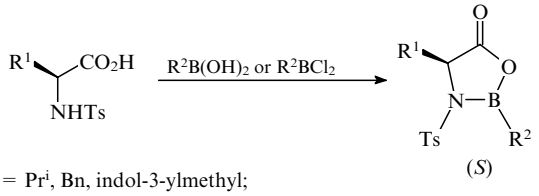

(*S*)

R^1 = Pr^i, Bn, indol-3-ylmethyl;
R^2 = Me, Bu, Ph, 3,5-$(CF_3)_2C_6H_3$, CH_2Bn.

Using negative ion mass spectrometry,[186, 187] it was shown that this reaction is accompanied by the formation of side products **128** and **129** (for R = H) or **130** (for R^1, R^2 = Alk, Ar).

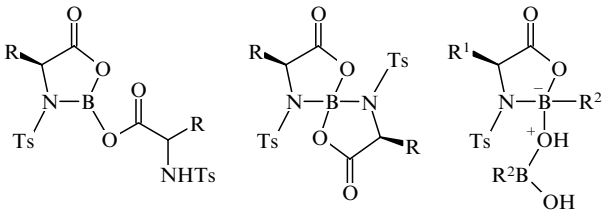

128 **129** **130**

Quantum-chemical methods were used to study the adducts formed upon coordination of formaldehyde with *N*-tosyl-1,3,2-oxazaborolidin-5-ones[183,188] and to determine the energies of their formation.[189] These calculations confirmed the previous assumption[190] on the possible formation of B–O···H–C and B···O=C bonds. The structures of the aldehyde adducts with *N*-tosyl-1,3,2-oxazaborolidin-5-ones were finally established only after the appearance of the publication by Corey *et al.*[191] devoted to X-ray diffraction analysis of some stable adducts where the existence of a hydrogen bond B–O···H–C between the oxygen atom of the 1,3,2-oxazaborolidine ring and the hydrogen atom of the aldehyde group was confirmed. According to Corey *et al.*,[191] the formation of such a non-trivial hydrogen bond is possible due to the high acidity of the hydrogen atom of the H–C(O) group upon coordination of its oxygen atom to the boron atom. This hydrogen bond is the structure-forming element in the rigid structure **131** resulting from the *re*-frontal attack of the nucleophile and governing the enantioselectivity of the aldol condensation and the Diels–Alder reaction (see below) catalysed by 1,3,2-oxazaborolidines (in this case, by compound **127c**).[191]

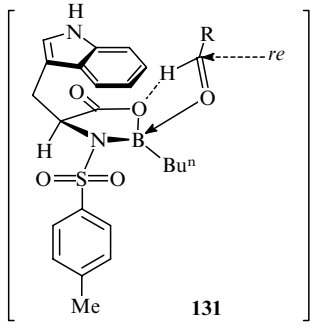

131

Other examples of the Mukaiyama-type aldol condensation of a series of aldehydes R^1CHO (R^1 = Ph, Pr^n, Pr^i, PhC≡C) with (*Z*)- and (*E*)-enol silyl ethers **132** are considered in the review.[185]

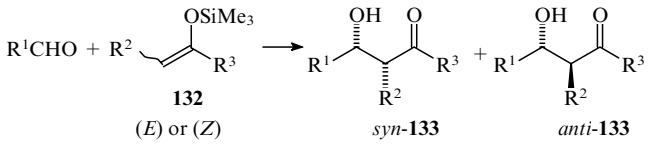

132 (*E*) or (*Z*) *syn*-**133** *anti*-**133**

R^1 = Ph, Pr^n, Pr^i, PhC≡C; R^2 = Me, R^3 = Ph, $R^2–R^3$ = $(CH_2)_4$.

The predominant formation of the *syn*-isomers **133** in this reaction is in accord with the model of the transition state **131**. The ratio of the *syn*-**133**:*anti*-**133** products in the condensation of benzaldehyde with trimethylsilyloxycyclohexene [$R^2–R^3$ = $(CH_2)_4$, *E*-isomer] in the presence of the catalyst **127e** was 78:22 with the total yield 99% (*ee* of compound *syn*-**133** was 89%),[185] while that in the condensation of propanal with the (*Z*)-isomer of trimethylsilyl ether **132** (R^2 = Me, R^3 = Ph) was > 99:1 with the total yield 99% (*ee* of compound *syn*-**133** was > 99%). These reactions were carried out in propionitrile at −78 °C for 12 h in the presence of 5 mol.%–10 mol.% of the catalysts **127a–e** (the catalyst **127e** manifested the highest efficiency).

Kiyooka *et al.*[172,192–204] have carried out a comprehensive analysis of the 1,3,2-oxazaborolidin-5-one catalysed Mukaiyama reaction and applied this methodology to the synthesis of bicyclic acetals, *e.g.*, compound **134**[195] and some natural compounds, *e.g.*, compound **135** which is a precursor of the macrolide acutiphycin, the key intermediate of the polyene macrolide filipin and the non-proteinogenic *N*-benzyloxycarbonylgalantinic acid.[201,205–207]

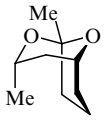

134

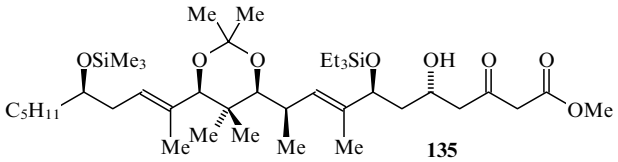

135

These reactions were carried out in the presence of stoichiometric amounts of 1,3,2-oxazaborolidine (*S*)-**125a** and its (*R*)-enantiomer (Schemes 8 and 9).

Three aldol condensations in the multistep synthesis of compound **135** (Scheme 9) were performed in the presence of the catalyst (*S*)-**125a** and the last one, in the presence of (*R*)-**125a**, which ensured the desired orientation of the asymmetric centres in the molecule **135**. It was found that the relative configuration of the stereocentres is governed by the stereochemistry of the oxazaborolidine and does not virtually depend on the nature of the substrate. According to Corey,[191] the structure of the transition complex formed in the Mukaiyama reaction catalysed by compound (*S*)-**125a** differs from that of the complex **131**. In this case, *si*-frontal attack of the nucleophile occurs resulting in predominant formation of *anti*-isomers.

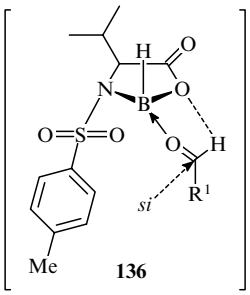

136

The *anti*:*syn* ratio varies from 2:1 to 10:1 [the use of (*R*)-**125a** results in the predominant formation of *syn*-isomers].[172,204] The isopropyl group in the complex **136** is *trans* relative to the tosyl group and *cis* relative to the B–H bond; the hydrogen bond C–H···O–B formed ensures fixation of the addition of the aldehyde to the catalyst **125a** thus providing high diastereoselectivity of its condensation with enol silyl ethers.

Scheme 8

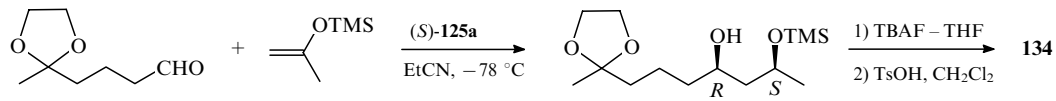

TBAF — Bu^n_4NF.

syn

Scheme 9

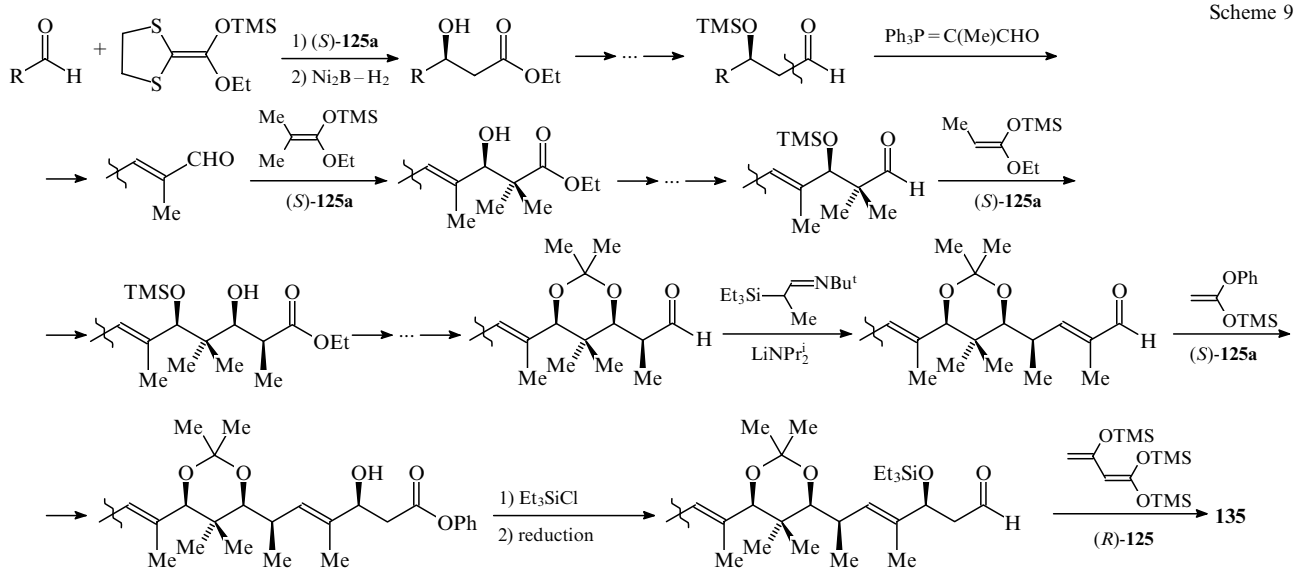

R = $CH_3(CH_2)_4$.

1,3,2-Oxazaborolidine **138** (0.2 equiv.) was used as a catalyst in the enantioselective aldol condensation of the silyl ether **137**.[208]

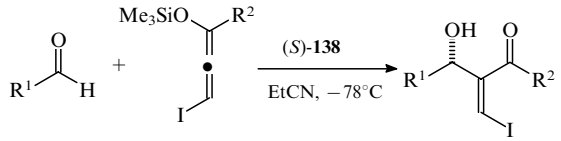

137

(60% – 70%, *ee* 61% – 98%)

R^1 = Me, Ph; R^2 = Me, Et; (*S*)-**138** = 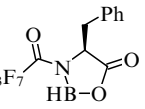

The Mukaiyama reaction in the presence of chiral 1,3,2-oxazaborolidin-5-ones **139a**–**d** was used in the synthesis of (2*R*,3*S*)-3-(4-methoxyphenyl)glycidate **140**, a key intermediate in the synthesis of the calcium antagonist diltiazem.[209]

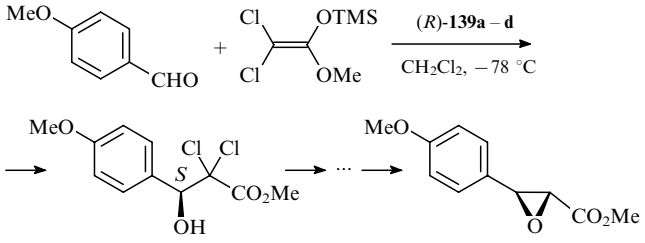

(*ee* 96%) (–)-**140** (*ee* > 96%)

(*R*)-**139a**–**d** = 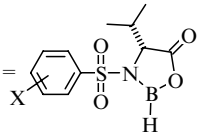

X = *p*-Me (**a**), *o*-NO_2 (**b**), *p*-NO_2 (**c**), *p*-OMe (**d**).

2. Enantioselective opening of the dioxolane ring

Desymmetrisation of *meso*-1,2-diols by asymmetric ring opening of 1,3-dioxolanes and other cyclic acetals under the action of chiral 1,3,2-oxazaborolidin-5-ones has been described by Harada *et al.*[210–215] In these reactions, 1,3,2-oxazaborolidin-5-one [*e.g.*, (*S*)-**126**] plays the role of a stereodifferentiating agent with respect to the enantiotopic oxygen atoms in the cyclic acetal and is predominantly coordinated to one of them. Treatment of this complex with a nucleophile results in the dioxolane ring opening.

Treatment of commercial 2,3-butanediol, which represents a mixture of *meso*- and *dl*-isomers (~ 2 : 1), with 3-phenylpropynal yields 68% of a mixture of acetals, 2-phenylethynyl-1,3-dioxolane isomers, *viz.*, *syn*-**141**, *anti*-**141** and *rac*-**141** (63 : 3 : 34).[210]

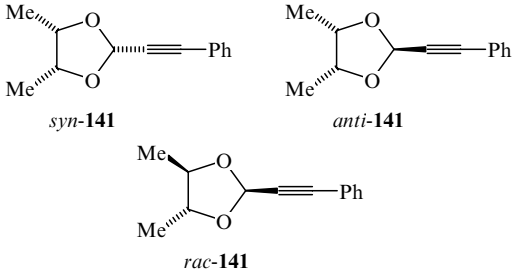

syn-**141** *anti*-**141**

rac-**141**

Treatment of this mixture with $Me_2C{=}C(SBu^t)OSiMe_3$ in the presence of 10 mol.% of the catalyst (*S*)-**126** at –78 °C results in the opening of the acetal ring of *syn*-**141** and the formation of the product **142** (yield 64%, *ee* 96%) (the diastereomeric acetal *anti*-**141** is not cleaved under these conditions).‡ The *anti*-**141** – *rac*-**141** mixture (7 : 93) is isolated after termination of the reaction.

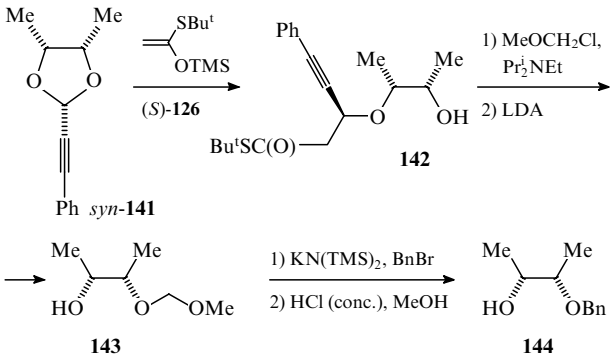

142

143 **144**

Thus a mixture of *meso*- and *dl*-forms of butanediol yields derivatives of optically active diols **143** and **144**.[210] Such desymmetrisation of *meso*-acetals is undoubtedly useful, since various 1,2-diols are available as mixtures of *meso*- and *dl*-forms (*e.g.*, they

‡ The phenylethynyl substituent appeared to be a suitable functional group, which allows one to perform all transformations in the highest optical yield.

can be prepared by SmI_2-induced reductive dimerisation of aldehydes).[210]

The desymmetrisation of bisacetals **145**[212] and diols **146** has also been described.[213]

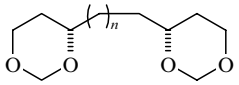

145 (n = 0, 1)

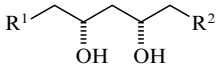

146

R^1 = OBn; R^2 = H, Me, Bu, OBn

(*S*)-**147** and (*S*)-**148a**,**b** can be used as catalysts along with (*S*)-**126.**[212,214]

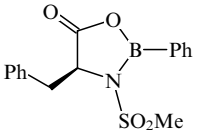

(*S*)-**147**

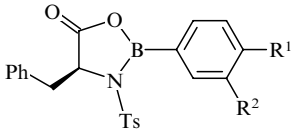

(*S*)-**148a**,**b**

148a: R^1 = H, R^2 = Cl;
148b: R^1 = Cl, R^2 = H.

All these catalysts play the role of contact ion pairs in enantiodifferentiating coordination of acetals with chiral substituted 1,3,2-oxazaborolidin-5-ones.[215]

3. Atroposelective opening of the lactone ring

In developing methods for the synthesis of natural naphthyltetrahydroisoquinoline alkaloids, Bringmann *et al.*[216–221] proposed the use of atroposelective opening of the lactone ring of 1,3-dimethylbenzo[*b*]naphtho[1,2-*d*]pyran-6-one (**149**). This method is a convenient procedure for the synthesis of atropoisomers.

The atroposelective reduction of lactone **149** by the complex (*S*)-**5**·BH_3 was studied first.[216–218] This lactone exists in two forms, *viz.*, (*P*)-**149** and (*M*)-**149**§ which are configurationally unstable and are easily interconverted. They form (*P*)-**150** and (*M*)-**150** complexes with the catalyst (*S*)-**5**·BH_3, respectively.

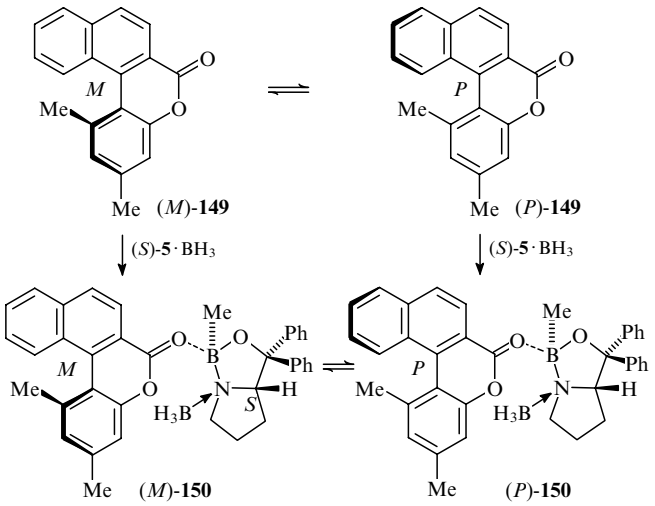

It was found that it is in the complex (*M*)-**150** that the enantioselective hydride transfer with subsequent formation of compound (*M*)-**151** takes place at −78 °C, which is due to the peculiarities of the spatial structure of the complex (*M*)-**150**. The isomeric complex (*P*)-**150** is not reduced under these conditions, it is first converted into (*M*)-**150** and then into (*M*)-**151**. Thus, the kinetic separation of two atropoisomers and their conversion into the same product, *viz.*, (*M*)-**151** (*ee* 97%), take place.[216–218]

§ For the (*P*) and (*M*) nomenclature of atropo-hindered biaryls, see Ref. 222.

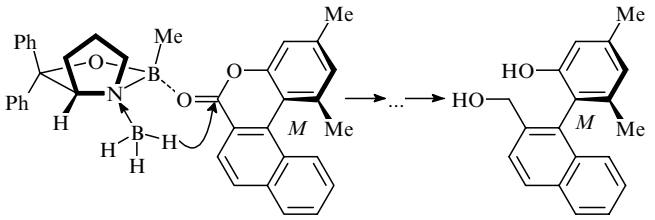

(*M*)-**150** (*M*)-**151**

This method was used by Bringmann for the total synthesis of naphthylisoquinoline alkaloids korupensamines. A mixture of lactones **152a** and **152b** (**152a** : **152b** = 4 : 96) was used as starting compounds, their reduction accompanied by kinetic resolution gives the key intermediate **153**.[219]

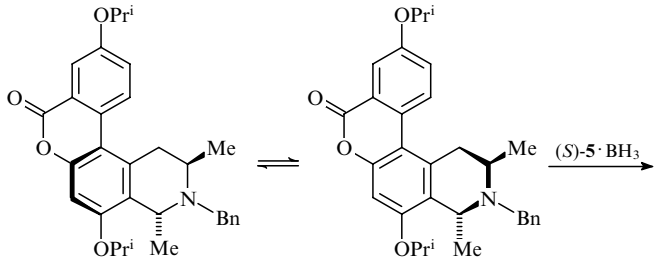

152a **152b**

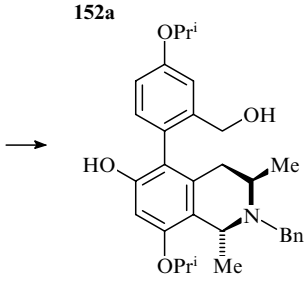

153

The reduction of the racemic lactone **154** proceeds with high enantioselectivity in a similar way (k_{rel} = 50).[220] As in the case of compound **149**, only the (*M*)-isomer is reduced under these conditions; the configurationally stable isomer (*P*)-**154** remains in the reaction mixture and can be separated. A procedure was developed which allowed isolation of the product (*M*)-**155** and the starting compound (*P*)-**154** in 33% and 30% yields (*ee* 93% and 95%, respectively) at ~ 33% conversion.[220] After separation, the enantiomer (*P*)-**154** can be reduced to (*P*)-**155** using $LiAlH_4$. This conversion allows the preparation of both enantiomers of 2,2′-dihydroxymethyl-1,1′-binaphthyl **155**.

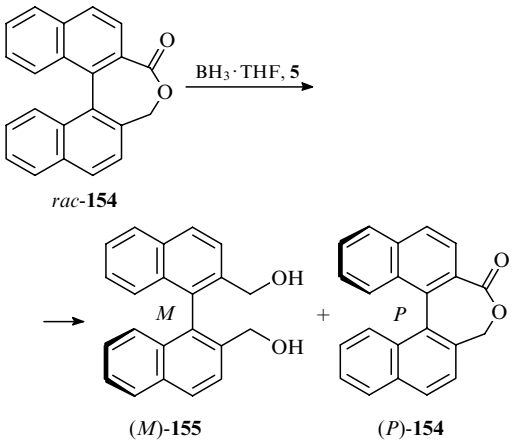

rac-**154**

(*M*)-**155** (*P*)-**154**

The reactions described in this section were also studied using quantum-chemical methods.[218,221]

4. Cycloaddition reactions

The Diels–Alder reaction is one of the most popular reactions in organic synthesis. It is known that Lewis acids form complexes with the oxygen atom of the carbonyl group of dienophiles and thus increase its electrophilicity and facilitate the reaction. In this context, the idea of gaining control over the enantioselectivity of the Diels–Alder reaction using chiral 1,3,2-oxazaborolidines seems to be justified. One of the pioneering works [184] devoted to the use of 1,3,2-oxazaborolidines in the Diels–Alder reaction describes model reactions of acrolein, methacrolein and crotonaldehyde with cyclopentadiene.

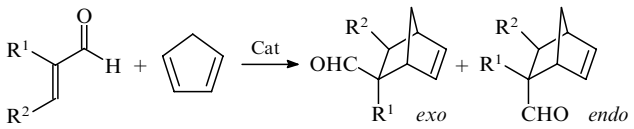

$R^1 = R^2 = H$; $R^1 = Me$, $R^2 = H$; $R^1 = H$, $R^2 = Me$.

The *exo* : *endo* ratio for methacrolein ($R^1 = Me$, $R^2 = H$) is 99 : 1 (*ee* of the *exo*-isomer is 86%), that for crotonaldehyde ($R^1 = H$, $R^2 = Me$) is 7 : 93 (*ee* of the *endo*-isomer is 59%). These reactions are catalysed by (*S*)-**125a** and (*S*)-**156**. The best results were obtained with the spatially hindered catalyst (*S*)-**156**. The use of (*S*)-**127a**–**c** and (*R*,*R*)-**157** as catalysts in the Diels–Alder reactions was first proposed by Corey.[223]

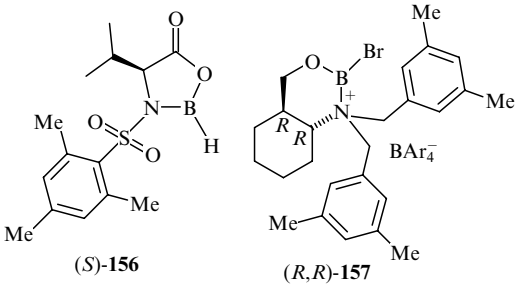

(*S*)-**156** (*R*,*R*)-**157**

It has already been noted that high enantio- and diastereoselectivity of the Mukaiyama aldol condensations are determined by the complexation of 1,3,2-oxazaborolidin-5-ones with aldehydes and the formation of a stable intramolecular hydrogen bond C–H···O–B.[191] The same was observed for the reaction of the aldehydes $R^2CH=CR^1CHO$ with cyclopentadiene in the presence of the catalyst (*S*)-**127c** (the structure of the intermediate **158** formed is similar to that of the intermediate **131**).

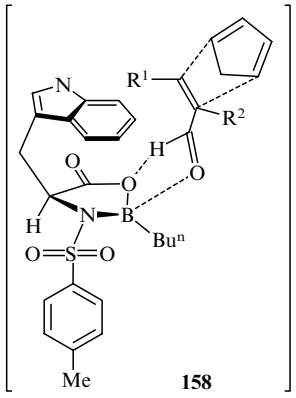

158

The structure of the complex **158** determines the regio- and stereoselectivity of the Diels–Alder reaction.

An increase in the Lewis acidity of the catalyst increases the stability of the 1,3,2-oxazaborolidine–aldehyde complex and, correspondingly, the enantioselectivity of the reaction. Recent studies by Corey have shown [224] that this effect can be attained if 1 equiv. of CF_3SO_3H (TfOH) is added to the reaction mixture.

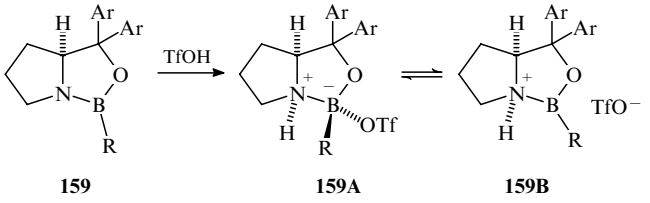

159 **159A** **159B**

R = Me, Bu, Ph, 2-MeC_6H_4, 1-naphthyl;
Ar = Ph, 2-naphthyl, 3,5-$Me_2C_6H_3$.

^{1}H NMR spectroscopy has shown that two forms of the catalyst **159**, *viz*., **A** and **B**, exist in solution at equilibrium at −78 °C in the presence of TfOH.[224]

The coordination of the electron-deficient methacrolein in the complex **160** occurs in such a way that its donor–acceptor π–π interaction with the π-electrons of the aromatic ring of the Ar-substituent in the *cis*-position of the C(5) atom of 1,3,2-oxazaborolidine **159** is possible.[224] As a result, the enantioselectivity of the reaction increases. Thus the bulky 3,5-dimethylphenyl group (as an Ar substituent) effectively shields the rear-side attack by the enal.

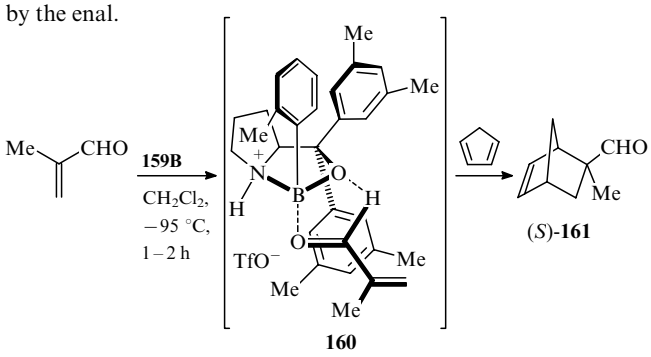

160

The addition of 6 mol.% of TfOH is sufficient to obtain good results. The yield of the product **16** is 73%–98%, the *exo* : *endo* ratio varies from 83 : 17 to 93 : 7 and *ee* varies from 75% to 91%. The best results were obtained when the catalyst **159** where R = 2-MeC_6H_4 and Ar = 3,5-$Me_2C_6H_3$ was used. In this case, the yield of the product **161** was 99%, *ee* was 96%, the *exo* : *endo* ratio was 89 : 11. This reaction does not occur in the presence of the spatially hindered catalysts **159** (R = 2-$Pr^iC_6H_4$, 2,6-$Me_2C_6H_3$). The addition of $MeSO_3H$ instead of CF_3SO_3H does not favour the reaction (in this case, the yields of the products do not exceed 30%).

Along with [4 + 2]-cycloaddition 1,3-dipolar cycloaddition was also studied.[180, 183, 225–230] However, the use of 1,3,2-oxazaborolidin-5-ones in the 1,3-dipolar cycloaddition did not give any positive results. When the reaction of diphenylnitrone **162** with the ketene acetals **163a**,**b** was carried out in the presence of the catalysts (*S*)-**164a**,**b** (20 mol.%), the yields of the products **165a**,**b** did not exceed 10%, although the enantioselectivity of the reaction was rather high: *ee* was 74% (for **165a**) and 62% (for the *cis*-isomer of **165b**).[226, 227]

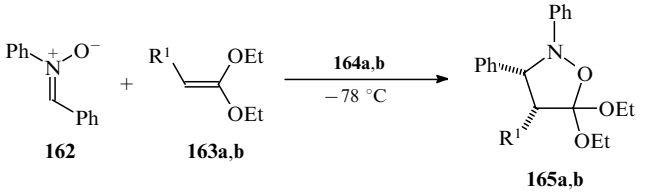

162 **163a**,**b** **165a**,**b**

R^1 = H (**163a**, **165a**), Me (**163b**, **165b**);

164a,**b** = 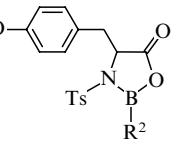 [R^2 = H (**164a**), Bu (**164b**)].

The 1,3-dipolar cycloaddition of the nitrone **162** to the electron-enriched alkene **163** is an example of a reaction with reverse electronic requirements. In this reaction, the catalyst **164** was used for the enantioselectivity control, since it was believed that a prominent role in such reactions is played by the donor–acceptor π–π interactions of the catalyst and the reagent in the transition state. The benzyloxy group of the catalyst **164** meets this requirement, since it interacts with the phenyl groups of the nitrone **162**.[227]

The enantioselectivity of this reaction drops drastically with an increase in temperature: at −78 °C, compound **165b** is formed with *ee* 62%, while at 25 °C *ee* is 38%. The product yields and reaction stereoselectivity also depend on the solvent.[227] Thus the reaction in THF catalysed by compound **164a** yields the isomer (−)-**165b** with *ee* 62%, whereas the reaction carried out in diphenyl ether, nitrobenzene or nitroethane gives the isomer (+)-**165b** with *ee* 79%. The yields of (−)- and (+)-**165b** are 33% and 60%, respectively.

The 1,3-dipolar cycloaddition of the nitrone **162** to the enal **166** in the presence of the catalyst (*R*)-**167** or **168a**,**b**[230] yields a mixture of isomers *cis*-**169** and *trans*-**169** in the *cis* : *trans* ratio of 1 : (8–9). In this case, the product yields are 44%–67%. The enantioselectivity of this reaction is rather low: the enantiomeric excess of *cis*-**169** in the reaction catalysed by (*R*)-**167** is 57%, while *ee* of *trans*-**169** in the presence of catalysts **168a** and **168b** are 8% and 19%, respectively.

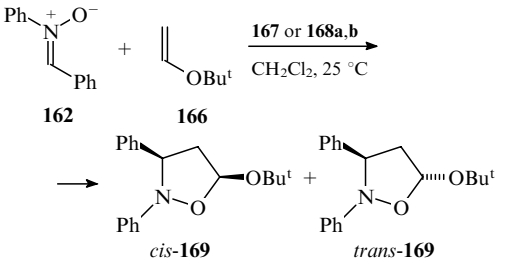

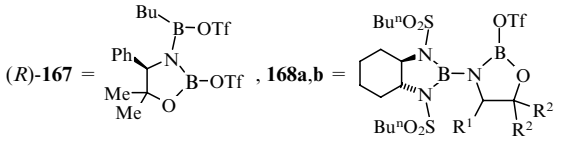

R^1 = Ph, R^2 = Me (**168a**);
R^1 = Bu^t, R^2 = H (**168b**).

The catalysis of the Diels–Alder reaction by 1,3,2-oxazaborolidines covalently bound to a polymeric matrix is also possible.[231, 232]

5. Miscellaneous reactions

The asymmetric allylation of imines **170a**–**h** by triallylborane in the presence of chiral amino alcohols R^2OH (**171**–**178**) has been described by Itsuno *et al.*[233]

The yields of 1-phenylbut-3-enylamine (**179**) vary from 12% to 90%. Depending on the nature of the imine used, either the (*S*)- or the (*R*)-isomer **179** with *ee* 10%–72% is formed. The best yields of (*S*)-phenylbut-3-enylamine (**179**) (64%–93%, *ee* 78%–96%) were obtained if (1*R*,2*S*)-norephedrine derivatives

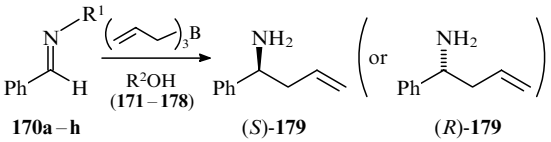

170a–**h** (*S*)-**179** (*R*)-**179**

R^1 = *p*-MeOC$_6$H$_4$ (**170a**), Tr (**170b**), OMe (**170c**), OAc (**170d**), SPh (**170e**), Ts (**170f**), P(O)Ph$_2$ (**170g**), SiMe$_3$ (**170h**);

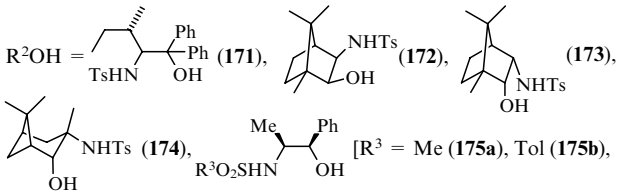

o-NO$_2$C$_6$H$_4$ (**175c**), 1-naphthyl (**175d**), 2-naphthyl (**175e**)],

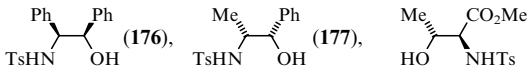

175a–**d** were used as catalysts. In the authors' opinion, this reaction occurs *via* the intermediate 2-allyloxazaborolidines of the type **180**.

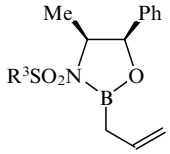

180

The chelate compounds **181** and **182** based on borates incorporating (*S*)-Pro were used for effective resolution of racemic 1,1′-bi-2-naphthol into enantiomers.[234]

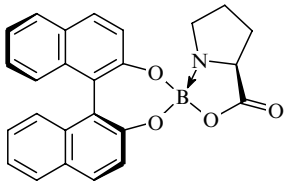

181

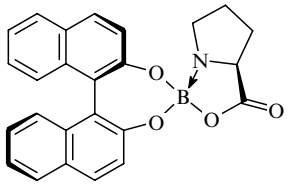

182

The use of oxazaborolidines for enantiomeric cleavage of epoxides by amines has been described.[235]

V. Reduction by immobilised 1,3,2-oxazaborolidines

Immobilised (polymer-bound or solid-phase) catalysts have a number of advantages over homogeneous catalysts, *e.g.*, they are easily separated from the reaction mass and can be used repeatedly.[158]

Several approaches to the synthesis of immobilised oxazaborolidines are known. First, the reaction of chloromethylated cross-linked polystyrene with amino alcohols containing phenol-type linkers (particularly, with tyrosine derivatives [156, 231, 236, 237]) yields the immobilised amino alcohol **183**, its reaction with $BH_3 \cdot THF$ affords the immobilised oxazaborolidine **184**.

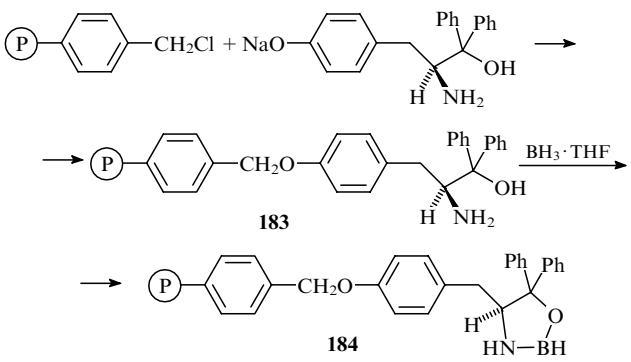

Second is *N*-alkylation or *N*-acylation of chiral amino alcohols by a reactive polymeric reagent with subsequent reaction of the intermediate **185** formed with $BH_3 \cdot THF$.[231, 232, 237–241]

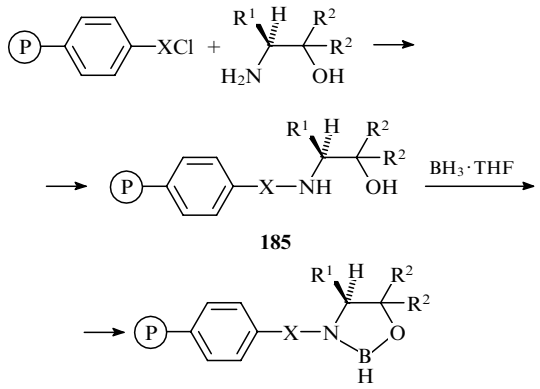

185

X = CH_2, SO_2; R^1 = Alk; R^2 = H, Alk, Ar.

The third approach entails suspension radical copolymerisation of the chiral monomer **186**, containing an amino alcohol fragment with styrene and divinylbenzene[156, 231, 242–244] in the presence of $BH_3 \cdot THF$.

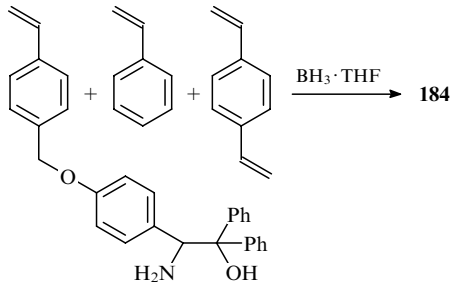

186

The enantiomeric excess in the reduction of butyrophenone by $BH_3 \cdot THF$ to (*R*)-1-phenylbutan-1-ol in the presence of the system **183** was 88%. The best results (*ee* 92% – 97%) were achieved in the reduction of acetophenone in the presence of the catalyst **187**.[156]

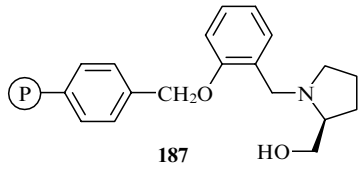

187

The immobilised reagent **184** was also used in the reduction of ketoxime ethers;[156] however, in this case the optical yields did not exceed 26%. The addition of Lewis acids ($AlCl_3$, $ZnCl_2$, $BF_3 \cdot OEt_2$) accelerated the reduction and increased the optical yields to 42% – 67%.[158]

Later,[158] a copolymer of a chiral monomer **188** with styrene and divinylbenzene was synthesised. With the molar content of the chiral ligand of 20% and of divinylbenzene of 10% (or 2%) (the degree of cross-linking), this compound catalysed the asymmetric reduction of acetophenone *O*-methyloxime to (*R*)-2-phenylethylamine by $BH_3 \cdot THF$ in 60% (or 65%) yield and *ee* 82% (or 96%). Repeated (5 times) use of the catalyst is possible without any loss of stereoselectivity (*ee* ~ 95%) for the divinylbenzene content of 2%.

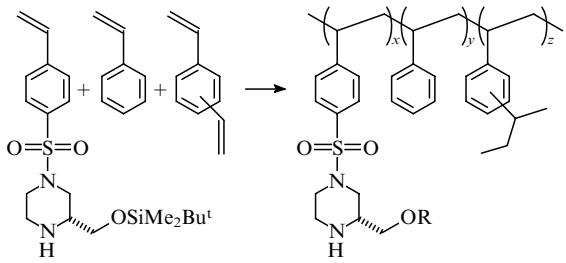

188 (R = $SiMe_2Bu^t$, H)

Immobilised 1,3,2-oxazaborolidines **189** can also be prepared from immobilised boronic acid.[237, 245–247]

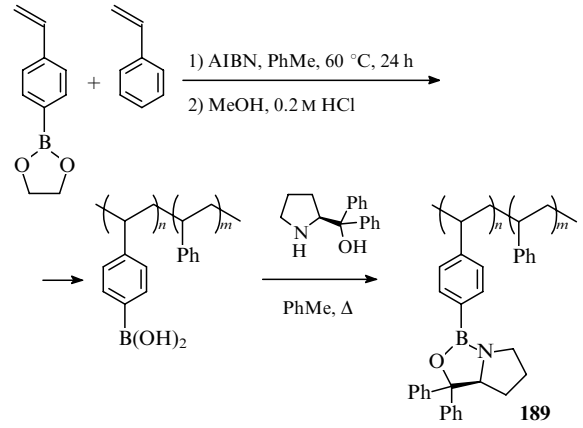

AIBN is azobisisobutyronitrile.

The boronic acid residue can be introduced into polystyrene using the following reaction sequence:[245–247]

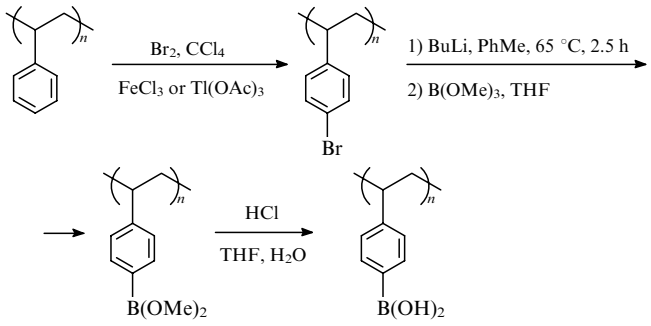

Copolymerisation of a mixture of 2-vinylthiophene, styrene and *p*-divinylbenzene is also used for the synthesis of immobilised boronic acid.[247, 248] The resulting thiophene-containing polymer reacts smoothly with n-butyllithium to give the corresponding thiophene-lithiated product, which makes the bromination step unnecessary and increases the final yield of the catalyst. Subsequent synthesis of the polymer containing oxazaborolidine groups can be carried out *in situ* using the system $NaBH_4$ – Me_3SiCl (or $BF_3 \cdot OEt_2$).[239] Reduction of ketones in the presence of this catalytic system is carried out in THF[239–241, 247] or in toluene[241] (the optimum temperatures are 60 – 110 °C, the amount of the catalyst is 0.1 – 0.2 equiv. per equiv. of the substrate; the yields of the secondary alcohols are 87% – 98%, the optical purity is 86% – 96%).[240, 249] The reduction by heterogeneous polymeric catalysts is usually carried out in flow reactors; otherwise, the separation of the catalyst by filtration is necessary. Repeated use[250] and fivefold regeneration[241] of the catalyst with an insignificant (up to 5% *ee*) loss of enantioselectivity are possible.

The synthesis of immobilised 1,3,2-oxazaborolidines by copolymerisation of compounds **190** or **191** with styrene and

p-divinylbenzene resulting in the polymeric catalysts **192** and **193** has recently been described.[249] The reduction of acetophenone by the $BH_3 \cdot THF$ complex in the presence of the catalyst **193** gave (*R*)-1-phenylethanol in 100% yield and with *ee* 84.8%, whereas the reduction of pinacoline affords the (*R*)-isomer of the corresponding secondary alcohol with *ee* 88.4%.

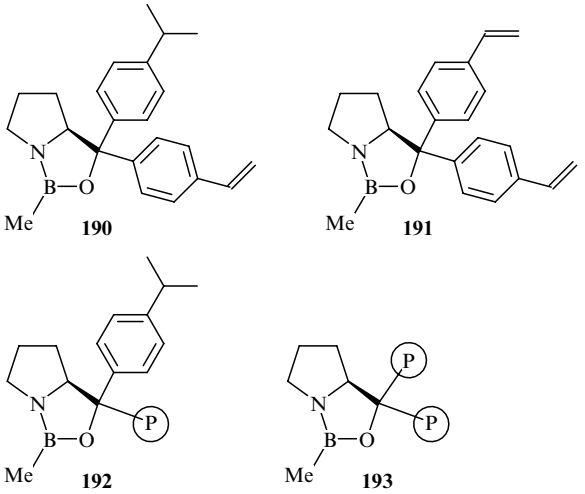

190 **191** **192** **193**

These data suggest that in some cases heterogeneous polymer-bound 1,3,2-oxazaborolidines compare well with homogeneous catalysts in efficiency.[240,245] It should be noted, however, that high values of *ee* were obtained only for polymers with a low (up to 2%) degree of cross-linking, *i.e.*, with low mechanical stability, which limits their industrial application.[238,241] An increase in the extent of cross-links hampers the diffusion of the substrate and the reducing agent within the polymer and thus increases the contribution of competitive non-catalytic reduction of the substrate and decreases its enantioselectivity.[245] This may account for the low selectivity of the reduction carried out in the presence of heterogeneous catalysts prepared by suspension copolymerisation.[245] This has prompted an idea to use homogeneous microgels soluble in organic solvents (THF, toluene) as carriers for oxazaborolidines.[237,245,251,252] To this end, the polymer **194** was prepared, which can be converted *in situ* into homogeneous immobilised oxazaborolidine manifesting a strong catalytic effect. The polymer **194** is formed upon palladium-catalysed hydrosilylation of the allyloxyprolinol derivative (2*S*,4*R*)-**195** by a copolymer of methylhydrosiloxane with dimethylsiloxane. In the presence of this catalyst, aromatic ketones are reduced to secondary alcohols with *ee* 89% – 98% (yields 83% – 89%).[251]

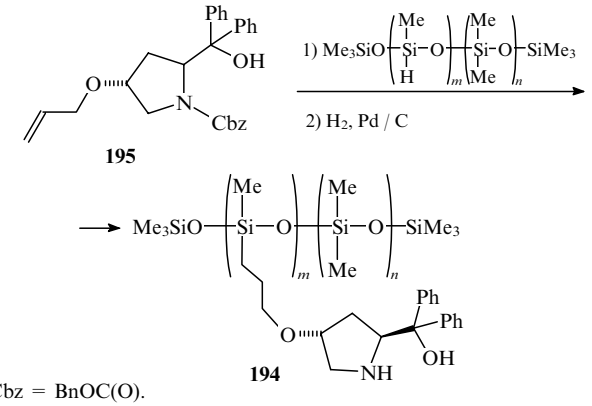

195 **194**

Cbz = BnOC(O).

Reaction products are separated from polymeric catalysts by nanofiltration in a membrane reactor.[237,252] Since the conversion of the ketone reaches ~ 100%, the solvent is distilled off at the outlet of the reactor; the reaction products are isolated by vacuum distillation.[252] The catalyst remains in the reactor and can be used in the next conversion cycle.

The preparation of a homogeneous polymeric microgel, which contains an oxazaborolidine fragment based on cheap (*S*)-diphenylalaninol, is a remarkable achievement of the Wulff group.[245] The radical polymerisation was carried out in strongly dilute solutions to prevent macrogel formation; ethylene dimethacrylate was used as a cross-linking agent. The reduction of aromatic ketones in the presence of this catalyst gives alcohols with *ee* 87% – 94%.[245] The weak spot of the given technology is the low activity of the microgels prepared using this method [the number of moles of the product per mole of the catalyst (turnover number) is 10 – 50]. The Kragl group[237] have succeeded in increasing the turnover number of the catalyst to 560. Later, the productivity of the membrane reactor was increased to 1.4 kg litre^{-1} day^{-1}; the deactivation rate of the catalyst was 1.8% per hour.[252] The efficiency of this catalytic system can be judged from the fact that the efficiency of enzymatic reduction of the same ketones by alcohol dehydrogenase is significantly lower (88 g litre^{-1} day^{-1}), which is attributed to low solubility of the enzyme in water.[252] On the whole, the use of homogeneous microgels in asymmetric catalysis is becoming more and more popular; considerable progress in this area should be expected in the near future.

A heterogeneous catalyst based on nickel boride nanoparticles coated with oxazaborolidine has been developed[253] aimed at combination of the advantages of a heterogeneous (easy separation of the catalyst) and homogeneous (high efficiency) catalysis. The catalyst with the formula $NiB_{2-0.1}$ (oxazaborolidine)$_{0.1}$ was synthesised *in situ* from (1*S*,2*R*)-(+)-2-amino-1,2-diphenylethanol or (1*R*,2*S*)-(−)-norephedrine and nickel salts $NiI_2 \cdot 6\ H_2O$ or $NiCl_2 \cdot 6\ H_2O$. This catalyst reduces acetophenone rapidly and with high enantioselectivity (*ee* of the alcohol is 90%) and can be used repeatedly. To ensure good selectivity, the ketone should be added to a catalyst – $BH_3 \cdot THF$ mixture at a very slow rate.

Catalytic reduction of aromatic ketones by the complex $BH_3 \cdot SMe_2$ in the presence of 0.1 equiv. of a chiral dendrimer based on 3,5-dihydroxybenzyl alcohol or 4,4-bis(4-hydroxyphenyl)pentanol with (*S*)-2-amino-3-(4-hydroxyphenyl)-1,1-diphenylpropan-1-ol linked through the phenolic group has been described.[254] The yields of the alcohols are 75% – 82%, *ee* is 82% – 96%. Homogeneous dendrimeric catalysts seem promising, since their application gives higher values of *ee* than the heterogeneous polymeric systems.[254]

The use of immobilised catalysts of the type **187** in enantioselective Diels – Alder reactions,[231,232] aldol condensation[242] and for addition of diethylzinc to aldehydes has been described.[247]

VI. 1,3,2-Oxazaborolidine analogues

1. 1,3,2-Diazaborolidines

1,3,2-Oxazaborolidine analogues, particularly diazaborolidines **196** – **198** recommended by Corey,[255,256] are widely used in asymmetric synthesis.

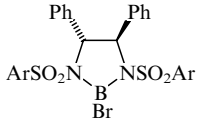

196, **197**

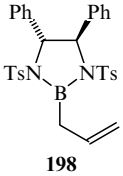

198

Ar = *p*-MeC_6H_4 (**196**), *p*-$NO_2C_6H_4$ (**197**)

Compounds **196** and **197** catalyse stereoselective aldol condensation,[255] whereas compound **198** is a highly efficient enantioselective allylating reagent for the synthesis of chiral allylic alcohols with *ee* > 90%.[256]

It is known that the introduction of a trifluoromethyl group into the aromatic ring of the arylsulfonyl residue increases the Lewis acidity of the boron atom. This fact was used in the design of an effective catalyst of aldol condensation, **199**. Corey *et al.* used compound **199** for the enantioselective synthesis of aldehydes [257, 258] and D-*threo*-*N*-acetylsphingosine.[259]

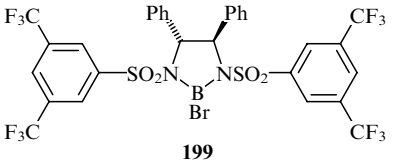

199

1,3,2-Diazaborolidine **200** was recommended as a catalyst for enantioselective reduction of prochiral ketones by boranes,[260] however, the *ee* in the reduction of acetophenone was low (40%). Two types of complexes of compound **200** with borane, *viz.*, **201a** and **201b**, were detected in THF by ^{11}B NMR spectroscopy; their competition accounts for low optical yields of the alcohol in this reaction. The use of compound **202** as a catalyst with a tosyl group at the nitrogen atom has made it possible to increase the enantioselectivity [the yield of (*S*)-1-phenylethanol was 95%, *ee* was 72%].

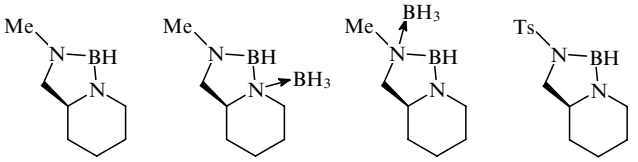

200 **201a** **201b** **202**

Chiral diamines **203**–**205** were recommended as an alternative to amino alcohols in the enantioselective reduction of prochiral ketones.[261]

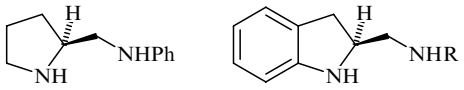

203 **204**, **205**

R = Ph (**204**), cyclo-C_6H_{11} (**205**).

Compound **204** appeared to be the most efficient of them.

The introduction of electron-withdrawing groups (*e.g.*, CF_3) into the aromatic ring has led to more efficient catalysts; of those, compound **206** appeared to be the best in the reduction of acetophenone [the yield of (*S*)-1-phenylethanol was 88%, *ee* was 92%].

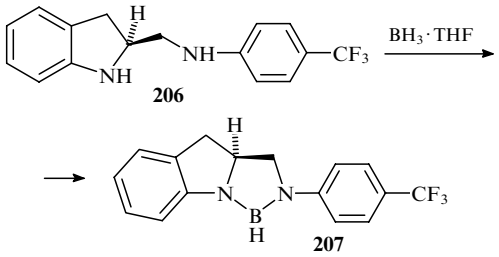

206 **207**

This reduction was carried out in THF at −15 °C in the presence of 0.15 equiv. of the chiral diamine and 1 equiv. of $BH_3 \cdot THF$, the reaction time was 2 h. This reaction is believed to proceed *via* 1,3,2-diazaborolidine **207** formed *in situ*. Other aromatic ketones were reduced in 88%–96% yields and with *ee* 82%–92%.[261] Thus, the electron-withdrawing groups increase the acidity of the boron atom, which results in its better coordination to the ketone carbonyl and, as a consequence, increases the optical yield of the final product.

Synthesis of heteroborolidines from pseudoephedrine (**208**) and ephedrine (**209**) has been described.[262–264] It was found that pseudoephedrine reacts with urea to give oxazolidinone **210**, which is converted into 1,3,2-oxazaborolidine **211** upon subsequent treatment with borane (this reaction is yet another method for the synthesis of 1,3,2-oxazaborolidines).

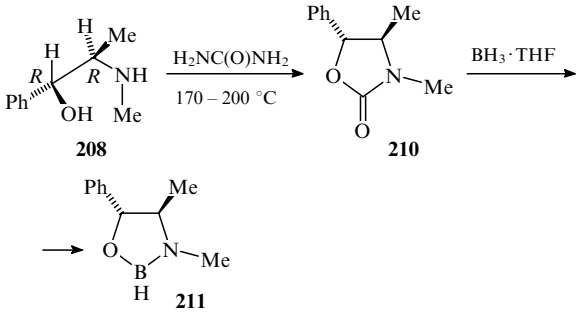

208 **210** **211**

Ephedrine reacts with urea in a different way. Intramolecular cyclisation of ephedrine **209** and subsequent nucleophilic attack by the cyanate ion formed from urea at 170–200 °C on the intermediate **212** gives *cis*-imidazolidinone **213** which yields 1,3,2-diazaborolidine **214** after reduction with borane.[262] The stereochemistry of compounds **212** and **214** was established by heteronuclear $^1H/^{13}C$ NMR and that of compound **213**, by X-ray diffraction analysis.

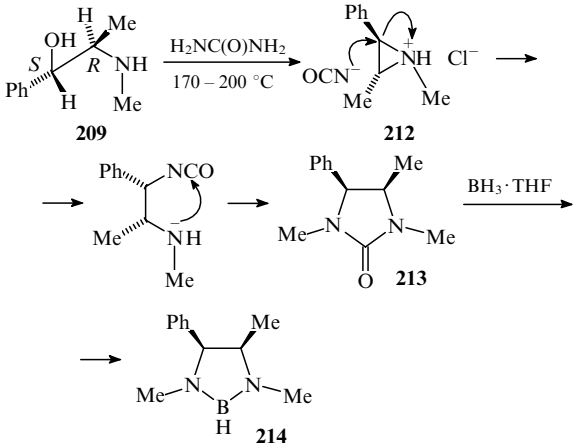

209 **212** **213** **214**

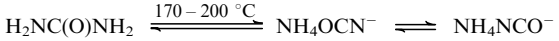

2. 1,3,2-Oxathia- and 1,3,2-azathiaborolidines

1,3,2-Azathiaborolidines (*e.g.*, **215**) [263, 264] and 1,3,2-oxathiaborolidines (*e.g.*, **216**) can be used, along with 1,3,2-oxazaborolidines, as catalysts in enantioselective ketone reduction reactions.[265, 266] 1,3,2-Azathiaborolidine **215** was synthesised from pseudoephedrine.[263, 264]

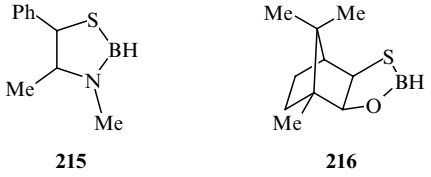

215 **216**

Compound **216** catalyses the reduction of acetophenone by the complex $BH_3 \cdot SMe_2$ to (*S*)-1-phenylethanol with *ee* 92%.

* * *

The present review demonstrates that chiral 1,3,2-oxazaborolidines occupy a prominent place in the arsenal of modern reagents for asymmetric synthesis owing to their high efficiency in enantioselective reduction of prochiral ketones, imines and oxime ethers. Being representatives of chiral Lewis acids, 1,3,2-oxazaborolidines can also be used as effective catalysts in stereoselective Diels–Alder reactions, aldol condensation, cleavage of acetals and atroposelective resolution of spatially hindered lactones. This trend has been developing especially intensively in the past decade and entails a search for novel highly efficient catalysts, their application in the production of enantiomerically pure drugs, their modification by immobilisation on polymers and dendrimers and broadening of the range of reactions catalysed by them.

References

1. S Wallbaum, J Martens *Tetrahedron: Asymmetry* **3** 1475 (1992)
2. L Deloux, M Srebnik *Chem. Rev.* **93** 763 (1993)
3. V K Singh *Synthesis* 605 (1992)
4. M Wills, J K Studley *Chem. Ind.* 552 (1994)
5. E J Corey, C J Helal *Angew. Chem., Int. Ed.* **37** 1986 (1998)
6. S Itsuno, in *Organic Reactions* Vol. 52 (New York: Wiley, 1998) Ch. 2, p. 395
7. S Itsuno, in *Comprehensive Asymmetric Catalysis I-III* (Eds E N Jacobsen, A Pfaltz, H Yamamoto) (Berlin: Springer, 1998) Ch. 6.4, p. 290
8. A Hirao, S Itsuno, S Nakahama, N Yamazaki *J. Chem. Soc., Chem. Commun.* 315 (1981)
9. S Itsuno, A Hirao, S Nakahama, N Yamazaki *J. Chem. Soc., Perkin Trans. 1* 1673 (1983)
10. S Itsuno, M Nakano, K Miyazaki, H Masuda, K Ito, A Hirao, S Nakahama *J. Chem. Soc., Perkin Trans. 1* 2039 (1985)
11. E J Corey, R K Bakshi, S Shibata *J. Am. Chem. Soc.* **109** 5551 (1987)
12. E J Corey, S Shibata, R K Bakshi *J. Org. Chem.* **53** 2861 (1988)
13. E J Corey, R K Bakshi, S Shibata, C P Chen, V K Singh *J. Am. Chem. Soc.* **109** 7925 (1987)
14. E J Corey, M Azimioara, S Sarshar *Tetrahedron Lett.* **33** 3429 (1992)
15. J M Brunel, M Maffei, G Buono *Tetrahedron: Asymmetry* **4** 2255 (1993)
16. A Lang, H Nöth, M Schmidt *Chem. Ber.* **130** 241 (1997)
17. J W Emsley, J Feeney, L H Sutcliff, in *High Resolution Nuclear Magnetic Resonance Spectroscopy* Vol. 2 (Oxford, New York: Pergamon Press, 1966)
18. D J Mathre, A S Thompson, A W Douglas, K Hoogsteen, J D Carroll, E G Corley, E J J Grabowski *J. Org. Chem.* **58** 2880 (1993)
19. E J Corey, J O Link *Tetrahedron Lett.* **30** 6275 (1989)
20. D K Jones, D C Liotta, I Shinkai, D J Mathre *J. Org. Chem.* **58** 799 (1993)
21. L P Linney, C R Self, I H Williams *J. Chem. Soc., Chem. Commun.* 1651 (1994)
22. V Nevalainen *Tetrahedron: Asymmetry* **3** 1563 (1992)
23. V Nevalainen *Tetrahedron: Asymmetry* **5** 289 (1994)
24. M Li, A Tian *J. Mol. Struct. (Theochem)* **544** 25 (2001)
25. M Li, A Tian *J. Mol. Struct. (Theochem)* **544** 37 (2001)
26. V Nevalainen, R Uggla, M R Sundberg *Tetrahedron: Asymmetry* **6** 1431 (1995)
27. G J Quallich, J F Blake, T M Woodall *J. Am. Chem. Soc.* **116** 8516 (1994)
28. E J Corey, J O Link, R K Bakshi *Tetrahedron Lett.* **33** 7107 (1992)
29. A W Douglas, D M Tschaen, R A Reamer, Y-J Shi *Tetrahedron: Asymmetry* **7** 1303 (1996)
30. E J Corey, R K Bakshi *Tetrahedron Lett.* **31** 611 (1990)
31. S T Kerrick, P Beak *J. Am. Chem. Soc.* **113** 9708 (1991)
32. J V B Kanth, M Periasamy *Tetrahedron* **49** 5127 (1993)
33. D J Mathre, T K Jones, L C Xavier, T J Blacklock, R A Reamer, J J Mohan, E T T Jones, K Hoogsteen, M W Baum, E J J Grabowski *J. Org. Chem.* **56** 751 (1991)
34. G J Quallich, T M Woodall *Tetrahedron Lett.* **34** 4145 (1993)
35. C Dauelsberg, J Martens *Synth. Commun.* **23** 2091 (1993)
36. Z -X Shen, J Lu, Q Zhang, Y-W Zhang *Tetrahedron: Asymmetry* **8** 2287 (1997)
37. X Li, R Xie *Tetrahedron: Asymmetry* **8** 2283 (1997)
38. S Hanessian, E Jnoff, A M Griffin *Can. J. Chem.* **80** 885 (2002)
39. J G H Willems, F J Dommerholt, J B Hammink, A M Vaarhorst, L Thijs, B Zwanenburg *Tetrahedron Lett.* **36** 603 (1995)
40. A V Rama Rao, M K Gurjar, P A Sharma, V Kaiwar *Tetrahedron Lett.* **31** 2341 (1990)
41. J Martens, C Dauelsberg, W Behnen, S Wallbaum *Tetrahedron: Asymmetry* **3** 347 (1992)
42. K Stingl, J Martens, S Wallbaum *Tetrahedron: Asymmetry* **3** 223 (1992)
43. S Wallbaum, J Martens *Tetrahedron: Asymmetry* **2** 1093 (1991)
44. I K Youn, S W Lee, C S Pak *Tetrahedron Lett.* **29** 4453 (1988)
45. Y H Kim, D H Park, I S Byun *J. Org. Chem.* **58** 4511 (1993)
46. E J Corey, C-P Chen, G A Reichard *Tetrahedron Lett.* **30** 5547 (1989)
47. B D Simone, D Savoia, E Tagliavini, A Umani-Ronchi *Tetrahedron: Asymmetry* **6** 301 (1995)
48. S Jones, J C C Atherton *Tetrahedron: Asymmetry* **11** 4543 (2000)
49. Y Hong, Y Gao, X Nie, C M Zepp *Tetrahedron Lett.* **35** 6631 (1994)
50. I Reiners, J Martens *Tetrahedron: Asymmetry* **8** 277 (1997)
51. A S Demir, I Mecitoglu, C Tanyeli, V Gülbeyaz *Tetrahedron: Asymmetry* **7** 3359 (1996)
52. M Falorni, C Collu, G Giacomelli *Tetrahedron: Asymmetry* **7** 2739 (1996)
53. M Masui, T Shioiri *Tetrahedron* **51** 8363 (1995)
54. M Masui, T Shioiri *Synlett* 49 (1996)
55. M Nakagawa, T Kawate, T Kakikawa, H Yamada, T Matsui, T Hino *Tetrahedron* **49** 1739 (1993)
56. G B Jones, S B Heaton, B J Chapman, M Guzel *Tetrahedron: Asymmetry* **8** 3625 (1997)
57. M P Sibi, G R Cook, P Liu *Tetrahedron Lett.* **40** 2477 (1999)
58. A V Rama Rao, M K Gurjar, V Kaiwar *Tetrahedron: Asymmetry* **3** 859 (1992)
59. WO PCT 9 532 937; *Chem. Abstr.* **124** 231 486 (1996)
60. C M Bellucci, A Bergamini, P G Cozzi, A Papa, E Tagliavini, A Umani-Ronchi *Tetrahedron: Asymmetry* **8** 895 (1997)
61. R Hett, C H Senanayake, S A Wald *Tetrahedron Lett.* **39** 1705 (1998)
62. US P. 6 005 133; *Ref. Zh. Khim.* 19 N 27P (2001)
63. H Tlahuext, R Contreras *Tetrahedron: Asymmetry* **3** 1145 (1992)
64. Eur. P. 713 848; *Chem. Abstr.* **125** 114 285 (1996)
65. Z Shen, W Huang, J Feng, Y Zhang *Tetrahedron: Asymmetry* **9** 1091 (1998)
66. R Berenguer, J Garcia, J Vilarrasa *Tetrahedron: Asymmetry* **5** 165 (1994)
67. H Tlahuext, R Contreras *Tetrahedron: Asymmetry* **3** 727 (1992)
68. I Reiners, J Martens *Tetrahedron: Asymmetry* **8** 27 (1997)
69. I Reiners, J Wilken, J Martens *Tetrahedron: Asymmetry* **6** 3063 (1995)
70. M Shimizu, S Yamada, Y Fujita, F Kobayashi *Tetrahedron: Asymmetry* **11** 3883 (2000)
71. B T Cho, Y S Chun *J. Org. Chem.* **63** 5280 (1998)
72. M Shimizu, Y Ikari, A Wakabayashi *J. Chem. Soc., Perkin Trans. 1* 2519 (2001)
73. T Fujisawa, Y Onogawa, M Shimizu *Tetrahedron Lett.* **39** 6019 (1998)
74. G-S Yang, J-B Hu, G Zhao, Y Ding, M-H Tang *Tetrahedron: Asymmetry* **10** 4307 (1999)
75. T Inoue, D Sato, K Komura, S Itsuno *Tetrahedron Lett.* **40** 5379 (1999)
76. J Zhao, X Bao, X Liu, B Wan, X Han, C Yang, J Hang, Y Feng, B Jiang *Tetrahedron: Asymmetry* **11** 3351 (2000)
77. B Kaptein, H Elsenberg, A J Minnaard, Q B Broxterman, L A Hulshof, J Koek, T R Vries *Tetrahedron: Asymmetry* **10** 1413 (1999)

78. T K Jones, J J Mohan, L C Xavier, T J Blacklock, D J Mathre, P Sohar, E T T Jones, R A Reamer, F E Roberts, E J J Grabowski *J. Org. Chem.* **56** 763 (1991)
79. E J Corey, J O Link *Tetrahedron Lett.* **33** 4141 (1992)
80. Y-J Shi, D Cai, U-H Dolling, A W Douglas, D M Tschaen, T R Verhoeven *Tetrahedron Lett.* **35** 6409 (1994)
81. D M Tschaen, L Abrahamson, D Cai, R Desmond, U-H Dolling, L Frey, S Karady, Y-J Shi, T R Verhoeven *J. Org. Chem.* **60** 4324 (1995)
82. K R K Prasad, N N Joshi *Tetrahedron: Asymmetry* **7** 3147 (1996)
83. G B Stone *Tetrahedron: Asymmetry* **5** 465 (1994)
84. E J Corey, J O Link, S Sarshar, Y Shao *Tetrahedron Lett.* **33** 7103 (1992)
85. C J Helal, P A Magriotis, E J Corey *J. Am. Chem. Soc.* **118** 10 938 (1996)
86. C Meier, W H G Laux *Tetrahedron: Asymmetry* **6** 1089 (1995)
87. E J Corey, K Y Yi, S P T Matsuda *Tetrahedron Lett.* **33** 2319 (1992)
88. E J Corey, J O Link *J. Am. Chem. Soc.* **114** 1906 (1992)
89. M Periasamy, J V B Kanth, A S B Prasad *Tetrahedron* **50** 6411 (1994)
90. A M Salunke, E R Burkhardt *Tetrahedron Lett.* **38** 1523 (1997)
91. B T Cho, W K Yang, O K Choi *J. Chem. Soc., Perkin Trans. 1* 1204 (2001)
92. S M Nettles, K Matos, E R Burkhardt, D R Rouda, J A Corella *J. Org. Chem.* **67** 2970 (2002)
93. R Hett, R Stare, P Helquist *Tetrahedron Lett.* **35** 9375 (1994)
94. R Hett, Q K Fang, Y Gao, Y Hong, H T Butler, X Nie, S A Wald *Tetrahedron Lett.* **38** 1125 (1997)
95. B T Cho, Y S Chun *Tetrahedron: Asymmetry* **10** 1843 (1999)
96. J S Yadav, P T Reddy, S R Hashim *Synlett* 1049 (2000)
97. G J Quallich, K N Keavey, T M Woodall *Tetrahedron Lett.* **36** 4729 (1995)
98. B T Cho, D J Kim *Tetrahedron: Asymmetry* **12** 2043 (2001)
99. A Barco, S Benetti, P Bergamini, C De Risi, P Marchetti, G P Pollini, V Zanirato *Tetrahedron Lett.* **40** 7705 (1999)
100. C -P Chen, K Prasad, O Repic *Tetrahedron Lett.* **32** 7175 (1991)
101. B Jiang, Y Feng, J Zheng *Tetrahedron Lett.* **41** 10281 (2000)
102. T S Kaufman *Tetrahedron Lett.* **37** 5329 (1996)
103. C E Garrett, K Prasad, O Repič, T J Blacklock *Tetrahedron: Asymmetry* **13** 1347 (2002)
104. E J Corey, C J Helal *Tetrahedron Lett.* **36** 9153 (1995)
105. G J Quallich, T Woodall *Tetrahedron Lett.* **34** 785 (1993)
106. K R K Prasad, N N Joshi *Tetrahedron: Asymmetry* **8** 173 (1997)
107. E J Corey, C J Helal *Tetrahedron Lett.* **37** 5675 (1996)
108. K Manju, S Trehan *Tetrahedron: Asymmetry* **9** 3365 (1998)
109. M Morr, C Proppe, V Wray *Leibigs Ann.* 2001 (1995)
110. O W Goging, R P Bansal *Synth. Commun.* **25** 1155 (1995)
111. M P DeNinno, R J Perner, L Lijewski *Tetrahedron Lett.* **31** 7415 (1990)
112. J Bach, R Berenguer, J Garcia, M Lupez, J Manzanal, J Vilarrasa *Tetrahedron* **54** 14947 (1998)
113. K P K Prasad, N N Joshi *J. Org. Chem.* **61** 3888 (1996)
114. D J Aldous, W M Dutton, P G Steel *Tetrahedron: Asymmetry* **11** 2455 (2000)
115. C-W Lin, C-C Lin, Y-M Li, A S C Chan *Tetrahedron Lett.* **41** 4425 (2000)
116. O K Choi, B T Cho *Tetrahedron: Asymmetry* **12** 903 (2001)
117. J Bach, R Berenguer, J Farrás, J Garcia, J Meseguer, J Vilarrasa *Tetrahedron: Asymmetry* **6** 2683 (1995)
118. T Konoike, Y Araki *Tetrahedron Lett.* **33** 5093 (1992)
119. H Dumartin, Y Le Floc'h, R Grée *Tetrahedron Lett.* **35** 6681 (1994)
120. P Wipf, S Lim *J. Am. Chem. Soc.* **117** 558 (1995)
121. S J Amigoni, L J Toupet, Y Le Floc'h *J. Org. Chem.* **62** 6374 (1997)
122. D B Smith, A M Waltos, D G Loughead, R J Weikert, D J Morgans Jr, J C Rohloff, J O Link, R Zhu *J. Org. Chem.* **61** 2236 (1996)
123. R Berenguer, M Cavero, J Garcia, M Muñoz *Tetrahedron Lett.* **39** 2183 (1998)
124. J Bach, R Berenguer, J Garcia, T Loscertales, J Manzanal, J Vilarrasa *Tetrahedron Lett.* **38** 1091 (1997)
125. K C Nicolaou, P Bertinato, A D Piscopio, T K Chakraborty, N Minowa *J. Chem. Soc., Chem. Commun.* 619 (1993)
126. E J Corey, K S Rao *Tetrahedron Lett.* **32** 4623 (1991)
127. L F Tietze, H Shirok *J. Am. Chem. Soc.* **121** 10264 (1999)
128. E J Corey, H Kigoshi *Tetrahedron Lett.* **32** 5025 (1991)
129. E J Corey, A V Gavai *Tetrahedron Lett.* **28** 3201 (1988)
130. A F Simpson, P Szeto, D C Lathbury, T Gallagher *Tetrahedron: Asymmetry* **8** 673 (1997)
131. K A Parker, M W Ledeboer *J. Org. Chem.* **61** 3214 (1996)
132. E J Corey, C J Helal *Tetrahedron Lett.* **37** 4837 (1996)
133. H-G Schmalz, H Jope *Tetrahedron* **54** 3457 (1998)
134. H-G Schmalz, J Hollander, M Arnold, G Dürner *Tetrahedron Lett.* **34** 6259 (1993)
135. J Wright, L Frambes, P Reeves *J. Organomet. Chem.* **476** 215 (1994)
136. L Schwink, P Knochel *Tetrahedron Lett.* **38** 3711 (1997)
137. E J Corey, X-M Cheng, K A Cimprich *Tetrahedron Lett.* **32** 6839 (1991)
138. R Romagloni, E C Roos, H Hiemstra, M J Moolenaar, W N Speckamp, B Kaptein, H E Shoemaker *Tetrahedron Lett.* **35** 1087 (1994)
139. M Ostendorf, R Romagloni, I C Pereiro, E C Roos, M J Moolenaar, W N Speckamp, H Hiemstra *Tetrahedron: Asymmetry* **8** 1773 (1997)
140. M Shimizu, Y Nishigaki, A Wakabayashi *Tetrahedron Lett.* **40** 8873 (1999)
141. A S Thompson, G R Humphrey, A M DeMarco, D J Mathre, E J J Grabowski *J. Org. Chem.* **58** 5886 (1993)
142. E J Corey, J O Link *J. Org. Chem.* **56** 42 (1991)
143. E J Corey, G A Reichard *Tetrahedron Lett.* **30** 5207 (1989)
144. J W Hilborn, Z-H Lu, A R Jurgens, Q K Fang, P Byers, S A Wald, C H Senanayake *Tetrahedron Lett.* **42** 8919 (2001)
145. V L Ponzo, T S Kaufman *Tetrahedron Lett.* **36** 9105 (1995)
146. J Garcia, M López, J Romeu *Tetrahedron: Asymmetry* **10** 2617 (1999)
147. B M Stoltz, T Kano, E J Corey *J. Am. Chem. Soc.* **122** 9044 (2000)
148. J Morrison (Ed.) *Asymmetric Synthesis. Analytical Methods* Vol. 1 (New York: Academic Press, 1983)
149. D Enders, U Reinhold *Tetrahedron: Asymmetry* **8** 1895 (1997)
150. F Fache, E Schulz, M L Tommasino, M Lamaire *Chem. Rev.* **100** 2159 (2000)
151. S Itsuno, Y Sakurai, K Ito, A Hirao, S Nakahama *Bull. Chem. Soc. Jpn.* **60** 395 (1987)
152. E Fontaine, C Namane, J Meneyrol, M Geslin, L Serva, E Roussey, S Tissandié, M Maftouh, P Roger *Tetrahedron: Asymmetry* **12** 2185 (2001)
153. B T Cho, Y S Chun *Tetrahedron: Asymmetry* **3** 1583 (1992)
154. R D Tillyer, C Boudreau, D Tschaen, U-H Dolling, P J Reider *Tetrahedron Lett.* **36** 4337 (1995)
155. M Shimizu, M Kamei, T Fujisawa *Tetrahedron Lett.* **36** 8607 (1995)
156. S Itsuno, M Nakano, K Ito, A Hirao, M Owa, N Kanda, S Nakahama *J. Chem. Soc., Perkin Trans. 1* 2615 (1985)
157. S Itsuno, Y Sakurai, K Shimizu, K Ito *J. Chem. Soc., Perkin Trans. 1* 1859 (1990)
158. S Itsuno, T Matsumoto, D Sato, T Inoue *J. Org. Chem.* **65** 5879 (2000)
159. B T Cho, Y S Chun *J. Chem. Soc., Perkin Trans. 1* 3200 (1990)
160. M Masui, T Shioiri *Tetrahedron Lett.* **39** 5195 (1998)
161. M Masui, T Shioiri *Tetrahedron Lett.* **39** 5199 (1998)
162. M Shimizu, K Tsukamoto, T Fujisawa *Tetrahedron Lett.* **38** 5193 (1997)
163. M Shimizu, K Tsukamoto, T Matsutani, T Fujisawa *Tetrahedron* **54** 10265 (1998)
164. US P. 5 442 118; *Chem. Abstr.* **124** 55 545 (1996)
165. B B Lohray, V Bhusan *Angew. Chem., Int. Ed. Engl.* **31** 729 (1992)
166. C H Heathcock, in *Asymmetric Synthesis* Vol. 3 (Ed. J D Morrison) (New York: Academic Press, 1984) p. 111

167. C H Heathcock, in *Comprehensive Organic Synthesis* Vol. 2 (Eds B M Trost, I Fleming) (Oxford: Pergamon Press, 1991) p. 133
168. M Kim, S F Williams, S Masamune, in *Comprehensive Organic Synthesis* Vol. 2 (Eds B M Trost, I Fleming) (Oxford: Pergamon Press, 1991) p. 239
169. T Mukaiyama, K Banno, K Narasaka *Chem. Lett*. 1011 (1973)
170. T Mukaiyama, K Banno, K Narasaka *J. Am. Chem. Soc*. **96** 7503 (1974)
171. T Mukaiyama, in *Organic Reactions* Vol. 28 (New York: Wiley, 1974) p. 203
172. S Kiyooka, H Kira, M A Hena *Tetrahedron Lett*. **37** 2597 (1996)
173. T Bach *Angew. Chem., Int. Ed. Engl*. **33** 417 (1994)
174. C Gennari, G Pain, D Moresca *J. Org. Chem*. **60** 6248 (1995)
175. E M Carreira, R A Singer, W Lee *J. Am. Chem. Soc*. **116** 8837 (1994)
176. K Furuta, T Maruyama, H Yamamoto *J. Am. Chem. Soc*. **113** 1041 (1991)
177. E J Corey, T P Loh, T D Roper, M D Azimioara, M C Noe *J. Am. Chem. Soc*. **114** 8290 (1992)
178. E J Corey, T P Loh *J. Am. Chem. Soc*. **113** 8966 (1991)
179. M Takasu, H Yamamoto *Synlett* 194 (1990)
180. D Sartor, J Saffrich, G Helmchen *Synlett* 197 (1990)
181. D Sartor, J Saffrich, G Helmchen, C J Richards, H Lambert *Tetrahedron: Asymmetry* **2** 639 (1991)
182. E R Parmee, O Tempkin, S Masamune, A Abiko *J. Am. Chem. Soc*. **113** 9365 (1991)
183. I Simpura, V Nevalainen *Tetrahedron: Asymmetry* **10** 7 (1999)
184. C-M Yu, J-Y Lee, K Chun, I-K Choi, S-K Kang *Chem. Commun*. 2698 (2001)
185. K Ishihara, S Kondo, H Yamamoto *J. Org. Chem*. **65** 9125 (2000)
186. T Mansikka, V Nevalainen, I Simpura, J Kokkonen, R Kostiainen *Tetrahedron: Asymmetry* **10** 1437 (1999)
187. V Nevalainen, T Mansikka, R Kostiainen, I Simpura, J Kokkonen *Tetrahedron: Asymmetry* **10** 1 (1999)
188. Y Kaneko, S-i Kiyooka *Mem. Fac. Sci. Kochi Univ. C* **15** 9 (1994); *Ref. Zh. Khim*. 23 B 297 (1995)
189. L Salvatella, M F Ruiz-López *J. Am. Chem. Soc*. **121** 10772 (1999)
190. E J Corey, J J Rohde *Tetrahedron Lett*. **38** 37 (1997)
191. E J Corey, T W Lee *Chem. Commun*. 1321 (2001)
192. S-i Kiyooka, Y Kaneko, M Komura, H Matsuo, M Nakano *J. Org. Chem*. **56** 2276 (1991)
193. S-i Kiyooka, Y Kaneko, K-i Kume *Tetrahedron Lett*. **33** 4927 (1992)
194. Y Kaneko, H Matsuo, S-i Kiyooka *Tetrahedron Lett*. **35** 4107 (1994)
195. S-i Kiyooka, Y Kaneko, Y Harada, H Matsuo *Tetrahedron Lett*. **36** 2821 (1995)
196. S-i Kiyooka, M A Hena *Tetrahedron: Asymmetry* **7** 2181 (1996)
197. S-i Kiyooka, T Yamagichi, H Maeda, H Kira, M A Hena, M Horiike *Tetrahedron Lett*. **38** 3553 (1997)
198. S-i Kiyooka, H Maeda *Tetrahedron: Asymmetry* **8** 3371 (1997)
199. M A Hena, S Terauchi, C-S Kim, M Horiike, S-i Kiyooka *Tetrahedron: Asymmetry* **9** 1883 (1998)
200. S-i Kiyooka, H Maeda, M A Hena, M Uchida, C-S Kim, M Horiike *Tetrahedron Lett*. **39** 8287 (1998)
201. M A Hena, C-S Kim, M Horiike, S-i Kiyooka *Tetrahedron Lett*. **40** 1161 (1999)
202. S-i Kiyooka, K A Shahid *Tetrahedron Lett*. **41** 2633 (2000)
203. S-i Kiyooka *J. Synth. Org. Chem. Jpn*. **55** 313 (1997); *Ref. Zh. Khim*. 9 Zh 278 (1998)
204. S-i Kiyooka *Rev. Heteroat. Chem*. **17** 245 (1997)
205. S-i Kiyooka, M A Hena *J. Org. Chem*. **64** 5511 (1999)
206. S-i Kiyooka, M A Hena, F Goto *Tetrahedron: Asymmetry* **10** 2871 (1999)
207. S-i Kiyooka, K Goh, Y Nikamura, H Takesue, M A Hena *Tetrahedron Lett*. **41** 6599 (2000)
208. G Li, H-X Wei, B S Phelps, D W Purkiss, S H Kim *Org. Lett*. **3** 823 (2001)
209. R Imashiro, T Kuroda *Tetrahedron Lett*. **42** 1313 (2001)
210. M Kinugasa, T Harada, A Oku *Tetrahedron Lett*. **39** 4529 (1998)
211. T Harada, T Egusa, M Kinugasa, A Oku *Tetrahedron Lett*. **39** 5531 (1998)
212. T Harada, T Egusa, A Oku *Tetrahedron Lett*. **39** 5535 (1998)
213. T Harada, T Nakamura, M Kinugasa, A Oku *Tetrahedron Lett*. **40** 503 (1999)
214. T Harada, H Yamanaka, A Oku *Synlett* 61 (2001)
215. T Harada, T Nakamura, M Kinugasa, A Oku *J. Org. Chem*. **64** 7594 (1999)
216. G Bringmann, T Hartung *Angew. Chem., Int. Ed. Engl*. **31** 761 (1992)
217. G Bringmann, T Hartung *Tetrahedron* **49** 7891 (1993)
218. G Bringmann, D Vitt *J. Org. Chem*. **60** 7674 (1995)
219. G Bringmann, M Ochse, R Gotz *J. Org. Chem*. **65** 2069 (2000)
220. G Bringmann, J Hinrichs *Tetrahedron: Asymmetry* **8** 4121 (1997)
221. G Bringmann, J Hinrichs, J Kraus, A Wuzik, T Shulz *J. Org. Chem*. **65** 2517 (2000)
222. M Nógrádi *Stereoselective Synthesis* (Weinheim: VCH, 1987)
223. Y Hayashi, J J Rohde, E J Corey *J. Am. Chem. Soc*. **118** 5502 (1996)
224. E J Corey, T Shibata, T W Lee *J. Am. Chem. Soc*. **124** 3808 (2002)
225. K V Gothelf, K A Jörgensen *Chem. Commun*. 1449 (2000)
226. J-P G Seerden, A W A S Reimer, H W Scheeren *Tetrahedron Lett*. **35** 4419 (1994)
227. J-P G Seerden, M M M Kuypers, H W Scheeren *Tetrahedron: Asymmetry* **6** 1441 (1995)
228. J-P G Seerden, M M M Boeren, H W Scheeren *Tetrahedron* **53** 11843 (1997)
229. M Meske *J. Prakt. Chem*. **339** 426 (1997)
230. P Bayón, P de March, M Figueredo, J Font, J Medrano *Tetrahedron: Asymmetry* **11** 4269 (2000)
231. S Itsuno, K Kamahori, K Watanabe, T Koizumi, K Ito *Tetrahedron: Asymmetry* **5** 523 (1994)
232. K Kamahori, K Ito, S Itsuno *J. Org. Chem*. **61** 8321 (1996)
233. S Itsuno, K Watanabe, T Matsumoto, S Kuroda, A Yokoi, A El-Shehawy *J. Chem. Soc., Perkin Trans. 1* 2011 (1999)
234. Z Shan, Y Xiong, D Zhao *Tetrahedron* **55** 3893 (1999)
235. C Puigjaner, A Vidal-Ferran, A Moyano, M A Pericas, A Riera *J. Org. Chem*. **64** 7902 (1999)
236. S Itsuno, K Ito, T Maruyama, N Kanda, A Hirao, S Nakahama *Bull. Chem. Soc. Jpn*. **59** 3329 (1986)
237. G Giffels, J Beliczey, M Felder, U Kragl *Tetrahedron: Asymmetry* **9** 691 (1998)
238. S Itsuno, K Ito, A Hirao, S Nakahama *J. Chem. Soc., Perkin Trans. 1* 2887 (1984)
239. B Altava, M I Burguete, M Collado, E Garcna-Verdugo, S V Luis, R V Salvador, M J Vicent *Tetrahedron Lett*. **42** 1673 (2001)
240. J Hu, G Zhao, Z Ding *Angew. Chem., Int. Ed*. **40** 1109 (2001)
241. J Hu, G Zhao, G Yang, Z Ding *J. Org. Chem*. **66** 303 (2001)
242. S-i Kiyooka, Y Kido, Y Kaneko *Tetrahedron Lett*. **35** 5243 (1994)
243. S Itsuno, Y Sakurai, K Ito, A Hirao, S Nakahama *Polymer* **28** 1005 (1987)
244. C Caze, N ElMoualij, P Hodge, C J Lock, J Ma *J. Chem. Soc., Perkin Trans. 1* 345 (1995)
245. C Schunicht, A Biffs, G Wulff *Tetrahedron* **56** 1693 (2000)
246. C Caze *React. Funct. Polym*. **26** 85 (1995); *Chem. Abstr*. **124** 144 896 (1996)
247. N ElMoualij, C Caze *Eur. Polym. J*. **31** 193 (1995)
248. C Caze, N ElMoualij, P Hodge, C J Lock *Polymer* **36** 621 (1995)
249. M D Price, J K Sui, M J Kurth, N E Schore *J. Org. Chem*. **67** 8086 (2002)
250. C Franot, G B Stone, P Engeli, C Spöndlin, E Waldvogel *Tetrahedron: Asymmetry* **6** 2755 (1995)
251. M Felder, G Giffels, C Wandrey *Tetrahedron: Asymmetry* **8** 1975 (1997)
252. S Rissom, J Beliczey, G Giffels, U Kragl, C Wandrey *Tetrahedron: Asymmetry* **10** 923 (1999)

253. K Movlinger, M López, J Court *Tetrahedron: Asymmetry* **11** 2263 (2000)
254. C Bolm, N Derrien, A Seger *Chem. Commun*. 2087 (1999)
255. E J Corey, R Imwinkelried, S Pikul, Y B Xiang *J. Am. Chem. Soc.,* **111** 5493 (1989)
256. E J Corey, R S Kania *J. Am. Chem. Soc*. **118** 1229 (1996)
257. E J Corey, C M Yu, S S Kim *J. Am. Chem. Soc*. **111** 5495 (1989)
258. E J Corey, S Choi *Tetrahedron Lett*. **41** 2769 (2000)
259. E J Coreyr S Choi *Tetrahedron Lett*. **41** 2765 (2000)
260. O Froelich, M Bonin, J-C Quirion, H-P Husson *Tetrahedron: Asymmetry* **4** 2335 (1993)
261. M Asami, S Sato, H Watanabe *Chem. Lett*. 990 (2000)
262. A Cruz, E Geníz, R Contreras *Tetrahedron: Asymmetry* **9** 3991 (1998)
263. A Cruz, A Flores-Parra, H Tlahuext, R Contreras *Tetrahedron: Asymmetry* **6** 1933 (1995)
264. A Cruz, D Mactas-Mendoza, E Barragan-Rodrtguez, H Tlahuext, H Nlth, R Contreras *Tetrahedron: Asymmetry* **8** 3903 (1997)
265. T-K Yang, D-S Lee *Tetrahedron: Asymmetry* **10** 405 (1999)
266. J-C Fiaud, F Mazé, H B Kagan *Tetrahedron: Asymmetry* **9** 3647 (1998)

Russian Chemical Reviews **73** (6) 609 – 619 (2004) © 2004 Russian Academy of Sciences and Turpion Ltd

DOI 10.1070/RC2004v073n06ABEH000879

Oxy acids of halogens HOHal

I V Nikitin

Contents

I.	Introduction	609
II.	Hypofluorous acid	609
III.	Hypochlorous acid	612
IV.	Hypobromous acid	614
V.	Hypoiodous acid	616

Abstract. The key methods for the synthesis of the acids HOF, HOCl, HOBr and HOI are considered. The results of investigations of the structures and properties of these acids are described. Possible participation of the HOHal acids in the destruction of stratospheric ozone is discussed. The bibliography includes 207 references.

I. Introduction

The aim of this review is to characterise a group of relatively little-known triatomic compounds of general formula HOHal belonging to the group of oxy acids of halogens. There are several types of oxy acids of halogens; however, only the triatomic acids HOHal are known for all halogens including fluorine, which forms hypofluorous acid. It is customary to use the suffix 'vatistaya' when naming the HOHal acids in the chemical literature written in Russian; its English equivalent is the suffix 'ous', which is used throughout the text of the review. Sometimes the compounds in question are called halogen hydroxides.

All the HOHal acids are unstable. They display a powerful oxidising action. The 'eldest' is hypochlorous acid, HOCl, whose salts have been known since the late 18th or early 19th century ('eau de Javelle', 'eau de Labarraque'). Salts of hypochlorous acid, *e.g.*, bleaching powder, calcium hypochlorite and sodium hypochlorite have found wide applications in the home and in industry as oxidants, bleaching agents, degassing agents and disinfectants. The chemistry of aqueous solutions of hypochlorous acid and its salts had been well studied by the mid-twentieth century. The acids of general formula HOHal have attracted considerable attention since the synthesis of hypofluorous acid and mainly in connection with the development of atmospheric chemistry. Possible involvement of halogen-containing small molecules† in the catalytic cycles of destruction of stratospheric ozone gave an impetus to investigations on the spectroscopic characteristics, photochemistry and reactivity (in particular, under conditions that simulate stratospheric conditions) of these species. Studies on the properties of hypofluorous acid and other hypohalous acids HOHal have also been reported. These new data are complementary to scarce information on these acids available from books on inorganic chemistry and handbooks.

I V Nikitin Institute of Problems of Chemical Physics, Russian Academy of Sciences, 142432 Chernogolovka, Moscow Region, Russian Federation. Fax (7-096) 576 40 09. Tel. (7-096) 522 35 70.
E-mail: led@icp.ac.ru

Received 2 October 2003
Uspekhi Khimii **73** (6) 662 – 672 (2004); translated by A M Raevskiy

II. Hypofluorous acid

Hypofluorous acid has long been considered a 'non-existent' compound [2] though its synthesis does not require hard-to-access starting compounds or unusual equipment.

Production of hypofluorous acid in the form of a complex with HF in the course of photolysis of a mixture of H_2O with F_2 in a low-temperature nitrogen matrix at 14 and 20 K was detected by IR spectroscopy in 1968.[3] The first synthesis of HOF was reported in 1971.[4]

HOF is synthesised from gaseous fluorine and liquid water or ice by bubbling fluorine through water one time at 223 – 233 K. Sometimes the reaction of fluorine with water is carried out in a recirculating system.

$$F_2 + H_2O \longrightarrow HOF + HF.$$

In spite of low reaction rate and low yield of HOF, the amount of the acid thus obtained can vary from several tens to several hundreds of milligrams.[2] The by-products of the reaction are oxygen difluoride, OF_2, and oxygen. It was assumed [5,6] that oxygen difluoride is produced in the reaction

$$F_2 + HOF \longrightarrow OF_2 + HF.$$

Later on, this assumption was confirmed experimentally. Using tracers (^{18}O and ^{18}F), it was shown that the OF_2 molecule contains one fluorine atom from the hypofluorous acid molecule and one fluorine atom from the F_2 molecule.[7] The reaction of fluorine with D_2O gave deuterated hypofluorous acid.

Noteworthy is that oxygen difluoride is not an anhydride of hypofluorous acid (no acid is produced upon dissolution of this compound in water). This differentiates OF_2 from dichlorine monoxide which gives hypochlorous acid upon dissolution in water.

Photolysis of a mixture of H_2O with F_2 in argon matrix produces HOF in the form of a complex with HF.[3] A thorough study of photolysis of $H_2O - F_2$ mixtures in solid argon at 12 K revealed the formation of complexes HF – HOF, FH – FOH and FH – OHF, the first-mentioned complex being the most stable.[8]

† The review [1] concerns tetraatomic compounds of halogens Hal_2O_2, which are of interest for atmospheric chemistry.

Hypofluorous acid is stable at the boiling temperature of liquid nitrogen but decomposes into HF and O_2 (sometimes, explosively) on heating. The half-life of HOF is $\sim$30 min at room temperature;[2] however, it increases to $\sim$3 h in a passivated IR spectroscopic cell.[9] The melting temperature of HOF is 156 K while its boiling temperature is somewhat lower than room temperature. The vapour pressure of HOF is at most 1 Torr at 194 K and nearly 5 Torr at 209 K (more accurate vapour pressure measurements are impossible because of the decomposition of the acid).[4]

The HOF molecule is a slightly asymmetrical prolate rotor characterised by the rotational constants $A_0 = 585\,628.93$, $B_0 = 26\,757.53$ and $C_0 = 25\,514.10$ MHz (see Refs 10, 11) and by the parameter $\kappa = 2[B-1/2(A+C)]/(A-C) = -0.9955$. The rotational constant values were repeatedly refined (see Refs 9, 12, 13). The rotational constants of the $H^{16}OF$ molecule are as follows: $A_e = 19.663796$, $B_e = 0.9003148$ and $C_e = 0.8608167$ cm^{-1}.[13]

An X-ray diffraction study [14] showed that the single crystal of HOF belongs to the orthorhombic crystal system. The lattice constants are $a = 4.075$, $b = 5.040$ and $c = 5.939$ Å; the space group is $P2_12_12_1$. The single crystal was grown by slow cooling of the HOF sample down to 113 K. Table 1 lists the experimental (obtained by X-ray analysis [14] and microwave spectroscopy [10, 11]) and calculated [15] bond lengths and bond angles in the HOF molecule.

Table 1. Bond lengths and bond angles in the HOF molecule.

Method	r(O–F) /Å	r(O–H) /Å	HOF angle /deg	Ref.
X-Ray analysis	1.442	0.78	101	14
Microwave	1.442	0.964	97.2	10
spectroscopy	1.442	0.966	96.78	11
TZP CCSD [a]	1.4356	0.9664	97.72	15

[a] *Ab initio* calculations using the Triple-Zeta-Plus-Polarisation Coupled Cluster Method with Single and Double Excitations.

The HOF molecule has a large dipole moment, $\mu_{exp} = 2.23 \pm 0.10$ D.[16] *Ab initio* calculations gave the values of 2.18 D (see Ref. 17) and 2.032–2.182 D (see Ref. 15).

Hypofluorous acid forms no associates in the gas phase (at least at pressures below 160 Torr) [18] but undergoes association in the condensed phase. Initially, it was hypothesised [18, 19] that the HOF molecules are linked together through O–H...F bridges; however, this assumption was rejected.[20] Taking into account the fact that the oxygen atom in the HOF molecule bears a larger negative charge compared to the fluorine atom owing to withdrawal of the electron density from the hydrogen atom, one could expect the formation of O–H...O bridges. It was reported [20] that in self-association of hypofluorous acid involving O–H...O bridges the HOF molecules form zig-zag chains or large cycles, $(HOF)_n$.[20] An X-ray diffraction study [14] confirmed the presence of nearly linear bridges O–H...O [O–H...O 163°, r(H...O) = 2.895 Å] in the single crystal of HOF (Fig. 1).

An IR spectroscopic study of photochemical reactions of hypofluorous acid in low-temperature matrices revealed the formation of dimers, $(HOF)_2$, and, probably, other oligomers of HOF.[21] It was concluded [21] that the HOF molecules form dimers $(HOF)_2$ linked through the O–H...O bridge (acyclic dimer). *Ab initio* calculations [22] showed that the O–H...O bridge in the dimer is stronger than the O–H...F bridge. Other *ab initio* calculations [23] revealed two stable $(HOF)_2$ structures differing in orientation of the constituent HOF molecules, namely, a linear structure of C_1 symmetry (molecules are linked together through both O–H...O and O–H...F bridges) and a cyclic structure of C_2 symmetry (here, molecules form dimers involving two O–H...F bridges). The linear structure is more stable, though the energy of the cyclic structure is only 0.35 kcal mol^{-1} higher.

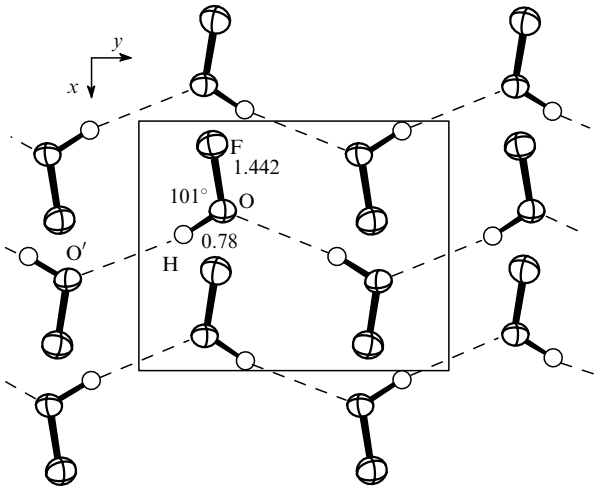

Figure 1. Crystal structure of HOF.[14]

The vibrational spectrum of HOF molecules has been thoroughly studied [9, 13, 18, 19, 21, 24, 25] (see Table 2).

Gaseous hypofluorous acid is characterised by intense absorption in the region $\lambda < 300$ nm; no pronounced absorption maximum is observed.[21] According to calculations,[26] the absorption spectrum of HOF exhibits two maxima, one in the region $\lambda < 200$ nm and the other in the region $\lambda > 200$ nm.

The ^1H and ^{19}F NMR spectra of hypofluorous acid were recorded [27] shortly after the pioneering synthetic study. The chemical shift of the F atom is 403 ppm (171 K) or 402 ppm (193 K) relative to gaseous fluorine at 298 K. The proton chemical shift is −16.0 ppm (193 K) or −12.1 ppm (293 K) relative to gaseous methane at 298 K. Fast proton exchange between HOF and HF present in the sample was demonstrated for the liquid phase.

The mass spectrum of HOF exhibits a peak of a molecular ion.[4] Photoionisation of hypofluorous acid at $\lambda = 77.5$ nm produces HOF^+, OH^+ and O^+ ions with the relative intensities of 100, 37 and 44 arbitrary units, respectively.[28] The first ionisation potential of the HOF molecule is 12.71 ± 0.01 eV [28] and nearly coincides with the adiabatic ionisation potential (12.69 ± 0.03 eV) determined from the HeI photoelectron spectrum of hypofluorous acid.[29] GAUSSIAN-2 (G2)‡ calculations [30] of the adiabatic ionisation energy of HOF gave a value of 12.71 eV.

The enthalpy of formation of hypofluorous acid determined in the study on photoionisation of HOF is -22.8 ± 1 (0 K) or -23.5 ± 1 kcal mol^{-1} (298 K).[28] A more accurate value is $\Delta H^\circ(HOF) = -19.9$ kcal mol^{-1} (0 K);[32] however, it was refined [33] and a new value of −19.5 kcal mol^{-1} (0 K) was reported. The results of some calculations very closely approach the experimental value of the enthalpy of formation of HOF (Table 3).

The adiabatic bond dissociation energy, $D_0(HO-F)$, of HO–F (50.4 kcal mol^{-1}) [28] was then recalculated. The refined $D_0(HO-F)$ value is 47.5 kcal mol^{-1} (see Ref. 32). Table 3 lists the bond dissociation energies reported in different studies. The atomisation energy of HOF obtained from G2 calculations [31] is 149.7 kcal mol^{-1}.

Proton affinity calculations for the HOF molecule were carried out for protonation at the O atom and at the F atom [routes (1) and (2), respectively].

$$HOF + H^+ \longrightarrow H_2OF^+ \quad (1)$$

‡ For G2 calculations, see Ref. 31.

Table 2. Main vibrational frequencies of HOF molecule.

Method	Spectrum recording conditions	ν /cm^{-1}			Ref.
		ν_1 (O–H, stretching vibration)	ν_2 (bending vibration)	ν_3 (O–F, stretching vibration)	
IR spectroscopy	gas phase	3578.5	1354.8	889.0	24
	low-temperature matrix	3537.1	1359.0	886.0	25
	the same	3572	1350	888	21
	HOF film, 78 K	3370	1397	885	19
High resolution FT-IR spectroscopy	H^{16}OF	3577.92580	1353.40466	889.07974	9, 13
Raman spectroscopy	77 K	3359	–	884	18

Table 3. Enthalpies of formation of HOF molecule (kcal mol^{-1}) and bond dissociation energies (kcal mol^{-1}) in the HOF molecule.

Computational method	ΔH°(HOF) (T /K)	D_0(HO–F)	D_0(H–OF)	Ref.
GAUSSIAN 1 (G1) [a]	–19.9 (0)	47.5	–	32
Refined values	–19.5 (0)	47.3	97.0	33
G2	–21.1 (298)	48.1	–	30
Quantum-chemical calculations				
B3LYP	–20.43±1.92 (298.15)	45.91	95.00	34
B3PW91	–20.35±1.34	46.20	115.05	34
CCSD(T)	(298.15)	45.77	98.17	34

[a] For G1 calculations, see Ref. 35.

and

$$HOF + H^+ \longrightarrow HOFH^+. \quad (2)$$

The former process was found to be preferred (Table 4).[30, 36–39] The O–F interatomic distance in the $HOFH^+$ and H_2OF^+ molecules is respectively longer and shorter than in the HOF molecule.[30, 36] According to G2 calculations, protonation of HOF at the oxygen atom is 18 kcal mol^{-1} more energetically favourable than protonation at the F atom.[34] (Protonation of other HOHal acids at the oxygen atom is also more energetically favourable.[30])

The possibility of using hypofluorous acid as the starting reagent in the synthesis of other compounds was studied by Appelman and co-workers.[2, 5, 6, 40–42] shortly after the synthesis of HOF. Hypofluorous acid appeared to be an excellent donor of oxygen atoms; however, the short lifetime of HOF at temperatures close to room temperature hampers the wide use of this compound.

Table 4. Proton affinity energy of the HOF molecule (298 K).

Computational method	Proton affinity energy /kcal mol^{-1}		Ref.
	protonation at the O atom	protonation at the F atom	
G2	135.2	116.8	30
	133.8	115.9	37
DFT/PW91 [a]	141.5	122.6	39

[a] *Ab initio* density functional calculations with the Perdew–Wang functional (PW91).

Photolysis of HOF in low-temperature matrices is thought to proceed as concerted elimination of HF to produce O(^{1}D) or O(^{3}P).[21]

$$HOF \xrightarrow{h\nu} O + HF.$$

In the case of non-inert matrices, the oxygen atoms enter in the reaction with the matrix molecules or with the dopant. For instance, photolysis of HOF in argon matrices doped with PF_3, AsF_3 or H_2O produces OPF_3, $OAsF_3$ or H_2O_2, respectively.

The possibility of using hypofluorous acid as oxidant has been thoroughly studied by Rozen and co-workers.[43–58] It was found that bubbling gaseous fluorine diluted with N_2 through a vigorously stirring mixture of acetonitrile with distilled water (usually, 10 : 1 or 20 : 1 by volume) at 263 or 258 K results in an oxidising solution with the oxidant concentration exceeding 1 mol litre^{-1}. Shortly after, it was established that the active component is the complex MeCN · HOF. The half-life of this complex is longer than 10 h at 273 K or 3 to 4 h at room temperature. This indicates that acetonitrile stabilises hypofluorous acid formed in the reaction of fluorine with water (HOF retains its oxidising properties).

^{19}F NMR and IR spectroscopies confirmed that HOF and acetonitrile form a rather stable 1 : 1 complex.[59] An X-ray diffraction study[60] of the complex MeCN · HOF carried out at 143 K revealed that the HOF and MeCN molecules are linked *via* a linear hydrogen bridge, O–H...N, 2.81 Å long (interatomic distance H...N is 1.71 Å).

Reactions involving the complex MeCN · HOF proceed under mild conditions at temperatures between 273 K and room temperature. A feature of these processes is their high rates (the reactions are completed in a few seconds to several minutes). In many cases, the product yields are as high as 90% to 100%. Often, compounds obtained using this complex cannot be synthesised by other methods.[54] Hydrogen fluoride formed as a by-product can be readily neutralised with calcium hydroxide.[56]

Complex MeCN · HOF is used for fast and efficient epoxidation of various olefins.[43, 45, 47, 49] The time taken to convert cyclooctene into epoxycyclooctane by the reaction with the complex MeCN · HOF at 273 K is shorter than 1 min; this also holds for the epoxidation of *trans*-stilbene.[45] Epoxidation of $C_4F_9CH=CH_2$ proceeds at a lower rate while sterically hindered $C_4F_9CH=CHC_4F_9$ does not enter into reaction.[47] Since the oxygen atom of the oxirane ring is supplied by the HOF molecule, it is possible to obtain epoxides containing tracers (^{17}O or ^{18}O isotopes) when using labelled water to synthesise HOF. This method allows the oxygen isotopes to be introduced into other compounds.[44–46, 48]

Reactions of anthracene and phenanthrene with MeCN · HOF produce quinones,[50] while pyrene, 2-acetylphenanthrene and 9-acetylphenanthrene are converted into epoxides.[57] Complex MeCN · HOF is used for the oxidation of aromatic amines[46] and aliphatic amines[48] to corresponding nitro compounds and for the oxidation of amino acid esters into nitrate esters.[51] The oxidation of AlkOMe ethers involves elimination of methanol, the ethers

with Alk = n-C_nH_{2n+1} being oxidised to acids (*via* aldehydes) while those with Alk = *sec*-C_nH_{2n+1} are oxidised to ketones and lactones.[54]

MeCN·HOF readily oxidises both aliphatic and aromatic sulfides to sulfones.[56] The reactions proceed at 198 K and involve an intermediate formation of sulfoxides that can be isolated in high yields.[56] Under these conditions, thiophenes are converted into corresponding *S*-dioxides.[52]

Thus, the complex MeCN·HOF is an efficient oxygen transfer agent. The oxidation reactions with participation of this complex proceed under mild conditions and in some cases at very high rates. The complex offers yet another remarkable advantage as a reactant, namely, no isolation, purification or other specific operations are needed when using it.

III. Hypochlorous acid

Traditionally, hypochlorous acid is synthesised by the reaction of chlorine with an aqueous suspension of yellow (red) mercury oxide or with moist mercury oxide powder.

$$HgO + 2Cl_2 + H_2O \longrightarrow 2HOCl + HgCl_2.$$

Hydrochloric acid formed in the reaction of chlorine with water (for the kinetics of hydrolysis of chlorine, see Ref. 61) reacts with mercury oxide, thus shifting the equilibrium in the reaction (3) to the right and giving an aqueous hypochlorous acid solution.

$$Cl_2 + H_2O \rightleftharpoons HOCl + HCl, \qquad (3, -3)$$

$$HgO + 2HCl \longrightarrow HgCl_2 + H_2O.$$

The reaction of chlorine with mercury oxide in the absence of water is known as a method for the synthesis of dichlorine monoxide. An approximate reaction equation has the form

$$2Cl_2 + HgO \longrightarrow Cl_2O + HgCl_2.$$

Being an anhydride of hypochlorous acid, Cl_2O is readily soluble in water, thus producing HOCl.

$$Cl_2O + H_2O \rightleftharpoons 2HOCl. \qquad (4, -4)$$

At room temperature, the equilibrium mixture $H_2O-Cl_2O-HOCl$ is stable over a period of a few hours.[62, 63] The equilibrium constant for the gas-phase reaction (4, −4) of hydrolysis of Cl_2O at room temperature ($K = 0.25$) calculated [62] in a study of the UV spectrum of HOCl appeared to be overestimated as compared to the results obtained in more recent studies.[63–66]

T/K	K	Method	Ref.
298	0.25	UV	62
298	0.082	UV	63
295 ± 3	0.068	IR	64
298	0.092 ± 0.011	LPMS-DFS [a]	65
298	0.10 ± 0.01	UV	66

[a] LPMS-DFS stands for Low-Pressure Mass Spectrometry–Discharge Flow System.

Hypochlorous acid is also synthesised by the reaction of aqueous sodium hypochlorite solution with aqueous solutions of magnesium sulfate heptahydrate or anhydrous $MgSO_4$.[67–70]

The acid HOCl was obtained in the reaction of hydrogen chloride with calcium hypochlorite powder.[71] The interaction between hydrogen fluoride diluted with N_2 and calcium hypochlorite powder also results in hypochlorous acid.[72, 73]

$$2HF + Ca(OCl)_2 \longrightarrow 2HOCl + CaF_2.$$

Gaseous HOCl is obtained by bubbling gaseous chlorine diluted with helium through an aqueous suspension of $CaCO_3$ (see Ref. 65).

$$2Cl_2 + H_2O + CaCO_3 \longrightarrow 2HOCl + CO_2 + CaCl_2.$$

The acid thus formed is immediately converted to the gas phase to prevent its decomposition into Cl_2O and H_2O. Sodium hydrocarbonate can be used instead of calcium carbonate; in this case, the reaction proceeds at a higher rate.[74]

The reaction of chlorine with concentrated hydrogen peroxide solution in alkali medium produces excited dioxygen in 100% yield.[75–77]

$$Cl_2 + H_2O_2 + 2OH^- \longrightarrow O_2(^1\Delta) + 2H_2O + 2Cl^-.$$

The main goal of investigations on the properties of HOHal acids carried out in the last decades is to study the behaviour of these compounds in the Earth's atmosphere and to establish their role in the destruction of stratospheric ozone.

Formation and decomposition reactions of HOCl in the stratosphere have been the subject of scientific research since the 1980s. Most studies are concerned with the radical–radical reaction $ClO^{\bullet} + HO_2^{\bullet}$ and with hydrolysis of chlorine nitrate because both processes can produce HOCl.

Tentatively, a bimolecular reaction $ClO^{\bullet} + HO_2^{\bullet}$ results in the following products:[78, 79]

Reaction	Products	ΔH(298 K) /kcal mol^{-1}	Reaction channel
$ClO^{\bullet} + HO_2^{\bullet}$	$HOCl + O_2$	−46	(*a*)
	$HCl + O_3$	−15	(*b*)
	$ClOO^{\bullet} + OH^{\bullet}$	+2.9	(*c*)
	$OClO^{\bullet} + OH^{\bullet}$	+6.0	
	$HClO + O_2$	+17	

Hypochlorous acid is formed following route (*a*). At 210–300 K, the contribution of this channel to the overall reaction exceeds 95% while that of channel (*b*) is only 5 ± 2%.[79] Quantum-chemical calculations [80] also showed that route (*a*) is the most energetically favourable and that channel (*b*) is impracticable.§ The probability of a weakly endothermic reaction (*c*) is also low.

Hypochlorous acid is formed as a result of the reaction of radical $ClO^{\bullet}$ with the hydrogen atom of the radical $HO_2^{\bullet}$ and in a more complex way *via* decomposition of the cyclic intermediate OClOOH produced upon the attack of the Cl atom of the radical $ClO^{\bullet}$ on the terminal oxygen atom of the $HO_2^{\bullet}$ radical (see Refs 78, 79, 82–86). The former mechanism dominates at $T > 370$ K while the latter governs the reaction at temperatures below 270 K. The fast reaction $ClO^{\bullet} + HO_2^{\bullet} \longrightarrow HOCl + O_2$ is characterised by a rate constant of $(4.5-6.5) \times 10^{-12}$ cm^3 molecule^{-1} s^{-1} at 298 K.[78] Yet another estimate of the rate constant for this reaction is $(7.1 \pm 1.8) \times 10^{-12}$ cm^3 molecule^{-1} s^{-1} at 294 K.[81]

Chlorine nitrate is inert towards ozone; however, hydrolysis of $ClONO_2$ and its interaction with HCl which proceed on the surface of aerosol particles are followed by the formation of catalytically active molecules HOCl and Cl_2.[87, 88]

$$ClONO_2 + H_2O \longrightarrow HOCl + HNO_3,$$

$$ClONO_2 + HCl \longrightarrow Cl_2 + HNO_3.$$

The reaction of gaseous chlorine nitrate with water is very slow.[89] At the same time, hydrolysis of $ClONO_2$ adsorbed on the surface of aerosol particles proceeds at a much higher rate. This reaction was studied by many authors (see, *e.g.*, Refs 71, 89–112). The reaction rate is affected by several factors, namely, temperature, aerosol particle size, surface structure, $ClONO_2 : H_2O$ ratio, presence of unbound water. In type-I polar stratospheric clouds containing mainly nitric acid trihydrate, hydrolysis of chlorine nitrate proceeds at a lower rate compared to the process in type-II clouds (hexagonal ice Ih).[90] However, this reaction proceeds rapidly in water-enriched type-I clouds.[107] Solvation of $ClONO_2$

§ The contribution of channel (*b*) to the overall reaction $ClO^{\bullet} + HO_2^{\bullet}$ is at most 1%.[81]

causes a substantial decrease in the activation energy for the hydrolysis reaction.[105, 107, 109, 110]

Using a tracer technique, it was shown that hydrolysis of $ClONO_2$ on ice ($H_2{}^{18}O$) produces $H^{18}OCl$ rather than $H^{18}ONO_2$.[98] The presence of the ^{18}O isotope in the hypochlorous acid molecule indicates cleavage of the $Cl-ONO_2$ bond in the chlorine nitrate molecule upon hydrolysis. The positively charged chlorine atom (+0.08) in the $ClONO_2$ molecule appears to be more accessible to the attacking oxygen atom of the water molecule (−0.36) than the positively charged N atom (+1.34) shielded by oxygen atoms.[106]

One would assume that nucleophilic attack of the water molecule results in a reactive intermediate, H_2OCl^+, which can be rapidly hydrolysed in a sufficient amount of water.[89, 97, 106]

$$H_2O + ClONO_2 \longrightarrow H_2OCl^+ + ONO_2^-,$$

$$H_2O + H_2OCl^+ \longrightarrow H_3O^+ + HOCl.$$

However, another mechanism of hydrolysis was found to be preferred.

$$ClONO_2 + 3H_2O \longrightarrow HOCl\cdot NO_3^-\cdot H_3O^+\cdot H_2O.$$

This mechanism is 10 to 14 kcal mol^{-1} more energetically favourable.[107, 111] An IR spectroscopic study of the products of hydrolysis of $ClONO_2$ also gave no proofs of the formation of H_2OCl^+ ion (see Ref. 111). Hydrolysis of $ClONO_2$ on ice proceeds efficiently at 75–140 K.[105] At temperatures below 155 K, hypochlorous acid thus obtained is adsorbed on the surface of ice and then goes to the gas phase at 155–185 K.[104, 108] The measured enthalpy of adsorption of HOCl on ice is -8.5 ± 2 kcal mol^{-1}, which is close to the published experimental and calculated values (see Ref. 69). The HOCl molecule forms a hydrogen bond with the water molecule, thus acting as a proton donor.[103, 113]

Hypochlorous acid is also formed in the reaction of hydroxyl radicals with chlorine or dichlorine monoxide.

$$^{\bullet}OH + Cl_2 \xrightarrow{a} HOCl + Cl^{\bullet}$$
$$^{\bullet}OH + Cl_2 \xrightarrow{b} HCl + ClO^{\bullet}$$

$$^{\bullet}OH + Cl_2O \longrightarrow HOCl + ClO^{\bullet}. \quad (5)$$

The reaction with chlorine almost exclusively follows route *a*.[114] The rate constant for the reaction is 6.70×10^{-14} cm^3 $molecule^{-1}$ s^{-1} at 298 K (according to Ref. 114) and $(6.8 \pm 1.0) \times 10^{-14}$ cm^3 $molecule^{-1}$ s^{-1} at 293 K (according to Ref. 115).

The rate constant for reaction (5) in the temperature interval 236–383 K is inversely proportional to temperature:[116]

$$k_5 = (1.7 \pm 0.8) \times 10^{-12} \exp\left(\frac{420 \pm 170}{T}\right) \text{cm}^3 \text{ molecule}^{-1} \text{ s}^{-1}.$$

At 298 K and a total pressure of 2 Torr, one has $k_5 = (7.4 \pm 0.6) \times 10^{-12}$ cm^3 $molecule^{-1}$ s^{-1}. Probably, a long-lived cyclic compound HOClOCl is formed as an intermediate product of this reaction.[116]

The reaction of hydroxyl radicals with chlorine dioxide also produces hypochlorous acid.[117]

$$^{\bullet}OH + OClO^{\bullet} \longrightarrow HOCl + O_2.$$

The microwave and IR spectra of HOCl have been the subject of numerous experimental and theoretical studies.[110, 118–137] Table 5 lists the bond lengths and bond angles in the HOCl molecule reported by different authors.

The HOCl molecule is a nearly symmetrical prolate rotor characterised by the parameter $\kappa = -0.998$ (see Ref. 121) and rotational constants (for $HO^{35}Cl$) $A_e = 20.49760$, $B_e = 0.50735$ and $C_e = 0.49509$ cm^{-1} (see Ref. 133). CCSD(T)/TZ2P calculations[93] gave a value of 1.56 D for the dipole moment of the HOCl molecule.

Table 5. Experimental and calculated geometric parameters of the HOCl molecule.

Method	r(O–Cl) /Å	r(O–H) /Å	HOCl angle /deg	Ref.
Microwave spectroscopy	1.693	0.97	103	118
IR spectroscopy	1.6891	0.9643	102.96	126
IR spectroscopy	1.68897	0.96437	102.965	133
DFT/B3LYP/G-311G(3df)	1.700	0.965	103.4	138

Table 6 lists the main vibrational frequencies in the gas-phase high resolution IR spectra of hypochlorous acid.

Numerous studies (see, *e.g.*, Refs 26, 62, 63, 66, 74, 137, 139–146) concern the UV absorption spectrum and photolysis of gaseous HOCl. At room temperature, the absorption spectrum of the HOCl molecule in the region 200–380 nm exhibits two maxima at 242 and 304 nm [absorption cross sections, σ, are $(2.1 \pm 0.3) \times 10^{-19}$ and 0.61×10^{-19} cm^2, respectively].[66] A weak peak was also detected at 380 nm ($\sigma = 4 \times 10^{-21}$ cm^2); the long-wavelength absorption extends to 480 nm ($\sigma = 5.52 \times 10^{-23}$ cm^2).[146]

Table 6. Vibrational frequencies in the IR spectrum of the $HO^{35}Cl$ molecule.

Frequency	Numerical value /cm^{-1}	Assignment	Ref.
ν_1	3609.48013	O–H stretch	120
ν_2	1238.62460	bending vibration	125
ν_3	724.35807	Cl–O stretch	125

Photolysis of HOCl produces mainly $^{\bullet}OH$ and $^{\bullet}Cl$ radicals. Other decomposition channels ($O^{\bullet} + HCl$ or $H^{\bullet} + {}^{\bullet}OCl$) are of little importance or not involved.[140, 141, 144] Photodissociation of HOCl causes destruction of stratospheric ozone

$$HOCl + h\nu \longrightarrow {}^{\bullet}OH(^2\Pi) + Cl^{\bullet}(^2P)$$
$$^{\bullet}OH + O_3 \longrightarrow HO_2^{\bullet} + O_2$$
$$Cl^{\bullet} + O_3 \longrightarrow ClO^{\bullet} + O_2$$
$$HO_2^{\bullet} + ClO^{\bullet} \longrightarrow HOCl + O_2$$

$$2\,O_3 \longrightarrow 3\,O_2$$

The lifetime of hypochlorous acid in the stratosphere under photolysis conditions is at most 30 min.[140, 146] The lifetime of HOCl in the mid-stratosphere (no photolysis) could be as long as ~600 h.[65]

The EI mass spectrum of HOCl exhibits peaks of molecular ions at m/e 52 and 54 (two isotopes, ^{35}Cl and ^{37}Cl).[70] The adiabatic and vertical ionisation energies determined from the HeI photoelectron spectrum of hypochlorous acid are 11.12 ± 0.01 and 11.22 ± 0.01 eV, respectively.[147] A photoionisation mass spectrometric study[148] of HOCl gave an adiabatic ionisation energy of 11.12 ± 0.01 eV, which coincides with the published value.[147] Using this value, Thorn *et al.*[148] calculated the enthalpy of formation of $HOCl^+$ [$\Delta H^\circ_{298}(HOCl^+) = 238.2 \pm 0.9$ kcal mol^{-1}]

and the proton affinity energy of ClO [$PA_{298}(ClO) = 151.8 \pm 0.9$ kcal mol^{-1}].

The enthalpies of formation of HOCl reported in the studies carried out at different times differ only slightly from one another (the ΔH_0° are given in parentheses).

ΔH_{298}(HOCl) /kcal mol^{-1}	−17.9	−18.0	−18.0	−18.4	−19.0	(−16.7)	(−17.2)
Ref.	64	63	65	149	67	150	32

QCISD(T)/6-311 + + G(3df,3pd)//QCISD(T)/6-311G(2d,2p) calculations [151] led to $\Delta H_{298}^\circ(HOCl) = -19.9 \pm 2$ kcal mol^{-1}. The values obtained later on using other computational methods are −18.2 (G2 calculations for 298 K) [30] and −17.5 kcal mol^{-1} [MP4/6-311 + G(d,p)].[138]

An exactly measured bond dissociation energy, $D_0(^{35}Cl-OH)$, is 55.15 kcal mol^{-1} (19290.3 ± 0.6 cm^{-1}).[152, 153] *Ab initio* G2 calculations gave $D_0(HO-Cl) = 55.2$ (see Ref. 30) and 55.25 kcal mol^{-1} (see Ref. 138). The result of density functional calculations [138] [B3LYP/6-31G(d) approximation], 55.24 kcal mol^{-1}, is also close to the experimental data. The H−OCl bond is stronger than the HO−Cl bond; the dissociation energy $D_0(H-OCl)$ is 93.8 kcal mol^{-1} (see Ref. 33) or 92.9 kcal mol^{-1} (see Ref. 154).

According to calculations, the HOCl isomer is 51.6 ± 1.2 kcal mol^{-1} (0 K) more stable than the HClO isomer.[155] The electron affinity energy of the HOCl molecule is low, namely, 0.27 eV (6.23 kcal mol^{-1}).[70] Protonation of HOCl at the oxygen atom ($HOCl + H^+ \longrightarrow H_2OCl^+$) is energetically more favourable compared to protonation at the chlorine atom ($HOCl + H^+ \longrightarrow HOClH^+$). The G2 calculated proton affinity energy is 153.4 kcal mol^{-1} in the former and 139 kcal mol^{-1} in the latter case (298 K).[30] The corresponding values obtained from density functional (PW91) calculations are 157.7 (298 K) and 140.1 kcal mol^{-1} (0 K).[39] Yet another computational study [156] also revealed that protonation at the oxygen atom is 16.2 kcal mol^{-1} energetically more preferable. The geometric parameters of the H_2OCl^+ ion calculated [110] at the B3LYP/6-311 + + G(d,p) level are as follows: $r(O-Cl) = 1.772$ Å, $r(O-H) = 0.984$ Å, the H−O−H angle is 123.9° and the H−O−Cl angle is 111.0°. The O−Cl bond length was also estimated at 1.78 Å.[157]

The reaction of hypochlorous acid with hydrogen chloride proceeding on the surface of ice or in sulfate aerosols can be a source of active chlorine in the stratosphere.[68, 71–73, 94, 96, 108, 158]

$$HOCl + HCl \longrightarrow Cl_2 + H_2O.$$

It is assumed [73] that protonation of HOCl is followed by the reaction of H_2OCl^+ ion with Cl^- producing Cl_2 and H_2O. Besides, HOCl can participate in the formation of active bromine monochloride following the reaction

$$HOCl + HBr \longrightarrow BrCl + H_2O.$$

Table 7. Rate constants for reactions involving HOCl (298 K).

Reaction	k /cm^3 molecule^{-1} s^{-1}	Ref.
HOCl + NO → products	1.0×10^{-17} (see [a])	159
HOCl + O_3 → products	4.0×10^{-16} (see [a])	159
HOCl + OH → H_2O + ClO	$(1.7-9.5) \times 10^{-13}$	160
HOCl + H → products	$(5.0 \pm 1.4) \times 10^{-12}$	160
HOCl + H → products	$(3.5 \pm 0.7) \times 10^{-12}$	67
HOCl + H → HCl + OH	$(6.7 \pm 2.1) \times 10^{-13}$ (see [a])	67
HOCl + Cl → products	$(1.4 \pm 0.37) \times 10^{-12}$	67
HOCl + Cl → Cl_2 + OH	$(3.4 \pm 1.5) \times 10^{-13}$	67
HOCl + F → products	$(4.9 \pm 0.6) \times 10^{-11}$	67
HOCl + F → ClF + OH	$(1.2 \pm 0.4) \times 10^{-11}$	67

[a] Given is the upper bound.

However, this reaction is of little importance because the concentration of hydrogen bromide in the atmosphere is at most 2 ppt (1 ppt = 10^{-12}).[69]

Table 7 lists the rate constants for some reactions involving HOCl calculated using the microwave discharge technique and mass spectrometry.

IV. Hypobromous acid

The first syntheses of solutions of hypobromous acid date back to the 1860s (cited according to Refs 161 and 162). Aqueous HOBr solutions are prepared by slowly adding liquid bromine to an aqueous solution of silver nitrate at room temperature.[161, 162] Subsequent vacuum distillation gives solutions with HOBr concentrations of about 0.2 mol litre^{-1}. Hypobromous acid is also formed in the reaction of bromine with an aqueous suspension of yellow mercury oxide (for hydrolysis of bromine, see Ref. 163). The reaction is conducted by passing water vapour and bromine through a column filled with mercury oxide supported by glass beads.[164, 165] Yet another procedure for the synthesis of hypobromous acid involves prolonged stirring of bromine in excess of water in the presence of Ag_2O powder.[33] The reaction was reported to proceed better in the presence of Ag_2O rather than mercury oxide.[33] A solution of HOBr was also prepared by the reaction of bromine with a 0.5 N solution of sulfuric acid in the presence of silver sulfate.[166]

By analogy with HOCl, hypobromous acid can be synthesised in the reaction of Br_2O with water.

$$Br_2O + H_2O \rightleftharpoons 2\,HOBr. \qquad (6, -6)$$

However, unlike a rather stable (at room temperature) Cl_2O, dibromine monoxide is stable only at temperatures below 233 K. It is produced by the reaction

$$2\,Br_2 + HgO \longrightarrow Br_2O + HgBr_2,$$

the yield of Br_2O being at most 1%–2%.[167, 168]

The rate constant for the reaction (6, −6) at 298 K is 0.02 (see Ref. 167) or 0.037 ± 0.004 (see Ref. 168).

HOBr for spectroscopic studies is obtained by fast exothermic reaction of $^\bullet$OH radicals with molecular bromine.

$$^\bullet OH + Br_2 \longrightarrow HOBr + Br^\bullet, \qquad (7)$$

The rate constant for reaction (7) is $k_7 = (4.2 \pm 0.7) \times 10^{-11}$ cm^3 molecule^{-1} s^{-1} at 298 K (see Ref. 169). In the temperature range 262–303 K, reaction (7) proceeds barrierlessly or has a very low activation barrier (~1 kcal mol^{-1}).[115] A study of the UV absorption spectrum of gaseous HOBr revealed [170] that at room temperature more than 97% of the total amount of the $^\bullet$OH radicals generated by photolysis of H_2O_2 are consumed following route (7) and less than 3% of these radicals are consumed in the reaction

$$^\bullet OH + H_2O_2 \longrightarrow HO_2^\bullet + H_2O.$$

Similarly to the reaction $HO_2^\bullet + ClO^\bullet$, the radical–radical reaction $HO_2^\bullet + BrO^\bullet$ [reaction (8)] producing hypobromous acid should be taken into account in simulation of atmospheric processes resulting in the destruction of stratospheric ozone.

$$HO_2^\bullet + BrO^\bullet \longrightarrow HOBr + O_2 \qquad (8a)$$

$$HOBr + h\nu \longrightarrow Br^\bullet + {}^\bullet OH$$

$$Br^\bullet + O_3 \longrightarrow BrO^\bullet + O_2$$

$$^\bullet OH + O_3 \longrightarrow HO_2^\bullet + O_2$$

$$2\,O_3 \longrightarrow 3\,O_2$$

Reaction (8) mainly follows route (*a*), the contribution of reaction (8*b*)

$$HO_2^\bullet + BrO^\bullet \longrightarrow HBr + O_3 \qquad (8b)$$

is insignificant, namely, the rate constant ratio $k_{8b}:k_{8a}$ is at most 0.015 (at 233–298 K, according to Ref. 171) or 0.004 (at 298 K, according to Ref. 172). Different sources estimate the activation energy for reaction (8) at about -1 kcal mol^{-1}; however, the rate constants for this reaction obtained by different authors at 298 K are somewhat different, lying in the range $(1.4-3.4)\times10^{-11}$ cm^3 molecule^{-1} s^{-1} (see Ref. 173).

$k_8\times10^{11}$ /cm^3 molecule^{-1} s^{-1}	3.4 ± 1.0	3.3 ± 0.5	1.4 ± 0.3	2.0 ± 0.6	3.1 ± 0.8
Ref.	174	171	175	173	172

HOBr can be formed in the troposphere and in the lower stratosphere as a result of heterogeneous hydrolysis of bromine nitrate on sulfate aerosol particles and on polar stratospheric clouds.[176, 177]

$$BrONO_2 + H_2O \longrightarrow HOBr + HNO_3.$$

Hydrolysis of $BrONO_2$ in the dark causes accumulation of HOBr but in sunlight HOBr is rapidly photolysed; as a consequence, the lifetime of HOBr is $\sim$15 min in the lower stratosphere and a few seconds in the upper stratosphere.[177] Hydrolysis of $BrONO_2$ on ice produces Br_2O as the secondary product.[162, 178]

$$BrONO_2 + HOBr \longrightarrow Br_2O + HNO_3.$$

The HOBr molecule is a nearly symmetrical prolate rotor characterised by the parameter $\kappa = -0.99936$. The dipole moment of the HOBr molecule is 1.384 D.[179]

The geometric parameters extracted from the pure rotation spectrum of HOBr are as follows:[179] $r(O-Br) = 1.834$ Å, $r(O-H) = 0.961$ Å and the H–O–Br angle is 102.3°. The rotational constants (for HO^{79}Br) are as follows: $A = 613\,677.34$, $B = 10\,576.60290$ and $C = 10\,383.05728$ MHz.

The frequencies in the IR spectrum of the HOBr molecule are listed in Table 8.[180, 181]

Table 8. Vibrational frequencies in the IR spectrum of the HOBr molecule.

Frequency	Numerical value /cm^{-1}	Assignment	Ref.
ν_1	3614.903	O–H stretch	180
ν_2	1162.570	bending vibration	181
ν_3	620.18	O–Br stretch	181

The absorption spectrum of gaseous HOBr in the region 200–420 nm was first studied by Orlando and Burkholder[167] who reported two structureless bands with maxima at nearly 280 nm [absorption cross section, σ, is $(3.1\pm0.4)\times10^{-19}$ cm^2] and at nearly 350 nm [$\sigma = (6.1\pm1.0)\times10^{-20}$ cm^2]. Later on, the third band at about 440 nm ($\sigma\approx9\times10^{-21}$ cm^2) was detected.[164] *Ab initio* calculations[182] substantiated the possibility for HOBr to absorb in the visible region with a maximum at 477 nm. According to another study,[170] at 295 K the spectrum of HOBr exhibits three broad bands with maxima at 284, 351 and 457 nm and the corresponding absorption cross sections σ of $(25.0\pm1.2)\times10^{-20}$, $(12.4\pm0.6)\times10^{-20}$ and $(2.3\pm0.2)\times10^{-20}$ cm^2. The absorption of HOBr in the long-wavelength region must have a strong effect on the rate of photolysis of the acid.[183] Laser photolysis of HOBr at 363 nm produces Br($^2P_{3/2}$) atoms with a quantum yield greater than 0.95.[161] No HBr was found among the products of photolysis.

The adiabatic ionisation energy of HOBr is 10.62 ± 0.04 (according to Ref. 184), 10.638 ± 0.03 eV (photoionisation mass spectrometry data[33]) and 10.642 ± 0.005 eV (photoelectron spectroscopy data[185]). G2 calculations[186] gave nearly the same ionisation energy, *viz*., 10.65 eV.

Earlier, the enthalpy of formation of HOBr was estimated at -19 ± 2 kcal mol^{-1}. However, this value appeared to be strongly overestimated compared to the results obtained more recently. In particular, a new value of the enthalpy of formation of HOBr reported in an experimental study[184] is $\Delta H^\circ_{298} = -9$ kcal mol^{-1} while the results of study[33] are $\Delta H^\circ_0 \geqslant -10.93\pm0.42$ and $\Delta H^\circ_{298} \geqslant -13.43\pm0.42$ kcal mol^{-1}. The ΔH°_{298} values determined in spectroscopic investigations are -11 (see Ref. 167) and -14.3 ± 0.9 kcal mol^{-1} (see Ref. 187). G2 calculations gave $\Delta H^\circ_{300} = -14.2\pm1.6$ (see Ref. 188) and $\Delta H^\circ_{298} = -13.9$ kcal mol^{-1} (see Ref. 30). More recent density functional calculations[138] at the B3LYP/6-311G(3df,3pd) level led to $\Delta H^\circ_{298} = -14.8$ kcal mol^{-1}. Two recommended[154] values of the enthalpy of formation of HOBr are -11.9 ± 0.3 (0 K) and -14.5 ± 0.3 kcal mol^{-1} (298 K).

The HOBr isomer is more stable than the 'hypervalent' isomer HBrO (the enthalpy of HOBr → HBrO conversion calculated for 0 K is 56.3 kcal mol^{-1}).[189]

The bond dissociation energies in the hypobromous acid molecule are $D_0(HO-Br) = 48.45\pm0.42$ kcal mol^{-1} and $D_0(H-OBr) = 94.2$ kcal mol^{-1}.[33] G2 calculations gave the following results: $D_0(HO-Br) = 48.8$ (see Ref. 30) and 49.5 kcal mol^{-1} (see Ref. 154) and $D_0(H-OBr) = 95.5$ kcal mol^{-1} (see Ref. 154).

The proton affinity energy of HOBr in the case of protonation at the oxygen atom

$$HOBr + H^+ \longrightarrow H_2OBr^+$$

is estimated at 162.0 (298 K)[30] or 161.5 kcal mol^{-1} (see Ref. 190).

Decomposition channels of hypobromous acid in the atmosphere involve photolysis and the interaction with ground-state elemental oxygen O(^{3}P)[191]

$$HOBr + O \longrightarrow BrO^\bullet + {}^\bullet OH. \qquad (9)$$

Tracer (^{18}O isotope) experiments followed by mass spectrometric analysis of reaction products showed that elemental oxygen interacts with the bromine atom of the HOBr molecule (HOBr + ^{18}O ⟶ Br^{18}O$^\bullet$ + $^\bullet$OH).[161] At 298 K, the rate constant for reaction (9) is $(2.5\pm0.4)\times10^{-11}$ cm^3 molecule^{-1} s^{-1}, being nearly 200 times higher than the rate constant for analogous reaction involving HOCl.[191] In the temperature range 233–423 K the rate constant can be calculated by the equation[192]

$$k_9 = (1.4\pm0.5)\times10^{-10}\exp\left(-\frac{430\pm260}{T}\right)\ \text{cm}^3\ \text{molecule}^{-1}\ \text{s}^{-1}.$$

Reactions of HOBr with F(^{2}P) and Cl(^{2}P) atoms proceed even more rapidly. At 298 K, the rate constants for these reactions are $k(F) = (2.0\pm0.7)\times10^{-10}$ and $k(Cl) = (1.1\pm0.7)\times10^{-10}$ cm^3 molecule^{-1} s^{-1} (see Ref. 191).

Gas-phase titration of HOBr with chlorine atoms revealed that the reaction exclusively follows one of the two possible channels, namely, route *a*.[161]

$$HOBr + Cl \xrightarrow{a} BrCl + {}^\bullet OH$$
$$HOBr + Cl \xrightarrow{b} BrO^\bullet + HCl$$

Heterogeneous reactions

$$HOBr + HBr \longrightarrow Br_2 + H_2O,$$
$$HOBr + HCl \longrightarrow BrCl + H_2O$$

can also proceed in the atmosphere on the surface of ice at $T < 228$ K. These reactions produce photochemically active Br_2 and BrCl.[166, 193] The interaction of HOBr with the surface of ice prepared by freezing aqueous NaBr solutions at 233 or 248 K results in the formation of Br_2; if ice contains NaCl, BrCl is formed. In the presence of both NaBr and NaCl, BrCl is the only gaseous product at 233 K but raising the temperature to 248 K causes the formation of Br_2 and BrCl.[194]

V. Hypoiodous acid

The main source of atmospheric iodine is methyl iodide liberated by algae and phytoplankton, but small amounts of ethyl iodide are also present in the atmosphere.[195] Photolysis of iodides produces elemental iodine, which then reacts with ozone

$$I^{\bullet} + O_3 \longrightarrow IO^{\bullet} + O_2.$$

Radical $IO^{\bullet}$ can react with radical $HO_2^{\bullet}$, thus resulting in hypoiodous acid

$$IO^{\bullet} + HO_2^{\bullet} \longrightarrow HOI + O_2. \quad (10)$$

Under photolysis conditions, HOI regenerates the iodine atoms or enters in the reaction with nitrogen oxide, which also leads to regeneration of elemental iodine [196]

$$IO^{\bullet} + NO \longrightarrow I^{\bullet} + NO_2.$$

Hypoiodous acid is the most abundant inorganic compound of iodine in the troposphere at heights below 8 km. It is of great importance for tropospheric chemistry, especially in marine areas.[197] However, the presence of HOI in the stratosphere and its active role in the catalytic cycle of ozone destruction cannot be ruled out.[198]

Unlike HOF, HOCl and HOBr which are produced in the reactions of corresponding halogens with water, large amounts of hypoiodous acid can hardly be obtained by the reaction of iodine with water. It is a common practice to perform *in situ* synthesis of HOI using some other reactions when carrying out spectroscopic studies of the acid.

It was proposed [199] to synthesise hypoiodous acid in the reaction of hydroxyl radicals with iodine (HONO can be used as a source of $^{\bullet}OH$ radicals). The rate constant for the reaction $^{\bullet}OH + I_2$ is $(2.1 \pm 1.0) \times 10^{-10}$ cm^3 molecule^{-1} s^{-1} (294 K).[199] A fast reaction

$$^{\bullet}OH + I_2 \begin{cases} \xrightarrow{a} HOI + I \\ \xrightarrow{b} IO + HI \end{cases}$$

was also proposed as a possible source of HOI.[200] The rate constant for this reaction is 1.6×10^{-10} cm^3 molecule^{-1} s^{-1} (298 K). It should be noted that channel (*b*) plays an insignificant role because $k_b : k_a < 0.01$.[200]

Hypoiodous acid is produced by photolysis (254 nm) of gaseous mixtures $I_2-H_2O_2$, $CH_3I-H_2O_2$ and $CH_2I_2-H_2O_2$.[197] The IR spectra of all these systems exhibit two absorption bands centred at 3620 and 1068 cm^{-1} and assigned to the stretching (O–H) and bending vibrations of the HOI molecule, respectively.[197] Photolysis of H_2O_2 followed by the reaction of $^{\bullet}OH$ radicals with iodine was also used to obtain HOI.[201, 202]

HOI can also be synthesised in the reactions of microwave discharge generated hydroxyl radicals with iodine or CF_3I and in the reactions of C_2H_5I with O(^{3}P).[198] Reactions of O(^{3}P) with two-carbon and longer alkyl iodides, *e.g.*,

$$C_2H_5I + O \longrightarrow HOI + C_2H_4,$$

$$C_3H_7I + O \longrightarrow HOI + C_3H_6,$$

produce excited (vibrationally hot) HOI molecules.[203] A study on the mechanisms of these reactions using ethyl iodide isotopomers CH_3CD_2I and CD_3CH_2I showed that attack of the O(^{3}P) atom on the I atom followed by hydrogen abstraction from the methyl group results in the formation of HOI.[204] The reaction with methyl iodide containing only one carbon atom yields no hypoiodous acid.

Similarly to HOCl and HOBr, hypoiodous acid can be synthesised in the radical–radical reaction (10). The first study on the kinetics of this reaction was reported in 1991.[205] The rate constant, k_{10}, for the reaction was estimated at $(6.4 \pm 0.7) \times 10^{-11}$ cm^3 molecule^{-1} s^{-1} at 298 K. Another k_{10} value available in the literature [206] is $(1.03 \pm 0.13) \times 10^{-10}$ cm^3 molecule^{-1} s^{-1} (298 K). The absence of ozone among the reaction products was demonstrated; this indicates an insignificant contribution of the channel

$$IO^{\bullet} + HO_2^{\bullet} \longrightarrow HI + O_3$$

to the overall reaction.

The temperature dependence of the rate constant for reaction (10) reported for the temperature range $T = 274-373$ K in a recent kinetic study [207] is described by the equation

$$k_{10} = 9.3 \times 10^{-12} \exp\left(\frac{680}{T}\right) \text{ cm}^3 \text{ molecule}^{-1} \text{ s}^{-1}.$$

At 298 K, the k_{10} value is $(9.7 \pm 2.9) \times 10^{-11}$ cm^3 molecule^{-1} s^{-1}. An inversely proportional temperature dependence ($T = 273-353$ K) of the rate constant for reaction (10) was also reported in another study [197]

$$k_{10} = (2.2 \pm 0.6) \times 10^{-11} \exp\left(\frac{400 \pm 80}{T}\right) \text{ cm}^3 \text{ molecule}^{-1} \text{ s}^{-1}.$$

The authors [197] concluded that the $IO^{\bullet}$ and $HO_2^{\bullet}$ radicals react exclusively to produce HOI and O_2.

The lack of simple methods for synthesis of HOI and the instability of the acid (its lifetime in an IR spectroscopic cell is only 1–2 min at room temperature [197]) strongly hamper studies on the structure and chemical properties of this acid.

The HOI molecule is a symmetrical prolate rotor characterised by the rotational constants $A_0 = 20.935$, $B_0 = 0.27894$ and $C_0 = 0.27507$ cm^{-1} and by the parameter $\kappa = -0.9996$.[203] The vibrational frequencies of HOI are $\nu_1 = 3625.84$, $\nu_2 = 1068$ and $\nu_3 = 575$ cm^{-1}.[203] The internuclear distance, r(O–I), is 1.991 Å, the distance r(O–H) is assumed to be 0.9643 Å (by analogy with the corresponding distances in the HOCl and HOBr molecules) and the angle H–O–I is 105.4°. Another set of geometric parameters of the HOI molecule is as follows: r(O–H) ≈ 0.96 Å, r(O–I) ≈ 1.959–1.995 Å and the angle H–O–I is 102.4°.[33] MultiConfiguration Self-Consistent Field (MCSCF) calculations [137] gave r(O–H) = 1.0078 Å, r(O–I) = 2.1044 Å and an H–O–I angle of 103.73°.

The absorption spectrum of gaseous HOI in the region 278–494 nm has been studied at 298 K.[201, 202] The spectrum exhibits two broad bands with absorption maxima at 340.4 and 406.4 nm [absorption cross sections, σ, are $(3.85 \pm 0.4) \times 10^{-19}$ and $(3.30 \pm 0.3) \times 10^{-19}$ cm^{-2}, respectively][201] or at 338.4 and 404.8 nm ($\sigma = 3.99 \times 10^{-19}$ and 2.85×10^{-19} cm^{-2}, see Ref. 202). Compared to HOCl and HOBr, the absorption bands of gaseous HOI are more intense and shifted towards the long-wavelength region.[202] The reaction $O + C_2H_5I$ used as a source of HOI provided evidence for the formation of oxide I_2O that can be a product of the reaction $2HOI \rightarrow I_2O + H_2O$.[202]

Photolysis of HOI (355 nm, 295 K) produces $^{\bullet}OH$ radicals with a quantum yield close to unity.[201] The lifetime of HOI in the troposphere in sunlight was estimated at a few minutes.[201, 202]

The adiabatic ionisation energy of HOI predicted [33] based on the analysis of trends in the changes in the properties of OHal and HOHal (Hal = F, Cl, Br) is the lowest among the HOHal compounds (9.71–9.80 eV). The experimental ionisation energy (9.81 ± 0.02 eV) [198] is close to the predicted [33] value. G2 calculations led to a value of 9.89 eV.[30]

According to an early estimation,[199] the enthalpy of formation of HOI lies in the range from −18.4 to −24.4 kcal mol^{-1} (more recently,[206] the average value, -21.4 ± 3.0 kcal mol^{-1}, was recommended). Revision [33] of these results led to a considerably different enthalpy of formation of HOI lying between −8 and −9 kcal mol^{-1} (*cf.* $\Delta H_0^{\circ} = -10.7$ and $\Delta H_{298}^{\circ} = -11.7$ kcal mol^{-1} obtained from G2 calculations [30]). Yet another pair of recommended enthalpy values is as follows: $\Delta H_0^{\circ} = -13.2$ and $\Delta H_{298}^{\circ} = -14.3$ kcal mol^{-1}.[154]

The calculated bond dissociation energies are D_0(HO–I) = 43–44 and D_0(H–OI) = 94.5–95.2 kcal mol^{-1}.[33] G2 calculations [30] gave a value of

45.3 kcal mol^{-1} for D_0(HO—I). The bond dissociation energies recommended in another study,[154] D_0(HO—I) = 48.2 and D_0(H—OI) = 93.7 kcal mol^{-1}, differ only slightly from those listed above.

* * *

The main goal of the studies on the properties of gaseous hypochlorous, hypobromous and hypoiodous acids is to establish their role in the destruction of stratospheric ozone. Hypofluorous acid, which also belongs to this group of oxy acids of halogens, is of little importance for atmospheric processes; however, this compound is of interest for preparative chemistry.

References

1. I V Nikitin *Usp. Khim.* **71** 99 (2002) [*Russ. Chem. Rev.* **71** 85 (2002)]
2. E H Appelman *Acc. Chem. Res.* **6** 113 (1973)
3. P N Noble, G C Pimentel *Spectrochim. Acta, Part A* **24** 797 (1968)
4. M H Studier, E H Appelman *J. Am. Chem. Soc.* **93** 2349 (1971)
5. R C Thompson, E H Appelman, J C Sullivan *Inorg. Chem.* **16** 2921 (1977)
6. E H Appelman, R C Thompson *J. Am. Chem. Soc.* **106** 4167 (1984)
7. E H Appelman, A W Jache *J. Am. Chem. Soc.* **109** 1754 (1987)
8. T C McInnis, L Andrews *J. Phys. Chem.* **96** 2051 (1992)
9. H Bürger, G Pawelke, A Rahner, E H Appelman, I M Mills *J. Mol. Spectrosc.* **128** 278 (1988)
10. H Kim, E F Pearson, E H Appelman *J. Chem. Phys.* **56** 1 (1972)
11. E F Pearson, H Kim *J. Chem. Phys.* **57** 4230 (1972)
12. H Bürger, G Pawelke, S Sommer, A Rahner, E H Appelman, I M Mills *J. Mol. Spectrosc.* **136** 197 (1989)
13. H Bürger, G Pawelke, A Rahner, E H Appelman, L Halonen *J. Mol. Spectrosc.* **138** 346 (1989)
14. W Poll, G Pawelke, D Mootz, E H Appelman *Angew. Chem., Int. Ed. Engl.* **27** 392 (1988)
15. W Thiel, G Scuseria, H F Schaefer III, W D Allen *J. Chem. Phys.* **89** 4965 (1988)
16. S L Rock, E F Pearson, E H Appelman, C L Norris, W H Flygare *J. Chem. Phys.* **59** 3940 (1973)
17. H Kim, J R Sabin *Chem. Phys. Lett.* **20** 215 (1973)
18. H Kim, E H Appelman *J. Chem. Phys.* **76** 1664 (1982)
19. E H Appelman, W W Wilson *Spectrochim. Acta, Part A* **37** 385 (1981)
20. K O Christe *J. Fluor. Chem.* **35** 621 (1987)
21. E H Appelman, A J Downs, C J Gardner *J. Phys. Chem.* **93** 598 (1989)
22. N J S Peters *J. Phys. Chem. A* **102** 7001 (1998)
23. S Berski, J Lundell, Z Latajka, J Leszczyński *J. Phys. Chem. A* **102** 10768 (1998)
24. E H Appelman, H Kim *J. Chem. Phys.* **57** 3272 (1972)
25. J A Goleb, H H Claassen, M H Studier, E H Appelman *Spectrochim. Acta, Part A* **28** 65 (1972)
26. S Nambu, K Nakata, S Iwata *Chem. Phys.* **135** 75 (1989)
27. J C Hindman, A Svirmickas, E H Appelman *J. Chem. Phys.* **57** 4542 (1972)
28. J Berkowitz, E H Appelman, W A Chupka *J. Chem. Phys.* **58** 1950 (1973)
29. J Berkowitz, J L Dehmer, E H Appelman *Chem. Phys. Lett.* **19** 334 (1973)
30. M N Glukhovtsev, A Pross, L Radom *J. Phys. Chem.* **100** 3498 (1996)
31. L A Curtiss, K Raghavachari, G W Trucks, J A Pople *J. Chem. Phys.* **94** 7221 (1991)
32. J A Pople, L A Curtiss *J. Chem. Phys.* **90** 2833 (1989)
33. B Ruscic, J Berkowitz *J. Chem. Phys.* **101** 7795 (1994)
34. O N Ventura, M Kieninger, R E Cachau *J. Phys. Chem. A* **103** 147 (1999)
35. J A Pople, M Head-Gordon, D J Fox, K Raghavachari, L A Curtiss *J. Chem. Phys.* **90** 5622 (1989)
36. M Alcamí, O Mó, M Yañez, J-L M Abboud, J Elguero *Chem. Phys. Lett.* **172** 471 (1990)
37. A Luna, M Manuel, O Mó, M Yañez *J. Phys. Chem.* **98** 6980 (1994)
38. P Burk, I A Koppel, A Rummel, A Trummal *J. Phys. Chem.* **99** 1432 (1995)
39. T K Ghanty, S K Ghosh *J. Phys. Chem. A* **101** 5022 (1997)
40. R Bonnett, R J Ridge, E H Appelman *J. Chem. Soc., Chem. Commun.* 310 (1978)
41. E H Appelman, R C Thompson, A G Engelkeimer *Inorg. Chem.* **18** 909 (1979)
42. K G Migliorese, E H Appelman, M N Tsangaris *J. Org. Chem.* **44** 1711 (1979)
43. S Rozen, M Brand *Angew. Chem., Int. Ed. Engl.* **25** 554 (1986)
44. S Rozen, M Brand, M Kol *J. Am. Chem. Soc.* **111** 8325 (1989)
45. S Rozen, M Kol *J. Org. Chem.* **55** 5155 (1990)
46. M Kol, S Rozen *J. Chem. Soc., Chem. Commun.* 567 (1991)
47. M H Hung, B E Smart, A E Feiring, S Rozen *J. Org. Chem.* **56** 3187 (1991)
48. S Rozen, M Kol *J. Org. Chem.* **57** 7342 (1992)
49. M -H Hung, S Rozen, A E Feiring, P R Resnick *J. Org. Chem.* **58** 972 (1993)
50. M Kol, S Rozen *J. Org. Chem.* **58** 1593 (1993)
51. S Rozen, A Bar-Haim, E Mishani *J. Org. Chem.* **59** 1208 (1994)
52. S Rozen, Y Bareket *J. Chem. Soc., Chem. Commun.* 1959 (1994)
53. R Beckerbauer, B E Smart, Y Bareket, S Rozen *J. Org. Chem.* **60** 6186 (1995)
54. S Rozen, S Dayan, Y Bareket *J. Org. Chem.* **60** 8267 (1995)
55. S Rozen *Chem. Rev.* **96** 1717 (1996)
56. S Rozen, Y Bareket *J. Org. Chem.* **62** 1457 (1997)
57. S Rozen, Y Bareket, J Blum *Tetrahedron Lett.* **38** 2333 (1997)
58. S Dayan, Y Bareket, S Rozen *Tetrahedron* **55** 3657 (1999)
59. E H Appelman, O Dunkelberg, M Kol *J. Fluorine Chem.* **56** 199 (1992)
60. O Dunkelberg, A Haas, M F Klapdor, D Mootz, W Pool, E H Appelman *Chem. Ber.* **127** 1871 (1994)
61. T X Wang, D W Margerum *Inorg. Chem.* **33** 1050 (1994)
62. L T Molina, M J Molina *J. Phys. Chem.* **82** 2410 (1978)
63. H-D Knauth, H Alberti, H Clausen *J. Phys. Chem.* **83** 1604 (1979)
64. H Niki, P D Maker, C M Savage, L R Breitenbach *Chem. Phys. Lett.* **66** 325 (1979)
65. C A Ennis, J W Birks *J. Phys. Chem.* **89** 186 (1985)
66. J B Burkholder *J. Geophys. Res. D,* **98** 2963 (1993)
67. R Vogt, R N Schindler *Ber. Bunsen-Ges. Phys. Chem.,* **97** 819 (1993)
68. L T Chu, M-T Leu, L F Keyser *J. Phys. Chem.* **97** 12798 (1993)
69. L Chu, L T Chu *J. Phys. Chem. A* **103** 691 (1999)
70. T E Caldwell, K L Foster, T Benter, S Langer, J C Hemminger, B J Finlayson-Pitts *J. Phys. Chem. A* **103** 8231 (1999)
71. D R Hanson, A R Ravishankara *J. Phys. Chem.* **96** 2682 (1992)
72. D R Hanson, E R Lovejoy *J. Phys. Chem.* **100** 6397 (1996)
73. D J Donaldson, A R Ravishankara, D R Hanson *J. Phys. Chem. A* **101** 4717 (1997)
74. E A Mishalanie, C J Rutkowski, R S Hutte, J W Birks *J. Phys. Chem.* **90** 5578 (1986)
75. A M Held, D J Halko, J K Hurst *J. Am. Chem. Soc.* **100** 5732 (1978)
76. D M Storch, C J Dymek, L P Davis *J. Am. Chem. Soc.* **105** 1765 (1983)
77. I M Byteva, V S Chernikov *Zh. Fiz. Khim.* **63** 1208 (1989) [a]
78. D Buttar, D M Hirst *J. Chem. Soc., Faraday Trans.* **90** 1811 (1994)
79. M Finkbeier, J N Crowley, O Horie, R Müller, G K Moortgat, P J Crutzen *J. Phys. Chem.* **99** 16264 (1995)
80. N Kaltsoyannis, D M Rowley *Phys. Chem. Chem. Phys.* **4** 419 (2002)
81. G P Knight, T Beiderhase, F Helleis, G K Moortgat, J N Crowley *J. Phys. Chem. A* **104** 1674 (2000)
82. R M Stimpfle, R A Perry, C J Howard *J. Chem. Phys.* **71** 5183 (1979)
83. J P Burrows, R A Cox *J. Chem. Soc., Faraday Trans. 1* **77** 2465 (1981)
84. M Mozurkewich *J. Phys. Chem.* **90** 2216 (1986)
85. F C Cattell, R A Cox *J. Chem. Soc., Faraday Trans. 2* **82** 1413 (1986)

86. D W Toohey, J G Anderson *J. Phys. Chem.* **93** 1049 (1989)
87. S Solomon, R R Garcia, F S Rowland, D J Wuebbles *Nature* (*London*) **321** 755 (1986)
88. F S Rowland, H Sato, H Khwaja, S M Elliott *J. Phys. Chem.* **90** 1985 (1986)
89. J R Sodeau, A B Horn, S F Banham, T G Koch *J. Phys. Chem.* **99** 6258 (1995)
90. M-T Leu, S B Moore, L F Keyser *J. Phys. Chem.* **95** 7763 (1991)
91. C M Nelson, M Okumura *J. Phys. Chem.* **96** 6112 (1992)
92. J P D Abbatt, M J Molina *J. Phys. Chem.* **96** 7674 (1992)
93. J T Lee, J E Rice *J. Phys. Chem.* **97** 6637 (1993)
94. R Zhang, J T Jayne, M J Molina *J. Phys. Chem.* **98** 867 (1994)
95. J M Van Doren, A A Viggiano, R A Morris *J. Am. Chem. Soc.* **116** 6957 (1994)
96. R Zhang, M-T Leu, L F Keyser *J. Phys. Chem.* **98** 13563 (1994)
97. S F Banham, A B Horn, T G Koch, J R Sodeau *Faraday Discuss.* **100** 321 (1995)
98. D R Hanson *J. Phys. Chem.* **99** 13059 (1995)
99. T Schindler, C Berg, G Niedner-Schattenburg, V E Bondybey *J. Chem. Phys.* **104** 3998 (1996)
100. G N Robinson, D R Worsnop, J T Jayne, C E Kolb, P Davidovits *J. Geophys. Res. D,* **102** 3583 (1997)
101. R Oppliger, A Allanic, M J Rossi *J. Phys. Chem. A* **101** 1903 (1997)
102. L Ying, X Zhao *J. Phys. Chem. A* **101** 6807 (1997)
103. A Robinson Brown, D J Doren *J. Phys. Chem. B* **101** 6308 (1997)
104. S B Barone, M A Zondlo, M A Tolbert *J. Phys. Chem. A* **101** 8643 (1997)
105. B S Berland, M A Tolbert, S M George *J. Phys. Chem. A* **101** 9954 (1997)
106. T G Koch, S F Banham, J R Sodeau, A B Horn, M R S McCoustra, M A Chesters *J. Geophys. Res. D* **102** 1513 (1997)
107. R Bianco, J T Hynes *J. Phys. Chem. A* **102** 309 (1998)
108. A B Horn, J R Sodeau, T B Roddis, N A Williams *J. Phys. Chem. A* **102** 6107 (1998)
109. S C Xu, X S Zhao *J. Phys. Chem. A* **103** 2100 (1999)
110. J P McNamara, I H Hillier *J. Phys. Chem. A* **103** 7310 (1999)
111. R Bianco, W H Thompson, A Morita, J T Hynes *J. Phys. Chem. A* **105** 3132 (2001)
112. J Harnett, S Haq, A Hodson *J. Phys. Chem. A* **106** 9226 (2002)
113. K Johnsson, A Engdahl, P Ouis, B Nelander *J. Phys. Chem.* **96** 5778 (1992)
114. L M Loewenstein, J G Anderson *J. Phys. Chem.* **88** 6277 (1984)
115. R B Boodaghians, I W Hall, R P Wayne *J. Chem. Soc., Faraday Trans. 2* **83** 529 (1987)
116. P S Stevens, J G Anderson *J. Phys. Chem.* **96** 1708 (1992)
117. Z-F Xu, R Zhu, M C Lin *J. Phys. Chem. A* **107** 1040 (2003)
118. D C Lindsey, D G Lister, D J Millen *J. Chem. Soc., Chem. Commun.* 950 (1969)
119. A M Mirri, F Scappini, G Cazzoli *J. Mol. Spectrosc.* **38** 218 (1971)
120. J S Wells, R L Sams, W J Lafferty *J. Mol. Spectrosc.* **77** 349 (1979)
121. R L Sams, W B Olson *J. Mol. Spectrosc.* **84** 113 (1980)
122. H E G Singbeil, W D Anderson, R W Davis, M C L Gerry, E A Cohen, H M Pickett, F J Lovas, R D Suenram *J. Mol. Spectrosc.* **103** 466 (1984)
123. C M Deeley, I M Mills *J. Mol. Spectrosc.* **114** 368 (1985)
124. W D Anderson, M C L Gerry, R W Davis *J. Mol. Spectrosc.* **115** 117 (1986)
125. W J Lafferty, W B Olson *J. Mol. Spectrosc.* **120** 359 (1986)
126. C M Deeley *J. Mol. Spectrosc.* **122** 481 (1987)
127. L Halonen, T-K Ha *J. Chem. Phys.* **88** 3775 (1988)
128. M Carlotti, G Di Lonardo, L Fusina, A Trombetti, B Carli *J. Mol. Spectrosc.* **141** 29 (1990)
129. M-L Junttila, W J Lafferty, J B Burkholder *J. Mol. Spectrosc.* **164** 583 (1994)
130. C Azzolini, F Cavazza, G Grovetti, G Di Lonardo, R Frulla, R Escribano, L Fusina *J. Mol. Spectrosc.* **168** 494 (1994)
131. M Bellini, P De Natale, L Fusina, G Modugno *J. Mol. Spectrosc.* **172** 559 (1995)
132. T S Dibble, J S Francisco *J. Phys. Chem.* **99** 1919 (1995)
133. R M Escribano, G Di Lonardo, L Fusina *Chem. Phys. Lett.* **259** 614 (1996)
134. B Abel, H H Hamann, A A Kachanov, J Troe *J. Chem. Phys.* **104** 3189 (1996)
135. J Koput, K A Peterson *Chem. Phys. Lett.* **283** 139 (1998)
136. S Skokov, K A Peterson, J M Bowman *J. Chem. Phys.* **109** 2662 (1998)
137. B F Minaev *J. Phys. Chem. A* **103** 7294 (1999)
138. B S Jursic *J. Mol. Struct.* (*Teochem*) **467** 173 (1999)
139. M J Molina, T Ishiwata, L T Molina *J. Phys. Chem.* **84** 821 (1980)
140. P J D Butler, L F Phillips *J. Phys. Chem.* **84** 183 (1983)
141. A J Bell, P R Pardon, C G Hickman, J G Frey *J. Chem. Soc., Faraday Trans.* **86** 3831 (1990)
142. S Nanbu, S Iwata *J. Phys. Chem.* **96** 2103 (1992)
143. H Guo *J. Phys. Chem.* **97** 2602 (1993)
144. C G Hickman, N Shaw, M J Crawford, A J Bell, J G Frey *J. Chem. Soc., Faraday Trans.* **89** 1623 (1993)
145. A R Offer, G G Balint-Kurti *J. Chem. Phys.* **101** 10416 (1994)
146. R J Barnes, A Sinha, H A Michelsen *J. Phys. Chem. A* **102** 8855 (1998)
147. D Colbourne, D C Frost, C A McDowell, N P C Westwood *J. Chem. Phys.* **68** 3574 (1978)
148. R P Thorn Jr, L J Stief, S-C Kuo, R B Klemm *J. Phys. Chem. A* **103** 812 (1999)
149. R P Thorn Jr, L J Stief, S-C Kuo, R B Klemm *J. Phys. Chem.* **100** 14178 (1996)
150. R J Barnes, A Sinha *J. Chem. Phys.* **107** 3730 (1997)
151. J S Francisco, S P Sander *J. Chem. Phys.* **99** 6219 (1993)
152. R J Barnes, G Dutton, A Sinha *J. Phys. Chem. A* **101** 8374 (1997)
153. M R Wedlock, R Jost, T R Rizzo *J. Chem. Phys.* **107** 10 344 (1997)
154. P Hassanzadeh, K K Irikura *J. Phys. Chem. A* **101** 1580 (1997)
155. T J Lee *J. Phys. Chem.* **98** 3697 (1994)
156. J S Francisco, S P Sander *J. Chem. Phys.* **102** 9615 (1995)
157. H Egsgaard, L Carlsen *Int. J. Mass Spectrom. Ion Processes* **113** 233 (1992)
158. J P D Abbatt, J B Nowak *J. Phys. Chem. A* **101** 2131 (1997)
159. J-E L Cook, C A Ennis, T J Leck, J W Birks *J. Chem. Phys.* **74** 545 (1981)
160. C A Ennis, J W Birks *J. Phys. Chem.* **92** 1119 (1989)
161. T Benter, C Feldmann, U Kirchner, M Schmidt, S Schmidt, R N Schindler *Ber. Bunsen-Ges. Phys. Chem.,* **99** 1144 (1995)
162. A Allanic, P Oppliger, M J Rossi *J. Geophys. Res. D* **102** 23 529 (1997)
163. R C Beckwith, T X Wang, D W Margerum *Inorg. Chem.* **35** 995 (1996)
164. R J Barnes, M Look, J Coleman, A Sinha *J. Phys. Chem.* **100** 453 (1996)
165. J P D Abbatt, G C G Waschewsky *J. Phys. Chem. A* **102** 3719 (1998)
166. L Chu, L T Chu *J. Phys. Chem. A* **103** 8640 (1999)
167. J J Orlando, J B Burkholder *J. Phys. Chem.* **99** 1143 (1995)
168. O V Rattigan, D J Lary, R L Jones, R A Cox *J. Geophys. Res. D* **101** 23021 (1996)
169. G Poulet, G Laverdet, G Le Bras *Chem. Phys. Lett.* **94** 129 (1983)
170. T Ingham, D Bauer, J Landgraf, J N Crowley *J. Phys. Chem. A* **102** 3293 (1998)
171. M Larichev, F Maguin, G Le Bras, G Poulet *J. Phys. Chem.* **99** 15911 (1995)
172. Y Bedjanian, V Riffault, G Poulet *J. Phys. Chem. A* **105** 3167 (2001)
173. J M Cronkhite, R E Stickel, J M Nicovich, P H Wine *J. Phys. Chem. A* **102** 6651 (1998)
174. I Bridier, B Veyret, R Lesclaux *Chem. Phys. Lett.* **201** 563 (1993)
175. M J Elrod, R F Meads, J B Lipson, J V Seeley, M J Molina *J. Phys. Chem.* **100** 5808 (1996)
176. D J Lary, M P Chipperfield, R Toumi, T Lenton *J. Geophys. Res. D* **101** 1489 (1996)
177. D J Lary *J. Geophys. Res. D* **101** 1505 (1996)

178. A Aguzzi, M J Rossi *J. Phys. Chem. A* **106** 5891 (2002)
179. Y Koga, H Takeo S Kondo, M Sugie, C Matsumura, G A McRae, E A Cohen *J. Mol. Spectrosc.* **138** 467 (1989)
180. E A Cohen, G A McRae, T L Tan, R R Friedl, J W C Johns, M Noël *J. Mol. Spectrosc.* **173** 55 (1995)
181. G A McRae, E A Cohen *J. Mol. Spectrosc.* **139** 369 (1990)
182. J S Francisco, M R Hand, I H Williams *J. Phys. Chem.* **100** 9250 (1996)
183. B F Minaev, H Ågren *J. Mol. Struct.* (*Teochem*) **492** 53 (1999)
184. P S Monks, L J Stief, M Krauss, S C Kuo, R B Klemm *J. Chem. Phys.* **100** 1902 (1994)
185. B Ruscic, J Berkowitz *J. Chem. Phys.* **101** 9215 (1994)
186. L A Curtiss, M P McGrath, J-P Blaudeau, N E Davis, R C Binning Jr , L Radom *J. Chem. Phys.* **103** 6104 (1995)
187. M Lock, R J Barnes, A Sinha *J. Phys. Chem.* **100** 7972 (1996)
188. M P McGrath, F S Rowland *J. Phys. Chem.* **98** 4773 (1994)
189. T J Lee *J. Phys. Chem.* **99** 15 074 (1995)
190. T J Lee, J S Francisco *Chem. Phys. Lett.* **251** 400 (1996)
191. P S Monks, F L Nesbitt, M Scalon, L J Stief *J. Phys. Chem.* **97** 11699 (1993)
192. F L Nesbitt, P S Monks, W A Payne, L J Stief *Geophys. Res. Lett.* **22** 827 (1995)
193. J P D Abbatt *Geophys. Res. Lett.* **21** 665 (1994)
194. A K Huff, J P D Abbatt *J. Phys. Chem. A* **106** 5279 (2002)
195. Y Yokouchi, H Mukai, H Yamamoto, A Otsuki, C Saitoh, Y Nojiri *J. Geophys. Res. D* **102** 8805 (1997)
196. G P Knight, J N Crowley *Phys. Chem. Chem. Phys.* **3** 393 (2001)
197. I Barnes, K H Becker, J Starcke *Chem. Phys. Lett.* **196** 578 (1992)
198. P S Monks, L J Stief, D C Tardy, J F Liebman, Z Zhang, S-C Kuo, R B Klemm *J. Phys. Chem.* **99** 16566 (1995)
199. M E Jenkin, K C Clemitshaw, R A Cox *J. Chem. Soc., Faraday Trans. 2* **80** 1633 (1984)
200. L M Loewenstein, J G Anderson *J. Phys. Chem.* **89** 5371 (1985)
201. D Bauer, T Ingham, S A Carl, G K Moortgat, J N Crowely *J. Phys. Chem. A* **102** 2857 (1998)
202. D M Rowley, J C Mössinger, R A Cox, R L Jones *J. Atmos. Chem.* **34** 137 (1999)
203. J J Klaassen, J Lindner, S R Leone *J. Chem. Phys.* **104** 7403 (1996)
204. R A Loomis, J J Klaassen, J Lindner, P G Christopher, S R Leone *J. Chem. Phys.* **106** 3934 (1997)
205. M E Jenkin, R A Cox, G D Hayman *Chem. Phys. Lett.* **177** 272 (1991)
206. F Maguin, G Laverdet, G Le Bras, G Poulet *J. Phys. Chem.* **96** 1775 (1992)
207. J M Cronkhite, R E Stickel, J M Nicovich, P H Wine *J. Phys. Chem. A* **103** 3228 (1999)

[a] — *Russ. J. Phys. Chem. (Engl. Transl.)*

Russian Chemical Reviews **73** (7) 621 – 636 (2004) © 2004 Russian Academy of Sciences and Turpion Ltd

DOI 10.1070/RC2004v073n07ABEH000813

Synthesis of allylic alcohols from alkenes and their derivatives

A K Banerjee, P S Poon, M S Laya, W J Vera

Contents

I.	Introduction	621
II.	Reagents for epoxide cleavage	621
III.	Reagents for allylic oxidation	628
IV.	Reagents for the reduction of α,β-unsaturated carbonyl compounds	632
V.	Miscellaneous methods	633

Abstract. The reagents used to transform epoxides, alkenes and α,β-unsaturated carbonyl compounds into allylic alcohols are considered. The bibliography includes 127 references.

I. Introduction

The presence of an allyl alcohol fragment in the molecules of organic compounds offers extensive opportunities for further modification for obtaining diverse natural and synthetic physiologically active compounds. Among the numerous existing methods for the synthesis of allyl alcohols, cleavage of α-epoxides, allylic hydroxylation and reduction of α,β-unsaturated carbonyl compounds are used most frequently. This review is devoted to these methods; the information is classified according to the type of reagent used for the transformations. Attention is concentrated on the studies published during the last 10 – 15 years.

II. Reagents for epoxide cleavage

Epoxides are important intermediates in the synthesis of various organic compounds. This is due not only to the ease of their preparation but also to the polarity and strain of the oxirane ring, which makes epoxides highly reactive towards electrophiles, nucleophiles, acids, bases, various reducing agents and some oxidants.

1. Isohypsic cleavage of epoxides to allylic alcohols

This Section covers the reactions of epoxide cleavage that are not accompanied by redox transformations (isohypsic reactions).

One of the most popular methods for the synthesis of allylic alcohols is treatment of epoxides with strong bases, for example, alkali metal amides. The role of the base is to eliminate the proton from the α-position with respect to the oxirane ring (Scheme 1).[1 – 3]

Unfortunately, these reagents are of little utility for the cleavage of epoxides containing additional labile functional groups. A number of reagents found in recent years have markedly extended the scope of application of this strategy.

Scheme 1

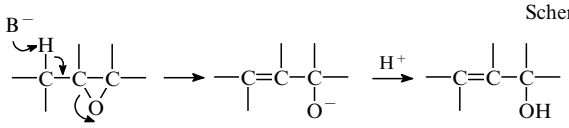

a. Methylmagnesium-*N*-cyclohexyl-*N*-isopropylamide

Falck and co-workers have shown[4] that methylmagnesium-*N*-cyclohexyl-*N*-isopropylamide [MeMgN(cyclo-C_6H_{11})Pr^i, NMA] induces efficient isomerisation of epoxides into allylic alcohols. This reagent is prepared by mixing toluene solutions of methylmagnesium bromide and lithium *N*-cyclohexyl-*N*-isopropylamide.

Examples of effective cleavage of epoxides **1** – **4** on treatment with MeMgN(cyclo-C_6H_{11})Pr^i to give allylic alcohols **5** – **8** are presented below.[4,5]

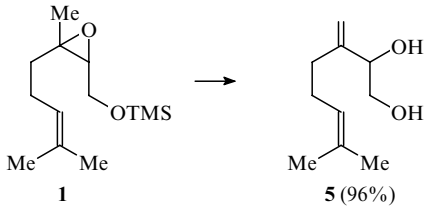

1 **5** (96%)

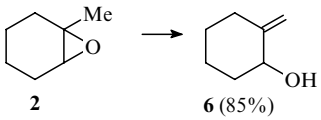

2 **6** (85%)

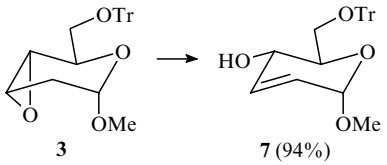

3 **7** (94%)

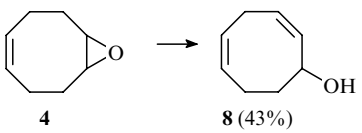

4 **8** (43%)

A K Banerjee, P S Poon, M S Laya, W J Vera Venezuelan Scientific Institute, Centre of Chemistry, Apartado 21827, Caracas 1020-A, Venezuela. Fax (58 -2) 504 13 50. Tel. (58-2) 504 13 24.
E-mail: abanerje@quimica.ivic.ve (A K Banerjee).
Tel. (58 -2) 504 13 29. E-mail: mlaya@quimica.ivic.ve (M S Laya).
Tel. (58-2) 504 13 85. E-mail: wvera@quimica.ivic.ve (W J Vera)

Received 16 June 2003
Uspekhi Khimii **73** (7) 675 – 691 (2004); translated by Z P Bobkova

Presumably, the formation of allylic alcohols from epoxides follows a β-elimination mechanism.[1–3]

Ethylmagnesium- and isopropylmagnesium-*N*-cyclohexyl-*N*-isopropylamides behave in a similar way, whereas the use of phenylmagnesium-*N*-cyclohexyl-*N*-isopropylamide results in low yields of allylic alcohols.

On treatment with NMA, cyclohexene oxide (**9**) and 2-(2-hydroxyethyl)-2-methyloxirane (**10**) are converted into saturated alcohols **11** and **12**.[4] In this case, oxirane is attacked by the methyl anion formed from the reagent.

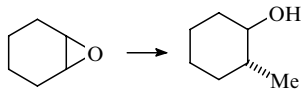

9 **11** (42%)

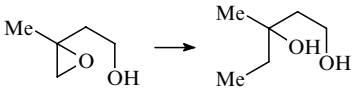

10 **12** (50%)

Smooth opening of the oxirane ring in labile epoxides of the oxylipin series containing carboxy and ester groups has also been effected using NMA.

b. Chiral lithium amides

It has been shown [6,7] that oxides of cyclic and acyclic alkenes can be cleaved under the action of chiral lithium amides **13a**–**h** to give the corresponding optically active alcohols.

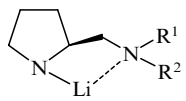

13a–**h**

R^1–R^2 = $(CH_2)_4$ (**a**), $(CH_2)_5$ (**b**), $(CH_2)_2O(CH_2)_2$ (**c**), $(CH_2)_2NMe(CH_2)_2$ (**d**), $R^1 = R^2$ = Et (**e**), Pr^i (**f**), R^1 = Et, $R^2 = Pr^i$ (**g**), R^1 = Bn, $R^2 = (CH_2)_2NBn_2$ (**h**).

For example, protected 3,4-epoxycyclopentanol (**14**) reacts with chiral lithium amides **13a** and **13c** to yield allylic alcohols **15** with a high enantiomeric excess (*ee* 89%–90%).[6]

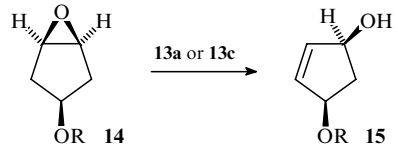

13a or **13c**

OR **14** OR **15**

R = THP (*ee* 90%) (THP is tetrahydropyran-2-yl), Bu^tMe_2Si (*ee* 89%).

Benzene, ether, toluene or THP can be used as solvents in this reaction (THF is the solvent of choice). This method has been used [8] in the synthesis of (−)-untenone A isolated from a sea sponge.

The transformation of epoxycyclohexane (**9**) on treatment with chiral lithium amides (**13a**,**b**,**d**–**h**) has been studied.[7,9] The enantiomeric excess of cyclohex-2-enol (**16**) varied from medium to high (40%–90%). The transformation of epoxycyclohexane was carried out in THF, ether, 1,2-dimethoxyethane (DME) and benzene; the best results were attained in THF.

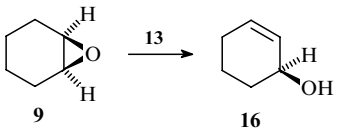

9 **16**

Amide **13**	Yield of **16** (%)	*ee* (%)
a	75–78	82–90
b	71	81
d	67	68
e	69	83
f	75	40
g	75	70
h	75	82

This reaction has also been carried out with symmetrical (*Z*)-4,5-epoxyoctane (**17**), which reacts with chiral lithium amide **13a** being converted into (*E*)-oct-5-en-4-ol (**18**) in 52% yield.[7] The yield of alcohol **18** can be increased to 60% by using additives, 1,5-diazabicyclo[4.3.0]non-5-ene (DBN) or 1,8-diazabicyclo[5.4.0]undec-7-ene (DBU).

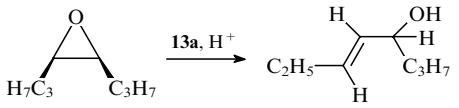

17 **18** (66%, *ee* 60%)

(*Z*)-2,3-Epoxybutane (**19**) and epoxycyclopentane (**20**) behave in a similar way being converted into compounds **21** and **22**.

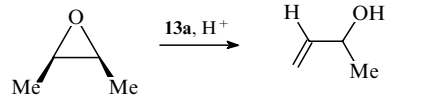

19 **21** (60%, *ee* 72%)

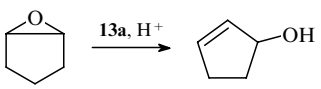

20 **22** (53%, *ee* 41%)

Colman *et al.*[10] used chiral diamines prepared on the basis of (1*R*,2*S*)- and (1*S*,2*S*)-norephedrine for opening of the oxirane ring.

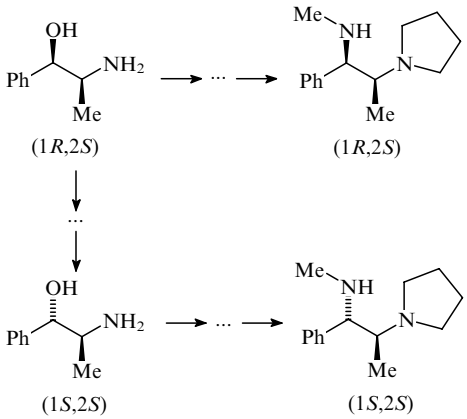

(1*R*,2*S*) (1*R*,2*S*)

(1*S*,2*S*) (1*S*,2*S*)

Opening of the oxirane ring in 4-amino-1,2-epoxycyclopentane under the action of chiral lithium amide obtained from (2*S*,3*aS*,7*aS*)-2-pyrrolidinomethyloctahydroindole has been reported.[11] A (1*S*,4*R*)-4-aminocyclopent-2-enol derivative has been synthesised with an enantiomeric excess of ~90%. O'Brien *et al.*[12] have used (*R*)-*N*-methyl-l-phenyl-2-pyrrolidinoethylamine to cleave the oxirane ring in the substituted epoxycyclopentane

(the enantiomeric excess of the alcohol was 60%). Several more examples of using chiral lithium amides for the synthesis of optically active compounds from prochiral epoxides have been reported.[13]

Using a large number of examples, Andersson and co-workers[14–16] have demonstrated efficient use of catalytic amounts of chiral diamines **23** and their derivatives for enantioselective transformation of *meso*-epoxides of cyclic and alicyclic olefins into optically active allylic alcohols.

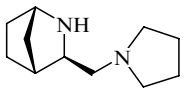

23

The reaction should be carried out in the presence of stoichiometric amounts of lithium diisopropylamide and up to 5 equiv. of DBU. Subsequently, it has been shown that this system of reagents is suitable for kinetic resolution of racemic epoxides (only one enantiomer reacts and, hence, the racemate is resolved).[17]

A recent study[18] describes the synthesis of chiral cyclohex-2-enol (**16**) from *meso*-epoxycyclohexane (**9**) with the use of chiral lithium amide.

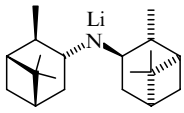

Johansson *et al.*[19] performed cleavage of the oxirane ring in epoxycyclohexane on treatment with chiral lithium amides formed from amines attached to a polymeric support.

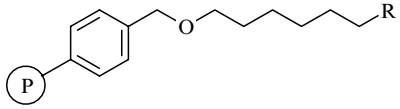

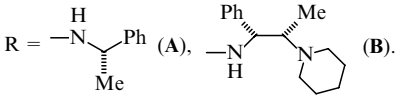

It was shown that immobilisation of ligand **A** on a support results in a markedly higher reaction enantioselectivity: the enantiomeric excess of (*S*)-**16** increases from 19% to 81%. Meanwhile, immobilisation of ligand **B** did not result in a desired increase in the enantioselectivity; conversely, the *ee* value decreased from 93% to 70%.

Thus, the above results demonstrate that chiral lithium amides are valuable reagents for the synthesis of chiral allylic alcohols from *meso*-epoxides of various structures.

c. Organoaluminium amides

The behaviour of organoaluminium amides in the transformation of epoxides into allylic alcohols differs somewhat from the behaviour of lithium dialkylamides. Aluminium derivatives have a relatively low basicity and a higher Lewis acidity; therefore, they are mainly coordinated to the oxygen atom of the epoxide ring. The subsequent proton elimination from the α-position takes place within this complex.[20]

Diethylaluminium 2,2,6,6-tetramethylpiperidide (DATMP) is the most promising reagent. Using this compound, oxiranes **24**–**26** were converted into allylic alcohols **27**–**29** in very high yields.

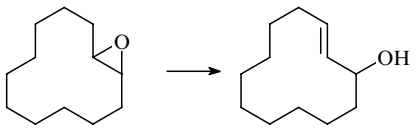

24 **27** (99%)

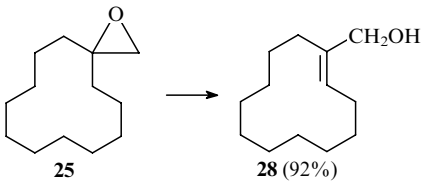

25 **28** (92%)

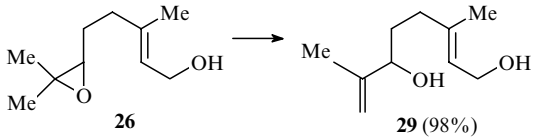

26 **29** (98%)

Benzene and hexane are the solvents of choice for the transformations of oxiranes into allylic alcohols on treatment with organoaluminium amides, because these solvents do not solvate aluminium amides. In ether, these reactions proceed in lower yields, while in THF, they barely take place. Other diethylaluminium amides Et_2AlNR_2 (R = Et, Pr^i, cyclo-C_6H_{11}) can also be used for converting oxiranes into allylic alcohols, but the reaction rates are markedly lower than that in the case of DATMP.

cis-Cyclododecene oxide reacts very slowly with DATMP, the corresponding allylic alcohol being formed in a low yield (~8%). Cycloalkene oxides with 5 to 8 carbon atoms in the ring do not react with DATMP.[20]

The structures of the allylic alcohols formed from oxiranes under the action of DATMP depend on the oxirane stereochemistry. For example, the transformation of *Z*-oxirane **30** gave methylene-type allylic alcohol **31** in 96% yield, while *E*-oxirane **32** was converted into allylic alcohol **33** with an internal double bond (yield 83%).[20]

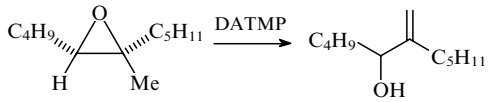

30 **31** (96%)

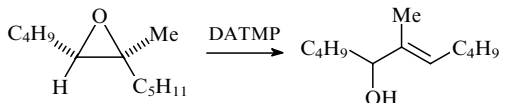

32 **33** (83%)

This reaction pattern is due to the fact that aluminium amides preferentially abstract the α-proton from the alkyl group that is located on the same side of the oxirane molecule as the hydrogen atom, because the aluminium-containing reagent attacks the substrate from the sterically less hindered side of the ring. This gives preferentially the allylic alcohol with the *E*-configured double bond.

d. Trimethylsilyl trifluoromethanesulfonate

Noyori and co-workers[21] have proposed the trimethylsilyl triflate (TMSOTf)–amine (DBU or lutidine) system for transformation of oxiranes into allylic alcohols. Trimethylsilyl triflate, which is a weak Lewis acid, activates the epoxide fragment; as a result, the amine basicity becomes sufficient for eliminating the hydrogen atom from the α-position relative to the oxirane ring. The reaction is carried out in benzene or toluene. The target allylic alcohols are formed initially as trimethylsilyl ethers. The trimethylsilyl group is removed by treatment with dilute hydrochloric acid or potassium fluoride in methanol. For example, oxiranes **34**–**38** were converted into allylic alcohols **39**–**43**.

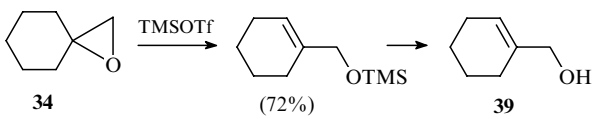

34 (72%) **39**

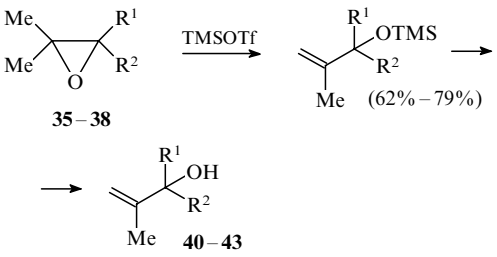

35 – 38 **40 – 43** (62% – 79%)

$R^1 = R^2 = H$ (**35**, **40**), Me (**36**, **41**); $R^1 = H$: $R^2 = CH(Me)CH_2C(O)Me$ (**37**, **42**), $(CH_2)_2CH(Me)CH_2CO_2Me$ (**38**, **43**).

The method has some limitations, in particular, it is inapplicable to the synthesis of allylic alcohols from mono- and 2,3-dialkyl-substituted oxiranes.

e. Trialkylsilyl iodides

The transformation of epoxides **44** – **47** into allylic alcohols **48** – **51** under the action of iodotrimethylsilane and 1,5-diazabicyclo[4.3.0]non-5-ene has been reported.[22]

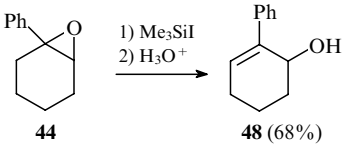

44 **48** (68%)

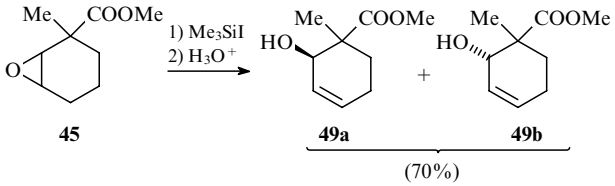

45 **49a** **49b** (70%)

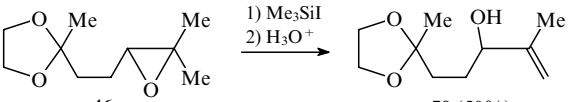

46 **50** (50%)

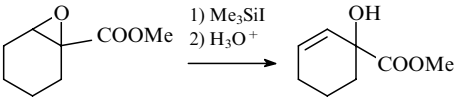

47 **51**

Allylic alcohols **48** – **50** were prepared in satisfactory yields (alcohol **51**, in a low yield). Triethylamine and diisopropylethylamine proved to be much less effective dehydrohalogenating agents than DBN. The reactions were carried out in acetonitrile. The initial ring opening in the epoxide rapidly occurs at room temperature, but dehydrohalogenation of the intermediate iodohydrin is completed only after heating the reaction mixture to the boiling point of the solvent. It is noteworthy that the ester and the ketal functional groups remain intact during the reaction, although they are known [23] to be reactive towards iodotrimethylsilane. In view of the mild reaction conditions, the ready accessibility of the reagents and the simple workup procedure for the reaction mixture, this method can make a good alternative to the Noyori method described above,[21] although the product yields are somewhat lower in this case, due to the formation of side deoxygenation products.

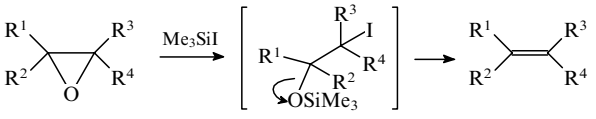

In the case of substituted oxiranes, the formation of deoxygenation products can be avoided by using Bu^tMe_2SiI in place of Me_3SiI;[24] however, this complicates somewhat the cleavage of the silyl ethers. This strategy was used to transform oxiranes **36** and **52** – **54** into the corresponding *tert*-butyl dimethylsilyl ethers in good yields. The protective group was removed by treatment of the ethers with tetraalkylammonium fluoride in moist DMSO or THF, or with potassium fluoride in the presence of catalytic amounts of 18-crown-6 ether; unsaturated alcohols **41** and **55** – **57** were thus liberated.

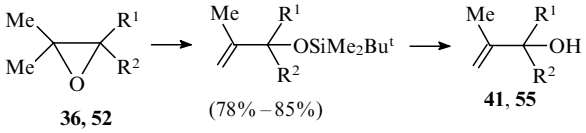

36, 52 (78% – 85%) **41**, **55**

$R^1 = R^2 = Me$ (**36**, **41**); $R^1 = H$, $R^2 = Et$ (**52**, **55**).

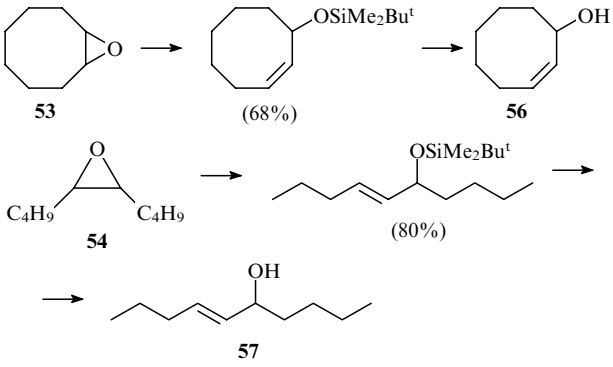

53 (68%) **56**

54 (80%)

57

The mechanism of the reaction of silyl iodides with oxiranes is not entirely clear.[25 – 27] The reaction furnishes a mixture of products of deoxygenation and ring opening (both silylated and non-silylated ones).

f. Selenols

The salts of selenols (usually, areneselenols) generated by various procedures easily cleave the epoxide ring giving rise to β-hydroxy selenides **58**.[28] Treatment of these products with mild oxidants gives selenium oxides **59**, which spontaneously split off ArSeOH with elimination of only the hydrogen atom located on the opposite side of the chain with respect to the oxygen function. This affords allylic alcohols **60**.[28] Most often, the products are formed in good yields.

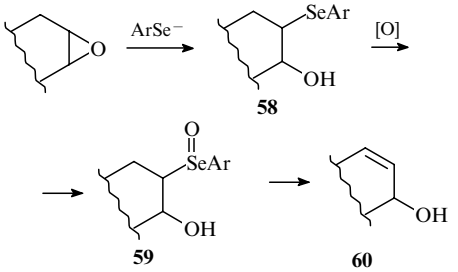

58 **59** **60**

The use of polystyrene-immobilised selenides for opening of the oxirane ring has been documented.[29]

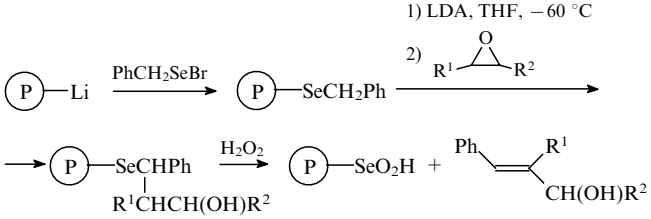

$R^1 = H$: $R^2 = Me$ (85%), Ph (86%), $PhOCH_2$ (84%);
$R^1 – R^2 = (CH_2)_4$ (77%).

g. Dimethylsulfonium methylide

Dimethylsulfonium methylide (DMSM, Corey's reagent) represents a special case among the reagents considered in this Section. This compound reacts with epoxides C_n to give homological allylic alcohols C_{n+1}. Evidently, DMSM serves as the source of an additional carbon atom.[30,31] Since the oxidation state of the starting compound does not change upon the reaction, this reaction should be classified as isohypsic.

Treatment of *cis*-epoxides **61**–**63** with excess DMSM gave allylic alcohols **64**–**66** in very high yields.[32]

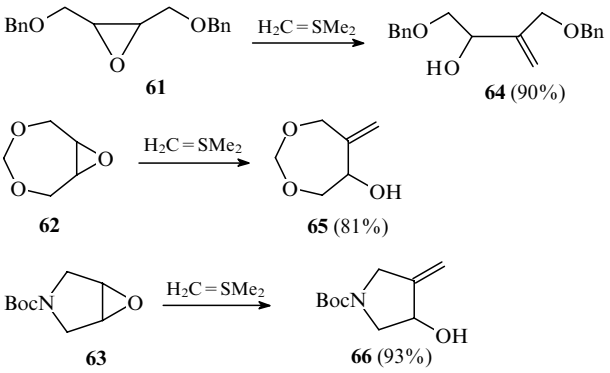

Noteworthy is the high chemoselectivity of this reaction: only the *cis*-isomers are cleaved, whereas the *trans*-isomers remain intact. Thus, the *cis*- and *trans*-isomers of the epoxides can be easily separated in this way. This method is widely used in the synthesis of natural products containing a fragment of 1,2-disubstituted allylic alcohol.

The reaction mechanism has been considered in relation to the cleavage of (*Z*)-2,3-epoxybutane (**19**). The nucleophilic addition of DMSM to epoxide **19** yields betaine intermediate **A**, which undergoes β-elimination of dimethyl sulfide. The elimination may follow either pathway *1* or pathway *2*. Both lead to the same allylic alcohol.

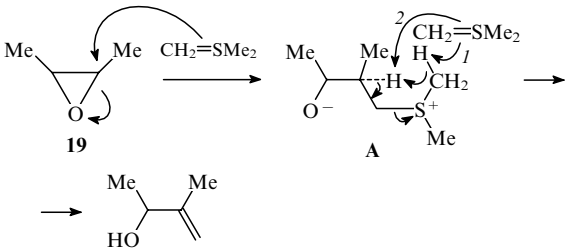

2. Reduction of epoxides, resulting in allylic alcohol

As noted above, oxiranes and allylic alcohols occur in the same oxidation state. Therefore, the reduction reactions considered in this Section are applied to epoxides that contain additional functional groups. The reducing reagents can be subdivided into two groups, *i.e.*, proper reductants and carbanionic synthons.

a. Samarium diiodide

It has been found[33] that treatment of functionalised vinyl-substituted oxiranes **67** with samarium diiodide in THF in the presence of a proton donor induces reductive opening of the oxirane ring, while functional groups such as keto, ester and nitrile groups remain intact. The reaction proceeds at a high rate at −90 °C and is complete, most often, over a period of five minutes.

The reaction mechanism (Scheme 2) includes the formation of radical anion **68**, which adds a proton, being converted into radical **69** containing an ester group. This compound isomerises to a conjugated radical, which produces conjugated dienolate **70** upon the addition of an electron. Regioselective protonation of dienolate **70** furnishes β,γ-unsaturated carbonyl compound **71**.

Scheme 2

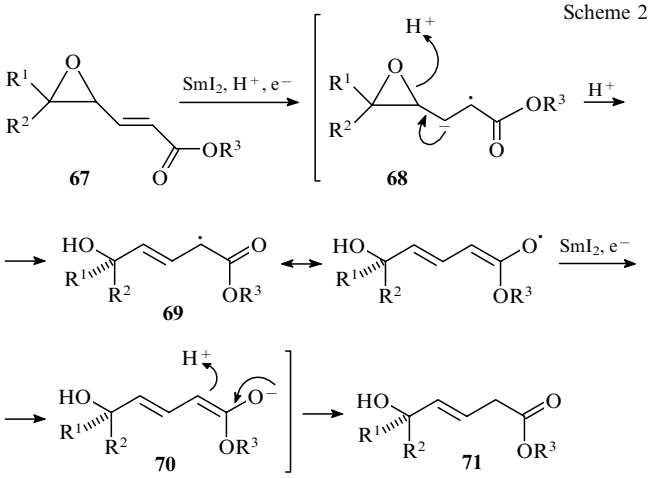

Since the reaction occurs in a nearly neutral medium, no shift of the equilibrium towards the conjugated isomer **70** is observed.

The reactions of epoxides **72**–**75** with samarium diiodide gave allylic alcohols **76**–**79** in very high yields.

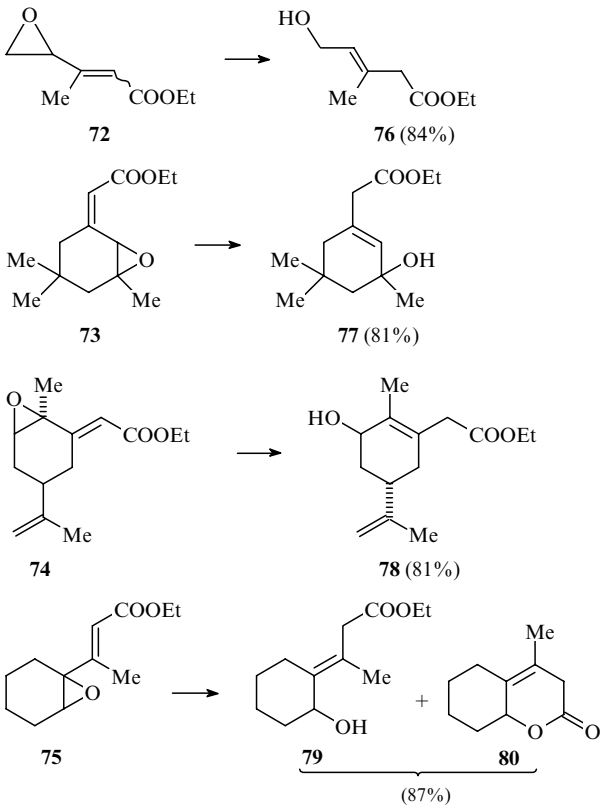

In addition to allylic alcohol **79**, cleavage of epoxide **75** yields lactone **80** (the ratio **79** : **80** = 1 : 1). In the case of epoxide **81**, the formation of 'allylic' lactone **82** becomes the predominant reaction route.

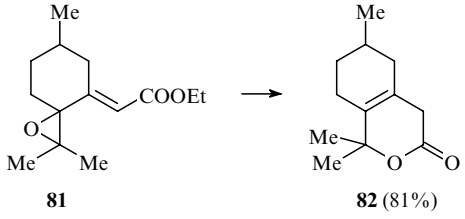

Apart from epoxides with ester groups, unsaturated epoxides with other electron-withdrawing groups can also participate in these reactions. Thus epoxides **83**–**86** were converted into allylic alcohols **87**–**90**.[33]

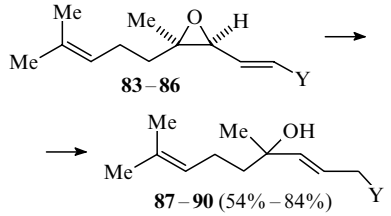

Y = COSEt (**83**, **87**), SO_2Ph (**84**, **88**), SPh (**85**, **89**), $PO(OEt)_2$ (**86**, **90**).

Okamura *et al.*[34] reported the synthesis of allylic alcohols from carvone (**91**) using samarium diiodide. Treatment of epoxy diacetate **92** with two equivalents of samarium diiodide and $Pd(PPh_3)_4$ in the absence of a proton donor yielded allylic alcohol **93**.

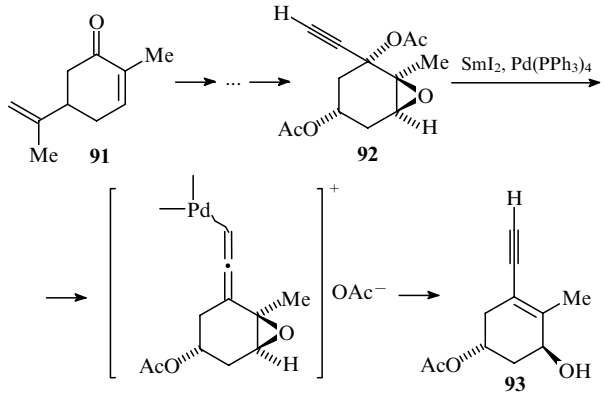

Thus, the reactions of samarium diiodide with epoxides constitute a promising method for the synthesis of diverse functionally substituted allylic alcohols. The use of chiral unsaturated epoxides in this reaction opens up the way to the synthesis of optically active compounds.

b. The reduction of α-haloepoxides catalysed by metal compounds

Epoxy halides **94**–**96** containing halogen atoms in the α-position to the oxirane ring react with sodium iodide and zinc dust in boiling methanol to give allylic alcohols **97**–**99** in high yields.[35] This strategy is used to prepare pure enantiomers by Sharpless asymmetric epoxidation of olefinic precursors.[36]

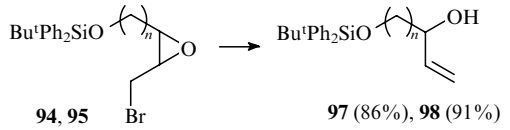

n = 1 (**94**, **97**), 2 (**95**, **98**)

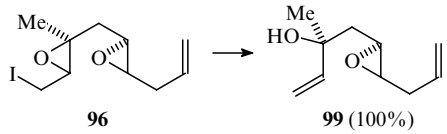

The same results were obtained upon the reduction of α-bromoepoxides **100**–**103** with a zinc/copper couple under sonochemical conditions.[37] The yields of allylic alcohols **104**–**107** were satisfactory. This method is applicable to oxirane ring opening not only in primary but also in secondary epoxy bromides.

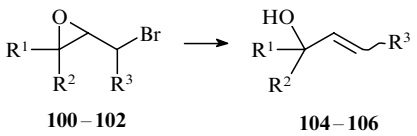

Compound	R^1	R^2	R^3	Yield of alcohol (%)
100, **104**	Alk	Me	H	94
101, **105**	H	Ph	H	95
102, **106**	H	Ph	Me	93

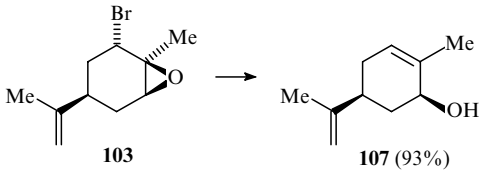

n-Butyllithium can also be used for the reductive cleavage of the oxirane ring in α-haloepoxides. By treatment of α-haloepoxides **103**, **108** and **109** with this reagent, allylic alcohols **107**, **110** and **111**, respectively, have been prepared.[35]

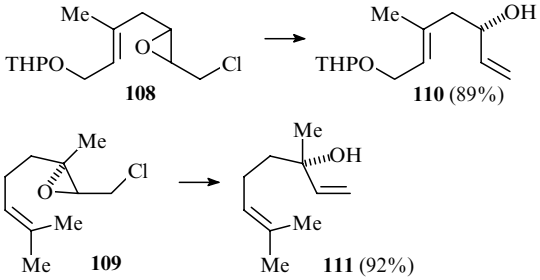

The reactions were carried out at −23 °C. In this case, the organolithium compound functions as a reducing agent rather than a C-nucleophile.

c. Bis(cyclopentadienyl)titanium chloride

It has been found[38] that α-hydroxyepoxides **112**–**115** react with Cp_2TiCl to give allylic alcohols **116**–**119** in good yields. Presumably, the reaction involves the intermediate formation of species **120**–**122** (Scheme 3).

Scheme 3

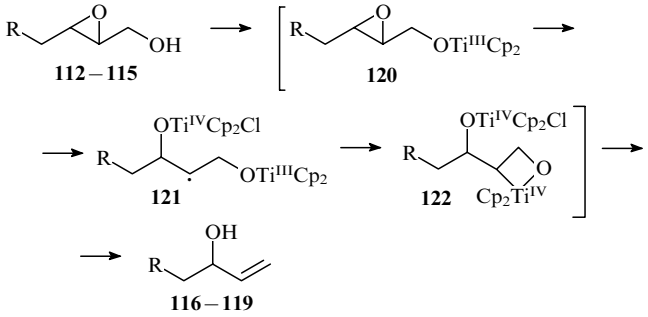

Compound	R	Yield of alcohol (%)
112, **116**	Bu	82
113, **117**	EtCH=CH	85
114, **118**	$CH_2=CH(CH_2)_2$	85
115, **119**	OBn	91

It is significant that the chirality of the starting epoxides at the 3-position is fully retained in allylic alcohols.

The starting optically active 2,3-epoxy alcohols are usually prepared by Sharpless asymmetric epoxidation[36] of isomeric allylic alcohols. Thus, the epoxidation–Cp_2TiCl reduction sequence represents a convenient protocol of an asymmetric

allylic rearrangement, which may yield multipurpose chiral synthons.[39]

The reagent Cp_2TiCl has also been used[40] to reduce vinylic epoxides to allylic alcohols.

d. Alkylmagnesium bromides

The Section deals with epoxide ring opening under the action of reagents serving as sources of additional carbon atoms.

As a further development of the research into alkylation of tosylhydrazones accompanied by elimination,[41] it has been shown[42] that α-epoxyaldehyde tosylhydrazones **123**–**127** can be converted into allylic alcohols **128**–**132** *via* the reaction with alkylmagnesium bromides.

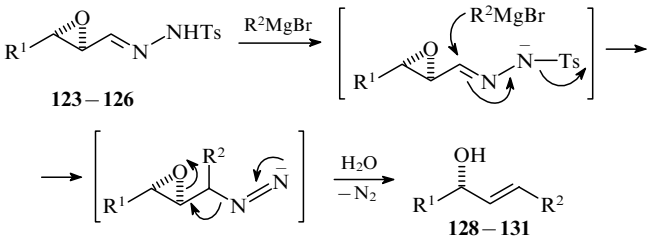

123–**126** **128**–**131**

Epoxide	R^1	R^2	Alcohol	Yield (%)
123	n-C_7H_{15}	Et	**128a**	66
		Bu	**128b**	68
		Ph	**128c**	58
124	OBn	Et	**129a**	64
		Bu	**129b**	65
		Ph	**129c**	70
125	Ph	Et	**130a**	62
		Bu	**130b**	65
126	$CH_2=CH(CH_2)_8$	Et	**131a**	71

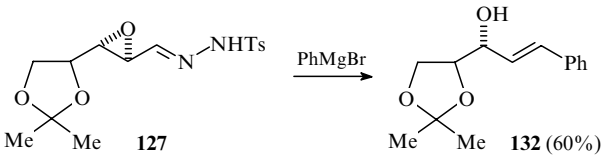

127 **132** (60%)

This reaction is also suitable for the preparation of optically active substances; for this purpose, the starting epoxy aldehydes are prepared by Sharpless asymmetric epoxidation.[43]

e. Organolithium compounds

Treatment of bicyclic α-methoxyepoxides **133**–**136** with various organolithium reagents leads to allylic alcohols **137**–**140**.[44]

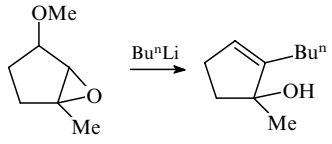

133 **137** (88%)

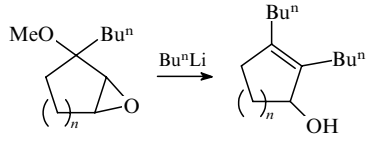

134, **135** **138** (85%), **139** (76%)

n = 1 (**134**, **138**), 2 (**135**, **139**).

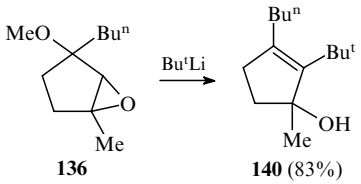

136 **140** (83%)

The reaction includes the formation of a carbene-like intermediate from the metallated oxirane followed by the insertion of alkyllithium and elimination of MeOLi.

Similar reactions involving 3,4-epoxydihydrofurans (**141**) and -pyrans (**142**) and derivative **143** result in diols **144**–**146**, containing an allylic alcohol fragment.[45]

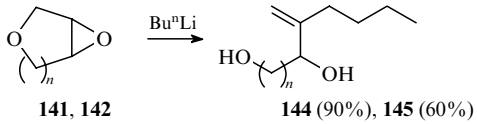

141, **142** **144** (90%), **145** (60%)

n = 1 (**141**, **144**), 2 (**142**, **145**).

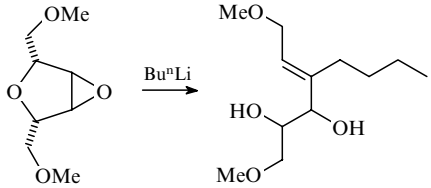

143 **146** (90%)

It is noteworthy that acyclic substrate **147** does not react to give the carbenoid, but is converted instead into the classical β-elimination product **148**.

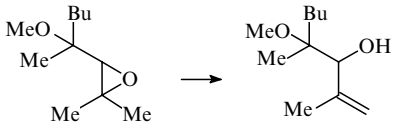

147 **148** (89%)

Hodgson *et al.*[46] reported the synthesis of unsaturated diols and amino alcohols containing an allylic alcohol fragment by cleavage of five- and three-membered heterocycles in the corresponding 3,4-epoxydihydrofurans and -pyrroles upon the reaction with alkyllithium in the presence of chiral diamines (Cat).

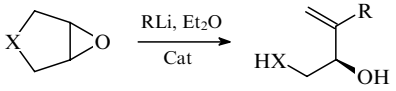

X = O, NSO_2Bu^t; R = Bu^n, Pr^i;

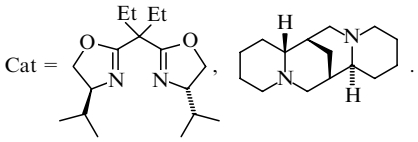

f. Lithium alkylcyanocuprates

Yet another method for the preparation of allylic alcohols is based on the reaction of vinylic epoxides with lithium organocuprates. A review by Marshall[47] contains numerous examples of opening of the oxirane ring in vinyloxiranes by means of these reagents.

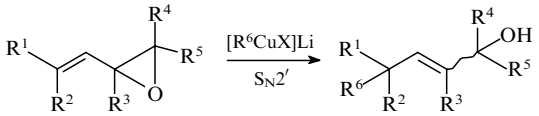

Thus the reaction of epoxycyclohexene **149** with lithium phenylcyanocuprate gives allylic alcohol **150** in a high yield. Alcohol **150** can be converted into the vinylic epoxide **151**, which is made to react with lithium methylcyanocuprate. This sequence of reactions can give allylic alcohol **152**.[48] If lithium methylcyanocuprate is used in the first step instead of phenylcyanocuprate, allylic alcohol **153** containing two methyl groups is formed.

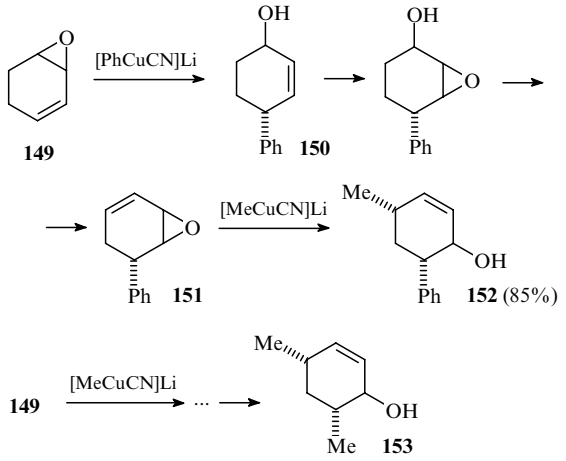

The readily available epoxycyclopentene **154** can also be involved in this reaction; allylic alcohols **155**–**157** were prepared by treatment of **154** with various alkylcyanocuprates.[49]

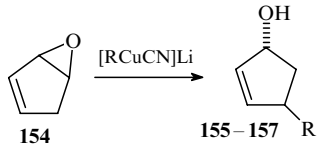

R = Bu^n (**155**, 95%), Bu^t (**156**, 88%), Me (**157**, 78%).

A similar reaction of lithium phenylcyanocuprate with epoxide **154** is non-regioselective and yields a mixture of isomeric phenylcyclopentenols **158** and **159** in 2 : 1 ratio and in an overall yield of 50%.

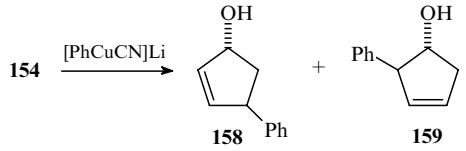

It was found that alkylcyanocuprates obtained from stabilised carbanions react with epoxycyclopentene **154** to give desired allylic alcohols in a low yield (17%). For example, with the use of cyanocuprate [Bu_3SnCH_2CuCN]Li, the yield of the alcohol does not exceed 5%.[48]

g. Synthesis of allylic alcohols from cyclic vinyl carbonates

This route is similar to the above-described method of synthesis of allylic alcohols from vinylic epoxides. Both reactions include a nucleophilic attack by the reagent on the double bond rather than on the centre bearing the leaving group (S_N2' mechanism).[50–52]

It was found[53] that many cyclic carbonates **160**–**163** react with organic cuprates [RCuCN]Li, [RCuCN]MgBr, RMgBr–CuI (Cat) (R = Me, Et, Bu^n) in the presence of $BF_3 \cdot Et_2O$ giving rise to alkylated (*E*)-allylic alcohols **164**–**167** with very high diastereoselectivities.

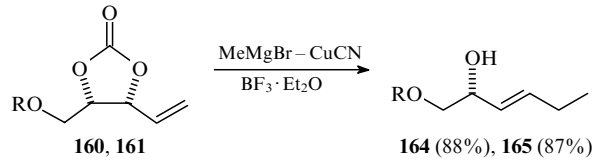

R = Bn (**160**, **164**), Bu^{t}Ph$_2$Si (**161**, **165**).

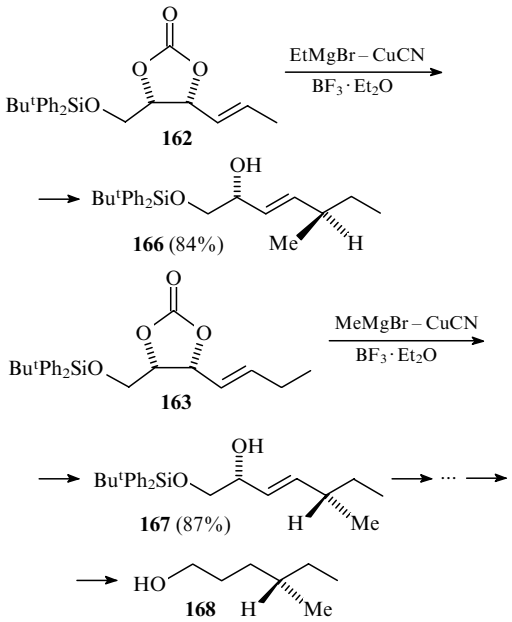

The configuration of the new stereocentre in molecule **167** was confirmed by transforming it into the known (*S*)-(+)-4-methylhexan-1-ol (**168**).[54] Cyclic sulfite **169** reacts with the MeMgBr–CuCN system in the presence of $BF_3 \cdot Et_2O$ in a similar way; the yield of the (*E*)-allylic alcohol **164** is 66%.

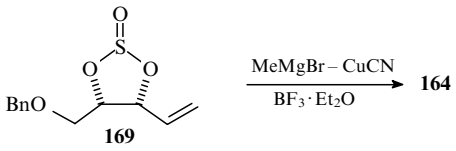

3. Miscellaneous methods for the synthesis of allylic alcohols from epoxides

To complete the Section, it is pertinent to mention some other methods used to prepare allylic alcohols from epoxides. Feringa and co-workers[55] have used the dialkylzinc–copper(II) triflate–chiral phosphoramidite system for oxirane ring opening in epoxides; this gave chiral alcohols. This procedure provided kinetic resolution of vinyloxirane isomers containing six- or seven-membered rings with *ee* values above 90%.[56] More detailed information on this topic is available from a review.[57] A recent publication[58] reports the reaction of phenylsulfonyl-substituted vinyl epoxides with various aromatic molecules (benzene, anisole, pyrrole, thiophene) in the presence of boron trifluoride etherate to give sulfonyl-containing allylic alcohols (Friedel–Crafts reaction).

III. Reagents for allylic oxidation

α-Oxidation of alkenes represents yet another strategy for the preparation of allylic alcohols. Below we consider the reagents used for this purpose.

1. Manganese(III) acetate in acetic acid

Alkenes are oxidised with manganese(III) acetate in acetic acid in the presence of metal halides to give allylic acetates,[59] which are readily transformed into allylic alcohols. For example, cyclopentene and cyclohexene can be converted into cyclopent- and cyclohex-2-enyl 3-acetates (**170**, **171**) in very good yields; hydrolysis of the acetates affords the corresponding alcohols **22** and **16**. Bicyclo[3.2.l]oct-2-ene (**172**) reacts with manganese acetate in a similar way to give acetate **173** in a good yield. Dihydronaphthalenes **174** and **175** were converted into acetates **176** and **177** but

the product yields were low.† Norbornene does not react with Mn(III) acetate. Manganese(III) acetate can be replaced by palladium,[60] thallium(III)[61] and lead[32] acetates.

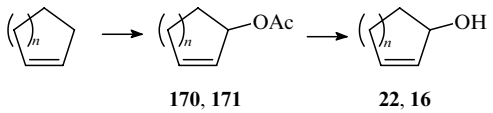

170, **171** **22**, **16**

n = 1 (**170**, **22**), 2 (**171**, **16**).

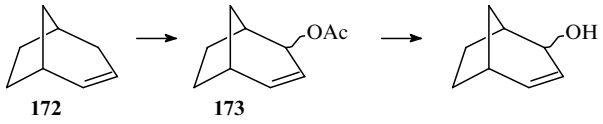

172 **173**

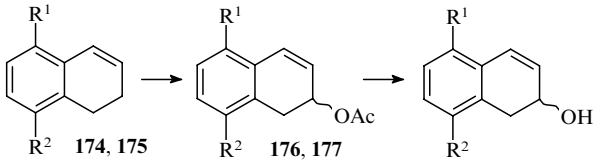

174, **175** **176**, **177**

R^1 = R^2 = Me (**174**, **176**), R^1 = H, R^2 = OMe (**175**, **177**).

It has been suggested that alkene oxidation involves the initial abstraction of a hydrogen atom to give a radical, which is rapidly oxidised to give allylic acetate. It is worth noting that this reaction gives good product yields for simple alkenes, whereas in the case of bicyclic alkenes, the yields of allylic acetates are not satisfactory.

2. Acetoxylation of vinylcycloalkenes in the presence of $PdCl_2$

Wagell and co-workers[62] reported the transformation of 4-vinylcyclohexene (**178**) into allylic acetate **179** upon the reaction with $CuCl_2$ or the $CuCl_2$ – LiCl – O_2 system in the NaOAc – AcOH medium in the presence of palladium chloride as a catalyst and an excess of triphenylphosphine (or bisphosphine $Ph_2PCH_2.CH_2PPh_2$) (Scheme 4). Despite variation of the reaction conditions, the yield of allylic acetate was low.

Scheme 4

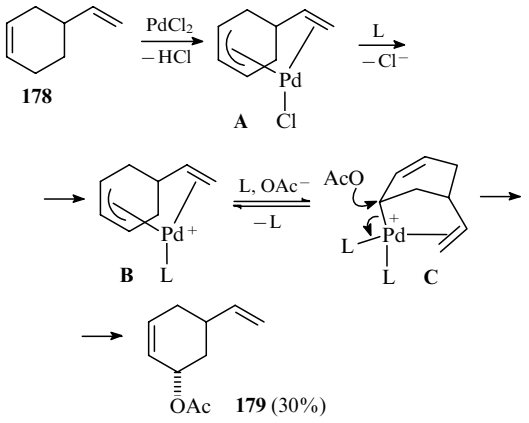

178 **A** **B** **C** **179** (30%)

The formation of compound **179** as the *trans*-isomer and high regioselectivity of the reaction can be explained in terms of the homogeneous catalysis mechanism. The reaction proceeds *via* intermediates **A** – **C**.

A model study has shown that the reaction route is determined by steric and stereoelectronic effects. The reasons for the formation of particularly the *trans*-isomer of compound **179** are related to the fact that triphenylphosphine (L), present in excess, blocks the metal atom in intermediate **C** and, hence, the weaker acetate ligand can approach the substrate only from the 'outside'.[63, 64]

In conformity with the proposed mechanism, the reaction stereochemistry is dictated by the vinyl group in compound **178**, and the phosphine ligand seems to be necessary for stabilisation of intermediate species **B** and **C**.

This reagent was also used to convert limonene (**180**) into allylic acetate **181**.[62]

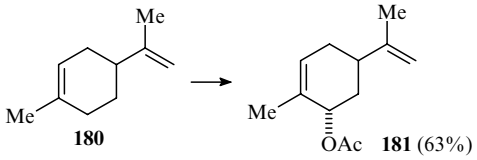

180 **181** (63%)

In this case, in view of the enhanced nucleophilicity of the vinyl group in limonene, acetoxylation can be carried out without a phosphine ligand.

3. Acetoxylation with palladium acetate-containing systems

Allylic acetoxylation of alkenes and cycloalkenes by treatment with palladium acetate in the presence of magnesium dioxide (oxidant) and benzoquinone (co-oxidant) in acetic acid has been reported.[65] This procedure was used to transform cycloalkenes **182** – **185** into the corresponding acetates **186** – **189** (in the case of cyclooctene **183**, the yield of allylic acetate **187** is moderate).

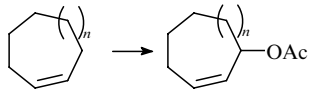

182 – **185** **186** – **189**

n = 1 (**182, 186**, 73%), 2 (**183**, **187**, 35%), 4 (**184**, **188**, 78%), 6 (**185**, **189**, 72%).

Asymmetrical alkenes, for example **190** – **194**, are also converted into the corresponding allylic acetates; the total yields of products are quite high but they are formed as isomer mixtures.

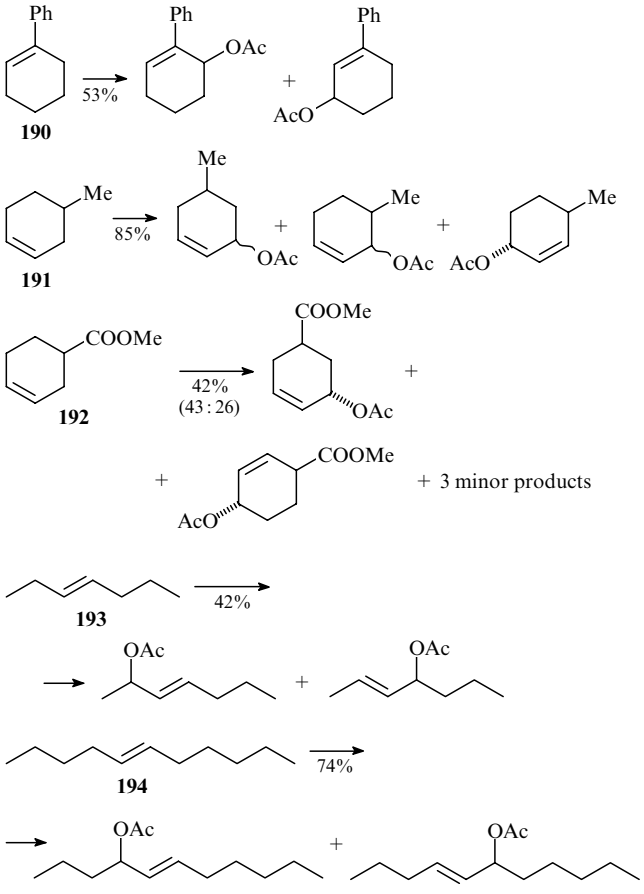

190 **191** **192** **193** **194**

Study of the reaction mechanism has shown that allylic acetoxylation either follows the 1,2-acetoxypalladation mecha-

† A K Banerjee, W J Vera, J A Azocar, unpublished data.

nism with subsequent β-elimination of palladium hydride or involves the formation of an alkene-η^3-allylic complex, which is subjected to a nucleophilic attack by the acetate. The contributions of both mechanisms depend on the alkene structure. For simple alkenes, the η^3-allylic mechanism is relatively unlikely.

Bystroem *et al.*[66] has performed allylic acetoxylation of alkenes by a procedure similar to that described in another study,[65] but using oxygen instead of MnO_2 and hydroquinone instead of benzoquinone. The reaction was carried in the presence of copper(II) acetate. Copper acetate can be replaced by manganese(III) or cobalt(II) acetate, although these are less efficient. Palladium acetate is an obligatory component; otherwise, the target product is not formed. The reaction rate increases with an increase in the amount of hydroquinone and does not change upon the replacement of hydroquinone by benzoquinone (in the latter case, the induction period almost disappears).

Instead of the hydroquinone (or benzoquinone)–copper acetate system, the reaction can be carried out with complex **195**, which contains a hydroquinone fragment.

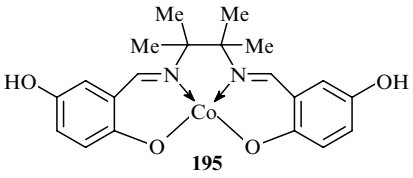

195

Acetoxylation of cyclohexene in the presence of complex **195** furnishes cyclohexenyl acetate **171** in 90% yield. The reaction occurs somewhat more slowly than with the copper acetate–hydroquinone system. The use of complexes **196** and **197** with similar structures affords acetate **171** in 68 and 19% yields, respectively. If the reaction is carried out in the presence of a mixture of compound **197** (5 mol %) and hydroquinone (10 mol %), the yield of product **171** increases to 80%.

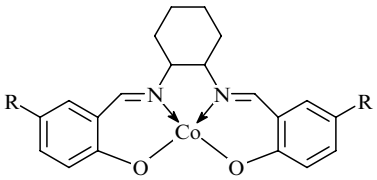

R = OH (**196**), H (**197**).

It is noteworthy that the acetoxylation of cycloalkenes we discuss has not been adequately studied (it has not been tested for all types of alkenes).

The acetoxylation of cyclohexene in the presence of system comprising 5 mol % of palladium acetate, 5 mol % of iron(III) nitrate and acetic acid under an oxygen atmosphere has been reported.[67] Cyclohexenyl acetate was obtained in a high yield (under an argon atmosphere, the acetate is formed in a low yield).[67] The addition of transition metal chlorides or acetates decreases the yield. The introduction of acetic anhydride results in a higher reaction rate. Non-symmetric 1-, 3 and 4-methylcyclohexenes are oxidised by palladium acetate or iron(III) nitrate giving rise to a mixture of isomeric products.

4. *N*-Bromosuccinimide

Brimple *et al.*[68] have developed an efficient method for the introduction of a hydroxyl group into the allylic position of unsaturated spiroketals using *N*-bromosuccinimide. Allylic bromination of unsaturated spiroketals with *N*-bromosuccinimide in tetrachloromethane furnishes bromo-derivatives containing an axial bromine atom. On treatment of these products with KO_2 and 18-crown-6 ether in a THF/DMSO mixture (10 : 1), the Br atom is replaced by an OH group by the S_N2 mechanism to give the alcohol with an equatorial hydroxyl group. This method was used to convert spiroketals **198**–**200** into bromo-derivatives **201**–**205**, which were then transformed into allylic alcohols **206**–**209**. It was found that allylic bromination of spiroketals **199** and **200** gives mixtures of isomeric products and bromide **205** does not enter into the substitution reaction to give the alcohol.

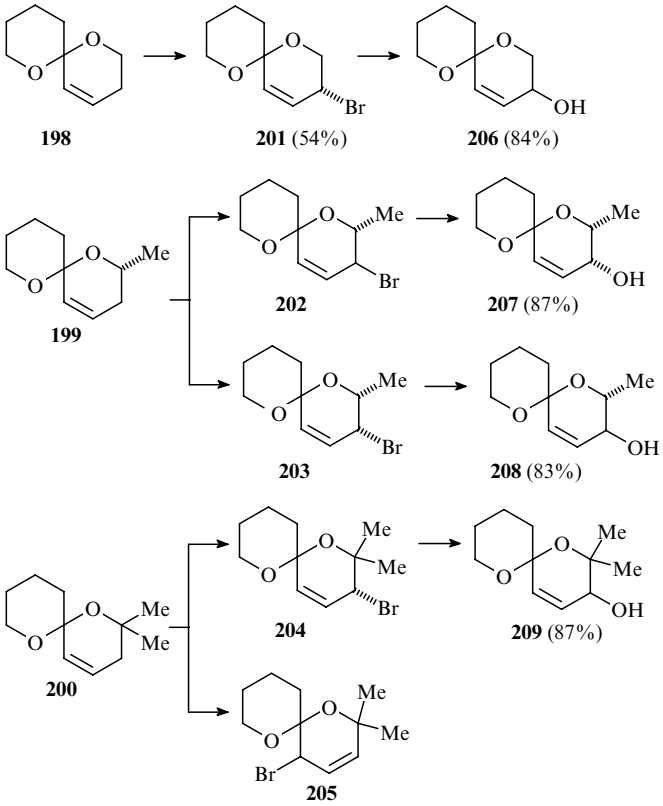

198 **201** (54%) **206** (84%)

199 **202** **207** (87%)

203 **208** (83%)

200 **204** **209** (87%)

205

Bernet *et al.*[69] have oxidised a bicyclic spiroketal at the allylic position by selenium dioxide.

5. *tert*-Butyl peroxybenzoate

Acyloxylation of alkenes with $Bu^tOOC(O)Ph$ or Bu^tOOH and carboxylic acids RCOOH (R = CF_3, CCl_3, Me, Bu^t, *etc.*) in the presence of catalytic amounts of copper compounds and chiral promoters, (*S*)- and (*R*)-prolines, has been reported.[70] This reaction yields optically active esters. For instance, allylic benzoates **210** and **211** have been prepared from cyclopentene and cyclohexene. Cycloalkenes with larger rings have also been introduced in this reaction.

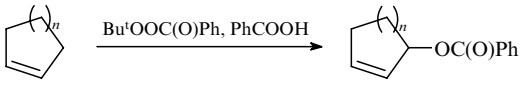

210–**213**

n = 1 (**210**, 39%, *ee* 56%), 2 (**211**, 59%, *ee* 37%), 3 (**212**, 27%, *ee* 23%), 4 (**213**, 32%, *ee* 4%).

Apart from proline (**214**) and its derivatives **215**, amino acids **216**–**218** were also used as chiral promoters, while acetonitrile or benzene were used as solvents.

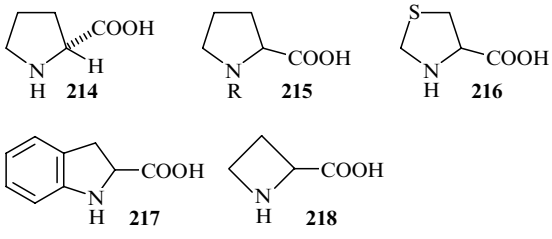

214 **215** **216**

217 **218**

The process enantioselectivity is dictated by the natures of the alkene and the auxiliary chiral reagent and depends little on the nature of the carboxylic acid.

Andrus *et al.*[71] have described allylic acyloxylation of alkenes with *tert*-butyl peroxybenzoate in the presence of catalytic amounts of copper compounds in boiling benzene. Thus cyclic alkenes and oct-1-ene react with $Bu^tOOC(O)Ph$ in the presence of chiral bisoxazoline complexes of copper(I) triflate **219**–**221**

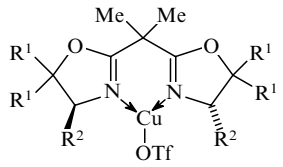

219: $R^1 = H$, $R^2 = Bu^t$;
220: $R^1 = Me$, $R^2 = Bu^t$;
221: $R^1 = Me$, $R^2 = Ph$.

219–**221**

to yield non-racemic allylic benzoates **210**, **211**, **213** and **222**.

In most experiments, acetonitrile served as the solvent, but in some cases (for example, in the synthesis of compound **222**), benzene was used. The reaction mechanism was considered taking oxidation of oct-1-ene as an example.

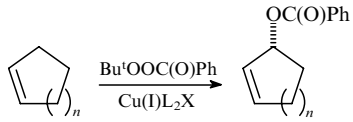

210, **211**, **213**

Benzoate	*n*	Yield (%)	*ee* (%)
210	1	44	70
211	2	62	67
213	4	62	67

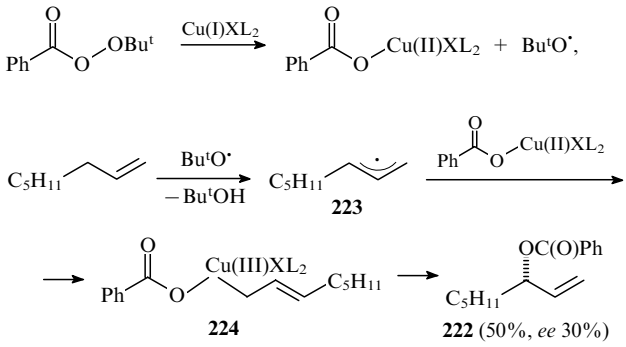

223

224

222 (50%, *ee* 30%)

X = OTf.

The reductive homolysis of the peroxide bond under the action of a copper(I) atom affords copper(II) benzoate and a *tert*-butoxyl radical. The latter splits off the allylic hydrogen atom from the olefin, which is converted into allylic radical **223**. This radical rapidly adds to copper(II) benzoate to give a copper(III) complex with the allylic ligand (**224**). The reaction ends in the rearrangement of complex **224** to give allylic ester **222** and to recover the copper(I)-containing catalyst.

Pfaltz *et al.*[72] have also utilised *tert*-butyl peroxybenzoate and copper(I) complexes obtained *in situ* from chiral bisoxazolines and Cu(I)OTf for the oxidation of cycloalkenes. They prepared cycloalk-2-enyl benzoates in satisfactory or good yields. For instance, the transformation products of cyclopentene and cycloheptene were isolated with an enantiomeric excess of 74% at 23 °C and 84% at a low temperature; in the case of cyclohexene, the enantioselectivity is somewhat lower (*ee* 64%–77%). Feringa and co-workers[73] have reported allylic oxidation of cyclohexene with a number of chiral Cu(II) complexes with amino acids.

It was found[74] that the copper(II) triflate complex with the tridentate tris(oxazoline) ligand **225** is an efficient chiral catalyst for the asymmetric allylic oxidation of various cycloalkenes with *tert*-butyl peroxybenzoate (Kharash — Sosnovsky reaction).

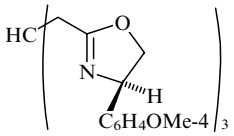

225

Cycloalkenyl benzoates are formed in this reaction in good yields and good enantioselectivities (*ee* > 81%). The reaction can be carried out in acetone, acetonitrile or 1,2-dichloroethane, the highest enantioselectivity being attained in the last-mentioned solvent.

The asymmetric allylic oxidation of cyclohexene and cyclopentene by treatment with *tert*-butyl 4-nitro-, 2-iodo- and 2,4,6-trichloro-substituted peroxybenzoates was also attempted for copper(I) hexafluorophosphate complexes with bis(*o*-tolyl)bisoxazolines **226a**–**d** and **227a**–**d**. This gave allyl benzoates with medium to high selectivities.[75]

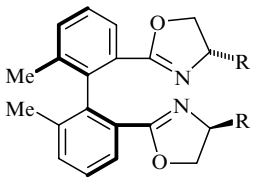

(*S*,*S*,*S*)-**226a**–**d**

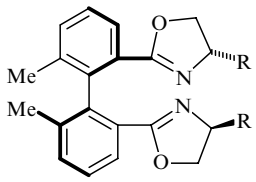

(*S*,*R*,*S*)-**227a**–**d**

R = Ph (**a**), Bu^t (**b**), Bn (**c**), Pr^i (**d**).

The highest selectivity was reached with 4-nitro-substituted *tert*-butyl peroxybenzoate and ligand **226a** (for cyclohexene, *ee* 73%) or **226c** (for cyclopentene, *ee* 72%).

Indian researchers[76] have used bisoxazoline ligand **228**. This allowed them to increase the enantioselectivity of allylic oxidation of cyclohexene to 86%.

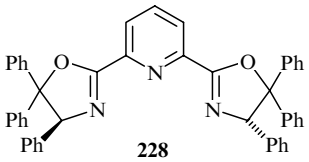

228

Catalytic allylic oxidation of α-pinene with *tert*-butyl hydroperoxide and hydrogen peroxide in the presence of transition metal salts has been reported.[77] It was found that oxidation of α-pinene with the Bu^tOOH–CuI system gives verbenone (**229**) as the major product, while the oxidation with the H_2O_2–$Pd(acac)_2$ system gives predominantly verbenol (**230**).

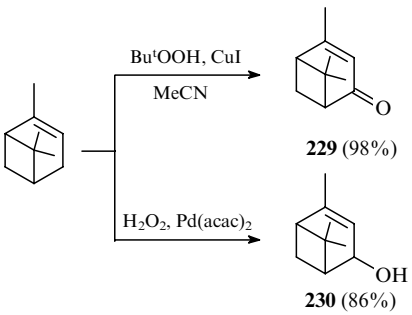

229 (98%)

230 (86%)

Other terpene alkenes (limonene, 3-carene) have also been involved in this reaction.

Sartori and co-workers[78] reported the use of the Cu-Na-HSZ-320 zeolite as an efficient and reusable catalyst for allylic oxidation

of alkenes into allylic alcohols on treatment with *tert*-butyl peroxybenzoate.

Catalytic allylic oxidation of alkenes with the use of the asymmetric version of the Kharash – Sosnovsky reaction is the subject of a review.[79]

6. Miscellaneous reagents for alkene α-oxidation

Oxidation of the methylene group in an allylic position with SeO_2 ‡ to give allylic alcohols has been reported.[79, 80]

The SeO_2-catalysed allylic oxidation with *tert*-butyl hydroperoxide as a stoichiometric reagent is more efficient.[28, 81] This reaction has been used for allylic hydroxylation of vinyl fluorides.[82] Photochemical synthesis of allylic alcohols from alkenes has also been described.[83] In this case, a benzene or pyridine solution of alkene or a conjugated diene is irradiated in the presence of oxygen and a sensitiser (methylene blue, some porphyrin derivatives); this gives a hydroperoxide, which is reduced to yield the allylic alcohol. By this method, one can convert alkenes into allylic alcohols with a shifted double bond.[84]

IV. Reagents for the reduction of α,β-unsaturated carbonyl compounds

Reduction of α,β-unsaturated carbonyl compounds (aldehydes, ketones, and esters) is a key method for the synthesis of allylic alcohols. However, the use of the most readily available reducing agents such as $NaBH_4$ or $LiAlH_4$ results in the partial or even complete reduction of the double bond;[85] therefore, other hydride reducing agents have been proposed for this purpose.[86, 87]

For example, $Li[(CH_2)_4NBH_3]$ has been used for selective reduction of ketones **231** – **233** into allylic alcohols **234** – **236**.[88, 89]

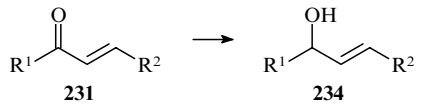

231 **234**

R^1 = H, R^2 = Ph (99%); R^1 = Me: R^2 = Ph (99%), n-C_5H_{11} (96%).

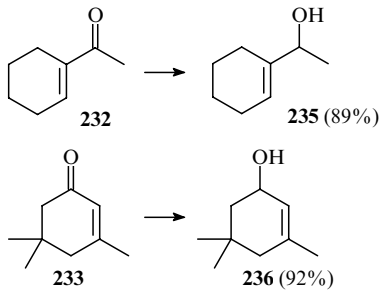

232 **235** (89%)

233 **236** (92%)

The ratio of 1,2- to 1,4-reduction products was > 99 : 1 in all cases.

Lithium aminoborohydrides are not pyrophoric; therefore, they are used in large-scale reduction processes.

Later, it was shown[90] that α,β-unsaturated ketones **237** are reduced with the $Bu_2SnH_2 - Bu_2SnF_2$ system in combination with HMPA to give allylic alcohols **238**.

237 **238**

R = H (75%), Me (89%), Ph (56%).

If HMPA is replaced by LiI, the C = C bond is reduced, while the keto group remains intact.

The synthesis of allyl vinyl alcohols **239** by treatment of α,β-unsaturated ketones with tetraallyltin (**240**) has been described.[91]

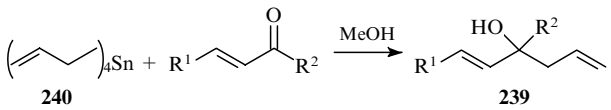

240 **239**

R^1 = H, R^2 = Et (73%); R^1 = Ph, R^2 = Me (91%),
$R^1 - R^2 = (CH_2)_3$ (65%).

Ranu and Das[92, 93] reported that the zinc borohydride – silica gel system is able to reduce conjugated ketones to allylic alcohols. For example, conjugated ketones **241**, **242** were converted into alcohols **243**, **244** in high yields.

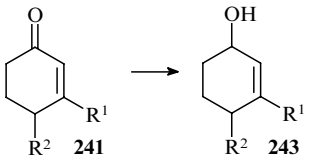

241 **243**

R^1 = R^2 = H (15%); R^1 = Me: R^2 = H (80%), COOEt (82%), COOMe (85%).

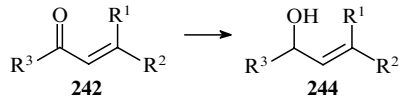

242 **244**

R^1 = H, R^2 = Me: R^3 = H (80%), Me (85%);
R^1 = H, R^2 = Ph: R^3 = H (82%), Me (85%);
R^1 = R^2 = R^3 = Me (79%).

The yield of the product of α-ionone reduction was 85%.

A recent publication[94] describes the formation of diastereomeric allylic alcohols **245** and **246** in 95 : 5 ratio (overall yield 80%) upon the diastereoselective reduction of *N*-Boc-protected δ-amino-α,β-unsaturated γ-ketoester **247** with $LiAlH(OBu^t)_3$ in EtOH at −78 °C under chelation control. The same reduction carried out with non-chelating NB-enantride in THF at −78 °C (so-called Felkin – Anh control) produces alcohols **245** and **246** in 5 : 95 ratio (overall yield 98%).

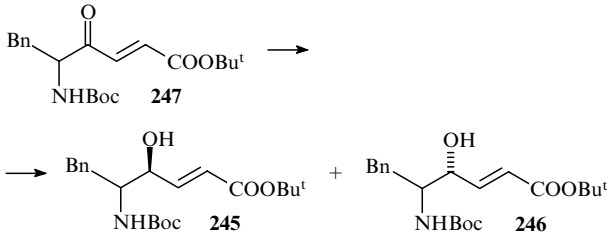

247

245 **246**

The reduction of ketoester **247** by standard reagents such as $NaBH_4 - CeCl_3$, $Zn(BH_4)_2$, Bu^i_2AlH (DIBAL-H) or a Bu^i_2AlH mixture with $ZnCl_2$ is non-selective.

Another study has also dealt with the reduction of enones to allylic alcohols.[95] It was shown that the reduction of amino-substituted enone obtained on the basis of L-serine with various reducing agents including L-selectride – THF, $LiAlH_4 - Et_2O$, $NaBH_4$ – MeOH, Red-Al – THF {Red-Al is $[(MeOCH_2.OCH_2)_2AlH_2]Na$} and so on results in a mixture of *syn*- and *anti*-isomers of aminoallylic alcohols in very high yields. The size of the hydride influences the diastereoselectivity of the reaction; the greater the hydride size, the higher the yield of the *syn*-isomer. The nature of the solvent also affects the isomer ratio.

Catalytic hydrogenation of the C = C – C = O fragment for the synthesis of allylic alcohols is normally difficult to arrange, especially under heterogeneous catalysis conditions. Nevertheless, a number of catalysts that increase the chemoselectivity and, in some cases, also the enantioselectivity of this reaction have been proposed in recent years.

‡ This reagent is also used in the synthesis of unsaturated carbonyl compounds.

The reduction of α,β-unsaturated ketones using isopropyl alcohol (as the source of hydrogen atoms) and a mixture of $CoO-ZrO_2$ oxides (as the catalyst) has been reported.[96]

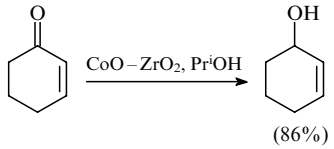

(86%)

$$R^1R^2C{=}CHCHO \xrightarrow{CoO-ZrO_2,\ Pr^iOH} R^1R^2C{=}CHCH_2OH$$

R^1 = H: R^2 = Pr^n (84%), Me (83%), Ph (80%);
R^1 = Me: R^2 = $(CH_2)_2CH{=}CMe_2$ (71%).

Iridium salts [for example, $Ir(acac)_3$] supported on various zeolites can be used as catalysts (Cat) instead of metal oxides. This method was used for chemoselective reduction of α- and β-ionones, testosterone, cholestenone, and so on.[97] For example,

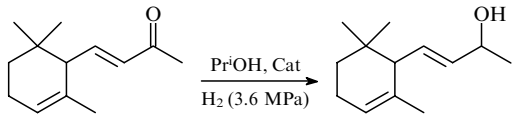

(75%, *ee* 71%)

High catalytic efficiency in the Meerwein–Ponndorf–Verley reduction of unsaturated ketones to allylic alcohols was found for Zr and Hf catalysts supported on mesoporous materials of the MCM-41 and MCM-48 type.[98]

Wills and co-workers [99] reported the efficient use of asymmetric transfer hydrogenation for the reduction of enones. Numerous catalyst systems have been developed for this process. The system ruthenium(II) complex–chiral monotosylated diamine (or β-aminoalcohol)–formic acid is used most often.

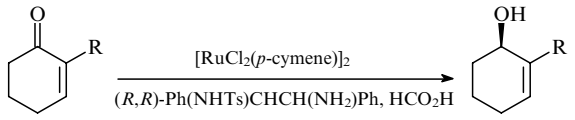

R = Ph (47%, *ee* 72%), OBn (78%, *ee* 99%),
$NHCO_2Me$ (54%, *ee* > 99%).

Other examples of catalytic hydrogenation of enones can be found in the review by Noyori.[100]

V. Miscellaneous methods

We have considered the most important reagents used to convert alkenes and their derivatives into allylic alcohols *via* cleavage of α-epoxides, allylic hydroxylation and reduction of α,β-unsaturated carbonyl compounds. This Section presents a brief discussion of other general methods for the synthesis of allylic alcohols.

1. Reactions of carbonyl compounds with alkenes and alkynes

The reaction of alkenylmagnesium halides with aldehydes or ketones (Normann method) is a well-known method for the synthesis of allylic alcohols. The addition of divinylzinc to carbonyl compounds also deserves attention.[101] Subsequently, this strategy has been developed in the field of metal complex catalysis.

The use of nickel(II) chloride and palladium(II) acetate as catalysts of the cross-coupling of iodoalkenes with aldehydes, resulting in the formation of allylic alcohols, has been reported.[102] It is important that double bond configuration in the product is the same as that in iodoalkene. Diastereoselective synthesis of allylic alcohols from α-substituted aldehydes by the Nozaki–Hiyama–Kishi reaction has been reported.[103] This transformation was used in the synthesis of (+)-herbarumin I.

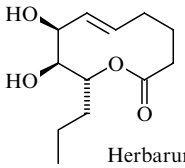

Herbarumin I

An efficient method for the synthesis of bromoallylic alcohols from 1-bromo-1-lithioethene and aldehydes or ketones has been reported.[104]

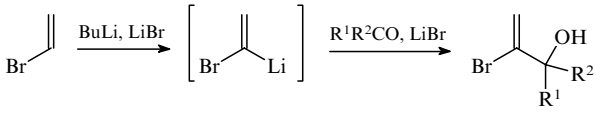

$R^1 = R^2$ = Me (77%); R^1 = Me, $R^2 = CH_2{=}CH$ (78%),
$CH_2{=}CH(CH_2)_2$ (84%), $CH_2{=}CHCMe_2CH_2CH_2$ (80%);
$R^1-R^2 = (CH_2)_5$ (85%); R^2 = H: R^1 = Et (46%), n-C_6H_{13} (50%),
Ph (81%), $CH_2{=}CH$ (74%).

Phosphines containing a ferrocene fragment proved to be efficient ligands for a number of catalytic reactions and a number of metal-catalysed asymmetric reactions.[105–107] It has been found [108] that P-chiral monodentate ferrocenylphosphines **248a–d** can be used as ligands in asymmetric catalytic reductive coupling of oct-4-yne with aldehydes **249a–c** to produce chiral allylic alcohols **250a–c** with high regio- and enantioselectivities.

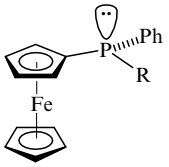

248a–d

R = Me (**a**), 4-$MeOC_6H_4$ (**b**), cyclo-C_6H_{11} (**c**), Bu^n (**d**);

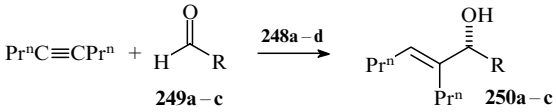

R = Ph (**a**), Pr^n (**b**), Pr^i (**c**).

Racemic allylic alcohols were also prepared *via* intramolecular [109, 110] and intermolecular [111] reductive coupling of alkynes and aldehydes. The reductive coupling of alkyne with aldehyde was also used to synthesise chiral allylic alcohols. Reductive coupling in the presence of stoichiometric amounts of transition metals has been studied by Takai and co-workers,[112] Negishi and co-workers,[113] Livinghouse and co-workers,[114] Takai and Utimoto and co-workers.[115, 116] For example,[112]

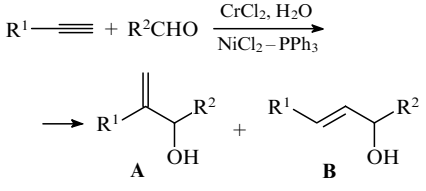

$R^1 = Ph(CH_2)_2$, R^2 = n-C_8H_{17} (82%, **A** : **B** = 95 : 5); R^1 = n-$C_{10}H_{21}$,
R^2 = Ph (99%, **A** : **B** = 94 : 6); R^1 = n-$C_{10}H_{21}$, R^2 = cyclo-C_6H_{11} (78%,
A : **B** = 90 : 10); $R^1 = HO(CH_2)_2$, $R^2 = Ph(CH_2)_2$ (83%, **A** : **B** = 99 : 1).

The use of a chiral titanium complex–alkyne system in the synthesis of chiral alcohols has been reported.[117]

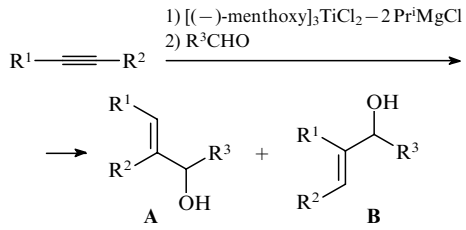

$R^1 = R^2 = n\text{-}C_5H_{11}$: R^3 = Et, Pr^i, cyclo-C_6H_{11};
$R^1 = Me_3Si$, R^3 = cyclo-C_6H_{11}: $R^2 = n\text{-}C_6H_{13}$, Ph.

The reaction between alkenyl triflates and aldehydes[118] induced by $CrCl_2$ in the presence of catalytic amounts of $NiCl_2$ is similar in essence. For example, triflates **251a–c** react with benzaldehyde in the presence of $CrCl_2$ and catalytic amounts of $NiCl_2$ in DMF to give the corresponding allylic alcohols **252a–c** in high yields. In ether and THF, which sparingly dissolve $CrCl_2$, this reaction barely proceeds. Other aldehydes can also be introduced in this reaction, for example, $C_8H_{17}CHO$ or $Pr^iCH=CHCHO$. In the presence of other catalysts such as $MnCl_2$, $FeCl_3$, $CoCl_2$ and $PdCl_2$, the yield of the target product decreases. In addition, decomposition of triflates is possible. Steric factors associated with the presence of substituents at the double bond can have a pronounced influence on the reaction route.

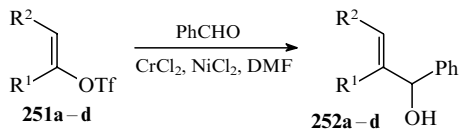

R^1 = Bu, R^2 = H (**a**); $R^1 = n\text{-}C_{10}H_{21}$, R^2 = H (**b**);
$R^1 - R^2 = (CH_2)_4$ (**c**); R^1 = Me, R^2 = Ph (**d**).

A mechanism including the reduction of nickel(II) chloride to nickel(0) with $CrCl_2$ has been proposed for this transformation. Nickel and triflates form organonickel compounds, which undergo transmetallation. The resulting organochromium compounds react with aldehydes.

For the synthesis of functionally substituted allylic alcohols, the Baylis–Hillman reaction is used. These alcohols are important intermediates in the synthesis of many natural compounds: alkaloids, pyrethroids, steroids, pheromones, and so on. In particular, allylpropargyl alcohols **253**[119] and 2-(α-hydroxybenzyl)cyclohex-2-enone (**254**)[120] have been synthesised in this way.

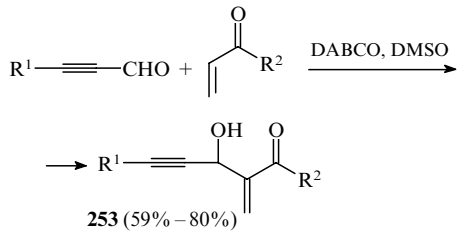

R^1 = Ph, $n\text{-}C_6H_{13}$; R^2 = Me, OEt; DABCO is diazabicyclooctane.

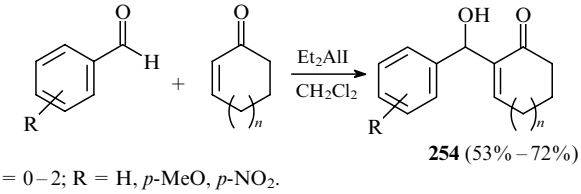

n = 0–2; R = H, *p*-MeO, *p*-NO_2.

2. [2,3]-Sigmatropic rearrangements of chalcogen oxides

It has been noted above that oxidative elimination of a selenium group is a general method for the synthesis of alkenes.[28] However, during the oxidation of allyl selenides, the intermediate selenium oxide undergoes a [2,3]-sigmatropic rearrangement involving the double bond, resulting in the selenenic ester of the rearranged allylic alcohol and finally in the corresponding allylic alcohol.

In the case of analogous sulfur compounds, this reaction is less typical, although some examples are known (see the review[121]). Thus on heating in the presence of trimethyl phosphite, allyl sulfoxide **255** is partially rearranged into the allyl ester of sulfenic acid **256**.[121] As a rule, the equilibrium in this reaction is largely shifted toward the sulfoxide, but on treatment of the reaction mixture with a thiophilic reagent (for example, trimethyl phosphite and diethylamine), the sulfenate is irreversibly converted into allylic alcohol **257**.

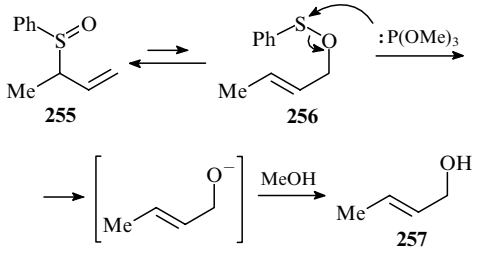

The transformation of sulfoxide **258** into allylic alcohol **259**, which is the racemic form of prostaglandin E (PGE_1), has been reported.[122]

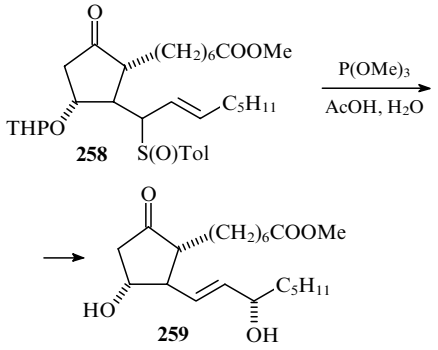

Other examples of rearrangement of sulfoxides and sulfones and the use of products of these rearrangements in total syntheses of natural compounds are given in the review by Prilezhaeva.[123]

3. Other methods

In conclusion, we would like to note that allylic alcohols are formed upon partial hydrogenation of many acetylenic alcohols. The appropriate reducing agents include $LiAlH_4$, Red-Al, hydrogen with special catalysts, for example Pd–$CaCO_3$ (Lindlar catalyst) and so on. The reduction of acetylenes **260–262** has resulted in the preparation of allylic alcohols **263–265**.[124–126]

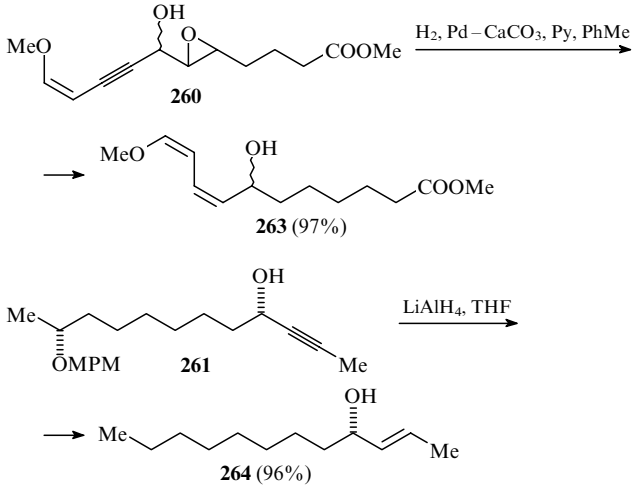

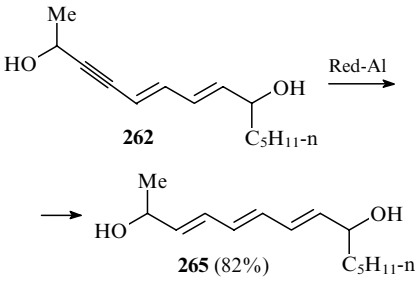

The reduction–oxygenation sequence induced by molecular oxygen and triethylsilane catalysed by cobalt(II) porphyrinate followed by treatment with trimethyl phosphite performs the transformation of compounds **266**, **267** into compounds **268**, **269**, containing an allyl alcohol fragment.[127]

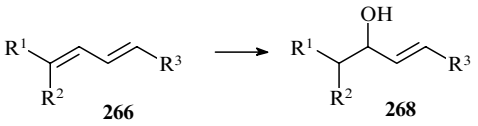

$R^1 = R^2 = Me$, $R^3 = COOEt$ (81%); $R^1 = Bu^n$, $R^2 = H$, $R^3 = CHO$ (54%); $R^1 = n\text{-}C_6H_{13}$, $R^2 = H$, $R^3 = COOBu^t$ (73%); $R^1 = Pr^n$, $R^2 = H$, $R^3 = COOEt$ (82%).

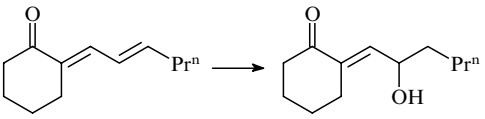

References

1. J K Crandall, M Apparu *Org. React.* **29** 345 (1983)
2. J G Smith *Synthesis* 629 (1984)
3. A S Rao, S K Paknikar, J G Kirtane *Tetrahedron* **39** 2323 (1983)
4. P Mosset, S Manna, J Viala, J R Falck *Tetrahedron Lett.* **27** 299 (1986)
5. J K Crandall, L H Chang *J. Org. Chem.* **32** 532 (1967)
6. M Asami *Tetrahedron Lett.* **26** 5803 (1985)
7. M Asami *Bull. Chem. Soc. Jpn.* **63** 721 (1990)
8. M Asami, T Ishizaki, S Inone *Tetrahedron Lett.* **36** 1893 (1995)
9. D Bhuniya, V K Singh *Synth. Commun.* **24** 375 (1994)
10. B Colman, S E de Sousa, P O'Brien, T D Towers, W Watson *Tetrahedron: Asymmetry* **10** 4175 (1999)
11. M Asami, M Ogawa, S Inoue *Tetrahedron Lett.* **40** 1563 (1999)
12. P O'Brien, T D Towers, M Voith *Tetrahedron Lett.* **39** 8175 (1998)
13. P O'Brien *J. Chem. Soc., Perkin Trans. 1* 1439 (1998)
14. M J Sodergren, S K Bertilsson, P G Andersson *J. Am. Chem. Soc.* **122** 6610 (2000)
15. M J Sodergren, P G Andersson *J. Am. Chem. Soc.* **120** 10760 (1998)
16. S K Bertilsson, P G Andersson *Tetrahedron* **58** 4665 (2002)
17. A Gayet, S K Bertilsson, P G Andersson *Org. Lett.* **4** 3777 (2002)
18. S V Malhotra *Tetrahedron: Asymmetry* **14** 645 (2003)
19. A Johansson, P Abrahamsson, Ö Davidson *Tetrahedron: Asymmetry* **14** 1261 (2003)
20. A Yasuda, H Yamamoto, H Nozaki *Bull. Chem. Soc. Jpn.* **52** 1705 (1979)
21. S Murata, M Suzuki, R Noyori *J. Am. Chem. Soc.* **101** 2738 (1979)
22. G A Kraus, K Frazier *J. Org. Chem.* **45** 2579 (1980)
23. M E Jung, M A Lyster *J. Org. Chem.* **42** 3761 (1977)
24. M R Detty *J. Org. Chem.* **45** 924 (1980)
25. G A Olah, S C Narang, B G B Gupta, R Malhotra *J. Org. Chem.* **44** 1247 (1979)
26. M E Jung, T A Blumenkopf *Tetrahedron Lett.* 3657 (1978)
27. T L Ho, G A Olah *Synthesis* 417 (1977)
28. K C Nicolaou, N A Petasis *Selenium in Natural Products Synthesis* (Philadelphia: CIS INC, 1984)
29. X Huang, W Xu *Tetrahedron Lett.* **43** 5495 (2002)
30. C Baylon, M P Heck, C Mioskowski *J. Org. Chem.* **64** 3354 (1999)
31. R J Davoille, D T Rutherford, S D R Christie *Tetrahedron Lett.* **41** 1255 (2000)
32. L Alcaraz, A Cridland, E Kinchin *Org. Lett.* **3** 4051 (2001)
33. G A Molander, B E La Belle, G Hahn *J. Org. Chem.* **51** 5259 (1986)
34. J M Aurrecoechea, W H Okamura *Tetrahedron Lett.* **28** 4947 (1987)
35. K C Nicolaou, M E Duggan, T Ladduwahetty *Tetrahedron Lett.* **25** 2069 (1984)
36. T Katsuki, K B Sharpless *J. Am. Chem. Soc.* **102** 5974 (1980)
37. L A Sarandeses, A Mouriño, J-L Luche *J. Chem. Soc., Chem. Commun.* 818 (1991)
38. J S Yadav, T Shekharam, V R Gadgil *J. Chem. Soc., Chem. Commun.* 843 (1990)
39. J S Yadav, V R Gadgil *J. Chem. Soc., Chem. Commun.* 1824 (1989)
40. J S Yadav, T Shekharam, D Srinivas *Tetrahedron Lett.* **33** 7973 (1992)
41. E Vedejs, J M Dolphin, W T Stolle *J. Am. Chem. Soc.* **101** 249 (1979)
42. S Chandrasekhar, M Takhi, J S Yadav *Tetrahedron Lett.* **36** 307 (1995)
43. Y Gao, R M Hannon, J M Klunder, S Y Ko, H Masamune, K B Sharpless *J. Am. Chem. Soc.* **109** 5765 (1987)
44. L Dehoux, E Doris, C Mioskowski *Chem. Commun.* 549 (1996)
45. D M Hodgson, M A H Stent, F X Wilson *Org. Lett.* **3** 3401 (2001)
46. D M Hodgson, C R Maxwell, T J Miles, E Paruch, M A H Stent, I R Matthews, F X Wilson, J Witherington *Angew. Chem., Int. Ed.* **41** 4313 (2002)
47. J A Marshall *Chem. Rev.* **89** 1503 (1989)
48. J P Marino, N Hatanaka *J. Org. Chem.* **44** 4467 (1979)
49. J P Marino, R F Pradilla, E Labrode *J. Org. Chem.* **52** 4898 (1987)
50. Y Yamamoto *Angew. Chem., Int. Ed. Engl.* **25** 947 (1986)
51. B H Lipshutz *Synlett* 119 (1990)
52. E Nakamura *Synlett* 539 (1991)
53. S K Kang, D H Lee, H S Sim, J S Lim *Tetrahedron Lett.* **34** 91 (1993)
54. K Mori, T Suguro, M Uchida *Tetrahedron* **34** 3119 (1978)
55. F Badalassi, P Crotti, F Macchia, M Pineschi, A Arnold, B L Feringa *Tetrahedron Lett.* **39** 7795 (1998)
56. H B Kagan, J C Fiaud *Top. Stereochem.* **18** 249 (1988)
57. O Molt, T Schrader *Synthesis* 2633 (2002)
58. S Brandange, J E Backvall, H Leijonmarck *J. Chem. Soc., Perkin Trans. 1* 2051 (2001)
59. J R Gilmore, J M Mellor *J. Chem. Soc.* 2355 (1971)
60. W Kitching, Z Rappaport, S Winstein, W G Young *J. Am. Chem. Soc.* **88** 2054 (1966)
61. G H Whitham *J. Chem. Soc.* 2232 (1961)
62. A Heumann, M Reglier, B Waegell *Angew. Chem., Int. Ed. Engl.* **21** 366 (1982)
63. B M Trost *Tetrahedron* **33** 2615 (1977)
64. B M Trost, T R Verhoeven, J M Fortunak *Tetrahedron Lett.* 2301 (1979)
65. S Hansson, A Heumann, T Rein, B Aakermark *J. Org. Chem.* **55** 975 (1990)
66. S B Bystroem, E M Larsson, B Aakermark *J. Org. Chem.* **55** 5674 (1990)
67. E M Larsson, B Aakermark *Tetrahedron Lett.* **34** 2523 (1993)
68. M A Brimble, M K Edmonds, G M Williams *Tetrahedron Lett.* **31** 7509 (1990)
69. B Bernet, P M Bishop, M Caron, T Kawamata, B L Roy, L Ruest, G Sauve, P Soucy, P Deslongchamps *Can. J. Chem.* **63** 2810 (1985)
70. A Levina, J Mazart *Tetrahedron: Asymmetry* **6** 147 (1995)
71. M B Andrus, A B Argade, X Chen, M G Pamment *Tetrahedron Lett.* **36** 2945 (1995)
72. A S Gokhale, A B E Mindis, A Pfaltz *Tetrahedron Lett.* **36** 1831 (1995)
73. M T Rispens, C Zondervan, B L Feringa *Tetrahedron: Asymmetry* **6** 661 (1995)

74. Y Kohmura, T Katsuki *Tetrahedron Lett*. **41** 3941 (2000)
75. M B Andrus, D Asgari *Tetrahedron* **56** 5775 (2000)
76. R M Kamble, G Sekar, V K Singh *Proc. Indian Natl. Sci. Acad.* **68** 423 (2002)
77. B A Allal, L El Firdoussi, S Allaoud, A Karim, Y Castanet, A Mortreux *J. Mol. Catal. A: Chem*. **200** 177 (2003)
78. S Carloni, B Frullanti, R Maggi, A Mazzacani, F Bigi, G Sartori *Tetrahedron Lett*. **41** 8947 (2000)
79. J Eames, M Watkinson *Angew. Chem., Int. Ed*. **40** 3567 (2001)
80. G Aranda, M BertranneDelahaye, R Azerad, M Maurs, M Cortes, H Ramirez, G Vernal, T Prange *Synth. Commun*. **27** 45 (1997)
81. M A Umbreit, K B Sharpless *J. Am. Chem. Soc*. **99** 5526 (1977)
82. T Ernet, G Haufe *Synthesis* 953 (1997)
83. R W Denny, A Nickon *Org. React*. **20** 133 (1973)
84. A K Banerjee, A Martin, T Nakano, A Usubillaga *J. Org. Chem*. **38** 3807 (1973)
85. R S Varma, G W Kabalka *Synth. Commun*. **15** 985 (1985)
86. J M Fortunato, B Ganem *J. Org. Chem*. **41** 2194 (1976)
87. E J Corey, J O Link *Tetrahedron Lett*. **30** 6275 (1989)
88. Y Okude, S Hirano, T Hiyama, H Nozaki *J. Am. Chem. Soc*. **99** 3179 (1977)
89. J C Fuller, E L Stangeland, C T Goralski, B Singaram *Tetrahedron Lett*. **34** 257 (1993)
90. T Moriuchi-Kawakami, H Matsuda, I Shibata, M Miyatake, T Suwa, A Baba *Bull. Chem. Soc. Jpn*. **72** 465 (1999)
91. S K Leitch, A McCluskey *Synlett* 699 (2003)
92. B C Ranu *Synlett* 885 (1993)
93. B C Ranu, A R Das *J. Org. Chem*. **56** 4796 (1991)
94. J Vabena, M Brisander, T Lejan, K Luthman *J. Org. Chem*. **67** 9186 (2002)
95. A M P Koskinen, P M Koskinen *Tetrahedron Lett*. **34** 6765 (1993)
96. S U Sonavane, R V Jayaram *Synlett* 146 (2004)
97. M De Bruyn, S Coman, R Bota, V I Parvulescu, D E De Vos *Angew. Chem., Int. Ed*. **42** 5333 (2003)
98. M De Bruyn, M Limbourg, J Denayer, G V Baron, V I Parvulescu, P J Grobet, D E De Vos, P A Jacobs *Appl. Catal. A* **254** 189 (2003)
99. J Hannedouche, J A Kenny, T Walsgrove, M Wills *Synlett* 263 (2002)
100. R Noyori *Angew. Chem., Int. Ed*. **41** 2008 (2002)
101. W Oppolzer, R N Radinov *Tetrahedron Lett*. **29** 5645 (1988)
102. H Jin, J-i Uenishi, W J Christ, Y Kishi *J. Am. Chem. Soc*. **108** 5644 (1986)
103. A A Sabino, R A Pilli *Tetrahedron Lett*. **43** 2819 (2002)
104. Y Y Novikov, P Sampson *Org. Lett*. **5** 2263 (2003)
105. K Tanaka, S Quio, M Tobisu, M M Lo, G C Fu *J. Am. Chem. Soc*. **122** 9870 (2000)
106. C J Richards, A J Locke *Tetrahedron: Asymmetry* **9** 2377 (1998)
107. R Shintani, M M Lo, G C Fu *Org. Lett*. **2** 3695 (2000)
108. E A Colby, T F Jamison *J. Org. Chem*. **68** 156 (2003)
109. J Montgomery *Acc. Chem. Res*. **33** 467 (2000)
110. X-Q Tang, J Montgomery *J. Am. Chem. Soc*. **122** 6950 (2000)
111. W S Huang, J Chan, T F Jamison *Org. Lett*. **2** 4221 (2000)
112. K Takai, S Sakamoto, T Isshiki *Org. Lett*. **5** 653 (2003)
113. K Takagi, C J Rousset, E-i Negishi *J. Am. Chem. Soc*. **113** 1440 (1991)
114. B C van Wagenen, T Livinghouse *Tetrahedron Lett*. **30** 3495 (1989)
115. K Takai, Y Kataoka, K Utimoto *J. Org. Chem*. **55** 1707 (1990)
116. Y Kataoka, J Miyai, K Oshima, K Takai, K Utimoto *J. Org. Chem*. **57** 1973 (1992)
117. Y Takayanagi, K Yamashita, Y Yoshida, F Sato *Chem. Commun*. 1725 (1996)
118. K Takai, M Tagashira, T Kuroda, K Oshima, K Utimoto, H Nosaki *J. Am. Chem. Soc*. **108** 6048 (1986)
119. P R Krishna, E R Sekhar, V Kannan *Tetrahedron Lett*. **44** 4973 (2003)
120. W Pei, H-X Wei, G Li *Chem. Commun*. 2412 (2002)
121. D A Evans, G C Andrews *Acc. Chem. Res*. **7** 147 (1974)
122. Y Masaki, K Hashimoto, K Kaji *Chem. Pharm. Bull*. **32** 3959 (1984)
123. E N Prilezhaeva *Usp. Khim*. **70** 1013 (2001) [*Russ. Chem. Rev*. **70** 897 (2001)]
124. E J Corey, J O Albright *J. Org. Chem*. **48** 2114 (1983)
125. S Takano, T Murakami, K Samizu, K Ogasawara *Heterocycles* **39** 67 (1994)
126. M Mladenova, M Alami, G Linstrumelle *Synth. Commun*. **26** 2831 (1996)
127. Y Matsushita, K Sugamoto, T Nakama, T Sakamoto, T Matsui, M Nakayama *Tetrahedron Lett*. **36** 1879 (1995)

Russian Chemical Reviews **73** (7) 637 – 669 (2004) © 2004 Russian Academy of Sciences and Turpion Ltd

DOI 10.1070/RC2004v073n07ABEH000856

Chemistry and biological activities of 1,8-naphthyridines †

V P Litvinov

Contents

I.	Introduction	637
II.	Synthetic methods and biological activities of 1,8-naphthyridine derivatives	637
III.	Physicochemical properties and reactivities of 1,8-naphthyridine derivatives	651
IV.	Conclusion	660

Abstract. Data on the synthetic methods, reactivities, biological activities and other practically important properties of 1,8-naphthyridine derivatives published over the last 15 years are analysed. The bibliography includes 759 references.

I. Introduction

Of the six isomeric pyridopyridines, 1,8-naphthyridine derivatives have received the most study in the last 15 years. This class of compounds has attracted considerable attention primarily because the 1,8-naphthyridine skeleton is present in many compounds which have been isolated from natural substances and exhibit various biological activities. The number of publications (including patents) devoted to the chemical and biological properties of 1,8-naphthyridines which were issued over this period is substantially larger than the number of studies on all other types of isomeric pyridopyridines published in the last 90 years. In the last two years, more than 900 publications appeared, among which were about 200 patents. Most of these studies were devoted to specific aspects of biological activity assays of 1,8-naphthyridine derivatives.

The present article, which completes a series of reviews of the chemistry of pyridopyridines,[1,2] summarises and analyses data on the synthesis methods, reactivities, biological activities and other practically important properties of 1,8-naphthyridine derivatives. For convenience of representation, the data are classified according to the types of the starting substrates, reagents or the nature of the compounds synthesised. In the discussion of the synthetic methods and chemical transformations, the principal data on biological activities of the compounds synthesised are considered. In my opinion, it is reasonable to cite a virtually complete bibliography, including patents, on the synthesis and properties of 1,8-naphthyridine derivatives. However, since the literature on these problems is voluminous, only general and promising synthetic methods and most typical reactions are covered in detail in the present review.

V P Litvinov N D Zelinsky Institute of Organic Chemistry, Russian Academy of Sciences, Leninsky prosp. 47, 119991 Moscow, Russian Federation. Fax (7-095) 135 53 28. Tel. (7-095) 135 88 37.
E-mail: vpl@ioc.ac.ru

Received 22 October 2003
Uspekhi Khimii **73** (7) 692 – 725 (2004); translated by T N Safonova

II. Synthetic methods and biological activities of 1,8-naphthyridine derivatives

Among 1,8-naphthyridine derivatives, 6-fluoro-substituted 1,8-naphthyridin-4-ones, which are aza analogues of fluoroquinolones, have attracted most attention in the last 15 years. Fluoroquinolone- and fluoronaphthyridonecarboxylic acids provided the basis for the design of highly efficient antibacterial drugs, such as norfloxacin (**1a**),[3] pefloxacin (**1b**),[4] ciprofloxacin (**1c**),[5] enoxacin (**1d**),[6] trovafloxacin (**1e**),[7–10] *etc*.

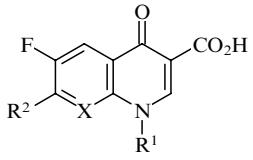

1a – e

X = CH: R^1 = Et, R^2 = piperazin-1-yl (**a**), *N*-methylpiperazin-1-yl (**b**); R^1 = cyclo-C_3H_5, R^2 = piperazin-1-yl (**c**); X = N: R^1 = Et, R^2 = piperazin-1-yl (**d**); R^1 = 2,4-$F_2C_6H_3$, R^2 = 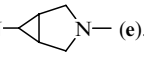 (**e**).

Fluoronaphthyridones are similar not only in biological activity but also in other properties to fluoroquinolones, whose chemistry has been studied in considerable detail.[11–15] The most commonly used method for the synthesis of fluoro-substituted 4-oxo-1,4-dihydro-1,8-naphthyridine-3-carboxylic acids is based on approaches developed for preparing fluoroquinolone analogues [16–20] and can be represented by the following scheme:

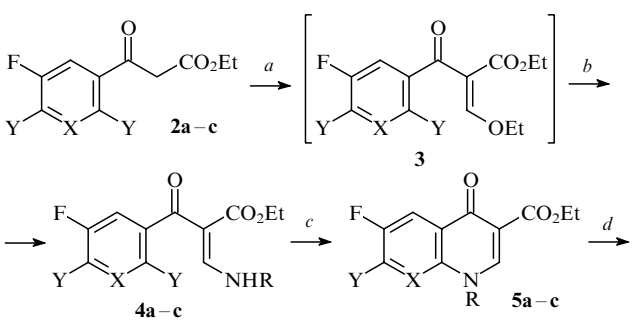

2a – c **3** **4a – c** **5a – c**

† Dedicated to Academician Oleg Nikolaevich Chupakhin on the occasion of his 70th birthday.

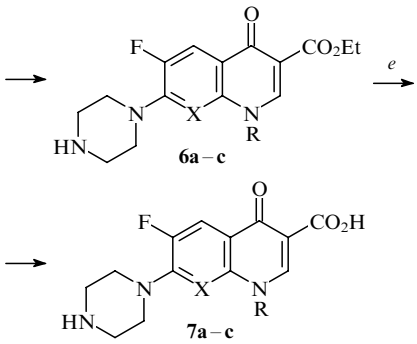

X = N (**a**), CH (**b**), CF (**c**); Y = Cl, F;

R = Et, Pr^i, cyclo-C_3H_5, Bu^t, CH_2=CMe, 4-FC_6H_4;

DBU is diazabicyclo[5.4.0]undec-7-ene;

(*a*) $HC(OEt)_3$, Ac_2O; (*b*) RNH_2, EtOH; (*c*) NaH, dioxane;

(*d*) $NH(CH_2CH_2)_2NH$, DBU, MeCN; (*e*) 1) NaOH, H_2O, Δ; 2) H^+.

Condensation of ethyl (2,6-dichloro-5-fluoronicotinoyl)acetate **2a** and analogous benzoyl derivatives **2b**,**c** with ethyl orthoformate in acetic anhydride followed by the reaction of intermediates **3** with a small excess of amine (ethanol, 20 °C) yields the corresponding enamino ketoesters **4a**–**c**. Heating of enamines **4b** with sodium hydride in dioxane gives rise to ethyl 4-oxo-1,4-dihydroquinoline-3-carboxylates **5b**. Cyclisation of enamines **4a**, which can be carried out according to three procedures, *viz*., by reaction with sodium hydride in dioxane, with potassium carbonate in acetonitrile or with *tert*-butylammonium fluoride in THF, affords naphthyridones **5a** in good yields.[16–26] The replacement of the halogen atom at position 7 of compounds **5a** under the action of amine in acetonitrile (in some cases, in the presence of DBU as a base) gives rise to esters **6a**, which are hydrolysed to form acids. This procedure was used for the synthesis of naphthyridonecarboxylic acids **7a** (R = Et,[21] Pr^i,[16] isoprenyl,[24] Bu^t,[22] cyclopropyl,[25] 4-fluorophenyl [19]).

The high synthetic potential of esters **2** is also exemplified by their reactions with thioformates. For example, the reaction of ethyl 2,6-dichloro-5-fluoronicotinoylacetate (**2a**) with phenyl *N*-cyclopropyliminochlorothioformate in the presence of one equivalent of sodium hydride in xylene proceeds through intermediate **8a** to give ethyl 7-chloro-1-cyclopropyl-6-fluoro-4-oxo-2-phenylthio-1,4-dihydro-1,8-naphthyridine-3-carboxylate (**9a**) in 51% yield.[24] An analogous treatment of ethyl 2,3,4,5-tetrafluorobenzoylacetate (**2c**) produces ethyl 1-cyclopropyl-6,7,8-trifluoro-4-oxo-2-phenylthio-1,4-dihydroquinoline-3-carboxylate (**9c**) in 42% yield. Oxidation of 3-carboxylic esters **9a**,**c** with *m*-chloroperoxybenzoic acid (*m*-CPBA) (CH_2Cl_2, 20 °C) affords ethyl 7-chloro-1-cyclopropyl-6-fluoro-4-oxo-2-phenylsulfinyl-1,4-dihydro-1,8-naphthyridine-3-carboxylate (**10a**) (83% yield) or ethyl 1-cyclopropyl-6,7,8-trifluoro-4-oxo-2-phenylsulfinyl-1,4-dihydroquinoline-3-carboxylate (**10c**) (78% yield), respectively. The regiospecific replacement of the sulfinyl group of sulfoxide **10a** with freshly prepared sodium hydrosulfide in aqueous THF gives rise to a 2-mercapto derivative, whose treatment (without purification) with hydroxylamine-*O*-sulfonic acid in the presence of sodium bicarbonate affords the hydrosulfamino derivative. The latter undergoes cyclisation to form 7-chloro-9-cyclopropyl-6-fluoro-2,3,4,9-tetrahydroisothiazolo[5,4-*b*]quinoline-3,4-dione (**11a**) (67% yield). The reaction of naphthyridinedione **11a** with an excess of piperazine (pyridine, 60 °C) produces 9-cyclopropyl-6-fluoro-7-(piperazin-1-yl)-2,3,4,9-tetrahydroisothiazolo[5,4-*b*]-[1,8]naphthyridine-3,4-dione (**12a**) in 98% yield. An analogous sequence of transformations of quinolinedione **11c** gives rise to 9-cyclopropyl-6,8-difluoro-7-(piperazin-1-yl)-2,3,4,9-tetrahydroisothiazolo[5,4-*b*]quinoline-3,4-dione (**12c**) (74%). Naphthyridinedione **12a** and quinolinedione **12c** exhibit higher antibacterial activity compared to ciprofloxacin **1c**.[24]

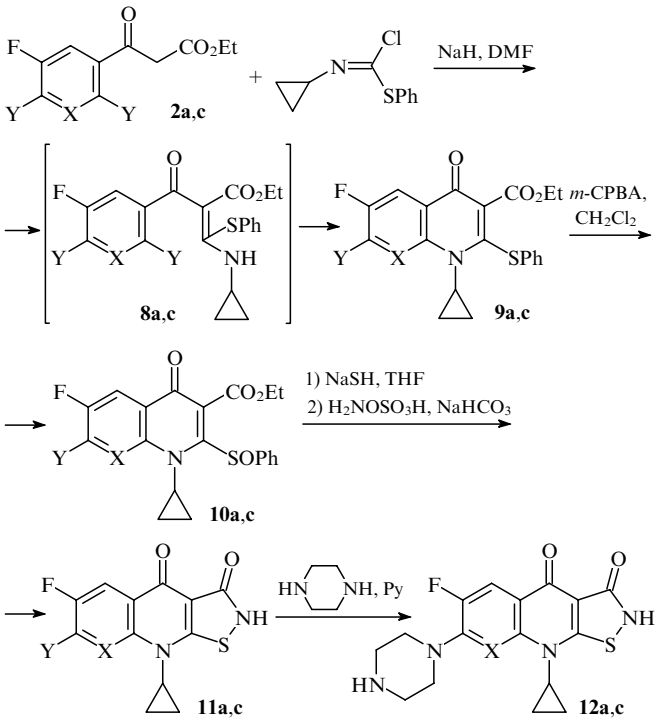

X = N, Y = Cl (**a**); X = CF, Y = F (**c**).

The reaction of ester **2a** with sodium hydride, carbon disulfide and methyl iodide in *N*,*N*-dimethylacetamide produces ketene dimethyl dithioacetal **13** (58% yield). The reactions of the latter with substituted amines **14** in toluene afford derivatives **15** in yields of up to 93%.[27] Their intramolecular cyclisation in the presence of potassium *tert*-butoxide gives rise to ethyl thiazolo-, oxazolo- and imidazolo[3,2-*a*][1,8]naphthyridine-4-carboxylates **16** (35%–92% yields). Condensation of ketene dithioacetal **13** with two equivalents of amines **14** allows one to prepare compounds **16** in one step. Acid hydrolysis of esters **16** gives the corresponding carboxylic acids **17** (55%–91% yields). The reactions of the latter with *N*-methylpiperazine are accompanied by the replacement of the chlorine atom at position 2 to form piperazine derivatives **18**, which exhibit *in vitro* antibacterial activity.

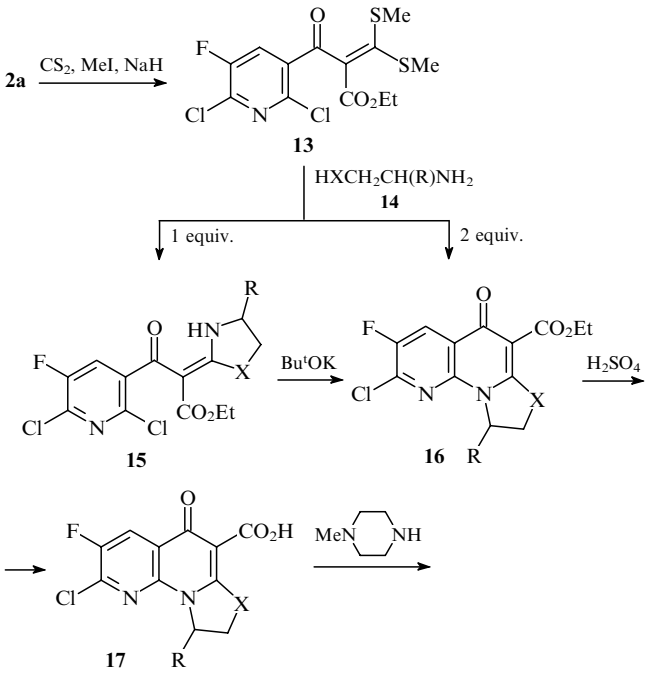

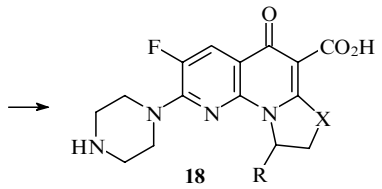

X = S,O, NMe; R = H, Me.

Ester **2a** was also used as the starting compound in the synthesis of previously unknown 7-substituted 6-fluoro-1-(1- or 2-naphthyl)-4-oxo-1,4-dihydro-1,8-naphthyridine-3-carboxylic acids **19**, which possess pronounced (comparable to that of the drug ataverdine) anti-HIV-RT activity.[28] The synthesis of acids **19** is illustrated by the following scheme:

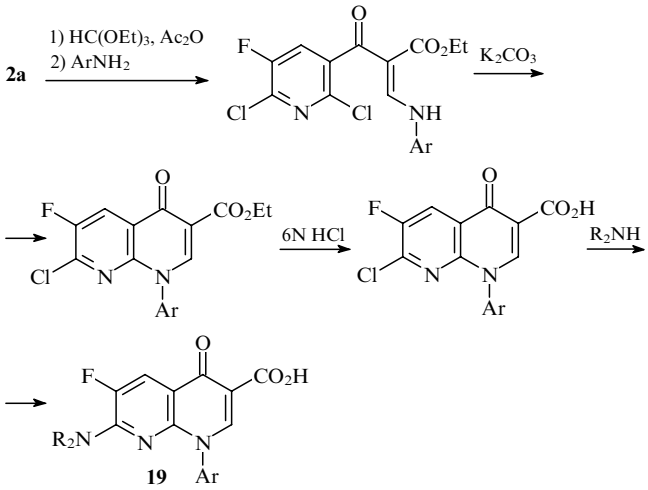

Ar = 1-naphthyl, 2-naphthyl; R_2NH = piperazine, 2-methylpiperazine, *N*-methylpiperazine, (2*R*,6*S*)-2,6-dimethylpiperazine, (3*S*)-3-aminopyrrolidine.

Ethyl (2-chloroquinolyl-3-carbonyl)acetates **20** served as the starting compounds for the preparation of benzo[*b*][1,8]naphthyridines **21**–**23**[29,30] possessing high antibacterial activity against Gram-positive bacteria. These compounds are used for the treatment of skin staphylococcus infections and water purification and also as preservatives and decontaminants.

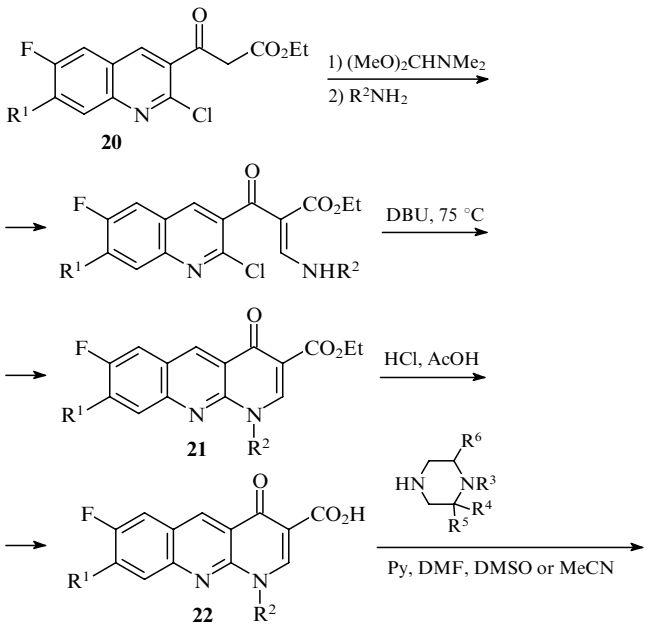

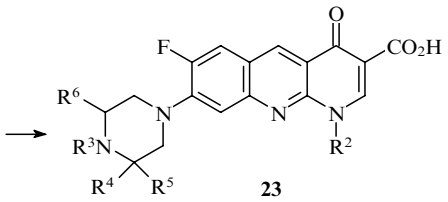

R^1 = F, Cl; R^2 = Me, MeO, cyclo-C_3H_5; R^3, R^4, R^5, R^6 = H, Alk.

A procedure was developed for the synthesis of 1-ethyl-(or cyclopropyl)-6-fluoro-4-oxo-1,4-dihydro-1,8-naphthyridine-3-carboxylic acid derivatives **24** containing the sulfinyl or sulfonyl group at position 7 of the naphthyridine system.[31,32] For example, heating (120–130 °C) of a mixture of ethyl 2-chloro-5-fluoronicotinate **25** and ethyl 3-(cyclopropylamino)propionate (**26a**) in DMF in the presence of Na_2CO_3 afforded diester **27a** (23%), the conversion of the starting nicotinate being 40%. Cyclisation of diester **27a** under the action of sodium hydride in toluene gave ethyl 1-cyclopropyl-6-fluoro-4-hydroxy-7-(*p*-tolyl)-1,2-dihydro-1,8-naphthyridine-3-carboxylate (**28a**), whose dehydrogenation with chloranil in toluene yielded 1,4-dihydro-4-oxo derivative **29a**. Alkaline hydrolysis of derivative **29a** gave 1-cyclopropyl-6-fluoro-4-oxo-7-(*p*-tolyl)-1,4-dihydro-1,8-naphthyridine-3-carboxylic acid (**30a**). In the reaction of the latter with an equimolar amount of *m*-chloroperoxybenzoic acid, the sulfide group is readily oxidised to the sulfoxide group. In the presence of a twofold excess of the peroxy acid, the sulfide group is oxidised to the sulfonyl group to form naphthyridonecarboxylic acids **24a**. This approach was used for the synthesis of analogous compound **24b** (R = Et) and the antibacterial drug enoxacin (**1d**).

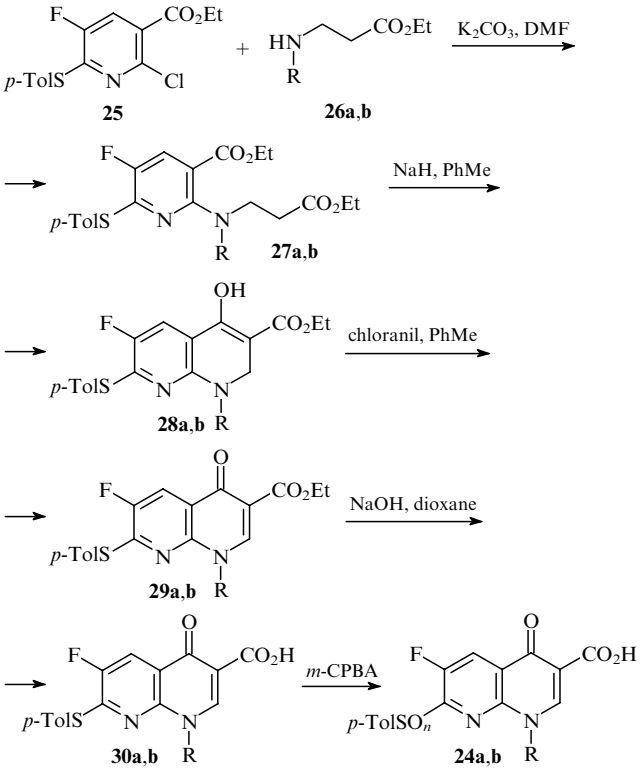

R = cyclo-C_3H_5 (**a**) Et (**b**); *n* = 1, 2; *p*-Tol is *p*-tolyl.

With the aim of studying the structure–antibacterial activity relationship, a series of new 7-substituted 6-fluoro-4-oxo-1,4-dihydro-1,8-naphthyridine-3-carboxylic acids **31** containing fluoro-substituted *tert*-butyl groups at the N(1) atom was synthesised.[22,23,33–35] For example, the reaction of intermediate **3** (X = N, Y = Cl) derived from ester **2a** with amines **32** in the presence of triethylamine in ethanol produces enamines **33**, whose

treatment with K_2CO_3 in acetonitrile results in their cyclisation to esters **34**. Condensation of the latter with amines upon refluxing in acetonitrile in the presence of DBU yields esters **35**, whose alkaline hydrolysis gives naphthyridonecarboxylic acids **31**. The latter exhibit high *in vitro* antibacterial activity against four types of Gram-positive bacteria and eight types of Gram-negative bacteria.[23] Examples of naphthyridonecarboxylic acids **31** are given in Table 1.

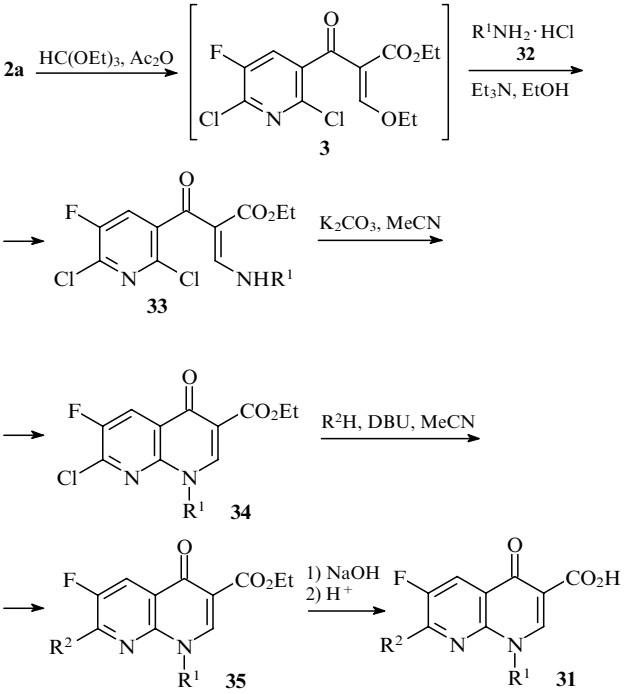

32: R^1 = Bu^t, FCH_2CMe_2, $(FCH_2)_2CMe$, $(FCH_2)_3C$.

6-Fluoro-4-oxo-1,4-dihydro-1,8-naphthyridine-3-carboxylic acid derivatives possess a very broad spectrum of biological activities, in particular, antibacterial action. Many compounds of this class exhibit high activity against various Gram-positive bacteria (*Staphylococcus aureus* ATCC 6538P, CMX 686B, FDA 209P JC-1; *Staphylococcus epidermidis* 3519, IAM 1296; *Streptococcus faecium* ATCC 8043, *Streptococcus pyogenes* 930) and Gram-negative bacteria (*Escherichia coli* Juhl, KC-14, K-12 C600; *Enterobacter aerogenes* ATCC 130048; *Klebsiella pneumoniae* 8045, PCI-602; *Pseudomonas aeruginosa* EZ, 5070, K799/WT; *Acinetobacter* CMX 669, AC54).[19,27]

Table 1. Substituted 1,8-naphthyridinecarboxylic acids **31**.

R^2	R^1	Yield (%)	Ref.
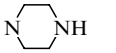	Bu^t	–	31
	FCH_2CMe_2	70	32
	$(FCH_2)_2CMe$	30	32
	$(FCH_2)_3C$	89	32
	Bu^t	–	36, 37
	FCH_2CMe_2	60	32
	$(CH_2F)_2CMe$	50	32
	$(CH_2F)_3C$	84	32
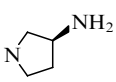	Bu^t	–	38
	$(FCH_2)CMe_2$	46	32
	$(FCH_2)_2CMe$	76	32
	$(FCH_2)_3C$	79	32
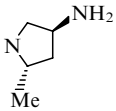	FCH_2CMe_2	65	32
	$(FCH_2)_3C$	78	32

These properties stimulated researchers to modify the 1,8-naphthyridine system by introducing various substituents using standard synthetic approaches. Biological activities of the compounds synthesised were tested, most publications being devoted to problems of analysis of toxicity, synergism of action of these compounds in various mixtures, elucidation of fine details of physiological actions of these compounds, *etc*. These aspects are beyond the scope of the present review, where only a bibliography of recent studies on fluoro-substituted 1,8-naphthyridones is given. Among these publications, numerous papers and patents concerned with the antibacterial drugs enoxacin (**1d**)[36–67] and trovafloxacin (**1e**)[68–187] are noteworthy.

In the literature (particularly, patent), other derivatives of fluorine-containing 1,8-naphthyridines have been described. For example, the review[188] was devoted to the synthesis, pharmacology, pharmokinetics and metabolism of 6-fluoronaphthyridinecarboxylic acids. Antibacterial[189–198] and antimicrobial[199,200] activities of these compounds were studied. These problems were also covered by many recent patents.[201–262]

Voluminous literature on 1,8-naphthyridine derivatives containing no fluorine is available. Explosion of interest in this class of heterocyclic compounds dates back to 1962, when Lesher and co-workers[263,264] synthesised 1-ethyl-7-methyl-4-oxo-1,4-dihydro-1,8-naphthyridine-3-carboxylic acid (**36**) (nalidixic acid) possessing strong antibacterial activity. The pharmacological properties of this compound are still being studied.[265–300]

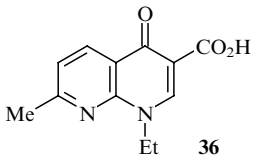

2-Chloronicotinoyl chloride (**37**) is widely used as the starting compound in the synthesis of various 1,8-naphthyridine derivatives. For example, its reactions with substituted 5-aminoacrylic acid anilides **38** produce aminomethylidene-1,8-naphthyridine-2,4-diones **39**.[301]

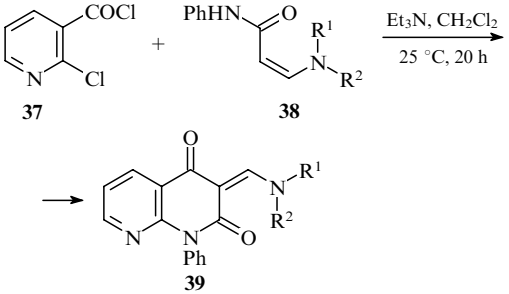

R^1 = H, Me; R^2 = Me, Et, Bn, 2-methyl-6-pyridyl.

The reactions of 2-chloronicotinoyl chloride (**37**) or 2-(3-chloroanilino)nicotinoyl chloride (**40**) with cyclic enamines (**41** and **42a**,**b**) in the presence of triethylamine afforded 1,8-naphthyridones **43** and **44a**,**b** possessing antiallergic, anti-inflammatory, antiulcerative and hypotensive actions.[302–306]

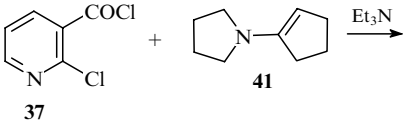

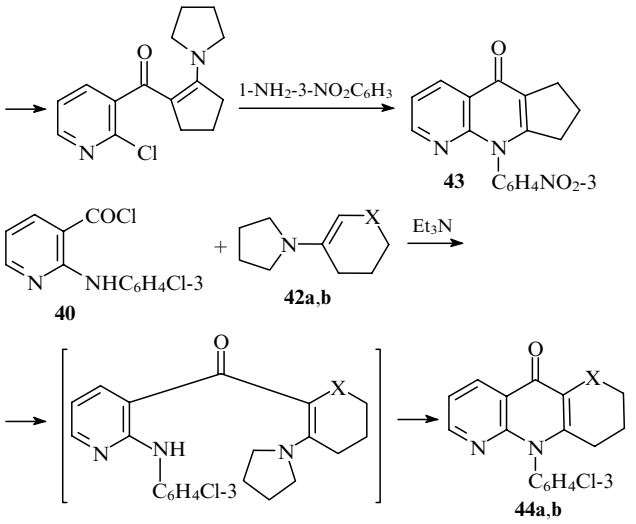

X = CH_2 (**a**), NAc (**b**).

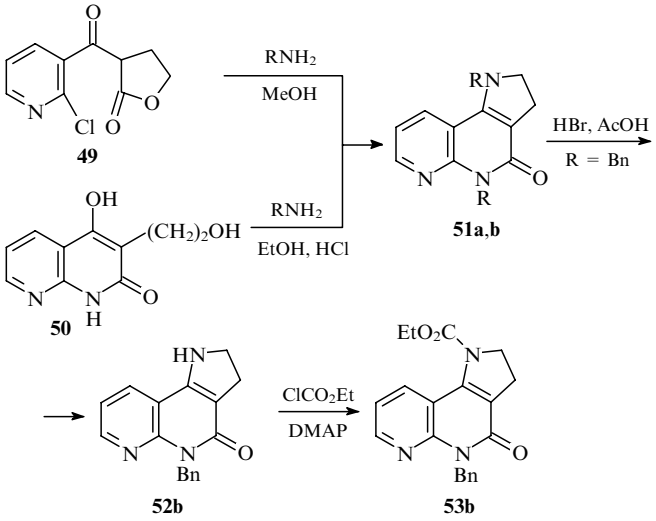

R = Ph (**a**), Bn (**b**); DMAP is 4-dimethylaminopyridine.

According to the ^{1}H NMR spectroscopic data, molecule **44a** is chiral. Naphthyridine **44a** exists as short-lived interconvertable atropoisomeric enantiomers, which form diastereomeric complexes with the shift-reagent [(*R*)-(−)-1-(9-anthryl)-2,2,2-trifluoroethanol]. The enantiomers were isolated in the individual form. The racemisation constant is 0.213 min^{-1} at 37 °C. The activation energy is E_a = 21.6 kcal mol^{-1}.[307]

The reaction of 2-chloronicotinoyl chloride **37** with di(benzothiazol-2-yl)methane (**45**) yielded fused naphthyridine system **46**.[308]

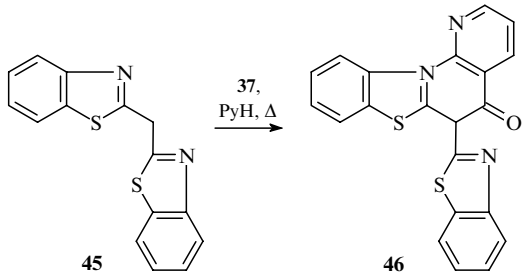

Imidazo[1,2-*a*][1,8]naphthyridine **47** was prepared by refluxing ethyl 2-chloronicotinate with 2-benzyl-4,5-dihydro-1*H*-imidazole (**48**) in toluene in the presence of sodium methoxide.[309]

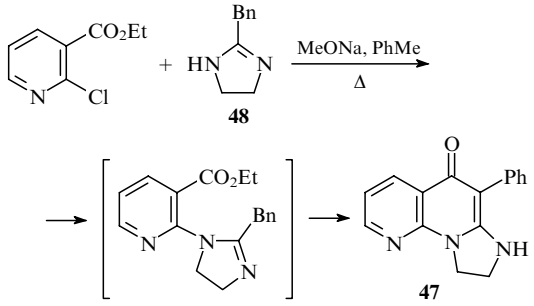

The reactions of 2-(2-chloronicotinoyl)butyrolactone (**49**) or 4-hydroxy-3-(2-hydroxyethyl)-1,8-naphthyridin-2-one (**50**) with amines (aniline or benzylamine) under an inert atmosphere afford pyrrolidinonaphthyridin-2-ones **51a**,**b**. Subsequent transformations of compound **51b** yield pyrrolidinonaphthyridones **52b** and **53b**. Derivatives **51a**,**b**, **52b** and **53b** possess anti-inflammatory and antihyperproliferative actions.[310, 311]

2-Aminopyridine and its derivatives are rather often used as the starting compounds in the synthesis of 1,8-naphthyridine derivatives.[312–353] For instance, the reaction of unsubstituted 2-aminopyridine with diethyl malonate in the presence of bases produces naphthyridinedione **54**, which exists as two tautomeric forms.[312, 313] Halogenation of compound **54** under various conditions (SO_2Cl_2, $POCl_3$, Br_2, I_2) gives rise to both 3-mono- and 3,3-dihalogen derivatives. The reactions of the latter with *o*-phenylenediamine and ethylene glycol form spiro-fused heterocycles **55** and **56**, respectively.[312]

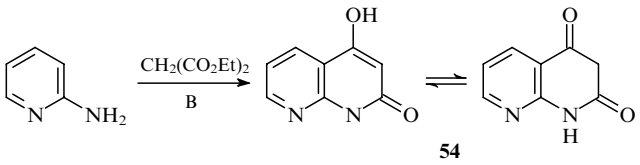

B is a base.

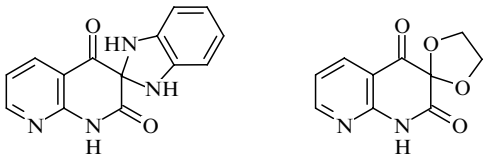

Substituted 2-aminopyridines, in particular, 2-amino-3-formylpyridine (**57**) and its derivatives, possess much higher synthetic potential.[316–319, 322–324, 326, 327, 331–333, 335, 336, 339, 353–356] For example, condensation of pyridine **57** in ethanol in the presence of piperidine as a base with compounds containing the active methylene group as well as with aldehydes, acyclic and cyclic ketones and diketones yielded 1,8-naphthyridines **58**–**61**, which were used as the starting compounds for the synthesis of derivatives **62**–**64**.[316, 318, 322–325, 349, 354] Naphthyridines **58** exhibit antibacterial and antihelmintic activities and are used in the synthesis of fungicides.[318, 323–325, 354] Compounds **59** are intermediates in the synthesis of some hypotensive drugs.[329] Naphthyridine **63** possesses herbicidal properties and is used for selective control of weeds in barley, wheat, maize, sorghum and rice crops.[349] 1,8-Naphthyridin-2-one derivative **62** is used for the treatment of memory disorders, in particular, Alzheimer's disease.[351]

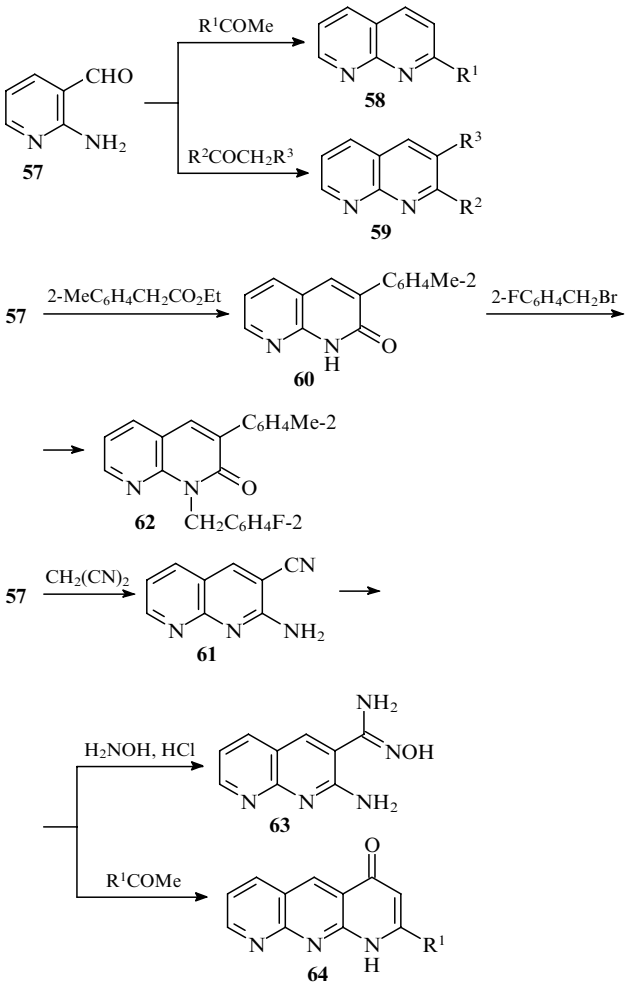

R^1 = Ph, 1-naphthyl, 2-pyridyl, 2-furyl, 2-thienyl, 2-HOC_6H_4, CH=CHPh; R^2 = Me, Ph; R^3 = Ph, COPh, CONHPh, MeCO.

There are numerous examples of the use of 2-amino-3-formylpyridine (**57**) in the synthesis of substituted 1,8-naphthyridines and their fused analogues. For instance, condensation of compound **57** with 2-acetyl-1-naphthol (**65**) in the presence of glacial acetic acid containing catalytic amounts of concentrated

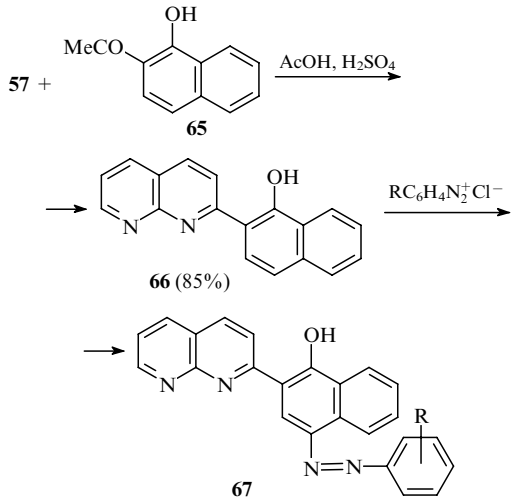

R = H, 2-Me, 4-Me, 3-MeO, 4-MeO, 3-OH, 3-NO_2, 3-Cl, 2-CO_2H, 3-CO_2H, 4-SO_3H, 4-SO_2NH_2.

H_2SO_4 afforded 2-(1,8-naphthyridin-2-yl)-1-naphthol (**66**).[323] Treatment of the latter with aryldiazonium salts gave 4-arylazo-2-(1,8-naphthyridin-2-yl)-1-naphthols (**67**) (60%–84% yields) possessing noticeable antibacterial activity.

2-Amino-3-(2-benzimidazolyl)-1,8-naphthyridine (**69**) was synthesised by the reaction of 2-amino-3-formylpyridine (**57**) with 2-cyanomethylbenzimidazole (**68**) in ethanol in the presence of trace amounts of piperidine.[316]

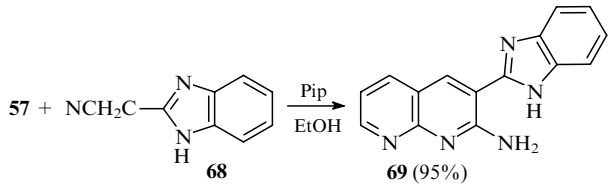

Pip is piperidine.

The reactions of aldehyde **57** with substituted 2-hydroxy-1-naphthyl styryl ketones **70**[318] or 1-hydroxy-2-naphthyl styryl ketones **71**[327] in glacial acetic acid in the presence of catalytic amounts of concentrated H_2SO_4 produce 8-aryl-8*H*-naphtho[1′,2′:5,6]pyrano[4,3-*b*][1,8]naphthyridines **72** or 6-aryl-6*H*-naphtho[2′,1′:5,6]pyrano[4,3-*b*][1,8]naphthyridines **73**, respectively. Compounds **72** and **73** showed no antibacterial activity.

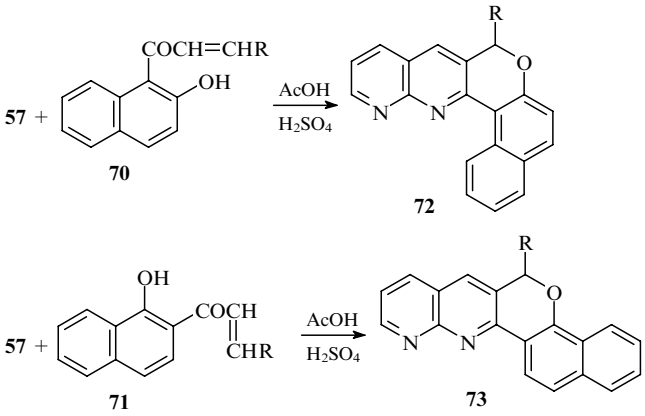

R = Ph, 4-$MeOC_6H_4$, 4-MeC_6H_4, 2-ClC_6H_4, 4-ClC_6H_4, 2-$NO_2C_6H_4$, 3-$NO_2C_6H_4$, 2-HOC_6H_4, 4-$Me_2NC_6H_4$, 1-naphthyl, 2-furyl, 2-thienyl.

Treatment of aminopyridinecarbaldehyde **57** with 7-azaindolinone **74** in toluene in the presence of piperidine affords pyrido[3′,2′:4,5]pyrrolo[3,2-*b*][1,8]naphthyridine (**75**).[334]

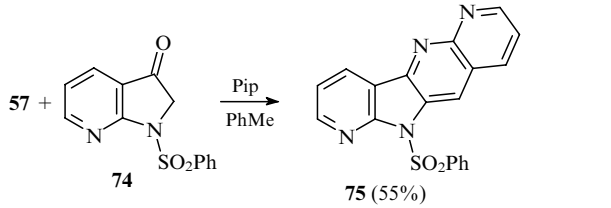

The same aminoaldehyde **57** was successfully used in the synthesis of polyannelated 1,8-naphthyridines. For example, 7,10-dihydrocycloocta[2,1-*b*:3,4-*b*′]di[1,8]naphthyridine (**77**) was prepared by the reaction of compound **57** with cyclooct-5-ene-1,2-dione (**76**) in ethanol in the presence of NaOH. The reaction of compound **77** with bromine in chloroform followed by debromination of adduct **78** with 1,5-diazabicyclo[4.3.0]non-5-ene (DBN) in toluene or DMSO produced cycloocta[2,1-*b*:3,4-*b*′]-di[1,8]naphthyridine (**79**), which is a new promising ligand system.[322, 333] The complex formation of ligand **79** with Cu(II) ions was studied.

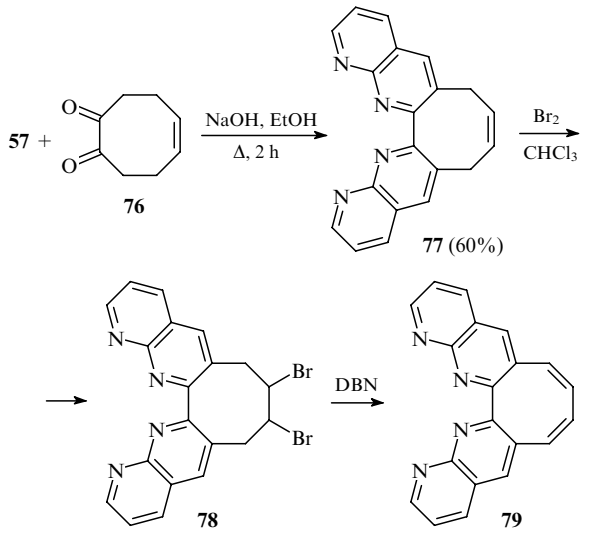

DBN is 1,5-diazabicyclo[4.3.0]non-5-ene.

Friedländer condensation of aminoaldehyde **57** with cyclic diketones **80** (anhydrous ethanol, KOH, refluxing under N_2, 4 h) gives rise to heptaannelated heterocyclic systems **81**.[335]

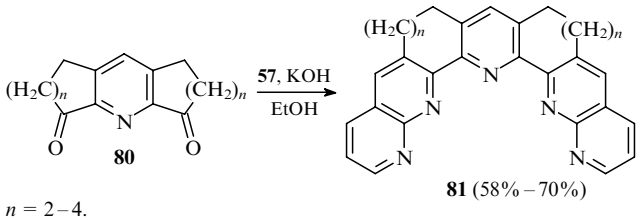

$n = 2-4$.

Analogous condensation with dione **82** in ethanol in the presence of piperidine as a base afforded a mixture of polyannelated bisnaphthyridines **83**–**85** in a total yield of 82% (Scheme 1).[336]

Under analogous conditions, α-aminopyridinealdehydes **86** react with activated and nonactivated ketones according to a cascade heterocyclisation scheme to form various 1,8-naphthyridine derivatives in satisfactory yields.

Treatment of compounds **86** with ethyl acetoacetate and piperidine in boiling ethanol affords aminonaphthyridine **87a** in 80% yield. Under the same conditions, the reactions with diethyl 3-oxoglutarate and *N*,*N*′-di-*tert*-butyl-3-oxoglutaramide produce naphthyridines **87b**,**c** in 35% and 40% yields, respectively. Condensation of aminoaldehyde **86** with diethyl malonate and 1,4-hexanedione affords naphthyridinone **88** and bis(aminonaphthyridine) **89**, respectively.[331]

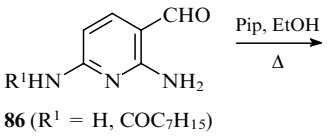

86 (R^1 = H, COC_7H_{15})

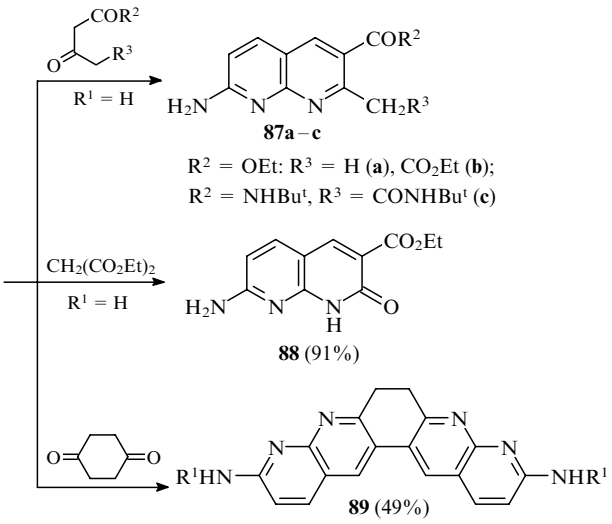

Analogous reactions with substituted 2-amino-3-formylpyridines as the starting substrates provide a promising approach to polyfunctional 1,8-naphthyridines, which are difficult to prepare. For example, refluxing of 6-amino-5-formyl-1,4-dimethyl-2-oxo-1,2-dihydropyridine-3-carbonitrile (**90**) and ethyl cyanoacetate in EtOH in the presence of piperidine produced the corresponding 1,8-naphthyridin-2-one (**91**).[353]

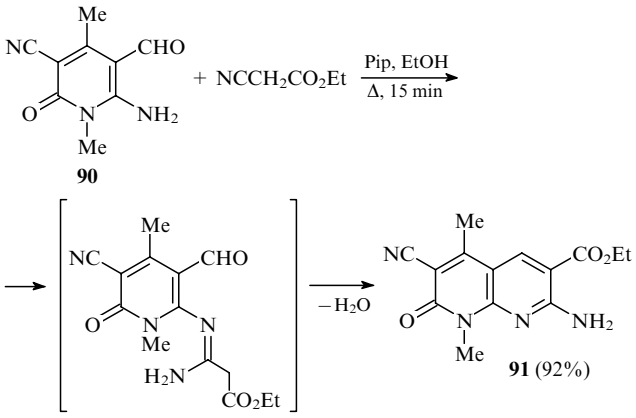

The use of 2-aminoaldehyde **92** in the synthesis of new polyfunctional heterocyclic systems **93** containing the 1,8-naphthyridine fragment serves as another example of this approach.[339] Deamination of amine **92** (*tert*-butyl nitrite, anhydrous $CuCl_2$, anhydrous MeCN) yields 2-chloro-3-formylpyridine **94**, whose treatment with secondary amine and triethylamine in THF gives rise to 2-dialkylamino-3-formylpyridines **95**. Knoevenagel condensation of compounds **95** with malononitrile in toluene (with the use of butylamine and ammonium acetate as catalysts) produces 2-dialkylamino-3-(2,2-dicyanovinyl)pyridine derivatives **96** in high yields. Thermolysis of the latter by boiling in a polar solvent (butanol or pentanol) or by heating in DMF or DMSO (140 °C) affords heterocyclic compounds **93** in yields from 10% to 100%.

Scheme 1

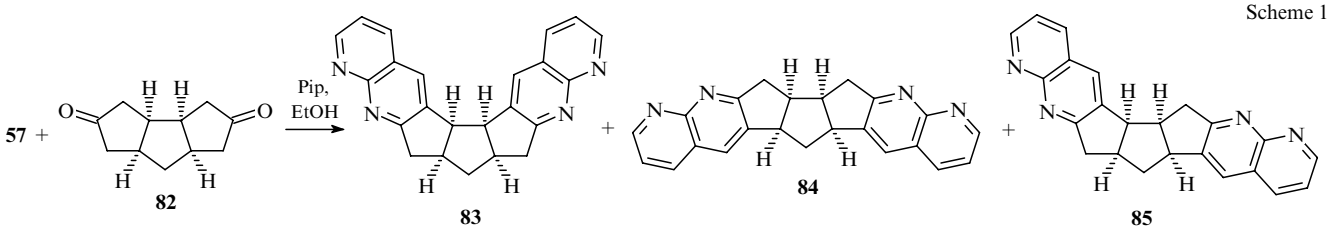

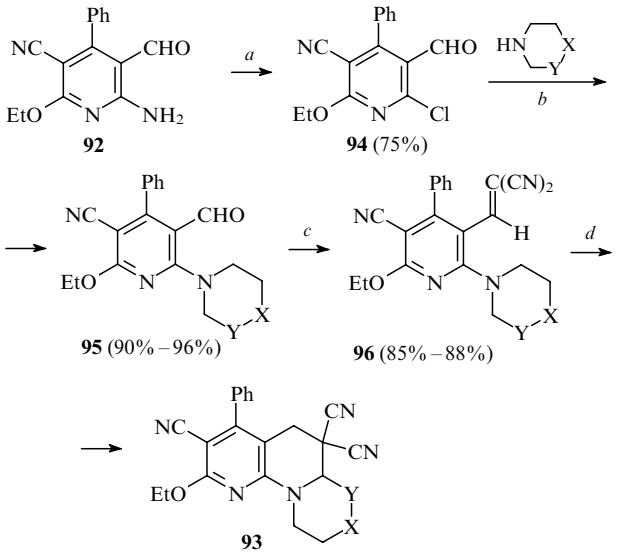

R = Pr^n, Bu^n; X = CH_2, $(CH_2)_2$, O, S; Y = CH_2, S.
(*a*) Bu^tONO, $CuCl_2$, MeCN, Δ, 15 min; (*b*) Et_3N, THF, Δ;
(*c*) 1) $CH_2(CN)_2$, Bu^nNH_2; 2) NH_4OAc, PhMe, Δ;
(*d*) RCH_2OH, Δ, 0.5 h – 7 days.

Substituted chloropyridine **94** was used as the starting compound in the synthesis of other derivatives of naphthyridine systems, such as isoindolo[2,1-*a*]-, isoquino[2,1-*a*]-, indolo[1,8,7-*a*,*b*]- and quino[1,9,8-*a*,*b*][1,8]naphthyridines.[340] The reactions of compound **94** with heterocyclic amines in the presence of triethylamine in THF or DMF produce the corresponding 2-dialkylamino-3-formylpyridine derivatives **97a**,**b** or 2-alkylarylamino-3-formylpyridine derivatives **98a**–**d** in 50%–95% yields. Knoevenagel condensation of the carbonyl groups of compounds **97a**,**b** or **98a**–**d** with malononitrile by refluxing in dichloromethane (2 h) in the presence of butylamine and ammonium acetate affords 2-dialkylamino- (**99a**,**b**) or 2-alkylarylamino-3-(2,2-dicyanovinyl)pyridine derivatives (**100a**–**d**, the yields of products **100a** and **100c** are 91%–95%), respectively. Heating of 2-dialkylamino derivatives **99a**,**b** and 2-alkylarylamino derivatives **100a**–**d** in polar solvents gives rise to tetracyclic compounds **101a**,**b** and **102a**–**d**, respectively.

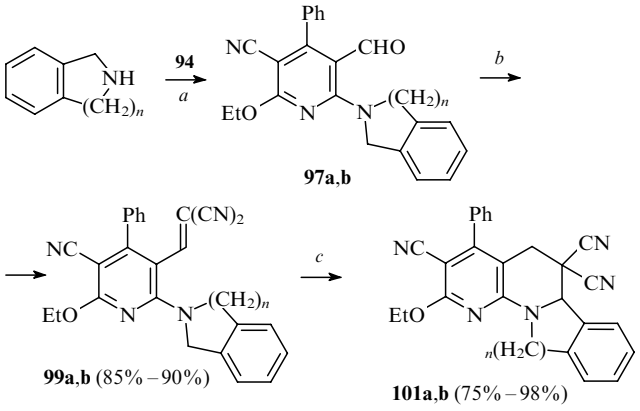

n = 1 (**a**), 2 (**b**);
(*a*) Et_3N, THF or DMF, Δ; (*b*) $CH_2(CN)_2$, $BuNH_2$, NH_4OAc;
(*c*) DMSO, 140 °C, 0.2 – 12 h.

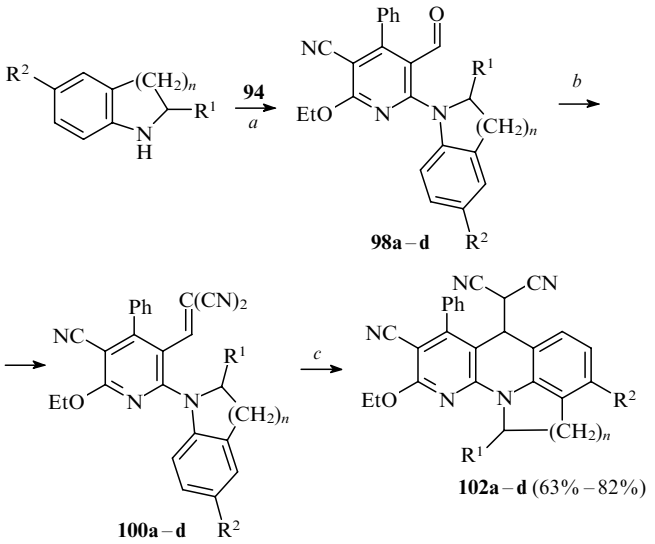

n = 1: R^1 = R^2 = H (**a**); R^1 = Me, R^2 = H (**b**);
n = 2: R^1 = R^2 = H (**c**); R^1 = Me, R^2 = F (**d**);
(*a*) Et_3N, THF or DMF, Δ; (*b*) $CH_2(CN)_2$, Bu^nNH_2, NH_4OAc;
(*c*) MeOH, Δ, 2 h.

N-Aryl-1,8-naphthyridines **103** possessing antiulcerative action were synthesised by Stobbe, Claisen or Knoevenagel condensations of substituted arylaminopyridinecarbaldehydes **104** with substituted carboxylic acids and their derivatives (esters, anhydrides, sodium salts).[343–347]

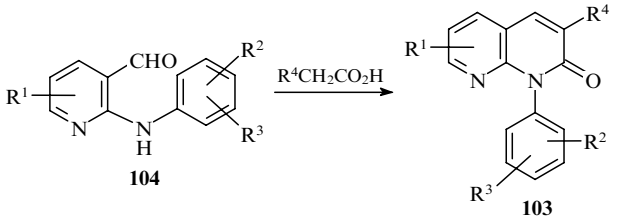

R^1 = H, Alk, cyclo-Alk, Hal, MeO, CF_3, NO_2; R^2, R^3 = H, Alk, Hal, CF_3, NO_2, MeO, MeS, $(CH_2)_nCN$, $(CH_2)_nCONH_2$;
R^4 = H, Alk, Alkenyl, NH_2, CO_2H, $HO_2C(CH_2)_n$, Ar, Het; *n* = 0–5.

With the aim of designing new potential antitumour drugs, procedures were developed for the synthesis of substituted 2-aryl-1,8-naphthyridin-4(1*H*)-ones using substituted 2-aminopyridines **105** and ethyl benzoylacetates **106** as the starting compounds.[314, 315] Their condensation in the presence of polyphosphoric acid (PPA) affords the corresponding pyridopyrimidinones **107**. Compounds **107** were also prepared by cyclisation of Schiff bases **108** with monochloroacetyl chloride in the presence of triethylamine. The subsequent thermal rearrangement of pyridopyrimidinones **107** at 350 °C gives rise to 2-phenyl-1,8-naphthyridin-4(1*H*)-ones **109**. An analogous approach was also used for the preparation of the corresponding 2-naphthyl-substituted 1,8-naphthyridinones.[352]

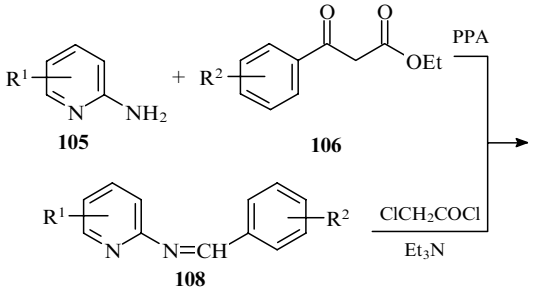

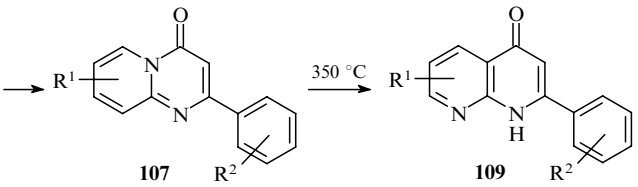

107 **109**

R^1 = H, Me, Cl, Br; R^2 = H, Me, F, Cl;
PPA is polyphosphoric acid.

Condensation of 2-aminopyridines **110a**,**b** with β-ketoesters or dicarboxylic esters provides a promising approach to the synthesis of 1,8-naphthyridines. The reaction is carried out at high temperature in polyphosphoric acid or Dowtherm.[357–367] For example, this procedure was used for the synthesis of 7-amino-2-hydroxy-1,8-naphthyridines **111**[357] and naphthyridones **112**.[359, 367]

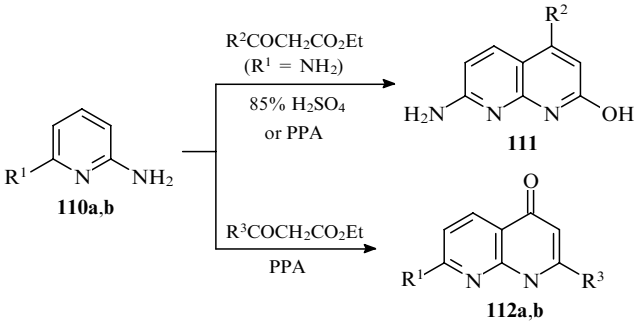

110a,**b** **111** **112a**,**b**

R^1 = Me (**a**), NH_2 (**b**); R^2 = Me, Pr, CF_3, $ClCH_2$, Ph;
R^3 = Me, Ph.

In some cases, pyrido[1,2-*a*]pyrimidines initially formed in analogous condensations (for example, compounds **113**–**115**) are isolated. Thermal isomerisation of these compounds affords oxo (**116**) or hydroxy derivatives (**117**, **118**) of 1,8-naphthyridines. Compounds **116**–**118** were subjected to subsequent transformations. For example, an additional ring was fused to naphthyridines **116** and **117**, and the successive reactions of naphthyridine **118** with $POCl_3$ and $N_2H_4 \cdot H_2O$ produced hydrazine **119**, which was transformed into amine **120**.[365]

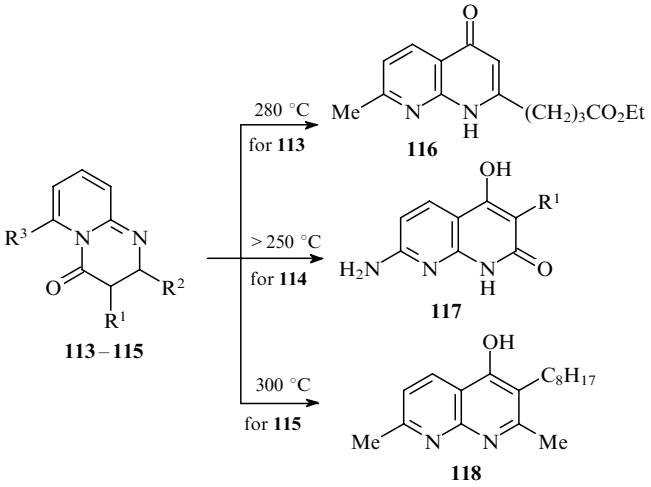

113–**115** **116** **117** **118**

R^1 = H, R^2 = $(CH_2)_3CO_2Et$, R^3 = Me (**113**);
R^1 = H, Alk, Ph; R^2 = OH, R^3 = NH_2 (**114**);
R^1 = *n*-C_8H_{17}, R^2 = Me, R^3 = Me (**115**).

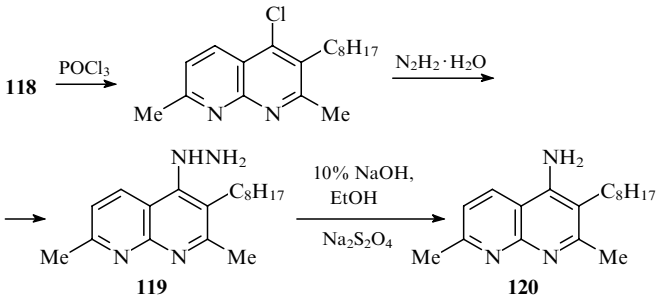

118 **119** **120**

Naphthyridine **111** (R^2 = $ClCH_2$) was covered by a patent as an agent reducing the phytotoxicity of herbicides belonging to cyclohexenones or phenoxyacetic acids.[362] Naphthyridone **112** (R^3 = Me) was used as an intermediate in the synthesis of compounds possessing antimalarial activity against *Plasmodium vinckei vinckei*.[361] Compounds **119** and **120** in doses of 0.1–5 kg hectare^{-1} exhibit fungicidal activity against phytopathogenic fungi (particularly, *Phycomyceten*) and are efficient against *Phytophtora infestans* on tomatoes and potatoes as well as against *Pseudoperonspora cubensis* on cucumbers.[363]

Other substituted pyridopyrimidines can also be used as starting compounds in the synthesis of 1,8-naphthyridine derivatives. For example, thermolysis of 4-oxo-4*H*-pyrido[1,2-*a*]pyrimidin-3-yl acrylates **121** afforded 2-substituted 1,8-naphthyridin-3-yl acrylates **122**, pyranonaphthyridines **123** or anthyridines **124** depending on the nature of the substituent at position 2 of the starting pyridopyrimidine.[365]

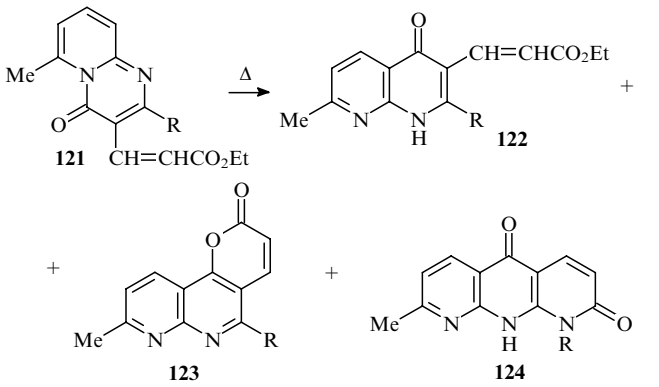

121 **122** **123** **124**

R = NHBu, Ph, Pip.

Other 2-aminopyridines were also successfully used in the synthesis of substituted 1,8-naphthyridines. For example, condensation of 2-amino-3-benzoylpyridine (**125**) with malonic acid derivatives in the presence of piperidine followed by hydrolysis of the reaction mixture affords 4-phenyl-1,8-naphthyridines **126** and **127**. Further hydrolysis of nitrile **127** gives amide **128**. Compounds **126** and **128** possess diuretic action.[330]

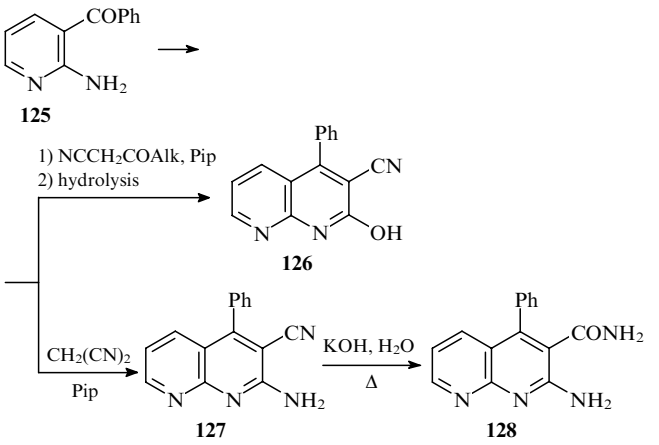

125 **126** **127** **128**

6,7,8,9-Tetrahydrobenzonaphthyridines **129** and **130** were prepared by condensation of 2-amino-3-acylpyridines **131**[366] or 2-amino-3-cyanopyridines **132**[367] with cyclohexanone.

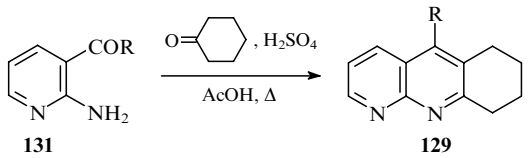

R = Me, Ph.

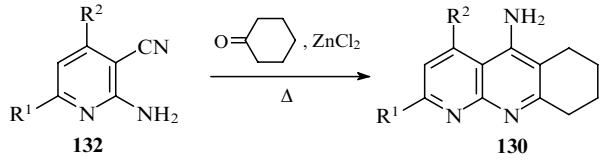

R^1, R^2 = Ph, 4-ClC_6H_4.

1,8-Naphthyridines can also be prepared by the reactions of substituted 2-alkylaminonicotinic acids with malonic acid derivatives. Cyclocondensation of nitriles **133** or esters **134** with $ClCOCH_2CO_2Et$ in anhydrous diethyl ether at 20 °C and then with EtONa in ethanol affords substituted 2-oxo-1,8-naphthyridine-3-carboxylic acids **135** and **136**, respectively. Compounds **135** were also synthesised by the reactions of nitriles **133** with a mixture of two equivalents of $(EtO_2C)_2CH_2$ and Na in anhydrous ethanol. Naphthyridinecarboxylic acids **135** and **136** were used in the synthesis of compounds which inhibit gastric secretion.[368]

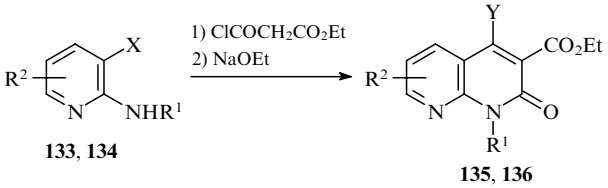

X = CN (**133**), CO_2Me (**134**); Y = NH_2 (**135**), OH (**136**);
R^1 = H, Me, Et, All; R^2 = H, Me.

Procedures were developed for the synthesis of various 1,8-naphthyridin-2-one derivatives based on condensation of methyl 2-arylaminonicotinates **137** and carbonyl compounds containing an activated methylene group. This method was used, for example, for the preparation of naphthyridones **138** and **139** exhibiting antiallergic, anti-inflammatory and antiulcerative actions.[369–385]

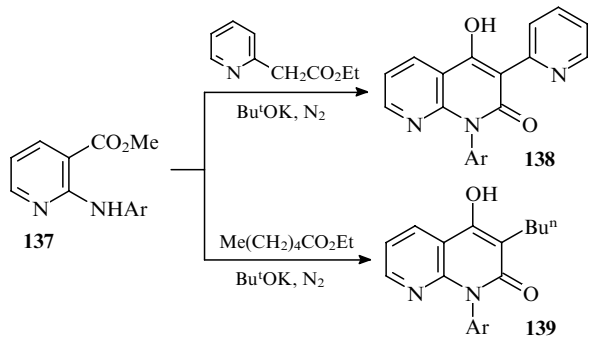

Ar = Ph, 4-$MeOC_6H_4$, 3,4-$(MeO)_2C_6H_3$, 4-FC_6H_4, 2,4-$F_2C_6H_3$, 2-Me-3-ClC_6H_3, 3-$MeSC_6H_4$.

2-Amino-3,5-dicyano-6-methoxy-4-(*p*-tolyl)pyridine (**140**) was used in the synthesis of 4-amino-1,8-naphthyridin-2(1*H*)-ones **141** and **142**. Condensation of compound **140** with methyl cyanoacetate in the presence of sodium amide or acetic anhydride in polyphosphoric acid yields naphthyridones **141** and **142**. Compound **143**, which was prepared by the reaction of aminonitrile **140** with hydrazine hydrate, underwent condensation with methyl cyanoacetate to form naphthyridone **144** (Scheme 2).[385]

4,6-Diaminopyridine-2(1*H*)-thione **148** was used as the starting compound for the synthesis of amino derivatives of 1,8-naphthyridine-2(1*H*)-thiones **145**–**147**.[386, 387] The reactions of **148** with malonic acid derivatives proceed in DMF in the presence of piperidine or in ethanol in the presence of triethylamine.

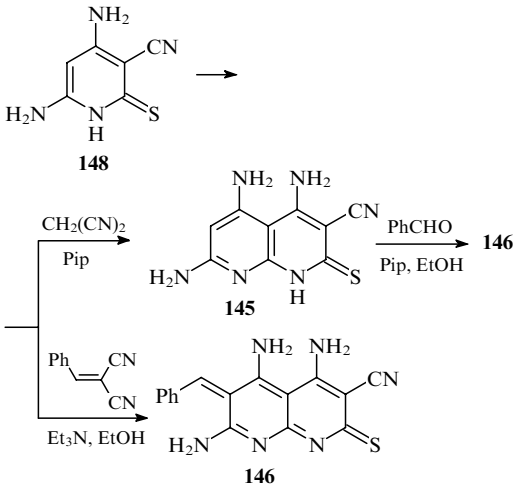

Scheme 2

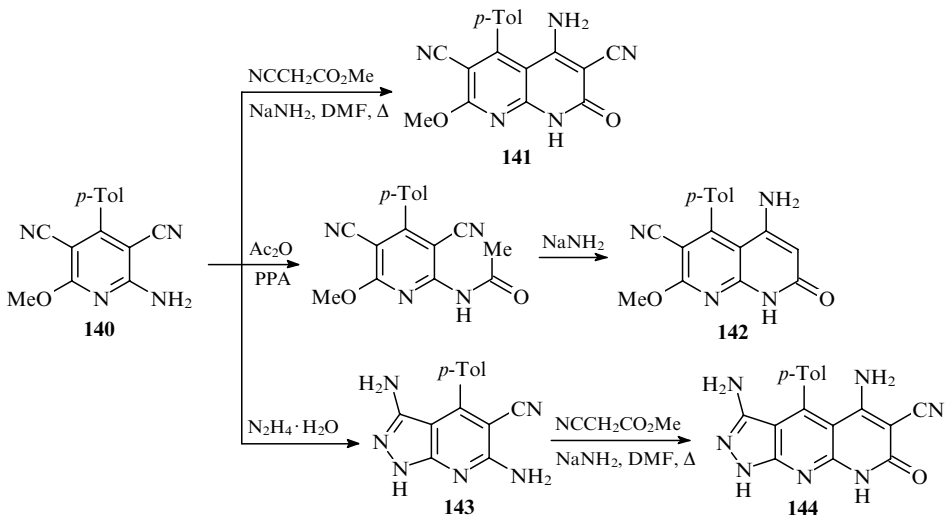

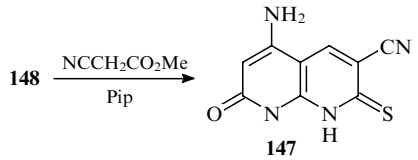

Ethyl 3-aminopyridine-2-carboxylate (**149**) reacts with 2-methoxyphenylacetyl chloride (**150a**) to form 1,5-naphthyridine (**151**). The analogous reaction of ethyl 2-aminopyridine-3-carboxylate (**152**) with ethyl 2-methoxyphenylacetate (**150b**) produces isomeric 1,8-naphthyridine (**153**).[388]

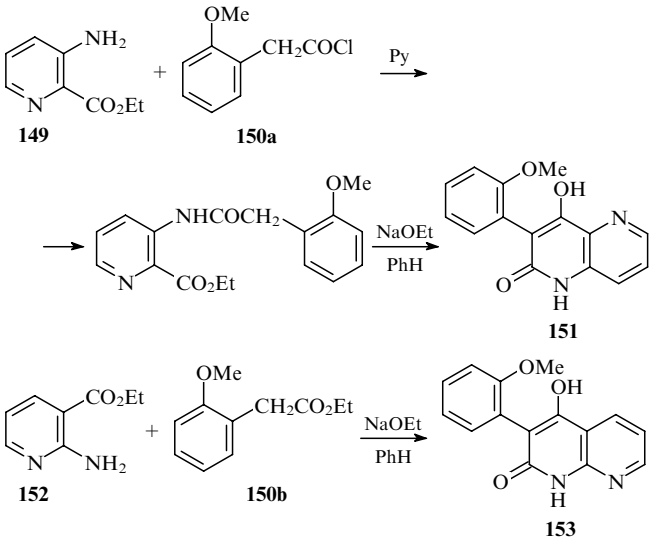

Cyclisation of substituted 2-(2-cyanophenylimino)piperidines **154** by refluxing in nitrobenzene in the presence of $ZnCl_2$ afforded 5-aminobenzonaphthyridines **155**, which were covered by a patent as drugs for the treatment of memory loss, aging and Alzheimer's disease.[389]

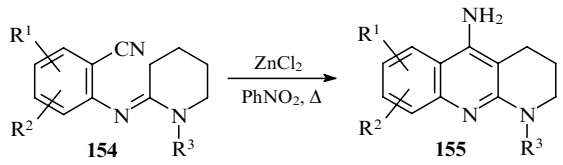

R^1 = H, 6-F, 6-Cl, 7-NO_2; R^2 = H, 8-Cl; R^3 = H, Ac, COPh.

A convenient regioselective procedure was developed for the synthesis of new heterocycles, *viz*., 5-phenyl-1*H*- (**156**) and 5-phenyl-3*H*-imidazo[4,5-*c*][1,8]naphthyridin-4(5*H*)-ones (**157**), starting from 2-phenylaminonicotinic acid (**158a**) or its methyl ester (**158b**).[390–394] Treatment of ester **158b** with trichloromethyl chloroformate in 1,2-dichloroethane at 80 °C affords *N*-phenyl-3-azaisatinic anhydride (**159**). The reaction of the latter with sodium hydride and ethyl nitroacetate in *N*,*N*-dimethylacetamide produces 4-hydroxy-3-nitro-1-phenyl-1,8-naphthyridin-2(1*H*)-one (**160**). Chlorination of naphthyridone **160** with phosphorus oxychloride gives rise to chloride **161**, which is transformed into the target naphthyridines by successive amination, reduction and cyclisation. Imidazonaphthyridones **156** and **157** are new non-steroid anti-inflammatory drugs possessing activity analogous to that of glucocorticoids (Scheme 3).

A new efficient procedure was proposed[368,395–398] for the synthesis of 3-substituted 1,8-naphthyridine-2,4-diones, which are of considerable pharmacological interest. The reactions of 2-methyl-4*H*-pyrido[2,3-*d*][3,1]oxazin-4-one (**162**) with compounds containing an active methylene group in the presence of potassium *tert*-butoxide in *tert*-butyl alcohol or in the presence of sodium hydride in anhydrous benzene produce 3-substituted 1-acetyl-1,2,3,4-tetrahydro-1,8-naphthyridine-2,4-diones **163** in yields of up to 87%.[399] Evidently, the reactions proceed through intermediates **164**.

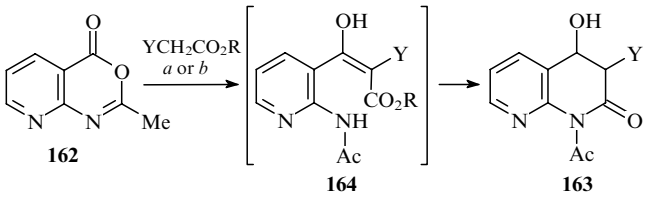

Y = EWG, R = Alk;

(*a*) Bu^tOK, Bu^tOH, 20 °C; (*b*) NaH, PhH, 20 °C

Amines of the isoquinoline series can be used as the starting compounds for the preparation of benzoannelated 1,8-naphthyridines. The reactions of 3-aminoisoquinolines **165** with ethyl acetoacetate form 4-methylbenzo[*c*][1,8]naphthyridin-2(1*H*)-ones **166** or their isomers **167** depending on the reaction conditions.[400–402]

Scheme 3

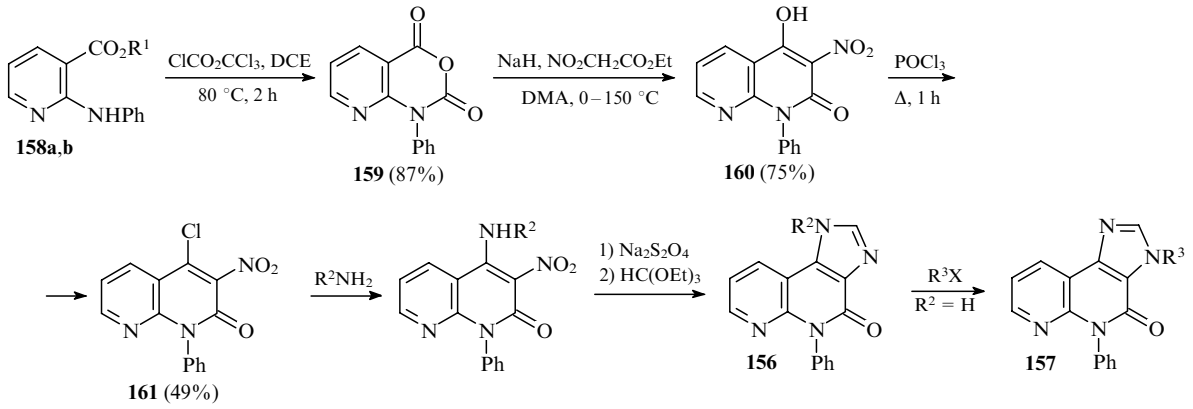

R^1 = H (**a**), Me (**b**); R^2 = H, Et, Pr^i, Bn; R^3 = Me, Et, Pr^n, Pr^i, Bu^n, Bu^t, C_6H_{13}, Bn, $CH(Me)C_6H_5$;

X = I, Cl, Br; DCE is 1,2-dichloroethane; DMA is *N*,*N*-dimethylacetamide.

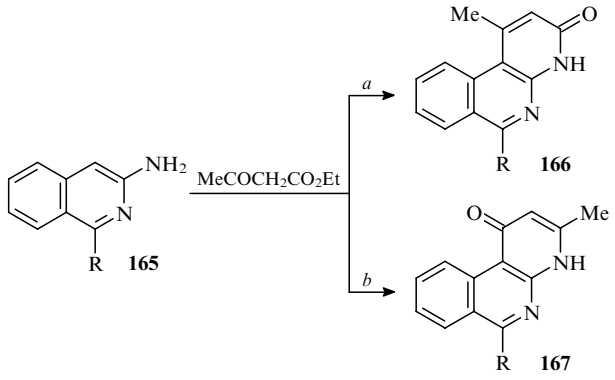

R = MeO, 4-MeC$_6$H$_4$O;

(*a*) AcOH, 150 °C; (*b*) $CaSO_4$, AcOH, EtOH.

Cyclocondensation of 3-amino-1-(*p*-tolyloxy)isoquinoline-4-carbaldehyde **168** with acetone or cyanoacetic acid derivatives in the presence of bases yields substituted benzo[*c*][1,8]naphthyridines **169**–**172**.[403]

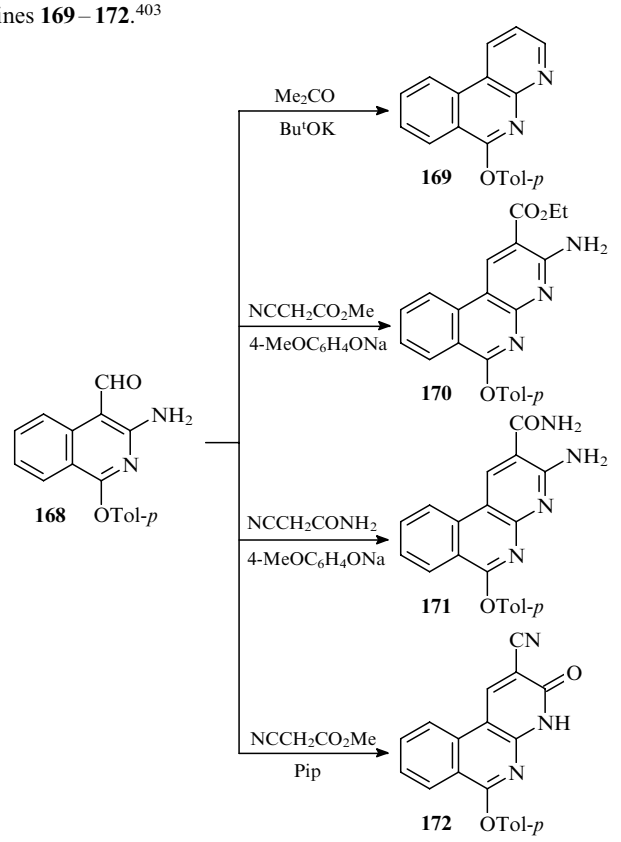

The reaction of ethyl 2-amino-5,6-dihydro-4*H*-cyclopenta[*c*]-nicotinate (**173a**, $n = 1$) with *N*,*N*-dimethylacetamide diethyl acetal produces 1,4-dihydro-4-oxo-1,8-naphthyridine derivative **174a**. Reactions with methylbutyro-, -valero- and -caprolactam diethyl acetals afford tetracyclic compounds **175a**. Similar reactions giving rise to naphthyridone **174b** ($n = 2$) and tetracyclic compounds **175b** were also performed using the cyclohexane analogue of compound **173**.[404]

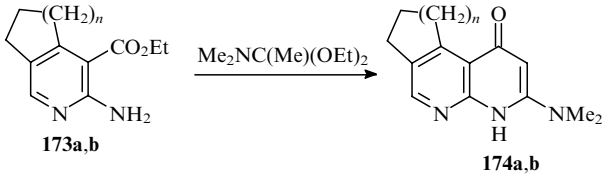

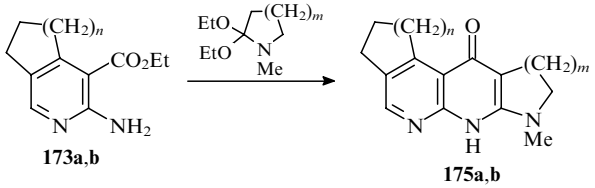

n = 1 (**a**), 2 (**b**); m = 1–3.

Protonation of naphthyridones **175a**,**b** was studied by UV and ^{1}H and ^{13}C NMR spectroscopy.[404] It was found that protonation occurs at the carbonyl group to give the cationic form **A**. In 70% DMF, the ionisation constants of naphthyridones **175a**,**b** depend on the size of the saturated cyclic fragments of the molecules, which is associated with steric factors, such as a change in steric accessibility of the polar groups of the cationic (**A**) and anionic (**B**) forms to solvation.[404]

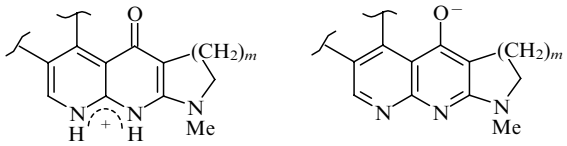

m = 1–3.

1,8-Naphthyridinones were also synthesised starting from 6-aminopyridin-2-one (**176**).[405] Its condensation with enones **177** in the presence of 2,3-dichloro-5,6-dicyano-1,4-benzoquinone (DDQ) in DMF afforded ethyl 2-oxo-1,8-naphthyridine-6-carboxylate (**178**). This naphthyridine was transformed into compound **179** in five steps. This compound was covered by a patent as a drug for the treatment of hyperlipoproteinemia, atherosclerosis and lowering of blood cholesterol levels.[405]

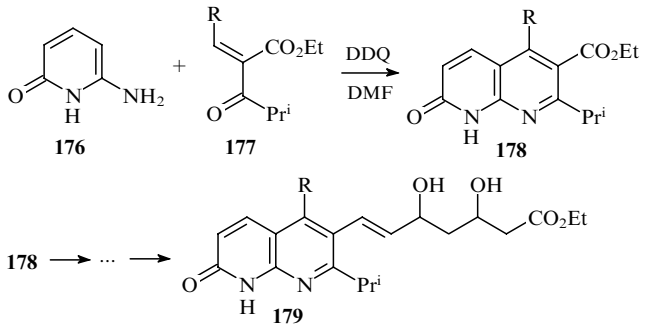

R = Ar, Het.

5,5-Dimethyl-5,10-dihydrobenzo[*b*][1,8]naphthyridines **181** were prepared in yields of up to 87% by intramolecular cyclisation of 2-arylamino-3-(1-hydroxy-1-methylethyl)pyridines **180** in polyphosphoric acid. Alkylation of benzonaphthyridines **181** with dialkylaminoalkyl halides in the presence of KOH in toluene gives rise to 10-substituted benzonaphthyridines **182** (yields of up to 88%), which are analogues of the corresponding acridines possessing a broad spectrum of biological activities.[406]

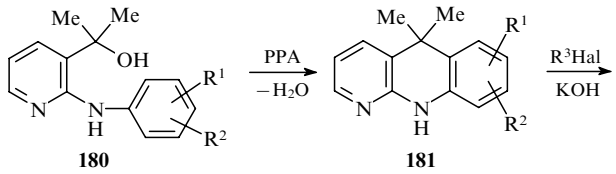

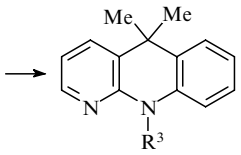

182

R^1 = H, 7-MeO, 7-EtO, 7-Cl, 8-Cl, 9-Cl; R^2 = H, 9-Me, 9-Cl; R^3 = $CH_2CR^4(CH_2)_nNR^5R^6$, n = 0, 1; R^4 = H, Me; R^5, R^6 = Me, Et, Pr^i, Bu^n, Bn; R^5-R^6 = $(CH_2)_5$, $(CH_2)_2O(CH_2)_2$, $(CH_2)_2NMe(CH_2)_2$, $(CH_2)_2N(CH_2CH_2OH)(CH_2)_2$, $(CH_2)_3CO(CH_2)_2$; Hal = Cl, Br.

Refluxing of 2-(3-ethoxycarbonyl-4-oxo-4,5-dihydrofur-2-yl)aminopyridines **183** in diphenyl ether leads to their cyclisation to furo[2,3-*b*][1,8]naphthyridine-3,4(2*H*,9*H*)-diones **184**, which exhibit antiallergic activity.[407]

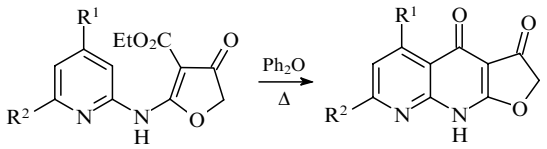

183 **184** (78%–85%)

R^1, R^2 = H, Me.

Cyclisation of substituted thiourea **185** occurs under the action of mercury oxide in methanol saturated with ammonia to give 1,8-naphthyridine derivative **186**.[408]

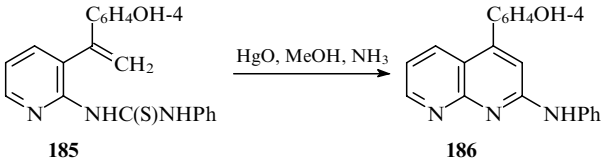

185 **186**

Photochemical cyclisation (DRL-400 mercury lamp, 60% *tert*-butyl alcohol, 20 °C, 10 h) of 8-chloro-1-(2-pyridylamino)naphthalene (**187**) was studied. The reaction proceeds non-selectively to form C–C and C–N bonds and produces new polyannelated heterocyclic systems, *viz*., 7*H*-7,8-diazabenzo[*de*]anthracene (**188**) containing the 1,8-naphthyridine fragment, dimer **189** and pyrido[1,2-*a*]perimidine (**190**). Compounds **188**–**190** were separated by chromatography on silica gel (Scheme 4).[409,410]

Hydroxy derivatives of the pyridine series were used as the starting compounds in the synthesis of annelated 1,8-naphthyridines. Benzo[*b*][1,8]naphthyridines **193** and **194** were synthesised

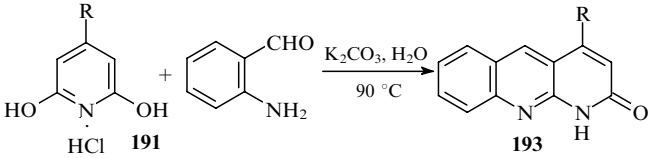

191 **193**

R = H, Me.

by Friedländer condensation of hydroxypyridines **191** and **192**, respectively, with 2-aminobenzaldehyde.[411]

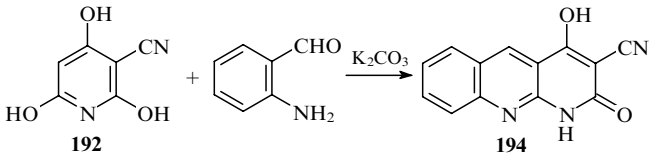

192 **194**

Imidazo[1,2-*a*]naphthyridines **195**–**197** were prepared by the reaction of 5-aminoimidazo[1,2-*a*]pyridine (**198**) with 1,1,3,3-tetramethoxypropane, acetoacetaldehyde dimethyl acetal or acetylacetone under the conditions of the Combes reaction (reaction with H_3PO_4, 2 h).[412]

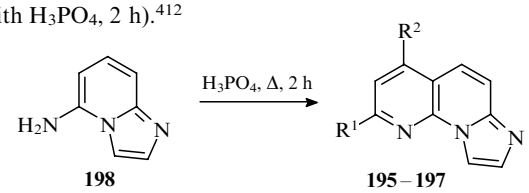

198 **195**–**197**

Reagent	Compound	R^1	R^2
$(MeO)_2CHCH_2CH(OMe)_2$	**195**	H	H
$MeCOCH_2CH(OMe)_2$	**196**	Me	H
$MeCOCH_2COMe$	**197**	Me	Me

Triazolonaphthyridines **199** and **200** were synthesised by condensation of Schiff base (**201**) of the 1,2,4-triazolo[4,3-*a*]pyridine series with malononitrile or its benzylidene derivative in the presence of organic bases (Scheme 5).[413]

The enamino fragment of hexahydroimidazo[1,2-*a*]pyridine-8-carboxylic acid **202** reacts with the triple bond of acetylenedicarboxylates to form compounds **203** in quantitative yields. Their

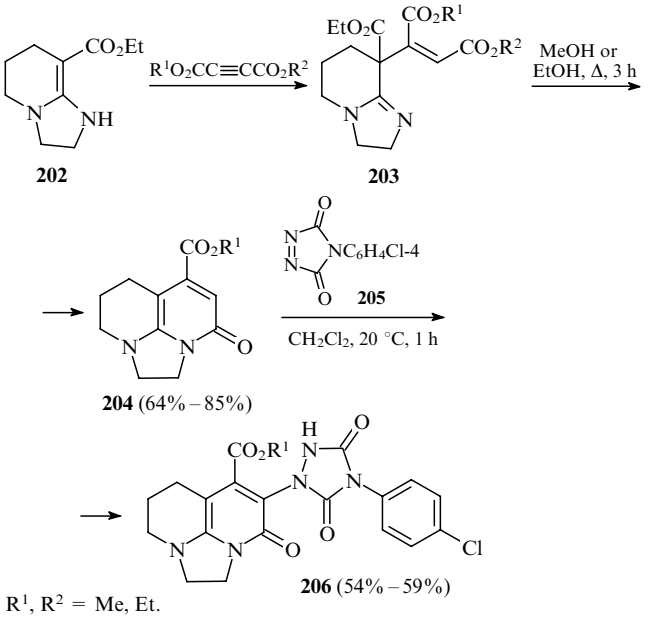

202 **203** **204** (64%–85%) **205** **206** (54%–59%)

R^1, R^2 = Me, Et.

cyclisation (20 °C, 2 days, then refluxing in MeOH or EtOH, 3 h) gives rise to partially hydrogenated imidazonaphthyridines **204**, which react with dione (**205**) to give 6-(1,2,4-triazolidin-1-yl)imidazo[1,2,3-*ij*][1,8]naphthyridines (**206**).[414]

Scheme 4

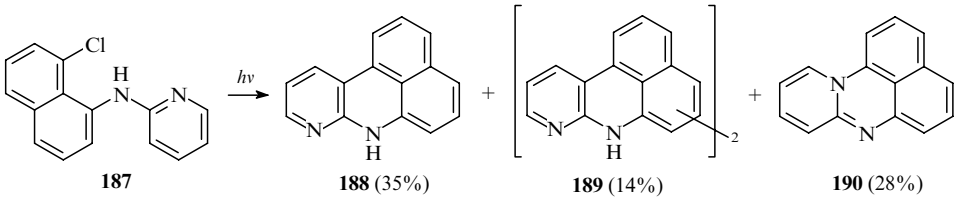

187 **188** (35%) **189** (14%) **190** (28%)

Scheme 5

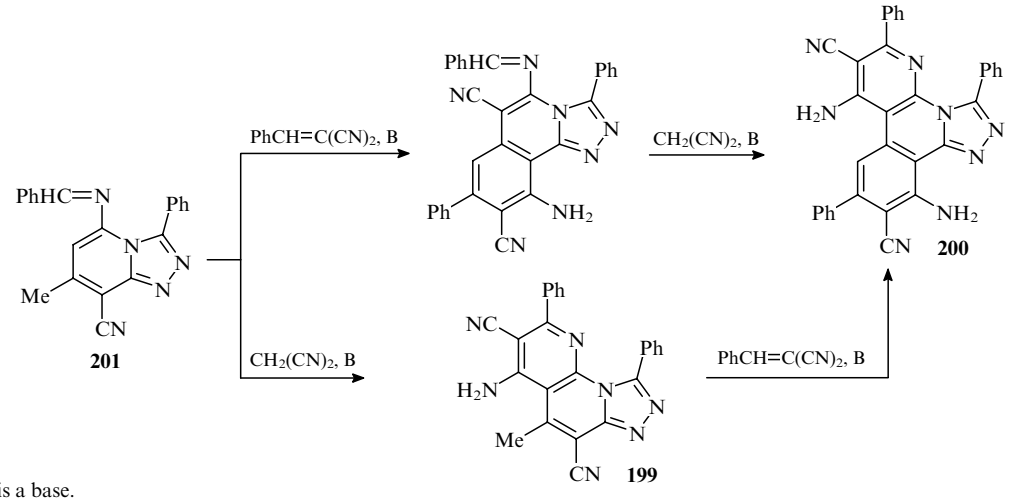

B is a base.

Hexahydroindolo[1,2-*a*]-1,8-naphthyridines **207** containing *cis*-fused rings were synthesised with high stereoselectivity by the electrochemical [4 + 2]-cycloaddition of 2-vinylindoles **208** and β-substituted enamines (**209**) of the tetrahydropyridine series in acetonitrile.[415]

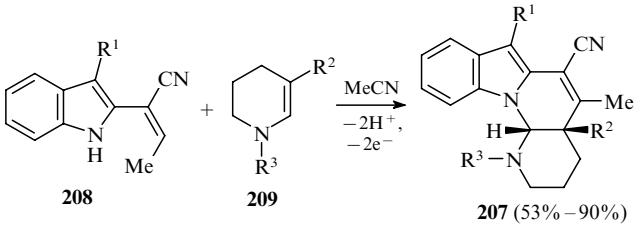

R^1 = Me, $(CH_2)_2OEt$; R^2 = CN, CO_2Me; R^3 = H, Me.

The Pictet–Spengler reaction of tryptamine with aldehyde **210** produces the bisindole derivative of decahydronaphthyridine-2,7-dione **211** along with two isomeric tryptamides **212a** (*cis*-1-Et) and **212b** (*trans*-1-Et).[416]

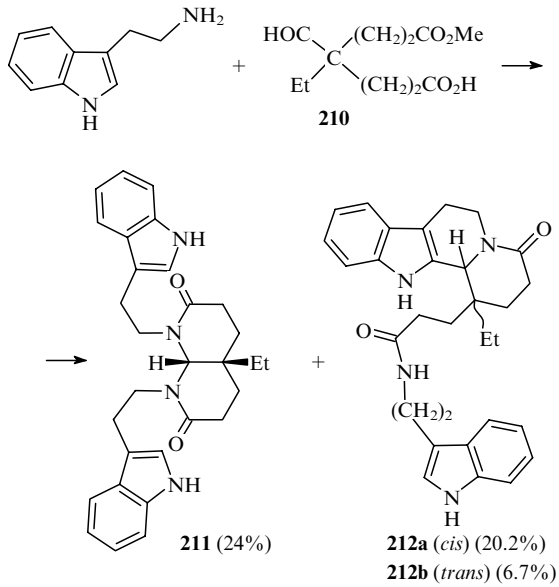

The reaction of imidazo[1,2-*a*]pyridine derivative **213** with a twofold excess of methyl vinyl ketone in acetonitrile proceeds with high stereoselectivity to form exclusively *cis*-dihydroxyimidazo[1,2,3-*ij*][1,8]naphthyridine **214**.[417]

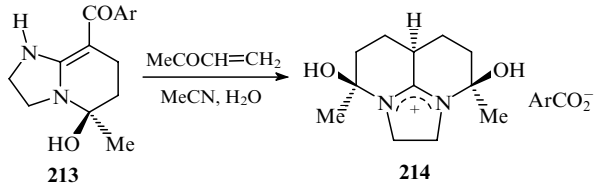

Ar = Ph, 2-furyl, 2-thienyl.

A one-step procedure was developed for the synthesis of the previously unknown dihydro-*1H*-1,9-diazaphenalene **215**, which also contains the 1,8-naphthyridine fragment.[418] The synthesis scheme involves O-allylation, condensation of the reaction product with ethyl azidoacetate and the Staudinger reaction with triphenylphosphine. This procedure was used for the preparation of iminophosphorane **217** from commercially available 2-hydroxy-3-methoxybenzaldehyde (**216**). The reactions of compound **217** with aromatic isocyanates produce carbodiimides **218**, whose thermolysis yields diazaphenalenes **215**.

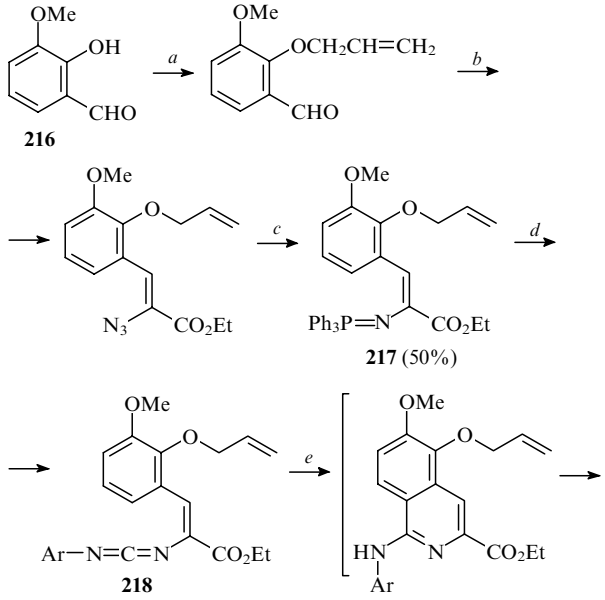

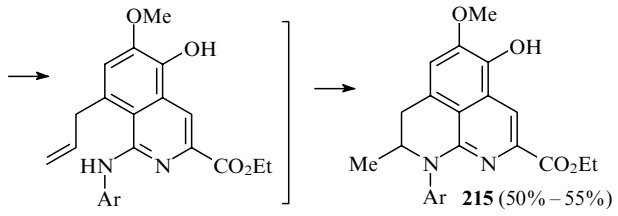

Ar = Ph, 4-MeC_6H_4, 4-$MeOC_6H_4$, 4-ClC_6H_4, 4-FC_6H_4;
(*a*) $BrCH_2CH=CH_2$, K_2CO_3, Me_2CO, Δ; (*b*) $N_3CH_2CO_2Et$, NaOEt, EtOH, −15 °C; (*c*) PPh_3, Et_2O, 20 °C; (*d*) ArNCO, PhMe, 20 °C, 1 h; (*e*) sealed tube, PhMe, 150–160 °C, 12 h.

Cyclisation of 1,1-bisanilino-2,2-dicyanoethylene (**219**) under the action of trifluoromethanesulfonic acid in dichloromethane giving rise to 11,12-diaminodibenzo[*b*,*g*][1,8]naphthyridine (**220**) provides an example of the synthesis of annelated 1,8-naphthyridines.[419]

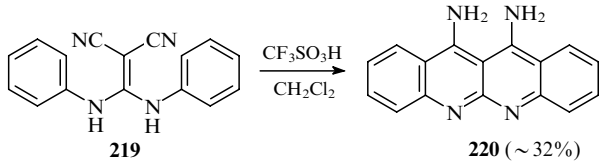

Condensation of iminium salt **221** with aniline in the presence of triethylamine occurs regioselectively. The subsequent replacement of the anion in the presence of 70% $HClO_4$ affords linearly annelated cycloadduct **222**.[420]

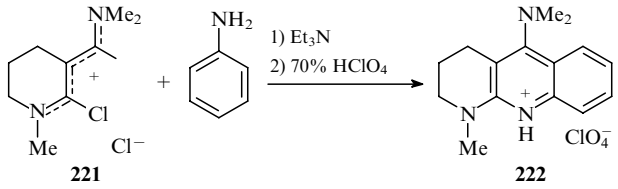

In the study,[421] diethyl 2,6-dimethylpyridine-3,5-dicarboxylate (**223**) was synthesised by the Hantzsch reaction of ethyl acetoacetate with hexamethylenetetramine (AcOH, 100 °C). In the course of the reaction, symmetrical bicyclic naphthyridine derivative **224** was detected. According to the X-ray diffraction data, the rings in compound **224** are *cis*-fused and adopt an envelope conformation. It was hypothesised that compound **224** is generated as a result of diene condensation of the intermediates, *viz*., 1,4-dihydropyridine **A** and heterodiene **B**, derived *in situ* from ethyl 2-methyleneacetoacetate and ammonia. The low yield of naphthyridine derivative **224** (2.3%) is attributable to its instability in AcOH. At 100 °C, the transformation of this derivative into pyridine **223** is completed in 0.5 h, although compound **224** is rather stable in EtOH, Pr^iOH and DMF.

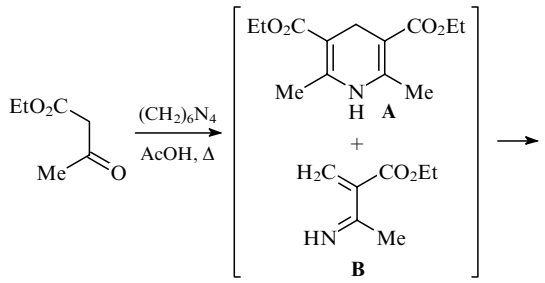

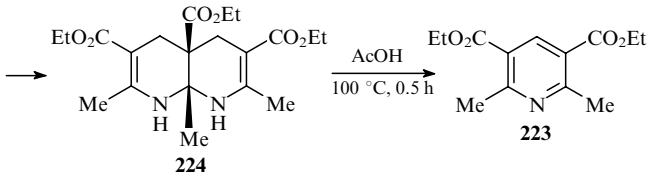

Hydrogenated 1,8-naphthyridines were synthesised by the reaction of dinitriles **225** with K_2CO_3 in aqueous alcohol. Intramolecular cyclisation affords 4*a*-aryl-8*a*-methyl-2,7-dioxo-1,8-naphthyridines **226**.[422]

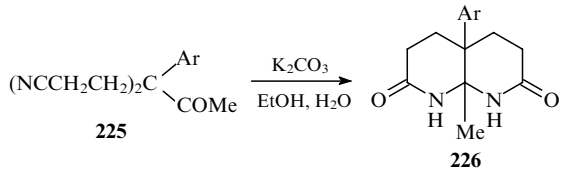

Ar = Ph, 3,4-$(MeO)_2C_6H_3$.

III. Physicochemical properties and reactivities of 1,8-naphthyridine derivatives

Data on the structures, physicochemical properties and reactivities of pyridopyridines, including 1,8-naphthyridine, published up to 1984 inclusive, have been analysed in sufficient detail in the reviews.[1,423–425]

1. Physicochemical properties

Studies on the physicochemical properties of 1,8-naphthyridines are being continued. 1,8-Naphthyridinium 1-tetraphenylborate,[426] 4-oxo-1,4-dihydro-1,8-naphthyridinium methanesulfonate[427] and some other derivatives[428–433] were studied by X-ray diffraction.

The behaviour of bromo-substituted isomeric naphthyridines, which include 2-amino-6-bromo-, 2-amino-3,6-dibromo- and 4-bromo-2-hydroxy-1,8-naphthyridines, was investigated by mass spectrometry.[434] It was demonstrated that fragmentation of aminobromonaphthyridines under electron impact follows three main pathways.

1. Elimination of the $Br^{\bullet}$ radicals followed by successive elimination of two HCN molecules (with high intensity) from the molecular ions.

2. Elimination of the HCN molecule followed by liberation of $Br^{\bullet}$ and HCN (with lower intensity).

3. Elimination of the HCN molecule can also be accompanied by competitive liberation of $Br^{\bullet}$ and HCN.

The fragmentation of bromohydroxynaphthyridines follows two main pathways: liberation of $Br^{\bullet}$ accompanied by elimination of CO and two HCN molecules or liberation of CO accompanied by competitive elimination of $Br^{\bullet}$, HCN and C_2H_2.

Mass spectra of aminonitro derivatives of naphthyridines were also studied.[435] Mass spectrometry was used for investigation of the structures and decomposition of the isomeric $[M-HCN]^{-\bullet}$ and $[M-2\,HCN]^{-\bullet}$ ions formed upon fragmentation of naphthyridines and benzoazines.[436] It was found that the $[M-2\,HCN]^{-\bullet}$ ions can exist as two isomeric forms, one of which is typical of naphthyridines, whereas the other is characteristic of benzoazines.

The absorption and transmission spectra of 1,8-naphthyridines were investigated in the region of 50 000–20 000 cm^{-1} in solutions and various mixed crystals at 4.2 and 300 K.[437] The $\pi^*-\pi$-band system of 1,8-naphthyridines is analogous to the corresponding bands in the spectra of the related naphthalene molecule taking into account perturbations caused by the replacement of the C atoms with N. The position of the long-wavelength

$\pi^* - \pi$ band at 27 000 cm^{-1} corresponds to that predicted based on calculations by the extended Hückel method. The bands at 31 600 – 31 900 cm^{-1} were tentatively assigned to the second $\pi^* - \pi$ transition.

With the aim of elucidating the influence of substituents on the absorption spectra, the UV spectra (in methanol) of 1,8-naphthyridines monosubstituted at positions 2 (Me, Cl, Br, OMe, OEt, SMe, NH_2, OH or SH as the substituent), 3 (Me, Cl, Br, NO_2 or NH_2 as the substituent) or 4 (Me, Cl, Br, OMe, OEt, OH or SH as the substituent) were examined.[438]

The electric dipole moment of 1,8-naphthyridine in benzene was determined (4.10 D).[439] The ESR spectrum of hexahydro-1,8-naphthyridinetetrazole was measured.[440]

Homonuclear 2D *J*-resolved ^1H NMR spectra of 2-(2-pyridyl)-1,8-naphthyridine were measured and a complete assignment of the resonances was made.[441]

The ^1H and ^{13}C NMR spectra of imidazo[1,2-*a*][1,8]naphthyridine were analysed based on the results of quantum-chemical calculations using the CNDO/2 method.[442]

Complexes of the antitumour antibiotics naphthyridinomycins with DNA were investigated by molecular mechanics methods (molecular simulation).[443] It was found that the nature of the substituent at the C(11) atom as well as the stereoconfiguration of the C(7) centre are of importance for biological activity of naphthyridinomycins. The antibacterial activities of various substituted 1,8-naphthyridines,[444] including 2-phenyl-1,8-naphthyridin-4-one derivatives, were calculated using the QSAR method.[445]

The character of deuterium distribution in isotope exchange products of 1,8-naphthyridine and its methyl, hydroxy, amino and nitro derivatives indicates that the rate and pathway of this process depend on the pH of the medium as well as the nature and position of the substituent.[446] In neutral D_2O and a D_2O – DCl mixture, deuterium atoms are replaced with protons exclusively at positions 2 and 7. In D_2O solutions containing NaOD, deuterium atoms are replaced with protons in all positions of the naphthyridine system. In neutral D_2O, the replacement of the protons in monomethyl-substituted 1,8-naphthyridines occurs predominantly in the *ortho* positions with respect to the nitrogen atoms (positions 7 and 2, 7). The high reactivity of these positions is determined by the inductive effect of the substituent.

A spectrophotometric procedure [447] and a modified gas-chromatographic method [448] were devised for analysis of nalidixic acid **36**. Drug forms for intramuscular injection [449] and sublimed drugs for parenteral use [450] are available. These drug forms contain the gyrase inhibitor from 1,4-dihydro-4-oxo-1,8-naphthyridine-3-carboxylic acid derivatives as the active component.

The complexation properties of naphthyridines are widely used for analytical purposes, primarily, in medicine. A highly sensitive diagnostic was proposed [431] for bacterial infectious diseases based on scanning electron microscopy. Complexes of antibiotics of the 1,8-naphthyridin-4-one series or their salts with ^{99m}Tc, ^{67}Ga, ^{111}In, ^{113m}In and other radionuclides are used for revealing inflammatory focus. These compounds are involved in parenteral drug forms.[451]

Polycyclic compound **227**, which forms stable complexes with urea, guanidine, amidines and their derivatives, is covered by patents.[452, 453] These complexes were used in biological investigations. Receptor betaine molecule **228** was constructed for diagnostic tests for blood (serum) creatinine and renal insufficiency.

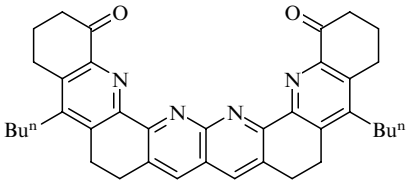

227

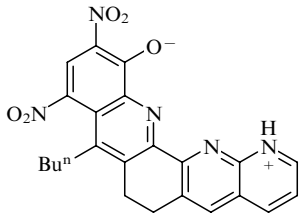

228

New guanine receptors were prepared based on 7-acetylamino-2-chloro-4-methyl-1,8-naphthyridine (**229**).[454] Amino alcohol **230** was prepared by the reaction of compound **229** with an excess of sodium 2-hydroxyethoxide. Compound **230** reacts with dicarboxylic acid chlorides **231** under high dilution conditions to form naphthyridine macrocycles **232**.

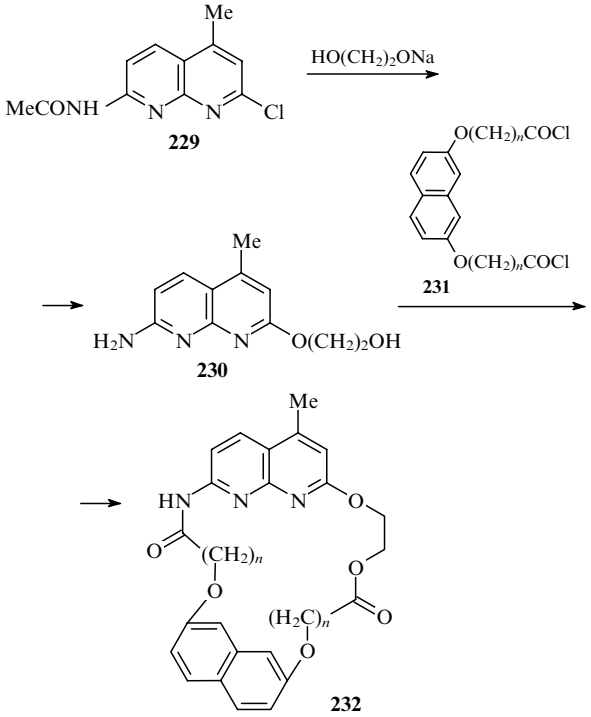

229

230

231

232

$n = 2, 3$.

It was demonstrated that the addition of 2′,3′,5′-tri-*O*-pentanoylguanosine (**233**) to a solution of macrocyclic compound **232** in $CDCl_3$ causes pronounced changes in the ^1H NMR spectra of both compounds: the resonances of the NH and NH_2 groups are shifted downfield, whereas all six resonances of the naphthalene system are shifted upfield. The assumed [454] structure of the complex consists of two molecules linked *via* three hydrogen bonds (analogous to the structure of complex **234**), and the naphthalene system forms a complex with guanine. The constant of association of compounds **232** and **233** is four times as high as that of the guanine complex with unsubstituted 1,8-naphthyridine.

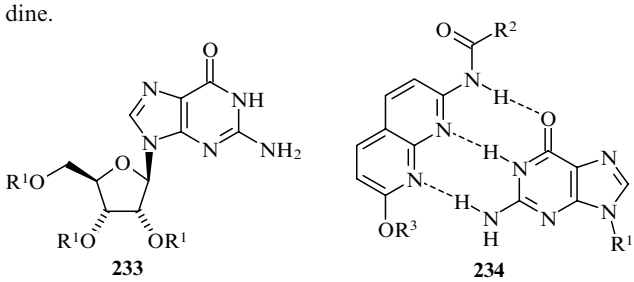

233 **234**

R^1 = C(O)Bu^n; R^2 = H, MeCO, Pr^nCO; R^3 = Cl, OEt, $O(CH_2)_2OH$.

The structures of other complexes based on 1,8-naphthyridine and pyrido[2,3-*b*][1,8]naphthyridine (1,9,10-anthyridine) derivatives containing three hydrogen bonds each were established.[331, 359, 362, 454–459]

1,9,10-Anthyridine was used for the synthesis of analogous stable complexes **235**–**237**.[456]

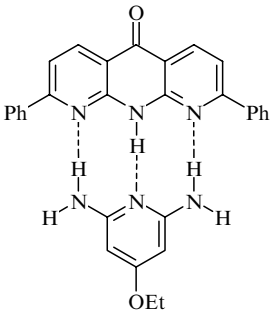

235

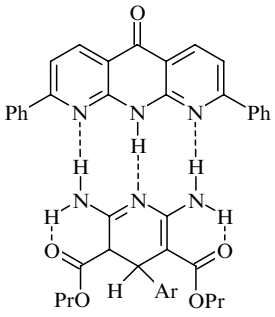

236

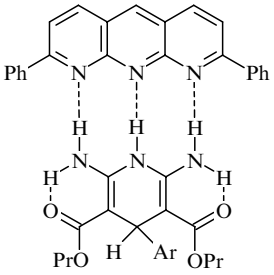

237

Ar = 2-$NO_2C_6H_4$ (**236**), 3-$NO_2C_6H_4$ (**237**).

In recent years, 1,8-naphthyridine derivatives have attracted growing interest as promising ligand systems, which coordinate metal ions of different groups of the Periodic table, such as Cu,[460–462] Au,[463, 464] Zn,[465–467] Hg,[468] Mo,[469, 470] Fe,[471] Co,[472] Ni,[473] Ru,[474–477] Rh,[478, 479] Pd,[480] Pt,[480, 481] Eu and Tr.[482] The crystal structures of some complexes were studied by X-ray diffraction analysis.

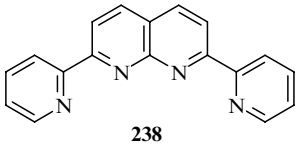

238

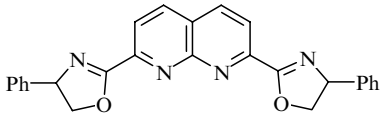

239

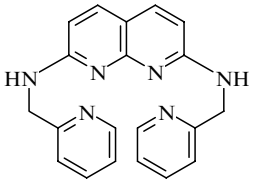

240

Various ligands based on 1,8-naphthyridines, including polydentate binuclear (compounds **238**,[460] **239**,[483] **240**[484]) and other compounds,[485, 486] were used for complexation with these metal ions.

2. Reactions of 1,8-naphthyridine derivatives

Among nitrogen-containing heterocyclic systems containing the 1,8-naphthyridine fragment, the above-mentioned 1,9,10-anthyridines, which are triaza analogues of anthracene, have attracted considerable attention. Earlier, these compounds have been synthesised according to multistep procedures starting from pyridine derivatives, such as 2,6-diaminopyridine,[487–491] 2,6-diamino-3,5-diformylpyridine,[492] *etc*.[493, 494] Later on, 1,8-naphthyridine derivatives became easily accessible,[316, 322, 358] which made it possible to simplify procedures.

Some transformations of 1,9,10-anthyridines were also described. 7-Nitroanthyridine-2,6-dione (**242**) or 3,7-dinitroanthyridine-2,6-dione (**243**) can be prepared by nitration of anthyridine-2,6-dione (**241**) with various amounts of a mixture of concentrated sulfuric and nitric acids (100 °C, 0.5–3 h). Treatment of nitro derivative **242** with sodium dithionite (in a 5% NaOH solution) gives rise to 7-aminoanthyridine-2,6-dione (**244**) in quantitative yield. The reaction with phosphorus pentasulfide in anhydrous pyridine produces 7-aminoanthyridine-2,6-dithione (**245**) (Scheme 6).[495]

3-Nitro-1,8-naphthyridines (**246**) and their derivatives were subjected to amination at position 4 using liquid ammonia and potassium permanganate[496] or liquid methylamine and potassium permanganate[497–499] as aminating systems. Amination of naphthyridines **246** (−7 °C, 0.5 h) affords 4-methylamino-3-nitro-1,8-naphthyridines (**247**) in 50%–90% yields.[497, 498] Quantum-chemical calculations demonstrated that the reaction is controlled by interactions of frontal molecular orbitals of the reagents.

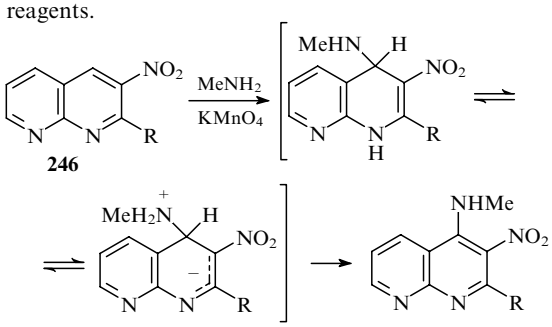

246 **247**

R = H, OH, OMe, Cl, NH_2, NHMe, NHPh.

The reaction of 1,8-naphthyridine with dichlorocarbene and dimethyl maleate followed by oxidation of the reaction mixture containing the intermediate cycloadduct with manganese dioxide

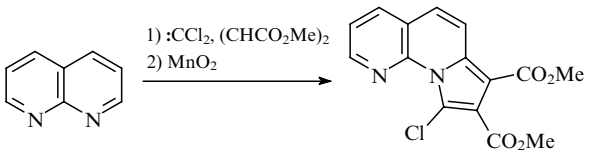

248

produced dimethyl 1-chloropyrrolo[1,2-*a*][1,8]naphthyridine-2,3-dicarboxylate (**248**) in 11% yield.[500]

Scheme 6

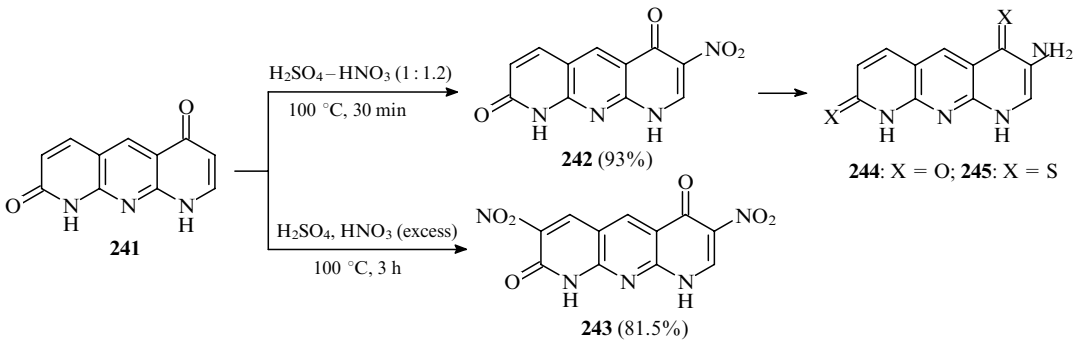

241 **242** (93%) **243** (81.5%) **244**: X = O; **245**: X = S

Dehydrogenation of 5,6,7,8-tetrahydro-1,9-diazaanthracene (**249**) over 20% Pd/C in diphenyl ether or *p*-cymene (250 °C, 3 h) affords 9,1-dihydro-1,9-diazaanthracene (**250**), whose oxidation with potassium dichromate in dilute H_2SO_4 (60 °C, 10 min) gives rise to benzo[*b*][1,8]naphthyridines (**251**). Oxidation of benzonaphthyridine **251** with peroxy acids yields 1,4-oxazepines **252** – **255**.[501, 502]

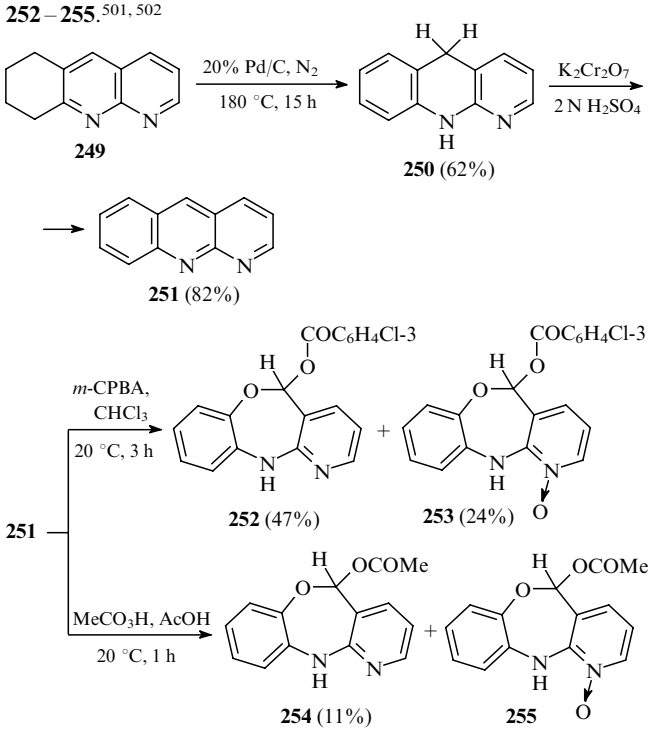

New bisnaphthyridines **256** and **257** containing the 5-amino-2,4-dimethylbenzo[*b*][1,8]naphthyridine or benzo[*b*][1,8]naphthyridone chromophores were synthesised in a phase-transfer system by the reaction of aminobenzonaphthyridine **258** or dihydrobenzonaphthyridone **259** with alkylene dibromides.[503] Such bisintercalates are of interest as potential antitumour drugs.

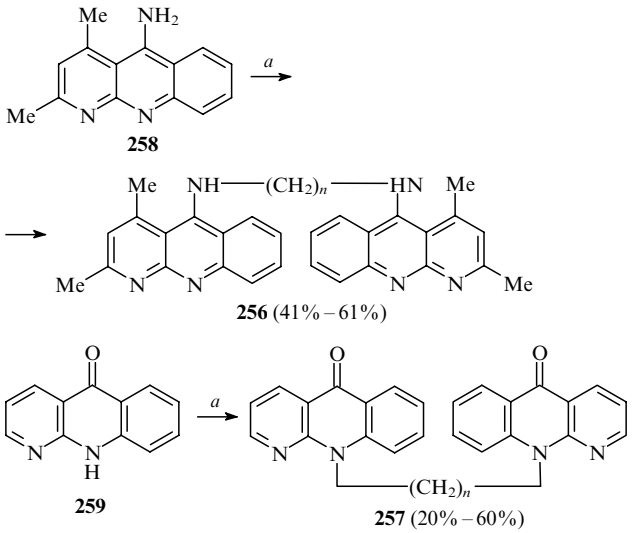

n = 3, 6, 8, 10; *a*) $Br(CH_2)_nBr$, TBAB, PhMe, 50% KOH, Δ; TBAB is tetrabutylammonium bromide.

Procedures were developed for the synthesis of new types of simple receptors based on substituted 1,8-naphthyridines. These receptors serve as carriers for transport of biologically important organic substrates (urea, amino acids, hydroxy acids) into cells. *N*-{6-[2-(7-Methyl[1,8]naphthyridin-2-yl)ethyl]pyridin-2-yl}acetamide (**260**) was prepared by the reaction of 2,7-dimethyl-1,8-naphthyridines **261** with n-butyllithium (2 equiv., THF, −78 °C) and 2-*N*-acetylamino-6-bromomethylpyridine (**262**). Another carrier, *viz*., *N*-(7-methyl[1,8]naphthyridin-2-yl)-*N*′-(6-methylpyridin-2-yl)isophthalamide (**263**), was synthesised from 2-amino-7-methyl-1,8-naphthyridine (**264**), 2-amino-6-methylpyridine (**110a**) and isophthaloyl chloride (**265**) in dry dichloromethane in the presence of triethylamine. *N*,*N*′-Bis(7-methyl[1,8]naphthyridin-2-yl)isophthalamide (**266**) was prepared from naphthyridines **264** and chloride **265** under analogous conditions. Isophthalamides **263** and **266** were used for the determination of L-(+)-tartartic acid as complexes (1 : 1) soluble in chloroform.[504, 505]

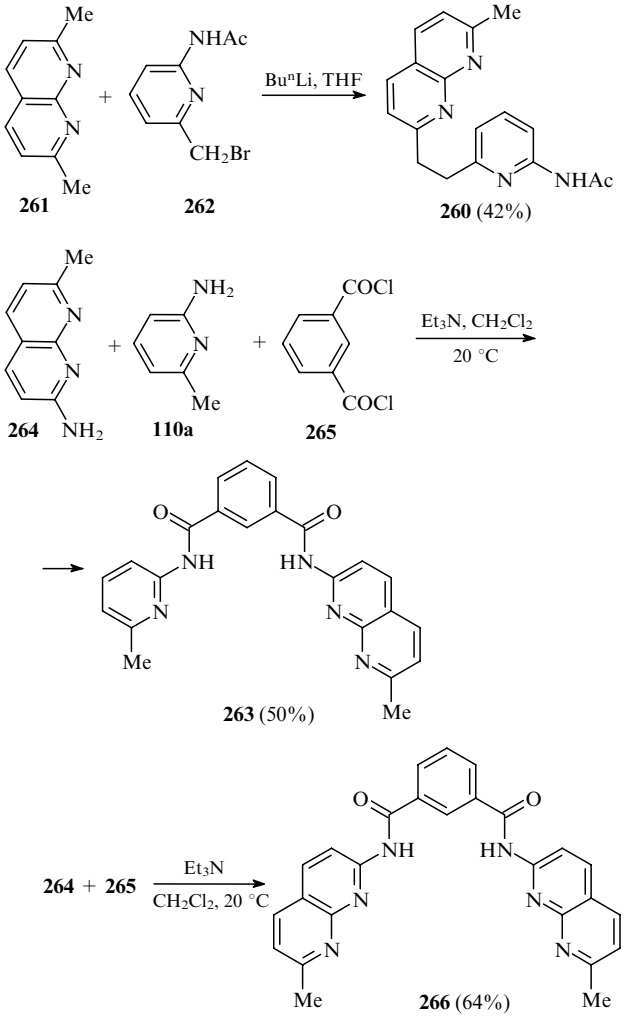

The new antitumour drug Ag-7352 (**267**) was designed based on 1,8-naphthyridin-4-one-3-carboxylic acid.[506, 507] An efficient stereospecific procedure was specially developed for the synthesis of (*S*,*S*)-3-methoxy-4-methylaminopyrrolidine, which is the key reagent in the synthesis of naphthyridine **267**.[508]

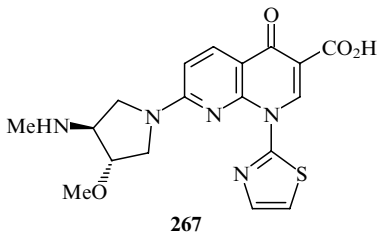

267

1,8-Naphthyridine derivatives were used for the preparation of polysiloxanes. New chiral stationary phase **268** was constructed on the basis of 2-*N*-(5,7-dimethyl-1,8-naphthyridin-2-yl)carboxamide.[509]

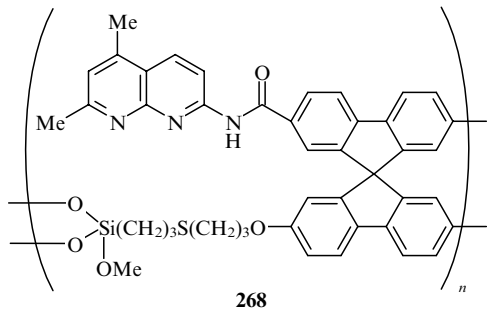

268

In studies of 1,8-naphthyridine derivatives possessing potential biological activities, a procedure was devised for the synthesis of a new tricyclic system containing the 1,8-naphthyridine fragment, *viz*., pyrimido-1,8-naphthyridines.[510, 511] The synthesis involves condensation of commercially available guanidine carbonate with ethyl nalidixate (**269**) to form *N*-[(1-ethyl-7-methyl-4-oxo-1,4-dihydro-1,8-naphthyridin-3-yl)carbonyl]guanidine hydrochloride (**270**). After pre-neutralisation with 10% NaOH, guanidine **270** readily undergoes cyclisation (EtOH, Δ, 1 h) to form the angularly annelated tricyclic system, *viz*., 6-ethyl-2-imino-8-methyl-2,3,4,6-tetrahydropyrimido[5,4-*c*][1,8]naphthyridin-4-one (**271**), which was isolated as the hydrochloride.[511] Treatment of guanidine **270** with an excess of sodium hydride in dry DMF at 20 °C afforded 2-amino-10-ethyl-8-methyl-1,4,5,10-tetrahydropyrimido[5,4-*b*][1,8]naphthyridine-4,5-dione (**272**), which was also isolated as the hydrochloride.

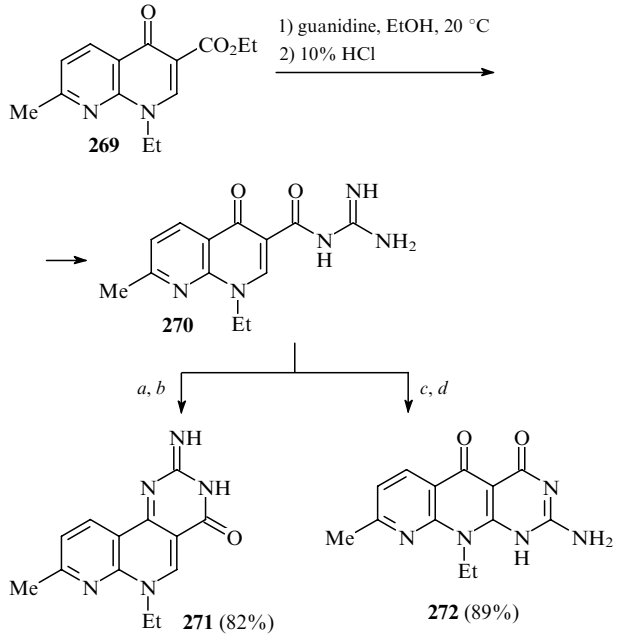

(*a*) EtOH, Δ, 1 h; (*b*) 10% HCl;

(*c*) NaH, DMF, 20 °C; (*d*) 10% HCl.

With the aim of searching for synthetic approaches to new 1,8-naphthyridin-2-one derivatives, transformations of ethyl 7-amino-1,4-dimethyl-2-oxo-1,2-dihydro-1,8-naphthyridine-6-carboxylate (**91**) were studied. Refluxing of this compound with *N*,*N*-dimethylformamide dimethyl acetal in dry toluene afforded 7-[(*N*,*N*-dimethylaminomethylene)amino]-1,8-naphthyridinone **273**. The reaction of naphthyridone **91** with triethyl orthoformate produced ethoxymethyleneamino derivative **274**. The reaction with hydrazine hydrate gave rise to 7-amino-3-cyano-1,4-dimethyl-2-oxo-1,2-dihydro-1,8-naphthyridine-6-carbohydrazide (**275**).[353]

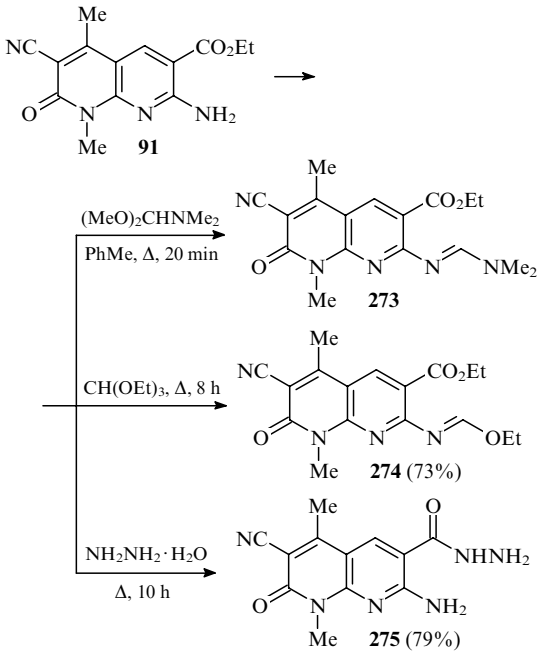

In the last 15 years, considerable attention has been given to variations of substituents in different positions of the molecule (predominantly at position 7), in particular, for the purpose of preparing new active fluoroquinolone and fluoronaphthyridone antibacterial drugs for peroral administration.[512–524] For example, esters of nalidixic acid (**276**) were used for this purpose.[523, 524] The reactions of these esters with *tert*-butoxybisdimethylaminomethane in Bu^{t}OH produce enamines **277**. The addition of the Vilsmeier reagent derived from DMF and thionyl chloride leads to the formation of enamines **278**. Treatment of the reaction mixture with hydrazine hydrate, hydroxylaminosulfonic acid or guanidine followed by hydrolysis of the reaction mixture gives rise to pyrazolyl- (**279**), isoxazolyl- (**280**) and pyrimidinyl-4-oxo-1,4-dihydro-1,8-naphthyridine-3-carboxylic acid derivatives (**281**).[524]

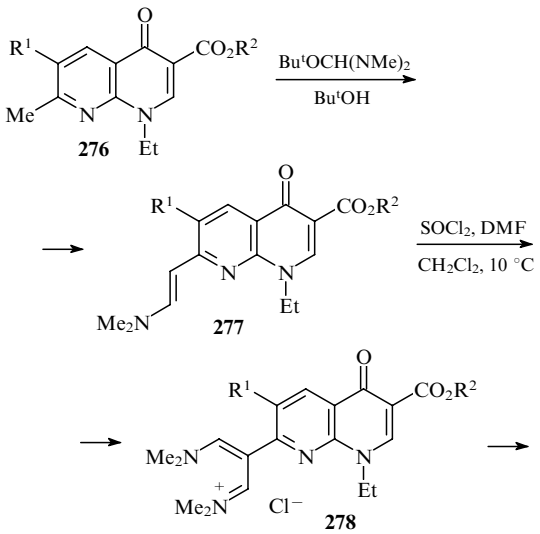

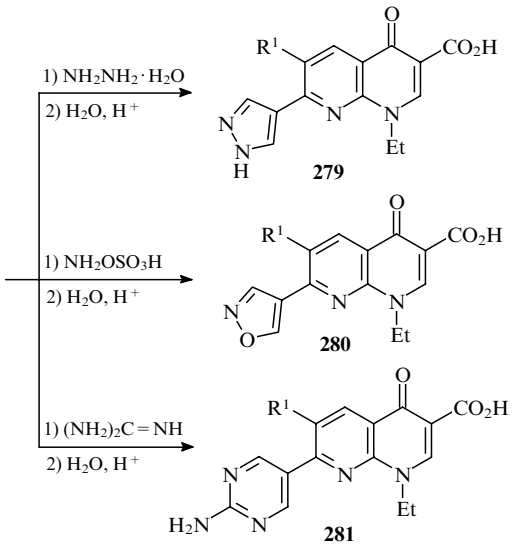

R^1 = H, F; R^2 = Me, Et.

The reaction of ethyl 1-ethyl-7-ethylsulfonyl-6-fluoro-4-oxo-1,4-dihydro-1,8-naphthyridine-3-carboxylate (**282**) with piperazine is accompanied by the replacement of the ethylsulfonyl group at position 7 to form 7-piperazino derivative **283a** in good yield.[521] Treatment of the starting ester **282** with morpholine and piperidine leads to the replacement of the fluorine atom at position 6 or the ethylsulfonyl group at position 7 to form a mixture of 6- and 7-substituted derivatives **283b**,**c** and **284b**,**c**.[523] The reaction of 7-chloro-1-ethyl-6-fluoro-4-oxo-1,4-dihydro-1,8-naphthyridine-3-carboxylic acid (**285**) with *N*,*N*′-dimethylethylenediamine in acetonitrile produces {*N*-methyl-*N*-[2-(methylamino)ethyl]}aminonaphthyridine **286**, which readily undergoes cyclisation upon heating in DMF to give 6-ethyl-1,4-dimethyl-9-oxo-1,2,3,4,6,9-hexahydropyrazino[2,3-*b*][1,8]naphthyridine-8-carboxylic acid (**287**).[523]

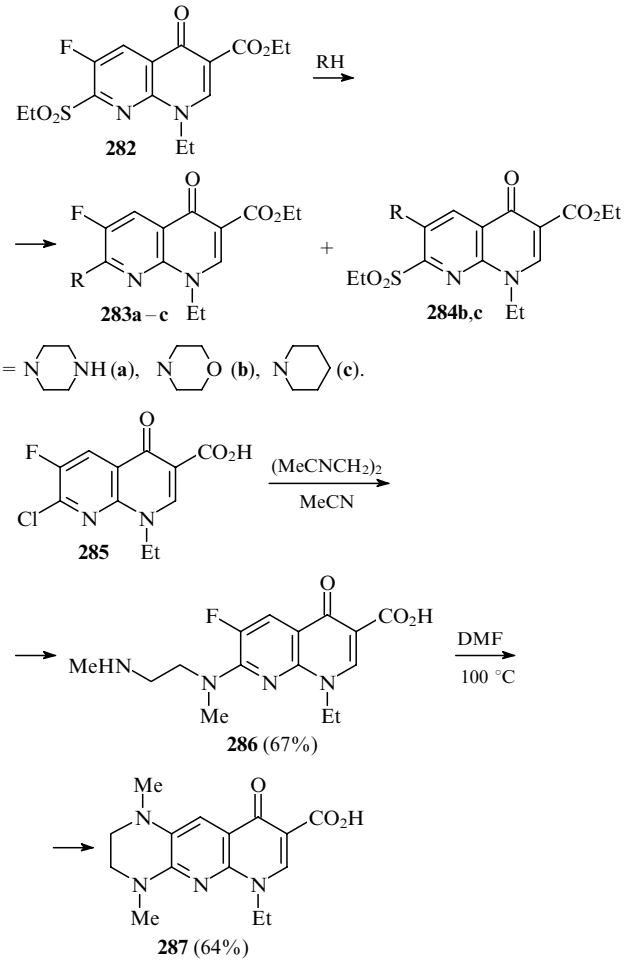

Selective reduction of the C(2)=C(3) bond in naphthyridone **9a** followed by treatment with Bu^iLi in THF and methylation affords compound **288**. Subsequent regeneration of the double bond occurs as a result of successive selenation, oxidation and *syn*-elimination to form naphthyridone **289**.[525] Earlier, an analogous scheme has been used for the synthesis of ethyl 7-chloro-1-ethyl-6-fluoro-2-methyl-4-oxo-1,4-dihydro-1,8-naphthyridine-3-carboxylate.[526]

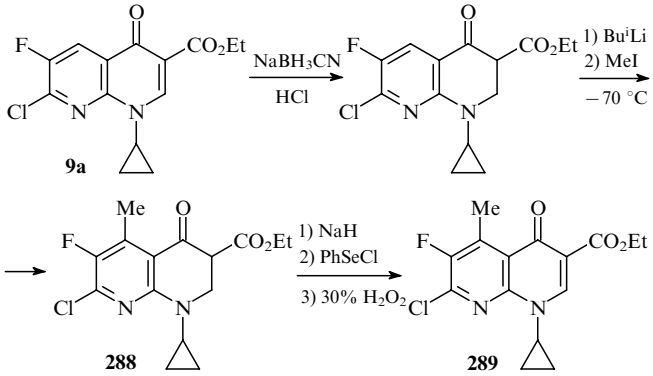

Thieno[2,3-*b*][1,8]naphthyridone **291** exhibiting antimicrobial and antitumour actions was synthesised starting from the 2-mercapto derivative of naphthyridone **290**.[527]

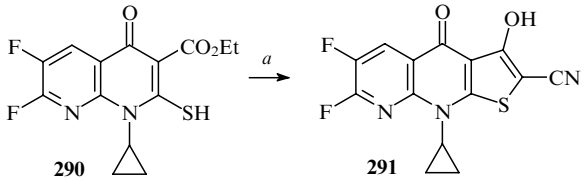

(*a*) 1) $BrCH_2CN$, THF, $NaHCO_3$; 2) $NaHSO_3$, THF, H_2O.

Procedures for the synthesis of compounds containing a five-membered heterocycle with a linearly fused 1,8-naphthyridine fragment (thiazolo[5,4-*b*]-,[528] imidazolo[4,5-*b*]-, triazolo[4,5-*b*]-,[529] oxazolo[5,4-*b*]-, thiadiazolo[5,4-*b*]-, isothiazolo[5,4-*b*]-, pyrazolo[3,4-*b*]-, thieno[2,3-*b*]-, furo[2,3-*b*]-1,8-naphthyridines[530]) were described and the antibacterial activity of these compounds was studied.

5-Ethyl-8-oxo-5,8-dihydrofuro[3,2-*b*][1,8]naphthyridine-2,7-dicarboxylic (**292**) and 5-ethyl-8-oxo-5,8-dihydrofuro[3,2-*b*][1,8]naphthyridine-7-carboxylic acids (**293**) were synthesised in the study.[531] Refluxing of a mixture of ethyl 1-ethyl-7-formyl-6-hydroxy-1,4-dihydro-4-oxo-1,8-naphthyridine-3-carboxylate (**294**), diethyl bromomalonate and K_2CO_3 in ethyl methyl ketone affords compound **295**. Successive treatment of the latter with K_2CO_3 in aqueous ethanol and 2 N NaOH gives dicarboxylic acid **292**. Selective decarboxylation of acid **292** on heating in dimethylformamide, dimethylacetamide or quinoline in the presence of copper compounds yields furonaphthyridinecarboxylic acid **293**.

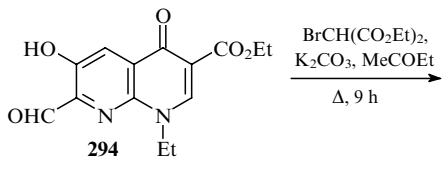

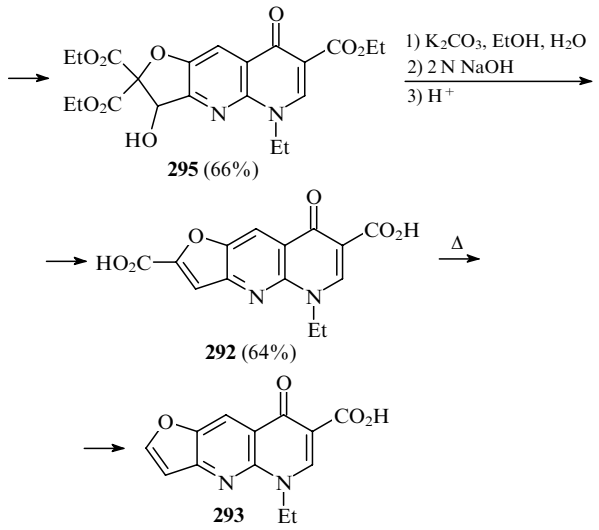

It was found [532] that 1,8-naphthyridine derivatives can react with adenosine receptors of subtypes A_1 and A_{2A}. This stimulated studies on the synthesis and investigation of the biological activities of various functionalised (particularly, at positions 1, 2, 4 and 7) naphthyridines. Alkylation and nucleophilic substitution of these compounds was studied. 7-Methyl-2-phenyl-1,8-naphthyridin-4-ol (**296**) is alkylated at position 1 with EtI and KOH in aqueous ethanol to form 1-ethyl-7-methyl-2-phenyl-1,8-naphthyridin-4(1*H*)-one (**297**).[533, 534] Refluxing of naphthyridone **296** with Lawesson's reagent in toluene affords 7-methyl-2-phenyl-4-thiol-1,8-naphthyridine (**298**). Treatment of 4-chloronaphthyridine **299** (which was prepared by the reaction of naphthyridone **296** with $POCl_3$) with sodium methoxide in methanol gave rise to 4-methoxy-7-methyl-2-phenyl-1,8-naphthyridine (**300**). Refluxing of compound **299** with PhONa in DMF produced 7-methyl-4-phenoxy-2-phenyl-1,8-naphthyridine (**301**). A series of other 1,8-naphthyridine derivatives was also prepared and their properties as A_1, A_{2A} and A_3 adenosine receptors were studied.[534]

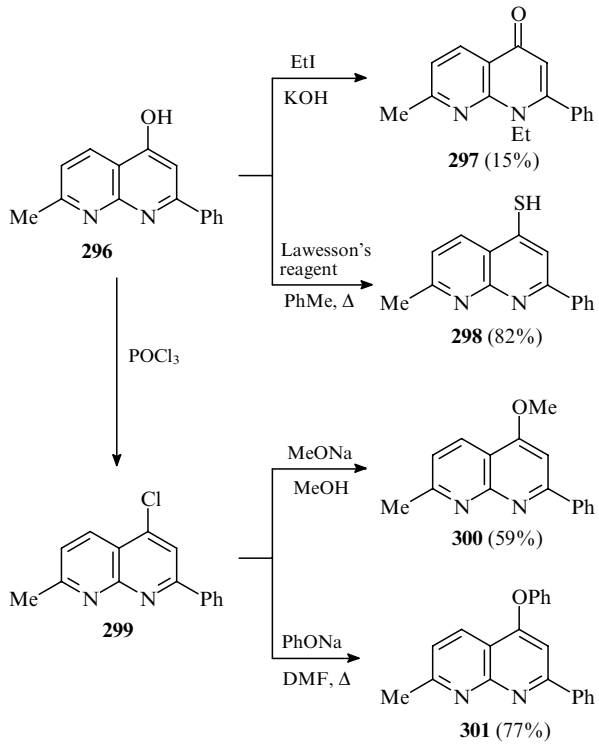

Along with substituted 1,8-naphthyridin-4-ones, derivatives containing the carbonyl group at position 2 were subjected to various transformations. For example, the reaction of 2-oxo-1,2-dihydro-1,8-naphthyridine-3-carbonitrile (**302**) with sodium azide and ammonium chloride in DMF produced tetrazolyl-1,8-naphthyridin-2-one **303**, which was covered by a patent as an anti-allergic drug.[535]

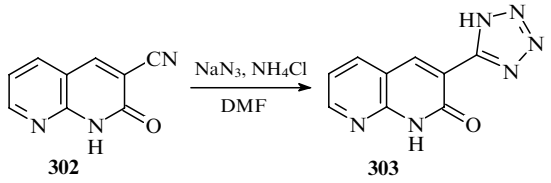

Imidazonaphthyridine **304** possessing anti-inflammatory action was synthesised by hydrogenation of 1-butyl-4-methylamino-3-nitro-1,8-naphthyridin-2(1*H*)-one (**305**) followed by cyclisation of diamino derivative **306** on heating with ethyl chloroformate.[536]

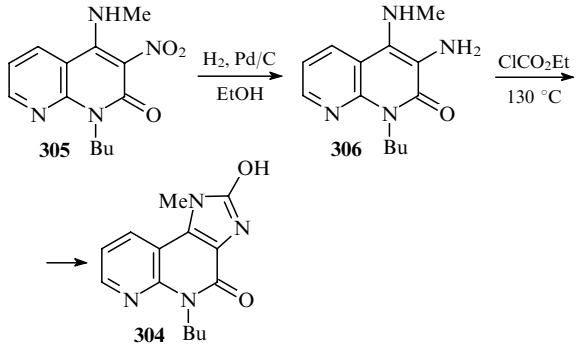

The reaction of 3-benzoyl-4-hydroxy-1-phenyl-1,8-naphthyridin-2(1*H*)-one (**307**) with hydrazine hydrate produces naphthyridone **308** possessing anti-inflammatory and broncholithic activities.[537]

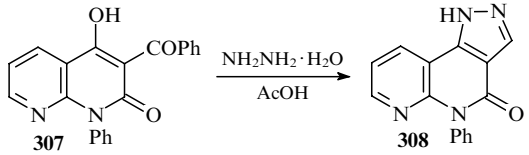

Numerous 3-(2-cyanovinyl)-substituted 1,8-naphthyridines **309** were prepared by refluxing 1,8-naphthyridine-3-carbaldehydes **310** with substituted acetonitriles in alcohol in the presence of catalytic amounts of pyridine. Compounds **309** were covered by a patent as promising starting compounds for the synthesis of new drugs for the treatment of cancer, psoriasis and atherosclerosis.[538]

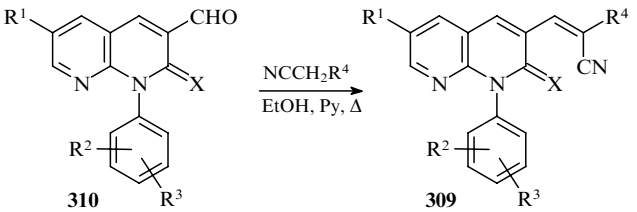

R^1 = H, AlkO, OH, Hal; R^2, R^3 = H, AlkO, AlkS, CF_3, HO, NO_2, CN, Hal; R^4 = Py, $CONH_2$, $CSNH_2$; X = NH, O, S.

Claisen–Schmidt condensation of 3-acetyl-2-methyl-1,8-naphthyridine (**311**) with aromatic aldehydes occurs in ethanol in the presence of KOH to give cinnamoyl-substituted 1,8-naphthyridines **312**. The latter undergo cyclisation under the action of hydrazine hydrate (AcOH, EtOH, Δ, 6 h) or phenylhydrazine (AcOH, Δ, 4 h) to form 3-(5-aryl-2-pyrazolin-3-yl)-1,8-naphthyridines (**313a**) (62%–84% yields) or 3-(5-aryl-1-phenyl-2-pyrazolin-3-yl)-2-methyl-1,8-naphthyridines (**313b**) (64%–86% yields), respectively, which exhibit pronounced antifungicidal activity.[539]

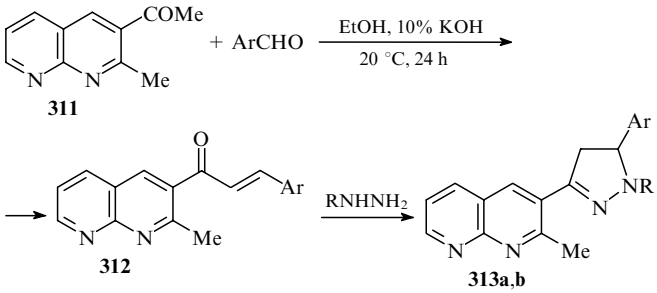

R = H (**a**), Ph (**b**); Ar = Ph, 3-MeC_6H_4, 4-MeC_6H_4, 2-$MeOC_6H_4$, 4-$MeOC_6H_4$, 4-HOC_6H_4, 2-ClC_6H_4, 4-ClC_6H_4, 3-$NO_2C_6H_4$, 4-$Me_2NC_6H_4$.

The reaction of *N*-aryl-2-methyl-1,8-naphthyridine-3-carboxamides **314** with $POCl_3$ (120 °C, 3 h) followed by the reaction of the imidoyl chloride **315** that formed with sodium azide afforded 3-(1-aryl-1*H*-tetrazol-5-yl)-1,8-naphthyridines **316**. However, assays of naphthyridines **316** demonstrated that these compounds do not exhibit the expected antibacterial activity.[540]

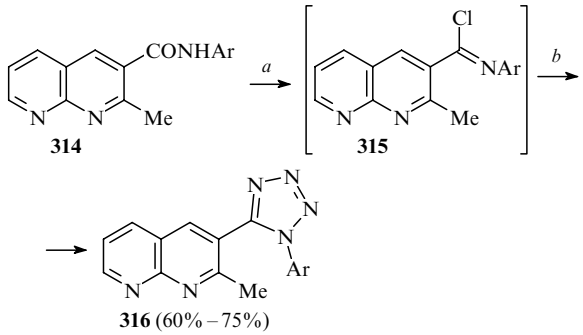

Ar = Ph, 2-MeC_6H_4, 3-MeC_6H_4, 4-MeC_6H_4, 2-$MeOC_6H_4$, 3-$MeOC_6H_4$, 4-$MeOC_6H_4$, 2-ClC_6H_4, 3-ClC_6H_4, 4-ClC_6H_4, 3-$NO_2C_6H_4$;
(*a*) $POCl_3$, 120 °C, 3 h; (*b*) NaN_3, AcONa, Me_2CO, H_2O, 20 °C, 24 h.

2-Methyl-1,8-naphthyridine-3-carboxylic acid hydrazide (**317**) served as the starting reagent for the synthesis of numerous 1,8-naphthyridine derivatives, such as 1,3,4-thiadiazol-2-yl- (**318**), 4*H*-1,2,4-triazol-3-yl- (**319**)[541] and 1,3,4-oxadiazol-2-ylnaphthyridines (**320**, **321**).[542] Compounds **321** can also be prepared by oxidative cyclisation of arylmethylidenehydrazides **322** with $FeCl_3$ in AcOH.[542]

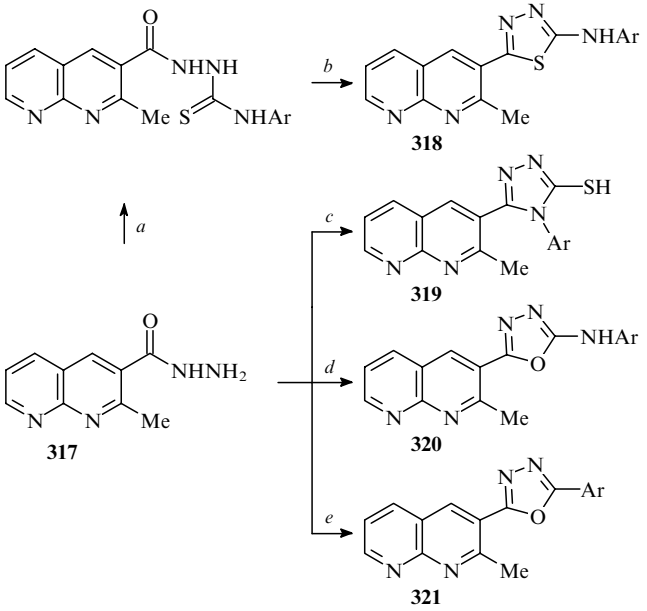

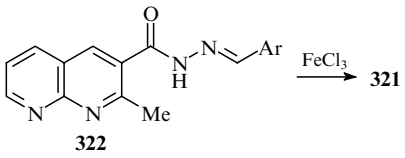

(*a*) ArNCS, EtOH; (*b*) concentrated H_2SO_4; (*c*) ArNCS, 2 N NaOH; (*d*) ArNCO, I_2, KI, 2 N NaOH; (*e*) $ArCO_2H$, 240 °C.

4-Formylpyrazole-1-substituted naphthyridines **323**[543] and compounds **324** and **325** containing complex heterocyclic substituents were synthesised starting from hydrazide **317**.[544]

Naphthyridines **318**–**321** and **323** exhibit bactericidal and fungicidal activities.[542, 543, 545]

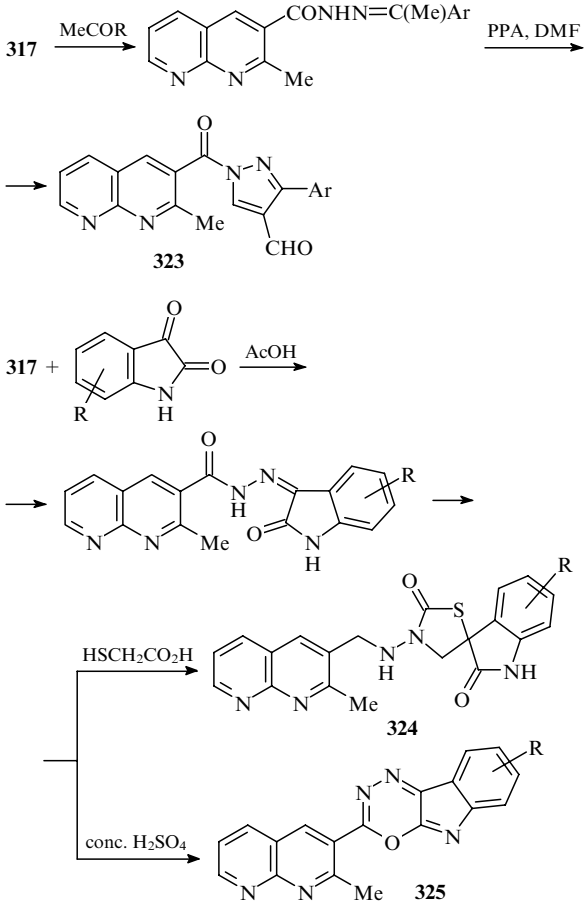

R = H, Me, Cl, Br.

Condensation of 2-amino-1,8-naphthyridine-3-carboxamide (**326**) with aromatic aldehydes in glacial acetic acid affords 2-aryl-1,2,3,4-tetrahydropyrimido[4,5-*b*][1,8]naphthyridin-4-ones **327**, whose oxidation with nitrobenzene in glacial acetic acid gives rise to 2-arylpyrimido[4,5-*b*][1,8]naphthyridin-4(3*H*)-ones **328**. Compounds **328** were also synthesised without intermediate isolation of naphthyridones **327** (condensation of amide **326** with aromatic aldehydes by refluxing in a mixture of nitrobenzene and glacial acetic acid).[546]

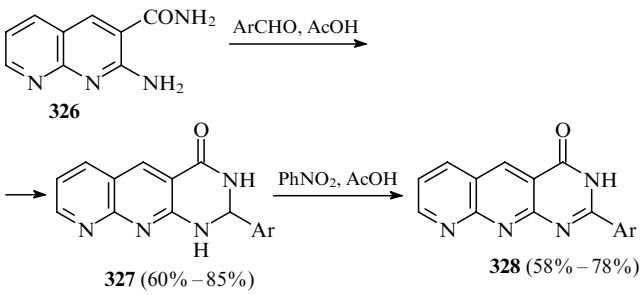

Ar = Ph, 2-MeC_6H_4, 4-MeC_6H_4, 2-$MeOC_6H_4$, 4-$MeOC_6H_4$, 2-ClC_6H_4, 3-ClC_6H_4, 4-ClC_6H_4, 2-$NO_2C_6H_4$, 3-$NO_2C_6H_4$, 4-$Me_2NC_6H_4$.

The reaction of 2-amino-5,7-dimethyl-1,8-naphthyridine (**329**) with 2-chlorophenyl sulfochloride produces sulfonamide **330**, which possesses herbicidal and growth-controlling properties.[547] Condensation of amine **329** with trichloroacetone affords a mixture of angular imidazo[1,2-*a*][1,8]naphthyridines **331** – **333** (Scheme 7).[548]

The reactions of substituted 3-nitro-1,8-naphthyridines **246** with chloromethyl phenyl sulfone (DMSO, 20 °C, 2 h) produce 3-nitro-4-(phenylsulfonylmethyl)-1,8-naphthyridines **334** in high yields. Quantum-chemical calculations by the MNDO method demonstrated that the pathway of this reaction, like that of amination (see above), is determined not by charge control but by the interaction between HOMO of the nucleophile and LUMO of the substrate.[549]

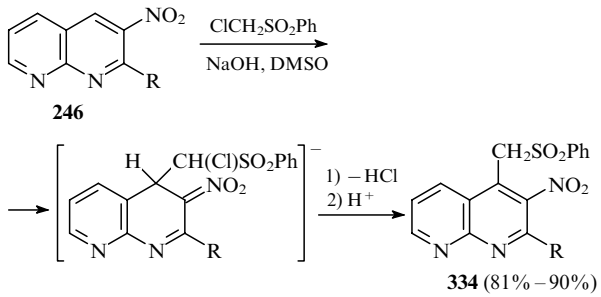

R = H, D, OH, OEt, Cl, NH_2.

Treatment of chloronaphthyridines **335** – **337** with diethanolamine (DEA) (120 °C) afforded the corresponding bis(2-hydroxyethyl)amino derivatives **338** – **340**. However, the expected antitumour activity of these compounds was not revealed.[550]

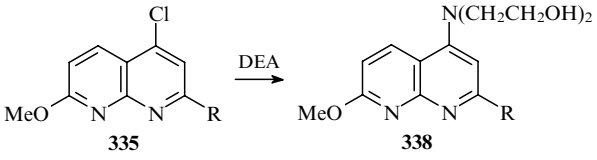

R = Me, Pr^n, Ph, CF_3, 4-$NO_2C_6H_4$.

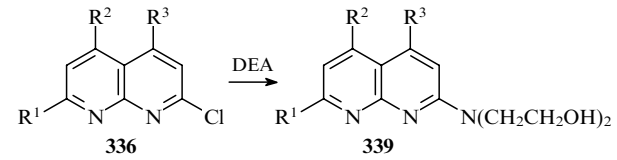

R^1 = Me, NH_2, OH; R^2 = H, Me; R^3 = H, Ph.

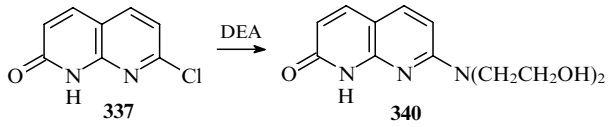

The reaction of ethyl 3-cyano-2-ethoxy-7-methyl-4-phenyl-1,8-naphthyridine-6-carboxamide (**341**) with dimethylformamide dimethyl acetal produces enamine **342**. Subsequent refluxing of the latter with ammonium acetate in ethanol leads to cyclisation to form tricyclic naphthyridine system **343**.[551]

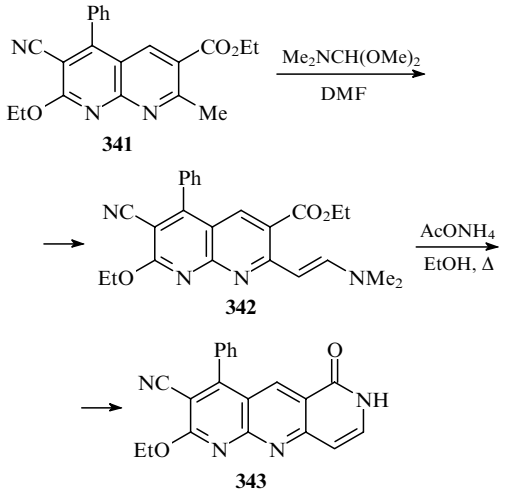

The study [552] was devoted to the transformations in a tetracyclic system containing the fused naphthyridines and benzimidazole ring. 5-Methoxybenzimidazo[1,2-*a*][1,8]naphthyridine-6-carbonitrile (**344**) was prepared by the reaction of 5-chlorobenzimidazo[1,2-*a*][1,8]naphthyridine-6-carbonitrile (**345**) with methanol in the presence of potassium carbonate. Upon heating to its melting point in DMF or in the absence of the solvent, compound **344** undergoes migration of the methyl group from the O atom to the N atom of the benzimidazole fragment to give 7-methyl-5-oxo-6-benzimidazo[1,2-*a*][1,8]naphthyridine-6-carbonitrile (**346**).

Scheme 7

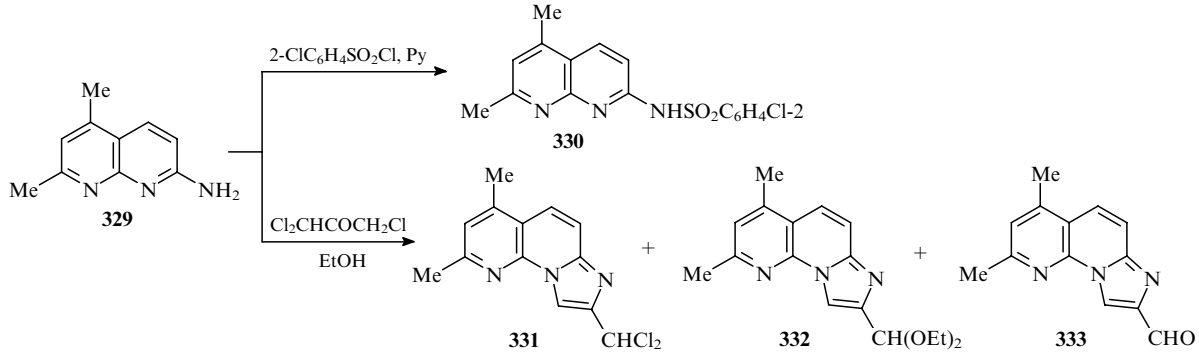

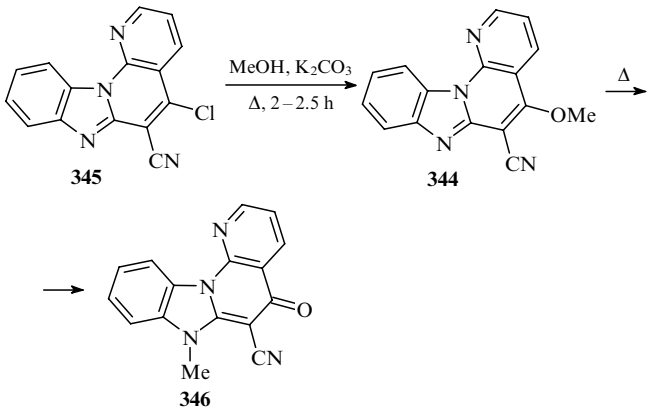

345 344 346

IV. Conclusion

The data surveyed in the present review convincingly demonstrate that the chemistry of pyridopyridines has attracted considerable interest. In the last decade, complex heterocyclic systems containing the 1,8-naphthyridine fragment have been synthesised and their reactions giving rise to functionalised naphthyridines have been investigated. The biological activities of 1,8-naphthyridine derivatives have received the most study. A detailed consideration of these studies is beyond the scope of the present review. For completeness of information, this review contains the bibliography, including patents [553–718] and papers,[719–752] published over the last 15 years, except for those in which 1,8-naphthyridine derivatives are used only in specific biochemical assays.

The activities exhibited by 1,8-naphthyridine derivatives are listed in Table 2. Several examples of the biological properties of this class of compounds are cited below.

With the aim of prolonging the action of nalidixic acid (**36**), which is used, in particular, for the treatment of infectious diseases, acid **36** was subjected to esterification with xanthine using dicyclohexylcarbodiimide in DMSO. The ester proved to be rather efficient against *Staphylococcus aureus* 209P.[753]

Naphthyridines **347** containing substituted pyridones at position 6 are used as components of cardiotonic drugs.[559]

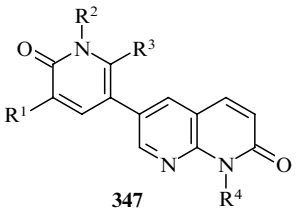

347

R^1 = H, Alk, AlkO, CHO, CN, NO_2, NH_2; R^2, R^3, R^4 = Alk, Ar.

The inotropic activities of 4-(2-hydroxyethylamino)-7-methyl-1,8-naphthyridine-3-carboxylic acid **348** and its chiral methyl derivative **349** were compared with those of known drugs having an analogous action (isoproterenol, adrenaline, histamine, *etc.*) with the use of isolated samples of guinea-pig myocardium. Biological assays demonstrated that compounds **348** and **349** are similar to heart glycosides in many respects.[754, 755]

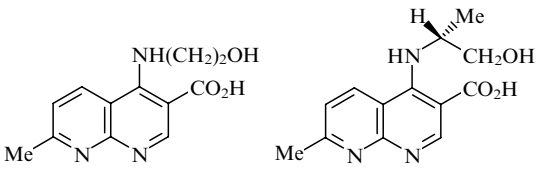

348 **349**

Table 2. Biological activities of 1,8-naphthyridine derivatives.

Activity	Ref.
Antibacterial	25, 137, 194, 195, 197, 215, 234, 236, 237, 241, 245, 247, 248, 253–256, 553, 568, 575, 614, 615, 617, 622, 623, 634, 635, 685, 689, 712, 718, 727, 732, 733, 735, 738–743
Antimicrobial	569, 578, 692, 693, 717, 740, 744, 750
Antiviral	586, 591, 598, 599
Anti-inflammatory	343, 571, 588, 750
Antitumour	583, 588, 712, 715
Antiulcerative	343
Antihypertensive	570, 594, 721, 723
Antidiabetic	588
Anticonvulsive	650
Antithrombotic	574, 580, 724, 725, 727, 750
Antiatherosclerotic	588, 631
Immunostimulating	567, 570, 571, 650
Analgetic	343, 584
Various receptor antagonists	254, 260, 534, 575, 577, 579, 581, 582, 585, 587, 588, 592, 593, 596, 597, 686, 746
Fungicidal [a]	363

[a] This type of activity was found against phytopathogenic fungi *Phytophtora infestans* on tomatoes, *Phytophtora castonuma* on apples and *Pseudoperonospora cubensis* on cucumbers.

Substituted 1,8-naphthyridin-2(1*H*)-ones **350** were tested as selective phosphodiesterase inhibitors.[756]

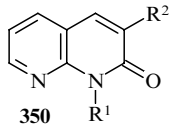

350

R^1 = Me, $(CH_2)_2Pr^i$, $(CH_2)_3OAc$, n-C_5H_{11}, Allyl, 2-$FC_6H_5CH_2$;
R^2 = H, Me, Ph, 2-Py, $(CH_2)_4OH$, $CH_2CH(OH)Me$.

Numerous substituted naphthyridines were studied and *N*-terminal aminohydroxy derivatives of β-amino acids **351** were demonstrated to inhibit renin.[566, 567] Naphthyridinedione **352** stimulates carotene biosynthesis;[757] (*E*)- and (*Z*)-*O*-(diethylamino)ethyl oximes of the naphthyridine series **353** are potential drugs for local anesthesia.[758] 1,8-Naphthyridine derivatives **354** exhibit high antihypertensive activity.[759]

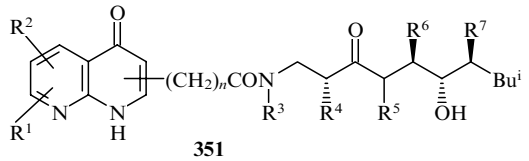

351

R^1, R^2 = H, Alk, OH, OAlk, Ar, CO_2H, NH_2; R^3, R^4 = H, Alk;
R^5 = H, Alk, cyclo-Alk, Bn; R^6 = Alk, cyclo-Alk, Ph;
R^7 = H, OH, OAlk, cyclo-Alk, NH_2.

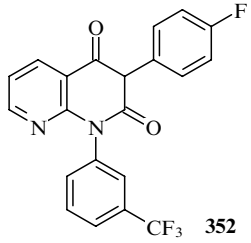

352

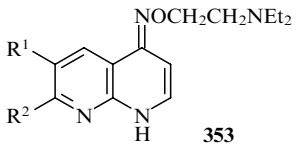

353

R^1 = H, Br;
R^2 = Me, OMe, OEt, Br.

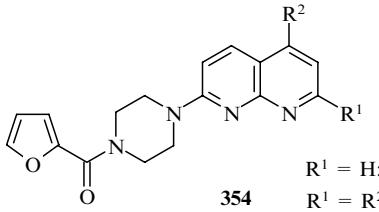

354

R^1 = H: R^2 = OH, OMe, NH_2;
R^1 = R^2 = Me, CF_3.

Of numerous compounds of the naphthyridine series covered by patents as various receptor inhibitors, cholesterol acyl transferase inhibitors **355**,[574, 580] integrin receptor antagonists **356** and **357**,[579, 581, 587, 588, 592, 593, 595, 596] vitronectin receptor antagonist **358**,[585] *etc*. are worthy of notice.

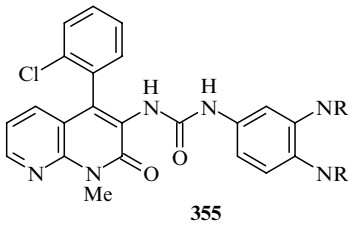

355

R = H, Alk, cyclo-Alk, Alkenyl.

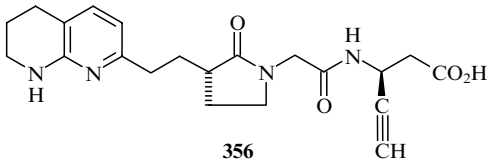

356

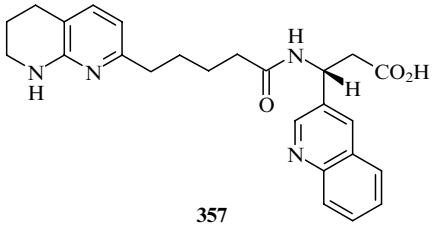

357

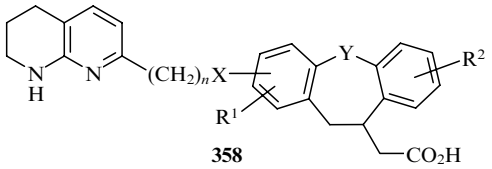

358

R^1 = H, Hal, C_1–C_6-Alk; R^2 = H, C_1–C_6-Alk;
X = Y = O, CH_2; n = 2, 3.

The present review, devoted to the chemistry and biological activities of 1,8-naphthyridine derivatives, will hopefully be of interest for organic chemists and biologists. Due to the presence of two geminal endocyclic nitrogen atoms, the 1,8-naphthyridine molecule is more promising for interactions with various biological receptors, coordination to metal ions and other intermolecular contacts compared to other isomeric pyridopyridines and the majority of known nitrogen heterocycles. In the immediate future it is hoped that new regio- and stereoselective procedures will be developed for the introduction of pharmacophoric groups at different positions of the naphthyridine molecule with the use of cascade heterocyclisation and combinatorial chemistry for the design of more efficient medical drugs possessing prolonged action or improved pharmokinetic characteristics. In particular, the design of the so-called dual action antibiotics, *viz*., systems consisting of β-lactam antibiotics of the penicillin and cefalosporin series and fluoroquinolonecarboxylic or fluoronaphthyridonecarboxylic acid derivatives, holds promise.

I thank Doctor S V Roman for help in collecting patent data.

This review has been written with the financial support of the Russian Foundation for Basic Research (Project No. 02-03-32063).

References

1. V P Litvinov, S V Roman, V D Dyachenko *Usp. Khim.* **69** 218 (2000) [*Russ. Chem. Rev.* **69** 201 (2000)]
2. V P Litvinov, S V Roman, V D Dyachenko *Usp. Khim.* **70** 345 (2001) [*Russ. Chem. Rev.* **70** 299 (2001)]
3. D Bouzard, in *Recent Progress in the Chemical Synthesis of Antibiotics* (Berlin, Heidelberg: Springler, 1999) p. 249
4. Y Goueffon, G Montay, F Roquet, M Pesson *C.R. Hebd. Seances Acad. Sci.* **292** 37 (1971)
5. K Sata, Y Matsura, M Inoue, T Une, Y Osada, H Ogawa, S Mitsuhaski *Antimicrob. Agents Chemother.* **22** 548 (1982)
6. T Miyamoto, H Egawa, J Matsumoto *Chem. Pharm. Bull.* **35** 2280 (1987)
7. P Urbaskova, J Trupl, H Hupkova, P C Appelbaum, M R Jacobs *Eur. J. Clin. Microbiol. Infect. Dis.* **15** 686 (1996); *Chem. Abstr.* **126** 16 683 (1997)
8. G W Kaatz, S M Seo, J R Aeschlimann, H H Houlihan, R-C Mercier, M J Rybak *Antimicrob. Agents Chemother.* **42** 254 (1998)
9. E Vilsmeier, T Goerz *Synthesis* 739 (1998)
10. K W Garey, G W Amdsen *Pharmacotherapy* **19** 21 (1999); *Chem. Abstr.* **130** 290 888 (1999)
11. R Wise, J M Andrews, I J Edwards *Antimicrob. Agents Chemother.* **23** 559 (1983)
12. R Albrecht *Prog. Drug Res.* **21** 9 (1983)
13. J T Smith *Pharm. J.* 299 (1984)
14. U Petersen, S Bartel, K-D Bremm, T Himmler, A Krebs, T Schenke *Bull. Soc. Chim. Belg.* **105** 683 (1996)
15. G A Mokrushina, S G Alekseev, V N Charushin, O N Chupakhin *Zh. Vsesoyuz. Khim. O-va im D I Mendeleeva* 447 (1991) [a]
16. D T W Chu, P B Fernandes, A K Claiborne, E Pihuleas, C W Nordeen, R E Maleczka, A G Pernet *J. Med. Chem.* **28** 1558 (1985)
17. Jpn. P. 6 0289 64; *Chem. Abstr.* **103** 71 202 (1985)
18. BRD P. 3 248 506; *Chem. Abstr.* **102** 6526 (1985)
19. D T W Chu, P B Fernandes, A K Claiborne, E H Gracey, A G Pernet *J. Med. Chem.* **29** 2363 (1986)
20. D T W Chu *J. Heterocycl. Chem.* **22** 1033 (1985)
21. J Matsumoto, T Miyamoto, A Minamida, Y Nishimura, H Egawa, H Nishimura *J. Med. Chem.* **27** 292 (1984)
22. D Bouzard, P Di Cesare, M Essiz, J P Jacquet, P Remuzon, A Weber, T Oki, M Masuyoshi *J. Med. Chem.* **32** 537 (1989)
23. P Remuzon, D Bouzard, P Di Cesare, M Essiz, J P Jacquet, J R Kiechel, B Ledoussal, R E Kessler, J Fung-Tomc *J. Med. Chem.* **34** 29 (1991)
24. J Matsumoto, Y Nishimura, A Minamida *Chem. Pharm. Bull.* **36** 1223 (1988)
25. BRD P. 3 508 816; *Chem. Abstr.* **105** 191 059 (1986)
26. D T W Chu, A K Claiborne *J. Heterocycl. Chem.* **27** 1191 (1990)
27. H Kondo, M Taguchi, Y Inoue, F Sakamoto, G Tsukamoto *J. Med. Chem.* **33** 2012 (1990)
28. Y-S Oh, S-H Cho *J. Heterocycl. Chem.* **35** 17 (1998)
29. Fr. P. 2 642 070; *Chem. Abstr.* **114** 62 082 (1991)
30. Fr. P. 2 642 071; *Chem. Abstr.* **114** 62 083 (1991)
31. Eur. P. 132 845; *Chem. Abstr.* **102** 220 858 (1985)
32. T Mijamoto, H Egawa, K Shibamori, J Matsumoto *J. Heterocycl. Chem.* **24** 1333 (1987)
33. D Bouzard, P Di Cesare, M Essiz, J P Jacquet, J R Kiechel, P Remuzon, A Weber, T Oki, M Masuyoshi, R E Kessler, J Fung-Tomc, J Desiderio *J. Med. Chem.* **33** 1344 (1990)
34. H Egawa, T Miyamoto, A Minamida, Y Nishimura, H Okada, H Uno, J Matsumoto *J. Med. Chem.* **27** 1543 (1984)
35. D Bouzard, P Di Cesare, M Essiz, J P Jacquet, P Remuzon, A Weber *Rev. Infect. Dis.* **11** (Suppl. 5) S912 (1989)
36. L Maftanova, D V Majtan *Folia Microbiol. (Prague)* **43** 104 (1998); *Chem. Abstr.* **128** 164 873 (1998)
37. A Hostacka, E Karelova *Arzneim.-Forsch.* **48** 185 (1998)

38. K G Naber, M Well, K Hollauer, D Kirchbauer, W Witte *Chemotherapy (Basel)* **44** 77 (1998)
39. Y Kashida, M Kato *Antimicrob. Agents Chemother.* **41** 2389 (1997)
40. K Kohno, M Niwa, M Nozaki, T Uematsu, H Fujimura *Gen. Pharmacol.* **29** 767 (1997)
41. K E Scheirer, N P Higgins *J. Biol. Chem.* **272** 27 202 (1997)
42. D Chadha, S P Agarwal *Indian J. Pharm. Sci.* **59** 101 (1997)
43. Faming Zhuanli Shenquing Gongkai Shuomingshu CN P. 1 145 258; *Chem. Abstr.* **128** 119 695 (1998)
44. M E Cavet, M West, N L Nicholas *Antimicrob. Agents Chemother.* **41** 2693 (1997)
45. T Kobayashi *Nagoya-Shiritsu Daigaku Igakkai Zasshi* **48** 131 (1998); *Chem. Abstr.* **128** 229 117 (1998)
46. S Sortino, G De Guidi, S Giuffrida, S Monti, A Velardita *Photochem. Photobiol.* **67** 167 (1998)
47. A A El-Shanawani *Chin. Pharm. J. (Taipei)* **49** 259 (1998); *Chem. Abstr.* **128** 262 040 (1998)
48. A Hostacka *Microbios* **91** 137 (1997); *Chem. Abstr.* **128** 280 745 (1998)
49. L J Martinez, R H Sik, C F Chignell *Photochem. Photobiol.* **67** 399 (1998)
50. H Xe, Y Li, Z Zhang *Fenxi Shiyanishi* **17** 71 (1998); *Chem. Abstr.* **130** 104 685 (1999)
51. E Fasani, A Profumo, A Albini *Photochem. Photobiol.* **68** 666 (1998)
52. V Majtan, L Majtanova *Microbios* **95** 117 (1998); *Chem. Abstr.* **130** 136 459 (1999)
53. M D Rose, J Bygrave, G W F Stubbings *Analyst* **123** 2789 (1998)
54. S-W Sun, A-C Wu *J. Liq. Chromatogr. Relat. Technol.* **22** 281 (1999); *Chem. Abstr.* **130** 158 506 (1999)
55. C Zhao, Y Shen, L Zhang *Tongji Yike Daxue Xuebao* **27** 391 (1998); *Chem. Abstr.* **130** 191 842 (1999)
56. G Zlotos, M Oehlmann, P Nickel, U Holzgrabe *J. Pharm. Biomed. Anal.* **18** 847 (1998)
57. T Perez-Ruiz, C Martinez-Lozano, A Sanz, E Bravo *Chromatographia* **49** 419 (1999)
58. T Takizawa, K Hashimoto, N Itoh, S Yamashita, K Owen *Hum. Exp. Toxicol.* **18** 38 (1999)
59. G Li, Q Chen, S Wang *Zhongguo Kangshengsu Zazhi* **25** 124 (2000); *Chem. Abstr.* **134** 2507 (2001)
60. G De Guidi, S Guiffrida, S Monti, P S Pisu, S Sortino, L L Costanzo *Int. J. Photoenergy* 13 (1999); *Chem. Abstr.* **134** 120 779 (2001)
61. B Hamel, N Mottet, M Audran, P Costa, F Bressole *J. Antimicrob. Chemother.* **46** 993 (2000)
62. A Blotz, L Michel, A Moysan, J Blumel, L Dubertret, J N Ahr, H-W Vohr *J. Photochem. Photobiol., B* **58** 46 (2000); *Chem. Abstr.* **134** 204 371 (2001)
63. Z Altkosar, G Altiokka, M Tuncel *Acta Pharm. Turc.* **43** 47 (2001); *Chem. Abstr.* **134** 344 686 (2001)
64. S Sauvaigo, T Douki, F Odin, S Caillat, J-L Ravant, J Cadet *Photochem. Photobiol.* **73** 230 (2001)
65. G Ackermann, V J Tang, A C Rodloff, J Silva *J. Antimicrob. Chemother.* **47** 722 (2001)
66. P-L Wang, L Chen, Y-F Fan *J. AOAC Int.* **84** 684 (2001); *Chem. Abstr.* **135** 170 895 (2001)
67. J-Y Fang, C-T Hwang, W-T Chiu, Y-Y Wang *Int. J. Pharm.* **219** 61 (2001)
68. Eur. P. 413 455; *Chem. Abstr.* **115** 232 216 (1991)
69. US P. 5 164 402; *Chem. Abstr.* **119** 117 227 (1993)
70. T D Gootz, K E Brighty, M R Anderson, B J Schmieder, S L Haskell, J A Sutcliffe, M J Castaldi, P R McGurik *Diagn. Microbiol. Infect. Dis.* **19** 235 (1994); *Chem. Abstr.* **122** 27 600 (1995)
71. K E Brighty, M J Castaldi *Synlett* 1097 (1996)
72. R A Fromtling, R A Castaner *Drugs Future* **21** 496 (1996)
73. M M Paris, S M Hickey, M Trujillo, S Shelton, G H McGracken *Antimicrob. Agents Chemother.* **39** 1243 (1995)
74. E J Giamarellos-Bourboulis, P Grecka, I Galani, H Gimarellou *Clin. Drug Invest.* **14** 330 (1997); *Chem. Abstr.* **128** 1833 (1998)
75. A P MacGowan, K E Bowker, H A Holt, M Wootton, D S Reeves *J. Antimicrob. Chemother.* **40** 503 (1997)
76. F Marco, M S Barrett, R N Jones *J. Antimicrob. Chemother.* **40** 605 (1997)
77. M E Ernst, E Ernst, M E Klepser *Am. J. Health-Syst. Pharm.* **54** 2569 (1997); *Chem. Abstr.* **128** 70 299 (1998)
78. C Y Chan, D S C Tsang, T L Chan, W W Yew, S W Cheung, A F B Cheng *Chemotherapy (Basel)* **44** 7 (1998)
79. D G Schick, H N Canawati, J Z Mongomerie *Diagn. Microbiol. Infect. Dis.* **29** 233 (1997); *Chem. Abstr.* **128** 125 717 (1998)
80. S H Zinner, D Gilbert, M N Dudley *Antimicrob. Agents Chemother.* **42** 72 (1998)
81. J Z Montgomerie, D G Schick *Antimicrob. Agents Chemother.* **42** 188 (1998)
82. P C Fuchs, A L Barry, S D Brown *J. Clin. Microbiol.* **36** 585 (1998); *Chem. Abstr.* **128** 178 043 (1998)
83. M P Montanari, M Prenna, M Mingoia, S Ripa, P E Varaldo *Chemotherapy (Basel)* **44** 85 (1998)
84. M A Visalli, S Bajaksouzian, M R Jacobs, P C Appelbaum *Diagn. Microbiol. Infect. Dis.* **30** 61 (1998); *Chem. Abstr.* **128** 202 922 (1998)
85. R B Jones, J Schwebke, E M Thorpe, Z A Dalu, P Leone, R B Johnson *Am. J. Med.* **104** 28 (1998); *Chem. Abstr.* **128** 212 763 (1998)
86. A A Firsov, A A Shevchenko, S N Vostrov, S H Zinner *Antimicrob. Agents Chemother.* **42** 659 (1998)
87. F -J Schmitz, J Verhoef, A Fluit, H-P Heinz, M E Jones *J. Antimicrob. Chemother.* **41** 311 (1998)
88. M C Struwig, P L Botha, L J Chalkley *Antimicrob. Agents Chemother.* **42** 2752 (1998)
89. A Gikas, I Spyridaki, A Psaroulaki, D Kofterithis, Y Tselentis *Antimicrob. Agents Chemother.* **42** 2747 (1998)
90. J Vincent, L Dogolo, B A Baris, S A Willavize, R Teng *Eur. J. Clin. Microbiol. Infect. Dis.* **17** 427 (1998); *Chem. Abstr.* **130** 20 177 (1999)
91. G Melnik, W H Schwesinger, R Teng, L C Dogolo, J Vincent *Eur. J. Clin. Microbiol. Infect. Dis.* **17** 431 (1998); *Chem. Abstr.* **130** 20 215 (1999)
92. P Leophonte, R J T Baldwin, N Pluck *Eur. J. Clin. Microbiol. Infect. Dis.* **17** 434 (1998); *Chem. Abstr.* **130** 20 257 (1999)
93. B O Doherty, R Danill *Eur. J. Clin. Microbiol. Infect. Dis.* **17** 441 (1998); *Chem. Abstr.* **130** 20 258 (1999)
94. F Tremolieres, F De Kock, N Pluck, R Daniel *Eur. J. Clin. Microbiol. Infect. Dis.* **17** 447 (1998); *Chem. Abstr.* **130** 20 259 (1999)
95. D Williams, S Hopkins *Eur. J. Clin. Microbiol. Infect. Dis.* **17** 454 (1998); *Chem. Abstr.* **130** 20 260 (1999)
96. J Garcia-de-Lomas, E Millas, M A Lozaro, M Bermejo, C Gimeno, D Navarro, S Sanchez *Eur. J. Clin. Microbiol. Infect. Dis.* **17** 420 (1998); *Chem. Abstr.* **130** 32 720 (1999)
97. K Weiss, M Laverdiere, C Restieri *J. Antimicrob. Chemother.* **42** 523 (1998)
98. D Pontani, H Washton, S Bouchillon, J Johnson *Eur. J. Clin. Microbiol. Infect. Dis.* **17** 413 (1998); *Chem. Abstr.* **130** 35 538 (1999)
99. E J Giamarellos-Bourboulis, H Sambatakon, P Grecka, H Giamarellon *Eur. J. Clin. Microbiol. Infect. Dis.* **17** 657 (1998); *Chem. Abstr.* **130** 35 542 (1999)
100. A A Firsof, S N Vostrov, A A Shevchenko, Yu A Portnov, S H Zinner *Antimicrob. Agents Chemother.* **42** 2841 (1998)
101. A Bauernfeind, R Jungwirth *Chemother J.* **7** 86 (1998)
102. H Seifert *Zentralbl. Bakteriol.* **288** 509 (1998); *Chem. Abstr.* **130** 122 059 (1999)
103. R N Jones, M A Pfaller, G V Doern *Diagn. Microbiol. Infect. Dis.* **32** 119 (1998); *Chem. Abstr.* **130** 136 444 (1999)
104. H D Isenberg, P Alperstein, K France *Diagn. Microbiol. Infect. Dis.* **32** 115 (1998); *Chem. Abstr.* **130** 136 443 (1999)
105. U Holzgrabe, P Heisig *Pharm. Unserer Zeit.* **28** 30 (1999); *Chem. Abstr.* **130** 148 159 (1999)
106. Y S Kim, Q Lin, L L Chow, H F Chambers, M G Tiuber *Antimicrob. Agents Chemother.* **42** 3325 (1998)
107. K G Naber, D Adam *Int. J. Antimicrob. Agents* **10** 255 (1998)
108. S Bomparde, L Ferrante, L Leone, S Ripa *Chromatographia* **49** 185 (1999)

109. R N Jones, M L Beach, M A Pfaller, G V Doern *Diagn. Microbiol. Infect. Dis.* **32** 247 (1998); *Chem. Abstr.* **130** 234 558 (1999)
110. J A Weigelt *Am. J. Surg.* **176** 4S (1998); *Chem. Abstr.* **130** 246 133 (1999)
111. B A Lipsky, C A Baker *Clin. Infect. Dis.* **28** 352 (1999)
112. J Vincent, R Teng, D K Dalvie, H L Friedman *Am. J. Surg.* **176** 8S (1998); *Chem. Abstr.* **130** 246 259 (1999)
113. E Melnik, W H Schwesinger, L C Dogolo, R Teng, J Vincet *Am. J. Surg.* **176** 14S (1999); *Chem. Abstr.* **130** 246 373 (1999)
114. M G Martines, M Maccato, C Van Hook, J Vincent *Am. J. Surg.* **176** 18S (1998); *Chem. Abstr.* **130** 246 374 (1999)
115. P E Donahue, D L Smith, A E Yellin, S J Mintz *Am. J. Surg.* **176** 53S (1998); *Chem. Abstr.* **130** 246 376 (1999)
116. S Roy, D Hemsell, S Gordon, D Godwin, M Pearlman, D Luke *Am. J. Surg.* **176** 62S (1998); *Chem. Abstr.* **130** 246 377 (1999)
117. S Roy, W Koltun, A Chatwani, M G Martens, R Dittrich, D R Luke *Am. J. Surg.* **176** 67S (1998); *Chem. Abstr.* **130** 246 378 (1999)
118. D J Williams, S Hopkins *Am. J. Surg.* **176** 74S (1998); *Chem. Abstr.* **130** 246 379 (1999)
119. I Trujillano-Martin, E Garcia-Svnchez, I M Martinez, M J Fresnadillo, J E Garcia-Sanchez, J A Garcia-Rodriguez *Antimicrob. Agents Chemother.* **43** 194 (1999)
120. J H Jorgensen, L M Weigel, M J Ferraro, J M Swenson, F C Tenover *Antimicrob. Agents Chemother.* **43** 329 (1999)
121. H Fukuda, K Hiramatsu *Antimicrob. Agents Chemother.* **43** 410 (1999)
122. M E Jones, M R Visser, M Klootwijk, P Heisig, J Verhoef, F-J Schmitz *Antimicrob. Agents Chemother.* **43** 421 (1999)
123. E Varon, C Janoir, M-D Kitzis, L Gutmann *Antimicrob. Agents Chemother.* **43** 302 (1999)
124. O Manzor, J Pawlak, L Saravolatz *J. Antimicrob. Chemother.* **43** 31 (1999)
125. J M Entenza, J Vouillamoz, M P Glauser, P Moreillon *Antimicrob. Agents Chemother.* **43** 77 (1999)
126. L O Clara, M A Biglica *Medicina (Buenos Aires)* **59** 17 (1998); *Chem. Abstr.* **130** 290 996 (1999)
127. P C Fuchs, A L Barry, S D Brown *Diagn. Microbiol. Infect. Dis.* **33** 33 (1999); *Chem. Abstr.* **130** 293 838 (1999)
128. M A Cohen, M D Huband *Diagn. Microbiol. Infect. Dis.* **33** 43 (1999); *Chem. Abstr.* **130** 293 839 (1999)
129. L Martinez-Martinez, F Fernández, E J Perea *J. Antimicrob. Chemother.* **43** 277 (1999)
130. M A Croco, D J Biedenbach, M A Pfaller, G V Doern, R N Jones *J. Antimicrob. Chemother.* **42** 672 (1998)
131. L Martinez-Martinez, F Fernández, A I Suárez, E J Perea *J. Antimicrob. Chemother.* **43** 227 (1999)
132. A A Firsov, S N Vostrov, O V Kononenko, S H Zinner, Yu A Portnov *Antimicrob. Agents Chemother.* **43** 498 (1999)
133. J A Orden, J A Ruiz-Santa-Quiteria, S Garcia, D Cid, R de la Fuente *Antimicrob. Agents Chemother.* **43** 510 (1999)
134. E Hershberger, J R Aeschlimann, T Moldovan, M J Rybak *Antimicrob. Agents Chemother.* **43** 717 (1999)
135. M O'Brien, T Quach, D Gilbert *Clin. Microbiol. Infect.* **5** 12 (1999); *Chem. Abstr.* **130** 322 829 (1999)
136. C H M Van Nispen, A I M Hoepelman, M Rozenberg-Arska, J Verhoef, L Purkins, S A Willarize *Am. J. Surg.* **176** 27S (1998); *Chem. Abstr.* **130** 332 320 (1999)
137. J Vincet, R Teng, S M Pelletier, S A Willavize, H L Friedman *Am. J. Surg.* **176** 28S (1998); *Chem. Abstr.* **130** 342 862 (1999)
138. J Vincent, T Hunt, R Teng, L Robarge, S A Willavize, H L Friedman *Am. J. Surg.* **176** 32S (1998); *Chem. Abstr.* **130** 332 830 (1999)
139. A B Onderdonk *Am. J. Surg.* **176** 39S (1998); *Chem. Abstr.* **130** 332 321 (1999)
140. R D Snyder, C S Cooper *Photochem. Photobiol.* **69** 288 (1999)
141. R Hakenbeck, in *The 1st International Moxifloxacin Symposium, Berlin, 1999* p. 21; *Chem. Abstr.* **133** 1498 (2000)
142. G L Mandell, E J Coleman *Antimicrob. Agents Chemother.* **44** 2561 (2000)
143. A King, J May, G French, I Phillips *J. Antimicrob. Agents* **45** (Suppl. S1) 1 (2000)
144. J Broskey, K Coleman, M N Gwynn, L McCloskey, C Traini, L Voelker, R Warren *J. Antimicrob. Agents* **45** (Suppl. S1) 95 (2000)
145. R N Jones L M Deshpande, M E Erwin, M S Barrett, M L Beach *J. Antimicrob. Agents* **45** (Suppl. S1) 67 (2000)
146. C Armbruster, B Robibaro, A Griesmacher, H Vorbach *J. Antimicrob. Chemother.* **45** 533 (2000)
147. B Heinemann, H Wisplinghoff, M Edmond, H Seifert *Antimicrob. Agents Chemother.* **44** 2211 (2000)
148. D R Snydman, N V Jacobus, L A McDermott, S E Supran *Antimicrob. Agents Chemother.* **44** 1710 (2000)
149. J L M Bellido, F J S Hernandez, M N G Zufiaure, J A Garcia-Rodriguez *J. Antimicrob. Chemother.* **46** 334 (2000)
150. G G Zhanel, J A Karlowsky, D E Low, D J Daryl *J. Antimicrob. Chemother.* **45** 655 (2000)
151. L M Ednoban, K L Credito, M Khantipong, M R Jacobs, P C Appelbaum *J. Antimicrob. Chemother.* **45** 633 (2000)
152. A E J M van der Bogaard, N London, E E Stobberingh *J. Antimicrob. Chemother.* **45** 663 (2000)
153. I Morrissey, J T George *J. Antimicrob. Chemother.* **45** (Suppl. S1) 107 (2000)
154. E Swiatlo, E Moore, J Watt, L S McDaniel *Int. J. Antimicrob. Agents* **15** 73 (2000)
155. L C Preheim, C Laurel, J Martha, M U Snitily *Infect. Dis. Ther.* 23 (2000); *Chem. Abstr.* **133** 83 907 (2000)
156. A Lubasch, I Keller, K Borner, P Koeppe, H Lode *Antimicrob. Agents Chemother.* **44** 2600 (2000)
157. E Hershberger, E A Coyle, G W Koatz, M J Zervos, M J Rybak *Antimicrob. Agents Chemother.* **44** 1921 (2000)
158. A M Sugar, X-P Lin *Antimicrob. Agents Chemother.* **44** 2004 (2000)
159. R Gozalbes, M Brun-Pascaud, R Garzia-Domenech, J Galvez, P-M Girard, J-P Doucet, F Derouin *Antimicrob. Agents Chemother.* **44** 2771 (2000)
160. M Tanaka, H Tunoe, O Mochida, A Kanayama, T Saika, I Kobayashi, S Naito *Diagn. Microbiol. Infect. Dis.* **38** 109 (2000); *Chem. Abstr.* **134** 97 689 (2001)
161. J C McNabb, R Quintiliani, C H Nightingale, D P Nicolau *Chemotherapy (Basel)* **46** 389 (2000)
162. L E T Stearne, C Kooi, W H F Goessens, I A J M Bakker-Woudenberg, I C Gyssens *Antimicrob. Agents Chemother.* **45** 243 (2001)
163. C M Bébéar, O Grau, A Charron, H Renaudin, D Gruson, C Bébéar *Antimicrob. Agents Chemother.* **44** 2719 (2000)
164. O J Yoin-Lambert, M Michea-Hamzehpour, T Kohler, F Chaun, F Faurisson, S Dantrey, C Vissuzaine, C Carbon, J-C Pechere *Antimicrob. Agents Chemother.* **45** 571 (2001)
165. US P. 6 184 380; *Chem. Abstr.* **134** 147 591 (2001)
166. P C Fuchs, A L Bary, S D Brown *Diagn. Microbiol. Infect. Dis.* **38** 243 (2000); *Chem. Abstr.* **134** 190 590 (2001)
167. D B Hoellman, L M Kelly, M R Jacobs, P C Appelbaum *Antimicrob. Agents Chemother.* **45** 589 (2001)
168. G Garcia-Calvo, A Molleja, M J Giménez, A Parra, E Nieto, C Ponte, L Aguilar, F Soriano *Antimicrob. Agents Chemother.* **45** 608 (2001)
169. S M Zakeri, H Meyer, G Meinhardt, W Reinishi, K Schrattbauer, M Knoefler, L H Block *Immunopharmacology* **48** 27 (2000)
170. I Morrisey, J T George *Int. J. Antimicrob. Agents* **17** 33 (2001)
171. M Takahata, M Shimakura, R Hori, K Kizawa, Y Todo, S Minami, Y Watanabe, N Narita *Antimicrob. Agents Chemother.* **45** 312 (2001)
172. J C Rodriguez, F Linares, G Royo *Chemotherapy (Basel)* **47** 39 (2001)
173. M B Kays, M Conkin *Pharmacotherapy* **20** 1310 (2000)
174. G Kronvall, M Rylander, M Waldere, L Lind-Brandberg, P Larsson, S Tornqvist, T Monsen *Scand. J. Infect. Dis.* **31** 573 (1999); *Chem. Abstr.* **134** 97 420 (2001)
175. D S Burgess, R W Hastings *Diagn. Microbiol. Infect. Dis.* **38** 37 (2000); *Chem. Abstr.* **134** 97 677 (2001)
176. J C Shobha, T R Kumar, N Deivanayagam, R B Singh, P Waghray, P A Babu, J Bhaduri, C C Sekhar *Clin. Drug Invest.* **20** 95 (2000); *Chem. Abstr.* **134** 157 225 (2001)

177. J M Blondeau, X Zhao, G Hansen, K Drlica *Antimicrob. Agents Chemother*. **45** 433 (2001)
178. T R Shultz, J W Tapsall, P A White *Antimicrob. Agents Chemother*. **45** 734 (2001)
179. E Fernandez-Moreira, D Balas, I Gonzalez, A G de la Campa *Microb. Drug Resist. (Larchmont, NY)* **6** 259 (2000); *Chem. Abstr*. **134** 322 468 (2001)
180. D Jonas, I Engels, C Friedhoff, B Spitzmüller, F D Daschner, U Frank *J. Antimicrob. Chemother*. **47** 147 (2001)
181. C Heer, K Stuerz, R R Reinhert, M Mader, R Nau *Infection (Munich)* **28** 13 (2000); *Chem. Abstr*. **134** 338 095 (2001)
182. M Klepser, E J Ernst, C R Petzold, P Rhomberg, G V Doern *Antimicrob. Agents Chemother*. **45** 673 (2001)
183. H W Horowitz, T-C Hsieh, M E Aguero-Rosenfeld, F Kalantarpour, I Chowdhury, G P Wormser, J M Wu *Antimicrob. Agents Chemother*. **45** 786 (2001)
184. D N Gilbert, S E Kohlhepp, K A Slama, G Grunkemeier, G Lewis, R J Dworkin, S E Slaughter, J E Leggett *Antimicrob. Agents Chemother*. **45** 883 (2001)
185. J C Fung-Tomc, B Minassian, B Kolek, E Huczko, L Aleksunes, T Stickle, T Washo, E Gradelski *Antimicrob. Agents Chemother*. **44** 3351 (2000)
186. K-T Luh, P-R Hsueh, L-J Teng, H-J Pan, Y-C Chen, J-J Lu, J-J Wu, S-W Ho *Antimicrob. Agents Chemother*. **44** 3374 (2000)
187. K E Aldridge, D Ashcraft, K Cambre, C L Pierson, S G Jenkins, J E Rosenblatt *Antimicrob. Agents Chemother*. **45** 1238 (2001)
188. A Granl, J Castaner *Drugs Future* **23** 1199 (1998)
189. J Matsumoto, J Nakano, T Miyamoto, T Hirose, A Minamida, H Egawa, Y Nishimura, K Chiba, H Okada, in *Proceedings of the 14th International Congress on Chemotherapy* (Tokyo: University Tokyo Press, 1985); *Chem. Abstr*. **106** 2758 (1987)
190. D Bouzard, P Di Cesare, M Essiz, J P Jacquet, B Ledoussal, P Remuzon, R E Kessler, J Fung-Tomc *J. Med. Chem*. **35** 518 (1992)
191. P Remuzon, D Bouzard, P Di Cesare, C Dussy, J P Jacquet, A Jaegly *J. Heterocycl. Chem*. **29** 985 (1992)
192. P Remuzon, D Bouzard, C Guiol, J P Jacquet *J. Med. Chem*. **35** 2898 (1992)
193. D Bouzard, P Di Cesare, P Hoffmann, J Fung-Tomc, R Kessler *Drugs Exp. Clin. Res*. **18** 291 (1992); *Chem. Abstr*. **119** 62 461 (1993)
194. J Kim, Y H Yoon, I H Cho, J M Lee, K Lee, J H Kim, K H Hong *Korean J. Med. Chem*. **6** 183 (1996); *Chem. Abstr*. **126** 186 005 (1997)
195. C Y Hong, Y K Kim, J H Chang, S H Kim, H Choi D H Nam, Y Z Kim, J H Kwak *J. Med. Chem*. **40** 3584 (1997)
196. C Y Hong, Y K Kim, J H Kwak *Bioorg. Med. Chem. Lett*. **8** 221 (1998)
197. R Singh, R Fathi-Afshar, G Thomas, M P Singh, F Higashitani, A Hyodo, N Unemi, R G Micetich *Eur. J. Med. Chem*. **33** 697 (1998)
198. L J V Piddock, M Jhonson, V Ricci, S L Hill *Antimicrob. Agents Chemother*. **42** 2956 (1998)
199. J W Babich, R H Rubin, W A Graham, R A Wilkinson, J Vincent, A J Fishman *Nucl. Med. Biol*. **23** 995 (1996); *Chem. Abstr*. **126** 128 755 (1997)
200. M G Cormican, R N Jones *Antimicrob. Agents Chemother*. **41** 204 (1997)
201. Eur. P. 9425; *Chem. Abstr*. **93** 168 305 (1980)
202. Eur. P. 27 752; *Chem. Abstr*. **95** 150 631 (1981)
203. Fr. P. 2 496 663; *Chem. Abstr*. **98** 53 859 (1983)
204. Fr. P. 2 500 833; *Chem. Abstr*. **98** 107 273 (1983)
205. Fr. P. 2 531 084; *Chem. Abstr*. **101** 55 088 (1984)
206. Jpn. P. 59 227 887; *Chem. Abstr*. **103** 22 618 (1985)
207. Jpn. P. 60 172 981; *Chem. Abstr*. **104** 88 622 (1986)
208. BRD P. 3 514 076; *Chem. Abstr*. **104** 129 888 (1986)
209. US P. 4 550 104; *Chem. Abstr*. **104** 168 455 (1986)
210. Ind. P. 154 878; *Chem. Abstr*. **104** 224 882 (1986)
211. BRD P. 3 426 486; *Chem. Abstr*. **105** 172 310 (1986)
212. Jpn. P. 61 148 179; *Chem. Abstr*. **105** 226 520 (1986)
213. Belg. P. 9 040 86; *Chem. Abstr*. **105** 208 850 (1986)
214. Eur. P. 191 451; *Chem. Abstr*. **105** 226 521 (1986)
215. Jpn. P. 61 126 082; *Chem. Abstr*. **106** 4995 (1987)
216. Jpn. P. 61 137 885; *Chem. Abstr*. **106** 4996 (1987)
217. Jpn. P. 61 282 382; *Chem. Abstr*. **106** 156 450 (1987)
218. Jpn. P. 61 152 682; *Chem. Abstr*. **107** 39 861 (1987)
219. Jpn. P. 62 840 85; *Chem. Abstr*. **107** 134 294 (1987)
220. US P. 4 767 762; *Ref. Zh. Khim*. 12 O 124P (1989)
221. WO PCT 8 802 627; *Chem. Abstr*. **110** 57 646 (1989)
222. Eur. P. 312 794; *Chem. Abstr*. **111** 194 747 (1989)
223. Jpn. P. 01 106 886; *Chem. Abstr*. **111** 232 778 (1989)
224. Eur. P. 321 191; *Chem. Abstr*. **112** 77 161 (1990)
225. US P. 4 880 814; *Chem. Abstr*. **112** 235 280 (1990)
226. BRD P. 4 120 646; *Chem. Abstr*. **118** 233 894 (1993)
227. WO PCT 9 222 550; *Chem. Abstr*. **118** 233 896 (1993)
228. WO PCT 9 313 090; *Chem. Abstr*. **120** 164 147 (1994)
229. BRD P. 4 303 657; *Chem. Abstr*. **121** 179 620 (1994)
230. WO PCT 9 633 992; *Chem. Abstr*. **126** 47 118 (1997)
231. BRD P. 19 519 822; *Chem. Abstr*. **126** 104 101 (1997)
232. WO PCT 9 700 268; *Chem. Abstr*. **126** 157 823 (1997)
233. Jpn. P. 0 912 546; *Chem. Abstr*. **126** 199 451 (1997)
234. WO PCT 9 708 191; *Chem. Abstr*. **126** 251 417 (1997)
235. WO PCT 9 711 068; *Chem. Abstr*. **126** 305 587 (1997)
236. Span. P. 2 095 809; *Chem. Abstr*. **127** 135 786 (1997)
237. WO PCT 9 731 919; *Chem. Abstr*. **127** 262 605 (1997)
238. US P. 5 663 181; *Chem. Abstr*. **127** 262 666 (1997)
239. Jpn. P. 09 288 105; *Chem. Abstr*. **128** 32 133 (1998)
240. Eur. P. 811 613; *Chem. Abstr*. **128** 61 434 (1998)
241. Jpn. P. 1 007 568; *Chem. Abstr*. **128** 93 222 (1998)
242. WO PCT 9 802 431; *Chem. Abstr*. **128** 140 620 (1998)
243. WO PCT 9 818 795; *Chem. Abstr*. **128** 321 632 (1998)
244. WO PCT 9 823 592; *Chem. Abstr*. **129** 41 087 (1998)
245. US P. 5 776 944; *Chem. Abstr*. **129** 122 580 (1998)
246. Jpn. P. 10 330 205; *Chem. Abstr*. **130** 91 663 (1999)
247. WO PCT 9 900 393; *Chem. Abstr*. **130** 110 281 (1999)
248. Jpn. P. 1 112 278; *Chem. Abstr*. **130** 124 998 (1999)
249. US P. 5 869 670; *Chem. Abstr*. **130** 168 355 (1999)
250. WO PCT 9 906 430; *Chem. Abstr*. **130** 168 660 (1999)
251. WO PCT 9 907 682; *Chem. Abstr*. **130** 182 367 (1999)
252. WO PCT 9 907 706; *Chem. Abstr*. **130** 182 368 (1999)
253. WO PCT 9 910 351; *Chem. Abstr*. **130** 196 646 (1999)
254. WO PCT 9 907 704; *Chem. Abstr*. **130** 196 577 (1999)
255. Jpn. P. 1 160 578; *Chem. Abstr*. **130** 223 178 (1999)
256. WO PCT 0 037 467; *Chem. Abstr*. **133** 74 014 (2000)
257. WO PCT 0 117 961; *Chem. Abstr*. **134** 220 700 (2001)
258. Eur. P. 1 057 828 Evropa; *Chem. Abstr*. **134** 21 491 (2001)
259. WO PCT 0 118 002; *Chem. Abstr*. **134** 222 702 (2001)
260. WO PCT 0 130 779; *Chem. Abstr*. **134** 326 520 (2001)
261. WO PCT 0 136 408; *Chem. Abstr*. **135** 5534 (2001)
262. WO PCT 0 132 655; *Chem. Abstr*. **134** 353 259 (2001)
263. G J Lesher, E J Froelich, M D Greutt, J H Bailey, R P Brundage *J. Med. Pharm. Chem*. **5** 1063 (1962)
264. Belg. P. 612 258; *Chem. Abstr*. **58** 7953 (1963)
265. R J Rowbury, M Goodson *J. Appl. Microbiol*. **85** 615 (1998)
266. H Aijima, H Nagata, K Tanaka, H Hoshi, M Itagaki, T Ryouke, Y D Xu *Nichidai Igaku Zasshi* **57** 327 (1998); *Chem. Abstr*. **130** 20 249 (1999)
267. V R Bari, U J Dhorda, M Sandareson *Anal. Chim. Acta* **376** 221 (1998)
268. L Martinez, C F Chignele *J. Photochem. Photobiol., B* **45** 51 (1998); *Chem. Abstr*. **130** 78 008 (1999)
269. Y Hiraku, H Ito, S Kawanishi *Biochem. Biophys. Res. Commun*. **251** 466 (1998); *Chem. Abstr*. **130** 47 297 (1999)
270. E Dahan-Grobgeld, Z Livneh, A F Maretzek, S Polak-Charcon, Z Eichenbaum, H Degani *J. Biol. Chem*. **273** 30 232 (1998)
271. I D Meras, T G Diaz, F S Lopez, M I R Caceres *J. Chromatogr., B* **718** 135 (1998)
272. C D Miranda, G Castillo *Sci. Total Environ*. **224** 167 (1998); *Chem. Abstr*. **130** 172 527 (1999)
273. A F Youssef, F A Omar, H A Elsherief,G E D A A Abuo-Rahma *Bull. Pharm. Sci., Assuit Univ*. **21** 15 (1998); *Chem. Abstr*. **130** 182 379 (1999)
274. Y Xu, H Huang, H Shen *Fenxi Huaxue* **26** 1494 (1998); *Chem. Abstr*. **130** 191 399 (1999)
275. C H-L Corre, P Y Donnio, M Bonnier, M F Travert, A Lacourt, J L Avril *Pathol. Biol*. **46** 587 (1998); *Chem. Abstr*. **130** 207 186 (1999)

276. M-L Wang, S-C Chen, S C Kuo *J. Liq. Chromatogr. Relat. Technol.* **22** 771 (1999); *Chem. Abstr.* **130** 227 833 (1999)
277. L J V Piddock, Y-F Jin, V Ricci, A E Asuquo *J. Antimicrob. Chemother.* **43** 61 (1999)
278. M Cormican, D Morris, G Corbett-Feeney, J Fljnn *Diagn. Microbiol. Infect. Dis.* **32** 317 (1998); *Chem. Abstr.* **130** 279 157 (1999)
279. P A Borrow, M A Lovell, G Szmolleny, C K Murphy *Avian Pathol.* **27** 586 (1998); *Chem. Abstr.* **130** 291 110 (1999)
280. M-L Wang, S-C Chen, S-C Kuo *Chin. Pharm. J. (Taipei)* **50** 313 (1998); *Chem. Abstr.* **130** 324 437 (1999)
281. J Li, J Zhang, R Lin, Q Yu, W Cao *Beijng Huagong Daxue Xuebao* **27** 85 (2000); *Chem. Abstr.* **134** 246 861 (2001)
282. L-F Capitan-Vallvey, O M A Al-Barbarawi, M A Osma, M D Fernandez-Ramos, R Avidad, V R Gonzalez *Analyst* **125** 2000 (2000)
283. A Pomeranz, A El-Khayam, Z Korzets, O J Kessler, L Godfrey, B Katz, B Wolach *J. Urol. (Baltimore)* **164** 1070 (2000); *Chem. Abstr.* **134** 125 574 (2001)
284. Y Hiraku, S Kawanishi *Arch. Biochem. Biophys.* **382** 211 (2000)
285. B B Kachro *Chromatography (Basel)* **47** 97 (2001)
286. C Bakermans, E L Madsen *J. Microbiol. Methods* **43** 81 (2000); *Chem. Abstr.* **134** 344 110 (2001)
287. S Yamanaka, M Ishihara, J Sugigama *Cellulose (Dordrecht)* **7** 213 (2000); *Chem. Abstr.* **134** 368 420 (2001)
288. H Deng, H Zhang, J Zhang, M Lin *Fenxi Huaxue* **29** 306 (2001); *Chem. Abstr.* **135** 40 334 (2001)
289. F Kasnya, M Hiasa, Y Kawai, K Igarashi, M Fukui *Biochem. Pharmacol.* **62** 363 (2001)
290. C Pope, M Ayroud, G Ollis, M Chirino-Trejo, N Smart, S Quessy, P Michel *Microb. Drug Resist. (Larchomont, NY)* **7** 197 (2001); *Chem. Abstr.* **135** 269 931 (2001)
291. H J Linde, M Schmidt, E Fuchs, U Reischl, H-H Niller, N Lenh *Antimicrob. Agents Chemother.* **45** 1553 (2001)
292. K Buyukguzel *J. Econ. Entomol.* **94** 21 (2001); *Chem. Abstr.* **135** 253 176 (2001)
293. J S Lee, Y J Jung, M J Doh, J M Kim *Drug Dev. Ind. Pharm.* **27** 331 (2001); *Chem. Abstr.* **135** 293 823 (2001)
294. M S Y Khan, P Raghuvanshi *Indian J. Chem., Sect. B* **40** 530 (2001)
295. J Szych, A Cieslik, J Paciorek, S Kaluzewski *Int. J. Antimicrob. Agents* **18** 37 (2001)
296. R K Singh *Indian J. Exp. Biol.* **39** 818 (2001); *Chem. Abstr.* **135** 315 768 (2001)
297. Jpn. P. 10 298 204; *Chem. Abstr.* **130** 39 984 (1999)
298. Br. P. 2 324 242; *Chem. Abstr.* **130** 134 169 (1999)
299. Jpn. P. 1 146 762; *Chem. Abstr.* **130** 234 607 (1999)
300. WO PCT 9917791; *Chem. Abstr.* **130** 278 956 (1999)
301. US P. 5 179 093; *Ref. Zh. Khim.* 9 O 38P (1994)
302. US P. 4 810 708; *Ref. Zh. Khim.* 5 O 105P (1990)
303. US P. 4 988 705; *Ref. Zh. Khim.* 15 O 96P (1992)
304. US P. 5 116 840; *Ref. Zh. Khim.* 20 O 41P (1993)
305. US P. 5 126 352; *Ref. Zh. Khim.* 5 O 70P (1994)
306. D Hesk, T Duelfer, S Hickey, D Hochman, D Koharski, P McNamara, S Saluja *J. Labelled Compd. Radiopharm.* **34** 680 (1994)
307. R J Friary, M Spangler, R Osterman, L Sculman *Chirality* **8** 364 (1996)
308. Yu M Volovenko, A G Nemazannyi, F S Babichev *Ukr. Khim. Zh.* **51** 750 (1985)
309. R Friary, J H Schwerdt, V Seidl, F J Villani *J. Heterocycl. Chem.* **27** 189 (1990)
310. US P. 4 859 669; *Chem. Abstr.* **112** 77 165 (1990)
311. US P. 4 996 212; *Chem. Abstr.* **115** 71 570 (1991)
312. E A Mohamed, R M Abdel-Rahman, Z El-Gendy, M M Ismail *J. Indian Chem. Soc.* **71** 765 (1994)
313. E A Mohamed, R M Abdel-Rahman, Z El-Gendy, M M Ismail *J. Serb. Chem. Soc.* **58** 1003 (1993)
314. K Chen, S-C Kuo, M-C Hsieh, A Mauger, C M Lin, E Hamel, K-H Lee *J. Med. Chem.* **40** 2266 (1997)
315. K Chen, S-C Kuo, M-C Hsieh, A Mauger, C M Lin, E Hamel, K-H Lee *J. Med. Chem.* **40** 3049 (1997)
316. K Mogilaih, K R Reddy, K V Reddy, B Sreenivasulu *J. Indian Chem. Soc.* **63** 345 (1986)
317. K R Reddy, K Mogilaiah, B Sreenivasulu *J. Indian Chem. Soc.* **61** 888 (1984)
318. K V Reddy, M K Vijayender, B Sreenivasulu *J. Indian Chem. Soc.* **63** 443 (1986)
319. K R Reddy, K Mogilaiah, B Sreenivasulu *J. Indian Chem. Soc.* **63** 984 (1986)
320. K R Reddy, K Mogilaiah, B Sreenivasulu *J. Indian Chem. Soc.* **64** 193 (1987)
321. K R Reddy, R G Rao, K Mogilaiah, B Sreenivasulu *J. Indian Chem. Soc.* **64** 443 (1987)
322. K R Reddy, M K Rajendar, B Sreenivasulu *J. Indian Chem. Soc.* **64** 709 (1987)
323. K R Reddy, K Mogilaiah, B Sreenivasulu *Indian J. Chem., Sect. B* **28** 362 (1989)
324. T M Chary, K Mogilaiah, B Sreenivasulu *J. Indian Chem. Soc.* **64** 488 (1987)
325. G R Rao, K Mogilaiah, K R Reddy, B Sreenivasulu *J. Indian Chem. Soc.* **64** 710 (1987)
326. G R Rao, K Mogilaiah, B Sreenivasulu *Indian J. Pharm. Sci.* **51** 182 (1989)
327. R G Rama, K Mogilaiah, B Sreenivasulu *Collect. Czech. Chem. Commun.* **54** 1716 (1989)
328. R K Rajendar, K Mogialiah, B Sreenivasulu *Collect. Czech. Chem. Commun.* **53** 643 (1988)
329. K Agarwal *J. Indian Chem. Soc.* **68** 85 (1991)
330. D H Lorne, R G Gedir, E M Hawes, D G Wibberley *Eur. J. Med. Chem.* **20** 381 (1985)
331. E E Fenlon, T J Murray, M H Baloga, S C Zimmerman *J. Org. Chem.* **58** 6625 (1993)
332. X C Wang, H N C Wong, T C W Mak *Tetrahedron Lett.* **28** 5833 (1987)
333. X C Wang, H N C Wong *Tetrahedron* **51** 6941 (1995)
334. E Desarbre, J Y Merour *Tetrahedron Lett.* **35** 1995 (1994)
335. R P Thumel, Y Jahng *J. Org. Chem.* **50** 2407 (1985)
336. G Mehta, C Prabhakar, N Radmaja, M A Viswamitra *J. Chem. Soc., Perkin Trans. 1* 1747 (1992)
337. J M Quintela, J Vilar, C Peinador, C Veiga, V Ojea *Heterocycles* **41** 1001 (1995)
338. J M Quintela, R M Arcas, C Veiga, C Peinador, J Vilar, V Ojea *Heterocycles* **43** 53 (1996)
339. V Ojea, C Peinador, J M Quintela *Synthesis* 798 (1992)
340. V Ojea, C Peinador, J Vilar, J M Quintela *Synthesis* 152 (1993)
341. Jpn. P. 60 112 790; *Chem. Abstr.* **103** 196 067 (1985)
342. Jpn. P. 60 126 284; *Chem. Abstr.* **104** 50 861 (1986)
343. Fr. P. 2 567 520; *Chem. Abstr.* **105** 208 847 (1986)
344. Fr. P. 2 592 649; *Chem. Abstr.* **108** 112 422 (1988)
345. Fr. P. 2 592 652; *Chem. Abstr.* **108** 112 423 (1998)
346. Fr. P. 2 592 651; *Chem. Abstr.* **108** 112 424 (1998)
347. Fr. P. 2 592 650; *Chem. Abstr.* **108** 112 425 (1998)
348. Fr. P. 2 650 279; *Chem. Abstr.* **114** 62 083 (1991)
349. BRD P. 3 907 938; *Chem. Abstr.* **114** 122 342 (1991)
350. WO PCT 9 412 499; *Chem. Abstr.* **121** 179 567 (1994)
351. Eur. P. 0 670 320; *Ref. Zh. Khim.* 1 O 68P (1997)
352. Fr. P. 2 641 783; *Ref. Zh. Khim.* 10 O 61P (1991)
353. R A Mekheimer *Synthesis* 103 (2001)
354. G R Rao, K Mogilaiah, B Sreenivasulu *Collect. Czech. Chem. Commun.* **54** 1716 (1989)
355. K Mogilaiah, R B Rao *Indian J. Chem., Sect. B* **40** 713 (2001)
356. Y Hsiao, N R Rivera, N Yasuda, D L Huges, P J Reider *Org. Lett.* **3** 1101 (2001)
357. P L Ferrarini, C Mori, G Primofiore, L Galzolari *J. Heterocycl. Chem.* **27** 881 (1990)
358. B D Schober, T Kappe *J. Heterocycl. Chem.* **25** 1231 (1998)
359. L W Deady, D M Werden *Synth. Commun.* **17** 319 (1987)
360. A Da Settimo P L Ferrarini, C Mori, G Primofiore, A Subissi *Farmaco* **41** 926 (1986)
361. P B Barlin, W-L Tan *Aust. J. Chem.* **37** 1065 (1984)
362. BRD P. 3 907 937; *Chem. Abstr.* **114** 81 808 (1991)
363. BRD P. 3 644 825; *Chem. Abstr.* **109** 170 409 (1988)
364. T R Kelly, G J Bridger, C Zhao *J. Am. Chem. Soc.* **112** 8024 (1990)
365. I Hermecz, A Horvath *J. Heterocycl. Chem.* **29** 559 (1992)
366. F Trecourt, F Marsais, T Gungor, G Queguier *J. Chem. Soc., Perkin Trans. 1* 2409 (1990)

367. C J Chandler, L W Deady, J A Reiss, V Tzimos *J. Heterocycl. Chem.* **19** 1017 (1982)
368. B E Bayoumy, S El-Bahaie, S El-Feky *Pol. J. Chem.* **65** 1265 (1991)
369. A A Santilli, A C Scotese, R F Bauer, S C Bell *J. Med. Chem.* **30** 2270 (1987)
370. P L Nyce, M Steinman *Synthesis* 571 (1991)
371. US P. 4 492 702; *Chem. Abstr.* **100** 121 036 (1984)
372. US P. 4 684 727; *Chem. Abstr.* **106** 213 924 (1987)
373. US P. 4 551 463; *Ref. Zh. Khim.* 12 O 142P (1986)
374. US P. 4 596 809; *Ref. Zh. Khim.* 7 O 118P (1987)
375. US P. 4 632 923; *Ref. Zh. Khim.* 20 O 131P (1987)
376. US P. 4 628 055; *Ref. Zh. Khim.* 17 O 131P (1987)
377. US P. 4 652 564; *Ref. Zh. Khim.* 1 O 125P (1988)
378. US P. 4 775 524; *Ref. Zh. Khim.* 16 O 47P (1989)
379. US P. 4 782 067; *Ref. Zh. Khim.* 17 O 88P (1989)
380. US P. 4 897 487; *Ref. Zh. Khim.* 6 O 62P (1991)
381. US P. 4 916 131; *Ref. Zh. Khim.* 6 O 50P (1991)
382. US P. 5 037 826; *Ref. Zh. Khim.* 2 O 98P (1993)
383. US P. 5 079 360; *Ref. Zh. Khim.* 7 O 67P (1993)
384. US P. 5 180 823; *Ref. Zh. Khim.* 11 O 34P (1994)
385. M Seada, M-A El-Behairy, H Jahine, F Hanafy *Oriental. J. Chem.* **5** 273 (1989)
386. S M Fahmy, R M Mohareb *Tetrahedron* **42** 687 (1986)
387. R M Mohareb, S M Fahmy *Z. Naturforsch. B: Chem. Sci.* **41** 105 (1986)
388. J L Chen, W Steiglich *J. Heterocycl. Chem.* **30** 909 (1993)
389. Eur. P. 430 485; *Chem. Abstr.* **115** 136 078 (1991)
390. G M Coppola, J D Fraser, G E Hardtmann, M J Shapiro *J. Heterocycl. Chem.* **22** 193 (1985)
391. T Kuroda, F Suzuki *J. Heterocycl. Chem.* **28** 2029 (1991)
392. T Kuroda, F Suzuki, T Tamura, K Ohmori, H Hosoe *J. Med. Chem.* **35** 1130 (1992)
393. F Suzuki, T Kuroda, T Tamura, S Sato, K Ohmori, S Ichikawa *J. Med. Chem.* **35** 2863 (1992)
394. A L Zografos, C A Mitsos, O Igglessi-Markopoulou *J. Org. Chem.* **66** 4413 (2001)
395. M H Sherlock, J J Kaminski, W C Tom, J F Lee, S-C Wong, W Kreutner, R W Brayant, A T McPhail *J. Med. Chem.* **31** 2108 (1988)
396. T Duefler, D Gala *J. Labelled Compd. Radiopharm.* **29** 651 (1991)
397. W Kreutner, J Sherwood, S Sehring, C Rizzo, R W Chapman, M I Siegel, R W Egan *J. Pharmacol. Exp. Ther.* **247** 997 (1988)
398. D J Blithyn, H-J Shue, E Carlon, J Spitler, W Kreutner *Bioorg. Med. Chem. Lett.* **4** 1327 (1994)
399. V Delieza, A Detsi, V Bardakos, O Igglessi-Markopoulou *J. Chem. Soc., Perkin Trans. 1* 1487 (1997)
400. L W Deady *Aust. J. Chem.* **37** 1135 (1984)
401. L E Deady, D M Werden *Aust. J. Chem.* **39** 667 (1986)
402. P Cherubim, L W Deady *Aust. J. Chem.* **43** 1469 (1990)
403. G Agriropoulos, L W Deady, M Dorkos *Aust. J. Chem.* **44** 481 (1991)
404. L T Guss, L S Khabarova, L V Ershov, G G Dvoryantseva, N N Proshina, V G Granik *Khim. Geterotsikl. Soedin.* 643 (1990) [b]
405. BRD P. 3 911 064; *Ref. Zh. Khim.* 23 O 48P (1991)
406. P Meisel, E Kretzschmar, R Bartsch *Pharmazie* **39** 671 (1984)
407. S-C Kuo, S-Y Tsai, H-T Li, C-H Wu, K Ishii, H Nakamura *Chem. Pharm. Bull.* **36** 4403 (1988)
408. M W Read, P S Ray *J. Heterocycl. Chem.* **32** 1595 (1995)
409. A N Frolov, M V Baklanov *Zh. Org. Khim.* **27** 2424 (1991)
410. A N Frolov, M V Baklanov *Mendeleev Commun.* 22 (1992)
411. J Reisch, M Scheer *Arch. Pharm.* **320** 1174 (1987)
412. P Vanelle, S Ghezali, J Maldonato, O Chavignon, A Gueiffier, J C Teulade, M P Crozet *Heterocycles* **36** 1541 (1993)
413. A W Erian *J. Chem. Res., Synop.* 8 (1993)
414. H Wamhoff, W Lamers *Synthesis* 111 (1993)
415. C F Gurtler, E Steckhan, S Blechert *J. Org. Chem.* **61** 4136 (1996)
416. L Szabo, E Szentirmay, E Baitz-Gacs, G Kalaus, C Szantay *Tetrahedron Lett.* **38** 115 (1997)
417. J-H Zhang, M-X Wang, Z-T Huang *Tetrahedron Lett.* **39** 9237 (1998)
418. P Molina, M Alajarin, A Vidal *J. Chem. Soc., Chem. Commun.* 7 (1990)
419. S Shi, F Wudl *J. Org. Chem.* **53** 5379 (1988)
420. G Toth, A Kovacs, I Bitter, H Duddeck *Liebigs Ann. Chem.* 1215 (1991)
421. M Balogh, I Hermecz, G Naray-Szabo, K Simon, Z Meszaros *J. Chem. Soc., Perkin Trans. 1* 753 (1986)
422. G Metz *Arch. Pharm.* **320** 285 (1987)
423. W W Paudler, T J Kress *Adv. Heterocycl. Chem.* **11** 123 (1970)
424. H C van der Plas, M Wozniak, H J W van den Haak *Adv. Heterocycl. Chem.* **33** 95 (1983)
425. W W Paudler, R M Sheets *Adv. Heterocycl. Chem.* **33** 147 (1983)
426. H Bock, T T H Van, H Schoedel *Monatsh. Chem.* **127** 391 (1996)
427. WO PCT 9 639 406; *Chem. Abstr.* **126** 117 960 (1997)
428. Y Besidsky, K Lutham, A Claesson, C J Fowler, I Csoregh, U Hacksell *J. Chem. Soc., Perkin Trans. 1* 465 (1995)
429. P W Codding, M B Szkaradzinska, A W Roszak, L J Aha, T J Hagen, J M Cook *Can. J. Chem.* **66** 2981 (1988)
430. B Pniewska, A Rykowski, R Anulewicz *Acta Crystallogr., Sect. C* **46** 417 (1990)
431. B Pniewska, R Anulewicz *Acta Crystallogr., Sect. C* **43** 2198 (1987)
432. M Datta, S S Hannan, A N Talukdar *Acta Crystallogr., Sect. C* **51** 978 (1995)
433. T Kurihara, M Katsuda, K Nasu, M Inoue, M Doi *Chem. Pharm. Bull.* **33** 5551 (1985)
434. E G Paronikyan, S N Sirakanyan, R G Paronikyan, A S Noravyan, in *Tezisy Dokladov Vsesoyuznogo Seminara 'Khimiya Fiziologicheski Aktivnykh Soedinenii', Chernogolovka, 1989* (Abstracts of Reports of the All-Union Seminar 'The Chemistry of Physiologically Active Compounds', Chernogolovka, 1989) p. 193; *Ref. Zh. Khim.* 8 O 95 (1990)
435. M Wozniak, B Szpakiewicz *Zesz. Nauk. UJ. Pr. Chem.* 87 (1989); *Ref. Zh. Khim.* 23 B 1158 (1990)
436. M S Bobyleva, N S Kulikov *Teoret. Eksperim. Khim.* **25** 626 (1989) [c]
437. P Wormell, A R Lacey *Chem. Phys.* **118** 71 (1987)
438. M Wozniak, M Tomula *Zesz. Nauk. UJ. Pr. Chem.* 30 (1987); *Ref. Zh. Khim.* 12 B 1209 (1988)
439. J H Markgraf, J F Skinner, G T Marshall *J. Chem. Eng. Data* **33** 9 (1988)
440. H Quast, A Fuss, W Neudling *Eur. J. Org. Chem.* 317 (1998)
441. E L Ezell, R P Thummel, G E Martin *J. Heterocycl. Chem.* **21** 817 (1984)
442. A Gueiffier, A Viols, Y Blache, J P Chapat, O Chavignon, J C Teulade, F Fauvelle, G Grassy, G Dauphin *J. Heterocycl. Chem.* **34** 765 (1997)
443. M B Cox, P Arjunan, S K Arora *J. Antibiotics* **44** 885 (1991)
444. J Li, R Lin, Q Yu, L Zhu *Yaoxue Xuebao* **33** 498 (1998); *Chem. Abstr.* **130** 261 449 (1998)
445. M Weight, M Wiese *Quant. Struct.-Act. Relat.* **19** 142 (2000); *Chem. Abstr.* **133** 83 863 (2000)
446. M Wozniak *Zesz. Nauk. UJ. Pr. Chem.* 179 (1988); *Ref. Zh. Khim.* 11 B 4040 (1989)
447. D M Shingbal, S Sarjyotishi *Indian Drugs* **26** 576 (1989)
448. S-M Wu, H-L Wu, S-H Chen *J. Chin. Chem. Soc.* **34** 7 (1987)
449. BRD P. 3 902 079; *Ref. Zh. Khim.* 14 O 199P (1990)
450. US P. 5 188 833; *Ref. Zh. Khim.* 12 O 126P (1994)
451. Br. P. 2 262 937 Angliya; *Ref. Zh. Khim.* 13 O 114P (1994)
452. US P. 5 030 728; *Chem. Abstr.* **115** 183 265 (1991)
453. US P. 5 283 333; *Chem. Abstr.* **121** 157 631 (1994)
454. A D Hamilton, N Pant *J. Chem. Soc., Chem. Commun.* 765 (1988)
455. T R Kelly, C Zhao, G J Bridger *J. Am. Chem. Soc.* **111** 3744 (1989)
456. T W Murray, S C Zimmerman *J. Am. Chem. Soc.* **114** 4010 (1992)
457. B Feibush, M Saha, K Onan, B Karger, R Giese *J. Am. Chem. Soc.* **109** 7531 (1987)
458. W L Jorgensen, J Pranata *J. Am. Chem. Soc.* **112** 2008 (1990)
459. J Pranata, S G Wierschke, W L Jorgensen *J. Am. Chem. Soc.* **113** 2810 (1991)

460. S C Zimmerman, B F Duer *J. Org. Chem.* **57** 2215 (1992)
461. W R Tikkanen, K Kruger, K D Bomben, W L Jolly, W C Kaska, P C Ford *Inorg. Chem.* **23** 3633 (1984)
462. M Malkawa, M Munakata, S Kitagawa, T Kuroda-Sowa, Y Suenaga, M Yamamoto *Inorg. Chim. Acta* **271** 129 (1998)
463. C Vu, D Walker, J Wells, S Fox *J. Heterocycl. Chem.* **39** 829 (2002)
464. M Munakata, S-G Yan, M Maekawa, M Akiyama, S Kitagawa *J. Chem. Soc., Dalton Trans.* 4257 (1997)
465. W-H Chan, K-K Cheung, T C W Mak, C-M Che *J. Chem. Soc., Dalton Trans.* 873 (1998)
466. C J Fahrni, A Pfalts, M Neuburger, M Zehnder *Helv. Chim. Acta* **81** 507 (1998)
467. N V Kaminskaia, C He, S J Lippard *Inorg. Chem.* **39** 3365 (2000)
468. C-M Che, C-W Wan, K-Y Ho, Z-Y Zhou *New. J. Chem.* **25** 63 (2001)
469. F Zamora, M Sabat, B Lippert *Inorg. Chim. Acta* **282** 237 (1998)
470. T Tanase, T Igoshi, K Kobayashi, Y Yamamoto *J. Chem. Res., Synop.* 538 (1998)
471. A Dossing, S Larsen, A van Lelieveld, R M Bruun *Acta Chem. Scand.* **53** 230 (1999)
472. P Barbaro, C Bianchini, M Rochi, D Masi, C Mealli *Acta Crystallogr., Sect. C* **48** 625 (1992)
473. Y Zhu, X Gan, N Tang, M Tan *Bull. Chem. Soc. Jpn.* **62** 1279 (1998)
474. H Aghabozorg, R C Palenik, C J Palenik *Inorg. Chem.* **24** 4214 (1985)
475. M Mintert, W S Sheldrick *J. Chem. Soc., Dalton Trans.* 2663 (1995)
476. A E M Boelrijk, T X Neenan, J Reedijk *J. Chem. Soc., Dalton Trans.* 4561 (1997)
477. T Mizukawa, K Tsuge, H Nakajima, K Tanaka *Angew. Chem., Int. Ed.* **38** 362 (1999)
478. Jpn. P. 2001 199 922; *Chem. Abstr.* **135** 107 144 (2001)
479. A Tiripicchio, F J Lahoz, L A Oro, M A Ciriano, B E Villarroya *Inorg. Chim. Acta* **111** L1 (1986)
480. J L Bear, L K Chau, M Y Chavan, F Lefoulon, R P Thummel, K M Kadish *Inorg. Chem.* **25** 1514 (1986)
481. B Oskui, M Mintor, W S Sheldrick *Inorg. Chim. Acta* **287** 72 (1999)
482. I Ara, J M Gasas, J Fornies, A J Rueda *Inorg. Chem.* **35** 7345 (1996)
483. S V Beltyukova, E I Tselik, A V Egorova *J. Pharm. Biomed. Anal.* **18** 261 (1998); *Chem. Abstr.* **130** 29 317 (1999)
484. C J Fahrni, A Pfaltz *Helv. Chim. Acta* **81** 491 (1998)
485. C He, S J Lippard *Tetrahedron* **56** 8245 (2000)
486. G R Newkome, K J Theriot, V K Majestik, P A Spruele, G R Baker *J. Org. Chem.* **55** 2838 (2000)
487. Jpn. P. 09 169 668; *Chem. Abstr.* **127** 181 140 (1997)
488. US P. 2 002 280; *Chem. Abstr.* **29** 4598 (1935)
489. T Takahashi, H Saikachi, T Sasaki *J. Pharm. Soc. Jpn.* **67** 221 (1947); *Chem. Abstr.* **46** 112 (1952)
490. S Carboni, A Da Settimo, G Pirisino *Gazz. Chim. Ital.* **96** 103 (1966)
491. S Carboni, A Da Settimo, I Tonnetti *J. Heterocycl. Chem.* **7** 875 (1970)
492. P Caluwe, T G Majewicz *J. Org. Chem.* **42** 3410 (1977)
493. S Carboni, A Da Settimo, D Segnini, I Tonetti *Gazz. Chim. Ital.* **96** 1443 (1966)
494. S Carboni, A Da Settimo, P L Ferrarini, I Tonetti, D Bertini *Gazz. Chim. Ital.* **97** 1274 (1967)
495. S Carboni, A da Settimo, P L Ferrarini, O Livi, I Tonetti *J. Heterocycl. Chem.* **9** 801 (1972)
496. M Wozniak, H C van der Plas, B van Veldhiizen *J. Heterocycl. Chem.* **20** 9 (1983)
497. M Wozniak, P Surjio, H C van der Plas *Khim. Geterotsikl. Soedin.* 1652 (1996) [b]
498. M Wozniak, M Grzegozek, P Surylo *Liebigs Ann. Chem.* 2601 (1997)
499. M Wozniak, M Grzegozek, P Surylo *Can. J. Chem.* **78** 950 (2000)
500. A F Khlebnikov, E I Kostik, Yu Kopf, E V Aleksandrov, R R Kostikov *Zh. Org. Khim.* **34** 754 (1998) [d]
501. I Takeuchi, K Asai, Y Hamada, K Masuda, H Suezawa, M Hirota, Y Kurono, K Hatano *Heterocycles* **43** 2139 (1996)
502. I Takeuchi, N Naga, T Kariyama, Y Hamada, H Matsuzaki *Heterocycles* **48** 2125 (1998)
503. C Alfloroaei, N Dulamita, M Vlassa, J Barbe, P Brouant *J. Heterocycl. Chem.* **37** 1289 (2000)
504. S Goswami, K Ghosh, R Mukherjee *J. Indian Chem. Soc.* **76** 661 (1999)
505. S Goswami, K Ghosh, R Mukherjee *Tetrahedron* **57** 4987 (2001)
506. K Tomita, Y Tsuzuki, K Shibamori, S Kashimoto, K Chiba, in *Book of Abstracts of the 217th ACS National Meeting, Anaheim, CA, 1999* p. 249
507. K Chiba, Y Tsuzuki, K Tomita, K Mizuno, Y Sato, in *Book of Abstracts of the 218th ACS National Meeting, New Orleans, LA, 1999* p. 127
508. Y Tsuzuki, K Chiba, K Hino *Tetrahedron: Asymmetry* **12** 1793 (2001)
509. J Suntze, F Diederich *Helv. Chim. Acta* **80** 897 (1997)
510. D Edmont, R Rocher, C Plisson, J Chenault *Bioorg. Med. Chem. Lett.* **10** 1831 (2000)
511. C Plisson, J Chenault *J. Heterocycl. Chem.*, **38** 467 (2001)
512. J S Wolfson, D C Hooper *Antimicrob. Agents Chemother.* **28** 581 (1985)
513. J S Wolfson, D C Hooper *Antimicrob. Agents Chemother.* **28** 716 (1985)
514. P B Fernandes, D T W Chu, in *Annual Reports on Medical Chemistry* Vol. 22 (Ed. D M Baily) (Orlano, FL: Academic Press, 1987) p. 117
515. J M Domagala, L D Hanna, C L Heifetz, M P Hutt, T F Mich, J P Sanchez, M Solomon *J. Med. Chem.* **29** 394 (1986)
516. J M Domagala, C L Heifetz, T F Mich, J B Nichols *J. Med. Chem.* **29** 445 (1986)
517. L Verbist *Pharm. Weekblad, Sci. Ed.* **8** 22 (1986)
518. C Rufer, H J Kessler, K Schwarz *Eur. J. Med. Chem.* **12** 27 (1977)
519. J P Sanchez, J W Rogowski *J. Heterocycl. Chem.* **24** 215 (1987)
520. S Nishigaki, N Mizushima, K Senga *Chem. Pharm. Bull.* **25** 349 (1977)
521. J Matsumoto, T Miyamoto, A Minamida, Y Nishimura, H Egawa, N Nishimura *J. Heterocycl. Chem.* **21** 673 (1984)
522. Jpn. P. 6 272 686; *Chem. Abstr.* **106** 213 981 (1987)
523. Y Nishimura, A Minamida, J Matsumoto *J. Heterocycl. Chem.* **25** 479 (1988)
524. J M Domagala, P Peterson *J. Heterocycl. Chem.* **26** 1147 (1989)
525. J S Kiely *J. Heterocycl. Chem.* **28** 541 (1991)
526. J S Kiley, S Huang, L E Lesheski *J. Heterocycl. Chem.* **26** 1675 (1989)
527. Jpn. P. 3 223 289; *Ref. Zh. Khim.* 15 O 103P (1993)
528. N Suzuki, R Dohmori *Chem. Pharm. Bull.* **27** 410 (1979)
529. N Suzuki, Y Tanaka, R Dohmori *Chem. Pharm. Bull.* **28** 235 (1980)
530. N Suzuki *Chem. Pharm. Bull.* **28** 761 (1980)
531. I Hayakawa, N Suzuki, K Suzuki, Y Tanaka *Chem. Pharm. Bull.* **32** 4914 (1984)
532. C J Muller, B Grahner, D Heber *Pharmazie* **49** 878 (1994)
533. S Carboni, A Da Settimo, P L Ferrarini, O Livi *Farmaco Ed. Sci.* **33** 315 (1978)
534. P L Ferrarini, C Mori, C Manera, A Martinelli, F Mori, G Saccomanni, P L Barili, L Betti, B Giannaccini, L Trincavelli, A Lucacchini *J. Med. Chem.* **43** 2814 (2000)
535. US P. 4 735 948; *Ref. Zh. Khim.* 5 O 107P (1989)
536. US P. 5 364 859; *Ref. Zh. Khim.* 6 O 73P (1996)
537. US P. 5 281 610; *Ref. Zh. Khim.* 11 O 56P (1995)
538. Fr. P. 2 706 898; *Ref. Zh. Khim.* 15 O 39P (1996)
539. M T Chary, K Mogilaiah, B Sreenivasulu *Collect. Czech. Chem. Commun.* **53** 1543 (1988)
540. K Mogilaiah, K R Reddy, G R Rao, B Sreenivasulu *Collect. Czech. Chem. Commun.* **53** 1539 (1988)
541. K R Reddy, K Mogilaiah, B Swamy, B Sreenivasulu *Acta Chim. Hung.* **127** 45 (1990)

542. M T Chary, K Mogilaiah, G R Rao, B Sreenivasulu *J. Indian Chem. Soc.* **67** 691 (1990)
543. R J Sudhakar, B Sreenivasulu, K Mogilaiah *Indian J. Chem., Sect. B* **34** 734 (1995)
544. H S Rani, K Mogialiah, R J Sudhakar, B Sreenivasulu *Indian J. Chem., Sect. B* **34** 1035 (1995)
545. K R Reddy, K Mogialiah, B Sreenivasulu *Nat. Acad. Sci. Lett.* **12** 193 (1990)
546. K R Reddy, K Mogilaiah, B Sreenivasulu *Indian J. Chem., Sect. B* **26** 1194 (1987)
547. BRD P. 3 804 990; *Ref. Zh. Khim.* 16 O 445P (1990)
548. O Chavignon, J C Teulade, M Madesolaire, A Gueiffier, J Blache, H Viols, J P Chapat, G Dauphin *J. Heterocycl. Chem.* **29** 691 (1992)
549. M Grzegozek, M Wozniak, A Baranski, H C van der Plas *J. Heterocycl. Chem.* **28** 1075 (1991)
550. P L Ferrarini, C Mori, G Biagi, O Livi, I Tonetti *J. Heterocycl. Chem.* **21** 417 (1984)
551. J Vilar, C Peinador, V M Carmen, V Ojea, J M Quintela *Heterocycles* **41** 111 (1995)
552. F S Babichev, Yu M Volovenko, A G Nemazannyi, B Nemaa *Khim. Geterotsikl. Soedin.* 273 (1989) [b]
553. US P. 4 510 000; *Ref. Zh. Khim.* 1O28P (1986)
554. US P. 5 235 054; *Ref. Zh. Khim.* 22 O 141P (1994)
555. US P. 5 434 147; *Ref. Zh. Khim.* 11 O 55P (1997)
556. US P. 5 329 002; *Ref. Zh. Khim.* 6 O 137P (1996)
557. US P. 4 695 572; *Ref. Zh. Khim.* 11 O 92P (1988)
558. US P. 5 273 978; *Ref. Zh. Khim.* 9 O 58P (1995)
559. US P. 4 866 074; *Ref. Zh. Khim.* 18 O 80P (1990)
560. US P. 4 760 073; *Ref. Zh. Khim.* 8 O 70P (1989)
561. US P. 4 866 061; *Ref. Zh. Khim.* 22 O 84P (1990)
562. US P. 4 882 332; *Ref. Zh. Khim.* 2 O 96P (1991)
563. US P. 5 011 860; *Ref. Zh. Khim.* 13 O 91P (1992)
564. US P. 4 452 800; *Ref. Zh. Khim.* 5 O 160P (1985)
565. US P. 5 126 341; *Ref. Zh. Khim.* 10 O 45P (1995)
566. US P. 5 179 102; *Ref. Zh. Khim.* 11 O 33P (1994)
567. US P. 5 215 996; *Ref. Zh. Khim.* 22 O 150P (1994)
568. US P. 4 477 449; *Chem. Abstr.* **102** 6457 (1985)
569. US P. 4 735 949; *Chem. Abstr.* **109** 110 273 (1988)
570. US P. 4 617 308; *Chem. Abstr.* **110** 114 695 (1989)
571. US P. 4 916 229; *Chem. Abstr.* **113** 40 659 (1990)
572. US P. 4 945 160; *Chem. Abstr.* **113** 231 222 (1990)
573. US P. 5 077 834; *Chem. Abstr.* **116** 59 210 (1992)
574. US P. 5 281 612; *Chem. Abstr.* **120** 270 366 (1994)
575. US P. 5 591 766; *Chem. Abstr.* **126** 162 259 (1997)
576. US P. 5 801 183; *Chem. Abstr.* **129** 216 627 (1998)
577. WO PCT 8 607 359; *Chem. Abstr.* **107** 154 317 (1987)
578. WO PCT 8 607 537; *Chem. Abstr.* **107** 183 554 (1987)
579. WO PCT 8 700 752; *Chem. Abstr.* **106** 213 924 (1987)
580. WO PCT 9 210 191; *Chem. Abstr.* **118** 6961 (1993)
581. WO PCT 9 210 492; *Chem. Abstr.* **118** 212 902 (1993)
582. WO PCT 9 404 505; *Chem. Abstr.* **120** 244 711 (1994)
583. WO PCT 9 425 438; *Chem. Abstr.* **122** 81 354 (1995)
584. WO PCT 9 601 260; *Chem. Abstr.* **124** 289 279 (1996)
585. WO PCT 9 637 475; *Chem. Abstr.* **126** 74 824 (1997)
586. WO PCT 9 638 445; *Chem. Abstr.* **126** 89 279 (1997)
587. WO PCT 9 704 755; *Chem. Abstr.* **126** 225 310 (1997)
588. WO PCT 0 912 546; *Chem. Abstr.* **126** 251 417 (1997)
589. WO PCT 9 727 856; *Chem. Abstr.* **127** 215 196 (1997)
590. WO PCT 9 805 661; *Chem. Abstr.* **128** 180 424 (1998)
591. WO PCT 9 807 428; *Chem. Abstr.* **128** 221 630 (1998)
592. WO PCT 9 808 840; *Chem. Abstr.* **128** 217 627 (1998)
593. WO PCT 9 818 795; *Chem. Abstr.* **128** 321 632 (1998)
594. WO PCT 9 823 615; *Chem. Abstr.* **129** 41 083 (1998)
595. WO PCT 9 831 359; *Chem. Abstr.* **129** 136 499 (1998)
596. WO PCT 9 835 967; *Chem. Abstr.* **129** 202 953 (1997)
597. WO PCT 9 839 322; *Chem. Abstr.* **129** 230 737 (1998)
598. WO PCT 9 902 527; *Chem. Abstr.* **130** 125 001 (1999)
599. WO PCT 9 915 508; *Chem. Abstr.* **131** 267 229 (1999)
600. WO PCT 9 929 318; *Chem. Abstr.* **131** 44 810 (1999)
601. WO PCT 9 930 709; *Chem. Abstr.* **131** 58 814 (1999)
602. WO PCT 9 931 061; *Chem. Abstr.* **131** 58 766 (1999)
603. WO PCT 0 033 838; *Chem. Abstr.* **133** 43 507 (2000)
604. WO PCT 0 046 215; *Chem. Abstr.* **133** 150 586 (2000)
605. WO PCT 0 050 424; *Chem. Abstr.* **133** 193 081 (2000)
606. WO PCT 0 072 801; *Chem. Abstr.* **134** 29 136 (2001)
607. WO PCT 0 078 317; *Chem. Abstr.* **134** 56 581 (2001)
608. WO PCT 0 155 719; *Chem. Abstr.* **135** 134288 (2001)
609. WO PCT 0 124 797; *Chem. Abstr.* **134** 295 810 (2001)
610. WO PCT 0 134 602; *Chem. Abstr.* **134** 366 793 (2001)
611. WO PCT 0 172 304; *Chem. Abstr.* **135** 251 947 (2001)
612. WO PCT 0 170 742; *Chem. Abstr.* **135** 257 228 (2001)
613. WO PCT 0 174 816; *Chem. Abstr.* **135** 288 769 (2001)
614. BRD P. 3 808 118; *Ref. Zh. Khim.* 12 O 440P (1991)
615. BRD P. 3 816 119; *Ref. Zh. Khim.* 15 O 39P (1990)
616. BRD P. 4 234 330; *Ref. Zh. Khim.* 20 O 114P (1995)
617. BRD P. 4 234 078; *Ref. Zh. Khim.* 20 O 115P (1995)
618. BRD P. 3 519 286; *Chem. Abstr.* **106** 196 270 (1987)
619. BRD P. 3 525 335; *Chem. Abstr.* **106** 144 013 (1987)
620. BRD P. 3 525 108; *Chem. Abstr.* **106** 176 189 (1987)
621. BRD P. 3 601 567; *Chem. Abstr.* **107** 236 747 (1987)
622. BRD P. 3 635 062; *Chem. Abstr.* **109** 110 457 (1988)
623. BRD P. 3 632 222; *Chem. Abstr.* **110** 29 107 (1989)
624. BRD P. 3 711 103; *Chem. Abstr.* **110** 114 497 (1989)
625. BRD P. 3 719 764; *Chem. Abstr.* **110** 155 810 (1989)
626. BRD P. 3 906 365; *Chem. Abstr.* **113** 97 462 (1990)
627. BRD P. 4 301 246; *Chem. Abstr.* **121** 157 539 (1994)
628. BRD P. 4 230 804; *Chem. Abstr.* **121** 157 629 (1994)
629. BRD P. 4 303 657; *Chem. Abstr.* **121** 179 620 (1994)
630. BRD P. 4 427 530; *Chem. Abstr.* **124** 289 280 (1996)
631. BRD P. 19 627 431; *Chem. Abstr.* **128** 128 005 (1998)
632. BRD P. 19 652 219; *Chem. Abstr.* **129** 81 718 (1998)
633. BRD P. 19 652 239; *Chem. Abstr.* **129** 81 719 (1998)
634. Fr. P. 2 583 418; *Ref. Zh. Khim.* 20 O 133P (1987)
635. Fr. P. 2 595 355; *Ref. Zh. Khim.* 11 O 166P (1988)
636. Fr. P. 2 592 880; *Ref. Zh. Khim.* 15 O 80P (1988)
637. Fr. P. 2 592 881; *Ref. Zh. Khim.* 15 O 81P (1988)
638. Fr. P. 2 592 882; *Ref. Zh. Khim.* 15 O 82P (1988)
639. Fr. P. 2 607 503; *Ref. Zh. Khim.* 8 O 48P (1989)
640. Fr. P. 2 607 504; *Ref. Zh. Khim.* 8 O 49P (1989)
641. Fr. P. 2 607 506; *Ref. Zh. Khim.* 10 O 100P (1989)
642. Pat 2 678 934; *Ref. Zh. Khim.* 2 O 28P (1994)
643. Fr. P. 2 678 931; *Ref. Zh. Khim.* 4 O 40P (1994)
644. Fr. P. 2 678 932; *Ref. Zh. Khim.* 4 O 41P (1994)
645. Fr. P. 2 678 933; *Ref. Zh. Khim.* 4 O 42P (1994)
646. Fr. P. 2 684 673; *Ref. Zh. Khim.* 9 O 41P (1994)
647. Fr. P. 2 695 389; *Ref. Zh. Khim.* 16 O 45P (1994)
648. Fr. P. 2 687 154; *Ref. Zh. Khim.* 21 O 35P (1994)
649. Fr. P. 2 548 664; *Chem. Abstr.* **103** 123 373 (1985)
650. Fr. P. 2 567 887; *Chem. Abstr.* **105** 191 056 (1986)
651. Fr. P. 8 802 627; *Chem. Abstr.* **108** 131 601 (1987)
652. Eur. P. 106 489; *Chem. Abstr.* **101** 72 740 (1984)
653. Eur. P. 134 165; *Chem. Abstr.* **103** 71 201 (1985)
654. Eur. P. 153 828; *Chem. Abstr.* **104** 88 512 (1986)
655. Eur. P. 153 580; *Chem. Abstr.* **104** 88 585 (1986)
656. Eur. P. 159 174; *Chem. Abstr.* **104** 148 850 (1986)
657. Eur. P. 207 420; *Chem. Abstr.* **106** 138 267 (1987)
658. BRD. P. 3 519 286; *Chem. Abstr.* **106** 196 270 (1987)
659. Eur. P. 255 908; *Chem. Abstr.* **108** 204 486 (1988)
660. Eur. P. 230 053; *Chem. Abstr.* **108** 112 498 (1988)
661. Eur. P. 305 744; *Chem. Abstr.* **111** 134 124 (1989)
662. Eur. P. 304 087; *Chem. Abstr.* **111** 153 777 (1989)
663. Jpn. P. 01 106 886; *Chem. Abstr.* **111** 232 778 (1989)
664. Eur. P. 326 916; *Chem. Abstr.* **112** 77 163 (1990)
665. Eur. P. 343 560; *Chem. Abstr.* **112** 235 326 (1990)
666. Eur. P. 343 524; *Chem. Abstr.* **113** 6178 (1990)
667. Eur. P. 357 047; *Chem. Abstr.* **113** 132 157 (1990)
668. Eur. P. 360 258; *Chem. Abstr.* **113** 153 051 (1990)
669. Eur. P. 362 759; *Chem. Abstr.* **114** 6305 (1991)
670. Eur. P. 391 185; *Chem. Abstr.* **114** 143 749 (1991)
671. Eur. P. 393 400; *Chem. Abstr.* **114** 164 195 (1991)
672. Eur. P. 388 298; *Chem. Abstr.* **114** 143 165 (1991)
673. Eur. P. 390 215; *Chem. Abstr.* **114** 247 291 (1991)
674. Eur. P. 391 169; *Chem. Abstr.* **114** 185 466 (1991)
675. Eur. P. 401 623; *Chem. Abstr.* **114** 207 234 (1991)
676. Eur. P. 394 120; *Chem. Abstr.* **114** 185 485 (1991)
677. Eur. P. 429 304; *Chem. Abstr.* **115** 183 131 (1991)
678. Eur. P. 520 277; *Chem. Abstr.* **119** 49 377 (1993)

679. Eur. P. 544 981; *Chem. Abstr.* **119** 139 201 (1993)
680. WO PCT 9 404 505; *Chem.Abstr.* **120** 244 711 (1994)
681. Eur. P. 589 318; *Chem. Abstr.* **121** 108 832 (1994)
682. Eur. P. 622 367; *Chem. Abstr.* **122** 105 892 (1995)
683. Eur. P. 671 391; *Chem. Abstr.* **124** 8852 (1996)
684. Eur. P. 721 948; *Chem. Abstr.* **124** 167 807 (1996)
685. Eur. P. 763 359; *Chem. Abstr.* **126** 282 813 (1997)
686. Eur. P. 1 065 207; *Chem. Abstr.* **134** 71 600 (2001)
687. Can. P. 2 094 082a; *Chem. Abstr.* **121** 157 628 (1994)
688. Hung. P. 185 285; *Ref. Zh. Khim.* 14 O 130P (1989)
689. Hung. P. 199465; *Ref. Zh. Khim.* 13 O 143P (1992)
690. Yugos. P. 39 892; *Ref. Zh. Khim.* 23 O 132P (1989)
691. Russ. P. 2 039 058; *Ref. Zh. Khim.* 3 O 40P (1996)
692. Pol. P. 125 298; *Chem. Abstr.* **105** 191 054 (1986)
693. Pol. P. 125 310; *Chem. Abstr.* **105** 191 055 (1986)
694. South Afr. P. 8 504887; *Chem. Abstr.* **105** 208 848 (1986)
695. Jpn. Appl. 32 181; *Ref. Zh. Khim.* 3 O 40P (1993)
696. Jpn. P. 6 032 790; *Chem. Abstr.* **103** 2 2 617 (1985)
697. Jpn. P. 61 152 682; *Chem. Abstr.* **105** 97 307 (1986)
698. Jpn. P. 62 234 082; *Chem. Abstr.* **106** 138 267 (1987)
699. Jpn. P. 6 233 176; *Chem. Abstr.* **106** 213 923 (1987)
700. Jpn. P. 6 270 370; *Chem. Abstr.* **107** 23 253 (1987)
701. Jpn. P. 6 272 616; *Chem. Abstr.* **107** 183 556 (1987)
702. Jpn. P. 63 685 866; *Chem. Abstr.* **109** 129 000 (1988)
703. Jpn. P. 63 104 977; *Chem. Abstr.* **109** 149 509 (1988)
704. Jpn. P. 63 203 679; *Chem. Abstr.* **110** 75 490 (1989)
705. Jpn. P. 1 100 165; *Chem. Abstr.* **111** 153 844 (1989)
706. Jpn. P. 1 110 603; *Chem. Abstr.* **111** 189 591 (1989)
707. Jpn. P. 01 165 584; *Chem. Abstr.* **112** 35 840 (1990)
708. Jpn. P. 01 128 978; *Chem. Abstr.* **112** 35 698 (1990)
709. Jpn. P. 02 115 181; *Chem. Abstr.* **113** 152 479 (1990)
710. Jpn. P. 02 115 182; *Chem. Abstr.* **113** 132 200 (1990)
711. Jpn. P. 02 264 724; *Chem. Abstr.* **114** 247 292 (1991)
712. Jpn. P. 03 223 289; *Chem. Abstr.* **116** 59 403 (1992)
713. Jpn. P. 0 459 726; *Chem. Abstr.* **117** 118 522 (1992)
714. Jpn. P. 0 692 963; *Chem. Abstr.* **121** 157 630 (1994)
715. Jpn. P. 09 221 424; *Chem. Abstr.* **127** 288 165 (1997)
716. Jpn. P. 1 160 578; *Chem. Abstr.* **130** 110 281 (1999)
717. Jpn. P. 11 147 883; *Chem. Abstr.* **131** 31 880 (1999)
718. Korean P. 9 701 159; *Chem. Abstr.* **133** 74 015 (2000)
719. G Makara, G M Keseru, A Kovaks *J. Chem. Soc., Perkin Trans. 2* 591 (1994)
720. R J Friary, M Spangler, R Osterman, L Schulman, J H Schwerdt *Chirality* **8** 364 (1996)
721. P L Ferrarini, C Mori, M Badawneh, C Manera, G Saccomanni, V Calderone, R Scatizzi, P L Barili *Eur. Med. Chem.* **32** 955 (1997)
722. P L Ferrarini, C Mori, M Badawneh, C Manera, A Martinelli, M Miceli, F Romagnoli, G Saccomanni *J. Heterocycl. Chem.* **34** 1501 (1997)
723. P L Ferrarini, C Mori, M Badawneh, V Calderoni, L Calzolari, T Loffredo, E Martinotti, G Saccomanni *Eur. Med. Chem.* **33** 383 (1998)
724. P L Ferrarini, C Mori, M Badawneh, F Franconi, C Manera, M Miceli, G Saccomanni *Farmaco* **55** 603 (2000)
725. P L Ferrarini, M Badawneh, F Fraconi, C Manera, M Miceli, C Mori, G Saccomanni *Farmaco* **56** 311 (2001)
726. J P Jacquet, D Bouzard, J-N Kiechel, P Remuzon *Tetrahedron Lett.* **32** 1565 (1991)
727. J P Jacquet, D Bouzard, P Di Cesare, N Dolnic, M Massoudi, P Remuzon *Heterocycles* **34** 2301 (1992)
728. K Mogilaiah, K Ragava Raju, B Srennivasulu *Indian J. Chem., Sect. B* **20** 821 (1981)
729. K Mogilaiah, B Srennivasulu *Indian J. Chem., Sect. B* **21** 479 (1982)
730. K Mogilaiah, B Srennivasulu *Indian J. Chem., Sect. B* **21** 582 (1982)
731. K Mogilaiah, K V Reddy, B Srennivasulu *Indian J. Chem., Sect. B* **22** 178 (1983)
732. K Mogilaiah, R B Rao *Indian J. Chem., Sect. B* **37** 139 (1998)
733. K Mogilaiah, R B Rao *Indian J. Chem., Sect. B* **37** 894 (1998)
734. K Mogilaiah, R B Rao *Indian J. Chem., Sect. B* **39** 145 (2000)
735. K Mogilaiah, D S Chowdary, R B Rao *Indian J. Chem., Sect. B* **40** 43 (2001)
736. K Mogilaiah, R B Rao *Indian J. Chem., Sect. B* **40** 235 (2001)
737. K Mogilaiah, R B Rao, G R Sudhakar *Indian J. Chem., Sect. B* **40** 336 (2001)
738. K Mogilaiah, P R Reddy *Indian. J. Chem., Sect. B* **40** 619 (2001)
739. K Mogilaiah, D S Chowdary, R B Rao *Indian J. Heterocycl. Chem.* **9** 311 (2000)
740. K Mogilaiah, H R Babu, R B Rao *Indian J. Heterocycl. Chem.* **10** 109 (2000)
741. S Nishigaki, N Mizushima, H Kanazava, M Ishiba, K Senga *J. Heterocycl. Chem.* **22** 1029 (1985)
742. Y Nishimura, A Minamida, J Matsumoto *Chem. Pharm. Bull.* **36** 1223 (1988)
743. A J Bridges, J P Sanchez *J. Heterocycl. Chem.* **27** 1527 (1990)
744. M Refai, M T Omar, M M Kamel, Z M Nofal, N S Ismail *Egypt. J. Pharm. Sci.* **37** 241 (1996); *Chem. Abstr.* **126** 251 088 (1997)
745. B Wang, I O Sutherland *Chem. Commun.* 1495 (1997)
746. Y Ikeura, T Tanaka, Y Kiyota, S Morimoto, M Ogino, T Ishimaru, I Kamo, T Doi, H Natsugari *Chem. Pharm. Bull.* **45** 1642 (1997)
747. H Guo *Yaoxue Xuebao* **33** 629 (1998); *Chem. Abstr.* **130** 81 432 (1999)
748. M M Kamel, M T Omar, W A Abdou, N S Ismail *Al-Azhar Bull. Sci.* **7** 161 (1996); *Chem. Abstr.* **128** 61 478 (1998)
749. N J Traynor, M D Barratt, W W Lovell, J Ferguson, N K Gibbs *Toxicol. in Vitro* **14** 275 (2000); *Chem. Abstr.* **133** 68 442 (2000)
750. G Roma, M Di Braccio, G Grossi, F Mattioli, M Ghia *Eur. J. Med. Chem.* **35** 1021 (2000)
751. S-X Zhang *Diss. Abstr. Int. B* **60** 6042 (2000); *Chem. Abstr.* **134** 216 876 (2001)
752. M A Cordoba, I L Roccia, M Marta de Luca, B C Pezzani, J A Basualdo *Microbiol. Immunol.* **45** 383 (2001); *Chem. Abstr.* **135** 177 909 (2001)
753. S Dumitriu, M Popa, M Dumitriu, T Pandele *J. Bioact. Compat. Polym.* **5** 310 (1990)
754. S Herzig, D Heber, A Mescheder, U Reifenstein-Herzig, T Thormann, M Verborg, K Mohr *Arzneim.-Forsch.* **44** 937 (1994)
755. D Heber, M Verborg *Arch. Pharm.* **324** 600 (1991)
756. A Matsuura, N Ashizawa, R Asakura, T Kumonaka, T Aotsuka, T Hase, C Shimizu, T Kurihara, F Kobayashi *Biol. Pharm. Bull.* **17** 498 (1994)
757. K Bowden, F P Malik, K E Pallett, J D Tomlinson *J. Chem. Res. Synop.* 305 (1991)
758. P L Ferrarini, C Mori, N Tellini *Farmaco* **45** 385 (1990)
759. A Da Settimo, P L Ferrarini, C Mori, G Primofiore, A Subissi *Farmaco* **41** 827 (1986)

[a] — *Mendeleev Chem. J. (Engl. Transl.)*
[b] — *Chem. Heterocycl. Compd. (Engl. Transl.)*
[c] — *Theor. Exp. Chem. (Engl. Transl.)*
[d] — *Russ. J. Org. Chem. (Engl. Transl.)*

Russian Chemical Reviews **73** (7) 671 – 699 (2004) © 2004 Russian Academy of Sciences and Turpion Ltd

DOI 10.1070/RC2004v073n07ABEH000838

Chiral phosphites as ligands in asymmetric metal complex catalysis and synthesis of coordination compounds

K N Gavrilov, O G Bondarev, A I Polosukhin

Contents

I.	Introduction	671
II.	P-Monodentate phosphites	672
III.	P,N-Bidentate compounds of phosphite nature	679
IV.	P,P-Bidentate phosphites	686
V.	Other groups of chiral phosphite ligands	693
VI.	Conclusion	694

Abstract. The data published during the last five years on the application of chiral derivatives of phosphorous acid in coordination chemistry and enantioselective catalysis are summarised and discussed. The effect of the nature of these ligands on the structure of metal complexes and on the efficiency of catalytic organic syntheses is shown. Hydroformylation, hydrogenation, allylic substitution and conjugate addition catalysed by transition metal complexes with optically active phosphites and hydrophosphoranes are considered. The prospects for the development of this field of research are demonstrated. The bibliography includes 215 references.

I. Introduction

Organic reactions catalysed by chiral transition metal complexes are the basis of modern asymmetric synthesis. This statement was substantiated by the fact that three leading researchers working in this field of chemistry were awarded the Nobel Prize in 2001. The key to obtaining high catalytic results is targeted synthesis of optically active ligands. Among them, of prime importance are phosphorus-containing compounds which are crucial to the progress of such avenues of organic synthesis as asymmetric reduction, isomerisation and formation of carbon – carbon and carbon – heteroatom bonds.[1] These ligands also play an important role in the development of concepts of the geometry and structure of complexes, mutual influence of intra-sphere ligands and the nature of coordination bond.[2] Initially, emphasis was placed on systems with P – C bonds, especially tertiary phosphines. We cannot but agree with Ansell and Wills[3] that this situation is unjust. Indeed, compounds with three P – O and (or) P – N bonds offer a number of considerable advantages.[3–5] First, they are synthetically accessible, because most of them can be synthesised rather simply and in high yield from a variety of optically active precursors. This makes possible a direct one-step phosphorylation of chiral compounds, whereas the synthesis of corresponding phosphine derivatives requires preliminary modification. Second, these compounds exhibit higher oxidative stability because of the absence of the P – C bond in the corresponding structures. This is of great importance in those cases where the oxidation of a phosphorus-containing ligand faces considerable difficulties, *e.g.*, in the synthesis of some types of coordination compounds and catalysis of hydroformylation. Third, these compounds possess a pronounced π-acceptor ability, which allows the coordinated phosphites to stabilise low oxidation states of metals used as complexing agents, thus enhancing their electrophilicity. By and large, replacement of carbon atoms by heteroatoms [oxygen and (or) nitrogen] in the first coordination sphere of phosphorus atom appeared to be a much more efficient tool for control of the chemical stability of ligands and their donor – acceptor properties and steric features compared to traditional introduction of various substituents into benzene rings of the PAr_2 fragment typical of most phosphine systems.

The aforesaid is responsible for an increase, in the last decade, in the number of communications concerned with applications of chiral derivatives of phosphorous acid in the synthesis of coordination compounds and in catalysis. Studies in the field reported before 1998 were summarised in two reviews.[6,7] Most of the P-monodentate ligands considered in these reviews were carbohydrate derivatives but some chiral amino alcohols and diols were also presented. No systematic investigations on their complexation were carried out at that time. The optical yields of catalytic reactions (hydrogenation, hydrosilylation, hydrocyanation) involving these compounds were at most 20% – 30%.[6] However, the first phosphorus-containing derivatives of BINOL (**1**) were synthetically available at that time.

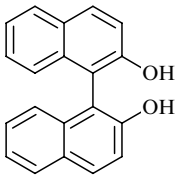

1 (BINOL)

Later on, these BINOL-based compounds were top-ranked among the P-monodentate phosphites (type **A**). The group of P,N-bidentate ligands (type **B**) comprised a few compounds containing sp^3-hybridised peripheral nitrogen atoms, *i.e.*, phosphites and phosphoramidites containing an amino group in the

K N Gavrilov S A Esenin Ryazan State Pedagogical University, ul. Svobody 46, 390000 Ryazan, Russian Federation. Fax (7-0912) 44 43 90. Tel. (7-0912) 77 28 54. E-mail: chem@ttc.ryazan.ru
O G Bondarev, A I Polosukhin A N Nesmeyanov Institute of Organoelement Compounds, Russian Academy of Sciences, ul. Vavilova 28, 119991 Moscow, Russian Federation. Fax (7-095) 135 64 71. Tel. (7-095) 135 25 48. E-mail: bond@ineos.ac.ru (O G Bondarev), apol73@yahoo.com (A I Polosukhin)

Received 31 March 2003
Uspekhi Khimii **73** (7) 726 – 756 (2004); translated by A M Raevskiy

substituent; for simplicity, hereafter we will call them 'aminophosphites' and 'aminophosphoramidites.' No interesting results were obtained when catalytic reactions were performed involving these species.[6] This also holds for the phosphite derivatives of alkaloids.[8] On the contrary, P,P-bidentate ligands (type **C**) have been the subject of numerous studies, which were carried out to gain a better insight into their coordination chemistry and revealed high catalytic efficiency of these compounds.

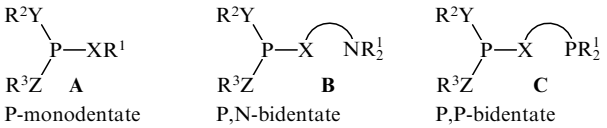

A **B** **C**

X, Y, Z = O or N.

The advances made before 1998 and fully considered in Ref. 7 are as follows: design of two groups of structures providing an enantioselectivity of up to 87% in Rh-catalysed hydroformylation of styrene

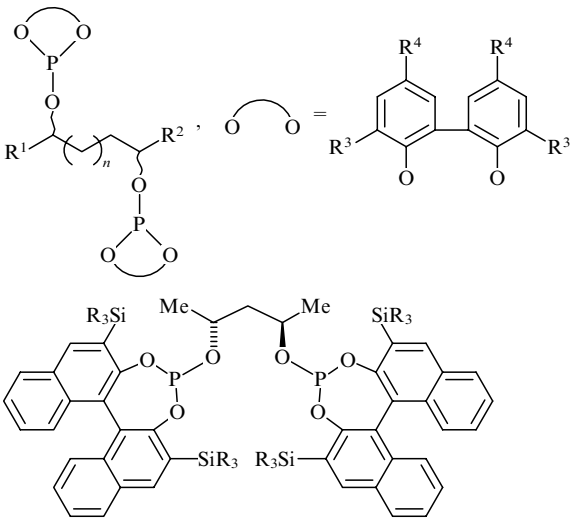

by van Leeuwen's group and a series of studies by Takaya *et al.* who first synthesised dissymmetric phosphine-phosphites BINAPHOS (**2**) and BIPHEMPHOS and their simplest derivatives.

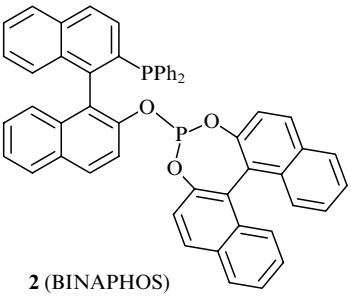

2 (BINAPHOS)

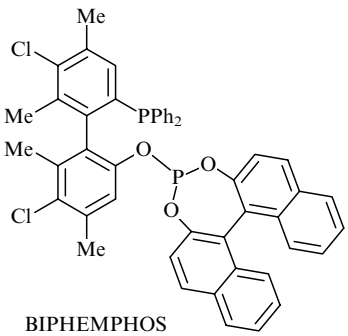

BIPHEMPHOS

The use of these compounds in Rh-catalysed hydroformylation of a broad spectrum of substrates (vinyl acetate, styrene and its homologues, *N*-vinylphthalimide, cyclic and fluorinated alkenes, 4-vinyl-β-lactam) allowed an *ee* of 87% – 98% to be achieved. They also demonstrated a high enantioselectivity in Pd-catalysed copolymerisation of alkenes and dienes with CO.

Based on analysis of the role played and niche occupied by chiral phosphites in the coordination chemistry and catalytic studies (see above), some predictions were made concerning further use of these compounds.[7] In particular, dissymmetric P,P-bidentate compounds based on amino alcohols, active use of P,N-bidentate systems in asymmetric catalysis and the development of new fields of application of phosphite ligands (hydrosilylation and hydroboronation of C=C bonds) were predicted. These predictions were fully substantiated by further progress in the field, which appeared to be so rapid that recently reported studies[6,7] are now in essence out of date. A large body of new experimental material requires systematisation and discussion. The aim of this review is to consider the data published during the last five years. The data are classified based on the structure (first of all, denticity) of chiral phosphite ligands. This approach seems to be quite logical because it allows the advances of asymmetric catalysis and coordination chemistry to be analysed from a unified standpoint based on the nature of the phosphorus-containing ligand. In addition, in discussing the material we tried to group the studies reported by researchers from the leading scientific schools together and to highlight the most important results concerned with catalytic processes.

II. P-Monodentate phosphites

1. Phosphite derivatives of BINOL

This group of ligands comprises axially chiral compounds (**3a**–**q**) and compounds containing additional C*-stereocentres in the exocyclic substituent (**3r**–**w**).

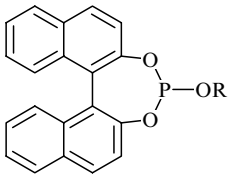

3a–**w** [(S_{ax}) and/or (R_{ax})]

Compound **3**	R	Compound **3**	R
a	Me	**n**	2-BrC_6H_4
b	Pr^i	**o**	2,6-$Me_2C_6H_3$
c	cyclo-C_5H_9	**p**	2,6-$Ph_2C_6H_3$
d	Bu^i	**q**	2-naphthyl
e	CH_2CHEt_2	**r**	(*S*)- or (*R*)-Bu^s
f	neopentyl	**s**	(*S*)- or (*R*)-CH(Ph)Me
g	Bn	**t**	(1*S*,2*R*)- or (1*R*,2*S*)-Ph(cyclo-C_6H_{11})
h	CH_2CH_2OMe	**u**	(1*S*,2*R*)- or (1*R*,2*S*)-(2-naphthyl)cyclohexyl
i	CH_2CH_2Cl	**v**	*O*-methyldianhydro-D-mannityl
j	CH_2CCl_3	**w**	menthyl
k	Ph		
l	4-$MeOC_6H_4$		
m	4-$CF_3C_6H_4$		

They are used in enantioselective processes resulting in the formation of C–C bonds and in hydrogenation of unsaturated esters. For instance, phosphites (S_{ax})-**3k**–**m** provided an *ee* of 32% – 96% in the Ir-catalysed allylic alkylation of esters of cinnamyl alcohol by dimethyl malonate. The highest enantioselectivity at a regioselectivity of 93 : 7 (branched : linear product) was demonstrated by ligand **3k** {$[IrCl(cod)]_2$ was used as precatalyst; cod = cyclooctadiene}.[9]

Asymmetric Cu-catalysed addition of Et_2Zn to acyclic enones $R^1-CH=CH-C(O)-R^2$ (R^1 and/or R^2 = Me, Pr^i, C_5H_{11}, Ph)

involving phosphites **3t**,**u** was studied.[10,11] It was found that enantioselectivity is governed by the axial chirality, namely, the enantiomeric excess was 56% to 87% for (R_{ax})-**3t**,**u** and at most 33% for (S_{ax})-**3t**,**u**. An odorant (*R*)-(−)-muscone was synthesised following reaction (1) using (R_{ax})-**3t** with a chemical yield of 53% and an optical yield of 79%.

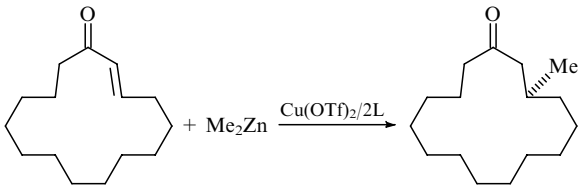

(1)

Tf = CF_3SO_2.

No less important were the results obtained in hydrogenation of prochiral esters **4a**,**b** [reaction (2)].

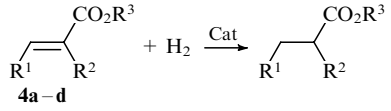

4a–**d** (2)

Compound **4**	R^1	R^2	R^3
a	H	CH_2CO_2Me	Me
b	H	NHAc	Me
c	4-AcO-3-$MeOC_6H_3$	NHAc	H
d	Ph	NHAc	Me

The optical yields of reactions involving (S_{ax})-**3a**,**b**,**k**,**n** were 89%–98% for compound **4a** and 70%–95% for compound **4b** {with $[Rh(cod)_2]^+BF_4^-$ as precatalyst}.[11] Noteworthy is that systems (S_{ax})-**3o**,**p** containing *ortho*-substituted exocyclic phenoxy groups appeared to be of low efficiency, namely, the optical yields in reaction (2) involving substrate **4a** were at most 39%. At the same time ligands bearing additional C*-stereocentres appeared to be excellent stereoselectors: hydrogenation of ester **4a** in the presence of (S_{ax})-**3v** and (R_{ax})-**3v** gave an *ee* of 95% to 98%; the optical yields in hydrogenation of esters **4a**,**b** using phosphites (S_{ax}, S_C)-**3s** and (S_{ax}, R_C)-**3s** were 93% to 99%.[12,13] Similarly, hydrogenation of substrate **4a** and in the presence of epimers (S_{ax})-**3w** and (R_{ax})-**3w** led to an *ee* of 91% to 95%.[14]

Phosphites **3a**–**j**,**r**,**s** also exhibited a high enantioselectivity (*ee* 75%–97%) in hydrogenation of enamides **5a**–**e** {also with $[Rh(cod)_2]^+BF_4^-$ as precatalyst, reaction (3)}.[15]

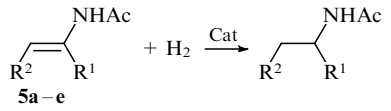

5a–**e** (3)

Compound **5**	R^1	R^2	Compound **5**	R^1	R^2
a	Ph	H	**d**	Ph	Me(*Z*)
b	4-ClC_6H_4	H	**e**	Ph	Me(*E*)
c	2-naphthyl	H			

Except for the reaction with ligand **3j** containing a CCl_3 group, which strongly withdraws the electron density and thus increases the π-acceptor ability of the P-centre, a 99%–100% conversion was obtained (*cf.* less than 5% for compound **3j**). Taking into account the above and the low cost of phosphite derivatives of BINOL (about 2% of the cost of the known P,P-bidentate phosphine ligand BINAP),[15] the conclusion about great prospects for industrial applications of these systems seems to be quite substantiated.

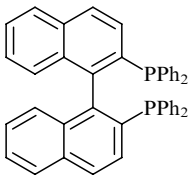

BINAP

Probably, this was the reason for the synthesis of phosphites **6a**,**b** with long-chain exocyclic substituents.[16]

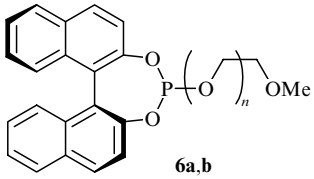

6a,**b**

n = 16 (**a**), 17 (**b**).

Being used with $[Rh(cod)_2]^+BF_4^-$, ligands **6a**,**b** accelerate hydroformylation of styrene under conditions of phase transfer catalysis. This example demonstrates the possibility of re-use of the catalytic system without loss of efficiency in spite of the low optical yield (17%).

2. Phosphoramidite derivatives of BINOL

Similarly to the phosphite systems, both axially chiral compounds (**7a**–**k**) and compounds containing additional C*-stereocentres (**7l**–**u**) were studied.

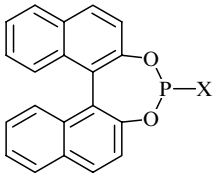

7a–**u** [(S_{ax}) and/or (R_{ax})]

Compound **7**	X	Compound **7**	X
a	NMe_2	**o**	(*R*)-bis(1-naphthylethyl)-amino
b	NEt_2		
c	NPr^i_2		
d	NBn_2	**p**	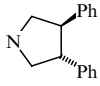
e	NMeBn		
f	$N(CH_2)_5$		
g	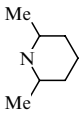	**q**	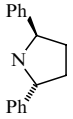
h		**r**	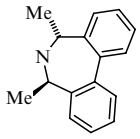
i			
j	$N(o\text{-}MeOC_6H_4)_2$		
k		**s**	(*S*)- or (*R*)- 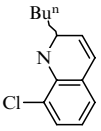
l		**t**	(*S*)- or (*R*)- 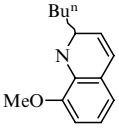

Compound **7**	X	Compound **7**	X
m		**u**	
n	(*S*)- or (*R*)-N(1-PhEt)$_2$		

Besides, ligands **8** based on the *ortho*-disubstituted derivatives of BINOL (**1**) were synthesised.

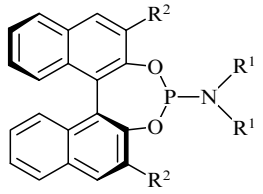

8a–e

Compound **8**	R^1	R^2	Compound **8**	R^1	R^2
a	Me	Me	**d**	Me	Br
b	Pr^i	Me	**e**	Me	Ph
c	$(CH_2CH_2)_2O$	Me			

Undoubtedly, the scientific school headed by Feringa is a leader in the field of synthesis and catalytic applications of ligands **7**. As early as 1994, Feringa reported the synthesis of the first compound in this class, **7a** (MonoPhos).[17] The main field of application of these phosphoramidites is processes involving formation of C–C bonds (first of all, by Cu-catalysed addition of organozinc reactants). For instance, reactions with participation of cyclic α,β-unsaturated ketones **9** [reaction (4)] were studied.

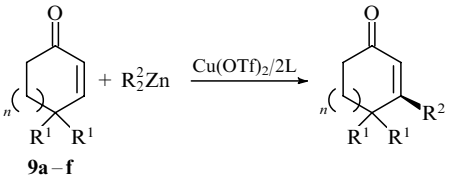

(4)

9a–f

Compound **9**	R^1	*n*	Compound **9**	R^1	*n*
a	H	1	**d**	H	3
b	H	0	**e**	Me	1
c	H	2	**f**	Ph	1

The results of these studies for Et_2Zn are summarised in Table 1. As can be seen, ligand (S_{ax},R_C)-**7n** provides the highest enantioselectivity.[18–20] Its homologue, (S_{ax})-**7o**, bearing bulkier naphthyl substituents is somewhat less efficient, but stereomer (S_{ax},S_C)-**7n** is much less efficient (*ee* 75%).[19] Systems containing no additional C*-stereocentres **7a–j** appeared to be the worst stereoselectors (the maximum optical yield in the reaction with substrate **9a** was 60%, see Table 1).[19]

Table 1. Comparative enantioselectivity of a number of P-monodentate chiral phosphoramidites in the Cu-catalysed asymmetric addition of Et_2Zn to cyclic enones [reaction (4)].

Substrate	*ee* (%)	
	ligand (S_{ax})-**7c**	ligand (S_{ax},R_C)-**7n**
9a [a]	60	98
9b	–	10
9c	55	98
9d	–	97
9e	81	98
9f	–	98

[a] The enantioselectivity provided by other ligands involved in the reaction with this substrate was also studied; the results obtained are as follows: 25% for S_{ax}-**7a**, 72% for S_{ax}-**7m** and 94% for S_{ax}-**7o**.

Reactions of other R_2Zn derivatives [R = Me, Pr^i , Bn, C_7H_{15}, $(CH_2)_5OAc$ and $Me_2CH(OEt)_2$] in the presence of compounds **9a** and (S_{ax},R_C)-**7n** were also characterised by high enantioselectivity (*ee* 94%–98%).[20,21] Therefore, it is quite logical that the most efficient ligand, (S_{ax},R_C)-**7n**, also provided excellent results in other related reactions of R_2Zn addition to cyclic aliphatic vinyloxiranes (*ee* up to 96%);[22] α,β-unsaturated nitroacetals (*ee* up to 92%);[23] 4,4-disubstituted cyclohexadienones (*ee* up to 99%);[24] cyclic unsaturated ketones (followed by aldol condensation to give bicyclic enones with an optical yields of up to 98%);[25] and to 4,4,5-trisubstituted cyclohexanones (*ee* up to 97%).[26] Systems R_2Zn/Cu(OTf)$_2$/2L [L = (S_{ax})-**7c**, (S_{ax})-**7l–o**] were employed to achieve enantioselective kinetic resolution of racemic cyclohex-2-enones.[27] Again, ligand (S_{ax},R_C)-**7n** was the best stereoselector and provided a greater than 99% optical purity of the product [*cf*. an *ee* of only 22% for (S_{ax})-**7c**]. A related kinetic resolution of racemic vinyloxiranes with phosphoramidite (S_{ax},R_C)-**7n** was also characterised by *ee* up to 99%.[28] Very high enantioselectivity achieved in the key stage of R_2Zn addition to cyclic enones under the action of Cu(OTf)$_2$/2L [L = (S_{ax},R_C)-**7n**] permitted the development of efficient procedures for the synthesis of optically pure bicyclic alcohols[29] and methyl ester of (–)-prostaglandin E_1.[30]

Phosphoramidite (S_{ax},R_C)-**7n** is also used in a promising reaction of synthesis of chiral alkenes. Namely, the optically active product was obtained at 85 : 15 regioselectivity (branched : linear products) and an *ee* of 77% [ligands (S_{ax})-**7c**, (S_{ax})-**7m**, (S_{ax})-**7o** provide an *ee* of at most 31%].[31]

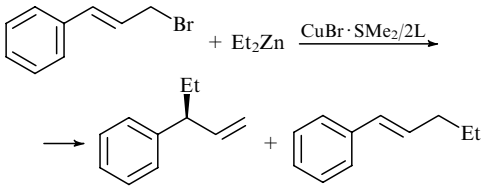

It should be noted that in some cases the best results were obtained using the (R_{ax},S_C)-**7n** enantiomer. A case in point is the addition of Et_2Zn to cyclic enones (*ee* up to 92%)[10] and a variety of nitroolefins (*ee* up to 94%).[32,33]

Recently synthesised[34] ligand (R_{ax})-**7q** can also be considered rather promising. Indeed, the addition of Et_2Zn to enone **9a** catalysed by Cu(OTf)$_2$/2L [reaction (4)] was performed with an optical yield of 93%. Besides, the catalytic synthesis of (*R*)-(–)-muscone involving ligand (R_{ax})-**7q** [reaction (1), see above] is characterised by much higher enantioselectivity (*ee* 95%)[34] compared to the reaction with phosphite (R_{ax})-**3t**.

By and large, phosphoramidites bearing additional C*-stereocentres are much better stereoinductors in reactions of Cu-catalysed addition of organozinc compounds. However, there are also a few exceptions. In particular, the reaction with chalcone showed an *ee* of 90% with ligand (S_{ax})-**7c** and only 75% with (S_{ax},R_C)-**7n**.[18,19]

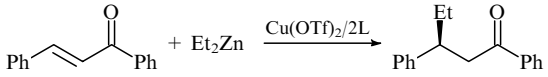

Efforts to obtain *ortho*-disubstituted phosphoramidites **8a–e** lacked support because the enantioselectivity showed by these compounds was no higher than that provided by their unsubstituted analogues **7a–u**.[18,19]

Note that, in spite of quite impressive catalytic results achieved using phosphoramidites **7a–q**, the coordination chem-

istry of these ligands is still poorly studied. Though a general scheme for the catalytic cycle of addition of organozinc reactants to cyclic enones has been reported,[19,20] no data confirming the structure of intermediates are available. The structure of catalytically active complexes is also unknown. Only Feringa and coworkers[18] earlier reported the synthesis and X-ray diffraction study of compound $CuI(L)_3$ [L = (S_{ax})-**7a**], while the course of complexation in the system $Cu(OTf)_2/2L$ is still to be clarified. We believe that one should expect publication of studies aimed at developing polymer-immobilised catalysts for asymmetric conjugate addition reactions. The first step along this line of investigation was reported recently.[35] Cu-Catalysed reaction of Et_2Zn with substrate **9a** [reaction (4)] using various modifications of the (R_{ax})-**7k** ligand covalently bound to hydroxymethylpolystyrene showed optical yields of up to 67%.

Phosphoramidite derivatives of BINOL (**1**) have also found applications in other reactions of C–C bond formation, in particular, Ir-catalysed allylic substitution.

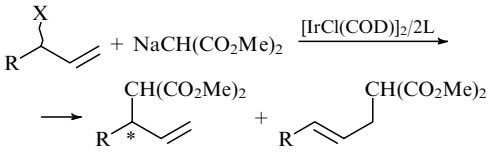

R = Me, CH_2CH_2Ph, Pr^i; X = OAc, Cl, OCO_2Et, $PO(OEt)_2$.

For instance, ligand (R_{ax})-**7a** usually provides a nearly 100% regioselectivity and an optical yield of up to 86% (R = CH_2CH_2Ph and X = OAc).[36,37] Very high chemical yields and regioselectivities are also observed in the presence of ligand (R_{ax},R_C)-**7n** in a related allylic amination reaction of a broad spectrum of substrates R–CH=CH–CH_2OCO_2Me by various amines (with enantioselectivities of 76%–97%).[38]

An interesting group of ligands **7s**,**t** was reported by Faraone *et al.*[39] The first communication was concerned with the synthesis and complexation of epimers **7s**. ^{31}P NMR and IR spectroscopy studies of the system $[RhCl(CO)_2]_2$/L [L = (S_{ax},R_C)-**7s**] revealed the formation of not only a conventional binuclear complex **10** but also its structural isomer **11** with a coordiation number of the Rh atom of 6.

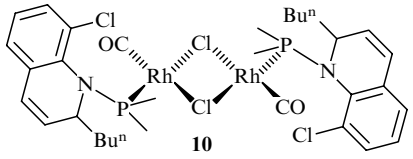

10

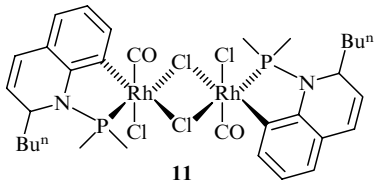

11

The formation of complex **11** involves oxidative addition of the ligand C–Cl bond to rhodium. In the case of epimer (S_{ax},S_C)-**7s** the process is sterically hindered and therefore only complex **10** is formed. The reactions of phosphoramidite (S_{ax},R_C)-**7s** with $[PdCl_2(PhCN)_2]$ or $[PtI_2(cod)]$ (at L : M = 2 mole ratio) resulted in corresponding complexes *cis*-$[MHal_2L_2]$. They were studied by ^{31}P and ^1H NMR, long-wavelength IR spectroscopy and X-ray analysis (complexes $[PtI_2L_2]$).[39]

The use of both epimers **7s** in Cu-catalysed addition of Et_2Zn to substrate **9a** [reaction (4)] led to different results. Namely, the optical yield obtained with the ligand (S_{ax},S_C)-**7s** is close to zero, but was 70% for (S_{ax},R_C)-**7s**.[40] This was ascribed to the different orientation of the chloroquinoline fragments in the intermediate copper complexes.

A similar situation was also observed for Ni-catalysed hydrovinylation of styrene.[41,42]

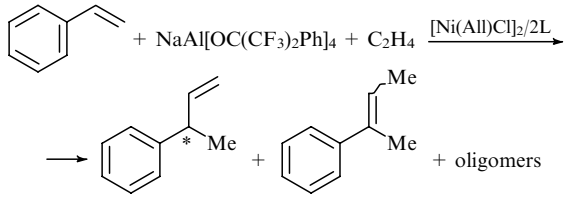

The reaction involving ligand (R_{ax},S_C)-**7s** results nearly exclusively in oligomeric side products, whereas epimer (R_{ax},R_C)-**7s** provides the synthesis of optically active product with nearly 100% regioselectivity and an *ee* of 87%. Related reactions using ligand (R_{ax},R_C)-**7t** and its epimer (R_{ax},S_C)-**7t** showed optical yields of only 8% and 56%, respectively. Nevertheless, the known ligand (R_{ax},S_C)-**7n** is more efficient than phosphites **7s**,**t** in this reaction, because it provides an optical yield of 95%.[41]

Recently, it was shown that phosphoramidite derivatives of BINOL (**1**) are excellent stereoselectors in not only C–C bond formation reactions but also other catalytic processes. For instance, the best results for hydrosilylation–oxidation of styrene (Ar = Ph, R = H), namely, an *ee* of 99%, were achieved using ligand (S_{ax},R_C)-**7n**.[43]

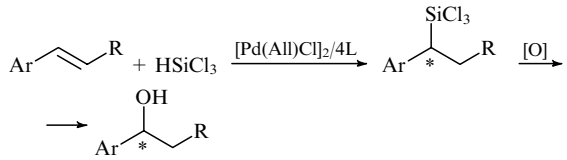

The optical yields of reactions with other aryl-substituted alkenes are also high (89%–98%). Systems without additional C*-stereocentres demonstrate much lower selectivities, *e.g.*, *ee*'s of 55% and 20% for the ligands (R_{ax})-**7a** and (R_{ax})-**7c**, respectively (with styrene as substrate).

At the same time the structurally simplest phosphoramidites (S_{ax})-**7a**,**b** appeared to be highly efficient ligands in asymmetric reduction. For instance, acetophenone is transformed in α-phenylethanol under the action of complex $BH_3 \cdot THF$ in the presence of catalytic amounts of ligand (S_{ax})-**7b** with an optical yield of up to 99%.[44] Catalytic hydrogenation of prochiral esters **4a** and **4b** following reaction (2) using the catalytic system $[Rh(cod)_2]^+BF_4^-$/2L [L = (S_{ax})-**7a**] is characterised by enantiomeric excesses of 94% and greater than 99%, respectively.[45] Hydrogenation of a large number of enamides [reaction (3)] using the same catalytic system showed optical yields of up to 96% (in particular, 95%, 93% and 89% for substrates **5a**, **5b** and **5d**, respectively).[46,47] The enantioselectivity obtained with derivatives of β-dehydroamino acids is as high as 99% [L = (S_{ax})-**7a**, (S_{ax})-**7e** and (S_{ax},R_C)-**7u**].[48]

Phosphoramidite derivatives of other chiral binaphthyldiols deserve separate consideration. Ligand **12**

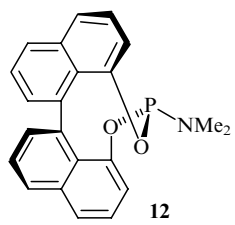

12

was successfully used in the reduction of acetophenone by complex $BH_3 \cdot THF$ (*ee* 96%) and in Cu-catalysed addition of Et_2Zn to enone **9a** [reaction (4), *ee* 83%].[49] For the latter reaction similar results were also shown by phosphoramidite (S_{ax})-**14b** based on H_8-BINOL (**13**), namely, the *ee* was 85% for substrate **9a** and 88% for substrate **9e**.[50]

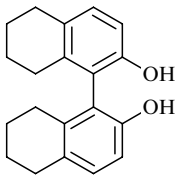

13 (H_8-BINOL)

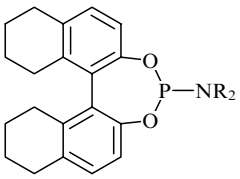

14a, **b** [(S_{ax}) and/or (R_{ax})]

R = Me (**a**), Pr^i (**b**).

The advantage of compound (R_{ax})-**14a** over its analogue **7a** is better solubility in organic solvents and a larger dihedral angle between the tetrahydronaphthalene fragments. It is quite logical that hydrogenation of α-dehydroamino acid esters [reaction (2) with $[Rh(cod)_2]^+BF_4^-$ as precatalyst] in the presence of (R_{ax})-**14a** is more efficient than the process involving ligand **7a**. For all substrates under study, the optical yields exceeded 90% (for compounds **4b**–**d**, it was 99% at nearly 100% conversion).[51,52] It should be noted that ester **4c** is a precursor of the known drug L-DOPA.

Recently,[53] a direct phosphorylation of (*S*)- or (*R*)-1,1′-spiroindan-7,7′-diol to give ligand **15a** was reported. Hydrogenation of substrate **4a** [reaction (2), *ee* 94%] and a number of methyl esters of α-dehydroamino acids in the presence of enantiomer (*S*)-**15a** with $[Rh(cod)_2]^+BF_4^-$ as precatalyst showed *ee* values of up to 99%.[53]

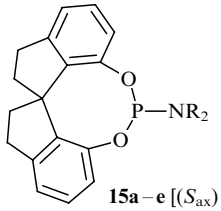

15a–**e** [(S_{ax}) and/or (R_{ax})]

R = Me (**a**), Et (**b**), Pr^i (**c**), cyclo-C_6H_{11} (**d**), CHMePh (**e**).

Ligand (*S*)-**15a** also possesses very high stereoinduction in $[Rh(cod)_2]^+BF_4^-$-catalysed hydrogenation of a series of prochiral enamides [reaction (3)]: the *ee* values obtained were between 91 and greater than 99%.[54] The dependence of enantioselectivity on the ligand structure can be illustrated by the following data:

Ligand	(S_{ax})-**7a**	(S_{ax})-**14a**	(S_{ax})-**15a**	(R_{ax})-**15a**	(S_{ax})-**15b**	(S_{ax})-**15c**
ee (%)	95	96	99	96	57	38

Thus, the optical yield dramatically decreases as the substituents at the nitrogen atom (compounds **15a**–**c**) become bulkier. Since the dihedral angle between the aromatic fragments in (S_{ax})-**15a** is larger than in (S_{ax})-**14a**, the enantiomeric excess provided by the former ligand was somewhat higher. Cu-Catalysed addition of Et_2Zn to enone **9a** [reaction (4)] involving ligands **15a**–**e** is also characterised by an *ee* of 98% [the NR_2 fragment of ligand **15e** has the (*R*,*R*)-configuration].[55]

Summarising the material presented in Sections II.1 and II.2, it should be noted that P-monodentate derivatives of BINOL and related binaphthyldiols are highly efficient in various asymmetric catalytic reactions. This first of all concerns Cu-catalysed addition of R_2Zn to unsaturated substrates and Rh-catalysed hydrogenation of C=C bonds. To date, the best results were obtained using phosphoramidite ligands. As applied to the processes mentioned above, phosphoramidite ligands are at least competitive with (and often better than) phosphites in the number of substrates and in stereoinduction achieved, being also active in Ni-catalysed hydrovinylation, Pd-catalysed hydrosilylation–oxidation and reduction of ketones by $BH_3 \cdot THF$ complex. All these reactions are characterised by high and very high optical yields.

3. Phosphites and phosphoramidites based on biphenyldiols

Interest in these systems is based on an attractive idea of replacing axially chiral derivatives of binaphthyldiols by much more accessible and inexpensive biphenyldiols. Though the corresponding ligands (*e.g.*, **16**) undergo atropoisomerisation, bonding to a metal stabilises the configuration of the biphenyl frame.[56]

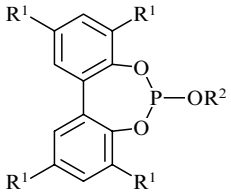

16a–**j**

Compound **16**	R^1	OR^2	Compound **16**	R^1	OR^2
a	H	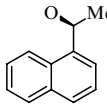	**g**	H	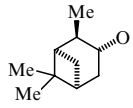
b	Bu^t		**h**	Bu^t	
c	H	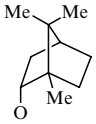	**i**	H	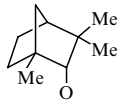
d	Bu^t		**j**	Bu^t	
e	H	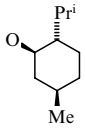			
f	Bu^t				

Complexation and catalysis using the $[Rh(cod)_2]^+BF_4^-$ system involving compounds **16a**–**j** have been studied.[57] ^{31}P NMR studies revealed a nearly 5:1 ratio of atropoisomers in the complexes $[Rh(cod)(L)_2]^+BF_4^-$ (*cf.* an equimolar mixture of unbound ligand atropoisomers). Unsubstituted structures (R^1 = H) provided higher enantioselectivity of hydrogenation of dimethyl itaconate (**4a**) following reaction (2); the enantiomeric excesses were 29% to 75% (the latter value was obtained with ligand **16i**) while at most 19% with $R^1 = Bu^t$.

Phosphoramidites **17a**–**d** were studied in Cu-catalysed addition of Et_2Zn to cyclic α,β-unsaturated ketones [reaction (4)] and nitroolefins.[58–60] Not only were a variety of substrates tested but also the reaction conditions varied [in particular, Cu(I) and Cu(II) salts used in the reactions].

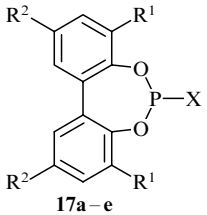

17a–**e**

Compound **17**	R^1	R^2	X
a	H	H	(*S*)- or (*R*)-N(1-PhEt)$_2$
	Me	Me	
c	H	H	(*S*)- or (*R*)-N(1-PhPr)$_2$
	Me	Me	
e	Bu^t	OMe	(*S*)- or (*R*)- 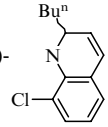

For instance, substrate **9a** provided an *ee* of 96% to 99% (93%–95% for substrate **9c**), which is comparable with the enantioselectivity of phosphoramidite (S_{ax},R_C)-**7n** (see Table 1). The asymmetric induction achieved with other substrates was strongly affected by the nature of the ligand. In particular, for Ph–CH=CH–NO_2 the ligand (*S*)-**17b** provides an *ee* of 82% [*cf.* only 48% obtained with (R_{ax}, S_C)-**7n**].[60] Unlike derivatives **16a**–**j**, there is no correlation between the stereoinduction achieved and the presence of substituents in the phenyl rings of compounds **17a**–**e**, though by and large systems with $R^1 = R^2 = Me$ appeared to be more efficient.

The asymmetrising potential of ligands **17a**–**d** has found applications in the synthesis of silyl ethers of cyclic enols[61] and in reactions of Grignard reagents with allyl chlorides,[62] which involve conjugate addition of R_2Zn to cyclohexenones.

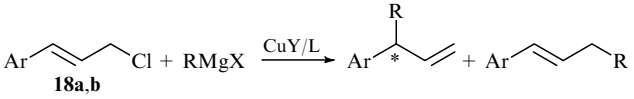

18a,**b**

Ar = Ph (**a**), 3-$MeOC_6H_4$ (**b**).

The reaction of EtMgBr with substrate **18a** shows an *ee* of up to 79% involving ligand (*S*)-**17a** and 54% with substituted ligand (*S*)-**17b** [*cf.* at most 49% provided by two BINOL derivatives, (S_{ax})-**7a** and (S_{ax}, S_C)-**7n**]. The best results, that is, an *ee* of 86% at 91 : 9 regioselectivity (branched : linear products) was obtained using ligand (*S*)-**17a** [substrate **18b**, Pr^iMgBr, CuTC (TC is thiophene-2-carboxylate)]. $[IrCl(cod)]_2$/2L-Catalysed allylic amination of Ph–CH=CH–CH_2OCO_2Me by benzylamine was characterised by an optical yield of 87%.[38]

Thus, biphenyldiol-based phosphoramidites **17a**–**d** successfully compete with analogous derivatives of BINOL (**1**). In contrast to ligand **7s**, the reaction of ligand **17e** with $[RhCl(CO)_2]_2$ proceeds selectively and results in a binuclear Rh(III) complex, which is similar to compound **11** and was studied by IR and ^{31}P NMR spectroscopies and by X-ray analysis.[39] The synthesis of compound *cis*-$[PdCl_2(L)_2]$ (L = ligand **17e**) was also reported in that study.[39]

4. TADDOL-based phosphites and phosphoramidites

This group comprises the ligands obtained by phosphorylation of (+)- or (−)-α,α,α′,α′-tetraaryl-1,3-dioxolane-4,5-dimethanol (TADDOL, **19**).

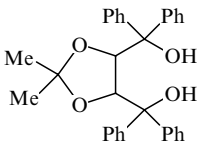

19 (TADDOL)

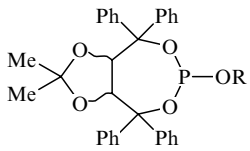

20a–**m** [(*S*) and/or (*R*)]

Compound **20**	OR	Compound **20**	OR
a	OMe	**i**	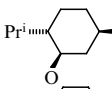
b	OBu^t		
c	O-cyclo-C_6H_{11}		
d	OPh	**j**	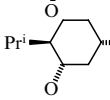
e	OH		
f	$OCH_2C{\equiv}C-SiMe_3$		
		k	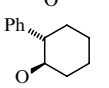
g	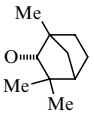		
		l	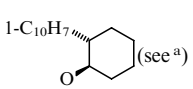 (see [a])
h	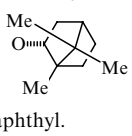		
		m	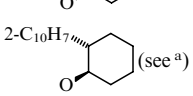 (see [a])

[a] $C_{10}H_7$ is naphthyl.

Initially, phosphites **20a**,**d** were employed in hydrosilylation of acetophenone followed by hydrolysis [reaction (5)].

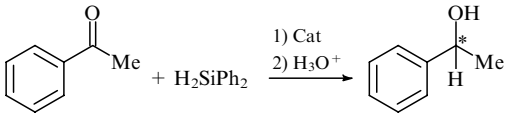

(5)

However, the optical yield appeared to be low {less than 25% with $[RhCl(cod)]_2$ as precatalyst}.[63] The enantioselectivity in Cu-catalysed addition of Et_2Zn to enone **9a** [reaction (4)] involving ligands **20a**–**f** was also low (*ee* less than 18%). Among phosphites with fragments of chiral alcohols, the best results in this reaction were provided by compounds (*S*)-**20m** (*ee* 86%) and (*S*)-**20k** (*ee* 96%).[64,65] Thus, in some cases the use of TADDOL-based phosphites leads to worse results compared to the use of, *e.g.*, phosphorus-containing BINOL derivatives. However, the stereoinduction achieved in conjugate addition to alkylidene malonates with L = (*S*)-**20m** can be as high as 73% and only 26% with ligand **7n**.[66]

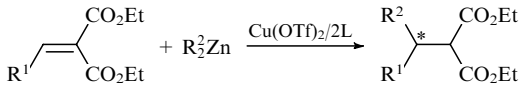

In a model reaction of Et_2Zn with enone **9a** [reaction (4), $Cu(OTf)_2$/2L], ligands **21a**–**h** provide an *ee* of 71%.[65,67]

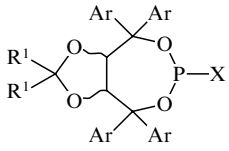

21a–**h** [(*S*) and/or (*R*)]

Compound **21**	R^1	Ar	X	Compound **21**	R^1	Ar	X
a	Me	Ph	NHMe	**g**	Me	2-MeC_6H_4	NMe_2
b	Me	Ph	NMe_2				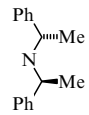
c	Me	Ph	NPr^i_2				
d	Me	Ph	NBn_2	**h**	Me	Ph	
e	Me	Ph	$N(CH_2)_5$				
f	$(CH_2)_4$	Ph	NMe_2				

In contrast to the situation for BINOL-based phosphoramidites, in this case the asymmetric induction increases as the substituents at the nitrogen atom become less bulkier. Because of this, the best results are provided by ligand **21b**.[67] It is of considerable importance that the reaction with substrate **9b** (also involving **21b**) shows[67] an *ee* of up to 62% [*cf.* 10% with (S_{ax},R_C)-**7n**, see Table 1]. The enantioselectivities of phosphites (*R*)-**21c** and (S_{ax},S_C)-**7n** in conjugate addition of R_2Zn to alkynylepoxides are comparable (*ee* 36% and 38%, respectively).[68] Recently,[69] ligand (*R*)-**21b** was successfully used in an intramolecular Heck reaction [reaction (6)]; the enantiomeric excess was 96% at 100% conversion.

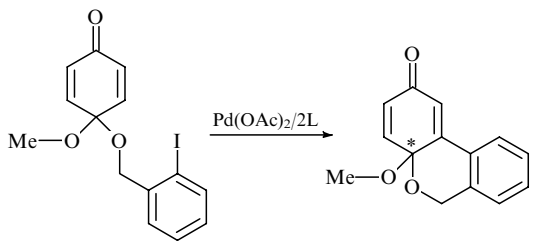

(6)

5. Phosphites and phosphoramidites based on carbohydrates and their derivatives

As mentioned above, the pioneering studies in this field were considered earlier.[6] Some examples were also presented in a review [70] concerned with complexes of platinum subgroup metals with carbohydrates. In spite of the fact that phosphorus-containing sugar derivatives are among the long-studied groups of chiral phosphite ligands, they still attract the attention of researchers. For instance, the reaction was reported [71] of compound **22a** with $[CuCl(CO)]_x$ to give a tetranuclear copper(I) complex $[\{CuCl(L)\}_4]$, which was studied by X-ray analysis. The structure of compound **22a** is characterised by a large Tolman cone angle ($\sim 180^\circ$). Because of this, the complex in CD_2Cl_2 solution is in equilibrium with $[\{CuCl(L)_2\}_2]$ dimer (^{31}P NMR data).

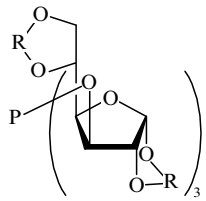

22a,**b**

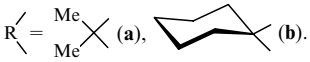

Ligands **22a**,**b** and **23a**–**d** are used in the synthesis of rhodium(I) complexes and in Rh-catalysed hydrosilylation of acetophenone by diphenylsilane [reaction (5), *ee* less than 58%].[72]

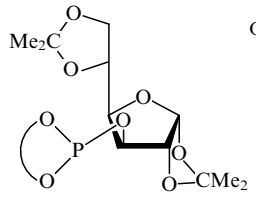

23a–**d**

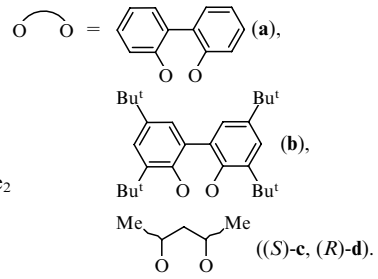

The reactions of compounds **22a**,**b** and **23b** with $[RhCl(cod)]_2$ result in mononuclear complexes [RhCl(cod)(L)]. Further increase in the L : Rh mole ratio (L = **22a**) is not accompanied by the formation of the desired product, $RhCl(L)_3$. Attempts at obtaining $RhCl(L)_3$ starting from $[RhCl(C_2H_4)_2]_2$ also failed. This is also associated with the large cone angle in ligand **22a**. Nevertheless, these two ligands can be in a *cis*-position relative to each other in the coordination sphere of rhodium, which was confirmed by the synthesis of complex $[Rh(acac)L_2]$. It was found that $[RhCl(cod)]_2$ is inefficient as a precatalyst in the hydrosilylation of acetophenone (*ee* at most 11%). The best result, *ee* 58% (see above), was obtained using the $[RhCl(C_2H_4)_2]_2$/6L system (L = compound **22b**).

Bicyclophosphites **24a**–**c** and **25** were proposed as efficient ligands for synthesis of coordination compounds. Complexes $[\{CuBr(L)\}_4]$, $[M(CO)_5(L)]$ (M = Cr, Mo) and *cis*-$[PtCl_2(L)_2]$ were synthesised using phosphites **24a**–**c**; and studied by IR spectroscopy, ^{31}P and ^{13}C NMR and by X-ray analysis.[73]

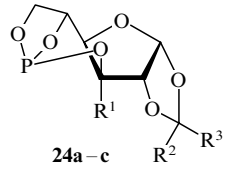

24a–**c**

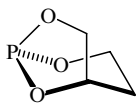

25

Compound **24**	R^1	R^2	R^3
a	H	Me	Me
b	H	H	CCl_3
c	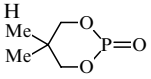	Me	Me

Phosphite **25** derived from (*S*)-1,2,4-butanetriol was employed in the synthesis of complexes with an open and a half-open titanocene.[74]

A novel group of phosphoramidites **26** and **27** [75,76] should be pointed out.

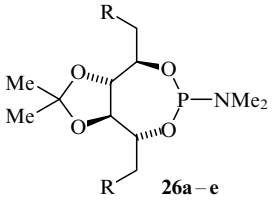

26a–**e**

R = H (**a**), Me (**b**), Et (**c**), Bu^i (**d**), Ph (**e**).

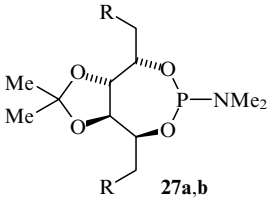

27a,**b**

R = H (**a**), Ph (**b**).

They were used to obtain cationic complexes of rhodium(I), $[Rh(cod)(L)_2]^+OTf^-$, and neutral complexes of palladium(II), *cis*-$[PdCl_2(L)_2]$. Two Pd complexes with L = **26a** and **27a** were studied by X-ray analysis. These coordination compounds were also studied by ^1H and ^{31}P NMR spectroscopy and by FAB mass spectrometry. It is unclear why the set of ^{31}P NMR spectral parameters does not include the $^1J(P,Rh)$ spin-spin coupling constants, which are useful for assessing the electron-donor ability of phosphorus-containing ligands.

Complexes $[Rh(cod)L_2]^+OTf^-$ (L = **26**, **27**) were studied as catalysts for the hydrogenation of unsaturated acids, namely, α-(*N*-acetylamino)cinnamic (*ee* up to 89%) and itaconic acid (*ee* up to 94%).[76] In both cases the best results were obtained using phosphoramidite **27b**, whereas its diastereomer **26e** is much less efficient and provides enantiomeric excesses of 36% and 61%, respectively.

6. Other P-monodentate chiral phosphites

Cyclic phosphites **28a**–**e** based on tartaric acid derivatives are also of interest.

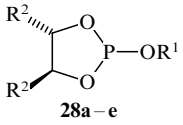

28a–**e**

Compound **28**	R^1	R^2	Compound **28**	R^1	R^2
a	(L)-menthyl	CO_2Et	**d**	(L)-menthyl	CO_2Pr^i
b	(D)-menthyl	CO_2Et	**e**	(L)-menthyl	$CONMe_2$
c	bornyl	CO_2Et			

They provided an *ee* of up to 40% in conjugate addition for Et_2Zn to enone **9a** [reaction (4)] and up to 65% in the reaction with benzylidenacetone [with the $Cu(OTf)_2$/2L catalytic system].[77] Though these optical yields cannot be considered high, ligands **28a**–**e** are much better stereoselectors than related phosphites **29a**–**c** whose efficiency in these reactions was characterised by an *ee* of at most 11%.[77]

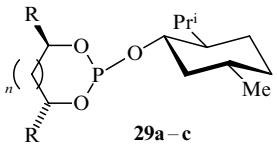

29a–**c**

R = Me: *n* = 1 (**a**), 0 (**b**); R = Ph, *n* = 0 (**c**).

Complexes **30a**,**b** and **31** were used as catalysts of acetophenone reduction by the $BH_3 \cdot THF$ adduct; however, the optical yield was at most 37%.[78]

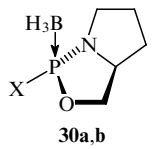

30a,**b**

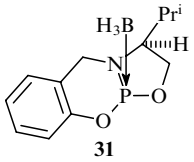

31

X = OPh (**a**), NMe_2 (**b**).

Mention also may be made of phosphites **32**–**34**.

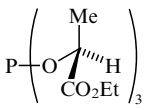

32

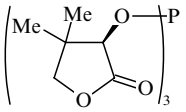

33

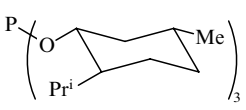

34

Ligands **32** and **33** were used in complexation with [Fe(chd)$(CO)_3$] (chd = 1,3-cyclohexadiene)[79] and [Ni$(cod)_2$] (see Ref. 80), respectively. Trialkyl phosphite **34** was involved in Cu-catalysed addition of Et_2Zn to enone **9a** [reaction (4), *ee* 36%].[77]

Thus, at present the catalytic potential of compounds **22**–**34** seems to be quite modest as compared to the potential of ligands based on BINOL (**1**) and TADDOL (**19**). However, we believe that it is not completely explored and considerable progress is possible in this field. A good example is provided by the successful use of phosphite **27b** in Rh-catalysed hydrogenation (see above).

III. P,N-Bidentate compounds of phosphite nature

The first synthesis of ligands belonging to this class and their complexation with rhodium(I) was reported in 1993.[81] Since then, methods of synthesis and the coordination chemistry of these compounds have been the subject of some studies;[5,6,8] however, they have been efficiently used in asymmetric catalysis only during the last five years. The introduction of the N-donor centre into the chiral ester or phosphorous acid amidoester molecule makes it possible to extend the field of application of P,N-bidentate compounds of phosphite nature. Therefore, the material presented in this Section is classified with emphasis on the nature of the nitrogen donor centre.

1. Phosphites and phosphoramidites containing an oxazoline fragment

The major contribution to the design of these systems was made by Pfaltz *et al.*[82,83] who proposed a broad spectrum of ligands **35**–**38** based on BINOL (**1**) and related structures.

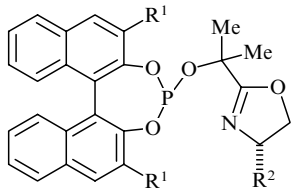

35a–**h** [(S_{ax}) and/or (R_{ax})]

Compound **35**	R^1	R^2	Compound **35**	R^1	R^2
a	H	Pr^i	**e**	Ph	Bu^t
b	H	Ph	**f**	4-PhC_6H_4	Bu^t
c	H	Bu^t	**g**	2,4,6-$Me_3C_6H_2$	Bu^t
d	Me	Bu^t	**h**	3,5-$Bu^t_2C_6H_3$	Bu^t

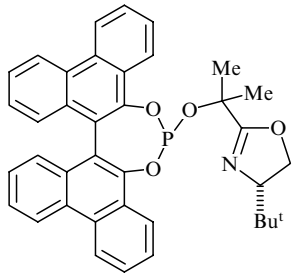

36 [(S_{ax}) and/or (R_{ax})]

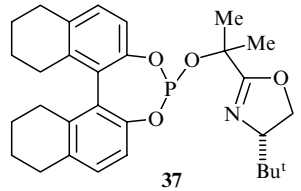

37

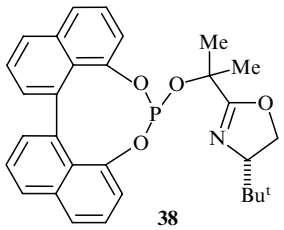

38

Pd-Catalysed allylic substitutions involving ligands **35a**–**d** and substrate **39a** [reaction (7)] showed the enantiomeric excesses lying between 7% and 92% and the yields of the branched products in the range 46%–76%.[82,83] The highest enantioselectivity was provided by ligand (S_{ax})-**35d**.[83]

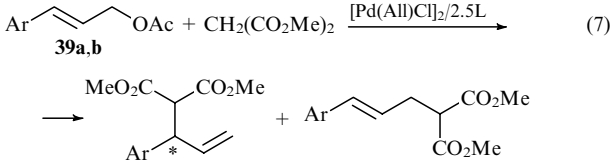

(7)

39a,**b**

Ar = Ph (**a**), naphthyl (**b**).

The asymmetric induction depends first of all on the configuration of the oxazoline fragment. Namely, the enantiomeric excess provided by the ligands is 79% for (R_{ax})-**35c** and 90% for (S_{ax})-**35c**, the product configurations in both cases being the same.[83] Substrate **39b** is characterised by greater steric requirements and makes it possible to achieve an *ee* of up to 96% at high regioselectivity and chemical yield [L = (S_{ax})-**35c**].[84] The structure of catalytically active complex {Pd(All)[(S_{ax})-**35c**]}$^+PF_6^-$ was confirmed by X-ray analysis.[82]

Oxazolinophosphites **35c**–**h** and **36**–**38** were studied in the Cu-catalysed addition of Et_2Zn to cyclic enones **9a**–**c** [reaction (4)].[85–87] The enantiomeric excesses obtained for different substrates are as follows: up to 90% for **9a** [L = (R_{ax})-**35d**], up to 94% for **7b** [L = (R_{ax})-**35f**] and up to 94% for **9c** [L = (S_{ax})-**36**]. The high enantioselectivity of the reaction involving enone **9b** should be pointed out, which could not be provided by other phosphites (*cf.* the data listed in Table 1). A study on the dependence of enantioselectivity on the ligand structure revealed no direct correlation between the optical yields and the size of substituents in the *ortho*-positions of the naphthyl rings. However, the presence of these substituents is a necessary condition for high stereoinduction.[85,87]

Both epimers of ligand **40** were also described.[88]

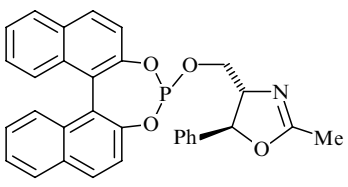

40 [(S_{ax}) and (R_{ax})]

^{31}P NMR spectroscopy, IR spectroscopy and electrospray mass spectrometry data showed that ligand **40** unexpectedly forms dimeric rather than chelate complexes of rhodium(I) with a 'head-to-tail' bridging bonding of the P,N-bidentate ligand and that the structures of the complexes depend on the absolute configuration of BINOL. This remarkable fact should be taken into account in analysis of applications of P,N-bidentate ligands as catalysts, the more so as the stereoinduction involving epimers **40** is also significantly different. Namely, ligands (R_{ax})-**40** and (S_{ax})-**40** provide an *ee* of up to 58% and at most 4%, respectively, in Rh-catalysed hydrosilylation of acetophenone [reaction (5)] .

As mentioned above, the enantioselectivity of oxazolinophosphites **35a**–**d** in Pd-catalysed allylic alkylation is to a great extent governed by the oxazoline fragment. This makes it possible to rule out the axially chiral template BINOL for ligand design purposes. In particular, compound **41** provides an *ee* of 83% in the reaction involving substrate **39a** [reaction (7)].[82]

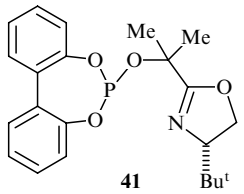

41

Moreover, acyclic ligands **42a**,**b** also appeared to be efficient.

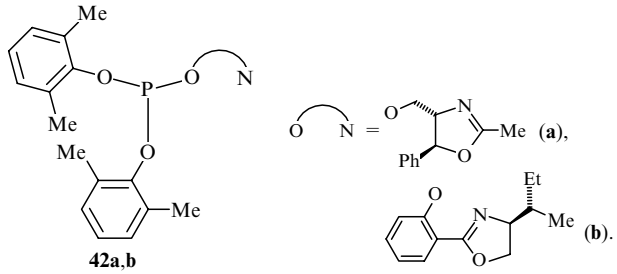

42a,**b**

Pd-Catalysed allylic substitutions of substrate **43** for dimethyl malonate [reaction (8)] and $NaSO_2$(*p*-Tol) [reaction (9)] respectively showed an *ee* of 85% {for $[Pd(All)Cl]_2$/2.5L, L = **42a**}[89] and an *ee* of 92% {for $[Pd(All)(\mathbf{42b})]^+BF_4^-$}.[90]

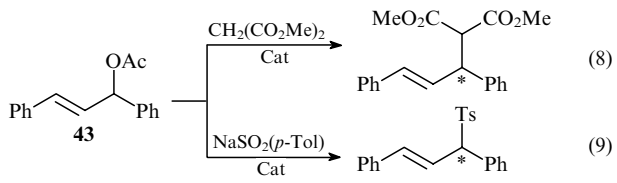

43

(8)

(9)

Chelate mononuclear complexes [RhCl(CO)(L)] with L = **42a**,**b** were synthesised. The complex with phosphite **42a** was studied by X-ray analysis.[89]

Systems based on chiral 1,2-diamines and TADDOL (**19**) and containing oxazoline fragments and phosphite cyclic groups were also synthesised. Oxazolinophosphoramidites **44a**–**g** were found to be highly efficient.

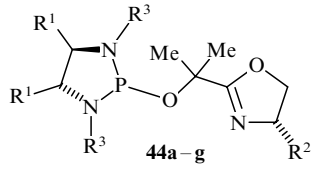

44a–**g**

Compound **44**	R^1	R^2	R^3
a	Ph	Bu^t	Ts
b	$(CH_2)_2$ (see [a])	Bu^t	Ts
c	Ph	Ph	Ts
d	Ph	Bu^t	(1-naphthyl)methyl
e	Ph	Bu^t	4-$MeOC_6H_4$
f	$(CH_2)_2$ (see [a])	Bu^t	4-$MeOC_6H_4$
g	Ph	Bu^t	4-biphenylyl

[a] Here, R^1-R^1.

They showed high enantioselectivities in Pd-catalysed substitution of substrates **39a** (*ee* up to 95%), **37b** (*ee* greater than 99%) [reaction (7)] and **43** (*ee* up to 88%) [reaction (8)] for dimethyl malonate. Additionally, Ir-catalysed hydrogenation of various vinylarenes showed an *ee* of greater than 99%.[91,92]

The catalytic system $[Pd_2(dba)_3\cdot CHCl_3]$/2L (L = **45**, dba = dibenzylideneacetone) provides an optical yield of 92% in the reaction of substrate **43** with $NaSO_2$(*p*-Tol) [reaction (9)].[93]

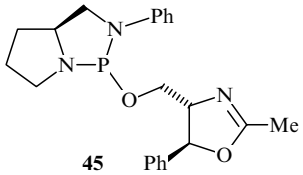

45

Note that in addition to three C*-stereocentres compound **45** also contains a P*-stereocentre in the (*R*)-configuration. In contrast to oxazolinophosphite **42b**, ligand **45** provides a lower stereoinduction in the cationic complex $[Pd(All)(\mathbf{45})]^+BF_4^-$ (*ee* 77%).

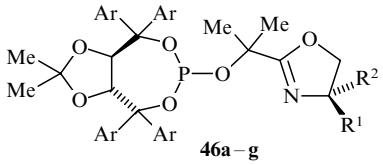

46a–**g**

Compound **46**	Ar	R^1	R^2	Compound **46**	Ar	R^1	R^2
a	Ph	H	Ph	**e**	2-naphthyl	Pr^i	H
b	Ph	Ph	H	**f**	Ph	H	Bu^t
c	Ph	H	Pr^i	**g**	2-naphthyl	H	Bu^t
d	Ph	Pr^i	H				

Ligands **46a**–**e** were used[94] in the synthesis of cationic complexes of rhodium(I) $[Rh(cod)(L)]^+BF_4^-$ (complex with L = **46b** was studied by X-ray analysis) and in hydrosilylation of a number of aliphatic and aromatic ketones {with $[RhCl(cod)]_2$ as precatalyst}. The best results were obtained with ligand **46d**, which provided the optical yields of 88% and 95% for the reduction of acetophenone and *tert*-butyl methyl ketone, respectively. Phosphite **46f** provides high optical yields in the Pd-catalysed substitution of substrate **39b** [reaction (7), *ee* 94%] while phosphites **46f**,**g** also behave analogously in Ir-catalysed hydrogenation of 4-$MeOC_6H_4C(Me)=CHMe$ (*ee* 95%).[91,92]

The use of ligand **46c** in Cu-catalysed addition of Et_2Zn to enone **9a** [reaction (4)] and to alkylidene malonates has also been reported; however, the enantioselectivities achieved were low (*ee* at most 22%).[65,66]

2. Phosphites and phosphoramidites containing pyridine fragments

As in the ligand group considered above, BINOL-based systems **47**–**49** are also known in this group. Phosphites **47a**–**e** and **48a**,**b** were found to be inefficient in the reaction of Pd-catalysed alkylation of substrate **43** by dimethyl malonate [reaction (8)]. They provided optical yields of at most 37%[95] while the use of ligands **47a**,**b** resulted in racemic product.[95,96] Multinuclear NMR studies (including 2D NOESY experiments) showed that this is due to the presence of different configurational isomers of the intermediate palladium complexes.[95,96]

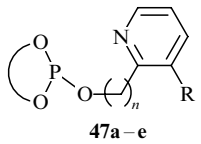

47a–e

n = 0, R = H (**a**);
n = 1: R = H (**b**), Me (**c**), Ph (**d**), Br (**e**).

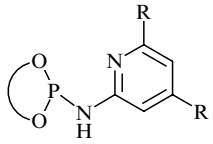

48a,b

R = H (**a**), Me (**b**).

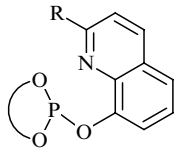

49a,b

R = H (**a**), Me (**b**).

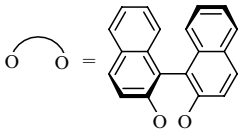

= S_{ax}-BNaph(O)$_2$.

Cu-Catalysed addition of Et_2Zn to enone **9a** [reaction (4)] in the presence of ligands **49a**,**b** also showed a moderate enantioselectivity (*ee* up to 51%).[40] Note that phosphite **49a** is used as a chelate-forming ligand in the synthesis of half-sandwich complexes of ruthenium(II) and rhodium(III), *e.g.*, [RhCl(η^5-C_5Me_5)(S_{ax}-**49a**)]$^+PF_6^-$ (see Ref. 97), which was studied by X-ray analysis. Yet another enantiomer, (R_{ax})-**49a**, was used in the substitution reaction involving substrate **43** and dimethyl malonate {reaction (8), with [Pd(All)Cl]$_2$ as precatalyst, *ee* 31%}.[98]

Quite interesting compounds **50a**,**b** [99, 100]

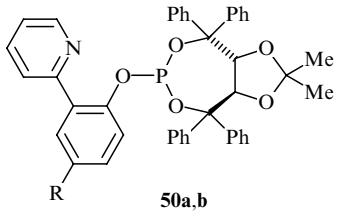

50a,b

R = H (**a**), OSiBu^{t}Me$_2$ (**b**).

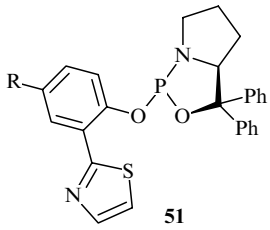

51

R = OSiBu^{t}Me$_2$.

were studied in the Rh-catalysed hydroboronation–oxidation of styrene.

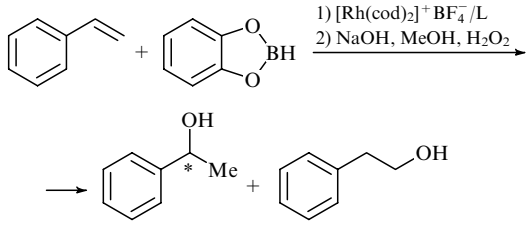

The optical yield was 59% at chemical yields in the range 52%–56% and regioselectivities (branched : linear product ratios) from 77 : 23 to 80 : 20.[100] Similar results were also obtained for compound **51** containing no pyridine fragment.[99, 100]

Shortening of the distance between the chiral fragment and the donor atoms of the ligand is known to favour a significant enhancement of stereoinduction. It is particularly appropriate if these atoms are stereocentres. A number of ligands **52**, **53** containing asymmetric phosphorus atoms were proposed by Buono *et al.*[101–103]

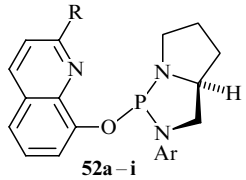

52a–i

Compound **52**	R	Ar	Compound **52**	R	Ar
a	H	Ph	**g**		Ph
b	Me	Ph			
c	Bu^t	Ph	**h**		Ph
d	Ph	Ph			
e	CN	Ph	**i**	H	1-naphthyl
f		Ph			

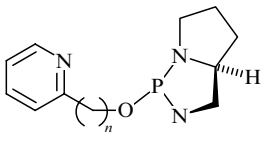

53a,b

n = 0 (**a**), 1 (**b**).

^{13}C NMR and X-ray diffraction studies of complex [Pd(All)(**52a**)]$^+ClO_4^-$ revealed the (*R*)-configuration of the P*-stereocentre.[101]

The classical allylic substitution in the reaction of substrate **43** with dimethyl malonate {reaction (8), catalytic system [Pd(All)Cl]$_2$/4L, L = **52a–h** or **53a**,**b**} is characterised by an optical yield of up to 87% and by nearly 100% conversion.[98, 102] The highest enantioselectivity was obtained with ligand **52a**, whereas the *ee* provided by its derivatives **52b–h** was at most 55%.[98] A related process, allylic amination of substrate **43** involving benzyl- and veratrylamines as nucleophiles (L = **52a–i** and **53a**,**b**) showed an *ee* of up to 94%.[103] Here, phosphite **52a** was also the most efficient (compound **52b–h** provided the enantiomeric excesses in the range 38%–78%).[98]

Phosphoramidite **52a** is also used in Pd-catalysed allylic amination of prochiral bicyclic diacetates (*ee* up to 89%),[104] Cu-catalysed Diels–Alder reactions (*ee* greater than 99% at 99% conversion)[105] and conjugate addition of Et_2Zn to cyclohexenone **9a** [reaction (4), *ee* up to 61%].[106]

Yet another example of the potential of ligand **52a** is provided by an elegant reaction to give quaternary C*-stereocentres by allylation of β-ketoesters.[107]

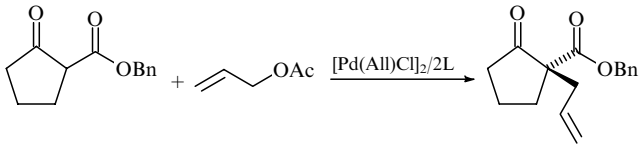

It is characterised by an *ee* of 95%; however, one should keep in mind that the enantioselectivity is quite 'sensitive' to the nature of the substrate and allylating agent. For instance, the optical yield in the reaction involving a homologous keto ester containing a six-membered ring was at most 17%.

The efficiency of ligand **52a** as stereoselector is most pronounced when comparing it with phosphoramidites **54–57**.

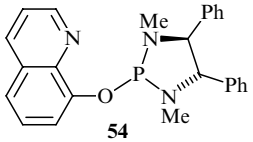

54

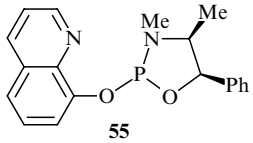

55

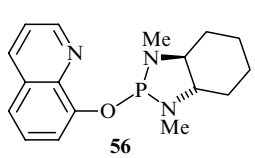

56

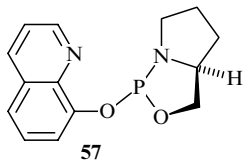

57

Studies of compounds **54**–**57** and (R_{ax})-**49a** in the catalytic processes mentioned above revealed low asymmetrising activities of these species. Namely, the optical yield of Pd-catalysed allylic substitution of substrate **43** for dimethyl malonate [reaction (8)] was at most 31% and 35% in the case of benzylamine; the enantiomeric excess in Cu-catalysed addition of Et_2Zn to enone **9a** [reaction (4)] was only 27%.[98]

Thus, most ligands containing a pyridine fragment possess low or moderate enantioselectivities. The exceptions are phosphoramidites **52a** and **53**; however, their efficiency may be due to the unique structure of the bicyclic phosphite centre rather than the nitrogen-containing fragment.

3. Aminophosphites and aminophosphoramidites

We begin our discussion of this group of ligands (type **B**) with phosphite derivatives of BINOL **58a**–**j**.

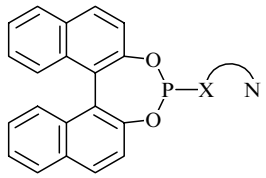

58a–**j** [(S_{ax}) and/or (R_{ax})]

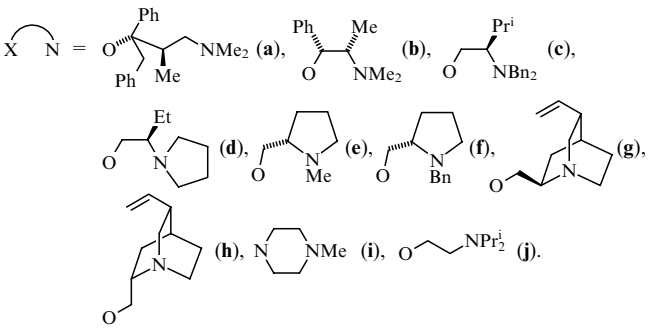

Reactions of compounds **58a**–**g** with $[RhCl(CO)_2]_2$ result in chelate mononuclear complexes [RhCl(CO)(L)]. It was shown that coordination of ligand **58c** proceeds non-selectively due to significant steric hindrances to chelation produced by benzyl substituents at the nitrogen atom. As a result, a *trans*-$[RhCl(CO)(L)_2]$ complex is formed in addition to the metal-containing chelate.[88]

Compounds **58a**,**b** were studied in Pd-catalysed alkylation of substrates **59** by dimethyl malonate {reaction (10), catalytic system $[Pd(All)Cl]_2/2L$}. The optical yield was at most 34%.[88]

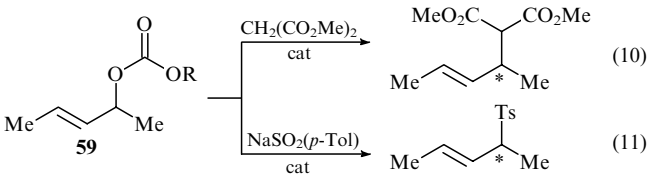

(10)

(11)

Similarly to this, phosphite **58h** showed a low enantioselectivity (*ee* 16%) in Rh-catalysed hydroformylation of styrene.[108] Cu-Catalysed addition of Et_2Zn to cyclic enone **9a** in the presence of ligand **58i** [reaction (4)] and Rh-catalysed hydrogenation of enamide **5a** in the presence of ligand **58j** [reaction (3)] result in racemates.[15,19] In this case, the attainment of an *ee* of 67% in the last-mentioned reaction involving a large group of polystyrene-immobilised systems [109] of general structural type **60** seems to be encouraging.

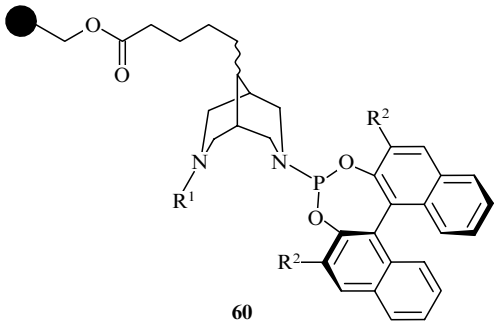

60

Acyclic aryl phosphites **61** are related to compounds **58**.

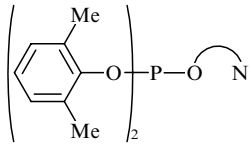

61a–**h**

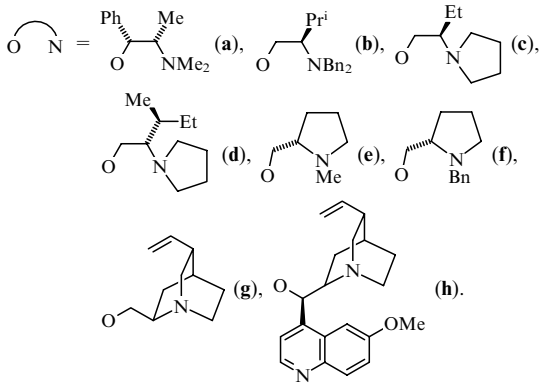

They were used to synthesise chelate complexes [RhCl(CO)(L)]. Similarly to the case of compound **58c**, complexes *trans*-$[RhCl(CO)(L)_2]$ are formed as side reaction products.[110] It is possible to overcome this difficulty and obtain individual metal-containing chelates using an original exchange reaction, which is considered below taking ligand **61b** as an example.

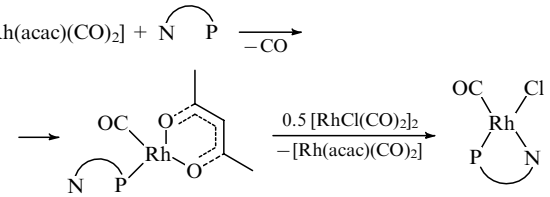

Unfortunately, aryl phosphites **61** are inefficient in Pd-catalysed allylic substitution of substrates **43** [reaction (8)] and **59** [reaction (10)] by dimethyl malonate,[110,111] in sulfonylation of substrate **59** under the action of $NaSO_2$(*p*-Tol) [reaction (11)] and in Rh-catalysed hydrosilylation of acetophenone [reaction (5)].[110] The enantiomeric excess in these reactions was at most 28%.

A quinine-based aryl phosphite **61h** was used in Pd-catalysed enantioselective rearrangement of allyl thiocarbamate, which proceeds at a 100% conversion and an *ee* of 47%.[112]

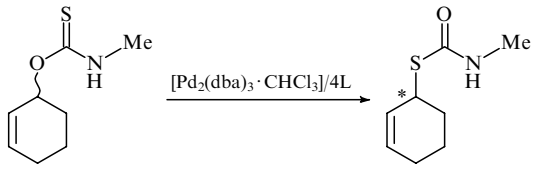

Noteworthy is that ligand **61g** is inefficient in this reaction (*ee* 2%). This is likely due to the large cone angle in structure **61h** ($\Theta = 190^\circ$) and to the presence of additional quinoline donor N atom.

Cu-Catalysed addition of Et_2Zn to cyclic enone **9a** [reaction (4)] in the presence of TADDOL-based phosphites **62** and phosphites **63** based on tartaric acid was also studied. The optical yields were rather low (*ee*s less than 38% for compounds **62a**–**e**[65] and less than 30% for compounds **63a**,**b**). In the latter case, the configuration of the product is controlled by the (*R*,*R*)-diethyl tartrate fragment.[77]

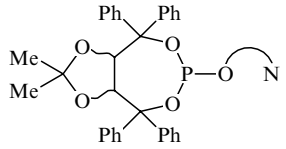

62a–**f** [(*S*) and/or (*R*)]

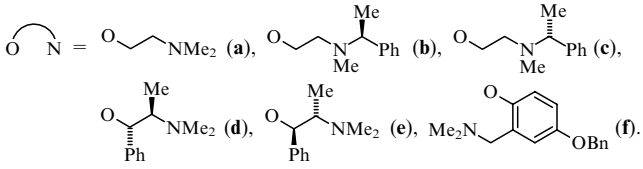

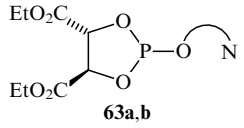

63a,**b**

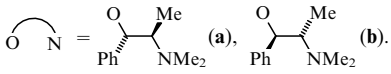

Low optical yield (20%) was also obtained in the methoxycarbonylation of $[Cr(o\text{-}Cl_2C_6H_4)(CO)_3]$ in the presence of complex $[PdCl_2(\mathbf{62f})]$.[113]

Nevertheless, the use of some aminophosphites permitted enhancement of the enantioselectivity. In particular, the first direct Pd-catalysed asymmetric synthesis of carboranes was reported[114] and a number of ligands were studied. The highest optical yield was 48% [reaction (12)].

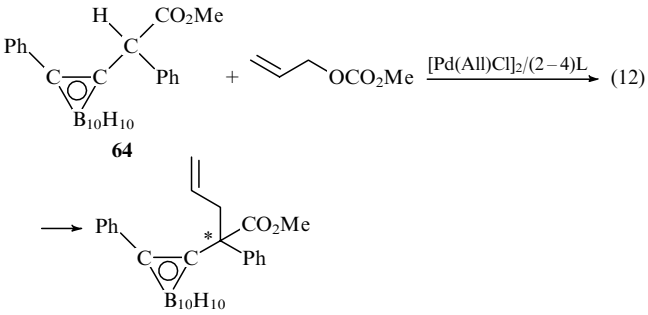

64

^{31}P NMR spectroscopy, IR spectroscopy and mass spectrometry studies of the catalytic system $[Pd(All)Cl]_2$/**65** revealed that phosphoramidite **65** behaves as a P-monodentate ligand, namely, a large amount of complex $[Pd(All)(L)_2]^+Cl^-$ is formed even at an L : Pd = 1 mole ratio (see Ref. 114).

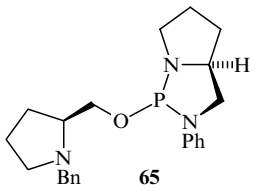

65

Palladium-catalysed allylic substitution reactions involving dimethyl malonate in the presence of phosphite derivatives of (2*R*)-2-pyrrolidin-1-ylbutan-1-ol (**66a**–**e**) were studied.[111]

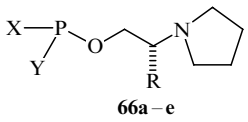

66a–**e**

Compound **66**	X—P / Y	R	Compound **66**	X—P / Y	R
a		Et	**d**		Et
b	$(Pr^iO)_2P$	Et			
c	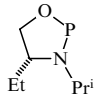	Et	**e**	$(Pr^iO)_2P$	Pr^i

In the case of substrate **43** [reaction (8)] the optical yield was at most 14%, being 61% for allyl acetate **39a** [reaction (7)] {with $[Pd(All)Cl]_2$ as precatalyst, the most efficient ligand was **66b**}.

Cu-Catalysed conjugate addition of Et_2Zn to cyclohexenone **9a** [reaction (4)] in the presence of aminophosphites **67** and **68** based on D-xylose and D-ribose, respectively, is characterised by similar enantioselectivity (*ee* up to 63%).[115]

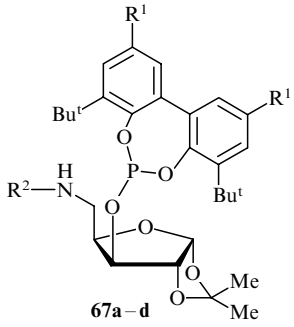

67a–**d**

Compound **67**	R^1	R^2
a	Bu^t	Bu^t
b	OMe	Bu^t
c	Bu^t	Pr^i
d	Bu^t	Ph

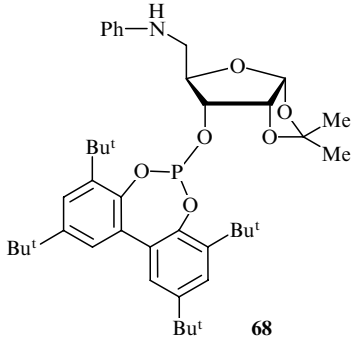

68

The best stereoselector was found to be ligand **67d**.

A number of chiral aminophosphites, which are used at present only in coordination chemistry of platinum metals, should be pointed out.

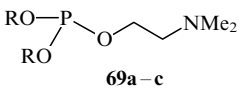

69a–c

R is bornyl (**a**), menthyl (**b**), cholesteryl (**c**).

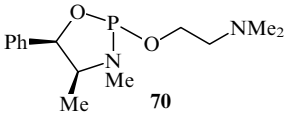

70

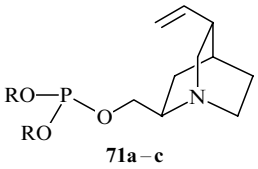

71a–c

R–R = $(CH_2)_2$ (**a**);
R = Pr^i (**b**), bornyl (**c**).

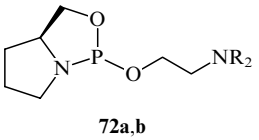

72a,b

NR_2 = NMe_2 (**a**), (**b**).

For instance, reactions of compounds **69a–c** with $[PdCl_2(cod)]$ afforded mononuclear chelate complexes $[PdCl_2(L)_2]$, whch were studied by multinuclear NMR spectroscopy, IR spectroscopy, sedimentation analysis and X-ray analysis (for ligand **69a**).[116,117] Aminophosphoramidite **70** also forms an analogous metal-containing chelate in the reaction with $[PdCl_2(cod)]$, whereas the reaction with $[PtCl_2(cod)]$ results in an exclusive product, a compound with P-monodentate bonding of the *cis*-$[PtCl_2(L)_2]$ ligand (according to ^{31}P, ^{13}C and ^{195}Pt NMR spectroscopy and IR spectroscopy).[118]

Similarly to compounds **66a–e** (see above), aminophosphites **71a–c** act as typical chelate-forming agents towards $[RhCl(CO)_2]_2$.[111,119] Ligands **71b,c** behave analogously in the reaction with $[PdCl_2(cod)]$. However, the reaction with phosphite **71a** results not only in chelate $[PdCl_2(L)]$ but also in products of composition $[PdCl_2(L)_2]$, which may be due to the insufficient strength of the metallacycle in the presence of a *spiro*-fragment in the chelate complex.[119]

The reaction of compound **72a** with $[RhCl(CO)_2]_2$ results in a metal-containing chelate [RhCl(CO)L], while ligand **72b** containing a piperidine nitrogen centre also forms a large amount of dimer $[RhCl(CO)L]_2$,[120,121] which has a 'head-to-tail' structure and a *trans*-orientation of the phosphorus and nitrogen atoms at the Rh atom.[121] A codeine-based aminophosphite **73** also forms a structurally similar dimer; in this case, the *trans*-dimer is in equilibrium with *cis*-$[RhCl(CO)(L)]_2$.[122]

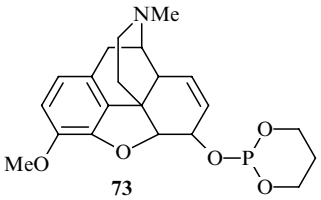

73

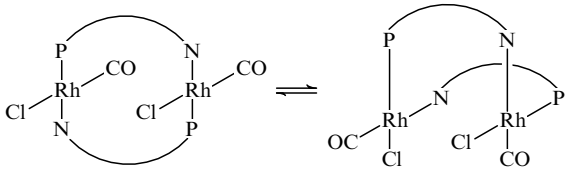

The equilibrium position is governed by the solvent, *viz*., in DMF the complex exists as a *trans*-isomer while a nearly equimolar mixture of the *cis*- and *trans*-isomers is observed in DMSO.

Thus, the coordination behaviour of ligands containing peripheral amino groups is ambiguous. *A priori*, they seem to be typical chelate-forming compounds; however, P-monodentate bonding is often observed. The choice of a particular type of bonding is controlled by the nature of the ligand, the starting metal complex and the solvent. Chelation-preventing factors first of all include the involvement of donor atoms in the five- and six-membered rings (see also Ref. 123) and the presence of bulky substituents at the nitrogen atom. Undoubtedly, these features should be taken into account when predicting and analysing the use of aminophosphites in catalysis. The enantioselectivities obtained to date cannot meet the requirements imposed by modern asymmetric catalysis. Therefore, further investigations and search for new, more efficient ligands are required.

4. Phosphite derivatives of Schiff bases

This is the 'youngest' group of P,N-bidentate derivatives of phosphorous acid, which has been little studied. First of all, aryl phosphite ligands **74** and **75** should be pointed out.

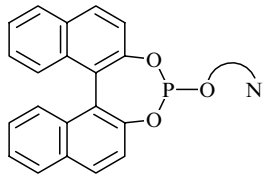

74a–f [(S_{ax}) and/or (R_{ax})]

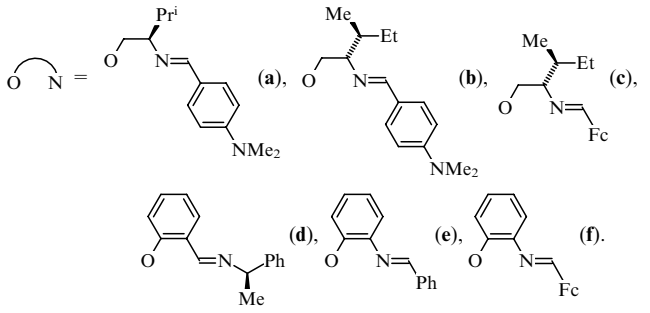

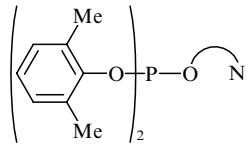

75a–g

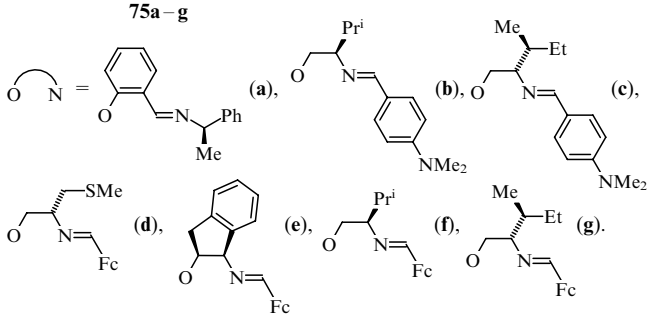

Ligands **74a–f** act as typical chelate-forming compounds towards $[RhCl(CO)_2]_2$ and the corresponding reactions result in complexes [RhCl(CO)L].[88] At the same time, particular reaction routes in complexation with Pd(II) are governed by the nature of the starting organometallic compound. For instance, the use of $[PdCl_2(MeCN)_2]$ or $[Pd(All)Cl]_2$ permits high yields of the corresponding metal-containing chelates, *e.g*., $[Pd(All)(L)]^+X^-$ [L = (R_{ax})-**74a**, (R_{ax})-**74c**, (S_{ax})-**74e**; X = Cl, BF_4]. On the contrary, the reaction with $[PdCl_2(cod)]$ proceeds non-selectively [this was shown taking ligands (R_{ax})-**74a** and (R_{ax})-**74f** as examples], resulting in chelates $[PdCl_2(L)]$ and large amounts of side products:

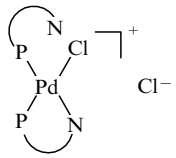

These results must be taken into account when choosing a starting metal complex for Pd-catalysed reactions involving aryl phosphites **74a**–**f**.

Ligands **75a**–**g** containing no cyclic phosphite fragments react with $[RhCl(CO)_2]_2$, $[PdCl_2(cod)]$ or $[Pd(All)Cl]_2$ to give exclusively mononuclear metal-containing chelates, which was also proved by X-ray analysis.[110]

Allylic alkylation of substrate **59** by dimethyl malonate {reaction (10) with $[Pd(All)Cl]_2$ as precatalyst} in the presence of compounds **74a**–**f** proceeds with an optical yield of up to 81% [the most efficient ligand is (R_{ax})-**74c**].[88] However, the presence of the BINOL fragment is not necessary for stereoinduction. Indeed, an *ee* of 82% was also achieved using acyclic aryl phosphite **75g**.[110] Moreover, additional axial chirality even decreases the enantioselectivity in Rh-catalysed hydrosilylation of acetophenone [reaction (5)], namely, ligand **75g** provides an *ee* up to 50%, whereas the epimers (S_{ax})-**74c** and (R_{ax})-**74c** can show at most 20%. Pd-Catalysed reaction of substrate **59** with $NaSO_2(p\text{-Tol})$ [reaction (11)] in the presence of ligand **75g** is also characterised by high enantioselectivity (*ee* 80%).[110]

It should be noted that, according to Ito,[124] substrate **59** is 'uncontrollable' and therefore the optical yields achieved (80%–82%) are in fact very high, thus indicating a great stereodiscriminating potential of phosphites containing Schiff bases. Unfortunately, attempts at realising this potential in other Pd-catalysed allylations have failed as yet. Namely, the enantioselectivity of asymmetric synthesis involving a carborane derivative **64** [reaction (12)] and ligands **74a**,**b** and **75b**,**c**,**f**,**g** was at most 32%.[125]

Systems with another structure at the phosphorus centre are also available.

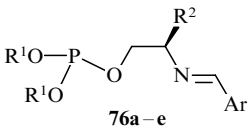

76a–**e**

Compound **76**	R^1	R^2	Ar
a	Pr^i	Et	Ph
b	Pr^i	Pr^i	4-$Me_2NC_6H_4$
c	bornyl	Et	Ph
d	cholesteryl	Pr^i	Ph
e	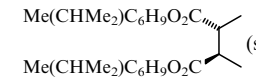 (see [a])	Pr^i	4-$Me_2NC_6H_4$

[a] Here, R^1-R^1; menthyl is $Me(CHMe_2)C_6H_9$.

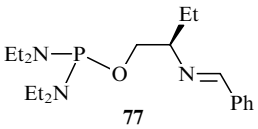

77

Similarly to phosphites **75a**–**g**, compounds **76a**–**e** and **77** behave in reactions with $[RhCl(CO)_2]_2$ and $[PdCl_2(cod)]$ as good chelate-forming compounds[89,126,127] {complexes [RhCl(CO)L] with L = **76a**,**c** were studied by X-ray analysis[126]}. The exception is ligand **76d** containing bulky cholesteryl fragments, which forms a side product $[PdCl_2(L)_2]$ in the reaction with $[PdCl_2(cod)]$.[89] Alkylation of substrate **43** by dimethyl malonate [reaction (8)] in the presence of compounds **76a**–**e** and $[Pd(All)Cl]_2$ is characterised by an *ee* of up to 76%, the best ligand being **76e**.[89,126]

By and large, a small (at the moment) group of phosphites containing Schiff bases appears to be more efficient in asymmetric catalysis than the best aminophosphites known so far. There are grounds for believing that in the future these new compounds will successfully compete with ligands containing oxazoline structural fragments.

It should be emphasised that all P,N-bidentate phosphites possess enhanced π-acceptor abilities (even as compared to the most electron-accepting phosphines containing an amino group in the substituent).[5] This affects the spectral characteristics of chlorocarbonyl rhodium complexes with these ligands. For instance, the spin–spin coupling constants ^1J(P,Rh) of such complexes are, on average, increased by 80–100 Hz and the ν(CO) frequencies are nearly 20–25 cm^{-1} higher. Direct correlations between the optical yields of hydrosilylation of ketones, allylation, hydroboronation–oxidation and the π-acceptor ability of the P,N-bidentate ligand should be pointed out (see Refs 5 and 128 and references cited therein). In some cases one should also take into account the σ-donor ability of nitrogen-containing fragments. In this connection a convenient spectral characteristic was suggested, which permits fast evaluation of the electronic effect of any P,N-bidentate ligand. This is the parameter ν_{Rh}, or the ν(CO) vibrational frequency of [RhCl(CO)L] complexes.[128] The steric characteristics are determined by another parameter, the cone angle at the phosphorus atom, which can be obtained with ease from the semiemirical AM1 calculations.[129]

5. Hydrophosphorane ligands

Hydrophosphoranes (HPs) form a rare and original group of phosphorus-containing ligands. At first glance, their structures contain no potential donor centres because phosphorus atoms have no lone electron pairs while the lone electron pairs of nitrogen or oxygen atoms must be involved in $p_\pi-d_\pi$-conjugation with d orbitals of the phosphorus atom. However, it is these compounds that show a variety of types of bonding to metal ions, namely, the P-, N-, P,N-, P,O- and N,N-coordination. Coordination chemistry of HPs has been analysed in detail in a separate review;[130] however, since then new information on complexation and catalysis involving chiral HPs has been reported. This first of all concerns hydrospirophosphoranes (HSPs) **78** and tricyclic hydrophosphoranes (TCHPs).

Hydrospirophosphoranes are typical chelate-forming compounds, which form metal-containing derivatives of their 'open' structures.[131–135]

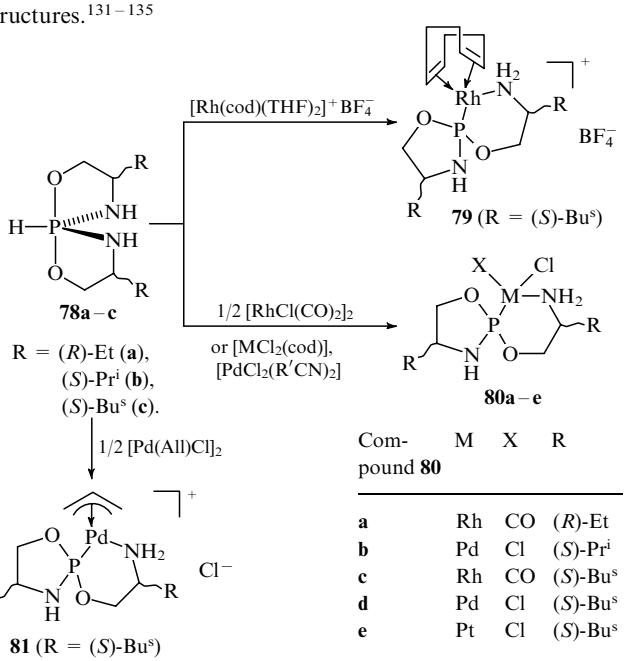

Compound **80**	M	X	R
a	Rh	CO	(*R*)-Et
b	Pd	Cl	(*S*)-Pr^i
c	Rh	CO	(*S*)-Bu^s
d	Pd	Cl	(*S*)-Bu^s
e	Pt	Cl	(*S*)-Bu^s

Complexes **79**–**81** are stable compounds. They were thoroughly studied by various methods of physicochemical analysis.[131,133–135] Unfortunately, they usually exist as equimolar mixtures of epimers with respect to the P*-stereocentre, which significantly reduces the scope of their application in asymmetric catalysis.

TCHPs (**82**) provide a source of richer coordination chemistry owing to a larger number of possible complexation routes. However, usually one route (sometimes, two routes) can be realised for a particular ligand; therefore, the corresponding

complexes retain, as a rule, their stereochemical individuality.[133–139]

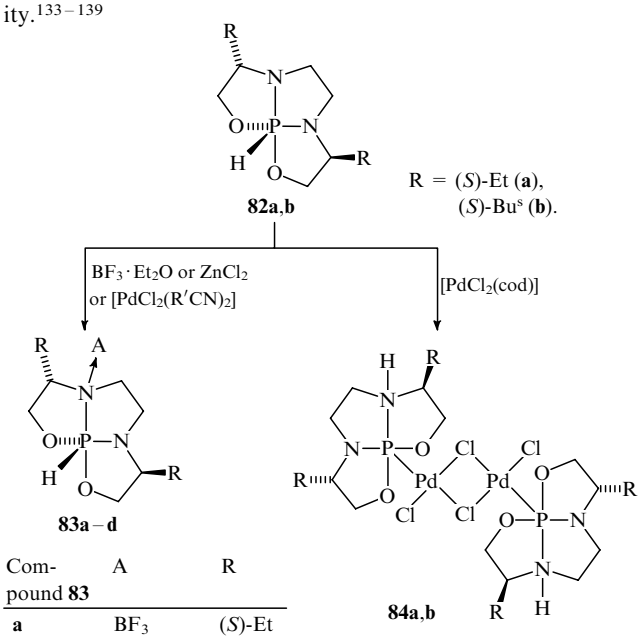

Compound **83**	A	R
a	BF_3	(*S*)-Et
b	$ZnCl_2$	(*S*)-Bu^s
c	PdCl(μ-Cl)	(*S*)-Et
d	PdCl(μ-Cl)	(*S*)-Bu^s

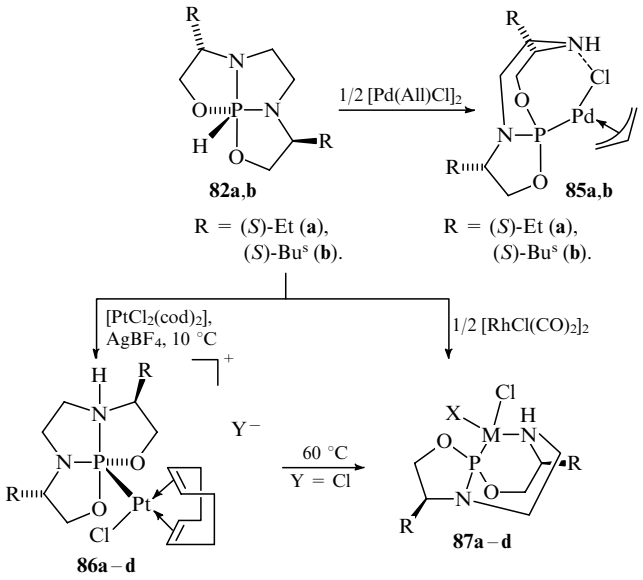

Compound **86**	Y	R
a	Cl	(*S*)-Et
b	BF_4	(*S*)-Et
c	Cl	(*S*)-Bu^s
d	BF_4	(*S*)-Bu^s

Compound **87**	M	X	R
a	Rh	CO	(*S*)-Et
b	Pt	Cl	(*S*)-Et
c	Rh	CO	(*S*)-Bu^s
d	Pt	Cl	(*S*)-Bu^s

Of considerable interest is to study the complexation mechanism of HPs. Here, two mechanisms are possible, one with and one without involvement of the P(III) tautomers of HPs.[130] In the former case, the role of the transition metal is in essence to shift the tautomeric equilibrium P(V) ⇄ P(III) by bonding to the structure with the tricoordinate phosphorus atom. The latter case is in fact a kind of metal complex catalysis of the opening of the hydrophosphorane structure. The first stage involves complexation at the apical donor atom of HPs (for BF_3 and $ZnCl_2$ this stage is simultaneously the last one, resulting in compounds **83a**,**b**). An important argument in favour of this stage is provided by a direct correlation between the Lewis basicity of HPs and their coordination activity.[133] This stage can be followed by oxidative addition – reductive elimination proceeding *via* agostic and metal hydride intermediates.[133, 135]

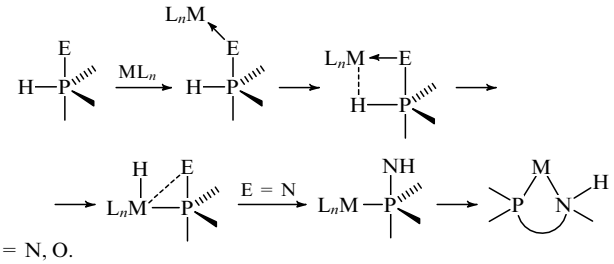

From this standpoint compounds **86a**,**c** can be treated as relatively stable intermediates that can be isolated at elevated temperature.[137, 139] Replacement of chloride counterion by non-nucleophilic tetrafluoroborate anion permits the synthesis of rather stable complexes **86b**,**d**, which were studied by various methods including X-ray analysis.[134, 139]

The choice between both complexation mechanisms of HPs and the structures of corresponding products depend first of all on the nature of the phosphorane and the Lewis acid. For instance, coordination of tetraoxohydrospirophosphorane **88** to rhodium(I) and palladium(II) involves a P(III) tautomer.[133]

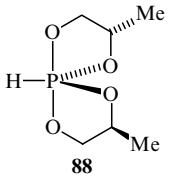

Compared to HSPs, tricyclic hydrophosphoranes are much more prone to retention of the phosphorane frame. At the same time, rhodium(I) and platinum(II) assist the opening of TCHPs more actively than palladium(II).

Hydrophosphoranes **78c** and **82a**,**b** were studied taking Pd-catalysed alkylation of substrate **43** by dimethyl malonate [reaction (8)] as an example.[135] Ligands **78c** and **82a** were found to be inefficient stereoselectors (the enantiomeric excess was 34% and 27%, respectively). A much higher optical yield (up to 74%) was achieved using compound **82b**. At present, this is the best result in asymmetric catalysis involving phosphorane ligands. Noteworthy is that the use of a catalytic system based on $[Pd(All)Cl]_2$ and ligands **82a**,**b** results in the formation of complexes **85a**,**b** with P-monodentate bonding of the 'open' forms of TCHPs. In contrast to this, complexation of $[PdCl_2(R'CN)_2]$ (R′ = Me, Ph) with ligand **82b** affords a mixture of compounds **83d** and **84b** with retention of the phosphorane structure of the ligand. Nevertheless, this system also provides a rather high enantioselectivity (*ee* up to 60%). We believe that these facts point to the great potential of tricyclic hydrophosphoranes as a specific group of chiral phosphorus-containing ligands.

IV. P,P-Bidentate phosphites

1. Phosphine-phosphites and phosphine-phosphoramidites

We begin this Section with consideration of these systems because the presence of two donor centres of different nature in such molecules makes them similar to the P,N-bidentate ligands considered above. Interest in these compounds is also due to the fact that they combine the two most important classes of chiral phosphorus-containing ligands, *viz*., phosphines and phosphites. First of all, studies aimed at unveiling the potential of the highly efficient ligand BINAPHOS (**2**) are noteworthy. Here, the research avenues are as follows: preparation of polymer-immobilised catalysts, the use of particularly valuable or 'hard-to-access' substrates and operation in supercritical CO_2.

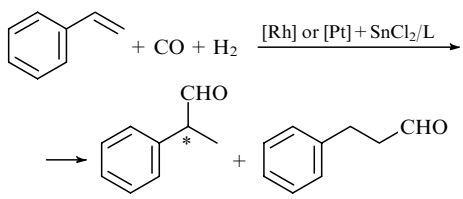

(13)

For instance, polymer-immobilised BINAPHOS provides an *ee* of 89% in Rh-catalysed hydroformylation of styrene [reaction (13)] at high conversion and regioselectivity (the mole fractions of different monomer units are shown in the Scheme).[140, 141]

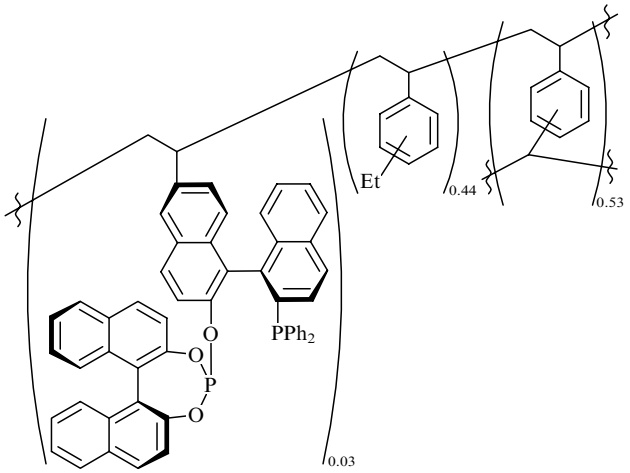

This polymeric ligand was also successfully used in hydroformylation of (*Z*)-but-2-ene, 3,3,3-trifluoropropene and vinyl acetate with optical yields of 89%–93% including solvent-free processes in the synthesis gas.[142]

BINAPHOS (**2**) has found new fields of application, namely, Rh-catalysed hydroformylation of (i) conjugated dienes, which provides a synthetic route to hard-to-access β,γ-unsaturated aldehydes (*ee* up to 97%),[143] and (ii) allylic alcohols followed by oxidation of intermediate lactols to lactones (*ee* up to 87%).[144] An *ortho*-substituted derivative of BINAPHOS was found to be appropriate for treating heterocyclic olefins (optimisaton of hydroformylation conditions for these substrates faces severe problems).

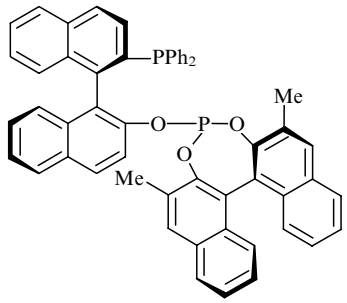

(*R*,*S*)-3,3′-Me-BINAPHOS

The use of this compound in the reaction shown below provided the enantiomeric excesses in the range 64% to 76%.[145]

X = O, NBoc, NAc.

New studies on the mechanism of catalytic hydroformylation involving BINAPHOS,[146] including quantum-chemical calculations[147] have been reported.

Pd-Catalysed copolymerisation of alkenes with CO has been improved;[148] the corresponding metal complex intermediates were studied by spectral methods.[149]

Compounds [M(BINAPHOS)$_2$] [M = Ni(0), Pd(0)] were synthesised and studied by ^{31}P NMR spectroscopy and FAB mass spectrometry.[150] Hydrocyanation of norbornene catalysed by a palladium complex results in an *exo*-nitrile with the highest enantioselectivity achieved so far (48%).

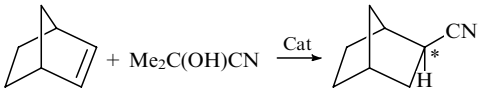

Recently, supercritical CO_2 has became popular as an ecologically safe and non-toxic medium for performing catalytic reactions. However, it has severe limitations due to the poor solubility of many phosphorus-containing ligands in CO_2. To enhance the solubility of BINAPHOS (**2**), a fluorinated derivative, (*R*,*S*)-3-H^{2}F^6-BINAPHOS, was synthesised.[151, 152]

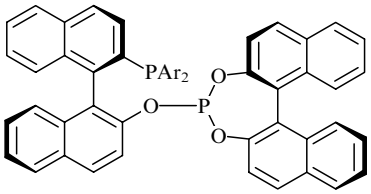

(*R*,*S*)-3-H^{2}F^6-BINAPHOS

Ar = $C_6H_4(CH_2)_2(CF_2)_6$-*m*.

A study on this ligand involved in Rh-catalysed hydroformylation in supercritical CO_2 showed that it demonstrates a high enantioselectivity (*ee* 88%–94%), conversion (>98%) and regioselectivity (branched : linear product ratio from 93 : 7 to 96 : 4) in reactions with different substrates, thus being highly competitive with (*R*,*S*)-BINAPHOS (**2**). Using multinuclear NMR spectroscopy, it was shown that supercritical CO_2 has no effect on the formation of the hydroformylation catalyst, [RhH(CO)$_2$L], and that the catalytic reaction in this medium proceeds by the same mechanism as reactions in organic solvents. (*R*,*S*)-3-H^{2}F^6-BINAPHOS was also found to be highly efficient in hydrogenation processes proceeding in supercritical CO_2 [an *ee* of 97% at 99% conversion was achieved for substrates **4a**,**b** in reaction (2)].

Fluorinated derivatives of BINAPHOS **89a**–**c** were obtained to be used in hydroformylation of styrene [reaction (13)] in supercritical CO_2 or in fluorine-containing solvents.

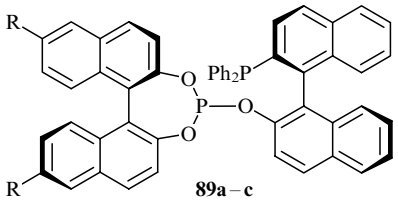

89a–**c**

R = n-$C_4F_9(CH_2)_3$ (**a**), n-$C_6F_{13}(CH_2)_3$ (**b**), n-$C_8F_{17}(CH_2)_3$ (**c**).

Ligand (*S*,*R*)-**89b** provided an *ee* up to 74% at 90 : 10 regioselectivity (branched : linear product) in supercritical CO_2.[153] Unfortunately, reactions in perfluorinated solvents were characterised by low (at most 11%) conversion of olefins at enantioselectivities of up to 94%.

Another interesting group of phosphine-phosphites comprises a series of ligands **90**–**93** containing both C*- and P*-stereocentres. These compounds were synthesised by van Leeuwen *et al.*[154–157]

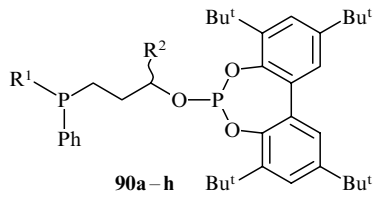

90a–h

Compound **90**	R^1	R^2	Compound **90**	R^1	R^2
(S_P,S_C)-**a**	1-naphthyl	Ph	(R_P,R_C)-**e**	Bu^t	Ph
(S_P,R_C)-**b**	1-naphthyl	Ph	(R_P,S_C)-**f**	Bu^t	Ph
(S_P,S_C)-**c**	2-anisyl	Ph	(R_P,rac_C)-**g**	Bu^t	Ph
(S_P,R_C)-**d**	2-anisyl	Ph	(R_P,R_C)-**h**	Bu^t	Me

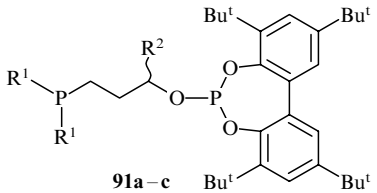

91a–c

Compound **91**	R^1	R^2
(S_C)-**a**	Bu^t	Ph
(S_C)-**b**	Ph	Ph
(S_C)-**c**	Ph	Me

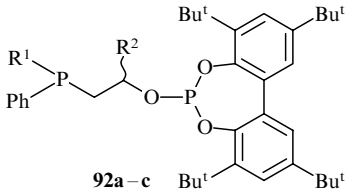

92a–c

Compound **92**	R^1	R^2
(R_P,S_C)-**a**	Bu^t	Ph
(R_P,R_C)-**b**	Bu^t	Ph
(S_C)-**c**	Ph	Me

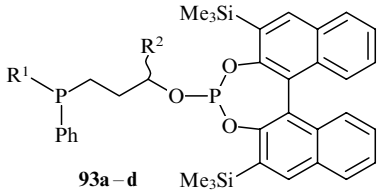

93a–d

Compound **93**	R^1	R^2
(S_P,S_C,R_{ax})-**a**	1-naphthyl	Ph
(S_P,S_C,S_{ax})-**b**	1-naphthyl	Ph
(R_{ax})-**c**	Ph	H
(S_{ax})-**d**	Ph	H

By varying positions and configurations of stereogenic centres it was established how these factors affect the enantioselectivity in catalytic processes.[154–157] Intermediates in the Rh-catalysed hydroformylation of styrene [reaction (13)] were also comprehensively studied by IR spectroscopy and ^{1}H and ^{31}P NMR spectroscopy. It was shown[154] that in trigonal-bipyramidal complexes [RhH(CO)$_2$L] the σ-donor phosphine centre occupies an apical position while the π-acceptor phosphite centre is in an equatorial position. The latter feature as well as manifestation of the so-called co-operative effect (the presence of chiral centres on the phosphine phosphorus atom and on atoms of the bridging group connecting two donor centres) are of great importance for achieving high enantioselectivity. Ligand **90a** used in reaction (13) provided an *ee* of up to 63%.

Cu-Catalysed addition of Et$_2$Zn and Et$_3$Al to cyclic enone **9a** [reaction (4)] in the presence of compounds **90**–**93** was also studied.[155] All reactions showed excellent conversions and regioselectivities at moderate optical yields (22% to 62%).

In addition, ligands **90**–**93** were studied in the alkylation of substrate **43** by dimethyl malonate [reaction (8)].[156] The best stereoselector, compound **90b**, provided an *ee* of 83%. The structure of one catalytically active complex, [Pd(All)(**92a**)], was refined by X-ray analysis. It was found that the Pd–C$_{All}$ bond in the *trans*-position relative to the phosphite phosphorus atom is 0.05 Å shorter than the bond in the *trans*-position relative to the phosphine phosphorus atom because of the greater π-acceptor ability of the phosphite centre. In the catalytic cycle, the nucleophile attacks the carbon atom of the allylic ligand in the *trans*-position relative to the phosphine P atom. Thus, a general trend is as follows: intermediates of allylic substitution containing heterobidentate ligands are attacked by nucleophiles at the *trans*-position with respect to the 'softer' (according to Pearson's HSAB principle) donor atom, namely, the phosphine centre in phosphine-phosphites or the phosphorus centre in P,N-bidentate compounds. It was shown that the enantioselectivity provided by compounds **90**–**93** depends on the structural parameters of the phosphite fragment of the ligand including the cone angle.[158]

Phosphine-phosphites **90**–**92** were also used in the asymmetric hydrogenation of substrates **4b**,**d** [reaction (2)] and gave an *ee* of up to 99% at nearly 100% conversion.[157] Similarly to allylic alkylation, the enantioselectivity is controlled by the structural parameters of the phosphite centre and of the C*-stereocentre present in the linker. Catalytically active complexes [Rh(cod)L]$^+$BF$_4^-$ were studied by multinuclear NMR spectroscopy. A double set of signals with similar values of the ^1J(P,Rh) spin–spin coupling constant was explained by either atropoisomerism of the phosphite centre or conformational isomerism of the chelate metallacycle. The joint action of both factors cannot also be ruled out. Note that this presents no obstacles to hydrogenation with excellent optical yields.

A series of phosphine-phosphite ligands **94** containing chiral phosphite and(or) phosphine fragments was synthesised.[159,160]

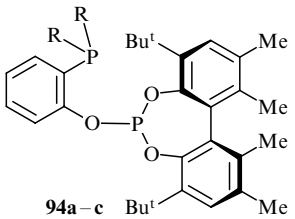

94a–c R = Ph (**a**), Me (**b**), Pr^i (**c**).

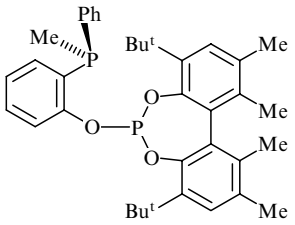

(S_{ax})-**94e**, (R_{ax})-**94f**

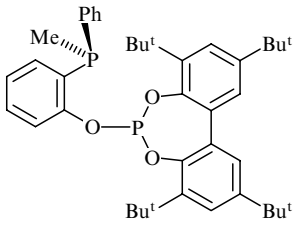

94d

The electronic properties of the donor centres were assessed by analysing the ^1J(P,Se) spin–spin coupling constants of corresponding diselenides. The weaker σ-donor ability of the phosphite moiety compared to the phosphine fragment was confirmed. This is also indicated by the magnitude of the ^1J(P,Rh) spin–spin coupling constant, which for the phosphine centre of complexes [RhCl(CO)L] is 120 Hz lower than for the phosphite centre. X-Ray diffraction studies revealed a *trans*-disposition of the phosphine centre and the carbonyl ligand.

Cationic complexes [Rh(cod)L]$^+$BF$_4^-$ were used in the asymmetric hydrogenation of esters **4a**,**d** [reaction (2)]. It was found that high enantioselectivity requires the presence of an axially chiral phosphite moiety and bulky substituents in the phosphine fragment. For instance, compounds **94a** and **94f** provide an *ee* of 99% (*cf.* at most 49% for ligand **94d**).

A group of phosphine-phosphite derivatives of D-xylose **95a–d** is noteworthy.[161]

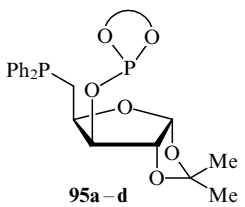

95a–d

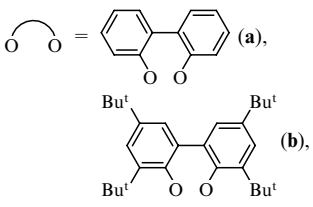

(R_{ax})-BNaph(O)$_2$ (**c**),
(S_{ax})-BNaph(O)$_2$ (**d**).

Using these compounds, a Rh-catalysed hydroformylation of styrene [reaction (13)] resulted in a product with a regioselectivity of up to 95 : 5 (branched : linear product) at moderate optical yields (*ee* up to 49%). The best stereoselector was ligand **95b** containing bulky *tert*-butyl substituents. The efficiency of phosphine-phosphites **95** in asymmetric addition of Et_2Zn to enone **9a** [reaction (4)] under the action of copper salts was even lower (the enantioselectivity was at most 19%).[162]

In contrast to this, compounds **95** were successfully used in the Rh-catalysed hydrogenation of substrates **4b**,**d** [reaction (2)] and ligand **95b** provided an *ee* of greater than 99%.[163] Similarly to phosphine-phosphites **90**–**92** (and for the same reasons), spectral analysis of rhodium complexes of compounds **95**, $[Rh(cod)L]^+BF_4^-$, revealed a double set of signals. The stereoinduction was also high.

An original approach is to increase the denticity of phosphine-phosphites by, *e.g.*, incorporating an additional phosphine centre.[164] In this case, Rh-catalysed hydrogenation of esters **4a**,**b** in the presence of ligands **96** and **97** resulted in racemic products. However, one must keep in mind that this is the first step in studies of tridentate phosphine-phosphite ligands.

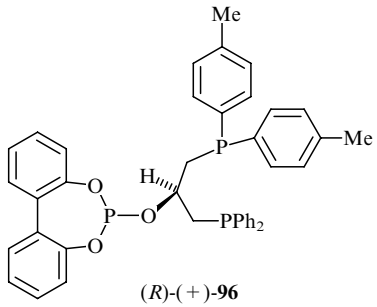

(*R*)-(+)-**96**

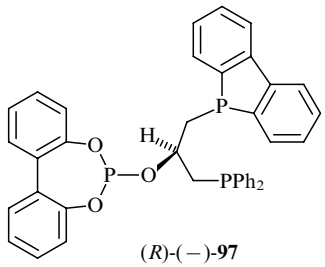

(*R*)-(−)-**97**

Yet another promising research avenue is the synthesis of phosphine-phosphoramidites. In particular, a series of quinoline derivatives **98a**–**d** was proposed.[165]

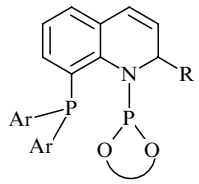

98a–**d** [(R_C) and/or (S_C)]

Compound **98**	Ar	R	
a	Ph	Bu^n	(R_{ax})-BNaph(O)$_2$
b	Ph	Bu^t	(R_{ax})-BNaph(O)$_2$
c	Ph	Bu^n	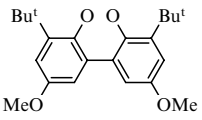
d	*m*-$F(CF_2)_6(CH_2)_2C_6H_4$	Bu^n	(R_{ax})-BNaph(O)$_2$

Mixtures of diastereomers were resolved by column chromatography. The first experiments revealed the efficiency of these systems in asymmetric catalysis. Ligand (R_{ax},S_C)-**98a** provided an *ee* of up to 74% at 96 : 4 (branched : linear product) regioselectivity and 79% conversion in hydroformylation of styrene [reaction (13)]. The use of its epimer, (R_{ax},R_C)-**98**, leads to a dramatic decrease in the enantioselectivity down to 5%. In contrast to this, epimer (R_{ax},R_C)-**98a** appeared to be more efficient in hydrogenation of unsaturated acid esters **4a**,**d** [reaction (2)] and provided an *ee* of 98%–99%.

The enantioselectivity of hydroformylation in the presence of aminophosphonite-phosphite **99** was somewhat lower (*ee* 58%).[166]

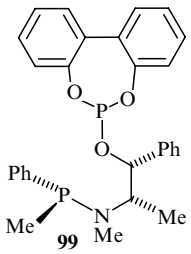

99

NMR and IR spectroscopy studies of catalytically active complexes $[RhH(CO)_2L]$ revealed that the amidophosphonite centre occupies an apical position while the phosphite centre is in an equatorial position. Summing up the results reported in Refs 154, 161 and 166, note that in complexes $[RhH(CO)_2L]$ with dissymmetric P,P-bidentate compounds the equatorial position is occupied by the phosphorus centre, which possesses more pronounced π-acceptor properties. The exception is BINAPHOS (**2**); however, this is due to steric reasons.[7]

Only one series of aminophosphonite-phosphite ligands **100a**–**d** based on the ephedrine moiety has been reported to date.[167]

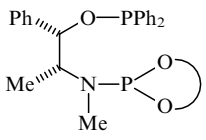

100a–**d**

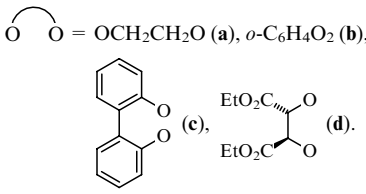

However, the enantioselectivity of Rh-catalysed hydroformylation of styrene [reaction (13)] in the presence of compounds **100a**–**d** was at most 20%. Mention may also be made of phosphonite-phosphite **101** providing an *ee* of up to 80% in Rh-catalysed hydrogenation of ester **4a** [reaction (2)].[168]

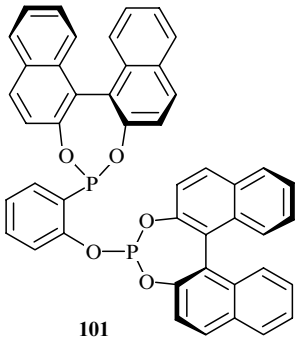

101

2. Phosphite-phosphoramidite and diphosphoramidites

Moving to phosphite-phosphoramidites makes it possible to have two different phosphorus centres in the ligand structure in the

absence of a fragment containing P–C bonds. This approach was realised taking ligands **102a–d** as examples.[167]

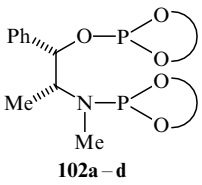

102a–d

O O = OCH_2CH_2O (**a**), *o*-$C_6H_4O_2$ (**b**),

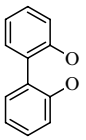

(**c**),

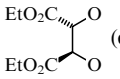

(**d**).

A chelate mononuclear complex $[PtCl_2(L)]$ with phosphite-phosphoramidite **102a** was obtained. However, ligands **102a–d** provided low enantioselectivities in Rh-catalysed hydroformylation of styrene [reaction (13)].

Phosphite derivatives **103** of available (*S*)-prolinol and (*S*)-oxyprolinol appeared to be somewhat better stereoselectors.[169]

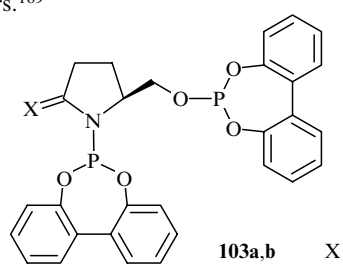

103a,**b** X = 2 H (**a**), O (**b**).

Platinum complexes of these compounds catalyse hydroformylation of styrene [reaction (13)] with an optical yield of up to 44%.

Even higher enantioselectivity (*ee* up to 65%) is provided by rhodium complexes of phosphite-phosphoramidites **104** and **105** based on D-xylose and D-ribose:[170]

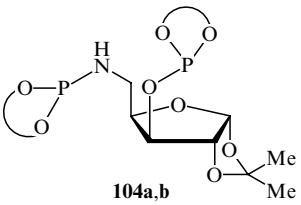

104a,**b**

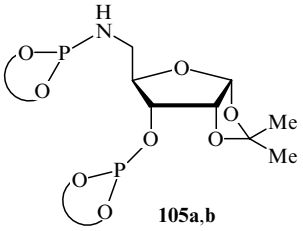

105a,**b**

O O = 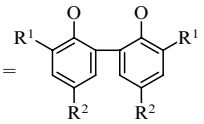 ; R^1 = Bu^t: R^2 = Bu^t (**a**), OMe (**b**).

Besides, compounds $[Rh(cod)L]^+BF_4^-$ (L = **104** and **104**) were used in asymmetric hydrogenation of substrates **4a**,**b**,**d** [reaction (2)].[171] They provided an *ee* of up to 99% at nearly 100% conversion. Similarly to hydroformylation, the chemical and optical yields depend on the absolute configuration of the C*(3)-stereocentre and on the nature of the *ortho*-substituents in the biphenyl fragment of the ligands.

Symmetrical (C_2) diphosphoramidites **106** and **107** have been reported recently.[172]

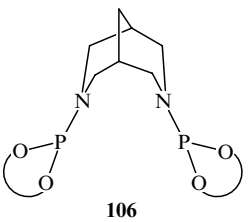

106

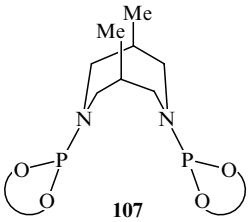

107

O O = (R_{ax})-BNaph(O)$_2$.

They provided an *ee* of up to 82% in Cu-catalysed addition of Et_2Zn to enones **9a**,**b** [reaction (4)] and up to 90% in Rh-catalysed hydrogenation of esters **4a**,**d** [reaction (2)].

A series of phosphoramidite derivatives of acyclic diamines comprises the following compounds:[173]

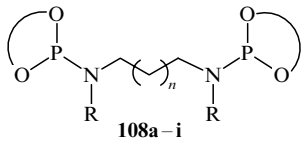

108a–i

Compound **108**	R	*n*	O O
a	Me	0	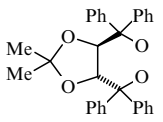
b	Me	1	
c	Me	0	(R_{ax})-BNaph(O)$_2$
d	Me	1	
e	Pr^i	1	
f		1	
g		1	
h		0	(S_{ax})-BNaph(O)$_2$
i		1	

Cu-Catalysed tandem 1,4-addition of Et_2Zn to cyclopentenone **9b** and aldol condensation with benzaldehyde proceed with optical yields of up to 83%. The best ligand is compound **108h**. Conjugate addition of Et_2Zn to enone **9a** [reaction (4)] showed an *ee* of up to 89% with the most efficient diamide ligand **108f** . Ligands **108a**,**b** containing no BINOL moiety are inefficient.

3. Diphosphites based on carbohydrates and their derivatives

We begin consideration of this type of ligands with diphosphites derived from D-xylofuranose **109** and D-ribofuranose **110**.[174–176]

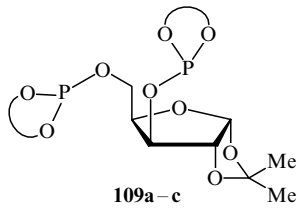

109a–c

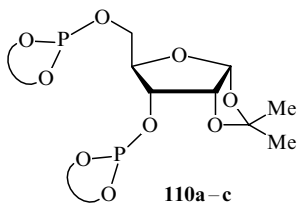

110a–c

O O = 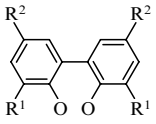 ; R^1 = R^2 = H (**a**); R^1 = Bu^t: R^2 = OMe (**b**), Bu^t (**c**).

Rh-Catalysed hydrogenation of itaconic acid, hydroformylation of styrene [reaction (13)], Cu-catalysed addition of Et_2Zn to cyclohexenone **9a** [reaction (4)] and Ir-catalysed hydrogenation of imines involving ligands **109** and **110** proceed with optical yields ranging between 50% and 60%. The best results were obtained [177] for allylic substitution of substrate **43** [reaction (8)] for dimethyl malonate (*ee* up to 90%) and benzylamine (*ee* up to 97%); both values were obtained in the presence of diphosphite **109c**). It was established that the stereoinduction is controlled by the configuration of the C*(3)-stereocentre of the furanose ring, while the nucleophile attacks the allylic carbon atom of the intermediate palladium complex, which is in the *trans*-position relative to the phosphite centre at the C(5) atom. Because of this, an increase in the size of substituents at the phosphite centre at the C(5) atom favours enhancement of enantioselectivity.

More efficient is a group of phosphite derivatives of 6-deoxy-D-allose, 6-deoxy-D-glucose, 6-deoxy-L-talose and 6-deoxy-L-idose **111**–**114**, which contain an additional C*-stereocentre.[178, 179]

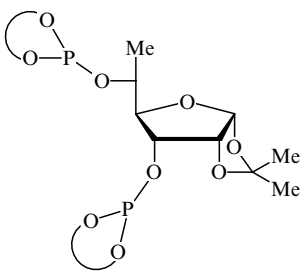

(1*R*,2*R*,3*R*,4*R*,5*R*)-**111a**–**h**

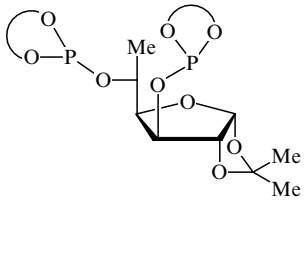

(1*R*,2*R*,3*S*,4*R*,5*R*)-**112a**–**h**

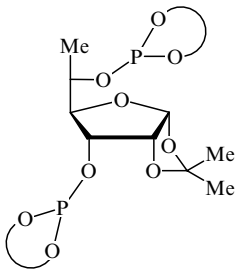

(1*R*,2*R*,3*R*,4*R*,5*S*)-**113a**–**h**

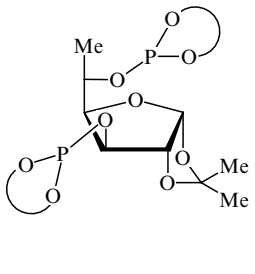

(1*R*,2*R*,3*S*,4*R*,5*S*)-**114a**–**h**

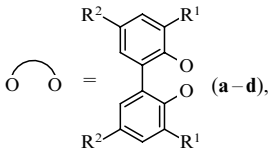

(**a**–**d**),

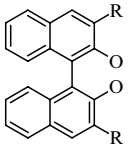

(**e**–**h**).

Compounds **111**–**114**	R^1	R^2
a	H	H
b	Bu^t	Bu^t
c	Bu^t	OMe
d	$SiMe_3$	H

Compounds **111**–**114**	R
(S_{ax})-**e**	H
(R_{ax})-**f**	H
(S_{ax})-**g**	$SiMe_3$
(R_{ax})-**h**	$SiMe_3$

These ligands provided an *ee* of up to 91% in the hydroformylation of styrene [reaction (13)] at amazingly high regioselectivity 99 : 1 (branched : linear products), which is comparable with the efficiency of the BINAPHOS (**2**) ligand. It was shown that the absolute configuration of the product depends on the configuration of the C*(3)-stereocentre while the enantioselectivity is controlled by the co-operative effect of the C*(3)- and C*(5)-stereocentres. NMR and IR spectroscopy studies of intermediates [$RhH(CO)_2L$] revealed that the best stereoselectors are those ligands which occupy two equatorial positions in the coordination sphere of the Rh atom. The dynamic equilibrium between the equatorial and equatorial-axial bonding reduces the enantioselectivity.

Rh-catalysed hydrogenation of substrates **4a**,**b**,**d** [reaction (2)] in the presence of diphosphite **111d** with bulky trimethylsilyl substituents showed an *ee* of greater than 99% at 100% conversion.[180] Compounds **111**–**113** provide an *ee* of up to 84% in Cu-catalysed addition of Et_2Zn to enone **9a** [reaction (4)].[181] The optical yields in Rh-catalysed hydrosilylation of acetophenone [reaction (5)] involving diphosphites **111**–**114** were lower (*ee* less than 51%).[182] However, trends common to this series of ligands can also be revealed. These are control of the configuration of the product by the stereochemistry of the C*(3) centre and favourable influence of both the co-operative effect of the C*(3) and C*(5) stereocentres and an increase in the size of the *ortho*- and *para*-substituents in the aromatic rings on the enantioselectivity.

The use of ligands **111**–**113** in the Pd-catalysed alkylation of substrate **43** by dimethyl malonate [reaction (8)] should be emphasised. A 100% conversion and an optical yield of 95% were achieved under standard experimental conditions in the presence of diphosphite **112c** and took only 10 min.[183] At present, this is the best result in Pd-catalysed allylic alkylation using P,P-bidentate phosphites.

A series of diphosphite ligands based on phenyl-β-D-glucopyranoside **115a**–**k** and their rhodium and platinum complexes were synthesised.[184] They were studied in hydroformylation of various substrates.

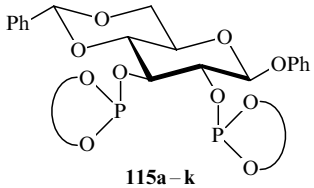

115a–**k**

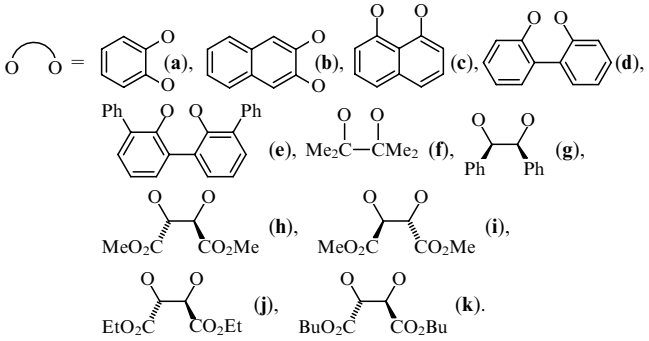

However, the asymmetric induction was low (*ee* 36% with allyl acetate as substrate).

The best stereoselectors in this group of ligands are diphosphite derivatives of dianhydro-D-mannite **116**.[185]

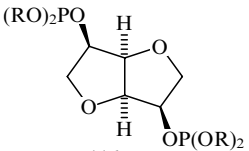

116a–**g**

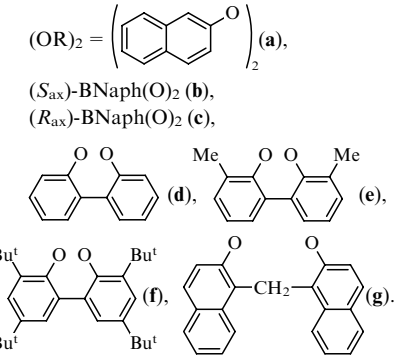

In particular, ligands **116e** and **116c** provide enantiomeric excesses of up to 98% and 96%, respectively, in Rh-catalysed hydrogenation of ester **4a** [reaction (2)]. In both cases the product has the same absolute configuration. A feature of ligands **116a**–**g** is that, in contrast to the general trend, an increase in the size of substituents in the *ortho*- and *para*-positions of the aromatic rings causes a dramatic decrease in enantioselectivity. For instance, the reaction in the presence of a catalyst based on compound **116f** results in a nearly racemic product.

4. Diphosphites based on BINOL and chiral diols

Chan *et al.*[186] proposed a series of aryl phosphite structures based on BINOL (**1**).†

† Ligand **117a** was described earlier (see Ref. 7 and references cited therein).

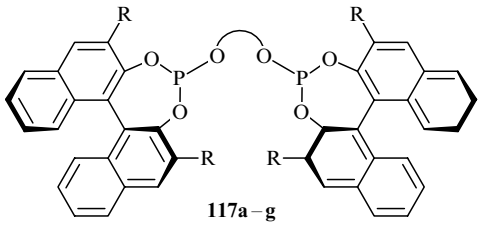

117a–g

Compound **117**	R	O O
a	H	(R_{ax})-BNaph(O)$_2$
b	Me	(R_{ax})-BNaph(O)$_2$
c	H	(R_{ax})-3,3′-Me$_2$-BNaph(O)$_2$
d	H	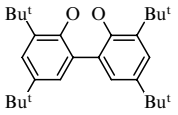
e	H	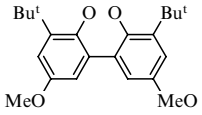
f	H	*o*-C$_6$H$_4$O$_2$
g	H	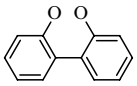

These compounds were studied in the Ni-catalysed hydrocyanation of alkenes. In particular, ligand **117d** provides an *ee* of 65% for styrene and an *ee* of 73% for vinyl acetate.

Cu-Catalysed addition of Et_2Zn to cyclic enone **9a** [reaction (4)] and to enone **9b** proceeds with optical yields of up to 90% and 89%, respectively. Diphosphites **117d**,**f** were found to be the best in both reactions.[187] α,β-Unsaturated lactones **118a**,**b** were also used as substrates.[188] The enantioselectivity of the reaction with lactone **118a** was as high as 92% at 100% conversion. Here, diphosphite **117d** also exhibited the best efficiency. However, passage to the five-membered ring in lactone **118b** was accompanied by a marked decrease in the stereoinduction (*ee* up to 56%). It should be noted that the structure of the catalytically active complex [Cu(MeCN)$_2$(**117d**)]$^+$OTf$^-$ was established by X-ray analysis.[188]

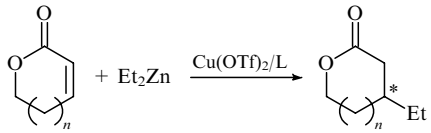

118a,**b**

n = 1 (**a**), 0 (**b**).

The conversion and enantioselectivity (*ee* up to 28%) provided by a complex [Rh(cod)L]$^+$BF$_4^-$ based on diphosphite **117a** (see Ref. 189) in hydroformylation of styrene [reaction (13)] were similar to those of the catalytic system [Rh(acac)(CO)$_2$]/**117a**. According to IR spectroscopy and ^{31}P and ^{1}H NMR data, this is due to the formation of the same intermediate [RhH(CO)$_2$L] in the catalytic cycle.

Ligand **117a** was also used in the Ir-catalysed hydrogenation of prochiral arylimines (*ee* up to 12%) [190] and in the Co-catalysed intramolecular Pauson–Khand reaction.[191]

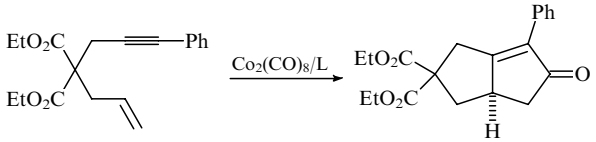

The cobalt-phosphite precatalyst and the cobalt-phosphite-alkyl intermediate of the catalytic process were detected by electrospray mass spectrometry and ^{31}P NMR spectroscopy. The best results (*ee* up to 75%) in reactions with various substrates were achieved using aryl-substituted 1,6-alkynes.

Two original dimeric rhodium complexes **119a**,**b** based on the ligands related to diphosphites **117a–g** are noteworthy.[192]

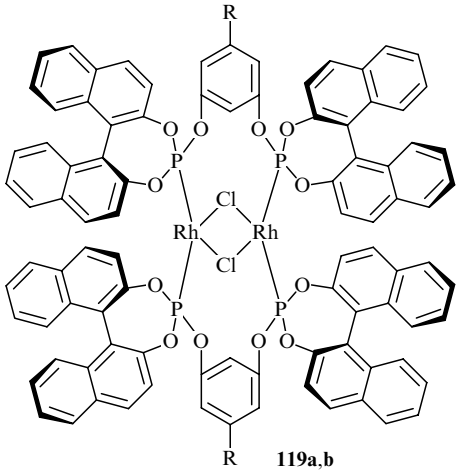

119a,**b**

R = H (**a**), OMe (**b**).

The structure of compound **119a** was established by X-ray analysis. Complexes **119a**,**b** showed low enantioselectivities (*ee* at most 20%) in the hydrosilylation of acetophenone [reaction (5)].

Unusual binuclear metal complexes **120a**,**b** containing twenty-eight-membered macrocycles [193] should also be pointed out.

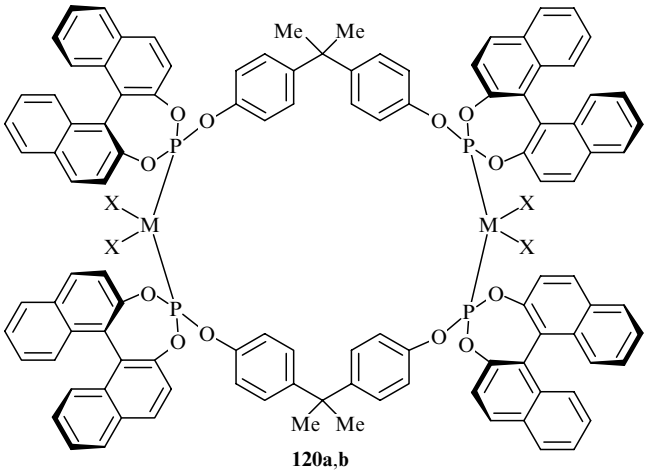

120a,**b**

M = Pd, X = Cl (**a**); M = Pt, X = I (**b**).

The synthesis of such compounds is closely related to the synthesis of chiral supramolecular structures.

Diphosphites **121a–c** based on H$_8$-BINOL (**13**) appeared to be excellent stereoselectors.[194] They provided an *ee* of 97%–99% at 92%–99% conversion in the Cu-catalysed addition of Et_2Zn to enones **9a–c** [reaction (4)].

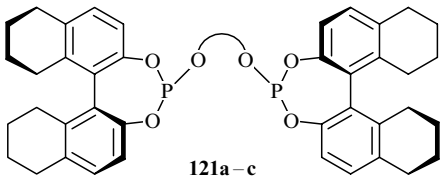

121a–c

O O = (R_{ax})-BNaph(O)$_2$ (**a**), (R_{ax})-H$_8$-BNaph(O)$_2$ (**b**), (S_{ax})-BNaph(O)$_2$ (**c**).

It was found that the configuration of reaction products and the enantioselectivity remain unchanged as the configuration of the bridging fragment of ligands changes. The optical and chemical yields are rather sensitive to the nature of the solvent. Namely, they increase after replacement of toluene and methylene chloride by diethyl ether possessing more pronounced electron-donor properties. Phosphite **121a** was also used in the addition of Me_2Zn to cyclic enone **9c** [reaction (4)], the optical yield being as high as 99%. This is the best result obtained for this reaction, which is the key stage of the synthesis of anticancer drug clavularin B. Ligand **121a** also exhibited a high efficiency in the reaction of Me_3Al with substrate **9a** (an *ee* of 96% was obtained at high conversion).[195]

The synthesis of diphosphites **122a**–**d** based on *cis*, *trans*-spiro[4.4]nonane-1,6-diol has been reported.[196]

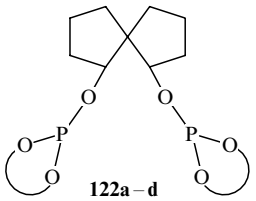

122a–**d**

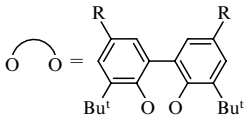

: R = Bu^t (**a**), OMe (**b**),

(S_{ax})-BNaph(O)$_2$ (**c**),

(R_{ax})-BNaph(O)$_2$ (**d**).

An attempt at obtaining their diastereomers based on *cis*,*cis*-spiro[4.4]nonane-1,6-diol failed because of steric hindrance (close disposition of bulky substituents). Therefore, only less sterically hindered phosphine-phosphite ligands **123a**,**b** were synthesised. Compounds **122a**–**d** and **123a**,**b** were studied in Rh-catalysed hydroformylation of styrene [reaction (13)] and showed a moderate enantioselectivity (*ee* up to 65%).

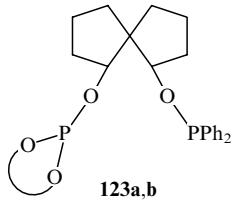

123a,**b**

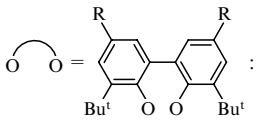

R = Bu^t (**a**), OMe (**b**).

At the same time one of the two ligands based on (2*R*,4*R*)-pentadiol **124a**,**b** provides an *ee* of up to 91% in Pt-catalysed hydroformylation of styrene [reaction (13)].[197]

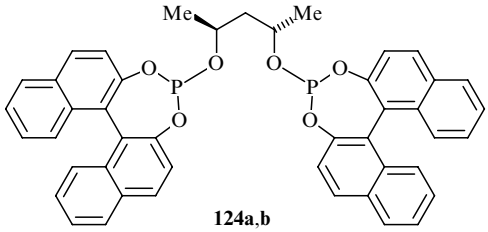

124a,**b**

(2*R*,4*R*)-bis(R_{ax}) (**a**), (2*R*,4*R*)-bis(S_{ax}) (**b**).

Noteworthy is that only diastereomer **124a** is efficient. Here we deal with the co-operative effect of the axial and central chiralities. Catalytically active *cis*-chelate complexes [$PtCl_2$(**124a**)] and [$PtCl(SnCl_3)$(**124a**)] were isolated and studied.

Diphosphites based on BINOL or atropoisomeric diphenyldiols and containing phosphorus centres were considered earlier. However, systems with cyclic phosphite moieties which are based on optically active aliphatic diols are also known. Two examples are provided by ligands **125a**,**b**.[198]

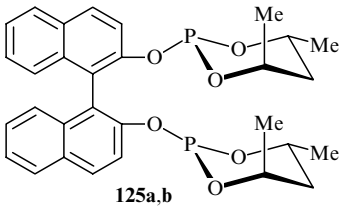

125a,**b**

(R_{ax})-bis(4*R*,6*R*) (**a**), (S_{ax})-bis(4*R*,6*R*) (**b**).

The corresponding *cis*-chelate complexes [$PtCl_2$(L)] and [$PtCl(SnCl_3)$L] were obtained and studied by multinuclear NMR spectroscopy and X-ray analysis. Both Pt- and Rh-catalysed hydroformylations of styrene [reaction (13)] in the presence of compounds **125a**,**b** show moderate regioselectivities and optical yields of at most 39%.

Diphosphite derivatives of sterically hindered chiral diols **126**, **127** are noteworthy. They contain, in particular, the dioxaphosphorinane rings in the hindered chair conformation.[199, 200]

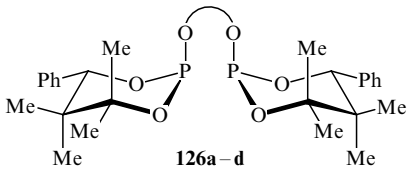

126a–**d**

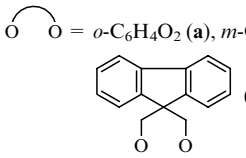

= *o*-$C_6H_4O_2$ (**a**), *m*-$C_6H_4O_2$ (**b**), $OCH_2CMe_2CH_2O$ (**c**),

(**d**).

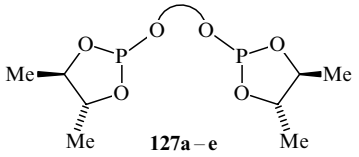

127a–**e**

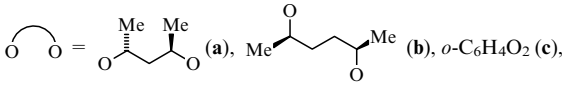

(**a**), (**b**), *o*-$C_6H_4O_2$ (**c**),

(R_{ax})-BNaph(O)$_2$ (**d**), (S_{ax})-BNaph(O)$_2$ (**e**).

The structures of compounds **126a** and **127d** were refined by X-ray analysis. Based on ligands **126a**–**d**, complexes [$Mo(CO)_4$L] and [$(BH_3)_2$L] were synthesised, which can be used in asymmetric catalysis, *e.g.*, hydroformylation and conjugate addition.

V. Other groups of chiral phosphite ligands

First of all, P,S-bidentate phosphites are of interest. The syntheses of ligand **128** and its complexes of compositions [Pd(alkene)L] (L = fumaronitrile, maleic anhydride, pentadienone)[201] and [Rh(cod)L]$^+$ BF_4^- (see Ref. 202) were reported. These compounds were thoroughly studied by multinuclear NMR spectroscopy, mass spectrometry and X-ray analysis.

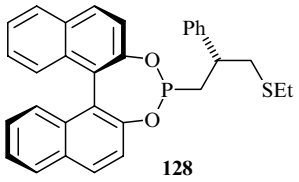

128

2D NMR (NOESY) studies revealed that [Pd(alkene)L] exists in solution in the form of two stereoisomers due to the relatively unhindered rotation of the alkene ligands. Phosphite **128** was used in the allylic substitution of unsymmetrical substrate **39a** for dimethyl malonate [reaction (7)] with $[RhCl(cod)]_2$, $[IrCl(cod)]_2$ and $[Pd(1,3\text{-}Ph_2All)Cl]_2$ as precatalysts. The highest stereoinduction was achieved using the rhodium complex (*ee* up to 81%) while the iridium and palladium compounds provided an *ee* of 68% – 70%.

A series of thioether-phosphite ligands **129a – e** based on xylofuranose was applied [162] in the Cu-catalysed conjugate addition of Et_2Zn to enone **9a** [reaction (4)].

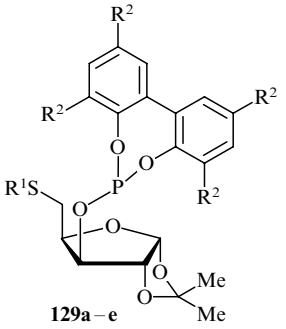

129a – e

Compound **129**	R^1	R^2
a	Me	Bu^i
b	Pr^i	Bu^t
c	Ph	Bu^t
d	Pr^i	H
e	Ph	H

In contrast to the P,P-bidentate systems, the optical yields achieved using ligands **129** appeared to be rather low (at most 41%). Ir-Catalysed hydrogenation of itaconic acid showed an enantioselectivity of up to 51%. Rh-Catalysed hydroformylation of styrene resulted in a racemic product. Probably, the reason is that the ligands are coordinated to the rhodium atom in a monodentate fashion (through the P atom).[203]

A formally P,P,P,N-tetradentate ligand **130** was successfully employed in the Rh-catalysed hydrosilylation of acetophenone [reaction (5) and provided an *ee* of up to 81%].[204]

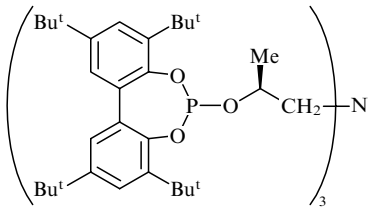

130

It should be emphasised that phosphite **130** coordinated to $[RhCl(cod)]_2$ behaves as a P,P-bidentate ligand. By and large there are a few phosphites that do not belong to the three major classes considered above.

VI. Conclusion

The material presented in this review shows that research on chiral phosphites is progressing rapidly. Over four hundred chiral phosphite compounds are used in asymmetric catalysis, in particular, hydrogenation of C=C and C=N bonds, hydroformylation, hydrosilylation of C=C and C=O bonds, hydroboronation – oxidation, allylic substitution, conjugate addition, hydrovinylation, hydrocyanation and in the Heck, Diels – Alder and Pauson – Khand reactions.

The most important results obtained in enantioselective catalysis using optically active phosphites are summarised in Table 2. As can be seen, considerable advances have been made in hydrogenation, conjugate addition and allylic substitution. On the other hand, the wide use of P-monodentate systems in hydroformylation of ketones and of P,P-bidentate systems in hydrosilylation of ketones seems to be appropriate. Processes in which chiral phosphites are of limited use as yet, namely, hydrosilylation – oxidation and hydroboronation – oxidation of C=C bonds, hydrovinylation and the named reactions mentioned above, deserve much greater attention. Finally, there are also reasons to pay attention to such asymmetric catalytic transformations that were performed up to now exclusively without using chiral phosphite ligands. To start with, examples are proton transfer, cross-coupling and enantioselective rearrangements.

There are a number of unsolved topical problems and potential 'growth points' of the chemistry of chiral phosphite ligands. In particular, studies on the mechanisms of catalytic reactions should be developed more intensively. The results obtained in this field will serve as a basis for recommendations concerned with the choice of experimental conditions and targeted synthesis of the most efficient ligands. Up to now, most of these problems are attacked empirically. Progress towards an understanding of the mechanism of hydroformylation and, to a lesser extent, of allylic substitution in the presence of P,P-bidentate phosphites has been made. Information on other reactions and other ligand groups is scarce. This especially holds for the popular class of P-monodentate phosphites. For instance, there is no theoretical understanding of the reasons for the high asymmetrising activity of these compounds in hydrogenation (earlier, P,P-bidentate chelation was assumed to be a necessary condition). The corresponding studies are in the early stage of development.[206]

At present, P-monodentate chiral phosphites are most widely used. However, different groups of ligands belonging to this class of compounds have been studied in different ways. Emphasis has been placed on compounds derived from BINOL (**1**) and TADDOL (**19**). For instance, the synthesis of a new group of esters and amidoesters of BINOL, **131** and **132**, was reported very recently.

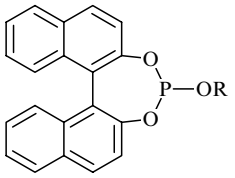

131a – f [(S_{ax}) and/or (R_{ax})]

R = Et (**a**), cyclo-C_6H_{11} (**b**), Bu^t (**c**), 9-fluorenyl (**d**),

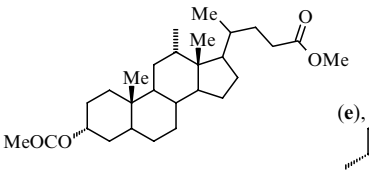

(**e**),

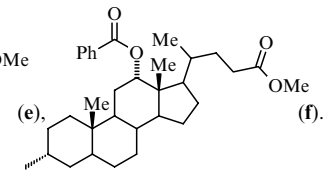

(**f**).

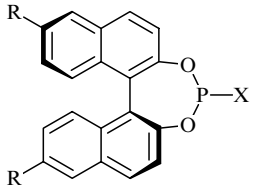

132a – c

Compound **132**	X	R
a	$N(CH_2)_4$	H
b	NMe(OMe)	H
c	NMe_2	Br

Ligands **131a – d** are used in Rh-catalysed combinatorial hydrogenation [207] while compounds **132a**,**b** are employed in the interesting reaction of conjugate addition of arylboronic acids to α,β-unsaturated substrates {with $[Rh(acac)(C_2H_4)_2]$ as precatalyst}.[208] Comparative studies of these systems and classical diphosphine ligands are in progress. In particular, the advantages of phosphoramidites not only in enantioselectivity but also in the catalytic activity in Rh-catalysed hydrogenation [reaction (2)] are revealed.[209] For instance, a 100% conversion of substrate **4d** in the

Table 2. Relative enantioselectivity of chiral phosphites in the most important catalytic reactions [listed are the maximum *ee* values (%)].

Ligand type	Hydrogenation of C=C bonds	Ref.	Hydroformylation	Ref.	Hydrosilylation of ketones	Ref.	Hydrosilylation or hydroboronation–oxidation of C=C bonds	Ref.	Allylic substitution	Ref.	Conjugate addition of R_2Zn to enones	Ref.
P-Monodentate												
Phosphites based on												
BINOL	99	12, 13	–		–		–		96	9	87	10, 11
biphenyldiols	75	57	–		–		–		–		–	
TADDOL	–		–		25	63	–		–		96	64, 65
carbohydrates	–		–		58	72	–		–		–	
Phosphoramidites based on												
BINOL	>99	45	–		–		99	43, 44	97	38	>99	27
biphenyldiols	–		–		–		–		87	38	99	58–60
TADDOL	–		–		–		–		–		71	67
carbohydrates	94	76	–		–		–		–		–	
P,N-Bidentate												
Oxazoline	>99	91, 92	–		95	94	–		>99	91, 92	94	85–87
Pyridine	–		–		–		59	100	95	107	61	106
Amine	67	109	16	108	94	205	–		61	111	63	115
Imine	–		–		50	110	–		82	110	–	
P,P-Bidentate												
Phosphine-phosphites	>99	163	97	143	–		–		83	156	62	155
Phosphine-phosphoramidites	99	165	74	165	–		–		–		–	
Phosphite-phosphoramidites	99	171	65	170	–		–		–		–	
Diphosphoramidites	90	172	–		–		–		–		89	172, 173
Diphosphites based on												
carbohydrates	>99	180	91	178, 179	51	182	–		97	177	84	181
BINOL and chiral diols	–		91	197	81[a]	204	–		–		99	194
P,S-Bidentate	51	203	0	203	–		–		81	201, 202	41	162

[a] For the formally P,P,P,N-tetradentate ligand **130**.

presense of phosphoramidite **132c** at an optical yield of the product of 94% takes less than 30 min.

The field of application of these ligands is extending continuously. Phosphoramidite (R_{ax},R_C)-**7n** was successfully (enantioselectivity up to 97%) used in a novel Ir-catalysed reaction of allylic etherification of achiral allylic carbonates with alkali metal phenolates.[210] It is of great importance that recent investigations in the field of Cu-catalysed addition of Me_2Zn to acyclic nitroalkenes (*ee* up to 98%)[211] opened novel routes to valuable bioactive compounds (Cyclamenol A, cryptophycins and β-methyl carbopenem antibiotics).

At the same time, increasing the number of phosphite (phosphoramidite) derivatives of BINOL and TADDOL obtained by varying the nature of exocyclic substituents is an extensive approach whose potential has been to a great extent exhausted. For instance, the enantioselectivity achieved in the Cu-catalysed addition of Et_2Zn to acyclic enones in the presence of phosphites **131e**,**f** (see Ref. 212) appeared to be lower (78%) than the enantioselectivity provided by the simpler ligands **3t**,**u**. We believe that it is more useful to extend the range of P-monodentate systems based on substituted diphenyldiols and, probably, on various mononuclear phenols. Here, two examples are provided by phosphoramidites **133a**,**b** based on axially chiral biphenyldiols.[208]

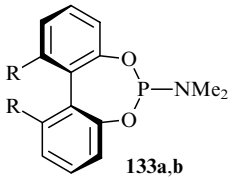

133a,**b** R = OMe (**a**), Ph (**b**).

The use of achiral phenols as, *e.g.*, in the synthesis of ligands **16** and **17** seems to be even more promising. These compounds, provided that BINOL and TADDOL are synthetically accessible ligands, undoubtedly are a step towards the synthesis of much simpler and inexpensive P-monodentate ligands.

A few monodentate systems containing P-stereocentres have been reported to date. However, it was established that ligands containing asymmetric donor atoms are of particular value for asymmetric induction. Therefore, synthesis of such ligands is a quite promising avenue of research in this field of catalysis.

Among P,N-bidentate phosphites, considerable attention should be paid to structures with oxazoline fragments and to phosphite derivatives of Schiff bases. This group of compounds can comprise convenient and efficient systems based on biphenyldiols as well as structures containing stereogenic phosphorus atoms.

We believe that relevant areas of catalytic applications should be found for a variety of aminophosphites. A recent example is provided by the use of ligands **134a–i** in Rh-catalysed hydrosilylation of prochiral ketones.[205]

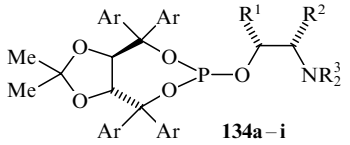

134a–i

Compound **134**	Ar	R^1	R^2	R^3
a	Ph	Ph	Me	H
b	Ph	Ph	Me	Me
c	Ph	H	H	Me
d	Ph	H	Me	Me
e	Ph	Ph	H	Me
f	Ph	Ph	Me	$(CH_2)_4$ (see [a])
g	Ph	Ph	Me	$(CH_2)_5$ (see [a])
h	Ph	Ph	Ph	Me
i	2-naphthyl	Ph	Me	Me

[a] Here, R^3-R^3.

The best results were obtained using aminophosphite **134b**. The enantiomeric excess was 80% and 94% for the reduction of acetophenone and β-naphthyl methyl ketone, respectively.

As mentioned above, phosphine-phosphites form one of the most efficient groups of P,P-bidentate ligands. Undoubtedly, studies on applications of these compounds in asymmetric catalysis will continue. However, we believe that the synthesis of ligands containing phosphorus centres of different natures and no fragments with P–C bonds is at least equally important. These compounds (phosphite-phosphoramidite, unsymmetrical bisphosphoramidites) can be obtained with ease by phosphorylation of the corresponding amino alcohols and diamines. The data listed in Table 2 point to considerable advances made in applications of these ligands in catalytic reactions.

No planar chiral phosphite ligands have been reported as yet, though this type of chiral phosphines has long been known and comprises a variety of compounds that are excellent stereoselectors.[1,5] Therefore, there are grounds to expect the synthesis of planar chiral phosphites, the more so since the procedure for the synthesis of appropriate starting compounds (*e.g.*, ferrocene series) has already been developed.[213]

In the field of coordination chemistry one can expect a continuation of research into complexation of the most important groups of ligands with catalytically active metals. At present, there are a large number of catalytically efficient phosphites whose complexes with transition metals have not been isolated and studied in detail. This particularly concerns the P-monodentate compounds. Their coordination behaviour was studied much less thoroughly than that of the P,P- and P,N-bidentate systems. The structure of rhodium, palladium and iridium compounds has been studied in more detail, while information on copper complexes is scarce. Obviously, for each group of ligands it is important to combine catalytic experiments and studies on the structure of catalytically active complexes and intermediates of the catalytic cycle.

Is seems appropriate to synthesise a series of related complexes with different ligands for each class of chiral phosphites. Based on their spectral characteristics, the electron-donor properties of ligands will be assessed, which is of great importance for the prediction of catalytic efficiency. Interest in the optically active phosphites continuously increases. This is also indicated by the recently published reviews concerned with the problems of asymmetric synthesis.[214,215] We can with certainty say that application of chiral phosphites has brought coordination chemistry and asymmetric catalysis into a novel epoch.

References

1. I Ojima (Ed.) *Catalytic Asymmetric Synthesis* (New York: Wiley, 2000)
2. Yu N Kukushkin *Reaktsionnaya Sposobnost' Koordinatsionnykh Soedinenii* (Reactivity of Coordination Compounds) (Leningrad: Khimiya, 1987)
3. J Ansell, M Wills *Chem. Soc. Rev.* **31** 259 (2002)
4. D J Wink, T J Kwok, A Yee *Inorg. Chem.* **29** 5006 (1990)
5. K N Gavrilov, A I Polosukhin *Usp. Khim.* **69** 721 (2000) [*Russ. Chem. Rev.* **69** 661 (2000)]
6. K N Gavrilov, I S Mikhel' *Koord. Khim.* **24** 883 (1998) [a]
7. K N Gavrilov, I S Mikhel' *Koord. Khim.* **25** 83 (1999) [a]
8. K N Gavrilov, D V Lechkin *Koord. Khim.* **24** 3 (1998) [a]
9. K Fuji, N Kinoshita, K Tanaka, T Kawabata *Chem. Commun.* 2289 (1999)
10. A Alexakis, C Benhaïm, X Fournioux, A van den Heuvel, J-M Levêque, S March, S Rosset *Synlett* 1811 (1999)
11. A Alexakis, C Benhaim *Eur. J. Org. Chem.* 3221 (2002)
12. M T Reetz, G Mehler *Angew. Chem., Int. Ed.* **39** 3889 (2000)
13. I V Komarov, A Börner *Angew. Chem., Int. Ed.* **40** 1197 (2001)
14. W Chen, J Xiao *Tetrahedron Lett.* **42** 2897 (2001)
15. M T Reetz, G Mehler, A Meiswinkel, T Sell *Tetrahedron Lett.* **43** 7941 (2002)
16. J A J Breuzard, M L Tommasino, M C Bonnet, M Lemaire *J. Organomet. Chem.* **616** 37 (2000)
17. R Hulst, N K de Vries, B L Feringa *Tetrahedron: Asymmetry* **5** 699 (1994)
18. A H M de Vries, A Meetsma, B L Feringa *Angew. Chem., Int. Ed. Engl.* **35** 2374 (1996)
19. L A Arnold, R Imbos, A Mandoli, A H M de Vries, R Naasz, B L Feringa *Tetrahedron* **56** 2865 (2000)
20. B L Feringa *Acc. Chem. Res.* **33** 346 (2000)
21. B L Feringa, M Pineschi, L A Arnold, R Imbos, A H M de Vries *Angew. Chem., Int. Ed. Engl.* **36** 2620 (1997)
22. F Badalassi, P Crotti, F Macchia, M Pineschi, A Arnold, B L Feringa *Tetrahedron Lett.* **39** 7795 (1998)
23. J P G Versleijen, A M van Leusen, B L Feringa *Tetrahedron Lett.* **40** 5803 (1999)
24. R Imbos, M H G Brilman, M Pineschi, B L Feringa *Org. Lett.* **1** 623 (1999)
25. R Naasz, L A Arnold, M Pineschi, E Keller, B L Feringa *J. Am. Chem. Soc.* **121** 1104 (1999)
26. R Imbos, A J Minnaard, B L Feringa *Tetrahedron* **57** 2485 (2001)
27. R Naasz, L A Arnold, A J Minnaard, B L Feringa *Angew. Chem., Int. Ed.* **40** 927 (2001)
28. F Bertozzi, P Crotti, F Macchia, M Pineschi, B L Feringa *Angew. Chem., Int. Ed.* **40** 930 (2001)
29. R Naasz, L A Arnold, A J Minnaard, B L Feringa *Chem. Commun.* 735 (2001)
30. L A Arnold, R Naasz, A J Minnaard, B L Feringa *J. Org. Chem.* **67** 7244 (2002)
31. H Malda, A W van Zijl, L A Arnold, B L Feringa *Org. Lett.* **3** 1169 (2001)
32. N Sewald, V Wendisch *Tetrahedron: Asymmetry* **9** 1341 (1998)
33. A Alexakis, C Benhaim *Org. Lett.* **2** 2579 (2000)
34. Y H Choi, J Y Choi, H Y Yang, Y H Kim *Terahedron: Asymmetry* **13** 801 (2002)
35. O Huttenloch, E Laxman, H Waldmann *Chem. Eur. J.* **8** 4767 (2002)
36. B Bartels, G Helmchen *Chem. Commun.* 741 (1999)
37. B Bartels, C Garcia-Yebra, F Rominger, G Helmchen *Eur. J. Inorg. Chem.* 2569 (2002)
38. T Ohmura, J F Hartwig *J. Am. Chem. Soc.* **124** 15164 (2002)
39. G Franciò, C G Arena, F Faraone, C Graiff, M Lanfranchi, A Tiripicchio *Eur. J. Inorg. Chem.* 1219 (1999)
40. C G Arena, G P Calabrò, G Franciz, F Faraone *Tetrahedron: Asymmetry* **11** 2387 (2000)
41. G Franciò, F Faraone, W Leitner. *J. Am. Chem. Soc.* **124** 736 (2002)
42. L J Gooven *Angew. Chem., Int. Ed.* **41** 3775 (2002)

43. J F Jensen, B Y Svendsen, T V la Cour, H L Pedersen, M Johannsen *J. Am. Chem. Soc.* **124** 4558 (2002)
44. M F P Ma, K Li, Z Zhou, C Tang, A S C Chan *Tetrahedron: Asymmetry* **10** 3259 (1999)
45. M van den Berg, A J Minnaard, E P Schudde, J van Esch, A H M de Vries, J G de Vries, B L Feringa *J. Am. Chem. Soc.* **122** 11539 (2000)
46. M van den Berg, R M Haak, A J Minnaard, A H M de Vries, J G de Vries, B L Feringa *Adv. Synth. Catal.* **344** 1003 (2002)
47. X Jia, R Guo, X Li, X Yao, A S C Chan *Tetrahedron Lett.* **43** 5541 (2002)
48. D Peña, A J Minnaard, J G de Vries, B L Feringa *J. Am. Chem. Soc.* **124** 14552 (2002)
49. P Müller, P Nurg, G Bernardinelli *Helv. Chim. Acta* **83** 843 (2000)
50. F-Y Zhang, A S C Chan *Tetrahedron: Asymmetry* **9** 1179 (1998)
51. O Zeng, H Liu, X Cui, A Mi, Y Yiang, X Li, M C K Choi, A S C Chan *Tetrahedron: Asymmetry* **13** 115 (2002)
52. O Zeng, H Liu, X Cui, A Mi, Y Yiang, X Li, M C K Choi, A S C Chan *Tetrahedron* **58** 8799 (2002)
53. Y Fu, J-H Xie, A-G Hu, H Zhou, L-X Wang, Q-L Zhou *Chem. Commun.* 480 (2002)
54. A-G Hu, Y Fu, J-H Xie, H Zhou, L-X Wang, Q-L Zhou *Angew. Chem., Int. Ed.* **41** 2348 (2002)
55. H Zhou, W-H Wang, Y Fu, J-H Xie, W-J Shi, L-X Wang, Q-L Zhou *J. Org. Chem.* **68** 1582 (2003)
56. K Nozaki, N Sakai, T Nanno, T Higashijima, S Mano, T Horiuchi, H Takaya *J. Am. Chem. Soc.* **119** 4413 (1997)
57. W Chen, J Xiao *Tetrahedron Lett.* **42** 8737 (2001)
58. A Alexakis, S Rosset, J Allamand, S March, F Guillen, C Benhaim *Synlett* 1375 (2001)
59. L M Urbaneja, A Alexakis, N Krause *Tetrahedron Lett.* **43** 7887 (2002)
60. A Alexakis, C Benhaim, S Rosset, M Humam *J. Am. Chem. Soc.* **124** 5262 (2002)
61. O Knopff, A Alexakis *Org. Lett.* **4** 3835 (2002)
62. A Alexakis, K Croset *Org. Lett.* **4** 4147 (2002)
63. J-I Sakaki, W B Schweizer, D Seebach *Helv. Chim. Acta* **76** 2654 (1993)
64. A Alexakis, J Vastra, J Burton, C Benhaim, P Mangeney *Tetrahedron Lett.* **39** 7869 (1998)
65. A Alexakis, J Burton, J Vastra, C Benhaim, X Fournioux, A van den Heuvel, J-M Levêque, F Mazé, S Rosset *Eur. J. Org. Chem.* 4011 (2000)
66. A Alexakis, C Benhaim *Tetrahedron: Asymmetry* **12** 1151 (2001)
67. E Keller, J Maurer, R Naasz, T Schader, A Meetsma, B L Feringa *Tetrahedron: Asymmetry* **9** 2409 (1998)
68. F Bertozzi, P Crotti, F Macchia, M Pineschi, A Arnold, B L Feringa *Tetrhedron Lett.* **40** 4893 (1999)
69. R Imbos, A J Minnaard, B L Feringa *J. Am. Chem. Soc.* **124** 184 (2002)
70. D Steinborn, H Junicke *Chem. Rev.* **100** 4283 (2000)
71. M Stolmar, C Floriani, G Gervasio, D Viterbo *J. Chem. Soc., Dalton Trans.* 1119 (1997)
72. A Suarez, A Pizzano, I Fernandez, N Khiar *Tetrahedron: Asymmetry* **12** 633 (2001)
73. E E Nifantyev, M P Koroteev, A M Koroteev, V K Belsky, A I Stash, M Yu Antipin, K A Lyssenko, L Cao *J. Organomet. Chem.* **587** 18 (1999)
74. D Vos, A M Arif, R D Ernst *J. Organomet. Chem.* **553** 277 (1998)
75. A Bayer, U Thewalt, B Rieger *Eur. J. Inorg. Chem.* 199 (2002)
76. A Bayer, D Murszat, U Thewalt, B Rieger *Eur. J. Inorg. Chem.* 2614 (2002)
77. A Alexakis, J Vastra, J Burton, P Mangeney *Tetrahedron: Asymmetry* **8** 3193 (1997)
78. J-M Brunel, O Chiodi, B Faure, F Fotiadu, G Buono *J. Organomet. Chem.* **529** 285 (1997)
79. A Bohac, M Lettrichova, P Hrnciar, M Hutta *J. Organomet. Chem.* **507** 23 (1996)
80. A Tillack, R Selke, Ch Fischer, D Bilda, K Kortus *J. Organomet. Chem.* **518** 79 (1996)
81. K N Gavrilov, E Yu Zhorov *Zh. Neorg. Khim.* **38** 1544 (1993) [b]
82. R Prêtöt, G C Lloyd-Jones, A Pfaltz *Pure Appl. Chem.* **70** 1035 (1998)
83. R Prêtöt, A Pfaltz *Angew. Chem., Int. Ed.* **37** 323 (1998)
84. A Pfaltz *J. Heterocycl. Chem.* **36** 1437 (1999)
85. A K H Knöbel, I H Escher, A Pfaltz *Synlett* 1429 (1997)
86. A Pfaltz *Synlett* 835 (1999)
87. I H Escher, A Pfaltz *Tetrahedron* **56** 2879 (2000)
88. K N Gavrilov, O G Bondarev, R V Lebedev, A I Polosukhin, A A Shyryaev, S E Lyubimov, P V Petrovskii, S K Moiseev, V N Kalinin, N S Ikonnikov, V A Davankov, A V Korostylev *J. Organomet. Chem.* **655** 204 (2002)
89. A I Polosukhin, O G Bondarev, S E Lyubimov, A V Korostylev, K A Lyssenko, V A Davankov, K N Gavrilov *Tetrahedron: Asymmetry* **12** 2197 (2001)
90. O G Bondarev, S E Lyubimov, A A Shiryaev, N E Kadilnikov, V A Davankov, K N Gavrilov *Tetrahedron: Asymmetry* **13** 1587 (2002)
91. R Hilgraf, A Pfaltz *Synlett* 1814 (1999)
92. A Pfaltz, J Blankenstein, R Hilgraf, E Hörmann, S McIntyre, F Menges, M Schönleber, S P Smidt, B Wüstenberg, N Zimmermann *Adv. Synth. Catal.* **345** 33 (2003)
93. K N Gavrilov, O G Bondarev, V N Tsarev, A A Shiryaev, S E Lyubimov, A S Kucherenko, V A Davankov *Izv. Akad. Nauk, Ser. Khim.* 116 (2003) [c]
94. D K Heldmann, D Seebach *Helv. Chim. Acta* **82** 1096 (1999)
95. C G Arena, D Drommi, F Faraone *Tetrahedron: Asymmetry* **11** 4753 (2000)
96. C G Arena, D Drommi, F Faraone *Tetrahedron: Asymmetry* **11** 2765 (2000)
97. D Drommi, F Faraone, G Franciò, D Belletti, C Graiff, A Tiripicchio *Organometallics* **21** 761 (2002)
98. G Delapierre, J M Brunel, T Constantieux, G Buono *Tetrahedron: Asymmetry* **12** 1345 (2001)
99. R Kranich, K Eis, O Geis, S Mühle, J W Bats, H-G Schmalz *Chem. Eur. J.* **6** 2874 (2002)
100. F Blume, S Zemolka, T Fey, R Kranich, H-G Schmalz *Adv. Synth. Catal.* **344** 868 (2002)
101. J M Brunel, T Constantieux, G Buono *J. Org. Chem.* **64** 8940 (1999)
102. J M Brunel, T Constantieux, A Labande, F Lubatti, G Buono *Tetrahedron Lett.* **38** 5971 (1997)
103. T Constantieux, J-M Brunel, A Labande, G Buono. *Synlett* 49 (1998)
104. G Muchow, J M Brunel, M Maffei, O Pardigon, G Buono *Tetrahedron* **54** 10435 (1998)
105. J M Brunel, B Del Campo, G Buono *Tetrahedron Lett.* **39** 9663 (1998)
106. G Delapierre, T Constantieux, J M Brunel, G Buono *Eur. J. Org. Chem.* 2507 (2000)
107. J M Brunel, A Tenaglia, G Buono *Tetrahedron: Asymmetry* **11** 3585 (2000)
108. C Saluzzo, J Breuzard, S Pellet-Rostaing, M Vallet, F LeGuyader, M Lemaire *J. Organomet. Chem.* **643** 98 (2002)
109. O Huttenloch, E Laxman, H Waldmann *Chem. Commun.* 673 (2002)
110. K N Gavrilov, O G Bondarev, R V Lebedev, A A Shiryaev, S E Lyubimov, A I Polosukhin, G V Grintselev-Knyazev, K A Lyssenko, S K Moiseev, N S Ikonnikov, V N Kalinin, V A Davankov, A V Korostylev, H-J Gais *Eur. J. Inorg. Chem.* 1367 (2002)
111. A I Polosukhin, O G Bondarev, A V Korostylev, R Hilgraf, V A Davankov, K N Gavrilov *Inorg. Chim. Acta* **323** 55 (2001)
112. O G Bondarev, K N Gavrilov, V N Tsarev, V A Davankov, G-I Gais *Izv. Akad. Nauk, Ser. Khim.* 1604 (2002) [c]
113. B Gotov, H-G Schmalz *Org. Lett.* **3** 1753 (2001)
114. O G Bondarev, K N Gavrilov, V N Tsarev, V A Davankov, R V Lebedev, S K Moiseev, V N Kalinin *Izv. Akad. Nauk, Ser. Khim.* 484 (2002) [c]
115. M Dieguez, A Ruiz, C Claver *Tetrahedron: Asymmetry* **12** 2861 (2001)
116. K N Gavrilov, I S Mikhel', K A Lysenko, M Yu Antipin, G I Timofeeva, A I Polosukhin, A V Korostylev *Zh. Neorg. Khim.* **42** 593 (1997) [b]
117. K N Gavrilov, A V Korostylev, G I Timofeeva, A I Polosukhin, O G Bondarev, P V Petrovskii *Koord. Khim.* **24** 610 (1998) [a]
118. I S Mikhel', K N Gavrilov, A I Rebrov *Zh. Neorg. Khim.* **44** 1634 (1999) [b]

119. A I Polosukhin, K N Gavrilov, O G Bondarev, A V Korostylev, P V Petrovskii, V A Davankov *J. Organomet. Chem.* **608** 89 (2000)
120. A I Polosukhin, O G Bondarev, S E Lyubimov, A A Shiryaev, K N Gavrilov *Koord. Khim.* **26** 400 (2000) [a]
121. A I Polosukhin, O G Bondarev, S E Lyubimov, A A Shiryaev, P V Petrovskii, K A Lysenko, K N Gavrilov *Koord. Khim.* **27** 630 (2001) [a]
122. K N Gavrilov, A V Korostylev, O G Bondarev, A I Polosukhin, V A Davankov *J. Organomet. Chem.* **585** 290 (1999)
123. A V Korostylev, O G Bondarev, A Yu Kovalevsky, P V Petrovskii, V A Davankov, K N Gavrilov *Inorg. Chim. Acta* **312** 117 (2001)
124. K Ito, R Kashiwagi, K Iwasaki, T Katsuki *Synlett* 1563 (1999)
125. R V Lebedev, S K Moiseev, O G Bondarev, M M Il'in, K N Gavrilov, V N Kalinin *Izv. Akad. Nauk, Ser. Khim.* 476 (2002) [c]
126. K N Gavrilov, A I Polosukhin, O G Bondarev, A V Korostylev, S E Lyubimov, A A Shiryaev, Z A Starikova, V A Davankov. *Mendeleev Commun.* 33 (2001)
127. K N Gavrilov, O G Bondarev, A I Polosukhin, S E Lyubimov, V N Tsarev *Koord. Khim.* **28** 152 (2002) [a]
128. K N Gavrilov, A I Polosukhin *Koord. Khim.* **26** 695 (2000) [a]
129. A I Polosukhin, A Yu Kovalevskii, K N Gavrilov *Koord. Khim.* **25** 812 (1999) [a]
130. K N Gavrilov, I S Mikhel' *Usp. Khim.* **65** 242 (1996) [*Russ. Chem. Rev.* **65** 225 (1996)]
131. K N Gavrilov, I S Mikhel', A I Polosukhin, A I Rebrov, G V Cherkaev, G I Timofeeva *Koord. Khim.* **23** 925 (1997) [a]
132. A I Polosukhin, A Yu Kovalevsky, A V Korostylev, V A Davankov, K N Gavrilov *Phosphorus, Sulfur Silicon Relat. Elem.* **159** 69 (2000)
133. K N Gavrilov, A V Korostylev, A I Polosukhin, O G Bondarev, A Yu Kovalevsky, V A Davankov *J. Organomet. Chem.* **613** 148 (2000)
134. O G Bondarev, I S Mikhel', V N Tsarev, P V Petrovskii, V A Davankov, K N Gavrilov *Izv. Akad. Nauk, Ser. Khim.* 110 (2003) [c]
135. K N Gavrilov, A I Polosukhin, O G Bondarev, S E Lyubimov, K A Lyssenko, P V Petrovskii, V A Davankov *J. Mol. Catal. A: Chem.* **196**/**1**–**2** 39 (2003)
136. K N Gavrilov, I S Mikhel', D V Lechkin, A I Rebrov, G V Cherkaev, G I Timofeeva, M G Vinogradov *Zh. Neorg. Khim.* **42** 1676 (1997) [b]
137. I S Mikhel', K N Gavrilov, D V Lechkin, A I Rebrov *Izv. Akad. Nauk, Ser. Khim.* 1416 (1997) [c]
138. K N Gavrilov, A V Korostylev, P V Petrovskiy, A Yu Kovalevsky, V A Davankov *Phosphorus, Sulfur Silicon Relat. Elem.* **155** 15 (1999)
139. I S Mikhel, O G Bondarev, V N Tsarev, G V Grintselev-Knyazev, K A Lyssenko, V A Davankov, K N Gavrilov *Organometallics,* **22,** 925 (2003)
140. K Nozaki, F Shibahara, Y Itoi, E Shirakawa, T Ohta, H Takaya, T Hiyama *Bull. Chem. Soc. Jpn.* **72** 1911 (1999)
141. K Nozaki, Y Itoi, F Shibahara, E Shirakawa, T Ohta, H Takaya, T Hiyama *J. Am. Chem. Soc.* **120** 4051 (1998)
142. K Nozaki, F Shibahara, T Hiyama *Chem. Lett.,* 694 (2000)
143. T Horiuchi, T Ohta, E Shirakawa, K Nozaki, H Takaya *Tetrahedron* **53** 7795 (1997)
144. K Nozaki, W -G Li, T Horiuchi, H Takaya *Tetrahedron Lett.* **38** 4611 (1997)
145. T Horiuchi, T Ohta, E Shirakawa, K Nozaki, H Takaya *J. Org. Chem.* **62** 4285 (1997)
146. T Horiuchi, E Shirakawa, K Nozaki, H Takaya *Organometallics* **16** 2981 (1997)
147. D Gleich, R Schmid, W A Herrmann *Organometallics* **17** 2141 (1998)
148. K Nozaki, Y Kawashima, K Nakamoto, T Hiyama *Macromolecules* **32** 5168 (1999)
149. K Nozaki, T Hiyama *Organometallics* **19** 2031 (2000)
150. T Horiuchi, E Shirakawa, K Nozaki, H Takaya *Tetrahedron: Asymmetry* **8** 57 (1997)
151. G Franciò, K Wittmann, W Leitner *J. Organomet. Chem.* **621** 130 (2001)
152. G Franciò, W Leitner *Chem. Commun.* 1663 (1999)
153. D Bonafoux, Z Hua, B Wang, I Ojima *J. Fluorine Chem.* **112** 101 (2001)
154. S Deerenberg, P C J Kamer, P W N M van Leeuwen *Organometallics* **19** 2065 (2000)
155. M Digguez, S Deerenberg, O Pemies, C Claver, P W N M van Leeuwen, P C J Kamer *Tetrahedron: Asymmetry* **11** 3161 (2000)
156. S Deerenberg, H S Schrekker, G P F van Strijdonck, P C J Kamer, P W N M van Leeuwen, J Fraanje, K Goubitz *J. Org. Chem.* **65** 4810 (2000)
157. S Deerenberg, O Pemies, M Digguez, C Claver, P C J Kamer, P W N M van Leeuwen *J. Org. Chem.* **66** 7626 (2001)
158. C A Tolman *Chem. Rev.* **77** 313 (1977)
159. A Suarez, A Pizzano *Tetrahedron: Asymmetry* **12** 2501 (2001)
160. A Suarez, M A Mendez-Rojas, A Pizzano *Organometallics* **21** 4611 (2002)
161. O Pemies, G Net, A Ruiz, C Claver *Tetrahedron: Asymmetry* **12** 3441 (2001)
162. M Digguez, O Pemies, G Net, A Ruiz, C Claver *J. Mol. Catal. A: Chem.* **185** 11 (2002)
163. O Pemies, M Digguez, G Net, A Ruiz, C Claver *J. Org. Chem.* **66** 8364 (2001)
164. J Scherer, G Huttner, H Heidel *J. Organomet. Chem.* **539** 67 (1997)
165. G Franciz, F Faraone, W Leitner *Angew. Chem., Int. Ed.* **39** 1428 (2000)
166. R Ewalds, E B Eggeling, A C Hewat, P C J Kamer, P W N M van Leeuwen, D Vogt *Chem. Eur. J.* **6** 1496 (2000)
167. O Lot, I Suisse, A Mortreux, F Agbossou, G Nowogrocki *J. Mol. Catal. A: Chem.* **164** 125 (2000)
168. M T Reetz, M Pastd *Tetrahedron Lett.* **41** 3315 (2000)
169. S Naili, I Suisse, A Mortreux, F Agbossou-Niedercorn, G Nowogrocki *J. Organomet. Chem.* **628** 114 (2001)
170. M Digguez, A Ruiz, C Claver *Tetrahedron: Asymmetry* **12** 2827 (2001)
171. M Digguez, A Ruiz, C Claver *Chem. Commun.* 2702 (2001)
172. O Huttenloch, J Spieler, H Waldmann *Chem. Eur. J.* **7** 671 (2001)
173. A Mandoli, L A Arnold, A H M de Vries, P Salvadori, B L Feringa *Tetrahedron: Asymmetry* **12** 1929 (2001)
174. O Pàmies, G Net, A Ruiz, C Claver *Tetrahedron: Asymmetry* **11** 1097 (2000)
175. O Pàmies, G Net, A Ruiz, C Claver *Tetrahedron: Asymmetry* **10** 2007 (1999)
176. E Guiu, B Munoz, S Castillon, C Claver *Adv. Synth. Catal.* **345** 169 (2003)
177. O Pàmies, G P F van Strijdonck, M Diéguez, S Deerenberg, G Net, A Ruiz, C Claver, P C J Kamer, P W N M van Leeuwen *J. Org. Chem.* **66** 8867 (2001)
178. M Diéguez, O Pàmies, A Ruiz, S Castilllon, C Claver *Chem. Eur. J.* **7** 3086 (2001)
179. M Diéguez, O Pàmies, A Ruiz, S Castilllon, C Claver *Chem. Commun.* 1607 (2000)
180. M Diéguez, A Ruiz, C Claver *J. Org. Chem.* **67** 3796 (2002)
181. M Diéguez, A Ruiz, C Claver *Tetrahedron: Asymmetry* **12** 2895 (2001)
182. M Diéguez, O Pàmies, A Ruiz, C Claver *Tetrahedron: Asymmetry* **13** 83 (2002)
183. M Diéguez, S Jansat, M Gomez, A Ruiz, G Muller, C Claver *Chem. Commun.,* 1132 (2001)
184. R Kadyrov, D Heller, R Selke *Tetrahedron: Asymmetry* **9** 329 (1998)
185. M T Reetz, T Neugebauer *Angew. Chem., Int. Ed.* **38** 179 (1999)
186. M Yan, Q-Y Xu, A S C Chan *Tetrahedron: Asymmetry* **11** 845 (2000)
187. M Yan, A S C Chan *Tetrahedron Lett.* **40** 6645 (1999)
188. M Yan, Z-Y Zhou, A S C Chan *Chem. Commun.* 115 (2000)
189. P Uriz, E Fernandez, N Ruiz, C Claver *Inorg. Chem. Commun.* **3** 515 (2000)
190. A Martorell, C Claver, E Fernandez *Inorg. Chem. Commun.* **3** 132 (2000)
191. S J Sturla, S L Buchwald *J. Org. Chem.* **67** 3398 (2002)

192. S Ini, A G Oliver, T D Tilley, R G Bergman *Organometallics* **20** 3839 (2001)
193. C G Arena, D Drommi, F Faraone, C Graiff, A Tiripicchio *Eur. J. Inorg. Chem.* 247 (2001)
194. L Liang, T T L Au-Yeung, A S C Chan *Org. Lett.* **4** 3799 (2002)
195. L Liang, A S C Chan *Tetrahedron: Asymmetry* **13** 1393 (2002)
196. Y Jiang, S Xue, K Yu, Z Li, J Deng, A Mi, A S C Chan *J. Organomet. Chem.* **586** 159 (1999)
197. S Cserépi-Szücs, J Bakos *Chem. Commun.* 635 (1997)
198. S Cserépi-Szücs, G Huttner, L Zsolnai, J Bakos *J. Organomet. Chem.* **586** 70 (1999)
199. A C Dros, A Meetsma, R M Kellogg *Tetrahedron* **55** 3071 (1999)
200. P Kruger, B Wederndorfer, H Werner *Z. Anorg. Allg. Chem.* **626** 2228 (2000)
201. K Selvakumar, M Valentini, P Pregosin *Organometallics* **18** 4591 (1999)
202. M Valentini, K Selvakumar, M Worle, P Pregosin *J. Organomet. Chem.* **587** 244 (1999)
203. O Pàmies, M Diéguez, G Net, A Ruiz, C Claver *Organometallics,* **19** 1488 (2000)
204. S D Pastor, S P Shum *Tetrahedron: Asymmetry* **9** 543 (1998)
205. S Yao, J-C Meng, G Siuzdak, M G Finn *J. Org. Chem.* **68** 2540 (2003)
206. M van den Berg, A J Minnaard, R M Haak, M Leeman, E P Schudde, A Meetsma, B L Feringa, A H M de Vries, C E P Maljaars, C E Willans, D Hyet, J A F Boogers, H J W Henderickx, J G de Vries *Adv. Synth. Catal.* **345** 308 (2003)
207. M T Reetz, T Sell, A Meiswinkel, G Mehler *Angew. Chem., Int. Ed.* **42** 790 (2003)
208. J-G Boiteau, R Imbos, A J Minnaard, B L Feringa *Org. Lett.* **5** 681 (2003)
209. D Pena, A J Minnaard, A H M de Vries, J G de Vries, B L Feringa *Org. Lett.* **5** 475 (2003)
210. F López, T Ohmura, J F Hartwig *J. Am. Chem. Soc.* **125** 3426 (2003)
211. A Duursma, A J Minnaard, B L Feringa *J. Am. Chem. Soc.* **125** 3700 (2003)
212. A Iuliano, P Scafato *Tetrahedron: Asymmetry* **14** 611 (2003)
213. A Togni, T Hayashi *Ferrocenes. Homogenous Catalysis, Organic Synthesis, Material Science* (Weinheim: VCH, 1995)
214. O Molt, T Schrader *Synthesis* 2633 (2002)
215. H-U Blaser, C Malan, B Pugin, F Spindler, H Steiner, M Studer *Adv. Synth. Catal.* **345** 103 (2003)

[a] — *Russ. J. Coord. Chem. (Engl. Transl.)*
[b] — *Russ. J. Inorg. Chem. (Engl. Transl.)*
[c] — *Russ. Chem. Bull., Int. Ed. (Engl. Transl.)*

Russian Chemical Reviews **73** (7) 701 – 733 (2004) © 2004 Russian Academy of Sciences and Turpion Ltd

DOI 10.1070/RC2004v073n07ABEH000835

Nucleosides and oligonucleotides containing 2′-reactive groups: synthesis and applications

T S Zatsepin, E A Romanova, T S Oretskaya

Contents

I.	Introduction	701
II.	Synthesis of modified nucleosides containing reactive groups in the 2′-position	701
III.	Synthesis of conjugates based on 2′-modified nucleosides and oligonucleotides	710
IV.	The use of nucleosides, nucleotides and oligonucleotides containing reactive groups in the 2′-position	722
V.	Conclusion	727

Abstract. The known methods for the synthesis of 2′-functionalised nucleosides, oligonucleotides and their conjugates are systematised. The applications of 2′-modified nucleosides and oligonucleotides are discussed. The bibliography includes 451 references.

I. Introduction

At present, the use of synthetic (including modified) oligonucleotides is unavoidable for progress in molecular biology and medicine. The interest in oligonucleotides and their derivatives as potential therapeutics able to influence, in one way or another, intracellular transformations of nucleic acids (NA) has been steadily increasing in the past decade. In addition, oligonucleotides are applied in antisense [1] and anti-gene [2] biotechnologies. The use of NA-based ribozymes [3] and aptamers [4] as well as RNA interference [5, 6] are no less promising trends.

Treatment of fragments of native NA with various chemical reagents usually results in statistical intrachain or terminal modifications. Incorporation of a modified fragment into a predetermined position of the oligomeric chain in the course of oligonucleotide synthesis is a more versatile approach which enables the introduction of reactive groups into heterocyclic bases, internucleotide phosphate groups or carbohydrate fragments. Obviously, nucleic acids should preserve their ability for complementary interactions. In this context, modification of functional groups involved in complementary interactions is undesirable, since it causes significant destabilisation of an NA duplex formed by the modified oligomer and complementary NA template.[7, 8] The C(5) atom of pyrimidine [9, 10] and the C(7) [11] or the C(8) atom [12] of purine nucleosides are sites of choice for the modification of heterocyclic bases, primarily because of minimum disturbances in the structures of the modified NA fragments obtained. The introduction of substituents into internucleotide phosphate groups results in the apperance of chiral centres and, as a consequence, the existence of two stereoisomers. Modification at the C(2′) atom of nucleosides seems to be especially promising, since the disturbances in the structures of DNA duplexes upon incorporation of thus modified fragments into the oligonucleotide structure are minimum. Besides, the introduction of reactive groups into the 2′-position allows the synthesis of nucleosides with both C(2′)-*exo*- and C(2′)-*endo*-conformations of the carbohydrate residue, directing the substituent to both minor and major grooves of the NA duplex.[13] The synthesis of 2′-modified oligonucleotides is reduced to the preparation of nucleoside phosphoramidite derivatives containing protected reactive groups with subsequent incorporation of the unit formed into the oligonucleotide chain by automated synthesis.

This review deals with the analysis of published papers devoted to the synthesis of nucleosides containing a reactive group in the 2′-position; this group is linked to the C(2′) atom either directly or through various linkers. Main attention is given to derivatives which can be incorporated into the oligonucleotide chain. The groups, which differ in reactivity from that of the functional groups of the natural nucleosides, will be referred to as the reactive groups. Here we do not consider modified nucleosides containing a single or a double C—C bond at the C(2′) atom, since these nucleosides, with only few exceptions, are not potential objects for conjugation with other compounds and incorporation into oligonucleotides.

The application of nucleosides and oligonucleotides containing reactive groups at the C(2′) atom is also discussed.

II. Synthesis of modified nucleosides containing reactive groups in the 2′-position

Numerous methods for the synthesis of nucleosides containing nucleophilic (amino or thio groups) and electrophilic (carboxy, aldehyde, *etc.*) groups in the 2′-position are known to date.

1. Synthesis of nucleosides containing nucleophilic groups

a. Synthesis of 2′-amino-2′-deoxynucleosides

Nucleophilic substitution at the C(2′) atom of activated nucleoside derivatives under the action of the azide ion and subsequent reduction of the azide to the amine is the most popular approach to the introduction of the amino group into the 2′-position of a nucleoside. The synthesis of nucleosides containing an azido group in the sugar moiety has been reviewed.[14] Here we shall consider only those papers which were not cited in that review [14] or were considered only briefly.

T S Zatsepin, E A Romanova, T S Oretskaya Department of Chemistry, M V Lomonosov Moscow State University, A N Belozersky Institute of Physicochemical Biology, M V Lomonosov Moscow State University, Leninskie Gory, 119992 Moscow, Russian Federation,
Fax (7-095) 939 31 81. Tel. (7-095) 939 48. E-mail: tsz@yandex.ru (T S Zatsepin), romanova@belozersky.msu.ru (E A Romanova).
Tel. (7-095) 939 54 11. E-mail: oretskaya@belozersky.msu.ru (T S Oretskaya)

Received 19 December 2003
Uspekhi Khimii **73** (7) 757 – 791 (2004); translated by R L Birnova

$O^2,2'$-Anhydrouridine (**1**) is most frequently used as an activated derivative for the synthesis of pyrimidine 2′-amino-2′-deoxyribonucleosides. The anhydronucleoside **1** can be prepared by different methods among which the reaction of uridine (**2**) with diphenyl carbonate in the presence of sodium hydrogencarbonate as a base is the most popular.[15,16] The reaction of compound **1** with a weak nucleophile (*e.g.*, the azide ion) yields the 2′-substituted nucleoside **3**. If a stronger nucleophilic agent, *e.g.*, ammonia, is used, the reaction involves the heterocyclic base and yields arabinoisocytidine (**4**).

The reduction of 2′-azido-2′-deoxyuridine (**3**) was used for the preparation of 2′-amino-2′-deoxyuridine (**5**) in 50% yield.[17] Subsequent modification of the heterocyclic base in compound **5** yields the analogous cytidine derivative **6**.

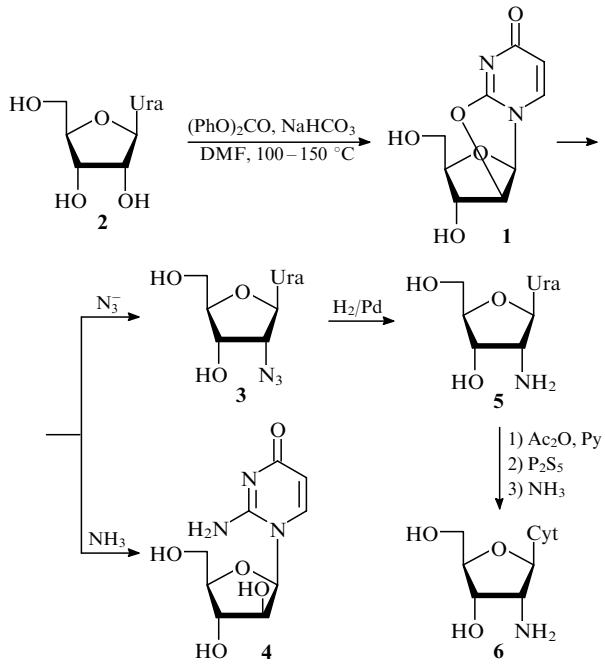

A similar procedure for the synthesis of pyrimidine 2′-amino-2′-deoxyribonucleosides starting from 5′-*O*-trityl- (see Ref. 18) and 3′,5′-di-*O*-benzoyl-$O^2,2'$-anhydrouridine was developed later.[19] In the latter case, partial deprotection of the 3′-hydroxy group took place.

The yield of compound **3** can be increased to 70% through *in situ* generation of lithium azide in the reaction of lithium fluoride with trimethylsilyl azide.[20,21] The addition of tetramethylethylenediamine to the reaction mixture favours the solubilisation of lithium azide in DMF due to its complexation with lithium ions, which increases the yield of the azido derivative **3** up to 80%. A similar effect was observed when a system Me_3SiN_3 – KF – 18-crown-6 was used.[20]

5′-*O*-Acetyl-2′,3′-*O*-(1-methoxyethylidene)uridine (**7**) was used as a starting compound in the synthesis of protected azidouridine **8**.[22] The generation of anhydrouridine occurs *in situ*. Nucleophilic substitution under the action of sodium azide in the presence of Me_3SiCl and Bu_4NCl results in compound **8** in 80% yield.

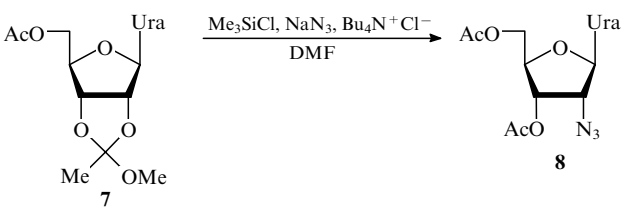

An alternative approach to the synthesis of 2′-amino-2′-deoxyribonucleosides has been developed.[23] The reaction of 5′-protected anhydrouridine **9** with trichloroacetonitrile affords trichloroacetimidate **10**; its subsequent hydrolysis with an ethanolic alkali yields the target product, *viz.*, 2′-amino-2′-deoxyuridine **11**.

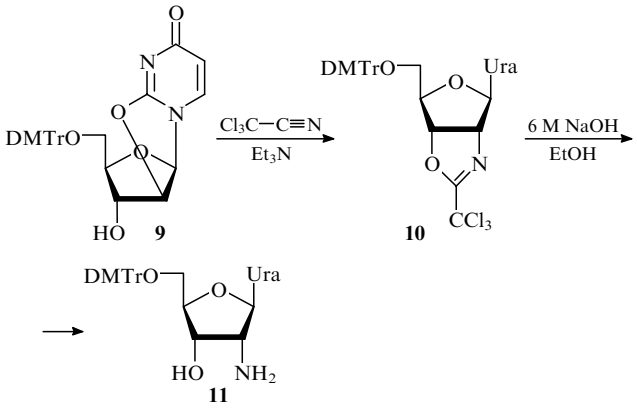

DMTr = $(4\text{-MeOC}_6H_4)_2PhC$.

This methodology gives access to pyrimidine 2′-alkoxyaminonucleosides **12**[24,25] and 2′-alkylaminonucleosides **13**[26,27] as well as 2′-hydroxyaminonucleosides.[28–30] The use of the *tert*-butyldiphenylsilyl protecting group for the 5′-hydroxy function allows the preparation of easily crystallisable products.

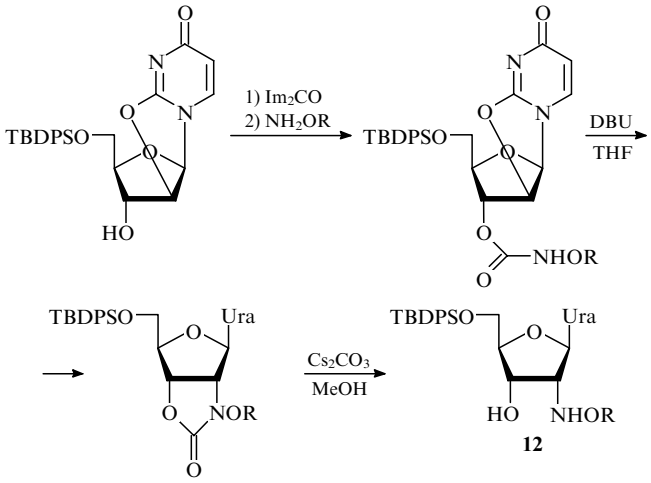

TBDPS = Bu^tPh_2Si; Im is imidazolyl; R = Me, Et, Bn, $(CH_2)_2OH$; DBU is 1,8-diazabicyclo[5.4.0]undec-7-ene.

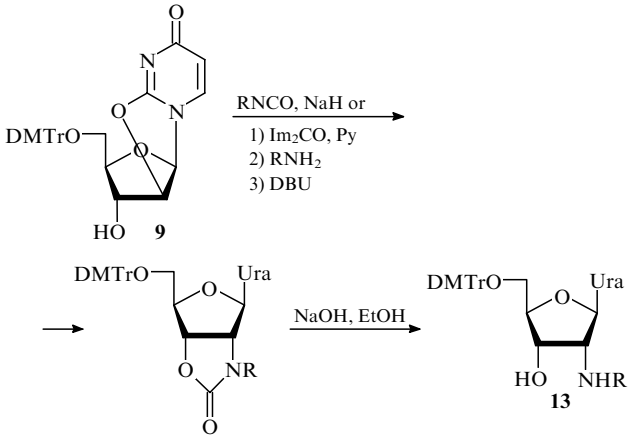

R = Et, $(CH_2)_7Me$, 2-$PyCH_2$, 2-$Py(CH_2)_2$.

5′-*O*-*tert*-Butyldiphenylsilyl-2′-tetrahydrofuranyloxyamino-2′-deoxyadenosine was prepared starting from mesylated arabinoadenosine **14** using a similar approach.[29]

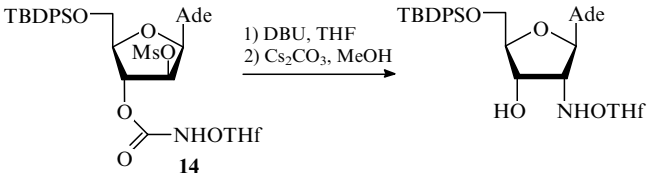

14

Ms = $MeSO_2$, THf is tetrahydrofuranyl.

Recently, Beigelman and co-workers [31] have developed an efficient scheme for the synthesis of protected 2′-amino-2′-deoxyribonucleosides. The starting arabinonucleosides **15a**–**c** with the tetraisopropyldisiloxane-1,3-diyl (TIPDS) [32] protecting group for 3′- and 5′-OH-groups were activated by treatment with trifluoromethanesulfonyl chloride. Nucleophilic substitution of the triflate group in the derivatives formed by treatment with phthalimides containing various substituents in the benzene ring resulted in 2′-phthalimido-2′-deoxynucleosides **16a**–**c** in 35%–70% yields. 4,5-Dichlorophthalimide proved to be the nucleophile of choice; its application did not result in the formation of side products such as 2′-deoxy-1′,2′-didehydronucleosides. This is a preparative and versatile method for the synthesis of purine and pyrimidine nucleosides.

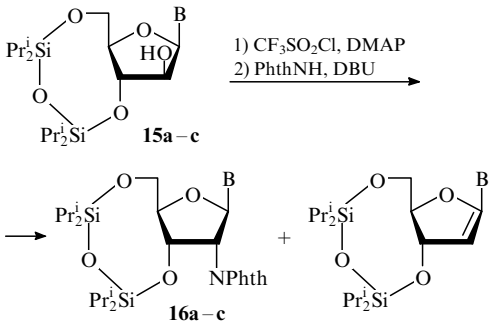

15a–**c** → **16a**–**c** +

B = Ura (**a**), Ade^{Bz} (**b**), Cyt^{Ac} (**c**); DMAP = 4-Me_2NPy;

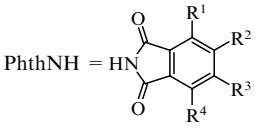

R^1	R^2	R^3	R^4
H	H	H	H
Cl	Cl	Cl	Cl
H	Cl	Cl	H
NO_2	H	H	H
H	NO_2	H	H

Realisation of a similar method has been described.[33,34] In this case, the triflate of the protected arabinoadenosine obtained in the first step was introduced in the reaction with lithium azide with subsequent reduction of the azido group.

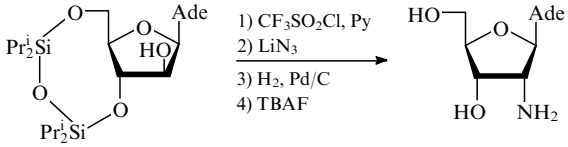

TBAF = $Bu_4N^+F^-$.

The nucleophilic substitution of 2′-*O*-sulfonyl groups in ribonucleoside derivatives, which also occurs with reversal of the configuration at the C(2′)-atom, is used for the synthesis of 2′-amino-2′-deoxyarabinonucleosides. Of this type of nucleoside, purine nucleosides are synthetically more accessible.

Starting from 3′,5′-di-*O*-tetrahydropyranyl-2′-*O*-trifluoromethylsulfonyladenosine (**17**), 2′-azido-2′-deoxy-β-D-arabinoadenosine **18** was prepared, which was reduced to the target nucleoside **19** after deprotection.[35]

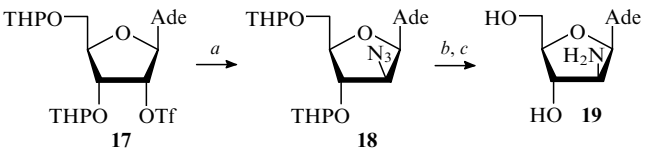

17 **18**

THP is tetrahydropyranyl, Tf = CF_3SO_2.
(*a*) NaN_3, (*b*) H^+, (*c*) Ph_3P, H_2O.

The same strategy was used in the synthesis of 2′-amino-2′-deoxy-β-D-arabinoadenosine (**19**) [36] and its analogues **20a**,**b** [37] from protected ribonucleosides **21a**–**c**.

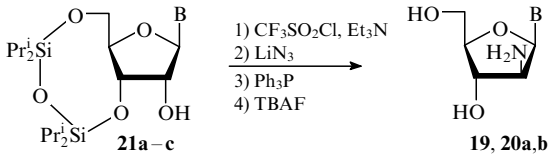

21a–**c** → **19**, **20a**,**b**

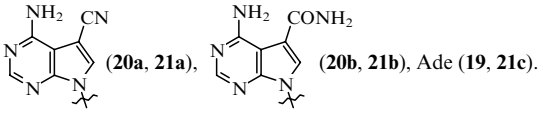

(**20a**, **21a**), (**20b**, **21b**), Ade (**19**, **21c**).

It should be noted that the glycosidic bond in the 2′-*O*-tosyl adenosine derivative is cleaved under the action of nucleophilic agents in DMF resulting in the liberation of adenine.[38] The nucleophilic substitution of the tosyloxy group under the action of NaN_3 in hexamethylphosphoramide has been carried out, however, with low yields [46% and 11% for 2′-*O*-(toluene-*p*-sulfonyl)adenosine and -guanosine, respectively].[39]

A scheme for the preparation of 2′-amino-2′-deoxyarabinoadenosine from the β-D-lyxoadenosine derivative **22** has been proposed.[40] The opening of the aziridine ring in the *N*-trifluoroacetyl derivative **23** occurred in a virtually regioselective manner; the yield of compound **24** was 49%.

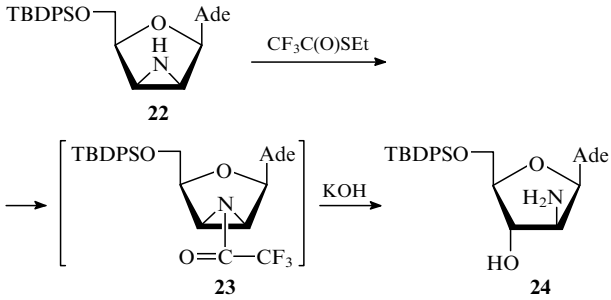

22 → **23** → **24**

Pyrimidine 2′-amino-2′-deoxyarabinonucleosides are synthetically less accessible and were prepared for the first time as late as 1989 using the reaction of protected ribouridine **25a** and ribothymidine **25b** with diphenyl phosphorazidate in the presence of diethyl azodicarboxylate (DEAD) and triphenylphosphine with subsequent reduction of the azido group. The presence of a benzoyl protecting group at the N^3-atom of the heterocyclic base is necessary for preventing the closure of the O^2,2′-anhydro ring, which yields 2′-amino derivatives with a ribo-configuration.[41,42]

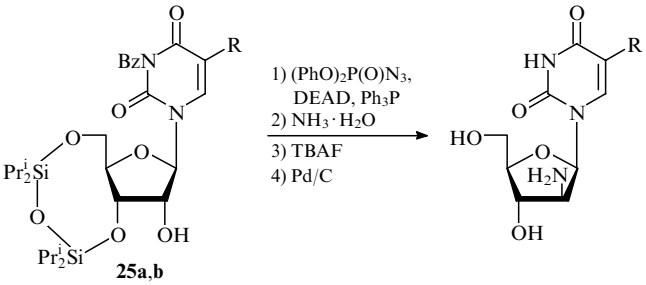

25a,**b**

R = H (**a**), Me (**b**).

An original scheme for the synthesis of 2′-arylamino-2′-deoxy-β-D-arabinouridines from the O^2,5′-anhydroderivative **26** has been developed.[43] Selective tosylation of the 2′-hydroxy group and subsequent treatment with aromatic amines yielded tricyclic compounds **27**, which were further hydrolysed with aqueous alkali. If aliphatic amines were used, the intermediate tricyclic compounds underwent degradation.

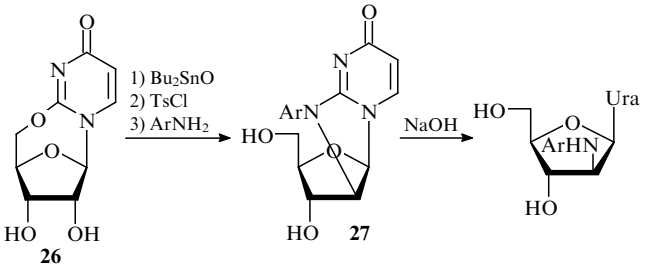

Ts = 4-$MeC_6H_4SO_2$; Ar = Ph, 4-MeC_6H_4.

The synthesis of 2′-amino-2′-deoxyadenosine from 9-(2,3-anhydro-D-lyxofuranosyl)adenine has been described.[44]

In all the methods for the synthesis of 2′-amino-2′-deoxynucleosides, the amino group was introduced using modification of activated derivatives of preformed nucleosides. An alternative strategy consists of glycosylation of heterocyclic bases by premodified sugars. First attempts to synthesise 2′-amino-2′-deoxyderivatives of purine nucleosides starting from D-altrose[45] and glucosamine[46] were unsuccessful. Glycosylation of purines by protected 2-azido-2-deoxyribose **28** was more successful; however, a mixture of α and β-anomers of the target 2′-azido-2′-deoxyribonucleosides was obtained (7- and 9-isomers are formed in the case of guanosine).[47]

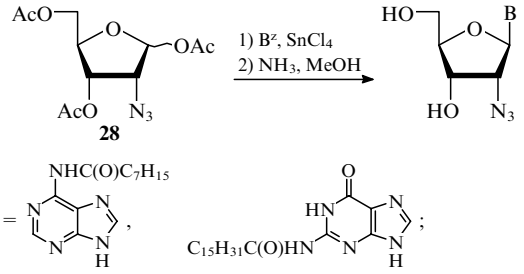

B = Ade (38%), Gua (21%).

Later, purine 2′-amino-2′-deoxynucleosides were synthesised by transglycosylation of protected adenine and guanine with 2′-trifluoroacetamido-2′-deoxyuridine.[48]

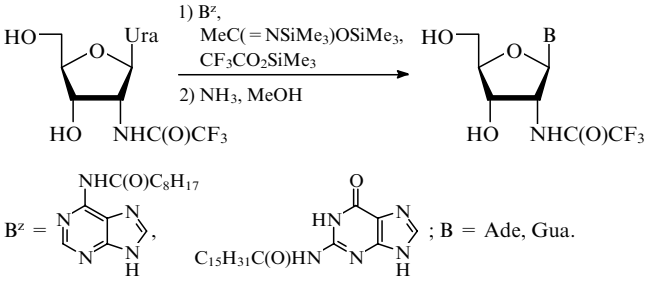

; B = Ade, Gua.

The condensation of 3-*O*-acetyl-2-azido-5-*O*-benzoyl-2-deoxy-D-arabinofuranosyl chloride, prepared from D-glucose by a multistep synthesis, with silylated cytosine afforded 1-(2-azido-2-deoxy-β-D-arabinofuranosyl)cytosine in 37% yield. This reaction was also accompanied by the formation of the α-anomer (yield 10%).[41]

Some examples are known of chemoenzymatic synthesis of modified nucleosides which combines classical methods of organic synthesis with the use of enzymes[49] and cell cultures.[50] Thus 2′-amino-2′-deoxyadenosine is produced by the bacteria *Actinomadura*.[51,52] Transglycosylation of hypoxanthine[53] and adenine[54] by 2′-amino-2′-deoxyuridine in a cell culture of *Ervinia herbicola* with a degree of conversion of up to 50% has been carried out. 2′-Amino-2′-deoxy-β-D-arabinoadenosine was converted into the corresponding inosine derivative under the action of adenosine deaminase.[55]

Synthesis of 2′-*O*-aminoalkylnucleosides

The preparation of 2′-*O*-aminoalkylnucleosides can be regarded as a special case of alkylation of the 2′-hydroxy group. The methods for the synthesis of 2′-*O*-alkylnucleosides have been reviewed.[56] In this Section, special attention will be given to the introduction and protection of the amino group.

2′-*O*-Aminoalkyl nucleosides **29** were first obtained in 1991 by Cook and co-workers[57] Free adenosine was alkylated with phthalimidoalkyl bromides in the presence of sodium hydride.[57–61]

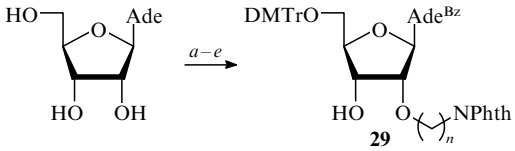

(*a*) $PhthN(CH_2)_nBr$, NaH, DMF; (*b*) Me_3SiCl, Py; (*c*) BzCl; (*d*) NH_4OH; (*e*) DMTrCl, Py; *n* = 2–6.

This reaction yields a mixture of 2′- and 3′-isomers which can be separated only after benzoylation of the exocyclic amino group of adenine and tritylation of the 5′-hydroxy group. Although the total yields of nucleosides **29** are low (10%–20%), the advantage of this method is that it does not require additional protection/deprotection steps and eliminates multiple chromatography of intermediates. In addition, the aminoalkyl group is introduced in one step, while the phthaloyl protecting group is stable under the conditions of the oligonucleotide synthesis and is removed by standard post-synthetic treatments with concentrated aqueous ammonia on heating. Trifluoroacetyl[62] or 2-cyanoethoxycarbonyl groups can be used instead of the phthaloyl protecting group.[63]

Nucleosides **30a–d** in which the amino groups are linked to the O(2′) atom through more complex linkers have also been used in oligonucleotide synthesis.[64]

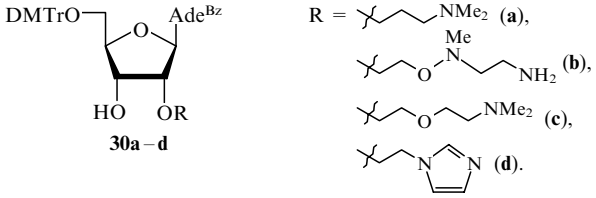

Unfortunately, direct alkylation of non-protected nucleosides is possible only in the case of adenosine and its analogues. Metal-directed alkylation of the *cis*-diol group permits one to increase the total yield of pyrimidine nucleosides **31a**,**b** to 46% (no base alkylation is observed), but the regiospecificity of the substitution is still low (a mixture of 2′- and 3′-isomers is formed in a 55 : 45 ratio).[65]

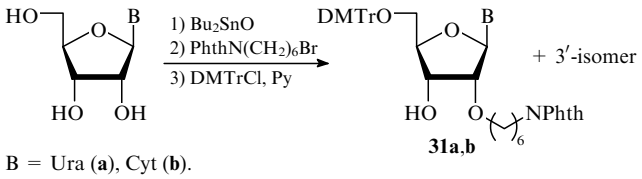

B = Ura (**a**), Cyt (**b**).

A method for the alkylation of O^2,2′-anhydrouridine **1** and thymidine **32** by boric acid esters has been developed.[63,66–69] The yields of compounds **33** and **34** are 15%–20%. The opening of the

Scheme 1

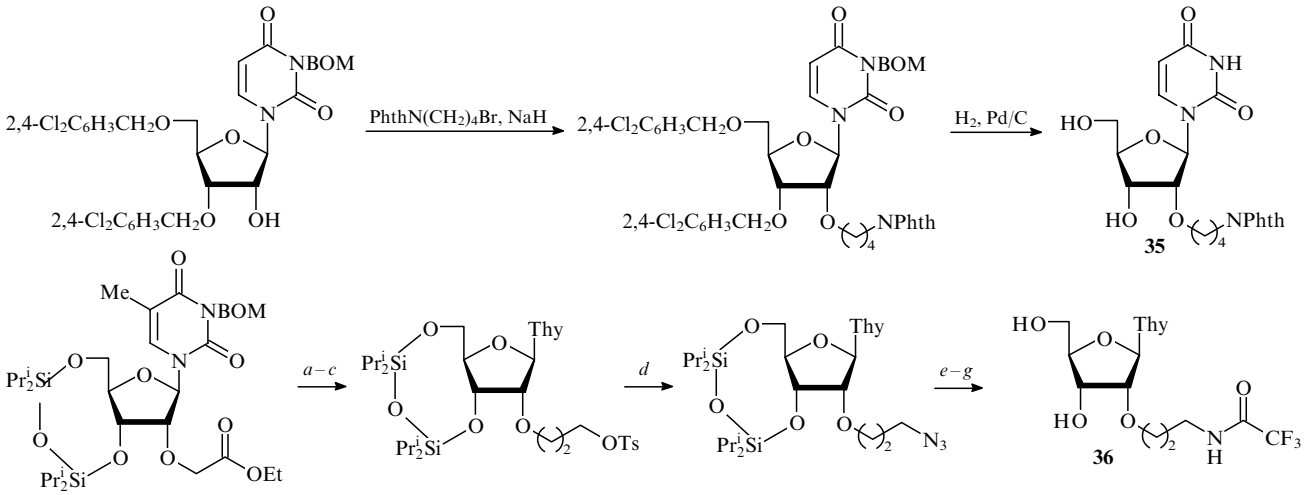

BOM = CH_2OBn; (*a*) $LiBH_4$, MeOH, THF; (*b*) TsCl, Et_3N, DMAP, CH_2Cl_2; (*c*) H_2, Pd/C; (*d*) NaN_3, DMF; (*e*) $SnCl_2$, MeOH; (*f*) $(CF_3CO)_2O$, Py; (*g*) TBAF, THF.

ring in compound **32** was achieved by treatment with phthalimidoethanol in the presence of titanium tetraisopropoxide.[70]

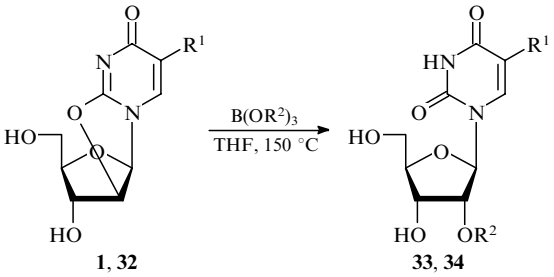

1, **32** **33**, **34**

1, **33**: R^1 = H; **32**, **34**: R^1 = Me; $R^2 = (CH_2)_n$NPhth; n = 2, 3.

A more standard version of the synthesis of 2′-*O*-aminoalkylnucleosides **35** and **36** based on protection of all the reaction centres with the exception of that to be modified has been published.[71,72] Here, all the synthetic steps are high-yielding, but the total yield is only 10%–25% due to the large number of steps (Scheme 1).

A similar synthesis of modified glycosides **37** and **38** with non-native aglycons has been carried out.[73]

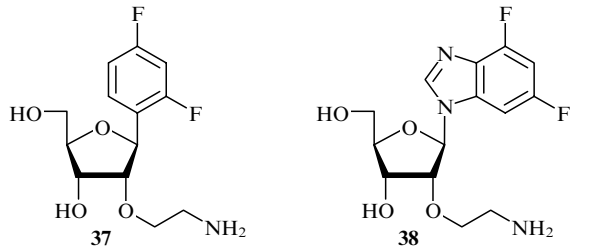

37 **38**

Sollogoub *et al.*[74] have performed alkylation of the protected riboside **39** with subsequent introduction of an amino group under conditions of the Mitsunobu reaction; glycosylation was carried out in the later steps of the synthesis (Scheme 2).

The aminoalkyl groups were attached to the O(2′) atom through a carbamoyl linker.[75–77] This approach provides high yields of the aminoalkylated derivatives **40**.

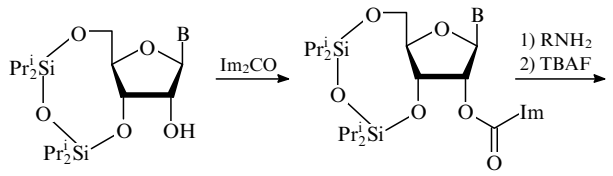

Scheme 2

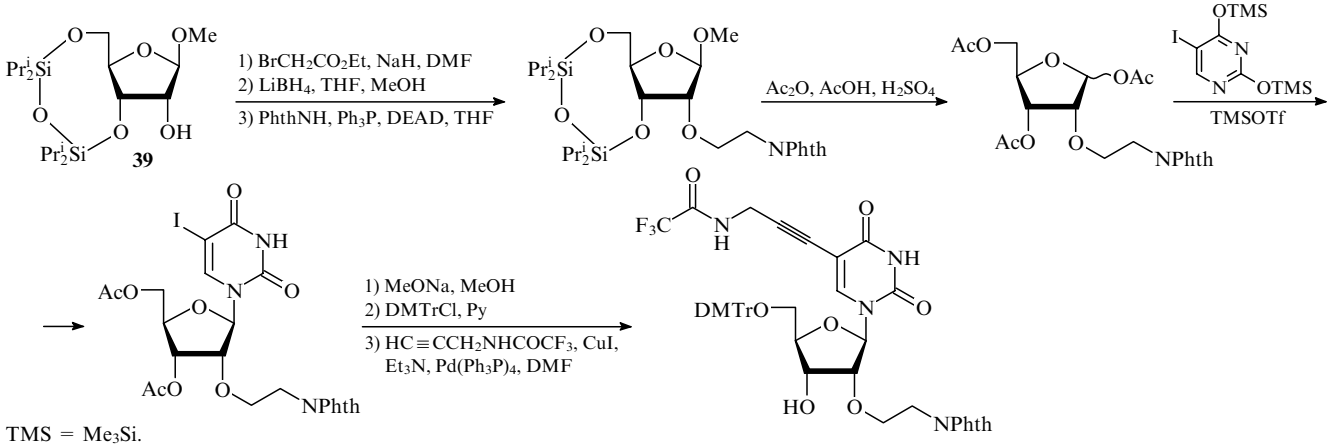

TMS = Me_3Si.

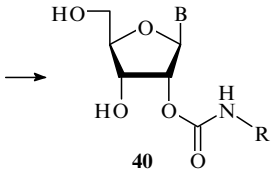

40

B = Cyt^{Bz}: R = $(CH_2)_6NHC(O)CF_3$;
B = Ura: R = $(CH_2)_2NPhth$, $CH_2(CH_2CH_2O)_3(CH_2)_2NH_2$, $CH_2(CH_2CH_2NH)_2(CH_2)_2NH_2$, $(CH_2)_3NH(CH_2)_2NH_2$, Leu-PheNH_2.

The carbamate of 3′,5′-protected arabinouridine was prepared in a similar way.[78]

Keller and Haner[79] have synthesised *N*-acylated 2′-*O*-(9-amino-2-oxo-3-azanonyl)thymidine **41** starting from the nucleoside **42** containing a glycolic acid fragment in the 2′-position.

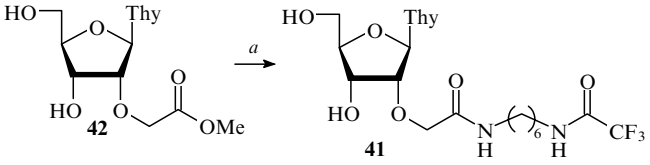

42 **41**

(*a*) $H_2N(CH_2)_6NHC(O)CF_3$.

c. Synthesis of nucleosides containing an aminooxy group

Treatment of nucleosides with *N*-hydroxyphthalimide under conditions of the Mitsunobu reaction is an optimum method for the introduction of an aminooxy group.[80] This method is well developed and the phthaloyl protecting group meets all the requirements for the automated oligonucleotide synthesis.

A possible approach to the introduction of the aminooxyethyl group into the 2′-position of protected thymidine **43a** and adenosine **43b** has been described.[81,82]

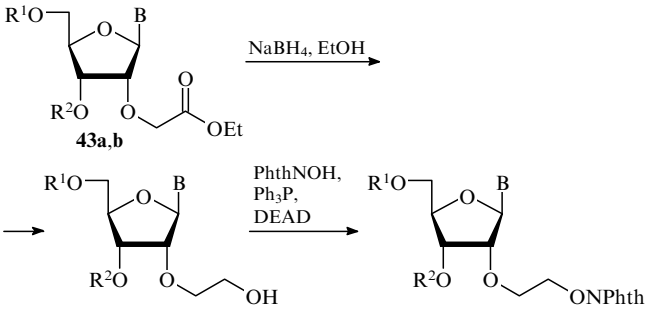

43a,**b**

B = Thy: $R^1 = R^2 = 2,4\text{-}Cl_2C_6H_3CH_2$ (**a**);
B = Ade: $R^1 - R^2 = (Pr^i_2Si)_2O$ (**b**).

Recently, a shorter route to the synthesis of pyrimidine 2′-*O*-(2-hydroxyethyl)nucleosides by alkylation of O^2,2′-anhydronucleosides by boric acid esters has been proposed.[83–85] The nucleosides thus prepared are intermediate compounds in the synthesis of protected 2′-*O*-(2-aminooxyethyl)nucleosides.

In an attempt to introduce the phthalimido group directly into the 2′-position of 3′,5′-*O*-protected nucleosides, the yields of the target products did not exceed 10% because of the low reactivity of the secondary hydroxy group under conditions of the Mitsunobu reaction. Nevertheless, the desired products **44a**,**b** were prepared by substitution of the 2′-*O*-trifluoromethylsulfonyl group in the arabinouridine derivatives **15a** and the arabinoadenosine derivatives **15b**.[86] This reaction occurs with inversion of the configuration of the C(2′) atom.

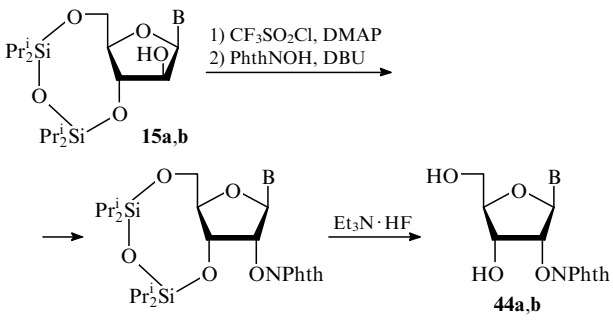

15a,**b** **44a**,**b**

B = Ura (**a**), Ade (**b**).

d. Synthesis of nucleosides containing a thiol group

In this subsection, we shall consider the synthesis of 2′-thionucleosides and 2′-*O*-mercaptoalkylnucleosides. A review[87] devoted to the synthesis of various thionucleosides has been published recently; however, methods for the synthesis of C(2′)-derivatives are not considered there.

The first attempts to carry out the reaction of free O^2,2′-anhydrouridine **1**[88] or its protected derivative **45**[89] with sodium ethanethiolate resulted in 3′-*S*-ethylthio-3′-deoxyxylouridine **46** as the main product.

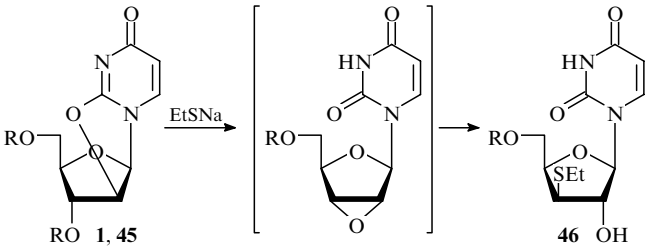

1, **45** **46**

1: R = H; **45**: R = Ac.

Later, it was found that preparation of the nucleoside 2′-thioderivatives **47a**–**e** by nucleophilic substitution at the C(2′) atom of the anhydronucleoside **1** requires the use of weaker nucleophiles, *e.g.*, thioacetic acid[90,91] and various thiols[92] and that the reaction was carried out in the presence of triethylamine or N^1,N^1,N^3,N^3-tetramethylguanidine. This approach was repeatedly used later.[93–96]

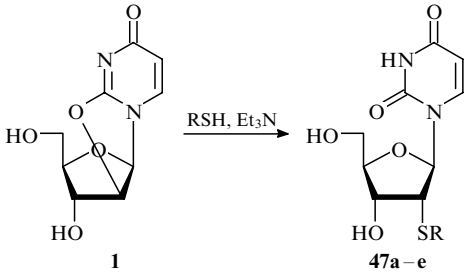

1 **47a**–**e**

R = Ac (**a**), Me (**b**), Et (**c**), Bn (**d**), 4-$MeOC_6H_4$ (**e**).

Recently, it was proposed that 2-(trimethylsilyl)ethanethiol in the presence of potassium carbonate can be used for the synthesis of pyrimidine 2′-thionucleosides.[97] The uridine **48** thus modified can be easily converted into the mixed disulfide **49** and the analogous cytidine derivatives **50** and **51**. The high cost of reagents is the main disadvantage of this method. An attempt to deprotect the thiol group in compound **48** with tetrabutylammonium fluoride yielded a complex mixture of reaction products.

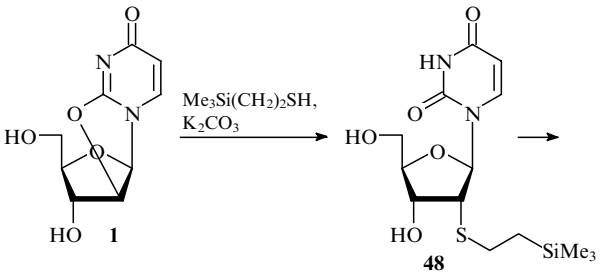

(*a*) Ac_2O, Py; (*b*) , $POCl_3$, Et_3N; (*c*) NH_3.

2′-Thiocytidine derivatives can be prepared not only by transamination of uridine,[93,97] but also by opening of the O^2,2′-anhydrocytidine ring.[98] An intramolecular attack of the 3′-*O*-dithiophosphate group at the C(2′) atom of substituted O^2,2′-anhydrocytidine **52** has been described.[98] This yields a mixture of 2′,3′-cyclodithiophosphate **53** and 2′,3′-cyclothiophosphate **54** which can be prepared from compound **53** by treatment with iodine.

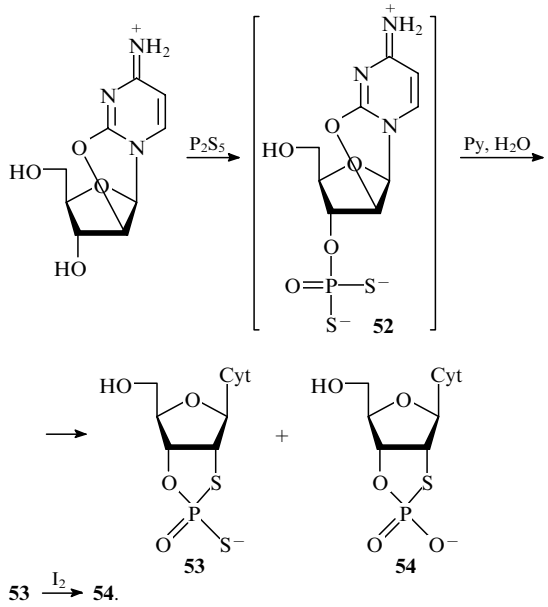

53 $\xrightarrow{I_2}$ **54**.

The synthesis of 2′-benzoylthioadenosine **55** by glycosylation of protected adenine with the ribose thioanalogue **56** has been described.[99]

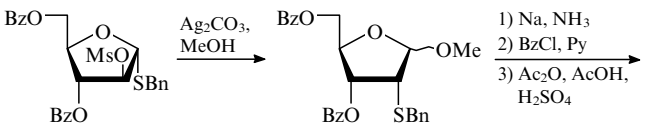

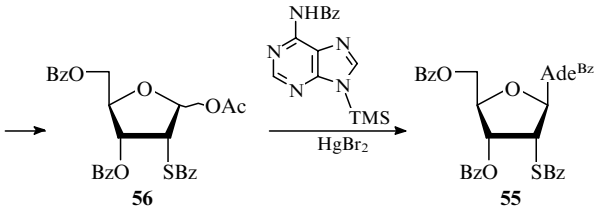

Although 2′-thionucleosides were first described about 25 years ago, they came into the routine practice of oligonucleotide synthesis only very recently.[93,100]

Two strategies are feasible for the synthesis of 2′-*O*-mercaptoalkylnucleosides, *viz*., the reaction of nucleosides with alkyl halides containing a protected thiol group,[101–103] or the preparation of 2′-*O*-hydroxyalkyl nucleosides with subsequent conversion of the hydroxy group into the thiol group.[104–107]

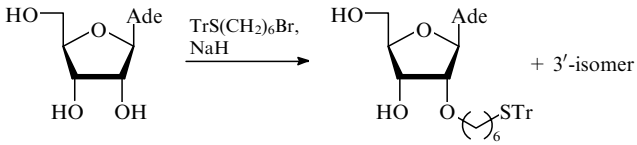

Tr = Ph_3C.

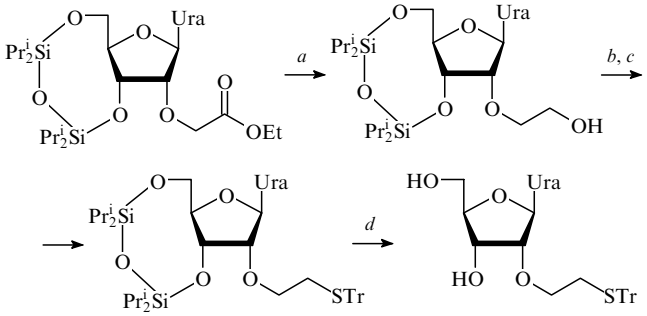

(*a*) $NaBH_4$, MeOH, Bu^tOH; (*b*) Ph_3P, CBr_4, MeCN; (*c*) TrSH, DBU, C_6H_6; (*d*) TBAF, THF.

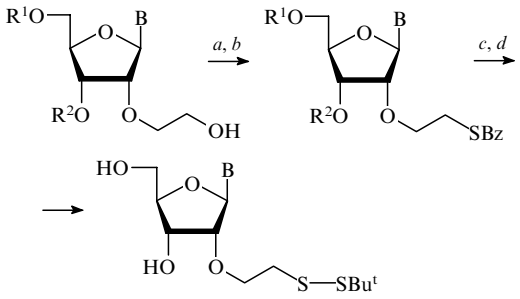

B = Ura, Cyt^{Bz}, $Gua^{Bu^iC(O)}$; $R^1 - R^2 = (Pr^i_2Si)_2O$, $R^1 = R^2 = Bu^tMe_2Si$.
(*a*) $MeSO_2Cl$, Py, CH_2Cl_2; (*b*) BzSH, Et_3N, DMF; (*c*) HF, MeCN; (*d*) 1-(*tert*-butylthio)hydrazine-1,2-dicarboxymorpholide, LiOH, MeOH, THF.

Moreover, target 2′-*O*-mercaptoalkyl nucleosides can be prepared *via* intermediate bromoalkyl nucleosides.[108]

2. Synthesis of nucleosides containing electrophilic groups

In contrast to nucleophilic groups, electrophilic groups (with the exception of monosubstituted phosphate and keto groups) cannot be directly introduced at the C(2′) atom of the nucleoside. This is due to the fact that such nucleosides are highly unstable and prone to β-elimination. Therefore, the use of linkers is the only possible approach to the attachment of electrophilic groups at the C(2′) atom of the nucleoside. A recently published review [109] devoted to the preparation of modified oligonucleotides containing electrophilic groups describes the synthesis of nucleosides containing

aldehyde and carboxy groups. Here we thought it expedient to highlight some aspects of the problem not touched upon in the above-cited review.

a. Synthesis of 2′-oxonucleosides

It has long been thought that 2′-oxo derivatives of nucleosides are highly unstable and undergo decomposition due to the high lability of the *N*-glycosidic bond.[110] Nevertheless, Robins and co-workers[111,112] succeeded in the oxidation of 3′,5′-protected uridine by CrO_3. Later, this approach was used by other authors.[113,114] Matsuda *et al.*[115–120] have performed the synthesis of protected 2′-oxonucleosides using the Swern oxidation by the oxalyl chloride–DMSO–triethylamine system.[121,122] This reaction requires protection of the heterocyclic base.[123,124] A recently published paper[125] deals with a comparison of various acylating reagents used in the Swern oxidation of 3′,5′-protected cytidine. It was shown that the use of trifluoroacetic anhydride provides the maximum yield of 2′-oxocytidine.

In 1990, Robins *et al.*[126] used the Dess–Martin 'periodinane' {1,1,1-triacetoxybenzo[*d*]-1,2-iodoxol-3(1*H*)-one} **57** for the oxidation of the 2′-hydroxy group.[127] At present, this is the method of choice,[128,129] since the reaction is selective and the product formed can be used in subsequent transformations without additional purification.

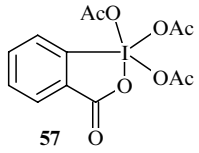

57

2′-Oxonucleosides are further used in the synthesis of the 2′-deoxy-2′-methylidene derivatives **58** by the Wittig reaction[130–133] or of the cyano derivatives **59**.[134,135] The modified nucleosides **58** and **59** are extensively employed in the therapy of cancer and viral diseases.[136,137] However, the introduction of these derivatives into the oligonucleotide chain results in significant destabilisation of the NA duplex;[138] therefore, their use in the synthesis of modified oligonucleotides is hardly justified.

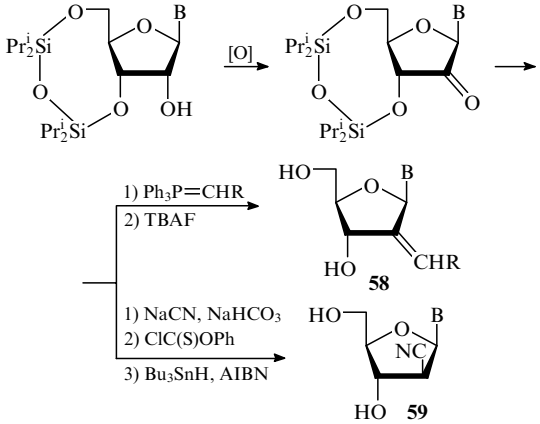

B is a free or protected heterocyclic base,
R = Alk.

b. Synthesis of nucleosides containing an aldehyde group

Synthesis of nucleosides containing an aldehyde group in the 2′-position is usually carried out by oxidative cleavage of their precursors (*vic*-diol derivatives) by sodium periodate.

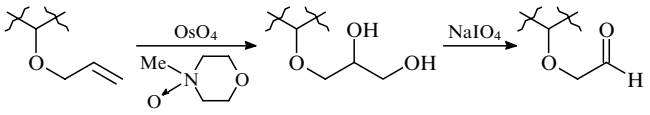

The choice of this strategy is determined by a number of factors. First, the oxidation of the vinyl group to the aldehyde group occurs under milder conditions than that of the primary hydroxy group. Second, if a nucleoside to be introduced into the oligonucleotide chain already contains an aldehyde group, the latter should be protected to prevent its reaction with the amino groups of heterocyclic bases and phosphorus(III) derivatives and oxidation by iodine. Unfortunately, no suitable protecting group has been found so far. Thus the *N*,*N*′-bis(3-chlorophenyl)imidazolidine protecting group[139] recommended for the protection of the aldehyde group of 5-formyl-2′-deoxyuridine has not found wide application, because its removal requires long-term treatment of the oligonucleotide **60** with 80% acetic acid, which leads to the degradation of even the most stable homothymidine oligonucleotides.

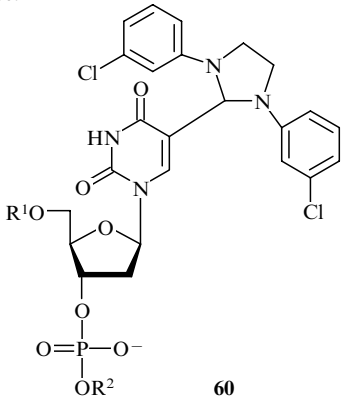

60

R^1 and R^2 are fragments of an oligodeoxyribonucleotide chain.

Studies by Glick and co-workers[105,106] who first performed the synthesis of the 2′-*O*-allyl pyrimidine nucleoside derivatives **61a**,**b**, their subsequent oxidation to the *vic*-diols **62a**,**b** and then cleavage to the aldehydes **63a**,**b**, represent an example of this methodology.

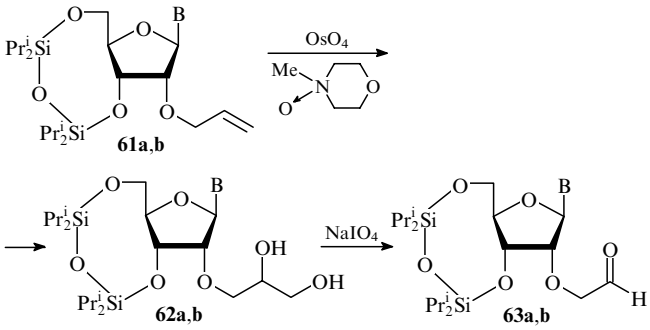

B = Ura (**a**), Cyt^{Bz} (**b**).

A similar approach was used in other studies[140,141] with the only exception that the *vic*-diol group of protected uridine **62a** was benzoylated into a 3′-phosphoroamidite derivative, which was then used in automated oligonucleotide synthesis. The aldehyde group was generated at the oligonucleotide level.

Martin[71] proposed the use of isopropylideneglycerol and glycidol toluene-*p*-sulfonates for the alkylation of the 2′-hydroxy group of the protected nucleoside **64**. The *vic*-diol fragment was generated upon acid hydrolysis of the isopropylidene protecting group in the modified uridine **65** or of the oxirane **66** (Scheme 3).

Scheme 3

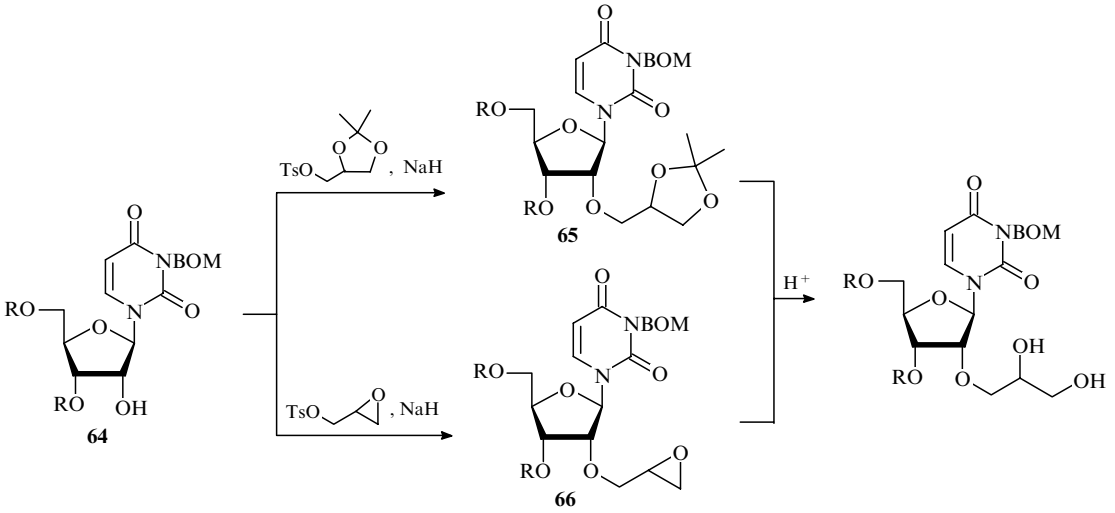

R = 2,4-$Cl_2C_6H_3CH_2$.

Mention should also be made of the recently published reviews [142–144] devoted to the synthesis and applications of nucleoside and oligonucleotide dialdehyde derivatives.

c. Synthesis of nucleosides containing a carboxy group

Studies devoted to the synthesis of 2′-*O*-alkoxycarbonyl methylnucleosides are generalised in the review.[109] Here, we shall consider only those publications which have not been included in that review [109] or demand additional discussion.

Alkylation of 3-*N*-(benzyloxymethyl)ribothymidine containing free hydroxy groups [145] occurred with high regiospecificity (the isomer ratio 2′ : 3′ was 9 : 1) (however, the yield of the 2′-isomer is not indicated).

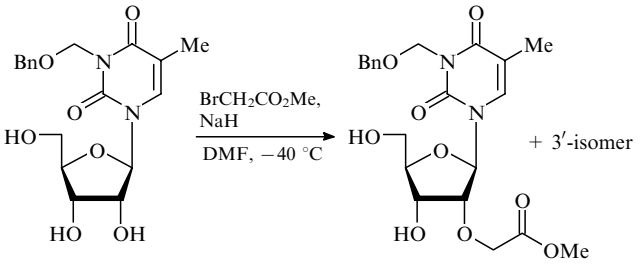

The preparation of 2′-methoxycarbonylmethylthio-2′-deoxyuridine **67** has been described.[94,95] The alkylation of the nonprotected derivative **68** by methyl bromoacetate partly involved the N(3) atom of the heterocyclic base.

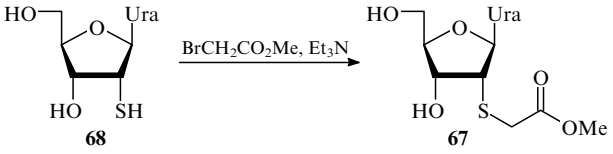

According to literature data,[146] the 2′-*S*-alkyl group is exposed to the major groove of the DNA duplex contrary to the 2′-*O*-alkyl group, which is exposed to the minor groove.[147] The difference in the arrangement of reactive groups in the NA duplexes allows preparation of conjugates with different properties from modified oligonucleotides and other molecules.

d. Synthesis of nucleosides containing other electrophilic groups

Studies by Sekine *et al.*[148,149] describe the synthesis of nucleosides and oligonucleotides containing a 2′-phosphate or a 2′-thiophosphate group. The 3′- and 5′-protected nucleosides **69a–d** were converted into the trivalent phosphorus derivatives **70a–d**; their subsequent oxidation with *tert*-butyl hydrogen peroxide or sulfur yielded 2′-phosphates **71a–d** and thiophosphates **72a–d**, respectively.

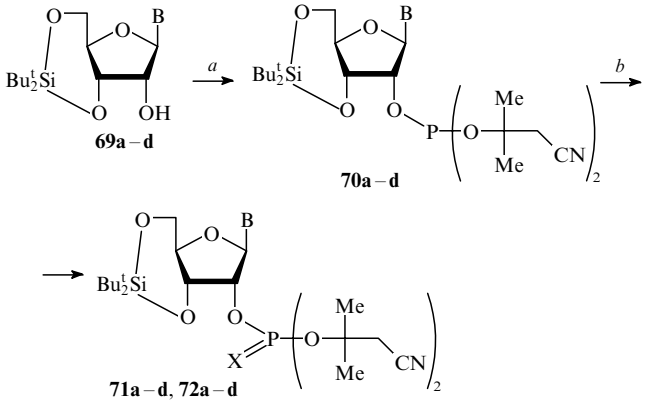

B = Ura^{Bz} (**a**), $Cyt^{Bu^tC(O)}$ (**b**), Ade^{Bz} (**c**); 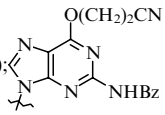 (**d**);
71a–d: X = O; **72a–d**: X = S;
(*a*) $Pr^i_2NP(OCMe_2CH_2CN)_2$, TetrH; (*b*) Bu^tO_2H or S_8;
TetrH is tetrazole.

The conversion of the 2′-amino group of modified uridine **73** into the isothiocyanate group, which can further be introduced into reactions with various nucleophiles, has been described.[150]

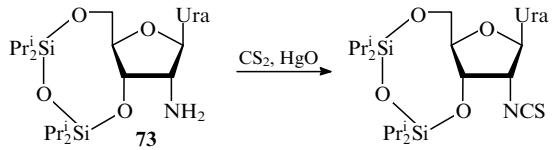

These data suggest that the methodology for synthesis of modified nucleosides containing free or protected reactive groups in the 2-position of the carbohydrate fragment is fairly well developed. The former are used for the preparation of conjugates with various compounds, whereas the latter are employed for the preparation of protected phosphoramidite derivatives for oligonucleotide synthesis.

III. Synthesis of conjugates based on 2′-modified nucleosides and oligonucleotides

Two, different in principle, approaches to the synthesis of NA, *viz*., chemical and enzymatic, are known. The overwhelming majority of 2′-modified oligonucleotides have been synthesised using the chemical approach. The latter implies initial preparation of protected nucleoside derivatives for automatic oligonucleotide synthesis. Natural $3' \rightarrow 5'$ internucleotide bonds are usually formed using 3′-phosphoramidite nucleoside derivatives, although some exceptions are possible. The dimethoxytrityl protecting group is widely used for the protection of the 5′-hydroxy group, whereas amino groups of heterocyclic bases are protected by groups that are labile in alkaline media. This approach enables the synthesis of oligomers containing up to 80 – 100 nucleotides. NA with longer chains are synthesised using chemical [151] or enzymatic [152] ligation.

The use of the enzymatic approach, which entails the incorporation of nucleoside 5′-triphosphates into NA using DNA and RNA polymerases, is confined to 2′-amino-2′-deoxy- [153] and 2′-alkoxyaminonucleosides.[154, 155] In addition, the substrate properties of pyrimidine 2′-amino-2′-deoxynucleoside triphosphates are inferior to the natural nucleoside triphosphates.[156]

Oligonucleotide 2′-conjugates can be prepared using three different approaches. The first of them includes the preparation of nucleoside conjugates with other compounds and their subsequent introduction into the automated oligonucleotide synthesis. The stability of phosphoramidite derivatives of conjugates in the course of the oligonucleotide synthesis and post-synthetic treatments is a prerequisite. The possibility of selective conjugation and no need for post-synthetic modifications of oligonucleotides are considered as advantages of this method. However, this requires considerable amounts of modified nucleosides, which significantly restricts the potential of this method.

The second approach consists of the conjugation of 2′-modified oligonucleotides immobilised on a polymeric support. To achieve this, a modified fragment containing a 2′-protected reactive group is incorporated into the oligonucleotide chain in the course of solid-phase chemical synthesis. The protecting group in this fragment should retain stability throughout the oligonucleotide synthesis and be selectively removed on its termination without any effect on the newly formed bonds in the protected oligonucleotide. 2′-Hydroxy and amino groups are protected either by the allyloxycarbonyl group, which is removed by palladium(0) complexes, or by the fluorenylmethoxycarbonyl group, which is removed upon treatment with morpholine or piperidine. The levulinoyl and phthaloyl groups are used for the protection of hydroxy and amino groups, respectively, and are removed by hydrazinolysis. Fluorenylmethyl protection, which is removed by treatment with morpholine or piperidine, is used for the carboxy group. Various photolabile protecting groups are also used for this purpose. The use of *tert*-butyldimethylsilyl and *tert*-butyldiphenylsilyl protecting groups is limited to automated synthesis on polystyrene carriers, since controlled-pore glass (CPG) support is destroyed upon removal of protecting groups under the action of the fluoride anion.

Conjugation is carried out after deprotection of the reactive group. Oligonucleotide conjugates immobilised on a polymeric support are washed to remove excess reagents, deprotected, and the product is split from the solid phase. The conjugation is usually carried out in anhydrous organic solvents, especially in the case of conjugates with hydrophobic compounds that are poorly soluble in aqueous and aqueous-organic media. Selective removal of 2-cyanoethyl protecting groups from phosphate groups by treatment with morpholine increases the hydrophilicity of the protected oligonucleotide and favours its conjugation in aqueous – organic media. The fact that protection of heterocyclic bases increases the lability of the *N*-glycosidic bond should also be taken into consideration.

The third approach entails the synthesis of oligonucleotide conjugates in solution. In this case, the protection of the reactive group in the 2′-position should be stable under conditions of oligonucleotide synthesis and be easily removed in the course of standard post-synthetic treatments. Side reactions with the imino and amino groups of heterocyclic bases, *e.g*., during the amide bond formation in compounds containing carboxy groups, can occur, which is a limitation of this method.

1. Synthesis of nucleoside 2′-conjugates

Three different approaches to the synthesis of nucleoside 2′-conjugates with various compounds are possible. The first of them entails direct attachment of various molecules to the 2′-hydroxy groups of nucleosides with formation of ether,[56] carbamate [76] or phosphotriester [157] bonds. The second approach consists of preliminary attachment, to the C(2′)-atom, of a linker containing an amino [57] or a carboxy group,[79] which is then made to react with another compound to form an amide bond. Acylation of 2′-amino-2′-deoxynucleosides is yet another route.

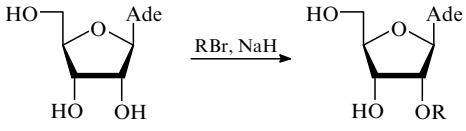

74a – c

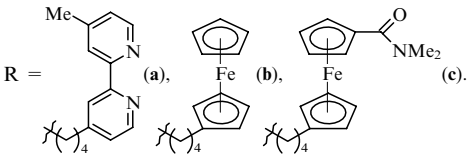

The preparation of the adenosine derivatives **74a – c** containing 2,2′-bipyridine and ferrocene residues linked to the O(2′) atom through a butylene bridge has been described.[158 – 160] The alkylation of adenosine occurs regiospecifically, the yields of 3′-derivatives are insignificant.

A similar alkylation procedure was used [161] for the introduction of an azobenzene fragment at the O(2′)-atom of protected uridine **25a**. The resulting derivative **75** was deprotected and incorporated into an oligonucleotide.

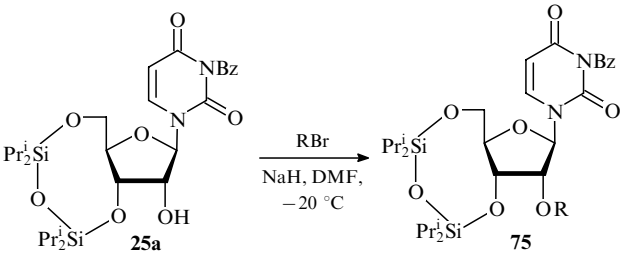

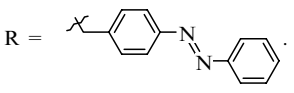

The alkylation of 3′,5′-protected uridine **76** by substituted methyl chlorides in the presence of potassium hydroxide was used for the introduction of polyaromatic molecules into the carbohydrate fragment of the nucleoside.[162, 163] It is of note that the heterocyclic base was not affected, compounds **77a**,**b** being the only reaction products.

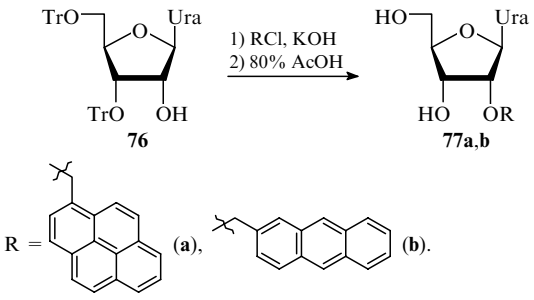

The metal-directed alkylation of uridine has been described.[164, 165] Prior to the reaction, the *vic*-diol system of N^3-benzoyluridine (**78**) was activated by dibutyltin oxide and the intermediate formed was introduced into the reaction with 2-bromomethylanthraquinone. The addition of caesium fluoride to the reaction mixture increases the proportion of the 2′-isomer **79**.

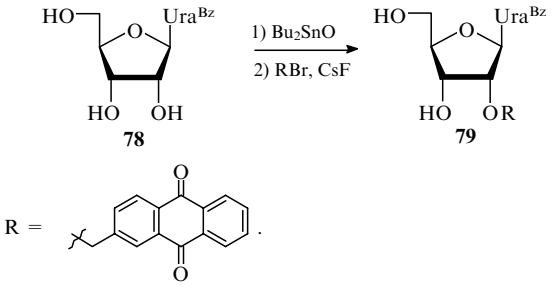

Chattopadhyaya and co-workers[166, 167] have developed a simple and convenient scheme for the attachment of a spermine C-homologue to a nucleoside through a 2′-phosphate group. The 2′-phosphoramidite **80** formed from the protected arabinouridine **15a** was made to react with the hydroxy derivative of the spermine analogue with subsequent oxidation of the phosphorus-containing fragment and deprotection of the hydroxy groups. In these studies, spermine was considered as a cationic constituent able to increase the stability of the NA duplex due to interaction with the phosphate groups of the opposite chain. Similarly, phenazine derivatives were attached to the O(2′)-atom of arabinouridine through a phosphate group.[157]

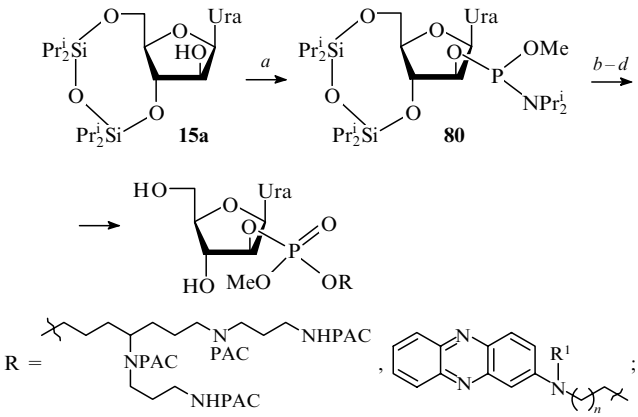

PAC = $PhOCH_2C(O)$; R^1 = PAC, Me; n = 2, 4, 6.
(*a*) $Pr^i_2NP(Cl)OMe$, Pr^i_2NEt; (*b*) ROH, TetrH;
(*c*) I_2, THF, Py, H_2O; (*d*) TBAF.

Yet another approach to the synthesis of nucleoside 2′-conjugates has been developed by Cook and co-workers.[168, 169] This included the introduction of fragments of various compounds into the 2′-position of uridine through an aminohexyl linker. This method was used in the synthesis, from one modified nucleoside, of hydrophobic derivatives **81a**–**d**[168, 169] as well as compounds with fluorescent (**81e**[170]) and electrochemical (**81f**[171]) labels suitable for incorporation into the oligonucleotide chain.

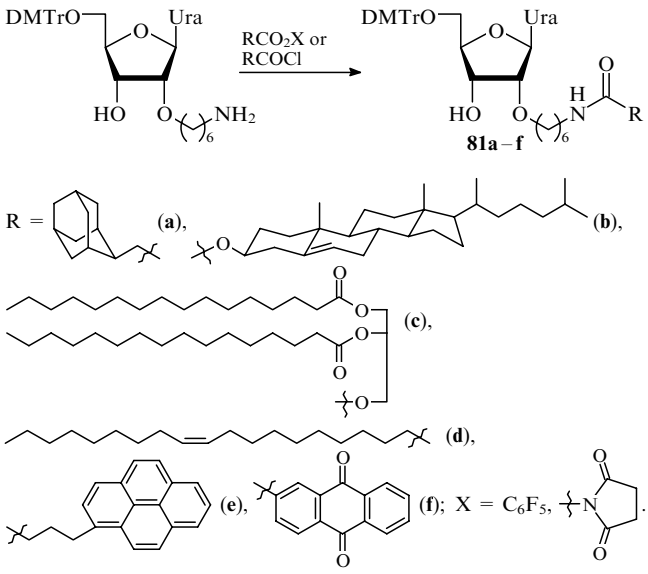

Cholesterol was attached to the modified nucleosides **82a**,**b**.[172] The resulting derivatives **83a**,**b** were introduced into a standard automated oligonucleotide synthesis. The presence of a cholesterol residue in the modified oligonucleotides strongly affects their pharmacodynamic properties.

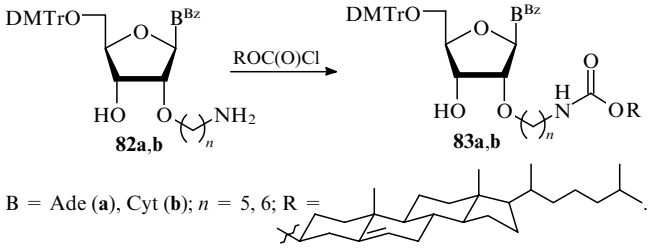

Keller and Haner[79, 173] have carried out reactions of 2′-*O*-(methoxycarbonylmethyl)nucleosides **42** and **84a**,**b** with 2-[(2-aminoethyl)amino]anthraquinone, octylamine and 6-(*N*,*N*-dimethylamino)hexylamine. The resulting nucleoside conjugates **85a**–**c** were first converted into phosphoramidite derivatives and then incorporated into the oligonucleotide chain. The presence of such modifications in oligonucleotide molecules increases the thermal stabilities of the respective NA duplexes in comparison with native analogues.

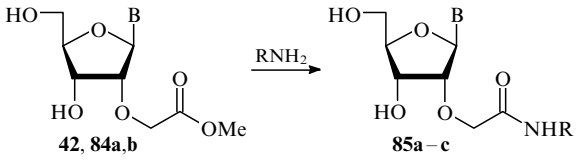

B = Cyt^{Bz} (**84a**, **85a**), Ade^{Bz} (**84b**, **85b**), Thy (**42**, **85c**);

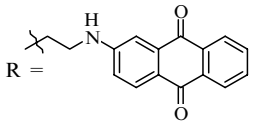

Starting from protected uridine **86** containing an activated 2′-carboxy group and protected 5-aminomethyl-2′-deoxyuridine **87**, Sekine and co-workers[174, 175] have synthesised the dinucleoside **88;** this was converted into a dinucleoside phosphate having a fixed conformation[174] and incorporated into the oligonucleotide **89** (Scheme 4).[175]

The synthesis of 2′-*O*-carboranylmethyluridine **90** starting from the propargyluridine derivative **91**[176, 177] or protected allofuranose **92** has been carried out.[178] In the latter case, the attach-

Scheme 4

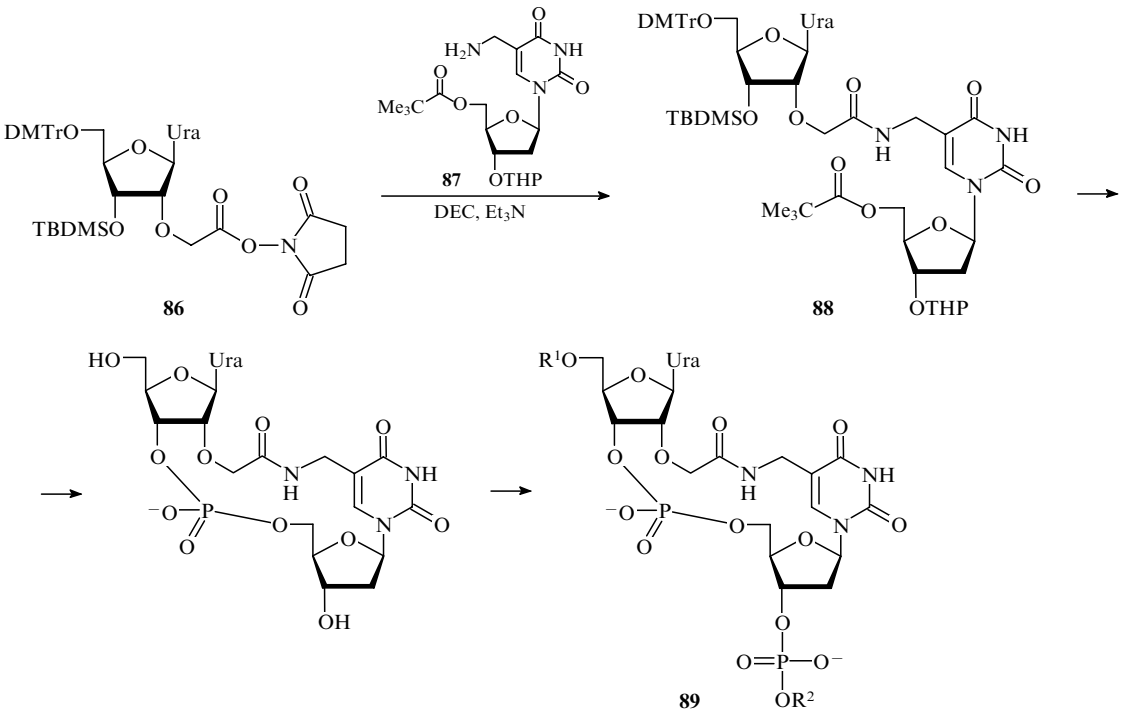

TBDMS = Bu^{t}Me$_2$Si; DEC = Me$_2$N(CH$_2$)$_3$N=C=NEt; R^1 and R^2 are fragments of an oligonucleotide chain.

ment of decaborane to the carbohydrate **92** gave first the 3′-isomer **93**; after removal of isopropylidene protecting groups and cleavage of the *cis*-diol system, this was transformed into a ribofuranose derivative and used for glycosylation.

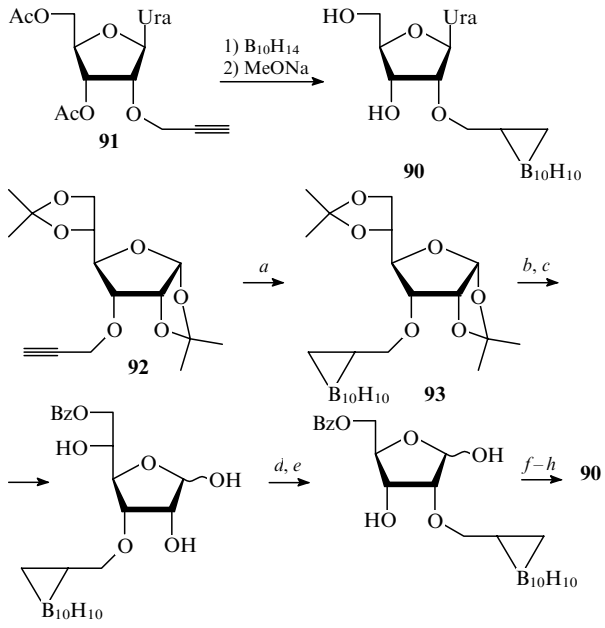

(*a*) $B_{10}H_{14}$; (*b*) H^+; (*c*) BzCl; (*d*) $NaIO_4$; (*e*) Py, H_2O, Δ; (*f*) Ac_2O, Py; (*g*) Ura^{TMS}, TMSOTf; (*h*) MeONa.

Carboranyl nucleosides are used in boron neutron-capture therapy of malignant tumours.[179,180] *In vivo* studies have shown[181] that the nucleoside **90** effectively penetrates into cells, but is not phosphorylated. The intracellular boron concentration varies from 5 to 35 μg g^{-1}, *i.e.*, is sufficient for the implementation of efficient boron neutron-capture therapy. Further studies have shown[182] that the incorporation of the nucleoside **90** into the oligonucleotide chain significantly decreases the stability of the DNA duplex, most probably due to the formation of a negatively charged *nido*-form of carborane under the action of ammonia upon standard post-synthetic treatments.

Synthesis of conjugates based on 2′-amino-2′-deoxyuridine **5** included the acylation of the amino group with acids activated by dicyclohexylcarbodiimide (DCC) or a mixture of 1-hydroxybenzotriazole (HOBT) with *O*-(benzotriazol-1-yl)-*N*,*N*,*N*′,*N*′-tetramethyluronium (HBTU) hexafluorophosphate. This approach was used for the introduction, into the 2′-position of the nucleoside, of various fluorescent labels, such as 6-dimethylamino-2-naphthalene (**94a**),[183,184] the dansyl group (**94b**),[185] coumarin (**94c**)[186] and pyrene (**94d**),[187] of the electrochemical label ferrocene (**94e**),[188–190] of phenanthroline (**94f**)[191] (chemical nuclease in the presence of multicharged metal ions) and of nalidixic acid **94g**;[192] the attachment of the latter to the 3′-end of an oligonucleotide significantly increases the thermal stability of the duplex formed.

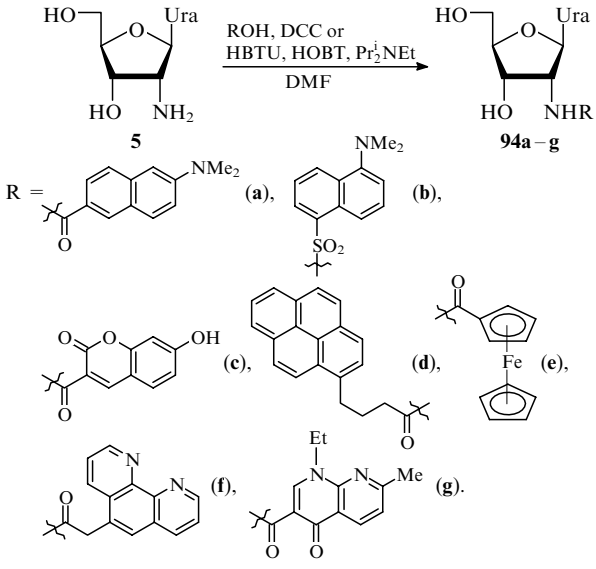

Protected 2′-amino-2′-deoxyuridine **11** was acylated with amino acids.[193] The derivatives **95a–d** obtained were converted into phosphoramidites and incorporated into ribozymes to increase catalytic activity and stability against nucleases.

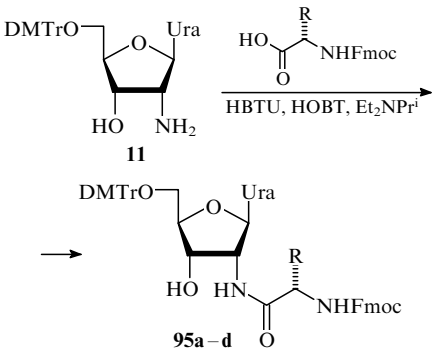

R = Me (**a**), Bn (**b**), $(CH_2)_4NHFmoc$ (**c**), CH_2CO_2Bn (**d**);

Fmoc = 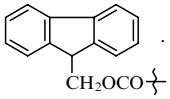

The protected 2′-amino-2′-deoxyuridine **95c** acylated with *N*-protected lysine served as a basis for the preparation of the bisconjugate **96** containing peracetylgalactosamine residues.[194] Unfortunately, subsequent reactions of the nucleoside phosphoramidite derivative **96** were strongly hampered due to steric hindrances.

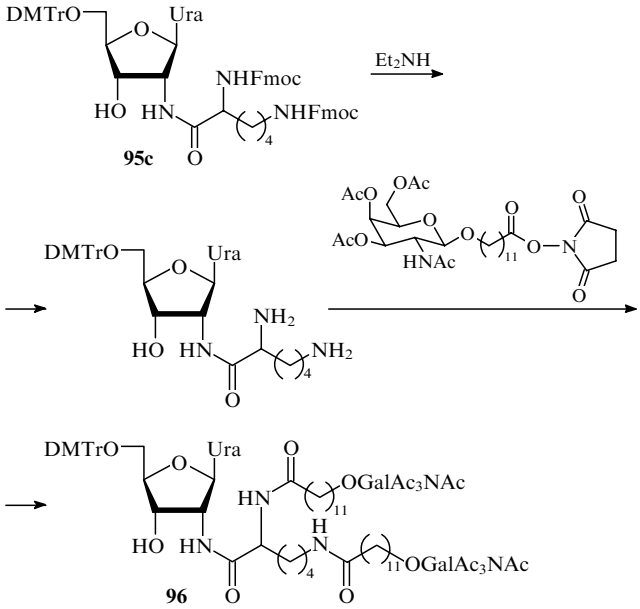

Acylation of free and protected 2′-amino-2′-deoxyadenosine with various aromatic acids in the presence of 1-(3-dimethylaminopropyl)-3-ethylcarbodiimide has been described.[34, 195]

An unusual version of the acylation of 2′-amino-2′-deoxyadenosine has been proposed.[196] Here, the role of acylating agents is played by activated *N*-sulfo-*N*-cyanomethylamides of carboxylic acids immobilised on a solid phase (safety catch linker).[197] Aminomethylated polystyrene containing 4-substituted benzoic or butyric acid residues were used as polymeric supports. The yields in this reaction are more than 95%.

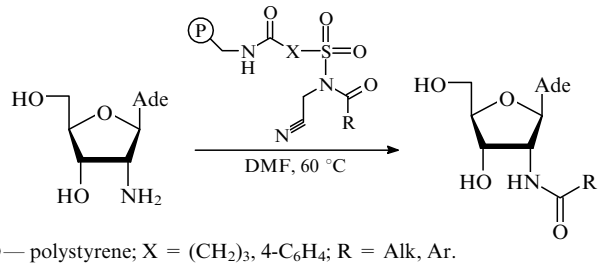

Ⓟ — polystyrene; X = $(CH_2)_3$, 4-C_6H_4; R = Alk, Ar.

This approach was used for the preparation of various 2′-aroyl derivatives of N^6-substituted 2′-amino-2′-deoxyadenosine and 2′,5′-diamino-2′,5′-dideoxyadenosine.[198–201]

An original procedure for the synthesis of the nucleoside **97** having a methoxalylamido fragment in the 2′-position by the reaction of protected 2′-amino-2′-deoxyuridine **11** with methoxalyltetrazole has been developed by Polushin.[202]

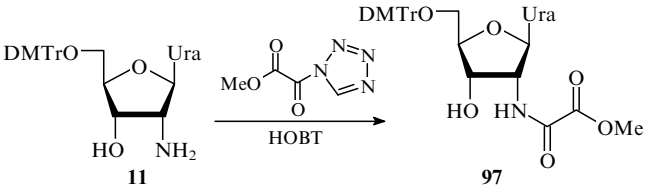

Later[203] 2′-succinimido-2′-deoxyuridine **98** and the dendrimers **99**, **100**[204] based on it were synthesised.

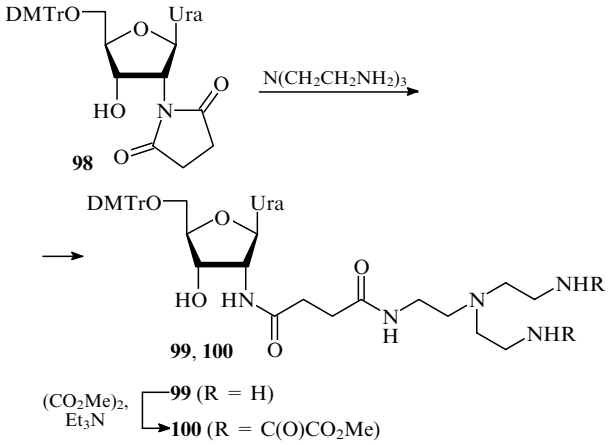

The imino derivative **101** synthesised starting from 2′-amino-2′-deoxyuridine **11** reacted *in situ* with bis(bipyridine)ruthenium(II) chloride.[205, 206] The resulting nucleoside **102** was converted into a phosphoramidite derivative and incorporated into the oligonucleotide chain; however, the yield in the condensation step was extremely low.[27] The yield in the immobilisation of the nucleoside **102** on a polymeric support using a succinate linker was comparable to those for non-modified nucleosides.[206] The complex **102** within the oligonucleotide is stable under the conditions of the post-synthetic treatments with saturated ammonia. Derivatives of the type **102** are the optimum reagents for modification of 3′- (see Ref. 206) and 5′-ends[207] of oligonucleotides, since they cause minimum changes in the structure of the DNA duplex.

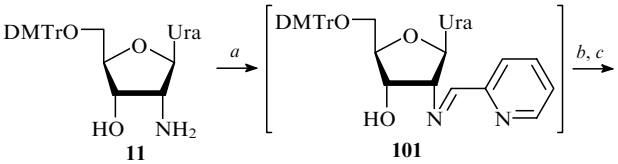

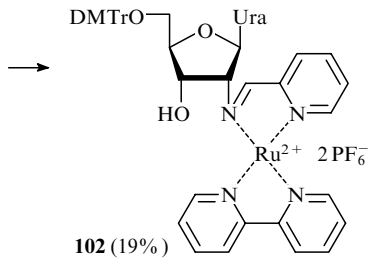

(*a*) 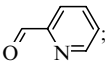 ; (*b*) $Ru(bpy)_2Cl_2$; (*c*) KPF_6; bpy is 2,2′-bipyridine.

The nucleoside **103** containing a picolylamino group in the 2′-position has recently been synthesised.[27] The introduction of such a modified fragment into the oligonucleotide chain decreases the thermal stability of the DNA duplex by 2–4 °C. These oligonucleotides can also be used for ruthenium chelation.

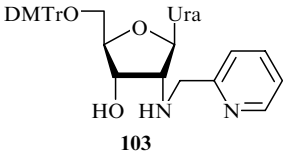

103

2. Solid-phase synthesis of oligonucleotide conjugates

The publications on this subject are few in number, although in some cases, *e.g.*, for incorporation of hydrophobic molecules, this method is the optimum and is the only possible solution for the construction of combinatorial libraries. The term 'combinatorial libraries' is used to encompass a set of conjugates containing identical cores (*e.g.*, oligonucleotides), but differing in the fragments of molecules attached to them. It is of note that such sets of conjugates are prepared simultaneously, *e.g.*, by treatment of an oligonucleotide containing the amino group with a mixture of activated carboxylic acids with subsequent separation of the reaction products. Combinatorial oligonucleotide libraries are extensively used in bioorganic chemistry and molecular biology, particularly, in the search for compounds that are highly resistant to nucleases.[208]

An alternative approach to the synthesis of conjugates based on immobilised oligonucleotides **104** containing a protected 2′-*O*-(6-aminohexyl)nucleoside has been described by Manoharan and co-workers [209] Selective removal of the allyloxycarbonyl protecting group by a palladium(0) complex and subsequent reaction of pyrenylbutyric acid ester with *N*-hydroxysuccinimide give compound **105a.** The internucleotide bonds and protecting groups of heterocyclic bases and internucleotide phosphates remained intact. Later, the same authors [210] carried out the synthesis of oligonucleotides **105b** containing a guanidine group attached to a 2′-*O*-aminohexyl linker (Scheme 5).

A recently published paper [211] describes the synthesis of the oligonucleotide conjugates **106a**,**b** with 3′-terminal 2′-acylamido groups. A nucleoside with an *N*-protected phenylalanylamide residue in the 2′-position was immobilised on a polymeric support through a standard succinate linker. The allyloxycarbonyl protecting group in compound **107** was selectively removed and the immobilised nucleoside was acylated and introduced into the standard oligonucleotide synthesis (Scheme 6).

Yet another approach to the attachment of an amino group to the 3′-end of an oligonucleotide entails the use of a 5′-phosphor-

Scheme 5

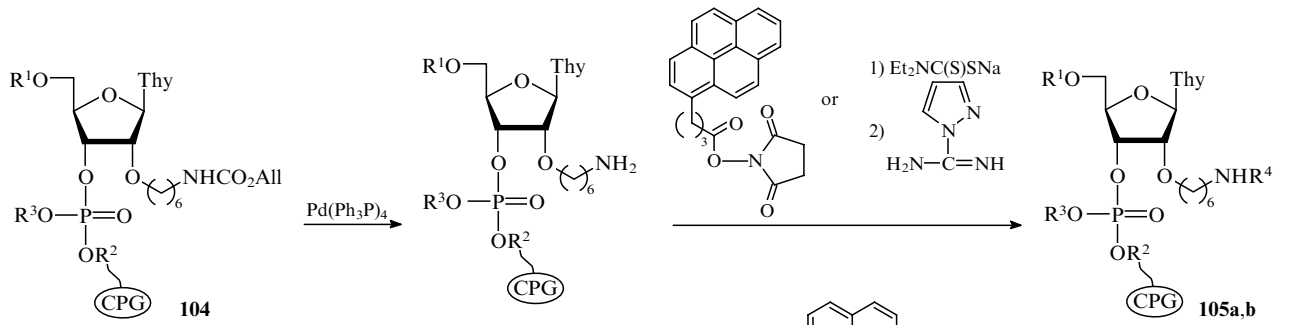

R^1 and R^2 are fragments of a protected oligonucleotide chain; $R^3 = (CH_2)_2CN$; CPG is controlled-pore glass.

R^4 = 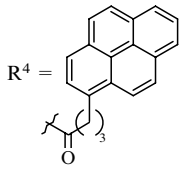 (**a**), 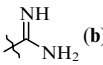 (**b**);

Scheme 6

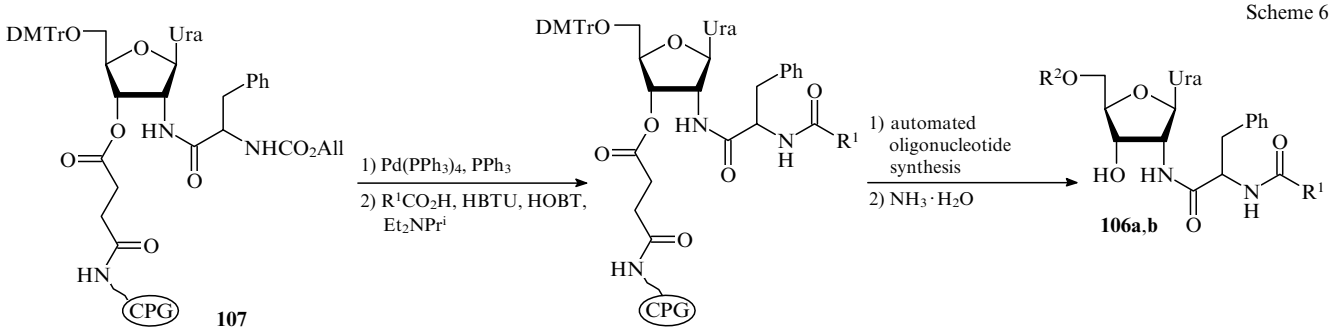

R^1 = 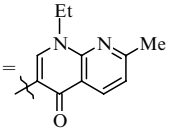 (**a**), 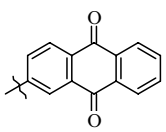 (**b**); R^2 is a fragment of an oligonucleotide chain.

Scheme 7

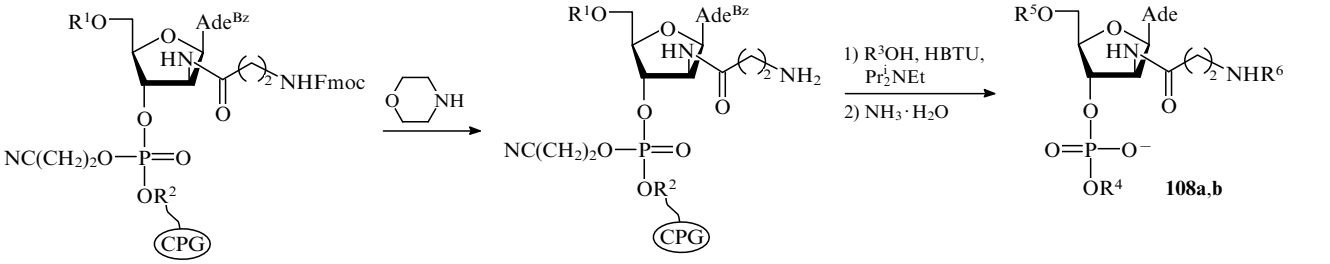

R^1 and R^2 are fragments of a protected oligonucleotide chain; R^3 = –Gly-LeuNHFmoc, –Gly-Phe-D-Ala-TyrNHFmoc; R^4 and R^5 are fragments of a deprotected oligonucleotide chain; R^6 = –Gly-LeuNH$_2$ (**a**), –Gly-Phe-D-Ala-TyrNH$_2$ (**b**).

amidite derivative of a modified nucleoside that is incorporated into the oligonucleotide chain by reversed (5′→ 3′) automated oligonucleotide synthesis.[211] High yields in the *N*-acylation step enable the construction of a combinatorial library and investigation of the resistance of 3′-oligonucleotide conjugates against nucleases.[208]

Synthesis of peptide–oligonucleotide conjugates has been described by Oretskaya and co-workers[212] The protected amino group of 2′-(β-alanyl)amido-2′-deoxyarabinoadenosine incorporated into oligonucleotides was selectively deprotected by morpholine or piperidine. Subsequent acylation with *N*-protected peptides and removal of protecting groups afforded the target conjugates **108a**,**b** with a degree of conversion of 80%–90% (Scheme 7).

Hwang and Greenberg[213, 214] have recommended the use of photo-removable 4,5-dimethoxy-2-nitrobenzyloxycarbonyl protection for the 2′-amino group of modified nucleosides. The reactivities of 2′-amino-2′-deoxy- and 2′-*O*-(4-aminobutyl)uridine groups of oligonucleotides in acylation reactions have been studied. In some cases, the yields of the products **109** and **110** were rather low (*e.g.*, the yield of the oligonucleotide–peptide conjugate **110b** was 30%) (Scheme 8).

Manoharan and co-workers[215] used phthaloyl protection (which is selectively removable by hydrazinolysis) of aminooxy groups of modified nucleosides. The aminooxy group is extremely reactive with respect to carbonyl compounds. This type of conjugation is extensively used in peptide chemistry.[216] The oximes thus prepared are stable over a broad pH range and can be reduced to *N*,*O*-disubstituted hydroxylamines which are even more stable under drastic conditions (Scheme 9).

Sawai and co-workers[94, 95] have proposed to simultaneously remove protecting groups and convert the ester group in a modified fragment into an amide group. In this way, dinucleoside monophosphates were prepared containing non-substituted (**111a**), *N*-alkyl (**111b**), *N*-aminoalkyl (**111c**) carbamoyl groups and a dendrimer (**111d**) in the 2′-position. It is of note that the yields of the target products were smaller in the case of more complex amines. When *N*-protected adenosine, cytidine and guanosine were used instead of thymidine and uridine, side transamination occurred.

Scheme 8

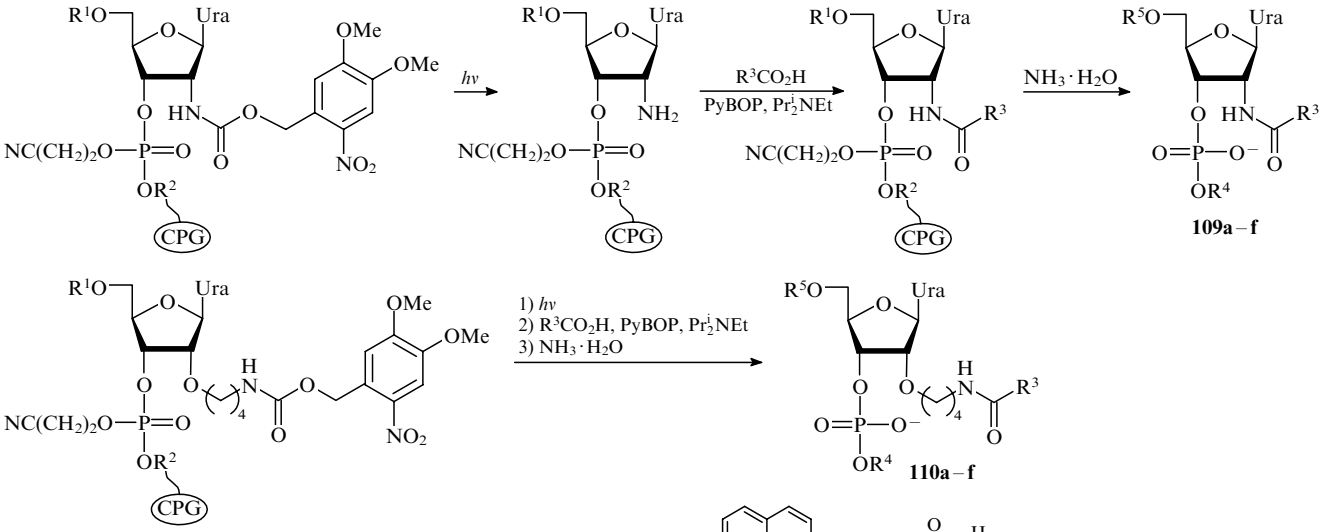

R^1 and R^2 are fragments of a protected oligonucleotide chain; R^3 = 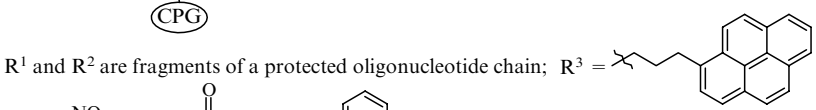 (**a**), 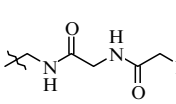 (**b**), 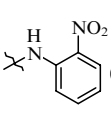 (**c**), 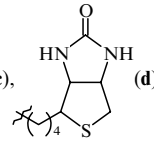 (**d**), 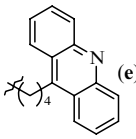 (**e**), 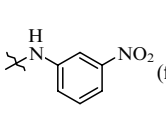 (**f**); R^4 and R^5 are fragments of a deprotected oligonucleotide chain;

PyBOP is benzotriazol-1-yloxytris(pyrollidino)phosphonium hexafluorophosphate.

Scheme 9

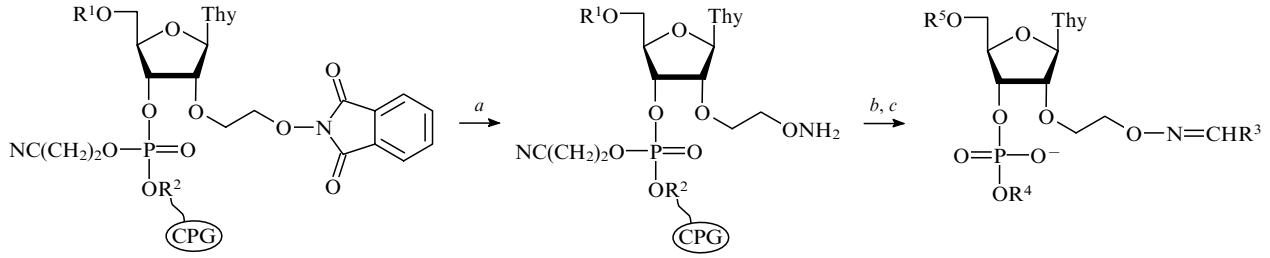

(*a*) $N_2H_4 \cdot H_2O$, Py, AcOH; (*b*) R^3CHO, DMF or MeCN; (*c*) $NH_3 \cdot H_2O$.

R^1 and R^2 are fragments of a protected oligonucleotide chain; R^3 = 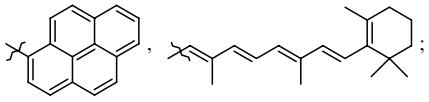
R^4 and R^5 are fragments of a deprotected oligonucleotide chain.

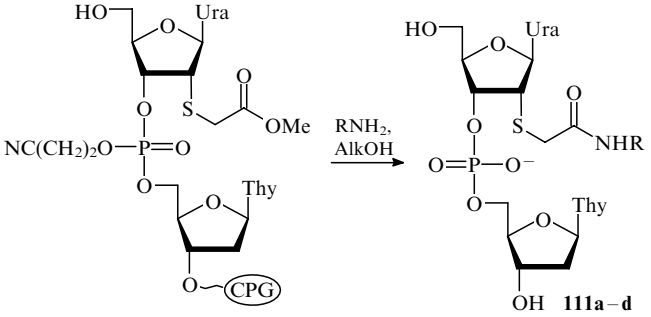

R = H (**a**), $(CH_2)_6Me$ (**b**), $(CH_2)_2NH_2$ (**c**), $(CH_2)_2N(CH_2CH_2NH_2)_2$ (**d**); Alk = Me, Et.

This methodology was further developed by Manoharan and co-workers [145] If primary amines were used, high yields of compounds **112a**–**c** were achieved within 24 h at room temperature, but the yield of compound **112d** in the reaction with dimethylamine was as low as 50%; at higher temperature, side products were formed.

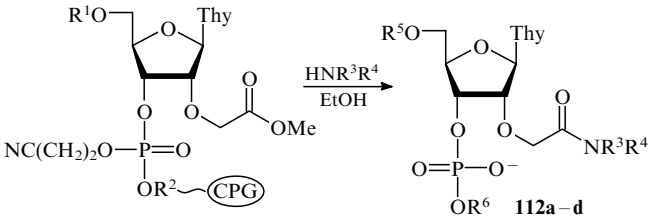

R^1 and R^2 are fragments of a protected oligonucleotide chain;
R^3 = H: R^4 = H (**a**), Me (**b**), $(CH_2)_2NMe_2$ (**c**); R^3 = R^4 = Me (**d**);
R^5 and R^6 are fragments of a deprotected oligonucleotide chain.

Polushin [202] has prepared a series of oligonucleotides **113** containing a methoxalylamido group in the 2′-position. This group is more electrophilic in comparison with ordinary ester group, which permits one to carry out reactions with amines under milder conditions without simultaneous splitting of the oligonucleotide from the polymer.

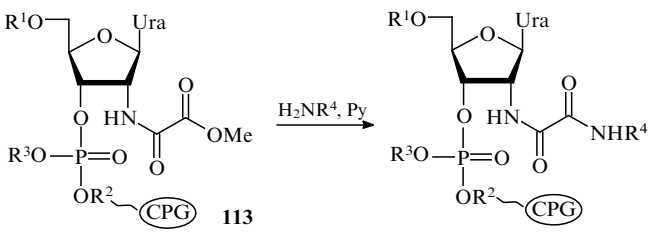

R^1 and R^2 are fragments of a protected oligonucleotide chain;
$R^3 = (CH_2)_2CN$; $R^4 = (CH_2)_{12}NH_2$.

In 2′-succinimido derivatives of 2′-deoxyuridine and -cytidine, the five-membered imide ring is opened upon reactions with various amines. [203, 204, 217]

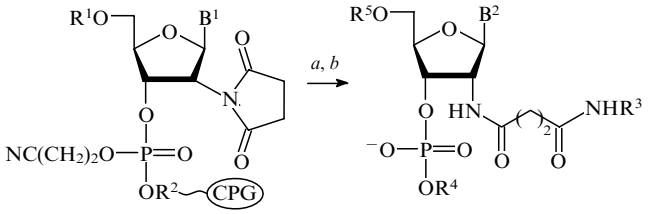

B^1 = Ura, Cyt^{Bz}; B^2 = Ura, Cyt; R^1 and R^2 are fragments of a protected oligonucleotide chain; R^3 = Me, $(CH_2)_2OH$, $(CH_2)_6OH$, $(CH_2)_3NMe_2$, $(CH_2)_n$Im; n = 2, 3; R^4 and R^5 are fragments of a deprotected oligonucleotide chain; (*a*) R^3NH_2; (*b*) $NH_3 \cdot H_2O$.

The same authors [204, 217] have described the synthesis of dendrimeric derivatives based on 2′-succinimido-2′-deoxyuridine incorporated into the oligonucleotide chain. The attachment of branched polyamines to a modified nucleoside fragment was followed by acylation of free amino groups with methoxalyltetrazole. Treatment of the dendrimer formed with histamine affords the conjugate **114** which is a potential chemical nuclease.

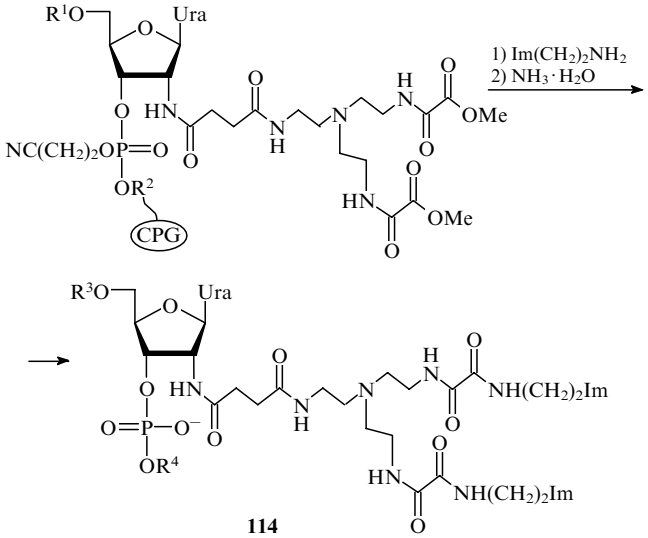

114

R^1 and R^2 are fragments of a protected oligonucleotide chain;
R^3 and R^4 are fragments of a deprotected oligonucleotide chain.

The incorporation of a bromoalkyl group into an oligonucleotide enables conjugation with nucleophiles, such as thiols and sodium azide. [108, 218] Thus the preparation of oligonucleotide conjugates with amines included initial synthesis of modified

oligonucleotides **115** immobilised on a polymeric support containing a ω-bromoalkyl group at the O(2′) atom.[219] These were treated with thioglycolic acid in the presence of a base. After the activation of the carboxy group in the acids formed, the latter reacted with various amines to yield compounds **116a–c**.

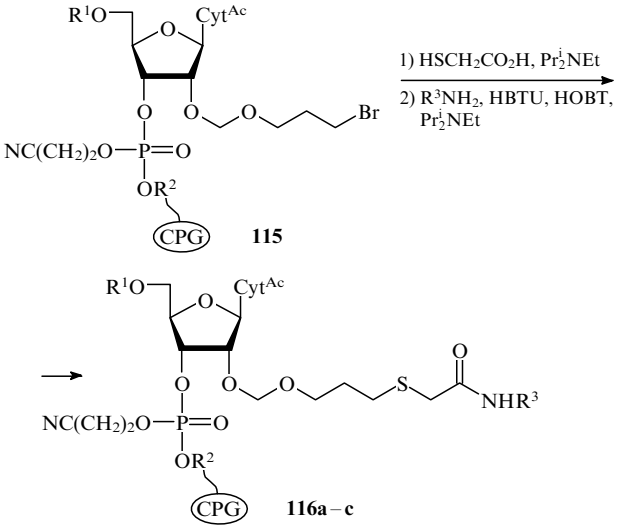

R[1] and R[2] are fragments of a protected oligonucleotide chain;

R[3] = 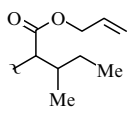 (**a**), Me (**b**), 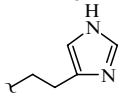 (**c**).

3. Solution synthesis of oligonucleotide conjugates

Oligonucleotides containing pyrimidine 2′-amino-2′-deoxyribonucleoside fragments have been especially extensively used for conjugation in solution. The amino group in the 2′-position has pK_a = 6.2,[220] which was confirmed by ^{1}H NMR (see Ref. 221) and ^{13}C NMR (see Ref. 222) spectroscopic data. This enables its selective acylation at appropriate pH precluding the involvement of amino groups of heterocyclic bases with pK_a from 3 to 5. The significant decrease in the melting temperature of the duplexes formed by 2′-amino-2′-deoxyribooligonucleotides with non-modified NA is the main disadvantage of this modification. Thus the melting temperature of a 15-membered duplex decreases by 2.7–13.8 °C depending on the structure of the duplex and the position of the modified fragment in the chain.[223]

The choice of a protecting group for the amino group of a modified fragment for the incorporation of 2′-amino-2′-deoxyribonucleosides into the oligonucleotide chain presents a problem. The use of trifluoroacetyl protection for this purpose was suggested, but the condensation of a commercially available 2′-trifluoroacetamido-2′-deoxyuridine phosphoramidite with a growing oligonucleotide chain occurs in a relatively low yield (~ 90% in 10 min),[224] which can be attributed to the high electronegativity of the trifluoroacetyl protecting group. This problem can be overcome by increasing the condensation time;[225] however, side reactions thus occur, which diminish the total yield of the oligonucleotide.[226] The trifluoroacetyl protecting group was also used for the protection of the amino group of 2′-amino-2′-deoxyguanosine.[227] The fluorenylmethoxycarbonyl protecting group meets all the requirements of oligonucleotide synthesis, but the thus protected 2′-amino-2′-deoxyuridine phosphoramidite derivative was unstable in an acetonitrile solution and was destroyed even in a solid state at −20 °C.[224, 228] Nevertheless, this group was used for protection.[229] The use of the phthalimide group was also proposed;[224] the latter was introduced with high yields and could be completely removed with standard post-synthetic treatments, but in this case the condensation efficiency could be increased by only 3%–5%. The use of the 2-(4-nitrophenyl)ethoxycarbonyl protecting group[230, 231] can hardly be called successful, since its removal demands preliminary 12-h treatment of the protected oligonucleotide with a 1 M solution of DBU in pyridine. The thus protected 2′-amino-2′-deoxynucleoside cannot be immobilised on a polymeric support using a succinate linker due to intramolecular $O \rightarrow N$ migration of the acyl group upon deprotection. The stability of the amide bond in the 2′-succinamide formed prevents the removal of the modified oligonucleotide from the polymeric support.

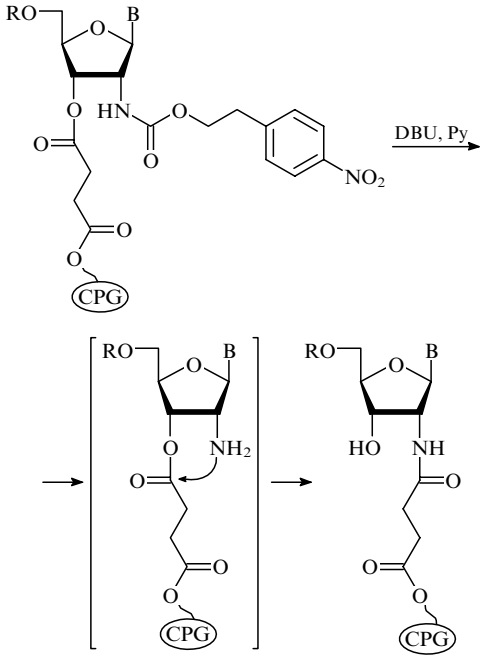

R is a fragment of a protected oligonucleotide chain;
B is a protected heterocyclic base.

A new approach, in principle, to the synthesis of oligonucleotides with 2′-amino-2′-deoxyribonucleoside fragments has been developed by Polushin *et al.*[232] The oligonucleotides **117** containing a 2′-azido-2′-deoxyuridine fragment were prepared using the phosphotriester method. The azido group was further reduced to the amino group by treatment with triphenylphosphine or tris(2-carboxyethyl)phosphine (TCEP) in the presence of water. However, this approach has not received wide application, since the solid-phase phosphotriester method is no longer used in oligonucleotide synthesis due to the lengthy reaction cycle and lower yields in the condensation step in comparison with the phosphoramidite method. Nevertheless, today it is the only approach which enables the synthesis of oligonucleotides containing 2′-amino-2′-deoxyribonucleoside fragments in the middle of the chain.

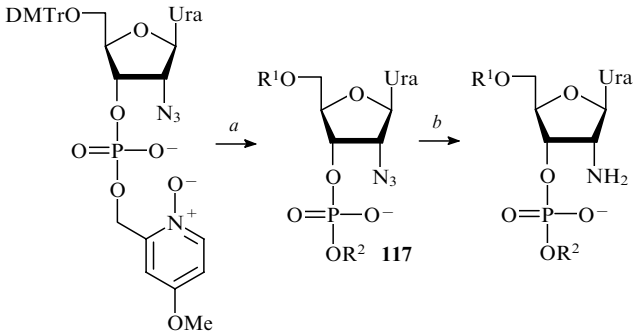

(*a*) is oligonucleotide synthesis; (*b*) Ph_3P or TCEP, H_2O, MeCN;
R[1] and R[2] are fragments of an oligonucleotide chain.

Synthesis of conjugates based on oligonucleotides containing 2′-amino groups is carried out using *N*-acylation in a borate, phosphate or carbonate buffer at pH 8–8.5. Under these con-

ditions, the amino groups of heterocyclic bases are protonated, which allows selective involvement of the 2′-amino group of the modified fragment. Activated carboxylic acids, isocyanates or isothiocyanates are used as acylating reagents. This approach was used for the preparation of conjugates (**118**–**120a**,**b**) with fluorescein isothiocyanate,[233–235] rhodamine 5-isocyanate,[222] a photochemically active diazirine derivative **120a**[236] and a spin label **120b**.[237]

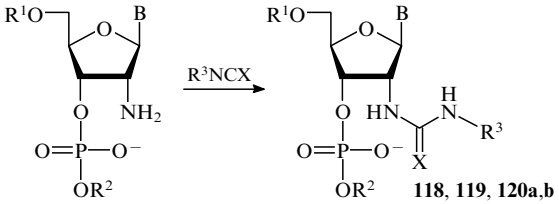

R^1 and R^2 are fragments of an oligonucleotide chain;
118: R^3 is fluorescein, X = S, B = Ura;
119: R^3 is rhodamine, X = O, B = Cyt.

120: R^3 = 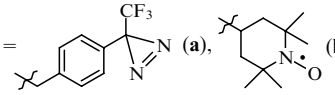 (**a**), (**b**); X = O, S; B = Ura.

Sigurdsson *et al.*[238–240] have prepared the conjugates **121** by the reaction of a 2′-amino-2′-deoxyuridine fragment of an oligonucleotide with 2-isothiocyanatoethyl 2-pyridyl disulfide.

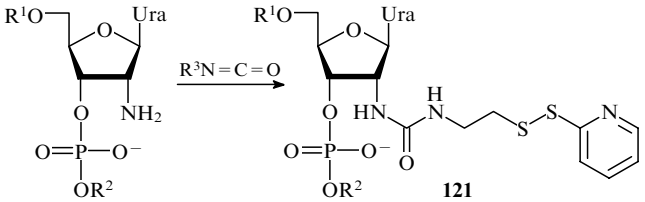

R^1 and R^2 are fragments of an oligonucleotide chain;

$R^3N{=}C{=}O$ = 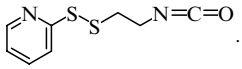 .

The oligonucleotides containing 2′-amino-2′-deoxyuridine[241–244] or 2′-(β-alanylamido-2′-deoxyarabinoadenosine[245,246] were used by Shabarova *et al.* in the synthesis of covalently bound duplexes **122** and **123**. In this case, a nonnucleoside fragment containing a carboxy group at the end of an extended linker was introduced into the complementary chain.

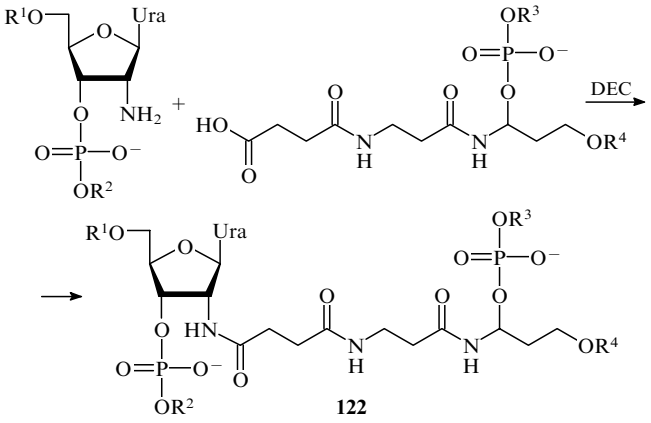

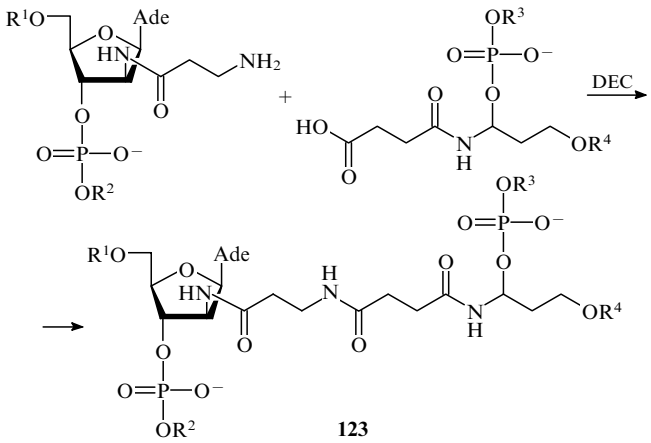

R^1, R^2, R^3 and R^4 are fragments of oligonucleotide chains.

Oligonucleotides **124**, where the chain units are linked by amide bonds in addition to phosphodiester bonds through linkers attached to the C(2′) atoms, have been synthesised.[247] The spatial proximity of carboxy and amino groups determined the high regioselectivity of this reaction, the yield of the target product **124** being 78%; the formation of side products was not observed (Scheme 10).

Substituted carboxylic acid esters of *N*-hydroxysuccinimide are often used as activated acylating agents. Silverman and Cech[248] have performed the acylation of oligonucleotides containing 2′-amino-2′-deoxyuridine using pyrenylacetic and pyrenylbutyric acid esters of *N*-hydroxysuccinimide; Weeks and coworkers[249–251] used biotinylbutyric ester for this purpose.

Conjugates of modified oligonucleotides containing 2′-amino-2′-deoxyuridine with histamine **125**[252] and the cobalt complex **126** have been synthesised.[253] In the latter case, the acylation was

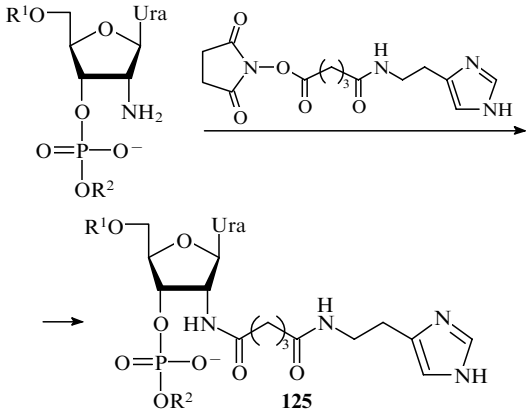

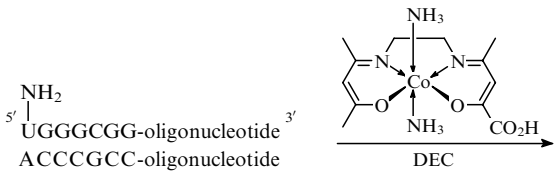

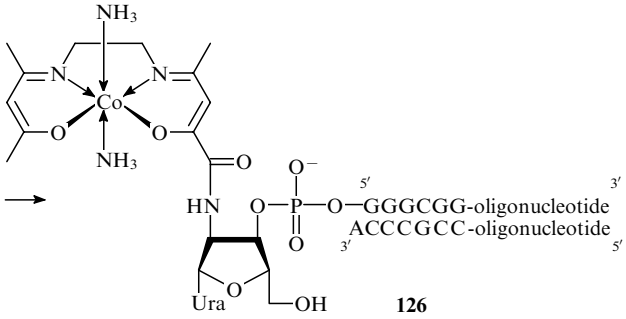

Scheme 10

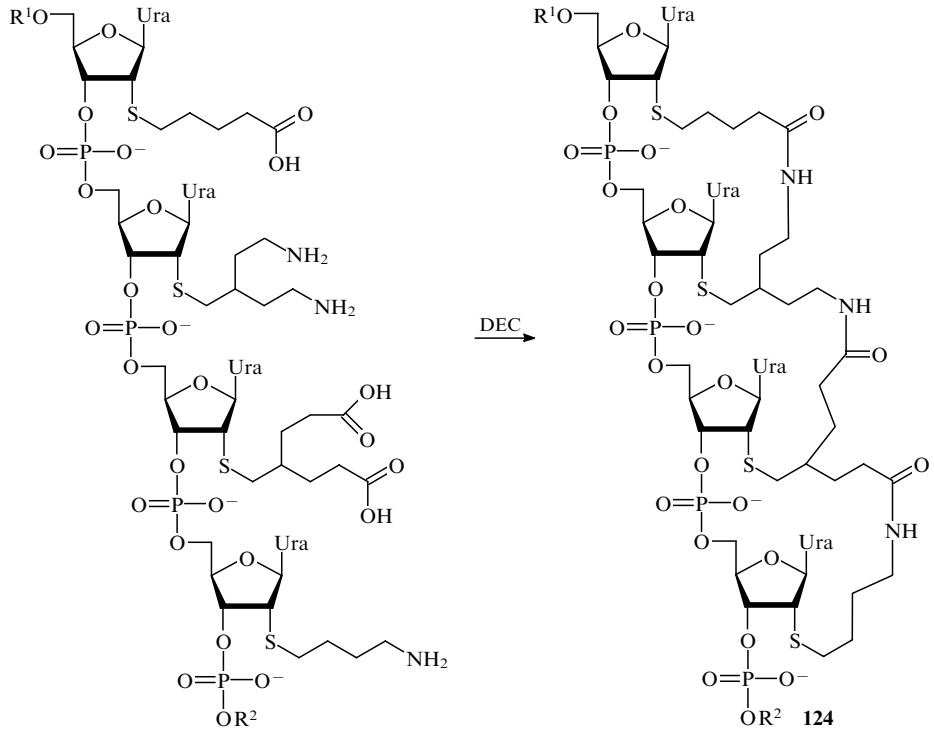

R^1 and R^2 are fragments of an oligonucleotide chain.

performed in the duplex in order to prevent the interaction of the carboxy group of the ligand with the amino groups of the heterocyclic bases.

Studies by Meade *et al.*[254, 255] are devoted to the synthesis of ruthenium complexes of 2′-amino-2′-deoxyribooligonucleotides. Complementary oligonucleotides containing 2′-amino-2′-deoxyuridine at the 5′-ends were modified by two ruthenium complexes differing in degree of oxidation. The complex formation was carried out within the DNA duplexes to prevent interaction of the ruthenium complexes with exocyclic amino groups of the heterocyclic bases. The modified DNA duplex was used for the study of photoinduced electron transfer along the DNA chain which plays an essential role in the damage and repair of DNA.[256, 257]

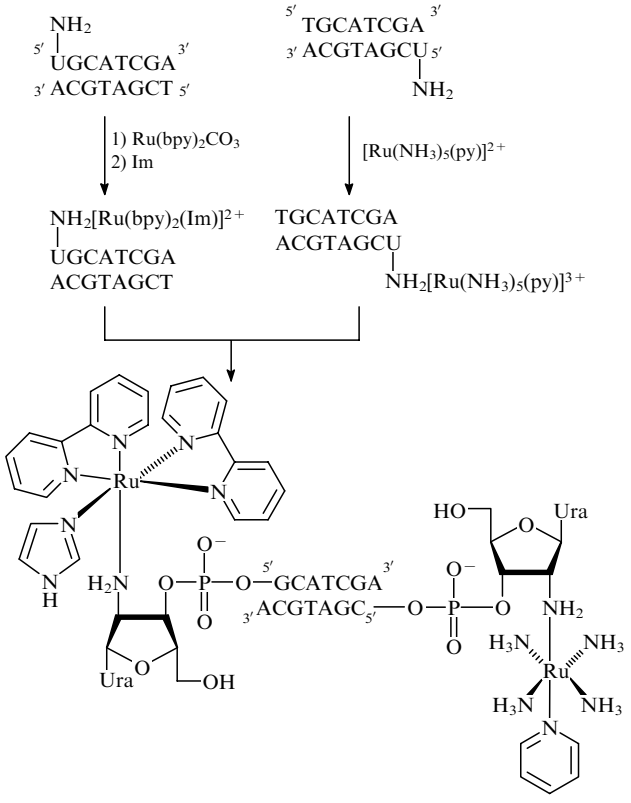

A series of conjugates **127a**–**d** were prepared by reactions of modified oligonucleotides containing 2′-*O*-(5-aminopentyl)uridine[65] and -adenosine[57] with various *N*-hydroxysuccinimide esters.

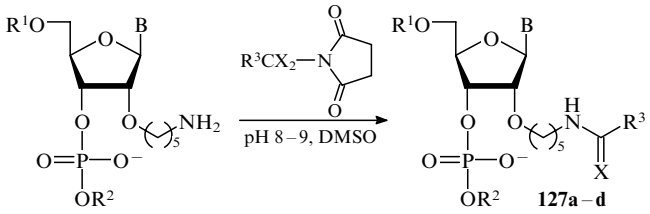

R^1 and R^2 are fragments of an oligonucleotide chain; B = Ade, Ura;

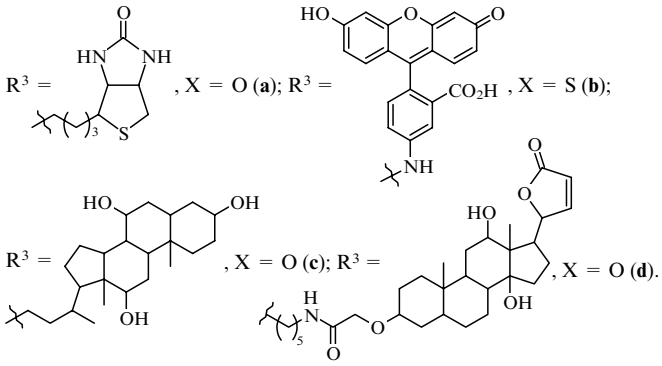

Acylation of the oligoribonucleotide **128** containing 2′-(β-alanylamido)-2′-deoxyuridine with a bifunctional reagent [3,3′-dithiobis(propionic) acid ester of *N*-hydroxysuccinimide] eventually allowed preparation of conjugate **129** containing a peptide linked to the C(2′) atom through a disulfide linker.[258] The disulfide bond can be cleaved by thiols, which simplifies the mass-spectrometric analysis of the conjugates with peptides.

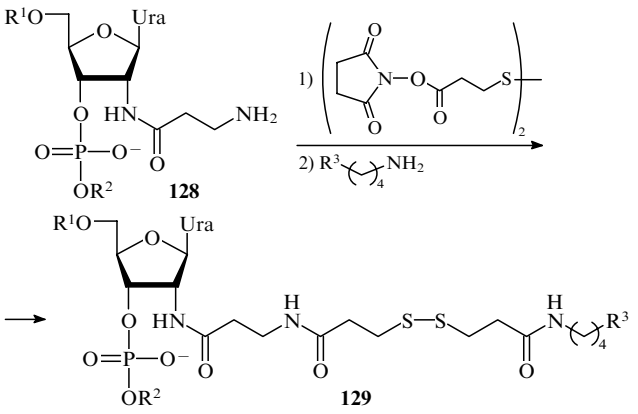

R^1 and R^2 are fragments of an oligonucleotide chain; R^3 is a fragment of the Tat-protein.

Conjugates of oligonucleotides containing 2′-*O*-(4-aminobutyl)ribothymidine with lanthanide complexes **130a**–**c**,[259] and conjugates of oligonucleotides containing 2′-*O*-(6-aminohexylcarbamoyl)cytidine linked with a porphyrin manganese complex (**131**) were synthesised in a similar way.[75]

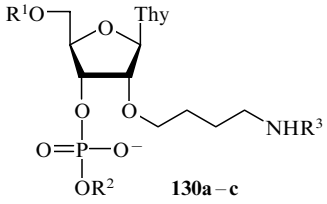

R^1 and R^2 are fragments of an oligonucleotide chain;

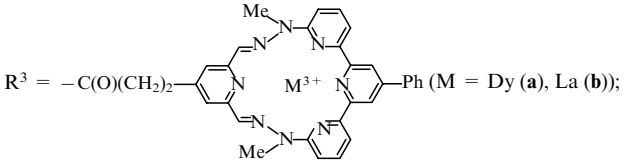

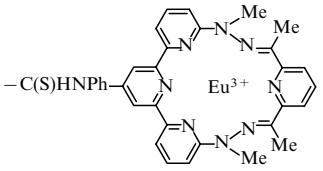

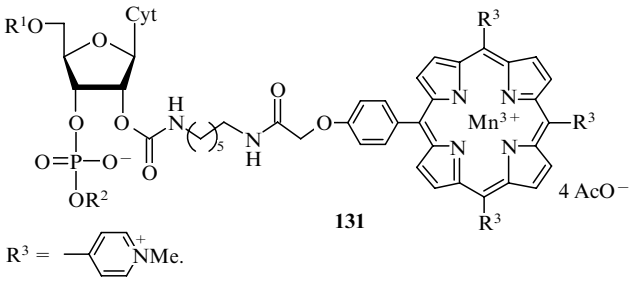

The presence, in modified oligonucleotides, of a thiol group, which can be involved in the formation of disulfide bonds, thioethers and thioesters offers broad opportunities for conjugation.[260]

2′-*O*-(6-Mercaptohexyl)adenosine incorporated into the oligomeric chain was converted into the conjugates **132a**–**d** using *S*-alkylation by iodoacetamidophenanthroline or addition of maleimide derivatives of fluorescein, pyrene and a phospholipid.

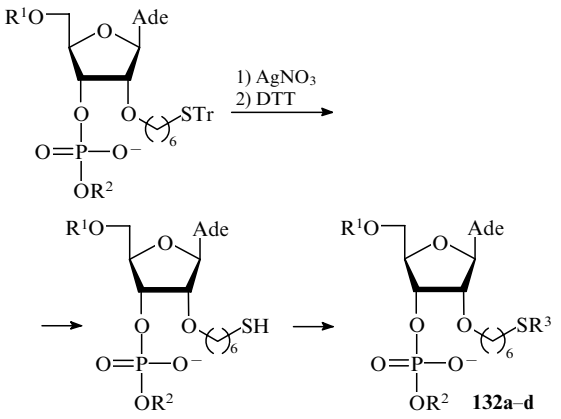

R^1 and R^2 are fragments of an oligonucleotide chain; DTT is dithiothreitol;

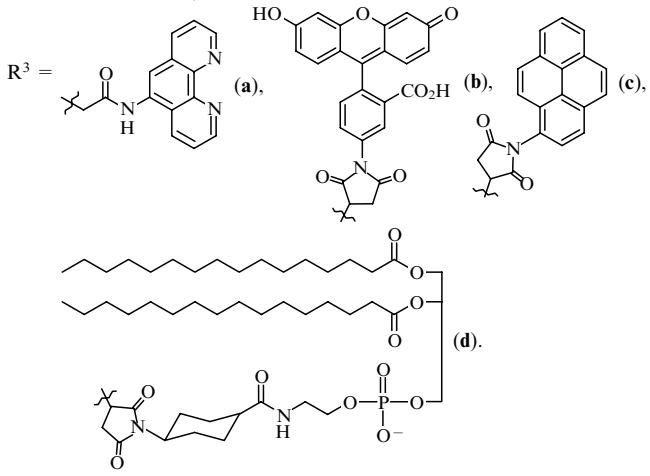

Sigurdsson *et al.*[238,240] have succeeded in synthesising cross-linked duplexes **133** and conjugates with the fluorescent label bimane **134**[239] starting from oligonucleotides **135** containing a thiol group as well as conjugates with glutathione **136** based on oligomers **121** containing an activated thiol group (Scheme 11).[239]

Covalent ‘homocross-linking’ of thiols **137** has been carried out; the duplexes formed were used for the study of the spatial structure of $tRNA^{Phe}$.[105,106]

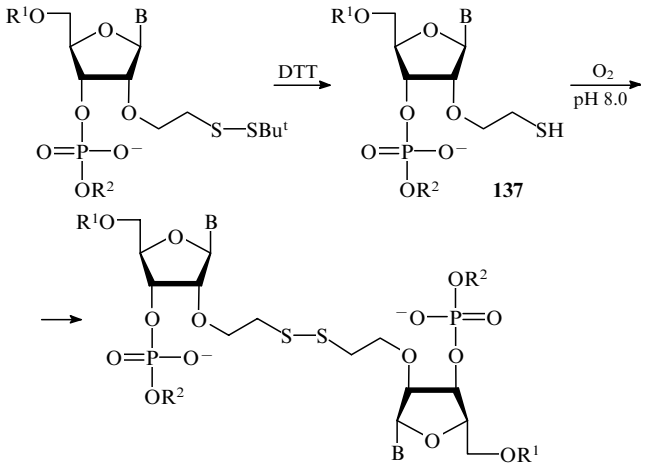

R^1 and R^2 are fragments of $tRNA^{Phe}$; B = Ura, Cyt.

The conjugates **138** containing a disulfide bond were formed in the thiol–disulfide exchange reaction.[261]

Scheme 11

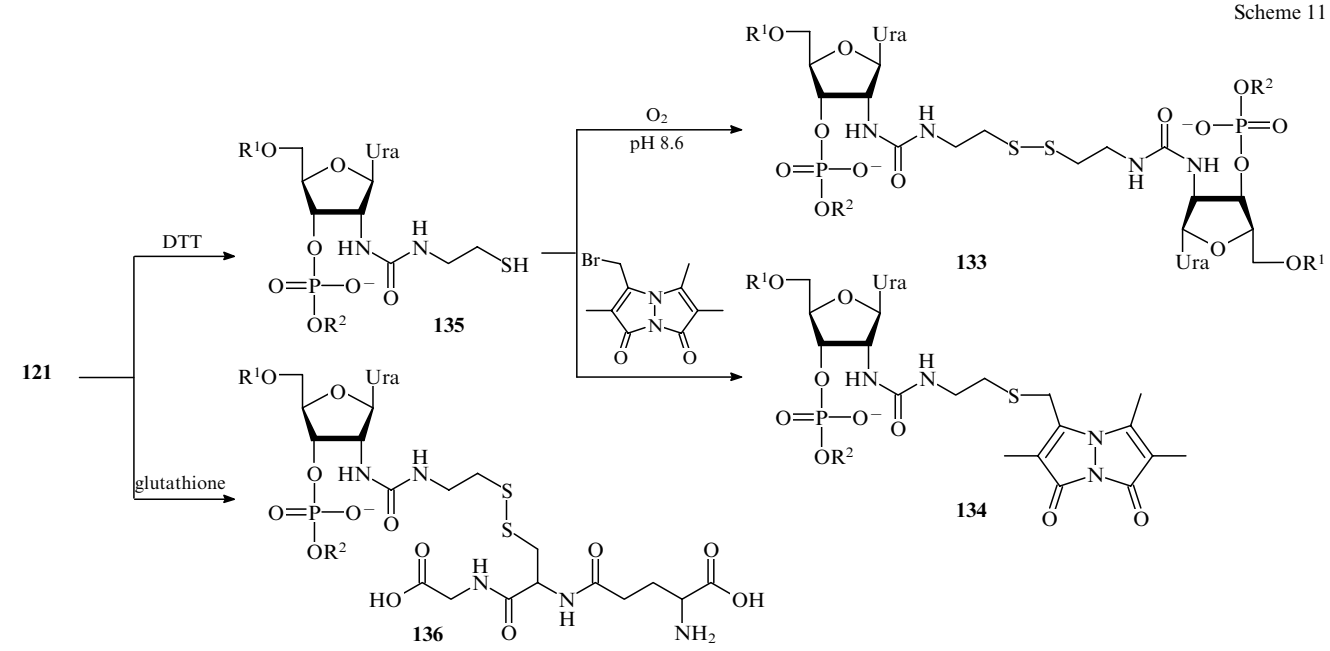

R^1 and R^2 are fragments of an oligonucleotide chain.

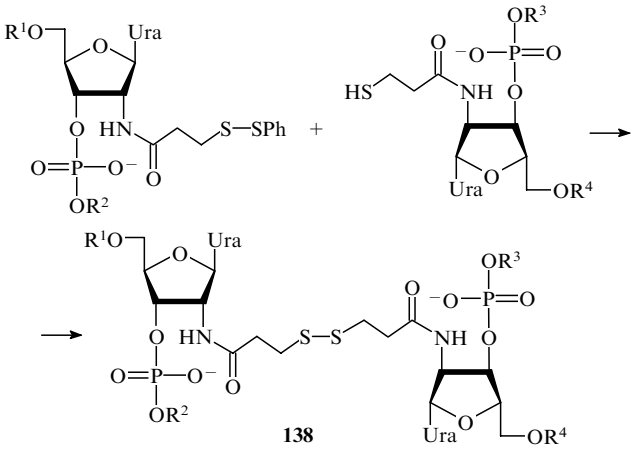

R^1, R^2, R^3 and R^4 are fragments of an oligonucleotide chain.

Hamm and Piccirilly [262] have synthesised oligonucleotides **139** containing 2′-*S*,3′-*O*-cyclophosphate at the 3′-end. The free 2′-thiol group was generated by treatment of the oligomers **139** with silver nitrate; subsequent reaction with iodoacetamide yielded the derivatives **140**. This approach can be used for modification of 2′-thionucleosides localised in the middle of the oligonucleotide chain.

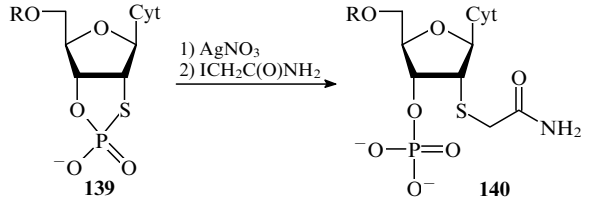

R is a fragment of an oligonucleotide chain.

No formation of side 1′,2′-episulfides was observed, which occurs in the case of 2′-thionucleotides in an alkaline medium.[263,264] Presumably, this reaction involves silver thiolate rather than a free thio group. It is of note that 2′-thiooligonucleotides are more stable in alkaline media than non-modified oligoribonucleotides.

Cook and co-workers [265–267] have prepared a cross-linked duplex by reductive amination of an AP site in the oligonucleotide **141** with an aminoalkyl substituent at the O(2′) atom of adenosine **142** in the opposite chain.

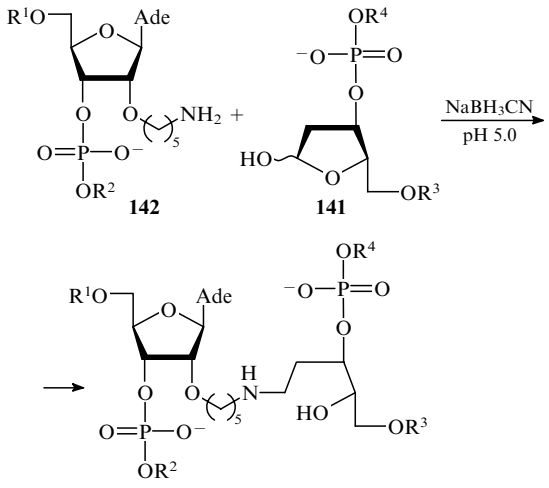

R^1, R^2, R^3 and R^4 are fragments of an oligonucleotide chain.

The addition of a series of 1,2-aminothiols, *O*-alkylhydroxylamines and hydrazides to oligonucleotides **143** containing an acetaldehyde residue at the O(2′) atom [268] yielded conjugates with peptides, pyrene, acridine and biotin. The hydrazones synthesised were unstable at neutral pH, which required their additional reduction to hydrazines with sodium cyanoborohydride. It is of note that this is the first example of simultaneous addition of several peptide residues to an oligonucleotide molecule owing to incorporation of several modified fragments into the chain.

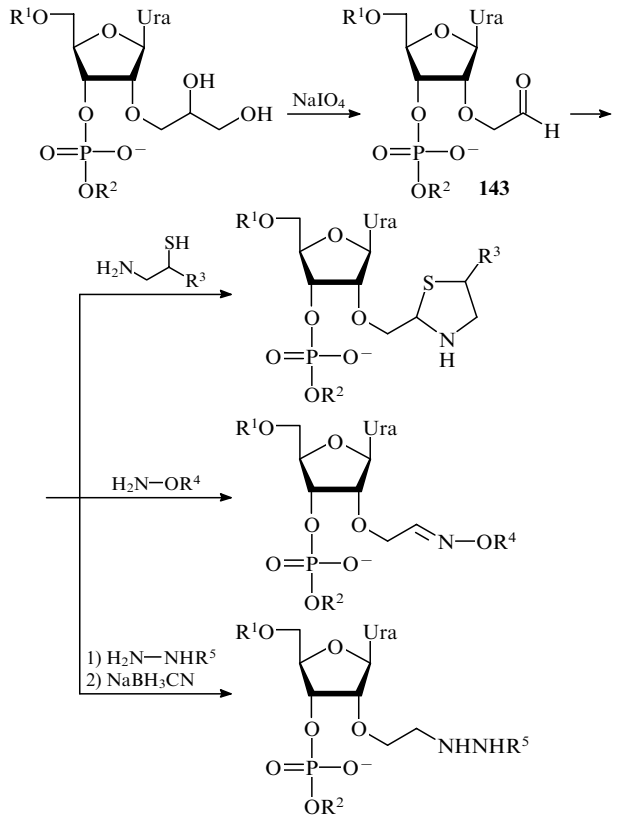

R^1 and R^2 are fragments of an oligonucleotide chain; R^3 = C(O)NHCH$_2$CO$_2$H, C(O)—CFSRAYPTPLRSKKT—OH, C(O)—GYGPKKKRKVGG—OH,

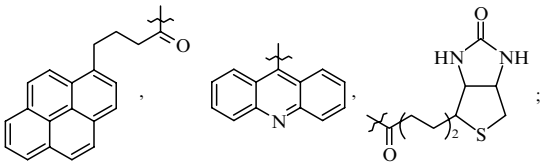

R^4 = CH$_2$C(O)–DPGYIGSR–OH;
R^5 = C(O)(CH$_2$)$_2$C(O)–DPGYIGSR–OH.

Sekine *et al.*[148] used oligonucleotides **144** and **145** containing 2′-phosphate and -thiophosphate groups for the introduction of biotin and biman to give the conjugates **146** and **147** containing the pyrophosphate and thiophosphate bonds, respectively. Later, it was shown[269] that the 2′-phosphate and -thiophosphate groups are easily and selectively removed on heating. Studies of the mechanism of this reaction have shown that the presence of a neighbouring 3′-phosphate group favours 2′-dephosphorylation.

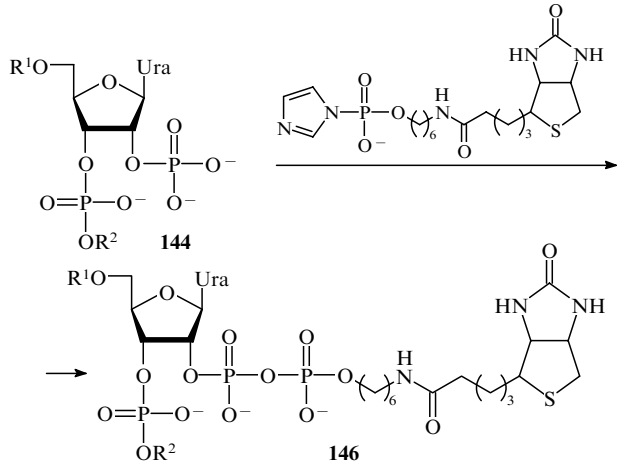

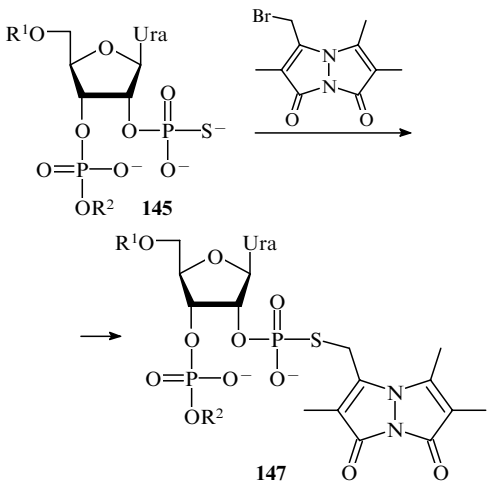

R^1 and R^2 are fragments of an oligonucleotide chain.

IV. The use of nucleosides, nucleotides and oligonucleotides containing reactive groups in the 2′-position

1. The use of nucleosides and nucleotides

2′-Modified nucleosides and nucleotides can find application as selective inhibitors of certain enzymes. To this end, a group able to react with amino acid residues in the active site of the enzyme and thus to irreversibly inhibit it is introduced into a nucleoside. This approach is effective in a case where the structure of the enzyme active site and the mechanisms of its functioning have been studied in detail.

The use of 5′-diphosphates of pyrimidine 2′-thio- and 2′-thiocyanatonucleosides for the inhibition of ribonucleoside diphosphate reductase has been suggested.[270–272] This enzyme plays a key role in the biosynthesis of 2′-deoxyribonucleosides from ribonucleosides by catalysing the reduction of ribose as a constituent of ribonucleoside diphosphates to 2-deoxyribose. This reaction requires two hydrogen atoms which are generated by thioredoxin, a reduced protein cofactor containing two free SH groups in the cysteine residues. The reduction of ribose is accompanied by the oxidation of the cysteine residues; these conditions favour the conversion of thioredoxin into a disulfide form. It was suggested[271,273] that 2′-thio- and 2′-thiocyanate nucleoside diphosphate derivatives react competitively with the cysteine residues in the active centre of the enzyme and thus induce its inhibition. Besides, 2′-methylidene-2′-deoxyribonucleosides were used for the inhibition of ribonucleoside diphosphate reductase.[274]

2′-Hydroxyamino-2′-deoxyribonucleosides able to generate free radicals manifested high anti-fibrosacroma activity *in vitro* and *in vivo*.[28–30] It is of interest that 3′-isomers of these nucleosides inhibit RNA synthesis and suppress tumour growth in mice.

2′-Acylamino-2′-deoxyadenosine derivatives containing aromatic acid residues[195,275–277] manifested high inhibiting activity towards glyceraldehyde-3-phosphate dehydrogenase from *Trypanosoma brucei* which is the cause of sleeping sickness.[278] Effective inhibition was induced even by submicromolar concentrations of the nucleosides. X-ray diffraction analysis has shown[279] that the binding of N^6,2′-modified adenosine to glyceraldehyde-3-phosphate dehydrogenase significantly changes the enzyme structure.

2. The use of 2′-modified oligonucleotides and their conjugates

a. Antisense and anti-gene biotechnologies

The main trend over the past 15–20 years was the use of modified oligonucleotides for suppression of gene expression by their interactions with cell DNA and RNA. This is achieved using antisense and anti-gene approaches and RNAi.

The antisense mechanism of oligonucleotide action implies their intracellular complexation with mRNA to yield hybrid duplexes which prevent translation due to the inhibition of mRNA binding to ribosomes,[280,281] reverse transcription [282] or processing of mRNA.[283,284] In some cases, such hybrid duplexes act as substrates for the RNAase H,[281] which catalyses hydrolysis of a ribonucleic component, and undergo 'decapitation' of the 5′-end of the RNA molecule,[285] sequence-specific cleavage of RNA [3,286–289] or covalent binding of the oligonucleotide to RNA.[290] The most recent achievements in antisense biotechnology have been described in the review.[291]

In contrast, the anti-gene mechanism entails either direct binding of a modified oligonucleotide to genomic DNA and formation of a triplex on a complementary sequence [2,292] or unwinding of the double helix and formation of a heterogeneous duplex or D-loop.[293] This results in the inhibition of transcription of the corresponding genes and an increase in the susceptibility of the DNA site to nucleases [294] and chemical reagents.[295–298] Both antisense and anti-gene mechanisms are based on enhanced affinities of modified oligonucleotides for the complementary sequence in comparison with their native counterparts.

The phenomenon of RNA interference was discovered in 1998;[299] it consists of the degradation of mRNA induced by a double-helical RNA, which is complementary to a certain region of the former, and, as a consequence, of inhibition of gene expression. Initially, extended RNA duplexes (300–1000 bp) were used for this purpose, but later it was shown [300,301] that RNA interference was induced by shorter (21–23 bp) duplexes. A strong intracellular effect is observed upon introduction of even very few copies of RNA duplexes into the cell, which can be due to their functioning in a catalytic mode. A salient advantage of short RNA duplexes is that in mammalian cells they do not elicit non-specific immune response, which involves interferon production and cell death as in the case of extended RNA duplexes. For this reason, short RNA duplexes are considered to be efficient selective inhibitors of expression of individual genes and promising candidates for medicinal drugs.

Unfortunately, even minor modifications of RNA, *e.g.*, substitution of inosine for guanosine,[302] introduction of 2′-*O*-methylated nucleotides [303] or addition of a non-complementary base pair,[304] completely abolish RNA interference. The introduction of 2′-amino-2′-deoxyuridine or 2′-fluoro-2′-deoxyuridine into the sense chain of an RNA duplex only slightly inhibits the RNA interference, whereas modification of an antisense chain is crucial.[302] Nevertheless, it was shown that modification of two 3′-terminal nucleotides is possible.[303] Studies of RNA interference in mammalian cells have demonstrated [305] that the introduction of 2′-fluoro-2′-deoxyuridine and conformationally protected 2′-*O*-4′-*C*-methylidene nucleosides into RNA duplexes has no effect on the efficiency of RNA interference. The activities of single-helical, 22-membered RNA (the so-called miRNA [306,307]) are being investigated; their mechanism of action is similar to RNA interference.[5,6,308,309]

A recently developed SELEX procedure [4,310,311] enables the selection of NA molecules with predetermined properties from combinatorial libraries containing up to 10^{25} individual molecules.[312,313] The choice of target NA molecules is based on their ability to form stable complexes with various proteins and their low-molecular-mass analogues. As a rule, these properties are inherent in RNA molecules containing 40–100 nucleotide units, termed as 'aptamers'. The introduction of modified nucleosides into the structure of aptamers [314] increases their conformational mobilities and resistance to nucleases. The structures of modified aptamers can be established using tandem mass spectrometry combined with ESI-MS electrospray ionisation.[315,316] SELEX is also used for the analysis of ribozyme libraries.[317]

The use of oligonucleotides as therapeutic drugs requires that they possess high resistance to nucleases, can efficiently be delivered to the cell, selectively bound to the targets and are free of side effects. Low cost and availability of modified oligonucleotides are no less important. Thus, the construction of efficient antisense and anti-gene agents demands simultaneous solution of many problems.

It has been shown [318,319] that inside the cell oligonucleotides are predominantly hydrolysed under the action of exogenous nucleases. Today, the problem of stability of oligonucleotides may be considered to be solved owing to the use of 2′-*O*-methylated nucleotides, conformationally locked nucleic acids [320,321] and various 3′-terminal modifications, which significantly increase the resistance of NA against nucleases.

The problem of targeted delivery of oligonucleotides to cells is much more complicated. Its solution is difficult due to the lack of clear understanding of the mechanisms of oligonucleotide penetration across cell membranes, which involves either non-specific adsorption on the surface of the cell membrane and subsequent diffusion or receptor-mediated endocytosis. In this respect, covalent [260,322] and non-covalent [323] oligonucleotide conjugates with peptides present considerable interest. No less attention is given to the use of liposomes as vehicles for targeted delivery of oligonucleotides, *e.g.*, anionic and neutral,[324,325] cationic,[326] pH-sensitive,[327] fusogenic (*i.e.*, able to penetrate through cell membranes),[328] folate receptor-targeted liposomes [329] and immunoliposomes.[330] Of interest are oligonucleotide glycoconjugates in which receptor-mediated endocytosis is effected through lectin receptors.[331] The intracellular distribution of these conjugates between the cytosol and the nucleus is determined by their interaction with intracellular lectins. Hydrophobic nanoparticles [332] and polyamidoamine dendrimers [333] are also used as cargos for oligonucleotide delivery. The transmembrane transport of thiophosphorylated oligonucleotides [334] and of hydrophobic oligonucleotide conjugates [64] has also been discussed.

The design of antisense analogues of nucleic acids allows modification of both the sugar–phosphate backbone and heterocyclic bases. 2′-*O*-Alkyloligonucleotides containing reactive groups and their conjugates with other compounds are especially widely used along with other 2′-modified oligonucleotides in antisense biotechnology. Thus it has been found [268] that the attachment of 10–15-membered peptides to the O(2) atom of the carbohydrate fragment through a linker virtually does not affect the binding of the antisense conjugate to TAR RNA. Moreover, the solution of quite a number of practical tasks demands the introduction of more complex groups into the 2-position of the carbohydrate fragment of NA. The synthesis of 2′-*O*-{2-[2-(*N*,*N*-dimethylamino)ethoxy]ethyl}oligonucleotides is an example.[69] The introduction of such a modification into the oligomer structure increases the thermal stability of duplexes with RNA due to the *gauche*-effect,[71] while the presence of a positive charge increases its resistance against nucleases.[335]

3′-Phosphoramidite derivatives of 2′-*O*-methylnucleosides are commercially available, which determines the wide application of 2′-*O*-methyl oligonucleotides with internucleotide thiophosphate and phosphodiester bonds in antisense biotechnology. High *in vitro* [336] and *in vivo* activities of such oligomers have been demonstrated in experiments on various cell lines [337–341] and in mice.[342] One of the most popular approaches [343] entails the synthesis of a chimeric oligonucleotide which is made up of 2′-*O*-alkylribonucleosides and 2′-deoxyribonucleosides linked through internucleotide thiophosphate bonds in the middle of the chain. RNA duplexes with such oligonucleotides serve as substrates for RNAase H. It should be noted that the simultaneous presence of thiophosphate groups and 2′-*O*-methylnucleotide units results in additive inhibition of gene expression.[340] A similar approach entails the activation of RNAase P.[341] This enzyme splits the 3′-terminal fragment of RNA within the duplex,[344] which occurs more selectively than traditional RNAase H.[345]

2′-*O*-Methoxyethylated RNAs are thought to be the most promising among other 2′-modified oligonucleotides.[346] It has been shown [347] that such oligomers penetrate more easily across cell membranes, are stable in blood plasma [348] and specifically inhibit gene expression.[349]

In addition, 2′-*O*-methoxyethylated RNAs are effective inhibitors of telomerase.[350] Moreover, the inhibition of 3′-polyadenylation of pre-mRNA by such oligonucleotides is the reason for the increased stability of mRNA and, correspondingly, for the hyperexpression of proteins.[351]

2′-*O*-Alkylated oligonucleotides have also found wide application in anti-gene biotechnology. It was shown that 2′-*O*-methyloligonucleotides form kinetically and thermodynamically more stable triplexes in comparison with native oligonucleotides,[352] which is due to the pre-organisation of the oligonucleotide structure, [*i.e.*, a more favourable C(3′)-*endo*-, C(2′)-*exo*-conformation of the carbohydrate fragment] and van der Waals interactions between the 2′-*O*-methyl groups and purine bases.[353] Conformationally fixed 2′-*O*,4′-*C*-methylidene oligonucleotides confer even higher stabilities on the triplexes under conditions close to physiological,[354] the best results being observed in the case of 2′-*O*-(2-aminoethyl)oligonucleotides.[355–357] NMR spectroscopic studies have shown that in this case the increased stability of the triplex is due to electrostatic interactions of the charged amino groups of the pyrimidine oligonucleotide with the phosphate groups of the opposite purine chain of DNA.[70, 358] The so-called *gauche*-effect,[359] which determines the magnitude of the torsion angles in the system X–C–C–Y (X and Y are electronegative substituents), contributes significantly to the stabilities of the triplexes. The presence of a *gauche*$^+$-effect for the 2′-*O*-aminoethyl group determines the conformation which is optimum for the interaction with the phosphate group of the opposite strand; this favours the pre-organisation of the oligonucleotide. The presence of a charged amino group is yet another factor which determines the stabilities of the triplexes at low concentrations of Mg^{2+} close to physiological;[357] this is not typical of triplex-forming oligonucleotides.[360] It should be noted that the incorporation of a large number of modified units[356] alleviates the inhibition of gene expression *in vivo*. It was suggested[357] that this is due to the increased hydrophobicity of the oligonucleotide owing to the partial neutralisation of the negative charges of phosphate groups and, as a consequence, its adsorption on cell membranes, hydrophobic proteins, *etc*. The decrease in the intracellular concentration of a modified oligonucleotide also diminishes its anti-gene effect. Recently, it has been shown[361] that such modified oligonucleotides are promising for site-specific mutagenesis *in vivo*. The incorporation of 2′-*O*-aminoethyl-5-propargylaminopyrimidine nucleosides into oligonucleotides[362] exerted an additive effect caused by the interaction of two amino groups, which provided further stabilisation of the triplexes with DNA.

b. Studies of DNA – protein interactions

The second line of the use of modified oligonucleotides is the study of protein – nucleic acid interactions. This includes, in particular, covalent binding of nucleic acids to proteins.[142, 143, 363] The most significant information about the structures of NA – protein conjugates can be obtained by X-ray diffraction analysis,[364] however, it is not always possible to isolate sufficient amounts of specific protein complexes with DNA and/or bring about their crystallisation. Besides, the results can be wrong due to differences in the conformations of macromolecules in solution or in crystalline form. NMR analysis of the structures of NA – protein complexes is an alternative approach.[365] However, the data obtained by NMR spectroscopy are often difficult to interpret. Site-specific mutagenesis[366, 367] and chemical modification of proteins are potent methods for the study of DNA – protein interactions, however, their application demands preliminary identification of a specific site in the protein molecule responsible for the interaction with NA. The use of the 'footprinting' technique allows the identification of DNA sequences recognised by DNA-binding proteins,[368] but cannot be used for the identification of specific protein sites interacting with NA. Covalent attachment of proteins to modified nucleic acids containing reactive groups not only allows the identification of the protein site interacting with NA, but sometimes enables the determination of the amino acid responsible for the binding.[363, 369] The changes in the NA structure are minimal in this case.

Changes in the physicochemical properties of individual oligonucleotide fragments can be caused by even minor disturbances in the geometry of the molecule; the effects of modification can be determined by kinetic methods.[370]

The interaction of a fragment of the Tat-protein with C(2′)-modified RNA has been studied.[258] It was shown that the conjugate **129** (see above) is formed in the reaction of the activated ester at the C(2′) atom of Urd(23) with the ε-amino group of Lys(51).

Oligonucleotides **148** containing a dialdehyde group in the 2′-position were used for the study of protein-NA interactions with restriction endonuclease *Eco*RII, DNA-methyltransferases *Eco*RII,[371] *Mva*I (see Refs 372–374) and T7 RNA polymerase.[373, 375] The use of modified oligonucleotides permits one to inhibit the enzyme activity without any effect on the ability of enzymes to bind the NA substrate. The interaction of oligonucleotides **148** with enzymes occurs in a selective manner and involves the ε-amino groups of lysine. The yields of the conjugates **149** are 3% – 5%.

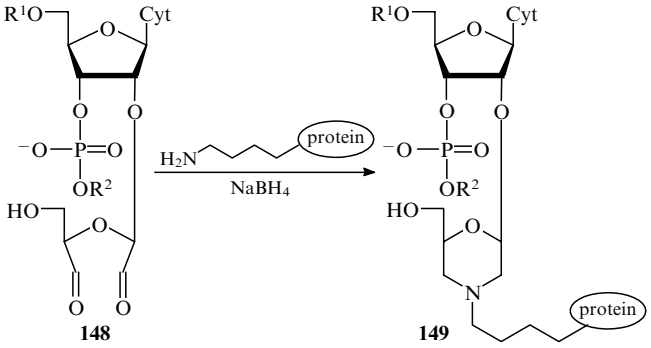

R^1 and R^2 are fragments of an oligonucleotide chain.

The covalent binding of modified oligonucleotides **143** containing 2′-*O*-(2-oxoethyl)uridine to the transcription factor NF-κB has been described.[376] This modification seems to be more preferable than the dialdehyde group, since its small size favours its interaction with the ε-amino groups of lysine closest to DNA.

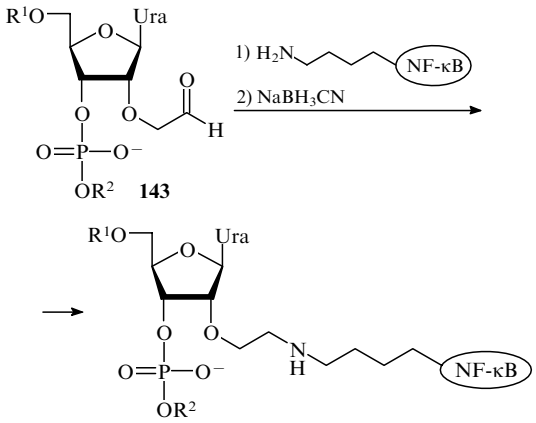

R^1 and R^2 are fragments of an oligonucleotide chain.

The covalently bound duplexes **122** and **123**[241–244] are extremely resistant against nucleases. Their interactions with the transcription factor NF-κB have been studied; the efficiency of the binding of the modified duplexes to the protein was higher than of native duplexes.[377] For a more detailed description of the synthesis and applications of covalently bound nucleic acids see Ref. 378.

Oligonucleotides **89** containing intrachain cross-links in the neighbouring nucleotide units [174, 175] have a chain kink at the modification site and structurally correspond to the U-turn of tRNA. These oligonucleotides can be used for the study of RNA – protein interactions.

It was suggested [253] that the transcription factor Sp1 could be selectively inhibited using irreversible binding of side histidine groups in the protein molecule to the cobalt atom of a metal complex covalently linked to the oligonucleotide.

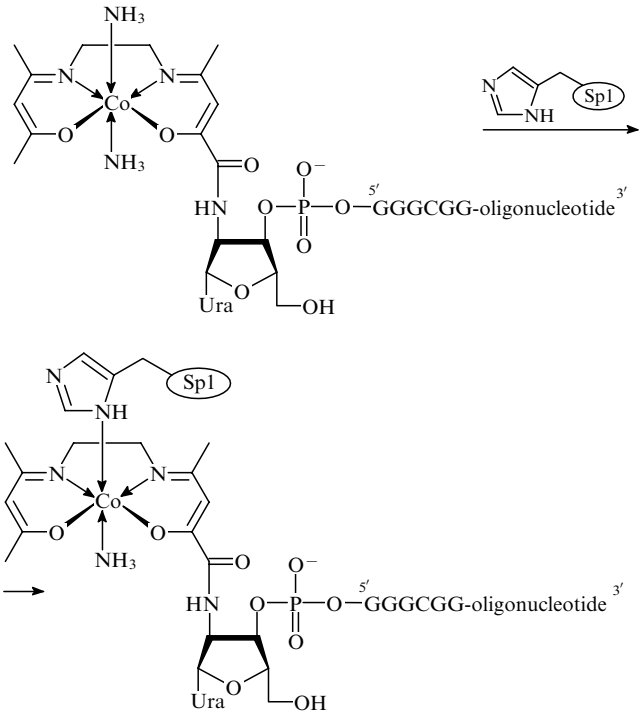

Ribonucleic acids containing 2′-amino-2′-deoxyribonucleotide fragments were repeatedly used as aptamers possessing higher binding constants to various proteins and receptors than native nucleic acids. The proteolytic enzyme elastase from human neutrophils,[379] the vascular endothelium growth factor,[380] the fibroblast growth factor,[381] the protein Rev HIV-1,[382] the human γ-interferon,[383] *N*-methylmesoporphyrin (a low-molecular-mass analogue of heme-containing proteins),[384, 385] as well as insulin [386] and acetylcholine receptors [387] served as the objects of this study. After incorporation of the 2′-amino group into RNA, the ability to form hydrogen bonds remains. In addition, the presence of such modifications has only marginal effect on the local structure of RNA molecules because of the similarity of the van der Waals radii of the amino and hydroxy groups.

Oligonucleotides containing 2′-amino-2′-deoxyribonucleotide fragments were also used in the study of the role of 2′-hydroxy groups in RNA – protein interactions. The interactions of DNA with ribonuclease H1 from *E.coli*,[388] of RNA with the bacteriophage MS2 membrane protein [389, 390] and uracyl-DNA glycosylase [391, 392] have been studied. Aurup *et al.*[393] have synthesised mRNA from 2′-amino-2′-deoxyribonucleoside-5′-triphosphates and demonstrated that such an mRNA cannot be translated *in vitro* and *in vivo*.

c. Study of the structures of nucleic acids

The fluorescent properties of oligonucleotides containing a methylpyrene residue at the O(2′) atom [162] have been studied.[394 – 396] It was shown that the pyrene residue intercalates between the heterocyclic bases in a duplex with DNA as can be evidenced from the shift in its fluorescence maximum. In contrast, duplexes with RNA are characterised by strongly enhanced emission, which suggests the localisation of the pyrene residue outside the duplex. These conclusions were confirmed by the data from the thermal stabilities of the duplexes and CD spectra. In addition, the fluorescence characteristics of pyrene-containing oligonucleotides appeared to be highly sensitive to the presence of mismatches.[396] These oligonucleotides can be used in structural analysis of RNA.[397 – 399]

The emission characteristics of modified oligonucleotides where pyrene was attached to the C(2′) atom of uridine through an extended linker [170] were studied in relation to the nature of the 3′-flanking nucleotide and the presence of a complementary chain, which made it possible to determine the electron transfer energies and conformational mobilities of heterocyclic bases in various single- and double-stranded structures.

Silverman *et al.*[187, 248, 400] have used a series of modified oligonucleotides with different lengths of linkers between the pyrene residue and the C(2′) atom in order to study intron folding of the *Tetrahymena* group I P4 – P6 domain. The folding was accompanied by an increase in fluorescence intensity, which suggested changes in the environment around the modified nucleotide. It was demonstrated that the folding of RNA occurs in different ways depending on the ionic strength and pH of the solution.

The use of oligonucleotides containing 2′-*O*-(*N*-pyrenylmethylcarbamoyl)uridine has been proposed recently.[78] The spatial approximation of modified nucleosides in the complementary chains results in the formation of a pyrene excimer in the major groove of a DNA duplex.[170] The use of a linker with low conformational mobility has made it possible to prepare derivatives possessing strong fluorescence.

Nakano and co-workers [183 – 186, 235] have published a series of papers devoted to the synthesis of oligonucleotides containing various fluorescent labels at the C(2′) atom. Hybridisation of oligonucleotides containing a 4-(*N*,*N*-dimethylamino)phenylsulfamide group with a complementary DNA chain was accompanied by an increase in fluorescence intensity.[184, 185] The fluorescent properties of oligonucleotide duplexes containing fluorophore pairs (dansyl – fluorescein and coumarin — fluorescein) in the opposite chains have been studied.[186, 235] Unfortunately, in the former case the quantum yield of the energy transfer was too low, which excludes the use of such oligonucleotides for fluorescence resonance energy transfer (FRET). The quantum yield for the coumarin – fluorescein pair amounted to 25%; the quenching of the fluorescence of the energy donor was observed only in the case where the acceptor was conjugated with a complementary oligonucleotide.

Electrochemical detection of the DNA structure is a promising approach to the study of mononucleotide polymorphism.[401 – 403] A series of patents [404, 405] and papers [159, 406, 407] devoted to different applications of modified oligonucleotides containing 2′-*O*-ferrocenylalkylnucleoside fragments for the electrochemical detection of mononucleotide polymorphism in DNA fragments have been published. DNA chips and devices based on them are now commercially available (eSensor™, eSensor™ 4800 Reader, Motorola Clinical Micro Sensors, USA). For a more detailed description of the synthesis and properties of ferrocene-containing oligonucleotides see Ref. 403.

The introduction of the anthraquinone residue at the C(2′) atom [164] increases the thermal stabilities of duplexes of modified oligonucleotides with DNA and RNA.[408] ^{1}H NMR spectroscopic studies have shown [409] that the anthraquinone residue linked to the C(2′) atom intercalates between heterocyclic base pairs. This property was used in the study of electron transfer mechanisms along the DNA chain.[165] In further studies, oligonucleotides containing 2′-*O*-anthraquinonylmethyluridine were used in development of a novel type of DNA sensor.[410, 411] The efficiency of the electron transfer was shown to increase drastically upon formation of a duplex between the anthraquinone-containing oligonucleotide immobilised on an electrode and the NA target.

Whittemore *et al.*[171, 412] have used oligonucleotides containing an anthraquinone residue attached through a 2′-*O*-aminohexyl linker for electrochemical detection of complementary NA mole-

cules on the electrode surface with the help of cyclic voltammetry. The use of a dropping mercury electrode [171] did not reveal any steady dependence of the voltammetric characteristics on the concentration of the NA under study, which can be attributed to the non-specific adsorption of the oligonucleotide on the mercury surface. In further studies,[412] an oligonucleotide containing a 5′-terminal thiol group was immobilised on the surface of a gold electrode. To minimise non-specific adsorption, the electrode surface was treated with 2-mercaptoethanol after which a complementary oligonucleotide containing an anthraquinone residue was added and the detection was begun. If is of interest that the UV spectroscopic data exclude intercalation of the anthraquinone residue between heterocyclic base pairs.[412]

Oligonucleotides containing a ruthenium complex at the C(2′) atom [206] were suggested as models for the study of electron transfer along the DNA chain. However, it was found that the oxidation of the guanosine residue within the duplex occurs in very low yields.

Recently published reviews are devoted to the use of thiol-containing oligoribonucleotides for the study of structures and functions of ribozymes [413] and the three-dimensional structure of RNA.[414, 415]

Sigurdsson *et al.*[238] unambiguously chose one of the two tertiary structures of a ribozyme containing covalently bound domains which have earlier been deduced from X-ray diffraction analysis data. This approach was further used to prove proximity of two domains of a hairpin ribozyme.[416]

A study of the formation of disulfide cross-links between modified oligonucleotide chains [261] has made it possible to estimate the rates of the thermal motions of structural elements of the ribozyme *Nhe*I. In further studies, the switch-over of the nuclease activity of ribozyme HHα10 to a ligating activity could be achieved through the use of similar modifications.[417, 418] A considerable increase in the ligation rate, which was not accompanied by changes in hydrolysis rates, was attributed to a sharp decrease in the thermal motions of the ribozyme domains,[417] structural changes in the catalytic site of the enzyme [418] and, as a consequence, in arrangement of the 2′-hydroxy and 3′-phosphate groups of the substrate.

Glick and co-workers [105, 106] have used disulfide bond formation between thiol-containing oligonucleotides for the study of the spatial structure of $tRNA^{Phe}$. It was found that the effects of covalent cross-links on the three-dimensional structure of tRNA are minimum. The kinetics and thermodynamics of the folding of $tRNA^{Phe}$ upon cleavage of disulfide cross-links due to thiol–disulfide exchange were studied.[419]

Modified 5S rRNA **120a**, which contains a photochemically active aryl(trifluoromethyl)diazirine group,[236] was used in the study of the spatial environment of 5S rRNA within the ribosome.

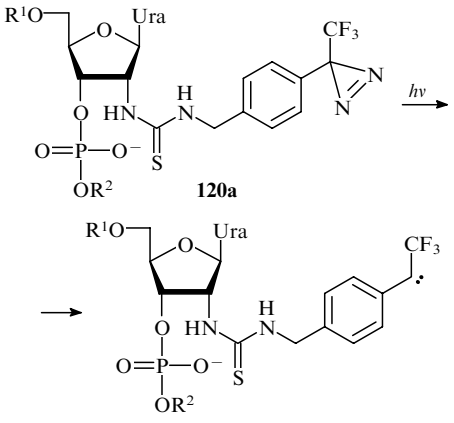

R^1 and R^2 are fragments of an oligoribonucleotide chain.

Upon UV irradiation, diazirine is converted into a highly reactive carbene which attacks even aliphatic C—H-bonds.[420] An analysis of the reaction products has made it possible to establish several contacts between 5S rRNA and 23S rRNA.

Buchmueller *et al.*[421, 422] have used oligoribonucleotides containing 2′-(4-azido-2-hydroxybenzamido)-2′-deoxyuridine for detecting non-equilibrium structures formed upon folding of RNA.

An interesting application for oligonucleotides containing pyrimidine 2′-amino-2′-deoxyribonucleosides has been proposed by Weeks and co-workers [249–251] who have demonstrated that the acylation rate of the 2′-amino group depends on the conformational mobility of the modified nucleotide fragment. This is maximum for a single-stranded NA and minimum for an ideal duplex. The kinetic and thermodynamic parameters of the acylation with the biotinylbutyric acid *N*-hydroxysuccinimide ester were established for all possible nucleotide pairs in DNA–DNA and DNA–RNA duplexes.[250, 251] The data obtained were used in further studies of the local structure of $tRNA^{Asp}$ (see Ref. 249) and detection of mononucleotide polymorphism.[251] It was shown in particular that the acylation rate of a 2′-amino-2′-deoxyribonucleoside incorporated into the anticodon loop of $tRNA^{Asp}$ (see Ref. 249) exceeds that of nucleosides involved in complementary interactions or representing elements of the tertiary structure.

It has been shown [423] that the acylation rate of the 2′-amino group is determined not only by the local conformational mobilities of oligonucleotides, but also by the chemical nature of the vicinal groups in the 3′-position. The reaction rate drops drastically in the presence of a phosphotriester group in the 3′-position of the 3′,5′-cyclophosphate group or upon substitution of threofuranose for the ribose residue. This suggests the involvement of the 3′-phosphate or the 3′-hydroxy group in the catalysis of the acylation reaction. The results obtained and the data from computer simulation prompted a conclusion on a possible catalytic role of the 2′-hydroxy group in the formation of a peptide bond in the peptidyl site of the ribosome.

Sigurdsson *et al.*[424, 425] have studied the effects of metal ions on the structure and interactions of modified TAR RNA with different fragments of the Tat-protein using RNA carrying a spin label in the 2′-position.[237] ESR studies have shown that the substitution of sodium ions for calcium ions does not influence the structure of TAR RNA, but weakens the interaction of a fragment of a mutant Tat-protein with definite nucleotide fragments. The introduction of several spin labels into the TAR RNA [426] enabled the investigation into the interactions of the latter with dyes, intercalators and antibiotics and the determination of binding sites for these molecules. In further studies, this modification was used for measuring the distances in double-helical RNA using ESR spectroscopy.[427]

d. Ribozymes

Ribozymes are short-chain RNA, which catalyse the sequence-specific cleavage of RNA, ligation and some other processes.[3] The hammerhead ribozyme is the best studied.[428–430] In this Section, we consider ribozymes that incorporate nucleosides containing reactive groups in the 2′-position.

The incorporation of 2′-amino-2′-deoxyribonucleosides,[228, 431–437] 2′-thionucleosides,[433, 435] 2′-aminooxynucleosides,[86, 433, 435] 2′-*O*-methyl- and 2′-*O*-allylnucleosides [438] into definite positions of the ribozyme significantly increases the resistance of RNA against nucleases with simultaneous preservation of, or a small decrease in, the catalytic activity. Similar results were obtained for the DNAzyme.[439]

However, it was found [440] that the catalytic activity of a ribozyme decreases significantly as a result of incorporation of certain substituents into the 2′-position. This effect does not depend on the size of the group incorporated, but rather is determined by the nature of the bond at the C(2′) atom. Some modifications, *e.g.*, 2′-acylamido and 2′-alkylcarbamoyl groups presumably prevent conformational changes in the ribozyme molecule in the catalytic act. This is confirmed by the data [441] on the lack of catalytic activity of a hammerhead ribozyme contain-

ing 2′-acetamido groups and the data of Beigelman *et al.*[193] on a substantial decrease in the catalytic activity upon acylation of 2′-amino-2′-deoxyuridine with amino acids (alanine, phenylalanine, lysine and asparagine).

According to Hamm *et al.*,[442] cleavage of an RNA substrate containing 2′-thiocytidine instead of native cytidine by the ribozyme dHH16 proceeds *via* an intermediate 1′,2′-episulfide by a mechanism similar to hydrolysis in an alkaline medium.[263, 264] Under these conditions, the cleavage rate of modified RNA decreases by two orders of magnitude in comparison with native oligoribonucleotides. Further studies of the properties of oligonucleotides containing 2′-thiocytidine units revealed[443] that this reaction requires the presence of manganese ions. Moreover, it does not occur in the absence of oxygen or in the presence of free radical scavengers in the reaction mixture.

The incorporation of several 2′-thiocytidine-5′-phosphate units into the ribozyme fully suppressed its catalytic activity.[444]

Schwans *et al.*[445] have synthesised a modified *Tetrahymena* group I intron P4–P6 domain using α-thiotriphosphates of 2′-thionucleosides. Isolation of RNAs, which differed from the native fragment in gel-electrophoretic mobilities, and subsequent cleavage of the thiophosphate groups in the modified RNAs by iodine has made it possible to determine the positions of 2′-hydroxy groups in the domain essential for its folding.

Stromberg *et al.*[446–448] have studied self-splicing of the intron IA2 of pre-mRNA formed during the expression of the gene *nrdB* of the bacteriophage T4. Attachment of guanosine to the 5′-end of the intron occurs, which was accompanied by cleavage of RNA with subsequent elimination of the guanosine residue from the intron sequence in the presence of metal ions. When 2′-amino-2′-deoxyguanosine was used as a cofactor instead of guanosine, the splicing rate decreased 20–25-fold. An analysis of the dependence of the cleavage rate of guanosine on pH, concentration and the nature of bivalent metal ions has made it possible to reveal the interactions of metal ions with 2′-hydroxy and 2′-amino groups. Similar studies of catalytic activities of *Tetrahymena* RNA have shown[449, 450] that the 2′-amino group and the bivalent metal ion compete for the same 5′-phosphate group in the active site of the ribozyme.

The modified ribozymes currently available represent complex structures which contain simultaneously 2′-*O*-methyl nucleosides, 2′-amino-2′-deoxyuridine, 2′-fluoro-2′-deoxynucleosides and thiophosphate internucleotide bonds.[451] The introduction of bulky substituents into the 2′-position significantly decreased the ribozyme activity;[229, 440] therefore, the use of such constructions seems to hold little promise.

V. Conclusion

At present, the synthesis of oligonucleotides containing reactive groups in the 2′-position and of their conjugates is a promising approach to targeted changes in the physicochemical and substrate properties of nucleic acid fragments. Among modified nucleosides, 2′-amino-2′-deoxyribonucleosides are especially popular. These can easily be incorporated into NA by chemical or enzymatic methods and then selectively acylated. This circumstance has determined the commercial availability of the pyrimidine 2′-amino-2′-deoxyribonucleoside phosphoramidite derivatives and 5′-triphosphates (TriLink BioTech, USA).

The methodology of preparation of modified oligonucleotides where the molecules or reactive groups are linked to the C(2′) or O(2′) atom has been developed fairly well. A vast number of publications are devoted to the synthesis of oligonucleotides containing nucleophilic groups, since in the majority of cases the corresponding phosphoramidite derivatives are commercially available.

Conjugates containing an amide bond are prepared by activation of the carboxy group using methods originally developed for peptide synthesis where the concentration of a compound containing a carboxy group exceeds that of the amino-containing component by an order of magnitude. It therefore seems expedient to perform the reactions of oligonucleotides bearing amino groups with an excess of carboxyl-containing compounds. Moreover, the presence of an amino group in the oligonucleotide chain fits well into the protocol of oligonucleotide synthesis, while the carboxy group needs to be deblocked prior to standard post-synthetic treatments.

Modified oligonucleotides where the thiol groups are attached to the O(2′) atom through various linkers are readily accessible and are used for the preparation of conjugates with a disulfide bond.

The reason for the rare employment of oligonucleotides containing an aldehyde or an oxo group is unclear. The synthesis and applications of aldehyde-containing oligonucleotides have been documented only in the past decade.[109] A commercially available modified polymeric carrier (Glen Research) for the synthesis of oligonucleotides with an aldehyde group at the 3′-end, has become popular. A 4-formylbenzoic activated ester designed for the incorporation of the aldehyde group into oligonucleotides containing an aliphatic amino group has recently become available (Trilink Biotech, USA).

These data altogether suggest that the aforementioned methods for the preparation of conjugates in solution and on polymeric supports are nearly equally efficient. In choosing a method for conjugation in solution, special attention should be given to the solubility of the reaction components and selectivity of the reaction, while the substances to be attached to the oligonucleotide should be easily separated from the reaction products by HPLC or gel electrophoresis. In the case of a solid-phase version, the bond formed and the molecule attached should retain stability under the conditions of post-synthetic treatments. The conjugation of nucleosides is less important but nevertheless promising in the synthesis of compounds carrying various reporter groups.

Analysis of the publications devoted to the use of 2′-modified oligonucleotides has demonstrated significant progress in many fields of molecular biology, antisense and anti-gene biotechnology and enzymology.

The authors thank Drs. A Yu Tomashevsky (University of Virginia, Charlottesville, VA, USA), O Yu Smirnova (German Cancer Research Centre, Heidelberg, Germany) and D A Stetsenko (Medical Research Council, Cambridge, UK) for their valuable assistance in the preparation of this review for publication. This review has been written within the framework of the Programme ‘Universities of Russia’ (Project No. UR.05.03.010) and with the financial support of the Wellcome Trust (Grant No. CRIG 069419) and the Russian Foundation for Basic Research (Project No. 03-04-48957).

References

1. D A Braasch, D R Corey *Biochemistry* **41** 4503 (2002)
2. D Praseuth, A L Guieysse, C Helene *Biochim. Biophys. Acta* **1489** 181 (1999)
3. E A Doherty, J A Doudna *Annu. Rev. Biochem.* **69** 597 (2000)
4. L Gold, B Polisky, O Uhlenberg, M Yarus *Annu. Rev. Biochem.* **64** 763 (1995)
5. P D Zamore *Nat. Struct. Biol.* **8** 746 (2001)
6. G J Hannon *Nature (London)* **418** 244 (2002)
7. J Telser, K A Cruikshank, L E Morrison, T L Netzel *J. Am. Chem. Soc.* **111** 6966 (1989)
8. E Bucci, L De Napoli, G Di Fabio, A Messere, D Montesarchio, A Romanelli, G Piccialli, M Varra *Tetrahedron* **55** 14435 (1999)
9. V A Korshun, E V Manasova, Yu A Berlin *Bioorg. Khim.* **23** 324 (1997) [a]
10. A F Nasonov, G A Korshunova *Usp. Khim.* **68** 532 (1999) [*Russ. Chem. Rev.* **68** 483 (1999)]
11. H Rosemeyer, N Ramzaeva, E M Becker, E Feiling, F Seela *Bioconjugate Chem.* **13** 1274 (2002)
12. M T Tierney, M W Grinstaff *Org. Lett.* **2** 3413 (2000)
13. M Manoharan *Biochim. Biophys. Acta* **1489** 117 (1999)

14. T Pathak *Chem. Rev.* **102** 1623 (2002)
15. J G Moffatt, in *Nucleoside Analogues. Chemistry, Biology and Medical Applications* Vol. A26 (Eds R T Walker, E De Clercq, F Eckstein) (New York: Plenum, 1979) p. 92
16. T Ueda, in *Chemistry of Nucleosides and Nucleotides* Vol. 1 (Ed. L B Townsend) (New York: Plenum, 1988) p. 50
17. J P H Verheyden, D Wagner, J G Moffatt *J. Org. Chem.* **36** 250 (1971)
18. T Sasaki, K Minamoto, T Siguira *J. Org. Chem.* **40** 3498 (1975)
19. T Sasaki, K Minamoto, T Siguira, M Niwa *J. Org. Chem.* **41** 3138 (1976)
20. G P Kirschenheuter, Y Zhai, W A Pieken *Tetrahedron Lett.* **35** 8517 (1994)
21. D P C McGee, C Vargeese, Y Zhai, G P Kirschenheuter, A Settle, C R Siedem, W A Pieken *Nucleosides Nucleotides* **14** 1329 (1995)
22. M W Logue, B H Han *J. Org. Chem.* **45** 5000 (1980)
23. D P C McGee, A Vaughn-Settle, C Vargeese, Y Zhai *J. Org. Chem.* **61** 781 (1996)
24. D P C McGee, D P Sebesta, S S O'Rourke, R L Martinez, M E Jung, W A Pieken *Tetrahedron Lett.* **37** 1995 (1996)
25. D P Sebesta, S S O'Rourke, R L Martinez, W A Pieken, D P C McGee *Tetrahedron* **52** 14385 (1996)
26. D P C McGee, A Vaughn-Settle *Nucleosides Nucleotides* **16** 1095 (1997)
27. E S Krider, J E Miller, T J Meade *Bioconjugate Chem.* **13** 155 (2002)
28. A Ogawa, S Shuto, O Inanami, M Kuwabara, M Tanaka, T Sasaki, A Matsuda *Bioorg. Med. Chem. Lett.* **8** 1913 (1998)
29. A Ogawa, M Tanaka, T Sasaki, A Matsuda *J. Med. Chem.* **41** 5094 (1998)
30. A Ogawa, S Shuto, M Tanaka, T Sasaki, S Mori, S Shigeta, A Matsuda *Chem. Pharm. Bull.* **47** 1000 (1999)
31. A Karpeisky, D Sweedler, P Haeberli, J Read, K Jarvis, L Beigelman *Bioorg. Med. Chem. Lett.* **12** 3345 (2002)
32. W T Markiewicz, M Wieworowski *Nucleic Acids Res. Spec. Publ.* 185 (1978)
33. M J Robins, S D Hawrelak, A E Hernandez, S F Wnuk *Nucleosides Nucleotides* **11** 821 (1992)
34. S Van Calenbergh, E van Den Eeckhout, P Herdewijn, A De Bruyn, C Verlinde, W G J Hol, M Callens, A van Aerschot, J Rozensky *Helv. Chim. Acta* **77** 631 (1994)
35. R Ranganathan, D Larwood *Tetrahedron Lett.* **19** 4341 (1978)
36. M J Robins, F Hansske, J S Wilson, S D Hawrelak, D Madej, in *Selective Modification and Deoxygenation at C2′ of Nucleosides* (Ed. J L Rideout) (New York, London: Academic Press, 1984) p. 278
37. S H Krawczyk, M Bernier-Rodriguez, M R Nassisri, E R Kern, L L Wotring, J C Drach, L B Townsend *J. Med. Chem.* **33** 3160 (1990)
38. D Wagner, J P H Verheyden, J G Moffatt *J. Org. Chem.* **39** 24 (1974)
39. A Sato, R Imai, N Nakamizo, T Hirata *Chem. Pharm. Bull.* **27** 821 (1979)
40. M J Robins, S D Hawrelak *Tetrahedron Lett.* **19** 3653 (1978)
41. A Matsuda, J Yasuoka, T Ueda *Chem. Pharm. Bull.* **37** 1659 (1989)
42. A Matsuda, J Yasuoka, T Sasaki, T Ueda *J. Med. Chem.* **34** 999 (1991)
43. K Minamoto, K Azuma, T Tanaka, H Iwasaki, S Eguchi, S Kadoya, R Moroi *J. Chem. Soc., Perkin Trans. 1* 2955 (1988)
44. R Mengel, H Wiedner *Chem. Ber.* **109** 433 (1976)
45. F J McEvoy, B R Baker, M J Weiss *J. Am. Chem. Soc.* **82** 209 (1960)
46. M L Wolfrom, M W Winkley *J. Org. Chem.* **32** 1823 (1967)
47. J B Hobbs, F Eckstein *J. Org. Chem.* **42** 714 (1977)
48. M Imazawa, F Eckstein *J. Org. Chem.* **44** 2039 (1979)
49. M Ferrero, V Gotor *Monatsh. Chem.* **131** 585 (2000)
50. T Utagawa *J. Mol. Catal., B* **6** 215 (1999)
51. K Matsuyama, Y Takahashi, M Yamashita, A Hirano, S Omura *J. Antibiot.* **32** 1367 (1979)
52. R J Suhadolnik, S Pornbanlualap, D C Baker, K N Tiwari, A K Hebbler *Arch. Biochem. Biophys.* **270** 374 (1989)
53. T Utagawa, H Morisawa, T Nakamatsu, A Yamazaki, S Yamanaka *FEBS Lett.* **119** 101 (1980)
54. T Utagawa, H Morisawa, S Yamanaka, A Yamazaki, Y Hirose *Agric. Biol. Chem.* **44** 1671 (1985)
55. M J Robins, R Zon, F Hansske, S F Wnuk *Can. J. Chem.* **75** 762 (1997)
56. T S Zatsepin, E A Romanova, T S Oretskaya *Usp. Khim.* **71** 586 (2002) [*Russ. Chem. Rev.* **71** 513 (2002)]
57. C J Guinosso, G D Hoke, S Frier, J F Martin, D J Ecker, C K Mirabelli, S T Crooke, P D Cook *Nucleosides Nucleotides* **10** 259 (1991)
58. M Manoharan, C J Guinosso, P D Cook *Tetrahedron Lett.* **32** 7171 (1991)
59. US P. 5 859 221 (1999)
60. US P. 5 872 232 (1999)
61. US P. 5 9143 96 (1999)
62. R H Griffey, B P Monia, L L Cummins, S M Freier, M J Greig, C J Guinosso, E A Lesnik, S M Manalili, V Mohan, S R Owens, B R Ross, H Sasmor, E Wancewich, K Weiler, P D Weeler, P D Cook *J. Med. Chem.*, **39** 5100 (1996)
63. M Manoharan, T P Prakash, I Barber-Peoc h, B Bhat, G Vasquez, B S Ross, P D Cook *J. Org. Chem.* **64** 6468 (1999)
64. M Manoharan *Antisense Nucleic Acid Drug. Dev.* **12** 103 (2002)
65. M Manoharan, K M Tivel, L K Andrade, P D Cook *Tetrahedron Lett.* **36** 3647 (1995)
66. B S Ross, R H Springer, Z Tortorici, S Dimock *Nucleosides Nucleotides* **16** 1641 (1997)
67. M Manoharan, T P Prakash, I Barber-Peoc h, B Bhat, G Vasquez, B S Ross, P D Cook *Nucleosides Nucleotides* **18** 1199 (1999)
68. T P Prakash, M Manoharan, A W Kawasaki, A S Fraser, E A Lesnik, N Sioufi, J M Leeds, M Teplova, M Egli *Biochemistry* **41** 11 642 (2002)
69. M Prhavc, T P Prakash, G Minasov, M Egli, M Manoharan *Org. Lett.* **5** 2017 (2003)
70. M J J Blommers, F Natt, W Jahnke, B Cuenoud *Biochemistry* **37** 17 714 (1998)
71. P Martin *Helv. Chim. Acta* **78** 486 (1995)
72. B Cuenoud, F Casset, D Husken, F Natt, R M Wolf, K-H Altmann, P Martin, H E Moser *Angew. Chem., Int. Ed.* **37** 1288 (1998)
73. A E Klopfer, J W Engels *ChemBioChem* **5** 707 (2004)
74. M Sollogoub, B Domingues, K R Fox, T Brown *Chem. Commun.* 2315 (2000)
75. I Dubey, G Pratviel, B Meunier *J. Chem. Soc., Perkin Trans. 1* 3088 (2000)
76. M Prhavc, E A Lesnik, V Mohan, M Manoharan *Tetrahedron Lett.* **42** 8777 (2001)
77. V A Korshun, D A Stetsenko, M J Gait. *J. Chem. Soc., Perkin Trans. 1* 1092 (2002)
78. N N Dioubankova, A D Malakhov, D A Stetsenko, M J Gait, P E Volynsky, R G Efremov, V A Korshun *ChemBioChem* **4** 841 (2003)
79. T H Keller, R Haner *Helv. Chim. Acta* **76** 884 (1993)
80. O Mitsunobu *Synthesis* 1 (1981)
81. A M Kawasaki, M D Casper, T P Prakash, S Manalili, H Sasmor, M Manoharan, P D Cook *Tetrahedron Lett.* **40** 661 (1999)
82. A M Kawasaki, M D Casper, T P Prakash, S Manalili, H Sasmor, M Manoharan, P D Cook *Nucleosides Nucleotides* **18** 1419 (1999)
83. T P Prakash, A M Kawasaki, G Vasquez, A S Fraser, M D Casper, P D Cook, M Manoharan *Nucleosides Nucleotides* **18** 1381 (1999)
84. T P Prakash, M Manoharan, A M Kawasaki, E A Lesnik, S R Owens, G Vasquez *Org. Lett.* **2** 3995 (2000)
85. T P Prakash, A M Kawasaki, A S Fraser, G Vasquez, M Manoharan *J. Org. Chem.* **67** 357 (2002)
86. A Karpeisky, C Gonzalez, A B Burgin, L Beigelman *Tetrahedron Lett.* **39** 1131 (1998)
87. S Chambert, J-L Decout *Org. Prep. Proced. Int.* **34** 27 (2002)
88. D M Brown, D B Parihar, Sir A Todd, S Varadarajan *J. Chem. Soc.* 3028 (1958)

89. Y Furukawa, Y Yoshioka, K Imai, M Honjo *Chem. Pharm. Bull.* **18** 554 (1970)
90. R Ranganathan *Tetrahedron Lett.* **18** 1291 (1977)
91. M Imazawa, T Ueda, T Ukita *Chem. Pharm. Bull.* **23** 604 (1975)
92. K J Divakar, C B Reese *J. Chem. Soc., Perkin Trans. 1* 1625 (1982)
93. M L Hamm, J A Piccirilly *J. Org. Chem.* **62** 3415 (1997)
94. H Ozaki, S Momiyama, K Yokotsuka, H Sawai *Nucleic Acids Symp. Ser.* **42** 47 (1999)
95. H Ozaki, S Momiyama, K Yokotsuka, H Sawai *Tetrahedron Lett.* **42** 677 (2001)
96. K J Divakar, A Mottoh, C B Reese, Y S Sanghvi *J. Chem. Soc., Perkin Trans. 1* 969 (1990)
97. S Chambert, I Gautier-Luneau, M Fontecave, J-L Decout *J. Org. Chem.* **65** 249 (2000)
98. A D Patel, W H Schrier, J Nagyvary *J. Org. Chem.* **45** 4830 (1980)
99. K J Ryan, E M Acton, L Goodman *J. Org. Chem.* **36** 2646 (1971)
100. C B Reese, C Simons, Z Pei-Zhuo *J. Chem. Soc., Chem. Commun.* 1809 (1994)
101. M Manoharan, L K Johnson, K L Tivel, R H Springer, P D Cook *Bioorg. Med. Chem. Lett.* **3** 2765 (1993)
102. M Manoharan, K L Tivel, B Ross, P D Cook *Gene* **149** 147 (1994)
103. US P. 5 578 718 (1996)
104. M E Douglas, B Beijer, B S Sproat *Bioorg. Med. Chem. Lett.* **4** 995 (1994)
105. J T Goodwin, S E Osborne, E J Scholle, G Glick *J. Am. Chem. Soc.* **118** 5207 (1996)
106. E J Maglott, G Glick *Nucleic Acids Res.* **26** 1301 (1998)
107. C W Gundlach IV, T R Ryder, G D Glick *Tetrahedron Lett.* **38** 4039 (1997)
108. X Wu, S Pitsch *Bioconjugate Chem.* **10** 921 (1999)
109. A V Kachalova, E M Zubin, T S Oretskaya *Usp. Khim.* **71** 1171 (2002) [*Russ. Chem. Rev.* **71** 1041 (2002)]
110. U Brodbeck, J G Moffatt *J. Org. Chem.* **35** 3552 (1970)
111. F Hansske, M J Robins *Tetrahedron Lett.* **24** 1589 (1983)
112. F Hansske, D Madej, M J Robins *Tetrahedron* **40** 125 (1984)
113. A Tronchet, R Benhamza, G Bernardinelli, M Geoffroy *Tetrahedron Lett.* **31** 531 (1990)
114. T-S Lin, M-Z Luo, M-C Liu, R H Clarke-Kazenburg, Y-C Cheng, W H Prusoff, W R Mancini, G I Birnbaum, E J Gabe, J Giziewicz *J. Med. Chem.* **34** 2607 (1991)
115. A Matsuda, K Takenuki, H Itoh, T Sasaki, T Ueda *Chem. Pharm. Bull.* **35** 3967 (1987)
116. A Matsuda, H Itoh, K Takenuki, T Sasaki, T Ueda *Chem. Pharm. Bull.* **36** 945 (1988)
117. T Ueda, A Matsuda, Y Yoshimura, K Takenuki *Nucleosides Nucleotides* **8** 743 (1989)
118. K Takenuki, A Matsuda, T Ueda, T Sasaki, A Fujii, K Yamagami *J. Med. Chem.* **31** 1063 (1988)
119. K Takenuki, H Itoh, A Matsuda, T Ueda *Chem. Pharm. Bull.* **38** 2947 (1990)
120. A Matsuda, K Takenuki, T Sasaki, T Ueda *J. Med. Chem.* **34** 234 (1991)
121. K Omura, A K Sharma, D Swern *J. Org. Chem.* **41** 957 (1976)
122. K Omura, D Swern *Tetrahedron* **34** 1651 (1978)
123. J R McCarthy, D P Matthews, D M Stemerick, E W Huber, P Bey, B J Lippert, R D Snyder, P S Suncara *J. Am. Chem. Soc.* **113** 7439 (1991)
124. D P Matthews, R A Persichetti, J S Sabol, K T Stewart, J R McCarthy *Nucleosides Nucleotides* **12** 115 (1993)
125. R B Appell, R J Duguid *Org. Process Res. Dev.* **4** 172 (2000)
126. V Samano, M J Robins *J. Org. Chem.* **55** 5186 (1990)
127. D B Dess, J C Martin *J. Org. Chem.* **48** 4155 (1983)
128. D P Kjell, B J Slattery *Nucleosides Nucleotides,* **16** 469 (1997)
129. M Dunkel, V Reither *Bioorg. Med. Chem. Lett.* **9** 787 (1999)
130. K Takenuki, A Matsuda, T Ueda, T Sasaki, A Fujii, K Yamagami *J. Med. Chem.* **31** 1064 (1988)
131. A E A Hassan, S Shuto, A Matsuda *J. Org. Chem.* **62** 11 (1997)
132. R Buff, J Hunziker *Helv. Chim. Acta* **85** 224 (2002)
133. M Sukeda, S Shuto, I Sugimoto, S Ichikawa, A Matsuda *J. Org. Chem.* **65** 8988 (2000)
134. A Matsuda, Y Nakajima, A Azuma, M Tanaka, T Sasaki *J. Med. Chem.* **34** 2917 (1991)
135. A Azuma, Y Nakajima, N Nishizono, N Minakawa, M Suzuki, K Hanaoka, T Kobayashi, M Tanaka, T Sasaki, A Matsuda *J. Med. Chem.* **36** 4183 (1993)
136. K Hanaoka, M Suzuki, T Kobayashi, F Tanzawa, K Tanaka, T Shibayama, S Miura, T Ikeda, H Iwabuchi, A Nakagawa, Y Mitsuhashi, M Hisaoka, M Kaneko, A Tomida, Y Wataya, T Nomura, T Sasaki, A Matsuda, T Tsuruo, S Kurakata *Int. J. Cancer* **82** 226 (1999)
137. T Takahashi, A Nakashima, J Kanazawa, K Yamaguchi, S Akinaga, T Tamaoki, M Okabe *Cancer Chemother. Pharmacol.* **41** 268 (1998)
138. S M Freier, K H Altmann *Nucleic Acids Res.* **25** 4429 (1997)
139. A Matsuda, M Inada, H Nara, E Ohtsuka, A Ono *Bioorg. Med. Chem. Lett.* **3** 2751 (1993)
140. A V Kachalova, T S Zatsepin, E A Romanova, D A Stetsenko, M J Gait, T S Oretskaya *Nucleosides Nucleotides Nucleic Acids* **19** 1693 (2000)
141. T S Zatsepin, A V Kachalova, E A Romanova, D A Stetsenko, M J Gait, T S Oretskaya *Bioorg. Khim.* **27** 45 (2001) [a]
142. O M Gritsenko, E S Gromova *Usp. Khim.* **68** 267 (1999) [*Russ. Chem. Rev.* **68** 241 (1999)]
143. B S Ermolinskii, S N Mikhailov *Bioorg. Khim.* **26** 483 (2000) [a]
144. E Efimtseva, S N Mikhailov *Biokhimiya* **67** 1374 (2002) [b]
145. T P Prakash, A M Kawasaki, E A Lesnik, S R Owens, M Manoharan *Org. Lett.* **5** 403 (2003)
146. A Fraser, P Wheeler, P D Cook, Y S Sanghvi *J. Heterocycl. Chem.* **30** 1277 (1993)
147. M Egli *Angew. Chem., Int. Ed. Engl.* **35** 1894 (1996)
148. M Sekine, H Tsuruoka, S Iimura, H Kusuoku, T Wada, K Furusawa *J. Org. Chem.* **61** 4087 (1996)
149. H Tsuruoka, K Shohda, T Wada, M Sekine *J. Org. Chem.* **65** 7479 (2000)
150. A Zehl, D Cech *Liebigs Ann. Chem.* 595 (1997)
151. N G Dolinnaya, Z A Shabarova *Sov. Sci. Rev. D, Physicochem. Biol.* **13** 1 (1995)
152. J C Leitzel, D G Lynn *Chem. Rec.* **1** 53 (2001)
153. H Aurup, D M Williams, F Eckstein *Biochemistry* **31** 9636 (1992)
154. W Pieken *Ciba Found. Symp.* **209** 218 (1997)
155. B E Eaton, W A Pieken *Annu. Rev. Biochem.* **64** 837 (1995)
156. M J Kujau, A Siebert, S Wolfl *J. Biochem. Biophys. Methods* **35** 141 (1997)
157. E Zamaratski, J Chattopadhyaya *Tetrahedron* **54** 8183 (1998)
158. C J Yu, H Wang, H Yowanto, J C Kim, L H Donilon, C Tao, M Strong, Y Chong *J. Org. Chem.* **66** 2937 (2001)
159. C J Yu, Y Wan, H Yowanto, J Li, C Tao, M D James, C L Tam, G F Blackburn, T J Meade *J. Am. Chem. Soc.* **123** 11 155 (2001)
160. J K Bashkin, J Xie, A T Daniher, U S Sampath, J L-F Kao *J. Org. Chem.* **61** 2314 (1996)
161. H Asanuma, T Yoshida, T Ito, M Komiyama *Tetrahedron Lett.* **40** 7995 (1999)
162. K Yamana, Y Ohashi, K Nunota, M Kitamura, H Nakano, O Sangen, T Shimidzu *Tetrahedron Lett.* **32** 6347 (1991)
163. K Yamana, R Aota, H Nakano *Tetrahedron Lett.* **36** 8427 (1995)
164. K Yamana, Y Nishijima, T Ikeda, T Gokota, H Ozaki, H Nakano, O Sangen, T Shimidzu *Bioconjugate Chem.* **1** 319 (1990)
165. D Ly, L Sanii, G B Schuster *J. Am. Chem. Soc.* **121** 9400 (1999)
166. C Sund, N Puri, J Chattopadhyaya *Tetrahedron* **52** 12 275 (1996)
167. C Sund, N Puri, J Chattopadhyaya *Nucleosides Nucleotides* **16** 755 (1997)
168. M Manoharan, K L Tivel, P D Cook *Tetrahedron Lett.* **36** 3651 (1995)
169. M Manoharan, K L Tivel, T P Condon, L K Andrade, I Barber-Peoch, G Inamati, S Shash, V Mohan, M J Graham, C F Bennet, S T Crooke, P D Cook *Nucleosides Nucleotides* **16** 1129 (1997)
170. M Manoharan, K L Tivel, M Zhao, K Nafisi, T L Netzel *J. Phys. Chem.* **99** 17461 (1995)

171. N A Whittemore, A N Mullenix, G B Inamati, M Manoharan, P D Cook, A A Tuinman, D C Baker, J Q Chambers *Bioconjugate Chem.* **10** 261 (1999)
172. M Manoharan, G Inamati, K L Tivel, B Conklin, B S Ross, P D Cook *Nucleosides Nucleotides* **16** 1141 (1997)
173. T H Keller, R Haner *Nucleic Acids Res.* **21** 4499 (1993)
174. K Seio, T Wada, K Sakamoto, S Yokoyama, M Sekine *J. Org. Chem.* **63** 1429 (1998)
175. K Seio, T Wada, K Sakamoto, S Yokoyama, M Sekine *Helv. Chim. Acta* **83** 162 (2000)
176. A K M Anisuzzaman, F Alam, A H Soloway *Polyhedron* **9** 891 (1990)
177. W Tjaks, A K M Anisuzzaman, L Liu, A H Soloway, R F Barth, D J Perkins, D M Adams *J. Med. Chem.* **35** 1628 (1992)
178. W Tjaks, A K M Anisuzzaman, A H Soloway *Nucleosides Nucleotides* **11** 1765 (1992)
179. R F Barth, A H Soloway, R G Fairchild, R M Brugger *Cancer* **70** 2995 (1992)
180. A H Soloway, W Tjarks, B A Barnum, F G Rong, R F Barth, I M Codogni, J G Wilson *Chem. Rev.* **98** 1515 (1998)
181. L Liu, R F Barth, W Tjarks, A H Soloway, A K M Anisuzzaman *Anticancer Res.* **16** 113 (1996)
182. A B Olejniczak, M Koziolkiewicz, Z J Lesnikowski *Antisense Nucleic Acid Drug Dev.* **12** 79 (2002)
183. T Mitsui, H Hayashi, K Yamana, H Nakano *Nucleic Acids Symp. Ser.* 69 (1997)
184. K Yamana, T Mitsui, H Hayashi, H Nakano *Tetrahedron Lett.* **38** 5815 (1997)
185. K Yamana, Y Ohashi, K Nunota, H Nakano *Tetrahedron* **53** 4265 (1997)
186. T Mitsui, H Nakano, K Yamana *Tetrahedron Lett.* **41** 2605 (2000)
187. S K Silverman, M L Deras, S A Woodson, S A Scaringe, T R Cech *Biochemistry* **39** 12465 (2000)
188. US P. 6 090 933 (2000)
189. US P. 6 096 273 (2000)
190. US P. 6 221 583 (2001)
191. L Milne, D M Perrin, D S Sigman *Proc. Natl. Acad. Sci. USA* **97** 3136 (2000)
192. O P Kryatova, W H Connors, C F Bleczinski, A A Mokhir, C Richert *Org. Lett.* **3** 987 (2001)
193. J Matulic-Adamic, L Beigelman, L W Dudycz, C Gonzalez, N Usman *Bioorg. Med. Chem. Lett.* **5** 2721 (1995)
194. J Matulic-Adamic, V Serebryany, P Haeberli, V R Mokler, L Beigelman *Bioconjugate Chem.* **13** 1071 (2002)
195. A M Aronov, S Suresh, F Buckner, W van Voorhis, C L M J Verlinde, F R Opperdoes, W G J Hol, M H Gelb *Proc. Natl. Acad. Sci. USA* **96** 4273 (1999)
196. A Link, S van Calenbergh, P Herdewijn *Tetrahedron Lett.* **39** 5175 (1998)
197. B Backes, A A Virgilio, J A Ellmann *J. Am. Chem. Soc.* **118** 3055 (1996)
198. A Golisade, S van Calenbergh, A Link *Tetrahedron* **56** 3167 (2000)
199. J C Bressi, C L M J Verlinde, A M Aronov, M L Shaw, S S Shin, L N Nguyen, S Suresh, F S Buckner, W C van Voorhis, I D Kuntz, W G J Hol, M H Gelb *J. Med. Chem.* **44** 2080 (2001)
200. A Golisade, J C Bressi, S van Calenbergh, M H Gelb, A Link *J. Comb. Chem.* **2** 537 (2000)
201. A Golisade, C Herforth, L Quirijnen, L Maes, A Link *Bioorg. Med. Chem.* **10** 159 (2002)
202. N N Polushin *Tetrahedron Lett.* **37** 3231 (1996)
203. US P. 5 902 879 (1999)
204. N N Polushin *Collect. Czech. Chem. Commun. Symp. Ser.* **2** 145 (1999)
205. J J Rack, E S Krider, T J Meade *J. Am. Chem. Soc.* **122** 6287 (2000)
206. E S Krider, J J Rack, N L Frank, T J Meade *Inorg. Chem.* **40** 4002 (2001)
207. N L Frank, T J Meade *Inorg. Chem.* **42** 1039 (2003)
208. K L Dombi, U E Steiner, C Richert *J. Comb. Chem.* **5** 45 (2003)
209. I Barber-Peoc'h, M Manoharan, P D Cook *Nucleosides Nucleotides* **16** 1407 (1997)
210. M A Maier, I Barber-Peoc'h, M Manoharan *Tetrahedron Lett.* **43** 7613 (2002)
211. W H Connors, S Naranayan, O P Kryatova, C Richert *Org. Lett.* **5** 247 (2003)
212. E M Zubin, E A Romanova, E M Volkov, V N Tashlitsky, G A Korshunova, Z A Shabarova, T S Oretskaya *FEBS Lett.* **456** 59 (1999)
213. J-T Hwang, M M Greenberg *Org. Lett.* **1** 2021 (1999)
214. J-T Hwang, M M Greenberg *J. Org. Chem.* **66** 363 (2001)
215. H Salo, P Virta, H Hakala, T P Prakash, A M Kawasaki, M Manoharan, H Lönnberg *Bioconjugate Chem.* **10** 815 (1999)
216. J P Tam, J C Spetzler *Biomed. Peptides Proteins Nucleic Acids* **1** 123 (1995)
217. N Polushin, A Malykh, O Malykh, M Zenkova, N Chumakova, V Vlassov, S Kozyavkin *Nucleosides Nucleotides Nucleic Acids* **20** 507 (2001)
218. V Banuls, J-M Escudier, C Zedde, C Claparols, B Donnadieu, H Plaisancie *Eur. J. Org. Chem.* 4693 (2001)
219. X Wu, S Pitsch *Helv. Chim. Acta* **83** 1127 (2000)
220. W Gueschlbauer, K Jankowski *Nucleic Acids Res.* **8** 1421 (1980)
221. L-S Kan, R Bauman, P Bhan, P S Miller *J. Chin. Chem. Soc. (Taipei)* **40** 469 (1993)
222. H Aurup, T Tuschl, F Benseler, J Ludwug, F Eckstein *Nucleic Acids Res.* **22** 20 (1994)
223. C Hendrix, B Devreese, J Rozenski, A van Aershot, A De Bruyn, J van Beeumen, P Herdewijn *Nucleic Acids Res.* **23** 51 (1995)
224. L Beigelman, A Karpeisky, J Matulic-Adamic, P Haerberli, D Sweedler, N Usman *Nucleic Acids Res.* **23** 4434 (1995)
225. P S Miller, P Bhan, L-S Kan *Nucleosides Nucleotides* **12** 785 (1993)
226. F Wincott, A Di Renzo, C Shaffer, S Grimm, D Tracz, C Workman, D Sweedler, N Usman *Nucleic Acids Res.* **23** 2677 (1995)
227. F Benseler, D M Williams, F Eckstein *Nucleosides Nucleotides* **11** 1333 (1992)
228. O Heindenreich, F Benseler, A Fahrenholz, F Eckstein *J. Biol. Chem.* **269** 2131 (1994)
229. M Scherr, C Klebba, R Haner, A Ganser, J W Engels *Bioorg. Med. Chem. Lett.* **7** 1791 (1997)
230. G Walcher, W Phleiderer *Helv. Chim. Acta* **79** 1067 (1996)
231. B Greiner, W Phleiderer *Helv. Chim. Acta.* **81** 1528 (1998)
232. N N Polushin, I P Smirnov, A N Verentchikov, J M Coull *Tetrahedron Lett.* **37** 3227 (1996)
233. L G Kuznetsova, E M Volkov, E A Romanova, V N Tashlitskii, T S Oretskaya, Z A Shabarova *Bioorg. Khim.* **17** 1289 (1991) [a]
234. L G Kuznetsova, E A Romanova, E M Volkov, V N Tashlitskii, T S Oretskaya, N F Krynetskaya, Z A Shabarova *Bioorg. Khim.* **19** 455 (1993) [a]
235. K Yamana, T Mitsui, H Nakano *Tetrahedron* **55** 9143 (1999)
236. P Sergiev, S Dokudovskaya, E Romanova, A Topin, A Bogdanov, R Brimacombe, O Dontsova *Nucleic Acids Res.* **26** 2519 (1998)
237. T E Edwards, T M Okonogi, B H Robinson, S T Sigurdsson *J. Am. Chem. Soc.* **123** 1527 (2001)
238. S T Sigurdsson, T Tuschl, F Eckstein *RNA* **1** 575 (1995)
239. S T Sigurdsson, F Eckstein *Nucleic Acids Res.* **24** 3129 (1996)
240. S Alefelder, S T Sigurdsson *Bioorg. Med. Chem.* **8** 269 (2000)
241. S I Antsypovich, E M Volkov, T S Oretskaya, E A Romanova, V N Tashlitskii, M Blyumenfel'd, Z A Shabarova *Bioorg. Khim.* **21** 774 (1995) [a]
242. S I Antsypovich, T S Oretskaya, E M Volkov, E A Romanova, V N Tashlitsky, M Blumenfeld, Z A Shabarova *Nucleosides Nucleotides* **15** 923 (1996)
243. S I Antsypovich, T S Oretskaya, E A Romanova, E M Volkov, V N Tashlitskii, M Vasser, Z A Shabarova *Bioorg. Khim.* **22** 264 (1996) [a]
244. S I Antsypovich, T S Oretskaya, E A Romanova, E M Volkov, V N Tashlitsky, M Vasser, Z A Shabarova *FEBS Lett.* **378** 224 (1996)

245. E M Zubin, S I Antsypovich, T S Oretskaya, E A Romanova, E M Volkov, V N Tashlitskii, Z A Shabarova *Bioorg. Khim.* **23** 809 (1997) [a]
246. E M Zubin, S I Antsypovich, T S Oretskaya, E A Romanova, E M Volkov, N G Dolinnaya, Z A Shabarova *Nucleosides Nucleotides* **17** 425 (1998)
247. L Zhu, P S Lukeman, J W Canary, N C Seeman *J. Am. Chem. Soc.* **125** 10178 (2003)
248. S K Silverman, T R Cech *Biochemistry* **38** 14224 (1999)
249. S I Chamberlin, K M Weeks *J. Am. Chem. Soc.* **122** 216 (2000)
250. D M John, K M Weeks *Chem. Biol.* **7** 405 (2000)
251. D M John, K M Weeks *Biochemistry* **41** 6866 (2002)
252. M Beban, P S Miller *Bioconjugate Chem.* **11** 599 (2000)
253. A Y Louie, T J Meade *Proc. Natl. Acad. Sci. USA* **95** 6663 (1998)
254. T J Meade, J F Kayyem *Angew. Chem., Int. Ed. Engl.* **34** 352 (1995)
255. E S Krider, T J Meade *J. Bioinorg. Chem.* **3** 222 (1998)
256. D B Hall, R E Holmin, J K Barton *Nature (London)* **382** 731 (1996)
257. P J Dandliker, R E Holmin, J K Barton *Science* **275** 1465 (1997)
258. M A Farrow, F Aboul-ela, D Owen, A Karpeisky, L Beigelman, M J Gait *Biochemistry* **37** 3096 (1998)
259. J Hall, D Husken, R Haner *Nucleic Acids Res.* **24** 3522 (1996)
260. D A Stetsenko, A A Arzumanov, V A Korshun, M J Gait *Mol. Biol.* **34** 998 (2000) [c]
261. S B Cohen, T R Cech *J. Am. Chem. Soc.* **119** 6259 (1997)
262. M L Hamm, J A Piccirilly *J. Org. Chem.* **64** 5700 (1999)
263. R Johnson, C B Reese, Z Pei-Zhuo *Tetrahedron* **51** 5093 (1995)
264. C L Dantzman, L L Kiesseling *J. Am. Chem. Soc.* **118** 11 715 (1996)
265. M Manoharan, L K Andrade, P D Cook *Org. Lett.* **1** 311 (1999)
266. US P. 5 719 271 (1998)
267. US P. 5 543 507 (1996)
268. T S Zatsepin, D A Stetsenko, A A Arzumanov, E A Romanova, M J Gait, T S Oretskaya *Bioconjugate Chem.* **13** 822 (2002)
269. H Tsuruoka, K Shohda, T Wada, M Sekine *J. Org. Chem.* **62** 2813 (1997)
270. L L H De Fallois, J L Decout, M Fontecave *J. Chem. Soc., Perkin Trans. 1* 2587 (1997)
271. J Coves, L L H De Fallois, L Le Pape, J-L Decout, M Fontecave *Biochemistry* **35** 8595 (1996)
272. M Fontecave *Cell Mol. Life Sci.* **1** 684 (1998)
273. B Roy, S Chambert, M Lepoivre, A M Aubertin, J Balzarini, J L Decout *J. Med. Chem.* **46** 2565 (2003)
274. J Stubbe, W A van der Donk *Chem. Biol.* **2** 793 (1995)
275. C L M J Verlinde, M Callens, S van Calenbergh, A Van Aershot, P Herdewiijn, V Hannaert, P A Michels, F R Opperdoes, W G J Hol *J. Med. Chem.* **37** 3605 (1994)
276. S van Calenbergh, C L M J Verlinde, J Soenens, A De Bruyn, M Callens, N M Blaton, O M Peeters, J Rozensky, W G J Hol P Herdewiijn *J. Med. Chem.* **38** 3838 (1995)
277. A M Aronov, C L M J Verlinde, W G J Hol, M H Gelb *J. Med. Chem.* **41** 4790 (1998)
278. D H Smith, J Pepin, A H Stich *Br. Med. Bull.* **54** 341 (1998)
279. S Suresh, J C Bressi, K J Kennedy, C L M J Verlinde, M H Gelb, W G Hol *J. Mol. Biol.* **309** 423 (2001)
280. E Uhlmann, A Peyman *Chem. Rev.* **90** 543 (1990)
281. J F Milligan, M D Matteucci, J C Martin *J. Med. Chem.* **36** 1923 (1993)
282. C Boiziau, N T Thuong, J J Toulme *Proc. Natl. Acad. Sci. USA* **89** 768 (1992)
283. M Kulka, C C Smith, L Aurelian, R Fishelevich, K Meade, P Miller, P O P Ts'o *Proc. Natl. Acad. Sci. USA* **86** 6868 (1989)
284. B Mestre, A Arzumanov, M Singh, F Boulme, S Litvak, M J Gait *Biochim. Biophys. Acta* **1445** 86 (1999)
285. B F Baker, H Khalili, N Wei, J R Morrow *J. Am. Chem. Soc.* **119** 8749 (1997)
286. D S Wilson, J W Szostak *Annu. Rev. Biochem.* **68** 611 (1999)
287. G M Emilsson, R R Breaker *Cell. Mol. Life Sci.* **59** 596 (2002)
288. B N Trawick, A T Daniher, J K Bashkin *Chem. Rev.* **98** 939 (1998)
289. V N Silnikov, V V Vlassov *Usp. Khim.* **70** 562 (2001) [*Russ. Chem. Rev.* **70** 491 (2001)]
290. D G Knorre, V V Vlassov, V F Zarytova *Biochimie* **65** 785 (1985)
291. C F Bennett *Antisense Nucleic Acid Drug Dev.* **12** 215 (2002)
292. J Sung, T Garestier, C Helene *Curr. Opin. Struct. Biol.* **6** 327 (1996)
293. N Schmid, J-P Behr *Tetrahedron Lett.* **36** 1447 (1995)
294. V Demidov, M Frank-Kamenetskii, M Egholm, O Buchardt, P E Nielsen *Nucleic Acids Res.* **21** 2103 (1993)
295. K G Ragunathan, H-J Schneider *Angew. Chem., Int. Ed. Engl.* **35** 1219 (1996)
296. D S Sergeyev , T S Godovikova, V F Zarytova *Nucleic Acids Res.* **23** 4400 (1995)
297. T J Povsic, P B Dervan *J. Am. Chem. Soc.* **112** 9428 (1990)
298. E A Lukhtanov, M A Podyminogin, I V Kutyavin, R B Meyer, H B Gamper *Nucleic Acids Res.* **24** 683 (1996)
299. A Fire, S Xu, M K Montgomery, S A Kostas, S E Driver, C C Mello *Nature (London)* **391** 806 (1998)
300. S M Elbashir, J Hardworth, W Lendeckel, A Yalcin, K Weber, T Tuschl *Nature (London)* **411** 494 (2001)
301. S M Elbashir, W Lendeckel, T Tuschl *Genes Dev.* **15** 188 (2000)
302. S Parrish, J Fleenor, S Xu, C Mello, A Fire *Mol. Cell* **6** 1077 (2000)
303. S M Elbashir, J Martinez, A Patkaniowska, W Lendeckel, T Tuschl *EMBO J.* **20** 6877 (2001)
304. A D J Scadden, C W J Smith *EMBO Rep.* **2** 1107 (2001)
305. D A Braasch, S Jensen, Y Liu, K Kaur, K Arar, M A White, D R Corey *Biochemistry* **42** 7967 (2003)
306. H Grosshans, F J Slack *J. Cell Biol.* **156** 17 (2002)
307. E G Moss *Curr. Biol.* **12** R688 (2002)
308. M T McManus, P A Sharp *Nature Rev. Genet.* **3** 737 (2002)
309. S Gottesman *Genes Dev.* **16** 2829 (2002)
310. A M Kopylov, V A Spiridonova *Mol. Biol.* **34** 1097 (2000) [c]
311. T Hermann, D J Patel *Science* **287** 820 (2000)
312. C Tuerk, L Gold *Science* **249** 505 (1990)
313. A D Ellington, J W Szostak *Nature (London)* **346** 818 (1990)
314. W Kusser *J. Biotechnol.* **74** 27 (2000)
315. J L Beck, M L Colgrave, S F Ralph, M M Sheil *Mass Spectrom. Rev.* **20** 61 (2001)
316. C G Huber, H Oberacher *Mass Spectrom. Rev.* **20** 310 (2001)
317. V K Jayasena, L Gold *Proc. Natl. Acad. Sci. USA* **94** 10 612 (1997)
318. C Cazenave, M Chevrier, T T Nguyen, C Helene *Nucleic Acids Res.* **15** 10 507 (1987)
319. P S Eder, R J Devine, J M Dagle, J A Walder *Antisense Res. Dev.* **1** 141 (1991)
320. H Orum, J Wengel *Curr. Opin. Mol. Ther.* **3** 239 (2001)
321. A N Elayadi, D R Corey *Curr. Opin. Investig. Drugs* **2** 558 (2001)
322. C H Tung, S Stein *Bioconjugate Chem.* **11** 605 (2000)
323. R I Mahato, Y Takakura, M Hashida *J. Drug Target* **4** 337 (1997)
324. R L Juliano, S Akhtar *Antisense Res. Dev.* **2** 165 (1992)
325. A R Thierry, A Dritschilo *Nucleic Acids Res.* **20** 5691 (1992)
326. C R Dass *J. Pharm. Pharmacol.* **54** 3 (2002)
327. P Milhaud, J P Bolgartz, B Lebleu *Drug Delivery* **3** 67 (1996)
328. M Fresta, R Chillemi, S Spampinato, S Scuito, G Puglisi *J. Pharm. Sci.* **87** 616 (1998)
329. S Wang, R J Lee, G Cauchon, D G Gorenstein, P S Low *Proc. Natl. Acad. Sci. USA* **92** 3318 (1995)
330. M P Selvam, S M Buck, R A Blay, R E Mayner, P A Mied, J S Epstein *Antiviral Res.* **33** 11 (1996)
331. M Monsigny, P Midoux, R Mayer, A C Roche *Biosci. Rep.* **19** 125 (1999)
332. G Lambert, E Fattal, P Couvreur *Adv. Drug Deliv. Rev.* **47** 99 (2001)
333. S W Poxon, P M Mitchell, E Liang, J A Hughes *Drug Delivery* **3** 255 (1996)
334. I Lebedeva, L Benimetskaya, C A Stein, M Vilenchik *Eur. J. Pharmacol. Biopharmacol.* **50** 101 (2000)
335. M Teplova, S T Wallace, V Tereshko, G Minasov, A M Symons, P D Cook, M Manoharan, M Egli *Proc. Natl. Acad. Sci. USA* **96** 14 240 (1999)

336. A Arzumanov, A P Walsh, V K Rajwanshi, R Kumar, J Wengel, M J Gait *Biochemistry* **40** 14 645 (2001)
337. J C Schmitz, D Yu, S Agrawal, E Chu *Nucleic Acids Res.* **29** 415 (2001)
338. P Sazani, S H Kang, M A Maier, C Wei, J Dillman, J Summerton, M Manoharan, R Kole *Nucleic Acids Res.* **29** 3965 (2001)
339. V Dapic, P J Bates, J O Trent, A Rodger, S D Thomas, D M Miller *Biochemistry* **41** 3676 (2002)
340. T C Mou, D M Gray *Nucleic Acids Res.* **30** 749 (2002)
341. M Ma, L Benimetskaya, I Lebedeva, J Dignam, G Takle, C A Stein *Nat. Biotechnol.* **18** 58 (2000)
342. M Rydh-Rinder, O G Berge, T Hokfelt *Brain Res. Mol. Brain. Res.* **86** 23 (2001)
343. B P Monia, E A Lesnik, C Gonzalez, W F Lima, D McGee, C J Guinosso, A M Kawasaki, P D Cook, S M Freier *J. Biol. Chem.* **268** 14 514 (1993)
344. G Krupp *Biochimie* **75** 135 (1993)
345. B Larrouy, C Boiziau, B Sproat, J J Toulme *Nucleic Acids Res.* **23** 3434 (1995)
346. M Teplova, G Minasov, V Tereshko, G B Inamati, P D Cook, M Manoharan, M Egli *Nat. Struct. Biol.* **6** 535 (1999)
347. O Khatsenko, R Morgan, L Truong, C York-Defalco, H Sasmor, B Conklin, R S Geary *Antisense Nucleic Acid Drug Dev.* **10** 35 (2000)
348. R S Geary, T A Watanabe, L Truong, S Freier, E A Lesnik, N B Sioufi, H Sasmor, M Manoharan, A A Levin *J. Pharmacol. Exp. Ther.* **296** 890 (2001)
349. P Sazani, F Gemignani, S H Kang, M A Maier, M Manoharan, M Persmark, D Bortner, R Kole *Nat. Biotechnol.* **20** 1228 (2002)
350. D R Corey *Oncogene* **21** 631 (2002)
351. T A Vickers, J R Wyatt, T Burckin, C F Bennett, S M Freier *Nucleic Acids Res.* **29** 1239 (2001)
352. H Torigoe, R Shimizume, A Sarai, H Shindo *Biochemistry* **38** 14 653 (1999)
353. J L Asensio, R Carr, T Brown, A N Lane *J. Am. Chem. Soc.* **121** 11 063 (1999)
354. H Torigoe, Y Hari, M Sekiguchi, S Obika, T Imanishi *J. Biol. Chem.* **276** 2354 (2001)
355. A M Stutz, J Hoeck, F Natt, B Cuenoud, M Woisetschlager *J. Biol. Chem.* **276** 11 759 (2001)
356. N Puri, A Majumdar, B Cuenoud, F Natt, P Martin, A Boyd, P S Miller, M M Seidman *J. Biol. Chem.* **276** 28991 (2001)
357. N Puri, A Majumdar, B Cuenoud, F Natt, P Martin, A Boyd, P S Miller, M M Seidman *Biochemistry* **41** 7716 (2002)
358. T Carlomango, M J J Blommers, J Meiler, B Cuenoud, C Griesinger *J. Am. Chem. Soc.* **123** 7364 (2001)
359. K B Wiberg *Acc. Chem. Res.* **29** 229 (1996)
360. S W Blume, J Lebowitz, W Zacharias, V Guarcello, C A Mayfield, S W Ebbinghous, P Bates, D E Jones, J Trent, N Vigneswaran, D M Miller *Nucleic Acids Res.* **27** 695 (1999)
361. A Majumdar, N Puri, B Cuenoud, F Natt, P Martin, A Khorlin, N Dyatkina, A J George, P S Miller, M M Seidman *J. Biol. Chem.* **278** 11 072 (2003)
362. M Sollogoub, R Darby, B Cuenoud, T Brown, K R Fox *Biochemistry* **41** 7224 (2002)
363. G Ya Sheflyan, E A Kubareva, E S Gromova *Usp. Khim.* **65** 765 (1996) [*Russ. Chem. Rev.* **65** 709 (1996)]
364. V Pingoud, E Kubareva, G Stengel, P Friedhoff, J M Bujnicki, C Urbanke, A Sudina, A Pingoud *J. Biol. Chem.* **277** 14 306 (2002)
365. A Pingoud, A Jeltsch *Eur. J. Biochem.*, **246** 1 (1997)
366. O V Vorob'eva, S A Vasil'ev, A S Karyagina, T S Oretskaya, E A Kubareva *Mol. Biol.* **34** 1074 (2000) [c]
367. K M Meisenheimer, T H Koch *Crit. Rev. Biochem. Mol. Biol.* **32** 101 (1997)
368. E A Kubareva, E M Volkov, N L Vinogradova, I A Kanevsky, T S Oretskaya, S A Kuznetsova, M G Brevnov, E S Gromova, G A Nevinsky, Z A Shabarova *Gene* **157** 167 (1995)
369. S S Parikh, G Walcher, G D Jones, G Slupphaug, H E Krokan, G M Blackburn, J A Tainer *Proc. Natl. Acad. Sci. USA* **97** 5083 (2000)
370. M Ghosh, N V Kumar, U Varshney, K V Chary *Nucleic Acids Res.* **28** 1906 (2000)
371. O M Gritsenko, E V Koudan, S N Mikhailov, B S Ermolinsky, A van Aerschot, P Herdewijn, E S Gromova *Nucleosides Nucleotides Nucleic Acids* **21** 753 (2002)
372. S N Mikhailov, B S Ermolinsky, E V Efimtseva, M G Brevnov, O M Gritsenko, E S Gromova, A van Aerschot, P Herdewijn *Nucleosides Nucleotides* **18** 1469 (1999)
373. S N Mikhailov, B S Ermolinsky, E V Efimtseva, G P Moiseyev, V L Tunitskaya, E E Rusakova, S N Kochetkov, O M Gritsenko, E S Gromova, A van Aerschot, P Herdewijn *Collect. Czech. Chem. Commun., Symp. Ser.* **2** 141 (1999)
374. O M Gritsenko, S N Mikhailov, E V Efimtseva, A van Aerschot, P Herdewijn, E S Gromova *Nucleosides Nucleotides Nucleic Acids* **19** 1805 (2000)
375. V L Tunitskaya, E E Rusakova, L V Memelova, S N Kochetkov, A van Aerschot, P Herdewijn, E V Efimtseva, B S Ermolinsky, S N Mikhailov *FEBS Lett.* **442** 20 (1999)
376. D V Turutin, T S Zatsepin, M A Timchenko, E A Kubareva, T S Oretskaya *Mol. Biol.* **36** 877 (2002) [c]
377. S Antsypovich, E Kubareva, V Tashlitsky, T Oretskaya, Z Shabarova *Eur. J. Biochem.* **255** 414 (1998)
378. S I Antsypovitch, T S Oretskaya *Usp. Khim.* **67** 274 (1998) [*Russ. Chem. Rev.* **67** 245 (1998)]
379. Y Lin, Q Qiu, S C Gill, S D Jayasena *Nucleic Acids Res.* **22** 5229 (1994)
380. L S Green, D Jellinek, C Bell, L A Beebe, B D Feistner, S C Gill, F M Jucker, N Janjic *Chem. Biol.* **2** 683 (1995)
381. D Jellinek, L S Green, C Bell, C K Lynnot, N Gill, C Vargeese, G Kirschenheuter, D P C McGee, P Abesinghe, W A Pieken *Biochemistry* **34** 11363 (1995)
382. J S Nelson, L Giver, A D Ellington, R L Letsinger *Biochemistry* **35** 5339 (1996)
383. M F Kubik, C Bell, T Fitzwater, S R Watson, D M Tasset *J. Immunol.* **159** 259 (1997)
384. N Teramoto, H Ichinary, N Kawazoe, Y Imanishi, Y Ito *Biotechol. Bioeng.* **75** 463 (2001)
385. N Kawazoe, N Teramoto, H Ichinari, Y Imanishi, Y Ito *Biomacromolecules* **2** 681 (2001)
386. S W Lee, B A Sullenger *J. Exp. Med.* **184** 315 (1996)
387. S W Lee, B A Sullenger *Nat. Biotechnol.* **15** 41 (1997)
388. S Iwai, S Kataoka, M Wakasa, E Ohtsuka, H Nakamura *FEBS Lett.* **368** 315 (1995)
389. N Baidya, O C Uhlenbeck *Biochemistry* **34** 12 363 (1995)
390. D Dertinger, T Dale, O C Uhlenbeck *J. Mol. Biol.* **314** 649 (2001)
391. E A Kubareva, N L Vasilenko, O V Vorobjeva, E M Volkov, T S Oretskaya, G A Korshunova, G A Nevisky *Biochem. Mol. Biol. Int.* **46** 597 (1998)
392. A E Sudina, E M Volkov, E A Kubareva *Moscow University Chem. Bull. Suppl.* **41** 122 (2000)
393. H Aurup, A Siebert, F Benseler, D Williams, F Eckstein *Nucleic Acids Res.* **22** 4963 (1994)
394. K Yamana, T Gokota, H Ozaki, H Nakano, O Sangen, T Shimidzu *Nucleosides Nucleotides* **11** 383 (1992)
395. K Yamana, R Iwase, S Furutani, H Tsuchida, H Zako, T Yamaoka, A Murakami *Nucleic Acids Res.* **27** 2387 (1999)
396. K Yamana, H Zako, K Asazuma, R Iwase, H Nakano, A Murakami *Angew. Chem., Int. Ed.* **40** 1104 (2001)
397. R Iwase, S Furutani, T Yamaoka, K Yamana, A Murakami *Nucleic Acids Symp. Ser.* **35** 117 (1996)
398. R Iwase, H Tsuchida, T Yamaoka, K Yamana, A Murakami *Nucleic Acids Symp. Ser.* **36** 205 (1997)
399. R Iwase, K Mahara, K Yamana, A Yamaoka, A Murakami *Nucleic Acids Symp. Ser.* **42** 115 (1999)
400. B T Young, S K Silverman *Biochemistry* **41** 12271 (2002)
401. E Palecek, M Fojta *Anal. Chem.* **73** 74A (2001)
402. A E Beilstein, M T Tierney, M W Grinstaff *Comments Inorg. Chem.* **22** 105 (2000)
403. T S Zatsepin, S Yu Andreev, T Hianik, T S Oretskaya *Usp. Khim.* **72** 602 (2003) [*Russ. Chem. Rev.* **72** 537 (2003)]
404. US P. 6 063 573 (2000)
405. US P. 6 071 699 (2000)
406. E K Wilson *Chem. Eng. News* **76** 47 (1998)

407. R M Umek, S W Lin, J Vielmetter, R H Terbrueggen, B Irvine, C J Yu, J F Kayyem, H Yowanto, G F Blackburn, D H Farkas, Y P Chen *J. Mol. Diagn.* **3** 74 (2001)
408. K Yamana, T Mitsui, J Yoshioka, T Isuno, H Nakano *Bioconjugate Chem.* **7** 715 (1996)
409. H M Desmukh, S P Joglekar, A D Broom *Bioconjugate Chem.* **6** 578 (1995)
410. K Yamana, S Kumamoto, H Nakano, Y Matsuo, Y Sigue *Chem. Lett.* 1132 (2001)
411. K Yamana, S Kumamoto, T Hasegawa, H Nakano, Y Sigue *Chem. Lett.* 506 (2002)
412. V Kertesz, N A Whittemore, G B Inamati, M Manoharan, P D Cook, D C Baker, J Q Chambers *Electroanalysis (N.Y.)* **12** 889 (2000)
413. S T Sigurdsson *Methods* **18** 71 (1999)
414. G Glick *Biopolymers* **48** 83 (1998)
415. S T Sigurdsson *Methods Enzymol.* **318** 165 (2000)
416. D J Earnshaw, B Masquida, S Muller, S T Sigurdsson, F Eckstein, E Westhof, M J Gait *J. Mol. Biol.* **274** 197 (1997)
417. T K Stage-Zimmermann, O C Uhlenbeck *Nat. Struct. Biol.* **8** 863 (2001)
418. K F Blount, O C Uhlenbeck *Biochemistry* **41** 6834 (2002)
419. E J Maglott, J T Goodwin, G D Glick *J. Am. Chem. Soc.* **121** 7461 (1999)
420. G A Korshunova, N V Sumbatyan, A N Topin, M T Mchedlidze *Mol. Biol.* **34** 966 (2000) [c]
421. K L Buchmueller, B T Hill, M S Platz, K M Weeks *J. Am. Chem. Soc.* **125** 10850 (2003)
422. K L Buchmueller, K M Weeks *Biochemistry* **42** 13869 (2003)
423. S I Chamberlin, E J Merino, K M Weeks *Proc. Natl. Acad. Sci. USA* **99** 14688 (2002)
424. T E Edwards, T M Okonogi, S T Sigurdsson *Chem. Biol.* **9** 699 (2002)
425. T E Edwards, S T Sigurdsson *Biochem. Biophys. Res. Commun.* **303** 721 (2003)
426. T E Edwards, S T Sigurdsson *Biochemistry* **41** 14 843 (2002)
427. O Schiemann, A Weber, T E Edwards, T F Prisner, S T Sigurdsson. *J. Am. Chem. Soc.* **125** 3434 (2003)
428. F Burlina, A Favre, J-L Fourrey *Bioorg. Med. Chem.* **5** 1999 (1997)
429. D J Earnshow, M J Gait *Biopolymers* **48** 39 (1998)
430. M J Fedor *J. Mol. Biol.* **297** 269 (2000)
431. W A Pieken, D B Olsen, F Benseler, H Aurup, F Eckstein *Science* **253** 314 (1991)
432. O Heidenreich, F Benseler, A Fahrenholz, F Eckstein *J. Biol. Chem.* **269** 2131 (1994)
433. L Beigelman, J A McSwiggen, K G Draper, C Gonzalez, K Jensen, A M Karpeisky, A S Modak, J Matulic-Adamic, A B DiRenzo, P Haeberli, D Sweedler, D Tracz, S Grimm, F E Wincott, V G Thackray, N Usman *J. Biol. Chem.* **270** 25 702 (1995)
434. T C Jarvis, F E Wincott, L J Alby, J A McSwiggen, L Beigelman, J Gustofson, A DiRenzo, K Levy, M Arthur, J Matulic-Adamic, A Karpeisky, C Gonzalez, T M Woolf, N Usman, D T Stinchcomb *J. Biol. Chem.* **271** 29 107 (1996)
435. D J Earnshaw, M L Hamm, J A Piccirilli, A Karpeisky, L Beigelman, B S Ross, M Manoharan, M J Gait *Biochemistry* **40** 7350 (2001)
436. A Beaudry, J DeFoe, S Zinnen, A Burgin, L Beigelman *Chem. Biol.* **7** 323 (2000)
437. S P Zinnen, K Domenico, M Wilson, B A Dickinson, A Beaudry, V Mokler, A T Daniher, A Burgin, L Beigelman *RNA* **8** 214 (2002)
438. G Paolella, B S Sproat, A I Lamond *EMBO J.* **11** 1913 (1992)
439. M Cieslak, J Niewiarowska, M Nawrot, M Koziolkiewicz, W J Stec, C S Cierniewski *J. Biol. Chem.* **277** 6779 (2002)
440. K F Blount, N L Grover, V Mokler, L Beigelman, O C Uhlenbeck *Chem. Biol.* **9** 1009 (2002)
441. C Hendrix, M Mahieu, J Anne, S van Calenbergh, A van Aerschot, J Content, P Herdewijn *Biochem. Biophys. Res. Commun.* **210** 67 (1995)
442. M L Hamm, J P Schwans, J A Piccirilli *J. Am. Chem. Soc.* **122** 4223 (2000)
443. M L Hamm, D Nikolic, R B van Breemen, J A Piccirilli *J. Am. Chem. Soc.* **122** 12 069 (2000)
444. K Raines, P A Gottlieb *RNA* **4** 340 (1998)
445. J P Schwans, C N Cortez, J M Olvera, J A Piccirilli *J. Am. Chem. Soc.* **125** 10012 (2003)
446. R Stromberg, S Hahne, A S Sjogren, B M Sjoberg *Biochem. Biophys. Res. Commun.* **183** 842 (1992)
447. A S Sjogren, E Pettersson, B M Sjoberg, R Stromberg *Nucleic Acids Res.* **25** 648 (1997)
448. A S Sjogren, R Stromberg, B M Sjoberg *Nucleic Acids Res.* **25** 3543 (1997)
449. S Shan, D Herschlag *Biochemistry* **38** 10 958 (1999)
450. S Shan, G J Narlikar, D Herschlag *Biochemistry* **38** 10 976 (1999)
451. D V Morrissey, P A Lee, D A Johnson, S L Overly, J A McSwiggen, L Beigelman, V R Mokler, L Maloney, C Vargeese, K Bowman, J T O'Brien, C S Shaffer, A Conrad, P Schmid, J D Morrey, D G Macejak, P A Pavco, L M Blatt *J. Viral Hepat.* **9** 411 (2002)

[a] — *Russ. J. Bioorg. Chem. (Engl. Transl.)*
[b] — *Biochemistry (Engl. Transl.)*
[c] — *Mol. Biol. (Engl. Transl.)*

Russian Chemical Reviews **73** (8) 735 – 736 (2004) © 2004 Russian Academy of Sciences and Turpion Ltd

DOI 10.1070/RC2004v073n08ABEH001076

Department of Chemistry of the Kyiv National Taras Shevchenko University

This issue of the Journal is devoted to the 170th anniversary of the Kyiv National Taras Shevchenko University (KNU) and comprises reviews written by professors and researchers of the Department of Chemistry of KNU and reflecting traditional and novel trends of research carried out at the Department.

The Kyiv University was founded in 1834. Chemistry was taught at the University from the moment of its foundation; research activities were also begun at that time. In 1904, a special building was built for the University chemists and the next year a department of chemistry was established within the University structure. Many prominent chemists, such as S M Reformatsky, A K Babko, A M Golub, A T Pilipenko, O V Palladin, I V Pyatnitsky, A I Kiprianov, K B Yatsimirsky, F S Babichev, Yu K Delimarsky and V N Yeremenko have worked there at different times. To date, the research staff of the Department of Chemistry comprises 208 people including 68 professors and 140 researchers.

The Department takes an active part in comprehensive research programmes of the KNU and the European Union. It maintains and develops constant collaboration with leading research centres in Russia, Poland, USA, Germany, Great Britain, France and Italy. An agreement for joint activities in 2001 – 2005 concluded between the departments of chemistry of the Kyiv National Taras Shevchenko University and M V Lomonosov Moscow State University is aimed at the design of new generations of functional materials, polymers, flocculants and drugs. The Division of Inorganic Chemistry collaborates with Wroclaw (Poland) and Leipzig (Germany) Universities. The studies at the Division of High-Molecular Compounds are carried out within the framework of collaboration programmes between KNU, Gdansk University and Radom Technical University (Poland), the Research Centre LG Gable (Korea) and the Charles Sadron Institute (France). The Division of Organic Chemistry collaborates with Toulouse University (France). The researchers of the Division of Physical Chemistry are carrying out joint research with their colleagues from York University (Great Britain).

The Department of Chemistry takes an active part in the organisation and holding of various national and international conferences; in particular, it was the organiser of the 21st International Chugaev Conference in June 2003 dedicated to the 130th anniversary of L A Chugaev.

The Department of Chemistry of KNU consists of five divisions, *viz*., the Divisions of Inorganic Chemistry, Analytical Chemistry, Organic Chemistry, Physical Chemistry and Chemistry of High-Molecular Compounds. Future chemists are trained there in nine specialities.

Studies devoted to the synthesis and structural analysis of coordination compounds and studies of complexation reactions of transition metals in various media occupy a significant place in the research activities of the Division of Inorganic Chemistry. Its major achievements include the development of a direct (one-step) synthesis of coordination compounds from metal powders and metal oxides, which has enabled easy preparation of a series of novel compounds which cannot be synthesised by traditional methods. The results of these studies have been generalised in the monograph by V V Skopenko, A D Garnovskii, V M Kokozey *et al*., 'Direct Synthesis of Coordination Compounds' (1997).

Considerable attention in the past decade has been given to metal complexes with amide, hydrazide, oxime and carbacylphosphoramidate ligands possessing interesting catalytic and

physical properties. These investigations are considered in the review by V V Skopenko, V M Amirkhanov, T Yu Sliva, I S Vasilchenko, E L Anpilova and A D Garnovskii 'Various types of metal complexes based on chelating β-diketones and their structural analogues'.

Yet another trend of research at the Division of Inorganic Chemistry is related to the design of novel inorganic materials possessing non-linear optical and specific electrophysical properties. In particular, studies of the regularities of phase formation of phosphates in solution-melt media of multicomponent systems and under solid-phase interaction conditions; synthesis of heterosubstituted crystalline templates of double phosphates and study of relationships between compositions, structures and properties of novel compounds are under way. Studies into the synthesis of complex phosphates under conditions of hydrothermal interaction are carried out jointly with the Institute of Magnetism of the National Academy of Sciences of the Ukraine. This trend of research is represented in the review by V V Skopenko, V V Lisnyak, N V Stus and N S Slobodyanik 'Phosphate tungsten bronzes'.

The traditional trends of research at the Division of Analytical Chemistry include studies of extraction and sorption processes which serve as the basis for the development of the most advanced methods of environmental analysis and control. The approach including the design, analysis and applications of solid-phase analytical reagents is also being developed successfully. Unique adsorbents for selective solid-phase concentration and separation of metal ions, pesticides, antibiotics and phenols in environmental objects and biological fluids and selective membranes for chemical and biological sensors have been designed. These problems are surveyed in the monographs by Yu V Kholin and V M Zaitsev 'Complexes on the surface of chemically modified silica' (1997) and by V M Zaitsev 'Complex-forming silica: synthesis and structures of graft layers and surface chemistry'. Other studies are concerned with the practical application of a novel concentration procedure, *viz*., micellar extraction or microcomponents from aqueous solutions using non-ionic surfactants. These studies gave an impetus to the development of methods for determining surfactants and toxic organic compounds in natural and waste waters.

The main lines of research at the Division of Organic Chemistry include asymmetric synthesis of organic compounds, stereochemistry, studies into mechanisms of chemical reactions, synthesis and investigation of heterocyclic and biologically active compounds, chemistry of proteins and carbohydrates and computer chemistry. The review by A A Pokholenko, Z V Voitenko and V A Kovtunenko 'Pyrido- and pyrimidoisoindoles: methods of synthesis and properties' summarises the data on the synthesis, physical and chemical properties of pyrido- and pyrimidoisoindoles with unusual electronic structures.

One of the most modern trends of research, *viz*., calculation of atomic clusters using most advanced computer programmes, is being intensively developed at KNU. In recent years, research activities of KNU investigators have been focused on the design of fluorescent probes and ionic indicators as well as peptidomimetics and peptide models. A systematic search for biologically active compounds is under way. This line of research is discussed in the review by I V Komarov, A O Grigorenko, A V Turov and V P Khilya 'Conformationally rigid cyclic α-amino acids in the design of peptidomimetics, peptide models and biologically active compounds'.

Studies into physicochemical, adsorption and catalytic properties of metal-containing systems as well as thermodynamic and structural studies of metal and oxide melts are traditional subjects of investigation at the Division of Physical Chemistry. These include studies of interactions of gas molecules with surfaces of solids including melts. An important role of heterogeneity and polymorphism in adsorption-catalytic properties of melts has been demonstrated and the microheterogeneity phenomenon in melts has been established. The oxidation mechanisms of small molecules (CO, H_2, CH_4) on surfaces of metal catalysts have been investigated and some novel classes of metal-containing catalytic systems have been discovered. The theoretical grounds for the mechanisms underlying the effects of non-ionogenic water-soluble polymers on electronic-surface properties and aggregate resistance of coarse-dispersion systems have been developed. Structure–activity relationships of ice-forming compositions of various chemical nature have been established based on an analysis of a mosaic model of a hydrophilic-hydrophobic surface. Of special noting is the synthesis of adsorption-semiconducting gas sensors, development of various devices based on them and determination of thermodynamic characteristics of various novel binary and ternary metal systems containing aluminium, germanium, silicon, *etc*.

The main trend of research at the Division of High-Molecular Compounds is the synthesis and modification of polymers, monomers and other compounds and their use in the design of polymeric compositions possessing unique properties. Novel polymeric materials for microelectronic engineering have been developed. Numerous polymeric photosemiconductors, polymeric solid electrolytes, photosensitive polymers and compositions and biologically active polymers have been prepared.

The interest in heteropolymeric systems, such as intermolecular polycomplexes (InterPC) as well as block and graft polymers has increased considerably in the past decade due to the explosive development of nanophase materials science. The review by T B Zheltonozhskaya, N E Zagdanskaya, O V Demchenko, L N Momot, N M Permyakova, V G Syromyatnikov and L R Kunitskaya 'Graft copolymers with chemically complementary components as a special class of high-molecular-weight compounds' deals with the description of modern concepts and novel approaches to the study of graft copolymers. The long-standing experience of researchers of the Division in the synthesis of photosensitive compounds and their applications in photopolymeric engineering is generalised in the review by V G Syromyatnikov, P A Kondratenko, A Yu Kolendo *et al*., 'Structures, properties and applications of photosensitive organic azides and pentazadienes' to be published in one of the next issues of 'Russian Chemical Reviews'.

The size of this issue cannot encompass the whole range of research carried out at the Department of Chemistry. Therefore, all those who are interested in more detailed information about KNU and the Department of Chemistry are invited to visit our web-sites: http://www.univ.kiev.ua and http://www.chem.univ.kiev.ua

N S Slobodyanik, Corresponding Member
of the National Academy of Sciences of the Ukraine
Dean of the Department of Chemistry of KNU

Russian Chemical Reviews **73** (8) 737 – 752 (2004) © 2004 Russian Academy of Sciences and Turpion Ltd

DOI 10.1070/RC2004v073n08ABEH000909

Various types of metal complexes based on chelating β-diketones and their structural analogues

V V Skopenko, V M Amirkhanov, T Yu Sliva, I S Vasilchenko, E L Anpilova, A D Garnovskii

Contents

I.	Introduction	737
II.	Metal complexes of β-diketones	738
III.	Modified β-diketonates	744
IV.	Conclusion	749

Abstract. Data on the synthesis and structures of β-diketonates and their N,P-containing structural analogues are generalised and described systematically. The possibility of creating diverse metal complexes with various modes of coordination of typical chelating ligands is discussed. The bibliography includes 200 references.

I. Introduction

Chelating systems **1**, which form, most often, six-membered metal-containing rings **2**, are among the most widely used ligands in modern coordination chemistry.[1–3]

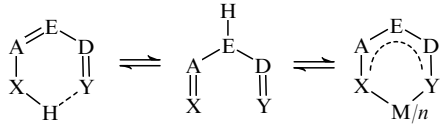

1a **1b** **2**

The metal complexes **2** formed by ligands **1** are mainly represented by β-diketonates (X = Y = O; A, D, E = CR, where R = H, Alk, Ar, Het),[4–9] their aza analogues (X = O, NR; Y = NR; A, D = CR, N; E = CR, where R = H, Alk, Ar)[10,11] and hetero analogues (X, Y = O, S, Se; A = CR, PR_2; D = PR_2; E = CR, where R = H, Alk, Ar).[2,3,12,13] Other examples of these ligands are compounds **3**, which are used to prepare metal chelates **4** (X, Y = O, S, Se; A = CR^1, PR^1_2; D = PR^1_2, where R^1 = H, Alk, Ar, NR^2_2, OR^2; R^2 = H, Alk, Ar, ArAlk).[14,15]

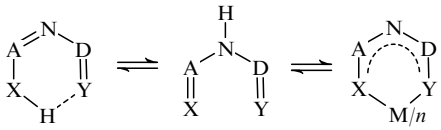

3a **3b** **4**

Although metal chelates **2** and **4** arouse the steady interest of researchers, equally important are other coordination capabilities of ligands **1** and **3**, which are not limited to the formation of chelates (intracomplex compounds†) containing the ligand as a bidentate X,Y-donor anion. This aspect of the chemistry of metal complexes of these ligands has been considered in detail only for β-diketonates **2** (X = Y = O; A = D = E = CR). The possible modes of coordination in mono-, di- and polynuclear β-diketonate complexes can be illustrated by structures **5** – **27**.[5,9,16–24]

O- and O,O-coordination

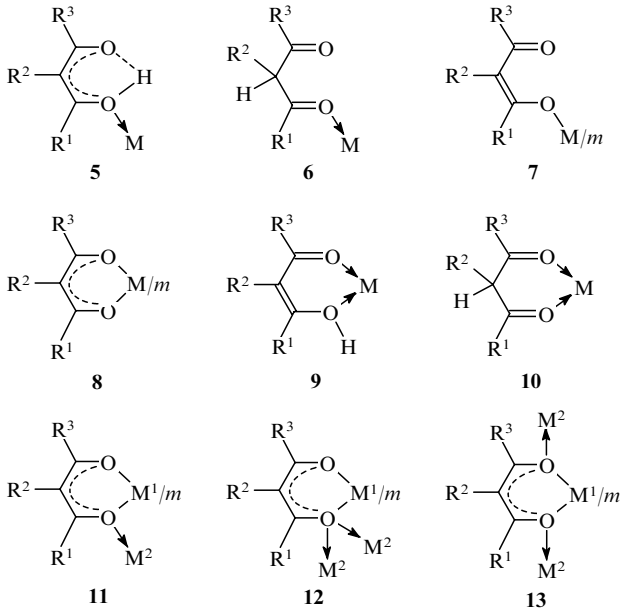

5 **6** **7**

8 **9** **10**

11 **12** **13**

† The notion 'intracomplex compound' taken from early publications (see, for example, Refs 8 and 14) is used in Russian and German literature to emphasise the fact that these compounds have been obtained from ring-forming ligands with an intramolecular H-bond, for example, from acetylacetone. More generally, the complexes with metal-containing rings are called chelates.[2]

V V Skopenko, V M Amirkhanov, T Yu Sliva Department of Chemistry, Kyiv National Taras Shevchenko University, ul. Vladimirskaya 64, 01033 Kyiv, Ukraine. Fax (38-044) 220 83 91. Tel. (38-044) 220 86 91, (38-044) 239 32 20 (V V Skopenko). Tel. (38-044) 239 33 92.
E-mail: v.amyrkhanov@clariant.com.ua (V M Amirkhanov)
I S Vasilchenko, E L Anpilova, A D Garnovskii Research Institute of Physical and Organic Chemistry, Rostov State University, Prosp. Stachki, 194 /2, 344090 Rostov-on-Don, Russian Federation. Fax (7-863) 243 46 67. Tel. (7-863) 243 47 76. E-mail: vas@ipoc.rsu.ru (I S Vasilchenko), jane@fss.rost.ru (E L Anpilova). Tel. (7-863) 243 47 76.
E-mail: garn@ipoc.rsu.ru (A D Garnovskii)

Received 1 March 2004
Uspekhi Khimii **73** (8) 797 – 813 (2004); translated by Z P Bobkova

O- and O,O-coordination

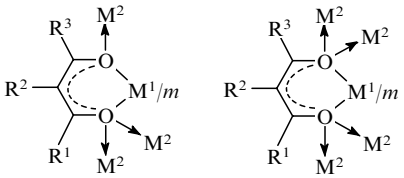

14 **15**

C-, C,C- and C,C,C-coordination

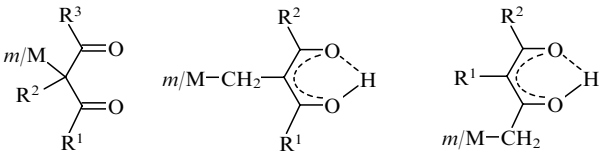

16 **17** **18**

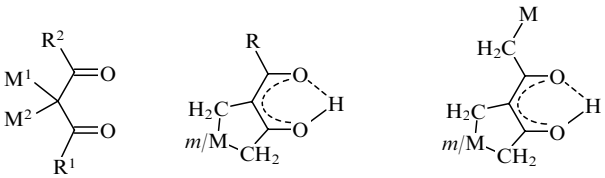

19 **20** **21**

C,O- and C,O,O-coordination

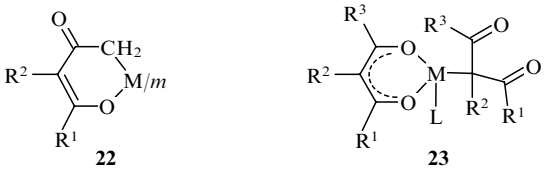

22 **23**

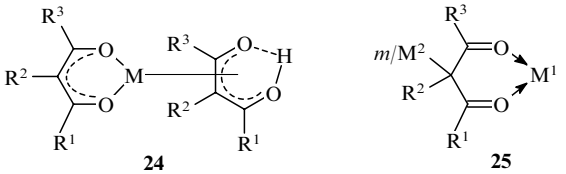

24 **25**

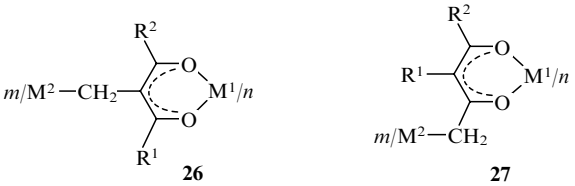

26 **27**

Study of the coordination modes of typical chelating ligands is important for the understanding of their ambident properties.[20–24] Therefore, this review surveys the published data (obtained mainly during the last 10 years) concerned with the ability of ligands **1** and **3** to form metal complexes in which the coordination bonds can be localised in different ways.

II. Metal complexes of β-diketones

Coordination compounds of β-diketones are prepared either by classical methods (by reactions of various compounds, most often salts, of complexing metals with β-diketonate ligands) or by specific reactions (gas-phase synthesis and electrosynthesis[2–5]). The type of the metal complex to be formed plays an important role in the transformations considered below.

1. Chelates formed by β-diketones

The chelates of β-diketones (β-diketonates) containing the monodeprotonated O,O′-anion of the ligand[25] are synthesised most often by the reactions of ligand systems **28** with metal salts in water, aqueous organic solvents, or in solvent mixtures.

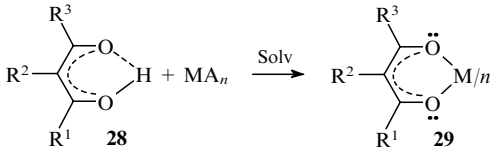

28 **29**

Solv is solvent.

β-Diketonates **29** for metals of virtually all Groups of the Periodic Table have been prepared in this way. Due to the enormous number of publications on this topic, only some examples of such syntheses are cited in this review.‡

Silver(I) β-diketonates **29** are formed in 20%–66% yields upon the reaction[26]

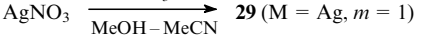

28, **29**: $R^1 = Bu^t$, $R^2 = H$, $R^3 = Bu^t$, $SiMe_3$.

The data on the syntheses of β-diketonates of Group II elements (Be, Ca, Mg, Ba, Sr) are summarised in a recent review.[9] The synthesis of beryllium β-diketonate **30** is described in more detail in another study.[27]

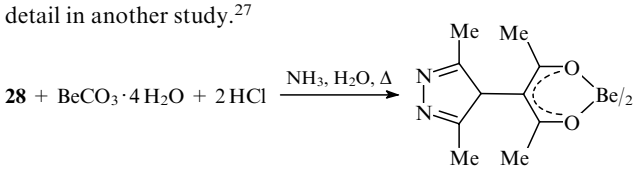

30

β-Diketonates of Group III metals are prepared using metal halides. In particular, aluminium and indium chelates have been obtained in this way.[28]

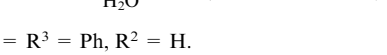

8, **28**: $R^1 = R^3 = Ph$, $R^2 = H$.

An enormous number of coordination compounds of transition metals have been synthesised on the basis of aliphatic and aromatic β-diketones.[1–8] It should be emphasised that chelates **31**–**34**, similar in structure to chelate **8**, have also been synthesised by reactions of 3d-metal salts with β-diketones containing nitrile,[29] pyrazole,[30] 1,2-benzothiazine 1,1-dioxide[31] and ferrocenyl[32] substituents, respectively.

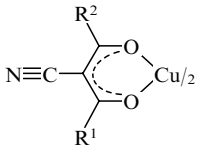

31: $R^1 = R^2 = Me, Bu^t$

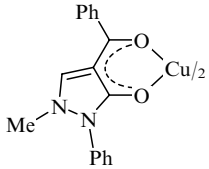

32

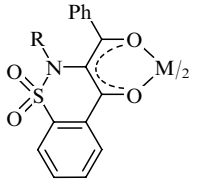

33: R = H, Me;
M = Co, Ni, Cu, Zn

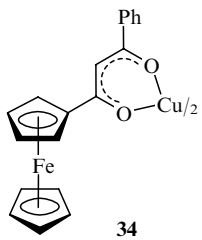

34

‡ The Cambridge Structural Data Base contains structures of more than 1500 β-diketonates and related fragments as parts of monomeric and polymeric coordination compounds.

The relatively simple transformations considered above can be complicated by solvolysis, resulting in the formation of adducts and decomposition of complexes (especially, in the case of hydrolysis). Therefore, these syntheses are carried out using anhydrous organic solvents; for example, β-diketonate **35** was synthesised in anhydrous benzene.[33]

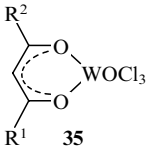

35

R^1, R^2 = Me, Ph, 4-$MeOC_6H_4$.

Apart from salts, metal oxides can also be used in complexation reactions.[2–4,9] These syntheses have been long known [34] and still have not lost their significance. For example, complexes **29** ($R^1 = R^3 = CF_3$; R^2 = H; M = Ag; m = 1),[35] **36**,[36] **37** [34] and **38** [37] can be prepared from silver, tin, molybdenum and lanthanum oxides, respectively.

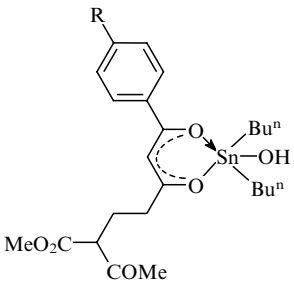

36: R = H, Bu^t, NO_2, Cl

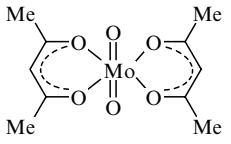

37

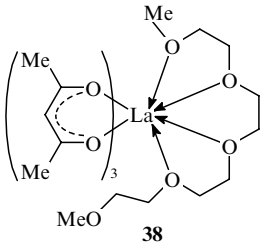

38

The reactions of ligands with metal alkoxides proved to be quite efficient for the synthesis of Group IV metal (Ti, Zr, Hf) β-diketonates.[9]

$$n\,(\beta\text{-diketone}) + M(OR)_4 \xrightarrow{Solv} M(\beta\text{-diketone})_n(OR)_{4-n} + n\,ROH$$

This reaction has been used, in particular,[38] to prepare zirconium and hafnium complexes with 2,2,6,6-tetramethylheptane-3,5-dione (LH), with the composition $M(OPr)_2L_2$, ML_4 and $M_2(OPr)_6L_2$, the synthesis being carried out in hexane.

Metal exchange reactions are often used to prepare β-diketonates **8**.[4,9] β-Diketonates of Group I metals are usually employed as the starting compounds for the exchange with d or f elements. Recently, this method has been used to synthesise mono-β-diketonates of rhodium(I) and iridium(I) **39** dicarbonyls having liquid-crystalline and nonlinear-optical properties. These complexes were prepared by replacement of potassium or sodium in acetylacetonates by platinum metals.[39]

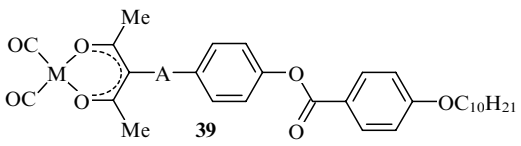

39

M = Rh^I, Ir^I; A = CH_2, CO_2, OOC.

The syntheses of mixed-ligand complexes of lanthanides (La, Sm, Er) described as $LaL_3(bipy)_2$, $[SmL_3(bipy)]bipy$, $ErL_3(phen)$ (bipy is 1,1′ -bipyridyl, phen is *o*-phenanthroline) proceed through the preliminary formation of the caesium salt of 1,1,1,5,5,5-hexafluoropentane-2,4-dione (LH).[40]

Thallium acetylacetonate has been used to prepare rhodium complex **40**.[41]

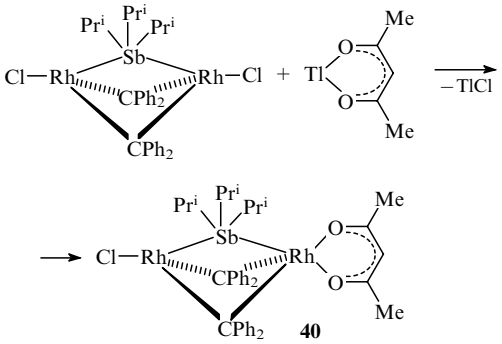

40

It is noteworthy that in some cases, reactions of β-diketone salts give products absolutely different from those formed in the syntheses from free ligands. In particular,[42] the reaction of gadolinium trichloride with the sodium salt of β-diketone (LNa) gave tetramer **41**, whereas a similar reaction of LH affords mononuclear complex **42**.

$$4\,GdCl_3 + 12\,LNa + 10\,H_2O \xrightarrow{H_2O-EtOH} Gd_4(OH)_4L_8(H_2O)_6 + 4\,LH + 12\,NaCl$$

41

$$GdCl_3 + 3\,LH \xrightarrow[-3\,HCl]{Me_2CO} GdL_3(Me_2CO)_2 \xrightarrow[-Me_2CO]{H_2O} GdL_3(Me_2CO)(H_2O)$$

42

The solid-state syntheses of β-diketonates **43** from salts of complex-forming elements and alkali metal β-diketonates deserve attention.[43–46]

$$PrCl_3 + 3\,M(acac) \longrightarrow Pr(acac)_3 + 3\,MCl$$

43

M = Li, Na; acac is acetylacetonate.

Numerous β-diketonates similar in structure to complex **8** have been prepared by ligand exchange.[4,5] In particular, metal complexes **44** were synthesised in this way.[47]

$$[M(OEt)_2(EtOH)_4]_n + 2n\,LH \longrightarrow [ML_2]_n + EtOH$$

44

M = Ca, Ba,Sr; LH = **28**: $R^1 = R^3$ = Me, Bu^t, Ph, CF_3; R^2 = H.

In addition to the above-mentioned polymeric complexes, this transformation carried out in the presence of triglyme (TG) and tetraglyme (TeG) furnished monomeric products, $BaL_2(TeG)$, $SrL_2(TG)$ and $SrL_2(TeG)$.[47]

Nickel β-diketonates **45** have been synthesised by the reaction of bis(η^3-allyl)nickel with β-diketones.[48]

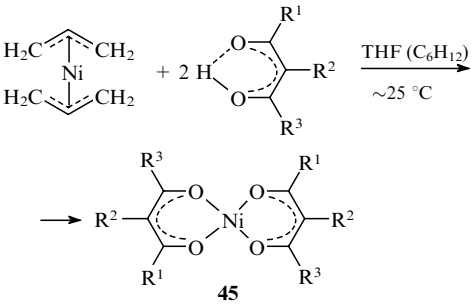

45

$R^1 = R^3$ = Me; R^2 = Me, Ph, Bn, $H_2C{=}CHR^4$ (R^4 = C_6H_8, C_6H_{12}, $C_{12}H_{24}$).

Mixed-ligand ruthenium(II) acetylacetonates **46** have been prepared by chlorine exchange reaction in ruthenium(III) complexes with 2,6-bis(pyrazolyl)pyridines.[49]

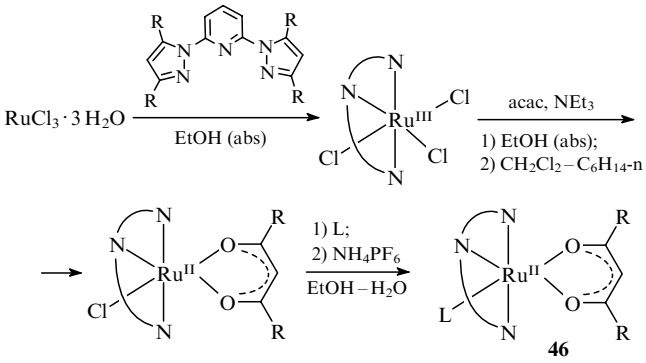

R = Me, Ph, CF_3; L = 4,4′-bipy, MeCN, Py, imidazole, pyrazine.

This approach has also been used for the synthesis of ruthenium(II) binuclear complexes with bridging bis-diketonate ligands.[50, 51] On refluxing for 6 h, these ligands replace H^- in the carbonyl hydride complexes of ruthenium to give coordination compounds **47**.

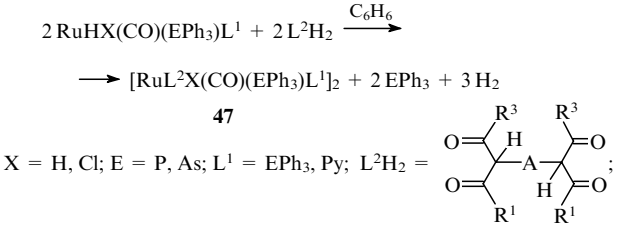

X = H, Cl; E = P, As; L^1 = EPh_3, Py; L^2H_2 = ;

A = CR^2R^4 (R^2, R^4 = H, Ph), S; R^1, R^3 = Me, Ph.

It appears of interest to use this approach to replace the ligands in β-diketonate complexes by other chelating compounds. The transformations [52, 53] giving rise to complexes **48** and **49** are examples of such syntheses.

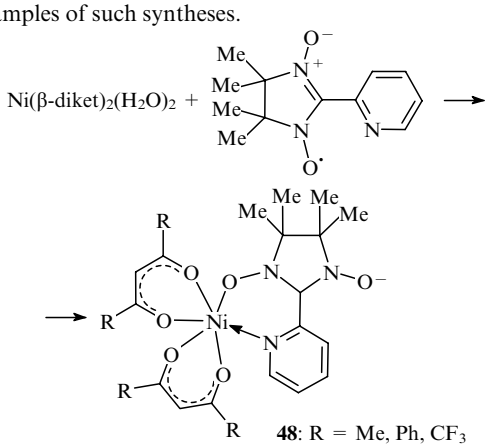

48: R = Me, Ph, CF_3

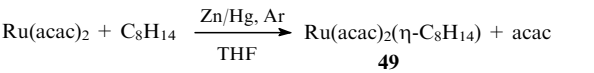

C_8H_{14} is cyclooctene.

By replacing the cyclooctene ligand by other ligands, acetylacetonate **49** has been converted [53] into a series of different-ligand complexes: $Ru(acac)_2Py_2$, $Ru(acac)_2$(bipy), $Ru(acac)_2(NCBu^t)_2$, $Ru(acac)_2(\eta^2\text{-}C_8H_{14})_2(NCMe)$, $Ru(acac)_2(NMe_3)_2$, $Ru(acac)_2(PPh_3)_2$, $Ru(acac)_2(PMePh_2)_2$, $Ru(acac)_2(PAlk_3)_2$, $Ru(acac)_2[P(OMe)_3]_2$; $Ru(acac)_2$ $[P(OPh)_3]_2$, $Ru(acac)_2[Ph_2P(CH_2)_mPPh_2]$ (m = 1–3), $Ru(acac)_2(\eta^2\text{-}C_8H_{14})_2(SbPh_3)$, $Ru(acac)_2(SbPh_3)_2$, $Ru(acac)_2$. .$(CO)(NMe_3)$, $Ru(acac)_2(CO)(PPh_3)$ and $Ru(acac)_2(CO)(AsPh_3)$.

The ligand exchange reactions yielding monoacetylacetonate binuclear rhodium complexes **50**–**52** are shown in Scheme 1.[54]

Ruthenium mono- (**53**) and binuclear (**54**) tris-chelates were prepared in a similar way.[55]

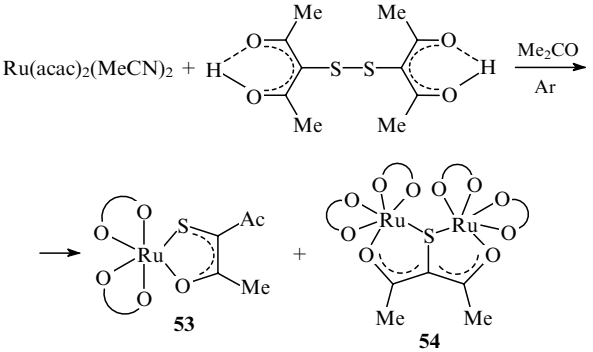

The acetylacetonate ligands can be rather easily completely replaced. This underlies the acetylacetonate method for the synthesis of metal complexes with diverse ligands,[56, 57] widely used in the coordination chemistry of gold.[57]

To our knowledge, no classical template syntheses of β-diketonates in which the β-diketonate ligand system is constructed from components on a metal template (*cf.* the studies [2, 3, 58–60]) have been reported. However, template syntheses of the second type, *i.e.*, the reactions of coordinated ligands (modification of ligand systems), [2, 3, 61–63] are represented rather extensively in the chemistry of metal complexes of β-diketones.[2–5] This is attributable to the ability of β-diketonates **8** devoid of substituents at the C(3) atom of the quasi-aromatic ligand system to undergo electrophilic substitution at this atom.[4, 5, 9]

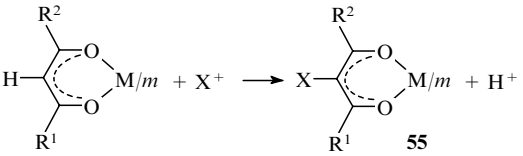

The halogenation, formylation, acylation and Mannich reactions and the introduction of thiocyanate and chlorosulfenyl

Scheme 1

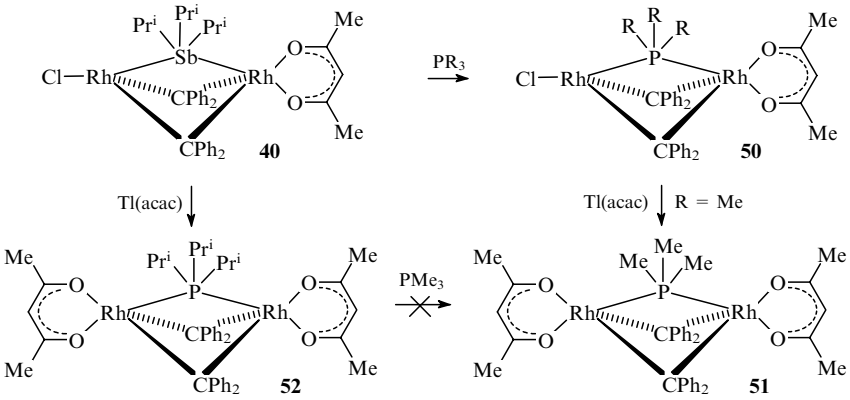

Scheme 2

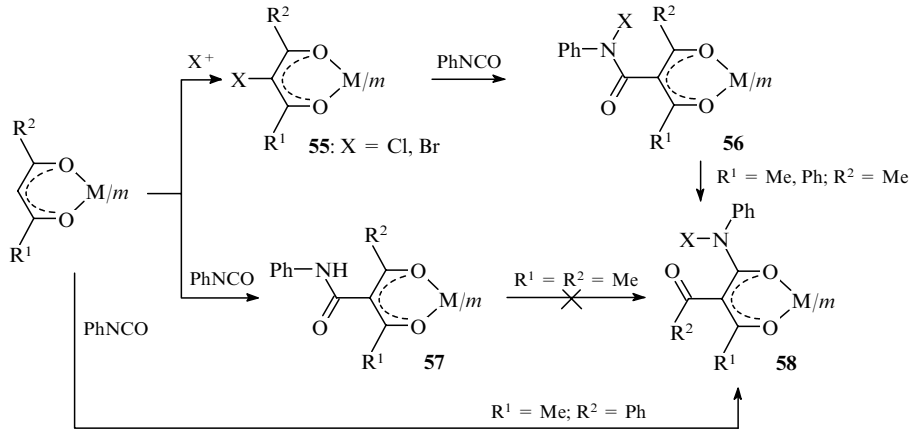

groups occur according to this route.[5] Nitrile[29] and phenyl isothiocyanate[64] fragments can be introduced in the ligand system in a similar way. The presence of a substituent X in complex **55** also allows one to modify β-diketone ligand systems. Scheme 2 shows transformations of this type, resulting in complexes **56**–**58**.[64]

An important role in the modification of the coordination sphere belongs to the reactions of β-diketonates with N-, P-, O- and S-donors involving a coordinatively unsaturated complexing metal, giving rise to adducts **59**.

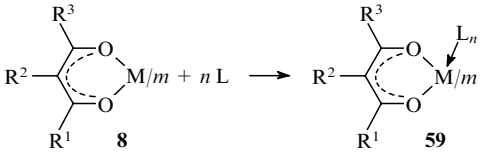

m = 1–3; *n* = 1, 2.

These reactions have been used to prepare adducts of silver(I) β-diketonates with tributyl- and triphenylphosphines,[26] cobalt(II) with pyrazine and 4,4′-bipyridyl,[65] rhodium(I) with cyclooctadiene[32] and iridium(II) with triallylphosphines and -stibines.[66]

In recent years, the interest in β-diketonate adducts with biradical bases such as complexes **60**[67] and **61**[68] has grown due to the development of new molecular magnets.

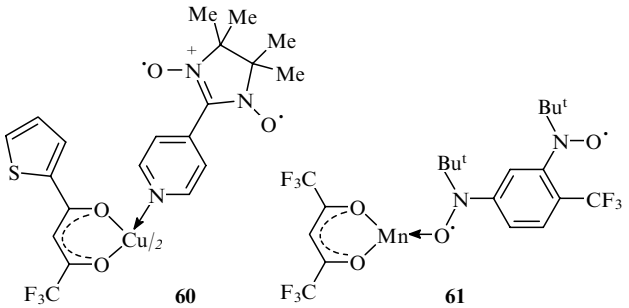

Adducts similar to compound **59** (in particular, complexes **62**[26] and **63**[69]), can also be formed in template reactions.

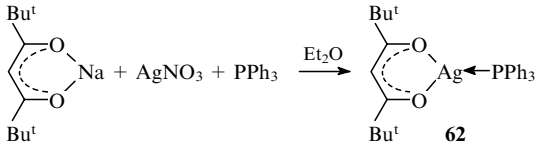

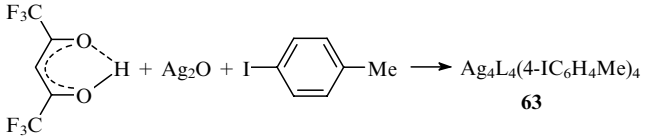

The direct method for the synthesis of β-diketones from ligands and zerovalent metals[2,3,4,9] is mainly applied for Group IA and IIA elements of the Periodic Table. This technique was used to prepare magnesium, calcium, barium and strontium β-diketonates (see the review[9] and references cited therein). Among more recent publications, noteworthy are papers devoted to the syntheses and structural studies of mononuclear chelates of barium **64**[70] and strontium **65**.[71]

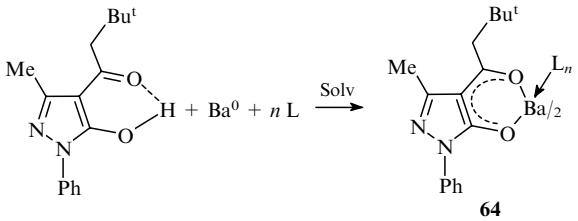

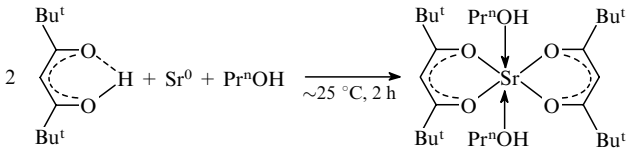

Some transition metals (Co, Fe, Ni, Cu) can also directly react with β-diketones. In these syntheses, iron is activated by atmospheric oxygen, whereas cobalt, copper and nickel are activated by the addition of N- or P-bases into the reaction mixture.[72–74] This method has been used to prepare[74] the β-diketonate complex of monovalent copper **66**, which has been structurally characterised.

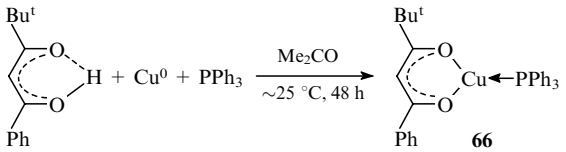

Direct one-step syntheses of β-diketonates from zerovalent metals in the gas phase[2,3,72,73,75–78] and under conditions of electrolysis[2,3,72,73,76,79] are especially efficient.

Gas-phase syntheses of β-diketonates have been developed for both non-transition and transition metals (M = Al, Sn, Pb, Ti, Zr, Hf, Co, Mn, Cr, Fe, Ni, Pd, Cu, Dy, Ho, Eu) which are evaporated *in vacuo* at 1000–2500 °C (see Refs 72, 73 and 78). A special setup for the gas-phase synthesis of β-diketonates has been designed.[73,80] Using this setup, chelates **8** of some metals (Ti, Zr, Hf, Co, Cr, Ni, Cu) can be obtained in almost quantitative yields (~90%–100%). The gas-phase syntheses of β-diketonates have been reported,[75,80] the latter publication being devoted to the synthesis of mononuclear calcium, strontium and barium trifluoro- and hexafluoroacetylacetonates (**8**: R^1 = H, CF_3;

R^2 = H; R^3 = CF_3; M = Ca, Sr, Ba; m = 2) from metals, metal oxides or fluorides.

The electrochemical method for the synthesis of β-diketonates implies anodic dissolution of the complexing metal in organic or aqueous–organic solvents containing the corresponding β-diketones (LH) and conductive additives.[2, 3, 72, 73, 75, 79–88] Graphite, platinum or some other metals, for example, nickel, are suitable as the cathode.[85–88] A systematic study of the electrochemical synthesis of β-diketonates has been reported.[75] The syntheses were carried out in 15%–20% solutions of ligands in aqueous (60%) methanol or ethanol, acetonitrile or DMF in the presence of LiCl, LiBr, NH_4Cl or Bu_4NBF_3. This gave β-diketonates ML_2 (M = Co, Mn, Ni), ML_3 (M = Al, In, Ga, Co, Fe), ML_4 (M = Zr, Hf), ML_2Solv (M = Ni, Fe), ML_3Cl (M = Ti, Zr), $TiL_3(OMe)$ and $ZrL_3(OMe)$ in yields of 60% to 90%. Several other publications [85–88] describe cobalt,[88] uranium [86] and dysprosium [85, 87] complexes obtained in an undivided electrolytic cell in ethanol. A synthesis carried out under an inert atmosphere (Ar, He) yields uranium β-diketonates UL_4, whereas in the presence of oxygen, the reaction gives UO_2L_2 (LH is acetyl- or benzoylacetone). The resulting cobalt and dysprosium β-diketonates are described as $CoL_2(EtOH)$ and Dy_3L_n (n = 1, 0.5). The use of the electrochemical method together with the chemical method (platinum cathode, methanol, Et_4NClO_4) furnishes chelates **32** (M = Co, Ni, Cu, Zn) in 17%–85% yields.[31] A promising approach is the use, in the electrochemical synthesis, of alkali metal β-diketonates in acetonitrile without any other conductive additives.[89] In this case, sodium β-diketonates can be obtained in the first stage and, subsequently, electrochemical replacement of sodium by a transition metal takes place.

β-Diketonates **8** can also be synthesised under boundary friction conditions (tribochemical mechanosynthesis);[72, 73] however, the preparative value of this method (see, for example, Ref. 90) is still obscure.

Since coordinatively unsaturated β-diketonates **8** are able to form adducts **59**–**66** with bases (see also a number of publications [91–95]), it appears of interest to convert them into heteronuclear complexes **67** .[96–99]

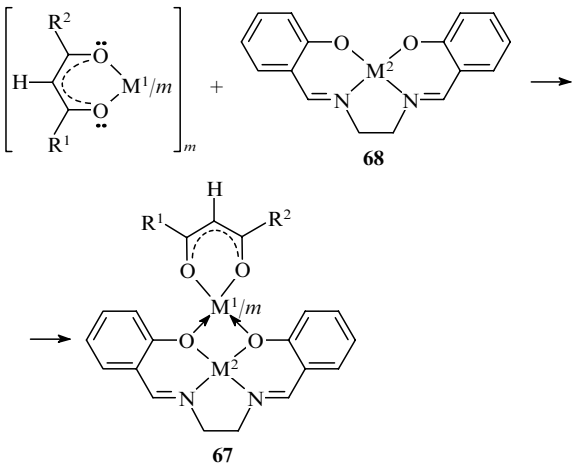

68

67

R^1 = Me, CF_3, Bu^t; R^2 = Me, CF_3;
M^1 = Mg, Ba, La, Y, Gd; M^2 = Cu, Ni; m = 2, 3.

In this reaction, *o*-hydroxyazomethine chelates **68** act as ligands.[10, 99, 100]

Similar procedures have been used to prepare bi- [101, 102] and trinuclear [103] complexes based on lanthanide (La, Gd) β-diketonates and transition metal *N*,*N*′-bisacetylacetone iminates.

The heteronuclear complexes in question were characterised by X-ray diffraction; they present considerable interest as molecular ferromagnets [96] and as precursors for the production of films and coatings by vapour deposition of heterometallic materials.[97–99, 101–103]

Note that fragment **8** can be incorporated in more complex structures (see, for example, Ref. 9).

2. Complexes with neutral β-diketonate ligands

Complexes of this type are few; they have been studied by X-ray diffraction.[2, 3, 16–18, 21]

The mononuclear complex $MnBr_2(LH)_2$ (**69**) [104, 105] and the binuclear complex $[ReCl(CO)_3(L'H)]_2$ (**70**) [106, 107] correspond to structure **5**. Complexes with monodentate O-coordination corresponding to structure **7** have been discussed in the literature.[17, 18]

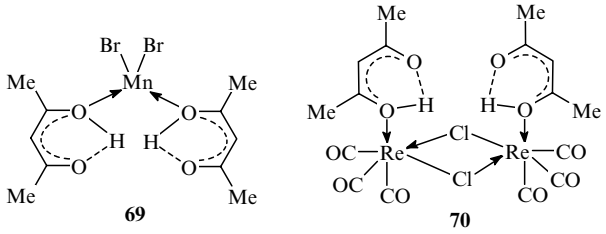

69 **70**

Compound **69** was synthesised without a solvent,[105] while compound **70** was prepared in benzene.[107] Apparently, the enol tautomer of the ligand is stabilised in these complexes.[104, 106]

It was found that the complexes $NiBr_2(LH)_2$ (**71**) [108] and $Ni(LH)_2(ClO_4)_2(H_2O)_2$ (**72**) have the same structure as chelate **10**.[109, 110]

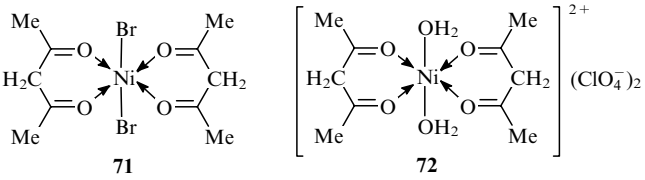

71 **72**

It should be emphasised that all hydrogen atoms in the structure of **72** have been located and the presence of a CH_2 group has been proven reliably. This indicates that the ligand exists in the keto form.

The data concerning other molecular complexes of β-diketones with mercury, tin, titanium, zirconium, manganese, cobalt, vanadium, rhenium, chromium, nickel, platinum, uranyl and europium halides and acetates are summarised in reviews.[17, 18] Only the results of elemental analysis (the composition was established to be MA_2L) and IR spectra were reported for these complexes, which precludes exact determination of their structures, in particular, distinguishing between the structures **9** and **10**.

3. Polynuclear complexes of O,O-coordinated β-diketones

The greatest number of structures of the type **11**–**15** is known among β-diketonates of Group IIA elements (Ca, Mg, Sr, Ba).[2, 3, 9, 21] In addition, worth mentioning are the dimer $[Ba_2L_4(NH_3)_4]$,[111] the trimer $[CaL_2]_3$,[112] the tetramer $[BaL_2]_4$,[9, 113–115] and the pentanuclear $Ba_5L_9Cl(H_2O)_7$ [116] and hexanuclear $Ba_6L_{10}(O_2)(H_2O)_6$ [117] complexes, which contain simultaneously structural elements of **8** and fragments of chelates **11**.

The syntheses of these polynuclear complexes are based on the ability of β-diketones to behave not only as Lewis acids but also as bases due to the oxygen electron pairs not involved in the coordination.[9, 113–120]

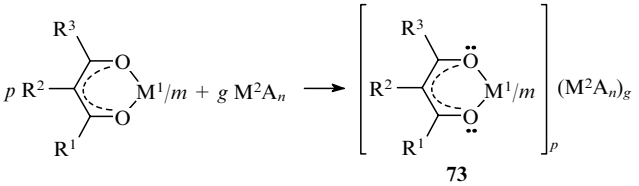

73

A is anion.

The formation of structures **73** can in principle be regarded as a sort of oligomerisation of metal β-diketonate monomers through M—O coordination, as in complex **74**.

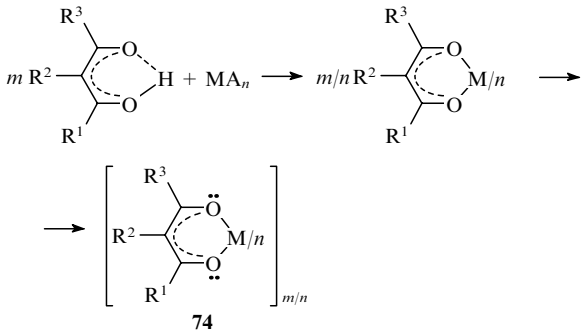

74

This transformation underlies the synthesis of a series of heterometallic complexes, for example, β-diketonates and other metal chelates **75** (metal exchange in the β-diketonate fragment and the transformation of the heterocyclic ligand system)[121] or alkoxides **76**[122] as well as the template reaction giving rise to complex **77**.[123]

$$2\,CuL^1_2 + 2\,CdL^2_2(phen) \xrightarrow[\Delta,\ 1\ h]{MeCN} (Cd_2L^1_2)(\mu^3\text{-}L^3_2)[Cu_2(phen)]_2$$

75

L^1H is 1,1,1,5,5,5-hexafluoroacetylacetone, L^2H is pyridine-2-thione, L^3H is 1,3,5-tris(trifluoromethyl)-1,3,5-trioxycyclohexane trianion;

$$BaL_4 + Bi(OEt)_3 \xrightarrow[\sim 25\ ^\circ C]{C_6H_5Me} Bi_4Ba_4(\mu^4\text{-}O_2)_2(\mu^3\text{-}OEt)_8(\mu\text{-}OEt)_4(\eta^2\text{-}L)_4$$

76

LH is 2,2,6,6-tetramethylheptane-3,5-dione;

$$Cu(OMe)_3 + H_2L^1 + BaL^2_2 \xrightarrow[25\ ^\circ C,\ 4\ h]{CH_2Cl_2} Ba_2Cu_2L^1_4L^2_4$$

77

H_2L^1 is 2,2-thiodiethanol, L^2H is 1,1,1,5,5,5-hexafluoroacetylacetone.

The complex $(Pr_2CuL^1_3)HL^2_2(L^3_4)(\mu^6\text{-}O)$ was synthesised under similar conditions.

4. β-Diketonates with M—C- and M—C,O-coordination

β-Diketonate complexes of these types are represented by structures **16**, **18** and **23** studied by X-ray diffraction and reported in monographs[2–4, 16, 18, 124] and reviews.[5, 17, 20–24] Therefore, we will consider only the synthetic aspect of the design of this type of complex with unusual localisation of the coordination bonds.

As emphasised in a monograph,[124] the M—C-coordination, which is found, for example, in compound **16**, is observed in the complexes of β-diketones with Mn^I, Rh^I, Au^I, Pt^{II}, Pt^{III}, *i.e.*, with soft metals, which is consistent with Pearson's hard–soft acid–base (HSAB) principle.[2, 3, 125, 126] Examples of such compounds are mercury(II) complexes **78**[127, 128] and **79**[129, 130] and gold(I) complex **80**.[131–135]

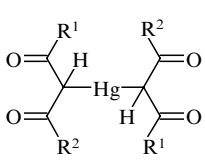

78: R^1, R^2 = Me, Bu^t

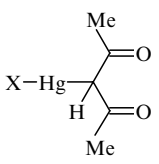

79: X = $MeCO_2$, Cl

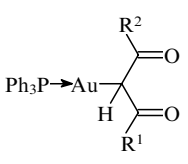

80: R^1 = Me, Bu^t, Ph; R^2 = Me, Bu^t, Ph, Fc (Fc is ferrocenyl)

Compound **78** was prepared in a quantitative yield by the following reaction:[127]

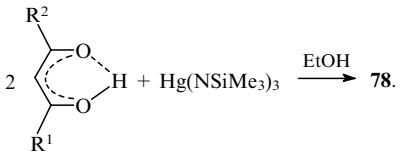

Subsequently,[128] complex **78** (R^1 = Bu^t; R^2 = n-C_3F_7) has been prepared using mercury(II) acetate. The structure of the resulting complex was studied by ^1H NMR spectroscopy and mass spectrometry, demonstrating the presence of keto–enol tautomerism (acetone, −60 to 40 °C).

Compounds **80** have been prepared in 46%–100% yields[135] upon the following transformation:

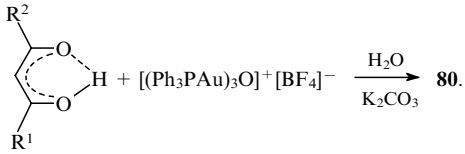

Other complexes with the structure of compound **16** have been discussed in reviews.[16–18, 136] Complexes with the structure of chelate **18** have been reported.[17, 18, 137]

The general method for the synthesis of complexes with the structure of chelate **23** is based on the reactions of β-diketonates **8** (M = Pt, Pd, Au) with organic amines and phosphines.[2, 3, 17, 18, 138, 139] This approach has received the most study in relation to the transformation of palladium diketonate **81** into complex **82**.[139–144]

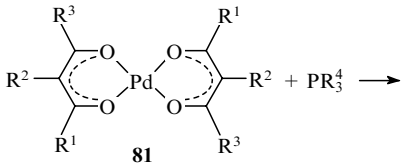

81

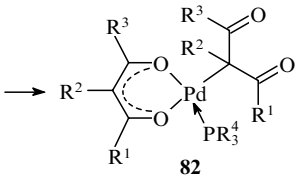

82

R^1–R^4 = H, Alk, Ar.

The M—C coordinated β-diketonate fragment is a part of trinuclear complexes $M[PtCl(acac)(acac\text{-}C^3)]_2$ where M = Mn^{II}, Fe^{II}, Co^{II}, Ni^{II}, Pd^{II}, Cu^{II}, Zn^{II}, Cd^{II}, VO and UO_2.[17, 18]

Other possible modes of coordination of β-diketone ligands have been confirmed experimentally,[16–18, 124] namely, C—O coordination as in chelate **22**; η^2(C,C′)- and μ^1(C)-coordinations in complex **83**; η-allylic coordination in complexes **84** and **85**; η^3(O,O′)-bridging coordination in complex **86**; and η^3(C,O)-bridging coordination in complex **87**.

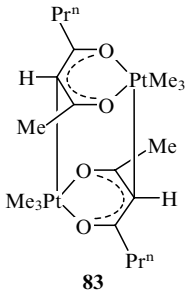

83

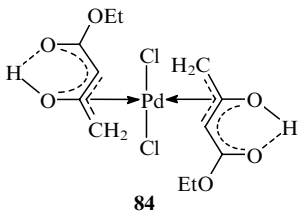

84

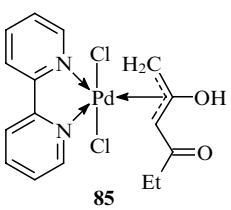

85

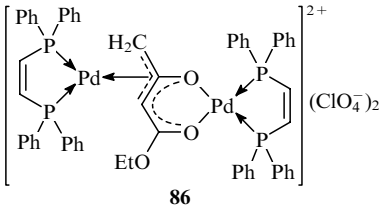

86

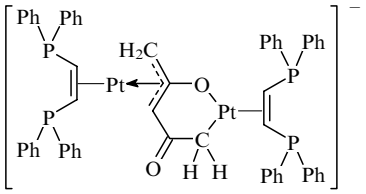

87

Binuclear compound **88** with the C—M-coordination, as in structure **19**, has been described and structurally characterised.[145]

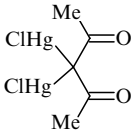

88

The compound **88** is the only example of a binuclear C-coordinated complex of β-diketone.

III. Modified β-diketonates

β-Diketone ligands are modified by altering the C—C—C fragment or replacing the oxygen atoms by N-, P-, S- and Se-donor centres. This gives rise to diverse ambident ligand systems. N,P-Containing analogues of β-diketones and chalcogen-substituted derivatives **3** (A = CR, D = PR^1R^2; X, Y = O, S) have been studied during the last decade.

1. N,P-Substituted β-diketonates

Among the potential polydentate ligands with N,O-donor centres, noteworthy are *N*-carbacylphosphoramidates (CAPh) **3** (A = CR, D = PR_2, X = Y = O), which have become readily available owing to the phosphazo reaction developed by Academician Kirsanov and co-workers.[146] Since CAPh are weak NH-(compound **89**) or OH-acids (compound **90**), they are able, similarly to β-diketones, to enter into the metal coordination sphere in either the deprotonated or the neutral form.[147]

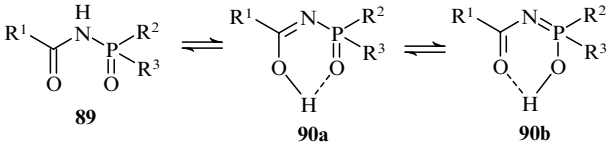

89 **90a** **90b**

R^1, R^2, R^3 = Alk, Ar, Het.

The complexes with CAPh, like β-diketonates, exist most often as structure **4** (A = CR, D = PR^1R^2, X = Y = O). This structure was proved for thallium complex **91** prepared by the following transformation (the crown ether was used to restrict the susceptibility of Tl^+ complexes to di- and polymerisation).[148]

$$Tl_2CO_3 + 2\,HL + 2\,(18\text{-crown-}6) \longrightarrow$$

$$\longrightarrow 2\,Tl(18\text{-crown-}6)L + CO_2\uparrow + H_2O$$

91

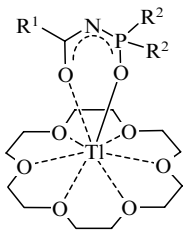

91: $R^1 = CCl_3$, $R^2 = OMe$

Structures of this type are widely represented in the series of lanthanide complexes.

In most lanthanide complexes, CAPh in the acid form is coordinated in the O,O′-bidentate mode (structures of chelates **4**, **8**). This was shown by X-ray diffraction[147] for neodymium complexes **92** and **93**.

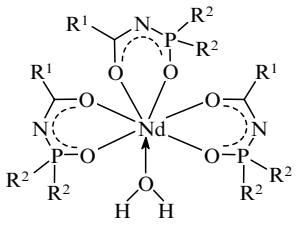

92: $R^1 = CCl_3$, $R^2 = N(C_2H_4)_2O$

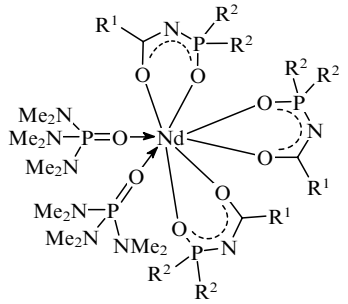

93: $R^1 = CCl_3$, $R^2 = OMe$

Complexes $LnL_3 \cdot Q$ with CAPh ligands, for example, **94** [$R^1 = CCl_3$; $R^2 = N(C_2H_4)_2O$, OPh, OMe; Q is α,α′-bipyridyl or 1,10-phenanthroline] have been prepared and structurally characterised.[149, 150]

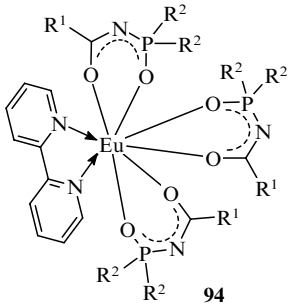

94

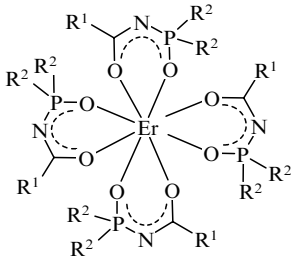

95

In the anionic complex of erbium **95**, the ligands are also coordinated in the bidentate chelating mode through the oxygen atoms of the phosphoryl and carbonyl groups.[151–153]

The homoligand anionic tetrakis-complexes M[LnL_4] with the ester type CAPh ligands have been synthesised from methanolic solutions in the following way:[151]

$$LnA_3 + 4\,NaL \longrightarrow Na[LnL_4] + 3\,NaA$$

A = Cl^-, NO_3^-.

Heteroligand cationic complexes of lanthanides have been prepared by metal exchange[2,3] from the sodium salt of *N*,*N*′-tetraethyl-*N*″-trichloroacetylphosphortriamide (NaL):[154]

$$Ln(NO_3)_3 + (3-n)\,NaL + m\,HMPA + n\,NaBPh_4 \longrightarrow$$

$$\longrightarrow [LnL_{3-n}(HMPA)_m](BPh_4)_n + 3\,NaNO_3\downarrow$$

$m = 2, 4$; $n = 1, 2$.

The synthesis was carried out in isopropyl alcohol in the presence of a dehydrating agent, ethyl orthoformate. According to electronic spectroscopy, the coordination polyhedron is a distorted octahedron.

The deliberate synthesis of binuclear complexes of lanthanides proceeds successfully when coordinatively unsaturated tris-complexes are used as structural elements and potential bridging ligands. For example, in the case of γ,γ′-bipyridyl, compounds of the type $(CAPh)_3Ln(\gamma,\gamma'\text{-bipy})Ln(CAPh)_3$ (**96**) were obtained;[155] in these products, the central atom is heptacoordinated, being O,O′-chelated by the ligand (structure **4**).

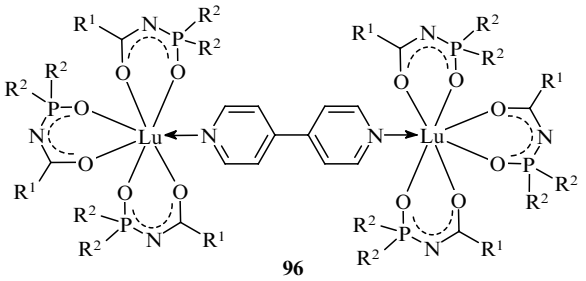

96

$R^1 = CCl_3$, $R^2 = OMe$.

The influence of the nature of the central lanthanide atom on the composition and structure of its complexes with these ligands was demonstrated in relation to $Nd_2(CAPh)_6(\gamma,\gamma'\text{-bipy})_3$ (**97**).[147] In this case, neodymium is octacoordinated.

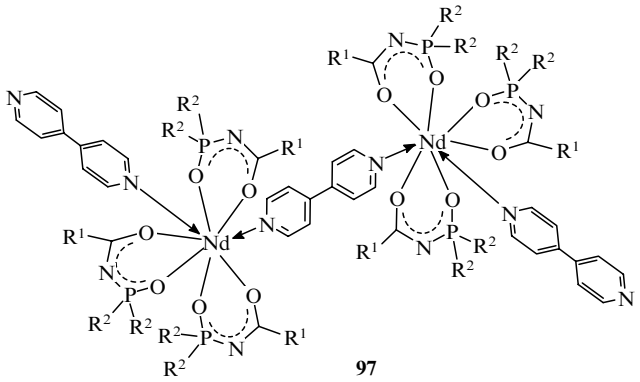

97

$R^1 = CCl_3$, $R^2 = NEt_2$.

The structure of chelate **4** (or **8**) is characteristic of CAPh complexes with transition metals, for example, the complex with iron(III) (**98**).[156]

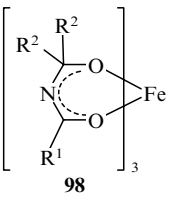

98

$R^1 = CCl_3$, $R^2 = NEt_2$, $N(C_2H_4)_2O$.

These compounds are known as not only monomeric (**98**) but also bi- and oligonuclear structures. Oligomerisation of the coordination polyhedra can take place by coordination of simple fragments such as alkoxy groups by the metal. For example, in the structure of dimeric chromium(III) complex (**99**), deprotonated CAPh ligands are coordinated in the bidentate chelating mode, the bridging functions being performed by two alkoxyl groups.[157]

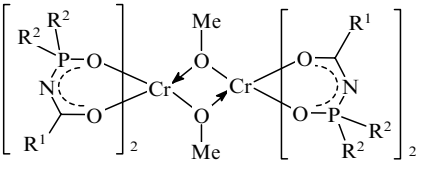

99

$R^1 = CCl_3$, $R^2 = OMe$.

Cobalt and nickel complexes crystallise as tetramers **100** with the composition $Me_4L_4(OMe)_4(HOMe)_4$ in which the tetramer core is formed by four Co atoms and by four O atoms of the methoxy groups.[147]

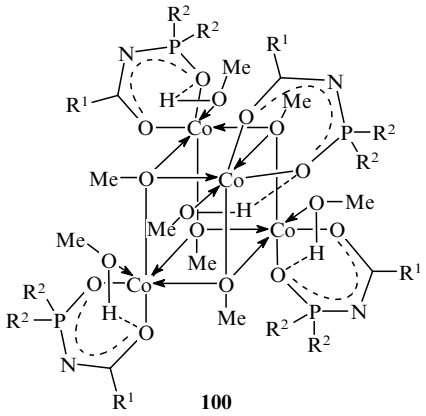

100

$R^1 = Ph$, $R^2 = NEt_2$.

Dioxane molecules and morpholine substituents can also function as bridges; this gives rise to dimeric copper(II) complexes **101** and **102** and polymeric complexes **103**.[158]

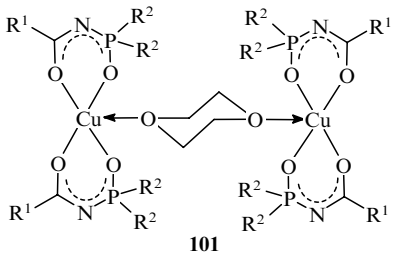

101

$R^1 = CCl_3$, $R^2 = NEt_2$.

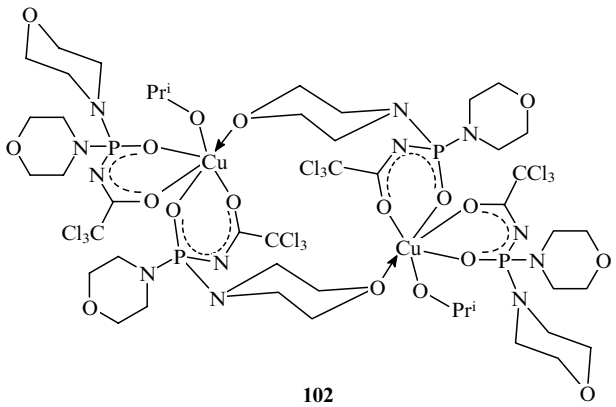

102

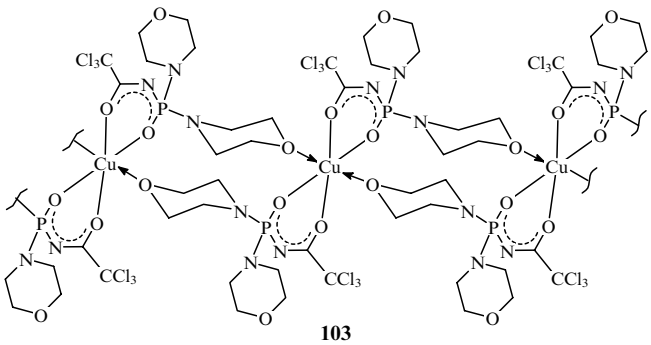

103

In the complexes of neutral CAPh with lanthanides, the ligand is monodentate, being coordinated through the oxygen atom of the phosphoryl group (similarly to structure **6**). These compounds

are prepared by direct reactions of the ligands (HL = CAPh) with lanthanide salts.[159]

$$LnA_3 \cdot n\,H_2O + 3\,HL \longrightarrow LnA_3(HL)_3 + n\,H_2O$$

A = Cl^-, NO_3^-.

In the case of complex $PrCl_3(HL)_3$, the *fac*-isomer **104** has been isolated; its structure was proved by X-ray diffraction.[160]

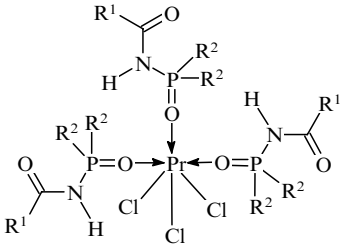

104

$R^1 = CCl_3$, $R^2 = NEt_2$.

The nitrate groups in the compound $Eu(NO_3)_3(HL)_3$ (**105**), which is similar to complex **6** in structure, are arranged in three mutually perdicular planes due to the directing action of the intramolecular hydrogen bonds.[161, 162]

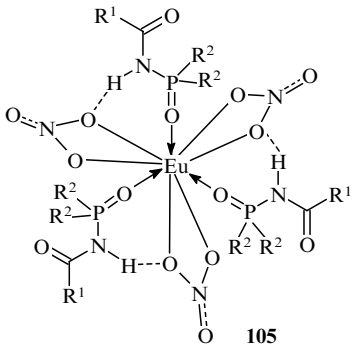

105

$R^1 = CCl_3$, $R^2 = NEt_2$.

The synthesis of complex $Nd(NO_3)_3(HL)_2(H_2O)_2$ (**106**) can be considered as an example of supramolecular self-organisation,[163, 164] whose driving force is the formation of hydrogen bonds with participation of the NH proton.[165]

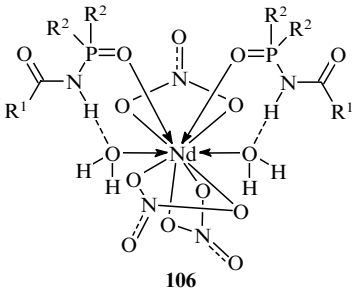

106

$R^1 = CCl_3$, $R^2 = N(C_2H_4)_2O$.

The supramolecular self-organisation typical of complexes formed by neutral CAPh (structure **6**) is manifested in the coordination compounds of uranyl $UO_2(NO_3)_2(HL)_2$ (**107**) in which the coordination polyhedron is a hexagonal bipyramid. The equatorial oxygen atoms are arranged in a virtually ideal plane.[166]

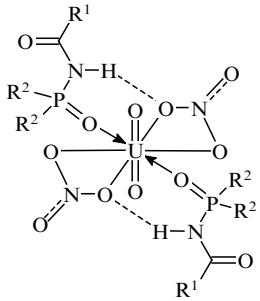

107: $R^1 = CCl_3$, $R^2 = NEt_2$

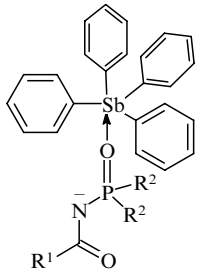

108: $R^1 = CCl_3$, $R^2 = OMe$

The monodentate coordination with participation of the phosphoryl oxygen atom has been established by X-ray diffraction also for the antimony complex **108**.[147]

The coordination compound $Ce(NO_3)_3(HL)_2$ (**109**) is the first example of bidentate chelating coordination of neutral CAPh (as in chelate **10**) realised through the phosphoryl and carbonyl oxygen atoms.[167]

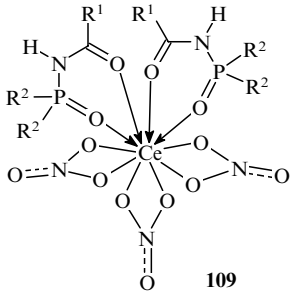

109

Among the coordination compounds of CAPh, structures with tridentate ligands similar to chelate **11** are represented rather widely. These include, in particular, complexes of Group IA metals.

Compounds of complex-forming alkali metals with some CAPh can be prepared in high yields by direct reaction of the ligands with metal salts in aqueous alcohols, for example:[147]

$$2\,HL + M_2CO_3 \longrightarrow 2\,ML + CO_2\uparrow + H_2O$$

M = Na, K, Rb, Cs.

Metal complexes with CAPh are also prepared by the reaction of ligands with the alkoxides of complexing metals in alcohols.[168–174]

$$HL + MOR \longrightarrow ML + HOR$$

The sodium and thallium complexes M_2L_2 crystallise as centrosymmetrical dimers **110**,[147] formed through the bridging oxygen atoms of the phosphoryl groups (the coordination mode is the same as in chelate **11**).

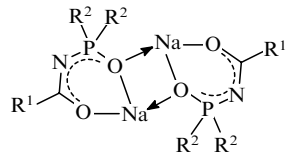

110

$R^1 = CCl_3$, $R^2 = OMe$.

The tendency of CAPh to form associates has been demonstrated in relation to the synthesis of the anionic $(PPh_4)_2[Na_4L_6]$ (**111**) complex [147] carried out in anhydrous acetonitrile.

$$2\,(PPh_4)Br + 6\,NaL \longrightarrow (PPh_4)_2[Na_4L_6] + 2\,NaBr\downarrow$$

111

Compound **111** contains two tetraphenylphosphonium cations and the $[Na_4L_6]^{2-}$ anion. The complex anion is composed of four sodium ions connected to one another by bi- and tridentate bridging oxygen atoms of the phosphoryl groups of the ligands (the coordination mode is the same as in chelate **12**).

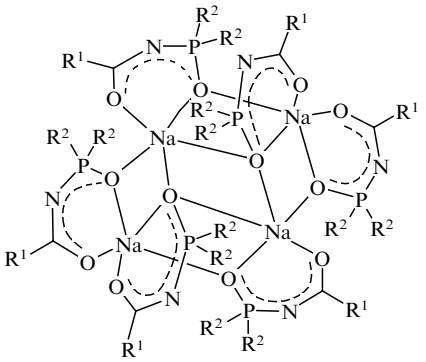

111

$R^1 = CCl_3$, $R^2 = OMe$.

The unit cell of complex Rb_4L_4 (**112**) contains four Rb^+ ions linked by bridging oxygen atoms of the phosphoryl and carbonyl groups,[147] *i.e.*, the mode of coordination is the same as in chelate **11**.

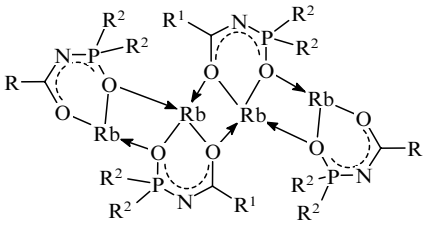

112

112: $R^1 = CCl_3$, $R^2 = OMe$.

The structures with mixed coordination of the ligands, similar to chelates **4** (or **8**) and **11**, are also encountered [147, 173] both in lanthanide complexes **113** and in cobalt(II) and nickel(II) complexes **114**.[175, 176]

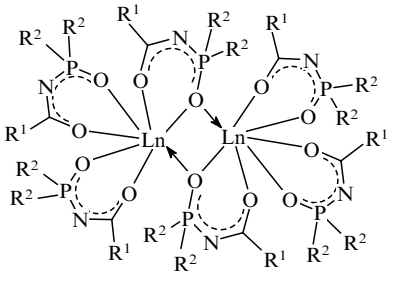

113

$R^1 = CCl_3$, $R^2 = NEt_2$.

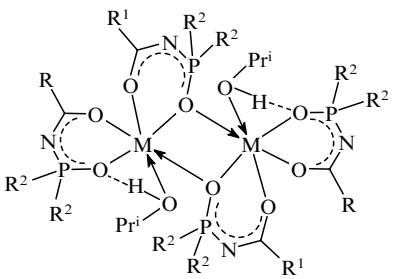

114

$R^1 = CCl_3$, $R^2 = OMe$; $M = Co^{2+}$, Ni^{2+}.

The complexes **113** were prepared in the following way:

$$2\,Ln(NO_3)_3 + 6\,NaL \longrightarrow Ln_2L_6 + 6\,NaNO_3\downarrow$$

Ln = La, Ce – Nd, Sm – Yb, Y.

Only one complex of CAPh with ligand coordination similar to that observed in compound **16** is currently known. The structure of this complex was proved by X-ray diffraction. This is the silver complex $Na[AgL_2]$ (**115**) prepared by metal exchange from acetonitrile solutions.[147]

$$2\,NaL + AgNO_3 \longrightarrow Na[AgL_2] + NaNO_3\downarrow$$

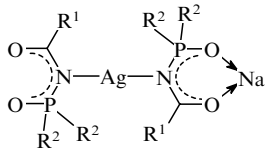

115

115: $R^1 = CCl_3$, $R^2 = OMe$.

The coordination of CAPh in this case can be compared with C-coordination of β-diketones, for example, the coordination found in compound **78**.[2, 3]

2. Metal complexes of N,P-derivatives of thio- and bisthiodiketones

The ligand systems and complexes in which structural analogues of β-diketones containing the XCNPY fragment (X = S, Y = O; X = O, Y = S; X = Y = S; X = O, Y = Se; X = Se, Y = O) are present as ligands in the coordination sphere (**116**, **117**) have been surveyed in sufficient detail.[177, 178]

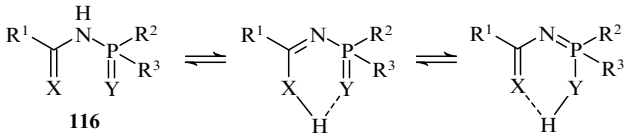

116 **117a** **117b**

X, Y = O, S, Se; R^1, R^2, R^3 = Alk, Ar, Het.

The metal complexes **116** and **117** mainly exist as structures **4** (A = CR; D = PR^1R^2; X, Y = O, S), which are classical for β-diketonates (chelates **8**). The structures of complexes **118** – **126** were confirmed by X-ray diffraction; these compounds are described below.

The synthesis and structure of copper and lead chelates ML_2 (**118**) with *N*-diisopropoxyphosphorylthiobenzamide (the MO_2S_2 coordination unit), characterised by a square planar and tetrahedral environments of the central atom, respectively, have been reported.[179, 180] The Cu^{2+} complexes were obtained from malachite (basic copper carbonate) in solutions of *N*-(thio)phosphorylated thioamides followed by reprecipitation from benzene with hexane. The Pb^{2+} compounds were synthesised by the reactions of alkali metal salts of the ligands dissolved in aqueous alcohols with lead salts or oxides.

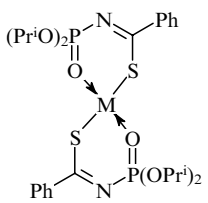

118: M = Cu, Pb

A bidentate O,S-coordination has also been found for copper(I) chelate **119**.[181]

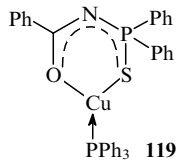

119

A number of studies are devoted to complex compounds containing the MS_4 coordination unit (structure **4**: A = CR, D = PR_2, X = Y = S). The syntheses of cobalt, nickel and palladium chelates with S-donor ligands of the type $R^1C(S)NHP(S)R^2_2$ were first described back in 1969.[182] The conclusions about the structures of the resulting compounds **120** were drawn from data of IR spectroscopy and magnetic chemistry (the square-planar environment for Ni^{2+}, Pd^{2+} and the tetrahedral environment for Co^{2+}).

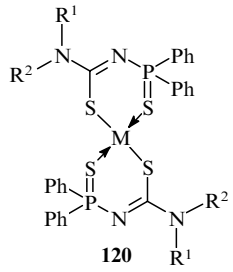

120

R^1 = Ph, R^2 = H; R^1 = R^2 = Et; M = Co, Ni, Pd.

Later on, data on the structure of an analogous nickel complex with *N*-(diphenylthiophosphoryl)methylthiourea (**120**, M = Ni) were documented.[183]

It should be emphasised that the reaction of platinum(II) chloride with diphenylthiophosphorylthiourea in CH_2Cl_2 results in complex **121**, whose coordination sphere contains bidentate chelating ligands coordinated in either deprotonated (structures **4**, **8**) or neutral (structure **10**) form. The exchange reaction of platinum(II) or zinc(II) chloride with the potassium salt of the ligand gives the usual chelates with square planar (**122**) and tetrahedral (**123**) structures, respectively.[181]

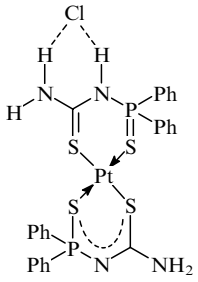

121

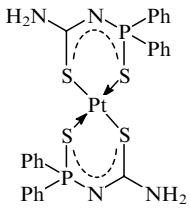

122

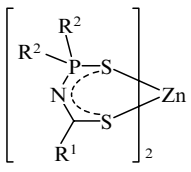

123

The reaction of *N*-(diisopropoxythiophosphoryl)thiobenzamide with mercury oxide in organic solvents gives mercury chelate **124**.[184]

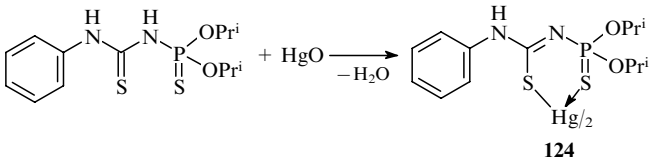

124

The central mercury atom in complex **124** forms a distorted tetrahedral environment.

On the basis of EPR and electronic spectroscopy studies, structures have been proposed for binuclear copper complexes (**125**); in addition, the electrochemical behaviour of these complexes has been studied.[185, 186]

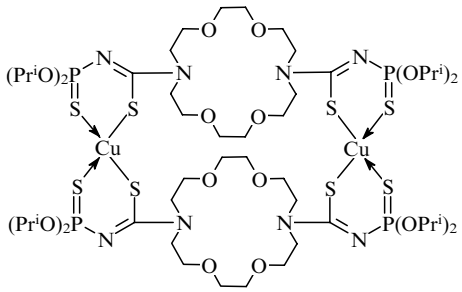

125

A method for the synthesis has been described and X-ray diffraction analysis has been performed for the tetrameric Ag(I) complex **126** in which the ligands are coordinated in the same way as in structure **11**.[187]

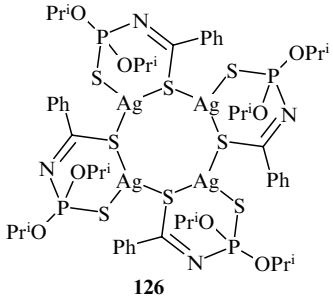

126

The formation of this tetramer is due to the presence of lone electron pairs at the donor sulfur atoms in mononuclear complexes, for example, in **121**–**123**. This is also quite usual for classical β-diketonates.[21, 188]

3. Coordination compounds of the N,P,P-derivatives of β-diketones and their chalcogen-containing analogues

Like the coordination compounds addressed in the preceding Sections, complexes of azobisphosphorus-containing analogues of β-diketones (their tautomers correspond to structures **89**–**91**, **116**, **117**) are represented, most often, by chelates with structure **4** (A = D = PR_2; X = O, Y = S, Se; X = S, Y = S, Se).[189–199] The structures **127** can be found in the six-membered chelates of indium,[189] palladium,[190, 195] platinum,[190] zinc[190] and cadmium.[190]

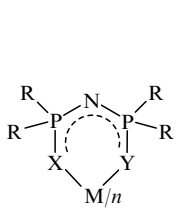

127

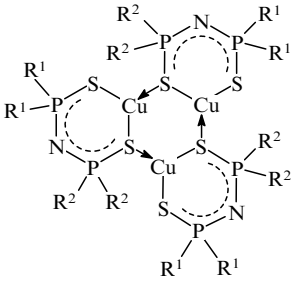

128: R^1 = Pr^i: R^2 = Pr^i, Ph, OPh

Of particular interest is the fact that the indium[189] and palladium[194] complexes were prepared directly from the corresponding zerovalent metals (synthetic strategies of this type are widely used in modern coordination chemistry[2, 3]).

Other modes of coordination are also known for complexes of these ligands. For example, in the case of platinum complexes, in addition to the coordination as in chelate **4** (**127**: X = O, Y = S), a structure with monodentate S-coordination of the metal atom is also formed.[195] A similar structure has been found for the gold complex,[195] which could be expected in terms of Pearson's HSAB principle (in view of the softness of the metals in question).[2, 3, 125, 126]

According to X-ray diffraction data, the trimeric copper complexes synthesised from compound **3** (A = D = PR_2, X = Y = S) and $CuCl_2$ in methanol occur as structure **128**[196] with the same coordination mode of the metal as found in chelate **11** .

In relation to the problem of competitive reactivity of ligands **3**, tellurium complexes are of interest.[197, 198] Not only tellurium complexes with a ligand coordination usual[20–24] for chelates, as in **127** (M = Te; X = S; Y = Se; n = 2) and **129**, have been described, but also complexes with the monodentate ligand bound through the S-donor centre at the phosphorus atom. This type of ligand coordination is embodied in structure **4** (A = D = PEt_2; X = Y = S).

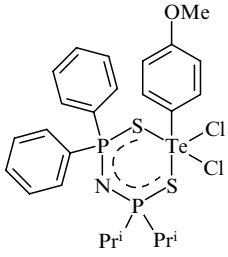

129

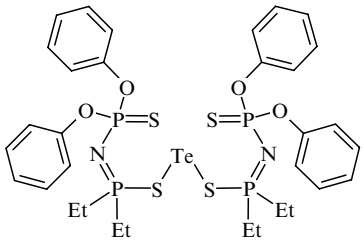

130

Complex **129** is of interest due to the fact that, according to X-ray diffraction data, the tellurium central atom is pentacoordinated, whereas in **130**, the same complex-forming element has a coordination number equal to two.

In conclusion, we would like to note that the material covered in this Section can be substantially extended by the data reported in the recent publication.[198]

IV. Conclusion

In writing this review, we have not set ourselves the task of embracing all the possible methods for the preparation of metal complexes of β-diketonates and their analogues. For example, we did not consider the coordination compounds of mono- and disubstituted nitrogen analogues of β-diketones, namely, β-aminovinyl ketones (**1**: A = E = D = CR^1; X = O; Y = NR^2) and β-aminovinylimines (**1**: A = E = D = CR^1; X = Y = NR^2), which have been studied rather comprehensively (see, for example, an exhaustive review [11]). All the complexes described in that review are chelates coordinated in the same manner as in chelate **2** (A = E = D = CR^1; X = O, NR^2; Y = NR^2). Meanwhile, in view of the data [10, 200] attesting to different modes of coordination of Schiff's bases in metal chelates (bidentate N,O-chelation by the anionic form of the ligand) and in molecular complexes (O-monodentate coordination of the neutral ligand), one should expect the formation of various types of complexes also for β-aminovinyl ketones and β-aminovinylimines.

This situation is typical of fairly well-known metal chelates of mono- and dithio-β-diketones (**1**: A = E = D = CR; X = O, Y = S; X = Y = S)[2, 3] and phosphorus-containing analogues of β-diketones (**1**: A = E = CR; D = PR_2; A = D = PR_2, E = CR; X, Y = O, S, Se).[12]

The material outlined in this review indicates that a number of β-diketonate ligands can be coordinated according to different modes. Therefore, metal complexes of different types can be prepared. We hope that further research will bring new data on the complexation of such ligands and will thus contribute to the development of deliberate strategies for the synthesis of complex compounds with specified coordination units on the basis of typical chelating ligands.

This review was prepared with financial support from the Russian Foundation for Basic Research (Project NSh-945.2003.3).

References

1. F A Cotton, G Wilkinson, C A Murillo, M Bochman *Advances Inorganic Chemistry* (6th Ed.) (New York: Wiley, 1999)
2. A D Garnovskii, I S Vasilchenko, D A Garnovskii *Sovremennye Aspekty Sinteza Metallokompleksov. Osnovnye Ligandy i Metody* (Modern Aspects of the Synthesis of Metal Complexes. The main Ligands and Methods) (Rostov-on-Don: LaPo, 2000)
3. L M Blanco, A D Garnovskii, D A Garnovskii, B I Kharisov, M A Mendes-Rojas, I S Vasilchenko *Synthetic Coordination and Organometallic Chemistry* (Eds A D Garnovskii, B I Kharisov) (New York: Marcel Dekker, 2003)
4. R C Mehrotra, R Bohra, D P Gaur *Metal β-Diketonates and Allied Derivatives* (London: Academic Press, 1978)
5. A R Siedle, in *Comprehensive Coordination Chemistry* Vol 2 (Ed. G Wilkinson) (Oxford: Pergamon Press, 1987) p. 365
6. D A Thornton *Coord. Chem. Rev.* **104** 173 (1990)
7. L I Martynenko (Ed.) *β-Diketonaty Metallov* (Metal β-Diketonates) (Vladivostok: Far-Eastern State University, 1990, 1991) Vols 1, 2
8. L I Martynenko, N P Kuz'mina, A N Grigor'ev *Ros. Khim. Zh.* **40** (4–5) 110 (1996) [a]
9. D J Otway, W S Rees Jr *Coord. Chem. Rev.* **210** 279 (2000)
10. A D Garnovskii, I S Vasilchenko *Usp. Khim.* **71** 1064 (2002) [*Russ. Chem. Rev.* **71** 943 (2002)]
11. L Bourget-Merle, M F Lappert, J R Severn *Chem. Rev.* **102** 3031 (2002)
12. L D Popov, A A Shvets, V A Kogan *Koord. Khim.* **15** 1299 (1989) [b]
13. P Bhattacharyya, J D Woollins *Polyhedron* **14** 3367 (1995)
14. E G Il'in, Yu A Buslaev *Ros. Khim. Zh.* **40** (4–5) 66 (1996) [a]
15. A D Garnovskii, I E Uflyand, I S Vasilchenko, A I Uraev, A S Burlov, A V Bicherov, E L Anpilova, O Yu Korshunov *Ros. Khim. Zh.* **48** 5 (2004) [a]
16. L M Shkol'nikova, M A Porai-Koshits, in *Kristallokhimiya (Itogi Nauki i Tekhniki)* [Crystal Chemistry (Advances in Science and Engineering Series)] (Moscow: Izd. VINITI, 1982) Vol. 16, p. 117
17. S Kawaguchi *Coord. Chem. Rev.* **70** 51 (1986)
18. S Kawaguchi, in *Variety in Coordination Modes of Ligands in Metal Complexes* (Berlin: Springer, 1988)
19. A D Garnovskii, D A Garnovskii, I S Vasilchenko *Zh. Neorg. Khim.* **37** 1474 (1992) [c]
20. A D Garnovskii, D A Garnovskii, A S Burlov, I S Vasilchenko *Ros. Khim. Zh.* **40** (4–5) 19 (1996) [a]
21. A D Garnovskii, D A Garnovskii, I S Vasilchenko, A S Burlov, A P Sadimenko, I D Sadekov *Usp. Khim.* **66** 434 (1997) [*Russ. Chem. Rev.* **66** 389 (1997)]
22. A D Garnovskii *Zh. Neorg. Khim.* **43** 1491 (1998) [c]
23. A D Garnovskii, A P Sadimenko, M I Sadimenko, D A Garnovskii *Coord. Chem. Rev.* **173** 31 (1998)
24. A D Garnovskii, B I Kharisov, L M Blanco, D A Garnovskii, A S Burlov, G I Bondarenko *J. Coord. Chem.* **46** 365 (1999)
25. *Ros. Khim. Zh.* **40** (Spec. Issue) (1996) [a]
26. S C Ngo, K K Banger, P J Toscano, J T Welch *Polyhedron* **21** 1289 (2002)
27. I Boldog, E B Rusanov, A N Chernega, J Sieler, K V Domasevitch *Angew. Chem., Int. Ed.* **40** 3435 (2001)
28. O T H Le, S Umetani, M Matsui *J. Chem. Soc., Dalton Trans.* 3835 (1997)
29. C M Silvernail, G Yap, R D Sommer, A L Rheingold, V W Day, J A Belot *Polyhedron* **20** 3113 (2001)
30. G J Goetz-Grandmont, A Tayeb, D Matt, J-P Brunette *Acta Crystallogr., Sect. C* **51** 53 (1995)
31. A V Bicherov, B I Kharisov, L M Blanco, O Yu Korshunov, E L Koroleva, A S Burlov, G S Borodkin, V P Kurbatov, I E Uflyand, A D Garnovskii *J. Coord. Chem.* **54** 337 (2001)
32. W C du Plessis, T G Vosloo, J C Swarts *J. Chem. Soc., Dalton Trans.* 2507 (1999)
33. V S Sergienko, A B Ilyukhin, Yu V Kovalenko, V L Abramenko *Koord. Khim.* **20** 842 (1994) [b]

34. G Brauer (Ed.) *Handbuch der Praparative Anorganischen Chemie* (Stuttgart: Ferdinand Enke Verlag, 1981)
35. A Bailey, T S Corbitt, M J Hampden-Smith, E N Duesler, T T Kodas *Polyhedron* **12** 1785 (1993)
36. D A Nieto-Alvarez, F Jiménez-Cruz, T Mancilla *Polyhedron* **21** 417 (2002)
37. G Malandrino, I L Fragalà, S Aime, W Dastrù, R Gobetto, C Benelli *J. Chem. Soc., Dalton Trans*. 1509 (1998)
38. K A Fleeting, P O'Brien, D J Otway, A J P White, D J Williams, A C Jones *Inorg. Chem*. **38** 1432 (1999)
39. J Barberá, A Eldugue, R Giménez, F J Lahoz, J A López, L A Oro, J L Serrano, B Villacampa, J Villalba *Inorg. Chem*. **38** 3085 (1999)
40. D R van Staveren, G A van Albada, J G Haasnoot, H Kooijman, A M Manotti-Lanfredi, P J Nieuwenhuizen, A L Spek, F Ugozzoli, T Weyhermüller, J Reedijk *Inorg. Chim. Acta* **315** 163 (2001)
41. T Pechmann, C D Brandt, C Röger, H Werner *Angew. Chem*. **114** 2398 (2002)
42. J C Plakatouras, I Baxter, M B Hursthouse, K M A Malik, J Mc Alocese, S R Drake *J. Chem. Soc., Chem. Commun*. 2455 (1994)
43. G V Trembovskii, L I Martynenko, I A Murav'eva *Zh. Neorg. Khim*. **30** 1163 (1985) [c]
44. A P Borisov, L A Petrova, V D Makhaev *Zh. Obshch. Khim*. **62** 15 (1992) [d]
45. A P Borisov, L A Petrova, T P Karpova, V D Makhaev *Zh. Neorg. Khim*. **41** 411 (1996) [c]
46. I G Zaitseva, N P Kuz'mina, L I Martynenko, V D Makhaev, A P Borisov *Zh. Neorg. Khim*. **43** 805 (1998) [c]
47. S R Drake, S A S Miller, M B Hursthouse, K M A Malik *Polyhedron* **12** 1621 (1993)
48. A Döhring, R Goddard, P W Jolly, C Krüger, V P Polyakov *Inorg. Chem*. **36** 177 (1997)
49. S J Slattery, W D Bare, D L Jameson, K A Goldsby *J. Chem. Soc., Dalton Trans*. 1347 (1999)
50. K Karvembu, K Natarajan *Polyhedron* **21** 219 (2002)
51. K Karvembu, K Natarajan *Polyhedron* **21** 1721 (2002)
52. T Yoshida, T Suzuki, K Kanamori, S Kaizaki *Inorg. Chem*. **38** 1059 (1999)
53. M A Bennett, G Chung, D C R Hockless, H Neumann, A C Willis *J. Chem. Soc., Dalton Trans*. 3451 (1999)
54. T Pechmann, C D Brandt, H Werner *Angew. Chem*. **112** 4069 (2000)
55. T Hashimoto, A Endo, N Nagao, G P Satô, K Natarajan, K Shimizu *Inorg. Chem*. **37** 5211 (1998)
56. H Hennig *Z. Chem*. **11** 81 (1971)
57. J Vicente, M T Chicote *Coord. Chem. Rev*. **193–195** 1143 (1999)
58. N V Gerbeleu *Reaktsii na Matritsakh* (Template Reactions) (Kishinev: Shtiintsa, 1980)
59. N V Gerbeleu, V B Arion *Templatnyi Sintez Makrotsiklicheskikh Soedinenii* (Template Synthesis of Macrocyclic Compounds) (Kishinev: Shtiintsa, 1990)
60. N V Gerbeleu, V B Arion, J Burgess *Template Synthesis of Macrocyclic Compounds* (Weinheim: Wiley-VCH, 1999)
61. D S Black, in *Comprehensive Coordination Chemistry* Vol. 2 (Ed. G Wilkinson) (Oxford: Pergamon Press, 1987) p. 415
62. E C Constable *Metal and Ligand Reactivity. An Introduction to the Organic Chemistry Metal Complexes* (Weinheim: VCH, 1995)
63. A J L Pombeiro, V Yu Kukushkin, in *Comprehensive Coordination Chemistry II* Vol. 1 (Eds J A McCleverty, T J Meyer) (Oxford: Elsevier, 2003) p. 585
64. S A Samath, N Raman, K Jeyasubramanian, S K Pamalingam *Polyhedron* **11** 33 (1992)
65. B-Q Ma, S Gao, T Yi, G-X Xu *Polyhedron* **20** 1255 (2001)
66. C Grünwald, M Laubender, J Wolt, H Werner *J. Chem. Soc., Dalton Trans*. 833 (1998)
67. I Yeltsov, V Ovcharenko, V Ikorskii, G Romanenko, S Vasilevsky *Polyhedron* **20** 1215 (2001)
68. A Rajca, S Rajca, J Wongsriratanakul, C R Ross II *Polyhedron* **20** 1669 (2001)
69. J Powell, M J Horvath, A Lough, A Phillips, J Brunet *J. Chem. Soc., Dalton Trans*. 637 (1998)
70. C Pettinari, F Marchetti, A Cingolani, D Leonesi, S Troyanov, A Drozdov *J. Chem. Soc., Dalton Trans*. 1555 (1999)
71. H O Davies, J J Brooks, A C Jones, T J Leedham, J F Bickley, A Steiner, P O'Brien, A J P White, D J Williams *Polyhedron* **20** 2397 (2001)
72. V V Skopenko, A V Garnovskii, V N Kokozei, A S Kuzharov, G Gokhon-Zorrilla, A S Burlov, O Yu Vasil'eva, V A Pavlenko, B I Kharisov, B M Kherets, L M Blanko, D A Garnovskii *Pryamoi Sintez Koordinatsionnykh Soedinenii* (Direct Synthesis of Coordination Compounds) (Ed. V V Skopenko) (Kiev: Venturi, 1997)
73. A D Garnovskii, B I Kharisov, V V Scopenko, L M Blanco, B M Jerez, V N Kokozay, A S Kuzharov, D A Garnovskii, O Yu Vassilyeva, A S Burlov, V A Pavlenko *Direct Synthesis of Coordination and Organometallic Compounds* (Eds A D Garnovskii, B I Kharisov) (Amsterdam: Elsevier, 1999)
74. R-N Yang, D-M Wang, Y-G Liu, D-M Jin *Polyhedron* **20** 585 (2001)
75. E A Mazurenko, Doctoral Thesis in Chemical Sciences, Institute of Organic and Inorganic Chemistry, Academy of Sciences, Ukr.SSR, Kiev, 1987
76. A D Garnovskii, B I Kharisov, G Gojon-Zorrilla, D A Garnovskii *Usp. Khim*. **64** 215 (1995) [*Russ. Chem. Rev*. **64** 201 (1995)]
77. A D Garnovskii , B I Kharisov, G Gojon-Zorrilla, D A Garnovskii, A S Burlov *Koord. Khim*. **23** 243 (1997) [b]
78. B I Kharisov, A D Garnovskii, L M Blanko, A S Burlov, A Garcia-Luna *J. Coord. Chem*. **49** 113 (1999)
79. A D Garnovskii, L M Blanko, B I Kharisov, D A Garnovskii, A S Burlov *J. Coord. Chem*. **48** 219 (1999)
80. A P Purdy, A D Berry, R T Holm, M Fatemi, D K Galskill *Inorg. Chem*. **28** 2799 (1989)
81. J Grobe, M Kein, B Schneider *Z. Naturforsch., B* **35** 428 (1980)
82. A P Tomilov, I N Chernykh, Yu M Kargin *Elektrokhimiya Elementoorganicheskikh Soedinenii. Elementy I, II, III Grupp Periodicheskoi Sistemy i Perekhodnye Metally* (Electrochemistry of Organoelement Compounds. Elements of Groups I, II, III of the Periodic System and Transition Metals) (Moscow: Nauka, 1985)
83. J Grobe, in *Electrochemical Synthesis* (Ed. R D Little) (New York: Marcel Dekker, 1991)
84. D G Tuck, in *Molecular Electrochemistry in Inorganic, Bioinorganic and Organometallic Compounds* (Dordrecht: Kluwer, 1993) p. 15
85. N N Kostyuk, V L Shirokii, I I Vinokurov, N A Maier *Zh. Obshch. Khim*. **64** 1432 (1994) [d]
86. N N Kostyuk, T A Kolevich, V L Shirokii, D S Umreiko *Koord. Khim*. **15** 1704 (1989) [b]
87. N N Kostyuk, V L Shirokii, T A Dik, N N Vinokurov, D S Umreiko *Koord. Khim*. **17** 1573 (1991) [b]
88. N N Kostyuk, V L Shirokii, I I Vinokurov, N A Maier *Zh. Neorg. Khim*. **37** 68 (1992) [c]
89. M A Méndez-Rojas, F Cordova-Lozano, G Gojon-Zorrilla, E Gonzáles-Vergana, M A Quiroz *Polyhedron* **18** 2651 (1999)
90. A S Kuzharov, V V Suchkov, L A Komarchuk *Zh. Fiz. Khim*. **57** 1748 (1983) [e]
91. A Dhammani, R Bohra, R C Mehrotra *Polyhedron* **17** 163 (1998)
92. H-Y Shen, D-Z Liao, Z-H Jiang, S-P Yan, B-W Sun, G-L Wang, X-K Yao, H-G Wang *Polyhedron* **17** 1953 (1998)
93. X-F Chen, S-H Liu, C-Y Duan, Y-H Xu, X-Z You, J Ma, N-B Min *Polyhedron* **17** 1883 (1998)
94. M A Ersteruelas, F J Lahoz, M Martin, A Martinez, L A Oro, A C Puerta, P Valerga *J. Organomet. Chem*. **577** 265 (1999)
95. W Simanko, K Mereiter, R Schmid, K Kirchner, A M Trzeciak, J J Ziolkowski *J. Organomet. Chem*. **602** 59 (2000)
96. I Romade, O Kahn, Y Jeannin, F Robert *Inorg. Chem*. **36** 930 (1997)
97. A S Alikhanyan, I P Markelova, N P Kuz'mina, A Gleiz, M Khul've, G L Sanz, I L Eremenko *Zh. Neorg. Khim*. **44** 969 (1999) [c]

98. N P Kuz'mina, A Yu Rogachev, F M Spiridonov, E M Dedlovskaya, V A Ketsko, A Gleiz, Dzh Batiston *Zh. Neorg. Khim.* **45** 1468 (2000) [c]
99. A D Garnovskii, A P Sadimenko, A I Uraev, I S Vasilchenko, D A Garnovskii *Koord. Khim.* **26** 334 (2000) [b]
100. A D Garnovskii, B I Kharisov, L M Blanco, A B Sadimenko, A I Uraev, I S Vasilchenko, D A Garnovskii *J. Coord. Chem.* **55** 1119 (2002)
101. M V Ryazanov, S I Troyanov, I P Markelova, A S Alikhanyan, N P Kuz'mina *Zh. Neorg. Khim.* **46** 256 (2001) [c]
102. N P Kuz'mina, M V Ryazanov, V A Ketsko, A N Gleiz *Zh. Neorg. Khim.* **47** 30 (2002) [c]
103. N Kuzmina, M Ryazanov, I Markelova, A Alihanyan, A N Gleizes *Eur. J. Inorg. Chem.* **701** (2001)
104. S Koda, S Ooi, H Kuroya, Y Nakamura, S Kawaguchi *J. Chem. Soc., Chem. Commun.* 280 (1971)
105. Y Nakamura, K Isobe, H Morita, S Yamazaki, S Kawaguchi *Inorg. Chem.* **11** 1573 (1972)
106. M C Fredette, C J L Lock *Can. J. Chem.* **51** 1116 (1973)
107. M C Fredette, C J L Lock *Can. J. Chem.* **53** 2481 (1975)
108. S Koda, S Ooi, H Koroya, K Isobe, Y Nakamura, S Kawaguchi *J. Chem. Soc., Chem. Commun.* 1321 (1971)
109. K Alzenhofer, T G Hewitt *Z. Kristallogr.* **134** 54 (1971)
110. R E Cramer, S W Cramer, K F Cramer, M A Chudyk, K Seff *Inorg. Chem.* **16** 219 (1977)
111. W S Rees, M W Carris, W Hesse *Inorg. Chem.* **30** 4479 (1991)
112. V-C Arunasalam, S R Drake, M B Hursthouse, K M A Malik, S A S Miller, D M P Mingos *J. Chem. Soc., Dalton Trans.* 2435 (1996)
113. A A Drozdov, S I Troyanov *Polyhedron* **11** 2877 (1992)
114. N P Kuz'mina, A A Drozdov, T V Zolotova, G N Kupriyanova, F P Pisarevskii, Yu T Struchkov *Koord. Khim.* **20** 743 (1994) [b]
115. A A Drozdov, A Pozhitkov, S I Troyanov, A P Pisarevsky *Polyhedron* **15** 1731 (1996)
116. A A Drozdov, S I Troyanov, A P Pisarevsky, Yu T Struchkov *Polyhedron* **13** 1445 (1994)
117. A A Drozdov, S I Troyanov, A P Pisarevsky, Yu T Struchkov *Polyhedron* **13** 2459 (1994)
118. N Novnanian, J Galloy, P Miele *Polyhedron* **14** 297 (1995)
119. L I Martynenko, N P Kuz'mina, A N Grigor'ev *Koord. Khim.* **21** 515 (1995) [b]
120. C Pettinari, F Marchetti, A Drozdov, in *Comprehensive Coordination Chemistry II* Vol. 1 (Ed. A B P Lever) (Oxford: Elsevier-Pergamon Press, 2003) p. 97
121. R Castro, M L Durvn, J A Garsia-Vvzguaz, J Romero, A Sousa, A CastiKheiras, W Hiller, J Strihle *Polyhedron* **11** 1195 (1992)
122. S Parola, R Papiernik, L G Hubert-Pfalzgraf, C Bois *J. Chem. Soc., Dalton Trans.* 737 (1998)
123. S R Breeze, S Wang, J E Greedan, N P Raju *J. Chem. Soc., Dalton Trans.* 2327 (1998)
124. V N Peshkova, N V Mel'chakova *β-Diketony* (β-Diketones) (Moscow: Nauka, 1986)
125. R G Pearson *J. Am. Chem. Soc.* **85** 3533 (1963)
126. A D Garnovskii, A P Sadimenko, O A Osipov, G V Tsintsadze *Zhestko-Myagkie Vzaimodeistviya v Koordinatsionnoi Khimii* (Hard – Soft Interactions in Coordination Chemistry) (Rostov-on-Don: Rostov-on-Don State University, 1986)
127. R Allmann, K Flatau, H Musso *Chem. Ber.* **105** 3067 (1972)
128. R H Fish *J. Am. Chem. Soc.* **96** 6664 (1974)
129. R Allmann, H Musso *Chem. Ber.* **106** 3001 (1973)
130. L E McCandlish, J W Macklin *J. Organomet. Chem.* **99** 31 (1975)
131. L G Kuz'mina *Koord. Khim.* **20** 540 (1994) [b]
132. L G Kuz'mina *Koord. Khim.* **20** 547 (1994) [b]
133. L G Kuz'mina *Koord. Khim.* **20** 633 (1994) [b]
134. L G Kuz'mina *Koord. Khim.* **21** 374 (1995) [b]
135. K I Grandberg, L G Kuz'mina, E I Smyslova, A I Zinin, D P Kut'ko, V P Dyadchenko *Zh. Neorg. Khim.* **41** 231 (1996) [c]
136. D Gibson *Coord. Chem. Rev.* **4** 225 (1969)
137. Z Kanda, Y Nakamura, S Kawaguchi *Inorg. Chem.* **17** 910 (1978)
138. S Baba, T Ogura, S Kawagushi *Bull. Chem. Soc. Jpn.* **47** 665 (1974)
139. S Komiya, J K Kochi *J. Am. Chem. Soc.* **99** 3695 (1977)
140. G V Ratovskii, O V Burlakova, V S Tkach, F K Shmidt *Koord. Khim.* **16** 997 (1990) [b]
141. L B Belykh, T V Dmitrieva, S V Zinchenko, F K Shmidt *Koord. Khim.* **21** 476 (1995) [b]
142. O V Tyukalova, G V Ratovskii, L B Belykh, F K Shmidt *Zh. Obshch. Khim.* **67** 58 (1997) [d]
143. L B Belykh, T V Dmitrieva, F K Shmidt *Koord. Khim.* **25** 528 (1999) [b]
144. F K Shmidt, L B Belykh, T V Goremyka *Koord. Khim.* **28** 98 (2002) [b]
145. L E McCandlish, J W Macklin *J. Organomet. Chem.* **99** 31 (1975)
146. A V Kirsanov (Ed.) *Fosfazosoedineniya* (Phosphazo Compounds) (Kiev: Naukova Dumka, 1965)
147. V M Amirkhanov, Doctoral Thesis in Chemical Sciences, Kyiv National University, Kyiv, 2002
148. V A Trush, K V Domasevitch, V M Amirkhanov, J Sieler *Z. Naturforsch., B* **54** 451 (1999)
149. V A Ovchinnikov, V M Amirkhanov, K V Domasevich, I Siler, V V Skopenko *Zh. Neorg. Khim.* **46** 615 (2001) [c]
150. M Borzechowska, V Trush, I Turowska-Tyrk, W Amirkhanov, J Legendziewicz *J. Alloys Compd.* **341** 98 (2002)
151. V M Amirkhanov, V A Trush, A A Kapshuk, V V Skopenko *Zh. Neorg. Khim.* **41** 2052 (1996) [c]
152. V M Amirkhanov, V V Skopenko, V S Dradrakh, V A Trush, V A Ovchinnikov, A V Turov *Zh. Neorg. Khim.* **45** 341 (2000) [c]
153. V Amirkhanov, V Ovchynnikov, J Legendziewicz, A Graczyk, J Hanuza, L Macalik *Acta Phys. Pol. A* **90** 455 (1996)
154. V M Amirkhanov, V A Ovchinnikov, A N Rekhta, A Ya Grytskiv, V V Skopenko *Koord. Khim.* **24** 368 (1998) [b]
155. V A Trush, J Swiatek-Kozlowska, V V Skopenko, V M Amirkhanov *Z. Naturforsch., B* **56** 249 (2001)
156. E A Trush, V A Ovchynnikov, K V Domasevitch, J Swiatek-Kozlowska, V Ya Zub, V M Amirkhanov *Z. Naturforsch., B* **57** 746 (2002)
157. V A Trush, Candidate Thesis in Chemical Sciences, Kyiv, Kyiv National University, 2003
158. V A Trush, V M Amirkhanov, V A Ovchynnikov, J Swiatek-Kozlowska, K A Lanikina, K V Domasevitch *Polyhedron* **22** 1221 (2003)
159. V M Amirkhanov, V A Ovchinnikov, A V Turov, V V Skopenko *Koord. Khim.* **23** 139 (1997) [b]
160. V M Amirkhanov, V A Ovchinnikov, A A Kapshuk, V V Skopenko *Zh. Neorg. Khim.* **40** 1869 (1995) [c]
161. V M Amirkhanov, A A Kapshuk, V A Ovchinnikov, V V Skopenko *Zh. Neorg. Khim.* **41** 1470 (1996) [c]
162. K E Gubina, J A Shatrava, V A Ovchynnikov, V M Amirkhanov *Polyhedron* **19** 2203 (2000)
163. J-M Lehn *Supramolecular Chemistry. Concepts and Perspectives* (Weiheim: VCH, 1995)
164. J W Steed, J L Atwood *Supramolecular Chemistry* (Chichester: Wiley, 2000)
165. V A Ovchynnikov, T P Timoshenko, V M Amirkhanov, J Sieler, V V Skopenko *Z. Naturforsch., B* **55** 262 (2000)
166. V M Amirkhanov, J Sieler, V A Trush, V A Ovchynnikov, K V Domasevich *Z. Naturforsch., B* **52** 1194 (1997)
167. K E Gubina, V A Ovchynnikov, V M Amirkhanov, H Fischer, R Stumpf, V V Skopenko *Z. Naturforsch., B* **55** 576 (2000)
168. V V Polovinko, V D Rudzevich, V M Amirkhanov *Zh. Neorg. Khim.* **39** 640 (1994) [c]
169. V M Amirkhanov, V A Trush *Zh. Obshch. Khim.* **65** 1120 (1995) [d]
170. V M Amirkhanov, V A Ovchinnikov, V A Trush, V V Skopenko *Zh. Org. Khim.* **32** 376 (1996) [f]
171. V A Ovchynnikov, V M Amirkhanov, T P Timoshenko, *Z. Naturforsch., B* **53** 481 (1998)
172. V M Amirkhanov, V A Ovchynnikov, T Glowiak, H Kozlowski *Z. Naturforsch., B* **52** 1331 (1997)
173. K E Gubina, V A Ovchynnikov, V M Amirkhanov, T Yu Sliva, V V Skopenko, T Glowiak, H Kozlowski *Z. Naturforsch., B* **54** 1357 (1999)

174. K E Gubina, V A Ovchynnikov, V M Amirkhanov, V V Skopenko, O V Shishkin *Z. Naturforsch., B* **55** 495 (2000)
175. V V Skopenko, V M Amirkhanov, V A Ovchinnikov, A V Turov *Zh. Neorg. Khim.* **41** 611 (1996) [c]
176. E A Bundya, V M Amirkhanov, V A Ovchynnikov, V A Trush, K V Domasevitch, J Sieler, V V Skopenko *Z. Naturforsch., B* **54** 1033 (1999)
177. N G Zabirov, F M Shamsevaleev, R A Cherkasov *Usp. Khim.* **60** 2189 (1991) [*Russ. Chem. Rev.* **60** 1128 (1991)]
178. T Q Ly, J D Woollins *Coord. Chem. Rev.* **176** 451 (1998)
179. N G Zabirov, V N Solov'ev, F N Shamsevaleev, R A Cherkasov, A N Chekhlov, A G Tsifarkin, I V Martynov *Zh. Obshch. Khim.* **61** 657 (1991) [d]
180. A L Kon'kin, V G Shtyrlin, N G Zabirov, A V Aganov, L E Zapechel'nyuk, S V Kashevarov, A V Zakharov *Zh. Neorg. Khim.* **41** 1156 (1996) [c]
181. D J Birdsall, J Green, T Q Ly, J Novosad, M Necas, A M Z Slawin, J D Woollins, Z Zak *Eur. J. Inorg. Chem.* 1445 (1999)
182. I Ojima, T Iwamoto, T Onishi, N Inamoto, K Tamaru *J. Chem. Soc., Chem. Commun.* 1501 (1969)
183. T Iwamoto, F Ebina, H Nakazawa, C Nakatsuka *Bull. Chem. Soc. Jpn.* **52** 1857 (1979)
184. N G Zabirov, V N Solov'ev, F M Shamsevaleev, R A Cherkasov, I V Martynov *Zh. Obshch. Khim.* **61** 1748 (1991) [d]
185. A L Kon'kin, V G Shtyrlin, N G Zabirov, I A Litvinov, A T Gubaidullin, R R Garipov, A V Aganov, A V Zakharov *Phosphorus Sulfur Silicon Relat. Elem.* **147** 449 (1999)
186. L G Shaidarova, A V Gedmina, N A Ulakhovich, G K Budnikov, N G Zabirov *Zh. Obshch. Khim.* **72** 1662 (2002) [d]
187. V N Solov'ev, A N Chekhlov, N G Zabirov, I V Martynov *Dokl. Akad. Nauk* **341** 502 (1995) [g]
188. C Pettinari, A Drozdov, F Marchetti, in *Comprehensive Coordination Chemistry II* Vol. 1 (Eds J A McCleverty, T J Mayer) (Oxford: Elsevier, 2003) p. 97
189. G L Abbati, M C Aragoni, M Arca, F A Devillanova, A C Fabretti, A Garau, F Isaia, V Lippolis, G Verani *J. Chem. Soc., Dalton Trans.* 1515 (2003)
190. D Cupertino, D J Birdsall, A M Z Slawin, J D Woollins *Inorg. Chim. Acta* **290** 1 (1999)
191. P Bhattacharyya, A M Z Slawin, M B Smith *J. Chem. Soc., Dalton Trans.* 2467 (1998)
192. A M Z Slawin, M B Smith, J D Woollins *J. Chem. Soc., Dalton Trans.* 1537 (1998)
193. A M Z Slawin, M B Smith *New J. Chem.* **23** 777 (1999)
194. G L Abbati, M C Aragoni, M Arca, F A Devillanova, A C Fabretti, A Garau, F Isaia, V Lippolis, G Verani *J. Chem. Soc., Dalton Trans.* 1105 (2001)
195. C S Browning, D H Farrar, D C Frankel, J J Vittal *Inorg. Chim. Acta* **241** 111 (1996)
196. M Necas, M R S J Foreman, J Marek, J D Woollins, J Novosad *New J. Chem.* **25** 1256 (2001)
197. D J Birdsall, J Novosad, A M Z Slawin, J D Woollins *J. Chem. Soc., Dalton Trans.* 435 (2000)
198. P Sekar, J A Ibers *Inorg. Chem.* **42** 6294 (2003)
199. D J Birdsall, A M Z Slawin, J D Woollins *Inorg. Chem.* **38** 4152 (1999)
200. A D Garnovskii, A L Nivorozhkin, V I Minkin *Coord. Chem. Rev.* **126** 1 (1993)

[a] — *Mendeleev Chem. J. (Engl. Transl.)*
[b] — *Russ. J. Coord. Chem. (Engl. Transl.)*
[c] — *Russ. J. Inorg. Chem. (Engl. Transl.)*
[d] — *Russ. J. Gen. Chem. (Engl. Transl.)*
[e] — *Russ. J. Phys. Chem. (Engl. Transl.)*
[f] — *Russ. J. Org. Chem. (Engl. Transl.)*
[g] — *Dokl. Chem. (Engl. Transl.)*

Russian Chemical Reviews **73** (8) 753 – 770 (2004) © 2004 Russian Academy of Sciences and Turpion Ltd

DOI 10.1070/RC2004v073n08ABEH000898

Phosphate tungsten bronzes

V V Skopenko, V V Lisnyak, N V Stus, N S Slobodyanik

Contents

I.	Introduction	753
II.	Methods of synthesis	753
III.	Crystal structure	757
IV.	Electronic structure	764
V.	Electrophysical properties	766
VI.	Conclusion	767

Abstract. Theoretical and experimental data on the synthesis, structure, properties and applications of phosphate tungsten bronzes accumulated to date are systematised. Attention is focussed on interrelations between structural features and electrophysical properties of these compounds. Prospects for practical applications of phosphate tungsten bronzes are discussed. The bibliography includes 138 references.

I. Introduction

Recently, interest in macroscopic quantum phenomena such as superconductivity and laser effect has grown rapidly. Research into and application of these phenomena introduces fundamental concepts of quantum mechanics into everyday life.[1,2] Intensive studies of oxide bronzes (low-dimensional metallic conductors) have been carried out in the last ten to fifteen years. This is, in particular, due to the fact that these compounds possess macroscopic quantum properties, *e.g.*, electronic instabilities responsible for initiation of spin density waves (SDW) and charge density waves (CDW).[3–8]

The term 'oxide bronzes' was introduced by Friedrich Wohler in 1824 to name a series of oxide compounds of tungsten. Currently, the term is used for crystalline compounds of general formula M_xEO_n, where M is usually an alkali metal and E is a transition metal. Characteristic of the oxide bronzes are intense colour and metallic luster. These compounds can possess metallic or semiconducting properties. Usually, bronzes retain the structure of the starting oxide EO_2 or EO_3 when the element E can be in an oxidation state of less than 4 or less than 6, respectively, and are characterised by certain homogeneity regions.[9] Electrons of the dopant cations inserted into the starting oxide can be delocalised over the entire structure, thus being responsible for the onset of metallic-type conductivity. The semiconducting properties are due to the interaction of polyvalent metal ions through bridging oxygen atoms.

Oxide bronzes can exhibit high anisotropy (low dimensionality) of electronic conductivity owing to peculiarities of their crystal and electronic structures. For quasi-one-dimensional compounds the conductivity along a particular crystallographic direction is several orders of magnitude higher than along two other directions while for quasi-two-dimensional compounds the conductivities along two particular crystallographic directions are several orders of magnitude higher than the conductivity along the third direction. The crystal structures of the oxide bronzes represent three-dimensional frameworks; because of this, the dimensionality of electronic conductivity can be lower than the dimensionality determined from crystallographic data.

Many transition metal oxides (among them, superconducting copper oxides are best known) possess low-dimensional properties. This also holds for both molybdenum and tungsten oxide bronzes which undergo transitions to the CDW state.[10,11] Minor variations of thermodynamic parameters (temperature, pressure, chemical potential, *etc.*) can cause significant changes in the physical properties of compounds. Because of this 'thermodynamic susceptibility' these inorganic materials can serve as model objects in studies of various instabilities.

The available models for mechanisms of the onset of CDW are inadequate. Therefore, systematic studies are carried out of CDW in compounds which exhibit low-dimensional electrophysical properties but have different compositions and structures. Among the widely used model objects are the phosphate tungsten bronzes containing perovskite-type layers built of ReO_3-type corner-sharing WO_6 octahedra separated by layers comprised of monophosphate groups or diphosphate units. Redistribution of the electron density between the phosphate groups and the layers of WO_6 octahedra in the phosphate tungsten bronzes gives rise to a partially filled conduction band composed of hybridised p- and d-AOs. These structural features are also responsible for the metallic conductivity of bronzes and for two kinds of electronic instabilities, namely, Peierls transitions leading to the CDW state [12–18] and the superconducting state instabilities.[18,19]

II. Methods of synthesis

At present, three main groups of the phosphate tungsten bronzes are known. These are the monophosphate tungsten bronzes (MPTBs) of general formula $A_x(PO_2)_4(WO_3)_{2m}$ with pentagonal (MPTBp) [20–23] or hexagonal (MPTBh) [24,25] structural channels and the diphosphate tungsten bronzes (DPTBs) of general for-

V V Skopenko, V V Lisnyak, N V Stus, N S Slobodyanik Department of Chemistry, Kyiv National Taras Shevchenko University, ul. Vladimirskaya 64, 01033 Kyiv, Ukraine. Fax (38-044) 239 32 20. Tel. (38-044) 220 86 91, (38-044) 239 32 20 (V V Skopenko). Tel. (38-067) 977 95 62. E-mail: lisnyak@chem.univ.kiev.ua (V V Lisnyak). Tel. (38-044) 239 33 14. E-mail: stus@chem.univ.kiev.ua (N V Stus). Tel. (38-044) 234 51 85 (N S Slobodyanik)

Received 14 January 2004
Uspekhi Khimii **73** (8) 814 – 832 (2004); translated by A M Raevskiy

mula $A_x(P_2O_4)_2(WO_3)_{2m}$ (A is a vacancy or a monovalent or divalent cation) with hexagonal channels (DPTBh).[26, 27] Studies on phase formation in the systems $P_2O_5-WO_3-W$ and $A_2O-P_2O_5-WO_3-W$ began in the 1980s in connection with the search for new functional materials for semiconductor electronics.[28–34]

It should be noted that the phosphate tungsten bronzes are prone to form the intergrowth phases. This trend becomes more pronounced as the parameter m increases. Therefore, the MPTBp compounds with $m > 14$, MPTBh compounds with $m > 7$ and DPTBs with $m > 10$ have not been synthesised as regular single crystals.

1. Synthesis of polycrystals

Polycrystalline powders and small single crystals of a number of the phosphate tungsten bronzes were first obtained by solid-state reactions starting from tungsten trioxide, acid ammonium orthophosphates of different degree of substitution and metallic tungsten taken in the stoichiometric ratio. Here, choosing an optimum regime of synthesis of compounds of specified compositions is a challenge. Usually, the interaction of reagents involves two stages, (1) melting of tungsten trioxide with ammonium orthophosphate monohydrate in the temperature range 573–890 K for 24–48 h[20, 22, 24, 27] to form some intermediate ammonium-containing compounds and low-melting glasses[35] and (2) interaction of the product obtained with fine-grained tungsten powder at temperatures 1000–1473 K in inert atmosphere (evacuated ampoules) over a period of several weeks. In most cases the starting components are taken in a ratio that provides the desired stoichiometry of the reaction product. This technique permits the synthesis of powders and small crystals of good quality, which are often used for growth of single crystals.[36, 37]

Reduction by transition metals (in particular, tungsten) in multicomponent oxide systems is a nonequilibrium process. This leads to coexistence of the regions suitable for crystallisation of individual compounds and broad heterogeneous-heterophase regions in which co-crystallisation of several phases occurs in narrow temperature and concentration ranges.[25, 38, 39] The compositions of the compounds formed in multicomponent oxide systems strongly depend on the synthesis conditions, *i.e.*, the ratio of the starting reagents, their dispersion, temperature, presence of temperature gradients, duration of the reaction and on the presence of modifiers.

Unfortunately, no optimised general methods of preparation of polycrystalline phosphate tungsten bronzes are available as yet. It should be noticed that often crystallisation of compounds differing in composition and structure occurs under identical experimental conditions.

2. Growth of single crystals

One of the most widely used methods of growth of single crystals of the phosphate tungsten bronzes involves the use of various transport reactions (in the presence of temperature gradients) in the temperature range from 850 to 1473 K. Using this technique, it is possible to grow high-quality single crystals with typical dimensions $(1-3)\times(0.6-3)\times(0.1-0.75)$ mm over a period of one to three weeks.[40, 41] Here, the role of the transporting agents can be played by iodine, phosphorus pentaoxide and by the ammonium and some alkali metal iodides, bromides or chlorides. The method was optimised to obtain the following members of the MPTBp family: $(PO_2)_4(WO_3)_4$, $(PO_2)_4(WO_3)_8$ and $(PO_2)_4(WO_3)_{12}$.[42–44]

The possibility of control of chemical transport reactions using methods of chemical thermodynamics[45] (in particular, using the CVTRANS program package[46]) make this single-crystal growth technique attractive for both laboratory and large-scale applications.

Flux growth of crystals of phosphate tungsten bronzes using low-melting phosphate–tungsten and phosphate–tungstate–molybdate systems[38] and complex fluxes containing a glass-forming component (*e.g.*, SiO_2 and GeO_2[21, 38, 47, 48]) was found to be less promising owing to uncontrollable inclusion of impurities that deteriorate the electrophysical properties of materials.

At present, there are many methods of synthesis of polycrystals and single crystals of MPTBp compounds which crystallise in the form of plane-parallel plates with high reflectivity. Tables 1 and 2 list the synthesis conditions and characteristics of a number of MPTBp crystals.[49–55]

Table 1. Synthesis conditions and characteristics of $(PO_2)_4(WO_3)_{2m}$ crystals with $m = 2$ and 4.

m	Starting components	Synthesis conditions	Crystal colour, habit, size /mm	Ref.
Conditions for solid-phase synthesis of polycrystals				
2	$WOP_2O_7 + W$ (1 : 2)	1573 K	blue plates	49
4	$(NH_4)_2HPO_4 + WO_3 + W$ (see [a])	873 K, 1223 K (48 h), 1273 K	purple plates	50, 51
4	$(NH_4)_2HPO_4 + WO_3 + W$ (see [a])	1173 K, 1250 K	red plates	22
Conditions for synthesis of single crystals				
2	$P_2O_5 + W + WO_3$ (see [a])	heating of furnace from 873 to 1473 (1523) K for 6 h, storage for four days	dark brown plates, $2\times0.75\times0.2$	52
2	$P + WO_3$ (see [a, b])	1273–1173 K	maroon	43
2	$P_2O_5 + W + WO_3 + SiO_2$ (5 : 3 : 3 : 2)	1523 K (two or three days), 1373 K	maroon plates, $0.12\times0.09\times0.05$	21, 38
4	$(NH_4)_2HPO_4 + WO_3 + W$ (see [a])	heating from 873 to 1273 K at a rate of 200 K h^{-1}, two-zone furnace 1473/1273 K (a week), cooling down to 298 K	purple plates, $3\times3\times0.2$	50, 51
4	$(NH_4)_2HPO_4 + WO_3 + Tl_2CO_3 +$ + W (see [c])	573 (24 h), two-zone furnace, 1343 K (hot zone), $\Delta T = 130$ K (see [d])	purple plates, $1.5\times0.6\times0.3$	52

Note. Here and in Tables 2, 3 in the column 'Synthesis conditions' we present the parameters of the heat treatment regimes, *viz.*, temperatures and durations of corresponding stages (in parentheses). At the first temperature (often, the time of stay at this temperature is not reported in the original studies), the mixtures of the metal trioxide and metal phosphate (in some cases) and metal carbonate (in other cases) were initially heated. At the second temperature, metallic tungsten was added and the system was kept until complete interaction between the metal and other components. At the third temperature, particular bronzes were synthesised (cooling is accompanied by bronze crystallisation).

[a] The starting reagent ratio was calculated with respect to the stoichiometry of the reaction product. [b] Obtained with 0.5 mol.% I_2 as transporting agent. [c] Calculated with respect to the stoichiometry of the compound $TlP_4W_4O_{20}$; obtained with 5 mol.% KI as transporting agent. [d] ΔT is the temperature difference between the hot and cold zones.

Table 2. Synthesis conditions and characteristics of $(PO_2)_4(WO_3)_{2m}$ crystals with $m > 4$.

m	Starting components	Synthesis conditions	Crystal colour, habit, size /mm	Ref.
Conditions for solid-phase synthesis of polycrystals				
5	$(NH_4)_2HPO_4 + WO_3 + W$ (calculated with respect to the stoichiometry of the compound $P_4W_8O_{32}$)	873 K, 1223 K (48 h), 1273 K, cooling down to 300 K	blue-purple	50
5 4 + 6	$(NH_4)_2HPO_4 + WO_3 + W$ (calculated with respect to the stoichiometry of the compound $P_4W_{10}O_{38}$)	673 K, 1373 K (seven days)	dark blue 0.006 mm thick	53, 54
6	$(NH_4)_2HPO_4 + WO_3 + W$ (see [a])	873 K, 1173 K (few days)	prismatic	20
6	$(NH_4)_2HPO_4 + WO_3 + W$ (see [a])	923 K, 1273 K (four days), cooling at a rate 0.6 K h^{-1} down to 500 K	dark blue plates, $5.26 \times 3.1 \times 1.42$	38
7	$(NH_4)_2HPO_4 + WO_3 + W$ (calculated with respect to the stoichiometry of the compound $P_4W_{14}O_{50}$)	873 K (10 h), heating with a 100 K increment, two-zone furnace, 1473/1273 K (a week), cooling down to 600 K	dark blue plates	28
8	$(NH_4)_2HPO_4 + WO_3 + W$ (see [a])	873 K, 1173 K (few days)	purple-red plates	20
10	$(NH_4)_2HPO_4 + WO_3 + W$ (see [a])	873 K (12 h), 1273 K (48 h)	black plates, $1.5 \times 0.5 \times 0.3$	55
12	$(NH_4)_2HPO_4 + WO_3 + W$ (see [a])	873 K (12 h), 1273 K (48 h)	blue plates, $0.125 \times 0.07 \times 0.003$	51
Conditions for synthesis of single crystals				
5	$(PO_2)_4(WO_3)_8$ (see [b])	heating from 873 to 1273 K at a rate of 200 K h^{-1}, two-zone furnace, 1473/1273 K (a week), cooling down to 298 K	blue-purple plates with golden edges, $3 \times 3 \times 0.2$	50
7	$(PO_2)_4(WO_3)_{12}$ (see [b])	873 K (10 h), 873 K, two-zone furnace, 1473/1273 K (a week), cooling down to 600 K	purple plates, $0.69 \times 0.15 \times 0.075$	54
10	$(PO_2)_4(WO_3)_{20}$ (see [b])	two-zone furnace, 1473/1273 K (two weeks), $\nabla T = 10$ K cm^{-1} (see [c]), cooling down to 600 K	black plates, $1.5 \times 0.5 \times 0.3$	55
12	$(PO_2)_4(WO_3)_{24}$ (see [b])	two-zone furnace, 1473/1273 K (two weeks), $\nabla T = 10$ K cm^{-1} (see [c])	blue plates, $0.125 \times 0.07 \times 0.003$	51

[a] The ratio of the starting reagents was calculated with respect to the stoichiometry of the reaction product. [b] Recrystallisation from a mixture of compounds obtained by solid-phase synthesis. [c] ∇T is the temperature gradient.

3. Peculiar features of the synthesis of compounds $A_x(PO_2)_4(WO_3)_{2m}$ and $A_x(P_2O_4)_2(WO_3)_{2m}$

One of the most widely used methods of synthesis of compounds of the families $A_x(P_2O_4)_2(WO_3)_{2m}$ and $A_x(PO_2)_4(WO_3)_{2m}$ (Tables 3 and 4) is melting of stoichiometric mixtures of ammonium orthophosphates and tungsten trioxide (if A is a vacancy) and metal carbonates (if A is a monovalent or divalent metal) followed by interaction of the glass obtained with metallic tungsten in inert atmosphere.

The use of the flux technique to obtain these compounds has some peculiar features because the glass formation region is limited and the reaction is carried out at the liquid–metal interface. It should be noted that high reactivity of melts towards the crucible materials at $1153 \leqslant T \leqslant 1270$ K causes enrichment of the system with silicates or aluminates. Therefore, the synthesis of pure phases and studies on phase formation in the systems in question become much more complicated. The phase diagrams of pseudoquaternary systems were constructed only for a few isothermal sections in narrow concentration ranges, *viz.*, $KWO_3-WO_3-PWO_5$,[25] $Li_xWO_3-WO_3-PWO_5$,[38] $Na_xWO_3-WO_3-PWO_5$,[38] $K_4P_8W_4O_{32}-P_8W_4O_{32}-Na_4P_8W_4O_{32}$ and $K_4P_4W_{12}O_{44}-P_4W_{12}O_{44}-Na_4P_4W_{12}O_{44}$.[40, 68] The phase diagrams of the two last-mentioned systems exhibit broad multiphase regions, which casts some doubt upon their correctness.

In addition to the classical method of synthesis (see above) there is a variety of methods based on the chemical or electrochemical intercalation of cations into the MPTBp or MPTB frameworks containing cations in the structural channels. A number of sodium- and lithium-containing derivatives were obtained using the redox reactions with such organometallic reducing agents as LiC_4H_9 and $NaC_{10}H_8$.[28] In this case filling of the perovskite-type cavities in the bronze structure by cations occurs in contrast to the high-temperature methods of synthesis. Using the simplest electrochemical cells, $(+)|A|AClO_4Y|[(PO_2)_4(WO_3)_{2m}/A_x(PO_2)_4(WO_3)_{2m}]|(-)$ (A = Li, Na; Y = propylene carbonate), it is possible to control the synthesis of materials with different degrees of filling of structural channels with cations and to perform ion exchange by simple charge–discharge cycles.[28] Intercalation of cations to obtain compounds of the $A_x(P_2O_4)_2(WO_3)_{2m}$ family can also be achieved *via* chemical vapour transport reactions. For instance, the $A_x(PO_2)_4(WO_3)_8$ crystals were synthesised by reactions of the Group Ia element or Tl(I) iodides with $(PO_2)_4(WO_3)_{2m}$.[69]

4. Peculiarities of phase formation in the systems containing inserted polyvalent metal cations

Recently, numerous studies aimed at obtaining phosphate tungsten bronzes modified by homovalent and heterovalent substitution have been carried out. The compositions and crystallographic parameters of a number of compounds obtained are listed in Table 5.

At present, the absence of the phosphate molybdenum bronzes similar in structure and properties to the phosphate tungsten bronzes is a paradox with no explanation, though mixed molybdenum–phosphate bronzes are known.

The use of molybdenum as the reducing agent in mixed nitrate–phosphate systems leads to formation of low-melting fluxes and to shift of the heat treatment regimes towards lower

Table 3. Synthesis conditions and characteristics of crystals $A_x(PO_2)_4(WO_3)_{2m}$ and $A_x(P_2O_4)_2(WO_3)_{2m}$ obtained by solid-phase synthesis [melting of the components $A_2CO_3 + (NH_4)_2HPO_4 + W + WO_3$ (A = Na, K, Rb, Cs) and $BaCO_3 + (NH_4)_2HPO_4 + W + WO_3$ taken in the stoichiometric ratios].

Composition	Starting components	Synthesis conditions	Crystal colour, habit, size /μm	Ref.
Conditions for solid-phase synthesis of polycrystals				
$Na_{1.4}(PO_2)_4(WO_3)_8$	$Na_2CO_3 + (NH_4)_2HPO_4 + W + WO_3$	773 K, 1173 K (three days)	light-brown with copper reflection needles, $30 \times 48 \times 456$	56
$Na_{2.2}(PO_2)_4(WO_3)_{12}$	$Na_2CO_3 + (NH_4)_2HPO_4 + W + WO_3$	773 K, 1173 K (three days)	purple needles, $48 \times 60 \times 380$	56
$Na_2(PO_2)_4(WO_3)_{2m}$ ($4 \leqslant m \leqslant 13$) and $Na_3(PO_2)_4(WO_3)_{14}$	$Na_2CO_3 + (NH_4)_2HPO_4 + W + WO_3$	873 K, 1273 K (few days)	–	57
$K_x(PO_2)_4(WO_3)_8$ ($0.75 \leqslant x \leqslant 2$)	$K_2CO_3 + (NH_4)_2HPO_4 + W + WO_3$	873 K (12 h), 1223 K (48 h), cooling down to 298 K	purple needles	58
$K_x(PO_2)_4(WO_3)_{12}$ ($1 \leqslant x \leqslant 2$)	$K_2CO_3 + (NH_4)_2HPO_4 + W + WO_3$	873 K (12 h), 1223 K (48 h), cooling down to 298 K	dark purple rods, $60 \times 30 \times 10$	41
$K_x(P_2O_4)_2(WO_3)_{20}$ ($x \leqslant 0.25$)	$K_2CO_3 + (NH_4)_2HPO_4 + W + WO_3$	1173 K, 1373 K (ten to fifteen days), cooling for two days down to 300 K	dark blue plates, $14 \times 90 \times 262$	59
$K(P_2O_4)_2(WO_3)_{2m}$ ($5 \leqslant m \leqslant 10$)	$K_2CO_3 + (NH_4)_2HPO_4 + W + WO_3$	873 K, 1373 K (fifteen days)	dark blue and black	6
$K_x(P_2O_4)_2(WO_3)_{2m}$ ($4 \leqslant m \leqslant 10$, $x = 2$) ($2 \leqslant m \leqslant 20$, $1.5 \leqslant x \leqslant 4$)	$K_2CO_3 + (NH_4)_2HPO_4 + W + WO_3$	823 K, 1173 – 1473 K (four to eight days)	the same	60
$Rb(P_2O_4)_2(WO_3)_{2m}$ ($4 \leqslant m \leqslant 10$)	$Rb_2CO_3 + (NH_4)_2HPO_4 + W + WO_3$	873 K, 1373 K (fifteen days)	"	60
$Rb_{1.6}(P_2O_4)_2(WO_3)_6$	$Rb_2CO_3 + (NH_4)_2HPO_4 + W + WO_3$	900 K, 1230 K (eight days)	needles, $10 \times 76 \times 144$	61
$Rb_{0.44}(P_2O_4)_2(WO_3)_{14}$	$Rb_2CO_3 + (NH_4)_2HPO_4 + W + WO_3$	900 K, 1270 K (a week)	plates, $120 \times 18 \times 96$	62
$Rb_x(P_2O_4)_2(WO_3)_{16}$ ($1.6 \leqslant x \leqslant 2$)	$Rb_2CO_3 + (NH_4)_2HPO_4 + W + WO_3$	1173 K	plates, $18 \times 75 \times 280$	48
$Cs(P_2O_4)_2(WO_3)_4$	$Cs_2CO_3 + (NH_4)_2HPO_4 + W + WO_3$	1173 K, 1230 K (15 h)	maroon needles, $28 \times 40 \times 144$	63
$Ba(P_2O_4)_2(WO_3)_{16}$	$BaCO_3 + (NH_4)_2HPO_4 + W + WO_3$	873 K, 1473 K (48 h)	plates, $120 \times 18 \times 96$	27
$Ba(P_2O_4)_2(WO_3)_{2m}$ ($m = 6-10$)	$BaCO_3 + (NH_4)_2HPO_4 + W + WO_3$	(1173 – 1473), (six to twenty-one days), cooling down to 300 K	–	64
Conditions for synthesis of single crystals				
$K_x(PO_2)_4(WO_3)_8$ ($0.75 \leqslant x \leqslant 2$)	$K_x(PO_2)_4(WO_3)_8$ ($0.75 \leqslant x \leqslant 2$)	two-zone furnace, 1473 K/1273 K (a week), cooling down to 298 K (see [a])	purple plates, $60 \times 30 \times 10$	58
$K_x(PO_2)_4(WO_3)_8$ ($0.86 \leqslant x \leqslant 1.94$)	$K_x(PO_2)_4(WO_3)_8$ ($0.86 \leqslant x \leqslant 1.94$)	two-zone furnace, 1473 K/1273 K, (a week), cooling down to 298 K (see [a])	copper-coloured needles, $100 \times 20 \times 4$	8, 16
$K_x(PO_2)_4(WO_3)_{12}$	$K_x(PO_2)_4(WO_3)_{12}$	two-zone furnace, 1473 K/1273 K (a week), cooling down to 298 K (see [a])	purple plates, $60 \times 30 \times 10$	41
$Cs(P_2O_4)_2(WO_3)_4$	$Cs_2CO_3 + (NH_4)_2HPO_4 + W + WO_3$	923 K (see [b]), 1223 K (two weeks), cooling at a rate of 3 K h^{-1}	golden plates, $15 \times 20 \times 30$	65

[a] Stepwise cooling of the system (five steps of 200 K each). [b] Gas transport reaction with 5 mol.% KBr.

temperatures (673 – 873 K). It should be noted that the phase crystallisation processes in the $A_2CO_3 - H(NH_4)_2PO_4 - WO_3(MoO_3)$ systems and the structure of the resulting are strongly dependent on the composition, structure and physicochemical features (namely, differences between the thermochemical properties of the starting oxides and the melts formed, the type of short-range order in melts and the size of clusters comprised of the MO_6 octahedra) of the glasses formed in these systems.[71–77] Usually, the use of complex systems leads to the formation of compounds with mixed frameworks that differ from the frameworks of the phosphate tungsten bronzes.[70–77]

For instance, a $Na_{1+x}(Mo_{0.15}W_{1.85})O_5(PO_4)$ phase was crystallised in the system $Na_2CO_3 - H(NH_4)_2PO_4 - WO_3 - Mo$ in the temperature interval 673 – 903 K.[74] The framework of this phase is comprised of infinite ribbons analogous to those observed in the monophosphate tungsten bronzes $(PO_2)_4(WO_3)_8$ (see Ref. 50) and

Table 4. Existence regions of the compounds $A_x(PO_2)_4(MO_3)_{2m}$ and $A_x(P_2O_4)_2(MO_3)_{2m}$ (A is a monovalent or divalent cation or a vacancy; M = W, Mo).

System	Composition	Ref.
$MoO_3-(NH_4)_2HPO_4-WO_3-W$	$(PO_4)_2(W_{1-x}Mo_xO_3)_6$ ($0 \leqslant x < 0.26$),	66
$Li_2CO_3-(NH_4)_2HPO_4-WO_3-W$	$Li_x(P_2O_4)_2(WO_3)_6$ ($x \leqslant 0.167$),	66
$Na_2CO_3-(NH_4)_2HPO_4-WO_3-W$	$Na_2(PO_2)_4(WO_3)_{2m}$ ($4 \leqslant m \leqslant 10$), $Na_3(PO_2)_4(WO_3)_{14}$, $Na_2(PO_2)_4(WO_3)_{2m}$ ($m \leqslant 13$)	27, 56, 57
	$Na_x(PO_2)_4(WO_3)_{2m}$ ($2 \leqslant m \leqslant 20$; $1.1 \leqslant x \leqslant 4$, $m = 4$); $Na_x(PO_2)_4(WO_3)_{12}$ ($1.1 \leqslant x \leqslant 4$), pure phases $Na_x(PO_2)_4(WO_3)_{2m}$ ($m \leqslant 13$, $m \neq 5$)	57
	$Na_x(P_2O_4)_2(WO_3)_6$ ($x \leqslant 0.22$)	66
	$Na_x(PO_2)_4(WO_3)_8$ ($1.1 \leqslant x \leqslant 1.5$, 2), $Na_x(PO_2)_4(WO_3)_{12}$ ($1.6 \leqslant x \leqslant 4$),	57
$K_2CO_3-(NH_4)_2HPO_4-WO_3-W$	$K_x(P_2O_4)_2(WO_3)_{20}$ ($x \leqslant 0.25$)	26
	$K(P_2O_4)_2(WO_3)_{2m}$ ($5 \leqslant m \leqslant 10$)	60
	$K_2(P_2O_4)_2(WO_3)_{2m}$ ($2 \leqslant m \leqslant 20$); $K_x(P_2O_4)_2(WO_3)_{2m}$ ($x > 1$, MPTBh; $x \leqslant 1$, DPTBh); compounds formed in the system K–W–P–O are as follows: MPTBp ($x = 0$), DPTBp ($x = 1$), MPTBh ($x = 2$); $1.75 \leqslant x \leqslant 3$, $m = 4-10$, $m \neq 5$; mixtures of the compounds with $m = 9$ and 10; mixtures of the MPTBh compounds and K_xWO_3 ($x = 3$, $m \leqslant 10$); mixtures of the compounds WO_3, K_xWO_3 and DPTBh ($x = 3$, $m > 10$)	60
$Rb_2CO_3-(NH_4)_2HPO_4-WO_3-W$	$Rb(P_2O_4)_2(WO_3)_{2m}$ ($4 \leqslant m \leqslant 10$)	60
	$Rb_{1.6}(P_2O_4)_2(WO_3)_6$	61
	$Rb_{0.44}(P_2O_4)_2(WO_3)_{14}$	62
	$Rb_x(P_2O_4)_2(WO_3)_{16}$ ($1.6 \leqslant x \leqslant 2$)	48
$BaCO_3-(NH_4)_2HPO_4-WO_3-W$	$Ba_x(PO_2)_4(WO_3)_{2m}$ ($6 \leqslant m \leqslant 10$; $m = 11-17$)	27
	$Ba(P_2O_4)_2(WO_3)_{2m}$ ($m = 6-10$)	64
$Cs_2CO_3-(NH_4)_2HPO_4-WO_3-W$	$Cs(P_2O_4)_2(WO_3)_4$	63, 65
	$Cs_{1-x}(P_2O_4)_2(WO_3)_4$ ($0 \leqslant x \leqslant 0.46$)	67
$Cs_2CO_3-Rb_2CO_3-(NH_4)_2HPO_4-WO_3-W$	$Cs_xRb_y(P_2O_4)_2(WO_3)_4$ ($0.72 \leqslant x \leqslant 0.97$, $0.16 \leqslant y \leqslant 0.33$)	67
$Cs_2CO_3-Na_2CO_3-(NH_4)_2HPO_4-WO_3-W$	$Cs_{0.89}Na_{0.17}(P_2O_4)_2(WO_3)_4$	67
$Cs_2CO_3-MoO_3-(NH_4)_2HPO_4-WO_3-W$	$Cs(P_2O_4)_2(W_{1-x}MO_xO_3)_4$ ($0. \leqslant x \leqslant 0.26$)	67
$PbCO_3-(NH_4)_2HPO_4-WO_3-W$	$Pb_x(PO_2)_4(WO_3)_{2m}$ [$6 \leqslant m \leqslant 10$; $x = 0.66$ ($m = 7$)]	7

Table 5. Systems studied and crystallographic characteristics of the phases obtained.

System	Composition	Space group	Unit cell parameters [a]					Ref.
			a /Å	b /Å	c /Å	β /deg	Z	
$CsNO_3-(NH_4)_2HPO_4-WO_3-W-V_2O_5$	$Cs_5VW_4O_9VO_4(PO_4)_4$	$Cmc2_1$	14.948	20.008	9.942	–	4	70
$RbNO_3-(NH_4)_2HPO_4-WO_3-Mo-MoO_3$	$Rb_2Mo_2WO_5(PO_4)_3$	$P2_1/n$	10.756	9.493	15.478	108.99	4	71
$K_2CO_3-(NH_4)_2HPO_4-WO_3-Mo-MoO_3$	$K_{6.6}Mo_{2.36}W_{3.64}O_{15}(PO_4)_4$, $K_7Mo_{6-x}W_xP_4O_{31}$ ($2 \leqslant x \leqslant 4$)	$R\bar{3}$	17.545	15.714	–	–	6	72
$Na_2CO_3-(NH_4)_2HPO_4-WO_3-Mo-MoO_3$	$Na_{0.75}(Mo_{0.42}W_{0.58})(Mo_{0.75}W_{0.25})O_3(PO_4)_2$, $Na_xMo_{2-y}W_yP_2O_{11}$ ($0.25 \leqslant x \leqslant 1$, $1.75 \leqslant y \leqslant 0.25$)	$P2_1/m$	7.200	6.369	9.123	106.29	2	73
	$Na_{1.3}(Mo_{0.15}W_{0.15})(W_{1.7})O_5(PO_4)_2$, $Na_2Mo_yW_{2-y}PO_9$ ($0.15 \leqslant y \leqslant 0.75$)	$P2_12_12_1$	4.853	8.516	16.646	–	4	74
$Li_2CO_3-(NH_4)_2HPO_4-WO_3-Mo-MoO_3$	$LiMo_{0.68}W_{1.32}O_3(PO_4)_2$	$C2/m$	8.142	6.361	7.728	102.45	2	75
	$Li_{0.5}MoWO_3(PO_4)_2$	$P2_1/m$	7.735	12.655	8.324	105.97	4	76
	$(Mo_xW_{2-x})O_3(PO_4)_2$ ($0 \leqslant x \leqslant 1.25$)	$P2_1/m$	7.827	12.538	7.833	92.36	2	77

[a] Data of single-crystal X-ray diffraction studies.

$A_x(PO_2)_4(WO_3)_8$ (see Ref. 56) but the fashion in which the ribbons are connected by PO_4 tetrahedra and the shape of channels where the sodium atoms reside are different. One metal position in the MO_6 octahedra is occupied by tungsten atoms only while the other is occupied by the statistically disordered molybdenum and tungsten atoms.[74] The framework of the compound $K_{6.6}Mo_{2.36}W_{3.64}O_{15}(PO_4)_4$ is built of $[MO_5]_\infty$ (M = W, Mo) spiral chains with alternating *cis*- and *trans*-bonds M–O–M. The chains are connected through PO_4 tetrahedra.[72]

Most mixed molybdenum–tungsten phosphates contain isolated MO_6 octahedra or M_2O_{11} bioctahedra. These are, *e.g.*, compounds $Cs_5VW_4O_9VO_4(PO_4)_4$,[70] $Rb_2Mo_2WO_5(PO_4)_3$,[71] $Na_{0.75}(Mo_{0.42}W_{0.58})(Mo_{0.75}W_{0.25})O_3(PO_4)_2$ (Ref. 73) and $Li_{0.5}MoWO_3(PO_4)_2$.[75,76]

In contrast to molybdenum, niobium does form the niobium phosphate bronzes. This permits the synthesis of mixed bronzes $(Nb_{0.787}W_{0.213})_4O_4(PO_4)_4$ (see Ref. 78) and $K_{3.75}Nb_{8.5-x}.W_xO_{14}(PO_4)_4$.[79] At the same time, compounds of the family $A_x(NbW)_5O_9(PO_4)_3$ (A = Li, K, Rb and Cs)[80] obtained in the systems $A_2CO_3-H(NH_4)_2PO_4-WO_3-W-Nb_2O_5$ contain distorted perovskite-type layers in which some WO_6 octahedra are replaced by PO_4 tetrahedra.

III. Crystal structure

Unlike the oxide tungsten bronzes A_xWO_3 (A = Li, Na, K, Rb, Cs) (Fig. 1 *a–c*) containing three-dimensional frameworks built of WO_6 octahedra, two families of the phosphate tungsten

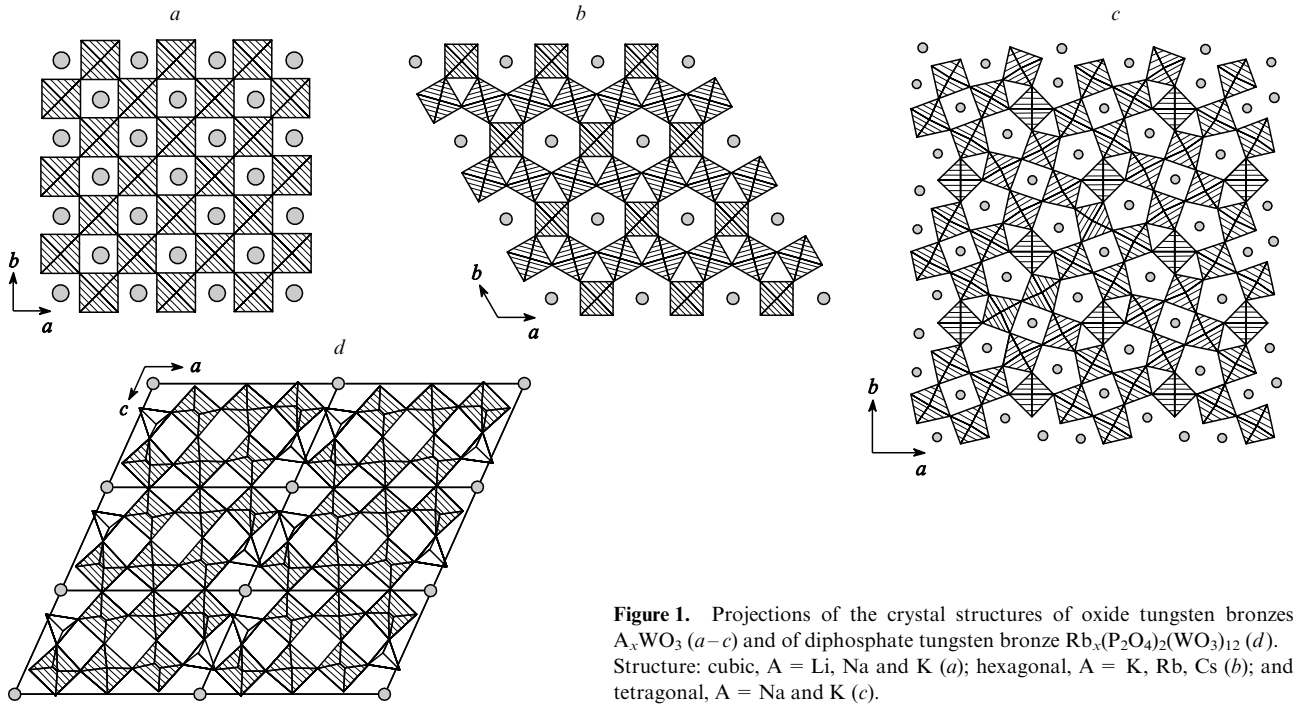

Figure 1. Projections of the crystal structures of oxide tungsten bronzes A_xWO_3 (*a*–*c*) and of diphosphate tungsten bronze $Rb_x(P_2O_4)_2(WO_3)_{12}$ (*d*). Structure: cubic, A = Li, Na and K (*a*); hexagonal, A = K, Rb, Cs (*b*); and tetragonal, A = Na and K (*c*).

bronzes, $A_x(PO_2)_4(WO_3)_{2m}$ and $A_x(P_2O_4)_2(WO_3)_{2m}$ (A is a vacancy or Na, K, Rb, Cs, Pb and Ba), contain chains or layers comprised of WO_6 octahedra connected by phosphate groups (see, *e.g.*, Fig. 1 *d*).

Because of (i) redistribution of the electron density in the mixed framework formed by the WO_6 octahedra and PO_4 tetrahedra and (ii) insertion of additional cations the oxidation state of the tungsten atoms in the phosphate tungsten bronzes usually varies between 5 and 6. Sharing of 4d electrons of the tungsten atoms and their delocalisation over the system of the W–O–W–O bonds lead to quasi-metallic electrophysical properties of the oxide and phosphate tungsten bronzes.[29,30]

The frameworks of the phosphate tungsten bronzes comprise corner-sharing WO_6 octahedra connected in the same manner as in the ReO_3-type cubic oxide tungsten bronzes (Fig. 2). In contrast to the oxide bronzes the perovskite-type blocks built of WO_6 octahedra in the frameworks of the phosphate tungsten bronzes are linked by PO_4 tetrahedra or by diphosphate units, P_2O_7. Depending on the value of the parameter *m*, these blocks can be chains (for the first members of each series with $m = 2$, see Fig. 3) or layers with the thickness increasing with *m*.

The frameworks of both the monophosphate and diphosphate tungsten bronzes containing perovskite-type layers are built based on similar principles. Namely, linear (DPTBs) or zigzag (MPTBs) slabs comprised of corner-sharing WO_6 octahedra are linked together to form infinite ribbons of composition W_mO_{4m+1} and W_mO_{4m+2}, respectively. The ribbons are connected in such a way

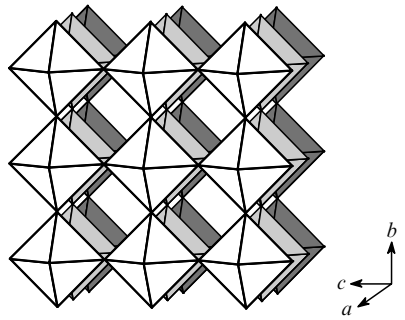

Figure 2. Structure of ReO_3.

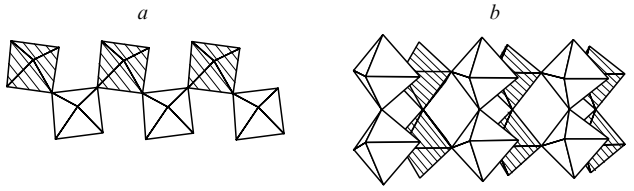

Figure 3. $(WO_5)_\infty$ chains in the structure of $(PO_2)_4(WO_3)_4$ (*a*) and $(WO_4)_\infty$ chains in the structure of $Rb_{0.5}(P_2O_4)_2(WO_3)_4$ (*b*).

that the first tungsten atom of each ribbon is bound to the third tungsten atom of the preceding ribbon through an axial oxygen atom. This results in the formation of perovskite-type layers containing corner-sharing octahedra only (the examples for $m = 4$ are shown in Fig. 4).

Usually, the layer thickness is expressed *via* the length of the linear chains of WO_6 octahedra and running along the directions of the perovskite crystallographic axes directed from the centre of an octahedron towards its vertices. The number of octahedra in two adjacent chains running along the $[001]_{per}$ axis (hereafter the subscript 'per' refers to the perovskite structure) is the same ($m/2$) for the even members of the series or differs by unity ($[(m+1)/2]$ and $[(m-1)/2]$) for the odd ones. The length of a chain of WO_6 octahedra along the $[010]_{per}$ and $[100]_{per}$ crystallographic directions equals *m* for any value of this parameter.

The orientation of the layer of octahedra can be determined with respect to the perovskite crystallographic axes; these layers are parallel to the $(112)_{per}$ plane in MPTBs and to the $(102)_{per}$ plane in DPTBs (see Fig. 4).

The phosphate or diphosphate groups are more strongly bound to one layer of WO_6 octahedra, namely, the PO_4 tetrahedra share three vertices with this layer, being connected to the adjacent layer through one vertice; while P_2O_7 units share four and two vertices, respectively. Therefore, the phosphate groups can be treated as constituents of the layer of octahedra. Different lengths of the bonds between adjacent oxygen atoms in WO_6 octahedra [$d(O-O) \approx 2.7$ Å] and in PO_4 tetrahedra [$d(O-O) \approx 2.5$ Å] lead to distortion of the octahedra linked to the phosphate groups. The structure distortion decreases on going towards the midpoint of the layer of octahedra. The inserted monovalent and divalent

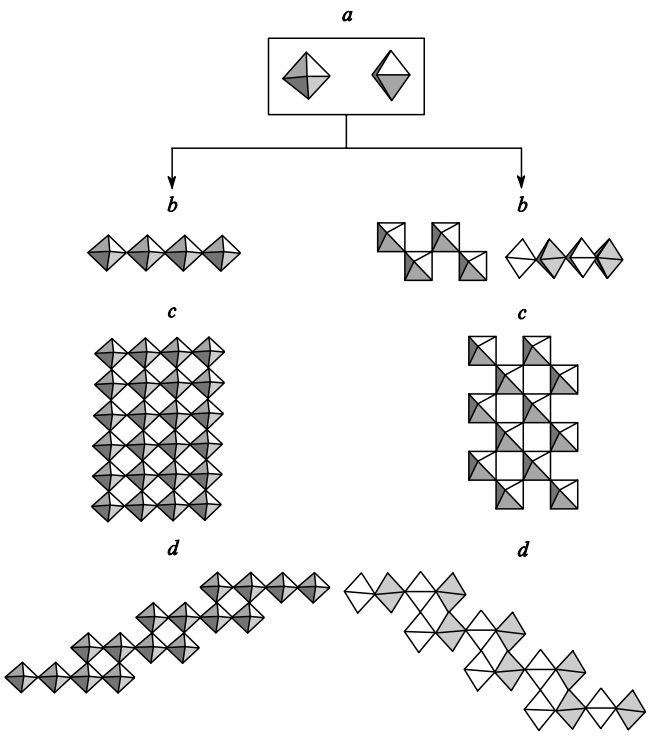

Figure 4. Structures of perovskite-type layers in the DPTB (on the left) and MPTB (on the right) compounds.
Isolated octahedra (*a*); W_4O_{21} blocks (*b*); W_4O_{17} units (on the left) and W_4O_{18} ribbons (on the right) (*c*); and the W_4O_{15} (on the left) and W_4O_{16} (on the right) layers (*d*) built of layers running normal to the plane of this Figure.

metal cations can be located within cavities of the framework which are connected by 'windows' of different shape and size.

Structural phase transitions in the phosphate tungsten bronzes can occur owing to the possibility of small tilts of octahedra in the perovskite-type layers and to ordering of the inserted cations within cavities of the framework.

1. Structural features of monophosphate tungsten bronzes

Two adjacent $W_mO_{4m}(PO_2)_2$ layers in the structure of the monophosphate tungsten bronzes $A_x(PO_2)_4(WO_3)_{2m}$ (A is a vacancy or Na, Ag, K, Pb) can be connected in two ways (see Fig. 5). In the first case, the layers are related by translation; all octahedra in the structure have the same orientation and cavities connected by hexagonal 'windows' are formed at the junction. In the second case, the layers are related by rotation about a twofold axis and cavities connected by pentagonal 'windows' are formed at the junction. Therefore, different (parallel or antiparallel) mutual orientations of layers lead to two families of the monophosphate tungsten bronzes with somewhat incorrect names, *viz*., the MPTBs with hexagonal and pentagonal channels (MPTBh and MPTBp, respectively). The frameworks of the monophosphate tungsten bronzes contain two types of cavities differing in shape and size. Cavities delimited by eighteen oxygen atoms (O_{18}) are surrounded by eight WO_6 octahedra and four PO_4 tetrahedra. The layer of octahedra contains perovskite-type cavities framed by twelve oxygen atoms (O_{12}) and connected by tetragonal 'windows'. All the structural data available at the moment indicate that monovalent or divalent cations be located only in the O_{18} cavities, whereas positions in the O_{12} cavities remain unoccupied.

Both MPTBp and MPTBh are structurally similar to the Magnéli phases containing perovskite-type layers built of MoO_6 octahedra isostructural to the W_4O_{16} layers of the monophosphate tungsten bronzes with $m = 4$. In γ-Mo_4O_{11} and η-Mo_4O_{11}, the layers built of octahedra are linked through MoO_4 tetrahedra similarly to the MPTBp and MPTBh, respectively.

Intercalation of lithium and sodium into different-type phosphate tungsten bronzes was first studied by Wang and Greenblatt [28] who reported the possibility of nearly complete filling of the perovskite cavities. However, these results require confirmation. Unfortunately, no structural studies of the bronzes obtained were performed.

The variety of symmetry types in the case of MPTB structures is due to small tilts of octahedra in the perovskite-type layer. In contrast to the WO_3 structure which permits tilting of the corner-sharing octahedra relative to three perovskite crystallographic axes, only tilting with respect to the $[001]_{per}$ direction is possible for the MPTBs. If the phosphate tungsten bronzes contain inserted cations, small tilts of octahedra in the perovskite-type

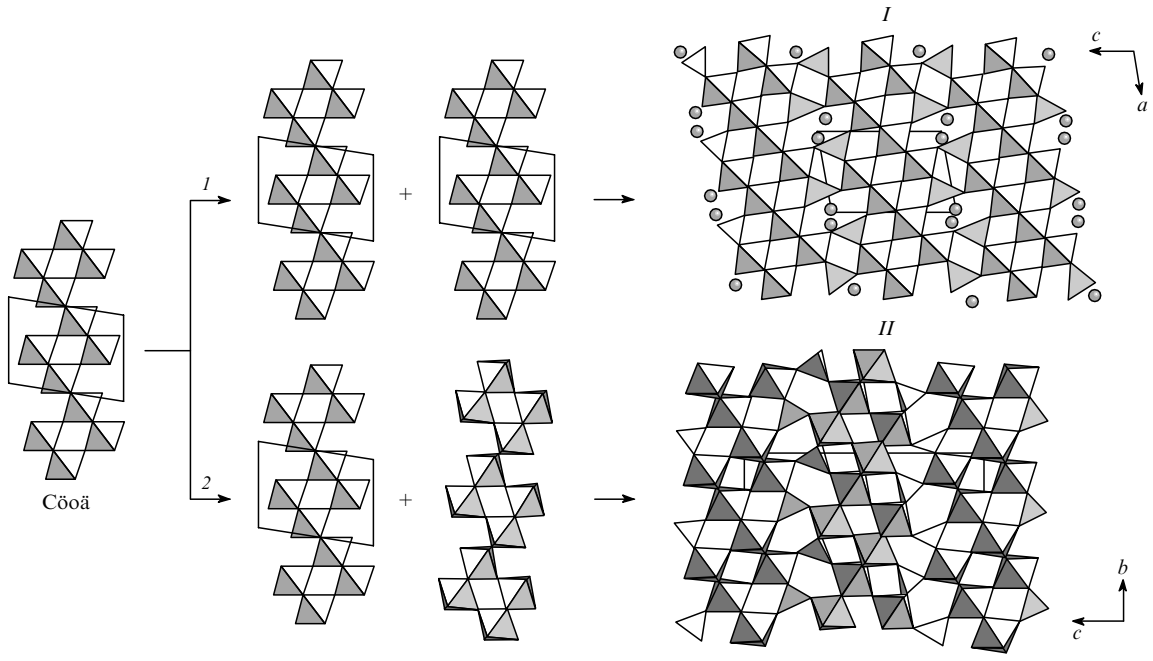

Figure 5. Parallel (*1*) and antiparallel (*2*) orientation of layers in the structures of the MPTBh (*I*) and MPTBp (*II*) compounds with $m = 4$.

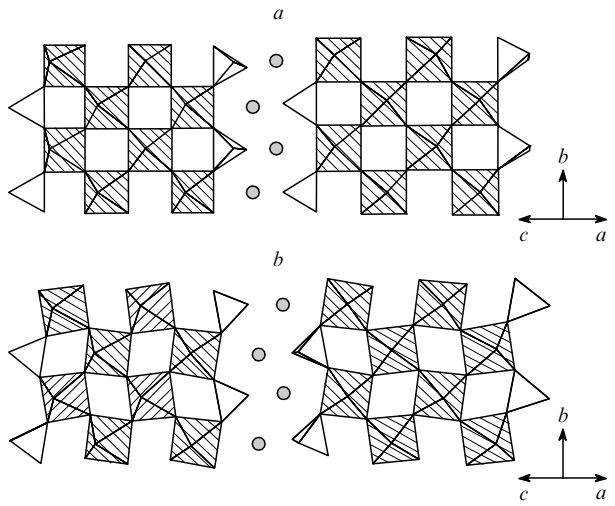

Figure 6. $(PO_2)_2(W_4O_{18})$ chains in the structures of $K_x(PO_2)_4(WO_3)_4$ (*a*) and $Na_x(PO_2)_4(WO_3)_4$ (*b*).

layer cause displacements of the cations located in the cavities and thus changes in the cavity shapes. Among the $A_x(PO_2)_4(WO_3)_{2m}$ bronzes (A = K, Na), small tilts by about 8.5° occur only in the sodium-containing compounds, whereas octahedra in the perovskite-type layer of the potassium-containing MPTBh are untilted (Fig. 6 *a*). In the $Na_x(PO_2)_4(WO_3)_{2m}$ bronze with $x < 4$ all octahedra in the linear chain running along the $[001]_{per}$ direction are rotated in one direction; correspondingly, octahedra in the four adjacent chains are rotated in the opposite direction (Fig. 6 *b*).

2. Monophosphate tungsten bronzes with pentagonal channels

Most of the MPTBp compounds have a general formula $(PO_2)_4(WO_3)_{2m}$. Structural features of this family of bronzes have been studied in most detail. The structure of the MPTBp with $m = 2$ contains the $(WO_5)_\infty$ chains instead of layers. In spite of this two tetrahedra and three octahedra also form pentagonal 'windows' similarly to other MPTBp compounds (Fig. 7). The unit cell parameters (in a standard setting) of the MPTBp compounds with the same thickness of the layer of octahedra are related to the perovskite unit cell parameters as follows:

$$a_{MPTBp} \approx a_{per}\sqrt{2},\ b_{MPTBp} \approx b_{per}\sqrt{3},$$

$$c_{MPTBp} \approx K + m a_{per}\cos 35^\circ \text{ (see Ref. 68)},$$

$$a_{MPTBp} \| [1\bar{1}0]a_{per},\ b_{MPTBp} \| [11\bar{1}]a_{per},\ c_{MPTBp} \| [112]a_{per}.$$

Here K is a constant related to the size of the PO_4 tetrahedron ($K \approx 2 \times 2.45$ Å) and 35° is the angle between the c_{MPTBp} axis and the $[001]_{per}$ axis. The unit cell thus defined has an orthorhombic symmetry with the a and b lattice constants being independent of m value. The c lattice constant linearly increases as m increases. The a_{MPTBp} and b_{MPTBp} parameters (~5.3 Å and ~6.55 Å, respectively) are close to the doubled face height and doubled edge length of the WO_6 octahedron, respectively.

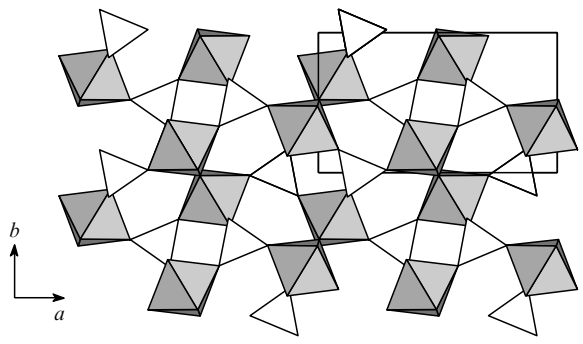

Figure 7. Projection of the crystal structure of $(PO_2)_4(WO_3)_4$.

In addition to the standard setting, a unit cell setting with the crystallographic axes running parallel to the perovskite axes is also used. If two layers of different thickness (m and m') alternate, the bronze unit cell becomes monoclinic with the following parameters [51]

$$d_{001} = K + 0.5(m + m')a_{per}\cos 35^\circ,$$

$$\tan \alpha_{MPTBp} = \frac{d_{001}}{0.5}(m - m')a_{per}\sin 35^\circ,$$

$$c_{MPTBp} = \frac{d_{001}}{\sin \alpha_{MPTBp}},$$

$$a_{MPTBp} = a_{per}\sqrt{2},$$

$$b_{MPTBp} = a_{per}\sqrt{3}.$$

Only one member of the MPTBp family (compound with $m = 5$) was obtained as two polymorphs. The structure of the first polymorph is characterised by regular alternation of the layers comprised of four and six octahedra, while the structure of the second polymorph is built of identical layers comprising five octahedra each. The structures of other MPTBp compounds contain layers of the same thickness, though irregular intergrowth of phases with different m occurs not infrequently [according to high-resolution transmission electron microscopy (HRTEM) data]. The probability of formation of the intergrowth phases increases as the m value increases.

The symmetry of many members of the MPTBp family is reduced with respect to an ideal structural type due to the possibility of small tilting of octahedra and to a different fashion of layer connection. Only one type of tilting is realised within the perovskite-type layer, the directions of tilting in two adjacent layers being the same or opposite. Taking into account different symmetry of the bronzes with the even and odd m values, the MPTBp compounds can crystallise in four structural types. The unit cell parameters of the MPTBp bronzes with the reliably (X-ray) established structures are listed in Table 6.

Most of the structures of MPTBp compounds studied by single-crystal X-ray diffraction analysis are characterised by symmetries lower than orthorhombic one. Studies of the MPTBp bronzes with large m values revealed satellite reflections indicating structure modulation at room temperature. The modulated structure of compound $(PO_2)_4(WO_3)_{20}$ with $m = 10$ was refined.[55] Structure modulation in the bronzes with small m values occurs only at low temperatures. For instance, a synchrotron radiation study of $(PO_2)_4(WO_3)_8$ (a compound with $m = 4$) at 20 K revealed structure modulation. All the MPTBp studied exhibited small tilting of octahedra, the tilt angle (8°) approaching that characteristic of WO_3.[89]

It has long been accepted that intercalation of cations into an MPTBp matrix is impossible and that crystallisation in the presence of inserted cations leads to the MPTBh compounds. The first members of the MPTBp families of composition $Na_x(PO_2)_4(WO_3)_{2m}$ with $0 \leqslant x \leqslant 1$ (isolated as individual compounds only for $m = 6$) were obtained only recently in the studies of phase relations in the systems $K_4(PO_2)_4(WO_3)_{2m}-Na_4(PO_2)_4.(WO_3)_{2m}-(PO_2)_4(WO_3)_{2m}$ with $m = 4$ and 6.[40] The $A_x(PO_2)_4.(WO_3)_{2m}$ bronzes were synthesised by intercalating monovalent cations (A = Li, Na, Ag, K) into the MPTBp structures.[90]

Changes in the structure of the MPTBp compound with $m \leqslant 14$ as a function of temperature have been reported in several studies (see, *e.g.*, Refs 2 and 15). A number of phase transitions related to periodic lattice distortions were detected at different

Table 6. Crystallographic parameters of the $(PO_2)_4(WO_3)_{2m}$ compounds with $m = 2-14$ obtained from single-crystal X-ray diffraction studies.

Composition	m	Space group	Unit cell parameters				Ref. [a]
			a /Å	b /Å	c /Å	angle /deg	
$P_4W_4O_{20}$	2	$P2_1cn$	5.231(3)	6.552(2)	11.117(1)	–	21, 54 (49, 38, 52)
$P_4W_8O_{32}$	4	$P2_12_12_1$	5.285(2)	6.569(1)	17.351(3)	–	50, 51 (15, 23, 38, 81–83)
$P_4W_{10}O_{38}$	5	$P2_1/n$	5.283(2)	6.574(39	20.451(1)	$\beta = 90.40(2)$	50 (23, 38, 84, 86)
$P_4W_{10}O_{38}$	6+4	$P2_1$	5.2850(2)	6.5656(2)	20.573(15)	$\alpha = 96.18(1)$	54 (23)
$P_4W_{12}O_{44}$	6	$P2_12_12_1$	5.2927(1)	6.5604(1)	23.549(3)	–	20 (15, 23, 82, 83, 87, 88)
$P_4W_{14}O_{50}$	7	$P2_1/n$	5.293(1)	6.571(3)	26.65(2)	$\beta = 90.19(1)$	54 (23, 82, 87, 88)
$P_4W_{16}O_{56}$	8	$P2_12_12_1$	5.2943(1)	6.5534(0)	29.700(4)	–	20 (2, 23, 85)
$P_4W_{18}O_{62}$	9	$P\bar{1}$	5.283(1)	6.571(3)	32.79(2)	$\alpha = 90.0(1)$, $\beta = 90.2(2)$, $\gamma = 89.78(1)$	81 (2, 20, 23, 83, 85)
$P_4W_{20}O_{68}$	10	$P2_1$	5.332(1)	6.551(2)	35.82(2)	$\beta = 90.6(2)$	55 (2, 38, 81, 83, 85)
$P_4W_{24}O_{80}$	12	$P2_12_12_1$	5.312(1)	6.5557(8)	42.196(8)	–	51 (81)
$P_4W_{28}O_{92}$	14	$P2_1/n$	5.321(1)	6.543(2)	48.00(5)	$\gamma = 91.04(2)$	81 (2, 38)

[a] Given in parentheses are the references to alternative solutions to the corresponding structures (including X-ray phase analysis data).

temperatures. These transitions correspond to anomalies of the temperature dependence of the electronic properties.

3. Monophosphate tungsten bronzes with hexagonal channels

The monophosphate tungsten bronzes with hexagonal channels have a general formula $A_x(PO_2)_4(WO_3)_{2m}$ (A = Na, Ag, K, Pb, Tl). In accord with the general framework build-up pattern, the unit cell symmetry cannot be higher than monoclinic one. Usually, the monoclinic cell is set in such a way that the twofold axis runs along the b direction. The unit cell parameters in the standard setting are as follows:[25]

$$a_{\mathrm{MPTBh}} \approx \sqrt{3}\, a_{\mathrm{per}}\,,\ b_{\mathrm{MPTBh}} \approx \sqrt{2}\, a_{\mathrm{per}}\,,$$

$$c_{\mathrm{MPTBh}} \sin\beta \approx 0.5\, K\ + 0.5\, m\, a_{\mathrm{per}} \cos 35^\circ,$$

$$a_{\mathrm{MPTBh}} || [11\bar{1}]_{\mathrm{per}}\,,\ b_{\mathrm{MPTBh}} || [1\bar{1}0] a_{\mathrm{per}}\,,\ c_{\mathrm{MPTBh}} || [112]_{\mathrm{per}}\,.$$

The parameters a_{MPTBh} and b_{MPTBh} are nearly 6.55 and 5.3 Å, respectively. Members of this series of bronzes with odd m values and most compounds containing sodium and lead are characterised by doubling of the c constant compared to the value calculated using the relation given above. The crystallographic parameters of MPTBh compounds obtained using data of X-ray studies are listed in Table 7.

The tilt angle of octahedra in the MPTBh bronzes depends on the size and content of inserted cations. For instance, all $Na_x(PO_2)_4(WO_3)_{2m}$ compounds with $x < 2$ are characterised by a tilt angle of nearly 8.5°. This angle decreases to 6.5° for the $Pb_x(PO_2)_4(WO_3)_{2m}$ bronzes with $6 \leqslant m \leqslant 10$. No tilt of octahedra was found in $Na_4(PO_2)_4(WO_3)_8$ and $K_x(PO_2)_4(WO_3)_{2m}$. These differences can be explained by the larger size of potassium ions and by the impossibility of redistribution of sodium cations in the cavities when all positions in $Na_4(PO_2)_4(WO_3)_8$ are occupied. At the same time each compound probably exists in two forms, a high-temperature form with non-tilted octahedra and a low-temperature form with tilted octahedra. At present, only the MPTBh compounds with alternation of the tilt direction from one layer to another are available. In the case of small tilts of octahedra the oxygen atom through which layers are linked virtually retains its position. This permits the formation of various intergrowth phases (layers with different m values and the MPTBh and MPTBp compounds), twins and defects.

The outermost (with respect to the centre of the perovskite-type layer in the MPTBh bronzes) WO_6 octahedra share their corners with three PO_4 tetrahedra and three WO_6 octahedra, the next octahedron shares its corners with one PO_4 tetrahedron and five WO_6 octahedra while other WO_6 octahedra are connected to one another only. The degree of distortion of the octahedra (in particular, the scatter of the W–O bond lengths) increases from the centre of the layer towards its periphery, being consistent with the increase in the formal oxidation state of the tungsten atoms calculated using data on the W–O bond lengths. In contrast to this, the average number of conduction electrons increases on going towards the centre of the layer.

All cations (sodium, potassium and lead) occupy a part of the O_{18} cavity near the phosphate groups. As the cation size increases, the average A–O distance also increases (2.68, 2.74 and 2.83 Å for Na, Pb and K, respectively), which is due to distortion of the perovskite-type layer. Positions of the sodium and lead cations differ only slightly. The decrease in the tilt angle of WO_6 octahedra in the Pb-containing structure was ascribed to the increase in the A–O bond lengths and to the steric effect of the lone electron pair whose location was established by Roussel *et al.*[51] Potassium cations are characterised by the smallest scatter of the K–O distances.

Arrangement of sodium cations in the MPTBh and MPTBp frameworks can be followed taking the structures of $Na_{1.7}(PO_2)_4(WO_3)_{12}$ (see Ref. 57) and $Na_4(PO_2)_4(WO_3)_8$ (see Ref. 91) as examples. The O_{18} cavities in the MPTBh structure are connected to four identical cavities by large hexagonal windows and by small rhombohedral windows delimited by two WO_6 octahedra and two PO_4 tetrahedra. The O_{18} cavities in the MPTBp structure are linked to four identical cavities by pentagonal windows. The surface areas of cavities are much larger than those of windows. One half of the cavity is the same for both MPTBh and MPTBp compounds while the other half can be matched by rotation about a twofold axis. On average the corresponding O–O distances in two O_{18} cavities differ by about 1.6%. In both cases the sodium ion is bound to oxygen atoms of the phosphate groups; usually, this ion is treated as an octacoordinate species (for comparison with the potassium-containing MPTB). In this case, the sodium atoms occupy significantly different positions and the scatter of the Na–O bond lengths is rather large. In the $Na_{1.7}(PO_2)_4(WO_3)_{12}$ bronze the sodium ion is displaced from the cavity centre by 1.11 Å; four Na–O bond lengths lie between 2.45 and 2.64 Å while the other four Na–O bond lengths fall within the interval 2.85 to 3.02 Å. In the $Na_4(PO_2)_4(WO_3)_8$ structure the coordination number of the sodium atom decreases to six. The edge-sharing distorted pentagonal pyramids NaO_6 form zigzag chains running along the [010] direction with a Na–Na separation of 3.211 Å (Fig. 8).[91] In the MPTBp structure the sodium ion is displaced from the centre of the O_{18} cavity by 1.5 Å, seven Na–O bond lengths are in the range from 2.37 to 2.64 Å while the eighth Na–O bond length is equal to 2.82 Å.

Table 7. Crystallographic characteristics of the compounds $A_x(PO_2)_4(WO_3)_{2m}$ with $m = 4-7$ and $A_x(P_2O_4)_2(WO_3)_{2m}$ with $m = 4-10$ obtained from single-crystal X-ray diffraction studies.

Composition	m	Space group	Unit cell parameters				Ref.
			a /Å	b /Å	c /Å	angle /deg	
Compounds $A_x(PO_2)_4(WO_3)_{2m}$							
$K_{0.84}P_4W_8O_{32}$	4	$P2_1/m$	6.6702(5)	5.3228(8)	8.9091(8)	$\beta = 100.546(7)$	8, 13, 16, 25, 53, 58
$Na_4P_4W_8O_{32}$	4	$P2_1/m$	6.6065(2)	5.2711(2)	8.8898(2)	$\beta = 99.5898(2)$	91
$Na_{1.5}P_4W_{10}O_{38}$	4	$P2_1/c$	6.6702(5)	5.277(4)	17.788(11)	$\beta = 99.64(5)$	33, 57, 86, 92
$K_{2.01}P_4W_{10}O_{38}$	6	$P2_1/m$	6.6736(2)	5.3543(3)	11.9005(5)	$\beta = 92.615(3)$	25, 41
$Na_{1.7}P_4W_{12}O_{44}$	6	$P2_1/c$	6.588(2)	5.291(1)	23.775(17)	$\beta = 93.47(4)$	37, 56, 57, 86
$K_{1.4}P_4W_{14}O_{50}$	7	$A2/m$	6.660(2)	5.3483(3)	27.06(5)	$\beta = 97.20(2)$ $\alpha = 89.62(1)$	8, 59
$Na_{1.7}P_4W_{14}O_{50}$	7	$A\bar{1}$	6.575(2)	5.304(1)	27.076(3)	$\beta = 96.17(1)$ $\gamma = 90.26(1)$ $\alpha = 90.208(6)$	27, 57
$Pb_{0.66}P_4W_{14}O_{50}$	7	$A1$	6.6015(3)	5.3156(4)	27.039(2)	$\beta = 96.757(5)$ $\gamma = 89.867(5)$	93
Compounds $A_x(P_2O_4)_2(WO_3)_{2m}$							
$RbP_4W_8O_{32}$	4	$A2/m$	10.181(6)	7.519(1)	17.156(4)	$\beta = 113.32(3)$	94
$KP_4W_{10}O_{38}$	5	–	11.061(1)	7.500(1)	17.133(2)	$\beta = 93.78(2)$	60
$RbP_4W_{10}O_{38}$	5	–	11.091(2)	7.522(2)	17.140(2)	$\beta = 93.78(1)$	60
$KP_4W_{12}O_{44}$	6	$A2/m$	14.006(2)	7.530(2)	17.056(2)	$\beta = 114.30(1)$	34, 60
$RbP_4W_{12}O_{44}$	6	$A2/m$	13.991(3)	7.530(1)	17.122(2)	$\beta = 114.22(1)$	61
$BaP_4W_{12}O_{44}$	6	$A2/m$	14.103(3)	7.494(1)	17.027(5)	$\beta = 114.19(1)$	23
$KP_4W_{14}O_{50}$	7	$P2_1/c$	14.618(4)	7.508(3)	17.098(4)	$\beta = 98.99(2)$	34, 60
$RbP_4W_{14}O_{50}$	7	$P2_1/c$	14.638(4)	7.534(3)	17.070(5)	$\beta = 99.00(2)$	60
$RbP_4W_{14}O_{50}$	7	$P2_1/c$	15.723(4)	7.528(6)	17.118(4)	$\beta = 113.42(2)$	62
$BaP_4W_{14}O_{50}$	7	$A2/m$	14.713(3)	7.484(2)	17.175(7)	$\beta = 99.41(3)$	23
$KP_4W_{16}O_{56}$	8	$P2_1/c$	16.208(8)	7.540(4)	17.087(8)	$\beta = 93.92(4)$	22
$RbP_4W_{16}O_{56}$	8	$P2_1/c$	16.209(11)	7.547(3)	17.095(7)	$\beta = 93.99(4)$	22
$RbP_4W_{16}O_{56}$	8	$P2_1/c$	16.194(3)	7.5438(8)	17.095(4)	$\beta = 93.82(2)$	48
$BaP_4W_{16}O_{56}$	8	$A2/m$	17.910(2)	7.480(2)	17.0606(9)	$\beta = 114.74(1)$	27
$BaP_4W_{16}O_{56}$	8	$A2/m$	18.271(4)	7.491(2)	17.346(4)	$\beta = 117.46(2)$	23
$TlP_4W_{16}O_{56}$	8	$P2_1/c$	16.208(8)	7.540(4)	17.087(8)	$\beta = 93.92(4)$	22
$KP_4W_{18}O_{62}$	9	$P2_1/c$	18.143(2)	7.532(2)	17.120(3)	$\beta = 101.54(1)$	60
$RbP_4W_{18}O_{62}$	9	$P2_1/c$	18.069(2)	7.556(2)	17.163(3)	$\beta = 102.53(2)$	60
$KP_4W_{20}O_{68}$	10	$P2_1/c$	21.386(2)	7.534(2)	16.968(1)	$\beta = 113.57(2)$	60
$KP_4W_{20}O_{68}$	10	$P2_1/c$	19.589(3)	7.5362(4)	16.970(3)	$\beta = 91.864(14)$	22
$RbP_4W_{20}O_{68}$	10	$P2_1/c$	21.395(2)	7.552(3)	17.063(5)	$\beta = 113.93(3)$	60
$BaP_4W_{20}O_{68}$	10	$A2/m$	23.193(4)	7.487(2)	17.175(7)	$\beta = 99.41(3)$	23

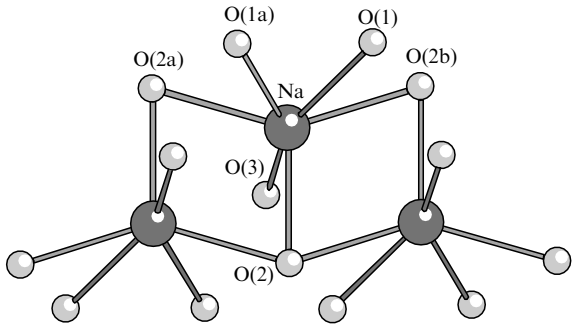

Figure 8. $(NaO_5)_\infty$ chains in the structure of $Na_4(PO_2)_4(WO_3)_8$.

4. Diphosphate tungsten bronzes

Diphosphate tungsten bronzes with hexagonal and pentagonal channels are described by a general formula $A_x(P_2O_4)_2(WO_3)_{2m}$ (A = K, Rb, Cs, Tl, Ba, *etc.*) with integer m values ($4 \leqslant m \leqslant 10$). The frameworks of the simplest members of the DPTB family, compounds $A_x(P_2O_4)_2(WO_3)_4$ (A = Rb, Tl, Ba), contain infinite chains built of ReO_3-type WO_6 octahedra running along the [001] direction of an orthorhombic unit cell. The chains are linked together by diphosphate units. As a result, octagonal channels with a large cross section running along the [001] direction are formed (Fig. 9 *a*); channels with a smaller cross section run along the [010] direction (Fig. 9 *b*). The DPTBs with $m \geqslant 4$ contain characteristic hexagonal channels extending along the [010] direction (see Fig. 1 *d*).

Ordering of cations in the cavities was studied[95] by X-ray diffuse scattering taking the bronze $Cs_{1-x}(P_2O_4)_2(WO_3)_4$ as an example. At 298 K, Cs^+ ions are locally ordered in the lattice along the direction of the channel; however, no correlation between the arrangements of these ions in adjacent channels was found. The period of one-dimensional incommensurate concentration waves depends on stoichiometry with respect to Cs^+ cations. At low temperatures, the degree of intrachannel ordering of Cs^+ cations increases and interchannel ordering appears. Kinetic effects preclude long-range three-dimensional ordering even at low temperatures. Due to the phase shift between the concentration waves of Cs^+ cations in different channels their electrostatic repulsion is minimum. Occurrence of Anderson-type transition in $Cs_{1-x}P_8W_8O_{40}$ (at small x) due to the change in the degree of disorder of ceasium was confirmed by the character of the temperature dependence of electrophysical properties.[95]

In the structure of $(WO_3)_6(P_2O_4)_2$ three nonequivalent WO_6 octahedra differ in the number of bonds with other WO_6 octa-

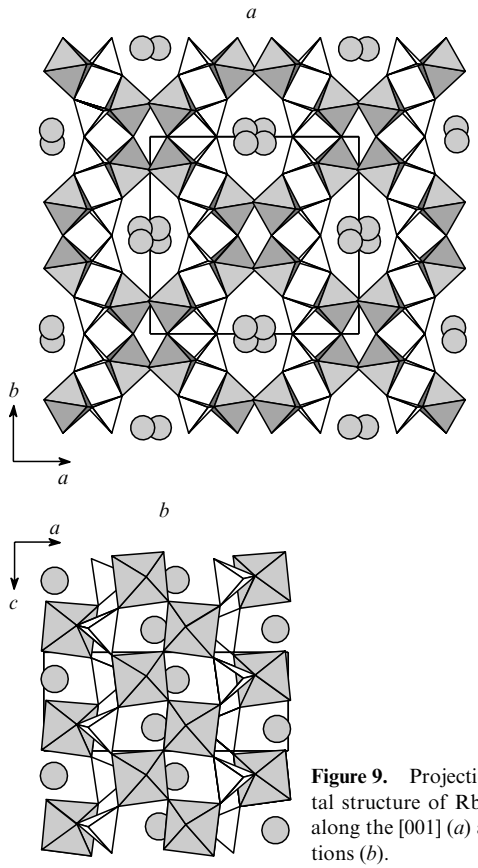

Figure 9. Projections of the crystal structure of $Rb(P_2O_4)_2(WO_3)_4$ along the [001] (*a*) and [010] directions (*b*).

hedra and PO_4 tetrahedra, which equals (5 + 1), (4 + 2) and (3 + 3), respectively. The magnitudes of displacement of the tungsten atoms from the centre of gravity of the octahedron and difference of the W—O bonds in the octahedra increase as the number of bonds with tetrahedra increases. In contrast to all other phosphate tungsten bronzes the structure of $(P_2O_4)_4(WO_3)_{12}$ comprises zigzag-shaped W_6O_{28} chains connected through not only the diphosphate units (P_2O_7) but also immediately through oxygen atoms to form a three-dimensional framework. The structure can be described as a ReO_3-type framework in which one of the four MO_6 octahedra is replaced by the diphosphate unit. Infinite perovskite-type W_3O_{14} ribbons running along the [001] direction are shown in Fig. 10. Two types of channels, *viz*., pentagonal and distorted hexagonal ones extend along the [001] direction (Fig. 11). Three types of face-sharing cavities delimited by thirteen, fourteen and fifteen oxygen atoms can be distinguished in the structure. The O_{13} cavities are formed by six WO_6 octahedra and three PO_4 tetrahedra while O_{14} cavities are formed by six octahedra and two diphosphate units. Elongated O_{15} cavities are formed

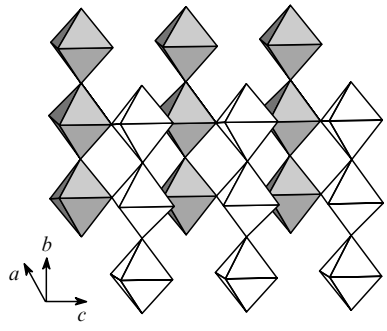

Figure 10. $(W_3O_{14})_\infty$ chains in the structure of $(P_2O_4)_2(WO_3)_6$.

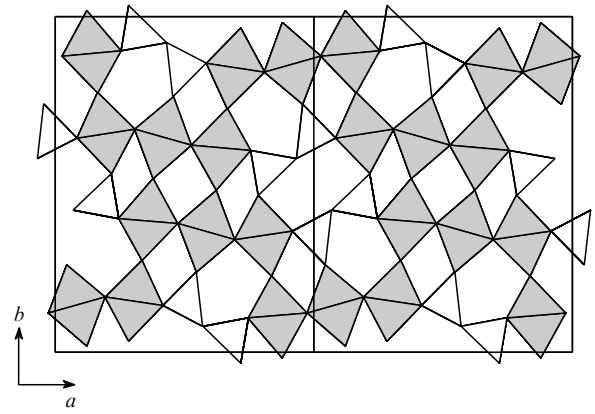

Figure 11. Projection of the crystal structure of $(P_2O_4)_2(WO_3)_6$ along the [001] direction.

by five octahedra and three diphosphate groups. Perovskite-type cavities O_{12} also exist.

The unit cell parameters of the DPTBh compounds with even *m* values ($m > 6$) in the standard setting are [64]

$$a_{\mathrm{DPTBh}} \approx K + 0.5\ a_{\mathrm{per}}\, m,$$

$$b_{\mathrm{DPTBh}} = 2\, a_{\mathrm{per}},$$

$$c_{\mathrm{DPTBh}} = \sqrt{2}\, a_{\mathrm{per}},$$

where $K \approx 2.6$ Å, $\beta \approx 116.6^\circ$.

It should be noted that only the parameter *a* depends on *m* and is related to the layer thickness. For the DPTBh compounds with odd *m* values the unit cell parameters are as follows:[68]

$$a_{\mathrm{DPTBh}} \approx K + a_{\mathrm{per}}[1 + 0.25(m-1)^2],$$

$$b_{\mathrm{DPTBh}} = 2\, a_{\mathrm{per}},$$

$$c_{\mathrm{DPTBh}} = \sqrt{2}\, a_{\mathrm{per}},$$

where $K \approx 2.6$ Å, $\beta \approx 116 - \omega$, $\omega = \arctan[2/(m+1)]$.

Stacking of layers of the same thickness along the *a* direction leads to monoclinic symmetry of the structure. The unit cell parameters of DPTBh, obtained using X-ray diffraction and phase analyses are listed in Table 7.

The diphosphate tungsten bronzes with pentagonal channels were not synthesised as individual phases; however, DPTBp microcrystals containing non-parallel domains with ReO_3-type structure of different thickness (with large *m* values) were found by HRTEM. The tungsten diphosphate WP_2O_7 (see Ref. 96) can be considered as a zeroth member of this class of DPTBs ($m = 2$). Its framework comprises isolated octahedra and zigzag channels with pentagonal windows.

5. Structural defects in phosphate tungsten bronzes

Phosphate tungsten bronzes have been the subject of intensive HRTEM studies. Using this method, it is impossible to reveal small distortions of polyhedra in a real structure with respect to the ideal structural type; however, it is possible to determine non-stoichiometric defects, intergrowth phases, domains and changes in the content of inserted cations in channels.

Structural defects in MPTBs can be divided into two groups. The first group of defects is due to the distribution of planes built of phosphate groups with respect to layers built of the WO_6 octahedra. The second group of defects is due to distribution of PO_4 groups within the phosphate planes.

Electron micrographs of the MPTBs with $m = 4 + 6$ and $m > 12$ usually exhibit certain intergrowth phases of different members of this family of compounds. Bronzes with $m > 13$ were not synthesised as regular single crystals. The compound with $m = 5$ behaves in an unusual manner compared to other phosphate bronzes.[23, 59, 64, 86] Usually, the number of octahedra in the

defect layer approaches that in the main phase. The intergrowth phases can form in both the phosphate [36, 37, 59, 64] and the oxide bronzes in which a shear deformation is possible.

The MPTBh crystals exhibit two kinds of growth defects, (i) separation of the crystal into two regions and (ii) growth of small domains of different thickness on the crystal faces.[57] Often, these domains are somewhat disoriented relative to the main part of the crystal and separated by a clearly seen boundary. In some cases, small domains are poorly crystallisable or amorphous.

A model for connection of these domains through a coherent boundary involving PO_4 tetrahedra, P_2O_7 units in the eclipsed conformation [similar to those found in the structure of $(P_2O_4)_2(WO_3)_6$, see Ref. 97] and edge-sharing WO_6 octahedra was proposed.[57] The boundary is nearly parallel to the hexagonal channel. This model cannot be considered as exclusive; however, structural units employed by the model, *viz.*, the PO_4 and P_2O_7 groups and the edge-sharing WO_6 octahedra are available at any point of the domain boundary.

Changes in the order of alternation of PO_4 tetrahedra and WO_6 octahedra cause two types of defects. Characteristic of the first type of defects is the appearance of additional hexagonal or pentagonal channels. They are observed in the perovskite-type layers containing more than thirteen octahedra [23] and appear only in a part of the layer. The contrast produced by these channels is somewhat different from that produced by the matrix (due to distortions in the framework region adjacent to the defect); however, the content of cations in these channels cannot be determined with certainty. If additional channels in crystals pass throughout the layer, two adjacent layers characterised by small m values appear in the matrix with large m value. This type of defects was found only in the sodium-containing MPTBh.

Additional pentagonal channels characteristic of the MPTBp compounds can appear at the boundary between two MPTBh domains with different orientation of WO_6 octahedra. Correspondingly, hexagonal channels typical of the MPTBh compounds can appear at the boundary between two domains in the MPTBp crystal. A quite rare case is a shear defect along the direction perpendicular to the channel axes.

The potassium- and sodium-containing MPTBh compounds with relatively high alkali metal contents ($x \approx 2$ for K and $x = 3$ for Na) exhibit local variations of the cation concentrations, which lead to distortion of the framework and manifest themselves in periodic changes in the contrast of hexagonal channels.

The nature of cations residing in hexagonal channels affects both the homogeneity region and the structure of the MPTBh compounds. Sodium-containing MPTBh compounds are more stable than their potassium-containing analogues. The sodium-containing bronzes are characterised by a greater variety of defects; a compound with $m = 5$ was stabilised.

A number of the diphosphate tungsten bronzes $Ba_x(P_2O_4)_2(WO_3)_{2m}$ were studied by X-ray diffraction analysis and electron microscopy. Electron diffraction studies showed that, in contrast to the DPTBs containing alkali metal cations, the barium-containing DPTBs exhibit the A-type of the Bravais lattice, superstructural reflections and higher stability. These differences are due to the large covalent component of the bonds between barium and oxygen atoms of the framework. Many $Ba_x(P_2O_4)_2(WO_3)_{2m}$ crystals are characterised by irregular intergrowth. At the same time, ordered intergrowth were observed for the bronzes with $m = 8$ and 9.

IV. Electronic structure

The electronic structures of phosphate tungsten bronzes were calculated by the extended Hückel method. This semiempirical approach is suitable for a more or less satisfactory description of the energy bands of crystals under study but does not allow a reliable geometry optimisation. The research strategy involves analysis of the model fragments (either finite or infinite) of a crystal structure as they become more complicated. To make the electronic structure calculations more exact, information on the band structure of the model systems is used along with the structural data obtained for real compounds.

1. Electronic structure calculations of diphosphate tungsten bronzes

The crystal structure of the first member of the DPTB series, $Cs_{0.5}(P_2O_4)_2(WO_3)_4$ ($m = 2$), is built of isolated W_4O_{18} chains. This compound is expected to possess quasi-one-dimensional electronic properties. The electron count is 1.125 d electrons per tungsten atom and 4.5 d electrons per W_4O_{18} unit. The t_{2g}-levels of $Cs_{0.5}(P_2O_4)_2(WO_3)_4$ are by and large identical to those of an ideal W_4O_{18} chain. The presence of two chains in the unit cell causes a doubling of the bands with a small splitting in each pair of bands. The main feature of the t_{2g}-bands of $Cs_{0.5}(P_2O_4)_2(WO_3)_4$ is that the Fermi level crosses a one-fourth filled one-dimensional delocalised band, whereas the fully filled localised bands and the unfilled delocalised bands are above and below the Fermi level, respectively.[7, 68]

The electronic structure of $Cs_{0.5}(P_2O_4)_2(WO_3)_4$ (see Refs 7, 66 and 67) is similar to that of the lithium bronze $Li_{0.9}Mo_6O_{17}$. In both compounds d electrons are localised within M_4O_{18} (M = W, Mo) chains that are connected in a different way, namely, through diphosphate groups in the former and through Mo_4O_{14} chains built of corner-sharing MoO_6 octahedra and MoO_4 tetrahedra in the latter case. The W_4O_{18} chains in $Cs_{0.5}(P_2O_4)_2(WO_3)_4$ are shielded more weakly than the Mo_4O_{18} chains in $Li_{0.9}Mo_6O_{17}$, so that the conduction electrons are more susceptible to the electric fields created by cations.

Thus, order–disorder transitions of the caesium cations can influence the conducting properties of bronzes. Partial interchannel ordering of cations is observed at a temperature close to the metal–semiconductor transition temperature. Probably, an increase in the resistivity at 24 K is due to the CDW created as a result of one-fourth filling of the one-dimensional bands.[7] As the electron density in the partially filled delocalised bands increases, the shielding (see above) also increases and the conduction electrons become less susceptible to the electric fields created by cations. The $Tl_yCs_x(P_2O_4)_2(WO_3)_4$ phases with $x + y > 0.5$ are isostructural to $Cs_{0.5}(P_2O_4)_2(WO_3)_4$; here, the high-temperature resistivity maximum at 160 K indicating a transition to the CDW state disappears as the sum $x + y$ increases.[7]

The three-dimensional framework of $(P_2O_4)_2(WO_3)_6$ (a DPTB with $m = 3$) contains a system of corner-sharing WO_6 octahedra. Zigzag W_6O_{28} chains are linked by $W'''O_6$ octahedra. According to Zachariasen-type group structure analysis of the W–O bond lengths, the oxidation states of the tungsten atoms W′, W″ and W‴ are 5.19, 5.10 and 5.71, respectively. The band structure of the $W_{12}O_{48}$ framework is similar to that of an isolated W_6O_{28} chain except for the delocalised π-bands in $W_{12}O_{48}$ that cross the Fermi level in all three directions. Therefore, π-orbitals of the $W'''O_6$ octahedra provide not only intrachain but also interchain π-interaction. Therefore, the bronze $(P_2O_4)_2(WO_3)_6$ must possess a three-dimensional metallic conductivity, which was confirmed experimentally. The Zachariasen-type analysis showed that the partially filled delocalised bands are to a great extent composed of the orbitals of the W′ and W″ tungsten atoms.

The $(P_2O_4)_2(WO_3)_6$ bronze significantly differs from the purple bronze $Li_{0.9}Mo_6O_{17}$ in the number of d electrons in the M_4O_{18} (M = Mo, W) chain. Namely, in $Li_{0.9}Mo_6O_{17}$ there are 5.8 electrons per formula unit of the M_4O_{18} chain and the lower lying bands are completly filled, while in the tungsten bronze there are only four electrons and both bands (π and δ) are partially filled. According to calculations, $(P_2O_4)_4(WO_3)_{12}$ must behave as a one-dimensional metal provided that the Fermi level is higher than the π-band upon filling of bands with additional electrons. According to experimental data, the $(Li,Na)_x(P_2O_4)_2(WO_3)_6$ ($x < 0.5$) bronzes containing up to five electrons per formula unit in both (π and δ) bands [7, 67] exhibit a three-dimensional metallic conductivity. Thus, group-structure analysis of the systems $Li_{0.9}Mo_6O_{17}$

and $(P_2O_4)_2(WO_3)_6$ reveals a similar pattern of the distribution of d electrons but different conductivity. This is due to the fact that two types of different-dimensionality bands correspond to the same energy. In these cases, the dimensionality of conductivity strongly depends on the degree of band filling.

For the DPTB compound with $m = 4$, layers built of corner-sharing WO_6 octahedra are similar to Mo_4O_{15} layers in the Magnéli phase Mo_8O_{23}. However, in these structures layers are connected in a different manner, *viz*., through diphosphate groups in the DPTB compound and by Mo_4O_{14} chains built of edge-sharing MoO_6 octahedra in Mo_8O_{23}. Real DPTBs have more complex structures because connection of the layers of WO_6 octahedra by P_2O_7 groups causes small distortions of the octahedra and leads to a unit cell four times larger than that of an ideal W_4O_{15} layer. The average valence corresponding to the oxidation state of tungsten in DPTBs increases with the layer thickness, being equal to $[6-(8+x)/4m]$ in the $(P_2O_4)_2(WO_3)_{2m}$ compounds. At $m = 4$, the number of d electrons per tungsten atom equals 0.625, which is close to the value of 0.5 obtained from calculations for molybdenum atoms in a Mo_4O_{15} layer of the Mo_8O_{23} structure. Therefore, these two systems are structurally similar and exhibit similar electrical properties. No alternation of short and long O–Mo–O bonds along the *b* direction occurs in DPTBs (in contrast to Mo_8O_{23}), so all three t_{2g}-orbitals of tungsten atoms can form low-lying t_{2g}-bands.

The band structures of an ideal W_4O_{17} chain and W_4O_{15} layer have also been calculated. The lowest-lying d-type energy states of the W_4O_{17} chains are four localised bonding δ-bands composed of x^2-y^2-orbitals and eight delocalised π-bands. Four of the delocalised bands are nearly degenerate. The dispersion relations for the t_{2g}-bands along the W_4O_{17} chain of the W_4O_{15} layer are similar to those calculated for a single chain except for the splitting of the four degenerate bands into two groups. The x^2-y^2 orbitals can be involved in interchain π-antibonding interaction and, hence, form a band that is delocalised along the *c* direction. In addition, there are bands originating from the antibonding interaction of the metal d-orbitals with the oxygen p-orbitals along the *b* direction.

The Fermi level calculated for 2.5 electrons in the unit cell crosses the δ- and π-bands originating from the interaction of AOs along the *c* and *b* axes, respectively.[7] Therefore, the system must behave as a two-dimensional metal, *i.e*., possess a metallic conductivity in two directions. However, the Fermi level crosses these bands in such a way that the conductivity along the *b* direction is higher than along the *c* direction. It should be noted that the two-dimensional metallic character of this system is due to the presence of two one-dimensional bands in two mutually perpendicular directions rather than essentially two-dimensional bands.

The band structures calculated for actual W–O layers in $Rb_2(P_2O_4)_2(WO_3)_8$, $Rb_{0.9}(P_2O_4)_2(WO_3)_{12}$ and $Rb_{0.87}(P_2O_4)_2 \cdot (WO_3)_8$ are qualitatively similar to the band structures of an ideal W–O layer. More complex band structure can be a consequence of the doubling of the unit cell (doubling of the parameters *b* and *c*). Hence, all these systems must be two-dimensional metals with the highest conductivity along the *b* direction, which is consistent with experimental data.

A number of bands exhibit a plateau in the vicinity of the Fermi level, which indicates a high density of states. The Fermi level population, $n(E_F)$, can be changed by increasing or decreasing its energy. The increase in $n(E_F)$ can be responsible for the observed increase in the conductivity of both electron-deficient and electron-enriched systems $K_xRb_y(P_2O_4)_2(WO_3)_{12}$ $(x + y < 1)$ and $KSn_x(P_2O_4)_2(WO_3)_{12}$ $(x > 0)$, respectively, compared to the conductivity of $K(P_2O_4)_2(WO_3)_{12}$.[66,67] However, a theoretical model[66] predicts an increase in the conductivity only for the electron-deficient systems $A_{1-x}(P_2O_4)_2(WO_3)_{14}$ $(x > 0)$.

2. Electronic structure calculations of monophosphate tungsten bronzes

The electronic properties of $P_4W_4O_{20}$ differ from those of other MPTBp compounds with $m > 2$. The crystal structure of $P_4W_4O_{20}$ contains no perovskite-type layers; it comprises only the zigzag W_2O_{10} chains built of corner-sharing octahedra. Lithium–molybdenum bronze $Li_{0.9}Mo_6O_{17}$ contains similar Mo_2O_{11} chains. The energy level diagram calculated for $P_4W_4O_{20}$ is similar to that obtained for $Li_{0.9}Mo_6O_{17}$ and exhibits both localised (in *ab* planes) and delocalised (along *c* axis) t_{2g}-bands formed as a result of the interaction of d electrons of tungsten atoms. The t_{2g}-bands are filled with two d electrons (two tungsten(V) atoms in the W_2O_{10} chain per unit cell). The last band is nearly half-filled, while the nearly degenerate localised bands are one-fourth filled. Calculations also predicted a magnetic moment created by electrons in the narrow bands, metallic properties of the compound and its electronic instability.

Perovskite-type layers in the MPTBs with $m > 2$ are characterised by nonuniform distribution of d electrons whose concentration increases from the centre of the layer towards its periphery.

The monophosphate tungsten bronzes are two-dimensional metals similar to their structural analogues, γ-Mo_4O_{11} and η-Mo_4O_{11}. The transport properties and electronic instabilities of the W–O and Mo–O layers in the Magnéli phases are different. The Mo–O layers have a larger number of d electrons due to the difference in the oxidation state of the atom in a tetrahedral environment [Mo(VI) in the Magnéli phases and P(V) in the MPTBs]. Changes in the topology of the Fermi surface as a function of the number of d electrons in the unit cell and the thickness of the perovskite-type layer have been studied.[7] The electronic band structures of the MPTBs were calculated by the extended Hückel tight binding method using the modified Wolfsberg–Helmholtz approximation.[6,7]

The electronic band structures of different MPTBs obey an identical pattern, being similar to the band structure calculated for an ideal layer built of regular WO_6 octahedra. An example of this layer is provided by, *e.g*., a W_4O_{16} layer with W–O distances of 1.916 Å. The average oxidation state of the tungsten atoms in $(PO_2)_4(WO_3)_{2m}$ is $(6m-2)/m$. Therefore, each layer of WO_6 octahedra contains two d electrons per unit cell irrespective of *m* value. In the $A_x(PO_2)_4(WO_3)_{2m}$ bronzes containing monovalent cations each layer has $(2 + x/2)$ electrons in the unit cell to fill the t_{2g}-bands (Fig. 12).[67] Two Magnéli phases, γ-Mo_4O_{11} and η-Mo_4O_{11}, are characterised by $N = 4$, the $A_2(PO_2)_4(WO_3)_{2m}$ compounds are characterised by $N = 3$ while $N = 2$ for the MPTBp compounds. At $N \leqslant 4$, only two bottom bands are partially filled, one of them being one-dimensional while the other (consisting of two subbands) is a two-dimensional one.

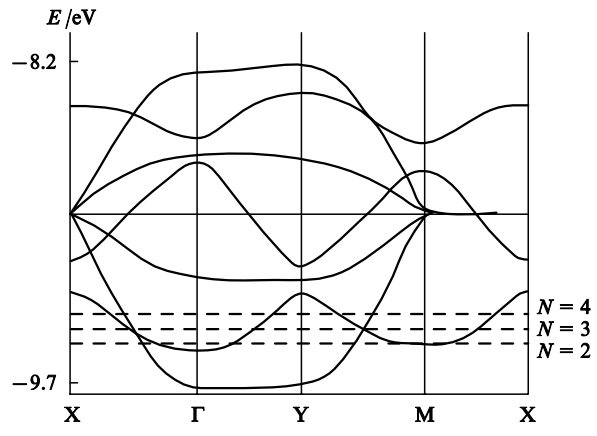

Figure 12. Dispersion relations for the t_{2g}-bands in a perfect W_4O_{16} layer. Dashed lines denote the Fermi levels at different numbers of d electrons in the unit cell (*N*).

Table 8. Peierls transition temperatures and the modulation wave vectors of some MPTBp compounds.

m	T_P /K		Modulation wave vector $\boldsymbol{q}^{(m)}$ (see [a])	Ref.
	T_{P1}	T_{P2}		
4	80(1)	52(1)	$\boldsymbol{q}_1^{(4)} = [0.330(5), 0.295(5)]$, $\boldsymbol{q}_2^{(4)} = [0.340(5), 0.000(5)]$	14, 47, 99 – 102, 104, 106
5	83(5)	60(2)	$\boldsymbol{q}_1^{(4)} = [0.32(1), 0.29(1), 0.0(1)]$, $\boldsymbol{q}_2^{(4)} = [0.36(1), 0.00(5), 0.0(1)]$	98
4 + 6	158(2)	–	$\boldsymbol{q}_1^{(4)} = [0.330(5), 0.295(5)]$, $\boldsymbol{q}_2^{(4)} = [0.33(4), 0.00(4)]$	103, 104
6	120(1)	62(1), ~ 30 [b]	$\boldsymbol{q}_1^{(6)} = [0.385(5), 0.000(5)]$, $\boldsymbol{q}_2^{(6)} = [0.310(5), 0.295(5)]$, $\boldsymbol{q}_3^{(6)} = [0.29(2), 0.11(2)]$	14, 18, 33, 100 – 102, 104, 106
7	183 – 188	47 – 60	$\boldsymbol{q}_1^{(7)} = [0.260(3), 0.073(3), 0.27(5)]$, $n = 1 - 7$	18, 19 100, 101, 104, 106
	188(1)	60(1)	$n\boldsymbol{q}_2^{(7)} = n[0.12(1), 0.03(1), 0.15(5)]$, $n = 1, 3, 5$	
8	≈220	~200	$\boldsymbol{q}_1^{(8)} = [0.47(2), 0.02\ (1), 0.15(10)]$, $n\boldsymbol{q}_2^{(8)} = n[0.19(2), 0.03(1), 0.15(5)]$, $n = 1 - 6$ (see [c])	104, 105
9	565(5)	330(5)	$\boldsymbol{q}_0^{(9)} = [0.50(1), 0.00(1), 0.0(2)]$, $\boldsymbol{q}_1^{(9)} = [0.17(1), 0.00(1), 0.0(2)]$	104, 105
10 (see [d])	≈450		$\boldsymbol{q}^{(10)}$ (300 K) = [0.43(1), 0.00(1), 0.0(1)], $\boldsymbol{q}^{(10)}$ (300 K) = [0.14(1), 0.00(1), 0.0(1)]	47, 104
11	560(5)	–	$n\boldsymbol{q}^{(11)}(T) = 1, 2, 3$; $\boldsymbol{q}^{(11)}$ (300 K) = [0.43(1), 0.00(1), 0.0(1)]	81
12	535(5)	500(5)	$\boldsymbol{q}_1^{(12)} = [0.12(1), 0.00(2), 0.0(2)]$, $\boldsymbol{q}_0^{(12)} = [0.50(1), 0.00(1), 0.5(2)]$	47, 104, 105
13	550(5)	–	$n\boldsymbol{q}_1^{(13)} = [0.053(8), 0.016(10)]$, $n = 1, 2$;	17, 104, 105
	510(5)	–	$\boldsymbol{q}_0^{(13)} = [0.50(1), 0.00(1), 0.0(2)]$, $\boldsymbol{q}_2^{(13)} = [0.178(8), 0.145(10)]$	
	160(10)	–		
14	≈695 – 730	–	$\boldsymbol{q}_0^{(14)} = [0.50(1), 0.00(1), 0.5(2)]$	104, 105

[a] Presented in units of the reciprocal cell. [b] The T_{P3} value. [c] In the case of short-range order in the crystal. [d] The crystal was doped with 0.2% Ge.

3. The Fermi surfaces

The Fermi surface of an ideal one-dimensional metal consists of two parallel planes separated by the Fermi wave vector $2\boldsymbol{k}_F$. A Peierls transition (metal – insulator transition) causes destruction of this Fermi surface. The Fermi surfaces of quasi-two-dimensional (2D) conductors are of more complex shape.[10] In this case a Peierls transition causes a partial destruction of the Fermi surface; as a consequence, metal – metal transitions are observed. Transitions to the CDW state or between two CDW states are a consequence of the interaction between a phonon and the energy states of conduction electrons. Pre-transitional phenomena observed in the MPTBp compounds above the Peierls transition temperature (T_P) indicate that CDW-type instability is due to the quasi-one-dimensional electronic structure of these compounds. Large flat areas of the Fermi surface which include bands of different orientation can be calculated using the extended Hückel tight binding approximation.[6, 7, 10] X-Ray diffuse scattering experiments [14, 17 – 19, 47, 81, 98 – 106] allowed the Fermi vectors for each quasi-one-dimensional area of the Fermi surface to be determined (Table 8).

The Fermi surface was first imaged by high-resolution photoemission UV spectroscopy in a study of MPTBp compounds with $4 \leqslant m \leqslant 12$.[104] The Fermi surface of $(PO_2)_4(WO_3)_8$ contains quasi-one-dimensional bands,[104, 107] which is consistent with the results of earlier band structure calculations.[66, 67, 108]

V. Electrophysical properties

The electric and magnetic properties of MPTBp polymorphs with $m = 2$ [the α- and β-phases of $(PO_2)_4(WO_3)_4$] were first studied by Kinomura *et al.*[49] Both phases exhibit semiconducting properties in the temperature range 77 – 420 K. The monoclinic β-phase is characterised by higher conductivity. The results of preliminary magnetisation measurements with α-phase and β-phase polycrystals in the temperature interval 77 – 500 K revealed nonzero local magnetic moments.

The magnetic susceptibility (2 – 300 K, in a 5000 G field) and the resistivity (50 – 390 K) of oriented MPTBp single crystals were experimentally studied by Greenblatt *et al.*[52] In this temperature range, the resistivity shows a semiconducting behaviour. At 298 K, the resistivity measured along different crystallographic axes is $R_c = 5 \times 10^{-3}$, $R_b = 4 \times 10^{-2}$ and $R_a = 1 \times 10^{-1}$ Ω cm. At $T < 50$ K, the resistivity is $\geqslant 10^4$ Ω cm. Seebeck effect measurements at 300 K showed electrons as the main type of charge carriers (*n*-type conduction). Experiments revealed a semiconducting rather than the predicted metallic type of conductivity along the *c* axis (though the conductivity at 298 K approaches a value characteristic of metals).

The temperature dependence of the magnetic susceptibility (χ) in the samples exhibits the onset of antiferromagnetic ordering at 15 K. In the temperature range 50 – 300 K the dependence of $1/\chi$ on T obeys the Curie – Weiss law with $\theta = -34.6$ K. The effective magnetic moment in this temperature range is 0.88 μ_B. The large deviation of this dependence from the linear one at $T < 50$ K is likely due to the change in the type of magnetic exchange interaction upon structural phase transition.

A large anisotropy of the Neel temperature (T_N) was found along the *b* direction ($T_N \approx 16$ K), along the *c* direction ($T_N \approx 20$ K) and along the *a* direction at low temperatures the temperature dependence of χ exhibits a plateau with $\chi_{max} = 1.12 \times 10^{-2}$ cm^3 mol^{-1} at 4.6 K. Taking into account a rather low activation energy for conductivity along the *a* axis ($E_a = 0.084$ eV at 50 – 200 K), the conductivity can be described in terms of the hopping of small polarons in the narrow conduction bands originating from the overlap of 5d-orbitals of the tungsten atom and 2p-orbitals of the oxygen atom.

The crystal structure of the monophosphate tungsten bronze $(PO_2)_4(WO_3)_4$ comprises isolated chains built of WO_6 octahedra with the lowest (for this class of compounds) oxidation state of tungsten. Along $(WO_5)_\infty$ chains (*c* axis direction) the magnetisation is much lower while the conductivity is much higher than along other axes.

CDW-type electronic instabilities are also possible in bronzes. At 298 K, high semimetallic conductivity along one-dimensional chains built of WO_6 octahedra implies a transition to the metallic state, *i.e.*, a CDW-type instability at $T > 390$ K, as was predicted by Canadell and Whangbo.[109]

At present, the properties of the $(PO_2)_4(WO_3)_{2m}$ bronzes with $4 \leqslant m \leqslant 14$ have been a subject of most intensive studies.[3, 10, 88, 99] It was established that the critical temperature of Peierls transition and the resistivity at room temperature increase with the thickness of the layer of WO_6 octahedra. This is consistent with the simple models proposed for the monophosphate tungsten bronzes with $m = 4 - 12$.[16, 84, 98] At the same time, the MPTBp compounds with

$m = 4$ and 6 are treated as typical CDW-compounds while the compounds with $m = 7$ exhibit anomalous electrophysical properties.

The electrophysical properties of the bronzes $(PO_2)_4(WO_3)_{2m}$ are closely related to the character of the Fermi surface. Some studies take into account the role of electron – phonon interaction. In particular, a rather high resistivity at room temperature should be ascribed to an increase in the contribution of electron – phonon (or electron – electron) interaction, which can be due to the presence of the CDW satellites corresponding to anharmonic CDW modulation. With allowance for this fact the electrophysical properties of certain phosphate tungsten bronzes should be described using the bipolaron model rather than the traditionally used CDW model.[110]

The results of studies on the bronzes with $m = 10$ and 12 indicate that the critical temperatures of transitions to the CDW state increase as the m value increases. It should be noted that crystals were grown using glass-forming oxides. This was accompanied by doping the crystals (with *e.g.*, germanium). Due to the different electronic structures of the impurity and the host atoms it is possible to change the density of states at the Fermi level. A Ge $\leftrightarrow$ P substitution of tetrahedral positions was also proposed;[47] we believe that the Ge $\leftrightarrow$ W substitution [38] is also possible, though the impurity concentration is rather low and no significant changes in the temperature of transition to the CDW state are expected.

An increase in the resistivity at room temperature with increasing m is comparable with the decrease in the charge carrier concentration evaluated using a simple Drude model. The average number of electrons in the samples with $m = 4$ and 12 was estimated at 7×10^{27} and 3×10^{27} m^{-3}, respectively. However, this provides no explanation for the fact that the resistivity increases by two orders of magnitude in the temperature interval from 4 to 300 K and undoubtedly indicates that the band theory, as applied to the crystals in question, is of limited use. This is confirmed by the conductivity of these crystals at room temperature ($\sigma_{300\ K} = 10^2\ \Omega\ cm^{-1}$ for $m = 12$), which approaches the lowest possible value of the metallic type conductivity. It should be noticed that the electrophysical properties of the compounds $(PO_2)_4(WO_3)_{2m}$ with large m values can be described in terms of the theory of Fermi liquid.[108]

Experiments with single crystals of the bronzes with $7 < m \leqslant 12$ showed that the Peierls transition temperatures and the resistivity at room temperature increase as m increases, as is expected in accord with the known models. Diffraction intensity measurements of the CDW satellites for $m = 7$ revealed two transitions at $T_{P1} = 183 - 188$ K and $T_{P2} = 47 - 60$ K. The transition temperatures depend on the method of growth of single crystals (chemical vapour transport reactions or solid-phase synthesis) and on the purity of the starting components. The T_{P1} transition, which is accompanied by considerable changes in the resistivity, seems to be a first-order phase transition.[88]

At $T \leqslant 180$ K, the temperature dependences of the resistivity and intensity of the CDW satellites exhibit a large hysteresis. This means that the CDW state is metastable below T_{P1}. The low-temperature transition affects the transport properties of the compound only after the onset of magnetoresistance at 6 T. This transition was detected during specific heat measurements using a relaxation technique.[17] The enthalpy and entropy of this transition to the CDW state are $\Delta H_{P2} = 220$ J mol^{-1} and $\Delta S_{P2} = 5.5$ J mol^{-1} K^{-1}, respectively.

Based on the X-ray diffraction data, two families of CDW satellites at $\boldsymbol{q}_1 = a^*/2\,(T_{P1} \approx 445\ K)$ and $\boldsymbol{q}_2 = a^*/3\,(T_{P2} = 324\ K)$ were found for the compound with $m = 9$.[85] The temperature dependences show that the resistivity at 300 K and the critical temperatures of transition to the CDW state increase as m increases.

It should be noted that the resistivity ($R_{300\ K}$) increases by two orders of magnitude on going from $m = 4$ to $m = 12$. However, the compound with $m = 7$ exhibits an abnormally high resistivity ($R_{300\ K} = 30$ mΩ cm). The temperature T_P monotonically increases by about an order of magnitude for the whole series of compounds with $4 \leqslant m \leqslant 12$ including the bronze with $m = 7$.[47]

Structural studies confirmed the onset of the CDW state in the $(PO_2)_4(WO_3)_{2m}$ compounds with $m = 10$ and 12 at room temperature. For the compound with $m = 10$ the CDW wave vector [$\boldsymbol{q} = (3/7)a^*$ in the undoped sample] is shifted towards $\boldsymbol{q} = a^*/2$ in the Ge-doped samples.[85]

CDW-satellites with $\boldsymbol{q} = a^*/2$ in these bronzes characterise a phase with $m = 12$. However, the nature of the low-temperature resistivity anomaly in these compounds has not been studied as yet.

The phases with $m = 4$ and 6 are regular and undergo a CDW transition. The MPTBp compound with $m = 7$ possesses anomalous properties. The higher $R_{300\ K}$ value corresponds to strong electron – phonon or electron – electron interaction, which is indirectly confirmed by the presence of the CDW satellite harmonics, which indicate an anharmonic CDW modulation. In this context the phenomenon should be described using the bipolaron model.[107]

X-Ray diffuse scattering data obtained for the phases with $m = 4$ and 6 showed that two different CDWs coexist in the temperature intervals 40 – 60 and 75 – 85 K.[3, 88] The large magnetoresistance at low temperatures along the direction perpendicular to perovskite-type layers was ascribed to the existence of unfilled states on the Fermi surface in the CDW state.[100]

To study how the population of energy levels influences the CDW character, the conductivity, magnetoresistance, Hall effect, thermoelectric power and specific heat were studied using a number of $K_x(PO_2)_4(WO_3)_8$ samples with $0.8 < x < 1.94$ [$K_x(PO_2)_4(WO_3)_8$ is an MPTBh compound].[8] All the compounds studied exhibit anomalous dependences of the Curie temperature (T_c) on x. The $T_c(x)$ curve plotted using the conductivity data for $x = 1.3$ passes through a maximum at $T = 170$ K. Based on the results of X-ray diffraction studies of the samples,[13, 58] the observed $T_c(x)$ dependence can be explained as a manifestation of nonmonotonic behaviour of the density of electronic states upon variation of energy. In contrast to transitions in the undoped monophosphate bronze $(PO_2)_4(WO_3)_8$, transitions in $K_x(PO_2)_4(WO_3)_8$ are not determined by conventional Peierls-type charge density instability and cannot be treated only in the framework of the Bloch – Grüneisen model for collisions between charge carriers and phonons.[8, 16]

VI. Conclusion

The phosphate tungsten bronzes exhibiting unusual electrophysical properties and electronic instabilities are studied by various physical and crystallographic methods. A number of MPTBp compounds forms several CDW states. The properties of the MPTBh and DPTBh compounds strongly depend on the type and concentration of inserted cations, affecting the number of electrons in the partially filled conduction band. Peculiarities of the crystal and electronic structures of these compounds permit independent variation of the thickness of the conducting layer and the degree of filling of the conduction band. This opens up great prospects for targeted design of materials with preset electrophysical properties.

Topology features of the Fermi surface in the phosphate tungsten bronzes are studied using modern quantum-chemical calculations and experimental methods.[89, 104, 111 – 114]

The range of phosphate tungsten bronzes is continuously being extended as a result of elaboration of new methods of synthesis. Systematisation of information on the structure – property relations will be useful for development of software for computer simulation of electrophysical properties of these complex systems.

Recently, the phosphate tungsten bronzes have found some fields of practical application. Materials based on the tungsten and molybdenum oxides are now widely used in electrochromic

cells, optical devices, as secondary batteries, in gas sensors and as catalysts of various processes.[115–130] This is also possible for the phosphate tungsten bronzes that exhibit catalytic activity in some oxidation and isomerisation reactions.[131–133]

The first MOSFET-like device employing the motion of CDW in $Rb_{0.3}MoO_3$ was fabricated recently. However, it is of limited use because a single crystal is used as the working substance.[134]

Particular emphasis is placed on practical applications of the dimensionality effects, in particular, for film heterostructures (single-phase epitaxial films grown by pulse-laser deposition), which exhibit a coherent CDW transport. Nonlinear behaviour of these films in weak electromagnetic fields leads to extremely high dielectric constant (from $>10^8$ at low frequencies to 10^3 at microwave frequencies) and is of considerable interest for modern electronics.[135] At present, no devices employing the phosphate tungsten bronzes are available because of the lack of supported bronze thin films. However, first attempts at obtaining such films have been made by the authors of this review.[136–138]

One can assume that the CDW transition temperatures and the resistance of oriented thin films of the phosphate tungsten bronzes can be controlled by synthesis of layers of specified thickness. This allows fabrication of controllable heterostructures made of these new functional materials using, in particular, lithography techniques. Submicrometre-scale structures and nanostructures based on phosphate tungsten bronzes will also permit implementation of new possibilities in the studies of the influence of the dimensionality on the CDW phenomenon.

References

1. J Bardeu *Phys. Today* **12** 25 (1990)
2. A Ottolenghi, J-P Pouget *J. Phys. I* **6** 1059 (1996)
3. M Greenblatt *Int. J. Mod. Phys. V* **7** 4045 (1993)
4. C Schlenker *Low-Dimensional Electronic Properties of Molybdenum Bronzes and Oxides* (Dordrecht: Kluwer Academic, 1989)
5. G Gruner (Ed.) *Density Waves in Solids, Frontiers of Physics Series* (Reading, MA: Addison Wesley, 1994)
6. E Canadell, M-H Whangbo *Phys. Rev. V* **43** 1894 (1991)
7. E Canadell, M Whangbo *Chem. Rev.* **91** 965 (1991)
8. P Roussel, D Groult, C Hess, Ph Labbe, C Schlenker *J. Phys.: Condens. Mater.* **9** 7081 (1997)
9. J Rouxel (Ed.) *Crystal Chemistry and Properties of Materials with Quasi-one-dimensional Structures* (Dodrecht, Boston, Lancaster, Tokyo: Kluwer Academic, 1986)
10. M-H Whangbo, E Canadell, P Foury, J R Pouget *Science* **252** 96 (1991)
11. S Adams *J. Solid State Chem.* **149** 75 (2000)
12. C Schlenker, C Hess, C Letouze, J Dumas *J. Phys. I* **6** 2061 (1996)
13. J Dumas, U Beierlein, S Drouard, C Hess, D Groult, Ph Labbe, P Roussel, G Bonfait, E Gomez Marin, C Schlenker *J. Solid State Chem.* **147** 320 (1999)
14. C Hess, C Schlenker, J Dumas, M Greenblatt, Z S Teweldemedhin *Phys. Rev. B* **54** 4581 (1996)
15. P Foury, J R Pouget, Z S Teweldemedhin, E Wang, M Greenblatt, D Groult *J. Phys. IV* **3** C2-133 (1993)
16. S Drouard, J Dumas, P Foury, J P Pouget, P Roussel, C Schlenker, D Groult *Synth. Met.* **103** 2636 (1999)
17. J Lehmann, C Schlenker, C Letouze, A Rotger, J Dumas, J Marcus, Z S Teweldemedhin, M Greenblatt *J. Phys. IV* **3** C2–243 (1993)
18. C Hess, C Shlenker, G Bonfait, T Ohm, C Paulsen, D Dumas, Z Teweldemedhin, M Greenblatt, J Marcus, M Almeida *Solid State Commun.* **104** 663 (1997)
19. C Hess, C Shlenker, G Bonfait, J Marcus, T Ohm, C Paulsen, J Dumas, J L Tholence, M Greenblatt, M Almeida *Physica C* **282–287** 955 (1997)
20. Ph Labbe, M Goreaud, B Raveau *J. Solid State Chem.* **61** 324 (1986)
21. S L Wang, C C Wang, K H Lii *J. Solid State Chem.* **82** 298 (1989)
22. J P Giroult, M Goreaud, Ph Labbe, B Raveau *Acta Crystallogr., Sect B: Struct. Crystallogr. Cryst. Chem.* **37** 2139 (1981)
23. B Domenges, M Hervieu, B Raveau, R J D Tilley *J. Solid State Chem.* **54** 10 (1984)
24. M Hervieu, B Domenges, B Raveau *J. Solid State Chem.* **58** 233 (1985)
25. B Domenges, M Hervieu, B Raveau, M O'Keeffe *J. Solid State Chem.* **72** 155 (1988)
26. Ph Labbe, D Ouachee, M Goreaud, B Raveau *J. Solid State Chem.* **50** 163 (1983)
27. M Lamire, Ph Labbe, M Goreaud, B Raveau *J. Solid State Chem.* **71** 342 (1987)
28. E Wang, M Greenblatt *J. Solid State Chem.* **68** 38 (1987)
29. E Wang, M Greenblatt, in *Extended Abstract Papers of the 197th American Chemical Society National Meeting, Dallas, TX, 1989* p. 520
30. C Schlenker, J Dumas, M Greenblatt, S Van Smalen (Eds) *Physics and Chemistry of Low Dimensional Inorganic Conductors. NATO-ASI. Ser. B: Physics* (New York: Plenum, 1996) Vol. 354
31. E Wang, M Greenblatt, I Rachidi, E Canadell, M-H Whangbo *J. Solid State Chem.* **81** 173 (1989)
32. E Wang, M Greenblatt, I Rachidi, E Canadell, M-H Whangbo *J. Solid State Chem.* **80** 266 (1989)
33. E Wang, M Greenblatt, I Rachidi, E Canadell, M-H Whangbo, S Vadlamannati *Phys. Rev. B* **39** 12969 (1989)
34. E Wang, M Greenblatt, I Rachidi, E Canadell, M-H Whangbo, S Vadlamannati *Phys. Rev. B* **40** 11964 (1989)
35. V V Lisnyak, N S Slobodyanik, V Ya Zub *Ukr. Khim. Zh.* **65** 78 (1999)
36. M Hervieu, B Raveau *Chem. Scr.* **22** 117 (1983)
37. M Hervieu, B Raveau *Chem. Scr.* **22** 123 (1983)
38. V V Lisnyak, Candidate Thesis in Chemical Sciences, Kiev National University, Kiev, 2001
39. V V Lisnyak, V S Sudavtsova, N V Stus, M S Slobodyanik, in *The 6th International School-Conference Phase Diagrams in Materials Science, Kiev, 2001* p. 76
40. P Roussel, D Groult, A Maignan, Ph Labbe *Chem. Mater.* **11** 2049 (1999)
41. P Roussel, S Drouard, D Groult, Ph Labbe, J Dumas, C Schlenker *J. Mater. Chem.* **9** 973 (1999)
42. H Mathis, R Glaum, R Gruehn *Acta. Chem. Scand.* **45** 781 (1991)
43. R Gruehn, R Glaum *Angew. Chem., Int. Ed.* **112** 706 (2000)
44. M Lenz, R Gruehn *Chem. Rev.* **97** 2967 (1997)
45. H Mathis, R Galum, R Gruehn, in *7 Vortrastagung der GDCh-Fachgruppe, Festkorperchemie, Bonn, 1994* p. 87
46. R Galum, O Trappe *Das Computerprogramm CVTRANS zur Modellierung Chemischer Transportexperimente* (Gießen: Universität Gießen, 1999)
47. C Schlenker, C Letouze, C Hess, A Rltger, J Dumas, J Marcus, M Greenblatt, Z S Teweldemedhin, A Ottolenghi, P Foury, J P Pouget *Synth. Met.* **70** 1263 (1995)
48. J P Giroult, M Goreaud, Ph Labbe, B Raveau *Acta Crystallogr., Sect. B: Struct. Crystallogr. Cryst. Chem.* **36** 2570 (1980)
49. N Kinomura, M Hirose, N Kumada, F Muto, T Ashida *J. Solid State Chem.* **77** 156 (1988)
50. P Roussel, P Foury-Leylekian, B Domenges, D Groult, Ph Labbe, J-P Pouget *Eur. Phys. J. B* **12** 497 (1999)
51. P Roussel, G Mather, B Domenges, D Groult, Ph Labbe *Acta Crystallogr., Sect. B: Struct. Sci.* **54** 365 (1998)
52. Z S Teweldemedhin, K V Ramanujachary, M Greenblatt *J. Solid State Chem.* **95** 21 (1991)
53. J P Giroult, M Goreaud, Ph Labbe, B Raveau *J. Solid State Chem.* **44** 407 (1982)
54. P Roussel, Ph Labbe, D Groult, B Domenges, H Leligny, D Grebille *J. Solid State Chem.* **122** 281 (1996)
55. P Roussel, Ph Labbe, H Leligny, D Groult, P Foury-Leylekian, J P Pouget *Phys. Rev. B* **62** 176 (2000)
56. A Benmoussa, D Groult, Ph Labbe, B Raveau *Acta Crystallogr., Sect C: Cryst. Struct.Commun.* **40** 573 (1984)
57. B Domenges, M Hervieu, B Raveau *Acta Crystallogr., Sect. B: Struct. Sci.* **46** 610 (1990)

58. S Drouard, D Groult, J Dumas, R Buder, C Schlenker *Eur. Phys. J. V* **16** 593 (2000)
59. B Domenges, M Goreaud, Ph Labbe, B Raveau *J. Solid State Chem.* **50** 173 (1983)
60. M Hervieu, B Raveau *J. Solid State Chem.* **43** 299 (1982)
61. J P Giroult, M Goreaud, Ph Labbe, B Raveau *Acta Crystallogr., Sect. B: Struct. Crystallogr. Cryst. Chem.* **37** 1163 (1981)
62. J P Giroult, M Goreaud, Ph Labbe, B Raveau *Acta Crystallogr., Sect. B: Struct. Crystallogr. Cryst. Chem.* **38** 2342 (1982)
63. M Goreaud, Ph Labbe, B Raveau *J. Solid State Chem.* **56** 41 (1985)
64. B Domenges, M Hervieu, B Raveau *Acta Crystallogr., Sect. B: Struct. Sci.* **40** 249 (1984)
65. E Wang, M Greenblatt *J. Solid State Chem.* **76** 340 (1988)
66. E Canadell, I Rachidi, E Wang, M Greenblatt, M-H Whangbo *Inorg. Chem.* **28** 2455 (1989)
67. E Wang, M Greenblatt, I Rachidi, E Canadell, M-H Whangbo *Inorg. Chem.* **28** 2452 (1989)
68. P Roussel, O Perez, Ph Labbe *Acta Crystallogr., Sect. B: Struct. Sci.* **57** 603 (2001)
69. V V Lisnyak, N V Stus, A M Solomon, in *Anniversary Fedorov Session FS2003, St Petersburg, 2003* p. 57
70. F Berrah, A Leclaire, A Guesdon, M M Borel, J Provost, B Raveau *J. Solid State Chem.* **141** 155 (1998)
71. A Leclaire, M M Borel, J Chardon, B Raveau *J. Solid State Chem.* **130** 48 (1997)
72. A Leclaire, M M Borel, J Chardon, B Raveau *J. Solid State Chem.* **127** 1 (1996)
73. A Leclaire, M M Borel, J Chardon, B Raveau *J. Solid State Chem.* **120** 353 (1995)
74. A Leclaire, M M Borel, J Chardon, B Raveau *J. Solid State Chem.* **124** 224 (1996)
75. A Leclaire, M M Borel, J Chardon, B Raveau *J. Solid State Chem.* **128** 215 (1997)
76. A Leclaire, M M Borel, J Chardon, B Raveau *Mater. Res. Bull.* **31** 1257 (1996)
77. A Leclaire, M M Borel, J Chardon, B Raveau *J. Solid State Chem.* **128** 191 (1997)
78. D Mezaoui, A Laclaire, M M Borel, B Raveau *Z. Kristallogr.* **212** 837 (1997)
79. A Leclaire, M M Borel, D Mezaoui, H Rebbah, B Raveau *C.R. Acad. Sci., Ser. IIc* **323** 679 (1996)
80. D Mezaoui, M M Borel, A Leclaire, H Rebbah, J Provost, B Raveau *J. Solid State Chem.* **136** 305 (1998)
81. P Roussel, Ph Labbe, D Groult *Acta Crystallogr., Sect. B: Struct. Sci.* **56** 377 (2000)
82. P Foury, J-P Pouget *Int. J. Mod. Phys. B* **7** 3973 (1993)
83. P Foury, J-P Pouget, Z Tewldemedihin, E Wang, M Greenblatt *Synth. Met.* **55–57** 2605 (1993)
84. P Foury, J-P Pouget, P Roussel, D Groult *Synth. Met.* **103** 2624 (1999)
85. A Ottolenghi, P Foury, J P Pouget, Z S Teweldemedhin, M Greenblatt, D Groult, J Marcus, C Schlenker *Synth. Met.* **70** 1301 (1995)
86. A Benmoussa, Ph Labbe, D Groult, B Raveau *J. Solid State Chem.* **44** 318 (1982)
87. P Foury, J P Pouget, E Wang, M Greenblatt *Synth. Met.* **43** 3973 (1991)
88. P Foury, J P Pouget, E Wang, M Greenblatt *Europhys. Lett.* **16** 485 (1991)
89. J Ludecke, A Jobst, S van Smaalen *Europhys. Lett.* **49** 357 (2000)
90. N V Stus, V V Lisnyak, M S Slobodyanik, in *Proceedings of the 20th European Crystallographic Meeting on Crystallography in Natural Science and Technology, Krakow, 2001* Vol. 1, p. 252
91. N V Stus, V V Lisnyak, M S Slobodyanik *J. Alloys Compd.* **325** 73 (2001)
92. A Benmoussa, D Groult, B Raveau *Rev. Chim. Miner.* **21** 710 (1984)
93. P Roussel, A C Masset, B Domenges, A Maignan, D Groult, Ph Labbe *J. Solid State Chem.* **139** 362 (1998)
94. J P Giroult, M Goreaud, Ph Labbe, B Raveau *Rev. Chim. Miner.* **20** 829 (1983)
95. P Foury-Leylekian, J P Pouget, M Greenblatt, E Wang *Eur. Phys. J. B* **2** 157 (1998)
96. V V Lisnyak, N V Stus, N S Slobodyanik, N M Belyavina, V Ya Markiv *J. Alloys Compd.* **309** 83 (2000)
97. B Domenges, M Goreaud, Ph Labbe, B Raveau *Acta Crystallogr., Sect. B: Struct. Crystallogr. Cryst. Chem.* **38** 1724 (1982)
98. U Beierlein, C Schlenker, J Dumas, D Groult, Ph Labbe, E Balthes, E Steep *Synth. Met.* **103** 2593 (1999)
99. Z S Teweldemedhin, K V Ramanujachary, M Greenblatt *Phys. Rev. B* **46** 7897 (1992)
100. A Rötger, J Lehmann, C Schlenker, J Dumas, J Marcus, Z S Teweldemedhin, M Greenblatt *Europhys. Lett.* **25** 23 (1994)
101. A Rötger, C Schlenker, J Dumas, E Wang, Z S Teweldemedhin, M Greenblatt *Synth. Met.* **56** 2670 (1993)
102. C Letouze, C Bonfait, C Shlenker, J Dumas, M Almeida, M Greenblatt, Z S Teweldemedhin *J. Phys. I* **5** 437 (1995)
103. C Hess, C LeTouze, C Schlenker, J Dumas, D Groult *Synt. Met.* **86** 2157 (1997)
104. N Witkowski, M Garnier, D Purdie, Y Baer, D Malterre, D Groult *Solid State Commun.* **103** 471 (1997)
105. C Hess, C Letouze, C Schlenker, J Dumas, D Groult, J Marcus *Synt. Met.* **86** 2419 (1997)
106. C Hess, A Ottolenghi, J P Pouget, C Shlenker, J L Hodeau, J Marcus *Synth. Met.* **86** 2169 (1997)
107. H Guyot, N Motta, J Marcus, S Drouard, B Balaska, in *Proceedings of the 19th European Conference on Surface Science (ECOSS-19), Madrid, 2000* Vol. 1, p. 54
108. E Canadell, M-H Whangbo *Int. J. Mod. Phys. B* **7** 4005 (1993)
109. E Canadell, M-H Whangbo *J. Solid State Chem.* **86** 131 (1990)
110. C M Varma, P B Littlewood, S Schmitt-Rink *Phys. Rev. Lett.* **63** 1996 (1989)
111. Y F Yan, M Kleman, C LeTouze, J Marcus, C Schlenker, in *Extended Abstract of the 13th International Conference on Electronic Microscopy* (Eds B Jouffrey, C Collieux) (Paris: Les Editions de Physique, 1994) Vol. IIB, p. 909
112. Y Yan, M Kleman, C Letouze, J Marcus, C Schlenker, A Buffat *Europhys. Lett.* **30** 49 (1995)
113. E Sandre, P Foury-Leylekian, S Ravy, J-P Pouget *Phys. Rev. Lett.* **86** 5100 (2001)
114. O Perez, P Roussel, H Guyot *Tech. Rep. Institut Max von Laue – Paul Langevin (Grenoble)* **1** 23 (2000)
115. X W Lou, H C Zeng *Inorg. Chem.* **42** 6169 (2003)
116. G R Patzke, F Krumeich, R Nesper *Angew. Chem., Int. Ed.* **41** 2446 (2002)
117. Y Xia, P Yang, Y Sun, Y Wu, B Mayers, B Gates, Y Yin, F Kim, H Yan *Adv. Mater.* **15** 353 (2003)
118. C N R Rao, A K Cheetham *J. Mater. Chem.* **11** 2887 (2001)
119. C N R Rao, G U Kulkami, P J Thomas, P P Edwards *Chem. Eur. J.* **8** 29 (2002)
120. N I Kovtyukhova, T E Mallouk *Chem. Eur. J.* **8** 4354 (2002)
121. C G Granqvist *Sol. Energy Mater. Sol. Cells* **60** 201 (2000)
122. I Turyan, U Q Krasovec, B Orel, T Saraidorov, R Reisfeld, D Mandler *Adv. Mater.* **12** 330 (2000)
123. W M Qu, W Wlodarski *Sens. Actuators, B,* **64** 42 (2000)
124. X Z Li, F B Li, C L Yang, W K Ge *J. Photochem. Photobiol., A* **141** 209 (2001)
125. C Santato, M Odziemkowski, M Ulmann, J Augustynski *J. Am. Chem. Soc.* **123** 10 639 (2001)
126. T Millner, J Neugebauer *Nature (London)* **163** 601 (1949)
127. J Pfeifer, E Badaljan, P Tekula-Buxbaum, T Kovacs, O Geszti, A L Toth, H-J Lunk *J. Cryst. Growth* **169** 727 (1996)
128. H Qi, C Wang, J Liu *Adv. Mater.* **15** 411(2003)
129. Y B Li, Y Bando, D Golberg, K Kurashima *Chem. Phys. Lett.* **367** 214 (2003)
130. Z Liu, Y Bando, C Tang *Chem. Phys. Lett.* **372** 179 (2003)
131. V K Yatsimirsky, V V Lisnyak, N V Stus, N S Slobodyanik, in *Proceedings of the 5th European Congress of Catalysis, Limerick, 2001* p. 37
132. V V Lisnyak, N S Slobodyanik, V K Yatsimirsky, N A Boldyreva, in *Studies in Surface Science and Catalysis* Vol. 130 (Eds A Corma, F V Melo, S Mendioroz, J L G Fierro) (Amsterdam, London, New York, Paris, Geneva, Bern, Tokyo, Seoul, Sydney: Elsevier, 2000) p. 3807

133. V V Lisnyak, N S Slobodyanik, V K Yatsimirsky, in *Proceedings of the 4th European Congress of Catalysis, International Conference on CO Catalyst, Remini, 1999* p. 837
134. T L Adelman, S V Zaitsev-Zotov, R E Thorne *Phys. Rev. Lett.* **74** 5264 (1995)
135. H S J van der Zant, O C Mantel, C Dekker, J E Mooij, C Traeholt *Appl. Phys. Lett.* **68** 3823 (1996)
136. V V Lisnyak, N V Stus, M S Slobodyanik, in *Proceedings of International Conference Functionalized Materials: Synthesis, Properties and Application, Kyiv, 2002* p. 55
137. V V Lisnyak, N V Stus, M S Slobodyanik, in *Proceedings of International Conference Functionalized Materials: Synthesis, Properties and Application, Kyiv, 2002* p. 144
138. V V Lisnyak, N V Stus, V S Sudavtzova, P Popovich, N S Slobodyanik, in *Science for Materials in the Frontier of Centuries Advantages and Challenges* Vol. 2. (Ed. V Skorohod) (Kyiv: European Material Research Society, National Academy of Science of Ukraine, Frantsevich Institute for Problem of Material Science, 2002) p. 233

Russian Chemical Reviews **73** (8) 771 – 784 (2004) © 2004 Russian Academy of Sciences and Turpion Ltd

DOI 10.1070/RC2004v073n08ABEH000906

Pyrido- and pyrimidoisoindoles: methods of synthesis and properties

A A Pokholenko, Z V Voitenko, V A Kovtunenko

Contents

I.	Introduction	771
II.	Methods of synthesis of pyrido- and pyrimidoisoindoles	771
III.	Electronic structures and spectral characteristics of aromatic azinoisoindoles	779
IV.	Chemical properties	779
V.	Biological activity	783

Abstract. The data on the synthesis, structures and chemical properties of pyrido- and pyrimidoisoindole derivatives with an azine ring annelated to a pyrrole ring, which have been published over the last two decades, are generalised. The structure of the π-electron system and the high reactivities of azinoisoindoles are discussed. Special attention is given to aromatic pyrido- and pyrimidoisoindoles. The bibliography includes 86 references.

I. Introduction

The heterocyclic isoindole system attracts the attention of chemists involved in both synthetic and theoretical chemistry. A combination of high reactivity with pronounced aromatic properties is the main distinguishing feature of isoindole derivatives.[1–3] Several quantum-chemical approaches to the estimation of aromaticity and description of the 10π-electron system of the isoindole ring have been proposed. It was found that the concept based on the calculation of valence activities of its fragments reflects the structures and properties of such *ortho*-quinoid heteroaromatic compounds in the most adequate way.[4,5] This concept was confirmed experimentally for isoindole derivatives using X-ray diffraction analysis[4] and mass spectrometry.[6]

The present review is devoted to the methods of synthesis and chemical properties of three types of isoindole systems fused at the pyrrole ring and containing a junction nitrogen atom, *viz*., pyrido[2,1-*a*]- (**1**),† pyrimido[2,1-*a*]- (**2**) and pyrimido[6,1-*a*]isoindole (**3**) derivatives.

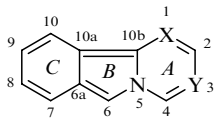

1: X = Y = CH;
2: X = N, Y = CH;
3: X = CH, Y = N

The annelation, to the electron-donating isoindole ring, of an additional acceptor azine ring strongly influences the structures and reactivities of these tricyclic systems, and unusual chemical properties can be expected. To date, investigations of *a*-fused isoindole systems are scarce. Some publications are devoted to original approaches to the synthesis of such derivatives, their biological activities and other useful properties. A review[2] devoted to the synthesis and properties of simple isoindoles provides but few examples of preparation of fused isoindole systems. Thus a small chapter in the monograph[1] published in 1983 is virtually the only literature source devoted to the chemistry of azinoisoindoles, whereas a recently published review[7] deals with the description of fused triazolo- and tetrazoloisoindoles. The present review surveys the data on the methods for the synthesis and properties of pyrido- and pyrimidoisoindoles published over the last two decades and includes some earlier publications, which enables the comprehensive presentation and systematisation of the data published on the subject.

II. Methods of synthesis of pyrido- and pyrimidoisoindoles

The uniqueness of the chemistry of azinoisoindoles can well be illustrated by some specially developed synthetic methods. As a rule, the starting compounds contained a benzene ring (*C*) to which a heterocyclic system [a pyrrole (*B*) or an azine (*A*) ring or both rings simultaneously] was attached. The data on the annelation of the benzene ring to indolizine derivatives (or their aza analogues) yielding azinoisoindoles are unavailable in the literature published over the last two decades, although several syntheses of this kind were described earlier.[1]

1. Synthesis of pyrido[2,1-*a*]isoindole derivatives

a. Closure of the pyrrole ring with formation of the N(5) – C(6) bond

The closure of the pyrrole ring with the concomitant formation of the N(5) – C(6) bond is one of the general approaches to the synthesis of aromatic isoindole systems. There are only a few examples of the synthesis of pyrido[2,1-*a*]isoindoles prepared by this method. Thus the intramolecular alkylation of the pyridine nitrogen atom is based on the formation of 2-[(*o*-halogenomethylaryl)]pyridines and has only been applied to the synthesis of pyrido[2,1-*a*]isoindole[8] and its methyl derivative.[9] Treatment of pyridines **4** with HBr affords pyrido[2,1-*a*]isoindolium bromide **5** in good yields. The dehydrobromination of the salt **5** (R^1 = H) with an aqueous solution of sodium carbonate gives a base (**1**) which is unstable in air, but can be used for further conversions.

A A Pokholenko, Z V Voitenko, V A Kovtunenko Department of Chemistry, Kyiv National Taras Shevchenko University, ul. Vladimirskaya 64, 01033 Kyiv, Ukraine. Fax (38-044) 235 12 73. Tel. (38-044) 239 34 93. E-mail: palek@mail.univ.kiev.ua (A A Pokholenko), z_voitenko@mail.univ.kiev.ua (Z V Voitenko), vkovtunenko@mail.univ.kiev.ua (V A Kovtunenko)

Received 1 March 2004
Uspekhi Khimii **73** (8) 833 – 848 (2004); translated by R L Birnova

† These systems can also be regarded as benzo[*a*]indolizine derivatives; however, in general, we shall consider isoindole as the base fragment.

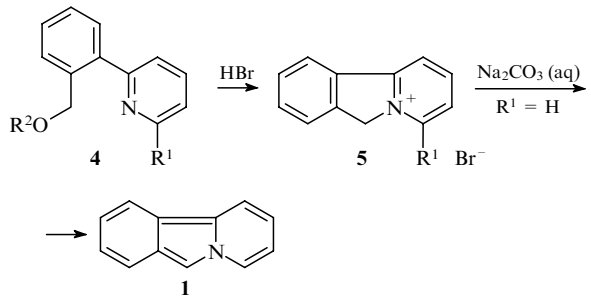

R^1, R^2 = H, Me.

A heptacyclic heteroaromatic system with a junction nitrogen atom containing a pyrido[2,1-*a*]isoindole fragment has been synthesised.[10] Upon thermal decarboxylation of quinaldinic acid (**6**) in the presence of *meso*-benzanthrone (**7**), the intermediate 2-(7-hydroxy-7-benzanthryl)quinoline (**8**) eliminates a water molecule and cyclises into compound **9**.

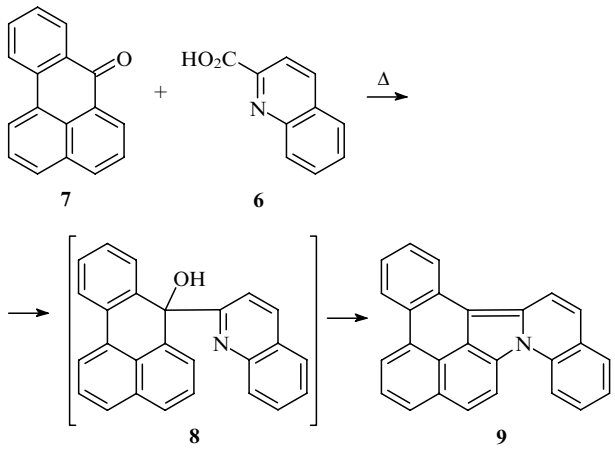

In this case, the formation of the N(5)–C(6) bond is preceded by the formation of the C(10a)–C(10b) bond, which results in the closure of the pyrrole ring and the formation of a fused pyrido[2,1-*a*]isoindole system.

b. Closure of the pyrrole ring with formation of the C(10a)–C(10b) bond

The most popular procedures for the synthesis of the pyridoisoindole system are based on the use of readily available *N*-substituted pyridine derivatives as the starting compounds. Two main types of cyclisation mechanisms are possible: one of them involves the formation of an ionic intermediate, while the second consists of the formation of a radical intermediate. Reactions *via* organometallic intermediates can be singled out into a separate group.

The Kröhnke cyclisation of pyridinium ylides. This cyclisation was discovered by Kröhnke[11] and is characteristic of ylides generated from pyridinium salts **10**. This served as the basis for the development of a general method for the formation of an isoindole fragment of nitrogenous heterocycles which was considered in detail in the monograph. [1] On treatment with a base, *e.g.*, an excess of piperidine in DMSO, pyridinium ylide **11** is converted into pyridoisoindole **12**.

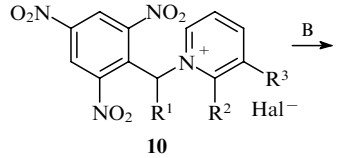

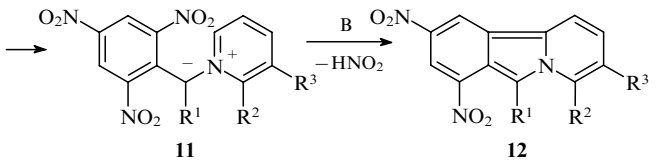

R^1 = H, ArCO; R^2, R^3 = H, Alk; B is a base.

This procedure, *viz*., short-term heating in aqueous methanol with 2 equiv. NaOH, is used for the preparation of 7,9-dinitropyrido[2,1-*a*]isoindole **12a** (R^1, R^2, R^3 = H) in 97% yield.

Cyclisation of radicals generated from aryl halides. Two approaches to the generation of free radicals, *viz*., photochemical and initiator-induced, are considered below.

Intramolecular photocyclisation enables the preparation of pyridoisoindoles containing halogens and alkyl substituents in both benzene and pyridine rings. The pyrido[2,1-*a*]isoindolium salt **5** (R^1 = R^2 = H) was synthesised for the first time by cyclisation of the isomeric pyridinium salts **13** (R^1 = R^2 = H) and **14** (R^1 = R^2 = H) upon UV irradiation of their aqueous solutions.[12]

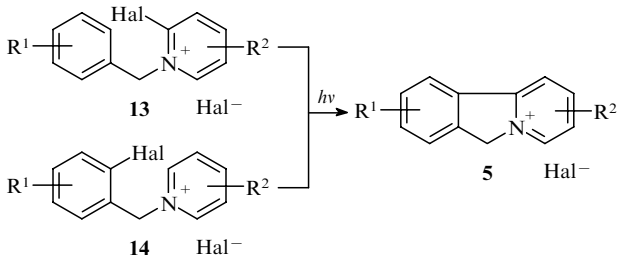

Hal = Cl, Br; R^1, R^2 = H, Me, Cl, Br.

Later, this method was extended to substituted pyridinium salts.[13, 14] The best yields of reaction products were obtained upon monochromatic irradiation of the substrate at the absorption wavelengths of the starting salt (~260–280 nm).[14] It was found that *N*-benzyl-2-halogenopyridinium salts **13** are more reactive than their isomers **14**. The effects of the substituents in the benzene and pyridine rings on the reaction rates and product yields have been investigated. No photocyclisation takes place, if the benzene ring of the starting salt contains a nitro group [12] or if alcohols, *e.g.*, methanol or ethanol, are used as solvents.[14]

The intermediates and products of laser-induced flash photolysis (a laser pulse at 266 nm) of the isomers **13** and **14** have been studied [15] and the following reaction mechanism has been proposed: the initial photohomolytic cleavage of the C–Hal bond is followed by radical arylation and proton elimination (Scheme 1).

Scheme 1

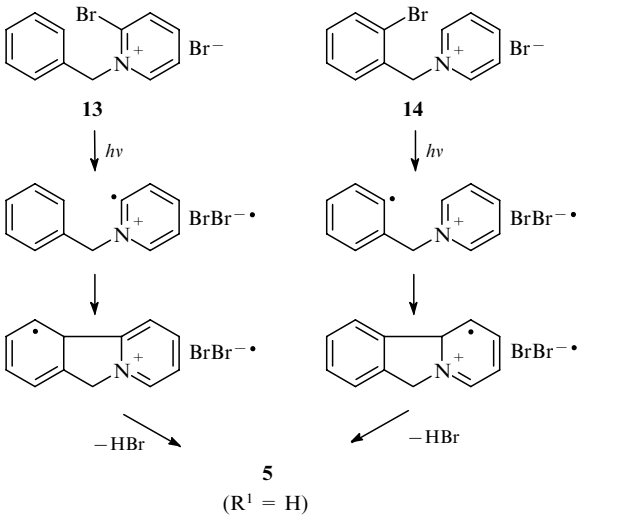

A method for the preparation of pyridoisoindoles by radical cyclisation of the corresponding *N*-(*o*-bromobenzyl)pyridone derivatives in the presence of an initiator has been developed.[16] Thus treatment of aryl bromide **15** with azobisisobutyronitrile (AIBN) and Bu_3SnH (benzene, 80 °C) results in the generation of an aryl radical which is intramolecularly attached to the pyridone ring at position 6. Retention of the double bond in compound **16** is interpreted as spontaneous oxidation of the intermediate radical addition product. This reaction occurs through a non-chain mechanism, so the initiator is used in an equimolar amount.

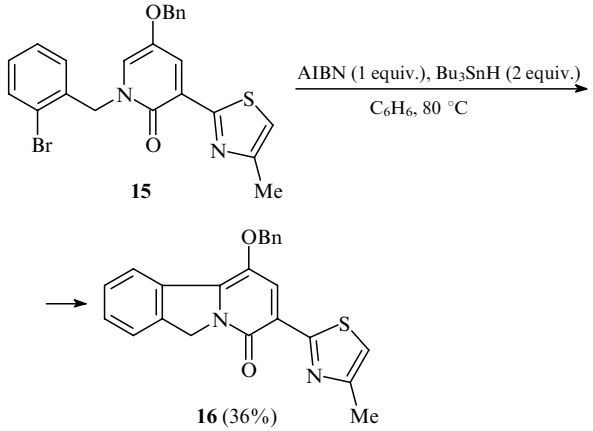

Hydrogenated pyrido[2,1-*a*]isoindoles are formed similarly from tetrahydro- and dihydropyridine derivatives containing a 5,6-double bond. Thus starting from *N*-(*o*-halobenzyl)pyridines **17** compounds **18** are formed under radical initiation conditions, whereas derivatives **19** (R = H) give rise to the isomers **20** and **21** in total yields 34% – 52%.[17] In these reactions, reductive debromination affords compounds **22** and **23** as side products (Scheme 2).

N-(*o*-Iodobenzyl and *o*-iodobenzoyl)-3,4-dihydro-2-pyridones (**24** and **25**, respectively) also undergo cyclisation under the action of the system Bu_3SnH – AIBN.[18] This reaction requires catalytic amounts of the initiator; the reaction time increases to 8 – 10 h, and the corresponding products **26** and **27** are formed in high yields.

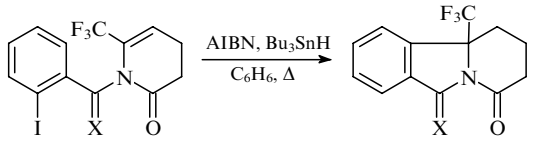

X = 2 H (**24**, **26**); O (**25**, **27**).

The radical cyclisation of 2-substituted 2,3-dihydro-4-pyridones **28** containing an *o*-bromobenzoyl group at the nitrogen atom occurs in good yields and with high diastereoselectivities. The pyridonoisoindolinones **29** formed were isolated as *trans*-isomers with a pseudo-axial position of the substituent R. The stereochemistry of the derivative **29a** was confirmed by data from X-ray diffraction analysis.[19]

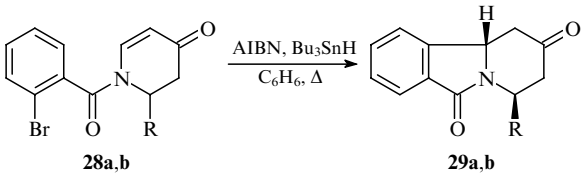

R = Ph (**a**, 91%), Me (**b**, 86%).

In contrast to the previous examples, *N*-benzoylpiperidines **30** do not contain a double bond as the site for the addition of a phenyl radical. However, these substrates can eliminate the hydrogen atom from the α-position to the nitrogen atom with a subsequent attack of the benzene ring. Such products were isolated from the reaction mixture upon radical cyclisation of compounds **30** under the action of the system AIBN – Bu_3SnH.[20] A stepwise formation of two radical intermediates, **31** and **32**, eventually resulting in the pyridoisoindole derivatives **33** was suggested.

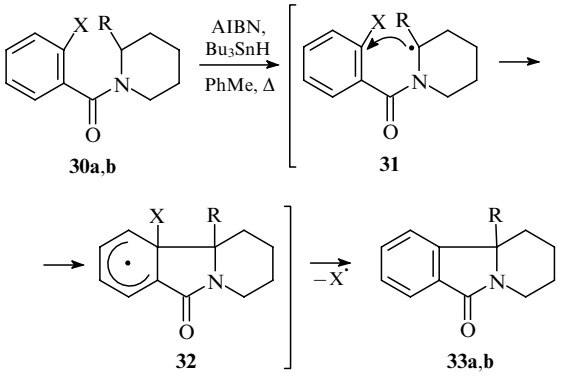

X = H, R = All (**a**, 10%); X = I, R = $CH_2C{\equiv}CSiMe_3$ (**b**, 18%).

This approach was used in the synthesis of a series of pyrido[1,2-*a*]isoindoles containing various functional groups in the pyridine ring.[21]

Intramolecular cyclisation of organometallic intermediates. The Heck intramolecular cyclisation is the most popular reaction of this type. Cyclisation of arylpalladium intermediates involving the double bonds of the tetrahydropyridine ring is the key step of this reaction. An unsuccessful attempt at cyclisation of substituted aryl bromide **15** under conditions of the Heck reaction has been described.[16] The use of the system $Pd(OAc)_2$ – PPh_3 – K_2CO_3 –

Scheme 2

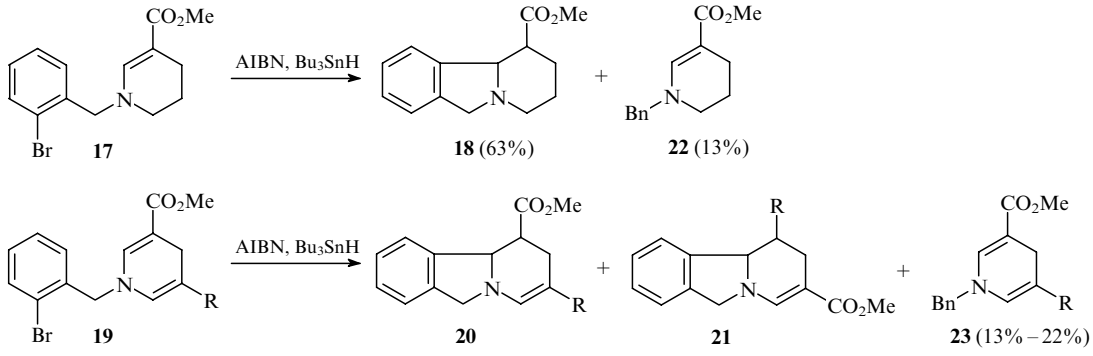

R = H, CO_2Me.

Et_4NCl led only to the reduction and decomposition of the substrate.

However, the intramolecular cyclisation using arylpalladium reagents was successfully applied to *N*-acyltetrahydropyridones **34** (see Refs 22 and 23).

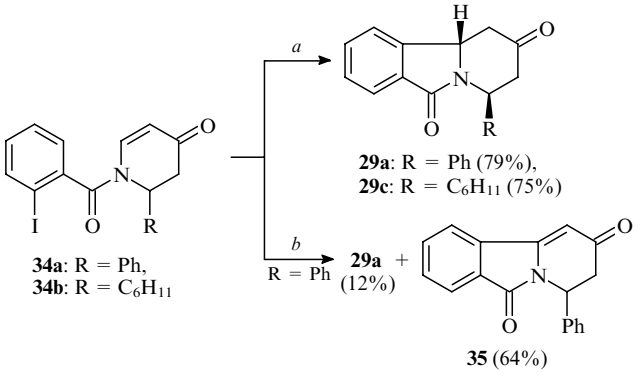

(*a*) $(Ph_3P)_2Pd(OAc)_2$, HCO_2H, Et_3N, DMF, 80 °C;

(*b*) $(Ph_3P)_2Pd(OAc)_2$, Bu_4NBr, NaOAc, molecular sieves 4 Å, DMF, 80 °C.

In the presence of formic acid (conditions *a*), this reaction occurs regio- and stereoselectively and yields only the *trans*-diastereomer **29** as in the case of the radical cyclisation of this substrate.[19] In the absence of a proton source (conditions *b*), the dehydrogenated derivative **35** is the main product. The carbonyl group of the amide bond is essential in this reaction; in its absence, only the dehalogenation of the substrate takes place.[22]

The competitive formation of three isomeric tetrahydropyrido[2,1-*a*]isoindolones **36**–**38** is observed in the intramolecular cyclisation of *N*-(*o*-iodobenzoyl)-2-methyltetrahydropyridine **39** *via* arylpalladium complexes. However, by varying reaction conditions one can change the ratio of the reaction products and even make this process regiospecific.[24, 25]

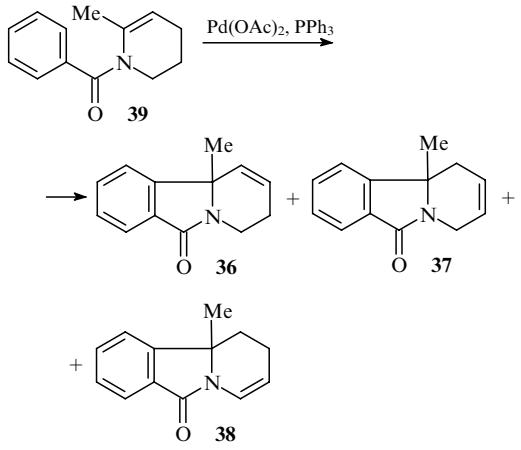

Conditions	*T* /°C	Time	Yield (%)	Selectivity (%)			Ref.
				36	**37**	**38**	
MeCN	–	–	–	39	34	27	24
K_2CO_3, Et_4NCl, DMF	30	2 h	72	68	32	–	25
TlOAc, MeCN	80	4 days	65	100	–	–	24

The cyclisation mechanism of 2-substituted *N*-(2-lithiobenzoyl- and 2-lithiobenzyl)-2,3-dihydro-4-pyridones formed upon treatment of substituted pyridones **34** and **40**, respectively, with butyllithium is similar to that of the Heck reaction. Rapid substitution of lithium for the halogen is followed by intramolecular nucleophilic addition.[26] This reaction is characterised by a high degree of stereoselectivity (compounds **29** and **41** were isolated as *trans*-isomers) and has found sufficiently broad synthetic application.

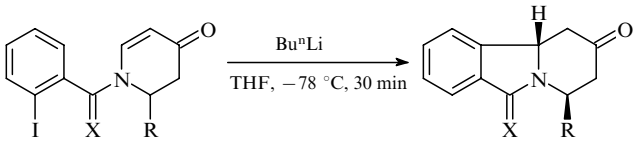

X = O (**29**, **34**); 2 H (**40**, **41**).

Compound	X	R	Yield (%)
29	O	Ph	91
	O	C_6H_{11}	86
	O	$CH_2=CH$	89
	O	$CH\equiv C$	88
	O	$C_4H_9C\equiv C$	86
41	2 H	H	50

c. Closure of the pyrrole ring with simultaneous formation of the C(5) – C(6) and C(10a) – C (10b) bonds

Heterocyclisation involving dehydrobenzene is an approach to the construction of the azinoisoindole system. 1,3-Dipolar addition of 4-substituted pyridinium dicyanomethylides **42** to dehydrobenzene results in 2-R-6-cyanopyrido[2,1-*a*]isoindoles **43** in moderate yields.[27–30] Dehydrobenzene can be generated by pyrolysis of diphenyliodonium-2-carboxylate or reaction of anthranilic acid with isoamyl nitrite. The derivatives **43** formed can themselves be used as 1,3-dipolar reagents (see Section IV.1.c). 6-Cyanopyrazino[2,1-*a*]isoindole is prepared from pyrazinium dicyanomethylide in a similar way, whereas pyrimidinium dicyanomethylide does not generate the corresponding heterocycles under these conditions.

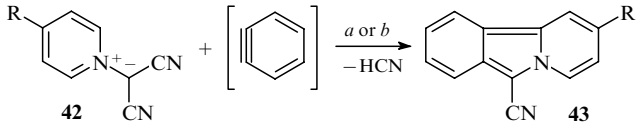

R = H, Me, Ph, COPh, COMe, CO_2Me;

(*a*) 190–200 °C; (*b*) chloroform – acetone, Δ.

d. Closure of the pyridine ring with formation of the C(1) – C(10b) bond

This methodology for the synthesis of a pyrido[2,1-*a*]isoindole structure is based on the use of *N*-substituted phthalimides and their analogues as the starting compounds. Two heterocyclisation principles are possible depending on the type of the intermediate formed.

Radical cyclisation. Several examples of cyclisations yielding saturated pyridoisoindoles are documented. Thus irradiation of the phthalimide derivative **44** results in photochemical triplet-sensitised decarboxylation. The intermediate biradical generated upon the electron transfer (the SET-mechanism) from the carboxylate anion to one of the carbonyl groups of the phthalimide eliminates CO_2 and undergoes cyclisation to give compound **45**.[31, 32] Irradiation of *N*-[4-(trimethylsilyl)butyl]phthalimide **46** in acetonitrile yields a mixture of products, since these conditions favour the simultaneous realisation of two mechanisms, *viz*., intramolecular abstraction of the hydrogen atom by the carbonyl group of phthalimide resulting in the formation of the biradical **47** followed by its subsequent conversions and cleavage of the trimethylsilyl group with a single-electron transfer resulting in the biradical **48**. If the reaction is carried out in an acetonitrile – water (35% of water) mixture, the second mechanism predominates and compound **45** is the only product (yield 94%) (Scheme 3).[33]

Scheme 3

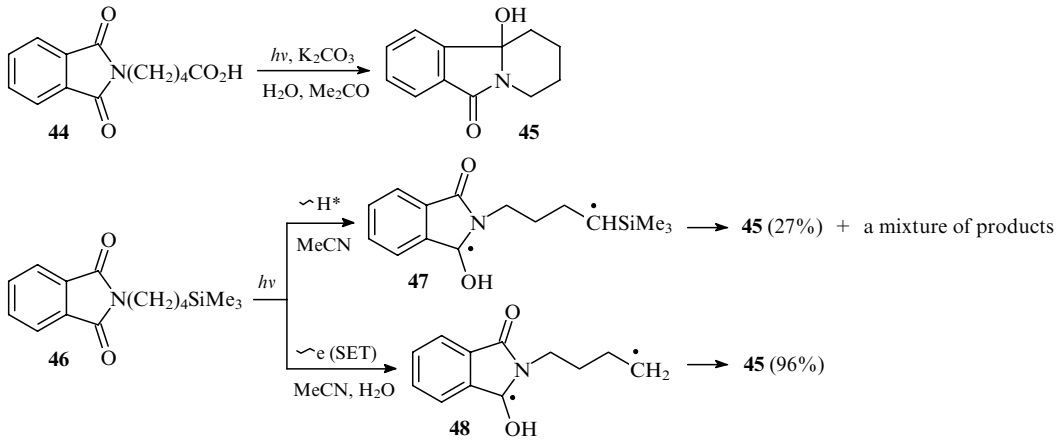

Cyclisation of the imide **49** under the action of SmI_2 (radical reduction) and subsequent spontaneous dehydration result in compound **50**.[34]

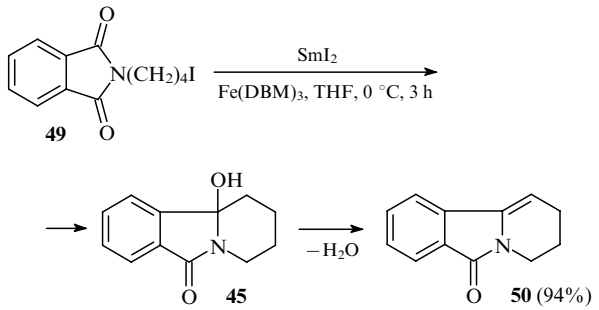

DBM is dibenzoylmethane.

Six-membered *exo*-cyclisation of the α-aminoacyl radical generated upon cleavage of the phenylthio group from phthalimidine **51** yields a functionalised saturated pyrido[2,1-*a*]isoindole derivative **52**.[35]

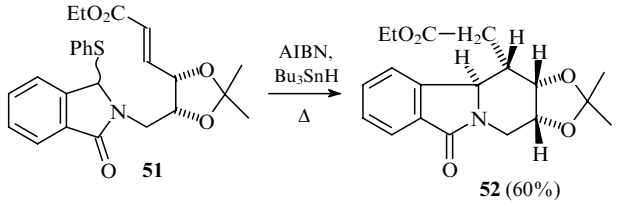

Cyclisation involving anionic intermediates. Among other reactions of formation of the pyridoisoindole system, this method is illustrated by the largest number of examples. Under the action of bases, substituted phthalimidine **53**, which is structurally close to the aforementioned derivative **51**, generates the α-aminoacyl-α-sulfoaryl anion **54**, which undergoes a Michael-type intramolecular addition to the double bond of the α,β-unsaturated ester substituent.[36] The tricyclic sulfone **55** is reduced to partially saturated isoindolone **56** upon treatment with Raney nickel.

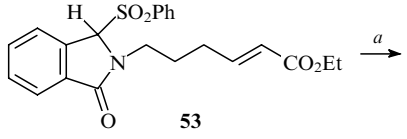

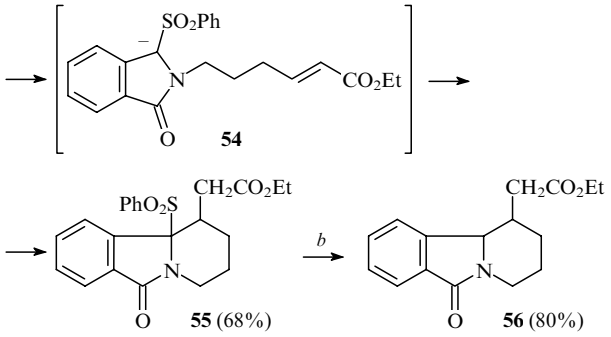

(*a*) NaH, DMSO, THF, 20 °C, 20 min;
(*b*) Ni/Re, EtOH, ultrasound, 5 min.

The formation of a nitrogen-containing tetracyclic system, which incorporates a pyridoisoindole fragment, was observed [37] in the recyclisation of the Michael addition products of a lithium derivative of the oxazoline **57** to α,β-unsaturated esters.

The adduct of the oxazoline anion to (*Z*)-ω-phthalimidopent-2-enoate **58**, *i.e.*, compound **59**, is converted into the tetracycle **60** in high yield under acidic conditions.[37]

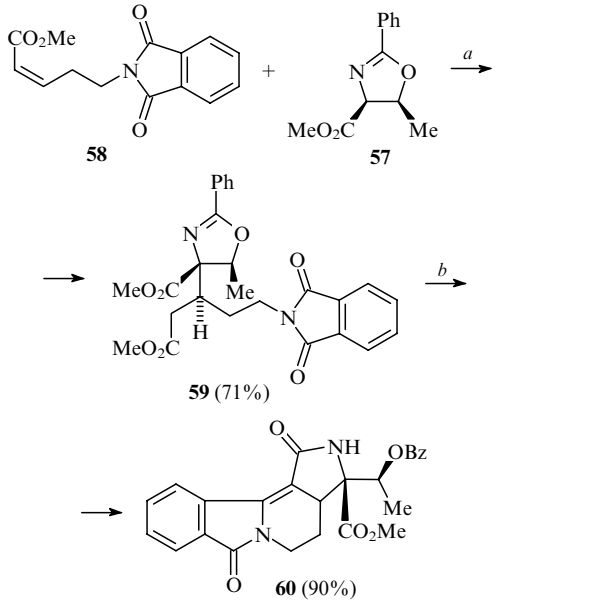

(*a*) LDA, DME, −78 °C; (*b*) CF_3CO_2H, Na_2SO_4, H_2O, THF.

Studies of alkylation of *N*-(3-bromopropyl)phthalimide **61** under the action of an excess of the anions **62** have shown that the closure of the pyridine ring in the intermediate phosphonates **63**

formed occurs by the Horner – Wadsworth – Emmons reaction to yield the pyridoisoindole derivatives **64**.[38]

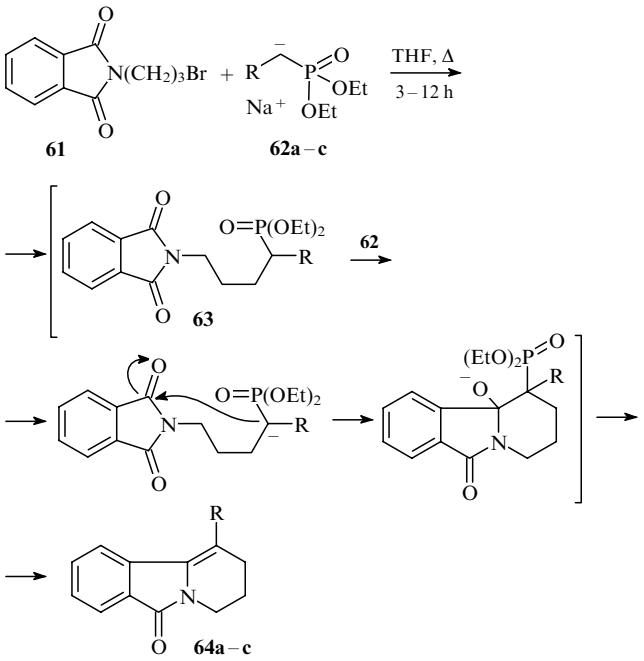

R = P(O)(OEt)$_2$ [**a** (78%)], CO_2Et [**b** (92%)], CN [**c** (95%)].

Closure of the C(1) – C(10b) bond of the pyridoisoindole system was also observed upon intramolecular cyclisation of ketone-stabilised sulfur ylides with a phthalimide substituent.[39–41] For example, cyclisation of the ylide **65** (prepared in four steps from β-alanine) in the presence of an equimolar amount of benzoic acid gave substituted pyrimidoisoindoledione **66**.[40]

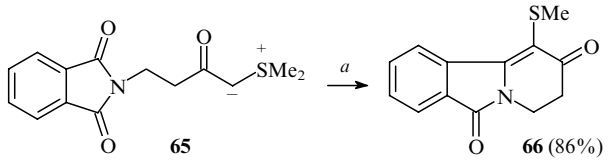

(*a*) $PhCO_2H$, PhMe, Δ.

Asymmetric mono-C-alkylation of chiral amidine **67** with 1,4-dichlorobutane gave compound **68**; the latter underwent easy intramolecular cyclisation to give an optically active hydrogenated pyridoisoindole **69** following hydrazinolysis.[42]

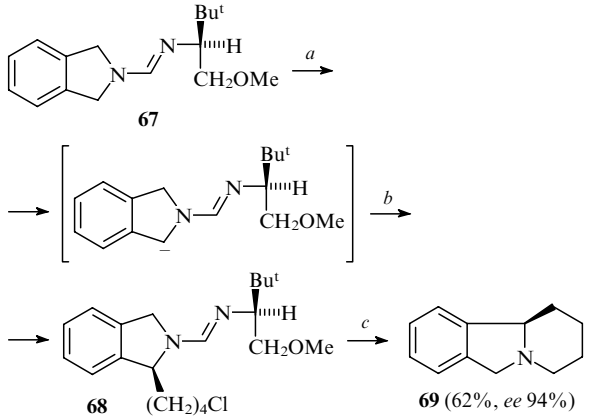

(*a*) Bu^{n}Li, THF, −78 °C; (*b*) $Cl(CH_2)_4Cl$, THF, −100 °C, 30 min; (*c*) N_2H_4, 20 °C, 5 – 10 min.

Pyridoisoindoles were also synthesised from substituted isoindole; in this case, the pyridine ring is 'made complete' using an addition reaction. Thus 3-ethoxy-1-methyl-1*H*-isoindole **70** reacts with dimethyl acetylenedicarboxylate (DMAD) (molar ratio 1 : 2) at room temperature to give 1,2,3,4-tetramethoxycarbonyl-6-methylpyrido[2,1-*a*]isoindole **71**.[43]

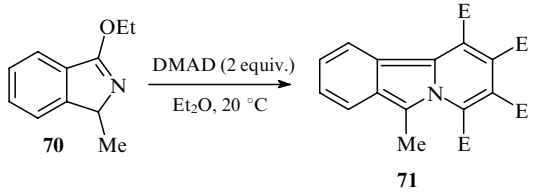

E = CO_2Me.

Hence, this method allows one to synthesise both saturated and aromatic pyridoisoindole derivatives.

e. Simultaneous closure of two rings

In this Section, we provide examples of several different approaches to the formation of a pyridoisoindole system. Thus aryl iodide **72** enters the so-called 'tandem' reaction with simultaneous closure of both heterocyclic rings, *viz*., pyrrole and pyridine, under conditions of the Heck reaction.[44] In terms of a hypothetical mechanism of such a double cyclisation, a palladium complex plays the role of a catalyst. Treatment of the starting iodide with palladium acetate in the presence of triphenylphosphine (2 equiv.) yields an arylpalladium intermediate where the palladium atom migrates from the aryl carbon atom to the alkyl carbon atom. This alkylpalladium complex contains no hydrogen atoms in the β-position with respect to the palladium atom which might be eliminated; therefore, it reacts with the second double bond present in the molecule. These conditions favour the transfer of the palladium atom to another alkyl carbon atom, its subsequent splitting as the initial palladium complex and formation of hydrogenated pyridoisoindolone **73**.

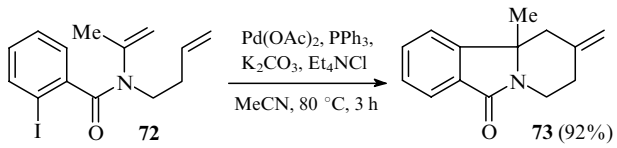

Synthesis of isoindolo[2,1-*b*]isoquinoline **74** where simultaneous formation of two heterocyclic rings also occurs has been described.[45] Heating of dry diammonium salt of 2,2′-dicarboxydeoxybenzoin **75** results in its cyclisation into 5,7-dihydroisoindolo[2,1-*b*]isoquinoline-5,7-dione **76**, which is reduced to the heteroaromatic system **74** in a two-step reaction.

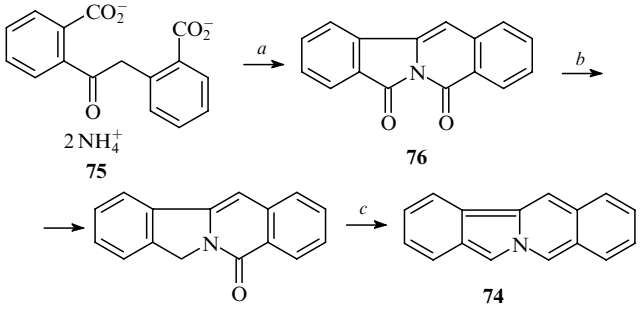

(*a*) Ph_2NH, 240 °C; (*b*) Zn, HCl, AcOH; (*c*) $LiAlH_4$, Et_2O, Δ, 3 h.

Treatment of 2- or 3-methylcrotonic acid **77** with lithium diethylamide gives the dianions **78**; their reactions with phthalodinitrile result in 6-iminopyrido[2,1-*a*]isoindolones **79**.[46] The yields of the conversion products depend on the type of the unsaturated acid used.

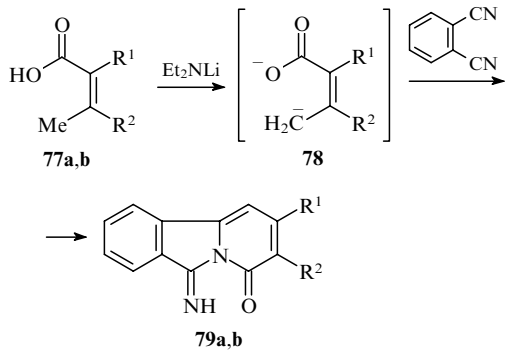

R^1 = Me, R^2 = H (*E*) [**a** (9%)]; R^1 = H, R^2 = Me [**b** (39%)].

The intramolecular Diels–Alder reaction in the substrates **80** also afforded partially saturated pyridoisoindoles. The starting molecule contains a piperidine ring, while the pyrrole and aliphatic rings are being constructed. The decahydropyrido-[2,1-*a*]isoindole structure is formed in a quantitative yield as a mixture of two diastereomeric pairs **81** (*cis*- and *trans*-isomers, the latter being predominant). This reaction occurs quantitatively both upon heating and under the action of a catalyst ($TiCl_4$).[47,48]

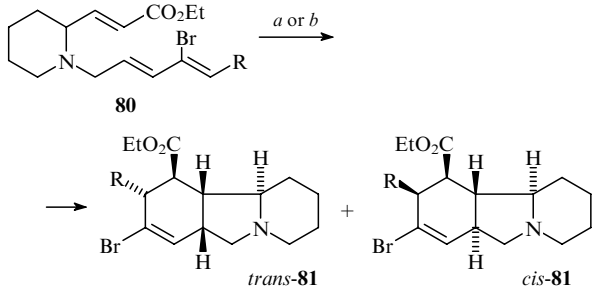

R = Me, Pr^i;

(*a*) PhMe, Ar, 100–150 °C, 16.5 h; (*b*) $TiCl_4$, CH_2Cl_2, 20 °C, 1 day.

2. Synthesis of pyrimido[2,1-*a*]isoindole derivatives

Systems containing fused isoindole and pyrimidine rings have received much less attention than pyrido[2,1-*a*]isoindoles. However, pyrimido[2,1-*a*]isoindole derivatives have recently been synthesised using both novel reactions and traditional approaches.

a. Closure of the pyrrole ring

Houlihan *et al.*[49] have performed synthesis of a series of 6-aryl-substituted 2,3,4,6-tetrahydropyrimido[2,1-*a*]isoindol-6-oles **82**. The *N*,*o*-dilithium derivatives prepared by treatment of 2-phenyl-1,4,5,6-tetrahydropyrimidines **83** with butyllithium reacted with methyl esters of halo-substituted benzoic acids. Compounds **82** represent structural analogues of the medicinal drug Mazindol (see Section V).

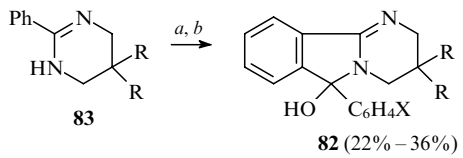

X = Cl, F; R = H, Me;

(*a*) Bu^nLi, THF, 50 °C, 3 h; (*b*) $XC_6H_4CO_2Me$, THF, 50 °C, 6 h.

Not only was this approach to the construction of the isoindole structure employed in the synthesis of annelated pyrimidine analogues, but it was also extended to imidazole and diazepine derivatives.[49]

b. Closure of the pyrimidine ring

Conventional cyclisation of thiolactams **84** into amidines[50] has recently been used for the synthesis of a series of the derivatives **85** containing a hydrogenated pyrimido[2,1-*a*]isoindole system with hydroxyalkyl substituents in positions 4 and/or 6.[51,52] This reaction includes several steps, *viz*., *S*-methylation of the starting thiolactam with methyl iodide to yield a methylthioimmonium salt, deprotection of the terminal amino group by treatment with trifluoroacetic acid and final spontaneous cyclisation into amidine **85** following deprotonation of the intermediate ammonium salt with a base.

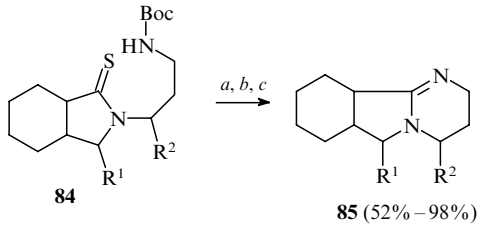

R^1 = R^2 = CH_2OH; R^2 = H: R^1 = $(CH_2)_2OH$, $CH_2CH(Ph)OH$;

(*a*) MeI, 20 °C, 17 h; (*b*) CF_3CO_2H, CH_2Cl_2, 0 °C;

(*c*) Et_3N or NaOH (solid), CH_2Cl_2, 0 °C, 2 h.

In the reactions of chiral starting thiolactams, enantiomerically pure hydroxyamidines **85** are formed, which proved to be very useful as catalysts in the asymmetric addition of nucleophiles to α,β-unsaturated ketones.

Cyclisation starting from 1-aminoisoindole. Construction of the pyrimidine ring fused to isoindole can also be performed starting from 1-aminoisoindole or its salts containing an N–C=N fragment. This methodology was initially applied to 1-aminoisoindolium perchlorate **86**. The pyrimido[2,1-*a*]isoindolium salts **87** substituted in the pyrimidine ring were prepared by its condensation with β-diketones **88**.[53,54]

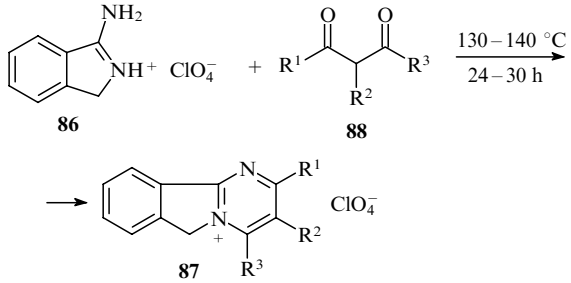

R^1, R^2, R^3 = H, Me, Et.

The 1-aminoisoindole base reacts similarly with β-oxo esters **89** to give both 2-oxo (**90**) and 4-oxo isomers (**91**).[55,56] A detailed investigation into this reaction has made it possible to select the conditions for the isolation of each of the isomers. Thus it was found that the yield of 4-oxo derivatives increases with temperature.

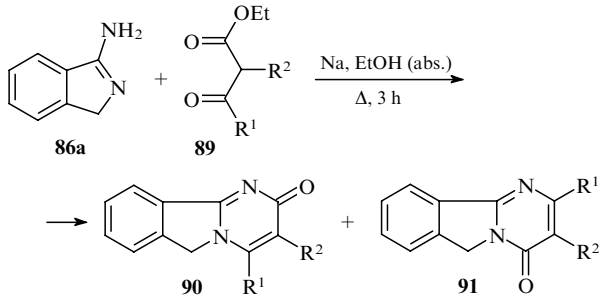

R^1–R^2 = $(CH_2)_n$; *n* = 3, 4.

c. Simultaneous closure of pyrrole and pyrimidine rings

Condensation of *o*-acylbenzoic acids and related compounds with 1,3-diamino derivatives, which results in simultaneous closure of the pyrrole and pyrimidine rings, is the most efficient approach to the synthesis of the pyrimido[2,1-*a*]isoindole system and was

detailed in the monograph.[1] Here, the most typical examples of synthesis based on this approach are mentioned.

1,3-Diaminopropane **92** reacts with *o*-acylbenzoic acids **93**, *o*-acylbenzaldehydes **94** and phthalic anhydride **95** (but not with phthaloyl dichloride or phthalates[57]) to give hexahydropyrimido[2,1-*a*]isoindol-6-ones **96** or the tetrahydro derivatives **97** and **98**, respectively. This reaction usually occurs upon boiling of the reaction mixture in toluene or xylene with azeotropic distillation of water in the presence of catalytic amounts of toluene-*p*-sulfonic acid (for **93**, the yields exceed 60%).

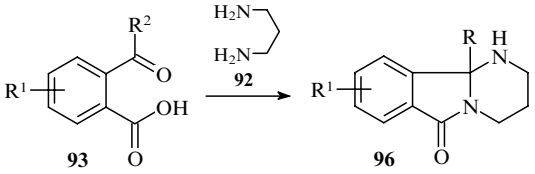

R^1 = H, Alk; R^2 = Alk, Ar.

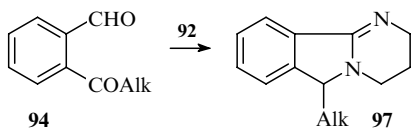

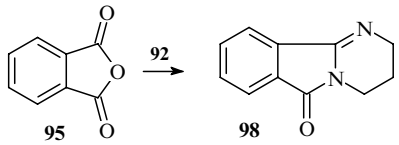

Carbonylation of 2-bromobenzaldehyde **99** with 1,3-diaminopropane **92** in the presence of a palladium catalyst also results in hexahydropyrimido[2,1-*a*]isoindol-6-ones.[58]

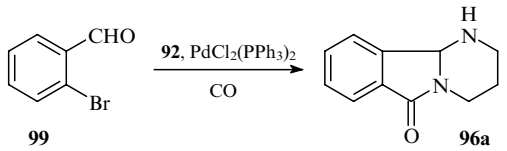

Heterocyclisation of carbene **100** formed upon gas-phase thermolysis of phenyltriazolo[1,5-*a*]pyrimidine **101** can also be related to this type. Pyrimido[2,1-*a*]isoindole **102** is the main reaction product.[59,60]

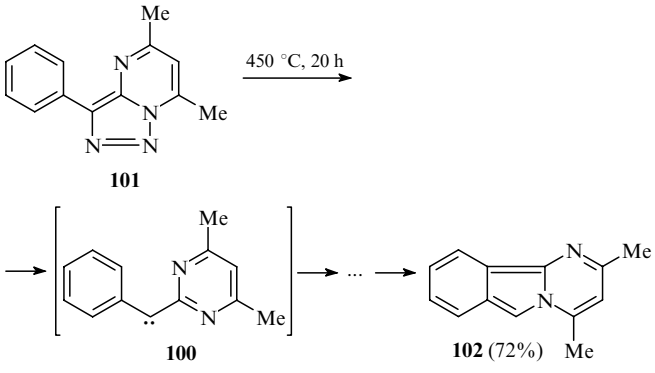

3. Synthesis of pyrimido[6,1-*a*]isoindole derivatives

The aromatic system of pyrimido[6,1-*a*]isoindole has not been synthesised so far; only a few examples of preparation of partially saturated derivatives of this heterocycle have been described. Thus cyclisation of diamides prepared by acylation of amine **103** leads to the closure of the azine ring of the pyrimido[6,1-*a*]isoindole **104**. Upon heating with phosgene, this amine forms compound **105**. The cyclic structure of the products **104** and **105** is confirmed by an upfield shift of a signal for the axial proton at the C(4) atom in the ^{1}H NMR spectra in comparison with the non-cyclic structure.[61]

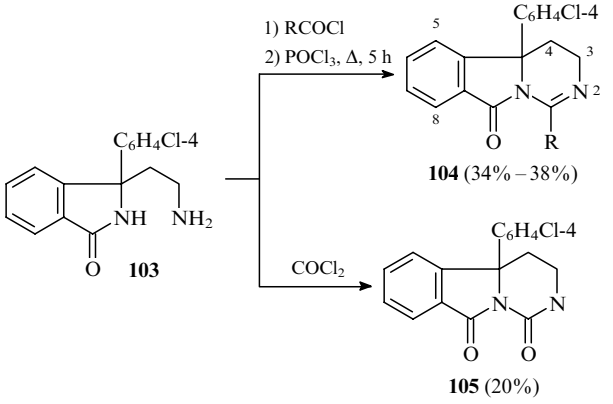

R = H, Me, 4-ClC_6H_4, CH_2Ph.

Treatment of pyrimidone **106** with formic and orthophosphoric acids results in the closure of the pyrrole ring and the formation of pyrimido[6,1-*a*]isoindole derivatives **107**.[62] Although the mechanism of this reaction has not been studied in detail, it can be assumed with a high degree of certainty that in acidic medium the arylmethyl carbocation, which is formed first, attacks either the carbon atom or the nitrogen atom of the enamine fragment. The direction of this reaction is determined by the presence, in the pyrimidine ring, of the *N*-methylpiperazine group which manifests electron-donating properties and induces strong activation of the nitrogen atom at position 1.

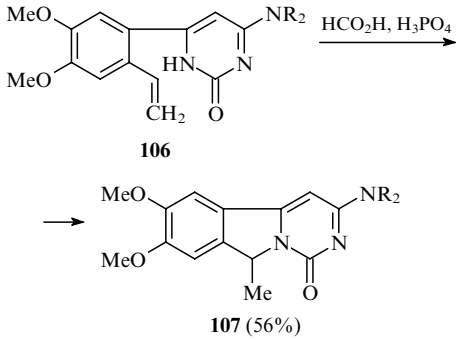

NR_2 is *N*-methylpiperazin-1-yl.

Treatment of the 1-(*o*-bromobenzoyl)pyrimidine derivatives **108** with Bu_3SnH or $(Me_3Si)_3SiH$ in the presence of catalytic amounts of AIBN afforded a series of tricyclic pyrimido[6,1-*a*]-isoindolinetriones **109** in good yields.[63] This synthetic approach is similar to the above-described radical heterocyclisation and allows the formation of the C(10a)–C(10b) bond and the closure of the pyrrole ring of hydrogenated pyrido[2,1-*a*]isoindolediones (see Section II.1.b).

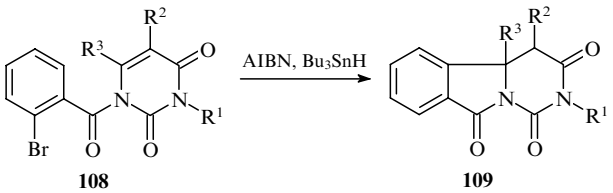

R^1	R^2	R^3	Yield (%)
Bu^s	Me	H	50
H	H	H	59
H	H	Me	80
H	H	CF_3	59

Thus, the choice of a synthetic procedure is determined by the structure of the desired azinoisoindolines.

III. Electronic structures and spectral characteristics of aromatic azinoisoindoles

Quantum-chemical calculations of aromatic azinoisoindoles **1**–**3** have demonstrated that these compounds can be regarded as 14π-electron aromatic systems characterised by a high degree of internuclear conjugation and localisation of double bonds in both six-membered rings, *i.e.*, azine and benzene. The highest negative π-charge of the systems **1**–**3** is on the carbon atom 6 of the pyrrole ring and exceeds that on the nitrogen atoms.[5] These peculiarities of the electronic structure are responsible for the changes in the chemical properties of azinoisoindole compounds in comparison with isoindole itself.

It is of note that annelation of the quinazolone fragment to the side *a* of isoindole yields the corresponding isomeric 18π -electron isoindoloquinazolones **110** and **111**, which can be presented as two weakly interacting π-fragments, one of which represents the 10π-electron fragment of isoindole.

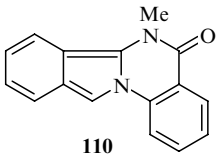

110

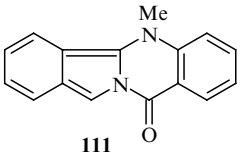

111

Consequently, their chemical behaviour should be similar to that of 1,2-disubstituted non-fused isoindoles.[5] The ability of isoindoloquinazolones to be involved in [4 + 2]cycloaddition reactions to give 1 : 1 adducts confirms this statement.

It is known that simple isoindoles behave as dienes in the Diels–Alder reaction involving the pyrrole ring.[1,2] Based on the results of quantum-chemical calculations, Kovtunenko *et al.*[64] attempted to predict the behaviour of various fused isoindoles in this reaction and in a competitive Michael addition in the α-position of the pyrrole ring. These calculations allowed one to suggest high activities of the compounds studied as dienes; the addition of dienophiles to all the azinoisoindoles under study (as in the case of isoindole) occurs most probably to the pyrrole diene fragment, *i.e.*, at positions 6 and 10b. The values of the static reactivity indices suggest that the activities of azinoisoindoles in both synchronous and non-synchronous cycloaddition reactions decrease in the following order: **110** = **111** > **1** > **3** > **2**.

No special studies of the spectral properties of azinoisoindoles have been carried out; however, the structures of all the derivatives synthesised were confirmed by ^{1}H NMR or, in some cases, ^{13}C NMR spectroscopy. Comparative data on the NMR spectra for six 2-R-6-cyanopyrido[2,1-*a*]isoindoles **43** are available.[29] Detailed assignment of signals in the ^{1}H and ^{13}C NMR spectra of benzo[1,2]pyrrolizino[3,4,5-*a*,*b*]isoquinolines (**112**)[65] and indolizino[3,4,5-*a*,*b*]isoindoles (**113**) was carried out based on the results of COSY, HMQC and HMBC experiments and the nuclear Overhauser effects.[66]

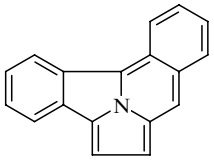

112

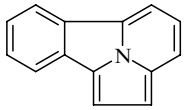

113

Matsumoto *et al.*[67] have measured the ESR spectra of the radical cations derived from benzo[*a*]isoindolo[1,2,3-*cd*]indolizine (1,2,3,4-dibenzocyclo[2,2,3]azine) **114** (R = H) upon its oxidation with $AgClO_4$ in dichloromethane at room temperature. It was found that despite high resonance stabilisation of the benzene rings these compounds containing a pyridoisoindole fragment as a structural element are related to the 18π-electron conjugated system.

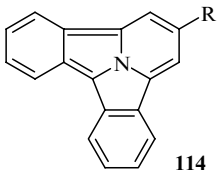

114

R = H, D, Me, Ph, PhCO.

The redox potentials of the derivatives of compounds **114** have been studied.[68,69] It was shown that the presence of an electron-withdrawing substituent in this heteroaromatic system increases their oxidation potentials in comparison with the unsubstituted compound **114** (R = H), whereas the electron-donating and phenyl groups decrease it.

The mass-spectrometric behaviour of some fused isoindole derivatives has been described.[6] Studies of the fragmentation patterns of molecular ions of pyrido[2,1-*a*]- and pyrimido[2,1-*a*]-isoindoles suggest their aromaticity. The specific pathways of their fragmentation under electron impact have been studied.

IV. Chemical properties

1. Reactions of pyrido[2,1-*a*]isoindoles

Like isoindole, aromatic pyrido[2,1-*a*]isoindoles demonstrate high reactivities. Reactions with electrophiles and addition of unsaturated compounds are the most characteristic for aromatic pyridoisoindoles.

a. Reactions with electrophiles

Aromatic pyrido[2,1-*a*]isoindoles as such are unstable compounds, therefore, the stable 6*H*-protonated forms, *i.e.*, pyridoisoindolinium salts of the type **5**, are usually employed in reactions with electrophilic reagents. The electrophilic attack occurs at the most electron-excessive position 6 of the pyrrole ring. Examples of such reactions (acylation, arylation, diazotisation, *etc.*) are described in the monograph.[1]

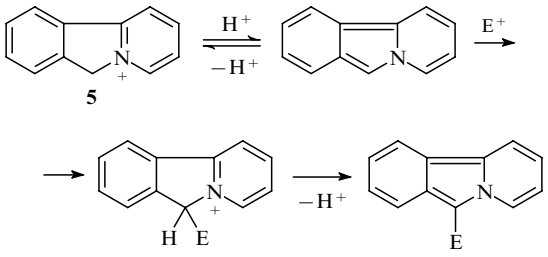

5

The reaction of 4-methylpyridoisoindolinium salt **5** (R^2 = 4-Me) with 2,3-dihydroxy-1,4-dioxane as the glyoxal synthon in ethanol in the presence of triethylamine (the molar ratio of the reagents is = 1 : 1 : 1), which yields compound **115** as a double condensation product at the side methyl group and at position 6 of pyridoisoindole,[9] can also be assigned to reactions of this kind. Apparently, the initial deprotonation involves the more CH-acidic methyl group.

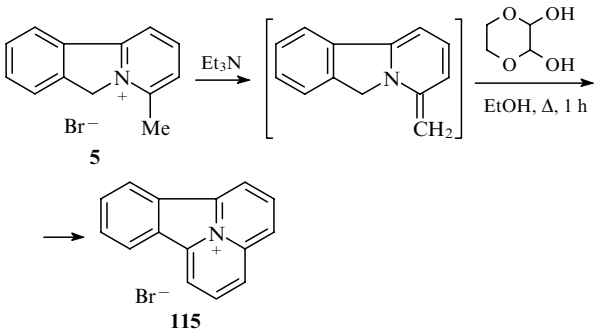

115

b. Addition of electron-deficient alkenes

The formation of the cyclic adducts **116** upon reactions of pyrido[2,1-*a*]isoindole **1** with compounds containing an activated double bond, *viz*., maleic, fumaric and acrylic esters and acrylonitrile, at 0 °C was established by ^{1}H NMR spectroscopy.[8] Spectral analysis revealed that the dienophile adds to the substrate at positions 4 and 6 in accordance with the [3 + 2](8π + 2π)-cycloaddition mechanism. These cycloadducts are extremely labile and at room temperature are gradually converted into the Michael adducts at position 6, *viz*., compounds **117**. Oxidation of the cycloadducts **116** with chloranil yields the indolizino[3,4,5-*ab*]-isoindole derivatives **118**.

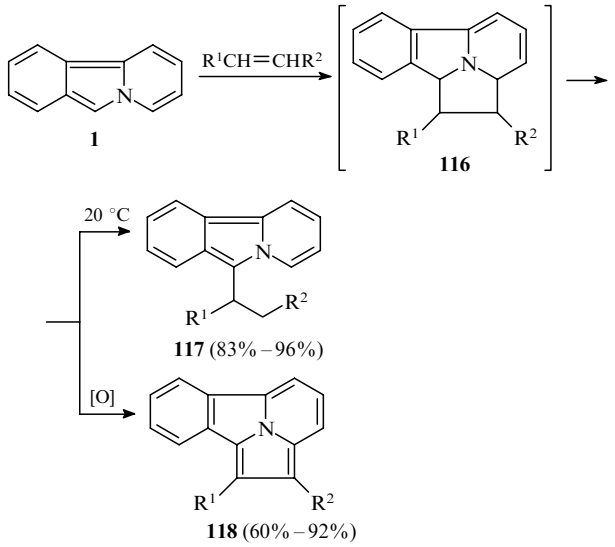

R^1 = H: R^2 = CN, CO_2Me; R^1 = R^2 = CO_2Me.

Unexpectedly, the reaction of pyrido[2,1-*a*]isoindole **1** with (*E*)-1-(4-methoxyphenyl)-2-nitroethene and *N*-(*p*-tolyl)maleimide (**119a**) at 0 °C gave directly the corresponding Michael adducts **117**. Thus, the cycloadducts represent kinetic products.[8]

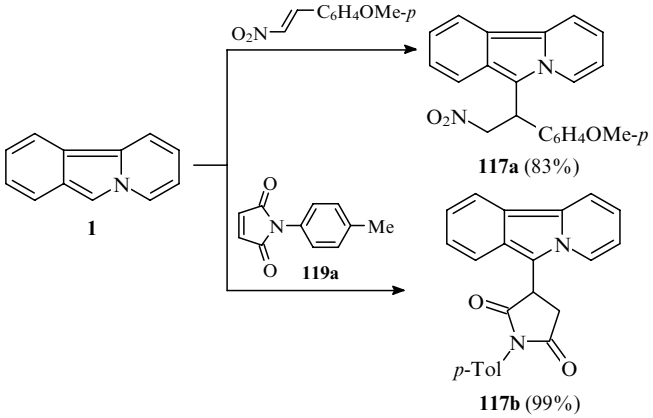

Recently, it has been shown that the reaction of pyrido[2,1-*a*]-isoindole **1** with maleinimides (2 equiv.) under conditions of thermodynamic control (boiling in propan-2-ol) yields the 1 : 2 adducts **120**. Their structures were investigated by spectroscopic methods and X-ray diffraction analysis, which revealed that the reaction is quite unusual. The following mechanism has been proposed: after the formation of the Michael adduct at position 6 of one alkene molecule (**121**) (the latter is similar to compound **117b**), the second maleimide molecule is added at positions 6 and 10b (the Diels – Alder reaction). The 7-azanorbornene system in the intermediate **122** is very sterically strained due to simultaneous annelation of three rings. This leads to the rearrangement of the bonds, which is accompanied by opening of two rings, aromatisation of the pyridine fragment and formation of an exocyclic double bond.[70, 71] Such a rearrangement has been documented for neither simple isoindole systems nor for fused systems.

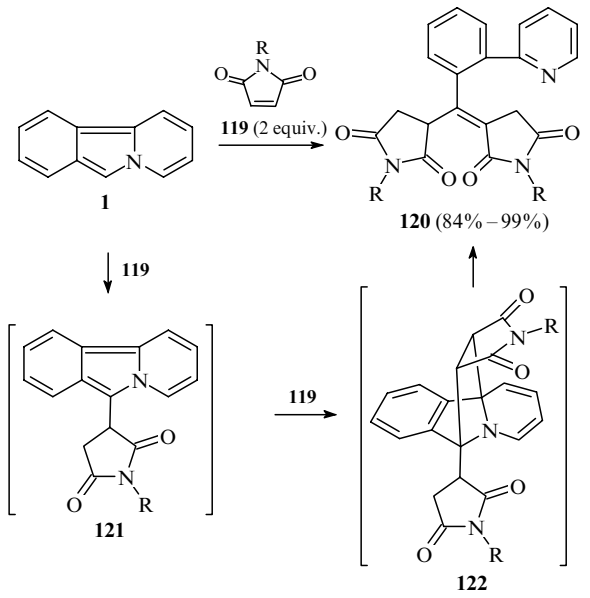

R = H, Ph, 4-MeC_6H_4, 4-$MeOC_6H_4$, 4-$NO_2C_6H_4$, Bn, naphthyl.

The conversion products **120** present interest with regard to their stereochemistry. In the solid state, they have a 'twisted' double bond (the winding angle is equal to 7 – 10°), whereas in solution they represent a mixture of atropodiastereomers due to the presence of an asymmetric carbon atom and hindered rotation around the C – C bond between the exocyclic double bond and the 2-(α-pyridyl)phenylene fragment.[70] This phenomenon was studied in detail using ^{1}H NMR spectroscopy and the possibility of atropoisomerism in this type of compounds was confirmed by quantum-chemical calculations.[72]

c. Reactions with activated alkynes

These reactions have already been mentioned in the section devoted to the synthesis of pyrido[2,1-*a*]isoindoles. Thus the preparation of 2-substituted 6-cyanopyrido[2,1-*a*]isoindoles using 1,3-dipolar addition of dehydrobenzene to 4-substituted pyridinium dicyanomethylides **42** is accompanied by the formation of benzo[*a*]isoindolo[1,2,3-*cd*]indolizines **114** as side products. Although the yields of the latter did not exceed 4% and no corresponding compounds were isolated in the case of R = CO_2Me, it is evident that 6-cyanopyrido[2,1-*a*]isoindole **43** was further coupled with dehydrobenzene with the elimination of HCN.[29, 30]

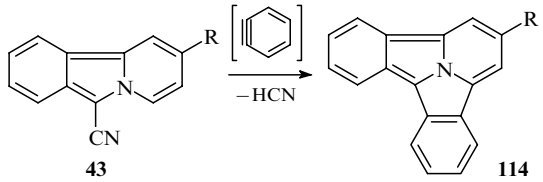

R = H, Me, Ph, PhCO, CO_2Me, MeCO.

It is of interest that the change in the mode of generation of dehydrobenzene (the reaction of anthranilic acid with isoamyl nitrite was used instead of pyrolysis of diphenyliodonium-2-carboxylate) and the decrease in the reaction temperature increase the yield of the corresponding benzoyl derivative of benzo[*a*]-isoindolo[1,2,3-*cd*]indolizine **114** (R = PhCO) (up to 17%) without any significant changes in the yields of the products with other substituents.[30] If compounds **43** isolated in the individual state reacted with dehydrobenzene generated by pyrolysis of diphenyliodonium-2-carboxylate, the yields of the products **114** were 18% – 39%.

6-Cyanopyrido[2,1-*a*]isoindoles **43** as 1,3-dipolar agents also add alkynes activated by at least one electron-withdrawing group at positions 4 and 6.[27, 29, 73, 74] The yields of compounds **123** (sometimes, in a mixture with their precursors **124**) depend on the nature of the alkyne and reaction conditions; regioisomers **123** in various ratios are obtained from non-symmetrical alkynes.[74]

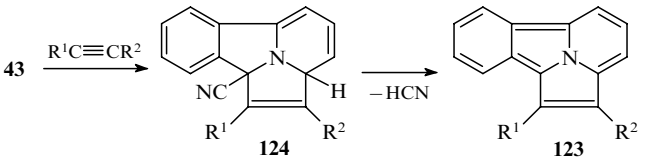

R^1, R^2 = H, COMe, COPh, CO_2Me, CO_2Bu^t, Ph, $SiMe_3$.

Numerous examples of reactions of fused pyridoisoindoles with dimethyl and diethyl acetylenedicarboxylates are documented. It was found[43] that isoquinolino[3,2-*a*]isoindole **125** reacts with diethyl acetylenedicarboxylate with the formation of benzoindolizino[3,4,5-*a*,*b*]isoindole **126**.

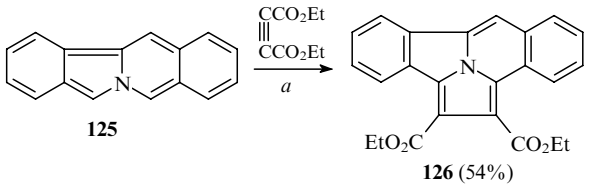

(*a*) 10% Pd/C, hydroquinone, PhMe, Δ, 14 h.

The data on the reaction of 6-cyanoisoindolo[1,2-*ab*]-isoquinoline **127** with dimethyl acetylenedicarboxylate are contradictory. Thus a product similar to the tetracycle **123** is formed in the presence of acetic acid (yield 26%),[75] whereas adducts with the composition 1 : 2 are formed in its absence (see Refs 73 and 75). The data on the structures of the latter are ambiguous. According to Matsumoto *et al.*,[73] they represent [5 + 2]-cycloaddition products which undergo further rearrangements into pyrroles **128** (3-cyanoindolizines react with DMAD in a similar way to yield pyrroles), whereas Tominaga *et al.*[75] prepared [3 + 2 + 2]-cycloadducts that underwent subsequent [1,5]-hydride shift, *i.e.*, compound **129** (an analogous reaction of 3-cyanoindolizine with DMAD has been described [73]) (Scheme 4).

Pyrido[2,1-*a*]isoindole itself reacts with DMAD involving positions 4 and 6, which is followed by a hydride shift.[8] Such structural conversion violates aromaticity of the benzene ring in favour of isoindole **130** with a quinoid structure containing a chain of conjugated double bonds.

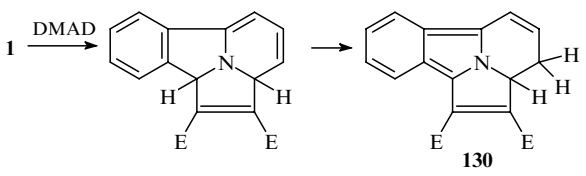

In contrast to the above examples, 1,2,3,4-tetramethoxycarbonyl-6-methylpyrido[2,1-*a*]isoindole **71** (for the synthesis, see above) reacts with DMAD at positions 1 and 4 as a diene to give the adduct **131**.[43] This result is quite unexpected: it could not be predicted either on the basis of the general theoretical concepts of the Diels – Alder reaction (since the isoindole fragment possesses more pronounced donor properties than the pyridine one and geometrical considerations suggest that the triple bond is preferably added synchronously to the five-membered pyrrole ring) or on the basis of calculations of the reactivity indices of such derivatives.[64]

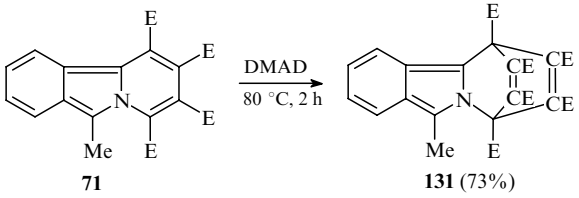

2. Chemical properties of pyrimido[2,1-*a*]isoindoles

These systems are still insufficiently studied; nevertheless, reactions with pyrimidino[2,1-*a*]isoindoles or their fused derivatives as substrates can be found in the literature.

a. Reactions with electrophiles

Electrophilic substitution of 2,4-dimethylpyrimido[2,1-*a*]isoindole **132** at position 6 occurs upon its treatment with phenyl isothiocyanate or acetic anhydride.[54]

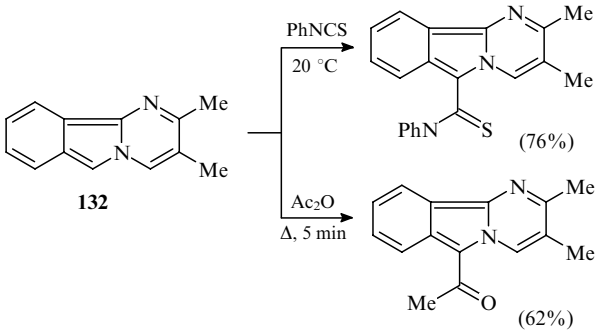

Scheme 4

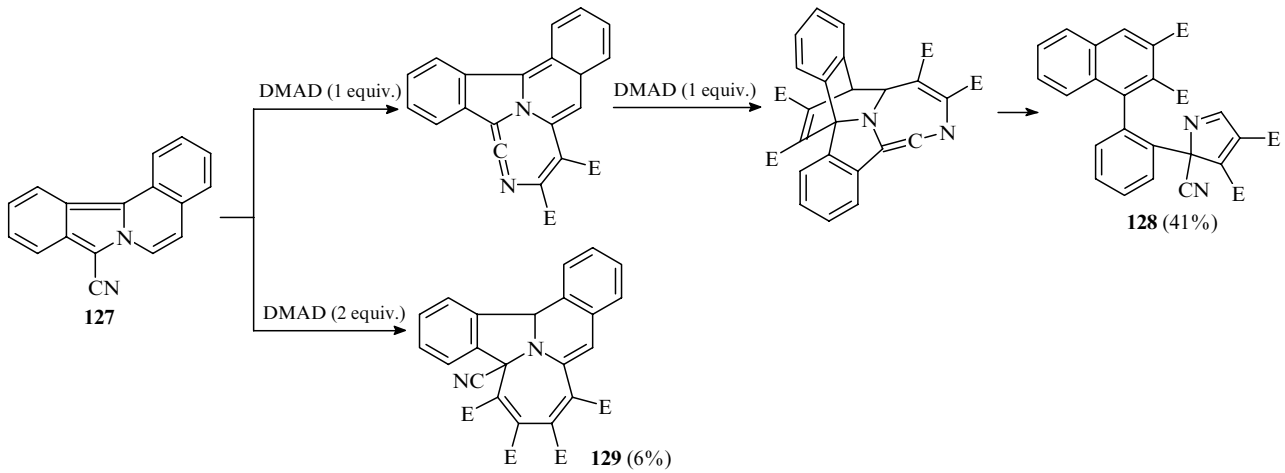

Rearrangement of pyrimido[2,1-*a*]isoindol-2-ones (**90**) into 4-isomers (**91**) was observed in 1985[76] and their properties including reactions with electrophilic reagents were studied. The rearrangement takes place upon heating of compounds **90** with sulfur in DMF. A similar reaction occurred upon heating with selenium; however, it was less efficient. The mechanism of this rearrangement has not been established yet.[77]

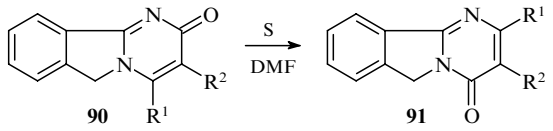

R^2 = H: R^1 = Me, Ph; R^1–R^2 = $(CH_2)_n$; n = 3, 4.

Presumably, in the initial step sulfur electrophilically attacks the position 6 of isoindole. The hemithioaminal formed undergoes recyclisation (*via* thioaldehyde) into an intermediate, which yields the isomer **91** following extrusion of sulfur.

Among other reactions with electrophiles, protonation and methylation of both isomers have been studied. According to IR spectroscopic data, compounds **90** are protonated at the oxygen atom in the formation of hydrobromides, while compounds **91** undergo protonation at the nitrogen atom at position 1. In reactions with dimethyl sulfate or methyl toluene-*p*-sulfonate, pyrimido[2,1-*a*]isoindol-4-ones **91** are methylated at the nitrogen atom at position 1. The structure of the methylation products of the 2-isomers depends on reaction temperature: at temperatures up to 100 °C, methylation occurs at the oxygen atom, whereas that at 130 °C occurs at the nitrogen atom at position 1 (see Ref. 78). Pyrimido[2,1-*a*]isoindol-2-ones **90** differ from the 4-isomers in having lower chromatographic mobilities and lower stretching vibration frequency of the C=O group in the IR spectra. Pyrimido[2,1-*a*]isoindol-4-ones **91** are characterised by a bathochromic shift in the UV spectra.[79] Other differences in physicochemical properties of these isomers have also been established.[79,80]

b. Reactions with activated unsaturated compounds

Recently, it has been found that reaction of 2,4-dimethylpyrimido[2,1-*a*]isoindole **133** with maleimides **119** yields a mixture of products (Scheme 5) from which benzo[*f*]isoindole derivatives **134** were isolated.[81,82] Their yields depended on the reaction conditions and the nature of the substituent in the imide fragment. A mechanism for the formation of these products was proposed in which extrusion of the bridging nitrogen atom from the intermediate Michael–Diels–Alder adducts **135** was the key step (see Scheme 5).

Interesting results were obtained in the study of reactions of isoindolo[2,1-*a*]quinazolin-5-ones **110** formally containing a pyrimido[2,1-*a*]isoindole fragment with maleimide derivatives. If the reagents are used at equimolar ratios, the rearranged adducts **136** are formed in high yields. This reaction occurs upon heating or brief boiling of the reactants in various solvents ($CHCl_3$, CH_2Cl_2, EtOH, Pr^iOH, PhMe). In order to establish the mechanism of this conversion under conditions of kinetic control, the intermediates **137**, which represent *endo*-Diels–Alder adducts, were isolated in the pure state. The conversion of the intermediate **137** into the final product **136** *via* the *exo*-isomer was confirmed by ^{1}H NMR spectroscopy.[83–85]

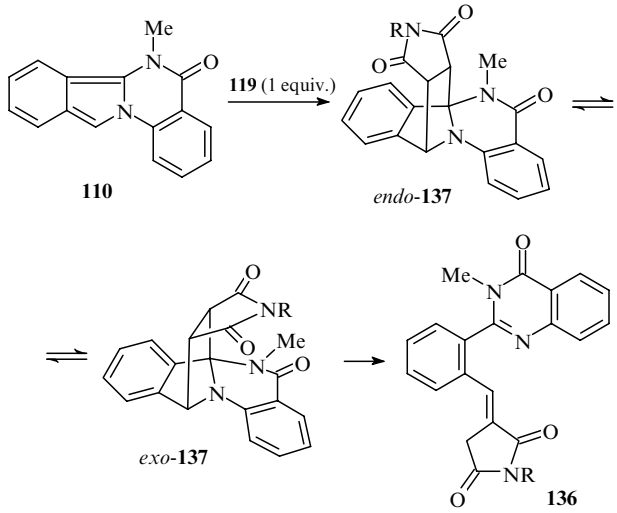

R = H, Bn, Ar.

With 2 equiv. of maleimide, the reaction under similar conditions follows another pathway: the Michael addition at the α-position of the pyrrole ring is the primary step, and the Michael adduct formed is involved in the Diels–Alder addition with the formation of stable tricyclic 7-azanorbornenes **138**. The structures of the products **136** and **138** were confirmed by X-ray diffraction analysis. No such rearrangement was observed for simple iso-

Scheme 5

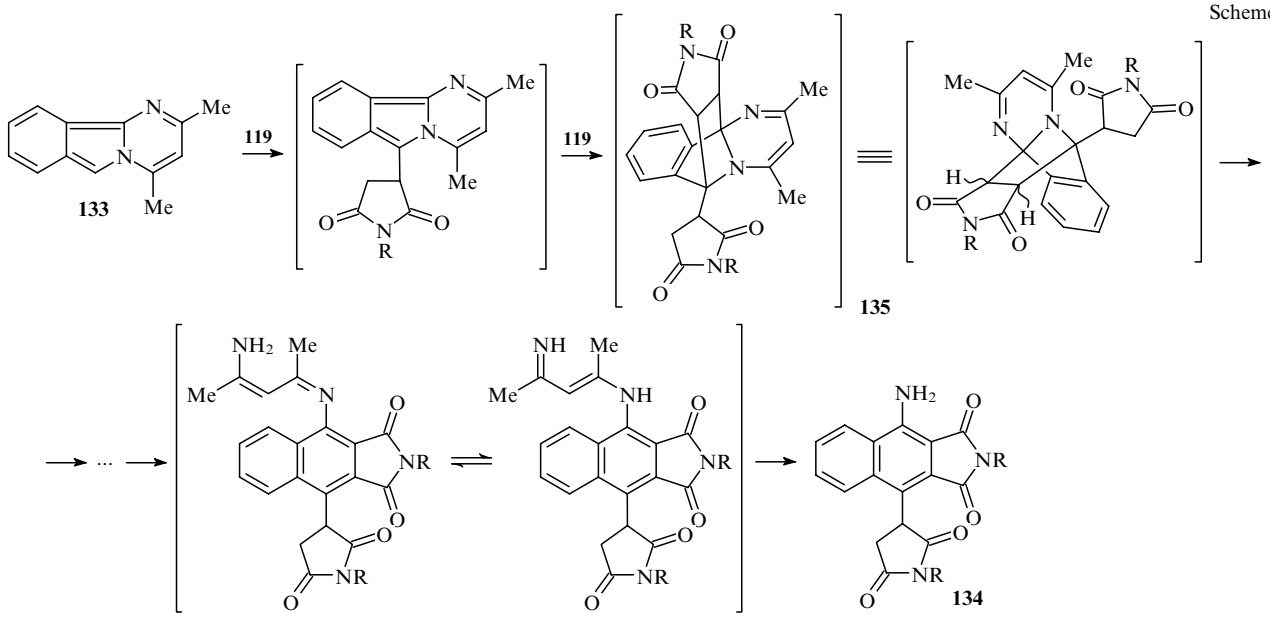

R = H, 4-MeC_6H_4, 2-MeC_6H_4, 4-$MeOC_6H_4$, 1-naphthyl.

indoles (including fused ones). Compounds **138** appeared to be the first stable representatives of tricyclic 7-azanorbornene derivatives.

Compound **110b**, which represents the adduct of compound **110a** with maleimide, contains a succinimide fragment as a substituent R and can further react with maleimides. The adducts **138** or **139** formed may contain various substituents in the imide fragments.

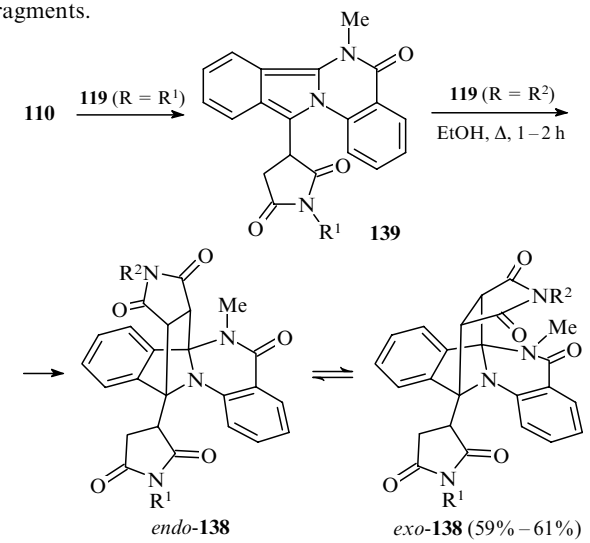

R^1, R^2 = H, Bn, Ar.

The reaction of 6-methyl-5,6-dihydroisoindolo[2,1-*a*]quinazolin-5-one **110a** with DMAD affords the Michael adduct **140**.

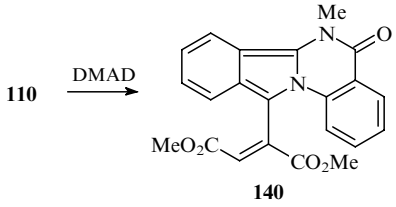

Studies of the chemical properties of various azinoisoindole compounds are under way.

V. Biological activity

Various isoindole derivatives have found application in many areas, particularly for production of polymeric materials possessing valuable properties or as biological markers and analytical reagents for chemistry and medicine. Numerous biologically active substances with a broad spectrum of activity have been found among compounds with the isoindole structure. Tricyclic isoindole derivatives (including azinoisoindoles) manifest antiviral, anti-inflammatory, analgesic and other physiological activities.[1]

Various analogues of Mazindol **141** (a psychotropic drug recently introduced into clinical practice) have been extensively investigated in the past decade. They include a series of partially unsaturated azinoisoindoles **83**, which manifested high activity in neuronal tests.[49]

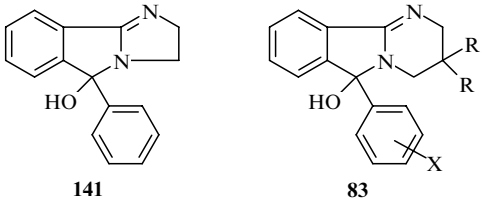

R = H: X = H, 2-F, 3-F, 4-F, 3-Cl, 4-Cl; R = Me, X = 4-Cl.

Compounds **83** inhibit the reverse capture of dopamine more efficiently than cocaine and Mazindol and by several orders of magnitude more selectively than serotonin.

Compound **16**, an analogue of known $GABA_A$ receptor agonists, was synthesised within the framework of a search for tricyclic non-sedative anxiolytic agents of the pyridine series.[21] This compound appeared to be efficient for both therapy and prophylaxis of CNS diseases.

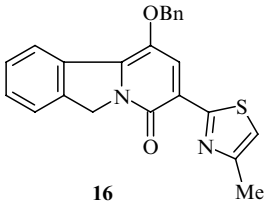

Among other newly established biological properties of pyrimidoisoindoles, special mention can be made of the bactericidal activity of the fused derivative **140**.[86]

Other examples of practical applications of isoindole derivatives can be found in the monograph [1] and reviews.[2, 7]

* * *

It should be noted in conclusion that despite the sufficiently large number of examples of formation of the pyridoisoindole system published in the literature, the portion of direct syntheses of aromatic pyrido[2,1-*a*]isoindoles is extremely small. Deprotonation of the corresponding 6*H*-salts is still the main route to the synthesis of aromatic pyrido[2,1-*a*]isoindole derivatives. Pyrimido[2,1-*a*]isoindole and its derivatives are studied to an even lesser extent, while aromatic pyrimido[6,1-*a*]isoindole systems are presently unknown.

It thus appears that the azinoisoindoles considered above are insufficiently studied, although calculations and the recently described reactions with dienophiles demonstrate their high synthetic potential. Of particular interest is the possibility of a transition to various classes of organic compounds as a result of recently discovered rearrangements. The known reactions of azinoisoindoles with maleimides suggest their high reactivities in addition reactions occurring at position 6 of the pyrrole fragment.

Systematic synthetic, spectroscopic (including X-ray diffraction analysis) and biological studies into pyrido- and pyrimidoisoindole derivatives and the products of their diverse conversions represent a promising field of research in the chemistry of heterocyclic compounds.

References

1. F S Babichev, V A Kovtunenko *Khimiya Izoindola* (The Chemistry of Isoindoles) (Kiev: Naukova Dumka, 1983)
2. V A Kovtunenko, Z V Voitenko *Usp. Khim.* **63** 1064 (1994) [*Russ. Chem. Rev.* **63** 997 (1994)]
3. F S Babichev, V A Kovtunenko, A K Tyltin *Usp. Khim.* **50** 2073 (1981) [*Russ. Chem. Rev.* **50** 1087 (1981)]
4. V A Kovtunenko, Z V Voitenko, V L Sheptun, A K Tyltin, A I Chernega, Yu T Struchkov, F S Babichev *Khim. Geterotsikl. Soedin.* 1497 (1984) [a]
5. V A Kovtunenko, Z V Voitenko, V L Sheptun, L I Savranskii, A K Tyltin, F S Babichev *Ukr. Khim. Zh.* **51** 976 (1985)
6. P B Terent'ev, V A Kovtunenko, Z V Voitenko, T T Kucherenko, V V Ishchenko, A K Tyltin, F S Babichev *Khim. Geterotsikl. Soedin.* 923 (1991) [a]
7. Z V Voitenko, T V Egorova, V A Kovtunenko *Khim. Geterotsikl. Soedin.* 1171 (2002) [a]
8. S Kajigaeshi, S Mori, S Fujisaki, S Kanemasa *Bull. Chem. Soc. Jpn.* **58** 3547 (1985)
9. M Fourmique, K Boubekeur, P Batail, K Bechgaard *Angew. Chem., Int. Ed. Engl.* **28** 588 (1989)

10. W Bradley, H E Nursten *J. Chem. Soc.* 4027 (1955)
11. W Augstein, F Kröhnke *Justus Liebigs Ann. Chem.* **697** 158 (1966)
12. A Fozard, C K Bradsher *Tetrahedron Lett.* **7** 3341 (1966)
13. A Fozard, C K Bradsher *J. Org. Chem.* **32** 2966 (1967)
14. Y-T Park, C-H Joo, C-D Choi, K-S Park *J. Heterocycl. Chem.* **28** 1083 (1991)
15. Y-T Park, N W Song, Y-H Kim, C-G Hwang, S K Kim, D Kim *J. Am. Chem. Soc.* **118** 11 399 (1996)
16. A Nadin, T Harrison *Tetrahedron Lett.* **40** 4073 (1999)
17. A L J Beckwith, S W Westwood *Tetrahedron* **45** 5269 (1989)
18. T Okano, T Sakaida, S Eguchi *J. Org. Chem.* **61** 8826 (1996)
19. A L J Beckwith, S P Joseph, R T A Mayadunne *J. Org. Chem.* **58** 4198 (1993)
20. M Ikeda, Y Kugo, T Sato *J. Chem. Soc., Perkin Trans. 1* 1819 (1996)
21. WO PCT 98/50384; *Chem. Abstr.* **130** 13 918 (1999)
22. D L Comins, S P Joseph, Y-m Zhang *Tetrahedron Lett.* **37** 793 (1996)
23. S Berteina, A D Mesmaeker *Synlett* 1227 (1998)
24. R Grigg, V Sridharan, P Stevenson, T Worakun *J. Chem. Soc., Chem. Commun.* 1697 (1986)
25. R Grigg, V Loganathan, V Santhakumar, V Sridharan, A Teasdale *Tetrahedron Lett.* **32** 687 (1991)
26. D L Comins, Y-m Zhang *J. Am. Chem. Soc.* **118** 12 248 (1996)
27. K Matsumoto, T Ushida, T Sugi, Y Yagi *Chem. Lett.* 869 (1982)
28. K Matsumoto, T Ushida, T Sugi, T Kobayashi *Heterocycles* **20** 1525 (1983)
29. K Matsumoto, T Ushida, K Aoyama, M Nishikawa, T Kuroda, T Okamoto *J. Heterocycl. Chem.* **25** 1793 (1988)
30. K Matsumoto, H Katsura, T Uchida, K Aoyama, T Machiguchi *J. Chem. Soc., Perkin Trans. 1* 2599 (1996)
31. M Oelgemoller, A G Griesbeck, W Kramer, F Nerowski *J. Inf. Rec.* **24** 87 (1998)
32. A G Griesbeck, A Henz, W Kramer, J Lex, F Nerowski, M Oelgemoller *Helv. Chim. Acta* **80** 912 (1997)
33. U C Yoon, S W Oh, S M Lee, S J Cho, J Gamlin, P S Mariano *J. Org. Chem.* **64** 4411 (1999)
34. D-C Ha, C-S Yun, E Yu *Tetrahedron Lett.* **37** 2577 (1996)
35. R Clauss, R Hunter *J. Chem. Soc., Perkin Trans. 1* 71 (1997)
36. F A Luzzio, D-A P Zacherl *Tetrahedron Lett.* **39** 2285 (1998)
37. S Jaroch, R T Matsuoka, L E Overman *Tetrahedron Lett.* **40** 1273 (1999)
38. J-P Gourves, H Couthon, G Sturtz *Eur. J. Org. Chem.* 3489 (1999)
39. F Z Galin, S N Lakeev, G A Tolstikov *Khim. Geterotsikl. Soedin.* 1693 (1989) [a]
40. F Z Galin, S N Lakeev, G A Tolstikov *Izv. Akad. Nauk, Ser. Khim.* 165 (1996) [b]
41. L M Khalilov, V S Sultanova, S N Lakeev, F Z Galin, L F Chertanova, G A Tolstikov *Izv. Akad. Nauk SSSR, Ser. Khim.* 2298 (1991) [b]
42. A I Meyers, B Santiago *Tetrahedron Lett.* **36** 5877 (1995)
43. H Hennige, R Kreher, J Uhrig *Synthesis* 842 (1982)
44. B Burns, R Grigg, V Sridharan, P Stevenson, S Sukirthalingam, T Worakun *Tetrahedron Lett.* **30** 1135 (1989)
45. J C Godfrey *J. Org. Chem.* 581 (1959)
46. E M Brun, S Gil, R Mestres, M Parra *Synlett* 1088 (1999)
47. A Tsirk, S Gronowitz, A-B Hörnfeldt *Helv. Chim. Acta* **80** 1483 (1997)
48. A Tsirk, S Gronowitz, A-B Hörnfeldt *Tetrahedron* **54** 9529 (1998)
49. W J Houlihan, J W Boja, V A Parrino, T A Kopajtic, M J Kuhar *J. Med. Chem.* **39** 4935 (1996)
50. B Yde, N M Yousif, U Pedersen, I Thomsen, S-O Lawesson *Tetrahedron* **40** 2047 (1984)
51. M Ostendorf, S van der Neut, F P J T Rutjes, H Hiemstra *Eur. J. Org. Chem.* 105 (2000)
52. M Ostendorf, J Dijkink, F P J T Rutjes, H Hiemstra *Eur. J. Org. Chem.* 115 (2000)
53. A K Tyltin, V A Kovtunenko, F S Babichev *Khim. Geterotsikl. Soedin.* 990 (1979) [a]
54. F S Babichev, A K Tyltin, V A Kovtunenko, Z V Levitskaya *Ukr. Khim. Zh.* **47** 627 (1981)
55. F S Babichev, A K Tyltin, V A Kovtunenko, A V Turov *Ukr. Khim. Zh.* **48** 641 (1982)
56. V A Kovtunenko, V V Ishchenko, A K Tyltin, A V Turov, F S Babichev *Khim. Geterotsikl. Soedin.* 1368 (1985) [a]
57. C H Gaozza, H Grinberg, S Lamdan *J. Heterocycl. Chem.* **9** 883 (1972)
58. C S Cho, L H Jiang, S C Shim *Synth. Commun.* **28** 849 (1998)
59. C Mayor, C Wentrup *J. Am. Chem. Soc.* **97** 7467 (1975)
60. C Wentrup *Chimia* **31** 258 (1977)
61. M K Eberle, L Brzechffa *J. Heterocycl. Chem.* **25** 445 (1988)
62. B Lal, R M Gidwani *Tetrahedron* **49** 255 (1993)
63. W Zhang, G Pugh *Tetrahedron Lett.* **40** 7591 (1999)
64. V A Kovtunenko, Z V Voitenko, L I Savranskii, A K Tyltin, F S Babichev *Khim. Geterotsikl. Soedin.* 216 (1988) [a]
65. L W Castle, Y Tominaga, R N Castle *J. Heterocycl. Chem.* **31** 1209 (1994)
66. L W Castle, Y Tominaga, R N Castle *J. Heterocycl. Chem.* **32** 1033 (1995)
67. K Matsumoto, J Yamauchi, T Uchida *Heterocycles* **23** 2773 (1985)
68. J Yamauchi, T Uchida, K Matsumoto *Heterocycles* **31** 1785 (1990)
69. K Matsumoto, H Katsura, J Yamauchi, T Uchida, K Aoyama, T Machiguchi *Bull. Soc. Chim. Fr.* **133** 891 (1996)
70. Z V Voitenko, O A Pocholenko, O O Chkarov, O V Shishkin, S V Shishkina, A Dall'Ava, M Vedrenne, M Sanchez, J-G Wolf *Eur. J. Org. Chem.* **7** 1401 (2001)
71. Z V Voitenko, A A Pokholenko, O O Shkarov, V A Kovtunenko, F S Babichev *Khim. Geterotsikl. Soedin.* **416** 211 (2002) [a]
72. Z V Voitenko, O I Ostrovskaia, in *Proceedings of International Conference 'The 5th World Congress of Theoretically Oriented Chemists', London, 1999* p. 561
73. K Matsumoto, T Uchida, T Kato, M Toda, K Aoyama, H Konishi *Heterocycles* **31** 593 (1990)
74. Y Tominaga, Y Shiroshita, H Gotou, Y Matsuda *Heterocycles* **24** 3071 (1986)
75. Y Tominaga, Y Shiroshita, Y Matsuda, A Hosomi *Heterocycles* **26** 2073 (1987)
76. F S Babichev, V A Kovtunenko, V V Ishchenko, A K Tyltin, T A Yudina *Khim. Geterotsikl. Soedin.* 1691 (1985) [a]
77. V A Kovtunenko, V V Ishchenko, A K Tyltin, F S Babichev *Dokl. Akad. Nauk SSSR* **299** 373 (1988) [c]
78. V A Kovtunenko, V V Ishchenko, A K Tyltin, F S Babichev *Dokl. Akad. Nauk USSR, Ser. B.* (11) 41 (1987)
79. V A Kovtunenko, V V Ishchenko, A K Tyltin, F S Babichev *Dokl. Akad. Nauk SSSR* **294** 375 (1987) [c]
80. V V Ishchenko, V A Kovtunenko, A K Tyltin, V V Trachevskii, V Vshetechka, F S Babichev *Ukr. Khim. Zh.* **56** 517 (1990)
81. V O Kovtunenko, O A Pokholenko, Z V Voitenko, R V Karbovs'ka, A K Tyltin *Vestn. Kievskogo Un-ta, Ser. Khim.* (39–40) 90 (2003)
82. Z V Voitenko, O A Pokholenko, R V Karbovs'ka, O T Il'kun, V O Kovtunenko, J G Wolf, in *Book of Abstracts of the 12-eme Journee Chimie Grand Sud-Ouest, Montpellier (France), 2002* p. 3-03
83. Z V Voitenko, V P Samoilenko, V A Kovtunenko, V Yu Gurkevich, A K Tyltin, M V Shcherbakov, O V Shishkin *Khim. Geterotsikl. Soedin.* 669 (1999) [a]
84. Z V Voitenko, V P Samoilenko *Khim. Geterotsikl. Soedin.* 218 (2002) [a]
85. V P Samoylenko, Z V Voitenko, B Donnadieu, J-J Bonnet *Tetrahedron* **58** 6103 (2002)
86. V P Samoilenko, P M Luazo, Z V Voitenko, in *Vseukrainskaya Nauchno-Prakticheskaya Konferentsiya 'Sovremennye Tekhnologii Organicheskogo Sinteza i Meditsinskoi Khimii', Khar'kov, 2003* (All-Ukrainian Research and Practical Conference 'Modern Technologies of Organic Synthesis and Medical Chemistry', Khar'kov, 2003) p. 68

[a] — *Chem. Heterocycl. Compd. (Engl. Transl.)*
[b] — *Russ. Chem. Bull., Int. Ed. (Engl. Transl.)*
[c] — *Dokl. Chem. (Engl. Transl.)*

Russian Chemical Reviews **73** (8) 785 – 810 (2004) © 2004 Russian Academy of Sciences and Turpion Ltd

DOI 10.1070/RC2004v073n08ABEH000912

Conformationally rigid cyclic α-amino acids in the design of peptidomimetics, peptide models and biologically active compounds

I V Komarov, A O Grigorenko, A V Turov, V P Khilya

Contents

I.	Introduction	785
II.	Conformationally constrained and conformationally rigid molecules	786
III.	Principles of the design of peptidomimetics and peptide models comprising conformationally rigid amino acids	786
IV.	Conformationally rigid cyclic and spirocyclic amino acids with three- and four-membered rings	788
V.	Bi- and polycyclic conformationally rigid amino acids with an endocyclic nitrogen atom	797
VI.	Bi- and polycyclic conformationally rigid amino acids with an exocyclic nitrogen atom	803
VII.	Conclusion	807

Abstract. A class of conformationally rigid cyclic α-amino acids that can be used in the synthesis of peptidomimetics, peptide models and biologically active compounds is surveyed. The rigid frameworks of such amino acids enable 'fixation' of strictly defined torsion angles and hence prediction and deliberate tuning of the conformation of a polypeptide chain. Recent data on the structures and methods of the synthesis of such amino acids are presented. The bibliography includes 259 references.

I. Introduction

Synthesis of compounds with constrained conformational flexibility increasingly attracts the attention of chemists. It is commonly assumed that restriction of the conformational flexibility of molecules by structural modifications may serve as an efficient tool in the studies of, and control over, properties of various compounds. In particular, by 'fixing' a ligand molecule in the so-called biologically active conformation, one can achieve high efficiency and selectivity of its interaction with the corresponding receptor. Restriction of the conformational flexibility of chiral ligands in metal complex catalysts allows enhancement of the enantioselectivity of catalytic asymmetric reactions.[1]

The vast majority of studies which make use of this approach relate probably to the synthesis of peptidomimetics and peptide models. Synthesis of peptidomimetics is aimed at improvement of the properties of natural peptides, first of all, of their biological activities,[2] whereas that of peptide models, at studies of the properties of peptides and proteins. For instance, peptidomimetics with improved pharmacological characteristics (solubility, bioselectivity, resistance to *in vivo* degradation, *etc*.) can be prepared by modifying structures of amino acid constituents of a bilogically active natural peptide. Compounds utilised in studies of the mechanism of the enzyme catalysis may be mentioned as examples of peptide models.[3]

Both peptidomimetics and peptide models may have either peptide or non-peptide nature. A key principle of their design consists of the incorporation of conformationally constrained or rigid analogues of natural amino acids into the peptide chain.

Up to now, numerous conformationally constrained and rigid amino acids, as well as peptidomimetics and artificial peptides on their base, have been synthesised. Methods for the preparation of these compounds and their biochemical properties have been surveyed in a number of reviews.[4 – 15] Nevertheless, issues related to the structural features and conformational properties of these compounds as well as to the design of peptidomimetics and peptide models with conformationally constrained amino acids have not been adequately addressed so far. The goal of the present review is to span this gap.

Among the whole range of the known amino acids that are characterised by restricted conformational flexibility, conformationally rigid α-amino acids deserve particular mention. Hereinafter, substances the molecules of which exist in a unique conformation, are referred to as conformationally rigid α-amino acids (CRA).† These also encompass amino acids where only a specific fragment is rigid. Conformationally rigid amino acids have several advantages in the design of peptidomimetics and peptide models over amino acids that are conformationally constrained but not rigid. Rigid molecules or molecular fragments are characterised by 'fixed' bond and torsion angles, which are either known or can be calculated with sufficient accuracy by molecular mechanics. The values of these angles are virtually independent of the structure and conformation of the remaining part of the polypeptide chain. Furthermore, rigid fragments formed by CRA can impose a specific chain conformation on their immediate proximity. This simplifies the design of peptidomimetics or artificial peptides with desired characteristics.

This approach limits the number of amino acids applicable in the design, however the structural diversity of CRA is fairly broad as will be shown below. Many of the theoretically possible CRA have not been synthesised so far and one goal of the present review is to draw the attention of chemists to their synthesis.

I V Komarov, A O Grigorenko, A V Turov, V P Khilya Department of Chemistry, Kyiv National Taras Shevchenko University, ul. Vladimirskaya 64, 01033 Kyiv, Ukraine. Fax (38-044) 226 12 73. Tel. (38-044) 239 33 15. E-mail: ik214@yahoo.com (I V Komarov), gregor@univ.kiev.ua (A O Grigorenko), vkhilya@hotmail.com (V P Khilya). Tel. (38-044) 239 33 21. E-mail: nmrlab@univ.kiev.ua (A V Turov)

Received 18 March 2004
Uspekhi Khimii **73** (8) 849 – 876 (2004); translated by Ya V Zubavichus

† In the present review, the generalised meaning of the term conformation is adopted, *viz*., a conformation is understood as any spatial mutual arrangement of nuclei comprising a molecule, which can be realised without disturbing integrity of the molecule.[16 – 19]

Since the term 'conformational rigidity' is central in this review, it deserves a dedicated consideration.

II. Conformationally constrained and conformationally rigid molecules

Two terms 'conformationally constrained (restricted)' and 'conformationally rigid' frequently occur in the scientific literature and are commonly considered as being intuitively obvious. L-Proline (**1**) and its bicyclic analogue 2,4-methanoproline (**2**) may be taken as examples of a conformationally constrained and a conformationally rigid molecule, respectively.

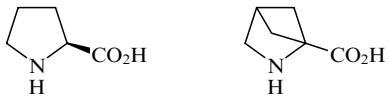

1 **2**

The presence of a five-membered ring in **1** substantially restricts the conformational flexibility of both the L-proline molecule and peptides containing its residue. Nevertheless, there exists a set of proline conformations such that transitions between them do not require significant energy expenditure.[20] The molecule of **2**, a proline analogue, is regarded as rigid, because its conformational mobility is severely restricted by the methylene bridge. Nevertheless, it does not comply with the strict definition of CRA given in the preceeding section, as it can still adopt more than one conformation.

The Chemical Encyclopaedic Dictionary [21] gives the following definition of the term 'rigid molecule': 'A characteristic feature of rigid molecules is that a transition from one of their equilibrium conformations to another requires a considerable energy (>100 kJ mol^{-1})... Only transpositions of nuclei which are realised by rigid rotations or mirror reflections of the molecule as a whole without cleavage of chemical bonds are allowed in rigid molecules'. The major drawback of this definition, in our opinion, is that it poses a specific value of the maximum energy of a configurational (conformational) transition, *i.e.*, 100 kJ mole^{-1}. Even neglecting the arbitrariness in the selection of this value, this definition can hardly be applied to a particular molecule since the exact energy profile of its conformational transitions is typically unknown.

It would be appropriate here to refer to aromatic and heteroaromatic compounds. For a long time (see, for instance, Refs 21–23), it has been believed that they represent rigid structures. However, recent theoretical and experimental studies have revealed substantial flexibility of benzene [24] and pyridine [25] rings: a change in the torsion angle by 20° in these aromatic systems results in an energy increase of not more than 13 kJ mol^{-1}. Alkenes and fragments with a triple bond cannot also be classified as conformationally rigid. According to a recent theoretical and experimental studies,[26] bond and torsion angles in unsaturated compounds can experience noticeable distortions at energy not exceeding 20 kJ mol^{-1}.

Alternatively, the conformational rigidity may be defined in a more strict and versatile way using a topological approach based on the graph theory. Within this approach, rigid molecules were described as rigid graphs with edges of fixed lengths.[27] Note that various conformationally rigid molecules can be constructed theoretically using the graph theory; these molecules, however, can prove to be unstable or non-existent in reality. The three-membered ring **3** is evidently classified as conformationally rigid. The graph **4** is also rigid but unsubstituted tetrahedrane with this skeleton is so unstable that all attempts at its synthesis undertaken so far have failed.[26]

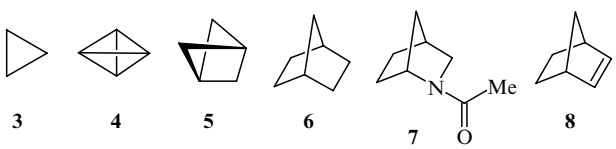

3 **4** **5** **6** **7** **8**

At resent, there is no uniform criterion of conformational rigidity, therefore, the attribution of a particular amino acid to conformationally rigid ones is based in the following discussion primarily on literature data concerning their structures and conformational mobilities. Analysis of the published data allowed us to conclude that cyclic and polycyclic cages with fixed torsion and bond angles in their CR_4 fragments and those involving sp^2- and sp-hybridised atoms are regarded as rigid most frequently. For the former class, this is due to large force constants of both bonds and angles, while the latter class lies beyond the scope of the present review. In particular, polycyclic molecules with bridges involving 0 or 1 atom (*e.g.*, the molecule **5**) are referred to as rigid. Polycyclic molecules with two-atomic bridges are also often considered as rigid in the literature (*e.g.*, compound **6**), especially in those cases where the structure is additionally 'reinforced' by an amide group or by multiple bonds (*e.g.*, the structures **7** and **8**).

The following structural types of CRA will be considered as rigid in the following discussion:

(1) mono- and spirocyclic compounds with three- and four-membered rings;

(2) bicyclic compounds with short bridges comprising from 0 to 2 atoms;

(3) tri- and polycyclic compounds with sufficiently short bridges.

In the next sections, the major attention will be paid to conformationally rigid analogues of natural α-amino acids. This is primarily due to the fact that the design of conformationally constrained peptidomimetics or peptide models typically implies replacement of natural amino acids in the native peptide by structurally most similar analogues; the so-called 'topomers' or 'topologically equivalent' amino acids. The principles of such a 'topographic' design of peptides have been formulated quite recently.[28, 29] Evidently, in this case, the results of conformational and biological studies can be more easily interpreted since earlier experimental data on related natural amino acids can be used for comparison.

The synthesis of CRA that are not close analogues of natural α-amino acids is also of substantial practical and theoretical interest. The molecules of CRA can contain two or more fragments of natural amino acids (such amino acids are referred to as 'chimeric').

The literature data search has been accomplished using electronic databases, *viz.*, Beilstein Crossfire, SciFinder and the Cambridge Structural Database (CSD).[30]

III. Principles of the design of peptidomimetics and peptide models comprising conformationally rigid amino acids

The design of peptidomimetics and peptide models comprising CRA is based on the knowledge of the features of the secondary structure elements of peptides. The three major types of secondary structures of peptides adopted currently include helices (*I*), β-folded structures (*II*) and bends (*III*) (Fig. 1).[28, 31–33]

Conformations of polypeptide chains corresponding to each of the secondary structure elements can be described in terms of the torsion angles φ, ψ and ω whereas the conformation of side chains of amino acids can be described in terms of the torsion angles χ_1, χ_2, χ_3, and so forth (Fig. 2).

The most typical (*i.e.*, mean or standard) values of the torsion angles φ, ψ and ω for the secondary structure elements of peptides and proteins determined as a result of analysis of numerous experimental structural data and computer simulations are summarised in Table 1.[28, 32] Based on the values of the torsion angles φ, ψ and ω given in Table 1, it is possible to predict in the first approximation the effects of a replacement of a natural amino acid by its conformationally rigid analogue with fixed torsion

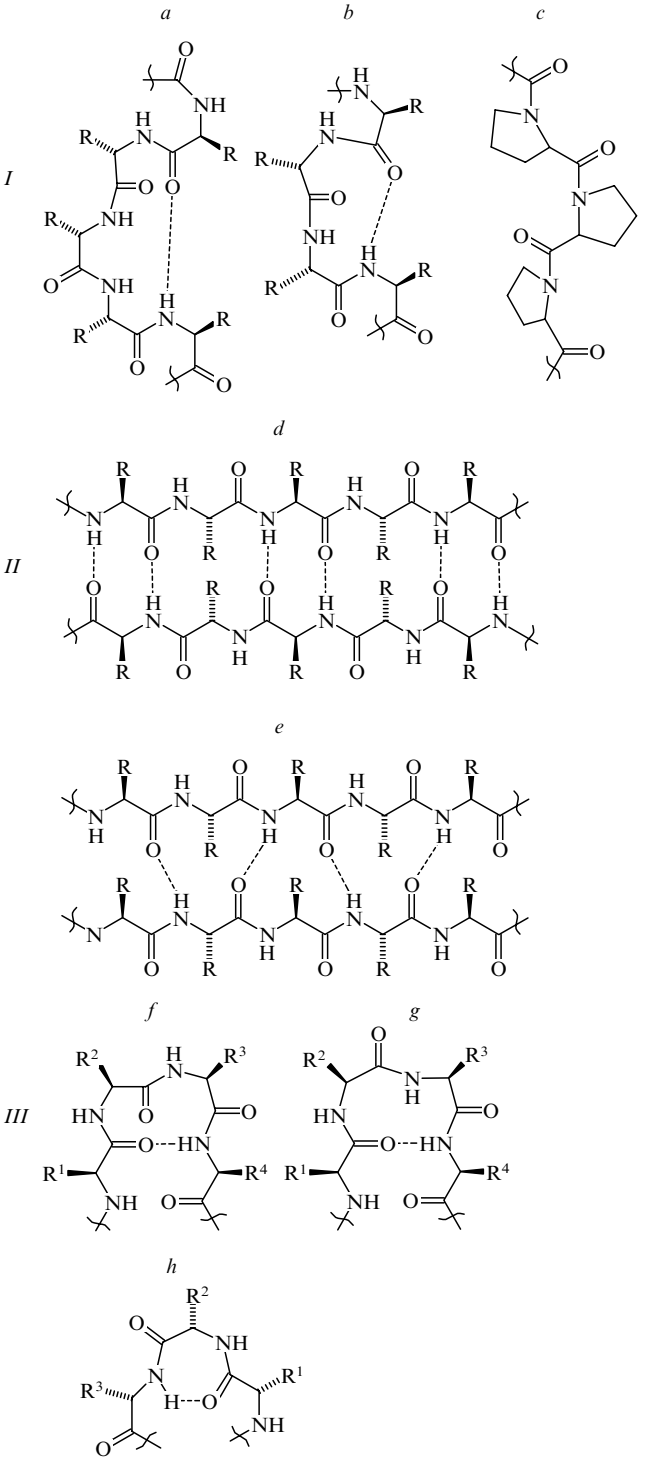

Figure 1. Elements of the secondary structure of peptides and proteins: (*I*) helices: α-helix (right-handed) (*a*), 3_{10}-helix (right-handed) (*b*), polyproline II helix (left-handed) (*c*); (*II*) β-folded structures: antiparallel (*d*), parallel (*e*); (*III*) bends: type I β-bend (*f*), type II β-bend (*g*), γ-bend (*h*).

angles (most frequently, it is the torsion angle φ that is fixed) on the conformation of the peptide fragment. It is noteworthy that the torsion angles exert a decisive influence on the conformation of the whole fragment involving CRA. If torsion angles at the peptide bond formed by a CRA are close to the respective torsion angles of a secondary structure element of the native peptide, stabilisation of this structure element is expected. Otherwise, this will be destabilised and a change of its conformation can be predicted with a sufficient degree of accuracy.

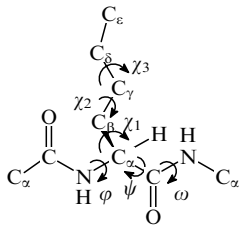

Torsion angle	Notation
$C-N-C_\alpha-C$	φ
$N-C_\alpha-C-N$	ψ
$C_\alpha-C-N-C_\alpha$	ω
$N-C_\alpha-C_\beta-C_\gamma$	χ_1
$C_\alpha-C_\beta-C_\gamma-C_\delta$	χ_2
$C_\beta-C_\gamma-C_\delta-C_\varepsilon$	χ_3

Figure 2. The torsion angles φ, ψ, ω and χ in peptides.

Table 1. Mean values of the torsion angles φ, ψ and ω (deg.) typical of different elements of the secondary structure of peptides and proteins.

Secondary structure element	φ	ψ	ω
Helices			
α-helix	−57	−47	180
3_{10}-helix	−60	−30	180
polyproline I helix	−83	158	0
polyproline II helix	−76	146	180
β-Folded structures			
parallel	−119	113	–
antiparallel	−139	135	–
extended chain	180	180	–
β-Bends [a]			
type I	−60 (φ_{i+1}); −90 (φ_{i+2})	−30 (ψ_{i+1}); 0 (ψ_{i+2})	
type I′	60 (φ_{i+1}); 90 (φ_{i+2})	30 (ψ_{i+1}); 0 (ψ_{i+2})	
type II	−60 (φ_{i+1}); 80 (φ_{i+2})	120 (ψ_{i+1}); 0 (ψ_{i+2})	
type II′	60 (φ_{i+1}); −80 (φ_{i+2})	−120 (ψ_{i+1}); 0 (ψ_{i+2})	
type III	−60 (φ_{i+1}); −60 (φ_{i+2})	−30 (ψ_{i+1}); −30 (ψ_{i+2})	
type III′	60 (φ_{i+1}); 60 (φ_{i+2})	30 (ψ_{i+1}); 30 (ψ_{i+2})	
γ-Bend	−65 (φ_{i+1})	120 (ψ_i); 80 (ψ_{i+1}); −120 (ψ_{i+2})	

[a] By definition, a β-bend involves four amino acid residues. They are enumerated as *i*th to $i+3$th residue starting from the N-end. The indices of the torsion angles correspond to this enumeration.

This also holds for the torsion angles χ that characterise spatial arrangement of the peptide side chains. Knowledge of these torsion angles is exceptionally important for the understanding of the functions of the peptides. Unfortunately, studies devoted to the torsion angles χ in natural peptides are rather scarce.

In some cases, 'stereolibraries' of CRA have been compiled, which represent diastereomeric series of amino acids that are close structural analogues of the corresponding natural amino acids. In these series, strictly fixed torsion angles vary from one compound to another. Synthesis of a series of peptidomimetics or peptide models on the basis of such a library enables elucidation of the relationships between the properties of peptides and their conformations and thus increases the efficacy of the search for biologically active compounds and drugs.

However, the conformation of a peptide fragment does not depend only on the torsion angles in the CRA residue. Any structural modification (even a minor one) of a natural amino acid affects to a certain extent all the angles describing the conformation of a peptide fragment close to modification. As an

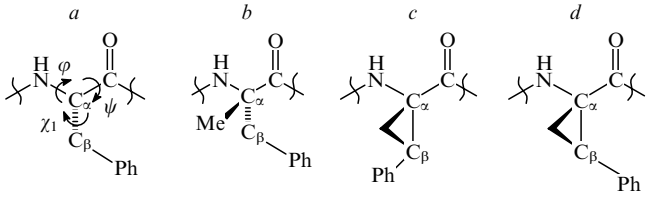

Figure 3. Structural modifications of the L-phenylalanine residue.

example, let us consider a diasteriomeric series of amino acid analogues of L-phenylalanine (Fig. 3).

Replacement of an L-phenylalanine residue (Fig. 3 *a*) in a peptide chain by its α-methyl derivative (Fig. 3 *b*) sterically hinders the free rotation around the bonds $C_\alpha-N$, $C_\alpha-C$ and $C_\alpha-C_\beta$. This modification influences the torsion angles φ, ψ and χ to nearly the same extent. Introduction of rigid analogues of L-phenylalanine containing a cyclopropane moiety (Figs 3 *c* and 3 *d*) results in the fixation of the angle χ_1. This also affects the angles φ and ψ: the L-phenylalanine analogue shown in Fig. 3 *c* is characterised by hindered rotation around the $C_\alpha-N$ bond while that shown in Fig. 3 *d* is characterised by hindered rotation around the $C_\alpha-C$ bond. Additionally, the well-known 'unsaturated' character of the cyclopropane ring results in a decrease in the torsion angle ψ due to the conjugation between the ring and the carbonyl group π-system. Unfortunately, no detailed conformational analysis of this kind for peptide fragments has been performed for almost all known CRA.

Let us now discuss the effects of changes in the torsion angle ω on the conformation of the peptide fragment in the proximity of modification. What is important is that the angle ω does not adequately reflect structural features of the peptide bond NH–CO in all cases. In an ideal case (the $C_\alpha-C-N-C_\alpha$ fragment is planar), this angle is 0° for the *cis*-configuration of the peptide bond and 180° for the *trans*-configuration. In the majority of amino acid residues constituting natural proteins, the peptide bonds have the *trans*-configuration although bonds with the *cis*-configuration are also encountered sometimes. Furthermore, the NH–CO fragment can be non-planar. The *cis*–*trans*-isomerisation of peptide bonds is closely related to many biologically important processes, primarily, to folding and unfolding.[34, 35] It has been shown that amides of cyclic amino acids with a nitrogen atom in the ring (these amino acids form tertiary amides in peptides) are characterised by noticeable pyramidalisation of the nitrogen and carbon atoms of the bond NH–CO and by 'twisting' around this bond. The following parameters have been suggested for quantitative description of the conformation of such a non-planar amide fragment: the twist angle τ [τ is the angle between the planes defined by the atoms C(1)NC(2) and OC(3)C(4)];[36–39] parameters ω_0(N) and ω_0(C), which reflect pyramidalisation of bonds at the nitrogen and carbon atoms, respectively; and the tilt angle (δ) between the N–C(3) bond and the plane defined by the C(1)C(2)N atoms. The substantial pyramidalisation of bonds at the nitrogen atom and 'twisting' of the amide bond can be achieved in rigid systems, such as

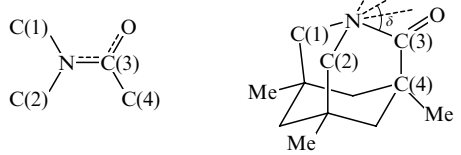

[$\tau = \delta = 0°$, ω_0 (N) = 360°]

9 [$\tau = 90°$, $\delta = 57°$, ω_0 (N) = 326°]

$\tau = [\angle C(4)C(3)NC(2) + \angle OC(3)NC(1)]/2$;
ω_0 (N) = ∠C(1)NC(2) + ∠C(2)NC(3) + ∠C(1)NC(3).

derivatives of 1-azaadamantan-2-one **9**. Thus, angles τ, pyramidalisation parameters ω_0(N) (hereinafter ω_0) and tilt angles δ will be discussed for peptide fragments bearing CRA (provided that the respective information is given in the original papers).

Finally, in the design of peptidomimetics and peptide models based on CRA, one should take into account changes in the chemical properties of the respective peptide fragments induced by the substitution of CRA for natural amino acids.

IV. Conformationally rigid cyclic and spirocyclic amino acids with three- and four-membered rings

The major types of known fragments of CRA, the conformational rigidity of which is due to the presence of small (three- and four-membered) rings are as follows:

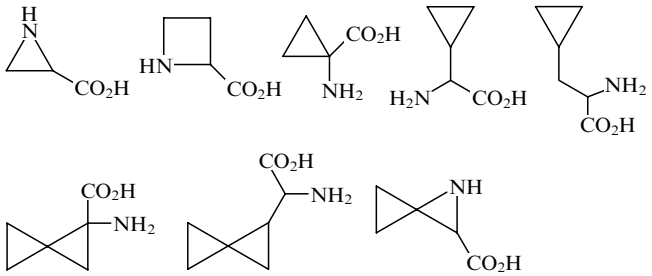

It is of note that the four-membered ring in azetidine-2-carboxylic acid is conformationally flexible but it acquires rigidity in peptides due to involvement of the nitrogen atom of the azetidine ring in the amide bond. Therefore, azetidine-2-carboxylic acid is also classified as a CRA.

A common feature of the CRA described in this section is a significant angle strain within the small rings, which strongly affects not only the structure but chemical properties of both the acids and their derivatives.

1. Aziridine-2-carboxylic acid and its derivatives

Aziridine-2-carboxylic acid (**10**)‡ may be regarded both as α- and β-amino acid with the angles φ and χ strictly fixed.

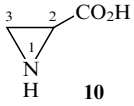

10

Unfortunately, there have been only a few structural studies of derivatives of the acid **10**, and no single-crystal X-ray diffraction data on peptides containing this residue have been published so far. Nevertheless, conformational properties of such peptides may be judged from the single-crystal X-ray diffraction studies of compounds **11** and **12**.[34]

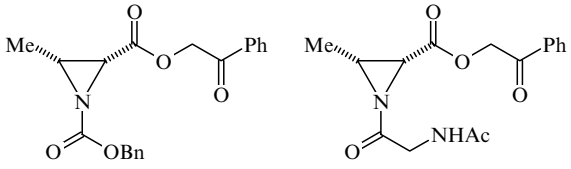

11 **12**

The experimental results suggest significant pyramidalisation of the nitrogen atom, which is evidently a consequence of the angle strain in the three-membered ring. The angle δ in **11** and **12** amounts to 37–38°, *i.e.*, the nitrogen atom is virtually tetrahedral as in the case of sp^3-hybridisation.

‡ The residue of aziridine-2-carboxylic acid in peptides is denoted as Azy.

Single-crystal X-ray diffraction studies of **11**, **12** and aziridine amides demonstrate that the steric strain within the three-membered ring results not only in pyramidalisation of bonds at the nitrogen atom but in the twisting of the amide bond as well. These compounds can serve as models in studies of the transition state of the *cis*–*trans*-isomerisation of amides, *i.e.*, the process that plays a key role in the folding of protein molecules.

Twisting of the amide bond can lead to substantial changes in the properties of this amide fragment as has been demonstrated in a case study of a derivative of 1-azaadamantan-2-one (**9**).[39] In particular, it was found that twisting results in increased reactivity of the amide bond with respect to nucleophiles and in substantial basicity of the nitrogen atom (pK_a of **9** in water is 5.2). According to calculations,[40] aziridine amides undergo protonation at the nitrogen atom under physiological conditions in contrast to unstrained amides that are very weak bases. This fact is of great importance in the design of peptidomimetics and peptide models comprising Azy.

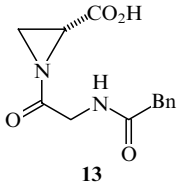

13

In a study on *N*-(phenylacetyl)glycyl-D-aziridine-2-carboxylic acid (**13**),[41] it was found that this compound with a non-planar amide group was a substrate for β-lactamases, which confirmed a hypothesis on the evolution of DD-peptidases into β-lactamases. As a result of this evolution, the enzyme active site is modified so as to provide more efficient binding of non-planar β-lactams (which are natural substrates for β-lactamases) with respect to unstrained planar amides.

The structure of several peptides containing aziridine-2-carboxylic acid residues can be inferred from spectroscopic data. For instance, NMR studies of solutions of the tripeptides **14** and **15**, which contain 3-Ph-Azy residues (a conformationally rigid analogue of phenylalanine) and L-proline, have shown that the terminal amino acid residues form a 10-membered ring involving the hydrogen bonds NH···OC typical of β-bends.[42]

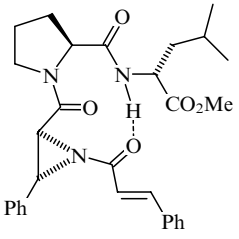

14

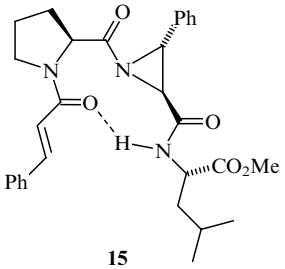

15

The tripeptide **15** has been utilised as a model compound to rationalise high diastereoselectivity of epoxidation of double bonds in peptides based on *N*-cinnamoyl-L-proline derivatives catalysed by cobalt(II).[43] It was suggested that the major reason for the stereoselectivity of the epoxidation is the presence of γ- and β-bends in these peptides, which directs the attack of the reagent strictly from one side of the double bond plane. High diastereoselectivity of the epoxidation reaction of the tripeptide **15**, the conformation of which in the region of β-bends is similar to that in the above peptides, has justified this hypothesis.

The model studies described above are scarce and by no means systematic. Quite another property of derivatives of aziridine-2-carboxylic acid, *viz*., the ease of opening of the strained three-membered ring under the action of nucleophiles, is exploited more frequently.§ This property makes it possible to use aziridine-2-carboxylic acid and its derivatives as irreversible inhibitors of enzymes. For instance, the acid **10** itself was used as an inhibitor of cysteine proteases. It selectively deactivates the thiol group and does not react with other nucleophilic groups present in the active sites of the proteases.[44]

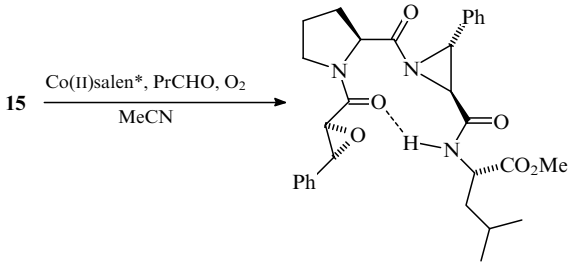

Co(II)salen* is a polyaniline-supported Co(II)-salen complex.

Unfortunately, Azy-containing peptides are toxic due to its high reactivity, which prevents their use as drugs.

Later, a number of inhibitors of cysteine proteases based on aziridine-2,3-dicarboxylic acid (Azi, **16**–**18**) derivatives were discovered. A common structural feature of these inhibitors is the presence of a peptide fragment and a reactive aziridine ring. The peptide fragment binds to the active site of the enzyme and the aziridine ring irreversibly reacts with the thiol group.[45,46] Unfortunately, the influence of the rigid residue of aziridine-2,3-dicarboxylic acid on the conformation of the molecules under study has not been analysed, although it is the conformation of the inhibitor that can define the efficiency of its binding to the active site of the enzymes.

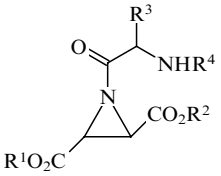

16

R^1 = Et, H; R^2 = Et, Bn; R^3 is an amino acid residue; R^4 is a protecting group, an amino acid or a peptide residue.

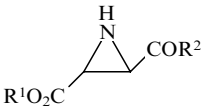

17

R^1 = Et, H; R^2 is an amino acid or a peptide residue.

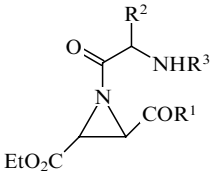

18

R^1 is an amino acid or a peptide residue; R^2 is a side chain of an amino acid; R^3 is a protecting group.

Recently, the influence of free carboxylic groups in molecules of similar inhibitors on the inhibition efficiency has been investigated.[47]

Among other inhibitors studied, 2-(2-carboxyethyl)- (**19**)[48] and 2-(4-amino-4-carboxybutyl)aziridine-2-carboxylic acids (**20**)[49] are worth noting. They act as irreversible inhibitors of glutamate racemase and diaminopimelic acid epimerase, respectively.

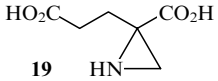

19

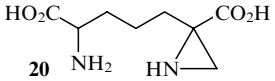

20

A number of methods for the preparation of aziridinecarboxylic acid and its derivatives have been developed and the major

§ It is of note that the residues of aziridine-2-carboxylic acid or its derivatives in peptides are additionally activated due to the presence of an electron-withdrawing carboxyl group linked to the nitrogen atom.

attention has been paid to the stereoselective syntheses. The development of new methods for the synthesis of these compounds was encouraged by their potential use as convenient precursors of alkaloids, β-lactam antibiotics and other biologically active compounds rather than as conformationally rigid analogues of natural amino acids in the synthesis of peptidomimetics and peptide models.[7] These methods are primarily based on the ease and selectivity of the nucleophilic opening of the aziridine ring.

The basic method for the synthesis of aziridinecarboxylic acid and its derivatives consists of cyclisation of α-amino β-hydroxy acids (Scheme 1), in particular, of serine and threonine.[50–52] (The starting chiral α-amino β-hydroxy acids can be produced from tartaric acid.[53])

Scheme 1

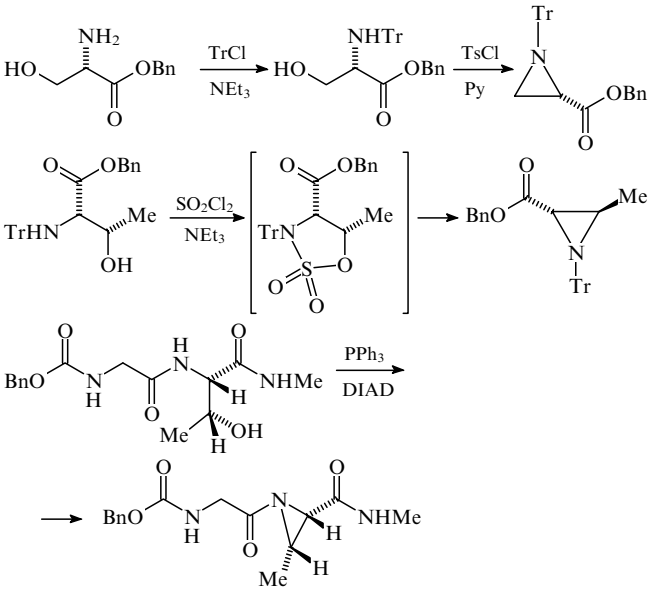

Tr = Ph_3C, Ts = $SO_2C_6H_4Me$-4,
DIAD is diisopropyl azodicarboxylate.

Cyclisation is most frequently performed under conditions of the Mitsunobu reaction (see Scheme 1). For the synthesis of substituted aziridinecarboxylic acids, reactions of sulfinylimides with lithium α-bromoenolates (the aza-Darzen reaction) are typically exploited.[54]

Chiral aziridinecarboxylic acids are prepared through asymmetric synthesis. The current approaches are represented in Scheme 2. The key stage in these transformations is the Sharpless catalytic asymmetric epoxidation (pathway *a*)[55,56] or asymmetric aziridination of a C=C double bond (pathway *b*).[57]

Scheme 2

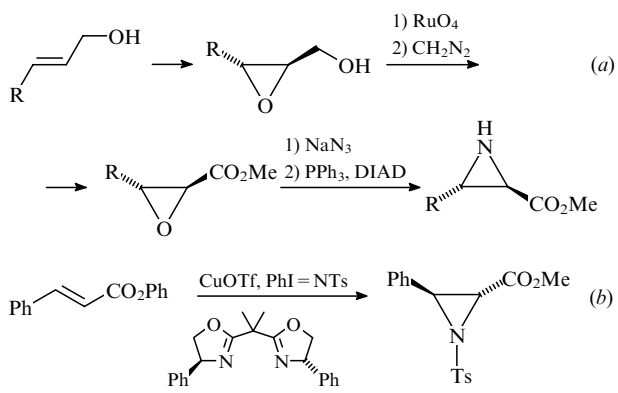

Tf = CF_3SO_2.

Syntheses using chiral auxiliary groups, *e.g.*, (4*S*,5*R*)-1,5-dimethyl-4-phenylimidazolidin-2-one, for the stereoselectivity control are worth mentioning. A scheme of the synthesis of aziridine-2-carboxylic acid derivatives by the Gabriel–Cromwell reaction used to build up the aziridine ring is shown below.[58,59]

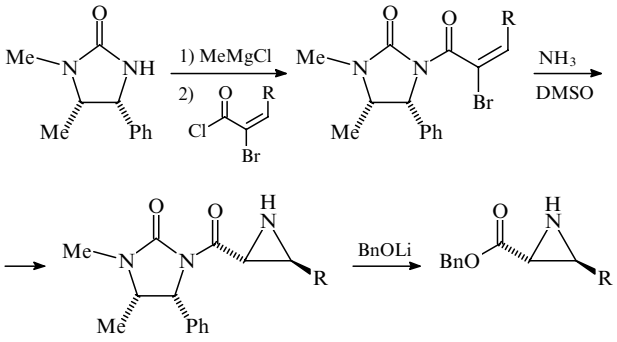

2. Azetidine-2-carboxylic acid and its derivatives

The residue of azetidine-2-carboxylic acid (**21**), when incorporated into a peptide chain, loses its mobility and becomes (φ,χ)-rigid because the nitrogen atom becomes involved in the amide bond.¶ (The Aze residue is the closest homologue of Pro.)

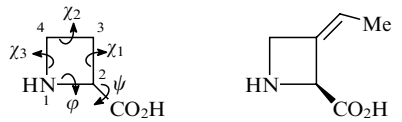

21 **22**

The amino acid **21** has been found in nature.[60] The unique amino acid **22** (polyoximic acid) was isolated from fungicide antibiotic polyoxines (peptide nucleosides).[61] It is noteworthy that the configuration of the exocyclic double bond in **22** was first erroneously assigned as *E*, but later its *Z* configuration was reliably established by structural studies and synthesis.[62]

Following structural elucidation of **21**, it was suggested that the biological activity of peptides containing the Aze residue is determined by the peculiarities of their secondary structures, and the conformational properties of azetidine-2-carboxylic acid differ from those of proline and other natural amino acids. Further structural studies have confirmed this suggestion. Compounds **23**–**26**, which are derivatives of azetidine-2-carboxylic acid[63–65] and *trans*-polyoximic acid,[66] have been used as model substances in the evaluation of conformational features of Aze in peptides.

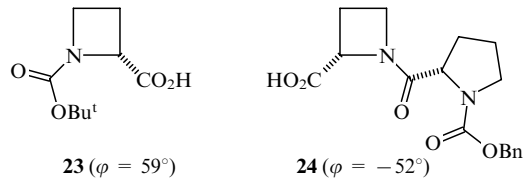

23 (φ = 59°) **24** (φ = −52°)

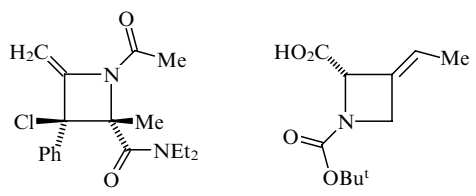

25 (φ = 56°) **26** (φ = −67°)

The azetidine rings in compounds **23**–**26** are virtually planar, which justifies the assignment of the Aze residue to conformationally rigid fragments.

¶ The residue of azetidine-2-carboxylic acid in peptides is denoted as Aze or, less frequently, Azt.

The absolute values of the torsion angle φ in **23**–**26** ($\sim 55^\circ$) are smaller by approximately 20° than in proline ($\sim 75^\circ$), which may be responsible for the differences in conformations of Aze- and Pro-containing peptides. Pyramidalisation of the nitrogen atom in Aze is substantially less pronounced than in a more strained Azy residue; the same is true for the angle δ, which is $\sim 5^\circ$ in **23**–**26** according to X-ray diffraction data. On the other hand, the Aze residue is more strained than Pro, which is reflected in a decrease in the energy barrier to the *cis*–*trans* isomerisation of the peptide bond. According to the results of dynamic NMR studies, the energy barrier to the *cis*–*trans* isomerisation in two model peptides, Ala-Aze-$NHC_6H_4NO_2$-4 and Ala-Gly-Aze-$NHC_6H_4NO_2$-4, is lower than in related peptides Ala-Pro-$NHC_6H_4NO_2$-4 and Ala-Gly-Pro-$NHC_6H_4NO_2$-4 by 10 kJ mol^{-1}.[67]

Taking into account the rigidity of the Aze unit, one should expect that substitution of Aze for Pro in peptides will inevitably affect conformation of the secondary structure elements in those fragments that previously contained proline.[68] Proline residues are often encountered in the $(i+1)$th positions of β-bends.[68] NMR studies of model tetrapeptides **27**–**29** using the NOESY technique showed that all these peptides reveal β-bends, although the distance between terminal amino acid residues in the azetidine-containing peptide ($n = 0$) is longer than in its proline-containing analogue ($n = 1$).[69]

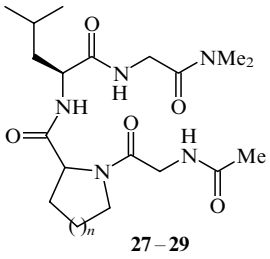

27–**29**

$n = 0$ (**27**), 1 (**28**), 2 (**29**).

Introduction of 3- or 4-substituted Aze residues into peptides offers extended possibilities of control over the conformation of their side chains owing to the strictly fixed torsion angles χ in Aze. The values of these angles in several peptides containing the Aze residue have been reported.[64, 70]

Although a method for the preparation of racemic azetidine-2-carboxylic acid starting from γ-butyrolactone was developed rather long ago,[71–73] the synthesis of enantiomerically pure azetidine-2-carboxylic acid was accomplished only in 2003.[74] There are only a few efficient stereoselective methods for the preparation of its derivatives substituted at positions 3 or 4.

The isomers of azetidine-2-carboxylic acid **30** and **31** (which may be considered as glutamic acid analogues) were synthesised using a method similar to that applied for unsubstituted acid **21** (Scheme 3).[75]

Intramolecular nucleophilic cyclisation has also been used to construct the azetidine ring.[76] In particular, intramolecular nucleophilic substitution of the Cl atom in **32** yielded two diastereomers of 3-phenylazetidine-2-carboxylic acid † **33** and **34** (Scheme 4).

Scheme 3

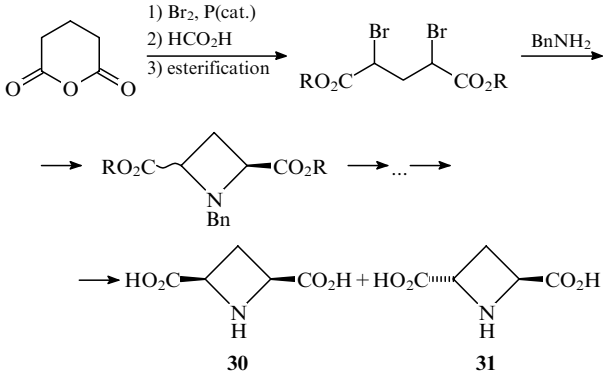

30 **31**

Scheme 4

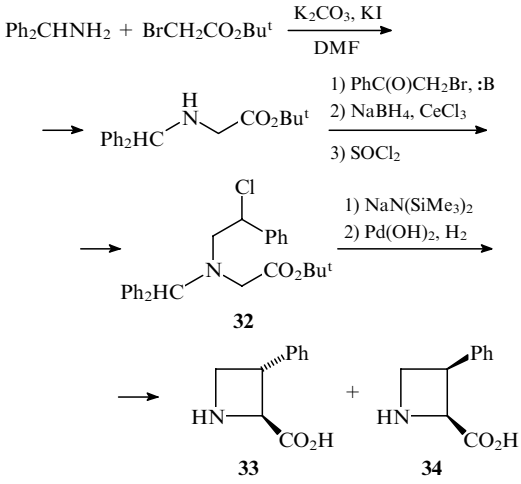

32

33 **34**

In both cases, racemic diastereomeric products were separated using liquid chromatography on silica gel.

Intramolecular nucleophilic cyclisation has also been utilised in the synthesis of 3,3-dimethylazetidine-2-carboxylic acid (an analogue of Leu).[77]

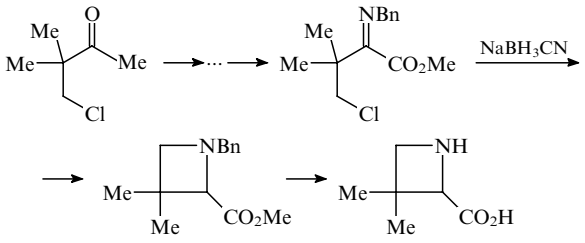

Recently, asymmetric synthesis of 2-cyanoazetidines **35**, precursors of substituted azetidine-2-carboxylic acids, has been accomplished. In this case, the cyclisation was realised through the stereoselective intramolecular Michael addition.[78] The use of optically pure β-amino alcohols as the starting compounds provided enantiomerically pure target amino acids (Scheme 5).

Taking into account that a four-membered ring is substantially less strained than a three-membered ring, one could expect that azetidine-2-carboxylic acid derivatives would appear more suitable for the design of peptidomimetics and peptide models than highly reactive aziridine-2-carboxylic acid derivatives. However, the lack of general stereoselective methods for synthesis of azetidine-2-carboxylic acid derivatives prevented their wide use. The unsubstituted amino acid **21** is the only exception which is available in multigram quantities either synthetically or from natural sources.

The acid **21** was frequently introduced into peptidomimetics in the course of systematic search for new drugs. An investigation into the structure–activity relationship for tripeptide inhibitors of thrombin (*i.e.*, the enzyme that plays an important bioregulative role in blood coagulation) [79] may be mentioned as an example. In particular, it was shown that the inhibition activity of tripeptides is strongly affected by the conformation of the central amino acid residue. Taking this into account, modification of a known thrombin inhibitor, *viz.*, Boc-D-Phe-Pro-Arg-H, by replacing the constituent amino acid residues by their conformationally constrained analogues was carried out.[79] Substitution of conformationally rigid Aze for Pro in this tripeptide resulted in a twofold increase in the inhibitory activity. Conversely, substitution of conformationally flexible residue of pipecoline-2-carboxylic acid

† 3-Phenylazetidine-2-carboxylic acid is a phenylalanine (Phe) analogue.

Scheme 5

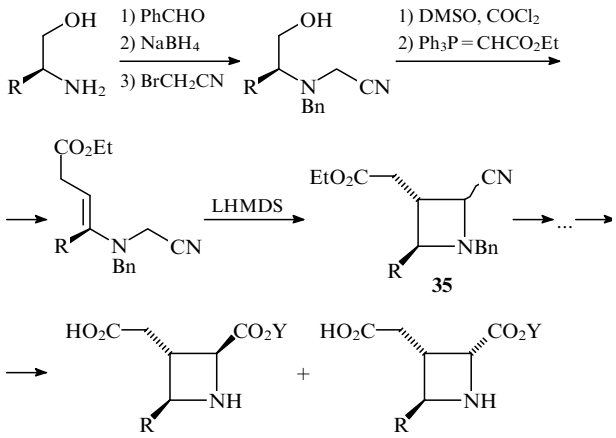

LHDMS is lithium hexamethyldisilazanide.

for Pro decreased the inhibitory activity by about two orders of magnitude.

3. 1-Aminocyclopropanecarboxylic acid and its derivatives

In contrast to aziridine-2-carboxylic acid and its derivatives described above, 1-aminocyclopropanecarboxylic acid (**36**, ACC) and its derivatives are very often used as CRA in the synthesis of peptidomimetics and peptide models.

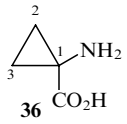

36

To date, cyclopropane analogues (also referred to as 2,3-methanologues or cyclopropanologues of α-amino acids) of all natural amino acids have been synthesised together with numerous artificial α-amino acids with a cyclopropane ring. Furthermore, starting from these amino acids, an array of peptides have been prepared and their structures, conformations and biological activities have been investigated. There are several reasons for such popularity of ACC and its derivatives. Primarily, it is due to the fact that the conformational rigidity of ACC derivatives (for ACC derivatives, the torsion angle χ_1 is fixed) is achieved by a minor structural modification of the respective conformationally flexible analogues, *viz*., through introduction of a methylene bridge between the α- and β-carbon atoms. This simplifies interpretation of results of conformational and biochemical studies.

Introduction of substituents into the cyclopropane ring provides the structural diversity of this type of CRA, which makes it possible to produce arrays of stereoisomeric amino acids (*i.e*., 'stereolibraries' of CRA).

For instance, 3-substituted ACC exists as four stereoisomers **A**–**D**. The residue of each of the stereoisomers introduced into a peptide is characterised by a specific torsion angle χ_1, which can easily be estimated using molecular mechanics calculations.

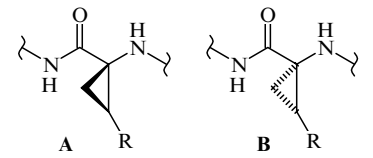

cis-Methanologues ($\chi_1 \approx 0°$)

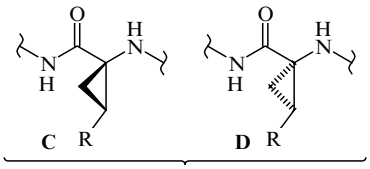

trans-Methanologues ($\chi_1 \approx -145°$ and $145°$, respectively)

For amino acids with a long side chain (*e.g*., for arginine, Arg), two types of methanologues **37** and **38** can be obtained, which differ from each other in the length of the side chain. This increases the number of available topomers of the natural amino acids.

The cyclopropane fragments in the compounds **37** (2,3-methanoarginine, cyclo-Arg) and **38** (cyclo-Arg′) were introduced by insertion of a methylene bridge across the $C_\alpha - C_\beta$ bond and by formation of a $C_\alpha - C_\gamma$ bond, respectively. As a result, cyclo-Arg is characterised by a fixed angle χ_1 whereas in cyclo-Arg′, it is the angles χ_1 and χ_2 that are fixed. Therefore, the conformational mobility of the amino acid **38** is less than that of **37**.

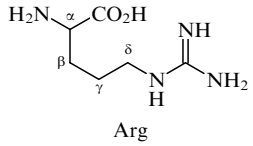

Arg

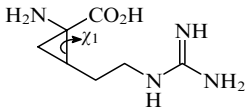

37 (cyclo-Arg)

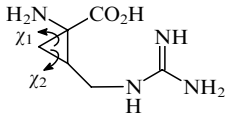

38 (cyclo-Arg′)

Yet another reason for the wide application of ACC and its derivatives in the design of peptidomimetics and peptide models is their accessibility. A number of efficient ways of their synthesis have been developed (including syntheses in gram quantities).

Finally, it is worth noting that 1-aminocyclopropanecarboxylic acid (**36**) itself and some of its derivatives occur in nature. The acid **36** is a precursor of ethylene, a plant hormone, furthermore, it is an important metabolite of methionine in plants.[80] Alkyl-substituted ACC, *i.e*., coronamic acid (**39a**, R = Et) and norcoronamic acid (**39b**, R = Me) have been isolated from hydrolysates of bacterial toxins coronatine and norcoronatine (in *Pseudomonas coronafaciens* and *Pseudomonas syringae*).[81,82] Carnosadine (**40**), which is an arginine analogue, has been isolated from the red alga *Grateloupia carmasa*.[83,84]

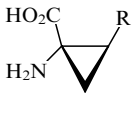

39a,**b**

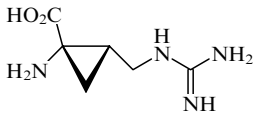

40

Although the number of the known methanologues of natural amino acids is presently quite large, there have been only a few detailed structural and conformational studies of peptides that include these acids. The most studied peptides are those containing methanologues of methionine,[85–87] phenylalanine[88,89] and diphenyl-substituted ACC.[90–92] A number of conformational features have been revealed for the peptides based on ACC derivatives due to the presence of strained conformationally rigid three-membered rings. X-ray diffraction study of model dipeptides R^1CO-L-Pro-c_3Phe-NHR^2 (c_3Phe stands for phenyl-substituted 1-aminocyclopropanecarboxylic acids) **41a**,**b** (see Refs 88, 89) and **42** (see Ref. 92) has shown that the torsion angle χ_1 is virtually constant over this series of compounds and equal, on average, to $7\pm3°$ and $136\pm1°$ for the two diastereomers. The deviations of the angles φ and ψ from the respective mean values are due to steric repulsion of substituents in the cyclopropane rings of dipeptides **41a**,**b** and **42a**,**b** from the atoms that

form the polypeptide chain. The absolute value of φ in **41a**,**b**, **42a**,**b**, **43**–**45** is, on average, 83°; and the scatter of this value is quite small, *i.e.*, ~7° (see Refs. 89, 90, 92–95). In the majority of cases, the angle ψ is close to 0°. This suggests that the ACC residue in peptides is not only χ-rigid but φ-rigid as well. X-Ray diffraction study of **45** (which is a 2,3-methanologue of proline) has shown[95] that the angle φ (−76°) virtually does not differ from that in L-Pro. Thus, cyclo-L-Pro can be used as a conformationally rigid proline analogue in the design of peptidomimetics and peptide models.

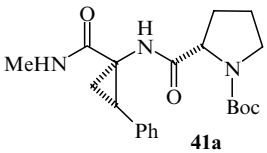

41a

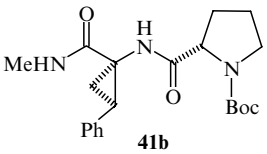

41b

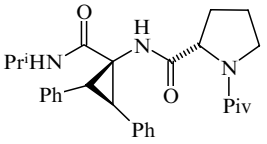

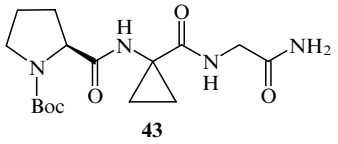

43

42a (2*R*,3*R*), **42b** (2*S*,3*S*)

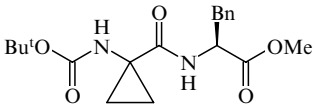

44

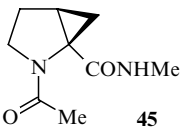

45

Compound	Torsion angles /deg			Ref.
	φ	ψ	χ_1	
41a	89	−4.5	135	88
41b	77	−11	−4	89
42	86	−20	7 (138)	92
43	84	−8.5	–	93
44	−84.5	0	–	94
45	−76	−7	–	95

From the aforementioned mean values of the torsion angles φ and ψ it was possible to conclude that peptides bearing ACC residues tend to form β-bends with the ACC residues in the $(i + 2)$th position.[93,94] Undoubtedly, the conformation of peptides in solutions can be different; therefore, the peptides were studied using not only X-ray diffraction, but NMR and IR spectroscopy and computer simulations as well.[88,89] It was concluded that 2,3-methanophenylalanine (a phenylalanine analogue) induces formation of β-bends in peptides, the type of the bend (β-I or β-II) being governed by the orientation of the substituent (Ph) at the C(3) atom of the cyclopropane ring, which is dictated by the strictly fixed torsion angle χ_1. For the model dipeptides **41a**,**b**, it has been shown experimentally for the first time that the orientation of the side chain can induce a specific conformation of the polypeptide chain.

The influence of methionine *cis*- and *trans*-methanologues on the conformation of peptides has been elucidated for the peptidomimetics **46a**,**b** as examples.[85–87] The conformation of **46a**,**b** in solutions has been studied using NMR and circular dichroism spectroscopy supplemented with computer simulations.[86,87] It was found that introduction of methionine methanologues into peptides gives rise to γ-bends irrespective of the isomer. Presumably, the tendency to form γ-bends relates not only to fixed values of the torsion angles φ and ψ, but to a larger value of the N−C_α−C(O) bond angle (117°) as well, which, in these compounds, substantially exceeds the corresponding values typical of residues of unstrained amino acids (~ 112° according to the CSD data).

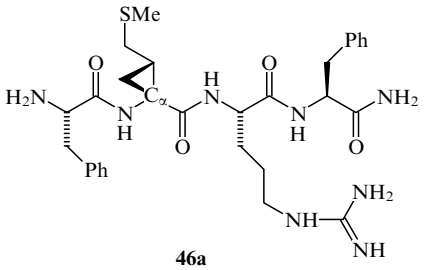

46a

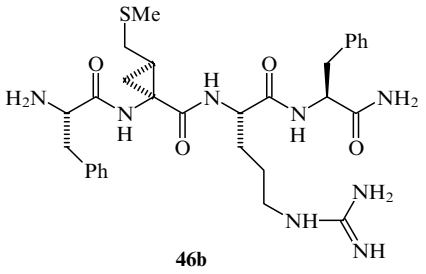

46b

The synthesis of methanologues of natural and other amino acids with a cyclopropane ring has been recently surveyed.[4,6] Therefore, in the present review we shall just outline the known methods for the preparation of ACC and discuss in more detail only methods developed in recent years.

Among the most frequently applied methods of synthesis of ACC, the following are the most popular: bisalkylation (*a*), addition of oxosulfonium ylides (*b*) and 1,3-dipolar cycloaddition of diazomethane (*c*) (Scheme 6).[6]

Scheme 6

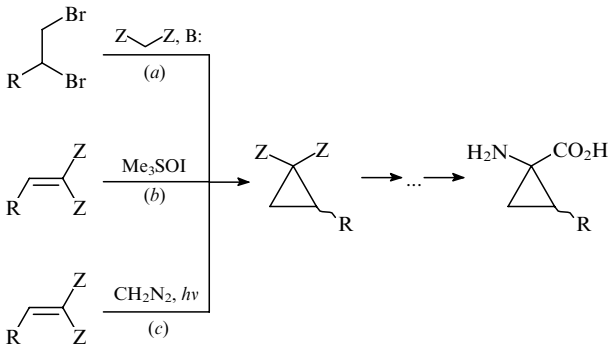

Z is an electron-withdrawing group.

For the preparation of optically active amino acids, diastereo- and enantioselective syntheses have been developed, which make use of chiral auxiliary groups. Essentially, these syntheses exploit asymmetrical versions of the reactions *a*–*c* (Scheme 6). For instance, the bisalkylation (*a*) was conducted with a chiral glycine equivalent, *i.e.*, the Schollkopf bislactim esters (**47**),[96] the Seebach imidazolidinones (**48**)[6] or 1,3-oxazolidine chiral derivatives (**49**).[6] The diastereoselective addition of oxosulfonium ylides to derivatives of tetrahydrooxazinone **50** (*b*) has led to methanologues of amino acids. The 1,3-dipolar cycloaddition of diazomethane (*c*) was realised for a terpenoid derivative **51**.[6]

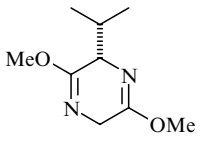

47

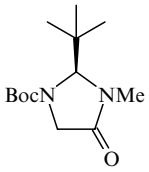

48

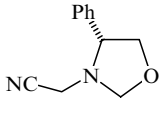

49

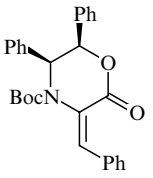

50

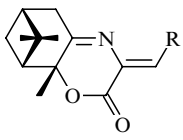

51

Elaboration of the synthetic routes that allowed preparation of ACC and its derivatives in multigram quantities is a significant achievement in this field. Among such routes, preparation of (2*R*,3*R*)-cyclo-Phe catalysed by rhodium complexes is worth a special note.[6]

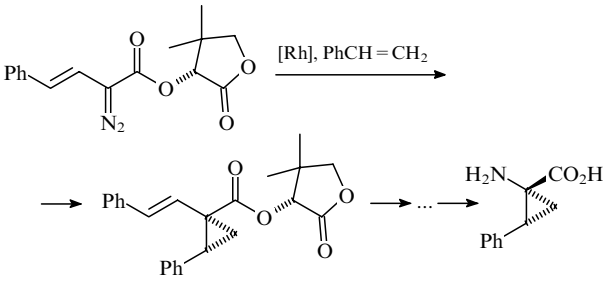

Syntheses of ACC derivatives including cyclo-Met, cyclo-Arg, cyclo-Arg′, cyclo-Glu, cyclo-Gln and cyclo-Lys starting from a chiral lactone **52** proved to be extremely efficient. This lactone can be synthesised from D-mannitol, which is an accessible natural chiral compound.[6] The strategy of the synthesis of ACC derivatives starting from the lactone **52** is illustrated in Scheme 7 with (*Z*)-cyclo-Met as an example.

Scheme 7

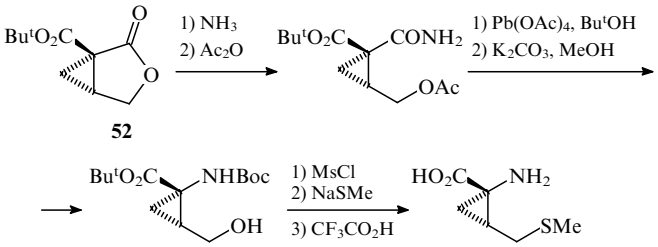

52

In a series of recent studies, available chiral compounds have been used as the starting materials in the stereoselective synthesis of ACC derivatives. In particular, starting from the optically active alcohols **53** and **54**, *allo*-norcoronamic acid (**55**) and (2*S*,3*R*)-methanoproline (**56**), respectively, were synthesised (Scheme 8). The key step in these syntheses was the condensation of the corresponding cyclic sulfates with methyl benzylideneglycinate.[97, 98]

Several methanologues of natural amino acids have been prepared by functionalisation of a dihydroxy-derivative **57** synthesised starting from D-glyceraldehyde.[99]

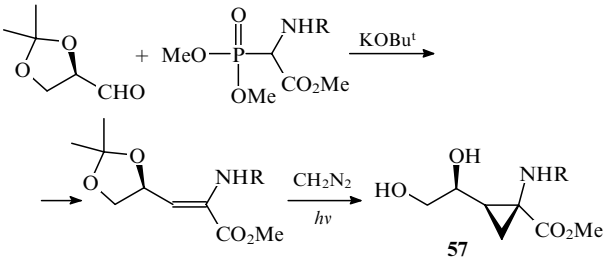

57

Transition metal complexes are often used in the stereoselective syntheses of ACC derivatives both as catalysts and reagents. The use of palladium complexes in the synthesis of functionalised cyclopropane derivatives [100, 101] and the stereoselective cyclopropanation of alkenes by Fischer dialkylaminocarbene complexes [102] have been reported.

Scheme 8

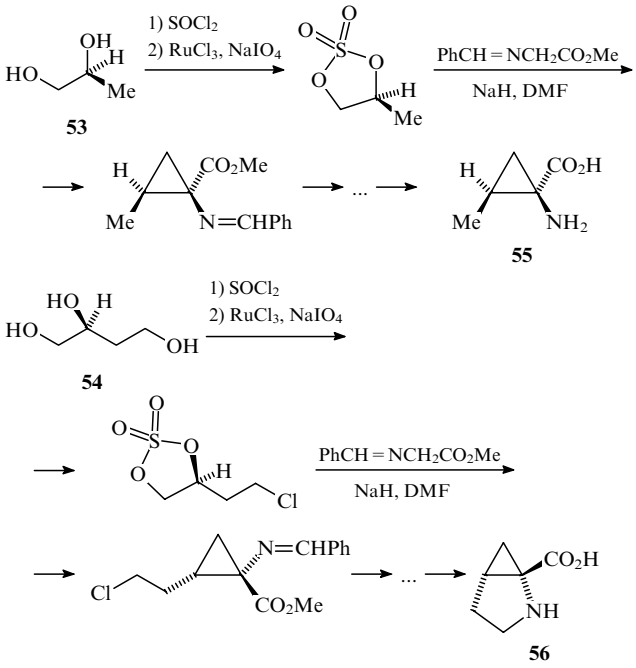

53

55

54

56

ACC, its derivatives and peptidomimetics or peptide models based on them have been the subject of numerous biochemical studies. The most prominent examples will be given here. As has been mentioned above, ACC is a precursor in the biosynthesis of ethylene. This reaction is catalysed by the iron-containing enzyme ACC oxidase. Two mechanisms of functioning of this enzyme have been suggested,[103] *viz*., nitrene- and radical-mediated ones. Recently, convincing arguments in favour of the free radical-mediated biochemical conversion of ACC into ethylene have been obtained. The formation of penta-1,4-diene upon oxidation of 2-cyclopropyl-substituted ACC (**58**) in the presence of this enzyme may be considered as an indirect proof of this suggestion.[104]

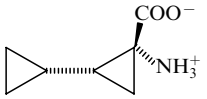

58

Russian scientists have observed [105] formation of tetrachlorophenoxy radicals upon enzymatic oxidation of ACC *in vitro* in the presence of an inhibitor, *viz*., tetrachlorohydroquinone, which also supports the radical mechanism of ACC oxidase action. ACC itself,[106] its various alkyl derivatives,[107–109] cyclo-Pro [95] and the respective hydroxamic acid [110] have been used to study the topology of the active site of ACC oxidase and the mechanism of its action.

An interesting example of studies aimed at the elucidation of factors responsible for the sweet taste of asparagine-containing dipeptides is the use of peptides containing ACC or its alkyl-substituted derivatives. Substitution of an ACC residue or its homologues, *i.e*., 1-aminocycloalkanecarboxylic acids **59**–**63**, for an L-Phe residue in Aspartame® (L-Asp-L-Phe-OMe) made it possible to reveal the dependence of the taste properties of the respective dipeptides on the steric volume of the C terminal residue. In particular, substitution of the ACC residue (**36**) and its homologues **59** and **60** for L-Phe retains the sweet taste of the dipeptide. At the same time, substitution of the residues **61** and **62** for L-Phe yields bitter dipeptides whereas the peptide containing a residue of **63** is tasteless.[111]

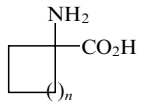

59 – 63

n = 1 (**59**), 2 (**60**), 3 (**61**), 4 (**62**), 5 (**63**).

Later, conformations of similar dipeptides containing residues of methyl-, dimethyl- and trimethyl-derivatives of ACC were analysed.[112] It was concluded that the observed changes in taste of the dipeptides are defined by their conformation, which depends upon the configuration of the cyclopropane-containing CRA in the dipeptide.

4. 3,4-Methanologues of α-amino acids

3,4-Methano-α-amino acids **64** are structural isomers of the 2,3-methano-α-amino acids discussed above.

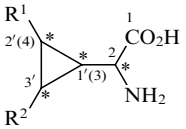

64

Molecules of 2,3-methanoamino acids are characterised by the fixed torsion angles $\chi_{1(2)}$ whereas their 3,4-cyclopropyl analogues reveal strictly fixed torsion angles $\chi_{2(3)}$. The presence of a cyclopropane fragment in such amino acids imposes only small restrictions on the angle χ_1 and does not influence significantly the angles of the peptide chain in the corresponding peptides. An exception to this tendency is the respective proline analogue, one isomer of which, *viz*., *cis*-3,4-methylene-L-proline (**65**), has been found in nature. Its structure has been confirmed by X-ray diffraction study and synthesis.[113]

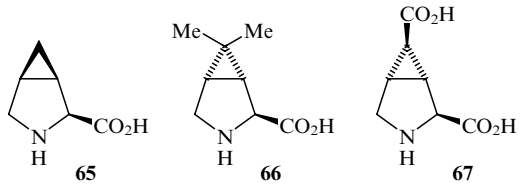

65 **66** **67**

In the 3,4-methanologue of proline, the torsion angles φ and χ are also fixed. This property was successfully employed in the design of mimetics of the polyproline II helix, which plays an important role in the processes of intracellular signal transmission.[114] The chimeric amino acids **66** and **67** have been investigated. They may be considered as analogues of both proline and leucine (the former) and proline and glutamic acid (the latter). A detailed conformational analysis of di- and tripeptides containing residues of **66** and **67** has shown that the torsion angles φ, ψ, χ_1 and χ_2 therein are $-70°$, $131°$, $-57°$ and $-158°$, respectively. These values agree with angles typical of the left-handed helix conformation of polyproline II (see Table 1).[115, 116] This conformational analysis was performed on the basis of the NMR data (for **66**) and results of computer simulations (for **66**, **67**). It is noteworthy that the calculations using molecular mechanics (MM) and *ab initio* (HF/6-31G* basis set) approaches yielded virtually identical geometric parameters of these two molecules. This illustrates an important advantage of the use of CRA in the design of peptidomimetics: the structure of their peptide fragments can be predicted on the basis of simple computational methods.

Compilation of 'stereolibraries', *i.e*., diastereomeric series of amino acids differing from each other in the configuration of chiral centres, is also possible for 3,4-methanologues. For instance, 2′-substituted derivatives have eight stereoisomers while 2′,3′-disubstituted amino acid analogues have sixteen isomers.

The large number of stereoisomers of 3,4-methanologues has been used in a study of neuroreceptors activated by L-glutamic acid. At present, several types of receptors that interact with L-glutamic acid are known. It has been suggested that L-glutamic acid interacts with different receptors adopting different conformations. This hypothesis was strongly supported by the synthesis and investigation of all diastereomers of 2-(carboxycyclopropyl)-glycine (CCG) **68**.[117, 118]

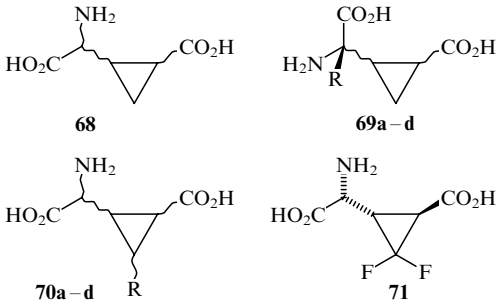

68 **69a – d** **70a – d** **71**

R = Alk (**a**), Ph (**b**), CH_2OMe (**c**), CO_2H (**d**).

It was established that in many cases the diastereomers CCG interact with different neuroreceptors selectively. Synthesis and biological studies of α-substituted derivatives of CCG, compounds **69a – d** [119, 120] as well as the compilation of 'stereolibraries' for 2′,3′-disubstituted derivatives **70a – d** [121 – 125] and the synthesis of difluoro-substituted derivative **71** [126] provided further confirmation of this hypothesis and a significant contribution to the understanding of mechanisms of neurophysiological processes. All 16 stereoisomers of 2′-carboxy-3′-phenylcyclopropylglycine (**70b**) have been synthesised.

Analogues of other natural amino acids, such as valine, serine,[127] homophenylalanine,[128] arginine,[129] proline [130] and ornithine [131] (**72 – 75**, **65** and **76**) have also been synthesised.

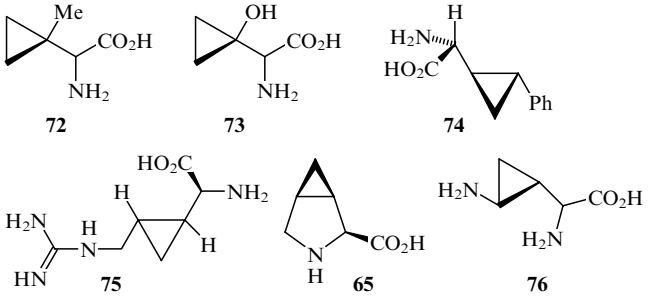

72 **73** **74** **75** **65** **76**

Methods for the synthesis of 3,4-methanologues of amino acids are analogous to those of 2,3-methanologues. Similarly, the key step of these syntheses usually consists of the build up of a cyclopropane ring. In this respect, major efforts were aimed at the optimisation of the respective tranformations to the suitable level of diastereoselectivity. The most frequently applied method is cyclopropanation of a C=C double bond, *i.e*., addition of carbenes or carbenoids. The synthesis of D-2-(carboxycyclopropyl)glycine can be mentioned as an example of this approach.[118]

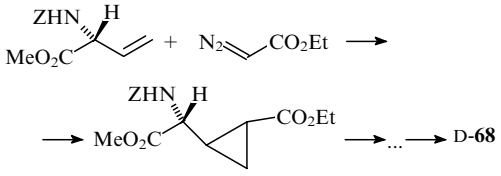

For the preparation of glycine derivatives (*e.g.*, of **70**), the Michael addition followed by elimination of hydrogen bromide was also applied to form a cyclopropane ring (Scheme 9).[121]

Scheme 9

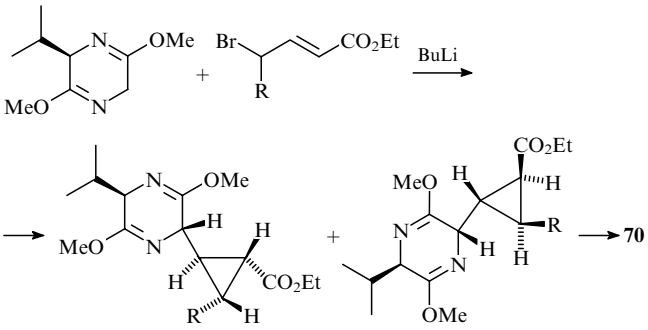

An original route to the synthesis of substances from this class of CRA has been suggested by de Meijere *et al.*[127] This involves 1,4-addition of nucleophiles to 2-chloro-2-cyclopropylideneacetates with subsequent substitution of azide for chloride, reduction and deprotection.

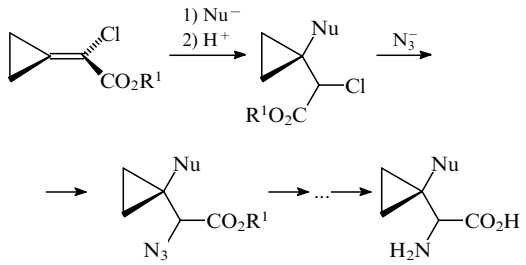

Nu = H, Me, NH_2, CH_2CO_2H, SMe.

The key step of the synthesis of proline 3,4-methanologues [130] is the formation of the pyrrolidone ring as a result of the intramolecular insertion of a carbene (*viz.*, cyclopropylidene) at the C–H bond.

Yet another new original approach to the synthesis of carboxycyclopropylglycine derivatives consists of the addition of stabilised C-nucleophiles to tricarbonyl(1-methoxycarbonylpentadienyl)iron cation.[132]

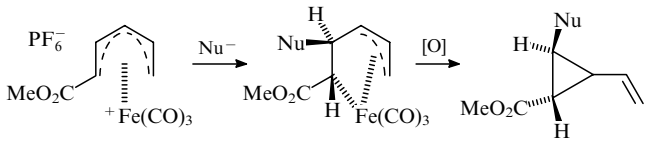

Nu is a glycine synthon.

5. 4,5-Methanologues of α-amino acids

4,5-Methano-α-amino acids (**77**) are used in the synthesis of peptidomimetics and biologically active substances substantially less frequently. It is no surprise since only the torsion angle χ_3, which is situated quite far from the peptide chain, is strictly fixed in these molecules.

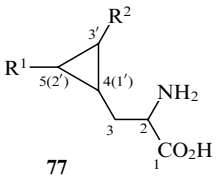

77

4,5-Methanologues of amino acids can be classified as CRA only formally. The presence of a cyclopropane moiety in 4,5-methano-α-amino acids imposes only small constrains on the torsion angle χ_2 and virtually does not affect the torsion angles φ and ψ within the polypeptide chain as well as the angle χ_1 in the respective peptides.

Although 4,5-methanologues of amino acids have attracted insignificant attention from researchers, they are quite abundant in nature. In particular, the compound **78**, the so-called hypoglycine A, occurs in some unripe fruits.[133] Another derivative, *trans*-(2-aminocyclopropyl)alanine (**79**), is the key component of a novel antitumour antibiotic Belastosin A.[134] Yet another derivative, *trans*-(2-nitrocyclopropyl)alanine (**80**), represents a rare example of a naturally occurring substance bearing a nitro group;[135] it is a component of a macrolide antibiotic Hormaomycine.

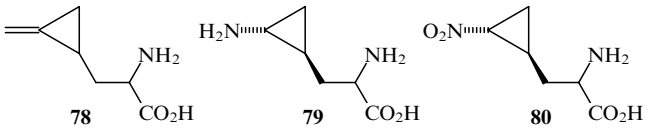

This class of compounds also includes the recently synthesised 2-aminoadipic acid analogue **81** [136] as well as chimeric amino acids **82** and **83**, which may be regarded as analogues of glutamic acid and proline simultaneously (the acid **83** also contains a fragment of α-cainic acid **84**, which is a naturally occurring non-proteinogenic amino acid).[137]

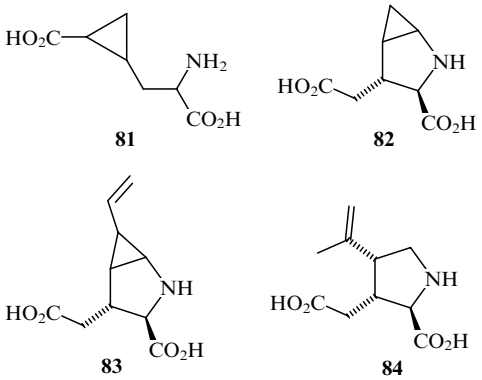

As in the case of 3,4-methanologues, the key step in the synthesis of compounds **78**–**83** is the construction of a cyclopropane ring or of a bicyclic core in the case of **82** and **83**. For the synthesis of **80**, the three-membered ring was formed using alkylation of nitromethane (the Henry reaction).

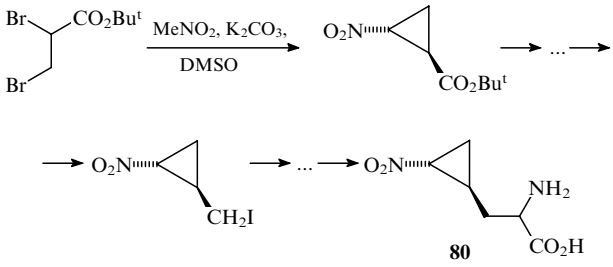

In the synthesis of compounds **82** and **83**, the five-membered and three-membered rings are built up consecutively. For instance, the acid **82** was synthesised according to Scheme 10.

Scheme 10

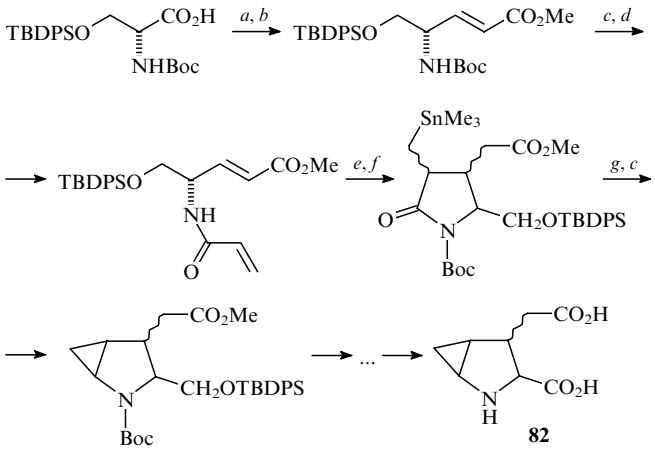

TBDPS is *tert*-butyldiphenylsilyl;
(*a*) Bu^i_2AlH; (*b*) $Ph_3P=CHCO_2Me$; (*c*) CF_3CO_2H; (*d*) $CH_2=CHCOCl$; (*e*) Me_3SnCl, $NaBH_3CN$, azobisisobutyronitrile; (*f*) Boc_2O, 4-dimethylaminopyridine, Et_3N; (*g*) $LiBHEt_3$.

6. Spiro[2.2]pentane derivatives

Three types of spirocyclic CRA (compounds **85**–**87**) have been synthesised.

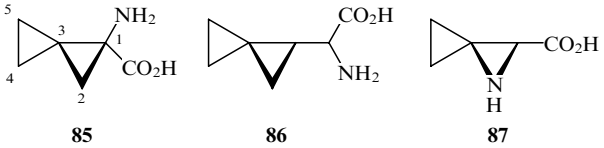

85 **86** **87**

The molecule **85** with a spiro[2.2]pentane skeleton is characterised by the bond lengths and angles strongly distorted with respect to standard mean values.[26, 138] In particular, the C–C bonds involving the spiroatoms C(3) are shortened on average by 0.07 Å, while the bond angles are distorted even more strongly (the values lie in the range from 59° to 135°).

No structural data on the compound **87** with a 1-azaspiro-[2.2]pentane framework have been published. The torsion angles in the molecule **85** have been reported by Pelliciari *et al.*,[138] the corresponding values for **87** can be estimated only approximately.

Compounds with spiro[2.2]pentane and 1-azaspiro[2.2]pentane frameworks are synthesised by different routes.

In particular, two consecutive [2 + 1]cycloaddition reactions involving carbene or carbenoid intermediates have been used for the preparation of 2-aminospiro[2.2]pentane-2-carboxylic acid (Scheme 11).[139]

Scheme 11

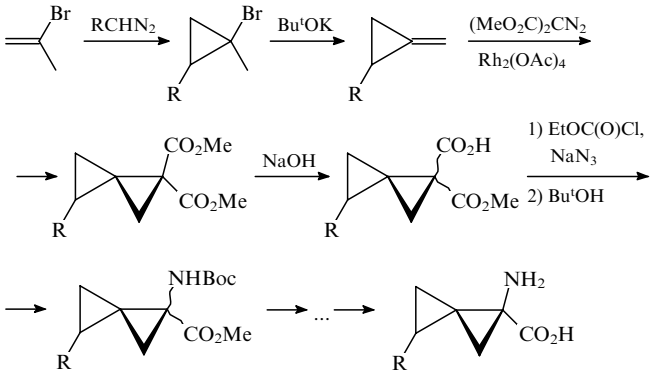

This route was also applied to the synthesis of compounds **85**, **86** and 4-carboxy-substituted derivative **88**, an analogue of glutamic acid. The latter compound was obtained in the form of four diastereomeric pairs.

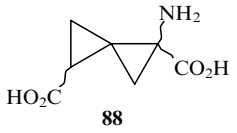

88

It is of note that compound **85** is unstable and spontaneously rearranges into a cyclobutane derivative **89** in aqueous solution in 2 weeks.[139]

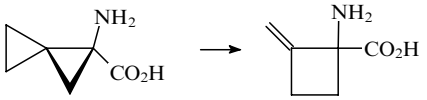

85 **89**

1-Azaspiro[2.2]pentane-2-carboxylic acid (**87**) is formed by the reaction of methyl(chloro)cyclopropylideneacetate with primary amines or ammonia.

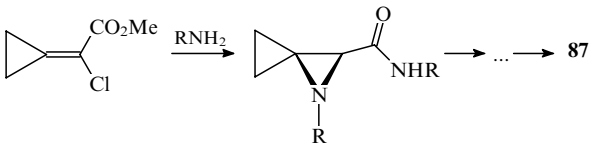

The amino acid **87** has proven to be relatively stable, it has been used to prepare a glycine-containing dipeptide.[140]

Diastereomers of compound **88** have been extensively studied as regards their binding to typical ionotropic and metabotropic glutamic acid receptors. Since the results of the biological assays were negative in all cases, one may assume that all these compounds are characterised by a spatial configuration of functional groups energetically unfavourable for glutamic acid. Weak binding was observed only with ionotropic *N*-methyl-D-aspartate (NMDA) receptor.[138]

V. Bi- and polycyclic conformationally rigid amino acids with an endocyclic nitrogen atom

Amino acids discussed in this and following sections represent bi- or polycyclic structures, which enable fixation of a larger number of torsion angles as compared to the monocyclic CRA discussed above.

This Section is devoted to amino acids possessing an amine nitrogen atom incorporated into a polycycle. Consequently, the torsion angle φ is strictly fixed in all corresponding peptides. Furthermore, the torsion angle χ_1 (and very often other angles χ as well) is fixed.

It is convenient to classify these amino acids according to the ring containing the nitrogen atom. There are only a few published examples of compounds possessing three- and four-membered C_nN rings (n = 2, 3). In addition to the spirocyclic compounds considered above, 2-azabicyclo[2.1.0]pentane-3-carboxylic acid (also referred to as 3,4-methanoazetidine-2-carboxylic acid **90**) has been reported.[141]

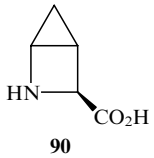

90

On the other hand, amino acids with larger C_nN rings ($n \geqslant 6$) are not rigid (furthermore, such amino acids are rare). Therefore, only amino acids with five- and six- membered C_nN rings ($n = 4$, 5), which are proline and pipecolic acid analogues, respectively, will be discussed below.

1. Proline analogues

Proline occupies a special place among proteinogenic amino acids due to its unique structure. In this amino acid, the amine nitrogen atom is involved in the five-membered ring, which gives rise to the following changes in the conformation of a proline-containing polypeptide chain:

— due to the absence of a hydrogen atom at the nitrogen atom, the latter cannot form hydrogen bonds;

— the *trans*-configuration of a polypeptide chain becomes only slightly more favourable than the *cis*-configuration;[142–144]

— due to steric hindrance, the values of the torsion angle φ within the five-membered ring vary in the range of $-75^\circ \pm 30^\circ$ (see Ref. 20) (the range of possible values of the torsion angle ψ is also limited due to steric requirements);

— due to significant steric strains, the nitrogen atom is substantionally pyramidalised and the amide bond is twisted;[142, 145]

— the polypeptide loses its capability to form α-helices and thus the tendency towards formation of β-bends is strengthened (especially in the case of the *cis*-configuration of the peptide bond), which explains the higher content of proline in active and peptide-binding sites of enzymes.[144]

It is of note that the above features are typical to a certain extent of all amino acids having an endocyclic nitrogen atom involved in the polypeptide chains. These are more pronounced for amino acids with strained rings.

In order to confer conformational rigidity on the proline ring, it is necessary to introduce bridges with a length of 1 or 2 atoms into the molecule. When such a bridge links two adjacent positions in the ring, proline methanologues are formed, which were considered above. Other examples of theoretically possible bicyclic amino acids representing proline analogues are shown below (hereinafter, the structural types that have not been reported in the literature to date are given in parentheses):

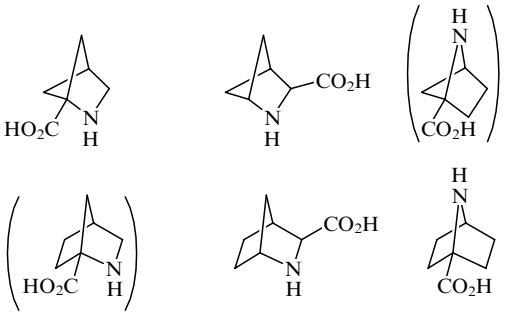

Polycyclic proline analogues with more than two rings will be discussed separately.

a. 2-Azabicyclo[2.1.1]hexane derivatives

2-Azabicyclo[2.1.1]hexane-1-carboxylic acid (**2**) or 2,4-methanoproline (atom enumeration in parentheses corresponds to that for proline) was isolated in 1980 from the seeds of legume *Ateleia herbert smithii* among other new amino acids.[146] Recently, this acid has also been isolated from the plant *Bocoa alterna*.[147]

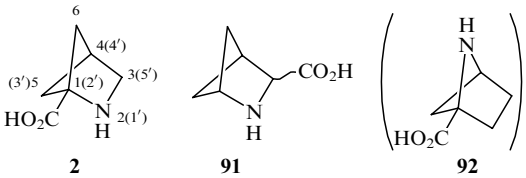

2 **91** **92**

2,4-Methanoproline (**2**) is one of a few naturally occurring proline analogues; the residue of this amino acid in peptides is denoted as 2,4-MePro. In addition to 2,4-methanoproline, two other proline analogues having an azabicyclo[2.1.1]hexane skeleton are possible, *viz*., 3,5-methanoproline (*exo*-**91**) and 2,5-methanoproline (**92**).

exo-3,5-Methanoproline and 2,4-methanoproline **2** have been synthesised quite recently,[148] whereas no synthesis of their 5-aza-analogue **92** has been reported so far.

The bond lengths in the molecule of 2-azabicyclo[2.1.1]hexane-1-carboxylic acid (**2**) are very similar to those in proline but the bond angles in the two molecules are somewhat different (Table 2).[145, 149] The largest difference is observed for the C(2′)–C(3′)–C(4′) and C(2′)–C(6)–C(4′) angles due to the strain in the cyclobutane moiety. The differences in the C(3′)–C(4′)–C(5′) and C(3′)–C(4′)–C(6) angles are probably caused by a specific distortion of the framework, which will be discussed below.

Table 2. The values of the bond angles in 2,4-methanoproline and proline (atom enumeration corresponds to that in proline).

Angle	Value (deg)	
	2,4-MePro	Pro
N–C(5′)–C(4′)	97.0	103
C(3′)–C(4′)–C(5′)	103.1	103
C(3′)–C(4′)–C(6)	100.5	103
C(2′)–C(3′)–C(4′)	82.4	103
C(2′)–C(6)–C(4′)	81.9	

Polypeptides containing a 2,4-MePro residue are characterised by fixed torsion angles φ and χ (the values of these angles may be found elsewhere [149, 150]).

No structural data on 3,5-methanoproline have been published. However, owing to the rigidity of its bicyclic framework, its structural parameters can be predicted on the basis of respective data for the 2,4-isomer.

One may conclude that the angle φ in the 2,4-MePro residue should be 0° assuming the symmetry of the 2-azabicyclo[2.1.1]-hexane framework and planarity of the amide moiety. However, the experimental value of this angle determined for *N*-acetyl-2,4-methanoproline-*N*′-methylamide (**93**)‡ is 29° (see Ref. 150).

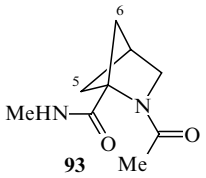

93

The observed deviation from the ideal value of 0° is due to distortion of the 2-azabicyclo[2.1.1]hexane framework of **93**, which results in the non-equivalency of the C(5) and C(6) atoms.

The sum of the bond angles at the nitrogen atom in **93** is 356°, *i.e*., virtually no pyramidalisation of the nitrogen atom occurs. This supports the above suggestion that the distortion of the angle φ originates in the deformation of the framework. Numerous structural data on the unsubstituted acid **2** in solutions suggest that the molecules of **2** exist in the form of two interconverting enantiomers, which means, strictly speaking, that they are not rigid.

‡ This type of compounds are quite often applied to prepare peptide models in order to estimate the torsion angles in the respective polypeptide chain.

The value of the angle φ in peptides containing an *exo*-3,5-methanoproline (**91**) residue should be -60° taking into account the fact that the bicyclic framework is symmetrical and the amide bond is planar. However, the bicyclic framework is expected to be distorted in this case as well.

The tilt angle (δ) of the amide bond (at the tertiary nitrogen atom) in compound **93** is 16° and the twist angle $\tau = 10^\circ$.

The torsion angle ω in compound **93** is equal to -178° (this molecule adopts the *trans*-conformation in crystals). As has been shown, the *trans*-isomer of **93** is more stable than the *cis*-isomer both in the solid state and in solutions.[149, 150]

There are several approaches to the synthesis of 2,4-methanoproline. All of them are based on the [2+2]-cycloaddition reaction.

Earlier,[151–153] the photochemical cyclisation of the diene **94** was employed (the only difference between several suggested procedures consisted of the routes for the preparation of the diene **94**).

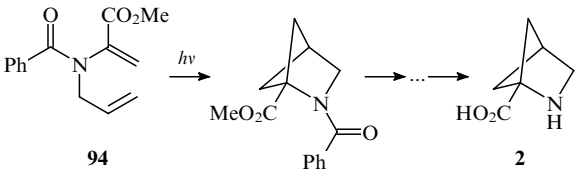

94 **2**

Alternatively, a recently suggested method for the synthesis of 2,4-methanoproline includes [2+2]-cycloaddition with dichloroketene followed by cyclisation.[154]

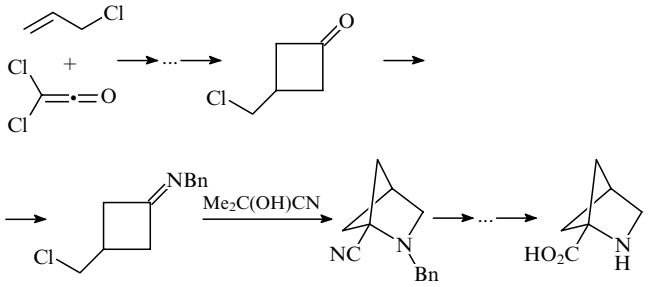

Rearrangement of 2-azabicyclo[2.2.0]hex-5-enes following addition of bromine[155] is rarely used for the preparation of 2,4-methanoproline due to difficulties associated with the introduction of a 1-carboxy group. Nevertheless, this reaction is a very promising method for the formation of the 2-azabicyclo[2.1.1]-hexane framework.

Although 2-azabicyclo[2.1.1]hexane has been known for a long time, it has rarely been used for the synthesis of amino acids. For instance, carboxylation of unsubstituted 2-azabicyclo[2.1.1]-hexane cannot be regarded as a method for the preparation of 2,4-methanoproline since it yields an equimolar mixture of 2,4- and 3,5-methanoprolines (it is of note, however, that it is exactly by this route that the 3,5-isomer **91** has been produced).[148]

Only one functionalised 2,4-methanoproline derivative, *viz*., glutamic acid analogue **95**, has been synthesised to date. It is formed in the photochemical [2+2]-cyclisation of the respective diene precursor[156] (similar to the synthesis of the acid **2** from the diene **94**).

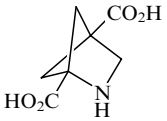

95

Like other functionalised proline analogues, the amino acid **95** is chimeric since it simultaneously mimics glutamic acid and proline.

The biological activity of 2,4-methanoproline and its derivatives is quite well explored. In particular, 2,4-methanoproline has been introduced in place of proline into oligopeptides bradykinin and angiotensin II[157] that are neurotransmitters playing a crucial role in the regulation of blood pressure and heart functioning. Unfortunately, the synthetic analogues proved less active than the original oligopeptides. Compound **95** has been tested as an inhibitor of a sodium-dependent glutamate transport protein.[156]

b. Derivatives of 2-azabicyclo[2.2.1]heptane-3-carboxylic and 7-azabicyclo[2.2.1]heptane-1-carboxylic acids

Compounds with the norbornane framework are widely employed in the synthesis of diverse conformationally rigid substances. In particular, aza-derivatives of norbornane have been used in the design of CRA analogous to proline. In principle, there are three possible variants of incorporation of proline into the norbornane framework (compounds **96**–**98**).

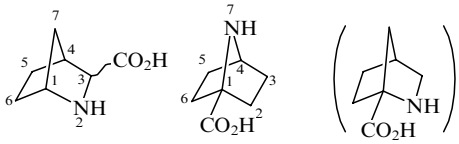

96 **97** **98**

To date, only 2-azabicyclo[2.2.1]heptane-3-carboxylic (**96**) and 7-azabicyclo[2.2.1]heptane-1-carboxylic (**97**) acids along with some of their derivatives have been synthesised.

2-Azabicyclo[2.2.1]heptane-3-carboxylic acid (**96**) (its residue in peptides is denoted as Abh) has been known for a relatively long time.[158] It was one of the first artificial conformationally rigid analogues of proline.

An analysis of X-ray diffraction data on proline[145] and the acid **96**[159] has revealed important differences in the bond angles within the pyrrolidine rings of the two substances despite similarity of the respective bond lengths. The values of the bond angles (in deg.) in model peptides containing Pro and Abh residues are given below.

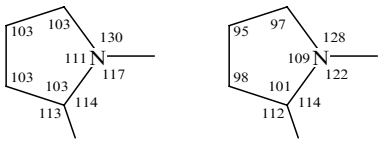

Pro Abh

Owing to the rigid framework of 2-azabicyclo[2.2.1]heptane-3-carboxylic acid, peptides with an Abh residue are characterised by the fixed torsion angle φ. The same is valid for the torsion angles χ (the values of these torsion angles for the *exo*-isomer **96** are given elsewhere,[159, 160] similar values are expected for the *endo*-isomer).

Assuming that the bicyclic framework of **96** is symmetrical and the amide bond is planar, the torsion angle φ should be equal to -60°. Although there have been no dedicated investigations on this topic, the available data for **99** ($\varphi = -39^\circ$)[160] and **100** ($\varphi = -73^\circ$)[159] allow one to suggest that the real value of this torsion angle in **96** will deviate from the ideal value (-60°). The large deviation of the torsion angle φ from -60° observed for **99** can be partly attributed to the presence of a six-membered ring.

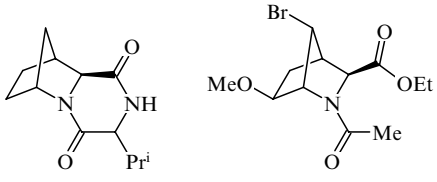

99 **100**

The nitrogen atoms in **99** and **100** are characterised by insignificant pyramidalisation ($\omega_0 \approx 358^\circ$), however, the respec-

tive peptide bonds are non-planar. The non-planarity of the amide bonds is evidenced by the values of the angles δ and τ: $\delta = 14°$, $\tau = 8°$ and $\delta = 14°$, $\tau = 6°$ for **99** and **100**, respectively.

The compound **100** in crystals adopts the *trans*-conformation ($\omega = -177°$). No data on the amide bond configuration in solutions of **100** are available.

The principal method for the synthesis of 2-azabicyclo[2.2.1]-heptane-3-carboxylic acid is the Diels–Alder reaction of cyclopentadiene (as a diene) and imine (as a dienophile) that is normally generated *in situ*.[158, 161, 162]

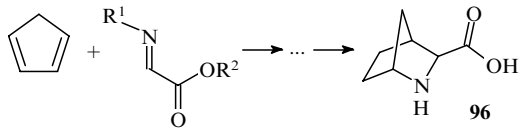

96

Using this reaction, optically active 2-azabicyclo[2.2.1]heptane-3-carboxylic acid (*exo*-**96**) can be produced in gram quantities.[161]

Substituted amino acids are usually prepared by a modification of the double bond formed at the cycloaddition stage.

Other routes to the synthesis of the amino acid **96** are based on different intramolecular cyclisations but they found only limited applications.[163]

Despite the apparent simplicity of the preparation of 2-azabicyclo[2.2.1]heptane-3-carboxylic acid derivatives, there are only a few known representatives of this class. In addition to the unsubstituted compound **96**, only analogues of homoserine and glutamic acid have been reported, *i.e.*, **101** (along with its protected derivatives) [164] and **102,**[163] respectively.

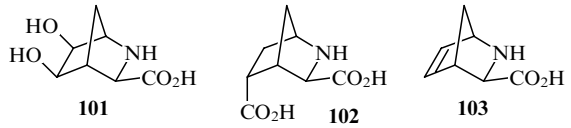

101 **102** **103**

Compound **103** has also been synthesised. Since it tends to rearrange in acidic media, it was isolated only in the protected form.[165]

2-Azabicyclo[2.2.1]heptane-3-carboxylic acid (**96**) is widely employed in asymmetric synthesis.[166] It has also been used for the preparation of analogues of fragments of the tumour growth factor TGFα (see Ref. 167) and inhibitors of prolylendopeptidase § **104**–**107** (see Ref. 168).

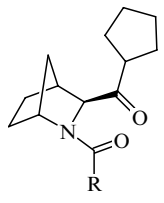

104–**107**

R = $Ph(CH_2)_3$ (**104**), PhCHCH$_2$CHCH$_2$ (**105**), (cyclo-C_3H_5)$_2$CH$(CH_2)_3$ (**106**), Bu^{t}O (**107**).

In contrast to 2-azabicyclo[2.2.1]heptane-3-carboxylic acid (**96**), 7-azabicyclo[2.2.1]heptane-1-carboxylic acid (**97**) has been prepared only quite recently.[169, 170]

An analysis of structural data indicates that the bond lengths and bond angles in 7-azabicyclo[2.2.1]heptane are virtually identical to those in proline (except for the angles at the nitrogen atom).[145] Certain differences in the latter (by up to 7° as compared to proline) are due to the pyramidalisation of the nitrogen atom.

An analysis of the dihedral angles shows that the angle φ as well as all angles χ in the 7-azabicyclo[2.2.1]heptane molecule are fixed (the values of these angles can be found elsewhere [171, 172]).

The theoretical value of the angle φ calculated under the assumption that the framework is symmetrical and the amide bond is planar is equal to 0°. For the sake of structural elucidation of peptides, a series of model oligopeptides with a residue of **97** (for this residue, a notation Ahc is adopted) has been synthesised. According to X-ray diffraction data, the angle φ in the protected dipeptides Piv-Ahc-L-Ser-NHMe (**108**) and Piv-L-Ser-Ahc-NHMe (**109**) strongly deviates from the theoretical value of 0°, similarly to the aforementioned case of dipeptides with a 2,4-methanoproline residue: $\varphi = -36°$ (for **108**), 40° and 44° (for two crystalline modifications of **109**). Compound **110** is characterised by an even larger deviation ($\varphi = \pm 51°$).[172]

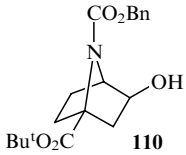

110

The norbornane framework in **108**–**110** is undistorted and the deviation of the angle φ from the idealised value of 0° occurs due to the pyramidalisation at the nitrogen atom. Strictly speaking, the molecules again lose rigidity as regards the angle φ.

The torsion angle ω_0 is 346° in the case of Piv-Ahc-L-Ser-NHMe. Such a low value of ω_0 is observed only in a few amides (*e.g.*, in aziridine derivatives). The amide bond in **108** is characterised by the following values: $\delta = 34°$, $\tau = 5°$. For **110**, the respective parameters are 335° (ω_0), 43° (δ) and 17° (τ).

In the crystals of **110**, the angle ω is 133°, which corresponds to the *trans*-configuration. Meanwhile, the angle ω is close to ±180° in all the dipeptides studied.

Introduction of an Ahc residue into a peptide chain in place of proline stabilises the β-bend (type I).[171]

There are several approaches to the synthesis of the 7-azabicyclo[2.2.1]heptane framework. The amino acid **97** has been prepared for the first time using a radical cyclisation of 1-(*o*-bromobenzoyl)-2-(prop-2-enyl)pyrrolidines,[169, 170] which yields a series of by-products, including 8-azabicyclo[3.2.1]octane derivatives. This method is inefficient for the synthesis of the amino acid **97**; it is used solely for the preparation of 7-azabicyclo[2.2.1]heptane unsubstituted at position 1.

Another method utilises a nucleophilic substitution reaction that is accompanied by formation of a bond between the nitrogen and carbon C(4) atoms. To form the 6-membered ring, the Diels–Alder reaction is applied, in which the Danishefsky diene [CH_2=C(OSiMe_3)CH=CH-OMe] or 3-methoxy-1,3-butadiene are used as the dienes and 2-acylamidoacrylates as the dienophiles. The general scheme of the synthesis is depicted below.[173–177]

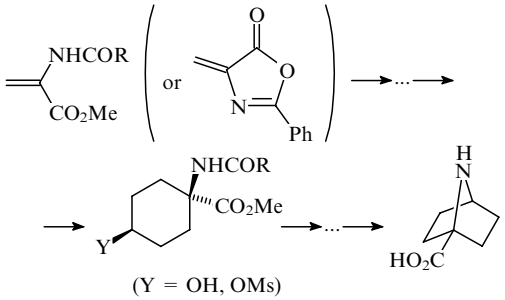

(Y = OH, OMs)

This method is especially convenient for the synthesis of 2-substituted derivatives.

Yet another approach to the synthesis of 7-azabicyclo[2.2.1]-heptane-1-carboxylic acid has been suggested,[172] which implies

§ Prolylendopeptidase is the only enzyme capable of splitting the C-terminal peptide bond formed by the proline residue. This enzyme splits neuropeptides involved into the learning and remembering processes; thus it is one of the targets within the scope of curing of the Alzheimer decease and amnesia.

formation of a bond between the C(1) and C(6) atoms as a result of alkylation of the respective enolate anion.

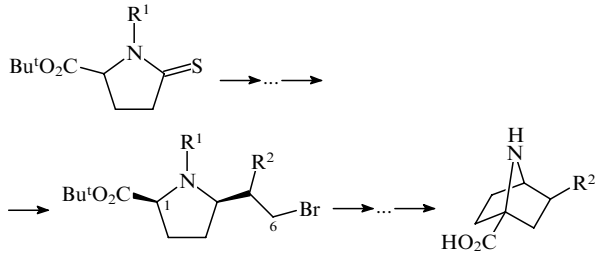

This method has been used to produce a number of chimeric 3-substituted amino acids.

It should be noted that all amino acids having a 7-azabicyclo[2.2.1]heptane framework, except for the unsubstituted amino acid **97**, are chimeric since they always mimic proline in addition to the natural amino acid representing their most direct analogue. In particular, 2- and 3-substituted chimeric acids **111**–**121** have been synthesised, which are analogues of phenylalanine, 4-hydroxyproline, glutamic acid, homophenylalanine, ornithine, arginine, lysine and serine.[172–174, 177, 178]

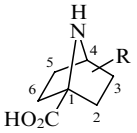

111–**121**

R = 2-Ph (**111**),[174] 2-CH_2CO_2H (**112**),[177] 3-OH (**113**),[177] 3-Ph (**114**),[172] 2-CO_2H (**115**),[173] 2-Pr^n (**116**),[173] 3-CO_2H (*exo*- and *endo*-**117**),[172] 2-OH (*exo*- and *endo*-**118**),[178] 3-CH_2NH_2 (*exo*- and *endo*-**119**),[172] 3-$CH_2NHC(=NH)NH_2$ (*exo*- and *endo*-**120**),[172] 3-$CH_2CH_2NH_2$ (**121**).[172]

Only protected derivatives of the amino acids **117**, **119**–**121** have been prepared.[172]

The unsubstituted amino acid **97** has been utilised in the synthesis of peptidomimetics. In particular, substitution of Ahc for Pro in the peptide Ac-D-Phe-Pro-boroArg-OH (**122**, DuP714), a thrombin inhibitor, yielded the peptidomimetic **123**. This peptidomimetic manifested the 30-fold lower thrombin affinity than the original peptide **122**, which allowed the authors to conclude[179] that the conformation of the model compound in the bound state does not correspond to that of the object being modeled.

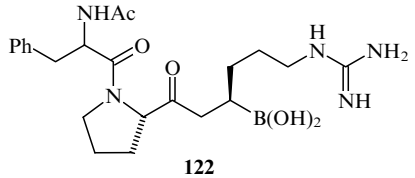

122

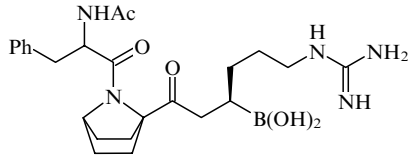

123

A benzyl derivative of the amino acid **113** has been introduced into a proline-containing inhibitor of HIV-I protease. The mimetic obtained manifested quite a high degree of binding to the enzyme.[180]

c. Other proline analogues

As has been mentioned above, the bridges in bicyclic CRA should include 0, 1 or 2 atoms, the presence of sp^2-hybridised atoms in the bridge enhances the conformational rigidity of the CRA molecule. For bridges containing a π-bond, lengths of up to three atoms are possible. For instance, compound **124**[181, 182] with a 2,5-bridge is classified as a CRA.

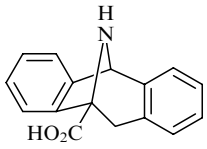

124

Compound **124** has been prepared as a potential ligand for the NMDA receptor but it can be formally regarded as a proline analogue.

The tricyclic amino acids **125**–**127** can also be considered as proline analogues.

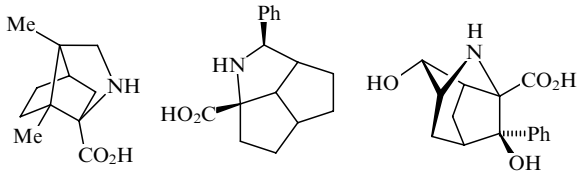

125 **126** **127**

Compound **125** has been prepared in several steps starting from camphor.[183] The molecule **125** is extremely rigid. This fact makes **125** very promising for the synthesis of peptidomimetics.

The tricyclic compound **126** is produced by intramolecular [3 + 2]-cycloaddition. This is a key intermediate in the synthesis of guanidine alkaloids.[184] It was isolated only in the protected form.

Compound **127** is of particular interest. It has the full right to be named a 'hyperchimeric' amino acid since it is an analogue of eight natural amino acids: proline, serine, homoserine, phenylalanine, threonine, isoleucine, valine and 4-hydroxyproline.[185]

No structural data on **124**–**127** are available, although the results of an X-ray diffraction study of the amino acid **128** (which is a precursor of **127**) have been published.[185]

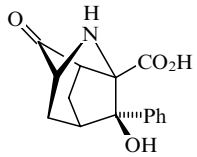

128

2. Pipecolic acid analogues

Pipecolic acid **129** is a non-natural cyclic α-amino acid that represents a proline homologue.

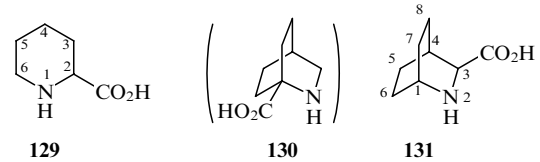

129 **130** **131**

To confer rigidity on the pipecolic acid framework, it has to be included into a bicycle with the bridge linking positions 2 and 5 (or 3 and 6). The case of a bridge containing only one atom has been discussed above since it is the 2-azanorbornane framework. In the case of a bridge containing two atoms, two structural types **130** and **131** are possible.

To date, only compound **131** with a carboxy group at the position 3 has been synthesised. Compound **130** has not been

reported although its β-lactam derivative has been characterised.[186]

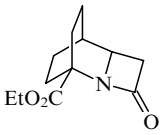

2-Azabicyclo[2.2.2]octane-3-carboxylic acid (**131**) is quite often used as a substitute for the proline residue although it is actually an analogue of pipecolic acid (for the residue of this acid, a notation Abo is adopted). This acid can be rather easily prepared in the enantiomerically pure form.

No dedicated structural studies on the 2-azabicyclo[2.2.2]octane framework of **131** have been conducted so far, although its amide **132** (see Ref. 187), tosyl derivative **133** (see Ref. 188) and the drug Zabicipril (S 9650-3) **134** (see Ref. 189) have been studied using X-ray diffraction.

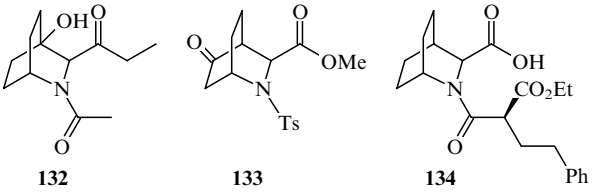

132 **133** **134**

An analysis of these structural data indicates that the C–C bonds of the piperidine rings within the 2-azabicyclo[2.2.2]octane framework are slightly (approximately by 0.03 Å) longer than in pipecolic acid;[190] no substantial difference in the bond angles is observed.

Formally, the two piperidine rings in **131**, *i.e.*, C(1)NC(3)C(4)C(5)C(6) and C(1)NC(3)-C(4)C(8)C(7), can be distinguished. According to experimental results,[190] the absolute values of the torsion angles in these rings are not identical, which indicates that the framework is somewhat distorted (as in the case of 2,4-methanoproline).

Theoretically, the value of the angle φ in derivatives of 2-azabicyclo[2.2.2]octane-3-carboxylic acid assuming the symmetrical framework and the undistorted amide bond is -60°. According to X-ray diffraction data, this value is -65° in **133** (*i.e.*, the deviation from the idealised value is small). In Zabicipril **134**, the respective torsion angle is -63°.

The pyramidalisation parameter (ω_0) of the nitrogen atom in **132** is 359.7°. Distortion of the amide bond is also insignificant ($\tau = 4^\circ$ and $\delta = 9^\circ$), *i.e.*, the amide bond in derivatives of 2-azabicyclo[2.2.2]octane is virtually planar.

According to X-ray diffraction data, the amide bond is characterised by the *trans*-configuration in **132** and **134** ($\omega = -172^\circ$ and 174° for **132** and **134**, respectively).

The amino acid **131** and its derivatives can be prepared using several methods. As in the case of azanorbornane, the basic method for the construction of this framework is the Diels–Alder reaction.[189, 191]

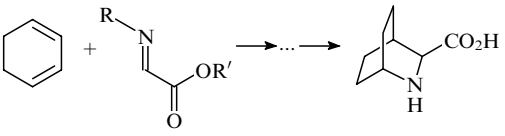

Functionalised derivatives can be produced by modification of the double bond that is formed in the cycloaddition reaction.[191]

Among other synthetic routes, the following are worth a special note: the reaction of 1,2-dihydropyridines with dienophiles,[192] the intramolecular Dieckmann and Michael reactions,[193] intramolecular S_N2 epoxide opening.[194]

Despite the apparent simplicity of these syntheses, only a few chimeric amino acids with the 2-azabicyclo[2.2.2]octane framework have been prepared, including dihydroxy-substituted acid **135**, its protected derivatives and unsaturated acid **136**.[191]

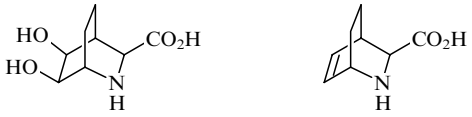

135 **136**

Derivatives of 2-azabicyclo[2.2.2]octane-3-carboxylic acid are widely applied in asymmetric synthesis.[191, 195]

Numerous peptidomimetics have been synthesised based on Abo, in particular, the aforementioned Zabicipril **134**, which represents an efficient inhibitor of angiotensin converting enzyme (ACE), which plays a crucial role in blood pressure regulation.[196] The angiotensin II mimetic **134** is a promising antihypertensive drug.[189] This represents an example of a successful drug design: the peptidomimetic obtained retains activity of the native peptide and it is more stable against biodegradation, which gives rise to a strong prolongation effect.

The amino acid **131** along with the aforementioned acid **96** (Abh) and conformationally constrained but not rigid perhydroindole-2-carboxylic acid **137** (Phi) are often used in complex investigations of peptidomimetics as regards their biological activity.

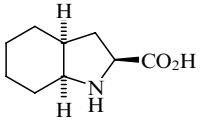

137

For instance, these amino acids have been utilised to mimic the prolylendopeptidase inhibitor SUAM 1221 (**138**), which is a proline derivative.[168]

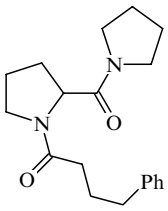

138

In addition to modifications involving the side chain of the acid residue,¶ different substitutes for the central proline residue were tested. The best results were achieved when the proline resudue was replaced by the Phi residue, although Abo and Abh also gave promising results.

The same amino acids have been probed as substitutes for proline in the tripeptides Val-Pro-Val and Val-Pro-Lys in the search for efficient selective inhibitors of the human leucocyte elastase (HLE).[197] The synthetic peptidomimetics manifested high potential as long-lasting inhibitors of pulmonary tissue degradation related to HLE.

Furthermore, the amino acid **131** has been used for the preparation of antagonists for the tetrapeptide tachykinin. Introduction of an Abo residue into the peptidomimetic resulted in prolongation of the activity of the synthetic antagonist.[198]

Among other analogues of pipecolic acid, the polycyclic compounds **139** and **140** are of special interest. The polycyclic compound **139** is an analogue of pipecolic and glutamic acids. It has been produced as a protected derivative in a small yield by the reaction of substituted bicyclo[2.2.2]hexadiene with *o*-iodoaniline catalysed by palladium(II).[199]

¶ These modifications were conducted within the principles of the strict conformational fixation (by introduction of cyclopropane fragments), which yielded positive results in some cases.

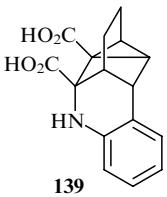

139

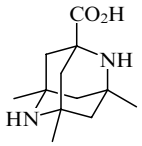

140

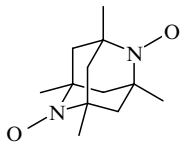

141

Compound **140** is formed as an intermediate in the synthesis of a biradical **141**, an organic ferromagnetic species.[200] It may be assumed that the presence of an additional nitrogen atom would impart particular properties to the biologically active substances produced on its base.

It is of note that the non-functionalised 2-azaadamantane derivative **142** has not been prepared so far despite the fact that adamantane is frequently used in the synthesis of CRA. Only a homologue of 2-azaadamantane **143** has been reported,[201] which is not conformationally rigid, however.

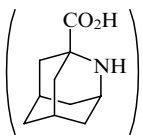

142

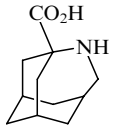

143

VI. Bi- and polycyclic conformationally rigid amino acids with an exocyclic nitrogen atom

In the case of bi- and polycyclic amino acids discussed above, the conformational rigidity is achieved by inclusion of the nitrogen-containing ring into a polypeptide chain. In contrast, the torsion angles of the polypeptide chain are not fixed for cyclic amino acids with an exocyclic nitrogen atom, although the respective amino acids are χ-rigid.

There are several rigid bicyclic cages, in particular, bicyclo[1.1.1]pentane (**A**), bicyclo[2.1.1]hexane (**B**), norbornane (**C**), bicyclo[2.2.2]octane (**D**) and bicyclo[2.2.0]hexane (**E**) with bridge lengths not more than two atoms (cyclopropane derivatives have been thoroughly discussed above and thus are not mentioned here):

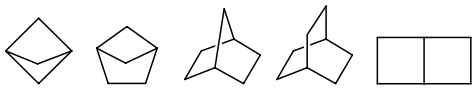

A **B** **C** **D** **E**

The respective amino acids are known for all these bicyclic systems (except for bicyclo[2.2.0]hexane):

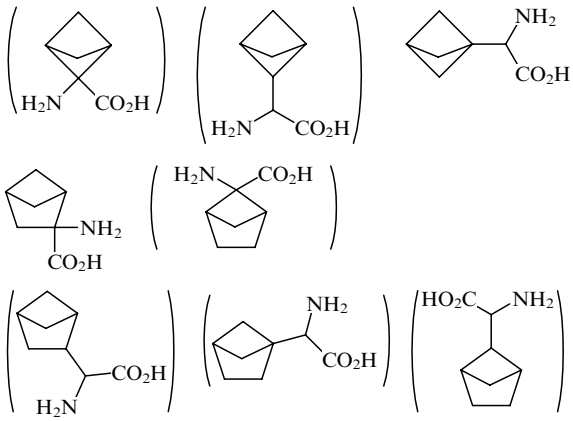

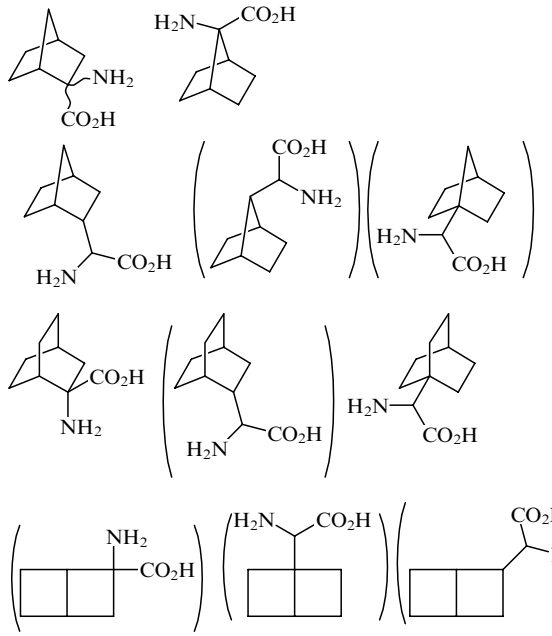

It can be noted that these bicyclic cages fix either all torsion angles χ or only some of them. Therefore, for further discussion, it is convenient to differentiate between the χ_1-rigid amino acids and other χ_n-rigid amino acids ($n \geqslant 2$).

In addition to the bicyclic amino acids, polycyclic amino acids are also known. However, examples of these are scarce (these include derivatives of adamantane, cubane and fullerene C_{60}).

1. Norbornane derivatives

2-Aminonorbornane-2-carboxylic acid (**144**) (its residue in peptides is denoted as Bch) has been known from the mid-1950's,[202, 203] whereas synthesis of its trimethyl derivative, the camphor analogue **145**, was reported even earlier.[204] Potential biological activity of **144** was discussed following its preparation.[205]

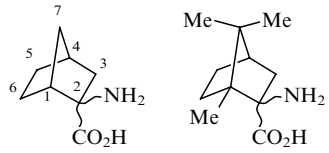

144a,**b** **145a**,**b**

The values of the torsion angles in the bicyclo[2.2.1]hexane cage are given elsewhere.[206, 207] Introduction of functional groups into the norbornane framework gives rise to only minor changes in the torsion angles (by not more than 15°). Only the angles involving the substituents are mostly affected. No distinct effect of the norbornane fragment on the torsion angles within the polypeptide chain has been revealed.

Methods for the synthesis of norbornane-based amino acids have been recently surveyed,[11, 12] therefore, we shall just mention them. The most popular method is based on the Diels–Alder cycloaddition reaction of cyclopentadiene to derivatives of α,β-unsaturated α-amino acids.[202, 203, 208–216]

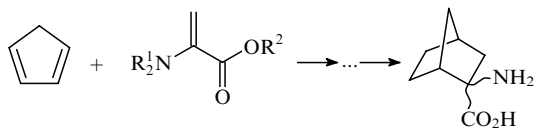

Dienophiles substituted at the β-position can also be employed in this reaction. Diastereo- and enantioselective modifications of this method have been elaborated.

Another approach utilises the classical Strecker and Bucherer–Lieb reactions [204, 205, 217, 218] starting from 2-norbornanone, which in turn is produced by the Diels–Alder reaction.

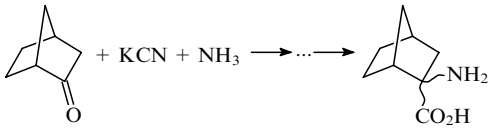

Numerous CRA with the norbornane cage have been prepared. In addition to the unsubstituted acid **144**, various functionalised derivatives **146**–**155** (which represent analogues of phenylalanine,[208, 209, 217] tyrosine,[217] aspartic acid,[211, 212] serine,[213] methionine,[219] glutamic acid [211, 219–221]), including polyhydroxy-compounds **156a**–**d** [216] have been prepared. All of these compounds are fully χ-rigid (except for **152**, which is χ_1-rigid).

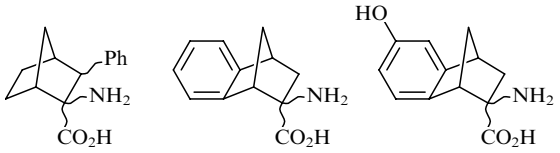

146a–d **147a,b** **148a,b**

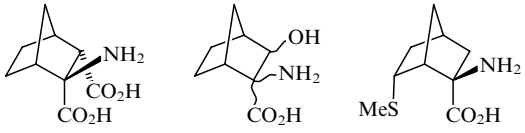

149 **150a,b** **151**

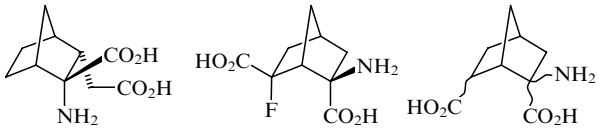

152 **153** **154a–d**

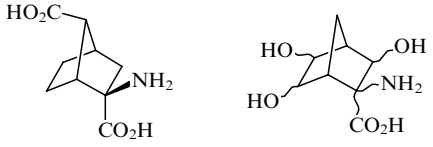

155 **156a–d**

For the synthesis of 3-substituted derivatives, the respective substituted cyclopentadienes are used, 6- and 7-substituted derivatives are produced by functionalisation of the double bond.

The unsaturated derivative **157** has been prepared only in the protected form.

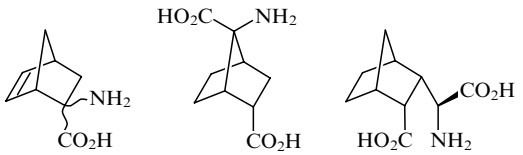

157 **158** **159**

7-Aminonorbornane-2,7-dicarboxylic acid **158** has been synthesised, which is also an analogue of glutamic acid.[221]

Among norbornylglycine derivatives, only the acid **159** is known,[211] which is also a glutamic acid analogue †. This type of amino acids are not χ_1-rigid, that is why probably they attract only limited interest.

The biological activity of the unsubstituted 2-aminonorbornane-2-carboxylic acid (**144**) has been studied. For instance, it has been shown that this acid is selectively transported into nearly all cells by sodium-independent systems responsible for the transport of hydrophobic amino acids.[223] The acid is almost excluded from the metabolism and thus it can be accumulated in tissues. The Bch residue mimics most closely the properties of leucine (and, to a lesser extent, of isoleucine and valine), which makes it possible to monitor pathways of leucine transport in tissues through the use of ^{14}C-labeled Bch or to inhibit this transport. In particular, with the help of the acid **144**, the sodium-independent transport systems of phenylalanine and leucine have been shown to be identical. Furthermore, it was demonstrated that the transport system is selective to one of the diastereomers **144a** or **144b**.

The diastereomers **144a** and **144b**, as was established in the course of the study of their transport, manifest hypoglycaemic activity (that is also typical of leucine [224]), and the effect of a decrease in the glucose concentration in blood was long-lasting. As a side effect, concentrations of at least five amino acids in blood plasma were observed to decrease. Physiological tests on rats showed that the acid **144** is non-toxic; it was almost completely excreted with urine.

Another activity was observed for the acid **144** introduced into rat mitochondria: Bch stimulates the glutamine catabolism by activating mitochondrial glutaminase (this activity was not observed for leucine).[225] The processes of insulin release and glutaminase activation under action of Bch are coupled.[226]

The biological activity of the acid **154**, which is a glutamic acid analogue, has also been studied. The activity of this acid towards metabotropic glutamic acid receptors mGluR1 and mGluR2 has been revealed.[220]

2. Bicyclo[2.2.2]octane derivatives

Amino acids with the bicyclo[2.2.2]octane framework are best studied as regards the number of derivatives synthesised. The unsubstituted acid **160** [227] as well as its derivatives **161**–**164** [203, 228–231] have been prepared and characterised.

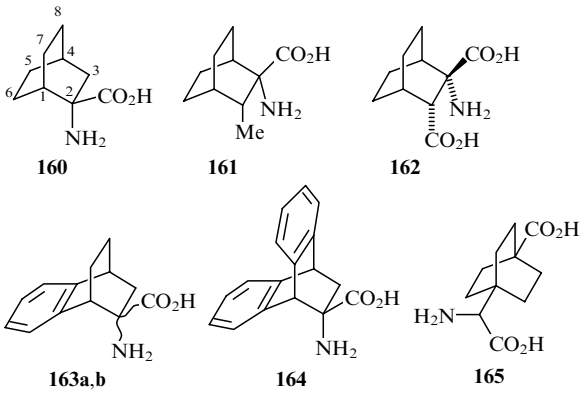

160 **161** **162**

163a,b **164** **165**

The values of the torsion angles in the bicyclo[2.2.2]octane cage are given elsewhere.[228, 232] An analysis of the structural data indicates that amino acids with a bicyclo[2.2.2]octane framework are characterised by distorted torsion angles (especially, in the case of bulky substituents).

Another amino acid **165**, in which the C_α atom is exocyclic with respect to the bicyclo[2.2.2]octane framework, has been reported.[233]

Methods for the synthesis of amino acids with a bicyclo[2.2.2]octane cage are generally similar to those of norbornane derivatives, which have been discussed above. They include the Diels–Alder reaction of 1,3-cyclohexadiene with α,β-dehydroalanines, the Strecker and Bucherer reactions.[228–230] The acid **165** is formed by alkylation of enolates (Scheme 12).

The unsubstituted amino acid **160** manifests biological activity analogous to 2-aminonorbornane-2-carboxylic acid **144** .[234] Compounds **163a,b** have been investigated as analogues of phenylalanine in the inhibition of phenylalanylhydroxylase and phenylalanyldecarboxylase.

† Synthetic glutamic acid analogues attracts significant interest and thus they are especially numerous.[222]

Scheme 12

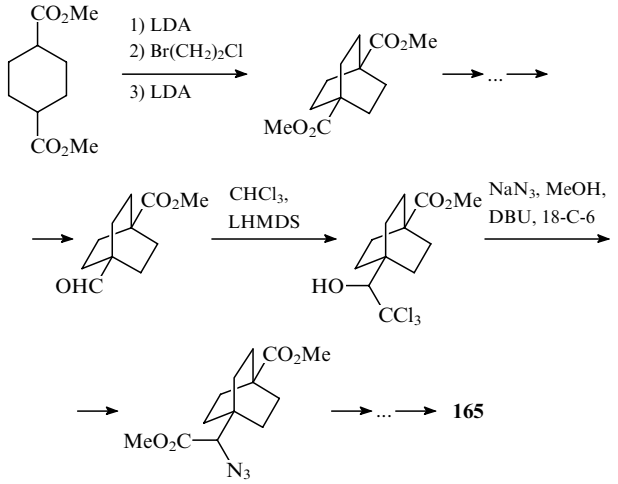

3. Derivatives of bicyclo[1.1.1]pentane and bicyclo[2.1.1]hexane

To date, only one CRA **166** with a bicyclo[1.1.1]pentane framework [235] and one acid **167** (four diastereomers) with the bicyclo[2.1.1]hexane framework [236, 237] are known. They both may be considered as analogues of glutamic acid.

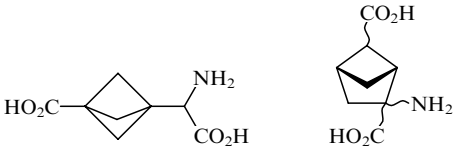

166 **167a–d**

Values of the torsion angles in bicyclo[1.1.1]pentane [238, 239] and bicyclo[2.1.1]hexane [240, 241] have been reported. These two frameworks deserve special consideration since they are extremely rigid and characterised by relatively small steric volume. Therefore, one may hope that other amino acids with these cages will be synthesised in the future, although the synthesis of such compounds is challenging. The diastereomers **167a–d** were prepared by an intramolecular photochemical [2 + 2]-cycloaddition from the appropriately substituted 1,5-diene [236] or by a contraction of the norbornane system through photochemical decomposition of α-diazoketones.[237] The amino acid **166** has been synthesised *via* [1.1.1]propellane **168** (Scheme 13).[235]

Binding of the amino acids **166** and **167** to the corresponding receptor has been elucidated. Compound **166** proved to be a fairly efficient selective antagonist of the glutamate metabotropic

Scheme 13

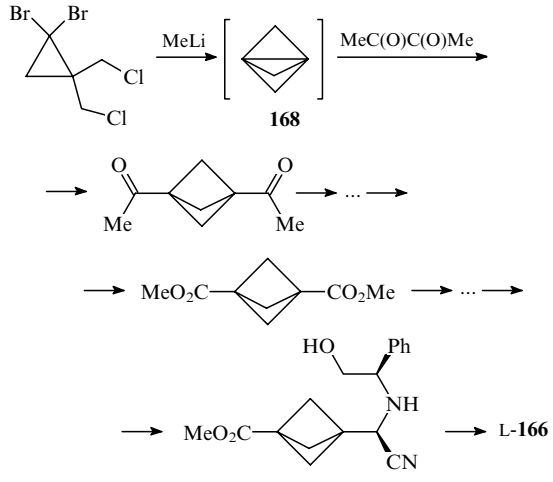

receptors mGluR1 and one of the diastereomers **167a–d** was active as a common antagonist of all the mGluR receptors tested.

4. Fullerene derivatives

Over the last decade, numerous studies related to a greater or lesser extent to fullerene C_{60} have appeared. Taking into account the rigidity of the buckminsterfullerene cage, its introduction into side chains of amino acids is expected to lead to strict fixation of the torsion angles χ. However, due to specific restrictions related to the structure of the C_{60} molecule as well as to available methods of fullerene functionalisation, only χ_2-rigid CRA are known to date, which have been prepared by introduction of functional groups at adjacent positions of the fullerene cage.

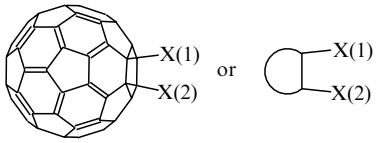

In these compounds, the fullerene cage strictly fixes only one dihedral angle, *viz*., X(1)–C(1)–C(2)–X(2). Ideally, this angle should be close to 0° but no structural data on this class of CRA are available.

There are two ways to introduce an α-amino acid fragment into the fullerene cage.

The first one is based on the [3 + 2]-cycloaddition reaction, which gives rise to proline analogues.[242, 243] Protected proline analogues **169** with R = H (see Ref. 242) or Ph (see Ref. 243) have been produced.

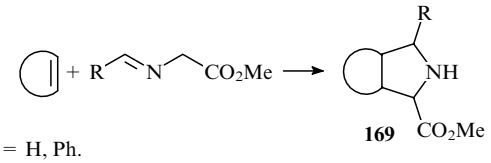

169

R = H, Ph.

Alternatively, proline analogues can be prepared by the direct photochemical reaction of fullerene with amino acid esters.[244] The products formed in this reaction are similar to those considered above but the mechanisms of the two reactions are distinctly different. The photochemical reaction proceeds through formation of radical intermediates. It has been applied to prepare protected proline analogue **169** with R = CO_2Me.[244]

The second way is based on a reaction that looks similar to [2 + 1]-cycloaddition but follows a different mechanism.[245]

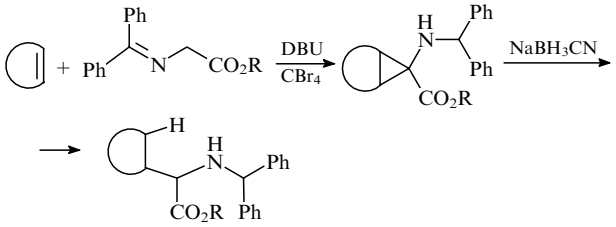

This method has been applied to prepare 1,2-dihydro[60]fullerenylglycine (**170**) and aminomethano[60]fullerenecarboxylic acid (**171**).

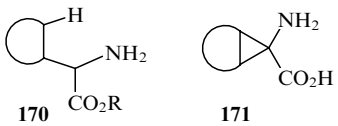

170 **171**

Furthermore, this method has been successfully exploited in the synthesis of bismethano[60]fullerenylglycines, which yield monosubstituted 1,2-dihydrofullerene upon reduction.

The amino acids mentioned in this Section are characterised by a wide range of interesting biological properties, and are especially promising in such fields as photodynamic therapy,

developments of HIV protease inhibitors[246] and antibacterial drugs.[247]

5. Miscellaneous conformationally rigid polycyclic amino acids

In the previous sections, CRA with side chains representing quite bulky carbon cages devoid of any functional groups have been considered. Biological properties of these compounds have been described in detail with 2-aminonorbornane-2-carboxylic acid as an example. It has been shown that such CRA may be regarded as analogues of hydrophobic proteinogenic amino acids, in particular, of isoleucine, and they are superior in some respects to the latter. First, they do not metabolise. Second, owing to the conformational rigidity, they are quite compact despite their relatively high molecular mass. Third, they are characterised by higher lipophilicity, which allows them to penetrate through various intra- and intercellular barriers. Thus, it is not surprising that the search for new cage amino acids continues. New structures can provide new capabilities for the design of *ad hoc* amino acids with specific conformations of their side chains.

Adamantane and cubane, which are characterised by highly symmetrical frameworks, take a special place among polycyclic hydrocarbons. While an appreciable number of studies have been devoted to the synthesis of adamantane-based CRA, cubane has been slipping the attention of researchers so far.

The values of the torsion angles within the adamantane cage of the corresponding amino acids and their derivatives are given elsewhere;[248,249] the respective data on the cubane cage are reported in Refs 250, 251. The experimental data indicate that the adamantane and cubane cages are essentially undistorted.

Three unsubstituted amino acids with the adamantane cage are known to date, *viz*., 2-aminoadamantane-2-carboxylic acid (**172**),[252,253] (1-adamantyl)glycine (**173**)[254] and 3-(1-adamantyl)-alanine (**174**)[255] (the latter can be classified as CRA only formally; such a remote χ_3-rigidity plays only a minor role) and 1,3-adamantylidenediglycine (**175**).[256] Derivatives of the acids **172**–**174** methylated at bridgehead carbon atoms have also been prepared.

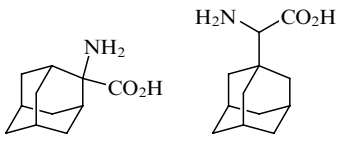

172

173

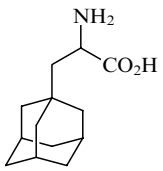

174

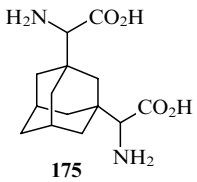

175

Compounds containing the adamantane cage have been used as the starting materials in the syntheses of the amino acids **172**–**174**. In particular, the amino acid **172** was synthesised from 2-adamantanone by the classical Strecker and Bucherer–Lieb reactions.[252,253] Compounds **173** and **174** have been prepared starting from adamantylacetic and adamantylpropionic acids, respectively, by α-halogenation (*e.g*., according to the Hell–Volhard–Zelinsky reaction) followed by substitution of the amino group for the halogen atom.[255] Compound **175** has been prepared similarly.[256]

In the case of cubane, only one CRA **176** is known, which is a glutamic acid analogue.[257]

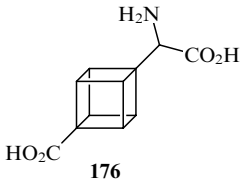

176

Its synthesis has been performed starting from dimethylcubanedicarboxylate using a method similar to that used for the preparation of bicyclo[1.1.1]pentane (**166**) considered above.

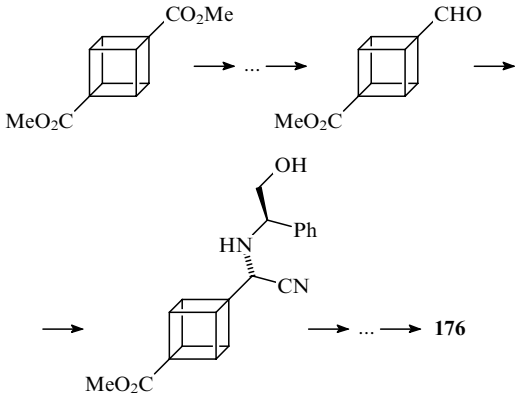

(1-Adamantyl)glycine (**173**) is an active inhibitor of leucine and methionine transport (like 2-aminonorbornane-2-carboxylic acid), however, its introduction into neoplasmatic cells did not produce the anticipated antitumour effect.[254]

Introduction of the amino acid **173** into small peptides yields model compounds which at room temperature predominantly adopt a conformation typical of the γ-bend.[258] This is very unusual since CRA typically stabilise various β-bends.

Compounds **173**–**175** manifest antiviral activity, which is, however, solely due to the presence of the adamantyl substituent.[255] A study of binding of compound **176** to metabotropic glutamate receptors has revealed that it represents a selective antagonist of mGluR1.[257]

The consideration of polycyclic amino acids with an exocyclic nitrogen atom will be incomplete, if we omit another unique substance, *viz*., pentacyclic CRA **177**, which is a pentacyclo[5.4.0.0^{2,6}.0^{3,10}.0^{5,9}]undecane derivative.[259]

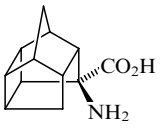

177

Compound **177** has been prepared by a multistep synthesis starting from the adduct of cyclopentadiene and *p*-benzoquinone.

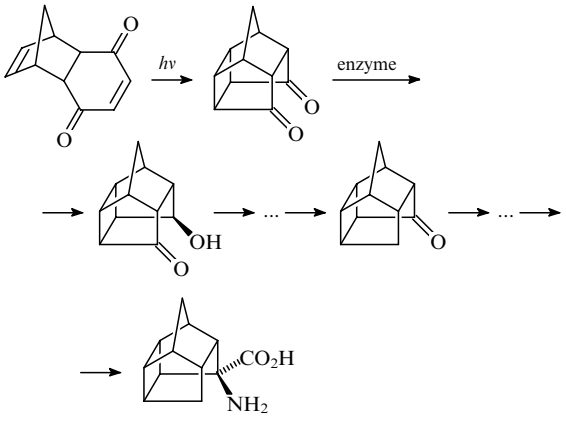

VII. Conclusion

Nowadays, the assortment of conformationally rigid cyclic amino acids which can be utilised in the design of peptidomimetics, peptide models and biologically active compounds, is quite wide. Some of the theoretically possible structures have not been realised so far, therefore, we expect that this list will soon be extended with new CRA suitable for the design. Furthermore, new stereoselective routes to the synthesis of the known amino acids will be elaborated since much research effort is put into this field. The primary reason for these efforts is that CRA enable preparation of peptides with high selectivity of their biological activities and degradation stability and thus are of significance as potential drugs. Introduction of CRA residues into the polypeptide chain has advantages within the context of the design of peptidomimetics and peptide models due to the particular conformational rigidity of these residues. CRA residues are able to stabilise or conversely destabilise specific elements of the secondary structure of peptides. This allows prediction of conformations of the peptides within a certain confidence level and thus gives a partial control over their biological function.

References

1. E N Jacobsen (Ed.) *Comprehensive Asymmetric Catalysis* (Heidelberg: Springer, 1999)
2. J Gante *Angew. Chem., Int. Ed. Engl.* **33** 1699 (1994)
3. A J Kirby *Angew. Chem., Int. Ed. Engl.* **35** 707 (1996)
4. S H Stammer *Tetrahedron* **46** 2231 (1990)
5. A Alami, M Calmes, J Daunis, R Jacquier *Bull. Soc. Chim. Fr.* **130** 5 (1993)
6. K Burgess, K-K Ho, D Moye-Sherman *Synlett* 575 (1994)
7. D Tanner *Angew. Chem., Int. Ed. Engl.* **33** 599 (1994)
8. M Goodman, H Shao *Pure Appl. Chem.* **68** 1303 (1996)
9. S Hanessian, G McNaughton-Smith, H-G Lombart, W D Lubell *Tetrahedron* **53** 12789 (1997)
10. C Cativiela, M D Díaz-de-Villegas *Tetrahedron: Asymmetry* **9** 3517 (1998)
11. S E Gibson, N Guillo, M J Tozer *Tetrahedron* **55** 585 (1999)
12. C Cativiela, M D Díaz-de-Villegas *Tetrahedron: Asymmetry* **11** 645 (2000)
13. L Peterlin-Mašič, D Kikelj *Tetrahedron* **57** 7073 (2001)
14. K-H Park, M J Kurth *Tetrahedron* **58** 8629 (2002)
15. K Undheim, J Efskind, G B Hoven *Pure Appl. Chem.* **75** 279 (2003)
16. V I Sokolov *Vvedenie v Teoreticheskuyu Stereokhimiyu* (Introduction to Theoretical Stereochemistry) (Moscow: Nauka, 1982)
17. N S Zefirov *Zh. Vses. Khim. O-va im D I Mendeleeva* **22** 261 (1977) [a]
18. D H R Barton, R Cookson *Quart. Rev.* **10** 44 (1956)
19. S I Miller *Adv. Phys. Org. Chem.* **6** 185 (1968)
20. A A Adzhubei, M J E Sternberg *J. Mol. Biol.* **229** 472 (1993)
21. I L Knunyants (Ed.) *Khimicheskii Entsiklopedicheskii Slovar'* (Chemical Encyclopaedia) (Moscow: Sov. Entsiklopediya, 1983)
22. G Ferenczy, L Harsányi, B Rozsondai, I Hargittai *J. Mol. Struct.* **140** 71 (1986)
23. L Clowney, S C Jain, A R Srinivasan, J Westbrook, W K Olson, H M Berman *J. Am. Chem. Soc.* **118** 509 (1996)
24. O V Shishkin, K Yu Pichugin, L Gorb, J Leszczynski *J. Mol. Struct.* **616** 159 (2002)
25. O V Shishkin, L Gorb, J Leszczynski *Chem. Phys. Lett.* **330** 603 (2000)
26. I V Komarov *Usp. Khim.* **70** 1123 (2001) [*Russ. Chem. Rev.* **70** 991 (2001)]
27. M F Thorpe, P M Duxbury (Eds) *Rigidity Theory and Applications* (New York: Kluwer Academic, 1999)
28. Yu A Ovchinnikov *Bioorganicheskaya Khimiya* (Bioorganic Chemistry) (Moscow: Prosveshchenie, 1987)
29. V J Hruby, F Al-Obeidi, W Kazmierski *Biochem. J.* **268** 249 (1990)
30. F H Allen, J E Davies, J J Galloy, O Johnson, O Kennard, C F Macrae, E M Mitchell, G F Mitchell, J M Smith, D G Watson *J. Chem. Inf. Comput. Sci.* **31** 187 (1991)
31. K I Varughese, A R Srinivasan, C H Stammer *Int. J. Pept. Protein Res.* **26** 1673 (1985)
32. G D Rose, L M Gierasch, J A Smith *Turns in Peptides and Proteins. Advances in Protein Chemistry* (New York: Academic Press, 1985)
33. J B Ball, R A Hughes, P F Alewood, P R Andrews *Tetrahedron* **49** 3467 (1993)
34. H Shao, X Jiang, P Gantzel, M Goodman *Chem. Biol.* **1** 231 (1994)
35. G Fischer *Angew. Chem., Int. Ed. Engl.* **33** 1415 (1994)
36. J D Dunitz, F K Winkler *Acta Crystallogr., Sect. B* **31** 251 (1975)
37. S Yamada *Angew. Chem., Int. Ed. Engl.* **32** 1083 (1993)
38. V Somayaji, R S Brown *J. Org. Chem.* **51** 2676 (1986)
39. A J Kirby, I V Komarov, N Feeder *J. Chem. Soc., Perkin Trans. 2* 522 (2001)
40. S J Cho, C Z Cui, J Y Lee, J K Park, S B Suh *J. Org. Chem.* **62** 4068 (1997)
41. B P Murphy, R F Pratt *Biochemistry* **30** 3640 (1991)
42. E N Prabhakaran, J P Nandy, S Shukla, A Tewari, S K Das, J Iqbal *Tetrahedron Lett.* **43** 6461 (2002)
43. J P Nandy, E N Prabhakaran, S K Kumar, A C Kunwar, J Iqbal *J. Org. Chem.* **68** 1679 (2003)
44. L Moroder, H-J Musiol, R Scharf *FEBS Lett.* **299** 51 (1992)
45. V Martichonok, C Plouffe, A C Storer, R Ménard, J B Jones *J. Med. Chem.* **38** 3078 (1995)
46. T Schirmeister *J. Med. Chem.* **42** 560 (1999)
47. T Schirmeister, M Peric *Bioorg. Med. Chem.* **8** 1281 (2000)
48. M E Tanner, S C Miao *Tetrahedron Lett.* **35** 4073 (1994)
49. F Gerhart, W Higgins, C Tardif, J B Ducep *J. Med. Chem.* **33** 2157 (1990)
50. K Nakajima, F Takai, T Tanaka, K Okawa *Bull. Chem. Soc. Jpn.* **51** 1577 (1978)
51. P Wipf, C P Miller *Tetrahedron Lett.* **33** 6267 (1992)
52. E Kuyl-Yeheskiely, M Lodder, G A van der Marel, J H van Boom *Tetrahedron Lett.* **33** 3013 (1992)
53. D Tanner, C Birgersson, H K Dhaliwal *Tetrahedron Lett.* **31** 1903 (1990)
54. F A Davis, H Liu, P Zhou, T Fang, G V Reddy, Y Zhang *J. Org. Chem.* **64** 7559 (1999)
55. J Legters, L Thijs, B Zwanenburg *Tetrahedron Lett.* **30** 4881 (1989)
56. J Legters, L Thijs, B Zwanenburg *Recl. Trav. Chim. Pays-Bas* **111** 1 (1992)
57. D A Evans, M M Faul, M T Bilodeau, B A Anderson, D M Barnes *J. Am. Chem. Soc.* **115** 5328 (1993)
58. G Cardillo, L Gentilucci, C Tomasini, M P V Castejon-Bordas *Tetrahedron: Asymmetry* **7** 755 (1996)
59. G Cardillo, L Gentilucci, A Tolomelli *Chem. Commun.* 167 (1999)
60. L Fowden *Adv. Enzym.* **29** 89 (1967)
61. K Isono, K Asahi, S Suzuki *J. Am. Chem. Soc.* **91** 7490 (1969)
62. S Hanessian, J-M Fu, Y Tu, K Isono *Tetrahedron Lett.* **34** 4153 (1993)
63. M Cesari, L D'llario, E Giglio, G Perego *Acta Crystallogr., Sect. B* **31** 49 (1975)
64. R H Blessing, G D Smith *Acta Crystallogr., Sect. B* **38** 1203 (1982)
65. P J S S van Eijk, W P Trompenaars, D N Reinhoudt, S Harkema *Recl. Trav. Chim. Pays-Bas* **107** 52 (1988)
66. S Hanessian, J-M Fu, J-L Chiara, R di Fabio *Tetrahedron Lett.* **34** 4157 (1993)
67. D Kern, M Schutkowski, T Drakenberg *J. Am. Chem. Soc.* **119** 8403 (1997)
68. P Y Chou, G D Fasman *J. Mol. Biol.* **115** 135 (1977)
69. T Hayashi, T Asai, H Ogoshi *Tetrahedron Lett.* **38** 3039 (1997)
70. M Teng, J W Lauher, F W Fowler *J. Org. Chem.* **56** 6840 (1991)
71. R M Rodebaugh, N H Cromwell *J. Heterocycl. Chem.* **5** 309 (1968)
72. R M Rodebaugh, N H Cromwell *J. Heterocycl. Chem.* **6** 435 (1969)

73. H H Wasserman, B H Lipshutz, A W Tremper, J S Wu *J. Org. Chem.* **46** 2991 (1981)
74. F Couty, G Evano, N Rabasso *Tetrahedron: Asymmetry* **14** 2407 (2003)
75. A P Kozikowski, W Tückmantel, I J Reynolds, J T Wroblewski *J. Med. Chem.* **33** 1561 (1990)
76. D J Blythin, M J Green, M J R Lauzon, H-J Shue *J. Org. Chem.* **59** 6098 (1994)
77. N De Kimpe, M Boeykens, D Tourwé *Tetrahedron* **54** 2619 (1998)
78. A Carlin-Sinclair, F Couty, N Rabasso *Synlett* 726 (2003)
79. R T Shuman, R B Rothenberger, C S Campbell, G F Smith, D S Gifford-Moore, J W Paschal, P D Gesellchen *J. Med. Chem.* **38** 4446 (1995)
80. L F Burroughs *Nature* (*London*) **179** 360 (1957)
81. S Sakamura, A Ichihara, K Shiraishi, H Sato, K Nishiyama, R Sakai, A Furusaki, T Matsumono *J. Am. Chem. Soc.* **99** 636 (1977)
82. R E Mitchell *Phytochemistry* **24** 1485 (1985)
83. T Wakamiya, H Nakamoto, T Shiba *Tetrahedron Lett.* **25** 4411 (1984)
84. T Wakamiya, Y Oda, H Fujita, T Shiba *Tetrahedron Lett.* **27** 2143 (1986)
85. K Burgess, K-K Ho, B M Pettitt *J. Am. Chem. Soc.* **116** 799 (1994)
86. K Burgess, C-Y Ke *J. Org. Chem.* **61** 8627 (1996)
87. K Burgess, K-K Ho, B M Pettitt *J. Am. Chem. Soc.* **117** 54 (1995)
88. A I Jiménez, R Vanderesse, M Marraud, A Aubry, C Cativiela *Tetrahedron Lett.* **38** 7579 (1997)
89. A I Jiménez, C Cativiela, A Aubry, M Marraud *J. Am. Chem. Soc.* **120** 9452 (1998)
90. D Moye-Sherman, S Jin, I Ham, D Lim, J M Scholtz, K Burgess *J. Am. Chem. Soc.* **120** 9435 (1998)
91. D Moye-Sherman, S Jin, S M Li, M B Welch, J Reibenspies, K Burgess *Chem. Eur. J.* **5** 2730 (1999)
92. A I Jiménez, C Cativiela, M Marraud *Tetrahedron Lett.* **41** 5353 (2000)
93. N Fabiano, G Valle, M Crisma, C Toniolo, M Saviano, A Lombardi, C Isernia, V Pavone, B Di Blasio, C Pedone, E Benedetti *Int. J. Pept. Protein Res.* **42** 459 (1993)
94. E Benedetti, B Di Blasio, V Pavone, C Pedone, A Santini, V Barone, F Fraternali, F Lelj, A Bavoso, M Crisma, C Toniolo *Int. J. Biol. Macromol.* **11** 353 (1989)
95. F L Switzer, H Van Halbeek, E M Holt, C H Stammer, M E Saveit Jr *Tetrahedron* **45** 6091 (1989)
96. U Schöllkopf, U Groth, C Deng *Angew. Chem., Int. Ed. Engl.* **20** 798 (1981)
97. A Hercouet, B Bessières, M Le Corre *Tetrahedron: Asymmetry* **7** 283 (1996)
98. A Hercouet, B Bessières, M Le Corre *Tetrahedron: Asymmetry* **7** 1267 (1996)
99. J M Jiménez, J Rifé, R M Ortuño *Tetrahedron: Asymmetry* **7** 537 (1996)
100. K Estieu, J Ollivier, J Salamn *Tetrahedron Lett.* **36** 2975 (1995)
101. P Dorizon, G F Su, G Ludvig, L Nikitina, R Paugam, J Ollivier, J Salaün *J. Org. Chem.* **64** 4712 (1999)
102. J Barluenga, F Aznar, I Gutiérrez, S García-Granda, M A Llorca-Baragaño *Org. Lett.* **4** 4273 (2002)
103. A M Serebryanyi, G A Krashennikova, L V Vakhnina *Biokhimiya* **60** 1005 (1995) [b]
104. M C Pirrung, G M McGeehan *Angew. Chem.* **97** 1074 (1985)
105. A M Serebryanyi, V I Binyukov, V V Kasparov, N K Tatarskaya, A L Kovarskii *Dokl. Akad. Nauk* **370** 770 (2000) [c]
106. J Zhou, A M Rocklin, J D Lipscomb, L Que Jr, E I Solomon *J. Am. Chem. Soc.* **124** 4602 (2002)
107. N E Hoffman, S F Yang, S F Ichihara, S Sakamura *Plant Physiol.* **70** 195 (1982)
108. J E Baldwin, R M Adlington, B J Rawlings *Tetrahedron Lett.* **26** 481 (1985)
109. M C Pirrung, G M McGeehan *J. Org. Chem.* **51** 2103 (1986)
110. M C Pirrung, J Cao, J Chen *J. Org. Chem.* **60** 5790 (1995)
111. J W Tsang, B Schmied, R Nyfeler, M Goodman *J. Med. Chem.* **27** 1663 (1984)
112. Y-F Zhu, T Yamasaki, J W Tsang, S Lok, M Goodman *J. Org. Chem.* **57** 1074 (1992)
113. Y Fujimoto, F Irreverre, J M Karle, I L Karle, B Witkop *J. Am. Chem. Soc.* **93** 3471 (1971)
114. G Siligardi, A F Drake *Biopolymers* **37** 281 (1995)
115. R Zhang, J S Madalengoitia *J. Org. Chem.* **64** 330 (1999)
116. A Mamai, R Zhang, A Natarajan, J S Madalengoitia *J. Org. Chem.* **66** 455 (2001)
117. K Shimamoto, M Ishida, H Shinozaki, Y Ohfune *J. Org. Chem.* **56** 4167 (1991)
118. R Pellicciari, B Natalini, M Marinozzi, J B Monahan, J P Snyder *Tetrahedron Lett.* **31** 139 (1990)
119. D Ma, Z Ma, J Jiang, Z Yang, C Zheng *Tetrahedron: Asymmetry* **8** 889 (1997)
120. P L Ornstein, T J Bleisch, M B Arnold, R A Wright, B G Johnson, D D Schoepp *J. Med. Chem.* **41** 346 (1998)
121. A Mazón, C Pedregal, W Prowse *Tetrahedron* **55** 7057 (1999)
122. R Pellicciari, M Marinozzi, B Natalini, G Costantino, R Luneia *J. Med. Chem.* **39** 2259 (1996)
123. S Shimamoto, Y Ohfune *J. Med. Chem.* **39** 407 (1996)
124. D Ma, Y Cao, W Wu, Y Jiang *Tetrahedron* **56** 7447 (2000)
125. M Marinozzi, R Pellicciari *Tetrahedron Lett.* **41** 9125 (2000)
126. A Shibuya, M Kurishita, C Ago, T Taguchi *Tetrahedron* **52** 271 (1996)
127. L Wessjohann, N Krass, D H Yu, A de Meijere *Chem. Ber.* **125** 867 (1992)
128. P de Frutos, D Fernández, E Fernández-Alvarez, M Bernabé *Tetrahedron Lett.* **32** 541 (1991)
129. D Fishlock, J G Guillemette, G A Lajoie *J. Org. Chem.* **67** 2352 (2002)
130. V V Tverezovsky, M S Baird, I G Bolesov *Tetrahedron* **53** 14 773 (1997)
131. J Zindel, A de Meijere *Synthesis* 190 (1994)
132. Y K Yun, K Godula, Y Cao, W A Donaldson *J. Org. Chem.* **68** 901 (2003)
133. J E Baldwin, R M Adlington, D Bebbington, A T Russel *Tetrahedron* **50** 12 015 (1994)
134. M Brandl, S I Kozhushkov, K Loscha, O V Kokoreva, D S Yufit, J A K Howard, A de Meijere *Synlett* **12** 1741 (2000)
135. O V Larionov, T F Savel'eva, K A Kochetkov, N S Ikonnokov, S I Kozhushkov, D S Yufit, J A K Howard, V N Khrustalev, Y N Belokon, A de Meijere *Eur. J. Org. Chem.* 869 (2003)
136. R Pellicciari, B Natalini, M Marinozzi, B M Sadeghpour, A A Cordi, T H Lanthorn, W F Hood, J B Monahan *Farmaco* **46** 1991 (1243)
137. S Hanessian, S Ninkovic, U Reinhold *Tetrahedron Lett.* **37** 8971 (1996)
138. R Pelliciari, M Marinozzi, E Camaioni, M del C Nùnez, G Costantino, F Gasparini, G Giorgi, A Macchiarulo, N Subramanian *J. Org. Chem.* **67** 5497 (2002)
139. A de Meijere, K Ernst, B Zuck, M Brandl, S I Kozhushkov, M Tamm, D S Yufit, J A K Howard, T Labahn *Eur. J. Org. Chem.* 3105 (1999)
140. M Tamm, M Thutewohl, C B Ricker, M T Bes, A de Meijere *Eur. J. Org. Chem.* 2017 (1999)
141. *Agric. Biol. Chem.* **43** 2279 (1979)
142. S S Zimmerman, H A Scheraga *Macromolecules* **9** 408 (1976)
143. D E Stewart, A Sarkar, J E Wampler *J. Mol. Biol.* **214** 253 (1990)
144. S H Choi, Y J Yu, J K Shin, M S Jhon *J. Mol. Struct.* **323** 233 (1994)
145. A Avenoza, J H Busto, J M Peregrina, F Rodríguez *J. Org. Chem.* **67** 4241 (2002)
146. E A Bell, M Y Qureshi, R J Pryce, D H Janzen, P Lemke, J Clardy *J. Am. Chem. Soc.* **102** 1409 (1980)
147. G C Kite, H Ireland *Phytochemistry* **59** 163 (2002)
148. G R Krow, S B Herzon, G L Lin, F Qiu, P E Sonnet *Org. Lett.* **4** 3151 (2002)
149. L Piela, G Nëmethy, H A Scheraga *J. Am. Chem. Soc.* **109** 4477 (1987)
150. S Talluri, G T Montellione, G van Duyne, L Piela, J Clardy, H A Scheraga *J. Am. Chem. Soc.* **109** 4473 (1987)

151. P Hughes, M Martin, G Clardy *Tetrahedron Lett*. **21** 4579 (1980)
152. P Hughes, G Clardy *J. Org. Chem*. **53** 4793 (1988)
153. M C Pirrung *Tetrahedron Lett*. **21** 4577 (1980)
154. T Rammeloo, C V Stevens, N De Kimpe *J. Org. Chem*. **67** 6509 (2002)
155. G R Krow, G Lin, D Rapolu, Y Fang, W S Lester, S B Herzon, P E Sonnet *J. Org. Chem*. **68** 5292 (2003)
156. C S Esslinger, H P Koch, M P Kavanaugh, D P Philips, A R Chamberlin, C M Thompson, R J Bridges *Bioorg. Med. Chem. Lett*. **8** 3101 (1998)
157. P Juvvadi, D J Dooley, C C Humblet, G H Lu, E A Lunney, R L Panek, R Skeean, G R Marshall *Int. J. Pept. Protein Res*. **40** 163 (1992)
158. D E Gaitanopoulous, J Weinstok *J. Heterocycl. Chem*. **22** 957 (1985)
159. M B Hursthouse, K M A Malik, D E Hibbs, S M Roberts, A J H Seago, V Sik, R Storer *J. Chem. Soc., Perkin Trans. 1* 2419 (1995)
160. M Jäger, K Polborn, W Steglich *Tetrahedron Lett*. **36** 861 (1995)
161. V I Tararov, R Kadyrov, Z Kadyrova, N Dubrovina, A Börner *Tetrahedron: Asymmetry* **13** 25 (2002)
162. H Waldmann, M Braun *Liebigs Ann. Chem*. 1045 (1991)
163. L Bunch, T Liljefors, J R Greenwood, K Frydenvang, H Bräuner-Osborne, P Krogsgaard-Larsen, U Madsen *J. Org. Chem*. **68** 1489 (2003)
164. P Pinho, P G Andersson *Chem. Commun*. 597 (1999)
165. T Kobayashi, K Ono, H Kato *Bull. Chem. Soc. Jpn*. **65** 61 (1992)
166. P Brandt, P G Andersson *Synlett* **8** 1092 (2000)
167. J M Mellor, N G J Richards, K J Sargood, D W Anderson, S G Chamberlin, D E Davies *Tetrahedron Lett*. **36** 6765 (1995)
168. B Portevin, A Benoist, G Rèmond, Y Hervg, M Vincent, J Lepagnol, G De Nanteuil *J. Med. Chem*. **39** 2379 (1996)
169. T Sato, T Mori, T Sugiyama, H Ishibashi, M Ikeda *Heterocycles* **37** 245 (1994)
170. T Sato, Y Kugo, E Nakaumi, H Ishibashi, M Ikeda *J. Chem. Soc., Perkin Trans. 1* 1801 (1995)
171. J A Campbell, H Rapoport *J. Org. Chem*. **61** 6313 (1996)
172. F Theobald, N Rodier, T Lakhlifi, A Sedqui, B Laude *Acta Crystallogr., Sect. C* **46** 1074 (1990)
173. A Avenoza, C Cativiela, J H Busto, J M Peregrina *Tetrahedron Lett*. **36** 7123 (1995)
174. E Buñuel, A M Gil, M D Díaz-de-Villegas, C Cativiela *Tetrahedron* **57** 6417 (2001)
175. A Avenoza, C Cativiela, J H Busto, M A Fernández-Recio, J M Peregrina, F Rodrígues *Tetrahedron* **57** 545 (2001)
176. A Avenoza, C Cativiela, M A Fernández-Recio, J M Peregrina *Synthesis* 165 (1997)
177. B P Hart, H Rapoport *J. Org. Chem*. **64** 2050 (1999)
178. A Avenoza, J I Barriobero, J H Busto, C Cativiela, J M Peregrina *Tetrahedron: Asymmetry* **13** 625 (2002)
179. W Han, J C Pelletier, L J Mersinger, C A Kettner, C N Hodge *Org. Lett*. **1** 1875 (1999)
180. W Han, J C Pelletier, C N Hodge *Bioorg. Med. Chem. Lett*. **8** 3615 (1998)
181. J A Monn, K C Rice *Tetrahedron Lett*. **30** 911 (1989)
182. J A Monn, A Thurkauf, M V Mattson, A E Jacobson, K C Rice *J. Med. Chem*. **33** 1069 (1990)
183. M V Gorichko, O O Grygorenko, I V Komarov *Tetrahedron Lett*. **43** 9411 (2002)
184. L E Overman, J E Tellew *J. Org. Chem*. **61** 8338 (1996)
185. P Wessig *Synlett* **9** 1465 (1999)
186. G M Bright, M F Dee, M S Kellogg, *Heterocycles* **14** 1251 (1980)
187. H-J Teuber, C Tsaklakidis, J W Bats *Liebigs Ann. Chem.,* 461 (1992)
188. T N Birkinshaw, A B Tabor, A B Holmes, P Kaye, P M Mayne, P R Raithby *J. Chem. Soc., Chem. Commun*. 1599 (1988)
189. M Vincent, C Pascard, M Cesario, G Rémond, J-P Bouchet, Y Charton, M Laubie *Tetrahedron Lett*. **33** 7369 (1992)
190. I D Rae, C L Raston, A H White *Aust. J. Chem*. **33** 215 (1980)
191. W Maison, D Küntzer, D Grohs *Synlett* **11** 1795 (2002)
192. H Tomisawa, H Nakano, H Hongo *Chem. Pharm. Bull*. **36** 1692 (1988)
193. T Imanishi, N Yagi, M Hanaoka *Chem. Pharm. Bull*. **33** 4202 (1985)
194. M Asaoka, N Ohkura, M Yokota, S Sonoda, H Takei *Heterocycles* **38** 2455 (1994)
195. M J Södergren, P G Andersson *Tetrahedron Lett*. **37** 7577 (1996)
196. D H Rich *Compr. Med. Chem*. **2** 400 (1990)
197. B Portevin, M Lonchampt, E Canet, G De Nanteuil *J. Med. Chem*. **40** 1906 (1997)
198. N Kucharczyk, C Thurieau, J Paladino, A D Morris, J Bonnet, E Canet, J E Krause, D Regoli, R Couture, J L Fauchere *J. Med. Chem*. **36** 1654 (1993)
199. K Saito, K Ono, M Sano, S Kiso, T Takeda *Heterocycles* **57** 1781 (2002)
200. R Chiarelli, A Rassat, P Rey *J. Chem. Soc., Chem. Commun*. 1081 (1992)
201. T Sasaki, S Eguchi, T Okano *J. Org. Chem*. **46** 4474 (1981)
202. S Umezawa, M Kinoshita, H Yanagisawa *Bull. Chem. Soc. Jpn*. **40** 209 (1967)
203. M Kinoshita, H Yanagisawa, S Dot, E Kaji, S Umezawa *Bull. Chem. Soc. Jpn*. **42** 194 (1969)
204. H L Hoyer *Chem. Ber*. **83** 491 (1950)
205. H S Tager, H N Christensen *J. Am. Chem. Soc*. **94** 968 (1972)
206. R S Glass, M Sabahi, W P Singh *J. Org. Chem*. **57** 2683 (1992)
207. E Bunuel, C Cativiela, M D Díaz-De-Villegas, J A Gálvez *Acta Crystallogr., Sect. C* **53** 626 (1997)
208. A Avenoza, C Cativiela, J A Mayoral, M A Roy *Tetrahedron* **45** 3923 (1989)
209. C Cativiela, M D Díaz-de-Villegas, J A Mayoral, A Avenoza, J M Peregrina *Tetrahedron* **49** 677 (1993)
210. E Buñuel, C Cativiela, M D Díaz-de-Villegas *Tetrahedron* **49** 7287 (1993)
211. J Ezquerra, C Pedregal, I Collado, B Yruretagoyena, A Rubio *Tetrahedron* **51** 10107 (1995)
212. E Buñuel, C Cativiela, M D Díaz-de-Villegas *Tetrahedron: Asymmetry* **7** 1521 (1996)
213. F Clerici, M L Gelmi, A Gambini *J. Org. Chem*. **65** 6138 (2000)
214. B A Burkett, C L L Chai *Tetrahedron Lett*. **41** 6661 (2000)
215. F Clerici, M L Gelmi, A Gambini *J. Org. Chem*. **66** 4941 (2001)
216. T Abellán, B Mancheño, C Nájera, J M Sansano *Tetrahedron* **57** 6627 (2001)
217. W J Layton, S L Smith, P A Crooks, T Deeks, R D Waigh *J. Chem. Soc., Perkin Trans. 1* 1283 (1984)
218. H Ito, A Saito, A Kakuuchi, T Taguchi *Tetrahedron* **55** 12741 (1999)
219. R S Glass, M Hojjatie, M Sabahi, L K Steffen, G S Wilson *J. Org. Chem*. **55** 3797 (1990)
220. F Tellier, F Acher, I Brabet, J-P Pin, R Azerad *Bioorg. Med. Chem*. **6** 195 (1998)
221. F Tellier, F Acher, I Brabet, J-P Pin, R Azerad *Bioorg. Med. Chem. Lett*. **5** 2627 (1995)
222. H Bräuner-Osborne, J Egebjerg, E Ø Nielsen, U Madsen, P Krogsgaard-Larsen *J. Med. Chem*. **43** 2609 (2000)
223. H N Christinsen, M R Handlogten, I Lam, H S Tager, R Zand *J. Biol. Chem*. **244** 1510 (1969)
224. H N Christinsen, A M Cullen *J. Biol. Chem*. **244** 1521 (1969)
225. J Zaleski, D F Wilson, M Ereciñska *J. Biol. Chem*. **261** 14091 (1986)
226. U Panten, S Zielmann, J Langer, B J Zunkler, S Lenzen *Biochem. J*. **219** 189 (1984)
227. S G Pine, G Safaeri *J. Chem. Res*. **3** 160 (1996)
228. E Bunuel, C Cativiela, M D Díaz-De-Villegas, J A Gálvez *Acta Crystallogr., Sect. C* **52** 2292 (1996)
229. W J Layton, S L Smith, P A Crooks, T Deeks, R D Waigh *J. Chem. Soc., Perkin Trans. 1* 1283 (1984)
230. G L Grunewald, S H Kuttab, M A Pleiss, J B Mangold, P Soine *J. Med. Chem*. **23** 754 (1980)
231. S Kotha, A K Ghosh, M Behera *Indian J. Chem., Sect. B*. **41** 2330 (2002)
232. E Buñuel, C Cativiela, M D Díaz-de-Villegas *Tetrahedron* **51** 8923 (1995)

233. S R Baker, T C Hancox *Tetrahedron Lett*. **40** 781 (1999)
234. R Zand, O Z Sellinger, R Water, R Harris *J. Neurochem*. **23** 1201 (1974)
235. R Pelliciari, M Raimondo, M Marinozzi, B Natalini, G Costantino, C Thomsen *J. Med. Chem*. **39** 2874 (1996)
236. A P Kozikowski, D Steensma, G L Araldi, W Tückmantel, S Wang, S Pshenichkin, E Surina, J T Wroblewski *J. Med. Chem*. **41** 1641 (1998)
237. P Conti, A P Kozikowski *Tetrahedron Lett*. **41** 4053 (2000)
238. P Luger, M Weber, G Szeimies, M Pätzel *J. Chem. Soc., Perkin Trans. 2* 1956 (2001)
239. R E Marsh *Acta Crystallogr., Sect. B* **53** 317 (1997)
240. B Tinant, J-P Declercq *Acta Crystallogr., Sect. C* **46** 904 (1990)
241. R H Blaauw, J-F Briére, R de Jong, J C J Benningshof, A E van Ginkel, J Fraanje, K Goubitz, H Schenk, F P J T Rutjes, H Hiemstra *J. Org. Chem*. **66** 233 (2001)
242. L Gan, D Zhou, C Luo, H Tan, C Huang, M Lm, J Pan, Y Wu *J. Org. Chem*. **61** 1954 (1996)
243. L-H Shu, G-W Wang, S-H -Wu , H-M Wu, X-F Lao *Tetrahedron Lett*. **36** 3871 (1995)
244. L Gan, J Jiang, W Zhang, Y Su, Y Shi, C Huang, J Pan, M Lü, Y Wu *J. Org. Chem*. **63** 4240 (1998)
245. G A Burley, P A Keller, S G Pyne, G E Ball *J. Org. Chem*. **67** 8316 (2002)
246. T Da Ros, M Prato *Chem. Commun*. 663 (1999)
247. F Pellarini, D Pantarotto, T Da Ros, A Giangaspero, A Tossi, M Prato *Org. Lett*. **3** 1845 (2001)
248. L Quere, G Longfils, R Boigegrain, B Labeeuw, D Gully, F Durant *Bioorg. Med. Chem. Lett*. **8** 653 (1998)
249. L Quéré, R Boigegrain, F Jeanjean, D Gully, G Evrard, F Durant *J. Chem. Soc., Perkin Trans. 2* 2639 (1996)
250. O Ermer, J Lex *Angew. Chem., Int. Ed. Engl*. **26** 447 (1987)
251. H Irngartinger, S Strack, F Gredel *Liebigs Ann. Chem*. 311 (1996)
252. H T Nagasawa, J A Elberling, F N Shirota *J. Med. Chem*. **16** 823 (1973)
253. M Paventi, F L Chubb, J T Edward *Can. J. Chem*. **65** 2114 (1987)
254. K Bott *Tetrahedron Lett*. **9** 3323 (1968)
255. P A Krasutskii, I G Semenova, M I Novikova, A G Yurchenko, N A Leont'eva, T V Veselovskaya *Khim.-Farm. Zh*. **7** 825 (1985) [d]
256. P A Krasutskii, I G Semenova, M I Novikova, A G Yurchenko *Zh. Org. Khim*. **21** 1905 (1985) [e]
257. R Pellicciari, G Costantino, E Giovagnori, L Matolli, I Brabet, J-P Pin *Bioorg. Med. Chem. Lett*. **8** 1569 (1998)
258. Y Kuroda, H Ueda, H Nozawa, H Ogoshi *Tetrahedron Lett*. **38** 7901 (1997)
259. F J C Martins, A M Viljoen, H G Kruger, L Fourie, J Roscher, A J Joubert, P L Wessels *Tetrahedron* **57** 1601 (2001)

[a] — *Mendeleev Chem. J. (Engl. Transl.)*
[b] — *Biochemistry (Moscow) (Engl. Transl.)*
[c] — *Dokl. Chem. (Engl. Transl.)*
[d] — *Pharm.-Chem. J. (Engl. Transl.)*
[e] — *Russ. J. Org. Chem. (Engl. Transl.)*

Russian Chemical Reviews **73** (8) 811 – 829 (2004) © 2004 Russian Academy of Sciences and Turpion Ltd

DOI 10.1070/RC2004v073n08ABEH000901

Graft copolymers with chemically complementary components as a special class of high-molecular-weight compounds

T B Zheltonozhskaya, N E Zagdanskaya, O V Demchenko, L N Momot, N M Permyakova, V G Syromyatnikov, L R Kunitskaya

Contents

I.	Introduction	811
II.	Intramolecular polycomplexes	812
III.	Complex formation of covalently non-bound polymeric partners as a criterion of chemical complementarity between components of graft copolymers	813
IV.	Matrix effects in free-radical graft copolymerisation	815
V.	System of intramolecular main chain – graft and graft – graft bonds as the main factor of stabilisation of the structures of intramolecular polycomplexes	817
VI.	Influence of grafting density on the bulk structure and solution behaviour of intramolecular polycomplexes	818
VII.	Characteristic features of the structures and properties of intramolecular polycomplexes depending on the graft length	823
VIII.	Functional capabilities of intramolecular polycomplexes	824
IX.	Conclusion	826

Abstract. The review surveys the synthesis, bulk structures, solution behaviour and functional capabilities of graft copolymers containing chemically complementary polymer components. The influence of a system of intramolecular bonds between the main and grafted chains and between the adjacent grafted chains on the properties of graft copolymers is analysed. Such graft copolymers are shown to belong to a special class of polymer compounds referred to as intramolecular polycomplexes. The bibliography includes 204 references.

I. Introduction

Graft copolymers are considered as promising heteropolymeric functional materials. These compounds are widely used for controlling stability of disperse systems,[1–7] as compatibilisers for improving compatibility of polymer mixtures,[8–12] as matrix binders in biotechnological processes, macromolecular therapeutic systems [13–19] and paper production,[20] as semipermeable membranes,[21–23] thickeners,[24–28] film-forming coatings,[29,30] protective coatings,[31–33] lyophilising coatings,[34–40] physical gels [41] and agents of drag reduction of turbulent flow.[42–44] Such heteropolymeric systems have attracted growing interest in recent years owing to impressive progress in developing new nanoreactor catalytic processes [45,46] and nanophase technologies for the construction of composite polymeric materials, including controlled growth of metal nanoparticles in the presence of polymer matrices [47,48] and grafting of polymer chains onto the surface of inorganic nanoparticles.[49–59] The interest in graft copolymers is associated with considerable possibilities for controlling their structures and properties through variations in the chemical nature and length of polymer components and through changes in the number (density) and distribution of grafted chains.

A combination of chemically complementary (which are able to interact cooperatively) polymeric partners in the macromolecules of graft copolymers offers considerable possibilities for varying their properties and functions. Since such copolymers have features in common with intermolecular polycomplexes, they can be considered as a special class of high-molecular-weight compounds referred to as intramolecular polycomplexes. In the present review, we discuss the characteristic features of the bulk structure, solution behaviour and functional capabilities of such intramolecular polycomplexes.

In the late 1950s, Mino and Kaizerman [60,61] were among the first to perform the directed synthesis of graft copolymers. However, comprehensive and theoretically supported knowledge of the relationship between the chemical nature of polymer components and the molecular architecture of graft copolymers and the structure – properties relationship is lacking. In early studies, this problem was difficult to solve because of difficulties associated with the preparation of graft copolymers with desired structures and the lack of efficient methods for the determination of their molecular parameters. However, fundamental studies in this field are still few in number in spite of the well-developed synthetic base and modern methods for investigation of these compounds. The reason is that most attention has been focused on practical applications of graft copolymers and, hence, exclusively properties of copolymers which are of interest from a practical standpoint, have been investigated.

Nevertheless, not only the main molecular architectures (described as stars, combs and brushes) of graft copolymers [62–64] but also the major factors influencing their structures and solution behaviour were revealed. Among such factors are the chemical nature and thermodynamic compatibility of polymer components, the number (density), length and distribution of grafted chains along the main chain and the nature of the solvent and its

T B Zheltonozhskaya, N E Zagdanskaya, O V Demchenko, L N Momot, N M Permyakova, V G Syromyatnikov, L R Kunitskaya Department of Chemistry, Kyiv National Taras Schevchenko University, ul. Vladimirskaya 64, 01033 Kyiv, Ukraine. Fax (038-044) 239 31 00. Tel. (38-044) 239 34 11. E-mail: zheltonozhskaya@ukr.net (T B Zheltonozhskaya), nzagdanska@mail.ru (N E Zagdanskaya), odemch@ukr.net (O V Demchenko), momot_lesya@ukr.net (L N Momot), permyakova@ukr.net (N M Permyakova), larisa_kunitskaya@alsi.kiev.ua (L R Kunitskaya). Tel. (38-044) 239 33 00. E-mail: svg@univ.kiev.ua (V G Syromyatnikov)

Received 26 January 2004
Uspekhi Khimii **73** (8) 877 – 896 (2004); translated by T N Safonova

selectivity (or non-selectivity) to individual polymer components.[63–69] As demonstrated below, a system of intramolecular main chain – graft and graft – graft bonds plays an important role in the structures of graft copolymers which form intramolecular polycomplexes. In addition, hydrophobic interactions between the binding regions of active groups of the polymer components, which facilitate shrinkage and association of coils, play a significant role in stabilisation of the structures of graft copolymers in an aqueous medium.

A relatively small number of publications were devoted to analysis of the properties of graft copolymers depending on the density and molecular mass of grafted chains and thermodynamic compatibility between polymer components in the last 15 years.[62–64, 70–76] The results of investigations of graft copolymers which form intramolecular polycomplexes were not analysed at all. Systematic studies of this class of polymer compounds have been carried out only for poly(vinyl alcohol)-graft-polyacrylamide (PVA-g-PAA) copolymers. Hence, in the present review emphasis is given to these graft copolymers. Published data on the synthesis, structures and properties of other graft copolymers containing chemically complementary polymer components are considered in relation to the data for PVA-g-PAA.

II. Intramolecular polycomplexes

Poly(vinyl alcohol)-graft-polyacrylamide copolymers and polysaccharide-graft-PAA copolymers were among the first graft copolymers containing chemically complementary components to be synthesised.[60, 61, 77–79] Initially, the specific rheological properties of such copolymers, in particular, significant drag reduction of turbulent flow (combined with high resistance to degradation) in dilute solutions[42, 77, 80] and high viscosity in semidilute solutions,[81] have attracted researchers' attention. Later on, yet another characteristic feature of these copolymers, *viz*., their high flocculating ability, was discovered.[5, 82, 83] It was believed that these properties are determined by a combination of the properties of polymer components involved in graft copolymers and the branched structures of copolymer macromolecules. Subsequently, graft copolymers of this type were studied over many years in parallel with copolymers containing non-interacting (incompatible) or weakly interacting polymer components without classifying them as a special group.

The possible existence of strong intramolecular interactions (hydrogen bonds), which are responsible for the properties of poly(vinyl alcohol)-graft-poly(*N*-vinylpyrrolidone) copolymers (PVA-g-PVPD) was mentioned for the first time in the study.[84] In contrast to a number of other graft copolymers, the characteristic viscosity [η] of PVA-g-PVPD in aqueous solutions decreases compared to this parameter for the starting polymer (PVA). The low value of [η] is retained over a wide temperature range. However, the addition of dimethylformamide (DMF), which facilitates destruction of H-bonds, leads to rapid swelling of the PVA-g-PVPD macromolecules.

Essentially similar effects were noted earlier.[85] The cited study was devoted to comparative investigation of the physicochemical properties of acetylcellulose-graft-PAA copolymers (AC-g-PAA) and the corresponding polymer mixtures. Actually, the solubility of the graft copolymer in aqueous solutions of acetic and formic acids, which are good solvents for both polymer components, decreases as the degree of grafting of PAA increases from 27.6% to 38.1%. Besides, the reduced viscosities of mixtures of the above-mentioned polymers are substantially lower than the calculated additive values throughout the composition range, which is unambiguously indicative of complex formation between polymers. However, the authors of the cited study have not yet interpreted these results in the context of strong interactions between AC and PAA.

Strong intramolecular interactions were revealed in the PVA-g-PVPO graft copolymers, where PVPO is poly(vinylpyridine *N*-oxide), and in mixtures of these polymers [thermodynamic studies of solvent (water) vapour sorption according to Tager's method].[86] The negative free energies of mixing and the negative values of the Flory – Huggins parameter (χ_{12}), which characterises thermodynamic affinity between polymers in a particular solvent, were observed throughout the composition range of the mixture and the graft copolymer. For the copolymers with PVPO contents of 0.39 and 0.43, the parameter χ_{12} is -1.9 and -3.8, respectively. The thermodynamic parameters of the PVA-g-PVPO copolymers also have smaller values compared to those of a mixture of the constituent polymers. From this it was concluded that compatibility between the polymer components in the graft copolymer is higher than that in their mixture.[86]

The presence of strong interactions between the main and side chains in the graft copolymers of poly(acrylic acid) (PAAc) or poly(methacrylic acid) (PMAA) onto PVA and the graft copolymers of poly(ethylene glycol) (PEG) onto PMAA was noted in the studies.[87–89] In particular, grafting of PMAA onto PVA by free-radical polymerisation in the presence of a Ce(IV) salt as an initiator was accompanied by precipitation of the copolymer[87] due to hydrogen bonding between the polymer components. In this case, the composition of the PVA-g-PMAA graft copolymer was close to equimolar. The influence of complex formation between PMAA and PEG involved in the cross-linked PMAA-g-PEG graft copolymer on hydrogel swelling and release of a drug dissolved in the hydrogel was considered.[88] It was demonstrated that hydrogen bonding hinders swelling of the hydrogel and decreases its permeability. In the presence of PEG and PMAA in an equimolar ratio, the rates of hydrogel swelling and release of the dissolved compound from the hydrogel appeared to be minimal. The complex character of association of graft copolymers based on PAAc and poly(*N*,*N*-dimethylacrylamide) (PDMAA) in solutions was noted in the study.[90] Spherical aggregates with a diameter of 150 nm, which are stabilised through both intramolecular and intermolecular H-bonds between the polymer components, were found to be formed from the PAAc-g-PDMAA molecules in an aqueous medium.

Attempts were made to analyse interactions between free and covalently bound polymer partners[91] and reveal changes in thermodynamic affinity between polymer components with increasing grafting density.[92] The thermodynamics of equilibrium complex formation between linear macromolecules and chemically complementary oligomers in dilute solutions was studied[91] for oligomers covalently end-bound to macromolecules and for mixtures of free components in solution. The polymer conformations were calculated using a general statistically mechanical approach (with a simple random walk model). The free energy of an oligomer involved in a complex was calculated using the method of generating functions. In this case, the lengths of loops, binding parts and tails were not restricted. The results of modelling of free oligomers were compared with the results obtained for oligomers covalently linked to macromolecules. Theoretical analysis provided an explanation for many experimental data, in particular, for the dependence of the part of the complex-bound oligomer links on the binding energy and the length of its chain and also for an increase in efficiency of complex formation in the presence of covalent bonds between the polymer reagents.

The influence of the grafting density on interactions between components of a binary layer of graft polymers (for amphiphilic diblock copolymers adsorbed at the liquid – liquid interface) was examined in the study.[92] The ratio of the Flory radius R_F, which characterises free isolated grafted chains in a particular solvent, to the distance D between the centres of the adjacent grafts was demonstrated to be of particular importance. The equality $D = R_F$ was considered as the overlap threshold for coils of

grafted chains. The system was shown to behave as a two-dimensional regular solution, in which the interaction parameter between components χ_{12} decreases with increasing D. Two regions in which χ_{12} decreases depending on the grafting density were revealed. In the region of D which does not reach the overlap threshold ($D > R_F$), χ_{12} decreases according to the law

$$\chi_{12} = \left(\frac{R_F}{D}\right)^2,$$

but at a high grafting density ($D < R_F$), χ_{12} changes according to the equation

$$\chi_{12} \approx \left(\frac{R_F}{D}\right)^{3/4}$$

or

$$\chi_{12} \approx \left(\frac{R_F}{D}\right)^{5/3}$$

depending on the starting theoretical premises (boundary conditions). Therefore, according to the predictions of this theory, interactions between the components of the binary layer should become weaker with increasing grafting density, the most substantial weakening occurring at $D > R_F$.[92]

It should be noted that the specific features of these copolymers were ignored in most other studies devoted to the synthesis and properties of graft copolymers containing chemically complementary polymer components, such as the above-mentioned PVA and PAA,[60, 61, 78, 93, 94] polysaccharides (dextran, starch, hydroxymethylcellulose and carboxymethylcellulose) and PAA[43, 77, 79, 81, 95–100] or poly(*N*-isopropylacrylamide) (PIPAA),[101, 102] PVA and PAAc,[89, 103] poly(ethylene oxide) (PEO) and PAA,[104] PAA,[105] the copolymer of acrylic acid (AAc) and acrylamide (AA)[106] or PIPAA,[107] chitosan and PAA [14] and, finally, PAA and PIPAA.[21, 108]

However, graft copolymers with strong intramolecular interactions serve as highly efficient flocculants,[5, 109] are used as degradation-resistant agents of drag reduction of turbulent flow [44, 110] and possess abnormally high binding ability.[88] The latter property of graft copolymers containing interacting polymer components was confirmed, in particular, by the results of the study,[111] where complex formation of individual PMAA with Cu^{2+} ions was compared with that of PMAA involved in the AC-g-PMAA graft copolymer. The constant of complex formation of the grafted chains with copper ions ($\sim 10^{6.5}$) was determined by potentiometric titration of the starting aqueous-salt solution of AC-g-PMAA ($c_{NaCl} = 0.1$ mol dm^{-3}) and of the same solution in the presence of Cu^{2+} ions (the concentration was varied from 5×10^{-5} to 5×10^{-3} mol dm^{-3}). This complex formation constant is higher than that for individual PMAA. The authors reasonably attributed the higher complex formation ability of PMAA grafted onto AC to specific conformational effects in the macromolecules of this copolymer.

Based on analysis of the data published in the literature and the results of our investigations of graft copolymers [44, 112] and intermolecular polycomplexes,[113] we hypothesised that graft copolymers containing the chemically complementary main and grafted chains belong to a special class of polymer compounds referred to as intramolecular polycomplexes.[114] This assumption was confirmed by the results of comprehensive investigation of the formation, structures, behaviour in solution and functional capabilities of the PVA-g-PAA graft copolymers depending on the grafting density and the molecular mass of the grafted chains. Further, we consider the synthesis and properties of graft copolymers which form intramolecular polycomplexes. Initially, let us determine which polymers could be assigned to the class under consideration and discuss the criteria to be used.

III. Complex formation of covalently non-bound polymeric partners as a criterion of chemical complementarity between components of graft copolymers

It is known that the spontaneous formation of intermolecular complexes through a cooperative system of bonds of a particular nature (Coulombic interactions, hydrogen bonds, donor–acceptor bonds, van der Waals contacts) is a distinguishing feature of pairs of chemically complementary polymers.[115, 116] The formation of a cooperative system of bonds causes a sharp shift of the equilibrium at the macromolecular level toward the formation of a polycomplex. The stability constant K_v of intermolecular polycomplexes increases as a power function of the number of links v (or length) in the polymer chain.[116] For cooperative interactions to occur, a particular critical chain length, which depends on the energy of a single bond, is required. In addition, the interacting macromolecules must be structurally and conformationally complementary.[115–117] The nature of the solvent is of considerable importance. The solvent molecules must neither compete with active groups of the polymers nor shield them, *i.e.*, must not hinder the formation of a network of intermolecular bonds.[116]

From the above, it can be concluded that heterogeneous block-type polymers (graft and block copolymers) containing chemically and structurally complementary polymer blocks of sufficient length can be involved in intramolecular cooperative interactions. These heterogeneous polymers belong to a class of intramolecular polycomplexes. The criterion for assigning particular graft and block copolymers to this class of compounds is spontaneous complex formation of covalently non-bound polymer components. It should be noted that the average number of units in the main chain between the adjacent grafts should be considered as the average length of the reacting blocks in graft copolymers.

Using the above criterion, it is easy to demonstrate that the assumption of chemical complementarity of a series of polymer components of graft copolymers, which was made in Section II, is justified. Actually, spontaneous complex formation between covalently non-bound polyacids (PAAc, PMAA), on the one hand, and polyalcohols (PVA), polyesters (PEO), polyamides (PAA) and polysaccharides (for example, methylcellulose, hydroxyethylcellulose or chitosan), on the other hand, was observed.[115, 118–121] Chemical complementarity between PVA and PAA was proved in our special investigations (data on complex formation between these polymers have been lacking in the literature). This was the first necessary step in studies of the PVA-g-PAA graft copolymers which form intramolecular polycomplexes.

In several studies (see, for examples, Refs 93 and 122), only selected properties of mixtures of PVA and PAA were characterised and no conclusions about the formation of intermolecular polycomplexes between these polymers were drawn. The low value of K_{AB} (0.3) for this system determined by viscosimetry is indicative of a low degree of overlapping between the molecules of the types A (PVA) and B (PAA) in dilute aqueous solutions.[93] The phase separation in the PVA–PAA–H_2O system was observed [122] at certain polymer ratios. However, this effect was not interpreted as a consequence of formation of intermolecular polycomplexes. Taking into account the above-mentioned facts, we studied the PVA–PAA system in an aqueous solution and in the bulk state by varying the molecular mass and chemical structure of the polymeric components with the use of viscosimetry, IR spectroscopy, high-speed sedimentation, gel chromatography, differential scanning calorimetry (DSC) and benzene solubilisation.[123–129] Let us briefly consider the principal results of these studies.

The formation of intermolecular polycomplexes in the PVA–PAA system at $M_{PAA} \gg M_{PVA}$ (*i.e.*, the PAA macromolecules can be considered as matrices with respect to PVA) was estab-

lished by a conventional viscosimetric method. The deviation of the ratio of the specific viscosity of mixture to the sum of specific viscosities of the individual components from unity served as the criterion for the presence of interactions between the polymers.[124] For a relatively low-molecular-weight sample of PVA ($M_v = 4 \times 10^4$), this ratio was smaller than unity, which was indicative of the formation of compact particles of intermolecular polycomplexes. For higher-molecular-weight samples of PVA ($M_v = 8 \times 10^4$ and 1.2×10^5), this ratio was larger than unity, *i.e.*, more and more friable particles of intermolecular polycomplexes appeared. Further studies of this system by high-speed sedimentation and gel chromatography demonstrated that these polycomplexes had a constant composition, which was independent of the PVA to PAA ratio in solution[124, 128] and of the molecular parameters of PVA (in the range under consideration) but decreased from $\varphi_{char} = 9$ to $\varphi_{char} = 4$ $kg_{PVA}\,(kg_{PAA})^{-1}$ (φ_{char} is the characteristic composition) as $M_{v\,PAA}$ increased from 2.72×10^6 to 4.4×10^6 (see Refs 124 and 127–129). Therefore, particles of polycomplexes contained a substantial excess of the PVA molecules. In addition, macromolecules of individual PVA and PAA were aggregated in water. These aggregates were destroyed in the process of complex formation. Taking into account this fact, a substantial excess of PVA in intermolecular polycomplexes was accounted for by interactions of the long PAA macromolecules with partially destroyed aggregates of PVA.

Interaction between the polymers through hydrogen bonding was established by IR spectroscopy.[124, 126, 127] Two of the most important regions of the IR spectra of thin films of PAA and the intermolecular polycomplex are shown in Fig. 1. The results of computer separation of overlapping bands in the Amide I and Amide II regions by the spline-function method are presented in Fig. 2. Detailed analysis of the positions and relative intensities of the bands in the spectra of the PAA film and the intermolecular polycomplexes revealed the following structures of H-bonds: a small amount of 'open' dimers of COOH groups (these groups are derived from the amide groups of PAA upon their partial hydrolysis) characterised by the band $\nu_{C=O} = 1724$ cm^{-1}; a small amount of free amide groups characterised by the Amide I band at 1707 cm^{-1}; a substantial amount of *trans*-multimers of amide groups characterised by the Amide I bands at 1692 (terminal C=O groups of *trans*-multimers) and 1679 cm^{-1} (H-bonded C=O groups of *trans* aggregates); a large amount of *cis*–*trans*-multimers of amide groups characterised by the Amide I band at 1661 cm^{-1}. In addition, the spectra of the intermolecular polycomplexes show an individual band at 1670 cm^{-1} (see Fig. 2*a*) assigned to H-bonds between PVA and PAA. With the aim of revealing changes in the structure of these polycomplexes relative to PAA, the numbers of amide groups forming one or other system of H-bonds were compared. Quantitative calculations were carried out taking into account the following facts:[127, 129] (1) similar shifts of Amide I bands of bound amide groups in the intermolecular polycomplexes and PAA relative to the band of the free amide groups; (2) the absence of substantial orientational effects in thin films of these polymers;[130] (3) the Bouguer–Lambert–Beer law

$$B_i = A_i l c_i ,$$

where B_i is the apparent integral absorption coefficient of the ith Amide I band in the IR spectrum, A_i is the true integral absorption coefficient of the absorption band, l is the film thickness and c_i is the molar concentration of amide groups, which are in the ith state, in the film.

To reduce to a minimum the effect of the difference in the film thickness along the light path and the difference in the number of acrylamide units in the films of PAA and intermolecular polycomplexes, the coefficient B_i was normalised to the apparent integral absorption coefficient B_0 of the vibration band ν_{C-H} of the methylene groups, which is proportional to the concentration of the polymer compound, and to the mole fraction of the acrylamide units in the polymer sample ($X_{n\,AA}$). The calculated $B_i/B_0X_{n\,AA}$ ratios (Table 1) are proportional to the mole fraction of the amide groups in the ith state. In addition to the above-

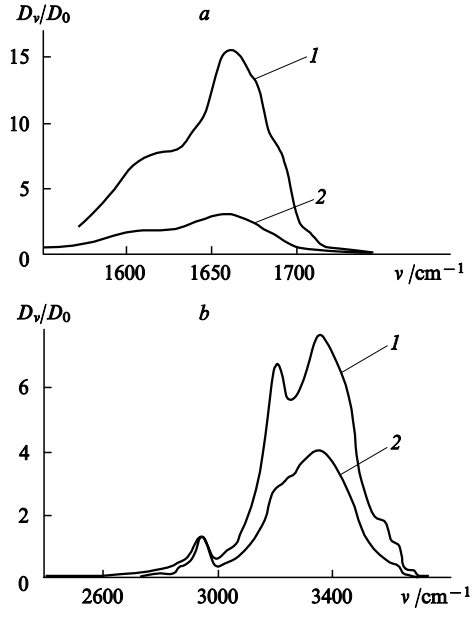

Figure 1. Reduced IR spectra of PAA films (*1*) and the PVA–PAA intermolecular polycomplex at $\varphi = \varphi_{char} = 4$ $kg_{PVA}\,(kg_{PAA})^{-1}$ (*2*) in the Amide I and Amide II regions (*a*) and in the region of C–H, N–H and O–H vibration frequencies (*b*);
D_0 is the amplitude of the band of the internal standard (C–H vibrations of the methylene groups); $T = 293$ K, $l = 7$–9 μm; $M_{v\,PAA} = 4.4 \times 10^6$, $M_{v\,PVA} = 4 \times 10^4$.

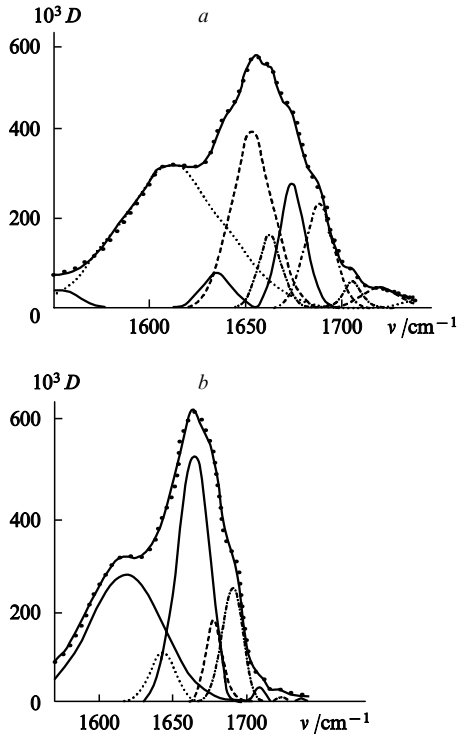

Figure 2. Results of computer processing of the IR spectra of the intermolecular complex at $\varphi = \varphi_{char}$ (*a*) and PAA (*b*) in the Amide I and Amide II regions.
Experimental (points) and calculated (solid lines) contours of overlapping bands; the contours of separated bands are presented below.

Table 1. Reduced apparent integral absorption coefficients of the Amide I absorption bands ($B_i/B_0X_{n\,PAA}$) and the effective lengths of *trans*-multimers of amide groups (β) for PAA and the PVA–PAA intermolecular polycomplex.

$B_i/B_0X_{n\,AA}$ for ν (cm^{-1})					$\beta = \frac{B_{1679}}{B_{1692}}$
1661	1670	1679	1692	1707	
Sample — PAA					
8.37	–	1.33	2.64	0.16	0.50
Sample — PVA–PAA (see [a])					
5.69	1.31	2.47	2.28	0.32	1.08

[a] $M_{v\,PAA} = 4.4 \times 10^6$ (hydrolysis degree is ~1%), $M_{v\,PVA} = 4 \times 10^4$.

mentioned parameters, Table 1 gives the effective lengths of the *trans*-multimers of amide groups (parameter β).

As can be seen from Table 1, complex formation between PAA and PVA is accompanied by destruction of a substantial amount of *cis*–*trans*-multimers of amide groups (band at ~1661 cm^{-1}), hydrogen bonding between the polymers (band at ~1670 cm^{-1}) and a slight decrease in the amount of *trans*-multimers of amide groups (band at ~1692 cm^{-1}) with a simultaneous increase in their length by a factor of more than 2. In our opinion, an increase in the rigidity of the polyacrylamide chain upon complex formation with PVA is attributable to appearance of the following sequence of H-bonds between segments of these polymers:[129]

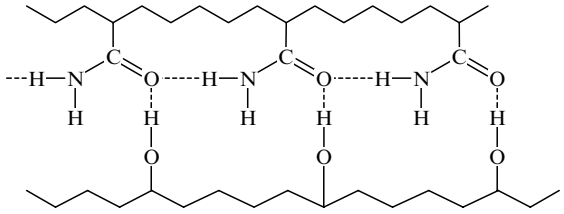

The conclusion about interactions of PAA with PVA aggregates in solutions was completely confirmed by the results of comparative structure studies of PVA–PAA mixtures with $\varphi = \varphi_{char}$ and $\varphi = 1\ kg_{PVA}(kg_{PAA})^{-1}$ and the individual polymers in the bulk state.[123, 125, 127–129] Studies were carried out by DSC (Fig. 3). Actually, the PVA microcrystalline domains distributed in regions of the polymer component compatibility were found in the structures of polymer mixtures with a characteristic composition (curve *3′*) prepared from solutions. Evidently, the compatibility regions in the structures of intermolecular polycomplexes are attributable to the presence of segments of the polymer components linked to each other, whereas the microcrystalline regions occur due to the presence of PVA aggregates in the polycomplexes formed. In solid mixtures with composition $\varphi = 1$ (curve *4*), microregions formed by segments of excessive PAA, which was not involved in intermolecular polycomplexes, were revealed along with the above-mentioned two types of domains.[129] This is indicative of a constant composition of the polycomplex and the occurrence of disproportionation in this system (the presence of completely filled and free matrices).

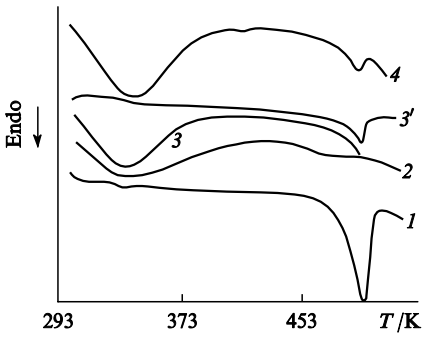

Figure 3. DSC thermograms of PVA (*1*), second scanning; PAA (*2*), first scanning; a PVA–PAA mixture at $\varphi = \varphi_{char} = 4\ kg_{PVA}(kg_{PAA})^{-1}$ (*3*), first scanning; the mixture of the same composition (*3′*), second scanning; the mixture at $\varphi = 1\ kg_{PVA}(kg_{PAA})^{-1}$ (*4*).

It was found that the stability of compact particles of intermolecular polycomplexes containing PVA with $M_v = 4 \times 10^4$ in water depends substantially on hydrophobic interactions. The volume of hydrophobic regions in the particle of the intermolecular polycomplex, which was determined by benzene solubilisation, was 408 nm^3 (see Refs 127 and 128).

The reaction of PVA with PAA in water was assigned to the known type of matrix + oligomer reactions [118, 131]

$$P_1\ (\text{matrix}) + n\,P_2 \longrightarrow$$
$$\longrightarrow \text{intermolecular polycomplex } (P_1 + n\,P_2),$$

where the PAA macromolecules act as a matrix, whereas the PVA aggregates, which are destroyed only partially, act as an oligomer (P_2). The constancy of the composition of the intermolecular complex and the existence of free matrices at $\varphi < \varphi_{char}$ are indicative of the non-uniform distribution of the oligomers between the matrices upon complex formation, *i.e.*, two levels of cooperativity take place in this reaction.[127, 128] The first level is associated with the formation of a cooperative system of H-bonds between the individual chains of the PVA aggregates and the corresponding regions of the PAA macromolecule, and the second level occurs due to interactions between the PVA aggregates onto the PAA chain (Fig. 4).

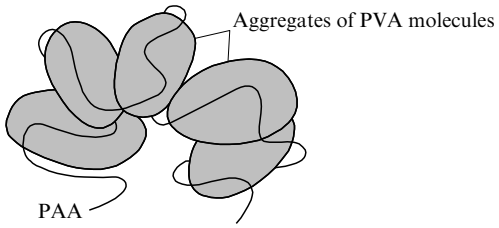

Figure 4. Schematic representation of a particle of the PVA–PAA intermolecular polycomplex.

Thus, not only chemical complementarity between PVA and PAA was established but also self-assembly of small aggregates of one polymer component at the long chains of another component analogously with the known effect of self-assembly of protein globules at the chains of oppositely charged polyelectrolytes was demonstrated.[132]

IV. Matrix effects in free-radical graft copolymerisation

The synthesis of graft copolymers has been widely discussed in the literature in recent years.[72, 133–152] Let us consider the main approaches to the synthesis of graft copolymers. The first approach includes methods based on free-radical or ionic graft copolymerisation involving the transformation of the main chain into a macroinitiator as the initial step.[72, 133–145, 151] Macroinitiators can be produced with the use of redox systems involving variable-valence metals,[134–137] irradiation of chains with high-energy particles,[138–140] atom-transfer reactions [141, 142] and chemical or thermal activation of particular groups (including double

bonds) at the main chain.[141–145, 151] The second approach includes methods of polymerisation or copolymerisation involving macromonomers.[146–148] The third approach is based on the chain transfer to polymer.[149, 150] Finally, methods were developed for chemical cross-linking of the pre-formed grafts to active groups of the main chain.[152] It should be noted that many studies devoted to the kinetics and mechanisms of graft copolymerisation (see, for example, Refs 153 and 154) dealt with graft copolymers containing chemically complementary polymer components. However, the question about the possible influence of strong interactions between the main and grafted chains on the properties of these compounds has remained beyond the scope of these investigations.

At the same time, the matrix synthesis of polymers through interactions of the growing (daughter's) chain with a matrix, *viz*., a chemically complementary chain, of another chemical nature was well known.[47] Hence, it is reasonable to suggest that many processes of the synthesis of graft copolymers containing strongly interacting polymer components (in particular, graft copolymerisation) would belong to matrix processes. This aspect has received proper attention in studies of free-radical graft copolymerisation of PAA onto PVA. The PVA-g-PAA copolymers were synthesised by free-radical graft copolymerisation using a Ce(IV) salt as the initiator. The general scheme of the reaction is as follows:[129]

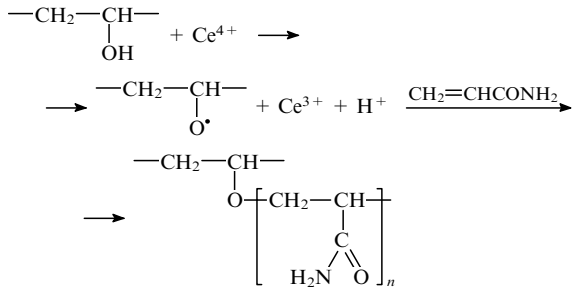

Until recently, the mechanism of grafting of PAA onto hydroxy-containing polymers (including PVA) was believed to be well understood.[77, 78, 81, 96, 155] This mechanism involves the formation of Ce(IV) complexes with several OH groups of the main chain as the first step [156] followed by decomposition of these complexes to form macroinitiators of free-radical graft copolymerisation.

The aim of the study [129] was to synthesise two series of graft copolymers. In each series, only one of the two major parameters responsible for the properties of graft copolymers, *viz*., the number (N) or molecular mass of the grafted chains, was varied. For this purpose, the ratio between the molar concentrations of the Ce^{4+} ions and PVA units (α) was initially varied holding the ratio (γ) between the molar concentrations of the Ce^{4+} ions and the monomer (acrylamide) constant. In a series of the PVA-g-PAA(1–3) copolymers † thus prepared, N was increased from 25 to 49 and the grafted chains in samples 1–3 had comparable molecular masses ($M_v \sim 1 \times 10^5$). In another series of the PVA-g-PAA(4–6) copolymers, N was increased from 25 to 42, and the molecular mass of the grafted chains was decreased from 3.72×10^5 to 1.63×10^5. Then the ratio γ was varied with α held constant. As a result, a series of the PVA-g-PAA(8–10) samples was prepared, in which the molecular mass of the grafted chains varied from 3.72×10^5 to 5.1×10^5 at $N = 9$.[129] In addition, the PVA-g-PAA(7) sample with $N = 4$ and $M_v = 1.12 \times 10^6$ was synthesised.[112] It should be noted that in all the copolymers synthesised, $M_{v\,PVA} = 8 \times 10^4$.

Taking into account thermodynamic affinity between PVA and PAA and the phenomenon of matrix polymerisation of monomers of the same chemical nature in the presence of complementary macromolecules of another chemical nature,[47, 155] it was hypothesised that free-radical graft copolymerisation of PAA onto PVA belongs to the category of matrix processes. This assumption was also supported by the results of the study,[157] in which the matrix effect (an increase in the growth rate of the PMAA chain by an order of magnitude) was observed in the course of grafting of PMAA onto starch granules. In order to confirm or refute this hypothesis, the kinetics of this reaction was compared with that of homopolymerisation of acrylamide performed under analogous experimental conditions.[158] The purpose was to reveal the kinetic matrix effect.[47] The kinetic parameters of the reaction, such as the time of the initial slow step (τ_0), *viz*., the initiation step, and the rates of polymerisation v_p^{20} and v_p^{60} at the conversions $K = 20\%$ and 60%, respectively, were determined by dilatometry.[158] In one series of experiments, the ratio α was increased with γ held constant (Fig. 5, Table 2). As mentioned above, this led to an increase in the grafting density in the graft copolymers [samples PVA-g-PAA(1–3)]. In another series of experiments, the ratio of α was held constant, whereas γ was decreased, the graft length being increased at constant N [samples PVA-g-PAA(8–10)]. The results of these investigations demonstrated that the rate of graft copolymerisation increases compared to the rate of homopolymerisation of acrylamide (see Table 2).[158] However, when the density of the growing daughter's chains became too high [see the data for PVA-g-PAA(3) in Table 2], the matrix effect disappeared.

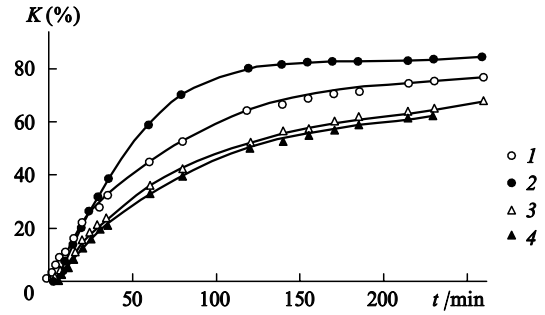

Figure 5. Plot of the monomer conversion *vs*. the reaction time of AA homopolymerisation (*1*) and graft copolymerisation of PAA onto PVA with increasing grafting density (*2–4*).
$T = 298$ K; α and γ are given in Table 2.

Table 2. Reagent ratios and the kinetic parameters for AA homopolymerisation and graft copolymerisation of PAA onto PVA.

Polymer	α (see [a])	τ_0 /min	$10^4 v_p^{20}$ (see [b])	$10^4 v_p^{60}$ (see [b])	K(%) (see [c])
PAA	1.000 [d]	8	0.95	0.48	60
PVA–PAA(1)	0.014	2	1.85	0.99	73
PVA–PAA(2)	0.027	3	1.96	1.69	82
PVA–PAA(3)	0.055	5	0.99	0.48	62

[a] For all polymers, the parameter γ was 10^{-3}. [b] In mol dm^{-3} s^{-1}. [c] The conversion after 200 min. [d] The molar ratio between Ce^{4+} and ethanol.

Therefore, not only the kinetic matrix effect was established in the synthesis of PVA-g-PAA but also its relation to the density of the growing chains was revealed. Actually, a decrease in τ_0 (compared to that for homopolymerisation of acrylamide) and a virtually twofold increase in the growth rate of the PAA chains in the graft copolymer were observed at relatively low α (< 0.055), *i.e*., in the presence of a small amount of grafted chains (small N) in the final copolymer. At $\alpha = 0.055$, the kinetic parameters of graft copolymerisation were virtually equal to those determined from the kinetic curves of homopolymerisation of acrylamide (see

† The sample numbers are given in parentheses.

Table 2). This important result can be attributable, first, to the fact that an increase in N leads to a decrease in the average length of the reacting block of the matrix (*i.e.*, the average distance between the adjacent grafted chains at the main chain), which is accessible for complex formation with the growing PAA chains, and, second, to an increase in steric hindrance to binding of grafted chains to the main chain.[158] By contrast, in the synthesis of the PVA-g-PAA(8 – 10) samples characterised by constant N and different graft lengths, the kinetic matrix effect was observed at all ratios γ and constant $\alpha = 0.014$.[158]

Investigations revealing the kinetic matrix effect and its dependence on the density of growing chains were the first step in studies of the new phenomenon, the so-called matrix graft copolymerisation. In the next step, the structural matrix effect, which is also characteristic of matrix processes, should be established.[47]

V. System of intramolecular main chain – graft and graft – graft bonds as the main factor of stabilisation of the structures of intramolecular polycomplexes

The determination of the detailed structure and the number of intermolecular bonds in intermolecular polycomplexes is of great importance for an understanding of the mechanism of complex formation of polymers at the level of single contacts between active groups. Studies devoted to these problems, most of which were carried out by IR and NMR spectroscopy, are well known (see, for example, Refs 159 – 161). The above methods allow one also to reveal the dependence of the state of these polycomplexes on different factors, in particular, on the pH of the medium [162] and temperature.[163, 164] These studies are of particular importance for polycomplexes between non-ionic polymers, in which the number of bonds is impossible to estimate by simpler methods, for example, by potentiometric titration (which can be employed in investigations of polyelectrolytes).[113, 115 – 117]

Intramolecular bonds in graft copolymers, including those containing chemically complementary components, were not studied in detail, although IR and NMR spectroscopy was used in many investigations (see Refs 14, 103, 142, 144 and 165). The aim of these investigations has been to prove the formation of graft copolymers. However, studies of systems of intramolecular bonds and changes in these systems depending on the number (density) and molecular mass (length) of grafted chains are of fundamental importance for graft copolymers, which form intramolecular polycomplexes, the more so as these systems are formed already in the course of the synthesis of these copolymers (matrix effect). Hence, considerable attention has been given to this problem in studies of the PVA-g-PAA graft copolymers. Let us briefly discuss these results.

The validity of the assignment of graft copolymers to intramolecular polycomplexes was confirmed primarily by IR spectroscopy.[114, 129, 166] The IR spectra of thin films of PVA-g-PAA(1 – 3) (which differ in N) were thoroughly analysed using computer separation of vibrational bands in the Amide I and Amide II regions by the spline-function method, and the structures of the macromolecules of the graft copolymers were demonstrated to be stabilised by an extensive hydrogen bond network, including H-bonds between the main chain and grafted chains (as in the case of the corresponding intermolecular polycomplex) and H-bonds between the units of the grafted chains (*cis* – *trans*-multimers of amide groups).[129, 166] An increase in N led to substantial changes in this hydrogen bond network (Fig. 6).[129] Actually, in the PVA-g-PAA macromolecules containing a relatively small number of grafted chains ($N \leqslant 25$), the number of main chain – graft H-bonds was large, whereas the number of graft – graft H-bonds was relatively small (see Fig. 6 *a*). As N increased from 25 to 49 in the series of the copolymers under study, steric hindrance to thermodynamic affinity between PVA and PAA became more substantial. As a result, the number of H-bonds between the main chain and the grafts decreased, whereas the number of H-bonds between the drawn together grafted chains increased (see Fig. 6 *c*). In the case of an intermediate value of N ($N = 31$), H-bonds of both types occurred (see Fig. 6 *b*), which was unambiguously established by IR spectroscopy.[129]

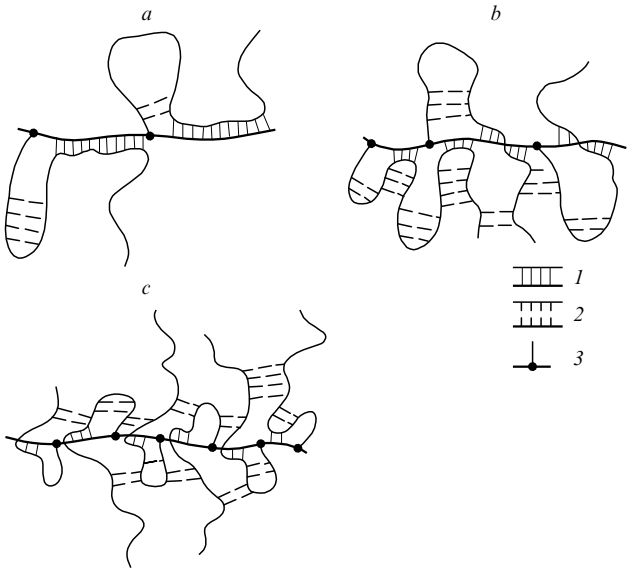

Figure 6. Redistribution of H-bonds in the PVA-g-PAA macromolecules at $N \leqslant 25$ (*a*), $N = 31$ (*b*) and $31 \leqslant N \leqslant 49$ (*c*).
(*1*) main chain – grafted chain H-bonds, (*2*) grafted chain – grafted chain H-bonds, (*3*) graft.

The influence of the molecular mass of the grafted chains on the hydrogen bond network was studied for a series of PVA-g-PAA(8 – 10) samples, in which N was held constant ($N = 9$). For this purpose, the spectra of thin films of the copolymers in the Amide I and Amide II regions were processed by the spline-function method. The spectra of these graft copolymers show all the Amide I bands which were observed in the spectra of the PVA – PAA intermolecular polycomplexes, including a band at 1670 cm^{-1} assigned to a sequence of H-bonds between PVA and PAA (see Section III).[167] Thus, it was proved that intramolecular polycomplexes are formed in macromolecules of the samples of the copolymers containing grafted chains of different lengths. It was found that the largest number of the main chain – graft H-bonds and the smallest number of the graft – graft H-bonds are characteristic of the PVA-g-PAA(9) sample containing the grafted chains with an intermediate molecular mass ($M_{v\,PAA}$ =

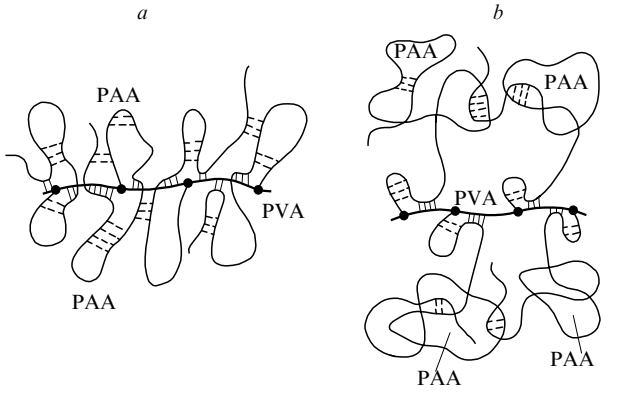

Figure 7. Scheme illustrating detachment of grafted chains from the main chain.
(*a*) $M_{v\,PAA} < M^*$, (*b*) $M_{v\,PAA} > M^*$; for notations of the elements in the scheme, see Fig. 6.

4.3×10^5). At $M_{v\,PAA} > 4.3 \times 10^5$, the hydrogen bond network in the copolymer changed as follows: the number of the main chain – graft H-bonds sharply decreased and the rigidity of the grafted chains, which was estimated from the increase in the effective length of the *trans*-multimers of amide groups, increased by a factor of more than 5. In fact, the effect of 'detachment' and stretching of the grafted chains in different directions away from the main chain was observed for polymers in which the molecular mass (length) of the grafted chains was higher than some critical value M^* (Fig. 7).[129, 167]

The above-described changes in the hydrogen bond network in PVA-g-PAA with increasing N and molecular masses of the grafted chains are reflected in all the properties of the intramolecular complexes under study.

VI. Influence of grafting density on the bulk structure and solution behaviour of intramolecular polycomplexes

The bulk structures of graft copolymers were studied in much less detail compared to their structures in solution and the structures of block copolymers. The majority of publications were devoted to graft copolymers containing thermodynamically incompatible components,[168–177] although studies of the bulk structures of graft copolymers containing chemically complementary main and grafted chains were also reported (see, for example, Ref. 25). To reveal the general and specific features of the bulk structure of PVA-g-PAA compared to the structures of other graft copolymers, let us discuss the results of the above-mentioned studies. It is known that incompatibility of components in linear block copolymers causes microphase separation to form the following regular supercrystalline structures: planar lamellas (if components are present in similar amounts), cylindrical or spherical domains, which are formed from the minor component as the percentage of the major polymer increases.[62] The state of the interface between the domains (sharp or extended) is determined by the molecular mass of the blocks. The higher the molecular mass, the higher the degree of segregation (degree of microphase separation) of the blocks and, correspondingly, the sharper the interface. The shift of the glass transition temperature of a separate microphase relative to T_g of the corresponding homopolymer is most often used as the measure of segregation of the blocks.[172, 174] A decrease in the degree of segregation of the blocks (an increase in the compatibility of the components of a block copolymer) is reflected in an increase in the shifts of T_g for the 'hard' and 'soft' microphases along the temperature scale toward each other.

In the case of star-like graft copolymers consisting of f branches, each of which is a diblock copolymer (for example, based on isoprene or butadiene as a 'soft' block and styrene or α-methylstyrene as a 'hard' block), the molecular masses of the blocks have a much lesser effect on the structure compared to the density of branches or the order of arrangement of the hard and soft blocks in the star (in the centre or at the periphery).[168–172] In particular, it was demonstrated[168–171] that the density of the branches (for f from 2 to 18) influences the structures of the star-like copolymers of isoprene (inner part of branching) and styrene (outer part of branching) with $w_{isoprene}/w_{styrene} = 0.7/0.3$ and the molecular mass of the grafted chains of $(2.3–10) \times 10^4$. Covalently non-bound branchings form a cylindrical supercrystalline structure, *viz*., long cylindrical domains of polystyrene (PS) in a polyisoprene (PIP) matrix. This structure was retained at a low density of branches ($f < 6$ and $M_n = 3.3 \times 10^4$). At higher values of f, the star structure sharply changed (both PS and PIP phases became uninterrupted). The PS blocks formed two interpenetrating tetrahedral lattices in a continuous matrix consisting of the PIP blocks. The role of the order of arrangement of the blocks in the star was considered in the study.[172] It was demonstrated that the microphases in the structures were nearly completely separated when the branched elastomeric block was located in the centre. By contrast, mixing of the components was observed when the hard block served as the branched central block.

The structures of traditional graft copolymers, in which one component serves as the main chain and another component serves as a graft, are determined not only by the density and the order of arrangement of the hard and soft blocks but also by the molecular mass of the grafted chains. This fact was supported by the results of the studies.[173–177] The authors of these studies reached the following common conclusion: the mutual mixing of the main and grafted chains increases with decreasing graft length and grafting density. Actually, irregular fractal-like microregions were observed in the structure of the PEA-g-PS graft copolymer, where PEA is poly(ethyl acrylate), at a low grafting density (on average, one grafted chain per main chain), whereas ordered lamellar microdomains were observed at a high density of rigid grafted chains (on average, three grafts per PEA chain).[173] Study of the PB-g-PS copolymer (PB is polybutadiene) by DSC revealed the effect of mutual mixing of the components (a substantial decrease in the glass transition temperature of PS in the copolymer compared to T_g of the homopolymer and a decrease in the crystallinity of PB) at a low grafting density.[174] However, this effect disappeared upon repeated heating of the sample (second scan). The glass transition temperature T_g for the PS microphase even increased (was 6–7 K higher than that of individual PS) with increasing grafting density. A substantial decrease in the difference between T_g for polydimethylsiloxane (PDMS) and PS was observed also for the PS-g-PDMS graft copolymers characterised by a low molecular mass of the grafts and low grafting density.[174] The degree of microphase separation also increased as each of these parameters increased. Analogous effects were observed for the graft copolymers of PEO onto PEA, PS, polyamide 12, copolymers of MA or MMA (MA is maleic anhydride and MMA is methyl methacrylate) and styrene and the ethylene – vinyl alcohol copolymer.[175–177] In all cases, the crystallinity of the PEO chains increased as the number of these chains grafted onto the main chain and their length increased.

X-Ray diffraction study of graft copolymers containing chemically complementary components, such as ST-g-PAA and AM-g-PAA (ST is starch and AM is amylose), revealed substantial mutual mixing of the main and grafted chains over a wide grafting-density range.[25] As a result, the main chain became uncrystallisable.

The structures of the PVA-g-PAA graft copolymers were studied by DSC[123, 129] and these results were compared with the analogous data for the individual polymers. In the case of a relatively small number of grafted chains ($N \leqslant 25$), the DSC thermograms (Fig. 8) show only one heat capacity jump, *i.e*., one glass transition (curves *1* and *2*), whose temperature $T_g = 459.5–463.5$ K (depending on the sample) was between the corresponding glass transition temperatures of PVA ($T_g = 331.5$ K) and PAA ($T_g = 464$ K). Taking into account the low PVA content in the graft copolymers (2.4 mass % –

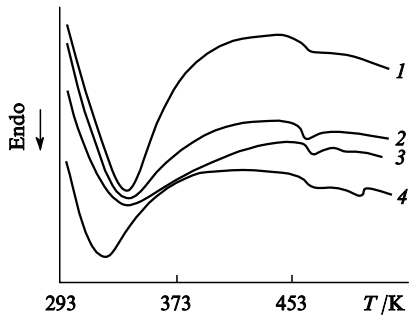

Figure 8. DSC thermograms (first scanning) for samples of PVA-g-PAA(7) (*1*), PVA-g-PAA(1) (*2*), PVA-g-PAA(2) (*3*) and PVA-g-PAA(3) (*4*).

4.0 mass %), this fact is indicative of complete compatibility of the polymer components in these samples of the copolymers and homogeneity of their structures. However, the second heat capacity jump appears in the thermograms of PVA-g-PAA at $N > 25$. This is indicative of the microphase separation in the structures of the copolymers. The height and temperature of the second heat capacity jump (second glass transition), which persisted after repeated heating–cooling cycles, increased with increasing N (see Fig. 8, curves *3* and *4*). It was established that microphase separation in the copolymers with a high grafting density is determined by the presence of compatibility regions of the polymer components along with domains formed by segments of grafted chains, which do not interact with the main chain because of steric hindrance. From the above, it can be concluded that compatibility between the main and grafted chains in graft copolymers which form intramolecular polycomplexes, is attained only for N smaller than some critical value N^* (in the series of graft copolymers under study, $N^* \approx 25$).[129]

Yet more evidence for the existence of intramolecular polycomplexes in the PVA-g-PAA(1–3) macromolecules and redistribution of hydrogen bonds with increasing N was obtained in the study of resistance of the copolymers to thermooxidative destruction by dynamic thermogravimetric analysis (DTGA). The mass-loss curves (TG curves) were processed on a computer to determine simultaneously three formally kinetic parameters of destruction steps (the total activation energy E, the reaction order n in each step and the frequency factor Z).[129, 166, 178] Three steps of thermooxidative destruction were revealed for all samples of the copolymers and for individual PVA and PAA (Fig. 9). The first step involves chemical transformations without participation of oxygen (dehydration of PVA chains, imidisation of PAA and some other conversions), as evidenced by endothermic effects in the DTA curves.

In the second step of destruction of the copolymers and PAA as well as at the end of the first step of PVA destruction, oxidation of polymer chains and accumulation of free radicals took place, which was immediately reflected in the sign of thermal effects in the DTA curves (the exothermic effect was observed instead of the endothermic effect). Bulk decomposition of the alkyl, alkoxy and peroxy radicals formed in the second step together with complete decomposition of polymer chains occurred in the final third step of destruction and was accompanied by the maximum exothermic effects.[129, 179]

The temperatures of the destruction onset (T_d) of most copolymers are intermediate between T_d for individual PVA and PAA. In the series of PVA-g-PAA(1–3) copolymers, the following changes in the parameters of destruction were observed with increasing N: a rise in the temperature of the destruction onset, an increase in the temperature ranges of the first (accompanied by the endothermic effect) and third (accompanied by the maximum endothermic effect) steps of destruction and an increase (by 92 °C) in the overall temperature range of destruction. The above-described effects are indicative of a substantial increase in resistance of graft copolymers to thermooxidative destruction with increasing number of grafted chains. Analysis of possible chemical transformations and free-radical processes in all steps of thermooxidative destruction of the polymers and the results of experimental studies of water solubility of polymer samples after thermal treatment under various conditions demonstrated that interchain cross-links, such as main chain–graft (interchain esters) and graft–graft (interchain imides) cross-links, are formed in the graft copolymers and PAA already before the onset of destruction and in its first step. Apparently, interchain cross-links formed in the PVA-g-PAA macromolecules with a low (Fig. 10 *a*) and high (Fig. 10 *b*) grafting density have different effects on further destruction. In the latter case, cross-linking between the adjacent grafted chains facilitates more substantial stabilisation of the coil as a whole. The cross-linked coil becomes poorly accessible for oxygen, and elimination of gaseous destruction products of the main and grafted chains is decelerated. This is the reason why thermal stability of the copolymers increases with increasing grafting density.[129, 179]

Interesting information was obtained in calculations of the formally kinetic parameters E, n and Z for the first step of destruction involving chemical transformations without the participation of oxygen (Table 3). In particular, for samples of the

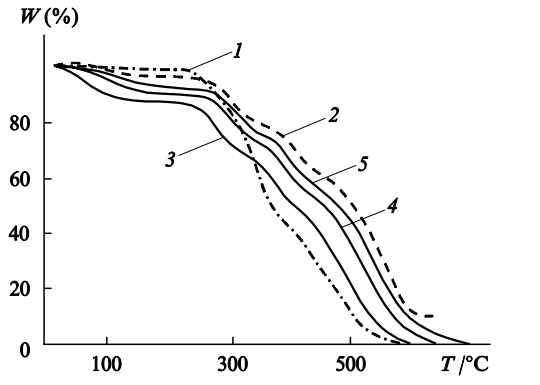

Figure 9. TG curves for PVA ($M_v = 4 \times 10^4$) (*1*), PAA ($M_v = 4.4 \times 10^6$) (*2*), PVA-g-PAA(1) (*3*), PVA-g-PAA(2) (*4*) and PVA-g-PAA(3) (*5*).

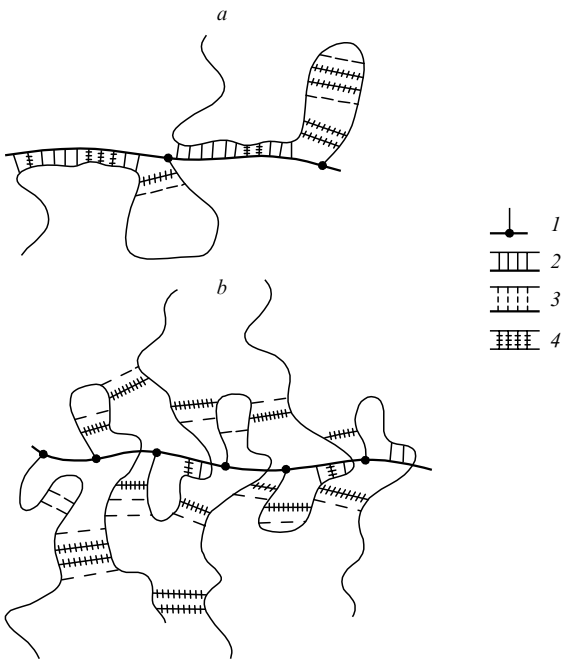

Figure 10. Schematic representation of interchain cross-links in the PVA-g-PAA macromolecules with low (*a*) and high (*b*) grafting density. (*1*) graft, (*2*) H-bonds between the main and grafted chains, (*3*) H-bonds between the units of PAA, (*4*) cross-links between the chains.

Table 3. Kinetic parameters of the first step of thermooxidative destruction of graft copolymers with different grafting densities.

Sample	E /kJ mol^{-1}	n	Z /s^{-1}	k /s^{-1} (see [a])
PVA	59.2	0.83	6.11×10^3	0.064
PAA	143.9	1.15	1.34×10^{12}	0.113
PVA-g-PAA(1)	182.2	2.36	6.9×10^{16}	0.174
PVA-g-PAA(2)	172.2	2.31	1.09×10^{15}	0.149
PVA-g-PAA(3)	139.1	1.63	6.05×10^{11}	0.140

[a] The rate constant calculated by the Arrhenius equation.

graft copolymers with $N \leqslant 25$, the parameters E, n and Z appeared to be substantially larger than the corresponding values for PAA. However, these parameters approach the corresponding parameters characteristic of PAA as N increases from 25 to 49. It is known that the parameters E and n for complex chemical processes [involving many competitive and(or) successive reactions] are integrated values. Hence, the above-mentioned substantial increase in these parameters in the first step of destruction of a PVA-g-PAA sample with a low grafting density (compared to PAA) is indicative of a specific structure in the macromolecules of these copolymers. The presence of intramolecular polycomplexes stabilised predominantly through main chain – graft H-bonds complicates chemical transformations and causes a sharp increase in the parameters E, n and Z in the first step of destruction of graft copolymers.[129, 179]

It should be noted that the results of systematic studies of thermal stability of graft copolymers and its relation to the grafting density, the molecular mass of grafted chains and thermodynamic affinity between polymer components are virtually absent from the literature. Using the results of investigations for PVA-g-PAA, we attempted to analyse the influence of not only the molecular mass of grafts and the grafting density but also of chemical complementarity between the polymer components on thermooxidative destruction of the graft copolymers. Of a few studies devoted to these problems, two investigations on thermal destruction (under an inert atmosphere) of graft copolymers containing chemically complementary components, such as ST (or AM) and PAA,[25] PVA and the AA – MMA copolymer,[103] are noteworthy. Thermal treatment of the ST-g-PAA and AM-g-PAA graft copolymers, in which only the molecular mass of the grafted chains was varied, was accompanied by several characteristic effects, such as a rise in the temperatures of the onset and completion of destruction with increasing molecular mass of PAA and an increase in thermal stability (extension of the temperature range of destruction) of graft copolymers compared to that of individual ST and AM.[25] An increase in thermal stability of the PVA-g-P(AA-co-MMA) graft copolymers compared to that of PVA was evidenced by the DTGA data obtained in the study.[103] Unfortunately, the authors of the cited studies did not report analogous results for individual PAA, which did not allow us to compare thermal stabilities of the graft copolymers and PAA. Resistance of the α-cellulose-g-PMMA graft copolymers, where PMMA is poly(methyl methacrylate), to destruction was examined by DTGA.[180] According to the results of an X-ray diffraction study, the components of these copolymers weakly interact with each other. In contrast to the above-described data, it was found that thermal stability of the α-cellulose-g-PMMA graft copolymers decreases with increasing amount of grafted PMMA. However, this fact remains to be explained.

Let us consider the change in ability of PVA-g-PAA to swell and dissolve in water depending on the number N of grafted chains. In the course of swelling and dissolution, all characteristic features of the chemical structures of the polymers, their molecular, supermolecular and macroscopic structures, the phase state and thermodynamic affinity for a particular solvent reveal themselves. The results of investigations of these properties are widely used for characterisation of the structures of graft copolymers.[21, 34, 63, 88, 104, 144] These studies are of particular importance for copolymers containing chemically complementary polymer components, because the formation of a cooperative system of bonds between these components sharply decreases accessibility of the active groups of the components for a solvent. Swelling and dissolution of films of PVA-g-PAA(1 – 3) and (for comparison) PAA in water (the thickness of the film of the copolymer was ~ 23 μm) were studied using a specially developed procedure.[181, 182] It should be noted that samples of the graft copolymers and PAA were characterised by the virtually equal amounts of hydrophilic groups (0.0141 – 0.0143 mol g^{-1}). However, the behaviour of the graft copolymers in the course of swelling and dissolution in water differs substantially from that of PAA. The PVA-g-PAA(1) sample with a low grafting density ($N = 25$) appeared to be the least hydrophilic of all the polymers under study. Among the above-mentioned three copolymers, this sample has the largest number of main chain – graft H-bonds. As N increased, the rates of swelling and dissolution of the films increased, the thickness of the polymer layer that remained undissolved (after 24 h) decreased and the degree of its swelling diminished due to a decrease in the number of H-bonds between the main and grafted chains. Therefore, thermodynamic affinity of the copolymers for water increased with increasing N.

The state of PVA-g-PAA in aqueous solutions was studied [129, 166, 183] by static light scattering. The molecular and thermodynamic parameters of the light-scattering coils were determined from the Zimm plots by the double extrapolation method. Only samples of PVA-g-PAA(2, 3) with $N \geqslant 31$, which spontaneously dissolved in water at room temperature, were examined. It was found that the PVA-g-PAA(2) and PVA-g-PAA(3) macromolecules occur as aggregates even in dilute solutions, which is attributable to low values of the second virial coefficient A_2. The latter, though it increases with increasing N (Table 4), remains close to zero, which is typical of θ solvents. This result is reasonable taking into account that PVA-g-PAA is an intramolecular polycomplex. Solubility of the copolymers in water noticeably increases with increasing N, as evidenced by an increase in A_2 and a decrease in both Z and $\langle R^2 \rangle_z^{1/2}$. Such behaviour of the graft copolymers in solutions is consistent with the above-described effect of a successive decrease in the number of main chain – graft H-bonds with increasing grafting density.

It was demonstrated [129, 183] that the grafting density influences substantially the hydrodynamic and optical characteristics of PVA-g-PAA(1 – 3) in water. Studies by viscosimetry and light scattering (by determining the depolarisation coefficients of scattered light) showed that the characteristic viscosity of solutions and the Huggins constant decrease, whereas the crossover concentration and optical anisotropy of the coils in water increase with increasing number of grafts.

Table 4. Molecular and thermodynamic characteristics of graft copolymers with different grafting densities.

$10^{-6} M_w$ (see [a])	$10^{-6} M_{w\,PVA\text{-}g\text{-}PAA}$	N	Z [b]	$10^{11} A_2$ /m^3 mol kg^{-2}	$\langle R^2 \rangle_z^{1/2}$ /nm (see [c])
Sample of PVA-g-PAA(2)					
29.07	2.49	37	12	−2.04	362
Sample of PVA-g-PAA(3)					
7.84	3.92	49	2	3.46	193

[a] The mass-average molecular mass of scattering particles. [b] Number of macromolecules in the aggregate. [c] The z-average radius of gyration of the coil.

In aqueous solutions of intermolecular polycomplexes, segregation of the bound parts of active groups of polymers through hydrophobic interactions gives rise to compact particles of the polycomplexes with developed hydrophobic regions [115, 131] or leads to phase separation of the system analogously to that observed for stoichiometric polyelectrolyte complexes.[116] Hence, it was of interest to examine this stabilisation factor in the intramolecular polycomplexes under consideration. The contribution of hydrophobic interactions to stabilisation of the structures of intramolecular polycomplexes in water was estimated by benzene solubilisation.[129, 183] The results of these studies not only confirmed that such stabilisation occurs but also demonstrated that the role of this factor substantially decreases with increasing N. Actually, the volume of hydrophobic regions in the PVA-g-PAA(1 – 3) series decreased from 794 to 98 nm^3 (per macromolecule) as N increased from 25 to 49, which correlates with

improvement of thermodynamic quality of water serving as the solvent for this series of polymers.

Therefore, a decrease in the grafting density in the PVA-g-PAA copolymers in an aqueous medium is accompanied by strong aggregation (self-assembly) of the coils of the graft copolymers to form increasingly dense and hydrophobic particles of intramolecular polycomplexes. A substantial increase in the density of aggregates with decreasing N is supported by the fact that the changes in the parameters Z and $\langle R^2 \rangle_z^{1/2}$ (see Table 4) in going from PVA-g-PAA(2) to PVA-g-PAA(3) occur at substantially different rates. Analysis of the published data demonstrated that a decrease in viscosity of aqueous solutions of the graft copolymers with increasing grafting density is typical also of other copolymers involving chemically complementary components, for example, of the dextran-g-PAA copolymer.[81, 96] However, taking into account all the above, this fact is attributable to the influence of the grafting density on complex formation between the main and grafted chains rather than to the known fact that an increase in branching leads to deterioration of thermodynamic quality of a solvent for branched macromolecules.[184, 185]

The results obtained for PVA-g-PAA provide a new insight into the fundamental principles of the state-of-the-art statistical theories of graft copolymers, which have been developed in the context of general theoretical analysis of a series of similar systems commonly referred to as polymer brushes.[62] Evidently, these theories are valid for graft copolymers containing incompatible or weakly interacting polymer components.

According to these theories, the role of the main chain (matrix) is reduced to merely a spatial factor (a 'sphere' and a 'cylinder' for star-like and comb-like graft copolymers, respectively), while the possible contributions of interactions between the main and grafted chains to the free energy are ignored. Hence, it was concluded that the state of grafted chains at a low grafting density, *i.e.*, in the absence of their overlapping, should be close to the state of an isolated chain in the same solvent.[62] As demonstrated above, an opposite situation is observed for the PVA-g-PAA graft copolymers. As the grafting density decreases, the grafted chains nestle against the main chain, which is accompanied by sharp deterioration of the quality of the solvent, segregation of hydrophobic binding regions of active groups and aggregation of macrocoils. In fact, the macrocoil as a whole undergoes collapse. However, only collapse of grafted chains is considered in the above-mentioned statistical theories.[62] This is yet another drawback restricting application of such theories to graft copolymers which form intramolecular polycomplexes. It should be noted that the effect of shrinkage of particles of intermolecular polycomplexes through strong interactions between polymeric partners (collective collapse) is well known.[47, 115–117]

Therefore, the collapse of a macrocoil as a whole, which occurs due to complex formation of the main and grafted chains, and the collapse of the main or grafted chains, which occurs due to incompatibility of the polymer components (for example, in a selective solvent), should be distinguished for graft copolymers which form intramolecular polycomplexes. Our results agree with the predictions made in the study.[92] Actually, a decrease in the grafting density leads to strengthening of thermodynamic affinity between PVA and PAA.

Investigation of the changes in the state of the PVA-g-PAA macromolecules in solution induced by factors able to destroy an H-bond network (*i.e.*, intramolecular polycomplex) is of special interest. Among these factors, the temperature[186–188] and the hydrodynamic shear field[189, 190] were examined. The complex extreme dependence $[\eta] = f(T)$ was found and the Huggins constant was demonstrated to decrease in parallel with increasing temperature. A sharp decrease in $[\eta]$ to a minimum (Fig. 11 *a*) and the corresponding sharp increase in the Huggins constant (Fig. 11 *b*) in a narrow temperature range of 303–308 K, which is virtually independent of N, are indicative of the possible conformational transition in the copolymer macromolecules. Analogous extreme temperature dependences of $[\eta]$ were observed

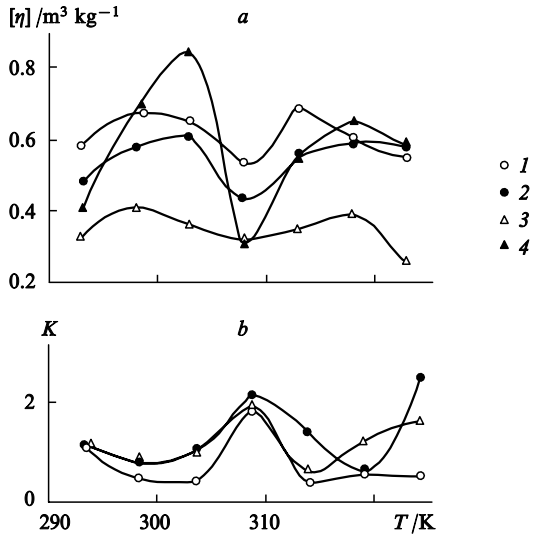

Figure 11. Temperature dependences of the characteristic viscosity (*a*) and the Huggins constant (*b*) for PVA-g-PAA(7) (*1*), PVA-g-PAA(4) (*2*), PVA-g-PAA(5) (*3*) and PVA-g-PAA(6) (*4*) (c = 0.4 kg m^{-3}).

also for a series of other graft copolymers containing chemically complementary polymer components, for example, for AC-g-PAA in acetic and formic acids,[85] DAC-g-PAA (DAC is diacetylcellulose) in formic acid [70] and PVA-g-PEO in water.[105]

The occurrence of the conformational transition in the macromolecules of PVA-g-PAA(7) (for this sample, the largest decrease in $[\eta]$ was observed) was confirmed by the results of investigations of solutions of this copolymer by quasielastic laser light scattering.[186–188] The correlation function of scattered light in a dilute solution of the graft copolymer was measured at different temperatures. The diffusion-coefficient distribution was calculated from these data using the corresponding regularisation procedure. The bimodal distribution on the diffusion coefficients was revealed (Fig. 12). Taking into account the rigid structure of coils of the copolymer, the characteristic narrow molecular-mass distribution and the criterion $\boldsymbol{q}R_g > 1$ ($\boldsymbol{q}$ is the scattering vector and R_g is the radius of gyration of macroparticles), which was maintained in the experiment, the bimodality of the distribution curves was interpreted as a sum of two exponential contributions to the normalised correlation function. The contributions are attributable to translational motion and translational-rotational motion of scattering particles,[129, 188]

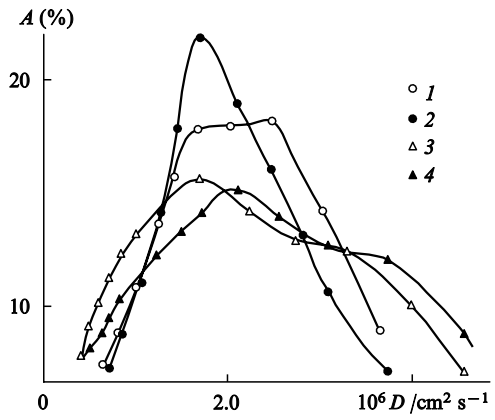

Figure 12. Distribution curves on the diffusion coefficients for PVA-g-PAA(7) at 298 (*1*), 303 (*2*), 308 (*3*) and 313 K (*4*).
A is the contribution of particles characterised by a particular diffusion coefficient to the total scattering intensity.

Table 5. Diffusion parameters of PVA-g-PAA(7) at different temperatures.

T /K	$10^{10} D_t$ /m^2 s^{-1}	$10^{-3} D_r$ /s^{-1}
298	1.8	3.5
303	1.7	2.6
308	1.7	8.2
313	2.1	7.4

$$g_1(t) = A_0(\boldsymbol{q})\exp(-\Gamma_0 t) + A_1(\boldsymbol{q})\exp(-\Gamma_1 t).$$

Here $\Gamma_0 = D_t\boldsymbol{q}^2$ and $\Gamma_1 = D_t\boldsymbol{q}^2 + 6\,D_r$ are the time constants of the exponential components of the correlation function, D_t and D_r are the effective coefficients of translational and rotational diffusion. Changes in the temperature caused the following changes in the state of the PVA-g-PAA(7) macromolecules. An increase in the temperature to $\sim$303 K led to swelling of the macrocoils due to partial cleavage of the main chain – graft H-bonds, which was accompanied by a decrease in asymmetry of the coils (increase in D_r, see Table 5) and, correspondingly, to a decrease in the contribution of the translational-rotational mode to the total scattering intensity. In the range $\sim 303 < T < 308$ K, the rupture of a large number of H-bonds led to a sharp contraction (collapse) of the coils and an increase in their asymmetry (an increase in D_r, see Table 4) because of poor solubility of PVA in water compared to PAA. This transformation was referred to as an intramolecular polycomplex $\rightleftarrows$ segregated state transition (Fig. 13).[186] A further increase in the temperature was accompanied by swelling of asymmetrical coils. The depth of conformational changes, which can be estimated as a decrease in the characteristic viscosity, was found to depend on N. The smallest changes were observed for PVA-g-PAA(6), which is characterised by the largest grafting density ($N = 42$) compared to all the other samples prepared in this experiment. This result can be attributable to substantial stretching of the main chain with a high grafting density.[62] Consequently, the ability of the main chain to be contracted on collapse is limited due to volume effects. It should be noted that no changes in [η] were observed [34] for the PVA-g-PVPD copolymer containing strongly interacting polymer components, and low viscosity persisted over a wide temperature range. Evidently, the reason is stability of intramolecular hydrogen bonding at high temperatures (in the temperature range under study).

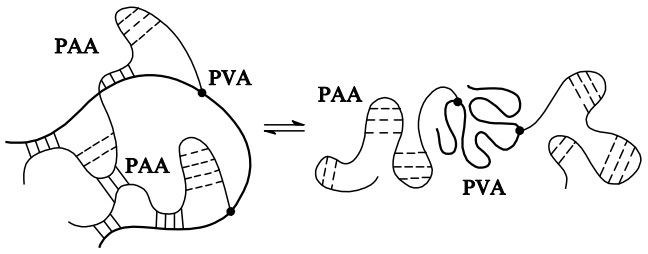

Figure 13. Scheme of the conformational transition in the PVA-g-PAA macromolecules on heating.
For notations of the elements in the scheme, see Fig. 6.

The influence of hydrodynamic shear field on the structure of PVA-g-PAA in solutions was studied on a rheo-viscometer equipped with coaxial cylinders. A non-traditional behaviour of solutions of the copolymers was observed in hydrodynamic fields.[189, 190] This is illustrated by Figs 14 and 15, which show the dependences of the effective viscosity of solutions of PVA-g-PAA(2) on the shear rate gradient and the concentration dependences of the reduced viscosity of these solutions. At relatively high

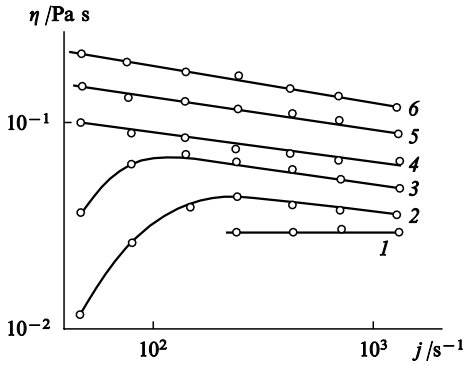

Figure 14. Plot of the effective viscosity of solutions of PVA-g-PAA(2) *vs.* the shear rate gradient.
The concentrations of the solutions /kg m^{-3}: (*1*) 0.5, (*2*) 1, (*3*) 2, (*4*) 3, (*5*) 4, (*6*) 5; $T = 298$ K.

concentrations ($c \approx 3-5$ kg m^{-3}), typical non-Newtonian flow was observed for all copolymers. At lower concentrations ($c \approx 1-3$ kg m^{-3}), the flow curves have a maximum, whose position is determined by N and c. In a dilute solution ($c \approx 0.5$ kg m^{-3}), the viscosities at small shear rate gradients j were initially low to an extent that they were beyond the sensitivity limits of the instrument. However, the viscosity of the solution sharply increased (ten – hundred times) at a critical value of j^*.[189, 190] The largest value of j^* (243 s^{-1}) is characteristic of the PVA-g-PAA(2) copolymer. According to the IR spectroscopic data, this copolymer had the largest number of main chain – graft and graft – graft bonds (see Fig. 6 *b*). It should be emphasised that all flow curves were completely reversible. A substantial reversible increase in viscosity of solutions with increasing j (negative thixotropy) indicates that the PVA-g-PAA macromolecules exhibit viscoelastic properties due to destruction of an H-bond network (destruction of the intramolecular complex) induced by the hydrodynamic field.

The critical concentration c^*, below which the intramolecular polycomplex was destroyed, was determined from the concentration dependences of the reduced viscosity of solutions of the copolymers at different j, which were calculated with the use of flow curves.[189, 190] The critical concentrations c^* in the PVA-g-PAA(1 – 3) series changed in parallel with the crossover concentration and increased from 2 to 4 kg m^{-3} with increasing grafting density. Hence, two levels of reversible destruction of PVA-g-PAA in solutions induced by the hydrodynamic shear field were revealed. At the first level, a network of pinnings is destroyed. In the second deeper level, the intramolecular polycomplexes along with primary aggregates are destroyed (Fig. 16).

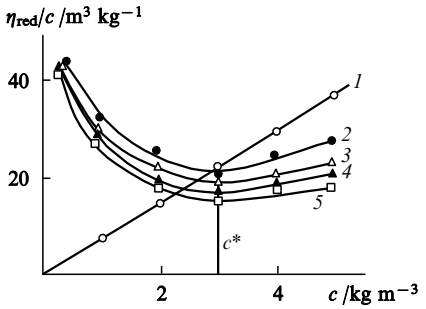

Figure 15. Concentration dependences of the reduced viscosity of solutions of PVA-g-PAA(2) at j of 49 (*1*), 146 (*2*), 437 (*3*), 729 (*4*) and 1312 (*5*) s^{-1};
η_{red} is the reduced viscosity, c and c^* are the concentration and the critical concentration of the solutions, respectively.

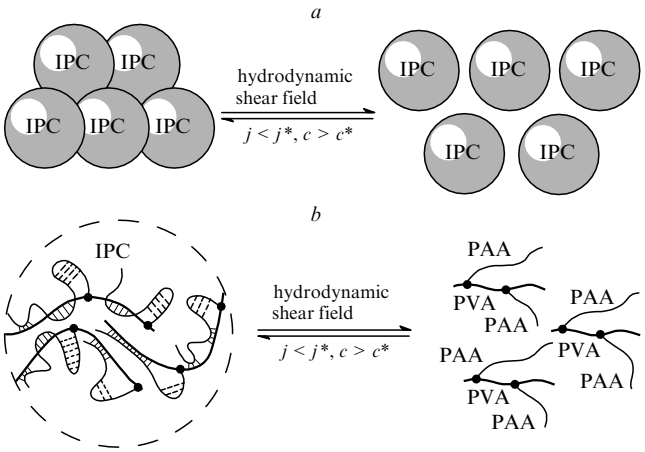

Figure 16. First (*a*) and second (*b*) levels of destruction of PVA-g-PAA structure induced by hydrodynamic shear field.
IPC is intramolecular polycomplex.
The critical values are marked with an asterisk.

Interestingly, rheological studies revealed exclusively non-Newtonian (pseudoplastic) flow for a series of other graft copolymers containing chemically complementary polymer components. These results were obtained, in particular, for the dextran-g-PAA,[81,96] ST-g-PAA, AM-g-PAA,[25] PVA-g-PMAA,[87] P(AA-co-AA)-g-PEO[106] and PAA-g-PEO copolymers.[105] However, taking into account high molecular masses of the samples under study ($\sim 2-6\times10^6$), high concentrations of the solutions used in measurements ($\sim 2-30$ kg m^{-3}) and the fact that PVA-g-PAA exhibits viscoelastic properties only in dilute solutions, the above-described result for these graft copolymers seems to be reasonable.

VII. Characteristic features of the structures and properties of intramolecular polycomplexes depending on the graft length

The molecular mass (length) of grafted chains is an important parameter, which allows one to control the structure and properties of graft copolymers. However, the role of this parameter is poorly understood. First attempts to reveal the influence of this factor on the thermodynamic properties and behaviour of graft copolymers in solutions have been made in the studies.[68,70] The 'pure' influence of the molecular mass of grafted chains is difficult to reveal because of the necessity to prepare and study samples, which should be characterised by the same grafting density and a narrow molecular-mass distribution of the grafts. This problem has attracted increasing interest in recent years because graft copolymers can be synthesised starting from macromonomers with controlled chain length. The results of the studies[148,176] devoted to the influence of the molecular mass and the grafting density of PEO on the bulk structures of PMA-g-PEO [PMA is poly(methyl acrylate)], PMMA-g-PEO and PS-g-PEO were discussed above. Among investigations of graft copolymers in solutions, several interesting systematic studies have been undertaken to reveal the role of the molecular mass and the density and distribution of hydrophobic hydrocarbon grafted chains (in comb-like copolymers with PEO[26] or with the AA – MA copolymer[27,28]) in their aggregation in an aqueous medium. Studies by static light scattering, fluorescence spectroscopy and rheology demonstrated that an increase in the concentration of solutions was accompanied by a characteristic transition from intramolecular aggregation of hydrophobic branchings to intermolecular aggregation for all the above-mentioned copolymers. This transition was shifted to lower concentrations and was attended by a sharper and sharper increase in viscosity of the solution as the length and number of neighbouring hydrophobic tails increased. In many other studies (see, for example, Ref. 31), the molecular mass and the number of grafted chains (PMMA) in graft copolymers were varied with the aim of solving single-purpose problems (in particular, for the purpose of enhancing the strength of two-component polyurethane coatings). Analogous systematic studies of the role of the molecular mass of grafted chains in graft copolymers containing chemically complementary components are few.

When studying the structure and state of the PVA-g-PAA(8 – 10) samples which are characterised by the constant number but different molecular masses of the PAA chains, in solutions, our main interest was to elucidate how the effect of 'detachment' of the grafted chains from the main chain at $M_{v\,PAA} > M^*$ (which was revealed by IR spectroscopy) is reflected in the properties of the copolymers.

The above-mentioned phenomenon was confirmed primarily by the structure studies of these copolymers by DSC.[191] The DSC thermograms of the PVA-g-PAA(8, 9) samples with $M_{v\,PAA} \leqslant 4\times10^5$ show only one heat capacity jump (Fig. 17, curves *1* and *2*), *i.e.*, these copolymers are characterised by complete compatibility of the polymer components. The DSC thermogram of the PVA-g-PAA(10) sample with $M_{v\,PAA} = 5.1\times10^5$ has already two heat capacity jumps (curve *3*), which is indicative of the microphase separation in the structure of this copolymer. One microphase ($\sim 85\%$) corresponds to regions of compatibility of the polymer components, whereas another microphase ($\sim 15\%$) corresponds to domains formed by segments of PAA, which are 'detached' from the main chain.[129,191]

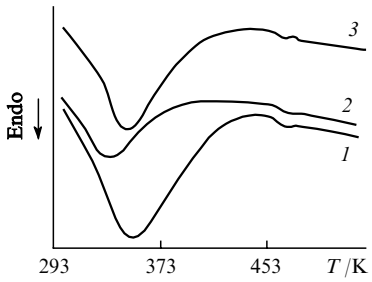

Figure 17. DSC thermograms for PVA-g-PAA(8) (*1*), PVA-g-PAA(9) (*2*) and PVA-g-PAA(10) (*3*).

Three main steps of thermooxidative destruction were revealed for these copolymers by TGA.[191] The temperatures of the onset of destruction of the copolymers were close to the analogous temperature for PAA but lower than that for PVA. The parameters of destruction changed with increasing $M_{v\,PAA}$ as follows: (1) the temperature of the onset of destruction rose; (2) the temperature of completion of destruction increased; (3) the temperature range of the first step of destruction (accompanied by the endothermic effect) became narrower; (4) the temperature range of the third step of destruction (accompanied by the maximum exothermic effect) decreased; (5) the overall temperature range of destruction decreased.

Hence, an increase in the molecular mass of the grafted chains led, on the one hand, to a slight growth of thermal stability of the copolymers (an increase in the temperature of the onset of destruction) but, on the other hand, to an increase in the rate of their complete decomposition. The latter fact is indicative of loosening of the PVA-g-PAA structure with increasing $M_{v\,PAA}$, due to which different elements of the structure become more accessible for oxygen, removal of gaseous decomposition products becomes easier and, that is why, thermooxidative destruction is accelerated. These data actually confirm the effect of 'detachment' of the grafts from the main chain. The parameters E, n and Z of the first two steps of destruction were calculated using

computer processing of the TG curves. In the first step, in which chemical processes occur without the involvement of oxygen, the parameters E, n and Z pass through a maximum for PVA-g-PAA(9) with $M_{v\,PAA} = 4.3 \times 10^5$ with increasing $M_{v\,PAA}$. This fact is in complete agreement with the maximum number of the main chain – graft H-bonds in this graft copolymer compared to those in all other samples of PVA-g-PAA under study and indicates that complicated chemical transformations occur in the first step of destruction of this copolymer.

The properties of copolymers containing grafted chains with different molecular masses were studied also by light scattering.[167] All samples of the series under consideration are water-soluble at room temperature. According to the results obtained with the use of the Zimm plots (Table 6), the thermodynamic quality of water with respect to the copolymers was improved (the parameter A_2 increased) with increasing $M_{v\,PAA}$. At the same time, the number of macromolecules in aggregates and their radius of gyration reached minimum values for PVA-g-PAA(9), which was characterised by an intermediate value of $M_{v\,PAA}$ (4.3×10^5) and existed in water in the molecular-disperse state. Two other copolymers occurred as aggregates, which differed from each other in the packing density of segments. It was demonstrated [129, 167] that loose swollen aggregates of the copolymer containing grafted chains with the highest molecular mass ($M_{v\,PAA} = 5.1 \times 10^5$) were formed due to 'detachment' of the grafted chains from the main chain and improvement of the quality of the solvent, in contrast to compact aggregates of PVA-g-PAA(8) with $M_{v\,PAA} = 3.72 \times 10^5$.

Table 6. Results obtained by light scattering for graft copolymers containing grafted chains with different molecular masses ($N = 9$).

Sample	$10^{-6} M_w$	$10^{-4} M_{w\,PVA\text{-}g\text{-}PAA}$	Z	$10^9 A_2$ (see [a])	$\langle R^2 \rangle_z^{1/2}$ /nm
PVA-g-PAA(8)	6.92	3.46	2	1.18	299
PVA-g-PAA(9)	3.81	3.81	1	1.55	253
PVA-g-PAA(10)	18.83	4.71	4	1.66	777

[a] In m^3 kmol kg^{-2}.

The depolarisation coefficients of scattered light were determined at $\theta = 0$ and $c = 0$ (θ is the scattering angle and c is the concentration of the solution), and aggregates (or macromolecules) of all samples of the copolymers in the series under consideration were demonstrated to be optically isotropic in water (the optical anisotropy is equal to zero).[129, 167] According to the results of viscometric measurements at 298 K, an increase in $M_{v\,PAA}$ in the series of PVA-g-PAA(8 – 10) leads to a successive increase in the Huggins constant, and the parameter $[\eta]$ passes through a small minimum. These results correlate qualitatively with the data obtained by static light scattering.

The results of measurements of benzene solubilisation in solutions of the copolymers were somewhat unexpected.[192] Actually, an increase in $M_{v\,PAA}$ to 4.3×10^5 did not lead to a substantial change in the amount of benzene in the bound state. However, a further increase in the molecular mass of the grafted chains to 5.1×10^5 led to a sharp increase in solubilisation. To account for this effect, the contributions to solubilisation determined, first, by dispersion interactions of benzene with hydrophobic regions (the contribution of S_d) and, second, by binding of benzene to proton-donor groups of the polymer through H-bonding (the contribution of S_H) were considered.[129, 192] Then the UV spectra of benzene in water and solutions in ethanol, PAA and the PVA-g-PAA(10) sample containing the grafted chains of maximum length were measured. These studies revealed an increase in the intensity of the characteristic absorption band of benzene at $\lambda = 260$ nm in solutions of the graft copolymer. Taking into account this fact, it was concluded that the above effect is associated with a sharp increase in the amount of H-bound benzene in swollen coils of this sample of PVA-g-PAA.

Investigation of the temperature dependence of $[\eta]$ in solutions of the above-mentioned samples of the graft copolymers demonstrated [192] that the PVA-g-PAA(10) sample, in which the grafted chains are 'detached' from the PVA chain, has the lowest temperature of the onset of conformational transition. The deepest conformational changes (a sharp decrease in $[\eta]$ in the transition region) took place in the macromolecules of the copolymer characterised by the intermediate value of $M_{v\,PAA}$ (4.3×10^5). As mentioned above, these macromolecules possessed the largest number of main chain – graft H-bonds.

VIII. Functional capabilities of intramolecular polycomplexes

It is known that intermolecular polycomplexes can adsorb various organic compounds, ions, colloidal particles and biopolymers from solutions.[115 – 117, 131, 193] Such versatility is due to the fact that these polycomplexes contain hydrophobic binding regions of the polymer components and hydrophilic cavities formed by loops of non-bound polymer units and, in addition, to the possibility of self-adjustment of the system, *i.e.*, changes in the hydrophilic – hydrophobic balance in the polycomplex particle in the course of sorption, due to which the best results can be obtained.[115, 116, 193] However, intermolecular polycomplexes have drawbacks as binding agents because of the existence of a complex formation equilibrium at the macromolecular level. Hence, these complexes can be destroyed to individual components in highly dilute solutions,[115] under the action of strong competitive agents [116] or under changes in external conditions (for example, temperature or pH of the solution).[115 – 117] In this respect, intramolecular polycomplexes, in which the interacting polymer components are additionally linked by covalent bonds, hold more promise. Due to the absence of an equilibrium at the macromolecular level, intramolecular polycomplexes are not destroyed to individual polymers even under conditions of competitive binding of the sorbed compound to just one of the components. Presently, high binding ability of intramolecular polycomplexes is used for the construction of macromolecular therapeutic systems providing prolonged action of drugs.[14, 16, 21, 88, 103]

Films of the PVA-g-PAA intramolecular polycomplex can efficiently (and selectively) adsorb phenol from water (Fig. 18). Detailed investigation of this phenomenon [194, 195] made it possible to construct highly efficient sensors for measuring phenol in natural water.

Graft copolymers containing chemically complementary polymer components are promising as flocculants. Actually, a higher flocculating ability of the graft copolymers of PAA onto oxyethylcellulose and amylopectin compared to PAA with the same molecular mass was observed in the study.[196] Later on, graft

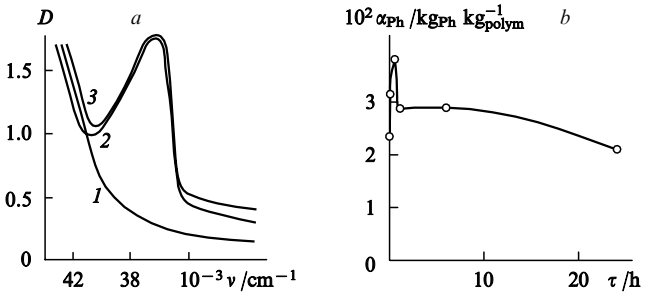

Figure 18. UV spectra (*a*) of the starting thermally treated film of PVA-g-PAA(2) (*1*) and a film kept in an aqueous solution of phenol ($c = 10$ kg m^{-3}) for 4 (*2*) and 5 (*3*) min and the change in the amount of phenol in the bound state (α_{Ph}) at $T = 293$ K calculated from the above data (*b*).

copolymers of acrylamide and acrylic acid onto water-soluble cellulose derivatives were tested and covered by patents as flocculants for clearing of water and conditioning of precipitates of waste-water treatment facilities.[5]

Numerous examples of the use of graft copolymers as flocculants were offered in the literature. In particular, graft copolymers of PAA onto polysaccharides, such as sodium alginate, starch and its components (amylose and amylopectin), were studied.[6, 7, 109, 110, 197, 198] Their flocculating ability was tested using kaolin suspensions, waste waters from the pulp-and-paper industry and waste waters obtained upon iron ore processing and in the course of concentration of 10% iron ore slurry. It was found that the copolymer of PAA grafted onto branched amylopectin is the most efficient of all the flocculants studied.[109, 110, 197] A series of samples of this copolymer containing different amounts of grafted chains with different molecular masses was studied. Unfortunately, detailed characteristics of these copolymers are lacking in the literature. However, it was noted that both a decrease in the grafting density and an increase in the graft length lead to enhancement of the flocculating effect.

Highly efficient non-ionic Unicomfloc^{intra} flocculants were developed based on the PVA-g-PAA intramolecular polycomplex for clarification of highly turbid clay suspensions [199] and preparation of drinking water at water treatment plants.[200] The effect of one sample of these flocculants in coagulative–flocculative clearing of river water is compared with that of the known Magnafloc LT-27 flocculant (Allied Colloids, UK) in Table 7. The efficiency of the individual coagulant (aluminium sulfate) and coagulant–flocculant pairs was estimated taking into account the main characteristics of the quality of water, such as turbidity, chromaticity, permanganate oxidisability and the content of residual aluminium. The advantages of the Unicomfloc^{intra} flocculants are their ability to perform complex purification of water from suspended substances of both natural and anthropogenic origin, such as phenol [201, 202] and ^{137}Cs radionuclides.[203]

Semidilute aqueous solutions of the PVA-g-PAA intramolecular polycomplex exhibit a substantial negative thixotropic effect. Thus, these solutions become thickened on slight stirring and occur in this state for several hours. As mentioned above, the reason is that a hydrodynamic field induces reversible destruction of the polycomplex. Substantial reversible thickening of solutions of the copolymers induced by a hydrodynamic shear field can serve as a basis for the development of a special type of thickening agents providing high viscosity of a solution only for a desired period of time.

Graft copolymers containing chemically complementary main and grafted chains are highly efficient agents for drag reduction of turbulent flow.[42, 44, 82, 112] For example, PVA-g-PAA samples containing a small polymer additive at $Re = 5 \times 10^3 - 5 \times 10^4$ show a drag reduction of turbulent flow $W \approx 60\%$ (Fig. 19 *a*). A somewhat higher efficiency in drag reduction of turbulent flow ($W \approx 65\% - 68\%$ at $Re = 1.4 \times 10^4$) was achieved with the use of particular samples of CMC-g-PAA (CMC is carboxymethylcellulose) and ST-g-PAA.[82] The activity of the above copolymers decreases substantially with increasing density and decreasing molecular mass of the grafted chains. It is important that solutions of these graft copolymers not only exhibit high hydrodynamic activity but are also resistant to degradation induced by turbulent flow (see Fig. 19 *b*, curve *1*), as distinguished from solutions of high-molecular-weight PEO (curve *2*) and PAA.[204] It should be noted that the time interval between two adjacent points in the curves in Fig. 19 *b* corresponds to the time during which a polymer solution was passed once through a capillary of a rheometer, and the total number of points corresponds to the number of repeated cycles of exposure of the solution to turbulent flow. Hence, resistance of solutions of PVA-g-PAA (as well as of CMC-g-PAA, ST-g-PAA and other graft copolymers, which form intramolecular polycomplexes) to degradation is determined by the fact that the macromolecules of the copolymers can rapidly and virtually completely restore their original molecular and supermolecular structures under conditions when the action of a strong hydrodynamic field is periodically interrupted. Reversibility of destruction of PVA-g-PAA in solution, which is also observed in usual rheological experiments, distinguishes these graft copolymers from PEO and PAA and is indicative of the existence of a special force, which restores the system to its original state after termination of the action of a hydrodynamic field. Undoubtedly, this is thermodynamic affinity between the main and grafted chains.

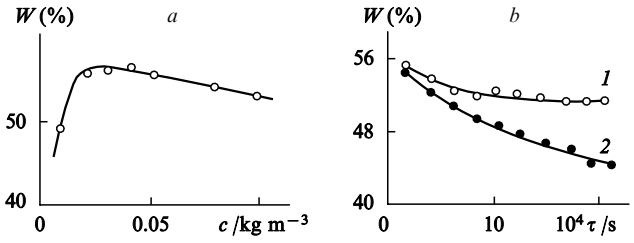

Figure 19. Drag reduction of turbulent flow *vs.* the concentration of PVA-g-PAA(7) (*a*) and the time of hydrodynamic field action of solutions of PVA-g-PAA(7) (*1*) and PEO (*2*) ($M_v = 6 \times 10^6$ at $T = 293$ K) (*b*).

Table 7. Efficiency of the clearing effect of the coagulant (aluminium sulfate) and different coagulant–flocculant pairs {a water sample from the Desna river: $T = 15$ °C, the turbidity was 4.3 mg dm^{-3}, the chromaticity was 37 deg (Cr–Co scale), the alkalinity was 3.65 mg-equiv. dm^{-3}, pH 8.2, $[NH_3] = 0.26$ mg dm^{-3}, the permanganate oxidisability was 9.1 mg dm^{-3}}.

Sample of a flocculant	Amount /mg dm^{-3} (see [a])		Turbidity /mg dm^{-3}	Chromaticity /deg (Cr–Co scale)	Oxidisability /mg dm^{-3}	c_{Al} /mg dm^{-3} (see[b])
	$Al_2(SO_4)_3$	flocculant				
–	–	–	2.5[c]	31	9.1	–
–	5	–	1.3	23	9.1	0.39
–	10	–	0.8	15	8.1	0.25
–	20	–	0.5	11	7.2	0.16
Magnafloc LT-27	5	0.1	1.3	17	7.2	0.32
	10	0.1	0.8	13	5.7	0.25
	20	0.1	0.3	9	5.0	0.15
Unicomfloc^{intra}	5	0.1	1.0	13	5.8	0.28
	10	0.1	0.5	9	5.2	0.17
	20	0.1	0	5	4.8	0.09

[a] The concentration of chlorine water was 4.8 mg dm^{-3}. [b] The concentration of residual aluminium. [c] The parameters of the starting water after clarification for 3 h.

IX. Conclusion

To summarise, graft copolymers containing chemically complementary main and grafted chains, such as PVA-g-PAA, belong to a special class of polymer compounds, which may be classified as intramolecular polycomplexes. Their structures and properties in the bulk state and solutions are determined by intramolecular H-bonds of the main chain – graft and graft – graft types. The formation of intramolecular polycomplexes occurs, evidently, already in the course of free-radical graft copolymerisation of PAA onto PVA. Hence, the synthesis of PVA-g-PAA belongs to the category of matrix processes. At a too-high density of the growing grafted chains (about three grafts per 100 units of the main chain), the matrix effect (which is reflected in an increase in the rate of graft copolymerisation compared to that of AA homopolymerisation) decreases.

An increase in the density and(or) molecular mass of the grafted chains is accompanied by redistribution of H-bonds in the PVA-g-PAA macromolecules toward a decrease in the number of main chain – graft bonds and an increase in the number of bonds between the grafted chains. As a result, the structure of graft copolymers in the bulk state retains homogeneity only up to some critical mutually dependent values of N^* and M^*. At higher N and(or) molecular masses of the grafted chains, the structures of the copolymers contain ordered microregions (domains) formed by segments of PAA along with compatibility regions of the polymer components. Due to steric hindrance (at $N > N^*$) and(or) overlapping and interactions between long grafted chains (at $M_{PAA} > M^*$) at large distances from the main chain, these PAA segments cannot realise their thermodynamic affinity for PVA, and, hence, the PAA segments form an individual microphase in the PVA-g-PAA structure. Evidently, this type of microphase separation cannot be considered as a criterion for thermodynamic incompatibility between polymer components involved in graft copolymers.

Thermodynamic affinity between the main and grafted chains is responsible for reversibility of cleavage of an H-bond network and, correspondingly, destruction of the molecular and supermolecular structure of the PVA-g-PAA macromolecules in solution induced by temperature and hydrodynamic shear field. This fact is responsible for high resistance of solutions of PVA-g-PAA and other analogous graft copolymers to degradation in turbulent flow.

Graft copolymers which form intramolecular polycomplexes composed of chemically complementary polymer components additionally linked by covalent bonds, possess high binding ability. This provides, in particular, high flocculating ability of PVA-g-PAA as well as of the known graft copolymers of PAA onto polysaccharides in clearing of various suspensions and natural water.

References

1. A Holmberg, L Piculell, B Wesslen *J. Phys. Chem.* **100** 462 (1996)
2. A Holmberg, P Hansson, Z Piculell, P Linse *J. Phys. Chem. B.* **103** 10 807 (1999)
3. Y Lu, H Xie *Acta Polym. Sci.* 325 (2000)
4. H D Bijsterbosh, M A Cohen Stuart, G J Fleer *J.Colloid Interface Sci.* **210** 37 (1999)
5. V A Molotkov, V I Kurlyankin, S I Klenin, G V Shishkina, in *Vsesoyuznaya Konferentsiya 'Koagulyanty i Flokulyanty v Ochistke Prirodnykh i Stochnykh Vod' (Tez. Dokl.), Kiev, Odessa, 1988* [All-Union Conference 'Coagulants and Flocculants in Treatment of Natural and Waste Waters' (Abstracts of Reports), Kiev, Odessa, 1988] p. 140
6. T Tripathy, R P Bhagat, R P Singh *Eur. Polym. J.* **37** 125 (2001)
7. R P Singh, T Tripathy, G P Karmakar, S K Rath, N C Karmakar, S R Pandey, K Kannan, S K Jain, N T Lan *Curr. Sci.* **78** 798 (2000)
8. J Z Willett, M A Kotnis, G S O'Brien, G F Fanta, S H Gordon *J. Appl. Polym. Sci.* **70** 1121 (1998)
9. F J Hua, C P Hu *J. Polym. Sci., Part A* **37** 3568 (1999)
10. D Gersappe, D Irvine, A C Balazs, Y Lin, J Sokolov, M Rafailovich, S Schwatz, D G Periffer *Science* **265** 1072 (1994)
11. D Li, D Jia, P Zhou *J. Appl. Polym. Sci.* **93** 420 (2004)
12. J Zhou, F Yan *J. Appl. Polym. Sci.* **93** 948 (2004)
13. P Artursson, L Brown, J Dix, P Goddard, K Petrak *J. Polym. Sci., Part A* **28** 2651 (1990)
14. X-H Peng, J-P Du, M-J Wang, Q Lu *Fine Chem.* **17** 137 (2000)
15. R Maureen *Chem. Eng. News* **77** 63 (1999)
16. D M Disley, J Blyth, D C Cullen, H-X You, S Eapent, C R Lowe *Biosens. Bioelectron.* **13** 383 (1998)
17. I Castellano, I Goni, M C Ferrero, A Munoz, R Jimenez-Castellanos, M Gurruchaga *Drug Dev. Ind. Pharm.* **25** 1249 (1999)
18. I Castellano, I Goni, M Gurruchaga, I Goni *Carbohydr. Polym.* **34** 83 (1997)
19. C Ming-Qing, S Takeshi, A Mitsuru *Polym. Adv. Technol.* **10** 120 (1999)
20. US P. 5 374 336; *Ref. Zh. Khim.* 7 F 127P (1996)
21. N Kubota, T Matsuhara, Y Eguchi *J. Appl. Polym. Sci.* **70** 1027 (1998)
22. T Nonaka, T Yoda, S Kurihara *J. Polym. Sci., Part A* **36** 3097 (1998)
23. A Zouahri, A Elmidaoui, B Ameduri, Y Hervaud, B Boutevin *Eur. Polym. J.* **38** 2247 (2002)
24. C L McCormick *J. Macromol. Sci. A* **22** 955 (1985)
25. G P Karmakar, R P Singh, in *Proceedings of the SPE International Symposium on Oilfield Chemistry, Houston, TX, 1997* p. 739
26. F Liu, Y Frere, J Francois *Polymer* **42** 2969 (2001)
27. G L Smith, C L McCormick *Macromolecules* **34** 918 (2001)
28. G L Smith, C L McCormick *Macromolecules* **34** 5579 (2001)
29. E I Kuryatnikov, V N Kislenko *Zh. Prikl. Khim.* **73** 1530 (2000) [a]
30. S Kovuttikulrangsie, K Sahakaro, C Intarakong, P Klinpituksa *J. Appl. Polym. Sci.* **93** 833 (2004)
31. Y Matsuno, T Adachi, N Numa *Prog. Org. Coat.* **35** 117 (1999)
32. Md I H Mondal, R Alam, Md Abu Sayeed *J. Appl. Polym. Sci.* **92** 3622 (2004)
33. N Abidi, E Hequet *J. Appl. Polym. Sci.* **93** 145 (2004)
34. G C Eastmond, M Gibas, W F Pacynko, J Paprotny *J. Membr. Sci.* **207** 29 (2002)
35. N I Shtan'ko, V Ya Kabanov, P Yu Apel', O L Orelovich, A I Vilenskii, A L Tolstikhina *Preprint of Joint Institute for Nuclear Research, Dubna, 1999* No. R18-99-281
36. I Iosito *Khemen* **27** 777 (1989); *Ref. Zh. Khim.* 15 S 286 (1990)
37. A Bismarck, M Pfaffemoschke, M Selimovic, J Springer *Colloid Polym. Sci.* **276** 1110 (1998)
38. L P Razumovskii, N Yu Mosina, T V Druzhinina, V G Zaikov, G S Gal'braikh *Zh. Prikl. Khim.* **64** 2373 (1991) [a]
39. O H Kwon, Y C Nho, K D Park, Y H Kim *J. Appl. Polym. Sci.* **71** 631 (1999)
40. M Gurruchaga, I Goni, M Valero, G M Guzman *Polymer* **33** 2860 (1992)
41. C Wan-Lin, S R Kenneth *Macromolecules* **32** 6298 (1999)
42. S Ungeheuer, H-W Bewersdorff, R P Singh *J. Appl. Polym. Sci.* **37** 2933 (1989)
43. S R Deshmukh, K Sudhakar, R P Singh *J. Appl. Polym. Sci.* **43** 1091 (1991)
44. N P Mel'nik, T B Zheltonozhskaya, L N Momot, I A Uskov *Dokl. Akad. Nauk Ukr. SSR, Ser. B* (11) 50 (1988)
45. G Carrot, J C Valmalette, C J G Plummer, S M Scholz, J Dutta, H Hofmann, J G Hilborn *Colloid Polym. Sci.* **276** 853 (1998)
46. H El-Hamshary, S Al-Sigeny *J. Appl. Polym. Sci.* **93** 630 (2004)
47. I M Papisov *Vysokomol. Soedin., Ser. B* **39** 562 (1997) [b]

48. A D Pomogailo, A S Rozenberg, I E Uflyand *Nanochastitsy Metallov v Polimerakh* (Metal Nanoparticles in Polymers) (Moscow: Khimiya, 2000)
49. N Tsubokawa, T Umeno *J. Jpn. Soc. Colour Mater.* **64** 751 (1991)
50. Y Shirai, N Tsubokawa *React. Funct. Polym.* **32** 153 (1997)
51. N Tsubokawa, K Kawatsura, T Kanemaru, H Fukui *J. Jpn. Soc. Colour Mater.* **71** 156 (1998)
52. Y Shirai, K Kawatsura, N Tsubokawa *Prog. Org. Coat.* **36** 217 (1999)
53. J Liu, R Pelton, A N Hrymak *J. Colloid Interface Sci.* **227** 408 (2000)
54. Y Shen, S Zhy, R Pelton *Macromolecules* **34** 5812 (2001)
55. O B Shibanova, Yu G Medvedevskikh, S A Voronov, V S Tokarev, M Stamm, E M Antipov *Vysokomol. Soedin., Ser. A* **44** 424 (2002) [b]
56. M L Rong, Q L Ji, M Q Zhang, K Friedrich *Eur. Polym. J.* **38** 1573 (2002)
57. M-I Baraton, F Chancel, L Merhari *Nanostruct. Mater.* **9** 319 (1997)
58. Ukr. P. 36 528; *Promislova Vlastnist'* (6) (2003)
59. Ukr. P. 44 968 A; *Promislova Vlastnist'* (3) (2002)
60. G Mino, S A Kaizerman *J. Appl. Polym. Sci.* **31** 122 (1958)
61. J R Elliott (Ed.) *Macromolecular Syntheses* (New York, London, Sydney: Wiley, 1966)
62. T M Birshtein, V M Amoskov *Vysokomol. Soedin., Ser. C* **42** 2286 (2000) [b]
63. J Ruhe, M Ballauff, M Biesalski, P Dziezok, F Grohn, D Johannsmann, N Houbenov, N Hugenberg, R Konradi, S Minko, M Motornov, R R Netz, M Schmidt, C Seidel, M Stamm, T Stephan, D Usov, H Zhang *Adv. Polym. Sci.* **165** 79 (2004)
64. A Hult, M Johansson, E Malmstrom *Adv. Polym. Sci.* **143** 1 (2003)
65. Z Tuzar, P Kratochvil *Adv. Colloid Interface Sci.* **6** 201 (1976)
66. K M Munmaya *J. Macromol. Sci., Part C* **22** 471 (1982 – 1983)
67. D J McDowall, B S Gupta, V T Stannett *Prog. Polym. Sci.* **10** 1 (1983)
68. E A Bekturov, S A Tashmukhamedov, Kh I Akbarov, in *Monomery i Polimery* (Monomers and Polymers) (Alma-Ata: Nauka, 1985) p. 110
69. S A Tashmukhamedov, Kh I Akbarov, R S Tillaev *Usp. Khim.* **55** 1920 (1986) [*Russ. Chem. Rev.* **55** 1094 (1986)]
70. S A Tashmukhamedov, R S Tillaev, Kh I Akbarov, G Khamrakulov *Termodinamicheskie Svoistva Rastvorov Privitykh Sopolimerov* (Thermodynamic Properties of Solutions of Graft Copolymers) (Tashkent: FAN, 1989)
71. S A Ezzell, C L McCormic, in *Water Soluble Polymers. Synthesis, Solution Properties and Applications (ACS Sym. Ser.)* No. 467 (Eds S Shalaby, C L McCormic, J B Butler) (Washington, DC: American Chemical Society, 1991) p. 130
72. K A Devis, K Matyjaszewski *Adv. Polym. Sci.* **159** 1 (2002)
73. J J Freire *Adv. Polym.Sci.* **143** 35 (1999)
74. Forster, V Abetz, A H E Muller *Adv. Polym. Sci.* **166** 173 (2004)
75. J Bohrisch, C D Eisenbach, W Jaeger, H Mori, A H E Muller, M Rehahn, C Schaller, S Traser, P Wittmeyer *Adv. Polym. Sci.* **165** 1 (2004)
76. A Hill, F Candau, J Selb *J. Progr. Colloid Polym. Sci.* **84** 61 (1991)
77. R A Wallace, D G Young *J. Polym. Sci., Part A-1* **4** 1179 (1966)
78. D Staszewska *Makromol. Chem.* **176** 2481 (1975)
79. V I Kurlyankina, S I Klenin, S Ya Lyubina, V A Molotkov, A V Troitskaya, I Ya Strelina *Vysokomol. Soedin., Ser. A* **18** 997 (1976) [a]
80. R H Wade *A Study of Molecular Parameters Influencing Polymer Drug Reduction. Report NUC TP473, Naval Undersea Center, San Diego, CA, 1975*
81. C L McCormick, L S Park *J. Polym. Sci., Polym. Chem. Ed.* **19** 2229 (1981)
82. S R Deshmukh, R P Singh *J. Appl. Polym. Sci.* **32** 6133 (1986)
83. N P Mel'nik, L N Momot, I A Uskov *Dokl. Akad. Nauk Ukr. SSR, Ser. B* (6) 48 (1987)
84. S A Tashmukhamedov, Sh A Azizov, A Sh Karabaev, E T Tsagaraev, R S Tillaev, Kh U Usmanov *Vysokomol. Soedin., Ser. A* **18** 2171 (1976) [b]
85. S A Tashmukhamedov, B U Sagdullaev, P P Larin, R S Tillaev, Kh U Usmanov *Vysokomol. Soedin., Ser. A* **16** 1395 (1974) [b]
86. F F Nurgalieva, Z G Sagdieva, S A Tashmukhamedov, R S Tillaev *Vysokomol. Soedin., Ser. B* **28** 37 (1986) [b]
87. A A Sarkisyan, G A Gabrielyan, L S Gal'braikh in *Vodorastvorimye Polimery i Ikh Primenenie (Tez. Dokl. 3 Vsesoyuz. Konf.), Irkutsk, 1987* [Water-Soluble Polymers and Their Applications (Abstracts of Reports of the Third All-Union Conference), Irkutsk, 1987] p. 44
88. N A Peppas, J Klier *J. Controlled Release* **16** 203 (1991)
89. T R Fang, L C Ji, J G Yu, L Y Wang, S X Xu *Polym. Bull.* **29** 71 (1992)
90. T Shibanuma, T Aoki, K Sanui, N Ogata, A Kikuchi, Y Sakurai, T Okano *Macromolecules* **33** 444 (2000)
91. A B Scranton, J Klier, N A Peppas *J. Polym. Sci. B* **29** 211 (1991)
92. A Halperin *Europhys. Lett.* **4** 439 (1987)
93. D Staszewska, M Bohdanecky *Eur. Polym. J.* **17** 245 (1981)
94. I Kaur, S Maheshwari, A Gupta, B N Mistra *J. Appl. Polym. Sci.* **58** 835 (1995)
95. D H Staszewska *Polim.-Tworz. Wielkoczasteczkowe* **31** 301 (1986)
96. C L McCormic, L S Park *J. Appl. Polym. Sci.* **30** 45 (1985)
97. S I Klenin, S F Bartoshevich, L G Revel'skaya, V I Kurlyankina *Vysokomol. Soedin., Ser. B* **28** 534 (1986) [b]
98. S F Bartoshevich, E N Bykova, V A Molotkov, S I Klenin *Vysokomol. Soedin., Ser. B.* **31** 747 (1989) [b]
99. S F Bartoshevich, G V Shishkina, V E Potapenko, V A Molotkov, S I Klenin *Vysokomol. Soedin., Ser. A* **31** 2477 (1989) [b]
100. B Abd El-Hady, M M Ibrahim *J. Appl. Polym. Sci.* **93** 271 (2004)
101. J-M Chem, W-F Lee, M-Y Hsieh *J. Appl. Polym. Sci.* **92** 3651 (2004)
102. H Kubota, N Shiobara *React. Funct. Polym.* **37** 219 (1998)
103. S Mishra, A Panda, B C Singh *J. Appl. Polym. Sci.* **73** 677 1999)
104. L J Bromberg *J. Phys. Chem. B* **102** 10736 (1998)
105. S C De Vos, M Moller *Macromol. Shem., Macromol. Symp.* **73** 223 (1993)
106. K Ulbrich, C Konak, Z Tuzar, J Kopecek *Makromol. Chem.* **188** 1261 (1987)
107. J Virtanen, C Baron, H Tenhu *Macromolecules* **33** 336 (2000)
108. N Chourdakis, G Bokias, G Staikos *J. Appl. Polym. Sci.* **92** 3466 2004)
109. S K Rath, R P Singh *J. Appl. Polym. Sci.* **66** 1721 (1997)
110. R P Singh, G P Karmakar, S K Rath, N C Karmakar, S R Pandey, T Tripathy, J Panda, K Kanan, S K Jain, N T Zan *Polym. Eng. Sci.* **40** 46 (2000)
111. F F Nurgalieva, Z G Sagdieva, R S Tillaev *Vysokomol. Soedin., Ser. A* **32** 772 (1990) [b]
112. N P Mel'nik, T B Zheltonozhskaya, L N Momot, I A Uskov, M M Matveenko *Ukr. Khim. Zh.* **56** 539 (1990)
113. T B Zheltonozhskaya, L N Podolyak, B V Eremenko, I A Uskov *Vysokomol. Soedin., Ser. A* **29** 2487 (1987) [b]
114. T B Zheltonozhs'ka, N P Mel'nik, L M Momot, I O Uskov *Ukr. Khim. Zh.* **59** 658 (1993)
115. V A Kabanov, I M Papisov *Vysokomol. Soedin., Ser. A* **21** 243 (1979) [b]
116. V A Izumrudov, A B Zezin, V A Kabanov *Usp. Khim.* **60** 1570 (1991) [*Russ. Chem. Rev.* **60** 792 (1991)]
117. J Xia, P Z Dubin, in *Macromolecular Complexes in Chemistry and Biology* Ch. 15 (Ed. P Z Dubin) (Berlin, Heidelberg: Springer, 1994) p. 247
118. E P Ageev, S L Kotova, E E Skorikova, A B Zezin *Vysokomol. Soedin., Ser. A* **38** 323 (1996) [b]
119. T V Budtova, N G Bel'nikevich, N P Ivanova, V A Kuznetsova, E F Panarin, Yu N Panov, A Ya Sorokin, S Ya Frenkel' *Vysokomol. Soedin., Ser. A* **33** 1664 (1991) [b]

120. V Yu Baranovskii, G S Georgiev, V A Kabanov *Vysokomol. Soedin., Ser. A* **31** 486 (1989) [b]
121. O V Nikolaeva, Z F Zoolshoev, T V Budtova, Yu V Brestkin, S Ya Frenkel' *Vysokomol. Soedin., Ser. B* **37** 1945 (1995) [b]
122. R J Hefford *Polymer* **25** 979 (1984)
123. O V Demchenko, N V Kutsevol, T B Zheltonozhskaya, V G Syromyatnikov *Macromol. Symp.* **166** 117 (2001)
124. T Zheltonozhskaya, L Momot, N Permyakova, O Demchenko, S Philipchenko, V Syromyatnikov, in *Polymers of Special Applications, Radom, Poland, 2002* p. 250
125. O Demchenko, T Zheltonozhskaya, N Permyakova, V Syromyatnikov, in *Polymers of Special Applications, Radom, Poland, 2002* p. 127
126. N M Permyakova, T B Zheltonozhskaya, O V Demchenko, L N Momot, S A Filipchenko, V G Syromyatnikov *Ukr. Khim. Zh.* **68** 57 (2002)
127. N Permyakova, T Zheltonozhskaya, O Demchenko, L Momot, S Filipchenko, N Zagdanskaya, V Syromyatnikov *Pol. J. Chem.* **76** 1347 (2002)
128. N M Permyakova, T B Zheltonozhskaya, O V Demchenko, L N Momot, S A Filipchenko, N E Zagdanskaya, V G Syromyatnikov *Ukr. Khim. Zh.* **68** 123 (2002)
129. T B Zheltonozhskaya, Doctoral Thesis in Chemical Sciences, Kyiv National University, Kyiv, 2003
130. T B Zheltonozhskaya, N P Mel'nik, L N Momot, V I Pavlov, N V Kutsevol, B V Eremenko *Bionika* **26** 123 (1993)
131. I M Papisov, A A Litmanovich *Macromolecular Reactions* (New York: Wiley, 1995)
132. V A Izumrudov, S Kh Lim. *Vysokomol. Soedin., Ser. A* **44** 793 (2002) [b]
133. T C Chung *Prog. Polym. Sci.* **27** 39 (2002)
134. K C Gupta, S Sahoo *J. Macromol. Sci. A.* **37** 447 (2000)
135. I Casinos *Polymer* **33** 1304 (1992)
136. M J Yanjarappa, S Sivaram *Prog. Polym. Sci.* **27** 1347 (2002)
137. J Gao, J Yu, W Wang, L Chang, R Tian *J. Macromol. Sci. A* **35** 483 (1998)
138. E-S A Hegazy *Polymer* **33** 96 (1992)
139. M Ohralander, R Palmgren, A Wiesen, A-C Albertsson *J. Polym. Sci.* **37** 1659 (1999)
140. O Sanli, S Aytemiz, I Unal Halil *J. Macromol. Sci. A* **34** 1003 (1997)
141. S Liu, A Sen *Macromolecules* **33** 5106 (2000)
142. H Chang-guo, W Xiao-long, H Zhi-giang, Y Sheng-kang *J. Funct. Polym.* **13** 169 (2000)
143. A Hebeish, A Waly, F A Abdel-Mohdy, A S Aly *J. Appl. Polym. Sci.* **66** 1029 (1997)
144. B Hazer *J. Macromol. Sci.: Macromol. Rep. A* **32** 477 (1995)
145. S-D Lee, F Sanda, T Endo *J. Polym Sci.* **37** 1041 (1999)
146. K Matyjaszewski, K L Beers, A Kern, S G Gaynor *J. Polym. Sci. A* **36** 823 (1998)
147. K Ishizu, K Tsubaki, A Mori, S Uchida *Progr. Polym. Sci.* **28** 27 (2003)
148. H-Q Xie, D Xie *Prog. Polym. Sci.* **24** 275 (1999)
149. E I Kuryatnikov, V N Kislenko, A A Berlin *Vysokomol. Soedin., Ser. B* **40** 1219 (1998) [b]
150. K E Russell *Prog. Polym. Sci.* **27** 1007 (2002)
151. G P Belov, D G Belov, N G Vasilenko, A M Muzofarov, D K Polyakov, A V Rebrov, N P Bessonova, E V Konyukhova, A N Ozerin *Vysokomol. Soedin., Ser. A* **39** 396 (1997) [b]
152. A R Eckert, S E Webber *Macromolecules* **29** 560 (1996)
153. V N Kislenko, A A Berlin *Vysokomol. Soedin., Ser. A* **33** 546 (1991) [b]
154. V N Kislenko *J. Colloid Interface Sci.* **209** 136 (1999)
155. J Yong Tan *Prog. Polym. Sci.* **19** 561 (1994)
156. B A Dolgoplosk, E I Tinyakova *Okislitel'no-Vosstanovitel'nye Sistemy kak Istochniki Svobodnykh Radikalov* (Redox Systems as Sources of Free Radicals) (Moscow: Nauka, 1972)
157. P Aravindakshan, A Bhatt, V G Kumar *J. Appl. Polym. Sci.* **66** 397 (1997)
158. N E Zagdanskaya, T B Zheltonozhskaya, V G Syromyatnikov *Voprosy Khim. Khim. Tekhnol.* **3** 53 (2002)
159. V V Annenkov, N L Mazyar, V A Kruglova *Vysokomol. Soedin., Ser. A* **43** 1308 (2001) [b]
160. P Smith, A Eisenberg *Macromolecules* **27** 545 (1994)
161. T B Zheltonozhskaya, V M Kharlanov, G S Pop, B V Eremenko, I A Uskov *Ukr. Khim. Zh.* **59** 987 (1993)
162. Q Liu, J R Du Wijn, C A Van Blitterswijk *Eur. Polym. J.* **33** 1041 (1997)
163. G T Zhumadilova, A D Gazizov, L A Bimendina, S E Kudaibergenov *Polymer* **42** 2985 (2001)
164. X Zhang, K Takegoshi, K Hikichi *Polymer* **33** 718 (1992)
165. J-P Gao, Z-C Li, M-Z Huang *J. Appl. Polym. Sci.* **55** 1291 (1995)
166. T Zheltonozhskaya, O Demchenko, N Kutsevol, L Momot, V Syromyatnikov, in *Polymers of Special Applications, Radom, Poland, 2002* p. 242
167. T Zheltonozhskaya, O Demchenko, I Rakovich, J-M Guenet, V Syromyatnikov *Macromol. Symp.* **203** 173 (2003)
168. D B Alward, D J Kinning, E Z Thomas *Macromolecules* **19** 215 (1986)
169. D J Kinning, E L Thomas, D B Alward, L J Fetters, D L Handlin *Macromolecules* **19** 1288 (1986)
170. E L Thomas, D B Alward, D J Kinning, D C Martin *Macromolecules* **19** 2197(1986)
171. T Hashimoto, Y Ijishi *J. Chem. Phys.* **89** 2463 (1988)
172. N M Bol'bit *Vysokomol. Soedin., Ser. A* **35** 255 (1993) [b]
173. M Rabeony, D G Peiffer, S K Behal, M Disko, W D Dozier *J. Chem. Soc., Faraday Trans.* **91** 2855 (1995)
174. V A Bershtein, V M Egorov, in *Differentsial'naya Skaniruyushchaya Kalorimetriya v Fizikokhimii Polimerov* (Differential Scanning Calorimetry in Physical Chemistry of Polymers) (Leningrad: Khimiya, 1990) p. 119
175. H Derand, P Sannasch, B Wesslen *J. Polym. Sci. A.* **36** 803 (1998)
176. H-Q Xie, J Liu, D Xie *Eur. Polym. J.* **25** 1119 (1989)
177. L Yan, X Hongquan *Petrochem. Technol.* **21** 295 (1992)
178. O V Demchenko, T B Zheltonozhskaya, V V Shilov, Yu P Gomza, V G Syromyatnikov, in *Proceedings of the 2nd International Conference on Carpathian Euroregion Ecology, Miskolc-Lillafured, Hungary, 1997* p. 190
179. N V Kutsevol, T B Zheltonozhskaya, O V Demchenko, L R Kunitskaya, V G Syromyatnikov *Vysokomol. Soedin., Ser. A* **46** 839 (2004) [b]
180. P Das, C N Saikia, N N Dass *J. Appl. Polym. Sci.* **92** 3471 (2004)
181. O V Demchenko, T G Ezhova, T B Zheltonozhskaya, V V Skripka, V G Syromyatnikov, in *Materialy Kompleksa Nauchnykh Meropriyatii Stran SNG* (Proceedings of the Set of Scientific Actions of the Commonwealth of Independent States) (Odessa: NPO 'VOTUM', 1997) Pt. 2, p. 45
182. O O Romankevich, T G Ezhova, O V Demchenko, T B Zheltonozhskaya, V L Budzinskaya, V G Syromyatnikov, in *Rozvitok Virobnitstva Novikh Visokoefektivnikh Koagulyantiv i Flokulyantiv ta Tekhnologii ikh Vprovadzhennya u Praktiku Ochishchennya Prirodnikh i Stichnikh Vod (Trudy Nauchno-Prakticheskoi Konferentsii), Kiev, 1998* [Development of Production of New High-Performance Coagulants and Flocculants and Technology of Their Practical Application for Treatment of Natural and Waste Waters (Proceedings of Scientific and Practice Conference), Kyiv, 1998] p. 27
183. T B Zheltonozhskaya, O O Romankevich, N V Kutzevol, V G Syromyatnikov, in *Proceedings of the 2nd International Conference on Carpathian Euroregion Ecology, Miscolc-Lillafured, Hungary, 1997* p. 149
184. J F Douglas, J Rovers, K F Freed *Macromolecules* **23** 4168 (1990)
185. C Ioan, S Ioan *J. Macromol. Sci., Pure Appl. Chem. A* **32** 1589 (1995)
186. T B Zheltonozhskaya, N P Melnik, S G Ostapchenko, D A Gavruschenko, B V Eremenko *Ukr. Polym. J.* **4** 37 (1995)

187. T Zheltonozhskaya, N Kutsevol, N Melnik, V Syromyatnikov, in *Polymers of Special Applications, Radom, Poland, 2002* p. 60
188. N Kutsevol, T Zheltonozhskaya, N Melnik, J-M Guenet, V Syromyatnikov *Macromol. Symp.* **203** 201 (2003)
189. T B Zheltonozhskaya, O V Demchenko, N V Kutsevol, T V Vitovetskaya, V G Syromyatnikov *Macromol. Symp.* **166** 255 (2001)
190. T B Zheltonozhs'ka, N V Kutsevol, T V Vitovets'ka, O V Demchenko, V G Syromyatnikov *Ukr. Khim. Zh.* **68**121 (2002)
191. O Demchenko, T Zheltonozhskaya, J-M Guenet, S Filipchenko, V Syromyatnikov *Macromol. Symp.* **203** 183 (2003)
192. N Zagdanskaya, L Momot, T Zheltonozhskaya, J-M Guenet, V Syromyatnikov *Macromol. Symp.* **203** 193 (2003)
193. V A Kabanov *Vysokomol. Soedin., Ser. A* **36** 183 (1994) [b]
194. O V Demchenko, T B Zheltonozhskaya, V G Syromyatnikov, N V Strilchuk, V N Yashchuk, V Yu Kudrya *Funct. Mater.* **7** 711 (2000)
195. V Yu Kudrya, V N Yashchuk, L P Paskal, T B Zheltonozhskaya, O V Demchenko *Macromol. Symp.* **166** 249 (2001)
196. R S Burr, C F Fanta, W M Doane *Starke* **27** 313 (1975)
197. S K Rath, R P Singh *Colloids Surf., A* **139** 129 (1998)
198. T Thipathy, R P Singh *Eur. Polym. J.* **36** 1471 (2000)
199. Ukr. P. 23 743; *Promislova vlastnist'* (11) (2001)
200. Ukr. P. 29 933; *Promislova vlastnist'* (3) (2002)
201. O V Demchenko, T B Zheltonozhskaya, N V Kutsevol, V G Syromyatnikov, I I Rakovich, O O Romankevich *Chem. Inz. Ekol.* **8** 463 (2001)
202. N V Kutsevol, T B Zheltonozhskaya, O V Demchenko, L N Momot, N M Permyakova *Chem. Inz. Ekol.* **8** 679 (2001)
203. S Filipchenko, T Zheltonozhskaya, O Demchenko, T Vitovetskaya, N Kutsevol, L Sadovnikov, O Romankevich, V Syromyatnikov *Chem. Inz. Ekol.* **9** 1521 (2002)
204. S I Klenin, S Ya Lyubina, I A Baranovskaya, E N Bykova, B P Makogon, V A Molotkov *Vysokomol. Soedin., Ser. A* **32** 439 (1990) [b]

[a] — *Russ. J. Appl. Chem. (Engl. Transl.)*
[b] — *Polym. Sci. (Engl. Transl.)*

Russian Chemical Reviews **73** (9) 831 – 846 (2004) © 2004 Russian Academy of Sciences and Turpion Ltd

DOI 10.1070/RC2004v073n09ABEH000914

Development of inorganic chemistry as a fundamental for the design of new generations of functional materials

Yu D Tretyakov

Contents

I.	Introduction	831
II.	Chemistry of ionic and molecular precursors	832
III.	Crystal chemical design of novel inorganic compounds and preparation of materials based on them	834
IV.	Inorganic nano- and supramolecular chemistry	835
V.	Chemistry of compounds with variable compositions	836
VI.	Chemistry of elements in unusual oxidation states	837
VII.	Chemistry of inorganic biomaterials	838
VIII.	Inorganic synthesis of functional materials using sonication, hydrothermal treatment and microwave irradiation	841
IX.	Conclusion	844

Abstract. The lines of research in the field of inorganic chemistry that are closely related to the design of novel functional materials are analysed. Special attention is given to areas of inorganic materials chemistry that have been developed most intensely at the Division of Inorganic Chemistry of the Department of Chemistry and at the Department of Materials Science of the Moscow State University over the past decade. The bibliography includes 135 references.

I. Introduction

Much of the actual knowledge which constitutes the basis of modern inorganic chemistry was obtained rather long ago; however, in the second half of the 20th century inorganic chemistry faded into the background of extraordinary achievements in organic chemistry and the chemistry of living systems. The progress in electronic engineering,[1] photonics,[2] sensorics[3] and spintronics,[4] which is impossible without the development of new generations of functional materials, has resulted in a kind of renaissance in inorganic chemistry in the past 10 – 15 years.

An active search for ways of utilisation of virtually all chemical elements systematised as the Periodic Table aimed at the development of novel materials and technologies is under way. The increasing applications of the most recently discovered chemical elements, *e.g.*, rhenium, technetium and francium, to say nothing of plutonium, americium and other actinides, provide illustrative examples.

The transition from chemical elements to materials is extremely complicated, and even the development of methods of combinatorial chemistry[5,6] does not allow one to master a multitude of combinations of the elements. Just for elements having stable isotopes, the number of such combinations exceeds 7×10^{23}. This increases by many orders of magnitude considering that the majority of the existing functional materials are developed on the basis of metastable (rather than thermodynamically stable) states of substances which are indefinably numerous for each particular compound with a fixed composition.

Obviously, the method of random enumeration of compositions is inefficient in the design of novel materials, and a significantly more pronounced effect is produced owing to the use of various approaches based, in particular, on the progress in inorganic chemistry. Despite the well-established traditions in the development of inorganic chemistry in Russia, the range of research in the field of inorganic synthesis in our country has recently narrowed considerably due to the limited experimental facilities of many research groups wich have no access to modern high-precision equipment, such as electron microscopes, synchrotron radiation sources, squid magnetometers, high-resolution NMR spectrometers, *etc*. This is all the more distressing taking into account the outstanding contribution of Russian scientists to the development of modern inorganic chemistry. Suffice it to mention the investigations by D I Mendeleev, N S Kurnakov, L A Chugaev and I I Chernyaev and more recent studies by A V Novoselova, I V Tananaev, V I Spitsyn and many others.

At present, the inorganic chemistry of materials is being developed especially intensively at such research centres as the N S Kurnakov Institute of General and Inorganic Chemistry of the RAS (Moscow), the A V Nikolaev Institute of Inorganic Chemistry of the Siberian Branch of the RAS (Novosibirsk), the Institute of Solid State Chemistry of the Urals Branch of the RAS (Ekaterinburg), the I V Grebenshchikov Institute of Silicate Chemistry of the RAS (Saint-Petersburg) as well as by divisions of inorganic chemistry of the largest classical and technical Russian universities including the M V Lomonosov Moscow State University (MSU).

In writing the present review and other reviews published in this issue of the Journal, the authors did not set themselves the task encompassing all the trends in contemporary inorganic chemistry, which is impossible in principle. They have consciously confined the range of scientific problems to those directly related to the design of novel functional materials and appropriate to their own research experience gained at the Division of Inorganic Chemistry of the Department of Chemistry and the Department of Materials Science of MSU over the past 10 – 15 years.

It may be hoped that despite the inevitable subjectivity, the reviews presented in this issue will provide an insight into modern

Yu D Tretyakov Department of Chemistry and Department of Materials Science, M V Lomonosov Moscow State University, Leninskie Gory, 119992 Moscow, Russian Federation. Fax (7-095) 939 09 98. Tel. (7-095) 939 20 74. E-mail: yudt@inorg.chem.msu.ru

Received 9 March 2004
Uspekhi Khimii **73** (9) 899 – 916 (2004); translated by R L Birnova

inorganic chemistry as a fundamental for the design of new generations of functional materials. The main research trends touched upon in the present review are as follows:

— chemistry of ionic and molecular precursors;
— crystal chemical design of novel inorganic compounds and design of materials based on them;
— inorganic nano- and supramolecular chemistry;
— chemistry of non-stoichiometric compounds;
— chemistry of elements in unusual oxidation states;
— inorganic chemistry of biomaterials and implants;
— inorganic synthesis of functional materials using ultrasonic, hydrothermal and microwave methods.

II. Chemistry of ionic and molecular precursors

The design of materials with a definite range of structure-dependent properties on the basis of chemical compounds (rather than merely the synthesis of chemical compounds) is the ultimate goal for a wide range of inorganic chemists engaged in the development and perfection of functional materials. Such properties depend on the real structure of a material beginning with the structure of the unit cell and ending with the peculiarities of polycrystalline (ceramic) structures with their characteristic defects (dislocations, crystallite boundaries, pores and cracks). Different structural levels are mutually related. The possibility of control over such relationships is considered in reviews [7,8] within the framework of approaches of non-linear dynamics. The latter can be used for the description of the evolution of physicochemical systems under non-equilibrium conditions determined by specific interactions of these systems with the environment. It has been shown [9] that some factors, among which the unambiguity and reproducibility of the original states of chemical precursors are critical, should be taken into consideration in the optimisation of the reaction zone for the synthesis of materials. The more complex are the systems the more difficult this is to attain. Here, we define the complexity of a system as both its chemical and phase compositions and activities of its precursors determined by their chemical and thermal prehistories, *i.e.*, the effect of 'topochemical memory'.[10]

If a material, which is the target product of chemical and phase conversions, is multicomponent, additional requirements for homogeneity and ability to preserve it upon transition to the target product are imposed on its precursors. It is for this reason that solid-phase synthesis, which seems to be technologically the simplest and has been widely employed previously for the manufacture of magnetic dielectrics and piezoceramics, is fairly ineffective in the preparation of many functional materials. Thus the synthesis of manganese–zinc ferrites with high magnetic permeability was carried out by the reaction:

$$1/3\,MnCO_3 + 2/3\,ZnO + Fe_2O_3 = Mn_{0.33}Zn_{0.67}Fe_2O_4 + 1/3\,CO_2.$$

It was found, however, that in many cases the combination of traditional processes, such as mechanical blending, compaction of precursor mixtures and high-temperature annealing ($\sim$1200 °C), does not allow preparation of a single-phase product. An increase in temperature results in inevitable losses of volatile zinc oxide and dissociation of iron(III) oxide to form magnetite. These processes significantly deteriorate the composition and properties of the product due to considerable magnetic and dielectric losses, especially at ultrahigh frequencies. Repeated grinding and heating at constant temperatures lead to further contamination of the product with the mill materials, which markedly decreases the magnetic permeability of the target ferrites.

The problem of reproducibility and enhancement of functional properties of solid-phase synthetic products can be overcome by combining the solid-phase synthesis and thermolysis. In this case, mechanical mixtures or co-precipitated salts of various oxoacids [11] including sulfates, carbonates, nitrates, oxalates, acetates, citrates, formates and stearates are used as chemical precursors. The use of salt solid solutions obtained under equilibrium or non-equilibrium conditions was next step forward. It has been found [12,13] that schoenite-type salts of the general formula $M^{2+}A^{+}(RO_4)_2\cdot 6\,H_2O$ (M = Mg, Mn, Ni, Co, Fe, Cu, Zn; A is an alkali metal or NH_4; R = S, Se, Te, Cr) or alum-type salts $A^{+}M^{3+}(SO_4)_2\cdot H_2O$ (where A is an alkali element or NH_4; M = Fe, Cr, Co) are the most convenient for equilibrium crystallisation.

The ability to form continuous solid solutions at any ratios of the reaction components and good solubility in water, which decreases drastically upon cooling, were used as a basis for the development of original methods for the preparation of highly homogenous isomorphic salt mixtures. These methods are based on isoconcentration evaporation of the solvent or isoconcentration elimination of micro-oversaturation of the solution.

The practical implementation of these processes has become possible due to extensive studies [12] of equilibrium diagrams of ternary (salt 1 – salt 2 – water) and more complex systems and determination of thermodynamic distribution coefficients of salt components between co-existing liquid and solid phases aimed at selecting the conditions for equilibrium crystallisation of salt solid solutions the cationic compositions of which are identical to those of the ferrites to be synthesised. The transition from the salt precursor to the target product occurs upon thermolysis using a reaction of the type:

$$(Ni_{1/3}Fe_{2/3})SO_4\cdot(NH_4)_2SO_4\cdot 6\,H_2O =$$
$$= 1/3\,NiFe_2O_4 + 2\,SO_2 + 2\,NH_3 + 3/2\,O_2 + 7\,H_2O.$$

The conditions of this reaction predetermine, to a large extent, the feasibility of preparation of a polycrystalline material with a preset ceramic structure and structure-dependent properties.

The cryochemical method may be regarded as a versatile procedure for the preparation of salt-like multicomponent precursors. The cryochemical technology [13–15] is based on a balanced combination of heating and cooling processes, the latter being used to prevent the uncontrollable changes in intermediate and target products (Fig. 1). Rapid freezing (*e.g.*, in liquid nitrogen) of solutions containing metal salts as constituents of materials to be synthesised and dispersed in the form of mono- or polydispersed drops is a crucial step in the cryochemical technology. Frozen

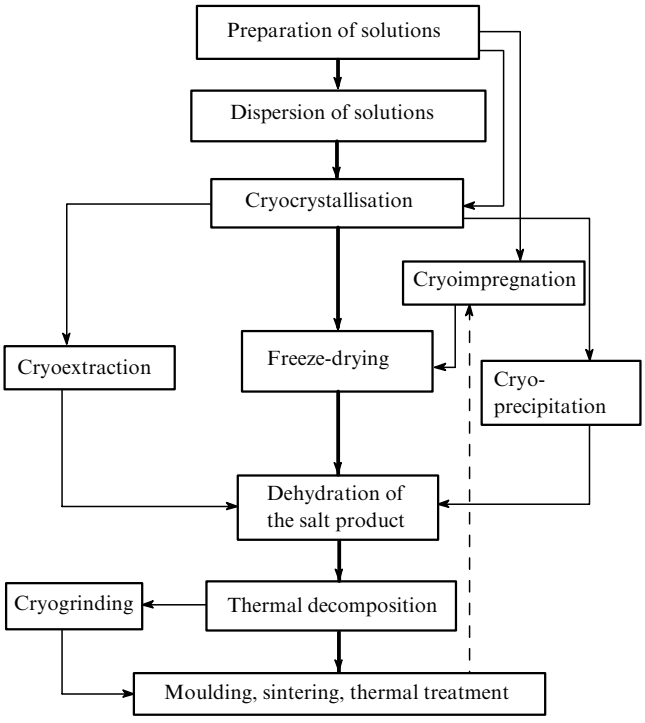

Figure 1. Processes of cryochemical technology.

solutions of salts in the form of cryogranules are usually subject to freeze-drying; its optimum conditions provide the preparation of highly homogenous salt precursors. The rate of cryocrystallisation exceeds that of solid phase formation by several orders of magnitude when other known non-equilibrium methods (*e.g.*, solvent replacement by desalting from aqueous solutions with non-aqueous solvents, such as acetone, ethanol or methanol) are used for the preparation of salt precursors.

The wide application of cryochemical technology was preceded by fundamental investigations of cryocrystallisation, freeze-drying, cryoprecipitation, cryoextraction, cryodispersion and some original cryocalorimetric procedures.[13–16] The cryochemical synthesis of salt precursors underlies the preparation of various functional materials (Fig. 2). Dispersed powders prepared by thermal decomposition of salt precursors are distinguished by microplasticity, high reactivity and sintering ability in addition to their chemical homogeneities.

The so-called topochemical memory, *i.e.*, the ability of solid-phase chemical conversion products to store ('to remember') information about their origin and to transfer it upon subsequent topochemical reactions, is a characteristic feature of salt-like ionic precursors. A real structure, which is usually formed under non-equilibrium conditions and affects significantly the properties of functional materials obtained as polycrystalline ceramics, seems to be the most probable candidate for 'storing' and 'delivering' information in solids.[10]

Studies related to the chemistry of molecular precursors are extremely important for the design of thin-film materials by molecular deposition. In order to solve the global problem of the increase in the density of information recording in silicon chips, it is necessary to replace the 'natural' oxide (SiO_2) by oxides with higher dielectric constants. The most probable candidates are HfO_2, ZrO_2 and Ln_2O_3. Preparation of films of such oxides on the surface of silicon by MOCVD (Metal-Organic Chemical Vapour Deposition) requires development of molecular precursors possessing high volatilities and relative thermal stabilities as well as abilities to undergo hydrolysis, pyrohydrolysis or other decomposition reactions leading to the formation of amorphous oxides on the surface of silica. The main idea realised at the Laboratory of Coordination Chemistry of MSU [17] consists of the use of novel molecular precursors based on metal complexes with complete saturation of the coordination sphere with ligands that form relatively weak donor–acceptor bonds. Saturation (and, as a consequence, volatility) was provided by the introduction of an additional neutral ligand (*e.g.*, phenanthroline); charged ligands were chosen on the basis of quantum-chemical calculations of the energies of the metal–ligand bonds.

Complexes with organic ligands were also successfully used for the solution of yet another vital task, *viz.*, preparation of thermoprotective (barrier) coatings for gas-turbine unit blades. It was shown [18] that deposition of coatings from vapours of β-diketonates of appropriate metals using ZrO_2 (Y_2O_3) is the most

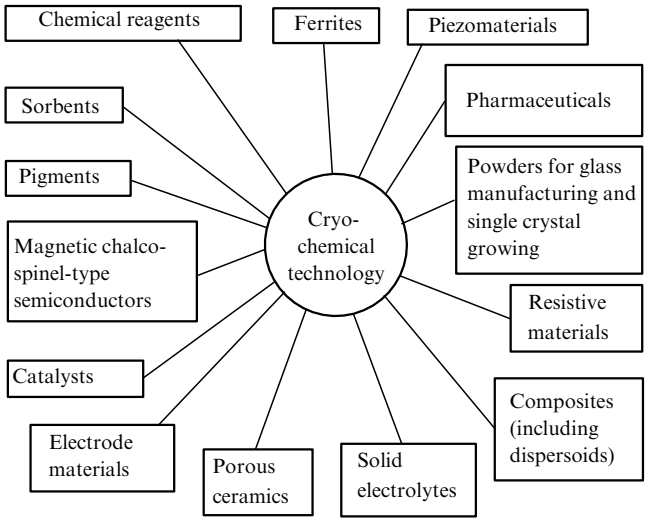

Figure 2. The main products prepared by cryochemical technology.

efficient approach which allows radical reduction of the production cost owing to the use of inexpensive acetylacetonates. As for the problem of insufficient volatility of polymeric $Y(acac)_3$, it is solved by co-evaporation with volatile $Zr(acac)_4$, its small portions being fed gradually into the evaporator. The well-known synergistic effect is observed, *i.e.*, joint evaporation is more complete than separate.

A series of novel REE mixed-ligand complexes including Tb(III) complexes with some aromatic acid derivatives to be used as luminescent materials for an organic light emitting diode (OLED) have been synthesised. An OLED represents a multilayer unit constructed using planar technology. The material of the working layer should not only possess bright electroluminescence, but also be temperature-resistant (since OLED is spontaneously heated during operation) and form smooth films upon deposition on the surface of the substrate, *i.e.*, be readily soluble in organic solvents, to moisten the surface of the anodic layer and be resistant to cracking. Such luminescent materials are prepared by mixed-ligand complex formation using neutral ligands.

Spectral characteristics of the terbium salicylate complex $Tb(sal)_3 \cdot H_2O$ with triphenylphosphine (TPPO) obtained by the reaction

$$Tb(sal)_3 \cdot H_2O + TPPO \xrightarrow{EtOH-C_6H_6} Tb(sal)_3 \cdot (TPPO)_2$$

are shown in Fig. 3 as an example.

Terbium salicylate is stable at temperatures up to 120 °C, whereas the complex $Tb(sal)_3 \cdot (TPPO)_2$ retains stability up to

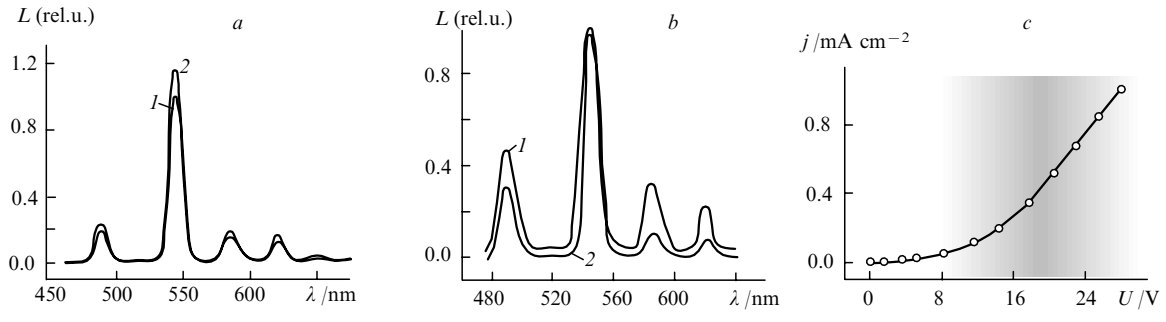

Figure 3. Spectral characteristics of $Tb(sal)_3 \cdot H_2O$, $Tb(sal)_3 \cdot (TPPO)_2$ (*a*) and OLED based on $Tb(sal)_3 \cdot (TPPO)_2$ (*b, c*).
(*a*) Luminescence spectra of $Tb(sal)_3 \cdot H_2O$ (*1*) and $Tb(sal)_3 \cdot (TPPO)_2$ (*2*); (*b*) photo- (*1*) and electroluminescence (*2*) spectra of OLED; (*c*) voltammetric characteristics of OLED (the luminescence zone is shown in grey).

200 °C, the surface roughness of the former being 66 nm, that of the latter being 9 nm.

One of the latest successful investigations related to molecular precursors was carried out by Romanov *et al.*[19] These authors have synthesised a mixed-ligand complex niobium isopropoxide–dipivaloylmethanate and used it, along with dipivaloylmethanate potassium *tert*-butoxide, for the preparation, by the MOCVD method, of epitaxial films of potassium niobate $KNbO_3$ characterised by extremely high values of non-linear optical and piezoelectric constants.

III. Crystal chemical design of novel inorganic compounds and preparation of materials based on them

Antipov and co-workers[20] have developed a concept of intergrowth structures and used it in a search for novel oxide materials. This was achieved through the use of structural design which had proved to be efficient in the preparation of novel high-temperature superconductors based on complex copper oxides. The latter contain structures derived from perovskite (ABO_3) or a perovskite-like fragment as one of the structural components of intergrowth structures. The prediction and synthesis of novel superconductors were carried out by selecting various intergrowth structures. Such a synthesis is, to a certain extent, similar to that of organic compounds; however, its realisation demands an analysis of infinite two-dimensional layers forming structural units rather than of isolated groups of atoms as in the case of organic molecules.

The geometric commensurability of structurally different fragments in the plane *ab* is a prerequisite for the formation of intergrowth structures. By varying the cationic compositions of the units and the formal degree of oxidation of copper ions, one can vary the geometrical sizes of the units and obtain the desired compounds using an appropriate synthetic procedure. In predicting the compositions of intergrowth structures, attention should be given to crystal chemical characteristics of the cations, their chemical similarities and electron neutrality of the elementary cell as a whole. The choice of a synthetic procedure is determined by the chemical peculiarities of the starting compounds and the degree of oxidation of the cations in the target structure.

This approach was used for the preparation of more than 100 novel complex copper oxides among which about 30 oxides possess superconducting properties.[21]

The search for novel superconductors was carried out among compounds comprising an anion-deficient perovskite-like structure, *viz.*, $A_n(Cu,M)_nO_{3n-\delta}$, and a series of novel oxides was obtained. The 'structural substitution' approach was also used in the synthesis of novel compounds where prototypes with a layer sequence corresponding to the formula $(CuO_2)(M\square)(CuO_2)$ served as the basis of the structure. In the structures of novel compounds, this fragment was rearranged into the sequence $(CuO_2)(A_2O_2)(CuO_2)$ the (A_2O_2) block in which has the structure of fluorite.

Crystal chemical simulation has made it possible to predict the existence and to synthesise a new family of superconductors, *viz.*, $HgBa_2Ca_{n-1}Cu_nO_{2n+2+\delta}$ with record values of T_c. The transition temperatures for superconduction of the phases $HgBa_2Ca_{n-1}Cu_nO_{2n+2+\delta}$ depend on the content of oxygen (δ) and the number of CuO_2 layers (n). A progressive increase in T_c on going from the first member of the homologous family (97 K) to the second (127 K) and third (135 K) members is followed by its decrease for the fourth (127 K), fifth (110 K) and sixth (107 K) members. The T_c value for $HgBa_2Ca_2Cu_3O_{8+\delta}$ at 23.5 GPa was found to be equal to 157 K. The possibility, in principle, of a transition into the superconducting state at $T_c = 150-160$ K at atmospheric pressure has been demonstrated for compounds with the Cu–O distances corresponding to those in the $HgBa_2Ca_{n-1}Cu_nO_{2n+2+\delta}$ complexes under external pressure. The fact that the anionic sublattice may contain fluorine atoms along with oxygen atoms significantly expands the area of a search for Cu-containing oxofluoride superconductors. Xenon difluoride, which was employed for the first time as a mild fluorinating agent by Abakumov,[22] has a number of advantages over traditional fluorine sources. First, XeF_2 is solid at room temperature, which permits its precise quantification to attain a required level of fluorination and desired copper oxidation state; second, XeF_2 is less aggressive than gaseous fluorine, which excludes the use of sophisticated equipment and, third, no reaction products that could contaminate the target material are formed from XeF_2. Altogether, more than twenty novel cuprates including superconductors, such as $YBa_2Cu_3O_6F_2$ ($T_c = 94$ K) and $Y_2Ba_4Cu_7O_{14}F_2$ ($T_c = 62$ K), have been synthesised. Special mention should be made of the synthesis of $HgBa_2Ca_2Cu_3O_8F_{0.32}$; here, the introduction of fluorine caused anisotropic chemical compression and a record-high elevation of T_c (138 K).

The method of structural design was successfully used for the simulation of structures of novel complex manganites that sometimes possess colossal magnetoresistance.[23]

Epitaxial stabilisation of unstable oxide phases in the form of thin films developed by Kaul *et al.*[24] is a new in principle approach to the design of novel materials. Based on the results of thermodynamic simulation, direct syntheses of the novel phases RBO_3 (R = REE; B = Ni, Co, Mn, Fe, In) have been carried out. Some of them are ferroelectrics ($RFeO_3$ and $RMnO_3$); in others ($RNiO_3$, $RCoO_3$), a transition 'metal–insulator' is possible; ($R_3Fe_5O_{12}$) is a magnetic material. It was found that epitaxial stabilisation can successfully be used in the technology of preparation of thin-film materials for microelectronics. This technology was used as a basis for realisation of the local epitaxy principle during photolithographic formation of planar heterostructures.

A detailed study of epitaxial ratios of various structural types has made it possible to significantly expand the potential of heteroepitaxy. This method was used,[24] in particular, for the design of nanodomain epitaxial structures based on REE manganites characterised by high tunnel magnetoresistance values. It was shown that nanodomain epitaxial structures are formed as a result of self-organisation of a system that is crystallised at the nanolevel. Provided the energetically identical heteroepitaxial approaches exist, these structures can be used as a basis for the manufacture of inexpensive, highly sensitive magnetic field sensors.

The fundamental physicochemical problems related to the design of HTSC materials based on nonstoichiometric phases $R_{1+x}Ba_{2-x}Cu_3O_z$ with predetermined compositions, homogeneities and structures conferring desired structure-dependent properties, are considered in recent reviews.[25,26] TTT diagrams (Time–Temperature–Transformation) have been developed for the first time and the efficiency of their use in the design of HTSC materials has been demonstrated based on the results of systematic studies of temperature- and time-dependent changes in these phases.

The properties of manganites manifesting colossal magnetoresistance, which make them promising components of various magnetic sensors and novel magnetic information-recording devices, depend critically on structural parameters. Compositions with extremely high sensitivities to the magnetic field, light and other factors including changes in the isotopic composition have been obtained for the first time.[27,28] Optimisation of chemical compositions of manganites was carried out with due regard to the results of physical simulation of electron transfer processes. The phases $(La_{1-x}Pr_x)_{0.7}CaO_3MnO_3$ in the form of ceramics and thin epitaxial films have been studied in detail. It was found that unusually high sensitivities of electric resistances of critical compositions to the light and electric and magnetic fields are related to the competition between the metallic and charge-ordered states. The material synthesised by Babushkina *et al.*[28] ($x = 0.75$) manifests an anomalously high isotope effect upon the substitution of ^{18}O for ^{16}O and a transition from the metal-type con-

ductivity to a dielectric state. The magnetoresistances of film materials depend on elastic stresses generated upon their epitaxial fusion with the substrate. Critical compositions of the system $R_{1-x}Sr_xMnO_3$ are characterised by extremely high magnetostriction concomitant with a strong magnetocalorific effect. Such phases present considerable interest for the design of magnetic and mechanical sensors and Freon-free refrigerating plants having high coefficients of efficiency.

Needless to say, the ideology of the construction of functional materials is not confined to a crystal chemical design of novel inorganic compounds. Suffice it to remember the system of physicochemical principles formulated by the author of the present review rather long ago [29] and successfully used for the optimisation of properties of many functional materials, such as ferrites, magnetic semiconductors based on chalcospinels, electronic-ionic conductors of the oxide bronze type, complex silver chalcogenides and lanthanoidates, ceramic electrolytes with unipolar conductivities with respect to anions, cations and hydrogen as well as piezoceramic materials and flexible piezocomposites based on them.[30] This system comprises the following principles:

periodicity (properties of compounds of elements arranged according to the increase in their atomic numbers change periodically);

physicochemical analysis (principles of continuity, conformity and compatibility of components of an equilibrium system);

limitation of the number of independent parameters of states (among the multitude of parameters of state that characterise an equilibrium system comprising material-forming solid phases, only very few are independent according to the Gibbs' phase rule);

disordering and variability of composition (diverse defects are formed in crystalline lattices of solids at any temperature different from the absolute zero, while any solid-phase compounds with non-molecular types of bonds have variable compositions);

complication of composition (properties of a system change as a result of its chemical, structural and phase complication);

homogeneity (properties of solid-phase materials are sensitive to the degree of their homogeneities at both micro- and macrolevels);

equivalence of disorder sources (under equilibrium conditions, materials acquire specific defects which ensure a maximum increase in the entropy at minimum energy expenditures);

similarity of responses to physicochemical effects (necessary changes in the properties of materials can be achieved under the influence of various physicochemical factors);

nonequivalence of volume and surface;

metastable diversity (the number of non-equilibrium states of materials is indefinitely large; these states can be kinetically stable in solid phases).

The aforementioned principles constitute the system which defines possible approaches to the solution of material-science problems from the point of view of a chemist. Initially, no preference to these principles can be given, they represent a specific set of alternatives. However, when a specific problem is concerned, a decisive (key) principle is isolated from the system for a particular step by analysis of physicochemical conditions and used for the solution of problems aimed at the practical realisation of this principle. The next step towards the solution of the entire problem entails return to the system of principles, isolation and realisation of the next alternative, and so on.

IV. Inorganic nano- and supramolecular chemistry

In 2000, a national programme for investigations and developments in the field of nanotechnologies which has the name 'The National Nanotechnology Initiative' was set up in the USA. In the 2001 budget, the financing for its realisation constituted \$500 M, *i.e.*, significantly larger than, for example, the sum allocated for investigations in the field of high-temperature superconductivity immediately after its discovery in 1986. This is not surprising, however, since it is with nanotechnology that the next industrial revolution is associated. Amazingly, many research groups in Russia manage to carry on successful research in the field of nanomaterials and nanotechnologies with financial support which is three orders of magnitude smaller than that in the USA.

The interest in nanomaterials is associated with their unusual physical properties which are not characteristic of bulk materials. For example, a decrease in the size of semiconductor particles below a certain critical level can lead to the change in the width of a band gap, the generation of a second harmonic and dimensional quantisation of energy levels. At the same time, it is known that the predisposition of free nanoparticles to aggregation restricts their practical application. In this context, the development of methods for preparation of nanocomposites, *i.e.*, nanoparticles incorporated into an inert matrix, which protects the particles from environmental factors and thus prevents their aggregation, appears to be of crucial importance.

A promising method of matrix isolation of nanoparticles is based on chemical modification of lamellar double hydroxides (LDH) [31] with the general formula $M^{2+}_{1-x}M^{3}_{x}(OH)_2[(X^{n-})_{x/n}\cdot m\,H_2O]$. These compounds are made up of positively charged hydroxide layers $M^{2+}_{1-x}M^{3}_{x}(OH)^{x+}_{2}$ and interstitial anions X^{n-}. The method for the synthesis of nanocomposites is related to the chemical modification of these anions. The reaction zone is surrounded by hydroxide layers, so the conditions for the synthesis of the nanophase are similar to those observed in a two-dimensional nanoreactor.

The unique characteristics of lamellar double hydroxides open up broad opportunities for the design of nanocomposite materials based on them. Magnetic (based on metallic iron, cobalt and nickel) and semiconducting (based on MS, M = Pb, Zn, Cd) nanomaterials prepared from anion- and cation-substituted hydrotalcite, $Mg_{1-x}Al_x(OH)_2[(CO_3)_{x/2}\cdot m\,H_2O]$, using the above-mentioned method were the subjects of investigation.[32–35] Some of the factors influencing the structures and properties of nanocomposites synthesised have been established. Thus the dependences of the composition, size distribution, morphology and anisotropy of the nanostructures on the structure and composition of LDH used as a lamellar matrix were revealed. Conditions for chemical modification of substituted LDH also have a pronounced effect on the composition and structure of the nanophase formed inside the matrix.

In addition to LDH, a family of silica-based mesoporous molecular sieves has been recommended as a template for the synthesis of nanocomposite materials with a nanophase endowed with predetermined properties.[36] The structure of silica is characterised by the presence of a highly ordered system of pores with the diameters ranging from 20 to 100 Å. It is of note that such specific features of the aforementioned mesoporous materials as uniform size distribution of pores, extremely high specific surface ($\sim$1000 $m^2\ g^{-1}$) and broad variability of a pore size, make them especially attractive for investigators. By virtue of its ordered structure, mesoporous SiO_2 can be used as a template in the synthesis of metal and semiconductor nanoparticles as well as polyaniline and carbon fibres.

Currently, the main attention of specialists in inorganic supramolecular chemistry is focused on the design of supramolecular ensembles manifesting specific properties. Of considerable interest are ideally ordered ensembles, their structure being determined by the structure of the backbone of the 'host' (receptor), while the functional properties are determined by the nature of the 'guest' (substrate). The diversity of physical properties is due to structural peculiarities of the 'guest' structures including magnetic ordering of d^1-, d^3- and d^9-centres, spin transitions in d^6-centres, electron transitions with valence fluctuations and dynamic effects.

The properties related to dynamic effects are employed in the design of novel thermoelectrical materials. Semiconducting clathrates provide an example of compounds that are studied to this end.[37] The crystalline structure of a clathrate includes the backbone of the 'host' with 'guest' atoms with the coordination numbers of 20 and 24 in its cavities. The 'guest' atoms are not

bound to the 'host' backbone by covalent bonds and oscillate inside the cage with frequencies ensuring effective scattering of heat-conducting phonons. This results in a very low heat conductivity (as in the case of glasses). At the same time, the covalently bound backbone ensures high concentrations and mobilities of charge carriers, which accounts for high electroconductivity. A combination of these two features makes clathrates promising compounds for the design of effective thermoelectric materials. It has been found [38] that abnormal magnetisation and thermal capacities of tin-containing clathrates observed at $\sim$250 K are not associated with ordinary phase transitions. These data point to the possibility, in principle, of independent optimisation of electro- and heat-conducting properties determined by the structure of the backbone and the dynamics of guest molecules, respectively.

A new trend in inorganic supramolecular chemistry is related to controlled self-assembly of ordered supramolecular ensembles under conditions of high-temperature reactions where reaction systems are complex and heterophasic and are not subject to analysis. Such processes are based on the mutual adjustment of the 'host' and the 'guest' where the 'guest' is a template for the formation of a definite topology and geometry of the 'host' backbone and it itself changes its parameters in accordance with the 'host' requirements. It has been found [39] that weak 'guest–host' interactions are decisive in such self-assembly. Being limited by van der Waals forces, these interactions control the reciprocal arrangement of the 'guests' and the particles forming the 'host' backbone in the first step. If the 'guest' and the 'host' match each other, the formation of ideally ordered supramolecular ensembles takes place where hosts are recognised by 'guests' of various compositions and occupy their predetermined specific sites. As an illustration, Fig. 4 shows the structure $[Hg_6P_4](TiCl_6)Cl$ formed as a result of self-assembly of $TiCl_6^{3-}$ and Cl^- in the cavities of the backbone of $[Hg_6P_4]^{4+}$.

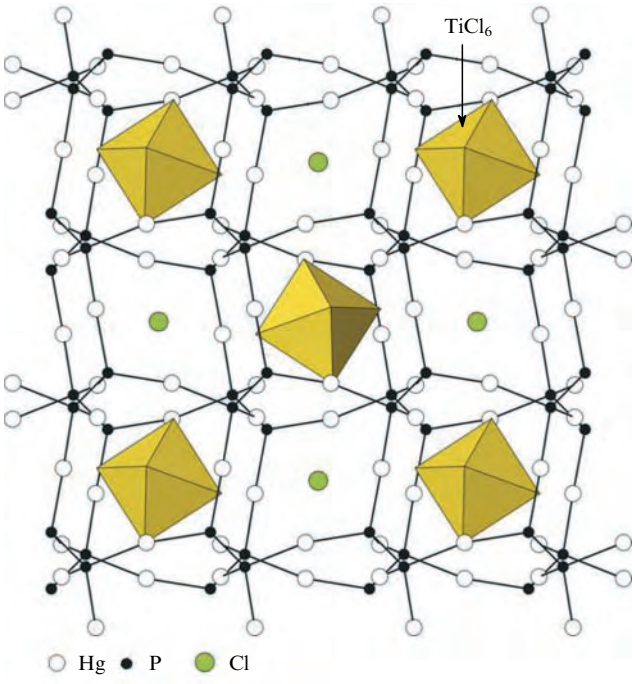

Figure 4. The structure of $[Hg_6P_4](TiCl_6)C1$ prepared by high-temperature synthesis.
The structure was formed by self-assembly of TiC_6^{3-} and Cl^- in the cavity of a three-dimensional cage of $[Hg_6P_4]^{4+}$.

V. Chemistry of compounds with variable compositions

The formation of chemical compounds with variable compositions, which have the name 'berthollides', was discovered over 100 years ago by N S Kurnakov who studied silicate and metallic systems. Later, it was found that compositional variability is an intrinsic property of inorganic solid-phase compounds with ionic bonds predominating. Depending on the nature of the elements constituting inorganic compounds, the area of their existence is either very broad (*e.g.*, titanium and iron monoxides) or, *vice versa*, extremely narrow (*e.g.*, alkali metal halides, zinc, lead and cadmium chalcogenides). In any case, a deviation from stoichiometry is a critical factor in the formation of binary and more complex crystals.

Using statistical thermodynamics methods, Schottky and Wagner [40] have established a correlation between the defects of crystal lattices of inorganic compounds and their non-stoichiometries and proved the inevitable existence of the latter in any ionic crystal. Minor deviations from stoichiometry are usually described within the framework of disordering models with formation of non-interacting vacancy-type point defects, incorporated atoms or antistructural defects. Defect formation is accompanied by pronounced changes in electrical, magnetic, optical, thermal and mechanical properties of solid-phase compounds; therefore, an analysis of their non-stoichiometries is one of the most important directions in inorganic chemistry of solids.[41]

The development of methods for coulometric titration in reversible electrochemical circuits with solid electrolytes possessing ionic (anionic or cationic) conductivity [42] has led to considerable progress in the study of non-stoichiometry, in particular of compounds manifesting a narrow range of homogeneity. Quasichemical models of defect formation in inorganic compounds were successfully employed for the description of functional properties of semiconductors and ferrites. For example, the results of studies of non-stoichiometry as a function of oxygen pressure and temperature using a quasichemical approximation have provided a clue to the solution of problems related to directed doping of ferrites.[43]

Defect formation in ferrospinels MFe_2O_4 can be described by the following system of equations:

$$O \rightleftharpoons e' + h^{\bullet}, \qquad K_1 = np,$$

$$Fe_{Fe}^{x} \rightleftharpoons Fe_i^{\bullet\bullet\bullet} + V_{Fe}^{\prime\prime\prime}, \qquad K_2 = [Fe_i^{\bullet\bullet\bullet}][V_{Fe}^{\prime\prime\prime}],$$

$$M_M^{x} \rightleftharpoons M_i^{\bullet\bullet} + V_M^{\prime\prime}, \qquad K_3 = [M_i^{\bullet\bullet}][V_M^{\prime\prime}],$$

$$M_M^{x} + Fe_{Fe}^{x} \rightleftharpoons M_{Fe}^{\prime} + Fe_M^{\bullet}, \qquad K_4 = [M_{Fe}^{\prime}][Fe_M^{\bullet}],$$

$$O \rightleftharpoons V_M^{\prime\prime} + 2V_{Fe}^{\prime\prime\prime} + 4V_O^{\bullet\bullet}, \qquad K_5 = [V_M^{\prime\prime}][V_{Fe}^{\prime\prime\prime}]^2[V_O^{\bullet\bullet}]^4,$$

$$O_O^{x} \rightleftharpoons 1/2\,O_2 + V_O^{\bullet\bullet} + 2e', \qquad K_6 = [V_O^{\bullet\bullet}]n^2p_{O_2}^{1/2},$$

$$Fe_2O_3 \rightleftharpoons 2Fe_{Fe}^{x} + 3O_O^{x} + V_O^{\bullet\bullet} + V_M^{\prime\prime}, \qquad K_7 = [V_O^{\bullet\bullet}][V_M^{\prime\prime}]a_{Fe_2O_3}^{-1},$$

$$3[Fe_i^{\bullet\bullet\bullet}] + 2[M_i^{\bullet\bullet}] + [Fe_M^{\bullet}] + 2[V_O^{\bullet\bullet}] + p = [M_{Fe}^{\prime}] + 3[V_{Fe}^{\prime\prime\prime}] + 2[V_{Fe}^{\prime\prime\prime}] + n.$$

In addition to activity ($a_{Fe_2O_3}$), temperature (T) and partial oxygen pressure (p_{O_2}), the role of variables is played by the concentrations of all possible types of point defects, *viz.*, $[M_i^{\bullet\bullet}]$, $[Fe_i^{\bullet\bullet\bullet}]$, $[M_{Fe}^{\prime}]$, $[Fe_M^{\bullet}]$, $[V_O^{\bullet\bullet}]$, $[V_M^{\prime\prime}]$, $[V_{Fe}^{\prime\prime\prime}]$, n, p, which can be calculated as functions of the parameters of state. Whilst the quasichemical approach is not strictly accurate, its practical utility leaves no doubt.

Figure 5 shows a defect formation diagram plotted in the coordinates $\log[i]-f(\log p_{O_2})$ at constant values of T and $a_{Fe_2O_3}$, where $[i]$ is the concentration of the defects of the ith type. From the diagram it follows that changes in thermal treatment and sintering regimes of ferrites can underlie the transitions from electron to hole conductivity and the predominance of ionic conductivity for compositions close to stoichiometric.

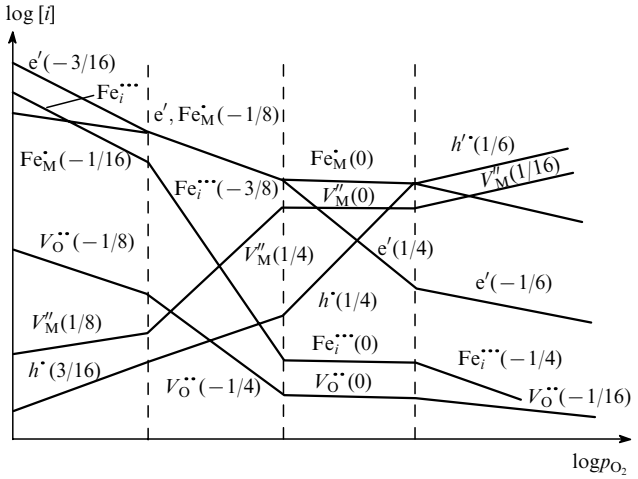

Figure 5. A diagram of defect formation in a crystal lattice of a ferrospinel at constant temperature and constant activity of Fe_2O_3. The individual segments of the dependences show the predominant defects; the numbers in parentheses indicate the slopes.

Passage to inorganic compounds with more pronounced non-stoichiometries casts doubts on the existence of a strict correlation between the non-stoichiometry index and the concentration of predominant point defects as is implied by the quasichemical approximation.

Changes in the structures of binary or more complex crystals as a result of increasing non-stoichiometries have a different origin. Sometimes, they are related to the formation of associates, the simplest being bivacancies, to a spatial ordering of superstructure-type defects and finally to annihilation of point defects accompanied by changes in the types of bonds of coordination polyhedra and formation of the so-called crystallographic-shift structures of the type of homologous series: M_nO_{3n-1} where n = 8, 9, 10, 11, 12 and 14. However, the concept of discrete compositional changes resulting necessarily from rearrangements of coordination polyhedra upon crystallographic shift (CS) is questionable.

According to Anderson,[44] there exist many systems possessing infinitely adaptable structures, *i.e.*, the phases that maintain a high level of structural organisation despite continuous composition changes by virtue of changes in the repetition frequencies of CS planes or orientation of the latter with the preservation of fragments of the matrix structure rather than involvement of point defects. The former process is discrete and gives rise to the formation of various homologues of the same series, while the latter is continuous. Their combination ensures the continuity of compositional changes within the same order. An infinitely adaptable structure was found, for example, in phases with variable compositions of $Y(OF)_{2.13-2.22}$, solid solutions ($TiO_2-Cr_2O_3$) and cerium–cadmium alloys.

The imperfections of structural patterns, *e.g.*, coherent intergrowth of sites with different orientations of CS planes, are predominant defects in the case of non-stoichiometric phases with a high level of structural organisation. These defects, which are commonly referred to as Wadsley defects, strongly affect the properties of solid phases and their behaviour under the action of various chemical and physical agents.

It is clear that the compositions and structures of non-stoichiometric compounds do not always correspond to the equilibrium conditions of their formation. On the contrary, very often the conditions of synthesis, thermal treatment and existence of such compounds are far from equilibrium and the net result is determined by the rates of processes involved. For example, nickel monoxide prepared by thermolysis of nickel nitrate at moderate heating temperatures may contain excess oxygen up to the composition $NiO_{1.5}$, whereas nickel monoxide synthesised in air under equilibrium conditions has the composition NiO_{1-x}, where $x = f(T, p_{O_2})$. At 1373 K and $p_{O_2} = 2 \times 10^{-9}$ atm, the value of x is equal to 1.8×10^{-8}.

Undoubtedly, the fundamental principles of chemistry of non-stoichiometric compounds considered above are valid for any newly produced functional materials, be they superconducting cuprates, manganites with superhigh magnetic resistance or cerates manifesting high proton conductivity. At the same time, any of these materials have specific features of their own and demand analysis of their non-stoichiometries as in the case of semiconducting or ferrite systems.

The design of superconducting materials able to maintain high levels of critical currents in strong magnetic fields has become possible owing to the passage from yttrium–barium cuprate $YBa_2Cu_3O_z$ with strict cationic stoichiometry to neodymium–barium cuprate $Nd_{1-x}Ba_{2-x}Cu_3O_z$ with a broad range of homogeneity for both oxygen and cations. It was found also that a change in the cationic composition within the homogeneity zone is accompanied by evolution of the structure from 123 *via* 336 to the superstructure 213.[45] The use of a TTT diagram, which characterises the behaviour of a metastable, slowly evolvable system, is necessary because of an extremely low rate of cationic ordering in neodymium–barium cuprates.

VI. Chemistry of elements in unusual oxidation states

The design of novel functional materials based on chemical elements in unusual oxidation states is a nontrivial process, at least because the unusual oxidation state is equivalent to the instability of a particular state of an element. Hence, the phenomenon of the appearance of one or another unusual oxidation state of a chemical element is insufficient from the practical point of view, one should also be sure that the lifetime of a chemical element in an unusual oxidation state is commensurate with the period of functioning of the material containing this element. A significant contribution to the chemistry of elements in unusual oxidation states has been made by researchers of the Institute of Chemical Physics of the RAS and the Department of Chemistry of the MSU. The former have succeeded in obtaining Np(VII), Pu(VII), Am(VII), Cm(VI), Cm(V) (see Ref. 46) and a series of actinides and lanthanides in lower oxidation states,[47] the latter have demonstrated the possibility of existence of Tm(IV) and found that the tetrad effect characteristic of lanthanides and actinides is more significant for 'distant' lanthanides than for 'near' lanthanides in solid compounds.[48]

At first, the values of extremely high oxidation states for transition metals of Groups 3–11 of the Periodic System correlate with the group number, but then this correlation is absent, which is determined by the electronic structure or, more precisely, by disturbances in the fine balance between binding and loosening forces in atomic orbitals and increasing instabilities of the corresponding compounds in their extremal oxidation states.

'Matrix' systems formed upon crystallisation from homogeneous media (solutions, melts), co-precipitation or solid-phase synthesis present the greatest interest for specialists in materials sciences. Matrix systems containing Fe(IV), Fe(V), Fe(VI) and Co(VI) were prepared by reactions of binary oxides with dopant oxides.[49]

An alternative approach consists of the so-called constitutional substitution where the doping ion occupies the host metal positions of the matrix; the properties of which predetermine the oxidation state of the doping ion. Thus Fe(V) is stabilised in vanadium pentaoxide; this oxidation state unusual for iron is formed upon dissolution of trivalent iron oxide in a melt of vanadium pentaoxide. However, the formation of Fe(V) could be observed only after quenching of the samples into metallic mercury.

The formation of matrix systems under conditions of oxidative synthesis (sintering of Group 3–11 metal oxides with alkali

metal peroxides) revealed certain peculiarities of the final products which are determined by the properties of the matrix metal and the mechanisms of reactions. Thus it was found that the final products prepared with the use of molybdate and tungstate matrices contained extrinsic magnetics, *i.e.*, Mo(V)- and W(V)-containing exchangeable clusters of the ferro- and antiferromagnetic type. The initial steps of the reactions may involve the formation of bronze-type derivatives, trace amounts of which are partly stabilised in final products and elicit the corresponding magnetic responses.[50]

Yet another line of research related to the synthesis of bismuth derivatives in lower oxidation states has been described.[51] The authors have succeeded in preparation of homonuclear polycations of the types Bi_5^{3+}, Bi_8^{5+} and Bi_9^{5+}. A fragment of the crystal structure and the main structural elements of compound $Bi_{10}Nb_3Cl_{18}$ synthesised upon heating of a $Bi-BiCl_3-NbCl_5$ mixture to 550 °C are shown in Fig. 6. In the structure of this compound, the polycations Bi_9^{5+} are surrounded by octahedral counteranions $NbCl_6^{2-}$ containing Nb(IV). Usually, it is $NbCl_6^-$ ions containing Nb(V) that are more stable.

The crystal structure of compound Ni_8Bi_8SI synthesised by Baranov *et al.*[52,53] contains unusual bimetallic infinitely one-dimensional cationic columns of $[Ni_8Bi_8SI]_\infty^+$ which are made up of square nickel antiprisms surrounded by a sheath of bismuth atoms (Fig. 7). In this compound, nickel and bismuth atoms exist in unusually low oxidation states, which are responsible for the formation of such an unusual system of metallic bonds between the metal atoms. This structure can be regarded as consisting of a set of 'molecular' metal wires (a thread of nickel antiprisms) enclosed in an insulating matrix (a sheath of bismuth atoms). According to its physical properties, this compound represents a one-dimensional metallic conductor and a Pauli paramagnet.

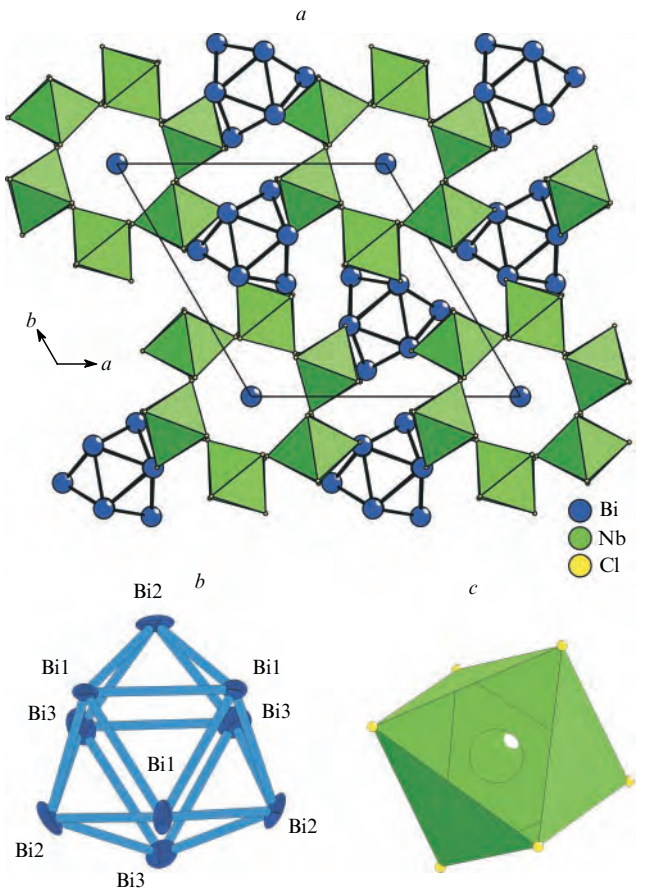

Figure 6. A fragment of the crystal structure (*a*) and the main structural elements (*b*, *c*) of $Bi_{10}Nb_3Cl_{18}$.

VII. Chemistry of inorganic biomaterials

Natural ageing of biomaterials, the building elements of any living organism, shortens their lifetime. What is most surprising is that ageing problems are inherent in such strong, at first glance,

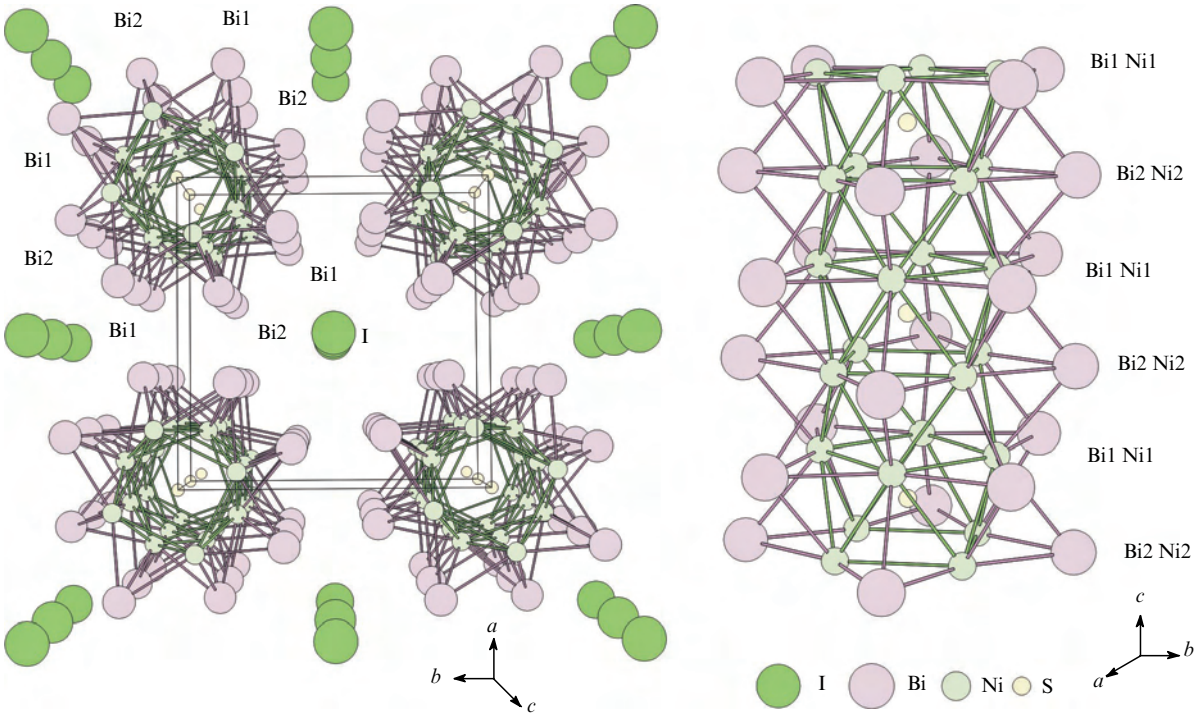

Figure 7. The crystal structure of Ni_8Bi_8SI.

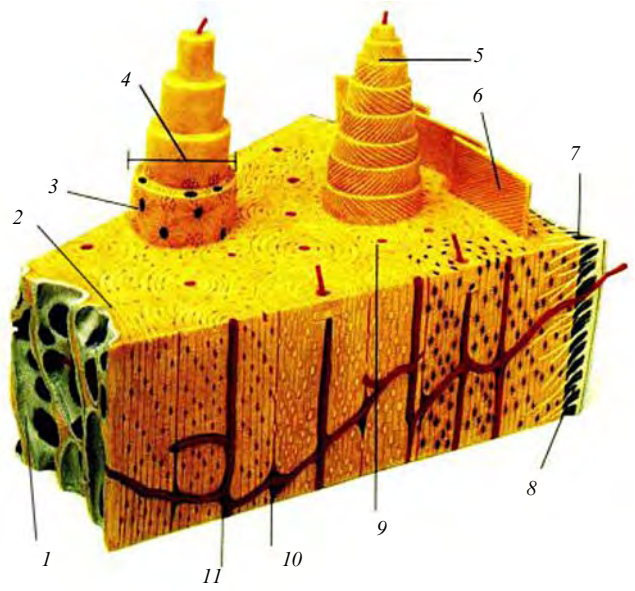

Figure 8. The levels of structural organisation of the bone tissue. (*1*) Internal bone tissue membrane, (*2*) intermediate plate, (*3*) osteocyte (bone cell), (*4*) osteon (Haversian system), (*5*) Haversian plate, (*6*) outer plate, (*7*) the Sharpie fibre, (*8*) peroosteum, (*9*) Haversian canal, (*10*) lacuna, (*11*) the Volkmann vessel.

natural materials as bone and dental tissues. From the standpoint of materials science, the bone tissue is a composite material which comprises both inorganic and organic components,[54–57] *viz*., hydroxyapatite $Ca_{10}(PO_4)_6(OH)_2$ (63 mass %) and the protein collagen (20 mass %), respectively (Fig. 8). In addition to Ca^{2+} and PO_4^{3-}, bone tissue contains appreciable amounts of Na^+, Mg^{2+}, K^+, Cl^-, F^- and CO_3^{2-} ions. The physicochemical character of the interactions between bone components, which ensures, in particular, its high strength properties, has not been finally established yet. Even the use of modern biotechnological approaches does not permit one to construct a full analogue of the natural bone tissue. Therefore, the use of artificial materials (implants) is still the only way to restore functioning of large regions of damaged bones.

Metal alloys based on low-toxic titanium are used in those cases where it is required to restore the bones of parts of the body exposed to heavy cyclic loads (*e.g*., hip joints). In other cases, preference is given to ceramic or composite materials based on calcium phosphates; their chemical compositions are similar to that of bone.[54–58] Among other modern trends in the field of implant design, special mention should be made of 'regeneration', *viz*., synthesis and application of materials able to stimulate regenerative processes in damaged tissues owing to their active interaction with the organism.[54] Such implants cannot be prepared without a thorough knowledge of mechanisms of reactions occurring in bone tissues in all steps of their evolution.

It is believed that not only the chemical composition, but also the morphology of synthetic hydroxyapatite (HAP) crystals are important characteristics that determine the response of the organism to the exogenous material of an implant. In this context, an ideal material should possess the chemical composition and granulometric properties similar to those of a bone biomineral, *e.g*., non-stoichiometric hydroxyapatite, $Ca_{10-x}(HPO_4)_x.(PO_4)_{6-x}(OH)_{2-x}$ ($0 < x < 1$). Its crystals have the shapes of plates ($40 \times 20 \times 5$ nm) with an axis c lying in the crystal plane (sp.gr. $P6_3/m$ of the hexagonal system; $a = b = 9.432$ Å, $c = 6.881$ Å) (Fig. 9).[55]

Calcium phosphate-based ceramic materials prepared by high-temperature treatment are routinely used in clinical practice.[59–62] Strong hydroxyapatite ceramic materials are chemically

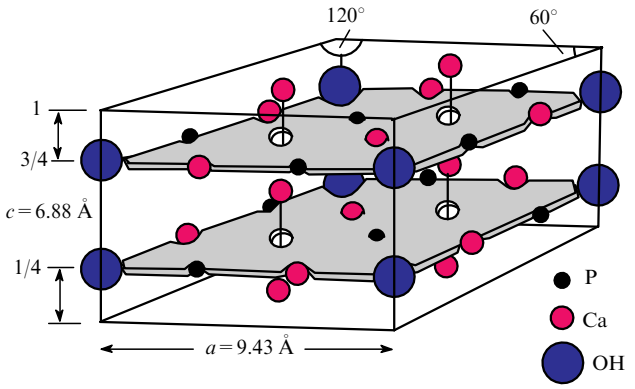

Figure 9. A simplified representation of a unit cell of hydroxyapatite.

inert, which significantly decelerates the resorption of the material and inhibits the growth of the contact bone tissue. Large specific surfaces of calcium phosphates prepared by solution methods (up to 100 $m^2\ g^{-1}$) make them more reactive in comparison with their high-temperature counterparts ($\sim 1\ m^2\ g^{-1}$). The results of the use of calcium phosphate-containing cements and biphasic composite materials suggest that in some cases the use of materials that could serve as bioapatite 'sources' *in vivo* is a simpler and more efficient approach (Fig. 10).[54, 59, 61]

Large-scale production of materials strictly corresponding to calcium phosphates of biological origin as regards their chemical and structural characteristics is very problematic. Nevertheless, there is every reason to believe that chemical and morphological match of a biomaterial and a bone mineral is one of the basic principles in the design of novel materials for biomedical purposes. Deviations of the compositions and sizes of artificial crystals from those of their natural counterparts can be employed for the directional synthesis of biomaterials with predetermined bioactivities. The practical implementation of such a programme requires the elucidation of a quantitative relationship, first, between chemical composition and micromorphology of calcium phosphate crystals and parameters of their solution synthesis and, second, between micromorphological parameters and bioactivity of the material.

The existing methods for the synthesis of HAP enable the preparation of highly dispersed powders with particle shapes varying unpredictably in a rather broad range, *viz*., from equiaxial to needle-shaped, depending on conditions.[55, 56, 63] Nevertheless, no explicit and quantitative information about the effects of parameters of HAP synthesis on the morphology of the target

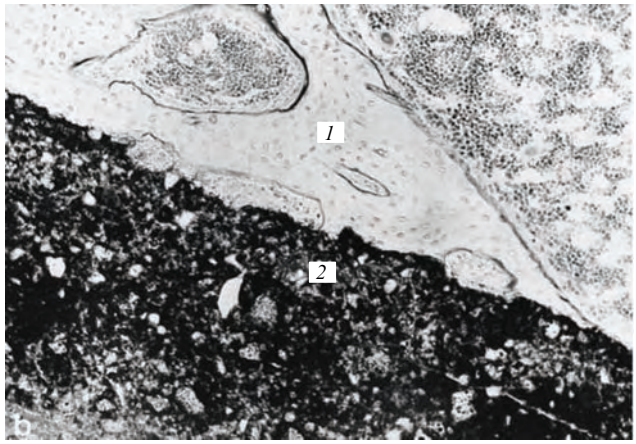

Figure 10. Formation of new bone tissue at the boundary of a cement implant with the composition 75% $Ca_3(PO_4)_2$ + 20% $Ca_4P_2O_9$ + 5% $CaHPO_4$.[62] (*1*) New tissue, (*2*) implant.

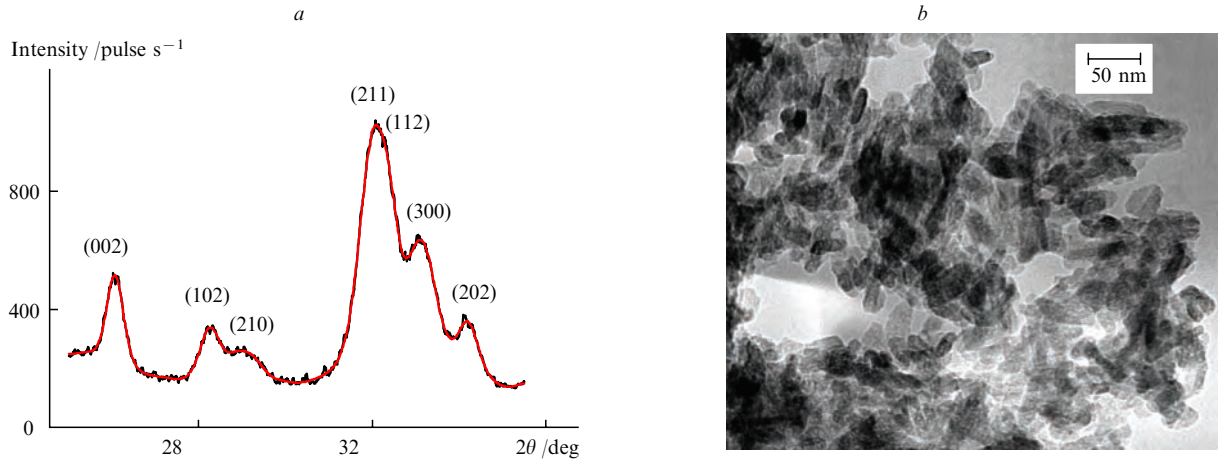

Figure 11. The results of studies of HAP powders using a multiprofile X-ray analysis (*a*) and transmission electron microscopy (*b*);[64] (*a*): crystal size 55 × 18 nm, the numbers in parentheses indicate Miller indexes.

product is available. It is noted that samples of calcium phosphate powders prepared according to one synthetic procedure elicit different responses of an organism up to a complete rejection of the material. This brings forth a vast variety of chemical and materials science-related problems connected with the synthesis of calcium phosphates with predetermined compositions and micromorphological characteristics as well as with prediction of their bioactivities *in vitro* and development of methods for the bioactivity correction by chemical modification of the synthetic product.

In practice, synthesis of HAP is mainly carried out in aqueous solutions and the existing methods can be classified into three main groups: (1) precipitation in solutions with constant or variable composition; (2) hydrothermal synthesis and (3) hydrolysis of calcium phosphates.[55, 56, 58, 63, 64] Precipitation of HAP from aqueous alkaline solutions yields fine-crystalline calcium hydroxyapatite.

$$10\,CaX_2 + 6\,M_2HPO_4 + 8\,MOH = Ca_{10}(PO_4)_6(OH)_2 + 20\,MX + 6\,H_2O,$$

where M = Na, K, NH_4, H; X = Cl, NO_3, CH_3COO, OH.

The formation of HAP is usually preceded by precipitation of amorphous calcium phosphate.[57, 65] The degree of crystallinity of the precipitated HAP increases with temperature and duration of ageing, while its non-stoichiometry, *i.e.*, the deviation of the Ca/P ratio from 1.67, increases with a decrease in pH, temperature and duration of synthesis.[55] The hydroxyapatite powders prepared by solution methods have a large specific surface ($\sim$100 m^2 g^{-1}) and a small size of crystallites ($\sim$100–200 nm). The size and the habitus of crystals depend on a number of factors, such as duration of crystallisation, temperature, composition of solution, degree of supersaturation, ionic strength, pH, the order of addition and mixing rates of reactants.[55, 56, 58, 64] The diversity of morphology of HAP crystals can be attributed to the fact that the synthesis is performed under strictly non-equilibrium conditions; the shape of the crystals strongly depends on the presence of admixtures.[65–68] In the presence of carbonate ions in the solution, carbonate apatite crystals of type A [$Ca_{10}(PO_4)_6(OH)_{2-x}\cdot(CO_3)_{x/2}$] or type B [$Ca_{10-x}Na_x(PO_4)_{6-x}(CO_3)_x(OH)_2$] differing in shape (plates or needles) depending on the carbonate content are formed.

As was mentioned above, the micromorphology of HAP powders is an important property which largely determines the areas of application of calcium phosphate-based biomaterials. It is of note that the choice of experimental conditions for the synthesis of HAP crystals of predetermined morphology implies knowledge of the contribution of each parameter (factor) of synthesis to, and of the result of their mutual action (interaction of factors) on, the two characteristic sizes of anisotropic HAP crystals, *viz.*, along and perpendicular to the axis [001]. This information, which has not been explicitly and quantitatively documented in the literature concerning the methods of apatite synthesis, is considered in a review.[64] A systematic study of effects of various parameters of HAP synthesis by precipitation from salt solutions (initial concentration of reagents, pH and temperature) on the sizes and shapes of the crystals formed has been carried out. The morphological characteristics of HAP crystals were established through mutual application of a comprehensive X-ray diffraction analysis and transmission electron microscopy (Fig. 11).

Mathematical models based on the results of statistical analysis of morphological characteristics of crystals allowed quantitation of various factors on HAP synthesis by precipitation. These factors (separately and in combination) determine ionic equilibria in solutions, since changes in temperature, pH and initial concentrations of solutes induce changes in the concentrations of ionic forms as can be judged from the calculations on activities of ions and ion pairs. One can state that there is a tendency towards an increase in the size of HAP crystals as the activities of the ion associates of $CaPO_4^-$ and $CaOH^+$ in solutions increase. The formation of HAP occurs in two steps. Amorphous calcium phosphate is formed from ion associates with the composition $Ca_9(PO_4)_6$ (the 'Pozner clusters') by a sol–gel transition mechanism in the first, relatively fast step. This has a mesoporous structure and hydroxyapatite nanocrystals formed in the second step by an AFC dissolution–HAP precipitation mechanism inherit porosity.[64, 65]

The use of hydrolytic reactions of calcium orthophosphates of the type

$$3\,Ca_3(PO_4)_2 + H_2O = Ca_9HPO_4(PO_4)_5OH$$

is yet another convenient approach to the synthesis of HAP crystals with different micromorphological features (needles, plates) [55, 63, 69, 70] (Fig. 12).

The sizes of HAP crystals obtained upon heating of solutions exceed significantly those synthesised by precipitation ($\sim$0.5–5 μm and $\sim$20–100 nm, respectively). It was noted above that materials with particles of submicrometric sizes are preferable for practical use. If HAP are prepared by hydrolysis of poorly soluble calcium orthophosphates [$CaHPO_4$, $CaHPO_4\cdot 2\,H_2O$, α- and β-$Ca_3(PO_4)_2$, $Ca_8(HPO_4)_2(PO_4)_4\cdot 5\,H_2O$, $Ca_4(PO_4)_2O$], the composition of the solution can be considered as being quasi-equilibrium, this depending on the solubility product of the solid phase. Like the majority of heterogenous processes, hydrolysis of calcium orthophosphates is characterised by a low rate, since the layer of the product formed blocks the surface of the starting material. The reaction can be accelerated by increasing the temperature and/or activating the

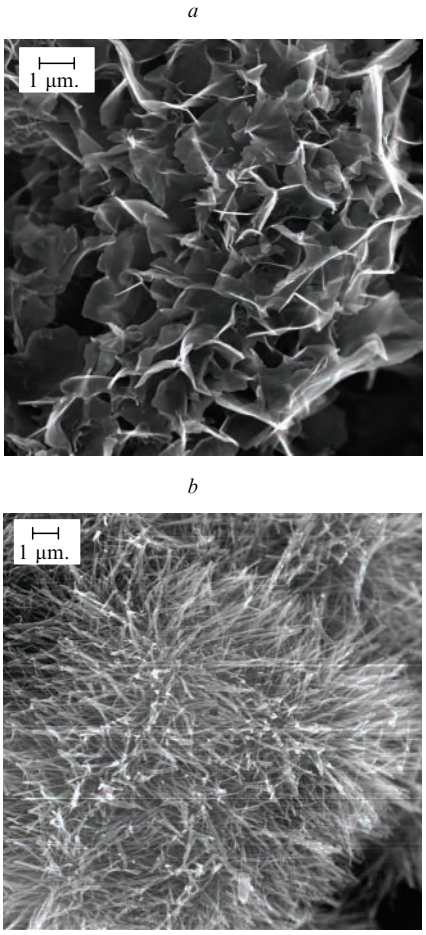

Figure 12. Micrographs of samples prepared by hydrolysis of α-$Ca_3(PO_4)_2$ at 40 (*a*) and at 100 °C (*b*).

reagent surface by sonication. It was shown that the conversion rate of a $CaHPO_4 - Ca(OH)_2$ mixture into HAP upon sonication of the suspension is 20% – 30% per 1 h, which is comparable with the rate of HAP synthesis from the same mixture at 60 °C. This is accompanied by the formation of aggregates consisting of spherical hydroxyapatite particles with a diameter of ~100 – 300 nm.[64]

The biological activities of calcium phosphates can be increased by increasing the specific surfaces of the powders and decreasing the sizes of the crystallites as well as by changing the physicochemical characteristics of the surface. An alternative approach consists of chemical modification of calcium phosphates aimed at preparing materials able to undergo active resorption upon interaction with body fluids. In this context, special attention is given to the development of methods for the synthesis of carbonate-containing hydroxyapatite $Ca_{10-0.5x}(PO_4)_{6-x}(CO_3)_x(OH)_2$ as well as silicon-containing hydroxyapatite, $Ca_{10}(PO_4)_{6-x}(SiO_4)_x(OH)_{2-x}$.[64,68] The latter can be synthesised by precipitation of HAP from solution using a reaction of amorphous calcium phosphate with tetraethoxysilane in an alkaline medium. It was found that silicon-containing HAP is more soluble in weakly acidic solutions than non-substituted hydroxyapatite.[64]

The very fact of design of materials stimulating osteogenesis suggests that the nearly half a century-old history of intense application of biomaterials has led to the comprehension that regeneration and replacement of bone tissue is an extremely complex and ambiguous problem. The use of one or another material depends on both the biomedical characteristics of a bone defect and, perhaps, the clinical case. Therefore, the solution of this problem is possible only if a broad range of biomaterials is available, while the choice of a maximum suitable material, which meets all the specific requirements, is the key to success.

VIII. Inorganic synthesis of functional materials using sonication, hydrothermal treatment and microwave irradiation

Inorganic synthesis of functional materials always requires the activation of the starting reactants whatever the mechanisms of chemical transformations involved. The simplest method is heating; its efficiency is estimated from the activation energy in the Arrhenius equation. However, this parameter, which is determined experimentally as a temperature coefficient of the reaction rate, has a physical meaning only if it is associated with a particular elementary process which limits the reaction rate in a given temperature range.

In real systems used in the synthesis of functional materials, chemical interactions involve at least two fundamental processes, *viz*., the chemical reaction itself and transfer of a substance to the reaction zone. Since the latter occurs owing to diffusion and the diffusional mobility of components of the solid is determined by the imperfection of its structure, it can be expected that the defects influence substantially the conditions of the solid-phase synthesis. This in turn suggests that the rate and direction of chemical transformations can be controlled through physical actions, which occur either simultaneously with the thermal activation or separately. It is often recommended that high-temperature factors are excluded, since both the reactants and the reaction products may be subject to undesirable changes which include:

— dissociation of the solid-phase product of inorganic synthesis, *e.g*., thermal dissociation of ferrites having a spinel structure according to the reaction:

$$6\,MFe_2O_4 \longrightarrow 4\,Fe_3O_4 + 6\,MO + O_2\,.$$

The magnetic and dielectric properties of the material are usually deteriorated by the reaction products;

— changes in the composition of reaction products due to the loss of volatile components, especially in gaseous media containing water vapour and CO_2. These changes are substantial, *e.g*., in the synthesis of solid electrolytes based on alkali metal polyaluminates and lithium-containing ferrites.

The efficacy of sonication in reactions occurring in various reaction systems in the synthesis of materials [71,72] depends on the phase state of a system. In liquid-phase systems (solutions, melts), cavitation, *i.e*., the formation, oscillation and collapse of microvesicles, is the main result of sonication which leads to the formation of short-living hot zones with characteristic temperatures up to ~5000 K and pressures up to 1000 atm. In some cases, 'collapse' of cavitation vesicles is accompanied by formation of intense microcurrents of fluids and potent shock waves, which enhance the mass transfer. As a consequence, in physicochemical systems (both homogenous and heterogenous) decomposition of volatile compounds, like metal carbonyls, acceleration of redox reactions, formation of stable emulsions and suspensions and disaggregation of particles in colloid solutions take place. Sonication of liquid-phase systems has proved to be efficient in classical reactions of organic and inorganic synthesis [73,74] as well as in the synthesis of amorphous and crystalline metal, oxide and carbide nanopowders.[75,76]

In solid-phase systems, sonication is efficient only if a certain power threshold of acoustic vibrations is exceeded concomitantly with a significant (by one or two orders of magnitude) increase in the number of dislocations and in the values of effective diffusion coefficients and the formation of new interphase contacts.[77,78] As a consequence, sonication of reaction mixtures may change the reaction mechanism, decrease considerably the apparent activation energy and the temperature of vigorous interactions of the reactants.[79–81] Acoustic activation of solid-phase processes enables synthesis of various oxide materials [80,81] and active forms of

precursors [82] and, in some special cases, directed modulation of the structure-dependent properties of solid-phase products.[83]

It has been found [83] that the concentration of structural defects in sonicated compounds depends non-linearly on the amplitude of input acoustic vibrations and the temperature. The defectiveness of samples increases significantly (by more than one order of magnitude), in a definite temperature interval and at a definite ultrasound volume, *i.e.*, the acoustic and thermal effects are synergistic.

At fixed temperatures, a significant (2–3-fold) increase in effective diffusion coefficients of carbon in steels is observed only at definite acoustic input vibration amplitudes.[84] Similarly, at fixed ultrasound volume the defectiveness of simple metal oxides increases anomalously, however, only in a narrow temperature range.[85] It is of note that the temperature range corresponding to the maximum activation is determined by the chemical nature of the oxides that undergo sonication. Thus it has been shown that in high-temperature sonication of iron(III) oxide ultrasonic generation and annihilation of defects and their thermal annealing compete.[85] The rates of each of these processes depend differently on temperature; therefore, the defectiveness of α-Fe_2O_3 and the corresponding reactivity change non-linearly reaching a maximum at $\sim$800 °C.

Combination of different factors allows one to change both the kinetics and the mechanisms of solid-phase reactions. Studies of interactions in the system $Fe_2O_3 + Li_2CO_3$ have shown [79] that superposition of an acoustic field at definite temperatures induces changes in the reaction mechanism, *viz.*, the chemical interaction at the interphase becomes a limiting step, whereas under normal conditions this reaction is limited by the formation of nuclei and their progressive diffusion-dependent growth. In turn, the reaction rate increases significantly with a change in the reaction mechanism and an increase in the mass transfer rate. It is noteworthy that in this case the temperature, which corresponds to the maximum effect of the ultrasound, is lower than the temperature of the onset of the reaction in the system under ordinary conditions, *i.e.*, sonication allows one to reduce significantly (by 100–150 °C) the temperature of synthesis. Studies of solid-phase reactions of ferrite formation

$$LiFeO_2 + 2\,Fe_2O_3 \xrightarrow{530-650\ ^\circ C} LiFe_5O_8\,,$$

$$ZnO + Fe_2O_3 \xrightarrow{600-800\ ^\circ C} ZnFe_2O_4\,,$$

$$NiO + Fe_2O_3 \xrightarrow{600-800\ ^\circ C} NiFe_2O_4$$

have shown [86, 87] that temperatures of the onset of the reaction decrease by 50–200 °C in the case of sonication, while the time of synthesis of monophasic ferrites diminishes 1.5–2-fold. A change in the reaction mechanism is due to a direct formation of the reaction zone in the acoustic field; its most characteristic feature is the presence of a well-defined initial step of a sonochemical reaction mediated by a special mechanism of formation of intercrystallite contacts in the ultrasonic field.

Of special interest are studies of effects of sonication on hydrothermal synthesis of simple and complex oxides and chalcogenides.[88] First of all, it has been established [89] that sonication causes cavitation both in hydrothermal solutions and ordinary liquid media the intensity of which at 250 °C is 70%–80% of that observed at 25 °C. Cobalt, titanium and zirconium oxides as well as ferrites $Ni_{1-x}Zn_xFe_2O_4$ were used as subjects in these studies. Hydrothermal treatment and sonication of a suspension of an amorphous gel of $Co(OH)_2$ in water at 250 °C yielded the phase Co_3O_4; no such phase was formed without sonication. Most probably, sonolysis of water in hydrothermal solutions gives rise to hydrogen peroxide which induces the oxidation of Co(II) into Co(III). The particle sizes of the oxide products of hydrothermal synthesis in an ultrasonic field are significantly smaller than those of an analogous product synthesised without sonication (Fig. 13).

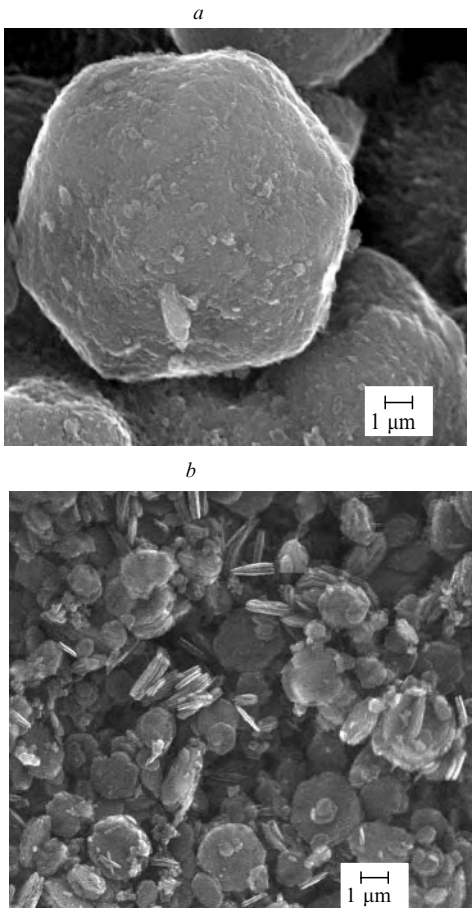

Figure 13. Micrographs of products of hydrothermal syntheses in the absence (*a*) and in the presence of an ultrasonic field (*b*).

Hydrothermal treatment of amorphous gels $ZrO_2 \cdot n\,H_2O$ and $TiO_2 \cdot n\,H_2O$ and simultaneous sonication result in a significant increase in the rates of their crystallisation, whereas sonication of products of hydrothermal synthesis favours the formation of thermodynamically more stable phases (Fig. 14).[90]

Although the idea of large-scale application of microwave heating for domestic and technological purposes was realised rather long ago [91] and numerous studies were undertaken in the past decade on the microwave-induced synthesis and sintering of functional materials,[92, 93] the physicochemical nature of the processes occurring in microwave synthesis still remains obscure. Oxides, hydroxides, salts or their mixtures were used as precursors for various functional materials including ferrites, manganites, cobaltites, nickelates and cuprates subject to microwave radiation.[94–96]

According to theoretical concepts on the interaction of microwave radiation with matter,[97] effective absorption of energy requires the presence in the matter of either dipoles capable of changing their orientation and rotating under the action of microwave radiation, or free charge carriers able to move in an applied microwave field. Many inorganic salts possess low electronic, hole or ionic conductivities. At the same time, water molecules, which are present in the crystal lattices of crystal hydrates, and some anions have high dipole moments. Thus, in the majority of salt systems the most probable mechanism of absorption of microwave radiation is related to dipoles.

It has been found experimentally [94] that compounds devoid of chemically bound water (carbonates, nitrates and oxalates of alkali and alkaline-earth elements) virtually do not adsorb microwave radiation. In contrast, crystal hydrates of inorganic salts interact with a microwave field, the mode of this interaction being

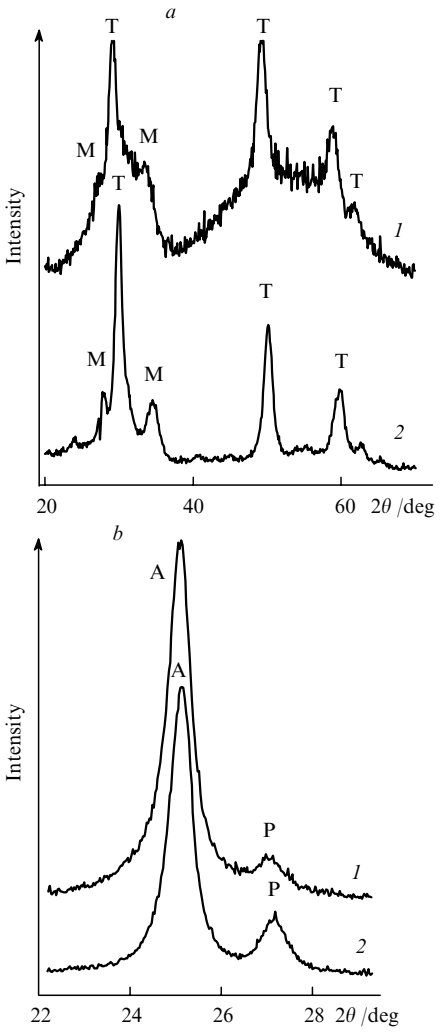

Figure 14. X-ray diffraction spectra of products of hydrothermal treatment of $ZrO_2 \cdot n\,H_2O$ (*a*) and $TiO_2 \cdot n\,H_2O$ (*b*) performed at 250 °C for 3 hours without (*1*) and with (*2*) sonication.
Designations: T, tetragonal phase of ZrO_2; M, monoclinic phase of ZrO_2; A, anatase; P, rutile.

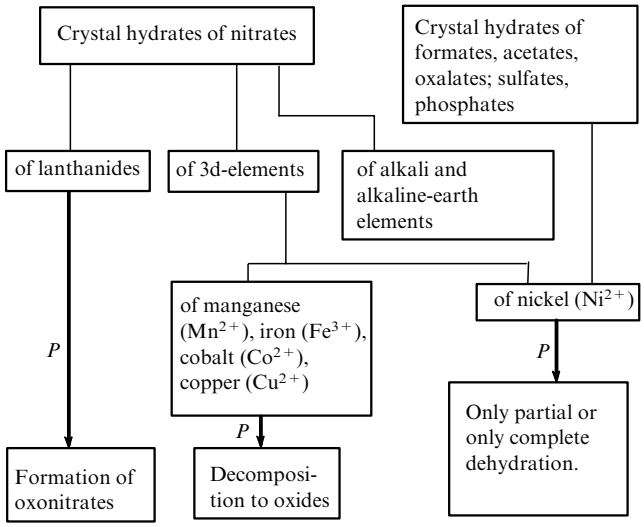

Figure 15. Interaction of crystal hydrates with microwave radiation. *P*, energy of a microwave field.

dependent on the chemical nature of the cations (Fig. 15). Later, it was shown that the decomposition of crystal hydrates in the microwave field to oxides takes place only if the oxide formation occurs prior to the removal of all the water present in the system. Of all the salt crystal hydrates tested in this study,[94] only 3d-metal nitrate crystal hydrates meet this requirement and can be used as active (with respect to microwave radiation) components in the synthesis of complex oxide phases. A generalised scheme of interaction of metal salt crystal hydrates with microwave radiation is shown in Fig. 16. Studies of salt precursors have demonstrated the expediency of *in situ* application of microwave treatment of salt mixtures in solid-phase reactions, since highly dispersed oxide particles formed upon decomposition of salt mixtures and distributed uniformly throughout the reaction bulk react actively with one another.

Specific 'non-thermal' effects of microwave radiation caused by generation of ionic currents on intercrystallite and interaggregate boundaries make a significant contribution to diffusional processes occurring in the solid-phase reactions; the intensity of ionic currents increases in highly dispersed systems. Consequently, microwave irradiation of a reaction mixture can be accompanied by an increase in the rate and a decrease in the temperature of solid-phase interactions. It is this effect that is observed in synthesis of functional materials.[98–105]

However, it would be erroneous to think that microwave-induced synthesis always makes use of salt precursors able to convert microwave energy into thermal energy starting from room temperature. It is known that the energy (*P*) absorbed by an object placed into a uniform microwave field is expressed by the equation:

$$P = 2\pi f \varepsilon_0\, K \tan\delta\, |E|^2,$$

where f is the microwave frequency, ε_0 is the vacuum permittivity, K is the dielectric constant of the sample, $\tan\delta$ is the dielectric loss tangent and E is the microwave field intensity in the sample under assay. The K and δ values depend on temperature and on the nature of the phases used as precursors. For example, the mixture $SrCO_3 - Co(NO_3)_2 \cdot 6\,H_2O - Fe_2O_3$ used in the synthesis of $SrFeCo_{0.5}O_y$, a promising electron-ionic conductor, can absorb low-wavelength energy only in those cases where microwave irradiation is preceded by ordinary heating as a result of which the oxidative thermolysis of cobalt nitrate yields Co_3O_4. The latter effectively absorbs microwave energy and favours rapid heating of the entire reaction mixture to temperatures above 1000 °C, although other components of the reaction mixture ($SrCO_3$, Fe_2O_3) are inert in the microwave field and are thermally activated only upon interaction with Co_2O_3.[106]

Non-stoichiometric oxides of the type TiO_{2-x} or Ta_2O_{5-x},[107] hydroxides or basic salts[95] as well as amorphous carbon used as soot[108] or a highly dispersed metal[109] can be used as active components for microwave irradiation. In the manufacture of compact piezoelectric ceramic materials of the type $(Ba,Sr)TiO_3$ (see Ref. 110) or ion-conducting ceramic materials of the type Na-β-alumina,[111] the powdered precursor with the identical composition is synthesised by ordinary heating, whereas sintering is performed in a microwave field.

And, finally, the use of the so-called monomodal microwave heating[112,113] based on the propagation of an electromagnetic beam from a magnetron along a waveguide where a standing wave is established opens up radically new opportunities for inorganic synthesis, for it allows one to focus the microwave energy in a small volume of the reaction mixture and to initiate very rapidly chemical and structural transformations that are impossible in the case of ordinary thermal or multimodal microwave heating.

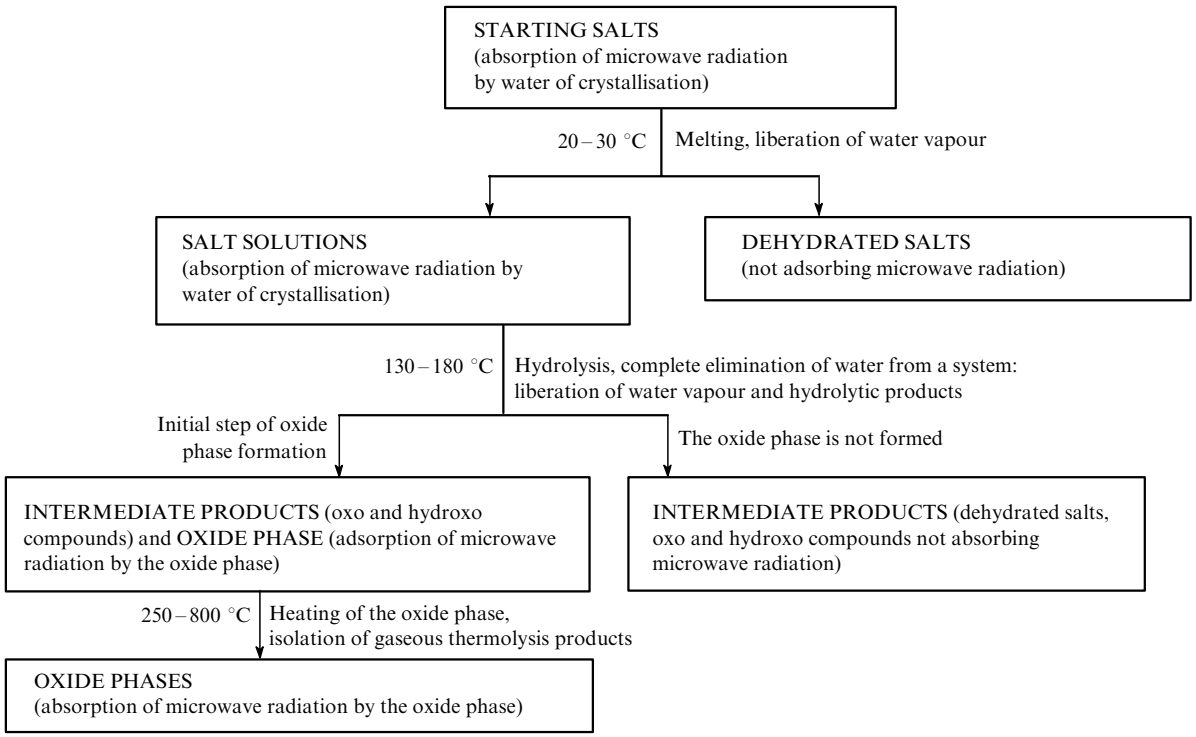

Figure 16. A scheme of the interaction of metal salt crystal hydrates with microwave radiation.

IX. Conclusion

In the past two decades, inorganic chemistry has experienced impressive changes owing to its integration with physical chemistry, physics of solids, organic chemistry and biochemistry and the use of advanced instrumental methods. The range of subjects of inorganic chemistry has been extended considerably. Now, these encompass not only chemical compounds, but also materials, sometimes even those which contain, along with an inorganic component, organic, polymeric or biopolymeric fragments. At present, studies of the majority of subjects are carried out at several levels. In addition to crystal or molecular structures, they involve electronic and magnetic structures of various compounds, specific defects of their crystal structures, distribution of microadmixtures, structures of interfaces in multicrystalline compounds, nanostructures, micro- and mesopore structures and surface structures as well as the effects of the aforementioned organisational levels of a substance on its properties. Special mention should be made of the unusual extension of the range of the impact of different kinds of energy on substances aimed at determining their limit characteristics and the development of methods for the construction of novel materials.

The spectrum of problems considered in this review does not encompass all the trends in inorganic chemistry related to the design of novel functional materials. For example, the problem of organisation of the reaction zone in the synthesis of materials considered in the review [7] was mentioned only briefly. Neither was the problem of the development of microcomposite materials based on superconducting cuprates [114] discussed in proper detail. In addition to the functional inorganic materials considered in the present review, the subjects under study at the Division of Inorganic Chemistry of the Department of Chemistry and the Department of Materials Science of MSU include:

— inorganic structures as materials for gas sensors;†

— barrier materials based on $BaMO_3$ (M = Zr, Hf, Th, Ce, Ti);[116, 117]

— luminescent nanocomposites based on $A^{IV}B^{VI}$;[118, 119]

— low-dimensional structures and superlattices;[120, 121]

— new generations of semiconductors and semiconductor heterostructures;[122 – 124]

— oxygen-conducting membranes and solid electrolytes;[125, 126]

— materials for lithium current sources;[127 – 129]

— magnetic nanocomposites based on glassy matrices;[130]

— photonic crystals;[131]

— ceramic pigments based on hydroxyapatites containing copper ions in an unusual linear coordination.[132]

It should be mentioned in conclusion that other promising trends of research related primarily to the development of molecular electronics,[133] spintronics [134] and biocrystal systems [135] require active participation of inorganic chemists. Taking into account the extreme dynamism shown by the scientific community towards the design of novel functional materials, it has become necessary to follow closely the new trends in this field which are especially successfully documented in journals such as 'MRS Bulletin', 'Advanced Materials', 'Materials Today' and 'Materials Chemistry'. Unfortunately, no domestic analogues are available so far.

The author thanks his colleagues at the Division of Inorganic Chemistry of the Department of Chemistry and the Department of Materials Science of MSU for valuable assistance in the preparation of this review for publication. The contributions of

† A review devoted to this subject [115] will be published in the next issue of 'Russian Chemical Reviews'.

Drs A V Lukashin, A G Veresov, A R Kaul and E A Goodilin are especially highly appreciated.

References

1. M Van Rossum *Microelectron. Eng.* **34** 125 (1996)
2. E Suhir *Microelectron. J.* **31** 839 (2000)
3. N Yamazoe, N Miura, in *Chemical Sensor Technology* (Ed. S Yamanchi) (Tokyo: Kidansha, 1992)
4. H Ohno *Science* **291** 840 (2001)
5. H Koinuma, H N Aiger, Y Matsumoto *Sci. Technol. Adv. Mater.* **1** 1 (2000)
6. Y K Yoo, X-D Xiang *J. Phys.: Condens. Matter* **14** R49 (2002)
7. Yu D Tretyakov *Usp. Khim.* **72** 731 (2003) [*Russ. Chem. Rev.* **72** 651 (2003)]
8. Yu D Tretyakov *Z. Phys. Chem.* **207** 93 (1998)
9. Yu D Tretyakov *Dokl. Akad. Nauk* **388** 1 (2003) [a]
10. N N Oleinikov, E A Goodilin, Yu D Tretyakov, in *Rossiiskaya Nauka. Vystoyat' i Vozrodit'sya* (Russian Science. Hold out and Reappear) (Moscow: Nauka, 1997)
11. Yu D Tretyakov *Tverdofaznye Reaktsii* (Solid-Phase Reactions) (Moscow: Khimiya, 1978)
12. Yu D Tretyakov, Doctoral Thesis in Chemical Sciences, Moscow State University, Moscow, 1965
13. Yu D Tretyakov, N N Oleynikov, O A Shlyaktin *Cryochemical Technology of Advanced Materials* (London: Chapman and Hall, 1997)
14. Yu D Tretyakov, O A Shlyakhtin *J. Mater. Chem.* **9** 1 (1999)
15. Yu D Tretyakov, A P Mozhaev, N N Oleinikov *Osnovy Kriokhimicheskoi Tekhnologii* (Foundations of Cryochemical Technology) (Moscow: Vysshaya Shkola, 1987)
16. S V Naumov, A P Mozhaev, I V Gordeev, Ya A Kesler, N A Fomkin, V I Pershin *Zh. Fiz. Khim.* **56** 556 (1982) [b]
17. S V Eliseeva, O V Morozov, O V Kotova, K V Anikin, A G Vitukhnovskii, N P Kuz'mina, in *XXI Mezhdunarodnaya Chugaevskaya Konferentsiya po Koordinatsionnoi Khimii (Tez. Dokl.), Kiev, 2003* [International Chugaev Conference on Coordination Chemistry (Abstracts of Reports), Kyiv, 2003] p. 252
18. G Wahl, Ch Metz, S Samoilenkov *J. Phys. IV* **11** 3 (2001)
19. M B Romanov, I E Korsakov, A R Kaul, S Yu Stefanovich, I A Bolshakov, G Wahl *Adv. Mater.: J. CVD* (2004) (in the press)
20. A M Abakumov, E A Antipov, L M Kovba, E M Kopnin, S N Putilin, R V Shpanchenko *Usp. Khim.* **64** 769 (1995) [*Russ. Chem. Rev.* **64** 719 (1995)]
21. E V Antipov, Doctoral Thesis in Chemical Sciences, Moscow State University, Moscow, 1997
22. A M Abakumov, M G Rozova, E A Ardashnikova, E V Antipov *Usp. Khim.* **71** 442 (2002) [*Russ. Chem. Rev.* **71** 383 (2002)]
23. A M Abakumov, M G Rozova, E V Antipov *Usp. Khim.* **73** 917 (2004) [*Russ. Chem. Rev.* **73** 847 (2004)]
24. A R Kaul, O Yu Gorbenko, A A Kamenev *Usp. Khim.* **73** 932 (2004) [*Russ. Chem. Rev.* **73** 861 (2004)]
25. Yu D Tretyakov, E A Goodilin *Usp. Khim.* **69** 3 (2000) [*Russ. Chem. Rev.* **69** 1 (2000)]
26. Yu D Tretyakov, E A Goodilin *J. Inorg. Chem.* **46** (Suppl. 3) 203 (2001)
27. O Yu Gorbenko, A R Kaul, N A Babushkina, L M Belova, B Guettler *Aust. J. Phys.* **52** 269 (1999)
28. N A Babushkina, L M Belova, O Yu Gorbenko, A R Kaul, A A Bosak, V I Ozhegin, K I Kugel *Nature (London)* **391** 159 (1998)
29. Yu D Tretyakov *Izv. Akad. Nauk SSSR, Neorg. Mater.* **21** 693 (1985) [c]
30. Yu D Tretyakov, Yu D Metlin *Zh. Vsesoyuz. Khim. O-va im. D I Mendeleeva* **36** 265 (1991) [d]
31. A V Lukashin, S V Kalinin, A A Vertegel, Yu D Tretyakov *Dokl. Akad. Nauk* **369** 781 (1999) [a]
32. A V Lukashin, N G Zhuravleva, A A Eliseev, S V Kalinin, A A Vertegel, Yu D Tretyakov *Dokl. Akad. Nauk* **383** 504 (2002) [a]
33. A V Lukashin, M V Chernysheva, A A Vertegel, Yu D Tretyakov *Dokl. Akad. Nauk* **388** 200 (2003) [a]
34. M P Nikiforov, M V Chernysheva, A V Lukashin, A A Vertegel, Yu V Maksimov, S V Novichikhin, I P Suzdalev, Yu D Tretyakov *Dokl. Akad. Nauk* **391** 53 (2003) [a]
35. A V Lukashin, A A Vertegel, A A Eliseev, M P Nikiforov, P Goernert, Yu D Tretyakov *J. Nanopart. Res.* **5** 455 (2003)
36. Yu D Tretyakov, A V Lukashin, A A Eliseev *Usp. Khim.* **73** 974 (2004) [*Russ. Chem. Rev.* **73** 899 (2004)]
37. M M Shatruk, K A Kovnir, A V Shevelkov, I A Presniakov, B A Popovkin *Inorg. Chem.* **38** 3455 (1999)
38. L N Reshetova, J V Zaikina, A V Shevelkov, K A Kovnir, M Lindsjo, L Kloo *Z. Anorg. Allg. Chem. B* **628** 2145 (2002)
39. A V Olenev, O S Oleneva, M Lindsjo, L Kloo, A V Shevelkov *Chem. Eur. J.* **9** 3201 (2003)
40. W Schottky, C Wagner *Z. Phys. Chem. B* **11** 163 (1931)
41. Yu D Tretyakov *Khimiya Nestekhiometricheskikh Okislov* (The Chemistry of Non-Stoichiometric Oxides) (Moscow: Moscow State University, 1974)
42. Yu D Tretyakov, A F Maiorova, Yu M Berezovskaya, in *Electrical Properties of Oxide Materials* (Eds J Nowothy, C C Sorroll) (Zürich: Trans. Tech. Publ., 1997) p. 283
43. O A Malykh, A P Mozhaev, V P Shabatin *Vestn. Mosk. Univ., Ser. 2: Khim.*; article deposited at the VINITI, No. 2543-85 (Moscow, 1985)
44. J S Anderson *J. Chem. Soc., Dalton Trans.* **12** 1335 (1973)
45. E A Goodilin, Doctoral Thesis in Chemical Sciences, Moscow State University, Moscow, 2003
46. N N Krot, A D Gel'man *Dokl. Akad. Nauk SSSR* **177** 124 (1967) [a]
47. N B Mikheev *Zh. Neorg. Khim.* **47** 558 (2002) [e]
48. Yu M Kiselev *Zh. Neorg. Khim.* **39** 1266 (1994) [e]
49. Yu M Kiselev *Zh. Neorg. Khim.* **48** 2050 (2003) [e]
50. Yu A Koksharov, V A Avdei, V D Dolzhenko, Yu M Kiselev *Mendeleev Commun.* 2004 (in the press)
51. A N Kuznetsov, P I Naumenko, B A Popovkin, L Kloo *Izv. Akad. Nauk, Ser. Khim.* **10** 1989 (2003) [f]
52. A I Baranov, A V Shevelkov, A V Olenev, B A Popovkin, L Kloo, in *High Temperature Superconductors and Novel Inorganic Materials Engineering MSU HTSC-VI, Moscow, St Petersburg, 2001* PIII-11
53. A I Baranov, L Kloo, A V Olenev, B A Popovkin, A I Romanenko, A V Shevelkov *J. Am. Chem. Soc.* **123** 12 375 (2001)
54. L L Hench *J. Am. Ceram. Soc.* **81** 1705 (1998)
55. W Suchanek, M Yoshimura *J. Mater. Res.* **13** 94 (1998)
56. A G Veresov, V I Putlyaev, Yu D Tretyakov *Ros. Khim. Zh.* **44** 32 (2000) [d]
57. S V Dorozhkin, M Epple *Angew. Chem., Int. Ed.* **41** 3130 (2002)
58. V P Orlovskii, G E Sukhanova, Zh A Ezhova, G V Rodicheva *Zh. Vses. Khim. O-va im D I Mendeleeva* **36** 683 (1991) [d]
59. M Vallet-Regi *J. Chem. Soc., Dalton Trans.* 97 (2001)
60. R H Doremus *J. Mater. Sci.* **27** 285 (1992)
61. M Bohner *Eur. Spine J.* **10** 114 (2001)
62. K DeGroot *J. Ceram. Soc. Jpn.* **99** 943 (1991)
63. T Kanazava *Neorganicheskie Fosfatnye Materialy* (Inorganic Phosphate Materials) (Kiev: Naukova Dumka, 1998)
64. A G Veresov, Candidate Thesis in Chemical Sciences, Moscow State University, Moscow, 2003
65. A V Soin, A G Veresov, V I Putlyaev *Vestn. Voronezh. GTU, Ser. Materialoved.* **1.12** 36 (2002)
66. A Ito, N Kanzaki, K Onuma, G Treboux, S Tsutsumi *J. Phys. Chem. B* **104** 4189 (2000)
67. E D Eans, A W Hailer *Calcif. Tissue Int.* **66** 449 (2000)
68. G V Rodicheva, V P Orlovskii, V I Privalov, S M Barinov, F Rustikelli, S Oskarsson *Zh. Neorg. Khim.* **46** 1798 (2001) [e]
69. K S TenHuisen, P W Brown *J. Am. Ceram. Soc.* **82** 2813 (1999)
70. A G Veresov, N V Plohih, O V Sinitsina, V I Putlyaev, Yu D Tretyakov, in *Solid State Chemistry (Abstracts of Reports), Oslo, 2001* p. 109
71. K S Suslick, G J Price *Annu. Rev. Mater. Sci.* **29** 295 (1999)
72. T J Meson *Ultrasonics Sonochem.* **10** 175 (2003)
73. M Chanon, J L Luche, in *Synthetic Organic Chemistry* (Ed. J-L Luche) (New York: Plenum, 1998) p. 376

74. M A Margulis *Sonochemistry and Cavitation* (Luxemburg: Gordon and Breach, 1995)
75. K Yang, J Zhu, J Zhu, S Huang, X Zhu Ma *Mater. Lett.* **57** 4639 (2003)
76. K S Suslick, M Fang, T Hyeon *J. Am. Chem. Soc.* **118** 11 960 (1996)
77. N A Tyapunina, E K Naimi, G M Zinenkova *Deistvie Ul'trazvuka na Kristally s Defektami* (Ultrasound Action on Crystals with Defects) (Moscow: Moscow State University, 1999)
78. O V Bubnovskaya, Candidate Thesis in Physical and Mathematical Sciences, Moscow State University, Moscow, 1997
79. A E Baranchikov, V K Ivanov, N N Oleinikov, Yu D Tretyakov *Zh. Neorg. Khim.* **48** 42 (2003) [e]
80. A E Barantchikov, A N Baranov, V K Ivanov, N N Oleynikov, Yu D Tretyakov *Solid State Ionics* **141 – 142** 689 (2001)
81. V M Kuznetsov, A N Baranov, N N Oleinikov, Yu D Tretyakov *Dokl. Akad. Nauk* **352** 355 (1997) [a]
82. B B Khanukaev, N S Khanukaeva *Zh. Fiz. Khim.* **72** 1607 (1998) [b]
83. O V Abramov *Vozdeistvie Moshchnogo Ul'trazvuka na Zhidkie i Tverdye Metally* (Effect of Powerful Ultrasound on Liquid and Solid Metals) (Moscow: Nauka, 2000)
84. A V Kulemin *Ul'trazvuk i Diffuziya v Metallakh* (Ultrasound and Diffusion in Metals) (Moscow: Metallurgiya, 1978)
85. V M Kuznetsov, Candidate Thesis in Chemical Sciences, Institute of General and Inorganic Chemistry, Moscow, 1999
86. A E Baranchikov, V K Ivanov, N N Oleinikov, Yu D Tretyakov *Zh. Neorg. Khim.* **48** 1828 (2003) [e]
87. A E Baranchikov, V K Ivanov, G P Murav'eva, N N Oleinikov, Yu D Tretyakov *Dokl. Akad. Nauk* (2004) [a] (in the press)
88. R Walton *Chem. Soc. Rev.* **31** 230 (2002)
89. P E Meskin, A E Baranchikov, V K Ivanov, E V Kisterev, A A Burukhin, B R Churagulov, N N Oleinikov, Sh Komarneni, Yu D Tretyakov *Dokl. Akad. Nauk* **389** 207 (2003) [a]
90. P E Meskin, Y V Kolenko, A E Baranchikov, V K Ivanov, B R Churagulov, N N Oleynikov *Mater. Res. Soc. Symp. Proc.* **389** L8.12.1 (2004)
91. R V Decareau *Microwaves in the Food Processing Industry* (New York: Academic Press, 1985)
92. D E Stein (Ed.) *Microwave Processing of Materials* (Washington, DC: National Academy Press, 1994)
93. E T Thostenson, T-W Chou *Composites, A* **30** 1055 (1999)
94. A S Vanetsev, Candidate Thesis in Chemical Sciences, Moscow State University, Moscow, 2004
95. P Kalyani, N Kalaiselvi, N G Renganathan *J. Power Sources* **123** 53 (2003)
96. R K Sahu, M L Rao, S S Manohazan *J. Mater. Sci.* **36** 4099 (2001)
97. R E Newnham, S J Jang, M Xu *Ceram. Trans.* **21** 51 (1991)
98. M Kato, K Sakakibara, Y Koike *Appl. Supercond.* **5** 33 (1997)
99. B Vaidhyanathan, D K Agrawal, T R Stout, Y Fang *Mater. Lett.* **42** 207 (2000)
100. H Yan, X Huang, L Chen *J. Power Sources* **81 – 82** 647 (1999)
101. Y-F Liu, X-Q Liu, G Y Meng *Mater. Lett.* **48** 176 (2001)
102. R K Satu, M L Rao, S S Manoharan D Elefant, P Verges, A Gueth, C M Schneider *J. Mater. Res.* **17** 3090 (2002)
103. Y-P Fu, K-Y Pan, C-H Lin *J. Alloys Compd.* **349** 228 (2003)
104. J-J Zhu, J-M Zhu, X-H Liao, J-L Fang, M-G Zhou, H Y Chen *Mater. Lett.* **53** 12 (2002)
105. T Kodaira, K Miyazawa, T Ikeda, Y Kiyozumi *Micropor. Mesopor. Mater.* **29** 329 (1999)
106. D Huo, J Zhang, Z Xu, Y Yang, H Yang *J. Am. Ceram. Soc.* **85** 510 (2002)
107. J P Cheng, D K Agrawal, S Komarneni, M Mathias, R Roy *Mater. Res. Innovat.* **1** 44 (1997)
108. M H Bhat, A Miura, P Vinatier, A Levasseur, K J Rao *Solid State Commun.* **125** 557 (2003)
109. M Higuchi, K Katayama, Y Azuma, M Yukawa, M Suhara *J. Power Sources* **119 – 121** 258 (2003)
110. W Yang, A Chang, B Yang *J. Mater. Synth. Proc.* **10** 363 (2002)
111. R Subasri, T Mathews, O M Sreednaran, V S Raghunathan *Solid State Ionics* **158** 199 (2003)
112. M Gasgnier, A Petit, M-F Gardette, E Riviere, S Launay, A Dworkin, S Toscani *J. Alloys Compd.* **309** 219 (2000)
113. M Gasgnier, J Osterero, A Petit *J. Alloys Compd.* **275**/**277** 41 (1998)
114. P E Kazin, Yu D Tretyakov *Usp. Khim.* **72** 960 (2003) [*Russ. Chem. Rev.* **72** 849 (2003)]
115. R B Vasiliev, L I Ryabova, M N Rumyantseva, A M Gaskov *Usp. Khim.* **73** 1019 (2004) [*Russ. Chem. Rev.* **73** 939 (2004)]
116. Yu D Tretyakov, T E Os'kina, A L Vinokurov *Materialovedenie* **9** 47 (2000)
117. A L Vinokurov, O A Shlyakhtin, A V Orlov, Yu D Tretyakov *Dokl. Akad. Nauk* **384** 634 (2002) [a]
118. N G Zhuravleva, A A Eliseev, A V Lukashin, A A Vertegel, Yu D Tretyakov *Vestn. Voronezh. GTU, Ser. Materialoved.* **1.8** 11 (2000)
119. A V Lukashin, A S Vyacheslavov, A A Vertegel, Yu D Tretyakov *Dokl. Akad. Nauk* **385** 71 (2002) [a]
120. D O Charkin, P S Berdonosov, A M Moisejev, R R Shagiakhmetov, V A Dolgikh, P Lightfoot *J. Solid State Chem.* **146** 527 (1999)
121. P S Berdonosov, D O Charkin, A M Kusainova, C H Hervoches, V A Dolgikh, P Lightfoot *Solid State Sci.* **2** 553 (2000)
122. L G Bychkova, O I Davarashvili, M I Enukashvili, V P Zlomanov *Fizika* **7** 621 (2002)
123. V P Zlomanov *Mater. Sci. Semicond. Proc.* **16** 368 (2003)
124. L V Yashina, V I Shtanov, Z G Yanenko *J. Cryst. Growth* **252** 68 (2003)
125. N V Lyskov, Yu G Metlin, V V Belousov, Yu D Tretyakov *Solid State Ionics* **166** 207 (2004)
126. A G Dedov, Yu V Ivanina, V A Ketsko, E V Kruglyakov, N T Kuznetsov, A S Loktev, I I Moiseev, N N Oleinikov, K V Parkhomenko *Khim. Tekhnol.* **2** 8 (2003)
127. A Burukhin, O Brylev, P Hany, B R Churagulov *Solid State Ionics* **151** 259 (2002)
128. O A Brylev, O A Shlyakhtin, A V Egorov, T L Kulova, A M Skundin, S V Pouchko *NATO Sci. Ser. II* **61** 497 (2002)
129. A V Egorov, O A Brylev, O A Shlyakhtin, T L Kulova, A M Skundin, Yu D Tretyakov *NATO Sci. Ser. II* **61** 633 (2002)
130. D D Zaitsev, P E Kazin, Yu D Tretyakov, M Yanzen *Neorg. Mater.* **39** 12 1869 (2003) [c]
131. A S Sinitsky, A V Knot'ko, Yu D Tretyakov *Solid State Ionics* (2004) (in the press)
132. A S Karpov, J Nuss, M Jansen, P E Kezin, Y D Tretyakov *Solid State Sci.* **5** 1277 (2003)
133. R H Reuss, B R Chalamala *MRS Bull.* **28** 11 (2003)
134. S A Chambers, Y K Yoo *MRS Bull.*, **28** 10 (2003)
135. N Hampp *Chem. Rev.* **100** 1755 (2000)

[a] — *Dokl. Chem. (Engl. Transl.)*
[b] — *Russ. J. Phys. Chem. (Engl. Transl.)*
[c] — *Inorg. Mater. (Engl. Transl.)*
[d] — *Mendeleev Chem. J. (Engl. Transl.)*
[e] — *Russ. J. Inorg. Chem. (Engl. Transl.)*
[f] — *Russ. Chem. Bull., Int. Ed. (Engl. Transl.)*

Russian Chemical Reviews **73** (9) 847 – 860 (2004) © 2004 Russian Academy of Sciences and Turpion Ltd

DOI 10.1070/RC2004v073n09ABEH000917

Complex manganese oxides with the brownmillerite structure: synthesis, crystal chemistry and properties

A M Abakumov, M G Rozova, E V Antipov

Contents

I.	Introduction	847
II.	General information on the crystal structure of brownmillerites $A_2BB'O_5$	848
III.	Synthesis of Mn-containing brownmillerites	851
IV.	The crystal structure of $A_2MnB'O_{5+\delta}$ (A = Ca, Sr; B′ = Ga, Al; $\delta \approx 0$)	851
V.	Specific pattern of the oxidation of brownmillerites $A_2MnGaO_{5+\delta}$ (A = Ca, Sr)	854
VI.	Complex oxofluorides $Sr_2MnGaO_{5-x}F_{1+x}$	856
VII.	Magnetic and transport properties of brownmillerites $A_2MnB'O_{5+\delta}$ (A = Ca, Sr; B′ = Ga, Al) and their derivatives	857
VIII.	The oxide $Ca_{2.5}Sr_{0.5}GaMn_2O_8$ as the second member of the homologous series of brownmillerite-like structures	858
IX.	Conclusion	858

Abstract. Structural features and methods for the synthesis of complex manganese oxides with the brownmillerite structure $A_2MnB'O_{5+\delta}$ (A = Ca, Sr; B′ = Ga, Al) and of their derivatives are surveyed. Modern approaches to the description of crystal structures containing various types of chains of tetrahedra are considered and possible ordering patterns of these chains are discussed. The effects of the electronic structure and crystal chemical properties of the B′ cations on the possibility of formation of a layered ordered structure is noted. The emphasis is placed on the anion non-stoichiometry of the brownmillerite phases and the influence of the excess oxygen (fluorine) on the structure of the compounds. A comparative analysis of properties of oxygen- and fluorine-doped brownmillerites is given. The data on the magnetic structures, transport and magnetoresistive properties of Mn-containing brownmillerites are generalised. The bibliography includes 74 references.

I. Introduction

Among complex manganese oxides, oxides with a general stoichiometry $Ln_{1-x}A_xMnO_3$ (where Ln is a rare-earth cation and A = Ca, Sr, Ba) are most thoroughly studied primarily due to the fact that many representatives of this class manifest colossal magnetoresistance† (see Refs 1 – 6). These compounds possess perovskite-like structures (Fig. 1 *a*) and are characterised by complex correlations between their compositions, crystal structures and physical properties. The magnetic and electronic properties of manganites are usually interpreted within the double exchange theory, which considers the electron transfer between adjacent Mn^{3+} (in the high-spin state $t_{2g}^3e_g^1$) and Mn^{4+} ($t_{2g}^3e_g^0$) ions through the Mn – O – Mn bond chain.[7,8] A specific type of structural distortion of the perovskite lattice is realised owing to cooperative tilts and rotations of the MnO_6 octahedra, which is defined by the ratio of the radii of the cations in the sublattices A and B. Additionally, a deformation of the MnO_6 octahedra due to the Jahn – Teller effect (which is typical of Mn^{3+} cations in the high-spin electronic configuration) is superimposed on the cooperative distortion of the 3-dimensional framework. The situation can be further complicated if the deformation is static, *i.e.*, the

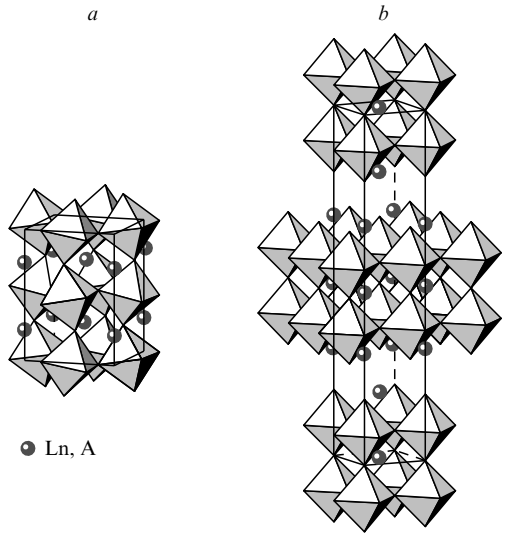

Figure 1. The crystal structures of $Ln_{1-x}A_xMnO_3$ (space group *Pnma*, $GdFeO_3$ structural type) (*a*) and $Ln_{2-x}A_{1+x}Mn_2O_7$ {$[(Ln,A)MnO_3]_n$.$[(Ln,A)O]$} (*b*).
Manganese atoms are in the centres of octahedra.

A M Abakumov, M G Rozova, E V Antipov Department of Chemistry, M V Lomonosov Moscow State University, Leninskie Gory, 119992 Moscow, Russian Federation. Fax (7-095) 939 09 98. Tel. (7-095) 939 52 44. E-mail: abakumov@icr.chem.msu.ru (A M Abakumov), rozova@icr.chem.msu.ru (M G Rozova). Tel. (7-095) 939 33 75. E-mail: antipov@icr.chem.msu.ru (E V Antipov)

Received 9 March 2004
Uspekhi Khimii **73** (9) 917 – 931 (2004); translated by Ya V Zubavichus

† Magnetoresistance is a change in the electrical resistance of a sample in an external magnetic field. Quantitatively, it is described by the magnetoresistive effect, which is given by the formula MR (%) = $100[(R_0 - R_H)/R_H]$, where R_0 and R_H are resistivities of the sample in the absence and in the presence of the external magnetic field with a strength H at a certain temperature, respectively. The term colossal magnetoresistance is applied to situations when the electrical resistivity changes in a magnetic field by a few orders of magnitude.

effect of orbital ordering takes place, and/or charge ordering occurs, being mainly observed at a doping level corresponding to the Mn^{3+} to Mn^{4+} ratio equal to unity (see Refs 9, 10). Nevertheless, a common feature of compounds $Ln_{1-x}A_xMnO_3$ is the retention of the spatial perovskite framework formed by vertex-sharing MnO_6 octahedra.

The discovery of colossal magnetoresistance in complex oxides $Ln_{2-x}A_{1+x}Mn_2O_7$ (Ln = La, Pr, Nd; A = Ca, Sr) stimulated studies of this phenomenon in other manganites with anisotropic layered structures.[11–15] The oxides $Ln_{2-x}A_{1+x}Mn_2O_7$ belong to the homologous series of the Ruddlesden–Popper phases with a general stoichiometry $A_{n+1}B_nO_{3n+1}$; their crystal structures may be described as intergrowth structures formed by regularly alternating perovskite and rock salt motifs, *i.e.*, $[(Ln,A)MnO_3]_n[(Ln,A)O]$ (Fig. 1 *b*). In terms of their electrical properties, the Ruddlesden–Popper phases are quasi-two-dimensional since conducting perovskite units (formed by vertex-sharing MnO_6 octahedra) are separted from each other by insulating blocks with the rock salt structure. These phases are convenient model objects for elucidation of the magnetic and electronic properties of complex manganites as a function of the dimensionality of the framework of the Mn–O–Mn bonds. Furthermore, the two-dimensional layered manganites represent a natural structural matrix suitable for the realisation of the colossal magnetoresistance by the mechanism of tunnelling of the conductivity electrons through the insulating blocks which separate the conducting perovskite fragments.

Complex manganites are similar to a certain extent to high-temperature superconducting (HTSC) cuprates as regards the possible formation of layered structures owing to the similarity in the crystal chemical properties of the cations Cu^{2+} and Mn^{3+}. Indeed, both cations are of the Jahn–Teller type due to partial filling of their e_g orbitals and thus it is a distorted octahedral environment (most often an axially elongated one) formed by oxygen atoms that is typical of them. The radii of octahedrally coordinated cations Cu^{2+} and Mn^{3+} (the latter being in the high-spin state) are also similar: $r(Mn^{3+}) = 0.79$ Å while $r(Cu^{2+}) = 0.87$ Å. Some of the axial oxygen atoms can be relatively easily removed from both the octahedrally coordinated Cu^{2+} and Mn^{3+} cations thus converting the coordination polyhedra into tetragonal pyramids. However, the square planar environment, which is often encountered in the structures of complex copper oxides, is not typical of manganese. Taking into account this close similarity, it is of no surprise that some layered perovskite-like complex manganese oxides have close analogues among HTSC cuprates. Perovskite and rock salt fragments are the major building blocks of layered cuprates as well. The known high-temperature superconducting cuprates $La_{2-x}A_xCuO_4$ (A = Sr, Ba) belong to the homologous series of the Ruddlesden–Popper phases $A_{n+1}B_nO_{3n+1}$ ($n = 1$) and have a structural analogue among manganites ($LaSrMnO_4$).[16, 17] A series of manganites including $Bi_{2-x}Pb_xSr_2MnO_{6+\delta}$ ($x = 0$, 1; the so-called 2201 phases)[18, 19] and $Bi_{2-x}Pb_xSr_{1.5}Ca_{1.5}Mn_2O_{9-\delta}$ (the 2212 phase) have been synthesised by analogy with the HTSC cuprates.[20] Another series of compounds with the composition $Bi_2Sr_2MnO_{6+\delta}$ (where δ is varied over a wide range), which correspond to an oxidation state of manganese in the range of $+2.7 < V_{Mn} < +3.3$ (see Ref. 21), have been prepared under high pressure.

The analogy between complex oxides of copper and manganese can be extended even further. According to one of the crystal chemical prerequisites to the formation of a layered perovskite-like structure with two different cations in the sublattice B, ordering of the cations is favoured by the difference in their coordination of oxygen atoms. The structure of brownmillerite $A_2BB'O_5$ represents a possible version of such a perovskite-derived layered structure. Formally, this anion-deficient structure is formed as a result of ordering of the anion vacancies giving rise to a regular alternation of the BO_2 and $B'O$ layers, which are characterised by the octahedral and tetrahedral coordination of the B and B′ cations, respectively (Fig. 2).

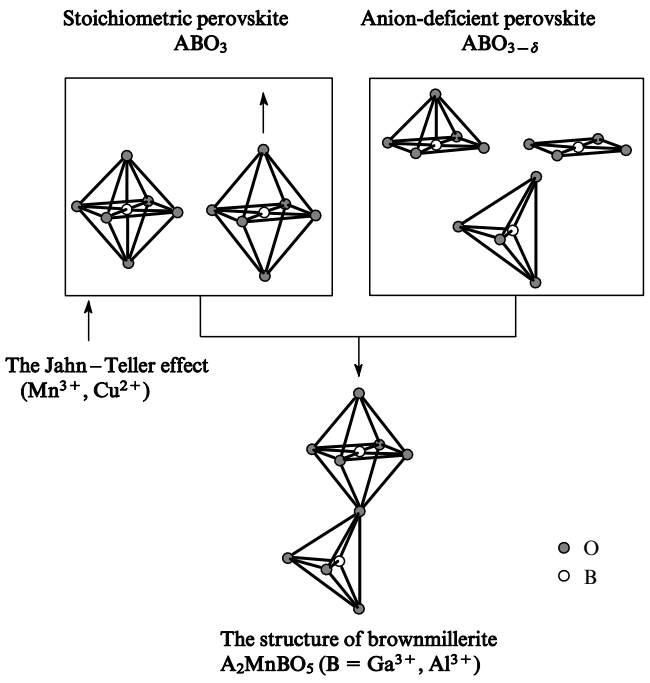

Figure 2. A scheme of formation and bonding of the coordination polyhedra BO_6 (an axially elongated octahedron) and $B'O_4$ (a tetrahedron) in the brownmillerite structure.

Since complex copper oxides with this structure are known, *viz.*, $LnACuGaO_5$ (Ln = La, Pr, Nd; A = Ca, Sr),[22–25] we have suggested that the synthesis of analogous manganese compounds is also possible. Taking into account different formal oxidation states of copper and manganese, the stoichiometry of manganites with the brownmillerite structure should be A_2MnGaO_5 ($V_{Mn} = +3$). An Al-containing analogue, *viz.*, Ca_2MnAlO_5, has been reported but it was considered only as a cement component rather than a potential magnetoresistant material.[26] An attractive feature of the brownmillerite structures as model objects in studies of magnetic and transport properties of layered manganites as a function of their composition and manganese oxidation state is its broad capability of 'tuning' changes in the anion stoichiometry and manganese valence. The preferable octahedral coordination of manganese atoms in oxidation states from +3 to +4 ensures retention of the perovskite-like MnO_2 layer whereas anion vacancies within the tetrahedral $B'O$ layers allow variations in the anion stoichiometry. The present review surveys different aspects of the synthesis of brownmillerites $A_2MnB'O_{5+\delta}$ (A = Ca, Sr; B′ = Ga, Al) and related compounds, their crystal structures and magnetic properties.

II. General information on the crystal structure of brownmillerites $A_2BB'O_5$

Brownmillerite $A_2BB'O_5$ is an anion-deficient analogue of perovskite ABO_3, which crystallises in the orthorhombic system and has unit cell parameters related to the unit cell parameter a_{per} of cubic perovskite as $a \approx \sqrt{2}a_{per}$, $b \approx 4a_{per}$, $c \approx \sqrt{2}a_{per}$. The structure of brownmillerite may be described as a result of regular alternation of the layers AO, BO_2 and $B'O$ along the unit cell axis *b* giving rise to the following layer sequence: BO_2–AO–$B'O$–AO–BO_2 (which constitutes half a repeat period along the *b* axis). The anion vacancies are ordered and localised in the $B'O$ layer, which can be formally produced from a perovskite $B'O_2$ layer (Fig. 3 *a*) by removal of half the oxygen atoms so as to form chains of anion vacancies going along the *a*

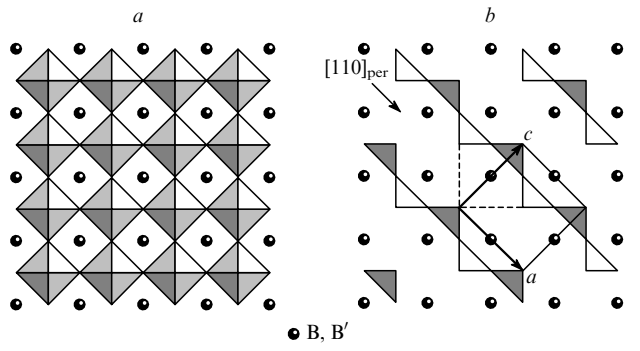

Figure 3. The structures of the BO_2 layers in the perovskite structure (*a*) and B′O layers in the structure of brownmillerite $A_2BB'O_5$ (*b*).
A cations are situated above and below the layer, the unit cell of perovskite is marked with dashes.

axis or, alternatively, along the [110] crystallographic direction of the parent perovskite (Fig. 3 *b*). The chains of vacant anion sites alternate with chains of sites occupied by oxygen atoms along the direction $c = [\bar{1}10]_{per}$. Owing to this ordered arrangement of anion vacancies, the coordination environment of the B′ cations is converted from octahedral to tetrahedral.

Thus, alternating layers of BO_6 octahedra and $B'O_4$ tetrahedra can be distinguished in the crystal structure of brownmillerite. The $B'O_4$ tetrahedra in the B′O layers are linked to each other through shared vertices to form chains along the *a* axis. The oxygen atoms in the B′O layers are shifted from their positions in the ideal cubic perovskite structure due to cooperative rotations of the tetrahedra in the chains around the *b* axis that is equivalent to the [001] direction of the parent perovskite (Fig. 4). As a result of the formation of the anion vacancies and cooperative shifts of oxygen atoms, the coordination number of the cations A (that are located between these layers) decreases from 12 to 8 + 2 (this notation means that two out of ten A−O bond lengths are substantially larger than the others).

The $B'O_4$ tetrahedra with opposite directions of rotation, *i.e.*, clockwise (CW) and counterclockwise (CCW), alternate along the chains of tetrahedra (see Fig. 4). These chains can adopt two configurations, *viz.*, left (L) and right (R), which are mirror reflections of each other.[27,28] If the vector $[\bar{1}10]_{per}$ translates a CW-tetrahedron of one chain into a CW-tetrahedron of another chain, both chains possess the same configuration (either L or R). On the contrary, if the vector $[\bar{1}10]_{per}$ translates a CW-tetrahedron of one chain into a CCW-tetrahedron of another chain or *vice versa*, these two chains possess different configurations. Mutual

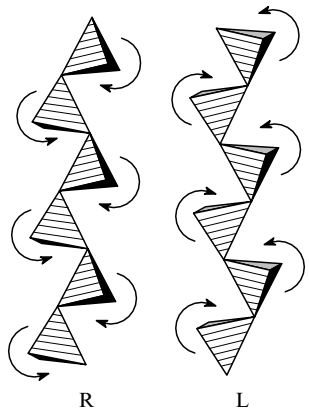

Figure 4. Chains of tetrahedra in the brownmillerite structure.
The arrows show directions of rotation of the respective tetrahedra.

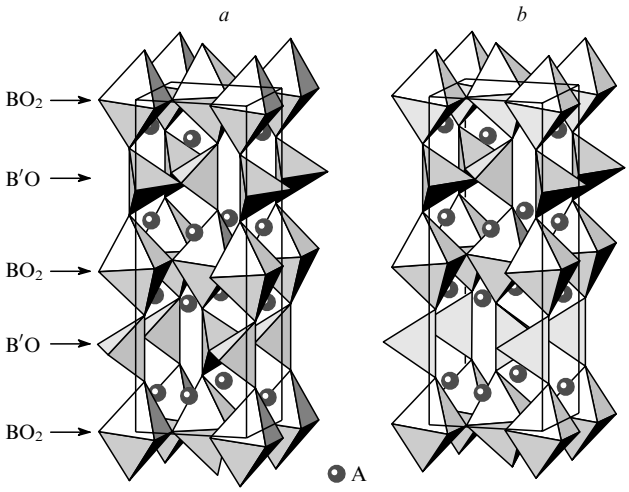

Figure 5. Crystal structures of two brownmillerite modifications with the space groups *I2mb* (*a*) and *Pnma* (*b*).

conversions of the L- and R-chains change neither the coordination polyhedra of the cations A, B and B′ nor respective interatomic distances since the space group of the parent perovskite includes the symmetry operations realising such conversions.[27,28] Hence, the L- and R-chains should be energetically equivalent and with similar probabilities of their formation.

For the majority of brownmillerites, three variants of space symmetry, which correspond to different ways of ordering the chains of tetrahedra belonging to the two configurations, are considered. In the case of completely random arrangement of the L- and R-chains, the structure belongs to the space symmetry group *Imma*. If only one type of chain is present, the structure belongs to the noncentrosymmetrical group *I2mb* (Fig. 5 *a*). Regular alternation of the B′O layers formed exclusively by either L- or R-chains gives rise to the space group *Pnma* (Fig. 5 *b*). However, the pattern of ordering of the chains of tetrahedra can be more complicated than the above three variants. Ordering of the L- and R-chains of tetrahedra can occur within one B′O layer thus increasing the repeat period along the *c* axis. Superstructural reflections corresponding to the regular alternation of the chains of tetrahedra along this axis have indeed been observed for brownmillerites such as Sr_2CuGaO_5,[29] $Ba_2In_2O_5$ [30] as well as for related phases $LnSr_2GaCu_2O_7$ (where Ln is a rare-earth element, the so-called Ga1212 phases), which contain GaO layers with brownmillerite-like chains of tetrahedra.[27,28]

A unified model encompassing all types of such superstructural ordering has been proposed by Lambert *et al.*[31] According to this model, the brownmillerite structure may be regarded as a lattice commensurately modulated with respect to the starting orthorhombic unit cell (with the unit cell parameters $a \approx \sqrt{2}a_{per}$, $b \approx 4a_{per}$ and $c \approx \sqrt{2}a_{per}$) by a modulation vector $\boldsymbol{q} = \gamma c^*$ giving rise to the (3 + 1)-dimensional space group $Imma(00\gamma)s00$.‡ In this case, the pattern of alternation of the chain of tetrahedra in the structure can be unambiguously described by a step function of the occupancy modulation. This function is defined in (3 + 1)-dimensional space by an interval on the a_4 axis with a width $\Delta(x_4)$ centred at x_4^0. An atom is assigned an occupancy of 1 if its x_4 coordinate lies inside the interval Δ, while an occupancy of 0 is assigned if the coordinate lies beyond it. In order to determine the widths and centres of the intervals defining the step functions of the occupancy modulation, it is necessary to apply the symmetry operations of the (3 + 1)-dimensional space group $Imma(00\gamma)s00$

‡ Fundamentals of space groups with the dimensionality > 3 as applied to description of modulated structures (supplied with a detailed reference list) are given in the International Tables for Crystallography.[32]

to all oxygen atoms in the B′O layer taking into account that the change in the configuration of a chain of tetrahedra should not change the composition of the layer or result in defects in the sequential arrangement of tetrahedra along the chain. For a cross-section of the brownmillerite structure on the $(x, 1/4, z)$ plane, which corresponds to the plane of the B′O layer, the sequence of atoms O*a*–Ga1–O*c*–Ga1 corresponds to the R-chain of tetrahedra, while the sequence Ga2–O*b*–Ga2–O*d* corresponds to the L-chain (Fig. 6). Since only one chain can be present in a specific point of the crystal lattice, the interval width Δ of the step function is equal to 1/2 for all atoms in this layer. The atoms O*a* and O*c* belong to the same chain of tetrahedra and thus they should be present in the structure simultaneously. Phases of the step function for these atoms should be equal, *i.e.*, $t(\mathrm{O}a) = t(\mathrm{O}c)$. This gives rise to the following relation between the coordinate t of the centre of the step function domain and the γ component of the modulation vector (see Fig. 6 for the case of $\gamma = 1/2$).

$$t = \frac{1-\gamma}{4}.$$

Taking into account that $t = x_4 - \boldsymbol{q}\,\boldsymbol{r}_{\mathrm{av}}$ (where $\boldsymbol{r}_{\mathrm{av}}$ is a vector defining the position of an atom in the average structure), the coordinate x_4^0 of the domain centre for the chain O*a*–Ga1–O*c*–Ga1 is given by

$$x_4^0(\mathrm{R}) = \frac{1-\gamma}{4} + \gamma z\,.$$

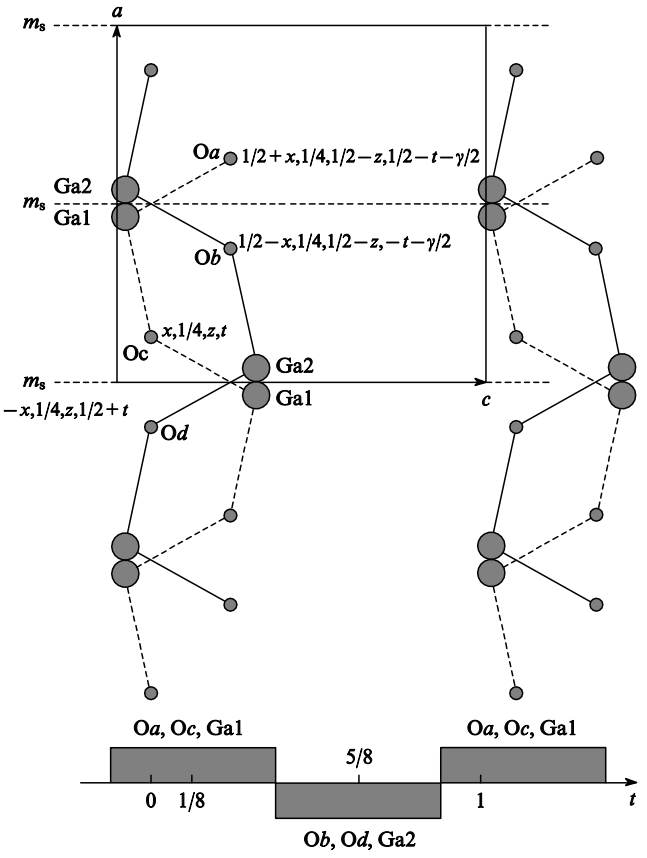

Figure 6. Arrangements of atoms in the B′O layer $(x, 1/4, z)$ for R- and L-chains of tetrahedra.
The sequence O*a*–Ga1–O*c*–Ga1 (dashed line) corresponds to the R-chain; the sequence Ga2–O*b*–Ga2–O*d* (solid line) corresponds to the L-chain; for the oxygen atoms, four-dimensional coordinates (x, y, z, t) are given; the positions of domains of the step function of the occupancy modulation are given for $\gamma = 1/2$.

The chain Ga2–O*b*–Ga2–O*d* is symmetrically related to the chain O*a*–Ga1–O*c*–Ga1 through a mirror plane m_s, which shifts the modulation phase by 1/2

$$x_4^0(\mathrm{L}) = \frac{1-\gamma}{4} + \gamma z + 1/2\,,$$

i.e., since $\Delta(x_4) = 1/2$, the two chains cannot be present at the same point of the crystal structure simultaneously. A translation by one repeat period of the parent structure along the *c* axis (*i.e.*, between two neighbouring chains in the layer) shifts the modulation phase by γ. Therefore, the sequence of alternation of the L- and R-chains can be unambiguously defined by the γ component of the modulation vector. This model is applicable for any values of the γ component. The three-dimensional symmetry group of a specific structure can be derived from the symmetry operations of the (3+1)-dimensional space group *Imma*(00γ)*s*00 for any rational γ and initial phase t of the modulation (Table 1).[31] As is clearly seen from Table 1, the brownmillerite structures with the space groups *I*2*mb* and *Pnma* correspond to two limiting cases, *viz.*, $\gamma = 0$ and $\gamma = 1$.

Table 1. Three-dimensional space groups corresponding to the brownmillerite structures with the modulation vector $\boldsymbol{q} = \gamma c^*$, (3+1)-dimensional space group *Imma*(00γ)*s*00 and different possible combinations of γ and t (r, s, v, τ, μ are integers).

$\gamma = r/s$ ($r < s$)	Space group at		
	$t = v/2s$	$t = (2v+1)/4s$	other t
$\gamma = 0$	*I*2*mb*	*I*2*mb*	*I*2*mb*
$r = 2\tau$, $s = 2\mu + 1$	$I2_1/m$	*I*2*mb*	*Im*
$r = 2\tau + 1$, $s = 2\mu + 1$	*Pnma*	*Pnmb*	$Pnm2_1$
$s = 2\mu$	*Pcmb*	*Pcma*	$Pcm2_1$
$\gamma = 1$	*Pnma*	*Pnmb*	$Pnm2_1$

The crystal structure of brownmillerite is a suitable matrix to accomodate the Jahn–Teller cations in its octahedral sites. A common feature of brownmillerites contaning transition metals is the elongation of two axial B—O distances in the BO_6 octahedra as compared to four equatorial distances. This distortion is due to alternation of the vertex-sharing BO_6 octahedra and $B'O_4$ tetrahedra along the *b* axis rather than to the electronic structure of the B cation. Since the B′—O distances are shorter than the B—O distances owing to the smaller coordination number, a decrease in the $B'-O_{ax}$ bond length has to be compensated by the respective elongation of the $B-O_{ax}$ bond. In fact, axial distortions of the BO_6 octahedra are observed not only for cations manifesting the Jahn–Teller effect, such as Cu^{2+}, but also for cations devoid of this property (Table. 2). Brownmillerites contaning Fe^{3+} (electronic configuration d^5) may serve as an example. Filling an octahedral cavity with a Jahn–Teller cation favours the formation of the brownmillerite structure owing to stabilisa-

Table 2. The B—O bond lengths (B = Cu, Fe) in copper- and iron-containing brownmillerites.

Oxide	$d(B-O_{eq})$ /Å	$d(B-O_{ax})$ /Å	Ref.
$LaCaCuGaO_5$	1.916–1.922	2.406	24, 25
$LaSrCuGaO_5$	1.888–1.934	2.436–2.478	22, 23
$PrSrCuGaO_5$	1.731–2.112	2.494	23
$NdSrCuGaO_5$	1.913–1.930	2.407–2.409	23
$Ca_2Fe_2O_5$	1.957–1.970	2.114–2.130	33–35
$Sr_2Fe_2O_5$	1.940–2.028	2.202–2.217	36, 37
Ca_2FeAlO_5	1.942–1.954	2.217	38
Ca_2FeGaO_5	1.954–1.959	2.128	39

tion of a distorted octahedral environment. Therefore, possible retention of the oxidation state +3 for the manganese cations should be taken into account when selecting a method for the synthesis of Mn-containing brownmillerites.

III. Synthesis of Mn-containing brownmillerites

The ceramic method is typically applied for the synthesis of Mn-containing brownmillerites $A_2MnB'O_5$ (A = Ca, Sr; B′ = Ga, Al). The temperature and partial pressure of oxygen at which the solid-state reaction is performed strongly influence the phase composition of the reaction products and degree of ordering of the manganese and B′ cations over octahedral and tetrahedral sites. Monophasic $Ca_2MnB'O_5$ with fully ordered manganese and B′ cations (according to the neutron diffraction data) is obtained in a ceramic synthesis starting from $CaCO_3$, manganese oxides (Mn_2O_3, MnO_2) or manganese oxalate and B'_2O_3 oxides conducted at 1200–1250 °C in a flow of an inert gas (N_2).[40,41] Synthesis of the same products in air requires higher temperatures (1300–1350 °C) in order to stabilise the phase at elevated partial oxygen pressure. An analysis of IR spectra of Ca_2MnAlO_5 suggested that an increase in the temperature of the synthesis favours partial disordering of the manganese and aluminium cations.[26] When the synthesis of Ca_2MnGaO_5 is performed in air at 1300 °C, a perovskite phase (presumably with disordered positions of manganese and gallium cations) is formed as an admixture.[40] Disordering of these cations (up to 5% of the Mn cations occupy Ga positions) is also observed in the synthesis of Sr_2MnGaO_5 at 1350 °C in a flow of nitrogen.[41,42] Meanwhile, $SrCaMnGaO_5$ with the fully ordered structure can be prepared at 1200 °C in a flow of argon.[43]

Taking all the above data into account, one may conclude that the formation of the ordered layered brownmillerite structure is favoured by a decrease in the temperature of the solid-state reaction and in the partial oxygen pressure. The latter is necessary to preserve the formal +3 oxidation state of the manganese cations and the overall anion stoichiometry, which should be identical or close to the nominal stoichiometry of brownmillerite, *i.e.*, $A_2MnB'O_5$ [this makes it possible to utilise differences in the coordination environment of the manganese (octahedral) and B′ (tetrahedral) cations to stabilise the ordered layered phase]. For instance, an increase in the coordination number of the B′ cations to 6 gives rise to disordered perovskite phases with a three-dimensional framework of octahedra despite the retention of the manganese oxidation state $V_{Mn} = +3$. In particular, the compounds Ln_2MnGaO_6 (Ln = La, Nd) are characterised by an orthorhombic structure (which belongs to the structural type of $GdFeO_3$) with manganese and gallium cations statistically occupying octahedral sites.[44,45] A similar situation was revealed for solid solutions with a common stoichiometry $La_{2-x}Sr_xMnGaO_6$ ($x = 0.7$), which crystallise in the monoclinic system (sp. gr. $I2/c$) and are characterised by an oxidation state of manganese other than +3.[46,47] A change in the Mn/Ga stoichiometric ratio also prevents formation of the layered brownmillerite structure. Solid solutions $SrMn_{1-x}Ga_xO_{3-\delta}$ ($0 \leqslant x \leqslant 0.33$) have a disordered cubic perovskite structure whereas for $0.33 < x < 0.5$, a two-phase region was found.[48]

We have suggested that the optimum conditions for the formation of brownmillerites Ca_2MnGaO_5 and Sr_2MnGaO_5 could be achieved provided that the synthesis is performed in evacuated sealed quartz tubes starting from CaO (SrO) preformed by decomposition of the respective carbonates in a dynamic vacuum (10^{-2} mbar, 900 °C), Mn_2O_3 and Ga_2O_3. The use of highly reactive oxides of alkaline-earth metals at a low partial oxygen pressure in the tube allows the preparation of monophasic ordered brownmillerites at 1000 °C.[40,49,50] The samples containing alkali-metal oxides have to be handled in a glove box free of water vapour and CO_2.

Brownmillerites containing manganese in an oxidation state slightly above +3 can be prepared by the heterovalent substitution of a bivalent cation for a trivalent one in the B′ sublattice. A series of solid solutions $Ca_2MnGa_{1-x}Zn_xO_{5+\delta}$, where $x = 0.1$ ($\delta = 0.075$, $V_{Mn} = +3.25$) or $x = 0.2$ ($\delta = 0.08$, $V_{Mn} = +3.36$) have been synthesised; phases with an increased manganese oxidation state are formed when the synthesis is performed at 1200 °C in air.[40] The manganese atoms in the original brownmillerite $Ca_2MnGaO_{5+\delta}$ with $\delta = 0$ can be further oxidised by annealing at low temperature and high partial oxygen pressure. Insertion of oxygen into this compound proceeds under drastic conditions ($T = 415$ °C, $p_{O_2} = 80$ atm); no complete oxidation of manganese to $V_{Mn} = +4$ occurs, the maximum reachable value of δ is 0.39.[40] Annealing $Sr_2MnGaO_{5+\delta}$ under milder conditions ($T = 415$ °C, $p_{O_2} = 1-20$ atm) gives rise to almost complete oxidation to $\delta = 0.47-0.505$. $Sr_2MnGaO_{5+\delta}$ with an intermediate value of the oxygen overstoichiometry index $0 < \delta < 0.5$ can be prepared by reduction of fully oxidised $Sr_2MnGaO_{5.5}$ in a closed circuit with a preset partial oxygen pressure.[51] In this method, the annealing is performed in a circulating flow of an argon–oxygen mixture; the required partial oxygen pressure is kept constant using a Cu/Cu_2O getter and controlled by an electrochemical cell with a solid oxygen-ionic electrolyte. A series of phases with $\delta = 0.13$ ($\log p_{O_2} = -5.19$), $\delta = 0.41$ ($\log p_{O_2} = -4.04$) and $\delta = 0.46$ ($\log p_{O_2} = -1.12$) have been synthesised at 415 °C using this method. A biphasic region corresponding to a mixture of a reduced and an oxidised phase with $\delta = 0.13$ and 0.41, respectively, was observed in the range of $0.13 < \delta < 0.41$.

IV. The crystal structure of $A_2MnB'O_{5+\delta}$ (A = Ca, Sr; B′ = Ga, Al; $\delta \approx 0$)

Unit cell parameters and space groups of Mn-contaning brownmillerites corresponding to different oxygen overstoichiometry indices are listed in Table 3. Based on X-ray powder diffraction data,[26] a primitive orthorhombic unit cell was suggested for Ca_2MnAlO_5. A subsequent low-temperature neutron diffraction study of this phase has given the space group $I2mb$.[41] For the Ga-containing analogue, *i.e.*, $Ca_2MnGaO_{5.045}$, formation of the *Pnma* modification of brownmillerite was unambiguously established by electron diffraction and X-ray powder diffraction.[40] Refinement of the crystal structure of $Ca_2MnGaO_{5.045}$ within the *Pnma* model using the Rietveld method resulted in a good correspondence between the experimental and calculated X-ray powder diffraction patterns.

Nevertheless, the real structure of $Ca_2MnGaO_{5.045}$ proved to be much more complicated than the idealised *Pnma* model, as evidenced by neutron diffraction and high-resolution electron microscopy (HREM). While the *Pnma* model provides a reasonable description of the experimental X-ray diffraction pattern, the neutron diffraction pattern can be fitted within this model only with large reliability factors. Systematic underestimation of the calculated intensities of reflections with $h + k + l = 2n$ and a nonmonotonic dependence of the FWHMs of reflections on the interplanar distance indicate the co-existence of two brownmillerite polymorph modifications with the space groups *Pnma* and *I2mb* in the sample. If the *I2mb* phase is taken into account in the fitting procedure, the fit quality is significantly improved. However, the Fourier difference maps for the *Pnma* phase still reveal extra maxima corresponding to incomplete ordering of the chains of tetrahedra (89% of one type of chain and 11% of another type within one layer instead of 100% of a certain type of chain, which has to be observed in the case of the ideal *Pnma* model). These results of structure refinement using neutron diffraction data can be interpreted as indicating the simultaneous presence of the *Pnma* and *I2mb* domains in the crystal structure of $Ca_2MnGaO_{5.045}$. The HREM data fully support this model.[40] Figure 7 shows two HREM micrographs of $Ca_2MnGaO_{5.045}$ along the crystallographic direction [101] and their Fourier images corresponding to the *Pnma* and *I2mb* phases. Reflections of the hkl, $k \neq 2n$ type are clearly resolvable in Fig. 7 *a* but absent in Fig. 7 *c*, so that the

Table 3. The crystallographic data for brownmillerites $A_2MnB'O_{5+\delta}$ (A = Ca, Sr; B′ = Ga, Al).

Composition	Unit cell parameters /Å			Space group	Oxygen overstoichiometry index		T /K	Ref.
	a	b	c		value	method [a]		
$Ca_2MnAlO_{5+\delta}$	5.244(2)	14.904(2)	5.465(1)	see [b]	–		293	26
	5.23135(8)	14.9533(3)	5.46258(9)	*I2mb*	0	TGA, ND	2	41
$Ca_2MnGaO_{5+\delta}$	5.2685(4)	15.301(1)	5.4686(5)	*Pnma*	0.045	CA, ND	293	40
	5.2712(7)	15.267(1)	5.4722(6)	*Pnma*	0.09	CA	293	40
	5.302(1)	14.940(4)	5.428(2)	*Pnma*	0.39	CA	293	40
$Ca_2MnGa_{0.9}Zn_{0.1}O_{5+\delta}$	5.278(1)	15.216(4)	5.479(1)	*Pnma*	0.075	CA	293	40
$Ca_2MnGa_{0.8}Zn_{0.2}O_{5+\delta}$	5.278(1)	15.163(5)	5.486(1)	*Pnma*	0.08	CA	293	40
$SrCaMnGaO_{5+\delta}$	5.3196(2)	15.7817(6)	5.4925(2)	*I2mb*	0.035	CA, ND	290	43
	5.30562(6)	15.7705(2)	5.48090(7)	*I2mb*	0.035	CA, ND	2	43
$Sr_2MnGaO_{5+\delta}$	5.4023(5)	16.130(2)	5.5645(7)	*I2mb, Imma*	−0.03	CA	293	51
	5.3717(6)	16.234(2)	5.5033(6)	*Imma*	0	TGA	293	42
	5.35450(2)	16.2256(6)	5.4888(2)	*Imma*	0	TGA, ND	2	41
	5.3863(1)	16.1971(3)	5.5257(1)	*I2mb, Imma*	0.01	CA, ND	293	52
	5.3894(4)	16.193(1)	5.5348(4)	*Imma*	0.025	CA	293	51
	5.3700(5)	16.240(2)	5.4976(4)	*Imma*	0.13	CA	293	51
	5.3628(3)	8.0193(8)	5.4066(3)	*Bmmm*	0.41	CA	293	51
	5.3666(6)	7.959(2)	5.3861(5)	*Bmmm*	0.46	CA	293	51
	3.7995(1)	–	7.9209(3)	*P4/mmm*	0.505	CA	293	51
	5.3834(2)	5.3652(2)	7.9448(2)	*Cmmm*	0.5	TGA, ND	293	48

[a] TGA stands for thermogravimetric analysis, ND stands for neutron diffraction, CA stands for chemical analysis. [b] Primitive orthorhombic lattice.

apparent repetition period along the b axis for the *I2mb* phase appears half as long as that for the *Pnma* phase (b = 15.3 Å).

In addition to crystallites strictly corresponding to one of the two variants (either *Pnma* or *I2mb*), the HREM data revealed crystallites with narrow extended domains of the *I2mb* phase embedded into the *Pnma* matrix. Thus, the real structure of $Ca_2MnGaO_{5.045}$ represents a mixture of the polymorph modifications *Pnma* and *I2mb*, both at the level of separate crystallites (which manifests itself in the structure refinement using neutron diffraction data as a contribution from the *I2mb* phase) and narrow domains within one crystallite (which manifests itself in the neutron diffraction data as the presence of differently oriented chains within the *Pnma* phase).

Substitution of strontium atoms for calcium in $Ca_2MnGaO_{5+\delta}$ suppresses formation of the *Pnma* modification. The crystal structure of $SrCaMnGaO_{5.035}$ was successfully refined using neutron diffraction data within the fully ordered *I2mb* model.[43] A similar model was applied to refine the structure of $Sr_2MnGaO_{5+\delta}$ ($\delta < 0$) from X-ray[49] and neutron powder diffraction data.[52, 53] However, it was found that it is the *Imma* structural model with a disordered arrangement of the L- and R-chains of tetrahedra that better reproduces the neutron diffraction pattern for Sr_2MnGaO_5. The difference between the fit qualities obtained for this compound within the *I2mb* and *Imma* models is not as significant as in the case of Ca_2MnAlO_5.[41, 52] This can be seen from a comparison of the corresponding integral discrepancy factors χ^2 (see Ref. 41):

Oxide	Sr_2MnGaO_5	Sr_2MnGaO_5	Ca_2MnAlO_5	Ca_2MnAlO_5
Sp. gr.	*Imma*	*I2mb*	*Imma*	*I2mb*
χ^2	3.30	5.28	27.5	2.99

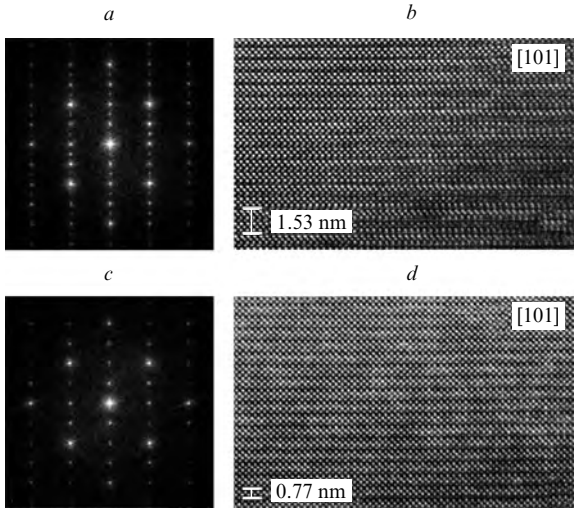

Figure 7. HREM micrographs (a, c) and respective Fourier images for $Ca_2MnGaO_{5.045}$ along the crystallographic direction [101] (b, d) showing domains of the *Pnma* (a, b) and *I2mb* (c, d) phases.

Actually, the ordering of the chains of tetrahedra in Sr_2MnGaO_5 has a more complicated character as compared with the idealised *I2mb* and *Imma* models. An electron diffraction study of Sr_2MnGaO_5 has revealed superstructural reflections corresponding to ordering of the L- and R-chains in the GaO layers along the axis c.[54] These reflections can be indexed assuming a modulation vector of $\boldsymbol{q} = (1/2)c^*$, which corresponds to a sequence of alternating chains of tetrahedra L–R–L–R–L along the c axis according to the Labmert model (see section II). Alternatively, this structure can be described in the orthorhombic space group *Pcmb* with a doubled c parameter (Fig. 8). This model was confirmed using HREM.[54] In addition to the regularly ordered fragments of the *Pcmb* phase, domains with another type of shift of the ordered layers of tetrahedra, which corresponded to a monoclinic unit cell (a = 17.100 Å, b = 5.406 Å, c = 11.118 Å, β = 108.97°, sp. gr. $P2/c$) (Fig. 9), were revealed together with numerous defects due to disturbed alternation sequences of the L- and R-chains of tetrahedra.

These two examples, *viz*., $Ca_2MnGaO_{5+\delta}$ and $Sr_2MnGaO_{5+\delta}$ demonstrate that structural analysis of brownmillerite phases can become very complicated due to the multitude of ordering patterns of the chains of tetrahedra. Even neutron powder diffraction, which is quite sensitive to the positions of oxygen atoms, is often insufficient to determine the real structure of brownmillerites and thus it should be applied in a combination

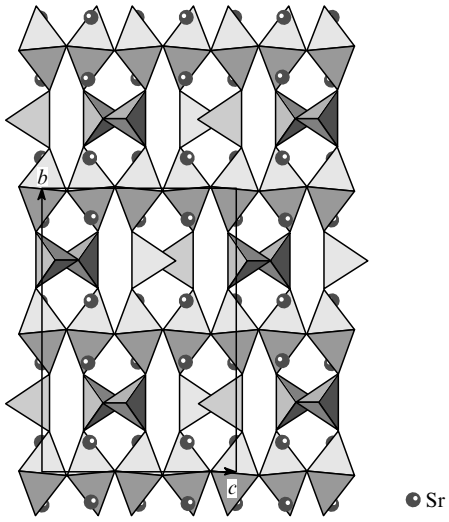

Figure 8. A model of the crystal structure of Sr_2MnGaO_5 with the chains of tetrahedra ordered according to the L – R – L – R pattern.
The two different projections of the GaO_4 tetrahedra correspond to the two chain types.

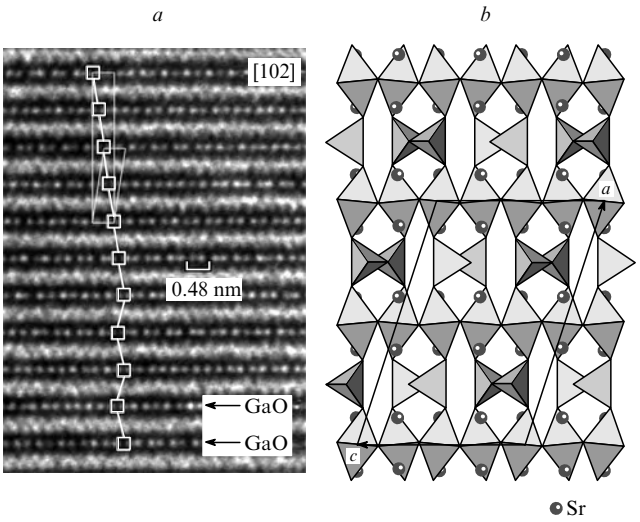

Figure 9. HREM micrographs of defects in the structure of Sr_2MnGaO_5 (*a*) and a model of this structure in the monoclinic space group $P2/c$ (*b*).

with local diffraction methods, *e.g.*, electron diffraction as implemented in transmission electron microscopes and HREM. High-temperature electron diffraction makes it possible to determine the influence exerted by the synthesis and annealing conditions on the character of ordering of the chains of tetrahedra. The electron diffraction patterns for the [010]* zone of Sr_2MnGaO_5 in the temperature range from room temperature to ~900 °C are shown in Fig. 10.[54] It is clearly seen that at 620 °C, the intensity of satellite reflections corresponding to the superstructure $\boldsymbol{q} = (1/2)c^*$ decreases and stripes of diffuse scattering oriented along the c^* axis appear. At 665 °C, the satellites completely disappear while the stripes of diffuse scattering remain, which suggests the loss of long-range ordering in the arrangement of the chains of tetrahedra at this temperature. Ordering is completely destroyed at ~900 °C (Fig. 10 *d*). This temperature is lower than the minimum temperature required for the synthesis of Mn-containing brownmillerites (1000 °C). This means that specific ordering of the chains of tetrahedra is realised not at the temperature of the synthesis of the sample but rather during its subsequent cooling. Hence, the exact character of the ordering should depend on the cooling rate.

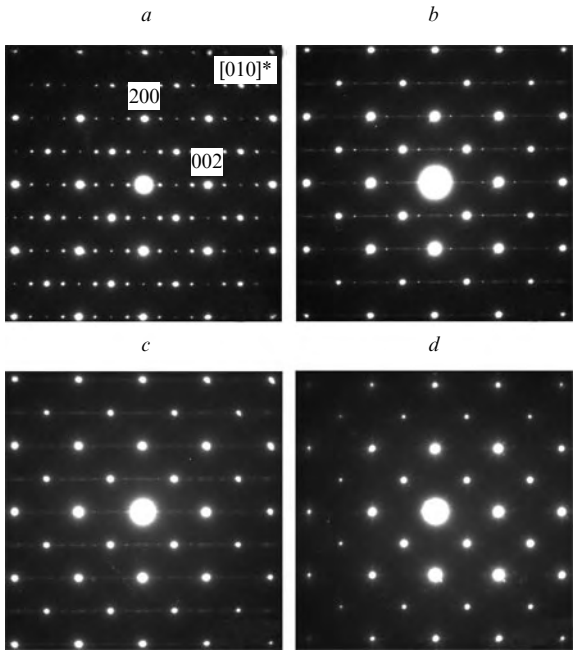

Figure 10. Electron diffraction patterns for the [010]* zone of Sr_2MnGaO_5 at room temperature (*a*), 620 °C (*b*), 665 °C (*c*) and 905 °C (*d*).

All brownmillerites $A_2MnB'O_{5+\delta}$ (A = Ca, Sr; B′ = Ga, Al; $\delta \approx 0$) are characterised by strong distortions of the MnO_6 octahedra. The lengths of the equatorial and axial Mn – O bonds for various members of this family, as determined by neutron diffraction, are listed in Table 4. A direct comparison of the bond lengths would not be informative since the respective values were determined for compounds with different oxygen content at different temperatures. However, a tendency that two axial Mn – O bonds are substantially longer than four equatorial ones is apparent for all the structures. Such a deformation of the coordination polyhedron is typical of the Jahn – Teller high-spin Mn^{3+} cation with the electronic configuration $t_{2g}^3e_g^1$. It is of note that the length of an axial Mn – O bond depends on the mean radius of cations in the sublattice A: it increases from 2.239 Å for A = Ca to 2.308 Å for A = Sr, Ca and further to 2.368 Å for A = Sr. As will be shown below, the bond length is also dependent on the oxidation state of manganese.

Table 4. The Mn – O bond lengths in the structures of brownmillerites $A_2MnB'O_{5+\delta}$ (A = Ca, Sr; B′ = Ga, Al) with $\delta \approx 0$.

Composition	d(Mn – O)$_{eq}$ /Å	d(Mn – O)$_{ax}$ /Å	δ	T/K	Ref.
$Ca_2MnAlO_{5+\delta}$	1.888(2) × 2	2.249(1) × 2 1.909(2) × 2	0	2	41
$Ca_2MnGaO_{5+\delta}$	1.899(4) × 2 1.918(4) × 2	2.239(3) × 2	0.045	293	40
$SrCaMnGaO_{5+\delta}$	1.890(6) × 2 1.941(6) × 2	2.308(2) × 2	0.035	290	43
	1.888(6) × 2 1.932(6) × 2	2.299(2) × 2	0.035	2	43
$Sr_2MnGaO_{5+\delta}$	1.9302(1) × 4	2.368(3) × 2	0.01	293	52
	1.91872(7) × 4	2.375(1) × 2	0	2	41

V. Specific pattern of the oxidation of brownmillerites $A_2MnGaO_{5+\delta}$ (A = Ca, Sr)

An increase in the formal oxidation state of manganese in $A_2MnGaO_{5+\delta}$ as a result of a heterovalent substitution in the cation sublattice or insertion of oxygen atoms converts the electronic configuration of Mn from $t_{2g}^3e_g^1$ to $t_{2g}^3e_g^0$ and is accompanied by a suppression of the Jahn–Teller effect and decrease in the axial Mn–O bond lengths in the MnO_6 octahedra. In the case of $Ca_2MnGaO_{5+\delta}$ and solid solutions based on it, these bond lengths decrease monotonically with an increase in the oxidation state of manganese (V_{Mn}).[40, 55]

Oxide	$Ca_2MnGaO_{5.045}$	$Ca_2MnGa_{0.8}Zn_{0.2}O_{5.08}$	$Ca_2MnGaO_{5.39}$
V_{Mn}	+3.09	+3.36	+3.78
d(Mn–O) /Å	2.239(3)	2.221(9)	1.873(9)

In the latter compound, the MnO_6 octahedra are axially compressed (*i.e.*, the axial Mn–O bonds are shorter than the equatorial ones). Since the axial Mn–O bonds are oriented nearly parallel to the *b* axis, their contraction results in a decrease in the *b* parameter of the unit cell. In the case of $Ca_2MnGaO_{5+\delta}$ and $Ca_2MnGa_{1-x}Zn_xO_{5+\delta}$, the *b vs.* V_{Mn} function is nearly linear (Fig. 11). Therefore, the *b* parameter is sensitive to changes in the oxidation state of manganese. The range of oxygen nonstoichiometry possible for Ca_2MnAlO_5 has not been studied, however, one may assume that this compound can be characterised by variable oxygen content, since the *b* parameter for a sample prepared in air [26] is significantly smaller than the respective value for a sample prepared in an inert atmosphere,[41] which assumes that the oxidation state is higher for the products synthesised in air.

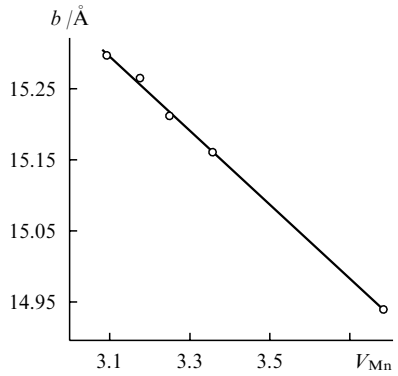

Figure 11. Changes in the *b* parameter as a function of V_{Mn} for $Ca_2MnGaO_{5+\delta}$ and $Ca_2MnGa_{1-x}Zn_xO_{5+\delta}$.

A heterovalent substitution of Zn for Ga leads to a substantial change in the *b* parameter alone while the *a*, *c* parameters and the degree of the orthorhombic distortion of the unit cell change insignificantly, mainly due to variation of the mean radii of cations occupying B and B′ positions. On the contrary, insertion of excess oxygen (*i.e.*, an increase in the index δ) gives rise to a significant decrease in the degree of the orthorhombic distortion, which is reflected in an increase in the *a* parameter coupled with a decrease in the *c* parameter (see Table 3). This occurs because the geometry of a part of the anion-deficient $GaO_{1+\delta}$ layers changes when extra oxygen atoms appear. An electron diffraction and HREM study has shown that insertion of oxygen into the $Ca_2MnGaO_{5+\delta}$ structure proceeds inhomogeneously.[40] Oxidation affects only half of the anion-deficient GaO layers giving rise to an ordered arrangement of GaO_2 and GaO□ (□ is the anion vacancy) (Fig. 12). The idealised structure of the oxidised material can be represented by the following layer sequence:

$GaO_2–CaO–MnO_2–CaO–GaO□–CaO–MnO_2–CaO–GaO_2$,

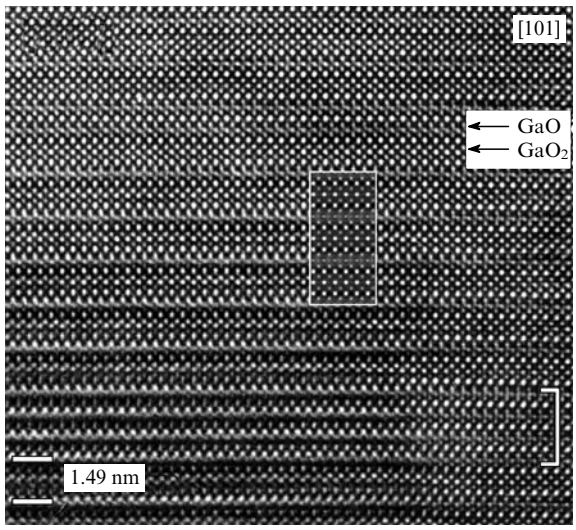

Figure 12. HREM micrographs of $Ca_2MnGaO_{5.39}$ along the crystallographic direction [101].
The square bracket shows a domain of the starting reduced phase with the *I2mb* structure, the inset in the centre shows an image calculated theoretically for the $Pmc2_1$ model.

two adjacent Ga layers are not symmetrically related to each other. Such a structure can be described in the noncentrosymmetrical space group $Pmc2_1$, which is actually a noncentrosymmetrical subgroup of the group *Pnma*. The resultant unit cell parameters relate to the unit cell parameters of the original cubic perovskite as $a \approx 4a_{per}$, $b \approx c \approx \sqrt{2}a_{per}$. The ordered disposition of the GaO□ and GaO_2 layers is violated by the slabs of the starting reduced phase with the *I2mb* structure. The structure of a completely oxidised compound is described by an idealised formula $Ca_2MnGaO_{5.5}$ [$Ca_4(Mn_2Ga)GaO_{11}$], which corresponds to the third member of the homologous series of the brownmillerite structures $A_{n+1}B_nB'O_{3n+2}$ (n = 3, Fig. 13). In this structure, triple layers of BO_6 octahedra (B = Mn, Ga) are separated by a layer of $B'O_4$ tetrahedra (B′ = Ga). According to the above stoichiometry, the oxidation state of manganese in these fragments should be +4, however the mean oxidation state of manganese was +3.78 in a sample oxidised at p_{O_2} = 80 atm due to the presence of areas with the original *I2mb* structure corresponding to $V_{Mn} \approx +3$. Probably, the phase with the ideal

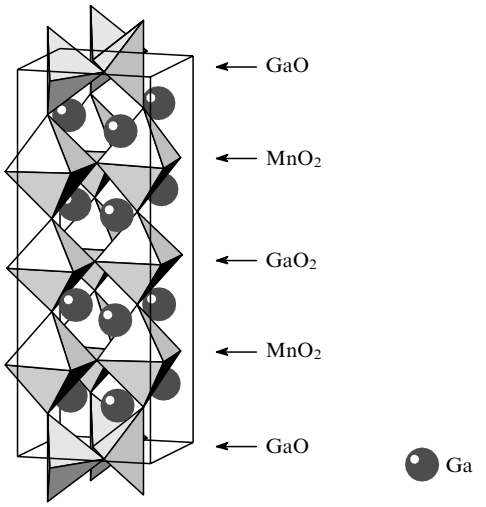

Figure 13. A model of the crystal structure of a completely oxidised phase $Ca_2MnGaO_{5.5}$.

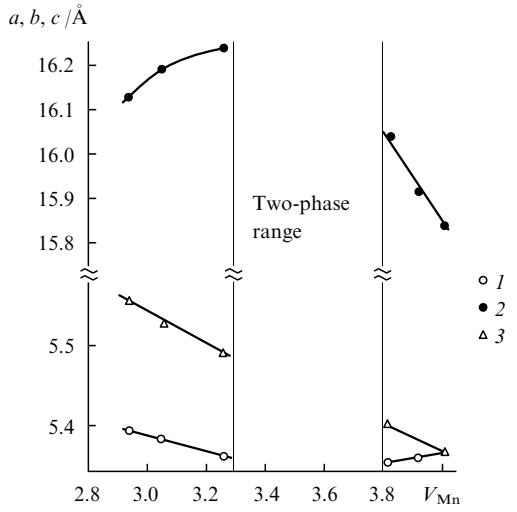

Figure 14. Changes in the unit cell parameters *a* (*1*), *b* (*2*) and *c* (*3*) as a function of the manganese oxidation state in $Sr_2MnGaO_{5+\delta}$.

stoichiometry $Ca_2MnGaO_{5.5}$ can be prepared at a higher partial oxygen pressure and longer duration of annealing.

The oxide $Sr_2MnGaO_{5+\delta}$ is characterised by a more complex dependence of the unit cell parameters on the oxidation state of manganese V_{Mn} and oxygen content.[51,56] The unit cell volume, degree of its orthorhombic distortion and *c* parameter decrease regularly with an increase in δ (Fig. 14, see Table. 3). The *a* and *b* parameters behave differently in two ranges of the manganese oxidation state, *viz*., $+2.94 \leqslant V_{Mn} \leqslant +3.26$ (the weakly oxidised range) and $+3.82 \leqslant V_{Mn} \leqslant +4.01$ (the strongly oxidised range). In the weakly oxidised range, the *a* parameter decreases whereas the *b* parameter increases. Conversely, in the strongly oxidised range, the *a* parameter increases whereas the *b* parameter decreases. The unit cell vectors and the space group also undergo changes. In the weakly oxidised range, the brownmillerite structure is retained. In the strongly oxidised range, the intensity of the *hkl* reflections with $k \neq 2n$ becomes zero, which corresponds to a transition to a new unit cell with the following parameters: $a \approx c \approx \sqrt{2}a_{per}$, $b \approx 2a_{per}$ and space group *Bmmm*. A progressive decrease in the degree of the orthorhombic distortion for $Sr_2MnGaO_{5.505}$ ultimately gives rise to a tetragonal unit cell with $a \approx a_{per}$, $c \approx 2a_{per}$ and space group *P*4/*mmm* (Fig. 15). For the oxidised phase $Sr_2MnGaO_{5.5}$, an orthorhombic structure was established[48] based on the neutron diffraction data (see Table 3). It is likely that discrepancies in the crystallographic symmetry suggested for this compound by different authors (see Refs 48, 51, 52, 56) arise due to different procedures used for the preparation of different samples or variable oxygen content in these samples, which lies within the accuracy limits of the available determination methods.

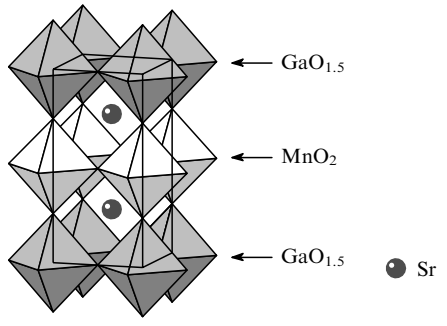

Figure 15. The crystal structure of $Sr_2MnGaO_{5.5}$.

The character of structural changes that occur upon oxidation of $Ca_2MnGaO_{5+\delta}$ and $Sr_2MnGaO_{5+\delta}$ is similar to that induced by insertion of fluorine atoms into the structure of brownmillerite $LaACuGaO_5$ (A = Ca, Sr).[57] In the case of A = Sr, fluorination of $LaACuGaO_5$ yields a tetragonal phase with $a \approx a_{per}$, $c \approx 2a_{per}$, whereas in the case of A = Ca, the orthorhombic symmetry is retained although the degree of the orthorhombic distortion substantially decreases. Similarly, oxidation of Mn-containing brownmillerites gives rise to a tetragonal structure only for A = Sr. According to X-ray diffraction, the structure of the tetragonal phase $Sr_2MnGaO_{5.5}$ is similar to that of oxofluoride $LaSrCuGa(O,F)_{6-\delta}$ (see Refs 53, 57). Probably, the differences in the oxidation of the Ca- and Sr-containing phases are due to steric hindrance associated with insertion of overstoichiometric oxygen atoms. The coordination number of the A cation in the tetragonal structure *P*4/*mmm* should be equal to 12 provided all anion sites are fully occupied or 11 if 1/4 of the oxygen atoms in the Ga layer are absent as in the case of $Sr_2MnGaO_{5.5}$. Realisation of large coordination numbers is difficult in the case of a Ca system (the ionic radius of Ca^{2+} is 1.35 Å) but possible for the larger Sr^{2+} ion (the ionic radius is 1.44 Å). Meanwhile, fluorination of $LaACuGaO_5$ can be represented as anion exchange $O^{2-} \rightarrow 2F^-$, which does not affect the oxidation state of copper. As a result, strong Jahn–Teller distortions of the CuO_6 octahedra are retained in the structure of oxofluorides $LaACuGa(O,F)_{6-\delta}$ and the perovskite subcell undergoes elongation in the direction perpendicular to the CuO_2 layers owing to orbital ordering. Insertion of oxygen into manganites with the brownmillerite structure proceeds oxidatively and results in suppression of the Jahn–Teller deformation.

In the case of $Sr_2MnGaO_{5+\delta}$, oxygen is inserted into every GaO layer, in contrast to the case of $Ca_2MnGaO_{5+\delta}$. According to a refinement of the crystal structure of $Sr_2MnGaO_{5.46}$, the coordination number of gallium atoms increases from 4 to 5 and their coordination polyhedron is a distorted trigonal bipyramid, although oxygen atoms are not completely ordered in the $GaO_{1+\delta}$ layer. Ordering of oxygen atoms and anion vacancies at certain values of δ can be observed by electron diffraction. For $Sr_2MnGaO_{5.41}$, such ordering lowers the symmetry to the monoclinic space group *P*2/*m* ($a = 10.813$ Å, $b = 8.019$ Å, $c = 8.486$ Å, $\beta = 108.57°$). A structural model of this oxide has been developed based on the analogy between the $GaO_{1+\delta}$ layers and anion-deficient $MnO_{1.5}$ layers in the compounds $A_2B_2O_5$ (A = Ca, Sr, La; B = Mn, Cu),[58–61] $Ca_2MnO_{3.5}$[62] and $Sr_2MnO_{3.5}$ (see Ref. 63). The $Mn(Cu)O_{1.5}$ layers consist of vertex-sharing $Mn(Cu)O_5$ tetragonal pyramids (Fig. 16 *a*,*b*). A probable arrangement of the GaO_5 polyhedra, which agrees with the unit cell parameters and space group symmetry of $Sr_2MnGaO_{5.41}$, is shown in Fig. 16 *c*. In order to convert tetragonal pyramids into GaO_5 trigonal bipyramids, both gallium and oxygen atoms have to be slightly shifted (Fig. 16 *d*).

The observed changes in the unit cell parameters of $Sr_2MnGaO_{5+\delta}$ as a function of the oxygen overstoichiometry δ can be rationalised taking into account the following trends:

— the mean radius of manganese cations decreases with an increase in the oxidation state from +3 to +4 [$r(Mn^{3+}) = 0.79$ Å, $r(Mn^{4+}) = 0.68$ Å];

— the Jahn–Teller distortions of the MnO_6 octahedra are suppressed;

— the degree of distortion of the MnO_2 layers is decreased owing to a smaller tilt angle of the MnO_6 octahedra with respect to the *a* axis;

— the mean Ga–O bond length increases with an increase in the coordination number of gallium atoms due to the appearance of additional oxygen atoms in the Ga layer.

A decrease in the degree of the orthorhombic distortion with an increase in δ occurs as a result of interactions between gallium and inserted oxygen atoms. When the latter occupy vacant anion sites within the $GaO_{1+\delta}$ layer, the distance between two nearest gallium atoms and the additional oxygen atom from neighbouring

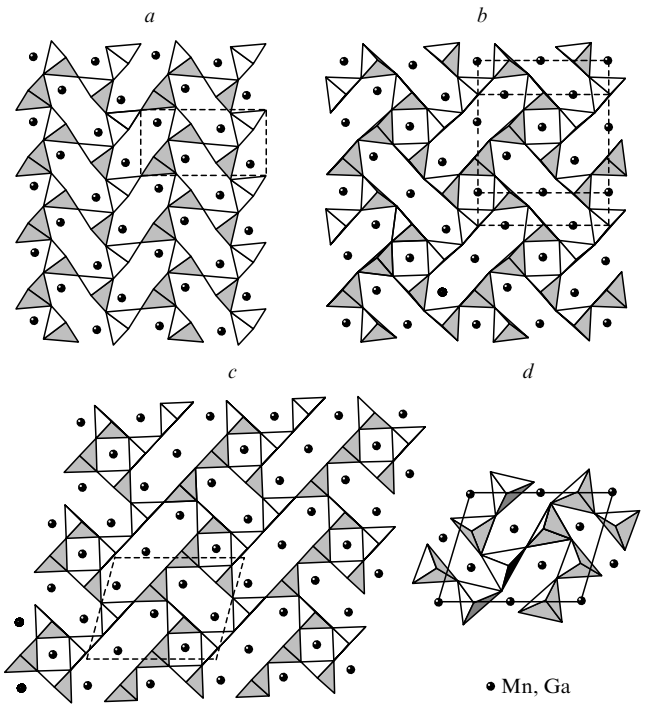

Figure 16. Arrangement of layers composed of the MnO_5 tetragonal pyramids in the structures of $Ca_2Mn_2O_5$, $Ca_2MnO_{3.5}$ (*a*) and $Sr_2MnO_{3.5}$ (*b*) and of the GaO_5 tetragonal pyramids in the structures of $Sr_2MnGaO_{5.41}$ (*c*) (*d* shows the conversion of a GaO_5 tetragonal pyramid into a trigonal bipyramid).

chains of tetrahedra becomes too large. In order to decrease this distance, the gallium atoms from the neighbouring chains shift towards the positions of the B cations in the original perovskite structure thus giving rise to a decrease in the distance between the chains of tetrahedra and the unit cell parameter *c*, the latter being almost linearly dependent on V_{Mn} and, consequently, on δ. The two opposite trends contribute to the change in the parameter *a*. With an increase in the manganese oxidation state in $Sr_2MnGaO_{5+\delta}$, the equatorial Mn – O bond length decreases.

δ	−0.003	0.025	0.13	0.46	0.47
$d(Mn-O)_{eq}$ /Å	1.945(20)	1.9243(5)	1.9222(4)	1.9010(1)	1.8998(1)

In the weakly oxidised range, this leads to a decrease in the *a* parameter and is accompanied by an increase in the degree of distortion of the chains of tetrahedra owing to cooperative rotation of the GaO_4 tetrahedra around the *b* axis by a larger angle, which is reflected in the change in the Ga – O – Ga bond angle from 134.4(5)° in $Sr_2MnGaO_{4.97}$ to 131.4(5)° in $Sr_2MnGaO_{5.025}$. However, further decrease in the degree of the orthorhombic distortion and formation of the tetragonal structure in the strongly oxidised range requires an increase in the Ga – O – Ga angle [*e.g.*, this angle is 165.8(4)° in $Sr_2MnGaO_{5.46}$], which finally leads to an increase in the *a* parameter in this range.

With an increase in the manganese oxidation state, axial distortions of the MnO_6 octahedra progressively decrease affecting the axial Mn – O bond lengths

δ	−0.03	0.025	0.13	0.46	0.5
$d(Mn-O)_{ax}$ /Å	2.411(4)	2.372(5)	2.225(8)	1.983(6)	1.956(3)

Since the axial Mn – O bonds are oriented along the *b* axis, a decrease in the respective unit cell parameter might be expected. Notwithstanding, the *b* parameter increases in the weakly oxidised range. The reason for this is a decrease in the degree of distortions of the MnO_2 layers due to a smaller tilt angle of the MnO_6 octahedra around the *a* axis. The Mn – O – Mn bond angle in the MnO_2 plane increases from 169.5(10)° (δ = −0.03) to 173.7(3)° (δ = 0.025), 176.8(5)° (δ = 0.13) and becomes equal to 180° for δ = 0.46, 0.47, 0.505. Simultaneously, the axial Ga – O bond elongates: 1.816(5) Å (δ = −0.03), 1.847(5) Å (δ = 0.025), 1.977(9) Å (δ = 0.13). As a result of this elongation and subsequent orientation of the axial Mn – O bond lengths parallel to the *b* axis, the *b* parameter in the weakly oxidised range increases despite shortening of the axial Mn – O bond.

VI. Complex oxofluorides $Sr_2MnGaO_{5-x}F_{1+x}$

In addition to oxygen atoms, fluorine atoms can also be used to modify the composition of the anion sublattice and the manganese oxidation state in brownmillerite Sr_2MnGaO_5. Oxygen and fluorine atoms are similar in terms of their crystal chemical properties. Their anions have similar ionic radii (r_{F^-} = 1.29 Å, $r_{O^{2-}}$ = 1.35 Å for the coordination number of 2). Several examples of successful insertion of fluorine into the structures of complex manganese oxides resulting in respective oxofluorides have been reported, including $Sr_2Mn_2O_{5-x}F_{1+x}$,[64] $LaSrMnO_4F$ (Ref. 65) and $La_{1.2}Sr_{1.8}Mn_2O_7F_2$.[66] As has been shown recently,[57] fluorine-derivatives of copper-contaning brownmillerites $LaACuGaO_5$ (A = Ca, Sr) can be synthesised using XeF_2 as a fluorinating agent. A similar method was applied to the synthesis of oxofluorides $Sr_2MnGaO_{5-x}F_{1+x}$. A detailed discussion of the utilisation of xenon difluoride for the fluorination of complex oxides and analysis of the processes accompanying fluorination may be found in a recent review.[67] Oxofluorides $Sr_2MnGaO_{5-x}F_{1+x}$ were synthesised starting from completely oxidised $Sr_2MnGaO_{5.5}$ at 500 – 600 °C using an anion exchange reaction, which gives rise to a decrease in the formal oxidation state of manganese.[56, 68]

$$Sr_2MnGaO_{5.5} + \frac{1+x}{2}XeF_2 \longrightarrow$$

$$\longrightarrow Sr_2MnGaO_{5-x}F_{1+x} + \left(\frac{1}{2}+x\right)[O] + \frac{1+x}{2}Xe.$$

Chemical reduction in the reaction with xenon difluoride is achieved owing to involvement of the walls of the copper tube that is used as the reactor. Oxygen evolved upon anion exchange is adsorbed by the walls giving rise to the Cu/Cu_2O getter, which regulates the partial oxygen pressure in the course of the reaction. Oxofluorides $Sr_2MnGaO_{5-x}F_{1+x}$ crystallise in the tetragonal system (sp. gr. *P*4/*mmm*) with the following unit cell parameters: $a \approx a_{per}$, $c \approx 2a_{per}$ (Table 5). According to a calculation of the bond valence sum and crystal lattice energy, partial substitution of fluorine for oxygen and insertion of excess fluorine atoms takes place in the Ga layers. Consequently, all vacancies in these layers become filled giving rise to the stoichiometry $GaO_{1-x}F_{1+x}$. It is of interest to analyse changes in the behaviour of the compound Sr_2MnGaO_5 doped with either fluorine or oxygen as a function of the manganese oxidation state. The changes in the Mn – O bond lengths for the fluorinated and oxidised phases are plotted in Fig. 17 *a*. In both cases, the equatorial Mn – O bonds in the MnO_6 octahedra elongate with a decrease in V_{Mn} (which is equivalent to a decrease in δ or an increase in the fluorine content) from 1.8998 Å (V_{Mn} = +4) to 1.9222 Å (V_{Mn} = +3.26, δ = 0.13)[51]

Table 5. The crystallographic data for oxofluorides $Sr_2MnGaO_{5-x}F_{1+x}$.

Fluorination conditions	Unit cell parameters /Å		V_{Mn}
	a	*c*	
Starting oxide (without XeF_2)	3.8003(7)	7.948(3)	+4.00
1 : 1 XeF_2, 500 °C, 10 h	3.8557(3)	7.7843(8)	+3.78
1 : 1 XeF_2, 600 °C, 20 h	3.865(1)	7.779(3)	+3.54
1 : 3 XeF_2, 600 °C, 20 h	3.8794(3)	7.7328(6)	+3.39

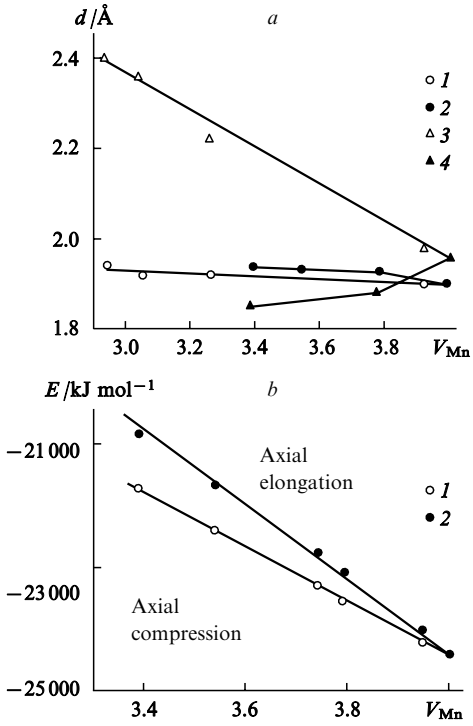

Figure 17. Changes in the $(Mn-O)_{eq}$ (*1*, *2*) and $(Mn-O)_{ax}$ (*3*, *4*) bond lengths in $Sr_2MnGaO_{5+\delta}$ (*1*, *3*) and $Sr_2MnGaO_{5-x}F_{1+x}$ (*2*, *4*) (*a*) and in the crystal lattice energy for $Sr_2MnGaO_{5-x}F_{1+x}$ in the case of axially compressed (*1*) and axially elongated (*2*) MnO_6 octahedra (*b*) as a function of the manganese oxidation state.

and further to 1.9411 Å ($V_{Mn} = +3.39$, $x_F = 0.61$) owing to an increase in the ionic radius of manganese upon reduction.

In the case of $Sr_2MnGaO_{5+\delta}$ ($\delta \approx 0.5$), reduction is also accompanied by an elongation of the axial Mn–O bonds due to the Jahn–Teller effect. Conversely, a progressive compression of the MnO_6 octahedra with a decrease in the manganese oxidation state is observed for solid solutions $Sr_2MnGaO_{5-x}F_{1+x}$. The axial Mn–O bonds in $Sr_2MnGaO_{4.78}F_{1.22}$ [*viz.*, 1.876(8) Å] are significantly shorter than in $Sr_2MnGaO_{5.5}$ [1.956(3) Å]. Thus, the reductive fluorination leads to a change in the type of Jahn–Teller effect from axially elongated to axially compressed. Presumably, this is due to competitive changes in the lattice energy and stabilisation energy associated with the Jahn–Teller distortion of the octahedral environment of manganese atoms.

In manganites $Sr_2MnGaO_{5+\delta}$ doped with oxygen, the axial elongation of the MnO_6 octahedra is partly compensated by shortening of the axial Ga–O bonds due to a decrease in the coordination number of gallium to 4. For solid solutions $Sr_2MnGaO_{5-x}F_{1+x}$, the axial Ga–O bond lengths remain constant upon variation of the composition of the solid solution since all anion sites in the Ga layer are already occupied and thus the coordination number of gallium atoms does not change. Therefore, in this case, the elongation of the axial Ga–O bond coupled with the lack of a compensating contraction should result in too long Sr–O bonds and thus in inevitable losses in the crystal lattice energy (Fig. 17 *b*).

The change in the type of Jahn–Teller distortion on going from $Sr_2MnGaO_{5.5}$ to $Sr_2MnGaO_{5-x}F_{1+x}$ should give rise to a change in the type of orbital ordering, as it was established for solid solutions $Nd_{1-x}Sr_xMnO_3$.[69] A change in the strontium/neodymium stoichiometric ratio and, consequently, in the manganese oxidation state results, at $x = 0.6$, in a change in the type of Jahn–Teller distortion from axially compressed [$0.55 < x < 0.6$, $d(Mn-O)_{eq} = 1.948$ Å, $d(Mn-O)_{ax} = 1.906$ Å] to axially elongated [$x > 0.6$, $d(Mn-O)_{eq} = 1.894$ Å, $d(Mn-O)_{ax} = 1.955$ Å]. The reason for the change in the type of Jahn–Teller distortion is the change of the type of orbital ordering from $d(x^2-y^2)$ to $d(z^2)$, which, in turn, is accompanied by a change in the magnetic structure from type A (antiferromagnetically ordered ferromagnetic planes) to type C (ferromagnetically ordered antiferromagnetic planes) and a metal–dielectric transition at $x = 0.6$.

VII. Magnetic and transport properties of brownmillerites $A_2MnB'O_{5+\delta}$ (A = Ca, Sr; B′ = Ga, Al) and their derivatives

Despite differences in the crystal structures of brownmillerites $A_2MnB'O_{5+\delta}$ (A = Ca, Sr; B′ = Ga, Al) with $\delta \approx 0$ due to different ordering patterns of the chains of tetrahedra, their magnetic structures are essentially similar. These phases convert into an antiferromagnetic state at $T_N = 150-180$ K. The respective saturated magnetic moments (μ) and the Néel temperatures (T_N), as determined by neutron diffraction for several compositions, are listed in Table 6. The magnitudes of the magnetic moments are in good agreement with the theoretical values for Mn^{3+} (which is characterised by the electronic configuration $3d^4$, $t_{2g}^3e_g^1$). The magnetic moments of manganese atoms are oriented perpendicular to the MnO_2 layers. All reduced brownmillerites reveal the G-type antiferromagnetic structure, which implies that the magnetic unit cell conforms to the crystallographic one and the magnetic moments of adjacent manganese atoms are antiparallel not only in the MnO_2 layers but between the layers as well (Fig. 18 *a*).

The magnetic interaction in the brownmillerite structure has a three-dimensional character despite the fact that the distances between adjacent Mn atoms along the *b* axis are approximately twice as large as in the *ac* plane. The three-dimensional character of the magnetic ordering assumes significant superexchange interactions between consecutive MnO_2 layers along the *b* direc-

Table 6. The magnetic characteristics of brownmillerites $A_2MnB'O_{5+\delta}$ (A = Ca, Sr; B′ = Ga, Al).

Oxide	μ /μ_B	T_N /K	Ref.
Ca_2MnAlO_5	3.53(2)	152	41
Ca_2MnGaO_5	3.61(5)	160	52
$SrCaMnGaO_5$	3.30(2)	180	43
Sr_2MnGaO_5	3.16(6)	183	52
	3.26(3)	180	41
$Sr_2MnGaO_{5.5}$	2.1(1)	110	52

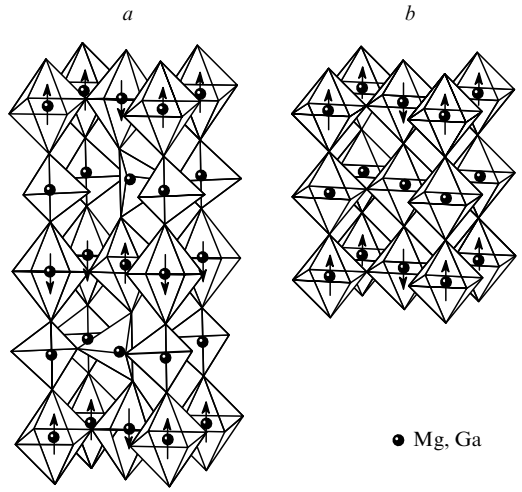

Figure 18. The magnetic structure of Sr_2MnGaO_5 (G-type) (*a*) and $Sr_2MnGaO_{5.5}$ (C-type) (*b*).

tion of the orthorhombic unit cell. The involvement of the superexchange interactions is directly supported by the NQR data.[55] The frequency of the local magnetic field on a gallium atom exceeds the calculated frequency of a dipole field by two orders of magnitude. This suggests that the experimentally observed local field has a dominant contact character and is induced by the superexchange interactions between manganese ions through a 'nonmagnetic' GaO_4 tetrahedron. The magnetic structure of $Sr_2MnGaO_{5.5}$, although also antiferromagnetic, is different from that of the reduced compound. In this structure, the MnO_2 layers (in which manganese atoms are ordered antiferromagnetically) are coupled ferromagnetically, which corresponds to type C of the perovskite magnetic structures (Fig. 18 *b*). The magnetic unit cell remains tetragonal although its volume is twice as large as that of the crystallographic cell. The parameters of the magnetic and crystallographic unit cells relate to each other by the following equations: $a_m = \sqrt{2}a_c$, $c_m = c_c$. The changes in the magnetic structure type on going from Sr_2MnGaO_5 to $Sr_2MnGaO_{5.5}$ occur due to the appearance of extra oxygen atoms in the Ga layers, which additionally stabilise the type C magnetic structure due to more distant 'diagonal' superexchange interactions through the GaO_6 octahedra.[52] Interactions through the $Ga(O,F)_6$ octahedra in $Sr_2MnGaO_{5-x}F_{1+x}$ [$T_N = 70$ K, $\mu = 1.5(1)\ \mu_B$] also give rise to ferromagnetic ordering of antiferromagnetic planes.[70] Nevertheless, in contrast to Sr_2MnGaO_5 and $Sr_2MnGaO_{5.5}$, the orientation of the magnetic moments in oxofluorides is parallel to the MnO_2 layers rather than perpendicular to them, which can be explained assuming the change in the orbital ordering type. This was suggested based on the analysis of interatomic distances in the structures of oxofluorides.[68]

According to neutron diffraction and muon resonance spectroscopy, $Sr_2MnGaO_{5.5}$ is characterised by an inhomogeneous magnetic structure below 180 K. This manifests itself in the appearance of small domains ($\sim$40 Å) with the type G magnetic structure embedded into a matrix with the type C structure.[52] When the oxygen overstoichiometry index δ is decreased to 0.41, the local magnetic order of the type G is replaced by co-existence of two regular magnetic structures: an antiferromagnetic type G structure is formed at $T = 140$ K while an admixture of a type C phase appears at $T = 110$ K.[71] The co-existence of these two long-range magnetic structures was observed for $Sr_2MnGaO_{5.5}$ as well (see Ref. 48). It is the local ordering of oxygen atoms in the $GaO_{1+\delta}$ layer giving rise to differences in the character of interactions between adjacent MnO_2 layers that should be considered as the most probable reason for this phenomenon. Indeed, such an ordering, which results in the symmetry lowering to monoclinic system, was experimentally established for $Sr_2MnGaO_{5.41}$ (see Refs 51, 56).

Complex oxides $Ca_2MnGaO_{5.045}$, $Ca_2MnGa_{1-x}Zn_xO_5$ ($x = 0.1-0.2$)[55] and $SrCaMnGaO_5$ (see Ref. 43) are insulators. Their electrical resistance as a function of temperature follows the normal activation law with sufficient accuracy. $SrCaMnGaO_5$ manifests magnetoresistance that amounts to 85% in a field of 6 T and up to 90% in a field of 13 T at 159 K.[43]

VIII. The oxide $Ca_{2.5}Sr_{0.5}GaMn_2O_8$ as the second member of the homologous series of brownmillerite-like structures

The homologous series of brownmillerite structures $A_{n+1}B_nB'O_{3n+2}$ is formally constructed by adding a certain number of octahedral layers to the brownmillerite structure. The *n*th member of the series contains blocks composed of *n* layers of BO_6 octahedra separated from each other by a layer of $B'O_4$ tetrahedra. The second member of the manganese-containing homologous series, which corresponds to stoichiometry $Ca_{2.5}Sr_{0.5}GaMn_2O_8$, was synthesised at 1100 °C in air.[72] Since the formal oxidation state of manganese in this compound is +3.5, the synthesis does not require an inert atmosphere. This

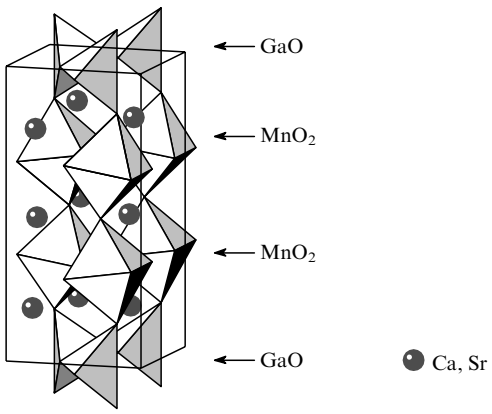

Figure 19. The crystal structure of $Ca_{2.5}Sr_{0.5}GaMn_2O_8$.

oxide crystallises in the orthorhombic system [sp. gr. $Pcm2_1$, $a = 5.4294(1)$ Å, $b = 11.3722(3)$ Å, $c = 5.2983(1)$ Å] (Fig. 19). In this structure, the MnO_6 octahedra are distorted but the character of the distortion differs from that in brownmillerite. An MnO_6 octahedron is characterised by five shorter [1.857(10) – 1.950(4) Å] and one longer [2.163(5) Å] Mn – O bonds. The elongated axial Mn – O bond is directed towards the layer of tetrahedra whereas the short axial bond is responsible for the Mn – O – Mn bonding between the layers of octahedra. Apparently, such an atomic arrangement provides the optimum coordination of the A cations located between the octahedral layers. This oxide converts between 150 K and 125 K into an antiferromagnetically ordered state with the magnetic moments oriented perpendicular to the MnO_2 layers [$\mu = 3.09(1)\ \mu_B$]. Within the MnO_2 layer, the neighbouring manganese atoms interact antiferromagnetically whereas adjacent octahedral layers and their pairs separated from each other by a GaO layer interact ferromagnetically. The transition into the magnetically ordered state is accompanied by an abrupt decrease in the electrical resistance (which, notwithstanding, remains too high to refer this transition to a dielectric – metal transition) with the magnetoresistance effect being about 50% in a field of 80 kŒ.[72]

Reduction of manganese in $Ca_{2.5}Sr_{0.5}GaMn_2O_8$ by means of partial substitution of trivalent cations for bivalent cations of alkaline-earth metals gives rise to a structural transformation resulting in a new type of anion ordering, which has been observed for the first time in the crystal structure of $Sr_{0.7}Y_{0.3}CoO_{2.62}$ (see Ref. 73). The oxide $Y_{0.8}Sr_{2.2}GaMn_2O_{7.9}$ is characterised by a tetragonal unit cell with the following parameters: $a = 7.6373(3)$ Å and $c = 15.6636(10)$ Å, sp. gr. $I4/mmm$.[74] This structure is composed of alternating octahedral and tetrahedral layers; the B sites are statistically occupied by manganese and gallium atoms with manganese atoms preferably occupying the octahedral sites. The structure of $Y_{0.8}Sr_{2.2}GaMn_2O_{7.9}$ contains isolated squares of vertex-sharing tetradera instead of chains of tetrahedra typical of the brownmillerite structure. The coordination environment of the B cations within this layer is supplemented by additional oxygen atoms situated between the squares of tetrahedra giving rise to a total coordination number of 5.[74] Presumably, the driving force for the formation of this structure is ordering of crystallographically non-equivalent Sr^{2+} and Y^{3+} cations.

IX. Conclusion

It is the differences in the ionic radii, electronic structures and typical coordination polyhedra of various cations differing in their crystal chemical properties that can be deliberately exploited in the design and synthesis of layered perovskite-like compounds. This idea is demonstrated in the present review by the example of complex oxides $A_2MnB'O_{5+\delta}$ (A = Ca, Sr; B′ = Ga, Al) having

the brownmillerite structure. A method for the synthesis of such complex oxides has to provide the optimum conditions (including a proper choice of composition, temperature and partial oxygen pressure) for ordering of cations. The presence of anion vacancies in the brownmillerite structure enables chemical modifications of the structure and adjustments of properties by variations of the anion stoichiometry under mild conditions not affecting the initially achieved ordered arrangement of cations. The brownmillerite structure is capable of adapting to changes in the anion composition (owing to the anion-deficient B′O layers); it is characterised by stable octahedral environment of manganese atoms in the oxidation states +3 and +4; it allows preparation of various members of the homologous series $A_{n+1}B_nB'O_{3n+2}$ manifesting magnetoresistance (for $n = 1, 2$). Thanks to all these features, browmillerite-like complex oxides of manganese should be considered as highly promising objects for the synthesis of novel magnetoresistive materials.

The current review has been written with partial financial support from the 'Petroleum Research Fund' (Project No. 38459-AC5), the INTAS (Grant for young scientists YSF 03-55-1035) and the 'Federal Programme in Support of the Leading Scientific Schools of the Russian Federation' (Project NSch-2033.2003.03). The authors are grateful to colleagues from the Laboratory for Inorganic Crystal Chemistry at the Department of Chemistry, MSU and Laboratory for Electron Microscopy at Antwerp University (EMAT, RUCA) for help in the research work and fruitful discussions. A M Abakumov also acknowledges financial support from the Charitable fund of the Russian Academy of Sciences.

References

1. R V Helmot, J Wecker, B Holzapfel, L Schultz, K Samwer *Phys. Rev. Lett.* **71** 2331 (1993)
2. S Jin, T H Tiefel, M McCormack, R A Fastnacht, R Ramesh, L H Chen *Science* **264** 413 (1994)
3. C N R Rao, A K Cheetham *Science* **272** 369 (1996)
4. A P Ramirez *J. Phys.: Condens. Matter* **9** 8171 (1997)
5. Y Tokura, Y Tomioka, H Kuwahara, A Asamitsu, Y Morimoto, M Kasai *J. Appl. Phys.* **79** 5288 (1996)
6. J M D Coey, M Viret, S von Molnar *Adv. Phys.* **48** 167 (1999)
7. J B Goodenough *Phys. Rev.* **100** 564 (1955)
8. J B Goodenough *J. Appl. Phys.* **81** 5330 (1997)
9. D I Khomskii, G A Sawatsky *Solid State Commun.* **102** 87 (1997)
10. C N R Rao, A Arulraj, P N Santosh, A K Cheetham *Chem. Mater.* **10** 2714 (1998)
11. Y Morimoto, A Asamitsu, H Kuwahara, Y Tokura *Nature (London)* **380** 141 (1996)
12. T Kimura, Y Tomioka, H Kuwahara, A Asamitsu, M Tamura, Y Tokura *Science* **274** 1698 (1996)
13. P D Battle, S J Blundell, M A Green, W Hayes, M Honold, A K Klehe, N S Laskey, J E Millburn, L Murphy, M J Rosseinsky, N A Samarin, J Singleton, N A Sluchanko, S P Sullivan, J F Vente *J. Phys.: Condens. Matter* **8** L427 (1996)
14. R Seshardi, C Martin, A Maignan, M Hervieu, B Raveau, C N R Rao *J. Mater. Chem.* **6** 1585 (1996)
15. H Asano, J Hayakawa, M Matsui *Phys. Rev. B* **56** 5395 (1997)
16. G Blasse *J. Inorg. Nucl. Chem.* **27** 2863 (1965)
17. A Benabad, A Daoudi, R Salmon, C Le Flem *J. Solid State Chem.* **22** 121 (1977)
18. J M Tarascon, Y Le Page, W R McKinnon, E Tselepis, P Barboux, B G Bagley, R Ramesh *Mater. Res. Soc. Symp. Proc.* **156** 317 (1989)
19. M Catti, G Dalba, P Fornasini, M Molgg *J. Solid State Chem.* **112** 392 (1994)
20. M Herview, C Michel, D Pelloquin, A Maignan, B Raveau *J. Solid State Chem.* **132** 420 (1997)
21. T P Beales, M Molgg, J R Gorton, D C Sinclair *Mater. Res. Bull.* **31** 1543 (1996)
22. J T Vaughey, J B Wiley, K R Poppelmeier *Z. Anorg. Allg. Chem.*, **598**/**599** 321 (1991)
23. G Roth, P Adelmann, R Knitter, S Massing, Th Wolf *J. Solid State Chem.* **99** 376 (1992)
24. A L Kharlanov, I Bryntse, E V Antipov, A V Luzikova *Acta Chem. Scand.* **47** 434 (1993)
25. A V Luzikova, A L Kharlanov, E V Antipov, H Müller-Bushbaum *Z. Anorg. Allg. Chem.* **620** 326 (1994)
26. F Puertas, M T Blanco Varela, R Dominguez *Cem. Concr. Res.* **20** 429 (1990)
27. T Krekels, O Milat, G Van Tendeloo, S Amelinckx, T G N Babu, A J Wright, C Greaves *J. Solid State Chem.* **105** 313 (1993)
28. O Milat, T Krekels, G Van Tendeloo, S Amelinckx *J. Phys. I* **3** 1219 (1993)
29. M L Ruiz-Gonzalez, C Prieto, J Alonso, J Ramirez-Castellanos, J M Gonzalez-Calbet *Chem. Mater.* **14** 2055 (2002)
30. P Berastegui, S Hull, F J Garcia-Garcia, S-G Eriksson *J. Solid State Chem.* **164** 119 (2002)
31. S Lambert, H Leligny, D Grebille, D Pelloquin, B Raveau *Chem. Mater.* **14** 1818 (2002)
32. *International Tables for Crystallography* Vol. 1 (London: Kluwer Academic, 1999) p. 899
33. A A Colville *Acta Crystallogr., Sect. B* **26** 1469 (1970)
34. J Berggren *Acta Chem. Scand.* **25** 3616 (1971)
35. P Berastegui, S-G Eriksson, S Hull *Mater. Res. Bull.* **34** 303 (1999)
36. C Greaves, A J Jacobson, B C Tofield, B E F Fender *Acta Crystallogr., Sect. B* **31** 641 (1975)
37. M Schmidt, S G Campbell *J. Solid State Chem.* **156** 292 (2001)
38. A A Colville, S Geller *Acta Crystallogr., Sect. B* **27** 2311 (1971)
39. R Arpe, R von Schenck, H Müller-Bushbaum *Z. Anorg. Allg. Chem.* **410** 97 (1974)
40. A M Abakumov, M G Rozova, B Ph Pavlyuk, M V Lobanov, E V Antipov, O I Lebedev, G Van Tendeloo, D V Sheptyakov, A M Balagurov, F Bouree *J. Solid State Chem.* **158** 100 (2001)
41. A J Wright, H M Palmer, P A Anderson, C Greaves *J. Mater. Chem.* **12** 978 (2002)
42. A J Wright, H M Palmer, P A Anderson, C Greaves *J. Mater. Chem.* **11** 1324 (2001)
43. P D Battle, A M Bell, S J Blundell, A I Coldea, D J Gallon, F L Pratt, M J Rosseinsky, C A Steer *J. Solid State Chem.* **167** 188 (2002)
44. J Toepfer, J B Goodenough *Eur. J. Solid State Inorg. Chem.* **34** 467 (1997)
45. E J Cussen, M J Rosseinsky, P D Battle, J C Burley, L E Spring, J F Vente, S J Blundell, A I Coldea, J Singleton *J. Am. Chem. Soc.* **123** 1111 (2001)
46. A I Coldea, S J Blundell, I M Marshall, C A Steer, J Singleton, F L Pratt, L D Noailles, M J Rosseinsky, L E Spring, P D Battle *Phys. Rev. B* **65** 054 402 (2001)
47. P D Battle, S J Blundell, J B Claridge, A I Coldea, E J Cussen, L D Noailles, M J Rosseinsky, J Singleton, J Sloan *Chem. Mater.* **14** 425 (2002)
48. E N Caspi, M Avdeev, S Short, J D Jorgensen, B Dabrowski, O Chmaissem, J Mais, S Kolesnik *J. Solid State Chem.* **177** 1456 (2004)
49. A M Abakumov, M G Rozova, B Ph Pavlyuk, M V Lobanov, E V Antipov, O I Lebedev, G Van Tendeloo, O L Ignatchik, E A Ovtchenkov, Yu A Koksharov, A N Vasil'ev *J. Solid State Chem.* **160** 353 (2001)
50. A M Abakumov, M G Rozova, A M Alekseeva, M V Lobanov, E V Antipov, O I Lebedev, G Van Tendeloo, D V Sheptyakov, A M Balagurov *Z. Anorg. Allg. Chem.* **628** 2233 (2002)
51. A M Abakumov, M G Rozova, A M Alekseeva, M L Kovba, E V Antipov, O I Lebedev, G Van Tendeloo *Solid State Sci.* **5** 871 (2003)
52. V Yu Pomyakushin, A M Balagurov, T V Elzhov, D V Sheptyakov, P Fisher, D I Khomskii, V Yu Yushankhai, A M Abakumov, M G Rozova, E V Antipov, M V Lobanov, S J L Billinge *Phys. Rev. B* **66** 184 412 (2002)
53. D V Sheptyakov, A M Abakumov, E V Antipov, A M Balagurov, S J L Billinge, P Fisher, L Keller, M V Lobanov, B Ph Pavlyuk, V Yu Pomyakushin, M G Rozova *Appl. Phys. A* **74** S1734 (2002)

54. A M Abakumov, A M Alekseeva, M G Rozova, E V Antipov, O I Lebedev, G Van Tendeloo *J. Solid State Chem.* **174** 319 (2003)
55. M V Lobanov, Candidate Thesis in Chemical Sciences, Moscow State University, Moscow, 2000
56. E V Antipov, A M Abakumov, A M Alekseeva, M G Rozova, J Hadermann, O I Lebedev, G Van Tendeloo *Phys. Status Solidi A* 1 (2004)
57. J Hadermann, G Van Tendeloo, A M Abakumov, B Ph Pavlyuk, M Rozova, E V Antipov *Int. J. Inorg. Mater.* **2** 493 (2000)
58. K R Poeppelmeier, M E Leonowicz, J M Longo *J. Solid State Chem.* **44** 89 (1982)
59. K R Poeppelmeier, M E Leonowicz, J C Scanlon, J M Longo, W B Yelon *J. Solid State Chem.* **45** 71(1982)
60. V Caignaert, N Nguyen, M Hervieu, B Raveau *Mater. Res. Bull.* **20** 479 (1985)
61. N R Khasanova, F Izumi, Z Hiroi, M Takano, Q Huang, A Santoro *Acta Crystallogr., Sect. C* **52** 2381 (1996)
62. M E Leonowicz, K R Poeppelmeier, J M Longo *J. Solid State Chem.* **58** 71 (1985)
63. L J Gillie, A J Wright, J Hadermann, G Van Tendeloo, C Greaves *J. Solid State Chem.* **167** 145 (2002)
64. M V Lobanov, A M Abakumov, A V Sidorova, M G Rozova, O G D'yachenko, E V Antipov, J Hadermann, G Van Tendeloo *Solid State Sci.* **4** 19 (2002)
65. L D Aikens, R K Li, C Greaves *Chem. Commun.* **21** 2129 (2000)
66. C Greaves, J L Kissick, M G Francesconi, L D Aikens, L J Gillie *J. Mater. Chem.* **9** 111 (1999)
67. A M Abakumov, M G Rozova, E I Ardashnikova, E V Antipov *Usp. Khim.* **71** 443 (2002) [*Russ. Chem. Rev.* **71** 383 (2002)]
68. A M Alekseeva, A M Abakumov, M G Rozova, E V Antipov, J Hadermann *J. Solid State Chem.* **177** 731 (2004)
69. R Kajimoto, H Yoshizawa, H Kawano, H Kuwahara, Y Tokura, K Ohoyama, M Ohashi *Phys. Rev. B* **60** 9506 (1999)
70. V Pomjakushin, D Sheptyakov, P Fischer, A Balagurov, A Abakumov, M Alekseeva, M Rozova, E Antipov, D Khomskii, V Yushankhai *J. Magn. Magn. Mater.* (2004) (in the press)
71. V Pomjakushin, D Sheptyakov, P Fischer, A Balagurov, A Abakumov, M Alekseeva, M Rozova, E Antipov *Phys. Rev. B* (2004) (in the press)
72. P D Battle, S J Blundell, P N Santhosh, M J Rosseinsky, C Steer *J. Phys.: Condens. Matter* **14** 13 569 (2002)
73. S Ya Istomin, J Grins, G Svensson, O A Drozhzhin, V L Kozhevnikov, E V Antipov, J P Attfield *Chem. Mater.* **15** 4012 (2003)
74. L J Gillie, H M Palmer, A J Wright, J Hadermann, G Van Tendeloo, C Greaves *J. Phys. Chem. Solids* **65** 87 (2004)

Russian Chemical Reviews **73** (9) 861 – 880 (2004) © 2004 Russian Academy of Sciences and Turpion Ltd

DOI 10.1070/RC2004v073n09ABEH000919

The role of heteroepitaxy in the development of new thin-film oxide-based functional materials

A R Kaul, O Yu Gorbenko, A A Kamenev

Contents

I.	Introduction	861
II.	Epitaxial stabilisation	861
III.	Variant structures	874
IV.	Conclusion	878

Abstract. The methods of synthesis of new oxide compounds and thin-film materials based on the use of heteroepitaxy are considered. The thermodynamic model and the theory of the epitaxial stabilisation phenomenon are outlined, the role of thermodynamic and structure-geometric factors determining the possibility of epitaxial stabilisation of unstable phases is interpreted. The use of epitaxial stabilisation for the design of heterostructures with specific electric properties is demonstrated. The characteristic features of the structural relations between the film and substrate materials, resulting in the formation of thin films with different numbers of variants, are discussed. The bibliography includes 128 references.

I. Introduction

Epitaxy, *i.e.*, oriented growth of a crystal on another crystal, has long been used to synthesise thin-film materials. This is the simplest and the most economical way of preparing structurally perfect film materials, which successfully replace single crystals with large diameters. Numerous examples of using epitaxial processes in elementary semiconductors are known, in particular, heteroepitaxy of silicon films on the surface of a sapphire single crystal, preparation of films of the Si_xGe_{1-x} solid solution on the surface of single crystal silicon plates, silicon autoepitaxy on silicon plates and so on. By means of epitaxy, one can produce materials with different widths of the forbidden gap. The most impressive results in the design of semiconductor materials of the $A^{III}B^{V}$ family for optoelectronics were attained using this method. Epitaxy was used to obtain layers with a low concentration of defects and periodic structures with alternation of numerous layers with diverse compositions several nanometers thick. For the synthesis of such structures, a MOC-hydride process has been developed and special highly automated equipment has been designed (in particular, AIXTRON equipment has found extensive application).

A R Kaul, O Yu Gorbenko Department of Chemistry, M V Lomonosov Moscow State University, Leninskie Gory, 119992 Moscow, Russian Federation. Fax (7-095) 939 14 92. Tel. (7-095) 939 14 92.
E-mail: kaul@inorg.chem.msu.ru (A R Kaul),
gorbenko@inorg.chem.msu.ru (O Yu Gorbenko)
A A Kamenev YUKOS Research and Development Centre, Leninsky prosp. 55/1, Building 2, 119333 Moscow, Russian Federation.
Fax (7-095) 730 61 02. Tel. (7-095) 730 61 01 (2-26)

Received 9 March 2004
Uspekhi Khimii **73** (9) 932 – 953 (2004); translated by Z P Bobkova

Unlike the epitaxy of semiconductors, the epitaxy of oxides is far from being well-developed in both theoretical and engineering aspects, although the demand for oxide materials in semiconductor engineering was realised long ago. This lag is due to a number of reasons, most of all, to the great diversity of structures and chemical properties of oxides. It often remains unknown whether it is possible to perform epitaxial intergrowth of oxides corresponding to different structural types and having different lattice parameters. The necessity of using high temperature and, most often, a high partial pressure of oxygen promotes side chemical reactions of oxides, in particular, those with the products of surface oxidation of semiconductors. These circumstances appreciably complicate the preparation of epitaxial oxide materials. In addition, the structural and chemical diversity of oxides accounts for more diverse manifestations of the epitaxy (compared to those for semiconductors) and opens up new prospects for the application of this phenomenon.

This review deals with two original methods for the preparation of new thin-film oxide materials, namely, epitaxial stabilisation of unstable phases and the design of variant structures. The review mainly presents the studies carried out by researchers engaged in the chemistry and physics of thin oxide films at the Chair of Inorganic Chemistry of the Department of Chemistry of the M V Lomonosov Moscow State University.

II. Epitaxial stabilisation

1. The principles of epitaxial stabilisation

The last 15 years have seen intensive research into the preparation of epitaxial films of multicomponent complex oxides. The attention of researchers was focused on perovskite-type or related compounds, which possess unique properties. These include high temperature semiconductors of the $RBa_2Cu_3O_{7-\delta}$ (R is lanthanide) and Bi – Ca – Sr – Cu – O families, the $Pb(Ti,Zr)O_3$ and $(Ba,Sr)TiO_3$ ferroelectrics, materials with colossal magnetoresistance $La_{1-x}(Ca,Sr)_xMnO_3$, and electron – ion conductors $La_{1-x}(Sr,Ca)_xCoO_3$.

Much effort was devoted to methods for the preparation of multicomponent oxide films, such as metal organic chemical vapour deposition (MOCVD), pulse laser deposition (PLD), magnetron sputtering, *etc*. Despite the difference, these methods have one feature in common — the mass transfer processes that underlie them are incongruent, *i.e.*, during the substance transfer from the target or the gas phase onto the substrate, the ratio of the cationic components changes to some extent. This often violates the stoichiometry of the cationic composition of the films and usually gives rise to second phases (inclusions). In order to obtain single-phase epitaxial films, the composition of the target or the

flow of volatile components should be consistently corrected based on the results of elemental analysis of films.

Examination of phase analysis data for off-stoichiometric epitaxial films has shown that impurity phases often differ from those expected relying on the known phase diagrams of the systems under consideration. In addition, it was found that the growth of single-phase epitaxial films often takes place under thermodynamic conditions (P_{O_2} and T) where this compound as a bulk material (polycrystalline powder, ceramics or a single crystal) is thermodynamically unstable. These phenomena are of a common nature and can be explained by phase stabilisation due to the epitaxy on the substrate or due to the epitaxy at the interface between two phases formed simultaneously (the matrix and the inclusion).

The relationship between the formation of metastable phases and the epitaxy was first noted by Dankov [1,2] when growing oxide layers on metals. Later, van der Merwe [3,4] performed a comprehensive theoretical analysis of the growth of epitaxial layers. The data they obtained were summarised to formulate the structural and size compliance principle (the Dankov–van der Merwe principle). As applied to epitaxial stabilisation, this principle can be outlined as follows: the competitive formation of new phases on a substrate surface would predominantly yield phases congruent to the substrate. In Russian publications, this is called more often the Dankov–Konobeevskii principle.

The appearance of metastable phases on the single crystal surface may be of both thermodynamic and kinetic nature. The Dankov–van der Merwe principle is apparently applicable both to systems in which the particle diffusion in the growing layer is sufficient for ensuring a phase equilibrium and to systems in which diffusion is retarded.

In the systems we are interested in, epitaxial films of complex oxides grow, most often, at high temperatures ($\sim 600-900\,^{\circ}C$), *i.e.*, the thermodynamic factor predominates. Depending on the structural correspondence between the film and the substrate, either epitaxial or polycrystalline films are formed. Experiments show that the phase composition of the polycrystalline films does not differ from that predicted by equilibrium phase diagrams for the given elemental composition and the number of phases obeys the Gibbs phase rule. In addition, the phase composition is reproduced in successive experiments on film preparation and does not change during long-term annealing at the film deposition temperature. These findings prove that the polycrystalline oxide layers formed on the substrates in the above-indicated temperature range are quite close to true thermodynamic equilibrium,† although film growth from the gas phase is undoubtedly a non-equilibrium process.

As regards epitaxial films produced under the same conditions, their phase composition is also reproducible and also does change after long-term annealing at the temperature of film growth. However, the phase composition of the epitaxial films, unlike that of polycrystalline films, often does not correspond to that predicted relying on the equilibrium phase diagram. However, epitaxial films are much closer to an ideal single crystal and have a lower free energy than polycrystalline films of the identical composition, as they do not have an extensive internal surface typical of polycrystals. Thus, one can state that the observed deviations of the phase composition of the oxide epitaxial films from that predicted on the basis of equilibrium phase diagrams constructed for bulk states are due to thermodynamic factors. These deviations are related to the formation of new equilibrium phase relations in the film material. This is caused by the decrease in the system free energy following a decrease in the contribution of the free energy of the film/substrate interface in the case where they are structurally coherent.

The epitaxial stabilisation (ES) can be defined, from the thermodynamic standpoint, as extension of the $P-T-x$ space of the thermodynamically stable existence of the epitaxial phase with respect to the bulk state of this phase free from a substrate.

Table 1 presents examples of epitaxial stabilisation which shows itself as metamorphism of simple and complex oxides, the formation of new oxide phase and as the stabilisation of compounds containing metals in unstable oxidation states.

This Table is not meant to be exhaustive, giving only the epitaxial phases formed upon epitaxial stabilisation of the thermodynamic origin. It is noteworthy that most of the researchers cited were prone to treat the results they obtained as a curiosity observed for unknown reasons in a particular system rather than a predictable phenomenon of the thermodynamic nature.

In the next Sections, we consider the theoretical foundations of the epitaxial stabilisation and demonstrate, using our studies as examples, that this phenomenon can be utilised for the synthesis of new solid-state compounds and new materials.

The greater part of the data included in Table 1 refer to the polymorphism of simple oxides. This is due to several reasons: first, the preparation of the phases of simple oxides is not complicated by the necessity of controlling the cationic composition; second, selection of the $P_{O_2}-T$ conditions for their synthesis is more obvious than in other cases; third, highly symmetric single-crystal substrates can be used in their synthesis.

Examples of preparing new compounds with complex compositions due to the ES are scarce since the necessary conditions unknown in advance, namely, the stochiometric ratio of the cations, the $P_{O_2}-T$ film growth conditions, and the similarity of growing film and substrate parameters, are unlikely to be simultaneously fulfilled by chance. The choice of these conditions should be deliberate.

2. The thermodynamic model of epitaxial stabilisation

Let us consider the formation of a new phase nucleus on the surface of a single crystal during deposition from the gas phase. The Gibbs energy (ΔG_f) of the formation of this nucleus‡ is described by the equation:

$$\Delta G_f = \Delta g_V V + \sigma S + \Delta G^{El}, \quad (1)$$

where Δg_V is the specific volume Gibbs energy, J m^{-3}; σ is the surface tension, N m^{-1}; V and S are the volume and the surface area of the nucleus, respectively; ΔG^{El} is the contribution of elastic tension arising in the nucleus due to the compressive or tension effect of the substrate. Note the difference between the units of measurement of the free Gibbs energy (ΔG_f) and the specific volume Gibbs energy (Δg_V), the former being related to one nucleus of the phase and expressed in J and the latter being related to the unit volume of the phase and measured in J m^{-3}. The Δg_V value can be determined directly from the standard thermodynamic parameters, while ΔG_f is calculated from Eqn (1) and takes into account the energetic contributions of the volume and the surface of the nucleus and stress in the nucleus. For a thermodynamically stable phase, $\Delta g_V < 0$, while the energy contribution of the nucleus surface to the Gibbs energy is always positive ($\sigma S > 0$), which hampers the growth of the nucleus.

Now we consider in more detail the contributions of all components to ΔG_f using the Little and Zangwill formalism.[49]

To simplify the manipulation, we will make a number of model assumptions which do not influence the results. We consider the influence of epitaxy on the growth of an oxide film in which a polymorphic transition of the $A' \rightarrow A''$ type, where A' is a phase coherent to the substrate and A'' is a non-coherent phase, may take place. For conservation of the amount of substance, as a first approximation, one can neglect the difference between the densities ρ of the two competing polymorphic forms A' and A''.

† This statement implies impossibility of further solid-state transformations in the layer.

‡ The calculation of the free energy of formation of a nucleus is a routine procedure in consideration of nucleation thermodynamics.[48]

Table 1. Epitaxial stabilisation of oxide phases in thin films.

Epitaxially stabilised phases (structural type)	Substrate [a] [misfit of the unit cell parameters of the film and the substrate $(a_f - a_s)/a_s$]	Equilibrium phases formed in bulk materials under the same conditions (structural type)	Film thickness /nm	Film deposition method	Remarks	Ref.
Metamorphism						
Simple oxides						
TiO_2 (anatase)	(001)$SrTiO_3$ (−3.1%)	TiO_2 (rutile)	1000	MOCVD, molecular beam epitaxy (MBE)	deposition on the leucosapphire (Al_2O_3) with different orientation on the surface under the same conditions gives rutile	5–9
	(001)$LaAlO_3$ (−0.2%)	TiO_2 (rutile)	$n \times 10$	MBE		10
	$La_{0.5}Sr_{0.5}CoO_3$ (−0.5%)	TiO_2 (rutile)	–	PLD		11
	(001)MgO (−10.1%)	TiO_2 (rutile)	1000	MOCVD		6
	(110)MgO (−10.1%, 12.9%)	TiO_2 (rutile)	1000	MOCVD		6
ZnO (sphalerite)	ZnS/(001)GaAs	ZnO (wurtzite)	560	MBE from organometallic compounds		12
Mn_3O_4 (cubic spinel)	(001)MgO	Mn_3O_4 (hausmannite, tetragonal spinel)	–	MOCVD		13
WO_3 (tetragonal phase)	*R*-Al_2O_3 (10.3%, 2.5%)	WO_3 (orthorhombic phase)	30	electron beam evaporation		14
γ-Fe_2O_3	(001)MgO (−0.9%)	α-Fe_2O_3	100	MBE	deposition on the leucosapphire (*a*-, *c*- and *R*-Al_2O_3) under the same conditions gives α-Fe_2O_3	15
Complex oxides						
$BaRuO_3$ (perovskite)	(001)$SrTiO_3$	$BaRuO_3$ (hexagonal, 9R)	100	radio frequency sputtering		16, 17
$Sr(Ru_{0.5}Sn_{0.5})O_3$ (perovskite)	(001)$KTaO_3$ (0.25%)	$Sr(Ru_{0.5}Sn_{0.5})O_3$ (hexagonal, 4H or 9R)	600	PLD		18
$BaTi_{1-x}Nb_xO_3$ (x = 0.01–0.15) (hexagonal)	*R*-Al_2O_3 (17%)	$BaTi_{1-x}Nb_xO_3$ (x = 0.01–0.15) (perovskite)	60	PLD	deposition on (001)$SrTiO_3$ gives perovskite	19
β-BaB_2O_4	*c*-Al_2O_3, *R*-Al_2O_3	α-BaB_2O_4	–	PLD	deposition on (001)Si gives α-BaB_2O_4	20
$PbZr_{1-x}Ti_xO_3$ (pyrochlore)	(001)CeO_2/*R*-Al_2O_3 (3.8%)	$PbZr_{1-x}Ti_xO_3$ (perovskite)	–	PLD	deposition on (001)$SrTiO_3$ and (001)LiF gives perovskite	21
Epitaxial stabilisation of new oxide phases						
Complex oxides						
$Bi_3Fe_5O_{12}$ (garnet)	(001)$Gd_3(Sc,Ga)_5O_{12}$, (111)$Gd_3(Sc,Ga)_5O_{12}$ (<0.5%)	$BiFeO_3$ + $Bi_2Fe_4O_9$	<1000	reaction deposition from ion beams		22, 23
				plasma sputtering, radio frequency sputtering		24, 25
				PLD		22, 26, 27
Ba_2RuO_4 (K_2NiF_4 type)	(001)$SrTiO_3$ (2.1%)	no data	150	PLD	no Ba_2RuO_4 phase is formed on the substrates: (001)MgO, (001)$MgAl_2O_4$, (001)$LaSrGaO_4$, (001)$LaAlO_3$, (001)$LaAlO_3$–Sr_2AlTaO_6	28
Epitaxial stabilisation of oxide phases with metal atoms in unusual oxidation states						
Simple oxides						
CrO_2 (rutile)	TiO_2 (rutile) in different orientations (2%–4%), *c*-Al_2O_3 (−7.1%, 6.0 %)	Cr_2O_3 (corundum)	1000	MOCVD	$T \leqslant 550$ °C, P_{O_2} = 1 bar, CrO_2 is not formed on SiO_2 (quartz)	29–35

Table 1 (continued).

Epitaxially stabilised phases (structural type)	Substrate [a] [misfit of the unit cell parameters of the film and the substrate $(a_f - a_s)/a_s$]	Equilibrium phases formed in bulk materials under the same conditions (structural type)	Film thickness /nm	Film deposition method	Remarks	Ref.
Epitaxial stabilisation of oxide phases with metal atoms in unusual oxidation states						
Simple oxides						
MnO (NaCl type)	c-Al_2O_3, (111)MgO	Mn_3O_4	500	PLD	T = 700 °C, P_{O_2} = $= 10^{-4}$ mbar	36
Fe_3O_4 (spinel)	(001)MgO (0.4%)	Fe_2O_3 (corundum)	–	MBE	corundum grows on c-Al_2O_3	37–39
Fe_3O_4 (spinel)	(001)MgO (0.4%)	Fe	–	MBE	Fe grows on c-Al_2O_3	37–39
$Fe_{3-\delta}O_4$ ($0 < \delta < 0.33$) (spinel)	(001)MgO (0.4%–0.8%)	Fe_2O_3 (corundum)	–	MBE	corundum grows on c-Al_2O_3	15, 37–46
$Fe_{1-x}O$ (NaCl type)	(001)MgO (2.3%)	Fe + Fe_3O_4	–	MBE	T = 450 °C	45
Complex oxides						
$LaCuO_{3-\delta}$ (δ = 0.5) (orthorhombic phase)	(001)$SrTiO_3$ (−2.3%, −0.6%)	$LaCuO_{3-\delta}$ ($0.2 < \delta < 0.5$) (monoclinic phase)	300	PLD	T = 650–750 °C, P_{O_2} = 0.26 mbar	47

[a] The orientations of the perovskite substrates are given in the cubic system.

This assumption does not introduce a significant error but eliminates the necessity of knowing the density or the molar volume (V'_M) of the coherent phase in the absence of stresses (in particular, the latter value is difficult to estimate for a material obtained only as a stressed film).

Assume that new-phase nuclei having a square base with side d and height h are formed on the surface of a single-crystalline substrate representing a two-dimensional lattice with a square unit cell. The relative misfit of the crystal lattice parameters of the substrate and the film at the interface will be defined as

$$\varepsilon = (a_f - a_s)/a_s = \Delta a/a_s ,$$

where a_f and a_s are the unit cell parameters of the growing film and the surface, respectively. Let us consider the case where the film occurs in a uniformly strained state. The expressions for calculating the Gibbs energies for the formation of unit nuclei of the coherent ($\Delta G'_f$) and non-coherent phases ($\Delta G''_f$) can be written as

$$\Delta G'_f = \Delta g'_V d^2 h + (\sigma^s_c)' d^2 + (\sigma^V)'(d^2 + 4dh) + h\frac{\mu}{1-\nu}\varepsilon^2 d^2, \quad (2)$$

$$\Delta G''_f = \Delta g''_V d 2h + (\sigma^s_{ic})'' d^2 + (\sigma^V)''(d^2 + 4dh). \quad (3)$$

The subscripts c and ic refer to the coherent and non-coherent states of the interface, respectively, and the superscripts s and V refer to the nucleus / substrate and nucleus / surrounding gas phase interfaces, respectively. The last term in Eqn (2) is the contribution of the epitaxial stress energy of the nucleus of the coherent phase. This includes the shear modulus μ and Poisson's ratio ν.

The nucleus of the non-coherent phase A″ occurs in a relaxed (*i.e.*, unstressed) state, because it is not bound epitaxially to the substrate. Therefore, Eqn (3) does not have a term corresponding to the stress energy in the nucleus. It is worth mentioning that the surface tension at the non-coherent nucleus/substrate interface is much higher than at the coherent nucleus/substrate interface, $(\sigma^s)' \ll (\sigma^s)''$. The surface tensions at the interfaces between A′ and A″ and the surrounding vapour phase can be taken to be equal: $(\sigma^V)' = (\sigma^V)''$.

We will assume that the non-coherent phase A″, which is free from the substrate, is thermodynamically more stable than the coherent phase A′ under the $P_{O_2} - T$ conditions of film preparation, *i.e.*,

$$\Delta g''_V < \Delta g'_V .$$

[On the substrate, the relative stability of the phases may change due to the pronounced differences between $(\sigma^s)'$ and $(\sigma^s)''$.] By subtracting Eqn (2) from Eqn (3), we get the expression for the Gibbs energy that characterises the stability of one polymorphic form with respect to the other one. Dividing both equations into d^2 (for simplification) gives the equation for determining the Gibbs energy of unit surface of the nucleus ($\Delta E_f = \Delta G_f/d^2$). Hence,

$$\Delta E = \Delta E''_f - \Delta E'_f = \quad (4)$$
$$= h\left[(\Delta g''_V - \Delta g'_V) - \frac{\mu}{1-\nu}\varepsilon^2\right] + \left[(\sigma^s_{ic})'' - (\sigma^s_c)'\right].$$

To take into account the difference between the densities of phases A′ and A″, the difference $(\Delta g''_V - \Delta g'_V)$ should be replaced by

$$\frac{\Delta g''_V V''_M - \Delta g'_V V'_M}{V'_M} = \frac{\Delta G_t}{V'_M},$$

where ΔG_t is the free energy of the solid-state transition per mole.

Equation (4) reflects the opposite effects of two contributions to the Gibbs energy, the surface and the volume ones. Indeed, the first term (the total contribution of the volume energy) is always negative, whereas the second term (the total contribution of the surface energy and the epitaxial stress) is always positive. If the ratio of these contributions is such that $\Delta E > 0$, the condition of epitaxial stabilisation of the coherent phase A′ is fulfilled, although in the free state, this phase is less stable than the non-coherent phase A″. Thus, the ΔE value is the energy of epitaxial stabilisation.

As can be seen from Eqn (4), the misfit between the unit cell parameters of the phase being stabilised and the substrate is a highly significant parameter. The dependence of ΔE on the misfit parameter ε follows a quadratic law, whereas the dependences on the difference between the specific Gibbs energies and the difference between the interface energies with the substrate are linear. The variation of the ES *vs.* film thickness is also linear. The equilibrium condition for the two polymorphic forms A′ and A″ ($\Delta E = 0$) is met at a critical film thickness (h_c):

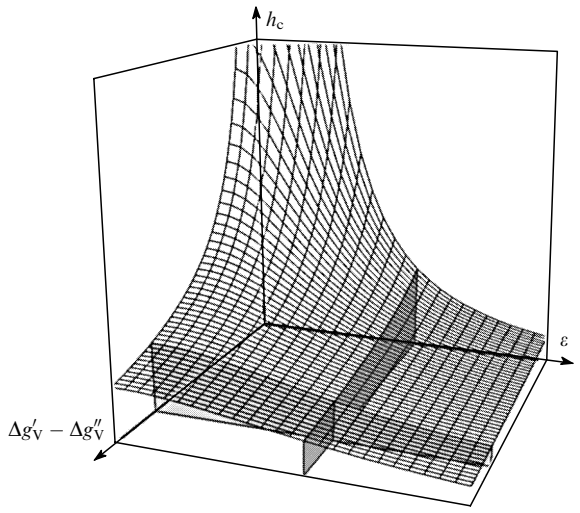

Figure 1. Critical film thickness (h_c) *vs.* the misfit of the unit cell parameters at the substrate/epitaxial film interface (ε) and *vs.* the difference between the specific volume energies of the unstable and stable phases.

$$h_c = \frac{(\sigma^s_{ic})'' - (\sigma^s_c)'}{(\Delta g'_V - \Delta g''_V) + [\mu/(1-\nu)]\varepsilon^2}. \quad (5)$$

Figure 1 shows a draft view of the dependence of the critical film thickness on the misfit of the cell parameters at the film/substrate interface and on the difference between the specific volume energies of the stable and unstable phases.

When the difference between specific volume energies of the competing polymorphic forms and the misfit between the cell parameters of the substrate and the stabilised form are small, the critical film thickness may be fairly large. Estimation of the h_c value from Eqn (5) shows that for a difference between the free energies of the phases of ~ 10 kJ mol^{-1} (this value is usual for polymorphic forms at a moderate deviation of the thermodynamic conditions from the polymorphic transition point), $\varepsilon \approx 0.01$ and for interfacial energies taken from published sources (presented below, see Ref. 50), the critical thickness of the stabilised layer amounts to tens of nanometres.

Interface (i)	Coherent (c)	Semicoherent (sc)	Non-coherent (ic)
σ^s_i /mJ m^{-2}	5–200	200–800	800–2500

When the film thickness is about several tens of nanometres, the model of uniformly strained film is no longer realistic. Stress relaxation in a non-uniformly strained film occurs through the formation of misfit dislocations. In this case, Eqn (4) should be supplemented by a term taking into account the non-uniformity of stresses. For simplicity, we assume that the Burgers vector of the misfit dislocation is equal to the unit cell parameter of the film a_f. Then the expression for ΔE has the form

$$\Delta E = h\left[(\Delta g''_V - \Delta g'_V) - \frac{\mu}{1-\nu}\left(\varepsilon - \frac{a_f}{l}\right)^2\right] + \quad (6)$$
$$+\left[(\sigma^s_{ic})'' - (\sigma^s_c)'\right] - \frac{1}{l}\left[E_{core} + \frac{\mu}{1-\nu}Ka_f^2 \exp\left(-\frac{4\pi h}{l}\right)\right],$$

where l is the distance between the neighbouring misfit dislocations, E_{core} is the energy of the dislocation nucleus and K is the pre-exponential factor. In the limit, $l = a_f/\varepsilon$, which corresponds to full relaxation of the epitaxial stress and disappearance of the term taking into account the contribution of uniform stresses from Eqn (6). When $h > a_f/\varepsilon$, the exponential term in the expression for non-uniform stress also disappears and the remaining addend, which does not depend on the film thickness, can be introduced as a correction for the interfacial energy [this correction transforms the energy of a coherent interface (σ_c) into the energy of a semicoherent interface (σ_{sc})]:

$$\Delta E = h(\Delta g''_V - \Delta g'_V) + [(\sigma^s_{ic})'' - (\sigma^s_{sc})']. \quad (7)$$

The term $[(\sigma^s_{ic})'' - (\sigma^s_{sc})']$ in Eqn (7) is positive, while the term depending on the film thickness is negative. The contribution of the surface energy $[(\sigma^s_{ic})'' - (\sigma^s_{sc})']$ to the Gibbs energy is lower in the case of a non-uniformly strained film than for a uniformly strained film with a coherent interface due to the higher energy of the semicoherent interface. However, the first (positive, 'destabilising') term also decreases in this case due to disappearance of the stress contribution. Thus, the epitaxial stabilisation can also take place in the growth of relaxed films on semicoherent substrates. In other words, epitaxial stresses in the film are not obligatory for the epitaxial stabilisation. Taking the difference between the Gibbs energies of the polymorphic forms to be, as in the previous case, 10 kJ mol^{-1} and substituting the interfacial energies into Eqn (7), one can estimate the critical thickness of the stabilised phase. The result is of the order of tens of nanometres.

The experience in preparation of thin films indicates that the phase non-coherent to the substrate always grows as a polycrystal. The internal interfaces in a polycrystalline materials make a substantial contribution to the Gibbs energy. This contribution (so-called excessive Gibbs energy), which has not yet been included in the energy balance of two polymorphic phases, undoubtedly affects the epitaxial stabilisation. Assuming that the average grain size in the non-coherent phase equals r and the average energy of the boundaries of chaotically oriented grains equals σ''_{gb} and taking into account the fact that the number of grains on unit surface equals d^2/r^2 ($d \gg r$), we obtain a relation for the total energy of the grain boundaries of the non-coherent phase concentrated on unit surface area of the substrate

$$E_{gb} = \frac{2h\,\sigma''_{gb}}{r}. \quad (8)$$

By substituting the E_{gb} value as an additional term for the non-coherent phase energy, into Eqn (7), we get an expression for the epitaxial stabilisation energy

$$\Delta E = h\left[(\Delta g''_V - \Delta g'_V) + \frac{2\,\sigma''_{gb}}{r}\right] + [(\sigma^s_{ic})'' - (\sigma^s_{sc})']. \quad (9)$$

It should be noted that the surface tension σ''_{gb} in a polycrystalline film is of the same order of magnitude as σ_{ic}, and, hence, the influence of polycrystallinity, which increases ΔE, may become prevailing. The role of this factor appreciably increases with a decrease in the grain size. As the polycrystalline film of the stable phase grows, the grain size does not remain constant but increases; however, under steady-state conditions of growth, this increase follows the law $r \propto \sqrt[n]{h}$ ($n \geqslant 2$). Therefore, the increase in the grain size does not much decrease the excessive free energy of the intergrain boundaries and, finally, does not interfere with the preparation of the epitaxially stabilised phase as films with a large critical thickness.

In order to verify the applicability of Eqns (7) and (9) for the calculation of ΔE, we will consider the results of calculations of the polymorphic transition TiO_2(anatase) → TiO_2(rutile) (Fig. 2). It follows from the data of Table 1 that the TiO_2(anatase) film grows on the (001)$LaAlO_3$ surface epitaxially to form a semicoherent interface. According to the above data, the energy of the semicoherent interface between the thin film and the substrate can be taken to be $(\sigma^s_{sc})' = 800$ mJ m^{-2}. A hypothetical film of the stable rutile phase could grow in the polycrystalline form under these conditions. The energy of the non-coherent interface between such a film and a substrate $(\sigma^s_{ic})''$ can amount to 2500 mJ m^{-2}; the non-coherent intergrain boundaries σ''_{gb} have the same energy. The difference between the specific volume energies $(\Delta g''_V - \Delta g'_V)$ calculated using the published value of the Gibbs energy for the TiO_2(anatase) → TiO_2(rutile) transition (-5 kJ mol^{-1}) [51, 52] and

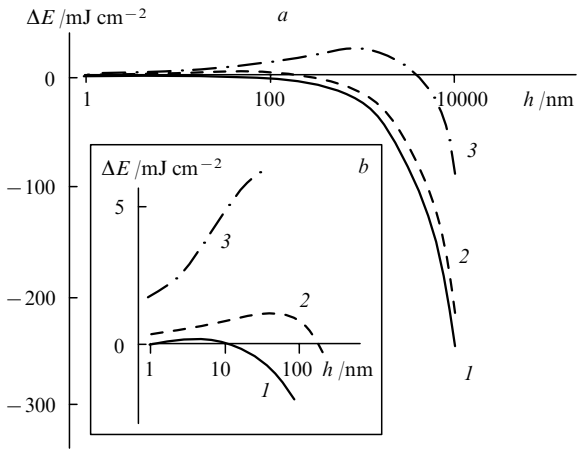

Figure 2. Results of model calculations for the TiO_2(anatase) → TiO_2(rutile) polymorphic transition using Eqns (7) (curve *1*) and (9) (curves *2* and *3*) (*a*). The inset (*b*) shows the enlarged view of the initial course of curves *1*–*3*;
r/μm: ∞ (*1*), 25 (*2*), 1 (*3*).

the theoretical density values for rutile and anatase (4.25 and 3.89 g cm^{-3}, respectively), is equal to 243.7 J cm^{-3}.

It can be seen from Fig. 2 that the anatase epitaxial film is thermodynamically more stable than the rutile polycrystalline film when the film thickness is smaller than the critical value h_c, corresponding to the condition $\Delta E = 0$. With the reasonable assumption that the rutile film can be formed by crystallites with the size $\sqrt{h}$, we finally get that the critical thickness of an epitaxially stabilised film of anatase can reach 4 μm! Although the exact value of h_c depends on the numerical values $(\sigma^s_{ic})''$, $(\sigma^s_{sc})''$ and σ''_{gb} used for calculations, this calculation still proves the theoretical possibility of preparing stabilised phases as epitaxial films with a sufficient thickness for many practical applications. In other words, the epitaxial stabilisation can be an efficient tool for the preparation of new functional materials.

Undoubtedly, crystallisation under real conditions is much more complicated than is described in terms of the above model. First of all, this model does not take into account any kinetic effects, resulting in accumulation of non-equilibrium point and extended defects in the epitaxial films (stacking faults, antiphase boundaries, development of mosaic block low-angle boundaries) and ultimately in the inevitable disappearance of the epitaxy following an increase in the film thickness. Apparently, these kinetic effects rather than the value we calculated from thermodynamic considerations are responsible for restriction of the stabilised phase thickness. Thus, the growth of films under conditions favourable for acceleration of diffusion processes and crystallisation, in particular, the growth at a temperature exceeding the Tamman temperature,§ or implementation of the liquid-phase growth mechanism (for example, vapour–liquid–crystal or the liquid-phase epitaxy) would promote the formation of stabilised phases as epitaxial films with the critical thickness predicted by the thermodynamic model outlined above.

This model can be applied not only to a polymorphic transformation of two phases but also to more complicated phase ensembles; however, considering such ensembles requires much more complicated equations but does not reveal any new significant aspects of epitaxial stabilisation.

§ The Tamman temperature is the temperature above which intensive self-diffusion occurs in a solid. As a rule, the Tamman temperature is taken to be 0.6 T_m (the Tamman rule).

3. Preparation of epitaxial oxide films by MOCVD

Metal organic chemical vapour deposition (MOCVD) is a promising and efficient method for the preparation of films of simple and complex oxides.

The MOCVD method has a number of obvious advantages over the high-vacuum physical (physical vapour deposition, PVD) methods, in particular,

— relatively low cost,
— relatively low requirements to the vacuum equipment,
— the possibility of high deposition rate,
— remarkable versatility as regards the variation of the elemental composition of films.

These advantages make the MOCVD method very attractive for the modern technology of films and coatings. A substantial progress in the development of this method as applied to the production of films of simple and complex oxides has been attained during the last 15 years. This was largely due to the advent of methods for the preparation of epitaxial films of high-temperature superconductors (HTSC), especially those of the $RBa_2Cu_3O_{7-\delta}$ family.[53] The superconducting properties of films are highly sensitive to minor changes in the composition and structure; therefore, the problem of preparing HTSC with reproducible properties is much more challenging than the problem of preparing other thin-film materials. The advances attained in MOCVD syntheses of HTSC films stimulated the extension of this method to many other functional oxide materials often having rather complex elemental composition.

The heterogeneous MOCVD process consists of several consecutive stages: evaporation or sublimation of the starting compounds (volatile organometallic compounds), their transfer through the gas phase (often complicated by gas-phase reactions) and, finally, oxidative thermolysis on the substrate with simultaneous crystallisation of the product. Each stage is complicated. In the case of multicomponent films, the difference between the chemical and thermal properties of compounds used to transport each of the starting components results in a substantial incongruence of the process, *i.e.*, in different stoichiometric ratios of the metallic components in the vapour of the starting compounds and in the film. This is the major syntetic challenge in the preparation of multicomponent films.[54, 55]

Nevertheless, the synthesis of new volatile compounds with improved properties (more stable and more volatile) for a large number of metals, perfection of batching and vaporisation techniques and the design of more advanced reactors with optimised thermal fields and gas dynamics turned MOCVD into an advanced process technology.

Most often, metal dipivaloylmethanates $M(dpm)_n$ or their adducts with *o*-phenanthroline were used as the starting compounds for the synthesis of the thin films of manganites $R_{1-x}M_xMnO_3$ (R = La–Lu; M = Ca, Sr, Pb, Na), nickelates $RNiO_3$ (R = La, Pr, Nd, Sm, Gd), cobaltates $RCoO_3$ (R = Tm, Lu), ferrites $RFeO_3$ (R = Eu–Lu), garnets $R_3Fe_5O_{12}$ (R = Nd, $Nd_{1-x}La_x$), indates $RInO_3$ (R = La–Lu), ruthenates $(Ca,Sr)RuO_3$ and superconductive cuprates $RBa_2Cu_3O_{7-\delta}$ (R = Lu, Ho, Y, Gd) considered in this review. These compounds were evaporated as microbatches fed successively to the evaporating chamber; thus, the flash vaporisation principle, which minimises the thermal degradation of the precursors, was implemented. Various special devices (feeders) were used for the supply of precursors: aerosol, vibratory, belt, frictional and screw feeders. The precursor vapours were transported by an argon–oxygen stream to tubular reactors heated by the external resistance furnace or induction method.

The temperature of the substrates (usually single crystals cut along a definite plane and polished) was varied, depending on the system, in the 650–900 °C range and the oxygen pressure was 1–7 mbar. The total pressure in the reactors (maintained constant in each experiment) was in the range 3–20 mbar. The

MOCVD conditions are described in more detail in our original publications.[53, 56–60]

4. Epitaxial stabilisation of unstable compounds RMO_3 (R is lanthanide, M = Mn, Ni, Co, Fe, In)

Manganites $RMnO_3$. In the series of $RMnO_3$, phases with the perovskite structure are formed under ambient pressure only for lanthanides with great ionic radii (R = La–Dy), whereas elements with smaller ionic radii (Y, Ho–Lu) form hexagonal structures with the same stoichiometry.[61] The corresponding perovskites $RMnO_3$ (Y, Ho–Lu) were prepared only under high pressure.[62] However, the situation can change upon the change in the contribution of the surface free energy. Thus the $YMnO_3$ nanoparticles synthesised under normal pressure are no longer hexagonal but have a perovskite structure.[63]

We attained epitaxial stabilisation of the perovskite phase $RMnO_3$ (R = Y, Ho, Tm, Lu) by MOCVD deposition of the $RMnO_3$ films onto the (001)$LaAlO_3$ and (001)$SrTiO_3$ substrates.[64] The orthorhombically distorted perovskite $YMnO_3$ was also prepared by PLD on a substrate.[65]

The most efficient stabilisation takes place on the $LaAlO_3$ substrate because this is characterised by a minimum misfit (~0.5%) between the unit cell parameters and the growing perovskite film. Using this substrate, 100–200-nm thick perovskite films were prepared (T = 750 °C). Under the same conditions, no perovskite phase is formed on the $(1\bar{1}02)Al_2O_3$ and (111)$ZrO_2(Y_2O_3)$ substrates. The resulting perovskite films were structurally identical to those formed in the polycrystalline state at high pressure: their perovskite structure experienced substantial orthorhombic distortion (orthorhombicity parameter ~5%, space group *Pnma*). The distortion of the perovskite structure gave rise to twinning in the films. According to powder X-ray diffraction and high-resolution transmission electron microscopy (HREM) of film cross-sections, the unit cell parameters are always doubled along the substrate plane (Figs 3, 4) and the direction of doubling of the cell parameter in each successive domain is changed by 90°. This type of twinning reduces the stress arising in the film due to the misfit in the cell parameters of the film and the substrate because this markedly decreases the energy of the film/substrate interface, in conformity with the theory developed by Little and Zangwill.[49]

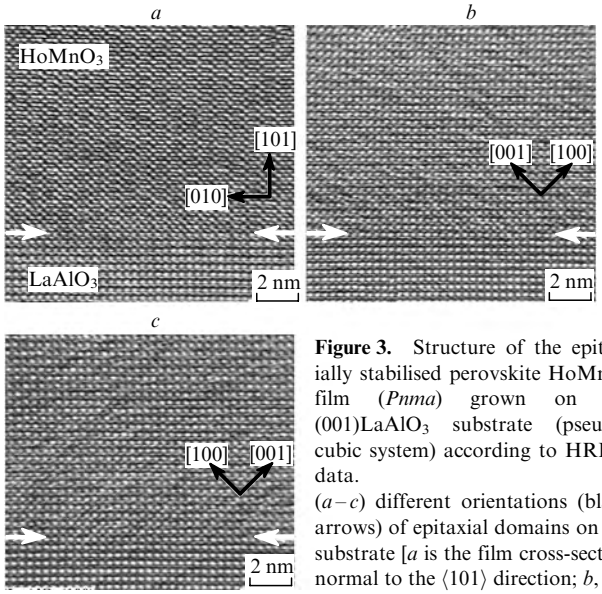

Figure 3. Structure of the epitaxially stabilised perovskite $HoMnO_3$ film (*Pnma*) grown on the (001)$LaAlO_3$ substrate (pseudocubic system) according to HREM data.
(*a*–*c*) different orientations (black arrows) of epitaxial domains on the substrate [*a* is the film cross-section normal to the ⟨101⟩ direction; *b*, *c* is the same normal to the ⟨010⟩ direction.] Here and below, light arrows designate the film/substrate boundary.

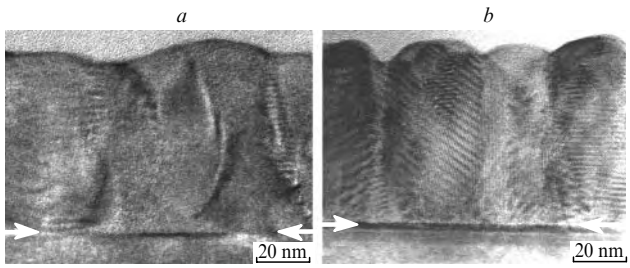

Figure 4. Photomicrograph of the cross-section of $HoMnO_3$ (*a*) and $LuMnO_3$ (*b*) perovskite films on the (001)$LaAlO_3$ substrate (TEM data).

The size of domains correlates with the misfit of the crystal lattice parameters between the film and the substrate at the interface; an increase in the misfit results in a decrease in the size of domains. For example, much more extended domains are formed in the perovskite $HoMnO_3$ films (Fig. 4*a*) than in $LuMnO_3$ films (Fig. 4*b*).

The results of investigations of the real structure of $RMnO_3$ perovskite films confirm the conclusion drawn above, namely, that a stress in the lattice is not a necessary factor of epitaxial stabilisation, as some researchers believe [see, for example, A Zunger, D Wood *J. Cryst. Growth* **98** 1 (1989)].

Compounds $RMnO_3$ with a hexagonal structure of the $LuMnO_3$ type (space group $P6_3cm$) stable under ambient pressure are formed only for lanthanide cations with small ionic radii (R = Ho–Lu, Y). Their structure can be represented as a close packing of oxygen ions (ABCACB) in which the Mn^{3+} ions occupy positions with C.N. 5 (a five-vertex trigonal bipyramid), while the R^{3+} ions occur in positions with C.N. 7 (a seven-fold one-cap octahedron).[57] The interest in these compounds is due to the fact that they crystallise in space group $P6_3cm$. It is known that compounds that belong to this structural type can exhibit ferroelectric properties. In particular, $YMnO_3$ is a promising ferroelectric, which could find application in electronics.[66]

The complex oxide $DyMnO_3$ ($r_{Dy} > r_{Ho}$), prepared under usual solid-state synthesis conditions, has a stable perovskite structure. For this compound to crystallise in the hexagonal phase, heat treatment at a temperature of ⩾1600 °C with subsequent quenching is required.[63] The greater the lanthanide ionic radius, the higher the temperature of the perovskite-to-hexagonal phase transition. Indeed, for $GdMnO_3$, the temperature of this polymorphic transition should be as high as about 2800 °C (determined by extrapolation), which knowingly exceeds the melting point of this compound and other manganites. In other words, $RMnO_3$ with R = Gd and larger lanthanide ions cannot exist as stable bulk samples in a hexagonal modification; however, these can be obtained as thin films using epitaxial stabilisation.[67]

On the basis of the available structural data for stable hexagonal phases, (111)$ZrO_2(Y_2O_3)$ was concluded to be the substrate of choice for the synthesis of hexagonal epitaxial films. In this case, the crystallographic positions of oxygen atoms at the substrate/hexagonal $RMnO_3$ interface perfectly coincide and the misfit parameter ε is a minimum [the films deposited on the (001)$LaAlO_3$, (001)MgO and (001)$ZrO_2(Y_2O_3)$ substrates had purely perovskite structures]. The X-ray diffraction patterns of the $DyMnO_3$, $GdMnO_3$ and $EuMnO_3$ films on the (111)$ZrO_2(Y_2O_3)$ substrate (Fig. 5) contained both symmetric (00*l*) and asymmetric (111), (112) reflections typical of a hexagonal structure of the $LuMnO_3$ type (asymmetric reflections are not shown in Fig. 5). It should be noted that the intensity of the (00*l*) reflections from the hexagonal phase decreases on passing from Dy to Eu and becomes zero for Sm; conversely, the intensity of the perovskite reflections increases in the same sequence. This means that the $DyMnO_3$ film grows as a purely hexagonal phase, the $EuMnO_3$ and $GdMnO_3$ films contain the hexagonal phase coexisting with the perovskite one (this was confirmed by recording the

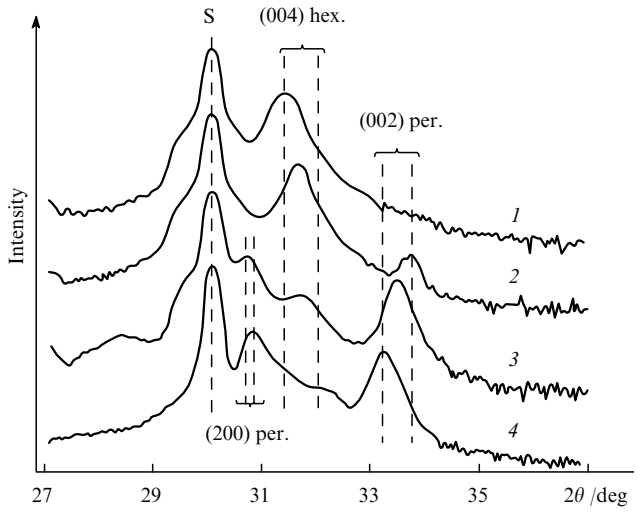

Figure 5. X-Ray diffraction patterns ($Cu_{K\alpha}$) of the $RMnO_3$ films grown on (111)$ZrO_2(Y_2O_3)$. R = Dy (*1*), Gd (*2*), Eu (*3*), Sm (*4*). Here and below, the reflections marked by S correspond to the substrate.

pole figures), and the $SmMnO_3$ film contains only the perovskite phase.

The hexagonal phase is *c*-oriented [as follows from X-ray φ-scanning spectra (Fig. 6) and pole figure images] and has the following epitaxial relations:

$$(001)_{hex}\,\langle 1\bar{1}0\rangle_{hex}\,RMnO_3 \parallel (111)\langle 1\bar{1}0\rangle\,ZrO_2(Y_2O_3),$$

i.e., the hexagonal (001) plane is parallel to the (111) plane of the substrate; the direction $\langle 1\bar{1}0\rangle_{hex}$ of $RMnO_3$ and $\langle 1\bar{1}0\rangle$ of the cubic substrate are also parallel.

Figure 7 shows the model of the epitaxial growth (polyhedral image) of the hexagonal $RMnO_3$ phase on (111)$ZrO_2(Y_2O_3)$.

It should be noted that an increase in the film thickness to 300 nm entailed an increase in the intensity only of perovskite reflections and not of reflections from the hexagonal phase. This indicates that the hexagonal phase grows only in the region adjacent to the substrate, while away from the substrate (in the upper part of the film), the usual perovskite phase is formed, stable in the bulk materials with this composition.

By extrapolating the available thermodynamic data on lanthanide manganites[68] to the region of epitaxially stabilised phases, one can estimate the thermodynamic effect of the ES for manganites with the perovskite and hexagonal structures (Fig. 8).

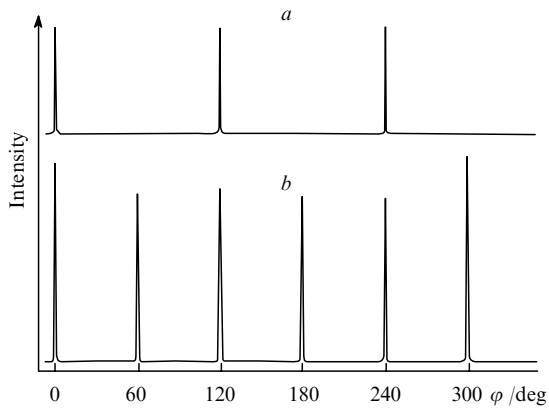

Figure 6. X-Ray diffraction spectra (φ-scanning) of the (111)$ZrO_2(Y_2O_3)$ substrate (*a*) and the $DyMnO_3$ film (*b*).
(*a*) {100}, χ = 55°, FWHM = 0.25°; (*b*) {112}, χ = 61°, FWHM = 0.55° (FWHM is the full width at half maximum, χ is the slope angle).

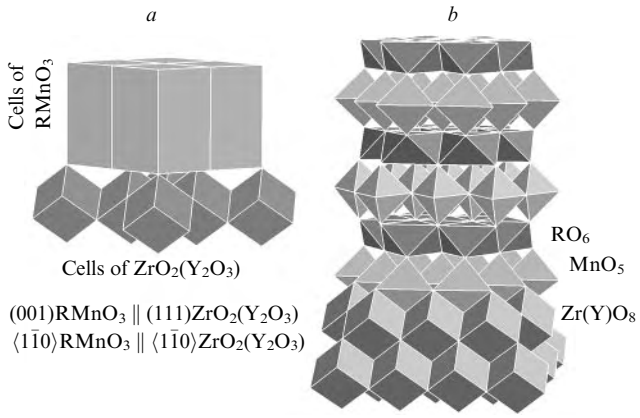

Figure 7. Model of the epitaxial growth of the $RMnO_3$ hexagonal phase on (111)$ZrO_2(Y_2O_3)$ (polyhedral image).
(*a*) Correlation of the substrate and film unit cells; (*b*) packing of the layers.

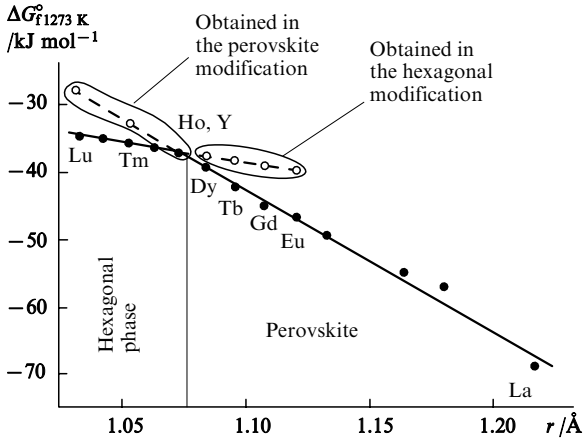

Figure 8. Gibbs energy of the formation of $RMnO_3$ (R is lanthanide) by the reactions $1/2\,R_2O_3 + 1/3\,Mn_3O_4 + 1/12\,O_2 = RMnO_3$ *vs.* ionic radius of the lanthanide (from Ref. 68).
The dashed lines represent the extrapolation to the epitaxial stabilisation region.

It can be stated that the ES of a thermodynamically less stable phase is possible if the difference between the Gibbs energies of the formation of the polymorphic forms does not exceed 10–15 kJ mol^{-1}, because in this case, the difference between the Gibbs energies can be counterbalanced by the decrease in the free energy of the system due to the low energy of the coherent interface between the epitaxial film and the substrate. The critical thickness of the stabilised phase decreases with an increase in the energy difference between the stable and unstable phases: even in thin films of the $GdMnO_3$ hexagonal phase, the upper layer has a perovskite structure. In the $EuMnO_3$ films, the layer of the stabilised hexagonal phase is even thinner.

We have also prepared previously unknown orthoferrites with the hexagonal structure, $RFeO_3$ (R = Eu, Er, Tm, Yb, Lu),[69] by stabilising them on the (111)$ZrO_2(Y_2O_3)$ substrate and confirmed, as in the case of manganites, the key conclusions of the thermodynamic model of ES. It was shown that these compounds may, in principle, exhibit ferroelecteric properties.[69]

The nickelates $RNiO_3$. A general structure–thermodynamics relationship for series of perovskite compounds has now been established, in particular, deformation of the perovskite structure with a decrease in the tolerance factor is accompanied by a decrease in the thermodynamic stability of compounds.[70] In the series of lanthanide perovskites (nickelates and cobaltites), this is manifested as an increase in the equilibrium pressure of oxygen

(for T = const) following a decrease in the lanthanide ionic radius. The solid-state synthesis of $RNiO_3$ powder or ceramics, except for $LaNiO_3$, requires high pressure P_{O_2}, which reaches 100 bar for the last members of the lanthanide row.

Using the ES, we succeeded in preparing thin epitaxial films of $RNiO_3$ (R = Pr, Nd, Sm, Gd) at a reduced oxygen pressure, which did not exceed 20 mbar.[71] The formation of perovskite phases was observed only for substrates having a perovskite structure ($LaAlO_3$, $SrTiO_3$), whereas the films grown on MgO and $ZrO_2(Y_2O_3)$ consisted of a mixture of the R_2O_3 and NiO oxides. Single-phase $RNiO_3$ films were prepared only on the $LaAlO_3$ substrate, which is most consistent with nickelates as regards the crystal lattice parameter ($\varepsilon = 0.2\% - 0.7\%$), whereas on the $SrTiO_3$ substrate with greater ε ($\varepsilon \approx 3\%$), phases of simple nickel and lanthanide oxides are formed in addition to $RNiO_3$ perovskite (Fig. 9). The content of the epitaxial perovskite $RNiO_3$ phase in the films prepared by MOCVD under identical conditions decreased with a decrease in the ionic radius of R^{3+}, due to the decrease in the perovskite stability in the same series.[72, 73] The least stable nickelate we studied, $GdNiO_3$, could be obtained only on $LaAlO_3$. These experiments revealed a clear-cut correlation between the thermodynamic properties of nickelates (the measure of their instability) and the critical film thickness for stabilised phases, which is consistent with the ES theory considered above.[67] After the critical thickness had been attained, a layer of the R_2O_3 and NiO oxide mixture started to grow on the surface of the perovskite phase.

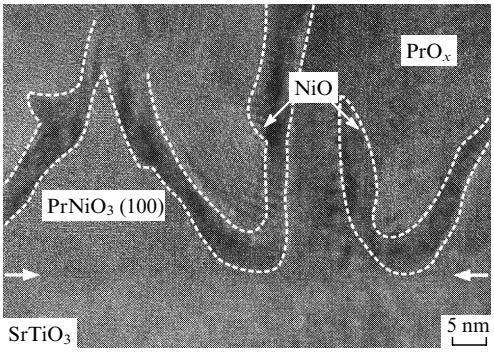

Figure 9. Cross-section of the $PrNiO_3/(100)SrTiO_3$ film in the (100) plane obtained by HREM (see the comments in the text).

Important information was gained from a HREM study of cross-sections of nickelate films. It was found that the atomically smooth interface between the epitaxial $RNiO_3$ film and the $LaAlO_3$ substrate is not distorted by misfit dislocations, which indicates unambiguously the presence of epitaxial compression stresses in the films, resulting in the tetragonal deformation of the film crystal lattice. Previously, this type of deformation has been found by X-ray diffraction.[74] It was demonstrated that nickelates crystallise in an orthorombic group of symmetry *Pnma*. It was shown that epitaxial films of nickelates (like manganite films) consist of orthorhombic domains; the axis directed along the doubled cell parameter can be oriented along the three orthogonal axes (Fig. 10) ¶ and the ε parameters for all the possible domain orientations are virtually equal. In this case, the formation of orthorhombic domains (twins) in nickelate films does not eliminate the epitaxial stresses (the situation opposite to that described above for $RMnO_3$ perovskite films). As a result, the anisotropic epitaxial stresses represent one more factor (in addition to the misfit of the lattice parameters at the film/substrate interface) to restrict the critical thickness of the stabilised phase.

¶ Note that orthorhombic distortions in lanthanide nickelates are much less pronounced than in manganites.

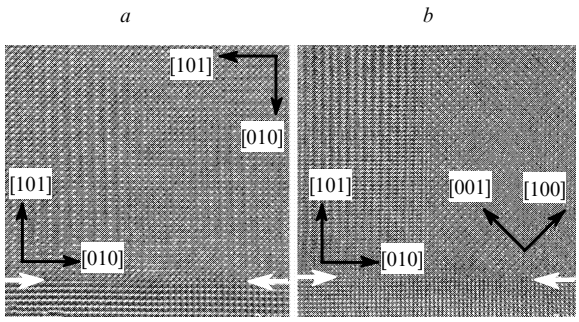

Figure 10. Domain structure of the $SmNiO_3/(001)LaAlO_3$ film (according to HREM data).
(*a*, *b*) Different domain orientations are shown.

An HREM study of the cross-sections of the films has also shown that the perovskite phase coexists, in some range of thicknesses, with simple oxide phases (see Fig. 9) and the volume fraction of perovskite gradually decreases with an increase in the film thickness. This result attests to the limitation of the model in which the phase composition sharply changes as the film reaches the critical thickness h_c and, conversely, validates the idea put forward by Little and Zangwill,[49] which predicts gradual transition from the epitaxially stabilised phase to phases stable as bulk materials.

The cobaltates $RCoO_3$. In the series of $RCoO_3$ perovskites, the border of high-temperature stability of phases at $P_{O_2} = 1$ bar is situated between Yb and Tm; hence, the last members of the row, $YbCoO_3$ and $LuCoO_3$, can be obtained by solid-state synthesis only under an elevated pressure of oxygen.[75] An estimate of the Gibbs energy for the reactions

$$Co_3O_4 + R_2O_3 + O_2 \longrightarrow RCoO_3$$

R = Tm – Lu

by extrapolation of the linear dependence of $\Delta G^\circ_{1100\,K}$ on the tolerance factor[76] obtained for more stable cobaltates gives positive values. In particular, the $\Delta G^\circ_{1100\,K}$ value for the least stable $LuCoO_3$ is equal to 8 kJ mol^{-1}, which confirms that this compound is unstable under solid-state synthesis conditions.

We attempted to prepare $LuCoO_3$ films by epitaxial stabilisation without using a high pressure of oxygen. The films were synthesised by MOCVD at 700 – 850 °C and P_{O_2} = 6.5 mbar on single-crystalline substrates, $(001)CaGdAlO_4$, $(001)LaAlO_3$, $(001)SrTiO_3$ and (001)MgO,[77] whose parameters ε were 0.3%, 3%, 6% and 14%, respectively. The X-ray diffraction patterns of $LuCoO_3$ films (Fig. 11), obtained on different substrates at the same temperature, imply a dependence of the formation of $LuCoO_3$ on the ε value. Indeed, a film of the Lu_2O_3 and Co_3O_4 oxide mixture grew on the non-coherent MgO substrate, while the films grown on more coherent $SrTiO_3$, $LaAlO_3$ and $CaGdAlO_4$ substrates were epitaxial $LuCoO_3$ films with the perovskite structure in the (001) orientation with an admixture of simple oxides, the content of the admixture decreasing on passing from $SrTiO_3$ to $CaGdAlO_4$ (one should note a low intensity of reflections from polycrystalline phases in the films). Similar results were obtained in the synthesis of $TmCoO_3$ films. However, the films of more stable $GdCoO_3$ with $\Delta G^\circ_{1100\,K} < 0$ [76] were also grown on MgO, moreover, in the polycrystalline form, *i.e.*, without the directing effect of the substrate.

An increase in the temperature of film deposition resulted in disappearance of the perovskite phase due to an increase in the equilibrium oxygen pressure above cobaltates. However, in this case, too, the behaviours of the films grown on different substrates were markedly dissimilar: the film stabilisation energy was correlated with ε. On the $CaGdAlO_4$ substrate, the perovskite phase was observed even at 820 °C, whereas on $SrTiO_3$, this phase did

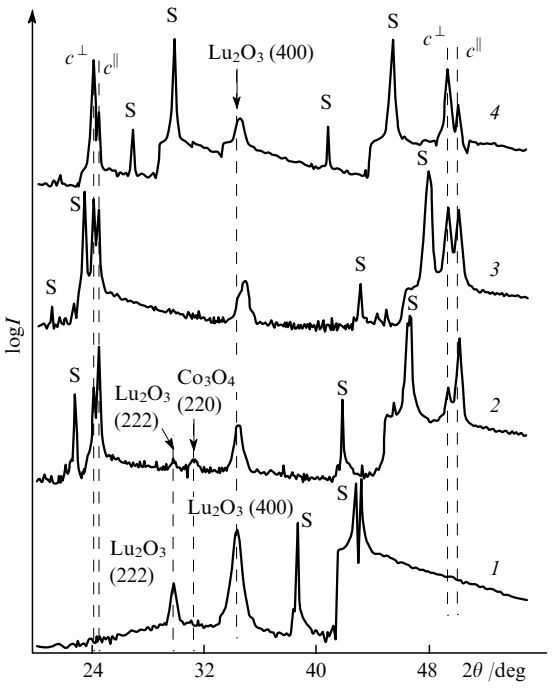

Figure 11. X-Ray diffraction patterns of the $LuCoO_3$ films grown on various substrates (S is the substrate reflections, $c^{\parallel}$, $c^{\perp}$ are perovskite reflections).
Substrate [ε (%)]: (*1*) (001)MgO (14), (*2*) (001)$SrTiO_3$ (6), (*3*) (001)$LaAlO_3$ (pseudo-cubic notation) (3), (*4*) $CaGdAlO_4$ (0.3).

not exist above 800 °C. The process of disappearance of the stabilised $LuCoO_3$ film on raising the deposition temperature differed from the process of disappearance of the bulk dissociating oxide: the latter disappeared immediately after some threshold $P_{O_2}-T$ conditions (equilibrium dissociation conditions). In the case of films, the intensity of X-ray reflections from $LuCoO_3$ gradually decreases with temperature rise; this is in line with the decrease in the critical thickness of the stabilised phase following a decrease in the thermodynamic stability of this phase [*i.e.*, with an increase in $\Delta g''_V - \Delta g'_V$, see Eqn (9)].

Evidently, even at the optimal temperature of film deposition (750 °C) on the most coherent substrate, an admixture-free $LuCoO_3$ perovskite phase can be obtained only in a limited range of thicknesses. When the film thickness is ~100 nm, the films contain only the perovskite phase, whereas ~400-nm thick films contain pronounced amounts of Lu_2O_3 and Co_3O_4 impurities. These are equilibrium phases (under film deposition conditions) of the bulk polycrystalline Lu–Co–O system formed in the upper layers of the $LuCoO_3$ films as they exceed the critical thickness.

The essential orthorhombicity inherent in the $RCoO_3$ phases is responsible for the doubling of the diffraction peak for the cubic perovskite. The orientation of the orthorhombic domains in epitaxially stabilised films depends on the nature of the substrate. According to X-ray diffraction data, two types of domains are formed in the $LuCoO_3$ films: in the first-type domains ($c^{\parallel}$), the doubled parameter (*i.e.*, the *c* axis within the *Pbnm* group) is directed along the substrate surface, while in second-type domains ($c^{\perp}$), it is perpendicular to the substrate. It was found that the fraction of $c^{\parallel}$-type domains increases in the series $CaGdAlO_4$–$LaAlO_3$–$SrTiO_3$, whereas the fraction of $c^{\perp}$-type domains decreases in this series (see Fig. 11). This regularity was interpreted by mininisation of the misfit between the film and substrate parameters through giving preference to either type of domains. This raised the question of whether both types of domains originate simultaneously during film deposition, or twinning occurs during cooling of the films. The X-ray diffraction analysis of the films quenched after deposition at 800 °C has shown that single-domain films of the $c^{\parallel}$ type originate and grow on $SrTiO_3$, and $c^{\perp}$ type films grow on $LaAlO_3$ (Fig. 12). The structure of twin domains is formed during cooling, apparently according to the martensite mechanism. Twinning is a way of decreasing thermomechanical stresses arising at the film/substrate interface on slow cooling.[77]

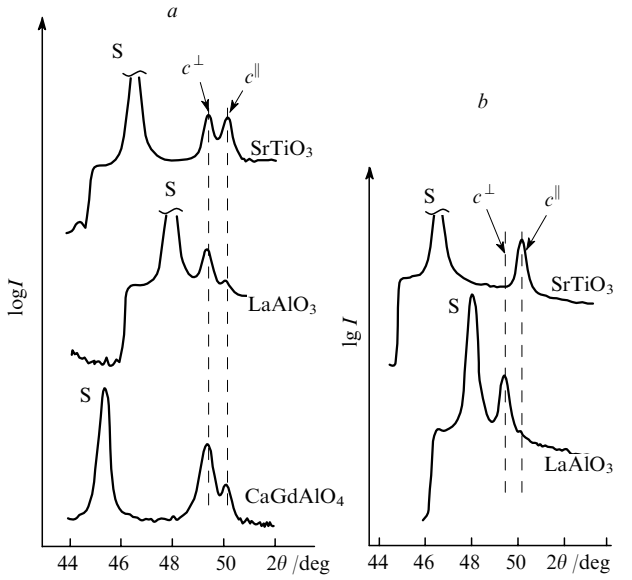

Figure 12. Sections of the X-ray diffraction patterns of the $LuCoO_3$ films on various substrates.
(*a*) X-ray diffraction patterns of the films slowly cooled after deposition; (*b*) X-ray diffraction patterns of the films hardened after deposition on the substrate at 800 °C in air. The reflection (220) refers to type $c^{\perp}$ domain and (004), to type $c^{\parallel}$ domain.

The indates $RInO_3$. The lanthanide indates of the composition $RInO_3$, existing in the bulk state, can be divided into three groups in terms of the structure, namely, perovskites, hexagonal phases and fluorite type phases. The compounds $RInO_3$ with R = La–Sm can be prepared as perovskites by the conventional solid-state synthesis, whereas the homologues with R = Eu–Dy form hexagonal phases under the same conditions. Under the action of high pressure (65 kbar), these phases can turn into perovskites.[78] The compounds $RInO_3$ with R = Y and Ho are solid solutions of the fluorite type, which also acquire a perovskite structure under the action of high pressure.[79] No data on the phase formation in the R–In–O systems (R = Er–Lu) have been reported.

We attempted to synthesise indates $RInO_3$ (R = Eu–Lu) with the perovskite structure without using high pressure but by means of the ES.

As the substrate for growing $RInO_3$ films, we chose $SrTiO_3$, which best fits the known perovskites $RInO_3$ as regards the cell parameter. We have grown $RInO_3$ films (R = Eu–Lu) on this substrate. Figure 13 shows X-ray diffraction spectra of the resulting films, which confirm their perovskite structure [reflections (001) and (002)], and the photomicrograph of the $NdInO_3/SrTiO_3$ film, which proves that the h_c value is greater than 80 nm. The decrease in the intensity of perovskite reflections (002) upon a decrease in the ionic radius of R^{3+} indicates that the stability of perovskites decreases with an increase in the tolerance factor and that the critical thickness of the stabilised perovskite phases decreases as they become less stable in the form of bulk materials. It was found that the conductivity of the resulting thin films of lanthanide indates can be appreciably changed by heterovalent doping. The doped films can be used in gas sensors.

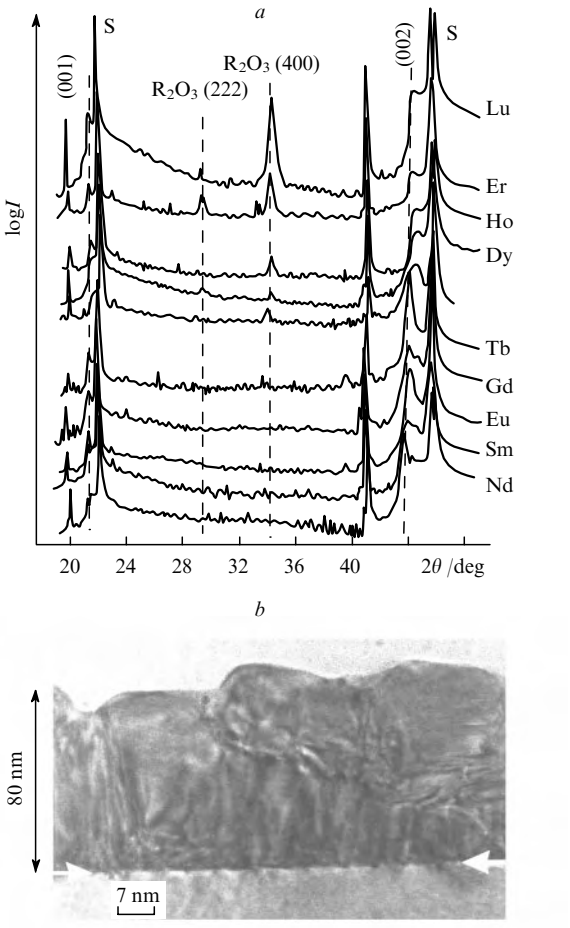

Figure 13. X-Ray diffraction patterns of the $RInO_3$ films (R = Nd – Lu) grown on $SrTiO_3$ (*a*) and photomicrograph of the $NdInO_3/SrTiO_3$ film (*b*) obtained by HREM.

The garnets $R_3Fe_5O_{12}$. A necessary condition for the formation of a garnet structure is fulfillment of the criterion $r_{M^{3+}} : r_{Fe^{3+}} \leqslant 1.7$, which means that ferrogarnets are formed only in those cases where the ionic radius of the lanthanide is not larger than 1.14 Å, *i.e.*, only for R = Sm – Lu, Y. The elements of the beginning of the row (La, Ce, Pr, Nd) do not form garnets in the conventional solid-state synthesis, although $Nd_3Fe_5O_{12}$ can be synthesised at high pressure.[80]

We managed to prepare (by means of the ES) thin films of garnet-type solid solutions $(La_xNd_{1-x})_3Fe_5O_{12}$ on the $(111)Gd_3Ga_5O_{12}$, $(210)Gd_3Ga_5O_{12}$, $(111)Nd_3Ga_5O_{12}$ and $(111)(Y_{0.8}Ca_{0.9}Tm_{0.7}Sm_{0.6})(Ge_{0.2}Fe_{0.8})_5O_{12}$ substrates with a garnet structure; the orientation of the garnet films corresponded to the substrate orientation (no garnet phase was formed in films with the same composition on substrates with the perovskite or MgO structure).

The photomicrographs of the $(La_xNd_{1-x})_3Fe_5O_{12}$ films (Fig. 14) give an idea of the critical film thickness of stabilised garnets. In the case of $Nd_3Fe_5O_{12}$, the film thickness was unexpectedly great (more than 3.6 μm, Fig. 14 *b*). It was found that the film thickness decreases with an increase in the La concentration in the solid solution (Fig. 14 *c*). When the critical thickness is exceeded, $RFeO_3$ and Fe_2O_3 equilibrium phases start to grow on the surface of the stabilised phase of the garnet.

The concentration ranges of stability of the garnets $(La_xNd_{1-x})_3Fe_5O_{12}$ grown on substrates with the garnet structure were determined using powder X-ray diffraction and HREM (Fig. 14). It was found that films with the garnet structure are formed only in the range of $0 < x < 0.66$. Differences in the

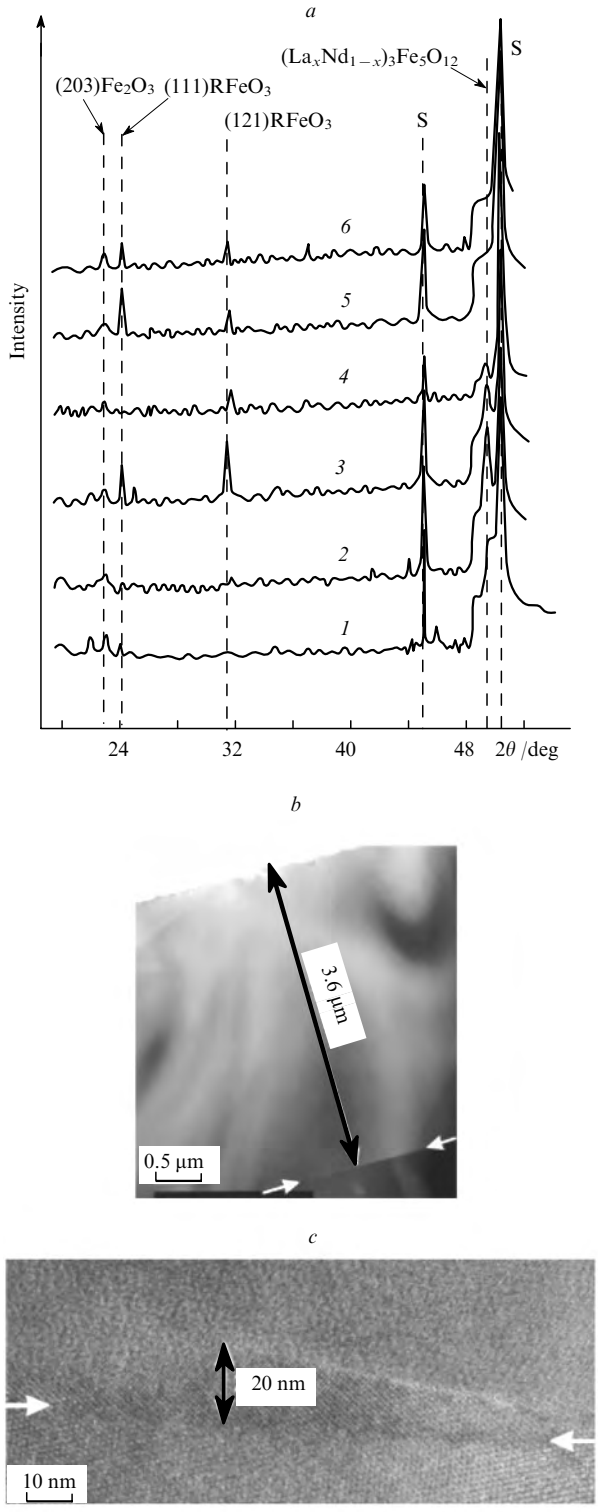

Figure 14. Formation of garnet phases $(La_xNd_{1-x})_3Fe_5O_{12}$.
(*a*) X-ray diffraction patterns of films on the $(111)Gd_3Ga_5O_{12}$ substrate, $x = 0$ (*1*), 0.37 (*2*), 0.5 (*3*), 0.66 (*4*), 0.7 (*5*), 0.75 (*6*);
(*b*, *c*) photomicrographs (TEM) of the cross-sections of films recorded along the ⟨110⟩ direction; $x = 0$ (*b*) and 0.66 (*c*).

substrate material do not much influence the stability limits of the $(La_xNd_{1-x})_3Fe_5O_{12}$ phases.

Epitaxially stabilised lanthanide-derived ferrogarnets, which are soft ferromagnetic materials, can find application in devices for amplification of an external magnetic field and in thin-film magnetooptical devices.

5. Application of epitaxial stabilisation for the development of functional heterostructures (selective epitaxy)

Epitaxial stabilisation can be used successfully for the design of multilayer heterostructures in selective epitaxy processes. The selective epitaxy is performed on specially prepared areas of the substrate which are characterised by structural coherence with the stabilised phase. On those substrate sections where the coherence condition is not fulfilled, products would crystallise that correspond to the equilibrium bulk state of the system. An example of such application of the ES is reported in our study [81] aimed at designing a heterostructure composed of numerous alternating lanthanide manganite and nickelate ribbons. This heterostructure shows an unusual temperature dependence of the resistivity (Fig. 15, curve *1*), because it combines the manganite phase (curve *2*), characterised by a sharp decrease in the resistivity on the dielectric–metal transition, and the nickelate phase (curve *3*), whose resistivity, conversely, sharply increases below the temperature of the metal–dielectric transition. As a result, the temperature behaviour of the resistivity of this heterostructure exhibits a sharp minimum.

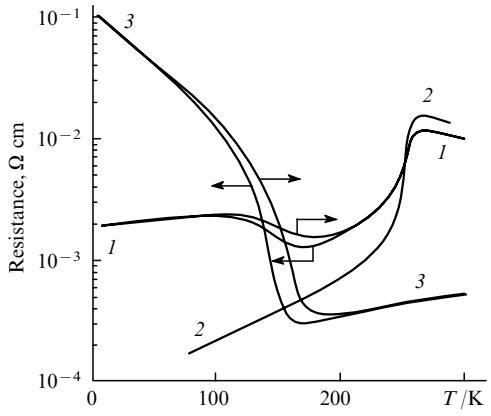

Figure 15. Temperature dependence of the resistance of the $NdNiO_3$–$La_{0.7}Ca_{0.3}MnO_3$ heterostructure (*1*) and its components $La_{0.7}Ca_{0.3}MnO_3$ (*2*) and $NdNiO_3$ (*3*).

The heterostructure was formed using MOCVD and photolithography (Fig. 16). First, the epitaxial $(La,Pr)_{0.7}Ca_{0.3}MnO_3$ layer was formed on the $LaAlO_3$ substrate (Fig. 16 *a*). Then this layer was etched with H_2O_2 and H_2SO_4 solutions through a photolitographic mask (Fig. 16 *b*), a polycrystalline layer of CuO was applied on it (Fig. 16 *c*), and the spots meant for $NdNiO_3$ were etched with an HCl solution (Fig. 16 *d*). The etching resulted in exposure of areas on the surfaces of the perovskite substrate and the manganite layer; hence, during the subsequent deposition of $NdNiO_3$, perovskite phase grew epitaxially exactly on these areas (Fig. 16 *e*), while an equilibrium mixture of the Nd_2CuO_4 and NiO phases with high resistivity was situated on the surface bearing the remaining CuO (structurally non-coherent to perovskite). The current that was passed along the substrate surface ran succesively through the alternating manganite and nickelate regions.

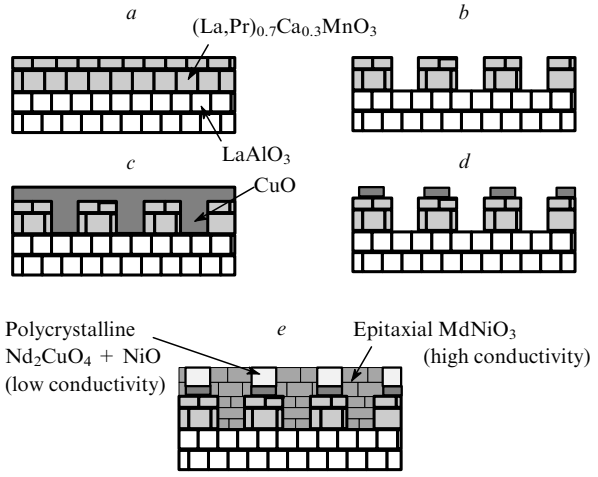

Figure 16. Formation of the manganite/nickelate heterostructure [for the description of stages (*a*–*e*), see the text].

It should be noted that in the epitaxial stabilisation of these heterostructures, one should take into account the stressed state of the substrate ($LaAlO_3$) surface and the buffer layer [$(La,Pr)_{0.7}Ca_{0.3}MnO_3$]: with the same deposition conditions and the same composition of the deposited components, different types of these stresses may completely change the phase composition of the deposited layer. Thus the epitaxial $NdNiO_3$ films obtained on a buffer manganite layer, $(La,Pr)_{0.7}Ca_{0.3}MnO_3$, which was, in turn, deposited on the perovskite $LaAlO_3$ and $SrTiO_3$ substrates were substantially dissimilar. Quite perfect epitaxial layers of $NdNiO_3$ up to a thickness of 200 nm were obtained on the $(La,Pr)_{0.7}Ca_{0.3}MnO_3/LaAlO_3$ substrates, whereas in the case of $(La,Pr)_{0.7}Ca_{0.3}MnO_3/SrTiO_3$, the perovskite phase contained simple oxides even at early stages of the growth (films with a similar phase composition were grown on the $SrTiO_3$ substrate without a buffer layer [82]). The epitaxial quality of the $(La,Pr)_{0.7}Ca_{0.3}MnO_3$ buffer layer grown on both substrates was equally high; however, the epitaxial stresses in the layers had opposite signs on different substrates, namely the buffer layer on $LaAlO_3$ experienced compression and that on $SrTiO_3$ underwent stretching in the substrate plane. This is indicated unambiguously by comparison of the lattice parameters of the non-deformed $(La,Pr)_{0.7}Ca_{0.3}MnO_3$ layer ($a = 0.385$ nm) with those of the $(La,Pr)_{0.7}Ca_{0.3}MnO_3/LaAlO_3$ ($a = 0.383$ nm) and $(La,Pr)_{0.7}Ca_{0.3}MnO_3/SrTiO_3$ ($a = 0.387$ nm) layers. The lattice parameter of the compressed $(La,Pr)_{0.7}Ca_{0.3}MnO_3/LaAlO_3$ layer is much closer to that of $NdNiO_3$ ($a = 0.381$ nm) than the parameter of the stretched layer, which accounts for the better properties of the former in stabilisation of the nickelate perovskite phase.

6. Effect of the epitaxy on the mutual solubility of oxides

The change in the phase equilibria in oxide systems under the influence of epitaxy is encountered rather often. However, we have not yet mentioned the possibility of extending the homogeneity regions for the cations of the epitaxially stabilised phases.† Below we consider several typical examples.

$R_{1-x}MnO_{3+\delta}$ (R = La, Nd). The perovskite $R_{1-x}MnO_{3+\delta}$ phases formed by lanthanides with a great ionic radius can be markedly non-stoichiometric as regards the cations,[83] the excess negative charge being counterbalanced by the transition $Mn^{3+} \rightarrow Mn^{4+}$. The maximum allowable lanthanide deficiency in the $R_{1-x}MnO_{3+\delta}$ ceramic samples corresponds to the subscript $x = 0.1-0.15$ (the x value depends on the conditions of high-temperature treatment; the highest non-stoichiometry can be attained under oxidative conditions). The epitaxial $R_{1-x}MnO_{3+\delta}$ films prepared by MOCVD on the $LaAlO_3$ and $SrTiO_3$ substrates allow a much higher deficiency of lanthanide ions. For example, single-phase perovskite $R_{1-x}MnO_{3+\delta}$ films (R = La, Nd) with $x \leqslant 0.3$ have been synthesised.[84]

$Zn_{1-x}M_xO$ (M = Mg, Mn). In wurtzite (ZnO), zinc can be partially replaced by other cations with similar ion radii such as Mg^{2+}, Cd^{2+} or Mn^{2+}. In ceramic $Zn_{1-x}Mg_xO$ samples, the x value does not exceed 0.02–0.04,[85] while in single-phase (0001)$Zn_{1-x}Mg_xO$ epitaxial films obtained by MBE at

† In this case, the term 'stabilised phases' is used to mean not only phases that cannot be obtained in the bulk state under the given thermodynamic conditions but also stable phases whose thermodynamic properties have changed in the epitaxially bound state.

550 °C,[86–88] the x values reach 0.22 and for the films obtained by PLD at 700–750 °C,[88] $x \leqslant 0.36$. The difference in the mutual solubility of the ZnO and MgO oxides in ceramics and epitaxial films is emphasised by the fact that two-phase ceramic pellets were used as targets (the sources of ZnO and MgO vapours). The epitaxial films were grown on the $(0001)Al_2O_3$ substrate. The film thickness reached 150 nm[86–88] and $\leqslant$500 nm.[89] The epitaxial relations for the ZnO–MgO solid solution reported in the literature[89]

$$(0001)[\bar{1}2\bar{1}0]Zn_{1-x}Mg_xO \parallel (0001)[01\bar{1}0]Al_2O_3$$

coincide with those for the films of pure ZnO grown on sapphire.[90] This mutual orientation of the film and the substrate corresponds to a misfit of the parameters $\varepsilon = 15\%$ which induces a substantial dislocation density at the interface.[89] In addition, it was shown that the $Zn_{0.85}Mg_{0.15}O$ film is stable during annealing (1000 °C, $P_{O_2} = 1$ bar, 1 h), whereas the film with the composition $Zn_{0.78}Mg_{0.22}O$ decomposes under the same conditions to give an equilibrium mixture of the wurtzite solid solution $Zn_{0.85}Mg_{0.15}O$ and the solid solution $Mg_{0.46}Zn_{0.54}O$ with the NaCl structure.[88] Thus, the extension of the wurtzite solid solution in the ZnO–MgO system markedly increases as a result of the ES.

The synthesis of epitaxial films of wurtzite doped with manganese oxide, $(0001)Zn_{1-x}Mn_xO/(0001)Al_2O_3$, has been reported.[91] Films several hundred nanometres thick were obtained at 600 °C. It was found that the unit cell parameters of wurtzite (a and c) increased monotonically with an increase in the Mn content up to $x = 0.35$; this markedly exceeds the solubility level of manganese oxide in zinc oxide in equilibrium bulk systems, which corresponds to $x_{lim} = 0.13$.[92]

$Ni_xFe_{3-x}O_4$. Nickel oxide NiO, like iron oxide Fe_3O_4 (spinel type), can grow epitaxially on the MgO substrate; however, the parameters of Fe_3O_4 are in better agreement with the substrate parameters; therefore, the spinel type solid solution $Ni_xFe_{3-x}O_4$ is stabilised on the substrate. The limiting nickel content in the solution is higher than in equilibrium polycrystalline solid solutions under the same conditions. The distribution of the Ni and Fe atoms over tetrahedral and octahedral positions of the spinel structure differs appreciably from that in the bulk materials.[93] This indicates that the ES can substantially influence the degree of inversion of spinels and, correspondingly, their magnetic properties.

$BaRuO_3$–$SrRuO_3$. From consideration of the equilibrium phase diagram of the $BaRuO_3$–$SrRuO_3$ binary system, one can predict the formation of two immiscible solid solutions, namely, the perovskite solution based on $SrRuO_3$ and stable up to Ba : Sr = 1 : 1 and a hexagonal (polytype 9R) solution based on $BaRuO_3$ and stable up to Ba : Sr = 9 : 1.[94] The preparation of a continuous series of solid solutions of the perovskite type, from $SrRuO_3$ to $BaRuO_3$, by radio frequency sputtering on the $SrTiO_3$ substrate has been reported.[17] However, an attempt to prepare $BaRuO_3$ as a perovskite on the $(001)KTaO_3$ perovskite substrate ($a = 0.3989$ nm) failed. This may be due to the fact that $BaRuO_3$ in the perovskite form experiences pronounced tetragonal distortions; as a result, its lattice becomes more consistent with the $SrTiO_3$ lattice than with the $KTaO_3$ lattice.

These examples provide the conclusion that solid solutions in epitaxial films are more extended than the same solid solutions in powders, ceramics, single crystals or polycrystalline films. The degree to which the ES extends the homogeneity regions depends on the coherence of the structures of the resulting film and the substrate and on the enthalpy of formation of the solid solution. If the consideration is restricted to the formation of regular solid solutions for which $\Delta H = x_A x_B Q$ (where x_A and x_B are the mole fractions of the components, Q is the energy parameter of interaction independent of the composition), it can be stated that the smaller the Q value (which is always positive), the more pronounced the effect of epitaxial extension of the solubility limits. In some cases, continuous solid solutions can be prepared.

7. The effect of epitaxy on the reactivity of thin films

The set of experimental data considered in this review attests that the $P–T–x$ space of thermodynamically stable existence is greater for the epitaxial phase than for its substrate-free bulk state. This implies that the chemical potential of the epitaxially bound phase (μ_{el}) is lower than the standard chemical potential (μ^0) of the same phase. In view of the fact that

$$\mu_{el} = \mu^0 + RT\ln a_{el},$$

the thermodynamic activity of the phase in the epitaxial state is given by $a_{el} < 1$. Thus, the epitaxial binding of some phase by a coherent substrate has the same consequence (namely, a decrease in the thermodynamic activity of the phase) as the formation of a solid solution or a chemical compound by this phase. A decrease in the thermodynamic activity of the phase in the epitaxial state ($a_{el} < 1$) implies a decrease in its reactivity compared to that of the substrate-free phase. It should be emphasised that this conclusion is valid not only for the 'unusual phases' which can arise under these conditions only owing to the ES but also for any epitaxial phases, no matter whether they are stable in the free (bulk) state.

The chemical consequences of the reduced thermodynamic activity may vary. In particular, the dissociation equilibrium

$$ABO_x \rightleftharpoons AO + BO_{x-1} + O_2$$

would be shifted more appreciably to the left in the case of epitaxial films than for the same phases in the bulk state at the same $P_{O_2}–T$ conditions (in other words, at the same temperature, the equilibrium pressure of oxygen P_{O_2} above an epitaxial film is lower than that above a powder or ceramic with the same composition).

In those cases where the growing phase is not stoichiometric for oxygen and dissociation does not result in the phase decomposition

$$ABO_x \rightleftharpoons ABO_{x-\delta} + \delta/2\,O_2,$$

one can expect that the epitaxial and bulk phases brought to equilibrium under the same $P_{O_2}–T$ conditions would differ in the oxygen content.‡

This conclusion may appear defamatory for the common practice of investigation of the dependence of the functional properties of films on the oxygen non-stoichiometry. Since the direct determination of the oxygen content in thin films is an exceptionally complicated analytical problem yet unsolved, the amount of oxygen is usually determined in the corresponding powders or ceramics, which can be easily analysed by both chemical and physical methods (the oxygen content in epitaxial films is considered to be the same as in powders and in ceramics after identical heat treatment). The observed differences between the functional properties (first of all, electric and magnetic ones) of epitaxial films and ceramics with the composition as close as possible to that of the films are interpreted most often as being due to different microstructures and/or stressed states of the films; however, the role of differences in the oxygen non-stoichiometry also cannot be neglected.

The problem becomes even more complicated if one takes into account the dependence of the thermodynamic properties of the epitaxial layer on its thickness; obviously, the difference $\mu^0 - \mu_{el}$ in each section parallel to the substrate plane should decrease on moving away from the film/substrate interface toward the upper surface of the film. For a non-stoichiometric oxide, this means, in particular, that the content of oxygen in an epitaxial film would vary along the thickness coordinate. Unfortunately, due to the lack of experimental data, this aspect can be discussed only as a problem definition.

‡ The quantitative difference between the oxygen contents is difficult to predict, because the uncertainties in the estimation of the energy benefit from the epitaxial growth in particular systems are rather high.

Below we elucidate how the decrease in the phase reactivity in the epitaxial state would influence the solid-state reactions involving them. We demonstrated that in the epitaxial heterostructures $YBa_2Cu_3O_{7-\delta}/CeO_2/R\text{-}Al_2O_3$, no chemical interaction takes place between the $YBa_2Cu_3O_{7-\delta}$ superconductor and the $(001)CeO_2$ buffer layer grown epitaxially on the *R*-sapphire, not even during the long-term high-temperature annealing (Fig. 17 *a*).[95,96] In addition, it is well known [97] that polycrystalline CeO_2 reacts with $YBa_2Cu_3O_{7-\delta}$ according to the reaction

$$3\,CeO_2 + 2\,YBa_2Cu_3O_{7-\delta} \longrightarrow 3\,BaCeO_3 + Y_2BaCuO_5 + 5\,CuO.$$

The Gibbs energy of this reaction calculated for conditions similar to the conditions of MOCVD [98] under which the epitaxial heterostructures were obtained ($T = 820$ °C and $P_{O_2} = 2$ mbar) equals -5 kJ mol^{-1}. This reaction will not take place if ΔG becomes positive. This will happen when $a_{CeO_2} \approx 0.83$. Apparently, such decrease in the activity of CeO_2 occurs during its epitaxial growth on *R*-sapphire.

If polycrystalline CeO_2 is replaced by ZrO_2, the following reaction will proceed at the $YBa_2Cu_3O_{7-\delta}/ZrO_2$ interface

$$3\,ZrO_2 + 2\,YBa_2Cu_3O_{7-\delta} \longrightarrow 3\,BaZrO_3 + Y_2BaCuO_5 + 5\,CuO.$$

The replacement of polycrystalline ZrO_2 by the epitaxial one does not terminate the reaction. The reason can be understood from thermodynamic considerations: the Gibbs energy ΔG for this reaction calculated for the MOCVD conditions [98] is equal to -30 kJ mol^{-1}. This energy remains negative even if $a_{ZrO_2} = 0.83$, *i.e.*, the reaction does not stop. It is of interest that the product of reaction of ZrO_2 with $YBa_2Cu_3O_{7-\delta}$, namely, compound $BaZrO_3$, which separates the superconductor layer from the ZrO_2 substrate, belongs to the perovskite type and, therefore, it forms epitaxial interfaces with both the $YBa_2Cu_3O_{7-\delta}$ film and the substrate (Fig. 17 *b*).

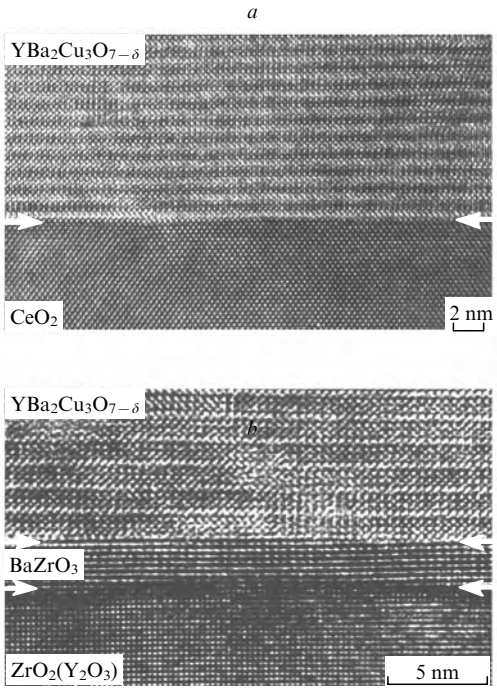

Figure 17. Images of the cross-sections of the $YBa_2Cu_3O_{7-\delta}$ films on CeO_2 (*a*) and on $ZrO_2(Y_2O_3)$ (*b*) (the images were obtained by HREM). (*a*) no chemical reaction takes place at the interface between the $YBa_2Cu_3O_{7-\delta}$ superconductor and the CeO_2 buffer layer, (*b*) a $BaZrO_3$ layer is formed at the interface.

III. Variant structures

During the last 15–20 years, vast experimental material has been accumulated on the heteroepitaxy of simple and complex oxides of various structures. The diversity of the crystal structures formed in the heteroepitaxy of oxides gives rise to a series of interesting phenomena not involved in classical metallic and semiconductor systems. For example, a definite type of orientational relations between an epitaxial film and a single-crystalline substrate can often be realised in different ways.

The orientational relations in heteroepitaxial systems are usually analysed in terms of the concept of coincident site lattices (CSL). Within the framework of this concept, the two-dimensional crystal lattices (site networks) of the film and the substrate are compared in the region of their contact.[99–101] Usually, an idealised view of the surface structure is invoked, *i.e.*, the structure of the surface of each crystal is regarded as being identical to the structure of a similar crystallographic plane inside the crystal, the rearrangement effects that took place on the exposed surface being ignored.[102] This simplification proved to be quite satisfactory, because the energy of the epitaxial surface is much lower than the energy of the free surface of the crystal. Therefore, the surface rearrangement is hampered due to overlaying of the epitaxial film.

Despite the diversity of the CSL sizes and shapes, they can always be reduced to one of five types of two-dimensional lattices (Fig. 18) corresponding to four types of symmetry (in the same way as three-dimensional lattices can be reduced to one of the 14 Bravais lattices, which form six systems). In the simplest case, the type of two-dimensional CSL coincides with the type of the two-dimensional lattice of the film and substrate site networks in the contact region. For example, for the epitaxial growth of the $(001)CeO_2$ film (fluorite structure) on the $(001)SrTiO_3$ substrate (perovskite structure), the site network and the CSL are square lattices. For $(001)CeO_2$, [100] and [010] are the CSL vectors, while for $(001)SrTiO_3$, these are [110] and [1$\bar{1}$0], respectively, *i.e.*, the *a* parameter of the CSL is $\sqrt{2}$ times greater than the lattice parameter of $SrTiO_3$.[103] In the example considered, this epitaxial relation is the only one possible; no other epitaxial relations arise in this case.

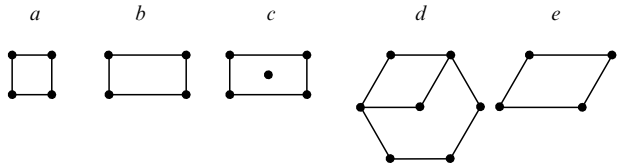

Figure 18. Types of two-dimensional lattices: primitive square (*a*), primitive orthogonal (*b*), centred orthogonal (*c*), primitive hexagonal (*d*), primitive oblique (*e*).

If the three-dimensional crystal lattices of the film and the substrate belong to different systems but the two-dimensional lattices correspond to the same system, in this case, too, only one epitaxial relation is realised. As an example, consider the $(001)TiO_2$ epitaxial films with a tetragonal anatase structure grown on perovskite substrates of the $(001)SrTiO_3$ type. This gives rise to the only possible square CSL with a spacing corresponding to that of the square site networks in the contact plane of the film and the substrate.[5,11,104]

Thus, a single variant of the CSL arises in those cases where the site networks of the film and the substrate in the contact plane correspond to the same system. If they are different, several variants of CSL fully equivalent from geometric and energetic standpoints may appear. The greatest possible number of variants is dictated by the order of the principal normal axis of the site

network that has a higher symmetry. It can be easily demonstrated that several equivalent CSL containing 2, 3, 4 and 6 epitaxial orientations can exist. The number of variants decreases if any additional symmetry elements in the film and substrate site networks coincide in the contact region (*e.g.*, symmetry planes parallel to the principal normal axis). The standard methods for determination of the number of variants of the epitaxial growth and orientation include X-ray diffraction (pole figures, φ-scanning), electron diffraction and transmission electron microscopy.

The formation of the variant structures is related genetically to the xenotaxy phenomenon (literally, this means a foreign growth on the surface), which represents the formation of a CSL, at the film/substrate interface, whose two-dimensional symmetry is lower than that allowed by the symmetry conditions. This situation is possible in the case where the low-symmetry configuration is clearly preferred from the energy standpoint. A low-symmetry CSL on a substrate site network with a higher symmetry also gives rise to variant structures. Depending on the relationship between the interface energies for the same film/substrate pair, different types of xenotaxy can arise, resulting in different variant structures.

Let us consider a simple example. During the deposition of films of the $RBa_2Cu_3O_{7-\delta}$ high-temperature superconductors (R is a lanthanide) on single-crystalline perovskite substrates in a pseudo-cubic (001) orientation (so-called *c*-orientation), the epitaxial growth of a film in the (100) orientation (*a*-orientation) is often observed. The smaller the misfit between the substrate and film lattice parameters (*i.e.*, the better the CSL coincidence), the easier the switching from the thermodynamically preferred growth along the (001) direction to the growth along the (100) direction (Fig. 19).[105–107] The site network of the perovskite substrate in the (001) plane is square. The $RBa_2Cu_3O_{7-\delta}$ site network in the (100) plane and the CSL are orthogonal and the ratio of their unit cell edges is close to 1 : 3. The maximum number of variants of the epitaxial growth for this case is 4, but the condition of collinearity of the perovskite and $RBa_2Cu_3O_{7-\delta}$ site networks reduces the possible number of variants to two:

$$(001)[100]SrTiO_3 \parallel (100)[001]RBa_2Cu_3O_{7-\delta}$$

and

$$(001)[010]SrTiO_3 \parallel (100)[001]RBa_2Cu_3O_{7-\delta}.$$

The existence of structural variants in the *a*-oriented $RBa_2Cu_3O_{7-\delta}$ films is responsible for the substantial difference between their electric properties and those of the *c*-oriented films with the same chemical composition. The critical current density in two-variant *a*-oriented $RBa_2Cu_3O_{7-\delta}$ films does not exceed 10^5 A cm^{-2} at 77 K, whereas in the monovariant *c*-oriented samples, this value reaches $\geqslant 10^6$ A cm^{-2} (see the studies [108, 109]). This difference is not at all due to the poor crystallinity of the two-variant structure compared to the monovariant one; conversely, the X-ray diffraction and HREM data indicate unambiguously that the *a*-oriented films are structurally more perfect (in particular, the integral width of the X-ray rocking curves is several times smaller for these films than for the *c*-oriented $RBa_2Cu_3O_{7-\delta}$ films). The decrease in the critical current density is due to the fact that in the HTSC structure, the superconducting carriers move efficiently only in the CuO_2 planes normal to the *c* axis. Thus, in the *c*-oriented films, the superconductive planes are stretched along the substrate plane. In the two-variant structure with the *a*-orientation, more intricate routes for the supercurrent are formed, *i.e.*, 'superconducting tapes', perpendicular to the substrate plane; this decreases the supercurrent critical density.

More complex variant structures are formed on the deposition of films of the perovskite series (for example, manganites $R_{1-x}A_xMnO_3$ (R is lanthanide, A is the alkaline earth element), cobaltites $R_{1-x}Sr_xCoO_3$ and ruthenates $CaRuO_3$ and $SrRuO_3$) [58] on substrates with the fluorite structure. The fluorite site network in the (001) plane is square. On the given surface these perovskites form an orthogonal site network in the (110) plane. The vectors of the orthogonal CSL are as follows: for the (001)$ZrO_2(Y_2O_3)$ fluorite, $[1\bar{1}0]$ and $4\times[\bar{1}\bar{1}0]$; for the (110) perovskites, $[1\bar{1}1]$ and $3\times[1\bar{1}\bar{2}]$ (Fig. 20). The similarity of the lengths of the body diagonal in the perovskite cube $[1\bar{1}\bar{2}]$ and the face diagonal in the fluorite cube $[1\bar{1}1]$ is the crucial factor for this type of epitaxial growth. However, a better dimensional fit may be observed in the perpendicular direction to the interface. For example, in the growth of (110)$La_{0.7}Ca_{0.3}MnO_3$ films on the surface of (001)$ZrO_2(Y_2O_3)$, the misfit in the CSL is 8% for the $[1\bar{1}0]$ and $[1\bar{1}1]$ pair and 2% for the $[\bar{1}\bar{1}0]$ and $[1\bar{1}\bar{2}]$ pair. The number of epitaxial variants for this case is 4 (Fig. 20). These variants are fully equivalent from the geometric and energetic standpoints. The HREM data (Fig. 21) indicate that these growth variants occur in the film as nanodomains (f1 and f2) with a characteristic size of 20–50 nm (Fig. 21 *c*). Interestingly, their lateral size almost does not change with thickness and the mutual coherence of the domains along the substrate surface normal is retained throughout the whole film thickness (Fig. 21 *d*).[110]

The formation of four-variant structures in the epitaxy of perovskites on the (001)fluorite has also been reported in a

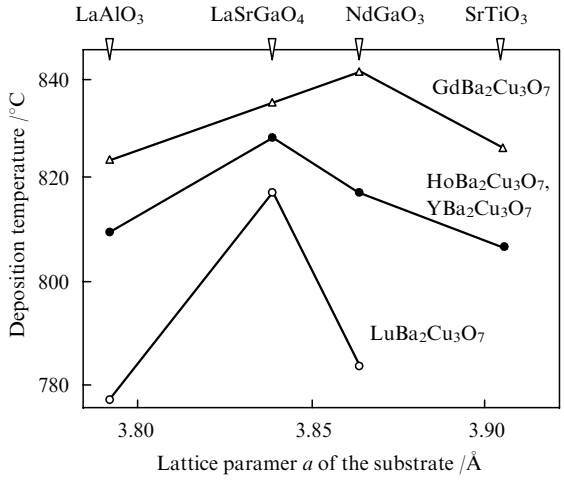

Figure 19. Temperature regions corresponding to the *c*-oriented epitaxial growth (above the line) and the growth with mixed *c* + *a*-orientation (below the line) of the $RBa_2Cu_3O_{7-\delta}$ films on substrates with a small (< 2%) misfit of parameters at the interface.

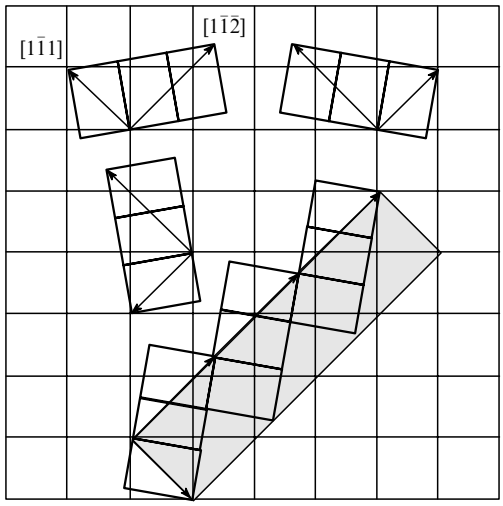

Figure 20. Four variants of perovskite growth on the (100)fluorite. The hatched region shows the CSL unit cell.

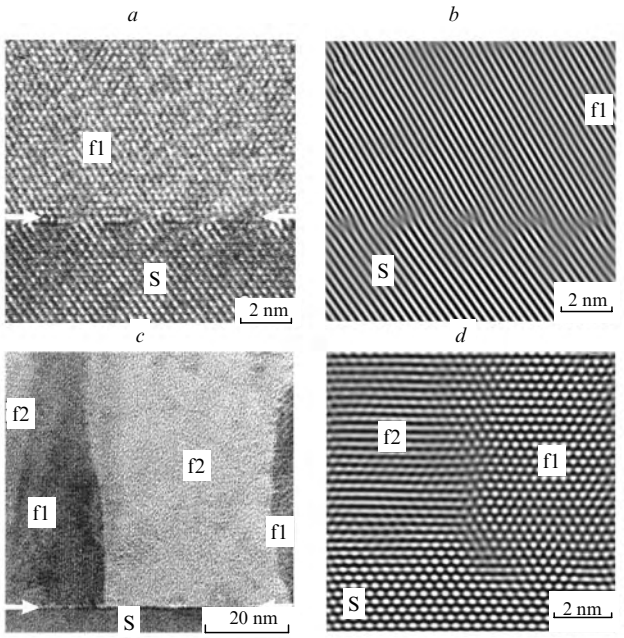

Figure 21. HREM study of the variant $(La_{0.5}Pr_{0.5})_{0.7}Ca_{0.3}MnO_3$ film on $(001)ZrO_2(Y_2O_3)$. In all cases, the $[110]ZrO_2(Y_2O_3)$ area is shown: (*a*) epitaxial stresses completely relax at the film/substrate interface, (*b*) Fourier image of the same region of the interface, (*c*) orientational growth modes (domains f1 and f2) in a low resolution, (*d*) coherence of the oriented variants along the film growth direction.

number of studies [111–114] dealing with the preparation of epitaxial films of the $Ba_{0.5}Sr_{0.5}TiO_3$, $Bi_{3.25}La_{0.75}Ti_3O_{12}$ and $SrBi_2TaO_9$ ferroelectrics with a ferroelectric polarisation axis oriented normal to the surface of the (001)silicon substrate. For solving this highly topical problem, epitaxial film heterostructures of the $(100)Bi_{3.25}La_{0.75}Ti_3O_{12}/(110)SrRuO_3/(001)ZrO_2(Y_2O_3)/(001)Si$ type were prepared. The conductive layer of the $SrRuO_3$ perovskite had a four-variant structure; as a result, $Bi_{3.25}La_{0.75}Ti_3O_{12}$ a layered phase derived from perovskite grown on $SrRuO_3$, had 8 options of arrangement in the plane parallel to the substrate.

A large number of boundaries between numerous structural variants may have an adverse effect on the ferroelectric properties; therefore, the possibility of affecting the pattern of the variant structure by changing the CSL on the surface of the $ZrO_2(Y_2O_3)$ single crystal through its slight $(1-5^\circ)$ deviation from the (001) plane has been studied.[114] This expedient proved to be most efficient when the deviation was performed along the [110] direction; the number of epitaxial variants in the $(110)SrRuO_3$ film decreased to two. Obviously, this approach could also find application in the studies of other heteroepitaxial systems.

A multivariant growth motif is also observed in the deposition of $La_{0.7}Ca_{0.3}MnO_3$ on $(111)ZrO_2(Y_2O_3)$. In this case, the body diagonal of the perovskite cube also corresponds to the face diagonal of the fluorite cube at the interface. In this case, the vectors of the orthogonal CSL determined from X-ray diffraction and HREM data are $[\bar{1}01]$, $3\times[1\bar{2}1]$ for $(111)ZrO_2(Y_2O_3)$ and $[1\bar{1}1]$, $4\times[1\bar{1}\bar{2}]$ for the (110)perovskite. The misfit of the CSL equals 8% for the $[\bar{1}01]$ and $[1\bar{1}1]$ pair and 0% for the $[1\bar{2}1]$ and $[1\bar{1}\bar{2}]$ pair. The theoretical number of equivalent epitaxial variants for this case is six, and all these are actually encountered in the film (Fig. 22).

A direct consequence of the formation of epitaxial variant structures is the presence in the film of a high density of special high-angle boundaries. The set of angle orientations of such boundaries is strictly fixed and their concentration does not change over the film thickness. This represents the basic difference between the variant structures and polycrystalline materials in which the angle orientations of the boundaries make a broad

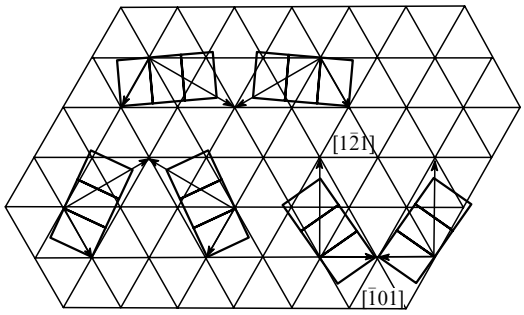

Figure 22. Six variants of the growth of perovskite on the (111)fluorite.

spectrum even in highly textured materials and the concentration of the boundaries themselves is not very high.

The epitaxial multivariant structure of the manganites is responsible for their interesting electrophysical properties which are not inherent in monovariant epitaxial films. First of all, this refers to the appearance of a substantial magnetoresistance (the change in the electric resistance of the material in a magnetic field) in weak magnetic fields over a broad temperature range below the Curie point.[115] This is due to the spin-dependent tunnelling of charge carriers through special high-angle boundaries. This is characteristic of the epitaxial films of manganites grown on bicrystalline perovskite substrates.[116]

The appearance of a substantial magnetoresistance in weak magnetic fields is of considerable interest as regards the manufacture of high-sensitivity magnetic field sensors. In the design of such sensors, one can use both the appearance of sharp maxima of positive magnetoresistance (*MR*) in the region of technical magnetisation (*i.e.*, magnetisation related to the re-orientation of magnetic domains) in fields weaker than 100 Œ and the appearance of great negative magnetoresistance ($\sim 30\%$) related to the tunnelling effect in fields of 100–5000 Œ (Fig. 23).

Both effects are also manifested in the traditional polycrystalline materials; however, the former requires much stronger fields (about 500–1000 Œ) and has a lower field gradient,[117] while the latter is much smaller in magnitude.[118] This is due to the fact that the structural coherence of high-angle boundaries implies a compression of the tunnelling barrier following an increase in the field strength,[119] which is impossible for non-coherent boundaries. We found that the magnitude of the tunnelling effect increases with an increase of the off-orientation angle of the neighbouring nanodomains in films with a variant structure.[109]

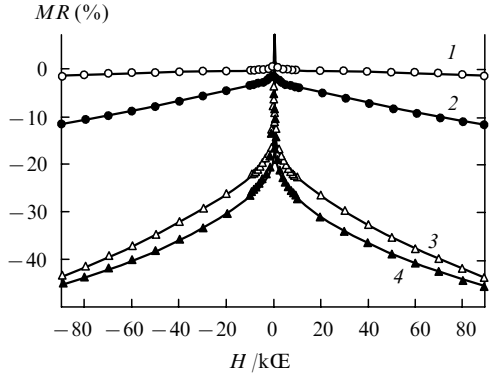

Figure 23. Magnetoresistance (*MR*) in the $(110)La_{0.7}Ca_{0.3}MnO_3$ epitaxial films grown on different substrates (temperature, 10 K). Substrate: (*1*) $(110)SrTiO_3$, (*2*) $(110)ZrO_2(Y_2O_3)$, (*3*) $(001)ZrO_2(Y_2O_3)$, (*4*) $(111)ZrO_2(Y_2O_3)$. Real structure of the obtained film: (*1*) monodomain, (*2–4*) multidomain with small-angle (*2*) and high-angle (*3*, *4*) boundaries (in the order of increasing off-orientation angle).

In particular, in the (110)perovskite films with a variant structure, the tunnelling magnetoresistance increases on passing from (001)$ZrO_2(Y_2O_3)$ to (111)$ZrO_2(Y_2O_3)$.

Tunnelling structures are often designed using epitaxial films of manganites on bicrystalline perovskite substrates. The films are grown on a special boundary produced, for example, by diffusion welding of two halves of a single-crystalline substrate. The structure of this boundary is inherited by the epitaxial film. Obviously, for practical application, multivariant structures on single-crystalline substrates have essential advantages over monovariant epitaxial structures on bicrystalline substrates. First, they are much less expensive and second, the whole surface of a variant film rather than only the bicrystalline boundary region can be used for the preparation of magnetic sensors.

Our further research has demonstrated that the field sensitivity of the variant structures based on manganite films can be increased through deposition of a layer of a soft ferromagnet (based on $MnFe_2O_4$) on a layer of the variant structure formed on the (111)$ZrO_2(Y_2O_3)$ substrate (Fig. 24, *cf.* curves *3*, *4* and *5*, *6*).

The variant structures also appear in films with other types of epitaxial interface. For example, a study of an In_2O_3 film (bixbyite cubic structure, $a = 1.0117$ nm) on (001)MgO (NaCl type, $a = 0.4213$ nm)[120] has shown that domains with the (111)In_2O_3 ‖ (001)MgO orientation, which split into four variant structures in the substrate plane, predominate in these films. In all of these structures, the diagonals of the cube faces of In_2O_3 and MgO are parallel: $[1\bar{1}0]In_2O_3$ ‖ [110]MgO, $[\bar{1}10]In_2O_3$ ‖ [110]MgO, $[110]In_2O_3$ ‖ $[1\bar{1}0]$MgO and $[110]In_2O_3$ ‖ $[\bar{1}10]$MgO. The same type of variant structure is typical of isostructural Y_2O_3 films on (001)MgO (Fig. 25 *a*).[121, 122] In both films (In_2O_3 and Y_2O_3), some of the crystallites are oriented with the (001) axis normal to the substrate; these crystallites are monovariant (Fig. 25 *b*). The ratio of the (111)- and (001)-oriented domains depends on the film deposition temperature and on the oxygen pressure in the evaporation chamber,[123] although the role of the latter is not quite clear. Probably, oxygen influences the rate of film deposition, which often switches the (111)-growth to the (001)-growth for cubic crystals. The formation of the variant structures has an essential influence on the conductivity of In_2O_3 films, because high-angle boundaries of the domains create additional resistance to the carrier transport. This circumstance should be taken into account when using In_2O_3 as a conductive layer on single-crystalline substrates.

Now we consider the growth of films with a rutile structure (TiO_2, CrO_2, RuO_2, SnO_2) on substrates of the fluorite and perovskite type. The length of the diagonal of the tetragonal face in the RuO_2 structure is close to the length of the edge of the fluorite cube [in $ZrO_2(Y_2O_3)$ and CeO_2] and to the length of the face diagonal of the perovskite cube [in $LaAlO_3$].[123] The orientation of the (100)RuO_2 ‖ (001)substrate film gives rise to four epitaxial modes of the growth (Fig. 26). In the RuO_2 film on *a*-sapphire, the (100)RuO_2 ‖ (0001)substrate orientation gives rise to three growth patterns with a common motif at the interface, $[010]RuO_2 \parallel [11\bar{2}0]Al_2O_3$, $[010]RuO_2 \parallel [\bar{2}110]Al_2O_3$ and $[010]RuO_2 \parallel [1\bar{2}10]Al_2O_3$.[124] It is noteworthy that the same film orientation takes place in the growth of rutiles on *R*-sapphire; however, the *R* plane has only one vector of the $[1\bar{2}10]Al_2O_3$ type; therefore, the epitaxy is monovariant: $(101)[010]MO_2 \parallel (\bar{1}012)[1\bar{2}10]Al_2O_3$.

The variant structures in the CrO_2 films with the rutile structure, as those in the manganites described above, show the tunnelling magnetoresistance effects, although they are weaker in magnitude.[125]

It follows from the foregoing that the variant structures (with high-angle domain boundaries) are actually heteroepitaxial nanostructures resulting from self-assembly on the substrate surface occurring in particular orientational relations with the growing film. They are to be distinguished from the mosaic single crystals in which the low-angle domain structures predominate and no rigid restrictions on the mutual orientation angle are involved.

Meanwhile, the variant structures have common features with single-crystalline twins. Whereas the prediction of a twin structure requires only crystal parameters, a variant epitaxial structure can be determined only with known crystallographic data for the film and the substrate and their epitaxial relations. Only in rare cases, does a variant structure correspond to twins known for this

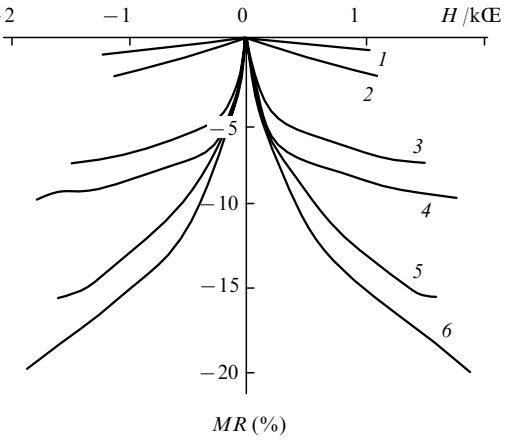

Figure 24. Magnetoresistance $MR = \{[R(H) - R(0)]/R(0)\} \cdot 100\%$ of films and heterostructures on different substrates.
(*1*) $(La_{0.7}Sr_{0.3})MnO_3$/MgO, (*2*) $(La_{0.7}Sr_{0.3})MnO_3$/(001)$SrTiO_3$, (*3*) $(La_{0.7}Sr_{0.3})MnO_3$/(110)$ZrO_2(Y_2O_3)$, (*4*) $MnFe_2O_4$/$(La_{0.7}Sr_{0.3})MnO_3$/(110)$ZrO_2(Y_2O_3)$, (*5*) $(La_{0.7}Sr_{0.3})MnO_3$/(111)$ZrO_2(Y_2O_3)$, (*6*) $MnFe_2O_4$/$(La_{0.7}Sr_{0.3})MnO_3$/(111)$ZrO_2(Y_2O_3)$.

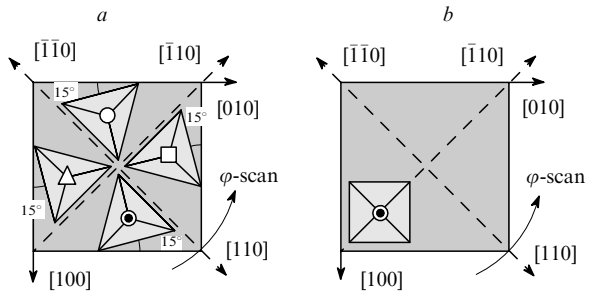

Figure 25. Modes of the epitaxial growth of Y_2O_3 on (001)MgO.[121, 122]
(*a*) Four modes of the growth of (111) domains, (*b*) monovariant growth of the (001) domains.

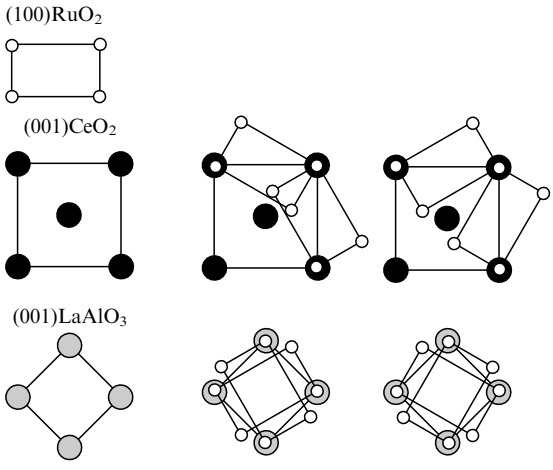

Figure 26. Four modes of the RuO_2 growth on the (001)CeO_2 fluorite and (001)$LaAlO_3$ perovskite.

crystal. This is usually the case for systems where the number of variants is reduced due to coincidence of some additional symmetry elements, as in *a*-oriented structures of $RBa_2Cu_3O_{7-\delta}$ related to each other by the (013) twinning plane.

It has been noted above that many perovskites tend to grow in the (110) orientation on fluorite substrates, for example, on $(001)ZrO_2(Y_2O_3)$. However, there are some exceptions. The $BaTiO_3$ epitaxial films have the (111) orientation on this substrate, which implies four epitaxial growth modes with a common motif: the length of the face diagonal of the perovskite cube is close to the length of the edge of the fluorite cube. These conditions are violated upon the change in the ratio of the lattice parameters of the film and the substrate. For example, deposition of $BaTiO_3$ on a buffer layer of the cubic praseodymium oxide (with the lattice parameter $a = 0.546$ nm) results in switching of the orientation of the $BaTiO_3$ film to (001), which provides the least misfit between the CSL parameters and the (001) layer of praseodymium oxide.[126]

Of considerable interest is further research into the kinetics of formation of variant structures and the possibility of controlling the nanodomain size, shape and arrangement on the substrate surface. The experimental data available to date attest to a dependence of the nanodomain size on the diffusive mobility of the film components. This in the MOCVD deposition of the $RBa_2Cu_3O_{7-\delta}$ films under conditions where the figurative point of the crystallising system occurs near the solidus surface, the domains of variant structures can grow to submicron dimensions. Some published data may be indicative of the possibility of controlling the shape anisotropy of the variant nanodomains. For the three-variant $(100)RuO_2$ structure on $(0001)Al_2O_3$, the following correlation was established: nanodomains with an average size of 30 nm are most extended along the direction of the least misfit of the CSL and least extended along the greatest misfit of the CSL. If this dependence is general, this would allow effective control of the shape of nanodomains through a change in the substrate material (and, hence, the parameter *a* of the substrate) by doping or deposition of buffer layers. The question concerning the possibility of fixing the arrangement of epitaxial variant structures on the substrate surface remains open. Apparently, interesting results could be provided by using vicinal or single-crystalline substrates with an artificial relief (graphoepitaxy).

Generally, variant structures represent a new group of thin-film materials whose physical properties (including electrical and magnetic ones) are determined at the nano-size level and differ appreciably from the properties of both monovariant epitaxial films and polycrystalline materials. Further research into these structures will promote extension of the scope of their application in the modern micro- and nanoelectronics.

IV. Conclusion

We would like to emphasise once again that the epitaxial stabilisation of oxide films discussed in this review is an equilibrium phenomenon, *i.e.*, the growing oxide phase exists in an external equilibrium with the substrate and the gas-phase oxygen and also in an internal (in the case of phase assembly) solid-state equilibrium. If the decrease in the Gibbs energy of the film/substrate system caused by epitaxy is greater in magnitude than the ΔG value of any solid-state process involving the phase growing on a substrate surface (a polymorphic transition, redox reaction, *etc.*), one can expect that phase equilibria in an epitaxial film would differ from the phase equilibrium in the same system without epitaxy. In particular, with epitaxial stabilisation, the 'unusual' simple or complex oxide phases that require high pressure, high temperature or high oxygen pressures to be formed can be prepared without resorting to these extrem conditions. In multiple phase films, the epitaxial relations of separate phases with the matrix phase in whose bulk they grow and/or with the substrate can give rise to stable phase assemblies differing from those dictated by the equilibrium phase diagram. All these phenomena can be regarded as being due to the change in the thermodynamics of the system under the action of epitaxy rather than to manifestation of slow kinetics of the surface reaction, which precludes attainment of the Gibbs energy minimum during the film growth. The effect of epitaxy on the thermodynamics of the growing phase is enhanced with an increase in the coherence of the film structure and the substrate. In the case of a perfect fit of the structures, the critical thickness of the stabilised phase reaches a maximum value.

This review considers examples of ES, taken mainly from our studies on gas-phase epitaxy; however, the ES phenomena are equally typical of the liquid-phase epitaxy (from aqueous solutions and melts), electrocrystallisation,§ and, perhaps, solid-state epitaxy. Moreover, the ES can be detected not only in the preparation of thin films or in the solid-state chemistry, but also in mineralogy (examples of pseudomorphism in minerals are frequently encountered [128]).

The understanding of the nature of the ES attained to date allows one to use this phenomenon for deliberate synthesis of unstable compounds as thin epitaxial films, which can soundly be expected to be a success. The films of epitaxially stabilised phases are of considerable interest not only as objects for the study of the fundamental properties of materials but also as real materials with potentially useful properties. The selective epitaxy based on the ES can find application in the preparation of complex heterostructures. It is beyond doubt that involving new types of single crystalline substrates in the practice of epitaxial stabilisation would give rise to new oxide compounds and materials.

The variant epitaxial structures have not yet received adequate attention. Meanwhile, they represent a new class of nanostructures in which self-assembly of nanodomains is due to the energetic degeneracy of various geometric modes of epitaxy. By conscious selection of substrates, one can change the number and the mutual orientation of epitaxial variant structures in the film. The considered examples of enhancement of the magnetoresistance in the doped lanthanum manganite films represent the first achievements made owing to the targeted design of high-angle boundaries of the epitaxial variant structures. Even now, one can state that this approach would diversify and, in some cases, markedly enhance the properties of materials (magnetic, electric, including ferroelectric, and optical properties) depending on the structure of internal interfaces.

In conclusion, the authors are happy to thank the colleagues who actively participated in various stages of the research covered in this review: Drs. I E Graboi, S V Samoilewnkov, M A Novozhilov and A A Bosak and students S Antonov, A Mikhailov and O Boitsova for their inestimable contribution to the experiments.

This work was carried out with partial financing by the Russian Foundation for Basic Research (Project Nos 02-03-33258 and 04-03-32505), the Volkswagen Stiftung (Grant I/77821) and the NWO Program of the Russia – Holland cooperation.

References

1. P D Dankov *Dokl. Akad. Nauk SSSR* **24** 773 (1939)
2. P D Dankov *Zh. Fiz. Khim.* **23** 1025 (1949)
3. F C Frank, J H van der Merwe *Proc. R. Soc. London, Ser. A* **198** 205 (1949)
4. J H van der Merwe *J. Appl. Phys.* **34** 117 (1963)
5. S Chen, M G Mason, H J Gysling, G R Paz-Pujalt, T N Blanton, T Castro, K M Chen, C P Fictorie, W L Gladfelter, A Franciosi, P I Cohen, J F Evans *J. Vac. Sci. Technol. A* **11** 2419 (1993)

§ The deposition of metals at potentials lower than the thermodynamic deposition potential [127] is apparently closely related to the ES.

6. S Tokita, N Tanaka, H Saitoh *Jpn. J. Appl. Phys.* **39** L169 (2000)
7. G S Herman, Y Gao *Thin Solid Films* **397** 157 (2001)
8. W Sugimura, A Yamazaki, H Shigetani, J Tanaka, T Mitsuhashi *Jpn. J. Appl. Phys.* **36** 7358 (1997)
9. C K Ong, S J Wang *Appl. Surf. Sci.* **185** 47 (2001)
10. M Murakami, Y Matsumoto, K Nakajima, T Makino, Y Segawa, T Chikyow, P Ahmet, M Kawasaki, H Koinuma *Appl. Phys. Lett.* **78** 2664 (2001)
11. B H Park, L S Li, B J Gibbons, J Y Huang, Q X Jia *Appl. Phys. Lett.* **79** 2797 (2001)
12. A B M A Ashrafi, A Ueta, A Avramescu, H Kumano, I Suemune, Y-W Ok, T-Y Seong *Appl. Phys. Lett.* **76** 550 (2000)
13. O Yu Gorbenko, I E Graboy, V A Amelichev, A A Bosak, A R Kaul, B Güttler, V L Svetchnikov, H W Zandbergen *Solid State Commun.* **124** 15 (2002)
14. L J LeGore, O D Greenwood, J W Paulus, D J Frankel, R J Lad *J. Vac. Sci. Technol., A* **15** 1223 (1997)
15. Y Gao, Y J Kim, S Thevuthasan, S A Chambers, P Lubitz *J. Appl. Phys.* **81** 3253 (1997)
16. N Fukushima, K Sano, T Schimizu, K Abe, S Komatsu *Appl. Phys. Lett.* **73** 1200 (1998)
17. N Fukushima, K Sano, T Schimizu, K Abe, S Komatsu *Mater. Res. Soc. Symp. Proc.* **494** 35 (1998)
18. H-M Christen, L A Boatner, J D Budai, M F Chisholm, L A Gea, D P Norton, C Gerber *Appl. Phys. Lett.* **70** 2147 (1997)
19. M N Khan, H-T Kim, T Kusawake, H Kudo, K Ohshima, H Uwe *J. Appl. Phys.* **86** 2307 (1999)
20. H B Liao, R F Xiao, P Yu, G K L Wong, J Q Zheng *J. Vac. Sci. Technol., A* **14** 2651 (1996)
21. L H Hamedi, N Lemee, M Guilloux-Viry, A Perrin, in *The 7th European Conference on Solid State Chemistry (Abstracts of Reports), Madrid, 1999* Vol. 1, p. 77
22. N Adachi, V P Denysenkov, S I Khartsev, A M Grishin, T Okuda *J. Appl. Phys.* **88** 2734 (2000)
23. T Okuda, T Katayama, H Kobayashi, N Kobayashi *J. Appl. Phys.* **67** 4944 (1990)
24. A Thavendrarajah, M Pardavi-Horvath, P E Wigen, M Gomi *IEEE Trans. Magn.* **25** 4015 (1989)
25. S Mino, M Matsuoka, A Tate, A Shibukawa, K Ono *Jpn. J. Appl. Phys.* **31** 1786 (1992)
26. M Y Chern, J -S Liaw *Jpn. J. Appl. Phys.* **36** 1049 (1997)
27. N Watanabe, N Takahashi, K Tsushima *Mater. Chem. Phys.* **54** 173 (1998)
28. Y Jia, M A Zurbuchen, S Wozniak, A H Carim, D G Schlom, L-N Zou, S Briczinski, Y Liu *Appl. Phys. Lett.* **74** 3830 (1999)
29. P G Ivanov, S M Watts, D M Lind *J. Appl. Phys.* **89** 1035 (2001)
30. F Y Yang, C L Chien, E F Ferrari, X W Li, G Xiao, A Gupta *Appl. Phys. Lett.* **77** 286 (2000)
31. X W Li, A Gupta, T R McGuire, P R Duncombe, G Xiao *J. Appl. Phys.* **85** 5585 (1999)
32. X W Li, A Gupta, G Xiao *Appl. Phys. Lett.* **75** 713 (1999)
33. A Gupta, X W Li, S Guha, G Xiao *Appl. Phys. Lett.* **75** 2996 (1999)
34. K Suzuki, P M Tedrow *Solid State Commun.* **107** 583 (1998)
35. R G Egdell, E Brand, D Kellett *J. Mater. Chem.* **9** 2717 (1999)
36. W Neubeck, L Ranno, M B Hunt, C Vettier, D Givord *Appl. Surf. Sci.* **139** 195 (1999)
37. T Fujii, M Takano, R Katano, Y Bando, Y Isozumi *J. Appl. Phys.* **66** 3168 (1989)
38. T Fujii, M Takano, R Katano, Y Bando, Y Isozumi *J. Cryst. Growth* **99** 606 (1990)
39. M Takano, T Fujii, Y Bando, in *New Functionality Materials, C, Synthetic Process and Control of Functionality Materials* (Eds T Tsuruta, M Doyama, M Seno) (Amsterdam: Elsevier, 1993) p. 745
40. Y Gao, Y J Kim, S A Chambers, G Bai *J. Vac. Sci. Technol., A* **15** 332 (1997)
41. D M Lind, S D Berry, G Chern, H Mathias, L R Testardi *J. Appl. Phys.* **70** 6218 (1991)
42. D M Lind, S D Berry, G Chern, H Mathias, L R Testardi *Phys. Rev. B* **45** 1838 (1992)
43. D M Lind, S P Tay, S D Berry, J A Borchers, R W Erwin *J. Appl. Phys.* **73** 6886 (1993)
44. F C Voogt, T Hibma, P J M Smulders, L Niesen *J. Cryst. Growth* **174** 440 (1997)
45. Y Gao, Y J Kim, S A Chambers *J. Mater. Res.* **13** 2003 (1998)
46. F C Voogt, T Fujii, P J M Smulders, L Niesen, M A James, T Hibma *Phys. Rev. B* **60** 11 193 (1999)
47. A Gupta, B W Hussey, A M Guloy, T M Shaw, R F Saraf, J F Bringley, B A Scott *J. Solid State Chem.* **108** 202 (1994)
48. V M Ievlev, A V Bulgakov, V I Trofimov, in *Rost i Substruktura Kondensirovannykh Plenok* (Growth and Substructure of Condensed Films) (Voronezh: Voronezh State University, 2000) p. 20
49. S Little, A Zangwill *Phys. Rev. B* **49** 16 659 (1994)
50. A P Sutton, R W Balluffi *Interfaces in Crystalline Materials* (Oxford: Calendron Press, 1995)
51. I Barin *Thermochemical Data of Pure Substances* Pt. 2 (Weinheim: VCH, 1989)
52. R C West (Ed.) *Handbook of Chemistry and Physics* (Boca Raton, FL: CRC Press, 1986)
53. S V Samoylenkov, O Yu Gorbenko, I E Graboy, A R Kaul, O Stadel, G Wahl, H W Zandbergen *J. Phys. IV* **9** 621 (1999)
54. B Schulte, M Maul, P Häussler, H Adrian *Appl. Phys. Lett.* **62** 633 (1993)
55. Y Q Li, J Zhao, C S Chern *Physica C* **195** 161 (1992)
56. S V Samoylenkov, O Yu Gorbenko, A R Kaul, A R Kuzhakhmetov, S A Zhgoon, G Wahl *Non-Linear Electromagn. Syst.* **13** 87 (1998)
57. O Yu Gorbenko, I E Graboy, A R Kaul, H W Zandbergen *J. Magn. Magn. Mater.* **211** 97 (2000)
58. O Yu Gorbenko, A R Kaul, A A Molodyk, V N Fuflyigin, M A Novozhilov, A A Bosak, U Krause, G Wahl *J. Alloys Compd.* **251** 337 (1997)
59. A A Molodyk, M A Novozhilov, I E Graboy, O Yu Gorbenko, I E Korsakov, A R Kaul *Electrochem. Soc. Proc.* **97** 1152 (1997)
60. A R Kaul, B V Seleznev *J. Phys. IV* **3** 375 (1993)
61. H L Yakel, W C Kohler, E F Bertaut, E F Forrat *Acta Crystallogr.* **16** 957 (1963)
62. A Waintal, J Chenavas *Mater. Res. Bull.* **2** 819 (1967)
63. G Szabo Ph.D. Thesis, University of Lyon, Lyon, 1969
64. A A Bosak, A A Kamenev, I E Graboy, S V Antonov, O Yu Gorbenko, A R Kaul, C Dubourdieu, J P Senateur, V L Svechnikov, H W Zandbergen, B Hollaender *Thin Solid Films* **400** 149 (2001)
65. P A Salvador, T D Doan, B Mercey, B Raveau *Chem. Mater.* **10** 2592 (1998)
66. N Fujimura, T Ishida, T Yoshimura, T Ito *Appl. Phys. Lett.* **69** 1011 (1996)
67. A A Bosak, C Dubourdieu, J-P Sénateur, O Yu Gorbenko, A R Kaul *J. Mater. Chem.* **12** 800 (2002)
68. T Atsumi, T Ohgushi, N Kamegashira *J. Alloys Compd.* **238** 35 (1996)
69. A A Bossak, I E Graboy, O Yu Gorbenko, A R Kaul, M S Kartavtseva, V L Svetchnikov, H W Zandbergen *Chem. Mater.* **16** 1751 (2004)
70. P Lacorre, J B Torrance, J Pannetier, A I Nazzal, P W Wang, T C Huang *J. Solid State Chem.* **91** 225 (1991)
71. M A Novojilov, O Yu Gorbenko, I E Graboy, A R Kaul, H W Zandbergen, N A Babushkina, L M Belova *Appl. Phys. Lett.* **76** 2041 (2000)
72. Yu D Tretyakov, A R Kaul, V K Portnoy *High Temp. Sci.* **9** 61 (1977)
73. Y Kanke, A Navrotsky *J. Solid State Chem.* **141** 424 (1998)
74. O Yu Gorbenko, M A Novojilov, I E Graboy, V A Amelichev, A A Bosak, I V Nikulin, A R Kaul, B Guettler, G Wahl, N A Babushkina, L M Belova, H W Zandbergen *Int. J. Inorg. Mater.* **3** 1303 (2001)
75. G Demazeau, M Pouchard, P Hagenmuller *C. R. Acad. Sci., Ser. C* **277** 107 (1973)
76. A Yu Kropanev, A N Petrov *J. Inorg. Chem.* **28** 1667 (1983)
77. M A Novojilov, G E Adamov, A R Kaul, I E Graboy, H W Zandbergen, in *Processes for Micro- and Nanotechnologies (Proceedings of NATO ASI Series), Kaunas, 2001* p. 20
78. N V Porotnikov, O I Kondratov, K I Petrov, O V Sidorova *Zh. Neorg. Khim.* **25** 3224 (1980) [a]

79. C W F T Pistorius, G J Kruger *J. Inorg. Nucl. Chem.* **38** 1471 (1976)
80. K I Portnoi, N I Timofeeva *Kislorodnye Soedineniya Redkozemel'nykh Elementov* (Oxygen Compounds of Rare Earth Elements) (Moscow: Metallurgiya, 1986)
81. V A Amelitchev, M A Novojilov, O Yu Gorbenko, A R Kaul, B Güttler, in *Thin Films Depositions of Oxide Multilayers (Industrial-Scale Processings)* (Vilnius: Vilnius University Press, 2000) p. 91
82. O Yu Gorbenko, I E Graboy, M A Novozhilov, A R Kaul, G Wahl, V L Svetchnikov *J. Phys. IV* **11** 247 (2001)
83. J A M van Roosmalen, P van Vlaanderen, E H P Cordfunke, W L IJdo, D J W IJdo *J. Solid State Chem.* **114** 516 (1995)
84. B Bochu, J Chenavas, J C Joubert, M Marezio *J. Solid State Chem.* **11** 88 (1974)
85. J F Sarver, F L Katnack, F A Hummel *J. Electrochem. Soc.* **106** 960 (1959)
86. A Ohtomo, M Kawasaki, T Koida, M Masubuchi, H Koinuma, Y Sakurai, Y Yoshida, T Yasuda, Y Segawa *Appl. Phys. Lett.* **72** 2466 (1998)
87. Y Matsumoto, M Murakami, Z W Jin, A Ohtomo, M Lippmaa, M Kawasaki, H Koinuma *Jpn. J. Appl. Phys.* **68** L603 (1999)
88. A Ohtomo, R Shiroki, I Ohkubo, H Koinuma, M Kawasaki *Appl. Phys. Lett.* **75** 4088 (1999)
89. A K Sharma, J Narayan, J F Muth, C W Teng, C Jin, A Kvit, R M Kolbas, O W Holland *Appl. Phys. Lett.* **75** 3327 (1999)
90. E Millon, O Albert, J C Loulergue, J Etchepare, D Hulin, W Seiler, J Perriere *J. Appl. Phys.* **88** 6937 (2000)
91. T Fukumura, Z Jin, A Ohtomo, H Koinuma, M Kawasaki *Appl. Phys. Lett.* **75** 3366 (1999)
92. C H Bates, W B White, R Roy *J. Inorg. Nucl. Chem.* **28** 397 (1966)
93. C L Chang, G Chern, C L Chen, H H Hsieh, C L Dong, W F Pong, C H Chao, H C Chien, S L Chang *Solid State Commun.* **109** 599 (1999)
94. P C Donahue, L Katz, R Ward *Inorg. Chem.* **5** 335 (1966)
95. H W Zandbergen, E Connolly, I E Graboy, V L Svetchnikov, A R Kaul *Physica C* **329** 37 (2000)
96. K Fröhlich, J Šouc, A Rosová, D Machajdík, I E Graboy, V L Svetchnikov, A Figueras, F Weiss *Supercond. Sci. Technol.* **10** 657 (1997)
97. I E Korsakov, Candidate Thesis in Chemical Sciences, Moscow State University, Moscow, 1993
98. G F Voronin, in *Materials and Crystallographic Aspects of T_c Superconductivity (Proceedings of NATO ASI Series), Erice, Italy, 1993* p. 194
99. H Grimmer *Acta Crystallogr.* **32** 783 (1976)
100. B K Vanshtein, A A Chernov, L A Shuvalov (Eds) *Sovremennaya Kristallografiya* (Modern Crystallography) (Moscow: Nauka, 1980)
101. V M Kosevich, V M Ievlev, L S Palatnik, A I Fedorenko *Struktura Mezhkristallitnykh i Mezhfaznykh Granits* (Structure of Intergrain Boundaries and Interfaces) (Moscow: Metallurgiya, 1980)
102. A Somorjia, in *Introduction to Surface Chemistry and Catalysis.* (New York: Wiley, 1994) p. 667
103. H Nagata, T Tsukahara, S Gonda, M Yoshimoto, H Koinuma *Jpn. J. Appl. Phys.* **30** L1136 (1991)
104. A A Bosak, A N Botev, O Yu Gorbenko, I E Graboy, S V Samoylenkov, A R Kaul, C Dubordieu, J P Senateur *J. Phys. IV* **11** 93 (2001)
105. Y Y Erokhin, O Yu Gorbenko, I E Graboy, A R Kaul, S Pozigun, W Decker, R Stolle, G Wahl, in *Proceedings of the VIth Trilateral German-Russian-Ukrainian Seminar on HTSC, Dubna, 1994* p. 407
106. S V Samoylenkov, O Yu Gorbenko, A R Kaul, S V Papucha, N A Mirin, V V Maleev, I E Graboy, in *Proceedings of the XIVth International Conference on CVD and EUROCVD-XI, Paris, 1997* Vol. 97-25, p. 990
107. C V Samoilenkov, O Yu Gorbenko, A R Kaul, I E Graboy, S A Zhgun, in *Materialy X Mezhdunarodnogo Simpoziuma 'Tonkie Plenki v Elektronike', Yaroslavl', 1999* (Proceedings of the Xth International Symposium 'Thin Films in Electronics', Yaroslavl', 1999) p. 65
108. T Hashimoto, M Sagoi, Y Mizutani, J Yoshida, K Mizushima *Appl. Phys. Lett.* **60** 1757 (1992)
109. Z Trajanovic, C J Lobb, M Rajeswari, I Takeuchi, C Kwon, T Venkatesan *Phys. Rev. B* **56** 925 (1997)
110. O Yu Gorbenko, A R Kaul, A A Bosak, I E Graboy, H W Zandbergen, V L Svetchnikov, N A Babushkina, L M Belova, K I Kugel *Solid State Commun.* **114** 407 (2000)
111. S Y Hou, J Kwo, R K Watts, J-Y Cheng, D K Fork *Appl. Phys. Lett.* **67** 1387 (1995)
112. H N Lee, S Senz, A Visinoiu, A Pingolet, D Hesse, U Gosele *Appl. Phys., A: Mater. Sci. Process* **71** 101 (2000)
113. H N Lee, D Hesse, N Zakharov, U Gosele *Science* **296** 2006 (2002)
114. D Hesse, S K Lee, X H Zhu, N Zakharov, H N Lee, in *The 14th International Conference on Crystal Growth in Conjunction with the 12th International Conference on Vapour Growth and Epitaxy (Book of Abstracts), Grenoble, 2004* p. 395
115. O Yu Gorbenko, A A Bosak *Sensor* **1** (2) 28 (2002)
116. K Steenbeck, T Eick, K Kirsch, K O'Donnell, E Steinbeiß *Appl. Phys. Lett.* **71** 968 (1997)
117. C Dubourdieu, M Audier, H Roussel, J P Sénateur, J Pierre *J. Appl. Phys.* **92** 379 (2002)
118. K-K Choi, T Taniyama, Y Yamazaki *J. Appl. Phys.* **90** 6145 (2001)
119. S P Isaac, N D Mathur, J E Evetts, M G Blamire *Appl. Phys. Lett.* **72** 2038 (1998)
120. H Sieber, S Senz, D Hesse *Thin Solid Films* **303** 216 (1997)
121. R J Gaboriaud, F Pailloux, J Pacaud, P O Renault, J Perriere, A Huignard *Appl. Phys., A: Mater. Sci. Process* **71** 675 (2000)
122. R J Gaboriaud, F Paumier, F Pailloux, P Guerin *Mater. Sci. Eng. B* **109** 34 (2004)
123. Q X Jia, X D Wu, G Song, S R Foltyn *J. Vac. Sci. Technol., A* **14** 1107 (1996)
124. Q Wang, W L Gladfelter, D F Evans, Y Fan, A Franciosi *J. Vac. Sci. Technol., A* **14** 747 (1996)
125. U Rüdiger, M Rabe, K Samm, B Özyilmaz, J Pommer, M Fraune, G Güntherodt, S Senz, D Hesse *J. Appl. Phys.* **89** 7699 (2001)
126. O Yu Gorbenko, A R Kaul, G Wahl *Chem. Vap. Depos.* **3** 193 (1997)
127. L J Buller, H D Abruna *Chem. Rev.* **101** 1897 (2001)
128. V S Urusov, V L Tauson, V V Akimov *Geokhimiya Tverdogo Tela* (Geochemistry of Solids) (Moscow: GEOS, 1997)

[a] — *Russ. J. Inorg. Chem. (Engl. Transl.)*

Russian Chemical Reviews **73** (9) 881 – 898 (2004) © 2004 Russian Academy of Sciences and Turpion Ltd

DOI 10.1070/RC2004v073n09ABEH000920

Structural and microstructural features of functional materials based on cuprates and manganites

Yu D Tretyakov, E A Goodilin, D V Peryshkov, D M Itkis

Contents

I.	Role of the d-elements in design of new materials	881
II.	Crystal structures of cuprates and manganites	882
III.	Local structure and defects	885
IV.	Chemical properties and phase diagrams	887
V.	Single crystals	889
VI.	Microstructure and new methods of preparation of ceramic composites	890
VII.	Geometrical control of mutual orientation of crystallites (graphotexturing)	892
VIII.	Fields of practical applications of cuprates and manganites	895

Abstract. The review considers characteristic features of the crystal structure, phase relations, microstructure and physical properties of the most important classes of modern cuprate and manganite materials including high-temperature superconductors, CMR magnetic semiconductors and superionic conductors. The bibliography includes 189 references.

I. Role of the d-elements in design of new materials

In design of modern functional materials possessing nonlinear magnetic and electric properties an important role is played by the transition elements capable of being in different oxidation states and spin states.[1,2] Among oxide materials, there are two most promising classes which have become the subjects of intensive research recently. These are high-temperature superconductors (HTSC)[3–8] and 'colossal magnetoresistive' (CMR) materials.[9–11] Open framework structures have also attracted close attention of researchers.[12,13] Often, these classes of compounds comprise complex oxides of copper and/or manganese. Peculiarities of the properties of these elements and their oxides are of crucial importance for practical applications because they allow one to trace how the chemical properties of the d-elements influence the functional properties of materials.

In a rather short time, large-scale research on high-temperature superconductivity has contributed largely to modern inorganic chemistry, physical chemistry, solid state chemistry and materials science.[3] High-temperature superconducting cuprates represent one of the most promising classes of ceramic materials possessing structure-sensitive properties. They are still complex and very interesting objects that are far from being studied comprehensively. Methodological approaches and experimental basis of inorganic chemistry and solid state chemistry are of particular importance for carrying out basic research on these compounds.

The ability of manganese to form complex framework structures built of joined MnO_6 octahedra and filled with different types of cations located in the framework cavities predetermines the variety of manganese-containing oxide materials.[14] For instance, hollandite, $BaMn_8O_{16}$, is one of the most prominent and well-known examples of compounds with a specific tunnel structure, which provides the possibility of using this phase as a catalyst, solid electrolyte, matrix for nuclear waste disposal and an electrode material.[13,15]

The magnetic, magnetotransport and other practically important physical properties of manganites are to a great extent governed by the ability of manganese to be present in the structure simultaneously in different oxidation states, by electron exchange between Mn^{3+} and Mn^{4+} and, sometimes, by the spin and charge ordering.[9–11] The discovery of the CMR effect in the manganites with perovskite structure, $R_{1-x}A_xMnO_{3-\delta}$ [R is a rare-earth element (REE) and A is an alkali or alkaline-earth metal[9–11]] was followed by a new flare of interest in studies of manganite systems in connection with the possibility of using them in magnetometers, reading heads for high-density magnetic recording, data storage devices, metal detectors, sensors, *etc.*[11] Perovskite-type manganites of compositions $CaCu_xMn_{7-x}O_{12}$ exhibit some features such as specific magnetoresistance mechanism different from that observed in conventional perovskites, the possibility for a rather high magnetoresistance to be achieved at relatively low magnetic fields and smooth temperature dependences of these parameters (in contrast to manganites $AMnO_3$). This offers great prospects for practical applications of these phases.[16–19] The temperature and the magnetic field dependences of the magnetoresistance indicate a large contribution of intergrain tunnelling to the total magnetoresistance of $CaCu_xMn_{7-x}O_{12}$ compounds. Generally, the tunnelling magnetoresistance depends on the microstructure, in particular, on the grain size, mutual orientation of grains and on the surface area of grain boundaries. Optimisation of these characteristics requires elaboration of novel methods of synthesis of these materials.[20] Thus, similarly to superconducting cuprates, complex oxides of alkaline-earth metals and manganese are of particular interest for inorganic chemistry and materials science.

This review concerns the main methods of preparation of modern functional materials and the 'composition – treatment –

Yu D Tretyakov, E A Goodilin, D V Peryshkov, D M Itkis Department of Chemistry and Department of Materials Science, M V Lomonosov Moscow State University, Leninskie Gory, 119992 Moscow, Russian Federation. Fax (7-095) 939 09 98. Tel. (7-095) 939 20 74.
E-mail: yudt@inorg.chem.msu.ru (Yu D Tretyakov).
Tel. (7-095) 939 47 29. E-mail: goodilin@inorg.chem.msu.ru (E A Goodilin), pyoryshkov@inorg.chem.msu.ru (D V Peryshkov), itkis@inorg.chem.msu.ru (D M Itkis)

Received 9 March 2004
Uspekhi Khimii **73** (9) 954 – 973 (2004); translated by A M Raevskiy

structure – property' correlations. We also summarise here the results of theoretical and experimental studies on fabrication of ceramic materials and coatings based on superconducting cuprates, cupromanganite-based CMR magnetic semiconductors and superionic conductors based on the manganites with framework structures.†

II. Crystal structures of cuprates and manganites

The main structureal types of superconducting cuprates are as follows:

oxygen-deficient perovskites characterised by the presence of 'infinite CuO_2 layers' separated by (La,Ca) – vacancy layers [*e.g.*, (Sr,Ca)CuO_2, see Fig. 1 *a*], substitution solid solutions $Nd_{1+x}Ba_{2-x}Cu_3O_z$ based on the triple perovskite-type unit cell CuO_{1-z} – BaO – CuO_2 – Nd – CuO_2 – BaO – CuO_{1-z} with different types of ordering of the heavy cations and the oxygen sublattice (Fig. 1 *b*,*c*);

intergrowth structures characterised by intergrowth of the perovskite units containing superconducting CuO_2 planes, NaCl [*e.g.*, La_2CuO_4 (Fig.1 *d*), $Bi_2Sr_2CaCu_2O_8$ (Fig. 1 *e*), $Pb_2SrYCu_3O_8$], fluorite bloks, *etc.*;

homologues, *i.e.*, phases with different numbers of CuO_2 layers [*e.g.*, $HgBa_2CaCu_2O_{6+z}$ and $HgBa_2Ca_2Cu_3O_{8+z}$ phases (Fig. 1 *f*)] or CuO layers (*e.g.*, $RBa_2Cu_3O_7$, $R_2Ba_4Cu_7O_{14}$, $RBa_2Cu_4O_8$);

low-dimensional structures formed by differently joined planar CuO_2 units [*e.g.*, $Sr_{14}Cu_{24}O_{48}$ (Fig. 1 *g*), $Sr_2Cu_3O_5$ (Fig. 1 *h*), $LaCuO_{2.5}$ (Fig. 1 *i*)].

Almost all HTSC are complex layered copper-containing oxides containing oxygen-deficient perovskite-type structural fragments.[5,7,8,106–108] The structure and properties of the HTSC are strongly influenced by the Jahn – Teller effect and ordering of ions.[3,7,8] The former effect is responsible for the formation of low-coordinated copper polyhedra in the structure while the latter causes local distortions and charge transfer between structural blocks.

In a planar CuO_2 layer the copper atoms form a square network while the oxygen atoms are located on the lines connecting the sites of the copper atoms. The $3d_{x^2-y^2}$ electrons of the copper atoms and the $2p_{x,y}$ electrons of the oxygen atoms form the in-plane bonds in the layer. These electrons are delocalised and do not belong to a particular atom. Below the critical temperature, superconductivity arises on 'doping' the CuO_2 layers with an optimum amount of charge carriers[6] in the absence of strong structural distortions. The phases with nearly ideal planar CuO_2 layers are, *e.g.*, mercury-containing[106] HTSC and 'infinite-layer' structures.[8] The onset of superconductivity requires that the formal oxidation state of copper in the layers containing shared electrons be in the ranges from +2.05 to +2.25 (hole-doped superconductors) or from +1.8 to +1.9 (electronic superconductors). The length of the in-plane Cu – O bond must be 0.19 to 0.197 nm provided that the distance between adjacent copper atoms is 0.380 to 0.394 nm. For any member of a homologous series the dependence of T_c on the charge carrier concentration passes through an extremum, while the highest transition temperature is usually observed for the homologue with an optimum number of the superconducting planes.[21,107]

It is believed that transition to the superconducting state occurs as a result of formation of a Cooper pair (a boson) provided that the motion of two charge carriers is correlated.[108] In the early stage of research into the HTSC mechanism it was assumed that the Cooper pair is a pair of holes that polarise the lattice. The electron – phonon interaction and symmetry of the ordering parameters in terms of the Ginzburg – Landau superconductivity theory (d-, s- or mixed type) are still the subject of wide speculation.[109] At present, the most probable mechanism of superconductivity considers a two-hole charge carrier and magnetically ordered spin moments of the copper atoms in the localisation region of the Cooper pair (sometimes, this is called a magnetic polaron or a 'spin bag'). In this case the coherence length of the charge-carrier wave function is rather small and different along the main crystallographic directions.[108] The Bose 'liquid' flows through a HTSC crystallite without dissipation provided that the critical current density (the critical magnetic field) is not exceeded; otherwise, the Cooper pairs are destroyed and the HTSC passes to the normal (resistive) state.

The structures of famous superconductors are built of alternating CuO_2 planes and 'dielectric' BaO, SrO, TlO, BiO, PbO, HgO, $Ca^{\square}$, *etc.*, layers.[5,7,8,107] In the intergrowth structures the non-superconducting units often act as specific charge reservoirs that ensure the formation and transfer of charge to the superconducting planes by insertion (or removal) of extra oxygen and by heterovalent doping. This is responsible for crucial importance of another structural parameter, *viz.*, the length of the bond between the copper atoms and oxygen atoms in the neighbouring layers. These bonds are usually much longer (more than 0.22 nm) than the in-plane bonds. In other words, the structures of superconducting cuprates contain unequal chemical bonds Cu – O, namely, strong bonds in the plane of the CuO_2 layer and much weaker bonds perpendicular to these layers.

The 'infinite-layer' superconducting structures obtained under high pressure[8] (see Fig. 1 *a*) and 'ladder'-type cuprates (see Fig. 1 *g* – *i*)[110,111] are of interest from the standpoint of both fundamental superconductivity theory and crystal chemistry. Both families of cuprates are low-dimensional, strongly correlated systems built of differently connected planar $(CuO_2)_n$ units with variable dimension (1D – 2D) and width (in the case of ribbon-like structures). As a consequence. they exhibit unique features of the spin and magnetic interactions.

The structure types characteristic of manganites are as follows: perovskite [$CaMnO_3$ (Fig. 2 *a*)], spinel [Li_2MnO_4 (Fig. 2 *b*)]; homologues, Ruddlesden – Popper phases $(R_{1-x}A_x)_{n+1}Mn_nO_{3n+1}$ [R is a rare-earth element and A is an alkali-earth element; $n = 1$ (Fig. 2 *c*) and 2 (Fig. 2 *d*)] characterised by intergrowth of different numbers of perovskite-type blocks $(R_{1-x}A_x)MnO_3$ and $NaCl(R_{1-x}A_x)O$ units; layered and chain manganites [birnessite $K_{0.5}Mn_2O_{4.3}(H_2O)_{0.5}$ (Fig. 2 *e*) and $Ba_6Mn_5O_{16}$ (Fig. 2 *f*)]; and tunnel structures related to pyrochlore [$Tl_2Mn_2O_7$ (Fig. 2 *g*)], pyrolusite [β-MnO_2 (Fig. 2 *h*)], hollandite [$A_{2-x}Mn_8O_{16}$, where A = Ba, Sr, Ca, *etc.* (Fig. 2 *i*)], todorokite [$MMn_6O_{12}\cdot 3H_2O$, where M = K, Ca, Mn, *etc.* (Fig. 2 *j*)], ramsdelite R-MnO_2 (Fig. 2 *k*) and psylomelane [$Ba_{0.66}Mn_5O_{10}(H_2O)_{1.35}$ (Fig. 2 *l*)].

Most simple manganese oxides have framework or layered structures (see Fig. 2).[2,12] The oxide Mn_3O_4 has a distorted spinel structure at room temperature which undergoes a transition in the cubic polymorph (γ-Mn_3O_4) at temperatures above 1170 °C. In the structure of hausmannite (β-Mn_3O_4) the distance from the cation to each of the two anions along the [001] direction is 16% longer than the distance from the cation to any anion in the (001) plane (at room temperature). Compounds γ-Mn_2O_3 and Mn_3O_4

† These investigations are carried out by the research staff of the Department of Chemistry, M V Lomonosov Moscow State University, in collaboration with domestic and foreign research centres. The research avenues are as follows: crystal chemistry of HTSC[21–23] and modification (fluorination)[24–30] of the superconducting phases and CMR manganites; synthesis of homologues of mercury-containing HTSC[31–38] and determination of their crystal chemical features[39–42] and physical properties;[43–45] single-crystal structure refinements;[46–48] studies on thermodynamics of HTSC systems[49,50] including mercury-containing HTSC;[51,52] studies on non-stoichiometry (with respect to oxygen) in and phase stability of manganites;[53] preparation of microcomposites based on bismuth-containing HTSC phases,[54–57] CMR manganite ceramics;[58–61] fabrication of thin films and heterostructures[62–71] based on HTSC or CMR manganites with preset microstructure and defect content;[72–82] studies on giant isotope effect[83–86] and magnetooptical properties of manganites;[87–90] stabilisation effect in film structures;[91] and determination of the local structure of complex oxide phases.[92–95] Detailed reports on the research avenues mentioned above can be found in Refs 5, 11, 96 – 107.

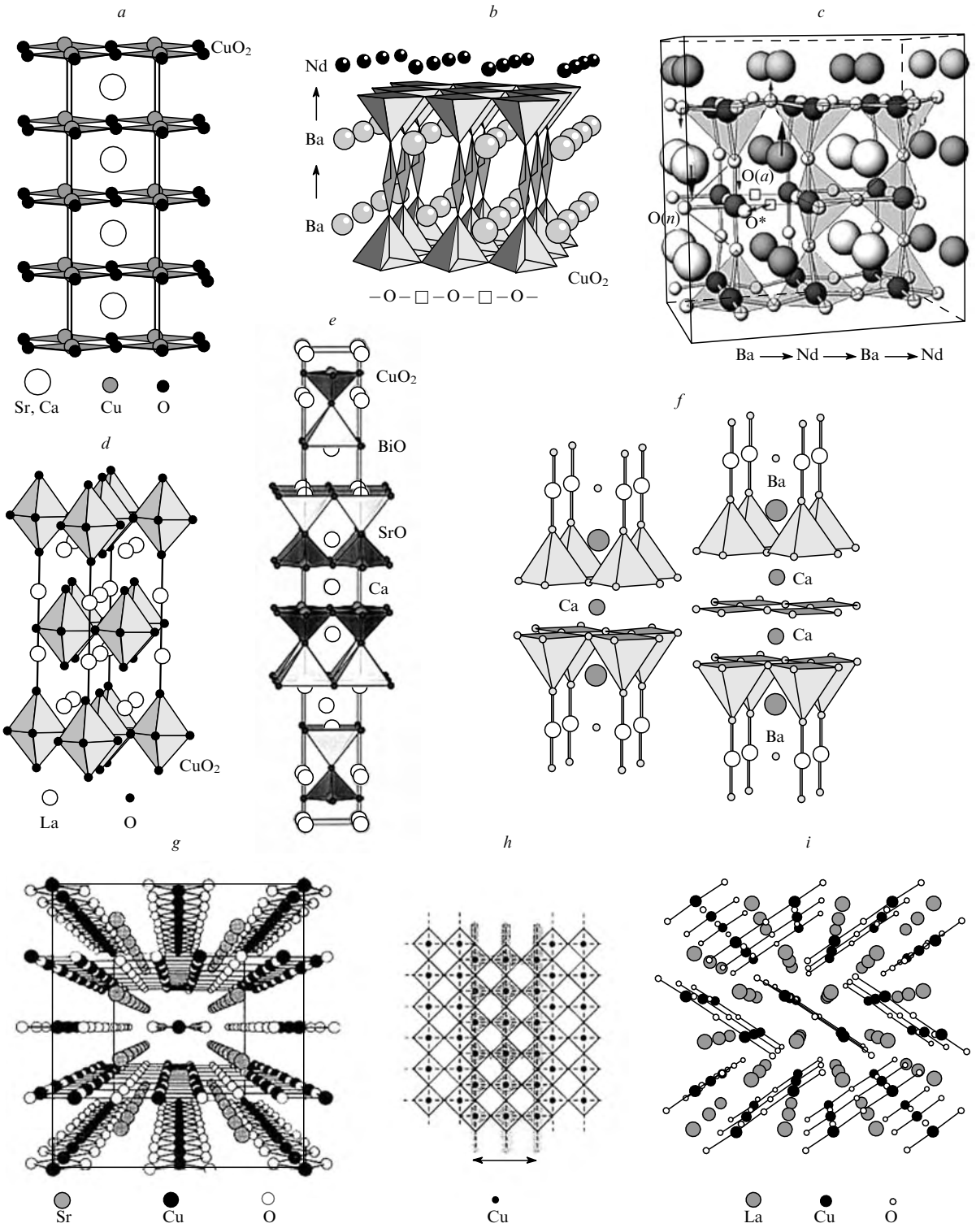

Figure 1. Main structures of superconducting cuprates.[7,8] (Sr, Ca)CuO_2 (*a*), $NdBa_2Cu_3O_z$ (*b*), $Nd_2BaCu_3O_z$ (*c*), La_2CuO_4 (*d*), $Bi_2Sr_2CaCu_2O_8$ (*e*), $HgBa_2CaCu_2O_{6+z}$ (on the left) and $HgBa_2CaCu_3O_{8+z}$ (on the right) (*f*), $Sr_{14}Cu_{24}O_{48}$ (*g*), $Sr_2Cu_3O_5$ (*h*), and $LaCuO_{2.5}$ (*i*).

are characterised by the same type of tetragonal distortion; MnO is isostructural to NaCl. The oxide Mn_5O_8 is described by the formula $Mn_2^{2+}Mn_3^{4+}O_8$. The structure of Mn_5O_8 can be represented by CdI_2-type layers in which 25% of the metal sites are vacant and the Mn^{2+} ions located above and below the vacant positions connect the layers to form a three-dimensional framework.

Depending on the fashion in which the MnO_6 octahedra are joined, tunnels of different shape and size are formed. The presence of tunnels usually leads to high anisotropy of the structure and in some cases to ionic conductivity. For instance, hollandite, cryptomelane, coronadite and α-MnO_2 belong to minerals described by a general formula $A_x(Mn^{4+}, Mn^{3+})_8(O^{2-},OH^-)_{16}$, where A is a large cation, usually, Ba^{2+} (hollandite) or K^+ (cryptomelane). The structure of hollandite comprises double chains of edge-sharing MnO_6 octahedra, which results in the formation of 2×2 tunnels. The structure of psylomelane, $(Ba,H_2O)_2Mn_5O_{10}$, is built of doubled and tripled chains of octahedra and large 2×3 tunnels filled with Ba^{2+} ions and water molecules. Dehydration of this compound by heating to

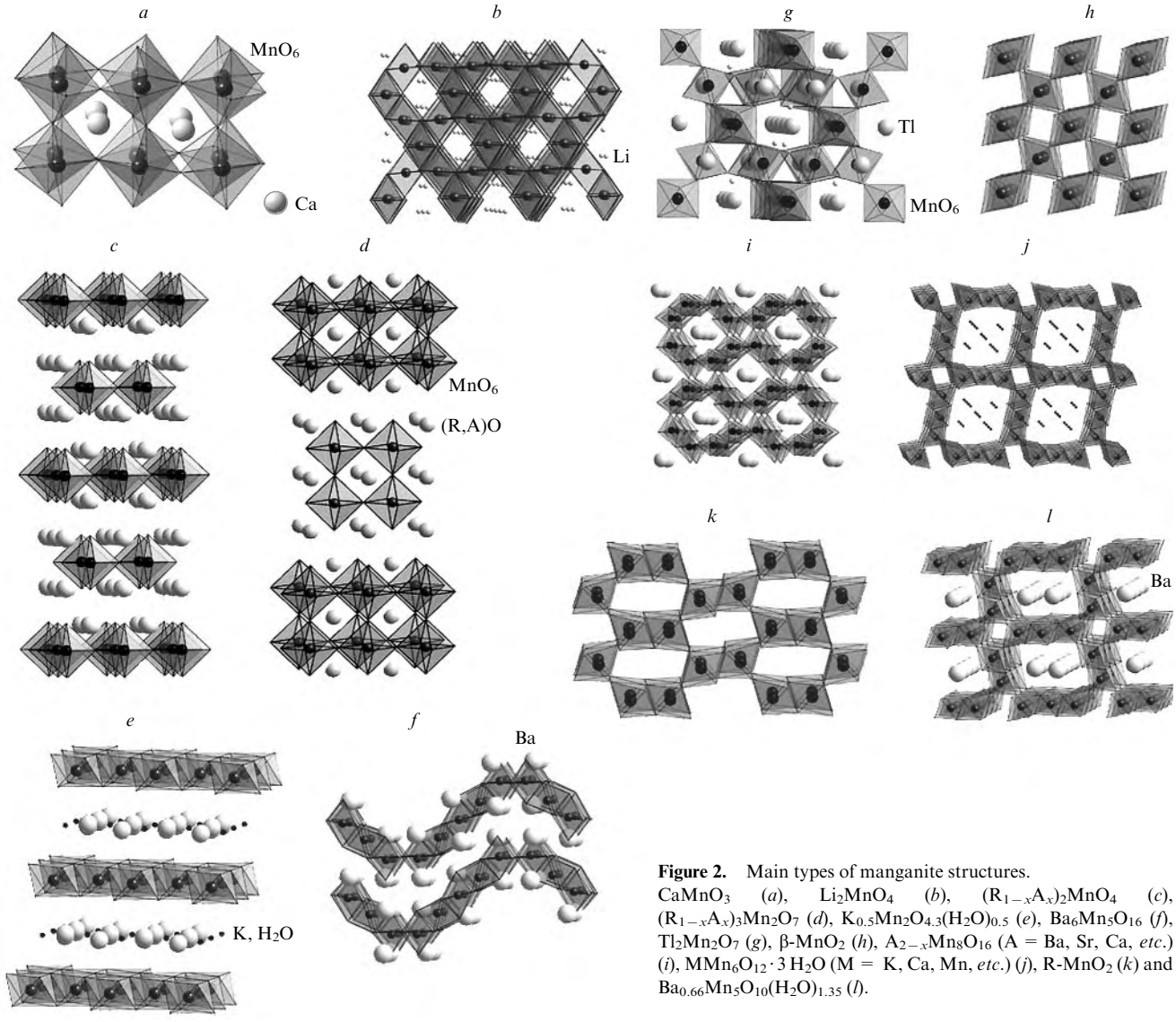

Figure 2. Main types of manganite structures. $CaMnO_3$ (*a*), Li_2MnO_4 (*b*), $(R_{1-x}A_x)_2MnO_4$ (*c*), $(R_{1-x}A_x)_3Mn_2O_7$ (*d*), $K_{0.5}Mn_2O_{4.3}(H_2O)_{0.5}$ (*e*), $Ba_6Mn_5O_{16}$ (*f*), $Tl_2Mn_2O_7$ (*g*), β-MnO_2 (*h*), $A_{2-x}Mn_8O_{16}$ (A = Ba, Sr, Ca, *etc.*) (*i*), $MMn_6O_{12}\cdot 3\,H_2O$ (M = K, Ca, Mn, *etc.*) (*j*), R-MnO_2 (*k*) and $Ba_{0.66}Mn_5O_{10}(H_2O)_{1.35}$ (*l*).

~550 °C is followed by its transformation in hollandite [12] with a disordered structure, which is due to the fact that the large tunnels enclosed on four sides by chains or ribbons of the manganese–oxygen octahedra are partially filled with cations. Tunnels in the todorokite structure are built of tripled 3 × 3 chains of edge-sharing octahedra and contain different numbers of Na, Ca and K atoms; tunnels of more complex shape can also form.[12]

The structure of birnessite, δ-MnO_2, is built of layers comprised of edge-sharing MnO_6 octahedra separated by layers containing water molecules and OH groups (see Fig. 2 *e*). The main structural feature of the manganites $BaMn_3O_5(OH)$ and $BaMn_2O_3(OH)_2$ are ribbons composed of four parallel chains of MnO_6 octahedra.[112] Layered manganites $Ba_4Mn_3O_{10}$ and $Ba_6Mn_5O_{16}$ containing no water molecules are also known.[113] Barium ions stabilise Mn(IV) in the structure. All compounds mentioned above can be obtained *via* 'molecular templates' in the synthesis of manganese oxides and their derivatives by 'soft chemistry' methods (see note ‡).[12]

‡ Here, the term 'soft chemistry methods' covers thermal decomposition of salt and hydroxide components, sol–gel technique, cryochemical or hydrothermal synthesis, which permit fabrication of materials with preset granulometric composition, stoichiometry, *etc.*, at rather low temperatures.

Compounds with a perovskite structure form a broad class of practically valuable materials. Distortion of an ideal perovskite structure in manganites appears due to three factors, namely, cooperative rotation of octahedra about a certain axis, Jahn–Teller distortion of MnO_6 octahedra and displacement of cations from their positions.[2] Thus, the initially cubic perovskite structure can experience a tetragonal, orthorhombic, rhombohedral or monoclinic distortion.

Phases of compositions $A_2Mn_2O_7$ (A = Dy–Lu, Sc, In, Tl) with pyrochlore-type structures [114] have cubic face-centred unit cells. Their structures represent frameworks built of vertex-sharing MnO_6 octahedra with the Mn–O–Mn angle of about 135°. In the structures of $A_2Mn_2O_7$ compounds the atoms A occupy centres of the hexagonal rings formed by the oxygen atoms (O) of MnO_6 octahedra and the oxygen atoms (O′) located above and below the ring plane (see Fig. 2 *g*). Thus, the environment of the atom A can be represented by a distorted cube. The MnO_6 octahedra are distorted, being in fact a kind of trigonal antiprisms; however, this is not a Jahn–Teller distortion characteristic of $R_{1-x}A_xMnO_3$ compounds.

Compounds $(R_{1-x}A_x)_{n+1}Mn_nO_{3n+1}$ belong to the Ruddlesden–Popper phases,[115] *i.e.*, layered manganites with a coherent intergrowth structure of perovskite-type units (the number of layers in the perovskite unit is *n*) and NaCl-type blocks (see

Fig. 2 *e*, *f*). The limiting case $n = \infty$ corresponds to the perovskite structure; the case $n = 1$ corresponds to the K_2NiF_4 structure.

III. Local structure and defects

The possibility of fabrication of cuprate- and manganite-based materials with preset functional properties and solution to the problem of 'anomalous' states of the phases with irreproducible fluctuations of functional properties [116–122] are to a great extent related to control of the cation ordering in the crystal lattices of solid solutions (Fig. 3).

Detailed studies showed that the physical properties of HTSC phases are often governed by the prehistory of samples.[116, 120, 121, 123–125] For instance, $Nd_{1+x}Ba_{2-x}Cu_3O_y$ solid solutions synthesised at low temperatures are characterised by cation disordering; therefore, the degree of local structural distortions in mixed REE–barium cuprates can be controlled by varying the temperature and duration of isothermal annealing (see Fig. 3 *a*). To establish an optimum regime of fabrication of superconducting materials, one should construct TTT-diagrams for different states of solid solutions, *viz*., ceramics, single crystals and films. This approach can also be used for efficient control of solid-phase decomposition of HTSC-cuprates, which can lead to the formation of microinclusions (efficient pinning centres).

Difficulties in studies of cation disordering using diffraction techniques (in particular, X-ray powder diffraction) are associated with integral character of information obtained in the experiments; in this case, investigations of local structural distortions by other methods can be more informative. To perform quantitative analysis of the local structure of high-temperature superconductors and manganites, it is appropriate to employ not only transmission electron microscopy but also efficient methods based on anomalous absorption of radiation, in particular, Mössbauer spectroscopy [119–122] and X-ray spectroscopic analysis [Extended X-ray Absorption Fine Structure (EXAFS)[116, 117]]. The EXAFS technique permits reliable determination of the average distances, coordination numbers and degree of disordering of the coordination environment in different clusters in solid solutions. Valuable additional information suitable for estimation of parameters of the nearest oxygen environment and the valent state of the probe atoms (^{57}Fe, *etc*.) can be extracted from the Mössbauer spectra. Raman spectroscopy provides important information on the local symmetry and force constants of the metal–oxygen bonds.[116, 117] Using Raman spectroscopy and Mössbauer spectroscopy, it is possible to study disordering of light atoms (*e.g*., oxygen atoms), thus complementing information obtained by powder X-ray diffraction methods in structure refinements.

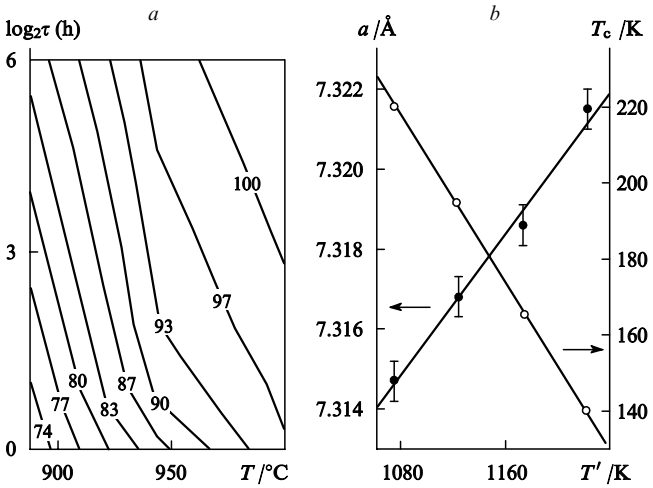

Figure 3. TTT-diagram § for the HTSC phase of $NdBa_2Ca_3O_7$ (*a*) and the lattice parameters and the temperature of magnetic ordering (T_c) of cupromanganite $CaCuMn_6O_{12}$ samples plotted *vs*. synthesis temperature (T') (*b*). Shown in the isolines are the superconducting transition temperatures (in per cent with respect to $T_c = 94$ K).

§ The Time–Temperature–Transformation diagram.

Mössbauer spectroscopy belongs to the most efficient and widely used methods of investigation of the local structure of HTSC phases.[126] The technique precludes on-site studies of defectivenes of the cation sublattice because parameters of hyperfine interactions depend mainly on the state of the first coordination sphere (oxygen environment) of the iron probe atoms occupying positions of copper atoms. At the same time the character of distortions of the oxygen polyhedra surrounding copper atoms is to a great extent governed by the extent of occupation of barium positions by other cations (*e.g*., neodymium ions in the $Nd_{1+x}Ba_{2-x}Cu_3O_z$ solid solution [5]). Schemes presented in Fig. 4 are convenient for establishment of correspondence between parameters of Mössbauer spectra and particular types of coordination polyhedra of the iron atoms occupying positions of copper atoms.[119, 120]

With heterovalent substitution of neodymium for barium the isomer shifts of the corresponding components increase (see Fig. 4) owing to stabilisation of the Fe^{3+} ions occupying the Cu1 positions in the substitutional solid solutions characterised by charge transfer between the dielectric block and the superconducting planes. An increase in the quadrupole splitting of spectral doublets is due to displacement of the apical oxygen O3, which is also characteristic of substitutional solid solutions. A spectral component associated with the $Fe_{Cu1}(III)O_{3+1}$ polyhedron, an unusual distorted configuration of the oxygen environment of the Fe atom occupying the Cu1 position [2 O(*a*) + O(*n*) + O*, see Fig. 1] should be pointed out. This component is characteristic [119, 127] only of annealed samples of the Nd213 : Fe solid solution with superstructural ordering of neodymium and barium atoms.

The main feature of the Mössbauer spectra of the pseudocubic phase $Nd_{1+x}Ba_{2-x}Cu_3O_z$ and substitutional solid solution Nd336 is the presence of components associated to the $Fe(IV)_{Cu1}O_6$ polyhedron.[116–120] These components originate from replacement of neodymium atoms by barium atoms.[118, 119] The $Fe(IV)_{Cu1}O_6$ octahedra are distorted owing to asymmetry of the second coordination sphere comprised of Ba atoms occupying their proper positions and Nd atoms occupying positions of Ba atoms. An increase in the formal oxidation state of iron atoms (decrease in isomer shift) can be explained by the formation of an associate of defects, $Fe(IV)_{Cu1}O_6-Nd_{Ba}$ (Fig. 5). In this case heterovalent substitution of Nd^{3+} for Ba^{2+} leads to displacement of apical oxygen atoms and occupation of vacant oxygen (O4) positions; as a consequence, the coordination sphere of the iron atoms occupying the Cu1 positions takes the shape of a distorted octahedron. No transfer of the excess local positive charge to the $Cu2O_2$ plane occurs, which increases the effective charge on the ^{57}Fe probe atoms. These data confirm the hypothesis that partial exchange of neodymium and barium in their proper crystallographic positions is possible in the pseudocubic phase $NdBa_2Cu_3O_7$ (see Fig. 5 *a*).

At high temperatures, the experimental temperature dependences of the magnetic susceptibility of the CMR manganites $CaCu_xMn_{7-x}O_{12}$ with $x > 0$ obey the Curie–Weiss law. However, the plots show clearly seen downward curvature typical of ferrimagnetics over a broad temperature interval.[16–20] The parameter of the cubic unit cell and the magnetic ordering temperature of the single-phase samples with identical cation and anion compositions depend on the synthesis temperature (see Fig. 3).

These correlations are due to specific structural features of solid solutions. For instance, the $CaCu_xMn_{7-x}O_{12}$ solid solution

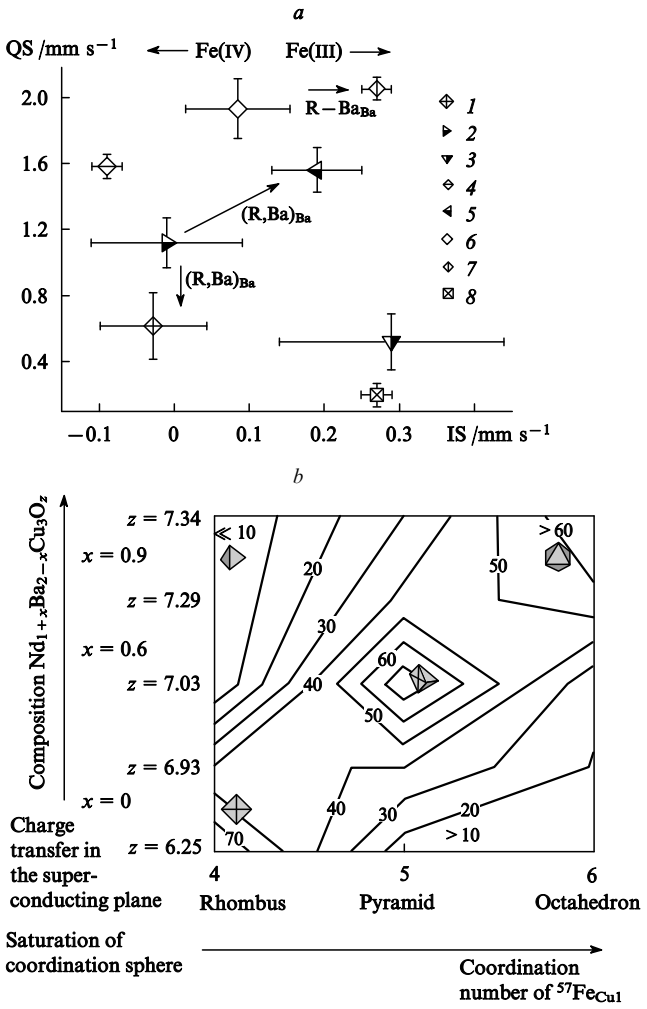

Figure 4. Schematic illustration of the results of Mössbauer spectroscopy studies of mixed REE–barium cuprates (*a*) and a generalised scheme of changes in the iron–oxygen polyhedra (a square, distorted rhombus, pyramid or octahedron) in the Cu1 position in the solid solution phase $Nd_{1+x}Ba_{2-x}Cu_3O_z$ with increasing x and z upon oxidation of samples (*b*). (*a*) Distorted octahedron (Cu1) (*1*), pyramid (Cu1) (*2*), pyramid (Cu2) (*3*), tetrahedron, twins (Cu1) (*4*), distorted pyramid (Cu1) (*5*), rhombus (Cu1) (*6*), distorted rhombus (Cu1) (*7*), and octahedron (Cu1) (*8*); QS is the quadrupole splitting and IS is the isomer shift; shown in the isolines are the contributions of the corresponding coordination numbers of the probe iron atoms (in per cent) (*b*).

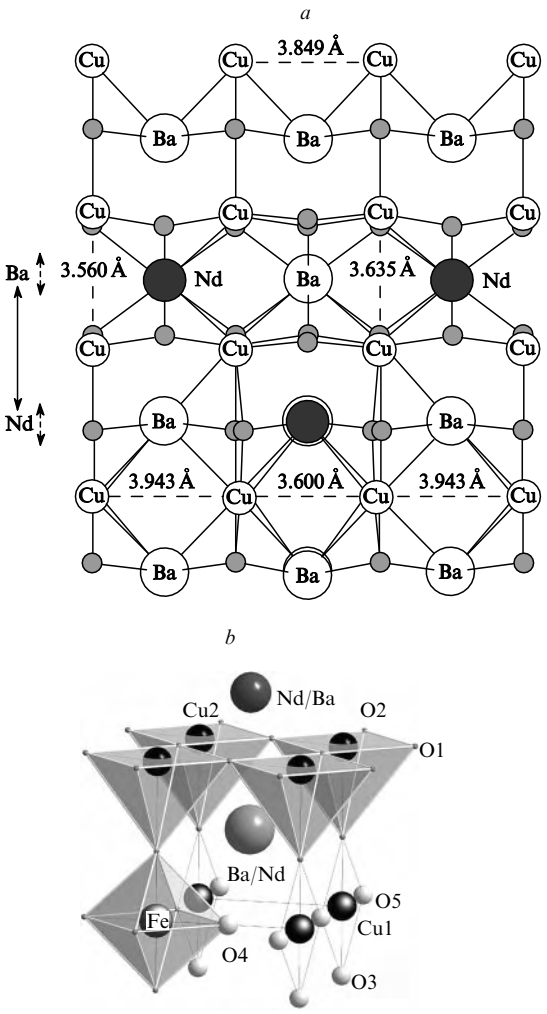

Figure 5. General model of defect (*a*) and a model of associated defects (*b*) $Fe(IV)_{Cu1}O_6-Nd^{3+}_{Ba^{2+}}$, which forms upon doping the substitutional solid solution $Nd_{1+x}Ba_{2-x}Cu_3O_z$ with iron in the case of antistructural disordering of neodymium and barium.

(Fig. 6 *a*) belongs to perovskite-type compounds [16–18] of general formula $AC_3B_4O_{12}$ (A is an alkali metal, alkaline-earth metal or REE cation; B = Mn^{4+}, Mn^{3+}, Ti^{4+}, Ru^{4+} or Ge^{4+}; C = Cu^{2+} or Mn^{3+}). In their framework structures, tunnels are filled with Ca^{2+}, Mn^{3+} and Cu^{2+} cations. The Mn^{3+} ions are also constituents of distorted MnO_6 octahedra occupying the unit cell vertices while the Mn^{4+} cations occupy ideal octahedral positions.

The solid solution (except for the composition with $x = 0$) crystallises in the cubic system (space group $Im\bar{3}$). This is accompanied by doubling of the parameter of ideal perovskite unit cell. The oxidation state of manganese in the B-position depends on the Cu^{2+}/Mn^{3+} ratio (x value) in the solid solution. Magnetic ordering arises as a result of interaction between the Cu^{2+} and Mn^{3+} magnetic sublattices, which depends on the occupation of crystallographic positions by cations and is governed by the procedure employed for sample preparation.

Yet another phase whose properties depend on the sample prehistory is $Ba_6Mn_{24}O_{48}$ with a composite structure (see Fig. 6 *b*) related to the known rutile and hollandite structures.[128] The crystal structure of $Ba_6Mn_{24}O_{48}$ can be represented as a combination of two sublattices, *viz*., a $[Mn_{24}O_{48}]$ framework containing randomly distributed Mn(IV) and Mn(III) and a sublattice of Ba^{2+} chains located within tunnels of the manganese–oxygen framework. Both sublattices have a tetragonal symmetry and the following parameters: $a \approx 18.2$ and $c \approx 2.8$ Å for Mn and $a \approx 18.2$ and $c \approx 4.6$ Å for Ba. The manganese sublattice comprises double columns of edge-sharing $Mn3O_6$ and $Mn1O_6$

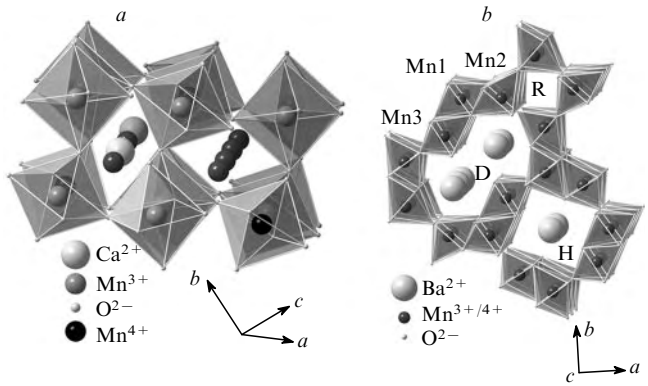

Figure 6. Fragments of the crystal structures of manganites $CaMn_7O_{12}$ (*a*) and $Ba_6Mn_{24}O_{48}$ (*b*).

octahedra and single columns of $Mn2O_6$ octahedra that join the double columns. This results in the formation of double (D), hollandite-type (H) or rutile-type (R) tunnels. Barium cations in the Ba sublattice are partially disordered and can be displaced along the z axis. In addition, barium cations located in the D-type tunnels form domains with a characteristic size of a few nanometres.

The Mössbauer spectra of $CaMn_{6.86}Fe_{0.14}O_{12}$ recorded at 300 K are superpositions of two doublets with similar chemical shifts;[122] small quadrupole splittings of both components confirm that all Fe probe atoms occupy octahedral positions. The Mössbauer spectrum of $Ba_6Mn_{23.76}Fe_{0.24}O_{48}$ is more complicated and can be described as a superposition of four doublets with different quadrupole splittings and equal contributions.

Because the Fe probe atoms have the same oxidation state (+3), both types of the Mössbauer spectra of manganites can be described using a model of continuous distribution of the electric field gradient, P (Fig. 7).[122] A symmetric narrow distribution obtained for $CaMn_7O_{12}$ indicates that the Fe^{3+} cations occupy positions with similar quadrupole splittings and have nearly identical nearest environments. In contrast to the flexible, readily deformable $CaMn_7O_{12}$ framework comprised of vertex-sharing octahedra, the octahedra in the $Mn1O_6-Mn3O_6$ unit of $Ba_6Mn_{24}O_{48}$, which confine the D- and H-type tunnels, are joined rigidly; as a result, distortions typical of these units are imposed on the probe atoms.

The composite structure of $Ba_6Mn_{24}O_{48}$ and the charge redistribution due to specific features of the distribution of barium cations lead to additional local distortions (see Fig.7 *b*).[122] Because of this, the Mössbauer spectrum of $Ba_6Mn_{24}O_{48}$ is best described using the model of continuous distribution of the electric field gradient; the distribution curve exhibits two broadened peaks whose positions correspond to the quadrupole splittings of the ^{57}Fe probe atoms that replace the manganese atoms in the double and single columns. Thus, parameters of spectral components of the Mössbauer spectra are strongly dependent on distortions of polyhedra in the starting structure and are governed by the fashion in which the polyhedra are connected and by the cation distributions within the framework cavities.

Unique information, which can be obtained by analysing the Mössbauer spectra, also concerns some features of the magnetic ordering in these systems. Most of Mössbauer spectroscopy studies of manganites were carried out using $R_{1-x}A_xMnO_3$ phases. The main goal was to investigate their magnetotransport properties as a function of the Mn^{3+}/Mn^{4+} ratio which varied by changing the type and amount of the divalent cation inserted into the perovskite structure.[129–133] Because manganese and iron have similar ionic radii, replacement of Mn^{3+}/Mn^{4+} by Fe^{3+} in the CMR manganites leaves the unit cell parameters almost unchanged but affects the Mn–O–Mn angle, which in turn influences the exchange interaction. Nevertheless, by doping with iron one can obtain information on the localised spin moment in the magnetic ordering region. Establishment of the role of structural distortions in the temperature-induced variations of the magnetotransport properties is also of great importance;[129, 130] therefore, Mössbauer spectroscopy studies allow one to obtain valuable information on specific features of the physical properties of manganites.

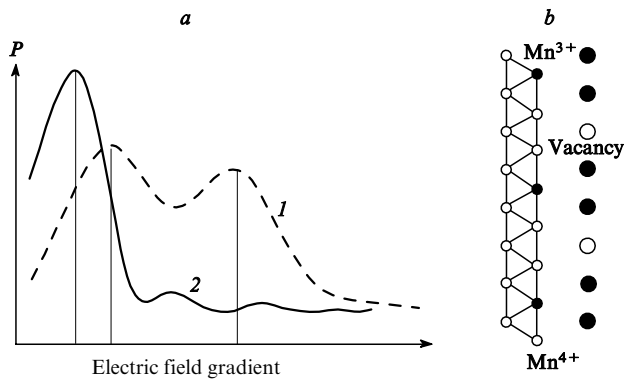

Figure 7. Mössbauer spectra of $Ba_6Mn_{23.76}{}^{57}Fe_{0.24}O_{48}$ (*1*) and $CaMn_{6.86}{}^{57}Fe_{0.14}O_7$ (*2*) samples processed using a model of continuous distribution of electric field gradient (*a*) and a scheme of local changes in the oxidation state of manganese in the case of incomplete filling of tunnels by barium ions (*b*).

IV. Chemical properties and phase diagrams

Difficulties in fabrication of manganite and especially HTSC materials are associated with complex chemical compositions and structures of these compounds (in some cases this is responsible for their thermal and chemical instability). Phase relations in the cuprate and manganite systems depend, in particular, on the size of the cations present in the framework formed by the manganese–oxygen or copper–oxygen polyhedra and on the existence of solid solutions with heterovalent substitution (Figs 8–10).

The $CaMn_2O_4-MnO_x$ polythermal section of the system Ca–Mn–O is characterised by the presence of a large number of phases with different $CaO:MnO_x$ ratios (1:2, 1:3, 1:7 and 1:8; adapted using the data taken from Ref. 134). It was shown [135] that the phase relations in the $BaO-MnO_x$ system are strongly different from those found in the $CaO-MnO_x$ system and the existence regions of compound $Ba_6Mn_{24}O_{48}$ and hollandite $Ba_{2-x}Mn_8O_{16}$ were also determined (see Fig. 8). Thus, changes in the ionic radii of alkaline-earth metal cations (Ca^{2+} or Ba^{2+}) lead to significant changes in the phase relations.

A scheme of phase relations for the polythermal section $CaMn_7O_{12}-CaCu_3Mn_4O_{12}$ of the system Ca–Mn–Cu–O is shown in Fig. 9.[20] The solid solution $CaCu_xMn_{7-x}O_{12}$ with a different degree of substitution ($0 \leqslant x \leqslant 1.5$) is formed in the temperature interval $750 \leqslant T \leqslant 1060$ °C. The highest degree of substitution ($x = 1.5$) is achieved at ~850 °C, whereas the $CaCuMn_6O_{12}$ phase ($x = 1$) exists in a broad temperature range from 750 to 1000 °C. At ~1060 °C, the complex oxide $CaMn_7O_{12}$ decomposes into marokite $CaMn_2O_4$ and hausmannite Mn_3O_4. At 750–1050 °C, the $CaCu_xMn_{7-x}O_{12}$ solid solution with the maximum degree of substitution is in equilibrium with $CuMn_2O_4$ and CuO.

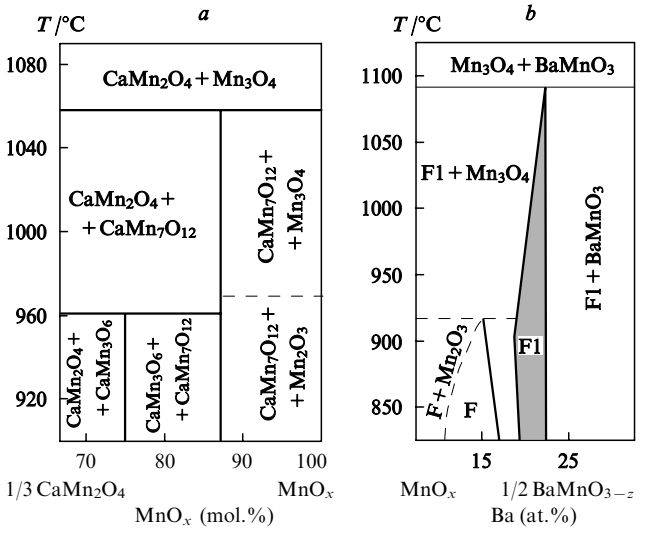

Figure 8. Polythermal section $CaMn_2O_4-MnO_x$ (*a*) and a scheme of phase relations in the system Ba–Mn–O (*b*).
$p_{O_2} = 1$ (*a*) and 0.21 atm (*b*).

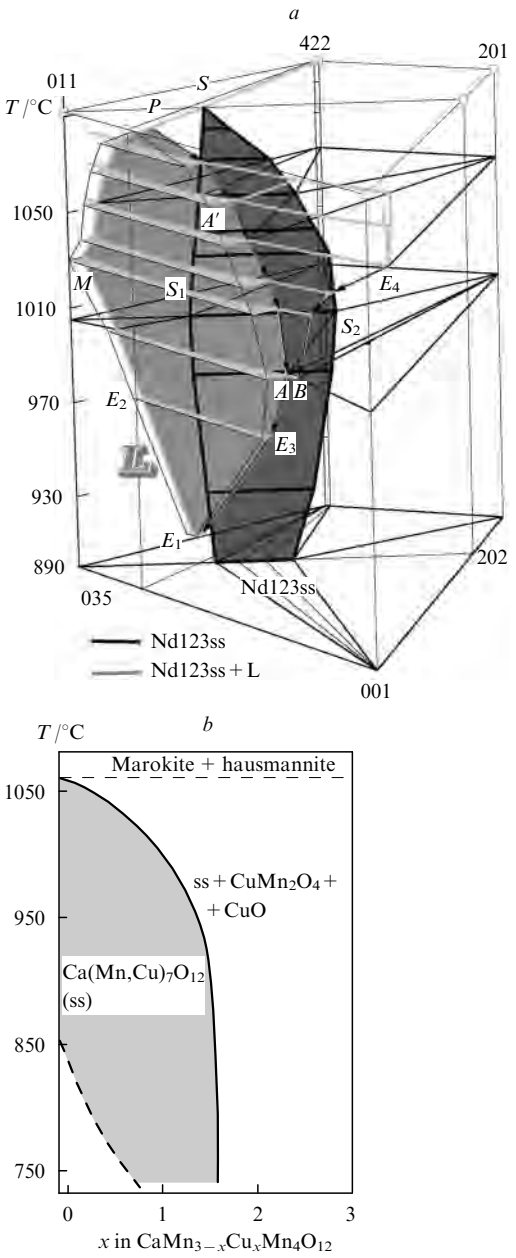

Figure 9. Three-dimensional model for phase relations in the $NdO_{1.5}$–BaO–CuO_x system at $p_{O_2} = 0.21$ atm (*a*) and a scheme of $CaMn_7O_{12}$–$CaCu_3Mn_4O_{12}$ polythermal section at $p_{O_2} = 1$ atm (*b*). The region of the $Nd_{1+x}Ba_{2-x}Cu_3O_z$ solid solution (S_1SS_2 is the high-temperature bound of the stability region) is shown by dark grey and the fraction of the liquid surface, which is in equilibrium with the solid solution phase ($E_1E_2MPA'AE_3$), is shown in light grey. Connodes for the two-phase region (solid solution – melt) are not shown. A and B are the points of peritectic decomposition of the limiting solid solution (Nd123ss + Nd_2CuO_4 + L) and the Nd_2CuO_4–CuO–(BaO) eutectic, the point A′ corresponds to passage from the equilibrium Nd123ss + 201 + L to the equilibrium Nd123ss + 422 + L; E_1, E_4 are eutectics in the binary systems $BaCuO_2$–CuO and Nd_2CuO_4–CuO, respectively.

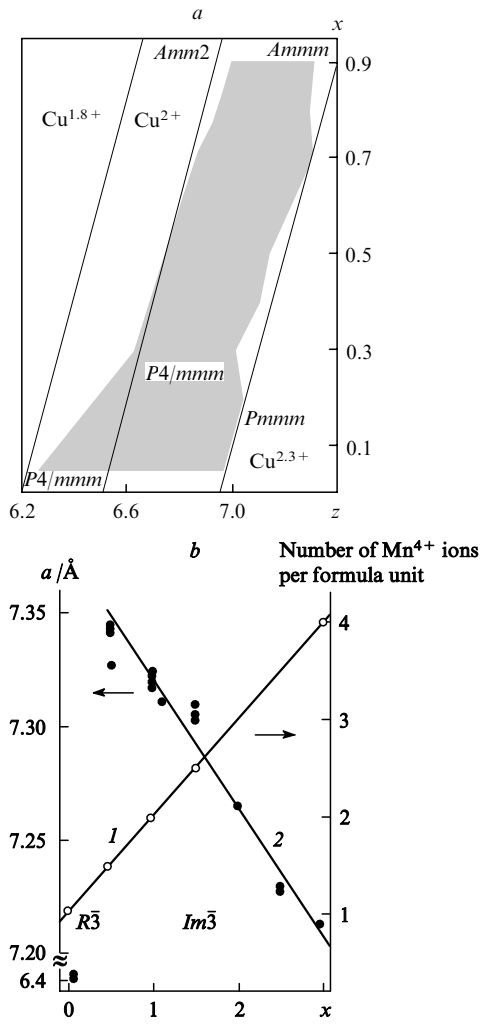

Figure 10. Average oxidation states of copper as functions of the cation and anion compositions of the $Nd_{1+x}Ba_{2-x}Cu_3O_z$ solid solution (*a*); dependences of the average oxidation state of manganese in the $CaCu_xMn_{7-x}O_{12}$ solid solution upon replacement of Mn^{3+} by Cu^{2+} (*1*) and of the lattice parameter (*2*) on *x* (*b*). The region of existence of the solid solution within its cationic and anionic composition ranges is shown in grey. Shown are the space groups of symmetry of the phases.

Phase relations in the supersolidus regions of the systems containing transition elements can be illustrated [4, 5, 136] taking the family of HTSC cuprates $RBa_2Cu_3O_z$ as an example (see Fig. 9). When considering the systems R_2O_3–BaO–CuO_n–O_2, the following deserves particular attention: the partial pressure of oxygen (especially in the coexistence regions of the solid and liquid phases) [137, 138] and the possibility of formation of substitutional solid solutions in which barium atoms are replaced by REE atoms due to rather large ionic radii of the early REE (La, Pr, Nd, Sm, Eu, Gd). For instance, the existence region of the solid solution $Nd_{1+x}Ba_{2-x}Cu_3O_z$ has a 'classical shape' and the limiting phases of compositions 123 and 213, $-0.1 < x < 1.0$ (see Fig. 9 *a*), are characterised by peritectic melting and a maximum decomposition temperature [5, 136] achieved at $x \approx 0.1$. Equilibria with the liquid phase in the solid solution – melt region and reasons for changes in the types of secondary phases ($Nd_4Ba_2Cu_2O_{10}$ and Nd_2CuO_4) formed in the course of peritectic decomposition have been studied in detail. [4, 136–140]

A good example of thoroughly studied materials with a broad region of cation and anion homogeneity is provided by HTSC cuprates (see Fig. 10 *a*). The existence region of solid solutions can be divided into three regions. [4, 136, 137, 141] Compounds with $0 < x < 0.3$ have tetragonal unit cells after quenching and orthorhombic unit cells after oxygenation, the unit cell constants *a* and $c/3$ ($a < c/3$) monotonically decrease as Ba^{2+} ions are replaced by ions with smaller radius (Nd^{3+}). At $0.3 < x < 0.6$, the unit cell is always tetragonal irrespective of the oxygen content ($a \approx c/3$). At $0.6 < x < 0.9$, the phase has an orthorhombic unit cell due to superstructural ordering of neodymium and barium ions. Interrelation between the cation and anion ordering was confirmed by the T–x–z-diagrams. [137] The range of the average oxidation

states of copper in the solid solution varies in accord with the concentration phase transitions; the lower the degree of substitution, the broader the range (see Fig. 10 *a*).

In the $Ca(Mn,Cu)_7O_{12}$ solid solution an increase in the degree of substitution of copper(II) for manganese(III) causes a reduction of the upper bound of the stability region of the solid solution from 1060 to ~950 °C (see Fig. 9 *b*) due to an increase[20] in the Mn^{4+} content (see Fig. 10 *b*). The lattice constant of the cubic solid solution (space group $Im\bar{3}$) decreases obeying the Vegard law (see Fig. 10 *b*). This is consistent with the heterovalent substitution of Mn^{3+} ions for Cu^{2+} ions, which causes an increase in the Mn^{4+} content in the phase and, hence, a decrease in size and in degree of distortion of the manganese–oxygen framework. Thus, the oxidation states of copper and manganese play the key role in stabilities of cuprate and manganite phases.

V. Single crystals

Construction of phase diagrams is an important stage in experimental studies of the growth of single crystals. Cuprate and manganite single crystals with preset chemical homogeneity, size, shape, concentrations of defects and impurities (Figs 11 and 12) are necessary for both basic and applied research and, in particular, for studies on crystallisation mechanisms of multicomponent melts. The advantage of these single crystals is the possibility of investigating the anisotropy of properties on different crystal faces. This is widely used in structural analysis, spectroscopy, oxygen diffusion studies, atomic force microscopy, in the determination of fundamental physical constants,[4] *etc*.

Single crystals of HTSC materials were obtained using almost all known melt growth techniques modified to allow for specific features of HTSC:[4, 138, 142–147] spontaneous crystallisation from solution in melt, Bridgman method, zone melting and the Kyropulos and Czochralski methods (see Fig. 11). Distinctive features of most of them are multicomponent composition of crystallising systems and a variety of interfacial interactions.[4] The mechanisms of crystallisation and growth of faces of HTSC crystals in different crystallographic directions seem not to be specific to the systems in question, being also different for each method mentioned above. The most commonly encountered growth mechanisms are the Frank–Kabrer mechanism and layer-by-layer growth.[4]

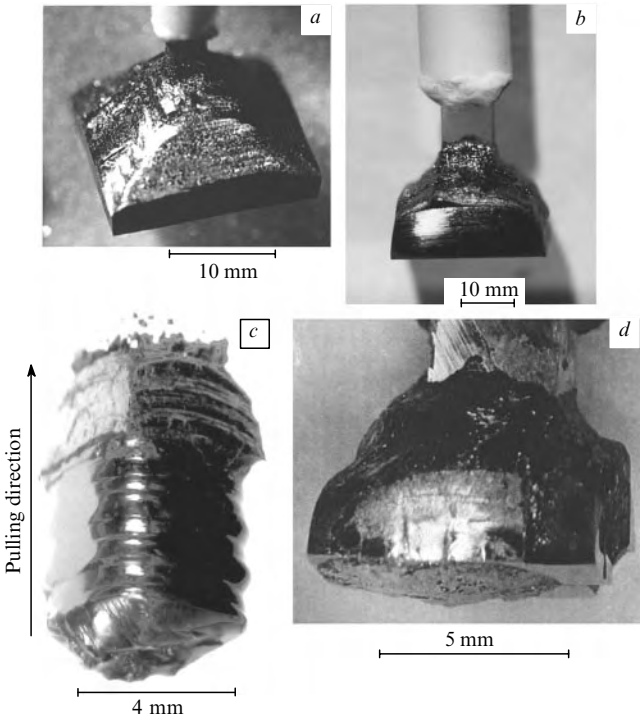

Figure 11. Photographs of the crystals of mixed REE–barium cuprates of different compositions grown using the modified Czochralski method (courtesy of Prof. Y Shiohara, SRL ISTEC, Japan).[142–145] One of the largest superconducting $NdBa_2Cu_3O_7$ crystals (*a*); large superconducting $YBa_2Cu_3O_7$ crystal grown using the modified Czochralski method (*b*); a cylindrical crystal of the superconducting phase $YBa_2Cu_3O_7$ grown in an automated growth setup (*c*); and a $Nd_{1.85}Ba_{1.15}Cu_3O_7$ crystal possessing a semiconductor-type temperature dependence of resistance (*d*).

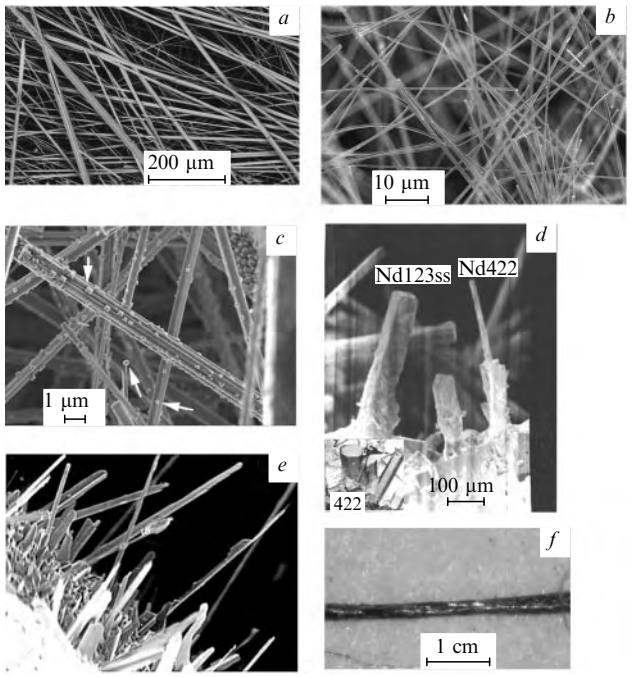

Figure 12. Micrographs of cuprate and manganite whiskers.
Hollow hollandite whiskers ($Ba_{2-x}Mn_8O_{16}$) obtained by isothermal evaporation of chloride fluxes (*a*); $Ba_6Mn_{24}O_{48}$ whiskers with a tunnel structure oriented along the growth direction, obtained by isothermal evaporation of KCl (*b*); the same crystals after storage in molten $LiNO_3$ at 300 °C (ion exchange causes replacement of barium in the channels by lithium; the arrows show octahedral spinel Li_2MnO_4 crystals oriented along the etching pits of the whiskers) (*c*); high-temperature superconducting $Nd_{1+x}Ba_{2-x}Cu_3O_z$ and $Nd_4Ba_2Cu_2O_{10}$ whiskers formed in the polythermal regime; superconducting $Bi_2Sr_2CaCu_2O_8$ whiskers (*e*) and a wire prepared by pulling of the glue mass containing $Ba_6Mn_{24}O_{48}$ filaments (*f*).

Anisotropy of the rate of growth of mixed REE–barium superconducting cuprates along the main crystallographic directions depends on the REE type and on crystallisation conditions in a very complicated manner.[4] This can be due to the crystallographic anisotropy, different energies of crystal faces and different growth mechanisms; the anisotropy of growth also causes changes in the face morphology and crystal habit (see Fig. 11). For instance, crystals grown by spontaneous crystallisation usually have a shape of thin plates with the smallest thickness along the ⟨001⟩ direction, because at high cooling rates ('kinetic control') the growth rate of the {100} faces is nearly five times higher than the growth rate of the {001} faces. A decrease in the melt cooling rate down to 0.5–1.0 deg h^{-1} causes the formation of thick prisms-parallelepipeds and even isometric crystals. Under these conditions not only the {100}, {010} and {001} faces but also the {101}, {011} and {111} faces grow, *i.e*., the crystal grows under thermodynamic control.

The method of top-seeded crystal pulling from a supercooled melt is characterised by rather low supersaturations; here, an important role is played by the hydrodynamic conditions and the temperature and concentration distributions near the growing crystal.[142, 143] By controlling the pulling rates and growth aniso-

tropy it is possible to grow various 'bulk' single crystals including pyramidal crystals with extending base, large isometric crystals with small edge angularity, pyramidal crystals with 'concave' low face and cylindrical crystals (see Fig. 11). Other crystallisation techniques allow growth of single crystals in the form of needles, plates and parallelepipeds.[4,5]

Considerable advances have been made in the field of single-crystal growth due to the development of a method of continuous growth of mixed REE–barium cuprate crystals,[142] in which the growing single crystal is fed under steady-state conditions owing to separation of the crystal growth zone ($T < T_p$) and the Y_2BaCuO_5 dissolution zone ($T > T_p$, T_p is the peritectic temperature) by a melt layer. In the presence of a temperature gradient (~ 3 deg cm^{-1}), diffusion and convective transport of yttrium-saturated melt occurs across this layer. To prevent the crystal contamination with the crucible material, crucibles made of yttria (generally, an REE oxide) are often used. Growth of Nd123 single crystals by the modified Czochralski method is performed in the presence of small temperature gradient.[143,144] Because of much higher solubility of neodymium oxide in the melt here we deal with isothermal crystal growth from supercooled melt in a crucible made of neodymium oxide. The modified Czochralski method is versatile and allows one to grow single crystals of almost all R123 (R = Y, Nd, Sm, Pr) phases and $(R^1R^2)Ba_2Cu_3O_z$ (R^1 = Y, R^2 = Sm, Nd), $Nd_{1+x}Ba_{2-x}Cu_3O_z$, $Pr_{1+x}Ba_{2-x}Cu_3O_z$, $Nd_{1+x}Ba_{2-x}Cu_{3-y}Ga_yO_z$, $YBa_2Cu_{3-y}Zn_yO_z$, *etc.*, solid solutions.[4,143] Using the floating zone technique, superconducting Pr123 crystals were obtained at reduced partial pressure of oxygen.[148] Recently, considerable attention has been paid to the development of methods of preparation of single-crystalline HTSC 'whiskers' (see Fig. 12).[149–152] These crystals can possess unique electrophysical and mechanical properties.

Experimental difficulties in growing manganite single crystals are caused by high melting temperatures of these compounds (~ 2000 °C) and low solubility in conventional high-temperature solvents. In most cases this problem is solved using an IR heated floating zone technique[153] because it excludes the interaction between the crystal and the container material. To grow manganite crystals, it is necessary that the feed rod have the same density along the whole length and homogeneous composition. The feed rods are produced by hot pressing and sintering appropriate components at ~ 1100 °C. This allows one to avoid melt penetration into pores of the sample (due to the capillary effect) and to stabilise the melt composition in the growth zone. The seeds used are both dense polycrystalline samples and pre-oriented single crystals. For instance, $La_{1-x}A_xMnO_3$ (A = Sr, Ca; $x = 0-0.3$), $Nd_{0.7}Sr_{0.3}MnO_3$, $La_{0.5}Ca_{0.5}MnO_3$ and $Nd_{1-x}(Sr,Pb)_xMnO_3$ rods (crystals) nearly 5 mm in diameter are usually grown at a growth zone rate of 5 to 7 mm h^{-1}. The floating zone method is also efficient for growth of single crystals of the Ruddlesden–Popper phases[154] possessing highly anisotropic properties due to their structural features. At the same time this technique is unsuitable for the synthesis of manganites $R_{1-x}A_xMnO_3$ (A is an alkali metal) owing to high volatility of A_2O oxides and of thermally unstable phases related to pyrolusite MnO_2 and hollandite.

Using traditional spontaneous crystallisation technique, it is possible to grow alkaline-earth manganite crystals. For instance, isotropic $Ln_{1-x-y}Sr_xPb_yMnO_3$ (Ln = La, Pr, Nd) crystals with a volume of up to 3 cm^3 are obtained using Bi_2O_3, PbF_2 and PbO as fluxes. $Sr_4Mn_3O_{10}$ crystals were flux grown with $SrCl_2 + SrF_2$.[155] An alternative to spontaneous crystallisation is electrolysis of manganite solutions in a molten mixture of Cs_2MoO_4 and MoO_3 using platinum electrodes in crucibles made of stabilised zirconia.[156] This technique was employed to obtain plate-like, strontium-doped lanthanum manganite crystals with a surface area of 0.25 to 4 mm^2. The temperature of the process was reduced to 1000 °C (alkali metal doped manganite crystals grow at 980–1000 °C).

Often, crystals of metastable or thermally unstable phases, *e.g.*, $BaMnO_3$, $BaMn_2O_3(OH)_2$ and $BaMn_3O_3OH$ are grown using the hydrothermal method.[112,157] This permits preparation of manganites with tunnel structures (pyrolusite, ramsdelite, hollandite and todorokite, see Fig. 2) starting from a layered manganite with the structure of sodium-containing birnessite treated with LiCl, KCl, $MgCl_2$ or $BaCl_2$ solutions; the size and shape of tunnels in the structure depend on the type of the cation inserted.[12]

MnO_2 and Mn_3O_4 nanowires were grown using hydrothermal method or microemulsions.[158,159] A simple method called isothermal evaporation of chloride fluxes was developed[135] to obtain filaments of potentially one-dimensional superionic conductors $BaMn_8O_{16}$ and $Ba_6Mn_{24}O_{48}$ with tunnel structures (see Fig. 12). The method not only provides a means of transportation of the components required for crystal growth by the 'vapour–liquid–crystal' mechanism but also allows an important problem of selection of the crystals obtained from solvent (flux) to be solved. The optimum temperature for growth of $Ba_6Mn_{24}O_{48}$ crystals from KCl is 950 °C. At $T < 900$ °C, an impurity of hollandite whiskers was always observed, while at $T > 950$ °C, hausmannite was formed, which is consistent with the phase diagram (see Fig. 8 *b*). Within the limits of experimental error for local X-ray spectroscopic analysis the crystals obtained were chemically homogeneous along the length and contained less than 1 at.%–2 at.% of flux components (K, Cl). These phases with anisotropic unit cells were also observed in the form of (i) 'pseudo-single-crystalline' whiskers with small-angle boundaries, (ii) hollow needles, (iii) dendrites and (iv) 'bundles' (see Figs 12 *a–c*). The $Ba_6Mn_{24}O_{48}$ whiskers were 1 to 5 μm thick, the hollandite whiskers were somewhat thicker ($\sim 20-50$ μm).

VI. Microstructure and new methods of preparation of ceramic composites

Methods of fabrication of polycrystalline materials with improved functional properties are based on the concept of a real structure characterised by a number of hierarchic levels of organisation.[5] As shown above, the fundamental properties of compounds are determined by the crystal structure and its local distortions. Individual crystallites comprised of certain units separated by extended defects form the mesoscopic level of structural organisation. The macroscopic level is formed by ensembles of crystallites and pores.

Superconducting phases with controllable superconducting transition temperature can be synthesised in a different manner.[5] At the same time improvement of such important characteristics of superconducting materials as the critical current density, J_c, and its stability in high magnetic fields faces reasonable difficulties. The superconducting transition temperatures of HTSC ceramics much exceed those of metallic superconductors while the coherence length of ceramics (0.2 nm) is an order of magnitude smaller than that of intermetallides. The thickness of grain boundaries in polycrystalline HTSC ceramics is greater than the coherence length; therefore, the magnitude of current flowing along the ceramic samples is strongly dependent on the intergrain contacts. In addition, layered crystal structures of almost all high-temperature superconductors cause their physical properties to be highly anisotropic; this requires texturing of polycrystalline materials. High-temperature superconductors are type II superconductors; therefore, under some conditions the external magnetic field can penetrate into the bulk of a sample in the form of Abrikosov vortices trapped in non-superconducting inclusions (pinning centres).[5,160] To achieve high critical current densities (greater than 10^5 A cm^{-2}) and stabilise them in the magnetic fields of 1 to 10 T, one should create efficient pinning centres, which is a practically important problem in the materials science of HTSC.

The magnetoresistance, as the phenomenon of relative change of electrical resistance in an external magnetic field, has long been known.[9–11] Intrinsic magnetoresistive effects are due to the properties of a particular compound; the tunnelling magnetoresistive effects are related to the specific features of interfaces and

various natural or artificial inhomogeneities. A commonly accepted model for the mechanism of intrinsic magnetoresistance involves the concept of double exchange first proposed by Ziner,[161] which has been successfully used to explain the magnetoresistance effect in $R_{1-x}A_xMnO_3$ solid solutions. The experimentally observed magnetoresistance is also explained by the influence of additional factors, in particular, the electron–phonon interaction and dynamic Jahn–Teller effect for Mn^{3+} (see Ref. 162). A model by Millis, Littlewood and Shraiman [163] includes local rearrangement of the crystal lattice, because hopping of charge carriers between the lattice sites occupied by the manganese ions produces a charge fluctuation and the charge carrier in the crystal becomes a charged magnetoelastic polaron.

The model of double exchange is inapplicable to pyrochlore-type manganites and cupromanganites [16–19, 114] because of the absence of the Mn^{3+} ions or large deviation of the Mn–O–Mn angle from 180°. In this connection alternative models for description of the CMR phenomemon have been developed. These are, *e.g.*, the magnetic impurity theory [164] and a model based on the concept of one-electron σ-bonding between the manganese and oxygen ions due to high covalency of the manganese–oxygen bond, which leads to the formation of a strongly correlated electronic state.[165]

The intrinsic magnetoresistance of polycrystalline materials is only a part of the total magnetoresistance. Indeed, in most of these materials the magnetoresistance effect manifests itself in wide temperature and magnetic field ranges rather than near the Curie point in high magnetic fields. In this connection the existence of the tunnelling magnetoresistance was hypothesised.

Peculiarities of the microstructural organisation of polycrystalline materials (see above) make traditional methods of solid-phase synthesis of cuprates and manganites inefficient for fabrication of materials with good operating characteristics. Hence, it was reasonable to elaborate new methods of synthesis of cuprates and manganites, *e.g.*, techniques involving mechanically activated reactants [166] and melt technologies [5, 160] permitting an integrated treatment of the real structure of a material.

A method of fabrication of $RBa_2Cu_3O_z$-based superconducting materials (Fig. 13) at record low temperatures (500–600 °C) during unique short reaction times (10–30 min) was proposed.[166, 167] The starting reactants were [166] copper(I) oxide obtained using 'soft' chemistry methods and a mixed oxide '$YBa_2O_{3.5}$' (containing BaO_2). Both compounds were mechanically activated in a ball mill and then 'warm' pressed at 250 °C. A feature of the technique is the use of oxides as reactants which react without liberation of gaseous products that could break the intergrain contacts in the reaction mixture. In addition, the mixed REE–barium oxide is a source of the yttrium and barium ions with low diffusion mobilities, whereas the copper(I) oxide is a source of the copper ions characterised by higher diffusion coefficients. Different reactants contain different cations; this provides high chemical potential gradients of the components, unambiguous direction of the diffusion processes in the system and, by and large, a high driving force of the formation of a superconductor. Pilot experiments were carried out on fabrication of superconducting aluminum-sheathed tapes with an oxide wire which becomes a superconductor ($T_c \approx 45–85$ K) after low-temperature synthesis at 600 °C using a procedure of mechanical activation of 'two-powder' precursors proposed in Ref. 166.

To prevent reduction of manganese to an oxidation state lower than +3 in the synthesis of a family of manganites, high oxygen pressure is required. For instance, phases in the system Ca–Mn–Cu–O are usually synthesised under oxygen pressures of 0.18–50 000 atm in sealed quartz ampoules or autoclaves.[16–18] The use of mechanically activated reactants, which is similar to that described above for the HTSC phases,[20] appeared to be efficient for the synthesis of cupromanganites. Clearly, pressing of mechanically activated powders at elevated temperatures (250–400 °C) to a great extent promotes a subsequent solid-phase reaction and permits the obtaining of complex manganese oxides

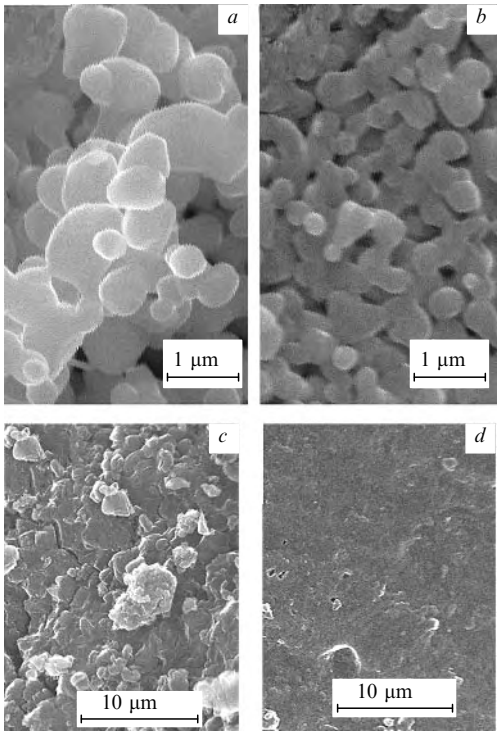

Figure 13. Changes in the morphologies of the ceramic samples of CMR manganites $CaCuMn_6O_{12}$ (*a*, *b*) and HTSC cuprates $YBa_2Cu_3O_z$ (*c*, *d*) obtained using mechanically activated reagents pressed at 250 °C. Duration of mechanical activation of the phases, min: 15 (*a*, *c*) (pressing under different loads), 120 (*b*) and 240 (*d*).

in the form of ceramics (see Figs 13 *a*,*b*) with improved magnetotransport properties at so low temperatures that Mn(IV) appears to be stable at a standard partial pressure of oxygen $p_{O_2} = 0.21–1$ atm.

Microstructural features have a strong effect on the transport properties of HTSC ceramics;[4, 5] this is also characteristic of manganites and cupromanganites. In spite of the fact that the CMR is intrinsic in mixed-valence manganites, a decrease in the grain size can make the role of the grain boundaries more important and favour charge transport due to the spin-polarised intergrain tunnelling. This can provide an explanation for 200% to 300% variation of the magnetoresistance of samples of the same composition $CaCuMn_6O_{12}$, which were synthesised under the same conditions but had different microstructures (Fig. 14).

Melt techniques have provided the best route to HTSC-materials.[4, 5] A feature of the melt-produced, coarse-grained HTSC ceramics is the presence of ensembles of pseudo-single-crystal domains of size 0.5 to 5 cm. Each domain is an aggregate of $RBa_2Cu_3O_z$ lamellae (5–50 nm), which are aligned and separated by small-angle boundaries through which electric current can flow. The microstructure of the melt textured HTSC ceramics is characterised by the presence of different types of extended defects such as twin boundaries, highly disperse inclusions of the non-superconducting phase, dislocations, microcracks and macrocracks.

Thus, melt-produced HTSC ceramics can be considered as a system possessing pronounced 'co-operative' superconducting properties due to specific crystallisation mechanisms. Pseudo-single-crystal domains form macroscopic aggregates capable of carrying heavy currents, because at the microstructural level they represent a system with pure superconducting boundaries and biaxially textured crystallites. High concentration of defects favours the formation of efficient pinning centres.

In addition to coarse-grained ceramics (Fig. 15 *a*) modern methods permit fabrication of HTSC-materials of complex

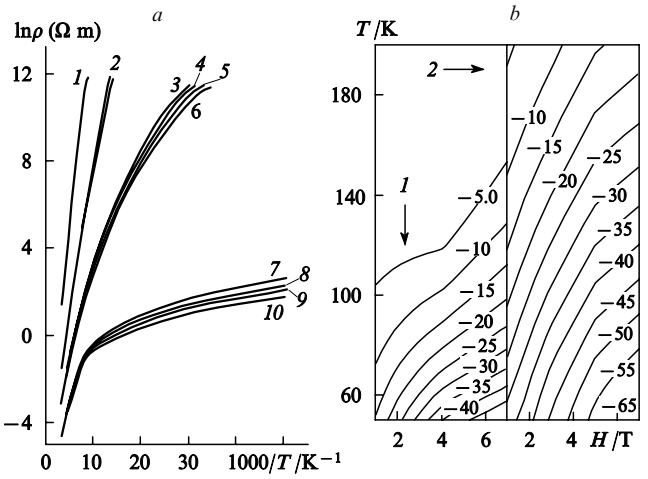

Figure 14. Magnetoresistive properties of the ceramic samples of $CaCu_xMn_{7-x}O_{12}$ solid solutions prepared using mechanically activated reactants (*a*) and the magnetoresistive effect in $CaCuMn_6O_{12}$ samples with different microstructures (*b*).
$x = 0$ (*1*), 0.5 (*2*), 1.0 (*3*–6), 1.5 (*7*–*10*); $T_c = 194$ (*1*–*6*) and 245 K (*7*–*10*); $H = 0$ (*3*, *7*), 1 (*4*, *8*), 3 (*5*, *9*) 5 T (*6*, *10*) (*a*); the microstructures of the samples *1* and *2* are shown in Figs 13 *a* and 13 *b*, respectively; figures in the isolines illustrate the magnetoresistive effect in % (*b*).

shape and(or) in the form of thick-film coatings (Figs 15 *b*–*e*).[168–174] These methods include saturation of a fabric obtained from yttria filaments or a ceramic 'foam' prepared using Y_2BaCuO_5 powder, organic binder and a polymer matrix with high-temperature cuprate melt.[168–173] On cooling of the Y_2BaCuO_5–melt system the non-superconducting REE oxides are transformed in the superconducting mixed REE–barium cuprate due to the reaction with the melt. Introduction of oriented seeds initiates directed crystallisation of the superconducting phase in the form of ceramics, fabric, foam, *etc.* (Figs 15 *b*,*c*). Studies on 'glueing' of individual geometrically matched blocks of dense coarse-grained ceramics into complex structures using mixed REE–barium cuprates, silver-containing and fluorine-containing fluxes with low melting temperatures (Fig. 15 *d*)[174] deserve particular attention. A unique method of directed crystallisation of mixed REE–barium cuprates on metallic substrates in artificially induced concentration gradient of the rare-earth elements was developed [175] (Fig. 15 *e*).

The use of the concentration gradients [175] is an efficient method of control of the crystallite orientations in thick films because of large local supersaturations (supercooling) produced in the system. The entire starting film can be in the form of a layer of a vapour deposited Y_2BaCuO_5 phase, which is then saturated with a melt. A seed strip of a polycrystalline $NdBa_2Cu_3O_z$ powder is arranged along the main layer. On the opposite side, an Yb_2BaCuO_5 strip is arranged to increase the concentration gradient and to preclude the formation of the HTSC phase in the adjacent region.

Cooling of the system after saturation with the melt is accompanied by nucleation of crystallites of the HTSC phase near the seed strip. Similarly to seeds, the HTSC crystallites have arbitrary initial orientations and growth directions. The direction in which crystals grow at the highest rate 'survives', *i.e.*, geometrical selection of crystallites occurs. As a result, the spatial evolution of the whole ensemble of crystallites beyond the transient zone of certain length occurs concertedly along the same direction. Experimental confirmation (see Fig. 15 *e*) of the efficiency of thick film texturing using a concentration gradient opens up great prospects for the development of new technologies of fabrication of highly oriented layers of functional materials with anisotropic properties.

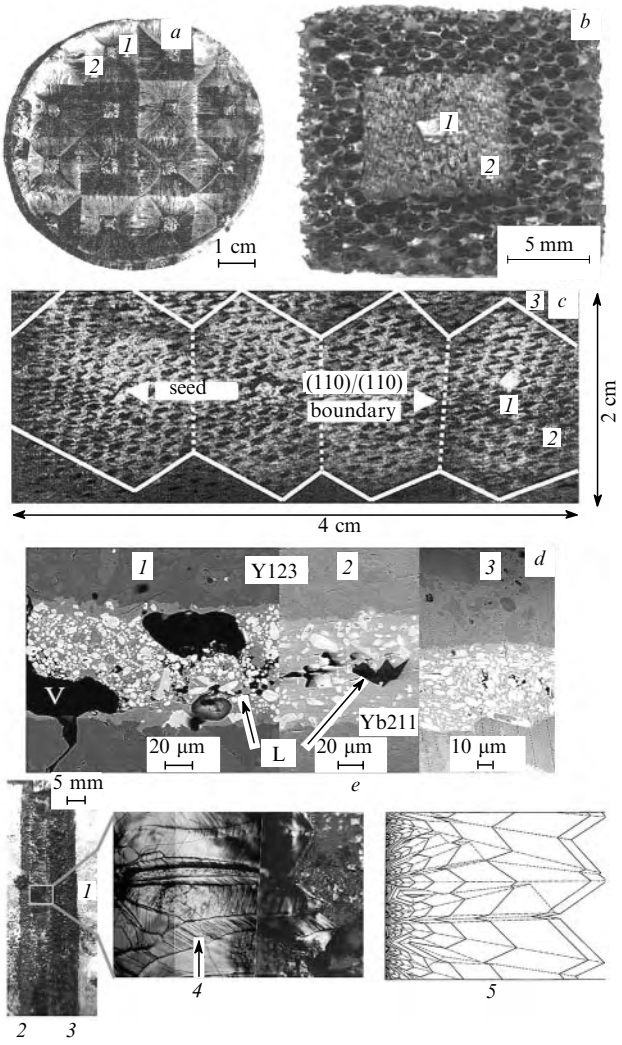

Figure 15. Coarse-grained superconducting samples of melt-solidified mixed REE–barium cuprates (courtesy of Prof. G Schmitz, ACCESS e.V., Germany).
(*a*) $YBa_2Cu_3O_z$ ceramics: mutually oriented $NdBa_2Cu_3O_z$ seed crystals (*1*) and pseudo-single-crystal blocks (*2*); (*b*) superconducting ceramic $YBa_2Cu_3O_z$ 'foam': $NdBa_2Cu_3O_z$ seed crystal (*1*) and pseudo-single-crystal domain (*2*); (*c*) HTSC-samples with a fabric structure obtained by infiltration technique using seeds (*1*), oriented domains (*2*) and a polycrystalline domain (*3*); (*d*) joining of pseudo-single-crystal superconducting mixed REE–barium cuprates using low-melting ytterbium–barium cuprates: polished surfaces of $YBa_2Cu_3O_z$ blocks (*1*); the same with an external pressure of 20 kPa applied (*2*); the same with PtO_2 added to reduce the size of crystallites of the secondary phases (V are structural voids and L is the liquid phase) (*3*); (*e*) spontaneous directed crystallisation in the presence of concentration gradient: substrate (silver–palladium alloy) (*1*); a seed strip of polycrystalline $NdBa_2Cu_3O_z$ with high temperature of peritectic melting, obtained by screen printing (*2*) and an $YbBa_2Cu_3O_z$ or Yb_2BaCuO_5 strip to induce the concentration gradient of the rare-earth element. The rectangle indicates a region of the Y_2BaCuO_5 layer impregnated with the cuprate melt in which crystallites of the superconducting $(Y,Nd,Yb)Ba_2Cu_3O_z$ solution grow on cooling (*3*), general view of superconducting crystallites at higher magnification (*4*) and graphic reconstruction of the grain selection process (*5*).

VII. Geometrical control of mutual orientation of crystallites (graphotexturing)

Modern functional materials (superconductors, piezoelectrics, giant-magnetoresistance materials, *etc.*) are usually characterised by high crystallographic anisotropy of physical properties. Therefore, the desired operating characteristics of a layer can be in some

cases improved by several orders of magnitude due to biaxial texturing. A good example of the texturing effect is provided by mixed REE – barium cuprates, for which an in-plane misorientation of only 5 – 10° can cause a decrease in the density of the intergrain transport current by 10 to 100 times. Texturing of modern functional materials is related to various aspects of crystal growth in complex oxide systems. New methods of preparation of textured HTSC-coatings [176 – 178] include, in particular, the use of artificial relief of the surface of a substrate (graphotexturing, Figs 16 – 19).

At present, of particular interest is fabrication of highly textured coatings on long-length substrates or surfaces of complex shape. This problem has been inufficiently studied because of numerous technical difficulties. Most well-studied methods of deposition of textured thin films involve epitaxy.[5] High absolute values of functional parameters can also be achieved using bulk ceramic materials, which are textured using the temperature, magnetic field or electric field gradients.[4, 5] However, in these cases the specific characteristics of materials are much worse than those of the films due to imperfect texture and the presence of various macroscopic defects. A drawback of epitaxy or gradient crystallisation is that they do not allow fabrication of samples of complex shape due to a complicated procedure for preparation of substrates, which must meet severe requirements (in the case of thin films), and to brittleness of ceramics and difficulties in mechanical treatment of this material (bulk samples).

In this situation a reasonable compromise is to use thick films. To attain high specific and absolute values of the functional parameters of thick films, one should follow a hybrid approach, *i.e.*, the orientation effect of substrate (*cf.* thin films) and melt growth of large grains (*cf.* bulk materials). Unfortunately, the 'molecular' nature of epitaxy makes it efficient only for films less than 1 μm thick while conventional methods of preparation of thick films cannot be used for complete biaxial texturing.[179] In the case of thick films the orientation effect of the substrate must be based on other principles (Fig. 19). Melt crystallisation should also be modified to retain the continuity and shape of the initial layer, which undergoes melting and crystallisation, and to minimise the chemical interaction between the film and substrates.

The appearance of a film texture is a result of two main processes, *viz.*, superficial nucleation characterised by certain arrangement and orientation of seeds owing to short-range molecular fields (saturation of 'uncompensated surface bonds') and/or the motion and mutual adjustment of the 'building blocks' from the nutrient medium due to, *e.g.*, external fields and forces (see Fig. 19). As a consequence, there are two film texturing methods.

The first approach is practically implemented in the form of gas-phase or liquid-phase heteroepitaxy on single-crystalline or biaxially textured substrates. This technique is most widely used for preparation of thin films of new functional materials and heterostructures.[4, 5] However, it has significant drawbacks such as a complicated film deposition procedure, poor scaling, low performance, high cost of the deposition procedure and substrates, low deposition rate and impossibility of film deposition on two-sided items of complex shape. These drawbacks are typical of even the most recently developed methods, such as the Ion Beam Assisted Deposition (IBAD), Rolling Assisted Biaxially Textured Substrate (RABiTS) and Inclined Substrate Deposition (ISD) techniques.[180]

The second approach is independent of the substrate nature and, similarly to texturing of ceramics, does not use external factors such as thermal or magnetic field gradients and single seeds or multiseeds (see Fig. 19). Because of this, it imposes virtually no limitation on the film thickness. Usually, practical implementation of this approach requires a condensed medium, *e.g.*, a melt or a solution, to provide high thick film growth rates. The scaling problem can be solved using the principles of self-organisation or self-assembly of polycrystalline layers of multicomponent functional materials, which permit simultaneous mutual correlated

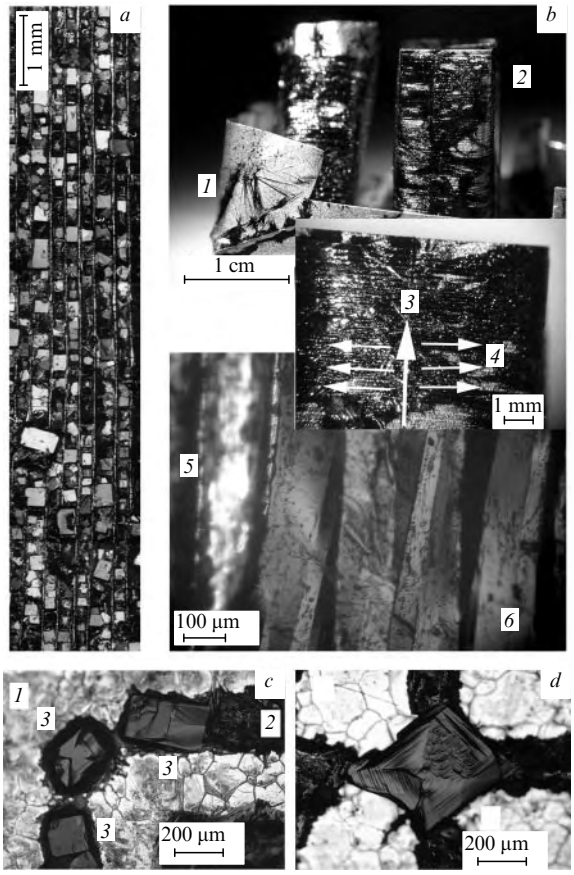

Figure 16. Micrographs of graphotextured HTSC phases.
(*a*) Biaxial texturing of polycrystalline yttrium – barium cuprate layer owing to the use of symmetrical surface relief: nearly 75% of 220 crystallites are oriented with respect to periodic striped relief (and to one another) due to nucleation near the relief elements;
(*b*) biaxially textured HTSC $Bi_2Sr_2CaCu_2O_8$ samples fabricated using silver tapes with artificial surface relief: a silver bath containing a peritectic melt of the HTSC phase (*1*), a cylinder coated with a textured HTSC layer (*2*), vertical grooves that help the melt to move upwards across the surface of the sample due to the action of capillary forces (*3*), horizontal grooves to provide (i) spillover of the melt across the surface and (ii) mutual orientation of the HTSC grains during crystallisation (*4*), a groove (*5*), ensemble of oriented crystallites (*6*);
(*c*) screen printing on silver substrate (*1*) with necessary surface structure (*2*) using an Y_2BaCuO_5 suspension followed by melt infiltration. Yttrium – barium cuprate crystallites formed on cooling (*3*) reproduce the pattern of the elements of the initial surface relief;
(*d*) surface relief (rectangular grid), which favours spontaneous formation of ⟨110⟩-oriented crystallites of mixed REE – barium cuprates (*4*).

growth on all portions of the ribbon surface. At present, these ideas are also used in nanotechnology, namely, self-assembling of monolayers causing a spontaneous formation of complex structures from the necessary building blocks; the phenomenon involves different-level energy interactions and imposition of limitations upon certain degrees of freedom of the system.[179] Research in the field of semiconductor engineering is aimed at using 'orientation filters' of the growing grains to control their growth in the desired direction.[181]

Artificial epitaxy (graphoepitaxy) was proposed nearly four decades ago for organic crystals and a number of semiconductors.[182] The method is based on the orientation effect of a microrelief created on the surface of a substrate. The relief is characterised by a certain symmetry and a period that can be several orders of magnitude greater than the lattice constant of the material. Therefore, crystals can be 'forced' to adopt a necessary

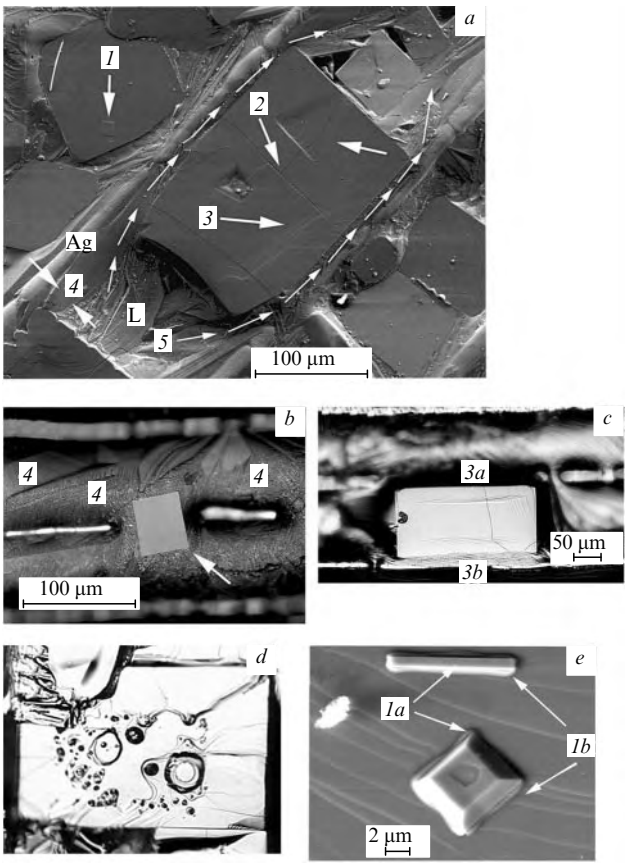

Figure 17. Micrographs of graphotextured mixed REE–barium cuprates.
Orientation of crystallites by the relief walls (*a*), a mobile crystallite solidified from melt in the early stage of growth (*b*), immobilisation of crystallite near the wall (*c*), face growth morphologies (*d*,*e*).
Notations: (*1*) barium cuprate on a crystallite face of mixed REE–barium cuprate, which interacts with growth steps (*1a*,*b*); (*2*) cracks; (*3*) (*3a*,*b*) growth steps moving from the periphery towards the centre in the case of capillary flow of the melt near the meniscus (*4*) between the relief walls and the crystallite [the direction of motion of the liquid phase, L, is shown by arrows (*5*)].

orientation by imposing necessary geometrical constraints on their growth. A few communications have been reported concerning the use of specific substrates, 'atomic' graphoepitaxy or application of photolithography for creation of the surface microrelief and influence of defects in the substrate on the morphology of HTSC films on polycrystalline silver.[183–185] Graphoepitaxy is efficient only for thin layers ($\sim$1 μm) and, correspondingly, only for small crystallites of size nearly 1 to 10 μm, whose orientation can be effectively controlled using methods of conventional thin-film epitaxy.

Optimisation of the deposition techniques and heat treatment regimes suitable for biaxial texturing of thick HTSC films has been the subject of recent studies.[176–178] It was established that the artificial relief must meet the following requirements: it must contain only those most efficient elements, which induce oriented growth of crystallites, and provide specified geometric constraints on the growth of crystallites in the case where the symmetry (habit) of crystallites matches the symmetry of artificial relief elements. Of great importance is also to provide conditions for nucleation near the elements of the artificial relief (otherwise, a reduced efficiency will be attained).

The artificial relief is a controllable parameter, which provides the possibility for crystallisation to occur in the desired direction. The microstructures of the samples (see Fig. 17) can be explained taking into account the effect of the artificial relief of the surface

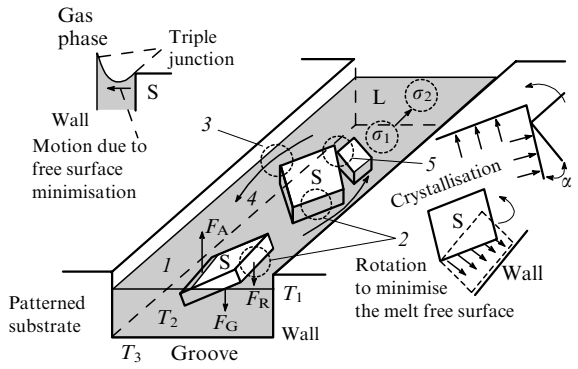

Figure 18. A model for orientation of growing crystallites.
T_1 is the temperature of the substrate surface contacting the gas phase and re-emitting heat, T_2 is the melt temperature inside the artificial relief elements (*1*), T_3 is the temperature in the bulk of the substrate, F_A is the Archimedian force, F_G is the gravity force, F_R is the surface tension force in the melt film (*2*) near crystallites (the resultant force stabilises small crystallites on the melt surface and drives them horizontally), meniscus (*3*), interacting crystallites (crystallisation pressure or a change in the meniscus shape) (*4*, *5*); σ is the surface tension depending on the component concentrations (Marangoni effect).

on the elementary processes occurring in the system on crystallisation, *viz*., nucleation, face growth of individual crystallites and interactions in the ensemble of the growing crystallites.

Elements of an artificial relief, which provides imposition of 'favourable' constraints on the growth of crystallites, are in fact a kind of geometrical template. A static effect of the template disturbs isotropy of the crystallising system and, finally, leads to desired orientation of crystallites in the ensemble. Unfortunately, such a template is a necessary but not sufficient condition for the formation of biaxially textured layers.

Stochastic nucleation and chaotic growth of a large number of crystallites can be among undesired factors, which preclude the growth and(or) motion of those crystallites, which could be oriented due to the effect of the artificial relief. Correspondingly, the number of crystallites per element of the artificial relief depends on both the probability density of nucleation and the characteristic size of the artificial relief elements.

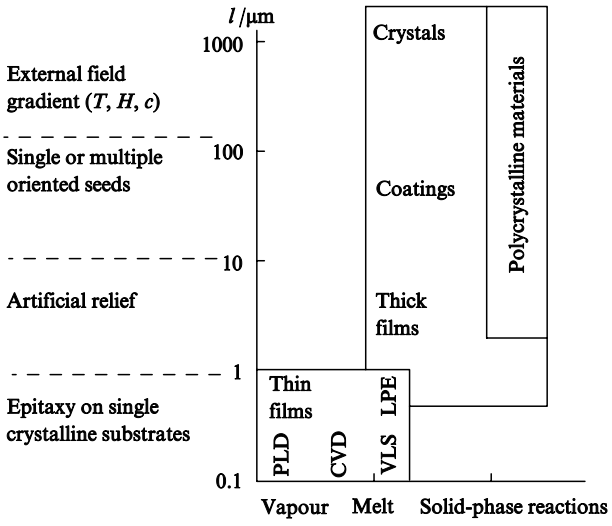

Figure 19. Main texturing techniques of polycrystalline HTSC-materials as functions of the thickness of the superconducting layer and deposition technique. Notations: PLD is Physical Layer Deposition, CVD is Chemical Vapour Deposition, VLS is Vapour Liquid Solid (mechanism) and LPE is Liquid Phase Epitaxy.

The most efficient orientation of HTSC-crystallites is attained using a simple striped relief (see Fig. 16).[176, 178] It provides (i) efficient geometric constraints on the crystal growth in the form of parallel walls of narrow grooves, (ii) a desired symmetry corresponding to the habits of the growing mixed REE–barium cuprate crystals and (iii) the density of the ensemble of crystallites, which is nearly independent of the cooling rate (because the crystallite size is limited to the groove width). At present, about 75% to 90% of the crystallites of sub-millimetre size can be readily and reproducibly aligned with a misorientation angle of less than 10° on substrates with artificial relief.

Artificial epitaxy does not use epitaxial relations for orientation of crystallites, because the technique is based on specific aspects of wetting, surface tension and meniscus, heterogeneous nucleation, redistribution of melt components, capillary effects, effects of crystallisation pressure and the topographic effect of the walls of relief elements, local temperature gradients,[176, 182] *etc*. (see Fig. 18). Clearly, high mobilities of the medium and particles in melt must provide a nearly instantaneous adjustment of orientations of the growing embryo-crystals floating on the melt surface, controlled by the relief elements, whereas the kinetics of the process depends on the adhesion, wetting of the crystallites and substrate and capillary forces and surface tension forces. The process under consideration can be practically implemented using various mechanical, electric and thermal effects that appear due to the creation of the artificial relief. The technique is convenient when using various materials and arbitrary substrates and can lead to nearly complete texturing of a polycrystalline layer in accord with the symmetry of the superficial pattern. Probably, the results reported in Refs 176–178 are among the first successful attempts to apply the method based on graphoepitaxy principles in texturing thick polycrystalline layers of complex, multicomponent systems.

VIII. Fields of practical applications of cuprates and manganites

The most promising field of practical application of the HTSC cuprates considered is design of materials for heavy-current engineering, in particular, fault current limiters (FCL). The material characteristics for an optimum FCL must be as follows:[172, 186] negligible resistance in the normal operating mode, sufficiently high resistance to limit the fault current, and high switching rate between the superconducting and resistive states. Additionally, as the fault currents are exceeded, a large amount of Joule heat releases after transition of the system to the resistive state. Therefore, the ability of the material to absorb the dissipated energy without damage should be considered as an extra necessary condition. This is possible in the case of, *e.g*., a good contact between the superconducting elements and the liquid cooling agent (this depends on the specific features of the cooling system and on the shape of the superconducting element). Respectively, high-temperature superconductors with a fabric structure having a well-developed system of regular pores (see Figs 15 *b*,*c*) to improve the contact with liquid nitrogen can be of considerable practical interest.¶

By creating a periodic and symmetrical artificial surface relief using ribbons made of commercial polycrystalline untextured silver as substrate it is possible to attain a nearly 90% mutual orientation of melt-grown HTSC crystallites in the *ab* plane.[176–178] These samples can be used as 'seed ribbons' and 'smart' seeds and for fabrication of items of complex shape. In the last-mentioned case (see Fig. 16 *b*) using a prototype device (artificially patterned HTSC coils) it was shown that the method including capillary 'suction' of melt, spillover of the melt across the surface and biaxial graphotexturing of the superconducting cuprate grains formed on cooling can be efficient in large-scale production of thick HTSC films on cheap metallic substrates in a uniform thermal field. It is possible to produce a batch of samples during one heat treatment cycle.

Growth of large superconducting crystals is mainly of academic interest to elaborate the crystal growth technique, to determine the growth mechanism and crystal parameters, *etc*. The fundamental physical characteristics can be successfully measured using small crystals. Owing to high cost and lower critical currents, the superconducting crystals can compete with neither coarse-grained ceramics used in heavy current devices nor thin films used as active elements in microelectronics.

At the same time neodymium–barium cuprate crystals with the limiting content of neodymium replacing the barium ions seem to be promising as substrate materials for fabrication of thin superconducting films. These crystals possess good dielectric properties and a small mismatch between their lattice parameters and those of the superconducting phases of other mixed REE–barium cuprates.[187] In this case, growth of large $Nd_{1.85}Ba_{1.15}Cu_3O_z$ crystals by the Czochralski method is worthwhile because the necessary surface area of polished substrates can reach a few square centimetres per device and large-scale production of this type of substrate can lead to considerable reduction of the high cost of devices for superconducting microelectronics.

This type of substrate offers some additional advantages such as chemical homogeneity (achieved using the modified Czochralski method), sufficiently high chemical stability (even in moist atmosphere), low degree of non-stoichiometry with respect to oxygen and orthorhombic unit cell. Morphology disturbance of the deposited HTSC-films at temperatures of *tetragonal–orthorhombic* transition can be prevented by oxygenation of the samples, because the anisotropy of the $R_2BaCu_3O_z$ lattice constants in the *ab* plane can act as an anisotropic strain field, which suppresses formation of twin defects in the superconducting film being deposited.

The $CaCu_xMn_{7-x}O_{12}$ solid solution can be considered as a candidate for the material to be used in magnetoresistive devices and spintronics.[188] The conductivity of $CaCu_xMn_{7-x}O_{12}$ (see Fig. 14) varies over a wide range depending on the x value and the magnetoresistance effect exhibits no pronounced thermal features. Ceramic samples synthesised from mechanically activated reactants showed the record (for this system) magnetoresistance effect of 65% at 35 K and 5 T.[20] Correspondingly, composites based on the CMR and HTSC-phases offer good prospects for practical application.[189]

Inorganic fibres provide a convenient means for fabrication of new types of materials in the form of, *e.g*., ion-conducting or catalytically active 'felts', multifilament wires or fabric (see Fig. 12 *e*). Tunnels in the structure of barium–manganese whiskers $Ba_6Mn_{24}O_{48}$ and the direction of their growth coincide. This permits practical implementation of structurally determined anisotropy of one-dimensional superionic conductivity. Usually, whiskers contain no dislocations and possess improved mechanical properties owing to the low defectiveness. In addition, studies on the behaviour of $Ba_6Mn_{24}O_{48}$ whiskers in lithium nitrate melt (see Fig. 12 *c*) showed that lithium penetrates into the structure of $Ba_6Mn_{24}O_{48}$ as a result of exchange reaction, thus inducing contraction of the unit cell along the normal to the growth direction of the whiskers. Because of this whiskers can be more stable than ceramic samples with respect to charge–discharge cycles when used as electrode materials.

Thus, the fundamental physical properties of cuprates, manganites and cupromanganites reflect the complex chemistry of copper and manganese, which predetermines structural and chemical features of these compounds. Methods of synthesis of materials with desired structures, microstructures and functional properties must be chosen allowing for this fact.

The review has been written with financial support from the Russian Foundation for Basic Research (Project Nos 04-03-32183a, 04-03-32827a and 04-03-08078ofia), the Programme 'Leading Scientific Schools' and 'Russian Universities' and from

¶ 'Super Foams' (HTSC foams) (Fig. 15) seem to have even greater prospects for being used as FCL.

the M V Lomonosov Moscow State University in the framework of Interdisciplinary Research Projects. The authors express their gratitude to N N Olejnikov, I A Presnyakov, E V Antipov, A M Abakumov, N R Khasanova, M A Novozhilov, I S Bezverkhij, V A Knot'ko and M V Makarova (Department of Chemistry, M V Lomonosov Moscow State University), E I Givargizov (Institute of Crystallography, Russian Academy of Sciences), V V Petrykin (TIT, Japan), G Schmitz and E Reddy (ACCESS e.V., Germany) and Y Shiohara (SRL ISTEC, Japan) for fruitful discussions of the results obtained.

References

1. M P Attfield *Annu. Rep. Sect. A: Inorgan. Chem.* **98** 435 (2002)
2. A Wells *Structural Inorganic Chemistry* (London: Oxford University Press, 1984)
3. D A Cardwell, D S Ginley (Eds) *Handbook of Superconducting Materials* Vols 1, 2 (Bristol, Philadelphia: IoP Publ., 2002)
4. Y Shiohara, E A Goodilin, in *Handbook on the Physics and Chemistry of Rare-Earths* Vol. 30, Ch. 189 (Eds K A Geschneidner Jr, L Eyring, M B Maple) (Amsterdam: Elsevier, 2000) p. 67
5. Yu D Tretyakov, E A Goodilin *Usp. Khim.* **69** 3 (2000) [*Russ. Chem. Rev.* **69** 1 (2000)]
6. B J Batlogg, R Buhrman, J R Clem *J. Supercond.* **10** 583 (1997)
7. J M S Skakle *Mater. Sci. Eng. R* **23** 1 (1998)
8. R J Cava, F J DiSalvo, L E Brus *Prog. Solid State Chem.* **30** 1 (2002)
9. B Raveau, A Maignan, C Martin, M Hervieu *Chem. Mater.* **10** 2641 (1998)
10. C N R Rao, A K Cheetham, R Mahesh *Chem. Mater.* **8** 2421 (1996)
11. O Yu Gorbenko, A A Bosak *Sensor* **2** 28 (2002)
12. Q Feng, H Kanoh, K Ooi *J. Mater. Chem.* **9** 319 (1999)
13. H Sato, T Enoki, J I Yamaura, N Yamamoto *Phys. Rev. B* **59** 12 836 (1999)
14. S Barbato, J L Gautier *Electochim. Acta* **46** 2767 (2001)
15. A Dyer, M Pillinger, J Newton, R Harjula, T Moller, S Amin *Chem. Mater.* **12** 3798 (2000)
16. Z Zeng, M Greenblatt, J E Sunstrom, M Croft, S Khalid *J. Solid State Chem.* **147** 185 (1999)
17. Z Zeng, M Greenblatt, M Croft *Phys. Rev. B* **58** 595 (1998)
18. I O Troyanchuk, L S Lobanovsky, N V Kasper, M Hervieu, A Maignan, C Michel, H Szymczak, A Szewczyk *Phys. Rev. B* **58** 14 903 (1998)
19. R Weht, W E Pickett *Phys. Rev. B* **65** 014415 (2001)
20. E A Pomerantseva, D M Itkis, E A Goodilin, M V Makarova, M V Lobanov, N N Oleinikov, Yu D Tretyakov *Dokl. Akad. Nauk* **388** 344 (2003) [a]
21. E V Antipov, L N Lykova, L M Kovba *Zh. Vsesoyuz. Khim. O-va im. D I Mendeleeva* **34** 458 (1989) [b]
22. N R Khasanova, A L Kharlanov, E V Antipov, L M Kovba, A A Gippius, V V Moshchalkov *Physica C* **190** 522 (1992)
23. A V Mironov, A M Abakumov, E V Antipov *Rigaku J.* **19**–**20** 23 (2003)
24. S N Putilin, E V Antipov, A M Abakumov, M G Rozova, K A Lokshin, D A Pavlov, A M Balagurov, D V Sheptyakov, M Marezio *Physica C* **338** 52 (2000)
25. G Van Tendeloo, O I Lebedev, R V Shpanchenko, E V Antipov *J. Electron Microsc.* **1** 23 (1997)
26. E V Antipov, S N Putilin, R V Schpanchenko, V A Alyoshin, M G Rozova, A M Abakumov, D A Mikhailova, A M Balagurov, O Lebedev, G Van Tendeloo *Physica C* **282**–**287** 61 (1997)
27. A M Abakumov, V L Aksenov, V A Alyoshin, E V Antipov, A M Balagurov, D A Mikhailova, S N Putilin, M G Rozova *Phys. Rev. Lett.* **80** 385 (1998)
28. A M Abakumov, M G Rozova, R V Shpanchenko, M L Kovba, S N Putilin, E V Antipov, O I Lebedev, G Van Tendeloo, E M Kopnin, J Karpinski *Physica C* **301** 155 (1998)
29. P N Oleinikov, R V Shpanchenko, M G Rozova, A M Abakumov, E V Antipov, I Khadermann, G Van Tendeloo *Zh. Neorg. Khim.* **46** 197 (2001) [c]
30. A M Alekseeva, A M Abakumov, M G Rozova, E V Antipov, J Hadermann *J. Solid State Chem.* **177** 731 (2004)
31. I F Voloshin, D A Emelianov, S O Klimonsky, V D Kuznetsov, A V Lyashenko, Yu D Tretyakov *Dokl. Akad. Nauk* **392** 779 (2003) [a]
32. S N Putulin, I Bryntse, E V Antipov *Mater. Res. Bull.* **26** 1299 (1991)
33. S N Putilin, E V Antipov, O Chmaissem, M Marezio *Nature (London)* **362** 226 (1993)
34. S N Putilin, E V Antipov, M Marezio *Physica C* **212** 266 (1993)
35. E V Antipov, S M Loureiro, C Chaillout, J J Capponi, P Bordet, J L Tholence, S N Putilin, M Marezio *Physica C* **215** 1 (1993)
36. M Nunez-Regueiro, J L Tholence, E V Antipov, J J Capponi, M Marezio *Science* **262** 97 (1993)
37. J J Capponi, J L Tholence, C Chaillout, M Marezio, P Bordet, J Chenavas, S M Loureiro, E V Antipov, E M Kopnin, M F Gorius, M Nunez-Regueiro, B Souletie, P Radaelli, F Gerhards *Physica C* **235**–**240** 146 (1994)
38. V A Alyoshin, D A Mikhailova, E V Antipov *Physica C* **271** 197 (1996)
39. A M Balagurov, D V Sheptyakov, V L Aksenov, E V Antipov, S N Putilin, P G Radaelli, M Marezio *Phys. Rev. B* **59** 7209 (1999)
40. O Chmaissem, Q Huang, E V Antipov, S N Putilin, M Marezio, S M Loureiro, J J Capponi, J L Tholence, A Santoro *Physica C* **217** 265 (1993)
41. G Van Tendeloo, C Chaillout, J J Capponi, M Marezio, E V Antipov *Physica C* **223** 219 (1994)
42. V L Aksenov, A M Balagurov, B N Savenko, V P Glazkov, I N Goncharenko, V A Somenkov, E V Antipov, S N Putilin, J J Capponi *High Pres. Res.* **14** 127 (1995)
43. G Fuchs, K A Nenkov, A Attenberger, K Luders, M Baenitz, C Ecker, K Kajikawa, E V Antipov, H R Khan *Physica C* **355** 299 (2001)
44. P Schilbe, K Lmders, M Baenitz, D A Pavlov, I Bryntse, A Abakumov, E V Antipov *Physica C* **391** 298 (2003)
45. P Schilbe, K Lmders, M Baenitz, D A Pavlov, A Abakumov, E V Antipov *Physica C* **388**–**389** 247 (2003)
46. J Karpinski, S M Kazakov, M Augst, A Mironov, M Mali, J Roos *Phys. Rev. B* **64** 094 518 (2001)
47. P Bordet, F Duc, S Le Floch, J J Capponi, E Alexandre, M Rosa-Nunes, S Putilin, E V Antipov *Physica C* **271** 189 (1996)
48. D V Fomichev, O G D'yachenko, A V Mironov, E V Antipov *Physica C* **225** 25 (1994)
49. S F Pashin, E V Antipov, L M Kovba, Yu Ya Skolis *Sverkhprovodimost: Fiz. Khim. Tekh.* **2** 102 (1989)
50. D A Mikhailova, V A Alyoshin, E V Antipov, J Karpinski *J. Solid State Chem.* **146** 151 (1999)
51. V A Alyoshin, D A Mikhailova, E V Antipov, A S Monayenkova, A A Popova, L A Tiphlova, J Karpinski *J. Alloys Compd.* **284** 108 (1999)
52. V A Alyoshin, D A Michailova, E B Rudnyi, E V Antipov *Physica C* **383** 59 (2002)
53. S N Mudretsova, A F Maiorova, A A Bosak, O Yu Gorbenko, A R Kaul, N A Babushkina, L M Belova *Zh. Fiz. Khim.* **74** 1765 (2000) [d]
54. P E Kazin, D D Zaitsev, Yu D Tretyakov *Dokl. Akad. Nauk* **385** 355 (2002) [a]
55. P E Kazin, A S Karpov, Yu D Tretyakov, M Jansen *Solid State Sci.* **3** 285 (2001)
56. P E Kazin, Yu D Tretyakov, V V Lennikov, M Jansen *J. Mater. Chem.* **11** 168 (2001)
57. P E Kazin, A A Kovalevskii, V V Poltavets, Yu D Tretyakov, M Yanzen *Neorg. Mater.* **37** 1383 (2001) [e]
58. M V Lobanov, A M Balagurov, V Ju Pomjakushin, P Fisher, M Gutmann, A M Abakumov, O G D'yachenko, E V Antipov, O I Lebedev, G Van Tendeloo *Phys. Rev. B* **61** 8941 (2000)
59. O A Shlyakhtin, Y-J Oh, Yu D Tretyakov *Solid State Commun.* **117** 261 (2001)
60. O A Shlyakhtin, Y-J Oh, Yu D Tretyakov *J. Eur. Ceram. Soc.* **20** 2047 (2000)

61. A M Abakumov, A V Mironov, V A Govorov, M V Lobanov, M G Rozova, E V Antipov, O I Lebedev, G Van Tendeloo *Solid State Sci.* **5** 1117 (2003)
62. O Yu Gorbenko, A R Kaul, I V Pogosova, S N Polyakov, E V Kolosova, S A Pozigun, V I Scritny *Mater. Sci. Eng. B* **17** 157 (1993)
63. W Decker, Yu Erokhin, O Gorbenko, I Graboy, A Kaul, A Nurnberg, M Pulver, R Stolle, G Wahl *J. Alloys Compd.* **195** 291 (1993).
64. O Yu Gorbenko, W Decker, G Wahl *J. Phys. IV* **3** 25 (1993)
65. W Decker, A Nurnberg, M Pulver, R Stolle, G Wahl, Yu Erokhin, O Gorbenko, I Graboy, A Kaul *Physica C* **209** 195 (1993)
66. O Yu Gorbenko, V N Fuflyigin, Yu Yu Erokhin, I E Graboy, A R Kaul, Yu D Tretyakov, L Klippe, G Wahl *J. Mater. Chem.* **4** 1585 (1994)
67. S V Samoilenkov, O Yu Gorbenko, A R Kaul, Yu D Tretyakov *Sverkhprovodimost* **8** 113 (1995)
68. S V Samoylenkov, O Yu Gorbenko, A R Kaul *Physica C* **267** 74 (1996)
69. S V Samoylenkov, O Yu Gorbenko, A R Kaul, Y A Rebane, V L Svetchnikov, H W Zandbergen *J. Alloys Compd.* **251** 342 (1997)
70. S O Klimonsky, S V Samoilenkov, O Yu Gorbenko, D A Emelianov, A V Lyashenko, S R Lee, A R Kaul, Yu D Tretyakov, D G Andrianov, A V Kalinov, I F Voloshin *Physica C* **383** 37 (2002)
71. G A Tsirlina, S N Putilin, O A Petrii, E V Antipov, Ya G Ponomarev, Kh T Rakhimov *Sverkhprovodimost: Fiz. Khim. Tekh.* **4** 1580 (1991)
72. O I Lebedev, G Van Tendeloo, A M Abakumov, S Amelinckx, B Leibold, H-U Habermeier *Philos. Mag. A* **79** 1461 (1999)
73. O Yu Gorbenko, A R Kaul, N A Babushkina, L M Belova *J. Mater. Chem.* **7** 747 (1997)
74. O Yu Gorbenko, R V Demin, L I Koroleva, A R Kaul, R Shimchak *Fiz. Tv. Tela* **40** 290 (1998) [f]
75. N A Babushkina, L M Belova, D I Khomskii, K I Kugel, O Yu Gorbenko, A R Kaul *Phys. Rev. B* **59** 6994 (1999)
76. O Yu Gorbenko, A A Bosak, V A Amelichev, A Yu Ganin, I E Graboy, A R Kaul, G Wahl, H W Zandbergen *J. Phys. IV* **9** 659 (1999)
77. O Yu Gorbenko, A R Kaul, A A Bosak, I E Graboy, H W Zandbergen, V L Svetchnikov, N A Babushkina, L M Belova, K I Kugel *Solid State Commun.* **114** 407 (2000)
78. A A Bosak, O Yu Gorbenko, A R Kaul, I E Graboy, C Dubourdieu, J P Senateur, H W Zandbergen *J. Magn. Magn. Mater.* **211** 61 (2000)
79. M Bibes, O Gorbenko, B Martinez, A Kaul, J Fontcuberta *J. Magn. Magn. Mater.* **211** 47 (2000)
80. O Yu Gorbenko, I E Graboy, A R Kaul, H W Zandbergen *J. Magn. Magn. Mater.* **211** 97 (2000)
81. V A Amelitchev, B Güttler, O Yu Gorbenko, A R Kaul, A A Bosak, A Yu Ganin *Phys. Rev. B* **63** 104 430 (2001)
82. B Guettler, V A Amelitchev, O Yu Gorbenko *Phase Transitions* **76** 63 (2003)
83. N A Babushkina, L M Belova, O Yu Gorbenko, A R Kaul, A A Bosak, V I Ozhogin, K I Kugel *Nature (London)* **391** 159 (1998)
84. L M Belova, N A Babushkina, O Yu Gorbenko, A R Kaul, K I Kugel, D I Khomskii *Physica B* **284–288** 1434 (2000)
85. N N Loshkareva, Yu P Sukhorukov, E A Gan'shina, E V Mostovshchikova, R Yu Kumaritova, A S Moskvin, Yu D Panov, O Yu Gorbenko, A R Kaul *Zh. Eksp. Teor. Fiz.* **119** 533 (2001) [g]
86. A M Balagurov, V Yu Pomjakushin, D V Sheptyakov, V L Aksenov, N A Babushkina, L M Belova, O Yu Gorbenko, A R Kaul *Eur. Phys. J. B* **19** 215 (2001)
87. M Baran, S L Gnatchenko, O Yu Gorbenko, A R Kaul, R Szymczak, H Szymczak *Phys. Rev. B* **60** 9244 (1999)
88. Yu P Sukhorukov, N N Loshkareva, E A Gan'shina, A R Kaul, O Yu Gorbenko, K A Fatieva *Pis'ma Zh. Tech. Fiz.* **25** 6 (1999) [h]
89. E A Gan'shina, O Yu Gorbenko, A G Smechova, A R Kaul, N A Babushkina, L M Belova *J. Phys.: Condens. Matter* **12** 2857 (2000)
90. T Mertelj, A A Bosak, O Yu Gorbenko, A R Kaul, D Mihailovic *Int. J. Mod. Phys. B* **14** 3584 (2000)
91. A A Bosak, A A Kamenev, I E Graboy, S V Antonov, O Yu Gorbenko, A R Kaul, C Dubourdieu, J P Senateur, V L Svechnikov, H W Zandbergen, B Hollinder *Thin Solid Films* **400** 149 (2001)
92. A A Gippius, E V Antipov, O Klein, K Lüders *Physica B* **284–288** 935 (2000)
93. A A Gippius, E N Morozova, E V Antipov, A M Abakumov, M G Rozova, K Lmders, W Hoffmann, G Buntkowsky, O Klein *Phys. Rev. B* **61** 14370 (2000)
94. A A Gippius, E V Antipov, W Hoffmann, K Lüders, G Buntkowsky *Phys. Rev. B* **59** 654 (1999)
95. W Hoffmann, H Breitzke, M Baenitz, M Heinze, K Lmders, G Buntkowsky, H H Limbach, E V Antipov, A A Gippius, O Loebich, H R Khan, M Paranthaman, J R Thompson *Physica C* **227** 225 (1994)
96. Yu D Tretyakov *Usp. Khim.* **72** 731 (2003) [*Russ. Chem. Rev.* **72** 651 (2003)]
97. Yu D Tretyakov *Khim. Ros.* **9** 11 (2000)
98. P E Kazin, Yu D Tretyakov *Usp. Khim.* **72** 960 (2003) [*Russ. Chem. Rev.* **72** 849 (2003)]
99. O Yu Gorbenko, V N Fuflygin, A R Kaul *Sverkhprovodimost: Issled. Razrab.* **5–6** 38 (1995)
100. O Yu Gorbenko, S V Samoilenkov *Sverkhprovodimost* **8** 800 (1995)
101. A M Abakumov, M G Rozova, E I Ardashnikova, E V Antipov *Usp. Khim.* **71** 442 (2002) [*Russ. Chem. Rev.* **71** 383 (2002)]
102. E V Antipov, V A Aleshin *Zh. Neorg. Khim.* **47** 530 (2002) [c]
103. A M Abakumov, M G Rozova, S N Putilin, E V Antipov *Naukoemkie Tekhnol.* **1** 50 (2003)
104. S M Loureiro, J J Capponi, E V Antipov, M Marezio, in *Studies of High Temperature Superconductors* Vol. 25 (New York: Nova Science Publisher, 1997) p. 229
105. E V Antipov, A M Abakumov, S N Putilin *Supercond. Sci. Technol.* **15** R31 (2002)
106. A M Abakumov, E V Antipov, L M Kovba, E M Kopnin, S N Putilin, R V Shpanchenko *Usp. Khim.* **64** 769 (1995) [*Russ. Chem. Rev.* **64** 719 (1995)]
107. E V Antipov, Doctoral Thesis in Chemical Sciences, Moscow State University, Moscow, 1997
108. A A Kiselev (Ed.) *Vysokotemperaturnaya Svekhprovodimost'. Fundamental'nye i Prikladnye Issledovaniya* (High-Temperature Superconductivity. Fundamental and Applied Investigations) (Leningrad: Mashinostroenie, 1990) No. 1
109. H B Brom, J Zaanen, in *Handbook of Magnetic Materials* (Ed. K H J Buschow) (Amsterdam: Elsevier, 2003) p. 379
110. A Läuchli, G Schmid, M Troyer *Phys. Rev. B* **67** 100 409(R) (2003)
111. T M Rice *Z. Phys. B* **103** 165 (1997)
112. O Tamada, H Paulus, H Fuess, N Yamamoto, S Muranaka *J. Solid State Chem.* **108** 112 (1994)
113. V G Zubkov, A P Tyutyunnik, I F Berger, V I Voronin, G V Bazuev, C A Moore, P D Battle *J. Solid State Chem.* **167** 453 (2002)
114. M A Subramanian, A P Ramirez, G H Kwei *Solid State Ionics* **108** 185 (1998)
115. M M Cruz, M D Carvalho, A Casaca, G Bonfait, F M Costa, M Godinho *J. Magn. Magn. Mater.* **226–230** 800 (2001)
116. V V Petrykin, E A Goodilin, J Hester, E A Trofimenko, N N Oleynikov, M Kakihana, Yu D Tretyakov *Physica C* **340** 16 (2000)
117. V V Petrykin, E A Goodilin, J Hester, E A Trofimenko, M Kakihana, N N Oleynikov, Y D Tretyakov *Physica C* **357** 388 (2001)
118. E A Goodilin, I A Presnyakov, M V Tarasov, S N Mudretsova, A F Maiorova, J Hester, N N Oleinikov, Yu D Tretyakov *Dokl. Akad. Nauk* **373** 160 (2000) [a]
119. K V Didenko, D V Peryshkov, E A Goodilin, I A Presnyakov, E A Pomerantseva, Yu D Tretyakov *Dokl. Akad. Nauk* **387** 343 (2002) [a]
120. D V Peryshkov, E A Goodilin, M V Makarova, E A Pomerantseva, S N Mudretsova, A F Maiorova, Yu D Tretyakov *Dokl. Akad. Nauk* **387** 491 (2002) [a]

121. D V Peryshkov, E A Goodilin, M V Makarova, S N Mudretsova, A F Maiorova, Yu D Tretyakov *Dokl. Akad. Nauk* **383** 651 (2002) [a]
122. E A Pomerantseva, D M Itkis, I A Presnyakov, E A Goodilin, J Hester, N N Oleinikov, Yu D Tretyakov *Dokl. Akad. Nauk* **387** 207 (2002) [a]
123. M F Limonov, E A Goodilin, X Yao, S Tajima, Y Shiohara, Yu E Kitaev *Phys. Rev. B* **58** 12368 (1998)
124. Yu D Tretyakov, E A Goodilin *Curr. Appl. Phys.* **3** 377 (2003)
125. Yu D Tretyakov, E A Goodilin *Physica B* **321** 249 (2002)
126. Z Hommonay, in *Mössbauer Spectroscopy of Sophisticated Oxides* (Eds A Vertes, Z Hommonay) (Budapest: Akademiai Kiado, 1997) p. 159
127. A V Kravchenko, E A Goodilin, I S Bezverkhii, D M Predtechenskaya, N N Oleinikov, Yu D Tretyakov *Zh. Neorg. Khim.* **45** 983 (2000) [c]
128. Ph Boullay, M Hervieu, B Raveau *J. Solid State Chem.* **132** 239 (1997).
129. H H Hamdeh, J C Ho, S A Oliver, J G Lin, S Y Lin, P C Kuo, C Y Huang *J. Magn. Magn. Mater.* **232** 175 (2001)
130. F Studer, N Nguyen, O Toulemonde, A Ducouret *Int. J. Inorg. Mater.* **2** 671 (2000)
131. I D Fawcett, M V Gabriel, M Greenblatt, M Croft, I Nowik *Solid State Sci.* **2** 821 (2000)
132. A Nath, V Chechersky, R L Greene *J. Solid State Chem.* **155** 116 (2000)
133. V Chechersky, A Nath, I Isaac, J P Franck, K Ghosh, R L Greene *Phys. Rev. B* **63** 52411 (2001)
134. H S Horowitz, J M Longo *Mater. Res. Bull.* **13** 1359 (1978)
135. E A Goodilin, E A Pomerantseva, O Yu Gorbenko, V V Petrykin, V V Poltavets, A V Knot'ko, A M Abakumov, N N Oleinikov, Yu D Tretyakov, M Kakikhana *Dokl. Akad. Nauk* **372** 100 (2000) [a]
136. Yu D Tretyakov, E A Goodilin *Zh. Neorg. Khim.* **46** 203 (2001) [c]
137. E Goodilin, A Oka, J G Wen, Y Shiohara, M Kambara, T Umeda *Physica C* **299** 279 (1998)
138. E Goodilin, M Kambara, T Umeda, Y Shiohara *Physica C* **289** 37 (1997)
139. M Kambara, M Tagami, X Yao, E Goodilin, Y Shiohara, T Umeda *J. Am. Ceram. Soc.* **81** 2116 (1998)
140. E Goodilin, M Kambara, T Umeda, Y Shiohara *Physica C* **289** 251 (1997)
141. E A Goodilin, N N Oleynikov, G Yu Popov, V A Shpanchenko, E V Antipov, G V Balakirev, Yu D Tretyakov *Physica C* **272** 65 (1996)
142. Y Yamada, M Nakamura, Y Shiohara, S Tanaka *J. Cryst. Growth* **148** 241 (1995)
143. M Kambara, X Yao, M Nakamura, Y Shiohara, T Umeda *J. Mater. Res.* **12** 2866 (1997)
144. X Yao, Y Shiohara *Supercond. Sci. Technol.* **10** 249 (1997)
145. M Egami, Y Shiohara, in *Advances in Superconductivity* Vol. 9 (Eds S Nakajima, M Murakami) (Tokyo: Springer, 1997) p. 809
146. X Yao, E A Goodilin, T Izumi, Y Shiohara *J. Mater. Res.* **16** 529 (2001)
147. X Yao, E Goodilin, Y Yamada, H Sato, Y Shiohara *Appl. Superconduct.* **6** 175 (1998)
148. Z Zou, J Ye, K Oka, Y Nishihara *Phys. Rev. Lett.* **80** 1074 (1998)
149. H Zhang, G Wang, H Wu *J. Cryst. Growth* **154** 293 (1995)
150. E A Goodilin, A P Soloshenko, V V Lennikov, A V Knot'ko, N N Oleynikov, Y D Tretyakov, in *Proceedings of the First Regional Conference on Magnetic and Superconducting Materials, MSM'99* (Eds M Akhavan, J Jensen, K Kitazawa) (Singapore: World Scientific, 2000) p. 167
151. E A Goodilin, A P Soloshenko, V V Lennikov, A V Knot'ko, D A Vetoshkin, N N Oleinikov, Yu D Tretyakov *Zh. Neorg. Khim.* **45** 917 (2000) [c]
152. S Lee, K-J Kwon, W-S Kim, S-I Lee *Physica C* **251** 149 (1995)
153. C Kloc, S W Cheong, P Matl *J. Cryst. Growth* **191** 294 (1998)
154. R Suryanarayanan, G Dhalenne, A Revcolevschi, W Prellier, J-P Renard, C Dupas, W Caliebe, T Chatterji *Solid State Commun.* **113** 267 (2000)
155. V A Cherepanov, L Yu Barkhatova, V I Voronin *J. Solid State Chem.* **134** 38 (1997)
156. W H McCarroll, K V Ramanuajachary, I D Fawcett, M Greenblatt *J. Solid State Chem.* **145** 88 (1999)
157. D Zhu, H Zhu, Y Zhang *J. Crystal Growth.* **249** 172 (2002)
158. X Wang, Y Li *Chem. Eur. J.* **9** 300 (2003)
159. C Xu, X Zhao, G Wang *J. Nanosci. Nanotech.* **3** 406 (2003)
160. E A Goodilin, N N Oleinikov, S R Li, Yu D Tretyakov *Zh. Neorg. Khim.* **39** 1043 (1994) [c]
161. C Zener *Phys. Rev.* **82** 403 (1951)
162. R V Krishnan, A Banerjee *J. Phys.: Condens. Matter* **12** 3835 (2000)
163. A J Millis *Nature (London)* **392** 147 (1998)
164. E L Nagaev *Usp. Fiz. Nauk* **168** 918 (1998) [*Physics-Uspekhi* **41** 831 (1998)]
165. M V Krasil'nikova *Zh. Tekhn. Fiz.* **72** 30 (2002) [i]
166. E A Goodilin, D V Pyorishkov, A V Knot'ko, V V Lennikov, N N Oleynikov, Y D Tretyakov *Physica C* **349** 278 (2001)
167. E A Goodilin, G Yu Popov, N N Oleinikov, G P Murav'eva, P E Kazin, Yu D Tretyakov *Dokl. Akad. Nauk* **344** 773 (1995) [a]
168. E S Reddy, G J Schmitz *Supercond. Sci. Technol.* **15** L21 (2002)
169. E S Reddy, J G Noudem, E A Goodilin, M Tarka, G J Schmitz *Supercond. Sci. Technol.* **16** 402 (2003)
170. J G Noudem, E S Reddy, E A Goodilin, M Tarka, M Noe, G J Schmitz *Physica C* **372 – 376** 1631 (2002)
171. E S Reddy, E A Goodilin, M Tarka, M Zeisberger, G J Schmitz *Physica C* **372 – 376** 1200 (2002)
172. J G Noudem, E S Reddy, M Tarka, M Noe, E A Goodillin, G J Schmitz *Physica C* **366** 93 (2002)
173. G J Schmitz, E S Reddy, E A Goodilin *Physica C* **378 – 381** 607 (2002)
174. J G Noudem, E S Reddy, E A Goodilin, M Tarka, M Noe, G J Schmitz *Physica C* **372 – 376** 1187 (2002)
175. G J Schmitz, O Kugeler *Physica C* **275** 205 (1997)
176. E A Goodilin, E S Reddy, J G Noudem, M Tarka, G J Schmitz *J. Cryst. Growth.* **241** 512 (2002)
177. E A Goodilin, E S Reddy, J G Noudem, M Tarka, G J Schmitz *Physica C* **372 – 376** 842 (2002)
178. Yu D Tretyakov, E A Goodilin, E S Reddi, G J Schmitz *Kristallografiya* **49** 283 (2004) [j]
179. F Schreiber *Prog. Surface Sci.* **65** 151 (2000)
180. S Tanaka *Physica C* **392 – 396** 1 (2003)
181. H Tanabe, C M Chen, H A Atwater *Appl. Phys. Lett.* **77** 4325 (2000)
182. E I Givargizov, in *Handbook of Crystal Growth* Pt. 3b (Ed. D T J Hurle) (Amsterdam: Elsevier, 1994) p. 941
183. H U Habermeier *J. Supercond.* **13** 871 (2000)
184. S Miyazawa, M Mukaida *Appl. Phys. Lett.* **64** 2160 (1994)
185. W D Dozier, C E Platt *App. Phys. Lett.* **62** 2048 (1993)
186. M Chen, L Donzel, M Lakner, W Paul *J. Eur. Ceram. Soc.* **24** 1815 (2004)
187. F M Saba, M Tagami, E A Goodilin, Y Shiohara, Y Enomoto *IEEE Trans. Appl. Supercond.* **10** 1662 (2000)
188. S A Wolf, D D Awschalom, R A Buhrman, J M Daughton, S von Molna, M L Roukes, A Y Chtchelkanova, D M Treger *Science* **294** 1488 (2001)
189. O Yu Gorbenko, I E Graboy, A A Bosak, V A Amelichev, A Yu Ganin, A R Kaul, G Wahl, H W Zandbergen *J. Phys. IV* **9** 659 (1999)

[a] — *Dokl. Chem. (Engl. Transl.)*
[b] — *Mendeleev Chem. J. (Engl. Transl.)*
[c] — *Russ. J. Inorg. Chem. (Engl. Transl.)*
[d] — *Russ. J. Phys. Chem. (Engl. Transl.)*
[e] — *Inorg. Mater. (Engl. Transl.)*
[f] — *Phys. Solid State (Engl. Transl.)*
[g] — *J. Exp. Theor. Phys. (Engl. Transl.)*
[h] — *J. Tech. Phys. Lett. (Engl. Transl.)*
[i] — *J. Tech. Phys. (Engl. Transl.)*
[j] — *Crystallogr. Rep. (Engl. Transl.)*

Russian Chemical Reviews **73** (9) 899 – 921 (2004) © 2004 Russian Academy of Sciences and Turpion Ltd

DOI 10.1070/RC2004v073n09ABEH000918

Synthesis of functional nanocomposites based on solid-phase nanoreactors

Yu D Tretyakov, A V Lukashin, A A Eliseev

Contents

I.	Introduction	899
II.	Methods for the synthesis of nanomaterials	899
III.	Synthesis of nanoparticles in amorphous matrices	901
IV.	Synthesis of nanoparticles in ordered matrices	901

Abstract. Approaches to the synthesis of functional nanocomposites based on zero-, one- and two-dimensional solid-state nanoreactors formed by zeolite cages, pores of mesoporous matrices, or interlayer cavities in layered compounds are considered. It is demonstrated that the use of solid-state nanoreactors opens up extensive opportunities for designing nanocomposites with specified physicochemical properties and makes it possible to avoid the aggregation of nanoparticles and to protect them from exposure to external factors, thus essentially facilitating the practical utility of these materials. The bibliography includes 304 references.

I. Introduction

The upsurge of interest in nanomaterials and nanotechnologies observed in the past decade manifests itself as a yearly growth (in geometrical progression) in the number of publications on this topic.[1] The unique properties of compounds in the nanocrystalline state [2] made it possible not only to create totally new generations of materials and devices but also to change the fundamental views about the world around us.[3, 4]

The reduction of particles to nanometre sizes changes considerably the properties of materials obtained on this basis, such as the melting point, heat capacity, electric conductance, *etc.*[5, 6] Furthermore, such materials acquire new optical, magnetic and electronic properties.[7, 8] In general, these changes are more prominent the smaller the particle sizes.[9]

The term 'nanoparticle' or 'nanosized particle' has appeared in scientific literature over ten years ago; however, there is no common opinion as to the size below which particles should be considered as nanosized. Quite different definitions of nanosizes can be found in the literature, namely, from a few nanometres to several hundred nanometres.[10] Sometimes, the definition of nanoparticles is related to the emergence of new properties other than the properties of the bulk phase rather than to the particle size.[11] It is believed that the size of nanoparticles is comparable to the correlation radius of some physical phenomenon (*e.g.*, the free-path length of electrons or phonons, the coherence length in a superconductor or the size of a magnetic domain or a solid-phase nucleus).[12] In such case, particles are characterised by quantum-size effects that depend both on the nature of the substance and on its properties. The majority of scientists believe that the maximum size of nanoparticles is 100 nm; however, they do admit that this is a purely arbitrary value, which is only necessary to provide a formal classification.[2, 13]

Two types of nanoparticles are usually distinguished: i, clusters or nanocrystals; and ii, nanoparticles as such. The first type comprises particles with well-defined structures and with sizes of 1 – 5 nm containing up to 1000 atoms, while the second type comprises nanoparticles with sizes of 5 – 100 nm consisting of $10^3 - 10^6$ atoms.[14] However, the latter definition is valid only for isotropic (spherical) nanoparticles, whereas nanowires and layered particles containing many more atoms and having one or two linear dimensions do not satisfy this definition, though they are typical nanoparticles as regards their properties. Owing to such differences in the linear sizes of nanoparticles, it is expedient to subdivide them into one-, two-, and three-dimensional nanoparticles (1D, 2D and 3D, respectively).[11] Lately, a distinction of geometrical and physical dimensionality of nanoparticles appeared.[15] It should be noted that if a nanoparticle has complex shape and structure, it is the size of its structural element rather than the linear size (which can often be much larger than 100 nm) that serves as the characteristic size. Such particles are called nanostructures. They are also subdivided into one-, two- and three-dimensional (zero-dimensional) particles (Fig. 1), depending on the anisotropy of the geometrical elements.

Owing to their unique physicochemical properties, nanoparticles are widely used in the creation of functional nanomaterials; among these, a special role belongs to magnetic and semiconducting nanomaterials due to the exceptional role of the latter in the progress of information technology. For example, superparamagnetic materials based on nanocrystalline transition metals (*e.g.*, Fe, Co and Ni) are used in memory devices with ultra-high data storage density;[16] nanomaterials based on semiconductors (*e.g.*, $A^{II}B^{VI}$ and $A^{IV}B^{VI}$) have unique optical properties and show promise as active elements in lasers with adjustable wavelength, elements of nonlinear optics, and nanoelectronic devices.[17]

II. Methods for the synthesis of nanomaterials

Numerous methods have been developed by now for the synthesis of nanomaterials, both in the form of powders and as inclusions in porous or solid matrices. In this case, ferro- and ferrimagnetics, metals, semiconductors, dielectrics *etc.* can serve as nanophases.

Yu D Tretyakov, A V Lukashin, A A Eliseev Department of Chemistry and Department of Materials Science, M V Lomonosov Moscow State University, Leninskie Gory, 119992 Moscow, Russian Federation.
Fax (7-095) 939 09 98. Tel. (7-095) 939 20 74.
E-mail: yudt@inorg.chem.msu.ru (Yu D Tretyakov).
Tel. (7-095) 939 59 31. E-mail: alex@inorg.chem.msu.ru
(A V Lukashin), eliseev@inorg.chem.msu.ru (A A Eliseev)

Received 9 March 2004
Uspekhi Khimii **73** (9) 974 – 998 (2004); translated by S S Veselyi

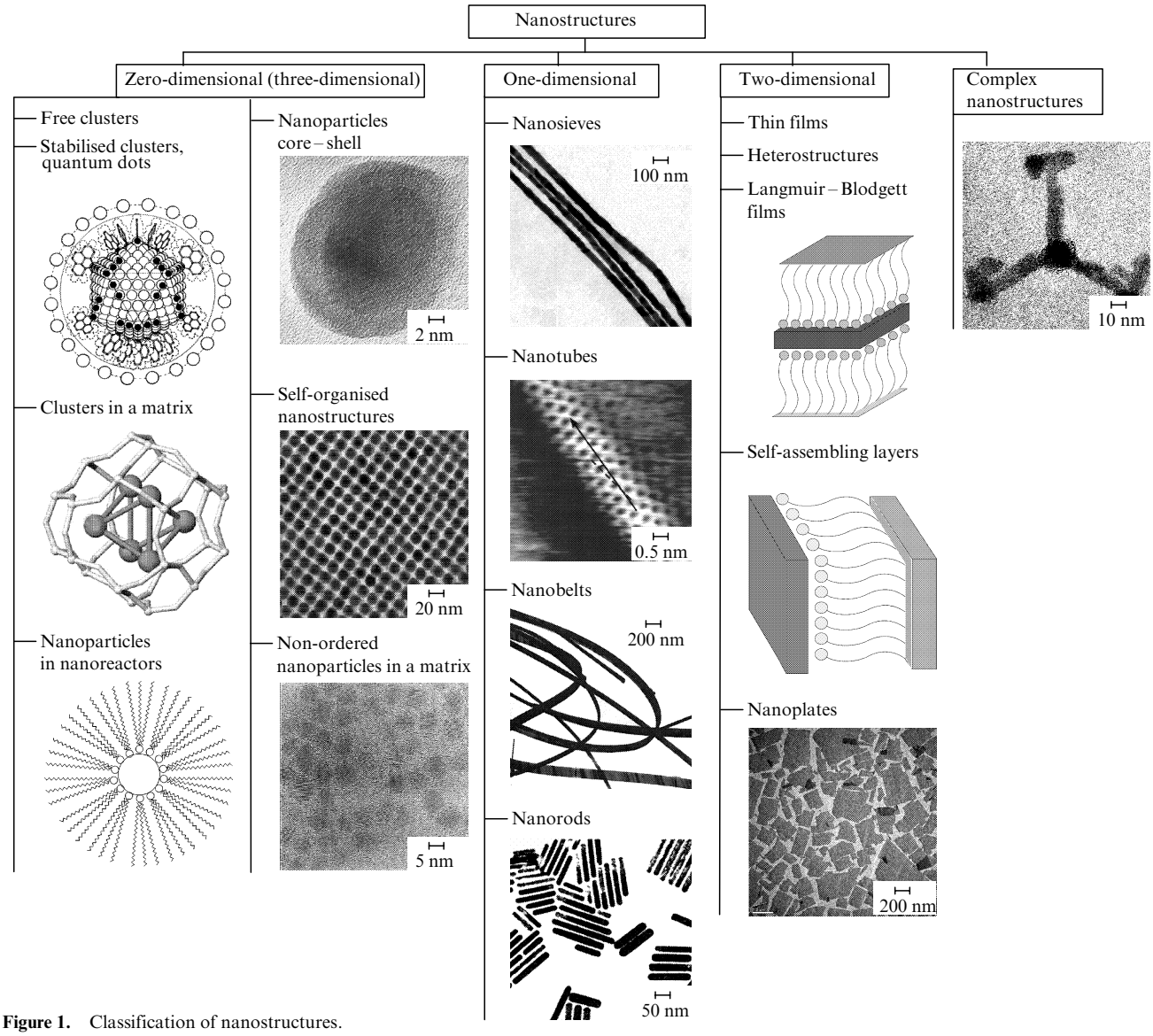

Figure 1. Classification of nanostructures.

According to Fendler,[18] the following conditions are of primary importance in the synthesis of nanomaterials:

1. The systems should be non-equilibrium. Virtually all nanosystems are thermodynamically unstable; they are obtained under conditions that are far from equilibrium, which allows one to achieve spontaneous nucleation and avoid the growth and aggregation of the nanoparticles formed.

2. Uniformity of nanoparticles. The high chemical uniformity of a nanomaterial is ensured if separation of components does not occur during the synthesis, either within a single nanoparticle or between the nanoparticles.

3. Monodispersity of nanoparticles. The properties of nanoparticles depend very strongly on their sizes; therefore, the synthesis of materials with good functional characteristics requires that particles with a sufficiently narrow size distribution be used.

It will be shown below that these conditions are not always mandatory. For example, solutions of surface-active compounds (micellar structures, Langmuir – Blodgett films, liquid – crystal phases) are thermodynamically stable but still give rise to various nanostructures.

All methods for the synthesis of nanomaterials can be tentatively separated into several large groups. The first group includes the so-called high-energy methods based on the rapid condensation of vapours under conditions precluding the aggregation and growth of the particles formed. The methods of this group mostly differ in the techniques of evaporation and stabilisation of the nanoparticles formed. Evaporation can be carried out by means of plasma excitation (plasma-arc), laser radiation (laser ablation), electric arc (carbon arc), or thermal exposure.[19, 20] Condensation was carried out either in the presence of a surfactant that slows down the growth of particles upon adsorption on their surfaces (vapour trapping); or on a cold matrix where the growth of particles is limited by the diffusion rate;[21] or in the presence of an inert component, which allows directed syntheses of nanocomposite materials with various microstructures.[22] If the components are mutually insoluble, the nanoparticle size can be controlled by thermal treatment.[19]

The second group includes mechanochemical methods (ball-milling), which make it possible to obtain nanocomposites by milling together mutually insoluble components in planetary mills or by decomposition of solid solutions to give new phases under exposure to mechanical stress.[23]

The third group of methods is based on the formation of spatially confined systems, that is, nanoreactors (micelles, droplets, films, *etc.*).[24–26] They also include synthesis in reverse micelles,[27] in Langmuir – Blodgett films[28] and in adsorbed layers.[29] Obviously, the size of the particles formed in this case cannot exceed the size of the corresponding nanoreactor,[30] hence these methods make it possible to obtain monodisperse systems. The biomimetic[31] and biological methods for nanoparticle syn-

thesis, where biomolecules (proteins, DNA, *etc.*) serve as nanoreactors, can also be attributed to this group.

The fourth group includes the methods based on the formation of ultramicrodisperse colloidal particles in solutions by polycondensation in the presence of surfactants that prevent aggregation.[32]

The fifth group comprises chemical methods for the synthesis of highly-porous and finely-dispersed structures (Rieke metals, Raney nickel) based on the removal of one component from a microheterogeneous system as a result of a chemical reaction or anodic dissolution. The traditional synthesis of nanocomposites by quenching a glass or salt matrix with a dissolved compound, which results in crystallisation of this compound in the matrix (glasses modified by semiconducting or metallic nanoparticles)[33] can also be classified as such a method. In this case, a compound can be introduced in a matrix in two ways: by adding it to a melt (solution) followed by quenching or by direct introduction into a solid matrix using ion implantation.[34]

Sol–gel synthesis is among the most widespread chemical methods for the synthesis of nanomaterials. It is used to obtain homogeneous oxide systems; chemical modifications of the latter (reduction, sulfidising, *etc.*) gives nanoparticles of the corresponding material in a matrix.[35–39] It should be noted that the sol–gel method makes it possible to obtain nanomaterials with improved functional properties by monitoring the composition and structure of the intermediate products.[40–42] It is also attractive because it can be implemented under laboratory conditions.[24] However, this method suffers considerable drawbacks. First, it does not ensure the formation of monodisperse particles. Second, it does not allow one to obtain anisotropic systems that can be synthesised in nanoreactors, such as two- and one-dimensional nanostructures as well as spatially ordered structures consisting of nanoparticles arranged at equal distances from each other or of parallel nanoplates interlaid with an inert matrix. Finally, in certain cases the required nanocomposite cannot be obtained due to the chemical reaction of particles with a gel-forming agent.

It should be noted that the use of free nanoparticles and nanostructures as materials is quite difficult due to the metastability of compounds in the nanocrystalline state. As noted above, this is caused by an increase in the specific surface of particles with a decrease in their linear dimensions to nanometres resulting in an increase in the chemical reactivity of a compound and in the enhancement of aggregation processes. In order to prevent the aggregation of nanoparticles and to protect them from external factors (*e.g.*, oxidation by atmospheric oxygen), nanoparticles are enclosed in a chemically inert matrix.[43]

Analysis of literature data shows that dozens of methods for matrix isolation of nanostructures have already been developed; these can be arbitrarily separated into two groups: i, synthesis of free nanoparticles followed by incorporation into an inert matrix and ii, direct formation of nanostructures in the bulk of a matrix in the course of its chemical modification.[12,44]

The first group of methods is easy to implement but the choice of the matrices is limited considerably. As a rule, polymeric organic compounds that do not have very high thermal stability and do not always have the required physical properties (*e.g.*, high optical transparency) are used as the matrices.[45] Furthermore, aggregation of nanoparticles during the incorporation cannot be prevented.[46]

The second group of methods makes it possible not only to avoid these drawbacks but also to directly monitor the parameters of nanoparticles in a matrix during the stage of their formation and even to change these parameters during the exploitation of a material. Matrices used for these purposes should contain structural cavities that can be occupied by compounds, subsequent modification of which would result in the formation of nanoparticles in these cavities.[47] In other words, these cavities should confine the zone of a reaction involving the compounds incorporated in them, *i.e.*, serve as specific nanoreactors. Obviously, it is possible to synthesise nanostructures with different morphology and anisotropy by choosing compounds with different shapes of their structural cavities.

The syntheses of nanomaterials with the use of porous oxide matrices (usually SiO_2 or Al_2O_3)[48,49] can serve as examples. However, due to the disordering of the porous structure of such matrices and the rather wide pore size distribution, it is almost impossible to obtain satisfactorily formed nanosystems by this method. Nanocomposites obtained in porous oxide matrices are usually employed in catalysis where the requirements for the monodispersity of particles are not too high.[50] Moreover, the rigid porous structures of such matrices do not allow the size and morphology of particles to be changed during the synthesis; as a rule, the latter parameters depend very strictly on the pore size and morphology,[51] that is, a very limited range of nanostructures can be obtained in a single type of matrix.

Sometimes, fast directed formation of nanoparticles in a matrix is achieved using additional physical effects, such as ultrasonic treatment as well as microwave and laser irradiation.[52–54]

III. Synthesis of nanoparticles in amorphous matrices

The first practical experience in obtaining nanoparticles in amorphous matrices, *viz.*, the preparation of coloured glass, dates back to the age of ancient Egypt.[4] However, the mechanism of colouring in such amorphous matrices was established only 100 years ago.[55] At present, crystallisation of glass is the main method for the synthesis of nanoparticles in amorphous matrices. It is known that the nucleation and growth of crystals in an amorphous matrix depend both on the heat treatment conditions of a glass and on its composition. The crystal size can be controlled by creating a certain concentration of nuclei, which is achieved by heat treatment of a glass at a relatively low temperature. The subsequent growth of crystals occurs at the higher temperature of annealing. It should be noted that the matrix composition changes during the crystallisation and hence the diffusion mobility of ions that constitute the crystalline phase also changes (decrease in the diffusion coefficient slows down the growth of particles and favours the formation of smaller particles of the disperse phase, whereas an increase in the diffusion coefficient favours the formation of larger particles).

Glass crystallisation has been used to obtain diverse nanoparticles of semiconducting, magnetic and catalytically active materials.[56–59] In particular, glasses doped with nanoparticles of semiconductors are widely used as optical filters. In the first place, they are attractive owing to their nonlinear optical properties, such as a considerable resonance effect, a dependence of the position of the absorption edge on the particle size, the doubling of the incident radiation frequency (generation of the second harmonic), *etc.*[60] The possibility of utilising glasses containing nanoparticles of high-coercivity magnetic phases (barium and strontium hexaferrites) as a medium for data recording and storage was considered.[61–68]

However, the glass crystallisation method does not provide nanoparticles with a sufficiently narrow size distribution, which is necessary for the manifestation of the quantum confinement effects or for the utilisation of such nanoparticles in technology.[66] This problem is solved by using porous materials with ordered pore structures, such as mesoporous silica and zeolites having one-dimensional channels or two-dimensional cavities.[67–69] It these cases, nanoparticles of filiform, layered or spherical shapes (depending on the type of the porous structure) with narrow size distributions were obtained.[67,70,71]

IV. Synthesis of nanoparticles in ordered matrices

Ordered matrices (or nanoreactors) are usually classified in accordance with the dimensionality of the pores they contain. Let us successively consider the synthesis of nanoparticles in zero-, one- and two-dimensional nanoreactors.

1. Synthesis of nanoparticles in zero-dimensional nanoreactors

Zero-dimensional nanoreactors are materials characterised by open porosity with an ordered arrangement of spherical pores. Such materials primarily include zeolites, *i.e.*, natural and synthetic aluminosilicates with the composition $M^{i}_{x}M^{ii}_{y}(Al_{x+2y}Si_{z}O_{2x+4y+2z})\cdot n\,H_2O$.[72] More than 150 types of zeolites, including about 30 natural ones, are known to date. Zeolite structures are built of $[SiO_4]^{4-}$ and $[AlO_4]^{5-}$ tetrahedra connected by common vertices into a three-dimensional framework penetrated by cavities and channels where water molecules and cations of alkaline (M^{i}) and alkaline-earth metals (M^{ii}) are located.

Unlike the framework atoms bound by covalent bonds, the cations located in the channels are bound with a matrix only electrostatically and can easily be exchanged for other cations in aqueous solutions.

Isomorphous replacement of aluminium atoms belonging to the framework by atoms of other elements, such as B, Ga, Fe, Co, Ti, or V, and exchange of cations incorporated in the pores allow one to modify the properties of zeolites in a desired direction. There are several factors that determine the possibility of isostructural replacement:[73]

— the similarity of the radii of the replaced and replacing atoms (the larger the difference in the radii the less energetically favourable the replacement);

— the replacement of a smaller atom by a larger one is possible provided that the coordination of the latter is smaller, and *vice versa*;

— the similarity of the electronegativities and ionisation potentials of the replaced and replacing atoms;

— the achievement of the minimum free energy during isomorphous replacement with retention of the coordination number.

The structures of zeolites are more open than those of other tectosilicates. The TO_4 tetrahedra (primary assembly units) form rings of various sizes and the rings are connected to give more complex structures (secondary assembly units). Each type of zeolites is characterised by a definite set of secondary assembly units. [It should be noted that the Si—O—Si angle can vary in rather a wide range (135–165°); as a result, the existence of silicon–oxygen rings with different numbers of atoms becomes possible.] Rings with five oxygen atoms, in which the Si—O—Si angle is about 145°, are more typical of zeolites with a high silicon content. Zeolites with a high aluminium content, which incorporate many Si—O—Al bonds, are mostly built of rings containing three or six oxygen atoms. The structures of natural zeolites most often contain rings with four or six oxygen atoms.

The classification of zeolites is rather a complex task. Each individual structure is described by the structural code comprising three Latin letters, *viz.*, the so-called IZA-code accepted by the International Zeolite Association Structure Commission (http://www.iza-structure.org/databases/). This code is applicable both to aluminosilicates and to some other compounds with similar structures containing atoms of elements (Si, Al, P, Ga, Ge, B, Be, *etc.*) in a tetrahedral environment.

The most general approach to the synthesis of zeolites is based on the joint hydrolysis of silicon compounds and compounds of a three-charged metal (most commonly aluminium) in the presence of an alkali and a quaternary amine (template). Organosilicon compounds that readily undergo hydrolysis, sodium silicate and silica gel with large surface area ($>200\ m^2\ g^{-1}$) are the most common sources of silicon atoms, whereas metal salts (sulfates, nitrates or chlorides) or alkoxides (isopropoxides, butoxides) are most commonly used as the sources of M^{3+} ions.

The schemes for the synthesis of zeolites with different compositions and structures are almost the same. The gels containing silicon and aluminium compounds are aged for prolonged periods of time below the crystallisation temperature (often under hydrothermal conditions) in the presence of templates. This time is necessary for a zeolite with a required structure to be formed in a high yield. The aging conditions and the nature of the templates play a decisive role in the structures of the zeolites formed.[74] The presence of template molecules increases the crystallinity of the aluminosilicate framework and affects its structure. Zeolites of some structural types can also be formed without a template. The structural type of the resulting zeolite also depends on the nature and concentration of the source of the three-charged metal.

The negative charge of the matrix in a zeolite is compensated by ions of alkaline metals, ammonium and/or alkylammonium (depending on the reagents used in the synthesis). Metal cations are generally removed by washing or by ion exchange for NH_4^+, since the presence of metal cations decreases the thermal stability of the matrices obtained. In order to remove the template, the ready zeolites are burnt off in a stream of oxygen at 500–550 °C, which converts them into the so-called H-form. The Si : Al ratio in zeolites is determined by standard methods of quantitative analysis.

Zeolites and similar porous materials are used as ion exchangers, selective adsorbents, catalysts and catalyst supports. The preparation of nanocomposite materials for catalytic purposes (isomerisation of aromatic hydrocarbons, treatment of NO and NO_2 gases) based on zeolites is a promising field of application of zeolites, hence it is not surprising that the majority of works in this field deal with the synthesis of nanoparticles of metals belonging to the 8–11th groups of the Periodic system. Zeolites of the FAU, LTA, SOD and MFI types are most commonly used as the matrices due to their accessibility and the facility of synthesis.[75–82] It should be noted that these matrices have a number of unique properties that are important for the directed synthesis of nanomaterials. Their structures are stable over a broad temperature range. The number of cations in the pores determined by the Al : Si ratio can be easily controlled during the synthesis, which allows one to vary the concentration of the reaction centres in the matrix.

Due to the open porosity of zeolites and the high diffusion rate of gases in the pores, chemical reactions involving intercalated cations can be carried out at elevated temperatures (*e.g.*, reduction with hydrogen required for the preparation of magnetic nanocomposites) almost without destruction of the matrix that confines the reaction zone. These properties open up rich possibilities for the chemical design of nanocomposite materials based on zeolites.

Nanomaterials based on zeolite Y (FAU type) are the most popular.[76, 77, 79–85] The structure of a Y-zeolite consists of the following secondary assembly units: 6-6 (hexagonal prism), 6-2 (hexagon and square with a common edge), 6 (hexagon) and 4 (square) (Fig. 2). The main structural motif of FAU zeolites consists of an octahedron truncated by a cube, *i.e.*, a sodalite cell or a small β-cage with an internal diameter of 0.66 nm comprising four-membered (the free diameter is less than 0.1 nm) and six-membered rings (the diameter is ~0.22 nm) from T-atoms. The vertices of the polyhedron contain 24 T-atoms, whereas the oxygen atoms are located between them. Connection of such polyhedrons through hexagonal prisms (cage diameter 0.36 nm) consisting of T- atoms gives the structures of zeolites (X and Y). They are charactised by a cubic symmetry (*Fm*3*m*) with lattice parameters of $a = 24.345$ Å (Fig. 3). The structure contains different types of cages: the α-cage (supercage) is the largest (its diameter is 1.2 nm) and is surrounded by eight truncated octahedrons; the β-cage (sodalite cage) is limited by a truncated octahedron; and the γ-cage is a hexagonal prism (see Fig. 2).

The main method for the preparation of nanocomposite materials based on zeolites involves the exchange of Na^+, H^+ and NH_4^+ cations contained in zeolites for cations of other metals in aqueous solutions followed by the reduction of the metal with hydrogen. For example, the preparation of a copper-containing zeolite by ion exchange of copper nitrate with a NaY-zeolite or by annealing a mixture of a NaY-zeolite with copper chloride at 420 °C was reported.[86] In the case of solid-phase annealing, the starting zeolite NaY was first stabilised by adding NaBr in order

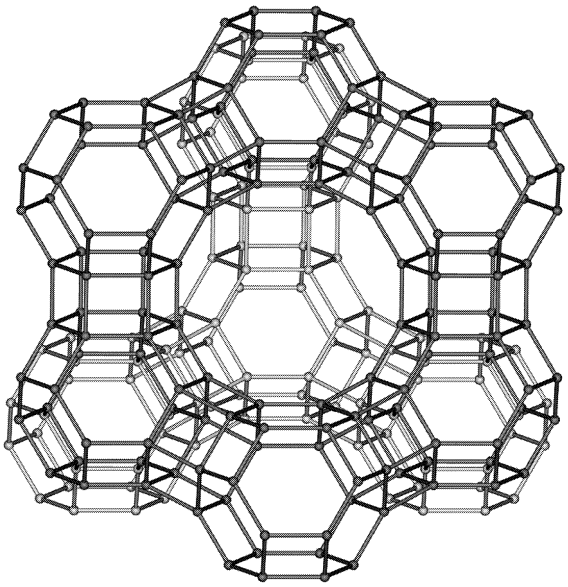

Figure 2. Structure of zeolite Y.

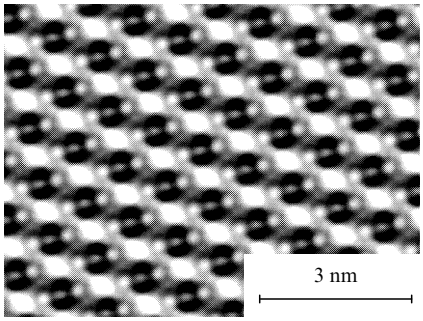

Figure 3. A photomicrograph of a NaY crystal along the [110] direction obtained by transmission electron microscopy (TEM).[76]

to fill the β-cages. This made it possible to introduce copper into α-cages and to increase the thermal stability of matrices. The reduction was carried out in a hydrogen atmosphere at temperatures of 300 – 600 °C. In both cases, the resulting copper particles (3 – 7 nm) were larger than the α-cages and the porous structure of the zeolite was damaged.

Au/NaY and Au-Fe/NaY nanocomposites were obtained in a similar way.[79, 82] Again, the nanoparticles resulting from the reduction of the metals were much larger than the size of the zeolite's α-cage.

Lanthanide-containing zeolites of the FAU structural type are formed upon ionic exchange of cations within zeolites with chlorides or nitrates of rare-earth metals.[83] Annealing at 500 °C of zeolites modified by this method gives oxides of rare-earth metals and results in a partial replacement of aluminium atoms in the zeolite structure by rare-earth atoms, which improves the thermal stability of the zeolite. At sufficiently high concentrations of lanthanides, their oxides are also formed outside the zeolite.

Aside from metal salts, complex cations can also be used. For example, the $Pd(NH_3)_4Cl_2$ complex was used[87] to obtain a palladium-containing zeolite. A Y-zeolite was soaked with a solution of the complex, annealed at 500 °C in a stream of oxygen and reduced with hydrogen at 400 °C. Samples with an overall palladium content from 1% to 10% were obtained using this method; at high palladium concentrations, the size of the nanoparticles that formed exceeded the size of the Y-zeolite cavity, which resulted in the destruction of the porous structure. In contrast, the sample containing 1% of palladium retained the structure of the original zeolite and its pores contained palladium particles with sizes about 1 nm.

Guillemot *et al.*[80] described the synthesis of gold nanoparticles with diameters of ~2 nm in a Y-zeolite matrix by soaking the zeolite with the $Au(en)_2Cl_3$ complex (en is ethylenediamine) followed by decomposing the complex at 250 °C in a stream of helium. According to X-ray photoelectron spectroscopy (XPS), the particles of gold occupied the α-cages of the zeolite.

Publications on the synthesis of nanoparticles of intermetallides† using zeolites have recently appeared. This method was used to obtain (Pt, Pd)-substituted zeolites.[88] Ammonia complexes of palladium and platinum were incorporated in a Y-zeolite by ion exchange. Thermolysis of metal complexes in a stream of oxygen at 300 °C followed by reduction in a stream of hydrogen at 300 °C produced nanoparticles of an alloy containing ~40% of platinum; however, data about the arrangement of the nanoparticles in the zeolite matrix are not available.

An Au – Pd intermetallide was obtained in a Y-zeolite using the $[Au(en)_2]^{3+}$ complex as the source of gold and $Pd(NH_3)_4^{2+}$ as the source of palladium.[89] Ion exchange was carried out in two stages. In the first stage, the palladium complex was introduced in the zeolite matrix; thermolysis of this complex in oxygen was accompanied by the formation of Pd atoms and their transfer to β-cages that are more favourable in terms of coordination. After that, ion exchange with the gold complex and reduction of the composite were carried out. The alloy was formed in the α-cage of the zeolite. Depending on the Au : Pd ratio and the composition of the starting zeolite, particles with sizes from 1 to 3 nm were obtained. Prolonged annealing resulted in the melting of the nanoparticles and their simultaneous growth (to 3.5 – 4 nm) as well as in a partial destruction of the porous structure of the zeolite.

Lázaro *et al.*[78] suggested a very interesting approach to the synthesis of clusters in zeolite cages based on the incorporation of hydrophobic compounds. Iron pentacarbonyl was used as the starting hydrophobic compound due to its ability to form iron clusters upon decomposition *in vacuo*; a dehydrated FAU-zeolite was used as the zeolite. Homogeneous incorporation of the carbonyl into the structure of the dehydrated zeolite could be expected, since the absence of internal OH groups on the cage walls makes their surfaces close to hydrophobic. In order to synthesise nanoparticles, a dehydrated NaY-zeolite was first soaked with iron pentacarbonyl at 77 °C and the pentacarbonyl was then thermally decomposed in a high vacuum. This resulted in superparamagnetic iron clusters with particle sizes from 1.5 to 2.0 nm (according to data from Mössbauer spectroscopy, more than 90% of the iron in the zeolite existed in the metallic state). Clusters were formed in pores, and the zeolite structure was not destroyed.

Carlsson *et al.*[76] studied the arrangement of iron oxide clusters in a Y-zeolite. The clusters were obtained by oxidation of iron pentacarbonyl in the matrix at low temperatures.[90] According to chemical analysis and electron diffraction data, the composition of iron oxide clusters is Fe_6O_n. The clusters are arranged in the β-cavities of the zeolite (Fig. 4); they are octahedra of iron atoms with a distance of 3.6 ± 0.15 Å between the latter. There are 76 $FeO_{1.5}$ units per unit cell of the zeolite.

It should be noted that the synthesis of nanocomposites in zeolites is not limited to matrices of the FAU structural type. There are a fair number of works dealing with the synthesis of nanocomposites in zeolites of the MFI structural type (as well as of the ZSM, MAS and other types) that correspond to one-dimensional nanoreactors.

An unconventional physical approach to the intercalation of chemical compounds into a zeolite matrix is described in a series of

† Nanoparticles of intermetallides are usually obtained by the substitution of ions in solutions containing either both cations or cationic complexes in the required ratio.

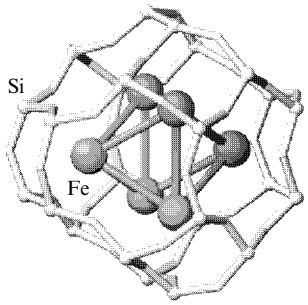

Figure 4. Schematic representation of a cluster in the β-cage of a Y-zeolite.[76]

works.[75, 91, 92]. Au_2Cl_6 was incorporated in dehydrated NaY through the gas phase in a high vacuum and then the gold was reduced to the 1+ oxidation state. As a result, AuCl clusters were formed in the zeolite pores.

It was also found to be rather promising to obtain functional optical materials based on nanoparticles of binary compounds in zeolite matrices. In such materials, it was possible to combine the properties of free nanoparticles with the solid-phase properties of the matrix. It should be noted that the open porosity of the zeolite matrix usually simplifies the reactions of compounds intercalated in it with gaseous reagents. For example, Garcia *et al.*[93] described a procedure for the preparation of a CdS/mordenite (MOR) composite. To do so, the starting zeolite $Na_8[Al_8Si_{40}O_{96}] \cdot 24\,H_2O$ (mordenite with a two-dimensional system of channels 0.65×0.70 nm and 0.26×0.57 nm) was treated with a cadmium nitrate solution, and sulfidised in a stream of hydrogen sulfide. The resulting nanocomposite contained cadmium sulfide particles with a diameter of ~60 nm that were much larger than the pore size. Although the zeolite lost crystallinity, the resulting nanocomposite partially retained the structural elements corresponding to the original mordenite structure. A NiS/Y nanocomposite was obtained in a similar way.[85] An NaY zeolite was placed in a $NiCl_2$ solution, dried (He, 400 °C, 2 h) and sulfidised (10% H_2S/H_2, 2 h) at different temperatures ($T = 25-400$ °C). In this case, the formation of large sulfide particles was observed as well.

A more successful example of using zeolites as nanoreactors is described in Ref. 84. Mixed sulfides of cobalt and molybdenum in a Y-zeolite were obtained by successive replacement of Na^+ ions by cobalt ions followed by incorporation of molybdenum hexacarbonyl into the zeolite in a stream of CO. According to chemical analysis, there are about two $Mo(CO)_6$ molecules per α-cage of the zeolite. The overall composition of the sample obtained at this stage is described by the formula Co(4 mass %)Mo(10 mass %)NaY. After that, the sample was sulfidised in a stream of H_2S at different temperatures (25–400 °C). The sizes of the resulting particles of mixed sulfides were 1–2 nm.

Zeolites are also widely employed as matrices for the synthesis of luminescent nanoparticles.[94]

At present, the complexity of studying the distribution of nanoparticles in a matrix by direct observation methods, such as transmission electron microscopy (TEM), is the main problem in the preparation of nanocomposites based on zeolites. Therefore, syntheses of nanocomposites isolated in matrices are most commonly based on matrices with ordered porous structures and with pore sizes of 2–50 nm. Such matrices include mesoporous molecular sieves and porous alumina.

2. Synthesis of nanoparticles in one-dimensional nanoreactors

The scope of materials that can be used as one-dimensional solid-state nanoreactors is not vast. It includes MFI-type zeolites, mesoporous molecular sieves and mesoporous structures based on alumina.

a. Zeolites of the MFI structural type

MFI type zeolites have an ordered system of channels with diameters ranging within 0.54–0.56 nm and with hexagonal packing (Fig. 5).[74, 95–100] Metal nanoparticles in channels of MFI-zeolites are usually obtained by ion exchange of protons (zeolite in the H^+-form) for metal cations or complexes followed by mild reduction in a stream of hydrogen.

It should be expected that the reduction of metal cations in the matrices of such zeolites would produce anisotropic nanoparticles (unfortunately, the size distribution of particles and their anisotropy were not studied due to the difficulties resulting from the small sizes of the channels).

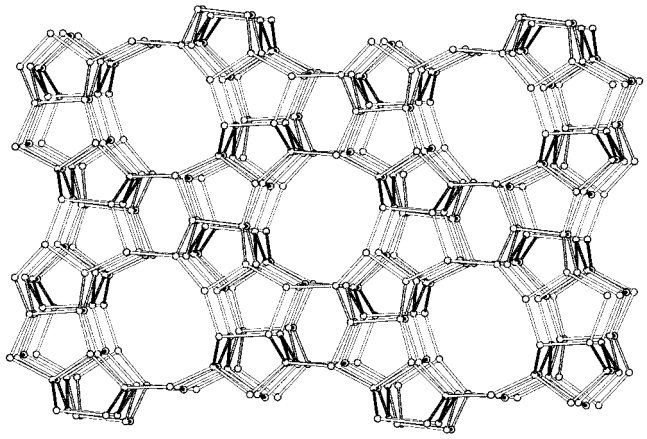

Figure 5. Structure of a zeolite with the MFI structural type.

b. Mesoporous molecular sieves

Mesoporous molecular sieves have been discovered by researchers of the Mobile Research and Development Corporation (USA) in 1992.[101] They synthesised a family of SiO_2-based molecular sieves (MCM-41) with a uniform and highly ordered distribution of pores, the size of which could be strictly controlled in the range from 2 to 10 nm, and with an extremely large specific surface area (~1000 $m^2\ g^{-1}$).

The template method is the most popular method for synthesising mesoporous SiO_2. A template is a centre around which the main structural units of a matrix are arranged and its framework is formed. Removal of a template produces a cavity with the same size and shape as those of the template. The accuracy of the 'printout' after the removal of the template depends on several factors: the nature of the template–matrix interaction, the ability of the matrix to assume the outlines of the template, the relative size of the template and the structural units of the matrix. The scheme of template synthesis is shown in Fig. 6.

Although the discovery of molecular sieves dates back to 1992, a 'template synthesis' was first described in 1949 in a study of gel formation by tetraethoxysilane (TEOS) in the presence of the methyl orange indicator (template). The silica gel formed upon condensation of TEOS selectively adsorbed methyl orange. Since that time, this rather simple and elegant method has become popular for the synthesis of numerous organic and inorganic materials.[30]

Let us consider the synthesis of molecular sieves for mesoporous SiO_2 (MCM) as an example. Samples of MCM are obtained by the polycondensation of silicon compounds [$Si(OMe)_4$ or $Si(OEt)_4$] in the presence of a template. Various molecules can serve as the template,[101–106] *e.g.*, noncovalently bound organic surfactants [as a rule, cetyltrimethylammonium bromide ($C_{16}H_{33}NMe_3Br$) is used].

Bifunctional molecules of cetyltrimethylammonium bromide are amphiphilic, *i.e.*, they contain a hydrophilic head group and a hydrophobic 'tail'. In aqueous solution, such molecules combine

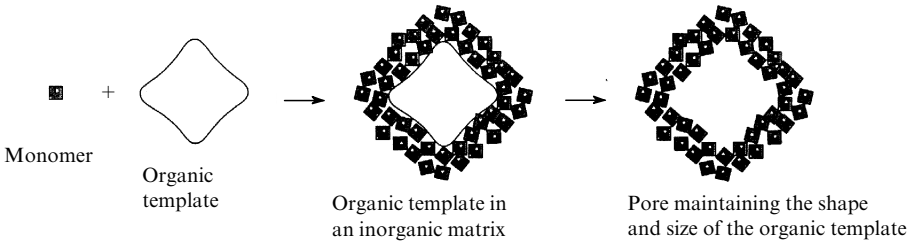

Figure 6. Scheme of template synthesis.

into micelles, in which the hydrophilic head groups form the external surface, whereas the hydrophobic 'tails' are oriented towards the centre. The extent of micellisation and the shape of micelles depend on the surfactant concentration. At high surfactant concentrations, micelles are aggregated into liquid-crystal phases the structure of which depends on the solution temperature and concentration. Figure 7 shows the phase diagram of the $H_2O-C_{16}H_{33}NMe_3Br$ system.[30]

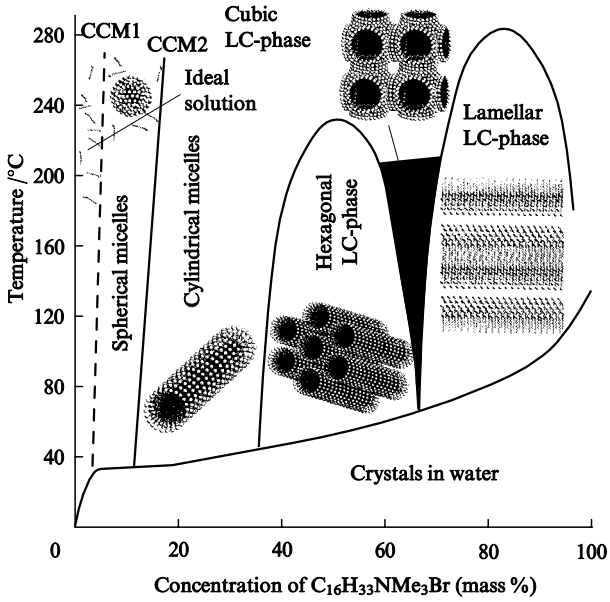

Figure 7. Schematic phase diagram of the $C_{16}H_{33}NMe_3Br-H_2O$ system (LC phase designates the liquid-crystal phase).[30]

A reaction mixture containing an aqueous solution of the surfactant, a tetraalkoxysilane and an acid (or alkali) is kept for a few hours at a constant temperature (80 °C). Hydrolysis of the tetraalkoxysilane produces mesoporous silica around the surfactant micelles.

Parameters affecting the gel formation include the pH of the solution, the nature and concentrations of the template and the organosilicon compound, the temperature, the type of the catalyst, *etc.*[103] Particular importance is attributed to the pH of the medium, more exactly, the ζ-potential that characterises the electrostatic interaction between the colloid particles and determines the structure of the polycondensation products. In the case of acid catalysis, the hydrolysis of a tetraalkoxysilane is probably the limiting step, whereas the condensation is relatively fast. As a result, weakly branched sol particles are formed.

Different types of template–matrix binding are possible. In our case, the template–matrix interaction occurs due to electrostatic forces, hydrogen bonds or van der Waals bonds.

Sodium silicate is sometimes used as the source of silicon.[105, 107] The types of mesoporous phases obtained by the method described are presented in Table 1 and in Fig. 8.

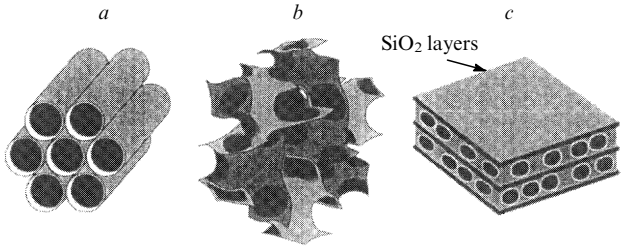

Figure 8. Possible structures of MCM-phases.[112] (*a*) hexagonal, (*b*) cubic, (*c*) lamellar.

Hydrothermal synthesis is an alternative method for the synthesis of mesoporous silica. A reaction mixture containing an aqueous solution of a surfactant and amorphous silica is subjected to prolonged hydrothermal treatment at about 150 °C. Such treatment results in the dissolution of silica accompanied by the rearrangement of its structure. Hydrolysed silicon oxide forms mesophases around the surfactant micelles.[113]

In the syntheses of MCM-41, the surfactant concentration in the starting solution is nearly always maintained below the critical micelle concentration (CMC1) (see Fig. 7), *i.e.*, the liquid-crystal phase is absent in the solution before the addition of a silicon source. This means that SiO_2 and a surfactant are mutually assembled into an organic–inorganic liquid-crystal phase during the reaction. It is assumed that ion exchange of the surfactant with multiply charged oligomeric silicate ions is the first step of the

Table 1. Types of mesoporous SiO_2 phases obtained by the template method.

Type of mesoporous SiO_2 phase	Template	Pore structure	Pore diameter /nm	Ref.
MCM-41	$C_nH_{2n+1}N^+Me_3X^-$ ($n = 6-22$, X = Hal, OH)	hexagonal (Fig. 8 *a*)	2–10	101
MCM-48	the same	cubic (Fig. 8 *b*)	2–5	108
MCM-50	"	lamellar (Fig. 8 *c*)	4	109
BSA-15	triblock-copolymers	hexagonal	5–30	104
MSU-V	$H_2N(CH_2)_nNH_2$ ($n = 12-22$)	hierarchic lamellar	1.3–2.7	110
MAS-5	$C_{16}H_{33}N^+Me_3Br^-$	hexagonal	3	111

formation of mesoporous materials if charged surfactants are used. Silicate ions are polydentate and can bind several surfactant molecules by shielding the repulsion forces between the head groups of the surfactant molecules, thus allowing micelles to increase in size. This effect is well known for simple surfactant–water systems. For example, the addition of electrolytes to $C_{16}H_{33}NMe_3Br$ solutions results in a transition from spherical to cylindrical micelles.[114] Hence, the interaction of surfactant micelles with silicate polyanions produces micellar rods encapsulated in silicate, which then spontaneously build a hexagonal structure.

It should be noted that this mechanism does not operate if neutral surfactants are used as templates. They have a much stronger tendency to form aggregates in water than charged surfactants (the CMC values for charged surfactants are about two orders higher than those of neutral surfactants with the same number of carbon atoms in the alkyl chain). The tendency of neutral surfactants towards aggregation combined with their tendency towards interaction with SiO_2 particles with the formation of hydrogen bonds is sufficient to create mesophases.[115]

The process for the preparation of porous amorphous silica usually includes three stages: synthesis of a gel, drying, and removal of the template. The diameter of pores in MCM-41 can be controlled during the synthesis by varying the type of the reagents used and the conditions of the synthesis. Drying of gels results in only a small shrinkage of pores and has only a small effect on their size, but considerably affects the gel structure. The method and conditions for template removal affect the final size of the pores but not their mutual arrangement. There is still no clear understanding about how the porosity can be controlled at each stage of the preparation of mesoporous SiO_2 (synthesis → drying → template removal) but certain factors determining the porosity have been studied quite thoroughly. For example, the pore size in the SiO_2–surfactant system can be roughly controlled by changing the surfactant 'tail' length. It was found that in the series of surfactants $C_nH_{2n+1}NMe_3Br$, n = 8, 10, 12, 14, 16, 18, the pore size in the resulting product increased by ~0.45 nm (Fig. 9 *a*,*b*) with each increase in n ($\Delta n = 2$). Yet another way to change the pore size is to introduce in the system a non-polar organic solvent [*e.g.*, mesitylene (Fig. 9 *c*,*d*)],[101,116] which is incorporated in the hydrophobic part of micelles during the synthesis, thus increasing their diameter.

The type of the template–matrix interaction affects the thickness of the SiO_2 walls. The silicate mesophases prepared using neutral surfactants have thicker pore walls ($\geqslant$1.7 nm) than the mesophases synthesised on the basis of ionic surfactants (0.8–1.3 nm).[115] There is no strong electrostatic interaction in the case of neutral surfactants; probably, this fact favours the further ordering and provides a product with thicker walls.

The capillary adsorption of gases at their liquid–gas transition temperatures is one of the main methods for the study of mesoporous phases. The results obtained by this method show that the specific surface areas of mesoporous phases are large (~1000 $m^2\ g^{-1}$) and the pore size distribution is narrow (Fig. 10). A detailed study of the gas adsorption in mesoporous matrices[117] showed that the pore size distribution can be calculated from data on the gas partial pressure above a sample (p/p_0) using a modified Kelvin equation:

$$r(p/p_0) = \frac{2V_L}{RT\ln(p/p_0)} + d(p/p_0) + 0.3,$$

where $r(p/p_0)$ is the pore size (nm); V_L is the molar volume of the gas used; γ is the surface tension factor of its liquid phase [$\gamma(N_2) = 8.88 \times 10^{-3}$ N m^{-1}],[117] $d(p/p_0)$ is the thickness of the liquid film adsorbed on the sample (calculated using the Harkins–Jura equation),[117] and 0.3 is the correction for the non-ideality of the system.

Studies of MCM-41 phases by electron microscopy and small-angle X-ray scattering (SAXS) showed that the samples have strictly ordered structures of pores uniformly distributed by size (Figs 9, 11).[118]

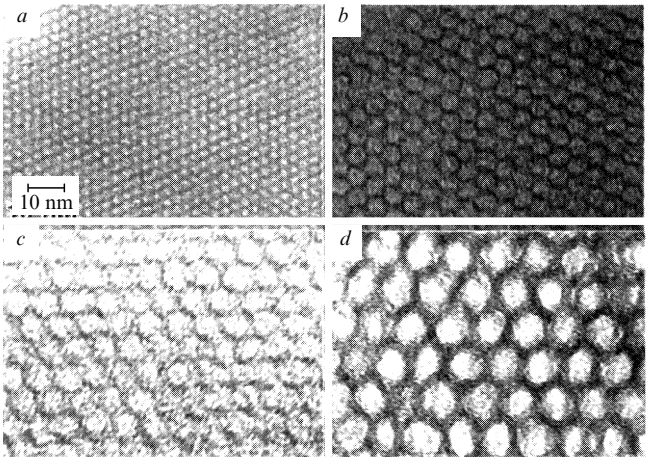

Figure 9. Photomicrographs of MCM-41 samples obtained by TEM.[101] (*a*) $C_8H_{17}NMe_3Br$ template, d = 2 nm; (*b*) $C_{16}H_{33}NMe_3Br$ template, d = 4 nm; (*c*) $C_{16}H_{33}NMe_3Br + Me_3C_6H_3$ template ($C_{16}H_{33}NMe_3Br$: $Me_3C_6H_3$ = 2), d = 6.5 nm; (*d*) same as above ($C_{16}H_{33}NMe_3Br$: $Me_3C_6H_3 > 3$), d = 10 nm.

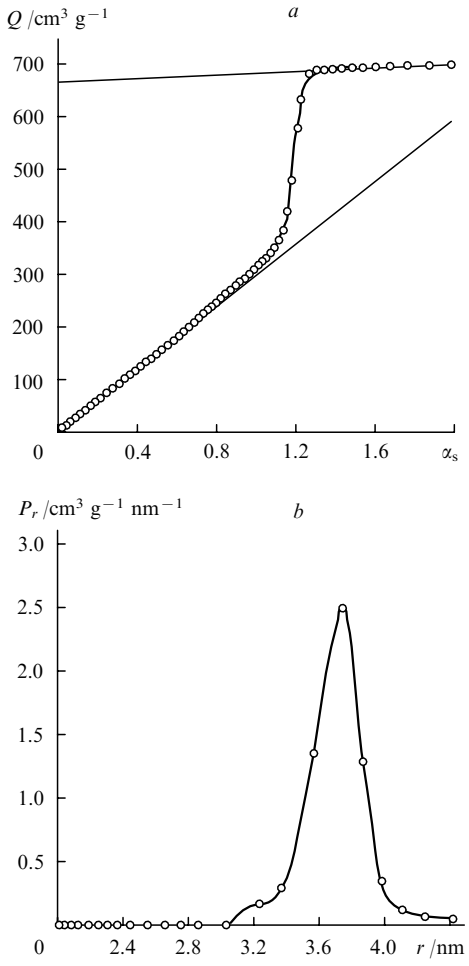

Figure 10. Standard adsorption curve (*a*) and pore size distribution (*b*) typical of MCM-41 molecular sieve.
Notation: α_s is standard adsorption, Q is amount of adsorbed gas, r is pore size, P_r is pore size distribution.

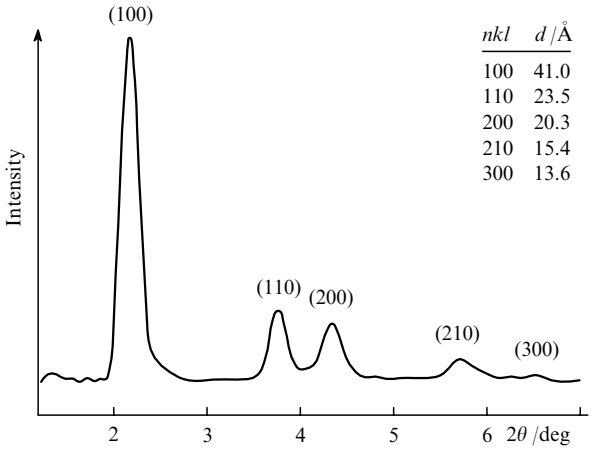

Figure 11. Small-angle X-ray scattering of an MCM-41 matrix.

All these facts make it possible to use materials based on mesoporous silica as catalyst supports, membranes, selective adsorbents, sensor materials and matrices for the preparation of various functional composite materials.

Films of mesoporous silica are of considerable interest since they can be used as media with low dielectric constants in the deposition of multiple-layer integrated circuits. Magnetic nanocomposites based on such films can be used for development of high-density information carriers.

There are various methods for the preparation of mesoporous SiO_2, many of which involve the chemical deposition of films from solutions. Obviously, the formation of mesophases in the synthesis of films occurs similarly to the synthesis of the corresponding bulk samples.

The orientation of films with respect to the plane of the substrate is one of the most important characteristics of films. In the case of mesoporous silica, special attention is paid to the mutual arrangement of the mesopores. As a rule, they are oriented parallel to a substrate, since the film – substrate interaction energy is a maximum for this orientation of micelles. For example, MCM-41 films have the (100)-orientation almost in all cases.‡ Syntheses of oriented films of mesoporous silica on glass, polymeric, graphite, mica and silicon substrates have been described.[119–121]

The ordering of pores in the substrate plane (*i.e.*, the formation of the rolling texture) is much more rare and is only possible if the substrate has a particular direction. The synthesis of epitaxial films of mesoporous SiO_2 on a Si (110) substrate can be

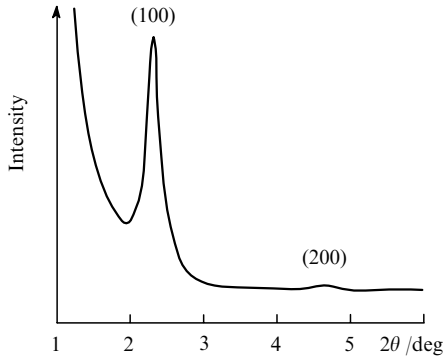

Figure 12. X-Ray diffraction pattern of a mesoporous silica film obtained on a Si (110) matrix.[119]

‡ It should be noted that the films formed at the liquid – gas interface also have the (100)-orientation.

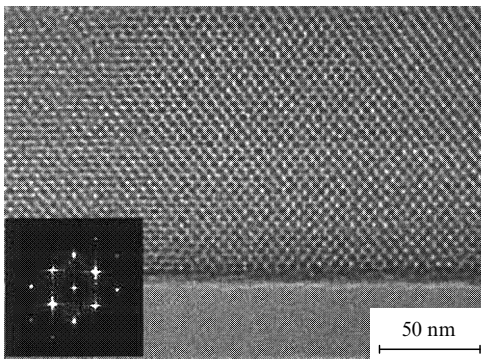

Figure 13. Photomicrograph of the cross section of a mesoporous silica film on a Si (110) matrix (the inset shows electron diffraction data).[119]

mentioned as an example.[119] Figure 12 shows the X-ray diffraction data for such films. The presence of the (100) and (200) diffraction maxima at 2θ values of 2.3° and 4.5° and the absence of the (110) peak suggest that the mesopores are oriented parallel to the substrate. Texture measurements showed that the pores in the substrate plane are oriented parallel to the [100] direction. These results are also confirmed by transmission electron microscopy data for a chip from a sample and by electron diffraction data (Fig. 13). At the same time, the SiO_2 films obtained on Si (100) and Si (111) substrates are not oriented in the substrate plane.

c. The use of mesoporous SiO_2 for the synthesis of nanocomposites

The application range of mesoporous phases and materials based on them is very broad due to their unique properties, such as the large specific surface area, the ordered system of mesopores, the uniform pore size distribution, the high diffusion rate of gases into the material bulk, *etc*. Mesoporous phases find use as catalysts [122] and catalyst supports;[123] matrices for conductive polyaniline [124] and carbon fibres;[125] tiny reactors for redox reactions;[126] selective membranes;[127] adsorbents with large surface area;[101] and porosity standards.[101]

In terms of structural parameters, the nanostructures synthesised inside cylindrical pores are subdivided into bulk nanoparticles, nanowires and nanotubes.[128] The methods for the synthesis of SiO_2-based nanocomposites can be classified into two groups. The first group includes the methods based on the impregnation of a porous material with metal salts followed by the chemical modification of the composite. For example, the synthesis of Ag and Cu nanoparticles in the mesoporous MCM-48 phase grade (mesoporous SiO_2 with cubic structure) was described.[39] MCM-48 samples were impregnated with solutions of $AgNO_3$ and $CuNO_3$ in ethanol and then dried to remove the solvent. During the evaporation of the solvent, the Ag^+, Cu^+ and NO_3^- ions were adsorbed on the silica surface. Reduction of the resulting composites resulted in Ag and Cu nanoparticles (Fig. 14) with sizes (~10 nm) exceeding the pore diameter of mesoporous silica (~3 nm). Presumably, in this case nanoparticles formed outside

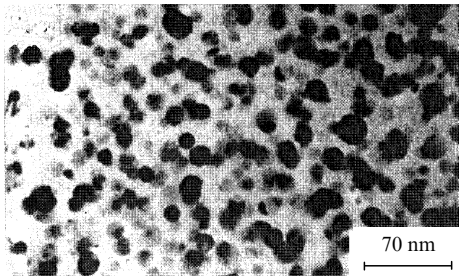

Figure 14. A TEM photomicrograph of mesoporous SiO_2 with incorporated Cu and Ag particles (Ag : Cu = 1 : 3).[39]

the pores. This probably resulted from low hydrophilicity of the inner surfaces of the mesopores [101] that complicated their impregnation with aqueous solutions.[129] As a result, the method for the synthesis of nanocomposites based on the impregnation of mesoporous silica with solutions of metal salts resulted in the formation of large particles.

The second group of methods is based on modifying mesoporous silica with metal complexes (in particular, complexes that form chemical bonds with silicon or oxygen atoms). The complexes can be incorporated in SiO_2 through the gas phase, by impregnation or by electrochemical treatment.

Jinwoo *et al.*[130] described the preparation of filiform Pd particles in the pores of mesoporous silica by incorporation of palladium hexafluoroacetylacetonate through the gas phase into the pores of an MCM-48 or MCM-41 matrix. Before the process, the matrices were annealed for 8 h at 400 °C. The precursor was incorporated into the pores *in vacuo* at 55 °C (as a result, the colour of the sample changed from white to yellow). The subsequent reduction of the palladium complex at 150 °C in a 10% H_2/N_2 mixture gave palladium nanowires (Fig. 15).

Incorporation of siloferrocenophane $[Fe(C_5H_4)_2SiMe_2]$ into the channels of mesoporous silica followed by polymerisation gave iron-containing particles.[128] It should be noted that the polymerisation of siloferrocenophane is accompanied by the formation of a chemical bond between the silicon atom of the complex and the oxygen atoms of mesoporous silica (Fig. 16 *a*), which allows one to decrease the mobility of the complex within the porous structure. Subsequent pyrolysis of the resulting composites in a stream of nitrogen at 900 °C results in the formation of iron monowires in a silica matrix (Fig. 16 *b*,*c*). Unfortunately, the nanoparticles obtained had nonuniform lengths (they filled the pores only partially) and thicknesses (the thickness nonuniformity can be explained by the partial melting of nanocrystalline iron during the annealing).

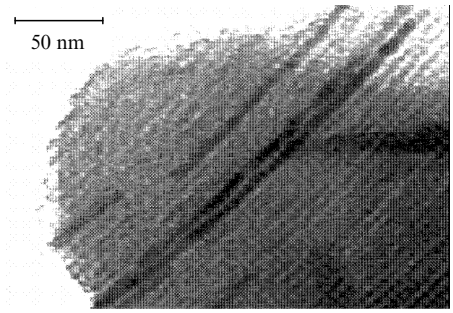

Figure 15. A TEM photomicrograph of Pd nanowires in an MCM-41 matrix.[130]

In the context of the synthesis of uniform particles, the study by Leon *et al.*[129] is of considerable interest. It reports the synthesis of germanium nanoparticles in a mesoporous silica matrix; these particles reproduce the shape and size of the pores. The nanoparticles were obtained by incorporation of Ge_2H_6 into the matrix through the gas phase at a high pressure (5–40 atm) at room temperature followed by thermal decomposition.

The synthesis of nanocomposites by incorporation of a metal complex into a mesoporous matrix in a liquid phase was described by Parala *et al.*[131] The nanoparticles of CdSe were obtained by impregnation of an MCM-41 mesoporous matrix with a solution of Me_2Cd and $(Bu_3P)_2Se$ in tributylphosphine followed by heating to 325 °C in trioctylphosphine oxide. As a result, CdSe nanoparticles with sizes of 3–5 nm formed inside the porous structure of MCM-41.

An alternative method for the synthesis of filiform iron nanoparticles was reported by Napolskii *et al.*[132] A nonpolar iron complex capable of decomposing at low temperatures with weak aggregation of nanoparticles was incorporated into the hydrophobic part of a liquid-crystalline micelle ($C_{16}H_{33}NMe_3Br$) in a mesoporous silica matrix (Fig. 17). $Fe(CO)_5$ was chosen as such a complex. The carbonyl complex was decomposed *in vacuo* under UV irradiation. The particles of metallic iron resulting from the decomposition (Fig. 18 *a*) were shown [133, 134] to contain a considerable fraction of amorphous iron; therefore, it was suggested to additionally crystallise iron particles in the channels of mesoporous silica by annealing in hydrogen flow at moderate temperatures.

The particles obtained after the annealing were characterised by a high anisotropy parameter, which was assessed using two independent methods: the temperature dependence of magnetic susceptibility and the small-angle polarised neutron scattering.[135–137] It was found that decomposition of $Fe(CO)_5$ at high temperatures resulted in a more complete crystallisation of iron, hence the nanocrystals grew lengthwise. Since the diameter of the nanoparticles does not change, this increases the geometrical anisotropy factor. For an iron-containing sample reduced at 375 °C, the anisotropy parameter equals 40, the coercive force is $\sim$450 Œ, and the saturation magnetisation is $\sim$3 emu g^{-1}. Thus, not only nanoparticles were obtained in the pores of mesoporous silica but also their distribution was made homogeneous.

A different approach to the synthesis of nanoparticles in the pores of mesoporous SiO_2 based on the hydrophilisation of the internal surfaces of a silica matrix by ethylenediamine was implemented by Zhang *et al.*[138] The nanoparticles of ZnO (a wide-gap semiconductor) § were obtained by adsorption of Zn^{2+}

§ The interest in ZnO nanoparticles is primarily due to the possibility of employing the latter in elements of short-wave electrooptical devices.

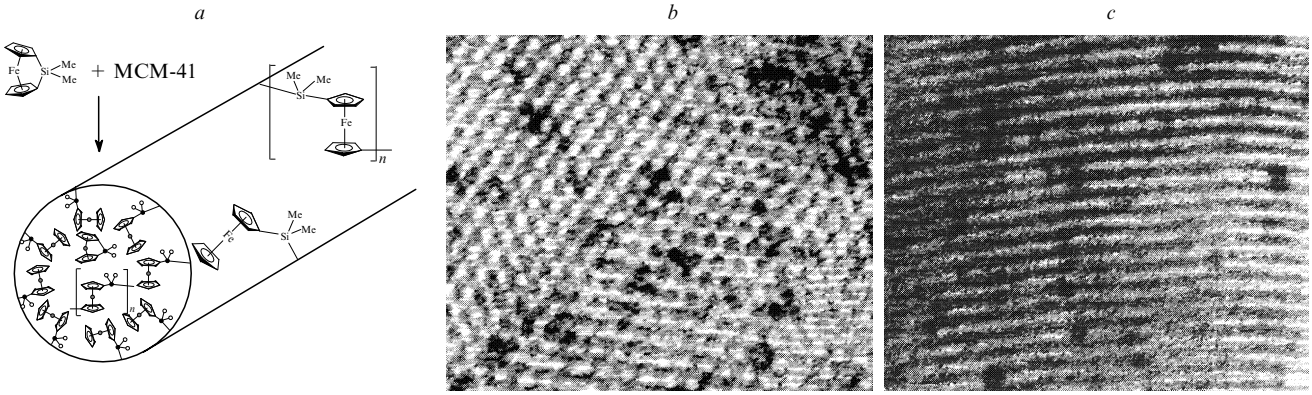

Figure 16. Scheme of the synthesis of iron nanowires in an MCM-41 matrix (*a*) and photomicrographs (*b*, *c*) of the resulting composites (*b* is cross section, *c* is longitudinal section).[128]

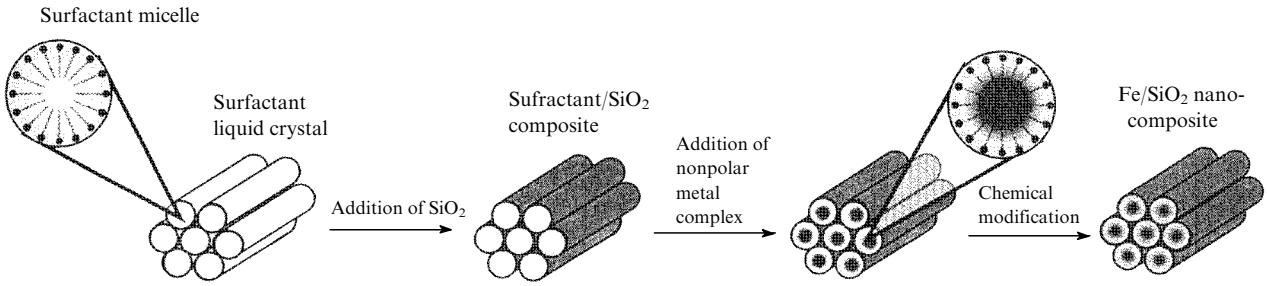

Figure 17. Scheme of synthesising iron nanowires in a mesoporous silica matrix.[132]

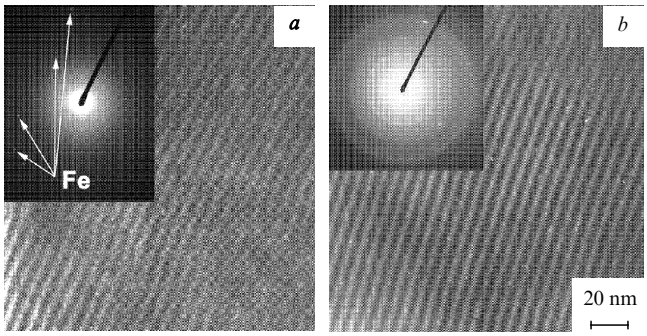

Figure 18. TEM image and electron diffraction (shown in the insets) of iron nanowires in a mesoporous silica matrix obtained by UV irradiation *in vacuo* (*a*) and additional crystallisation at 375 °C (*b*).[133]

cations on a porous silica surface modified with *N*-[3-(trimethoxysilyl)propyl]ethylenediamine followed by annealing in air at 600 °C. In principle, functional groups can be attached to both the internal and external surface of silica. In the latter case, this results in larger ZnO particles on the matrix surface. However, since the major part of the surface of mesoporous silica consists of the internal surfaces of the pores, the reaction of Zn^{2+} cations with ethylenediamine mostly occurs inside the porous structure. TEM data confirm the presence of zinc oxide nanoparticles in the pores of the mesoporous matrix and the absence of large particles on the external surface (Fig. 19). The content of zinc oxide in the samples reaches 9 mass %.

The absorption spectra suggest that the absorption edge of ZnO nanoparticles is shifted to the short-wave region (290 nm), whereas that of macrocrystalline ZnO is at 370 nm (3.1 eV). The considerable blue shift in the absorption spectra is caused by an

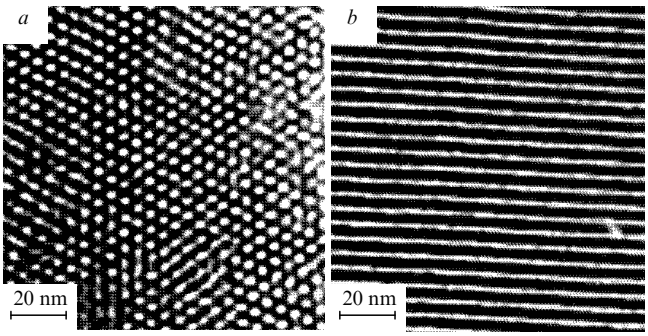

Figure 19. TEM image of ZnO particles in a mesoporous silica matrix;[139] (*a*) cross section, (*b*) longitudinal section.

increase in the band gap, which in turn is a manifestation of the quantum confinement effect. Studies of the photoluminescent properties of zinc oxide nanoparticles show the presence of a rather intense light emission in the blue part of the spectrum ($\sim$460 nm). The suggested method was tried for syntheses of other compounds, but it succeeded only in the case of cobalt oxide. Particles of precious metals such as silver, gold and palladium, as well as particles of nickel and copper oxides, could not be obtained using the method described above.

Particular interest is attracted by the synthesis of one-dimensional nanoparticles utilising films of mesoporous silica, including magnetic nanocomposites for data storage devices with ultra-high density of recording.

The rapid development of information technologies in the past years has necessitated the storage and processing of huge amounts of information, which has required that new devices with ultra-high areal density be created. Principally new magnetic materials with high-precision properties and nonlinear magnetic characteristics have been developed for these purposes.

According to literature data, ferromagnetic nanosized structures are the most promising magnetic materials for storage devices. However, materials based on spherical nanoparticles have low blocking temperatures and a near-zero coercive force at room temperature; therefore, it was suggested to use anisotropic nanoparticles.[139]

Yet another important requirement for magnetic materials based on nanoparticles is that magnetised nanoparticles must be firmly 'fixed' in a matrix to prevent their movement, aggregation and chemical interactions. This can be achieved by synthesising magnetic nanoparticles in nanoreactors. Utilisation of such particles instead of metallic alloys makes it possible to avoid the use of a protective layer on the magnetic data medium and thus to increase the resolution capability of the reading head.

Napolskii *et al.*[132] and Eliseev *et al.*[140] considered the prospects of magnetic nanocomposites obtained on the basis of epitaxial mesoporous SiO_2 films in storage devices with ultrahigh data density. It is known that mesoporous SiO_2 forms epitaxial films on certain supports [*e.g.*, on Si (110)]. It was found that the incorporation of a magnetic material (*e.g.*, iron) into the pores results in an ordered system of magnetic nanoparticles a few nanometres in diameter and several hundred nanometres long (Fig. 20).

Such particles are isolated from each other by silica walls; therefore, exchange interactions between them are sufficiently low.[141] Their geometrical anisotropy is yet another advantage that allows one to stabilise the magnetic moment of a separate particle and increase the coercive force. One more advantage should also be mentioned: the system of magnetic particles in a mesoporous silica reproduces the dimensions, shape and arrangement of pores, hence it is also ordered. This allows a reading head (for example, the tip of a magnetic force microscope) to be positioned with high precision when reading or writing data.[132]

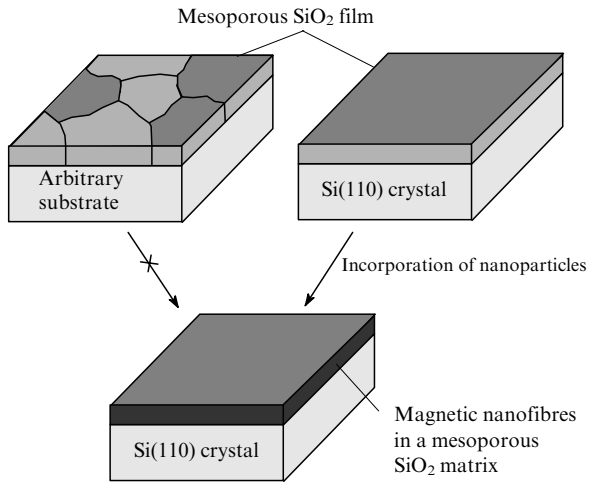

Figure 20. Scheme of growing of epitaxial films of Fe/SiO_2 nanocomposites for devices with ultra-high recording density.

d. Mesoporous aluminosilicates

Mesoporous materials based on silica with an ordered pore arrangement, in which a fraction of silicon atoms are replaced by aluminium atoms, are promising matrices for the synthesis of nanocomposites. Partial replacement of Si atoms by Al atoms in the silica structure creates a negative charge on the matrix, which is proportional to the amount of incorporated aluminium. Cations of transition metals can play the role of positively charged counterions located inside the pores; the number of such ions can be controlled by changing the content of aluminium in the matrix. Reduction of transition metal cations allows one to obtain nanocomposites with a predefined content of a metal phase in the aluminosilicate matrix.

Sasaki *et al.*[142, 143] synthesised platinum nano wires using mesoporous aluminosilicate FSM-16 with a hexagonal arrangement of pores ~ 3 nm in diameter. The matrix was annealed in an oxygen flow at 500 °C, impregnated with an H_2PtCl_6 solution and reduced under UV irradiation in the presence of a propan-2-ol vapour. This gave platinum nanowires 150 – 500 nm long (Fig. 21).

Subsequent utilisation of aluminosilicates for synthesising filiform nanoparticles of transition metals showed [141] that the morphology of nanoparticles in the samples depends on the Si : Al ratio in the aluminosilicate matrices. Nanocomposites containing filiform particles were obtained using aluminosilicate matrices with a small content of aluminium (< 10 mol.%). At higher aluminium concentrations in the matrix, not only nanofibres but also spherical particles with sizes of 3 – 10 nm formed; in this case, the total amount of the transition metal in the nanocomposite decreased. This is presumably explained by the formation of aluminium polyhydroxocomplexes that close the pores and prevent the incorporation of metal ions.

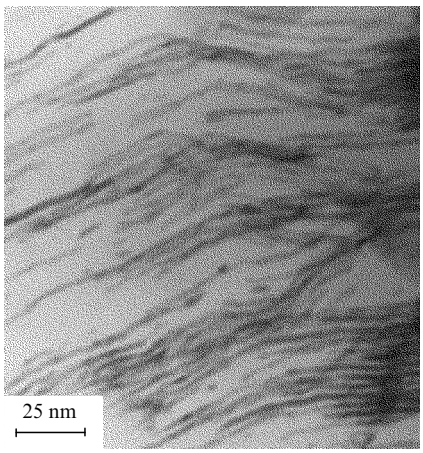

Figure 21. HRTEM photomicrograph of Pt nanowires in an FSM-16 matrix.[143]

Kolesnik *et al.*[144] and Eliseev *et al.*[145] compared the ion-exchanging properties of mesoporous aluminosilicates containing from 5 mol.% to 33 mol.% of aluminium obtained by cohydrolysis of silicon and aluminium compounds or by the hydrothermal method. It was shown that the parameters of ordering of the aluminosilicate structures depend on the hydrolysis rates of silicon and aluminium compounds.[146] It was found that $\sim 90\%$ of the overall number of aluminium atoms present in the reaction mixture are incorporated into the aluminosilicate structure, whereas the remaining 10% form polyhydroxocomplexes and block the pores.

e. Porous alumina

Films of porous alumina obtained by anodic oxidation are intensely studied in the context of their possible utilisation as templates in order to form nanostructured composites. The structures of such films contain an ordered pore system with the closest hexagonal packing, where the pores are arranged at right angles to the substrate surface. Their diameters and distance between the neighbouring pores can be varied in a broad range. The technology for the synthesis of porous alumina and its utilisation as a protective oxide coating has a long history. However, fundamental studies on the processes of self-organisation of nanostructures in a porous alumina matrix started only ten years ago. The latest achievements in the assembly of nanostructures using porous alumina were reviewed by Shingubara.[147] He also considered the utilisation of the resulting nanomaterials as high-density data storage media, functional nanosystems demonstrating quantum confinement effects, high-sensitivity chemical sensors, electronic devices with nanometre sizes and biochemical membranes. The main attention in our review will be given to synthetic approaches to the formation of nanocomposites with ordered structures of active sites in the porous alumina matrix.

The anodic oxidation of aluminium and its alloys in acidic electrolytes have been intensively studied for a long time due to their wide industrial utilisation. An early work [148] describes the structure of the porous alumina cell and the dependence of the lattice cell size on the voltage. A number of publications [149 – 151] report the assumed mechanism of the formation of mesopores during the electrolytic dissolution of aluminium. (Unfortunately, the nature of the nanopore self-organising process has not so far been established unambiguously.) Thompson *et al.*[151] studied the effect of several processes on the formation of nanoporous alumina, including the growth of alumina at the aluminium/alumina interface due to the transfer of Al^{3+}, OH^- and O^{2-} ions from the internal side of the oxide film to the external side, as well as the dissolution and deposition of alumina at the oxide film – solution interface. It is stated [152] that the morphology and conditions for the formation of a hexagonal ordered pore structure in alumina obtained by the anodic oxidation of aluminium in oxalic and sulfuric acids [153] are determined by the dependence of the coefficient of volume expansion of alumina on the anodising voltage and by the oxide formation rate. Nielsch *et al.*[154] assumed that the self-organisation of a structure requires a 10% porosity of the material, irrespective of other anodisation conditions. In other words, it is possible to obtain ordered porous alumina with any size of the lattice cell, provided that the applied voltage and the pH of the electrolyte satisfy the '10% porosity' rule. At present, the difference between the densities of alumina and metallic aluminium is also considered as an important factor for the formation of an ordered porous structure. Since the density of the oxide (~ 3900 kg m^{-3}) exceeds considerably the density of pure alumi-

nium (2698 kg m^{-3}) and electrochemical oxidation occurs only in a thin layer at the oxide film/metal interface, the increase in the density leads to the formation of an ordered porous structure.

The recent outburst of interest in the study of porous alumina was caused by the work by Masuda and Fukuda [155] who described the synthesis of a highly ordered porous alumina structure by two-stage oxidation. Initially, alumina with a highly ordered porous structure at the lower film boundary was obtained by the anodic oxidation of high-purity aluminium for 160 h at 0 °C in 0.3 M oxalic acid at a constant voltage of 40 V. The subsequent selective dissolution of the film in a mixture of 85% H_3PO_4 (35 ml $litre^{-1}$) and CrO_3 (20 g $litre^{-1}$) [156] at 80 °C gave aluminium with highly ordered relief of the surface. The second anodic oxidation of aluminium with such a roughened surface gave an oxide with a highly ordered nanopore structure. Such alumina can be used as a nanoreactor.

Figure 22 shows a typical structure of porous alumina obtained by two-stage anodic oxidation. Scanning electron microscopy data show the hexagonal packing of the nanopores. The mean pore diameter is 36 nm and the distance between the pore centres is ~90 nm. A cross-section of the porous structure (see the inset in Fig. 22) demonstrates the formation of the so-called 'barrier layer' ~30 nm thick with periodic roughness of the aluminium support. The neighbouring pores are separated by side walls ~50 nm thick.

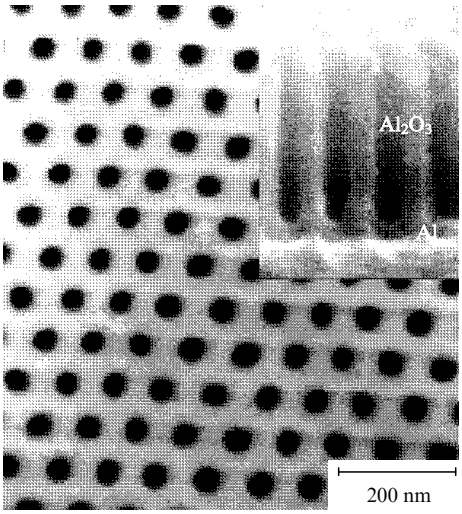

Figure 22. Typical structure of porous alumina obtained by two-stage anodic oxidation. The inset demonstrates the cross section of the film.

The choice of the acid in which the aluminium surface is subjected to anodic oxidation determines the size and geometric arrangement of the nanopores. The anodising voltage (V_a) which provides the formation of a porous alumina with highly ordered pore structure also depends on the acid.

Acid	V_a /V	D_{pore} /nm	D_{cell} /nm
H_2SO_4	25–27	>13	~55
$(COOH)_2$	40	>25	~90
H_3PO_4	195	>200	~500

The dependence of the mean cell size and the diameter of the pores on the voltage of anodic oxidation is shown in Fig. 23 for oxalic acid as the electrolyte.[157] The maximum ordering of the pores is achieved at a voltage of 40 V. The ordering increases with an increase in the duration of the first oxidation and the acid concentration. Masuda *et al.*[158, 159] also studied the conditions of the self-organisation of the porous structure of alumina obtained by the anodic oxidation of aluminium in sulfuric and phosphoric acids.

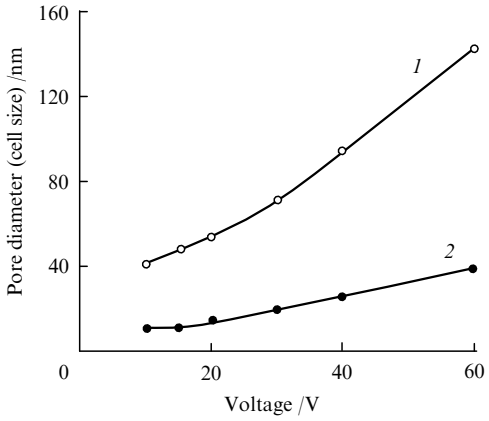

Figure 23. Dependence of the mean cell size (*1*) and pore diameter (*2*) on the anodic oxidation voltage in oxalic acid solution.[157]

Additional etching of the resulting porous material in appropriate acids makes it possible to widen the pores. The cell size of porous alumina differ slightly depending on the electrolyte used (at equal voltages). For example, the cell size in alumina obtained by anodic oxidation at 30–40 V in sulfuric acid is slightly smaller than in that obtained in oxalic acid.

Japanese researchers [160, 161] controlled the formation of mesopores by pretreatment of the starting aluminium surface. To do so, periodic mechanical defects were applied on an aluminium surface (by pressing aluminium with a silicon carbide having a preset surface periodicity at the mesolevel). The press-form was prepared using lithography and dry etching. This approach made it possible to obtain a well-ordered (by depth) pore structure (the ordering zone was 1 mm).

Yet another surface pretreatment method utilises the tip of an atomic force microscope (AFM) to apply defects on aluminium surface.[162] Using a diamond tip, it was found possible to create periodic depressions with a preset depth and geometric arrangement on aluminium surface. This method makes it possible to vary the structure of mesopores in a broad range. In particular, it was used to obtain a thin layer of alumina with a tetragonal pore packing. (As the thickness of the oxide coating increases, the porous structure tends to organise a hexagonal pore packing with a distance of ~90 nm between the pores.) The effect of the distance between the neighbouring defects on the organisation of the porous structure was studied. It was shown that the distance between the neighbouring pores could be varied from 65 to ~100 nm at a constant anodisation voltage of 40 V and that even a small mechanical strain ($\sim 5 \times 10^{-5}$ N) was sufficient for a controlled formation of mesopores by this method.

Alumina with an ordered mesopore structure was used for the synthesis of various nanomaterials. Porous alumina films are used as masks for etching certain materials, as templates for making polymer 'imprints' and as porous matrices for incorporating functional materials by electrochemical, sol–gel and CVD deposition.

Ion or plasma etching of semiconducting materials can serve as examples of the first process. In this case, the porous oxide structure of alumina is copied onto a substrate with a sufficiently high reproducibility.[163–165] Making an 'imprint' of a porous structure on a metal substrate by polymerisation of poly(methyl methacrylate) in the pores of alumina followed by dissolving alumina and sputter-deposition of a metal is a similar process (in this case, porous alumina plays the role of the template).[155] Incorporation of functional components into mesopores of an alumina matrix by electrochemical, sol–gel or CVD deposition is the most popular method for the synthesis of nanocomposites.

Studies of magnetic materials based on porous alumina were started a quarter of a century ago.[166–168] The main purpose of these studies was to create magnetic materials with ultrahigh data

density. The data density on modern data recording media reaches 100 Gb inch^{-2}, and the trend of the growth in the data carrier capacity has been maintained for over four decades. Currently, the possibility of creating materials with data density exceeding 1 Tb inch^{-2} is being studied.

Arrays of densely packed magnetic FePt nanoparticles (Fig. 24) is among the most promising magnetic materials;[169, 170] however, such particles with sizes of about 5–10 nm are in a superparamagnetic state and hence have a zero coercive force at room temperature. Ordered structures could not be obtained from these strongly anisotropic nanoparticles. Free FePt nanoparticles are generally unstable and tend to aggregation, which results in the necessity of creating a protective surface layer; the latter certainly decreases the prospects of using such structures as data media.

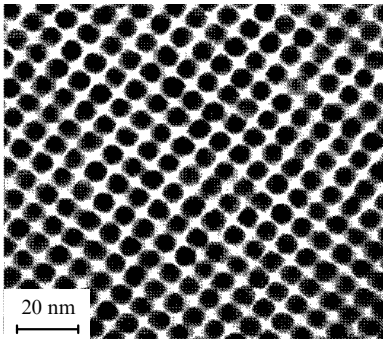

Figure 24. Array of densely packed magnetic FePt nanoparticles.[170]

It could be expected that magnetic nanofibres incorporated in a porous alumina matrix would satisfy the requirements for state-of-the-art data media. The simplicity of creating structures with high geometric anisotropy in the direction perpendicular to the substrate plane makes porous alumina very promising for the development of magnetic materials. Numerous publications are known that deal with the synthesis and study of nanoparticles of nickel,[171–176] iron,[172, 175, 177, 178] cobalt,[172, 175, 179–181] platinides,[173] lead [178] and alloys such as CoFe [182] and NiCo.[183]

Pulse deposition and electrodeposition with alternate current are the most efficient methods to synthesise metals in a porous alumina (deposition with direct current is accompanied by breakdown of the double electric layer, which results in the formation of large particles on the alumina surface). The use of electrodeposition of functional materials into alumina pores encounter a serious problem due to the existence of an Al_2O_3 barrier layer between the aluminium substrate and the lower boundary of a pore. Therefore, various methods have been developed for the removal of the barrier layer.[171, 184] The method for decreasing the barrier layer thickness by gradually decreasing the anodic potential [166] is recognised as the most successful. Yet another problem is that the formation of nanoparticles occurs at the porous structure–substrate interface and diffusion of solution ions to this interface is hindered; because of this, an important role in electrodeposition belongs to the time between successive deposition pulses.[171]

Magnetic Co nanowires with diameters of 10 to 60 nm and with distances of 60 to 120 nm between the adjacent wires (Fig. 25 *a*) were obtained using a porous alumina matrix synthesised by the anodic oxidation in oxalic or sulfuric acid. An HRTEM study of the cross-section of an array of nanofibres showed that the fibres consisted of partially aggregated cobalt nanoparticles (Fig. 25 *b*).[79]

An important advantage of the alumina matrix as a nanoreactor is that it is possible to obtain ferromagnetic fibres of different lengths by varying the duration of electrodeposition. Figure 26 shows the magnetic reversal curves for Co nanowires 5,

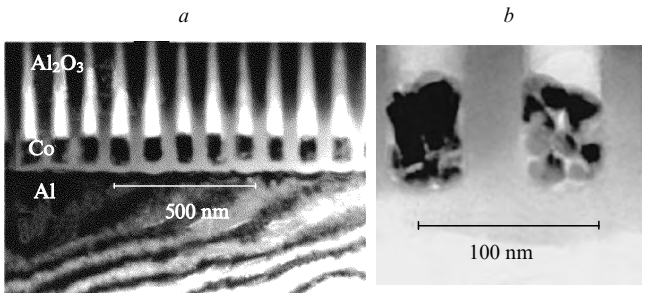

Figure 25. Cross section of an array of magnetic cobalt particles in a porous alumina matrix (*a* and *b* designate different magnifications).[79]

60 and 220 nm long. There are apparent differences in the magnetic anisotropy of such nanowires: cobalt nanowires ~5 nm long have a preferential anisotropy in the substrate plane, whereas longer wires (220 nm) are characterised by anisotropy in the direction perpendicular to the substrate. Thus, the magnetic anisotropy of ferromagnetic wires is mainly determined by the shape of the particles; this behaviour is typical of all ferromagnetic compounds. For iron fibres, there is a critical diameter corresponding to the maximum coercive force (2640 Œ) at room temperature [177] (at 5 K, no maximum on the 'coercive force–fibre diameter' plot was found).

In the $Fe_{1-x}Co_x$ system ($0 < x < 1$) obtained by controlled electrodeposition of the components,[182] a transition from the *bcc* crystal structure (Co content ~33%) to a mixed *hcp–fcc* structure (cobalt content ~67%) was observed. However, the coercive force was found to be almost the same for nanowires of both compositions and 9 nm in diameter: ~2900 Œ (for $Fe_{0.67}Co_{0.33}$) and ~2850 Œ (for $Fe_{0.33}Co_{0.67}$). Thus, the size and anisotropy of nanoparticles are the main factors determining the magnetic characteristics of ferromagnetic particles in the nanometre region.

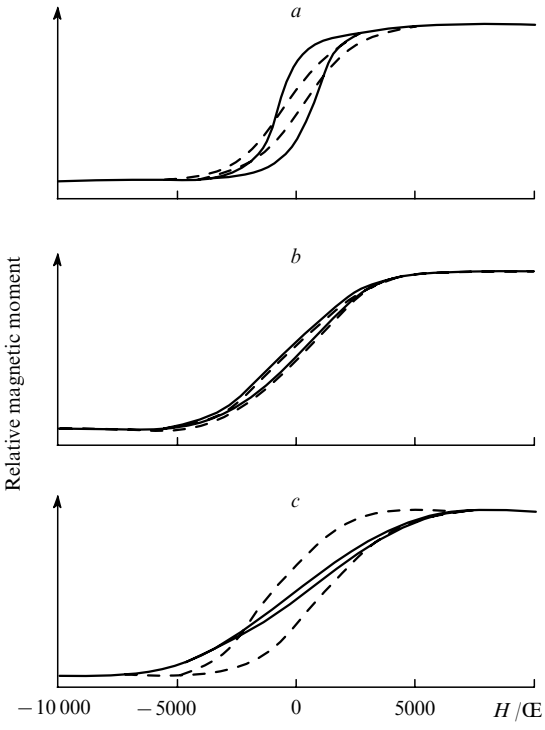

Figure 26. Magnetisation reversal curves for cobalt nanowires 5 nm (*a*), 60 nm (*b*) and 220 nm long (*c*) in a porous alumina matrix (solid line: the field is directed at right angle to the matrix plane; dashed line: the field is directed parallel to the matrix plane).

At the same time, decrease in the nanofibre diameter to 9 nm does not result in superparamagnetism. Calculations show that achieving a data density of about 1 Tb inch^{-2} requires that the distance between the adjacent nanofibres does not exceed 25 nm. This density has not been achieved to date.

In addition, optical nanostructured materials based on porous alumina arouse much interest because they possess a high luminescence intensity. Although the pore sizes in mesoporous alumina exceed the characteristic size required for the quantum confinement effect, it still has good luminescent properties that are not typical of bulk materials. First, porous alumina itself has luminescence in the blue region of the spectrum with a maximum intensity at 460 nm.[185] This emission band appears due to the formation of ionised oxygen vacancies (F^+-centres) in the strongly defective porous structure. The emission intensity can be further intensified by annealing the film at elevated temperatures.

High emission intensities were observed when the structure of mesoporous alumina was filled with zinc oxide. ZnO nanoparticles were synthesised in the matrix by hydrolysis of $Zn(OBu)_2$ in an aqueous medium.[186] The maximum luminescence intensity (485 nm) of zinc oxide nanoparticles approximately coincides with the maximum of irradiation from pure nanostructured ZnO, but the emission intensity of ZnO nanoparticles incorporated in a porous alumina matrix is almost 20 times higher, probably due to the increase in the number of ionised oxygen vacancies in ZnO nanoparticles located inside the alumina pores.

Several publications are available on the synthesis of optically active CdS nanowires prepared by electrodeposition;[187] and Bi_2Te_3;[188] titania doped with terbium or erbium (the sol–gel method);[189, 190] GaN nanoparticles (the sol–gel method),[164, 191] as well as dyes such as Rhodamine 6G and aluminium 8-hydroxyquinolinate[192] in a porous alumina matrix. It was suggested[184] to use anodised alumina for making electroluminescent materials; the aluminium substrate served as the cathode and a layer of conductive glass (ITO) served as the anode (the optically active component was incorporated into the pores). All these studies show the prospects of utilising nanostructures based on porous alumina films as electroluminescent materials.

Yet another use of porous alumina is related to the synthesis of two-dimensional photonic crystals. It is well known that photon band gap appears only if there is a highly ordered porous structure in sufficiently large areas. For this reason, the technology of aluminium pretexturing followed by anodic oxidation was developing in recent years.[157, 160, 161] This approach made it possible to obtain two-dimensional photonic crystals with a photon band gap in the visible spectral region.[193–197]

Porous alumina can be used to create field emitters based on carbon nanotubes. To do so, nanoparticles of metallic cobalt are electrochemically deposited in the pores of alumina (cobalt particles commonly used as catalysts for growth of carbon and carbon nitride nanotubes).[198–205] A photomicrograph of such an emitter is shown in Fig. 27.

Films of porous alumina are also promising as membrane materials. The transport of lithium ions[206] and other one-, two-[207] and trivalent cations[208] depends on the pore diameter, the pH of the medium and the ionic strength of the solution, as well as on the hydraulic permeability[209] of membranes. It is well known that the conductance of porous alumina considerably depends on the humidity. In view of this, an attempt was made to use a cell consisting of a layer of porous alumina compressed between metallic electrodes as a humidity sensor.[210] It was found that in the range from 50 to 100 ppm^{-1}, there is an almost linear dependence of the capacitance of this element on the air humidity, *i.e.*, such sensors are highly sensitive to humidity.

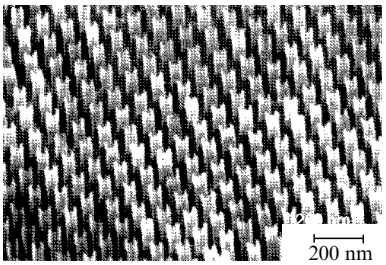

Figure 27. A scanning photomicrograph of a field emitter based on nanotubes synthesised in the pores of alumina.

It follows from the examples considered above that porous alumina is very a promising material for creating nanomaterials for magnetic data storage media, electronic devices, sensors and biomembranes. At present, methods for the synthesis of porous alumina with a pore diameter of $\leqslant 5$ nm are being developed in order to study quantum confinement effects, along with methods for the synthesis of porous membranes on solid semiconducting substrates characterised by high mechanical stability.

3. Synthesis of nanoparticles in two-dimensional nanoreactors. Layered double hydroxides

For two-dimensional nanoreactors, it is most efficient to use layered structures with variable dimensions of the structural cavities. The layers in such compounds are bound by weak van der Waals forces, hence the interlayer distance can be varied easily. Moreover, a layered structure allows one to accelerate considerably the diffusion of gases in the interlayer space and thus facilitate the chemical modification of layered compounds.[211, 212]

Several dozens of studies on the synthesis of nanocomposites using layered matrices have been published (see, *e.g.*, Refs 213–219). The compounds with negatively charged layers and cations in the interlayer space, *viz.*, aluminosilicates, are utilised the most widely. However, such compounds are generally nonstoichiometric, strongly hydrated and have cross-links between the layers; this complicates considerably the synthesis of nanomaterials on their basis and adversely affects the reproducibility of the results.[220, 221] This certainly prevents systematic studies on the mechanisms of nanostructure formation in layered matrices.

Layered double hydroxides (LDHs) with the composition $M^{2+}_{1-x}M^{3+}_x(OH)_2[X^{n-}_{x/n}\cdot m\,H_2O]$ (X is an anion) are the most widespread two-dimensional nanoreactors.[222] To date, compounds with $M^{2+} = Mg^{2+}$, Zn^{2+}, Fe^{2+}, Co^{2+}, Ni^{2+}, Cu^{2+}, Cd^{2+}, Sn^{2+}, Mn^{2+}, Pd^{2+}, Pt^{2+} and $M^{3+} = Al^{3+}$, Fe^{3+}, Cr^{3+}, Mn^{3+}, Ga^{3+}, In^{3+}, Bi^{3+}, Y^{3+}, La^{3+}, V^{3+}, Rh^{3+}, Ir^{3+} and Ru^{3+} have been obtained (see Refs 223–230). As a rule, the radii of the M^{2+} and M^{3+} cations participating in the formation of a layered structure should not differ more than 1.5-fold.[231] Virtually any anion or anionic complex can serve as the X^{n-} anion.[232] The structure of an LDH is a system of positively charged hydroxide layers $[M^{2+}_{1-x}M^{3+}_x(OH)_2]^{x+}$ and anions located in the interlayer space (Fig. 28).[233, 234] In addition to anions, the interlayer space commonly contains labile water molecules.[235] The LDH structure as a whole is stable due to the electrostatic interaction between the positively charged hydroxide layers and the interlayer anions bearing negative charges.

LDHs with the compositions $Li_{1-x}M^{3+}_x(OH)_2.[X^{n-}_{(2x-1)/n}\cdot m\,H_2O]$ $(x > 0.5)$[236] and $M^{2+}_{1-x}M^{4+}_x(OH)_2.[X^{n-}_{2x/n}\cdot m\,H_2O]$, where $M^{4+} = Zr^{4+}$, Ti^{4+}, Sn^{4+} or Se^{4+}, are also known (see Refs 237, 238). Moreover, cation-substituted layered hydroxides have been synthesised that contain several cations in oxidation states 2+ and/or 3+, *e.g.*, $M^{2+}_{1-x-y}(M')^{2+}_yM^{3+}_x(OH)_2[X^{n-}_{x/n}\cdot m\,H_2O]$ or $M^{2+}_{1-x-y}M^{3+}_x(M')^{3+}_y.(OH)_2[X^{n-}_{(x+y)/n}\cdot m\,H_2O]$.[239–241]

The vast majority of LDHs crystallise in the trigonal (rhombohedral) system. Hydrotalcite, a natural mineral with the composition $Mg_6Al_2(OH)_{16}[CO_3\cdot 4\,H_2O]$, has this structure. Compounds with the general formula $Mg_{1-x}Al_x(OH)_2[X^{n-}_{x/n}\cdot m\,H_2O]$ and with rhombohedral unit cells are called hydrotalcite-like compounds. Samples with the hydro-

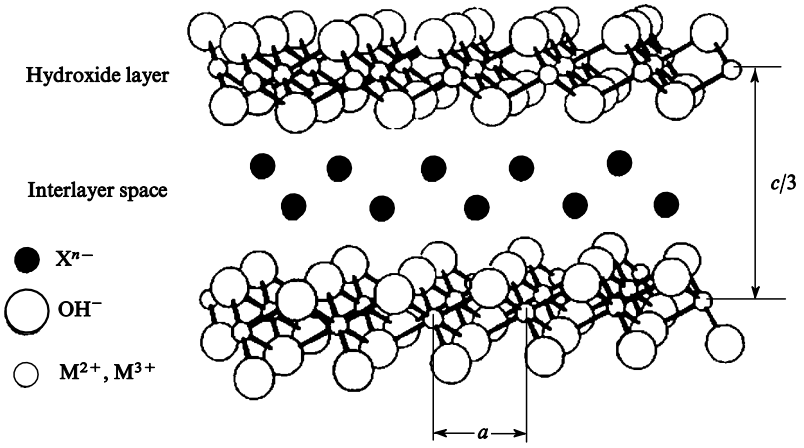

Figure 28. Structure of layered double hydroxides.

talcite structure and with x from 0.05 to 0.4 and m from 0 to 2 were obtained under laboratory conditions.

It should be noted that the arrangement of anions in the interlayer space can vary.[232, 242, 243] For example, the synthesis of LDHs with intercalated polyoxometallates, which have cylindrical symmetry, can result in two types of structures, *viz*., those with parallel and perpendicular arrangement of anions with respect to the hydroxide layers.[244] As a rule, anions are located in the interlayer space in such a way that its dimensions are minimised. However, as the $M^{3+}:M^{2+}$ ratio increases, the positive charge of the hydroxide layers also increases and more anions are required to compensate for it. If the charge of the anions is small, they can fail to fit in the interlayer space due to steric hindrance. Therefore, as the concentration of anions in the interlayer space increases, they need to be grouped into structures that are packed more densely. This is achieved either by arrangement of cylindrical anions at right angles to the hydroxide layers or by arrangement of anions in the interlayer space in two layers parallel to the hydroxide layers; in any case, this results in an increase in the interlayer distance. As a rule, if the unit cell parameter c and the anion size are known, it is possible to determine exactly which type of structure will be realised in a specific case.[245]

Layered double hydroxides have a number of unique properties that are important for the directed synthesis of nanomaterials. The stability of the layered structure of LDHs in a wide range of cation and anion sizes is among these properties. For example, samples of Mg-Al-LDHs containing various anions with sizes from 0.3 to 5 nm in the interlayer distance have been obtained. Furthermore, the number of anions present in the interlayer space of an LDH is determined by the $M^{z+}:M^{3+}$ ratio, which is easy to control during the synthesis. This makes it possible to obtain LDHs with preset stoichiometric compositions and hence to vary the concentration of reaction centres in a matrix.

The thermal stability of LDHs is yet another important property (thermal decomposition of LDHs occurs with retention of their layered structure). As a result, chemical reactions involving anions located in the interlayer space (*e.g*., reduction with hydrogen required for the preparation of magnetic nanocomposites) can be performed at elevated temperatures almost without destruction of the matrix that confines the reaction zone.

These properties open up rich possibilities for the chemical design of nanocomposite materials based on LDHs. First, the wide choice of cations makes it possible to choose a matrix that would satisfy the entire set of properties required from a material. For example, a diamagnetic matrix can be chosen for the synthesis of magnetic nanomaterials, or a matrix that is optically transparent in a specific spectral region can be selected for the preparation of optical nanocomposites. Second, by varying the $M^{2+}:M^{3+}$ cation ratio (*i.e*., the x value) and selecting a particular anionic complex and a chemical modification method, it is possible to vary widely the size and shape of nanoparticles.

Coprecipitation of hydroxides of M^{2+} and M^{3+} metals with an alkali from solutions of their salts at a controlled pH is the main method for synthesising LDHs.[246] To obtain an LDH with desired anions in the interlayer space, the coprecipitation is carried out in the presence of these anions in the initial solution:

$$(1-x)\,M^{2+} + x\,M^{3+} + 2\,OH^- + (x/n)\,X^{n-} \longrightarrow$$
$$\longrightarrow M^{2+}_{1-x}M^{3+}_{x}(OH)_2[X^{n-}_{x/n}].$$

It should be taken into account that if two or more types of anions are present in the solution, one of them will be incorporated preferentially.[247] The ability of anions to undergo preferential incorporation into the interlayer space is often called the selective intercalation constant of an anion. It depends both on the nature of the LDHs and on the conditions of the synthesis (pH, temperature).

A number of techniques are used to obtain LDHs with different anions in the interlayer space. LDHs in the carbonate or chloride form are usually utilised as the starting compounds.

Coprecipitation in the presence of an anion (the method described above). This method is very easy to implement but it does not allow one to obtain LDHs containing just one type of anions in the interlayer space. For this reason, it is only used where the required anion has a high selective intercalation constant.

Direct exchange of anions. This method is based on the anion-exchange properties of LDH.[248] If hydrotalcite (the carbonate form of LDH) is placed in a solution containing the required anion X^{n-}, partial exchange of carbonate ions for X^{n-} occurs, *i.e*., intercalation of the required anion into the interlayer space:

$$Mg_{1-x}Al_x\,(OH)_2[(CO^{2-}_3)_{x/2}] + (x/n)\,X^{n-} \rightleftharpoons$$
$$\rightleftharpoons Mg_{1-x}Al_x(OH)_2[X^{n-}_{x/n}] + (x/2)\,CO^{2-}_3.$$

Since the CO^{2-}_3 anions have a high selective intercalation constant, their complete displacement requires that hydrotalcite be repeatedly treated with a solution of X^{n-} (see Ref. 249). The main advantages of the ion-exchange method include its simplicity and the possibility of obtaining practically pure anion-substituted LDHs. However, the use of the ion exchange method does not allow one to obtain LDHs with large anions that generally have low selective intercalation constants. According to Drezdzon,[250] anion exchange is practically impossible if the size of X^{n-} exceeds 0.6–0.7 nm.

Syntheses of LDHs containing large anionic complexes by anion exchange usually involve sonication. For example, the synthesis of Mg-Al- and Zn-Al-LDHs containing anionic complexes of heteropolymetallates with sizes up to 1.5 nm by

exchange of NO_3^- anions for the corresponding anionic complexes on ultrasonic treatment of the system was described.[251,252]

Interaction of an X^{n-} solution with layered double oxides (LDOs). The method is based on the so-called 'memory effect' that is shown by LDOs obtained by thermal decomposition of LDHs. This effect was found by Chibwe and Jones[253] who showed that treatment of Mg-Al-LDOs with a dilute solution of a salt results in their rehydration to give LDHs with solution anions intercalated into the interlayer space:[254]

$$Mg_{1-x}Al_x(OH)_2[(CO_3)_{x/2}] \xrightarrow{150\ ^\circ C} \longrightarrow Mg_{1-x}Al_xO_{1+x/2} + H_2O + (x/2)\,CO_2,$$

$$Mg_{1-x}Al_xO_{1+x/2} + (x/n)\,X^{n-} + (1+x/2)\,H_2O \longrightarrow Mg_{1-x}Al_x(OH)_2[X^{n-}_{x/n}] + x\,OH^-.$$

Melt technique is based on the intercalation of carboxylate anions into LDHs. This method was implemented by heating a mixture of a solid carboxylic acid and hydrotalcite (or the corresponding LDO) at a rate of no more than 10 deg min^{-1} to a temperature $\sim$10 °C higher than the melting point of the acid.[255] The mixture was kept for 8 h at this temperature and then cooled to room temperature at a rate of $\sim$10 deg min^{-1}.

Many functional properties of materials based on LDHs are related to the special properties of anions intercalated into them. For example, the high reactivity of catalysts based on LDHs is usually due to the catalytic properties of the intercalated ions or products of their thermal decomposition. Depending on the nature of the anion, LDHs can show various magnetic, optical and electrophysical properties. For example, the presence of polymeric anions in the interlayer space induces unusual viscoelastic properties.[248,256]

Due to the sufficiently high interlayer distance in LDHs, diffusion of gases into the interlayer space occurs rather fast. This property is very important for the creation of catalysts and sensor materials with short response times. Moreover, the large interlayer distance makes it possible to perform the chemical modification of LDHs with various gaseous reagents without damaging the layered structure.

Layered double hydroxides are widely employed as catalysts for various organic reactions. Hydrotalcite-like LDHs with intercalated ions of polyoxometallates and Ni-containing LDHs obtained by thermal decomposition or reduction of various nickelates to metallic nickel by treatment with hydrogen are used most widely.[257–259]

Tichit *et al.*[260] describes a hydrogenation catalyst obtained by reduction of $Ni_{2.82}Al(OH)_{7.64}[(NO_3)_{0.17}(CO_3)_{0.41}\cdot 2.46\,H_2O]$ with hydrogen (T = 700 °C). It is a composite consisting of particles of metallic nickel and Al_2O_3; the sizes of these particles are several hundred nanometres. This catalyst is currently among the best nickel-based hydrogenation catalysts.[261]

There are several reasons that explain the popularity of LDH-based catalysts. First, owing to the high specific surface area and the presence of a rather wide interlayer space, they show a high catalytic activity. Second, a hydroxide matrix is an inert carrier for polyoxometallates that does not impair their catalytic properties over the entire lifetime of the catalysts. Third, both hydrotalcite-like LDH-catalysts in the polyoxometallate form and Ni-containing LDH-catalysts can operate at temperatures up to 800 °C without losing their catalytic properties and without a considerable decrease in the specific surface. Finally, the bulk distribution of the catalytic sites (polyoxometallates or metallic nickel) in such catalysts is very homogeneous, which increases the relative catalytic activity per unit mass. Moreover, the preparation of LDH-based catalysts is not too difficult. In fact, LDH-catalysts with polyoxometallate ions intercalated into them became strong competitors for classic oxide catalysts (SiO_2, Al_2O_3) impregnated with salts of various polyoxometallates.[262–264]

Some LDHs find use as solid electrolytes and electrodes due to the ionic conductance they possess.[265–268] The rather high ionic conductance of LDHs results from the high mobility of anions in the interlayer space. For example, the conductance of $Zn_2Cr(OH)_6[Cl\cdot m\,H_2O]$ at 17 °C is $10^{-3}\ \Omega^{-1}\ cm^{-1}$. Replacement of chloride ions by other anions decreases the conductance of this LDH to $10^{-4}\ \Omega^{-1}\ cm^{-1}$ (see Ref. 269). The authors called such compounds 'quasi-two-dimensional' electrolytes due to their high ionic conductance and layered structure. The ionic conductance of LDHs enables their practical application in sensors.[270,271]

The existence of rigid hydroxide layers that confine the interlayer space in the LDH structure creates conditions for the synthesis of nanosystems similar to conditions for their synthesis in nanoreactors.

The possibility of synthesising nanostructures with the use of LDHs was studied by a number of scientific groups. For example, the synthesis of a composite of cadmium sulfide nanoparticles and a solid solution of cadmium and zinc sulfides in the interlayer space of LDHs was reported.[272] An Mg-Al-LDH with intercalated $Cd(edta)^{2-}$ complex was used as the starting compound. The latter was obtained by treatment of an Mg-Al-LDO with an aqueous solution containing the above complex. Unfortunately, the EDTA-complex of cadmium used in this study was contaminated with nitrate ions that were also intercalated into the interlayer space. As a result, a compound with the composition $Mg_{0.654}Al_{0.346}(OH)_2[\{Cd(edta)\}_{0.075}(NO_3)_{0.196}\cdot 1.13\,H_2O]$ was obtained.

The size of the interlayer space in this compound was 0.285 nm (X-ray diffraction data). Since this distance matched the size of the Cd complex in the planar four-coordinate state (0.280 nm), it was assumed that the $Cd(edta)^{2-}$ complex was arranged in the interlayer space parallel to the hydroxide layers. The substituted LDH was sulfidised with sodium sulfide. The formation of cadmium sulfide follows from the change in the LDH colour from white to yellow and the appearance of cadmium sulfide reflections in the X-ray diffraction diagram. In fact, according to X-ray data, the interlayer distance in the LDH virtually did not change during the sulfidising, while the reflections of cadmium sulfide broadened considerably. Presumably, the sulfide was formed in the interlayer space of the LDH as plates no thicker than the interlayer distance (0.285 nm). However, this conclusion disagrees with spectrophotometric analysis data, according to which the absorption band edge for the samples obtained lies in the region of 460–480 nm; these values correspond to particles larger than 10 nm. This fact probably suggests that cadmium sulfide is most likely formed not only in the interlayer space but also on the surfaces of LDH particles. This conclusion is supported by the fact that sulfidising inevitably involves the anion exchange of interplanar ions for sulfide ions from the solution. In this case, sulfidising of the deintercalated cadmium complex should occur directly on the surfaces of the LDH particles.

Sato *et al.*[213,219,273–275] obtained nanosized cadmium and zinc sulfides using other layered compounds such as montmorillonite $\{(Na,K,Ca)(Al,Fe,Mg)[(Si,Al)_4O_{10}](OH)_2\cdot n\,H_2O\}$, $H_4Nb_6O_{17}$ and $H_2Ti_4O_9$.

Isupov *et al.*[276–281] studied the thermolysis of Li-Al-LDHs containing EDTA-complexes of certain transition metals. They showed that the thermal decomposition of $LiAl_2(OH)_6[\{M(edta)\}_{0.5}\cdot 2\,H_2O]$ (M = Cu, Co, Ni) *in vacuo* in an Li-Al oxide matrix resulted in nanoparticles of the transition metal M and that the size and morphology of the nanoparticles depended on the metal selected and on the decomposition conditions.

Thermolysis of Cu-containing LDHs at 400 °C gives spherical copper particles with sizes of 2–5 nm (in the interlayer space of the matrix) and 5–80 nm (on the surface), whereas thermolysis of Ni-containing LDHs gives spherical nickel particles with a $\sim$5 nm diameter and a very narrow size distribution. An increase

in the thermolysis temperature to 800 °C results in a growth in the particle size to 15 nm with a simultaneous broadening of the distribution. At the same time, thermolysis of Co-containing LDHs at 400–800 °C results in large (~100 nm) metal particles in the shape of disks, the size and morphology of which is virtually independent of the thermolysis temperature. It was shown that the reduction of the metal in the complex starts almost simultaneously with the end of the dehydration of the layered matrix. The formation of nanosized particles was explained by the influence of the matrix on the reduction process. Unfortunately, no conclusions were made concerning the reasons for the changes in the dependence of the size and morphology of the nanoparticles on the metal chosen and on the thermolysis conditions. It should be noted that decomposition of LDHs is accompanied by pyrolysis of the organic ligand to give amorphous carbon; as a result, final product is considerably contaminated with admixtures of metal carbides and the material loses its functional properties.

The formation of LDHs and the synthesis of nanocomposites on their basis were also studied by Tretyakov *et al.*[66, 282–292]

They performed[286, 291, 292] a detailed study of the anisotropy of iron and nickel nanoparticles obtained by reduction of anion-substituted Mg-Al-LDHs with different compositions in a stream of hydrogen at different temperatures (300–1000 °C). Based on electron microscopy data and magnetic measurements, the concentration dependences of the transverse and longitudinal anisotropy of metal nanophase reduced at different temperatures (see Ref. 66) were plotted. It was shown that, depending on the composition of the starting anion-substituted LDHs, metal nanoparticles with different dimensionality, *viz.*, from one- to three-dimensional, were formed in this system. An increase in the content of the metal complex in the LDH matrix resulted in a decrease in the dimensionality of the nanoparticles that formed and an increase in the anisotropy factor. It should be noted that the reduction temperature almost did not affect the morphology of the nanoparticles formed: an increase in the reduction temperature increased only the mean size of the nanoparticles, whereas their anisotropy changed insignificantly.

Yet another direction of studies by this group of researchers involved the synthesis of semiconducting nanostructures in the MS/Mg–Al–O system (M = Pb, Zn, Cd).[289, 290, 293, 294] They showed that direct sulfidising of Pb, Zn and Cd complexes intercalated in LDH in a stream of hydrogen sulfide at room temperature is unsuitable for the synthesis of MS/LDH nanocomposites. Therefore, they suggested using LDH systems where the formation of sulfides resulted from the decomposition of an intercalated sulfur-containing metal complex. Thiosulfate, thiocyanate and diethyldithiocarbamate compounds of Pb, Zn and Cd were used as such complexes. Decomposition of the latter ($T_{decomp} < 200$ °C)¶ in the interlayer space occurred without degradation of the LDH structure. For example, PbS/LDHs were obtained by thermal (100–200 °C) or photochemical (UV irradiation at 77 K) decomposition of $Mg_3Al(OH)_8 \cdot [\{Pb(S_2O_3)_2\}_{0.5} \cdot m\,H_2O]$.[290]

A considerable amount of attention was paid to the optical properties of the products obtained. High-resolution spectroscopy in the visible and UV spectral regions showed that the absorption edge for the PbS/LDH samples obtained by thermal treatment was within 500–750 nm. An increase in the annealing temperature shifts the absorption edge to the long-wave region, which indicates an increase in the particle size. Calculations show that the particle size changes insignificantly and lies within 3–5 nm for all the samples obtained. The spectrum of the sample obtained by UV irradiation shows additional maxima at ~580, ~400 and ~300 nm (Fig. 29) [for comparison, Fig. 29 also shows the spectra for the sample obtained by thermal decomposition (dashed line)]. These values are in good agreement with the $1S_e-1S_h$, $1S_e-1P_h$ and $1S_h-1P_e$ exciton transitions of lead sulfide.

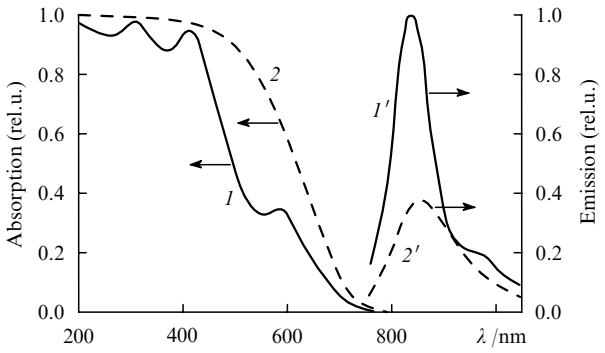

Figure 29. Absorption (*1*, *2*) and photoluminescence spectra (*1′*, *2′*) of PbS/LDH nanocomposites obtained by thermal decomposition at 200 °C (dashed line) and by decomposition under UV irradiation (solid line).[290]

These transitions are usually not observed in the spectra of PbS but they appear in the spectra of the PbS sol synthesised in the presence of polyvinyl alcohol.[295] Similar spectra were also obtained for nanoparticles of lead sulfide stabilised by protein molecules.[296] It is believed that the appearance of forbidden exciton transitions in PbS spectra is due to the modification of the nanoparticles' surfaces.

The photoluminescence spectra of the samples obtained by annealing at 200 °C and by UV photolysis are shown in the right part of Fig. 29. Each spectrum is characterised by the presence of two peaks at λ = 840 and 910–940 nm: the first one corresponds to the luminescent transition over the band gap, whereas the second one corresponds to the transition over the energy levels formed by surface defects. It should be noted that the integral intensity of the luminescence peak of the main state (transition over the band gap) for the sample obtained by UV irradiation is about four times higher than that for the sample obtained by annealing at T = 200 °C, which suggests that the quantum yield of luminescence increases.

The products of thermal and UV-induced decomposition of LDHs with intercalated $Pb(S_2O_3)_2^{2-}$ ions were studied by HRTEM.[290] A detailed study showed (Fig. 30)[290] that the PbS nanoparticles in the sample synthesised by UV photolysis have an amorphous shell, whereas those in the sample obtained by thermal

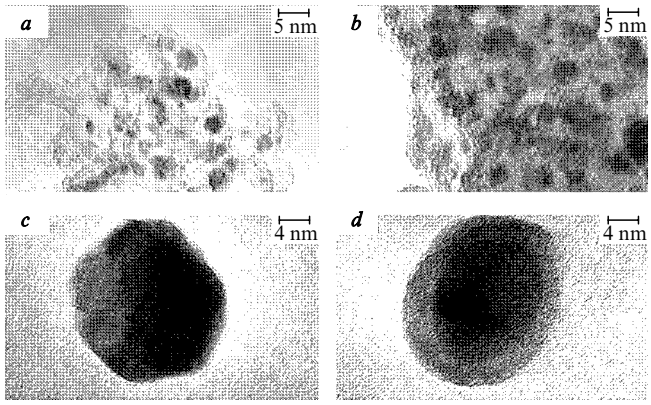

Figure 30. High-resolution electron photomicrographs of PbS particles in an LDH matrix obtained by thermal decomposition at 200 °C (*a*) and by decomposition under UV irradiation (*b*) (*c*, *d* are detailed photomicrographs of the largest particles).[290]

¶ It should be noted that in this case, the layered structure of the LDH affects the formation of semiconducting nanoparticles much more strongly than in the case where magnetic nanocomposites are synthesised by reduction at much higher temperatures than the destruction temperature of the LDH structure.

decomposition at 200 °C do not have such a shell. It is believed that the shell consists of amorphous sulfur that results from the UV-induced decomposition of the thiosulfate complex at low temperature; the absence of a similar shell in the sample obtained by thermal treatment is explained by the melting of elementary sulfur (m.p. = 119 °C). Most probably, the fact that nanoparticles of lead sulfide have an amorphous shell explains the appearance of exciton transitions in the absorption spectra and the increase in the photoluminescence intensity.

It should be noted that the optical properties of semiconducting nanoparticles depend not only on their composition, structure and size but also on the condition of the surface. It was shown that many defects on nanoparticle surfaces (*e.g.*, adsorbed atoms or structural point defects) can serve as potential holes or barriers for holes and electrons.[15] As a result, a change in the band structure and degradation of the optical properties of the nanosystem occur; the smaller the particles the more sensitive these changes to defects. In order to prevent such changes, passivation is used that makes it possible to bind the surface atoms with some other compound having a wider band gap.[297, 298] In other words, the particles are coated with a layer of an inert compound to give the so-called 'core–shell' nanoparticles. This improves considerably the optical properties of nanoparticles; as a result, these properties approach those of isolated nanoclusters.

The passivation effect is especially pronounced in luminescent properties of nanosystems.[299] In fact, the quantum yield of luminescence for coated nanoparticles of cadmium sulfide or selenide is considerably increased (almost by an order of magnitude) in comparison with free nanoparticles.[300, 301] According to literature data, the synthesis of nanoparticles in a shell is rather a complex multistage task. However, the authors succeeded in performing a one-stage synthesis of nanoparticles in a shell using anion-substituted LDHs. The interest in 'core–shell' systems is primarily related to the fact that the presence of a shell of a semiconductor with a large band gap or a dielectric results in the 'healing' of the majority of surface defects and an abrupt increase in the quantum yield of luminescence. Therefore, nanoparticles in shells show promise for creating lasers based on quantum points with adjustable wavelength and high generated power.

Yet another specific feature of LDHs is that destruction of the layered structure into separate hydroxide layers is possible. In fact, in the reaction of a dodecylsulfate-substituted Zn-Al-LDH $\{Zn_{0.67}Al_{0.33}(OH)_2[(C_{12}H_{25}SO_4)_{0.33}\cdot 2.1\,H_2O]\}$ with butanol at 120 °C, the layered structure is destructed in 24 h to give a colloid solution [302, 303] in which separate hydroxide layers are surrounded by surfactant molecules. Shaking this solution with aqueous solutions of salts results in sedimentation and recovery of the layered structure of the LDH (restructuring of the layered structure). In this case, solution anions are incorporated in the interlayer space. Hibino and Jones [304] described the destruction of the layered structure of an Mg-Al-LDH, which contained glycine anions in the interlayer space, on treatment with formamide. It was noted that the process occurred rather quickly even at room temperature.

A study of the reversible LDH for a pre-destructured sample of $Mg_2Al(OH)_6[(C_{12}H_{25}SO_4)\cdot m\,H_2O]$ showed that total recovery of the layered structure of the destructured LDH sample occurred in water and in aqueous solutions.

The reversible destruction of LDH into hydroxide layers may turn out to be rather promising for synthesising nanocomposite particles. It can be assumed that restructuring of a colloid solution of LDH layers in the presence of nanoparticles would result in the incorporation of the latter into the interlayer space of the LDH. In fact, the reaction of a colloid solution of a dodecylsulfate-substituted LDH in chloroform with a PbS sol gave a PbS/LDH nanocomposite.[289] The PbS particles formed in the matrix of the layered double hydroxide have sizes of 3–8 nm. The considerable broadening of the (00*l*) reflexes of the LDH and the low intensity of other reflexes suggest a violation of the mutual arrangement of the hydroxide layers due to intercalation of the PbS nanoparticles into the interlayer space. The accessibility of the starting reagents, the simplicity and cheapness of the synthesis, the facility of controlling the quantitative composition of the intermediates and final products and the possibility of incorporating various anions into the LDH structure make this method very promising for the synthesis of virtually any class of functional nanocomposites.

* * *

It should be noted in conclusion that utilisation of nanoreactors opens up rich possibilities for designing functional nanomaterials with predefined physicochemical characteristics that can find use in various fields of science and technology (*e.g.*, magnetic data storage devices, electronic devices, sensors, catalysts, membrane materials, *etc.*). A solid-state matrix makes it possible to avoid the aggregation of nanoparticles and protect them from external exposures, which facilitates considerably the application of such materials.

This review was financially supported in part by the Russian Foundation for Basic Research (Project No. 03-03-32182) and the programme for the State support of the leading scientific schools of the RF (Project NSh-2033.2003.3).

References

1. R W Siegel, E Hu, M C Roco (Eds) *Nanostructure Science and Technology: a Worldwide Study* (Washington, DC: NSTC, 2001)
2. A I Gusev, A A Rempel' *Nanokristallicheskie Materialy* (Nanocrystalline Materials) (Moscow: Fizmatlit, 2000)
3. M C Roco (Ed.) *Nanotechnology: Shaping the World Atom by Atom* (Washington, DC: American Chemical Society, 2000)
4. A S Edelstein, R S Cammarata (Eds) *Nanomaterials: Synthesis, Properties and Applications* (Bristol: Institute of Physics, 1998)
5. M Rieth, W Schommers, S Baskoutas *Mod. Phys. Lett. B* **14** 621 (2000)
6. I P Suzdalev, P I Suzdalev *Usp. Khim.* **70** 203 (2001) [*Russ. Chem. Rev.* **70** 177 (2001)]
7. K E Drexler *Nanosystems, Molecular Machinery, Manufacturing, and Computation* (New York: Wiley-Interscience, 1992)
8. R A Andrievskii, A M Glezer *Fiz. Met. Metalloved.* **89** 91 (2000) [a]
9. C Suryanarayana *Bull. Mater. Sci.* **17** 307 (1994)
10. R W Siegel, in *Springer Series in Materials Sciences* (Ed. F E Fujita) (Berlin: Springer, 1994) p. 65
11. P Moriarty *Rep. Prog. Phys.* **64** 297 (2001)
12. A D Pomogailo, A S Rozenberg, I E Uflyand *Nanochastitsy Metallov v Polimerakh* (Nanoparticles of Metals in Polymers) (Moscow: Khimiya, 2000)
13. C Suryanarayana, C C Koch *Hyperfine Interact.* **130** 5 (2000)
14. Y Kawazoe *Clusters and Nanomaterials: Theory and Experiment*. (Berlin: Springer, 2001)
15. A D Yoffe *Adv. Phys.* **50** 1 (2001)
16. P Marin, A Hernando *J. Magn. Magn. Mater.* **215** 729 (2000)
17. M Nogami, in *Sol-Gel Optics, Processing and Applications* (Ed. L C Klein) (Dordrecht: Kluwer Academic, 1994) p. 329
18. J H Fendler, I Dekany (Eds) *Nanoparticles in Solids and Solutions* (Dordrecht: Kluwer Academic, 1996)
19. J Lu, H Yang, S Yu, G Zou *Mater. Chem. Phys.* **45** 197 (1996)
20. P V Ananthapadmanabhan, K P Sreekumar, N Venkatramani, P K Sinha, P R Taylor *J. Alloys Compd.* **244** 70 (1996)
21. S R Shinde, A G Banpurkar, K P Adhi, A V Limaye , S B Ogale, S K Date, G Marest *Mod. Phys. Lett. B* **10** 1517 (1996)
22. A A Menovsky, J P Liu, H J Gelders, B J Harrison, H Ellermeyer, Y K Huang *Mater. Sci. Eng. A, Struct. Mater. Prop., Microstruct. Process.* **217** 227 (1996)
23. S BeginColin, F Wolf, G LeCaer *J. Phys. III* **7** 473 (1997)
24. B D Summ, N I Ivanova *Usp. Khim.* **69** 995 (2000) [*Russ. Chem. Rev.* **69** 911 (2000)]
25. J H Fendler *Chem. Mater.* **8** 1616 (1996)

26. P Vaqueiro, M A López-Quintela, J Rivas *J. Mater. Chem.* **7** 501 (1997)
27. M P Pileni, N Moumen, I Lisiecki, P Bonville, P Veilett, in *Nanoparticles in Solids and Solutions* (Eds J H Fendler, I Dekany) (Dordrecht: Kluwer Academic, 2002)
28. I Dekany, in *Nanoparticles in Solids and Solutions* (Eds J H Fendler, I Dekany) (Dordrecht: Kluwer Academic, 1996) p. 293
29. I Dekany, L Turi, G Vanko, G Lukasz, A Vertes, K Burger, in *Nanoparticles in Solids and Solutions* (Eds J H Fendler, I Dekany) (Dordrecht: Kluwer Academic, 1996) p. 555
30. N K Raman, M T Anderson, C J Brinker *Chem. Mater.* **8** 1682 (1996)
31. R S Kane, R E Cohen, R Silbey *Chem. Mater.* **8** 1919 (1996)
32. J H Fendler, F C Meldrum *Adv. Mater.* **7** 607 (1995)
33. R K Jain, R C Lind *J. Opt. Soc. Am. B* **73** 647 (1983)
34. K S Min, K V Shcheglov, C M Yang, H A Atwater, M L Brongersma, A Polman *Appl. Phys. Lett.* **68** 2511 (1996)
35. S V Kalinin, A V Lukashin, K V Tomashevich, A V Knot'ko, M P Nikiforov, S Yu Stefanovich, A A Vertegel, Yu D Tretyakov *Dokl. Akad. Nauk* **364** 207 (1999) [b]
36. S V Kalinin, A V Lukashin, M P Nikiforov, A A Eliseev, A A Vertegel, Yu D Tretyakov *Dokl. Akad. Nauk* **363** 777 (1998) [b]
37. E Cordoncillo, P Escribano, G Monros, M A Tena, V Orera, J Carda *J. Solid State Chem.* **118** 1 (1995)
38. M Nogami, Y Abe *Appl. Phys. Lett.* **65** 2545 (1994)
39. G De, L Tapfer, M Catalano, G Battaglin, F Caccavale, F Gonella, P Mazzoldi, R F Haglund Jr *Appl. Phys. Lett.* **68** 3820 (1996)
40. K Kang, A D Kepner, Y Z Hu, S W Kosh, N Peyghambarian, C-Y Li, T Takada, Y Kao, J D Mackenzie *Appl. Phys. Lett.* **64** 1487 (1994)
41. J Butty, N Peyghambarian, Y H Kao, J D Mackenzie *Appl. Phys. Lett.* **69** 3224 (1996)
42. J Butty, Y Z Hu, N Peyghambarian, Y H Kao, J D Mackenzie *Appl. Phys. Lett.* **67** 2672 (1995)
43. X H Jin, L Gao *J. Inorg. Mater.* **16** 200 (2001)
44. D Donescu *Mater. Plast.* **38** 3 (2001)
45. W Caseri *Macromol. Rapid Commun.* **21** 705 (2000)
46. P Gomez-Romero *Adv. Mater.* **13** 163 (2001)
47. A Huczko *Appl. Phys. A: Mater. Sci. Process.* **70** 365 (2000)
48. L Bronstein, E Krämer, B Berton, C Burger, S Förster, M Antonietti *Chem. Mater.* **11** 1402 (1999)
49. A A Eliseev, A V Lukashin, A A Vertegel, L I Heifets, A I Zhirov, Y D Tretyakov *Mater. Res. Innovat.* **3** 308 (2000)
50. P L J Gunter, J W Niemantsverdriet, F H Ribeiro, G A Somorjai *Catal. Rev. Sci. Eng.* **39** 77 (1997)
51. G Dantsin, K S Suslick *J. Am. Chem. Soc.* **122** 5214 (2000)
52. K W Gallis, C C Landry *Adv. Mater.* **13** 23 (2001)
53. D W Kim, A Blumstein, M Downey, J Kumar, S K Tripathy *Abstr. Pap. Am. Chem. Soc.* **220** 84 (2000)
54. N Herron *J. Inclusion Phenom. Mol. Recognit. Chem.* **21** 283 (1995)
55. J C Maxwell-Garnett *Philos. Trans. R. Soc. London* **203** 385 (1904)
56. K F Kelton *Int. J. Non-Eq. Process.* **11** 141 (1998)
57. H Sato, T Umeda *Mater. Trans., JIM* **34** 76 (1993)
58. S Komarneni *J. Sol-Gel Sci. Tech.* **6** 127 (1996)
59. H J Fecht *Mater. Trans., JIM* **36** 777 (1995)
60. B G Potter Jr, J H Simmons *Phys. Rev. B* **37** 10 838 (1988)
61. R L Comstock *J. Mater. Sci. Mater. Electron.* **13** 509 (2002)
62. A Morisako, T Naka, K Ito, U Takizawa, M Matsumoto, Y K Hong *J. Magn. Magn. Mater.* **242** 304 (2002)
63. S B Sohn, S Y Choi, I B Shim *J. Magn. Magn. Mater.* **239** 533 (2002)
64. R Müller, C Ulbrich, W Schuppel, H Steinmetz, E Steinbeiss *J. Eur. Ceram. Soc.* **19** 1547 (1999)
65. C K Lee, R F Speyer *J. Mater. Sci.* **29** 1348 (1994)
66. Yu D Tretyakov *Usp. Khim.* **72** 731 (2003) [*Russ. Chem. Rev.* **72** 651 (2003)]
67. G Ihlein, B Junges, U Junges, F Laeri, F Schuth, U Vietze *Appl. Organomet. Chem.* **12** 305 (1998)
68. A S Kovalenko, V G Il'in, O P Filippov *Teor. Eksp. Khim.* **33** 322 (1997) [c]
69. T J Pinnavaia *Adv. Chem. Ser. Mater. Chem.* **245** 283 (1995)
70. D Horváth, M Polisset-Thfoin, J Fraissard, L Guczi *Solid State Ionics* **141** 153 (2001)
71. A Fukuoka, N Higashimoto, Y Sakamoto, M Sasaki, N Sugimoto, S Inagaki, Y Fukushima, M Ichikawa *Catal. Today* **66** 23 (2001)
72. A A Kubasov *Tseolity — Kipyashchie Kamni* (Zeolites are Boiling Stones) (Moscow: Khimiya, 1998)
73. R Fricke, H Kosslick, G Lischke, M Richter *Chem. Rev.* **100** 2303 (2000)
74. K G Ione, L A Vostrikova *Usp. Khim.* **56** 393 (1987) [*Russ. Chem. Rev.* **56** 231 (1987)]
75. S Qui, R Ohnishi, M Ichikawa *J. Chem. Soc., Chem. Commun.* 1425 (1992)
76. A Carlsson, G Karlsson, J O Bovin, T Oku, Y Okamoto, N Ohnishi, O Terasaki *Eur. Phys. J. D* **9** 623 (1999)
77. Y Yamamoto, T Matsuzaki, S Tanaka, K Nishihira, K Ohdan, A Nakamura, Y Okamoto *J. Chem. Soc., Faraday Trans.* **93** 3721 (1997)
78. F J Lázaro, J L Garcia, V Schünemann, Ch Butzlaff, A Larrea, M A Zaluska-Kotur *Phys. Rev. B* **53** 13934 (1996)
79. Y M Kang, B Z Wan *Catal. Today* **35** 379 (1997)
80. D Guillemot, M Polisset-Thfoin, J Fraissard *Catal. Lett.* **41** 143 (1996)
81. Y M Kang, B Z Wan *Catal. Today* **26** 59 (1995)
82. Y M Kang, B Z Wan *Appl. Catal., A* **128** 53 (1995)
83. F E Trigueiro, D F J Monteiro, F M Z Zotin, E F Sousa-Aguiar *J. Alloys Compd.* **344** 337 (2002)
84. P W de Bont, M J Vissenberg, E J M Hensen, V H J de Beer, J A R van Veen, R A van Santen, A M van der Kraan *Appl. Catal., A* **236** 205 (2002)
85. P W de Bont, M J Vissenberg, E Boellaard, V H J de Beer, J A R van Veen, R A van Santen, A M van der Kraan *Hyperfine Interact.* **111** 39 (1998)
86. A Seidel, J Loos, B Boddenberg *J. Mater. Chem.* **9** 2495 (1999)
87. N Nishimiya, T Kishi, T Mizushima, A Matsumoto, K Tsutsumi *J. Alloys Compd.* **319** 312 (2001)
88. T Rades, M Polisset-Thfoin, J Fraissard *Top. Catal.* **11** 283 (2000)
89. A M Diamy, Z Randriamanantenasoa, J C Legrand, M PolissetThfoin, J Fraissard *Chem. Phys. Lett.* **269** 327 (1997)
90. Y Okamoto, H Kikuta, Y Ohto, S Nasu, O Terasaki, in *Progress in Zeolite and Microporous Materials. Studies in Surface Science and Catalysis* (Amsterdam: Elsevier, 1997) p. 2051
91. T M Salama, R Ohnishi, T Shido, M Ichikawa *J. Catal.* **162** 169 (1996)
92. T M Salama, T Shido, H Minagawa, M Ichikawa *J. Catal.* **152** 322 (1995)
93. H V Garcia, M H Velez, O S Garrido, J M M Duart, J Jimenez *Solid-State Electron.* **43** 1171 (1999)
94. G G Lindner, K Witke, H Schlaich, D Reinen *Inorg. Chim. Acta* **252** 39 (1996)
95. J F Jia, K S Pillai, W M H Sachtler *J. Catal.* **221** 119 (2004)
96. A Z Abdullah, M Z Abu Bakar, S Bhatia *Catal. Commun.* **4** 555 (2003)
97. J Perez-Ramirez, G Mul, F Kapteijn, J A Moulijn, A R Overweg, A Domenech, A Ribera, I W C E Arends *J. Catal.* **207** 113 (2002)
98. X T Li, C L Shao, S L Qiu, F S Xiao, W T Zheng, P L Ying, O Terasaki *Microporous Mesoporous Mater.* **40** 263 (2000)
99. X T Li, C L Shao, S L Qiu, F S Siao, W T Zheng, Z M Liu, O M Terasaki *Mater. Lett.* **48** 242 (2001)
100. Z J Li, M Flytzani-Stephanopoulos *J. Catal.* **182** 313 (1999)
101. J S Beck, J C Vartuli, W J Roth, M E Leonowicz, C T Kresge, K D Shmitt, C T W Chu, D H Olson , E W Sheppard, S B McCullen, J B Higgins, J L Schlenker *J. Am. Chem. Soc.* **114** 10 834 (1992)
102. Y Wei, D L Jin, T Z Ding, W H Shih, X H Liu, S Z D Cheng, Q Fu *Adv. Mater.* **10** 313 (1998)
103. S Sakka *Am. Ceram. Soc. Bull.* **64** 1463 (1985)
104. D Y Zhao, J L Feng, Q S Huo, N Melosh, G H Fredrickson, B F Chmelka, G D Stucky *Science* **279** 548 (1998)
105. A A Eliseev, A V Lukashin, L I Soboleva, A V Knot'ko, L I Kheifets, A A Vertegel, Yu D Tretyakov *Dokl. Akad. Nauk* **372** 770 (2000) [b]

106. L I Soboleva, A A Eliseev, A V Lukashin, A A Vertegel, Yu D Tretyakov *Vestn. Voronezh. GTU, Ser. Materialoved.* **1.8** 16 (2000)
107. H O Pastore, M Munsignatti, D R S Bittencourt, M M Rippel *Microporous Mesoporous Mater.* **32** 211 (1999)
108. J C Vartuli, K D Schmitt, C T Kresge, W J Roth , M E Leonowicz, S B McCullen, S D Hellring, J S Beck , J L Schlenker, D H Olson, E W Sheppard *Chem. Mater.* **6** 2317 (1994)
109. Z Gabelica, J M Clacens, R Sobry, G VandenBossche *Characterization of Hexagonal and Lamellar Mesoporous Silicas, Alumino- and Gallosilicates by Small-Angle X-Ray Scattering (SAXS) and Multinuclear Solid State NMR* (Amsterdam: Elsevier, 1995)
110. P T Tanev, Y Liang, T J Pinnavaia *J. Am. Chem. Soc.* **119** 8616 (1997)
111. Z T Zhang, Y Han, F S Xiao, S L Qiu, L Zhu, R W Wang, Y Yu, Z Zhang, B S Zou, Y Q Wang, H P Sun, D Y Zhao, Y Wei *J. Am. Chem. Soc.* **123** 5014 (2001)
112. T J Barton, L M Bull, W G Klemperer, D A Loy, B McEnaney, M Misono, P A Monson, G Pez, G W Scherer, J C Vartuli, O M Yaghi *Chem. Mater.* **11** 2633 (1999)
113. C F Cheng, D H Park, J Klinowski *J. Chem. Soc., Faraday Trans.* **93** 193 (1997)
114. F Quirion, L Magid *J. Phys. Chem.* **90** 5435 (1986)
115. P T Tanev, T J Pinnavaia *Science* **267** 865 (1995)
116. P Schmidt-Winkel, C J Glinka, G D Stucky *Langmuir* **16** 356 (2000)
117. M Kruk, M Jaroniec, A Sayari *Langmuir* **13** 6267 (1997)
118. C T Kresge, M E Leonowicz, W J Roth, J C Vartuli *Nature (London)* **359** 710 (1992)
119. H Miyata, K Kuroda *J. Am. Chem. Soc.* **121** 7618 (1999)
120. H Yang, A Kuperman, N Coombs, S MamicheAfara, G A Ozin *Nature (London)* **379** 703 (1996)
121. H Yang, N Coombs, I Sokolov, G A Ozin *J. Mater. Chem.* **7** 1285 (1997)
122. A Corma, V Fornes, M T Navarro, J Perez-Pariente *J. Catal.* **148** 569 (1994)
123. F Schuth *Ber. Bunsen.-Ges. Phys. Chem.* **99** 1306 (1995)
124. G-G Wu, T Bien *Science* **264** 1757 (1994)
125. G-G Wu, T Bien *Science* **266** 1013 (1994)
126. A Corma, V Fornes, H Garcia, M A Miranda, M J Sabater *J. Am. Chem. Soc.* **116** 9767 (1994)
127. US P. 5 364 797 (1994)
128. M J MacLachlan, P Aroca, N Coombs, I Manners, G A Ozin *Adv. Mater.* **10** 144 (1998)
129. R Leon, D Margolese, G D Stucky, P M Petroff *Phys. Rev. B* **52** 2285 (1995)
130. C Jinwoo, K Lee, H Kang, S L Oh, H-C Ri *Mater. Res. Soc. Symp. Proc.* **635** C. 3.3.1. (2001)
131. H Parala, H Winkler, M Kolbe, A Wohlfart, R A Fischer, R Schmechel, H von Seggern *Adv. Mater.* **12** 1050 (2000)
132. K S Napolskii, I V Kolesnik, A A Eliseev, A V Lukashin, A A Vertegel, Yu D Tretyakov *Dokl. Akad. Nauk* **386** 207 (2002) [b]
133. K S Napolskii, A A Eliseev, A V Knot'ko, A V Lukashin, A A Vertegel, Yu D Tretyakov *Vestn. Voronezh. GTU, Ser. Materialoved.* **1.11** 3 (2002)
134. A A Eliseev, K S Napolskii, A V Lukashin, Y D Tretyakov *J. Magn. Magn. Mater.* **272** (2004) (in the press)
135. E A Kelberg, S V Grigoriev, A I Okorokov, H Eckerlebe, N A Grigorieva, A A Eliseev, A V Lukashin, A A Vertegel, K S Napolskii *Physica B* **350** e305 (2004)
136. S V Grigoriev, A I Okorokov, H Eckerlebe, N A Grigorieva, A A Eliseev, A V Lukashin, K S Napolskii *Physica E* (2004) (in the press)
137. E A Kelberg, S V Grigoriev, A I Okorokov, H Eckerlebe, N A Grigorieva, W H Kraan, A A Eliseev, A V Lukashin, A A Vertegel, K S Napolskii *Physica B* **335** 123 (2003)
138. W-H Zhang, J-L Shi, L-Z Wang, D-S Yan *Chem. Mater.* **12** 1408 (2000)
139. R P Cowburn, D K Koltsov, A O Adeyeye, M E Welland *Europhys. Lett.* **48** 221 (1999)
140. A A Eliseev, K S Napolskii, D F Gorozhankin, A V Lukashin, Y D Tretyakov, N A Grigorieva, S V Grigoriev, A A Vorobiev, P Goernert *Mater. Res. Soc. Symp. Proc.* L.6.1 (2003)
141. A A Eliseev, K S Napolskii, A V Lukashin, Y D Tretyakov, in *Proceedings of the 13th NID Workshop, Athens, Greece, 2004* p. 77
142. M Sasaki, M Osada, N Sugimoto, S Inagaki, Y Fukushima, A Fukuoka, M Ichikawa *Microporous Mesoporous Mater.* **21** 597 (1998)
143. M Sasaki, M Osada, N Higashimoto, T Yamamoto, A Fukuoka, M Ichikawa *J. Mol. Catal. A: Chem.* **141** 223 (1999)
144. I V Kolesnik, A A Eliseev, A P Malakho, A V Garshev, V P Tarasov, A V Lukashin, Yu D Tretyakov *Dokl. Akad. Nauk* **396** (2004) [b] (in the press)
145. A A Eliseev, K S Napolskii, I V Kolesnik, Yu V Kolenko, A V Lukashin, P Goernert, Y D Tretyakov, in *Frontiers in Molecular Science and Technology of Nanocarbon, Nanosilicon and Biopolymer Integrated Nanosystems* (Eds E V Buzaneva, P Scharff) (Dordrecht: Kluwer Academic, 2004)
146. A A Eliseev, S V Kalinin, V I Privalov, A A Vertegel, Y D Tretyakov *J. Solid State Chem.* **147** 304 (1999)
147. S Shingubara *J. Nanoparticle Res.* **5** 17 (2003)
148. F Keller, M S Hunter, D L Robinson *J. Electrochem. Soc.* **100** 411 (1953)
149. T P Hoar, N F Mott *J. Phys. Chem. Solids* **9** 97 (1959)
150. J P O'Sullivan, G C Wood *Proc. R. Soc. London, Ser. A* **317** 511 (1970)
151. G E Thompson, R C Furneaux, G C Wood, J A Richardson, J S Goode *Nature (London)* **272** 433 (1978)
152. O Jessensky, F Muüler, U Gösele *J. Electrochem. Soc.* **145** 3735 (1998)
153. O Jessensky, F Müller, U Glsele *Appl. Phys. Lett.* **72** 1173 (1998)
154. K Nielsch, J Choi, K Schwirn, R B Wehrspohn, U Gösele *Nano Lett.* **2** 677 (2002)
155. H Masuda, K Fukuda *Science* **268** 1466 (1995)
156. G C Schwartz, V Platter *J. Electrochem. Soc.* **122** 1508 (1975)
157. S Shingubara, O Okino, Y Sayama, H Sakaue, T Takahagi *Jpn. J. Appl. Phys.* **36** 7791 (1997)
158. H Masuda, F Hasegwa, S Ono *J. Electrochem. Soc.* **144** L127 (1997)
159. H Masuda, K Yada, A Osaka *Jpn. J. Appl. Phys. Lett.* **37** L1340 (1998)
160. H Masuda, H Yamada, M Satoh, H Asoh, M Nakao, T Tamamura *Appl. Phys. Lett.* **71** 2770 (1997)
161. H Asoh, K Nishio, M Nakao, A Yokoo, T Tamamura, H Masuda *J. Vac. Sci. Technol., B* **19** 569 (2001)
162. S Shingubara, Y Murakami, K Morimoto, T Takahagi *Surf. Sci.* **532** 317 (2003)
163. J Y Liang, H Chik, A J Yin, J Xu *J. Appl. Phys.* **91** 2544 (2002)
164. L Chen, A J Yin, J S Im, A V Nurmikko, J M Xu, J Han *Phys. Status Solidi A* **188** 135 (2001)
165. M Nakao, S Oku, T Tamamura, K Yasui, H Masuda *Jpn. J. Appl. Phys.* **38** 1052 (1999)
166. T Kawai, S I Ishiguro, H Ohtaki *Bull. Chem. Soc. Jpn.* **53** 2221 (1980)
167. S Kawai, I Ishiguro *J. Electrochem. Soc.* **123** 1047 (1976)
168. R Ueda, S Kawai, I Ishiguro *J. Vac. Sci. Technol.* **12** 759 (1975)
169. S H Sun, C B Murray, D Weller, L Folks, A Moser *Science* **287** 1989 (2000)
170. S H Sun, E E Fullerton, D Weller, C B Murray *IEEE Trans. Magn.* **37** 1239 (2001)
171. K Nielsch, F Muller, A P Li, U Gosele *Adv. Mater.* **12** 582 (2000)
172. M Krlll, W J Blau, D Grandjean, R E Benfield, F Luis, P M Paulus, L J de Jongh *J. Magn. Magn. Mater.* **249** 241 (2002)
173. H Zeng, R Skomski, L Menon, Y Liu, S Bandyopadhyay, D J Sellmyer *Phys. Rev. B* **65** 4426 (2002)
174. H Zeng, S Michalski, R D Kirby, D J Sellmyer, L Menon, S Bandyopadhyay *J. Phys.: Condens. Matter* **14** 715 (2002)
175. P M Paulus, F Luis, M Kroll, G Schmid, L J de Jongh *J. Magn. Magn. Mater.* **224** 180 (2001)

176. M Zheng, L Menon, H Zeng, Y Liu, S Bandyopadhyay, R D Kirby, D J Sellmyer *Phys. Rev. B* **62** 12 282 (2000)
177. L Menon, M Zheng, H Zeng, S Bandyopadhyay, D J Sellmyer *J. Electron. Mater.* **29** 510 (2000)
178. R M Metzger, V V Konovalov, M Sun, T Xu, G Zangari, B Xu, M Benakli, W D Doyle *IEEE Trans. Magn.* **36** 30 (2000)
179. M Sun, G Zangari, R M Metzger *IEEE Trans. Magn.* **36** 3005 (2000)
180. H Zeng, M Zheng, R Skomski, D J Sellmyer, Y Liu, L Menon, S Bandyopadhyay *J. Appl. Phys.* **87** 4718 (2000)
181. G J Strijkers, J H J Dalderop, M A A Broeksteeg, H J M Swagten, W J M de Jonge *J. Appl. Phys.* **86** 5141 (1999)
182. L Menon, S Bandyopadhyay, Y Liu, H Zeng, D J Sellmyer *J. Nanosci. Nanotechnol.* **1** 149 (2001)
183. H Zhu, S G Yang, G Ni, D L Yu, Y W Du *Scr. Mater.* **44** 2291 (2001)
184. A V Kukhta, G G Gorokh, E E Kolesnik, A I Mitkovets, M I Taoubi, Y A Koshin, A M Mozalev *Surf. Sci.* **507** 593 (2002)
185. Y Du, W L Cai, C M Mo, J Chen, L D Zhang, X G Zhu *Appl. Phys. Lett.* **74** 2951 (1999)
186. G Shi, C M Mo, W L Cai, L D Zhang *Solid State Commun.* **115** 253 (2000)
187. Y H Wang, Y Q Xu, W L Cai, J M Mo *Acta Phys.-Chim. Sinica* **18** 943 (2002)
188. O Rabin, P R Herz, S B Cronin, Y Lin, A I Akinwande, M S Dresselhaus *Mater. Res. Soc. Symp. Proc.* **636** D. 4.7.1 (2001)
189. N V Gaponenko, O V Sergeev, E A Stepanova, V M Parkun, A V Mudryi, H Gnaser, J Misiewicz, R Heiderhoff, L J Balk, G E Thompson *J. Electrochem. Soc.* **148** H13 (2001)
190. N V Gaponenko, J A Davidson, B Hamilton, P Skeldon, G E Thompson, X Zhou, J C Pivin *Appl. Phys. Lett.* **76** 1006 (2000)
191. G S Cheng, L D Zhang, X G Zhu, S H Chen, Y Li, Y Zhu, G T Fei *Nanostruct. Mater.* **11** 421 (1999)
192. C X Xu, Q H Xue, Y Zhong, Y P Cui, L Ba, B Zhao, N Gu *Nanotechnology* **13** 47 (2002)
193. I Mikulskas, S Juodkazis, A Jagminas, S Meskinis, J G Dumas, J Vaitkus, R Tomasiunas *Opt. Mater.* **17** 343 (2001)
194. I Mikulskas, S Juodkazis, R Tomasiunas, J G Dumas *Adv. Mater.* **13** 1574 (2001)
195. R B Wehrspohn, J Schilling *MRS Bull.* **26** 623 (2001)
196. H Masuda, M Ohya, K Nishio, H Asoh, M Nakao, M Nohtomi, A Yokoo, T Tamamura *Jpn. J. Appl. Phys. Lett.* **39** L1039 (2000)
197. H Masuda, M Ohya, H Asoh, M Nakao, M Nohtomi, T Tamamura *Jpn. J. Appl. Phys. Lett.* **38** L1403 (1999)
198. T Iwasaki, T Motoi, T Den *Appl. Phys. Lett.* **75** 2044 (1999)
199. J Li, C Papadopoulos, J M Xu, M Moskovits *Appl. Phys. Lett.* **75** 367 (1999)
200. S L Sung, S H Tsai, C H Tseng, F K Chiang, X W Liu, H C Shih *Appl. Phys. Lett.* **74** 197 (1999)
201. S L Sung, S H Tsai, X W Liu, H C Shih *J. Mater. Res.* **15** 502 (2000)
202. J Li, C Papadopoulos, J Xu *Nature (London)* **402** 253 (1999)
203. X H Wang, Z Hu, Q Wu, Y Chen *Catal. Today* **72** 205 (2002)
204. Y C Sui, B Z Cui, R Guardian, D R Acosta, L Martinez, R Perez *Carbon* **40** 1011 (2002)
205. W C Hu, L M Yuan, Z Chen, D W Gong, K Saito *J. Nanosci. Nanotechnol.* **2** 203 (2002)
206. A Mozalev, S Magaino, H Imai *Electrochim. Acta* **46** 2825 (2001)
207. E A Bluhm, E Bauer, R M Chamberlin, K D Abney, J S Young, G D Jarvinen *Langmuir* **15** 8668 (1999)
208. E A Bluhm, N C Schroeder, E Bauer, J N Fife, R M Chamberlin, K D Abney, J S Young, G D Jarvinen *Langmuir* **16** 7056 (2000)
209. A T Shawaqfeh, R E Baltus *J. Membr. Sci.* **157** 147 (1999)
210. S Basu, S Chatterjee, M Saha, S Bandyopadhay, K K Mistry, K Sengupta *Sens. Actuators, B* **79** 182 (2001)
211. R Schöllhorn *Chem. Mater.* **8** 1747 (1996)
212. S Carlino *Chem. Br.* **33** 59 (1997)
213. T Sato, Y Fukugami, Y Shu *Scr. Mater.* **44** 1905 (2001)
214. J J Tunney, C Detellier *Chem. Mater.* **8** 927 (1996)
215. A S Zerda, A J Lesser *J. Polym. Sci., Part B: Polym. Phys.* **39** 1137 (2001)
216. D W Kim, A Blumstein, J Kumar, S K Tripathy *Chem. Mater.* **13** 243 (2001)
217. A Szucs, F Berger, I Dekany *Colloid Surf., A* **174** 387 (2000)
218. H R Fischer, L H Gielgens, T P M Koster *Acta Polym.* **50** 122 (1999)
219. T Sato, K Masaki, K I Sato, Y Fujishiro, A Okuwaki *J. Chem. Technol. Biotechnol.* **67** 339 (1996)
220. E P Giannelis *Appl. Organomet. Chem.* **12** 675 (1998)
221. Y Ma, W Tong, H Zhou, S L Suib *Microporous Mesoporous Mater.* **37** 243 (2000)
222. F Cavani, F Trifiro, A Vaccari *Catal. Today* **11** 173 (1991)
223. F Trifiro, A Vaccari, in *Comprehensive Supramolecular Chemistry* Vol. 7 (Eds J L Atwood, J E D Davies, D D MacNicol, F Vogtle, J M Lehn, G Alberti, T Beins) (Oxford: Pergamon Press, 1996)
224. F Basile, L Basini, G Fornasari, M Gazzano, F Trifiro, A Vaccari *Stud. Surf. Sci. Catal.* **118** 31 (1998)
225. C Barriga, J M Fernandez, M A Ulibarri, F M Labajos, V Rives *J. Solid State Chem.* **124** 205 (1996)
226. J M Fernández, C Barriga, M A Ulibarri, F M Labajos, V Rives *Chem. Mater.* **9** 312 (1997)
227. F M Labajos, V Rives, P Malet, M A Centeno, M A Ulibarri *Inorg. Chem.* **35** 1154 (1996)
228. M A Aramendia, V Borau, C Jimenez, J M Marinas, F J Romero, J R Ruiz *J. Solid State Chem.* **131** 78 (1997)
229. F M Vichi, O L Alves *J. Mater. Chem.* **7** 1631 (1997)
230. M A Aramendia, V Borau, C Jiménez, J M Marinas, F J Romero, F J Urbano *J. Mater. Chem.* **9** 2291 (1999)
231. M Bellotto, B Rebours, O Clause, J Lynch, D Bazin, E Elkaim *J. Phys. Chem.* **100** 8527 (1996)
232. V Rives, M A Ulibarri *Coord. Chem. Rev.* **181** 61 (1999)
233. A Roy, C Forano, K El Malki, J P Besse, in *Synthesis of Microporous Materials* Vol. 2 (Eds M L Occelli, H E Robson) (New York: Reinhold, 1992)
234. F C Hawthorne, S V Krivovichev, P C Burns *Rev. Mineral., Geochem.* **40** 1 (2000)
235. S H Han, C G Zhang, W G Hou, D J Sun, G T Wang *Chem. J. Chin. Univ.* **17** 1785 (1996)
236. C J Serna, J L Rendon, J E Iglesias *Clays Clay Miner.* **10** 180 (1982)
237. S Velu, D P Sabde, N Shah, S Sivasanker *Chem. Mater.* **10** 3451 (1998)
238. S Velu, K Suzuki, M Okazaki, T Osaki, S Tomura, F Ohashi *Chem. Mater.* **11** 2163 (1999)
239. S Velu, C S Swamy *J. Mater. Sci. Lett.* **15** 1674 (1996)
240. H B Friedrich, F Khan, N Singh, M van Staden *Synlett* 869 (2001)
241. F Basile, G Fornasari, M Gazzano, A Vaccari *Appl. Clay Sci.* **16** 185 (2000)
242. S P Newman, W Jones *New J. Chem.* **22** 105 (1998)
243. J Evans, M Pillinger, J J Zhang *J. Chem. Soc., Dalton Trans.* 2963 (1996)
244. S K Yun, T J Pinnavaia *Inorg. Chem.* **35** 6853 (1996)
245. E A Gardner, S K Yun, T H Kwon, T J Pinnavaia *Appl. Clay Sci.* **13** 479 (1998)
246. W T Reichle *Solid State Ionics* **22** 135 (1986)
247. S P Newman, W Jones *J. Solid State Chem.* **148** 26 (1999)
248. E L Crepaldi, J B Valim *Quim. Nova* **21** 300 (1998)
249. Y Israëli, T Taviot-Guého, J P Beese, J P Morel, N Morel-Desrosiers *J. Chem. Soc., Dalton Trans.* 791 (2000)
250. M A Drezdzon *Inorg. Chem.* **27** 4628 (1988)
251. C W Hu, X Zhang, Q L He, E B Wang, S W Wang, Q L Guo *Transition Met. Chem.* **22** 197 (1997)
252. F Kooli, W Jones, V Rives, M A Ulibarri *J. Mater. Sci. Lett.* **16** 27 (1997)
253. K Chibwe, W Jones *Chem. Mater.* **1** 489 (1989)
254. K Chibwe, W Jones *J. Chem. Soc., Chem. Commun.* 926 (1989)
255. S Carlino, M J Hudson *J. Mater. Chem.* **4** 99 (1994)
256. S B C Pergher, A Corma, V Fornes *Quim. Nova* **22** 693 (1999)
257. T Okuhara, N Mizuno, M Misono *Adv. Catal.* **41** 113 (1996)

258. A Corma *Chem. Rev.* **97** 2373 (1997)
259. I V Kozhevnikov *Chem. Rev.* **98** 171 (1998)
260. D Tichit, F Medina, B Coq, R Dutartre *Appl. Catal., A* **159** 241 (1997)
261. E D Rodeghiero, J Chisaki, E P Giannelis *Chem. Mater.* **9** 478 (1997)
262. D Tichit, A Vaccari *Appl. Clay Sci.* **13** 311 (1998)
263. D Tichit, F Fajula *Stud. Surf. Sci. Catal.* **125** 329 (1999)
264. B Sels, D De Vos, M Buntinx, F Pierard, A Kirsch-De Mesmaeker, P Jacobs *Nature (London)* **400** 855 (1999)
265. L Indira, P V Kamath *J. Mater. Chem.* **4** 1487 (1994)
266. P V Kamath, M Dixit, L Indira, A K Shukla, V G Kumar, N Munichandraiah *J. Electrochem. Soc.* **141** 2956 (1994)
267. G A Caravaggio, C Detellier, Z Wronski *J. Mater. Chem.* **11** 912 (2001)
268. M Morigi, E Scavetta, M Berrettoni, M Giorgetti, D Tonelli *Anal. Chim. Acta* **439** 265 (2001)
269. R Schöllhorn, B Otto *J. Chem. Soc., Chem. Commun.* 1222 (1986)
270. B Ballarin, M Morigi, E Scavetta, R Seeber, D Tonelli *J. Electroanal. Chem.* **492** 7 (2000)
271. E Scavetta, M Berrettoni, R Seeber, D Tonelli *Electrochim. Acta* **46** 2681 (2001)
272. T Sato, H Okuyama, T Endo, M Shimada *React. Solids* **8** 63 (1990)
273. Y Fujishiro, S Uchida, T Sato *Int. J. Inorg. Mater.* **1** 67 (1999)
274. T Sato, K I Sato, Y Fujishiro, T Yoshioka, A Okuwaki *J. Chem. Technol. Biotechnol.* **67** 345 (1996)
275. T Sato, K Masaki, T Yoshioka, A Okuwaki *J. Chem. Technol. Biotechnol.* **58** 315 (1993)
276. V P Isupov, K A Tarasov, L E Chupakhina, R P Mitrofanova, V V Boldyrev *Dokl. Akad. Nauk* **336** 209 (1994) [b]
277. V P Isupov, K A Tarasov, L E Chupakhina, R P Mitrofanova, L I Skvortsova, V V Boldyrev *Zh. Neorg. Khim.* **40** 22 (1995) [d]
278. V P Isupov, L E Chupakhina, R P Mitrofanova, K A Tarasov, A Y Rogachev, V V Boldyrev *Solid State Ionics* **101** 265 (1997)
279. V P Isupov, L E Chupakhina, R P Mitrofanova, K A Tarasov *Zh. Strukt. Khim.* **12** 454 (1998) [e]
280. K A Tarasov, V P Isupov, B B Bokhonov, Y A Gaponov, B P Tolochko, M R Sharafutdinov, S S Shatskaya *J. Mater. Synth. Process.* **8** 21 (2000)
281. K A Tarasov, V P Isupov, L E Chupakhina *Zh. Neorg. Khim.* **45** 1804 (2000) [d]
282. A V Lukashin, S V Kalinin, M P Nikiforov, N G Zhuravleva, A I Zhirov, V I Privalov, A A Vertegel *Mater. Res. Soc. Symp. Proc.* **547** 239 (1999)
283. A A Eliseev, A V Lukashin, A A Vertegel, Yu D Tretyakov *Vestn. Voronezh. GTU, Ser. Materialoved.* **1.8** 6 (2000)
284. A V Lukashin, S V Kalinin, M P Nikiforov, V I Privalov, A A Eliseev, A A Vertegel, Yu D Tretyakov *Dokl. Akad. Nauk* **364** 77 (1999) [b]
285. A A Eliseev, A V Lukashin, A A Vertegel, V P Tarasov, Yu D Tretyakov *Dokl. Akad. Nauk* **387** 777 (2002) [b]
286. A V Lukashin, A A Vertegel, A A Eliseev, M P Nikiforov, P Gornert, Y D Tretyakov *J. Nanoparticle Res.* **5** 455 (2003)
287. M P Nikiforov, M V Chernysheva, A V Lukashin, A A Vertegel, Yu V Maksimov, S V Novichikhin, I P Suzdalev, Yu D Tretyakov *Dokl. Akad. Nauk* **391** 53 (2003) [b]
288. A V Lukashin, M V Chernysheva, A A Vertegel, Yu D Tretyakov *Dokl. Akad. Nauk* **388** 200 (2003) [b]
289. A V Lukashin, A S Vyacheslavov, A A Vertegel, Yu D Tretyakov *Dokl. Akad. Nauk* **385** 71 (2002) [b]
290. A V Lukashin, A A Eliseev, N G Zhuravleva, S V Kalinin, A A Vertegel, Yu D Tretyakov *Dokl. Akad. Nauk* **383** 504 (2002) [b]
291. A V Lukashin, A A Vertegel, A A Eliseev, N G Zhuravleva, M P Nikiforov, Y D Tretyakov, in *Proceedings of the VIIIth European Conference on Solid State Chemistry, Oslo, Norway, 2001* p. 21
292. A V Lukashin, S V Kalinin, S R Lee, A V Knot'ko, A A Vertegel, Y D Tretyakov *NATO ASI Ser., Ser. 2* **17** 228 (2001)
293. A V Lukashin, A A Vertegel, N G Zhuravleva, Y D Tretyakov, in *Proceedings of the 2000 MRS Fall Meeting, Boston, USA, 2000* p. 236
294. N G Zhuravleva, A A Eliseev, A V Lukashin, A A Vertegel, Yu D Tretyakov *Vestn. Voronezh. GTU, Ser. Materialoved.* **1.8** 11 (2000)
295. X C Ai, L Guo, Y H Zou, Q S Li, H S Zhu *Mater. Lett.* **38** 131 (1999)
296. A A Patel, F X Wu, J Z Zhang, C L Torres-Martinez, R K Mehra, Y Yang, S H Risbud *J. Phys. Chem. B* **104** 11 598 (2000)
297. P Mulvaney, L M Liz-Marzán, M Giersig, T Ung *J. Mater. Chem.* **10** 1259 (2000)
298. F Caruso *Adv. Mater.* **13** 11 (2001)
299. M Kuno, J K Lee, B O Dabbousi, F V Mikulec, M G Bawendi *J. Chem. Phys.* **106** 9869 (1997)
300. X G Peng, M C Schlamp, A V Kadavanich, A P Alivisatos *J. Am. Chem. Soc.* **119** 7019 (1997)
301. M Danek, K F Jensen, C B Murray, M G Bawendi *Chem. Mater.* **8** 173 (1996)
302. M Adachi-Pagano, C Forano, J P Besse *Chem. Commun.* 91 (2000)
303. F Leroux, M Adachi-Pagano, M Intissar, S Chauvizhre, C Forano, J-P Besse *J. Mater. Chem.* **11** 105 (2001)
304. T Hibino, W Jones *J. Mater. Chem.* **11** 1321 (2001)

[a] — *Phys. Met. Metallogr. (Engl. Transl.)*
[b] — *Dokl. Chem. (Engl. Transl.)*
[c] — *Theor. Exp. Chem. (Engl. Transl.)*
[d] — *Russ. J. Inorg. Chem. (Engl. Transl.)*
[e] — *Russ. J. Struct. Chem. (Engl. Transl.)*

Russian Chemical Reviews **73** (9) 923 – 938 (2004) © 2004 Russian Academy of Sciences and Turpion Ltd

DOI 10.1070/RC2004v073n09ABEH000916

Semiconducting clathrates: synthesis, structure and properties

K A Kovnir, A V Shevelkov

Contents

I.	Introduction	923
II.	Crystal chemistry of semiconducting clathrates	925
III.	Electronic structures and properties of semiconducting clathrates	930
IV.	Methods for the synthesis of semiconducting clathrates	935
V.	Conclusion	935

Abstract. The review surveys different aspects of chemical studies of semiconducting clathrates belonging to a unique family of inclusion compounds. The classification, crystal and electronic structures, properties and methods for the synthesis of semiconducting clathrates are considered on the basis of analysis of recent publications. The prospects for fundamental research and the construction of new-generation materials based on semiconducting clathrates are discussed. The bibliography includes 161 references.

I. Introduction

The term 'clathrates' refers to compounds with a three-dimensional framework structure (host), whose cavities are occupied by isolated (in rare instances, one-dimensional infinite) associates of molecules, atoms or ions (guests), which do not form covalent bonds with the framework.[1] The crystal lattice of the host cannot exist in the absence of a guest. For the framework to be stabilised, cavities must be at least partially occupied. For this reason, clathrates are synthesised by co-crystallisation of a host and a guest. Generally, species included into a three-dimensional matrix cannot leave the latter without destruction of the overall architecture. The name 'clathrate' was first used by Powell in 1948 [2] (after the Latin word *clathratus*, which means 'enclosed or protected by cross bars of a grating'). Sometimes, the term 'clathrate' is used in a broader sense and applied not only to compounds in which the host has a three-dimensional structure (framework clathrates), but also to compounds with two-dimensional (layered clathrates or intercalates) and zero-dimensional (molecular clathrates) host structures. Examples are layered inclusion compounds of graphite and complexes of crown ethers with alkali metals. However, an extension of the term 'clathrate' to such systems is not commonly accepted.[2]

Over many years, only gas hydrates and compounds based on hydroquinone and urea have been assigned to clathrates, which have been considered as an exotic variety of inclusion compounds.[3] These compounds have attracted some interest from researchers because of their unusual structures. Certain silicates [4] and silicides [5] isostructural to gas hydrates and then germanides and stannides,[6] which were characterised in 1960 – 1980s, also aroused some interest. Only about two tens of papers have been published over the last 30 years.

The situation changed radically after the development of the Phonon Glass – Electron Crystal concept.[7] Taking into account this concept, particular inclusion compounds, which are poor conductors of heat (as amorphous compounds) and good conductors of electricity (as covalent semiconductors), can serve as a basis for the design of new-generation heat-saving materials.[8] In particular, this class of compounds includes clathrate germanides and stannides. The results of initial experiments published in 1998 [9] already confirmed that clathrates are promising new materials for thermoelectric cooling. This stimulated interest in semiconducting clathrates, as evidenced by a sharply increasing number of publications devoted to various aspects of the chemistry and physics of these compounds. In 2000, Bobev and Sevov published a brief review [10] concerned with the chemical aspects of clathrates. One year later, Nolas, Slack and Schjuman published a comprehensive review,[11] where the results of studies of the physical properties were discussed and related to the structural data.

Since that time, new types of clathrates have been synthesised. New data on the characteristic features of their crystal and electronic structures were obtained, which gave an insight into unusual transport properties of these compounds. Finally, clathrate silicides were found to exhibit superconducting properties. Therefore, the accumulated data on the crystal and electronic structures and the properties of semiconducting clathrates needed to be summarised. Our review is devoted to these problems. We consider the classification, crystal and electronic structures of semiconducting clathrates and some specific physical properties of these compounds determined by their structures. We also discuss prospects for gaining fundamental knowledge and constructing new materials.

Crystal hydrates of gases and liquids are the best known representatives of the clathrate family. Chlorine hydrate was discovered as early as 1811 by Davy, when he passed chlorine through water cooled to 2 – 3 °C.[12] In 1823, Faraday determined the composition of the new compound as $Cl_2 \cdot 10\,H_2O$,[1] which is close to the true composition $Cl_2 \cdot 7.25\,H_2O$. The crystal structure of chlorine hydrate was established by Allen as late as 1952.[13] In this compound, water molecules are linked by hydrogen bonds to form a three-dimensional framework (Fig. 1). Each water molecule is linked to four other water molecules. The framework contains polyhedral cavities. The oxygen atoms occupy the corners of these polyhedra, whereas the hydrogen atoms are

K A Kovnir, A V Shevelkov Department of Chemistry and Department of Materials Science, M V Lomonosov Moscow State University, Leninskie Gory, 119992 Moscow, Russian Federation. Fax (7-095) 939 09 98. Tel. (7-095) 939 12 00. E-mail: shev@inorg.chem.msu.ru (A V Shevelkov)

Received 9 March 2004
Uspekhi Khimii **73** (9) 999 – 1015 (2004); translated by T N Safonova

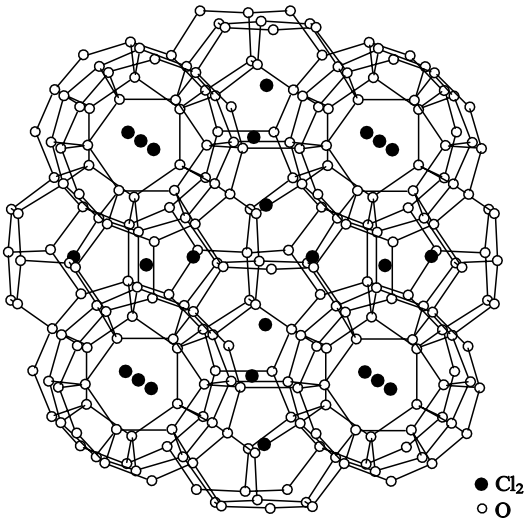

Figure 1. Crystal structure of chlorine hydrate $(Cl_2)_{6.34}[H_2O]_{46}$. Hydrogen atoms are omitted.

located at their edges. In the chlorine hydrate, there are 8 polyhedral cavities per 46 water molecules. If all cavities are occupied by chlorine molecules, the idealised formula is $(Cl_2)_8[H_2O]_{46}$. However, the true composition of the compound is close to $(Cl_2)_{6.34}[H_2O]_{46}$, and the chlorine molecules occupy cavities only partially. Strictly speaking, this compound cannot be assigned to hydrates based on its crystal structure. Nevertheless, this is the commonly accepted term, which is universally used in the literature.[1,3]

Numerous hydrates of other gases (for example, of noble gases Ar, Kr and Xe), gaseous and liquid inorganic compounds (N_2, O_2, CO_2, H_2S, PH_3, SO_2) and organic compounds [CH_4, CH_3Cl, C_2H_6, C_3H_8, $CHCl_3$, CH_3NO_2, cyclopentane, cyclobutanone, $(n\text{-}C_4H_9)_3SF$] were synthesised.[14] Clathrates in which compounds other than water (for example, phenol or hydroquinone) serve as the host are also known.[15] In all cases, the ratio of the cavity size in the host framework to the size of the guest molecules or atoms plays a decisive role in the formation of a clathrate structure, whereas the chemical nature of the guest molecules is of minor importance. Actually, small hydrogen, helium and neon molecules do not form such structures with water, whereas H_2S, PH_3, Cl_2 and Br_2, which have suitable sizes, are involved in such compounds even though they are chemically active and differ in acid-base and redox properties. It should be noted that the hydrogen hydrate can be prepared under high pressure, but the cavities in the framework formed by water molecules are occupied by clusters formed by two or four H_2 molecules, whose sizes match those of the cavities of different types.[16] All the above facts indicate that the size factor has a determining effect on the formation and stability of clathrates.

Prerequisites for the formation of clathrate structures are the presence of a host matrix built from tetrafunctional units (each unit forms four bonds within the matrix) and the ability of the corresponding guest species to occupy the cavities in the framework formed. In hydrates of gases and liquids, the host and guest atoms are formally uncharged, although it is these weak Coulombic interactions that play the major role in the stabilisation of the structure. All known hydrates crystallise in seven structural types, which differ in the type of polyhedra formed in the framework and the mode of their arrangement in the three-dimensional structure.[3]

Virtually all hydrates of gases and liquids decompose on heating, which strongly limits their application. Nevertheless, the possibility of using methane hydrate as a natural nanocrystalline container is discussed taking into account vast resources of methane, which exists as crystal hydrate on the World's Ocean Floor. There are plans to recover and transport these resources in the solid state.[17]

In addition to hydrates, there are about 120 inorganic compounds with clathrate structures, which are referred to as semiconducting clathrates. Our review is devoted to the latter compounds. In such clathrates, a three-dimensional framework is formed primarily by Group 14 elements (Si, Ge or Sn). These compounds are sometimes loosely (in our opinion) called 'intermetallic clathrates'.[18] It should be noted that the first compounds of this class, which were synthesised in the 1960s,[3] can be assigned to intermetallides because their frameworks consist of silicon atoms and the cavities are occupied by alkali metal cations. However, this is not correct for analogous compounds with pnicogens (P, As and Sb), tellurium and halogens (Cl, Br and I), which were also synthesised.[19–32] Therefore, the term 'intermetallic' can be applied only to some semiconducting clathrates. The term 'semiconducting' is also not perfect because the above compounds do not all have semiconducting properties (particular phases exhibit metallic conductivity). However, in our opinion, the term 'semiconducting' is more universal. Hereinafter, we shall use this term for all compounds of the class under consideration.

In contrast to hydrates, in which the host and guest atoms are formally uncharged, the framework and the guest atoms in semiconducting clathrates bear opposite charges. Besides, guests in semiconducting clathrates are always monoatomic. Compounds containing molecules or polyatomic ions as the guest are presently unknown.

1. Classification of semiconducting clathrates

Clathrate hydrates of gases and liquids crystallise in seven structural types, which are denoted by Roman numerals: type I clathrate, type II clathrate, ..., type VII clathrate.[3] Semiconducting clathrates crystallise only in three of these structural types, *viz.*, type I clathrate, type II clathrate and type III clathrate. Besides these, two structural types, which were not found for hydrates, are known as semiconducting clathrates. These types are referred to as the type VIII clathrate[33–35] and type IX clathrate.[36] Because of specific structural features, compounds of the latter type are sometimes called chiral clathrates.†

It should be noted that the distribution of semiconducting clathrates over the above structural types is essentially non-uniform. Almost 100 type-I clathrate compounds are known. About 10 compounds have the type-II clathrate structure, almost the same number of compounds have the type-IX clathrate structure, whereas only a few type-III clathrate and type-VIII clathrate compounds were synthesised.

Semiconducting clathrates can alternatively be classified according to the formal charge of the framework. The polyanionic and polycationic clathrates are distinguishable.[14,38] In polyanionic clathrates, the framework bears a negative charge and the guest atoms are positively charged (cations of alkali and alkaline-earth metals and europium). The reverse situation is observed for polycationic clathrates. In these compounds, the framework bears a positive charge and the guest atoms are negatively charged (halide anions).

2. Clathrate-forming polyhedra

The crystal structures of clathrates of any type contain a three-dimensional host framework, which is formed by tetrafunctional units and contains large cavities. The cavities in the framework are polyhedra with $n \geqslant 20$ vertices and regular pentagonal and hexagonal faces.[1,10,14] The polyhedra are denoted by the number of such faces.[39] For example, the notation [5^{12}] is used for a

† In a number of publications, type VIII clathrates are referred to as type III clathrates. This is incorrect because type III clathrates belong to the structural type of bromine hydrate $(Br_2)_{20}\square_{10}[(H_2O)_{172}]$,[1] for which semiconducting analogues are also known.[37] The structures of these compounds are radically different from chiral type VIII clathrates.

Table 1. Clathrate-forming polyhedra.

Name	Graphical representation	Notation	Number of penta/hexagons	Number of vertices	Observed in clathrates
Pentagonal dodecahedron	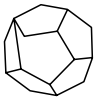	$[5^{12}]$	$\frac{12}{0}$	20	I, II, III VIII,[a] IX
Tetrakaidecahedron	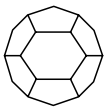	$[5^{12}6^2]$	$\frac{12}{2}$	24	I, III
Pentakaidecahedron	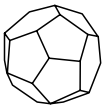	$[5^{12}6^3]$	$\frac{12}{3}$	26	III
Hexakaidecahedron	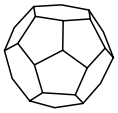	$[5^{12}6^4]$	$\frac{12}{4}$	28	II

[a] The type VIII clathrate contains distorted pentagonal dodecahedra.

pentagonal dodecahedron, *viz*., a 20-vertex polyhedron containing 12 pentagonal faces. The 24-vertex polyhedron (hexakaidecahedron) containing 12 pentagonal and 2 hexagonal faces is denoted by $[5^{12}6^2]$. Table 1 lists all polyhedra found in the structures of semiconducting clathrates.

A guest atom is located inside each polyhedron. The guest atom and the polyhedron are sometimes denoted by $G@E_x$.[1] This notation signifies that the guest atom G is located inside an *x*-vertex polyhedron formed by E atoms. For example, the notation $Cs@Sn_{20}$ represents the pentagonal dodecahedron consisting of tin atoms with a cesium atom inside.

The pentagonal dodecahedron is a Platonic body, in which all corners are equivalent and all faces are identical (in real structures, of the same type).[1] This polyhedron was found in the structures of clathrates of all types, except for type-VIII clathrate compounds. In the latter, the polyhedra are slightly distorted. Since the pentagonal dodecahedron has several fivefold axes, it is impossible to fill space with only these polyhedra, and it is necessary to combine these polyhedra with polyhedra which contain, in addition, hexagonal faces. Evidently, the total size of the cavity increases with increasing number of hexagonal faces, and the volumes of the polyhedra containing hexagonal faces are larger than the volume of the pentagonal dodecahedron.

II. Crystal chemistry of semiconducting clathrates

1. Type I clathrate

The type-I clathrate structure contains two types of polyhedra, *viz*., pentagonal dodecahedra $[5^{12}]$ and larger 14-face tetrakaidecahedra $[5^{12}6^2]$. The tetrakaidecahedra are linked to each other by sharing hexagonal faces to form a three-dimensional system of mutually perpendicular non-intersecting channels (Fig. 2). The pentagonal dodecahedra are enclosed in this system of channels and are isolated from each other. The unit cell contains 46 atoms of the framework and has 2 small and 6 large cavities. Therefore, the formula of the corresponding ideal clathrate is $G_2^{I}G_6^{II}[E_{46}]$ (G is a guest). All semiconducting clathrates, which crystallise in this structural type are listed in Tables 2 and 3.

Most type-I clathrate compounds crystallise in the cubic system in the centrosymmetrical space group *Pm*3*n*; 46 atoms of the framework occupy three positions, *viz*., 6*c*, 16*i* and 24*k*. The atoms in the 16*i* and 24*k* positions are present in the polyhedra of both types, whereas the atoms in the 6*c* position are present only in the bulkier tetrakaidecahedra (see Fig. 2). The atom in the 6*c* position is tetrahedrally coordinated by four atoms occupying the 24*k* position. The atom in the 16*i* position is tetrahedrally coordinated by three atoms occupying the 24*k* position and one atom occupying the 16*i* position. The atom in the 24*k* position is tetrahedrally coordinated by one atom occupying the 6*c* position, two atoms occupying the 16*i* position and one atom occupying the 24*k* position (Fig. 3 *a*).

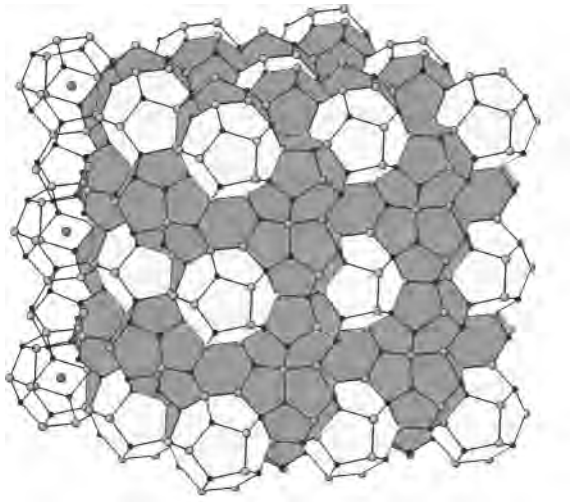

Figure 2. Polyhedral representation of the type-I clathrate structure.

In the structures of compounds of the general formula $X_8[Ge_{38}Z_8]$ (X = Cl, Br, I; Z = P, As, Sb), the centre of symmetry is absent. All these phases crystallise in the space group *P*43*n*, which is a non-centrosymmetrical analogue of the space group *Pm*3*n*.[19–21] Due to a loss of the centre of symmetry, the 16*i* position of the space group *Pm*3*n* is split into two eightfold 8*e* positions in the space group *P*43*n*. One of these positions is completely occupied by germanium atoms, whereas another one is occupied by pnicogen atoms. To our knowledge, the space

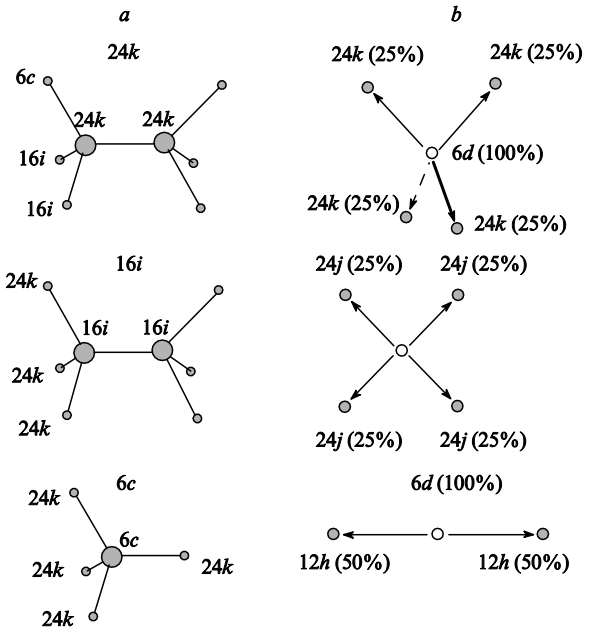

Figure 3. Atomic positions in the type-I clathrate structure. (*a*) Atoms of the clathrate framework, (*b*) disorder of the guest atoms in the 6*d* position.

Table 2. Type-I polyanionic clathrates.

Elements of the framework	Na, K, Rb, Cs as guest atoms	Ref.	Sr, Ba, Eu as guest atoms	Ref.
Compounds with a framework of silicon atoms				
p Metals	$Na_8[Si_{46}]$	3, 40 – 42	$Ba_{8-x}\square_x[Si_{46}]$	48 – 51
	$Na_{8-x}Ba_x[Si_{46}]$	43	$Ba_{7.7}\square_{0.3}[Si_{42.7}Ge_{3.1}\square_{0.2}]$	49
	$Na_xBa_6[Si_{46}]$	44	$Ba_{7.7}\square_{0.3}[Si_{39.3}Ge_{6.4}\square_{0.3}]$	49
	$K_{7.62}\square_{0.38}[Si_{46}]$	45	$Ba_{7.9}\square_{0.1}[Si_{33.3}Ge_{12.0}\square_{0.7}]$	49
	$Rb_{6.15}\square_{1.85}[Si_{46}]$	45	$Sr_8[Ga_{11}Si_{35}]$	52
	$K_8[Ga_8Si_{38}]$	46	$Sr_8[Ga_{12}Si_{34}]$	52
	$Rb_8[Al_8Si_{38}]$	47	$Ba_8[Ga_{16}Si_{30}]$	33, 47
	$Rb_8[Ga_8Si_{38}]$	46		
p and d Metals			$Ba_8[Ni_{1.8}Si_{44.2}]$	53
			$Ba_8[Pd_{2.5}Si_{43.5}]$	53
			$Ba_8[Pt_{2.7}Si_{43.3}]$	53
			$Ba_8[Cu_4Si_{42}]$	53
			$Ba_8[Ag_{3.8}Si_{42.2}]$	53
			$Ba_8[Au_6Si_{40}]$	53, 54
			$Ba_8[Au_6Si_{20}Ge_{20}]$	54
Compounds with a framework of germanium atoms				
p Metals	$K_8[Al_8Ge_{38}]$	55	$Ba_8[Ge_{43}\square_3]$	49, 61
	$Rb_8[Al_8Ge_{38}]$	56	$Ba_8[Al_{16}Ge_{30}]$	33, 47
	$K_8[Ga_8Ge_{38}]$	8	$Sr_8[Ga_{16}Ge_{30}]$	62
	$Rb_8[Ga_8Ge_{38}]$	57	β-$Eu_8[Ga_{16}Ge_{30}]$	34, 62,
	$Cs_8[Ga_8Ge_{38}]$	58		63
	$K_8[In_8Ge_{38}]$	59	$Ba_8[Ga_{4.44}Ge_{39.14}\square_{2.42}]$	64
	$Rb_8[In_8Ge_{38}]$	59	$Ba_8[Ga_{8.62}Ge_{36}\square_{1.38}]$	64
	$Cs_8[In_8Ge_{38}]$	60	$Ba_8[Ga_{12.35}Ge_{33.27}\square_{0.38}]$	64
			$Ba_8[Ga_{16}Ge_{30}]$	33, 34, 62, 65
			$Ba_8[Ga_{17}SbGe_{28}]$	66, 67
			$Ba_8[In_{16}Ge_{30}]$	68
			$Ba_8[Zn_8Ge_{38}]$	68
			$Ba_8[Cd_8Ge_{38}]$	68
			$Ba_8[Cd_4Ge_{40}\square_2]$	68
p and d Metals			$Ba_8[Ni_xGe_{46-x}]$	53
			$Ba_8[Pd_6Ge_{40}]$	53
			$Ba_8[Pt_xGe_{46-x}]$	53
			$Ba_8[Cu_xGe_{46-x}]$	53
			$Ba_8[Ag_6Ge_{40}]$	53
			$Ba_8[Au_6Ge_{40}]$	53, 54
Compounds with a framework of tin atoms				
p Metals	$K_{1.6}Cs_{6.4}[Sn_{44}\square_2]$	69	β-$Ba_8[Ga_{16}Sn_{30}]$	73
	$Rb_8[Sn_{44.6}\square_{1.4}]$	69	$K_{3.5}Ba_{4.5}[Ga_{12.5}Sn_{33.5}]$	47
	$Cs_8[Sn_{44}\square_2]$	8, 47, 70	$Ba_8Cu_{16}P_{30}$ (see[a])	74
	$K_8[Al_8Sn_{38}]$	47		
	$Rb_8[Al_8Sn_{38}]$	47		
	$K_8[Ga_8Sn_{38}]$	47		
	$Rb_8[Ga_8Sn_{38}]$	57		
	$Cs_8[Ga_8Sn_{38}]$	58		
	$Cs_8[Zn_4Sn_{42}]$	71		
	$Cs_8[Cd_4Sn_{42}]$	72		

[a] Compounds devoid of Group 14 elements.

Table 3. Type-I polycationic clathrates (halogen atoms as the guest).

Compounds with a framework of Ge atoms	Ref.	Compounds with a framework of Sn atoms	Ref.
P, As, Sb as a non-metal in the framework		P, As as a non-metal in the framework	
$I_8[Ge_{38}P_8]$	19 – 21	$I_8[Sn_{24}P_{19.3}\square_{2.7}]$	25
$Br_8[Ge_{38}P_8]$	20, 21	$Br_8[Sn_{24}P_{19.6}\square_{2.4}]$	31, 32
$Cl_8[Ge_{38}P_8]$	20, 21	$Br_xI_{8-x}[Sn_{24}P_{19.3}\square_{2.7}]$	31, 32
$I_8[Ge_{38}As_8]$	19 – 21, 23	$I_8[Sn_{14}In_{10}P_{21.2}\square_{0.8}]$	29
$Br_8[Ge_{38}As_8]$	20, 21, 23	$I_8[Sn_{10}In_{14}P_{22}]$	29
$Cl_8[Ge_{38}As_8]$	20, 21	$I_8[Sn_{17}Zn_7P_{22}]$	26, 75
$I_8[Ge_{38}Sb_8]$	20, 21	$Br_8[Sn_{17}Zn_7P_{22}]$	75
$Br_8[Ge_{38}Sb_8]$	20, 21	$I_8[Sn_{20}Zn_4P_{20.8}\square_{1.2}]$	75
$I_8[Ge_{14}Ga_{12}Sb_{20}]$	22	$I_8[Sn_{17}Cd_7P_{22}]$	75
Te as a non-metal in the framework		$I_8[Sn_{19.3}Cu_{4.7}P_{22}]$	28
$I_8[Ge_{46-x}Te_x]$	26	$I_8[Sn_{24}As_{19.3}\square_{2.7}]$	25
I as a non-metal in the framework		$I_8[Sn_{10}Ga_{14}As_{22}]$	75
$I_8[Ge_{43.33}I_{2.67}]$	24	$I_8[Sn_{17}Zn_7As_{22}]$	75
$I_8[Si_{44.5}I_{1.5}]$[a]	27, 30	$I_8[Sn_{19.3}Cu_{4.7}As_{22}]$	31
		$I_8[Sn_{17.6}Cu_{6.4}As_{22}]$	31

[a] A compound with a framework of Si atoms.

group *Pm*3*n*, in which the 16*i* position is occupied simultaneously by geranium and arsenic atoms, was described only for the $I_8[Ge_{38}As_8]$ phase in paper [23] published in 1982. However, the reliability of these data was not discussed in the cited study.

As can be seen from Table 2, there is a series of compounds of the general formula $A_8[E_{38}M_8]$ (A = Na, K, Rb, Cs, Ba; E = Si, Ge, Sn; M = Al, Ga, In, Zn, Cd), whose structures are also characterised by mixed occupancies of the positions of the framework by atoms of different types. However, the latter crystallise in the centrosymmetrical space group *Pm* 3*n*. It should be noted that the distribution of the heterometal atoms M over the positions of the framework in these compounds differs from that observed in pnicogen-containing clathrates in that the 'heteroatoms' either occupy predominantly the 6*c* position or are statistically distributed over all three positions, as exemplified by the $[Ge_{38}Ga_8]$ frameworks. In this case, the loss of an inversion centre cannot lead to additional ordering of the structure. Besides, the difference in the chemical nature of the atoms occupying the same position in the compounds under consideration is less significant than that in the case of the germanium/pnicogen pair.

The guest atoms in the type-I clathrate structure occupy the 2*a* and 6*d* positions, *viz*., the centres of the pentagonal dodecahedra and tetrakaidecahedra, respectively. According to the results of X-ray and neutron diffraction studies, the guest atoms show very large displacement parameters because of the absence of 'rigid' bonds between the framework and the guest. As expected, atoms execute larger-amplitude thermal motions in a larger space. For some compounds, it was proposed [9, 34, 76 – 79] that the guest atoms should be displaced from the 6*d* position to a position with a higher multiplicity and partial occupancy, *viz*., to 24*k* or 24*j* with 25% occupancy each or to 12*h* with 50% occupancy (Fig. 3 *b*). As can be seen from Fig. 3, the 6*d* position is tetrahedrally coordinated by the 24*k* positions, the 24*j* positions form a square about the *6d* position, and the 12*h* positions linearly coordinate the 6*d* position. However, this model of arrangement of the guest atoms in large polyhedra is possible only for a limited number of structures. In most cases, this model is incorrect because no displacements of the guest atoms from the 6*d* position were revealed in low-temperature X-ray diffraction experiments.[32, 80]

There are two modes of formation of a superstructure based on the crystal structures of type I clathrates (Fig. 4). One mode is observed in the $I_8[Sn_{14}In_{10}P_{21.2}\square_{0.8}]$ compound,[29] which crystallises in the tetragonal system in the space group $P4_2/m$. In this structure, the unit cell volume increases by a factor of five compared to the unit cell volume of the starting clathrate ($a_{super} \approx \sqrt{5}a_{clath}$, $b_{super} \approx \sqrt{5}b_{clath}$, $c_{super} \approx c_{clath}$), which is accompanied by partial ordering of vacancies in the clathrate framework. Ordering insures against mixed occupancy of the same position simultaneously by three- and four-coordinate metal atoms.

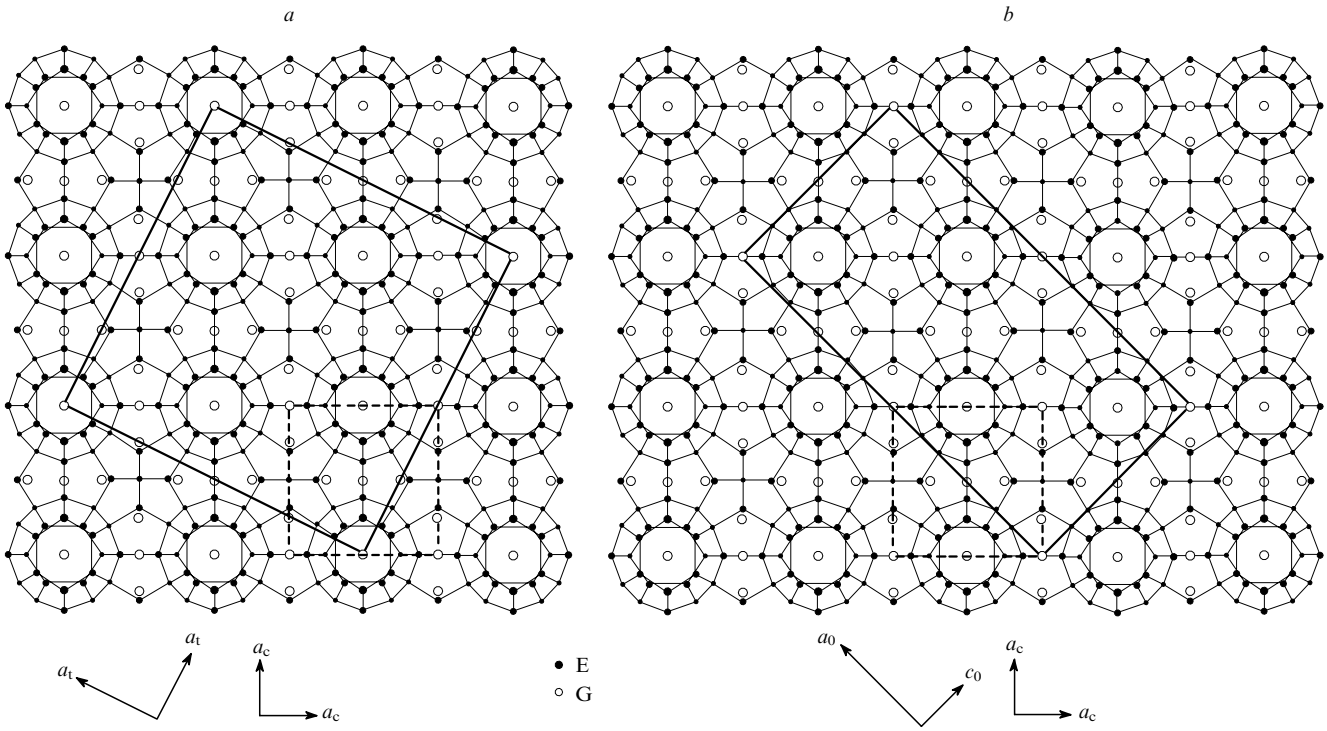

Figure 4. Superstructures of type I clathrates.
(*a*) The tetragonal superstruture $I_8[Sn_{14}In_{10}P_{21.2}\square_{0.8}]$, (*b*) the orthorhombic superstructure $Ba_8[Cu_{16}P_{30}]$; the initial cubic unit cell is indicated by dashed lines.

Another mode of formation of a superstructure is exemplified by the $Ba_8[Cu_{16}P_{30}]$ compound.[74] The latter is the only example of semiconducting clathrates, whose framework has no Group 14 elements. It crystallises in the orthorhombic system in the space group *Pbcn*, which is accompanied by an increase in the volume of the starting cubic unit cell by a factor of four ($a_{super} \approx \sqrt{2}a_{clath}$, $b_{super} \approx a_{clath}$, $c_{super} \approx 2\sqrt{2}a_{clath}$). In this compound, the copper atoms are always coordinated by four phosphorus atoms, whereas the phosphorus atoms have different coordination environments described as 3Cu + 1P, 2Cu + 2P and 1Cu + 3P. Evidently, this coordination of the copper atoms in the absence of a superstructure in the space group *Pm3n* can occur only if two positions are occupied by both the copper and phosphorus atoms.

Therefore, the formation of superstructures is, apparently, dictated by preferential coordination of atoms of different nature involved in the framework. Presumably, superstructures based on type I clathrates also occur in a number of other compounds (which prevents mixed occupancy of a position by atoms of different types). However, these types of ordering require a very large increase in the unit cell volume and, hence, may remain undetectable by conventional X-ray diffraction techniques.

2. Type II clathrate

The type-II clathrate structure also contains two types of polyhedra: pentagonal dodecahedra [5^{12}] and larger 16-face hexakaidecahedra [$5^{12}6^4$] (see Table 1). The type-I clathrate structure differs from the type-II clathrate structure (Fig. 5) in that the pentagonal dodecahedra in the former are not linked to each other, whereas these dodecahedra in the latter share faces and are packed in layers alternating in the order [ABC], which is typical of cubic close packing. The layers of pentagonal dodecahedra are linked to form a three-dimensional framework through hexakaidecahedra. The latter also share hexagonal faces and have a diamond-like arrangement in the cubic structure. The unit cell contains 136 atoms of the framework including 16 small and 8 large cavities. The formula of the corresponding ideal clathrate is $G^I_{16}G^{II}_8[E_{136}]$. As mentioned above, about 10 compounds have the type-II clathrate structure. This can be attributable to a large difference in the size of the polyhedra involved in the clathrate. As can be seen from Table 4, the type-II clathrate structure occurs either when compounds contain two cations, which differ substantially in size (for example, Na and Cs in $Na_{16}Cs_8[Ge_{136}]$) or when the guest atoms of one type occupy predominantly only one type of polyhedral cavity, whereas another type of cavity remains vacant. The type of the cavity being occupied depends on the size of the framework-forming element. In the case of tin, the large barium cations occupy only smaller cavities ($Ba_{16}\square_8[Ga_{32}Sn_{104}]$), whereas even rather small sodium cations occupy predominantly larger cavities in the framework formed by silicon atoms ($Na_x\square_{24-x}[Si_{136}]$, $x < 8$).

All compounds with the type-II clathrate structure crystallise in the cubic system in the centrosymmetrical space group *Fd3m*; 136 atoms of the framework occupy three positions, *viz.*, 8*a*, 32*e*

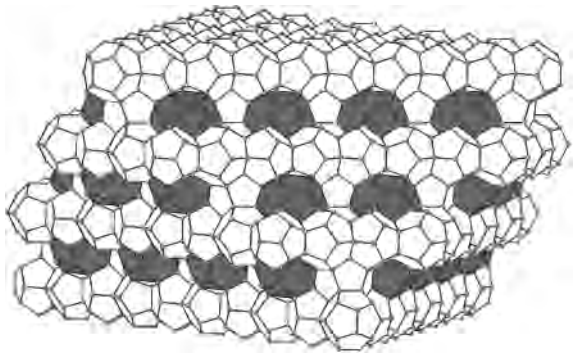

Figure 5. Overall view of the type-II clathrate structure.

Table 4. Compositions and structural features of polyanionic type-II clathrate phases.

Phase	Characteristics of the crystal structure	Ref.
$Na_x\square_{24-x}[Si_{136}]$	$1 < x < 23$; if $x < 8$, Na atoms occupy only larger cavities; at $x > 8$, smaller cavities begin to be filled	3, 40, 41, 81
$Na_x\square_{24-x}[Ge_{136}]$	$4 < x < 23$; if $x < 8$, Na atoms occupy only larger cavities; at $x > 8$, smaller cavities begin to be filled	82
$Cs_7\square_{17}[Si_{136}]$	Cs atoms occupy larger cavities	82
$Rb_8Na_{16}[Si_{136}]$	Rb atoms completely occupy larger cavities, Na atoms completely occupy smaller cavities	8
$Cs_8Na_{16}[Si_{136}]$	Cs atoms completely occupy larger cavities, Na atoms completely occupy smaller cavities	8, 83
$Rb_8Na_{16}[Ge_{136}]$	Rb atoms completely occupy larger cavities, Na atoms completely occupy smaller cavities	8
$Cs_8Na_{16}[Ge_{136}]$	Cs atoms completely occupy larger cavities, Na atoms completely occupy smaller cavities	8, 83
$Ba_{16}\square_8[Ga_{32}Sn_{104}]$	Ba atoms occupy only smaller cavities, and larger cavities are vacant	47, 84, 85

and 96*g*; 24 guest atoms occupy the 8*b* and 16*c* positions in the centres of the hexakaidecahedra and pentagonal dodecahedra, respectively. All positions of the framework in the type-II clathrate compounds (except for the $Ba_{16}\square_8[Ga_{32}Sn_{104}]$ compound) are occupied by atoms of one element. In the $Ba_{16}\square_8[Ga_{32}Sn_{104}]$ structure, the gallium and tin atoms are statistically distributed over all positions of the framework. Type II clathrates are characterised by full occupancies of the positions of the framework, whereas vacancies (if they are present) occur only in the guest positions (see Table 4).

3. Type III clathrate

Only two semiconducting clathrates with the type-III clathrate structure, *viz*., $Cs_{30}[Na_{2.5}Sn_{162.6}]$ and $Cs_{13.8}Rb_{16.2}[Na_{2.8}Sn_{162.3}]$, are known.[37] The structures of bromine hydrate $(Br_2)_{20}\square_{10}[(H_2O)_{172}]$ and dimethyl ether hydrate $(CH_3OCH_3)_{20}\square_{10}[(H_2O)_{172}]$ can be considered as prototypes of the type-III clathrate structure,[3] which consist of three types of polyhedra, *viz*., pentagonal dodecahedra $[5^{12}]$, larger tetrakaidecahedra $[5^{12}6^2]$ and even larger 15-face pentakaidecahedra $[5^{12}6^3]$ (see Table 1). Their ratio in the structure is 10 : 16 : 4, *i.e*., there are 30 polyhedra per unit cell. These polyhedra share faces to form a three-dimensional framework (Fig. 6) containing 172 atoms. The formula of the ideal type III clathrate is $G^{I}_{10}G^{II}_{16}G^{III}_{4}[E_{172}]$. Both compounds with the semiconducting type-III clathrate structure crystallise in the tetragonal system in the centrosymmetrical space group $P4_2/mnm$. All three types of cavities are completely occupied. In the $Cs_{30}[Na_{2.5}Sn_{162.6}]$ structure, all cavities are filled with cesium atoms. In the case of $Cs_{13.8}Rb_{16.2}[Na_{2.8}Sn_{162.3}]$, a situation, though more complicated, is also reasonable. In this structure, the largest pentakaidecahedra are occupied predominantly by cesium atoms, the smallest pentagonal dodecahedra are occupied predominantly by rubidium atoms, and the medium-sized tetrakaidecahedra are filled with cesium and rubidium atoms with equal probability.

The compositions of semiconducting type III clathrates differ slightly from the ideal composition, which is associated with the presence of vacancies in the framework. The reasons for the appearance of such vacancies and their amounts are discussed in detail below. The defect formation in the type-III clathrate structure differs from that in the type-I clathrate structure. In the type-III clathrate structure, vacancies are partially clusterised, *i.e*., a pair of tin atoms (Sn_2) is replaced by one sodium cation, which is located at the midpoint of the tin–tin bond (see Fig. 6). Hence, the formulas of the compounds under consideration can be written as $Cs_{30}[Na_{1.33x-10}Sn_{172-x}]$ and $Cs_{13.8}Rb_{16.2}.[Na_{1.33x-10}Sn_{172-x}]$ ($x \approx 9.6$).

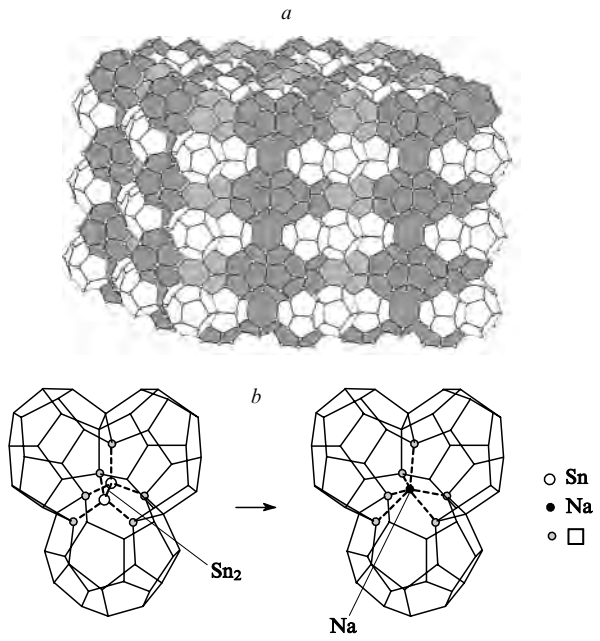

Figure 6. Type-III clathrate structure.
(*a*) Overall view, (*b*) formation of vacancies in the positions of tin atoms and replacement of these atoms with sodium atoms.

4. Type VIII clathrate

There are only two compounds, *viz*., α-$Eu_8[Ga_{16}Ge_{30}]$ (see Ref. 34) and α-$Ba_8[Ga_{16}\ Sn_{30}]$, with the type-VIII clathrate structure.[33,35] Both these compounds have a high-temperature β modification with the same composition and the type-I clathrate structure.[63] The type-VIII clathrate structure, unlike the type-I clathrate structure, has only one type of filled cavity (Fig. 7). These cavities can be described as distorted E_{20+3} polyhedra, which are derived from pentagonal dodecahedra as a result of the cleavage of three E–E bonds and the formation of nine new such bonds upon the addition of three additional E atoms. Since it is impossible to fill the complete space with this type of polyhedra, the structure also contains small eight-vertex cavities, which remain vacant. The formula of the ideal compound with the type-VIII clathrate structure is $G_8[E_{46}]$. Both known compounds crystallise in the cubic system in the non-centrosymmetrical space group $I43m$. The framework has 4 positions occupied by the E atoms of the framework (12*d*, 2*a*, 24*g* and 8*c*) and one guest position (8*c*). In both compounds, the gallium atoms are statistically mixed with Group 14 elements in all four positions of the framework. In studies,[34,35] the Ga : E ratio in the phases under consideration was demonstrated to be other than 16 : 30, *i.e*., these phases possess a certain homogeneity region and can contain a small excess of gallium. For the compound with E = Sn, this fact was established by X-ray diffraction.[35] In the case of E = Ge, non-stoichiometry was determined only on the basis of indirect evidence taking into account the physical properties of samples containing Ga and Ge in different ratios.[34]

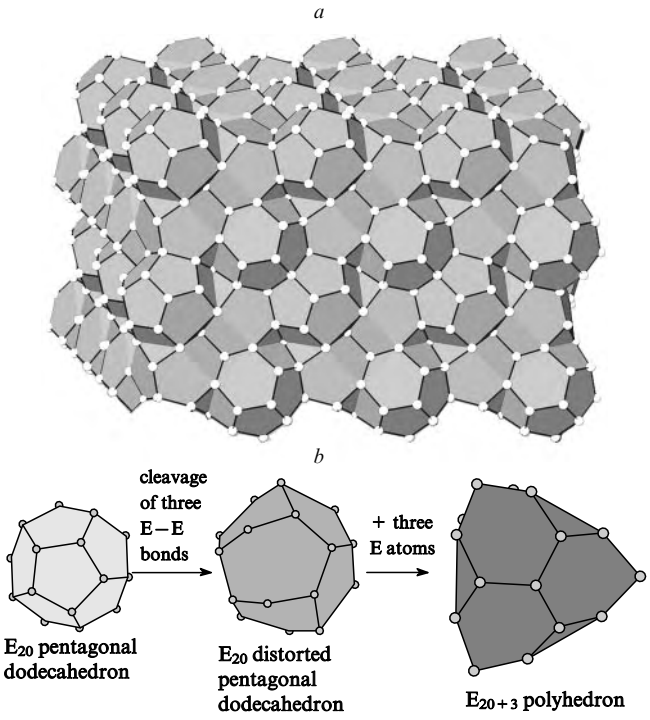

Figure 7. Type-VIII clathrate structure.
(*a*) Overall view, (*b*) scheme of distortions of the pentagonal dodecahedron.

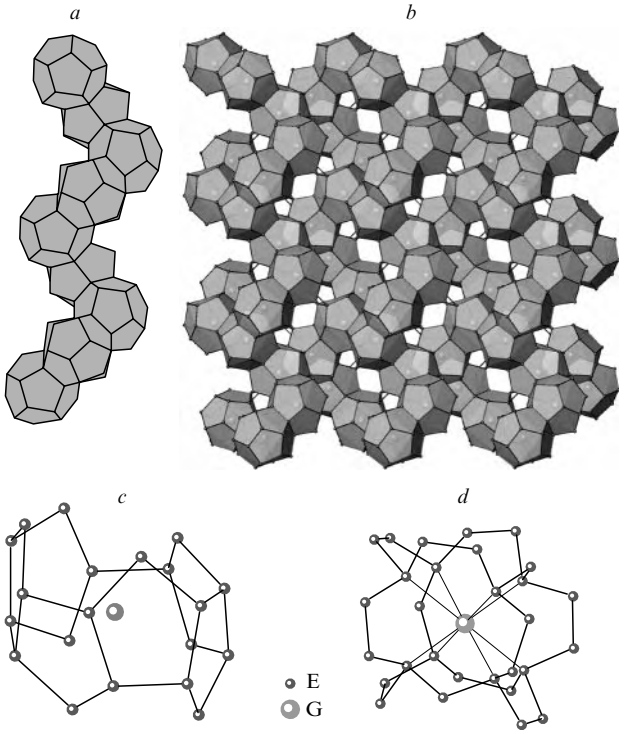

Figure 8. Type-IX clathrate structure.
(*a*) A chiral chain consisting of pentagonal dodecahedra, (*b*) a polyhedral representation of the structure, (*c*) the guest atom G^{II} in the open 20-vertex polyhedron, (*d*) the environment of the guest atom G^{III}.

5. Type IX clathrate

Type-IX clathrate compounds (or 'chiral' clathrates) crystallise in the cubic system in the non-centrosymmetrical space group $P4_132$. Eleven known compounds of this type are listed in Table 5. The main framework-forming polyhedron in the type-IX clathrate structure, like that in other clathrate structures, is a pentagonal dodecahedron. These polyhedra share faces to form a helix about each 4_1 axis (which accounts for the name 'chiral clathrate') (Fig. 8). The helical chains fill the space only partially, the channels between these chains being occupied by additional guest atoms of two types. The coordination of these atoms can be described as follows: one of these atoms is located in the 20-vertex open cavity and another atom is located in a distorted cube formed by the E atoms (see Fig. 8). The guest atoms located inside the pentagonal dodecahedra occupy the 8*c* position. Two other types of guest atoms can be described in different ways:

(1) both atoms completely occupy the 12*d* and 4*b* positions in the centres of the open twenty-vertex polyhedra and the cubes, respectively;[86–91, 94]

Table 5. Type-IX clathrate phases.

Framework-forming element	Phase	Ref.
Si	$Ba_6[Si_{25}]$	86
Ge	$Ba_6[Ge_{24}\square_1]$	87
	$Ba_{24}[Ge_{100}] \equiv Ba_6[Ge_{25}]$	88, 89
	$Na_2Ba_4[Ge_{25}]$	90
	$Ba_6[Ge_{23}Sn_2]$	87
	$Ba_6[Ge_{22}In_3]$	87
	$Ba_6[Ge_{21}In_4]$	36, 91
Sn	$K_6[Sn_{25}]$	92, 93
	$K_{7.4}[Sn_{25}]$	69
	$Rb_3Na_5[Sn_{25}]$	94
	$K_6[Sn_{23}Bi_2]$	92, 93

(2) the atoms in the centres of the open twenty-vertex polyhedra partially occupy the 24*e* position, and the atoms in the centres of distorted cubes completely occupy the 4*b* position;[69, 87, 92, 94, 95]

(3) both atoms partially occupy the 24*e* positions in the vicinity of the corresponding 12*d* and 4*b* positions.[93, 96]

It should be noted that the guest atoms in all models show large displacement parameters. In a number of studies (see, for example, Ref. 97), it was noted that a decrease in the temperature causes a phase transition accompanied by a change in the structure such that the atom is shifted from the 12*d* position to the 24*e* position with 50% occupancy.

The atoms of the framework occupy six positions, *viz*., three 24*e*, one 12*d* and two 8*c*. The type-IX clathrate structure differs essentially from all other types in that only 68 atoms of the framework (in two 24*e* positions and in the 12*d* and 8*c* positions) are four-coordinate, whereas 32 atoms (in the 24*e* and 8*c* positions) are three-coordinate. It should be noted that the type-IX clathrate structure has four formula units. The compositions of the clathrate phases given in Table 5 correspond to the compositions reported in the original studies. It can be seen that such compounds contain different amounts of guest atoms. This fact correlates with the electronic structures of semiconducting clathrates and is discussed in detail below.

6. Compounds structurally related to clathrates

Several compounds related to clathrates were described in the literature. The crystal structures of these compounds also contain the major polyhedron of clathrate structures, *viz*., the pentagonal dodecahedron. Examples are $Cs_3Na_{10}Sn_{23}$,[94] $Cs_2BaCu_8Te_{10}$,[98, 99] $Ba_{16}Na_{204}Sn_{310}$ (see Ref. 100) and $Te_{7+x}Si_{20-x}$ ($x \approx 2.5$).[101] The structure of the $Cs_3Na_{10}Sn_{23}$ compound contains layers of the face-sharing pentagonal dodecahedra $Cs@Sn_{20}$. These layers are analogous to the layers present in the type-II clathrate structure (see Fig. 5). In the $Cs_3Na_{10}Sn_{23}$ structure, these layers alternate with layers consisting of the $(Sn_4)^{4-}$ isolated tetrahedra, and the

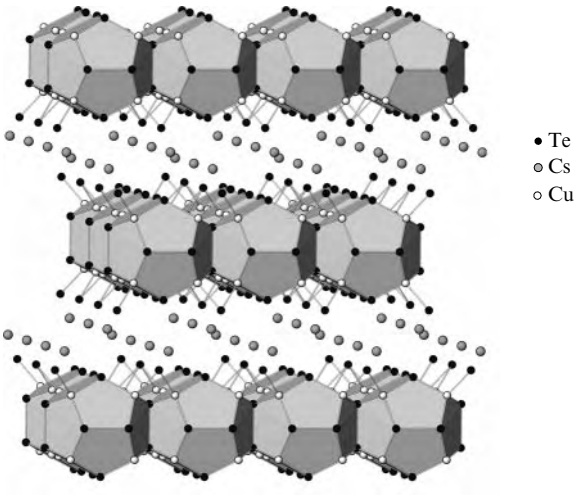

Figure 9. Crystal structure of $Cs_2BaCu_8Te_{10}$.

cavities between the polyhedra are occupied by sodium atoms. Another type of layer formed by the pentagonal dodecahedra is observed in the $Cs_2BaCu_8Te_{10}$ structure, in which the $Ba@Cu_8Te_{12}$ polyhedra share edges to form a layer. The layers are separated by cesium atoms (Fig. 9). The above-described compounds contain two-dimensional infinite fragments of clathrate structures.

The structures of the following two compounds have finite fragments. The structure of the $Ba_{16}Na_{204}Sn_{310}$ phase contains fragments of four vertex-sharing pentagonal dodecahedra $Ba@Sn_{20}$. Two other polyhedra of the host in this phase are the disordered $Na@Sn_{12}$ icosahedron and the 'empty' eight-vertex polyhedron Sn_8. The latter can be described as either a distorted cube or a distorted Archimedean antiprism. The space between the polyhedra is filled with sodium atoms. The structure of the $Te_{7+x}Si_{20-x}$ phase has the isolated pentagonal dodecahedra $Te@Te_{2.5}Si_{17.5}$, and the cavities between the latter are occupied by tellurium atoms. Interestingly, this compound is characterised by charge inversion, *viz*., the tellurium atoms, which are not involved in the polyhedron, bear a negative charge, *i.e*., they can formally be considered as Te^{2-} dianions.

A series of gallides and germanides of alkali, alkaline-earth and rare-earth metals, in which the positively charged guest metal atoms have rather high coordination numbers (from 14 to 19), were described in the literature.[102–115] Some researchers assigned these compounds to clathrate-like substances. However, in our opinion, it is unjustified to consider these compounds as related to clathrates because their crystal structures have no closed cavities and fragments of clathrate structures.

III. Electronic structures and properties of semiconducting clathrates

The electronic structures of semiconducting clathrates can qualitatively be described using the Zintl concept, *viz*.,the electron transfer from electropositive guest metal atoms to the framework formed by main-group atoms with localised covalent bonds.[38] Zintl phases are characterised by the strict correspondence between the crystal structure and electronic structures.

Classical Zintl phases are binary and ternary compounds, which contain alkali and alkaline-earth metals as cations and main-group elements from Groups 13–15 as anions and have structures of any complexity.[38] In such compounds, the cation donates electrons to the anion to form a closed-shell electronic configuration. The anion acquires an electron octet through the formation of two-centre two-electron homonuclear bonds and localised lone electron pairs. As a result, these compounds exhibit properties characteristic of Zintl phases. Evidently, if all atoms have closed-shell electronic configurations, all bonding and non-bonding (corresponding to lone electron pairs) states in the covalent anionic sublattice are filled, whereas all antibonding states are vacant. Correspondingly, Zintl phases exhibit semiconducting properties, even though they are polar intermetallides.

In addition to classical phases, there are the so-called metallic Zintl phases. These are compounds of Group 13 and 14 elements with alkali metals,[116] which can formally be described in terms of the Zintl concept. However, their properties differ from those predicted according to this concept. If the octet rule is obeyed, a change in the energy of interaction in going from a local level to an extended system can lead to the disappearance of a band gap and the appearance of metallic conductivity.[117,118] There are also 'non-traditional' Zintl phases. Among the latter are, for example, compounds containing transition metals, which cannot obey the octet rule but which can adopt the so-called closed-shell d-electron configurations (d^0, d^{10} and, sometimes, d^6 in an octahedral environment and d^8 in a square environment).[119,120] Inverted Zintl phases are generally assigned to 'non-traditional' phases. In such compounds, main-group elements form a cationic sublattice and acquire an electron octet, excess electrons being donated to eletronegative elements (halogens). This is accompanied by charge inversion: negatively charged halogen atoms are 'equivalent' to positively charged alkali and alkaline-earth metal cations in traditional Zintl phases.[38,121]

The detailed consideration of the Zintl concept and the properties of Zintl phases is beyond the scope of our review.‡ Here we demonstrate that most semiconducting clathrates are Zintl phases from the viewpoint of their formal electronic structures. However, some properties of these compounds cannot be explained in terms of the Zintl concept.

1. Type I clathrate

According to the Zintl concept, if the framework of the type I clathrate $A_8[E_{46}]$ is formed only by Group 14 atoms, which have four valence electrons and form four two-centre two-electron bonds, and has no vacancies, the $[E_{46}]$ framework should be electroneutral in the absence of guest atoms. The metal atoms A (alkali or alkaline-earth) placed in the polyhedral cavities in this framework acquire an electron octet due to donation of their valence electrons to the framework. A total of $8n$ electrons per formula unit (n is the valence of the A atom) are donated. Since these electrons occupy the antibonding conduction σ*-band of the host framework, the clathrate with the ideal composition $A_8[E_{46}]$ should exhibit metallic rather than semiconducting properties. Excess electrons in the σ*-band can be compensated in two different ways: by removal of some atoms of the framework or the partial replacement of the atoms of the framework by metal atoms having a smaller number of valence electrons.

In the former case, the removal of one E atom compensates four excess electrons. It is necessary to create $d = 8n/4$ vacancies in the framework. This situation is observed in alkali metal stannides ($d = 2$) of the general formula $A_8[Sn_{44}\square_2]$ (A = K, Rb, Cs) (see Table 2).[8,47,69,70]

In the case of heterovalent substitution, one heterometal atom M compensates $(14-z)$ excess electrons (z is the group number for the metal under consideration in the long-period form of the Periodic system of elements). The total number of metal atoms (y) required for the formation of the vacancy-free compound $A_8[M_yE_{46-y}]$ is calculated by the equation

$$y = \frac{8n}{14-z}.$$

The formulas of the ideal clathrates upon heterovalent substitution are given in Table 6.

Excess electron can also be compensated simultaneously through the formation of vacancies in the framework and hetero-

‡ These problems were discussed in detail in original studies.[38,121]

Table 6. Compositions with the type-I clathrate structure $A_8[M_yE_{46-y}]$, which were prepared by heterovalent substitution and obey the Zintl rule.

z	y	Composition ($n = 1$)	y	Composition ($n = 2$)
13	8	$A_8[M_8E_{38}]$	16	$A_8[M_{16}E_{30}]$
12	4	$A_8[M_4E_{42}]$	8	$A_8[M_8E_{38}]$
11	2.7	$A_8[M_{2.7}E_{43.3}]$	5.3	$A_8[M_{5.3}E_{40.7}]$
10	2	$A_8[M_2E_{44}]$	4	$A_8[M_4E_{42}]$

valent substitution. According to the Zintl concept, the coefficients y and d for the polyanionic clathrate $A_8[M_yE_{46-y-d}\square_d]$ are related by the equation

$$y(14-z) + 4d = 8n.$$

Such a 'twofold' compensation can be exemplified by the $Ba_8[Cd_4Ge_{40}\square_2]$ compound ($n = 2$, $z = 12$, $d = 2$, $y = 4$).[68]

In the case of heterovalent substitution of a p metal (Al, Ga, In, Zn or Gd) for a Group 14 element in polyanionic clathrates, the compositions determined by X-ray diffraction analysis are always identical to those predicted according to the Zintl concept (see Table 2). In some early studies, the synthesis of polyanionic clathrates, whose compositions do not satisfy the Zintl concept (for example, $K_8[Ga_{23}Sn_{23}]$ [122]), was mentioned. However, these data were not confirmed in later studies.[8, 46, 47, 55, 59] All clathrate compounds belonging to Zintl phases exhibit semiconducting and diamagnetic properties.[7, 9, 46, 47, 55–60, 68, 71, 72, 123]

Frameworks formed simultaneously by gallium and germanium atoms do not obey the Zintl principle. X-ray and neutron diffraction studies demonstrated that gallium atoms, unlike all other heteroatoms, are mixed with germanium atoms in all three positions of the clathrate frameworks.[8, 34, 57, 58, 62, 64, 65] Taking into account this fact, it can be hypothesised that the formation of phases, which exhibit metallic conductivity and whose compositions differ from those predicted in terms of the Zintl concept, is more favourable in mixed gallium-germanium systems.

Almost without exception, compounds prepared by heterovalent substitution of d metals for Group 14 elements do not satisfy the Zintl concept.[53] However, the compositions given in Table 2 were calculated on the assumption that all d-metal atoms are in the d^{10} state, although they can occur in other stable oxidation states. Besides, poor reliability factors ($R_1 \approx 6\%$–10%) may indicate that the structural features of the clathrate framework (for example, occupancies of atom positions) were not all established reliably.

The only europium-containing type I clathrate, *viz*., the β-$Eu_8[Ga_{16}Ge_{30}]$ phase,[34, 62, 124] is of particular interest. For this phase, the magnetic moment per europium atom is 7.9 μ_B, which corresponds to Eu^{2+}. Below 36 K, this phase behaves as a soft ferromagnetic material. At 36 K, ferromagnetic ordering (Fig. 10) occurs, which is accompanied by a stepwise change in the heat capacity.[34]

The compositions of binary clathrate silicides and the $Ba_8[Ge_{43}\square_3]$ compound deviate substantially from those predicted in terms of the Zintl principle. Recall that the Zintl concept is a simplified approach, according to which filling of electronic states can be considered on the basis of only formal oxidation states. Evidently, effects associated with the formation of energy bands in extended structures are ignored within the framework of this approach. The specificity of the electronic structures of clathrate silicides, which do not obey the Zintl rule, is apparently associated with the energy features of the atomic orbitals of silicon.[42, 82] The strength of the Si–Si bond (226 kJ mol^{-1}) [125] is substantially higher than that of the homoatomic bond between the germanium and tin atoms. Since the band gap in clathrates is small, the filling of the conduction band with excess electrons appears to be more favourable than the cleavage of the bonds between the silicon atoms and formation of vacancies in the clathrate framework. Consequently, there is no need for a strict

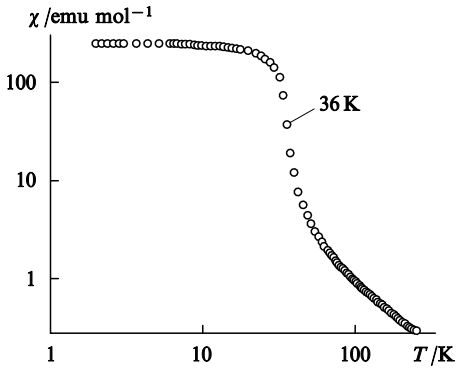

Figure 10. Temperature dependence of the magnetic susceptibility for β-$Eu_8[Ga_{16}Ge_{30}]$ according to the results of the study.[34]

correspondence between the composition of the compound and the number of electrons donated by the guest cation. Hence, many silicon-based clathrates have a wide non-stoichiometric region with respect to the cation. As an example we refer to $Rb_{8-x}Si_{46}$ ($x < 2$).[45] Such type I clathrates exhibit metallic conductivity and Pauli paramagnetism typical of metals.[126, 127]

In a series of studies, it was demonstrated that phases having no vacancies in the guest sublattice can be synthesised only under high pressure ($\sim$3 GPa).[48–51, 128] This method of synthesis allows one to prepare phases with unusual physical properties. Barium-containing silicides are low-temperature superconductors (T_c for $Ba_{7.76}\square_{0.24}[Si_{46}]$ is 9.0 K).[50, 51] This is the only example of superconductors with a framework formed by sp^3-hybridised silicon atoms. In studies,[50, 51] this fact was accounted for by partial overlapping of the s orbitals of the barium atoms with the orbitals of the atoms of the framework. An increase in the pressure leads to an increase in the amount of intercalated barium and an increase in the a parameter of the cubic unit cell. The partial replacement of barium with sodium or of silicon with germanium leads to a decrease in the superconducting transition temperature.[43, 44, 49]

The deviation of the composition of the germanium phase $Ba_8[Ge_{43}\square_3]$ (see Refs 49 and 61) from that predicted according to the Zintl concept ($Ba_8[Ge_{42}\square_4]$) is attributable to the fact that the formation of a large number of vacancies (four) in the framework is energetically less favourable than the formation of a smaller number of vacancies and doping of four excess electrons into the conduction band. Measurements of the resistive properties demonstrated that the $Ba_8[Ge_{43}\square_3]$ phase actually exhibits metallic conductivity.[61]

According to the Zintl concept, the framework of the inverse polycationic clathrates $X_8[E_{46}]$ (X is halogen) should donate eight excess electrons per formula unit to the X atoms. This is most easily achieved in the case of germanium compounds.[19–23] Each pnicogen atom in $X_8[Ge_{38}Z_8]$ (Z = P, As, Sb; X = Cl, Br, I) has 5 valence electrons, *i.e*., one electron more than the number of electrons required for the formation of four two-centre two-electron bonds. Correspondingly, 8 excess electrons are donated from eight pnicogen atoms to halogen atoms.

A different situation is observed in polycationic tin clathrates. The formula of ideal tin phosphide halide is $X_8[Sn_{24}P_{22}]$ (X = Br, I). Since each phosphorus atom donates one excess electron, while halogen atoms require only eight electrons to acquire an electron octet, the $X_8[Sn_{24}P_{22}]$ structure has $22-8 = 14$ excess electrons. These electrons can be compensated (as in the case of polyanionic clathrates) in two different ways: by the partial removal of the atoms of the framework or the partial replacement of the tin atoms with metal atoms having a smaller number of valence electrons.

In the former case, the removal of one phosphorus atom leads to compensation of five excess electrons. It is necessary to create $14/5 = 2.8$ vacancies. This corresponds to the $X_8[Sn_{24}P_{19.2}]$ com-

position, which is identical to that determined experimentally to within experimental error.[25, 31, 32]

In the case of heterovalent substitution, one heterometal atom M compensates $(14-z)$ excess electrons. To prepare the vacancy-free $X_8[M_ySn_{24-y}P_{22}]$ compound, the total number of metal atoms y can be calculated by the equation

$$y = \frac{14}{14-z}.$$

As can be seen from Table 3, the compositions of some vacancy-free tin phosphide halides, which were prepared by heterovalent substitution using p-metals (Ga, In, Zn, Gd) and even d-metals (Cu), are consistent with those predicted according to the Zintl concept.[26, 28, 29, 31, 75]

Excess electrons can be compensated simultaneously through the formation of vacancies in the framework and heterovalent substitution. In this case, according to the Zintl concept, the coefficients y and d for the polycationic clathrate $X_8[M_ySn_{24-y}P_{22-d}\square_d]$ are related by the equation

$$y(14-z) + 5d = 14.$$

The $I_8[Sn_{14}In_{10}P_{21.2}\square_{0.8}]$ ($z = 13$, $d = 0.8$, $y = 10$)[29] and $I_8[Sn_{20}Zn_4P_{20.8}\square_{1.2}]$ compounds ($z = 12$, $d = 1.2$, $y = 4$)[75] can serve as examples of the above-mentioned 'twofold' compensation.

The replacement of tin atoms with copper atoms in arsenide iodide can afford both a phase, which satisfies the Zintl principle ($I_8[Sn_{19.3}Cu_{4.7}As_{22}]$), and a phase containing an excess of copper ($I_8[Sn_{17.6}Cu_{6.4}As_{22}]$).[31] Since there are only a few tin arsenide iodides (see Table 3), the reasons for deviations from the Zintl principle remain unclear. There are two possible explanations: (1) the presence of transition metal atoms, which can adopt several stable electronic configurations; (2) as in the case of silicides, the cleavage of the As–As bonds and formation of vacancies are energetically less favourable than doping of excess electrons into the conduction band. A lack of data on the conductivity and magnetic susceptibility for these phases does not allow one to unambiguously decide between the above two schemes.

In the structures of all type I clathrates, vacancies are always located in the 6*c* position.[8, 25, 31, 32, 47, 49, 61, 64, 68–70] In this case, some atoms in the 24*k* position become three-coordinate. The presence of two types of tin atoms in the structures of alkali metal stannides was confirmed by ^{119}Sn NMR spectroscopy.[129] The distribution of the heterometal atoms over the positions of the framework in polyanionic clathrates differs from that observed in polycationic clathrates. In the former case, electropositive heterometals always fill first the 6*c* position and then the 16*i* position. The electronegative element (Sb) always fills the 24*k* position.[66, 67] Gallium, which is intermediate between the above-mentioned elements, can be mixed with Group 14 elements in all three positions of the framework.[8, 34, 57, 58, 62, 64, 65] In the case of polycationic clathrates, any heterometal occupies the 24*k* position together with tin,[26, 28, 29, 31, 75] which is accompanied by splitting of this position into two or three positions with partial occupancies, and some tin atoms are also three-coordinate. The coordination of tin atoms in polycationic clathrates can be confirmed not only by NMR spectroscopy but also by ^{119}Sn Mössbauer spectroscopy.[25, 26, 29, 75] In addition, the stereoactivity of the lone electron pairs on three-coordinate tin atoms can be judged from data on the quadrupole splitting of lines in the Mössbauer spectra.

The diamagnetic character of the temperature dependence of the magnetic susceptibility for certain polycationic type I clathrates, whose electronic structures obey the Zintl rule, is violated in the 200–250 K region, which is manifested in the appearance of a sharp jump in the curve $\chi(T)$.[32] As the field strength increases, this jump decreases up to its complete disappearance at $H \approx 5$ T. Low-temperature studies of the crystal structures of the $I_8[Sn_{24}P_{19.3}]$ and $Br_8[Sn_{24}P_{19.6}]$ compounds by X-ray diffraction analysis and Mössbauer, NMR, and X-ray photoelectron spectroscopy showed that a decrease in the temperature causes no structural changes.[32] Taking into account this fact, it can be concluded that a jump in the magnetic susceptibility curve is associated with either relaxation processes or a change in the mechanism of the electron–phonon interaction. Actually, the estimated value of the Debye temperature (below which, quantisation of thermal vibrations occurs) is 200–240 K. This conclusion is indirectly confirmed by the data on the temperature behaviour of the heat capacity of the $I_8[Sn_{24}P_{19.3}]$ phase. Thus, the maximum positive deviation from the Dulong–Petit law is observed at 250 K.[32]

An interesting and important transport property of semiconducting type I clathrates is their abnormally low heat conductivity.[7, 9, 34, 62, 72, 76, 78, 80, 123, 124, 130–132] At room temperature, the heat conductivity of many type I clathrates is 0.5–1.5 W m^{-1} K^{-1}, which is comparable to that of amorphous compounds. Moreover, a low-temperature region of the temperature dependence of the heat conductivity for most clathrates is typical of amorphous compounds (Fig. 11 *a*). This fact was initially explained by scattering of heat-carrying phonons by low-frequency vibrations of guest atoms inside the clathrate frameworks. Actually, calculations based on the Wiedemann–Franz law demonstrated that the electronic component of the heat conductivity is no higher than 6%–8%.[7, 9, 72, 78, 130] Consequently, the heat conductivity is determined primarily by its lattice component, and the guest atoms have high thermal parameters and can serve as efficient rattlers§ (Fig. 11 *b*). This mechanism is evidenced also by a slight decrease in the heat conductivity of most clathrates with decreasing temperature, which corresponds to a decrease in vibration amplitudes of the guest atoms.[80, 131] Such compounds are called phonon glasses, because glasses (in the general case, amorphous compounds) are characterised by a great number of structural irregularities, which effectively scatter pho-

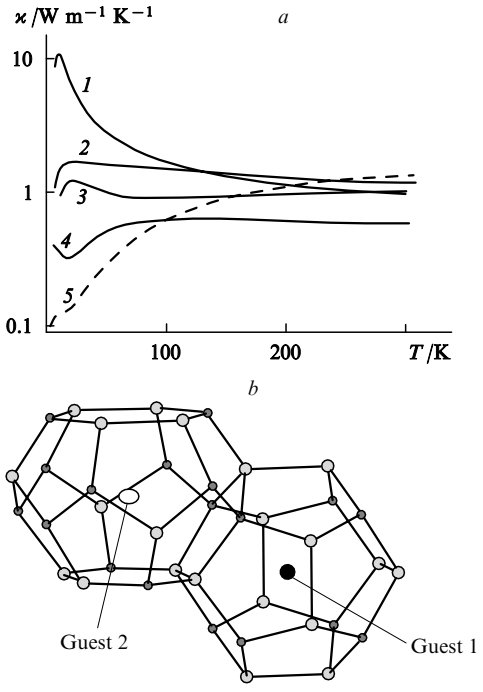

Figure 11. Temperature dependence of the heat conductivity for several type I clathrates (*a*) and anisotropic thermal displacements of the guest atoms in the clathrate polyhedra (*b*).
(*1*) $Cs_8[Sn_{44}\square_2]$, (*2*) $Rb_8[Zn_4Sn_{42}]$, (*3*) $I_8[Sn_{24}P_{19.3}\square_{2.7}]$, (*4*) β-$Eu_8[Ga_{16}Ge_{30}]$; data for vitreous silica (*5*) are given for comparison.

§ Weakly bound atoms or molecules, which can freely rotate or vibrate within a closed cavity and scatter heat-carrying phonons.

nons (the vibrational modes).[6] However, a detailed consideration of the temperature dependence of the heat conductivity showed that the region of this dependence below 50 K cannot be described as photon scattering by vibrations of guest atoms.[133] Two other possible mechanisms, *viz*., lattice relaxation and tunnelling of the guest atoms in a larger cavity to several nearby positions (see Fig. 3 *b*), were proposed.[34, 130, 133, 134] The characteristic features of a particular clathrate compound determine which process dominates.

The structures of the energy bands of type-I clathrate compounds were studied using various approximations, from the extended Hückel method to *ab initio* calculations.[9, 29, 38, 79, 135–144] Calculations showed that clathrates, which obey the Zintl rule, are narrow gap semiconductors. It appeared that the presence of vacancies predicted in terms of the Zintl concept is a necessary condition for the formation of semiconductors. If this condition is not met, one would expect the appearance of metallic properties.[29, 38, 141] For the polycationic clathrates, it was established that either orbitals of three-coordinate tin atoms having a lone electron pair or orbitals of heterometal atoms make the major contribution to the states in the vicinity of the Fermi level (Fig. 12).[29] The results of calculations for the $I_8[Sn_{24}P_{19.3}]$ phase agree well with the data from Mössbauer spectroscopy. The latter demonstrated that the lone electron pairs are not localised on tin atoms; instead, they form an extended band in the vicinity of the Fermi level.[29] Therefore, the properties of type I clathrates can be varied by changing the concentration of vacancies and performing various substitutions in the clathrate framework. Calculations also showed that the guest atoms in all type-I clathrate compounds are ionised.[29, 145] In particular, the charge on the halogen atoms in polycationic clathrates can be as high as -0.95, which is close to the corresponding oxidation state of the element. Arguments in favour of the atomic (non-ionised) state of the strontium atoms in $Sr_8[Ga_{16}\ Ge_{30}]$, which were adduced in several studies (see, for example, Ref. 77), were demolished in more recent studies.[144]

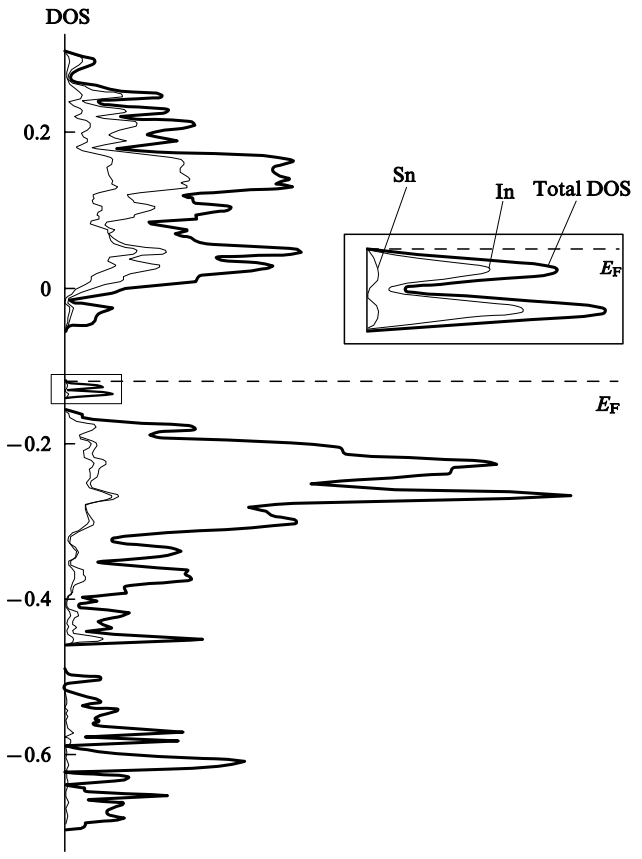

Figure 12. Plot of the density of states (DOS) for $I_8[Sn_{10}In_{14}P_{22}]$.[29]

2. Type II clathrate

In the framework of type-I clathrate compounds, as in the ideal type I clathrate, all atoms form four bonds. Correspondingly, all electrons donated by the guest atoms are excessive. Compensation of excess electron by replacing 32 tin atoms with gallium atoms occurs only in the $Ba_{16}\square_8[Ga_{32}Sn_{104}]$ compound (see Table 4).[47, 84, 85] This is sufficient for compensation of 32 electrons of 16 barium atoms. In all other cases, the compositions of the phases do not obey the Zintl rule. Such phases exhibit metallic conductivity and Pauli paramagnetism.[8, 83, 145, 146]

Studies of the band structures [126, 135, 146, 147] gave an insight into the electronic structures of type-II clathrate phases. Calculations for the hypothetical unfilled framework $[Si_{136}]$ showed that there is a strongly localised vacant nonbonding band with a capacity of 24 electrons in the vicinity of the Fermi level. The insertions of alkali metal (sodium) atoms into the polyhedral cavities in the framework of $Na_x[Si_{136}]$ is accompanied by ionisation of these atoms and filling of the nonbonding band with their valence electrons. If $x \geqslant 8$, the nonbonding band of the framework overlaps with the valence band. Hence, this compound must exhibit metallic properties. Correspondingly, at $x < 8$ silicide must possess semiconducting properties. However, the band gap between the valence and nonbonding bands is so narrow that it becomes smaller than kT at temperatures higher than 40 K, and $Na_x[Si_{136}]$ with $x < 8$ exhibits semiconducting properties only at low temperatures. Calculations of the band structures for silicides were confirmed by ^{29}Si and ^{23}Na NMR spectroscopy.[146, 147] The results of these calculations provide an explanation as to why the structure of the only barium-containing type II clathrate obeys the Zintl rule: the number of electrons donated by the barium atoms to the framework (32 electrons) is larger than the capacity of the nonbonding band (24 electrons), and doping of electrons into the conduction band is energetically unfavourable. That is why the type II clathrate, containing barium atoms as the guest, was synthesised only by partial heterovalent substitution of the atoms of the framework to compensate excess electrons.

It should be noted that silicon-based type II clathrates are characterised by very small compressibility comparable to that of silicon with a diamond-like structure.[148] Actually, the $Na_x[Si_{136}]$ compounds are not transformed into diamond-like silicon under high pressure; instead, they, like diamond-like silicon, are transformed into silicon with the structure of β-tin under a pressure of $\sim$11 GPa. The bulk modulum of $Na_x[Si_{136}]$ is only 8% smaller than that of diamond-like silicon. Hence, such clathrates hold considerable promise as superhard materials. Moreover, calculations demonstrated that carbon-based clathrates (if they will be synthesised) would be expected to have compressibility comparable to that of diamond and smaller than that of cubic boron nitride.[148, 149]

3. Type III clathrate

The general formula of type-III clathrate phases is $A_{30}[Na_{1.33x-10}Sn_{172-x}]$ ($x \approx 9.6$). The framework contains both isolated and 'clusterised' vacancies that formed upon the removal of a pair of bound tin atoms.[37] According to the Zintl concept, the presence of one isolated vacancy in the framework compensates four electrons. However, the removal of a pair of bound tin atoms compensates only six electrons. Actually, the removal of one tin atom gives rise to four three-coordinate tin atoms, each being involved in three bonds and having a lone electron pair. Five electrons are required for this coordination of the tin atom (three electrons for bonds with three other atoms and two electrons for the lone pair). Since the tin atom has only four electrons, one additional electron is necessary for each three-coordinate atom. Therefore, the removal of one tin atom compensates four electrons. The removal of a pair of tin atoms gives rise to only six three-coordinate atoms and, correspondingly, only six electrons are compensated (Fig. 13). It was demonstrated [37] that the ratio between the isolated and clusterised vacancies in the framework of type-III clathrate compounds, on the one hand, and the alkali

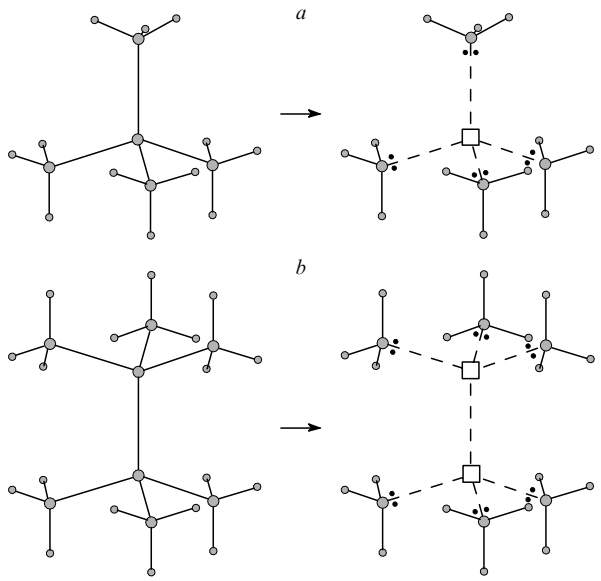

Figure 13. Clusterisation of the lone electron pairs of Group 14 elements in the case of formation of one (*a*) and two adjacent vacancies in the clathrate lattice (*b*).

metal atoms, on the other hand, is in complete agreement with the Zintl concept. Actually, magnetic measurements showed that both type-III clathrate compounds are diamagnetic.[37]

4. Type VIII clathrate

Type-VIII clathrate compounds are low-temperature polymorphs of type-I clathrate compounds.[63] The α phase (type VIII clathrate) of $Eu_8[Ga_{16}Ge_{30}]$[34] is stable up to 969 K, whereas the β phase (type I clathrate) is stable only over a narrow temperature range (969 – 972 K). At 972 K, the latter phase melts congruently. It should be noted that single-phase samples of the α and β phases were synthesised only using quenching to the corresponding temperatures (960 and 970 K for the α and β phases, respectively).

According to the Zintl concept, these compounds should have the same ideal composition: $A_8[Ga_{16}E_{30}]$ (A = Eu, Ba; E = Ge, Sn). However, the real compositions of these phases do not satisfy the Zintl rule. In early studies, the type-VIII clathrate compound in the Ba – Ga – Sn system was characterised as $Ba_8[Ga_{17.4}Sn_{28.8}]$.[33] More detailed investigation of the structure of this compound confirmed that its composition does not satisfy that predicted in terms of the Zintl concept. The refined composition of the phase is $Ba_8[Ga_{17.20(5)}Sn_{28.80(5)}]$.[35]

In the $Eu_8[Ga_{16}Ge_{30}]$ phase, as in other frameworks formed by gallium and germanium, the Ga : Ge ratio differs from 16 : 30.[133] The europium-containing α and β phases exhibit, on the whole, similar properties.[34] The magnetic moment per europium atom in the α modification also corresponds to Eu^{2+}. This phase is a soft ferromagnet and undergoes ferromagnetic ordering at 10.5 K. At this temperature, there is a jump in the temperature dependence of the heat capacity. A decrease in the temperature of ferromagnetic ordering compared to the analogous temperature for the type I clathrate is associated with the fact that the shortest Eu – Eu distances in the β phase are 5.23 Å, whereas the corresponding distances in the α phases are larger (5.56 Å).

5. Type IX clathrate

The type IX clathrate $A_6[E_{25}]$ is the only representative of clathrate compounds whose ideal framework contains three-coordinate atoms. Of the 25 atoms of the framework, 8 atoms are three-coordinate and 17 atoms are four-coordinate. Since each three-coordinate Group 14 atom requires one additional electron, the guest atoms should dope 8 electrons per formula unit into the framework to form an electroneutral compound. Among phases whose frameworks are formed exclusively by Group 14 atoms, the compositions of only two phases, *viz*., $Rb_3Na_5[Sn_{25}]$ (see Ref. 94) and $Ba_6[Ge_{24}\square_1]$,[87] obey the Zintl rule (see Table 5). In the latter phase, 4 excess electrons are compensated by the formation of one vacancy,[87] which is distributed over all positions of the framework in a complex fashion. It should be noted that the formation of this vacancy was not confirmed in other studies.[88, 89] By contrast, this phase was demonstrated to have no vacancies and its composition is inconsistent with the Zintl concept. Moreover, it was established[89] that it is impossible to synthesise a single-phase sample with composition $Ba_6[Ge_{24}\square]$.

Three phases, whose compositions obey the Zintl rule, *viz*., $Ba_6[Ge_{22}In_3]$,[87] $Ba_6[Ge_{21}In_4]$ (see Refs 36 and 91) and $K_6[Sn_{23}Bi_2]$,[92, 93] were synthesised by heterovalent substitution. In the first two phases, 4 excess electrons from the barium atoms are compensated by indium atoms (according to the Zintl concept, the four-coordinate indium atom compensates one electron, and the three-coordinated indium atom compensates two electrons). In the $Ba_6[Ge_{22}In_3]$ and $Ba_6[Ge_{21}In_4]$ phases, the indium atoms are distributed over all positions of the framework in a complex fashion. Hence, this distribution may also be considered as consistent with the Zintl concept. In the $K_6[Sn_{23}Bi_2]$ structure, the bismuth atoms occupy the three-coordinate positions of the framework. Each bismuth atom has 5 valence electrons, which are required for this coordination. Correspondingly, only 6 three-coordinate tin atoms remain in the framework, and six electrons from potassium atoms are sufficient for the formation of an electron-balanced compound. Phases whose electronic structures satisfy the Zintl rule, are diamagnetic narrow gap semiconductors.[36, 87, 91]

Compounds which do not obey the Zintl rule can be divided into two groups, *viz*., electron-excessive $Ba_6[Si_{25}]$ (+4*e*), $Ba_6[Ge_{25}]$ (+4e), $Ba_6[Ge_{23}Sn_2]$ (+4e) and $Na_2Ba_4[Ge_{25}]$ (+2e) and electron-deficient $K_6[Sn_{25}]$ (−2e).

The composition of potassium stannide with the type-IX clathrate structure has been initially characterised as $K_{7.4}[Sn_{25}]$.[69] However, the description of the positions and occupancies of the potassium atoms in this structure was doubtful, because the potassium atoms in this model were located at physically unreasonable short distances (2.92 Å). Later on, this phase was demonstrated to have a $K_6[Sn_{25}]$ composition.[92] To explain the fact that this composition does not satisfy the Zintl principle, the band structure of $K_6[Sn_{25}]^{2-}$ of the $K_6[Sn_{23}Bi_2]$ compound, which is isoelectronic to the Zintl phase, was calculated.[92, 93] This hypothetical structure is in complete agreement with the Zintl concept, and the calculations showed the typical semiconducting band structure with a band gap of ~1 eV. However, this band structure features an isolated filled band with a capacity of two electrons at the top of the valence band. Filling of this band influences primarily the interaction (repulsion) between 8 lone electron pairs of the tin atoms directed toward the centre of a distorted cube (see Fig. 8 *d*) and the potassium atom located in the centre of this cube. The repulsion is so high that a decrease in the number of electrons belonging to three-coordinate tin atoms is more favourable. Hence, the upper two-electron band in $K_6[Sn_{25}]$ is vacant. The replacement of two out of eight tin atoms with bismuth atoms (suppression of stereoactivity of the lone electron pair is more typical of the latter atoms) decreases repulsion between electrons giving rise to the classical Zintl phase $K_6[Sn_{23}Bi_2]$.[92, 93]

The band structures of electron-excessive phases were investigated.[95] In particular, the Fermi level was demonstrated to be located in the conduction band. According to the results of resistive measurements, such phases actually exhibit metallic conductivity.[86, 97, 150] The reason for the disorder in the guest sublattice (see the crystal structure of the type IX clathrate) was revealed. In the ordered structure, the Fermi level falls in a peak of the density of states. In the authors' opinion,[95] this fact may be indicative of the instability of the structure. Displacements of the

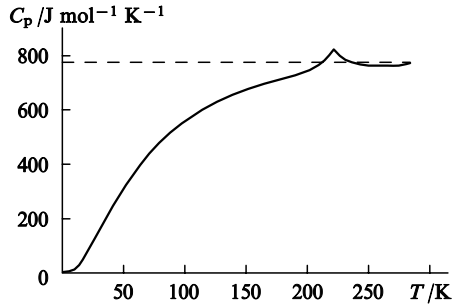

Figure 14. Temperature dependence of the heat capacity for $Ba_6[Ge_{25}]$.[97]

guest atoms from the ideal position to a partially occupied adjacent position leads to splitting of this peak into two peaks with larger and smaller energies. Therefore, a 'band' analogue of the Jahn–Teller effect is manifested in the crystal, and the density of states at the Fermi level substantially decreases.[95]

As expected, electron-excessive phases have metallic conductivity. A study of the heat capacity of the $Ba_6[Ge_{25}]$ phase revealed[97] a positive deviation from the Dulong–Petit law analogous to that observed for polycationic type I clathrates (Fig. 14). However, the authors of the cited study[97] explained this fact by a structural phase transition. At temperatures higher than the phase transition temperature, the barium atoms have high vibrations and can migrate from one partially occupied 24*e* position to another. A decrease in the temperature leads to 'freezing' of the barium atoms in the partially occupied 24*e* positions, which is indirectly confirmed by measurements of the temperature dependences of the electrical resistance, magnetic susceptibility and charge carrier mobility. In the $Na_2Ba_4[Ge_{25}]$ phase, 2/3 of barium atoms in the centres of the open 20-vertex polyhedra are replaced with sodium atoms. This phase is more ordered, and no structural transitions are observed in this phase down to 2 K.[97] Interestingly, both barium-containing germanides with the type-IX clathrate structure exhibit superconducting properties at low temperatures.[150] The superconducting transition temperatures T_c for the 'disordered' $Ba_6[Ge_{25}]$ phase and the 'ordered' $Na_2Ba_4[Ge_{25}]$ phase are 0.24 and 0.84 K, respectively. However, the temperature T_c of the disordered phase increases by a factor of more than 16 in response to external pressure (at 3.4 GPa, $T_c \approx 4.0$ K).[151] This fact was attributable to ordering of the barium atoms in the open cavities. Under high pressure, the barium atoms move from the partially occupied 24*e* positions to the 12*d* and 4*b* positions with 100% occupancy. The superconducting transition temperature for the ordered phase remains virtually unchanged under external pressure.[151] The above-mentioned compounds serve as examples of superconductors containing sp^3-hybridised atoms of p-elements.

IV. Methods for the synthesis of semiconducting clathrates

Since guest metal atoms (alkali metals, alkaline earth metals and europium) are highly reactive, polyanionic clathrates are generally synthesised under an inert gas (argon or helium) in sealed niobium or tantalum tubes, which are further placed in evacuated quartz tubes before annealing. Polycationic clathrates are more commonly synthesised simply in evacuated quartz tubes. It is more convenient to consider procedures for the synthesis of semiconducting clathrates for each particular main framework-forming element, *viz*., silicon, germanium or tin.

Silicon with a diamond-like structure has a very high melting point (1685 K) and, correspondingly, very low reactivity. Hence, the stoichiometric synthesis of binary clathrate silicides can be performed only at a high temperature under external pressure. For example, this procedure was used for the synthesis of $Ba_8[Si_{46}]$,[48–51] $Na_{8-x}Ba_x[Si_{46}]$,[43,44] $Ba_8[Si_{46-x-y}Ge_x\square_y]$ (see Ref. 49) and $Ba_{24}[Si_{100}]$.[86] The synthesis temperature was 1073–1573 K, and the pressure was 1.5–3 GPa. Another procedure for the synthesis involves thermal decomposition of binary silicides MSi (M = Na, K, Rb) to give $M_8[Si_{46}]$ or $M_x[Si_{136}]$ depending on the reaction conditions.[5,40,42,81,82] Heating to 500–700 K in the absence of dynamic vacuum can afford either type-I or type-II clathrate compounds with an x of ~ 10.[5,40–42] Under conditions of dynamic vacuum, syntheses produce primarily type II clathrate compounds. Depending on the reaction time, temperature and gas pressure, x can substantially be decreased (down to $x = 0.1$ at $\sim 10^{-3}$ Pa and 700 K).[152] Ternary clathrate silicides can be synthesised by the stoichiometric method. It should be noted that samples are usually pre-treated to enhance the reactivity of the starting compounds by performing either arc melting of the sample (for example, in the case of $Sr_8[Ga_xSi_{46-x}]$)[52] or heating of the sample to very high temperatures of 1300–1700 K (for example, in the case of $Ba_8[M_xSi_{46-x}]$, where M = Ni, Pd, Pt, Cu, Ag, Au),[53] generally, in an high-frequency furnace.

Germanium (T_m = 1210 K) is more reactive than silicon in spite of the fact that elemental germanium also has a diamond-like structure. Clathrate germanides can be synthesised by annealing stoichiometric amounts of the corresponding elements at 850–1250 K. As in the case of clathrate silicides, pre-treatment of samples is almost always required. For example, the $Ba_6[Ge_{25}]$ compound was prepared using arc melting[88] or induction heating.[89] The use of arc melting often leads to depletion of the reaction mixture due to evaporation of the most volatile metal and, correspondingly, to deviation from the starting stoichiometry. Because of this, this method is more often used for the synthesis of single crystals of clathrate compounds.[76,88] Single-phase samples are commonly synthesised using induction heating.[34,36,55–61,64,90,91] Since certain clathrate phases are stable only in a narrow temperature range (for example, β-$Eu_8[Ga_{16}Ge_{30}]$), the synthesis of such compounds involves quenching.[34]

Taking into account that the melting point of tin is low (505 K), stannides are generally prepared by annealing of a stoichiometric mixture of the elements without pre-treatment. In some instances, reaction mixtures containing an excess of tin are used. In such cases, tin serves also as a flux (for example, in the synthesis of the type IX clathrate $Rb_3Na_5[Sn_{25}]$).[91] The usual synthesis temperature is 600–700 K. Some tin-containing clathrates also cannot be prepared without quenching (for example, $Ba_8[Ga_{17.2}Sn_{28.8}]$).[33,35]

Polycationic clathrates are commonly synthesised by the simple stoichiometric method.[19–23,25,26,28,29,31,32] Elemental halogens are difficult to use because of their high volatility and also because chlorine and bromine are not solids under normal conditions. Therefore, halides of either metals or non-metals (MX_4, MX_2, TeI_4, ZX_3, where M = Ge, Sn; Z = P, As, Sb; X = Cl, Br, I) are usually used as the starting compounds. The synthesis temperatures vary from 670–830 K for tin-containing phases[25,26,28,29,31,32] to 1070 K for the $I_8[I_{1.5}Si_{44.5}]$ compound.[27,30] Polycationic clathrates can also be synthesised by the chemical transport reaction method. Since halogens and halides used as precursors are molecular compounds, they can serve as efficient transport agents. The chemical transport reaction method can be used for the preparation of single crystals and single-phase samples of polycationic clathrates. For example, single crystals of $Br_{2.4}I_{5.6}[Sn_{24}P_{19.2}\square_{2.8}]$ were grown in a temperature gradient of 825 – 725 K with the use of SnI_4 as the transport agent.[31,32]

V. Conclusion

Further studies of semiconducting clathrates will be aimed primarily at acquiring new fundamental knowledge and constructing new materials.

The fundamental scientific interest is associated primarily with the fact that particular type-I clathrate silicides [48, 50, 51] and type-IX clathrate germanides [150, 151] exhibit superconducting properties. Notwithstanding the fact that T_c for these compounds is no higher than 9.0 K, the occurrence of superconductivity in sp^3-hybridised systems is of obvious importance for a better understanding of this phenomenon. First data on the electron–phonon mechanism of superconductivity in clathrates were published as late as 2003.[153, 154]

An interesting field of investigation of semiconducting clathrates is concerned with elucidation of the reasons for the occurrence of such complicated structures, which are characterised by unusual filling of space with atoms and the unusual electron density distribution, and by the fact that the majority of these structures are thermodynamically stable and have diverse crystal structures. In particular, stability of the type-I clathrate compounds characterised by a distribution of the oppositely charged guest and host atoms was explained [155] in terms of periodic nodal surfaces (PNS),[155, 156] which allow one to relate the topology of the electron density distribution to the crystal structure. This method was also used for the description of the pathway of the phase transition between the α and β forms of $Eu_8[Ga_{16}Ge_{30}]$.[63]

Applied aspects of research on semiconducting clathrates are associated with the prospects of construction of new materials based on type-I clathrate compounds for thermoelectric cooling. The best currently available figure of merit (0.35) [157] is smaller than the maximum value (1.4) achieved for other types of inclusion compounds, *viz*., filled scutterudites.[132, 158] Nevertheless, there is no doubt that semiconducting clathrates hold promise,[11] and relative failures at the present stage of the investigation of these compounds are due to the fact that fundamental problems remain unsolved.[159, 160] Among such problems are the elucidation of the mechanisms of the abnormally low heat conductivity of clathrates and the prediction of fine changes in the electronic structure upon heterovalent substitution, including the prediction of the effective masses and concentrations of charge carriers.

Evidently, a combination of fundamental and applied studies [161] of semiconducting clathrates will contribute substantially to the development of inorganic and supramolecular chemistry, solid state chemistry and condensed matter physics.

This review has been written with the financial support of the Russian Foundation for Basic Research (Project Nos 00-03-32539a and 03-03-32514a), the European Commission (Fifth Framework Programme, Grant No. HPRN-CT-2002-00193) and the Russian National Science Foundation.

References

1. A Wells *Structural Inorganic Chemistry* (London: Oxford University Press, 1984)
2. H M Powell *Non-Stoichiometric Compounds* (Ed. L Mandelcorn) (New York: Academic Press, 1964)
3. J L Atwood, J E D Davies, P D MacNicol (Eds) *Inclusion Compounds* Vols 1, 2 (London: Academic Press, 1984)
4. B Kamb *Science* **148** 232 (1965)
5. J S Kasper, P Hagenmuller, M Pouchard *Science* **150** 1713 (1965)
6. Yu N Grin', L Z Melekhov, K A Chutonov, S P Yatsenko *Kristallografiya* **32** 497 (1987) [a]
7. G A Slack, in *CRC Handbook of Thermoelectrics* (Ed. D M Rowe) (Boca Raton, FL: CRC Press, 1995)
8. M A White *Properties of Materials* (Oxford: Oxford University Press, 1999)
9. G S Nolas, J L Cohn, G A Slack, S B Schjuman *Appl. Phys. Lett.* **73** 178 (1998)
10. S Bobev, S C Sevov *J. Solid State Chem.* **153** 92 (2000)
11. G S Nolas, G A Slack, S B Schjuman, in *Recent Trends in Thermoelectric Materials Research* (Ed. T M Tritt) (San Diego: Academic Press, 2001)
12. H Davy *Philos. Trans. R. Soc. London* **101** 155 (1811)
13. K W Allen *J. Chem. Soc.* 4131 (1959)
14. A Müller, H Reuter, S Dillinger *Angew. Chem., Int. Ed. Engl.* **34** 2328 (1995)
15. B Žemva, in *Encyclopedia of Inorganic Chemistry* Vol. 5 (Ed. R B King) (Chichester: Wiley, 1994)
16. W L Mao, H-k Mao, A F Goncharov, V V Struzhkin, Q Guo, J Hu, J Shu, R J Hemley, M Somayazulu, Y Zhao *Science* **297** 2247 (2002)
17. Yu A Dyadin, K A Udachin, I V Bondaryuk *Soedineniya Vklyucheniya* (Inclusion Compounds) (Novosibirsk: Novosibirsk State University, 1998)
18. Ya Mudryk, P Rogl, C Paul, S Berger, E Bauer, G Hilscher, C Godart, H Noël, A Saccone, R Ferro *Physica B* **328** 44 (2003)
19. H G von Schnering, H Menke *Angew. Chem., Int. Ed. Engl.* **84** 30 (1972)
20. H Menke, H G von Schnering *Naturwissenschaften* **59** 420 (1972)
21. H Menke, H G von Schnering *Z. Anorg. Allg. Chem.* **395** 223 (1973)
22. H Menke, H G von Schnering *Z. Anorg. Allg. Chem.* **424** 108 (1976)
23. T L Chu, S S Chu, R L Ray *J. Appl. Phys.* **53** 7102 (1982)
24. R Nesper, J Curda, H G von Schnering *Angew. Chem., Int. Ed. Engl.* **25** 369 (1986)
25. M M Shatruk, K A Kovnir, A V Shevelkov, I A Presnyakov, B A Popovkin *Inorg. Chem.* **38** 3455 (1999)
26. M M Shatruk, K A Kovnir, A V Shevelkov, in *The VIIth European Conference on Solid State Chemistry (Book of Abstracts), Madrid, 1999* p. O11
27. E Reny, S Yamanaka, C Cros, M Pouchard *Chem. Commun.* 2505 (2000)
28. M M Shatruk, K A Kovnir, A V Shevelkov, B A Popovkin *Zh. Neorg. Khim.* **45** 203 (2000) [b]
29. M M Shatruk, K A Kovnir, M Lindsjö, I A Presniakov, L A Kloo, A V Shevelkov *J. Solid State Chem.* **161** 233 (2001)
30. E Reny, S Yamanaka, C Cros, M Pouchard *J. Phys.: Condens. Matter* **14** 11 233 (2002)
31. L N Reshetova, J V Zaikina, A V Shevelkov, K A Kovnir, M Lindsjö, L Kloo *Z. Anorg. Allg. Chem.* **628** 2145 (2002)
32. K A Kovnir, J V Zaikina, A V Olenev, L N Reshetova, A V Shevelkov, E V Dikarev, N Senthikumaran, F Haarmann, M Baenitz, in *The IXth European Conference on Solid State Chemistry (Book of Abstracts), Stuttgart, 2003* p. 115
33. B Eisenmann, H Schäfer, R Zagler *J. Less-Common. Met.* **118** 43 (1986)
34. S Paschen, W Carillo-Cabrera, A Bentien, V H Tran, M Baenitz, Yu Grin, F Steglich *Phys. Rev. B* **64** 214 404 (2001)
35. W Carrillo-Cabera, R C Gil, V H Tran, Yu Grin *Z. Kristallogr.-New Cryst. Struct.* **217** 181 (2002)
36. R Kröner, R Nesper, H G von Schnering *Z. Kristallogr.-New Cryst. Struct.* **186** 164 (1989)
37. S Bobev, S C Sevov *J. Am. Chem. Soc.* **123** 3389 (2001)
38. M S Kauzlarich (Ed.) *Chemistry, Structure and Bonding of Zintl Phases and Ions* (New York: VCH, 1996)
39. F Liebau *Structural Chemistry of Silicates — Structure Bonding and Classification* (Berlin: Springer, 1985)
40. E Reny, P Gravereau, C Cros, M Pouchard *J. Mater. Chem.* **8** 2839 (1998)
41. G K Ramachandran, J Dong, J Diefenbacher, J Gryko, R F Marzke, O F Sankey, P F McMillan *J. Solid State Chem.* **145** 716 (1999)
42. G K Ramachandran, P F McMillan, J Diefenbacher, J Gryko, J Dong, O F Sankey *Phys. Rev. B* **60** 12 294 (1999)
43. H Kawaji, H Horie, S Yamanaka, M Ishikawa *Phys. Rev. Lett.* **74** 1427 (1995)
44. H Kawaji, K Iwai, S Yamanaka, M Ishikawa *Solid State Commun.* **100** 393 (1996)
45. G K Ramachandran, P F McMilan, J Dong O F Sankey *J. Solid State Chem.* **154** 626 (2000)
46. R Kröner, K Peters, H G von Schnering, R Nesper *Z. Kristallogr.-New Cryst. Struct.* **213** 667 (1998)
47. R Kröner, Doctoral Thesis in Chemical Sciences, University of Stuttgart, Stuttgart, 1989

48. S Yamanaka, E Enishi, H Fukuoka, M Yasukawa *Inorg. Chem.* **39** 56 (2000)
49. H Fukuoka, J Kiyoto, S Yamanaka *J. Solid State Chem.* **175** 237 (2003)
50. H Fukuoka, J Kiyoto, S Yamanaka *Inorg. Chem.* **42** 2933 (2003)
51. H Fukuoka, J Kiyoto, S Yamanaka *J. Phys. Chem. Solid* **65** 333 (2004)
52. M Imai, K Nishida, T Kimura, K Yamada *J. Alloys Compd.* **335** 270 (2002)
53. G Cordier, P Woll *J. Less-Common. Met.* **169** 291 (1991)
54. R F W Hermann, K Tanigaki, T Kawaguchi, S Kuroshima, O Zhou *Phys. Rev. B* **60** 13 245 (1999)
55. R Kröner, K Peters, H G von Schnering, R Nesper *Z. Kristallogr.-New Cryst. Struct.* **213** 675 (1998)
56. R Kröner, K Peters, H G von Schnering, R Nesper *Z. Kristallogr.-New Cryst. Struct.* **213** 669 (1998)
57. H G von Schnering, R Kröner, H Menke, K Peters, R Nesper *Z. Kristallogr.-New Cryst. Struct.* **213** 677 (1998)
58. R Kröner, K Peters, H G von Schnering, R Nesper *Z. Kristallogr.- New Cryst. Struct.* **213** 671 (1998)
59. R Kröner, K Peters, H G von Schnering, R Nesper *Z. Kristallogr.- New Cryst. Struct.* **213** 673 (1998)
60. H Menke, W Carrillo-Cabera, K Peters, E-M Peters, H G von Schnering *Z. Kristallogr.-New Cryst. Struct.* **214** 14 (1999)
61. W Carrillo-Cabera, J Curda, K Peters, S Paschen, M Baenitz, Yu Grin, H G von Schnering *Z. Kristallogr.-New Cryst. Struct.* **215** 321 (2000)
62. B C Sales, B C Chakoumakos, R Jin, J R Thompson, D Mandrus *Phys. Rev. B* **63** 245 113 (2001)
63. S Leoni, W Carrillo-Cabrera, Yu Grin *J. Alloys Compd.* **350** 113 (2003)
64. W Carrillo-Cabera, R C Gil, S Paschen, Yu Grin *Z. Kristallogr.-New Cryst. Struct.* **217** 183 (2002)
65. J D Bryan, V I Sdranov, G D Stucky, D Schmidt *Phys. Rev. B* **60** 3064 (1999)
66. S Latturner, X Bu, N Blake, H Metiu, G Stucky *J. Solid State Chem.* **151** 61 (2000)
67. S Latturner, J D Bryan, N Blake, H Metiu, G D Stucky *Inorg. Chem.* **41** 3956 (2002)
68. B Kuhl, A Czybulka, H-U Shuster *Z. Anorg. Allg. Chem.* **621** 1 (1995)
69. J-T Zhao, J D Corbett *Inorg. Chem.* **33** 5721 (1994)
70. H G von Schnering, R Kröner, M Baitinger, K Peters, R Nesper, Yu Grin *Z. Kristalogr.-New Cryst. Struct.* **215** 205 (2000)
71. G S Nolas, T J R Weakley, J L Cohn *Chem. Mater.* **11** 2470 (1999)
72. A P Wilkinson, C Lind, R A Young, S D Shastri, P L Lee, G S Nolas *Chem. Mater.* **14** 1300 (2002)
73. H G von Schnering, W Carrillo-Cabera, R Kröner, E-M Peters, K Peters *Z. Kristallogr.-New Cryst. Struct.* **213** 679 (1998)
74. J Dünner, A Mewis *Z. Anorg. Allg. Chem.* **621** 191 (1995)
75. M M Shatruk, Candidate Thesis in Chemical Sciences, Moscow State University, Moscow, 2000
76. B C Chakoumakos, B C Sales, D G Mandrus, G S Nolas *J. Alloys Compd.* **296** 80 (2000)
77. A Bentien, A E C Palmqvist, J D Bryan, S Latturner, G D Stucky, L Furenlid, B B Iversen *Angew. Chem., Int. Ed.* **39** 3613 (2000)
78. B C Chakoumakos, B C Sales, D G Mandrus *J. Alloys Compd.* **322** 127 (2001)
79. N P Blake, D Bryan, S Latturner, L Møllnitz, G D Stucky, H Metiu *J. Chem. Phys.* **114** 10 063 (2001)
80. G S Nolas, B C Chakoumakos, B Mahieu, G J Long, T J R Weakley *Chem. Mater.* **12** 1947 (2000)
81. C Cros, P Hagenmuller, M Pouchard *C. R. Acad. Sci.* **260** 4764 (1965)
82. C Cros, M Pouchard, P Hagenmuller *J. Solid State Chem.* **2** 570 (1970)
83. S Bobev, S C Sevov *J. Am. Chem. Soc.* **121** 3795 (1999)
84. R Kröner, R Nesper, H G von Schnering *Z. Kristallogr.-New Cryst. Struct.* **186** 172 (1989)
85. R Kröner, K Peters, H G von Schnering, R Nesper *Z. Kristallogr.-New Cryst. Struct.* **213** 664 (1998)
86. H Fukuoka, K Ueno, M Yasukawa *J. Organomet. Chem.* **611** 543 (2000)
87. S-J Kim, S Hu, C Uher, T Hogan, B Huang, J Corbett, M G Kanatzidis *J. Solid State Chem.* **153** 321 (2000)
88. H Fukuoka, K Iwai, S Yamanaka, H Abe, K Yoza, L Häming *J. Solid State Chem.* **151** 117 (2000)
89. W Carrillo-Cabera, J Curda, H G von Schnering, S Paschen, Yu Grin *Z. Kristallogr.-New Cryst. Struct.* **215** 207 (2000)
90. W Carrillo-Cabera, J Curda, K Peters, S Paschen, Yu Grin, H G von Schnering *Z. Kristallogr.-New Cryst. Struct.* **216** 183 (2001)
91. H G von Schnering, R Kröner, W Carrillo-Cabera, K Peters, R Nesper *Z. Kristallogr.-New Cryst. Struct.* **213** 665 (1998)
92. T F Fässler, C Kronseder *Z. Anorg. Allg. Chem.* **624** 561 (1998)
93. T F Fässler *Chem. Soc. Rev.* **32** 80 (2003)
94. S Bobev, S C Sevov *Inorg. Chem.* **39** 5930 (2000)
95. I Zerec, A Yaresko, P Thalmeier, Yu Grin *Phys. Rev. B* **66** 045 115 (2002)
96. V Petkov, T Vogt *Solid State Commun.* **127** 43 (2003)
97. S Paschen, V H Tran, M Baenitz, W Carrillo-Cabrera, Yu Grin, F Steglish *Phys. Rev. B* **65** 134 435 (2002)
98. X Zhang, Y Park, T Hogan, J L Schnidler, C R Kannewurf, S Seong, T Albright, M G Kanatzidis *J. Am. Chem. Soc.* **117** 10 300 (1995)
99. R Patschke, X Zhang, D Singh, J Schindler, C R Kannewurf, N Lowhorn, T Tritt, G S Nolas, M Kanatzidis *Chem. Mater.* **13** 613 (2001)
100. S Bobev, S C Sevov *J. Am. Chem. Soc.* **124** 3359 (2002)
101. N Jaussaud, M Pouchard, G Goglio, C Cros, A Ammar, F Weill, P Gravereau *Solid State Sci.* **5** 1193 (2003)
102. G S Smith, O Johnson, A G Tharp *Acta Crystallogr.* **18** 1085 (1965)
103. S P Yatsenko, E I Gladyshevskii, K A Chuntonov, Ya P Yarmolyuk, Yu N Grin' *Kristallografiya* **28** 809 (1983) [a]
104. F H Herbstein, R E Marsh *Acta Crystallogr., Sect. B* **39** 280 (1983)
105. A Czybulka, D Pinger, H U Schuster *Z. Anorg. Allg. Chem.* **579** 151 (1989)
106. O Zaharko, P Schobinger-Papamantellos, C Ritter, Y Janssen, E Brueck, F R de Boer, K H J Buschow *J. Phys.: Condens. Matter* **10** 2881 (1998)
107. G Venturini, A Verniere, B Malaman *J. Alloys Compd.* **291** 201 (1999)
108. R Welter, G Venturini *Acta Crystallogr., Sect. B* **55** 1969 (1999)
109. G Venturini, R Welter *J. Alloys Compd.* **299** 9 (2000)
110. G Venturini, A Verniere *J. Alloys Compd.* **305** 7 (2000)
111. U Schwarz, R Giedigkeit, R Niewa, M Schmidt, W Schnelle, R Cardoso, M Hanfland, Z Hu, K Klementiev, Yu Grin *Z. Anorg. Allg. Chem.* **627** 2249 (2001)
112. R Giedigkeit, R Niewa, W Schnelle, Yu Grin, R Kniep *Z. Anorg. Allg. Chem.* **628** 1692 (2002)
113. D Kaczorowski, Yu Grin *Solid State Commun.* **122** 637 (2002)
114. W Carrillo-Cabrera, S Paschen, Yu Grin *J. Alloys Compd.* **333** 4 (2002)
115. Yu Grin, W Schnelle, R Cardoso-Gil, O Sichevich, R Müllmann, B D Mosel, G Kotzyba, R Pöttgen *J. Solid State Chem.* **176** 567 (2003)
116. R Nesper *Prog. Solid State Chem.* **20** 1 (1990)
117. R Ramirez, R Nesper, H G von Schnering, M C Bohm *J. Phys. Chem. Solids* **48** 51 (1987)
118. C Zheng, R Hoffmann *Z. Naturforsch. B* **41** 292 (1986)
119. R Hoffmann, C Zheng *J. Phys. Chem.* **89** 4175 (1985)
120. T Y Kuromoto, S M Kauzlarich, D J Webb *Chem. Mater.* **4** 435 (1992)
121. A V Shevelkov, M M Shatruk *Izv. Akad. Nauk, Ser. Khim.* 337 (2001) [c]
122. W Westerhaus, H-U Schuster *Z. Naturforsch. B* **32** 1365 (1977)
123. G S Nolas, J L Cohn, J S Dyck, C Uher, J Yang *Phys. Rev. B* **65** 165 201 (2002)
124. G S Nolas, T J R Weakley, J L Cohn, R Sharma *Phys. Rev. B* **61** 3845 (2000)

125. D M Mingos *Essential Trends in Inorganic Chemistry* (Oxford: Oxford University Press, 1998)
126. J S Tse, K Uehara, R Rousseau, A Ker, C I Ratcliffe, M A White, G MacKay *Phys. Rev. Lett.* **85** 114 (2000)
127. G S Nolas, J-M Ward, J Gryko, L Qiu, M A White *Phys. Rev. B* **64** 153 201 (2001)
128. A Kitano, K Moriguchi, M Yonemura, S Munetoh, A Shintani, H Fukuoka, S Yamanaka, E Nishibori, M Takata, M Sakata *Phys. Rev. B* **64** 045 206 (2001)
129. F Haarmann, M Baitinger, Yu Grin, in *The IXth European Conference on Solid State Chemistry (Book of Abstracts), Stuttgart, 2003* p. 062
130. J L Cohn, G S Nolas, V Fessatidis, T H Metcalf, G A Slack *Phys. Rev. Lett.* **82** 779 (1999)
131. B C Sales, B C Chakoumakos, D Mandrus, J W Sharp *J. Solid State Chem.* **146** 528 (1999)
132. G S Nolas, M Kaeser, R T Littleton, T M Tritt *Appl. Phys. Lett.* **77** 1855 (2000)
133. S Paschen, V Pacheco, A Bentien, A Sanchez, W Carrillo-Cabrera, M Baenitz, B B Iversen, Yu Grin, F Steglich *Phys. B* **328** 39 (2003)
134. R C Zeller, R O Pohl *Phys. Rev. B* **4** 2029 (1971)
135. V I Smelyansky, J S Tse *Chem. Phys. Lett.* **264** 459 (1997)
136. J Zhao, A Buldum, J P Lu, C Y Fong *Phys. Rev. B* **60** 14 177 (1999)
137. N P Blake, L Müllnitz, G Kresse, H Metiu *J. Phys. Chem.* **111** 3133 (1999)
138. K Moriguchi, M Yonemura, A Shintani, S Yamanaka *Phys. Rev. B* **61** 9859 (2000)
139. D Connétable, V Timoshevskii, E Artacho, X Blase *Phys. Rev. Lett.* **87** 206 405 (2001)
140. K Moriguchi, S Munetoh, A Shintani, T Motooka *Phys. Rev. B* **64** 195 409 (2001)
141. C W Myles, J Dong, O F Sankey *Phys. Rev. B* **64** 165 202 (2001)
142. A Moewes, E Z Kurmaev, J S Tse, M Geshi, M J Ferguson, V A Trofimova, Y M Yarmoshenko *Phys. Rev. B* **65** 153 106 (2002)
143. L Møllnitz, N P Blake, H Metiu *J. Chem. Phys.* **117** 1302 (2002)
144. C Gatti, L Bertini, N P Blake, B B Iversen *Chem. Eur. J.* **9** 4556 (2003)
145. N F Mott *J. Solid State Chem.* **6** 348 (1973)
146. M Pouchard, C Cros, P Hagenmuller, E Reny, A Ammar, M Menètrièr, J-M Bassat *Solid State Sci.* **4** 723 (2002)
147. J Gryko, P F McMillan, R F Marzke, A P Dodokin, A A Demkov, O F Sankey *Phys. Rev. B* **57** 4172 (1998)
148. A San-Miguel, P Kèghèlian, X Blase, P Mèlinon, A Perez, J P Itiè, A Polian, E Reny, C Cros, M Pouchard *Phys. Rev. Lett.* **83** 5290 (1999)
149. S Saito, A Oshiyama, in *Recent Advances in the Physics and Chemistry of Fullerenes and Related Materials* Vol. 3 (Eds K M Kadish, R S Ruoff) (Pennington, NJ: Electrochemical Society, 1996) p. 457
150. F M Grosche, H Q Yuan, W Carrillo-Cabrera, S Paschen, C Langhammer, F Kromer, G Sparn, M Baenitz, Yu Grin, F Steglich *Phys. Rev. Lett.* **87** 247 003 (2001)
151. H Q Yuan, F M Grosche, W Carrillo-Cabrera, S Paschen, G Sparn, M Baenitz, Yu Grin, F Steglich *J. Phys.: Condens. Matter* **14** 11249 (2002)
152. J Gryko, P F McMillan, R F Marzke, G K Ramachandran, D Patton, S K Deb, O F Sankey *Phys. Rev. B* **62** R7707 (2000)
153. K Tanigaki, T Shimizu, K M Itoh, J Teraoka, Y Morimoto, S Yamanaka *Nature Mater.* **2** 653 (2003)
154. D Connetable, V Timoshevskii, B Masenelli, J Beille, J Marcus, B Barbara, A M Saitta, G-M Rignanese, P Melinon, S Yamanaka, X Blase *Phys Rev. Lett.* **91** 247 001 (2003)
155. H G von Schnering, R Nesper *Angew. Chem., Int. Ed. Engl.* **26** 1059 (1987)
156. H G von Schnering, R Nesper *Z. Phys. B: Condens. Matter* **83** 407 (1991)
157. B B Iversen, A E C Palmqvist, D E Cox, G S Nolas, G D Stucky, N P Blake, H Metiu *J. Solid State Chem.* **149** 455 (2000)
158. B C Sales, D Mandrus, B C Chakoumakos, V Keppens, J R Thompson *Phys. Rev. B* **56** 15 081 (1997)
159. A V Shevelkov *Vestn. Mosk. Univ., Ser. 2: Khim.* **44** 163 (2003) [d]
160. A Bentien, M Christensen, J D Bryan, A Sanchez, S Paschen, F Steglich, G D Stucky, B B Iversen *Phys. Rev. B* **69** 045 107 (2004)
161. F J DiSalvo *Science* **285** 703 (1999)

[a] — *Crystallogr. Rep. (Engl. Transl.)*
[b] — *Russ. J. Inorg. Chem. (Engl. Transl.)*
[c] — *Russ. Chem. Bull., Int. Ed. (Engl. Transl.)*
[d] — *Moscow Univ. Bull. (Engl. Transl.)*

Russian Chemical Reviews **73** (10) 939 – 956 (2004) © 2004 Russian Academy of Sciences and Turpion Ltd

DOI 10.1070/RC2004v073n10ABEH000921

Inorganic structures as materials for gas sensors †

R B Vasiliev, L I Ryabova, M N Rumyantseva, A M Gaskov

Contents

I.	Introduction	939
II.	Mechanism of gas sensitivity of semiconductor materials	940
III.	Mechanism of gas sensitivity of systems with heterojunctions	943
IV.	Conclusion	954

Abstract. Studies concerned with the design of new inorganic materials for gas sensors based on semiconductor structures are analysed. The influence of adsorbed molecules on the electronic state and electrical conductivity of the surface and inner interfaces in semiconductor materials is discussed. The mechanism of gas sensitivity is considered taking metal/insulator/semiconductor, semiconductor/insulator/semiconductor, metal/semiconductor, and semiconductor/semiconductor structures as examples. Specific features of the behaviour of heterostructures based on nanocrystalline metal oxides on single-crystalline silicon substrates with a SiO_2 dielectric layer are pointed out. The sensor properties of semiconductor structures in the detection of various molecules are described. The bibliography includes 114 references.

I. Introduction

Chemical sensors are among the most efficient environmental control, human physiology control and food quality control tools. Recently, design of new materials possessing a high and selective sensitivity to specific types of molecules has been a subject of intensive research. The authors of numerous publications on the subject (see, *e.g.*, reviews and monographs [1–7]) have paid considerable attention to fundamental concepts of adsorption mechanisms and to the character of electronic properties of the surface of oxide materials. This review mainly concerns problems related to processes occurring at interfaces of various semiconductor structures that are used as sensor elements. Usually, gas sensing elements of such structures are semiconductor metal oxides SnO_2, ZnO, WO_3 and In_2O_3.[7–17] The ability of these materials to detect gas molecules is due to their fundamental physical and chemical properties. The conductivity of wide-gap semiconductors in the temperature range 300 – 800 K is strongly dependent on the state of the surface. At these temperatures, redox reactions proceed on the oxide surfaces. The chemical properties of the surface also play an important role in the gas sensitivity mechanism. The oxide surfaces are characterised by good adsorption properties and high reactivities that are due to the presence of (i) free electrons in the conduction band, (ii) surface and bulk oxygen vacancies and (iii) reactive chemisorbed oxygen.[18,19]

In (traditional) resistive gas sensors the mechanism of gas sensitivity involves chemisorption on the surface accompanied by a change in the concentration of charge carriers (hereafter, carrier concentration) in the bulk of a semiconductor. The sensor response is a result of a change in the bulk conductance of a polycrystalline semiconductor material. The state of contacts between grains in the polycrystalline system contributes largely to the conductance. Such systems are extremely sensitive to trace amounts of oxidising or reducing agents present in the atmosphere. At the same time, information on the composition of the gas phase is insufficient due to the low selectivity of adsorption processes. The main goal of numerous studies aimed at improving the sensor parameters of materials is to optimise the electronic properties or the adsorption capacity of the materials. However, this approach is of limited use because resistive semiconductor gas sensors combine the functions of the sensing element (receptor) and signal transducer in the same material. Enhancement of sensitivity by changing the state of the surface leads to a change in the carrier concentration in the bulk of the semiconductor grain, *i.e.*, to a change in the parameters of the transducer. The receptor and transducer functions can be separated in those systems which include an interface between materials with different electronic properties. The conductance of such systems (the so-called heterostructures) is governed by the height of an energy barrier to charge carriers at the heterointerface. Chemisorption affects the electronic state of the interface, thus being responsible for the onset of gas sensitivity. Yet another advantage of the heterostructure gas sensors over resistive sensors is that they permit control of both the resistance and capacitance by varying the voltage and frequency of the reference signal.

The inorganic structures used for fabrication of various types of gas sensors are listed in Table 1.

Most often, gas sensors employ the so-called Schottky diodes (metal/semiconductor systems) as heterocontacts. The sensor properties of the Schottky diodes based on noble metals possessing catalytic properties (Pt, Pd; hereafter, catalytic metals) and single-crystalline silicon or silicon carbide have been studied in detail.[57] The Schottky diodes are extremely sensitive to trace amounts of hydrogen. The action mechanism of these systems

R B Vasiliev, L I Ryabova, M N Rumyantseva, A M Gaskov Department of Chemistry and Department of Materials Science, M V Lomonosov Moscow State University, Leninskie Gory, 119992 Moscow, Russian Federation. Fax (7-095) 939 09 98. Tel. (7-095) 939 54 71.
E-mail: romvas@inorg.chem.msu.ru (R B Vasiliev), roum@inorg.chem.msu.ru (M N Rumyantseva), gaskov@inorg.chem.msu.ru (A M Gaskov). Tel. (7-095) 939 11 51.
E-mail: mila@mig.phys.msu.ru (L I Ryabova)

Received 9 March 2004
Uspekhi Khimii **73** (10) 1019 – 1038 (2004); translated by A M Raevskiy

† This is the last review in a series of publications concerning the main avenues of research carried out at the Inorganic Chemistry Chair, Department of Chemistry and Department of Materials Science, M V Lomonosov Moscow State University [see *Russian Chemical Reviews* **73** (9) (2004)].

Table 1. Inorganic structures used in gas sensors.

Structure	Method of synthesis [a]	Molecules detected	Ref.
Metal/insulator/semiconductor			
$Pd/SiO_2/Si$	EBE	H_2, C_2H_5OH, $(CH_3)_2CO$, NO	20–22
$Pd/SiO_2/Si$	LIE	NH_3	23
$Pt/SiO_2/Si$	EBE	H_2	24
$Ru/SiO_2/Si$	EBE	H_2	25
$Ir/SiO_2/Si$	EBE	H_2	25
$Pd/SiO_2/SiC$	EBE	H_2	26
Semiconductor/insulator/semiconductor			
$SnO_2/SiO_2/Si$	SP	NH_3, C_2H_5OH	27
Metal/semiconductor			
Pd/Si	EBE	H_2	28–31
Pd/SnO_2	CVD	H_2, CO, O_2	32–34
Pd/TiO_2	EBE	H_2	35
Pd/TiO_2	TVE	H_2	36
Pt/SnO_2	CVD	NO_2	37
Pt/TiO_2	EBE	CO, O_2	38
Semiconductor/semiconductor			
PbS/Si	TVE	H_2	39
WO_3/Si	MS	NO	40
SnO_2(M)/Si	SP	NO_2, C_2H_5OH	41, 42
CuO/ZnO	SPS	CO, H_2, C_3H_8, H_2O	43–50
CuO/ZnO	MS	H_2, CO, H_2O	51
La_2CuO_4/ZnO	SPS	H_2, CO, H_2O	52, 53
CuO/SnO_2	MS	H_2S	54–56

[a] Notations: EBE is Electron Beam Evaporation, LIE is Laser Induced Evaporation, SP is Spray Pyrolysis, CVD is Chemical Vapour Deposition, TVE is Thermal Vacuum Evaporation, MS is Magnetron Sputtering and SPS is Solid-Phase Synthesis.

involves formation of a dipole layer at the metal/silicon interface. Yet another example is provided by a PbS/Si semiconductor/semiconductor heterojunction.[39] Its sensitivity to hydrogen is also due to the change in the carrier concentration in the PbS layer upon dissociative dissolution of hydrogen. The sensitivity of these systems to hydrogen is first of all associated with the impossibility of more complex molecules reaching the heterojunction region owing to limitations imposed on diffusion in crystalline systems. The use of porous nanocrystalline systems based on semiconductor oxides removes limitations on the diffusion of gas molecules.

In this review we will consider the electronic state of interfaces (surface and heterocontacts) in semiconductors under adsorption and the mechanisms of gas sensitivity of various types of heterostructures including those based on nanocrystalline metal oxides.

II. Mechanism of gas sensitivity of semiconductor materials

The mechanism of gas sensitivity in semiconductors has been studied in detail.[58–62] Materials used in resistive gas sensors are characterised by a reversible change in the conductivity depending on the gas phase composition. Accompanying processes can be divided into two main groups, *viz*., processes proceeding on the surface and in the bulk of the semiconductor material. The first group includes adsorption of gas molecules and chemical reactions on the surface and causes a change in the electronic state of the surface. The second group is associated with the change in the free carrier concentration in the near-surface layer as a result of electron exchange with the surface and also includes diffusion of atoms and variation of the concentration of bulk defects. All these changes caused by the interaction between the semiconductor material and the gas phase affect the carrier concentration and mobility (μ). In turn, changes in these parameters change the conductivity.

The electrophysical properties of a finite semiconductor are to a great extent determined by the presence of a specific class of energy levels (the so-called surface states) in the band structure. A comprehensive treatment of the surface states and interfaces has been given in a monograph [63] and a particular case of the surfaces of oxide materials was considered in Refs 64 and 65.

The interaction with the gas phase modifies the surface states. It should be noted that physisorption has little effect on the free carrier concentration and can influence only the electron work function needed to leave the semiconductor. Chemisorption is accompanied by charge exchange between the adsorbed molecule and the semiconductor. Consider an n-type semiconductor (SnO_2, ZnO, In_2O_3) in the framework of a simplest model.[66] Assume that there are no surface eigenstates on the surface of the semiconductor before adsorption (in the initial state) so that the energy bands are flat (Fig. 1). Depending on the electronegativity of the adsorbate molecule, the following types of chemisorption are possible:

(1) the electron affinity, A, of the adsorbate molecule is greater than the semiconductor work function, ϕ_{sc}; as a consequence, a surface acceptor level, E_{sa}, is formed, the near-surface layer of the semiconductor becomes depleted of electrons and the work function increases;

(2) the ionisation energy, I, of the adsorbate molecule is lower than the semiconductor work function, ϕ_{sc}; in this case, a surface donor level, E_{sd}, is formed, the near-surface layer of the semiconductor becomes enriched with electrons and the work function decreases.

The interfacial potential barrier, V_s, and the thickness, L, of the depletion layer, are given by:[67]

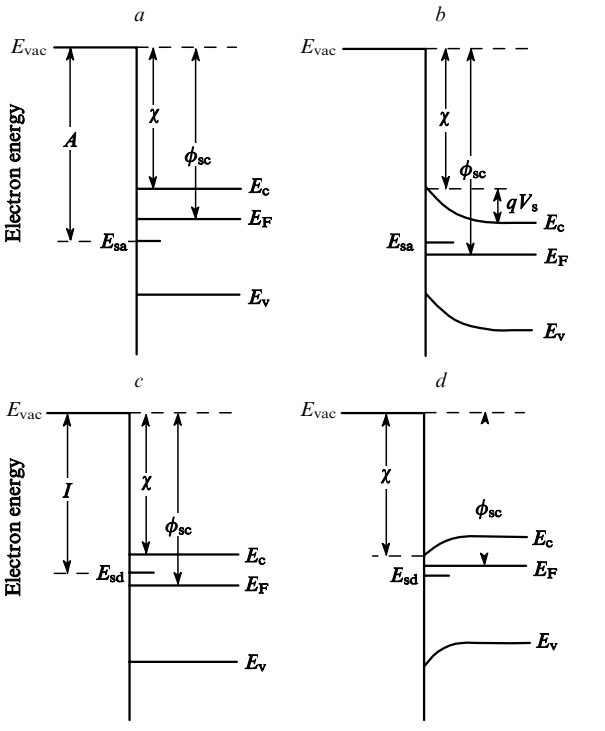

Figure 1. Band diagram of n-type semiconductor under adsorption of acceptor (*a*, *b*) and donor (*c*, *d*) molecules.[63]
Initial states (*a*, *c*) and final states (*b*, *d*); E_{vac} is the vacuum energy; E_c is the conduction band edge energy, E_v is the valence band edge energy, E_{sa} is the acceptor level, E_{sd} is the donor level, A is the electron affinity of the adsorbate, I is the ionisation energy of the adsorbate, χ is the electron affinity of the semiconductor and ϕ_{sc} is the semiconductor work function.

$$V_s = \frac{2\pi Q_s^2}{\varepsilon N_d} = \frac{2\pi (qN_s)^2}{\varepsilon N_d}, \quad (1)$$

$$L = L_D \left(\frac{eV_s}{kT}\right)^{1/2}, \quad (2)$$

where Q_s is the surface charge density, ε is the dielectric constant, N_d is the concentration of the donor impurity, q is the charge of the surface states, N_s is the density of the charged surface states, k is the Boltzmann constant, T is the absolute temperature and L_D is the Debye screening length

$$L_D = \left(\frac{\varepsilon kT}{2\pi e^2 N_d}\right)^{1/2}.$$

Typically, a doped semiconductor with $N_d \approx 10^{18}-10^{20}$ cm^{-3} and $N_s \approx 10^{13}$ cm^{-2} is characterised by $V_s \approx 1$ eV and $L \approx 1-100$ nm.[7]

Usually, semiconductor oxides used as gas sensors are polycrystalline materials with grain sizes ranging from 10 to 100 nm.[7] As the grain size decreases, the proportion of the surface atoms in the sensor material increases; correspondingly, the effective adsorption surface area and the contribution of the surface to the electrophysical properties also increase. The structure of a polycrystalline material is schematically shown in Fig. 2. Each grain is covered with a chemisorbed oxygen layer, which results in the formation of a near-surface layer depleted of charge carriers and intergranular potential energy barriers to charge carriers (the so-called double Schottky barriers). The conductivity of this system is determined by the electronic properties of the grain bulk and by transport of carriers through the barriers between grain contacts. Two mechanisms of conductivity of polycrystalline materials have been considered.[7]

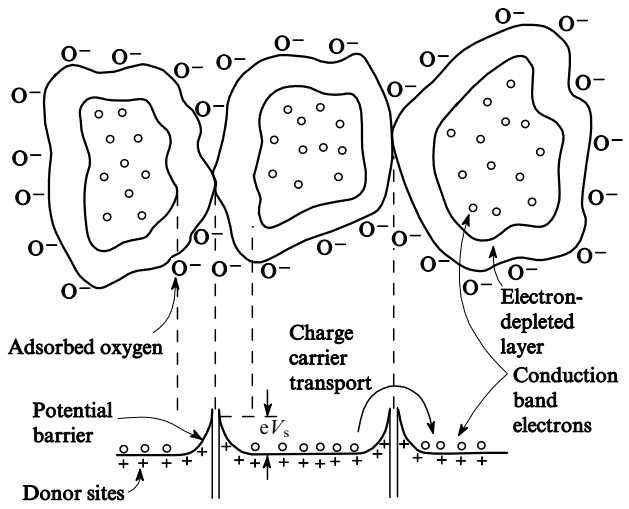

Figure 2. Polycrystalline oxide structure (above) and the corresponding band diagram (below).[59]

1. Surface trap limited conductivity mechanism. The conductivity is governed by the changes in the carrier concentration in the depletion layer and the potential energy barriers between grain contacts do not contribute to the conductivity. This mechanism is possible either in the case of surface conductivity (adsorption on a single-crystalline material) or when the intergranular barriers are low. The key parameter determining the conductivity is the thickness of the depletion layer.

2. Barrier-limited conductivity mechanism assumes a constant total carrier concentration and variable carrier mobilities. This mechanism is typical of all polycrystalline materials for which the energy of the intergranular barriers is higher than kT. The key parameter responsible for conductivity is the barrier height at grain boundaries.

It should be noted that depletion of charge carriers in the near-surface layer and formation of a surface potential barrier are characteristic of both mechanisms. However, in the former case charge carriers move along the interface or over the surface, whereas in the latter case they move through a potential barrier.

A method was proposed[7] for calculating the changes in the carrier concentration under adsorption proceeding by the first mechanism. The surface reactions considered were as follows:

$$\frac{m}{2}\,O_2 + e \underset{k_{-1}}{\overset{k_1}{\rightleftharpoons}} O_m^-, \quad (3)$$

$$O_m^- + m\,R \xrightarrow{k_2} m\,RO + e, \quad (4)$$

where R is the molecule of the reducing gas and m is the coefficient related to a particular form of chemisorbed oxygen (O_2^- or O^-). It should be noted that the existence of O^{2-} oxygen ions was also reported (see, *e.g.*, Ref. 68).

If a solid is in equilibrium with the gas phase, the equation for a surface coverage, $\theta = N_s/N_0$ (N_s is the number of occupied adsorption sites and N_0 is the total number of adsorption sites), with chemisorbed oxygen can be written as follows:

$$\theta = \frac{k_1 n (p_{O_2})^{m/2}}{k_{-1} + k_1 (p_{O_2})^{m/2} + k_2 (p_R)^m}, \quad (5)$$

where n is the equilibrium electron concentration.

In the case of adsorption on a thin film (film thickness, h, is less than the Debye screening length, L_D; *i.e.*, a totally depleted film) the conductivity (σ) is given by[7]

$$\sigma = \text{const} \exp\left[\frac{-(E_s - E_d)}{kT}\right] k_1^0 (p_{O_2})^{-m/2} \left[k_{-1}^0 + k_2^0 (p_R)^m\right], \quad (6)$$

where the first term (const) depends on the doping level, the conductivity of the bulk semiconductor and the number of adsorption sites on the surface; E_s is the ionisation energy of the surface state; E_d is the ionisation energy of the donor impurity and k_i^0 is the pre-exponent in the Arrhenius equation.

The conductivity is characterised by an activation energy ($E_s - E_d$), being also a power function of the partial pressures of oxygen and the reducing gas. The exponent is determined by the equilibrium forms of oxygen chemisorbed on the surface.

Similar schemes for calculating the electron concentration under equilibrium conditions were considered in other studies.[59, 60] Zemel[60] related the surface charge to the decrease in the surface concentration of oxygen vacancies ($V_O^\times$). In the course of chemisorption an oxygen ion occupies a position of the surface oxygen vacancy. The change in the surface concentration of ionised oxygen sites and the negative charge surface are given by

$$-\left[\Delta O_s^{2-}\right] = \left[V_{O_s}^\times\right] - \left[V_O^\times\right], \quad (7)$$

$$Q_s = -2e\left[\Delta O_s^{2-}\right]. \quad (8)$$

Assuming that the near-surface layer of each grain is electron-depleted, the expression for the effective electron concentration (n_{ef}) is as follows

$$n_{ef} = n_0 - \frac{\alpha Q_s}{eW}, \quad (9)$$

where n_0 is the bulk carrier concentration and α/W is the ratio of the grain surface area to the grain volume.

With the known average electron concentration[60] it is possible to estimate the surface charge density from relation (9). Polycrystalline SnO_2 with a carrier concentration of 10^{19} cm^{-3} and typical grain sizes of 10–100 nm becomes totally depleted of charge carriers at a surface charge density of 10^{13} cm^{-2}, which approx-

imately corresponds to one chemisorbed species per 100 surface atoms.

Generally, one should take into account a decrease in the electron concentration with shortening the distance from the surface. In this case, the effective carrier concentration is given by [69]

$$n_{\mathrm{ef}} = \frac{1}{d}\int n_0 \exp\left[\frac{-V(z)}{kT}\right] \mathrm{d}z, \tag{10}$$

where d is the grain diameter and $V(z)$ is the potential ($z = 0$ corresponds to surface and $z > 0$ corresponds to the grain bulk).

Consider the barrier-limited conductivity mechanism. As mentioned above, a double Schottky barrier is formed at each grain contact. For a unit contact the carrier current, j, is related to the barrier height, V_s, and the voltage applied, U, as follows [70]

$$j \propto \exp\left(\frac{-eV_s}{kT}\right)\sinh\left(\frac{eU}{2kT}\right). \tag{11}$$

In this case (assuming equal potential energy barriers between grain contacts) the conductivity of the polycrystalline system is exponentially related to the barrier height [71]

$$\sigma \propto \sigma_0 \exp\left(\frac{-eV_s}{kT}\right), \tag{12}$$

where σ_0 is a constant depending on the specific bulk conductivity of the grain.

The barrier height is proportional to the surface charge [see Eqn (1)]. Relation (12) predicts that a minor variation of the surface charge must cause significant changes in the conductivity of the polycrystalline material. At the same time a material with no potential energy barriers between grain contacts must be characterised by linear dependences of the carrier concentration and, correspondingly, conductivity on the surface charge. Therefore, systems with the barrier-limited conductivity mechanism seem to be attractive for design of materials for gas sensors. The gas sensing properties of polycrystalline ceramics with this conductivity mechanism have been studied.[72]

A number of studies on the Hall effect in polycrystalline oxides (SnO_2, ZnO) under adsorption of gaseous ethanol and nitrogen dioxide have been reported (see, *e.g.*, Refs 60, 73–75). This allowed the contribution of the carrier mobility to the conductivity of the material to be separated. It was found that the change in the carrier mobility is small compared to the change in the carrier concentration and makes an insignificant contribution to the electrical response of the material. Numerical calculations of the heights of the potential energy barriers between grain contacts as functions of the grain size and shape [58, 76] carried out for mobile donor atoms (high-temperature case) showed that the barrier height decreases substantially as the grain size decreases (Fig. 3). The shape of the grain has almost no effect on the barrier height; however, the formation of intergranular 'necks' affects this parameter. The profile of the potential inside two contacting grains connected by a neck of diameter D is shown in Fig. 4. A neck is a homogeneous contact region, which is not a charged interface between two grains. An increase in D causes a substantial decrease in the barrier height at the interface. Different types of intergranular necks are shown in Fig. 5. At $D > 2L$ (L is the thickness of the depletion layer) (Fig. 5 *a*), a conducting channel is formed (in this case adsorption affects only the diameter of this channel); at $D < 2L$ (Fig. 5 *b*) the barrier is too low but adsorption influences this parameter; and at $D = 0$ (double Schottky barrier) (Fig. 5 *c*), adsorption affects the barrier height (note that a zero neck radius does not mean the absence of contact between two grains).

Thus, the barrier-limited conductivity mechanism is possible only in rather large ($d \gg 2L_D$), *i.e.*, mostly ceramic crystalline samples. Sintering of samples leads to intergrowth of crystallites and redistribution of the bulk concentration of donor ions as a result of diffusion and can cause a decrease in the contribution of the barrier-limited conductivity mechanism.

The conductivity of a polycrystalline material with the barrier-limited conductivity mechanism was studied as a function of the partial pressure of gas.[7] The surface coverage with chemisorbed

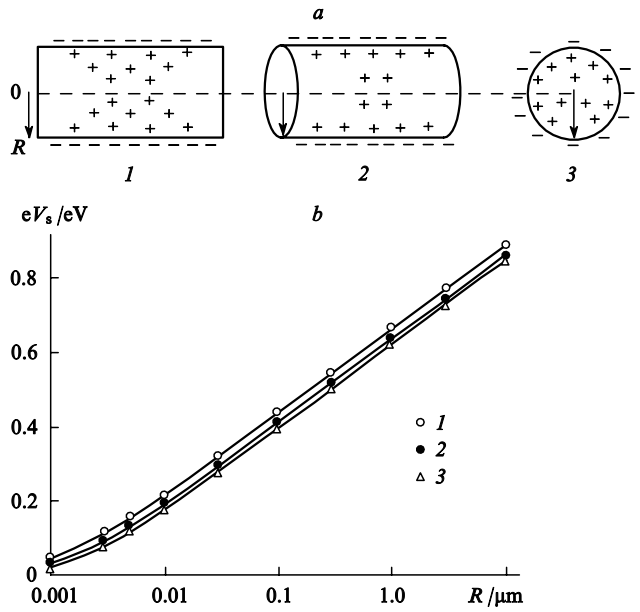

Figure 3. Grain geometries used in the solution of the Poisson equation (*a*) and intergranular barrier heights, eV_s, plotted *vs.* grain size, R, for totally depleted grains (*b*).[76]
Surface concentration of donor sites $N_{ds} = 10^{26}$ m^{-3}, $T = 573$ K. Grain shape: (*1*) slab (1D), (*2*) cylinder (2D) and (*3*) sphere (3D).

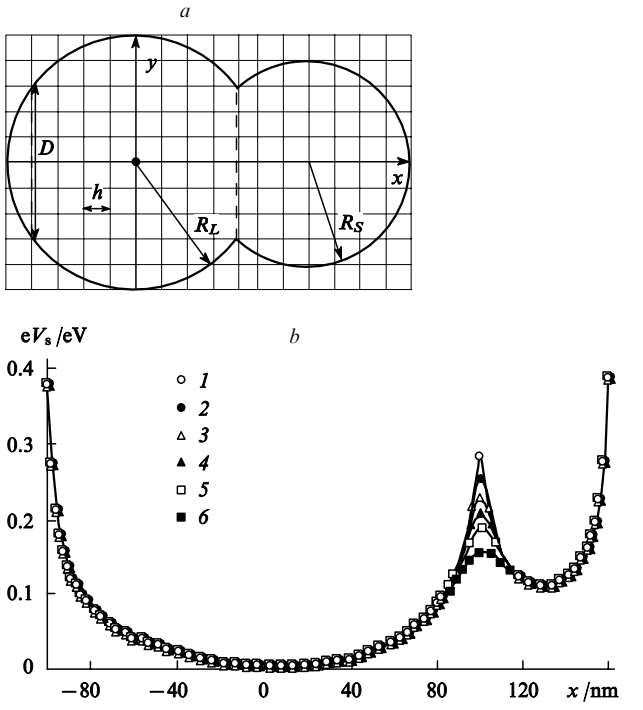

Figure 4. Schematic illustration of a contact between two grains (*a*) and calculated potential profile (*b*).
(*a*) D is the diameter of the contact circle in a neck; h is the mesh size used in the numerical solution; and R_L and R_S are the grain radii ($R_L = 100$ nm, $R_S = 30$ nm);[76]
(*b*) D /nm: 4 (*1*), 6 (*2*), 9 (*3*), 13 (*4*), 20 (*5*) and 28 (*6*).

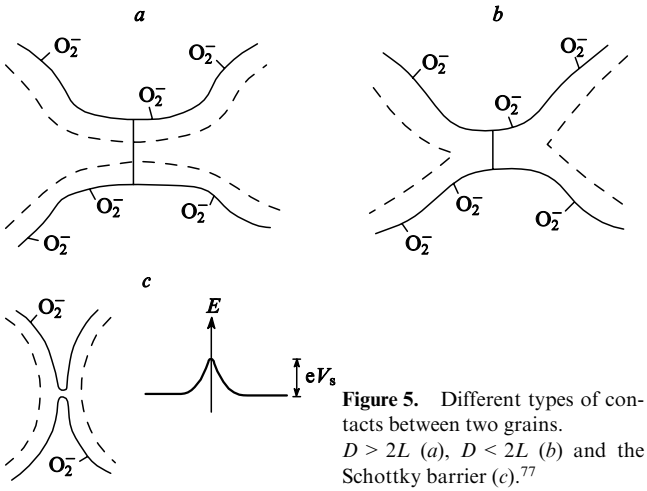

Figure 5. Different types of contacts between two grains. $D > 2L$ (*a*), $D < 2L$ (*b*) and the Schottky barrier (*c*).[77]

oxygen and the barrier height, V_s, at the interface between two grains are given by

$$\theta = k_1^0 N_d \exp\left[\frac{-(E_s - E_d)}{kT}\right] \exp\left(\frac{-eV_s}{kT}\right) \frac{(p_{O_2})^{m/2}}{k_{-1}^0 + k_2^0 (p_R)^m}, \quad (13)$$

$$V_s = \frac{kT}{e}\left\{\text{const} + \frac{m}{2} \ln p_{O_2} - \ln\left[k_{-1}^0 + k_2^0 (p_R)^m\right]\right\}, \quad (14)$$

where const depends on the Debye screening length. From this the relation for the conductivity is

$$\sigma \propto \frac{k_{-1}^0 + k_2^0 (p_R)^m}{(p_{O_2})^{m/2}}, \quad (15)$$

i.e., the barrier height is proportional to the logarithm of the partial pressure of gas, which corresponds to a power dependence of the conductivity. Thus, the conductivity depends on the partial pressure of gas in the same manner for both the barrier-limited conductivity mechanism and in the absence of potential energy barriers at interfaces between grains.[7] The reason is that electrons must overcome a potential barrier to be trapped on the surface. The interface coverage with chemisorbed oxygen varies only slightly with an increase in the partial pressure of oxygen. For instance, in a typical case $N_d \approx 10^{18}$ cm^{-3} and $N_s \sim 10^{15}$ cm^{-2} the maximum coverage is $\theta \approx 10^{-3}$.

In a vast majority of experimental studies the heights of the barriers between grains were determined from the temperature dependences of conductivity [see relation (12)]. The dependence of the average barrier height on the oxygen content in SnO_2 ceramics is shown in Fig. 6. As should be expected, in accord with relation (14) the average barrier height increases as the oxygen pressure increases. The experimental data on the barrier heights for polycrystalline SnO_2 are listed in Table 2.

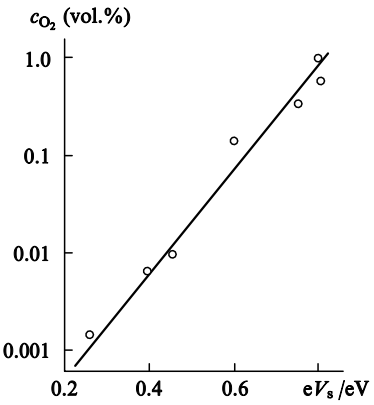

Figure 6. Average barrier height, V_s, in SnO_2 ceramic plotted *vs.* oxygen content in gas phase.[77]

Table 2. Intergranular barrier height in polycrystalline SnO_2.

eV_s /eV	T /K	p_{O_2} /atm	Ref.
Sintered ceramics			
0.64	770	1	78
0.62	770	1	79
Thin film			
0.73	700	10^{-2}	80
0.65	773	2.1×10^{-2}	81

Note that the barrier height calculated from the temperature dependence of conductivity corresponds to the activation energy for conductivity and is not directly related to the actual barriers between grains in the material. A proof of the barrier-limited conductivity mechanism is provided by the nonlinear current–voltage curve. However, there is a limitation associated with the fact that the potential applied is distributed along a chain of barriers connected in series. For small grains, nonlinear current–voltage curves are observed only at large potentials (this potential range is usually left out of consideration). A nonlinear current–voltage curve was obtained in experiments with tin dioxide ceramics.[77] The bulk and interface contributions to the conductivity of a polycrystalline material can also be separated using the complex impedance technique.[82,83] The complex impedance measurements of palladium-doped tin dioxide were reported.[84] Figure 7 presents the sensor response (calculated as the ratio of the resistance in gas to the resistance in air) plotted *vs.* the frequency of the reference signal. At low frequencies, a rather high sensitivity and near absence of high-frequency components were observed.

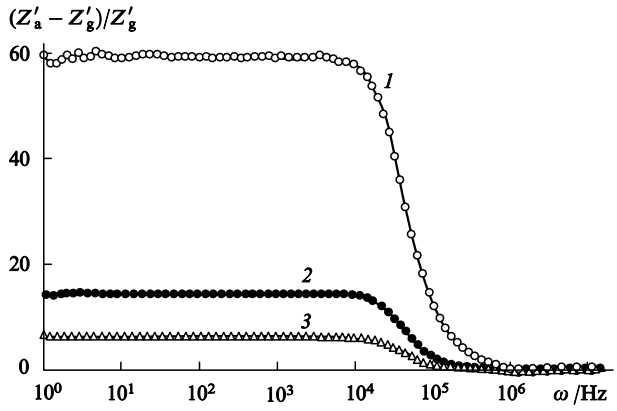

Figure 7. Sensor response, $[(Z'_a - Z'_g)/Z'_g]$, plotted *vs.* reference signal frequency, ω, for SnO_2(Pd) samples on an insulating support at 400 °C;[84] Z'_a is the resistance in air and Z'_g is the resistance in gas; gas concentration in air /ppm: (*1*) 80 (C_2H_5OH), (*2*) 1000 (CH_4) (*3*) and 300 (CO).

III. Mechanism of gas sensitivity of systems with heterojunctions

Systems with heterojunctions (heterostructures) are comprised of two or more layers with different chemical compositions and electronic properties. The main types of systems with heterojunctions are as follows:

— metal/insulator/semiconductor (MIS) structures,
— metal/semiconductor structures (Schottky diodes),
— semiconductor/insulator/semiconductor structures and
— semiconductor/semiconductor structures.

Interaction of heterostructures with the gas phase can lead to modification of the electronic states at the interface and in the bulk of the layers. In most cases the electrical response in heterostructures is associated with a change in the state of the interface and involves processes at the interface between three phases, *viz*., solid 1/solid 2/gas.[38] In this connection it is of importance whether the gas molecules can reach the heterointerface. This imposes some limitations on the composition and microstructure of materials for heterostructures and on the compositions of gases detected.

Two main mechanisms of gas sensitivity of heterostructures are as follows.

1. Change in the electron work function as a result of formation of a dipole layer by adsorbed molecules.

2. Change in position of the Fermi level in the bulk of the semiconductor.

These two mechanisms will be considered in detail taking the structures mentioned above as examples.

1. Methods of fabrication of heterostructures

Semiconductor heterostructures are often fabricated using various thin-film and ceramics growth techniques. Interrelations between the growth conditions and the compositions, crystal structures, morphologies and electrophysical properties of the materials that form a heterostructure have been reported in studies on CVD,[35,85–88] magnetron sputtering,[51,54,55,89] spray pyrolysis of organometallic and inorganic compounds,[27,90–94] thermal vacuum evaporation,[95] screen printing[96] and solid-phase synthesis.[43–47,52]

2. Metal/insulator/semiconductor structures

The gas sensitivity of the MIS structures is based on the change in the electron work function needed to leave the metal under adsorption of molecules at the metal/insulator interface. The metallic layer of the MIS structures is made of the catalytically active metals (Pt, Pd). In most cases silicon is used as the semiconductor because this allows dielectric oxide layers to be grown with ease on the Si surface upon thermal oxidation. In addition, the silicon support permits a ready incorporation of the MIS structures into electronic microchips. Except for some specific cases considered below the MIS structures are hydrogen sensitive. Figure 8 illustrates the interaction between $Pd/SiO_2/Si$ structures and hydrogen, which involves[20] adsorption of hydrogen molecules on the metal surface and subsequent palladium-catalysed dissociation of H_2 into atoms followed by diffusion of hydrogen atoms through the metal layer towards the metal/oxide interface. These processes can be represented as follows:

$$H_2 \underset{k_{-1}}{\overset{k_1}{\rightleftharpoons}} 2H_a, \qquad (16)$$

$$H_a \underset{k_{-2}}{\overset{k_2}{\rightleftharpoons}} H_b \underset{k_{-3}}{\overset{k_3}{\rightleftharpoons}} H_{ai}, \qquad (17)$$

where H_a is hydrogen adsorbed at the surface, H_b is hydrogen dissolved in the metal, H_{ai} is hydrogen adsorbed at the metal/oxide interface and k_i are the rate constants for these processes.

It should be emphasised that permeability of the palladium layer to hydrogen atoms is a necessary condition, which should be met to provide the possibility for these atoms to reach the M/SiO_2 interface and thus make corresponding structures gas sensitive. Hydrogen adsorption on the metal surface and at the M/SiO_2 interface leads to formation of the dipole layer.

In the band diagram of an MIS structure the formation of the dipole layer corresponds to the change in the metal work function by a value of $e\Delta V_s$. The change in the work function at the metal/gas interface was confirmed by photoemission spectroscopy[20] and by using a Kelvin probe.[21] Simultaneous registration of the change in the metal work function using the Kelvin probe technique and the ΔU value determined from the capacitance–voltage curves showed that these processes occur in parallel. This in turn confirms that the shift of the electrical characteristics is associated with the dipole layer and that this layer is formed at the metal/insulator rather than the insulator/semiconductor interface. The mechanism of formation of the dipole layer as a result of polarisation of hydrogen atoms is still to be clarified. It is assumed that ionisation of a hydrogen atom adsorbed at the M/SiO_2 interface accompanied by transition of an electron to the conduction band of the metal is the basis for this process.[20] In this case a dipole can be formed by a proton and a charge induced in the metal. According to calculations, the charges in the dipole are separated by about 1.4×10^{-3} nm and the adsorbed hydrogen atom has an unusually high dipole moment (2 D, which is atypical of hydrogen adsorption on metal surfaces).[24] It was assumed that hydrogen is adsorbed on the 'oxide side' of the interface. This is confirmed by the difference between the heats of adsorption on the metal surface (0.43 eV per atom) and at the metal/oxide interface (0.86 eV per atom). The bridging oxygen atom of the oxide can act as an adsorption site.

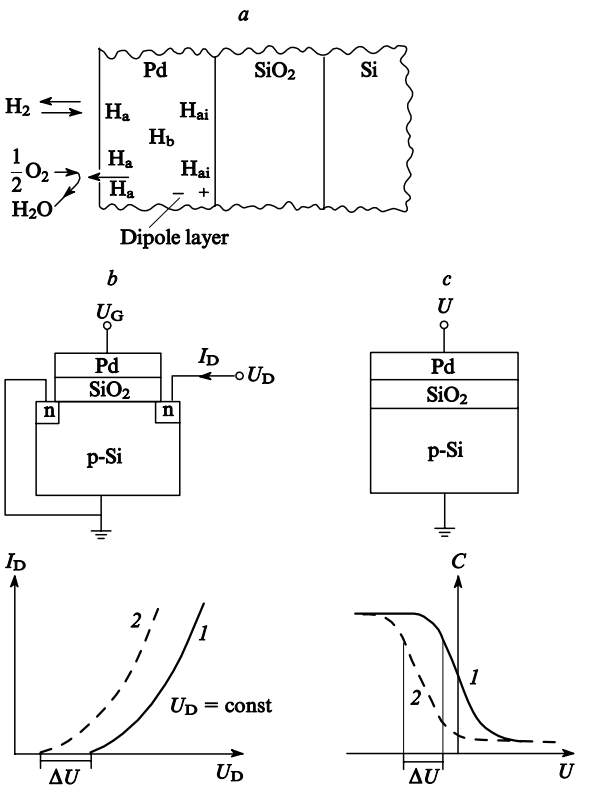

Figure 8. Brief description of the hydrogen sensitive MIS structure (taking a $Pd/SiO_2/Si$ structure as an example).[20]
Processes characterising the interaction with the gas phase (*a*), an MIS transistor and its current–voltage curve (*b*) and an MIS capacitor and its capacitance–voltage curve (*c*); in air (*1*) and under hydrogen (H_{ai}) adsorption at the Pd/SiO_2 interface (*2*).

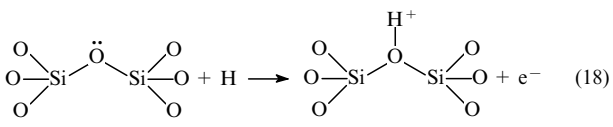

(18)

Lundstrom[25] analysed the temporal dependences of the sensor response and suggested co-existence of two types of hydrogen adsorption sites on the 'metal' side and on the 'oxide' side.

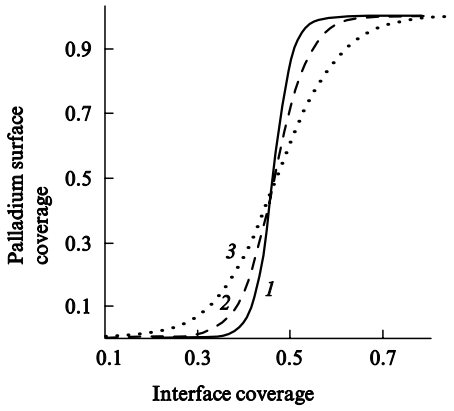

Figure 9. Relation between palladium surface coverage and Pd/SiO_2 interface coverage with hydrogen atoms.[24]
T/K: 223 (*1*), 423 (*2*) and 873 (*3*).

Since the heat of hydrogen adsorption at the metal/oxide interface is higher, hydrogen is mainly adsorbed at this interface. The results of calculations of the ratio between the specific concentrations of hydrogen at the surface and at the metal/oxide interface are shown in Fig. 9.[24] Thus, the structure can produce an electrical response even at very low specific surface concentration of hydrogen. In an inert atmosphere, this permits detection of extremely low hydrogen concentrations (at 10^{-3} ppb level).

The electrical response of the system is related to the partial pressure of hydrogen in an inert atmosphere as follows:[20]

$$\frac{1}{\Delta U} - \frac{1}{\Delta U_{\max}} = \frac{1}{\Delta U_{\max}} \left(\frac{\text{const}}{p_{H_2}} \right)^{1/2}, \qquad (19)$$

where

$$\text{const} = \frac{k_{-1}}{k_1} \left(\frac{k_{-2}k_{-3}}{k_2 k_3} \right)^2.$$

The results of calculations using Eqn (19) are in good agreement with the experimental dependences (Fig. 10). The maximum response, $\Delta U_{\max}$, corresponding to fully occupied adsorption sites is 0.5 V. The $\Delta U_{\max}$ value is determined by the concentration of active adsorption sites and depends on the state of the heterointerface.

As mentioned above, the MIS structures based on continuous metal films are sensitive to hydrogen or to molecules that can decompose at the surface and produce hydrogen. At the same time the sensitivity to hydrogen strongly depends on the presence of other gases that can be formed in the surface reactions, thus reducing the surface concentration of hydrogen. For instance, oxygen can react with adsorbed hydrogen as follows [20]

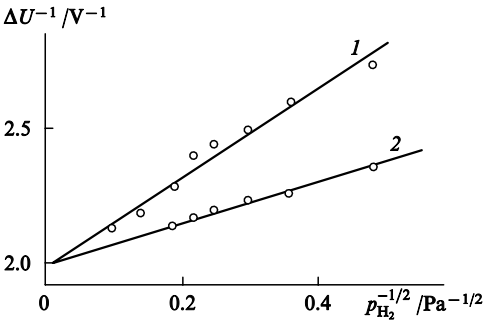

Figure 10. The response ΔU plotted *vs.* the partial pressure of hydrogen at 240 (*1*) and 280 °C (*2*).[20]

$$O_2 + 2H_a \longrightarrow 2(OH)_a, \qquad (20)$$

$$OH_a + H_a \longrightarrow H_2O, \qquad (21)$$

where H_a is the adsorbed hydrogen atom and $(OH)_a$ is the adsorbed hydroxy group.

Carbon and nitrogen monoxides also reduce the sensitivity to hydrogen [22,97] by blocking the adsorption sites.

MIS structures based on porous metal films can be sensitive to molecules having a permanent dipole moment, *e.g.*, NH_3,[23] ethanol, acetone and water.[98] The mechanism of formation of the dipole layer in this case is still poorly studied.

In addition to silicon-based structures, MIS structures based on silicon carbide (a material with a wider energy gap) have also been studied.[26] This permits operation at higher temperatures and reduces the poisoning effect of the working substance. Not only platinum- and palladium-based but also Ru- and Ir-based MIS structures are known.[25] Changes in the gas sensitivity are due to different catalytic activities of the metals; palladium-based systems were found to be the most efficient. The sensitivity to hydrogen was enhanced using a double metal layer (platinum on palladium);[98] however, the mechanism of this phenomenon has not been studied as yet.

3. Semiconductor/insulator/semiconductor structures

An example of the semiconductor/insulator/semiconductor structure is provided by a $SnO_2/SiO_2/Si$ structure fabricated using two methods, *viz.*, spray pyrolysis (SnO_2 layer)[27] and aerosol–gel (SiO_2 layer) techniques.[99,100] The capacitance–voltage curves of the $SnO_2/SiO_2/Si$ structures obtained under gas adsorption conditions are presented in Fig. 11. Curve *1* corresponds to the ground (low-capacitance; $C_{U=0}$ = 0.1 nF) state of the structure in N_2 atmosphere. In the presence of polar gas molecules, *e.g.*, H_2O, C_2H_5OH or NH_3, the capacitance in the forward branch of the capacitance–voltage curve substantially increases. Curves *2–4* were obtained after a 10 min exposure of the structure to different mixtures of the gases mentioned above with N_2. Prolonged exposure (> 10 h) leads to saturation of the signal of the gas sensor. Curve *5* corresponds to a saturation level of C = 5.8 nF obtained at zero bias after 24 h exposure to a mixture of N_2 with H_2O (1%) at room temperature. It should be noted that enhancement of the gas sensitivity corresponds to an increase in the capacitance in the forward branch of the capacitance–voltage curve rather than its shift along the voltage axis.

Changes in the capacitance on periodic change in the composition of the gas phase at zero potential are shown in Fig. 12. Each cycle involved a 1 h exposure of the structure to N_2 followed by a

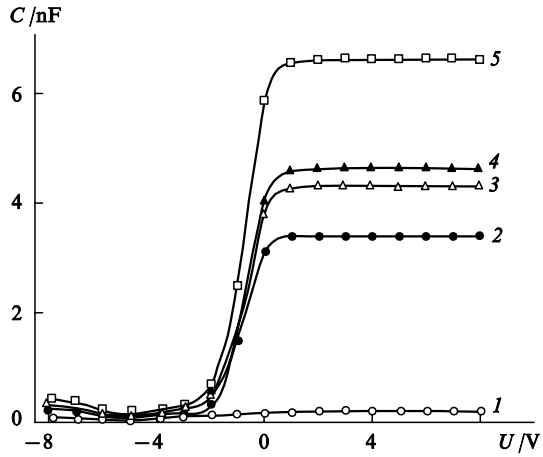

Figure 11. Typical capacitance–voltage curves of a $SnO_2/SiO_2/Si$ heterostructure in N_2 atmosphere (*1*), after 10 min exposures to mixtures of N_2 and C_2H_5OH (1%) (*2*), H_2O (1%) (*3*), NH_3 (1%) (*4*) and after 24 h exposure to a mixture of N_2 and H_2O (1%) (5) at 20 °C.[27]

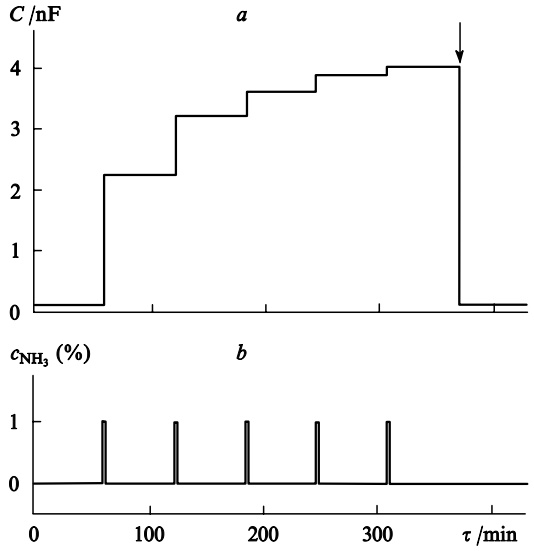

Figure 12. Time dependences of the capacitance of a $SnO_2/SiO_2/Si$ heterostructure on periodic change in the gas phase composition (*a*) and NH_3 concentration in nitrogen (*b*).[27]
Switching-on a 10 V electric pulse is arrowed.

2 min exposure to a mixture of N_2 with NH_3 (1%). As can be seen, the capacitance increases in proportion to the time of exposure to the gas mixture containing NH_3. An important feature of the structures studied is their ability to retain the capacitance $C(\tau)$ for a long time after removal of the active component from the gas mixture. This property is responsible for the 'memory' effect towards the external action and allows the structures in question to be used as dosimeters. The capacitance achieved in the atmosphere containing molecules analysed is retained on nearly 50 h exposure to N_2 or in air. Similar $C(\tau)$ dependences were observed for gas mixtures containing ethanol and water. The sensor response of the structure, S, calculated as $C(\tau)/C(\tau = 0)$ was 44, 33 and 58 rel. u. after 24-h exposure to gas mixtures of N_2 with 1% of NH_3, C_2H_5OH or H_2O, respectively. The system returned to the low-capacitance ground state (see curve *1* in Fig. 11) after application of a 10–15 V electric field pulse of direct polarity; the relaxation process was nearly 30 s long (Fig. 13).

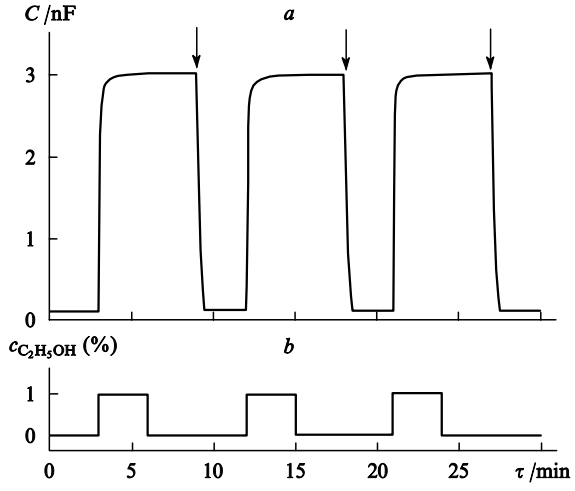

Figure 13. Time dependences of the capacitance of a $SnO_2/SiO_2/Si$ heterostructure on cyclic variation of the gas phase composition (*a*) and C_2H_5OH concentration in nitrogen (*b*).[27]
Switching-on a 10 V electric pulse is arrowed.

The properties of the $SnO_2/SiO_2/Si$ heterostructures significantly differ from those of other heterostructures. Of particular interest are the gas sensitivity mechanism and the relaxation process. Analysis of the capacitance–voltage curve of the $SnO_2/SiO_2/Si$ heterostructures (see Fig. 11) revealed their similarity to the curves obtained for the MIS structures. The direct branch corresponding to the gas sensitive state is of prime interest. A plateau in the direct branch corresponds to the capacitance of the SiO_2 dielectric layer, which is determined by its thickness (d), dielectric constant (ε) and the surface area (S)

$$C = \frac{\varepsilon\varepsilon_0 S}{d}. \tag{22}$$

An increase in the capacitance in the direct branch under adsorption of gas molecules is equivalent to the increase in the effective ε constant. The aerosol–gel grown SiO_2 layer plays a specific role. Silica thus produced differs from the thermally grown SiO_2, which is traditionally used as insulator in the MIS structures. The IR spectra of the aerosol–gel deposited SiO_2 layers indicate the presence of trace amounts of charged radicals (alkoxy groups and protons H^+) capable of forming mobile space charge regions.[100]

Similar heterostructures containing thermally grown SiO_2 produce no sensor signal. Hence, the gas sensitivity mechanism can involve changes in the proton concentration in the SiO_2 layer, which lead to an increase in the effective dielectric constant. All molecules studied can be involved in protonation of SiO_2. Water or ethanol can dissociate to give protons; the interaction of an ammonia molecule with a proton results in an ammonium ion.

Significant acceleration of the capacitance relaxation on application of electric field pulses can be due to migration and redistribution of protons in the SiO_2 layer. In this case the capacitance of the structure returns to the initial value. Proton migration in the SiO_2 layer in an electric field has been reported (see, *e.g.*, Refs 101 and 102).

Sensors based on $SnO_2/SiO_2/Si$ heterostructures can be of considerable interest as dosimeters. The possibility of controlling relaxation processes ('reset' of accumulated signal) by changing the electric field seems to be an advantage offered by these structures, because the performance of conventional gas sensors can be improved only by heating the structure, which usually limits the range of the operating temperatures to 200–400 °C.

4. Metal/semiconductor structures

Metal/semiconductor structures represent heterocontacts between a metal and a semiconductor with different electron work function. The condition for formation of a Schottky barrier at the heterointerface can be written as follows:[63]

$$\text{n-type semiconductor, } \phi_m > \phi_{sc}; \tag{23}$$

$$\text{p-type semiconductor, } \phi_m < \phi_{sc}, \tag{24}$$

where ϕ_m is the electron work function of the metal and ϕ_{sc} is the electron work function to the semiconductor.

Similarly to MIS structures, gas sensitive Schottky diodes usually employ catalytic metals. The semiconductor layer can be made of various materials including conventional (Si, GaAs) and oxide semiconductors (SnO_2, ZnO, TiO_2). Note that silicon-based Schottky diodes have a thin (20–30 Å) SiO_2 layer transparent to tunnelling. This precludes formation of silicides (*e.g.*, Pd_2Si) that are responsible for loss of sensitivity and reduces the density of proper surface states at the heterointerface.[28]

Usually, Schottky diodes are hydrogen sensitive (similarly to the MIS structures); however, sensitivity to other gases (O_2, CO, NO) has also been reported.

The current flowing through a Schottky diode is a nonlinear function of the voltage applied:[39]

$$j = \text{const}\ \exp\left(-\frac{e\phi_{ms}}{kT}\right)\left[\exp\left(\frac{e}{\beta kT}\right)-1\right] = \quad (25)$$

$$= j_s\left[\exp\left(\frac{eU}{\beta kT}\right)-1\right],$$

where j is the current density, ϕ_{ms} is the height of the Schottky barrier at the interface, U is the voltage applied, β is the non-ideality coefficient of the current–voltage curve and j_s is the saturation current density; the numerical value of the constant is related to the carrier transport mechanism (emission or diffusion).

The sensitivity of the Schottky diode to adsorption of gas molecules is associated with the change in the electron work function of the metal in the course of formation of the dipole layer. The mechanism of formation of the dipole layer in the Schottky diodes is similar to that considered for the MIS structures. The barrier height changes by $e\Delta V_s$ (Fig. 14) under adsorption conditions,[20] which leads to a change in the saturation current (typically, by two to three orders of magnitude at a hydrogen concentration of 100 ppm). For instance, a sensor response, $j_s(H_2)/j_s(\text{air})$, of 10^3 at a hydrogen concentration of 280 ppm in inert atmosphere was reported for a Pd/SiO_2/a-Si : H diode based on hydrogenated amorphous silicon.[29] The change in the barrier height under H_2 adsorption was directly measured for the Pd/SiO_2/a-Si : H diode using the temperature dependence of the reverse current and the capacitance–voltage ($C-U$) curve.[30] These two methods gave consistent results for the decrease in the barrier height (0.48 eV at a hydrogen concentration of 0.5 vol.%). At the same time the carrier concentration in the silicon layer obtained from the data of $C-U$ measurements remained unchanged.

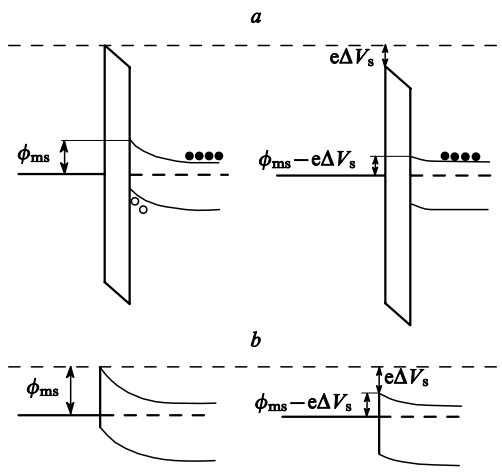

Figure 14. Band diagrams of Schottky diodes.
Metal/insulator/semiconductor structure (*a*) and metal/semiconductor structure (*b*). Shown is the change, $e\Delta V_s$, in the barrier height due to the formation of the dipole layer.[20]

Studies of the $Pd/SiO_2/Si$ diode revealed[28] clearly seen maxima in the reverse branch of the capacitance–voltage curve in the presence of trace amounts of hydrogen (*cf.* a monotonic change in air, Fig. 15). The appearance of peaks was associated with the interface states. The maximum capacitance corresponds to the case where position of the Fermi level matches that of the interface state (trap) and carriers become entrapped. According to calculations, the corresponding levels are 0.65 and 0.4 eV below the conduction band of Si.[31] The appearance of interface states was also reported in another study.[103] In the case of DC measurements the interface states are responsible for the tunnelling component of the electric current; *i.e.*, gas sensitivity is associated with electron tunnelling between the metal and the interface states of the semiconductor.

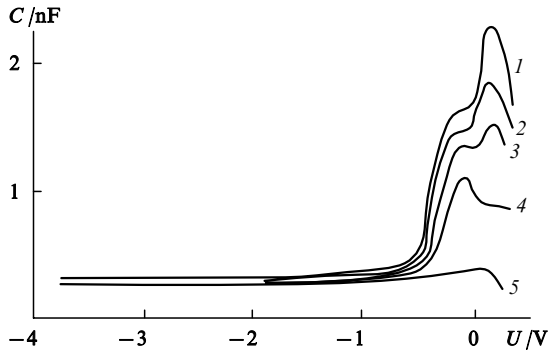

Figure 15. Capacitance–voltage curves of a $Pd/SiO_2/Si$ heterostructure in hydrogen (*1–4*) and oxygen (*5*) atmospheres at different frequencies at 70 °C.[28]
Frequency /Hz: 0.5 (*1*), 2 (*2*), 5 (*3*), 10 (*4*) and 0.5–10 (*5*).

The gas sensitivity mechanism of the Schottky diodes based on oxide layers (*e.g.*, a Pd/SnO_x heterocontact[32–34]) is different from that described above. Adsorption of gaseous O_2, CO and H_2 causes a change in the capacitance of the heterocontact and, hence, a shift of the $C-U$ curve by a value of ΔU. Similar results were obtained for platinum-based heterocontacts. At the same time the Ag/SnO_x heterocontact exhibited no gas sensitivity. The gas sensitivity mechanism was associated with chemisorption of oxygen molecules at the Pd/SnO_x interface and the formation of an electrical double layer by the negatively charged oxygen ions and positively charged ions in the near-surface region. The interaction with the gas causes changes in the concentration of chemisorbed oxygen and, correspondingly, in the ΔU value. This mechanism is supported by the linear dependence of ΔU on the partial pressure of oxygen plotted in the $\Delta U^{-1}-(p_{O_2})^{-1/2}$ coordinates. Similar dependences were obtained for CO adsorption. This sensitivity mechanism was also proposed for a Pt/TiO_2 Schottky diode.[38] Adsorption of oxygen changes the forward current flowing through the diode; the higher the partial pressure of O_2, the lower the current. The reverse is observed under CO adsorption. Processes occurring at the interface are illustrated by the band diagram shown in Fig. 16. Adsorption at the interface

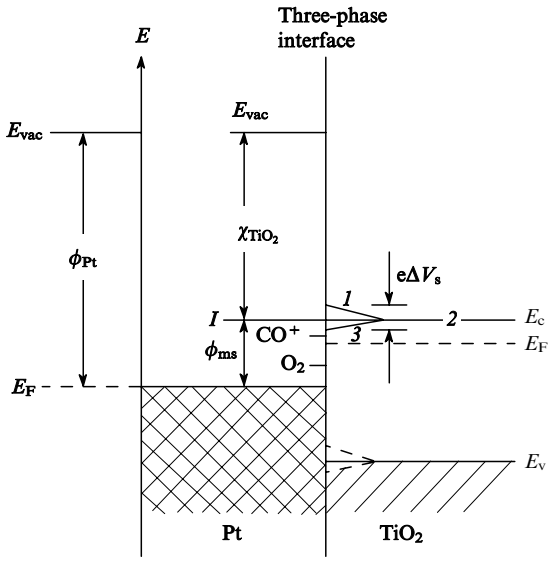

Figure 16. Band diagram of a Pt/TiO_2 heterojunction under adsorption of electron-donor (CO) and electron-acceptor (O_2) molecules.[38]
Depending on the occupation of the CO^+ and O_2^- surface states, the near-surface TiO_2 layer can be depleted of (*1*) or enriched with (*3*) electrons. Flat-band case (*2*).

leads to the formation of the O_2^- and CO^+ surface states lying 700 meV above and 133 meV below the Fermi level of the bulk TiO_2, respectively. As a consequence, the near-interface depletion layer of TiO_2 becomes even more depleted of or, correspondingly, enriched with charge carriers. The Schottky barrier becomes higher in the former and lower in the latter case. The role of the platinum/titanium dioxide interface should be emphasised. Annealing at 1070 K leads to disappearance of gas sensitivity and to linearisation of the nonlinear current – voltage curve. This can be due to platinum diffusion into the TiO_2 layer and formation of a transient layer.

An interesting example is provided by a Pd/TiO_2/n-Si diode structure [35] with extremely high sensitivity to hydrogen at room temperature, *viz*., 50 for 4 ppm and 10^5 for 10 000 ppm of H_2. The major contribution to the sensor response is assumed to come from the TiO_2 layer. Replacement of n-type silicon by p-type silicon caused a dramatic decrease in sensitivity (by two orders of magnitude). The change in the barrier height at the interface under hydrogen adsorption was estimated at 0.31 eV, which is comparable with the change in this parameter in the metal – SiO_2 – silicon systems. The Pd/TiO_2/n-Si structure can be treated as a semiconductor/semiconductor heterocontact rather than a Schottky diode.

A somewhat different mechanism of gas sensitivity was reported for a Pt/SnO_2 structure fabricated as a planar contact of specific shape.[37] The structure is highly sensitive to NO_2 traces (10^{-1} ppb) and has a rectified current – voltage curve. The current mainly changes at positive potentials. The mechanism of sensitivity was associated with extension of the depletion layer in tin dioxide under NO_2 adsorption. This leads to closure of the conducting channel and the forward current flowing through the structure dramatically decreases.

5. Semiconductor/semiconductor structures

Semiconductor/semiconductor heterostructures are of considerable interest for the design of gas sensing materials. Most of them are based on oxide semiconductors and usually comprise layers with different types of conductivity. The mechanisms of gas sensitivity of these structures are more intricate compared to the structures considered above and have no unambiguous interpretation. Two main mechanisms of gas sensitivity involve the formation of the dipole layer at the heterointerface and changes in the carrier concentration in a particular layer.

The basic relations for gas sensitivity of these heterostructures were reported by Zemel *et al*.[39] Consider a heterocontact between two semiconductors, S_1 and S_2. Let the electronic properties of S_1 be sensitive to the composition of the gas phase and let S_1 be also a kind of membrane providing diffusion of the gas molecules. Adsorption and subsequent molecular diffusion cause changes in the carrier concentration and, correspondingly, in position of the Fermi level of S_1 or lead to formation of the dipole layer at the heterointerface, which in turn is responsible for the change in the barrier height at the heterointerface.

The gas sensitivity of this system is affected by the carrier concentration in the S_1 layer and the thickness of this layer. Suppose that the current flowing through the heterojunction is given by Eqn (25), *i.e*., there is a well-defined saturation current governed by the height of the potential energy barrier. The relations listed below describe the change in the saturation current $\Delta j = j/j_0$ [j is the current under gas adsorption and j_0 is the current in the absence of adsorption (initial state)]:

degenerate semiconductor S_1, bulk effect

$$\Delta j = \exp\left(\frac{2}{3}\frac{e}{kT}\frac{\Delta c \phi_0}{n_0}\right); \tag{26}$$

non-degenerate semiconductor S_1, bulk effect

$$\Delta j = 1 + \frac{\Delta c}{n_0}; \tag{27}$$

degenerate and non-degenerate semiconductor S_1, a dipole layer at the interface

$$\Delta j = \exp\left(\frac{e}{kT}\Delta c Z_d^2\right). \tag{28}$$

Here Δc is the change in the concentration of electrically active states (bulk defects or dipolar molecules at heterointerface) due to adsorption of gas molecules, ϕ_0 is the initial barrier height at the heterointerface, n_0 is the initial carrier concentration in the S_1 layer and Z_d is the dipole moment of the adsorbed molecules.

The lower the carrier concentration in the sensitive layer, the higher the sensitivity of the heterojunction to adsorption of gas molecules in the case of bulk effect. Heterojunctions based on degenerate semiconductors (here, the carrier concentration is at least three orders of magnitude greater than the carrier concentration in non-degenerate semiconductors) are insensitive to gas molecules. However, if the dipole layer is formed, the sensitivity no longer depends on the carrier concentration, being determined only by the dipole moment of the adsorbed molecules. The effect of the charged surface states contributing to the capacitance is similar to the effect of the dipole layer.

A heterojunction operating by the mechanism of change in the space charge occurs in, *e.g*., the PbS/Si structure sensitive to hydrogen atoms.[39] Diffusion of hydrogen atoms towards the PbS causes an increase in the carrier (electron) concentration due to the fact that hydrogen atoms occupy positions of the lead vacancies. This leads to an increase in the height of the potential energy barrier at the heterointerface. The change in the reverse current as a function of the thickness, L, of the PbS layer is given by the following expressions

$$\Delta j = \frac{e[H_{Pb}]L}{Q_1} \text{ at } L < L_D, \tag{29}$$

$$\Delta j = \frac{[H_{Pb}]}{n_0} \text{ at } L > L_D, \tag{30}$$

where $[H_{Pb}]$ is the concentration of hydrogen atoms occupying positions of the lead vacancies, Q_1 is the uncompensated charge in the PbS layer, L_D is the Debye screening length for PbS and n_0 is the initial carrier concentration in the PbS layer.

Thickening of the PbS layer makes the material more sensitive and at $L > L_D$ the change in the reverse current is governed by the change in the carrier concentration. On the other hand, thickening of this layer makes the response time of heterostructures much longer.

Yet another example is provided by a Pt/n-SnO_2/p-diamond structure.[104] As the partial pressure of oxygen changes, the forward current also changes. The mechanism of gas sensitivity was associated with the change in the concentration of oxygen vacancies in the tin dioxide layer:

$$1/2\,O_2(gas) + V_O^{\bullet\bullet} + 2e = O_O^{\times}. \tag{31}$$

The role of platinum is to promote chemisorption of oxygen. It should be noted that the sensor response cannot be unambiguously related to the n-SnO_2/diamond heterointerface because platinum forms a Schottky barrier with tin dioxide and the height of this barrier also depends on the carrier concentration in SnO_2.

All systems considered above are sensitive at elevated temperatures. An example of a heterojunction, which is sensitive to NO at room temperature, is provided by the (Pt,Pd)/WO_3/Si system.[40] Adsorption of nitrogen monoxide causes an increase in the forward current. The authors [40] failed to determine which of the two heterointerfaces, (Pt, Pd)/WO_3 or WO_3/Si, is responsible for the onset of gas sensitivity. However, it was found that the WO_3 layer on insulator has a constant resistivity under NO adsorption. This can indicate that the mechanism of gas sensitivity is associated with the formation of charged states at the heterointerface or

with the formation of the dipole layer rather than the change in the carrier concentration in the WO_3 layer.

a. SnO_2(M)/Si structures

Heterostructures n-SnO_2(M)/p-Si (M = Cu, Pd, Ni) with a tin dioxide layer 1 μm thick were grown by aerosol pyrolysis ($SnO_{2(pyr)}$/Si) (see Ref. 41) and by magnetron sputtering ($SnO_{2(mag)}$/Si) (see Ref. 42) on a p-type single-crystalline silicon substrate (resistivity 10 Ω cm). A schematic view of the heterostructures studied is presented in Fig. 17. The dopant concentrations in the films synthesised were determined by local X-ray spectroscopic analysis. They are listed in Table 3.

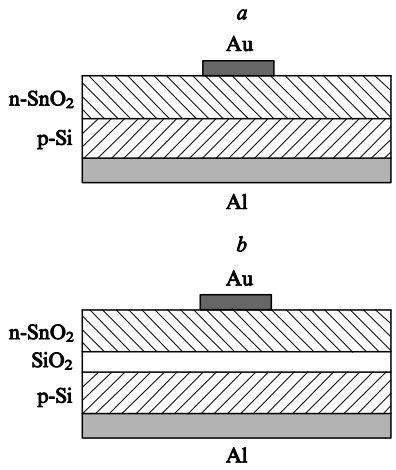

Figure 17. Schematic view of two heterostructures, n-SnO_2/p-Si (*a*) and n-SnO_2/SiO_2/p-Si (*b*).

The current – voltage curves of the $SnO_2(M)_{(pyr)}$/Si heterostructures measured in dry N_2 atmosphere at room temperature exhibit clearly seen portions of saturation current at reverse biases (Fig. 18). This points to the formation of a Schottky barrier at the heterojunction. The saturation current strongly depends on the type of dopant. The current – voltage curves of $SnO_{2(mag)}$/Si heterostructures are also rectifying in character; however, saturation of the reverse current is less pronounced.

Table 3. Main parameters of the current – voltage curves of heterostructures $SnO_2(M)_{(pyr)}$/Si.

Heterostructure	[M] (at.%)	j_s /μA cm^{-2}	β	R_s /Ω	E_a /eV
$SnO_{2(pyr)}$/Si		7.3	8.5	2×10^4	0.39 ± 0.02
$SnO_2(Ni)_{(pyr)}$/Si	0.8	9.0	10.7	5×10^3	0.51 ± 0.01
$SnO_2(Pd)_{(pyr)}$/Si	1.4	75.0	18.0	1×10^4	0.24 ± 0.03
$SnO_2(Cu)_{(pyr)}$/Si	0.6	88.0	13.5	3×10^3	0.27 ± 0.03

When analysing the current – voltage curves of the heterostructures under study, one should take into account that the surface area of the gold contact is much less than the surface area of the SnO_2 layer. Because of the 'current spreading' over the SnO_2 layer with a finite resistance the spreading resistance can contribute to the conductivity. Therefore, the current – voltage curves of the heterostructures cannot be exactly described by the relation (25). To allow for the current spreading, Eqn (25) was argumented with an additional parameter R_s (resistance connected in series with the Schottky barrier). Then, relation (25) takes the form

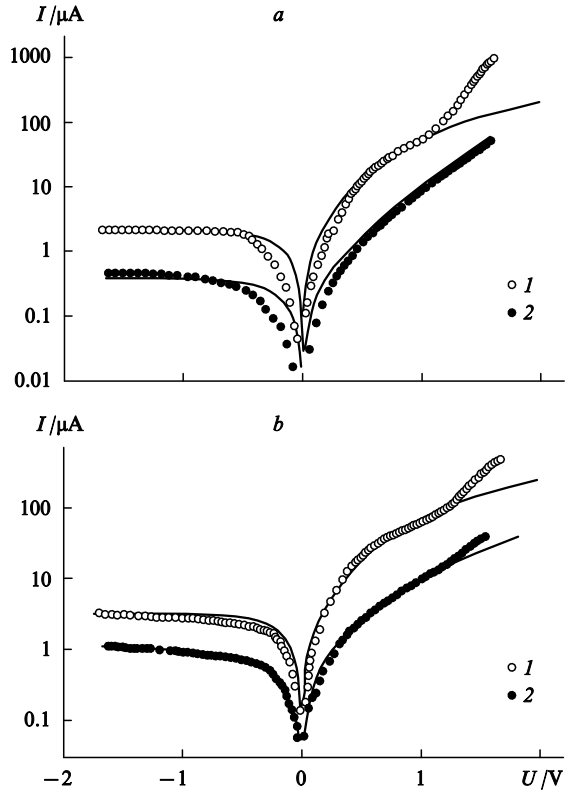

Figure 18. Capacitance – voltage curves of different heterostructures: $SnO_{2(pyr)}$/Si (*1*), $SnO_2(Ni)_{(pyr)}$/Si (*2*) (*a*) and $SnO_2(Cu)_{(pyr)}$/Si (*1*), $SnO_2(Pd)_{(pyr)}$/Si (*2*) (*b*) measured in dry nitrogen atmosphere.[91]
Full and open circles denote the experimental data and solid curves denote the results of calculations.

$$I = I_s\left\{\exp\left[\frac{e(U - IR_s)}{\beta kT}\right] - 1\right\}, \qquad (32)$$

where I is the current flowing through the heterostructure and I_s is the saturation current.

Thus, the current flowing through the heterostructure at a certain temperature depends on three parameters, *viz*., the saturation current, non-ideality coefficient, β, and the effective spreading resistance, R_s.

An attempt to describe the current – voltage curves of the magnetron sputtering fabricated heterostructures using relations (25) and (32) failed. The experimental U/j dependence obtained for the $SnO_{2(mag)}$/Si structure and the results of numerical simulation using the Schottky model with the parameters $j_s = 4.2$ μA cm^{-2} and $\beta = 15$ are shown in Fig. 19. As can be seen, the experimental and calculated data are inconsistent. For comparison we also present the experimental and calculated (with the parameters $j_s = 7.3$ μA cm^{-2} and $\beta = 8.5$) U/j dependences for the $SnO_{2(pyr)}$/Si heterostructure. Probably, in the magnetron sputtering fabricated heterostructures the contribution of the transient layers at the heterointerface to the formation of the Schottky barrier is greater than in the structures with the tin dioxide layer deposited by spray pyrolysis. This assumption is also consistent with the increase in the non-ideality coefficient ($\beta = 15$) of the structure in question. The formation of transient layers in the synthesis of films by magnetron sputtering was also reported by Golan *et al.*[105]

At reverse biases and at fixed U value, all the heterostructures studied exhibit an exponential dependence of the current on the reciprocal temperature. The activation energies, E_a, calculated from the equation

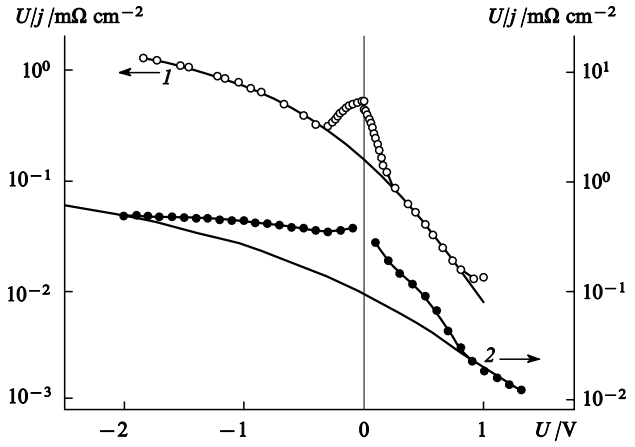

Figure 19. Impedance – voltage curves obtained for two heterostructures, $SnO_{2(pyr)}$/Si (*1*) and $SnO_{2(mag)}$/Si (*2*).[91]
Full and open circles denote the experimental data and solid curves denote the results of calculations.

$$I \propto \exp\left(\frac{E_a}{kT}\right),$$

are listed in Table 3. In the case of clearly seen saturation current the activation energy at reverse biases can be related to the barrier height. Among the spray pyrolysis fabricated structures, the maximum barrier height was found for $SnO_2(Ni)_{(pyr)}$/Si. The $SnO_{2(mag)}$/Si heterostructures are characterised by $E_a = (0.27 \pm 0.03)$ eV.

Changes in the barrier height at the heterointerface upon doping of the oxide layer can be due to the following reasons. Being an electron acceptor, copper can cause a dramatic increase in the film resistance, R, owing to compensation of donor oxygen vacancies.[106] Doping with nickel also leads to a substantial increase in the resistance and the appearance of activation-type portions in the temperature dependences of R. An increase in the nickel content causes a smooth increase in E_a up to 500 meV, which is most likely due to the increase in the intergranular barriers.[107] The activation energy of the copper-doped films reaches a value of 130 meV, which is comparable with the ionisation energy of oxygen,[108] and then remains unchanged with an increase in the dopant concentration. Doping of tin dioxide films with palladium was accompanied by the formation of metallic palladium clusters.[109] Since the palladium work function is greater than that of tin dioxide [63] doping can lead to depletion of charge carriers in the SnO_2 regions contacting Pd clusters and, correspondingly, to a decrease in the effective electron concentration in the tin dioxide layer. The decrease in the carrier concentration is supported by the high (compared to pure tin dioxide samples) resistance of the palladium doped structures. Thus, a decrease in the barrier height in the $SnO_2(M)_{(pyr)}$/Si heterostructures doped with copper and palladium correlates with the decrease in position of the Fermi level in the SnO_2 layer, which corresponds to the decrease in the carrier concentration. The increase in the barrier height in the nickel doped samples has no unambiguous explanation as yet.

Figure 20 presents the capacitance – voltage curves of the $SnO_2(Ni)_{(pyr)}$/Si heterostructures. A feature of these structures is a maximum of capacitance at positive biases, which can be associated with the contribution of an additional component corresponding to charge exchange between the interface states.[110–112] The character of changes in the capacitance – voltage curves at different frequencies of the reference signal confirms this assumption. Heterostructures fabricated by magnetron sputtering exhibit similar capacitance – voltage curves.

Adsorption of NO_2 and C_2H_5OH molecules strongly affects the electrophysical properties of the $SnO_2(M)_{(pyr)}$/Si heterostructures. Reproducible changes in the capacitance of the $SnO_2(Ni)_{(pyr)}$/Si heterostructure at zero potential on cyclic change in the gas phase composition from N_2 to $N_2 + C_2H_5OH$ (1%) mixture are shown in Fig. 21. The presence of ethanol molecules in the gas phase causes a substantial increase in the capacitance.

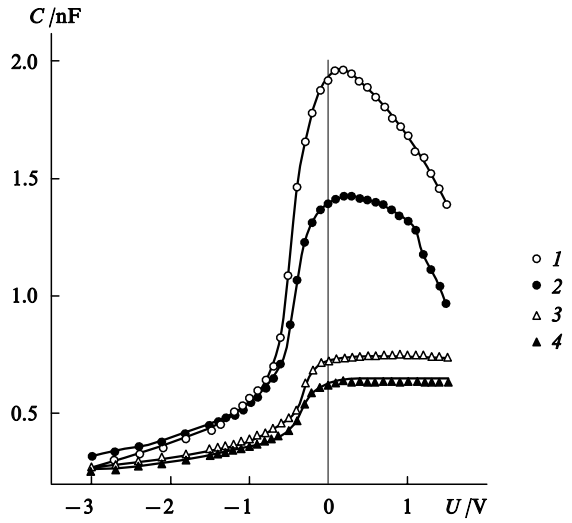

Figure 20. Capacitance – voltage curves of a $SnO_2(Ni)_{(pyr)}$/Si heterostructure at different frequencies.[92]
Signal frequency /kHz: 0.5 (*1*), 1 (*2*), 10 (*3*) and 20 (*4*).

The current – voltage curves of the $SnO_2(M)_{(pyr)}$/Si heterostructures change at both the forward and reverse biases. As an example, Fig. 22 presents the current – voltage curves of the $SnO_{2(pyr)}$/Si heterostructure in dry N_2 atmosphere (ground state) and in two mixtures, $N_2 + NO_2$ (0.1%) and $N_2 + C_2H_5OH$ (1%). Ethanol molecules were found to have an identical effect on all kinds of heterostructures, namely, the current considerably increases at forward biases and decreases at reverse biases. Adsorption of NO_2 molecules induces an opposite process for all heterostructures, *viz*., the current decreases at forward biases and increases at reverse biases. Changes in the saturation current at negative biases suggest a change in the barrier height at the heterointerface. Ethanol molecules adsorbed on the SnO_2 surface possess electron-donor properties.[64] Nitrogen dioxide molecules are electron acceptors and form a surface level in the band gap. The energy of this level is lower than that of the acceptor level of

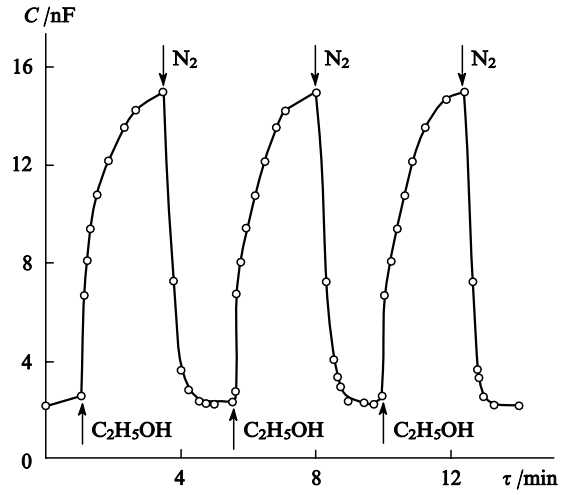

Figure 21. Periodic changes in the capacitance of a $SnO_2(Ni)_{(pyr)}$/Si heterostructure at 1 kHz on cyclic change in the gas phase composition from N_2 to $N_2 + C_2H_5OH$ (1%) mixture.[93]

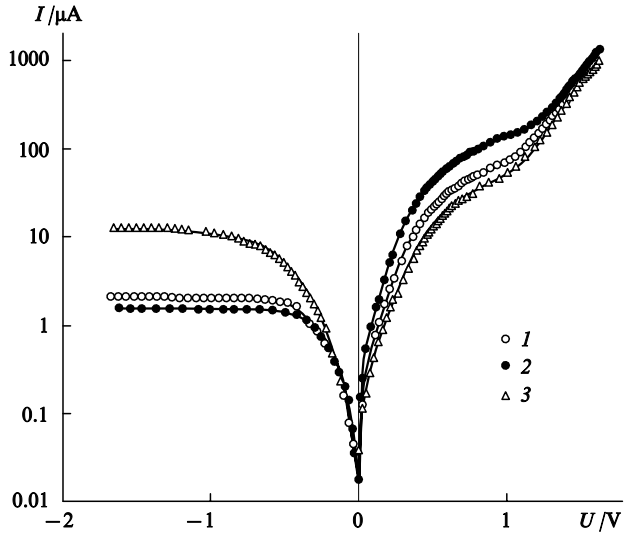

Figure 22. Current – voltage curves of a $SnO_{2(pyr)}$/Si heterostructure in different atmospheres: (*1*) N_2, (*2*) $N_2 + C_2H_5OH$ (1%) and (*3*) $N_2 + NO_2$ (0.1%).[93]

chemisorbed oxygen.[113] Thus, adsorption of NO_2 molecules causes a decrease in the effective carrier concentration and, correspondingly, a decrease in the barrier height. Adsorption of ethanol causes an opposite effect.

At forward biases, the change in the current flowing through the structure is to a great extent determined by spreading over the SnO_2 layer. A decrease in the tin dioxide resistance on adsorption of ethanol molecules leads to an increase in the effective spreading area, which governs the surface area of the working heterocontact. An increase in the SnO_2 resistance on adsorption of nitrogen dioxide leads to the opposite effect.

Adsorption of ethanol molecules causes an increase in the capacitance, the most pronounced effect being observed at positive biases. Modifications of the capacitance – voltage curves of the $SnO_2(Ni)_{(pyr)}$/Si structure in different atmospheres are shown in Fig. 23. The curve obtained in the presence of ethanol molecules has a clearly seen maximum whose position is shifted relative to the capacitance maximum for the curve obtained in the N_2 atmosphere. In the case of NO_2 adsorption the capacitance at forward biases decreases.

Thus, not only the change in the barrier height at the heterointerface but also the formation of the surface (interface) states influences the gas sensitivity. As mentioned above, the capacitance depends on charge exchange between the interface states responsible for the appearance of a maximum in the capacitance – voltage curve at forward biases. Changes in the capacitance peak amplitude under adsorption conditions (see Fig. 23) are characterised by the same features as the change in C upon variation of the frequency of the reference signal (see Fig. 20), which governs the contribution of charge exchange between the interface states. Therefore, the increase in the capacitance under ethanol adsorption can be associated with an increase in the density of electrically active surface states while the decrease in the capacitance under nitrogen dioxide adsorption can be due to a decrease in the density of the surface states.

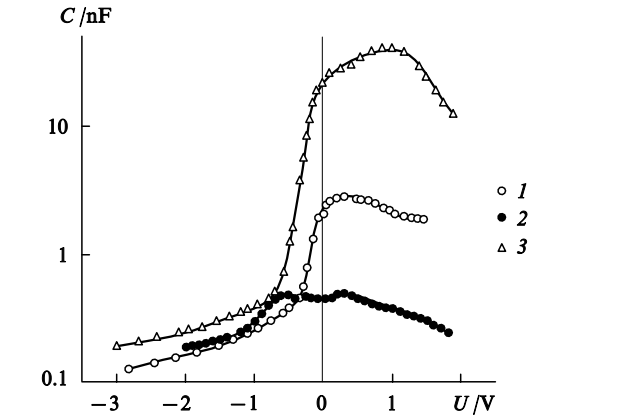

Figure 23. Capacitance – voltage curves of a $SnO_2(Ni)_{(pyr)}$/Si heterostructure in different atmospheres: (*1*) N_2, (*2*) $N_2 + C_2H_5OH$ (1%) and (*3*) $N_2 + NO_2$ (0.1%).[92]

The magnetron sputtering fabricated heterostructures behave in a significantly different manner under gas adsorption conditions. In NO_2-containing atmosphere, the current decreases at all forward and reverse biases. These changes in the shape of the current – voltage curves can be explained assuming that the major contribution to the conductivity of the structure comes from the resistance of the oxide layer rather than the heterojunction.

Additional information on changes in the current – voltage and capacitance – voltage curves can be obtained by analysing the voltage dependence of the sensor signal. The expression for the sensor signal has the form

$$S = \frac{r_1 - r_2}{r_2}, \; r_1 > r_2, \tag{33}$$

where r_1 and r_2 are the electrophysical characteristics of the sensor (current or capacitance) in N_2 atmosphere and in the gas mixture, respectively.

The sensitivities of the $SnO_2(Ni)_{(pyr)}$/Si heterostructure to NO_2 and C_2H_5OH calculated from the current – voltage and capacitance – voltage curves are presented in Fig. 24. The sensitivity – voltage plots exhibit non-monotonic changes. Clearly seen maxima are observed in both the $S(U)$ curves calculated using the capacitance – voltage curves under ethanol adsorption and in the $S(U)$ plots constructed using the current – voltage curves under NO_2 adsorption. The dependence of the sensitivity on the potential applied allows the best operating mode of a gas sensor to be chosen.

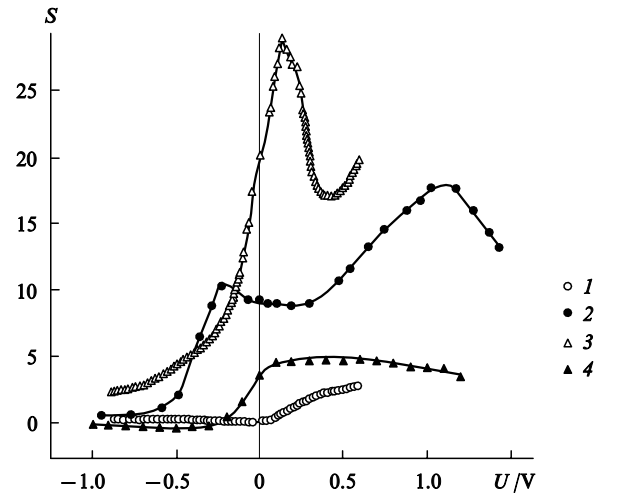

Figure 24. Sensitivity of a $SnO_2(Ni)_{(pyr)}$/Si heterostructure to C_2H_5OH (*1*, *2*) and NO_2 (*3*, *4*) plotted *vs.* voltage applied. Calculated using the current – voltage (*1*, *3*) and capacitance – voltage (*2*, *4*) curves.[93]
Gas concentration: C_2H_5OH (1%) and NO_2 (0.01%).

b. p-M_1O/n-M_2O structures

Considerable attention has been paid to studies of thin-film and ceramic n – p-heterojunctions based on semiconductor oxides

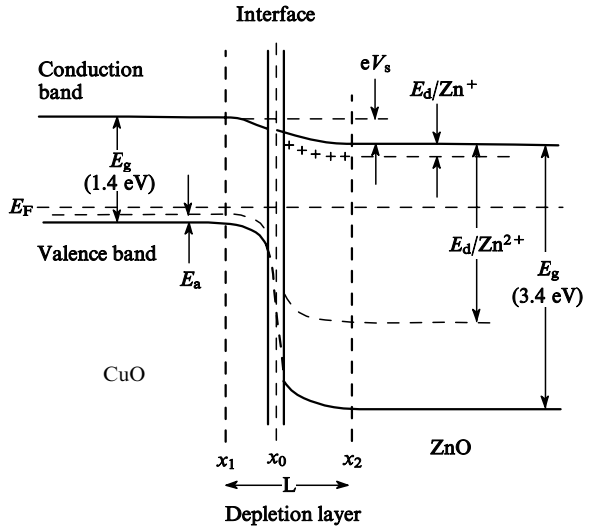

Figure 25. Band diagram of a CuO/ZnO heterojunction.[48]
E_d is the energy of the donor level and E_g is the energy gap width.

with different types of conductivity. These systems are H_2 and CO sensitive. The band diagram of a p-CuO/n-ZnO heterojunction is shown in Fig. 25. The energy barrier to carriers appears between the narrow-gap CuO with hole-type conductivity and the wide-gap ZnO with electronic conductivity. The heterojunction retains its rectifying characteristics over a wide temperature range (25–400 °C). Analysis of the current–voltage and capacitance–voltage curves showed that the energy barrier at the heterointerface cannot be correctly described by the Schottky model.[48] This is most likely due to the high concentration of surface states. If the gas phase contains CO and H_2 molecules, at elevated temperatures the current flowing through the heterojunction changes in both the forward and reverse branches and the sensitivity to CO is much higher than the sensitivity to H_2 at equal gas concentrations. The mechanism of selective sensitivity to CO was associated[68] with the following processes:

$$CO(gas) + h^+ \longrightarrow CO^+_{ads}(CuO\ surface), \quad (34)$$

$$1/2\,O_2(gas) + e^- \longrightarrow O^-_{ads}(ZnO\ surface), \quad (35)$$

$$CO^+_{ads} + O^-_{ads} \longrightarrow CO_2(CuO-ZnO\ heterointerface). \quad (36)$$

Analysis of complex impedance spectroscopy data showed that the interaction with CO molecules manifests itself in the form of additional capacitance and resistance components corresponding to the heterointerface.[48] It was assumed[49] that adsorption of CO molecules leads to the formation of additional interface states at the CuO/ZnO interface and that these states can be involved in tunnelling of charge carriers, which is responsible for the appearance of the additional component of electric current.

The sensitivity to CO can be enhanced by doping the CuO layer with alkali metals.[67] Metal cations increase the concentration of chemisorbed CO molecules, thus acting as additional adsorption sites. Another way of sensitivity enhancement is to anneal the CuO layer in inert atmosphere at 850 °C.[49] This is accompanied by partial reduction of CuO and an increase in the concentration of Cu^+ defects that also act as adsorption sites for CO molecules.

CuO/ZnO heterojunctions are sensitive to moisture content at room temperature. A change in the relative humidity from 0% to 90% causes the forward current to be changed by two orders of magnitude. Individual CuO and ZnO layers are insensitive to moisture content. A feature of these heterojunctions is a maximum in the dependence of sensitivity I_{H_2O}/I_{dry} (I_{H_2O} is the current in moist air and I_{dry} is the current in dry air) on the potential, which was associated[50] with electrolysis of water molecules. The

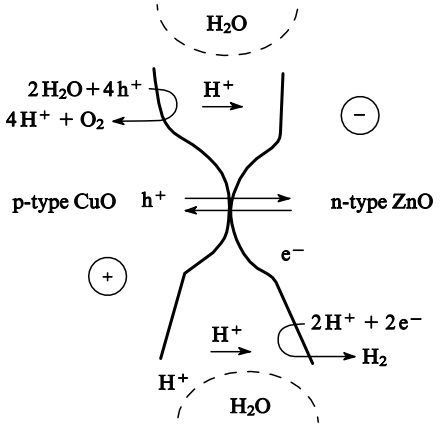

Figure 26. Schematic illustration of the mechanism of carrier transport through the CuO/ZnO heterointerface in the presence of water vapours.[53]

mechanism of gas sensitivity is schematically illustrated by Fig. 26. Two major processes are as follows:[53]

$$2\,H_2O + 4h^+ \longrightarrow 4\,H^+ + O_2\ (CuO\ surface), \quad (37)$$

$$2\,H^+ + 2e^- \longrightarrow H_2\ (ZnO\ surface). \quad (38)$$

In accord with this mechanism the adsorbed water molecules continuously leave the oxide surfaces. This permits shortening of the relaxation time of this heterojunction.

A La_2CuO_4/ZnO heterojunction exhibits a similar sensitivity to moisture content.[53] This structure is characterised by an increase in the forward current by four orders of magnitude upon changes in the relative humidity from 0% to 95%.

CuO/SnO_2 heterostructures (Fig. 27) were fabricated by magnetron sputtering of metals with subsequent thermal oxidation.[54, 55] The conditions for the oxidising annealing and the electrical properties of CuO films and the CuO/SnO_2 heterostructures, determined in each successive stage of annealing are listed in Table 4. The resistance of the CuO films changes non-monotonically in different stages of annealing. In the first stage (300 °C, 4 h) the resistance increases due to partial oxidation of the metal films.

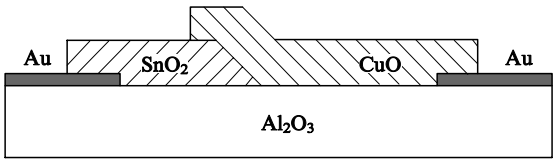

Figure 27. Schematic representation of a CuO/SnO_2 heterostructure.

Table 4. Electrical properties of CuO/SnO_2 heterostructures and CuO films in different stages of oxidising annealing.[55]

Stage	T/°C (see [a])	t/h (see [b])	Resistance at 25 °C/Ω		E_a/eV	
			CuO	CuO/SnO_2	CuO	CuO/SnO_2
0	–	–	1.0	1.5	–	–
1	300	4	5.1×10^6	2.3×10^6	0.22	–
2	300	2	1.5×10^6	1.8×10^6	–	–
3	400	10	1.9×10^5	3.1×10^5	0.16	0.14
4	450	10	1.5×10^5	7.3×10^5	–	–
5	500	10	1.3×10^5	2.2×10^7	0.14	0.19

[a] Annealing temperature. [b] Annealing duration.

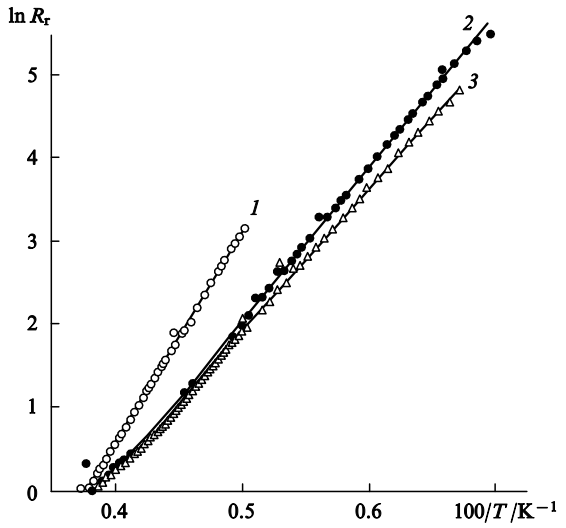

Figure 28. Relative resistance of CuO films in the first (*1*), third (*2*) and fifth (*3*) stages of annealing plotted *vs.* temperature.[55]

Subsequent thermal oxidation at 400 °C (10 h) and 500 °C (10 h) is accompanied by a decrease in the resistance. The temperature dependences of the relative resistance, $R_r = R(T)/R_{260\ K}$, of the CuO films are shown in Fig. 28. Linear plots obtained in the $\ln(R_r) - 1/T$ coordinates indicate the activation mechanism of conductivity. The activation energies, E_a, calculated using the relation

$$R \propto \frac{E_a}{RT},$$

decrease after each stage of annealing (see Table 4).

In the early stages of annealing (stages 1–3) the resistance of the heterostructures correlates with the data obtained for CuO films (Fig. 29). Further oxidation causes a substantial increase in the resistance of the heterostructures. The temperature dependences of the relative resistance of the heterostructures after the third stage and after complete oxidation at 500 °C are shown in Fig. 30. An increase in the resistance is accompanied by an increase in the activation energy. The temperature dependence of the resistance of the CuO/SnO_2 heterostructures after annealing at 400 °C exactly matches that of the CuO film after complete oxidation at 500 °C (see Fig. 30).

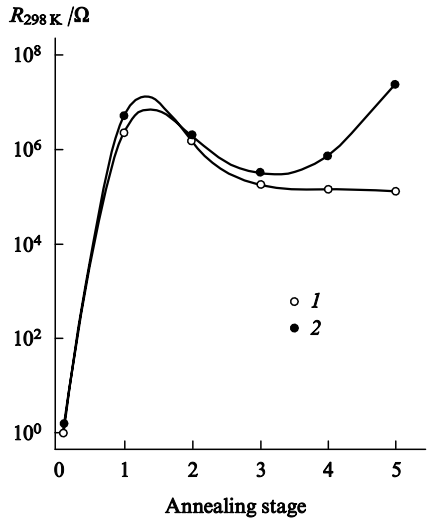

Figure 29. Changes in the resistance (T = 298 K) of CuO films (*1*) and CuO/SnO_2 heterostructures (*2*) in different stages of annealing.[55]

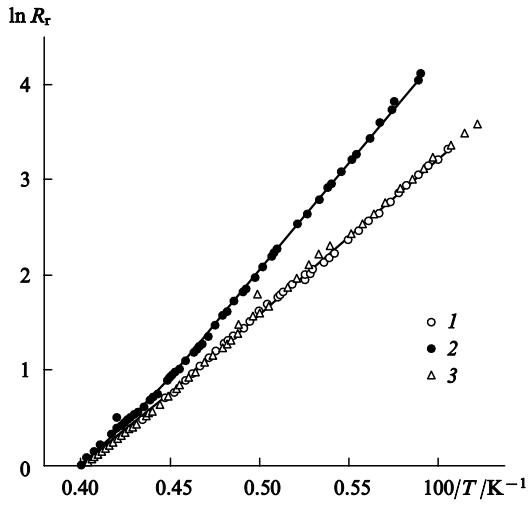

Figure 30. Relative resistance of CuO/SnO_2 (*1*), CuO/SnO_2 (*2*) and CuO film (*3*) samples in the third (*1*) and fifth (*2*, *3*) stages of annealing plotted *vs.* temperature.[55]

A secondary neutral mass spectrometry study [55] of the thickness distribution of the constituent elements of the CuO/SnO_2 heterostructures revealed three regions corresponding to CuO, SnO_2 and a transient layer at the CuO/SnO_2 interface. Therefore, the conductivity of these heterostructures can be described using an equivalent circuit including resistors connected in series and corresponding to CuO ($R1$), SnO_2(CuO) transient layer ($R2$) and SnO_2 ($R3$). Non-monotonic change in the resistance of the entire heterostructure during the oxidising annealing is governed by the contributions of different structural regions to the total resistance. In the initial stages of oxidation (stages 1–3) the CuO film is the most resistive element of the heterostructure. Further heating and an increase in the annealing duration lead to the formation of the SnO_2(CuO) transient layer whose resistance governs the conductivity of the entire heterostructure. The high resistance of the SnO_2(CuO) transient layer can be due to both the effect of compensation of intrinsic donor defects (oxygen vacancies) in SnO_2 by impurity acceptor sites, Cu_{Sn}, and the appearance of barriers at the n-SnO_2/p-CuO grain boundaries.

It should be noted that the CuO/SnO_2 heterostructures are characterised by linear current–voltage curves in all stages of annealing, though individual CuO and SnO_2 layers have p-type and n-type conductivities, respectively. This effect can be due to both the formation of the transient layer and the nanometre grain size of the contacting CuO and SnO_2 layers. The nanostructure has a very strong effect on electrical transport in semiconductors. For instance, gold contacts deposited on nanocrystalline SnO_2 are ohmic in character, whereas gold contacts deposited on single-crystalline SnO_2 form a Schottky barrier of 0.5 eV.[114] Thus, the interface between nanocrystalline materials can be transparent for tunnelling of charge carriers.

The sensor signals of the CuO/SnO_2 heterostructures in different stages of oxidising annealing were measured in a gas mixture containing 16.6 ppm of H_2S in N_2. The CuO/SnO_2 heterostructures annealed at 400 °C exhibit no sensitivity to H_2S (see curves *1* in Fig. 31 *a*,*b*). Raising the annealing temperature causes the appearance and amplification of the sensor signal (curves *2* and *3* in Fig. 31 *a*) with a maximum value of $S = 10^2$ observed after complete oxidation of the heterostructures at 500 °C over a period of 10 h. This maximum value is comparable with the magnitude of the sensor signal obtained for bulk doped SnO_2(CuO) films (curve *4* in Fig. 31 *b*). It should be noted that the CuO films exhibit no sensor sensitivity even when completely oxidised (curve *3* in Fig. 31 *b*). This indicates that the heterostructures become sensitive to H_2S only after formation of the SnO_2(CuO) transient layer

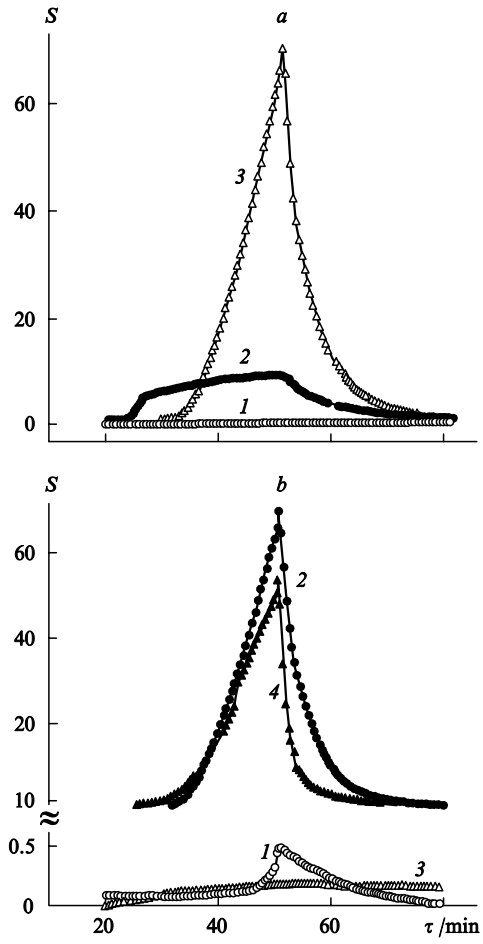

Figure 31. Sensitivities of materials to 16.6 ppm of H_2S in N_2 at 150 °C;[55] CuO/SnO_2 heterostructures in the third (*1*), fourth (*2*) and fifth (*3*) stages of annealing (*a*);
CuO/SnO_2 heterostructures in the third (*1*) and fifth (*2*) stages of annealing, CuO films (*3*) in the fifth stage of annealing and SnO_2(CuO) films (*4*) (*b*).

responsible for the appearance of the sensor signal. As the transient layer becomes the most resistive element of the equivalent circuit, the sensor sensitivity appears, the response signal reaching its maximum at the highest resistance of the heterostructure.

IV. Conclusion

Analysis of the available information on the properties of materials based on inorganic structures shows that interfaces in these objects are extremely sensitive to the state of the environment. Modern technologies offer great prospects for design of interfaces, especially in thin-film structures based on materials with different electronic properties. The vast majority of recent studies are concerned with MIS structures based on catalytic metals with well-studied mechanism of sensor sensitivity. Nevertheless, yet another type of structures, *viz*. those based on semiconductor oxides are also of interest. Porous nanocrystalline semiconductor oxides with large specific surface areas (150–200 $m^2\ g^{-1}$) are expected to extend the range of materials for gas sensors.

It should be noted that the possibility of detection and interpretation of the useful signal of the sensing elements can be significantly enhanced using gas sensors based on structures with heterojunctions. These structures are more complex systems compared to simple resistive transducers and offer a number of advantages. The main advantage is a much greater amount of information that can be read and, in some cases, stored. The amount of information is determined by the possibility of detecting the field and frequency dependent resistive and capacitance responses. Thus, one structure can be used instead of a chain or even an array of resistive transducers.

In spite of recent advances in using structures with heterojunctions as sensing elements of gas sensors, much is yet to be done. Considerable efforts should be made to solve the problem of degradation-induced instability of parameters of these structures. Development of methods of fast signal reset at room temperature is also of great importance. In this connection information on signal quenching by electric field pulses is of particular interest.

Pointing out the importance of applied aspects, we must also pay attention to interdisciplinary problems of basic research on interfaces under gas adsorption conditions. Studies on the chemical and physical mechanisms of processes occurring in various structures in static and high-frequency fields and in gas atmospheres of different compositions will find new fields of practical application of these processes.

The review has been written with financial support from the Russian Foundation for Basic Research (Project No. 03-03-32586) and from the Russian Federation Ministry of Science and Education (Russian Federation Presidential Grant MK-1710.2003.03).

References

1. T Seiyama, A Kato, K Fujiishi, M Nagatani *Anal. Chem.* **34** 1502 (1962)
2. V F Kiselev *Poverkhnostnye Yavleniya v Poluprovodnikakh i Dielektrikakh* (Surface Effects in Semiconductors and Dielectrics) (Moscow: Nauka, 1970)
3. J Janata (Ed.) *Solid State Chemical Sensors* (New York: Academic Press, 1985)
4. W Gopel, J Hesse, J N Zemel (Eds) *Sensors, a Comprehensive Survey* Vol. 2, Pt. 1 (Weinheim: Wiley-VCH, 1991)
5. B F Myasoedov, A V Davydov *Zh. Anal. Khim.* **45** 1259 (1990) [a]
6. E E Gutman *Zh. Fiz. Khim.* **58** 801 (1984) [b]
7. P T Moseley, B C Tofield (Eds) *Solid State Gas Sensors* (Bristol, Philadelphia: Alam Higer, 1987)
8. T Seiyama (Ed.) *Chemical Sensor Technology* (Amsterdam: Elsevier, 1988)
9. W Göpel *Sens. Actuators B* **16** 167 (1989)
10. W Göpel, K D Schierbaum *Sens. Actuators, B* **26**–**27** 1 (1995)
11. P T Moseley *Meas. Sci. Technol.* **8** 223 (1997)
12. J Watson, K Ihokura *Mater. Res. Soc. Bull.* **24** 14 (1999)
13. Y Shimizu, M Egashira *Mater. Res. Soc. Bull.* **24** 18 (1999)
14. G Martinelli, M C Carotta, E Traversa, G Ghiotti *Mater. Res. Soc. Bull.* **24** 30 (1999)
15. N Barsân, M Schweizer-Berberich, W Göpel *Fresenius J. Anal. Chem.* **365** 287 (1999)
16. D E Williams *Sens. Actuators, B* **57** 1 (1999)
17. N Barsân, U Weimar *J. Electroceram.* **7** 143 (2001)
18. N Yamazoe, J Tamaki, N Miura *Mater. Sci. Eng., B* **41** 178 (1996)
19. C Malagu, V Guidi, M Stefancich, M C Carotta, G Martinelli *J. Appl. Phys.* **91** 808 (2002)
20. I Lundstrom *Sens. Actuators* **1** 403 (1981)
21. I Lundstrom, D Soberberg *Sens. Actuators* **2** 105 (1981/1982)
22. J Fogelberg, H Dannetun, I Lundstrom, L G Petersson *Vacuum* **41** 705 (1990)
23. V I Filippov, A A Terentjev, S S Yakimov *Sens. Actuators, B* **28** 55 (1995)
24. L G Ekedal, M Eriksson, I Lundstrom *Acc. Chem. Res.* **31** 249 (1998)
25. I Lundstrom *Sens. Actuators, A* **56** 75 (1996)
26. P Tobias, P Martensson, A Baranzah, P Salomonsson, I Lundstrom, L Abom, A Lloyd-Spetz *Sens. Actuators, B* **47** 125 (1998)
27. R B Vasiliev, M N Rumyantseva, L I Ryabova, B A Akimov, M Labeau, M Langlet, A M Gaskov *Mater. Sci. Eng., B* **77** 106 (2000)

28. B Keramati, J N Zemel *J. Appl. Phys.* **53** 1091 (1982)
29. A D'Amico, G Fortunato, G Petrocco, C Coluzza *Appl. Phys. Lett.* **42** 964 (1983)
30. A D'Amico, G Fortunato, G Petrocco, C Coluzza *Sens. Actuators* **4** 349 (1983)
31. B Keramati, J N Zemel *J. Appl. Phys.* **53** 1100 (1982)
32. W P Kang, C K Kim *Sens. Actuators, B* **22** 47 (1994)
33. W P Kang, C K Kim *Appl. Phys. Lett.* **63** 421 (1993)
34. W P Kang, J F Xu, B Lalevic, T L Poteat *Sens. Actuators* **12** 349 (1987)
35. S J Fonash, Z Li, M J O'Leary *J. Appl. Phys.* **58** 4415 (1985)
36. D Dwivedi, R Dwivedi, S K Srivastava *Microelectron. J.* **29** 445 (1998)
37. U Hoefer, H Bottner, E Wagner, C D Kohl *Sens. Actuators, B* **47** 213 (1998)
38. K D Schierbaum, U K Kimer, W Göpel *Sens. Actuators, B* **4** 87 (1991)
39. J N Zemel, B Keramati, C W Spivak, A D'Amico *Sens. Actuators* **1** 427 (1981)
40. W Zhang, H Uchida, T Katsube, T Nakatsubo, Y Nishioka *Sens. Actuators, B* **49** 58 (1998)
41. M N Rumyantseva, A M Gaskov, L I Ryabova, J P Senateur, B Chenevier, M Labeau *Mater. Sci. Eng., B* **41** 333 (1996)
42. A S Ryzhikov, R B Vasiliev, M N Rumyantseva, L I Ryabova, G A Dosovitsky, A M Gilmutdinov, V F Kozlovsky, A M Gaskov *Mater. Sci. Eng., B* **96** 268 (2002)
43. S J Jung, H Ohsawa, Y Nakamura, H Yanagida, K Hasumi, O Okada *J. Electrochem. Soc.* **141** L53 (1994)
44. Y Nakamura, H Zhuang, A Kishimoto, O Okada, H Yanagida *J. Electrochem. Soc.* **145** 632 (1998)
45. S T Jun, G M Choi *Sens. Actuators, B* **17** 175 (1994)
46. K Hikita, M Miyayama, H Yanagida *J. Am. Ceram. Soc.* **77** 1961 (1994)
47. D J Choi, G M Choi *Sens. Actuators, B* **69** 120 (2000)
48. K Hikita, M Miyayama, H Yanagida *J. Am. Ceram. Soc.* **78** 865 (1995)
49. Y Ushio, M Miyayama, H Yanagida *Sens. Actuators, B* **17** 221 (1994)
50. D J Yoo, S J Park *J. Electrochem. Soc.* **143** L89 (1996)
51. Y Ushio, M Miyayama, H Yanagida *Sens. Actuators, B* **12** 135 (1993)
52. O Makimoto, T Arakawa *Sens. Actuators, B* **13**–**14** 585 (1993)
53. E Traversa *J. Am. Ceram. Soc.* **78** 2625 (1995)
54. R B Vasiliev, M N Rumyantseva, N V Yakovlev, A M Gaskov *Sens. Actuators, B* **50** 187 (1998)
55. R B Vasiliev, M N Rumyantseva, S E Podguzova, A S Ryzhikov, L I Ryabova, A M Gaskov *Mater. Sci. Eng., B* **56** 263 (1999)
56. M N Rumyantseva, M Labeau, J P Senateur, G Delabouglise, M N Boulova, A M Gaskov *Mater. Sci. Eng., B* **41** 228 (1996)
57. A L Spetz, L Uneus, H Svenningstorp, P Tobias, L G Ekendahl, O Larsson, A Goras, S Savage, C Harris, P Martensson, R Wigren, P Salomonsson, B Haggendahl, P Ljung, M Mattsson, I Lundstrom *Phys. Status Solidi A* **185** 15 (2001)
58. T Rantala, V Lantto *Surf. Sci.* **352**–**354** 765 (1996)
59. G Blazer, T Ruhl, C Diehl, M Ulrich, D Kohl *Physica A* **266** 218 (1999)
60. J N Zemel *Thin Solid Films* **163** 189 (1988)
61. S Strassler, A Reis *Sens. Actuators, B* **4** 465 (1983)
62. P K Clifford, D T Tuma *Sens. Actuators, B* **3** 233 (1982/1983)
63. F Bechstedt, R Enderlain *Semiconductor Surfaces and Interfaces. Their Atomic and Electronic Structures* (Berlin: Akademie Verlag, 1988)
64. V E Henrich, P A Cox *The Surface Science of Metal Oxides* (Cambridge: Cambridge University Press, 1996)
65. H Idriss, M A Barteau *Adv. Catal.* **45** 261 (1999)
66. A Meny, in *Surface Science: Recent Progress and Perspectives* (Eds T S Jayadevaiah, R Vanselow) (Cleveland: CRC Press, 1974)
67. A Zangwill *Physics at Surfaces* (Cambridge: Cambridge University Press, 1988)
68. D Kohl *Sens. Actuators* **18** 71 (1989)
69. H Geistlinger *Sens. Actuators, B* **17** 47 (1993)
70. K Mukae *Key Eng. Mater.* **125**–**126** 317 (1997)
71. E Souteyrand, in *Les Capteurs Chimiques* (Ed. C Pijolat) (Lyon: CMC2, 1997) p. 52
72. I A Myasnikov, V Ya Sukharev, L Yu Kupriyanov, S A Zav'yalov *Poluprovodnikovye Sensory dlya Fiziko-Khimicheskikh Issledovanii* (Semiconductor Sensors for Physico-chemical Investigations) (Moscow: Nauka, 1991)
73. K S Weissenrieder, J Muller *Thin Solid Films* **300** 30 (1997)
74. V Demarne, A Grisel, R Sanjines, D Rosenfeld, F Levy *Sens. Actuators, B* **47** 704 (1992)
75. R Sanjines, V Demarne, F Levy *Thin Solid Films* **193**/**194** 935 (1990)
76. T Rantala, V Lantto, T Rantala *Sens. Actuators, B* **47** 59 (1998)
77. J F McAlleer, P T Moseley, J O Norris, D E Williams *J. Chem. Soc., Faraday Trans. 1* **83** 1323 (1987)
78. V Lantto, P Romppainen, S Leppavuori *Sens. Actuators, B* **14** 149 (1988)
79. P K Clifford, D T Tuma *Sens. Actuators, B* **3** 255 (1982/1983)
80. R Sanjines, F Levy, V Demarne, A Grisel *Sens. Actuators, B* **1** 176 (1990)
81. G Sberveglieri, G Faglia, S Gropelli, P Nelli, A Taroni *Sens. Actuators, B* **7** 721 (1992)
82. J H Hwang, D S McLachlan, T O Mason *J. Electroceram.* **3** 7 (1999)
83. M J Verkerk, B J Middelhuis, A J Burgraaf *Solid State Ionics* **6** 159 (1982)
84. A Tadeev, Ph.D. Thesis, INPG, Grenoble 1999
85. S R Vishwakarma, Rahmatullah, H C Prasad *J. Phys. D: Appl. Phys.* **26** 959 (1993)
86. S V Slobodchikov, Kh M Salikhov, E V Russu *Fiz. Tekhn. Poluprovodn.* **33** 435 (1999)[c]
87. S V Slobodchikov, Kh M Salikhov, E V Russu *Fiz. Tekhn. Poluprovodn.* **35** 479 (2001)[c]
88. H Dib, Z Benamara, A Boudissa, B Zebentout, R Naoum, F Raoult *Microelectron. J.* **30** 679 (1999)
89. K Suga, N Koshizaki, K Yasumoto, E Smela *Sens. Actuators, B* **13**–**14** 598 (1993)
90. U R Chaudhuri, K Ramkumar, M Satyam *J. Appl. Phys.* **66** 1748 (1989)
91. R B Vasiliev, A M Gaskov, M N Rumyantseva, A S Ryzhikov, L I Ryabova, B A Akimov *Fiz. Tekhn. Poluprovodn.* **34** 993 (2000)[c]
92. R B Vasiliev, A M Gaskov, M N Rumyantseva, L I Ryabova, B A Akimov *Fiz. Tekhn. Poluprovodn.* **35** 436 (2001)[c]
93. R B Vasiliev, L I Ryabova, M N Rumyantseva, A M Gaskov, B A Akimov *Phys. Status Solidi A* **188** 1093 (2001)
94. M N Rumyantseva, O V Safonova, M N Bulova, L I Ryabova, A M Gaskov *Izv. Akad. Nauk, Ser. Khim.* **52** 1151 (2003)[d]
95. H Yan, G H Chen, W K Man, S P Wong, R W M Kwok *Thin Solid Films* **326** 88 (1998)
96. T Hyodo, T Mori, A Kawahara, H Katsuki, Y Shimizu, M Egashira *Sens. Actuators, B* **77** 41 (2001)
97. M Eriksson, L G Ekedal *Sens. Actuators, B* **42** 217 (1997)
98. I Lundstrom, A Spetz, F Winquist, U Ackelid, H Sundgren. *Sens. Actuators, B* **1** 15 (1990)
99. M Langlet, C Vautey, N Primeau *Thin Solid Films* **310** 47 (1997)
100. M Burgos, M Langlet, C Vautey *Thin Solid Films* **347** 184 (1999)
101. K Vanheusden, S P Karna, R D Pugh, W L Warren, D M Fleetwood, R A B Devine, A H Edwards *Appl. Phys. Lett.* **72** 28 (1998)
102. K Vanheusden, W L Warren, R A B Devine, D M Fleetwood, J R Schwank, M R Shaneyfelt, P S Winokur, Z J Lemnios *Nature (London)* **386** 587 (1997)
103. T Fare, A Spetz, M Armagarth, I Lundstrom *Sens. Actuators* **14** 369 (1988)
104. Y Gurbuz, W P Kang, J L Davidson, D V Kerns *Sens. Actuators, B* **35**–**36** 303 (1996)
105. A Golan, J Bregman, Y Shapira, M Eizenberg *J. Appl. Phys.* **69** 1494 (1991)
106. B A Akimov, A V Albul, A M Gaskov, V Yu Il'in, M Labo, M N Rumyantseva, L I Ryabova *Fiz. Tekhn. Poluprovodn.* **31** 400 (1997)[c]
107. B A Akimov, A M Gaskov, M Labo, S E Podguzova, M N Rumyantseva, L I Ryabova, A V Tadeev *Fiz. Tekhn. Poluprovodn.* **33** 205 (1999)[c]

108. S Samson, C G Fonstad *J. Appl. Phys.* **44** 4618 (1973)
109. M Gaidi, M Labeau, B Chenevier, J L Hazemann *Sens. Actuators, B* **48** 277 (1998)
110. J P Donnelly, A G Milnes *IEEE Trans. Electron Devices* **14** 63 (1967)
111. M J Madou, B H Loo, K W Frese, S R Morrison *Surf. Sci.* **108** 135 (1981)
112. A Turut, M Saglam, H Efeoglu, N Yalcin, M Yildrim, B Abay *Physica B* **205** 41 (1995)
113. J A Agapito, J P Santos *Sens. Actuators, B* **31** 93 (1996)
114. C J Fonstad, R H Rediker *J. Appl. Phys.* **42** 2911 (1971)

[a] — *Russ. J. Anal. Chem. (Engl. Transl.)*
[b] — *Russ. J. Phys. Chem. (Engl. Transl.)*
[c] — *Semiconductors (Engl. Transl.)*
[d] — *Russ. Chem. Bull., Int. Ed. (Engl. Transl.)*

Russian Chemical Reviews **73** (10) 957 – 989 (2004) © 2004 Russian Academy of Sciences and Turpion Ltd

DOI 10.1070/RC2004v073n10ABEH000895

Olefination of carbonyl compounds: modern and classical methods

V N Korotchenko, V G Nenajdenko, E S Balenkova, A V Shastin

Contents

I.	Introduction	957
II.	Addition of ylides or carbanions stabilised by heteroatoms in the α-position	958
III.	Condensation of carbonyl compounds with CH-acids	973
IV.	Reagents based on transition and non-transition metals	976
V.	Miscellaneous olefination methods	982
VI.	Conclusion	986

Abstract. The published data on the methods for alkene synthesis by olefination of carbonyl compounds are generalised and systematised. The main attention is given to the use of transition metals and organoelement compounds. The review covers the data on both classical and newly developed methods that are little known to chemists at large. The bibliography includes 276 references.

I. Introduction

Olefination of carbonyl compounds, *i.e.*, conversion of the carbonyl group into a double carbon – carbon bond, is one of the paramount strategies in the regioselective synthesis of substituted alkenes.[1 – 3]

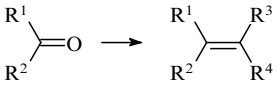

Thus many total syntheses of complex molecules, including natural compounds, involve the formation of a C = C bond by this particular route.[4] Olefination is the construction of an alkene from two different components, *viz.*, a carbonyl compound and an olefinating agent, which allows broad variation of the nature of substituents at the double bond.

Numerous reviews and monographs deal with separate classical olefination procedures; however, their collective description is virtually absent. A systematic consideration of the existing olefination methods is given only in *Comprehensive Organic Synthesis,* which covers the literature up to the year of 1999.[2] The handbook *Comprehensive Organic Transformations* contains a large set of olefination reactions with no comments.[5] The book *Preparation of Alkenes*[1] published in 1996 provides a brief description of the main olefination procedures, such as the Wittig, Peterson, Julia, Johnson and McMurry reactions, aldol condensation and reductive coupling of polyhaloalkanes with carbonyl compounds in the presence of chromium derivatives. In addition, this book describes some standard procedures for the synthesis of alkenes. Other reviews are devoted to the methods for the synthesis of individual types of unsaturated compounds. Thus the review[6] published in 1983 considers the use of various olefination procedures for the synthesis of stilbenes. The review[7] describes the McMurry and Barton – Kellog reactions and their application in the synthesis of sterically hindered alkenes. The review[8] deals with the addition reactions of CH-acids to aldehydes under conditions of phase transfer catalysis which sometimes yield alkenes. One of the chapters in the review[9] published in 2001 and devoted to the synthesis of conjugated dienes considers the use of olefination in the synthesis of dienes.

The striking progress in this field of organic synthesis is associated first of all with the use of various transition metals, reagents based on them and organoelement compounds; however, many novel olefination procedures are not mentioned in the reviews and monographs published so far. Besides, new modifications, reagents and catalysts of the classical reactions are being constantly developed, which has made it possible to extend the range of their practical applications and ensures higher yields, greater selectivity and milder reaction conditions.

The present review provides a comparative analysis of methods used for the olefination of carbonyl compounds and covers the literature published up to the end of 2003.

The carbonyl carbon atom bears a partial positive charge; therefore, general olefination procedures include, as a rule, the addition of various C-nucleophiles (both preformed and prepared *in situ*) to the carbonyl group. In this review, the methods used for converting the carbonyl group into the C = C bond are classified according to the type of nucleophilic species that attack the carbonyl carbon atom. Correspondingly, all olefination methods are divided into four groups, *viz.*, addition of ylides or carbanions stabilised by heteroatoms in the α-position to the carbonyl group (Section II); condensation of carbonyl compounds with various CH-acids (Section III); olefination with reagents based on metals (Section IV). Reactions not involving direct synthesis of alkenes, *e.g.*, the Grignard reaction, are excluded from consideration where possible. The methods not included in the first three groups are considered in Section V.

In describing the olefination reactions, we placed the main emphasis on both the preparative aspects and reaction mechanisms. The review displays the most recent modifications of the olefination reactions, since the traditional methods are considered

V N Korotchenko, V G Nenajdenko, E S Balenkova Department of Chemistry, M V Lomonosov Moscow State University, Leninskie Gory, 119992 Moscow, Russian Federation. Fax (7-095) 932 88 46. Tel. (7-095) 939 22 76. E-mail: vassili_k@mail.ru (V N Korotchenko), nen@acylium.chem.msu.ru (V G Nenajdenko, E S Balenkova)
A V Shastin Institute of Problems of Chemical Physics, Russian Academy of Sciences, 142432 Chernogolovka, Moscow Region, Russian Federation. Fax (7-096) 514 32 44. E-mail: shastin@icp.ac.ru

Received 26 December 2003
Uspekhi Khimii **73** (10) 1039 – 1074 (2004); translated by R L Birnova

in sufficiently great detail in the reviews.[10–35] The generally known data are cited only if they are of critical importance.

II. Addition of ylides or carbanions stabilised by heteroatoms in the α-position

This Section is devoted to the olefination methods based on the addition, to the carbonyl group, of ylides of the type **1** or of carbanions of the type **2** stabilised either by elements from Groups IIIA–VIIA of the Periodic System or by functional groups containing heteroatoms. Reactions of ylides **1** with carbonyl compounds yield the intermediates **3** with a betaine structure or the cyclic intermediates **4**. The addition of the carbanions **2** to the carbonyl group results in alkoxides of the corresponding β-hydroxy organoelement compounds **5**.

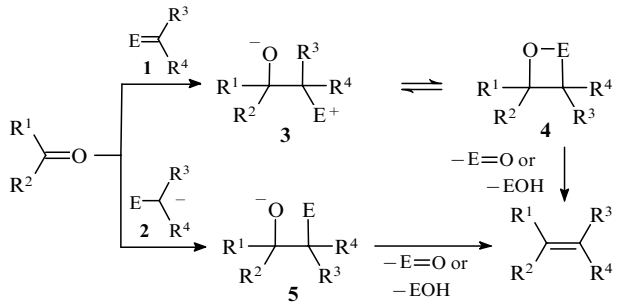

E is heteroatom or functional group.

Depending on the nature of the heteroatom, further transformations of the intermediates into the target alkenes occur in two routes. It is of note that the loss of the organoelement fragment usually occurs in the above-described reactions, which points to its subsidiary role. Elements with electronegativities lower than that of carbon (Table 1) and with high affinities for oxygen are eliminated from the intermediate compounds as the corresponding oxygen-containing products, *viz*., organoelement oxides and hydroxides. Thus, the olefinating agents can simultaneously act as the reducing agents.

If the electronegativity of an element is close to that of carbon or exceeds it (Cl, Br), the conversion of intermediate alkoxides of the type **5** into alkenes requires the use of additional reducing agents. In this case, the formation and reduction of the intermediate compounds **5** are carried out in succession. Very often, this is preceded by protection of the hydroxy group by silylation or acylation; in this case, it is protected compounds **6** that are subject to reduction.

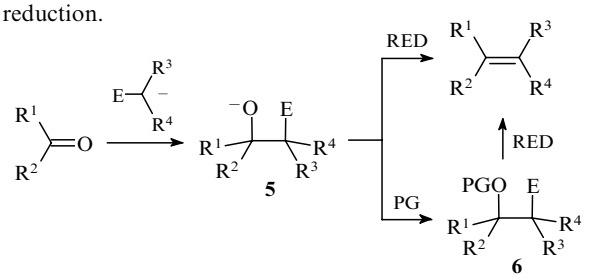

RED is a reducing agent, PG is protecting group.

The reaction of carbonyl compounds with isocyanides (Section II.3.a) is a special case. Here, the role of a reducing agent is played by the carbon atom of isocyanide, although the corresponding carbanion is stabilised by the nitrogen-containing functional group.

Table 1. The electronegativity and energy of the single bond E–O of Group IIIA–VIIA elements of the Periodic System.

Element	Group	Electronegativity [a]	Energy of the E–O bond /kcal mol^{-1} (see [b])	Reaction type
B	IIIA	2.01	124.3 (125.0)	addition with subsequent elimination
C	IVA	2.50	85.6	the same
Si	IVA	1.74	111.4 (108.0)	"
Ge	IVA	2.02	92.0 (86.8)	"
Sn	IVA	1.72	(85.5)	"
Pb	IVA	1.55	(95.1)	"
P	VA	2.06	86.0 (97.3)	"
N	VA	3.07	51.1	see [c]
As	VA	2.20	77.9 (114.0)	addition with subsequent elimination
Sb	VA	1.82	(75.0)	the same
Bi	VA	1.67	92.0 (81.0)	"
Te	VIA	2.01	(64.1)	"
S	VIA	2.44	(63.3)	use of an additional reducing agent
Se	VIA	2.48	(82.0)	the same
Cl	VIIA	2.83	49.2 (49.2)	"
Br	VIIA	2.74	(55.9)	"

[a] Data from Ref. 36; [b] data from Refs 37, 38, the data from Ref. 36 are given in parenthesis; [c] for details see Section II.3.a.

1. Reagents based on Group IIIA elements

A series of olefinating agents for the synthesis of alkenes based on organoboron compounds have been prepared.[1, 2, 10, 39] Thus the *gem*-lithioorganoboron reagent **7** synthesised *in situ* by metallation of *gem*-diborane **8** adds to benzaldehyde, aliphatic ketones and diaryl ketones to give an intermediate of type **9**.[40]

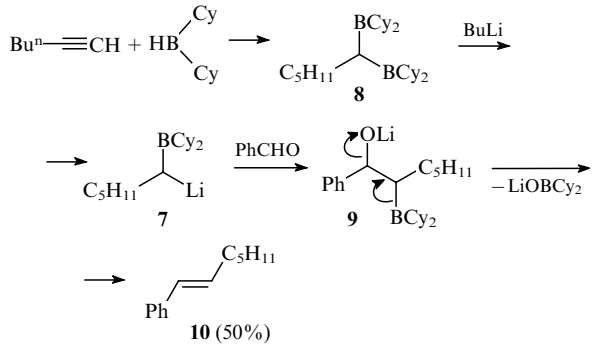

Cy is cyclo-C_6H_{11}.

Subsequent β-elimination of dialkyl borinate gives alkenes in 20%–50% yields; the *trans*-isomer of alkene **10** is formed predominantly from benzaldehyde. The high affinity of boron for oxygen is the driving force of this elimination (see Table 1). Thus, the organoboron reagent **7** acts simultaneously as the reducing agent. The necessity for the preliminary synthesis of *gem*-diborylalkane **8** is a significant disadvantage of this method.

The use of cyclic boronate **11** as an olefinating agent allows conversion of aldehydes and ketones into dithioacetals of homologous ketenes.[41]

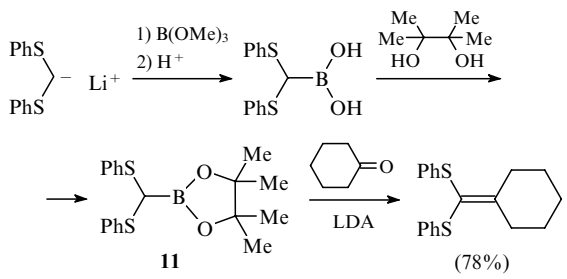

LDA is lithium diisopropylamide.

The addition of carbanions of type **12** stabilised by an α-boron atom to aromatic carbonyl compounds gives alkenes in good yields.[42,43]

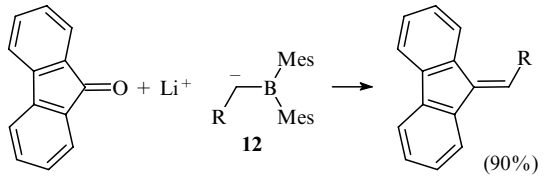

R = Me.

The carbanions **12** are prepared from dimesitylalkylboranes **13**, which in turn are synthesised from boron trifluoride etherate by successive addition of two equivalents of mesitylmagnesium bromide and subsequent treatment of compound **14** with Grignard reagents or organolithium compounds.[44]

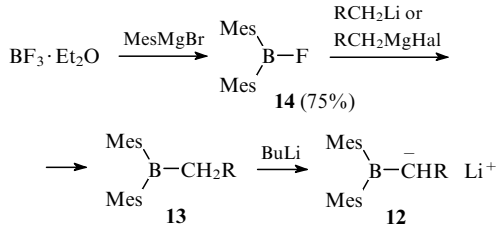

R = H, Alk.

In the case of aromatic aldehydes, the stereochemistry of alkene formation can be controlled by modifying the reaction conditions. Silylation of an intermediate alcohol and subsequent treatment of the silyl derivative **15** with hydrofluoric acid afford *E*-isomers of alkenes in high yields and with good stereoselectivity.

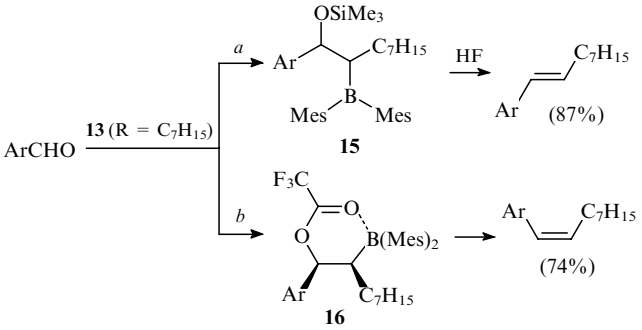

Ar = 4-MeOC$_6$H$_4$; (*a*) BuLi, Me$_3$SiCl; (*b*) BuLi, (CF$_3$CO)$_2$O.

Treatment of the intermediate alcohol with trifluoroacetic anhydride results in *Z*-isomers of alkenes; aromatic aldehydes containing electron-withdrawing groups in the *para*-position are an exception.[42] Presumably, the stereochemistry of this reaction is determined by coordination of the acyl oxygen atom to the boron atom in the intermediate **16**.

It was found that α-boron-substituted zinc organocyanocuprate **17**,[45] which reacts with a vast variety of electrophiles including carbonyl compounds, can be used as a convenient methylenating reagent. Its reactions with aldehydes in the presence of Lewis acids and subsequent thermolysis of the intermediate **18** yield terminal alkenes. The area of application of the reagent **17** includes aliphatic, aromatic and α,β-unsaturated aldehydes.

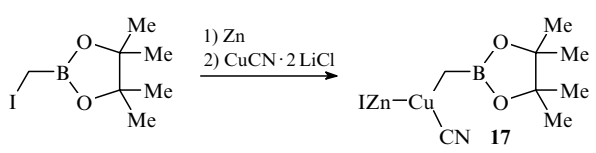

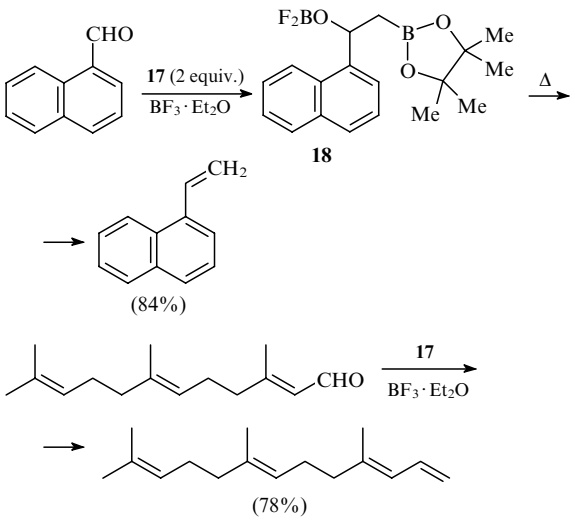

2. Reagents based on Group IVA elements

a. Silicon-based reagents: the Peterson olefination and related methods

The reaction of carbonyl compounds with carbanions stabilised by α-triorganylsilyl groups and subsequent elimination of the intermediate silanol is a general olefination method (the Peterson olefination).[1,2,11–15] Since the moment of its discovery in 1968,[46] this reaction has been used, along with the Wittig and the Julia reactions, in the synthesis of diverse alkenes. Silyl carbanions R$\overline{\text{C}}$HSiMe$_3$ **19** are employed as the olefinating agents. These are prepared by the Grignard reaction or by metallation of α-halogenosilanes, by deprotonation of silanes with strong bases as well as by addition of organometallic compounds to vinylsilanes. The deprotonation of silanes is favoured by the presence of other electron-withdrawing groups in the molecule. Aromatic, aliphatic and unsaturated aldehydes and ketones can be used as the carbonyl components.

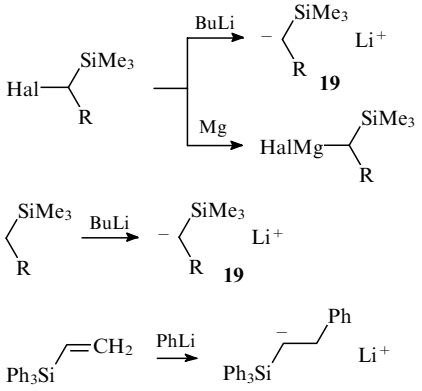

The addition of the α-silyl carbanion **19** to the carbonyl group yields the alkoxide intermediate **20**, which eliminates silanol and is converted into an alkene. The formation of a stable Si—O bond is a driving force of this reaction (see Table 1). If the intermediate **20** has an ionic nature (*e.g.*, if the role of a counterion is played by Na$^+$ or K$^+$, or the substituent R^3 represents an anion-stabilising group), silanol is spontaneously eliminated and an alkene is formed.[46,47] If the intermediate **20** has a covalent nature, *i.e.,* the role of a counterion is played by Li$^+$, Mg^{2+} or Al^{3+}, the corresponding β-hydroxy silanes **21** can be isolated.

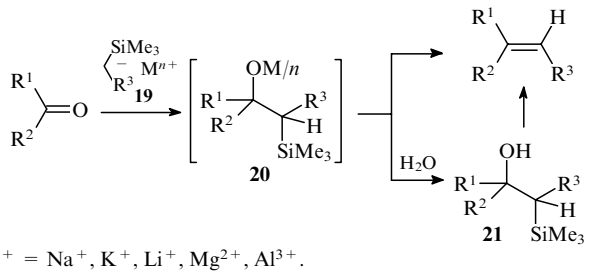

M^{n+} = Na^+, K^+, Li^+, Mg^{2+}, Al^{3+}.

The elimination of silanol from β-hydroxy silanes in the presence of acids or bases occurs according to different mechanisms and yields opposite alkene isomers.[13, 14, 48] Thus treatment of the β-hydroxy silane **22** with boron trifluoride etherate yields an *E*-isomer of oct-4-ene, whereas a *Z*-isomer is formed predominantly in the presence of KH.[48]

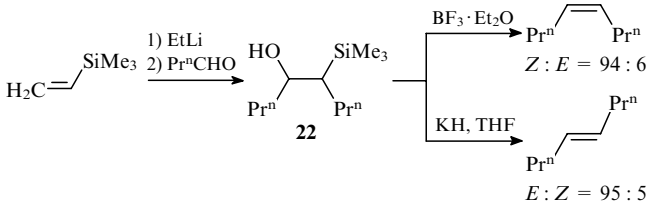

Such a stereoselectivity of the Peterson reaction is due to the fact that elimination of hydroxy- and trialkylsilyl groups in acidic media occurs from the thermodynamically most favourable *anti*-periplanar conformation of the *O*-protonated form of β-hydroxy silane **21**. In the presence of bases, alkenes having opposite geometries are formed from the intermediate siloxetane **23** by *syn*-elimination of silanol. The possibility of control over the geometry of reaction products is a main advantage of the Peterson olefination; however, the formation of β-hydroxy silanes **21** should be put under control in order to achieve stereoselectivity. Otherwise, the diastereomers formed have to be separated.

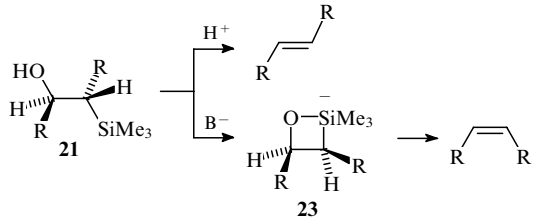

Lithium or magnesium salts of silicon-containing compounds are commonly used as the olefinating agents; however, several modern modifications of the Peterson reaction have been developed on the basis of transition-metal derivatives. In one of them, organometallic compounds **24**, **25** and **26** obtained *in situ* from transition-metal halides ($TiCl_4$, $CrCl_3$) and metallated silane (Me_3SiCH_2MgCl) or germane (Me_3GeCH_2MgCl) are used as the methylenating reagents.[49] Thus, the modified reagent actually represents an α-trimethylsilyl(germyl)-carbanion with a transition metal as a counterion. This family of reagents was used for the conversion of some aliphatic and aromatic aldehydes into terminal alkenes in high yields. Ketones do not enter into this reaction.

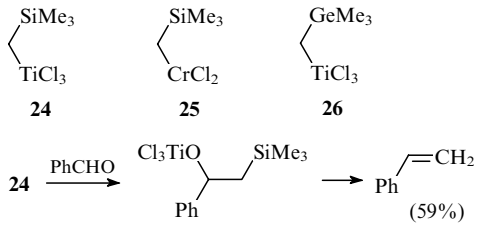

Apparently, the Peterson reaction with the system (trimethylsilyl)methyllithium (**27**) – cerium(III) chloride proceeds in a similar way.[50, 51] This system allows methylenation of a broad range of aldehydes and ketones including easily enolisable ones, since the basicities of organocerium reagents are much lower than that of the lithium derivative. Silanol is eliminated from the intermediate **28** under the action of HF or KF; the yields of the terminal alkenes are usually high (80% – 90%).

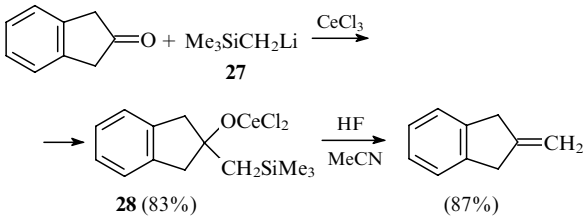

Some methods for the synthesis of various functionalised alkenes are based on the Peterson reaction. Thus a stabilised Peterson reagent, *viz*., ester α-silylenolate **29**, was used for the synthesis of α,β-unsaturated esters.[52] Compound **29** is easily prepared by deprotonation of the corresponding α-silylcarboxylates with strong bases like lithium diisopropylamide.

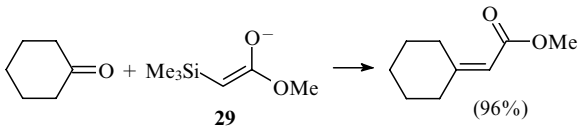

The polyfunctional anion **30** stabilised by trimethylsilyl and cyano groups is used in the synthesis of captodative alkenes of the type **31,** which contain both the donor (dimethylamino group) and acceptor (cyano group) substituents.[53] In the case of aliphatic aldehydes, this reaction occurs with high stereoselectivity and yields predominantly *E*-isomers of alkenes, whereas in the case of aromatic aldehydes and ketones the stereoselectivity of the reaction is lower.

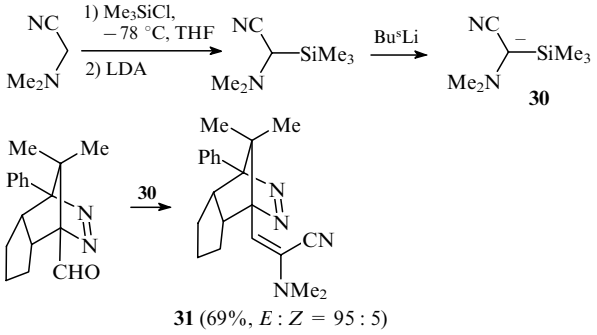

A comparison of the Peterson and the Wittig reactions, on the one hand, and the Peterson and the Horner – Wadsworth – Emmons (HWE) reactions, on the other hand, was carried out using the olefinating agents **32** and **33** stabilised by both silicon and phosphorus atoms. It was found that the reaction with benzophenone yields exclusively phosphorus-containing alkenes **34** and **35**.[12, 54, 55] Thus, the silyl groups are more prone to elimination than the phosphate groups. The vinyltriphenylphosphonium salt **34** can be used in particular in the synthesis of allenes of type **36**.

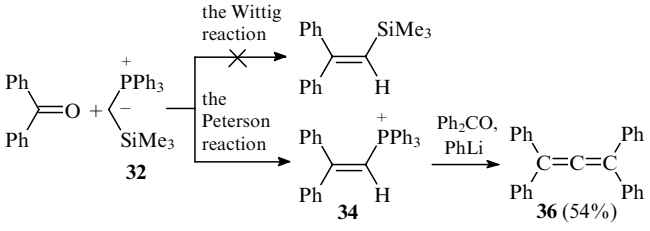

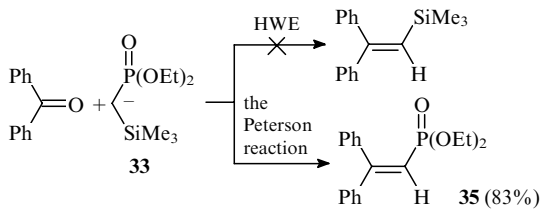

The mixed reagent **38**, which represents a carbanion stabilised simultaneously by sulfur and silicon atoms, was used in the synthesis of vinyl sulfides **37**.[55]

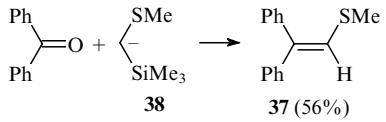

Stereoselective synthesis of unsaturated fluorine-containing sulfones **39** and **40** has been carried out using the organosilicon reagent **41**.[56] The olefination procedures make use of the previously synthesised reagent **41** or that prepared *in situ*.

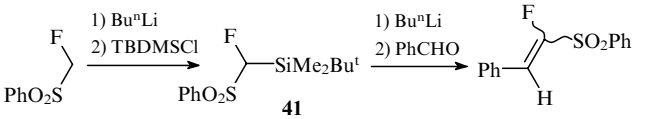

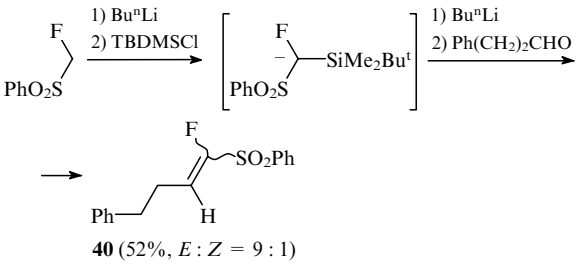

TBDMS is Bu^tMe_2Si.

The lithium salt of formamidine **42** containing a trimethylsilyl group was used in homologisation of carbonyl compounds.[57, 58] The reaction of the salt **42** with carbonyl compounds yields enamines **43** which can be further reduced to saturated amines or converted into the corresponding aldehydes.

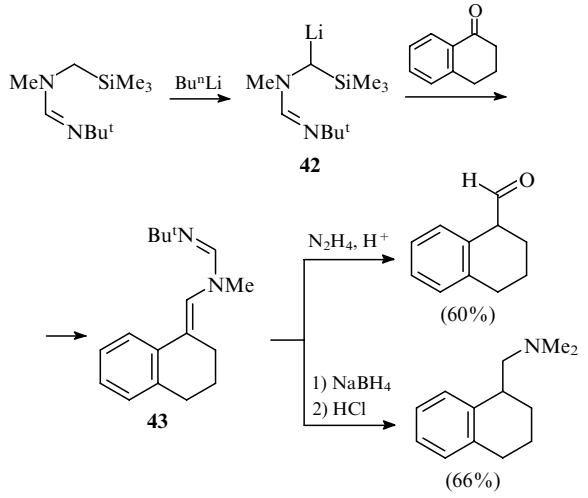

The use of the disilyl derivative **44** for olefination allows the preparation of α,β-unsaturated aldehydes.[59] The reactions with aldehydes yield *E*-isomers.

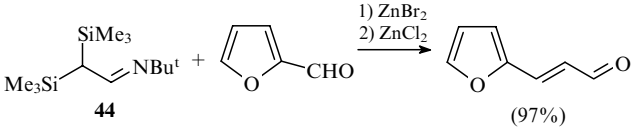

Triphenylsilylacetamides **45** can also be used as the olefinating agents. The reactions with aldehydes afford predominantly *Z*-isomers of the corresponding α,β-unsaturated amides **46**.[60]

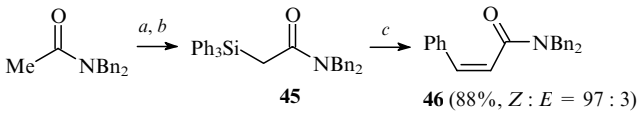

(*a*) LDA; (*b*) Ph_3SiCl; (*c*) PhCHO, KHMDS, THF, −78 °C;
KHMDS is potassium hexamethyldisilazanide.

The reagent **47** synthesised from trimethylsilylacetylene was used for the preparation of selenoamides of substituted cinnamic acids **48**.[61] The reactions of the selenoamide **47** with aromatic aldehydes in the presence of Bu^nLi result in *E*-isomers of unsaturated selenoamides **48**; the yields of the reaction products are virtually quantitative in most cases.

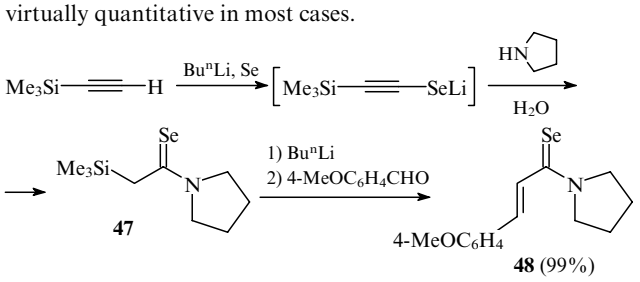

The reactions of aldehydes with α-silylthioacetamide **49** yield unsaturated thioamides **50** (*e.g.*, as 1 : 1 mixtures of isomers).[61]

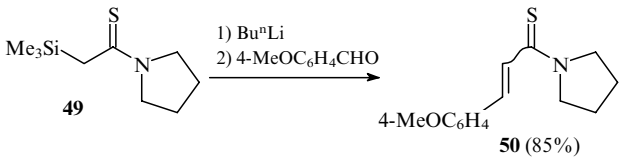

The olefination by *gem*-disilyl reagents **51** derived from imines **52** has been described.[62] This reaction occurs in the presence of tetrabutylammonium fluoride. Substituted benzaldehydes, pivalic and 2-methylcinnamic aldehydes were assayed as candidates for the carbonyl components. The carbanion **53** formed upon cleavage of a trimethylsilyl group under the action of the fluoride ion seems to play the role of an olefinating agent. The corresponding enamides **54** are obtained in good yields; however, the selectivity of the reaction is low.

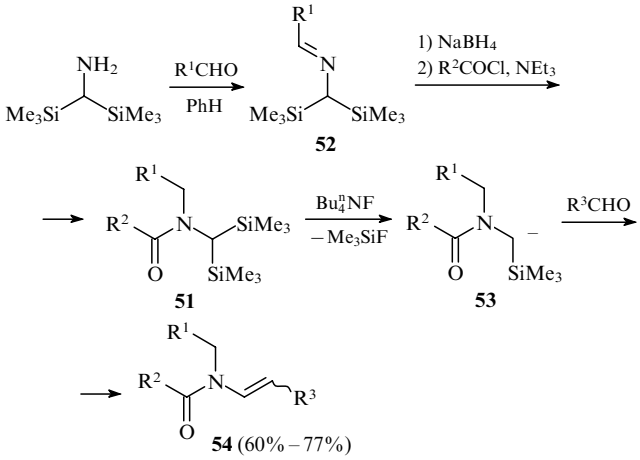

R^1 = Ar; R^2, R^3 = Alk, Ar.

Carbonyl compounds can be transformed into vinylsilanes **55** using *gem*-disilylmethane **56** containing a methoxy group at one of the silicon atoms.[63] Deprotonation of compound **56** and addition of the carbanion to the carbonyl group result in silicon-substituted alkenes. It is only the methoxysilyl group that is eliminated due to coordination of lithium to the oxygen atom in the intermediate.

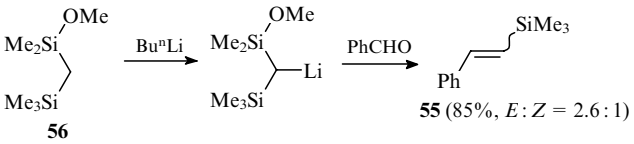

56

55 (85%, $E:Z = 2.6:1$)

b. Germanium-based reagents

An analogue of the Peterson reaction, which makes use of (trimethylgermyl)acetates **57**, has been described.[64] Their deprotonation affords carbanions **58** stabilised by the germanium atom, which add to aldehydes and ketones. Elimination of germanol (thermal or acid-induced) from intermediate diastereomeric β-hydroxy germanes **59** yields *E*-isomers of α,β-unsaturated esters. The reaction occurs with high stereoselectivity; both *threo*- and *erythro*-isomers **59** are converted into *E*-isomers of unsaturated compounds.

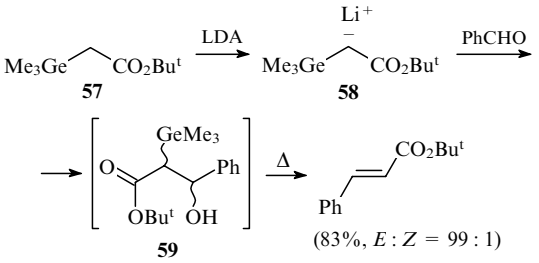

57 **58** **59**

(83%, $E:Z = 99:1$)

c. Tin- and lead-based reagents

A series of olefinating agents have been prepared based on organotin and -lead compounds.[65–76] Metallation of triphenylstannylmethyl iodide leads to triphenylstannylmethyllithium **60**, which adds to aldehydes and ketones to yield 2-triphenylstannylethanols **61**.[65] Subsequent thermal elimination of Ph_3SnOH gives terminal alkenes. This reaction may involve isolation of intermediate compounds **61** or be carried out as a one-pot synthesis. The total yield of alkenes is usually low (18%–62%), but can significantly be increased if the isolation step of intermediate stannyl ethanols **61** is excluded.

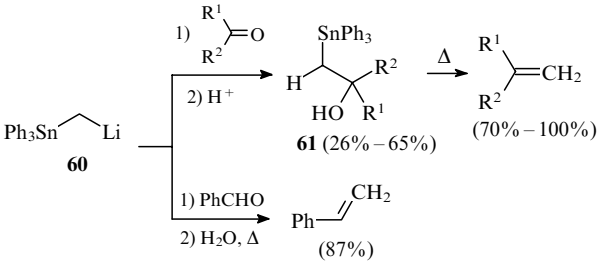

60

61 (26%–65%) (70%–100%)

(87%)

R^1 = Alk, Ar; R^2 = H, Alk.

The anions **62** and **63** stabilised simultaneously by the trimethylstannyl (**62**) or trimethylplumbyl (**63**) and phenylthio groups were used as olefinating agents.[66, 67]

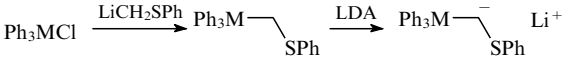

62, **63**

M = Sn (**62**), Pb (**63**).

The reagents **62** and **63** react with benzaldehyde to give diastereomeric pairs of phenylthio(triphenylstannyl)ethanols **64a**,**b** and phenylthio(triphenylplumbyl)ethanols **65a**,**b**. Separation of the diastereomers and subsequent thermal elimination or acid treatment yields *E*- or *Z*-isomers of β-(phenylthio)styrene **66**.

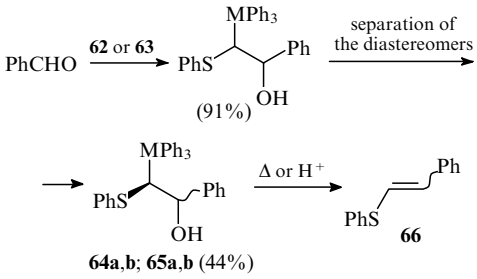

(91%)

64a,**b**; **65a**,**b** (44%) **66**

M	Alcohol	Configuration of **66** [yield (%)]	
		Δ	H^+
Sn	*threo*-**64a**	*E* (93)	*Z* (100)
	erythro-**64b**	*Z* (100)	*E* (95)
Pb	*threo*-**65a**	*E* (87)	*E* + *Z* (67)
	erythro-**65b**	*E* + *Z* (98)	*E* (83)

A method for the conversion of aromatic and aliphatic aldehydes into substituted alkenes by reductive addition of polyhalogeno compounds, such as tetrachloro- or tetrabromomethane, bromotrichloromethane, trichloroacetamide and trichloroacetonitrile, to aldehydes in the presence of a bimetallic system Pb–Al, has been developed.[68] This utilises aluminum foil as a reducing agent and lead halide as a catalyst. It was suggested[68] that the reaction proceeds *via* the organolead compound **67** formed upon oxidative addition of Pb^0 to the polyhalogenoalkane; subsequent reaction of the intermediate **67** with the carbonyl group yields the hydroxy derivatives **68**.

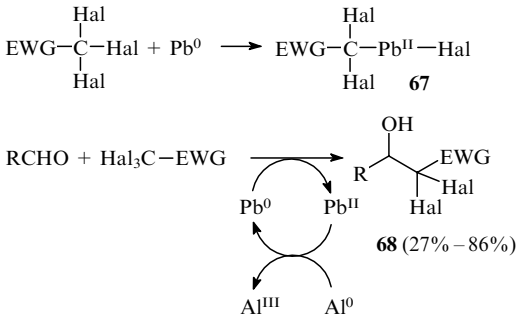

68 (27%–86%)

Hal = Cl, Br; EWG = Cl, Br, CN, $CONH_2$.

Reductive 1,2-elimination of the vicinal chlorine atom and the hydroxy group, which yields alkenes, was studied in the example of alcohols **68** based on CCl_4. The system $PbBr_2$–Al has proved to be an efficient reducing agent.[68]

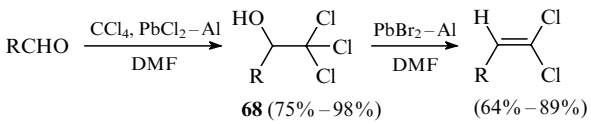

68 (75%–98%) (64%–89%)

3. Reagents based on Group VA elements

a. Carbanions stabilised by the isocyanide group

The isocyanide group can stabilise carbanions in the α-position.[69] The isocyanides **69** generate the carbanions **70** that add to the carbonyl groups of aldehydes and ketones to give the adducts **71**. Subsequent elimination of lithium cyanate, which proceeds *via* the oxazoline carbanion **72**, yields alkenes.

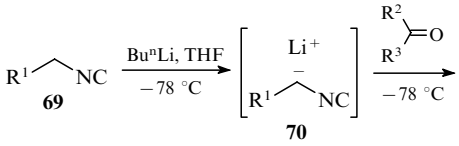

69 **70**

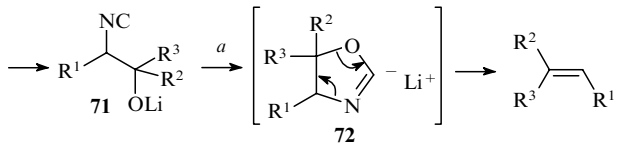

(*a*) from −78 to −20 °C.

This reaction usually proceeds with low yields and is highly sensitive to steric hindrance in both metallated isocyanide and the carbonyl compound. Thus the yield of tetraphenylethylene is much lower than that of styrene.

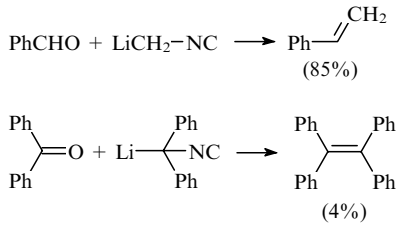

b. The Wittig reaction

A related group of methods is based on the Wittig reaction with phosphorus ylides and its modifications involving phosphonate anions (the Horner–Wadsworth–Emmons modification) or phosphine oxides (the Horner method).[2] The formation of P–O bonds, which proceeds with a considerable gain of energy, is the driving force of these reactions (see Table 1). At present, this methodology is the most general and efficient approach to the synthesis of alkenes. From the moment of its discovery in 1953, the Wittig reaction has been the subject of intense studies; its synthetic applications, the olefination mechanism and effects of various factors on its direction and stereochemistry have been rather extensively studied and are documented in many reviews and monographs.[2,16–21] In addition, the description of the Wittig reaction and its applications have been included in manuals of organic chemistry, therefore, there is no need to dwell upon them. This reaction has been used in the syntheses of numerous compounds including natural products.[70] A great number of publications are devoted to the theoretical studies of the reaction mechanism.[71,72] The Wittig reaction is general and applicable to aldehydes and ketones containing various functional substituents, such as nitro, hydroxy, alkoxy, amino and alkoxycarbonyl groups as well as halogen. The presence of double and triple bonds conjugated with the carbonyl group does not prevent the reaction. Phosphorus ylides (phosphoranes) **73** prepared by the treatment of phosphonium salts **74** with strong bases are used as the olefinating agents in the Wittig reaction; the phosphonium salts **74** are usually synthesised from phosphines and alkyl halides.

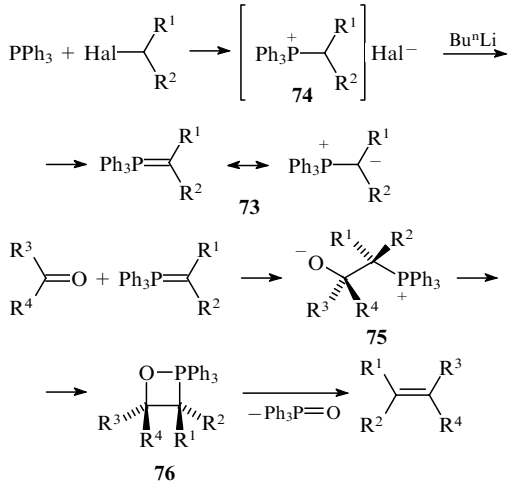

An alternative method for the synthesis of ylides includes reactions of phosphines with carbenes generated *in situ* upon catalytic decomposition of diazoalkanes [the so-called salt-free phosphorus ylides (Section V.3)]. Simple ylides (R^1, R^2 = H or Alk) are highly reactive and react with low active carbonyl substrates, such as ketones and esters, whereas the presence of electron-withdrawing groups (COR, CN, CO_2R, CHO) in the α-position of ylides makes these compounds more stable, but less reactive. It was found that the Wittig reaction proceeds through the formation of betaine **75**, its cyclisation into oxaphosphetane **76** and subsequent elimination of triphenylphosphine oxide.

Special mention should be made of the stereochemical result of the Wittig reaction. The so-called 'non-stabilised' phosphoranes react with aldehydes to yield predominantly (*Z*)-1,2-disubstituted alkenes. This method underlies a basic strategy in the synthesis of such compounds. In contrast, stabilised phosphoranes of the type Ph_3P = CH(EWG) yield *E*-isomers in reactions with aldehydes. These regularities have been reviewed in detail elsewhere.

In this Section, we consider the most recent applications of the Wittig reaction. The allyl vinyl ether **78** is the olefination product of veratric aldehyde with the olefinating agent **77** containing the allyloxy group.[73] Subsequent Claisen rearrangement gives the aldehyde **79**, which is further converted into the alkaloid mesembrine (**80**).

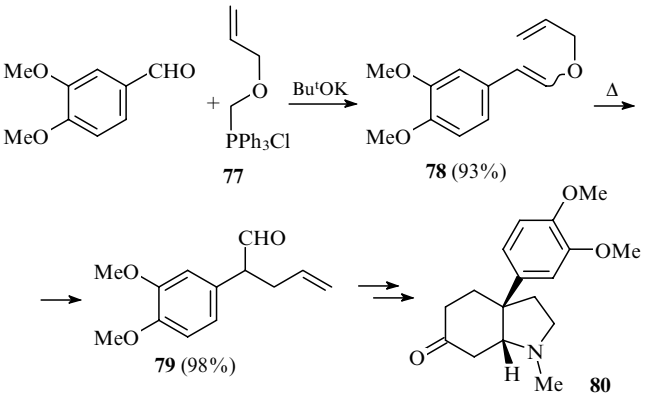

The phosphonium salt **81** was used in the synthesis of non-symmetrical divinyl ethers **82**.[74] The use of an excess base in the Wittig reaction ensures high yields of the target products.

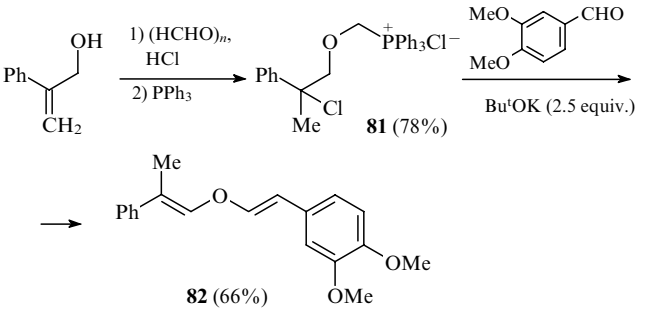

The use of the Wittig reaction in the synthesis of various cyclic systems is a promising methodology. Thus the reaction of the ylide **83** containing an aldehyde group with propiophenone enolate results in annelation and formation of the alcohol **84**, which is further dehydrated to give the substituted naphthalene **85**.[75] Various aromatic and aliphatic aldehydes and ketones were used as the carbonyl components in this reaction.

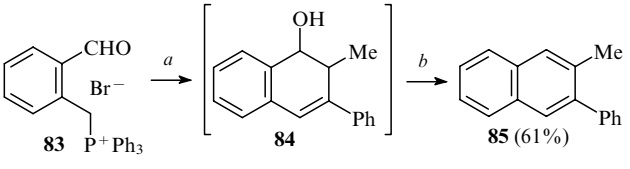

(*a*) PhCOEt, LDA; (*b*) TsOH.

The double Wittig reaction was used in the synthesis of the pheromone **86** (5,9-dimethylpentadecane).[76] The bisphosphonium salt **87** was sequentially introduced into a one-pot reaction with octan-2-one and hexan-2-one. Subsequent hydrogenation of the diene **88** yielded the pheromone **86** in the form of a racemic mixture of diastereomers.

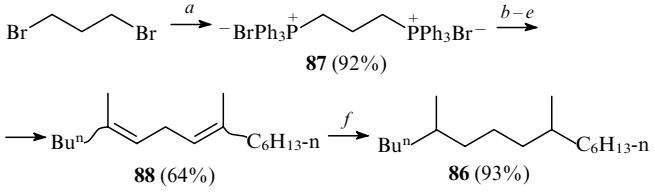

(*a*) PPh_3 (2.1 equiv.), DMF; (*b*) Bu^nLi (1.1 equiv.); (*c*) 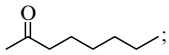 ;
(*d*) Bu^nLi (1.1 equiv.); (*e*) 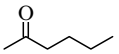 ; (*f*) H_2, Pd/C.

Preparation of aldehydes *in situ* by the oxidation of primary alcohols with *N*-methylmorpholine *N*-oxide in the presence of a catalytic amount of tetrapropylammonium perruthenate is a recent modification of the Wittig reaction.[77] This approach was used in the synthesis of the terminal alkene **89** from the alcohol **90**.

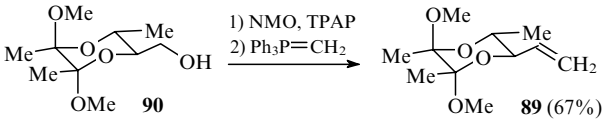

NMO is *N*-methylmorpholine *N*-oxide;
TPAP is tetrapropylammonium perruthenate.

It is not only aldehydes and ketones, but also esters, thiol esters, carboxylic anhydrides, amides and imides that can sometimes be used as substrates in the Wittig reaction.[16] Thus the intramolecular Wittig reaction was used by Woodward for the synthesis of the penicilline derivative **91**.[16,78]

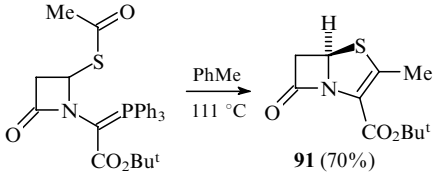

Cyanomethylenetrimethylphosphorane **92** was used in the synthesis of unsaturated nitriles from esters, lactones and imides.[79]

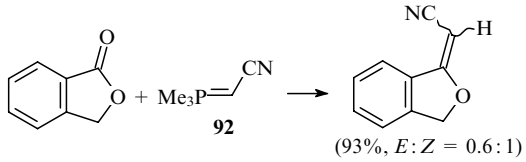

Despite its obvious versatility, the Wittig reaction has one disadvantage, *viz*., the necessity to use stoichiometric amounts of phosphines. Separation of reaction products from phosphine oxides complicates the experimental procedure. Other disadvantages include low stereoselectivity (in the case of allylic and benzylic ylides) and low reactivity of α,β-unsaturated and sterically hindered ketones.[80]

c. The Horner – Wadsworth – Emmons reaction

The Horner – Wadsworth – Emmons reaction (HWE) also known as a phosphonate modification of the Wittig reaction is widely employed in the synthesis of substituted alkenes.[1,2,16,18,22] In this case, the role of the nucleophile is played by the phosphonate anions **93** formed upon deprotonation of phosphonates **94** by strong bases, *e.g*., sodium hydride or potassium *tert*-butoxide. Anions of the type **93** are stronger nucleophiles than phosphorus ylides; therefore, the Horner – Wadsworth – Emmons method is efficient in the synthesis of alkenes from sterically hindered ketones which are not olefinated under the conditions of the classical Wittig reaction.[18] The second reaction product is dialkyl phosphate **95**, which is readily soluble in water; this, in turn, significantly facilitates the isolation of the target alkenes. However, the necessary presence of an anion-stabilising group in the α-position of the phosphonate reagent is a limitation of the method, which significantly narrows the area of its application in comparison with the classical Wittig reaction. Most commonly, the role of the stabilising group is played by the carboxy group; however, aryl or alkenyl groups and even halogens sufficiently stabilise the phosphonate anion.

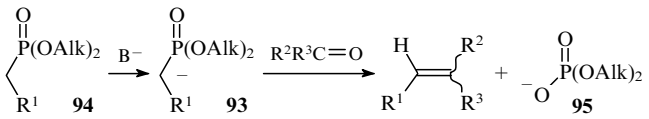

The mechanism of the Horner – Wadsworth – Emmons reaction is similar to that of the Wittig reaction and includes the formation of cyclic oxaphosphetanes. Variation of the olefination conditions and reagents allows one to synthesise *E*- and *Z*-alkenes with a high degree of stereoselectivity. *Z*-Isomers of alkenes are predominantly formed under conditions of kinetic control, *e.g*., at low temperatures, in weakly polar solvents (THF, CH_2Cl_2), under the action of strong bases containing a potassium atom (KHMDS, $KOBu^t$) for deprotonation and in the presence of crown ethers.[81] The use of bis(trifluoroethyl)phosphonates **96** and **97** also favours the formation of alkenes having a *Z*-configuration.

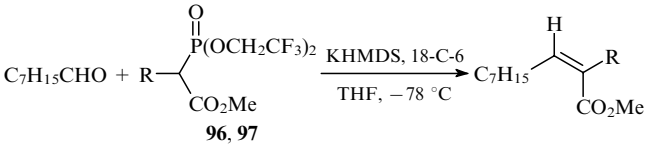

R = H (90%, *Z*:*E* = 12:1); R = Me (88%, *Z*:*E* = 46:1).

The optimum conditions for the synthesis of thermodynamically more stable *E*-isomers of alkenes are as follows: the reaction is to be carried out at 20 °C in polar solvents in the presence of lithium halides, amines are used as bases and phosphonates should contain bulky substituents.[82] Thus the olefination of aldehyde **98** with diethyl phosphonate **99** yields the *E*-isomer of the α,β-unsaturated ester **100**. Treatment of ketones with phosphonate anions under the conditions of the Horner – Wadsworth – Emmons reaction also yields both *E*- and *Z*-alkenes, although with lower stereoselectivity than in the case of aldehydes.

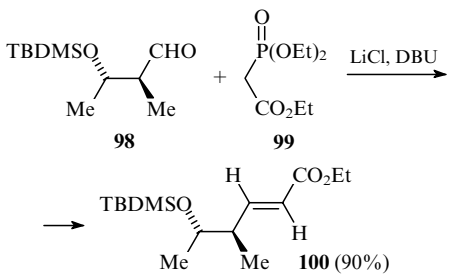

DBU is 1,8-diazabicyclo[5.4.0]undec-7-ene.

Thus by varying the reaction conditions and the structure of the phosphonate fragment, one can effectively control the stereochemistry of the olefination reaction.[83] The olefination of imidazolecarbaldehyde **101** with bis(trifluoroethyl) phosphonate **96** gives the unsaturated ester **102** with *Z*-configuration, whereas diethyl phosphonate **99** yields the *E*-isomer of the ester **103**.

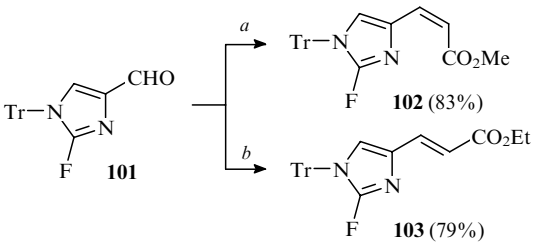

(*a*) $(CF_3CH_2O)_2P(O)CH_2CO_2Me$ (**96**), KHMDS, 18-C-6 (1.5 equiv.);

(*b*) $(Et_2O)_2P(O)CH_2CO_2Et$ (**99**), KHMDS, 18-C-6 (5 equiv.); Tr = Ph_3C.

Synthesis of dienylimidazoles **104** was effected using the reagent **105** containing an imidazole nucleus.[84] Alkenes are formed stereospecifically and the configuration of the newly formed double bond of diene **104** was *E*.

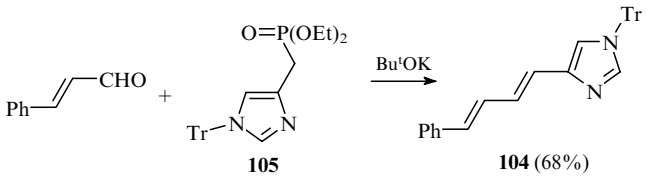

The use of potassium carbonate[85] or lithium hydroxide as promoters is a convenient modification of the Horner–Wadsworth–Emmons reaction.[86] Thus the addition of LiOH increases the stereoselectivity and prevents side reactions in the synthesis of unsaturated esters and nitriles.[86] This approach was used in the stereospecific synthesis of unsaturated nitriles **106**, where diethylphosphonoacetonitrile (**107**) was used as the olefinating agent. High stereoselectivity of this reaction is due to coordination of lithium in the transition state to the hydroxy group in the α-position of the substrate.

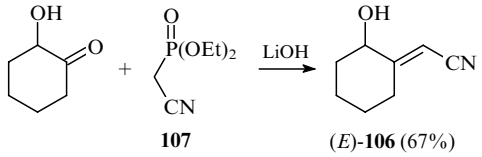

The reaction of benzaldehyde with methylenedi(phosphonate) **108** was used in the synthesis of allenes from carbonyl compounds.[87] The reaction of compound **108** with aldehydes gave the corresponding alkenylphosphonates **109**. Their subsequent treatment with LDA and the addition of the second carbonyl compound afford hydroxyalkenylphosphonates **110**, which can be converted into allenes **111** by treatment with potassium hydride.

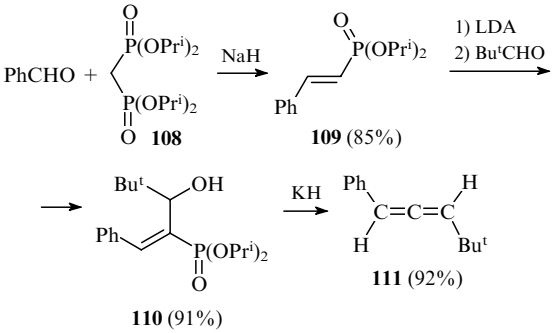

d. The Horner–Wittig reaction

The use of the reaction of phosphine oxides **112** with aldehydes in the presence of potassium *tert*-butoxide or sodium amide for the synthesis of alkenes was recommended by Horner.[2, 18, 88] In this case, the role of the olefinating agent is played by the phosphine oxide anion generated upon deprotonation of compound **112**. Its addition to the carbonyl group yields β-hydroxy phosphineoxide, which undergoes further *syn*-elimination of the anion $Ph_2PO_2^-$.

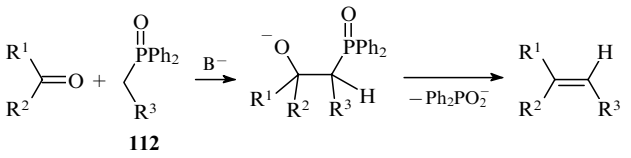

The corresponding phosphine oxides **112** can be prepared by thermal decomposition of alkyltriphenylphosphonium hydroxides **113**.[18]

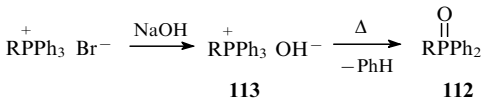

If sodium or potassium bases are used in the Horner–Wittig reactions, the elimination of $Ph_2PO_2^-$ from hydroxy phosphine oxide occurs *in situ*, whereas in the case of lithium bases β-hydroxy phosphine oxides can be isolated.[89] Upon subsequent treatment with other bases (NaH, KOH, $KOBu^t$), β-hydroxy phosphine oxides undergo *syn*-elimination resulting in alkenes, *Z*-isomers from the *erythro*-adducts and the corresponding *E*-isomers from the *threo*-adducts. Similar transformations were described for the adducts **114**.[89]

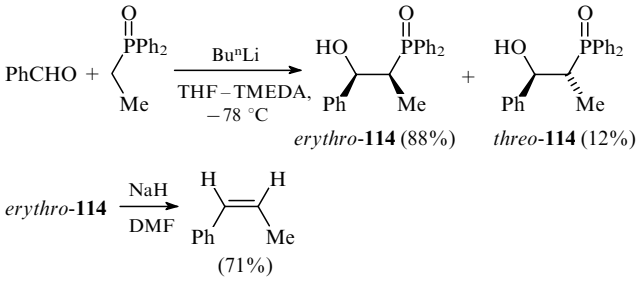

TMEDA is *N,N,N′,N′*-tetramethylethylenediamine.

The ratio of diastereomers of β-hydroxy phosphine oxides **114** can be changed by varying the nature of the solvent, the base and the reaction temperature.[89] In weakly polar solvents (THF, ether), *erythro*-diastereomers are formed predominantly at low temperatures (−78 °C) and in the presence of the system Bu^nLi–TMEDA, while mixtures of isomeric β-hydroxy phosphine oxides are usually formed at elevated temperatures and in more polar solvents. β-Hydroxy phosphine oxides enriched in the *threo*-stereomer are formed upon reduction of the corresponding β-oxophosphine oxides with sodium borohydride.[90]

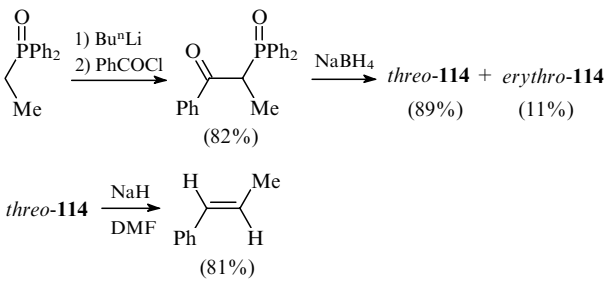

e. Arsenic-based reagents

Carbanions stabilised by arsenic and antimony are less commonly used in olefination reactions in comparison with their phosphorus analogues. Arsenic and antimony ylides containing electron-withdrawing groups are more reactive than the corresponding phosphoranes. Their reactions with aldehydes were used for the development of effective methods for the synthesis of some substituted alkenes the preparation of which by the Wittig reaction is either difficult or impossible. The properties and

applications of arsenic ylides (arsoranes) are described in a review.[91] The corresponding ylides are formed upon alkylation of triphenylarsine and subsequent deprotonation of the resulting arsonium salts. As a rule, olefination with arsenic ylides occurs stereospecifically. Arsenic ylides react with carbonyl compounds to give both alkenes and epoxides (this reaction route is more typical of sulfur ylides). Presumably, this is due to a lower affinity of arsenic for oxygen in comparison with phosphorus (see Table 1). Thus the reaction of arsorane **115** with 4-nitrobenzaldehyde yields a mixture of stilbene **116** and epoxide **117**.

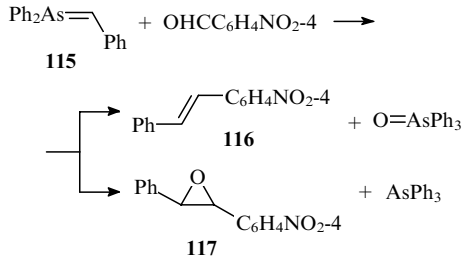

Ylides stabilised by electron-withdrawing groups manifest higher proneness for olefination, whereas more reactive ylides react with the predominant formation of epoxides.[91] Thus the ylide **118** derived from the ethyl 4-bromocrotonate **119** is used in the stereoselective synthesis of alka-2,4-dienoates **120** and 2,4,6-trienoates **121**.[92]

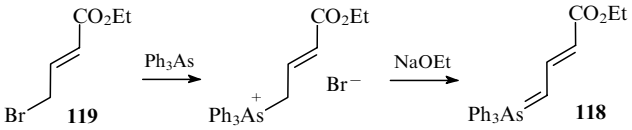

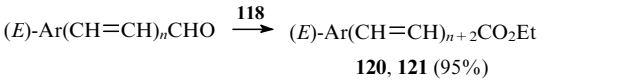

Ar = 4-ClC$_6$H$_4$, n = 0 (**120**); Ar = Ph, n = 1 (**121**).

Arsenic ylide **122**, the reaction product of triphenylarsine and bromoacetaldehyde **123**, reacts with phthalic aldehyde in the presence of potassium carbonate, to give the α,β-unsaturated aldehydes **124** in high yields; the nature of the carbonyl components can be varied over a broad range. This reaction is stereoselective; the ratio of the *E*- and *Z*-isomers of the target alkenes is no less than 97 : 3.[93]

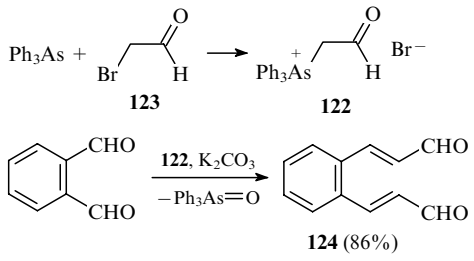

Arsenic ylide **125** generated from 4-chlorobenzyl bromide **126** was used in the stereoselective synthesis of *trans*-isomers of nonsymmetrical stilbenes [94] from diverse aromatic aldehydes containing both donor and acceptor substituents in the aromatic nucleus. The yields vary from 40% to 80%; it is the corresponding *trans*-stilbenes that were obtained in all cases.

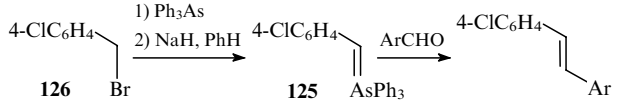

Ar = Ph, 3-NO$_2$C$_6$H$_4$, 4-NO$_2$C$_6$H$_4$, 4-MeC$_6$H$_4$, 4-MeOC$_6$H$_4$, 4-ClC$_6$H$_4$, 4-Me$_2$NC$_6$H$_4$, 3,4-(MeO)$_2$C$_6$H$_3$, 3,4-(MeO)$_2$-6-BrC$_6$H$_2$, 2-furyl.

(Pentafluorophenylmethylene)triphenylarsorane **127** obtained *in situ* by a reaction of methylenetriphenylarsorane **128** with hexafluorobenzene **129** gives stereospecifically non-symmetrical *E*-stilbenes **130** containing a perfluorophenyl substituent.[95]

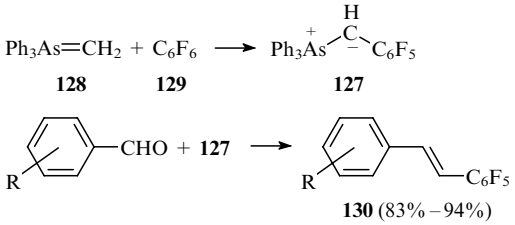

130 (83% – 94%)

f. Antimony-based reagents

The use of the system tributylstibine – ethyl bromoacetate as an olefinating agent allows transformation of some aromatic and aliphatic aldehydes and ketones into α,β-unsaturated esters.[96] A significant advantage of this method is the possibility to conduct the reaction in the absence of strong bases. A mixture of stibine **131** and ethyl bromoacetate (**132**) plays the role of an olefinating agent. Unfortunately, the mechanism of this reaction has not been reported, [96] but it is assumed that it resembles that of the Wittig reaction and involves the formation of antimony ylide **133**.

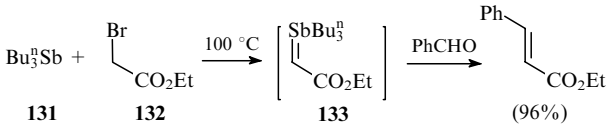

The reaction of antimony ylides **134** prepared by the copper(I) iodide-catalysed decomposition of α-diazo-β-dicarbonyl compounds with aromatic and aliphatic aldehydes and ketones yields α,β-unsaturated esters and ketones. As regards its outcome, this reaction is similar to the Knoevenagel reaction. In most cases, the yields are nearly quantitative. Studies of a relationship between the oxidation state of copper and the nature of the catalyst counterion and the yields of the target products revealed that copper(I) halides are the catalysts of choice.[97] Triphenylstibine should be used in equimolar amounts, and triphenylstibine oxide is formed as a second reaction product. A salient advantage of this method is that the ylide does not require strong bases for its generation. The use of derivatives of other Group VA elements (Ph_3As, Ph_3Bi) in this reaction is less efficient, whereas in the case of triphenylphosphine the target product is not formed at all. These results are different from the literature data on the olefination of carbonyl compounds by diazoalkanes in the presence of triphenylphosphine catalysed by such metals as rhodium and ruthenium (see Section V.3).

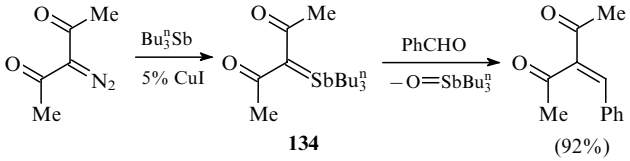

An alternative approach to the synthesis of antimony ylides **135** includes a reaction of tributylstibine **131** with *gem*-dibromomalonates **136**.[98] The quarternary antimonium salts **137** formed react with the second equivalent of stibine to yield stiboranes **135**. The latter play the role of olefinating agents which can be introduced into reactions with aliphatic ketones.

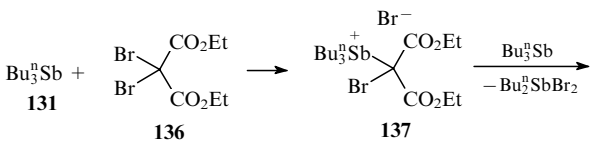

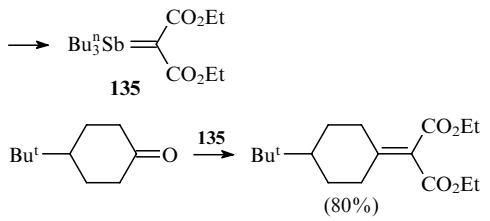

4. Reagents based on Group VIA elements

The olefination reactions considered in this Section include the addition, to the carbonyl group, of carbanions stabilised by a sulfo- or a sulfoximino group in the α-position as well as by selenium and tellurium.

a. The Julia reaction

The Julia reaction (also referred to as the Julia – Lythgoe reaction in the English-language literature) consists of the generation of carbanions **138** upon deprotonation of sulfones **139** by strong bases.[1, 2, 99–101] Subsequent addition of the anion **138** to the carbonyl group yields a mixture of diastereomeric β-hydroxy sulfones **140**. The reaction is accelerated in the presence of Lewis acids, such as boron trifluoride etherate[102] and magnesium bromide.[103] Then, the hydroxy group of β-hydroxy sulfones **140** is converted into a good leaving group (acetate, benzoate, *p*-toluenesulfonate); subsequent reduction of α-acyloxy sulfones **141** with sodium amalgam in methanol gives alkenes.[23]

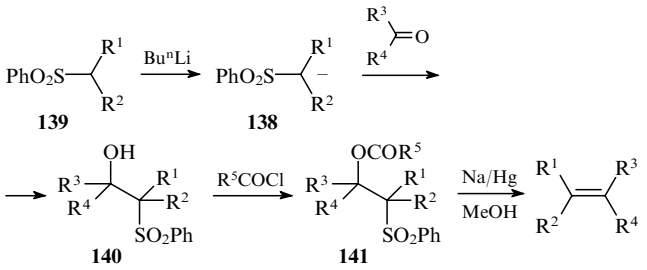

Sometimes, the modification step of the hydroxy group is omitted and β-hydroxy sulfones **140** are subjected to reductive elimination.[102] Thus the reduction of the adduct **142** with sodium amalgam gives the alkene **143** in high yield.

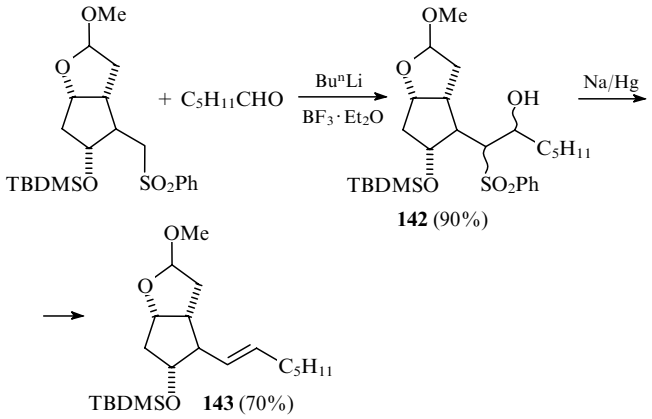

Reductive elimination occurs with high stereoselectivity: 1,2-disubstituted alkenes are formed exclusively as *E*-isomers.[2] It was shown that the geometry of the resulting alkene does not depend on the stereochemistry of the intermediate β-hydroxy sulfone; diastereomeric *erythro*- and *threo*-acetoxysulfones **144** are converted into the same *trans*-alkene,[104] which is one of the main advantages of the Julia reaction. High *E*-selectivity is explained by the fact that the intermediate anion **145** formed in the reductive elimination step has time to acquire a thermodynamically more favourable *trans*-configuration prior to the elimination of the acetate ion.

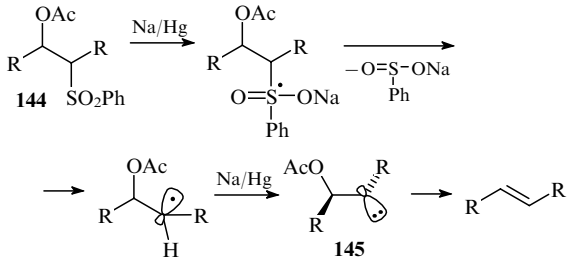

An alternative mechanism of reductive elimination includes preliminary formation of vinyl sulfones **146** and their subsequent reduction first to the vinyl radicals **147** and then to alkenes.[105]

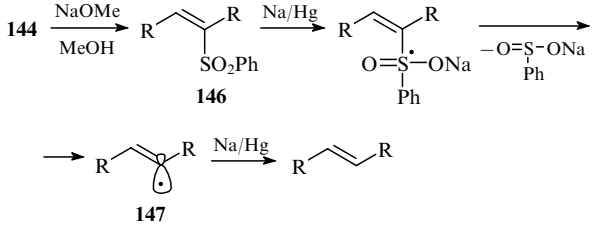

Toxic sodium amalgam can be replaced by other reducing reagents, such as magnesium or samarium iodide (the latter is generated *in situ* from samarium and iodine).[2, 105] In the latter case, β-acetoxy sulfone **148** is converted into vinyl sulfone **149** and then reduced with samarium iodide. Such a reduction usually occurs with high yields (69% – 95%) and high stereoselectivity and affords 1,2-disubstituted alkenes; however, the necessity to use nine equivalents of samarium iodide makes this method extremely expensive.

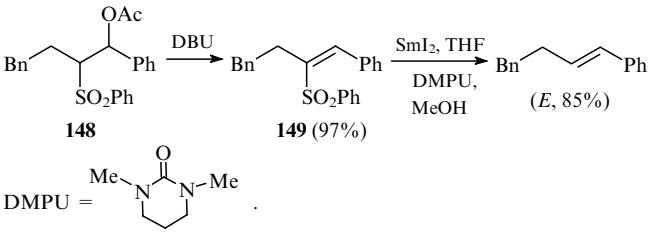

The Julia method is a convenient tool for the synthesis of alkenes; however, its main disadvantage is its multistep character. In addition, the synthesis of tri- and tetra-substituted alkenes proceeds in low yields. The use of disubstituted sulfones and aldehydes (rather than monosubstituted sulfones and ketones) is more preferable for the preparation of trisubstituted alkenes[1] due to reversibility of the reaction of a sulfone-derived anion with a ketone.[106, 107] A modified one-pot procedure, which includes acylation or silylation of β-hydroxy sulfones and reduction of the intermediates **150** and **151** with samarium iodide, allows the involvement of ketones into the reaction.[106, 107] However, the stereoselectivity of formation of trisubstituted alkenes is usually low; the *E* : *Z* ratio is ~2 : 1.

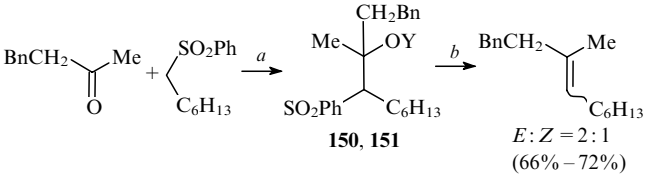

150: Y = Me_3Si (69%); **151**: Y = Bz (85%);
(*a*) 1) Bu^nLi, 2) Me_3SiCl or PhCOCl; (*b*) SmI_2, THF, HMPA;
HMPA is hexamethylphosphoramide.

This approach was used in the synthesis of the diene **152**, which contains a benzyloxy group at the terminal atom of the diene system.[107] Dienes like compound **152** are promising substrates for the Diels–Alder reaction.

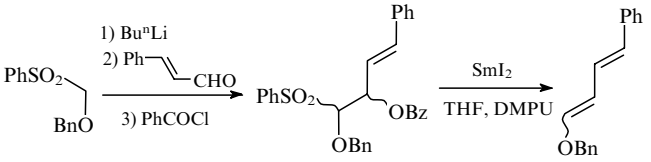

152 (82%, $E,E:E,Z = 1.7:1$)

The modification of the Julia reaction based on the use of benzothiazol-2-yl sulfones **153** as olefinating agents, has been named the Julia–Kocienski reaction. Upon addition of anions **154** to aldehydes, the adducts **155** are formed which undergo elimination of SO_2 resulting in the *trans*-isomers of 1,2-disubstituted alkenes and a lithium salt of 1,3-benzothiazol-2-one **156** as a side product.[108] The use of heteroaryl sulfones allows one to exclude the reductive elimination step.

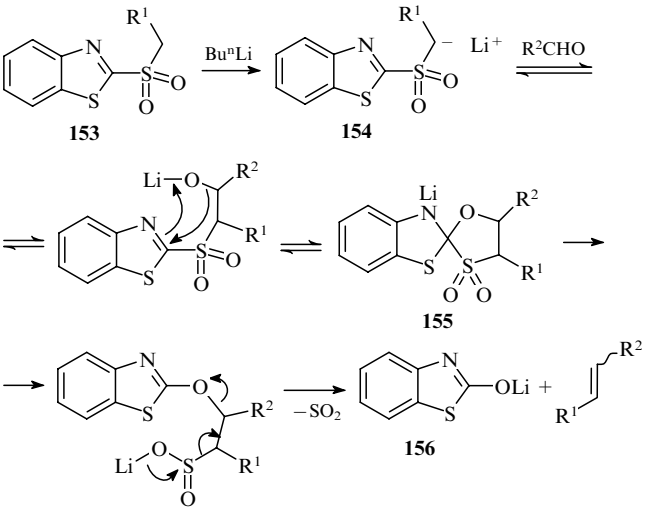

In a more recent study,[109] Kocienski suggested the use of sulfones **157** containing a phenyltetrazole system. These sulfones are more stable; the stereoselectivity of the reaction and the yields of the alkenes are higher than in the case of reagents containing a benzothiazole substituent.[109]

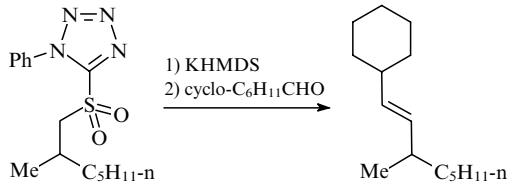

157 (59%, $E:Z = 99:1$)

Analogous reagents **158** and **159** contain a 1-*tert*-butyl-1*H*-tetrazol-5-yl system; the carbanion formed is additionally stabilised by a phenyl or vinyl group.[110] With these reagents, the yields of 1,2-disubstituted alkenes are higher than in the case of the reagent **157**; the formation of alkenes **160** and **161** proceeds with high *Z*-stereoselectivity.

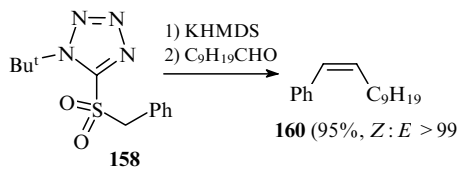

158

160 (95%, $Z:E > 99:1$)

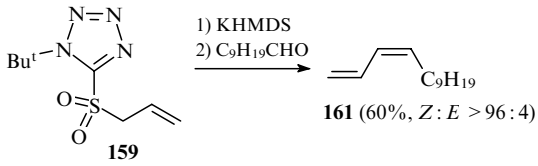

159

161 (60%, $Z:E > 96:4$)

The condensation of 2-pyridylsulfone **162** with α,β-unsaturated aldehydes occurs with predominant formation of *E,Z*-isomers of dienes. Compound **163** was obtained in 64% yield.[111]

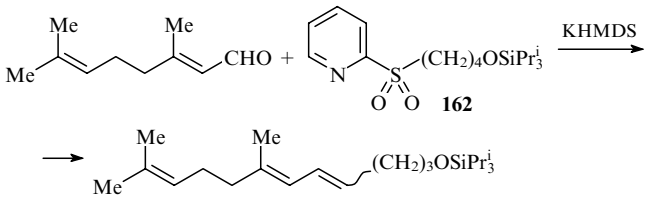

163 (64%; $E,Z:E,E = 88:12$)

β-Alkoxy sulfones **164a–c** can be used in the synthesis of enol ethers from aldehydes and ketones by the Julia–Kocienski reaction.[112] The formation of the ethers **165** occurs with low stereoselectivity, albeit in good yields.

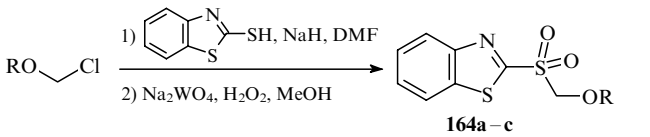

164a–c

R = Bn (**a**, 68%); 4-ClC_6H_4 (**b**, 80%); $MeOCH_2CH_2$ (**c**, 75%).

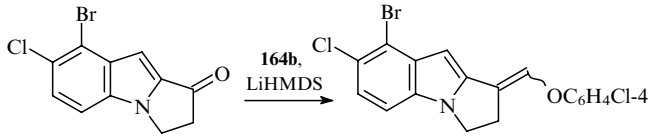

165 (85%, $E:Z = 74:26$)

LiHMDS is lithium hexamethyldisilazanide.

The sulfone **166** containing an electron-deficient arene fragment was used in yet another modification of the Julia–Kocienski reaction.[113] The addition of a carbanion generated from compound **166** to aldehydes and subsequent β-elimination of 3,5-bis(trifluoromethyl)phenoxide from the adduct **167** upon treatment with a base with concomitant liberation of SO_2 afford alkenes in high yields and with high *E*-stereoselectivities.

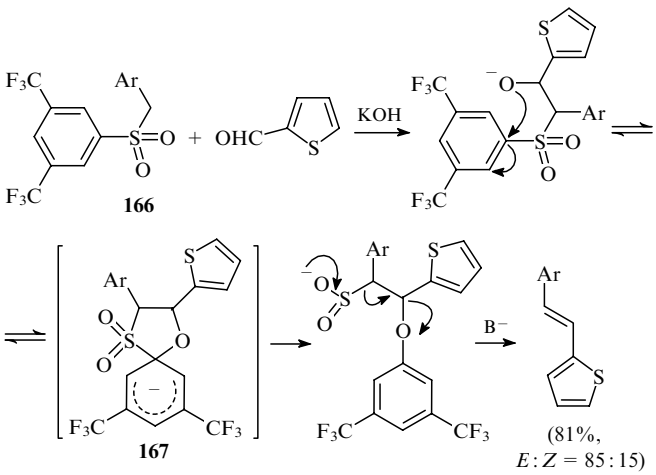

Ar = 3,5-$(MeO)_2C_6H_3$.

The Julia reaction can be used in the synthesis of conjugated polyenes from carbonyl compounds. Thus compound **168** prepared from hexylphenyl sulfone and the corresponding aldehyde was treated with a strong base, such as potassium *tert*-butoxide.[114]

The first step includes elimination of acetic acid and formation of the vinylic sulfone **169** which is rearranged into the allylic sulfone **170**. The latter undergoes 1,4-elimination to give a diene **171** (usually, with *E*,*E*-configuration).[115, 116] The intermediate vinylic sulfone **169** can be isolated upon treatment of **168** with an equimolar amount of a base. Subsequent cleavage of the sulfone requires a fourfold excess of potassium *tert*-butoxide and heating.

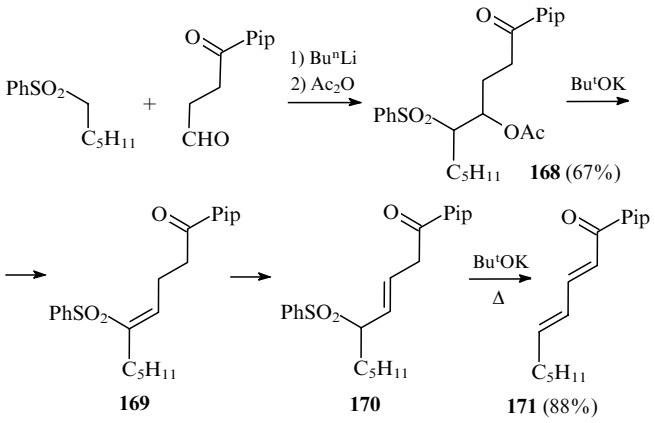

PiP is piperidin-1-yl.

The Julia method was used in the synthesis of many natural compounds including muscone and some retinoids.[2, 101, 117] Thus synthesis of retinol **172** involved the addition of β-cyclogeranyl sulfone **173** to the aldehyde **174**. The resulting β-hydroxy sulfone **175** was protected with a tetrahydropyranyl group; the product **176** was treated with potassium *tert*-butoxide. Subsequent elimination of the protected hydroxy group and the sulfone with concomitant rearrangement of multiple bonds yields the target compound **172** in which all the double bonds have a *trans*-configuration.

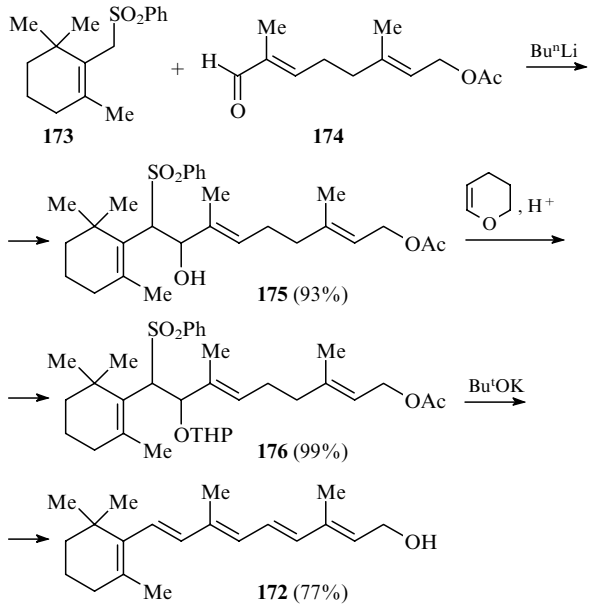

THP is tetrahydropyran-2-yl.

If the shift of double bonds in vinylic sulfones, *e.g.*, in compound **177**, is impossible, subsequent elimination yields acetylene **178**.[115]

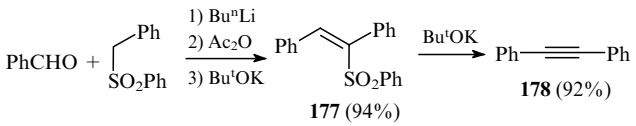

The addition of sulfones to dialdehydes allows one to synthesise non-symmetrical polyacetylenes.[118] Thus consecutive addition of two different sulfones (**179** and **180**) to the carbonyl groups of the dialdehyde **181** and elimination of the sulfonyl groups yield diacetylene **182** with different substituents.

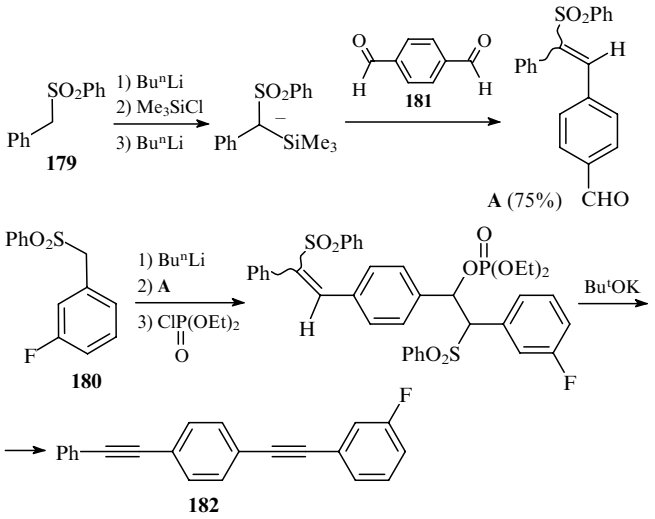

Benzyl phenyl sulfone α,α-dilithium derivative **183**, which is easily prepared by the double metallation of benzyl phenyl sulfone **184**, can be converted into an organodimagnesium compound **185** *in situ* using lithium – magnesium exchange upon treatment with magnesium iodide. The dimetallated sulfone **185** is a convenient olefinating agent, which reacts with aliphatic, aromatic and unsaturated aldehydes or ketones to give α,β-unsaturated sulfones **186** in good yields.[119] The sulfonyl group is removed using aluminium amalgam or the system $LiAlH_4 - CuCl_2$.[120] Unfortunately, in the majority of cases this reaction occurs non-stereoselectively and yields first a mixture of *E*- and *Z*-isomers of sulfones and then a mixture of the corresponding alkenes. The desulfonylation occurs in good yields (40% – 90%). Thus *trans*-stilbene is formed in 90% yield from the *Z*-sulfone **187**.[120]

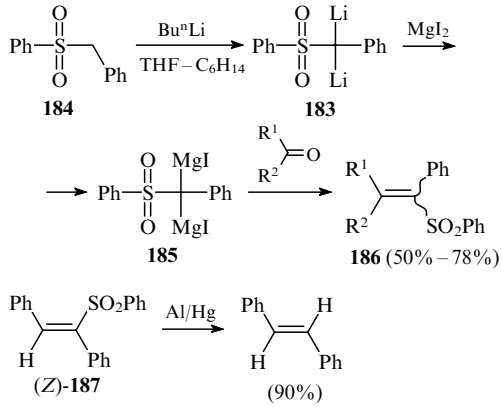

A sulfoxide modification of the Julia-type olefination reaction has been developed.[121, 122] In the case of sulfoxides **188,** the acidity of α-hydrogen atoms is lower than that of sulfones; this makes the corresponding carbanions more reactive as a result of which even ketones can be used as the carbonyl components in this reaction. Mesylation of the intermediate β-hydroxy sulfoxides **189** and reduction of the intermediates **190** by Grignard reagents or *tert*-butyllithium result in alkenes. In the case of an aliphatic substrate (*e.g.*, 3-phenylpropanal), the stereoselectivity of the reaction with all arylmethyl phenyl sulfoxides studied was low.

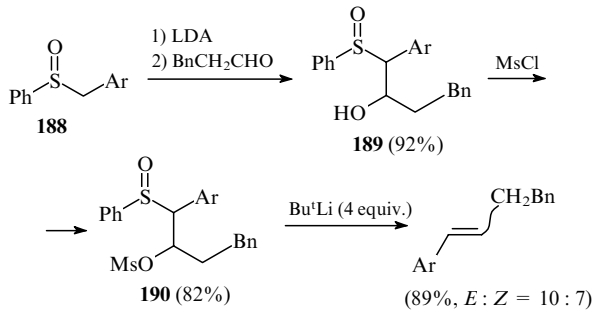

Ms = $MeSO_2$.

On going to aromatic aldehydes, non-symmetrical stilbenes are formed in this reaction exclusively as *trans*-isomers.[122] For example, the addition of sulfoxide **191** to 1-naphthaldehyde and mesylation of β-hydroxy sulfoxide **192** result in spontaneous elimination and formation of the *trans*-alkene **193**.

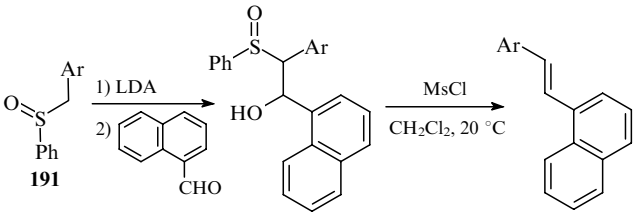

Ar = 4-$MeOC_6H_4$.

A recent modification of the Julia reaction consists of solid-phase synthesis.[123] A polymer containing pendent benzenethiol units is converted into the olefinating agent **194** by sequential *S*-alkylation and oxidation of the sulfide. Subsequent deprotonation and addition of anisaldehyde followed by benzoylation of the resulting β-hydroxy sulfone and reduction of compound **195** with samarium iodide yield the alkene **196** in 27% yield (starting from benzenethiol). The stereoselectivity of this reaction depends on the type of the acylating reagent (Ac_2O or PhCOCl) and the solvent used for reductive elimination.

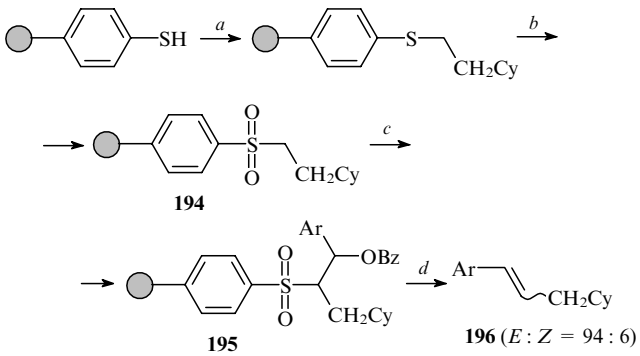

(*a*) 1) Bu^{t}OK (12 equiv.), 2) $CyCH_2CH_2OTs$ (2 equiv.), THF – DMSO (2 : 1), 20 °C; (*b*) *m*-CPBA (4 equiv.), CH_2Cl_2, 20 °C; (*c*) 1) Bu^{n}Li, 2) ArCHO, 3) PhCOCl; (*d*) SmI_2 (7 equiv.), THF, DMPU, 20 °C; Ar = 4-$MeOC_6H_4$; *m*-CPBA is *m*-chloroperbenzoic acid;

— polymeric support.

b. The Johnson reaction

In 1973, Johnson proposed to use sulfoximine **197** for methylenation of carbonyl compounds.[124, 125] The carbanion **198** prepared by deprotonation of the imine **197** with n-butyllithium appeared to be a strong C-nucleophile. Its addition to the carbonyl group of ketones yields β-hydroxy sulfoximine **199** which is further reduced with aluminium amalgam to the corresponding terminal alkene. The starting sulfoximine **197** can easily be prepared from methyl-phenyl sulfoxide.[124] The reaction can be carried out in a one-pot manner, without isolation of the intermediate **199**.[124] The Johnson reaction proved to be effective in the synthesis of terminal alkenes from both ketones and aldehydes. The carbanion **198** was found to be more nucleophilic than methylene triphenylphosphorane, this can be used in the synthesis of alkenes that cannot be prepared by the Wittig reaction.[2, 126]

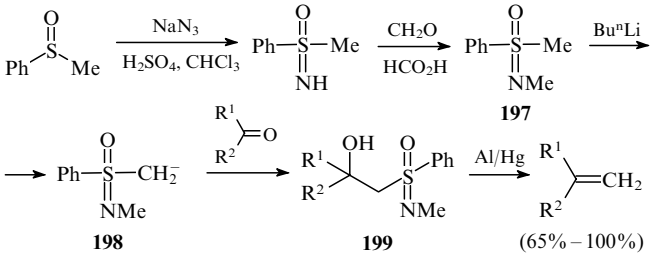

R^1 = Alk, Ar; R^2 = H, Alk.

The use of higher homologues of sulfoximines, *e.g.*, compound **200**, in reactions with aldehydes and ketones allows one to synthesise non-terminal alkenes; however, in this case the reaction occurs with low stereoselectivity.[125]

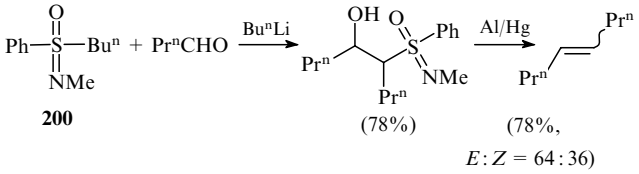

α-Fluoromethyl sulfoximine **201** was recommended as a convenient fluoromethyenating agent.[127] It was employed in the synthesis of a series of vinyl fluorides from aromatic and aliphatic aldehydes and ketones. This reaction is non-stereoselective and yields a mixture of alkene isomers in a 1 : 1 ratio.

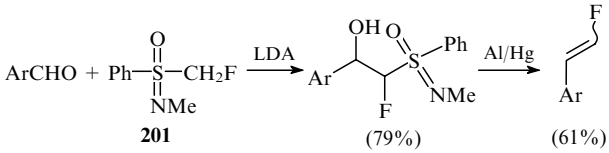

Ar = 4-$MeOC_6H_4$.

It should be noted that the Johnson reagent (sulfoximine **197**) contains an asymmetrical sulfur atom. The reaction of an individual *S*-enantiomer of the carbanion **198** with a racemic mixture of the ketone **202** (**202a**, **202b**), chromatographic separation of the intermediate diastereomeric β-hydroxy sulfoximines **203a**,**b** and subsequent reductive elimination of sulfoximine resulted in the alkene enantiomers **204a**,**b** in the optically pure state.[128]

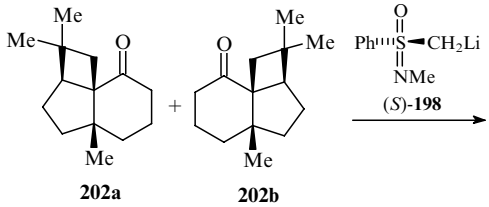

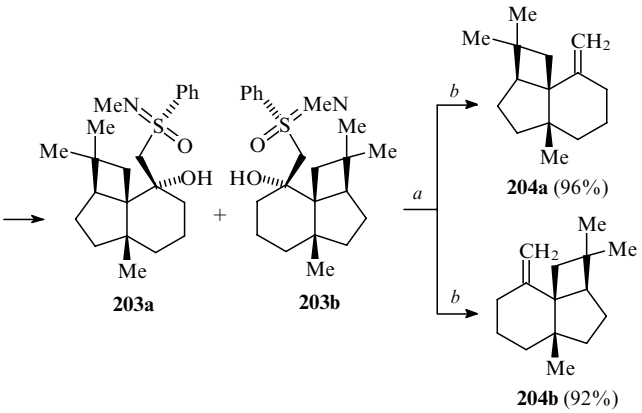

(*a*) separation of diastereomers; (*b*) Al/Hg.

c. Other sulfur-containing reagents

The carbanion **206** generated from thioanisole (**205**) adds to the carbonyl group of aliphatic and aromatic ketones to give β-phenylthioethanol **207**.[129] Benzoylation of the hydroxy group and subsequent reductive elimination of the ester and phenylthio groups yield terminal alkenes. Lithium in liquid ammonia,[129] the system $TiCl_4-Zn$ [2] or metallic titanium are used as the reducing agents.[130] Cage ketones can also be employed as the carbonyl components.[129]

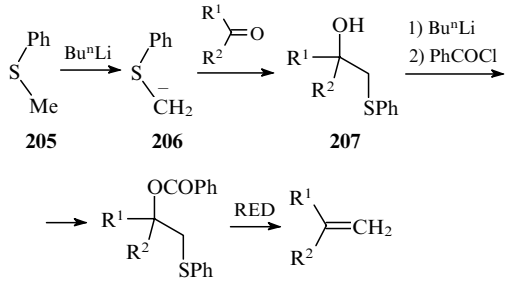

R^1, R^2 = Alk, Ar.

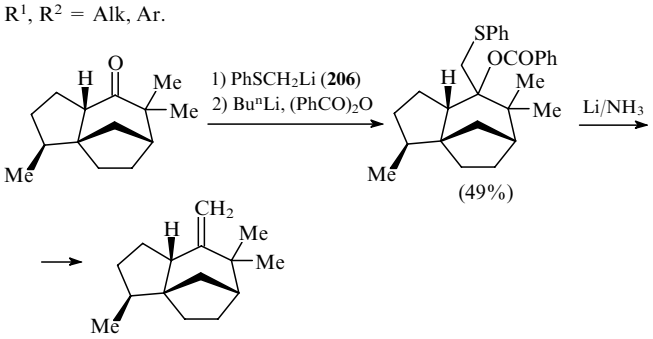

In the synthesis of thioaurones, *e.g.*, 2-(arylmethylidene)benzothiophen-3-ones **208**, 2-methylthiobenzoic acid or its methyl ester **209** were used as the olefinating agents.[131] This reaction is accompanied by anionic intramolecular cyclisation of the ester **209**, which yields the intermediate **210**; subsequent addition of the latter to the carbonyl group gives the alkene **208**. It should be noted that this reaction occurs stereospecifically and yields exclusively the *Z*-isomer of the alkene **208**. Other aliphatic and aromatic aldehydes can also enter into this reaction.[131]

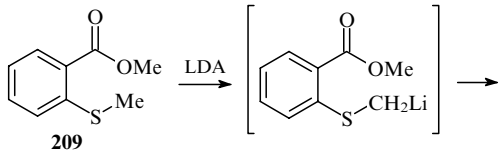

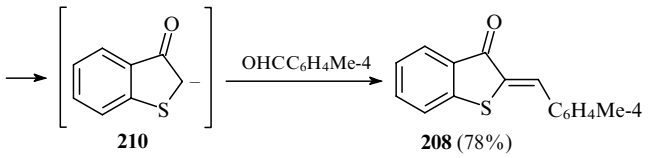

d. The Krief–Reich reaction

The olefination of carbonyl compounds by carbanions stabilised by selenium atoms is referred to as the Krief–Reich reaction.[2, 24, 132–134] The addition of carbanions prepared by deprotonation of alkyl aryl selenides **211** (see Ref. 3) or treatment of diselenoacetals with butyllithium,[135] to the carbonyl group results in β-hydroxy selenides **212**, which can further be converted into various products. In particular, alkenes are prepared by elimination of the hydroxy and selenyl fragments using methanesulfonyl chloride, $SOCl_2$ [134] or PI_3 in the presence of triethylamine.[135]

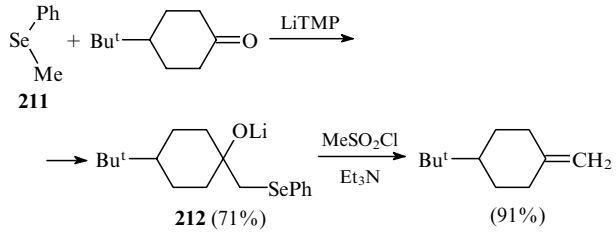

TMP is 2,2,6,6-tetramethylpiperidin-1-yl.

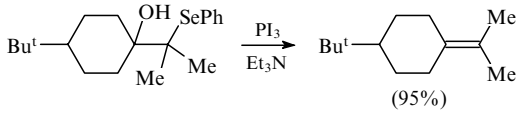

The modification of the OH-group of β-hydroxy selenide **213** by treatment with thionyl chloride results in its conversion into a good leaving group; elimination of the latter yields the selenonium cation **214**. An attack by an external nucleophile at the selenium atom of the cation **214** yields alkenes.[2, 136]

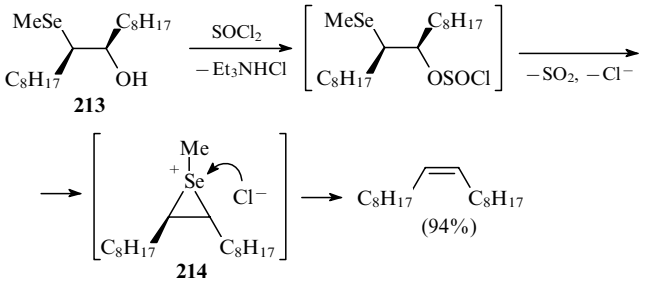

The Krief–Reich reaction was used in the synthesis of various types of alkenes including sterically hindered ones.[137]

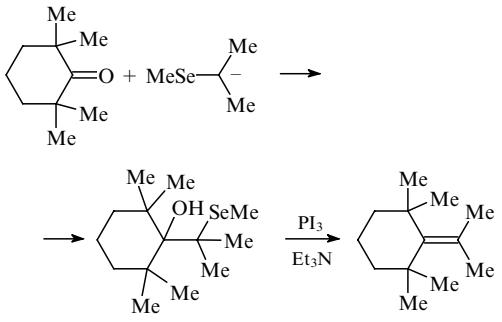

The Krief–Reich methodology can be used for cross-coupling of two different aldehydes.[132] Conversion of one of them into selenoacetal **215,** treatment of the latter with n-butyllithium and addition of the resulting carbanion to the second aldehyde result

in β-hydroxy selenide **216**. Subsequent elimination of the hydroxy and selenyl fragments yields alkenes.

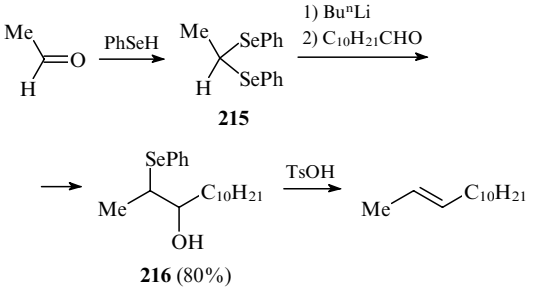

215

216 (80%)

d. Tellurium-based reagents

Tellurium ylides **217** containing an electron-withdrawing group (ester, cyano, keto, *etc.*) in the α-position are used in the synthesis of α,β-unsaturated esters, nitriles and ketones.[138, 139] To this end, aromatic aldehydes are treated with α-halo-substituted esters or nitriles in the presence of equimolar amounts of dibutyl telluride **218**. The corresponding tellurium ylides **217** are generated *in situ* by deprotonation of telluronium salts. This reaction results in good yields, it is highly stereoselective and gives predominantly *E*-isomers of alkenes. It is of note that reactions of tellurium ylides with carbonyl compounds yield olefination products, whereas reactions of sulfur ylides with the carbonyl group give epoxides.

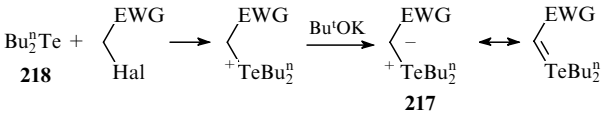

218 **217**

EWG = CO_2R, COR, CN; Hal = Cl, Br.

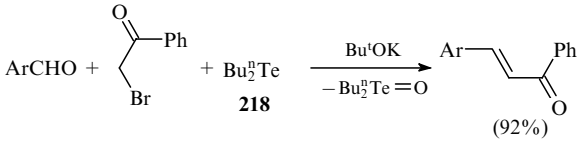

(92%)

Ar = 4-$NO_2C_6H_4$.

Both aldehydes and ketones can be used as the carbonyl components; however, in the case of non-symmetrical ketones the stereoselectivity of alkene formation is low.[139]

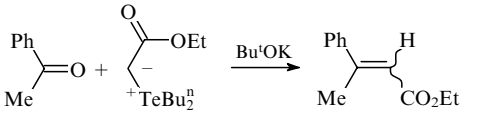

(68%, *E* : *Z* = 11 : 1)

In the presence of dibutyl telluride **218**, dibromomalonate **136** can be used as the olefinating agent in reactions with aromatic aldehydes.[140] The reaction mechanism is similar to that considered above for the olefination with tributylstibine (Section II.3.e) and includes the formation of the telluronium salt **219** as a result of the alkylation of dibutyl telluride. In the presence of a second equivalent of dibutyl telluride, the salt **219** reacts with aldehydes to give α,β-unsaturated malonates **220**.

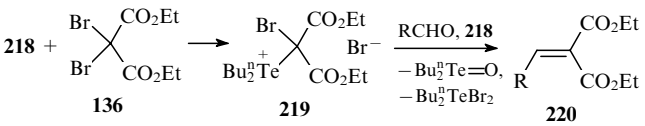

136 **219** **220** (84%–99%)

R = Alk, Ar, Het.

The copper-catalysed decomposition of diazo compounds in the presence of dialkyl or diaryl tellurides yields tellurium ylides **221**, which react with aldehydes to give alkenes.[141]

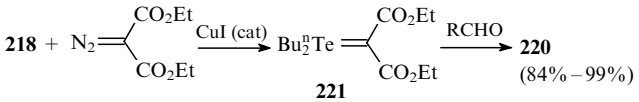

221 **220** (84%–99%)

R = Alk, Ar, Het.

A method for the synthesis of α,β-unsaturated esters, *e.g.*, the furan derivative **222**, has been developed where the telluride is coupled to polyethylene glycol (**223**).[142, 143] The tellurium derivative was used in catalytic amounts (2 mol.%), and equimolar amounts of triphenyl phosphite are required for the reduction of tellurium oxide formed. The yields of the target alkenes are usually close to quantitative; the stereoselectivity of the reaction is extremely high.

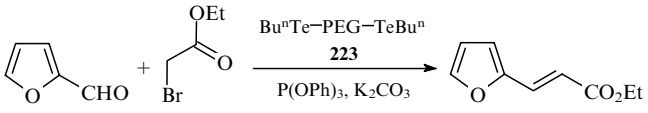

222 (96%, *E* : *Z* = 99 : 1)

PEG is polyethylene glycol.

5. Reagents based on Group VIIA elements

Addition of anions generated from tri-, di- and monohalomethanes to aldehydes and ketones $R^1R^2C{=}O$ and subsequent reduction of β-halogeno alcohols yields *gem*-dihaloalkenes $R^1R^2C{=}CHal_2$, vinyl halides $R^1R^2C{=}CHHal$ or terminal alkenes $R^1R^2C{=}CH_2$. This group of olefination methods was developed relatively recently, but nevertheless has rather a broad range of synthetic applications.

Reduction of aryltrichloromethylmethanols of the type **224** or their acetates,[144] with zinc in acetic acid (2–4 equiv.) or electrochemically is a convenient route to the synthesis of dichloroalkenes.[145] The corresponding alcohols are prepared by condensation of aldehydes with chloroform in the presence of phase-transfer catalysts [8, 145] or by a reaction of aldehydes with the trichloromethyl anion generated from trichloroacetic acid.[146]

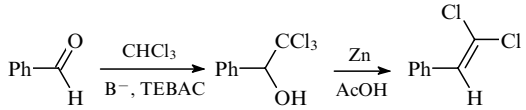

224 (87%)

TEBAC is triethylbenzylammonium chloride.

gem-Bromochloroalkenes and *gem*-dibromoalkenes can be prepared by a similar procedure using dibromochloromethane and bromoform, respectively.[147] Thus the addition of the tribromomethyl anion to ethyl phenyl ketone results in tribromomethylpropanol **225**. Subsequent acylation of the hydroxy group and reduction of the resulting ester **226** with Grignard reagent yield the dibromoalkene **227**. Other alkyl aryl and dialkyl ketones are also used as the carbonyl substrates.[147]

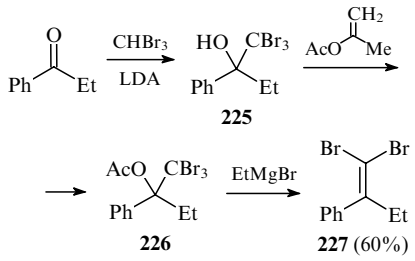

225 **226** **227** (60%)

Bromoalkenes **228** can be obtained from carbonyl compounds by treatment with dibromomethyllithium **229** generated *in situ* from dibromomethane and lithium dicyclohexylamide.[148] This reaction is applicable to a vast variety of aromatic and aliphatic aldehydes and ketones including α,β-unsaturated aldehydes and

ketones, which afford the corresponding bromo-substituted dienes. However, the stereoselectivity of the formation of bromoalkenes is usually low.

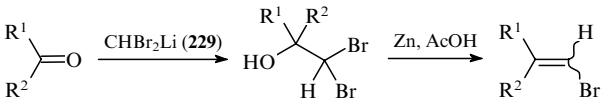

R^1, R^2 = Alk, Ar.

The reactions of carbonyl compounds with dihalomethanes (CH_2Cl_2, CH_2Br_2, CH_2BrCl) in the presence of lithium dicyclohexylamide and subsequent acidification of the reaction mixture yield the corresponding β,β-dihalo-substituted alcohols **230**; treatment of the latter with chlorotrimethylsilane in the presence of hexamethyldisilazane and pyridine gives the silylated derivatives **231**.[149] This reaction occurs with good yields and can be applied to both aliphatic and aromatic carbonyl substrates.

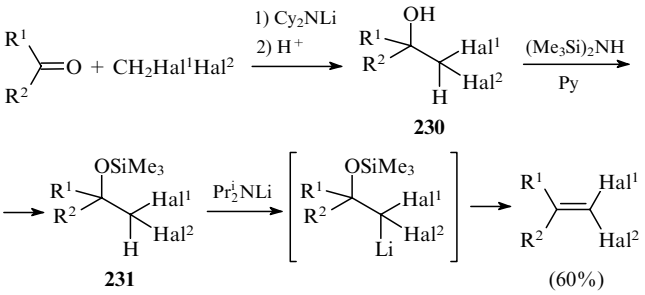

R^1 = H, Me, Et; R^2 = Et, C_7H_{15}, Ph; R^1–R^2 = $(CH_2)_3$, $(CH_2)_5$; Hal^1, Hal^2 = Cl, Br.

Subsequent treatment of compounds **231** with lithium diisopropylamide yields dihaloalkenes through C-deprotonation and β-elimination of silanol.

Silylation of an intermediate **232** derived from bromochloromethane and subsequent treatment of the silyl derivative **233** with n-butyllithium results in the chemoselective exchange bromine–lithium; elimination of silanol yields monohaloalkenes. However, the stereoselectivity of the synthesis of vinylic halides is very low: the isomer ratio is close to equimolar.

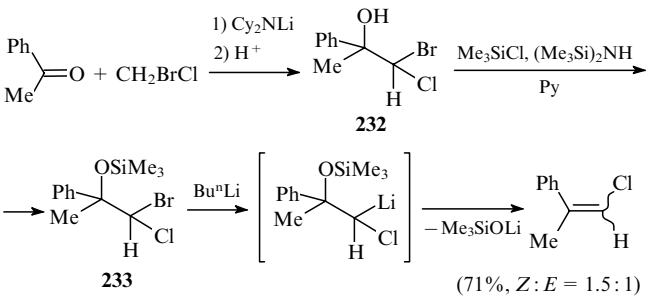

The use of chloromethyllithium **234** generated from chloroiodomethane as the olefinating agent in reactions with ketones results in terminal alkenes.[150] This reaction occurs *via* the intermediate **235**; subsequent reduction of the latter with lithium yields the target products.

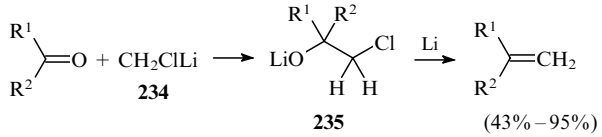

R^1, R^2 = Alk, Ar.

Thus condensation of polyhalomethyl anions with carbonyl compounds followed by acylation or silylation of intermediate alcohols and their subsequent reduction or elimination yield terminal alkenes or vinylic halides. However, the multistep character of this method is its disadvantage.

III. Condensation of carbonyl compounds with CH-acids

Compounds containing one or several electron-withdrawing groups at one carbon atom (CH-acids) are deprotonated in the presence of bases; the carbanions **236** formed add to the electrophilic carbon atom of the carbonyl group to give the alcohols **237**. If a CH-acid contains more than one hydrogen atom in the α-position relative to the electron-withdrawing group, the condensation products undergo dehydration resulting in the formation of alkenes **238** containing electron-withdrawing substituents. The presence of electron-withdrawing groups favours elimination according to the E1cb mechanism.

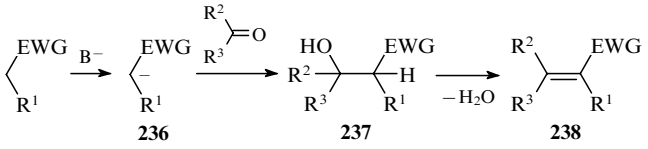

Many of the reactions described in this chapter were discovered as early as the 19th century; however, this branch of organic chemistry is still developing and novel modifications of the known reactions, reagents and catalysts continue to appear. A method for the synthesis of alkenes using carbanions stabilised by an electron-deficient aromatic system has been developed recently. Reactions of carbanions, which differ in the nature of substituents at the CH-acidic centre, are used in organic synthesis; these will be described in the chapters that follow.

1. Aldol condensation and its modifications

Reactions of enolate anions **239** generated from aldehydes and ketones with carbonyl compounds yield enals or enones **240**.[1,2] In these reactions, aldehydes and ketones play the role of both nucleophiles (the methylene component) and electrophiles (the carbonyl component). This allows both self-condensation and cross-coupling. Both bases and acids can be used as catalysts.

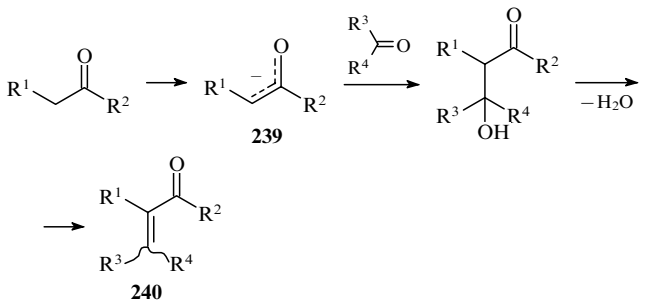

At present, direct chemo- and regioselective aldol condensation is based on the use of specially prepared metal enolates as well as of enol silyl ethers [151] and azaenolates.[152–154] Methods for the synthesis of enols and enolates as well as asymmetric syntheses based on them are documented in numerous reviews and monographs.[2,155–166] Thus conversion of one of the carbonyl compounds into an imine or a dimethylhydrazone by treatment with a primary amine or 1,1-dimethylhydrazine is a convenient procedure for modification of the aldol condensation.[2,152–154] Subsequent deprotonation of imines by non-nucleophilic bases yields azaenolates **241** and **242**, which act as the olefinating agents in the reaction with aldehydes and ketones.[3] The β-hydroxyimines formed are converted into α,β-unsaturated carbonyl compounds upon acid treatment. The condensation occurs stereospecifically and gives usually *trans*-isomers of alkenes.

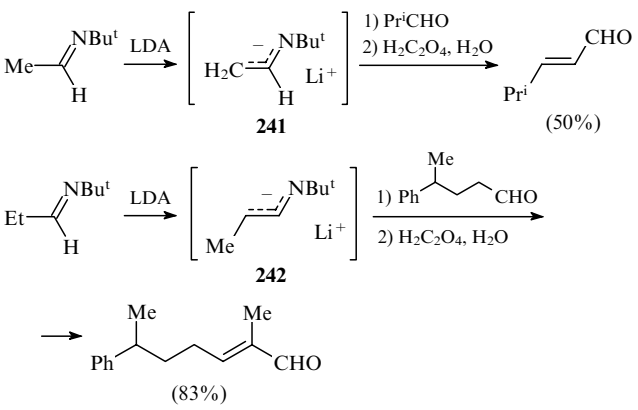

Preliminary conversion of a carbonyl compound, which plays the role of a nucleophilic component, into an enol silyl ether is yet another method for selective aldol cross-coupling.[151] In the case of non-symmetrical carbonyl compounds, enol ethers can be prepared regioselectively. Under conditions of kinetic control, a less substituted enol is formed predominantly, whereas under conditions of thermodynamic control a more stable substituted enol is the main product. Further reactions of enol silyl ethers with carbonyl compounds in the presence of Lewis acids yield β-hydroxy ketones or α,β-unsaturated ketones.[151]

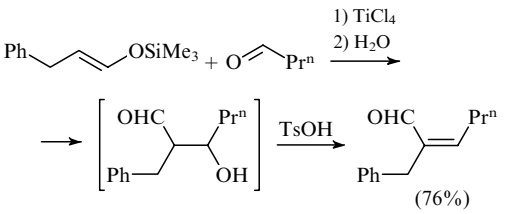

2. Condensation of aldehydes and ketones with esters

Esters $R^1CH_2COOR^2$ are used as nucleophilic components in condensations with carbonyl compounds, which yield α,β-unsaturated acids or esters.

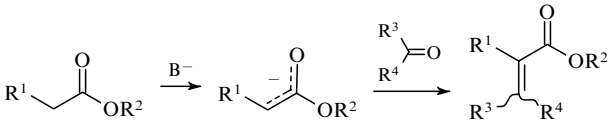

Esters usually require stronger bases for the generation of enolates than in the aldol condensation due to lower CH-acidity of hydrogen atoms in the α-position. This method is of a rather historical significance; the range of its application is fairly narrow due to drastic reaction conditions.[3] Modern approaches are based on the use of stronger bases of the LDA type, which allows complete deprotonation of the ester.

3. The Perkin reaction

Condensation of aromatic aldehydes and ketones with carboxylic anhydrides or their analogues is referred to as the Perkin reaction.[3,25] This reaction requires heating, sometimes rather significantly (up to 200–250 °C), of the reaction mixture. If an anhydride contains more than one α-hydrogen atom, dehydration takes place; the intermediate salt of β-hydroxy acid is never isolated. The role of a base in the Perkin reaction is always played by a sodium or potassium salt of the acid corresponding to the anhydride introduced into the reaction; however, in some versions, ammonia, triethylamine and some other amines are used. Aromatic aldehydes and their vinylogues ArCH=CHCHO are used as the carbonyl components. The Perkin reaction is a convenient procedure for the synthesis of substituted cinnamic acids from accessible aromatic aldehydes, the predominant formation of *E*-isomers is observed. However, at present this reaction has a rather historical significance, since it requires drastic conditions and often the yields of target products are low.

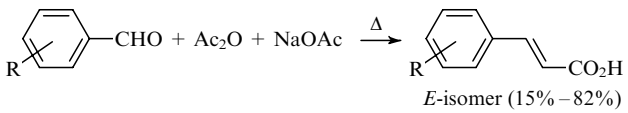

R = OH, OAlk, Hal, NO_2.

4. The Henry reaction

Condensation of carbonyl compounds with nitro derivatives is called the Henry reaction or the nitroaldol reaction.[2] It represents the most convenient method for the synthesis of nitro alcohols and nitro alkenes.[26–29,167] The nitroaldol reaction employs weak bases, since aliphatic nitro compounds are characterised by high CH-acidity. Amines, alkalis, carbonates and alkali metal alkoxides are usually employed as catalysts.

The reaction is often stopped at the step of a nitro alcohol; subsequent dehydration is carried out with dehydrating agents, such as dicyclohexylcarbodiimide, pivaloyl chloride, phthalic anhydride or methanesulfonyl chloride.[27] Thus the dehydration of the β-nitro alcohol **243** with dicyclohexylcarbodiimide in the presence of catalytic amounts of CuCl yields the nitro alkene **244**.[168]

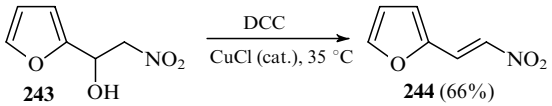

DCC is dicyclohexylcarbodiimide.

Aromatic aldehydes are directly converted into nitro alkenes **245** and **246** due to a considerable energy gain upon formation of the double bond conjugated to an aromatic system. The synthesis of alkenes **245** and **246** occurs in a stereoselective manner.[3]

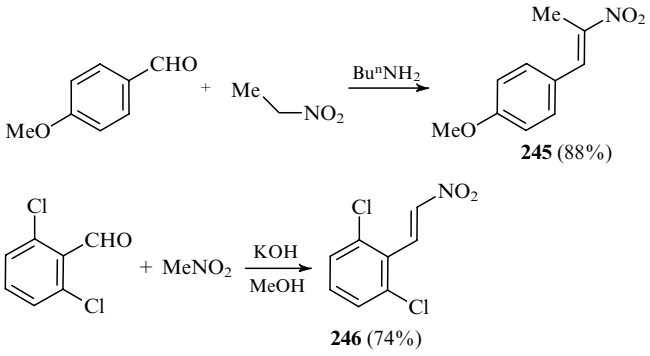

The olefination of ketones with nitromethane in the presence of ethylenediamine also results in unsaturated compounds.[27]

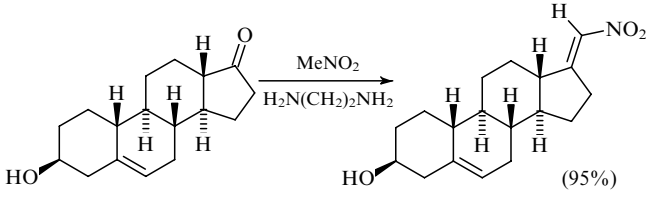

5. The Knoevenagel reaction

Reactions of aldehydes and ketones with compounds of the type $(EWG)_2CH_2$, which contain a reactive methylene group (1,3-diketones, 1,3-keto esters, malonates, ethyl cyanoacetate, malononitrile, *etc.*), are usually referred to as the Knoevenagel reaction,[3] although this definition is not quite correct.

In addition to 1,3-dicarbonyl compounds,[169,170] the Knoevenagel reaction widely employs alkyl cyanoacetates,[171] sulfonyl[172] and sulfinyl acetates,[173] as well as phosphonoacetates.[174]

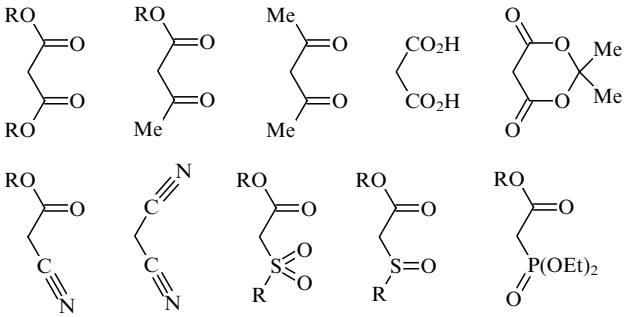

The generation of enolates from compounds containing two electron-withdrawing groups allows the use of weaker bases than the traditional aldol condensation, *viz*., amines, acetates as well as a mixture of $TiCl_4$ and pyridine.[174]

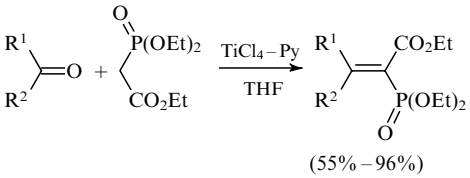

(55%–96%)

R^1, R^2 = Alk, Ar.

In one of the most recent modifications of the Knoevenagel reaction, ionic liquids are used as solvents. Thus condensation of diverse aromatic and aliphatic carbonyl compounds with ethyl cyanoacetate, acetylacetone and ethyl acetoacetate in 1-butyl-3-methylimidazolium tetrafluoroborate [(bmim)BF_4] was studied in the presence of ethylene diammonium diacetate (EDDA) as the catalyst.[173] This reaction is stereospecific and gives *E*-isomers of alkenes; in most cases, the yields of reaction products are virtually quantitative.

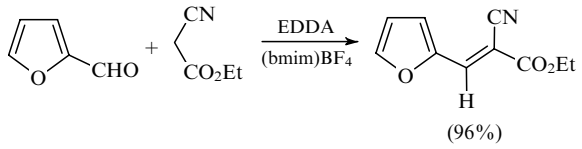

(96%)

The condensation of salicylic aldehydes with Meldrum's acid or malonic acid is widely used in the synthesis of substituted coumarin-3-carboxylic acids.[3] Its most recent version consists of a reaction of salicylic aldehydes of the type **247** with malononitrile **248** under heterogeneous conditions in the presence of an aqueous alkali or sodium hydrogen carbonate.[175] This results in substituted 3-cyanocoumarin **249**; its subsequent alkaline hydrolysis gives the coumarin-3-carboxylic acid derivative **250**. Both reaction steps occur in high yields.

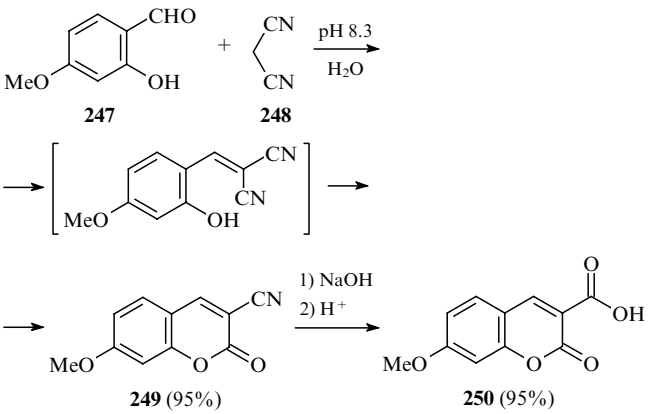

249 (95%) **250** (95%)

A three-component reaction representing the proline-catalysed condensation of aldehydes with Meldrum's acid **251** and subsequent Michael addition of ketone enolates to the adduct **252** formed, has been developed.[176] In this reaction, two C–C bonds are formed.

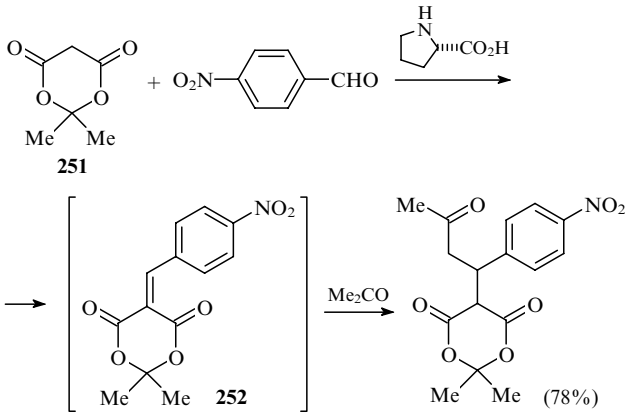

The use of malononitrile **248** in organic synthesis has been surveyed;[177–179] its condensation with carbonyl compounds is widely used in the synthesis of alkylidene- and arylidenemalononitriles. In particular, cyclopropyl-substituted dinitrile **253** was prepared in this manner.

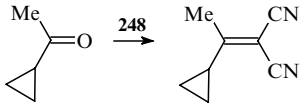

253 (81%)

And finally, special mention should be made of an original olefination procedure based on reductive addition, to the carbonyl group, of *gem*-dinitrile **254**, which is prepared by bisalkylation of malononitrile.[180] Reduction of *gem*-dinitrile **254** with lithium naphthalenide leads to the loss of one cyano group.The carbanion formed **255**, which is stabilised by the residual cyano group, is an effective nucleophile which reacts with a broad range of electrophiles including carbonyl compounds. The intermediate β-hydroxy nitrile **256** is further *O*-alkylated. Reductive elimination of the vicinal alkoxy- and cyano fragments by treatment of compound **257** with lithium 1-(dimethylamino)naphthalenide yields the corresponding alkene. This reaction results in the loss of both cyano groups. It is noteworthy that the possibility of synthesising tetrasubstituted alkenes from ketones is a significant advantage of this method.

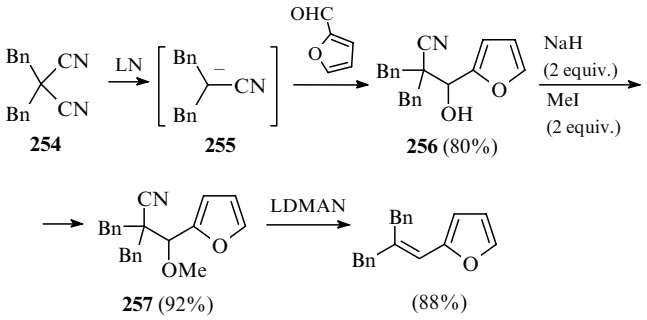

254 **255** **256** (80%)

257 (92%) (88%)

LN is lithium naphthalenide;
LDMAN is lithium 1-(dimethylamino)naphthalenide.

6. Condensation of carbonyl compounds with other CH-acids

Carbanions stabilised by an electron-deficient aromatic system can be used as olefinating agents.[2, 6, 181] Condensation of the corresponding CH-acids with aromatic aldehydes in the presence of bases is used for the preparation of non-symmetrical stilbenes or their heterocyclic analogues.[6] Pyridine, piperidine, alkali metal alkoxides and, less frequently, alkalis are commonly used as the bases.

Thus the reaction of aromatic aldehydes with 2-methylbenzothiazole **258** in the presence of aqueous alkali and a phase-transfer

catalyst yields olefination products, *viz*., 2-styrylbenzothiazoles **259**.[181]

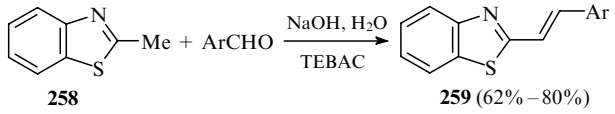

258 **259** (62% – 80%)

Ar = Ph, 2-ClC_6H_4, 4-ClC_6H_4, 4-MeC_6H_4, 4-$MeOC_6H_4$.

Synthesis of styrylthiazole is carried out in acetic acid in the presence of sodium acetate.[182] Protonation of the nitrogen atom of the heterocyclic base **260** increases the CH-acidity of the methyl group and favours its reaction with benzaldehydes. Lewis acids ($ZnCl_2$) and protic acids (HCl, H_3BO_3) can be used as catalysts.

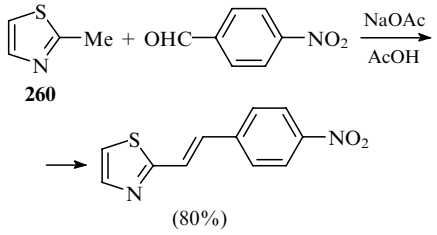

260

(80%)

Katritzky *et al*.[80, 183, 184] have proposed the use of *N*-alkylbenzotriazole anions **261** in the condensation of carbonyl compounds for the synthesis of allyl- and benzyl-substituted alkenes. The alcohols **262** formed containing a benzotriazole system are reduced to alkenes upon treatment with low-valence titanium derivatives; the heterocyclic system is thereby eliminated.

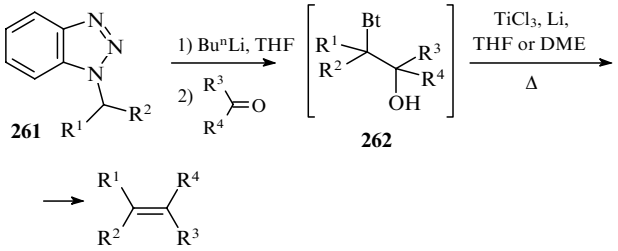

261 **262**

Bt is benzotriazol-1-yl.

The olefination proceeds in good yields (53% – 81%) and high *E*-stereoselectivity not only in the case of 1,2-disubstituted, but also tri- and tetrasubstituted alkenes. Thus stereoselectivity of the formation of the trisubstituted alkene **263**, which represents a heterocyclic analogue of stilbene, was fairly good.

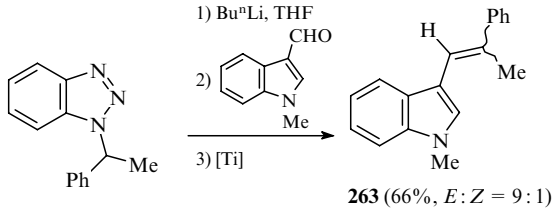

263 (66%, $E:Z = 9:1$)

Aliphatic and aromatic aldehydes and ketones as well as α,β-unsaturated carbonyl compounds were used as the carbonyl substrates. Unfortunately, the range of olefinating agents is limited to *N*-allyl- and *N*-benzylbenzotriazole derivatives.

This approach is used in the stereoselective synthesis of some conjugated dienes and trienes.[183, 184] Thus the reagent **264** was used to yield conjugated diene **265** and triene **266**:

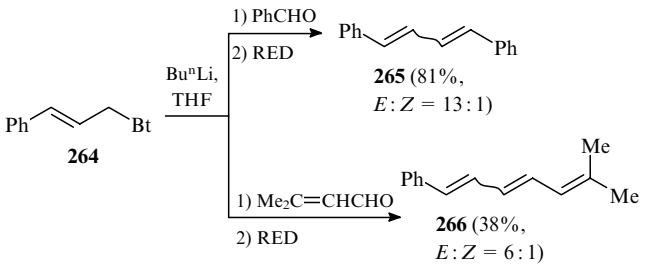

264

IV. Reagents based on transition and non-transition metals

A great diversity of methods for the olefination of carbonyl compounds is known which make use of reagents based on metals, in the first place, transition metals.[1, 3] In these reactions, metal compounds usually play the role of reducing agents. Reagents based on titanium, zinc and chromium are especially popular.

1. Reagents based on Group IIB metals

a. Zinc-based reagents

Reductive coupling of polyhaloalkanes with carbonyl compounds in the presence of zinc was used in the synthesis of various halogen-substituted alkenes.[185 – 187] It was shown that treatment of zinc with 1,1,1-trichloro-2,2,2-trifluoroethane gives a stable organozinc reagent **267**, its addition to aromatic and aliphatic aldehydes yields the corresponding alcohols. The latter can be reduced to trifluoromethyl-substituted alkenes by excess zinc. In the case of benzaldehyde, the yield of the reaction product **268** (over three steps) was 84%.[186, 187]

267

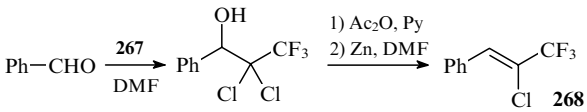

268

Diiodomethane was used as a methylenating agent in the synthesis of terminal alkenes from aromatic aldehydes in the presence of a zinc – copper couple.[188]

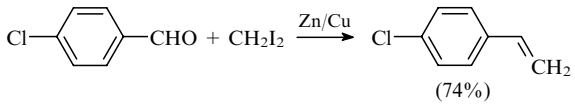

(74%)

The Oshima – Lombardo reaction includes methylenation of carbonyl compounds by dihalomethanes (CH_2I_2, CH_2Br_2) catalysed by $Zn-TiCl_4$ or $Zn-AlMe_3$ systems.[1, 189] A *gem*-organodizinc compound of the type $HalZnCH_2ZnHal$ (**269**, Hal = I, Br) is used as the olefinating agent.

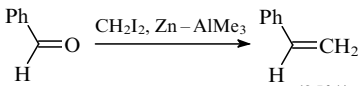

(85%)

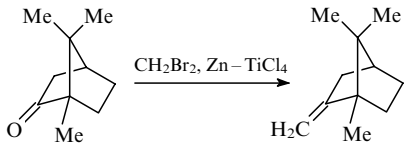

(92%)

It should be noted that the presence of ester or lactone fragments does not prevent methylenation of carbonyl groups.[190] Selective methylenation of the aldehyde group in the presence of the keto group and *vice versa* is a salient advantage of the Oshima – Lombardo reaction.[191] Thus the methylenation of a keto group, which does not affect an aldehyde group, can be performed following treatment of the substrate with tetrakis(diethylamino)titanium (this results in selective protection of the aldehyde group due to complex formation). The chemoselective methylenation of an aldehyde in the presence of a ketone is carried out using titanium isopropoxide or trimethylaluminium. This approach was demonstrated in a spectacular way in the selective methylenation of either keto or aldehyde groups of the keto aldehyde **270** to give isomeric oxo alkenes **271** and **272**, respectively.

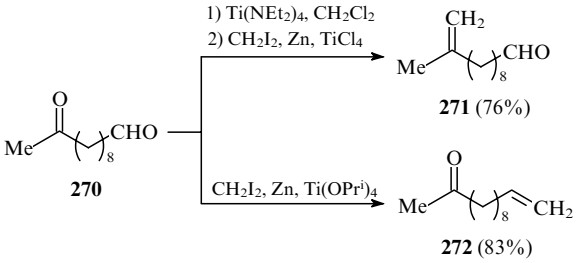

270 **271** (76%) **272** (83%)

The *gem*-organodizinc reagent **269** (Hal = I) was used in the synthesis of substituted allylic alcohols and amines from α-hydroxy and α-amino ketones.[192] Presumably, in this case coordination of the heteroatom to zinc takes place, which favours the methylenation reaction. The methylenation of substrates containing no such substituents in the α-position requires the presence of titanium salts.

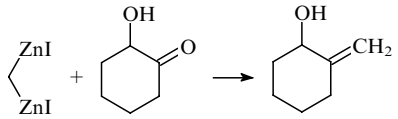

269 (90%)

Reductive coupling of carbonyl compounds in the presence of the system $InCl_3$ – Zn yields symmetrical alkenes; this reaction occurs stereospecifically and yields *E*-isomers.[193] Aromatic and aliphatic aldehydes and ketones are used as substrates. This process is similar to the McMurry reaction (see Section IV.3.a).

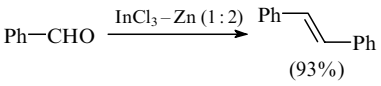

(93%)

The organozinc compound **73** was used in the stereoselective olefination of aromatic and unsaturated aldehydes. In the presence of a cobalt(I) complex, the reaction occurs under mild conditions and yields *E*-isomers of alkenes.[194]

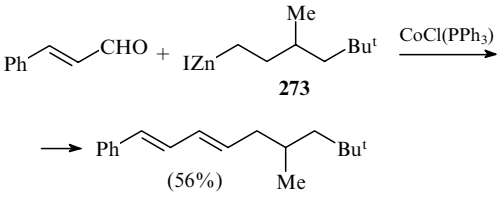

273

(56%)

The Reformatsky reaction represents the reaction of carbonyl compounds with α-halo-substituted esters **274** or their vinilogues $RCHHalCH=CHCO_2Et$ in the presence of zinc.[195] Its first step includes insertion of zinc into the C—Hal bond and formation of the organozinc intermediate **275** (the Reformatsky reagent), which represents zinc enolate. The intermediate organozinc compound is not isolated. β-Hydroxy esters are usually formed from aliphatic carbonyl compounds, which can easily be dehydrated into α,β-unsaturated esters. In the case of aromatic aldehydes and ketones, dehydration usually takes place directly in the reaction mixture.

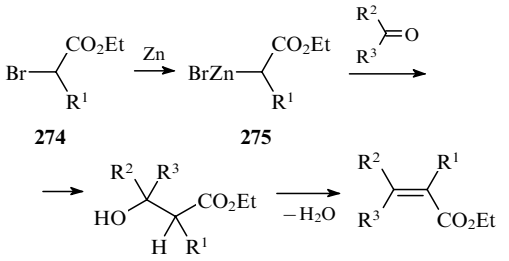

274 **275**

A mixed-type version of the Reformatsky and Peterson reactions based on the use of (halogeno)trimethylsilylacetate **276** is known.[196] The use of this reagent allows direct preparation of alkenes avoiding β-hydroxy derivatives.

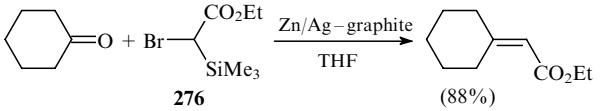

276 (88%)

b. Mercury-based reagents

A multistep synthesis of trifluoromethyl-substituted alkenes **268** using organomercurials as CF_3-group sources has been developed.[197] The organomercuric compound **277** prepared by treatment of phenylmercury chloride with halothane $CF_3CBrClH$ in the presence of potassium *tert*-butoxide served as the olefinating agent. Treatment of benzaldehyde with the reagent **277** in the presence of triphenylphosphine yields a mixture of *E*- and *Z*-isomers of the trifluoromethyl-substituted alkene **268** in an equimolar ratio. Low yields and high toxicities of the mercury compounds make this method inconvenient for application in synthetic practice.

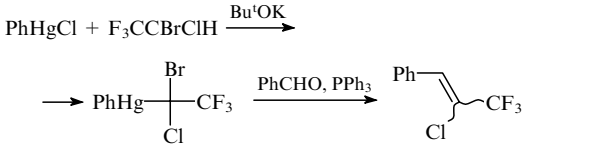

277 **268** (38%, $E:Z = 1:1$)

2. Reagents based on Group IIIB metals

The use of dicyclopentadienylyttrium chloride **278** as the olefinating agent yields fulvenes **279**.[198] Thus the reagent **278** acts as a synthetic equivalent of the cyclopentadienyl anion. The first step includes coordination of yttrium to the oxygen atom of the carbonyl group. Subsequent addition of cyclopentadienyl to the carbon atom and elimination of yttrium oxide give fulvenes **279**. Both aldehydes and ketones give high yields (57% – 96%) of reaction products.

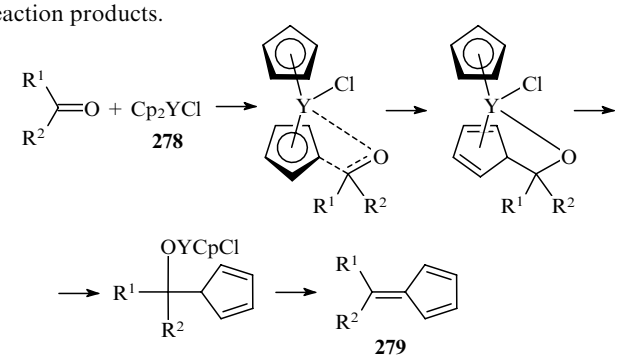

278 **279**

Cp is cyclopentadienyl.

3. Reagents based on Group IVB metals

a. The McMurry reaction

The McMurry reaction is the olefination of carbonyl compounds in the presence of low-valence titanium derivatives yielding various alkenes.[1] The formation of very strong Ti—O bonds is the driving force of this reaction. This reaction consists of reductive dimerisation of carbonyl compounds and gives symmetrical alkenes. The mechanism of the McMurry reaction and its synthetic applications have become the subject of intense studies which have been reviewed.[30–35] Both aldehydes and ketones are employed. Dimerisation of aromatic aldehydes is used for the synthesis of substituted stilbenes.[6]

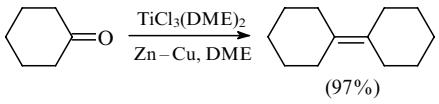

DME is 1,2-dimethoxyethane.

Various titanium derivatives playing the role of reducing agents can be prepared by *in situ* reduction of $TiCl_4$ or $TiCl_3$ with zinc, a zinc–copper alloy, lithium aluminium hydride and alkali metals. It is believed that zero-valent titanium is formed under these conditions. The first step of the McMurry reaction actually represents pinacol condensation; however, the *vic*-diols formed undergo further reduction to alkenes.

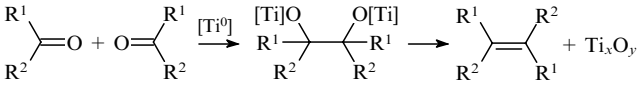

Functional groups, such as nitrile, amide, ester, *p*-toluenesulfonyl, *etc*., are not affected under the conditions of the McMurry reaction.[30] An epoxide or a *vic*-diol fragment present in the substrate is reduced to the alkene. Nitro groups, oximes and sulfoxides do not withstand the reaction conditions and are reduced.[30]

Reductive dimerisation according to McMurry was used for the preparation of a series of crowded alkenes containing bulky substituents, *e.g.,* adamantylideneadamantane (**280**),[30] tetraisopropylethylene (**281**)[199] and even di-*tert*-butyldiethylethylene (**282**).[200] Unfortunately, tetra-*tert*-butylethylene could not be prepared by this method.[30]

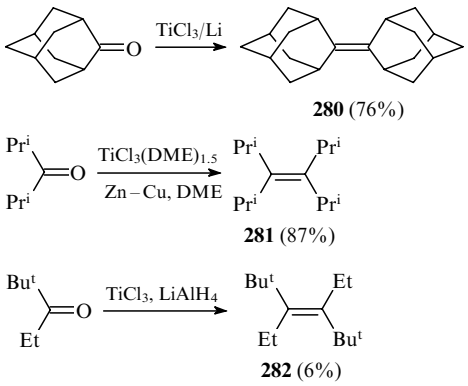

Reductive dimerisation of dicarbonyl compounds is a convenient method for the synthesis of cyclic alkenes with ring size varying from 3 to 36.[201] The synthesis of medium and large rings from dicarbonyl derivatives is carried out under high dilution; the ring closure proceeds in high yields and is highly stereoselective. Medium and large rings are usually formed with *E* configuration of the double bond.[199] Thus the endocyclic alkene **283** was prepared by the McMurry reaction.

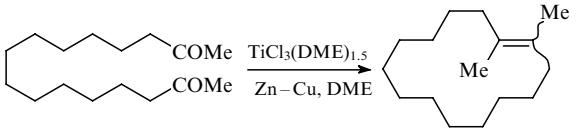

283 (82%, $E:Z = 92:8$)

It is unreasonable to prepare non-symmetrical alkenes by the McMurry reaction, since dimerisation of two carbonyl compounds gives all three possible alkenes. However, intramolecular coupling of substrates containing non-equivalent carbonyl groups represents a smooth access to non-symmetrical cycloalkenes. Thus the cyclisation of *o*-acylamino- or acyloxy-substituted benzophenones yields various indole and benzofuran derivatives.[202]

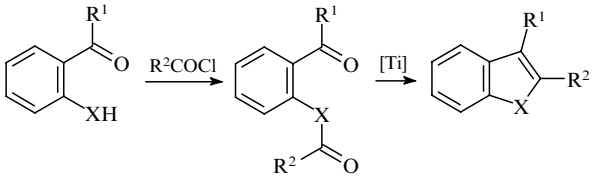

X = O, NH, NAlk; R^1 = Alk, Ar; R^2 = H, Alk, Ar, OAlk, $NAlk_2$.

The use of the McMurry reaction in the synthesis of substituted furans **284** and indoles **285** from compounds **286** and **287** has been described by Furstner *et al*.[203, 204]

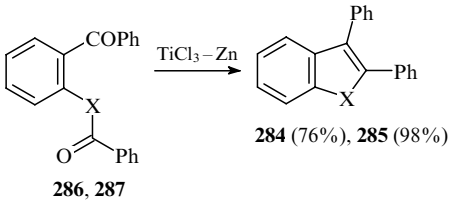

X = O (**284**, **286**); NH (**285**, **287**).

b. The Tebbe reaction

In 1978, Tebbe *et al*.[205] proposed to use metallacyclobutane **288** as a C_1-synthon, which became a popular reagent for olefination of carbonyl compounds. The Tebbe reagent is prepared *in situ* by the addition of commercially available titanocene dichloride to trimethylaluminium in toluene.[206] Under olefination conditions, the reagent **288** is converted into a highly reactive methylene-titanocene complex **289**. Donor ligands (*e.g*., THF or pyridine) are beneficial for the reaction, they favour elimination of the Lewis acid (Me_2AlCl) from the ring.[207]

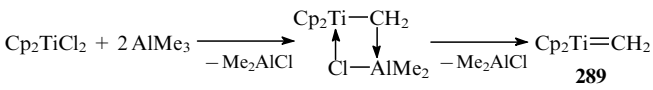

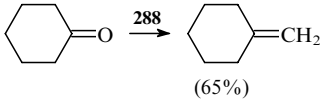

Carboxylic acid derivatives, *viz*., esters[208] and amides,[209] can be used as carbonyl components along with aldehydes and ketones. Thus, vinyl ethers and enamines can be obtained by the Tebbe reaction.

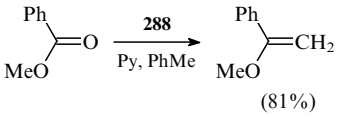

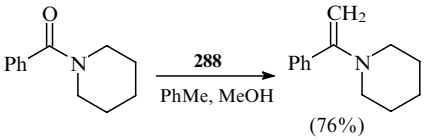

c. Dialkyltitanocenes

In 1990, Petasis and Bzowej[210] developed a new methylenating agent, *viz*., dimethyltitanocene Cp_2TiMe_2 (**290**), as an alternative to the Tebbe reagent. The advantages of this reagent include its stability and availability; besides, it does not contain aluminium. The Petasis reagent is prepared by mixing titanocene dichloride **291** with methyllithium. The area of its synthetic applications practically coincides with that of the Tebbe reagent.[211]

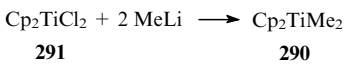

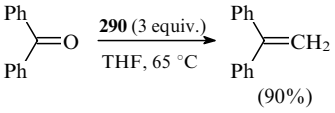

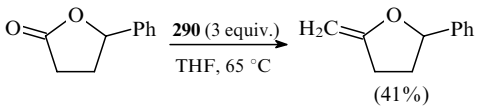

Several more olefinating agents have been developed based on titanocene dichloride **291**.[212,213] Thus the reactions of complex **291** with substituted benzylmagnesium chlorides yield dibenzyltitanocenes **292**.

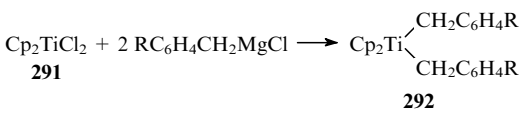

R = H, F, Cl, OMe.

The reactions of carbonyl compounds with the reagent **292** (R = H) yield aryl-substituted alkenes **293**.[212] Low stereoselectivity of this reaction is its main disadvantage.

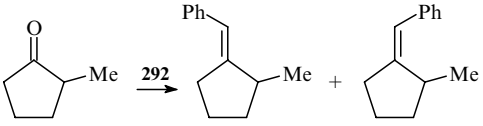

293 (75%, $E:Z$ = 1 : 1)

The reactions of a silicon-containing reagent **294** prepared from titanocene dichloride **291** with carbonyl compounds and carboxylic acid derivatives yield vinylsilanes **295**.[213,214]

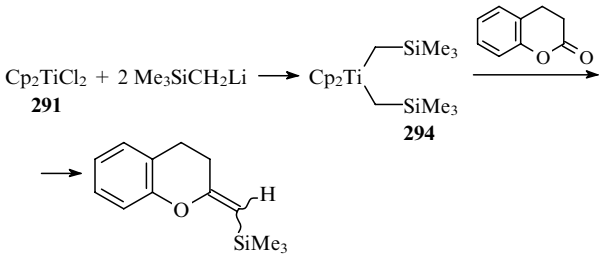

295 (83%, $Z:E$ = 2.5 : 1)

d. Miscellaneous titanium-based reagents

Reductive coupling of polyhalogeno compounds $CHal_2XY$ (Hal, X, Y = Cl, Br) with aldehydes and ketones is widely used in the synthesis of various substituted alkenes.

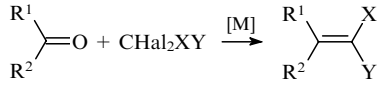

[M] is a reducing metal derivative in lower oxidation states.

Thus the olefination of aromatic and aliphatic aldehydes and ketones by *gem*-dihalo compounds has been described.[215–217] The titanium derivative **296** prepared *in situ* by reduction of titanocene dichloride **291** with magnesium in the presence of triethyl phosphite was used as the reducing agent.

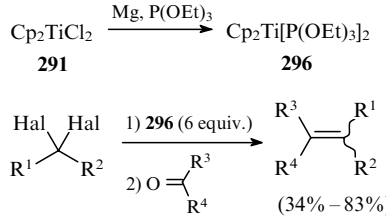

R^1, R^2 = H, Alk, Hal; Hal = Cl, Br; R^3 = Alk; R^4 = H, Alk, OAlk.

Aliphatic and aromatic aldehydes and ketones as well as esters and lactones can be used as carbonyl components. This is an undisputable advantage of the reaction, since it allows one to synthesise acyclic and cyclic vinyl ethers with different types of substitution at the double bond. Dichloro- and dibromoalkanes as well as chloroform and carbon tetrachloride are used as polyhaloalkane components. As a rule, the reaction proceeds stereoselectively and results in the predominant formation of a less sterically hindered alkene isomer. The reaction mechanism includes consecutive insertion of two molecules of the titanium derivative **296** into the C–Hal bond of the polyhaloalkane resulting in the intermediate **297**. Elimination of the Cp_2TiCl_2 molecule affords the titanium-carbene complex **298** which reacts with the carbonyl compound to give a dichloroalkene. The synthesis of dichloroalkenes can proceed in a different route, namely, *via* intermediate complexes of the type **299** prepared by addition of the organotitanium compound **297** to the carbonyl group. The necessity of using six equivalents of the reducing agent (compound **296**) is a serious disadvantage of this method.

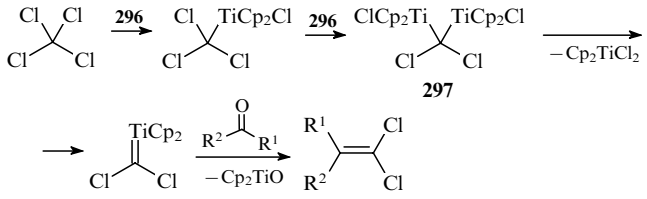

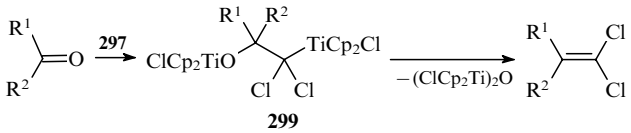

The use of the system dithioacetal – $Cp_2Ti[P(OEt)_3]_2$ (**296**) for olefination allows the transformation of carbonyl compounds into alkenes.[218,219] As in the case of polyhaloalkanes, the titanium-carbene complex is the key intermediate in this reaction. Intramolecular cyclisation of the titanium-carbene complex **300**, which contains simultaneously a dithioacetal fragment and an ester group, resulting in the cyclic vinyl ether **301**, is an example of such a reaction.[218]

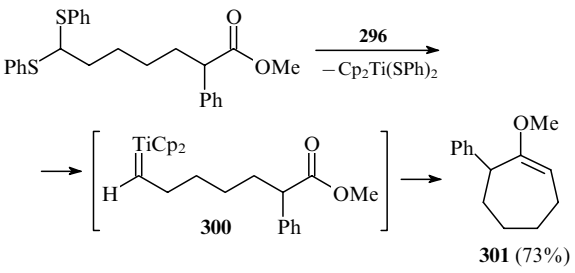

d. Zirconium-based reagents

The reaction of zirconocene dichloride **302** with dibromomethane in the presence of zinc yields a methylene-zirconium complex **303**, which was used as a methylenating agent in the synthesis of terminal alkenes.[220] Aliphatic, aromatic and α,β-unsaturated aldehydes and ketones were used as the carbonyl components.

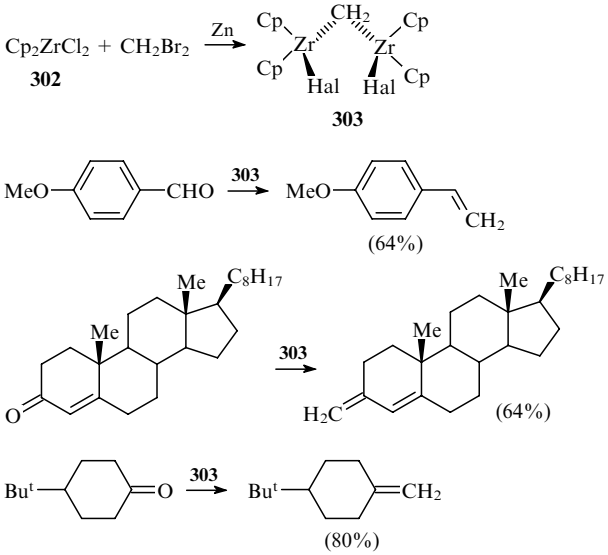

The hypothetical mechanism of this reaction includes coordination of the zirconium atom to the carbonyl oxygen atom and an attack of the nucleophilic carbon atom on the carbon atom of the carbonyl group. This reaction yields metallaoxacyclobutane **304**; subsequent rapid elimination of zirconocene oxide gives the target alkenes.[220]

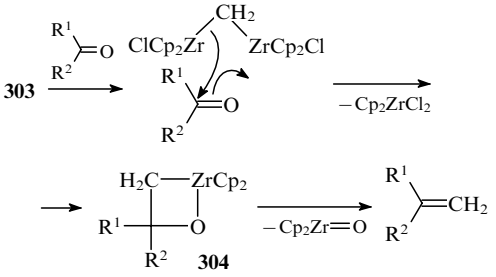

Alkylidenezirconium complexes **305** were used as olefinating agents for the introduction of longer-chain carbon fragments.[221,222] In contrast to the methylene complex **303**, these can be used in the synthesis of alkenes not only from ketones, but also from esters, lactones [222] and imidates.[223]

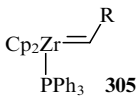

R = Bu^n, Bu^s, CH_2Bu^t, cyclo-C_5H_{11}.

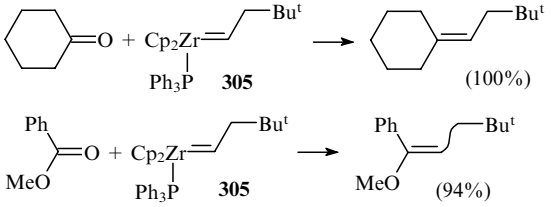

4. Reagents based on Group VB metals

Alkylidene complexes of nyobium and tantalum (the Schrock carbenes) manifest nucleophilic properties.[223,224] It was shown that the neopentylidenetantalum complex **306** formed upon reduction of compound **307** with neopentyllithium can be used for the introduction of the neopentylidene group into a broad range of carbonyl compounds.[225] Aldehydes, ketones, amides and esters were used as the carbonyl components of this reaction. The yields of alkenes varied from 35% to 90%. The neopentylideneniobium complex **308** manifests similar reactivity.

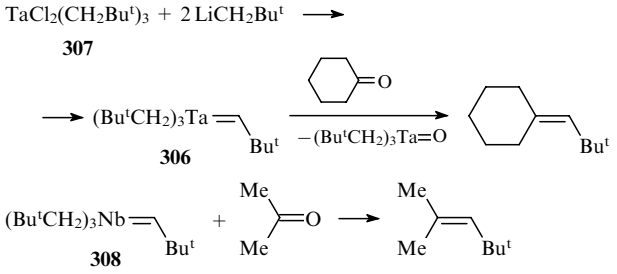

5. Reagents based on Group VIB metals

a. Chromium-based reagents

Reductive coupling of *gem*-dihalo compounds $CHal_2XY$ with aldehydes in the presence of chromium(II) chloride as the reducing agent is widely used in the synthesis of various alkenes.[1] It was found that reactions of such dihaloalkanes with aldehydes are stereoselective and give predominantly *E*-isomers of alkenes. Various substituted dihaloalkanes including those containing heteroatoms can be used as the olefinating components. This yields vinyl halides **309**,[226] vinylstannanes **310**,[227] vinylsilanes **311** and vinyl sulfides **312**.[228]

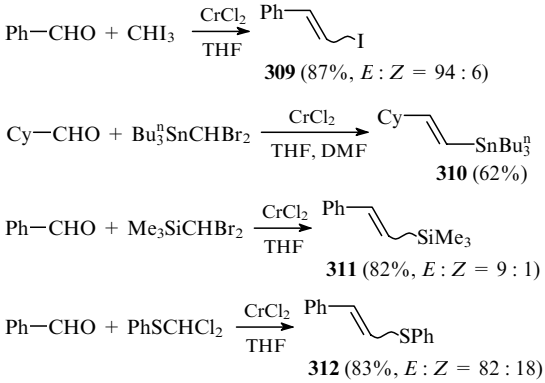

The mechanism of this reaction consists of substitution of chromium for two halogen atoms resulting in *gem*-organodichromium compounds **313**, which further add to the aldehyde. Subsequent elimination of a chromium(III) salt from the intermediate **314** yields alkenes.[1,226,229]

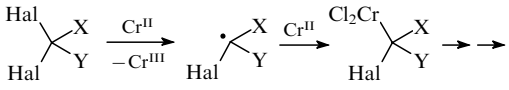

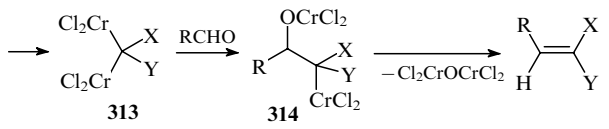

313 314

Hal = Cl, Br, I; X, Y = H, Alk, Hal, SR, $SnAlk_3$, $SiAlk_3$; R = Alk, Ar.

High yields and high stereoselectivity are indisputable advantages of this method. The disadvantages include the necessity of using six equivalents of the reducing agent and conducting the reaction in an inert atmosphere in dry solvents. The use of this method for the olefination of ketones has not been reported so far.

b. Molybdenum-based reagents

The methylene-molybdenum complex $Cl_3Mo{=}CH_2$ (**315**) prepared by treatment of molybdenum(V) chloride with methyllithium is a very mild methylenating agent. This reacts with aldehydes and ketones to give terminal alkenes in good yields.[230]

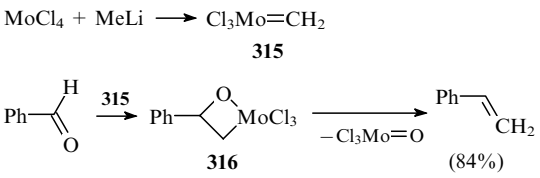

315 316 (84%)

Presumably,[230] this methylenation occurs *via* metallacyclobutane **316**. A family of methylenating agents **317**–**319** based on molybdenum have been synthesised. Reagents **315** and **317** have proved to be the most reactive.

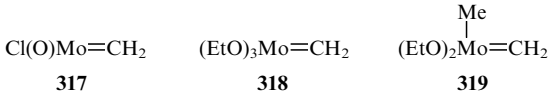

317 **318** **319**

c.Tungsten-based reagents

The tungsten-carbene complexes **320**–**322** are convenient reagents for the synthesis of sterically hindered (including exocyclic) alkenes.[231]

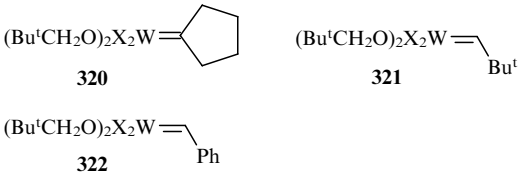

320 **321** **322**

X = OCH_2Bu^t, Cl, Br, I.

The role of a carbonyl component can be played by aromatic and aliphatic aldehydes, ketones, lactones and amides. The reaction is carried out using stoichiometric amounts of tungsten-carbene complexes. The yields are good in all cases.

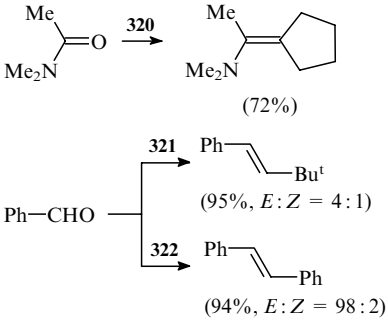

(72%) (95%, *E*:*Z* = 4:1) (94%, *E*:*Z* = 98:2)

Reductive dimerisation of aromatic aldehydes and ketones, which gives good yields of symmetrical alkenes, is carried out in the presence of low-valence tungsten derivatives (the so-called 'tungsten' version of the McMurry reaction)[232] prepared *in situ* by treatment of WCl_6 with butyllithium.

It was recommended[233] to perform the coupling of aldehydes and ketones with a reagent formed upon reduction of WCl_6 with lithium aluminium hydride (its structure is not reported by the authors) as a reducing agent. Coupling was shown to occur in moderate yields with both aliphatic and aromatic substrates. Studies of the reaction mechanism suggest that the tungsten-carbene complex **323** formed as a result of insertion of the reagent **324** (marked as [W] in the scheme) into the carbonyl group is involved in the formation of alkenes. Subsequent addition of the second aldehyde molecule to the complex **323** and fragmentation of the metallacyclobutane intermediate **325** results in alkenes.

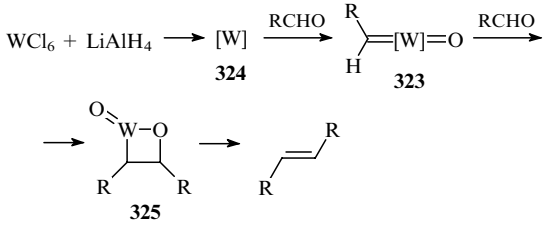

324 **323** **325**

The reaction of anisaldehyde with phenyldiazomethane in the presence of the reagent **324** gives *p*-methoxystilbene in low yield. In this case, the role of the olefinating agent is played by the diazo compound, while the tungsten-carbene complex **326** is a putative intermediate.[233]

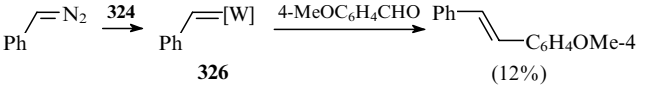

326 (12%)

The binuclear tungsten complex $W_2(OCH_2Bu^t)_6Py_2$ (**327**) was proposed for cross-coupling of two different carbonyl compounds.[234] Its reaction with acetone yields the complex $W_2(OCH_2Bu^t)_6(OCMe_2)Py_2$ (**328**). Subsequent treatment of aldehydes and ketones with the reagent **328** converts the carbonyl group into the isopropylidene group, *i.e.*, affords reductive cross-dimerisation products.

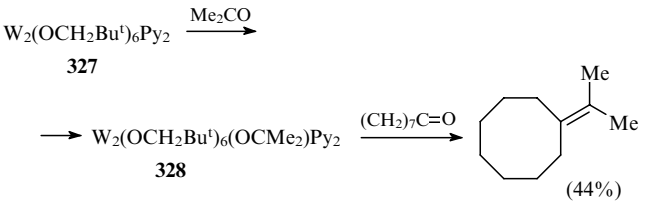

327 **328** (44%)

6. Uranium-based reagents

The metallacycle **329** based on uranium was proposed as a mild methylenating agent for cyclic and sterically hindered ketones as the carbonyl components.[235] It was shown that the olefination proceeds *via* intermediate six-membered metallacycles of the type **330**. High sensitivity of these complexes to moisture and air is a disadvantage.

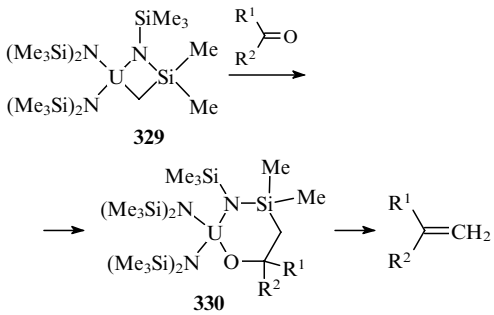

329 **330**

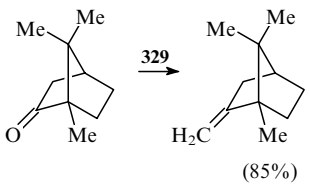

7. Reagents based on non-transition metals

Reductive coupling of carbonyl compounds with dihaloalkanes in the presence of non-transition reducing metals is also used in the synthesis. Presumably, the reactions of reducing metals with *gem*-dihaloalkanes afford *gem*-organodimetallic derivatives CH_2M_2, which yield the corresponding terminal alkenes in reactions with aldehydes and ketones.[39]

Dibromomethane and diiodomethane react with magnesium or magnesium amalgam to give *gem*-organodimagnesium compounds $CH_2(MgBr)_2$ (**331**) and $CH_2(MgI)_2$ (**332**). The latter proved to be convenient methylenating agents in the transformations of diverse carbonyl compounds into alkenes. These reactions usually give the products in high yields.[236]

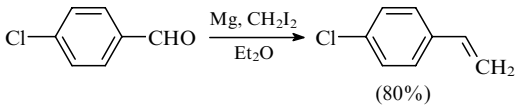

If benzylidene bromide $PhCHBr_2$ is used as the olefinating agent, the yield of the alkene is low. Therefore, this method can be used only for the incorporation of a methylene fragment.[236]

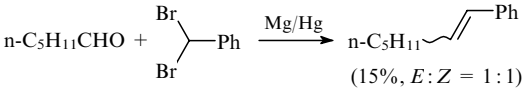

gem-Organodimagnesium compound **333** containing a trimethylsilyl group was successfully used in the synthesis of 1,1-diphenyl-2-trimethylsilylethylene **334** from benzophenone.[237] However, the yield of the expected reaction product with cyclohexanone was only 13%.

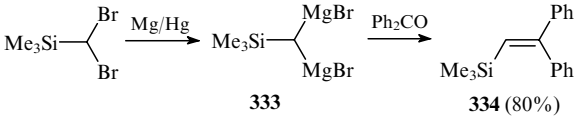

A method for the synthesis of terminal alkenes from ketones (including easily enolisable ones) using a family of *gem*-organodialuminium reagents of the type **335** and **336** has been developed.[238] The reagent **335** was prepared by boiling aluminum powder in dichloromethane in the presence of catalytic amounts of CH_2Br_2 as a primer.

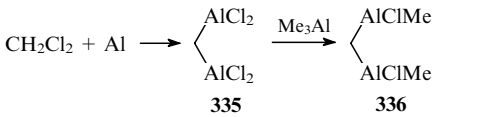

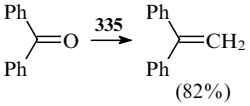

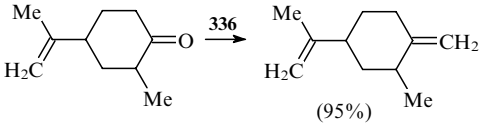

1,1-Bis(dichloroaluminio)hexane (**337**) prepared by the addition of two molecules of dichloroalane **338** to hex-1-yne was used in the synthesis of non-terminal alkenes from aromatic ketones.[39, 238]

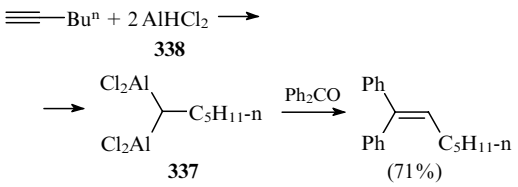

V. Miscellaneous olefination methods

1. The Barton – Kellogg reaction

The Barton – Kellogg olefination represents the condensation of diazo compounds **339** with carbonyl derivatives **340** resulting in thiadiazolines **341**. Subsequent heating of the latter in the presence of triphenylphosphine yields alkenes.[239] The Barton – Kellogg reaction can be regarded as a reductive coupling of two different carbonyl compounds, since diazo compounds **339** are usually prepared by oxidation of hydrazones.

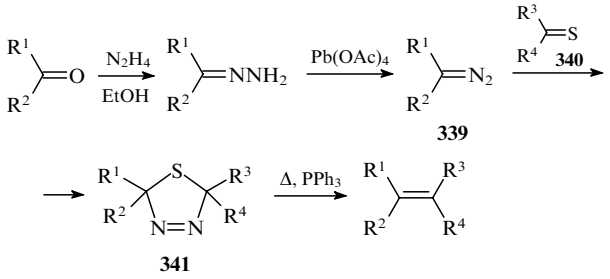

The Barton – Kellogg reaction was employed in the synthesis of sterically hindered alkenes. Thus bi(quadricyclylidene) **342** was prepared from the ketone **343** using this reaction sequence.[7]

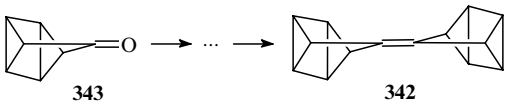

A version of the Barton – Kellogg reaction is known where the carbonyl compound is converted into a symmetrical azine **344**.[240, 241] Subsequent cyclisation upon treatment with hydrogen sulfide yields thiadiazolidine **345**; the latter is further oxidised to thiadiazoline **346** with lead tetraacetate. Thermolysis of compound **346** with simultaneous desulfurisation with triethyl phosphite yields a symmetrical alkene.

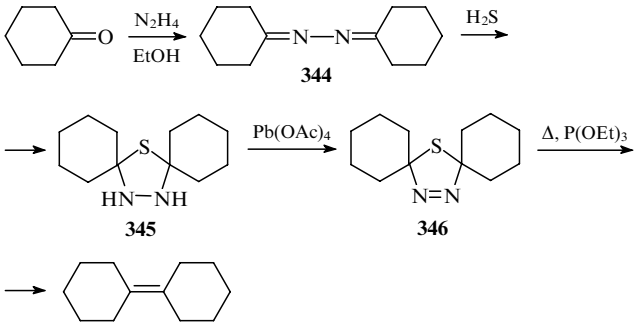

A procedure based on the use of selenocarbonyl compounds was effective in the synthesis of sterically hindered alkenes.[7, 24] Thus 2,2-di-*tert*-butyl-1,1-diphenylethylene (**347**) was prepared from di-*tert*-butylselone **348** and diphenyldiazomethane **349**.[24]

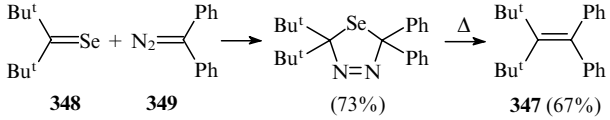

2. Thermal splitting of β-lactones

Thermal splitting of β-lactones **350** is a convenient method for the preparation of alkenes containing alkyl and aryl substituents at the double bond.[242] The corresponding lactones are formed by cyclisation of β-hydroxy acids under the action of benzenesulfonyl chloride in the presence of pyridine, while β-hydroxy acids are, in turn, prepared either by the condensation of dilithium derivatives of carboxylic acids with aldehydes and ketones or by the Reformatsky reaction. Thermolysis of β-lactones at 140–160 °C gives the corresponding alkenes in yields varying from moderate to quantitative.

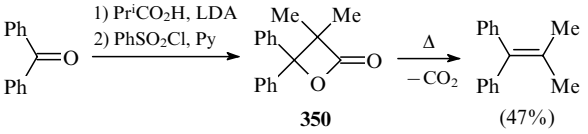

Sometimes, the formation of alkenes from β-hydroxy acids may take place *in situ* even in the step of lactone formation. It was found that the cyclisation of β-hydroxy acids in the presence of pyridine on gentle heating (45–55 °C) is accompanied by simultaneous decarboxylation of lactones, which yields almost exclusively *E*-stereoisomers of alkenes. Since the cyclisation of β-hydroxy acids results in the formation of the least sterically hindered lactones, *cis*-elimination of carbon dioxide yields the least hindered alkenes.

A two-step procedure for the synthesis of dichlorostyrenes from the corresponding aldehydes has been proposed.[243] The first step includes the [2 + 2]-cycloaddition of dichloroketene **351** to an aldehyde. The lactone **352** undergoes thermal decarboxylation to give the corresponding dichlorostyrene. The yields in the first step are 29%–83%, those in the second step are 23%–86%. In the case of aldehydes containing electron-withdrawing substituents, the yields are higher than from aldehydes containing donor groups.

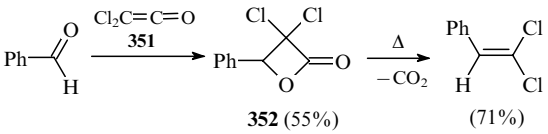

3. Olefination of carbonyl compounds by diazoalkanes in the presence of metal-complex catalysts

A method for the olefination of carbonyl compounds by stable diazoalkanes in the presence of stoichiometric amounts of triphenylphosphine catalysed by metal complexes based on rhenium,[244–251] ruthenium,[252,253] rhodium,[253] iron,[254–258] cobalt [259] and molybdenum,[260] has been developed.

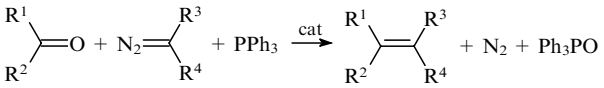

This reaction, which is analogous to the Wittig reaction, does not require strong bases for the synthesis of phosphorus ylides.[253] In the majority of cases, ylides are synthesised from stable diazoalkanes containing an electron-withdrawing group, although trimethylsilyldiazomethane was also employed.[253] The necessity to use stable diazocompounds and stoichiometric amounts of triphenylphosphine in this reaction poses certain restrictions on its synthetic application.

This version of olefination widely employs rhenium catalysts, *e.g.*, methyltrioxorhenium (**353**).[244,245] The olefination of carbonyl compounds upon treatment with ethyl diazoacetate or ethyl diazomalonate in the presence of equimolar amounts of triphenylphosphine and catalytic amounts of $MeReO_3$ has been described.[245] In the absence of the catalyst, no olefination occurs; the diazo compound reacts with the aldehyde to give a nonsymmetrical azine. It has been shown [246] that the rhenium(V) derivative **354** formed upon reduction of methyltrioxorhenium with triphenylphosphine plays the role of a true catalyst. Presumably, this reaction proceeds *via* the rhenium-carbene complex **355** as a key intermediate.[245,246] Subsequent [2 + 2]-cycloaddition of the carbonyl group to the carbene complex **355** results in metallacyclobutane **356**, the fragmentation of the latter yields an alkene.

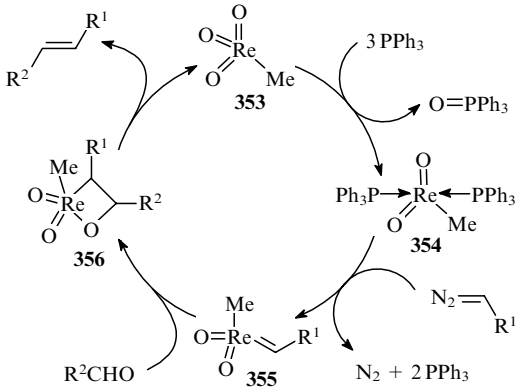

A binuclear rhenium(VII)–rhenium(V) complex **357** formed in the reaction of methyltrioxorhenium with triphenylphosphine [246] and an η^2-alkyne methyldioxorhenium complex [248] can be used as catalysts.

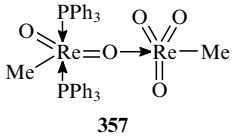

This method was used in the synthesis of α,β-unsaturated acid esters starting from aliphatic, aromatic and α,β-unsaturated aldehydes and cyclic ketones as the carbonyl components. *E*-Isomers of alkenes are formed in this reaction in high yields (80%–97%). In the case of aromatic aldehydes, the presence of electron-withdrawing substituents in the *para*-position relative to the carbonyl group favours the reaction.

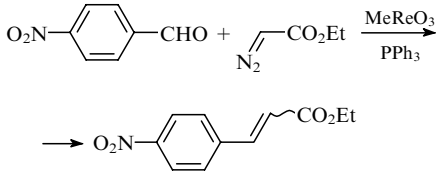

The ruthenium complex $RuCl_2(PPh_3)_3$ is yet another convenient catalyst for the olefination of aldehydes with ethyl diazoacetate in the presence of triphenylphosphine.[252] The mechanism of this reaction is not specified, but the formation of a ruthenium–carbene complex is conjectured. The stereoselectivity of this reaction is high both in the case of aliphatic and aromatic substrates; the ratio of *E*- and *Z*-isomers of α,β-unsaturated esters is no less than 9 : 1.

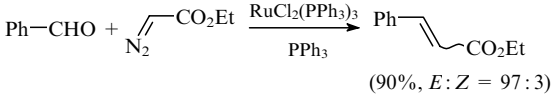

Trimethylsilyldiazomethane (**358**), in the presence of equimolar amounts of triphenylphosphine, was proposed for the methylation of aldehydes.[253] The choice of an optimum catalyst for this reaction, *viz.*, the Wilkinson catalyst $RhCl(PPh_3)_3$, was made based on the results of studies of catalytic activities of several rhodium and ruthenium complexes. This method proved to be suitable for the synthesis of terminal alkenes from various aldehydes. Functional or protective groups do not interfere with

this reaction. It is of note that the keto group of the substrate is not involved in the reaction. The yields of the alkenes are 60% – 98%.

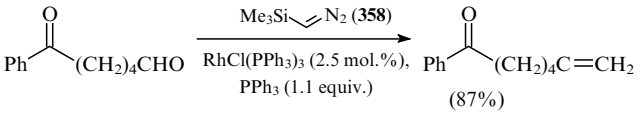

The olefination of aldehydes with ethyl diazoacetate in the presence of an iron(II) complex with tetra(*p*-tolyl)porphyrin [Fe^{II}(TTP)] proceeds with very high *trans*-stereoselectivity and in nearly quantitative yields.[254]

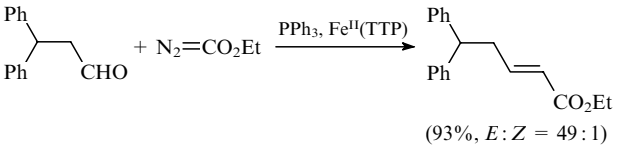

Presumably,[254] the mechanism of this reaction includes the formation of the iron carbene complex **359**, which is further involved in the transfer of carbene to triphenyl phosphine resulting in the ylide **360**. The olefination step itself is not included in the catalytic cycle.

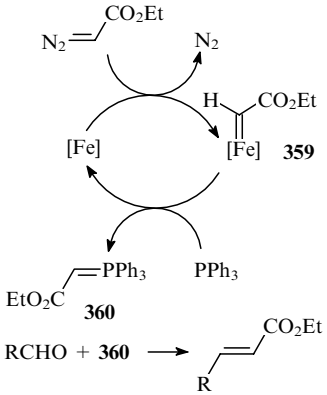

A similar olefination reaction is catalysed by the molybdenum complex $MoO_2(S_2CNEt_2)_2$.[260] This reaction proceeds with high stereoselectivity, but the yields of the corresponding alkenes are lower than in the catalysis by other metals. Aromatic, aliphatic and α,β-unsaturated aldehydes were used as the carbonyl components.

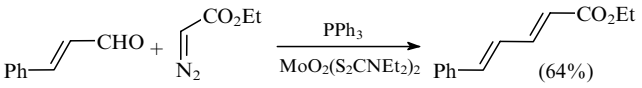

The reaction mechanism involves the formation of the molybdenum-carbene complex **361** which plays the role of the olefinating agent.

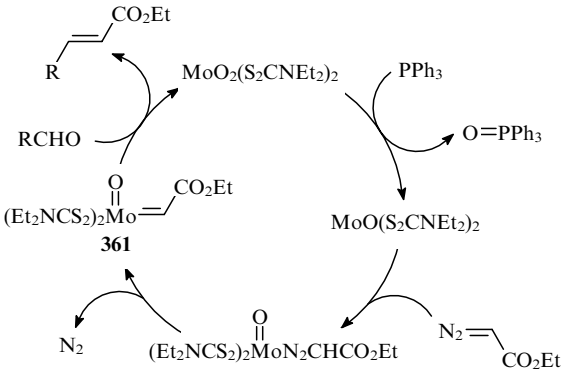

4. Catalytic olefination of hydrazones

A new, in principle, reaction of the catalytic olefination of hydrazones of carbonyl compounds was discovered in 1999.[261] It was found that the reaction of *N*-unsubstituted hydrazones of aromatic aldehydes **362** with *gem*-dihalo compounds $CHal_2XY$ in the presence of catalytic amounts of copper(I) chloride yields substituted alkenes. Symmetrical azines of the carbonyl derivatives **363** are formed as side products of transformations of hydrazones; this reaction is accompanied by evolution of nitrogen. Thus, a new double carbon – carbon bond is formed in this reaction.

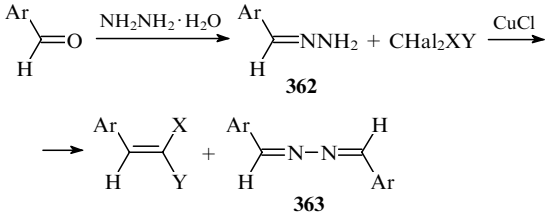

Ar = 4-$NO_2C_6H_4$, 4-ClC_6H_4, 4-$MeOC_6H_4$; Hal, X, Y = F, Cl, Br, I.

Since hydrazones are readily available, this reaction can be used as a simple two-step procedure for the synthesis of alkenes from carbonyl compounds.

In addition to copper salts, the oxidation of hydrazones with tetrachloromethane is catalysed by salts of other transition metals, such as silver, lanthanum, titanium, manganese, cobalt, rhodium, palladium and platinum. However, the highest yields of alkenes are obtained in the presence of CuCl.

This reaction served as the basis for the development of novel methods for the synthesis of various substituted alkenes. Thus the use of CCl_4 as the olefinating agent allows one to synthesise the corresponding dichloroalkenes.[262]

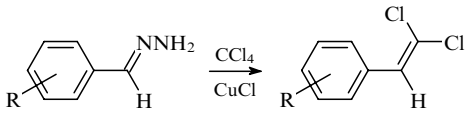

R = H (27%); 4-Cl (82%)

Substrates containing electron-withdrawing substituents in the aromatic nucleus (*e.g.*, chlorine, bromine, nitro and cyano groups) are converted into β,β-dichlorostyrenes in high yields. If hydrazones containing donor substituents or benzaldehyde hydrazone are used, the yields of dichloroalkenes are low. Low stabilities of the corresponding hydrazones are the main reason for the low yields of dichlorostyrenes in these cases.

A simplified procedure for the one-pot synthesis of dichloroalkenes directly from aldehydes, which obviates the preparation and isolation of hydrazones, has been developed.[263] Besides, in the case of donor substrates the yields of dichloroalkenes are significantly higher.

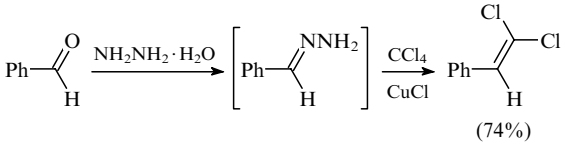

The area of synthetic applications of the catalytic olefination reaction is not confined to hydrazones of aromatic aldehydes; alkyl aryl ketone hydrazones can be converted into tetrasubstituted alkenes in good yields.[264]

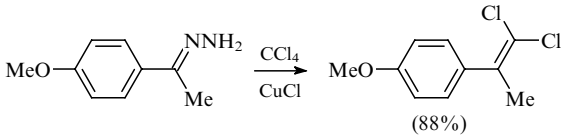

A mechanism of this reaction, which describes its catalytic cycle, has been proposed.[265–267] The first step includes oxidation of hydrazones **362** to the corresponding diazoalkanes **364** with copper(II) formed upon oxidation of CuCl with polyhaloalkanes. The diazo compounds **364** undergo further copper-catalysed fragmentation to give the copper-carbene complex **365**, the key intermediate of the olefination reaction. Further transformations of the complex **365** can proceed in two different routes. The reaction with polyhaloalkanes gives alkenes and is accompanied by regeneration of the catalyst (Cu^{II}) (the outer cycle). This reaction proceeds through oxidative addition of copper across the C—Hal bond and formation of the organocopper intermedate **366**. The side reaction, *i.e.*, the formation of azines **363**, occurs upon reaction of the complex **365** with the second molecule of diazoalkane **364** (the inner cycle).

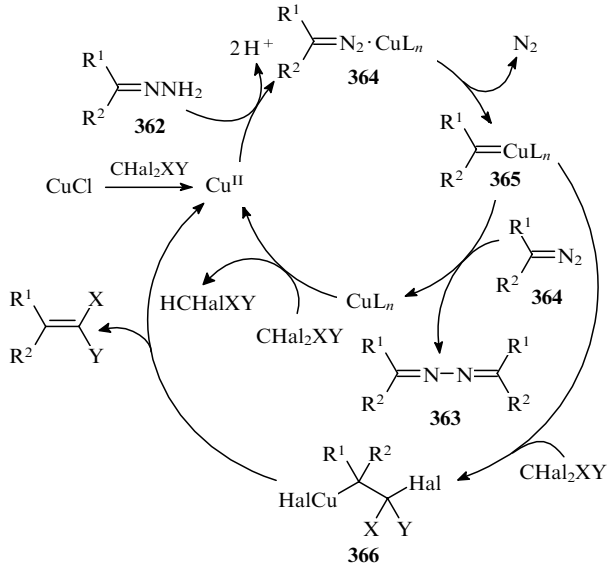

A salient advantage of this reaction is that the preparation of alkenes from carbonyl compounds does not require the use of external reducing agents, since this function is in fact fulfilled by hydrazine.

In addition to CCl_4, other polyhaloalkanes can be used as the olefinating agents; by varying the latter, one can obtain various types of alkenes. In particular, with CBr_4 as the olefinating agent, hydrazones of carbonyl compounds are converted into the corresponding dibromoalkenes.[264, 268, 269]

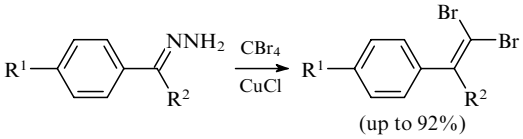

R^1 = H, MeO, Br; R^2 = H, Et.

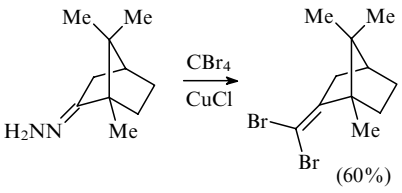

In the case of trihalomethanes (haloforms), the reaction with hydrazones yields monohalogenoalkenes. The reaction of the hydrazones of aromatic aldehydes with $CHBr_3$ leads to β-bromostyrenes stereoselectively (predominantly, *E*-isomers).[270]

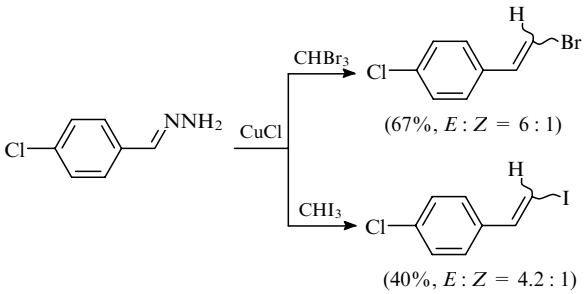

Reactions of hydrazones with iodoform proceed in a similar way. In this case, the corresponding vinyl iodides are formed as the reaction products.[271]

Fluorine-containing alkenes are formed if fluorochloroalkanes (Freons) are used as the olefinating agents. Thus reactions of hydrazones of aromatic aldehydes prepared *in situ* synthesised with Freons CCl_2FCClF_2 and CCl_3CF_3 yield fluoro alkenes **367** and **368**[272] (predominantly, less sterically hindered *Z*-isomers). The stereoselectivity of this reaction is rather high; the ratio of the isomers depends on the nature of the aromatic system and the position of the substituents in the benzene ring. Thus the stereoselectivity of the reaction increases in the case of donor substrates and decreases in the case of substrates containing electron-withdrawing groups.

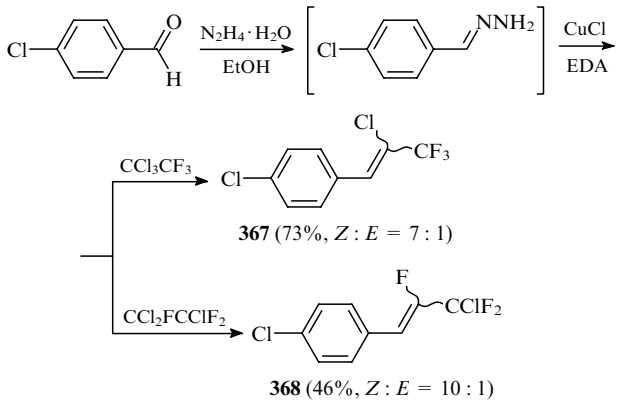

EDA is 1,2-ethylenediamine.

Dibromodifluoromethane and trichlorofluoromethane were used as fluorine-containing C_1-synthons in the catalytic olefination reaction, which afforded the corresponding *gem*-difluorostyrenes **369** (see Ref. 273) and chlorofluorostyrenes **370**.[274]

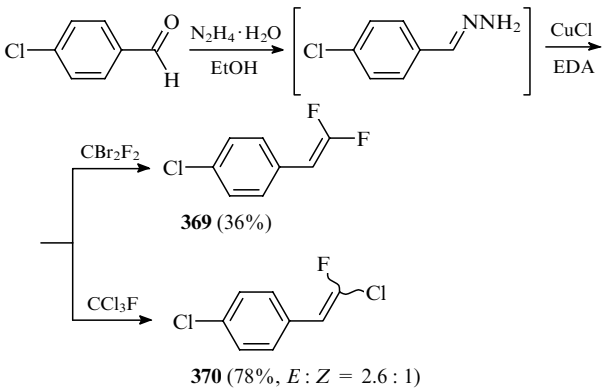

In the case of dibromotetrafluoroethane $CBrF_2CBrF_2$, the corresponding arylbromotetrafluoropropanes **371** (rather than unsaturated compounds) are formed as reaction products.

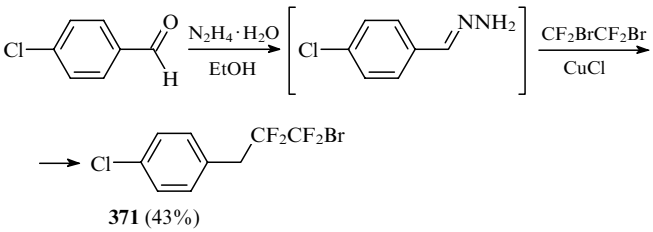

371 (43%)

It was found that in this case the abnormal course of this reaction is due to the high stability of the C–F bond. The reaction of the copper-carbene complex **365** with $CBrF_2CBrF_2$ yields the corresponding organocopper intermediate **372**; elimination of CuBrF from this intermediate is hardly likely and only the saturated compound **371** is formed.

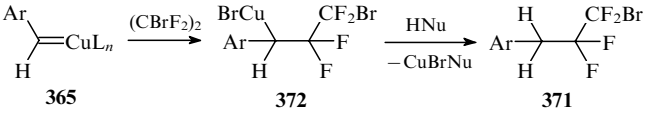

365 **372** **371**

Polyhalogenated reagents, such as CCl_3CO_2Et and CCl_3CN, are used in the synthesis of functionalised unsaturated compounds. Thus the reactions of hydrazones with ethyl trichloroacetate and trichloroacetonitrile give α-chlorocinnamates **373**[275] and α-chlorocinnamonitriles **374**.[276]

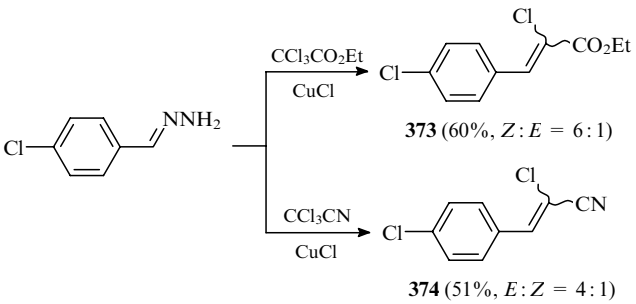

373 (60%, $Z:E = 6:1$)

374 (51%, $E:Z = 4:1$)

VI. Conclusion

A survey of the current literature demonstrates that the methods for olefination of carbonyl compounds are quite numerous and differ in the nature of the olefinating agents, reaction conditions, types of carbonyl substrates and, correspondingly, types of unsaturated compounds formed.

It is of note that the correct comparison of efficiencies of various olefination procedures is difficult, since many exotic chemical methods are more captivating than practical and have not received wide application because of their high cost, low availability of the corresponding reagents and certain inertiality of thought inherent in some synthetic chemists. Nevertheless, the present review gives an idea about both the wide arsenal and explosive development of this branch of synthetic organic chemistry.

This review has been written with the financial support of the Russian Foundation for Basic Research (Project No. 03-03-32052a).

References

1. J M J Williams (Ed.) *Preparation of Alkenes* (Oxford: Oxford University Press, 1996)
2. B M Trost, I Fleming (Eds) *Comprehensive Organic Synthesis* Vol. 1 (Oxford: Pergamon Press, 1999)
3. B M Trost, I Fleming (Eds) *Comprehensive Organic Synthesis* Vol. 2 (Oxford: Pergamon Press, 1999)
4. K C Nicolaou, E J Sorensen *Classics in Total Synthesis* (New York: VCH, 1996)
5. R C Larock *Comprehensive Organic Transformations: a Guide to Functional Group Preparations* (New York: VCH, 1989)
6. K B Becker *Synthesis* 341 (1983)
7. B M Lerman *Usp. Khim.* **64** 3 (1995) [*Russ. Chem. Rev.* **64** 1 (1995)]
8. G V Kryshtal', E P Serebryakov *Izv. Akad. Nauk, Ser. Khim.* 1867 (1995) [a]
9. A A Vasil'ev, E P Serebryakov *Usp. Khim.* **70** 830 (2001) [*Russ. Chem. Rev.* **70** 735 (2001)]
10. A Pelter *Izv. Akad. Nauk, Ser. Khim.* 1177 (1993) [a]
11. T-H Chan *Acc. Chem. Res.* **10** 442 (1977)
12. W P Weber *Silicon Reagents for Organic Synthesis* (Berlin: Springer, 1983)
13. D J Ager *Synthesis* 384 (1984)
14. D J Ager *Org. React.* **38** 1 (1990)
15. L F van Staden, D.Gravestock, D J Ager *Chem. Soc. Rev.* **31** 195 (2002)
16. P J Murphy, J Brennan *Chem. Soc. Rev.* **17** 1 (1988)
17. B E Maryanoff, A B Reitz *Chem. Rev.* **89** 863 (1989)
18. A W Johnson *Ylides and Imines of Phosphorus* (New York: Wiley, 1993)
19. T Rein, T M Pedersen *Synthesis* 579 (2002)
20. D J Burton, Z-Y Yang, W Qiu *Chem. Rev.* **96** 1641 (1996)
21. D J Burton *J. Fluorine Chem.* **100** 177 (1999)
22. J Boutagy, R Thomas *Chem. Rev.* **74** 87 (1974)
23. C Nájera, M Yus *Tetrahedron* **55** 10547 (1999)
24. T G Back (Ed.) *Organoselenium Chemistry* (New York: Oxford University Press, 1999)
25. J R Johnson, in *Organic Reactions* Vol. 1 (New York: Wiley, 1942)
26. H Feuer (Ed.) *The Chemistry of the Nitro and Nitroso Groups* (New York: Interscience, 1970)
27. A G M Barrett, G G Graboski *Chem. Rev.* **86** 751 (1986)
28. A G M Barrett *Chem. Soc. Rev.* **20** 95 (1991)
29. F A Luzzio *Tetrahedron* **57** 915 (2001)
30. J E McMurry *Chem. Rev.* **89** 1513 (1989)
31. J E McMurry *Acc. Chem. Res.* **7** 281 (1974)
32. D Lenoir *Synthesis* 883 (1989)
33. J E McMurry *Acc. Chem. Res.* **16** 405 (1983)
34. A Fürstner, B Bogdanovic *Angew. Chem., Int. Ed. Engl.* **35** 2442 (1996)
35. M Ephritikhine *J. Chem. Soc., Chem. Commun.* 2549 (1998)
36. A J Gordon, R A Ford *The Chemist's Companion* (New York: Wiley-Interscience, 1972)
37. J Emsley *The Elements* (Oxford: Clarendon Press, 1991)
38. D A Johnson *Some Thermodynamic Aspects of Inorganic Chemistry* (Cambridge: Cambridge University Press, 1982)
39. I Marek, J-F Normant *Chem. Rev.* **96** 3241 (1996)
40. G Cainelli, G Dal Bello, G Zubiani *Tetrahedron Lett.* **7** 4315 (1966)
41. A Mendoza, D S Matteson *J. Org. Chem.* **44** 1352 (1979)
42. A Pelter, B Singaram, J W Wilson *Tetrahedron Lett.* **24** 635 (1983)
43. A Pelter, D Buss, E Colclough, B Singaram *Tetrahedron* **49** 7077 (1993)
44. A Pelter, B Singaram, L Warren, W Wilson *Tetrahedron* **49** 2965 (1993)
45. M Sakai, S Saito, G Kanai, A Suzuki, N Miyaura *Tetrahedron* **52** 915 (1996)
46. D J Peterson *J. Org. Chem.* **33** 780 (1968)
47. P F Hudrilik, D J Peterson *Tetrahedron Lett.* **15** 1133 (1974)
48. P F Hudrilik, D J Peterson *J. Am. Chem. Soc.* **97** 1464 (1975)
49. T Kauffmann, R Konig, C Pahde, A Tannert *Tetrahedron Lett.* **22** 5031 (1981)
50. C R Johnson, B D Tait *J. Org. Chem.* **52** 281 (1987)
51. T Imamoto *Pure Appl. Chem.* **62** 747 (1990)
52. M B Gillies, J E Tonder, D Tanner, P-O Norrby *J. Org. Chem.* **67** 7378 (2002)
53. W Adam, C M Ortega-Schulte *Synlett* 414 (2003)
54. H Gilman, R A Tomasi *J. Org. Chem.* **27** 3647 (1962)
55. F A Carey, A S Court *J. Org. Chem.* **37** 939 (1972)
56. N Asakura, Y Usuki, H Iio *J. Fluorine Chem.* **124** 81 (2003)
57. A I Meyers, G E Jagdmann *J. Am. Chem. Soc.* **104** 877 (1982)
58. A L Meyers, P D Edwards, T R Bailey, G E Jagdmann *J. Org. Chem.* **50** 1019 (1985)
59. M Bellassoued, A Majidi *J. Org. Chem.* **58** 2517 (1993)

60. S Kojima, H Inai, T Hidaka, T Fukuzaki, K Ohkata *J. Org. Chem.* **67** 4093 (2002)
61. T Murai, A Fujishima, C Iwamoto, S Kato *J. Org. Chem.* **68** 7979 (2003)
62. C Palomo, J M Aizpurua, M Legido, J P Picard, J Dunogues, T Constantieux *Tetrahedron Lett.* **33** 3903 (1992)
63. T F Bates, S A Dandekar, J J Longlet, R D Thomas *J. Organomet. Chem.* **625** 13 (2001)
64. S Inoue, Y Sato *J. Org. Chem.* **56** 347 (1991)
65. T Kauffmann, R Kriegesmann, A Woltermann *Angew. Chem., Int. Ed. Engl.* **16** 862 (1977)
66. T Kauffmann, R Kriegesmann, A Hamsen *Chem. Ber.* **115** 1818 (1982)
67. T Kauffmann, R Konig, R Kriegesmann, M Wensing *Tetrahedron Lett.* **25** 641 (1984)
68. H Tanaka, S Yamashita, M Yamanoue, S Torii *J. Org. Chem.* **54** 444 (1989)
69. U Schollkopf, F Gerhart *Angew. Chem.* **80** 842 (1968)
70. K C Nicolaou, M W Harter, J L Gunzner, A Nadin *Liebigs Ann. Chem.* 1283 (1997)
71. F Mari, P M Lahti, W E McEwen *J. Am. Chem. Soc* **114** 813 (1992)
72. H Yamataka, S Nagase *J. Am. Chem. Soc.* **120** 7530 (1998)
73. M G Kulkarni, R M Rasne, S I Davawala, A K Doke *Tetrahedron Lett.* **43** 2297 (2002)
74. M G Kulkarni, A K Doke, S I Davawala, A V Doke *Tetrahedron Lett.* **44** 4913 (2003)
75. G A Kraus, P K Choudhury *Synlett* 97 (2004)
76. P H G Zarbin, J L Princival, E R de Lima, A A dos Santos, B G Ambrogio, A R M de Oliveira *Tetrahedron Lett.* **45** 239 (2004)
77. R N MacCoss, E P Balskus, S V Ley *Tetrahedron Lett.* **44** 7779 (2003)
78. I Ernest, J Gosteli, R B Woodward *J. Am. Chem. Soc.* **101** 6301 (1979)
79. T Tsunoda, H Takagi, D Takaba, H Kaku, S Ito *Tetrahedron Lett.* **41** 235 (2000)
80. A R Katritzky, J Li *J. Org. Chem.* **62** 238 (1997)
81. W C Still, C Gennary *Tetrahedron Lett.* **24** 4405 (1983)
82. B M Trost, P Metz, J T Hane *Tetrahedron Lett.* **27** 5691 (1986)
83. J Fan, B Dolensky, I H Kim, K L Kirk *J. Fluorine Chem.* **115** 137 (2002)
84. S Harusawa, S Koyabu, Y Inoue, Y Sakamoto, L Araki, T Kurihara *Synthesis* 1072 (2002)
85. J Villieras, M Rambaud *Synthesis* 300 (1983)
86. A Lattanzi, L R Orelli, P Barone, A Massa, P Iannece, A Scettri *Tetrahedron Lett.* **44** 1333 (2003)
87. H Inoue, H Tsubouchi, Y Nagaoka, K Tomioka *Tetrahedron* **58** 83 (2002)
88. L Horner, N M R Hoffman, H G Wippel, G Klahre *Chem. Ber.* **92** 2499 (1959)
89. A D Buss, S Warren *Tetrahedron Lett.* **24** 3931 (1983)
90. A D Buss, S Warren *J. Chem. Soc., Perkin Trans. 1* 2307 (1985)
91. D Lloyd, I Gosney, R A Ormiston *Chem. Soc. Rev.* **16** 45 (1987)
92. Y Huang, Y Shen, J Zheng, S Zhang *Synthesis* 57 (1985)
93. Y Huang, L Shi, J Yang *Tetrahedron Lett.* **26** 6447 (1985)
94. R S Tewari, S C Chaturvedi *Indian J. Chem., Sect. B.* **18** 359 (1979)
95. Y Shen, W Qui *Synthesis* 65 (1987)
96. Y Z Huarg, Y Shen, C Chen *Tetrahedron Lett.* **27** 2903 (1986)
97. Y Liao, Y-Z Huang *Tetrahedron Lett.* **31** 5897 (1990)
98. A P Davis, K M Bhattarai *Tetrahedron* **51** 8033 (1995)
99. M Julia, J M Paris *Tetrahedron Lett.* **14** 4833 (1973)
100. P R Blakemore *J. Chem. Soc., Perkin Trans. 1* **23** 2563 (2002)
101. E N Prilezhaeva *Usp. Khim.* **69** 403 (2000) [*Russ. Chem. Rev.* **69** 367 (2000)]
102. B Achmatowicz, E Baranowska, A R Daniewski, J Panowski, J Wicha *Tetrahedron Lett.* **26** 5597 (1985)
103. S J Danishefsky, H G Selnick, R E Zelle, M P DeNinno *J. Am. Chem. Soc.* **110** 4368 (1988)
104. P L Kocienski, B Lythgoe, S Ruston *J. Chem. Soc., Perkin Trans. 1* 829 (1978)
105. G E Keck, K A Savin, M A Weglarz *J. Org. Chem.* **60** 3194 (1995)
106. I E Marko, F Murphy, S Dolan *Tetrahedron Lett.* **37** 2089 (1996)
107. I E Markó, F Murphy, L Kumps, A Ates, R Touillaux, D Craig, S Carballares, S Dolan *Tetrahedron* **57** 2609 (2001)
108. J B Baudin, G Hareau, S A Julia, O Ruel *Tetrahedron Lett.* **32** 1175 (1991)
109. P R Blakemore, W J Cole, P J Kocienski A Morley *Synlett* 26 (1998)
110. P J Kocienski, A Bell, P R Blakemore *Synlett* 365 (2000)
111. A B Charette, C Berthelette, D St-Martin *Tetrahedron Lett.* **42** 5149 (2001)
112. S Surprenant, W Y Chan, C Berthelette *Org. Lett.* **5** 4851 (2003)
113. D A Alonso, C Najera, M Varea *Tetrahedron Lett.* **45** 573 (2004)
114. T Mandai, T Yanagi, K Araki, Y Morisaki, M Kawada, J Otera *J. Am. Chem. Soc.* **106** 3670 (1984)
115. J Otera, H Misawa, K Sugimoto *J. Org. Chem.* **51** 3830 (1986)
116. T Mandai, T Moriyama, K Tsujimoto, M Kawada, J Otera *Tetrahedron Lett.* **27** 603 (1986)
117. J Otera, H Misawa, T Onishi, S Suzuki, Y Fujita *J. Org. Chem.* **51** 3834 (1986)
118. F Ye, A Orita, A Doumoto, J Otera *Tetrahedron* **59** 5635 (2003)
119. V Pascali, A Umani-Ronchi *J. Chem. Soc., Perkin Trans. 1* 1166 (1973)
120. V Pascali, A Umani-Ronchi *J. Chem. Soc., Chem. Commun.* 351 (1973)
121. T Satoh, N Yamada, T Asano *Tetrahedron Lett.* **39** 6935 (1998)
122. T Satoh, N Hanaki, N Yamada, T Asano *Tetrahedron* **56** 6223 (2000)
123. J N P D'herde, P J DeClercq *Tetrahedron Lett.* **44** 6657 (2003)
124. C R Johnson, J R Shanklin, R A Kirchhoff *J. Am. Chem. Soc.* **95** 6462 (1973)
125. C R Johnson, R A Kirchhoff *J. Am. Chem. Soc.* **101** 3602 (1979)
126. H Niwa, K Wakamatsu, T Hida, K Niiyama, H Kigoshi, M Yamada, H Nagase, M Suzuli, K Yamada *J. Am. Chem. Soc.* **106** 4547 (1984)
127. M L Boys, E W Collington, H Finch, S Swanson, J F Whitehead *Tetrahedron Lett.* **29** 3365 (1988)
128. C R Johnson, N A Meanwell *J. Am. Chem. Soc.* **103** 7667 (1981)
129. R L Sowerby, R M Coates *J. Am. Chem. Soc.* **94** 4758 (1972)
130. S C Welch, J-P Loh *J. Org. Chem.* **46** 4072 (1981)
131. S G Cabiddu, S Cabiddu, E Cadoni, S De Montis, C Fattuoni, S Melis, M Usai *Synthesis* 875 (2002)
132. J Remion, W Dumont, A Krief *Tetrahedron Lett.* **17** 1385 (1976)
133. H J Reich, F Chow, S K Shah *J. Am. Chem. Soc.* **101** 6638 (1979)
134. H J Reich *Acc. Chem. Res.* **12** 22 (1979)
135. M Clarembeau, A Cravador, W Dumont, L Hevesi, A Krief, J Lucchetti, D Van Ende *Tetrahedron* **41** 4793 (1985)
136. J Remion, A Krief *Tetrahedron Lett.* **17** 3743 (1976)
137. D Labar, A Krief *J. Chem. Soc., Chem. Commun.* 564 (1982)
138. G Iwasaki, M Sano, M Sodeoka, K Yoshida, M Shibasaki *J. Org. Chem.* **53** 4862 (1988)
139. A Osuka, Y Mori, H Shimizu *Tetrahedron Lett.* **24** 2599 (1983)
140. Z-L Zhou, L-L Shi, Y-Z Huang *Synth. Commun.* **21** 1027 (1991)
141. Z-L Zhou, Y-Z Huang, L-L Shi *Tetrahedron* **49** 6821 (1993)
142. Z Z Huang, S Ye, W Xia, Y Tang *J. Chem. Soc., Chem. Commun.* 1384 (2001)
143. Z Z Huang, S Ye, W Xia, Y-H Yu, Y Tang *J. Org. Chem.* **67** 3096 (2002)
144. G M Zhdankina, G V Kryshtal', E P Serebryakov, L A Yanovskaya *Izv. Akad. Nauk, Ser. Khim.* 2868 (1988) [a]
145. A Merz *Angew. Chem.* **89** 54 (1977)
146. Z Wang, S Campagna, G Xu, M E Pierce, J M Fortunak, P N Confalone. *Tetrahedron Lett.* **41** 4007 (2000)
147. H Rezaei, J F Normant *Synthesis* 109 (2000)
148. D R Williams, K Nishitani, W Bennett, S Y Sit *Tetrahedron Lett.* **22** 3745 (1981)

149. J Barluenga, J L Fernandez-Simon, J M Concellon, M Yus *J. Chem. Soc., Perkin Trans. 1* 691 (1989)
150. J Barluenga, J L Fernandez-Simon, J M Concellon, M Yus *J. Chem. Soc., Perkin Trans. 1* 3339 (1988)
151. T Mukaiyama, K Banno, K Narasaka *J. Am. Chem. Soc.* **96** 7503 (1974)
152. J K Whitesell, M A Whitesell *Synthesis* 517 (1983)
153. R F Borch, A J Evans, J J Wade *J. Am. Chem. Soc.* **99** 1612 (1977)
154. N Ya Grigorieva, O A Pinsker *Usp. Khim.* **63** 177 (1994) [*Russ. Chem. Rev.* **63** 169 (1994)]
155. P Brownbridge *Synthesis* 85 (1983)
156. D Enders, M Klatt *Synthesis* 1403 (1996)
157. C Fehr *Angew. Chem., Int. Ed. Engl.* **35** 2567 (1996)
158. C J Cowden, I Paterson *Org. React.* **51** 1 (1997)
159. S G Nelson *Tetrahedron: Asymmetry* **9** 357 (1998)
160. R Mahrwald *Chem. Rev.* **99** 1095 (1999)
161. D Enders, J Adam, D Klein, T Otten *Synlett* 1371 (2000)
162. P Arya, H Qin *Tetrahedron* **56** 917 (2000)
163. M D Groaning, A I Meyers *Tetrahedron* **56** 9843 (2000)
164. D Cahard, P Duhamel *Eur. J. Org. Chem.* 1023 (2001)
165. C Palomo, M Oiarbide, J M Garcia *Chem.-Eur. J.* **8** 37 (2002)
166. A Job, C F Janeck, W Bettray, R Peters, D Enders *Tetrahedron* **58** 2253 (2002)
167. Y-J Jang, W-W Lin, Y-K Shih, J-T Liu, M-H Hwang, C-F Yao *Tetrahedron* **59** 4979 (2003)
168. P Knochel, D Seebach *Synthesis* 1017 (1982)
169. W Lehnert *Tetrahedron Lett.* **11** 4723 (1970)
170. E Campaigne, J C Beckman *Synthesis* 385 (1978)
171. C Su, Z-C Chen, Q-G Zheng *Synthesis* 555 (2003)
172. D A R Happer, B E Steenson *Synthesis* 806 (1980)
173. R Tanikaga, N Konya, T Tamura, A Kaji *J. Chem. Soc., Perkin Trans. 1* 825 (1987)
174. W Lehnert *Tetrahedron* **30** 301 (1974)
175. F Fringuelli, O Piermatti, F Pizzo *Synthesis* 2331 (2003)
176. B List, C Castello *Synlett* 1687 (2001)
177. A J Fatiadi *Synthesis* 165 (1978)
178. F Freeman *Chem. Rev.* **80** 329 (1980)
179. Yu A Sharanin, V K Promonenkov, V P Litvinov, in *Malononitril. Organicheskaya Khimiya (Itogi Nauki i Tekhniki)* [Malononitrille. Organic Chemistry (Advances in Science and Engineering Series)] (Moscow: Izd. VINITI, 1991) p. 20
180. T-Y Tsai, K-S Shia, H-J Liu *Synlett* 97 (2003)
181. V Dryanska, C Ivanov *Tetrahedron Lett.* **16** 3519 (1975)
182. S D Van Arnum, K Ramig, N A Stepsus, Y Dong, R A Outten *Tetrahedron Lett.* **37** 8659 (1996)
183. A R Katritzky, D Cheng, S A Henderson, J Li *J. Org. Chem.* **63** 6704 (1998)
184. A R Katritzky, D Toader *Synlett* 458 (2001)
185. M Fujita, T Morita, T Hiyama *Tetrahedron Lett.* **27** 2135 (1986)
186. M Fujita, T Hiyama, K Kondo *Tetrahedron Lett.* **27** 2139 (1986)
187. M Fujita, T Hiyama *Tetrahedron Lett.* **27** 3655 (1986)
188. H Hashimoto, M Hida, S Miyano *J. Organomet. Chem.* **10** 518 (1967)
189. K Takai, Y Hotta, K Oshima, H Nozaki *Tetrahedron Lett.* **19** 2417 (1978)
190. L Lombardo *Tetrahedron Lett.* **23** 4293 (1982)
191. T Okazoe, T Hibino, K Takai, N Nozaki *Tetrahedron Lett.* **26** 5581 (1985)
192. K Ukai, D Arioka, H Yoshino, H Fushimi, K Oshima, K Utimoto, S Matsubara *Synlett* 513 (2001)
193. D C Barman, A J Thakur, D Prajapati, J S Sandhu *Synlett* 515 (2001)
194. J-X Wang, Y Fu, Y Hu, K Wang *Synthesis* 1506 (2003)
195. R L Shriner, in *Organic Reactions* Vol. 1 (New York: Wiley, 1942)
196. A Fürstner *J. Organomet. Chem.* **336** C33 (1987)
197. D Seyferth, D C Mueller *J. Am. Chem. Soc.* **93** 3714 (1971)
198. C Quian, A Qui *Tetrahedron Lett.* **29** 6931 (1988)
199. J E McMurry, T Lectka, J G Rico *J. Org. Chem.* **54** 3748 (1989)
200. D Lenoir, D Malwitz, E Meyer *Tetrahedron Lett.* **25** 2965 (1984)
201. M Beller, C Bolm *Transition Metals for Organic Synthesis* Vol. 1 (New York: Wiley-VCH, 1998)
202. A Fürstner, A Hupperts, A Ptock, E Janssen *J. Org. Chem.* **59** 5215 (1994)
203. A Fürstner, A Hupperts, G Seidel *Org. Synth.* **76** 142 (1998)
204. A Fürstner *Pure Appl. Chem.* **70** 1071 (1998)
205. F N Tebbe, G W Parshall, G S Reddy *J. Am. Chem. Soc.* **100** 3611 (1978)
206. L F Cannizzo, R H Grubbs *J. Org. Chem.* **50** 2386 (1985)
207. J B Lee, R H Grubbs *J. Am. Chem. Soc.* **102** 6876 (1980)
208. S H Pine, R Zahler, D A Evans, R H Grubbs *J. Am. Chem. Soc.* **102** 3270 (1980)
209. S H Pine, R J Pettit, G D Geib, S G Cruz, C H Gallego, T Tijerina, R D Pine *J. Org. Chem.* **50** 1212 (1985)
210. N A Petasis, E I Bzowej *J. Am. Chem. Soc.* **112** 6392 (1990)
211. H Siebeneicher, S Doye *J. Prakt. Chem.* **342** 102 (2000)
212. N A Petasis, E I Bzowej *J. Org. Chem.* **57** 1327 (1992)
213. N A Petasis, I Akritopoulou *Synlett* 665 (1992)
214. N A Petasis, J P Staszewski, D-K Fu *Tetrahedron Lett.* **36** 3619 (1995)
215. T Takeda, R Sasaki, T Fujiwara *J. Org. Chem.* **63** 7286 (1998)
216. T Takeda, Y Endo, A Chandra Sheker Reddy, R Sasaki, T Fujiwara *Tetrahedron* **55** 2475 (1999)
217. T Takeda, K Shimane, K Ito, N Saeki, A Tsubouchi *Chem. Commun.* 1974 (2002)
218. M A Rahim, H Sasaki, J Saito, T Fujiwara, T Takeda *Chem. Commun.* 625 (2001)
219. T Takeda, J Saito, A Tsubouchi *Tetrahedron Lett.* **44** 5571 (2003)
220. J M Tour, P V Bedworth, R Wu *Tetrahedron Lett.* **30** 3927 (1989)
221. F W Hartner, J Schwartz, S M Clift *J. Am. Chem. Soc.* **105** 640 (1983)
222. S M Clift, J Schwartz *J. Am. Chem. Soc.* **106** 8300 (1984)
223. J P Collman, L S Hegedus, J R Norton, R G Finke *Principles and Applications of Organotransition Metal Chemistry* Vol. 2 (Mill Valley, CA: University Science Books, 1987)
224. R R Schrock *J. Chem. Soc., Dalton Trans.* 2541 (2001)
225. R R Schrock *J. Am. Chem. Soc.* **98** 5399 (1976)
226. K Takai, K Nitta, K Utimoto *J. Am. Chem. Soc.* **108** 7408 (1986)
227. D M Hodgson, L T Boulton, G N Maw *Tetrahedron* **51** 3713 (1995)
228. K Takai, Y Kataoka, Y Okazoe, K Utimoto *Tetrahedron Lett.* **28** 1443 (1987)
229. C E Castro, W C Kray *J. Am. Chem. Soc.* **88** 4447 (1966)
230. T Kauffmann, B Enner, J Sandler, R Wieschollek *Angew. Chem.* **95** 237 (1983)
231. A Aguero, J Kress, J A Osborn *J. Chem Soc., Chem. Commun.* 531 (1986)
232. K B Sharpless, M A Umbreit, M T Nieh, T C Flood *J. Am. Chem. Soc.* **94** 6538 (1972)
233. Y Fujiwara, R Ishikawa, F Akiyama, S Teranishi *J. Org. Chem.* **43** 2477 (1978)
234. M N Chisholm, J A Klang *J. Am. Chem. Soc.* **111** 2324 (1989)
235. A Dormond, A E Bouadili, C Moke *J. Org. Chem.* **52** 688 (1987)
236. F Bertini, P Grasselli, G Zubiani, G Cainelli *Tetrahedron* **26** 1281 (1970)
237. B J J van de Heisteeg, G Schat, M A G M Tinga, O S Akkerman, F Bickelhaupt *Tetrahedron Lett.* **27** 6123 (1986)
238. A M Piotrowski, D B Malpass, M P Boleslawski, J J Eisch *J. Org. Chem.* **53** 2829 (1988)
239. D H R Barton, B J Willis *J. Chem. Soc., Perkin Trans. 1* 305 (1972)
240. J Buter, S Wassenaar, R M Kellogg *J. Org. Chem.* **37** 4045 (1972)
241. F J Hoogesteger, R W A Havenith, J W Zwikker, L W Jenneskens, H Kooijman, N Veldman, A L Spek *J. Org. Chem.* **60** 4375 (1995)
242. A Waldemar, B Jaime, L Ju-Chao *J. Am. Chem. Soc.* **94** 2000 (1972)
243. H O Krabbenhoft *J. Org. Chem.* **43** 1305 (1978)

244. G S Owens, J Arias, M M Abu-Omar *Catal. Today* **55** 317 (2000)
245. W A Hermann, M Wang *Angew. Chem.* **103** 1709 (1991)
246. C C Romäo, F E Kühn, W A Hermann *Chem. Rev.* **97** 3197 (1997)
247. W A Hermann, P W Roesky, M Wang, W Scherer *Organometallics* **13** 4531 (1994)
248. B E Ledford, E M Carriera *Tetrahedron Lett.* **38** 8125 (1997)
249. A M Santos, C C Romao, F E Kuhn *J. Am. Chem. Soc.* **125** 2414 (2003)
250. R Harrison, A Mete, L Wilson *Tetrahedron Lett.* **44** 6621 (2003)
251. X Zhang, P Chen *Chem.-Eur. J.* 1852 (2003)
252. O Fujimura, T Honma *Tetrahedron Lett.* **39** 625 (1998)
253. H Lebel, V Paquet, C Proulx *Angew. Chem., Int. Ed.* **40** 2887 (2001)
254. G A Mirafzal, G Cheng, L K Woo *J. Am. Chem. Soc.* **124** 176 (2002)
255. S J Mahmood, C Brennan, M M Hossain *Synthesis* 1807 (2002)
256. Y Chen, L Huang, X P Zhang *J. Org. Chem.* **68** 3714 (2003)
257. G Cheng, G A Mirafzal, L K Woo *Organometallics* **22** 1468 (2003)
258. Y Chen, L Huang, X P Zhang *J. Org. Chem.* **68** 5925 (2003)
259. M-Y Lee, Y Chen, X P Zhang *Organometallics* **22** 4905 (2003)
260. X Lu, H Fang, Z Ni *J. Organomet. Chem.* **373** 77 (1989)
261. A V Shastin, V N Korotchenko, V G Nenajdenko, E S Balenkova *Izv. Akad. Nauk, Ser. Khim.* 2210 (1999) [a]
262. A V Shastin, V N Korotchenko, V G Nenajdenko, E S Balenkova *Tetrahedron* **56** 6557 (2000)
263. V G Nenajdenko, A V Shastin, V N Korotchenko, E S Balenkova *Izv. Akad. Nauk, Ser. Khim.* 1003 (2001) [a]
264. V N Korotchenko, A V Shastin, V G Nenajdenko, E S Balenkova *J. Chem. Soc., Perkin Trans. 1* 883 (2002)
265. V N Korotchenko, A V Shastin, V G Nenajdenko, E S Balenkova *Izv. Akad. Nauk, Ser. Khim.* 469 (2003) [a]
266. V N Korotchenko, A V Shastin, V G Nenajdenko, E S Balenkova *Zh. Org. Khim.* **39** 562 (2003) [b]
267. V G Nenajdenko, V N Korotchenko, A V Shastin, D A Tyurin, E S Balenkova *Izv. Akad. Nauk, Ser. Khim.* 1740 (2003) [a]
268. A V Shastin, V N Korotchenko, V G Nenajdenko, E S Balenkova *Synthesis* 2081 (2001)
269. V N Korotchenko, A V Shastin, V G Nenajdenko, E S Balenkova *Organic and Biomolecular Chemistry* **1** 1906 (2003)
270. A V Shastin, V N Korotchenko, V G Nenajdenko, E S Balenkova *Izv. Akad. Nauk, Ser. Khim.* 1334 (2001) [a]
271. A V Shastin, V N Korotchenko, G N Varseev, V G Nenajdenko, E S Balenkova *Zh. Org. Khim.* **39** 433 (2003) [b]
272. V N Korotchenko, A V Shastin, V G Nenajdenko, E S Balenkova *Tetrahedron* **57** 7519 (2001)
273. V G Nenajdenko, G N Varseev, V N Korotchenko, A V Shastin, E S Balenkova *J. Fluorine Chem.* **124** 115 (2003)
274. V G Nenajdenko, A V Shastin, V N Korotchenko, G N Varseev, E S Balenkova *Eur. J. Org. Chem.* 302 (2003)
275. V G Nenajdenko, O N Lenkova, A V Shastin, E S Balenkova *Synthesis* 573 (2004)
276. V G Nenajdenko, A V Shastin, I V Golubinskii, O N Lenkova, E S Balenkova *Izv. Akad. Nauk, Ser. Khim.* 218 (2004) [a]

[a] — *Russ. Chem. Bull., Int. Ed. (Engl. Transl.)*
[b] — *Russ. J. Org. Chem. (Engl. Transl.)*

Russian Chemical Reviews **73** (10) 991 – 1001 (2004) © 2004 Russian Academy of Sciences and Turpion Ltd

DOI 10.1070/RC2004v073n10ABEH000896

Oxide materials as positive electrodes of lithium-ion batteries

E V Makhonina, V S Pervov, V S Dubasova

Contents

I.	Introduction	991
II.	Lithium cobaltate and related materials	992
III.	Lithium nickelate and related materials	994
IV.	Lithium – manganese spinel and spinel-based materials	996
V.	Miscellaneous materials with average voltage of 4 V	998
VI.	The prospects of using metastable superstructures	998
VII.	Conclusion	999

Abstract. The published data on oxide materials as positive electrodes for lithium-ion batteries are described systematically. The mechanisms of structural changes in cathode materials occurring during the operation of lithium-ion batteries and the problems concerned with their selection are discussed. Modern trends in optimising cathode materials and lithium-ion batteries on the whole are considered. The bibliography includes 167 references.

I. Introduction

Whittingham[1] seems to be the first to demonstrate, by the example of Li_xTiS_2, that the process of electrochemical intercalation of lithium into the positive electrode structure can be utilised in rechargeable cells with lithium anodes. He described the reversible topotactic reaction of lithium insertion into titanium disulfide matrices in the $0 \leqslant x \leqslant 1$ composition range with a plateau at 2 V (with respect to metallic lithium) and a current density in the range 1 – 10 mA cm^{-2}. In the following several years, he and other authors studied a variety of materials with the aim of using them as positive electrodes in secondary lithium cells, *viz*., sulfides MoS_2 and $NiPS_3$, oxides V_2O_5 and MoO_3,[2] oxyhalide FeOCl,[2,3] oxide V_6O_{13},[4] sulfides $Ti_{1+x}S_2$ and TiS_3,[5] layered oxides MO_2 (M = Ti, V, Mn, Mo, W, Nb, Ru, Ir, Os)[6] and lithium cobaltate Li_xCoO_2.[7] Further development of lithium cells was impeded by the difficulties concerned with practical implementation of the reversible operation of negative electrodes made of metallic lithium and the choice of electrolytes. In the early 1980s, several authors[7–9] suggested to apply the principle of lithium electrochemical intercalation for negative electrodes as well. The substitution of reversible lithium intercalation host compounds for metallic lithium gave rise to a new generation of lithium batteries.

The development of a new kind of lithium battery was announced in 1990 by Sony Energetic Incorporated[10] and in 1991 and by Moli Energy Limited[11] and Bell Communications Research.[12] The basis for this was laid by Japanese scientists[13,14] who had discovered that certain carbon forms are capable of reversible lithium intercalation and can be used as materials for negative electrodes.

In these cells, the positive electrodes represented lithiated cobalt oxide (lithium cobaltate) $LiCoO_2$ (Sony), lithiated nickel oxide (lithium nickelate) (Moli) and lithium – manganese spinel $Li_xMn_2O_4$ (Bellcore). At first, these kinds of batteries were named 'rocking-chair' cells, which reflected their ability to transfer lithium from positive to negative electrode (charge) and back (discharge). At present, the conventional name is lithium-ion battery (LIB).

Commercial production of lithium-ion batteries with $LiCoO_2$ cathodes (voltage range 2.5 – 4.2 V, average voltage 3.6 V) was pioneered by Sony in 1991. The batteries had a high voltage level and the highest energy density (with respect to both mass and volume) among secondary cells of that time. Commercialisation of LIB has given powerful impetus to studies in this field, which included the search for new cathode materials. In the past decade, the number of publications on this subject has run into several thousands.[15] The reason for this lies in the fact that, despite all the merits of lithium cobaltate [high average voltage and high energy density, low self-discharge (the capacity fade in the discharged state at open circuit), simplicity of its industrial synthesis, good cyclability], its drawbacks came to light almost immediately. The latter are, first of all, the high cost and toxicity. Taking into account the volume of sales ($40 bln. per year) and the LIB market structure (cellular phones, video cameras, portable computers), these problems are certainly very serious. Moreover, the capacity of lithium cobaltate, even if having a high theoretical value (274 mA h g^{-1}), in practice does not exceed 150 mA h g^{-1}, because the discharge of Li_xCoO_2 involves a phase transition from its tetragonal form to a monoclinic one at $x \approx 0.5$; hence, stable cycling is possible only in the composition range $0.5 < x < 1$. Although lithium cobaltate is still used as the cathode material in the majority of commercial LIB, attempts to improve this material or find another one, cheaper and less toxic, have never stopped. According to the prognoses made by LIBES (Lithium Battery Energy Storage Technology Research Associa-

E V Makhonina N S Kurnakov Institute of General and Inorganic Chemistry, Russian Academy of Sciences, Leninsky prosp. 31, 119991 Moscow, Russian Federation. Fax/Tel. (7-095) 952 20 62. E-mail: evma@igic.ras.ru
V S Pervov Moscow State University of Engineering Ecology, ul. St. Basmannaya 21/4, 105066 Moscow, Russian Federation. Fax (7-095) 261 49 61. Tel. (7-095) 267 19 47. E-mail: pervov@igic.ras.ru
V S Dubasova Federal State Company 'Scientific Research Institute of Electrical Carbon Products', 142455 Elektrougli, Moscow Region, Russian Federation

Received 16 March 2004
Uspekhi Khimii **73** (10) 1075 – 1087 (2004); translated by T Ya Safonova

tion)[16] and such companies as SAFT,[17] the LIB production will continue to increase; however, the market structure is to change (for instance, according to certain estimates, the cellular phone market, the greatest LIB consumer, is close to saturation) as well as the requirements to LIB. The use of LIB in medicine and space technology (*e.g.*, for satellites) requires much longer service life (at least 15 years in place of the usual 3–5 years of present cells). Their use in military equipment will require not only the increased service life but also the wider rage of operation temperatures (now, it is from −20 to 60 °C) and the possibility of operating at high currents. The use of LIB as reserve power sources of autonomous power-consuming devices (including submarines and planes) and in electrical vehicles and cars with the so-called hybrid power sources (a combination of internal combustion engines with powerful rechargeable batteries) requires both the higher power level and lower costs. The high cost and the capacity fade during operation (the latter should not exceed 20% in 10 years) are the critical parameters in all application fields. All these problems are discussed in numerous publications devoted to materials for positive electrodes of LIB.

In addition to lithium cobaltate, the possible candidates for the cathode materials in LIB with average voltage of 4 V should also involve lithium nickelate $LiNiO_2$ and lithium-manganese spinel $LiMn_2O_4$. An analysis[18] has shown that it is these oxides that have the lithium intercalation potential in the required voltage range. That is why the mentioned compounds and their derivatives were studied most thoroughly. Thus, when analysing the literature data, it is reasonable to consider these three compounds separately while cathode materials based on different compounds united in a special group.

In should be stressed that, in fact, a cathode material represents a composite involving a certain carbon form (as a rule, carbon black) added with the aim of increasing the conductivity together with a binder represented most often by polyvinylidene fluoride. The content of these components in the material, the morphology of the latter, the particle size of the ingredients, and also the methods of cathode manufacturing (chemical method, cold pressing or film formation for polymeric LIB) have a great effect on the electrochemical behaviour of the resulting cathodes; however, these questions deserve special consideration and are beyond the scope of this review.

II. Lithium cobaltate and related materials

Depending on the synthetic method, two forms of $LiCoO_2$ can be obtained. A compound synthesised at high temperatures has a layered structure; that synthesised at low temperatures has the spinel structure. The majority of commercial LIB utilise the high-temperature form of stoichiometric lithium cobaltate, which can be cycled in the voltage range from 2.5 to 4.3 V and the composition range $0.5 < x < 1$ with the reversible capacity of 135–150 mA h g^{-1}. The upper voltage limit ($\sim$ 4.3 V) is chosen for a number of reasons, including safety requirements and the possibility of forming gaseous products. However, first of all, one has to take into account that a phase transition of $LiCoO_2$ from a layered hexagonal structure with rhombohedral symmetry (space group *R*3*m*) to monoclinic structure occurs at $x \approx 0.5$.

The structure of hexagonal $LiCoO_2$ (α-$NaFeO_2$ type, Fig. 1) consists of CoO_2 layers built of interlinked CoO_6 octahedra and separated by lithium-ion layers with octahedral coordination. The cation layers are located in voids of the almost perfect face-centred cubic sublattice of oxygen ions (alternating ABC layers, O3 structure). Other synthetic forms of lithium cobaltate differ in the arrangement of cations (also coordinated in octahedra) in the supercompact oxygen-ion packing. For instance, the low-temperature synthesis results in lithium cobaltate with the spinel structure.

The charging consists of the removal of lithium from the lithium cobaltate lattice by the reaction

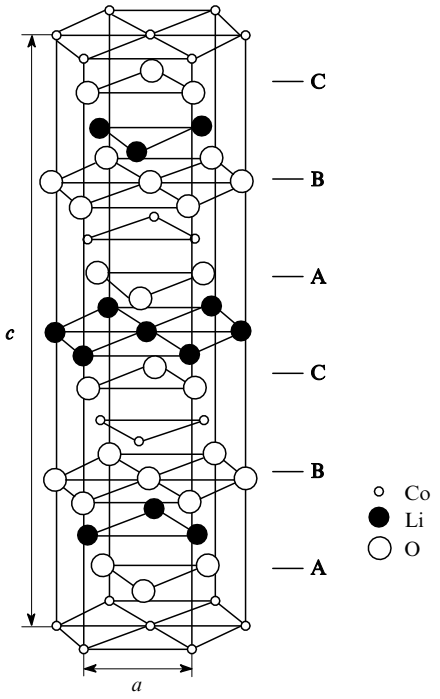

Figure 1. Crystal structure of lithium cobaltate with alternating ABC layers.

$$LiCoO_2 - (1-x)Li^+ - (1-x)e^- \longrightarrow Li_xCoO_2 .$$

As a result, the electrostatic repulsion of CoO_2 layers should become greater and the distance between the layers (the lattice parameter *c*) should increase. The discharge represents a reverse reaction. For a sufficiently long time, it was assumed that reversible cycling to voltages higher than 4.3 V, *i.e.*, up to the complete delithiation leading to CoO_2 is impossible, because removal of lithium should increase the repulsion between the CoO_2 layers and result in the structure failure (the hexagonal form O3 of cobalt oxide is unstable). Later, Amatucci *et al.*[19] have shown that the complete electrochemical delithiation can be achieved upon charging up to 5.2 V. Using a special cell designed for *in situ* XRD experiments, it was shown that upon complete delithiation a transition to a more organised truly hexagonal O1 structure isostructural to CdI_2 occurs rather than the expected decomposition of the original rhombohedral structure. Intercalation of lithium results immediately in the reverse phase transition.

As a whole, changes occurring in a single charge–discharge cycle of stoichiometric lithium cobaltate are sufficiently well studied (see Refs 19–21). In the *x* range from 1 (0.9, according to Ref. 19†) to $\sim$ 0.75–0.78, two hexagonal phases coexist (a wide plateau at 3.9 V in the charge–discharge curve). For *x* from 0.8 to 0.22–0.25, again a single hexagonal phase is present. In a very narrow interval, $x = 0.44–0.49$ (see Refs 20 and 21) (0.46–0.51, according to Ref. 19), the lattice symmetry changes to the monoclinic one; the appearance of this phase is associated with the ordering of ions in lithium layers. Phase transitions to the monoclinic structure and back to the hexagonal phase give rise to two small plateaux at approximately 4.08 and 4.15 V. Substantial changes occur upon reaching 4.2 V. At this voltage, the parameter *c* abruptly decreases indicating the gradual transition to the monoclinic symmetry at 4.5 V and $x = 0.22–0.25$.[19,20] The formation of this second monoclinic phase is explained by the Jahn–Teller effect due to the appearance of low-spin cobalt ions (d^5). Further deintercalation of lithium ions manifests itself, at

† According to data by Amatucci *et al.*,[19] in the *x* range from 1 to $\sim$0.9 the initial hexagonal phase is conserved.

first, by the co-existence of hexagonal and monoclinic phases. After a number of phase transitions,[19] the process is finished at 5.2 V with the formation of the well-crystallised hexagonal phase mentioned above. It should be noted that 95% of initial lithium can be intercalated back into the structure of electrochemically synthesised cobalt oxide.[19]

A relatively small number of studies deal with the changes in the $LiCoO_2$ crystal structure caused by long-term electrochemical cycling. X-ray diffraction, electron diffraction and transmission electron spectroscopy studies[22,23] have shown that after many charge–discharge cycles (~ 300) in the 3.0–4.3 V interval the layered structure of lithium cobaltate gradually gives way to the spinel structure (space group *Fd*3*m*). The lower electrochemical activity of the latter is partially responsible for the capacity fade upon prolonged cycling. Yet another reason for the cycling-induced capacity fade of lithium cobaltate is the change in the surface area of particles, which can reduce the cathode volume and break the electric contact with the active-substance particles. The above-mentioned phase transition at $x = 0.5$ makes the greatest contribution to the capacity fade during cycling in the 2.5–4.3 V range. Lithium cobaltate is very sensitive to overcharge. There are no theoretical limitations to the further polarisation of negative electrodes upon reaching the lithium electrode potential. As a result, a layer of metallic lithium which is highly reactive with respect to the electrolyte can deposit on the carbon surface.[24] This is also favoured by the low thermal stability of lithium cobaltate.[25] Hence, LIB based on lithiated cobalt oxide are equipped with electronic guarding devices, which impairs their specific characteristics and increases the cost of the finished articles.

The self-discharge of LIB with cathodes of lithiated cobalt oxide can be due to different processes, the main one being apparently the interaction of the electrode material with the solvent. However, despite the relatively high (~ 4.2 V) open circuit voltage (OCV) of LIB, their self-discharge is very low. The film formation on the negative electrode was shown to play an important role in the self-discharge process.[26] As was demonstrated[27] by using a method which allows separate determination of cathode and anode contributions,[28] the capacity fade may also be due to the phase transition from the hexagonal structure to spinel, which occurs on the surface of grains under the effect of increasing internal stresses.

In most publications, attempts were made to relate structural and electrochemical characteristics of the cathode material to the method of its preparation.[20,21,29–35] As was noted above, commercial LIB largely utilise the high-temperature (HT) form of $LiCoO_2$. As a rule, the latter is obtained by solid-state synthesis, *i.e.*, high-temperature annealing (700–850 °C) of cobalt carbonate or oxide with lithium oxide or hydroxide in air or in oxygen. This method has a number of drawbacks including the long time of synthesis, high energy consumption and the loss of lithium (it is evaporated in the course of long-term synthesis). As an alternative, sol–gel technologies were developed for the synthesis of lithium cobaltate.[29,30,33]. This method provides better homogeneity of the starting compounds and hence better uniformity of the resulting oxide, minimises the heat treatment time and requires much lower temperatures to produce the same HT form of $LiCoO_2$. As a rule, salts of lower carboxylic acids are used, and the synthesis is carried out in the presence of a chelating agent (citric, oxalic, malonic and other acids) and alcohol (*e.g.*, ethylene glycol). Annealing of the resulting gel at ~ 550 °C affords the high-quality final product.[29,33] According to the literature data, the HT form of $LiCoO_2$ obtained at lower temperatures by the sol–gel method exhibits somewhat better electrochemical characteristics: at the discharge to 2.8 V, its capacity reaches 150 mA h g^{-1}; moreover, the charge–discharge voltage is slightly lower, which is important in view of preventing the electrolyte decomposition.[30]

Among other methods for synthesising lithium cobaltate, mention should be made of a method with mechanochemical treatment, which allows the lower temperatures of final annealing,[31,32] a method employing cryochemical crystallisation,[34] a method of spraying[33] and synthesis in a microwave oven.[36] The mechanochemical synthesis of crystalline $LiCoO_2$ is complicated by its instability with respect to mechanochemical treatment and by redox processes which involve the gas phase.[31] It was shown that the formation of the HT-modification of $LiCoO_2$ can occur at 400 °C.[31] The important features of the resulting cathodic material are the uniform composition, morphology, particle size, texture, all of which strongly affect the electrochemical characteristics of fabricated positive electrodes. All the listed methods provide greater (as compared with the solid-state synthesis) homogeneity upon blending the initial substances and better uniformity of the final product with respect to both composition and particle size (including submicron particles), which defines the enhanced capacity, improves the cycling process and increases the possibilities of cycling at higher charge–discharge rates.[29–31,32–34] The advantages of the microwave synthesis include considerably reduced time of synthesis and, as a consequence, a decrease in lithium losses during this process.[36]

Several authors[37,38] reported on the impossibility of synthesising nonstoichiometric compositions of lithium cobaltate. However, according to other authors,[39–41] such compounds can be obtained. Later, the former authors[37,38] also described nonstoichiometric $LiCoO_2$.[42,43] The limit of the existence of solid solutions with excess lithium corresponds to $x = 1.15$. By iodometric titration, it was found that the valence of cobalt in Li_xCoO_2 remains equal to 3.0 up to $x = 1.15$ and decreases to 2.9 only for higher x. The electroneutrality of compounds with $1 < x < 1.15$ is maintained as a result of the decrease in the cobalt content.[42] It was shown that extra lithium gives rise to both cobalt and oxygen vacancies and affects the electrochemical characteristics of the material.[42,43] A small excess in lithium (up to $x = 1.1$) enhanced the capacity, improved the material cyclability and diminished irreversible losses in the first charge–discharge cycle; for higher x, the capacity was found to fade due to the decrease in the cobalt content.[42] In contrast to stoichiometric $LiCoO_2$, nonstoichiometric samples remained structurally homogenous and demonstrated no transition to the monoclinic phase,[41] so that the steps in the charge–discharge curve at 4.08 and 4.15 V ($x = 0.5$) were observed to disappear.[42,43] The results of these studies[41–43] confirmed the rather unexpected results of calculations[44–48] which derived that oxygen ions play the key role in the redox processes during electrochemical intercalation–deintercalation of lithium, notwithstanding the concepts of classical inorganic chemistry according to which delithiation should involve oxidation of cobalt to the tetravalent state. According to calculations, lithium extraction involves the transfer of electronic density to oxygen ions and changes in the hybridisation of oxygen and cobalt orbitals, while the charge of cobalt remains surprisingly constant. Thus, the so-called 'self-regulated' response is observed, *i.e.*, minimisation of the external impact by rehybridisation. The excess of lithium in Li_xCoO_2 gives rise to new states of oxygen ions and statistically distributed vacancies in cobalt and oxygen layers rather than to oxidation of cobalt.[41]

Using nonempirical calculation methods, the authors of theoretical studies cited above determined the average voltage of lithium intercalation into layered matrices of the same structure MO_2 to give $LiMO_2$ for different metal atoms (M = Co, Ni, Ti, V, Cu) and also for a constant chemical composition with different ordering in cations, which included different structures (lithium cobaltate: rhombohedral layered structure and spinel[47]). A detailed theoretical study was carried out for $LiCoO_2$.[49] The results of this study agree well with the experimental observations discussed above.[19–21]

A large number of studies dealt with properties of lithium cobaltate doped with different metals ($LiCo_{1-y}M_yO_2$) aimed at improving its electrochemical characteristics and simultaneously reducing the cost (see, *e.g.*, Refs 50–52). The use of such dopants as nickel, iron and manganese somewhat improved the cyclability of $LiCoO_2$ by stabilising its structure and lowering the probability

of phase transitions. Such metals as aluminium and magnesium were also tested as the dopants. Based on aforementioned ideas on the significant role of oxygen ions in the redox process, it was predicted and later confirmed experimentally that introduction of aluminium increases the charge–discharge voltage.[53,54] By studying the electrochemical characteristics of $LiCo_{1-y}Al_yO_2$ (y = 0.05–0.25), it was shown that aluminium, even if slightly affecting the theoretical and experimental specific capacity (*ca.* 120 mA h g^{-1} for the optimal composition $LiCo_{0.8}Al_{0.2}O_2$), substantially improves the cycling reversibility due to the formation of single-phase samples (the steps in the charge–discharge curve disappear).[30] The results mentioned above [53,54] on the increase in the average charge—discharge voltage were confirmed. Although high voltage is desirable for providing the high energy density of LIB, voltage above 4.2–4.5 V poses serious complications associated with the choice of electrolytes and the extensive practical application of such batteries. Of the materials considered, only $LiCo_{1-y}Ni_yO_2$ has a small niche in the LIB production.[35]

At present, the efforts of scientists engaged in industrial production of cathode materials based of lithium cobaltate are mainly concentrated on studies of their morphological properties and texture, elucidation of the dependence of their electrochemical characteristics on the particle size and size distribution and optimisation of the compositions and methods for fabrication of the cathode mass.[25] It was shown that smaller sizes of powder particles, more uniform size distributions [29–34,32–34,55] and the formation of small agglomerates of fine spherical particles [55] impart better electrochemical characteristics to cathode materials. As was mentioned above, physical characteristics of crystalline materials strongly depend on the synthetic method, the temperature interval chosen, the time of thermal treatment, starting compounds and sample prehistory.

We deliberately leave the questions associated with polymeric LIB beyond the scope of our survey, because the major relationships and trends found for cathode materials are also valid for compounds used in polymeric batteries. However, it is evident that characteristics of the latter should depend much more strongly on the material morphology, particle size and size distribution. For films, of great importance are the texture, the preferential orientation when films are applied on supports, the application method, *etc*. It should be taken into account that common polymeric electrolytes used in such LIB decompose at 3.8 V, which imposes certain limitations on the cathode materials used. All these problems require special consideration.

III. Lithium nickelate and related materials

Lithium nickelate was suggested as the cathode material almost simultaneously with lithium cobaltate,[11] its cost and toxicity are substantially lower as compared with cobaltate, whereas the experimental specific capacity is apparently among the highest known for this class of lithiated oxides $LiMO_2$ (185 and 210 mA h g^{-1} when charged to 4.1 and 4.2 V, respectively).[25] However, $LiNiO_2$ has not yet found use in commercial LIB. This is due first of all to the difficulties associated with the synthesis of such a compound with a stoichiometric or merely reproducible composition. In practice, the obtained compounds have a composition $Li_{1-x}Ni_{1+z}O_2$ where z depends on the conditions of synthesis and on average varies from 0.05 to 0.20.[56] Optimisation of the process can decrease z but has not yet provided values below 0.01–0.02.[25,56] The decrease in the lithium content in a compound lowers the specific capacity of the sample. Nonstoichiometry appears due to instability of trivalent nickel at high temperatures. 'Extra' nickel ions in the bivalent state occupy lithium positions. XRD data point to the ordered arrangement of lithium and nickel cations in the lithium layers;[56] hence, the more correct formula of lithium nickelate should indicate the occupied positions like $[Li_{1-z}Ni^{2+}_z]_{3a}[Ni^{3+}_{1-z}Ni^{2+}_z]_{3b}[O_2]_{6c}$ (rhombohedral structure $R3m$).[57] The presence of nickel ions in the lithium positions prevents free transport of lithium ions. Moreover, in the course of deintercalation, additional nickel ions were observed to occupy the lithium positions.[58] Electrostatic repulsion between lithium ions and extra nickel ions and reduction of the distance between the layers due to the presence of bi- and trivalent nickel substantially impair the reversibility of the charge–discharge process.[56,59,60] Furthermore, lithium nickelate is less stable with respect to overcharging (due to the greater cycling depth and structural changes).[61]

Lithium nickelate has the same structure of the α-$NaFeO_2$ type as lithium cobaltate, namely, the ordered rocksalt structure with alternating Li^+ and Ni^{3+} layers which occupy octahedral voids in the supercompact cubic packing of oxygen ions. However, for trivalent nickel (electronic configuration $t^6_{2g}e^1_g$), the Jahn–Teller effect is observed; hence, despite the identical structures, lithium nickelate and cobaltate behave differently. The distortion of NiO_6 octahedra due to the Jahn–Teller effect (different lengths of N—O bonds) was first discovered when analysing the fine structure of X-ray absorption spectra.[62] This distortion is of the local nature and cannot be observed in ordinary XRD spectra. Thus the lowering of the local symmetry from rhombohedral to monoclinic was observed. According to calculations,[63,64] the monoclinic distortion observed in the course of lithium deintercalation is due to the combined action of the Jahn–Teller cooperative effect and the ordering of the Li-ion vacancies. Ultimately, the lattice distortion has the decisive effect on the propensity of lithium nickelate to reversibly intercalate–deintercalate lithium. The phase diagram of Li_xNiO_2 calculated in the aforementioned studies [63,64] is in sufficient agreement with experimental results;[65–68] however, it should be stressed that the sequence of phase transitions in Li_xNiO_2 as a function of intercalation depth is not yet determined as reliably as for lithium cobaltate and certain discrepancies are still observed.[65–69] The number of individual phases detected in the system during the charge–discharge varies from three [67] to eight (according to *ab initio* calculations).[64] According to both experimental results [65–68] and calculations,[63,64] the rhombohedral phase exists in the $0.75 < x < 1$ range, whereas the monoclinic phase occurs at $0.4 < x < 0.75$. Within this range, lithium nickelate exhibits good electrochemical characteristics (the corresponding potential range is from approximately 3.6–3.65 to 3.9–4.0 V). Charging to 4.2 V substantially changes the Li_xNiO_2 structure, which is associated with great changes in its volume and the loss of charge–discharge reversibility.[66,68] The nickel dioxide phase $\square NiO_2$ (see ‡) (space symmetry $R3m$) is unstable in nonaqueous solvents at room temperature.[66] As in the case of cathodes based on lithium cobaltate, the surface of particles also changes, which results in the formation of microcracks and finally in the cathode failure.[70,71] The thermal behaviour of completely or partially charged Li_xNiO_2 was studied by differential scanning calorimetry (DSC).[72] It was shown that exothermal peaks of decomposition of delithiated phases for the samples with $x \leqslant 0.25$ are observed at temperatures above 180 °C, whereas the reaction begins at room temperature.

It was found [50] that doping with cobalt stabilises the lithium nickelate structure and minimises deviation from stoichiometry. The introduction of a 3d metal prevents lithium from ordering over the vacancies and weakens the monoclinic distortion, which results in a more stable structure. The charge–discharge curves for such samples are smoothed out, which points to the smaller number of phase transitions during intercalation–deintercalation. That is why the majority of scientists used this way for improving the electrochemical characteristics of lithiated nickel oxide and for studying the properties of doped lithium nickelates. Manganese,[73–80] cobalt,[50,81–86] iron,[87,88] aluminium,[72,89] titanium,[74,89] copper [89] and magnesium [90] were chosen as the dopants. Multicomponent systems with two dopants, *e.g.*, cobalt and gallium,[58] cobalt and aluminium,[61,91] cobalt and titanium,[92] cobalt and magnesium,[91] manganese and aluminium, manganese

‡ Symbol □ means vacancy.

and cobalt, manganese and magnesium, manganese and titanium,[80] gallium and magnesium,[93] and even systems with three dopants [92] were also studied.

According to the results of *in situ* X-ray spectroscopy with synchrotron emission, $LiNi_{1-y}Co_yO_2$ samples first undergo fast and almost complete oxidation of nickel, whereas cobalt is slowly oxidised at the end of charging.[83] Samples doped with cobalt exhibit higher thermal stability in the completely charged state and, hence, are more resistant towards overcharging.[80] For such systems, heat-induced (in the 50–150 °C range) structural changes were studied as a function of the cobalt content. For equal discharge depths (the same x) in $Li_xNi_{1-y}Co_yO_2$ ($y \leqslant 0.30$) in CD2032 coin cells, the temperature-induced changes in the $c:a$ ratio of the hexagonal lattice parameters (which reflects the degree of trigonal distortion) decrease with the increase in the cobalt content.[86] For cobalt-doped samples $LiNi_{1-y}Co_yO_2$, the smallest cycling-induced changes in the unit cell volume and reversible lithium intercalation–deintercalation at higher cycling rates in the range $0.2 \leqslant y \leqslant 0.4$ were observed.[50,94] At the same time, very good characteristics were reported for $LiNi_{0.5}Co_{0.5}O_2$,[85] $LiNi_{0.8}Co_{0.2}O_2$,[95] $LiNi_{0.85}Co_{0.15}O_2$ (see Ref. 83) and similar compositions. Solid solutions $LiNi_{1-y}Co_yO_2$ demonstrated good electrochemical characteristics for virtually all y values in the range $0.2 \leqslant y \leqslant 0.85$.

XRD and Mössbauer spectroscopy studies have shown that the introduction of Fe prevents the phase transition in solid solutions $Li(Ni_{1-y}Fe_y)O_2$ ($y \leqslant 0.30$) with rhombohedral structure.[87] Deintercalation up to $x = 0.12$ results only in oxidation of Ni^{2+}. As indicated by Mössbauer spectra, further deintercalation increases the oxidation state of iron and simultaneously trivalent nickel is oxidised to the tetravalent state. However, as the amount of introduced iron increases, the capacity is observed to substantially decrease, which can only be attributed to the decrease in the concentration of electrochemically active nickel. Moreover, the charge–discharge voltage of such samples is somewhat higher, which suggests that nickel oxidation in this compound is complicated as compared with pure lithium nickelate.

Kim and Amine [89] studied how the oxidation state of a dopant (bi-, tri- and tetravalent ions, namely, Cu^{2+}, Al^{3+}, Ti^{4+}) added to lithium nickelate affects the characteristics of the resulting material. Introduction of copper not only substantially decreased the specific capacity of samples (because copper is electrochemically inactive in this range), but also noticeably impaired their ability to reversibly intercalate–deintercalate lithium. Moreover, samples containing copper tend to form cubic lattices rather than layered structures. Introduction of aluminium resulted in the formation of stable solid solutions; however, the specific capacity of aluminium-containing substances also decreased with Al concentration, even if to the lesser extent than for copper; and the cycling reversibility was impaired. Finally, a 10%–20% titanium admixture, even if insignificantly (2.5%–5%) lowering the capacity (down to capacities of 187 and 161 mA h g^{-1} for 2.8 and 4.3 V, respectively), substantially improved the reversibility of the charge–discharge process (100 cycles). This can be explained by the fact that both nickel and bivalent copper can reside in the lithium layer, which impairs the electrochemical characteristics of the original nickelate. XRD analysis with Rietveld refinements have shown that in $Li_{1-x}(Ni_{1-y-z}Co_yMg_x)O_2$ bivalent magnesium ions occupy the positions of bivalent nickel in lithium layers.[91] Introduced trivalent aluminium was shown to substitute trivalent nickel ions in nickel layers and, at best, had no effect on the migration of Ni^{2+} ions to the lithium layers. Finally, Ti^{4+} ions compensate both the charge deficiency and the structural instability caused by the presence of Ni^{2+} ions in the lithium layers.

The information on the influence of aluminium added to lithium nickelate on the structural and electrochemical characteristics of the latter is ambiguous. It was shown that, in contrast to lithium nickelate, $Li(Ni_{1-x-y}Co_xAl_y)O_2$ demonstrates no phase transitions during cycling and can be deeply discharged (to voltages below 2.5 V), which increases the specific capacity and ensures its long shelf-life in the discharged state (its characteristics remained virtually unchanged after two years storage at 40 °C).[61] It was also noted that addition of aluminium has a positive effect on the thermal stability during lithium deintercalation.[61,92] However, the results of DSC studies [91] suggest that the thermal stability of multidoped samples $Li(Ni_{0.80}Co_{0.15}Al_{0.05})O_2$ reveals no dependence of the decomposition temperature on the nature and concentration of the second (after cobalt) dopant for equal degrees of lithium extraction. At the same time, the increase in the grain size enhanced the thermal stability regardless of the lithium extraction degree. It was also stated [72] that substitution of a fourth part of Ni atoms [$Li(Ni_{0.75}Al_{0.25})O_2$] suppresses the exothermal reaction of decomposition, making the resulting compound more resistant to overcharge. A cathode made of this material demonstrated a specific capacity up to 150 mA h g^{-1}; however, its characteristics can be improved by optimising the conditions of its synthesis and fabrication of the positive electrode.

In recent years, mixed lithiated oxides based on nickel and manganese were actively studied.[73–80] These compounds can be classified among both nickel-based materials ($LiNiO_2$) and manganese-based materials ($LiMnO_2$). At the same time, in contrast to lithium cobaltates and nickelates, lithiated manganese oxide ($LiMnO_2$) has a layered rhombohedral structure (space group *Pmnm*).[95] For a long time, due to different structures of lithium nickelate and lithium manganate, all attempts to obtain solid solutions in the Li–Ni–Mn–O systems with layered rhombohedral structures failed. A large body of data appeared only after Makimura and Ohzuku [73] proposed to synthesise these substances from a binary nickel–manganese hydroxide [$Ni(OH)_2$ and $Mn(OH)_2$ in the 1 : 1 ratio]. Later, the compound $LiNi_{0.5}Mn_{0.5}O_2$ was actively studied both experimentally and theoretically (*ab initio* calculations).[95] In the voltage range from 4.0 to 2.0 V, its specific capacity was 200 mA h g^{-1} with sufficiently good cyclability;[78] moreover, as compared with lithium nickelate, the material proved to be more resistant to heating. Samples of manganese–nickel oxides of other compositions were synthesised and studied.[75–77,79] Different synthetic methods were used, including those based on the sol–gel technology with organic acids as the chelating agents (*e.g.*, see Refs 75, 79). According to the results obtained (including those of nonempirical calculations [95]), $LiNi_{0.5}Mn_{0.5}O_2$ contains bivalent nickel and tetravalent manganese. Intercalation–deintercalation of lithium in the course of charge–discharge in the range between 4.0 and 2.0 V involves a two-electron process of nickel oxidation–reduction. The oxidation state of manganese remains unchanged. The absence of Mn^{3+} and Ni^{3+} ions which cause lattice distortion due to the Jahn–Teller effect and subsequent structural rearrangement makes this compound stable during cycling. It was found [77] that in the voltage range from 2.0 to 1.25 V one more lithium atom per formula unit can be inserted to give $Li_2Ni_{0.5}Mn_{0.5}O_2$ with hexagonal symmetry (space group *P3m*1). This compound has excellent cyclability but is unstable in air. However, the latter problem can be partially solved by synthesising composites based on it [*e.g.*, with Li_2TiO_3 (see Ref. 77)]. Presumably,[77] the form with the higher lithium content can be used for the development of a new kind of LIB in which the Li_2MO_2 phase is introduced to compensate the first-cycle irreversible losses.

Quite recently, an interesting compound, namely, $LiCo_{1/3}Ni_{1/3}Mn_{1/3}O_2$ was synthesised and studied.[96] This mixed oxide was obtained from a ternary hydroxide. It possesses very good characteristics: the specific capacity of *ca.* 200 mA h g^{-1} (2.5–4.5 V), insignificant capacity losses during 30 charge–discharge cycles and enhanced thermal stability.

Mention should be made of studies on partial substitution of fluoride or sulfide anions for oxygen anions in the oxygen sublattice of lithium nickelate. This substantially improved the reversibility of the charge–discharge process for layered $LiNiS_yO_{2-y}$ (see Ref. 97), although the sulfide anions added

lowered the specific capacity of the sample (the higher S^{2-} concentration, the lower the capacity). Ohzuku, Ueda and Kouguchi[98] suggested another way of improving cyclability which consists of introducing fluoride anion by adding HF to the original material. Similar results were obtained by other authors.[90] The synthesised samples of $Li_{1-z}Ni_{1+z}F_yO_{2-y}$ ($y = 0.015$, $z = 0.06$) demonstrated better cycling reversibility as compared with those nonsubstituted. The effect of dual doping with cations and anions was studied.[99] The compound $Li_{1.075}Ni_{0.755}Co_{0.17}$ $O_{1.9}F_{0.1}$ obtained by solid-phase synthesis demonstrated the best characteristics: initial capacity 182 mA h g^{-1} with only 2.8% lost during cycling (100 cycles). These results make it possible to assume that both cationic and anionic substitutions can contribute to the improvement of cyclability.

From the foregoing it is evident that for lithium nickelate the synthetic method still plays a greater role than for lithium cobaltate. Studies on the nature of starting materials, the synthesis temperature and the time of thermal treatment have shown that smaller deviations from stoichiometry are observed for more reactive starting materials and relatively low (600–700 °C) temperatures.[56] Under certain conditions,[56, 69] samples withstanding a large number of charge–discharge cycles (more than 50 cycles; capacity loss less than 0.12% per cycle) can be obtained.[69] The electrochemical behaviour of $LiNi_{1-y}Co_yO_2$ samples prepared by solid-phase synthesis was shown to be closely related to their particle size and size distribution.[82] The Coulomb efficiency in the first cycle is higher the smaller the particles, while the specific capacity remains virtually unchanged. As for lithium cobaltate, a comparison of samples obtained by solid-state synthesis and sol–gel methods confirmed that the latter method provides better homogeneity of starting reagents and the smaller particle size. As a rule, the starting compounds in the sol–gel method include aqueous solutions of nickel and metal-dopant salts, nickel hydroxide and a solution of ammonium hydroxide as the complex-forming agent. The ammonia concentration and pH of the solution were shown to be the most important synthetic parameters in view of preparing samples with desired properties.[84] Organic acids can also be used as the complex-forming agents in the sol–gel technology.[75, 79]

To increase the energy density of LIB, one should use materials possessing both high specific capacity and high density. The higher degrees of crystallinity and the greater particle size, the smaller bulk densities of materials, but simultaneously the lower specific capacities of samples. The bulk density is closely related to the morphology of particles, their sizes and size distribution. However, among materials with the same degrees of crystallinity, spherical particles have the highest bulk density. Thus, the characteristics of cathodes for nickel hydride batteries could be substantially improved when using $Ni(OH)_2$ with spherical particles was used.[84] Samples of cobalt-doped lithium nickelate $LiNi_{0.8}Co_{0.2}O_2$ with quasi-spherical particles and a narrow size distribution were synthesised.[84] This allowed the authors to increase the bulk density of $LiNi_{0.8}Co_{0.2}O_2$ up to 3.24 g cm^{-3} as compared with 2.3 g cm^{-3} for common commercial samples of this material. As compared with commercial samples produced by Merck (irregular crystals with a wide size distribution), $LiNi_{0.8}Co_{0.2}O_2$ samples with spherical particles demonstrated not only high bulk weight but also improved electrochemical characteristics when cycled in the range from 3.0 to 4.3 V (217 mA h g^{-1} in the first cycle and a discharge capacity of 172 mA h g^{-1} in further cycles, as compared with 210 and 165 mA h g^{-1}, respectively, for commercial samples).

IV. Lithium–manganese spinel and spinel-based materials

Among cathode materials under consideration, lithiated manganese oxides and their derivatives are the cheapest and most readily available. Their advantages also include a sufficiently high discharge voltage, high thermal stability especially in the discharged state and nontoxicity. That is why, the compounds of this class were the subject of active studies and wide speculations.

It should be noted that the Li–Mn–O system is much more complex as compared with Li–Co–O and Li–Ni–O systems, because it includes more than ten stable compounds with different structures that contain manganese in various oxidation states and have different degrees of defectiveness.[100] Figure 2 shows an isothermal section of the phase diagram for the Li–Mn–O ternary system (see Ref. 100) and also demonstrates the 'routes' of electrochemical insertion and extraction of lithium (designated by dashed lines with the corresponding average charge–discharge voltages written on the top) and the compounds involved (*T* and *C* designate tetragonal and cubic structures). Lithium intercalation–deintercalation is possible for samples located between λ-MnO_2 ($\square Mn_2O_4$, a stable compound) and $LiMn_2O_4$ (at 4 V), $LiMn_2O_4$ and $LiMnO_2$ ($Li_2Mn_2O_4$) (at 3 V), $Li_4Mn_5O_{12}$ and $Li_7Mn_5O_{12}$ (the latter two compositions can be represented as $LiMn_{1.67}Li_{0.33}O_4$ and $Li_2Mn_{1.67}$ $Li_{0.33}O_4$).

Among the compounds mentioned above, lithium–manganese spinel $LiMn_2O_4$ attracts the keen attention of scientists. Spinel is crystallised in the cubic system (space group *Fd*3*m*). The crystal structure of normal spinel $A[B_2]O_4$ is shown in Fig. 3. Oxygen anions form a supercompact cubic lattice where cations are localised in tetrahedral and octahedral voids. Two limiting positions are possible for cations. In normal spinels, atoms A occupy tetrahedral positions (8*a*), while cations B occupy octahedral positions (16*d*). In inverted spinels, atoms A and a half of atoms B are located in octahedral positions, the remaining atoms B occupy tetrahedral positions. Between these two versions, a continuous series of intermediate structures can be realised. It is a

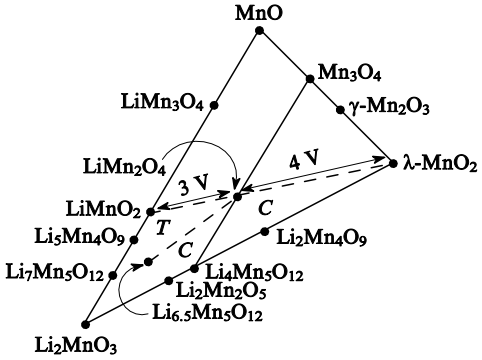

Figure 2. Isothermal section of a phase diagram for a ternary system Li–Mn–O.[100]

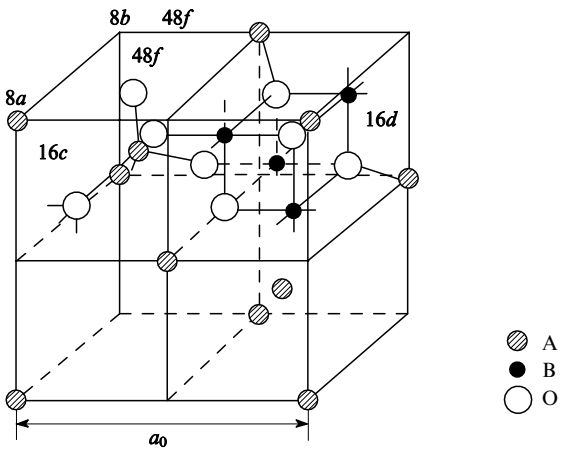

Figure 3. A scheme of $A[B_2]O_4$ spinel structure.

possibility to form different kinds of cationic positions and vacancies (defective structures) that determines the stability of spinel structures with different cations in variable valences. For the same reason, the spinel structure of $LiMn_2O_4$ can host lithium ions in both octahedral and tetrahedral positions.[101] Moreover, there is a 'hierarchy' of voids in the spinel structure, which suggests that discharge characteristics of cathodes based on these structures vary nonmonotonically in the absence of kinetic limitations.[102]

Indeed, electrodes with the working voltage of 4 V are formed when lithium is electrochemically intercalated–deintercalated into tetrahedral positions 8*a* of $Li_x\ Mn_2O_4$ spinel (for normal spinel).[103] For $x > 1$ (according to certain results,[100] at $x > 1.08$), lithium begins to migrate to octahedral positions. The process occurs at 3 V and results in the formation of a layered rhombohedral phase of $LiMnO_2$. In principle, if we consider the overall transition from λ-MnO_2 to $LiMnO_2$ from the theoretical viewpoint, the latter compound could be characterised as an excellent cathodic material with the theoretical capacity of 285 mA h g^{-1}. However, two different electrochemical mechanisms are responsible for the two plateaux at 3 and 4 V, *i.e.*, with a great voltage difference. From the viewpoint of practice, materials with such properties are of no interest.[25] The mentioned phase transition of the first kind was attributed to the increase in Mn^{3+} concentration, which strengthens the co-operative Jahn–Teller effect and gives rise to tetragonal distortions followed by structural changes.

As a whole, the following changes occur during the charge–discharge of a material with the stoichiometric composition $LiMn_2O_4$ in the range from 3.5 to 4.5 V.[104] At $\sim$ 4 V, lithium is electrochemically extracted and inserted in two stages divided by a small step of 0.1 V at $x = 0.45–0.6$ (4.05 and 4.15 V, respectively). The presence of this step is explained by the ordering of the remaining half of lithium ions over tetrahedral positions,[105] which contributes to the gradual specific capacity loss of the spinel. In the x range from 1 to 0.5, two phases coexist. For x below $\sim$ 0.5, also two $Li_xMn_2O_4$ cubic phases coexist, namely, with x equal to 0.15 and 0.4.[104]

Structural and phase transitions that occur during cycling, especially in the high voltage range, are accompanied by great changes in the cathode material bulk and, ultimately, cause irreversible changes in the cathode properties. Among the drawbacks of $Li_xMn_2O_4$ spinel, mention should be made of its relatively low theoretical specific capacity (148 mA h g^{-1}), the capacity loss during storage, especially at high temperatures, and the danger of its dissolution in inorganic solvents in the presence of moisture.

A spinel with nonstoichiometric composition $Li_{1+x}Mn_2O_4$ demonstrates much better cycling reversibility.[106] The disappearance of the step in the cycling curve suggests the homogeneous structure of nonstoichometric spinel. This is explained by the increase in manganese vacancies, which is responsible for certain strengthening of the Mn—O bond, and changes in the surrounding of lithium in tetrahedral positions.

It should be noted that the properties of lithium–manganese spinel strongly depend on the synthetic method.[18, 103, 106–111] Single-phase samples are obtained in the range $0.9 < x < 1.15$.[18] The parameter a of the spinel cubic lattice and the oxygen ion deficiency are shown to increase with an increase in the temperature of synthesis, or (when samples are prepared by quenching) with an increase in the quenching temperature and a decrease in quenching time. The loss of oxygen is responsible for tetragonal distortion of the spinel lattice. As the quenching temperature increases, the phase structure of $LiMnO_2$ spinel undergoes the following changes: first, a two-phase domain appears (840–890 °C), then, a domain of the existence of a single tetragonal phase is observed (895–910 °C) and, finally, above 910 °C, a domain of mixed phases (the main phase is rhombohedral $LiMnO_2$) occurs. The transition from the spinel phase to the tetragonal one is reversible. Spinels synthesised at low temperatures contain higher concentrations of oxygen and lower concentrations of trivalent manganese, which reduces the specific capacity of a sample to a certain extent but enhances its cyclability due to the weaker distortions associated with the Jahn–Teller effect.[107, 108] Moreover, both anionic and cationic kinds of nonstoichiometry were shown to depend not only on the temperature of synthesis but also on the nature of the starting compounds.[109, 110] The anionic nonstoichiometry has the greater effect on the properties of $LiMn_2O_4$, as compared with cationic nonstoichiometry (the Li/Mn ratio).[111] Certain publications[108, 112] reported good cyclability of samples made of disordered defective spinels with the nonstoichiometry Li/Mn < 1 (average cycling capacity of 120 mA h g^{-1}).

Different methods were used for the synthesis of lithium–manganese spinels, *viz.*, various versions of solid-phase synthesis,[103, 106, 109, 111] including those using the mechanical processing,[113–115] microwave synthesis,[116] sol–gel syntheses with different starting substances and chelating agents (*e.g.*, citric, polyacrylic and stearic acids),[107, 110, 117, 118] a method using the starting reagent in the form of an oil emulsion.[119] The development of synthetic methods is largely focused on the preparation of spinel phases nonstoichiometric in lithium and oxygen and more uniform with respect to composition and particle size.

The drawbacks of lithium–manganese spinels mentioned above can be eliminated by modifying their compositions (doping with cations and anions as in the case of lithium cobaltate and lithium nickelate) and surface as well as by using nonstoichiometric compositions.

Surface is modified in order to form a protective film preventing dissolution of the cathodic material in the electrolyte, *e.g.*, by encapsulating surface particles of $LiMn_2O_4$ in lithium borate. Another goal is to directly affect the active centres on the surface of lithium–manganese spinels, *e.g.*, by treating the surface with acetylacetone.[120] Moreover, the $LiMn_2O_4$ surface is often modified to compensate the losses in the first charge–discharged cycle. Thus by coating the $LiMn_2O_4$ surface with lithium cobaltate in the form of microemulsion, it is possible to reduce the specific capacity losses from 12% to 5% in 100 cycles.[121] To compensate the first-cycle losses, it was proposed[122] to add (to the bulk) Li_2CuO_2 which has an irreversible yet high specific capacity (320—340 mA h g^{-1}).

Numerous studies were devoted to modification of lithium–manganese spinels by doping. The following dopants were studied: Co,[108, 123–127] Ni,[81, 123, 124, 127–130] Cr,[124, 127, 129, 131–136] Fe,[123, 137] Al,[137, 138] Mg,[137, 139], Cu (see Ref. 137), *etc*. Simultaneous doping with two elements was also suggested.[137, 139, 140] These studies were carried out by various techniques: X-ray diffraction, X-ray photoelectron spectroscopy (XPS), ESR, Fourier-transform IR spectroscopy (FTIRS), EXAF spectroscopy, electron microscopy, neutron diffractometry, DSC and cyclic voltammetry. Electrochemical tests were also carried out.

In these publications, the effect of a metal M in $Li[Mn_{2-y}M_y]O_4$ was studied in the domains of existence of single-phase products with the spinel structure over the entire concentration range. In the majority it was shown that partial substitution for manganese in 16*d* positions weakens the distortion due to the Jahn–Teller effect, thus stabilising the spinel structure, and also reduces the specific capacity losses at high voltage (> 4 V). Moreover, as a rule, a step in the charge–discharge curve at $x \approx 0.5$ is 'smoothed', which apparently can be explained in the same way as for the case of nonstoichiometric spinel samples (the latter can be considered as lithium-doped), *i.e.*, by changes in the Mn—O bond strength and in the surrounding of lithium ions in tetrahedral positions. At high concentrations of an introduced substituent, the dopant ions can partly occupy the 8*a* positions of lithium [123, 137] (partially inversed spinel). The increase in the degree of substitution into 8*a* positions with an increase in the dopant concentration was shown to impede the migration of lithium ions and reduce the specific capacity of the cathode material.[137]

Doping (*e.g.*, with chromium) also increases the diffusion coefficient of lithium,[136] which allows one to increase the current density of the charge–discharge process. It should be noted that, in the voltage range from 2.5 to 4.5 V, oxidation–reduction of manganese occurs. In this case, doping is ineffective; hence, when improving the reversibility of electrochemical intercalation–deintercalation of lithium, it should be borne in mind that the lower capacities of materials the higher dopant concentrations (see, *e.g.*, Refs 125, 126, 134, 136).

Simultaneous introduction of anionic (S^{2-}) and cationic (Mg^{2+}) substituents is beneficial as regards reversibility but substantially reduces (up to 85 mA h g^{-1}) specific capacities of samples.[139]

Yet another feature of lithium–manganese spinel which has not been touched upon above, namely, the low-temperature transition to the other rhombic phase at 280–285 K deserves mention.[140, 141] Multidoping (with cobalt and nickel) makes it possible to suppress this phase transition,[141] because the latter is also caused by distortions due to the Jahn–Teller effect; this will allow using LIB at low temperatures.

Since the advent of electrolytes stable at high voltages, it has been found that cycling of doped samples up to 5.1–5.2 V gives rise to the second wide plateau (at $\sim$4.7–4.8 V) in the cycling curve.[81, 123, 127, 137] Its appearance is associated with redox transformations of the dopant metal,[123, 127] as was demonstrated by several techniques including the analysis of the fine structure of X-ray absorption spectra.[127] The reversibility of this process at $\sim$4.7–4.8 V strongly depends on the degree of crystallinity and the morphology of particles and takes the maximum value for quasispherical particles.

The role of the morphology of cathode-material particles, their sizes and size-distribution has been discussed in the previous Sections devoted to lithium cobaltate and lithium nickelate. Yet another study in which these problems are discussed in detail deserves mention.[142] It was shown that at high cycling rates of lithium–manganese spinel, it is the morphology of particles that plays the key role rather than their sizes. Hence, larger but porous particles with big surface areas exhibit better electrochemical characteristics, do not crack when cycled and do not affect greatly the cathode volume.

V. Miscellaneous materials with average voltage of 4 V

Although the main objective of this survey is to discuss cathode materials based on lithium cobaltate, lithium nickelate and lithium–manganese spinel, *i.e.*, compounds which are recognised to date as the main candidates for lithium-ion batteries,[143] a small group of different LIB materials with the voltage of 4 V also deserve discussion.

It should be noted that the efforts to apply materials based on layered manganese compounds never stop. These materials are often synthesised (for example, by ion exchange) in such a way as to make their structure as close to the structures of lithium cobaltate and lithium nickelate with good cyclability as possible.[73–80, 144–148] All of them, as a rule, are stabilised by introducing different dopants, *e.g.*, aluminium,[145] iron, manganese, cobalt,[146] chromium [147, 148] and, most often, nickel.[73–80] Properties of such materials are discussed in detail in section III using the example of nickel compounds.

Attempts were undertaken to develop cathodes based on the orthorhombic phase of $LiFeO_2$. However, the charge–discharge process in these compounds is irreversible due to the instability of Fe^{4+} in Li_xFeO_2 with respect to electrolyte.[25]

Recently, there was reported [149] a new cathode material in the Li–Co–Ti–O system. The resulting layered material has a structure resembling those of Li_2MnO_3 and Li_2TiO_3 and represents a solid solution of Li_2TiO_3 and Li_2CrO_2 with the general composition of Li_3CrTiO_5 ($Li[Li_{0.2}Cr_{0.4}Ti_{0.4}]O_2$). The samples were identified in the monoclinic system (space group $C2/m$). It was shown that this compound undergoes a redox process involving chromium (Cr^{3+}/Cr^{6+}) with a very good cycling reversibility in the voltage range from 2.0 to 4.8 V. Similar results (with electrochemically active chromium) were obtained for $LiMn_xCr_{1-x}O_2$.[148]

Recent publications discussed the prospects of using $LiFePO_4$.[150–153] This material is cheap, safe, has a high energy density and is sufficiently attractive as regards the working voltage (3.5 V); however, it has an extremely low electronic conductivity. Nevertheless, the introduction of a small amount (no more than 1%) of a dopant metal (Zn, Nb or Mg) was shown to increase the electronic conductivity by eight orders of magnitude.[151]

VI. The prospects of using metastable superstructures

The analysis of published data shows that most scientists tend to develop positive-electrode materials based on single-phase structures or solid solutions. However, as has already been noted in the previous section (see, *e.g.*, Ref. 77), the prospects of using complex multicomponent systems based on oxides of cobalt, nickel and manganese including multidoped systems are also considered. Thus in studies on the electrochemical behaviour of composites $LiMO_2 \cdot Li_2M'O_3$ (M = Co, Ni, Mn; M′ = Ti, Zr, Mn) [77, 154, 155] it was found that the addition of $Li_2M'O_3$ enhances the stability of the positive-electrode material. It was also shown [156] that the addition of $LiNi_{0.8}Co_{0.2}O_2$ to lithium–manganese spinel $Li_{1+x}Mn_{2-x}O_4$ inhibits spinel dissolution in the electrolyte and reduces capacity losses during storage at elevated temperatures. Mention should be made of several patents in which the materials for positive electrodes of lithium-ion batteries were developed on the basis of lithiated oxides. For instance, a mixture of $Li_xNi_yCo_zM_nO_2$ (M = Al, Ti, W, Cr, Mo, Mg, Ta, Si or their combinations) with lithium–manganese spinel $Li_xMn_{2-r}M'_rO_4$ (M′ = Cr, Ti, V, Ni, Co, Fe, Sn, Zn, Zr, Si or their combinations) was proposed to enhance the cycling stability of capacity characteristics and the stability with respect to overcharging.[157] A Japanese Patent of the Fuji Photo Film Company [158] also suggested using a mixture of two lithiated oxides, *viz.*, lithium cobaltate $Li_{1-y}CoO_2$ ($0.1 \leqslant y \leqslant 1$) and a spinel $Li_{2-x}Mn_2O_4$ ($0 \leqslant x \leqslant 1$). The materials were applied simultaneously on aluminium foil; one layer is expanded during the discharge, while the other is contracted. This material provided high initial capacity and stable cycling characteristics and eliminated the electrolyte leakage. Multiphase systems based on lithium–manganese spinel and lithiated oxides $LiNiO_2$, Li_2NiO_2, $LiNi_2O_4$, $Li_2Ni_2O_4$ and $LiNi_{1-x}M_xO_2$ (M = Co, Mn, Al) were suggested by scientists from the Japanese 'NEC Corporation'[159] with the aim of improving the cyclability, shelf life and safety of lithium-ion batteries. The authors of a patent [160] aimed at the development of LIB with enhanced high-temperature stability during discharge and overcharge and, at the same time, preservation of high energy characteristics suggested the use of a composite of the two following compounds as the positive-electrode material: $Li_xM_yO_4$ ($0 < x < 2$); $0.8 < y < 1.2$; M = Fe or Fe_zMn_{1-z}) and one of the lithiated oxides $LiCoO_2$, $LiNiO_2$ or $LiMn_2O_4$ with the potential of lithium intercalation–deintercalation higher than that of $Li_xM_yPO_4$.

From our viewpoint, along with analysing possible practical approaches to the development of such multiphase systems (and solid solutions), attempts should be made to understand the mechanisms of formation of these compositions and to study the processes that occur during the formation of eutectic compositions and solid solutions. It should be noted that, according to published data, eutectic compositions were never studied as candidates for cathode materials, although, undoubtedly, they are of interest. In recent years, a group that includes the authors of this review accomplished a number of studies aimed at elucidating self-organisation mechanisms for structures like supramolecular ensembles in the series of two-phase systems of oxides and

selenides. In a survey devoted to this problem,[161] we proposed to consider the structure of resulting eutectics and solid solutions as supramolecular structures formed due to self-organisation of incommensurable (which is also true for multiphase compositions of positive-electrode materials under discussion) interacting structures of components. Experimental studies of some eutectic oxide ($PbO-ZnO$, $PbO-Mo_2O_3$, $PbO-Y_2O_3$, $PbO-V_2O_5$)[162] and selenide ($GaSe-Ga_2Se_3$) (see Ref. 163) systems demonstrated that such self-organisation can occur and anomalous phases can form due to interaction of their components. The survey involved a theoretical part, in which the process of formation of supramolecular ensembles was considered within the framework of a static version of the Frenkel–Kontorova model for finite systems.[164–166] In this model, abstract thermodynamic criteria such as surface energy or surface tension are replaced by real parameters of interacting structures, *viz*., incommensurability, rigidity and interaction potential. The results of analytical and numerical simulations in terms of this approach allowed us to make certain very significant conclusions on how the mechanochemical processing affects the interacting substructures, to follow the variation of model parameters with temperature and characterise the excited states of the system, thus linking them with the synthetic conditions. It was shown that under certain conditions such systems demonstrate quite a number of very steady metastable states. Only the case of one-dimensional incommensurability was considered; however, the results obtained can be used for explaining certain phenomena observed for eutectic phases and solid solutions.

From our viewpoint, the presented approach to the problem of the formation of self-organised incommensurable interacting structures of eutectic compositions can be extended to multiphase materials for positive electrodes of lithium-ion batteries. The problem is how to choose a multiphase composition which when cycled would reversibly pass from one metastable structure to another without any substantial kinetic barriers and any significant changes in the crystal lattice volumes of these metastable structures. The understanding of self-organisation mechanisms in such multiphase compositions (including considerations in terms of the Frenkel–Kontorova model) opens up possibilities for optimising the methods of synthesising such structures and selecting their components.

VII. Conclusion

The researches directed at improving the performance of lithium-ion batteries constantly become more active. As mentioned above, the number of publications approaches several thousand.[15] Numerous patents devoted to this subject also deserve mention. Despite the incompleteness of selected information, the analysis carried out allowed us to follow the modern approaches to optimising lithium ion batteries. Optimisation of LIB concerns their reactor part as such and involves the materials for fabricating anodes and cathodes. It is noteworthy that in the past 3–4 years the number of publications devoted to negative-electrode materials became relatively smaller, while the number of studies dealing with cathode materials stayed at approximately the same level during the past 5–7 years.

In the field of cathode materials, the major research direction concerns the development of compounds or compositions that will allow us to change expensive, scarce and carcinogenic lithium cobaltate for cheaper, more available and safer materials. Moreover, the problems of improving the charge–discharge characteristics of the cathode material (capacity and energy), enhancing the reversibility and stability (structural and at elevated temperatures), increasing its charge and discharge rates, advancing the technology of electrode production and making the cell operation safer are posed.

For this purpose, the majority of leading research laboratories and companies tend to make positive-electrode materials more complex. Particularly, many studies were devoted to multidoping, *i.e*., simultaneous introduction of two and more dopants, including their combinations with anionic substituents. First of all, this concerns lithium–manganese spinel, when certain samples of substituted spinels are considered in terms of using them as the cathodes in the voltage region of 5 V. Much attention is paid to nickel–manganese oxides, including those doped with other elements $LiNi_{1-x-y}Mn_xM_yO_2$ (M = Al, Ti, W, Cr, Mo, Mg, Ta, *etc*.), and mixed ternary oxides $LiNi_{1-x-y}Mn_xCo_yO_2$ which are often multidoped as well.

In addition to compositions representing solid solutions, *e.g*., systems $xLi_2M'O_3(1-x)LiMO_2$ (M′ = Mn, Ti, Zr, Ru and M = Mn, Ni, Co), the group of M Thackeray[154, 155, 167] works on multiphase compositions which represent mixtures of different oxides. Finally, many laboratories all over the world actively study $LiFePO_4$,[167] *e.g*., as a component of multiphase systems.

The review is financially supported by the Russian Foundation of Basic Research (Project Nos 03-03-32467 and 02-03-32135).

References

1. M S Whittingham *J. Electrochem. Soc*. **123** 315 (1976)
2. M S Whittingham *Prog. Solid State Chem*. **12** 1 (1978)
3. P Palvadeau, L Coic, J Rouxel, J Portier *Mater. Res. Bull*. **13** 221 (1978)
4. D W Murphy, P A Christian, F J DiSalvo, J N Carides *J. Electrochem. Soc*. **126** 497 (1979)
5. G L Holleck, J R Driscoll *Electrochim. Acta* **22** 647 (1977)
6. D W Murphy, F J DiSalvo, J N Carides, J V Waszczak *Mater. Res. Bull*. **13** 1395 (1978)
7. K Mizushima, P C Jones, P J Wiseman, J B Goodenough *Mater. Res. Bull*. **15** 783 (1980)
8. M Lazzari, B Scrosati *J. Electrochem. Soc*. **127** 773 (1980)
9. J M Tarascon *J. Electrochem. Soc*. **132** 2089 (1985)
10. T Nagaura, K Tozawa *Prog. Batteries Solar Cells* **9** 209 (1990)
11. R Fong, U Von Sacken, J R Dahn *J. Electrochem. Soc*. **137** 2009 (1990)
12. J M Tarascon, D Guyomard *J. Electrochem. Soc*. **138** 2864 (1991)
13. R Kanno, Y Takeda, T Ichikawa, K Nakanishi, O Yamamoto *J. Power Sources* **26** 535 (1989)
14. M Mohri, N Yanagisawa, Y Tajima, H Tanaka, T Mitate, S Nakajima, M Yosida, Y Yoshimoto, T Suzuki, H Wada *J. Power Sources* **26** 545 (1989)
15. R N Kostoff, R Tshiteya, K M Pfeil, J A Humenik *J. Power Sources* **110** 163 (2002)
16. T Iwahori, Y Ozaki, A Funahashi, H Momose, I Mitsuishi, S Shiraga, S Yoshitake, H Awata *J. Power Sources* **81–82** 872 (1999)
17. M Broussely, in *Proceedings of the 5th China International Battery Fair (CIBF2001), Beijing, China, 2001* p. 113
18. D Guyomard, J M Tarascon *Solid State Ionics* **69** 222 (1994)
19. G G Amatucci, J M Tarascon, L C Klein *J. Electrochem. Soc*. **143** 1114 (1996)
20. J N Reimers, J R Dahn *J. Electrochem. Soc*. **139** 2091 (1992)
21. T Ohzuku, A Ueda *J. Electrochem. Soc*. **141** 2972 (1994)
22. H Wang, B Huang, D R Sadoway, Y-M Chiang *J. Electrochem. Soc*. **146** 473 (1999)
23. H Gabrisch, R Yazami, B Fultz *J. Power Sources* **119–121** 674 (2003)
24. I A Kedrinskii, V G Yakovlev *Li-Ionnye Akkumulyatory* (Li-Ion Accumulators) (Krasnoyarsk: IPK 'Platina', 2002)
25. M Broussely, P Biensan, B Simon *Electrochim. Acta* **45** 3 (1999)
26. M Broussely, S Herreyre, P Biensan, P Kasztejna, K Nechev, R J Staniewicz *J. Power Sources* **97–98** 13 (2001)
27. Y Ozawa, R Yazami, B Fultz *J. Power Sources* **119–121** 918 (2003)
28. R Yazami, Y F Reynier *Electrochim. Acta* **47** 1217 (2002)
29. Z S Peng, C R Wan, C Y Jiang *J. Power Sources* **72** 215 (1998)
30. C Julien, S Gastro-Garsia *J. Power Sources* **97–98** 290 (2001)
31. N V Kosova, V F Anufrienko, T V Larina, E T Devyatkina *Khim. Inter. Ustoich. Razvitiya* **9** 235 (2001) [a]

32. S-W Jang, H-Y Lee, S-J Lee, H-K Baik, S-M Lee *Mater. Res. Bull.* **38** 1 (2003)
33. C Julien, S S Michael, S Ziolkiewicz *Int. J. Inorg. Mater.* **1** 29 (1999)
34. O A Brylev, O A Shlyakhtin, I V Arkhangel'skii, in *Doklady Vserossiiskoi Konferentsii 'Khimiya Tverdogo Tela i Novye Materialy', Ekaterinburg, 1996* (Proceedings of the All-Russian Conference 'The Chemistry of Solid and New Materials', Ekaterinburg, 1996) p. 149
35. US P. 6 383 235 (2002)
36. H Yan, X Huang, Z Lu, H Huang, R Xue, L Chen *J. Power Sources* **68** 530 (1997)
37. M Menetrier, I Saadoune, S Levasseur, C Delmas *J. Mater. Chem.* **9** 1135 (1999)
38. N Imanishi, M Fujiyoshi, Y Takeda, O Yamamoto, M Tabuchi *Solid State Ionics* **118** 121 (1999)
39. M Carewska, S Scaccia, F Croce, S Arumugam, Y Wang, S Greenbaum *Solid State Ionics* **93** 227 (1997)
40. M P J Peeters, M J Van Bommel, P M C Neilen-ten Wolde, H A M Van Hal, W C Keur, A P M Kentgens *Solid State Ionics* **112** 41 (1998)
41. N V Kosova, V V Kaichev, V I Bukhtiyarov, D G Kellerman, E T Devyatkina, T V Larina *J. Power Sources* **119–121** 669 (2003)
42. N Imanishi, M Fujii, A Hirano, Y Takeda *J. Power Sources* **97–98** 287 (2001)
43. S Levasseur, M Menetrier, I Suard, C Delmas *Solid State Ionics* **128** 11 (2000)
44. G Ceder, M K Aydinol, A F Kohan *Comput. Mater. Sci.* **8** 161 (1997)
45. M K Aydinol, A F Kohan, G Ceder *J. Power Sources* **68** 664 (1997)
46. C Wolverton, A Zunger *Phys. Rev. B: Condens. Matter* **57** 2242 (1998)
47. C Wolverton, A Zunger *J. Electrochem. Soc.* **145** 2424 (1998)
48. C Wolverton, A Zunger *Phys. Rev. Lett.* **81** 606 (1998)
49. A Van der Ven, M K Aydinol, G Ceder, G Kresse, J Hafner *Phys. Rev. B: Condens. Matter* **58** 2975 (1998)
50. C Delmas, I Saadoune *Solid State Ionics* **53–56** 370 (1992)
51. R J Gummow, M M Thackeray *Solid State Ionics* **53–56** 681 (1992)
52. R Alcantara, P Lavela, J L Tirado, R Stoyanova, E Zhecheva *J. Electrochem. Soc.* **145** 730 (1998)
53. G Ceder, Y M Chiang, D R Sadoway, M K Aydinol, Y I Jang, B Huang *Nature (London)* **392** 694 (1998)
54. Y I Jang, B Y Huang, H F Wang, G R Maskaly, G Ceder, D R Sadoway, J M Chiang, H Liu, H Tamura *J. Power Sources* **81** 589 (1999)
55. G M Ehrlich, F J Puglia, R Gizendanner, B Hellen, C Marsh *J. Power Sources* **81–82** 863 (1999)
56. A Rougier, P Gravereau, C Delmas *J. Electrochem. Soc.* **143** 1168 (1996)
57. J Morales, C Perez-Vicente, J L Tirado *Mater. Res. Bull.* **25** 623 (1990)
58. M Balasubramanian, J McBreen *NSLS Activity Report, Brookhaven National Laboratory, 2001*
59. H Arai, S Okada, H Ohtsuka, M Ichimira, J Yamaki *Solid State Ionics* **80** 261 (1995)
60. A Hirano, R Kanno,Y Kawamoto, K Oikawa, T Kamiyama, F Izumi *Solid State Ionics* **86–88** 791 (1996)
61. M Broussely, Ph Blanchard, P Biensan, J P Planchat, K Nechev, R J Staniewicz *J. Power Sources* **119–121** 859 (2003)
62. T Ohzuku, T Yanagawa, M Kouguchi, A Ueda *J. Power Sources* **68** 131 (1997)
63. A Rougier, C Delmas, A V Chadwick *Solid State Commun.* **94** 123 (1995)
64. M E Arroyo y de Dompablo, G Ceder *Chem. Mater.* **15** 63 (2003)
65. M E Arroyo y de Dompablo, G Ceder *J. Power Sources* **119–121** 654 (2003)
66. L Croguennec, C Pouillerie, C Delmas *J. Electrochem. Soc.* **147** 1314 (2000)
67. T Ohzuku, A Ueda, M Nagayama *J. Electrochem. Soc.* **140** 1862 (1993)
68. W Li, J N Reimers, J R Dahn *Solid State Ionics* **67** 123 (1993)
69. R V Moshtev, P Zlatilova, V Manev, A Sato *J. Power Sources* **54** 329 (1995)
70. X Q Yang, X Sun, J McBreen *Electrochem. Commun.* **1** 227 (1999)
71. Z Zhang, D Fouchard, J R Rea *J. Power Sources* **70** 16 (1998)
72. J R Dahn, E W Fuller, M Obrovac, U Von Sacken *Solid State Ionics* **69** 265 (1994)
73. T Ohzuku, Y Makimura *Chem. Lett.* **8** 744 (2001)
74. H Arai, S Okada, Y Sakurai, J Yamaki *J. Electrochem. Soc.* **145** 4160 (1998)
75. S H Park, Y-K Sun *J. Power Sources* **119–121** 161 (2003)
76. L Zhang, H Noguchi, M Yoshio *J. Power Sources* **110** 57 (2002)
77. C S Johnson, J-S Kim, A J Kropf, A J Kahaian, J T Vaughey, M M Thackeray *J. Power Sources* **119–121** 139 (2003)
78. Y Makimura, T Ohzuku *J. Power Sources* **119–121** 156 (2003)
79. J-H Kim, Y-K Sun *J. Power Sources* **119–121** 166 (2003)
80. S-H Kang, K Amine *J. Power Sources* **119–121** 150 (2003)
81. A Ueda, T Ohzuku *J. Electrochem. Soc.* **141** 2010 (1994)
82. W Li, J C Currie *J. Electrochem. Soc.* **144** 2773 (1997)
83. M Balasubramanian, X Sun, X Q Yang, J McBreen *J. Electrochem. Soc.* **147** 2903 (2000)
84. J Ying, C Wan, C Jiang, Y Li *J. Power Sources* **99** 78 (2001)
85. I Belharouak, H Tsukamato, K Amine *J. Power Sources* **119–121** 175 (2003)
86. R V Chebiam, F Prado, A Manthiram *J. Electrochem. Soc.* **148** A49 (2001)
87. G Prado, A Rougier, L Fournès, C Delmas *J. Electrochem. Soc.* **147** 2880 (2000)
88. J R Mueller-Neuhaus, R A Dunlap, J R Dahn *J. Electrochem. Soc.* **147** 3598 (2000)
89. J Kim, K Amine *J. Power Sources* **104** 33 (2002)
90. A R Naghash, J Y Lee *Electrochim. Acta* **46** 2293 (2001)
91. S Albrecht, J Kümpers, M Kruft, S Malcus, C Vogler, M Wahl, M Wohlfahrt-Mehrens *J. Power Sources* **119–121** 178 (2003)
92. G T K Fey, J G Chen, V Subramanian *J. Power Sources* **119–121** 658 (2003)
93. A Yu, G V Subba Rao, B V R Chowdari *Solid State Ionics* **135** 131 (2000)
94. J Cho, H Jung, Y Park, G Kim, H S Lim *J. Electrochem. Soc.* **147** 15 (2000)
95. J Reed, G Ceder *Electrochem. Solid-State Lett.* **5** A145 (2002)
96. N Yabuuchi, T Ohzuku *J. Power Sources* **119–121** 171 (2003)
97. S H Park, Y-K Sun, R S Park, K S Nahm, Y S Lee, M Yoshio *Electrochim. Acta* **47** 1721 (2002)
98. T Ohzuku, A Ueda, M Kouguchi *J. Electrochem. Soc.* **142** 4033 (1995)
99. K Kubo, S Arai, S Yamada, M Kanda *J. Power Sources* **81** 599 (1999)
100. R J Gummow, M M Thackeray *J. Electrochem. Soc.* **141** 1178 (1994)
101. K West, G Vitins, R Koksbang *Electrochim. Acta* **45** 3141 (2000)
102. V S Pervov, E V Makhonina, I A Kedrinskii *Neorg. Mater.* **33** 1031 (1997) [b]
103. J M Tarascon, W R McKinnon, F Coowar, T N Bowmer, G Amatucci, D Guyomard *J. Electrochem. Soc.* **141** 1421 (1994)
104. T Ohzuku, M Kitagawa, T Hirai *J. Electrochem. Soc.* **137** 769 (1990)
105. A Van der Ven, C Marianetti, D Morgan, G Ceder *Solid State Ionics* **135** 21 (2000)
106. Y Xia, M Yoshio *J. Electrochem. Soc.* **143** 825 (1996)
107. A R Naghash, J Y Lee *J. Power Sources* **102** 68 (2001)
108. E V Makhonina, V S Dubasova, V S Pervov, A F Nikolenko, A S Fialkov *Neorg. Mater.* **37** 1259 (2001) [b]
109. T Nakamura, A Kajiyama *Solid State Ionics* **124** 45 (1999)
110. W Liu, G C Fartington, F Chaput, B Dunn *J. Electrochem. Soc.* **143** 879 (1996)
111. T Nakamura, A Kajiyama *Solid State Ionics* **133** 195 (2000)
112. M R Manchini, L Petrucci, F Ronci, P P Prosini, S Passerini *J. Power Sources* **76** 91 (1998)
113. N V Kosova, N F Uvarov, E T Devyatkina, E G Avvakumov *Solid State Ionics* **135** 107 (2000)
114. N V Kosova, E T Devyatkina, S G Kozlova *J. Power Sources* **97–98** 406 (2001)

115. W T Jeong, J H Joo, K S Lee *J. Power Sources* **119–121** 690 (2003)
116. H Yan, Kh Huang, L Chen *J. Power Sources* **81–82** 647 (1999)
117. S H Wu, H-L Chen *J. Power Sources* **119–121** 134 (2003)
118. A R Naghash, J Y Lee *J. Power Sources* **85** 284 (2000)
119. C-H Lu, S-W Lin *J. Power Sources* **93** 14 (2001)
120. G Amatucci, A D Pasquier, A Blyr, T Zheng, J-M Tarascon *Electrochim. Acta* **45** 255 (1999)
121. Z Liu, H Wang, L Fang, J Y Lee, L M Gan *J. Power Sources* **104** 101 (2002)
122. G Vitins, E A Raekelboom, M T Weller, J R Owen *J. Power Sources* **119–121** 938 (2003)
123. L Hernán, J Morales, L Sáncez, E Rodriguez Castellón, M A G Aranda *J. Mater. Chem.* **12** 734 (2002)
124. Y M Todorov, Y Hideshima, H Noguchi, M Yoshio *J. Power Sources* **77** 198 (1999)
125. Y-S Hong, C-H Han, K Kim, C-W Kwon, G Campet, J-H Choy *Solid State Ionics* **139** 75 (2001)
126. E Zhecheva, R Stoyanova, M Gorova, P Lavela, J L Tirado *Solid State Ionics* **140** 19 (2001)
127. Y Terada, K Yasaka, F Nishikawa, T Konishi, M Yoshio, I Nakai *J. Solid State Chem.* **156** 286 (2001)
128. Y-K Sun, D-W Kim, Y-M Choi *J. Power Sources* **79** 231 (1999)
129. M Hosoya, H Ikuta, M Wahira *Solid State Ionics* **111** 153 (1998)
130. Q Zhong, A Bonakdarpour, M Zhang, Y Gao, J R Dahn *J. Electrochem. Soc.* **144** 205 (1997)
131. C Sigala, A Le Gal La Salle, Y Piffard, D Guyomard *J. Electrochem. Soc.* **148** A812 (2001)
132. C Sigala, A Le Gal La Salle, Y Piffard, D Guyomard *J. Electrochem. Soc.* **148** A819 (2001)
133. C Sigala, A Le Gal La Salle, Y Piffard, D Guyomard *J. Electrochem. Soc.* **148** A826 (2001)
134. K Du, J Xie, J Wang, H Zhang *J. Power Sources* **119–121** 130 (2003)
135. H-S Moon, J-W Park *J. Power Sources* **119–121** 717 (2003)
136. D Zhang, B N Popov, R E White *J. Power Sources* **76** 81 (1998)
137. G T-K Fey, C-Z Lu, T P Kumar *J. Power Sources* **119–121** 332 (2003)
138. Y S Lee, N Kumada, M Yoshio *J. Power Sources* **96** 376 (2001)
139. S H Park, K S Park, S S Moon, Y K Sun, K S Nahm *J. Power Sources* **92** 244 (2001)
140. Y W Tsai, R Santhanam, B J Hwang, S K Hu, H S Sheu *J. Power Sources* **119–121** 701 (2003)
141. K Oikawa, T Kamiyama, F Izumi, B C Chakoumakos, H Ikuta, M Wakihara, J Li, Y Matsui *Solid State Ionics* **109** 35 (1998)
142. H Aikiyo, K Nakane, N Ogata, T Ogihara *J. Ceram. Soc. Jpn.* **109** 506 (2001)
143. A M Skundin, O N Efimov, O V Yarmolenko *Usp. Khim.* **71** 378 (2002) [*Russ. Chem. Rev.* **71** 329 (2002)]
144. J-M Kim, H-T Chung *J. Power Sources* **115** 125 (2003)
145. T A Eriksson, M M Doeff *J. Power Sources* **119–121** 145 (2003)
146. J M Paulsen, D Larcher, J R Dahn *J. Electrochem. Soc.* **147** 2862 (2000)
147. C Storey, I Kargina, Y Greencourt, I J Davidson, Y C Yoo, D Y Seung *J. Power Sources* **97–98** 541 (2001)
148. L Zhang, H Noguchi *Electrochem. Commun.* **4** 560 (2002)
149. S-T Myung, S Komaba, N Hirosaki, N Kumagai *Electrochem. Commun.* **4** 397 (2002)
150. M Thackeray *Nature Mater.* **1** 81 (2002)
151. S-Y Chung, J T Bloking, Y-M Chiang *Nature Mater.* **1** 123 (2002)
152. S Yang, Y Song, K Ngala, P Y Zavaliy, M S Whittingham *J. Power Sources* **119–121** 239 (2003)
153. A Yamada, M Hosoya, S-C Chung, Y Kudo, K Hinokuma, K-Y Liu, Y Nishi *J. Power Sources* **119–121** 232 (2003)
154. J-S Kim, C S Johnson, M M Thackeray *Electrochem. Commun.* **4** 205 (2002)
155. G J Moore, C S Johnson, M M Thackeray *J. Power Sources* **119–121** 216 (2003)
156. T Numata, C Amemiya, T Kumeuchi, N Shirakata, M Yonezawa *J. Power Sources* **97–98** 358 (2001)
157. US P. 6 379 842 (2002)
158. US P. 5 677 083; *Chem. Abstr.* **127** 150 991 (1997)
159. Eur. P. 1 117 145; *Chem. Abstr.* **132** 196 732 (2000)
160. Eur. P. 1 150 368; *Chem. Abstr.* **135** 346 864 (2001)
161. V S Pervov, I D Mikheikin, E V Makhonina, V D Butskii *Usp. Khim.* **72** 852 (2003) [*Russ. Chem. Rev.* **71** 759 (2003)]
162. V S Pervov, E V Makhonina *Usp. Khim.* **69** 528 (2000) [*Russ. Chem. Rev.* **69** 481 (2000)]
163. A Yu Zavrazhnov, D N Turchen, Zh V Dobrokhotova, V V Volkov, E V Makhonina, V S Pervov *Neorg. Mater.* **39** 149 (2004) [b]
164. I D Mikheikin, M Yu Kuznetsov, E V Makhonina, V S Pervov *Dokl. Akad. Nauk* **376** 785 (2001) [c]
165. I D Mikheikin, M Yu Kuznetsov, E V Makhonina, V S Pervov *J. Mater. Synth. Process.* **10** 51 (2002)
166. I D Mikheikin, M Yu Kuznetsov, E V Makhonina, V P Sakun, V S Pervov *Dokl. Akad. Nauk* **388** 501 (2003) [c]
167. *First-Guarter FY 2003. Report for the Batteries for Advanced Transportation Technologies (BATT) Program*; http://berc.lbl.gov/BATT/BATT.html

[a] — *Chem. Sust. Develop. (Engl. Transl.)*
[b] — *Inorg. Mater. (Engl. Transl.)*
[c] — *Dokl. Chem. (Engl. Transl.)*

Russian Chemical Reviews **73** (10) 1003 – 1031 (2004) © 2004 Russian Academy of Sciences and Turpion Ltd

DOI 10.1070/RC2004v073n10ABEH000846

Modelling of chemical conversion processes in multicomponent reciprocal salt systems

E S Gryzlova, N A Kozyreva

Contents

I.	Introduction	1003
II.	Conversion figures, conversion graphs and matrices	1004
III.	Methods of construction of conversion figures	1008
IV.	Practical applications of matrices and graphs in studies of complex systems	1017
V.	Practical applications of multicomponent salt melts	1026
VI.	Conclusion	1029

Abstract. The review surveys geometric and algebraic models of chemical conversion (exchange) processes occurring in multicomponent salt systems in the molten state. Thermochemical and matrix methods for the construction of conversion figures are described in detail. The practical applications of matrices and graphs in studies of complex systems are illustrated. There are good prospects for using multicomponent salt systems in thermal power sources and high-temperature processes, such as electrolytic aluminising of niobium and silver plating. The bibliography includes 62 references.

I. Introduction

Multicomponent reciprocal salt systems are involved as major components in many natural (rocks, minerals, glasses, salt lakes) and artificial (fertilisers, materials of construction) materials. Technologies for the production of salts, heat technology, manufacturing engineering (salt melts are used for chemical thermal treatment of metal and alloy products), metallurgy and foundry practice are the most important areas of applications of multicomponent systems. In the last quarter of the 20th century, salt systems found increasing application due to considerable growth in the production of semiconducting materials and progress in the nuclear industry, rocket technology with the use of autonomous power supply sources and other branches.

Investigation of reciprocal systems containing four or more components (unlike binary and ternary systems) requires a special approach. Prior to the experiment, it is necessary to carry out a theoretical examination of the composition diagram,[1–5] *viz*., to partition the diagram of an *n*-dimensional polytope, derive non-equilibrium and singular stars and reveal conversion elements.†

Geometric, matrix and algebraic models are widely used in analysis of reciprocal systems. Below we describe models of conversion (exchange) processes occurring in reciprocal systems. These models are based on interchange reactions in systems consisting of inorganic salts. Composition figures (polytopes) are generally partitioned without considering the formation of binary and triple salts. However, as will be demonstrated in the present review, phase diagrams of compositions corresponding to conversion elements, which were determined experimentally by differential thermal analysis (DTA), provide sufficient information also on complexation processes in multicomponent systems.

Non-equilibrium and singular stars, which are graphical models of reciprocal systems, reflect the compositions of simplex cells resulting from the partition of polytopes. Radishchev [2] considered a singular star as a stable complex of a system and defined it as a combination of geometric models of the system derived by partitioning the composition figures into simplexes. Therefore, a singular star consists of stable simplexes and is represented as a graph. Alekseeva and Dombrovskaya [5] characterised a singular star as an equilibrium chemical diagram. The latter is a geometric figure that represents a combination of components, which do not react with each other on mixing.

The partition of composition diagrams and location of the compositions of simplex cells in reciprocal systems are determined by exchange reactions occurring in these systems. According to the criterion proposed by Voskresenskaya,[2,3] the exchange reactions are shifted toward the formation of a salt pair, which is derived from another salt pair with heat evolution ($\Delta_f H_{298} < 0$). The validity of this criterion was confirmed by numerous experiments.[2,3]

The partition can be carried out in various ways, *e.g*., using geometric, matrix and combined (matrices + graphs) approaches. Methods were developed for partitioning polytopes into multidimensional figures consisting of any number of components with the use of tables of vertex indices in the absence of connections between salts [3] and taking into account the complex formation in terms of the graph theory.[4]

An intersection of non-equilibrium and equilibrium complexes of a system gives geometric elements, which model interchange reactions (the so-called conversion elements).

E S Gryzlova V I Vernadsky Institute of Geochemistry and Analytical Chemistry, Russian Academy of Sciences, ul. Kosygina 19, 117975 Moscow, Russian Federation. Fax (7-095) 938 20 54.
Tel. (7-095) 137 86 25. E-mail: elenagryzlova@hotbox.ru
N A Kozyreva The Higher Chemical College, Russian Academy of Sciences, Miusskaya pl. 9, 125047 Moscow, Russian Federation.
Fax (7-095) 978 85 27. Tel. (7-095) 978 85 27.
E-mail: deans@hcc.ru

Received 17 April 2004
Uspekhi Khimii **73** (10) 1088 – 1117 (2004); translated by T N Safonova

† In physicochemical analysis of multicomponent salt systems, the term 'conversion' is used to describe transformations of two salts into two other salts, both pairs having the same ion composition and different molecular compositions. The conversions of basic and secant elements are distinguished.

In systems containing no less than 9 salts, the basic elements are salt compositions corresponding to geometric figures, which serve as the basis of simplexes of a cyclic fragment of a star (triangles for quinary reciprocal systems consisting of nine salts, tetrahedra for senary reciprocal systems consisting of 12 salts, *etc.*).

The secant elements are geometric figures corresponding to metastable pairs of the starting salts, which react to form reaction products (a non-equilibrium partition), or stable salt pairs formed by exchange reactions (an equilibrium partition). The diagonals of a composition square of a system serve as secant elements for ternary reciprocal systems, two triangles serve as secant elements for quaternary reciprocal systems consisting of six salts, *etc.*

Non-equilibrium and equilibrium partitions can be represented in a matrix form as tables of vertex indices and matrices of reciprocal salt pairs. In matrices used in physicochemical analysis, both composition figures and exchange reactions occurring in the system as well as the reaction products and particular thermochemical relations are encoded. For example, a matrix referred to as a table of vertex indices [2,3] contains information on how many times each salt is formed in the system under consideration by exchange reactions. The composition of a system is expressed by ions rather by the formulas of salts, and the compositions of the salts are seen at the intersection of a row and a column of the matrix. For example, the table of vertex indices for the A,B//X,Y,Z,T system (A and B are cations; X, Y, Z and T are anions) is as follows:

	X	Y	Z	T
A	0	1	2	3
B	3	2	1	0

In this matrix, the AY salt is a product of one exchange reaction (1), and the BT salt is metastable (0), *i.e.*, the latter is the starting compound rather than a product of any reaction.

In a matrix of reciprocal salt pairs,[3] the numbers 1 and 0 signify stability and instability, respectively, of a salt pair. Compounds produced in an exchange reaction are denoted by unity. The number of unities is equal to the number of exchange reactions in the system. For example, the matrix for a quaternary reciprocal system A,B//X,Y,Z consisting of four salts is as follows:

	BX	BY	BZ
AX	0	1	1
AY	0	0	1
AZ	0	0	0

Radishchev [2] introduced the concepts of a point of complete conversion and a point of incomplete conversion for ternary reciprocal systems and the concept of a conversion line for quaternary reciprocal systems. These concepts are used in physicochemical analysis. Radishchev derived components of conversion figures of secant elements for reciprocal systems consisting of eight salts and considered the conversion of axial (basic) triangles and secant elements of quinary reciprocal systems consisting of nine salts. The further development of these concepts involved three lines.

1. The construction of conversion figures of basic elements.[3] Presently, this line of investigation has no practical application.

2. The construction and investigation of conversion figures of secant elements.[6] These figures reflect the main thermochemical relations and the energetics of exchange reactions.

3. The construction of conversion figures taking into account the formation of binary and ternary compounds involving salts. These figures are very complicated, and calculations for these systems can be carried out only on a computer. The energy characteristics of particular compositions can be estimated by calculation methods (these characteristics can also be estimated using conversion figures of secant elements, the procedure being more simple). This line of investigation has not been developed in detail.

The second line served as the basis for devising a conversion method for studying reciprocal multicomponent systems.[6] This method was used for solving a number of theoretical problems and practical tasks.[7,8] For example, this method made it possible to choose salt compositions characterised by the optimal heat-accumulation properties [8–10] and determine the final target products in complex mixtures.[11]

The first review on the conversion method was given in the monograph,[3] where the essence of this method was presented, procedures for deriving conversion elements were considered, examples of conversion figures and the prediction of phases, which crystallise from melts modelled by these figures, were offered, and a proximate method for studying multicomponent reciprocal systems was briefly described.

Phase complexes of systems were extensively studied by the conversion method in the late 1970s/early 1980s. Selected results were given in the monograph;[11] however, a systematic review was lacking. The practical application of the conversion method to the solution of applied problems (in particular, for heat accumulation) was described in the monograph.[8] More recent reviews on the modelling of conversion processes are lacking. This method was only briefly mentioned (a few references were given) in the monograph,[4] because the latter was devoted to an alternative methodology for studying complex salt systems.

Up to the mid-1990s, experimental data on conversion elements and their practical applications were accumulated.[11–18] Theoretical studies were devoted primarily to a combination of the conversion and matrix methods and examination of energy transfer processes in exchange reactions.[19–31] In this period, a method was devised for the construction of singular stars of tetrahedra from conversion elements; matrices of conversion figures and conversion graphs were derived; the structures of conversion figures of quinary reciprocal systems of the 3//3 series were refined; the fine energy structure of axial triangles of quinary reciprocal systems consisting of nine salts was revealed; the mechanism of transformation of a system from a non-equilibrium state to an equilibrium state was studied and intermediate stars of pentatopes and tetrahedra of reciprocal systems of the 3//3 series were derived; energy diagrams for the transformation from a non-equilibrium combination of three salts (a non-equilibrium triangle) to an equilibrium state (a stable axial triangle) were constructed; relationships between various models of conversion processes were revealed. Based on the conversion method, heat-accumulation compositions were developed, and studies of the behaviour of ionic liquids in multicomponent melts at various temperatures were started.

The concept of rational investigation of multicomponent reciprocal salt systems in melts was elaborated. This concept is based on thermochemical (energy) criteria and Kurnakov's correspondence principle.

The aim of the present review is to summarise data on the modelling of conversion processes in salt melts. Theoretical and experimental studies, which were performed in the last 20 years, were surveyed. The relationship between models used in studies of exchange equilibria was demonstrated. The conversion method of investigation of reciprocal systems was shown to be of importance in solving technological problems and developing fundamental sciences.

II. Conversion figures, conversion graphs and matrices

1. Ternary reciprocal systems

A stable secant complex of ternary reciprocal systems consisting of four salts is represented by one stable diagonal, which divides the composition square of a system into two ternary systems (Fig. 1). The stable AX – BY diagonal intersects the metastable AY – BX diagonal (a metastable secant complex) in the centre of

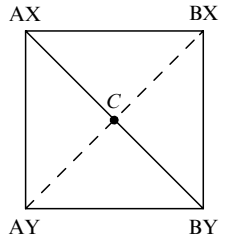

Figure 1. Composition square of the ternary reciprocal system A,B//X,Y with the full conversion point *C*.

the square, *viz*., at the point *C* (a point of complete conversion). At this point, salts of a metastable pair are completely transformed into a stable pair (complete conversion):

$$AY + BX = AX + BY.$$

An incomplete transformation of salts, *i.e*., incomplete conversion, corresponds to an arbitrary point of the composition figure, for example, on the metastable diagonal, but off the conversion point.

2. Quaternary reciprocal systems consisting of six salts

The conversion figure of a quaternary reciprocal system A,B,C//X,Y consisting of six salts of the 2//*n* (*n*//2) series contains two conversion lines denoted in the Fig. 2 as *EF* and *FT*. The points of complete conversion are *E*, *T* and *F*. The following exchange reactions correspond to these points:

for the point *E*: $CX + AY = AX + CY$, the first-stage reaction,

for the point *T*: $AX + BY = AY + BX$, the first-stage reaction,

for the point *F*: $CX + BY = BX + CY$, the second-stage reaction.

By summing these equations, we obtain

$$2\,CX + AY + 2\,BY + AX = AX + 2\,CY + 2\,BX + AY$$

or

$$CX + BY = CY + BX.$$

Hence, two first-stage reactions in the A,B,C//X,Y system are independent, whereas the reaction corresponding to the point of complete conversion *F* depends on the first-stage reactions.

The full conversion figure includes three points of complete conversion denoted as *E*, *F* and *T* (in accordance with the number of interchange reactions occurring in the system) and two conversion lines (see Fig. 2) converging to a common point corresponding to the second-stage reaction.

Since the conversion figure is a part of a composition figure, one can construct the phase diagram of the system under study using the lines of the conversion figures as the composition axis. The conversion figure is a polythermal section, which reflects the dependence of the melting point on the combination of salt pairs. This diagram displays salts, which initially crystallise from melts, secondary, tertiary, *etc*. crystallisation products and temperatures corresponding to invariant points.

If only vertices and edges of a conversion figure are displayed, one obtains a conversion graph. The vertices of this graph correspond to salt pairs or thermal effects of exchange reactions giving rise to these salts. In the latter case, the graph is referred to as an energy graph. This graph can be used for thermochemical calculations.

Each vertex of a conversion figure or a conversion graph corresponds to a reaction of a particular stage, and the degree of this vertex (*i.e*., the number of edges incident to this vertex) depends on the stage of the corresponding reaction. As a rule, the higher the stage, the larger the number of edges incident to the vertex of the graph corresponding to this reaction. Therefore, the number of reactions of a particular stage can directly be determined from the graph. The number of edges incident from vertices of conversion graphs for systems containing different numbers of salts are given in Table 1.

Rapid progress in computer technology made it possible to use matrix methods for displaying composition figures and physicochemical interactions in systems,[3] and, consequently, the use of the conversion method [6] for solving various applied problems on a computer caused a need to go from geometric objects, *viz*., graphs of conversion figures, to matrices of these figures.[32, 33]

It is known that each graph has its own adjacency matrix $A = (a_{ij})$ with dimensions $n \times n$, in which the element a_{ij} is equal to the number of edges of the graph connecting the vertices V_i and V_j. The distinguishing feature of the graphs of conversion figures is that they have no multiple edges. Hence, elements of rows and columns of the matrix can be only 1 or 0. The number of rows and columns in the matrix is determined by the number of vertices of the graph, *i.e*., the number of points of complete conversion of ternary reciprocal systems involved in the figure. For example, the graph of a conversion figure of any quaternary reciprocal system consisting of 6 salts can be expressed by a matrix, in which the points *A* and *C* correspond to first-stage reactions, and the point *B* corresponds to a second-stage reaction.

	A	*B*	*C*
A	0	1	0
B	1	0	1
C	0	1	0

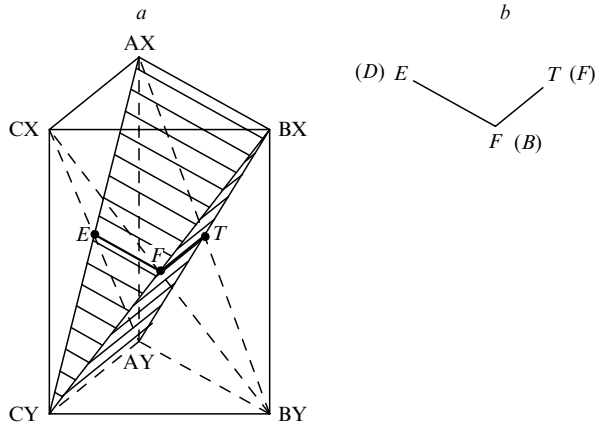

Figure 2. Arrangement of the conversion lines in the composition prism (*a*) and the conversion figure (*b*) of the quaternary reciprocal system A,B,C//X,Y (letters in parentheses correspond to a special case, *viz*., the Na,K,Ba//F,WO_4 system).

Table 1. Number of edges of conversion graphs incident to the points corresponding to reactions of particular stages for systems consisting of 4 – 12 salts.

Number of salts	Number of edges for the reaction of stage				
	I	II	III	IV	V
4	1	0	0	0	0
6	1	2	0	0	0
8	2	3	4	0	0
9 of the type					
A ⇄ B	2	5	5	8	0
C	3	3	0	8	0
D ⇄ E	2	6	0	0	0
10 (2//*n* series)	3	4	5	6	0
12 (2//*n* series)	4	5	6	7	8

The matrix of a conversion graph has the following properties.

1. The sum of the numbers in each row and each column is equal to the degree of the corresponding vertex of the graph (in the above matrix, the point *B* has two connections, and the points *A* and *C* each have one connection).

2. The matrix is symmetric with respect to the diagonal, whose elements are zero.

3. The matrix unambiguously defines the graph with an accuracy of up to isomorphous; hence, the corresponding graph can be constructed based on any matrix.

For practical use of a conversion figure, it is not necessary to construct the corresponding graph from the adjacency matrix. Geometric objects can completely be excluded, because the matrix of a conversion figure contains all necessary information. For example, the degree of a vertex of a graph defines not only the number of edges connecting this vertex to other vertices (*i.e.*, the number of conversion lines) but also the number of chemical reactions giving rise to the corresponding salt pair, as well as the reaction stage (the diagonal), on which the conversion point is located, and the compositions of simplexes of a singular star.

3. Quinary reciprocal systems consisting of eight salts of the 2//*n* (*n*//2) series

A conversion figure of a quinary reciprocal system consisting of eight salts (Fig. 3) contains six vertices (in accordance with the number of exchange reactions), eight conversion lines, two conversion triangles (*4–1–6* and *2–6–5*) and one conversion square (*3–5–6–4*). The third-stage reaction corresponds to the vertex 6, which has the largest number of connections to other vertices. The second-stage reactions correspond to the points *4* and *5*. The vertices *1*, *2* and *3* are the points of complete conversion of ternary reciprocal systems, in which first-stage reactions proceed.

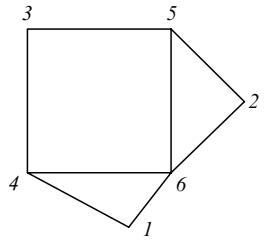

Figure 3. Conversion figure of a quaternary reciprocal system consisting of eight salts.

A conversion figure is a geometric model of chemical processes occurring in a system. This figure forms as the intersection of stable and metastable complexes or singular or non-equilibrium stars. Each element of the conversion figure (a point, a line, a plane, *etc.*) models exchange reactions taking place in the system. The point reflects a reaction of one salt pair (*i.e.*, one reaction), the line reflects an interaction between two salt pairs (two reactions), the plane reflects an interaction between three salt pairs (three reactions), *etc*. For systems including no less than 5 components, a fragment of the conversion figure enclosed by four conversion lines, which is commonly referred to as a conversion square, can be divided by the diagonal into two triangles.

Conversion triangles and squares have central points, which are points of complete conversion for a particular number of reactions. For each point of the conversion figure, a chemical reaction can be constructed. The number of salts involved in this reaction is equal to the number of these salts located at the vertices, which enclose this fragment of the conversion figure. The reaction equations include salts in stoichiometric amounts.

As an example we refer to the quinary reciprocal system Li,Na//Br,Cl,NO_3,SO_4 consisting of 8 salts. The thermochemical characteristics of this system are given in Table 2.

The matrix of the conversion graph for this system takes the form

	1	*2*	*3*	*4*	*5*	*6*
1	0	0	0	1	0	1
2	0	0	0	0	1	1
3	0	0	0	1	1	0
4	1	0	1	0	0	1
5	0	1	1	0	0	1
6	1	1	0	1	1	0

Table 2. Points of complete conversion and thermochemical relations for the quinary reciprocal system Li,Na//Br,Cl,NO_3,SO_4 .

Point	Ternary reciprocal system	Stable salt pair	Reaction	
			stage	*Q*
1	Li,Na//Cl,Br	LiCl + NaBr	I	Q_1
2	Li,Na//NO_3,SO_4	Li_2SO_4 + $NaNO_3$	I	Q_2
3	Li,Na//Cl,NO_3	$LiNO_3$ + NaCl	I	Q_3
4	Li,Na//Br,NO_3	$LiNO_3$ + NaBr	II	$Q_4 = Q_1 + Q_3$
5	Li,Na//Cl,SO_4	Li_2SO_4 + NaCl	II	$Q_5 = Q_2 + Q_3$
6	Li,Na//Br,SO_4	Li_2SO_4 + NaBr	III	$Q_6 = Q_1 + Q_2 + Q_3$

4. Senary reciprocal systems consisting of ten salts of the 2//*n* (*n*//2) series

The conversion figure of a senary reciprocal system shown in Fig. 4 *a*,*b* contains conversion points, lines, triangles and squares along with bulk elements, such as conversion tetrahedra

a

	Na_2SO_4	$NaNO_3$	NaCl	NaBr	NaI
Li_2SO_4	0	1	1	1	1
$LiNO_3$	0	0	1	1	1
LiCl	0	0	0	1	1
LiBr	0	0	0	0	1
LiI	0	0	0	0	0

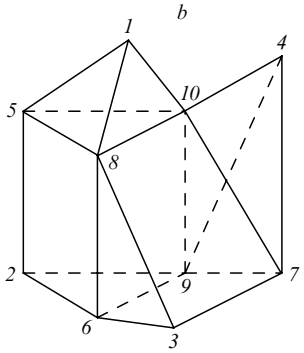

c

	I^-	Br^-	Cl^-	NO_3^-	SO_4^{2-}
Li^+	0	1	2	3	4
Na^+	4	3	2	1	0

Figure 4. Conversion graph inscribed in the matrix of mutual salt pairs (*a*), the conversion figure of secant tetrahedra (*b*) and the table of vertex indices (*c*) of the senary reciprocal system Li,Na//Cl,Br,I,NO_3,SO_4 consisting of ten salts.

(*1–5–10–8* and *4–7–9–10*) and triangular prisms (*4–7–10–8–6–3* and *5–8–10–9–6–2*). The point *10*, from which six conversion lines emerge, corresponds to a fourth-stage reaction. The points *8* and *9* (five lines) correspond to third-stage reactions. The points of complete conversion, from which four conversion lines emerge (the points *7*, *6* and *5* in Fig. 4 *b*), correspond to second-stage reactions.

Other vertices are points of complete conversion modelling first-stage reactions. The matrix table of vertex indices of the senary reciprocal system Li,Na//Br,Cl,I,NO_3,SO_4 is presented in Fig. 4 *c*.

5. Quinary reciprocal salt systems consisting of nine salts of the 3//3 series

Three thermochemical (five topological A, B, C, D, E) types of reciprocal quinary systems, *viz*., 9A ⇄ 9B, 9C ⇄ 9C′ and 9D ⇄ 9E, are known.[2] These pairs are characterised by the same set of reactions of particular stages (Table 3). However, their singular stars have different geometry (different topology) and, correspondingly, different notations.

Table 3. Number of reactions of particular stages for reciprocal systems of the 3//3 series.

Type of system	Number of reactions of a given stage			
	I	II	III	IV
9A ⇄ 9B	4	2	2	1
9C ⇄ 9C′	4	4	0	1
9D ⇄ 9E	6	3	0	0

The conversion figure of a reciprocal system of any thermochemical type of the 3//3 series is a graph, whose vertices correspond to points of complete conversion of ternary reciprocal systems involved in a more complex system (Figs 5–7). The lines of complete conversion of quaternary reciprocal systems serve as edges of the graph. For systems of the 2//*n* (*n*//2) series, the conversion figures contain no other conversion elements. Hence, the thermochemical type of the conversion figure coincides with the topological type. The structures of the conversion figures of quinary reciprocal systems of the 3//3 series are complicated,

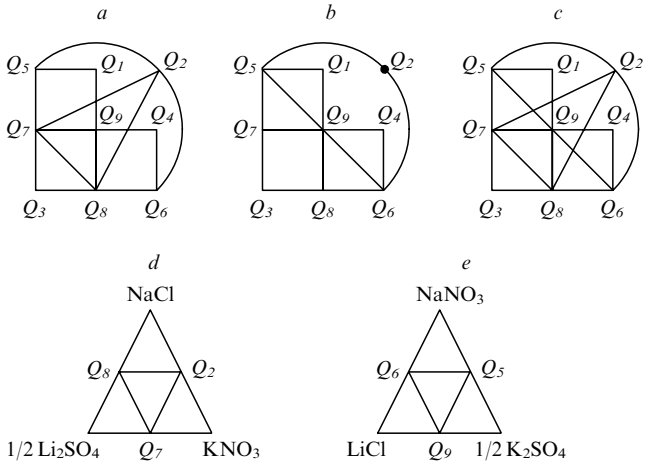

Figure 5. Conversion figures of quinary reciprocal systems consisting of nine salts of different topological types.
(*a*) 9A type; (*b*) 9B type; (*c*) 9A ⇄ 9B type; (*d*) the conversion lines $Q_9–Q_2–Q_7$ intersecting the axial stable triangle of the 9A ⇄ 9B-type Li,Na,K//Cl,NO_3,SO_4 system; (*e*) the conversion lines $Q_9–Q_5–Q_6$ intersecting the axial metastable triangle of the 9A ⇄ 9B-type Li,Na,K// Cl,NO_3,SO_4 system.

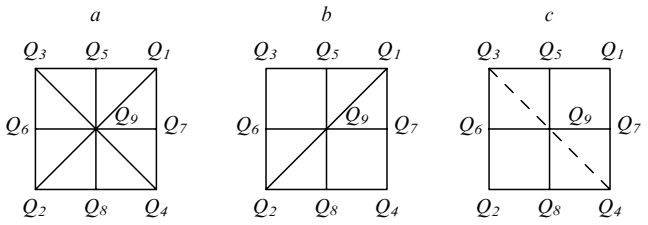

Figure 6. Conversion figures of the 9C-type quinary reciprocal system.
(*a*) The common conversion figure for the 9C ⇄ 9C′ equilibrium; (*b*) the conversion figure with the conversion lines $Q_1–Q_9–Q_2$ intersecting the axial stable triangle; (*c*) the conversion figure with the conversion lines $Q_3–Q_9–Q_4$ intersecting the axial metastable triangle.

because each topological type of these systems is characterised by its own conversion figure. It should be noted that the conversion figures of the same thermochemical type (9A ⇄ 9B, 9C ⇄ 9C′, 9D ⇄ 9E)[6,8] differ in the position of additional lines resulting from the intersection of axial (basic) triangles with conversion planes. Therefore, there are various topological types of conversion figures, which have a common thermochemical framework.

The number of edges incident to a vertex of a graph depends on the stage of the reaction, which is modelled by a particular conversion point. Systems of the 3//3 series differ in the characteristic features from 2//*n* (*n*//2) systems. For example, the points corresponding to second-stage reactions in 9B-type systems (see Fig. 5 *b*, the points Q_5 and Q_6) can have a larger number of connections than the points corresponding to third-stage reactions (the points Q_7 and Q_8 in Fig. 5 *b*).

The points of intersection of the first-stage diagonals in 9C-type systems also have different numbers of connections (Fig. 6, the points Q_1, Q_2, Q_3 and Q_4), which indicates that systems of the 3//3 series are more complicated than systems of the 2//*n* series.

From the thermochemical point of view, the conversion squares of 9C-, 9D- and 9E-type quinary reciprocal systems consisting of nine salts are equivalent, because they have diagonals corresponding to reactions of the same stages: I, II, II, IV (9C type); I, I, II, II (9D and 9E types). In 9A- and 9B-type systems, the conversion squares are thermochemically non-equivalent. For example, the conversion squares for 9A-type systems ($Q_1–Q_5–Q_7–Q_9$ and $Q_4–Q_6–Q_8–Q_9$) have the same sets of stages of the diagonals (I, II, III, IV), whereas the $Q_3–Q_7–Q_8–Q_9$ square differs from these squares (a set of stages of the I, III, III and IV diagonals). The same is true for 9B-type systems: the $Q_1–Q_5–Q_7–Q_9$ and $Q_4–Q_6–Q_8–Q_9$ squares are equivalent,

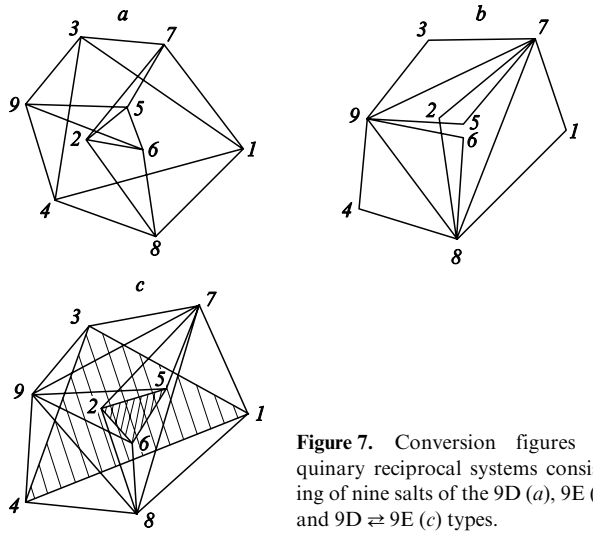

Figure 7. Conversion figures of quinary reciprocal systems consisting of nine salts of the 9D (*a*), 9E (*b*) and 9D ⇄ 9E (*c*) types.

whereas the $Q_3-Q_7-Q_9-Q_8$ square differs from the above two squares. This fact indicates that salts (or salt pairs) in the $Q_3-Q_7-Q_9-Q_8$ (9A type) and $Q_8-Q_9-Q_7-Q_3$ (9B type) squares are less reactive, and this region of the model (a conversion square) is characterised by a smaller number of reactions between salts, which are involved in pairs located at the vertices of this conversion square. The latter can be considered as the most stable square. The nature of the thermochemical non-equivalence of the conversion squares in 9A- and 9B-type systems (see Fig. 5 *a*,*b*) calls for a more detailed study.

Comparative investigation of conversion figures of systems belonging to different topological and thermochemical types may be useful in constructing mixtures of reciprocal salt systems possessing desired properties. Changes in the reactivity of a salt mixture upon the addition of a new component or the replacement of one component with another one can be predicted on the basis of conversion figures.

For example, the replacement of a component in a 9A-type system giving rise to a 9C-type system can lead to an increase in the reactivity of the salt system, because the conversion squares for 9A-type systems contain sets of higher-stage diagonals compared to the set of diagonals of the conversion squares for 9C-type systems. The reactivity of the mixtures can be further increased on going to 9D- or 9E-type systems (see Fig. 7).

Let us consider this relationship using real systems as examples.

a. Type 9A ⇄ 9B

Systems of the 9A ⇄ 9B thermochemical type are characterised by the occurrence of nine reactions (four first-stage reactions, two second-stage reactions, two third-stage reactions and one fourth-stage reaction). Topological conversion graphs for 9A- and 9B-type systems contain nine points corresponding to the number of exchange reactions (see Fig. 5 *a*,*b*), squares and triangles located on different planes of the three-dimensional space resulting from the intersection of secant tetrahedra of singular and non-equilibrium stars.[8]

The main framework of these figures is composed of lines corresponding to conversion figures of quaternary systems consisting of six salts. These lines connect nine vertices of the conversion figure. For example, these are the $Q_5-Q_7-Q_3$, $Q_6-Q_8-Q_3$, $Q_1-Q_9-Q_8$, $Q_4-Q_9-Q_7$, $Q_1-Q_5-Q_2$ and $Q_2-Q_6-Q_4$ lines in 9A-type systems (see Fig. 5 *a*). The inner lines, *viz*., Q_7-Q_8, Q_2-Q_8 and Q_2-Q_7 in 9A-type systems and Q_5-Q_6, Q_5-Q_9 and Q_6-Q_9 in 9B-type systems (see Fig. 5 *b*), are a special case. These lines intersect the planes of axial (stable and metastable) triangles (see Fig. 5 *d*,*e*). In Fig. 5 *c*, three conversion squares ($Q_1-Q_5-Q_7-Q_9$, $Q_3-Q_7-Q_9-Q_8$ and $Q_4-Q_6-Q_8-Q_9$) reflect chemical interactions in the quinary reciprocal system consisting of nine salts.

b. Type 9C ⇄ 9C′

The conversion figure of quinary systems of the 9C ⇄ 9C′ thermochemical type (see Fig. 6) contains nine vertices (in accordance with the number of points of complete conversion of ternary reciprocal systems involved in a quinary reciprocal system consisting of nine salts) and 16 lines, twelve of which are fragments of the conversion figures of all six reciprocal systems consisting of six salts involved in the quinary system.[8] Four lines emerging from the central point of the square (the point of intersection of the stable highest-stage diagonal with the corresponding metastable diagonal) are special lines. Both the stable and metastable axial triangles are divided into four triangles by these lines together with the conversion line of basic elements of a 9C ⇄ 9C′-type quinary reciprocal system consisting of nine salts.

c. Type 9D ⇄ 9E

The conversion figure of reciprocal systems of the 9D ⇄ 9E thermochemical type is a graph (see Fig. 7), whose vertices correspond to nine points of complete conversion of nine ternary reciprocal systems and edges correspond to 12 conversion lines of quaternary reciprocal systems consisting of six salts. The inner lines corresponding to interactions between all salts of the system are the *7–8*, *8–9*, *7–9* (E type); *5–6*, *5–2*, *2–6* (D type); *1–4*, *4–3*, *1–3* (common) lines, which intersect the planes of two stable axial triangles and one metastable triangle.

Nine diagonals (six first-stage diagonals and three second-stage diagonals) serve as thermochemical characteristics of 9D ⇄ 9E-type systems.

The thermal effects of the second-stage reactions can be expressed in a dual fashion as the sums of the thermal effects of first-stage reactions.

$$Q_2 + Q_3 = Q_1 + Q_5 = Q_7,$$

$$Q_1 + Q_6 = Q_2 + Q_4 = Q_8,$$

$$Q_4 + Q_5 = Q_3 + Q_6 = Q_9.$$

From these equations it follows that

$$Q_2-Q_1 = Q_5-Q_3 = Q_6-Q_4.$$

These relations can be used for solving problems associated with the construction of systems possessing the desired thermochemical characteristics of salt compositions.

III. Methods of construction of conversion figures

Several methods were developed for the construction of conversion figures, the so-called, geometric, thermochemical and matrix methods.

As mentioned above, the geometric method[2] is very complicated, because it requires the use of multidimensional geometry. According to this method, the conversion figures are constructed by intersecting stable and metastable complexes.

The thermochemical method[8] is based on thermochemical relations, which are used for the construction of an energy graph. Generally, the centre of this graph is occupied by a conversion point corresponding to the highest thermal effect, which is the sum of several thermal effects. This point has the largest number of thermochemical connections. For example, the point Q_9 for 9C ⇄ 9C′-type systems consisting of nine salts (see Fig. 6 *c*) has six connections and is connected to all points corresponding to reactions with independent thermal effects (first-stage reactions). The latter points have a minimum number of connections (three) and are connected to points corresponding to reactions with dependent thermal effects (as summands) and the point corresponding to the reaction with the highest thermal effect. The points corresponding to the thermal effects of second-stage reactions are connected to the points corresponding to first-stage reactions and the point corresponding to the reaction with the highest thermal effect. Three lines emerge from each of these points.

The conversion figure for systems of the 2//*n* type can be constructed from conversion figures of lower dimensionality. For example, the conversion figure of secant tetrahedra for systems of the 2//4 series can be constructed from the conversion figures of systems of the 2//3 series.

The matrix metod[8,33] will be discussed below.

1. The thermochemical method for the construction of conversion figures of systems of the 2//*n* (*n*//2) series

Conversion figures of systems of the 2//*n* (*n*//2) series are shown in Figs 1; 2 *a*,*b*; 3; 4 *a*,*b*.

Let us consider the method for the construction of conversion figures of a quaternary reciprocal system consisting of six salts using the Li,Na//Cl,NO_3,SO_4 system as an example. The conversion figure of reciprocal systems of the 2//3 (3//2) series is constructed based on thermochemical relations. The point of complete conversion corresponding to a second-stage reaction is connected by conversion lines to the points corresponding to first-stage reactions. The thermochemical relations for the Li,Na//

Table 4. Thermochemical relations for the Li,Na//Cl,NO_3,SO_4 system.

Ternary reciprocal system	Stable salt pair	Reaction [a]	
		stage	Q /kJ (mol equiv)$^{-1}$
Li,Na//Cl,SO_4	Li_2SO_4 + NaCl	II	$Q_3 = Q_1 + Q_2 = 26.78$
Li,Na//NO_3,SO_4	Li_2SO_4 + $NaNO_3$	I	$Q_1 = 7.95$
Li,Na//Cl,NO_3	$LiNO_3$ + NaCl	I	$Q_2 = 18.83$

[a] Hereinafter, the thermal effects of the reactions are given in kJ per mole of equivalents.

Cl,NO_3,SO_4 system are given in Table 4. The elements of the conversion figure of this system are listed in Table 5.

Three points of complete conversion correspond to the following chemical reactions:

point *B*: $2\,LiCl + Na_2SO_4 = Li_2SO_4 + 2\,NaCl - Q_3$,

point *C*: $2\,LiNO_3 + Na_2SO_4 = Li_2SO_4 + 2\,NaNO_3 - Q_1$,

point *A*: $2\,LiCl + 2\,NaNO_3 = 2\,LiNO_3 + 2\,NaCl - Q_2$.

The composition figures of systems of the 2//4 (4//2) series have three first-stage diagonals, two second-stage diagonals and one third-stage diagonal. The conversion figure of these systems consists of two triangles and one quadrangle connected in a particular manner.

Table 5. Conversion elements for the Li, Na//Cl,NO_3,SO_4 system.

Conversion element	Salt composition
Point *A*	$LiNO_3$, NaCl
Point *B*	Li_2SO_4, NaCl
Point *C*	Li_2SO_4, $NaNO_3$
Line *A* – *B*	Li_2SO_4, $LiNO_3$, NaCl
Line *B* – *C*	Li_2SO_4, NaCl, $NaNO_3$

The thermochemical relations in the quinary system Li,Na// Br,Cl,NO_3,SO_4 consisting of eight salts are given in Table 6. The elements of the conversion figure are shown in Fig. 8.

Table 6. Thermochemical relations for the Li,Na//Br,Cl,NO_3,SO_4 system.

Ternary reciprocal system	Metastable pair	Stable pair	Reaction	
			stage	Q
Li,Na//Cl,Br	LiBr + NaCl	LiCl + NaBr	I	Q_1
Li,Na// NO_3,SO_4	$LiNO_3$ + + Na_2SO_4	Li_2SO_4 + + $NaNO_3$	I	Q_2
Li,Na//Cl,NO_3	LiCl + $NaNO_3$	$LiNO_3$ + NaCl	I	Q_3
Li,Na//Br,NO_3	LiBr + $NaNO_3$	$LiNO_3$ + NaBr	II	$Q_4 = Q_1 + Q_3$
Li,Na//Cl,SO_4	LiCl + Na_2SO_4	Li_2SO_4 + NaCl	II	$Q_5 = Q_2 + Q_3$
Li,Na//Br,SO_4	LiBr + Na_2SO_4	Li_2SO_4 + NaBr	III	$Q_6 = Q_1 + Q_2 + Q_3$

The conversion figure for the Li,Na//Br,Cl,NO_3,SO_4 system is constructed based on the thermochemical relations taking into account the following facts. The centre of the conversion figure should be occupied by a point corresponding to the maximum thermal effect. This is the point *B* in Fig. 8 corresponding to intersection of the stable Li_2SO_4 – NaBr diagonal (a third-stage diagonal) and the metastable LiBr – Na_2SO_4 diagonal. The point *B* has the maximum number of connections to points of intersection of the lowest-stage diagonals (four connections).

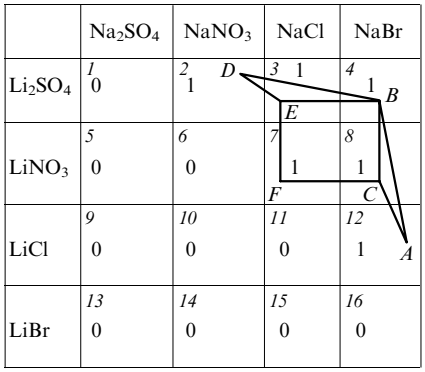

Figure 8. Conversion graph of the quaternary reciprocal system Li,Na// Cl,Br,NO_3,SO_4 inscribed in the matrix of mutual salt pairs.

These are the points *A* (a point of intersection of the first-stage diagonals LiCl – NaBr and LiBr – NaCl), *D* (a point of intersection of the first-stage diagonals Li_2SO_4 – $NaNO_3$ and $LiNO_3$ – Na_2SO_4), *E* (a point of intersection of the second-stage diagonals Li_2SO_4 – NaCl and LiCl – Na_2SO_4) and *C* (a point of intersection of the second-stage diagonals $LiNO_3$ – NaBr and LiBr – $NaNO_3$).

The points of intersection of second-stage diagonals (*E* and *C*) each have three connections to the points of intersection of first-stage diagonals (*A*, *D* and *F*) and the point of intersection of fourth-stage diagonals (*B*). Finally, the points of intersection of first-stage diagonals *A*, *D* and *F* each have two connections (see Fig. 8).

The conversion elements for the Li,Na//Br,Cl,NO_3,SO_4 system are given in Table 7.

The following reactions occur in the system:

point *A*: $2\,LiBr + 2\,NaCl =$ (1)

$= 2\,LiCl + 2\,NaBr - 6.69$ kJ (mol equiv)$^{-1}$,

point *B*: $2\,LiBr + Na_2SO_4 =$ (2)

$= Li_2SO_4 + 2\,NaBr - 33.47$ kJ (mol equiv)$^{-1}$,

point *C*: $2\,LiBr + 2\,NaNO_3 =$ (3)

$= 2\,LiNO_3 + 2\,NaBr - 25.52$ kJ (mol equiv)$^{-1}$,

point *D*: $2\,LiNO_3 + Na_2SO_4 =$ (4)

$= Li_2SO_4 + 2\,NaNO_3 - 7.95$ kJ (mol equiv)$^{-1}$,

Table 7. Conversion elements for the Li,Na//Br,Cl,NO_3,SO_4 system.

Conversion element	Salt composition
Point *A*	LiCl, NaBr
Point *B*	Li_2SO_4, NaBr
Point *C*	$LiNO_3$, NaBr
Point *D*	Li_2SO_4, $NaNO_3$
Point *E*	Li_2SO_4, NaCl
Point *F*	$LiNO_3$, NaCl
Line *A* – *B*	Li_2SO_4, NaBr, LiCl
Line *A* – *C*	$LiNO_3$, NaBr, LiCl
Line *B* – *C*	Li_2SO_4, $LiNO_3$, NaBr
Line *B* – *E*	Li_2SO_4, NaBr, NaCl
Line *B* – *D*	Li_2SO_4, $NaNO_3$, NaBr
Line *C* – *F*	$LiNO_3$, NaBr, NaCl
Line *D* – *E*	Li_2SO_4, $NaNO_3$, NaCl
Line *E* – *F*	Li_2SO_4, $LiNO_3$, NaCl
Triangle *A* – *B* – *C*	Li_2SO_4, $LiNO_3$, LiCl, NaBr
Triangle *B* – *E* – *D*	Li_2SO_4, $NaNO_3$, NaCl, NaBr
Plane *B* – *C* – *F* – *E*	Li_2SO_4, $LiNO_3$, NaCl, NaBr

point E: $2\,LiCl + Na_2SO_4 =$ (5)

$= Li_2SO_4 + 2\,NaCl - 26.78$ kJ (mol equiv)$^{-1}$,

point F: $2\,LiCl + 2\,NaNO_3 =$ (6)

$= 2\,LiNO_3 + 2\,NaCl - 18.83$ kJ (mol equiv)$^{-1}$.

By summing the reactions (1)–(6), we obtain the overall equation for the chemical reactions proceeding in a reciprocal system consisting of eight salts

$$6\,LiBr + 2\,LiCl + 3\,Na_2SO_4 + 2\,NaNO_3 = 3\,Li_2SO_4 + 2\,LiNO_3 + 2\,NaCl + 6\,NaBr.$$

The right-hand side of the equation represents the most stable salt composition. In the diagram of this system, this composition is modelled by a four-vertex sphenoid, which can include stable eutectic mixtures characterised by the highest thermal capacity.[8]

2. The thermochemical method for the construction of conversion figures of the 3//3 series

The principle for the construction of conversion figures of secant tetrahedra for reciprocal systems consisting of nine salts of various thermochemical types is analogous to that used for systems of the 2//n (n//2) series. Let us consider selected systems.

a. System Li,Cd,Na//Cl,NO$_3$,SO$_4$ (9A type)

The centre of the conversion graph (see Fig. 5 *a*) is occupied by the point Q_9 corresponding to intersection of fourth-stage diagonals (the $LiNO_3 + CdCl_2$ salt pair). This point has four thermochemical connections to the points Q_1, Q_4 (points of intersection of first-stage diagonals) and Q_7, Q_8 (points of intersection of third-stage diagonals). Data on the salt compositions corresponding to these points, the reaction stages and constituent thermal effects are given in Table 8. The points of intersection of third-stage diagonals Q_7 and Q_8 each have 5 connections: one connection between these points (Q_7-Q_8 lines), one connection to the point Q_9, one connection to the point Q_2, one connection to the point Q_3 (the latter three points correspond to first-stage reactions; the Q_3-Q_8, Q_3-Q_7 and Q_2-Q_7, Q_2-Q_8 lines) and connections to the points of intersections of second-stage diagonals (the Q_6-Q_8 and Q_5-Q_7 lines).

The following three connections correspond to the points of intersection of second-stage diagonals Q_5 and Q_6: two connections to the points of intersection of first-stage diagonals (the Q_1-Q_5, Q_2-Q_5, Q_2-Q_6 and Q_4-Q_6 lines) and connections to the points of intersection of third-stage diagonals (the Q_5-Q_7 and Q_6-Q_8 lines). The points of intersection of first-stage diagonals have the minimum number of connections (2) (except for the point Q_2). These points form the Q_1-Q_5, Q_2-Q_5, Q_1-Q_9, Q_2-Q_6, Q_2-Q_7, Q_2-Q_8, Q_3-Q_7, Q_3-Q_8 and Q_4-Q_6, Q_4-Q_9 lines.

Each of three conversion squares and the conversion triangle (see Fig. 5 *a*) are characterised by a particular set of stages of stable diagonals. These three conversion squares are thermochemically non-equivalent. The conversion square $Q_9-Q_8-Q_3-Q_7$ includes a point of intersection of fourth-stage diagonals, two points of intersection of third-stage diagonals and one point of intersection of first-stage diagonals. Consequently, these points correspond to the most stable salts of the system.

The relationships between the geometric elements of conversion and the chemical composition of the quinary reciprocal system Li,Cd,Na//Cl,NO$_3$,SO$_4$ are given in Table 9. The conversion figure of this system is characterised by the following features: the point of complete conversion of ternary reciprocal systems corresponds to crystallisation of two salts with different cations and anions; the conversion line of quaternary reciprocal systems corresponds to crystallisation of four salts with either three different cations and two different anions or with two different cations and three different anions; the planes, which characterise interactions in the quinary reciprocal system, correspond to crystallisation of four or five salts. (The conversion figure of the thermochemical type 9A ⇄ 9B is shown in Fig. 5 *c*.)

Table 8. Points of complete conversion and thermochemical relations for the Li,Cd,Na//Cl,NO$_3$,SO$_4$ system.

Point	Ternary reciprocal system	Stable salt pair	Reaction	
			stage	Q /kJ (mol equiv)$^{-1}$
1	Li,Cd//SO$_4$,NO$_3$	$LiNO_3 + CdSO_4$	I	$Q_1 = 2.51$
2	Li,Na//SO$_4$,NO$_3$	$NaNO_3 + Li_2SO_4$	I	$Q_2 = 7.95$
3	Na,Cd//Cl,SO$_4$	$Na_2SO_4 + CdCl_2$	I	$Q_3 = 12.55$
4	Li,Na//Cl,NO$_3$	$LiNO_3 + NaCl$	I	$Q_4 = 18.41$
5	Na,Cd//SO$_4$,NO$_3$	$NaNO_3 + CdSO_4$	II	$Q_5 = Q_1 + Q_2 = 10.46$
6	Li,Na//Cl,SO$_4$	$Li_2SO_4 + NaCl$	II	$Q_6 = Q_2 + Q_4 = 26.36$
7	Na,Cd//Cl,NO$_3$	$NaNO_3 + CdCl_2$	III	$Q_7 = Q_1 + Q_2 + Q_3 = 23.01$
8	Li,Cd//Cl,SO$_4$	$Li_2SO_4 + CdCl_2$	III	$Q_8 = Q_2 + Q_3 + Q_4 = 38.91$
9	Li,Cd//Cl,NO$_3$	$LiNO_3 + CdCl_2$	IV	$Q_9 = Q_1 + Q_2 + Q_3 + Q_4 = 41.42$

Table 9. Conversion elements for the Li,Cd,Na//Cl,NO$_3$,SO$_4$ system.

Reciprocal system	Conversion element	Salt composition
Li,Cd//NO$_3$,SO$_4$	point Q_1	$LiNO_3$, $CdSO_4$
Li,Na//NO$_3$,SO$_4$	point Q_2	Li_2SO_4, $NaNO_3$
Na,Cd//Cl,SO$_4$	point Q_3	Na_2SO_4, $CdCl_2$
Li,Na//Cl,NO$_3$	point Q_4	$LiNO_3$, NaCl
Cd,Na//NO$_3$,SO$_4$	point Q_5	$NaNO_3$, $CdSO_4$
Li,Na//Cl,SO$_4$	point Q_6	Li_2SO_4, NaCl
Na,Cd//Cl,NO$_3$	point Q_7	$NaNO_3$, $CdCl_2$
Li,Cd//Cl,SO$_4$	point Q_8	Li_2SO_4, $CdCl_2$
Li,Cd//Cl,NO$_3$	point Q_9	$LiNO_3$, $CdCl_2$
Li,Cd,Na//NO$_3$,SO$_4$	pair of lines $Q_1-Q_5-Q_2$	$LiNO_3$, Li_2SO_4, $NaNO_3$, $CdSO_4$
Na,Cd//Cl,NO$_3$,SO$_4$	pair of lines $Q_5-Q_7-Q_3$	$NaNO_3$, Na_2SO_4, $CdCl_2$, $CdSO_4$
Li,Na//Cl,NO$_3$,SO$_4$	pair of lines $Q_2-Q_6-Q_4$	$LiNO_3$, Li_2SO_4, NaCl, $NaNO_3$
Li,Na,Cd//Cl,SO$_4$	pair of lines $Q_6-Q_8-Q_3$	Li_2SO_4, NaCl, Na_2SO_4, $CdCl_2$
Li,Cd//Cl,NO$_3$,SO$_4$	pair of lines $Q_1-Q_9-Q_8$	$LiNO_3$, Li_2SO_4, $CdCl_2$, $CdSO_4$
Li,Na,Cd//Cl,NO$_3$	pair of lines $Q_4-Q_9-Q_7$	$LiNO_3$, NaCl, $NaNO_3$, $CdCl_2$
Li,Na,Cd//Cl,NO$_3$,SO$_4$	triangle $Q_8-Q_9-Q_7$	$LiNO_3$, Li_2SO_4, $NaNO_3$, $CdCl_2$
	triangle $Q_7-Q_3-Q_8$	Li_2SO_4, $NaNO_3$, Na_2SO_4, $CdCl_2$
	square $Q_4-Q_9-Q_8-Q_6$	$LiNO_3$, Li_2SO_4, NaCl, $CdCl_2$
	square $Q_1-Q_9-Q_7-Q_5$	$LiNO_3$, $NaNO_3$, $CdCl_2$, $CdSO_4$
	square $Q_7-Q_9-Q_8-Q_3$	Li_2SO_4, $NaNO_3$, $LiNO_3$, Na_2SO_4, $CdCl_2$

b. System K,Ba,Na//F,MoO$_4$,WO$_4$ (9B type)

For 9B-type systems (unlike 9A-type systems), the conversion figure of secant tetrahedra contains one conversion square

Table 10. Points of complete conversion and thermochemical relations for the K,Ba,Na//F,MoO_4,WO_4 system.

Point	Ternary reciprocal system	Stable salt pair	Reaction	
			stage	Q /kJ (mol equiv)$^{-1}$
1	Ba,Na// MoO_4,WO_4	Na_2WO_4 + + $BaMoO_4$	I	$Q_1 = 1.67$
2	K,Ba//F,MoO_4	$BaF_2 + K_2MoO_4$	I	$Q_2 = 2.51$
3	Na,K// MoO_4,WO_4	K_2WO_4 + + Na_2MoO_4	I	$Q_3 = 12.34$
4	Ba,Na//F,WO_4	$BaWO_4 + (NaF)_2$	I	$Q_4 = 19.04$
5	K,Ba// MoO_4,WO_4	K_2WO_4 + + $BaMoO_4$	II	$Q_5 = Q_1 + Q_3 = 14.01$
6	Ba,Na//F,MoO_4	$(NaF)_2 + BaMoO_4$	II	$Q_6 = Q_1 + Q_4 = 20.71$
7	K,Na//F,MoO_4	$(NaF)_2 + K_2MoO_4$	III	$Q_7 = Q_1 + Q_2 + + Q_4 = 23.22$
8	K,Ba//F,WO_4	$BaF_2 + K_2WO_4$	III	$Q_8 = Q_1 + Q_2 + + Q_3 = 16.52$
9	K,Na//F,WO_4	$(NaF)_2 + K_2WO_4$	IV	$Q_9 = Q_1 + Q_2 + + Q_3 + Q_4 = 35.56$

$Q_3-Q_7-Q_9-Q_8$ and five conversion triangles, $Q_1-Q_9-Q_5$, $Q_5-Q_7-Q_9$, $Q_4-Q_9-Q_6$, $Q_6-Q_8-Q_9$ and $Q_5-Q_6-Q_9$ (a degenerate triangle, see Fig. 5 *b*,*c*). The thermochemical relations for the K,Ba,Na//F,MoO_4,WO_4 system are given in Table 10.

The framework of the conversion graph for this system is constructed analogously to the conversion graph for 9A-type systems. The difference is that the former contains the additional Q_5-Q_6, Q_5-Q_9 and Q_6-Q_9 lines resulting from the intersection of the conversion figure with the axial triangle of the $(NaF)_2-K_2WO_4-BaMoO_4$ system. The point of intersection of fourth-stage diagonals Q_9 has the largest number of thermochemical connections (six connections) (see Fig. 5 *b*). The points Q_5 and Q_6, which correspond to second-stage reactions, each have four thermochemical connections. The points Q_7 and Q_8 corresponding to third-stage reactions each have three connections, and the points Q_1, Q_2, Q_3 and Q_4 corresponding to first-stage reactions each have two connections.

A chemical conversion reaction of the salts, which are located at the vertices of metastable figures, into salts located at the vertices of stable figures can be written for each point of the conversion figure. To follow the conversion in quinary reciprocal systems consisting of nine salts, one can use special diagrams put forward by Radishchev.[2] These diagrams can be constructed as follows: three-dimensional figures, which intersect each other (a pyramid and a sphenoid), are projected onto the plane of intersection of both spaces ‡ (giving rise to a conversion square, Fig. 9). The metastable and stable diagonals in this planar figure are indicated by dashed and solid lines, respectively.

For the K,Ba,Na//F,MoO_4,WO_4 system, this method gave one of conversion squares $B-Z-T-F$ of secant tetrahedra (see Fig. 9) resulting from the intersection of the metastable sphenoid $(KF)_2-Na_2WO_4-K_2MoO_4-BaWO_4$ and the stable pyramid $(NaF)_2-Na_2MoO_4-BaMoO_4-BaF_2-K_2WO_4$.

The equation for the central point of the conversion square $B-Z-T-F$ has the form

$$2\,(KF)_2 + 2\,Na_2WO_4 + 2\,K_2MoO_4 + 2\,BaWO_4 = \quad (7)$$
$$= (NaF)_2 + BaF_2 + BaMoO_4 + Na_2MoO_4 + 4\,K_2WO_4.$$

‡ The figures are located in different three-dimensional spaces involved in this four-dimensional space.

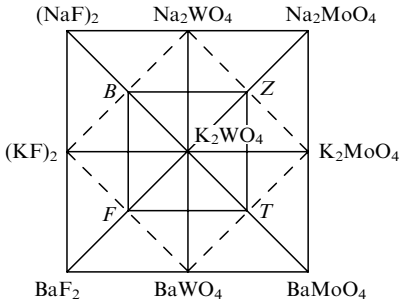

Figure 9. Conversion square $B-Z-T-F$ (a fragment of the conversion figure) of the 9B-type quinary reciprocal system Na,K,Ba//F,MoO_4,WO_4.

The right-hand side of the equation includes a metastable pair of salts, which react according to the equation

$$BaF_2 + Na_2MoO_4 = (NaF)_2 + BaMoO_4. \quad (8)$$

By summing the equations (7) and (8), we obtain

$$2\,(KF)_2 + 2\,Na_2WO_4 + 2\,K_2MoO_4 + 2\,BaWO_4 = \quad (9)$$
$$= 2\,(NaF)_2 + 4\,K_2WO_4 + BaMoO_4.$$

The exchange reactions afford salts, which form a stable axial triangle.

c. System Li,Na,K//Cl,Br,SO_4 (9C type)

Let us consider a procedure for the construction of a conversion figure based on stages of stable diagonals using the Li,Na,K// Cl,Br,SO_4 system as an example (see Fig. 6).

The thermal effects of the second-stage reactions giving rise to the stable $Na_2SO_4 + (KBr)_2$ (Q_5), $(LiCl)_2 + (KBr)_2$ (Q_6), $Li_2SO_4 + (KCl)_2$ (Q_7) and $Li_2SO_4 + (NaBr)_2$ (Q_8) pairs are the sums of two effects, and the thermal effect of the fourth-stage reaction [the stable $Li_2SO_4 + (KBr)_2$ pair (Q_9)] is the sum of four effects (Table 11). Hence, the conversion point corresponding to the second-stage reaction should have the following three connections: two connections to conversion points corresponding to first-stage reactions and one connection to the Q_9 point. Below are given the thermochemical connections for four points of complete conversion.

Table 11. Points of complete conversion and thermochemical relations for the Li,Na,K//Cl,Br,SO_4 system.

Point	Ternary reciprocal system	Stable salt pair	Reaction	
			stage	Q /kJ (mol equiv)$^{-1}$
1	K,Na//Cl,SO_4	$Na_2SO_4 + (KCl)_2$	I	$Q_1 = 3.56$
2	Li,Na//Cl,Br	$(LiCl)_2 + (NaBr)_2$	I	$Q_2 = 6.69$
3	Na,K//Cl,Br	$(KBr)_2 + (NaCl)_2$	I	$Q_3 = 7.53$
4	Li,Na//Cl,SO_4	$Li_2SO_4 + (NaCl)_2$	I	$Q_4 = 26.78$
5	K,Na//Br,SO_4	$Na_2SO_4 + (KBr)_2$	II	$Q_5 = Q_1 + Q_3 = 11.09$
6	Li,K//Cl,Br	$(LiCl)_2 + (KBr)_2$	II	$Q_6 = Q_2 + Q_3 = 14.22$
7	Li,K//Cl,SO_4	$Li_2SO_4 + (KCl)_2$	II	$Q_7 = Q_1 + Q_4 = 30.34$
8	Li,Na//Br,SO_4	$Li_2SO_4 + (NaBr)_2$	II	$Q_8 = Q_2 + Q_4 = 33.47$
9	Li,K//Br,SO_4	$Li_2SO_4 + (KBr)_2$	IV	$Q_9 = Q_1 + Q_2 + + Q_3 + Q_4 = 44.56$

Point of complete conversion	Thermochemical connections
Q_5	Q_1-Q_5, Q_3-Q_5, Q_5-Q_9
Q_6	Q_2-Q_6, Q_3-Q_6, Q_6-Q_9
Q_7	Q_1-Q_7, Q_4-Q_7, Q_7-Q_9
Q_8	Q_2-Q_8, Q_4-Q_8, Q_8-Q_9

The conversion graph presented in Fig. 6 *b*,*c* is constructed based on thermochemical relations in such a way that the central conversion point Q_9 is connected to the points of intersection of second-stage diagonals (the points Q_5, Q_6, Q_7 and Q_8) and the conversion points corresponding to first-stage reactions (Q_1, Q_2, Q_3 and Q_4) along the diagonal of the conversion square.

The main thermochemical framework of the conversion figure of secant tetrahedra for systems consisting of nine salts of any type can also be constructed from the conversion figures of quaternary reciprocal systems consisting of six salts, which are involved in this quinary system of the 3//3 series. The conversion lines of the quaternary reciprocal systems involved in the Li,Na,K//Cl,Br,SO_4 system are as follows:

System	Conversion line
Na,K//Cl,Br,SO_4	$Q_1-Q_5-Q_3$
Li,K//Cl,Br,SO_4	$Q_6-Q_9-Q_7$
Li,Na//Cl,Br,SO_4	$Q_2-Q_8-Q_4$
Li,Na,K//Cl,Br	$Q_3-Q_6-Q_2$
Li,Na,K//Cl,SO_4	$Q_4-Q_7-Q_1$
Li,Na,K//Br,SO_4	$Q_8-Q_9-Q_5$

The above-listed lines serve as the outer edges of the graphs and the inner lines dividing the figure into four smaller squares.

The conversion figure of a 9C-type quinary system (see Fig. 6 *b*,*c*) contains nine vertices (in accordance with the number of ternary reciprocal systems involved in the quinary system) and 14 lines, twelve of which are elements of the conversion figures of all six reciprocal systems consisting of six salts, which are involved in this quinary system. Two lines emerging from the central point of the square (the point of intersection of the most stable fourth-stage diagonal with the corresponding metastable diagonal) are special lines (Q_9-Q_1 and Q_9-Q_2, Fig. 6 *b*; Q_3-Q_9 and Q_4-Q_9, Fig. 6 *c*). These lines together with the conversion line of the basic elements of the 9C-type quinary reciprocal system consisting of nine salts divide the stable and metastable axial triangles into four triangles.

d. System Na,K,Ca//F,Cl,WO_4 (9D type)

Let us consider the construction of a conversion figure of the topological type D using the Na,K,Ca//F,Cl,WO_4 system as an example. The thermochemical characteristics of this system and the salt compositions for the conversion elements are given in Tables 12 and 13, respectively. The conversion figure of secant tetrahedra is shown in Fig. 7 *a*. The conversion graph of this system consists of three conversion planes and two conversion triangles: *9–6–8–4*, *2–7–1–8*, *9–3–7–5*, *3–4–1*, *2–6–5*. Each conversion square necessarily includes two points of intersection of second-stage diagonals and two points of intersection of first-stage diagonals [9D-type systems are characterised by the presence of six first-stage diagonals and three second-stage diagonals (see Table 12)]. The vertices of the conversion triangles *3–4–1* and *2–6–5* are the points of intersection of first-stage diagonals. The conversion squares (the main framework of the conversion figure) of this system are identical to the conversion squares of 9E-type systems. There are the following special six inner lines in the conversion figure of the Na,K,Ca//F,Cl,WO_4 system: *3–4*, *3–1*, *4–1*, *2–5*, *2–6* and *5–6*. These lines correspond to exchange reactions proceeding in the quinary reciprocal system consisting of nine salts and intersect the planes of the stable basic triangles $CaWO_4-(NaF)_2-(KCl)_2$ and $CaF_2-K_2WO_4-(NaCl)_2$.

Table 12. Thermochemical relations for the 9D-type quinary reciprocal system Na,K, Ca//F,Cl,WO_4 consisting of nine salts.

Metastable salt pair	Stable salt pair	Reaction	
		stage	Q /kJ (mol equiv)$^{-1}$
$CaF_2+Na_2WO_4$	$CaWO_4+(NaF)_2$	I	$Q_1=12.636$
$Na_2WO_4+(KCl)_2$	$K_2WO_4+(NaCl)_2$	I	$Q_2=22.720$
$(KF)_2+(NaCl)_2$	$(NaF)_2+(KCl)_2$	I	$Q_3=32.342$
$K_2WO_4+CaCl_2$	$CaWO_4+(KCl)_2$	I	$Q_4=40.710$
$CaWO_4+(KF)_2$	$K_2WO_4+CaF_2$	I	$Q_5=42.426$
$(NaF)_2+CaCl_2$	$CaF_2+(NaCl)_2$	I	$Q_6=50.794$
$Na_2WO_4+(KF)_2$	$K_2WO_4+(NaF)_2$	II	$Q_7=Q_2+Q_3=$ $=Q_1+Q_5=55.062$
$Na_2WO_4+CaCl_2$	$CaWO_4+(NaCl)_2$	II	$Q_8=Q_2+Q_4=$ $=Q_1+Q_6=63.430$
$(KF)_2+CaCl_2$	$CaF_2+(KCl)_2$	II	$Q_9=Q_4+Q_5=$ $=Q_3+Q_6=83.136$

Table 13. Salt compositions for conversion elements of the 9D-type Na,K,Ca//F,Cl,WO_4 system.

System	Conversion element	Salt composition
Na,Ca,K//F,WO_4	*1–7*	NaF, K_2WO_4, $CaWO_4$
Na,Ca//F,Cl,WO_4	*1–8*	NaF, NaCl, $CaWO_4$
Na,K//F,Cl,WO_4	*2–7*	NaF, NaCl, K_2WO_4
Na,Ca,K//Cl,WO_4	*2–8*	NaCl, K_2WO_4, $CaWO_4$
Na,Ca,K//F,Cl	*3–9*	NaF, KCl, CaF_2
Ca,K//F,Cl,WO_4	*4–9*	CaF_2, KCl, $CaWO_4$
Ca,K//F,Cl,WO_4	*5–9*	KCl, K_2WO_4, CaF_2
Na,Ca,K//F,Cl	*6–9*	NaCl, KCl, CaF_2
Na,K//F,Cl,WO_4	*3–7*	NaF, KCl, K_2WO_4
Na,Ca,K//F,WO_4	*5–7*	NaF, K_2WO_4, CaF_2
Na,Ca,K//Cl,WO_4	*4–8*	NaCl, KCl, $CaWO_4$
Na,Ca//F,Cl,WO_4	*6–8*	CaF_2, NaCl, $CaWO_4$

The points of intersection of second-stage diagonals each have four thermochemical connections. The points of intersection of first-stage diagonals *1–7*, *2–7*, *3–7*, *5–7*, *1–8*, *2–8*, *4–8*, *6–8*, *3–9*, *4–9*, *5–9*, *6–9* have the same number of connections (see Fig. 7 *a*). These 12 lines form the 9D ⇄ 9E-type framework of the conversion figure common to the two types. The salt compositions involved in the thermochemical 9D ⇄ 9E-type framework of the conversion figure belong to quaternary reciprocal systems.

The special conversion lines *2–5–6* and *1–3–4* correspond to the NaCl, K_2WO_4, CaF_2 and NaCl, KCl, $CaWO_4$ salt compositions, respectively in the Na,Ca,K//F,Cl,WO_4 system.

Hence, the conversion figure of secant tetrahedra for 9D-type quinary reciprocal systems consisting of nine salts is a graph containing nine points of complete conversion of ternary reciprocal systems, 12 lines (edges) corresponding to salt compositions of six salts and six special inner lines, which model an interaction in a system composed of nine salts.

e. System Na,Ba,Fe//Cl,S,SO_4 (9E type)

The conversion figure of reciprocal systems of the 3//3 series of the 9E topological type is a nine-point graph (see Fig. 7 *b*).

Nine points of complete conversion of ternary reciprocal systems serve as vertices of the graph, and 12 conversion lines of quaternary reciprocal systems consisting of six salts, which are constituents of the main thermochemical framework of the figure, serve as edges. Six triangular planes are sections of the composition prism for a quinary reciprocal system consisting of nine salts. The *8–7*, *9–8* and *7–9* diagonals intersecting the plane of the axial stable triangle are special inner lines of three conversion squares.

Nine diagonals (six first-stage diagonals and three second-stage diagonals) serve as the thermochemical characteristics of 9E-type systems. The thermal effects of a second-stage reaction can be expressed as the sums of the thermal effects of first-stage reactions:

$$Q_1 + Q_3 = Q_2 + Q_4,$$

$$Q_1 + Q_6 = Q_5 + Q_4,$$

$$Q_2 + Q_6 = Q_3 + Q_5.$$

From these equations it follows that

$$Q_6 - Q_5 = Q_4 - Q_1 = Q_3 - Q_2,$$

i.e., the thermal effects for six diagonals are related by the following condition: the differences for three pairs of thermal effects should be equal to each other. For example, these differences for the Na,Ba,Fe//Cl, S,SO_4 system are as follows:

$$Q_6 - Q_5 = 89.12 - 85.56 = 3.56 \text{ kJ (mol equiv)}^{-1},$$

$$Q_4 - Q_1 = 10.04 - 6.48 = 3.56 \text{ kJ (mol equiv)}^{-1},$$

$$Q_3 - Q_2 = 11.72 - 8.16 = 3.56 \text{ kJ (mol equiv)}^{-1}.$$

The main thermochemical characteristics of the Na,Ba,Fe//Cl,S,SO_4 system (9E type) are given in Table 14. The conversion graph of the 9E-type system consists of three conversion squares, which are divided by diagonals into six triangles. The diagonals of the conversion squares are the *7–8*, *8–9* and *7–9* lines, which correspond to the FeS + $(NaCl)_2$, FeS + $BaSO_4$ and $(NaCl)_2$ + $BaSO_4$ salt pairs, respectively. These lines intersect the stable axial triangle $(NaCl)_2$–FeS–$BaSO_4$ and characterise the chemical interaction in the quinary reciprocal system Na,Ba,Fe//Cl,S,SO_4. The conversion points *1*, *2*, *3*, *4*, *5* and *6* corresponding to first-stage reactions are involved in conversion squares (two points per square) and each have two thermochemical connections to conversion points corresponding to second-stage reactions. For example, the conversion square *4–9–6–8* includes the conversion points *4* and *6* (first-stage reactions) connected to the points *8* and *9* (second-stage reactions).

The points *7*, *8* and *9* each have six thermochemical connections (four connections to the points corresponding to first-stage reactions and two connections to each other). The points corresponding to second-stage reactions should be connected to other points, *viz*., the conversion points of first-stage reactions. For example, the point *9* is connected to the points *3* and *5* [the points of intersection of the first-stage diagonals $BaCl_2$ + FeS (Q_5) and $BaSO_4$ + $FeCl_2$ (Q_3)], and the point *8* is connected to the points *1* and *4* [the points of intersection of the first-stage diagonals $FeSO_4$ + $(NaCl)_2$ (Q_1) and $(NaCl)_2$ + BaS (Q_4)]. Finally, the point *7* corresponding to the second-stage reaction giving rise to the $(NaCl)_2$ + $BaSO_4$ pair (Q_7) is connected to the points *1* and *2* of the conversion square *2–7–1–8* and the points *3* and *5* of the conversion square *9–3–7–5*. All these constructions are determined by the thermochemical dependences of the second-stage reactions on the first-stage reactions. For example, the thermal effect of the second-stage reaction giving rise to the $BaSO_4$ + FeS pair is equal to the sum of the thermal effects of the first-stage reactions (see Table 14) Q_5 (the stable $BaCl_2$ + FeS pair) and Q_3 (the stable $BaSO_4$ + $FeCl_2$ pair)

$$Q_9 = Q_5 + Q_3 = 85.56 + 11.72 = 97.28 \text{ kJ (mol equiv)}^{-1}.$$

At the same time, this thermal effect is related to the thermal effects of the first-stage reactions yielding the $BaSO_4$ + Na_2S (Q_2) and Na_2SO_4 + FeS (Q_6) pairs

$$Q_9 = Q_2 + Q_6 = 8.16 + 89.12 = 97.28 \text{ kJ (mol equiv)}^{-1}.$$

Analogously, the thermal effect of the second-stage reaction giving rise to the $(NaCl)_2$ + FeS pair (Q_8) is equal to the sum of the thermal effects of the following first-stage reactions: $(NaCl)_2$ + BaS (Q_4) and $BaCl_2$ + FeS (Q_5) as well as $(NaCl)_2$ + $FeSO_4$ (Q_1) and Na_2SO_4 + FeS (Q_6)

$$Q_8 = Q_4 + Q_5 = Q_1 + Q_6 = 10.04 + 85.56 = \\ = 6.48 + 89.12 = 95.60 \text{ kJ (mol equiv)}^{-1}.$$

Analogously, the following equation can be written for Q_7:

$$Q_7 = Q_2 + Q_4 = Q_1 + Q_3 = 8.16 + 10.04 = \\ = 6.48 + 11.72 = 18.20 \text{ kJ (mol equiv)}^{-1}.$$

The above-considered methods for the construction of conversion figures of secant elements for quinary reciprocal systems consisting of nine salts of various thermochemical types are simple, convenient and do not require complicated tools of multidimensional geometry.

The general algorithm for the construction of conversion figures of secant tetrahedra for quinary reciprocal systems consisting of nine salts of various thermochemical types can be stated as follows:[8]

(1) the determination of stable diagonals in ternary reciprocal systems based on the thermal effects of exchange reactions;

(2) the determination of reaction stages and the constituent thermal effects;

(3) the determination of the thermochemical type of the system;

(4) the determination of the number of thermochemical connections for each point of complete conversion corresponding to the diagonal of the corresponding stage from the thermochemical relations in the system;

(5) the connection of nine points of complete conversion of ternary reciprocal systems, which correspond to intersections of diagonals of the stable and metastable complexes of the system, in accordance with the number of thermochemical functional connections revealed for each conversion point.

Table 14. Points of complete conversion and thermochemical relations for the Na,Ba,Fe//Cl,S,SO_4 system.

Point	Ternary reciprocal system	Stable salt pair	Reaction	
			stage	Q /kJ (mol equiv)$^{-1}$
1	Na,Fe//Cl,SO_4	$(NaCl)_2$ + $FeSO_4$	I	$Q_1 = 6.48$
2	Ba,Na//S,SO_4	Na_2S + $BaSO_4$	I	$Q_2 = 8.16$
3	Ba,Fe//Cl,SO_4	$BaSO_4$ + $FeCl_2$	I	$Q_3 = 11.72$
4	Na,Ba//Cl,S	$(NaCl)_2$ + BaS	I	$Q_4 = 10.04$
5	Ba,Fe//Cl,S	$BaCl_2$ + FeS	I	$Q_5 = 85.56$
6	Na,Fe//S,SO_4	Na_2SO_4 + FeS	I	$Q_6 = 89.12$
7	Na,Ba//Cl,SO_4	$(NaCl)_2$ + $BaSO_4$	II	$Q_7 = Q_2 + Q_4 = Q_1 + Q_3 = 18.20$
8	Na,Fe//Cl,S	$(NaCl)_2$ + FeS	II	$Q_8 = Q_5 + Q_4 = Q_1 + Q_6 = 95.60$
9	Ba,Fe//S,SO_4	$BaSO_4$ + FeS	II	$Q_9 = Q_2 + Q_6 = Q_3 + Q_5 = 97.28$

3. The matrix method for the construction of conversion figures

The thermochemical method is simple and convenient but requires the determination of the stages of stable diagonals, which is not always possible because of the lack of reliable data on the enthalpies of formation of salts. This gave impetus to the development of a procedure without this drawback. The matrix method is the most descriptive way of constructing conversion figures of secant elements.[8,32,33] This method does not require numerical values of the thermal effects of exchange reactions. To construct a conversion figure for reciprocal systems of the 2//n (n//2) series using matrices of reciprocal salt pairs, it is only necessary to know which salt pair is more stable. The presence (or the absence) of unities in cells of matrices of reciprocal salt pairs determines the sought-for thermochemical relations.

In the ternary reciprocal system A,B//X,Y, a stable diagonal in a four-cell matrix is denoted by unity. The conversion point of this system results from the intersection of the AX – BY and AY – BX diagonals, which occupy the cells 2 and 3, respectively. Since the conversion point belongs both to stable and metastable diagonals, it can be placed either in the cell 2 or in the cell 3. For convenience, let us display the point of complete conversion of the ternary reciprocal system in the cell occupied by the stable diagonal, *i.e.*, in the cell with unity.

	BX	BY
AX	1) 0	2) 0
AY	3) 1	4) 0

In the matrix of reciprocal salt pairs of a quaternary reciprocal system consisting of six salts, three cells are occupied by unities. A stable salt pair, *i.e.*, the unity located at the intersection of a row and column with two unities, forms a stable second-stage diagonal. The other two salt pairs denoted by unities correspond to first-stage diagonals.

	BX	BY	BZ
AX	0	0	1
AY	1	0	1
AZ	0	0	0

A conversion figure is constructed as follows: points corresponding to points of complete conversion of ternary reciprocal systems are placed in cells with unities. Then the points are connected by straight lines emerging from the point corresponding to the second-stage diagonal.

Let us consider the construction of a conversion figure of secant elements for more complex systems of the 2//*n* series, for example, for a quinary reciprocal system consisting of eight salts. This system is represented by a matrix consisting of 16 cells, six of which have unities and correspond to stable diagonals of ternary reciprocal systems. The matrix of reciprocal salt pairs for the Li,Na//Cl,Br,NO_3,SO_4 system is presented in Fig. 8.

For convenience, the conversion figure of the salt is placed in the matrix in such a way that the first row contains three unities, the second row has two unities, and the third row contains one unity, *i.e.*, in accordance with an increase in the stability of salts of the upper row and a decrease in the stability of salts of the left column. The unity in the fourth cell corresponds to a third-stage diagonal, unities in the third and eighth cells correspond to second-stage diagonals, and all other unities correspond to first-stage diagonals (see Fig. 8).

Conversion figures are constructed by connecting successively the points placed in cells with unities. The conversion point corresponding to the intersection of a stable third-stage diagonal and its metastable pair is connected by straight lines to the points in cells occupied by second-stage diagonals. The latter points, in turn, are connected to the point in the cell occupied by a first-stage diagonal. Therefore, the connection of four points located in the cells of the upper right part of the matrix by lines gives rise to a fragment of the conversion figure forming a quadrangle. Triangles result from the connection of points located in the first row and the last column of the matrix, respectively. The order in which the points are connected can be represented by the following scheme. The quadrilateral fragment of the conversion figure is $3 \to 4 \to 8 \to 7 \to 3$; the first triangle is $2 \to 3$ and $2 \to 4$; the second triangle is $8 \to 12$ and $4 \to 12$. In the case of this arrangement of unities and zeros in the matrix, the conversion figure always has the form shown in Fig. 8.

A conversion figure can be constructed in an alternative way. Let us consider this procedure with the use of the same Li,Na//Cl,Br,NO_3,SO_4 system consisting of eight salts as an example.

1. First, we write matrices of reciprocal salt pairs, which are constituents of quaternary reciprocal systems consisting of six salts.

	NaBr	Na_2SO_4	NaCl
LiBr	0	0	0
Li_2SO_4	1	0	1
LiCl	1	1	0

	NaBr	$NaNO_3$	NaCl
LiBr	0	0	0
$LiNO_3$	1	0	1
LiCl	1	1	0

	NaCl	$NaNO_3$	Na_2SO_4
LiCl	0	0	0
$LiNO_3$	1	0	1
Li_2SO_4	1	1	0

	NaBr	$NaNO_3$	Na_2SO_4
LiBr	0	0	0
$LiNO_3$	1	0	1
Li_2SO_4	1	1	0

2. Then we inscribe conversion figures for all quaternary reciprocal systems into the matrices by connecting the points corresponding to unities in rows and columns.

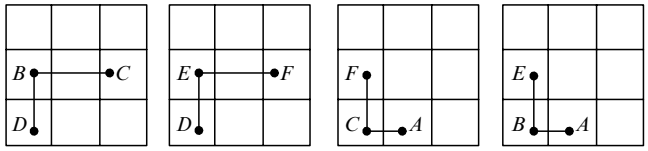

3. Finally, the conversion figures are transferred to a matrix of a quinary reciprocal system consisting of eight salts. The conversion figure for the Li,Na//Cl,Br,NO_3,SO_4 system is obtained automatically.

This procedure is particularly convenient for the construction of conversion figures for senary and more complex systems of the 2//*n* (*n*//2) series, because it substantially simplifies the determination of thermochemical relations.

The proposed algorithm is applicable only to systems of one thermochemical type, *viz.*, to systems of the 2//*n* (*n*//2) series. For systems consisting of nine salts of the 3//3 series, three matrices of the 2//3 (3//2) series involved in this quinary system should be considered.[32]

Conversion figures for various thermochemical types of quinary reciprocal systems are different. Hence, the algorithms for the construction of these figures are also different.

Let us consider the procedure for the construction using the Ba,K,Na//F,MoO_4,WO_4 system (the $B \rightleftarrows A$ thermochemical type) as an example. The thermochemical relations for this system are given in Table 15.

Table 15. Points of complete conversion and thermochemical relations for the Na,K,Ba//F,MoO_4,WO_4 system.

Point	Ternary reciprocal system	Stable salt pair	Reaction	
			stage	Q /kJ (mol equiv)$^{-1}$
1	Na,Ba//F,WO_4	$(NaF)_2 + BaWO_4$	I	$Q_4 = 19.04$
2	K,Ba//F,MoO_4	$K_2MoO_4 + BaF_2$	I	$Q_2 = 2.51$
3	Na,Ba// MoO_4,WO_4	$Na_2WO_4 +$ $+ BaMoO_4$	I	$Q_1 = 1.67$
4	Na,K// MoO_4,WO_4	$Na_2MoO_4 +$ $+ K_2WO_4$	I	$Q_3 = 12.34$
5	Na,Ba//F,MoO_4	$(NaF)_2 + BaMoO_4$	II	$Q_5 = Q_1 + Q_4 =$ $= 20.71$
6	K,Ba// MoO_4,WO_4	$K_2WO_4 +$ $+ BaMoO_4$	II	$Q_6 = Q_1 + Q_3 =$ $= 14.01$
7	K,Ba//F,WO_4	$BaF_2 + K_2WO_4$	III	$Q_7 = Q_1 + Q_2 + Q_3 =$ $= 16.52$
8	K,Na//F,MoO_4	$(NaF)_2 + K_2MoO_4$	III	$Q_8 = Q_1 + Q_2 + Q_4 =$ $= 23.22$
9	K,Na//F,WO_4	$(NaF)_2 + K_2WO_4$	IV	$Q_9 = Q_1 + Q_2 +$ $+ Q_3 + Q_4 = 35.56$

This system includes three quaternary reciprocal systems of the 3//2 series (Na,K,Ba//F,WO_4; Na,K,Ba//F,MoO_4; Na,K,Ba//MoO_4,WO_4) and three systems of the 2//3 series (Na,Ba//F,MoO_4,WO_4; K,Ba//F,MoO_4,WO_4; Na,K//F,MoO_4,WO_4). The matrices of reciprocal salt pairs and the matrices of conversion figures for these systems are given below (in the matrices of reciprocal salt pairs, the point numbers from the matrices of the conversion figures are given in parentheses).[11]

Let us write the matrix table consisting of 9 columns and 9 rows and then place unities from the matrices of the conversion figures in rows and columns. The conversion graph corresponding to this matrix belongs to the 9B topological type (Fig. 10).

	Z	*K*	*E*	*D*	*T*	*C*	*F*	*A*	*B*
Z(*1*)	0	0	0	0	1	0	0	0	1
K(*2*)	0	0	0	0	0	0	1	1	0
E(*3*)	0	0	0	0	1	1	0	0	0
D(*4*)	0	0	0	0	0	1	0	0	1
T(*5*)	1	0	1	0	0	1	1	0	1
C(*6*)	0	0	1	1	0	0	0	1	1
F(*7*)	0	1	0	0	1	0	0	1	1
A(*8*)	0	0	0	0	0	1	1	0	1
B(*9*)	1	0	0	1	1	1	1	1	0

Matrices of reciprocal salt pairs

	Na_2WO_4	K_2WO_4	$BaWO_4$
NaF	0	1(9)	1(1)
KF	0	0	0
BaF_2	0	1(7)	0

	Na_2MoO_4	K_2MoO_4	$BaMoO_4$
NaF	0	1(8)	1(5)
KF	0	0	0
BaF_2	0	1(2)	0

	Na_2WO_4	K_2WO_4	$BaWO_4$
Na_2MoO_4	0	1(4)	0
K_2MoO_4	0	0	0
$BaMoO_4$	1(3)	1(6)	0

	BaF_2	$BaMoO_4$	$BaWO_4$
NaF	0	1(5)	1(1)
Na_2MoO_4	0	0	0
Na_2WO_4	0	1(3)	0

	BaF_2	$BaMoO_4$	$BaWO_4$
KF	0	0	0
K_2MoO_4	1(2)	0	0
K_2WO_4	1(7)	1(6)	0

	KF	K_2MoO_4	K_2WO_4
NaF	0	1(8)	1(9)
Na_2MoO_4	0	0	1(4)
Na_2WO_4	0	0	0

Matrices of conversion figures

	1	7	9
1	0	0	1
7	0	0	1
9	1	1	0

	2	5	7
2	0	0	1
5	0	0	1
7	1	1	0

	3	4	6
3	0	0	1
4	0	0	1
6	1	1	0

	1	3	5
1	0	0	1
3	0	0	1
5	1	1	0

	2	6	8
2	0	0	1
6	0	0	1
8	1	1	0

	4	8	9
4	0	0	1
8	0	0	1
9	1	1	0

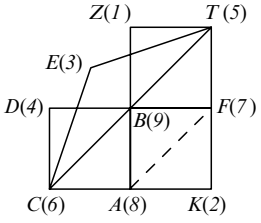

Figure 10. Conversion figure of the 9B-type quinary reciprocal system Na,K,Ba//F,MoO_4,WO_4.

A conversion graph can be constructed by the matrix method using an alternative procedure. In this case, stable salt pairs, which are determined from the melting diagram (if data on the enthalpies of formation of the salts are lacking) of ternary reciprocal systems, serve as the starting data. Let us consider the construction of a conversion graph using the quinary reciprocal system Ag,Li,Na//Cl,NO_3,SO_4 of the $9C \rightleftarrows 9C'$ type as an example. The thermochemical data for this system are given in Table 16. This system includes nine ternary reciprocal systems. Stable salt pairs for these systems are determined from experimental data.

Table 16. Thermochemical characteristics of the 9C-type quinary reciprocal system Ag,Li,Na//Cl,NO_3,SO_4.

Ternary reciprocal system	Stable salt pair	Reaction	
		stage	*Q*
Ag,Li//Cl,SO_4	AgCl + Li_2SO_4	IV	$Q_9 = Q_1 + Q_2 + Q_3 + Q_4 = Q_8 + Q_7 = Q_5 + Q_6$
Ag,Na//Cl,SO_4	AgCl + Na_2SO_4	II	$Q_8 = Q_3 + Q_4$
Li,Na//Cl,SO_4	NaCl + Li_2SO_4	II	$Q_7 = Q_1 + Q_2$
Ag,Li//Cl,NO_3	AgCl + $LiNO_3$	II	$Q_6 = Q_2 + Q_4$
Ag,Na//Cl,NO_3	AgCl + $NaNO_3$	I	Q_4
Li,Na//Cl,NO_3	NaCl + $LiNO_3$	I	Q_2
Ag,Li//NO_3,SO_4	$AgNO_3$ + Li_2SO_4	II	$Q_5 = Q_1 + Q_3$
Ag,Na//NO_3,SO_4	$AgNO_3$ + Na_2SO_4	I	Q_3
Li,Na//NO_3,SO_4	$NaNO_3$ + Li_2SO_4	I	Q_1

Two adjacency matrices (Fig. 11) are constructed from the matrices of reciprocal salt pairs of six reciprocal quaternary systems involved in the Ag,Li,Na//Cl,NO_3,SO_4 system.[33] In one matrix, the salts are arranged according to common cations (the cation matrix I), whereas the salts in another matrix are arranged according to common anions (the anion matrix II). As a result, the thermochemical characteristics of all six quaternary reciprocal systems, which are involved in the quinary reciprocal system of nine salts, are determined.

From the matrices I and II, it is evident that the AgCl and Li_2SO_4 salts each have four unities; the $AgNO_3$, $LiNO_3$, NaCl, $NaNO_3$ and Na_2SO_4 salts each have two unities; and the Ag_2SO_4 and LiCl salts have no unities.

Then the table of vertex indices is compiled (Table 17).

Table 17. Table of vertex indices for the 9C-type quinary reciprocal system Ag,Li,Na//Cl,NO_3,SO_4.

Metal	Cl	NO_3	SO_4	$\sum$
Ag	4	2	0	6
Li	0	2	4	6
Na	2[a]	2[b]	2[c]	6
$\sum$	6	6	6	18

Note. Here and in the figures presented below, the indices of different salts of the same metals are labelled a, b, c.

It is known that this type of system is characterised by one fourth-stage reaction, four first-stage reactions, and four second-stage reactions. The pair of salts, both of which are characterised by the presence of four unities in the corresponding adjacency matrices, AgCl – Li_2SO_4 (the thermal effect of the reaction is Q_9), corresponds to a fourth-stage reaction. The salt pairs produced in second-stage reactions are located at the intersection of rows and columns with two unities in the adjacency matrices I and II: AgCl – Na_2SO_4 (Q_8), NaCl – Li_2SO_4 (Q_7), AgCl – $NaNO_3$ (Q_6) and $AgNO_3$ – Li_2SO_4 (Q_5).

Other salt pairs are formed by first-stage reactions (Q_1, Q_2, Q_3 and Q_4). To determine the constituents of the thermal effects of the

I

	AgCl	$AgNO_3$	Ag_2SO_4	LiCl	$LiNO_3$	Li_2SO_4	NaCl	$NaNO_3$	Na_2SO_4
AgCl	0	0	0	0	1	1	0	1	1
$AgNO_3$	0	0	0	0	0	1	0	0	1
Ag_2SO_4	0	0	0	0	0	0	0	0	0
LiCl	0	0	0	0	0	0	0	0	0
$LiNO_3$	1	0	0	0	0	0	1	0	0
Li_2SO_4	1	1	0	0	0	0	1	1	0
NaCl	0	0	0	0	1	1	0	0	0
$NaNO_3$	1	0	0	0	0	1	0	0	0
Na_2SO_4	1	1	0	0	0	0	0	0	0

II

	AgCl	LiCl	NaCl	$AgNO_3$	$LiNO_3$	$NaNO_3$	Ag_2SO_4	Li_2SO_4	Na_2SO_4
AgCl	0	0	0	0	1	1	0	1	1
LiCl	0	0	0	0	0	0	0	0	0
NaCl	0	0	0	0	1	0	0	1	0
$AgNO_3$	0	0	0	0	0	0	0	1	1
$LiNO_3$	1	0	1	0	0	0	0	0	0
$NaNO_3$	1	0	0	0	0	0	0	0	1
Ag_2SO_4	0	0	0	0	0	0	0	0	0
Li_2SO_4	1	0	1	1	1	0	0	0	0
Na_2SO_4	1	0	0	1	0	0	0	0	0

Figure 11. Cation (I) and anion (II) adjacency matrices of the quinary reciprocal system Ag,Li,Na//Cl,NO_3,SO_4.

reactions, submatrices of quaternary reciprocal systems extracted from the adjacency matrices I and II should be considered. For the Ag,Li//Cl,NO_3,SO_4 system (in the upper right part of the cation matrix), the following reactions can be written:

$$AgNO_3 + LiCl = AgCl + LiNO_3 - Q_6$$

$$1/2\,Ag_2SO_4 + LiNO_3 = 1/2\,Li_2SO_4 + AgNO_3 - Q_5$$

$$1/2\,Ag_2SO_4 + LiCl = 1/2\,Li_2SO_4 + AgCl - Q_9$$

Hence, $Q_9 = Q_6 + Q_5$.

A consideration of the Ag,Li,Na//Cl,SO_4 system (the upper right semimatrix in the anion matrix) shows that $Q_9 = Q_7 + Q_8$. Other relations given in Table 16 are obtained in the same way.

Then the matrix of the conversion figure of the Ag,Li,Na//Cl,NO_3,SO_4 system is compiled (Fig. 12 *a*). This matrix includes unities from the matrices I and II along with two connections, *viz*., *1*–9 and *9*–*4*, resulting from the intersection of the stable (AgCl–Li_2SO_4–$NaNO_3$) and metastable (Ag_2SO_4–LiCl–$NaNO_3$) axial triangles of singular and non-equilibrium stars.

Once all necessary connections have been determined from the matrix of the conversion figure, one can construct the conversion graph of the quinary reciprocal system Ag,Li,Na//Cl,NO_3,SO_4 of the 9C type (Fig. 12 *b*).

Using the matrix of the conversion figure, one can find the salt compositions of secant tetrahedra and determine the total thermal effect for each tetrahedron.[8] For this purpose, it is necessary to perform a summation over the corresponding rows of the matrix. For example, the rows *5*, *3*, *8* and *9* should be summed for the

a

	1	*2*	*3*	*4*	*5*	*6*	*7*	*8*	*9*
1	0	0	0	0	1	0	1	0	1
2	0	0	0	0	0	1	1	0	0
3	0	0	0	0	1	0	0	1	0
4	0	0	0	0	0	1	0	1	1
5	1	0	1	0	0	0	0	0	1
6	0	1	0	1	0	0	0	0	1
7	1	1	0	0	0	0	0	0	1
8	0	0	1	1	0	0	0	0	1
9	1	0	0	1	1	1	1	1	0

b

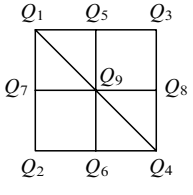

Figure 12. The matrix of the conversion figure (*a*) and the conversion figure (*b*) of the quinary reciprocal system Ag,Li,Na//Cl,NO_3,SO_4. (*1*) AgCl, (*2*) LiCl, (*3*) NaCl, (*4*) $AgNO_3$, (*5*) $LiNO_3$, (*6*) $NaNO_3$, (*7*) Ag_2SO_4, (*8*) Li_2SO_4, (*9*) Na_2SO_4; unity and zero in the cells of the matrix signify respectively the presence and the absence of a connection between stable salt pairs from the cation and anion matrices.

$Q_5 - Q_3 - Q_8 - Q_9$ square: $AgNO_3 - Li_2SO_4$ (Q_5), $AgNO_3 - Na_2SO_4$ (Q_3), $AgCl - Na_2SO_4$ (Q_8) and $AgCl - Li_2SO_4$ (Q_9). The salt composition of the tetrahedron is $AgNO_3 - Li_2SO_4 - AgCl - Na_2SO_4$, the total thermal effect of the reaction is $Q_9 + Q_8 + Q_5 + Q_3$. The results of summation are given in Table 18.

Table 18. Salt compositions of the secant tetrahedra for the quinary reciprocal system Ag,Li,Na//Cl,NO_3,SO_4.

Fragment of conversion figure	Salt composition of tetrahedron	Overall thermal effect of salts of tetrahedron
Square $Q_5 - Q_3 - Q_8 - Q_9$	$AgNO_3 - Li_2SO_4 - Na_2SO_4 - AgCl$	$Q_9 + Q_8 + Q_5 + Q_3$
Square $Q_2 - Q_7 - Q_9 - Q_6$	$LiNO_3 - Li_2SO_4 - NaCl - AgCl$	$Q_9 + Q_7 + Q_6 + Q_2$
Triangle $Q_1 - Q_9 - Q_7$	$NaNO_3 - Li_2SO_4 - NaCl - AgCl$	$Q_9 + Q_7 + Q_1$
Triangle $Q_1 - Q_5 - Q_9$	$AgNO_3 - Li_2SO_4 - NaNO_3 - AgCl$	$Q_9 + Q_5 + Q_1$
Triangle $Q_4 - Q_6 - Q_9$	$LiNO_3 - Li_2SO_4 - NaNO_3 - AgCl$	$Q_9 + Q_6 + Q_4$
Triangle $Q_4 - Q_8 - Q_9$	$NaNO_3 - Li_2SO_4 - Na_2SO_4 - AgCl$	$Q_9 + Q_8 + Q_4$

For the practical application of conversion figures, the corresponding graphs need not be constructed from the adjacency matrices. Geometric images can completely be omitted, because the matrix of the conversion figure contains all necessary information. For example, the degree of a vertex of a graph not only defines the number of connections of this vertex to other vertices (*i.e.*, the number of conversion lines) but also indicates the number of chemical reactions giving rise to a salt pair, the stage of diagonals, the intersection of which is occupied by a particular conversion point; the compositions of simplexes of a singular star, and the heat capacities of mixtures corresponding to secant elements of the singular star.

IV. Practical applications of matrices and graphs in studies of complex systems

Matrices of reciprocal salt pairs with inscribed conversion figures can be used for searching for salt mixtures, which are characterised by the highest energy capacity and are constituents of simplexes for systems of the 2//*n* (*n*//2) series.[8]

The thermochemical relations in a system can be judged from a matrix of reciprocal salt pairs with an inscribed conversion figure of secant elements, *i.e.*, such matrices allow one to determine the reaction stages yielding the corresponding salt pairs. It can easily be found out which simplex has a higher energy capacity. The larger the number of unities in the matrix that contains elements of a conversion figure (from which a simplex is obtained), the higher the total heat content of the salt mixture and, consequently, the higher all other energy characteristics.

All simplexes of a singular star of a system can be determined from the conversion figure inscribed into a matrix of reciprocal salt pairs, *i.e.*, triangulation can be performed without the use of tools of multidimensional geometry.

1. Construction of singular stars of secant tetrahedra of systems of the 2//*n* (*n*//2) series

Let us consider the determination of simplexes from a conversion figure inscribed into a canonical matrix b_0 of reciprocal salt pairs [11] for a system consisting of sodium, potassium and barium fluorides and tungstates (Fig. 13). In the Na,K,Ba//F,WO_4 system, $BaF_2 + K_2WO_4$, $(NaF)_2 + BaWO_4$ and $K_2WO_4 + (NaF)_2$ are stable pairs. The former two pairs are generated by first-stage

a

b_0	$(NaF)_2$	$(KF)_2$	BaF_2
Na_2WO_4	0	0	0
K_2WO_4	1	0	1
$BaWO_4$	1	0	0

b

$$\begin{pmatrix} a_{11} & a_{12} & a_{13} \\ a_{21} & a_{22} & a_{23} \\ a_{31} & a_{32} & a_{33} \end{pmatrix}$$

Figure 13. Conversion graph inscribed in the matrix of mutual salt pairs of the quaternary reciprocal system Na,K,Ba//F,WO_4 (*a*), and the general form of the matrix (*b*).

reactions, whereas the third pair is formed by a second-stage reaction. These pairs correspond to unities in cells of the matrix. Points are placed in cells with unities, and then the points are connected by solid lines to form the conversion figure of this system inscribed in the matrix (Fig. 13 *a*). The analysis of the conversion figure of the system starts with the determination of secant simplexes (triangles).

The vertices of the first triangle are determined from the row, which includes one of the lines a_{21} or a_{23}. This line corresponds to potassium tungstate, which forms stable pairs with sodium and barium fluorides.

Therefore, $K_2WO_4 - (NaF)_2 - BaF_2$ is one of the stable triangles. The vertices of the corresponding metastable triangle represent salts located in cells with zeros, which are symmetric to cells with unities relative to the zero diagonal. The cell a_{21} with unity is symmetric to the cell a_{12} with zero, and the cell a_{23} is symmetric to the cell a_{32}. Hence it follows that the $K_2WO_4 + (NaF)_2$ pair corresponds to the metastable $Na_2WO_4 + (KF)_2$ pair, and the stable $K_2WO_4 + BaF_2$ pair corresponds to the $BaWO_4 + (KF)_2$ pair. This gives rise to the metastable $Na_2WO_4 - (KF)_2 - BaWO_4$ triangle. The compositions of the stable $K_2WO_4 - (NaF)_2 - BaWO_4$ triangle and the metastable $(KF)_2 - Na_2WO_4 - BaF_2$ triangle are determined analogously from the conversion line in the column of the matrix.

The next stage involves the determination of tetrahedra of singular and non-equilibrium stars of the system. A stable sphenoid (irregular tetrahedron) is determined by salts corresponding simultaneously to all unities of the matrix (the overall conversion figure). In the case under consideration, this is the $K_2WO_4 - (NaF)_2 - BaWO_4 - BaF_2$ tetrahedron. The metastable sphenoid is formed by salts, which determine the row and column with three or two zeros [$BaWO_4 - BaF_2 - Na_2WO_4 - (KF)_2$]. Salts corresponding to the shared edge of the stable and metastable sphenoids are determined by the row and column with two zeros ($BaWO_4 - BaF_2$).

Stable tetrahedra correspond to salts, which occupy the cells of an entire row or column, through which conversion lines pass. For the system under consideration, these are the stable $K_2WO_4 - (KF)_2 - (NaF)_2 - BaF_2$ (row) and $(NaF)_2 - K_2WO_4 - Na_2WO_4 - BaWO_4$ (column) tetrahedra. Metastable tetrahedra are formed from columns and rows containing salts, which are located in cells with zeros, the cells being symmetric to cells with unities relative to the zero diagonal. The a_{21}, a_{22}, a_{23} row is symmetric to the a_{12}, a_{22}, a_{32} column, and the a_{11}, a_{21}, a_{31} column is symmetric to the a_{11}, a_{12}, a_{13} row. Hence, $K_2WO_4 - (KF)_2 - Na_2WO_4 - BaWO_4$ and $Na_2WO_4 - (NaF)_2 - (KF)_2 - BaF_2$ are metastable tetrahedra.

All elements of the stable and metastable complexes of the system are given in Table 19. The results obtained for the Na,K,Ba//F,WO_4 system according to the above-described procedure correlate well with the experimental data.[11]

Therefore, this method provides a simple and convenient way to determine secant elements of singular and non-equilibrium stars for reciprocal systems of the 2//*n* (*n*//2) series without the use

Table 19. Compositions of simplexes of the singular and non-equilibrium stars for the Na,K,Ba//F,WO_4 system.

Secant elements		Stable cells of singular star	Metastable cells of non-equilibrium star
stable	metastable		
$(NaF)_2-K_2WO_4-BaWO_4$	$(KF)_2-BaF_2-Na_2WO_4$	$(NaF)_2-K_2WO_4-BaWO_4-BaF_2$ $(NaF)_2-Na_2WO_4-BaWO_4-K_2WO_4$	$(KF)_2-Na_2WO_4-BaWO_4-BaF_2$ $(KF)_2-Na_2WO_4-BaF_2-(NaF)_2$
$(NaF)_2-K_2WO_4-BaF_2$	$Na_2WO_4-(KF_2)-BaWO_4$	$(KF)_2-NaF-BaF_2-K_2WO_4$	$(KF)_2-K_2WO_4-Na_2WO_4-BaWO_4$

of complicated geometric constructions. This method is rapid and allows one to study multicomponent systems (for example, systems containing 8, 10 or 12 salts).

The simultaneous determination of the energy characteristics of simplexes makes it possible (after the transformation of a conversion figure to an energy graph) to obtain a rapid semi-quantitative estimate of the energy capacities of salt compositions within one system. The estimation is performed as follows: the heats of melting of the salts involved in tetrahedra are added to the heats of exchange reactions occurring between the salts (taking into account whether the reaction is endothermic or exothermic, which is established by calculations or determined experimentally from DTA data). If the heats of melting of salts have similar values, the main difference in the energy capacity of salt mixtures is associated with the heats of reactions. Therefore, the energy capacity of a mixture depends on the number of exchange reactions that can occur between the salts. This value can easily be determined from the energy models (graphs).

For reciprocal systems containing six salts, the singular star consists of three tetrahedra divided by two secant triangles. Salt mixtures with the highest energy capacity are generally modelled by sphenoids, because they are intersected by two conversion lines, and, consequently, the salts belonging to the sphenoids are involved in three exchange reactions [in the case under consideration, the $(NaF)_2-BaWO_4-BaF_2-K_2WO_4$ sphenoid]. Other tetrahedra correspond to two exchange reactions. Hence, the overall thermal effect of the reaction of salts involved in a sphenoid is equal to twice the sum of the thermal effects of first-stage reactions.

It was experimentally established that a eutectic present in a sphenoid has the highest energy capacity.[8] Eutectics in systems consisting of six salts were found according to this procedure. The energy capacities of such eutectics are twice as high as those of foreign standards.[9,10] These eutectics were used as heat-accumulation mixtures in thermal chemical power sources.

2. Construction of systems with the desired direction of interchange reactions

Analysis of matrices of reciprocal salt pairs represents the basis for the rational choice of salts for the preparation of systems with the desired direction of exchange reactions. To prepare a quaternary reciprocal system consisting of six salts with the desired direction of interchange reactions, salts can be chosen using summary matrix tables of reciprocal salt pairs composed for particular groups of cations and anions.[3]

If the aim is to prepare a system characterised by the highest stability of a particular salt, the ions should be chosen using a matrix, in which this salt has two unities. In this case, the desired salt (for example, AX) is formed in the system according to the following reactions:

$$AY + BX = AX + BY,$$

$$AZ + BX = AX + BZ.$$

To construct a quinary reciprocal system consisting of nine salts, in which the desired salt is the most stable, one should be guided by the following principle. The chosen composition should be such that the desired salt has two unities in two of the three matrices compiled for the starting quaternary reciprocal systems or at least has two unities in one matrix and one unity in another matrix. For instance, the aim is to choose a salt composition of nine salts involving alkali metal halides and sulfates such that the exchange reactions are shifted toward the formation of lithium sulfate.

To solve this problem, cations, whose halides form stable pairs with lithium sulfate, are found from the matrix tables. All cations of Group I elements satisfy this requirement. If the choice is limited to lithium, sodium and potassium salts, a salt composition with the desired direction of exchange reactions can be constructed using a mixture of lithium, sodium and potassium chlorides, bromides and sulfates or a mixture of chlorides, iodides and sulfates of these alkali metals. In these cases, the following quinary reciprocal systems of nine salts are formed: Li,Na,K//Cl,Br,SO_4; Li,Na,K//Cl,I,SO_4; Li,Na,K//Br,I,SO_4.

In addition to lithium sulfate, the basic triangle for such systems involves a pair of sodium and potassium halides, which has unity in the third starting matrix. For the Li,Na,K//Cl,Br,SO_4 system, this is the KBr – NaCl pair, *i.e.*, the basic triangle has the composition $Li_2SO_4-KBr-NaCl$. This fact was confirmed by experimental data.[8] Lithium sulfate is formed according to the following equation:

$$2\,LiBr + K_2SO_4 + NaCl = Li_2SO_4 + 2\,KBr + NaCl.$$

The NaCl salt has crystallisation fields both in the non-equilibrium and basic triangles (Fig. 14).

For particular pairs of cations, reciprocal quaternary and quinary systems are conveniently constructed by setting up series of chemical reactivity (stability) of salts with these cations. For example, there are the following series of stability for systems involving lithium and sodium (stability increases from left to right):

LiI, LiBr, LiCl, $LiNO_3$, Li_2SO_4;

Na_2SO_4, $NaNO_3$, NaCl, NaBr, NaI.

To construct a quaternary reciprocal system of six salts characterised by the highest stability of a particular salt (for

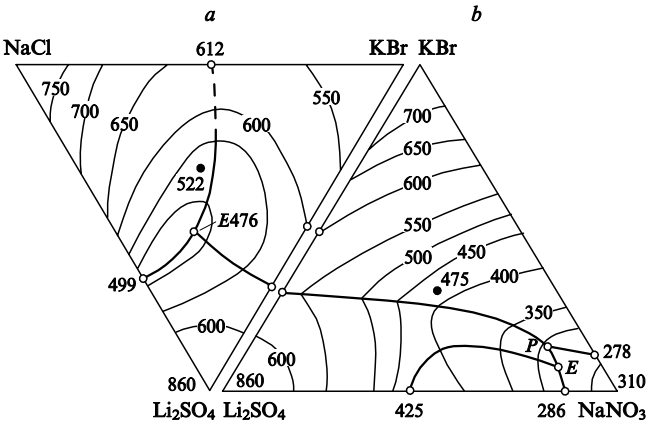

Figure 14. Axial stable triangles of the quinary reciprocal systems Li,Na,K//Cl,Br,SO_4 (*a*) and Li,Na,K//Br,NO_3,SO_4 (*b*).
E and *P* are quasiternary eutectic and peritectic points, respectively; the temperatures are given in degrees Centigrade.

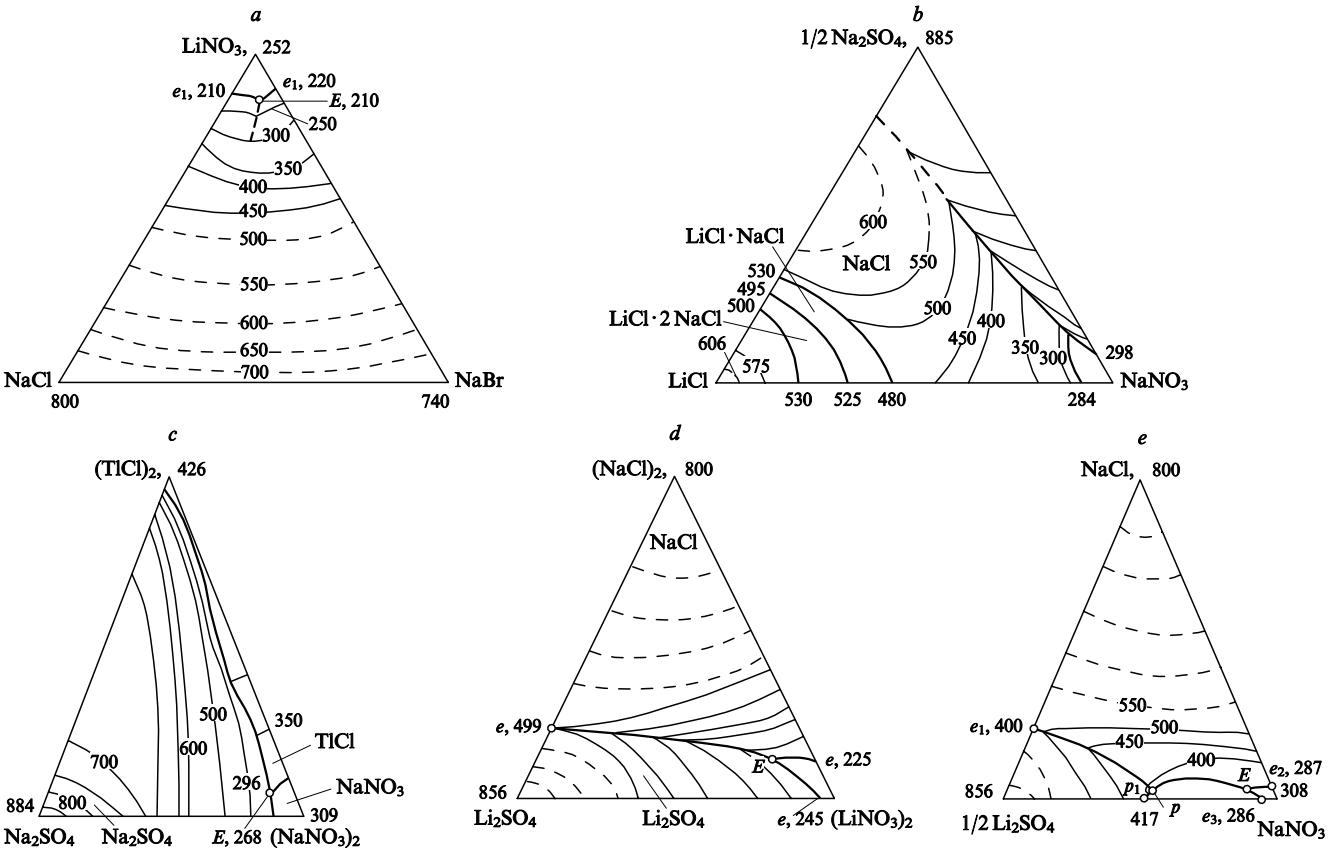

Figure 15. Sections of the quaternary reciprocal systems Li,Na//Cl,Br,NO_3 (*a*), Li,Na//Cl,NO_3,SO_4 (*b*), Na,Tl//Cl,NO_3,SO_4 (*c*) and Li,Na//Cl,NO_3,SO_4 (*d*, *e*); *e* and *p* are the saddle eutectic and peritectic points, respectively; the temperatures are given in degrees Centigrade.

example, lithium nitrate), a composition of salts, which are located in the left side of the series of stability (*i.e.*, lithium chlorides and bromides, chlorides and iodides, bromides and iodides), should be chosen. Actually, investigation of the quaternary reciprocal system Li,Na//Cl,Br,NO_3 demonstrated that $LiNO_3$ is the most stable salt in this system even in the presence of stable sodium salts (Fig. 15 *a*).

Let us consider another situation, where the aim is to change the direction of the exchange reaction in the reciprocal system Li,Na//Cl,NO_3,SO_4 consisting of six salts toward the formation of sodium sulfate.

The matrix of reciprocal salt pairs for this system has the form

		I		
		Na^+		
	c_0	Cl^-	NO_3^-	SO_4^{2-}
	Cl^-	0	0	0
Li^+	NO_3^-	1	0	0
	SO_4^{2-}	1	1	0

The main reaction

$$2\,LiCl + Na_2SO_4 = Li_2SO_4 + 2\,NaCl,$$

proceeding in this system can be shifted in the required direction by replacing one of the ions. In deciding on a cation to be replaced, one should choose an ion characterised by a reciprocal matrix. In the case under consideration, this is the type *c*, because the starting system has the matrix c_0. The thallium ion satisfies this requirement.

		II		
		Na^+		
	c	Cl^-	NO_3^-	SO_4^{2-}
	Cl^-	0	1	1
Tl^+	NO_3^-	0	0	1
	SO_4^{2-}	0	0	0

The main reaction in the Na,Tl//Cl,NO_3,SO_4 system is

$$2\,NaCl + Tl_2SO_4 = Na_2SO_4 + 2\,TlCl.$$

This fact can be confirmed by comparing the corresponding sections of the Li,Na//Cl,NO_3,SO_4 (Fig. 15 *b*) and Na,Tl//Cl,NO_3,SO_4 systems (Fig. 15 *c*).

In the former system, sodium sulfate is involved in the metastable $LiCl-Na_2SO_4-NaNO_3$ section. The liquidus surface of the section is shown in Fig. 15 *b*. It can be seen that the section is metastable, because it involves NaCl as the exchange product. After the replacement of the lithium ion with thallium, the section becomes stable.

The direction of the exchange reactions in quinary reciprocal systems consisting of 8 or 9 salts can be changed in the same manner as for reactions in quaternary reciprocal systems, except for the fact that one or two reciprocal matrices should be used.

Analysis of matrices of reciprocal salt pairs gives an idea of how one can influence the complexation processes. Let us consider the situation where complex compounds are formed by a stable salt produced by an exchange reaction. The complexation leads to a decrease in stability of the salt, and the yield of the salt in the reaction also decreases. To prevent complexation, it is necessary

to replace one component. For example, stability of lithium sulfate in the quaternary reciprocal system Li,Na//Cl,NO_3,SO_4 is low due to formation of $Li_2SO_4 \cdot Na_2SO_4$.

It is necessary to choose a salt composition, in which the $Li_2SO_4 \cdot Na_2SO_4$ compound has no effect on stability of the salt under consideration. It appeared that the stability of the desired salt can be increased within the same system by introducing an excess of lithium ions. For example, Li_2SO_4 is more stable in the presence of lithium nitrate (Fig. 15*d*). If it is required to replace a particular ion in a system with another ion, one should use an ion, the replacement of which leaves the main exchange reaction unaffected. In the Li,Na//Cl,NO_3,SO_4 system, the nitrate ion satisfies this requirement. This ion can be replaced with an anion or cation provided that the type of the matrix of reciprocal salt pairs remains unchanged. As can be seen from the series of chemical interactions of the cations, any cation to the left of lithium can be used for the replacement. Let us use potassium. In this case, the quaternary reciprocal system Li,K,Na//Cl,SO_4 is formed. The elementary matrix of this system is as follows:

	c_0	SO_4^{2-} Li^+	Na^+	K^+
	Li^+	0	0	0
Cl^-	Na^+	1	0	0
	K^+	1	1	0

In this matrix, lithium sulfate has two unities. This compound is formed by the reaction

$$K_2SO_4 + 2\,LiCl = Li_2SO_4 + 2\,KCl.$$

The $Li_2SO_4 \cdot Na_2SO_4$ compound in the Li,K,Na//Cl,SO_4 system occupies a small volume and is not manifested in the phase diagrams of stable sections.

The choice of salts, which promote immiscibility with retention of the direction of the exchange reaction toward the formation of the desired salt, is of practical interest. For instance, immiscibility in reciprocal systems can be used for extraction of salts from melts.

Suppose that there is a need to choose a salt composition, which consists of nine salts involving the Li^+ and Na^+ cations and is suitable for extraction of lithium sulfate from melts. Initially, information on which salts (in combination with lithium sulfate) lead to immiscibility can be extracted from the analysis of the data on ternary reciprocal systems. These salts are silver, cadmium and thallium chlorides. Then we choose cations, which have no effect on the stability of Li_2SO_4, based on series of chemical interactions for the halide – sulfate exchange.

For these cations, other anions can be included in the consideration (for example, nitrate ions, which do not decrease the stability of the salt of interest, in whatever combination desired). The procedure gives the following systems: Ag,Li,Na//Cl,NO_3,SO_4; Ag,Li,Na//Cl,Br,SO_4; Cd,Li,Na//Cl,NO_3,SO_4; Cd,Li,Na//Cl,Br,SO_4; Li,Na,Tl//Cl,NO_3,SO_4; Li,Na,Tl//Cl,Br,SO_4. Some of these systems were studied experimentally. For the Li,Na,Cd//Cl,NO_3,SO_4 system, the immiscibility region in the phase diagram of the axial stable triangle comprises 54.5% of the diagram.

3. Construction of singular stars of secant tetrahedra for systems consisting of nine salts

To construct singular stars, it is necessary to determine the salt compositions of secant tetrahedra. This can be done by interpreting elements of the graph (the conversion figure of this system).[8, 34, 35]

Let us consider the procedure for the determination of salt compositions of secant tetrahedra using the quinary reciprocal system Li,Na,K//Cl,Br,NO_3 consisting of nine salts as an example. This system belongs to the 9B topological type.[8, 23, 36] The conversion graph of this system is shown in Fig. 16. The stable salt pairs and elements of singular and non-equilibrium stars are given in Table 20.

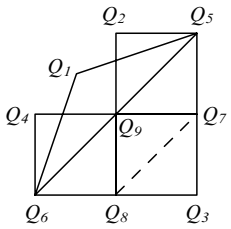

Figure 16. Conversion figure of the 9B-type quinary reciprocal system Li,Na,K//Cl,Br,NO_3.

Table 20. Elements of the conversion graph and salt compositions of secant tetrahedra for the quinary reciprocal system Li,Na,K//Cl,Br,NO_3.

Element of conversion graph	Stable salt pair	Element of singular star
Square	$LiNO_3 + KCl$ (Q_4)	pyramid
$Q_4 - Q_6 - Q_8 - Q_9$	$LiNO_3 + NaCl$ (Q_6)	$LiNO_3 - KCl - NaCl - NaBr - KBr$
	$LiNO_3 + NaBr$ (Q_8)	tetrahedra
	$LiNO_3 + KBr$ (Q_9)	$LiNO_3 - KCl - NaCl - KBr$
		$LiNO_3 - NaCl - NaBr - KBr$
Square	$KBr + NaNO_3$ (Q_2)	pyramid
$Q_2 - Q_5 - Q_7 - Q_9$	$KBr + NaCl$ (Q_5)	$KBr - LiNO_3 - LiCl - NaCl - NaNO_3$
	$KBr + LiCl$ (Q_7)	tetrahedra
	$KBr + LiNO_3$ (Q_9)	$KBr - LiNO_3 - LiCl - NaCl$
		$KBr - LiNO_3 - NaNO_3 - NaCl$
Square	$LiCl + NaBr$ (Q_3)	sphenoid
$Q_3 - Q_8 - Q_9 - Q_7$	$LiNO_3 + NaBr$ (Q_8)	$NaBr - KBr - LiNO_3 - LiCl$
	$LiNO_3 + KBr$ (Q_9)	
	$LiCl + KBr$ (Q_7)	
Triangle	$NaCl + KNO_3$ (Q_1)	tetrahedron-hemipyramid
$Q_1 - Q_5 - Q_6$	$KBr + NaCl$ (Q_5)	$LiNO_3 - KBr - NaCl - KNO_3$
	$NaCl + LiNO_3$ (Q_6)	

The salt compositions of the tetrahedra can be determined according to three procedures.

1. The procedure based on the thermochemical relations in a system. Individual squares and triangles of the conversion figure are considered. For each point of complete conversion, stable pairs and the corresponding stages of stable diagonals are written. For example, the point Q_4 for the conversion square $Q_4 - Q_6 - Q_8 - Q_9$ corresponds to the first-stage diagonal $LiNO_3 - KCl$, the point Q_6 corresponds to the second-stage diagonal $LiNO_3 - NaCl$, the point Q_8 corresponds to the third-stage diagonal $LiNO_3 - NaBr$, and the point Q_9 corresponds to the fourth-stage diagonal $LiNO_3 - KBr$. The $LiNO_3$ salt is repeated four times and, consequently, serves as the vertex of the pyramid, whose base is formed by the ternary reciprocal system Na,K//Cl,Br. The pyramid is composed of two tetrahedra, *viz.*, $LiNO_3 - KCl - NaCl - KBr$ and $LiNO_3 - NaCl - NaBr - KBr$, sharing the axial triangle $LiNO_3 - NaCl - KBr$. Analogously, the $LiNO_3 - NaNO_3 - NaCl - KBr$ and $LiNO_3 - LiCl - NaCl - KBr$ tetrahedra are determined from the conversion square $Q_2 - Q_5 - Q_7 - Q_9$.

2. The procedure based on chemical reactions described by conversion figures. By summing the reactions for points of complete conversion of ternary reciprocal systems, we obtain the reaction equation for the central point of the conversion square. For example, for the $Q_2 - Q_5 - Q_7 - Q_9$ square (see Fig. 16),

$$LiBr + KCl + NaBr + KCl + NaBr + KNO_3 + LiBr + KNO_3 =$$
$$= LiNO_3 + LiCl + 4\,KBr + NaCl + NaNO_3.$$

The salts formed in the reactions are placed at the vertices of the $KBr - LiNO_3 - LiCl - NaCl - NaNO_3$ pyramid, with the ternary reciprocal system Li,Na//Cl,NO_3 lying on its base. The salt

compositions of the tetrahedra involved in the pyramid can be derived from the reaction equations for the conversion triangles:

for the $Q_2-Q_5-Q_9$ triangle,

$$2\ KNO_3 + NaBr + NaBr + KCl + LiBr = \\ = 3\ KBr + LiNO_3 + NaCl + NaNO_3;$$

for the $Q_5-Q_7-Q_9$ triangle,

$$NaBr + LiBr + 2\ KCl + KNO_3 = \\ = 3\ KBr + LiNO_3 + NaCl + LiCl.$$

3. The geometric procedure.[8, 34] A fragment of the conversion figure, *viz*., a square or triangle, is displayed on the plane, and points of complete conversion are indicated. The conversion square is inscribed in a quadrangle (Fig. 17). The notations of salts common to each pair of points are placed at the vertices of the tetrahedron. For example, the NaBr salt is common to the points Q_3 and Q_8, $LiNO_3$ is common to the points Q_8 and Q_9, *etc*. The conversion triangle is inscribed in a tetrahedron parallel to one of its faces. A salt common to three points of complete conversion serves as a vertex of the resulting tetrahedron.

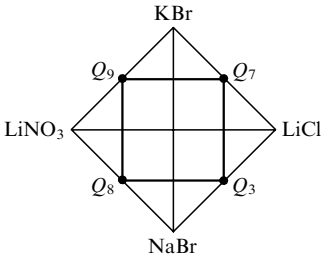

Figure 17. Geometric procedure for the determination of the salt compositions of the tetrahedra for the reciprocal system Li,Na,K// Cl,Br,NO_3 consisting of nine salts.

Once the salt compositions of the tetrahedra have been determined, the scheme of a singular star is constructed taking into account the reaction stages and constituents of the thermal effects.

The tetrahedra in the singular star are connected to each other in a particular manner. Schemes of singular stars of tetrahedra can be derived by analogy with singular stars of pentatopes.[8] Systems belonging to different topological types are characterised by different schemes (Fig. 18). In Fig. 18, the points correspond to the tetrahedron, and the line characterises the presence of three common salts involved in the tetrahedron. Hence, the triangle formed by stable diagonals serves as a connection unit between the tetrahedra.

Each topological type of a singular star of tetrahedra is characterised by a particular set of reaction stages.

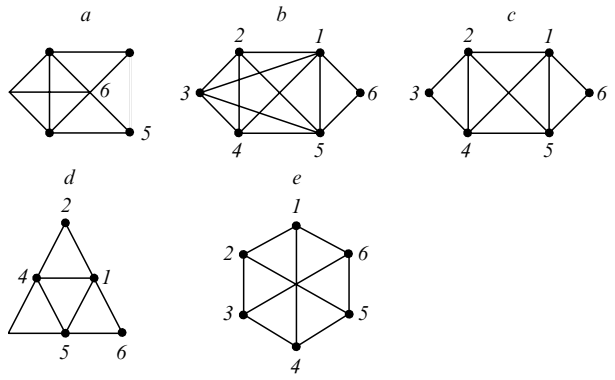

Figure 18. Schemes of singular stars of secant tetrahedra for quinary reciprocal systems of the topological types 9A (*a*), 9B (*b*), 9C (*c*), 9D (*d*) and 9E (*e*).

Schemes of connections between tetrahedra represent graphs with different arrangements of vertices corresponding to the topological type of the system. Analysis of such graphs allows one to reveal the reactivity of salts, which compose any tetrahedron of a singular star. The advantage of this procedure for the construction of graphs of singular stars of tetrahedra for systems of various topological types is that it clearly shows the relationships between the thermochemical relations, chemical reactions in the system as a whole and its constituents and the geometric elements of singular stars.

4. Proximate method for studying phase complexes of reciprocal salt systems in melts

According to Kurnakov's theory, the composition – property diagram of a system is formed at the intersection of the coordinate frame (the phase diagram of the system) with the phase complex. Triangulation methods allow one to construct a phase complex of a system after the construction and partitioning of the composition diagram.

The conversion method[6] enables one to study and construct phase diagrams of multicomponent reciprocal systems without preliminary investigation of the composition diagram, because conversion figures of secant elements can be constructed and analysed with the use of matrices of reciprocal salt pairs, sometimes without deducing singular and non-equilibrium stars.[8, 32, 33]

This method of studying phase complexes of reciprocal condensed systems reduces substantially the time of experimentation and, hence, is a proximate method, which allows one to solve a number of problems in serial technological investigations.[7] The essence of the method is that the minimum number of points in phase diagrams are studied experimentally. Differential thermal analysis (DTA) is used as the main method, which should be supplemented with methods for the determination of compositions of invariant points (zone melting, chemical analysis) and methods for the identification of phase compositions (powder X-ray diffraction analysis, microstructural analysis).

Investigation of a phase diagram is simplified due to a decrease in the amount of required data. With information only on binary systems and polymorphism of salts in hand, it is sufficient to study one point of complete conversion for a ternary reciprocal system. For quaternary reciprocal systems, two lines of complete conversion should be studied if experimental data on points of complete conversion of ternary reciprocal systems are available, and so forth.[11, 36]

The procedure for studying systems is as follows. Investigation of a ternary reciprocal system starts with the measurement of a thermogram of the point of complete conversion, *i.e*., the point corresponding to the equivalent ratio of a pair of salts, which have no ions in common. The thermogram is interpreted using data on the phase complex of binary systems.[36, 37] The first thermal effect corresponds to the onset of crystallisation of the phase, which crystallises at the point of complete conversion. The phase can be identified by microstructural analysis or otherwise. The second peak in the thermogram is assigned to co-crystallisation of the phases that form by the exchange reaction or complex formation. Data on binary systems give an indication of the irreversibly reciprocal character of a ternary reciprocal system, and the presence of two thermal effects in the thermogram confirms this suggestion. In this case, the temperatures of invariant points can be determined by thermographic analysis.[37]

In addition to the temperatures of invariant points, it is necessary to determine their compositions by zone melting followed by chemical analysis. Therefore, to reveal the phase complex of irreversibly reciprocal ternary systems, one needs to study several concentration points. Methods were developed for the calculation of crystallisation surfaces of ternary reciprocal systems and their sections.[38–42] Combinations of calculation and experimental methods were also used.[43–45]

The question about complexation in a ternary reciprocal system can also be solved using a thermogram for the point of

complete conversion, in which the thermal effects are observed. These effects accompany the following processes: the onset of crystallisation; co-crystallisation of a salt pair formed by an exchange reaction; co-crystallisation of a stable salt pair with a compound resulting from complexation.[37]

Thermograms of the points of complete conversion[11] are shown in Fig. 19. The Na,Ba//F,WO_4 system is irreversibly reciprocal, which was confirmed experimentally (Fig. 19 *a*). The Na,K//F,WO_4 system is complicated by the complexation process. The thermogram of the point of complete conversion of this system (Fig. 19 *b*) shows that the following competitive reactions proceed in the system

$$2\,KF + Na_2WO_4 = 2\,NaF + K_2WO_4,$$

$$3\,KF + Na_2WO_4 = 2\,NaF + KF\cdot K_2WO_4.$$

The compound is formed in the secondary reaction, which does not take place at the point of complete conversion. The overall phase complex of this system can be revealed by also studying points of incomplete conversion.[8, 11]

The conversion figure becomes more complicated as the number of components increases. Investigation of two lines of complete conversion, which include points of complete conversion of ternary reciprocal systems, is sufficient to obtain phase complexes of systems consisting of six salts.[46] The phase diagram of the Na,K,Ba//F,WO_4 system is shown in Fig. 20. The conversion lines *B*, *D* and *F* serve as the composition axis of this diagram. Based on analysis of the diagram, one can draw conclusions regarding the crystallisation volumes in the system under consideration, exchange and complexation reactions and invariant points.

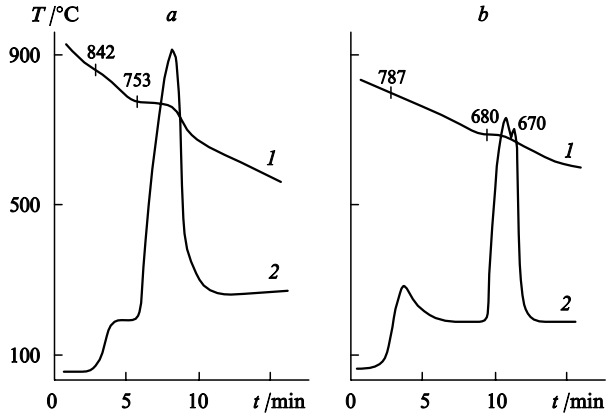

Figure 19. Thermograms of the points of complete conversions of the Na,Ba//F,WO_4 (*a*) and K,Ba//F,WO_4 (*b*) systems.
(*1*) Thermal analysis, (*2*) DTA.

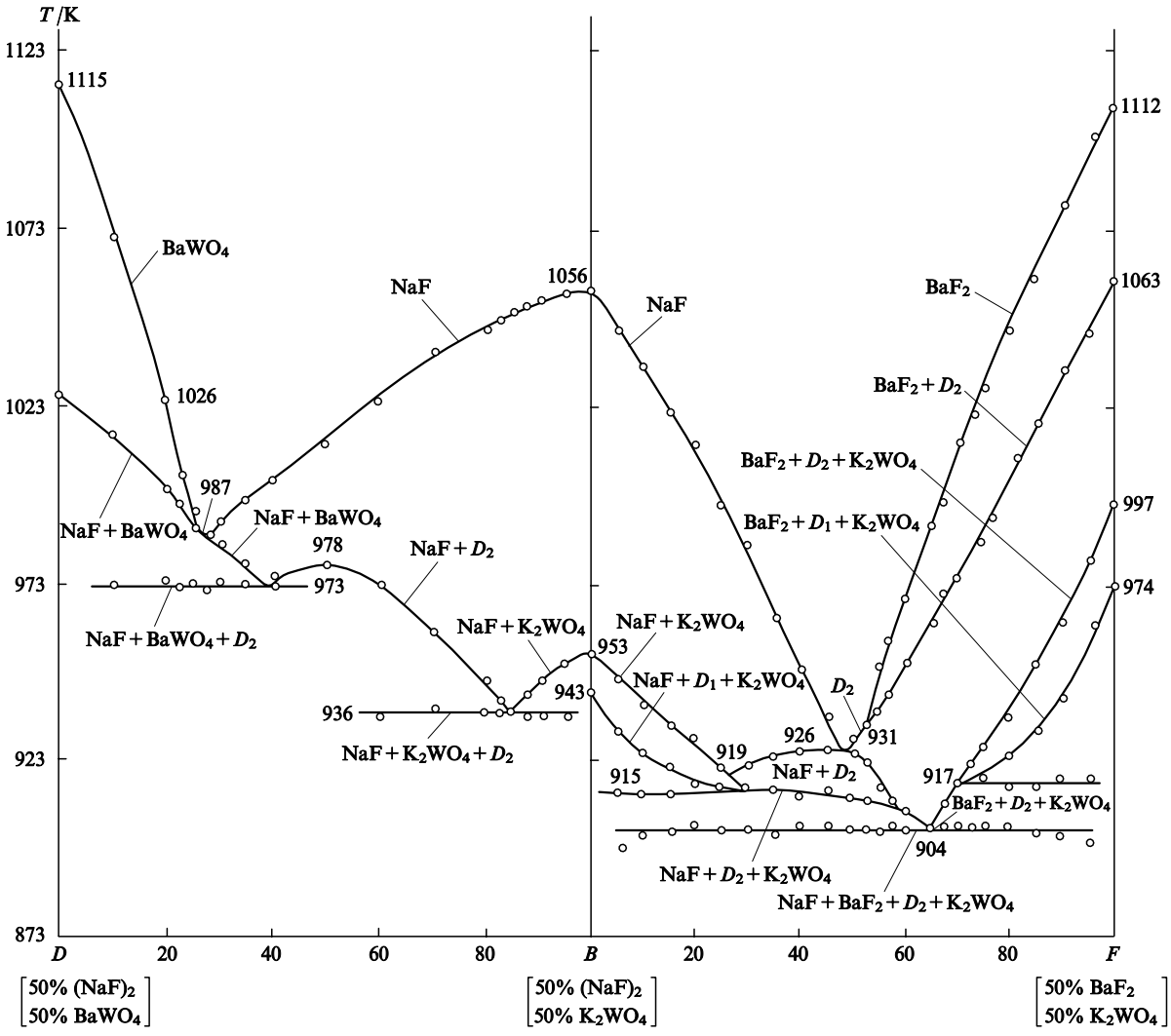

Figure 20. Temperature–composition diagram for the quaternary reciprocal system Na,K,Ba//F,WO_4.[11]
The composition axis represents the conversion lines *B*–*D* and *B*–*F* (see Fig. 2 *b*), $D_1 = KF\cdot K_2WO_4$, $D_2 = K_2WO_4\cdot BaWO_4$.

For example, the BaF_2, $BaWO_4$ and NaF salts are characterised by the largest volumes in the Na,K,Ba//F,WO_4 system. Experimental study of the conversion lines demonstrated that the following reactions occur in the system containing metastable salts in a stoichiometric ratio:

$$2\,KF + BaWO_4 = BaF_2 + K_2WO_4,$$

$$2\,KF + Na_2WO_4 = 2\,NaF + K_2WO_4,$$

$$BaF_2 + Na_2WO_4 = 2\,NaF + BaWO_4,$$

$$2\,KF + 2\,BaWO_4 = BaF_2 + K_2WO_4 \cdot BaWO_4,$$

$$3\,KF + Na_2WO_4 = 2\,NaF + KF \cdot K_2WO_4.$$

The $B-D$ line in Fig. 20 intersects the crystallisation fields of sodium fluoride, as evidenced by two branches of primary crystallisation intersecting at the point with coordinates 987 K and 27.5% of B. This point lies on the curve, which separates the crystallisation fields of NaF and $BaWO_4$ (Fig. 21). The curves of secondary crystallisation ($NaF + BaWO_4$), ($NaF + K_2WO_4 \cdot BaWO_4$) and ($NaF + K_2WO_4$) intersect at two points with the following coordinates: 973 K, 38.5% of B; and 936 K, 84% of B. These points correspond to quasiternary eutectics in the plane of the $(NaF)_2 - BaWO_4 - K_2WO_4$ triangle.

At 50% of B, a minimum is observed at 978 K in the curve of secondary crystallisation, and only two phases, *viz*., sodium fluoride and $K_2WO_4 \cdot BaWO_4$, are observable (see Fig. 20).

The results of powder X-ray diffraction analysis of the points of co-crystallisation of three phases on the $B-D$ line with $B > 50\%$ demonstrated that the following phases occur on this line: NaF, $K_2WO_4 \cdot BaWO_4$ and K_2WO_4. For melts with $B < 50\%$, the NaF, $K_2WO_4 \cdot BaWO_4$ and $BaWO_4$ phases were detected. The central point of the conversion line is characterised by crystallisation of two phases, *viz*., NaF and $K_2WO_4 \cdot BaWO_4$.

On the whole, the conversion lines and, consequently, the $(NaF)_2 - K_2WO_4 - BaWO_4$ triangle correspond to four phases, *viz*., NaF, K_2WO_4, $K_2WO_4 \cdot BaWO_4$ and $BaWO_4$ (see Figs 20, 21).

The $B-D$ line of complete conversion lies in the plane of the diagonal triangle $(NaF)_2 - K_2WO_4 - BaWO_4$, whose vertices correspond to salts formed by exchange reactions in the Na,K,Ba//F,WO_4 system. By summing the equations of the exchange reactions for the points B and D, we obtain the equation for the conversion line $B-D$.

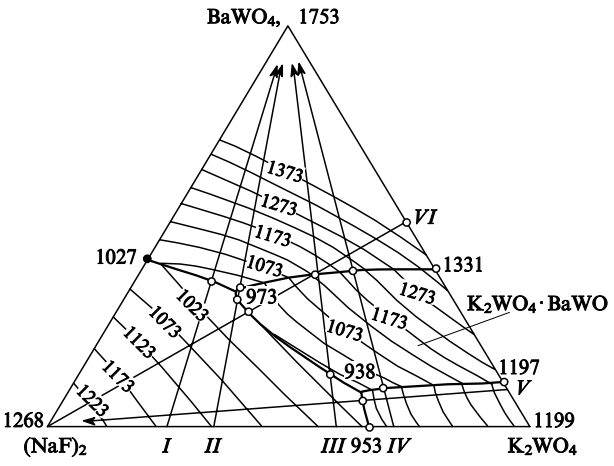

Figure 21. Phase diagram of the secant triangle $(NaF)_2 - BaWO_4 - K_2WO_4$ of the Na,K,Ba//F,WO_4 system.
Here and in Fig. 22, the temperatures are given in Kelvin (K); $I-VI$ denote the sections studied.

For the point B:

$$2\,KF + Na_2WO_4 = 2\,NaF + K_2WO_4,$$

for the point D:

$$BaF_2 + Na_2WO_4 = 2NaF + BaWO_4.$$

The following reaction corresponds to the central point of the $B-D$ line:

$$2\,KF + BaF_2 + 2\,Na_2WO_4 = 4\,NaF + K_2WO_4 + BaWO_4. \quad (10)$$

The data on the boundary elements show that K_2WO_4 and $BaWO_4$ taken in a ratio of 1:1 form the highly stable $K_2WO_4 \cdot BaWO_4$ compound

$$K_2WO_4 + BaWO_4 = K_2WO_4 \cdot BaWO_4. \quad (11)$$

By summing the latter two equations, we obtain

$$2\,KF + BaF_2 + 2\,Na_2WO_4 = 4\,NaF + K_2WO_4 \cdot BaWO_4. \quad (12)$$

Therefore, the following two phases should correspond to the central point of the conversion line $B-D$: NaF and $K_2WO_4 \cdot BaWO_4$. These compounds are stable products of exchange and complexation reactions.

The following equation is true for any other point of the conversion line $B-D$:

$$x(KF)_2 + (1-x)\,BaF_2 + Na_2WO_4 = (NaF)_2 + x\,K_2WO_4 + (1-x)\,BaWO_4. \quad (13)$$

Let us consider two cases: $x > 0.5$ and $x < 0.5$. Let $x = 0.6$. By summing the equations, we obtain

$$0.6(KF)_2 + 0.4BaF_2 + Na_2WO_4 = (NaF)_2 + 0.6K_2WO_4 + 0.4BaWO_4$$

$$0.4K_2WO_4 + 0.4BaWO_4 = 0.4(K_2WO_4 \cdot BaWO_4)$$

$$0.6(KF)_2 + 0.4BaF_2 + Na_2WO_4 = (NaF)_2 + 0.2K_2WO_4 + 0.4(K_2WO_4 \cdot BaWO_4).$$

Therefore, three phases, *viz*., NaF, K_2WO_4 and $K_2WO_4 \cdot BaWO_4$, should be observed at points on the conversion line $B-D$ with $B > 50\%$. This is consistent with the experimental data.

Let $x = 0.4$. Then

$$0.4(KF)_2 + 0.6BaF_2 + Na_2WO_4 = (NaF)_2 + 0.4K_2WO_4 + 0.6BaWO_4$$

$$0.4K_2WO_4 + 0.4BaWO_4 = 0.4(K_2WO_4 \cdot BaWO_4)$$

$$0.4(KF)_2 + 0.6BaF_2 + Na_2WO_4 = (NaF)_2 + 0.2BaWO_4 + 0.4(K_2WO_4 \cdot BaWO_4).$$

Hence, the NaF, $BaWO_4$ and $K_2WO_4 \cdot BaWO_4$ phases should be detected at the points on the conversion line $B-D$ with $B < 50\%$.

In addition to exchange reactions, the complexation reactions giving rise to the $KF \cdot K_2WO_4$ compound correspond to the conversion points B and F (see Fig. 20).

For the point B:

$$3\,(KF)_2 + 2\,Na_2WO_4 = 2\,(NaF)_2 + 2\,(KF \cdot K_2WO_4),$$

for the point F:

$$3\,(KF)_2 + 2\,BaWO_4 = 2\,BaF_2 + 2\,(KF \cdot K_2WO_4).$$

The following reaction corresponds to the central point of the conversion line $B-F$:

$$6\,(KF)_2 + 2\,BaWO_4 + 2\,Na_2WO_4 = \\ = 2\,(NaF)_2 + 2\,BaF_2 + 4\,(KF\cdot K_2WO_4)$$

or

$$3\,(KF)_2 + BaWO_4 + Na_2WO_4 = \\ = (NaF)_2 + BaF_2 + 2\,(KF\cdot K_2WO_4).$$

For any point on the $B-F$ line, the complex formation is described by the equation

$$3\,(KF)_2 + 2(1-x)\,BaWO_4 + 2x\,Na_2WO_4 = \\ = 2x\,(NaF)_2 + 2\,(KF\cdot K_2WO_4) + 2(1-x)\,BaF_2\,.$$

The reaction affords sodium fluoride, barium fluoride and $KF\cdot K_2WO_4$ for all x varying from 0 to 1.

However, the field of the $KF\cdot K_2WO_4$ compound is not observed in the plane of the diagonal triangle $(NaF)_2-BaF_2-K_2WO_4$ (Fig. 22), which is intersected by the conversion line $B-F$. From this it follows that a stable diagonal section with the $BaF_2-(NaF)_2$ edge and the third vertex $KF\cdot K_2WO_4$ should be present in the composition prism. This triangle was examined by the visual polythermal method.[46] The liquidus surface of this triangle consists of three crystallisation fields, *viz*., $(NaF)_2$, BaF_2 and $KF\cdot K_2\,WO_4$, intersecting at the point of crystallisation of three phases (a quasiternary eutectic point).

As can be seen from the phase diagrams of the conversion lines of the Na,K,Ba//F,WO_4 system, the central part of the composition prism includes the crystallisation volumes of stable components, which are products of exchange and complexation reactions: NaF, BaF_2, $BaWO_4$, K_2WO_4, $KF\cdot K_2WO_4$ and $K_2WO_4\cdot BaWO_4$.

The starting KF and Na_2WO_4 salts are absent in the phase diagrams, because they are metastable components and are consumed in the reaction.

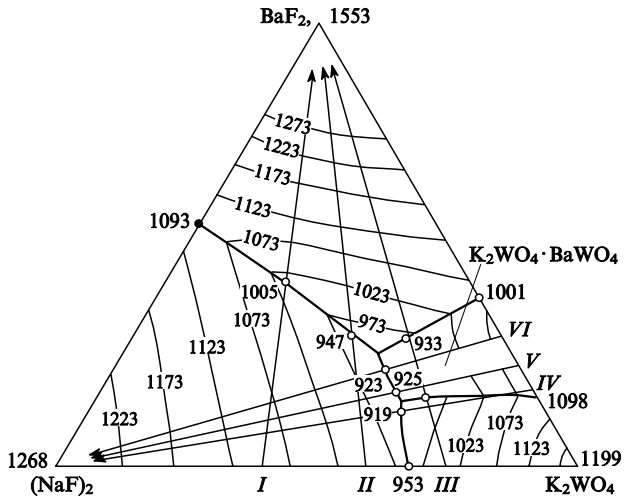

Figure 22. Phase diagram of the secant triangle $(NaF)_2-BaF_2-K_2WO_4$ of the Na,K,Ba//F,WO_4 system.

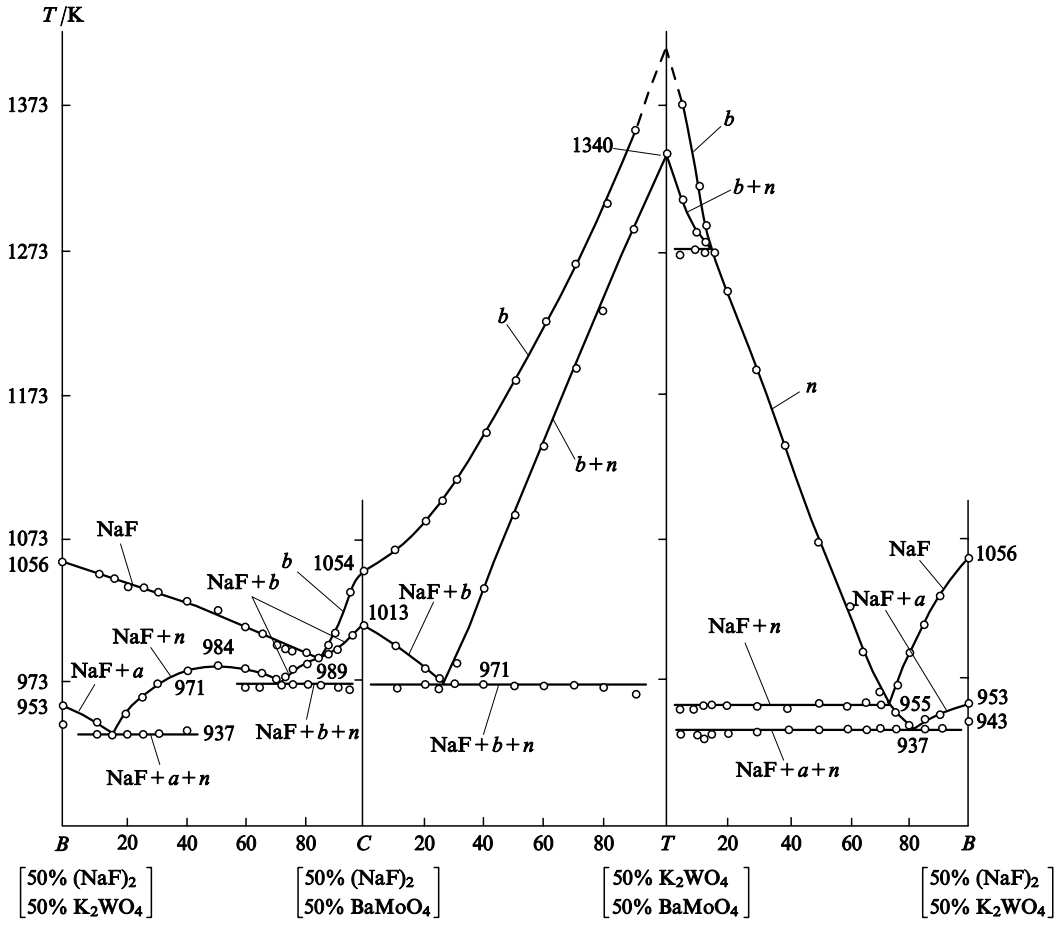

Figure 23. Temeprature–composition diagram for the quinary reciprocal system Na,K,Ba//F,MoO_4,WO_4.[11]
The composition axis represents the conversion lines $B-C$, $B-T$ and $C-T$ (see Fig. 10).

It should be noted that, in addition to two ternary invariant points, a quaternary eutectic point is present in the conversion lines.

The conversion figure of secant tetrahedra of quinary reciprocal systems consisting of nine salts represents a polythermal section and, consequently, the phase diagram of the system.

The conversion figure of the 9B ⇄ 9A-type quinary reciprocal system Na,K,Ba//F,MoO_4,WO_4 consisting of nine salts is shown in Fig. 10. The inner lines $C-T$, $B-T$ and $F-A$, $B-C$ of the conversion graph differ from other lines [46] in that the lines making up the conversion graph belong to none of the six prisms of the quaternary reciprocal systems, which bound the composition polytope of the quinary reciprocal system, and lie in the planes of the stable and non-equilibrium axial triangles.

The $B-C$, $B-T$ and $C-T$ lines intersect the stable axial triangle of the quinary reciprocal system Na,K,Ba//F,MoO_4,WO_4, and the $F-A$ line intersects the non-equilibrium triangle of this system.[46] Consequently, the crystallising phases involving all six ions correspond to these four lines. Hence, the lines were assigned to the quinary reciprocal system.

The $B-C$ line in Fig. 23 intersects the crystallisation volumes of NaF and the phase b (the $BaMoO_4-BaWO_4$ solid solution), as evidenced by two branches of primary crystallisation intersecting at the point with coordinates 989 K and 15.5% of B [the composition: 50% $(NaF)_2$, 43% $BaMoO_4$ and 7% K_2WO_4]. The curve of secondary crystallisation consists of the following three branches: NaF + a, NaF + b and NaF + n (a, the $K_2MoO_4-K_2WO_4$ solid solutions; b, the $BaMoO_4-BaWO_4$ solid solutions; n, the $K_2MoO_4\cdot BaMoO_4-K_2WO_4\cdot BaWO_4$ solid solutions). These branches intersect at the eutectic points of three phases: at 937 K and 28.5% B [33% $(NaF)_2$, 10% $BaMoO_4$ and 57% K_2WO_4], the solid phases NaF, a and n; at 971 K and 85% B [44% $(NaF)_2$, 39.5% $BaMoO_4$ and 16.5% K_2WO_4], the solid phases NaF, b and n.

The curve of secondary crystallisation has a maximum at 984 K and 50% B [44% $(NaF)_2$, 28% $BaMoO_4$ and 28% K_2WO_4], the solid phases NaF and n.[46] In Fig. 23, the conversion line $C-T$ intersects the crystallisation volume of the phase b, as evidenced by the curve of primary crystallisation (without extremes). Secondary crystallisation is represented by two branches, *viz.*, NaF – phase b and $n + b$, intersecting at the eutectic point of crystallisation of three phases, *viz.*, NaF, b and n (at 971 K and 27% T). The conversion line $B-T$ intersects the crystallisation volumes of NaF and the phases b and n. The branches of primary crystallisation intersect at two points with coordinates 1271 K and 15% B [7.5% $(NaF)_2$, 42.5% $BaMoO_4$ and 50% K_2WO_4], the solid phases b and n; and 955 K and 63% B [37% of $(NaF)_2$, 13% $BaMoO_4$ and 50% K_2WO_4], the solid phases NaF and n.

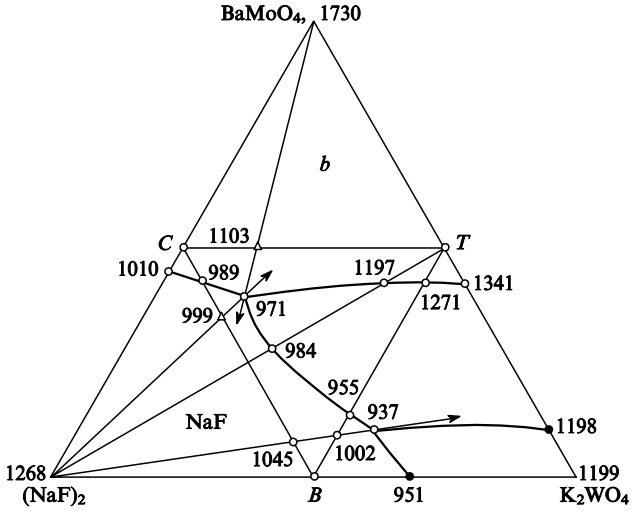

Figure 24. Phase diagram of the stable axial triangle $(NaF)_2-BaMoO_4-K_2WO_4$ of the Na,K,Ba//F,MoO_4,WO_4 system. Temperatures are given in Kelvin (K).

The phase diagram of the overall stable axial triangle can be constructed based on the data corresponding to the conversion lines $B-T$, $C-T$ and $B-C$ (Fig. 24).[11]

5. Stable tetrahedra of quinary reciprocal systems consisting of nine salts

The salt compositions of all tetrahedra of a singular star can be determined from a conversion figure of secant tetrahedra for quinary reciprocal systems of nine salts belonging to any topological type. Each point of the conversion figure of this system corresponds to an exchange reaction between stable and metastable salt pairs located at the vertices of the conversion graph.

The chemical interaction in the system under consideration can be described by reaction equations for the points lying in the planes of the conversion figure. Based on these equations, the crystallising phases in stable secant tetrahedra can be predicted.

The $A-B-C-D$ square of the conversion figure for the Na,K,Ba//F,MoO_4,WO_4 system is shown in Fig. 25. The equation for the central point of this square has the form

$$2(KF)_2 + 2Na_2MoO_4 + 2Na_2WO_4 + 2BaF_2 = 4(NaF)_2 + K_2MoO_4 + K_2WO_4 + BaMoO_4 + BaWO_4. \quad (14)$$

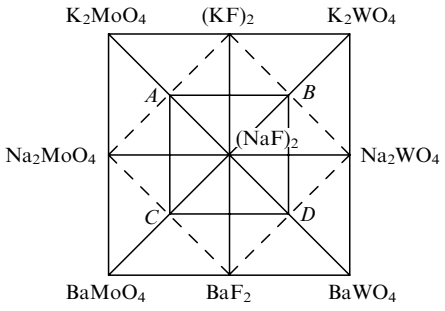

Figure 25. Conversion square $A-B-D-C$ (a fragment of the conversion figure) for the quinary reciprocal system Na,K,Ba//F,MoO_4,WO_4.

The right-hand side of this equation includes a metastable pair of salts, which react according to the equation

$$BaWO_4 + K_2MoO_4 = BaMoO_4 + K_2WO_4. \quad (15)$$

By summing Eqns (14) and (15), we obtain

$$2(KF)_2 + 2Na_2MoO_4 + 2Na_2WO_4 + 2BaF_2 = 4(NaF)_2 + 2BaMoO_4 + 2K_2WO_4. \quad (16)$$

Analysis of the data on the boundary elements demonstrated that crystallisation of $BaMoO_4$ and K_2WO_4 (taken in equivalent amounts) affords the phase n, *viz.*, the solid solutions of the $K_2MoO_4\cdot BaMoO_4-K_2WO_4\cdot BaWO_4$ compounds. Consequently, the latter reaction produces the phases NaF and n.

The central point of the conversion square $A-B-D-C$ coincides with the central point of the conversion line $B-C$ (see the diagrams of the conversion lines $B-T$, $C-T$ and $C-B$, Fig. 23). For this point, crystallisation of the phases NaF and n (the $K_2MoO_4-BaMoO_4$ and $K_2WO_4-BaWO_4$ solid solutions) was established experimentally. This fact is in complete agreement with the prediction of phases formed according to the above-given equation taking into account the data on the boundary elements.

The conversion square $A-B-D-C$ is divided by the $B-C$ line (the diagonal of the conversion square) into two triangles, $A-B-C$ and $B-D-C$. Each triangle is characterised by its own equation of the exchange reaction (Fig. 26).

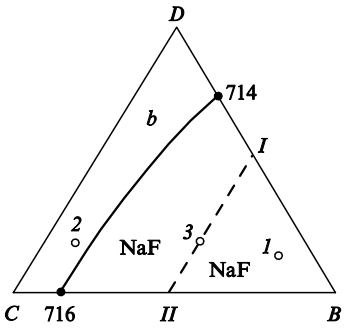

Figure 26. Phase diagram of a system represented by the conversion triangle $B-C-D$.

The composition of each point of the $B-C-D$ triangle can be expressed by the ratio between the B, C and D components, which reflect the transformation of a metastable salt pair into a stable pair. On the whole, the equation of exchange reactions for each point of the $B-C-D$ triangle can be written as follows:

$$x(Na_2MoO_4 + BaF_2) + y[(KF)_2 + Na_2WO_4] +$$
$$+ (1-x-y)(BaF_2 + Na_2WO_4) = x[BaMoO_4 + (NaF)_2] +$$
$$+ y[(NaF)_2 + K_2WO_4] + (1-x-y)[(NaF)_2 + BaWO_4].$$

After simple algebraic transformations, we obtain

$$x\,Na_2MoO_4 + (1-y)\,BaF_2 + y\,(KF)_2 + (1-x)Na_2WO_4 = \quad (17)$$
$$= (NaF)_2 + x\,BaMoO_4 + y\,K_2WO_4 + (1-x-y)\,BaWO_4.$$

Therefore, the exchange reactions afford stable salts located at the vertices of the secant tetrahedron, which is intersected by the conversion triangle $B-C-D$ (see Fig. 26). Let us analyse the possible reaction products for points on this triangle. Experimental studies demonstrated that the crystallisation surface of this triangle is represented by the fields of sodium fluoride and the phase b.

The triangle can be divided by the $I-II$ line, which connects the saddle points of the conversion lines $B-C$ and $B-D$, into two regions, $B-II-I$ and $I-II-C-D$. Particular stable phases correspond to both regions of the conversion triangle and the $I-II$ line. These phases are formed in the course of crystallisation of the products of the exchange reaction described by Eqn (17).

For each point of the $B-II-I$ region ($y > 0.5$, $x < 0.5$), the composition can be expressed as follows: y is the amount of the component B, x is the amount of the component C, the amount of the component D is $1-x-y$. Let us consider the arbitrarily chosen point 1, for which $x = 0.1$ and y = 0.7. The equation for this point has the form

$$0.1\,Na_2MoO_4 + 0.3\,BaF_2 + 0.7\,(KF)_2 + 0.9\,Na_2WO_4 = \quad (18)$$
$$= (NaF)_2 + 0.1\,BaMoO_4 + 0.2\,BaWO_4 + 0.7\,K_2WO_4.$$

If the $BaMoO_4 + BaWO_4$ and K_2WO_4 products are present in a ratio corresponding to the right-hand side of this equation, complete crystallisation affords the phases n (the $K_2MoO_4-BaMoO_4$ and $K_2WO_4-BaWO_4$ solid solutions) and a (the $K_2MoO_4-K_2WO_4$ solid solutions), as is obvious from the data on the boundary elements. Therefore, the following final reaction products correspond to the points in the $B-II-I$ region: NaF, the $K_2MoO_4-BaMoO_4$ and $K_2WO_4-BaWO_4$ solid solutions and the $K_2MoO_4-K_2WO_4$ solid solutions. For the point *2* in the $I-II-C-D$ region ($y < 0.5$) at $x = 0.7$ and $y = 0.1$, the equation has the form

$$0.7\,Na_2MoO_4 + 0.9\,BaF_2 + 0.1\,(KF)_2 + 0.3\,Na_2WO_4 = \quad (19)$$
$$= (NaF)_2 + 0.7\,BaMoO_4 + 0.2\,BaWO_4 + 0.1\,K_2WO_4.$$

At the above-mentioned ratio between the $BaMoO_4 + BaWO_4$ and K_2WO_4 products, crystallisation affords the phases NaF, b and n, as indicated by the data on the boundary elements. For the point *3* on the $I-II$ line ($y = 0.5$, $x = 0.5$) at $y = 0.5$, $x = 0.3$, the equation has the form

$$0.3\,Na_2MoO_4 + 0.5\,BaF_2 + 0.5\,(KF)_2 + 0.7\,Na_2WO_4 = \quad (20)$$
$$= (NaF)_2 + 0.3\,BaMoO_4 + BaWO_4 + 0.5\,K_2WO_4.$$

If $BaMoO_4 + BaWO_4$ and K_2WO_4 are present in equivalent amounts, crystallisation yields only the phase n. Consequently, the reaction affords NaF and n for all points on the $I-II$ line.

On the whole, the conversion triangle $B-C-D$ corresponds to products of the chemical reaction, *viz*., the phases NaF, b and n. This fact was confirmed experimentally.[46] Hence, the secant tetrahedron $(NaF)_2-BaMoO_4-BaWO_4-K_2WO_4$ corresponds to the crystallisation volumes of NaF, a, b and n (Fig. 27) intersecting along univariant curves. Quaternary invariant points are lacking.

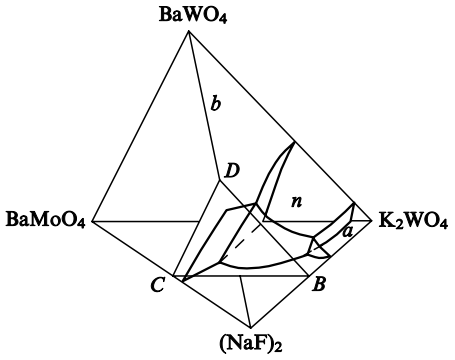

Figure 27. Crystallisation volumes of the $(NaF)_2-BaWO_4-K_2WO_4-BaMoO_4$ tetrahedron of the Na,K,Ba//F,MoO_4,WO_4 system.

The above-considered procedure can be used for determining the salt compositions and crystallisation volumes of all six secant tetrahedra of any quinary reciprocal system.[16,46]

V. Practical applications of multicomponent salt melts

The use of melts in various technological processes has attracted increasing attention in recent years. Considerable interest in molten salt systems as reaction media is associated with their specific properties, among which are their ability to dissolve many organic and inorganic compounds. Besides, these systems can intensify processes due to high heat- and mass-transfer coefficients, thermal conductivity and heat transfer; reacting compounds in these systems can occur in oxidation states, which are inaccessible in typical solutions; the density and viscosity of such reaction media are relatively low; the reaction products can easily be separated from the reaction mixtures; water as a solvent can completely be excluded from the technological scheme. (The growing problem of water deficiency needs urgent attention; hence, the above-mentioned possibilities are not only of scientific interest but are also sometimes technologically and economically advantageous.)

Electrochemistry, metallurgy and electrometallurgy are traditional areas of application of molten salt media. They also have promising applications in fuel cells and high-temperature information transformers, in single-crystal growth of optical materials and ferroelectric materials, in nuclear technology, as nuclear fuel, and as claddings for thermonuclear reactors. Inorganic synthesis in molten salts is yet another promising area of application of salt melts.[12] In many cases, reactions in molten salts proceed faster

and afford the target products in higher yields because of the highest possible concentrations of the reagents, one of which is the melt.[12]

The diversity of inorganic salts, all the more their mixtures, makes it possible to prepare a wide range of molten salt systems and, consequently, to carry out various syntheses in these media.[4,16–18,47] Actually, all main types of chemical reactions, *viz*., exchange, acid–base, redox and complexation reactions, have been performed in these media.

Systems containing eutectic composites, which are characterised by the constant melting points and compositions, are of great scientific interest. The melting points of the starting components of such systems decrease substantially already in binary systems.[48] In ternary systems, the melting points continue to decrease, the rate of decrease in the melting point being lower in quaternary systems. Nevertheless, even a slight decrease in the temperature of a eutectic composite (by 15–20 °C) may be of considerable practical importance for technological purposes.

Among salt melts, multicomponent reciprocal systems are of special interest. Reciprocal systems consisting of 4, 5, 6 or 7 components are the most difficult to study by methods of physicochemical analysis. These systems can be used for preparing materials possessing the desired combinations of properties, which is an important problem of applied chemistry. Hence, the rational choice of salt compositions is of considerable importance in improving conditions for the preparation of substances possessing the required characteristics.

1. Thermal chemical power sources

Ionic melts have found wide application in high-temperature power sources.[12]

Aqueous electrolytes are unsuitable for the construction of thermal chemical power sources, because certain electrode materials (alkali and alkaline-earth metals, halides) react with water. Salt melts serve as convenient electrolytes in high-temperature power sources.[13]

A molten electrolyte satisfying these requirements was designed on the basis of the quaternary reciprocal system Li,K,Ni//Cl,SO_4. The challenge was to find a low-melting electrolyte consisting of stable phases and exhibiting the required properties to use in chemical power sources.[13–15]

A procedure for revealing stable salt mixtures, which are modelled by tetrahedral simplexes in the composition diagram of a multicomponent system, and a procedure for the estimation of stability of such mixtures were described.[49]

A salt mixture is assumed to be stable, if the phase diagram obtained after heating the mixture above the melting point followed by crystallisation, includes crystallisation fields of salts produced by exchange reactions and crystallisation fields of double compounds formed by these salts, which are stable in the temperature range under consideration. A mixture is assumed to be metastable if the phase diagram has fields of the starting reactive salts involved in exchange reactions with each other and crystallisation fields of metastable double compounds, which decompose in the temperature range under consideration to yield reactive salts.

The procedure involves the following steps.

1. A composition figure of a multicomponent system is partitioned using one of the simplest procedures[11] with the aim of revealing tetrahedral simplexes, *i.e*., determining their salt compositions.

2. The possibilities of exchange reactions and complex formation for salts of each salt mixture are examined and estimated from the thermodynamical standpoint. It is most reasonable to study the regions of the conversion figure involved in this simplex.

3. If experimental data on the boundary subsystems are available, stability of the subsystems is estimated. Mixtures of three salts, which are modelled by triangles of ternary reciprocal systems, triangulating sections of quaternary reciprocal systems, *etc*., can serve as boundary subsystems of tetrahedra in reciprocal multicomponent systems consisting of six salts.

4. The stability of a salt mixture as a whole, which is modelled by a tetrahedron, is estimated from the data obtained in stages 2 and 3. If the mixture is estimated as metastable, further triangulation of the composition diagram is carried out and all of the procedure is repeated.

Let us apply this procedure to the quaternary reciprocal system Li,K,Ni//Cl,SO_4,[13] whose composition prism is divided into three tetrahedral simplexes by two triangular sections. The geometric partitioning is based on exchange reactions between the starting salts. The salt compositions of the tetrahedra can be determined from the matrix of reciprocal salt pairs with an inscribed conversion figure.[8] The composition prism of the quaternary reciprocal system Li,K,Ni//Cl,SO_4 along with the conversion figure $B-A-C$, the matrix of reciprocal salt pairs and the matrix of vertex indices is presented in Fig. 28. The stable tetrahedra of the singular star of the Li,K,Ni//Cl,SO_4 system are extracted from the matrix of reciprocal salt pairs:

$(LiCl)_2-(KCl)_2-NiCl_2-Li_2SO_4$,

$(KCl)_2-K_2SO_4-NiSO_4-Li_2SO_4$,

$NiCl_2-(KCl)_2-NiSO_4-Li_2SO_4$.

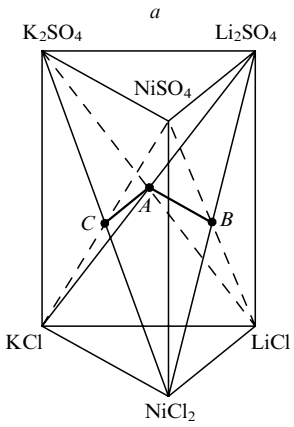

b

6	LiCl	KCl	$NiCl_2$
Li_2SO_4	0	1 *B*	1 *A*
K_2SO_4	0	0	0
$NiSO_4$	0	1 *C*	0

c

6	Cl	SO_4	∑
Li	0	2	2
K	2	0	2
Ni	1 [a]	1 [b]	2
∑	3	3	6

Figure 28. Models of the quaternary reciprocal system Li,Ni,K//Cl,SO_4. (*a*) The composition prism, (*b*) the matrix of reciprocal salt pairs with an inscribed conversion graph, (*c*) the matrix of vertex indices.

To predict stable phases crystallising from melts, the $(LiCl)_2-(KCl)_2-NiCl_2-Li_2SO_4$ tetrahedron with the conversion line $A-B$ was chosen (Fig. 29).[14]

The choice of the $(LiCl)_2-(KCl)_2-NiCl_2-Li_2SO_4$ tetrahedron was governed by the requirements imposed on chemical power sources. The stability of each boundary subsystem and the tetrahedron as a whole can be estimated from the morphological characteristics of the liquidus surface and the thermochemical relations in the quaternary reciprocal system Li,K,Ni//Cl,SO_4.

The $(KCl)_2-NiCl_2-Li_2SO_4$ face (Fig. 29). The conversion line $A-B$ intersecting the face reflects the exchange reactions in the Li,K,Ni//Cl,SO_4 system formed at the intersection of the stable triangle $(KCl)_2-NiCl_2-Li_2SO_4$ of a singular star with the corresponding metastable triangle $(LiCl)_2-NiSO_4-K_2SO_4$ of a non-equilibrium star.[14]

By summing the exchange reactions for the points of complete conversion A and B of the ternary reciprocal systems Li,K//Cl,SO_4 and Li,Ni//Cl,SO_4, we obtain

for the point A: $(LiCl)_2 + NiSO_4 = NiCl_2 + Li_2SO_4$

for the point B: $(LiCl)_2 + K_2SO_4 = (KCl)_2 + Li_2SO_4$

$$2\,(LiCl)_2 + NiSO_4 + K_2SO_4 = NiCl_2 + 2\,Li_2SO_4 + (KCl)_2\,. \quad (21)$$

This is the equation for the central point of the conversion line $A-B$. As can be seen from Eqn (21), the exchange equilibrium is shifted toward stable phases of the components of the face under consideration.

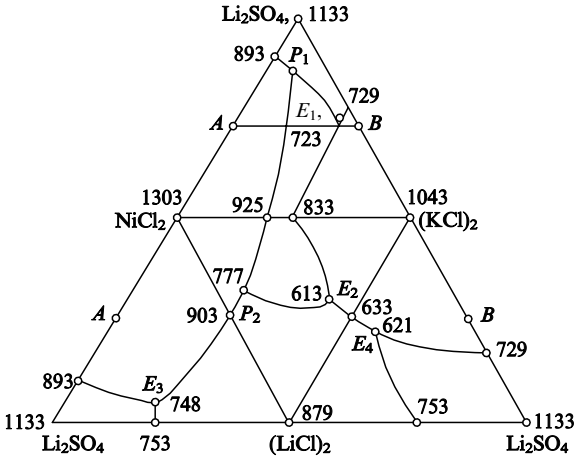

Figure 29. Development of the stable $(LiCl)_2-NiCl_2-Li_2SO_4-(KCl)_2$ tetrahedron of the quaternary reciprocal system Li,Ni,K//Cl,SO_4. The temperatures are given in Kelvin (K).

In addition to the exchange reaction, complex formation occurs in the Li,Ni//Cl,SO_4 system

$$(KCl)_2 + NiCl_2 = 2\,[KCl\cdot NiCl_2]. \quad (22)$$

By summing Eqns (21) and (22), we obtain

$$2\,(LiCl)_2 + NiSO_4 + K_2SO_4 + NiCl_2 = 2\,Li_2SO_4 + 2\,[KCl\cdot NiCl_2]. \quad (23)$$

The face of the $(KCl)_2-NiCl_2-Li_2SO_4$ tetrahedron is estimated as stable. Actually, the experiment gave the eutectic E_1 at 723 K and 51 mass% Li_2SO_4, 42 mass% KCl, 7 mass% $NiCl_2$ (see Fig. 29). The transition point P_1 has the following composition: 74 mass% Li_2SO_4, 13 mass% KCl and 13 mass% $NiCl_2$; the temperature is 833 K. The crystallisation surface of the $(KCl)_2-NiCl_2-Li_2SO_4$ system (the face of the tetrahedron) consists of the following four crystallisation fields: KCl, $NiCl_2$, Li_2SO_4 and $KCl\cdot NiCl_2$.[14]

The $(LiCl)_2-NiCl_2-Li_2SO_4$ face. As can be seen from Fig. 29, the point of complete conversion, which corresponds to the exchange reaction proceeding in the ternary reciprocal system Li,Ni//Cl,SO_4 [Eqns (21) and (23)], is located on the edge of the face. According to Eqn (21), $NiCl_2$ and Li_2SO_4 are stable phases. From the table of vertex indices, it follows that these salts are characterised by the highest indices. This prediction was confirmed experimentally. The crystallisation fields of the melting diagram converge at the eutectic point E_3 with coordinates 748 K, 45 mass% LiCl, 49.6 mass% Li_2SO_4 and 5.4 mass% $NiCl_2$. The LiCl, $NiCl_2$ and Li_2SO_4 compounds are solid phases.

The $(LiCl)_2-(KCl)_2-Li_2SO_4$ face. The exchange reaction giving rise to a stable pair of Li_2SO_4 and KCl salts [Eqn (21)], which are not involved in complex formation with the reactive K_2SO_4 and LiCl salts, occurs at the point of complete conversion B of the ternary reciprocal system Li,K//Cl,SO_4. The crystallisation surface of this system consists of crystallisation fields of the components; the eutectics occur at 621 K, 42 mass% LiCl, 50.5 mass% KCl and 7.5 mass% Li_2SO_4; LiCl, Li_2SO_4 and KCl are solid phases. Apparently, this section is stable (see Fig. 29).

The $(KCl)_2-NiCl_2-(LiCl)_2$ face. The melting diagram of the system was studied only partially because of decomposition of the mixtures containing large amounts of nickel chloride. The crystallisation surface of the $(KCl)_2-NiCl_2-(LiCl)_2$ system consists of four fields[14] belonging to the components and the incongruently melting $KCl\cdot NiCl_2$ compound (see Fig. 29).

Below are given the compositions, the equilibrium phases and the temperatures of invariant points of the $(KCl)_2-NiCl_2-(LiCl)_2$ system. This system is also stable.

Point	T/°C	Composition (mass%)			Equilibrium phases
		$NiCl_2$	LiCl	KCl	
E_2	340	3.5	42	54	LiCl, KCl, $KCl\cdot NiCl_2$
P_2	504	40	37.5	21.5	LiCl, $NiCl_2$, $KCl\cdot NiCl_2$

The $Li_2SO_4-(LiCl)_2-NiCl_2-(KCl)_2$ tetrahedron. Since the theoretical prediction of phases based on the boundary elements shows that all boundary systems of the tetrahedron are stable, the system, whose composition is represented by the $Li_2SO_4-(LiCl)_2-NiCl_2-(KCl)_2$ tetrahedron, should be stable. This assumption was confirmed experimentally.[15] The temperature and composition of the quaternary eutectic are 633 K, 39 mass% LiCl, 49.8 mass% KCl, 8 mass% Li_2SO_4, 3.2 mass% $NiCl_2$; the Li_2SO_4, LiCl, $NiCl_2$ and KCl solid phases.

2. High-temperature electrolytic aluminising of niobium

The quaternary reciprocal system Al,Ba,Na//F,Cl, *viz*., $BaCl_2$ (0.73%) – NaF (0.12%) – AlF_3 (0.15%), is used as a molten electrolyte for high-temperature electrolytic aluminising of niobium. The reaction of molten salts cannot be judged from the results of chemical analysis of a sample of the melt cooled and dissolved in water or acid. Chemical analysis provides only information on the concentrations of the ions dissolved in solution. Information on the true chemical reactions of molten salts in systems can be extracted from a phase complex, which is displayed in the melting diagram as crystallisation fields or volumes, lines of co-crystallisation and multiple points. This allows one to draw reliable conclusions about the reactions proceeding in systems at high temperatures. The quaternary reciprocal system Al,Ba,Na//F,Cl can be represented as a matrix of reciprocal salt pairs (Fig. 30 *a*), in which the conversion figure of secant triangles is inscribed. Using the conversion figure, the following secant triangles are extracted from the matrix: AlF_3-BaCl_2-NaCl and AlF_3-BaCl_2-NaF (elements of a singular star).

Data on the boundary elements are required to predict the crystallisation fields of these triangular sections. It is known that the NaF – AlF_3 subsystem contains two compounds, *viz*., Na_3AlF_6 and $5\,NaF\cdot 3\,AlF_3$, the $BaCl_2$ – NaF subsystem contains

a

6*b*	$AlCl_3$	$BaCl_2$	NaCl
AlF_3	0	1 *A*	1 *B*
BaF_2	0	0	0
NaF	0	1 *C*	0

b

	Cl^-	F^-	$\sum$
Al^{3+}	0	2	2
Ba^{2+}	2	0	2
Na^+	1 [a]	1 [b]	2
$\sum$	3	3	6

Figure 30. Models of the quaternary reciprocal system Al,Na,Ba//Cl,F. (*a*) The matrix of reciprocal salt pairs with an inscribed conversion graph, (*b*) the matrix of vertex indices.

the $BaCl_2 \cdot BaF_2$ compound, and the $AlF_3 - BaCl_2$ subsystem is characterised by a eutectic point (all data refer to the $AlF_3 - BaCl_2 - NaF$ system).

The required electrolyte can be chosen with the use of the phase diagrams of the triangular section of the Al,Ba,Na//F,Cl system. It was experimentally demonstrated that the liquidus surface of this stable triangular section consists of seven crystallisation fields: $BaCl_2$, NaF, AlF_3, BaF_2, Na_3AlF_6, $5\,NaF \cdot 3\,AlF_3$ and $BaCl_2 \cdot BaF_2$. Hence, the experimental results confirmed the predicted existence of three compounds in the $AlF_3 - BaCl_2 - NaF$ triangle of the singular star.

At the point of complete conversion *A*, the salt pairs undergo interchange according to the reaction

$$3\,BaF_2 + AlCl_3 = 2\,AlF_3 + 3\,BaCl_2.$$

The Na_3AlF_6 compound is formed at the point of complete conversion by the secondary reaction

$$2\,AlCl_3 + 12\,NaF = 2\,Na_3AlF_6 + 6\,NaCl.$$

At the point of complete conversion *C*, an exchange reaction and complex formation take place

$$BaF_2 + 2\,NaCl = 2\,NaF + BaCl_2,$$

$$4\,BaF_2 + 4\,NaCl = 2\,(BaF_2 \cdot BaCl_2) + 4\,NaF.$$

The conditions of the process are as follows: at a carbon anode, electrolysis is carried out at 900 °C; the thickness of an aluminium coating is 40 – 50 μm, the coating consists of Al, $NbAl_3$ and Nb_2Al.[12]

As can be seen from the matrix table of vertex indices (see Fig. 30 *b*), the $AlCl_3$ salt is most reactive and is completely consumed in the exchange reaction and the reaction giving rise to the compound, *i.e.*, this salt is absent in the melt (the index is 0). The system contains AlF_3 formed by the exchange reaction (the index of AlF_3 is 2). Barium chloride is consumed in the synthesis of the $BaF_2 \cdot BaCl_2$ compound and the exchange reaction yielding $BaCl_2$. The BaF_2 salt is most reactive (its index is 0). The $BaCl_2$ salt is stable and has the highest index (2). The latter salt is an exchange reaction product. The NaCl and NaF salts have the index 1. They are intermediate between the most reactive and stable salts.

From the above, it can be concluded that the composition of the electrolyte for high-temperature aluminising was chosen correctly.

3. Silver plating

Nitrate and halide – nitrate molten systems are used for electrolytic silver plating.[12] For example, the molten $AgI - NaNO_3 - KNO_3$ system is used for electrolytic silver plating. This system corresponds to a diagonal section of the composition prism of the quaternary reciprocal system Ag,K,Na//I,NO_3 consisting of six salts. The process occurs at 300 °C and at a current density of 50 A m^{-2}.

Electrolytic silver plating can be carried out with the use of a molten electrolyte developed on the basis of the quinary reciprocal system Ag,K,Na//Cl,Br,NO_3 consisting of nine salts, which belongs to the A ⇄ B thermochemical type.[21]

Let us construct the matrix table of vertex indices using the thermochemical relations for the salt pairs of the system. The stable axial triangle of a singular star with the highest indices in each row of the matrix can be determined from this matrix table.

9A	Br^-	Cl^-	NO_3^-	$\sum$
Ag^+	4	2	0	6
K^+	2	1	3	6
Na^+	0	3 [a]	3 [b]	6
$\sum$	6	6	6	18

This is the $AgBr - KNO_3 - NaCl$ triangle. The most stable salts formed by exchange (conversion) reactions are AgBr (the index is 4), KNO_3 (the index is 3) and NaCl (the index is 3 [a]). The $AgNO_3$ (the index is 0), NaBr (the index is 0) and KCl (the index is 1) salts are most reactive and are consumed in the interchange reaction

$$2\,AgNO_3 + 2\,KCl + 2\,NaBr = \\ = AgCl + KNO_3 + AgBr + NaNO_3 + KBr + NaCl.$$

The metastable salt pairs react further

$$AgCl + KBr = AgBr + KCl,$$

$$KCl + NaNO_3 = KNO_3 + NaCl.$$

Hence,

$$AgNO_3 + KCl + NaBr = AgBr + KNO_3 + NaCl.$$

As a result, stable salts forming a eutectic mixture should appear in the melt for electrolysis. It was experimentally demonstrated that a low-melting eutectic is formed in the $AgBr - KNO_3 - NaCl$ system at 513 K and 21.5% AgBr, 12% NaCl, 66.5% KNO_3.

A procedure for studying multicomponent reciprocal systems, which involves the experimental investigation of conversion elements, including elements of incomplete conversion, was also successfully used for solving some other problems, in particular, for preparing bronzes, rare-metal compounds, phase-transition materials, *etc.*[4, 50 – 53]

VI. Conclusion

Nowadays, the methodology of investigation of multicomponent systems involves the theoretical study of models of multicomponent systems followed by experimental examination of particular regions of phase diagrams and their construction as the necessary stages. This methodology can also serve as the basis for the development of important technological processes (construction of heat accumulators, heat carriers, galvanised coatings, *etc.*).

Modelling of multicomponent reciprocal salt systems provides a rational approach to solving numerous theoretical and practical problems. A conversion figure of secant elements plays a unique role, because it is common to non-equilibrium and equilibrium complexes and ensures spatial and physicochemical relationships between these complexes.

Conversion figures can be used in the analysis of the mechanisms of transformation from a non-equilibrium state of the system to equilibrium. These figures allow one to follow the sequence of transformations of the starting compounds into the final reaction products. In models, this is manifested as a spatial transformation from a non-equilibrium star through intermediate stars (containing partially non-equilibrium and partially equilibrium elements) to a singular (equilibrium) star. Conversion elements can be used for studying the structures of phase diagrams in more detail (determination of remarkable points and analysis of their metrics in various systems of coordinates, the polarity and symmetry in various multidimensional spaces).

The proximate analysis developed on the basis of the conversion method enables one to solve practical problems, such as the construction of a phase complex of a system with a minimum of experimental studies (investigation of a small number of compositions) as well as the construction of reciprocal systems with the desired direction of exchange reactions.

The practical value of the conversion method became evident after the development of media for electrolytic coatings and the preparation of low-melting composites, *viz.*, heat carriers and heat-accumulation composites, which are used to prolong the life of batteries with high energy characteristics. In particular, the composites, whose enthalpies of melting are almost twice as high as those of foreign standards, were constructed.

There are several directions of development of the conversion method for investigating reciprocal salt systems: construction and improvement of models; development of new methodological concepts; exploration of new areas of practical application of this methodology; integration of conversion models into scientific foundations of chemical disciplines.

The following theoretical problems are yet to be solved.

1. The thermodynamical description of conversion models taking into account the available data on the algebraic models of processes occurring in salt melts.[54, 55]

2. More detailed investigation of the energetics of exchange reactions using alternative models of multicomponent reciprocal salt systems, *viz*., energy diagrams and non-equilibrium, intermediate and singular stars.

3. Thermodynamical calculations of conversion processes at different temperatures.

4. The construction of models for the description of the behaviour of ionic liquids at different temperatures and the energy transfer performed by these liquids.

5. Study of the topology of the distribution of conversion elements over subspaces of the multidimensional space of the phase diagram of a multicomponent reciprocal system.

6. The development of models of conversion processes, involving complexation reactions.

The prospects of the development of the conversion method are tightly related to the worldwide scientific trends associated with investigations and applications of salt melts, which are reflected in papers presented at scientific conferences and symposia on molten salts.[56–62] Among these problems are investigations of the dynamic, structural, electrochemical and other properties of melts, thermodynamical modelling and calculations of phase diagrams, construction of models of ionic liquids and the energetics of melts, *etc*. The conversion method can be used for solving many of these problems.

References

1. N S Kurnakov *Izbrannye Trudy* (Selected Works) (Moscow: Academy of Sciences of the USSR, 1960) Vol. 1
2. V P Radishchev *Mnogokomponentnye Sistemy* (Multicomponent Systems) (Moscow: Institute of Organic and Inorganic Chemistry, Academy of Sciences of the USSR, 1964)
3. V I Posypaiko *Metody Issledovaniya Mnogokomponentnykh Solevykh Sistem* (The Methods of Investigation of Multicomponent Salt Systems) (Moscow: Nauka, 1978)
4. A S Trunin *Kompleksnaya Metodologiya Issledovaniya Mnogokomponentnykh Sistem* (Complex Methodology of Investigation of Multicomponent Systems) (Samara: Samara State Technology University, 1997)
5. E A Alekseeva, N S Dombrovskaya *Zh. Neorg. Khim.* **8** 407 (1963) [a]
6. V I Posypaiko, N A Vasina, E S Gryzlova *Dokl. Akad. Nauk SSSR* **223** 1191 (1975) [b]
7. V I Posypaiko, N A Vasina, E S Gryzlova, A S Trunin G E Shter *Dokl. Akad. Nauk SSSR* **241** 650 (1978) [b]
8. N A Vasina, E S Gryzlova, S G Shaposhnikova *Teplofizicheskie Svoistva Mnogokomponentnykh Solevykh Sistem* (Thermophysical Properties of Multicomponent Salt Systems) (Moscow: Khimiya, 1984)
9. E S Gryzlova, V V Chernyshev, I N Lepeshkov, I F Gladysheva *Zh. Neorg. Khim.* **34** 490 (1989) [a]
10. E S Gryzlova, V M Padalko, V V Chernyshev, I N Lepeshkov, I F Gladysheva *Zh. Neorg. Khim.* **34** 1817 (1989) [a]
11. V I Posypaiko, S A Tarasevich, E A Alekseeva *Prognozirovanie Khimicheskogo Vzaimodeistviya v Sistemakh iz Mnogikh Komponentov* (Prediction of Chemical Interaction in Systems with Many Components) (Moscow: Nauka, 1984)
12. Yu K Delimarskii *Ionnye Rasplavy i ikh Primenenie v Nauke i Tekhnike* (Ionic Melts and Their Applications in Science and Engineering) (Kiev: Naukova Dumka, 1984)
13. A A Safonov, F F Trush, M Yu Nakhshin, E S Gryzlova *Zh. Neorg. Khim.* **28** 1829 (1983) [a]
14. A A Safonov, F F Trush, M Yu Nakhshin, E S Gryzlova *Zh. Neorg. Khim.* **28** 538 (1983) [a]
15. A A Safonov, F F Trush, M Yu Nakhshin, E S Gryzlova *Zh. Neorg. Khim.* **28** 1344 (1983) [a]
16. A S Trunin, M A Loseva, A S Kosmynin *Vysokotemperaturnye Energoemkie Fazoperekhodnye Materialy na Osnove Solevykh Sistem* (High-Temperature Power-Energetic Phase-Transition Materials Based on Salt Systems) (Samara State Technology University, Samara, 1995); article deposited in VINITI, No. 2478-V95 (Moscow, 1995)
17. A M Gasanaliev, Doctoral Thesis in Chemical Sciences, Institute of Chemistry, Academy of Sciences of the Uz. SSR, Tashkent, 1990
18. O V Temirbulatova, Candidate Thesis in Chemical Sciences, Samara State Technology University, Samara, 1992
19. N A Kozyreva, E S Gryzlova, B F Myasoedov *Dokl. Akad. Nauk* **334** 64 (1994) [b]
20. E S Gryzlova, N A Kozyreva, B F Myasoedov *Dokl. Akad. Nauk* **334** 589 (1994) [b]
21. N A Kozyreva, E S Gryzlova, V T Orlova *Zh. Neorg. Khim.* **39** 1016 (1994) [a]
22. N A Kozyreva, E S Gryzlova, V T Orlova *Zh. Neorg. Khim.* **39** 1726 (1994) [a]
23. E S Gryzlova, N A Kozyreva, V T Orlova. *Dokl. Akad. Nauk* **345** 633 (1995) [b]
24. N A Kozyreva, E S Gryzlova *Zh. Neorg. Khim.* **41** 474 (1996) [a]
25. E S Gryzlova, N A Kozyreva, B F Myasoedov *Mendeleev Commun.* 228 (1994)
26. N A Kozyreva, E S Gryzlova *Zh. Neorg. Khim.* **41** 1198 (1996) [a]
27. N A Kozyreva, E S Gryzlova, V T Orlova *Zh. Neorg. Khim.* **42** 1373 (1997) [a]
28. N A Kozyreva, E S Gryzlova *Zh. Neorg. Khim.* **42** 1748 (1997) [a]
29. E S Gryzlova, N A Kozyreva *Zh. Neorg. Khim.* **45** 876 (2000) [a]
30. E S Gryzlova, N A Kozyreva, in *Proceedings of the EUCHEM 2000 Conference on Molten Salts. Progress in Molten Salt Chemistry 1 (Professor Niels Bjerrum Special Volume), Karrebeksminde, Denmark, 2000* p. 241
31. E S Gryzlova, N A Kozyreva *Zh. Neorg. Khim.* **46** 1921 (2001) [a]
32. N A Vasina, V I Posypaiko *Dokl. Akad. Nauk SSSR* **251** 620 (1980) [b]
33. N A Kozyreva, E S Gryzlova, Z M Dashevskii, B F Myasoedov *Dokl. Akad. Nauk* **325** 530 (1992) [b]
34. E S Gryzlova, N A Vasina, L M Vasil'chenko *Zh. Neorg. Khim.* **28** 2711 (1983) [a]
35. E S Gryzlova, N A Vasina, G E Shter, A S Trunin *Zh. Neorg. Khim.* **27** 1281 (1982) [a]
36. E S Gryzlova, V V Chernyshov, V M Padalko *Avtonom. Energet.* **1** 45 (1992)
37. E S Gryzlova, N A Kozyreva *J. Phase Equilib.* **22** 539 (2001)
38. T G Lupeiko, N I Tarasov, V N Zyablin *Matematicheskaya Model' Plavleniya Komponenta v Troinoi Vzaimnoi Sisteme* (Mathematical Model of Component Melting in a Ternary Reciprocal System) (Novocherkassk 1998); article deposited in the VINITI, No. 555-V98 (Moscow, 1998)
39. A D Pelton, P K Talley, R A Sharma *J. Phase Equilib.* **13** 384 (1992)
40. Y Dessureault, A D Pelton *J. Chem. Phys.* **88** 1811 (1991)
41. A D Pelton, P L Lin *CALPHAD* **7** 295 (1983)
42. A D Pelton, C W Bale, P L Lin *Can. J. Chem.* **62** 457 (1984)
43. M Chrenkova, O Patarak, V Danek *Chem. Pap.* **49** 167 (1995)
44. A S Kosmynin, Doctoral Thesis in Chemical Sciences, Samara State Technology University, Samara, 1999
45. A S Trunin, M Yu Belenov, M A Loseva, V A Lukinykh *Differentsiatsiya Chetyrekhkomponentnoi Vzaimnoi Sistemy Li,K//F,Cl,SO_4* (Differentiation of Four-Component Reciprocal System Li,K//F,Cl,SO_4) (St Petersburg, 1998); article deposited in the VINITI No. 658-V98 (Moscow, 1998)
46. G E Shter, Candidate Thesis in Chemical Sciences, Institute of Organic and Inorganic Chemistry, Academy of Sciences of the USSR, Moscow, 1976

47. A S Petrov, Candidate Thesis in Chemical Sciences, Institute of Organic and Inorganic Chemistry, Russian Academy of Sciences, Moscow, 1993
48. N A Kozyreva, E S Gryzlova *Mendeleev Commun*. 241 (1995)
49. N A Vasina, E S Gryzlova *Zh. Neorg. Khim*. **30** 748 (1985) [a]
50. A M Gasanaliev, M A Dibirov, M M Magomedov *Energeticheskaya Struktura Semikomponentnoi Vzaimnoi Sistemy iz 16 Solei* (Energetic Structure of a Seven-Component Reciprocal System of 16 Salts) (St Petersburg 1999); article deposited in the VINITI No. 1935-V99 (Moscow, 1999)
51. O V Temirbulatova, I K Garkushin, A S Trunin *Zh. Neorg. Khim*. **44** 493 (1999) [a]
52. Zh A Kochkarov, S N Lon'yaeva, G K Shurdumov, A S Trunin, A M Gasanaliev *Zh. Neorg. Khim*. **44** 1037 (1999) [a]
53. G K Shurdumov, Z A Cherkasov, Zh A Kochkarov *Zh. Neorg. Khim*. **44** 838 (1999) [a]
54. I Nerad *CODATA Project of the Institute of Inorganic Chemistry, Slovak Academy of Sciences, Bratislava, 1995*
55. U R Kattner *J. Mater*. **49** 14 (1997)
56. J E Enderby, in *Proceedings of the Euchem Research Conference on Molten Salts, Smolenice Castle, Slovakia, 1996* p. 26
57. E S Gryzlova, N A Kozyreva, in *Proceedings of the Euchem Research Conference on Molten Salts, Smolenice Castle, Slovakia, 1996* p. 27
58. A M Gasanaliev, B Yu Gamataeva, in *XVII Mendeleevskii S'ezd po Obshchei i Prikladnoi Khimii (Tez. Dokl.), Kazan, 2003* [The XVIIth Mendeleev Congress on General and Applied Chemistry (Abstracts of Reports), Kazan, 2003] Vol. 1, p. 221
59. E G Belov, A M Korobkov, S V Mikhailov, in *XVII Mendeleevskii S'ezd po Obshchei i Prikladnoi Khimii (Tez. Dokl.), Kazan, 2003* [The XVIIth Mendeleev Congress on General and Applied Chemistry (Abstracts of Reports), Kazan, 2003] Vol. 1, p. 123
60. N A Kozyreva, E S Gryzlova, in *Abstracts of the Molten Salts Conference EUCHEM-2004, Wroclaw University, Piechowice, Poland, 2004* p. 82
61. E S Gryzlova, N A Kozyreva, in *Abstracts of the Molten Salts Conference EUCHEM-2004, Wroclaw University, Piechowice, Poland, 2004* p. 134
62. R D Rogers, J D Holbrey, S K Spear, R P Swatlowski, in *Abstracts of the Molten Salts Conference EUCHEM-2004, Wroclaw University, Piechowice, Poland, 2004* p. 36

[a] — *Russ. J. Inorg. Chem. (Engl. Transl.)*
[b] — *Dokl. Chem. (Engl. Transl.)*

Russian Chemical Reviews **73** (11) 1033 – 1039 (2004) © 2004 Russian Academy of Sciences and Turpion Ltd

DOI 10.1070/RC2004v073n11ABEH000888

Spin catalysis as a new type of catalysis in chemistry

A L Buchachenko, V L Berdinsky

Contents

I.	Spin catalysis as a new chemical phenomenon	1033
II.	Discovery of spin catalysis	1033
III.	Theory of spin catalysis	1034
IV.	Two mechanisms of spin catalysis	1036
V.	Spin catalysis by radicals and high-spin molecules	1036
VI.	Paramagnetic ions as spin catalysts	1037
VII.	Spin catalysis in reactions with activation barriers	1038
VIII.	Coherent spin catalysis	1038

Abstract. A new phenomenon, spin catalysis, *i.e.*, stimulation of chemical reactions by removing the prohibitions imposed for reasons of electron angular momentum (spin) of reactants is considered. The physical and chemical mechanisms of this phenomenon are discussed. The nature of spin catalysts, the quantitative measure of catalytic effects and the types of chemical reactions susceptible to spin catalysis are considered. The bibliography includes 37 references.

I. Spin catalysis as a new chemical phenomenon

Spin catalysis consists of stimulation of chemical reactions by changing the electron angular momenta (spins) of the reactants. This phenomenon originates from the fundamental law of spin conservation, *viz* ., only those reactions are allowed in which the total spin of the products is identical to the total spin of the reactants; all other reaction channels are strictly forbidden.

The physical sense and role of spin catalysis consist of eliminating the spin forbiddenness, changing the reactant spins and opening reaction channels closed for spin reasons. These functions are performed by a spin catalyst, *viz*., a species with its own electron spin (an atom, radical or ion). When interacting with the reaction system, the catalyst combines its own spin with those of reactants; in such a united spin system, the initially closed reaction channels are opened, *i.e*, spin-allowed.[1,2]

Like other kinds of catalysis, spin catalysis is a purely kinetic phenomenon: a catalyst modifies the reactivities of reactants thus increasing the reaction rate (often, by several orders of magnitude). Spin catalysis manifests itself at two levels: for barrierless reactions, the pre-exponential factor in the rate constant expression (the total cross-section of the reaction) increases, while for reactions with activation barriers the low-barrier channels can be opened and the activation energy can be lowered (together with the increase in the pre-exponential factor in the aforementioned equation).

Many examples of the effect of paramagnetics on the rate and direction of chemical reactions can be cited. The mechanism of these effects remained unclear and often even intriguing (*e.g*., the effect of local activation in paramagnetic polymers) for a long time.[3] It is since the discovery of the spin catalysis phenomenon in the last decade that these effects have been clearly understood.

II. Discovery of spin catalysis

The first reliable and unambiguous proof of the existence of spin catalysis[4] was obtained from studies on photolysis of optically active *d,l*-diphenylpentanone (DPP), the dissociation scheme of which was reliably established.

$$\mathrm{Ph(Me)CH\overset{\overset{\mathrm{O}}{\|}}{C}CH(Me)Ph} \overset{h\nu}{\rightleftharpoons}$$

$$\rightleftharpoons [\mathrm{Ph(Me)\dot{C}H\ \dot{C}OCH(Me)Ph}] \longrightarrow \text{products.}$$

Photodissociation of the ketone occurs in the triplet state, giving rise to a triplet radical pair of acyl and alkyl radicals, which can either recombine (following the triplet – singlet conversion) to yield the original ketone or dissociate to give free radicals which can undergo further transformation to the molecular products (predominantly through decarbonylation of the acyl radical). The inversion of the alkyl radical in the pair results in the loss of optical activity for the regenerated ketone. By separating the optical isomers into *d,l*- and *meso*-DPP and estimating their yields as a function of chemical conversion of the ketone, we can determine with a high accuracy the probability of recombination of the radical pair (P_r).

This method proposed for measuring the cage recombination[5] was used in determination of P_r for DPP decomposition in benzene at 20 °C. Under these conditions, the value of P_r turned out to be very small, *viz.,* only ~ 0.03 (3%). Hence, the spin prohibition for recombination of triplet pairs is strictly fulfilled. (For comparison, it may be mentioned that the probability of cage recombination of similar singlet pairs is 10 – 20 times greater.)

The following fact was quite unexpected: in the presence of such a strong scavenger of carbon-centred radicals as the stable iminoxyl radical TEMPO (2,2,6,6-tetramethylpiperidine-1-oxyl),

A L Buchachenko N N Semenov Institute of Chemical Physics, Russian Academy of Sciences, ul. Kosygina 4, 117977 Moscow, Russian Federation. Fax (7-095) 938 24 84. Tel. (7-095) 939 74 90.
E-mail: spinchem@chph.ras.ru
V L Berdinsky Institute of Problems of Chemical Physics, Russian Academy of Sciences, 142432 Chernogolovka, Moscow Region, Russian Federation. Fax (7-095) 576 40 09. Tel. (7-096) 522 27 74.
E-mail: bvl@icp.ac.ru

Received 2 December 2003
Uspekhi Khimii **73** (11) 1123 – 1130 (2004); translated by T Ya Safonova

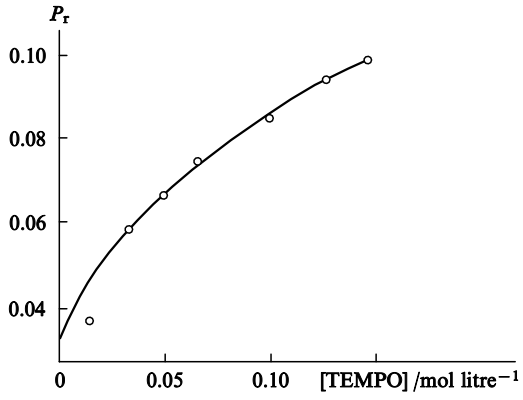

Figure 1. Probability of recombination of a triplet radical pair formed in the DPP photolysis as a function of concentration of TEMPO.[4] Points correspond to experiment, line corresponds to calculations.

the probability of recombination P_r increased with the increase in its concentration (Fig. 1).[4] This result contradicted the fact that in the presence of different strong but diamagnetic scavengers (*e.g.,* dodecanethiol) the P_r value decreased with an increase in the scavenger concentration. It is evident that the paramagnetic nitroxide catalyses the recombination of radicals; moreover, its catalytic function prevails over the traditional function of a potent radical scavenger.

The increase in P_r with an increase in the TEMPO concentration (see Fig. 1) implies that two spin-conversion channels coexist for a radical pair, namely, a direct channel induced by magnetic interactions within the pair (this provides only 3% of recombination) and a catalytic one. The contributions of these channels can be assessed quantitatively by analysing the following kinetic scheme:

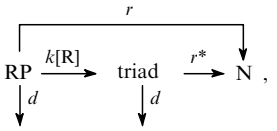

which takes into account both direct recombination of the pair to yield the product N (*meso*-DPP in the case of *d,l*-DPP) and catalytic recombination. The latter involves the integration of an iminoxyl radical R into the radical pair RP with the diffusion rate constant k, which is followed by spin conversion to give N. The meanings of constants r, r^* and d in the scheme are evident.

The following expression was derived[6] for such a scheme:

$$P_r = \frac{r}{r + d + k[R]} + \frac{r^*}{r^* + d}\,\frac{k[R]}{d + k[R]}. \qquad (1)$$

The terms in this equation define the contributions to the total probability of recombination made by the two channels, namely, a direct noncatalytic channel (for $[R] = 0$) and a catalytic channel *via* spin triads. The contributions are formed independently; the former channel defines the ratio $r/d = 3.4 \times 10^{-2}$, from which it follows that $r \ll d$. A numerical analysis of the catalytic contribution carried out by a trial-and-error procedure gives a stable solution at $d = 1.8 \times 10^8$ s^{-1}, $r = 6 \times 10^6$ s^{-1} and $r^* = 3.9 \times 10^7$ s^{-1}. For these parameters, the calculated P_r values coincide with those found experimentally (see Fig. 1) for all concentrations of the radical-catalyst.

The ratio for rate constants of catalytic and direct recombination r^*/r is 6.5, *i.e.,* the recombination rate constant for a given radical pair in the radical triad (in the presence of nitroxide as the third partner) is almost an order of magnitude higher than the recombination rate constant of the original (without nitroxide) radical pair. In other words, the third radical strongly catalyses the recombination of this pair, thus accelerating its conversion.

Such a remarkable conversion of a radical scavenger into a catalyst is the result of competition between the long-range potential responsible for spin exchange (and spin conversion) and the short-range potential of chemical bond formation. This effect is illustrated in Fig. 2: at an encounter between two radicals, namely, a catalyst and a partner of the pair, the exchange interaction of their unpaired electrons and spin conversion can begin even at great distances (l_{ex}), much larger than the distance required for the formation of a chemical bond (l_{ch}); the latter is formed at the Lennard-Jones contact of of rendezvous partners. In other words, sufficient overlap of wave functions, which induces the spin exchange, occurs long before the chemical contact of partners. Such a coordinate difference between two processes, namely, the spin exchange and the chemical reaction, is explained by their different energy scales: the exchange interaction frequency sufficient for spin conversion is of the order of magnitude of $10^8 - 10^{10}$ Hz, whereas chemical interaction is significant only at an exchange potential of no less than kT, *i.e.*, several orders of magnitude larger.

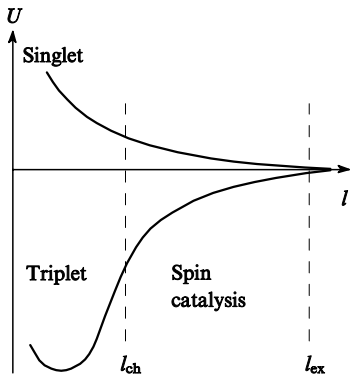

Figure 2. Potential energy (U) of triplet and singlet states of a radical pair as a function of the distance between unpaired electrons that form a chemical bond.

The relationship $l_{ex} > l_{ch}$ means that spin exchange is much more efficient than the reaction and its rate constant exceeds the cross-section of the chemical reaction. The efficiency of spin exchange (and spin catalysis) depends on details characterising the passage of the radical partners through the $l_{ex} - l_{ch}$ region (the time of their residence in this region, orientation dynamics, the extension of their orbitals and their spin delocalisation through solvent molecules).

Experiments on spin relaxation of muon-substituted radicals,[7] the transfer of spin polarisation between radicals[8–10] and other studies[11] directly confirmed the validity of the $l_{ex} > l_{ch}$ relationship. This problem is beyond the scope of this review and is not discussed below. Note that it is this relationship $l_{ex} > l_{ch}$ that is the key to the interpretation of spin catalysis as a chemical phenomenon; that is why organic paramagnetics are much more efficient spin catalysts than the chemical reactants.

III. Theory of spin catalysis

In fact, the theory of spin catalysis is a theory of spin states and spin transitions in multispin systems, namely, spin triads (where the third spin is that of the catalyst), four-spin systems (where the catalyst carries two spins, *e.g.,* an oxygen molecule or a Pr^{3+} ion), *etc.* The comprehensive theory of spin catalysis comprises two parts, namely, a static one, which studies new wave functions and spin states, and a dynamic one, which considers evolution of both the spin states and their population, and also time profiles. Both

parts are essential for the understanding of the physics of this phenomenon, purposeful selection of spin catalysts and prediction of the scope and limitations of catalysis.

1. Three-spin system

The three-spin system is a theoretical model of a radical triad (R^1,R^2,R^3), in which one of radicals (let it be R^3) is a spin catalyst, while the others, *i.e.*, R^1 and R^2, are the components of the reacting system, *e.g.*, a radical pair (note that these two spins can also pertain to any chemical bond which reacts in the presence of a spin catalyst, *e.g.*, to the π-bond of an alkene in its *cis–trans*-isomerisation or a carbene). Let the reacting spin pair (R^1 and R^2) be in the triplet state; the reaction product R^1R^2 is formed by recombination of the (R^1,R^2) pair in the singlet state. Hence, we have to find the probability of formation of R^1R^2 under the action of the spin of the third radical R^3. (Note that the problem is merely inversed if the original reacting spin pair is in the singlet state.)

If we neglect the Zeeman and hyperfine electron–nuclear interactions, the spin Hamiltonian of the triad can be presented as follows:[12]

$$H = -J_{12}(1/2 + S_1S_2) - J_{13}(1/2 + S_1S_3) - J_{23}(1/2 + S_2S_3). \quad (2)$$

This expression contains only exchange energies J_{ij} for pairs R^i and R^j ($i \neq j$; $i, j = 1, 2\ 3$); S_i and S_j are spin operators of spins i and j. Each spin in a triad has two spin states, so that the total number of states in the triad is eight (2^3). The exchange interaction (the spin-dependent part of the Coulomb interaction) splits these states into two groups: four quartet states Q with the total spin $S = 3/2$ and spin projections $S_z = \pm 3/2, \pm 1/2$ and four doublet states D and D' with the total spin of each state $S = 1/2$ and projections $S_z = \pm 1/2$. The spin functions of all four states are as follows:

$$|Q_{+3/2}\rangle = \alpha\alpha\alpha, \quad (3a)$$

$$|Q_{+1/2}\rangle = 3^{-1/2}(\alpha\alpha\beta + \alpha\beta\alpha + \beta\alpha\alpha), \quad (3b)$$

$$|Q_{-1/2}\rangle = 3^{-1/2}(\beta\beta\alpha + \beta\alpha\beta + \alpha\beta\beta), \quad (3c)$$

$$|Q_{-3/2}\rangle = \beta\beta\beta, \quad (3d)$$

$$|D_{+1/2}\rangle = 6^{-1/2}(\alpha\alpha\beta + \alpha\beta\alpha - 2\beta\alpha\alpha), \quad (4a)$$

$$|D_{-1/2}\rangle = 6^{-1/2}(\beta\beta\alpha + \beta\alpha\beta - \alpha\beta\beta), \quad (4b)$$

$$|D'_{+1/2}\rangle = 2^{-1/2}(\alpha\alpha\beta - \alpha\beta\alpha), \quad (4c)$$

$$|D'_{-1/2}\rangle = 2^{-1/2}(\beta\alpha\alpha - \beta\alpha\beta). \quad (4d)$$

These functions are eigenfunctions of energy and total spin; the energies of spin states are derived from the Schrödinger steady-state equation with the spin-Hamiltonian (2) and functions (3), (4)

$$E_Q = -(J_{12} + J_{13} + J_{23}), \quad (5)$$

$$E_D = 2^{-1/2}[(J_{12} - J_{13})^2 + (J_{12} - J_{23})^2 + (J_{13} - J_{23})^2]^{1/2}, \quad (6)$$

$$E_{D'} = -2^{1/2}[(J_{12} - J_{13})^2 + (J_{12} - J_{23})^2 + (J_{13} - J_{23})^2]^{1/2}. \quad (7)$$

Figure 3 illustrates the energy levels and spin transitions in a radical triad. In the quartet states, both the $R^1 + R^2$ recombination and scavenging reactions $R^1 + R^3$, $R^2 + R^3$ are spin-forbidden; these 'quartet' triads can only decompose due to diffusion or disappear due to some ' foreign' chemical reactions.

Of four doublet states in a triad, namely, $D_{\pm 1/2}$ and $D'_{\pm 1/2}$, only two ($D_{\pm 1/2}$) correspond to the singlet state of the reaction pair (R^1,R^2), *i.e.*, the $R^1 + R^2$ recombination occurs only in this state; the $D'_{\pm 1/2}$ state corresponds to the triplet state of the (R^1 , R^2) pair, for which recombination is forbidden. This is the point where spin catalysis is 'switched on', as a result of which the triads pass from non-reactive states D' to chemically active states D. This process is illustrated in Fig. 4. Let the exchange interaction be switched in the (R^1,R^2 ,R^3) triad between one of reacting pair partners, *e.g.*, R^2, and the spin catalyst R^3 . Then, the non-reactive state $D'_{+1/2}$ (corresponding to the triplet state of the reacting pair) is converted into a chemically active state $D_{+1/2}$ in which the (R^1,R^2) pair is a

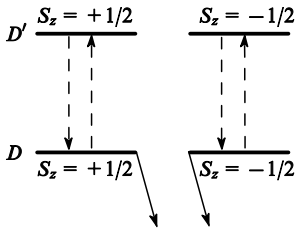

Figure 3. A scheme illustrating the doublet spin states of a radical triad. State D' corresponds to the triplet (chemically inert) state of the radical pair chosen (R^1 ,R^2); state D corresponds to the singlet (chemically active) state of the pair. Dashed lines indicate spin-catalytic $D' - D$ transitions.

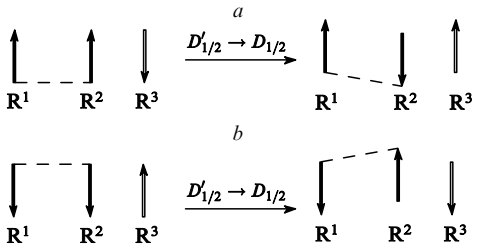

Figure 4. A scheme illustrating $D' - D$ transitions.
Triplet states of the radical pair (R^1,R^2) are transformed into the singlet state upon the interaction with a spin catalyst R^3; (*a*, *b*) are explained in the text.

singlet and hence can undergo recombination (see Fig. 4 *a*). This occurs due to the combining of S_2 and S_3 spins and their exchange (the mechanism of this process is shown below).

A spin catalyst converts $D'_{-1/2}$ into $D_{-1/2}$ by the same mechanism (see Fig. 4 *b*) and populates the chemically active singlet state of the (R^1,R^2) pair. Note that in these spin-catalytic processes neither the total spin S, nor its projection S_z, change. It is only the spin exchange within the triad that occurs in such a way that the chosen pair (R^1 ,R^2) undergoes a triplet–singlet conversion and becomes chemically active.

The spin exchange mechanism between a spin catalyst and an (R^1,R^2) pair partners can be clearly demonstrated in terms of the vector model. Let there be a triad in the $D'_{+1/2}$ state (Fig. 5 *a*), in which the chosen pair (R^1, R^2) is in a non-reactive triplet state (both its spins are oriented upwards, while the catalyst spin is directed downwards). Now, let the exchange interaction J_{23} between the radicals R^2 and R^3 be switched (say, as a result of their approach to one another within the triad). This interaction induces the precession of spins S_2 and S_3 around the total spin vector $S_2 + S_3$ (Fig. 5 *b*). In time τ such that $J_{23\tau} = \pi$, reorientation of S_2 and S_3 spins occurs (Fig. 5 *c*). Now, the triad is in the $D_{+1/2}$ state, *i.e.,* the (R^1 , R^2) pair becomes a singlet and is ready to react: its spins S_1 and S_2 are oppositely oriented, while the catalyst

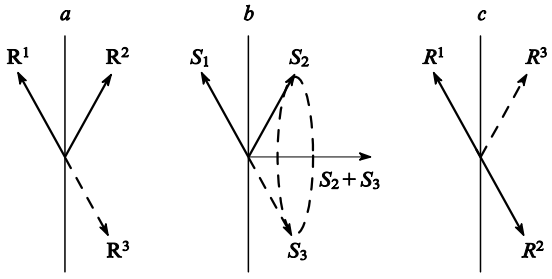

Figure 5. A vector model of spin conversion for a radical pair (R^1,R^2) from triplet to singlet state, induced by a spin catalyst R^3; (*a*, *b*) are explained in the text.

spin is oriented upwards. Moreover, both the triad total spin and spin projections are retained, whereas the chemical activity of the reacting system chosen changes dramatically.

2. Four-spin system

The spin dynamics in a four-spin triad (R^1,R^2,K) formed by a radical pair (R^1,R^2) and a third two-spin partner K, which may represent a biradical, a triplet molecule (*e.g*, O_2), a triplet carbene or a metal ion, resembles in principle the spin dynamics in the three-spin system.

Spin states of a four-spin system (the total number of states $2^4 = 16$) differ in energy, in total spin S and its projection S_z to the z axis and can be divided into three groups, *viz.,* five quintet states with the total momentum $S = 2$, nine states with the total momentum $S = 1$ (triplet states) and two four-spin singlet states ($S = 0$). Being induced by exchange interactions, the spin-catalytic triplet – singlet conversion of the (R^1,R^2) radical pair is only possible for the group of triplet states. The conservation laws for the total spin of the triad and the total spin of the catalyst prohibit the triplet – singlet conversion of the radical pair for triads in quintet and singlet states. The general theory of spin catalysis in the four-spin system was discussed in Ref. 13.

IV. Two mechanisms of spin catalysis

Two mechanisms were proposed for spin catalysis: the first was discussed in detail in the previous section and is realised due to the exchange (nonmagnetic) interaction of electron spins; the second mechanism is purely magnetic and realised due to interaction of spins as the magnetic dipoles.

When discussing the exchange mechanism in the previous section, we ignored the Zeeman and hyperfine interactions by assuming the absence of the magnetic field and magnetic nuclei in reactants. Including the Zeeman and hyperfine interactions does not affect the exchange mechanism. In this case, the energy levels of all eight states are modified only to a small extent, and additional channels of quartet – doublet spin conversion appear. Transitions $Q - D$ and $Q - D'$ forbidden in the absence of hyperfine coupling become partly allowed (like triplet – singlet transitions in isolated radical pairs). They create additional channels for populating the D and D' states of Q quartets. Populating these states increases the efficiency of spin catalysis; moreover, additional nuclear spin selectivity of spin-catalytic reactions and isotope fractionation are observed as side effects.[14] Spin transitions induced by hyperfine coupling can be reliably calculated in terms of spin chemistry (although it should be mentioned that these transitions are not directly related to spin catalysis).

Another mechanism of spin catalysis is purely magnetic and induced by the dipole – dipole interaction of electron spins. In contrast to the exchange mechanism, which stimulates only transitions between D and D' states, the dipole mechanism induces all transitions including $Q - D$ and $Q - D'$; moreover, the total spin and its projections are also changed (recall that both spin and its projections are retained for the case of exchange mechanism).

There is a clear criterion which allows distinguishing these two mechanisms: the exchange-induced spin catalysis is determined by the angular momentum (spin) of the catalyst, whereas the dipole-induced spin catalysis is unambiguously defined by the catalyst magnetic moment. The relative contributions of these mechanisms depend on the time of magnetic relaxation of the catalyst (T_1) and molecular dynamics, which modulates both spin and dipole interactions. Analysing the experimental results, we can see that the exchange mechanism contribution to spin catalysis prevails; the dipole effect is insignificant and operates only in exceptional cases.

V. Spin catalysis by radicals and high-spin molecules

The first clear example that opened up the spin catalysis as a new phenomenon in chemistry was discussed above (see Section III). Later, the spin-catalytic effect of the iminoxyl radical TEMPO in the recombination of a pair of isopropyl and acylisopropyl radicals was studied for photolysis of diisopropyl ketone by the method of chemically induced dynamic nuclear polarisation (CIDNP).[15]

Spin catalysis is also performed by biradicals. Interaction of alkyl radicals R with nitroxide biradicals B proceeds in two steps

$$B + R \xrightarrow{2k_B} M,$$

$$M + R \xrightarrow{k_M} MR.$$

The addition of R to any terminus of the biradical transforms it to a monoradical M, which in turn adds to another alkyl radical; the rate constants for these two reactions (k_B and k_M) should be strictly equal, because the radical fragments in the biradicals studied are absolutely identical. However, it turned out that the ratios k_B/k_M reliably measured for different biradicals and various radicals R always exceed unity [16] being equal to 1.1 – 1.5, *i.e*., the addition of the first radical occurs 1.1 – 1.5 times faster as compared with the second radical. It is evident that one of the radical fragments operates as the reactant, while the other operates as the spin catalyst accelerating the reaction of the former fragment. It is also clear that the catalysis proceeds for coiled conformations of flexible-chain biradicals — it is here that chains and nitroxide fragments are closer to one another and can form a spin triad with the reacting radical R. According to rough estimates, the fraction of coiled conformations is $\sim 10\%$; bearing in mind such a population of spin triads, we can assess the ratio of rate constants for catalytic and noncatalytic reactions, *viz*., $r^*/r \approx 2 - 5$ (this agrees with much more precise results shown in Section II).

The same result was obtained by Hayashi *et al*.;[17] with the only difference that all three triad partners were chemically bound within a single molecular system. In the photolysis of ketones, biradicals in the triplet state were generated by an intramolecular reaction of hydrogen abstraction (if Y = Me); for ketones where Y was a paramagnetic substituent (nitroxide fragment), this reaction generated triradicals.

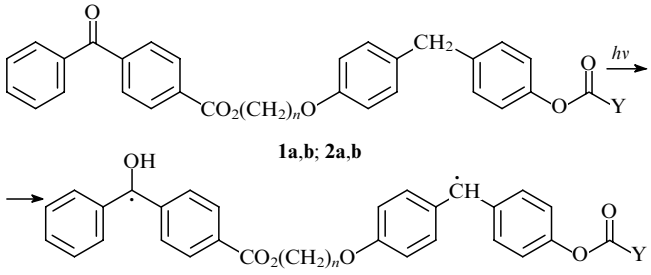

Compound	*n*	Y
1a	8	Me
1b	8	R˙
2a	2	Me
2b	2	R˙

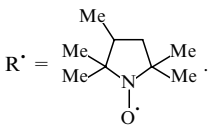

By studying the dynamics of intramolecular cyclisation of bi- and triradicals, it was discovered [17] that cyclisation rate constants in a triradical exceed similar constants for biradicals by an order of magnitude, although both cyclisation reactions are absolutely chemically identical. This is an example of spin catalysis where the third spin (on the nitroxyide fragment) induces the spin conversion of the triplet radical pair involved in cyclisation.

Similar examples of catalysis were observed for electron transfer reactions;[18] triplet radical pairs were found to be generated during photolysis. Their disproportionation (the reverse electron transfer) was dramatically accelerated in the presence of a spin label, *viz.*, a nitroxide fragment chemically attached to the radical-ion pair. In this case (as in the previous one), nitroxide was not involved in the reaction at all and served only as the spin catalyst inducing the triplet–singlet conversion of the reacting radical ion pair.

The function of the spin catalyst can be performed not only by bi- and polyradicals, but also by different high-spin molecules, *e.g.*, O_2. Thus catalytic effects of iminoxyl radicals and oxygen were observed in the reactions of 7-silanorbornadiene and dimethylsilane (carbene).[19—21]

VI. Paramagnetic ions as spin catalysts

Like iminoxyl radicals, paramagnetic ions can also catalyse barrierless reactions of radical recombination. An analysis of the spin-catalytic functions of ions was performed on the example of recombination of a triplet radical pair built of two benzyl radicals one of which is *para*-substituted in the phenyl ring; non-symmetrical dibenzyl represented the recombination product.[22] Figure 6 shows the dependence of its yield (the cage effect or recombination probability) on the lanthanide ion concentration in the micellar solution. This dependence is the same as for radicals (see Fig. 1); moreover, the spin-catalytic effect of ions is adequately described by Eqn (1). Figure 7 shows the rate constant ratio of catalytic and noncatalytic recombination r^*/r as a function of spin S_i; a clear correlation between the spin catalyst efficiency and its electron spin can be traced, which unambiguously suggests that the catalysis is governed by the exchange interaction between the radical pair and a paramagnetic ion. No correlation with the magnetic moments of ions was revealed, which additionally confirms the dominating role of the exchange mechanism in the catalysis.[23]

Figure 7 also shows the rate constant for cyclisation of a triplet biradical obtained by photodissociation of 2,10-diphenylcyclododecanone[24] as a function of the catalyst (lanthanide ion)

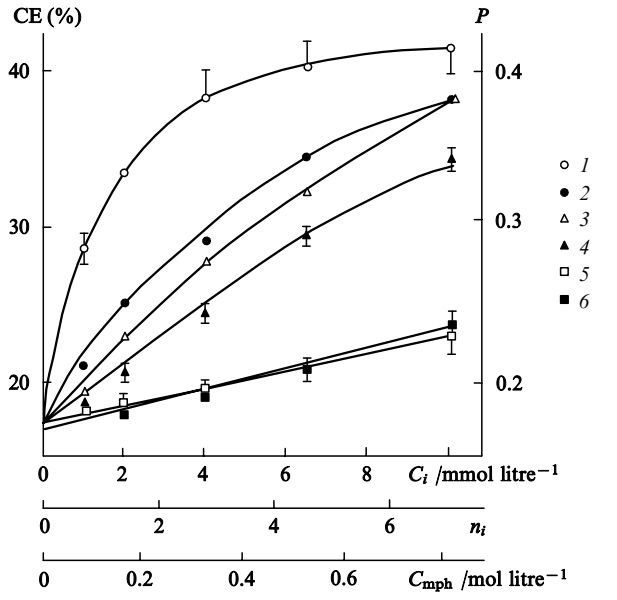

Figure 6. Dependences of the cage effect (CE) and the probability of recombination P for a triplet pair of benzyl radicals in micelles on the concentration of lanthanide ions. C_i is the concentration of ions in the micellar solution, C_{mph} is their concentration in the micellar phase; n_i is the average number of ions in each micelle; (*1*) $GdCl_2$, (*2*) $SmCl_3$, (*3*) $NdCl_3$, (*4*) $EuCl_3$, (*5*) $LaCl_3$, (*6*) $LuCl_3$.

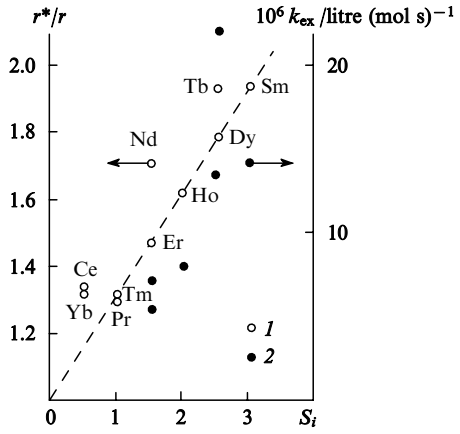

Figure 7. Dependences of (*1*) the rate constant ratio of catalytic and noncatalytic recombination of a radical pair ($PrCH_2$ CH_2Ph) and (*2*) the rate constant of catalytic recombination of the biradical on the catalyst electron spin (S_i).

spin. This dependence is also linear, which confirms the dominating contribution of the exchange mechanism of spin catalysis.

In addition to lanthanide ions, transition metal ions were also studied as spin catalysts of recombination of triplet pairs formed upon photolysis of naphthoquinones;[25] these ions proved to be potent catalysts, *viz.*, at the same level with Gd^{3+}, the best catalyst among lanthanides.

Table 1 shows the data on the efficiency of spin catalysts studied, which is represented as the ratio of rate constants for catalytic and noncatalytic recombination of radicals.

Table 1. Efficiency of spin catalysts.

Spin catalyst	r^*/r	Spin catalyst	r^*/r
Pr^{3+}	1.28	Tb^{3+}	1.93
Tm^{3+}	1.31	Gd^{2+}	4.4
Yb^{3+}	1.31	Co^{2+}	4.4
Ce^{3+}	1.34	Cu^{2+}	4.4
Er^{3+}	1.47	Fe^{2+}	5.3
Ho^{3+}	1.62	Mn^{2+}	5.7
Nd^{3+}	1.71	Ni^{2+}	5.7
Dy^{3+}	1.78	Cr^{3+}	6.2
Sm^{3+}	1.93	nitroxide	6.3

Diamagnetic ions (Sc^{3+}, La^{3+}, Zn^{2+}) or ions with zero angular momenta (Eu^{3+}) exhibit no catalytic effects. Lanthanide ions with unpaired electrons located in deep 4f electron shells and hence strongly shielded by upper electron layers are catalysts of low efficiency; the strongest catalyst is Gd^{3+} ($r^*/r = 4.4$). Note, by the way, that the latter ion drops out of the dependence shown in Fig. 7, its efficiency being higher than that predicted by the exchange mechanism. Probably, this is precisely that extraordinary case where the dipole-magnetic mechanism of spin catalysis operates together with the exchange mechanism.

Ions of transition metals with unpaired electrons in less shielded 3d electron shells display a catalytic activity substantially higher than that of lanthanide ions. Their activity increases systematically in the series from Co^{2+} to Cr^{3+} and approaches the highest value corresponding to the iminoxyl radical with an unpaired electron in the outer shell.

The quantitative hierarchy of spin catalysts with respect to their spin-catalytic activity agrees with a theory that predicts that the rate of spin conversion in a triad should be proportional to the exchange interaction energy of the catalyst with any partner of the

radical pair. Hence, it unambiguously follows that spin carriers with 'outer' unpaired electrons (radicals, oxygen) are much more potent spin catalysts than those spin carriers whose unpaired electrons are 'hidden' within the electron shell. However, being potent catalysts, the former function also as reactants (radical scavengers), whereas the latter are weak catalysts and as a rule chemically inactive, which is their practical advantage. In essence, the strategy of spin catalysis is to find a compromise between these two functions of spin catalysts, *viz*., to serve as a catalyst or a chemical reactant. This is not difficult to achieve by selecting suitable radicals or ions and varying their concentrations. Note that neither ionic radii nor the magnetic moments of ions are related to the catalytic activity. The absence of these dependences indicates that the exchange mechanism is the main driving force of spin catalysis.

VII. Spin catalysis in reactions with activation barriers

To this end, we analysed the spin catalysis in barrierless and low-barrier reactions such as recombination of radicals and disproportionation of radical ions. In reaction with activation barriers, spin catalysts not only increases the total reaction cross-section but also opens new earlier forbidden reaction channels.

A vivid example illustrating this idea is the spin catalysis of *cis*–*trans*-isomerisation of alkene derivatives. Rotation of one part of the molecule with respect to another by the angle π around the double bond occurs through a singlet channel but requires surmounting a high energy barrier ($\sim 50-60$ kcal mol^{-1}). The top of this barrier corresponds to the rotation angle $\pi/2$ where the parts of a molecule undergoing isomerisation are orthogonal to one another. However, there is another reaction trajectory along the reaction coordinate (the rotation angle φ) on the potential-energy surface of the triplet state of the molecule. At angles $\varphi = 0$, π, this surface lies well above the ground state energy; however, at $\varphi = \pi/2$ it has minima and lies well below the top of the singlet channel barrier. The overlap of singlet and triplet channels occurs at angles $\varphi \approx 40-50^\circ$ and $130-140^\circ$.

Kinetics of liquid-phase *cis*–*trans*-isomerisation of dimethyl maleate to dimethyl fumarate was studied.[26] Direct isomerisation proceeds slowly with a rate constant

$$k_d = 10^5 \exp\left(-\frac{27\,000}{RT}\right).$$

In the presence of stable iminoxyl radicals, isomerisation sharply accelerates, which is accompanied by neither their scavenging nor the formation of side products; moreover, the isomerisation rate is proportional to the concentration of iminoxyl radicals. For the unit concentration of iminoxyl (1 mol litre^{-1}), the rate constant of catalytic isomerisation is as follows:

$$k_c = 10^{12} \exp\left(-\frac{27\,000}{RT}\right).$$

A comparison of k_d and k_s constants provides grounds for the unambiguous explanation of these results. First, the identity of activation energies and their low values indicate that both the catalytic and noncatalytic reactions cross the coordinate $\varphi = \pi/2$ through the triplet channel; the spin-allowed singlet channel is too high to be surmounted for energy reasons.

Second, the small pre-exponential factor in the rate constant expression of the noncatalytic reaction suggests that the triplet channel of direct reaction is spin-forbidden. This prohibition is removed only partly due to the spin–orbit coupling along the reaction coordinate. Then, the spin changeover with the transition from the singlet channel to the triplet one at angles $\varphi\,40-50^\circ$ and $130-140^\circ$ is compensated for by the changes in the orbital angular momentum. However, in molecules containing carbon atoms, the spin–orbit coupling is very weak; hence, the triplet channel remains virtually closed.

In the catalytic reaction, a spin catalyst removes the spin-prohibition and opens the triplet channel of isomerisation; the latter becomes allowed so that for the unit concentration of the catalyst the pre-exponential factor in the expression for the catalytic reaction rate constant increases by seven orders of magnitude as compared with the similar factor for the non-catalytic reaction. The three-spin system susceptible to spin catalysis is formed by the catalyst spin and two electron spins of the double bond, which are weakly coupled in the coiled conformation and resemble the spin of a radical pair. The exchange interaction of the catalyst with this spin pair affords their triplet–singlet conversion by switching the reaction from the high-energy singlet channel to the low-energy triplet one.

Evidence for the spin catalyst interaction with the double bond by the exchange mechanism was obtained by analysing the paramagnetic shifts and paramagnetic broadening of NMR lines for dimethyl maleate in the presence of iminoxyl radicals.[27] It was reliably established that dimethyl maleate forms weakly bound complexes with nitroxide (the binding energy of $1-2$ kcal mol^{-1}), in which the spin density is transferred from the radical to the ligand (dimethyl maleate).[28,29] It is in this complex that the three-spin system is formed and the spin-catalytic event occurs.

Numerous examples of catalysing the *cis*–*trans*-isomerisation of alkenes by atoms and paramagnetic molecules (Br, I, NO, O_2, *etc*.) are known. McConnel referred to this phenomenon as 'paramagnetic catalysis',[30,31] although its physical sense had not yet been fully understood. Particularly, for Br and I atoms it had been assumed that the catalysis is realised due to spin–orbit coupling in their complexes with alkenes. The internal spin–orbit coupling in these atoms is substantial, whereas the intermolecular interaction should be weak and incapable of sustaining the efficient spin conversion of the alkene double bond, which always seemed puzzling. Now, however, it is clear that paramagnetic catalysis is, in fact, purely by spin catalysis in which the electron spin plays the key role.

Spin catalysis as a phenomenon may prove to be much more common than it seems at present. Charge separation and water oxidation during photolysis, C–H bond activation in CH_4 by metal complexes, ethylene activation by atoms and clusters, dissociative adsorption on metals, the performance of peroxidases, catalases and other metal enzymes — in many complex reactions involving spin carriers the role of spin catalysis in selecting the reaction pathways can turn out to be significant. This cannot be claimed for all cases, but the possibility of this should never be ignored.[6,32–36]

VIII. Coherent spin catalysis

The triad spin state D' corresponds to the non-reactive triplet state of a radical pair chosen (see Section III). The probability of spin conversion of D' to D in which this pair is in the chemically active singlet state is determined by the solution of a nonstationary Schrödinger equation. This solution is as follows:

$$\rho_{ss}(t) = \left(\frac{\Delta J}{\omega}\right)^2 \sin^2\left(\frac{\omega t}{2}\right). \tag{8}$$

Here, $c_{ss}(t)$ is the probability that the pair is in the singlet state, ΔJ is the difference in exchange energies of the spin catalyst and each partner of the radical pair

$$\Delta J = |J_{13} - J_{23}|; \tag{9}$$

ω is energy splitting of the doublet states D' and D, which is determined by equations (6) and (7)

$$\omega = 2[(J_{12}-J_{13})^2 + (J_{12}-J_{23})^2 + (J_{13}-J_{23})^2]^{1/2}. \tag{10}$$

It follows from equation (8) that both conjugated processes, *viz*., the doublet–doublet evolution of the triad and the triplet–

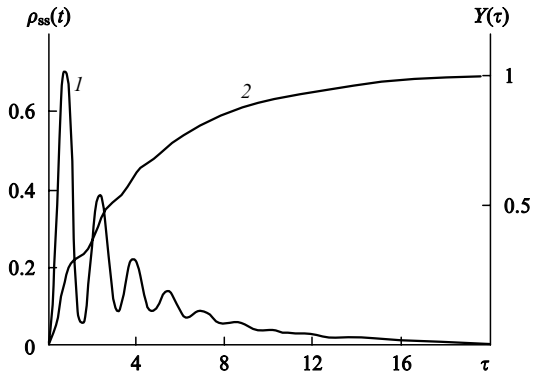

Figure 8. (*1*) Oscillating probability $\rho_{ss}(t)$ of the occurrence of (R^1,R^2) pair in the singlet state during its interaction with a spin catalyst R^3 and (*2*) the kinetics of accumulation of the recombination product.[37]

singlet conversion in the chosen pair of this triad, oscillate in time with a period $\mathbf{t} = \omega^{-1}$ (Fig. 8). In this case, both the total spin and its projection are retained.

The yield of reaction products (*e.g.*, as a result of recombination in ensembles of selected pairs) also oscillates in time with a frequency ω (Fig. 8). These oscillations (or quantum beats) can be observed in static triads with fixed distances between the partners, if the ensemble of these triads has been formed instantaneously and coherently, *i.e.*, in a fixed spin state and with the same phase. In such ensembles (or coherent wave packets), one can realise and observe the coherent spin catalysis with oscillating generation of the reaction product.[37]

A photosynthesis centre, *i.e.*, a molecular arrangement in which all the partners of a spin triad are rigidly organised, can serve as an example of a static triad. The photoinduced charge separation gives rise to a radical-ion pair, in which spin evolution is defined by the exchange interaction with Fe^{3+} ions as spin catalysts.

In non-rigid triads, the molecular motion induces random and incident changes in the distances between partners and modulates the exchange interaction, thus varying the frequencies of quantum beats. Ultimately, this motion modulates the phases and rates of spin evolution, upsetting coherency and suppressing quantum beats. The coherent spin catalysis has not yet been observed experimentally; however, it would be worthwhile to pursue its research in order to understand the structure and dynamics of spin triads.

* * *

Spin catalysis is the universal phenomenon typical of multispin molecular systems. This is observed in chemical reactions (both barrierless and with activation barriers), biological systems (primary light-accumulating reactions in photosynthesis centres, redox enzymes), in physical phenomena (the recombination of spin-oriented hydrogen atoms, which prevents their Bose-condensation, the spin conversion of positronium, the paramagnetic quenching of excited molecules). Scientists are often even unaware of its existence, although its abundance is much wider than seems at present. Any process of generation of radical or radical-ion pairs during catalytic or thermal decomposition or electron transfer can be accompanied by spin catalysis, so that such chemical catalysts as metal ions or metal complexes (especially, bi- and polynuclear) can also operate as spin catalysts. Such a coexistence of spin and chemical catalysis is also true for biocatalytic processes. Spin catalysis can also occur in heterogeneous processes such as hydrogenation, isomerisation, oxidation on zeolites, metals, oxides, *etc*.

The review was written with a financial support of the Russian Foundation of Basic Research (Project No. 02-03-32753), Program 'Integration', Federal Program 'Leading Scientific Schools of Russia' (Project NSh-1221.2003.03) and programs of the Division of Chemistry and Materials Science and the Presidium of the Russian Academy of Sciences.

References

1. A L Buchachenko, V L Berdinsky *Chem. Rev.* **102** 603 (2002)
2. A L Buchachenko *Pure Appl. Chem.* **72** 2243 (2000)
3. A A Berlin, S I Bass *Izv. Akad. Nauk SSSR, Ser. Khim.* 1492 (1962) [a]
4. E N Step, A L Buchachenko, N J Turro *J. Am. Chem. Soc.* **116** 5462 (1994)
5. V F Tarasov, N D Ghatlia, A L Buchachenko, N J Turro *J. Am. Chem. Soc.* **116** 228 (1994)
6. A L Buchachenko, V L Berdinsky *J. Phys. Chem.* **100** 18292 (1996)
7. H Dilger, M Schwager, P Tregenna-Piggott, E Roduner, I Reid, D Arseneau, J Pan, M Senba, M Shelley, D Flemming *J. Phys. Chem.* **100** 6561 (1996)
8. N J Turro, I V Khudyakov, D W Dwyer *J. Phys. Chem.* **97** 10530 (1993)
9. N J Turro, I V Khudyakov *Res. Chem. Intermed.* **25** 505 (1999)
10. N J Turro, I V Khudyakov *J. Phys. Chem.* **99** 7654 (1995)
11. D M Bartels, A D Trifunac, R G Lawler *Chem. Phys. Lett.* **152** 109 (1988)
12. A L Buchachenko, V L Berdinsky *Chem. Phys. Lett.* **242** 43 (1995)
13. V L Berdinsky, A L Buchachenko *Kinet. Katal.* **37** 659 (1996) [b]
14. A L Buchachenko, V L Berdinsky *Chem. Phys. Lett.* **298** 279 (1998)
15. I M Magin, V S Shevel'kov, A A Obynochny, A I Kruppa, T V Leshina *Chem. Phys. Lett.* **357** 351 (2002)
16. A L Buchachenko, L V Ruban, E N Step, N J Turro *Chem. Phys. Lett.* **233** 315 (1995)
17. Y Mori, Y Sakaguchi, H Hayashi *Chem. Phys. Lett.* **301** 365 (1999)
18. Y Mori, Y Sakaguchi, H Hayashi *J. Phys. Chem. A* **104** 4896 (2000)
19. M Taraban, O Volkova, A Kruppa, V Plusnin, V Grivin, Yu Ivanov, T Leshina, M Egorov, O Nefedov. *J. Organomet. Chem.* **566** 73 (1998)
20. M Taraban, A Kruppa, O Volkova, I Ovcharenko, R Musin, T Leshina, E Korolenko, K Kitahara *J. Phys. Chem. A* **104** 1811 (2000)
21. O Volkova, M Taraban, V Plusnin, T Leshina, M Egorov, O Nefedov *J. Phys. Chem. A* **107** 4001 (2003)
22. N J Turro, X Lei, I K Gould, M B Zimmt *Chem. Phys. Lett.* **120** 397 (1985)
23. V L Berdinskii, A L Buchachenko N J Turro *Kinet. Katal.* **39** 325 (1998) [b]
24. J Wang, K Welsh, K Waterman, P Fehler, C Doubleday, N J Turro *J. Phys. Chem.* **92** 3730 (1988)
25. Y Sakaguchi, H Hayashi *Chem. Phys. Lett.* **106** 420 (1984)
26. A L Buchachenko, L V Ruban, E G Rozantsev *Kinet. Katal.* **9** 915 (1968) [b]
27. N A Sysoeva, A V Karmilov, A L Buchachenko *Chem. Phys.* **7** 123 (1975)
28. N A Sysoeva, A V Karmilov, A L Buchachenko *Chem. Phys.* **15** 313 (1976)
29. N A Sysoeva, A V Karmilov, A L Buchachenko *Chem. Phys.* **15** 321 (1976)
30. H McConnell *J. Chem. Phys.* **20** 1043 (1952)
31. H McConnell *J. Chem. Phys.* **23** 2440 (1955)
32. B Minaev, H Agren *Coll. Czech. Chem. Commun.* **60** 339 (1995)
33. H Agren, O Vahtras, B Minaev *Adv. Quantum Chem.* **27** 71 (1999)
34. H Agren, B Minaev *Int. J. Quantum Chem.* **72** 581 (1999)
35. B Minaev, H Agren *J. Mol. Catal. A: Chem.* **149** 179 (1999)
36. P E M Siegbahn *J. Am. Chem. Soc.* **118** 1487 (1996)
37. A L Buchachenko, V L Berdinsky *Izv. Akad. Nauk, Ser. Khim.* 1646 (1995) [a]

[a] — *Russ. Chem. Bull., Int. Ed. (Engl. Transl.)*
[b] — *Kinet. Catal. (Engl. Transl.)*

Russian Chemical Reviews **73** (11) 1041 – 1064 (2004) © 2004 Russian Academy of Sciences and Turpion Ltd

DOI 10.1070/RC2004v073n11ABEH000855

Metal oxoalkoxides. Synthesis, properties and structures

N Ya Turova

Contents

I.	Introduction	1041
II.	Pathways of formation of oxoalkoxides from alkoxides	1043
III.	Properties of oxoalkoxides	1057
IV.	Structural types of oxoalkoxides	1057
V.	Oxoalkoxides as true precursors of oxide phases	1060

Abstract. The review surveys the pathways of formation of crystalline oligomeric oxoalkoxides $M_mO_n(OR)_p$, which are products of partially controlled (or uncontrolled) hydrolysis, oxidation, thermal decomposition of mono- and bimetallic alkoxides of the ortho series $M(OR)_n$ and $M_mM'_n(OR)_p$ or elimination of ethers from these compounds. The physicochemical properties of oxoalkoxides (solubility, the behaviour in solutions, volatility, *etc*.) differ considerably from the properties of the corresponding alkoxides. Hence, oxoalkoxides can be considered as immediate precursors of oxide materials produced by sol – gel technology. The $M_mO_n(OR)_p$ compounds are classified according to the sizes of associates. The crystal chemistry of alkoxides is discussed. The bibliography includes 249 references.

I. Introduction

Polymeric metal oxoalkoxides (OA) of the general formula $M_mO_n(OR)_p$, which are amorphous products of partial hydrolysis or thermolysis of alkoxides, have been used for years as heat-resistant insulating coatings, elastomers, resins for the production of plastics, lacquers, paints, enamels, *etc*. Andrianov,[1] who has made a considerable contribution to this area of chemistry, considered OA as 'polymers with inorganic main chains enclosed by OR groups',

$$-M(OR)_2-O-M(OR)_2-O-M(OR)_2-O-.$$

In the late 1950s, Bradley[2] studied hydrolysis of titanium alkoxides (and, in part, of zirconium alkoxides) primarily by ebullioscopy. He assigned structures to hydrolysis intermediates (which either occur in solution or exist in the amorphous state) based on his 'structural theory', according to which a metal atom has the maximum coordination number in the case of the lowest degree of association of $[MO_n(OR)_p]_x$. However, Bradley always emphasised that it is necessary to establish the structures by direct methods for solving this problem.

The present review is devoted to oligomeric crystalline oxoalkoxides belonging to a new class of oxo-bridged molecular compounds. These compounds have attracted considerable interest because they are immediate precursors in the 'sol – gel technology' of oxide materials, which is based on hydrolysis of alkoxides in organic solvents.[3]

$$M(OR)_n \xrightarrow{H_2O} MO_x(OR)_{n-2x} \xrightarrow{H_2O} M_2O_n\cdot y\,H_2O \xrightarrow[-H_2O]{} M_2O_n$$

The sol – gel method has assumed great importance, as evidenced by regular international conferences devoted to this problem. Beginning in 1981, information presented at these conferences was published in *J. Non-Cryst. Solids* and *J. Sol-Gel Sci. Technol*. The physicochemical fundamentals of various processes of sol – gel technology were discussed in the comprehensive monograph by Brinker and Scherer.[4] Applied aspects of this technology were covered in two collections of articles.[5, 6]

A substantial advantage of the alkoxide-based sol – gel technology is the possibility of deep purification of the starting compounds. Besides, mono- and bimetallic oxides are prepared as amorphous substances consisting of highly reactive nanosized particles. This allows one to perform ceramic sintering at lower temperatures compared to those used in alternative technologies. In the synthesis of complex oxides, the use of alkoxide solutions makes it possible to overcome the main difficulty of alternative methods, *viz*., the necessity of homogenising various metals at the molecular level. Subsequent hydrolysis and thermal treatment of such samples afford submicron particles. In particular, this method enables one to prepare particular composites inaccessible by direct reactions of oxides. Data on the compositions and structures of real particles involved in these processes are required to elucidate the mechanisms of formation of simple and complex oxide phases and to optimise the synthesis of materials based on these phases.

The class of oligomeric crystalline oxoalkoxides was discovered by the X-ray diffraction method. In the late 1960s, this method was used for establishing the structures of the partial hydrolysis products of titanium, niobium and zirconium alkoxides, *viz*., $Ti_7O_4(OEt)_{20}$,[7] $Nb_8O_{10}(OEt)_{20}$,[8] and $Zr_{13}O_8(OMe)_{36}$ (see Ref. 9) (Fig. 1 *a* – *c*). It was found that all oxo ligands in these molecules serve as bridges (even the Nb complex contains no terminal 'yl' oxygen atoms, which are typical of compounds with this metal). Oxo bridges were considered as units that formed upon condensation of two hydroxy groups resulting from the replacement of an OR group in the first step of hydrolysis.

X-Ray diffraction studies of OA revealed new molecules of various sizes and with different structures, which have greatly extended our knowledge of the crystal chemistry of metal alkoxo

N Ya Turova Department of Chemistry, M V Lomonosov Moscow State University, Leninskie Gory, 119992 Moscow, Russian Federation.
Fax (7-095) 932 88 46. Tel. (7-095) 939 33 39.
E-mail: natalie@inorg.chem.msu.ru

Received 16 June 2003
Uspekhi Khimii **73** (11) 1131 – 1154 (2004); translated by T N Safonova

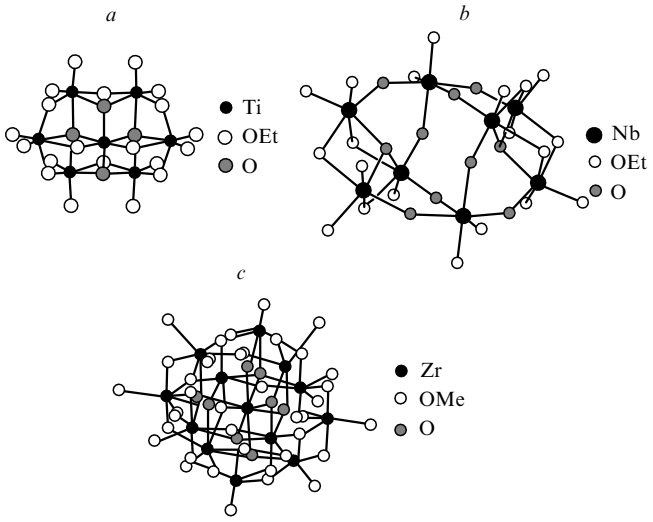

Figure 1. Metal–oxygen cores in the structures of $Ti_7O_4(OEt)_{20}$ (*a*),[7] $Nb_8O_{10}(OEt)_{20}$ (*b*)[8] and $Zr_{13}O_8(OMe)_{36}$ (*c*).[9]

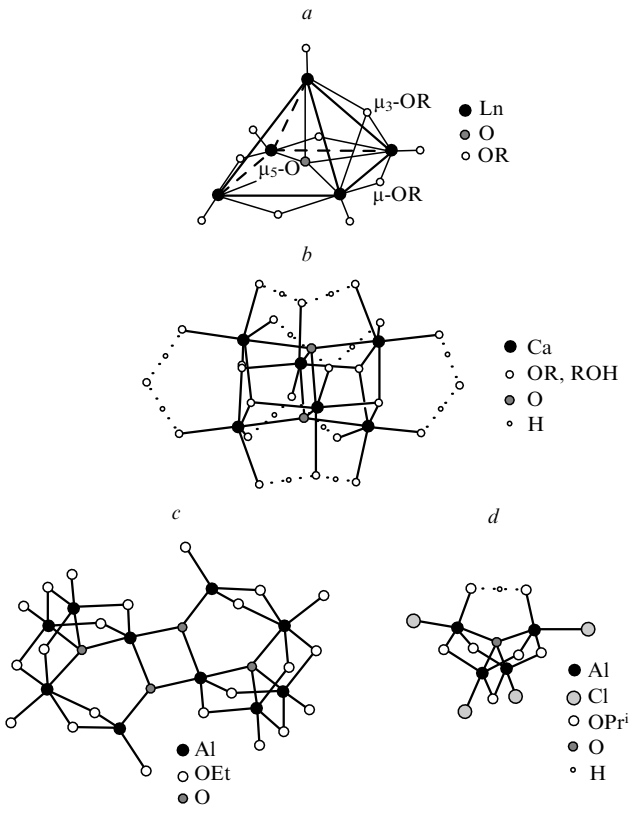

Figure 2. Metal–oxygen cores in the structures of $[M_5(\mu_5\text{-}O)(OR)_{13}]$ (M = Sc, Y, Ln, In, Al, Fe) (only one of four μ_3-OR groups is shown) (*a*),[10–15] $[Ca_6(\mu_4\text{-}O)_2(OEt)_8(EtOH)_{14}]$ (*b*),[16] $[Al_{10}(\mu_4\text{-}O)_2(\mu_3\text{-}O)_2(OEt)_{22}]$ (*c*)[17] and $[Al_4(\mu_4\text{-}O)(OPr^i)_6(Pr^iOH)Cl_4]$ (*d*).[18]

complexes. It appeared that many crystalline compounds, which were initially considered as alkoxides of the ortho series $M(OR)_n$, contain, in reality, oxo ligands generally with high dentate numbers. Examples of such compounds are 'isopropoxides' of rare-earth elements[10–14] and In,[14] 'iron(III) ethoxide'[15] (these compounds, in reality, contain the pentadentate oxo group $[M_5(\mu_5\text{-}O)(OR)_{13}]$) (Fig. 2 *a*), 'calcium ethoxide disolvate' $[Ca_6(\mu_4\text{-}O)_2(OEt)_8(EtOH)_{14}]$ (Fig. 2 *b*),[16] and 'crystalline aluminium ethoxide' $[Al_{10}(\mu_4\text{-}O)_2(\mu_3\text{-}O)_2(OEt)_{22}]$ (Fig. 2 *c*).[17] The '$AlCl(OPr^i)_2$' compound, which is a well-known catalyst and reducing agent used in organic chemistry, consists of the tetrahedral $[Al_4(\mu_4\text{-}O)(OPr^i)_6(Pr^iOH)Cl_4]$ molecules[18] (Fig. 2 *d*). Due to inclusions of organic solvents in the intercrystallite space and the formation of numerous solvates of OA with alcohols or hydrocarbons, the results of chemical analysis for OA are no different from those for $M(OR)_n$. For this reason, the present review deals only with compounds whose compositions were confirmed by the data on their structures. These compounds are listed in Tables 1–10 in order of increasing nuclearity. Unfortunately, space does not permit a discussion of abundant information on heteroleptic complexes, such as oxo alkoxo carboxides, oxo alkoxo β-diketonates, *etc*.

Table 1. Dinuclear oxoalkoxides.

Compound	Structure	Starting compounds, conditions of formation	Ref.
$[(OsO)O(OCMe_2CH_2NHBu^t)]_2$	two tetrahedra sharing a $(\mu\text{-}O)_2$ edge	$OsO_3(NBu^t) + Me_2C{=}CH_2$	19
$[Nd_2O(OCH_2Bu^t)_4]$	two tetrahedra sharing a $[(\mu\text{-}O)(\mu\text{-}OR)_2]$ face	–	20
$[Ti(\mu\text{-}O)(OC_6H_3Pr^i_2\text{-}2,6)_2 \cdot (NC_5H_4\text{-}4\text{-}NC_4H_8)]_2$ (see [a])	two trigonal bipyramids sharing a $(\mu\text{-}O)_2$ edge	$Ti(OC_6H_3Pr^i_2\text{-}2,6)_2[Bu^tNCBn_2]Py + H_2O$	21
$[Nb(\mu\text{-}O)(OC_6H_3Pr^i_2\text{-}2,6)_3]_2$	the same	$[Nb(OC_6H_3Pr^i_2\text{-}2,6)_3(CH_2C_6H_4Me\text{-}4)]_2 + H_2O$	22
$[Me_2NH_2]^+_2[(Mo^{V}O)(\mu\text{-}O)(OC_6F_5)_2]^-_2$	anion — two square pyramids sharing a $(\mu\text{-}O)_2$ edge	$Mo_2(NMe_2)_6 + C_6F_5OH$	23
$[(OsO)O(\eta^2\text{-}1,2\text{-}O_2C_2Me_4)]_2$	two square pyramids sharing a $(\mu\text{-}O)_2$ edge	$OsO_4 + Me_2C{=}CMe_2$	24
$[W_2O(OBu^t)(OSiMe_2Bu^t)_5Py_2]$	five-vertex polyhedron and an octahedron sharing a $[(\mu\text{-}O)(\mu\text{-}OR)]$ edge	$W_2(OSiMe_2Bu^t)_6 + Bu^tOH + NO + Py$	25
$[Li(THF)_3Nb(\mu\text{-}O)(OC_6H_3Me_2\text{-}2,6)_4]$	tetrahedron $[LiO(THF)_3]$ and the $[NbO(OR)_4]$ square pyramid sharing a $(\mu\text{-}O)$ vertex	$NbCl_3 + LiOC_6H_3Me_2\text{-}2,6$	26
$[Mo^{III}_2O(OCH_2Bu^t)_4(PMe_3)_4]$	five-vertex polyhedron and an octahedron sharing a $[(\mu\text{-}O)(\mu\text{-}OR)]$ edge	$Mo_2(OCH_2Bu^t)_6 + PMe_3 + H_2O$	27
$(MoO)_2O[O(CMe_2)_2O]_2[O(CMe_2)_2OH]_2$	$[(MoO)_2O(\eta^2\text{-}RO_2)_2(\eta^2\text{-}OROH)_2]$, two octahedra sharing a $(\mu\text{-}O)$ vertex	$MoO_3 + HO(CMe_2)_2OH$	28, 29

Table 1 (continued).

Compound	Structure	Starting compounds, conditions of formation	Ref.
$[(WO)O(RO_2)(OROH)]_2$, R = C_2Me_4, cyclo-C_7H_{12}, cyclo-C_8H_{14}	two octahedra sharing a $(\mu\text{-O})_2$ edge	$W(O_2R)_3 + H_2O$	30
$K_4[TiO(\eta^2\text{-}C_6H_4O_2\text{-}1,2)_2]_2 \cdot 9\,H_2O$	the same	$K_2Ti(C_6H_4O_2\text{-}1,2)_3 + H_2O$	31
$[(W^{VI}O)O(OSiMe_2Bu^t)_2Py]_2$	"	$W_2(OSiMe_2Bu^t)_6 + NO$	25
$[(Os^{VI}O)O(O_2C_6H_{10}\text{-cyclo})(C_7H_{13}N)]_2$	"	$OsO_4 + C_6H_{10} + C_7H_{13}N$	32
$[Ta_2O(OPr^i)_8(Pr^iOH)]$	two octahedra sharing a $[(\mu\text{-O})(\mu\text{-OR})]$ edge	electrochemical synthesis (Ta + Pr^iOH)	33, 34
$[Ta_2OCl_3(OC_6H_3Pr^i_2\text{-}2,6)_5]$	two octahedra sharing a $[(\mu\text{-O})(\mu\text{-Cl})_2]$ face	$TaCl_2(OC_6H_3Pr^i_2\text{-}2,6)_3$ + traces H_2O	35
$W^V_2O(OCH_2Bu^t)_8$	two octahedra sharing a $[(\mu\text{-O})(\mu\text{-OR})_2]$ face, W = W bond	$W_2(OCH_2Bu^t)_8$ + pyridine oxide	36
$M_2[(MoO_2)_2O(C_6H_4O_2\text{-}1,2)_2] \cdot n\,H_2O$, M = NH_4 (n = 2), Ba/2 (n = 5)	$[(MoO_2)_2O(\mu_3,\eta^2\text{-}RO_2)_2]^{2-}$, two octahedra sharing a $[\mu\text{-O}]_3$ face (from two RO_2 groups)	$M_2MoO_4 + C_6H_4(OH)_2\text{-}1,2$	37
$[Me_3NBn]_2[(WO_2)_2O(OMe)_4]$	two octahedra sharing a $[(\mu\text{-O})(\mu\text{-OR})_2]$ face	$[Me_3NBn]_2WO_4 + WO(OMe)_4$	38
$[(Re^{VI}O)_2O(OMe)_6]$	the same	$ReOCl_4 + MeOH + Et_3N$	39

[a] 4-NC_4H_8 is 4-pyrrolidino-.

Table 2. Trinuclear oxoalkoxides.

Compound	Structure	Starting compounds, conditions of formation	Ref.
Triangles $[M_3(\mu_3\text{-O})]$			
$[Sn_3O(OBu^i)_{10}(Bu^iOH)_2]$	three octahedra sharing a $[(\mu_3\text{-O})(\mu\text{-OR})]$ edge	$Sn(OBu^i)_4 + H_2O$	40
$[BiTi_2O(OPr^i)_8]$	two $[TiO_6]$ octahedra sharing a $[(\mu_3\text{-O})(\mu\text{-OR})_2]$ face and $[(\mu_3\text{-O})(\mu\text{-OR})]$ edges, Ψ-five-vertex polyhedron [:BiO_4]	$Ti(OPr^i)_4 + Bi(OPr^i)_3 + H_2O$	41
Triangles $[M_3(\mu_3\text{-O})(\mu_3\text{-X})]$, three $[M(\mu_3\text{-O})(\mu_3\text{-X})(\mu\text{-OR})_2(OR)_2]$ octahedra sharing $[(\mu_3\text{-O})(\mu_3\text{-X})(\mu\text{-OR})]$ faces			
$[Ti_3O(OMe)(OPr^i)_9]$	X = OMe	$Ti(OPr^i)_4 + H_2O + MeOH$ (h = 0.07)	42–44
$[Ti_3OCl(OCH_2Bu^t)_9]$	X = Cl	$TiCl_4 + NaOCH_2Bu^t$	42–44
$[Zr_3OCl(OCH_2Bu^t)_9]$	X = Cl	$ZrCl_4 + KOCH_2Bu^t$	42–44
$[Zr_3O(OH)(OBu^t)_9]$	X = OH	$ZrCl_4 + LiOBu^t$	44
$[Zr_3O(OBu^t)_{10}]$	X = OBu^t	prolonged storage of electrolyte	45
$[M^{IV}_3O(OR)_{10}]$ (M = Mo, W; R = Pr^i, CH_2Bu^t)	X = OR [a]	$M_2(OR)_6 + O_2$	46, 47
$[U_3O(OBu^t)_{10}]$	X = OBu^t (see [b])	$U_2(OBu^t)_8 + H_2O$	48
Triangles $[M_3(\mu_3\text{-O})(\mu_3\text{-X})]$, three $[M(\mu_3\text{-O})(\mu_3\text{-X})(\mu\text{-OR})_2(OR)_2]$ octahedra sharing $[(\mu_3\text{-O})(\mu_3\text{-X})(\mu\text{-OR})]$ faces			
$[Ba(Mo_2O_5)(OC_2H_4OMe)_4(MeOC_2H_4OH)]$	$[Ba(Mo_2O_5)_2(\mu_3,\eta^2\text{-OR})_2(\mu,\eta^2\text{-OR})_2(\eta^2\text{-ROH})]$, two Mo octahedra sharing a $[(\mu\text{-O})(\mu_3\text{-OR})_2]$ face, CN of Ba is 10	$Ba(OC_2H_4OMe)_2$ + + $MoO_2(OC_2H_4OMe)_2$	49
Ring			
$[W^{IV}_3O_2(OBu^t)_8]$	$[-W-(\mu\text{-O})-W=W-(\mu\text{-O})-]$, two W–W bonds, one W = W bond, CN of W are 3, 4, 5	$W_2(OBu^t)_6 + O_2$	50
Linear chain			
$[UO_2][U(\mu\text{-O})(OBu^t)_5]_2$	three octahedra sharing a $[(\mu\text{-O})(\mu\text{-OR})]$ edge	$UO_2Cl_2 + KOBu^t$	51
Angular molecule			
$Nb_3O_2[(CMe_2)_2O_2]_5[(CMe_2)_2O_2H]$	three $[Nb_3(\mu\text{-O})_2(\mu,\eta^2\text{-}O_2R)_2]_2[\eta^2\text{-}RO_2]_4H$ octahedra	$Nb(OEt)_5 + (CMe_2)_2(OH)_2$	52

Note. Accepted abbreviations: h = [H_2O] : [alkoxide], Ψ is an incomplete polyhedron with a localised electron pair, CN is the coordination number.
[a] The bond length M = M 2.53 Å; [b] the U···U distance is 3.57 Å.

II. Pathways of formation of oxoalkoxides from alkoxides

There are several main pathways of formation of oxo ligands in alkoxide molecules. Among them are hydrolysis and oxidation, thermolysis, desolvation of solvates $M(OR)_n \cdot m\,L$ and decomposition accompanied by elimination of ethers. Only the first two above-mentioned processes can be controlled. Although some authors persist in considering OA only as products of uncontrolled hydrolysis (and often do not discuss the origin of oxo

Table 3. Tetranuclear oxoalkoxides.

Compound	Structure	Starting compounds, conditions of formation	Ref.
Tetrahedra $[M_4(\mu_4\text{-}O)]$			
$[Al_4O(OPr^i)_6Cl_4(Pr^iOH)]$	$[Al_4(\mu_4\text{-}O)(\mu\text{-}OR)_5][H(\mu\text{-}OR)_2]Cl_4$, $[AlO_4Cl]$ trigonal bipyramids sharing $[O(\mu\text{-}OR)]$ edges	$Al(OPr^i)_3 + AlCl_3 + Pr^iOH$	18
$[Al_4O(OBu^i)_{10}(Bu^iOH)]$	pairs of $[AlO_5]$ trigonal bipyramids sharing $[(\mu_4\text{-}O)(\mu\text{-}OR)]$ edges	$Al(OBu^i)_3 + H_2O$	53, 54
$[Al_4O(OCH_2CF_3)_{10}(CF_3CH_2OH)]$	the same	$Al(OCH_2CF_3)_3 + H_2O$; $AlMe_3 + CF_3CH_2OH$	55
$[Y_4OCl_3(OBu^t)_7(THF)_3]$	$[Y(THF)_3(\mu\text{-}Cl)_3Y_3(\mu_4\text{-}O)(\mu_3\text{-}OR)(\mu\text{-}OR)_3(OR)_3]$; base of a tetrahedron consists of three $[YO_6]$ octahedra centred with μ_3-OR, CN of Y_{ax} is 7	$Y_3Cl_2(OBu^t)_7 \cdot 2\,THF + LiAlMe_4$	56
$[Ce_4^{IV}O(OPr^i)_{14}]$	two octahedra and two seven-vertex polyhedra sharing $[(\mu_4\text{-}O)(\mu\text{-}OR)_2]$ faces	$Ce(OPr^i)_4 \cdot Pr^iOH$ (70 °C, 10^{-3} mm Hg)	57
$[Lu_4O(OH)(OCMe_2CH_2OMe)_9]$	$[Lu_4(\mu_4\text{-}O)(\mu_3\text{-}OH)(\eta^2,\mu_3\text{-}OR)(\eta^2,\mu\text{-}OR)_3(\eta^1,\mu\text{-}OR)(\eta^1\text{-}OR)_4]$, two octahedra and two seven-vertex polyhedra	$Lu[N(SiMe_3)_2] +$ $+ MeOCH_2CMe_2OH$	58
$[Pb_4O(OSiPh_3)_6] \cdot PhH$	six $(\mu\text{-}OR)$ bonds along tetrahedron edges; $[:PbO_4]$ is a Ψ-trigonal bipyramid	$PbCp_2 + Ph_3SiOH + PhH$, Δ	59
$[Pb_2Ti_2O(OPr^i)_{10}]$	two $[:PbO_5]$ Ψ-octahedra and two $[TiO_6]$ octahedra	$Pb(OPr^i)_2 + Ti(OPr^i)_4$	60
$[Ce_4^{3.75+}O(OPr^i)_{13}(Pr^iOH)]$	'butterfly wings' — $[OCe_4]$; two octahedra are linked only *via* μ_4-O, two Ce seven-vertex polyhedra sharing $[O(\mu\text{-}OR)_2]$ faces	$[Ce(OPr^i)_4 \cdot Pr^iOH]$, UV irradiation	61
$[Pb_3ZrO(OBu^t)_8]$	'butterfly wings', a Zr octahedron and a Pb Ψ-tetrahedron are linked *via* μ_4-O, two Pb square pyramids sharing a $[(\mu\text{-}O)(\mu_3\text{-}OR)(\mu\text{-}OR)]$ face	$PbZr(OBu^t)_6 + Pb(OBu^t)_2$, Δ	62
$[Th_4O\{O(C_2H_4O)_4\}_3Cl_8] \cdot 3\,MeCN$	$[Th_4O(\eta^5,\mu\text{-}ORO)_3Cl_8]$, each $[O(C_2H_4O)_4]$ fragment is bound to one Th atom	$ThCl_4 + MeCN +$ $+ HO(C_2H_4O)_3C_2H_4OH$	63
$[NaBi_3O(OC_6F_5)_8THF]$	–	$BiCl_3 + NaOC_6F_5 + THF$	64
$[Li_2(NbO)_2O(OCMe_2CH_2OMe)_6]$	$[Li_2(NbO)_2(\mu_4\text{-}O)(\eta^2,\mu\text{-}OR)_4(\eta^2\text{-}OR)_2]$; two Nb octahedra; CN of Li is 5	–	65
Uncentred $[M_4]$ tetrahedron			
$[W_4^{III}O(OPr^i)_9Cl] \cdot 0.5\,Et_2O$	$[W_4(\mu\text{-}O)(\mu\text{-}OR)_2(OR)_7Cl]$; three W = W bonds, three W – W bonds, $[WO_4]$ square	$W_2(OPr^i)_6 + NaOPr^i + [Bu^n_2NH_2]Cl +$ $+ H_2O$ (traces) $+ Et_2O$	66
Cube $[M_4(\mu_3\text{-}O)_4]$			
$[(MoO)O(OSiMe_3)(Me_2NH)]_4$	cube $[M_4(\mu_3\text{-}O)_4]$	–	67
'Butterfly' — cluster of two $[M_3]$ triangles sharing a $[M_2]$ side			
$[Mo_4^{III}O(OCH_2Bu^t)_{10}Py]$	$[Mo_4(\mu_3\text{-}O)(\mu\text{-}OR)_4(OR)_6Py]$, one triangle is centred with μ_3-O; five Mo = Mo bonds, two OR groups at the end of one 'wing'; two OR and Py groups at the end of another 'wing'; one terminal OR group at each of the central atoms	$Mo_2(OCH_2Bu^t)_6 + O_2$	68
$[K(18^z\text{-}6)_2]^+[Mo_4O(OCH_2Bu^t)_{11}]^-$	one terminal OR group at each central Mo atom, two OR groups at one 'wing', three OR groups at another 'wing'	$Mo_2(OCH_2Bu^t)_6 + AsH_3 +$ $+ KOH + 18\text{-}C\text{-}6$ (see [a])	69
Rings of two dimers (two pairs of octahedra are linked to a ring *via* two μ-O groups)			
$[Nb_2Cl_4(OEt)_2(THF)_2]_2O_2$	$[Nb_2(\mu\text{-}Cl)(\mu\text{-}OR)Cl_3(OR)(THF)_2]_2(\mu\text{-}O)_2$	$NbCl_3 + EtOH + THF$	70
$[Re_2^V(OMe)_8]_2O_2$	$[Re_2(\mu\text{-}OR)_2(OR)_6]_2(\mu\text{-}O)_2$	electrochemical synthesis (Re + MeOH)	71
$[Re_2^{VI}O_3(OMe)_6]_2$	$[(ReO)_2(\mu\text{-}OR)_2(OR)_4]_2(\mu\text{-}O)_2$	the same	72
Planar $[M_4]$ rhombuses with two μ_3-L and four μ-L ['$Ti_4(OMe)_{16}$ type']			
$[Bi_4O_2(OBu^t)_8]$	Bi^1 five-vertex polyhedron, a Bi^2 tetrahedron	$Bi[N(SiMe_2)_2]_3 + Bu^tOH$	73
$[(V^VO)_4O_4(OMe)_4(bipy)_2]$	two $[V^1O(\mu_3\text{-}OR)_2(\mu\text{-}O)_2(OMe)]$ octahedra and two $[V^2O(\mu_3\text{-}OR)(\mu\text{-}O)_2bipy]$ octahedra	$V^{IV}O(sal\text{-}glu) \cdot H_2O$ [b] + bipy	74
$[Nb_4O_4\{O(Me_2C)_2O\}_2(OPr^i)_8]$	two $[Nb^1(\mu_3\text{-}O)_2(\mu\text{-}O)(OPr^i)(\eta^2,\mu\text{-}RO_2)]$ octahedra and two $[Nb^2(\mu_3\text{-}O)(\mu\text{-}O)(OPr^i)_3(\eta^2,\mu\text{-}RO)]$ octahedra	$Nb(OPr^i)_5 + (Me_2C)_2(OH)_2$	52
$[Ce_2Ti_2O_2(RO_2)_4(OPr^i)_4(Pr^iOH)_2]$, $R = (Me_2C)_2$	two $[Ti^1(\mu_3\text{-}O)_2(\eta^2,\mu\text{-}RO_2)_2]$ octahedra and two $[Ce^2(\mu_3\text{-}O)(\eta^2,\mu\text{-}RO)_2(OPr^i)_2(Pr^iOH)]$ octahedra	$Ce_2O[(Me_2C)_2O_2]_2[(Me_2C)_2O_2H]_2 +$ $+ Ti(OPr^i)_4$	75
$[Ce_2Nb_2O_2\{O(Me_2C)_2O\}_4(OPr^i)_6]$	two $[Nb^1(\mu_3\text{-}O)_2(\eta^2,\mu\text{-}RO_2)_2]$ octahedra and two $[Ce^2(\mu_3\text{-}O)(\eta^2,\mu\text{-}RO)_2(OPr^i)_3]$ octahedra	$Ce(OPr^i)_4(Pr^iOH) + [Nb_2O.$ $.\{(Me_2C)_2O_2\}_4\{(Me_2C)_2O_2H\}_2(OPr^i)]$	75

Table 3 (continued).

Compound	Structure	Starting compounds, conditions of formation	Ref.
Planar $[M_4]$ rhombuses with two μ_3-L and four μ-L ['$Ti_4(OMe)_{16}$ type']			
$[MgNbO(OMe)_5(MeOH)_2]_2$	two $[Mg^1(\mu_3\text{-}OR)_2(\mu\text{-}OR)_2(ROH)_2]$ octahedra and two $[(Mo^2O_2)(\mu_3\text{-}OR)(\mu\text{-}OR)(\mu\text{-}O)(OR)]$ octahedra	$Mg(OMe)_2$ + MeOH + + $Nb(OMe)_5$, Δ	76
$[(MoO_2)_4O_2(OMe)_4(Me_2CNOH)]$	two $[(Mo^1O_2)(\mu_3\text{-}OR)_2(\mu\text{-}OR)(\mu\text{-}O)]$ octahedra and two $[(Mo^2O_2)(\mu_3\text{-}OR)(\mu\text{-}OR)(\mu\text{-}O)(OR)]$ octahedra	$[Bu^n_4N]_4Mo_8O_{26}$ + MeOH + + Me_2CNOH	77
$[Bu^n_4N]^+_2[(MoO_2)_4O_2(OMe)_6]^{2-}$	the same	$[Bu^n_4N]_4Mo_8O_{26}$ + MeOH	78
$[Bu^n_4N]^+_2[(MoO_2)_2(MoO)_2O_4(OMe)_2.$ $.(C_6H_4O_2\text{-}1,2)_2]^-$	two $[(Mo^1O_2)(\mu_3\text{-}OR)_2(\mu\text{-}O)_2]$ octahedra and two $[(Mo^2O)(\mu_3\text{-}OR)(\mu\text{-}O)_2(\eta^2\text{-}ArO_2)]$ octahedra	$[Bu^n_4N]_4Mo_8O_{26}$ + + $C_6H_4(OH)_2$-1,2 + MeOH	78, 79
$[(Mo^VO)_4O_4(OPr^i)_4Py_4]$	two $[(Mo^1O)(\mu_3\text{-}O)_2(\mu\text{-}O)(\mu\text{-}OR)Py]$ octahedra and $[(Mo^2O)(\mu_3\text{-}O)(\mu\text{-}O)(\mu\text{-}OR)(OR)Py]$ octahedra, Mo = Mo bonds	$Mo_2(OPr^i)_6 + O_2$ + Py	80
$[(Mo^VO)_2OCl_2(OEt)_2L]_2$, L = EtOH, PMe_3	two $[(Mo^IO)(\mu_3\text{-}O)_2(\mu\text{-}OR)_2Cl]$ octahedra and two $[(Mo^2O)(\mu_3\text{-}O)(\mu\text{-}OR)_2ClL]$ octahedra, Mo — Mo bonds	$[(MoO)_2Cl_4(OEt)_2$ + EtOH] + + PMe_3 + SbF_3 + $Me_3SiC_3H_5$	81
$[(Mo^{V,VI}O)_4O_2Cl_4(OPr^n)_6]$	two $[(Mo^1O)O_2(\mu\text{-}OR)_2Cl]$ octahedra and two $[(Mo^2O)O(\mu\text{-}OR)_2(OR)Cl]$ octahedra, Mo — Mo bonds	$MeMoCl_2(OPr^n)_2 + Pr^nOH$	82
$[UO_2]_2[U_2O_2(OPh)_{10}(THF)_4]$	two $[(U^{VI(1)}O_2)(\mu_3\text{-}O)_2(\mu\text{-}OR)_2THF]$ pentagonal bipyramids and two $[U^{V(2)}(\mu_3\text{-}O)(\mu\text{-}OR)_2(OR)_3THF]$ pentagonal bipyramids	UCl_3 + NaOPh + THF	83
$[Re^{V,VI}_4O_6(OPr^i)_{10}]$	four $[Re_4(\mu_3\text{-}O)_2(\mu\text{-}O)_4(OR)_{10}]$ octahedra, five Re — Re bonds	electrochemical synthesis (Re + Pr^iOH)	84
$[LiNbO(OEt)_4(EtOH)]_2$	tetrahedron $[Li^2(\mu_3\text{-}OR)(\mu\text{-}OR)_2(ROH)]$ and the $[Nb^1(\mu_3\text{-}OR)_2(\mu\text{-}OR)_2(OR)O]$ octahedron	$LiNb(OEt)_5$ (decomposition in solution)	85
Linear chain of tetrahedra and octahedra			
$[(V^VO)(V^{IV}O)O(OEt)_3Phen]_2$ (see [c])	$[(V^VO)(OR)_2(\mu\text{-}O)(V^{IV}O)(\mu\text{-}OR)Phen]_2$	VCl_3 + NaSPh + EtOH + Phen	86
Zigzag molecule			
$[(Re^{VII}O_3)NbO(OMe)_4]_2$	$[(ReO_3)(\mu\text{-}O)Nb(OR)_3(\mu\text{-}OR)]_2$; Re — O — Nb angle $\approx 180^\circ$	$Re_2O_7 + Nb(OR)_5$	87
Octahedron is linked to a vertex of the $[M_3]$ triangle *via* a common $(\mu\text{-}OR)_3$ face			
$[W^{IV}_4O_2(OPr^i)_{12}]$	$[W_4(\mu\text{-}O)_2(\mu\text{-}OR)_3(OR)_9]$, along two ($\mu$-O) sides, W ≡ W bonds	$W_2(OPr^i)_6 + Me_2CO$	88

Note. Accepted abbreviations: ax is axial.
[a] 18-C-6 is 18-crown-6; [b] sal-glu is *N*-salicylideneglycinate; [c] Phen is phenathroline.

Table 4. Pentanuclear oxoalkoxides.

Compound	Structure	Starting compounds, conditions of formation	Ref.
Square pyramids $[M_5(\mu_5\text{-}O)]$ and $[M_5(\mu_5\text{-}OH)]$			
$[Ba_5O(OPh)_8(PhOH)(THF)_8]$	$[Ba_5H(\mu_5\text{-}O)(\mu_3\text{-}OR)_4(\mu\text{-}OR)_4(OR)_9(THF)_8]$, four μ_3-OR groups above lateral faces, four μ-OR groups along the base, CN of Ba_{ax} is 6, CN of Ba_{eq} is 7	Ba + PhOH + THF	89
$[Ba_5(THF)_4(H_2O)(OH)\{OCH(CF_3)_2\}_9]\cdot THF$	$[(BaTHF)_4Ba(H_2O)(\mu_5\text{-}OH)(\mu_3\text{-}OR)_4(\mu\text{-}OR)_4(OR)]\cdot THF$, four μ_3-OR groups above lateral faces, four μ-OR groups along the base	Ba + $(CF_3)_2CHOH$ + THF	90
$[(Ba_5(OH)(OC_6H_3Bu^t_2\text{-}3,5)_9(THF)_5]$	$[(BaTHF)_5(\mu_5\text{-}OH)(\mu_3\text{-}OR)_4(\mu\text{-}OR)_4(OR)]$; four μ_3-OR groups above lateral faces, four μ-OR groups along the base, OR group at Ba_{ax}, CN of Ba are 7, 8	Ba + 3,5-$Bu^t_2C_6H_3OH$ + + THF	91
$[M_5O(OPr^i)_{13}]$, M = In, Sc,Y, [Y4Pr], Pr, Er, Yb, Gd	$[M_5(\mu_5\text{-}O)(\mu_3\text{-}OR)_4(\mu\text{-}OR)_4(OR)_5]$; four μ_3-OR groups above lateral faces, four μ-OR groups along the base, CN of M is 6	electrochemical synthesis; M + Pr^iOH; MCl_3 + $NaOPr^i$; $Pr(OPr^i)_3\cdot Pr^iOH$ + Pr^iOH	10–14, 92, 93
$[Al_5O(OBu^i)_{13}]$	$[Al_5(\mu_5\text{-}O)(\mu\text{-}OR)_8(OR)_5]$; Al_{ax} — an octahedron, four Al_{eq} atoms — trigonal bipyramids, 8 μ-OR groups along all edges	$Al_4O(OBu^i)_{10}\cdot Bu^iOH$ + + DBU [b]	53
$[Fe_5O(OEt)_{13}]$	Fe_{ax} — an octahedron, four Fe_{eq} atoms — trigonal bipyramids, eight μ-OR groups along all edges	$FeCl_3$ + NaOEt	15

Table 4 (continued).

Compound	Structure	Starting compounds, conditions of formation	Ref.
Square pyramids $[M_5(\mu_4\text{-O})]$ with a centred base			
$[IBa(LiTHF)_4(OH)(OBu^t)_4]$	$[IBa(LiTHF)_4(\mu_4\text{-OH})(\mu_3\text{-OR})_4]$	$BaI_2 + LiOBu^t + H_2O + THF$	94
$[Sr_5O(OCH_2Bu^t)_8(Bu^tCH_2OH)(THF)_4]$	$[Sr_5(\mu_4\text{-O})(\mu_3\text{-OR})_4(\mu\text{-OR})_4(ROH)(THF)_4]$	$Sr + Bu^tCH_2OH + THF$	95
$[Eu^{III}Eu^{II}_4O_5(OAr)(ArOH)_5(MeCN)_8]$, Ar = $C_6H_3Pr^i_2$-2,6	$[Eu_5(\mu_4\text{-O})(\mu_3\text{-O})_4(\mu\text{-OAr})(\mu\text{-ArOH})(ArOH)_4(MeCN)_8]$, Eu^{III}_{ax} — an octahedron, CN of Eu^{II}_{eq} is 7	$Eu(OPr^i)_2 +$ + 2,6-$Pr^i_2C_6H_3OH$	96
$[Ti_3(OMe)_2(OPr^i)_9]^+[Fe^{II}_2Fe^{III}_2TiOCl_4(OPr^i)_9]^-$	$[(FeCl)_4Ti(\mu_3\text{-O})(\mu\text{-OR})_8(OR)]^-$ (see [a])	$FeCl_2 + KOPr^i +$ + $Ti(OPr^i)_4$ + MeOH	97
Trigonal bipyramids $[M_5(\mu_5\text{-O})]$			
$[Li(MgTHF)_4O(\mu\text{-}OC_6H_4Me\text{-}2)_7]$	two Mg_{ax} atoms; Mg — a trigonal bipyramid, Li — T-like coordination	$LiBu^n + MgBu^n_2 +$ + 2-$MeOC_6H_3OH$	98
$[Nd_5O(OPr^i)_{13}(Pr^iOH)_2]$	$[Nd_5(\mu_5\text{-O})(\mu_3\text{-OR})_2(\mu\text{-OR})_6(OR)_5(ROH)_2]$, two μ_3-OR groups above faces of two different pyramids, six *mer*-μ-OR groups, Nd — an octahedron	$Nd + Pr^iOH$ ($HgCl_2$)	10, 13, 99
$[Sm_4TiO(OPr^i)_{14}]$, $[(Tb_{0.9}Eu_{0.1})_4TiO(OPr^i)_{14}]$	two μ_3-OR groups above faces of two different pyramids, six *mer*-μ-OR groups, Ti — a trigonal bipyramid, Ln — an octahedron	$LnI_2 + NaTi(OPr^i)_5$, Ln = Sm, Tb, Eu	100, 101
Two $[MM'_2]$ triangles sharing an M vertex			
$Sr(Pr^iOH)_2[Ti_2O(OPr^i)_7]_2$	$Sr(ROH)_2[Ti_2(\mu_3\text{-O})(\mu\text{-OR})_2(OR)_5]_2$; $[Ti_2O(OR)_7]$ — two trigonal bipyramids sharing a $[(\mu_3\text{-O})(\mu\text{-OR})]$ edge	$Sr(OPr^i)_2 + Ti(OPr^i)_4 +$ + Pr^iOH	102
$[Ta_5O_7(OBu^t)_{11}]$	$[Ta_5(\mu_3\text{-O})_4(\mu\text{-O})_3(\mu\text{-OR})(OR)_{10}]$, $[Ta_5]$ is a trigonal pyramid	$Ta(OBu^t)_5 + H_2O$ (h = 1)	103
$[NaBi_4O_2(OC_6F_5)_9(THF)_2]$	$[NaBi_4(\mu_3\text{-O})_2(\mu\text{-OR})_7(OR)_2]$, $[NaBi_2(\mu\text{-OR})_3]$ ring in the centre	$BiCl_3 + NaOC_6F_5$	64
Rings containing five M atoms			
$[Mo^V_2Mo^{VI}Ta_2O_8(OPr^i)_{10}]$	Two $[Ta(\mu\text{-O})(\mu\text{-OR})_2(OR)_3]$ octahedra, one $[(Mo^VO)_2(\mu\text{-O})_2(\mu\text{-OR})_4]$ group (CN 5) and the $[(Mo^{VI}O_2)(\mu\text{-O})_2]$ tetrahedron	$Mo^V_4Ta_2O_8(OPr^i)_{14} +$ + O_2 traces	104

Note. Hereinafter, eq is equatorial.
[a] The authors considered the oxo ligand as tridentate taking into account the presence of three short bonds, *viz*., two $Fe_{eq}-O$ bonds and one $Ti_{ax}-O$ bond. [b] DBU is 1,8-diazabicyclo[5.4.0]undec-7-ene.

Table 5. Hexanuclear oxoalkoxides.

Compound	Structure	Starting compounds, conditions of formation	Ref.
Octahedra $[M_6(\mu_6\text{-O})]$			
$[Ba_6O(OC_2H_4OMe)_{10}(MeOC_2H_4OH)_4]$	$[Ba_6(\mu_6\text{-O})(\mu_3,\eta^2\text{-OR})_8(\eta^2\text{-ROH})_4(\mu\text{-OR})_2]$, a $[M_6]$ octahedron, μ_3-OR groups on eight faces, CN of Ba_{ax} is 8, CN of Ba_{eq} is 9	$Ba + MeOC_2H_4OH$	105
trans-$[Na_2Gd_4O(OBu^t)_{12}]$	$[Na_2\{Gd(OR)\}_4(\mu_6\text{-O})(\mu_3\text{-OR})_8]$, the $[NaO(\mu_3\text{-OR})_4]$ square pyramid in the axial position, the $[GdO(\mu_3\text{-OR})_4.$ $.(OR)]$ octahedron in the equatorial position	$GdCp_3 + NaOBu^t$	106
trans-$[K_4Zr_2O(OPr^i)_{10}]$	$[K_4Zr_2(\mu_6\text{-O})(\mu_3\text{-OR})_8(OR)_2]$, the $[ZrO(\mu_3\text{-OR})_4(OR)]$ octahedron in the axial position, the $[KO(\mu_3\text{-OR})_4]$ square pyramid in the equatorial position	$KH +$ '$Zr(OPr^i)_4$' $+ H_2O$	107
trans-$[K_4Zr_2O(OAr)_8(OEt)_4]$, Ar = C_6H_3OMe-2-All-4	$[K_4Zr_2(\mu_6\text{-O})(\mu_3\text{-OAr})_8(\mu\text{-OR})_2]$, K atoms are coordinated by eight OMe groups of eugenol	'$Zr(OEt)_4$' + + KOC_6H_3OMe-2-All-4	108
trans-$[M^I_4M^{III}_2O(OBu^t)_8]\cdot n$ THF, M^I = Na, K; M^{III} = Sb, Bi; n = 0, 1, 4	$[M_6(\mu_6\text{-O})(\mu_3\text{-OR})_8]$, M^I and M^{III} are disordered	$M(OBu^t)_3 + NaOBu^t + THF$ $(-Bu^t_2O)$	109
trans-$[Na_4Sb_2O(OSiMe_3)_8]$	$[M_6(\mu_6\text{-O})(\mu_3\text{-OR})_8]$, Na and Sb are disordered	$Sb(OSiMe_3)_3 + NaOSiMe_3$	110

Table 5 (continued).

Compound	Structure	Starting compounds, conditions of formation	Ref.
Octahedra [$M_6(\mu_6\text{-}O)$]			
cis-[$Na_4Bi_2O(OC_6F_5)_8(THF)_4$]	[$(NaTHF)_4Bi_2(\mu_6\text{-}O)(\mu_3\text{-}OR)_2(\mu\text{-}OR)_6$]	$2\,NaOC_6F_5 + Bi(OC_6F_5)_3 +$ + THF	111
[$V_6^{IV,V}O_7(OEt)_{12}$]	[$(VO)_6(\mu_6\text{-}O)(\mu\text{-}OR)_{12}$]	$VO(OEt)_3 + H_2O$ (traces)	112
$M_2[V_6^{IV,V}O_7(OH)_n\{MeC(CH_2O)_3\}_{(12-n)/3}]$, $n = 0, 3$; $M_2[(V^{IV,V}O)_6O_{7-n}(OH)_n\{RC(CH_2O)_3\}_2]$, R = NO_2, CH_2OH, Me, Et, Bn; $n = 0, 2, 4, 6$; $[M][(V^VO)_6O_6(OMe)_7]$, M = R_4N, Na	[$M_6(\mu_6\text{-}O)(\mu\text{-}O)_{12}O_6$], structural analogue of the [M_6O_{19}] 'large octahedron', μ-O groups along twelve edges of the octahedron	$V_2O_5 + V_2O_3 + NaVO_3 +$ + NH_4Cl + $MeC(CH_2OH)_3$ + + H_2O (Δ, high pressure)	113–117
[$Bu^n_4N]_{n-1}[M(WO)_5O_{13}(OMe)]$, M = Ti, Zr, Nb, Ta	analogue of the 'large octahedron', one terminal O atom is replaced by OMe	$M(OMe)_n + WO_4^{2-} +$ + MeOH + $(Bu^n_4N)Cl$	118
[$Bu^n_4N]_3[Nb_2W_4O_{18}(OR)$], R = Me, Et, Pr^i, Bu^t, $SiMe_3$	analogue of the 'large octahedron', $[Nb_2(WO)_2(WO_2)_2(\mu\text{-}O)_{12}(OR)]^{3-}$	$[HNb_2W_6O_{19}]^{3-}$ + ROH + + $(Bu^n_4N)Cl$	119
$[Me_4N]_2[Fe_6O\{MeC(CH_2O)_3\}_6]\cdot 4\,MeOH$ $[Me_4N]_2[Fe_6O\{MeC(CH_2O)_3\}(OMe)_6Cl_6]\cdot 2\,H_2O$	analogue of the 'large octahedron', one of three O atoms of the RO_3 ligand is μ-coordinated, two other O atoms are terminal	$FeCl_3 + [Me_4N]OMe +$ + $MeC(CH_2OH)_3$ + MeOH + H_2O	120, 121
$Tl_4Ti_2O(OR)_5(OEt)_5$, R = Et, Pr^i	[$Tl_4Ti_2(\mu_6\text{-}O)(\mu_3\text{-}OR)_8(OEt)_2$], Ti_{ax} atoms — distorted octahedron, Tl_{eq} atoms — Ψ-octahedra [a]	TlOEt + $Ti(OR)_4$, R = Et, Pr^i	122
Trigonal antiprism			
$[Mo_6^{3,3+}O(\mu\text{-}OEt)_{12}(OEt)_6]\cdot 4.8\,H_2O$	[$Mo_6(\mu_6\text{-}O)$]; μ-OR groups along nine edges and three μ-OR groups along diagonals of lateral faces	$Mo(OEt)_3 + H_2O$ (h = 15)	123
Uncentred [M_6] octahedra			
[$Sn_6O_4(OR)_4$], R = Me, Pr^i	[$Sn_6(\mu_3\text{-}O)_4(\mu_3\text{-}OR)_4$], μ_3-O and μ_3-OR groups alternate on eight octahedron faces	$Sn(OR)_2 + H_2O$, R = Me, Pr^i	124–126
[$Pb_6O_4(OR)_4$], R = Pr^i, Bu^t	[$Pb_6(\mu_3\text{-}O)_4(\mu_3\text{-}OR)_4$], μ_3-O and μ_3-OR groups alternate on eight octahedron faces	electrochemical synthesis ($Pb + Pr^iOH$); $Pb(OBu^t)_2 + H_2O$	127
[$Bi_6O_3(OC_6F_5)_{12}(THF)_2$]	[$Bi_6(\mu_4\text{-}O)(\mu_3\text{-}O)_2(\mu\text{-}OR)_{12}(THF)_2$]	$BiCl_3 + NaOC_6F_5 + THF$	64
[$La_2(MoO)_4(\mu_4\text{-}O)_4(\mu\text{-}OPr^i)_8(OPr^i)_6$]	[$La_2(MoO)_4(\mu_4\text{-}O)_4(\mu\text{-}OR)_8(OR)_6$], Mo atoms — octahedra, CN of La is 9	$La_5O(OPr^i)_{13}$ + + $MoO(OPr^i)_4$ ($-R_2O$)	128
Two [M_4] tetrahedra sharing an [M_2] edge			
$[Fe_6O_2(OMe)_{12}\{N(C_2H_4NH_2)_3\}_2]^{2+}\cdot$ $\cdot[CF_3SO_3]_2^-\cdot 2\,MeOH$	[$Fe_6(\mu_4\text{-}O)_2(\mu\text{-}OR)_8(OR)_4L_2]^{2+}$	$[Fe_3O_2(OH)N(C_2H_4NH_2)_3]^{4+}$ + + MeOH + CF_3SO_3H	129
Two cubes sharing an [$M_2(\mu_4\text{-}O)_2$] face			
$[Ca_6O_2(OEt)_8]\cdot 14\,EtOH$	[$Ca_6(\mu_4\text{-}O)_2(\mu_3\text{-}OR)_4(OR)_4$]; three terminal OR groups at the terminal Ca atom, two terminal OR groups at the central Ca atom	$Ca(OEt)_2 + EtOH +$ + $O_2 + H_2O$ (traces), Δ	16
Two [$M_3(\mu_n\text{-}O)$] triangles			
[$Gd_6O(MeOC_2H_4O)_{16}$]	[$Gd_6(\mu_4\text{-}O)(\eta^2,\mu_3\text{-}OR)_4(\eta^2,\mu\text{-}OR)_6(\eta^1,\mu\text{-}OR)_2(OR)_4$], two triangles in perpendicular planes sharing a μ_4-O vertex, CN of Gd are 7, 8	$Gd + MeOC_2H_4OH$	130
$[Ba_2Ti_4O(OMe)_{18}(MeOH)_7]\cdot MeOH$	[$Ba_2Ti_4(\mu_3\text{-}O)(\mu_3\text{-}OR)_6(\mu\text{-}OR)_2(OR)_{10}(ROH)_7]\cdot ROH$, [$BaTi_2(\mu_3\text{-}O)$] triangles sharing a [$Ba_2$] edge, CN of Ba is 9	$Ba + MeOH + Ti(OMe)_4$	131
[$Bi_6O_3(OC_6H_3Cl_2\text{-}2,6)_{12}$]	two [$Bi_3(\mu_3\text{-}O)(\mu\text{-}OR)_2(OR)_2$] triangles are linked *via* two μ_3-O groups and three μ-OR groups	$BiPh_3 + 2,6\text{-}Cl_2C_6H_3OH$	132
$[Hf_3O(OEt)_{10}(EtOH)]_2$	two [$Hf_3(\mu_3\text{-}O)(\mu\text{-}OR)_2(OR)_5$)] triangles are linked to each other to form a ring *via* two pairs of μ-OR groups	electrochemical synthesis ($Hf + EtOH$)	45

Table 5 (continued).

Compound	Structure	Starting compounds, conditions of formation	Ref.
Rings of two $[M_3(\mu_3\text{-O})]$ triangles linked *via* two linear μ-O groups			
$[MoTa_2O_4(OMe)_8]_2$	$[(MoO_2)Ta_2(\mu_3\text{-O})(\mu\text{-OR})_3(\mu\text{-O})(OR)_5]_2$	$MoO(OMe)_4 + 2\,Ta(OMe)_5 + H_2O$	133
$[IZnTa_2O_2(OPr^i)_7]_2$	$[IZnTa_2(\mu_3\text{-O})(\mu\text{-OR})_3(\mu\text{-O})(OR)_4]_2$	$ZnI_2 + KTa(OPr^i)_6$	134
$[Mo_3^{V}O_4Cl_4(OEt)_3]_2$	$[(MoOCl)_3(\mu_3\text{-O})(\mu\text{-OR})_3(\mu\text{-Cl})]_2$	$Mo_2Cl_4O_2(OEt)_2\cdot EtOH + Me_3SiC_3H_5\,(-C_3H_6)$	135
$[LiMo_2O_4(OC_2H_4OMe)(OPr^i)_4]_2$	$[Li(MoO_2)(MoO)(\eta^2,\mu_3\text{-}OC_2H_4OMe)(\mu_3\text{-OR})(\mu\text{-O}).(\mu\text{-OR})_2(OR)]_2$	$Li_2Mo_2O_4(OEt)_5\cdot EtOH + Pr^iOH + MeOC_2H_4OH$	136
$[NaMo_2O_4(OPr^i)_5(Pr^iOH)]_2$	$[Na(ROH)(MoO_2)(MoO)(\mu_3\text{-OR})_2(\mu\text{-OR})_2.(\mu\text{-O})(OR)]_2$	$MoO(OPr^i)_4 + NaOPr^i\,(-Pr^i_2O)$	137, 138
$[Ta_2(Re^{VI}O_4)O(OMe)_7]_2$	$[(ReO_3)(\mu\text{-O})Ta(\mu\text{-OR})_2Ta(OR)_3(\mu\text{-O})]_2$	$Re_2O_7 + Ta(OMe)_5$	139
Derivatives of $Ti_4(OMe)_{16}$ structural type			
$[Er_2Ti_4O_2(OEt)_{18}(EtOH)_2]$	$[Er_2Ti_4(\mu_4\text{-O})_2(\mu_3\text{-OR})_2(\mu\text{-OR})_8(OR)_8(ROH)_2]$, two $[Ti(\mu_3\text{-OR})(\mu\text{-OR})_2(OR)_2]$ fragments are bound to μ_3-O groups	$ErCl_3 + KOEt + Ti(OEt)_4 + H_2O$	140
$[NaBi_2O(OC_6F_5)_5THF]_2$	$[\{Na(THF)_2\}Bi_4(\mu_4\text{-O})_2(\mu\text{-OR})_{10}]$, two $\{Na(THF)\}$ fragments are bound to μ_3-O groups	$NaOC_6F_5 + Bi(OC_6F_5)_3 + THF$	64
$[Li_4(WO)_2O_2(OR)_6(ROH)]^{2+}[W_6O_{19}]^{2-}$, R = C_2H_4OMe	$[Li_4(WO)_2(\mu\text{-O})_2(\eta^2,\mu_3\text{-OR})_2(\eta^2,\mu\text{-OR})_4(\eta^2\text{-ROH})]^{2+}$, two $[Li(\mu\text{-O})(\eta^2\text{-ROH})]$ fragments are bound to terminal [WO] groups	$WO(OC_2H_4OMe)_4 + LiCl + O_2$	136
$[H_3Ba_6O(OBu^t)_{11}(R'O_2)(THF)_3]$, $R'O_2$ = $OCEt_2CH_2O$	$[Ba_5(\mu_5\text{-O})(\mu_3\text{-OR})_4(\mu\text{-OR})_3(OR)(THF)_3](\mu_3\text{-OR}).(\mu\text{-OR})_2Ba(\eta^2\text{-}R'O_2)]$, two Ba atoms are bound to three Ba atoms, $Ti_4(OMe)_{16}$ structural type with μ_5-O and μ-OR groups	$Ba + Bu^tOH + THF + HOCEt_2CH_2OH$	89
Zigzag chains			
$[Mo_3^{5.3+}O_5(OPr^i)_6]_2$ (A)	$[(Mo^{VI}O)(OR)_3(\mu\text{-OR})_2(Mo^{V}O)(\mu\text{-O})_2(Mo^{V}O)(\mu\text{-OR})_2]$, all Mo atoms are in a single plane; Mo = Mo bonds	$Mo_2(OPr^i)_6 + O_2$; $MoO(OPr^i)_4 \rightarrow A + Pr^i_2O + Pr^iOH + Me_2CO$	46, 141
$[Mo_2^{V}TaO_4(OPr^i)_7]_2$	$[(RO)_3Ta(\mu\text{-OR})_3(MoO)(\mu\text{-O})_2(MoO)(\mu\text{-OR})]_2$, Mo = Mo bonds	$MoO(OPr^i)_4 + Ta(OPr^i)_5$	104

[a] The authors considered this molecule as an octahedron centred only along the $Ti_{ax}-(\mu\text{-O})-Ti_{ax}$ direction taking into account a substantial difference in the Ti—O and Tl—O bond lengths.

Table 6. Heptanuclear oxoalkoxides.

Compound	Structure	Starting compounds, conditions of formation	Ref.
$[Ti_7O_4(OEt)_{20}]$	$[Ti_7(\mu_4\text{-O})_2(\mu_3\text{-O})_2(\mu\text{-OEt})_8(OEt)_{12}]$, six edge-sharing octahedra about the central $[TiO_4(\mu\text{-OEt})_2]$ octahedron	$Ti(OEt)_4 + H_2O$ (h = 0.5–0.7)	7, 142, 143
$[Ta_7O_9(OPr^i)_{17}]$	$[Ta_7(\mu_3\text{-O})_3(\mu\text{-O})_6(\mu\text{-OR})_4(OR)_{13}]$, two vertex-sharing $[Ta_4]$ tetrahedra are linked *via* one μ_3-O and two μ-OR groups	electrolyte (Ta + Pr^iOH), $Ta(OPr^i)_5 + H_2O$ (h = 0.5–1)	33, 34 103
$[Pb_7O_2(OPr^i)_{10}]$	fragment $[Pb_4(\mu_4\text{-O})(OR)_6]$ is linked to the $[Pb_3(\mu_3\text{-O})(\mu_3\text{-OR})(\mu\text{-OR})_2]$ chain *via* one μ_3-OR group and two μ-OR groups	$Pb(OPr^i)_2 + H_2O$	144
$[Pb_7O_2(OSiMe_3)_{10}]$	fragment $[Pb_4(\mu_4\text{-O})(OR)_6]$ is linked to the $[Pb_3(\mu_3\text{-O})(\mu_3\text{-OR})(\mu\text{-OR})_2]$ chain *via* one μ_3-OR group and two μ-OR groups	$Pb[N(SiMe_3)_2]_2 + Me_3SiOH\,[-(Me_3Si)_2O]$	145
$[Fe_7O(OH)(RO_3)_4Cl_6(MeCN)_2]$, R = $(CH_2)_3CCH_2OH$	$[Fe(OH)(MeCN)_2][Fe_6(\mu_6\text{-O})Cl_6(RO_3)_4]$, the $[Fe_6(\mu_6\text{-O})]$ octahedron is linked to the $[Fe(\mu_3\text{-O})_3(MeCN)_2(OH)]$ octahedron	$FeCl_2\cdot 4\,H_2O + V_2O_5 + C(CH_2OH)_4 + MeCN$,	146

Table 7. Octanuclear oxoalkoxides.

Compound	Structure	Starting compounds, conditions of formation	Ref.
Centred $[M_n(\mu_n\text{-O})]$ polyhedra			
$[Al_8O_2(OH)_2(OBu^i)_{18}]$	$[Al_4(\mu_4\text{-O})(\mu\text{-OH})(\mu\text{-OR})_5(OR)_4]_2$, two $[Al_4(\mu_4\text{-O})]$ tetrahedra sharing a $(\mu\text{-OR})_2$ edge	distillation of $Al_4O(OBu^i)_{10}$	53
$[K_2Sb_2O(OPr^i)_6]_2$	two $[K_2Sb_2(\mu_4\text{-O})(\mu_3\text{-OR})_6]$ tetrahedra are linked *via* the $[K_4(\mu_3\text{-OR})_8]$ group	$KSb(OPr^i)_4$, Δ	109
$[Ni_5Sb_3O_2(OEt)_{15}(EtOH)_4]$	$[Ni_5Sb_3(\mu_4\text{-O})_2(\mu_3\text{-OR})_4(\mu\text{-OR})_8(OR)_3(ROH)_4]$, $[Ni_4(\mu_3\text{-OR})_2(\mu_4\text{-O})_2]$ cube in the centre is surrounded by $[{:}SbO_4]$ groups of Ψ-octahedra and three Ni octahedra	$Sb(OEt)_3 + NiCl_2 + NaOEt$	147
$[Na_4Cr^{III}_4O_3(OPh)_{10}(TMEDA)_4]$ [a]	$[(Na_4(TMEDA)_4Cr_4(\mu_3\text{-O})_3(\mu_3\text{-OR})_4(\mu\text{-OR})_6]$; two $[NaCr_2(\mu_3\text{-O})]$ triangles, one $[Cr_3(\mu_3\text{-O})]$ and a $[Na(\mu\text{-OR})_3Cr]$ group; CN of Na and Cr is 5	$Na_4Cr^{II}_2(OPh)_8 +$ + TMEDA + O_2	148
$[Na_2Fe_6O(OMe)_{18}(MeOH)_6]$	$[Na(ROH)_3]_2[Fe_6(\mu_6\text{-O})(\mu_3\text{-OR})_6(\mu\text{-OR})_6(OR)_6]$; Na_{ax}	$FeCl_3 + NaOMe$	149
$[Pr_4O_2(OC_2H_4OMe)_8(OPMe_3)]_2$	spherical $[Pr_4(\mu_4\text{-O})_2(\eta^2,\mu_3\text{-OR})_2(\eta^2,\mu\text{-OR})_4(\eta^1,\mu\text{-OR})(OR).$ $.(OPMe_3)]_2$ molecule; CN of Pr are 7 and 8	$Pr[N(SiMe_3)_2]_3 +$ + $MeOC_2H_4OH$	150
Isopolyanion-type structures			
$[Ti_8O_6(OBn)_{20}]\cdot Et_2O$	$[Ti_8(\mu_3\text{-O})_4(\mu\text{-O})_2(\mu\text{-OR})_8(OR)_{12}]$	$Ti(OBn)_4 + H_2O$, $h = 1$	143
$[M_8O_{10}(OEt)_{20}]$, M = Nb, Ta	$[M_8(\mu_3\text{-O})_2(\mu\text{-O})_8(\mu\text{-OR})_6(OR)_{14}]$, two octahedra fragments $[M(\mu\text{-O})_4(OR)_2]$ are linked to each other to form a ring *via* two triads of $[M_3(\mu_3\text{-O})(\mu\text{-OR})_3(OR)_6]$ octahedra	$M(OEt)_5 + H_2O$ ($h = 1-1.25$) $NbO(EtO)_3$ ($-Et_2O$)	8, 103, 151, 152
$Na_4[Mo_8O_{24}(OMe)_4]\cdot 8\,MeOH$	$Na_4[(MoO_2)_6(MoO)_2(\mu_4\text{-O})_2(\mu_3\text{-O})_4(\mu\text{-O})_4(\mu\text{-OR})_2(OR)_2]$, structure is similar to $[Mo_8O_{26}]$ (metamolybdate)	$H_2MoO_4 + MeOH +$ + Na zeolite	153
$[Bu_4N]^+_2[Mo_8O_{20}(OMe)_4(RO_3)_2]^{2-}$, R = $MeC(CH_2)_3$	$[\{(MoO_2)_6(MoO)_2(\mu\text{-O})_6(\mu_3\text{-OMe})_2(\eta^3,\mu_3,\mu\text{-}(RO_3)\}_2(OMe)_2]^{2-}$, quadruples of octahedra sharing μ-O vertices	$[Bu_4N]_2Mo_2O_7 +$ + $MeC(CH_2OH)_3$	154
$[Bu_4N]^+_4[Mo^{V,VI}_8O_{24}(OMe)_2]^{4-}\cdot MeOH$	$[(Mo^{VI}O_3)_2(Mo^{VI}O_2)_2(Mo^{V}O)_4(\mu_3\text{-O})_2(\mu\text{-O})_8(\mu\text{-OR})_2]^{4-}$, $[Mo^{V}O_6]$ octahedron and $[Mo^{VI}O_4]$ tetrahedra, two Mo^V-Mo^V bonds	$[Bu_4N]_2Mo^{VI}_2O_7 + MeOH +$ + $Me_2C{=}NNH_2$	155
$[LiMo_4Ta_3O_{14}(OPr^i)_9(OC_2H_4OMe)_3]$	$[Li(MoO)_4Ta_3(\mu\text{-O})_{10}(\mu,\eta^3\text{-OR}')(OR)_9]$, $[LiMo_3O_4]$ cube is linked to three $[Ta(\mu\text{-O})_3(OR)_3]$ groups and one $[MoO(\mu\text{-O})_3]$ group	$LiMo_2O_4(OPr^i)_4(OC_2H_4OMe) +$ + $MoO(OPr^i)_4$	133
Rings			
$[Cu_4Zr_4O(OPr^i)_{18}]$	$[Cu_2Zr_2(\mu\text{-OR})_5(OR)_4]_2(\mu_4\text{-O})$, two eight-membered $[OCu_2(\mu\text{-OR})_2Zr_2(\mu\text{-OR})_3(OR)_4]$ rings sharing a μ_4-O vertex	$Cu_2Zr_2(OPr^i)_{10} + H_2O$	156
$[(Mo^VO)_4Cl_3O_2(OH)_3(OEt)_2(EtOH)_2]_2$	$[(MoO)_8Cl_6(\mu_3\text{-O})_4(\mu\text{-OH})_4(OH)_2(\mu\text{-OR})_4(ROH)_4]$; two rings consisting of four $[Mo_2(\mu_3\text{-O})]$ triangles sharing (μ-OH) vertices, Mo^V-Mo^V bonds	$(Mo^VO)_2Cl_4(OEt)_2 + SbF_3$	81, 157
Cuboidal-type structures			
$[LiTiO(OPr^i)_3]_4$	$[Li_4Ti_4(\mu_5\text{-O})_2(\mu_3\text{-O})_2(OPr^i)_4]$	$LiTi(OPr^i)_5 + H_2O$	158
$[Ba_4Ti_4O_4(OPr^i)_{16}(Pr^iOH)_4]$	$[Ba_4Ti_4(\mu_4\text{-O})_4(\mu_3\text{-OR})_2(\mu\text{-OR})_8(\mu\text{-OR})_6(ROH)_4]$	$BaTi_4(OPr^i)_{18}$ ($-Pr^i_2O$)	159
$[Mg_4Ta_4O_4(OBu^n)_{20}(Bu^nOH)_4]$	$[Mg_4Ta_4(\mu_4\text{-O})_4(\mu\text{-OR})_8(OR)_{12}(ROH)_4]$	$MgTa_2(OBu^n)_{12}$ ($-Bu^n_2O$)	160
$[Sr_4Ta_4O_4(OMe)_{20}(MeOH)_{10}]$	$[Sr_4Ta_4(\mu_4\text{-O})_4(\mu\text{-OR})_8(OR)_{12}(\mu\text{-ROH})_2(ROH)_8]$	$SrTa_2(OMe)_{12}$ ($-Me_2O$)	160
$[Ba_4M_4O_4(OEt)_{20}(EtOH)_6]$, M = Nb, Ta	$[Ba_4M_4(\mu_4\text{-O})_4(\mu_3\text{-OR})_4(\mu\text{-OR})_6(OR)_{10}(ROH)_6]$	$BaM_2(OEt)_{12}$ ($-Et_2O$)	85, 160
$[Mo_4Ta_4O_{16}(OPr^i)_{12}]$	vertices of the $[Mo_4Ta_4]$ cube are occupied by vertex-sharing $[(MoO)(\mu\text{-O})_3]$ tetrahedra and $[Ta(OR)_3(\mu\text{-O})_3]$ octahedra	$MoO(OPr^i)_4 + Ta(OPr^i)_5$	133
$H_x[Eu^{II}_8O_6(OC_6H_3Me_2\text{-}2,6)_{12}(OPr^i)_8]$	$H_x[Eu_8(\mu_4\text{-O})_6(\mu\text{-OAr})_{12}(OPr^i)_8]$, μ_4-O groups in the centres of faces, μ-OR are located along edges	$Eu + Pr^iOH + 2,6\text{-}Me_2C_6H_3OH$, Δ	96
$H_{10}[Eu_8O_8(OC_6H_3Me_2\text{-}2,6)_{10}.$ $.(OPr^i)_2THF]$	$H_{10}[Eu^{II}_6Eu^{III}_2(\mu_4\text{-O})_6(\mu\text{-O})_2(\mu\text{-OAr})_{10}(OPr^i)_2THF]$	$[Eu(OAr)_2(THF)_2] + Pr^iOH$	96

Table 7 (continued).

Compound	Structure	Starting compounds, conditions of formation	Ref.
Ribbon			
$[Cu_4^{II}Zr_4O_3(OPr^i)_{18}]$	$[Cu_4Zr_4(\mu_4\text{-}O)_3(\mu\text{-}OR)_{10}(OR)_8]$; $[Cu_4(\mu_4\text{-}O)(\mu\text{-}OR)_2]$ group in the centre of the molecule, two $[Cu_2Zr_2(\mu_4\text{-}O)(\mu\text{-}OR)_4(OR)_4]$ tetrahedra on opposite sides	$CuCl_2 + H_2O + K_4Zr_2O(OPr^i)_{10}$, $Cu_2^{I}Zr_2(OPr^i)_{10} + O_2$	157, 161
Two square pyramids $[M_5(\mu_5\text{-}O)]$ sharing one $[M_2]$ edge			
$[M_8O_2(OPh)_{12}(PhOH)_2L_6]\cdot 2\,PhMe$, $M_8 = Ba_8$ or $[Ba_2Sr_6]$, $L = OP(NMe_2)_3$	$[M_8(\mu_5\text{-}O)_2(\mu_3\text{-}OR)_8(\mu\text{-}OR)_4(\mu\text{-}ROH)_2L_6]$; μ_3-OR groups are above the centres of lateral faces, μ-OR groups are located along the base, CN of Ba are 6, 8	$Ba + PhOH + OP(NMe_2)_3$, $Ba + PhOH + Sr(OPh)_2 + OP(NMe_2)_3 + PhMe$	162
$[Eu_2^{III}Ba_6O_2(OPr^i)_{14}(Pr^iOH)_2(THF)_4]$	groups μ_3-OR are above the centres of lateral faces, μ-OR groups are located along the base, CN of Eu is 6, CN of Ba is 8	$Eu + Ba + Pr^iOH$, THF, Δ	163
Two $[M_4]$ tetrahedra linked by two μ-OR groups			
$[W_8^{III}O_4(OPr^i)_{16}]$	tetrahedra contain two W=W bonds and two W−W bonds, $[W_4(\mu\text{-}O)_2(\mu\text{-}OR)_2(OR)_6]_2$	decomposition of $W_4(OPr^i)_{10}$ $(-C_3H_8)$	164

[a] TMEDA = $(Me_2NCH_2)_2$.

Table 8. Nonanuclear oxoalkoxides.

Compound	Structure	Starting compounds, conditions of formation	Ref.
$[Ba_6Li_3O_2(OBu^t)_{11}(THF)_3]$	two $[M_6]$ octahedra sharing a $[Ba_3]$ face	$Ba + Bu^tOH + LiBu^n + THF$	165
$[Bi_9O_7(OC_6F_5)_{13}(THF)_2]$	$[Bi_6(\mu_3\text{-}O)_7(\mu_3\text{-}OAr)[Bi(OAr)_4]_3$; μ_3-O groups on seven faces of the $[Bi_6]$ octahedron, μ_3-OR groups on the eighth face; three of seven μ_3-O groups are coordinated to $[Bi(OR)_4]$	$[Bi(OC_6F_5)_3(PhMe)]_2\cdot 2\,PhMe +$ + THF	166
$[Fe_9O_3(OEt)_{21}]\cdot EtOH$	$[Fe_9(\mu_4\text{-}O)_2(\mu_3\text{-}O)(\mu\text{-}OR)_{15}(OR)_6(ROH)]$; two pentanuclear rings linked by μ_3-O and μ-OR groups and sharing an Fe atom	distillation of $Fe_5O(OEt)_{13}$ (200 °C, 0.01 mm Hg)	167
$H_{18}[Eu_9^{II}O_8(OAr)_{10}L_7][Eu_9O_9(OAr)_{10}L_6]$, Ar = 2,6-$Me_2C_6H_3$, L = THF	two types of monocapped cubes; μ_4-O groups in the centres of faces, three μ-OR groups along the edges	$Eu(OAr)_2(Pr^iOH)$, Δ, vacuum, THF	96

Table 9. Decanuclear oxoalkoxides.

Compound	Structure	Starting compounds, conditions of formation	Ref.
$[K_2(TMEDA)_2Li_8O(OBu^t)_8]$	$[K_2(\eta^2\text{-TMEDA})_2Li_8(\mu_8\text{-}O)(\mu_3\text{-}OR)_8]$	–	168
$[M_{10}(\mu_6\text{-}O)_2X_{26}]$ as structural analogues of $[V_{10}^{V}O_{28}]^{6-}$			
$Na_2[V_8^{IV}V_2^{V}O_{16}(RO_3)_4]\cdot n\,H_2O$, R = $HOCH_2C(CH_2)_3$	anion $[V_{10}(\mu_6\text{-}O)_2(\mu_3\text{-}O)_4(\mu\text{-}O)_{10}(\mu\text{-}OR)_4(OR)_8]^{n-}$, RO_3 groups on the surface of anions	$V_2O_5 + V_2O_3 + NaVO_3$	169
$[NH_4]_4[V_{10}^{IV}O_{16}(RO_3)_4]\cdot 4\,H_2O$ or $[Et_4N][V_{10}^{IV}O_{13}(RO_3)_5]$ [R = $EtC(CH_2)_3$] or $M_2[V_{10}^{IV}O_{14}(OH)_2(RO_3)_4]\cdot 2\,H_2O$ [M = Me_4N, Et_4N, Me_3NH; R = $HOCH_2C(CH_2)_3$]	the same	$R(OH)_3 + MCl + H_2O$, Δ, *P*	170
$M_2^{I}[Mn_{10}O_2(RO_3)_6Cl_8]\cdot 4\,MeOH\cdot 2\,H_2O$, R = $MeC(CH_2)_3$	anion $[Mn_{10}(\mu_6\text{-}O)_2[(OCH_2)_3CMe]_6Cl_8]^{2-}$	–	171
$[Fe_{10}O_2Cl_8(RO_3)_6]$, R = $EtC(CH_2)_3$	$[Fe_{10}(\mu_6\text{-}O)_2Cl_8(RO_3)_6]$	$FeCl_2\cdot 4\,H_2O + R(OH)_3$	146
$[(VO)_2Fe_8O_2Cl_6(RO_3)_6]$, R = $EtC(CH_2)_3$	$[(VO)_2Fe_8(\mu_6\text{-}O)_2Cl_6(RO_3)_6]$, two $[Fe_6(\mu_6\text{-}O)]$ octahedra sharing a $[Fe_2]$ edge	$FeCl_2\cdot 4\,H_2O + R(OH)_3 +$ + V_2O_5	146

Table 9 (continued).

Compound	Structure	Starting compounds, conditions of formation	Ref.
Other isopoly compounds			
$[Fe_{10}O_4Cl_8(OMe)_{14}(MeOH)_6]\cdot 2\,MeOH$	$[Fe_5(\mu_4\text{-}O)_2Cl_4(OR)_7(ROH)_3]_2\cdot 2\,ROH$	$FeCl_2$ + NaOMe + + $[NH_3OH]Cl$ + MeOH	172
$[LiTa_9O_{13}(OEt)_{20}(EtOH)]$	$[LiTa_9(\mu_4\text{-}O)(\mu_3\text{-}O)_3(\mu\text{-}O)_9(\mu\text{-}OR)_6(OR)_{15}(\mu_3\text{-}H)]$, Ta octahedra and a Li tetrahedron	by-product of electrochemical synthesis Ta + EtOH + LiCl	173
$[Mg(MeOH)_6]^{2-}[Mg_2Mo_8O_{22}(OMe)_6.$ $.(MeOH)_4]^{2-}\cdot 6\,MeOH$	anion $[Mg_2(Mo^{V,VI}O)_8(\mu_4\text{-}O)_2(\mu_3\text{-}O)_6(\mu\text{-}O)_6(\mu\text{-}OR)_6(ROH)_4]^{2-}$, $Mo^V = Mo^V$ bonds	$MoCl_5$ + $MgCl_2$ + + MeOH + NaOH	174
$[Na_4Zr_6O_2(OEt)_{24}]$	$[Na_2\{Zr(OR)\}_3(\mu_5\text{-}O)(\mu_3\text{-}OR)_2(\mu\text{-}OR)_7]_2$, two $[Na_2Zr_3(\mu_5\text{-}O)]$ trigonal bipyramids sharing a $[Na_2(\mu_3\text{-}O)_4]$ face	'$Zr(OEt)_4$' + $NaOSiMe_3$	44
$[Ba_4Cu^I_6O(OCEt_3)_{12}]$	$[Ba_4Cu_6(\mu_4\text{-}O)(\mu\text{-}OR)_{12}]$, six linear $[Cu(OR)_2]$ groups along edges of the $[OBa_4]$ tetrahedron	$Ba_2Cu^I_4(OCEt_3)_8 + O_2$	175
$[Al_{10}O_4(OEt)_{22}]$	$[Al_5(\mu_4\text{-}O)(\mu_3\text{-}O)(\mu\text{-}OR)_7(OR)_4]_2$; two pentanuclear rings are linked *via* the $[Al_2(\mu_3\text{-}O)_2]$ ring; CN of Al are 4, 5, 6	$Al(OEt)_3$, PhH, Δ	17
$[Al_{10}O_6(OPr^i)_{18}NH_3]$	$[Al_{10}(\mu_4\text{-}O)_2(\mu_3\text{-}O)_4(\mu\text{-}OR)_6(OR)_{12}NH_3]$; CN of Al are 4, 5, 6	$Al(OPr^i)_3 + NH_3$	176
$[Ti_{10}O_8(OEt)_{24}]\cdot PhMe$	$[Ti_{10}(\mu_4\text{-}O)_4(\mu_3\text{-}O)_2(\mu\text{-}O)_2(\mu\text{-}OEt)_{10}(OEt)_{14}]\cdot PhMe$	$Ti_7O_4(OEt)_{20}$ + + $Ti_8O_6(OR)_{20}$ + PhMe	143
$[Sr_6Ti_4O_4(OPr^i)_{20}]$	$[Sr_6Ti_4(\mu_4\text{-}O)_4(\mu_3\text{-}OR)_4(\mu\text{-}OR)_{12}(OR)_4]$; four μ_3-OR groups and four $[OTi(OR)_4]$ groups on eight faces of the $[Sr_6]$ octahedron; the $[SrO_6]$ octahedron	$Sr(OPr^i)_2 + Ti(OPr^i)_4$	102
$[Ni_6Sb_4O_4(OEt)_{16}(EtOH)_4]$	$[Ni_6Sb_4(\mu_4\text{-}O)_4(\mu\text{-}OR)_{16}(ROH)_4]$; Ψ-octahedra $[(\mu_4\text{-}O)Sb(\mu\text{-}OR)_4]$ on four faces of the $[Ni_6]$ octahedron, $[NiO_6]$ octahedra	$NiBr_2 + Sb(OEt)_3 + KOEt$	177
$[Pb_6Nb_4O_4(OEt)_{24}]$	$[Pb_6Nb_4(\mu_4\text{-}O)_4(\mu_3\text{-}OR)_4(\mu\text{-}OR)_{12}(OR)_8]$; four μ_3-OR groups and four $[ONb(OR)_5]$ octahedra on eight faces of the $[Pb_6]$ octahedron; the $[PbO_6]$ trigonal prism	$Pb_4O(OEt)_6 + Nb(OEt)_5$ $(-Et_2O)$	178
$[Me_4N]_4[Mn_{10}\{2,2\text{-}(OC_6H_4)_2\}_4O_4Hal_{12}]$, Hal = Cl, Br	$[Mn_{10}\{\mu,\mu\text{-}2,2\text{-}(OAr)_2\}_4O_4Hal_{12}]^{4-}$ is a structural analogue of adamantyl, CN of Mn are 5, 6	$MnCl_2 + C_6H_4(OH)_2$-2,2 + $[Me_4N]OH\cdot 5\,H_2O$	179

Table 10. Oxoalkoxides with nuclearity higher than 10.

Compound	Structure	Starting compounds, conditions of formation	Ref.
$[Al_{11}O_6(OR)_{21}]$, R = Pr^n, Pr^i	$[Al_{11}(\mu_4\text{-}O)_2(\mu_3\text{-}O)_2(\mu\text{-}O)_2(\mu\text{-}OPr^n)_{10}(\mu\text{-}OPr^i)_2(\mu\text{-}ROH)_2.$ $.(OPr^i)_8(OR)]$; two pentanuclear $[Al_5O_2(OX)_{10}]$ rings are linked *via* the $[Al(\mu_3\text{-}O)_2(\mu\text{-}O)_2(OR)]$ group	$Al(OPr^i)_3 + Ta(OPr^i)_5 + Pr^nOH$	180
$[Mn_7Sb_4O_4(OEt)_{18}(EtOH)_2]$	$[Mn_7Sb_4(\mu_5\text{-}O)_2(\mu_4\text{-}O)_2(\mu_3\text{-}OR)_2(\mu\text{-}OR)_{16}(ROH)_2]$	$Mn_2Sb_4(OEt)_{16} + H_2O$	181
$[Zr_3Mo_8O_{24}(OPr^i)_{12}(Pr^iOH)_4]$	$[Zr_3(MoO_2)_4(MoO)_4(\mu_3\text{-}O)_8(\mu\text{-}O)_4(\mu\text{-}ROH)_4(OR)]$	$Zr(OPr^i)_4\cdot Pr^iOH + MoO(OPr^i)_4$ $(-Pr^i_2O)$	182
$[Ti_{11}O_{13}(OPr^i)_{13}(OR)_5]$, R = Et, Pr^i	$[Ti_{11}(\mu_3\text{-}O)_{10}(\mu\text{-}O)_3(\mu\text{-}OR)_7(OR)_6(OEt)_5]$	$Ti(OPr^i)_4 + H_2O$ (h = 0.3 – 0.8)	183 – 185
$[Ti_{12}O_{16}(OPr^i)_{16}]$	$[Ti_{12}(\mu_3\text{-}O)_{14}(\mu\text{-}O)_2(\mu\text{-}OR)_4(OR)_{12}]$	$Ti(OPr^i)_4 + H_2O$, 100°C (h = 1)	183 – 185
$[Ti_{12}O_{16}(OPr^i)_{10}(OEt)_6]$	$[Ti_{12}(\mu_3\text{-}O)_{14}(\mu\text{-}O)_2(\mu\text{-}OR)_4(OR)_6(OEt)_6]$	$Ti(OPr^i)_4$ + AcOH	183 – 185
$[Mn_8Sb_4O_4(OEt)_{20}]$	$[Mn_8Sb_4(\mu_5\text{-}O)_4(\mu_3\text{-}OEt)_4(\mu\text{-}OEt)_{16}]$	$MnCl_2 + NaSb(OEt)_4$	186
$[Zr_{13}O_8(OMe)_{36}]$	$[Zr_{13}(\mu_4\text{-}O)_4(\mu\text{-}O)_4(\mu\text{-}OR)_{24}(OR)_{12}]$; Keggin-type $[Zr_{12}O_{36}]$ structure, the thirteenth Zr atom, $[ZrO_8]$ cube, in the centre; this cube is linked to twelve $[ZrO_2(\mu\text{-}OR)_4(OR)]$ seven-vertex polyhedra	$Zr(OMe)_4$ + MeOH + NaOH	9
$[Y_{14}Cl_{12}O_2(OBu^t)_{28}(THF)_4]$	four $[Y_3(\mu_3\text{-}OR)(\mu_3\text{-}Cl)(\mu\text{-}OR)_3(OR)_n(THF)_m]$ triangles are linked *via* μ_4-O and μ-Cl ligands and two $[Y(\mu\text{-}OR)_2(\mu\text{-}Cl)_2]$ groups	decomposition of $[Y_3Cl_2(OBu^t)_7(THF)_2]$	187

Table 10 (continued).

Compound	Structure	Starting compounds, conditions of formation	Ref.
Linear chain			
$[Li_8Y_8O_2Cl_4(OBu^t)_{24}]$	$[Li_4Y_4(\mu_4\text{-}O)(\mu_3\text{-}OR)_2(\mu\text{-}OR)_6(\mu\text{-}Cl)_2(OR)_4]_2$, two $[Li_2(\mu\text{-}OR)_2]$ groups in the centre are linked to two 'butterflies' *via* two μ-Cl	$YCl_3 + 2\,LiOBu^t + THF$	188
$[Ti_{16}O_{16}(OEt)_{32}]$	$[Ti_8(\mu_4\text{-}O)_2(\mu_3\text{-}O)_4(\mu\text{-}O)_2(\mu\text{-}OR)_8(OR)_8]_2$	$Ti(OEt)_4$ + EtOH, 100 °C, *P*	142, 189
$[V^{IV}_{16}O_{20}(\eta^3,\mu\text{-}O_3R)_8(H_2O)_4]\cdot 3\,H_2O$, R = $(CH_2)_3CCH_2OH$	$[\{(VO)_6V_2(\mu_5\text{-}O)_2(\eta^3,\mu\text{-}RO_3)_4(H_2O)_2\}_2(\mu\text{-}O)_4]\cdot 3\,H_2O$, four layers of $[V_2V_6]_2$ octahedra	$V_2O_5 + C(CH_2OH)_4 + MCl + H_2O$, Δ, *P*	190
$[Li_8Ta_8O_{14}(OEt)_{20}(EtOH)_8]\cdot 4\,EtOH$	$[Li_8Ta_8H_8(\mu_4\text{-}O)_2(\mu_3\text{-}O)_8(\mu\text{-}O)_4(\mu_3\text{-}OR)_2(\mu\text{-}OR)_{10}(OR)_{16}]\cdot 4\,ROH$	$LiTa_9O_{10}(OEt)_{20}(EtOH) + LiOEt$	173
$Ti_{17}O_{24}(OPr^i)_{20}$	Keggin-type structure, seventeenth Ti atom in the centre	$Ti(OPr^i)_4$ + AcOH	191
$[Ba_4Ti_{13}O_{18}(OC_2H_4OMe)_{24}]$	$[Ba_4Ti_{13}(\mu_5\text{-}O)_6(\mu_3\text{-}O)_{12}(\eta^2,\mu_3,\mu\text{-}OR)_{12}\,(\eta^1,\mu\text{-}OR)_{12}]$	$Ba(OR)_2 + Ti(OR)_4 + H_2O$ (h = 6)	192
$[Ti_{18}O_{28}(OBu^t)_{16}(Bu^tOH)]$	$[Ti_{18}(\mu_4\text{-}O)_4(\mu_3\text{-}O)_{20}(\mu\text{-}O)_4(OR)_{16}(ROH)]$	$Ti(OBu^t)_4 + H_2O$, 100 °C (h = 1.14)	193
$[Cu_{18}O_2(OSiMe_3)_{14}]$	$[Cu_{18}(\mu_4\text{-}O)_2(\mu\text{-}OR)_{14}]$; two intersecting $[Cu_9O_8]$ rings, μ_4-O in the centres	$CuOSiMe_3$, 80 °C, 10^{-3} mm Hg (−R_2O)	194
$Mn_{19}O_{12}(OR)_{14}(ROH)_{10}$, R = OC_2H_4OMe	$[Mn_{19}(\mu_3\text{-}O)_{12}(OR)_{14}(ROH)_{10}]$, CdI_2 structural type, layers of octahedra are linked *via* μ_3-O and μ_3-OR groups	$MnCl_2 + NaOC_2H_4OMe$	195
$[Ni_6Sb_{14}O_{18}(OEt)_{18}(EtOH)_2]$	–	$NiCl_2 + NaSb(OEt)_4$	147, 196
$M_7[Na(H_2O)_3Mo^V_{36}Mo^{VI}_6H_{15}O_{109}\cdot\{(OCH_2)_3CCH_2OH\}_7]$	framework of vertex- and edge-sharing Mo octahedra, the $[Na(H_2O)_3]$ group in the centre, RO_3 groups on the surface	$MoO_3 + Na_2MoO_4 + H_2O +$ $+ C(CH_2OH)_4 + Me_4NCl$, Δ, *P*	197
Polymeric linear chain			
$[Sr_2Sb_4O(OEt)_{14}]$	$[Sr_2Sb_4(\mu_4\text{-}O)(\mu\text{-}OR)_{14}]_\infty$ — a chain of alternating $[Sb(\mu\text{-}OR)_4]$ tetrahedra and $[Sr_2Sb_3(\mu_4\text{-}O)(\mu\text{-}OR)_{10}]$ groups, CN of Sb are 4, 5; CN of Sr is 7	$Sr(OEt)_2 + Sb(OEt)_3$	198

groups at all), the conditions of formation of the latter indicate that various decomposition processes can occur. In most cases, the appearance of oxo groups is associated with uncontrolled decomposition of alkoxides *in situ* in attempting to synthesise these compounds according to conventional methods.

Apparently, the most stable forms of OA exist in each system. For instance, single crystals of $Nb_8O_{10}(OEt)_{20}$ and $Ti_7O_4(OEt)_{20}$ prepared according to two procedures, *viz*., by the reactions of water with ethoxides or upon spontaneous decomposition, were demonstrated to be identical. For example, the $Nb_8O_{10}(OEt)_{20}$ compound was formed upon prolonged storage of liquid samples of $NbO(OEt)_3$ in tubes (the process is accompanied by elimination of Et_2O),[151] whereas $Ti_7O_4(OEt)_{20}$ was prepared by heating solutions of $Ti(OEt)_4$ in an autoclave to 100 °C,[142] *i.e*., in the complete absence of moisture.

Of special note is the synthesis of OA by alcoholysis of metal oxides or the synthesis of oxo metallates by exchange reactions with compounds which already contain oxo groups. Examples are the synthesis of $(MoO)_2O[(CMe_2)_2O_2]_2[O(CMe_2)_2OH]_2$ from MoO_3 and pinacol,[28,29] the formation of $[R_4N]_2\cdot[(MoO_2)_4O_2(OMe)_6]$ by methanolysis of metamolybdate $[Bu_4N]_4Mo_8O_{26}$,[78] the preparation of $[Bu_4N]_3[Nb_2W_4O_{18}(OR)]$ (R = Me, Et, Pr^i, Bu^t, $SiAlk_3$) by alcoholysis of the $[HNb_2W_4O_{19}]^{3-}$ heteropolyanion [118] and the hydrothermal synthesis of numerous hexa- and decanuclear molecular and anionic V(IV,V) and Mo(V,VI) complexes by reactions of metal oxides with MeOH and polyatomic alcohols.[113,115–117,169,170,197]

1. Hydrolysis

Pioneering X-ray diffraction studies of the structures of partial hydrolysis products of alkoxides marked the beginning of systematic studies of this reaction (which was generally monitored by ^{17}O, ^{1}H and ^{13}C NMR spectroscopy). Condensed titanium OA molecules were investigated by Day and co-workers,[42,143,183,193] Mosset and co-workers [142,189] and Sanchez and co-workers.[184,185,191] These molecules contain from three to eighteen metal atoms linked *via* polydentate oxo and alkoxy groups. Hydrolysis of alcoholic solutions at a $[H_2O]:[Ti(OEt)_4]$ ratio varying from 0.5 : 1 to 0.7 : 1 (h = 0.5–0.7) afforded crystals of $[Ti_{16}O_{16}(OEt)_{32}]$ [142,189] along with the above-mentioned $Ti_7O_4(OEt)_{20}$ [7,142] (see Fig. 1 *a*). Oxoisopropoxide $Ti_3O(OPr^i)_{10}$ is formed in solutions at h = 0.05–0.2. However, only the heteroleptic complex $[Ti_3(\mu_3\text{-}O)(\mu_3\text{-}OMe)(OPr^i)_9]$ was isolated in the crystalline state.[42] The octanuclear $[Ti_8O_6(OEt)_{20}]$ molecules exist in an alcoholic solution, but only a derivative of benzyl alcohol with the $[Ti_8O_6]$ core, *viz*., the $[Ti_8O_6(OBn)_{20}]\cdot Et_2O$ complex, was prepared in the crystalline state.[143] The decanuclear $[Ti_{10}O_8(OEt)_{24}]\cdot PhMe$ complex was also prepared from toluene solutions of oxoethoxides. Hydrolysis of $Ti(OPr^i)_4$ in solutions at 100 °C (in an autoclave) afforded a mixture of two isomers with composition $[Ti_{12}O_{16}(OPr^i)_{16}]$. At 20 °C, the solution contains $[Ti_{11}O_{13}(OPr^i)_{18}]$, which crystallises in the presence of EtOH to form $[Ti_{11}O_{13}(OPr^i)_{13}(OEt)_5]$.[183] The largest molecule of this group, *viz*., $[Ti_{18}O_{28}(OBu^t)_{16}(Bu^tOH)]$, was prepared by hydrolysis of $Ti(OBu^t)_4$ (h = 1.14).[193] Condensation of $Ti(OPr^i)_4$ in the presence of acetic acid to form $[Ti_{12}O_{16}(OPr^i)_{16}]$ [183,184] results from the reaction with water (generated in the course of esterification of an excess acid) and alcohol eliminated upon the replacement of OR groups with OAc.

Hydrolysis also gave rise to $[Sn_3O(OBu^i)_{10}(Bu^iOH)_2]$,[40] $[U_3O(OBu^t)_{10}]$,[49] a series of bimetallic complexes, *viz*., $[BiTi_2O(OPr^i)_8]$,[41] $[LiTiO(OPr^i)_3]_4$,[158] $[K_4Zr_2O(OPr^i)_{10}]$,[107] $[Cu_4Zr_4O_3(OPr^i)_{18}]$,[156] $[MoTa_2O_4(OMe)_8]_2$,[133] *etc*. Among these compounds, the barium titanium oxo cellosolve molecule

$[Ba_4Ti_{13}O_{18}(OC_2H_4OMe)_{24}]$ (prepared at $h = 6$) [192] has the maximum size.

Recently, the following oxoalkoxides were synthesised by controlled hydrolysis in alcoholic solutions of aluminium and tantalum alkoxides:[33, 34, 53–55, 103, 152] the tetrahedral $[Al_4(\mu_4\text{-}O)(OR)_{10}(ROH)]$ complexes (R = Bu^i, $h = 0.25$; CF_3CH_2, $h = 0.5$), $Ta_5(\mu_3\text{-}O)_4(\mu\text{-}O)_3(OBu^t)_{11}$ ($h = 1.0$), $Ta_7(\mu_3\text{-}O)_3(\mu\text{-}O)_6(OPr^i)_{17}$ ($h = 0.55$) and $Ta_8(\mu_3\text{-}O)_2(\mu\text{-}O)_8.(OEt)_{20}$ ($h = 0.5-1.0$) with isopolyanion-type structures.

Controlled hydrolysis of aryloxoalkyl derivatives, in which water replaces alkoxy groups, while aryloxy groups remain intact, is also of interest.

$$M(OAr)_nR_m + H_2O \longrightarrow [M(OAr)_nO_{m/2}]_2 + ROH$$

Examples are the $[TiO(OC_6H_3Pr^i_2\text{-}2,6)_2(NC_5H_4\text{-}4\text{-}NC_4H_8)]_2$ (see Ref. 21) and $[NbO(OC_6H_3Pr^i_2\text{-}2,6)_3]_2$ complexes.[22]

2. Oxidation

Many oxo complexes were synthesised by controlled oxidation of alkoxides of metals in the lowest oxidation states. For example, oxoalkoxides $[M^{IV}_3O(OR)_{10}]$ (R = Pr^i, CH_2Bu^t), $[(Mo^VO)_4O_4(OPr^i)_4Py_4]$, $[Mo^{5.3+}_3O_5(OPr^i)_6]_2$, $[Mo^{VI}O_2(OBu^t)_2]$ and $W^{VI}_2O_3(OR)_6$ (R = Pr^i, Bu^t, CH_2Bu^t) were isolated from the reaction products of $M_2(OR)_6$ (M = Mo, W) with oxygen.[46, 47, 80, 199, 200] In the case of $W_2(OR)_6$, NO {in the synthesis of $[W^{IV}_2O(OBu^t)(OSiMe_2Bu^t)_5Py_2]$ [25]} or acetone {in the synthesis of $[W^{IV}_4O_2(OPr^i)_{12}]$ [88]} were used as oxidants.

Oxidation of bimetallic copper(I) alkoxides, *viz*., $Ba_2Cu_4(OR)_8$ and $Cu_2Zr_2(OR)_{10}$, with oxygen produced the oxo ligands $[Ba_4Cu^I_6O(OCEt_3)_{12}]$ and $[Cu^{II}_4Zr_4O_3(OPr^i)_{18}]$, respectively.[156, 161, 175] In the former compound, the oxidation state of copper remained unchanged.

The $MoO_2(OEt)_4$, $WO(OR)_4$ and $NbO(OR)_3$ compounds (R = Me, Et, Bu^n) were prepared by passing dry air through coloured alcoholic solutions of electrolytes, which are anodic oxidation products of molybdenum, tungsten or niobium (which were subjected to partial reduction on the cathode).[136, 201, 202]

Uncontrolled oxidation with oxygen traces present in the gaseous phase or solvents is typical of alkali or alkaline-earth metal alkoxides. The primary reaction products contain peroxide groups OOR or OOH.[203] Decomposition of the latter by a radical mechanism results in the appearance of water molecules, as well as oxo and carboxy groups, in the coordination environment of the metal atom. This process is accompanied by the appearance of a yellow-brown colour, whose intensity sharply increases upon storage of samples or refluxing of their alcoholic solutions. For example, refluxing (in particular, in the course of dehydration of EtOH) of yellow alcoholic solutions of $Ca(OEt)_2$ over a long period of time afforded crystals of the oxo complex $Ca_6O_2(OEt)_8 \cdot 14\,EtOH$ (see Fig. 2 *b*).[16] Apparently, this colour is attributable to the presence of radicals, which was confirmed by ESR spectroscopy of coloured $Ba(OR)_2$ samples. The IR spectra of such products show the following new bands (regardless of the nature of the starting radical): ν(OH) band of ethanol molecules coordinated to OA and ν(COO) and δ(OCO) bands of the formate group generated from peroxides upon their decomposition. The tendency of alkoxides to oxidation increases in the series Li ≪ Cs, Mg ≪ Ba and Et < Bu^n ≪ Pr^i ≪ C_2H_4OMe,[204] which corresponds to the rate of formation of radicals (the rate was determined by ESR spectroscopy, in particular, for LiOR).[205]

Samples of M^IOAlk or $M^{II}(OAlk)_2$, which were prepared by the reactions of metals with a stoichiometric amount of alcohol in a hydrocarbon medium, appeared to be much more resistant to oxidation compared to those synthesised in alcoholic solutions or prepared by desolvation of $M(OR)_n \cdot x\,ROH$. Oxidation of the alkoxides in their synthesis in a hydrocarbon medium is, apparently, hindered by precipitation of the unsolvated $M(OR)_n$ compounds and insolubility of O_2 in hydrocarbons (as opposed to alcohols). Uncontrolled microhydrolysis is favourable for oxidation due, apparently, to the appearance of free alcohol in samples.[3]

An interesting procedure for the synthesis of OA is based on the addition of ketones to certain molecules, in particular, to $Ti(OR)_4$ ('oxolation') giving rise to large cluster molecules.[185]

3. Decomposition (thermolysis and elimination of ethers)

At rather high temperatures, volatile thermolysis products of alkoxides can contain alcohols, ethers, aldehydes, saturated and unsaturated hydrocarbons, *etc*. The structures of crystalline products provide evidence for condensation attendant on this process. For instance, refluxing of $Al(OEt)_3$ under a benzene layer for several days leads to thermal destruction of the polymeric molecules to give products which go into solution, resulting in crystallisation of $[Al_{10}O_4(OEt)_{22}]$ in low yield.[17] The hydrocarbon-soluble 'α form of aluminium ethoxide' (which is, in reality, OA) was synthesised (according to the Meerwein method) by the reaction of the metal with a stoichiometric amount of alcohol in a xylene solution at 140 °C; in this case decomposition of $Al(OEt)_3$ occurs already *in situ*.[206]

The $[Al_8O_2(OH)_2(OBu^i)_{18}]$ [53] and $[Fe_9O_3(OEt)_{21}] \cdot EtOH$ [167] complexes crystallise from vacuum distillation products of the lower-nuclearity oxo complexes $Al_4O(OBu^i)_{10}$ and $Fe_5O(OEt)_{13}$. Copper oxosilane oxide $[Cu_{18}O_2(OSiMe_3)_{14}]$ was prepared by distillation of $CuOSiMe_3$ [the formation of $(Me_3Si)_2O$ was established].[194] Evidently, the process is accompanied by destruction followed by condensation of the resulting fragments. Decomposition of $W_4(OPr^i)_{10}$ to $[W^{III}_4O_2(OPr^i)_8]_2$ occurs with elimination of propane.[164] Thermolysis of bimetallic isopropoxide $KSb(OPr^i)_4$ afforded crystalline $[K_2Sb_2O(OPr^i)_6]_2$ and Pr^i_2O. Refluxing of toluene solutions of $KM^{III}(OBu^t)_4$ (M^{III} = Sb, Bi) over a long period of time resulted in elimination of isobutylene and afforded the oxo complexes $[K_4M^{III}_2O(OBu^t)_8]$. It should be noted that Na-containing compounds with the same composition are generated already in the step of the reaction of $NaOBu^t$ with $M^{III}(OBu^t)_3$.[109]

If decomposition of alkoxides occurs at rather low temperatures, the reaction gives ethers as the major products. For instance, thermolysis of methoxides $Al(OMe)_3$, $Pb(OMe)_2$ and $NaAl(OMe)_4$ (at ~120 °C) afforded dimethyl ether as the only gaseous product.[206–208] Heating of an alcoholic solution of $Ti(OEt)_4$ in an autoclave at 100 °C led to crystallisation of $Ti_{16}O_{16}(OEt)_{32}$ and elimination of Et_2O.[142, 190]

Condensation with elimination of ethers

$$M-OR + RO-M \longrightarrow M-O-M + R_2O$$

proved to be one of the main pathways of spontaneous decomposition of alkoxides. The formation of oxo bridges is, undoubtedly, thermodynamically favourable and, in the case under consideration, is analogous to ageing of oxide hydrates accompanied by condensation of two hydroxy groups with elimination of a water molecule. This type of reaction was first described by Bradley and co-workers,[209] who prepared oxo complexes by transesterification of niobium ethoxide with *tert*-butyl alcohol

$$Nb(OEt)_5 + Bu^tOH \longrightarrow$$
$$\longrightarrow NbO(OBu^t)_3 + Nb_2O(OBu^t)_8 + Bu^t_2O + EtOH.$$

The proposed mechanism involves the heterolytic cleavage of the O–R bond followed by the attack of the resulting carbocation on the M–O bond of another OR group. Ethers (like other volatile decomposition products, for example, unsaturated hydrocarbons) are not always detectable against the background of alcohols.[14]

Evidently, the size ratio of the metal atom and the substituent (as well as the degree of branching of the latter) is an essential factor responsible for the resistance of ortho derivatives to decomposition. As an example, let us consider iron(III) alkoxides. In the known structures of alkoxides {except for $[Fe(OMe)_3 \cdot MeOH]_\infty$ and unstable $[Fe(OEt)_3]_\infty$}, the coordina-

tion environment of Fe atoms always involves oxo groups.[15, 129, 149, 172] However, in the presence of the $CHBu^t_2$, C_6HMe_4-2,3,4,6, $SiMe_3$ (see Ref. 3) or CMe_2Ph [15] substituents, the reactions afford stable structures of alkoxides of the ortho series containing tetrahedrally coordinated metal atoms. Of aluminium derivatives (the atomic radius of aluminium is substantially smaller than that of iron), polymeric alkoxides $Al(OR)_3$ (R = Me, Et) with a layered structure consisting of $[AlO_6]$ octahedra [isostructural with the corresponding $Fe(OR)_3$] appear to be quite stable. The same is true for the crystalline $[Al(OPr^i)_3]_4$ compounds (Al has coordination numbers of 4 and 6) and $[Al(OBu^t)_3]_2$ (containing tetrahedrally coordinated metal atoms). Analogous iron homologues do not crystallise at all and, according to the IR spectroscopic data, contain oxo groups.[3]

Apparently, this type of decomposition is the main pathway in various synthesis reactions of alkoxides resulting in the 'unexplainable' formation of oxo complexes. This decomposition is particularly characteristic of derivatives containing large Ba, Ln, Zr, Mo, W and U atoms. It should be emphasised that their lighter analogues form alkoxides of the ortho series under comparable conditions.

For instance, barium compounds virtually always contain oxo groups even in the presence of large ligands. Examples are $[Ba_5(\mu_5\text{-}O)(OPh)_8(PhOH)(THF)_8]$ [89] and $[Ba_6(\mu_6\text{-}O)(OR)_{10}\cdot(ROH)_4]$ (R = C_2H_4OMe).[105] The Ba atoms in these molecules have coordination numbers from 7 to 9. Analogous Sr or Ca derivatives, *viz*., $[Sr_4(OPh)_8(PhOH)_2(THF)_6]$ [210] and $Ca_9(OR)_{18}\cdot 2\,ROH$,[211] belong to the ortho series. In the latter compounds, the metal atoms are octahedrally coordinated (only in the calcium cellosolve, the peripheral Ca atoms have a coordination number of 7). Even the reaction of barium metal with phenol in the presence of orthophenoxide $[Sr(OPh)_2]_3\cdot 5\,OP(NMe_2)_3$ affords the bimetallic oxo complex $[Ba_2Sr_6(\mu_5\text{-}O)_2(OPh)_{12}(PhOH)_2\cdot\{OP(NMe_2)_3\}_6]$.[162] An increase in the size of metal atoms in going from Sr to Ba leads to an increase in the coordination number. Evidently, stable polyhedra are formed only if one oxo group is involved in the coordination environment of the metal atoms along with large ligands.

The appearance of oxo groups in these compounds is not associated with uncontrolled hydrolysis or oxidation. This is evidenced by high yields of products and good reproducibility of experiments which were carried out by different research groups under various conditions. The corresponding ortho forms $Ba(OAr)_2$ can be prepared only upon their stabilisation by chelation with crown ethers or amino alcohols or after the introduction of one more substituent into the phenoxy group in the *para* position with respect to the OH group.[91, 212–214]

The formation of oxo groups upon coordination of 'small' ligands to the Ba atom can be exemplified by barium alkoxotitanates. The most stable complexes in the $Ba(OR)_2$–$Ti(OR)_4$–ROH systems have the composition $Ba[Ti_2(OR)_9]_2$ (R = Et, Pr^i, Bu^n). In these complexes, the central Ba atom has a coordination number of 8.[215, 216] However, the use of a system consisting of methoxides leads to the formation of the $[Ba_2Ti_4(\mu_3\text{-}O)(OMe)_{18}\cdot(MeOH)_7]\cdot MeOH$ complex,[131] in which the coordination number of Ba increases to 9 due to additional coordination of one oxo group (Fig. 3). Evidently, eight 'small' OMe groups are inadequate to provide a stable polyhedron of the Ba atom, but only an oxygen atom can be coordinated instead of the ninth alkoxy group for steric reasons, resulting in elimination of an ether molecule. It should be emphasised that in all the molecules under consideration, the coordination environment of the metal atom involves only one oxo group.

An analogous situation is observed in the structures of rare-earth metal alkoxides, which can be exemplified by methyl cellosolves (R = C_2H_4OMe). Cerium-group metals form seven- and eight-vertex polyhedra involving oxo atoms: $[Pr_4(\mu_4\text{-}O)_2\cdot(OR)_8(OPMe_3)]_2$ (see Ref. 150) and $[Gd_6(\mu_4\text{-}O)(OR)_{16}]$.[130] By contrast, derivatives of yttrium-group metals $[M(OR)_3]_{10}$ (M = Y, Dy) contain no oxo ligands and occur as planar decanuclear rings with seven-coordinate metal atoms.[217, 218]

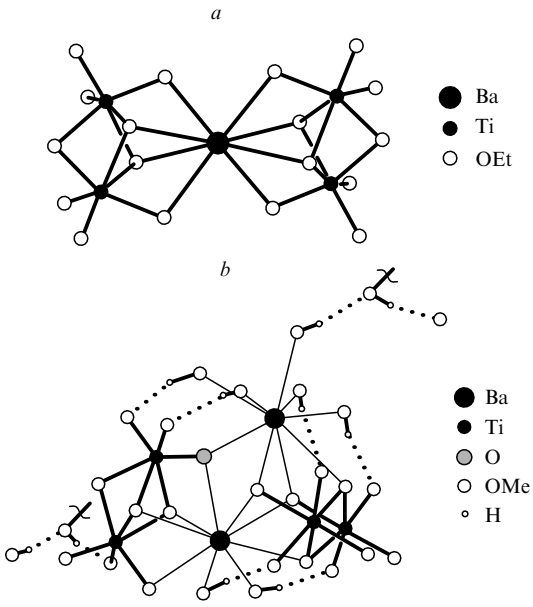

Figure 3. Metal–oxygen cores in the structures of $Ba[Ti_2(OR)_9]_2$ (*a*) [216] and $[Ba_2Ti_4(\mu_3\text{-}O)(OMe)_{18}(MeOH)_7]\cdot MeOH$ (*b*).[131]

Desolvation of the solvates $Ln(OR)_n\cdot m\,L$ (L = ROH, THF) is always attended by the formation of oxo groups. In certain cases, elimination of the corresponding ethers was observed.

Solvate	Reaction conditions	Reaction product	Ref.
$[La_3(OBu^t)_9L_2]$, L = Bu^tOH, THF	PhMe, Δ	$La_5O(OBu^t)_{13}$	219
$[Nd(OPr^i)_3(Pr^iOH)]_4$	25 °C, vacuum	$Nd_6O_5(OR)_8$	220
$[Ce(OBu^t)_4(THF)_2]$	20 °C, 72 h	$Ce_3O(OBu^t)_{10}$	221
$[Ce(OPr^i)_4(Pr^iOH)]_2$	70 °C, 10^{-3} mm Hg	$Ce_4O(OPr^i)_{14}$	57

The extremely unstable praseodymium solvate $Pr_3(OPr^i)_9\cdot(Pr^iOH)_2$ decomposes to $Pr_5O(OPr^i)_{13}$ already at low temperatures (in the course of drying).[92] Taking into account that the ortho forms $Ln(OAlk)_n$ (n = 3, 4) exist only as solvates with alcohols, THF or Py, it can be hypothesised that the widely occurring form of oxoalkoxides $Ln_5O(OR)_{13}$ (R = Pr^i, Bu^t) is generated as a result of desolvation of unstable solvates. Transesterification of the solvate $[Ce(OPr^i)_4(Pr^iOH)]_2$ with pinacol giving rise to $Ce_2O[O(CMe_2)_2O]_2[O(CMe_2)_2OH]_2$ (see Ref. 75) can also be assigned to this type of reaction.

Decomposition with elimination of ethers (detected) is very typical of lead and bismuth alkoxides. For example, polymeric $Pb(OPr^i)_2$ readily undergoes oligomerisation to form $Pb_4O\cdot(OPr^i)_6$, $Pb_6O_4(OPr^i)_4$ and $Pb_7O_2(OPr^i)_{10}$.[127, 144, 222, 223] In this connection, the complex formation of these compounds with other alkoxides is generally accompanied by the formation of the oxo complexes $[Pb_2Ti_2O(OPr^i)_{10}]$,[60] $[Pb_3Zr(\mu\text{-}O)(OBu^t)_8]$ [62] and $[Pb_6Nb_4(\mu_4\text{-}O)_4(OEt)_{24}]$ [178] [for Sn(II) alkoxides, only oxomethoxide, which was prepared by hydrolysis, is known [123]].

In various synthesis reactions and subsequent transformations, bismuth alkoxides also give oxo complexes. The exchange reactions of $BiCl_3$ with alkali metal alkoxides produce $[NaBi_4O_2(OC_6F_5)_9(THF)_2]$, $[Na_2Bi_4O_2(OC_6F_5)_{10}(THF)_2]$, $[NaBi_3O(OC_6F_5)_8(THF)]$ and $[Bi_6O_3(OC_6F_5)_{12}(THF)_2]$.[64] The complex formation of bismuth and sodium alkoxides affords $[Na_4Bi_2O(OBu^t)_8]$ [109] and $[Na_4Bi_2O(OC_6F_5)_8(THF)_4]$.[111] Alco-

Scheme 1

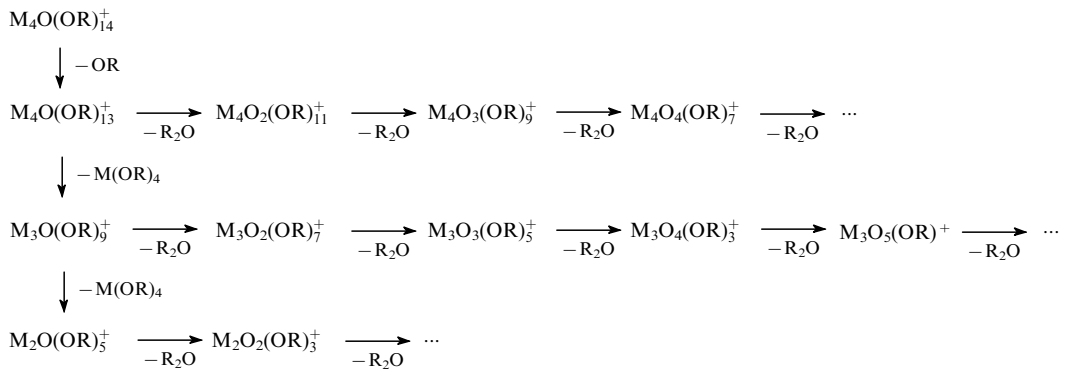

M = Zr, Hf; R = Et, Pr^i, Bu^n, Bu^i, Bu^t.

holysis of $BiPh_3$ or $Bi[N(SiMe_2)_2]_3$ is accompanied by the formation of $[Bi_6O_3(OC_6H_3Cl_2\text{-}2,6)_{12}]$[132] and $[Bi_4O_2(OBu^t)_8]$.[73] Transsolvation of $[Bi(OC_6F_5)_3(C_6H_6)]_2$ with tetrahydrofuran gives $[Bi_9O_7(OC_6F_5)_{13}(THF)_2]$.[166] Even hydrolysis of $Bi(OEt)_3$ in benzene occurs with elimination of ether.[224] Due to the high sensitivity of bismuth derivatives to moisture traces, the results of the synthesis of particular compounds depend on the origin of the starting reagents. For example, the reaction of $BiCl_3$ with $NaOC_6F_5$ in phenol purchased from Aldrich affords $[NaBi_3O(OC_6F_5)_8(THF)]$, whereas the reaction with the use of phenol purchased from Strem gives rise to $[NaBi_4O_2(OC_6F_5)_9(THF)_2]$ and $[Na_2Bi_4O_2(OC_6F_5)_{10}]$, which are products of deeper decomposition.[64]

Unexpectedly, it was found that zirconium and hafnium 'isopropoxides' (commercial reagents) prepared by desolvation of $[M(OPr^i)_4 \cdot Pr^iOH]_2$ contain several types of oxo complexes [for example, $M_3O(OR)_{10}$ and $M_4O(OR)_{14}$]. These samples also contain impurities of the undecomposed starting solvates. Hence, their empirical composition corresponds to the formula '$M(OR)_4$'. The presence of oxo complexes was detected by ^1H NMR spectroscopy and mass spectrometry of the $M(OR)_4 \cdot ROH$ compounds, in which fragmentation of all oligomers is attended by elimination of ether (Scheme 1).[225]

Crystals of $Zr_3O(OBu^t)_{10}$ and $[Hf_3O(OEt)_{10}(EtOH)]_2$ were grown by allowing electrolytes, which were prepared by anodic dissolution of metals in the corresponding alcohols,[45] to stand for a long period of time (Fig. 4).

Recently, the crystalline ortho form $[Zr(OPr^n)_4]_4$ has been isolated from commercial reagents containing primarily $Zr_3O(OPr^n)_{10}$ by vacuum distillation with unprecedented protection against moisture[226] [it should be noted that alkoxides $Ti(OAlk)_4$, unlike Zr and Hf derivatives, are quite stable]. In the study,[226] it was hypothesised that the formation of numerous oxoalkoxides $Ln_5O(OPr^i)_{13}$ is also associated with extremely high hygroscopicity of the corresponding ortho forms.

Condensation with elimination of ether is very typical also of rhenium,[227] molybdenum and, to a somewhat lesser extent, tungsten alkoxides. Of compounds belonging to the $Mo(OR)_6$ series, only highly unstable methoxide was isolated.[228–230] All oxoalkoxides $MoO(OR)_4$ are very prone to decomposition both in the free state and solutions to form polymeric compounds $MoO_2(OR)_2$ and ethers R_2O.[231] Numerous attempts to synthesise $W(OBu^t)_6$ led only to the formation of $WO(OBu^t)_4$, Bu^t_2O being detected among the reaction products.[232–234] Storage of the oily $MoO(OPr^i)_4$ compounds over a long period of time afforded crystalline $[Mo_3^{5,3+}O_5(OPr^i)_6]_2$ and Pr^i_2O (along with alcohol and acetone) as a result of a redox reaction.[141]

To summarise, it can be hypothesised that this type of decomposition is associated with the fact that metal atoms, which are coordinated only by alkoxy ligands and have no space for a new OR group, are coordinatively unsaturated. Hence, stable polyhedra are formed only in the presence of 'small' ligands, *viz*., an oxo group or solvate molecules (THF, ROH, MeCN, Py, *etc*.), in the coordination environment.

Decomposition of bimetallic alkoxides to oxo alkoxo metallates $M_mM'_nO_p(OR)_q$ containing heterometallic M–O–M′ bridges is of most importance among the reactions under consideration. Many complexes of this type are formed as a result of complexation of two alkoxides (*i.e*., decomposition occurs *in statu nascendi*). Attempts to isolate compounds devoid of oxo groups failed.

In most cases, alkali or alkaline-earth metal alkoxide is involved as one of the components. Examples are $[Li(MgTHF)_4O(\mu\text{-}OC_6H_4Me\text{-}2)_7]$,[98] $[LiTiO(OPr^i)_3]_4$,[158] $Sr(Pr^iOH)_2[Ti_2O(OPr^i)_7]_2$,[102] $[Sr_6Ti_4O_4(OPr^i)_{20}]$,[102] $[Na_2Zr_3O.(OEt)_{12}]_2$,[44] $[M_4Sb_2O(OBu^t)_8] \cdot n\,THF$[109] (M = Na, K; n = 0, 1, 4), $[Na_4Bi_2O(OBu^t)_8]$,[109] $[MgNbO(OMe)_5(MeOH)_2]_2$,[76] $[LiTa_9O_{10}(OEt)_{20}(EtOH)]$[173] and $Na_4[Mo_8O_{24}(OMe)_4] \cdot 8\,MeOH$.[153] However, processes are known where decomposition attends the complex formation of alkoxides of two transition metals, for instance, $[La_2(MoO)_4O_4(OPr^i)_{14}]$,[128] $[Zr_3Mo_8O_{24}.(OPr^i)_{12}(Pr^iOH)_4]$[182] (in these two cases, elimination of ether was observed), $[TaMo^V_2O_4(OPr^i)_7]_2$,[104] $[Er_2Ti_4O_2(OEt)_{18}.(EtOH)_2]$[140] and $[Cu_4Zr_4O(OPr^i)_{18}]$.[156]

The reactions of Ba and Nb (or Ta) ethoxides give rise to crystals of $[BaM^VO(OEt)_5(EtOH)_n]_4$ (M = Nb, Ta), although bimetallic complexes with composition $BaM^V_2(OEt)_{12}$ exist in freshly prepared solutions. By contrast, isopropoxides $[BaM^V_2(OPr^i)_{12}(Pr^iOH)_2]$ are not prone to decomposition and exist in the crystalline state.[85,160,235] The compound $[Ba_4Ti_4O_4(OPr^i)_{16}(Pr^iOH)_4]$ slowly crystallises from solutions of barium and titanium isopropoxides in isopropyl alcohol[159] [as mentioned above, the complexes in all solutions have the composition $BaTi_4(OR)_{18}$ (see Ref. 215)].

The influence of the nature of the substituent (steric factors) is observed, in particular, in the complexation of titanium and thallium(I) alkoxides. The reaction of two ethoxides and isopropoxides affords the octahedral $[Tl_4Ti_2O(OR)_{10}]$ molecules. However, even the partial introduction of OCH_2Bu^t groups gives rise to the ortho forms $TlTi_2(OR)_5(OCH_2Bu^t)_4$ (R = Et, Pr^i).[122]

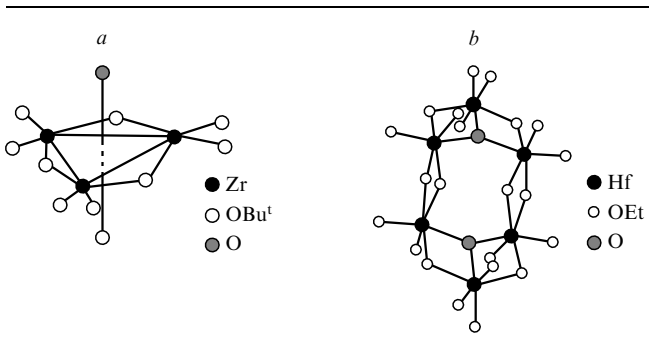

Figure 4. Metal–oxygen cores in the structures of $Zr_3O(OBu^t)_{10}$ (*a*) and $[Hf_3O(OEt)_{10}(EtOH)]_2$ (*b*).[45]

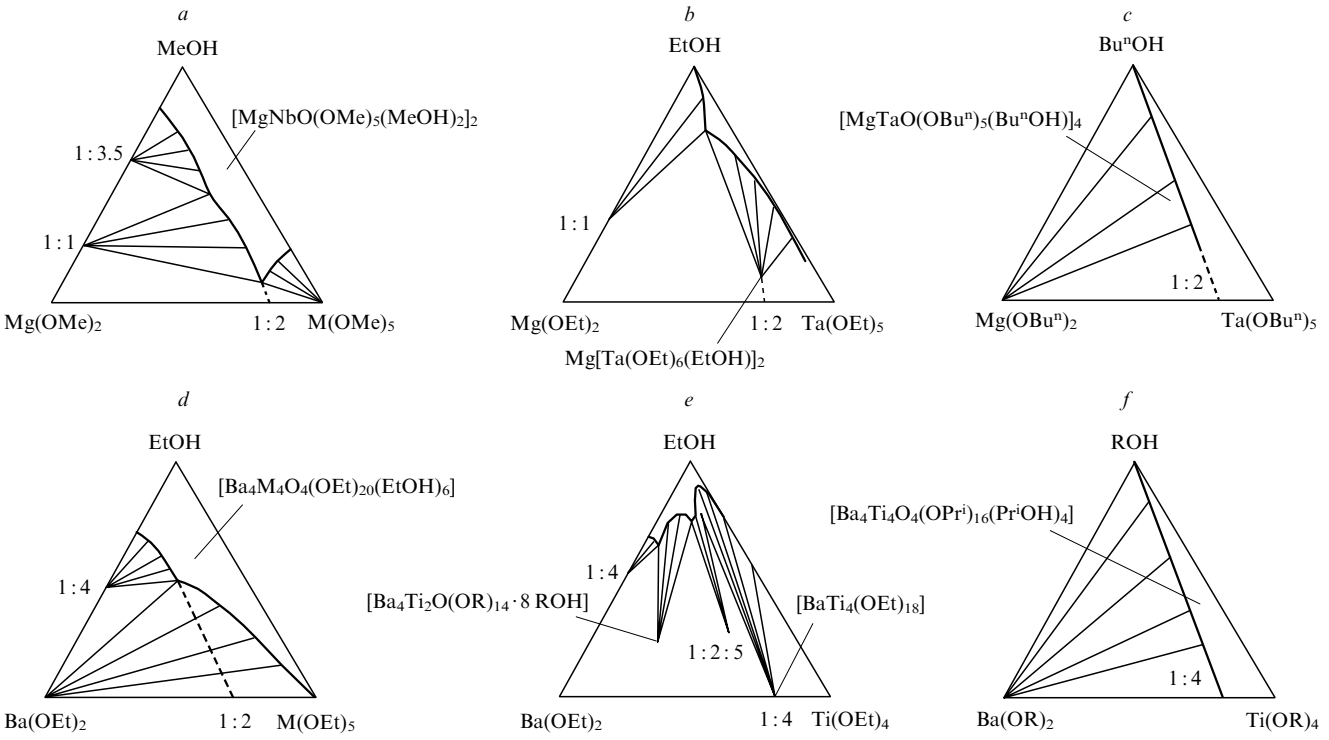

Figure 5. Solubility (20 °C) and the formation of bimetallic oxo complexes [76, 85, 159, 160] in the $Mg(OMe)_2-M(OMe)_5-MeOH$ (M = Nb, Ta) (*a*), $Mg(OEt)_2-Ta(OEt)_5-EtOH$ (*b*), $Mg(OBu^n)_2-Ta(OBu^n)_5-Bu^nOH$ (*c*), $Ba(OEt)_2-M(OEt)_5-EtOH$ (M = Nb, Ta) (*d*),[85, 235] $Ba(OEt)_2-Ti(OEt)_4-EtOH$ (*e*) and $Ba(OR)_2-Ti(OR)_4-ROH$ ($R = Pr^i$, Bu^n) (*f*)[215] systems.

Attempts to reveal a particular dependence of the decomposition pathway on the nature of metals and substituents failed. However, a comparison of the results of physicochemical analysis of the $M(OR)_m-M'(OR)_n-ROH$ systems (Fig. 5) with the results of structural studies of bimetallic oxo complexes demonstrated that crystallisation of OA occurs in systems (or concentration regions) where these compounds are least soluble. In these cases, $M_mM'_n(OR)_p$ are readily soluble or uncrystallisable products.

Molybdenum and tungsten derivatives are particularly prone to decomposition in the presence of alkali metal alkoxides. Judging from conductometric titration curves, the first step of the reactions of $MoO(OR)_4$ with NaOR in alcoholic solutions affords the addition products $NaMoO(OR)_5$ ($R = Et$, Pr^i). However, $[NaMo_2O_4(OR)_5(ROH)]_2$ [compounds of the $MoO_2(OR)_2$ series] crystallise from these solutions even if the reagents are present in a ratio $Na : Mo \leqslant 1 : 2$. In the presence of an excess of NaOR (compared to 1 : 2), the formation of Na_2MoO_4 is observed, and the crystallisation rate of this compound sharply increases with increasing concentration of NaOR. The process occurs with elimination of ether (which was detected chromatographically).[137, 138] Analogous results were obtained in the reactions of M^IOR with $WO(OR)_4$ or $WO_2(OR)_2$, but the rates of these reactions are substantially lower than that observed for $MoO(OR)_4$.[137]

The formation of oxo complexes [along with $M(OR)_n$ or instead of them] in the electrochemical synthesis of alkoxides is, apparently, attributable to decomposition of $M(OR)_n$ in the cathode compartment (presumably, due to local warming). Examples are the syntheses of $[M_5O(OPr^i)_{13}]$ (M = Sc, Y, La),[11, 93] $[Pb_6O_4(OPr^i)_4]$,[127] $[Hf_3O(OEt)_{10}(EtOH)]_2$,[45] $Ta_2O(OPr^i)_8 \cdot (Pr^iOH)$,[33, 34] $[LiTa_9O_{10}(OEt)_{20}(EtOH)]$,[173] a series of rhenium alkoxides $\{[Re_2^V(OMe)_8]_2O_2$,[71] $[Re_4^{VI}O_6(OMe)_{12}]$[72] and $[Re_4^{V,VI}O_6(OPr^i)_{10}]\}$[84] and numerous methyl cellosolves.[236]

Apparently, the above-described type of decomposition has a rather general character. For example, the synthesis of silane oxides $M(OSiMe_3)_2$ (M = Hg, Pb) by transesterification of $M(OR)_n$, alcoholysis of MCp_n or metathesis of $Pb[N(SiMe_3)_2]_2$ with Bu^tNCO is complicated by the formation of the oxo derivatives $Pb_4O(OSiPh_3)_6 \cdot PhH$,[59] $[Pb_7O_2(OSiMe_3)_{10}]$[145] and HgO[237] [with elimination of $(R_3Si)_2O$].

Heteroleptic complexes, in particular, alkoxo carboxylates, are even more prone to this type of decomposition[238, 239] than homoleptic alkoxides.

$$Sn(OR)_4 + Cd(OAc)_2 \longrightarrow$$
$$\longrightarrow Cd_4Sn_4O_2(OR)_{10}(OAc)_{10} + AcOR$$

$R = CH_2Bu^t$.

Since such complexes readily eliminate ester, they were proposed as precursors in the synthesis of complex oxides from the gaseous phase (CVD method):[240]

$$MM'_nO_x(OR)_y(R'COO)_z \longrightarrow MM'_nO_m + R'COOR.$$

Other examples of processes where the appearance of oxo groups cannot be related to the above-mentioned decomposition pathways of alkoxides, can be cited. In particular, transesterification of $Nb(OR)_5$ with pinacol affords $[Nb_3O_2\{O(CMe_2)_2O\}_5 \cdot \{O(CMe_2)_2OH\}]$ and $[Nb_4O_4\{\eta^2,\mu\text{-}O(CMe_2)_2O\}_2(OPr^i)_8]$.[52] By contrast, transesterification with ethylene glycol and methyl cellosolve gave rise to niobium compounds belonging to the ortho series.[241]

The formation of $[Al_4O(OBu^i)_{10}(Bu^iOH)]$,[53] $[Al_{10}O_6(OPr^i)_{18}NH_3]$[176] and $[K(18\text{-}C\text{-}6)_2]^+[Mo_4O(OCH_2 \cdot Bu^t)_{11}]^-$ (see Ref. 69) in the reactions with bases, such as DBU (1,8-diazabicyclo[5.4.0]undec-7-ene), NH_3 or KOH, may be associated with elimination of β-hydrogen atoms in radicals attended by elimination of alkenes.

Alcoholysis of chlorides, *viz.*, Lewis acids, can be accompanied by side reactions giving rise to HCl and water, which are responsible for the appearance of oxo groups {for example, in the $[Nb_2Cl_4(OEt)_2(THF)_2]_2O_2$ (see Ref. 70) and $[Th_4O \cdot \{(OC_2H_4)_4O\}_3Cl_8] \cdot 3MeCN$[63] molecules}. Presumably, the

same is also true for the formation of oxo complexes in numerous exchange reactions of chlorides in alcoholic solutions, where alcoholysis of MCl_n cannot be suppressed. Examples are the syntheses of $[IZnTa_2O_2(OPr^i)_7]_2$ [by the reaction of ZnI_2 with $KTa(OR)_6$],[134] $[Ti_3OCl(OCH_2Bu^t)_9]$ (from $TiCl_4$ and NaOR)[43] and $[Al_4O(OPr^i)_6Cl_4(Pr^iOH)]$ [from $AlCl_3$ and $Al(OR)_3$].[18]

Unfortunately, by-products of decomposition accompanied by the formation of OA have been thoroughly examined only in a few studies. The question about the relation between individual reactions is very complicated, particularly because oxidation and elimination of ethers are catalysed by water traces.

III. Properties of oxoalkoxides

Oxo complexes differ from alkoxides of the ortho series primarily in that the former compounds are not necessarily soluble in alcohols and hydrocarbons and they are much more prone to crystallisation. Numerous examples are known, where insoluble polymeric $M(OR)_n$ compounds undergo oligomerisation due to uncontrolled hydrolysis or oxidation. Solubility of these compounds sharply increases in alcohols and non-polar organic solvents. For instance, the replacement of OR groups in polymeric $Ba(OBu^n)_2$ up to the composition $BaO_{0.05}(OBu^n)_{1.9}$ leads to an increase in solubility in alcohols from 0% to ~40%.[204]

Crystalline oxo complexes go into an alcoholic solution only upon weak warming (or after mechanical grinding under an alcoholic layer). Cooling of such solutions generally leads to very slow crystallisation of $MO_m(OR)_n$ (even in the presence of a bottom phase), and crystals never precipitate in quantitative yields. Vacuum distillation of the mother liquor usually gives rise to a non-crystalline substance, which is compositionally different from crystals. In no case were the equilibrium values attained in the determination of the solubility of oxo complexes in alcohols. Polytherms measured on heating and cooling of solutions show a hysteresis.[151] The only exception is $Ta_2O(OPr^i)_8 \cdot Pr^iOH$, whose binuclear molecules apparently exist in an alcoholic solution.[33,34] These facts indicate that oxo complexes undergo solvolytic decomposition when going into solution to form fragments with different compositions and structures, and these fragments are involved in complex poly(oligo)merisation processes.

Certain information on the structures of fragments existing in the gaseous phase or alcoholic solutions can be obtained by their 'reconstruction' from the crystal structures of polynuclear complexes. For example, fragments of tetra-, penta- and hexanuclear oxo complexes can readily be distinguished in the $Al_{10}O_4(OEt)_{22}$ molecule (see Fig. 2 *c*).[17] These fragments were detected by mass spectrometry. The average degree of association [with respect to monomeric $Al(OR)_3$] is ~4.4. It should be noted that this value was obtained from the results of both mass spectrometry and cryoscopy in benzene, from which the decanuclear complex crystallises.[242] Analogously, the structures of molecules in amorphous $[NbO(OEt)_3]_n$ samples can be reconstructed from the data on the crystal structure of $Nb_8O_{10}(OEt)_{20}$ (see Fig. 1 *b*).[151]

The possibility of crystallisation of alkoxides of the ortho series from solutions containing oxo complexes is yet another consequence of the presence of particles with different compositions (including particles containing no oxo groups) in solutions of OA. For example, the starting solvate crystallises in low yield from an alcoholic solution of desolvation products of $[Zr(OPr^i)_4 \cdot Pr^iOH]_2$ containing, as mentioned above, $Zr_3O(OR)_{10}$ and $Zr_4O(OR)_{14}$.[225] Bimetallic alkoxides $ZrAl_2(OPr^i)_{10}$ and $LaNb_2(OPr^i)_{10}$ were prepared from solutions of the $Al(OPr^i)_3 - ZrO_n(OPr^i)_{4-2/n} - Pr^iOH$[243] or $Nb(OPr^i)_5 - La_5O(OPr^i)_{13} - Pr^iOH$ systems,[85] respectively, because they are apparently the least soluble of all the components and complexes present in these systems. In the presence of $Ti(OEt)_4$ or $Nb(OEt)_5$ (which add oxo groups), polymeric $Fe(OEt)_3$ precipitates from a solution containing iron oxoethoxide.[244]

Since oxoalkoxides undergo thermal destruction on heating, they are not, as a rule, transformed into the gaseous state. In some cases, mass spectra show low-intensity ions corresponding to fragmentation of the most stable molecules, for example, $[Ln_5O(OPr^i)_{13}]$[93,11,245] and $[Al_{10}O_4(OEt)_{22}]$.[17] The $[Na_4M_2O.(OBu^t)_8]$ complexes (M = Bi or Sb) sublime without decomposition at 180 and 120 °C (10^{-2} mm Hg), respectively.[109] In many cases, heating is accompanied by disproportionation of OA to form volatile $M(OR)_n$ and polymeric products containing a larger number of oxo groups per metal atom. This is the reason why $Ta(OPr^i)_5$ can be prepared by sublimation from the product of electrochemical synthesis $[Ta_2O(OPr^i)_8(Pr^iOH)]$[33] or by distillation of $Nb(OEt)_5$ from $[Nb_8O_{10}(OEt)_{20}]$.[151]

In conclusion, it should be noted that the reactivity increases substantially in going from alkoxides to oxo complexes. In many cases, high stability of one or both orthoalkoxides hinders their complexation. The replacement of inactive $M(OR)_n$ with the corresponding oxo complex substantially increases the reaction rate. For example, the reaction of $Ti(OPr^i)_4$ with partial hydrolysis products of polymeric $Pb(OPr^i)_2$ or $Bi(OPr^i)_3$ instead of these compounds as such proceeds rapidly at 20 °C to give $[Pb_2Ti_2O(OPr^i)_{10}]$[60] and $[BiTi_2O(OPr)_9]$, respectively.[41] Polymeric $Ba(OBu^n)_2$ reacts with alcoholic solutions of $Ta(OBu^n)_5$ only in the presence of traces of uncontrolled oxidation products to form highly soluble bimetallic oxo complexes. This allows one to prepare solutions of these two butoxides with different concentrations and any component ratio.[232] Under the same conditions, the reaction with $Ti(OBu^n)_4$ affords solutions with a ratio $Ba : Ti \gg 1 : 4$ (Fig. 5 *f*).[204] Zirconium, hafnium or tantalum isopropoxides react with $Al(OPr^i)_3$ only upon prolonged refluxing of alcoholic solutions, which is apparently accompanied by the appearance of OA particles.[243,246] Presumably, preliminary activation is not needed in reactions with M^IOR or $M^{II}(OR)_2$ due to the virtually unavoidable presence of microamounts of oxo groups in the samples.

IV. Structural types of oxoalkoxides

Since oxoalkoxides have various structures, it is convenient to consider these compounds in order of increasing nuclearity in their oligomeric molecules.

1. Binuclear OA

Binuclear oxoalkoxides (see Table 1) are represented by molecules consisting of two tetrahedra {$[(OsO)O(OCMe_2CH_2NHBu^t)]_2$,[19] $[Nd_2O(OCH_2Bu^t)_4]$[20]}, two five-vertex polyhedra, *viz*., trigonal bipyramids and tetragonal pyramids sharing a $(\mu\text{-O})_2$ edge {for example, $[Nb(\mu\text{-O})(OC_6H_3Pr^i_2\text{-}2,6)_3]_2$ (see Ref. 22)}, two octahedra sharing a μ-O vertex $[(MoO)_2O[O(CMe_2)_2O]_2.[O(CMe_2)_2OH]_2$[28]], sharing a $(\mu\text{-O})_2$ edge ($[(WO)O.(RO_2)(OROH)]_2$ (see Ref. 30), sharing a $[(\mu\text{-O})(\mu\text{-OR})]$ edge {$[Ta_2O(OPr^i)_8(Pr^iOH)]$[33,34]} or sharing a $[(\mu\text{-O})(\mu\text{-X})_2]$ face (X = OR, Cl) {for example, $[Ta_2OCl_3(OC_6H_3Pr^i_2\text{-}2,6)_5]$[35]}. The bonds between metals and oxo bridges are shorter than the M—(μ-OR) bonds and, in some cases, shorter than the terminal M—OR bonds. In the $[M_2(\mu\text{-OR})_2]$ rings of dimeric alkoxides, the M—(μ-OR)—M angles remain virtually constant (107–112°) and are independent of the nature of the metal atom, the substituent and the coordination polyhedron, whereas the M—(μ-O)—M angles in oxo complexes vary within a broad range {from 80.1° in the $[Mo^{III}_2O(OCH_2Bu^t)_4(PMe_3)_4]$ molecule[27] to 154–161° in the $[(WO)O(RO_2)(OROH)]_2$ molecule[30]}.

In the $[Ta_2O(OPr^i)_8(Pr^iOH)]$ complex,[33,34] the presence of one strong $Pr^iO\cdots HOPr^i$ hydrogen bond between the terminal ligands leads to a decrease in the distance between these ligands [O···O(H), 2.52 Å] and 'pushing off' of the OPr^i groups located on the opposite side of the equatorial plane (Fig. 6). Binuclear derivatives of metals in the lowest oxidation states, such as $[W^{IV}_2(\mu\text{-O})(\mu\text{-OBu}^t)(OSiMe_2Bu^t)_5Py_2]$,[25] $[Re^{VI}_2O_2(\mu\text{-O})(\mu\text{-OMe})_2.(OMe)_4]$[39] and $[(Mo^VO)(\mu\text{-O})(OC_6F_5)_2]^-_2$,[23] contain bridging groups along with M = M bonds (2.49–2.56 Å).

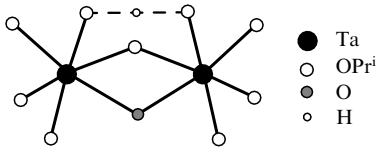

Figure 6. Metal–oxygen core in the structure of $[Ta_2O(OPr^i)_8.(Pr^iOH)]$.[33,34]

2. Trinuclear OA

Trinuclear oxoalkoxides (see Table 2) are represented by two types of triangles. In one type, the $[M_3]$ triangle is centred by a μ_3-O group on one side of the equatorial plane. In another (more widespread) type, there is not only a μ_3-O group but also a μ_3-X group located on the opposite side of the equatorial plane (X = OR, OH, Cl), resulting in the formation of the $[M_3(\mu_3\text{-}O).(\mu_3\text{-}X)(\mu\text{-}OR)_3]$ trigonal bipyramids (see Fig. 4 *a*) flattened along the threefold axis. In the $[Ti_3O(OMe)(OPr^i)_9]$ molecule,[42] the $(\mu_3\text{-}O)-Ti-(\mu_3\text{-}OMe)$ angles are 69°. In the $[W_3(\mu\text{-}O)_2(OBu^t)_8]$ molecules, the bonds in the triangle occur not only *via* the bidentate oxo groups but also *via* W–W single bonds and W=W double bonds (2.93 and 2.45 Å, respectively).[50]

In addition to triangular structures, there are also chain molecules, such as linear $[UO_2][U(\mu\text{-}O)(OBu^t)_5]_2$ (see Ref. 51) (as a result of the *trans* arrangement of two terminal groups in the central octahedron) and angular $[Nb_3O_2\{O(CMe_2)_2O\}_5.\{O(CMe_2)_2OH\}]$.[52]

3. Tetranuclear OA

Tetranuclear oxoalkoxides (see Table 3) are represented by two main groups, *viz*., tetrahedra and planar rhombuses consisting of four octahedra linked *via* two μ_3-ligands and four μ-ligands $[Ti_4(OMe)_{16}$ type [3]]. Apparently, a regular tetrahedron is present only in the $[Pb_4(\mu_4\text{-}O)(\mu\text{-}OSiPh_3)_6]$ molecule,[59] in which six μ-OR groups are located along its edges (Fig. 7 *a*). Taking into account the absence of one or several μ-OR groups in the $[Al_4.(\mu_4\text{-}O)(\mu\text{-}OR)_5X_5(ROH)]$ [X = OPr^i, Cl, OBu^i, OCH_2CF_3 (see Fig. 2 *d*)],[18,54,55] $[Pb_3Zr(\mu_4\text{-}O)(\mu_3\text{-}OBu^t)(\mu\text{-}OBu^t)_5(OBu^t)_2]$[62] and $[Ce_4^{3.75+}(\mu_4\text{-}O)(\mu_3\text{-}OPr^i)_2(\mu\text{-}OPr^i)_4(Pr^iO)_7(Pr^iOH)]$[61] structures, these compounds can be assigned to 'butterfly-type' molecules, in which the wings are additionally linked *via* an oxo group. In solvates of these molecules with alcohols, the wings are linked not only *via* an oxo group but also *via* a very short hydrogen bond between the terminal OR and ROH groups. In the distorted $[W_4(\mu\text{-}O)(\mu\text{-}OPr^i)_2(OPr^i)_7Cl]$ tetrahedron, the central μ_4-O group is absent, and the tungsten atoms are linked to each other *via* μ-OR and μ-O bridges and W=W and W–W bonds (2.45 and 2.9 Å, respectively).[66]

In $Ti_4(OMe)_{16}$-type molecules, four sides of the $[M_4]$ rhombus are additionally linked *via* μ groups, and two $[M_3]$ triangular fragments are linked by μ_3 ligands located on the opposite sides of the plane of the rhombus. These molecules involve two types of metal atoms. Metal atoms of one type are coordinated by two μ_3 groups, whereas metal atoms of another type are coordinated by only one μ_3 group (in Fig. 7 *b*, these atoms are denoted M^1 and M^2, respectively). The oxo ligands are generally located in μ_3 positions. Examples are the $[Bi_4(\mu_3\text{-}O)_2(OBu^t)_8]$[73] and $[(MoO)_4(\mu_3\text{-}O)_2(OEt)_4Cl_4(EtOH)_2]$[81] molecules. However, the reverse situation is observed in the $[(VO)_4O_4(OMe)_4(bipy)_2]$ (bipy is 2,2′-bipyridyl)[74] and $[(MoO_2)_4O_2(OMe)_4(Me_2CNOH)]$[77] complexes and the $[(MoO_2)_2(MoO)_2O_4(OMe)_2(C_6H_4O_2\text{-}1,2)_2]^-$ anion,[78,79] in which the OMe groups are in μ_3 positions, whereas the oxo groups are bidentate.

In the $[LiNbO(OEt)_4(EtOH)]_2$ (see Ref. 85) and $[MgNbO(OMe)_5(MeOH)_2]_2$ molecules,[76] the oxo ligands are terminal and are involved in the 'niobyl' groups (these groups occupy the M^1 and M^2 positions in two molecules, respectively).

Compounds containing more than four metal atoms occur, as a rule, as conglomerates of smaller stable fragments described above. However, there are several more types of penta-, hexa- and octanuclear associates (often *closo*) with high symmetry.

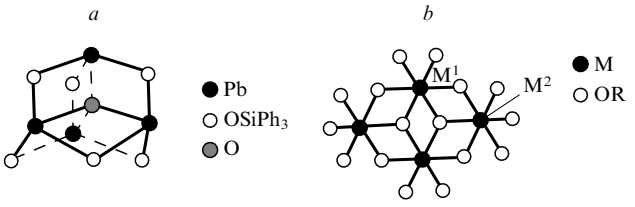

Figure 7. Metal–oxygen cores in the structures of $[Pb_4(\mu_4\text{-}O)(\mu\text{-}OSiPh_3)_6]$[59] (*a*) and $M_4(\mu_3\text{-}O)_2(\mu\text{-}OR)_4(OR)_n$ $[Ti_4(OMe)_{16}$ type] (*b*).

4. Pentanuclear complexes

Pentanuclear complexes (see Table 4) are represented by two main structural types, *viz*., clusters containing the $[M_5(\mu_5\text{-}O)]$ core and combinations of two $[M_2M']$ triangles.

In the molecules of isopropoxides $[Ln_5(\mu_5\text{-}O)(\mu_3\text{-}OR)_4(\mu\text{-}OR)_4(OR)_5]$ (Ln = Sc, Y, Er, Yb, [Y_4Pr], In),[10–14,92,93] the $[M_5O]$ group can be described as a tetragonal pyramid, in which four μ_3-OR ligands are located above the centres of lateral faces, and four μ-OR groups are located along the edges of the base (see Fig. 2,*a*). The $[Al_5O(OBu^i)_{13}]$ and $[Fe_5O(OEt)_{13}]$ molecules have the structure of $[M_5(\mu_5\text{-}O)(\mu\text{-}OR)_8(OR)_5]$ and differ from the above-described molecules in that they contain no μ_3-OR groups. In these molecules, eight μ-OR groups are located along all edges of the pyramid.[15,53]

In the $[Ln_5O(OPr^i)_{13}]$ molecules with the group $[M_5]$ = $[Sm_4Ti]$, the $[(Tb_{0.9}Eu_{0.1})_4Ti]$ molecule and the $[Nd_5(\mu_5\text{-}O)(OPr^i)_{13}(Pr^iOH)_2]$ solvate, the 'cluster' has a trigonal-bipyramidal structure. In these molecules, two μ_3-OR groups are located above faces of two different pyramids, whereas six μ-OR groups serve as bridges between two axial metal atoms and three equatorial metal atoms.[10,13,99–101] In the tetragonal-pyramidal molecules $[Sr_5(\mu_4\text{-}O)(OCH_2Bu^t)_8(Bu^tCH_2OH)(THF)_4]$[95] and $[Eu^{III}Eu^{II}_4O_5(OAr)(ArOH)_5(MeCN)_8]$ (Ar = $C_6H_3Pr^i_2$-2,6),[96] the oxo group is located in the centre of the base and is coordinated in a tetradentate fashion. Aggregates of this type are very stable, exist in solutions and the gaseous phase and have low reactivity, in particular, in complex formation with other metal alkoxides.

A combination of two corner-sharing triangles is observed exclusively in bimetallic complexes, the more electropositive metal atom being common to two triangles. In the $[NaBi_4(\mu_3\text{-}O)_2(\mu\text{-}OC_6F_5)_7(OC_6F_5)_2]$ molecule, the $[NaBi_2]$ triangles are centred by μ_3-O groups.[64] The $[Mo^V_2Mo^{VI}Ta_2O_8(OPr^i)_{10}]$ complex is the first example of molecule in which all five metal atoms are involved in a non-planar ring containing a Mo=Mo bond (2.58 Å) along with μ-O and μ-OR groups.[104]

5. Hexanuclear OA

Many compounds belonging to this group of mono- and bimetallic complexes (see Table 5) contain μ_6-O-centred or non-centred $[M_6]$ octahedral 'clusters'. In the $[Ba_6(\mu_6\text{-}O)(OC_2H_4OMe)_{10}.(MeOC_2H_4OH)_4]$,[105] *trans*-$[Na_2Gd_4(\mu_6\text{-}O)(OBu^t)_{12}]$[106] and *trans*-$[K_4Zr_2(\mu_6\text{-}O)(OPr^i)_{10}]$ molecules,[107] the μ_3-OR ligands are located on eight faces of the octahedron. Structural analogues of the 'large octahedron' $[M_6O_{19}]^{n-}$ = $[M_6(\mu_6\text{-}O)(\mu\text{-}O)_{12}O_6]$ (M = Nb, Ta, Mo, W), in which twelve μ-O groups are located along the edges and six μ-O groups are terminal, are also well known. Among them are numerous oxo alkoxo vanadates,[113–117] $[V^{IV,V}_6(\mu_6\text{-}O)(\mu\text{-}OEt)_{12}O_6]$, which is a microhydrolysis product of $VO(OEt)_3$ (see Ref. 112) and the $[Fe_6(\mu_6\text{-}O)\{MeC(CH_2O)_3\}_6]^{2-}$ and $[Fe_6(\mu_6\text{-}O)(OMe)_{18}]^{2-}$ anions[120,121] (Fig. 8 *a*).

Among octahedral clusters containing no μ_6-O groups, the $[M_6(\mu_3\text{-}O)_4(\mu_3\text{-}OR)_4]$ compounds (M = Sn, Pb; R = Me, Pr^i) with

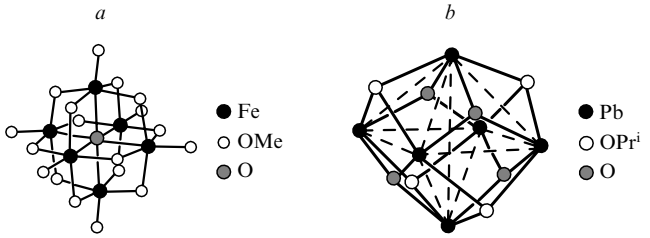

Figure 8. Metal–oxygen cores in the structures of $[Fe_6(\mu_6\text{-}O)(OMe)_{18}]^{2-}$ (*a*) [149] and $[Pb_6(\mu_3\text{-}O)_4(\mu_3\text{-}OPr^i)_4]$ (*b*).[127]

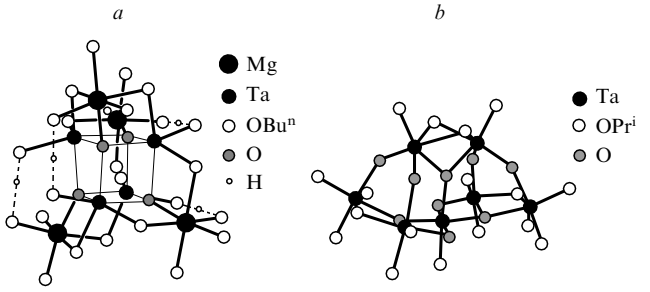

Figure 9. Metal–oxygen cores in the structures of $[Mg_4Ta_4O_4(OBu^n)_{20}(Bu^nOH)_4]$ (*a*) [160] and $[Ta_7O_9(OPr^i)_{17}]$ (*b*).[33, 103]

alternating oxo and OR ligands above the centres of the faces [124–127] [structural analogues of hydroxides of the same metals (see Fig. 8 *b*)] and the bimetallic $[La_2(MoO)_4(\mu_4\text{-}O)_4(\mu\text{-}OPr^i)_8(OPr^i)_6]$ complex,[128] in which four $[Mo_2La_2(\mu_4\text{-}O)]$ groups are located inside the octahedron, are of interest.

In yet another large group of hexanuclear complexes, two $[M_3(\mu_3\text{-}O)]$ triangles are linked to each other to form a ring *via* bidentate O or OR bridges. Examples are $[(MoO_2)Ta_2(\mu_3\text{-}O)(\mu\text{-}OMe)_3(\mu\text{-}O)(OMe)_5]_2$,[133] $[IZnTa_2(\mu_3\text{-}O)(\mu\text{-}OPr^i)_3(\mu\text{-}O)(OPr^i)_4]_2$ (see Ref. 134) and $[Hf_3(\mu_3\text{-}O)(\mu\text{-}OEt)_4(OEt)_6(EtOH)]_2$ (see Ref. 45, Fig. 4 *b*). In the $[Gd_3(OC_2H_4OMe)_8]_2(\mu_4\text{-}O)$ molecule, two triangles, which are perpendicular to each other, are linked *via* a tetradentate oxo group.[130]

In the bimetallic $[Er_2Ti_4O_2(OEt)_{18}(EtOH)_2]$ [140] and $[(NaTHF)_2Bi_4(\mu_3\text{-}O)_2(\mu\text{-}OC_6F_5)_{10}]$ [64] complexes, the $[Ti(\mu_3\text{-}OR)(\mu\text{-}OR)_2(OR)_2]$ and [NaTHF] groups, respectively, are additionally bound to two μ_3-O ligands of the core {$[Ti_4(OMe)_{16}]$ type}. Only the $[Ca_6(\mu_4\text{-}O)_2(\mu_3\text{-}OEt)_4(OEt)_4]\cdot 14\,EtOH$ molecule [16] contains two cuboidal tetramers sharing the $[Ca_2(\mu_4\text{-}O)_2]$ face (see Fig. 2 *b*). The $[Fe_6(\mu_4\text{-}O)_2(\mu\text{-}OMe)_8(OMe)_4.\{N(C_2H_4NH_2)_3\}_2]^{2+}$ cation [129] consists of two $[M_4]$ tetrahedra sharing the $[M_2]$ edge {the $[Fe_2(\mu_4\text{-}O)_2]$ group in the centre}. In the molecules $[(MoO)_3(\mu\text{-}O)_2(OPr^i)_6]_2$ (see Refs 46 and 141) and $[M^V(MoO)_2(\mu\text{-}O)_2(OPr^i)_7]_2$ (M^V = Nb, Ta),[104] the zigzag hexanuclear chains are linked *via* μ-O groups.

6. Oligomeric oxoalkoxides with nuclearity higher than six

The following structural types were found for oligomeric oxoalkoxides with nuclearity higher than six (see Tables 6–10): closed polyhedra, in which all atoms are bound to no more than two oxo groups; rings; condensed structures related to inorganic isopolyanions (metal atoms in the latter are coordinated by several oxo groups).

Among closed polyhedra, oxo complexes involving cuboidal cores (see Table 7) are of particular interest. The $[Li_4Ti_4(\mu_5\text{-}O)_2.(\mu_3\text{-}O)_2(OPr^i)_{12}]$ molecule consists of two cuboidal cores $[Li_2Ti_2O_3(OR)]$, which share the $[Ti_2(\mu_5\text{-}O)_2]$ face and are additionally linked *via* the 'external' trigonal bipyramids $[TiO(OR)_4]$.[158] A larger number of molecules contain one cube $[M^{II}_4(\mu_4\text{-}O)_4]$ in the centre. Examples are the $[Mg_4Ta_4O_4(OBu^n)_{20}(Bu^nOH)_4]$ (Fig. 9 *a*), $[Sr_4Ta_4O_4.(OMe)_{20}(MeOH)_{10}]$,[160] $[Ba_4M_4O_4(OEt)_{20}(EtOH)_6]$ (M = Nb, Ta) [85, 160] and $[Ba_4Ti_4O_4(OPr^i)_{16}(Pr^iOH)_{3.5}]$ [159] complexes.†

The M^{II} atoms are linked to the 'external' $[M'(OR)_m]$ groups (M' = Ti, Nb, Ta) *via* oxo ligands and two or more μ-OR groups. The coordination environment of the M^{II} atom also involves alcohol solvate molecules. In spite of the different nature (and even valence) of M' and R, these compounds are structurally very similar. The only difference is the orientation of the $[M'O(OR)_m]$ groups with respect to the cuboidal core. These groups can be located as continuations of edges (Mg–Ta), diagonals of faces (Ba–Nb) or body diagonals (Ba–Ti). It is reasonable to expect that the above-described structure would be observed also in other oxoalkoxides with a ratio $M^{II}:M^n = 1:1$. The complex $[Mg_4Ta_4O_4(OBu^n)_{20}(Bu^nOH)_4]$ is the first structurally characterised n-butoxide. Evidently, the cuboidal core (a matrix, on which an OA molecule is formed) prevents the hydrocarbon chain from knotting, which generally hinders crystallisation.

The same situation is observed in decanuclear molecules (see Table 9). In such molecules, the $[M_6]$ octahedral 'clusters' are located in the centre and the μ_3-OR and μ_4-O groups alternate on eight faces. The latter are involved in the $[(\mu_4\text{-}O)M'(OR)_5]$ octahedra. Examples are the $[Pb_6Nb_4O_4(OEt)_{24}]$,[178] $[Sr_6Ti_4O_4(OPr^i)_{20}]$ [102] and $[Ni_6Sb_4O_4(OEt)_{16}(EtOH)_4]$ [177] complexes. In all these complexes, the central octahedron is formed by more positive metals, *viz*., Pb, Sr and Ni, respectively. The $[Ba_4Cu_6(\mu_4\text{-}O)(\mu\text{-}OCEt_3)_{12}]$ molecule, in which the edges of the central $[(\mu_4\text{-}O)Ba_4]$ tetrahedron are linked *via* six linear $[Cu(\mu\text{-}OR)_2]$ groups,[175] can be considered as a tetrahedral analogue of the above-described structures. In the $[Fe_7O(OH)\{(OCH_2)_3CCH_2OH\}_4Cl_6(MeCN)_2]$ molecule,[146] the central $[Fe_6(\mu_6\text{-}O)]$ octahedron is linked to one $[Fe(OH)(MeCN)_2]$ group (see Table 6). In the $[Na_2Fe_6O(OMe)_{18}(MeOH)_6]$ complex [149] (with axial Fe atoms), the central octahedron is linked to two $[Na(ROH)_3]$ groups (see Table 7). In the structure of $[Bi_6(\mu_3\text{-}O)_7(\mu_3\text{-}OC_6F_5)[Bi(OC_6F_5)_4]_3(THF)_2]$,[166] the μ_3-O groups are located on seven faces of the $[Bi_6]$ octahedron {three of these groups are coordinated to $[Bi(OR)_4]$} and the eighth face is occupied by the μ_3-OR ligand (see Table 8).

Hepta-, octa-, deca- and octadecanuclear alkoxides (see Tables 6, 7, 9 and 10) form rings. The tetrahedral oxygen atom in the $[\{Cu_2Zr_2(OPr^i)_9\}_2(\mu_4\text{-}O)]$ molecule serves as a bridge between two eight-membered rings, each ring containing two linear $[CuO_2]$ groups and $[Zr(\mu\text{-}OR)_3Zr]$ octahedra.[156] One centrosymmetric ring, which consists of four $[Mo_2(\mu_3\text{-}O)]$ triangles linked to each other *via* μ-OH groups, is observed in the $[(MoO)_4O_2(OEt)_2(OH)_3Cl_3(EtOH)_2]_2$ molecule.[81, 157] The spherical $[Cu_{18}O_2(OSiMe_3)_{14}]$ molecule is formed by two intersecting μ_4-O-centred $[Cu_9O_8]$ rings.[194]

The pentanuclear $[M_5(\mu_4\text{-}O)(\mu_3\text{-}O)(\mu\text{-}OR)_6(OR)_4]$ rings, which differ only in the mode of binding to each other, were found in the structures of aluminium OA with nuclearity from 9 to 11. In the $[Al_{10}O_4(OEt)_{22}]$ molecule,[17] these rings are linked *via* the central $[Al_2(\mu_3\text{-}O)_2]$ group. In the $[Al_{11}O_6(OR)_{21}]$ complex (R = Pr^i, Pr^n), the rings are linked *via* the $[Al(\mu_3\text{-}O)_2(\mu\text{-}O)_2(OR)]$ group. In the $[Al_5Mg_4O_3(OH)_3(OPr^i)_8(acac)_6]$ molecule [180] (acac is acetylacetonate) and its structural analogue $[Fe_9O_3(OEt)_{21}]\cdot EtOH$,[167] the rings share the $[M(\mu_3\text{-}O)]$ edge and are additionally linked to each other *via* a μ-OH group. The $[Al_8O_2(OH)_2(OBu^i)_{18}]$ molecule [53] can be considered as a derivative of decanuclear oxoethoxide lacking one Al atom, which is not bound to the μ_4-O group, in each half of the molecule. Therefore, there is a homologous series of aluminium oxoalkoxides, including from octa- to undecanuclear molecules (Fig. 10).

† Taking into account the exceptionally short Ti–O bonds (1.71 and 1.79 Å), this structure can be considered as a combination of four ionic pairs $[Ba(ROH)]^{2+}_4[TiO(OR)_4]^{2-}_4$. In solution this complex, unlike molecular alkoxo titanates $Ba[Ti_2(OPr^i)_9]_2$, $[BaTi_2(OPr^i)_{10}]_2$ and $[BaTi_3.(OPr^i)_{14}]$,[247] can apparently exist as isolated ions or their associates.

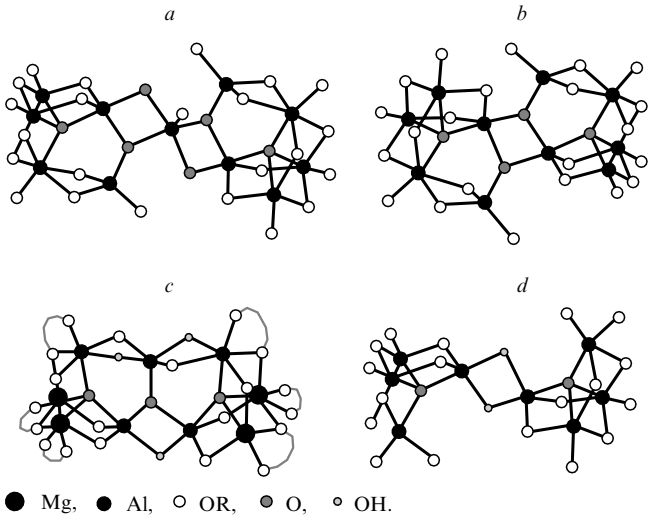

Figure 10. Comparison of the metal–oxygen skeletons in the molecules of undeca-, deca-, nona- and octanuclear aluminium oxoalkoxides — $[Al_{11}O_6(OPr^n)_{10}(OPr^i)_{10}(OR)(ROH)_2]$ (R = Pr^i, Pr^n) (*a*),[180] $[Al_{10}O_4(OEt)_{22}]$ (*b*),[17] $[Al_5Mg_4O_3(OH)_3(OPr^i)_8(acac)_6]$ (*c*)[180] and $[Al_8O_2(OH)_2(OBu^i)_{18}]$ (*d*).[53]

Many known oxo alkoxo complexes containing more than six metal atoms belong to condensed structures related to inorganic isopolyanions. All oxo groups in these compounds (except for 'yl' O atoms) serve as bridges (from bi- to hexadentate), and OR groups are either terminal ligands or bidentate bridges. Oxo alkoxo molybdates(VI) and (V,VI) and vanadates(IV), (V) and (IV,V), which are characterised by the closest packing of edge- and vertex-sharing octahedra, are worthy of notice. These compounds are analogous to metamolybdate $[Mo_8O_{26}]^{4-}$ (see Refs 154 and 155) and decavanadate $[V_{10}O_{28}]^{6-}$.[169, 170] Alkoxy groups of mono- or, more often, polyatomic alcohols $RC(CH_2O)_3$ are located on the surface of these compounds. Examples are the $[(MoO_2)_6(MoO)_2O_{10}(OMe)_4]^{4-}$ (see Ref. 153) and $[V^{IV}_{10}O_{13}\{EtC(CH_2O)_3\}_5]^-$ anions.[169] The $[Ta_7(\mu_3\text{-}O)_3(\mu\text{-}O)_6.(OPr^i)_{17}]$ molecule[33, 34, 103] consists of two vertex-sharing $[Ta_4]$ tetrahedra, which are additionally linked to each other *via* one μ_3-O group and two μ-OR groups (see Fig. 9 *b*). The structure of $[LiTa_9O_{13}(OEt)_{20}(EtOH)]$[173] contains Li atoms and two layers of rings consisting of the $[Ta_3O_7(OR)_6]$ and $[Ta_6O_6(OR)_{15}]$ octahedra, which are linked to each other *via* μ-O bridges. Apparently, the product of hydrothermal synthesis with composition $M_7[Na(H_2O)_3Mo^V_{36}Mo^{VI}_6H_{15}O_{109}\{(OCH_2)_3CCH_2OH\}_7]$[197] has the maximum size. The $[Na(H_2O)_3]$ group located in the centre of this molecule is surrounded by the $[Mo^V_6O_{24}]$ ring and the framework of the $[Mo^{V,VI}O]$ octahedra (see Table 10).

The spherical $[Zr_{13}O_8(OMe)_{36}]$[9] and $[Zr_3Mo_8O_{24}(OPr^i)_{12}.(Pr^iOH)_4]$[182] molecules also belong to the class of compounds under consideration. In these molecules, the $[ZrO_8]$ groups are located in the centre and OR groups are located on the surface (in the former complex, twelve OR groups serve as bridges). The $[Ba_4Ti_{13}O_{18}(OC_2H_4OMe)_{24}]$ molecule containing one central and twelve peripheral Ti octahedra {a structural analogue of the known $[Al_{13}O_4(OH)_{24}(H_2O)_{12}]^{7+}$ ion}[192] and the $[Mn_8Sb_4O_4(OEt)_{20}]$ molecule with the symmetry S_4 and two Mn octahedra in the centre belong to the same class of compounds (see Table 10).[186]

Unlike the structures with the closest packing of metal–oxygen polyhedra, the 'loose' $M_8O_{10}(OEt)_{20}$ molecules (M = Nb and Ta)[100, 148, 149] (see Fig. 1 *b* and Table 8) contain a cavity surrounded by pairs and triads of octahedra sharing a vertex and linked to each other *via* single octahedra.

Let us consider titanium oxoalkoxides, which have no analogues in inorganic chemistry, in more detail. The $Ti_7O_4(OEt)_{20}$ molecule, which is the first crystalline hydrolysis product of titanium ethoxide, can be considered as a condensation product of the $[Ti_4(OEt)_{16}]$ molecules and the $Ti(OEt)_2[(\mu\text{-}OEt)_2Ti(OEt)_3]_2$ trimer (the latter is present in solution).[248] This compound contains the linear $[Ti(\mu_4\text{-}O)(\mu\text{-}O)_2Ti]$ chain with the $[Ti(\mu_3\text{-}O).(\mu\text{-}O)Ti]$ groups located above and below this chain[7, 142] (see Fig. 1 *a* and Table 6). An analogous situation is observed in the structures of the large $[Ti_8O_6(OCH_2Ph)_{20}]\cdot Et_2O$, $[Ti_{10}O_8(OEt)_{24}]\cdot\cdot PhMe$,[143] $[Ti_{17}O_{24}(OPr^i)_{20}]$[191] and $[Ti_{18}O_{28}(OBu^t)_{16}(Bu^tOH)]$[193] molecules (first examples of Keggin-type structures containing Ti atoms). In these structures, chains composed of pairs or triads of edge-sharing octahedra are linked to each other *via* μ_4-O, μ_3-O and μ-OR bridges. The $[Ti_{16}O_{16}(OEt)_{32}]$ molecule[142, 189] contains two mutually perpendicular blocks consisting of eight octahedra. In each block, six octahedra form a NiAs-type layer, one octahedron is located above the layer, one octahedron is located below the layer, and a tetrahedral cavity is located in the centre of the molecule (see Table 10).

In summary, it can be concluded that most molecules belonging to the class of oxoalkoxides contain 4–10 metal atoms. A rather small number of dinuclear molecules have been described, and polymeric molecules are few in number, as opposed to alkoxides $M(OR)_n$, the majority of which belong to one of the latter two groups. Evidently, the reason is that OR bridges are, as a rule, bidentate (except for μ_3-OR groups on the surface of *closo*-aggregates $[M_n]$), whereas oxoalkoxide molecules contain oxo ligands with high dentate numbers (up to 8) responsible for coordination of metal atoms.

It should be noted that no cuboidal molecules of the $[M_4(\mu_3\text{-}X)_4]$ type were found in the class of tetranuclear oxo complexes {the only exception is $[(MoO)O(OSiMe_3)(Me_2NH)]_4$ (see Ref. 67)}, as opposed to orthoalkoxides, for which such molecules are very typical and these molecules are stable.

In many cases, the accumulated data allow one to predict the structures of unknown compounds of the ortho series with high probability.[3] At the same time, oxoalkoxides, on the whole, are characterised by high variability and unpredictability of molecular structures.

V. Oxoalkoxides as true precursors of oxide phases

It is quite apparent that oxo complexes (mono- and bimetallic) play a considerable role in the phase formation of simple and complex oxides and are true precursors. The M—O—M bridges in bimetallic oxo complexes provide homogeneity of the newly formed oxide phases at the molecular level.

The above-considered differences in the composition, stoichiometry, solubility and reactivity of ortho- and oxoalkoxides are widely used in the sol–gel synthesis of a series of very important composites. The synthesis of $BaTiO_3$ is the most prominent example. For the latter compound to be prepared, the starting solution must contain a precursor with a metal ratio of 1 : 1, which is attained only upon decomposition of $BaTi_4(OR)_{18}$ into oxoalkoxides $BaTiO_n(OR)_{6-2n}$. Otherwise the sol–gel synthesis affords a mixture of phases containing not only $BaTiO_3$ but also polytitanates and Ba_2TiO_4. The latter fact is attributable to the presence of free $Ba(OR)_2$ (along with a complex with 1 : 4 composition) in solutions containing Ba and Ti in a ratio of 1 : 1.[159, 215, 216] Therefore, for single-phase bimetallic oxides to be synthesised, it is necessary that the solution should contain not only components in a required ratio but also a complex with a specified stoichiometry.

Yet another aspect of the use of oxo complexes in the synthesis of crystalline oxide phases is associated with spontaneous decomposition of alkoxides at 20 °C accompanied by elimination of ethers (this method does not belong to the sol–gel technology). This procedure was employed for the preparation of Na_2MoO_4, Na_2WO_4, Li_2MoO_4, Li_2WO_4, γ-Bi_2MoO_6 and cubic solid solutions (δ* phase) of the Bi_2O_3–WO_3 system.[137, 224, 249] Alterna-

tively, the latter can be prepared by solid-phase synthesis. However, this method requires annealing at temperatures >700 °C over a long period of time. Crystallisation of oxide phases directly from solutions in organic solvents is unambiguously indicative of elimination of ether, whereas products prepared by the sol–gel method are amorphous and their crystallisation occurs only after dehydration by annealing.

References

1. K A Andrianov *Metal-Organic Polymers* (New York: Wiley, 1965)
2. D C Bradley, in *Inorganic Polymers* (Eds F G A Stone, W A G Grham) (New York: Academic Press, 1962)
3. N Ya Turova, E P Turevskaya, V G Kessler, M I Yanovskaya *The Chemistry of Metal Alkoxides* (Boston, Dordrecht, London: Kluwer Academic, 2002)
4. C J Brinker, G W Scherer *Sol-Gel Science. The Physics and Chemistry of Sol-Gel Processing* (San Diego, CA: Academic Press, 1990)
5. L C Klein (Ed.) *Sol-Gel Technology for Thin Films, Fibers, Preforms, Electronics and Specialty Shapes* (Park Ridge, NY: Noyes, 1988)
6. L C Klein (Ed.) *Sol-Gel Optics: Proceedings and Applications* (Boston, Dordrecht, London: Kluwer Academic, 1994)
7. K Watenpaugh, C N Caughlan *J. Chem. Soc., Chem. Commun.* 76 (1967)
8. D C Bradley, M B Hursthouse, P F Rodesiler *J. Chem. Soc., Chem. Commun.* 1112 (1968)
9. B Morosin *Acta Crystallogr., Sect. B* **33** 303 (1977)
10. O Poncelet, W J Sartain, L G Hubert-Pfalzgraf, K Folting, K G Caulton *Inorg. Chem.* **28** 263 (1989)
11. E P Turevskaya, A I Belokon, Z A Starikova, A I Yanovsky, E N Kiruschenkov, N Ya Turova *Polyhedron* **19** 705 (2000)
12. G Westin, M Kritikos, M Wijk *J. Solid State Chem.* **141** 168 (1998)
13. M Kritikos, M Moustiakimov, M Wijk, G Westin *J. Chem. Soc., Dalton Trans.* 1931 (2001)
14. D C Bradley, H Chudzynska, D M Frigo, M E Hammond, M B Hursthouse, M A Mazid *Polyhedron* **9** 719 (1990)
15. B J O'Keefe, S M Monnier, M A Hillmyer, W B Tolman *J. Am. Chem. Soc.* **123** 339 (2001)
16. N Ya Turova, E P Turevskaya, V G Kessler, A I Yanovsky, Yu T Struchkov *J. Chem. Soc., Chem. Commun.* 21 (1993)
17. A I Yanovsky, N Ya Turova, N I Kozlova, Yu T Struchkov *Koord. Khim.* **13** 242 (1987) [a]
18. N Ya Turova, A I Yanovsky, V G Kessler, N I Kozlova, Yu T Struchkov *Zh. Neorg. Khim.* **36** 2497 (1991) [b]
19. W P Griffith, N T McManus, A C Skapski *Inorg. Chim. Acta* **103** L15 (1985)
20. J Yingtai *J. Chin. Rare Earth Soc.* **11** 17 (1993)
21. J E Hill, P E Fanwick, I P Rotwell *Acta Crystallogr., Sect. C* **47** 541 (1991)
22. V M Visciglio, P E Fanwick, I P Rothwell *Acta Crystallogr., Sect. C* **50** 900 (1994)
23. R G Abbott, F A Cotton, L R Falvello *Inorg. Chem.* **29** 514 (1990)
24. F L Phillips, A C Skapski *J. Chem. Soc., Dalton Trans.* 2587 (1975)
25. M H Chisholm, C M Cook, K Folting, W E Streib *Inorg. Chim. Acta* **198–200** 63 (1992)
26. S K Park, S M Koo, Y E Lee *Polyhedron* **19** 1037 (2000)
27. T A Budzichowski, M H Chisholm, K Folting, K S Kramer *Polyhedron* **15** 3085 (1996)
28. C Knobler, B R Penfold, W T Robinson, C J Wilkins, S H Yong *J. Chem. Soc., Dalton Trans.* 248 (1980)
29. A J Matheson, B B Penfold *Acta Crystallogr., Sect. B* **35** 2707 (1979)
30. A Lehtonen, R Sillanpää *J. Chem. Soc., Dalton Trans.* 2119 (1994)
31. B A Borgias, S R Cooper, Y B Koh, K N Raymond *Inorg. Chem.* **23** 1009 (1984)
32. B A Cartwright, W P Griffith, M Schröder *J. Chem Soc., Chem. Commun.* 853 (1978)
33. N Ya Turova, A V Korolev, D E Tchebukov, A I Belokon, A I Yanovsky, Yu T Struchkov *Polyhedron* **15** 3869 (1996)
34. A I Yanovsky, N Ya Turova, A V Korolev, D E Chebukov, Yu T Struchkov *Izv. Akad. Nauk, Ser. Khim.* 125 (1996) [c]
35. G R Clark, A J Nielson, C E F Rickard *Polyhedron* **6** 1765 (1987)
36. J C Bollinger, M H Chisholm, D R Click, K Folting, C M Hadad, D B Tiedtke, P J Wilson *J. Chem. Soc., Dalton Trans.* 2074 (2001)
37. V V Tkachev, L O Atovmyan *Koord. Khim.* **2** 110 (1976) [a]
38. W Clegg, R J Errington, K A Fraser, D G Richards *J. Chem. Soc., Chem. Commun.* 1105 (1993)
39. P G Edwards, G Wilkinson, M.B.Hursthouse, K M Abdul Malik *J. Chem. Soc., Dalton Trans.* 2467 (1980)
40. H Reuter, M Kremser *Z. Anorg. Allg. Chem.* **615** 137 (1992)
41. S Parola, R Papiernik, L G Hubert-Pfalzgraf, S Jagner, M Hakansson *J. Chem. Soc., Dalton Trans.* 4631 (1997)
42. V W Day, T A Eberspacher, Y Chen, J Hao, W G Klemperer *Inorg. Chim. Acta* **229** 391 (1995)
43. T J Boyle, T M Alam, E R Mechenbier, B L Scott, J W Ziller *Inorg. Chem.* **36** 3293 (1997)
44. W J Evans, M A Ansari, J W Ziller *Polyhedron* **17** 869 (1998)
45. Z A Starikova, E P Turevskaya, N I Kozlova, N Ya Turova, D V Berdyev, A I Yanovsky *Polyhedron* **18** 941 (1999)
46. M H Chisholm, K Folting, J C Huffman, C C Kirkpatrick *Inorg. Chem.* **23** 1021 (1984)
47. M H Chisholm, K Folting, M Scheer *Polyhedron* **17** 2931 (1998)
48. F A Cotton, D O Marler, W Schwotzer *Inorg. Chim. Acta* **95** 207 (1984)
49. V G Kessler, N Ya Turova, A N Panov, Z A Starikova, A I Yanovsky, Yu T Struchkov *Polyhedron* **17** 4189 (1998)
50. M H Chisholm, C M Cook, K Folting *J. Am. Chem. Soc.* **114** 2721 (1992)
51. C J Burns, A P Sattelberger *Inorg. Chem.* **27** 3692 (1988)
52. L G Hubert-Pfalzgraf, V Abada, J Veissermann, J Roziére *Polyhedron* **18** 845 (1999)
53. I Abrahams, D C Bradley, H Chudzynska, M Motevalli, R A Sinclair *J. Chem. Soc., Dalton Trans.* 259 (2002)
54. R A Sinclair, W B Gleason, R A Newmark, J R Hill, S Hunt, P Lyon, J Stevens, in *Chemical Proceedings of Advanced Materials* (Eds L Hench, J K West) (New York: Wiley, 1992) p. 207
55. S A Sangokoya, W T Rennigton, J Byers-Hill, G H Robinson, R D Rogers *Organometallics* **12** 2429 (1993)
56. W J Evans, T J Boyle, J W Ziller *J. Am. Chem. Soc.* **115** 5084 (1993)
57. C Sirio, L G Hubert- Pfalzgraf, C Bois *Polyhedron* **16** 1129 (1997)
58. R Anwander, F C Munck, T Priermeier, W Scherer, O Runte, W A Herrmann *Inorg. Chem.* **36** 3545 (1997)
59. C Gaffney, P G Harrison, T J King *J. Chem. Soc., Chem. Commun.* 1251 (1980)
60. S Daniele, R Papiernik, L G Hubert-Pfalzgraf, S Jagner, M Hakansson *Inorg. Chem.* **34** 628 (1995)
61. K Yunlu, P S Gradeff, N Edelstein, W Kot, G Shalimoff, W E Streib, B A Vaartstra, K G Caulton *Inorg. Chem.* **30** 2317 (1991)
62. D J Teff, J C Huffman, K G Caulton *J. Am. Chem. Soc.* **118** 4030 (1996)
63. R D Rogers, A H Bond, M M Witt *Inorg. Chim. Acta* **182** 9 (1991)
64. K H Whitmire, C M Jones, M D Burkart, J C Hutchison, A L McKnight *Mater. Res. Soc. Symp. Proc.* **271** 149 (1992)
65. W A Herrmann *Angew. Chem., Int. Ed. Engl.* **34** 2187 (1995)
66. M H Chisholm, Ch E Hammond, J C Huffman, J D Martin *Polyhedron* **9** 1829 (1990)
67. G S Kim, D A Keszler, C W DeKock *Inorg. Chem.* **30** 574 (1991)
68. M H Chisholm, Y Yang, E Lobkovsky, J C Huffman *J. Cluster Sci.* **3** 151 (1992)
69. T A Budzichowski, M H Chisholm, K Folting, W E Streib, M Scheer *Inorg. Chem.* **35** 3659 (1996)
70. F A Cotton, M P Diebold, W J Roth *Inorg. Chem.* **24** 3509 (1985)
71. V G Kessler, A V Shevelkov, G V Khvorykh, G A Seisenbaeva, N Ya Turova, D V Drobot *Zh. Neorg. Khim.* **40** 1477 (1995) [b]
72. G A Seisenbaeva, V G Kessler, A V Shevelkov *J. Sol-Gel Sci. Technol.* **19** 285 (2000)

73. N N Sauer, E Garcia, R R Ryan *Mater. Res. Soc. Symp. Proc.* **180** 920 (1990)
74. I Cavaco, J C Pessoa, M T Duarte, P M Matias, R T Henriques *Polyhedron* **12** 1231 (1993)
75. L G Hubert-Pfalzgraf, V Abada, J Veissermann *Polyhedron* **18** 3497 (1999)
76. V G Kessler, E P Turevskaya, A I Belokon, N Ya Turova *Polyhedron* **21** 1629 (2002)
77. A Proust, P Gouzerh, F Robert *J. Chem. Soc., Dalton Trans.* 819 (1994)
78. H Kang, S Liu, S N Shaikh, T Nicholson, J Zubieta *Inorg. Chem.* **28** 920 (1989)
79. S Liu, S N Shaikh, J Zubieta *Inorg. Chem.* **26** 4303 (1987)
80. M H Chisholm, J C Huffman, C C Kirkpatrick, J Leonelli, K Folting *J. Am. Chem. Soc.* **103** 6093 (1981)
81. C Limberg, A J Downs, A J Blake, S Parsons *Inorg. Chem.* **35** 4439 (1996)
82. J A Beaver, M G B Drew *J. Chem. Soc., Dalton Trans.* 1376 (1973)
83. A J Zozulin, D C Moody, R R Ryan *Inorg. Chem.* **21** 3083 (1982)
84. P A Shcheglov, G A Seisenbaeva, D V Drobot, V G Kessler *Inorg. Chem. Commun.* **4** 227 (2001)
85. E P Turevskaya, N Ya Turova, A V Korolev, A I Yanovsky, Yu T Struchkov *Polyhedron* **14** 1531 (1995)
86. H Kumagai, M Endo, S Kawata, S Kitagawa *Acta Crystallogr., Sect. C* **52** 1943 (1996)
87. P A Shcheglov, D V Drobot, G A Seisenbaeva, S Govil, V G Kessler *Chem. Mater.* **14** 2378 (2002)
88. T P Blatchford, M H Chisholm, K Folting, J C Huffman *J. Chem. Soc., Chem. Commun.* 1295 (1984)
89. K G Caulton, M H Chisholm, S R Drake, K Folting, *J. Chem. Soc., Chem. Commun.* 1349 (1990)
90. H Vincent, F Labrise, L G Hubert-Pfalzgraf *Polyhedron* **13** 3323 (1994)
91. P Miele, J-D Foulon, N Hovnanian *Polyhedron* **12** 209 (1993)
92. G Westin, M Wijk, M Moustiakimov, M Kritikos *J. Sol-Gel Sci. Technol.* **13** 125 (1998)
93. N I Kozlova, N Ya Turova, E P Turevskaya *Koord. Khim.* **8** 639 (1982) [a]
94. K M Fromm, E D Gueneau, H Goesmann *Chem. Commun.* 2187 (2000)
95. T J Boyle, P G Clem, M A Rodriguez, B A Tittle, M D Heagy *J. Sol-Gel Sci. Technol.* **16** 47 (1999)
96. W J Evans, M A Greci, J W Ziller *Inorg. Chem.* **39** 3213 (2000)
97. G G Nunes, D M Reis, P Amorim, E L Sa, A S Mangrich, D J Evans, P B Hichcock, G J Leigh, F S Nunes, J F Soares *New J. Chem.* **26** 519 (2002)
98. K W Henderson, R E Mulvey, F B M Reinhard, W Clegg, L Horsburgh *J. Am. Chem. Soc.* **116** 10 777 (1994)
99. G Helgesson, S Jagner, O Poncelet, L G Hubert-Pfalzgraf *Polyhedron* **10** 1559 (1991)
100. S Daniele, L G Hubert-Pfalzgraf, J-C Daran, S Halut *Polyhedron* **13** 927 (1994)
101. M Moustiakimov, M Kritikos, G Westin *Acta Crystallogr., Sect. C* **54** 29 (1998)
102. A I Yanovsky, Z A Starikova, M I Yanovskaya, N M Kotova, N Ya Turova *Zh. Neorg. Khim.* **48** 1456 (2003) [b]
103. I Abrahams, D C Bradley, H Chudzynska, M Motevali, P O'Shaughnessy *J. Chem. Soc., Dalton Trans.* 2685 (2000)
104. A Johansson, M Roman, G A Seisenbaeva, L Kloo, Z Szabo, V G Kessler *J. Chem. Soc., Dalton Trans.* 387 (2000)
105. K G Caulton, M H Chisholm, S R Drake, K Folting, J C Huffman, W E Streib *J. Chem. Soc., Chem. Commun.* 1498 (1990)
106. H Schumann, G Kociok-Köhn, J Loebel *Z. Anorg. Allg. Chem.* **581** 69 (1990)
107. B A Vaartstra, W E Streib, K G Caulton *J. Am. Chem. Soc.* **112** 8593 (1990)
108. W J Evans, M A Ansari, J W Ziller *Inorg. Chem.* **38** 1160 (1999)
109. M Veith, E C Yu, V Huch *Chem.-Eur. J.* **1** 26 (1995)
110. M Baier, P Brissinger, J Blümel, H Schmidbaur *Chem. Ber.* **126** 947 (1993)
111. J I Jolas, S Hoppe, K H Whitmire *Inorg. Chem.* **36** 3335 (1997)
112. V G Kessler, G A Seisenbaeva *Inorg. Chem. Commun.* **3** 203 (2000)
113. Q Chen, D P Goshorn, C P Scholes, X L Tan, J Zubieta *J. Am. Chem. Soc.* **114** 4667 (1992)
114. A Müller, J Meyer, H Bogge, A Stammler, A Bolgi *Z. Anorg. Allg. Chem.* **621** 1818 (1995)
115. D Hou, G-S Kim, K S Hagen, C L Hill *Inorg. Chim. Acta* **211** 127 (1993)
116. M I Khan, Q Chen, J Zubieta, D P Goshorn *Inorg. Chem.* **31** 1556 (1992)
117. M I Khan, Q Chen, H Höpe, S Parkin, C J O'Connor, J Zubieta *Inorg. Chem.* **32** 2929 (1993)
118. W Clegg, M R J Elsegood, R J Errington, J Harvelock *J. Chem. Soc., Dalton Trans.* 681 (1996)
119. V W Day, W G Klemperer, C Schwartz. *J. Am. Chem. Soc.* **109** 6030 (1987)
120. K Hegetschweiler, H Schmalle, H M Streit, W Schneider *Inorg. Chem.* **29** 3625 (1990)
121. A Cornia, D Gatteschi, K Hegetschweiler, L Hausherr-Primo, V Gramlich *Inorg. Chem.* **35** 4414 (1996)
122. T J Boyle, C A Zechmann, T M Alam, M A Rodriguez, C A Hajar, B L Scott *Inorg. Chem.* **41** 946 (2002)
123. J A Hollingshead, R E McCarley *J. Am. Chem. Soc.* **112** 7402 (1990)
124. P G Harrison, B J Haylett, T J King *J. Chem. Soc., Chem. Commun.* 112 (1978)
125. Y Sasaki, N Miyazawa *Kin. Daigaku Rik. Kenk. Hokuku* **28** 237 (1992)
126. A M Domingos, G M Sheldrick *Acta Crystallogr., Sect. B* **30** 519 (1974)
127. A I Yanovsky, N Ya Turova, E P Turevskaya, Yu T Struchkov *Koord. Khim.* **8** 153 (1982) [a]
128. V G Kessler, N Ya Turova, A N Panov, A I Yanovsky, A P Pisarevsky, Y T Struchkov *Polyhedron* **15** 335 (1996)
129. V S Nair, K S Hagen *Inorg. Chem.* **31** 4048 (1992)
130. S Daniele, L G Hubert-Pfalzgraf, J-C Daran *Polyhedron* **15** 1063 (1996)
131. Z A Starikova, A I Yanovsky, N M Kotova, M I Yanovskaya, N Ya Turova, D Benlian *Polyhedron* **16** 4347 (1997)
132. S C James, N C Norman, A G Orpen, M J Quayle, U Weckenmann *J. Chem. Soc., Dalton Trans.* 4159 (1996)
133. A Johansson, V G Kessler *Polyhedron* **19** 1791 (2000)
134. S Boulmaaz, L G Hubert-Pfalzgraf, S Halut, J-C Daran *J. Chem. Soc., Chem. Commun.* 601 (1994)
135. C Limberg, S Parsons, A J Downs *J. Chem. Soc., Chem. Commun.* 497 (1994)
136. V G Kessler, A N Panov, N Ya Turova, Z A Starikova, A I Yanovsky, F M Dolgushin, A P Pisarevsky, Yu T Struchkov *J. Chem. Soc., Dalton Trans.* 21 (1998)
137. N Ya Turova, V G Kessler, S I Kucheiko *Polyhedron* **10** 2617 (1991)
138. V G Kessler, N Ya Turova, A I Yanovsky, Yu T Struchkov, M A Fedotov *Zh. Obshch. Khim.* **60** 2769 (1990) [d]
139. P A Shcheglov, G A Seisenbaeva, S Gohil, D V Drobot, V G Kessler *Polyhedron* **21** 2317 (2002)
140. G Westin, R Norrestam, M Nygren, M Wijk *J. Solid State Chem.* **135** 149 (1998)
141. V G Kessler, A V Shevelkov, L A Bengtsson-Kloo *Polyhedron* **17** 965 (1998)
142. R Schmid, A Mosset, J Galy *J. Chem. Soc., Dalton Trans.* 1999 (1991)
143. V W Day, T A Eberspacher, W G Klemperer, C W Park, F S Rosenberg *J. Am. Chem. Soc.* **113** 8190 (1991)
144. D J Teff, K G Caulton *Inorg. Chem.* **38** 2240 (1999)
145. C S Weinert, I A Guzei, A L Rheingold, L R Sita *Organometallics* **17** 498 (1998)
146. R Finn, J Zubieta *J. Cluster Sci.* **11** 461 (2000)
147. U Bemm, R Norrestam, M Nygren, G Westin *Inorg. Chem.* **31** 2050 (1992)
148. J J H Edema, S Gambarotta, J J Smeets, A L Spek *Inorg. Chem.* **30** 1380 (1991)
149. K Hegetschweiler, H Schmalle, H M Streit, V Gramlich, H U Hund, I Erni *Inorg. Chem.* **31** 1299 (1992)

150. L G Hubert-Pfalzgraf, S Daniele, A Bennaceur, J-C Daran, J Veissermann *Polyhedron* **16** 1223 (1997)
151. V G Kessler, N Ya Turova, A I Yanovsky, A I Belokon, Yu T Struchkov *Zh. Neorg. Khim.* **36** 1662 (1991) [b]
152. E P Turevskaya, N Ya Turova, A I Belokon, D E Chebukov *Zh. Neorg. Khim.* **43** 1065 (1998) [b]
153. E M McCarron III, R L Harlow *Acta Crystallogr., Sect. C* **40** 1140 (1984)
154. L Ma, S Liu, J Zubieta *J. Chem. Soc., Chem. Commun.* 440 (1989)
155. S Liu, J Zubieta. *Polyhedron* **8** 537 (1989)
156. J A Samuels, W-C Chiang, J C Huffman, K L Trojan, W E Hatfield, D V Baxter, K G Caulton *Inorg. Chem.* **33** 2167 (1994)
157. A J Blake, A J Downs, C Limberg, S Parsons *J. Chem. Soc., Dalton Trans.* 3263 (1995)
158. R Kuhlman, B A Vaartstra, W E Streib, J C Huffman, K G Caulton *Inorg. Chem.* **32** 1272 (1993)
159. A I Yanovsky, M I Yanovskaya, V K Limar, V G Kessler, N Ya Turova, Yu T Struchkov *J. Chem. Soc., Chem. Commun.* 1605 (1991)
160. Z A Starikova, A I Yanovsky, D E Chebukov, E P Turevskaya, N Ya Turova *Zh. Neorg. Khim.* **43** 1308 (1998) [b]
161. J A Samuels, B A Vaartstra, J C Huffman, K L Trojan, W E Hatfield, K G Caulton *J. Am. Chem. Soc.* **112** 9623 (1990)
162. K G Caulton, M H Chisholm, S R Drake, K Folting, J C Huffman *Inorg. Chem.* **32** 816 (1993)
163. W J Evans, D G Griorikos, M A Greci, J W Ziller *Eur. J. Inorg. Chem.* 453 (2002)
164. M H Chisholm, K S Kramer, W E Streib *J. Cluster Sci.* **6** 135 (1995)
165. H Bock, T Hauck, C Näther, N Rösch, M Staufer, O D Häberlen *Angew. Chem., Int. Ed. Engl.* **34** 1353 (1995)
166. C M Jones, M D Burkart, R E Bachman, D L Serra, S J Hwa, K H Whitmire *J. Chem. Soc., Chem. Commun.* 1638 (1992)
167. M Veith, F Grätz, V Huch *Eur. J. Inorg. Chem.* 367 (2001)
168. F M Mackenzie, R E Mulvey, W Clegg, L Horsburgh *Polyhedron* **17** 993 (1998)
169. M I Khan, Q Chen, D P Goshorn, J Zubieta *Inorg. Chem.* **32** 672 (1993)
170. M I Khan, Q Chen, D P Goshorn, H Höpe, S Parkin, J Zubieta *J. Am. Chem. Soc.* **114** 3341 (1992)
171. M Cavaluzzo, Q Chen, J Zubieta *J. Chem. Soc., Chem. Commun.* 131 (1993)
172. S Asirvatham, M A Khan, K M Nicholas *Inorg. Chem.* **39** 2006 (2000)
173. Z A Starikova, N Ya Turova, D E Chebukov, A I Yanovsky *Zh. Neorg. Khim.* **48** 1275 (2003) [b]
174. M Yu Antipin, L P Didenko, L M Kachapina, A E Shilov, A K Shilova, Yu T Struchkov *J. Chem. Soc., Chem. Commun.* 1467 (1989)
175. A P Purdy, C F George *Polyhedron* **17** 4041 (1998)
176. U M Tripathi, A Schier, H Schmidbaur *Z. Naturforsch. B* **53** 434 (1998)
177. U Bemm, R Norrestam, M Nygren, G Westin *Inorg. Chem.* **32** 1597 (1993)
178. R Papiernik, L G Hubert-Pfalzgraf, J-C Daran, Y Jeannih *J. Chem. Soc., Chem. Commun.* 695 (1990)
179. D P Goldberg, A Caneschi, S J Lippard *J. Am. Chem. Soc.* **115** 9299 (1993)
180. Z A Starikova, V G Kessler, N Ya Turova, D E Tcheboukov, E V Suslova, G A Seisenbaeva, A I Yanovsky *Polyhedron* **23** 109 (2004)
181. U Bemm, R Norrestam, M Nygren, G Westin *J. Solid State Chem.* **134** 312 (1997)
182. V G Kessler, A N Panov, A Yu Borissevitch, N Ya Turova *J. Sol-Gel Sci. Technol.* **12** 81 (1998)
183. V W Day, T A Eberspacher, W G Klemperer, C W Park *J. Am. Chem. Soc.* **115** 8469 (1993)
184. N Steunou, F Robert, F Ribot, K Boubekeur, C Sanchez *Inorg. Chim. Acta* **279** 144 (1998)
185. N Steunou, F Ribot, K Boubekeur, J Maquet, C Sanchez *New J. Chem.* **23** 1079 (1999)
186. U Bemm, R Norrestam, M Nygren, G Westin *Inorg. Chem.* **34** 2367 (1995)
187. W J Evans, M S Sollberger *Inorg. Chem.* **27** 4417 (1988)
188. W J Evans, M S Sollberger, T P Hanusa *J. Am. Chem. Soc.* **110** 1841 (1988)
189. A Mosset, J Galy *C.R. Acad. Sci., Ser. 2* **307** 1747 (1988)
190. M I Khan, Y-S Lee, C J O'Connor, J Zubieta *J. Am. Chem. Soc.* **116** 5001 (1994)
191. N Steunou, G Kickelbick, K Boubekeur, C Sanchez *J. Chem. Soc., Dalton Trans.* 3653 (1999)
192. J F Campion, D A Payne, H K Chae, J K Maurin, S R Wilson *Inorg. Chem.* **30** 3244 (1991)
193. C F Campana, Y Chen, V W Day, W G Klemperer, R A Sparks *J. Chem. Soc., Dalton Trans.* 691 (1996)
194. T Greiser, O Jarchow, K-H Klaska, E Weiss *Chem. Ber.* **111** 3360 (1978)
195. I A M Pohl, G Westin, M Kritikos *Chem.-Eur. J.* **7** 3438 (2001)
196. G Westin, M Nygren *J. Mater. Chem.* **4** 1275 (1994)
197. M I Khan, J Zubieta *J. Am. Chem. Soc.* **114** 10 058 (1992)
198. U Bemm, K Lashgari, R Norrestam, M Nygren, G Westin *J. Solid State Chem.* **108** 243 (1994)
199. M H Chisholm *Polyhedron* **2** 681 (1983)
200. M H Chisholm, K Folting, J C Huffman, C C Kirkpatrick, A L Ratermann *J. Am. Chem. Soc.* **103** 1305 (1981)
201. V G Kessler, E P Turevskaya, S I Kucheiko, N I Kozlova, N Ya Turova, I E Obvintseva, M I Yanovskaya, in *Better Ceramics through Chemistry VI (MRS Proceedings), Boston, 1994* Vol. 346, p. 3
202. V G Kessler, S Yu Vasil'ev, A I Belokon, N Ya Turova *Zh. Obshch. Khim.* **60** 2629 (1990) [d]
203. T G Brilkina, V A Shushunov *Reaktsii Metalloorganicheskikh Soedinenii s Kislorodom i Perekisyami* (Reactions of Organometallic Compounds with Oxygen and Peroxides) (Moscow: Nauka, 1966)
204. N Ya Turova, E P Turevskaya, M I Yanovskaya, N M Kotova, R R Shifrina *Zh. Neorg. Khim.* **38** 1137 (1993) [b]
205. E C Ashby, A B Goel, J N Argyropoulos *Tetrahedron Lett.* **23** 2273 (1982)
206. N Ya Turova, N I Kozlova, M I Yanovskaya *Koord. Khim.* **6** 508 (1980) [a]
207. E Amberger, R Hönigschmidt-Grossich *Chem. Ber.* **98** 3795 (1965)
208. M I Karpovskaya, N Ya Turova, A V Novoselova *Koord. Khim.* **3** 1296 (1977) [a]
209. D C Bradley, B N Chakravarti, A K Chatterjee, W Wardlaw, A Whitley *J. Chem. Soc.* 99 (1958)
210. S R Drake, W E Streib, M H Chisholm, K G Caulton *Inorg. Chem.* **29** 2707 (1990)
211. S C Goel, M A Matchett, M Y Chiang, W E Buhro *J. Am. Chem. Soc.* **113** 1844 (1991)
212. K G Caulton, M H Chisholm, S R Drake, K Folting, J C Huffman, W E Streib *Inorg. Chem.* **32** 1970 (1993)
213. K G Caulton, M H Chisholm, S R Drake, K Folting *Inorg. Chem.* **30** 1500 (1991)
214. S R Drake, D J Otway, M B Hursthouse, K M A Malik *Polyhedron* **11** 1995 (1992)
215. E P Turevskaya, M I Yanovskaya, V K Lymar', N Ya Turova *Zh. Neorg. Khim.* **38** 609 (1993) [b]
216. E P Turevskaya, V G Kessler, N Ya Turova, A I Yanovsky, Yu T Struchkov *J. Chem. Soc., Chem. Commun.* 2303 (1994)
217. O Poncelet, L G Hubert-Pfalzgraf, J-C Daran, R Astier *J. Chem. Soc., Chem. Commun.* 1846 (1989)
218. L G Westin, M Kritikos, A Caneschi *Chem. Commun.* 1012 (2003)
219. S Daniele, L G Hubert-Pfalzgraf, J Vaissermann *Polyhedron* **17** 4249 (1998)
220. O Poncelet, L G Hubert-Pfalzgraf *Polyhedron* **8** 2183 (1989)
221. W J Evans, T J Deming, J M Olofson, J W Ziller *Inorg. Chem.* **28** 4027 (1989)
222. R Papiernik, L G Hubert-Pfalzgraf, M C Massiani *Inorg. Chim. Acta* **165** 1 (1989)
223. R Papiernik, L G Hubert-Pfalzgraf, M C Massiani *Polyhedron* **10** 1657 (1991)

224. E P Turevskaya, V B Bergo, M I Yanovskaya, N Ya Turova *Zh. Neorg. Khim.* **41** 721 (1996) [b]
225. E P Turevskaya, N I Kozlova, N Ya Turova, A I Belokon, D V Berdyev, V G Kessler, Yu K Grishin *Izv. Akad. Nauk, Ser. Khim.* 752 (1995) [c]
226. V W Day, W G Klemperer, M M Pafford *Inorg. Chem.* **40** 5738 (2001)
227. A M Bol'shakov, M A Glushkova, Yu A Buslaev *Koord. Khim.* **4** 1075 (1978) [a]
228. E Jacob *Angew. Chem., Int. Ed. Engl.* **21** 142 (1982)
229. G A Seisenbaeva, L Kloo, P Werndrup, V G Kessler *Inorg. Chem.* **40** 3815 (2001)
230. G Tatzel, M Greune, J Weidlein, E Jacob *Z. Anorg. Allg. Chem.* **533** 83 (1986)
231. N Ya Turova, V G Kessler *Zh. Obshch. Khim.* **60** 113 (1990) [d]
232. D C Bradley, M H Chisholm, M W Extine, M E Stager *Inorg. Chem.* **16** 1794 (1977)
233. F A Cotton, W Schwotzer, E S Shamshoum *Inorg. Chem.* **23** 4111 (1984)
234. C I Kucheiko, N Ya Turova, N I Kozlova *Koord. Khim.* **11** 1656 (1985) [a]
235. D E Chebukov, N Ya Turova, A V Korolev, A I Belokon *Zh. Neorg. Khim.* **42** 1642 (1997) [b]
236. N Ya Turova, E P Turevskaya, V G Kessler, N I Kozlova, A I Belokon *Zh. Neorg. Khim.* **37** 50 (1992) [b]
237. H Schmidbaur, M Bergfeld, F Schindler *Z. Anorg. Allg. Chem.* **363** 73 (1968)
238. C D Chandler, G D Fallon, B O West *J. Chem. Soc., Chem. Commun.* 1063 (1990)
239. D C Bradley, I M Thomas *J. Chem. Soc., A* 3404 (1959)
240. J Caruso, M J Hampden-Smith *J. Sol-Gel Sci. Technol.* **8** 35 (1997)
241. L G Hubert-Pfalzgraf, V Abada, J Waissermann *J. Chem. Soc., Dalton Trans.* 2407 (1999)
242. H Ulich, W Nespital *Z. Phys. Chem.* **165** 294 (1933)
243. E P Turevskaya, D V Berdyev, N Ya Turova, Z A Starikova, A I Yanovsky, Yu T Struchkov, A I Belokon *Polyhedron* **16** 663 (1997)
244. T V Rogova, N Ya Turova, N I Kozlova *Koord. Khim.* **12** 762 (1986) [a]
245. D C Bradley, H Chudzynska, M B Hursthouse, M Motovalli *Polyhedron* **10** 1049 (1991)
246. D E Chebukov, N Ya Turova, A I Belokon *Zh. Neorg. Khim.* **44** 869 (1999) [b]
247. M Veith, S Mathur, V Huch *Inorg. Chem.* **36** 2391 (1997)
248. W R Russo, W H Nelson *J. Am. Chem. Soc.* **92** 1521 (1970)
249. I E Obvintseva, M I Yanovskaya, S I Kucheiko, N Ya Turova, R R Shifrina *Neorg. Mater.* **24** 790 (1988) [e]

[a] — *Russ. J. Coord. Chem. (Engl. Transl.)*
[b] — *Russ. J. Inorg. Chem. (Engl. Transl.)*
[c] — *Russ. Chem. Bull., Int. Ed. (Engl. Transl.)*
[d] — *Russ. J. Gen. Chem. (Engl. Transl.)*
[e] — *Inorg. Mater. (Engl. Transl.)*

Russian Chemical Reviews **73** (11) 1065 – 1089 (2004) © 2004 Russian Academy of Sciences and Turpion Ltd

DOI 10.1070/RC2004v073n11ABEH000877

The tris(trimethylsilyl)silyl group in organic, coordination and organometallic chemistry

A N Kornev

Contents

I.	Introduction	1065
II.	Steric and electronic effects of the $(Me_3Si)_3Si$ group	1065
III.	Tetrakis(trimethylsilyl)silane and its reactions	1066
IV.	Tris(trimethylsilyl)silane and its reactions	1067
V.	Tris(trimethylsilyl)silyl derivatives of elements of the main subgroups	1070
VI.	Tris(trimethylsilyl)silanides of d- and f-elements	1078
VII.	Photochemical reactions of hypersilyl derivatives	1082
VIII.	Rearrangements involving the tris(trimethylsilyl)silyl fragment	1084

Abstract. The published data on the synthesis, reactivities and applications of organic, coordination and organometallic compounds containing a $(Me_3Si)_3Si$ group are generalised and systematised. The bibliography includes 230 references.

I. Introduction

Among diverse organosilicon substituents of the type R_3Si, trialkylsilyl (Me_3Si, Et_3Si, Pr^i_3Si, Bu^t_3Si), triphenylsilyl (Ph_3Si) and tris(trimethylsilyl)silyl [$(Me_3Si)_3Si$] groups (hereinafter referred to as the TTS group)† attract the greatest attention of researchers. The choice of a particular group is usually determined not only by physicochemical characteristics of compounds that are essential for a specific goal, but also by commercial availability of their precursors. Until recently, compounds containing a TTS group were considered to be exotic. Significant progress has been achieved over the past decade in the development of methods for the synthesis and investigation of properties of TTS derivatives and their practical applications. Abundant experimental material accumulated thus far demands systematisation and generalisation. Yet another aim of this review is the discussion of specific characteristics of the TTS group, which differs markedly from other bulky substituents, such as [Bu^t_3Si (see Ref. 1), Pr^i_3Si (see Ref. 2) and Ph_3Si (see Ref. 3)], in its reactivity. This is due, first of all, to the high sensitivity of the highly polarisable Si – Si bond to nucleophilic and electrophilic reagents and to oxidation. In some cases, it can be activated by transition metals. In addition, molecules containing a system of Si – Si bonds can serve as precursors for silylenes when undergoing thermolysis or UV irradiation. Thus, the properties of the $(Me_3Si)_3Si$ group are rather specific and its functions are not confined solely to its use as a bulky substituent or a protecting group.

A N Kornev G A Razuvaev Institute of Organometallic Chemistry, Russian Academy of Sciences, ul. Tropinina 49, 603950 Nizhnii Novgorod, Russian Federation. Fax (7-831) 212 74 97.
Tel. (7-831) 212 66 52.
E-mail: akornev@imoc.sinn.ru

Received 30 September 2003
Uspekhi Khimii **73** (11) 1155 – 1180 (2004); translated by R L Birnova

II. Steric and electronic effects of the $(Me_3Si)_3Si$ group

1. Steric effect

The tris(trimethylsilyl)silyl group possesses a pronounced steric effect which is nevertheless weaker than that of its closest analogue, *viz*., the tris(*tert*-butyl)silyl group. A comparison of the structures of $(Me_3Si)_6Si_2$ (**1**) and $(Bu^t_3Si)_2$ (**2**) molecules shows that the distance between the central silicon atoms in compound **1** (2.40 Å) does not differ substantially from the average normal value (2.35 Å), whereas that in molecule **2** is 2.70 Å. Nevertheless, the conclusion that molecule **1** is sterically overcrowded can be drawn from the fact that some distances between the carbon atoms belonging to different $(Me_3Si)_3Si$ groups are as small as 3.52 Å, which is 12% smaller than the sum of the van der Waals radii of two methyl groups, 2.00 Å each.[3, 4]

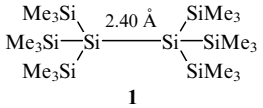

1

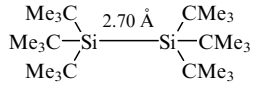

2

The steric effect of the TTS group was estimated using various methods including computation.[5] Thus the dynamic NMR method allowed determination of the barrier to rotation of the mesityl groups around the Mes – C bond in compounds $Mes_2C = C(OH)R$ [R = H, Me, Et, Pr^i, Bu^t, $(Me_3Si)_3Si$]. It was found that the steric effect of the TTS group on the coalescence of aromatic protons differs little from that of the *tert*-butyl group. Correlation and computational data suggest that the steric constant (E_s) of the TTS group varies from −1.46 to −1.6 (see Ref. 5), which is close to the E_s value for the Me_3C group (−1.54), but is significantly smaller than the corresponding value for the tris(trimethylsilyl)methyl group (−3.8) the van der Waals radius of which is close to that of the TTS group.[5] Such a pronounced difference in the steric constants is due to the greater distance between the TTS fragment and the reaction centre in comparison with the $(Me_3Si)_3C$ group owing to the difference in the lengths of the Si – Si and Si – C bonds.

† The term 'hypersilyl group' is generally accepted in the literature, this is also used in the present review.

2. Electronic effects of the $(Me_3Si)_3Si$ group

The tris(trimethylsilyl)silyl substituent can significantly stabilise the ground state of molecular ions. As can be seen from Table 1, the ionisation potentials of compounds containing a TTS group are much lower than those of their analogues due to significant delocalisation of the positive charge in the radical cations formed.

Table 1. The first ionisation potentials (I) of certain disilanes and benzene 1,4-derivatives.[6]

Compound	I /eV	Compound	I /eV
$F_3Si-SiF_3$	13.20	$H-C_6H_4-H$	9.24
$H_3Si-SiH_3$	10.53	$Me_3C-C_6H_4-CMe_3$	8.30
$Me_3Si-SiMe_3$	8.69	$(Me_3C)_3Si-C_6H_4-Si(CMe_3)_3$	7.45
$(Me_3Si)_4Si$	8.24	$(Me_3Si)_3Si-C_6H_4-Si(SiMe_3)_3$	7.37
$(Me_3Si)_3Si-Si(SiMe_3)_3$	7.79		

The changes in the ionisation potentials also agree with a decrease in the reduction half-wave potentials for Me_6Si_2 and $(Me_3Si)_4Si$ ($+1.400$ and $+1.320 \pm 0.005$ V, respectively),[7] which also suggests the somewhat greater proneness of tetrakis(trimethylsilyl)silane to oxidation.

A comparison of dissociation constants of carboxylic acids measured in 76% ethanol has shown[8] that tris(trimethylsilyl)silanecarboxylic acid [hypersilylcarboxylic acid, $(Me_3Si)_3SiCO_2H$] is weaker ($pK_a = 9.33$) than its closest analogues, *viz*., Me_3CCO_2H ($pK_a = 7.96$) and Ph_3SiCO_2H ($pK_a = 6.10$), which testifies to the σ-donor nature of the TTS group.

The tris(trimethylsilyl)silyl substituent can also stabilise the negative charge: more than half of the π-spin density in the 1,4-bis[tris(trimethylsilyl)silyl]benzene radical anion is localised on the $(Me_3Si)_3Si$ groups.[4] Studies on the phenyltris(trimethylsilyl)silane, $[(Me_3Si)_3SiPh]^{\bullet -}$ radical anion revealed that the TTS group behaves as a π-acceptor.[9]

Studies of electron affinities (EA) of a series of silyl radicals revealed that the radical $(Me_3Si)_3Si^{\bullet}$ has the highest value of EA (Table 2). The stability of silicenium anions increases significantly with an increase in the number of trimethylsilyl substituents at the central silicon atom.

Table 2. Electron affinities of silyl radicals.

Radical	EA /kcal mol^{-1}	Ref.
$(Me_3Si)_3Si^{\bullet}$	46.8	10
$(Me_3Si)_2HSi^{\bullet}$	44.7	10
$Me_2HSiMe_2Si^{\bullet}$	32.3	10
$Me_2HSi^{\bullet}$	24.7	11
$Me_3Si^{\bullet}$	22.4	11

It is known that silyl radicals exist predominantly in the pyramidal form with high configurational stability.[12] The rates of subsequent reactions of these radicals exceed their inversion rates. However, the fact that silyl radicals containing a Si–Si group yield racemic products[13] is in accord with an increasing deviation from planarity in the series:[14] $(Me_3Si)_3Si^{\bullet} < (Me_3Si)_2MeSi^{\bullet} < Me_3SiMe_2Si^{\bullet} < Me_3Si^{\bullet}$. The constants of the hyperfine coupling a (^{29}Si) in the ESR spectra change in the same order (Table 3).

Presumably, the stabilities of silyl radicals increase in the following order: $Me_3Si^{\bullet} < Me_3SiMe_2Si^{\bullet} < (Me_3Si)_2MeSi^{\bullet} < (Me_3Si)_3Si^{\bullet}$, mainly due to hyperconjugation with the β-Si–C bond.[21]

^{29}Si NMR spectroscopy has proved to be the most efficient method for obtaining information about the nature of the fragment linked to the TTS group and, correspondingly, about the electronic state of the TTS group itself. The values of experimentally determined chemical shifts vary in the range of more than 300 ppm (Table 4).

Table 3. Some parameters of the ESR spectra of silyl radicals.

Radical	a (^{29}Si) /Gauss	g	Ref.
$(Me_3Si)_3Si^{\bullet}$	64	2.0053	15, 16, 17
$(Me_3Si)_2MeSi^{\bullet}$	90	2.0045	18
$Me_3SiMe_2Si^{\bullet}$	137	2.0037	15, 16
$Me_3Si^{\bullet}$	181	2.0031	15, 16, 19, 20

Table 4. The chemical shifts (δ) in the ^{29}Si NMR spectra of central silicon atoms of some TTS derivatives.

Compound	δ (Si–$SiMe_3$)	Ref.
$(Me_3Si)_3SiK$	−195.8	22
$(Me_3Si)_3SiLi(THF)_3$	−185.4	23
$(Me_3Si)_3SiSnMe_3$	−136.6	24
$(Me_3Si)_3SiSiMe_3$	−135.6	22
$(Me_3Si)_3SiSi(SiMe_3)_3$	−129.5	22
$(Me_3Si)_3SiH$	−115.4	22
$(Me_3Si)_3SiEt$	−78.6	22
$(Me_3Si)_3SiHfCp^*Cl_2$ (see [a])	−49.77	25
Me_3SiK	−34.4	22, 26
$Me_3SiSiMe_3$	−20.5	22
$(Me_3Si)_3Si[B(C_6F_5)_4]$	+111.1	27
$[(Me_3Si)_3SiPh]^+$ (see [b])	+205.8	28
$(Me_3Si)_3Si^+$ (see [b])	+920.4	28

[a] Cp* is Me_5C_5; [b] calculated data.

The largest negative values of the chemical shifts (the high field) are characteristic of alkali metal hypersilanides where a considerable negative charge is localised on the central silicon atom. Contrariwise, the chemical shifts of the silicenium cations lie in the low field. The complex ion $[(Me_3Si)_3SiPh]^+$ formed upon dissolution of $(Me_3Si)_3Si[B(C_6F_5)_4]$ in benzene has the highest chemical shift for the TTS group hitherto known ($\delta = +111.1$). The calculated values of chemical shifts for the free ions $(Me_3Si)_3Si^+$ (in the gas phase) and $[(Me_3Si)_3SiPh]^+$, δ, are $+920.4$ and $+205.8$, respectively. It is suggested that the tris(trimethylsilyl)silicenium ion in benzene exists as a σ-complex $R_3Si-C_6H_6^+$ with a weak Si–C bond (13.6 kcal mol^{-1}).[28]

Quite naturally, the increasing applications of the Me_3Si group account for the progress in the chemistry of tris(trimethylsilyl)silane derivatives. By the time of the first synthesis of TTS derivatives, this group had widely been used in organic synthesis for protection of alcohols and enols.[29–32] Tetrakis(trimethylsilyl)silane and tris(trimethylsilyl)silane are the key compounds in the synthesis of numerous organometallic and organoelement compounds containing a TTS group; therefore, it seems expedient to begin with the consideration of methods for their synthesis and their reactivities.

III. Tetrakis(trimethylsilyl)silane and its reactions

The pioneering studies of the tris(trimethylsilyl)silyl group date back to 1964 when Gilman and Smith[33] synthesised tetrakis(trimethylsilyl)silane (**3**) by the reaction of chlorotrimethylsilane with $SiCl_4$ in the presence of metallic lithium in tetrahydrofuran.

$$4\ Me_3SiCl + SiCl_4 \xrightarrow[THF]{Li} (Me_3Si)_4Si$$

3 (70%)

In addition to compound **3**, this reaction yields an insoluble organosilicon polymer, which hampers the isolation of the target product.

It is known that tetrakis(trimethylsilyl)silane (**3**) is a side product in the preparation of tris(trimethylsilyl)silane (**4**);[34] however, it is often formed in substantial amounts due to exchange nucleophilic processes (see Section V.1.b).

$$Me_3SiCl\ (excess) + HSiCl_3 \xrightarrow[-10\ ^\circ C]{Li} \underset{\mathbf{4}\ (\sim 70\%)}{(Me_3Si)_3SiH} + \underset{\mathbf{3}\ (\sim 30\%)}{(Me_3Si)_4Si}$$

If this reaction is carried out at 20 °C, $(Me_3Si)_4Si$ is formed as the major product.

Compound **3** is stable in air and manifests high thermostability (m.p. 319–321 °C) (in a sealed capillary), sublimation temperature > 265 °C (at atmospheric pressure) and is easily sublimed *in vacuo*. The $(Me_3Si)_4Si$ molecule represents a virtually ideal sphere and has a rigid backbone with a tetrahedral symmetry.[35]

Tetrakis(trimethylsilyl)silane and other molecules containing a TTS fragment are easily obtained upon catalytic electrophilic rearrangements of linear polysilanes.[36]

$$Me(Me_2Si)_5Me \xrightarrow{AlCl_3,\ 1\%\ FeCl_3} \mathbf{3}\ (\sim 100\%)$$

Studies into the reactivity of $(Me_3Si)_4Si$ have shown that this is sensitive to both nucleophilic and electrophilic reagents. Treatment of compound **3** with methyllithium in THF results in elimination of the trimethylsilyl group in the form of tetramethylsilane and formation of a tris(trimethylsilyl)silyllithium–THF complex (**5**).[37]

$$\underset{\mathbf{3}}{(Me_3Si)_4Si} + MeLi \xrightarrow{THF-Et_2O} \underset{\mathbf{5}}{(Me_3Si)_3SiLi(THF)_3} + Me_4Si$$

The lithium derivative **5** is readily soluble in saturated and aromatic hydrocarbons, which is a prerequisite for subsequent syntheses.

Marschner[22] has prepared tris(trimethylsilyl)silylpotassium (**6**) in 80% yield by splitting the Si–Si bond with yet another strong nucleophile, *viz*., potassium *tert*-butoxide, in THF or dimethoxyethane (DME).[22]

$$\underset{\mathbf{3}}{(Me_3Si)_4Si} + Bu^tOK \longrightarrow \underset{\mathbf{6}}{(Me_3Si)_3SiK} + Bu^tOSiMe_3$$

Depending on the nature of the electrophile, treatment of silane **3** with strong electrophilic reagents results in cleavage of either Si–Si or Si–C bonds. Thus acetyl chloride reacts with compound **3** to eliminate four terminal methyl groups, which yields tetrakis(chlorodimethylsilyl)silane (**7**).[38]

$$\underset{\mathbf{3}}{(Me_3Si)_4Si} + 4\ MeC(O)Cl \xrightarrow{AlCl_3} \underset{\mathbf{7}}{(Me_2ClSi)_4Si} + 4\ Me_2CO$$

This reaction occurs in a stepwise manner in several steps, but the isolation and purification of the intermediate products present a considerable problem.

The reactions of halogens with silane **3** result in cleavage of the Si–Si bond.

$$\underset{\mathbf{3}}{(Me_3Si)_4Si} + 4\ Hal_2 \longrightarrow 4\ Me_3SiHal + SiHal_4$$

Hal = Cl, Br, I.

Compounds containing a $(Me_3Si)_3Si$ group and related compounds containing a $(Me_3Si)_3C$ group react with trifluoroacetic acid to yield different products.[39]

$$(Me_3Si)_3SiSiMe_2OMe + CF_3CO_2H \xrightarrow[-MeOH]{} (Me_3Si)_3SiSiMe_2O_2CCF_3,$$

$$(Me_3Si)_2C(SiMe_3)(SiMe_2OMe) \xrightarrow[-MeOH]{CF_3CO_2H} \underset{\mathbf{A}}{(Me_3Si)_2C^+(Me)(SiMe_2)_2\ CF_3CO_2^-} \xrightarrow[-CH_4]{CF_3CO_2H} (Me_3Si)_2C[SiMe_2OC(O)CF_3]_2.$$

Such a drastic difference is due to the formation, in the latter case, of intermediate cyclic silicenium cations **A** where elimination of methane occurs smoothly with simultaneous demethoxylation.[39]

IV. Tris(trimethylsilyl)silane and its reactions

Tris(trimethylsilyl)silane can be prepared by either direct synthesis from $HSiCl_3$ and Me_3SiCl or by acid hydrolysis of alkali metal silanides.[40]

$$(Me_3Si)_3SiLi + H_3O^+ \longrightarrow \underset{\mathbf{4}}{(Me_3Si)_3SiH} + Li^+ + H_2O$$

Despite its high cost, tris(trimethylsilyl)silane (TTSH, **4**) is becoming more and more popular as a versatile, mild and selective reducing agent for organic compounds.[41] Its efficiency exceeds those of other silicon hydrides. Presumably,[41] this can be attributed to the low dissociation energy of the Si–H bond in this compound in comparison with other organosilanes (Table 5).

Table 5. Dissociation energies (E_D) of the Si–H bond of some organosilanes.

$R-H \longrightarrow R^\bullet + H^\bullet$

Compound	E_D /kcal mol^{-1}	Ref.
$(Me_3Si)_3SiH$ (**4**)	79.0	10, 42
$Me_3SiSiMe_2H$	85.3	10, 42
Et_3SiH	90.1	10, 42
Me_3SiH	91.0	43, 44
F_3SiH	100.1	43, 44

1. Reduction of functional groups in organic compounds

Reduction with $(Me_3Si)_3SiH$ (**4**) is a radical-chain process. Di-*tert*-butyl peroxide and azobisisobutyronitrile (AIBN) are used as initiators. The mechanism of the Bu^tOOBu^t-induced reaction can be represented by the following scheme:

$$Bu^tOOBu^t \longrightarrow 2\ Bu^tO^\bullet,$$

$$Bu^tO^\bullet + \underset{\mathbf{4}}{(Me_3Si)_3SiH} \longrightarrow Bu^tOH + (Me_3Si)_3Si^\bullet,$$

$$(Me_3Si)_3Si^\bullet + RX \longrightarrow (Me_3Si)_3SiX + R^\bullet,$$

$$(Me_3Si)_3SiH + R^\bullet \longrightarrow RH + (Me_3Si)_3Si^\bullet.$$

The rate ratios of individual steps make it possible to maintain the chain of radical reactions in an optimum regime for the majority of substrates. The use of other silicon hydrides (trialkyl, aryl and chlorosilanes) for the reduction of functional groups is limited due to the high dissociation energies of their Si–H bonds, which prevent the formation of extended radical chains.

The reduction of organic halides takes place upon heating equimolar amounts of $(Me_3Si)_3SiH$ and a substrate in a solvent in the presence of ~5%–10% of the initiator at the temperature of its decomposition. In these reactions, the product yields are usually high for the majority of RX substrates (R = Alk; X = Cl, Br, I).[45–47]

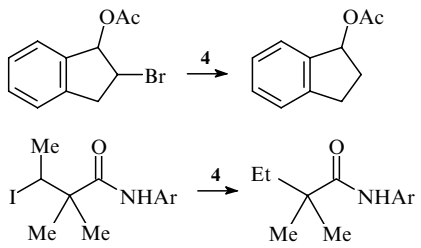

The selectivity of $(Me_3Si)_3SiH$ was found to be extremely high.

A detailed comparative study of the stereoselectivity of the reduction of organic *gem*-dichlorides with tris(trimethylsilyl)silane and tributylstannane has been carried out. It was found that despite numerous common features, these reagents manifest different stereoselectivities in certain cases. Thus the reduction of tetrachloride **8** with tributylstannane gives a mixture of isomers **9a** and **9b** in a ratio 1.3 : 1. At the same time, the reaction of compound **8** with tris(trimethylsilyl)silane gives a mixture of compounds **9a** and **9b** in a ratio 1.0 : 4.6.[48]

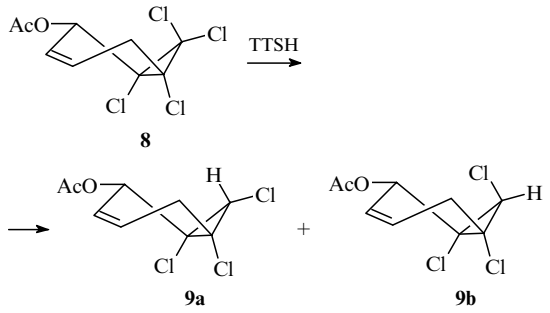

These observations are interpreted[48] as differences in the steric effects of substituents in the rigid-cage molecule $(Me_3Si)_3$. .SiH and in the molecule Bu_3SnH containing flexible mobile n-butyl groups. This hypothesis was confirmed by calculations of the geometry of the transition states.[48]

Despite the generally high reactivities of silyl radicals in halogen abstraction reactions from organic halides,[14] the radical $(Me_3Si)_3Si^{\bullet}$ manifests the lowest activity. The values of the absolute rate constants ($10^8 k$ litre mol^{-1} s^{-1}) in reactions with Me_3CBr decrease in the following order: $Et_3Si^{\bullet}$ (11.0) > $Ph_2Bu^tSi^{\bullet}$ (6.0) > $Me_3SiMe_2Si^{\bullet}$ (2.6) > $(Me_3Si)_3Si^{\bullet}$ (1.2).[14] The rate constants for each silyl radical decrease in the order: X = I > Br > Cl > F. Special mention should be made of the increasing role of electron-transfer reactions on going to polychloroalkanes; as a result, radical reactions occur spontaneously, *i.e.*, without any initiator. In the absence of exogenous radical initiators, $(Me_3Si)_3SiH$ reacts with carbon tetrachloride and bromoform. High yields of chlorotris(trimethylsilyl)silane are obtained on treatment of compound **4** with CCl_4 for 10 h at 20 °C. Trihalogenomethanes react in a similar way.[49]

$$(Me_3Si)_3SiH + CCl_4 \longrightarrow (Me_3Si)_3SiCl + CHCl_3,$$

$$(Me_3Si)_3SiH + CHX_3 \longrightarrow (Me_3Si)_3SiX + CH_2X_2$$

X = Cl, Br, I.

The spontaneous reaction of the hydride **4** with oxygen may result in its ignition in air. The mechanism of oxygen insertion into the Si–Si bond includes a series of intramolecular rearrangements.[41, 50]

$$(Me_3Si)_3Si^{\bullet} + O_2 \longrightarrow (Me_3Si)_3SiOO^{\bullet},$$

$$(Me_3Si)_3SiOO^{\bullet} \longrightarrow (Me_3Si)_2Si^{\bullet}OOSiMe_3,$$

$$(Me_3Si)_2Si^{\bullet}OOSiMe_3 \longrightarrow (Me_3Si)_2Si(O^{\bullet})OSiMe_3,$$

$$(Me_3Si)_2Si(O^{\bullet})OSiMe_3 \longrightarrow Me_3SiSi^{\bullet}(OSiMe_3)_2,$$

$$Me_3SiSi^{\bullet}(OSiMe_3)_2 + (Me_3Si)_3SiH \longrightarrow$$

$$\longrightarrow Me_3SiSiH(OSiMe_3)_2 + (Me_3Si)_3Si^{\bullet}.$$

In the absence of other substrates and under conditions of radical initiation, recombination of the tris(trimethylsilyl)silyl radical occurs to give hexakis(trimethylsilyl)disilane in high yield.[51]

$$\underset{\mathbf{4}}{(Me_3Si)_3SiH} \xrightarrow[130\ ^{\circ}C]{(Bu^tO)_2} \underset{(92\%)}{(Me_3Si)_3SiSi(SiMe_3)_3}$$

It is noteworthy that under these conditions radical recombination products are formed in trace amounts from simpler organosilicon hydrides (Me_3SiH or Me_5Si_2H).

Tris(trimethylsilyl)silane reduces functional groups containing a heteroatom: NC, SR, SeR (R = Alk, Ar).[46, 52, 53] The yields in these reactions are rather high.

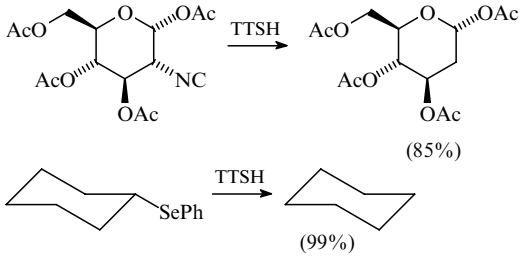

Upon treatment with 1 equiv. of $(Me_3Si)_3SiH$, 1,3-dithiolanes afford cleavage products of only one C–S bond.[54]

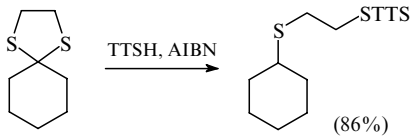

Under free-radical initiation conditions, carboxylic acid chlorides and phenyl selenoesters are reduced by tris(trimethylsilyl)silane to the corresponding aldehydes and alkanes.[55, 56]

$$RC(O)X + (Me_3Si)_3SiH \longrightarrow RC(O)H + RH + (Me_3Si)_3SiX$$

R = Alk, cyclo-Alk; X = Cl, SePh.

Tris(trimethylsilyl)silane is a convenient reagent for radical deoxygenation of alcohols following their conversion into *O*-phenoxythiocarbonyl derivatives.[57]

$$ROH + PhOC(S)Cl \xrightarrow[CH_2Cl_2]{Py} ROC(S)OPh \xrightarrow[AIBN]{\mathbf{4}} RH$$

The hydroxy group can also be reduced with $(Me_3Si)_3SiH$ *via* selenocarbonate derivatives.[58]

Successful application of tris(trimethylsilyl)silane as a promotor in multicomponent combination reactions of organic molecules is reported.[59, 60]

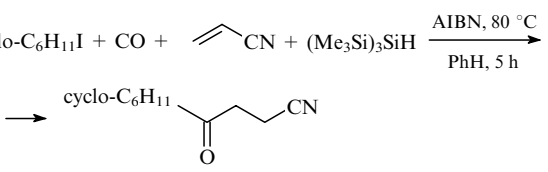

In the presence of AIBN, tris(trimethylsilyl)silane reacts with equimolar amounts of phosphine sulfides and phosphine selenides to give the corresponding phosphines in good yields.[7] Stereochemical studies with P-chiral phosphine sulfides have shown that this reduction occurs with retention of their configurations.[7]

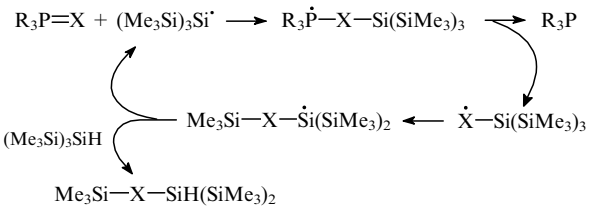

R = Me, Bu^n, Ph; X = S, Se.

However, no reaction of tris(trimethylsilyl)silane with phosphine oxides occurs even on heating to 150 °C.

2. Hydrosilylation reactions

In the presence of radical initiators, tris(trimethylsilyl)silane easily reacts with alkenes; the addition to the double bonds occurs against the Markownikoff rule.[61, 62]

$$(MeSi)_3SiH + Bu^nOCH{=}CH_2 \longrightarrow Bu^nOCH_2CH_2Si(SiMe_3)_3 \quad (92\%)$$

The addition of $(Me_3Si)_3SiH$ to prochiral alkenes containing ester groups occurs stereoselectively. The selectivity increases with a decrease in temperature, *viz*., the **10a** : **10b** isomer ratio is 19 : 1 at 60 °C, while that at −15 °C is 99 : 1.[61]

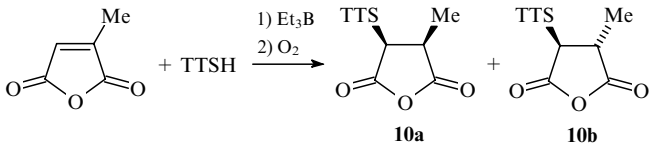

10a **10b**

The addition of $(Me_3Si)_3SiH$ to α-substituted chiral alkenes also occurs with high stereoselectivity.[63]

Generally, the activity of silyl radicals in addition reactions to the double bond of alkenes is high[46] (*e.g*., at 23 °C, $k = 10^6 - 10^8$ litre mol^{-1} s^{-1}), this decreases in the following order: $Et_3Si^{\bullet} > Me_3SiMe_2Si^{\bullet} > (Me_3Si)_3Si^{\bullet}$.

As a rule, the addition of trialkylsilyl radicals to alkenes is an irreversible exothermic reaction.[64] This general tendency notwithstanding, it was found that $(Me_3Si)_3Si^{\bullet}$ adds reversibly to many alkenes[65, 66] and catalyses their isomerisation. Thus treatment of each of the 1,5,9-cyclododecatriene isomers (**11**) with a $(Me_3Si)_3SiH - (Bu^tO)_2$ system at 143 °C affords a mixture of (*E*,*E*,*E*) : (*Z*,*E*,*E*) : (*Z*,*Z*,*E*) isomers in 80% yield and in a 78 : 22 : 2 ratio.

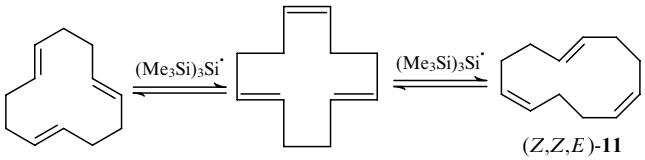

(*E*,*E*,*E*)-**11** (*Z*,*E*,*E*)-**11** (*Z*,*Z*,*E*)-**11**

Alkynes also react with tris(trimethylsilyl)silane according to a radical-chain mechanism.[61] The stereoselectivity of this reaction strongly depends on the nature of the substituents at the triple bond. For R = Ph, Y = CO_2Et or R = Bu^t, Y = H, the *Z* : *E* isomer ratio is 1 : 99. For R = Ph and Y = Alk, CN or CHO the stereoselectivity is much lower.[61]

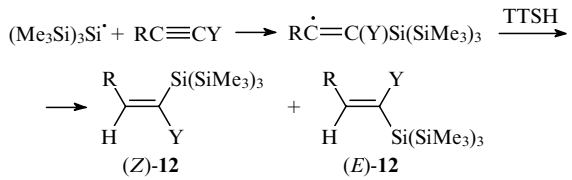

(*Z*)-**12** (*E*)-**12**

After termination of hydrosilylation reactions, the TTS group is removed using oxidative cleavage with 2,3-dimethylquinone and Bu_4NF or with bromine.[61]

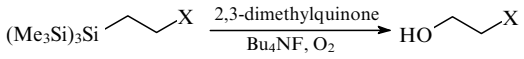

X = Ph, CN, CO_2H.

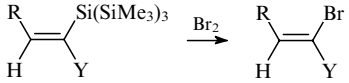

R = H, Bu^t, Ph; Y = CN, CO_2H.

The tris(trimethylsilyl)silyl radical adds easily to the carbonyl oxygen atom of aldehydes, dialkyl ketones and quinones,[67, 68] but the rate constants for these reactions were an order of magnitude lower than those of alkylsilyl radical reactions.

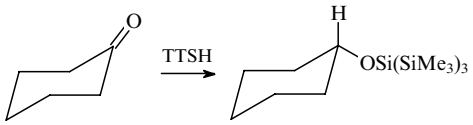

The tris(trimethylsilyl)silyl group is successfully employed in radical allylation reactions of the halogen-substituted organic compounds.[69]

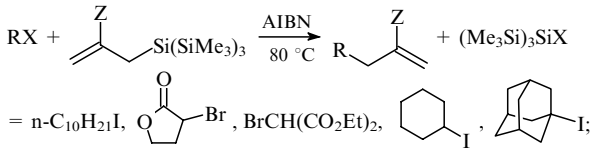

Z = H, Me, Cl, CN, CO_2Et.

The use of $(Me_3Si)_3SiH$ in the synthesis of nucleosides, α-amino acids and prostaglandins[69] seems to be more preferable than that of Bu_3SnH due to high toxicity of the latter.

Some examples of radical substitution of the Me_3Si group at the silicon atom are known.[70–72] Thus the carbon-centred radical in the intermediate **13** formed from the corresponding bromide by a chain reaction displaces in an intramolecular manner the trimethylsilyl fragment of the TTS group.

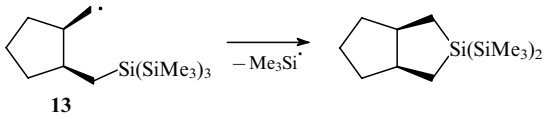

13

3. Polymerisation involving $(Me_3Si)_3SiH$

Tris(trimethylsilyl)silane was found to be one of the most efficient chain transmitters in the radical polymerisation of vinylic monomers.[73] The chain transfer constants (c_s) are listed in Table 6.

Chain transmitters result in a much more narrow molecular-mass distribution, which is broadened in their absence due to the gel effect. This circumstance is of considerable practical importance because of the lack, until now, of ways to significantly

Table 6. Chain transfer constants (c_s) through silicon hydrides in the bulk polymerisation of styrene and methyl metacrylate at 60 °C.[73]

Compound	$10^3\,c_s$	
	styrene	methyl metacrylate
Et_3SiH	7.3	4.23
Me_5Si_2H	14	56
$(Me_3Si)_2SiMeH$	92	706
$(Me_3Si)_3SiH$	550	8300

decrease the polydispersity of polymers prepared by radical polymerisation.

4. Acidity of $(Me_3Si)_3SiH$

It is known that silyl anions cause metallation of weak CH-acids,[37, 74, 75] but their generation by direct deprotonation of silanes with carbanions or alkali metal amides could not be detected. Only metallation of Et_3SiH by potassium hydride in dimethoxyethane or hexamethylphosphorotriamide is known.[76] Attempts to abstract the proton from $(Me_3Si)_3SiH$ using Bu^nLi, MeLi or Ph_3CLi in THF were unsuccessful and resulted in the destruction of the substrate. Such a deprotonation could be effected only when less nucleophilic $Ph_3CLi(Et_2O)_2$ in diethyl ether was used.[77]

$$Ph_3CLi(Et_2O)_2 + (Me_3Si)_3SiH \xrightarrow{Et_2O} Ph_3CH + (Me_3Si)_3SiLi$$

The acidity of tris(trimethylsilyl)silane in solution was established in reactions of the complex $(Me_3Si)_3SiLi(THF)_3$ (**5**) with various CH-acids.[78] Thus $(Me_3Si)_3SiH$ and 9-phenylxanthyllithium ($pK = 28.7$) form an equilibrium mixture in diethyl ether with a silane : silyl anion molar ratio of 12 : 7, which corresponds to $pK = 29.4$ for $(Me_3Si)_3SiH$.

The energy of deprotonation of $(Me_3Si)_3SiH$ in the gas phase was estimated to be equal to 350.8 kcal mol^{-1}, which is by $\sim$22 kcal mol^{-1} smaller than that of SiH_4 (372.8 kcal mol^{-1}) and significantly smaller than that of methane (416.6 kcal mol^{-1}).

The use of tris(trimethylsilyl)silane as a starting reagent in the synthesis of organoelement and organometallic compounds will be considered in subsequent chapters devoted to individual groups of elements.

V. Tris(trimethylsilyl)silyl derivatives of elements of the main subgroups

1. Elements of Groups IA – IIA

a. Preparation

The synthesis of $(Me_3Si)_3SiLi$ (**5**), first developed by Gilman and Smith,[37] was modified further.[23] The reaction rate depends on the procedure used for the preparation of methyllithium. The reaction with MeLi prepared from methyl iodide or bromide proceeds at a sufficiently high rate and is significantly slower, if methyl chloride has been used. Tris(trimethylsilyl)silyllithium was isolated and characterised as a colourless crystalline adduct with THF.[23, 35] This can be stored in an atmosphere of argon for several months. It is noteworthy that if the reaction is incomplete, a crystalline compound containing one tetrakis(trimethylsilyl)silane molecule per two lithium silanide molecules, $[(Me_3Si)_4Si][(Me_3Si)_3Si.Li(THF)_3]_2$, can be isoated from the reaction mixture.[35]

Tris(trimethylsilyl)silylpotassium (**6**) is yet another popular reagent. This is highly stable, can be stored at 20 °C for a long time and is highly reactive and its synthesis from tetrakis(trimethylsilyl)silane (**3**) is rather simple and convenient.[22]

Potassium, rubidium and caesium tris(trimethylsilyl)silanides can be prepared by treatment of $(Me_3Si)_3SiLi$ with *tert*-butoxides of the corresponding alkali metals.[79]

$$(Me_3Si)_3SiLi(THF)_3 + Bu^tOM \longrightarrow (Me_3Si)_3SiM + Bu^tOLi$$

M = K, Rb, Cs.

The solid reaction products can be separated by addition of crown ethers, which also determine the formation of contact or separated ion pairs. The following ionic compounds, *e.g.*, $K(18\text{-C-}6)Si(SiMe_3)_3$, $[K(12\text{-C-}4)_2][Si(SiMe_3)_3]$, $[Rb(15\text{-C-}5)_2].[Si(SiMe_3)_3]$, $[Cs(18\text{-C-}6)_2][Si(SiMe_3)_3]$ and $[Rb(18\text{-C-}6)_2].[Si(SiMe_3)_3][Rb(18\text{-C-}6)Si(SiMe_3)_3]_2$ were prepared in this way and their structures were established.[79]

Non-solvated $(Me_3Si)_3SiLi$ was prepared by substitution of lithium for mercury in a reaction of bis[tris(trimethylsilyl)-silyl]mercury with metallic lithium in toluene.[80]

$$[(Me_3Si)_3Si]_2Hg \xrightarrow{Li,\ PhMe} 2\,(Me_3Si)_3SiLi + Hg$$

Using ^7Li NMR spectroscopy, it was found that in hydrocarbon solvents the central silicon atom in $(Me_3Si)_3SiLi$ carrying a negative charge is associated with two lithium atoms, whereas the silicon atom in Me_3SiLi is associated with three lithium atoms.[80]

Non-solvated tris(trimethylsilyl)silanides of other alkali metals were prepared using transmetallation reactions of zinc tris(trimethylsilyl)silanide with an alkali metal in saturated hydrocarbons.[81]

$$[(Me_3Si)_3Si]_2Zn \xrightarrow{M} 2\,(Me_3Si)_3SiM + Zn$$

M = Na, K, Rb, Cs.

Tris(trimethylsilyl)silanides of alkali metals exist in a crystalline state as dimers with a nearly planar M_2Si_2 ring. The dimeric molecules are associated into a coordination polymer by abnormally short bonds between the alkali metal atom of one molecule and the methyl group of another molecule.[81]

b. Reactivities of tris(trimethylsilyl)silanides

Alkali metal silanides manifest extremely high reactivities. Many of them easily react even with the solvent. Potassium triethylsilanide, for example, deprotonates weak acids such as benzene or toluene. These reactions yield potassium hydride and triethylphenylsilane or benzyltriethylsilane, respectively.[82] The main advantage of alkali metal tris(trimethylsilyl)silanides is that they maintain high reactivities with respect to electrophilic sites without affecting the molecules of aromatic solvents (*e.g.*, benzene, toluene) and ethers. This can partly be due to the steric shielding of the nucleophilic centre and the simultaneous intramolecular stabilisation of the complex by $M\cdots CH_3$ interactions.[81]

Reactions of tris(trimethylsilyl)silylpotassium (**6**) with various electrophilic reagents proceed in high yields.[22]

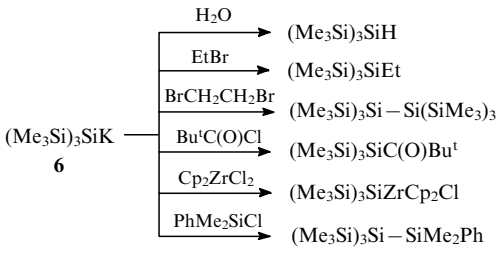

Tris(trimethylsilyl)silyllithium (**5**) lithiates hydrocarbons containing an active hydrogen atom.[37]

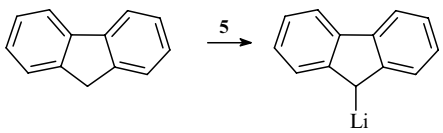

However, this reaction cannot be used for preparative purposes, since it is concomitant with side metathesis.

$$(Me_3Si)_3SiLi + (Me_3Si)_3SiH \longrightarrow (Me_3Si)_4Si + (Me_3Si)_2Si(H)Li$$

Treatment of magnesium bromide with 1 or 2 equiv. of lithium or potassium tris(trimethylsilyl)silanides in THF yielded the corresponding mono- $[(Me_3Si)_3SiMgBr(THF)_2]$ and disubstituted $\{[(Me_3Si)_3Si]_2Mg(THF)_2\}$ derivatives.[83] The crystalline complex $[(Me_3Si)_3Si]_2Mg(THF)_2$ is thermally highly stable and does not melt at temperatures up to 200 °C. However, in solution it slowly

(within 7 days) decomposes to give hexakis(trimethylsilyl)disilane and metallic magnesium.

$$[(Me_3Si)_3Si]_2Mg(THF)_2 \xrightarrow{C_6D_6} (Me_3Si)_3Si-Si(SiMe_3)_3 + Mg \quad (40\%)$$

Tris(trimethylsilyl)silylmagnesium bromide yields symmetrisation products upon addition of dioxane:

$$(Me_3Si)_3SiMgBr(THF)_2 + C_4H_8O_2 \longrightarrow [(Me_3Si)_3Si]_2Mg(THF)_2 + MgBr_2(C_4H_8O_2)$$

Since alkali metal tris(trimethylsilyl)silanides are used in the synthesis of diverse organoelement and organometallic compounds, their reactions will be considered in the appropriate sections.

2. Group IIIA elements

a. Boron

Silyl boranes constitute a small class of compounds due to instability of the Si–B bond. The tris(trimethylsilyl)silyl group has good potential for steric and electronic stabilisation of the electron-deficient boron atom. The reaction of lithium tris(trimethylsilyl)silanide with boron halides and alkylamides yields highly stable derivatives.[84]

$$n\,(Me_3Si)_3SiLi(THF)_3 + R_{3-n}BX_n \longrightarrow R_{3-n}B[Si(SiMe_3)_3]_n + n\,LiX$$

R = Me, Bu^t, bicyclo[3.3.1]nonane, Me_2N; X = Br, Cl.

Boron hydrides react with TTS-Li to give lithium salts:

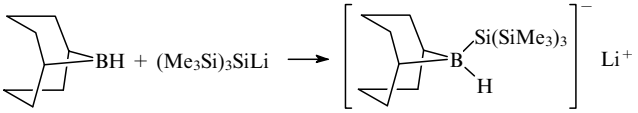

Upon methanolysis in acidic media, boroakylamides yield methoxyboranes with retention of the Si–B bond.[84]

$$[(Me_3Si)_3Si]_2BNMe_2 + HCl + MeOH \longrightarrow [(Me_3Si)_3Si]_2BOMe + [Me_2NH_2]Cl$$

Tris(trimethylsilyl)silyllithium reacts with aminodifluoroboranes to give substitution products.[85]

$$(Me_3Si)_3SiLi + F_2BN(R)SiMe_3 \longrightarrow (Me_3Si)_3SiB(F)N(R)SiMe_3 + LiF$$
14

R = Me, Et, Pr^i, Bu^t, $SiMe_3$.

The thermolysis of hypersilylaminofluoroboranes **14** results in stable iminoboranes **15**, which proved to be highly reactive compounds. They easily add water, methanol and even sterically hindered aromatic amines.[85]

$$(Me_3Si)_3SiB(F)N(R)SiMe_3 \xrightarrow{400-500\ ^\circ C} (Me_3Si)_3SiB{\equiv}N-R\ ,$$
14 **15**

$$(Me_3Si)_3SiB{\equiv}N-R + ArNH_2 \longrightarrow (Me_3Si)_3SiB(NHR)NHAr$$
15

R = $SiMe_3$, Bu^t; Ar = 2,4,6-$Me_3C_6H_2$.

b. Aluminium

Reactions of aluminium chloride, alkyl- and arylaluminium chlorides with TTS-Li give the corresponding hypersilyl derivatives.[86]

$$(Me_3Si)_3SiLi(THF)_3 + R_{3-n}AlCl_n \longrightarrow (Me_3Si)_3SiAlR_{3-n}AlCl_{n-1}(THF)$$

R = Me: n = 1 (81%); 3 (60%); R = Et: n = 1 (78%); 2 (83%).

It was shown that at low temperatures aluminium chloride forms a lithium adduct $[Li(THF)_4][(TTS)AlCl_3]$,[87] which decomposes at −15 °C. Trialkylaluminium gives a complex salt with TTS-Li.

$$(Me_3Si)_3SiLi(THF)_3 + R_3Al \xrightarrow{THF} [(Me_3Si)_3SiAlR_3]Li(THF)_n$$

R = Me, Et.

The reaction of lithium hypersilanide with tetrameric aluminium(I) bromide or iodide was used for the preparation of a tetranuclear complex of monovalent aluminium **16**.[88]

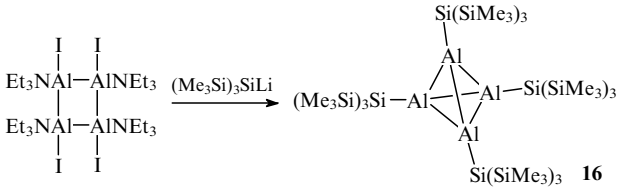

16

The interatomic distance Al–Al in compound **16** is equal to 2.602 Å, *i.e.*, is only slightly greater than the sum of the covalent radii (2.48 Å).

c. Gallium

In the past decade, the chemistry of silicon–gallium compounds has been developing especially intensely due to considerable interest in these compounds as precursors of materials for microelectronics.[89] In this context, much attention is being given to hypersilyl derivatives containing Si–Si and Si–Ga bonds initially.

The structurally characterised compounds with $(Me_3Si)_3SiGa$ fragments can be classified into three groups, *viz.*: (1) mononuclear gallium complexes containing a single Si–Ga bond of the type $(Me_3Si)_3Si-GaR_2$; (2) digallanes; (3) nuclear clusters containing gallium atoms surrounded by silyl substituents.

Compounds with Si–Ga bonds are prepared by reactions of the corresponding chlorides R_2GaCl with TTS-Li.

$$R_2GaCl + (Me_3Si)_3SiLi(THF)_3 \longrightarrow R_2Ga-Si(SiMe_3)_3 + LiCl$$
17

R = Me, Ph, 2,2,6,6-tetramethylpiperidine (tmpp).

The 2,2,6,6-tetramethylpiperidine derivative, $(tmpp)_2Ga$-TTS (**17**), is easily split at the Ga–N bond by treatment with water, EtOH, PhOH or HCl to give the corresponding derivatives, *viz.*, $[(Me_3Si)_3SiGa(OH)_2]_3$, $[(Me_3Si)_3SiGa(OEt)_2]_2$, $\{[(Me_3Si)_3Si.Ga(OPh)_3]^-[(tmpp)H_2^+]\}$ or $\{[(Me_3Si)_3SiGaCl_3]^-[(tmpp)H_2^+]\}$ where the coordination number of gallium is usually equal to 4.[90]

By virtue of their high proneness to form coordination compounds, gallium halides yield products with various compositions depending on the stoichiometric ratios of the components.[90,91] Two compounds with tentative compositions $Li[(Me_3Si)_3Si-GaCl_3](THF)_4$ and $(Me_3Si)_3Si-GaCl_2(THF)$[91] are formed at the $GaCl_3:(Me_3Si)_3SiLi$ ratio of 1 : 1 that could not be isolated in the pure state. The same reaction with two moles of $(Me_3Si)_3SiLi$ gives a structurally characterised ate-complex with lithium chloride **18**.[92] The TTS-$GaCl_2(THF)$ complex was prepared in the presence of an excess $GaCl_3$.[90]

$$(Me_3Si)_3SiLi + GaCl_3 \xrightarrow{THF} [(Me_3Si)_3Si]_2Ga(\mu\text{-}Cl)_2Li(THF)_2$$
18

Gallium(I, III) chloride, $Ga[GaCl_4]$, reacts with lithium tris(trimethylsilyl)silanide and, depending on the ratio of reagents, reaction temperature and the solvent type, yields a tetranuclear

cluster $[(Me_3Si)_3SiGaCl]_4$,[93] a homoleptic gallium(I) silanide, $[(Me_3Si)_3SiGa]_4$,[94] or gallium bis(hypersilyl)chloride, $[(Me_3Si)_3Si]_2GaCl$.[95] Larger clusters have been isolated, *e.g.*, the complex $Ga_{10}[Si(SiMe_3)_3]_6$ (**19**),[96] which represents two edge-shared octahedra one of which contains four TTS substituents, while the other one contains only two substituents.

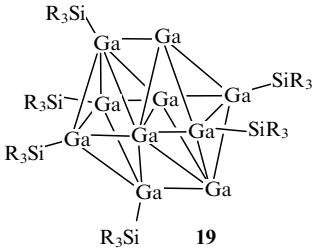

R = $SiMe_3$.

19

The reaction of Ga(I)Br with TTS-Li gives the cluster $Ga_{22}[(Me_3Si)_3Si]_8$ (**20**) which contains 22 gallium atoms;[97] the central gallium atom in this complex is surrounded by 13 different gallium atoms carrying eight $GaSi(SiMe_3)_3$ fragments on the outer side.

$$GaBr + (Me_3Si)_3SiLi(THF)_3 \longrightarrow$$
$$\longrightarrow [(Me_3Si)_3Si]_2GaBr_2 \cdot Li(THF)_2 + [(Me_3Si)_3SiGaBr]_4 +$$
$$+ Ga_{22}[(Me_3Si)_3Si]_8$$

20

The reactions of the cluster $[(Me_3Si)_3SiGaCl]_4$ with iron carbonylates, *e.g.*, $Na_2Fe(CO)_4$, $Na_2Fe_2(CO)_8$ and $Na_2Fe_3(CO)_{11}$, have been studied.[95] The reaction products, *viz.*, $(CO)_3Fe[Ga(TTS)]_3Fe(CO)_3$ and $(CO)_3Fe[Ga(TTS)]_2(\mu\text{-}CO).Fe(CO)_3$, represent $Fe_2(CO)_9$ derivatives where the bridging CO groups are partly or completely replaced by the $GaSi(SiMe_3)_3$ fragment.

d. Indium, thallium

Indium hypersilyl derivatives are not numerous. One of them is the ate-complex of indium bis(hypersilyl)chloride with LiCl , *viz.*, $[(Me_3Si)_3Si]_2In(\mu^2\text{-}Cl)_2Li$.[92] All attempts to obtain monovalent indium derivatives by reaction of indium(I) chloride with TTS-Li gave the same product, presumably, as a result of disproportionation of indium(I) chloride by the reaction:

$$3\,InCl \longrightarrow 2\,In + InCl_3.$$

The reaction of indium trichloride with TTS-Li at −60 °C yields $[(Me_3Si)_3Si]_2$ and metallic indium; however, at lower (−100 °C) temperatures, it is the bimetallic derivative $(TTS)_2In-In(TTS)_2$ that is formed.[98] A similar thallium derivative, *viz.*, compound **21**, was isolated by treatment of the monovalent thallium silylamide with potassium hypersilanide.[99]

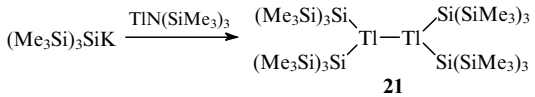

21

3. Group IVA elements

a. Carbon

Numerous compounds in which the hypersilyl group is bound to carbon are referred to in different sections of the present review. Let us give some additional examples.

The reaction of fullerene C_{60} with $(Me_3Si)_3SiLi$ in toluene at −78 °C and subsequent treatment of the reaction products with ethanol resulted in 1,16-bis[tris(trimethylsilyl)silyl]-C_{60}-fullerene in 69% yield. Its structure (in the form of a solvate with CS_2) was confirmed by X-ray diffraction analysis.[100]

The sterically overcrowded TTS derivatives present certain interest. Thus bis(hypersilyl)methoxymethane **22** is formed in the reaction of $(Me_3Si)_3SiLi$ with dichloromethoxymethane.[101, 102]

$$(Me_3Si)_3SiLi + Cl_2CHOMe \longrightarrow [(Me_3Si)_3Si]_2CHOMe$$

22 (35%)

The methoxy group in compound **22** is so strongly shielded that it is resistant to acid hydrolysis under drastic conditions;[101] the Si−C−Si angle is equal to 132.7°, which suggests steric overcrowding of this molecule. The reaction of TTS-Li with methyl formate afforded sterically overcrowded bis(hypersilyl)-methanol, $[(TTS)_2CHOH]$.

Treatment of hypersilyllithium with carbon dioxide and subsequent hydrolysis yielded thermally stable ($T_{decomp.}$ = 225 °C) hypersilylcarboxylic acid $(Me_3Si)_3SiCO_2H$.[8] Stable acylsilanes are formed in reactions of TTS-Li with acyl halides.[103]

$$(Me_3Si)_3SiLi + RC(O)Cl \longrightarrow (Me_3Si)_3SiC(O)R + LiCl$$

R = Bu^t, CEt_3, 1-adamantyl.

The properties of acylsilanes are considered in Section VIII. The tris(trimethylsilyl)silyl group confers stability also to the aldehyde $(Me_3Si)_3SiC(O)H$; however, this can be prepared exclusively using organometallic reagents (see Section VI.4).

b. Silicon

Treatment of $(Me_3Si)_3SiLi$ with various organosilicon halides was used for the preparation of derivatives of the type $(Me_3Si)_3SiSiR_2X$ (R = Cl, Me, Pr^i, Bu^t, Ph, X = Cl; R = $Bu^t(Me_3Si)N$, X = F)[104] as well as compounds of the type $(Me_3Si)_3SiR$, where R = $SiCl_3$, $SiMe_2H$, $SiPh_2Cl$.[39] Halogen or hydrogen atoms in the latter are fairly mobile and can easily be substituted by other functional groups, *e.g.*, OMe, I, OH, OAc, O_2CCF_3.[39]

Careful hydrolysis of disilane $(Me_3Si)_3SiSiCl_3$ allowed isolation of the thermally stable (m.p. = 210–213 °C) silanetriol $(Me_3Si)_3SiSi(OH)_3$, which exists as a hexamer in the crystalline state. The core of this spherical molecule consists of six associated silanetriol groups.[105]

Under mild conditions, lithium tris(trimethylsilyl)silanide reacts with stable silylene **23** to give the addition product **24**.[106]

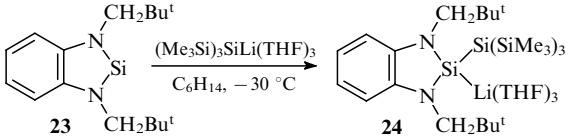

23 **24**

The tris(trimethylsilyl)silyl group plays a key role in the synthesis of branched polysilanes, since it allows one to elongate the chain by substitution of SiLi or SiCl for the terminal fragments SiMe.[107–109]

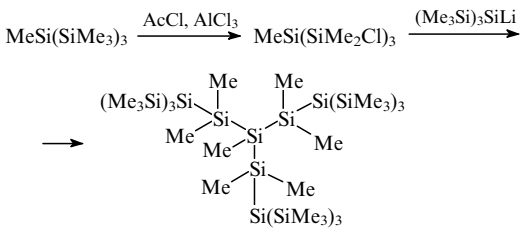

The synthesis of branched polysilanes has a number of specific features related to the steric factors and the ability of the Si−Si bond to be cleaved by nucleophilic reagents. Although some examples of Si−Si bond cleavage in disilanes[110, 111] resulting in Me_3SiM (M is an alkali metal) are known, this process never takes place in branched polysilanes. The formation of a silyl anion with a 'tertiary' silicon atom ($\equiv Si)_3Si^-$ is thermodynamically the most favourable process.

Splitting of branched polysilanes **25** under the action of methyllithium is mainly controlled by steric factors; MeLi largely attacks the least sterically hindered silicon atom (Table 7).[112]

Table 7. Relative yields (%) of the lithiation products of branched polysilanes $(Me_3Si)_3SiR$ **25**.[112, 113]

R	Route *a*	Route *b*
$SiMe_2H$	< 2	> 98
$SiMe_2Bu^t$	> 99	< 1
Si_2Me_5	70	30
$SiMe_2SiMe_2Bu^t$	98	2
$SiMe(SiMe_3)_2$	40	60
$Si(SiMe_3)_3$	< 2	> 98
$SiMeHSi(SiMe_3)_3$	< 2	> 98
$SiMe_2Si(SiMe_3)_3$	< 2	> 98

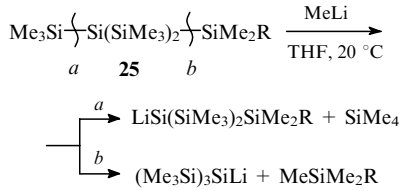

In branched chloropolysilanes, chlorine is relatively inactive; however, being an electronegative substituent, it stabilises 'tertiary' silyl anions. Therefore, at 0 – 30 °C (60% – 80%) the initial elimination of the trimethylsilyl group prevails.

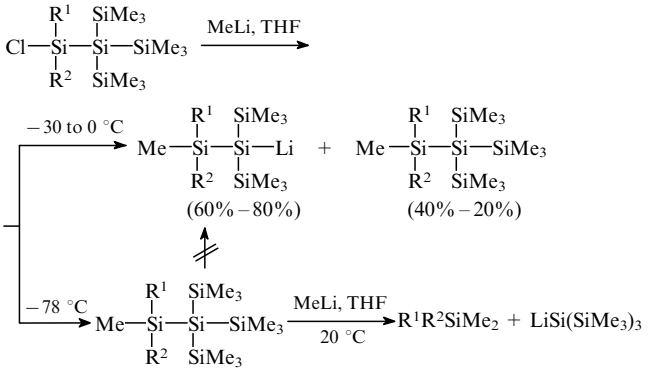

R^1, R^2 = Me, $SiMe_3$, $Si(SiMe_3)_3$.

The formation of disilenes as intermediates in this reaction is not excluded.[112] With a decrease in temperature down to −78 °C, the mobility of the TTS-group seems to decrease considerably and substitution of the methyl group for the chlorine atom becomes predominant.

The use of bulkier silyllithium reagents, such as Ph_3SiLi and TTS-Li as well as of Bu^tOK,[22] results in the cleavage of one or two peripheral Si – Si bonds.[113]

$$(Me_3Si)_3SiSi(SiMe_3)_3 \xrightarrow{RLi} (Me_3Si)_3SiSi(SiMe_3)_2Li + Li(Me_3Si)_2SiSi(SiMe_3)_2Li + RSiMe_3$$

R = Ph_3Si, $(Me_3Si)_3Si$.

$$(Me_3Si)_3SiSi(SiMe_3)_3 \xrightarrow{Bu^tOK} (Me_3Si)_3SiSi(SiMe_3)_2K + Bu^tOSiMe_3$$

The reaction of the resulting silyllithium derivatives with silicon halides constitutes the second step in the synthesis of branched polysilanes.

In one of the methods for the synthesis of bis(hypersilyl) derivatives, silyl triflate $(CF_3SO_3)_2SiH_2$ formed *in situ* from Ph_2SiH_2 and CF_3SO_3H is treated with tris(trimethylsilyl)silyllithium.[114]

$$2\,LiSi(SiMe_3)_3 + (CF_3SO_3)_2SiH_2 \longrightarrow (Me_3Si)_3Si-SiH_2-Si(SiMe_3)_3 \quad (19\%)$$

c. Germanium, tin, lead

A series of organotin TTS derivatives have been obtained in satisfactory yields by the reaction of $(Me_3Si)_3SiLi(THF)_3$ with alkyltin(IV) halides.[24]

$$R_{4-n}SnCl_n + n\,(Me_3Si)_3SiLi(THF)_3 \longrightarrow [(Me_3Si)_3Si]_nSnR_{4-n} + n\,LiCl$$

R = Me, Bu^n; n = 1, 2.

The reaction of lithium tris(trimethylsilyl)silanide with silicon, germanium and tin tetrachlorides provides an illustrative example of the steric effect of the TTS group on nucleophilic substitution. Silicon tetrachloride reacts with only 1 equiv. of $(Me_3Si)_3SiLi$ to yield $(Me_3Si)_3SiSiCl_3$;[104] $GeCl_4$ gives a dimer with a Ge – Ge bond, $[Cl_2GeSi(SiMe_3)_3]_2$,[115] while the substitution of two chlorine atoms in $SnCl_4$ affords $Cl_2Sn[Si(SiMe_3)_3]_2$.[24]

The reactions of trichlorosilane and germanium(II) silylamide with TTS-Li are more complicated and give cyclic compounds **26** and **27**, which formally represent the rearrangement products of tris(trimethylsilyl)silyl derivatives of bivalent silicon and germanium.[81]

$$2\,(Me_3Si)_3SiLi \xrightarrow[C_5H_{12},\ -30\ ^\circ C]{HSiCl_3} (Me_3Si)_2Si\langle Si(SiMe_3)_2 \rangle Si(SiMe_3)_2$$

26

$$2\,(Me_3Si)_3SiLi \xrightarrow[C_5H_{12},\ -30\ ^\circ C]{Ge[N(SiMe_3)_2]_2} (Me_3Si)_2Ge\langle Si(SiMe_3)_2 \rangle Si(SiMe_3)_2$$

27

Treatment of bivalent tin chloride with TTS-Li gives the ate-complex $[(Me_3Si)_3Si]_2Sn(\mu\text{-}Cl)Li(THF)_3$.[116]

The reaction of tris(trimethylsilyl)silyllithium with $PbCl_2$ occurs as a redox process resulting in metallic lead and hexakis(trimethylsilyl)disilane.[117]

$$PbCl_2 + 2\,(Me_3Si)_3SiLi(THF)_3 \longrightarrow (Me_3Si)_3SiSi(SiMe_3)_3 + 2\,LiCl + Pb$$

Chlorotriphenylplumbane reacts with TTS-Li to give a colourless crystalline thermostable product **28** in 81% yield.[118]

$$Ph_3PbCl + (Me_3Si)_3SiLi(THF)_3 \longrightarrow Ph_3PbSi(SiMe_3)_3 + LiCl$$

28

An attempt to obtain a bis(hypersilyl) derivative $Ph_2Pb[Si(SiMe_3)_3]_2$ resulted in diplumbane **29**.[118]

$$Ph_2PbCl_2 + 2\,(Me_3Si)_3SiLi(THF)_3 \longrightarrow (Me_3Si)_3Si-Pb(Ph_2)-Pb(Ph_2)-Si(SiMe_3)_3 + Si_2(SiMe_3)_6$$

29

Homoleptic hypersilanides of bivalent tin and lead were prepared by reactions of the corresponding silylamides with tris(trimethylsilyl)silyl derivatives of alkali metals.[119, 120]

$$[(Me_3Si)_2N]_2E + 2\,MSi(SiMe_3)_3 \longrightarrow [(Me_3Si)_3Si]_2E + 2\,(Me_3Si)_2NM$$

E = Sn, Pb; M = Na, K, Rb, Cs.

Di(hypersilyl)stannylene and -plumbene manifest amphoteric properties and behave as Lewis acids or bases. Quantum-chemical calculations of model compounds have demonstrated that the Lewis acidity of the carbenoids $(H_3Si)_2E$ (E = Sn, Pb) significantly exceeds that of the related diorganyl derivatives Me_2E, which increases their ability to form adducts (Lewis acid – base)

and dimers. The equilibrium between the monomeric and dimeric forms is more typical of di(hypersilyl)stannylene in solution, whereas in the crystalline state this compound is a dimer with an interatomic Sn–Sn distance of 2.825 Å. Di(hypersilyl)plumbene exists as a monomer both in solution and in the crystalline state, but forms adducts with other, less sterically overcrowded plumbenes. Such an interaction is also typical of di(hypersilyl)stannylene; it is of note that the formation of an adduct is accompanied by the migration of substituents.[119]

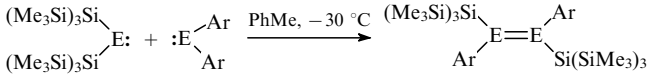

E = Sn, Pb; Ar = 2,4,6-$Me_3C_6H_2$; 2,6-$Me_2C_6H_3$.

Di(hypersilyl)stannylene and -plumbene react as Lewis bases with mesitylcopper. Hypersilylcopper **30** and mesityl(hypersilyl)-stannylene or -plumbene are the final reaction products.[121]

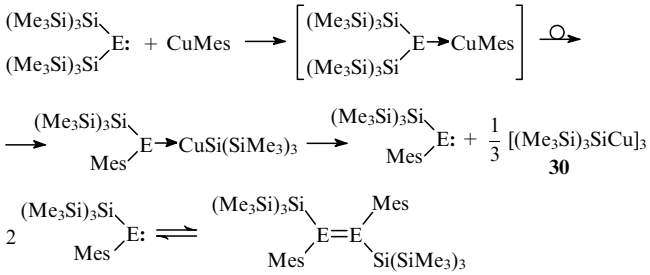

E = Sn, Pb.

In contrast to diarylstannylenes and -plumbenes, the dihypersilyl derivatives react faster with white phosphorus in toluene even at low temperatures (−30 °C).[119] Compounds containing Si–P bonds, $[(Me_3Si)_3SiP]_4Pb_4$ and $(Me_3Si)_3Si-P=P-Si(SiMe_3)_3$, are formed in the reaction of $Pb(TTS)_2$ in addition to the simple adduct $P_4[Pb(TTS)_2]_4$. $[(Me_3Si)_3SiP]_4Pb_4]$ has a cubane-like structure ($\delta\ ^{31}P = -506$).[119]

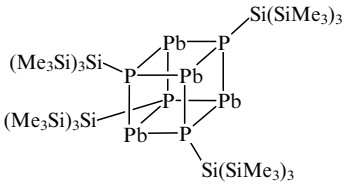

Organic azides form 1,3-addition products with di(hypersilyl)plumbene with simultaneous migration of the TTS group to the terminal nitrogen atom:[119]

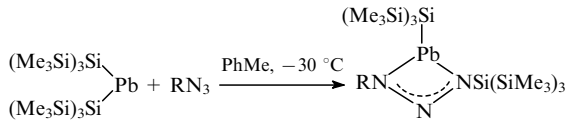

R = 1-adamantyl, Me_3Si.

Numerous reactions of di(hypersilyl)stannylenes and -plumbenes with various bases, including organic and silyl derivatives of alkali metals, have been studied.[119] However, only some of them yielded stable products. Thus di(hypersilyl)stannylene reacts with $(Me_3Si)_3SiNa$ in toluene to give $[(Me_3Si)_3Si]_3SnNa(PhMe)$ in a quantitative yield. At temperatures above −30 °C, tris(trimethylsilyl)silyl derivatives of alkali metals react with tin and lead silylamides in toluene to give toluene metallation products.

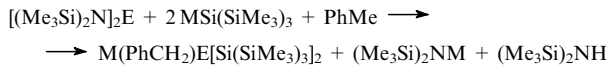

E = Sn, Pb; M = K, Rb, Cs.

4. Group VA elements

a. Nitrogen

Tris(trimethylsilyl)silyl derivatives of amines can be easily prepared by treatment of TTS halides with amines. Of particular interest in this respect is aminotris(trimethylsilyl)silane **31**, a highly stable compound which does not yield self-condensation products on heating.[122]

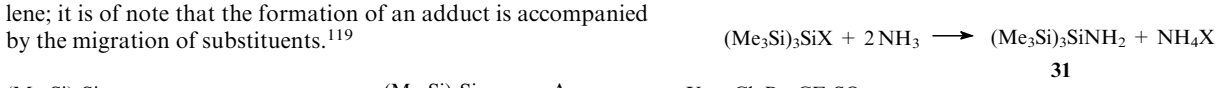

X = Cl, Br, CF_3SO_3.

b. Phosphorus

The Si–P bond is rather unstable. This has a certain effect on the chemistry of silicon–phosphorus compounds at large, on the chemistry of hypersilyl derivatives, in particular. The majority of reactions of lithium hypersilanide with phosphorus chlorides are accompanied by the formation of $(Me_3Si)_3SiCl$ (which is thermodynamically a very favourable product), and poly- or oligophosphines.[123–126]

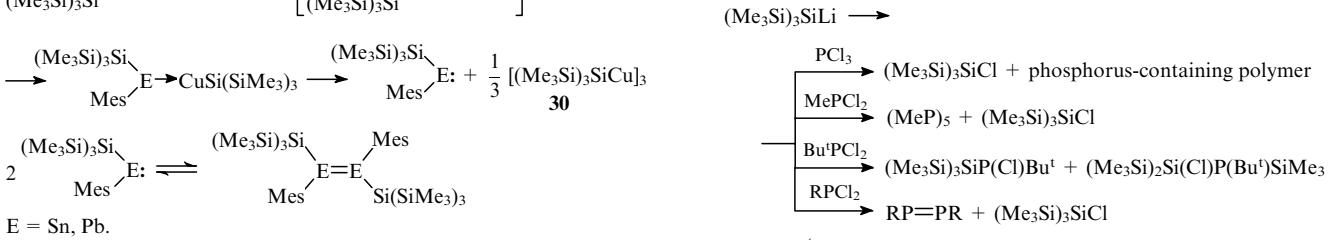

R = 2,4,6-$Bu^t_3C_6H_2$ (see [124]), $(Me_3Si)_3C$ (see [123]).

The complex of lithium tris(trimethylsilyl)silanide with THF (**5**) reacts with aminodifluorophosphines to give thermally stable derivatives **32a–d**.[127]

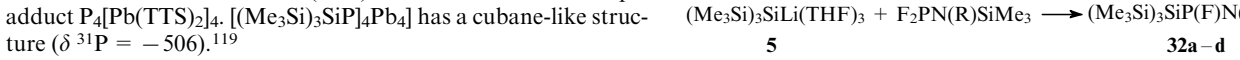

R = Bu^t (**a**), 2,4,6-$Me_3C_6H_2$ (**b**), $SiMe_3$ (**c**), 2-adamantyl (**d**).

Heating or distillation of compounds **32a–d** does not result in the elimination of Me_3SiF, whereas related tris(trimethylsilyl)-methyl derivatives are unstable and are readily converted into ylides $(Me_3Si)_2C=PN(R)SiMe_3$ (R = Bu^t, 2-adamantyl) upon elimination of fluorotrimethylsilane.[127]

The reaction of TTS-Li with 1-chloro-1*H*-phosphyrene **33** yielded the TTS-derivative **34**, which is relatively stable at 20 °C, but decomposes in light.[128]

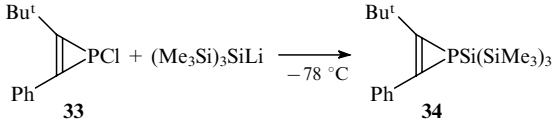

Sodium-potassium phosphide prepared from white or red phosphorus and a Na/K alloy reacts with chloro tris(trimethylsilyl)silane to give $[(Me_3Si)_3Si]_3P_7$ (**35**), a colourless crystalline compound in which the nortricyclane cell P_7 contains three TTS substituents.[129]

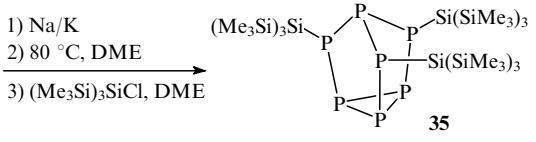

The phosphanortricyclanic cell is a relatively stable structure. Compounds of an analogous structure with other silyl substituents ($SiMe_3$, $SiPh_3$, $SiBu^t_3$) can be prepared as well.[129]

5. Group VIA elements

a. Oxygen

Tris(trimethylsilyl)silanol. Tris(trimethylsilyl)silanol, $(Me_3Si)_3Si.OH$, can be prepared by hydrolysis of TTS halides.

It is known that hydrolysis of halogenosilanes usually gives disiloxanes. The bulky TTS group prevents both the hydrolysis and subsequent condensation of silanols. Of the TTS halogen derivatives, only iodo- and bromosilanes are hydrolysed at satisfactory rates. Chlorotris(trimethylsilyl)silane does not react with water in neutral media. Its hydrolysis demands long-term (7 days) stirring of a TTS chloride solution in THF with 20% KOH. During this time, the greater part of the product is lost as a result of cleavage of the Si–Si bonds in the alkaline medium. An alternative method consists of long-term intense stirring of $(Me_3Si)_3SiCl$ with aqueous triethylamine in hexane.[130] In aqueous THF, bromotris(trimethylsilyl)silane is in an equilibrium with silanol and HBr; the latter is easily titrated with 5% NaOH. The equilibrium is shifted as a result of removal of HBr and the yield of $(Me_3Si)_3SiOH$ exceeds 90%.[131] Tris(trimethylsilyl)silanol is moderately sensitive to oxygen. Upon 1-month exposure to air, its content decreases by 30% with formation of a complex mixture of oxidation products.

Tris(trimethylsilyl)silanol differs from ordinary compounds of this class in thermal stability, this does not undergo condensation to disiloxane. In acidic media, substitution reactions take place instead of self-condensation, but in the case of ordinary silanols they proceed in the opposite direction.[131]

$$(Me_3Si)_3SiOH + HCl\,(aq.) \longrightarrow (Me_3Si)_3SiCl + H_2O,$$

$$(Me_3Si)_3SiOH + Me_3SiCl \longrightarrow (Me_3Si)_3SiCl + Me_3SiOH$$

Substitution reactions with carboxylic acids and primary alcohols (MeOH, EtOH) also take place.[132]

$$(Me_3Si)_3SiOH + MeC(O)OH \longrightarrow (Me_3Si)_3SiOC(O)Me + H_2O,$$

$$(Me_3Si)_3SiOH + EtOH \longrightarrow (Me_3Si)_3SiOEt + H_2O$$

However, in the case of isopropyl alcohol no reaction occurs, presumably due to steric hindrance. The esterification of tris(trimethylsilyl)silanol by carboxylic acids easily occurs even in an aqueous medium, since the reverse reaction (hydrolysis) is impossible in neutral or weakly acidic media.[132]

The IR spectrum of $(Me_3Si)_3SiOH$ contains intense absorption bands: a narrow band at 3660 cm^{-1} and a broad band around 3240–3600 cm^{-1}, which can be associated with the free and bound hydroxy groups, respectively.[130] The bands at 3443, 1080 and 1049 cm^{-1}, which relate to the protonated OH and SiO groups, are not detected in the Raman spectra. Such a difference is explained by changes in the symmetry due to dimer formation.[130]

Hypersilanolates $[(Me_3Si)_3SiO]_nML_m$. Alkali metal triorganylsilanolates are usually synthesised by treatment of triorganylsilanols with alkali metals or their hydrides.[133] However, alkali metal tris(trimethylsilyl)silanolates cannot be prepared by this method, since they either do not react with silanol or cause its destruction under more drastic conditions.[131,134] Lithium and sodium derivatives were prepared by treatment of tris(trimethylsilyl)silanol in hexane with butyllithium or sodium isopropoxide.[131]

$$(Me_3Si)_3SiOH + Bu^nLi \longrightarrow (Me_3Si)_3SiOLi + Bu^nH,$$

$$(Me_3Si)_3SiOH + Pr^iONa \longrightarrow (Me_3Si)_3SiONa + Pr^iOH$$

The thermal stabilities and reactivities of compounds containing $R_3Si-SiR_2OM$ groups depend on several factors, *viz*., the redox potential of a metal, its oxidation state, electron-donor properties of the polysilyl substituent, the degree of ionicity of the M–O bond and enthalpy of the rearrangement:

$$Si-Si-O-M \longrightarrow Si-O-Si-M.$$

Lanthanide derivatives with high affinities for oxygen and a moderately negative value of the standard redox potential appear to be the most stable compounds.

Thus the reaction of lanthanide silylamides with tris(trimethylsilyl)silanol gives gadolinium and lanthanum hypersilanolates **36a–f**.[135]

$$[(Me_3Si)_3N]_3Ln + 3\,(Me_3Si)_3SiOH + m\,L \longrightarrow [(Me_3Si)_3SiO]_3Ln(L_m) + 3\,(Me_3Si)_2NH$$

36a–f

Ln = Gd: L_m = $(THF)_2$ (**a**), $(MeCN)_2$ (**b**), 1,4-diazobicyclo[2.2.2]octane (**c**), (4,4′-bipiridyl)$_2$ (**d**), (4,4′-bipiridyl) (**e**);
Ln = La, L_m = $(THF)_4$ (**f**).

Homoleptic hypersilanolates, which contain no coordinating molecules, cannot be prepared because of their mobile equilibra and incomplete substitution. The bidentate ligand, 4,4′-bipyridyl, yields the coordination polymer **36e** upon coordination with the fragment $[(Me_3Si)_3SiO]_3Gd$, whereas 1,4-diazabicyclo[2.2.2]octane forms only a mononuclear complex **36c** at any ratio of the reagents due to steric hindrance. Gadolinium hypersilanolate **36a** absorbs only one mole of CO_2 to give $[(Me_3Si)_3SiO]_2Gd[OCOSi.(SiMe_3)_3](THF)_2$, whereas the analogous lanthanum complex **36f** yields the percarboxylate derivative $[(Me_3Si)_3SiOCO]_3La(THF)_2$.

Gadolinium and lanthanum hypersilanolates are stable at temperatures up to 200 °C. $(Me_3Si)_3SiOH$ and polylanthanosiloxane are the only decomposition products of compound **36a** at higher temperatures. It is noteworthy that thermolysis of more ionic lithium hypersilanolate, $(Me_3Si)_3SiOLi$, affords H_2, $(Me_3Si)_3SiH$ (55%), $Me_3SiOSi(SiMe_3)_3$ (10%) and $(Me_3Si)_3SiOH$ (13%).[131]

An increase in the redox potential on going from manganese to nickel and a simultaneous increase in the energy of the metal–silicon bond in the hypersilanolates of bivalent metals of Groups VII and VIII (Mn, Fe, Co, Ni) cause a significant decrease in their stability and increase their ability for intramolecular rearrangements eventually resulting in formation of the silicon–metal bond.

Cobalt(II) and iron(II) silanolates of the general formula **37a–k** were prepared by the reaction of tris(trimethylsilyl)silanol with the corresponding silylamides.[136] The reaction of $FeBr_2$ with $(Me_3Si)_3SiONa$ in dimethoxyethane was also used for the preparation of the ate-complex $(Me_3Si)_3SiOFe[\mu\text{-}OSi(SiMe_3)_3]_2.Na(DME)$ (**38**).[137]

$$[(Me_3Si)_2N]_2M + 2\,(Me_3Si)_3SiOH + L_n \longrightarrow [(Me_3Si)_3SiO]_2M(L_n) + 2\,(Me_3Si)_2NH$$

37a–l

M = Co: L_n is absent (**a**), L_n = THF (**b**), $(THF)_2$ (**c**), DME (**d**), $(MeCN)_2$ (**e**), $(PhCN)_2$ (**f**), 2,2′-bipyridyl (**g**), 4,4′-bipyridyl (**h**), $(Ph_3P)_2$ (**i**); M = Fe: L_n absent (**j**), L_n = 2,2′-bipyridyl (**k**), 4,4′-bipyridyl (**l**).

According to X-ray diffraction analysis, the homoleptic silanolates **37a**, **j** represent dimers in the crystalline state, but are monomers in solution (data from cryoscopic measurements in benzene). In contrast to other complexes, compound **37a** reversibly binds two THF molecules, which are easily removed *in vacuo* and upon dissolution in nonpolar solvents. 4,4′-Bipyridyl interacts with silanolates **37a**,**j** to give insoluble coordination compounds **37h**,**l**.[136]

It is of note that iron tris(trimethylsilyl)silanolates **37j**, **38** are pyrophoric in air, although they are in fact oxides. The oxidation of the Si–Si bonds proceeds at a high rate due to activation of the O_2 molecule on the coordinatively unsaturated iron atom. A detailed study of this oxidation in the example of compound **37j** revealed that oxygen is consumed in two routes, *viz*., in the

oxidation of the ligand (which is predominant) and in the oxidation of Fe(II) to Fe(III).[136]

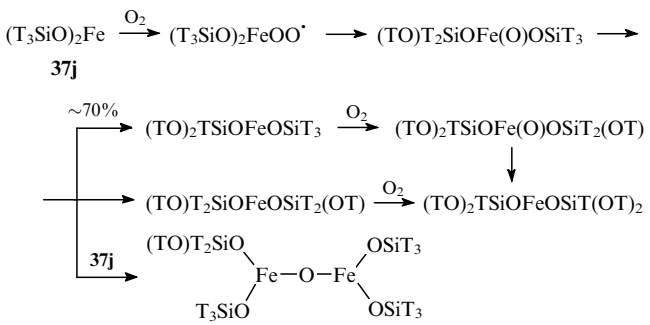

T = Me_3Si.

In the case of cobalt complexes, all of the oxygen is consumed for oxidation of the ligand.

The ate-complex of bivalent iron **38** reacts smoothly with tetracyanoethylene (TCE) to give Fe(III) hypersilanolate (**39**). Compound **39** does not react with oxygen.[137]

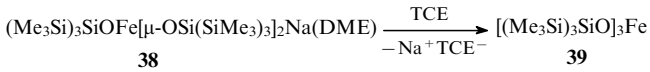

Under ordinary conditions, homoleptic cobalt silanolate **37a** adsorbs CO to give a complex with a tentative structure $(Me_3Si)_2(Me_3SiO)SiCo_x(CO)_y$. Compounds **37** are active as catalysts in the oligomerisaton of phenylacetylene. The reaction of equimolar amounts of silanolate **37f** and PhC≡CH results in the substitution of one silanolate group. Subsequent addition of PhC≡CH to the complex **40** yields 1,3,5-triphenylbenzene and polyphenylacetylene.

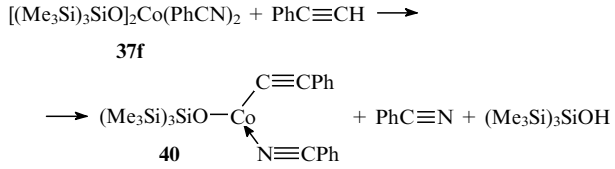

Thermal transformations of hypersilanolates have been studied. The decomposition of cobalt silanolate **37a** in solution begins at 40 °C. Acid hydrolysis of the solid thermolysis product gave Me_3SiH and $(Me_3Si)_3SiOSiH(SiMe_3)(OSiMe_3)$, which suggests a rearrangement occurs:

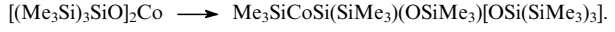

Thermolysis of $[(Me_3Si)_3SiO]_2Fe$ (**37j**) at 180–250 °C yields $(Me_3Si)_3SiOH$, $(Me_3Si)_3SiOSiMe_3$ and solid polyferro(Fe^{II})siloxane, whereas the ate-complex $(Me_3Si)_3SiOFe[\mu\text{-}OSi(SiMe_3)_3]_2.Na(DME)$ (**38**) gives silanes $[(Me_3Si)_3SiSi(SiMe_3)_3]$, $(Me_3Si)_4Si]$ and solid polyferri(Fe^{III})siloxane.[137] The reason for such a substantial difference is the presence, in the ate-complex, of sodium silanolate fragment possessing basic properties, which favours their disproportionation. Nickel hypersilanolates $LNi[OSi(SiMe_3)_3]_n$ cannot be synthesised because of smooth rearrangements leading to the formation of compounds with a Ni–Si bond.

For comparison, thermolysis of methoxytris(trimethylsilyl)silane, $(Me_3Si)_3SiOMe$, is accompanied by the formation of bis(trimethylsilyl)silylene (**41**).[138] Its further conversions depend on the reaction conditions. In the gas phase, compound **41** undergoes rearrangement into trisilylcyclopentane **42**.[139]

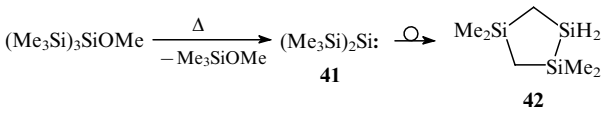

Thermolysis in the liquid phase yielded a totally different product, *viz*., octakis(trimethylsilyl)cyclotetrasilane (**43**).

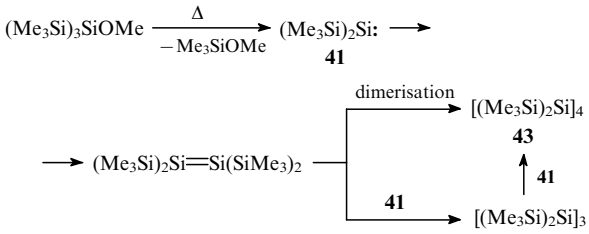

b. Chalcogens

Tris(*trimethylsilyl*)*silylchalcogenols* $(Me_3Si)_3Si-EH$ (E = S, Se, Te) *and their metal derivatives*. Chalcogens are easily inserted into the Si–Li bond of lithium hypersilanide to give the lithium derivatives **44a–c**.[140]

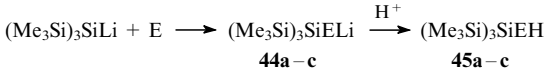

E = S (**a**), Se (**b**), Te (**c**).

Subsitution of lighter chalcogens for tellurium is a convenient approach to the synthesis of sulfur and selenium derivatives.[140]

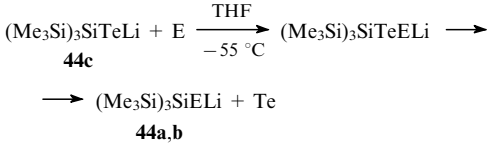

E = S, Se.

Acid hydrolysis of the lithium salts **44a–c** gives the corresponding chalcogenols **45a–c** in quantitative yields.[140,141] The acidic properties of hypersilylchalcogenols are increased, as expected, on going from sulfur to tellurium. The experimental values of pK_a for $(Me_3Si)_3SiEH$ are equal to 10.7 (**45a**, E = S), 8.3 (**45b**, E = Se) and 7.3 (**45c**, E = Te). The stretching vibration frequencies of the E–H bonds decrease significanly from sulfur to tellurium in the following order: 2557, 2294, 2017 cm^{-1}, respectively.[140]

Oxidation of the dimeric lithium hypersilyltellurolate–THF complex **44c**, like tellurol itself **45c**, gives hypersilyl ditelluride **46**.[142]

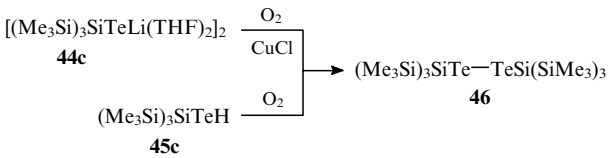

Tellurol **45c**, which possesses pronounced acidic properties, easily reacts with alkylmetal derivatives.[141]

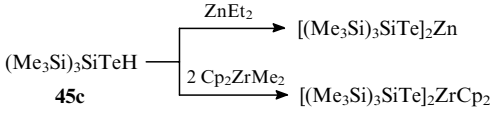

Hypersilylselenolates and -tellurolates of bivalent lanthanides (Yb, Eu, Sm) were prepared using reactions of the corresponding silylamides with hypersilylselenol or -tellurol and characterised as complexes with donor molecules.[143]

$$(THF)_2Ln[N(SiMe_3)_2]_2 + 2\,(Me_3Si)_3SiEH + n\,L \longrightarrow$$
$$\longrightarrow [(Me_3Si)_3SiE]_2Ln(L_n) + 2\,HN(SiMe_3)_2$$

E = Se, Te; Ln = Yb, Eu, Sm;
L = TMEDA, $n = 2$; L = $(Me_2PCH_2)_2$, $n = 1.5$;
TMEDA is *N*,*N*,*N*′,*N*′-tetramethylethylenediamine.

The thermally induced decomposition of ytterbium(II) hypersilylselenolate and -tellurolate results in their conversion into polycrystalline metal chalcogenides with elimination of bis(hypersilyl)chalcogen at 150–200 °C.

$$[(Me_3Si)_3SiE]_2Yb(TMEDA)_2 \longrightarrow [YbE] + E[Si(SiMe_3)_3]_2 + 2\,TMEDA$$

E = Se, Te.

Hypersilylselenolates $[(Me_3Si)_3SiSe]_3Ln(THF)_2$ (Ln = La, Sm, Yb) and -tellurolates $[(Me_3Si)_3SiTe]_3Ln(dmpe)_2$ [Ln = La, Ce, Y; dmpe is 1,2-bis(dimethylphosphino)ethane] of trivalent lanthanides with coordinating ligands were prepared in a similar way.[144] The homoleptic derivatives appeared to be significantly less stable. On storage, hypersilylselenides of Sm, Eu and Yb decompose, predominantly into the bivalent complexes $[(Me_3Si)_3SiSe]_2Ln$ and bis(hypersilyl)diselenide. An attempt to isolate homoleptic hypersilyltellurides of trivalent lanthanides yielded cluster compounds, $Ce_5Te_3[TeSi(SiMe_3)_3]_9$ in particular.[144]

First attempts at the synthesis of homoleptic tellurolate derivatives of transition metals of the first row were unsuccessful. Treatment of bivalent Cr, Mn, Fe, Co and Ni halides with 2 equiv. of $(Me_3Si)_3SiTeLi(THF)_2$ yielded ditelluride $[TeSi(SiMe_3)_3]_2$ and a pyrophoric residue of an unknown nature.[145] Reactions of metal silylamides $M[N(SiMe_3)_2]_2$ with $(Me_3Si)_3SiTeH$ gave oily products, no pure compounds could be isolated. It was the use of coordinating phosphine ligands that allowed the isolation and characterisation of individual complexes.[145]

$$M[N(SiMe_3)_2]_2 + 2\,(Me_3Si)_3SiTeH + n\,dmpe \longrightarrow$$
$$\longrightarrow [(Me_3Si)_3SiTe]_2M(dmpe)_n + 2\,HN(SiMe_3)_2$$

M = Mn, $n = 1$; M = Fe, $n = 2$.

Halides of Cr, Mn and Fe afford analogous compounds in reactions with lithium hypersilyltelluride in the presence of coordinating molecules. The redox reaction of the cobalt(II) bromide diphosphine complex with TTS-TeLi is an exception.

$$CoBr_2(PMe_3)_3 + 2\,(Me_3Si)_3SiTeLi(THF)_2 \longrightarrow$$
$$\longrightarrow \underset{\mathbf{47}}{Co[TeSi(SiMe_3)_3](PMe_3)_3} + 1/2\,[(Me_3Si)_3SiTe]_2$$

The Co(I) complex (**47**) actively absorbs 2 equiv. of CO at atmospheric pressure.[145]

$$\mathbf{47} + 2\,CO \longrightarrow (CO)_2Co[TeSi(SiMe_3)_3](PMe_3) + 2\,PMe_3$$

It should be noted that the electronegative silyltellurolate ligand in compound $[(Me_3Si)_3SiTe]_2Fe(dmpe)_2$ is highly labile and can be displaced into the outer coordination sphere with acetonitrile to give the salt $[Fe\{TeSi(SiMe_3)_3\}(dmpe)_2(MeCN)].[TeSi(SiMe_3)_3]$.

Vanadium hypersilylselenides[146] and -tellurides[147] were prepared starting from vanadium(III) amidobromide **48**.

$$[(Me_3Si)_2N]_2VBr + (Me_3Si)_3SiELi(THF)_2 \longrightarrow$$
$$\underset{\mathbf{48}}{\longrightarrow} [(Me_3Si)_2N]_2VESi(SiMe_3)_3$$

E = Se, Te.

Further substitution of the hypersilylselenol group for the silylamide groups gives the disproportionation products **49** and **50**.[148]

$$[(Me_3Si)_2N]_2VSeR + 2RSeH \longrightarrow \underset{\mathbf{51}}{[V(SeR)_3]} \longrightarrow \underset{\mathbf{49}}{\tfrac{1}{2}V(SeR)_2} + \underset{\mathbf{50}}{\tfrac{1}{2}V(SeR)_4}$$

R = $Si(SiMe_3)_3$.

The trivalent vanadium derivative **51,** which is formed first, can be isolated as adducts $[(Me_3Si)_3SiSe]_3V(L)$, where L is the donor molecule (pyridine, 2,6-dimethylisocyanobenzene, pyrazine).

An attempt to substitute the hypersilyltelluride groups for the silylamide groups in $[(Me_3Si)_2N]_2V-TeR$ by treatment with hypersilyltellurol gave only the tetrasubstituted product $V[TeSi.(SiMe_3)_3]_4$ (**52**) in 20% yield.[147] A similar derivative of tetravalent molybdenum $Mo[TeSi(SiMe_3)_3]_4$ (**53**) is formed upon treatment of tetrakis(*o*-tolyl)molybdenum with hypersilyltellurol.[147] Under the action of 1,2-bis(dimethylphosphino)ethane, compounds **52** and **53** easily undergo reductive elimination to give $[TeSi(SiMe_3)_3]_2$.

$$\underset{\mathbf{52,\ 53}}{M[TeSi(SiMe_3)_3]_4} \xrightarrow{dmpe} [TeSi(SiMe_3)_3]_2 + (dmpe)_2M[TeSi(SiMe_3)_3]_2$$

M = V (**52**), Mo (**53**).

In the presence of CO (1 atm), compound **53** readily eliminates two ditelluride molecules to give hexacarbonylmolybdenum.[147]

$$\underset{\mathbf{53}}{Mo[TeSi(SiMe_3)_3]_4} + 6\,CO \longrightarrow Mo(CO)_6 + 2\,[TeSi(SiMe_3)_3]_2$$

Homoleptic hypersilylchalcogenolates of Group IVB metals, *viz*., $M[ESi(SiMe_3)_3]_4$ (M = Ti, Zr, Hf), were prepared by treatment of the corresponding metal chlorides with TTS-ELi (E = S, Se, Te).[149] They represent thermally stable (m.p. > 220 °C) intensely coloured compounds. Treatment of zirconium and hafnium hypersilylselenides with the Lewis base bis(dimethylphosphino)methane (dmpm), yields binuclear complexes **54** the metal atoms in which are linked through selenide and phosphine bridges.[149]

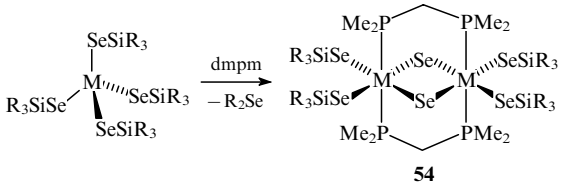

54

R = $SiMe_3$; M = Zr, Hf.

With dmpm, hypersilyltellorolates $[(Me_3Si)_3SiTe]_4M$ (M = Zr, Hf) form the mononuclear complexes $(dmpm)_2.[(Me_3Si)_3SiTe]_2M$ = Te, whereas ordinary octahedral complexes $[(Me_3Si)_3SiTe]_4M(2,6\text{-}Me_2C_6H_3NC)_2$ are formed under the action of 2,6-dimethylisocyanobenzene.

6. Group VIIA elements (TTS halides)

Chloro, bromo and iodo derivatives $(Me_3Si)_3SiX$ can be prepared by the reaction of tris(trimethylsilyl)silane with polyhalohydrocarbons (see Section IV.1).[49] They cannot be prepared by selective halogenation of $(Me_3Si)_4Si$ (**3**), since the reaction rates of intermediate compounds with halogens significantly exceed those of the starting silane. Tetrahalosilane and halotrimethylsilane are formed in these reactions. However, selective substitution of bromine for lithium atoms in lithium tris(trimethylsilyl)silanide can be effected at low temperatures.[150]

$$(Me_3Si)_3SiLi \xrightarrow[-78\ °C]{Br_2} (Me_3Si)_3SiBr + LiBr$$

Fluorotris(trimethylsilyl)silane was prepared by an exchange reaction of TTS bromide with antimony trifluoride.[151]

$$(Me_3Si)_3SiBr + 1/3\,SbF_3 \longrightarrow (Me_3Si)_3SiF + 1/3\,SbBr_3$$

Careful chlorination of chlorotris(trimethylsilyl)silane has led to dichlorobis(trimethylsilyl)silane in satisfactory yields.[151]

$$(Me_3Si)_3SiCl + Cl_2 \xrightarrow[-23\ ^\circ C]{C_5H_{12},\ N_2} (Me_3Si)_2SiCl_2 + Me_3SiCl \quad (94\%)$$

Tris(trimethylsilyl)silyl halides are highly thermally stable. The decomposition of $(Me_3Si)_3SiCl$ begins at 300 °C and formally yields insertion products of silylene $(Me_3Si)_2Si$ into the Si–Cl bond. $(Me_3Si)_3SiH$ behaves in a similar way.[138]

$$(Me_3Si)_3SiX \xrightarrow{\sim 300\ ^\circ C} (Me_3Si)_3Si-Si(SiMe_3)_2X$$

X = H (1 h, 67%), Cl (4 h, 30%).

The reactivities of halides $(Me_3Si)_3SiX$ with respect to nucleophilic reagents depend substantially on the halogen and decrease in the following order: X = I > Br > Cl > F. Hydrolysis of hypersilyl halides in the presence of bases gives stable silanol $(Me_3Si)_3SiOH$ (see Section V.5.a). Bromide $(Me_3Si)_3SiBr$ is the most convenient substrate for substitution reactions. Reactions involving this compound proceed at sufficiently high rates and in good yields.[150]

$$CpH \xrightarrow{Bu^nLi} CpLi \xrightarrow[-78\ ^\circ C]{TTS\text{-}Br} CpSi(SiMe_3)_3 \quad (98\%)$$

Hypersilyl chloride is highly inert and its reactions occur under more drastic conditions and require longer times. The reaction of $(Me_3Si)_3SiCl$ with the Grignard reagent gives a TTS derivative in low yield.[4]

$$p\text{-}BrC_6H_4Br \xrightarrow[2)\ TTS\text{-}Cl]{1)\ Mg,\ THF} p\text{-}(Me_3Si)_3SiC_6H_4Si(SiMe_3)_3 \quad (5\%)$$

Other reactions of TTS halides used as starting reagents in the synthesis of organometallic and organoelement compounds are considered in the sections that follow.

VI. Tris(trimethylsilyl)silanides of d- and f-elements

The $(Me_3Si)_3Si$ group is a convenient ligand and is used in the chemistry of transition metals. It provides sufficient steric protection of the metal centre, and the products formed possess good solubilities in organic solvents. Unique electron properties of the TTS group and its electronic 'amphoteric' character allow the preparation of various types of stable transition metal complexes. It should be remembered, however, that the TTS group itself (especially in the form of a TTS anion) is a very strong reducing agent. Therefore, its interactions with transition metal ions possessing a high redox potential are complicated by redox reactions. The use of metal complexes with stabilising ligands as the starting compounds and the correct choice of reaction conditions opens up the way to the synthesis of numerous TTS derivatives of d- and f-elements endowed with unique physical and chemical characteristics.

1. Group IB elements

a Copper

Upon reaction with copper(I) chloride, TTS-Li forms a complex $Li(THF)_4[Cu_5Cl_4(TTS)_2]$, which is stable at temperatures below −30 °C.[87] This compound may conventionally be regarded as an adduct of $[Li(THF)_4][Cu(TTS)_2]$ with four CuCl molecules. The central silicon atom in its TTS groups are coordinated simultaneously by two copper atoms. Other products of this redox reaction are Cu, $CuCl_2$ and LiCl.

Reactions of alkali metal tris(trimethylsilyl)silanides with copper *tert*-butoxide yield mixtures of complex silanides.[152]

$$MSi(SiMe_3)_3 \xrightarrow{Bu^tOCu} M[(Me_3Si)_3SiCuOBu^t] + (Me_3Si)_3SiCu + M[(Me_3Si)_3SiCuSi(SiMe_3)_3]$$

M = Li, Na, K, Cs.

The best results [the yield of $(Me_3Si)_3SiCu$ is > 60%] are obtained by metathesis of lead silanide with mesitylcopper (see Section V.3.c).[121] In the crystalline state, hypersilylcopper represents a planar cyclic trimer with a short Cu–Cu distance (2.384–2.415 Å).[121] The central silicon atoms in the hypersilyl groups act as bridging groups, each being linked with two copper atoms.

b. Silver

Tris(trimethylsilyl)silyl silver derivatives, $TTS\text{-}Ag(R_3P)_n$ (n = 1, R = Ph; n = 2: $R_3P = Ph_2PMe$, $Ph_2PTol\text{-}p$), were prepared by treatment of appropriate silver phosphine halides with TTS-Li.[153] The stabilities of these compounds increase with an increase in the number of phosphine substituents.

c. Gold

Of the TTS gold derivatives, the phosphine complexes $Ph_2MeP.AuTTS$ [154] and $TTSAuPh_2PCH_2CH_2PPh_2AuTTS$ (see Ref. 155) prepared by treatment of appropriate gold chlorides with TTS-Li in THF are especially well-characterised. The Au–Si bond is easily destroyed upon treatment with halogens, but withstands hydrolysis and methanolysis.[154] Presumably, the steric requirements for the two-coordinated gold atom are not very strict (in comparison with metals with greater coordination numbers); therefore, the length of the Au–Si bond in the TTS derivatives does not differ from that of other, less sterically hindered gold silanides.[154, 155]

2. Group IIB elements (Zn, Cd, Hg)

Compounds $(TTS)_2M$ (M = Zn, Cd, Hg) were prepared by treatment of bivalent metal halides with lithium tris(trimethylsilyl)silanide in ether.[156] In contrast to their trimethylsilyl analogues, TTS derivatives are thermally stable in the absence of air over a sufficiently long period of time. These compounds were found to be rather inert and did not react with metal halides such as $TaCl_5$, $TiCl_4$, $ZrCl_4$ and VCl_3. Hydrolysis of $(TTS)_2Zn$ is complete within several hours. Cadmium iodide forms an anionic complex $[Li(THF)_4][(Me_3Si)_3SiCd(I_3)CdSi(SiMe_3)_3]$ in a reaction with TTS-Li at 20 °C.[157]

$(TTS)_2Hg$ was synthesised using the Vyazankin method.[158]

$$2\,(Me_3Si)_3SiH + Bu^t_2Hg \longrightarrow [(Me_3Si)_3Si]_2Hg + 2\,Bu^tH$$

4

It is of note that a similar reaction of Bu^t_2Hg with tris(pentamethyldisilanyl)silane (**55**) yields a binuclear complex **56** where the organosilicon ligand has an umbrella shape 'covering' the mercury atoms.[159]

$$2\,(Me_5Si_2)_3SiH + Bu^t_2Hg \longrightarrow (Me_5Si_2)_3SiHg-HgSi(Si_2Me_5)_3 + 2\,Bu^tH$$

55 **56**

Upon heating to 180 °C, compound **56** eliminates one mercury atom to give $[(Me_5Si_2)_3Si]_2Hg$, whereas upon irradiation (λ > 330 nm) it generates a silyl radical $(Me_5Si_2)_3Si^\bullet$ stable at 20 °C.

3. Group IIIB elements, lanthanides, actinides

Tris(trimethylsilyl)silyl derivatives of Group IIIB elements, lanthanides and actinides are not numerous, only cyclopentadienyl complexes are known.[160] For example, the complex **57** containing a Sc–Si bond is extremely sensitive to oxygen and atmospheric moisture and easily absorbs two equivalents of CO to give the scandoxyketene derivatives **58** stabilised by donor molecules.[160]

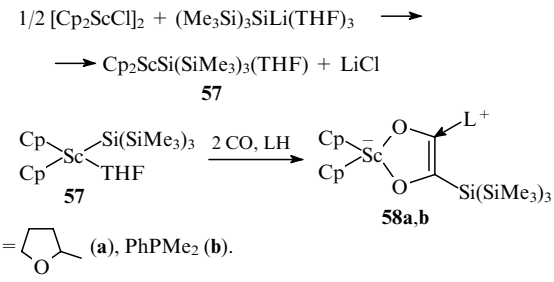

Heating of the complex **58a** *in vacuo* or carbonylation of compound **57** in a nonpolar medium gives the endione-diolate derivative **59**.

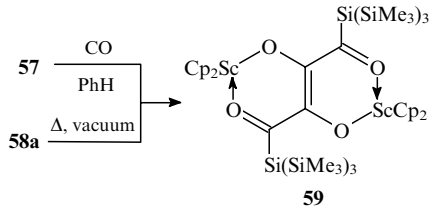

The addition of phenylacetylene to a solution of complex **57** in benzene results in the quantitative yield of $(Me_3Si)_3SiH$ and acetylenide **60**.[160]

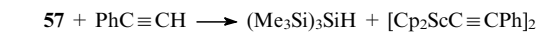

Isocyanides are inserted into the Sc–Si bond; the primary product **61** undergoes attack by a second isocyanide molecule resulting in migration of the Me_3Si group.[160, 161]

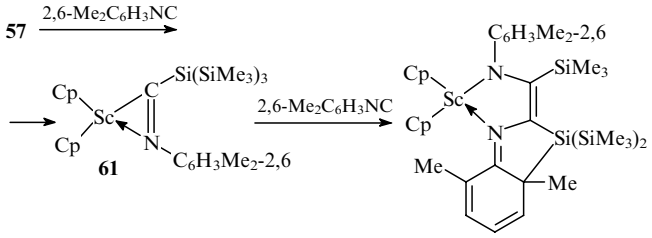

Carbon dioxide is easily incorporated into the Sc–Si bond of compound **57** to give the dimeric carboxylate **62**.[162]

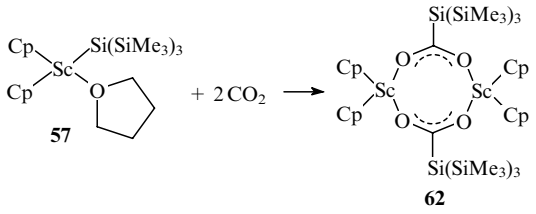

Compound **62** is unstable in solution and decomposes to the polymeric silanolate complex $[Cp_2ScOSi(SiMe_3)_3]_n$ with evolution of CO.[162]

The reaction of bis(pentamethylcyclopentadienyl)ytterbium with $(Me_3Si)_3SiLi$ in toluene results in substitution of the TTS group for one cyclopentadienyl ring.[163]

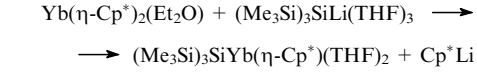

For as yet unknown reasons, silyl complexes of actinides are very difficult to isolate. The reaction of $Cp^*_2ThCl_2$ with TTS-Li yields the complex $Cp^*_2Th(TTS)Cl$ (**63**);[164] an attempt at its isolation results in its decomposition into $Cp^*_2ThCl_2$, $(Me_3Si)_3SiH$ and other products. Notwithstanding, carbonylation of compound **63** in solution with sequential insertion of two CO molecules and formation of the metalloxyketene derivative **64** takes place.[164]

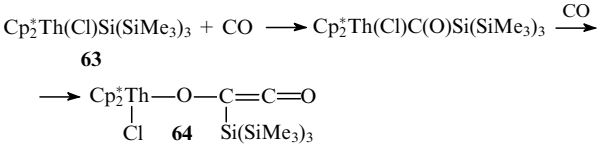

4. Group IVB elements (Ti, Zr, Hf)

Numerous TTS derivatives of Group IVB elements also containing cyclopentadienyl, alkyl, alkylamide or alkoxide substituents are known. The methods for the preparation of some of them are listed in Table 8.

Attempts to synthesise TTS titanium derivatives starting from $TiCl_4$ and TTS-Li gave predominantly a complex mixture of redox reaction products among which trimethylsilane and hexamethyldisilane were isolated.[165] Mixed titanium halogenoamides were used in the synthesis of the triamide complexes TTS-Ti$(NMe_2)_3$ and TTS-Ti$(NEt_2)_3$ (see Table 8). The resulting compounds are

Table 8. Conditions of the synthesis of TTS complexes of Group IVB transition metals.

Starting compound	Reaction product	Yield (%)	Reaction conditions	Ref.
$ClTi(NMe_2)_3$, TTS-Li	TTS-Ti$(NMe_2)_3$	40	C_6H_{14}, 20 °C, 0.5 h	165
$ClTi(NEt_2)_3$, TTS-Li	TTS-Ti$(NEt_2)_3$	–	C_6H_{14}, 20 °C, 0.5 h	166
$ClTi(CH_2SiMe_3)_3$, TTS-Li	TTS-Ti$(CH_2SiMe_3)_3$	–	C_6H_{14}	167
$ClZr(NMe_2)_3$, TTS-Li	TTS-Zr$(NMe_2)_3$	–	Et_2O	168
$(Bu^tO)_3ZrCl$, TTS-Li	TTS-Zr$(OBu^t)_3$	70	Et_2O, 0 °C, 12 h	169
$(Bu^tO)_3HfCl$, TTS-Li	TTS-Hf$(OBu^t)_3$	70	Et_2O, 0 °C, 12 h	169
Cp*$ZrCl_3$, TTS-Li	TTS-ZrCp*Cl_2	–	Et_2O, −78 °C	25
Cp*CpZrCl_2, TTS-Li	TTS-ZrCp*CpCl	62	PhH, 20 °C, 12 h	170
Cp*CpHfCl_2, TTS-Li	TTS-Hf(Cl)Cp*Cp	–	Et_2O, 20 °C	171
Cp_2ZrCl_2, TTS-Li	TTS-ZrCp_2Cl	70	Et_2O, 20 °C, 2 days	172
Cp*$ZrCl_3$, TTS-Li	TTS-ZrCpCl_2	–	Et_2O	25
(TTS)ZrCp_2Cl, MeMgBr	TTS-ZrCp_2Me	71	Et_2O, −78 to 20 °C	172
(TTS)ZrCp*CpCl, MeMgBr	TTS-ZrCp*CpMe	82	Et_2O, −78 to 20 °C	170
Cp_2ZrCl_2, TTS-K	$(TTS)_2ZrCp_2$	85	C_5H_{12}, 0–20 °C, 12 h	173
$(Bu^tCH_2)_3ZrCl$, TTS-Li	TTS-Zr$(CH_2Bu^t)_3$	–	C_6H_{14}	174, 175
Cp*$HfCl_3$, TTS-Li	TTS-HfCpCl_2	–	Et_2O	25
Cp_2HfCl_2, TTS-K	$(TTS)_2HfCp_2$	81	C_5H_{12}, 0–20 °C, 12 h	173

thermally stable and chemically inert.[166, 176] The triamide and trialkoxide complexes of zirconium and hafnium possess low reactivities and are inactive as catalysts of alkene polymerisation.[168, 169]

TTS zirconium and hafnium derivatives of the type TTS-MCp_nCl_{3-n} (n = 1, 2) present special interest by reason of their high reactivities and catalytic activities.

The complexes Cp*M(TTS)Cl_2 in which M = Zr (**65**) and Hf (**66**) are stable in argon, but are rapidly decomposed in humid air. Compounds **65** and **66** in C_6D_6 are thermally rather stable as follows from the NMR spectra recorded after storage at 95 °C for 1 day in tubes protected from light. However, these compounds rapidly decompose in light.

Tris(trimethylsilyl)silylzirconium and -hafnium derivatives **65** and **66** as well as CpCp*Zr(TTS)Cl (**67**) react with ethylene with insertion into the Si–M bond.[177]

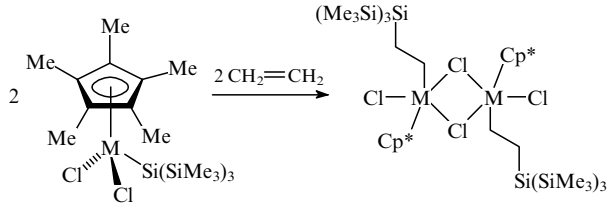

65, **66**

M = Zr, Hf.

At the same time, substituted alkenes (styrene, propene, trimethylsilylethylene) as well as diphenylacetylene do not react. The complex Cp_2Zr(TTS)Cl with non-substituted Cp ligands was found to be inert with respect to ethylene.

Compounds Cp*CpM(TTS)Cl **67** and **68** react with hydrogen and organosilanes with elimination of tris(trimethylsilyl)silane.[178]

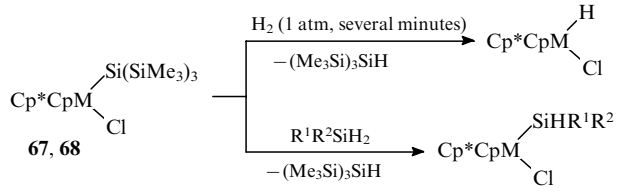

67, **68**

M = Zr (**67**), Hf (**68**); R^1 = H, Alk, Ar; R^2 = Alk, Ar.

The tris(trimethylsilyl)silyl group is the best leaving group for the metathesis in comparison with other R_3Si derivatives; therefore, compounds **67** and **68** are the most convenient reagents for the synthesis of novel d^0-hydridosilyl complexes in reactions with dihydrides.[171]

Dehydropolymerisation of primary silanes $RSiH_3$ in the presence of the TTS derivatives Cp*CpM(TTS)X (M = Zr, Hf; X = Me, Cl, $SiMe_3$) proceeds at a much faster rate than that with other analogous complexes.[178]

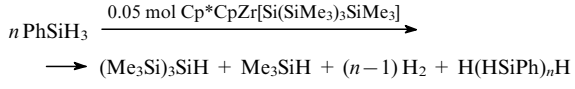

The hydride hafnocene complex **69** adds to molecules of unsaturated compounds with displacement of $(Me_3Si)_3SiH$.[179]

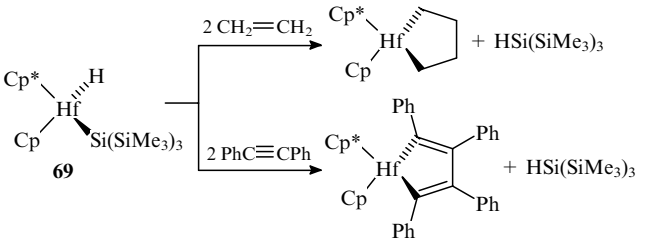

69

Compound **70** contains both trimethylsilyl and TTS groups, but one equivalent of CO is inserted exclusively into the Zr–$SiMe_3$ bond.[172]

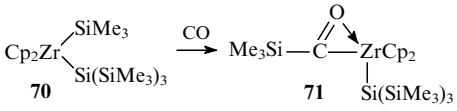

70 **71**

This fact is difficult to explain with account of the fact that, in the general case, CO is easily inserted into the $(Me_3Si)_3Si$–M bond, where M is a Group IVB metal. The reactivity of compound **71** is also unusual. Its treatment with HCl results in the quantitative evolution of $(Me_3Si)_3SiH$, but the use of benzoic acid causes elimination of the trimethylsilylcarbonyl group and formation of Cp_2Zr(TTS)(O_2CPh).[172] Carbon monoxide readily reacts across the Zr–Si bond of the spatially hindered CpCp*Zr(TTS)Cl molecule to give CpCp*Zr[C(O)TTS)]Cl,[170] but is not inserted into the Zr–Si bond within the Cp_2Zr(TTS)Cl complex.[172] This is attributed to the fact that the steric strains in the CpCp*Zr(TTS)Cl molecule exceed those in Cp_2Zr(TTS)Cl.[170]

The methyl derivative CpCp*Zr(TTS)Me (**72**) reacts with CO in a more complicated manner. The primary insertion product undergoes two sequential rearrangements eventually resulting in hydride-enolate **73**.[170]

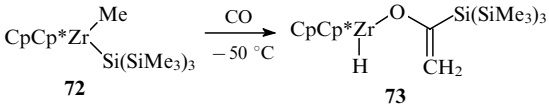

72 **73**

The complex **72** reacts with nitriles RCN to give the azomethine derivatives CpCp*ZrN = C(R)(TTS) (R = Me, CH = CH_2, Ph). Compound **72** reacts with pyridine to give the addition product **74**.[180]

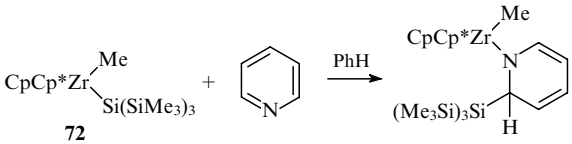

72 **74**

The analogous TTS zirconium complexes Cp_2Zr(TTS)Me and CpCp*Zr(TTS)Cl are significantly less reactive in reactions with nitriles and pyridine.

It was found that the insertion of CO into the Hf–Si bond of compound **75** results in an η^2-silylacyl derivative, which in turn gives rise to an insertion product **76** into the α-CH-bond of pyridine.[181]

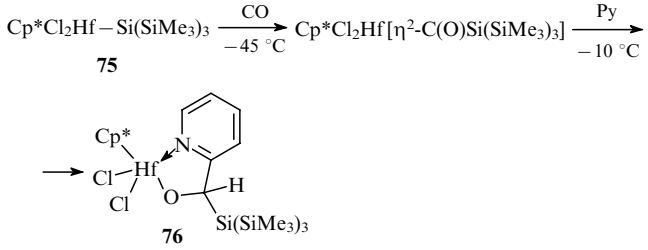

75 **76**

Protonation of the η^2-hypersilacyl zirconium complex **77** yields the organosilicon aldehyde **78**, which could not be prepared by any alternative methods.[182]

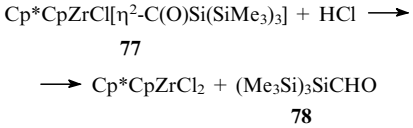

77 **78**

The insertion of isonitriles into the Zr–Si [182] bond is similar to that of carbon monoxide into the complex **70**.[175]

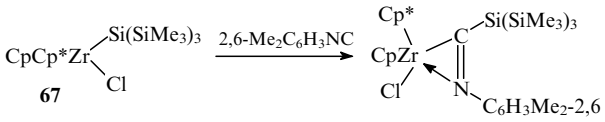

The tris(trimethylsilyl)silyl group was employed in the synthesis of 14-electron cationic complexes $[Zr(\eta\text{-}C_5H_4TTS)_2R]^+$ (R = Cl, Me), which proved to be efficient catalysts in ethylene polymerisation.[150] In the presence of a complex containing a tris(trimethylsilyl)silyl group in the cyclopentadienyl ring as a substituent, the polymerisation proceeds at a satisfactory rate. The molecular mass of the polymer (M_w = 126 000) was maximised in comparison with polymers prepared in the presence of catalysts of this series in which other substituents, *e.g.*, CH_2Ph and $CHPh_2$, were used instead of the TTS group.

Tris(trimethylsilyl)silylzirconium and -hafnium derivatives containing *tert*-butoxy groups instead of cyclopentadienyl ligands were found to be inactive with respect to CO, ethylene and $PhSiH_3$. However, both zirconium and hafnium complexes react with isocyanides to give the insertion products $[(Bu^tO)_3M(\eta^2\text{-}CNC_6H_3Me_2\text{-}2,6)(TTS)]$ (M = Zr, Hf).[169]

5. Elements of Groups VB – VIIIB

a. Tantalum

Group VB compounds are represented by tantalum complexes. The amidosilyl complexes **79** and **80** prepared from dichloride **81** are unstable and decompose even at 20 °C, which prevents their isolation.[183]

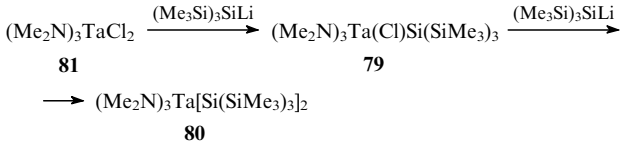

Stabilisation of neopentyl tantalum TTS complexes occurs owing to elimination of tris(trimethylsilyl)silane and formation of the alkylidene fragment (compound **82**).[175]

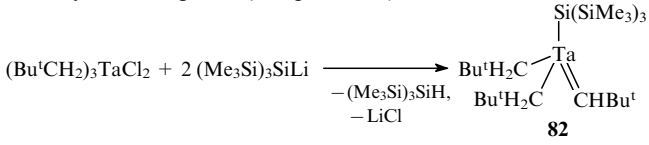

The reaction of the binuclear alkylidene – alkylidyne tantalum complex **83** with TTS-Li is also accompanied by elimination of tris(trimethylsilyl)silane. In this case, the bisalkylidyne complex **84** is formed.[184]

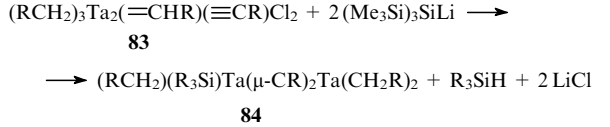

R = $SiMe_3$.

The reaction of 1 equiv. of CO with the tris(trimethylsilyl)silyl tantalum hydride complex **85** yields the addition product **86**, which isomerises within the next 24 h into the cyclic derivative **87**. This process involves the hydride, the carbonyl and the silyl groups.[185] The adduct **88** is formed in the presence of an excess of CO; its hydrolysis affords the organosilicon alcohol $(Me_3Si)_3SiCH_2OH$ in 90% yield.

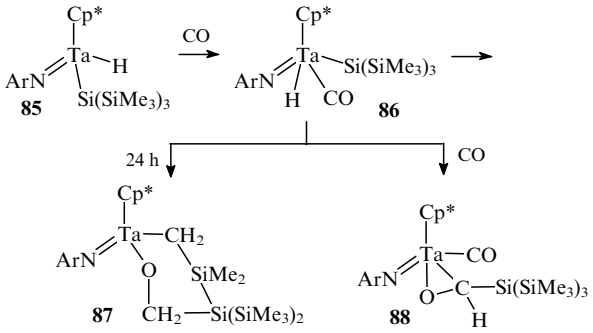

Ar = 2,6-$Pr^i_2C_6H_3$.

b. Chromium, manganese, iron

The reactions of lithium tris(trimethylsilyl)silanide with chromium(II), manganese(II) and iron(II) halides in a coordinating solvent yield the bishypersilyl complexes **89a – c** of the anionic type.[186]

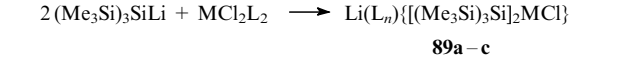

M = Cr (L = THF, *n* = 3) (**a**), Mn (L = DME, *n* = 2) (**b**), Fe (L = DME, *n* = 2) (**c**).

The iron and manganese complexes **89b,c** are rather thermally stable ($T_{decomp.}$ > 140 °C). The chromium complex **89a** was isolated and characterised only at temperatures below −20 °C.

All the low-coordination complexes obtained have high magnetic moments, which correspond to the high-spin configuration of metal atoms, but is uncommon to silyl transition-metal complexes.

c. Cobalt

Attempts to synthesise TTS cobalt derivatives by treatment of $CoCl_2$ with potassium tris(trimethylsilyl)silanide resulted in cobalt(II) cobalt(0) reduction products. However, $(Me_3Si)_3SiK$ reacts smoothly with cobalt silylamide to give the adduct **90**.[187]

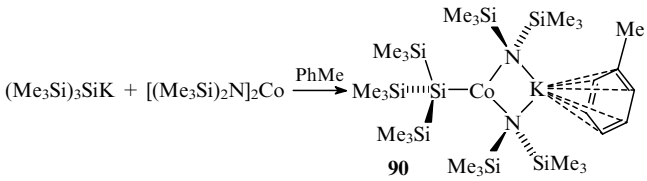

Compound **90** is stable in the crystalline state, but is rapidly decomposed in solution. The length of the Co–Si bond (2.513 Å) is the highest known value due to steric overcrowding of the complex **90**.

d. Carbonyl derivatives of Mn, Fe and Re

It is known that the reaction of metal carbonyls with silicon hydrides is one of the main approaches to the synthesis of compounds containing a silicon–metal bond [188] (see, *e.g.*, Refs 189 and 190).

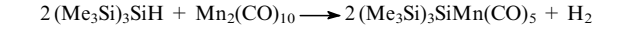

However, this method is not generally employed in the synthesis of polysilyl carbonyl derivatives because of the low yields of the target products, since the side reaction (*viz.*, the cleavage of the Si–Si bond) yields siloxanes and carbonylhydride metal clusters.[188, 191] An alternative approach consists of the reaction of anionic metal carbonyl complexes with TTS halides [191] or the reaction of carbonyl halides with tris(trimethylsilyl)silyllithium.[189, 191, 192]

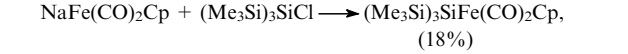

$$BrMn(CO)_4PPh_3 + (Me_3Si)_3SiLi \longrightarrow (Me_3Si)_3SiMn(CO)_4PPh_3, \quad (8\%)$$

$$BrM(CO)_nL + (Me_3Si)_3SiLi \longrightarrow (Me_3Si)_3SiM(CO)_nL$$

M = Mn, $(CO)_nL = (CO)_4PPh_3$; M = Re, $(CO)_nL = (CO)_5$.

d. Molybdenum, tungsten, rubidium

Treatment of molybdenum amidochloride, $(Me_2N)_4Mo_2Cl_2$, with TTS-Li yields the expected complex $(Me_2N)_4Mo_2(TTS)_2$, which contains a Mo≡Mo bond.[193]

Molybdenum bis(2,6-diisopropylphenylamido)dichloride (**91**) reacts with 1 equiv. of tris(trimethylsilyl)silyllithium to give the TTS derivative **92**.[194]

$$(2,6\text{-}Pr^iC_6H_3N{=})_2MoCl_2 + (Me_3Si)_3SiLi \longrightarrow$$
91

$$\longrightarrow (2,6\text{-}Pr^iC_6H_3N{=})_2Mo(Cl)Si(SiMe_3)_3 + LiCl$$
92

The complex **92** appeared to be non-reactive with respect to H_2, CO and C_2H_4, but reacted actively with 2,6-dimethylisocyanobenzene to give compound **93**, which is the isocyanide insertion product into the Mo–Si bond.[194]

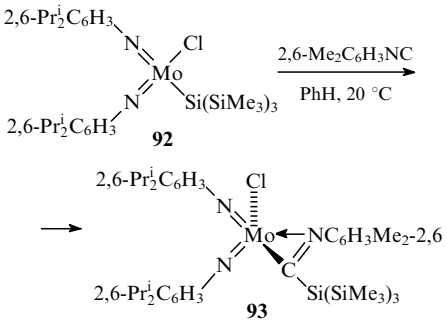

The alkylidyne tungsten complex $(Bu^tCH_2)_3W(\equiv CBu^t)(TTS)$ is prepared from the corresponding chloride, $(Bu^tCH_2)_3W(\equiv CBu^t)Cl$, by treating the latter with lithium tris(trimethylsilyl)silanides.[175]

In the reaction of TTS-Li with bis(cyclopentadienyl)tungsten dichloride (**94**), substitution of the TTS group for a hydrogen atom in the cyclopentadienyl ring occurs rather than formation of the expected complex containing a W–Si bond resulting in tungsten dihydride **95**.[195,196]

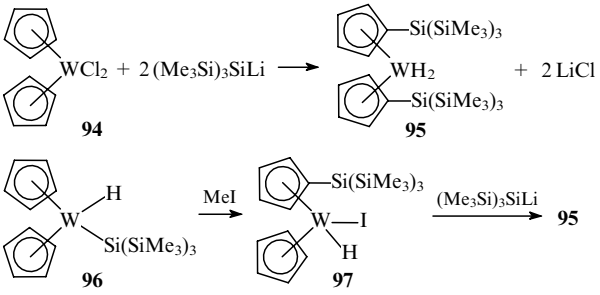

The silyl complex **96** prepared from $Cp_2W(H)Cl$ and $(Me_3Si)_3SiLi$ also reacts with methyl iodide to give the substitution product of the cyclopentadienyl ring **97**. Apparently, the molecular rearrangement of the tungsten complex does not require deprotonation of the Cp ring by a base; otherwise, $(Me_3Si)_3SiH$ would be formed as a side product.

It is of note that TTS-substituted cyclopentadiene, which can also be prepared by conventional methods from CpLi and $(Me_3Si)_3SiBr$, is used in the synthesis of metal complexes, *e.g.*, $[Cp\text{-}TTS)_2Zr]$.[150]

Stable η^5-sila- and η^5-germacyclopentadienylruthenium derivatives **98a,b** were synthesised using the TTS group in the ring as a stabilising substituent.[197,198]

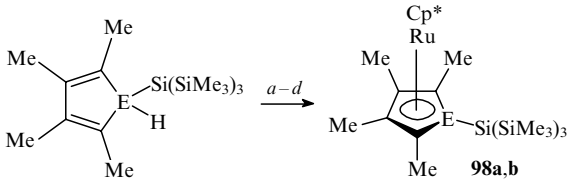

E = Si (**a**), Ge (**b**);
(*a*) $Cp^*Ru(OMe)_2$, (*b*) $Me_3SiOSO_2CF_3$ (2 equiv.), (*c*) 3 $NaBF_4$ (3 equiv.), (*d*) $LiSi(SiMe_3)_3$.

Synthesis of certain TTS derivatives of elements of Groups V–VIII is accompanied by rearrangements where the $(Me_3Si)_3Si$ fragment is destroyed, especially if the formation of metal silylene complexes is more preferable (see Section VIII).

VII. Photochemical reactions of hypersilyl derivatives

In comparison with linear derivatives, branched organooligosilanes, particularly $(Me_3Si)_4Si$, are little sensitive to UV light. However, if the TTS group is linked to a chromophore or an auxochromic group, the photoreactions involving the $(Me_3Si)_3Si$ fragment occur at noticeable rates.

Photolysis of aromatic TTS-containing compounds occurs through at least two pathways, *viz.*, with elimination of trimethylsilylphenylsilylene (route *a*) and with migration of the trimethylsilyl group into the aromatic ring (route *b*). The unstable intermediate **A** was identified following its reaction with 2,3-dimethylbuta-1,3-diene.[199,200]

Route *a*.

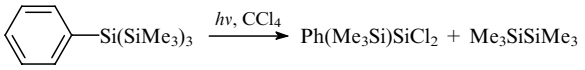

Route *b*.

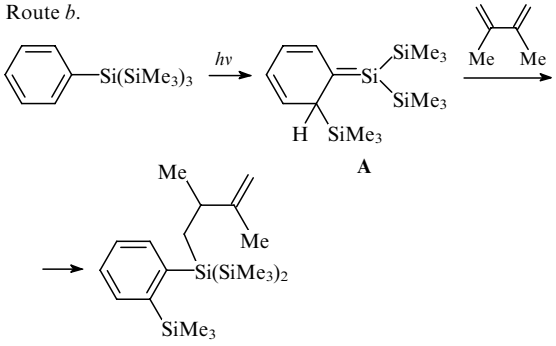

Photolysis (λ = 254 nm) of methoxytris(trimethylsilyl)silane **99** also proceeds non-selectively to yield methoxy(trimethylsilyl)silylene **100** and bis(trimethylsilyl)silylene **41** in a ~2 : 1 ratio.[201]

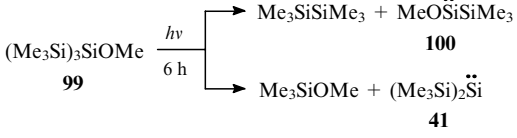

The silylenes formed were scavenged with traps, *e.g.*, buta-1,3-diene.

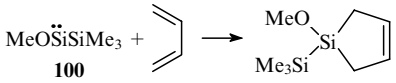

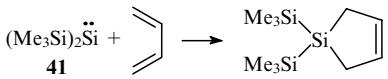

41

Photolysis of acyltris(trimethylsilyl)silanes is accompanied by migration of the trimethylsilyl group to the oxygen atom and the formation of silenes **101**, which undergo further conversions depending on the nature of the substituent in the acyl group and the reaction conditions.[202]

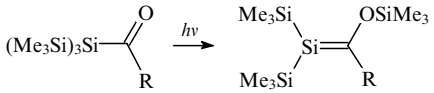

101

R = Me, Bu^t, 1-Ad (1-adamantyl), Ph, 2,4,6-$Me_3C_6H_2$.

The dimer **102a** of the 'head-to-head' type is formed in inert solvents for R = Ph.[203]

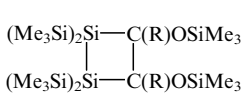

102a,**b**

R = Ph (**a**), Bu^t (**b**)

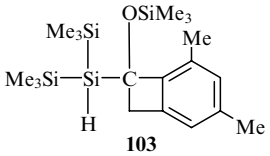

103

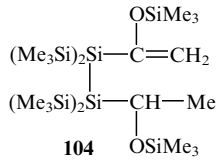

104

The bulkier *tert*-butyl group favours the formation of an equilibrium mixture of the dimer **102b** and the monomer **101** (R = Bu^t) in a 4 : 1 ratio.[203] The adamantyl substituent (R = 1-Ad) prevents dimerisation and a stable silene **101** is formed (R = 1-Ad).[103] However, in the case of yet another bulky substituent, *viz*., mesitylene, the sylene photochemical insertion product into the C–H-bond of one of the methyl groups (compound **103**) is formed.[202] If compound **101** contains α-protons in the substituent R (*e.g*., R = Me), the dimer undergoes disproportionation to give compound **104**.[203]

Photolysis of acylpolysilanes in the presence of methanol gives compounds **105** as the addition products to the double bond Si=C.[203]

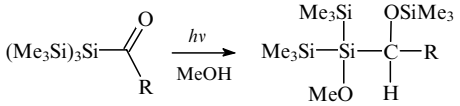

105

R = Me, Bu^t, Ph.

Unsaturated compounds (2,3-dimethylbutadiene, methylphenylacetylene) yield cyclic derivatives (*e.g*., compound **106**) as the addition products to the double bond Si=C of the photochemically generated silene **101**.[203]

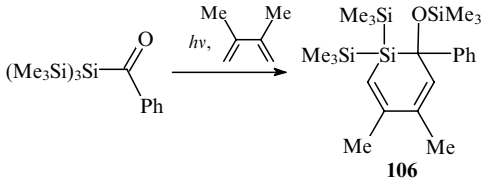

106

The photochemical reaction of benzophenone in a triplet state with tetrakis(trimethylsilyl)silane (**3**) affords two radical products, **107** and **108** (data from ESR spectroscopy).[203]

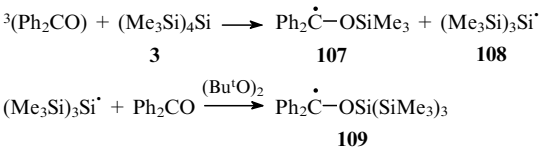

109

Photolysis of a benzophenone – tris(trimethylsilyl)silane mixture in the presence of di-*tert*-butyl peroxide yields exclusively the radical **109**. It should be noted that in contrast to $(Me_3Si)_3SiH$, $(Me_3Si)_4Si$ reacts with Bu^{t}O$^\cdot$ radicals generated upon photolysis of di-*tert*-butyl peroxide exclusively with abstraction of the hydrogen atom from the methyl groups to give the silylmethyl radicals $(Me_3Si)_3SiSiMe_2CH_2^\cdot$.

The photochemical reaction of 2,6-di-*tert*-butyl-1,4-benzoquinone **110** with tetrakis(trimethylsilyl)silane generates the radicals $(Me_3Si)_3Si^\cdot$ and $Me_3Si^\cdot$. The former adds exclusively to the oxygen atom of the quinone to give compound **111**, whereas the latter yields predominantly addition products at the carbon atom **112**. The addition product $Me_3Si^\cdot$ at the oxygen atom **113** is a minor component.[204]

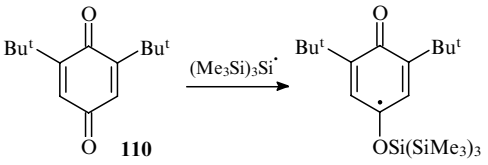

110 **111**

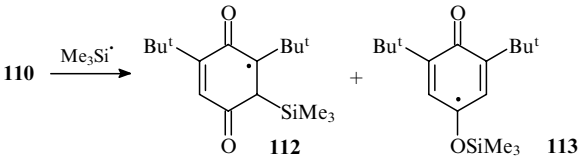

112 **113**

The tris(trimethylsilyl)silyl group can be used as a photolabile protecting group for the alcoholic function. The possibility of the use of the TTS group for this purpose was studied by Brook *et al*.[205, 206] Tris(trimethylsilyl)silyl ethers of primary and secondary alcohols were prepared in 70% to 97% yields by the reaction of tris(trimethylsilyl)silyl chloride with the corresponding alcohols in the presence of 4-dimethylaminopyridine (DMAP). The best yields are achieved in the case of more acidic alcohols. Tertiary alcohols do not react due to steric hindrance. Extremely high stability of the ethers formed with respect to aqueous bases, Grignard and Wittig reagents, butyllithium and caesium fluoride is their salient feature. Removal of the silyl protection was achieved by irradiation with UV light (254 nm; 30 min) in the presence of methanol or tetrabutylammonium fluoride

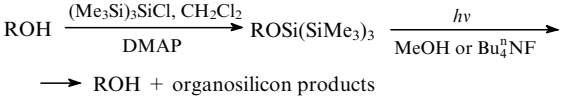

An obvious disadvantage of this silyl protection is the formation of heavy organosilicon products upon photolysis.

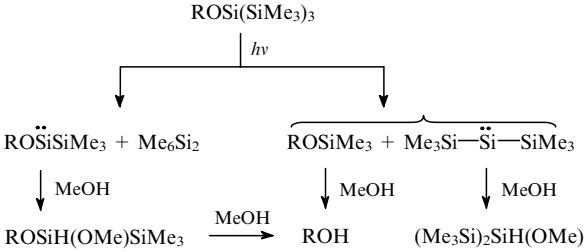

The use of chromatographic methods has made it possible to obtain desilylated alcohols in 80% – 90% yields.[205, 206]

VIII. Rearrangements involving the tris(trimethylsilyl)silyl fragment

The tris(trimethylsilyl)silyl group is 'milder', more mobile and more reactive in various rearrangements induced by acids, bases, light, heat and treatment with transition metals than other commonly used bulky groups (Bu^t_3C, Bu^t_3Si, Pr^i_3Si). It is of note that depending on the active site (charge) and modes of its stabilisation this group (or, to be more precise, its Si_3Si fragment) can be either destroyed or formed in different rearrrangements.

1. Migrations of silyl groups

In the presence of $AlCl_3$, permethylated polysilanes, $Me(Me_2Si)_nMe$ ($n = 4-10$) undergo skeletal rearrangements to give thermodynamically more stable branched isomers in nearly quantitative yields.[36]

$$Me(Me_2Si)_4Me \xrightarrow{AlCl_3} (Me_3Si)_3SiMe$$

$$Me(Me_2Si)_5Me \xrightarrow{AlCl_3} (Me_3Si)_4Si$$

Permethylated cyclopolysilanes also yield isomeric branched cyclosilanes under the action of $AlCl_3$ containing 1% $FeCl_3$.[207]

$$(Me_2Si)_5 \xrightarrow{AlCl_3} \not\rightarrow$$

$$(Me_2Si)_6 \xrightarrow{AlCl_3}$$

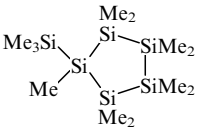

$$(Me_2Si)_7 \xrightarrow{AlCl_3}$$

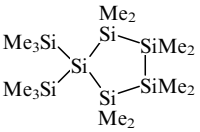

The photolytic rearrangement of the oligosilyl iron complex **114** produces the TTS fragment.[208]

$$(\eta^5\text{-Cp})Fe(CO)_2(SiMe_2)_4Me \xrightarrow{h\nu} (\eta^5\text{-Cp})Fe(CO)_2Si(SiMe_3)_3$$

114

This reaction occurs *via* the formation of silyl-silylene complexes $(\eta^5\text{-Cp})Fe(CO)(=SiMe_2)(Si_nMe_{2n+1})$ with subsequent migration of the silyl and methyl groups. The photochemical isomerisation of nonamethyltetrasilane, $H(SiMe_2)_4Me$, in the presence of catalytic amounts of $(\eta^5\text{-Cp})Fe(CO)_2SiMe_3$ or carbonyls $Fe(CO)_5$, $W(CO)_6$ initially results in $(Me_3Si)_3SiH$, which is further converted into the dimethylsilylene insertion product with insertion into the Si–H bond, $(Me_3Si)_3SiSiMe_2H$.[209] Thermal isomerisation in the presence of catalytic amounts of $(\eta^5\text{-Cp})Fe.(CO)(Ph_3P)SiMe_3$ gives exclusively tris(trimethylsilyl)silane.

Under the action of strong acids, such as HCl or H_2SO_4, 1-hydroxyalkyltris(trimethylsilyl)silanes **115** undergo isomerisation through a 1,2-Me_3Si–OH exchange to give trimethylsilylmethylsilanols **116**.[210,211]

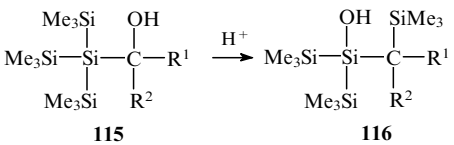

115 **116**

R^1 = H: R^2 = 4-MeC_6H_4, 4-$Pr^iC_6H_4$, Mes, 2-$Me_2NC_6H_4$, 2,4,6-$(MeO)_3C_6H_2$; $R^1 = R^2$ = Me.

Deprotonation of compounds **116** with sodium hydride results in migration of the trimethylsilyl group from the carbon atom to the oxygen atom.

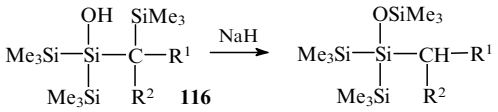

116

Silene **117** formed as a result of thermolysis of bis[tris(trimethylsilyl)silylcarbonyl]ethane **118** undergoes skeletal rearrangements to give the isomeric unsaturated compound **119**.[212]

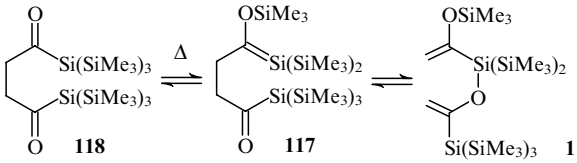

118 **117** **119**

2. Rearrangements of organoelement derivatives

Tris(trimethylsilyl)silanethiol **45a** undergoes smooth radical-induced skeletal rearrangement through a 1,2-shift of the Me_3Si group from the silicon atom to the sulfur atom eventually resulting in thiohydride **120**.[213]

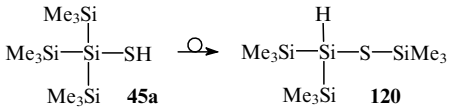

45a **120**

The migration of the Me_3Si group to the oxygen atom is energetically a very favourable process, this takes place in the autooxidation of tris(trimethylsilyl)silane (see Section IV.1)[50] as well as in its oxidation by alkyl nitrates.[214] The rearrangement of TTS-silanolate complexes into siloxysilyl complexes takes place in the thermolysis of transition metal hypersilylsilanolates.[136,137]

The reaction of $(Me_3Si)_3SiLi$ with *tert*-butyldichlorophosphine yields the expected product, *viz*., hypersilylphosphine **121**; however, its distillation (110–115 °C at 0.01 Torr) gives the rearrangement product **122**.[123]

$$(Me_3Si)_3SiLi + Bu^tPCl_2 \xrightarrow[-20\ ^\circ C]{THF} (Me_3Si)_3SiP(Cl)Bu^t \longrightarrow$$

121

$$\longrightarrow (Me_3Si)_2Si(Cl)P(SiMe_3)Bu^t$$

122

Alkyldichlorophosphines containing less bulky substituents, *e.g*., dichloromethylphosphine **123**, react with TTS-Li with elimination of tris(trimethylsilyl)chlorosilane.

$$(Me_3Si)_3SiLi + MePCl_2 \longrightarrow [(Me_3Si)_3SiP(Cl)Me] \longrightarrow$$

123

$$\longrightarrow (Me_3Si)_3SiCl + 1/5\,(MeP)_5$$

No formation of free phosphinydene took place in the presence of buta-1,3-diene in control experiments,[123] which is in favour of a bimolecular mechanism of splitting of tris(trimethylsilyl)chlorosilane.

Photochemical (λ = 280 nm) expansion of the three-membered phosphorus-containing ring **34** involving the tris(trimethylsilyl)silyl group is known.[128]

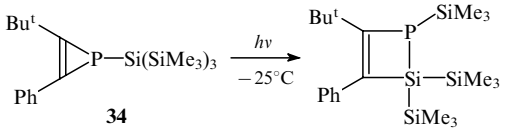

34

Low-valent transition metal complexes containing a TTS group are usually unstable; their stabilisation occurs at the expense of the migration of the silyl group.[215]

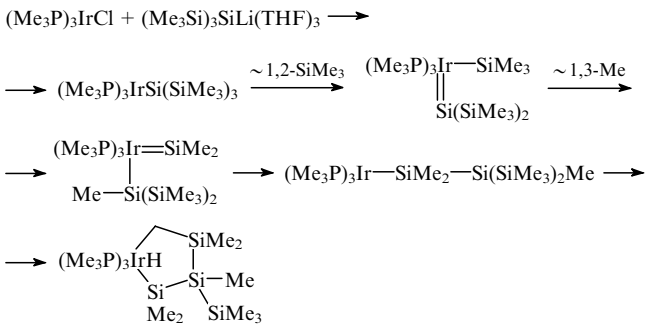

Similar migration is observed in the case of the TTS platinum complex **124**.[216, 217]

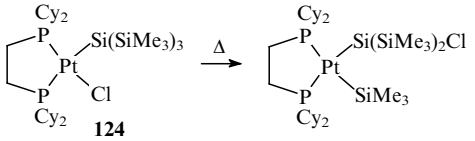

Cy is cyclohexyl.

Complex rearrangements of the TTS fragment, which first include migration of the trimethylsilyl and then of the methyl group, take place in the coordination sphere of the cyclopentadienylnickel derivative **125**.[218]

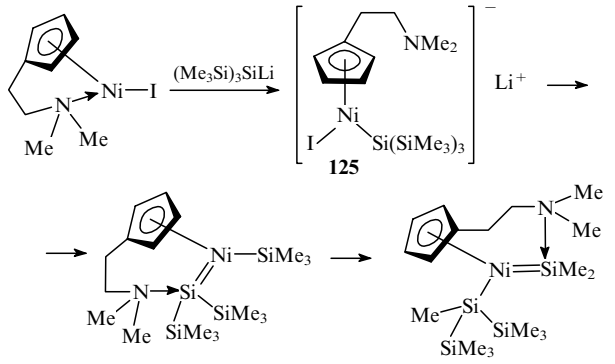

3. Migration of the trimethylsilyl group (the Peterson migration) and related processes in the series of hypersilyl derivatives

The formation of the O-nucleophilic centre in the β-position relative to the TTS group usually results in elimination of the trimethylsilanolate anion and formation of silaethenes **126**, which are further condensed to form disilacyclobutanes **127**.[219]

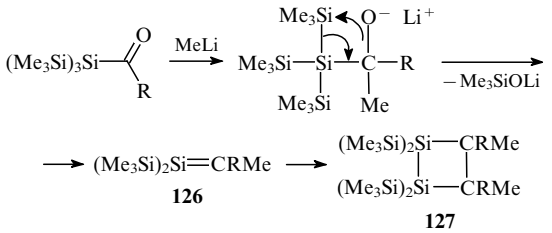

R = Me, Ph.

However, this reaction is extremely sensitive to steric factors. Under the action of methyllithium, compound **128** easily decomposes into *tert*-butyl methyl ketone and tris(trimethylsilyl)silyllithium.[219]

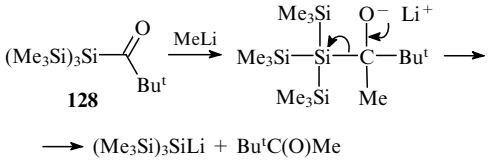

The introduction of a donor amino group that stabilises the intermediate silaethene **129** changes the direction of the dimerisation. In this case, the 'head-to-tail' dimer **130** is formed (Scheme 1).[220]

Apparently, triethylgermyllithium cannot add to the carbonyl group of 2-adamantyl tris(trimethylsilyl)silyl ketone **131** due to considerable steric hindrance. With the stoichiometric ratio of the reagents, the reaction product is silaenolate **132**; the half-conversion time is 12 h.[221, 222] In the presence of a twofold excess of triethylgermyllithium, silaenolate **132** is converted into trisilacyclobutane **133**.[222]

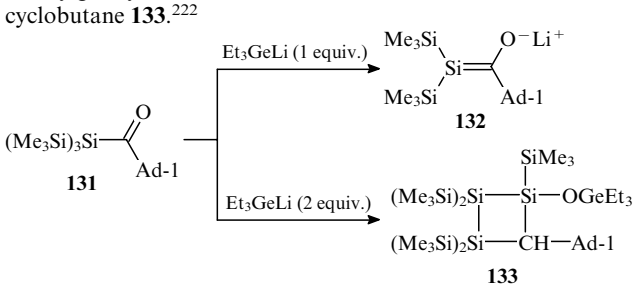

The Peterson elimination also occurs in the reaction of $(Me_3Si)_3SiLi(THF)_3$ with adamantanone in hexane and gives an unstable silene, which undergoes spontaneous dimerisation of the 'head-to-head' type to give disilacyclobutane **134**.[223]

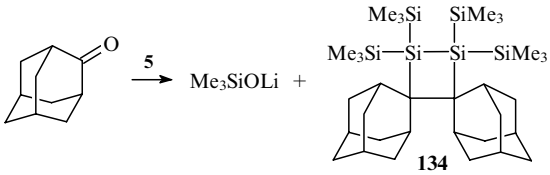

The reactions of tris(trimethylsilyl)silylcarboxylates $(Me_3Si)_3SiC(O)OR$ with lithium reagents have been studied in great detail.[224, 225] Depending on the nature of R and the reagent used, this reaction occurs through several main pathways, *viz.*: (1) formation of lithium tris(trimethylsilyl)silylcarboxylate; (2) elimination of the TTS group by a lithium reagent; (3) addition of a lithium reagent to the carbonyl group of carboxylates. In particular, the reaction of alkyl tris(trimethylsilyl)silacarboxylates **135** with $(Me_3Si)_3SiLi$ is accompanied by elimination of the Me_3Si group and formation of new silyllithium derivatives **136**.[225]

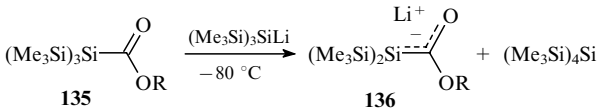

R = Cy, 1-Ad, Bn, *o*-Tol, Mes.

Scheme 1

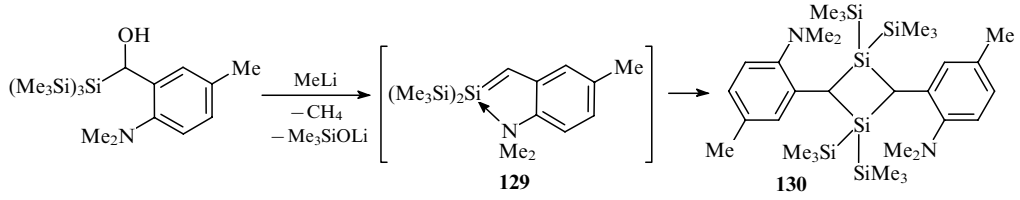

Hydrolysis, silylation and oxidation of silanoenolate **136** afford compounds **137**–**139**.

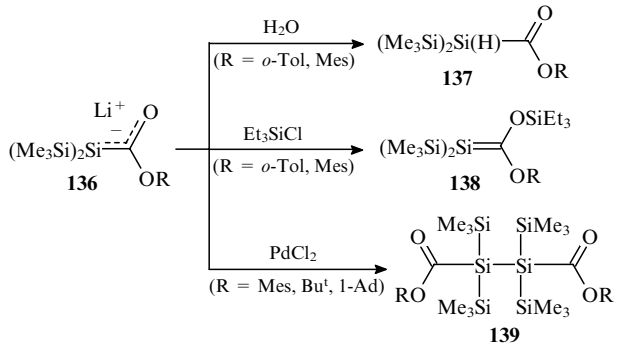

The reaction of tris(trimethylsilyl)silyllithium (**5**) with methyl formate[226] occurs *via* formylsilane **78** which adds the second molecule of $(Me_3Si)_3SiLi$. The intermediate lithium bis(trimethylsilyl)silylmethoxide **140** can be detected after hydrolysis as the corresponding bis(TTS)methanol **141**. Under the reaction conditions, compound **140** is further converted into the final product, *viz*., 1,2-bis[tris(trimethylsilyl)silyl]ethylene **142** in 60% yield.

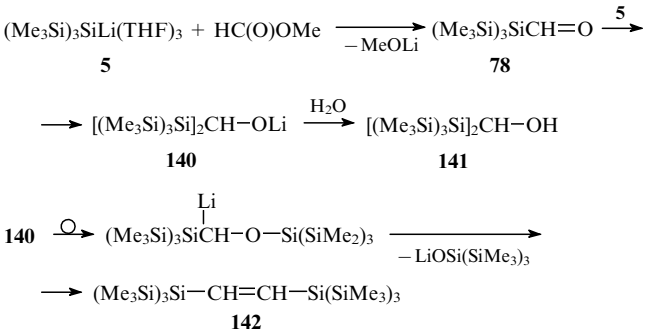

The reaction of ketenes **143** with tris(trimethylsilyl)silyllithium occurs with the migration of the anionic centre from the oxygen atom to the silicon atom, which eventually results in unexpected products **144** and **145**.[227]

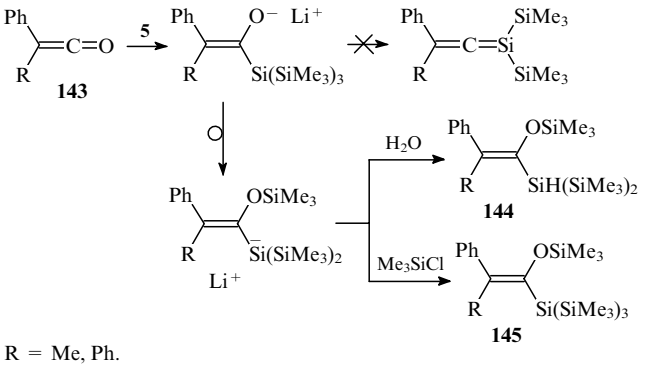

R = Me, Ph.

The synthesis of silanol **146** proceeds formally through elimination of (dimethylamino)trimethylsilane in accordance with the acid-induced Peterson reaction to give the intermediate silene $(Me_3Si)_2Si{=}CHSi(SiMe_3)_3$.[228]

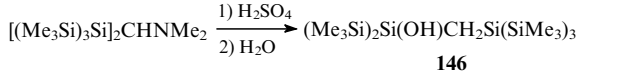

4. Thermal reactions of acylpolysilanes

Similar to photolysis, the thermolysis of acyltris(trimethylsilyl)silanes yields silaethenes.[229]

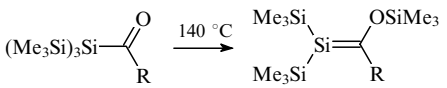

R = Me, But, 1-Ad, Ph, Mes.

Heating of acylsilanes in the presence of ketones affords products the composition of which is determined by the nature of the acyl substituent. This reaction consists of several consecutive insertion and rearrangement steps, which hinder significantly the prediction of the final products.[229]

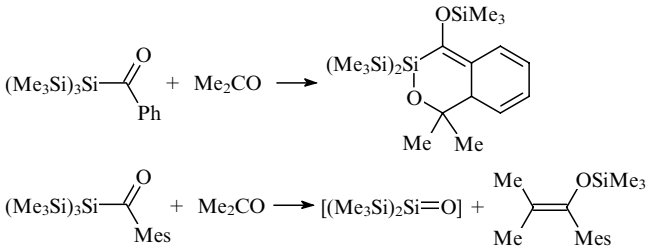

Acetyltris(trimethylsilyl)silane, $MeC(O)Si(SiMe_3)_3$, gives no adducts when heated with ketones, presumably due to rapid dimerisation of the silaethene formed.

An unusual system $(Me_3Si)_3SiC(O)(1\text{-Ad})-Ni(PEt_3)_4$ is reported,[230] which allows activation of the C−H bonds of aromatic compounds and of the Si−H bonds of silanes. Catalytic amounts of tetrakis(triethylphosphine)nickel catalyse the addition of RH (R = Ph, $PhMe_2Si$) to the silaethenes formed upon heating 1-adamantoyltris(trimethylsilyl)silane.

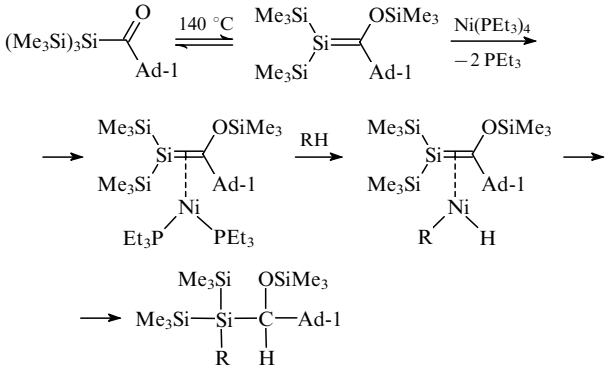

R = Ph, $PhMe_2Si$.

* * *

The data on the synthesis, reactivities and applications of tris(trimethylsilyl)silyl derivatives demonstrate the high potential of the $(Me_3Si)_3Si$ ligand in organic and organometallic chemistry and testify to the uniqueness of the TTS group. The present review is an attempt to draw a 'portrait' of the TTS group from different standpoints, which may facilitate the correct choice of this ligand for concrete experimental tasks. Currently, wide application of the TTS ligand is limited due to the high cost of the starting reagents, *viz*., $(Me_3Si)_3SiH$ and $(Me_3Si)_4Si$. It remains to be hoped that the rapid development of the chemistry of TTS derivatives in the next few years will make it possible to reduce the cost and to expand the range of the reagents based on them.

This review has been written with the financial support of the Russian Foundation for Basic Research (Project No. 02-03-07041-ano).

References

1. N Wiberg *Coord. Chem. Rev.* **163** 217 (1997)
2. C Rucker *Chem. Rev.* **95** 1009 (1995)
3. H Bock, K Ruppert, C Nither, Z Havlas, H-F Herrmann, C Arad, I Göbel, A John, J Meuret, S Nick, A Rauschenbach, W Seitz, T Vaupel, B Solouki *Angew. Chem., Int. Ed. Engl.* **31** 550 (1992)
4. H Bock, J Meuret, K Ruppert *Angew. Chem., Int. Ed. Engl.* **32** 414 (1993)
5. J Frey, E Schottland, Z Rappoport, D Bravo-Zhivotovskii, M Nakash, M Botoshansky, M Kaftory, Y Apeloig *J. Chem. Soc., Perkin Trans. 2* 2555 (1994)
6. H Bock, B Solouki, in *The Chemistry of Silicon Compounds* Pt. 1 (Eds S Patai, Z Rappoport) (Chichester: Wiley, 1989) p. 555
7. R Romeo, L A Wozniak, C Chatgilialoglu *Tetrahedron Lett.* **41** 9899 (2000)
8. O W Steward, G L Heider, J S Johnson *J. Organomet. Chem.* **168** 33 (1979)
9. H J Sipe Jr, R West *J. Organomet. Chem.* **70** 353 (1974)
10. E A Brinkman, S Berger, J I Brauman *J. Am. Chem. Soc.* **116** 8304 (1994)
11. R Damrauer, J A Hankin *Chem. Rev.* **95** 1137 (1995)
12. H Sakurai, M Murakami, M Kumada *J. Am. Chem. Soc.* **91** 519 (1969)
13. L H Sommer, L A Ulland *J. Org. Chem.* **37** 3878 (1972)
14. C Chatgilialoglu *Chem. Rev.* **95** 1229 (1995)
15. S W Bennet, C Eaborn, A Hudson, R A Jackson, K D J Root *J. Chem. Soc., A* 348 (1970)
16. J Cooper, A Hudson, R A Jackson *Mol. Phys.* **23** 209 (1972)
17. C Chatgilialoglu, S Rossini *Bull. Soc. Chim. Fr.* 298 (1988)
18. C Chatgilialoglu, A Guerrini, M Lucarini *J. Org. Chem.* **57** 3405 (1992)
19. P J Krusic, J K Kochi *J. Am. Chem. Soc.* **91** 3938 (1969)
20. J H Sharp, M C R Symons *J. Chem. Soc., A* 3084 (1970)
21. M Ballestri, C Chatgilialoglu, M Guerra, A Guerrini, M Lucarini, G Seconi *J. Chem. Soc., Perkin Trans. 2* 421 (1993)
22. C Marschner *Eur. J. Inorg. Chem.* 221 (1998)
23. G Gutekunst, A G Brook *J. Organomet. Chem.* **225** 1 (1982)
24. S P Mallela, R A Geanangel *Inorg. Chem.* **29** 3525 (1990)
25. J Arnold, D M Roddick, T D Tilley, A L Rheingold, S J Geib *Inorg. Chem.* **27** 3510 (1988)
26. G A Olah, R J Hunadi *J. Am. Chem. Soc.* **102** 6989 (1980)
27. J B Lambert, S Z Zhang, S M Ciro *Organometallics* **13** 2430 (1994)
28. C-H Ottosson, D Cremer *Organometallics* **15** 5495 (1996)
29. A E Pierce *Silylation of Organic Compounds* (Rockford: Pierce Chemical Co., 1968)
30. L H Sommer *Stereochemistry, Mechanism and Silicon* (New York: McGraw-Hill, 1965)
31. E J Corey, A Venkateswarlu *J. Am. Chem. Soc.* **94** 6190 (1972)
32. G Stork, P F Hudrik *J. Am. Chem. Soc.* **90** 4462 (1968)
33. H Gilman, C L Smith *J. Am. Chem. Soc.* **86** 1454 (1964)
34. H Bürger, W Kilian *J. Organomet. Chem.* **18** 299 (1969)
35. A Heine, R Herbst-Irmer, G M Sheldrick, D Stalke *Inorg. Chem.* **32** 2694 (1993)
36. M Ishikava, J Iyoda, H Ikeda, K Kotake, T Hashimoto, M Kumada *J. Am. Chem. Soc.* **103** 4845 (1981)
37. H Gilman, C L Smith *J. Organomet. Chem.* **14** 91 (1968)
38. H Sakurai, T Watanabe, M Kumada *J. Organomet. Chem.* **9** P11 (1967)
39. Y Derouiche, P D Lickiss *J. Organomet. Chem.* **407** 41 (1991)
40. H Gilman, J M Holmes, C L Smith *Chem. Ind.* **15** 848 (1965)
41. C Chatgilialoglu *Acc. Chem. Res.* **25** 188 (1992)
42. J M Kanabus-Kaminska, J A Hawari, D Griller, C Chatgilialoglu *J. Am. Chem. Soc.* **109** 5267 (1987)
43. D M Wetzel, K E Salomon, S Berger, J I Brauman *J. Am. Chem. Soc.* **111** 3835 (1989)
44. R Walsh *Acc. Chem. Res.* **14** 246 (1981)
45. C Chatgilialoglu, D Griller, M Lesage *J. Org. Chem.* **53** 3641 (1988)
46. M Ballestri, C Chatgilialoglu, K B Clark, D Griller, B Giese, B Kopping *J. Org. Chem.* **56** 678 (1991)
47. C Chatgilialoglu, D Griller, in *Organic Free Radicals* (Eds H Fisher, H Heimgartned) (Berlin: Springer, 1988) p. 25
48. Y Apeloig, M Nakash *J. Am. Chem. Soc.* **116** 10 781 (1994)
49. H Bürger, W Kilian, K Burczyk *J. Organomet. Chem.* **21** 291 (1970)
50. C Chatgilialoglu, A Guarini, A Guerrini, G Seconi *J. Org. Chem.* **57** 2207 (1992)
51. M Ishikawa, A Nakamura, M Kumada *J. Organomet. Chem.* **59** C11 (1973)
52. D P Curran, S Sun *Terahedron Lett.* **34** 6181 (1993)
53. A Krief, E Badaoui, W Dumont *Terahedron Lett.* **34** 8517 (1993)
54. P Arya, C Samson, M Lesage, D Griller *J. Org. Chem.* **55** 6248 (1990)
55. M Ballestri, C Chatgilialoglu, N Cardi, A Sommazzi *Terahedron Lett.* **33** 1787 (1992)
56. C Chatgilialoglu, M Lucarini *Terahedron Lett.* **36** 1299 (1995)
57. D Schummer, G Hofle *Synlett* 705 (1990)
58. L A Paquette, D Friedrich, E Pinard, J P Williams, D St Laurent, B A Roden *J. Am. Chem. Soc.* **115** 4377 (1993)
59. I Ryu, M Hasegawa, A Kurihara, A Ogava, S Tsunoi, N Sonoda *Synlett* 143 (1993)
60. I Ryu, K Nagahara, H Yamazaki, S Tsunoi, N Sonoda *Synlett* 643 (1994)
61. B Kopping, C Chatgilialoglu, M Zehnder, B Giese *J. Org. Chem.* **57** 3994 (1992)
62. K Miura, K Oshima, K Utimoto *Bull. Chem. Soc. Jpn.* **66** 2356 (1993)
63. W Smadja, M Zahouily, M Malacria *Terahedron Lett.* **33** 5511 (1992)
64. R A Jackson *J. Chem. Soc., Chem. Commun.* 573 (1974)
65. C Ferreri, M Ballestri, C Chatgilialoglu *Terahedron Lett.* **34** 5147 (1993)
66. C Chatgilialoglu, M Ballestri, C Ferreri, D Vecchi *J. Org. Chem.* **60** 3826 (1995)
67. A Alberti, C Chatgilialoglu *Tetrahedron* **46** 3963 (1990)
68. H Künzer, G Sauer, R Wiechert *Terahedron Lett.* **32** 7247 (1991)
69. C Chatgilialoglu, C Ferreri, M Ballestri, D P Curran *Terahedron Lett.* **37** 6387 (1996)
70. K J Kulicke, C Chatgilialoglu, B Kopping, B Giese *Helv. Chim. Acta* **75** 935 (1992)
71. K Miura, K Oshima, K Utimoto *Chem. Lett.* 2477 (1992)
72. K Miura, K Oshima, K Utimoto *Bull. Chem. Soc. Jpn.* **66** 2348 (1993)
73. S A Bulgakova, L M Mazanova, V V Semenov, Yu D Semchikov *Vysokomol. Soedin., Ser. A* **43** 1293 (2001) [a]
74. M A Hamid *Can. J. Chem.* **51** 2759 (1973)
75. M A Hamid *Can. J. Chem.* **50** 3761 (1972)
76. R Corriu, C Guerin *J. Chem. Soc., Chem. Commun.* 168 (1980)
77. R A Bartlett, H V R Dias, P P Power *J. Organomet. Chem.* **341** 1 (1988)
78. G Korogodsky, M Bendikov, D Bravo-Zhivotovskii, Y Apeloig *Organometallics* **21** 3157 (2002)
79. D M Jenkins, W J Teng, U Englich, D Stone, K Ruhlandt-Senge *Organometallics* **20** 4600 (2001)
80. M Nanjo, A Sekiguchi, H Sakurai *Bull. Chem. Soc. Jpn.* **71** 741 (1998)
81. K W Klinkhammer *Chem.-Eur. J.* **3** 1418 (1997)
82. E N Gladyshev, E A Fedorova, L O Yuntila, G A Razuvaev, N S Vyazankin *J. Organomet. Chem.* **96** 169 (1975)
83. J D Farwell, M F Lappert, C Marschner, C Strissel, T D Tilley *J. Organomet. Chem.* **603** 185 (2000)
84. W Biffar, H Noeth *Z. Naturforsch., B* **36** 1509 (1981)
85. M Haase, U Klingebiel, R Boese, M Polk *Chem. Ber.* **119** 1117 (1986)
86. M L Sierra, V S J de Mel, J P Oliver *Organometallics* **8** 2312 (1989)
87. A Heine, D Stalke *Angew. Chem., Int. Ed. Engl.* **32** 121 (1993)
88. A Purath, H Schnlckel *J. Organomet. Chem.* **579** 373 (1999)
89. N L Pickett, O Just, X Li, D G Vanderveer, W S Rees Jr *J. Organomet. Chem.* **582** 119 (1999)
90. G Linti, R Frey, W Kostler, H Urban *Chem Ber.* **129** 561 (1996)
91. F Schwan, S P Mallela, RA Geanangel *J. Chem. Soc., Dalton Trans.* 4183 (1996)

92. A M Arif, A H Cowley, T M Elkins, R A Jones *J. Chem. Soc., Chem. Commun.* 1776 (1986)
93. G Linti, W Köstler *Angew. Chem., Int. Ed. Engl.* **35** 550 (1996)
94. G Linti *J. Organomet. Chem.* **520** 107 (1996)
95. G Linti, W Köstler *Chem. Eur. J.* **4** 942 (1998)
96. M Kehrwald, W Kostler, G Linti, A Rodig, Th Blank, N Wiberg *Organometallics* **20** 860 (2001)
97. A Schnepf, E Weckert, G Linti, H Schnöckel *Angew. Chem., Int. Ed.* **38** 3381 (1999)
98. R Wochele, W Schwarz, K W Klinkhammer, K Locke, J Weidlein *Z. Anorg. Allg. Chem.* **626** 1963 (2000)
99. S Henkel, K W Klinkhammer, W Schwarz *Angew. Chem., Int. Ed. Engl.* **33** 681 (1994)
100. T Kusukawa, W Ando *Angew. Chem., Int. Ed. Engl.* **35** 1315 (1996)
101. E Jeschke, T Gross, H Reinke, H Oehme *Chem. Ber.* **129** 841 (1996)
102. T Gross, R Kempe, H Oehme *Chem. Ber.* **130** 1709 (1997)
103. A G Brook, S C Nyburg, F Abdesaken, B Gutekunst, G Gutekunst, R Krishna, M R Kallury, Y C Poon, Y M Chang, W N Winnie *J. Am. Chem. Soc.* **104** 5667 (1982)
104. M Haase, U Klingebiel *Z. Anorg. Allg. Chem.* **524** 106 (1985)
105. S S Al-Juaid, N H Buttrus, R I Damja, Y Derouiche, C Eaborn, P B Hitchcock, P D Lickiss *J. Organomet. Chem.* **371** 287 (1989)
106. X Cai, B Gehrhus, P B Hitchcock, M F Lappert, J C Slootweg *J. Organomet. Chem.* **651** 150 (2002)
107. A Sekiguchi, V Ya Lee, M Nanjo *Coord. Chem. Rev.* **210** 11 (2000)
108. J B Lambert, J L Pflug, C L Stern *Angew. Chem., Int. Ed. Engl.* **34** 98 (1995)
109. H Suzuki, Y Kimata, S Satoh, A Kuriyama *Chem. Lett.* 293 (1995)
110. H Sakurai, F Kondo *J. Organomet. Chem.* **92** C46 (1975)
111. H Sakurai, A Okada, M Kira, K Yonezawa *Terahedron Lett.* **12** 1511 (1971)
112. Y Apeloig, M Yuzefovich, M Bendikov, D K Bravo-Zhivotovskii *Organometallics* **16** 1265 (1997)
113. H Gilman, R L Harrell *J. Organomet. Chem.* **9** 67 (1967)
114. T Gross, H Reinke, H Oehme *Can. J. Chem.* **78** 1399 (2000)
115. S P Mallela, R A Geanangel *Inorg. Chem.* **30** 1480 (1991)
116. A M Arif, A H Cowley, T M Elkins *J. Organomet. Chem.* **325** C11 (1987)
117. S P Mallela, I Bernal, R A Geanangel *Inorg. Chem.* **31** 1626 (1992)
118. S P Mallela, R A Geanangel *Inorg. Chem.* **32** 602 (1993)
119. K Klinkhammer *Polyhedron* **21** 587 (2002)
120. K W Klinkhammer, W Schwarz *Angew. Chem., Int. Ed. Engl.* **34** 1334 (1995)
121. J Klett, K W Klinkhammer, M Niemeyer *Chem.-Eur. J.* **5** 2531 (1999)
122. M Westerhausen, W Schwarz *Z. Anorg. Allg. Chem.* **619** 1053 (1993)
123. A H Cowly, T H Newman *Organometallics* **1** 1412 (1982)
124. M Haase, U Klingebiel, *Z. Naturforsch., B* **41** 697 (1986)
125. M Haase, U Klingebiel *Angew. Chem.* **97** 335 (1985)
126. G Bertrand, C Couret, J Escudie, S Majid, J-P Majoral *Tetrahedron Lett.* **23** 3567 (1982)
127. M Haase, U Klingebiel, L Skoda *Z. Naturforsch., B* **39** 1500 (1984)
128. S Haber, R Boese, M Regitz *Angew. Chem.* **102** 1523 (1990)
129. H Siegl, W Krumlacher, K Hassler *Monatsh. Chem.* **130** 139 (1999)
130. B H Boo, H K Kang, S K Kang, S S Lee, D Kim, M H Lee *J. Organomet. Chem.* **436** 1 (1992)
131. A N Kornev, T A Chesnokova, V V Semenov, Yu A Kurskii *Izv. Akad. Nauk, Ser. Khim.* 1146 (1995) [b]
132. E V Zhezlova, T A Chesnokova, A N Kornev, in *Khimiya i Rrimenenie Fosfor-, Sera- i Kremniiorganicheskikh Soedinenii (Sb. Nauch. Trudov), S Peterburg, 1998* [The Chemistry and Application of Organophosphorus, Organosulfur and Organosilicon Compounds (Collection of Scientific Works), St Petersburg, 1998] p. 197
133. M G Voronkov, E A Maletina, V K Roman *Geterosiloksany* (Heterosiloxanes) (Novosibirsk: Nauka, 1984)
134. A G Brook, J J Chruscial *Organometallics* **3** 1317 (1984)
135. A N Kornev, T A Chesnokova, E V Zhezlova, L N Zakharov, G K Fukin, Yu A Kursky, G A Domrachev, P D Lickiss *J. Organomet. Chem.* **587** 113 (1999)
136. T A Chesnokova, E V Zhezlova, A N Kornev, Y V Fedotova, L N Zakharov, G K Fukin, Y A Kursky, T G Mushtina, G A Domrachev *J. Organomet. Chem.* **642** 20 (2002)
137. A N Kornev, T A Chesnokova, V V Semenov, E V Zhezlova, L N Zakharov, L G Klapshina, G A Domrachev, V S Rusakov *J. Organomet. Chem.* **547** 113 (1997)
138. Y S Chen, P P Gaspar *Organometallics* **1** 1410 (1982)
139. Y S Chen, B H Cohen, P P Gaspar *J. Organomet. Chem.* **195** C1 (1980)
140. P J Bonasia, V Christou, J Arnold *J. Am. Chem. Soc.* **115** 6777 (1993)
141. B O Dabbousi, P J Bonasia, J Arnold *J. Am. Chem. Soc.* **113** 3186 (1991)
142. P J Bonasia, D E Gindelberger, B O Dabousi, J Arnold *J. Am. Chem. Soc.* **114** 5209 (1992)
143. D R Cary, J Arnold *Inorg. Chem.* **33** 1791 (1994)
144. D R Cary, G E Ball, J Arnold *J. Am. Chem. Soc.* **117** 3492 (1995)
145. D E Gindelberger, J Arnold *Inorg. Chem.* **32** 5813 (1993)
146. C P Gerlach, J Arnold *Inorg. Chem.* **35** 5770 (1996)
147. S P Gerlach, S P Wuller, J Arnold *Chem. Commun.* 2565 (1996)
148. S P Gerlach, J Arnold *Inorg. Chem.* **37** 2393 (1998)
149. C P Gerlach, V Christou, J Arnold *Inorg. Chem.* **35** 2758 (1996)
150. M Bochmann, M L H Green, A K Powell, J Sassmannshausen, M U Triller, S Wocadlo *J. Chem. Soc., Dalton Trans.* 43 (1999)
151. B H Boo, P P Gaspar *Organometallics* **5** 698 (1986)
152. K W Klinkhammer, J Klett, M Niemer, in *The XIIth International Symposium on Organosilicon Chemistry (Abstracts of Reports), Sendai, Japan, 1999* 2B33
153. H Wagner, U Schubert *Chem. Ber.* **123** 2101 (1990)
154. J Meyer, J Willnecker, U Schubert *Chem. Ber.* **122** 223 (1989)
155. H Piana, H Wagner, U Schubert *Chem. Ber.* **124** 63 (1991)
156. J Arnold, T D Tilley, A L Rheingold, S J Geib *Inorg. Chem.* **26** 2106 (1987)
157. S P Mallela, F Schwan, R A Geanangel *Inorg. Chem.* **35** 745 (1996)
158. A K Hovland, T F Schaaf, J P Oliver *J. Organomet. Chem.* **120** 171 (1976)
159. D Bravo-Zhivotovskii, M Yuzefovich, M Bendikov, K Klinkhammer, Y Apeloig, *Angew. Chem., Int. Ed.* **38** 1100 (1999)
160. B K Campion, R H Heyn, T D Tilley *Organometallics* **12** 2584 (1993)
161. B K Campion, R H Heyn, T D Tilley *J. Am. Chem. Soc.* **112** 2011 (1990)
162. B K Campion, R H Heyn, T D Tilley *Inorg. Chem.* **29** 4355 (1990)
163. M M Corradi, A D Frankland, P B Hitchcock, M F Lappert, G A Lawless *J. Chem. Soc., Chem. Commun.* 2323 (1996)
164. N S Radu, M P Engeler, C P Gerlach, T Don Tilley, A L Rheingold *J. Am. Chem. Soc.* **117** 3621 (1995)
165. M V Ustinov, D A Bravo-Zhivotovskii, I D Kalikhman, V Yu Vitkovskii, N S Vyazankin, M G Voronkov *Metalloorg. Khim.* **2** 1259 (1989) [c]
166. Yu E Ovchinnikov, Yu T Struchkov, M V Ustinov, M G Voronkov *Izv. Akad. Nauk, Ser. Khim.* 1473 (1993) [b]
167. L H McAlexander, M Hung, L Li, J B Diminnie, Z Xue *Organometallics* **15** 5231 (1996)
168. Z Wu, J B Diminnie, Z Xue *Inorg. Chem.* **37** 6366 (1998)
169. R H Heyn, T D Tilley *Inorg. Chem.* **28** 1768 (1989)
170. F H Elsner, T D Tilley, A L Rheingold, S J Geib *J. Organomet. Chem.* **358** 169 (1988)
171. H G Woo, R H Heyn, T D Tilley *J. Am. Chem. Soc.* **114** 5698 (1992)
172. B K Campion, J Falk, T D Tilley *J. Am. Chem. Soc.* **109** 2049 (1987)
173. C Kayser, D Frank, J Baumgartner, C Marschner *J. Organomet. Chem.* **667** 149 (2003)

174. Z Wu, L H McAlexander, J B Diminnie, Z Xue *Organometallics* **17** 4853 (1998)
175. Z Xue, L Li, L K Hoyt, J B Diminnie, J L Pollitte *J. Am. Chem. Soc.* **116** 2169 (1994)
176. Yu E Ovchinnikov, V A Igonin, T V Timofeeva, S V Lindeman, Yu T Struchkov, M V Ustinov, D A Bravo-Zhivotovskii *Metalloorg. Khim.* **5** 1154 (1992) [c]
177. J Arnold, M P Engeler, F H Elsner, R H Heyn, T D Tilley *Organometallics* **8** 2284 (1989)
178. H G Woo, J F Walzer, T D Tilley *J. Am. Chem. Soc.* **114** 7047 (1992)
179. G L Casty, C G Lugmair, N S Radu, T D Tilley, J F Walzer, D Zargarian *Organometallics* **16** 8 (1997)
180. H-G Woo, T D Tilley *J. Organomet. Chem.* **393** C6 (1990)
181. J Arnold, H G Woo, T D Tilley, A L Rheingold, S J Geib *Organometallics* **7** 2045 (1988)
182. F N Elsner, H G Woo, T D Tilley *J. Am. Chem. Soc.* **110** 313 (1988)
183. Z Wu, J B Diminnie, Z Xue *J. Am. Chem. Soc.* **121** 4300 (1999)
184. X Liu, L Li, J B Diminnie, G P A Yap, A L Rheingold, Z Xue *Organometallics* **17** 4597 (1998)
185. U Burckhardt, T D Tilley *J. Am. Chem. Soc.* **121** 6328 (1999)
186. D M Roddick, T D Tilley, A L Rheingold, S J Geib *J. Am. Chem. Soc.* **109** 945 (1987)
187. Ya V Fedotova, T A Chesnokova, G K Fukin, A N Kornev, in *The XIVth FECHEM Conference on Organometallic Chemistry (Abstracts of Reports), Gdansk, Poland, 2001* p. 124
188. J Y Corey, J Braddock-Wilking *Chem. Rev.* **99** 175 (1999)
189. B K Nicholson, J Simpson, W T Robinson *J. Organomet. Chem.* **47** 403 (1973)
190. B K Nicholson, J Simpson *J. Organomet. Chem.* **32** C29 (1971)
191. B K Nicholson, J Simpson *J. Organomet. Chem.* **72** 211 (1974)
192. M C Couldwell, J Simpson, W T Robinson *J. Organomet. Chem.*, **107** 323 (1976)
193. M H Chisholm, H T Chiu, K Folting, J C Huffman *Inorg. Chem.* **23** 4097 (1984)
194. G L Casty, T D Tilley, G P A Yap, A L Rheingold *Organometallics* **16** 4746 (1997)
195. U Schubert, A Schenkel, J Müller *J. Organomet. Chem.* **292** C11 (1985)
196. U Schubert, A Schenkel *Chem. Ber.* **121** 939 (1988)
197. W P Freeman, T D Tilley, A L Rheingold *J. Am. Chem. Soc.* **116** 8428 (1994)
198. W P Freeman, T D Tilley, A L Rheingold, R L Ostrander *Angew. Chem., Int. Ed. Engl.* **32** 1744 (1993)
199. K Oka, R Nakao *J. Organomet. Chem.* **390** 7 (1990)
200. M Ishikawa, K-I Nakagawa, M Kumada *J. Organomet. Chem.* **178** 105 (1979)
201. P P Gaspar, Y S Chen, A P Helfer, S Konieczny, E C L Ma, S H Mo *J. Am. Chem. Soc.* **103** 7344 (1981)
202. A G Brook *J. Organomet. Chem.* **300** 21 (1986)
203. A G Brook, J W Harris, J Lennon, M E Sheikh *J. Am. Chem. Soc.* **101** 83 (1979)
204. A Alberti, S Dellonte, C Paradisi, S Roffia, G F Pedulli *J. Am. Chem. Soc.* **112** 1123 (1990)
205. M A Brook, S Balduzzi, M Mohamed, C Gottardo *Tetrahedron* **55** 10 027 (1999)
206. M A Brook, C Gottardo, S Balduzzi, M Mohamed *Tetrahedron Lett.* **38** 6997 (1997)
207. T A Blinka, R West *Organometallics* **5** 128 (1986)
208. K H Pannell, L J Wang, J M Rozell *Organometallics* **8** 550 (1989)
209. K H Pannell, M-C Brun, H Sharma, K Jones, S Sharma *Organometallics* **13** 1075 (1994)
210. K Sternberg, H Oehme *Eur. J. Inorg. Chem.* 177 (1998)
211. K Sternberg, M Michalik, H Oehme *J. Organomet. Chem.* **533** 265 (1997)
212. J Ohshita, K Yoshimoto, T Iida, A Kunai *J. Am. Chem. Soc.* **123** 8400 (2001)
213. M Ballestri, C Chatgilialoglu, G Seconi *J. Organomet. Chem.* **408** C1 (1991)
214. M Ballestri, C Chatgilialoglu, M Lucarini, G F Pedulli *J. Org. Chem.* **57** 948 (1992)
215. T D Tilley, in *The XXVIIIth Organosilicon Symposium (Abstracts of Reports), Gaisville, 1995* p. F1
216. L S Chang, M P Johnson, M J Fink *Organometallics* **8** 1369 (1989)
217. L S Chang, M P Johnson, M J Fink *Organometallics* **10** 1219 (1991)
218. R A Fischer, S Nlate, E Herdtweck *Angew. Chem., Int. Ed. Engl.* **35** 1861 (1996)
219. J Ohshita, Y Masaoka, M Ishikawa *Organometallics* **10** 3775 (1991)
220. D Hoffmann, T Gross, R Kempe, H Oehme *J. Organomet. Chem.* **598** 395 (2000)
221. I S Biltueva, D A Bravo-Zhivotovskii, I D Kalikhman, V Yu Vitkovskii, S G Shevchenko, N S Vyazankin, M G Voronkov *J. Organomet. Chem.* **368** 163 (1989)
222. D Bravo-Zhivotovskii, Y Apeloig, Y Ovchinnikov, V Igonin, Yu T Struchkov *J. Organomet. Chem.* **446** 123 (1993)
223. D Bravo-Zhivotovskii, V Braude, A Stanger, M Kapon, Y Apeloig *Organometallics* **11** 2326 (1992)
224. J Ohshita, E Nekoda, S Masaoka, M Ishikawa *J. Organomet. Chem.* **544** 49 (1997)
225. J Ohshita, H Sakurai, Y Tokunaga, A Kunai *Organometallics* **18** 4545 (1999)
226. T Gross, R Kempe, H Oehme *J. Organomet. Chem.* **534** 229 (1997)
227. A Naka, J Ohshita, A Kunai, M E Lee, M Ishikawa *J. Organomet. Chem.* **574** 50 (1999)
228. T Gross, R Kempe, H Oehme *Eur. J. Inorg. Chem.* 21 (1999)
229. M Ishikawa, S Matsui, A Naka, J Ohshita *Organometallics* **15** 3836 (1996)
230. J Ohshita, H Hasebe, Y Masaoka, M Ishikawa *Organometallics* **13** 1064 (1994)

[a] — *Polym. Sci. (Engl. Transl.)*
[b] — *Russ. Chem. Bull., Int. Ed. (Engl. Transl.)*
[c] — *Russ. J. Organomet. Chem. (Engl. Transl.)*

Russian Chemical Reviews **73** (11) 1091 – 1119 (2004) © 2004 Russian Academy of Sciences and Turpion Ltd

DOI 10.1070/RC2004v073n11ABEH000880

Physicochemical aspects of isomerisation of free radicals

E T Denisov, T G Denisova

Contents

I.	Introduction	1091
II.	Parabolic model of radical reactions	1092
III.	Migration of a hydrogen atom in alkyl radicals	1092
IV.	Isomerisation of alkoxyl radicals	1095
V.	Isomerisation of peroxyl radicals	1095
VI.	Cyclisation and ring opening in alkyl radicals	1095
VII.	Cyclisation and ring opening in aminyl radicals	1106
VIII.	Cyclisation and ring opening in oxygen-containing radicals	1111
IX.	Decomposition and ring opening in peroxoalkyl radicals to give epoxides	1114
X.	Migrations of aryl and vinyl groups in alkyl radicals	1114
XI.	Conclusion	1116

Abstract. Kinetic data on intramolecular abstraction of hydrogen atoms in alkyl, alkoxyl and peroxyl radicals are generalised and analysed. It is shown that the activation energies of these reactions are affected by ring strain. The kinetic parameters of mono- and bimolecular elimination reactions are compared. The difference between the activation energies of these reactions is interpreted using the model of intersecting parabolas. The same model is used to discuss the results of analysis of cyclisation of alkyl radicals; the ring strain energy is shown to play an important role in the activation of these reactions. It is noted that the difference between the electron affinities of the C, N and O atoms is clearly manifested in the cyclisation of aminyl and ω-formylalkyl radicals. The kinetic parameters of cyclisation and bimolecular radical addition reactions are compared. The experimental data on the transfer of the vinyl and aryl groups in alkyl radicals are analysed. The bibliography includes 146 references.

I. Introduction

The possible mechanisms of isomerisation of free radicals were discussed by N N Semenov back in 1958;[1] however, no quantitative kinetic data for these reactions were available at that time. The kinetics of these reactions has been studied rather intensively since the late 1970s.[2–4] Radical isomerisation reactions can be classified into (i) hydrogen atom migrations from one position to another; (ii) cyclisation reactions in radicals; (iii) ring opening reactions; (iv) cleavage of a peroxide bridge and epoxide formation; (v) migrations of aryl and vinyl groups in alkyl radicals.[2]

The isomerisation of alkyl radicals, for example

$$R^1C^{\bullet}H(CH_2)_nCH_2R^2 \longrightarrow R^1CH_2(CH_2)_nC^{\bullet}HR^2,$$

accompanied by migration of a hydrogen atom from one carbon to another is involved in chain processes of hydrocarbon cracking, photolysis and radiolysis,[5] radical polymerisation and oligomerisation of monomers,[6] and thermal and thermooxidative destruction of polymers.[7] These reactions affect appreciably both the overall process rates and the composition of products. The isomerisation of peroxyl radicals

$$R^1CH(OO^{\bullet})(CH_2)_nCH_2R^2 \longrightarrow R^1CH(OOH)(CH_2)_nC^{\bullet}HR^2$$

takes place during oxidation of hydrocarbons and yields bifunctional products (dihydroperoxides, dihydric alcohols, and so on) even at early oxidation steps.[8–10] These reactions play an important role in the oxidation of carbochain polymers.[7,11] Decomposition of peroxoalkyl radicals takes place during the oxidation of monomers[8,12] and is accompanied by cyclisation to give epoxides.

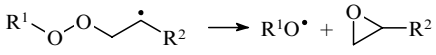

Alkyl radicals containing double bonds rapidly undergo intraradical cyclisation,[3] giving rise to cyclic radicals. The rings thus formed contain $n + 2$ or $n + 3$ carbon atoms.

$$C^{\bullet}H_2(CH_2)_nCH{=}CHR \longrightarrow \begin{cases} \text{cyclo-}[(CH_2)_{n+1}CH(C^{\bullet}HR)] \\ \text{cyclo-}[(CH_2)_{n+1}C^{\bullet}HCHR] \end{cases}$$

These reactions have been studied intensively during the last two decades. They are used in physical chemistry, for example, as a clock reaction in the method of competing reactions. For synthetic purposes, such reactions are employed to prepare diverse cyclic and spirocyclic compounds.[13–15]

Recently, we have analysed a number of classes of radical isomerisation reactions using the method of intersecting parabolas (MIP)[16–19] and have revealed some new features. Note that analysis of radical isomerisation reactions in terms of the MIP allows one to compare them with one another and with analogous bimolecular reactions involving radicals. This review presents the experimental kinetic parameters for radical isomerisation processes and the results of their analysis and comparison with reactions of other classes.

E T Denisov, T G Denisova Institute of Problems of Chemical Physics, Russian Academy of Sciences, 142432 Chernogolovka, Moscow Region, Russian Federation. Fax (7-096) 515 54 20. Tel. (7-096) 522 19 14. E-mail: edenisov@icp.ac.ru (E T Denisov), denisova@icp.ac.ru (T G Denisova)

Received 6 October 2003
Uspekhi Khimii **73** (11) 1181 – 1209 (2004); translated by Z P Bobkova

II. Parabolic model of radical reactions

The isomerisation reactions of free radicals

$$R^1C^{\bullet}H(CH_2)_nCH_2R^2 \longrightarrow R^1CH_2(CH_2)_nC^{\bullet}HR^2,$$

$$R^1CH(O^{\bullet})(CH_2)_nCH_2R^2 \longrightarrow R^1CH(OH)(CH_2)_nC^{\bullet}HR^2,$$

$$R^1CH(OO^{\bullet})(CH_2)_nCH_2R^2 \longrightarrow R^1CH(OOH)(CH_2)_nC^{\bullet}HR^2$$

are represented, within the framework of the MIP, as an intersection of the potential energy curves of the stretching vibrations of the reacting bonds, *i.e.*, the bond being cleaved and the bond being formed.[16, 20–23] The *y*-coordinate of the intersection point of these curves in the 'bond vibration amplitude–potential energy' coordinate system corresponds to the activation energy. The stretching vibration of the bond is taken to be harmonic.

The cyclisation reaction

$$Y^{\bullet}(CH_2)_nCH{=}CHR \longrightarrow \text{cyclo-}[(CH_2)_nYCH(C^{\bullet}HR)]$$

is represented, within the framework of the MIP, as an intersection of the potential energy curves of the stretching vibrations of the reacting bonds, *i.e.*, the C=C double bond to which the addition takes place and the C–Y bond that forms upon the addition of the Y atom having a free valence to a double-bond C atom.

The isomerisation reaction is described in terms of the MIP by the following parameters: the enthalpy (ΔH_e), the activation energy (E_e), the coefficients b and b_f ($2b^2$ is the force constant of the bond being cleaved, $2b_f^2$ is that of the bond being formed) and the overall elongation (r_e) of the bonds in the transition state. The reaction enthalpy (ΔH_e) includes the difference between the zero-point vibration energies of the reacting bonds

$$\Delta H_e = D_i - D_f + 0.5\,hN_A(v_i - v_f), \tag{1}$$

where D_i and D_f are the dissociation energies of the bond being cleaved (i) and the bond being formed (f), v_i and v_f are the stretching vibration frequencies of these bonds, respectively, h is the Planck constant, and N_A is Avogadro's number. The activation energy (E_e) also involves the zero-point vibration energy of the bond being cleaved and is related to the Arrhenius activation energy (E_a) as follows:

$$E_e = E_a + 0.5\,(hN_Av_i - RT). \tag{2}$$

Radical reactions of one class are described by equal pre-exponential factors A_{C-H} per C–H bond being attacked (n_i is the number of these bonds).[20] Therefore, from a known experimental rate constant of the reaction, one can calculate the activation energy

$$E_a = -RT\ln\left(\frac{k}{n_iA_{C-H}}\right). \tag{3}$$

Each class of radical reactions is described according to the MIP by the parameters $\alpha = b/b_f$ and br_e. The br_e parameter is related to the reaction enthalpy (ΔH_e) and the activation energy (E_e) by the equation

$$br_e = \alpha\sqrt{E_e - \Delta H_e} + \sqrt{E_e}. \tag{4}$$

This equation has been used to calculate the br_e parameter from experimental data. In addition to the α and br_e parameters, each class of radical reactions is characterised in terms of the MIP by a classical potential barrier (the activation energy which includes the zero-point vibration energy of the bond being attacked) to the thermally neutral reaction (E_{e0}) and the position ($r_0^{\neq}$) of the hydrogen atom in the transition state (TS) in the r_e segment at $E_e = E_{e0}$:

$$\sqrt{E_{e0}} = \frac{br_e}{1+\alpha}, \tag{5}$$

$$r_0^{\neq} = r_e(1+\alpha)^{-1}. \tag{6}$$

The values of α and b [measured in (kJ mol^{-1})$^{1/2}$ m^{-1}], $0.5\,hN_Av_i$ and $0.5\,hN_A(v_i - v_f)$ (both in kJ mol^{-1}) for different classes of radical isomerisation reactions accompanied by hydrogen migration are given below.

Reaction	α	$10^{-10}\,b$	$0.5\,hN_Av_i$	$0.5\,hN_A(v_i-v_f)$
$R^{\bullet}+H-C$	1.000	37.43	17.4	0.0
$RO^{\bullet}+H-C$	0.796	37.43	17.4	−4.3
$ROO^{\bullet}+H-C$	0.814	37.43	17.4	−3.8

The α and E_{e0} parameters can be used to calculate the activation energies of reactions of one class from their enthalpies. When α is close to 1 and the inequality $\Delta H_e(1-\alpha^2) \ll (br_e)^2$ holds, the dependence of the activation energy E_e on the enthalpy ΔH_e assumes the form

$$\sqrt{E_e} = \sqrt{E_{e0}} + \frac{\alpha\Delta H_e}{2(1+\alpha)\sqrt{E_{e0}}}. \tag{7}$$

For hydrogen transfer in alkyl radicals, the force constants of the outgoing and incoming bonds are equal; therefore, $\alpha = 1$. Thus, Eqn (7) assumes the form

$$\sqrt{E_e} = \sqrt{E_{e0}} + \frac{\Delta H_e}{4\sqrt{E_{e0}}}. \tag{8}$$

The contribution ΔE_H of the enthalpy to the activation energy of an individual reaction can be readily estimated from the formula

$$\Delta E_H = E_e - E_{e0}. \tag{9}$$

An important advantage of the MIP is the possibility to compare reactions of different classes through comparison of their characteristics such as the activation energy of the thermally neutral reaction (E_{e0}) and bond elongation (r_e) in the TS.

III. Migration of a hydrogen atom in alkyl radicals

The kinetic and thermodynamic parameters of hydrogen migration in alkyl radicals are summarised in Table 1.

The enthalpies of such reactions vary from −65 to +26 kJ mol^{-1} and the activation energies, from 12 to 40 kJ mol^{-1}. The transition states of these reactions are cyclic. The configuration of atoms in the TS of 1–4- and 1–5-migrations of a hydrogen atom calculated by the density functional theory (B3LYP)[17] is shown in Fig. 1.

Activation entropy of hydrogen migration. The formation of a cyclic TS eliminates the free rotation of alkyl fragments around the C–C bond. This results in a negative activation entropy ($\Delta S^{\neq}$). Comparison of the experimental pre-exponential factors A with the theoretical value [32] calculated from the formula

$$A = \frac{RT}{N_Ah}\exp\left(\frac{\Delta S^{\neq}}{R}\right), \tag{10}$$

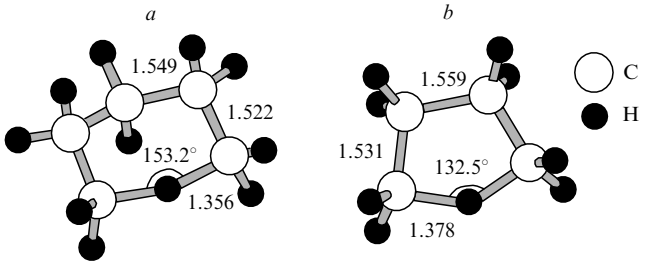

Figure 1. Geometric structure of the TS for hydrogen migration in the pentyl (*a*) and butyl (*b*) radicals based on quantum-chemical calculations (B3LYP).[17]
The bond lengths are in Å.

Table 1. Thermodynamic (D_i, D_f, ΔH) and kinetic (E_a) parameters of hydrogen migration in alkyl radicals.

Radical [a]	D_i (see [b])	D_f (see [b])	ΔH (see [b])	E_a (see [b])	Ref.
Six-membered ring					
$C^{\bullet}Cl_2(CH_2)_3(C-H)HMe$	413.0	388.7	24.3	39.9	24
$C^{\bullet}Cl_2(CH_2)_3(C-H)HEt$	414.5	388.7	25.8	39.0	24
$C^{\bullet}Cl_2(CH_2)_2SiEt_2(C-H)HMe$	413.0	388.7	24.3	44.8	25, 26
$C^{\bullet}H_2(CH_2)_3(C-H)HC(O)OMe$	398.8	422.0	−23.2	25.1	27
$(C-H)(O)CH_2CHBu^tCH_2C^{\bullet}H_2$	385.6	422.0	−36.4	12.5	28
$CH(O)(C-H)HCH_2CHBu^tCH_2C^{\bullet}H_2$	397.8	422.0	−24.2	17.1	28
Five-membered ring					
$C^{\bullet}H_2(CH_2)_2(C-H)HC(O)OMe$	398.8	422.0	−23.2	32.4	27
2-$[Me_2C(C-H)H_2]$-4,6-$Bu^t_2C_6H^{\bullet}_2$	422.0	474.0	−52.0	19.0	29–31
2,4,6-$Ad_3C_6H^{\bullet}_2$ (see [c])	408.8	474.0	−65.2	18.0	29, 31

[a] Here and in Tables 2, 3, 6, 7 and 8, the bond being attacked is designated by C—H; [b] in kJ mol^{-1}; [c] AdH is adamantane.

has shown that the $\Delta S^{\neq}$ value is exactly equal to the difference between the entropies of the linear and cyclic hydrocarbons:[18]

$$\Delta S^{\neq} = S(\text{cyclo-}C_nH_{2n}) - S(C_nH_{2n+2}).$$

The logarithms of the pre-exponential factors calculated from relation (10) are listed in Table 2.

Effect of the size of the ring formed in the transition state on the activation energy. The activation energy of hydrogen migration in an alkyl radical obviously depends on the reaction enthalpy.[20] What other factors influence the rate of migration of the hydrogen atom? This issue has been addressed in a study [16] where the br_e, r_e and E_{e0} parameters were calculated by the method of intersecting parabolas on the basis of experimental data. The activation energy for hydrogen migration in an alkyl radical was found to depend on the size of the ring formed in the TS. The reactions whose TS contain rings with equal numbers of carbon atoms are characterised by the same set of parameters ($\alpha = 1$, br_e, r_e and E_{e0}) and differ only in their activation enthalpies and energies. These parameters for the reactions

$$R^1C^{\bullet}H(CH_2)_nCH_2R^2 \longrightarrow R^1CH_2(CH_2)_nC^{\bullet}HR^2$$

are shown in Table 2. Below the classical potential barriers (E_{e0}) for such reactions are juxtaposed with the ring strain energies (E_{rsc}) in cycloalkanes (n is the number of carbon atoms in the TS ring).[33]

n	5	6	7
E_{e0} /kJ mol^{-1}	72.5 ± 0.9	52.0 ± 1.7	72.2
E_{rsc} /kJ mol^{-1}	26.7	0.7	26.8
$10^{10}\, r_e$ /m	0.455	0.385	0.454

It can be seen that the classical potential barriers to the reactions whose TS contain five- (72.5 kJ mol^{-1}) or seven-membered rings (72.2 kJ mol^{-1}) are markely higher than those for TS with six-membered rings (52.0 kJ mol^{-1}). Obviously, this is due to the difference between the ring strain: the higher the strain, the higher the activation energy. An empirical dependence between the E_{e0} and E_{rsc} values (expressed in kJ mol^{-1}) is as follows:

$$E_{e0} = 51.5 + 0.788\, E_{rsc}. \quad (11)$$

Thus, the dependence of the activation energy E_e on the ΔH and E_{rsc} values has the form [18]

$$\sqrt{E_e} = \sqrt{51.5 + 0.788E_{rsc}} + \frac{\Delta H}{4\sqrt{51.5 + 0.788E_{rsc}}}. \quad (12)$$

Table 2. MIP parameters for hydrogen migration in alkyl radicals.[16]

Radical $(R^1)^{\bullet}$	br_e /(kJ mol^{-1})$^{1/2}$	E_{e0}(m) [a] /kJ mol^{-1}	$10^{10}\, r_e$ /m	logA_{C-H} (s^{-1})	E_{e0}(b) [a] /kJ mol^{-1}
$(R^1)^{\bullet} \longrightarrow (R^2)^{\bullet}$ (Four-membered TS)					
$RC^{\bullet}H(CH_2)_3(C-H)HY$	23.85	142.2	0.637	11.16	74.8
$RC^{\bullet}H(CH_2)_3(C-H)HPh$	24.16	145.9	0.646	10.16	79.2
$RC^{\bullet}H(CH_2)_3(C-H)HCH=CH_2$	24.68	152.3	0.659	10.16	86.5
$(R^1)^{\bullet} \longrightarrow (R^2)^{\bullet}$ (Five-membered TS)					
$RC^{\bullet}H(CH_2)_2(C-H)HY$	17.03	72.5	0.455	10.55	74.8
$RC^{\bullet}H(CH_2)_2(C-H)HPh$	17.46	76.2	0.466	9.55	79.2
$RC^{\bullet}H(CH_2)_2(C-H)HCH=CH_2$	18.18	82.6	0.486	9.55	86.5
$(R^1)^{\bullet} \longrightarrow (R^2)^{\bullet}$ (Six-membered TS)					
$RC^{\bullet}H(CH_2)_3(C-H)HY$	14.42	52.0	0.385	9.95	74.8
$RC^{\bullet}H(CH_2)_3(C-H)HPh$	14.93	55.7	0.399	8.95	79.2
$RC^{\bullet}H(CH_2)_3(C-H)HCH=CH_2$	15.73	61.9	0.420	8.95	86.5
$(R^1)^{\bullet} \longrightarrow (R^2)^{\bullet}$ (Seven-membered TS)					
$RC^{\bullet}H(CH_2)_4(C-H)HY$	16.99	72.2	0.454	8.20	74.8
$RC^{\bullet}H(CH_2)_4(C-H)HPh$	17.42	75.9	0.465	7.20	79.2
$RC^{\bullet}H(CH_2)_4(C-H)HCH=CH_2$	18.14	82.3	0.485	7.20	86.5

[a] E_{e0}(m) and E_{e0}(b) are the classical potential barriers for the monomolecular cyclisation and bimolecular hydrogen abstraction, respectively.

Quantum-chemical calculations have shown[17] that in the TS for isomerisation of the butyl radical, the angle between the C, H and C atoms of the ring is about 21° smaller than the corresponding angle in the TS for pentyl radical isomerisation (see Fig. 1). Hence, the activation energy (determined by quantum-chemical calculations) for isomerisation of the butyl radical is higher than that for the pentyl radical by 31 kJ mol^{-1}. The results of quantum-chemical calculations for the ω-isomerisation of the butyl and pentyl radicals are presented below (the activation energies are expressed in kJ mol^{-1}; φ is the C···H···C angle).[17]

Reaction	E_a	$10^{10}\,r$(C···H) /m	φ /deg
$C^{\bullet}H_2(CH_2)_2Me \rightarrow Me(CH_2)_2C^{\bullet}H_2$	96.8	1.378	132.5
$C^{\bullet}H_2(CH_2)_3Me \rightarrow Me(CH_2)_3C^{\bullet}H_2$	65.8	1.356	153.2

Thus, the calculated parameters are in good agreement with experimental data.

Effect of the α-π-bond on the activation energy. Analysis of the experimental data on bimolecular reactions

$$(R^1)^{\bullet} + R^2H \longrightarrow R^1H + (R^2)^{\bullet}$$

indicates that a double bond or an aromatic ring present in the α-position relative to the bond being attacked results in a higher E_{e0} value (see Ref. 20). This effect is illustrated in Table 2, which presents the MIP parameters characterising hydrogen migration reactions in radicals with different structures.[16] Table 3 summarises the results of calculations, using this method, of the rate constants for the migration of hydrogen atoms from the β-, γ-, δ- and ε-positions with respect to the carbon atom with a free valence in different radicals.

Comparison of mono- and bimolecular hydrogen abstraction. Bimolecular reactions of hydrogen abstraction from hydrocarbon molecules by alkyl radicals have been analysed.[20] This allowed one to compare the classical potential barriers to monomolecular and bimolecular hydrogen abstraction reactions. The difference between the structures of these TS is obvious. In the bimolecular reaction, the C···H···C atoms of the reaction centre are arranged in one straight line. In an intramolecular hydrogen migration to the δ-position, which is accompanied by the lowest ring strain, the C···H···C atoms form an angle of 153° (quantum-chemical calculations, see Fig. 1).[16] According to the absolute reaction rate theory, the minimum repulsion between the atoms in the TS is attained in the reaction centre with a linear atom configuration;[1,32] it can therefore be expected that $E_{e0}(m) > E_{e0}(b)$. However, analysis of the experimental data using the MIP provides the opposite result: $E_{e0}(m) = 52$ kJ mol^{-1}, $E_{e0}(b) = 74.8$ kJ mol^{-1}, *i.e.*, $E_{e0}(m) < E_{e0}(b)$.[16] As shown by quantum-chemical calculations of the activation energy of the reactions

$$C_2H_5^{\bullet} + C_2H_6 \longrightarrow C_2H_6 + C_2H_5^{\bullet}$$

and

$$C^{\bullet}H_2(CH_2)_3Me \longrightarrow Me(CH_2)_3C^{\bullet}H_2,$$

the bimolecular reaction of the ethyl radical with ethane is characterised by $E_{e0} = 62.5$ kJ mol^{-1}, and the monomolecular migration of the H atom in the pentyl radical has $E_{e0} = 65.8$ kJ mol^{-1}, *i.e.*, the calculated activation energies of these two thermally neutral reactions are approximately equal.[17]

What is the reason for the fact that $E_{e0}(b) \geqslant E_{e0}(m)$? The answer can be derived from MIP considerations. In attaining the TS of mono- and bimolecular hydrogen abstraction, the following factors are important. In a bimolecular reaction whose TS has a linear reaction centre, C···H···C, the crucial role in the activation is played by the stretching vibration of the C–H bond being attacked. In this case, the activation energy depends on the force constant of the stretching vibration of the C–H bond being cleaved [$b = 37.43 \times 10^{10}$ (kJ mol^{-1})$^{1/2}$ m^{-1}]. In the case of intraradical migration of hydrogen, the situation is more complicated. The angular configuration of the C···H···C fragment needed for TS formation is attained through excitation of both the stretching vibration of the C–H bond being cleaved and the angular bending vibrations of the C–C–C and C–C–H bonds, which form a cyclic TS. There are five such bonds in a pentyl radical. The frequencies and the force constants of bending vibrations of the C–C–C bonds are much smaller than these parameters for the C–H bond. Owing to these 'soft' vibrations, this TS is attained more easily (as regards the energy expenditure), despite its seemingly less favourable angular configuration. In this case, the br_e parameter is the sum of $b_j r_{ej}$, where every partial parameter present in the $\Sigma b_j r_{ej}$ sum reflects the shifts of atoms in the TS induced by activation of vibrations of the corresponding bonds. Since the force constants of bending vibrations are lower than those of stretching vibrations, $\Sigma b_j r_{ej} < br_e$(b).

Polar effect. The polar interaction in the TS of bimolecular reactions is manifested in the reactions of halide-containing radicals with haloalkanes. The introduction of a halogen atom into a molecule or a radical not only changes the reaction enthalpy but also decreases the activation energy of the thermally neutral reaction.[20] The role of polar effect in the activation energy can be judged from the difference between the E_{e0} values of the reactions of radicals with a haloalkane and the corresponding hydrocarbon

$$\Delta E_{\mu} = E_{e0}(RX) - E_{e0}(RH). \qquad (13)$$

The data illustrating this effect for reactions of trichloromethyl radicals with a number of chloroalkanes are presented below.[19]

Compound	ΔE_{μ} /kJ mol^{-1}
CH_2Cl_2	−8.0
$CH_2ClCH_2CCl_3$	−18.8
$EtCCl_3$	−17.9
Pr^nCCl_3	−16.0

The polar interaction also shows itself in hydrogen migration (see Table 1). The E_{e0} and ΔE_{μ} values (in kJ mol^{-1}) calculated from experimental data for the hydrogen migration processes that involve the formation of a six-membered transition state are presened below.[19]

Table 3. Enthalpies, activation energies, and rate constants (k) for hydrogen migration in alkyl radicals calculated using the MIP relations.[16]

Radical	ΔH_e (see [a])	E_e(m) [b]	$k_{350\,K}$ (see [c])	E_e(b) [b]
$C^{\bullet}H_2CH_2(C-H)HMe$	−10.0	121.2	2.49×10^{-7}	54.0
$C^{\bullet}H_2(CH_2)_2(C-H)HMe$	−10.0	51.6	1.41×10^{3}	54.0
$C^{\bullet}H_2(CH_2)_3(C-H)HMe$	−10.0	31.1	4.07×10^{5}	54.0
$C^{\bullet}H_2(CH_2)_4(C-H)HMe$	−10.0	51.2	7.24×10^{3}	54.0
$MeC^{\bullet}H(CH_2)_3(C-H)HMe$	0	36.0	7.56×10^{4}	58.9
$MeC^{\bullet}H(CH_2)_3(C-H)Me_2$	−12.0	30.2	2.77×10^{5}	53.0
$MeC^{\bullet}H(CH_2)_2NH(C-H)HMe$	−33.4	20.6	1.50×10^{7}	43.2
$MeC^{\bullet}H(CH_2)_2NMe(C-H)HMe$	−44.9	16.0	7.30×10^{7}	38.2
$Me_2C^{\bullet}(CH_2)_2NH(C-H)Me_2$	−43.0	16.7	2.87×10^{7}	39.0
$Me_2C^{\bullet}(CH_2)_2NMe(C-H)Me_2$	−54.5	12.3	1.30×10^{8}	34.2
$MeC^{\bullet}H(CH_2)_3(C-H)HOH$	−14.6	29.0	8.38×10^{5}	51.8
$MeC^{\bullet}H(CH_2)_3(C-H)MeOH$	−20.5	26.2	1.10×10^{6}	49.0
$MeC^{\bullet}H(CH_2)_2C(O)(C-H)H_2$	−2.0	35.0	1.60×10^{5}	57.9
$MeC^{\bullet}H(CH_2)_2C(O)(C-H)HMe$	−14.2	29.1	8.09×10^{5}	52.0
$MeC^{\bullet}H(CH_2)_2C(O)(C-H)Me_2$	−19.3	26.8	8.92×10^{5}	49.6
$MeC^{\bullet}H(CH_2)_3(C-H)(O)$	−26.4	23.6	2.68×10^{6}	46.3
$MeC^{\bullet}H(CH_2)_3(C-H)HPh$	−43.3	20.1	1.78×10^{6}	43.1
$Me_2C^{\bullet}(CH_2)_3(C-H)MePh$	−45.3	19.3	1.17×10^{6}	42.3
$Me_2C^{\bullet}(CH_2)_3(C-H)HCH=CH_2$	−50.2	23.3	5.94×10^{5}	47.3
$Me_2C^{\bullet}(CH_2)_3(C-H)MeCH=CH_2$	−60.4	19.4	1.13×10^{6}	43.0

[a] Expressed in kJ mol^{-1}; [b] activation energies of mono- [E_e(m)] and bimolecular [E_e(b)] reactions expressed in kJ mol^{-1}; [c] in s^{-1}.

Reaction	E_{e0}	ΔE_{μ}
$C^{\bullet}H_2(CH_2)_3Me \rightarrow Me(CH_2)_3C^{\bullet}H_2$	52.0	0.0
$C^{\bullet}Cl_2(CH_2)_4Me \rightarrow CHCl_2(CH_2)_3C^{\bullet}HMe$	42.8	−9.2
$C^{\bullet}Cl_2(CH_2)_5Me \rightarrow CHCl_2(CH_2)_3C^{\bullet}HEt$	41.3	−10.7
$C^{\bullet}Cl_2(CH_2)_2SiEt_2CH_2Me \rightarrow CHCl_2(CH_2)_2SiEt_2C^{\bullet}HMe$	36.1	−15.9

Similar results were obtained by quantum-chemical calculations carried out by the B3LYP technique (the activation energies are expressed in kJ mol^{-1}; φ is the C···H···C angle).[19]

Reaction	E_a	$10^{10}\,r$(C···H) /m	φ /deg
$C^{\bullet}H_2(CH_2)_3Me \rightarrow Me(CH_2)_3C^{\bullet}H_2$	65.8	1.356	153.2
$C^{\bullet}Cl_2(CH_2)_3Me \rightarrow CHCl_2(CH_2)_3C^{\bullet}H_2$	50.8	1.350	101.5
$C^{\bullet}Cl_2(CH_2)_3CCl_2H \rightarrow CHCl_2(CH_2)_3C^{\bullet}Cl_2$	28.7	1.342	152.5

It can be seen that the polar effect markedly decreases the activation energy for hydrogen migration in chloroalkanes.

IV. Isomerisation of alkoxyl radicals

Alkoxyl radicals are highly active and rapidly enter into bimolecular hydrogen abstraction.[2,8]

$$R^1O^{\bullet} + R^2H \longrightarrow R^1OH + (R^2)^{\bullet}$$

In addition, alkoxyl radicals with rather long hydrocarbon chains ($>C_4$) also undergo intraradical hydrogen migration. Table 4 presents the rate constants for these reactions calculated from the ratio of the rate constants for RO$^{\bullet}$ isomerisation and RO$^{\bullet}$ destruction.[2]

Each of the reactions implies elimination of the hydrogen atom located in the γ-position, *i.e.*, the transition state contains a six-membered ring.

Table 4. Experimental rate constants and activation energies for hydrogen migration in alkoxyl radicals.

Reaction	E_a (see [a])	log$A$ (s^{-1})	$k_{350\,K}$ (see [b])	Ref.
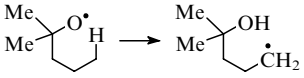	30.1	9.78	1.93×10^5	2
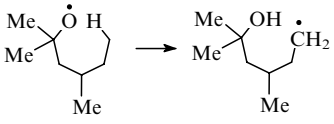	29.8	9.78	2.14×10^5	2
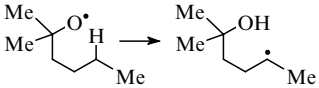	23.4	9.60	1.29×10^5	2
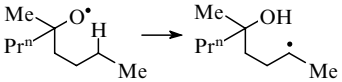	22.8	9.60	1.57×10^6	34
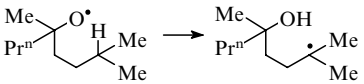	25.4	9.30	3.23×10^5	34
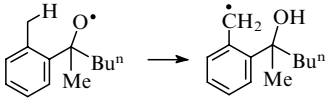	9.8	8.78	2.08×10^7	35

[a] Expressed in kJ mol^{-1}; [b] in s^{-1}.

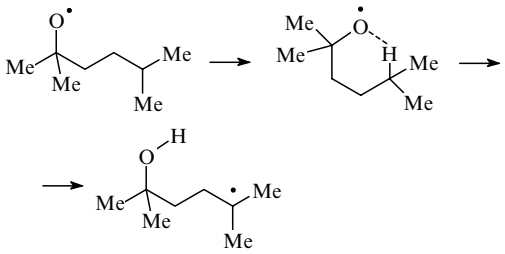

The kinetic parameters (br_e, E_{e0}, r_e and A_{C-H}) which describe this reaction in terms of the MIP are summarised in Table 5.

The hydrogen abstraction from the C−H bond located in the vicinity of the phenyl or vinyl group has a higher classical potential barrier (E_{e0}) due to stronger triplet repulsion.[20] However, the pre-exponential factor is smaller in this case due to entropy loss caused by the elimination of the free rotation of these groups in the TS. The activation energy of the thermally neutral isomerisation of alkoxyl radicals coincides with that of the bimolecular abstraction reaction:[16] E_{e0}(RO$^{\bullet}$ isomer.) = 53.4 kJ mol^{-1}, E_{e0}(RO$^{\bullet}$ + R^1H) = 53.2 kJ mol^{-1}. Thus, for the isomerisation with a non-linear TS, the relationship E(m) > E(b) expected theoretically does not hold either. The reason is apparently the same as in the case of hydrogen migration in alkyl radicals (see above).

Using MIP parameters, the activation energies and the rate constants for isomerisation of diverse alkoxyl radicals have been calculated.[16] The results of these calculations are summarised in Table 6.

V. Isomerisation of peroxyl radicals

The intraradical hydrogen migration also takes place in peroxyl radicals.[10,12,23] Hydrogen migrates from either β- or γ-position, *i.e.*, a TS with either six- or seven-membered ring is formed.

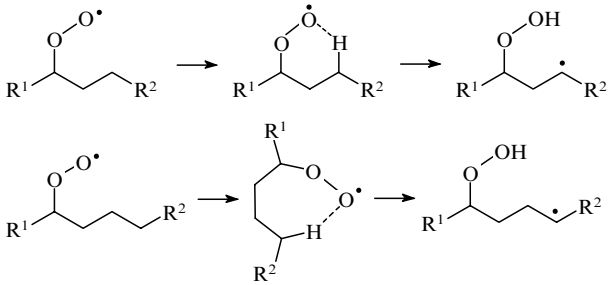

Experimental data on isomerisation of the alkyl and alkylaryl peroxyl radicals are listed in Table 7.

The MIP parameters for $RO_2^{\bullet}$ isomerisation calculated on the basis of these data are presented in Table 5. As in the case of isomerisation of alkoxyl radicals, in this case, too, the classical potential barriers (E_{e0}) are close to the E_{e0} values for the bimolecular reaction $RO_2^{\bullet}$ + RH (see Table 5). The activation energies E_{e0} of the reactions whose TS contain six- and seven-membered rings do not differ much. The activation energies and the rate constants for isomerisation of diverse peroxyl radicals calculated in terms of the MIP are summarised in Table 8.[16]

For these reactions, the E_a(m) values are close to E_a(b). The reason is apparently the same as in the case of isomerisation of the R$^{\bullet}$ and RO$^{\bullet}$ radicals.

VI. Cyclisation and ring opening in alkyl radicals

Alkyl radicals containing a multiple bond rapidly undergo intraradical cyclisation

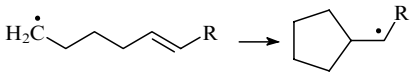

or

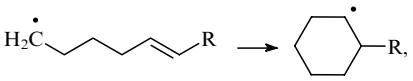

resulting in the formation of cyclic five- or six-membered radicals. These reactions have been intensively studied for the last 20 years. The experimental rate constants and the activation energies for the cyclisation of alkyl radicals are summarised in Table 9.

Recently, the experimental data have been analysed by means of the MIP protocol.[18] The ΔH_e, E_e and br_e values were calculated [see Eqns (1)–(4)] using the parameters presented below [b are expressed in (kJ mol^{-1})$^{1/2}$ m^{-1}, hN_Av_i and $hN_A(v_i-v_f)$ are in kJ mol^{-1}].

Attacked bond	α	$b\times10^{-10}$	$0.5hN_Av_i$,	$0.5hN_A(v_i-v_f)$
C=C	1.202	53.89	9.9	1.7
C≡C	1.542	69.12	12.7	4.5

The br_e, E_{e0} and r_e parameters and the experimental pre-exponential factors A are listed in Table 10.

The activation energy of cyclisation is undoubtedly affected by the reaction enthalpy. This is equal to the sum of the energy of formation of the new C–C bond and the strain energy of the newly formed ring (E_{rsc}) minus the energy of rupture of the C–C π-bond. Comparison of the br_e parameters for cyclisation reac-

Table 5. Kinetic parameters of the MIP for isomerisation of alkoxyl and peroxyl radicals.[16]

Radical ($R^1O^\bullet$)	br_e /(kJ mol^{-1})$^{1/2}$	E_{e0}(m) /kJ mol^{-1}	$10^{10}\,r_e$ /m	$\log A_{C-H}$ (s^{-1})	E_{e0}(b) /kJ mol^{-1}
$R^1O^\bullet \longrightarrow (R^2)^\bullet$ (Six-membered TS)					
$Me_2C(O^\bullet)(CH_2)_2(C-H)HR$	13.13	53.4	0.351	2.0×10^9	53.2
$Me_2C(O^\bullet)(CH_2)_2(C-H)HPh$	13.53	56.8	0.361	2.0×10^8	56.5
$Me_2C(O^\bullet)(CH_2)_2(C-H)HCH=CH_2$	14.17	62.2	0.379	2.0×10^8	62.0
$R^1O_2^\bullet \longrightarrow (R^2)^\bullet$ (Six-membered TS)					
$RCH(OO^\bullet)Y(C-H)HR$	13.23	53.2	0.353	2.0×10^9	56.3
$RCH(OO^\bullet)Y(C-H)HPh$	14.38	62.8	0.384	2.0×10^8	62.3
$RCH(OO^\bullet)Y(C-H)HCH=CH_2$	14.82	66.7	0.396	2.0×10^8	70.2
$R^1O_2^\bullet \longrightarrow (R^2)^\bullet$ (Seven-membered TS)					
$RCH(OO^\bullet)YCH_2(C-H)HR$	13.43	54.8	0.359	5.6×10^8	56.3
$RCH(OO^\bullet)YCH_2(C-H)HPh$	14.58	64.6	0.390	5.6×10^7	62.3
$RCH(OO^\bullet)YCH_2(C-H)HCH=CH_2$	15.02	68.6	0.401	5.6×10^7	70.2
$(R^2)^\bullet \longrightarrow R^1O_2^\bullet$ (Six-membered TS)					
$RCH(OO-H)YC^\bullet HR$	16.25	53.2	0.353	2.0×10^8	56.3
$RCH(OO-H)YC^\bullet HPh$	17.67	62.9	0.384	2.0×10^8	62.3
$RCH(OO-H)YC^\bullet HCH=CH_2$	18.21	66.8	0.396	2.0×10^8	70.2
$(R^2)^\bullet \longrightarrow R^1O_2^\bullet$ (Seven-membered TS)					
$RCH(OO-H)YCH_2C^\bullet HR$	16.50	54.8	0.359	5.6×10^7	56.3
$RCH(OO-H)YCH_2C^\bullet HPh$	17.91	64.6	0.389	5.6×10^7	62.3
$RCH(OO-H)YCH_2C^\bullet HCH=CH_2$	18.45	68.6	0.401	5.6×10^7	70.2

Table 6. Dissociation energies, enthalpies, activation energies and rate constants for hydrogen migration in alkoxyl radicals calculated using MIP relations.[16]

Radical	D_i (see [a])	ΔH_e (see [a])	E_e(m) [a]	$k_{350\,K}$ /s^{-1}	E_e(b) [a]
$Me_2C(O^\bullet)(CH_2)_2(C-H)H_2$	422.0	−19.5	29.3	2.5×10^5	29.1
$Me_2C(O^\bullet)(CH_2)_2(C-H)HMe$	412.0	−29.5	25.4	6.4×10^5	25.2
$Me_2C(O^\bullet)(CH_2)_2(C-H)Me_2$	400.0	−41.5	21.1	1.4×10^6	20.8
$Me_2C(O^\bullet)CH_2NH(C-H)HMe$	378.6	−62.9	14.0	3.3×10^7	13.7
$Me_2C(O^\bullet)CH_2NMe(C-H)HMe$	367.1	−74.4	10.5	1.1×10^8	10.3
$Me_2C(O^\bullet)CH_2NH(C-H)Me_2$	357.0	−84.5	7.7	1.4×10^8	7.5
$Me_2C(O^\bullet)CH_2NMe(C-H)Me_2$	345.5	−96.0	4.7	4.0×10^8	4.5
$Me_2C(O^\bullet)(CH_2)_2(C-H)HOH$	397.4	−44.1	20.1	3.9×10^6	19.9
$Me_2C(O^\bullet)(CH_2)_2(C-H)(OH)Me$	391.5	−50.0	18.1	3.9×10^6	17.9
$Me_2C(O^\bullet)CH_2C(O)(C-H)H_2$	410.0	−31.5	24.7	1.2×10^6	24.5
$Me_2C(O^\bullet)CH_2C(O)(C-H)HMe$	397.8	−43.7	20.3	3.8×10^6	20.1
$Me_2C(O^\bullet)CH_2C(O)(C-H)Me_2$	392.7	−48.8	18.5	3.4×10^6	18.3
$Me_2C(O^\bullet)(CH_2)_2(C-H)(O)$	385.6	−55.9	16.2	7.7×10^6	15.9
$Me_2C(O^\bullet)(CH_2)_2(C-H)HPh$	368.7	−72.8	14.0	3.3×10^6	13.7
$Me_2C(O^\bullet)(CH_2)_2(C-H)MePh$	354.7	−86.8	9.9	6.6×10^6	9.7
$Me_2C(O^\bullet)(CH_2)_2(C-H)HCH=CH_2$	349.8	−91.7	13.4	4.0×10^6	13.2
$Me_2C(O^\bullet)(CH_2)_2(C-H)MeCH=CH_2$	339.6	−101.9	10.6	5.2×10^6	10.4

[a] Expressed in kJ mol^{-1}.

Table 7. Experimental enthalpies, activation energies and rate constants for hydrogen migration in alkylperoxyl radicals.

Radical	ΔH (see [a])	E_a (see [a])	$k_{350\,K}$ /s^{-1}	n [b]	Ref.
PhCH($O_2^{\bullet}$)O(C−H)HPh	1.4	44.2	1.01×10^3	6	36–38
$Me_2C(O_2^{\bullet})CH_2$(C−H)Me_2	41.4	57.4	5.43	6	39
$Me_2C(O_2^{\bullet})O$(C−H)Me_2	32.2	55.2	11.6	6	36, 40
MeCH($O_2^{\bullet}$)CH_2(C−H)HMe	47.5	68.9	0.21	6	41
MeCH($O_2^{\bullet}$)CH_2(C−H)$HC_{10}H_{21}$-n	50.2	58.8	6.71	6	42
Me(C−H)$HCH_2CH(O_2^{\bullet})C_{12}H_{25}$-n	47.5	62.2	2.09	6	43
MeCH($O_2^{\bullet}$)CH_2(C−H)(O_2H)$C_{12}H_{25}$-n	26.0	48.3	1.24×10^2	6	43
$Me_2CHCH_2C(O_2^{\bullet})MeCH_2$(C−H)$Me_2$	41.4	54.5	14.72	6	44
$Me_2C(O_2^{\bullet})C$(O)(C−H)Me_2	34.1	59.0	3.13	6	45
[n-$C_6H_{13}C(O)OCH_2]_3CCH_2OC(O)CH_2CH(O_2^{\bullet})CH_2$(C−H)HEt	47.5	56.8	13.34	6	46
[n-$C_6H_{13}C(O)OCH_2]_3CCH_2OC(O)(CH_2)_3CH(O_2^{\bullet})CH_2$(C−H)$H_2$	56.5	56.9	19.34	6	46
Ph(C−H)(O_2H)OCH($O_2^{\bullet}$)Ph	1.4	47.7	15.22	6	38, 47
[n-$C_6H_{13}C(O)OCH_2]_3CCH_2OC(O)(CH_2)_2$(C−H)$HCH_2CH(O_2^{\bullet})$Me	50.2	56.8	13.34	6	46
[n-$C_6H_{13}C(O)OCH_2]_3CCH_2OC(O)CH_2CH(O_2^{\bullet})CH_2$(C−H)($O_2$H)Et	26.0	41.9	1.12×10^3	6	46
MeCH($O_2^{\bullet}$)$(CH_2)_2$(C−H)$HC_{11}H_{23}$-n	50.2	63.1	1.53	7	43, 48
EtC(O)$OCH_2Me_2CCH(O_2^{\bullet})OC$(O)(C−H)HMe	33.3	52.5	58.47	7	49
[EtC(O)$OCH_2]_3CCH(O_2^{\bullet})OC$(O)(C−H)HMe	33.3	53.5	41.47	7	49
Me(C−H)H$(CH_2)_2CH(O_2^{\bullet})C_{11}H_{23}$-n	47.5	62.3	2.02	7	43
MeCH($O_2^{\bullet}$)$(CH_2)_2$(C−H)(O_2H)$C_{11}H_{23}$-n	26.0	52.7	27.29	7	43
[EtC(O)$OCH_2]_2(CHCH_2)CCH(O_2^{\bullet})OC$(O)(C−H)HMe	33.3	53.4	42.92	7	49
[n-$C_6H_{13}C(O)OCH_2]_3CCH_2OC(O)CH_2CH(O_2^{\bullet})(CH_2)_2$(C−H)($O_2$H)Me	26.0	46.2	2.55×10^2	7	46
[n-$C_6H_{13}C(O)OCH_2]_3CCH_2OC(O)CH_2$(C−H)($O_2$H)$(CH_2)_2CH(O_2^{\bullet})$Me	26.0	47.0	1.93×10^2	7	46

[a] Expressed in kJ mol^{-1}; [b] the number of atoms in the TS ring.

Table 8. Enthalpies, activation energies and rate constants for hydrogen migration in alkylperoxyl radicals calculated using the MIP relations.[16]

Radical	ΔH_e (see [a])	ΔE_μ (see [a, b])	E_e(m) [a]	$k_{350\,K}$ /s^{-1}	E_e(b) [a]
$CH_2(OO^{\bullet})CMe_2$(C−H)H_2	56.5	0	64.3	1.5	67.2
MeCH($OO^{\bullet}$)CH_2(C−H)HMe	46.5	0	58.7	7.0	61.6
$Me_2C(OO^{\bullet})CH_2$(C−H)Me_2	41.4	0	55.9	9.2	58.9
MeCH($OO^{\bullet}$)NH(C−H)HMe	13.1	0	41.6	2.5×10^3	44.7
MeCH($OO^{\bullet}$)NMe(C−H)HMe	1.6	0	36.3	1.5×10^4	39.4
$Me_2C(OO^{\bullet})NH$(C−H)Me_2	−1.6	0	34.9	1.2×10^4	38.0
$Me_2C(OO^{\bullet})NMe$(C−H)Me_2	−13.1	0	30.0	6.6×10^4	33.1
CH(OH)($OO^{\bullet}$)CH_2(C−H)HOH	25.8	−2.2	45.5	6.4×10^2	48.6
MeC(OH)($OO^{\bullet}$)CH_2(C−H)MeOH	19.9	−2.2	42.6	8.7×10^2	45.7
$CH_2(OO^{\bullet})C$(O)(C−H)H_2	44.5	−15.4	42.2	3.1×10^3	45.1
MeCH($OO^{\bullet}$)C(O)(C−H)HMe	32.3	−15.4	35.7	1.9×10^4	38.7
$Me_2C(OO^{\bullet})C$(O)(C−H)Me_2	34.1	−15.7	36.3	7.7×10^3	39.3
C(O)($OO^{\bullet}$)CH_2(C−H)(O)	−20.5	−8.8	18.3	3.8×10^6	21.3
PhCH($OO^{\bullet}$)CH_2(C−H)HPh	−1.4	0	44.6	8.7×10^1	44.1
PhC($OO^{\bullet}$)CH_2(C−H)MePh	−3.9	0	43.5	6.3×10^1	43.0
CH_2=CHCH($OO^{\bullet}$)CH_2(C−H)HCH=CH_2	−15.7	0	42.4	1.9×10^2	45.9
CH_2=CHC($OO^{\bullet}$)$MeCH_2$(C−H)MeCH=CH_2	−19.0	0	41.2	1.5×10^2	44.5

[a] Expressed in kJ mol^{-1}; [b] ΔE_μ is the contribution of the polar interaction to the activation energy.

tions of various alkyl radicals (see Table 10) leads to the following conclusions.

1. The br_e parameter depends on the size of the ring formed.

2. This parameter does not depend (or slightly depends) on the number and the positions of substituents in the radical which undergoes cyclisation.

3. The br_e parameters of cyclisation are equal for radicals containing rings of the same size and chains, both composed of C atoms alone and incorporating also O and Si atoms.

4. For cyclisation reactions of perfluorinated radicals, the br_e parameters are higher.

5. Cyclisation that takes place through intramolecular attack of the radical on the triple bond is described by higher br_e parameters.

Effect of the ring strain energy on the activation energy. It follows from the data listed in Table 10 that, depending on the ring size, the activation energy of the thermally neutral cyclisation passes through a maximum, E_{e0} = 85.7 kJ mol^{-1}, which is attained upon the formation of a six-membered ring. The minimum value E_{e0} = 36.4 kJ mol^{-1} is observed for the formation of a three-membered ring. For radical cyclisation reactions resulting in three- to six-carbon rings, the following linear correlation is observed:

$$E_{e0} = 85.5 - 16.4\,(6 - n), \qquad (14)$$

where E_{e0} is expressed in kJ mol^{-1}, n is the number of C atoms in the ring.

Table 9. Experimental enthalpies, activation energies and rate constants for cyclisation of alkyl radicals.

Reactant	Product	ΔH /kJ mol^{-1}	T /K	$k_{298\,K}$ /s^{-1}	E_a /kJ mol^{-1}	Ref.
$n = 3$, log$A$ (s^{-1}) = 11.6						
$CH_2=CHCHMeC^{\bullet}H_2$		23.0	333 – 379	4.94×10^4	39.4	50
$CH_2=CHCH_2C^{\bullet}D_2$	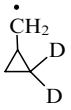	23.4	252 – 276	5.37×10^3	44.9	51
$Ph_2C=CHCH_2C^{\bullet}H_2$			277 – 309	2.01×10^7	24.5	52
$PhCH=CHCH_2C^{\bullet}H_2$			280 – 321	6.53×10^6	27.3	52
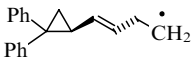	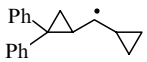		292 – 331	6.05×10^4	38.9	53
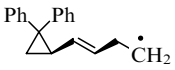	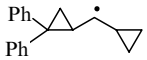		293 – 322	8.43×10^4	38.1	53
$n = 4$, log$A$ (s^{-1}) = 11.3						
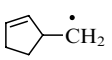		−24.8	338	8.3×10^4	34.8	54
$n = 5$, log$A$ (s^{-1}) = 10.2						
$CH_2=\,^{13}CH(CH_2)_3C^{\bullet}H_2$	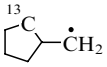	−64.4	313	1.8×10^5	29.7	55
$CH_2=CH(CH_2)_3C^{\bullet}H_2$	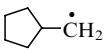	−64.4	188 – 373	3.75×10^4	32.1	56 – 59
$CH_2=CH(CH_2)_2CHMeC^{\bullet}H_2$	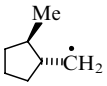	−66.7	318 – 373	4.57×10^5	25.9	60 – 62
$CH_2=CHCHMe(CH_2)_2C^{\bullet}H_2$	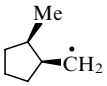	−66.3	298 – 373	7.74×10^4	30.3	60 – 62
$CH_2=CHCHMe(CH_2)_2C^{\bullet}H_2$	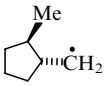	−69.8	298 – 373	3.74×10^5	26.4	60 – 62
$CH_2=CHCH_2CHMeCH_2C^{\bullet}H_2$	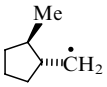	−66.7	318 – 373	2.40×10^5	27.5	60 – 62
$CH_2=CHCH_2CHMeCH_2C^{\bullet}H_2$	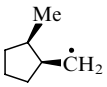	−63.2	318 – 373	2.40×10^5	27.5	60 – 62
$CH_2=CH(CH_2)_2CHMeC^{\bullet}H_2$	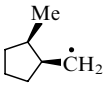	−63.2	318 – 373	2.40×10^5	27.5	60 – 62
$CH_2=CMe(CH_2)_3C^{\bullet}H_2$	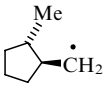	−65.3	298 – 338	2.22×10^4	33.4	56, 62, 63
$CH_2=CH(CH_2)_3C^{\bullet}HMe$	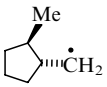	−66.8	298 – 338	1.03×10^5	29.6	56, 62
$MeCH=CMe(CH_2)_3C^{\bullet}H_2$	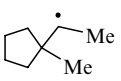	−61.7	338	3.3×10^5	30.3	56

Table 9 (continued).

Reactant	Product	ΔH /kJ mol^{-1}	T /K	$k_{298\,K}$ /s^{-1}	E_a /kJ mol^{-1}	Ref.
$n = 5$, log$A$ (s^{-1}) = 10.2						
$CH_2=CMe(CH_2)_3C^{\bullet}Me_2$	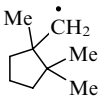	−43.8	313	6.2×10^4	32.4	63
$CH_2=CHCH_2CH(CH_2C^{\bullet}H_2)Pr^n$	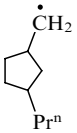	−64.4	353	6.6×10^6	22.8	60, 64
$CH_2=CPr^i(CH_2)_3C^{\bullet}H_2$	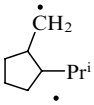	−61.6	338	2.5×10^4	37.5	60
$CH_2=CH(CH_2)_2CMe_2C^{\bullet}H_2$	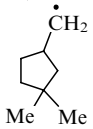	−64.4	298 – 353	2.81×10^6	21.4	64 – 66
$Me_2C=CH(CH_2)_3C^{\bullet}H_2$	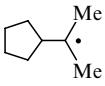	−69.3	338	2.6×10^6	24.5	56
$CH_2=CH(CH_2)_3C^{\bullet}HPr^n$	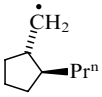	−66.8	338	8.5×10^5	27.6	56
$CH_2=CH(CH_2)_2CH(C^{\bullet}H_2)CH=CH_2$	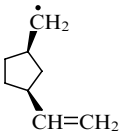	−60.9	353	7.8×10^5	29.1	60
$CH_2=CH(CH_2)_2CH(C^{\bullet}H_2)CH=CH_2$	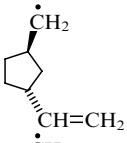	−64.4	353	1.4×10^6	27.3	60
$CH_2=CHCH_2CH(CH=CH_2)CH_2C^{\bullet}H_2$	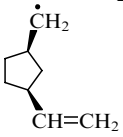	−60.9	353	2.2×10^6	26.1	60
$CH_2=CHCH_2CH(CH=CH_2)CH_2C^{\bullet}H_2$	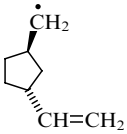	−64.4	353	6.6×10^5	29.6	60
$C^{\bullet}H_2CH_2CH(CH_2CH=CH_2)_2$	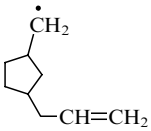	−65.4	303 – 357	1.88×10^6	22.4	67
$N\equiv CCH=CH(CH_2)_3C^{\bullet}H_2$	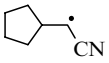	−107.4	223 – 324	1.72×10^8	11.2	68
$Ph_2C=CH(CH_2)_3C^{\bullet}H_2$	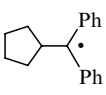	−112.5	226 – 317	5.35×10^7	14.1	69
$Ph_2C=CH(CH_2)_3C^{\bullet}H_2$	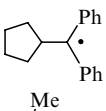	−112.5	236 – 317	4.08×10^7	14.8	70
$Ph_2C=CH(CH_2)_3C^{\bullet}HMe$	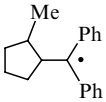	–	234 – 325	2.36×10^7	16.1	70

Table 9 (continued).

Reactant	Product	ΔH /kJ mol^{-1}	T /K	$k_{298\,K}$ /s^{-1}	E_a /kJ mol^{-1}	Ref.
$n = 5, \log A\ (s^{-1}) = 10.2$						
$Ph_2C{=}CH(CH_2)_3C^{\bullet}Me_2$	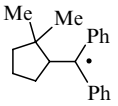	–	263 – 326	1.22×10^7	17.8	70
$Ph_2C{=}CH(CH_2)_3C^{\bullet}HOMe$	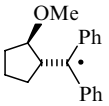	−106.7	273 – 313	3.87×10^7	14.9	71
$Ph_2C{=}CH(CH_2)_3C^{\bullet}HC(O)OEt$	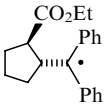	−98.1	273 – 313	6.55×10^7	13.6	72
$Ph_2C{=}CH(CH_2)_3C^{\bullet}MeC(O)OEt$	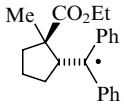	−87.6	273 – 333	4.39×10^5	26.0	72
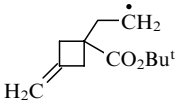	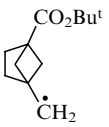	−61.6	274 – 383	2.71×10^5	27.2	73
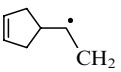		−51.2	366 – 403	3.91×10^3	37.7	74
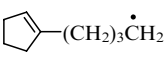		−61.9	338	1.2×10^5	33.0	56
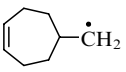		−53.8	280 – 470	1.67×10^5	28.4	75
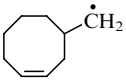		−56.4	280 – 470	6.86×10^4	30.6	75
$CH_2{=}CH(CH_2)_3C^{\bullet}(O)$		–	298	2.2×10^5		76
$MeCH{=}CH(CH_2)_2CHMeC^{\bullet}(O)$	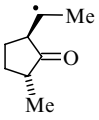	–	298	1.8×10^5	25.1	76
$MeCH{=}CH(CH_2)_2CHMeC^{\bullet}(O)$	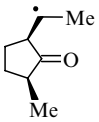	–	298	1.3×10^5	25.5	76
$CH_2{=}CH(CH_2)_2OC^{\bullet}H_2$	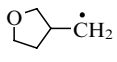	−65.7	180 – 220	3.32×10^4	32.4	65, 77
$CH_2{=}CMeCH_2OCH_2C^{\bullet}H_2$	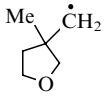	−62.9	313	2.0×10^5	29.3	78
$CH_2{=}CHCH_2OCH_2C^{\bullet}HMe$	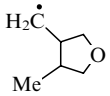	−96.1	338	8.8×10^6	21.1	79
$CH_2{=}CPhCH_2OCH_2C^{\bullet}H_2$	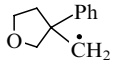	−61.6	313	1.7×10^5	29.7	78

Table 9 (continued).

Reactant	Product	ΔH /kJ mol^{-1}	T /K	$k_{298\,K}$ /s^{-1}	E_a /kJ mol^{-1}	Ref.
$n = 5, \log A\ (s^{-1}) = 10.2$						
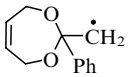	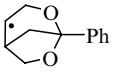	−92.7	298 – 423	4.96×10^5	25.7	80
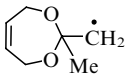	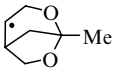	−92.7	272 – 394	8.38×10^5	24.4	80
$CF_2=CF(CF_2)_3C^{\bullet}F_2$	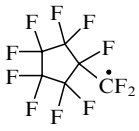	−136.8	231 – 353	4.22×10^5	26.1	81
$CF_2=CFO(CF_2)_2C^{\bullet}F_2$	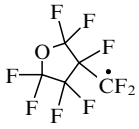	−137.9	303	3.5×10^6	21.2	82
$CH_2=CHCH_2OCF_2C^{\bullet}F_2$	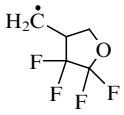	–	298	3.8×10^7	15.0	83
$CH_2=CHCH_2SiMe_2CH_2C^{\bullet}H_2$	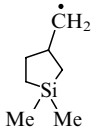	−64.4	298	1.0×10^3	36.6	58
$CH_2=CH(CH_2)_2SiMe_2C^{\bullet}H_2$	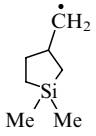	−64.4	298	7.5×10^3	38.7	58
$CH_2=CHSiMe_2(CH_2)_2C^{\bullet}H_2$	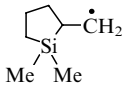	−64.4	298	7.5×10^4	34.9	58, 66, 84
$HC\equiv C(CH_2)_3C^{\bullet}H_2$		−75.9	298	2.8×10^4	32.8	62
$n = 6, \log A\ (s^{-1}) = 9.7$						
$CH_2=CH(CH_2)_3C^{\bullet}H_2$		−75.3	188 – 396	1.78×10^2	42.5	56 – 58, 61, 65
$CH_2=CH(CH_2)_4C^{\bullet}H_2$	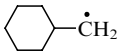	−92.5	338	2.5×10^4	34.3	85
$CH_2=CMe(CH_2)_3C^{\bullet}H_2$	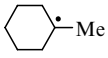	−108.3	298 – 338	8.57×10^3	32.9	56, 62
$CH_2=CH(CH_2)_3C^{\bullet}HMe$	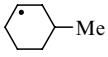	−97.6	338	9.7×10^3	36.9	56
$CH_2=CH(CH_2)_3C^{\bullet}Me_2$	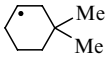	−87.6	298 – 338	9.68×10^3	32.6	56, 62, 86
$CH_2=CH(CH_2)_4C^{\bullet}HMe$	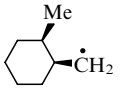	−82.7	298	2.1×10^3	33.9	62
$CH_2=CH(CH_2)_4C^{\bullet}HMe$	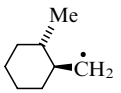	−90.5	298	5.7×10^3	36.4	62
$CH_2=CMe(CH_2)_3C^{\bullet}Me_2$	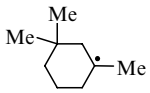	−105.1	313	5.4×10^4	29.7	56, 73
$MeCH=CMe(CH_2)_3C^{\bullet}H_2$	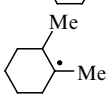	−92.2	338	6.0×10^4	31.8	56

Table 9 (continued).

Reactant	Product	ΔH /kJ mol^{-1}	T /K	$k_{298\,K}$ /s^{-1}	E_a /kJ mol^{-1}	Ref.
$n = 6$, $\log A$ (s^{-1}) = 9.7						
$CH_2=CH(CH_2)_3C^{\bullet}HPr^n$	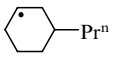	−97.6	338	4.1×10^3	39.4	56
$CH_2=CPr^i(CH_2)_3C^{\bullet}H_2$	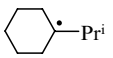	−103.9	338	8.0×10^4	31.0	62
$CH_2=CMe(CH_2)_2CMe_2C^{\bullet}H_2$	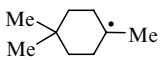	−105.0	318–373	2.17×10^4	30.6	64
$(CH_2=CHCH_2)_2CHCH_2C^{\bullet}H_2$	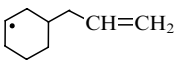	−95.3	333	2.3×10^5	27.6	71
$Ph_2C=CH(CH_2)_4C^{\bullet}HOMe$	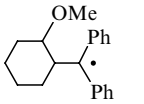	−133.0	283–323	1.51×10^5	25.8	71
$MeCH=CH(CH_2)_2CHMeC^{\bullet}(O)$	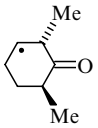	–	298	2.0×10^4	26.8	76
$MeCH=CH(CH_2)_2CHMeC^{\bullet}(O)$	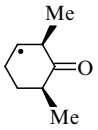	–	298	5.2×10^3	28.4	76
$PhCH_2CH=CH(CH_2)_2CHMeC^{\bullet}(O)$	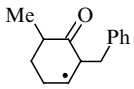	−84.8	353	2.0×10^5	29.7	87
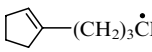		−89.3	338	3.0×10^4	33.7	56
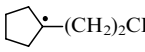		−76.8	338	6.7×10^4	31.5	56
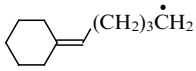	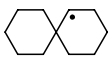	−89.5	338	1.0×10^6	23.8	56
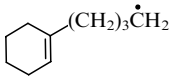	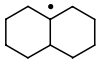	−89.4	338	5.3×10^4	32.2	56
$Ph_2C=CH(CH_2)_4C^{\bullet}HC(O)OEt$	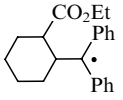	−124.5	273–313	1.99×10^7	13.7	73
$CH_2=CMeCH_2OCH_2C^{\bullet}H_2$	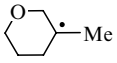	−80.0	313	4.6×10^3	36.2	78
$CH_2=CH(CH_2)_3CF_2C^{\bullet}F_2$	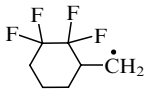	–	298	1.44×10^7	14.5	83
$CH_2=CHCH_2O(CF_2)_2C^{\bullet}F_2$	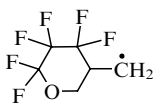	–	298	1.21×10^6	20.6	83
$CH_2=CHO(CH_2)_2CF_2C^{\bullet}F_2$	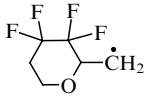	–	298	9.4×10^6	15.6	83
$CH_2=CH(CH_2)_2SiMe_2C^{\bullet}H_2$	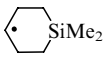	−95.3	298	1.6×10^4	34.0	58
$CH_2=CHSiMe_2(CH_2)_2C^{\bullet}H_2$		−95.3	298	7.5×10^4	34.7	58

Table 9 (continued).

Reactant	Product	ΔH /kJ mol^{-1}	T /K	$k_{298\,K}$ /s^{-1}	E_a /kJ mol^{-1}	Ref.
$n = 6$, log$A$ (s^{-1}) = 9.7						
$CH_2=CHCH_2SiMe_2CH_2C^{\bullet}H_2$	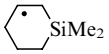	−95.3	298	1.4×10^4	34.9	66
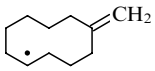		−136.2	313–396	9.97×10^8	4.0	88
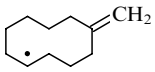		−149.6	313–396	3.21×10^9	1.1	88
$HC\equiv C(CH_2)_4C^{\bullet}H_2$	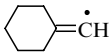	−58.9	333	4.6×10^4	32.1	59
$n = 7$, log$A$ (s^{-1}) = 9.1						
$CH_2=CH(CH_2)_4C^{\bullet}H_2$		−53.5	338	4.8×10^3	35.0	85
$CH_2=CH(CH_2)_5C^{\bullet}H_2$	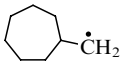	−64.6	338	8.3×10^2	39.9	85
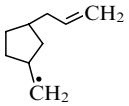		−73.4	338	3.0×10^3	37.7	67
$HC\equiv C(CH_2)_5C^{\bullet}H_2$	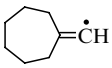	−85.3	333	2.5×10^3	36.3	59
$CH_2=CHO(CH_2)_2CF_2C^{\bullet}F_2$	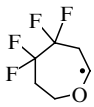	–	298	3.4×10^6	14.2	83
$n = 8$, log$A$ (s^{-1}) = 8.8						
$HC\equiv C(CH_2)_6C^{\bullet}H_2$	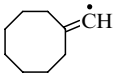	−58.5	333	1.2×10^2	42.8	59
$CH_2=CH(CH_2)_4CF_2C^{\bullet}F_2$	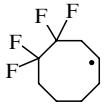	–	298	2.0×10^4	25.7	83
$CH_2=CH(CH_2)_2OC(O)CF_2C^{\bullet}F_2$	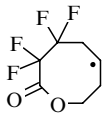	–	298	3.6×10^4	24.2	83
$n = 11$, log$A$ (s^{-1}) = 7.1						
$CH_2=CHC(O)O(CH_2)_6C^{\bullet}H_2$	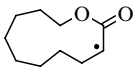	–	353	2.8×10^3	20.5	89
$n = 12$, log$A$ (s^{-1}) = 6.5						
$CH_2=CHC(O)O(CH_2CH_2O)_2CH_2C^{\bullet}H_2$	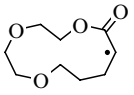	–	353	1.5×10^5	7.4	89
$CH_2=CMeC(O)O(CH_2CH_2O)_2CH_2C^{\bullet}H_2$	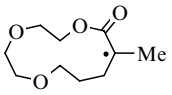	–	353	7.0×10^4	9.3	89
E-$MeCH=CHC(O)O(CH_2CH_2O)_2CH_2C^{\bullet}H_2$	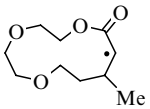	–	353	6.6×10^3	15.0	89

Table 9 (continued).

Reactant	Product	ΔH /kJ mol^{-1}	T /K	$k_{298\,K}$ /s^{-1}	E_a /kJ mol^{-1}	Ref.
$n = 12$, log$A$ (s^{-1}) = 6.5						
Z-(EtOC(O))CH=CHC(O)O(CH$_2$CH$_2$O)$_2$CH$_2$C$^{\bullet}$H$_2$	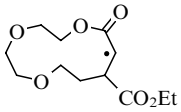	–	353	6.0×10^3	15.3	89
E-(EtOC(O))CH=CHC(O)O(CH$_2$CH$_2$O)$_2$CH$_2$C$^{\bullet}$H$_2$	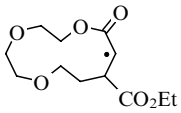	–	353	9.4×10^4	8.6	89
E-PhCH=CHC(O)O(CH$_2$CH$_2$O)$_2$CH$_2$C$^{\bullet}$H$_2$	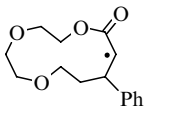	–	353	2.9×10^3	17.0	89
CH$_2$=C(C(O)OEt)CH$_2$O(CH$_2$CH$_2$O)$_2$CH$_2$C$^{\bullet}$H$_2$	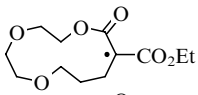	–	353	1.4×10^5	7.6	89
CH$_2$=CHC(O)O(CH$_2$)$_7$C$^{\bullet}$H$_2$	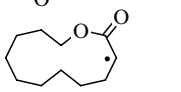	–	353	4.8×10^3	15.8	89

Table 10. MIP parameters for cyclisation of alkyl radicals and ring strain energies.[18,33]

n (see [a])	br_e (see [b])	E_{e0} (see [c])	E_{rsc} (see [c])	$10^{10}\,r_e$ /m	log$A$ (s^{-1})
3	13.28 ± 0.59	36.4	115.1	0.246	11.60
4	15.13	47.2	110.9	0.281	11.30
5	18.39 ± 0.60	69.7	26.7	0.341	10.20
6	20.39 ± 0.64	85.7	0.7	0.378	9.90
7	19.45 ± 0.66	78.0	26.8	0.361	9.10
5 (see [d])	21.38	94.3	26.7	0.397	10.20
5 (see [e])	22.98	81.7	26.7	0.332	10.20

[a] The number of atoms in the ring; [b] in (kJ mol^{-1})$^{1/2}$; [c] in kJ mol^{-1}; [d] for C_nF_{2n}; [e] for RC≡CR.

When a linear hydrocarbon is transformed into a cyclic one, a ring strain energy appears. This is due to the fact that the C–C–C angle best suited for sp^3-hybridisation (109°) decreases upon cyclisation, for example, to 60° in the case of cyclopropane, and this enhances the energy of the cyclic molecule. This strain in the formed ring may affect the E_{e0} value. The published [33] strain energies (E_{rsc}) for some rings are presented in Table 10; Fig. 2 juxtaposes the E_{e0} and E_{rsc} values.

The E_{e0} and E_{rsc} values (expressed in kJ mol^{-1}) obey the following linear correlation:

$$E_{e0} = (85.5 \pm 2.8) - (0.43 \pm 0.05)E_{rsc}\,. \qquad (15)$$

Thus, the higher the strain energy in the ring, the lower the classical potential barrier to the thermally neutral reaction. In addition, the higher the E_{rsc}, the higher the reaction enthalpy and, hence, the higher the activation energy of cyclisation, which depends on ΔH. Substitution of expression (14) into Eqn (4) followed by transformations gives an expression for calculating the activation energy E_e:

$$\sqrt{E_e} = 3.28\sqrt{194.4 - E_{rsc}}\left(1.202\sqrt{1 + \frac{0.208\Delta H_e}{194.4 - E_{rsc}}} - 1\right), \qquad (16)$$

which allows one to calculate the Arrhenius activation energy (E_a) of cyclisation from the reaction enthalpy ΔH ($\Delta H_e = \Delta H + 1.7$) and the strain E_{rsc} of the ring formed. Presented below are the results of calculation of the E_a values for the reactions

$$CH_2{=}CH(CH_2)_{n-2}C^{\bullet}HR \longrightarrow \text{cyclo-}[CHR(CH_2)_{n-2}CH(C^{\bullet}H_2)],$$

where $n = 3-10$ is the number of C atoms in the ring; the enthalpies and the activation energies are expressed in kJ mol^{-1}, $T = 350$ K.

n	ΔH_e	E_{rsc}	E_{e0}	E_a(calc)	E_a(exp)
3	21.7	115.1	36.4	38.9	44.9
4	16.7	110.1	54.1	38.1	34.8
5	–62.7	26.7	69.7	34.5	32.1
6	–90.8	0.7	85.7	33.5	34.3
7	–36.9	26.3	78.0	46.4	–
8	–19.8	40.6	–	48.7	–
10	–8.4	52.0	–	49.6	–

It can be seen that the lowest calculated E_a(calc) value corresponds to the formation of a six-membered ring, and starting from $n = 7$, the activation energy depends only slightly on the ring size. The influence of ΔH_e and E_{rsc} on the activation energy is largely compensated.

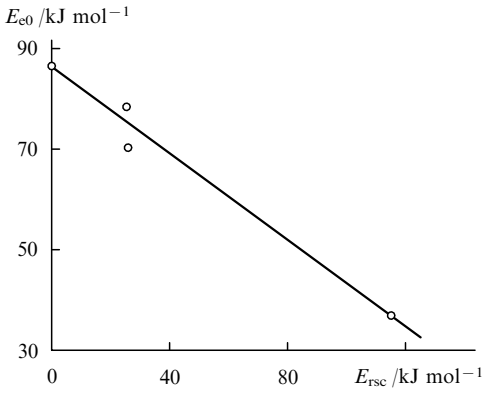

Figure 2. Activation energy of thermally neutral reaction (E_{e0}) *vs.* ring strain energy (E_{rsc}) for cyclisation of alkyl radicals.

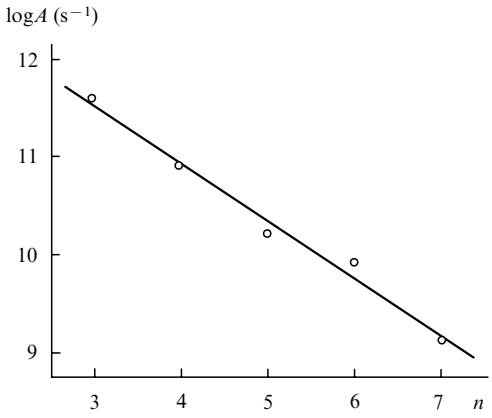

Figure 3. Dependence of log$A$ on the number (n) of carbon atoms in the ring for cyclisation of alkyl radicals.

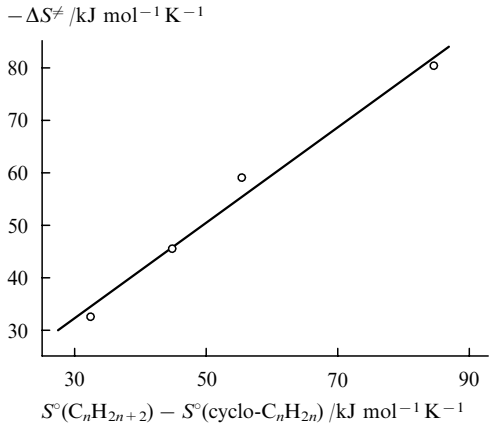

Figure 4. Correlation between the activation entropy ($\Delta S^{\neq}$) for cyclisation of alkyl radicals and the difference between the formation entropies (S°) of the corresponding linear and cycic hydrocarbons.

Effect of the ring size on the pre-exponential factor for cyclisation. As noted above (see Table 10), the pre-exponential factor for the radical cyclisation reaction depends on the size of the ring formed. Figure 3 shows the dependence of log$A$ on the number of atoms (n) in the ring of the resulting molecule.

For $n \geqslant 3$, this linear dependence is described by the relation

$$\log A\ (s^{-1}) = (13.34 \pm 0.21) - (0.60 \pm 0.04)\, n. \qquad (17)$$

This type of dependence of the pre-exponential factor on the ring size is due to the decrease in the activation entropy caused by the formation of a ring. The formation of a cyclic TS from a linear radical, for example, $CH_2{=}CH(CH_2)_{n-2}C^{\bullet}H_2$, eliminates free rotation of radical fragments around the corresponding C–C bonds. This results in a lower TS entropy compared to the starting radicals. The magnitide of this entropy change can be evaluated by comparing the S° values of the linear and the corresponding cyclic hydrocarbon molecules. The termination of rotation of one CH_2 group around a C–C bond decreases the entropy of a species by about 40 J mol^{-1} K^{-1}; therefore, the variation of log$A$ *vs.* n is linear. The entropies (S°) of the linear (C_nH_{2n+2}) and cyclic (cyclo-C_nH_{2n}) molecules, the difference between them (ΔS°) and the activation entropy ($\Delta S^{\neq}$) (J mol^{-1} K^{-1}) are presented below.

n	log$A$ (s^{-1})	$-\Delta S^{\neq}$	S°(cyclo-C_nH_{2n})	$S^{\circ}(C_nH_{2n+2})$	ΔS°
3	11.60	32.5	237.4	270.0	32.6
4	10.90	48.4	265.2	310.0	44.8
5	10.20	59.3	293.1	348.9	55.8
6	9.90	65.2	298.6	388.1	89.5
7	9.10	80.5	342.6	427.9	85.3

It can be seen that the difference $\Delta S^{\circ} = S^{\circ}$(cyclo-$C_nH_{2n}$) $- S^{\circ}(C_nH_{2n+2})$ increases with an increase in the ring size (for $n = 3-7$). This trend is caused by the following: the greater the number of C–C bonds in the ring around which the rotation takes place, the more pronounced the entropy loss that accompanies the cyclisation of a molecule or a radical. The cyclohexane ring provides an exception [$\Delta S^{\circ}(n = 6) > \Delta S^{\circ}(n = 7)$], probably, due to the presence of two conformations (a chair and a boat) where transition from one conformation to the other increases the entropy of the six-membered ring. It can be seen from Fig. 4 that the activation entropy ($-\Delta S^{\neq}$) depends linearly on the ΔS° value for $n = 3, 4, 5$ and 7; the reaction giving a cyclohexane ring ($n = 6$) is an exception. The variation of $\Delta S^{\neq}$ *vs.* ΔS° (both are in J mol^{-1} K^{-1}) is linear having a slope ratio close to unity (see Fig. 4):

$$-\Delta S^{\neq} = (5.36 \pm 0.08) + \\ + (0.90 \pm 0.08)\,[S^{\circ}(C_nH_{2n+2}) - S^{\circ}(\text{cyclo-}C_nH_{2n})]. \qquad (18)$$

This attests to a purely entropy influence of the ring size on the pre-exponential factor.

Role of the force constant in cyclisation reactions. The activation energy of the bimolecular elimination–addition reaction depends on the force constants on the reacting bonds.[20] The classical potential barrier to the thermally neutral reaction (E_{e0}) is determined, according to the MIP, by three parameters, namely, the total elongation of the reacting bonds (r_e) and the force constants of the bond being cleaved (b) and the bond being formed (b_f) [see Eqns (4), (5)]. The force constant of the triple C≡C bond is greater than that of the double C=C bond; therefore, it should be expected that the classical potential barrier (E_{e0}) to cyclisation involving a triple bond should be higher than that for cyclisation at a double bond. The data on cyclisation of the $CH_2{=}CH(CH_2)_3C^{\bullet}H_2$ and $HC{\equiv}CH(CH_2)_3C^{\bullet}H_2$ radicals confirm this assumption (see Table 10). This can also be seen from comparison of the MIP parameters [br_e in (kJ mol^{-1})$^{1/2}$, E_{e0} in kJ mol^{-1}, b in (kJ mol^{-1})$^{1/2}$ m^{-1}, r_e in m] for the cyclisation of radicals yielding a five-membered ring.

Bond	br_e	E_{e0}	$10^{-10}\,b$	$10^{10}\,r_e$
C=C	18.39	69.7	53.89	0.341
C≡C	22.98	81.7	69.12	0.332

Notably, the r_e parameters for reactions of these two classes are similar. Therefore, the difference between the activation energies of these reactions is due only to different force constants of the double and triple bonds.

Polar interaction. Cyclisation of perfluorinated radicals has a higher classical potential barrier than the cyclisation of hydrocarbon radicals (see Table 10): for $n = 5$, the E_{e0} values are 94.3 and 69.7 kJ mol^{-1}, respectively. The difference between the activation energies, $\Delta E_{e0} = 24.6$ kJ mol^{-1}, is rather high and characterises the contribution of the polar interaction of the C–F bonds to the TS energy.

Comparison of cyclisation with other reactions. Previously, bimolecular radical addition reactions have been analysed in terms of the MIP.[90] It appears pertinent to compare the kinetic parameters of these, rather similar reactions. Since the transition state of the bimolecular reaction is acyclic, these reactions should be compared most legitimately with the cyclisation resulting in a six-membered ring, devoid of bond strain, as the cyclic transition state. The parameters for these two types of reaction are listed below.

Parameter	Cyclisation ($n = 6$)	Bimolecular reaction
br_e /(kJ mol^{-1})$^{1/2}$	20.39 ± 0.64	20.01 ± 0.41
E_{e0} /kJ mol^{-1}	85.6 ± 2.7	82.6 ± 1.7
$10^{10}\, r_e$ /m	0.378 ± 0.012	0.371 ± 0.008
A	8.0×10^9 s^{-1}	5.0×10^8 litre mol^{-1} s^{-1}

It can be seen that the MIP parameters virtually coincide to within the error of determination. Thus, the activation energies of the bimolecular addition and the cyclisation giving rise to a six-membered ring do not differ much for the same enthalpy of the addition. Their rates are expected to be similar when the monomer concentration (c_m) is 16 mol litre^{-1}, where

$$A(\text{cycl}) = A(\text{b})\, c_m.$$

Section III outlines an analysis of intraradical hydrogen abstraction reactions

$$RCH(CH_2)_nC^{\bullet}H_2 \longrightarrow RC^{\bullet}(CH_2)_nMe.$$

It is of interest to compare isomerisations of radicals with hydrogen migration and with addition of the free valence to a double bond. The kinetic parameters [br_e in (kJ mol^{-1})$^{1/2}$, E_{e0} in kJ mol^{-1}, r_e in m], which describe the reactions of these two types giving rise to five-, six- and seven-membered rings in the TS are presented below.[90]

Type of reaction	n	br_e	E_{e0}	$10^{10}\, r_e$
Addition	5	18.39	69.7	0.341
Abstraction of H	5	17.03	72.5	0.455
Addition	6	20.39	85.7	0.378
Abstraction of H	6	14.42	52.0	0.385
Addition	7	19.45	78.0	0.361
Abstraction of H	7	14.40	51.8	0.385

From comparison of the activation energies of thermally neutral reactions, it can be seen that hydrogen abstraction is characterised by lower E_{e0} values than addition for rings with $n \geqslant 6$, while in the case of the five-membered ring, the E_{e0} values are similar (69.7 and 72.5 kJ mol^{-1}, respectively). The dependences of E_{e0} on the ring size are antiparallel: for addition reactions, the $E_{e0}(n = 6)$ value is the highest, whereas for abstraction, $E_{e0}(n = 6)$ is the lowest. Hence, ring strain has different effects on the height of the classical potential barrier E_{e0} of the intramolecular addition and hydrogen abstraction in alkyl radicals. The difference between the E_{e0} values is probably due to the following circumstance. In the addition reaction, the cyclic TS structure coincides with the cyclic structure of the product and differs from the initial linear structure of the reactant. In the intramolecular abstraction, only the TS has a cyclic structure, while both the reactant and the product are linear.

Thus, the activation energies and the rate constants for cyclisation of alkyl radicals are determined by the following three factors: the reaction enthalpy, the size of the ring formed and the force constants of the reacting bonds. The ring size influences both the reaction enthalpy and the classical potential barrier to the thermally neutral reaction. The activation entropy also depends on the number of atoms in the ring, being directly proportional to the loss of entropy upon transition from linear to ring hydrocarbon structure [see Eqn (18)].

Ring opening in the cyclic alkyl radicals is the reverse reaction with respect to cyclisation. Experimental data on these reactions are summarised in Table 11.

VII. Cyclisation and ring opening in aminyl radicals

Aminyl radicals containing a double bond in the alkyl substituent undergo cyclisation, like alkyl radicals, giving rise to heterocyclic alkyl radicals. This may give either five- or six-membered rings.

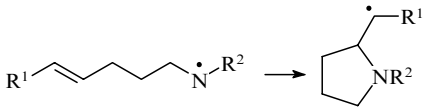

(A)

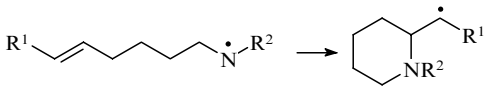

(B)

The aryl radicals with an imino group and a diazo group in the side chain also undergo cyclisation.

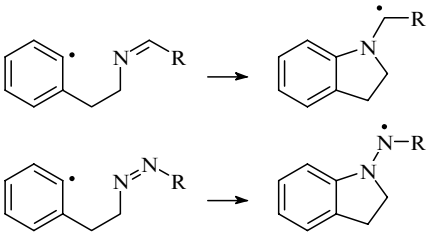

The experimental data on this type of isomerisation are summarised in Table 12. Cyclisation processes involving aminyl,

Table 11. Experimental activation energies, rate constants and pre-exponential factors for ring opening in alkyl radicals.

Reactant	Product	T /K	E_a /kJ mol^{-1}	log$A$ (s^{-1})	$k_{298\,K}$ /s^{-1}	Ref.
	$CH_2=CHCH_2C^{\bullet}H_2$	128 – 362	28.4	13.00	1.05×10^8	91 – 96
	$CH_2=CMeCH_2C^{\bullet}H_2$	310 – 58	31.0	13.15	5.20×10^7	96
	$CH_2=CHCH_2C^{\bullet}HMe$	310 – 378	25.5	13.00	3.39×10^8	50, 96
	$CH_2=CHCH_2C^{\bullet}HMe$	333 – 379	31.4	13.50	9.91×10^7	50, 96
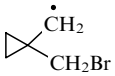	$BrCH_2C(=CH_2)CH_2C^{\bullet}H_2$	318	–	–	2.6×10^8	97
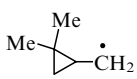	$CH_2=CHCH_2C^{\bullet}Me_2$	195 – 379	30.1	13.2	8.39×10^7	96, 98

Table 11 (continued).

Reactant	Product	T /K	E_a /kJ mol^{-1}	log$A$ (s^{-1})	$k_{298\,K}$ /s^{-1}	Ref.
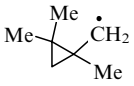	$CH_2=CMeCH_2C^{\bullet}Me_2$	310 – 358	26.8	12.85	1.42×10^{8}	96
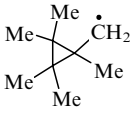	$CH_2=CMeCMe_2C^{\bullet}Me_2$	310 – 358	20.5	13.15	3.60×10^{9}	96
	$MeCH=CHCH_2C^{\bullet}H_2$	310 – 353	32.2	13.2	3.60×10^{7}	96, 99
	$Me_2C=CHCH_2C^{\bullet}H_2$	298 – 358	32.8	13.4	4.47×10^{7}	96,99,100
	$Me(Et)C=CHCH_2C^{\bullet}H_2$	233 – 382	42.1	14.5	1.31×10^{7}	101
	$MeCH=CEtCH_2C^{\bullet}H_2$	310	32.1	13.15	5.4×10^{7}	96
	$MeCH=CH(C^{\bullet}H_2)Pr^{n}$	310	28.0	12.85	1.4×10^{8}	96
	$MeCH=CHCH_2C^{\bullet}HEt$	310	23.4	12.85	8.6×10^{8}	96
	$Bu^{t}CH=CHC^{\bullet}H_2$	243	–	–	1.0×10^{3}	102
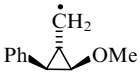	$CH_2=CHCH(OMe)C^{\bullet}HPh$	225 – 298	14.0	13.94	3.06×10^{11}	103, 104
	$CH_2=CHCH_2C^{\bullet}HPh$	225 – 298	13.0	13.90	4.18×10^{11}	103
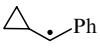	$PhCH=CHCH_2C^{\bullet}H_2$	315 – 353	52.7	14.0	5.79×10^{4}	99, 105
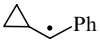	$PhCH=CHCH_2C^{\bullet}H_2$	280 – 321	47.7	13.3	8.69×10^{4}	52
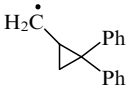	$CH_2=CHCH_2C^{\bullet}Ph_2$	225 – 298	8.4	13.10	4.24×10^{11}	104
	$Ph_2C^{\bullet}CH=CH_2$	351	–	–	4.0×10^{6}	106
	$C^{\bullet}H_2CH_2CH=CPh_2$	277 – 309	51.9	12.3	1.60×10^{3}	52
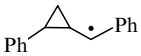	$PhC^{\bullet}HCH_2CH=CHPh$	313	–	–	3.8×10^{8}	107
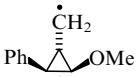	$PhC^{\bullet}HCH(OMe)CH=CH_2$	252 – 311	15.2	14.55	7.70×10^{11}	108
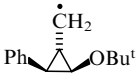	$PhC^{\bullet}HCH(OBu^{t})CH=CH_2$	257 – 311	16.4	14.54	4.63×10^{11}	108
	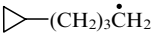	333 – 353	36.0	13.6	1.95×10^{7}	99
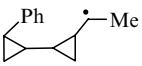	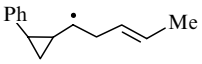	284	–	–	5.6×10^{7}	109
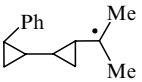	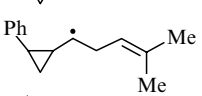	283	–	–	3.0×10^{7}	109
		200 – 303	22.2	13.1	2.10×10^{9}	96, 110

Table 11 (continued).

Reactant	Product	T /K	E_a /kJ mol^{-1}	log$A$ (s^{-1})	$k_{298\,K}$ /s^{-1}	Ref.
	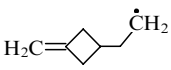	161 – 333	29.7	12.3	1.24×10^7	111, 112
	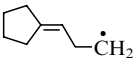	298 – 331	29.3	12.3	1.46×10^7	113
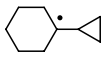	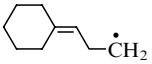	298	–	–	1.1×10^7	113
	$PhCH_2C^{\bullet}H_2$	108 – 198	11.7	9.2	1.41×10^7	114
	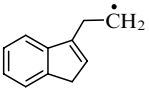	348	–	–	2.1×10^9	115
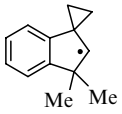	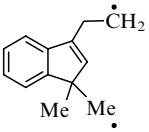	348	–	–	8.6×10^9	115
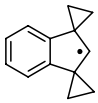	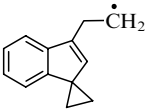	348	–	–	5.3×10^8	115
	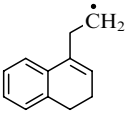	348	–	–	3.0×10^9	115
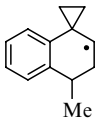	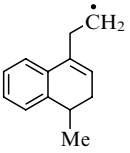	348	–	–	3.6×10^9	115
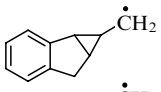	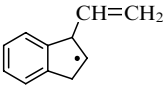	228 – 326	13.4	13.6	1.78×10^{11}	116
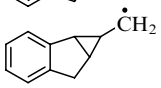	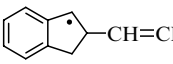	195 – 327	14.2	13.9	2.58×10^{11}	116
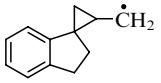	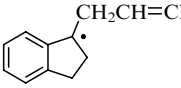	195 – 298	7.1	13.0	5.70×10^{11}	116
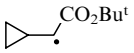	(*Z*)-Bu^{t}OC(O)CH = CHCH$_2$C$^{\bullet}$H$_2$	284 – 332	51.9	14.0	8.00×10^4	99
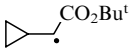	(*E*)-Bu^{t}OC(O)CH = CHCH$_2$C$^{\bullet}$H$_2$	284 – 332	44.8	13.7	7.04×10^5	99
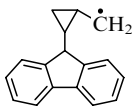	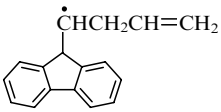	193 – 296	8.8	14.3	5.72×10^{12}	116
	$CH_2 = CH(CH_2)_2C^{\bullet}H_2$	148 – 363	48.3	13.43	9.20×10^4	117 – 119
	$CH_2 = CHC^{\bullet}HCH = CH_2$	214 – 298	42.2	12.23	6.81×10^4	111, 112
	$Me_2C = CH(CH_2)_2C^{\bullet}H_2$	273 – 333	58.1	13.63	2.79×10^3	117, 119

Table 11 (continued).

Reactant	Product	T /K	E_a /kJ mol^{-1}	log$A$ (s^{-1})	$k_{298\,K}$ /s^{-1}	Ref.
	$CH_2=CMe(CH_2)_2C^{\bullet}H_2$	333	54.4	14.90	2.30×10^6	117
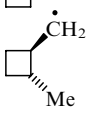	$CH_2=CH(CH_2)_2C^{\bullet}HMe$	333 – 363	48.5	15.06	3.62×10^6	117
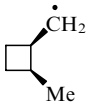	$CH_2=CH(CH_2)_2C^{\bullet}HMe$	333 – 363	44.8	15.26	2.55×10^7	117
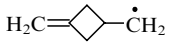	$CH_2=CHCH_2C(C^{\bullet}H_2)=CH_2$	211 – 400	48.1	12.9	2.94×10^4	119, 120
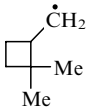	$Me_2C^{\bullet}(CH_2)_2CH=CH_2$	333 – 363	39.3	15.27	2.41×10^8	117
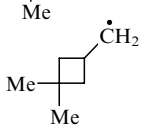	$CH_2=CHCH_2CMe_2C^{\bullet}H_2$	333 – 363	56.9	14.88	8.06×10^4	117
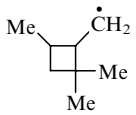	$CH_2=CHCHMeCH_2C^{\bullet}Me_2$	333 – 363	38.9	15.32	3.17×10^8	117
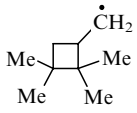	$CH_2=CHCH_2CMe_2C^{\bullet}Me_2$	333 – 363	42.2	15.37	9.40×10^7	117
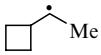	(*E*)-MeCH = $CH(CH_2)_2C^{\bullet}H_2$	333 – 363	54.4	14.54	1.01×10^5	117
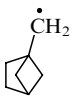	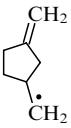	195 – 228	38.9	12.0	1.52×10^5	110
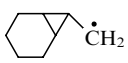	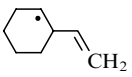	298	–	–	3.0×10^8	92
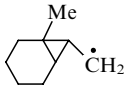	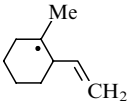	273	–	–	5.0×10^7	92
		413 – 493	56.5	13.6	4.97×10^3	121
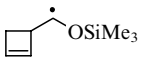	$CH_2=CHC^{\bullet}HCH=CHOSiMe_3$	214 – 247	45.1	12.23	2.11×10^4	118
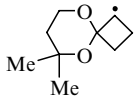	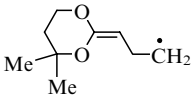	199 – 224	43.9	12.5	6.38×10^4	122

iminoalkyl and diazoalkyl radicals and resulting in five-membered rings are described, in terms of the MIP, by the parameters presented below [r_e in m, hN_Av and $hN_A(v_i - v_f)$ in kJ mol^{-1}].

Radical (n = 3, 4)	α	$10^{10}\,r_e$	$0.5\,hN_Av$	$0.5\,hN_A(v_i - v_f)$
$R^1CH=CH_2(CH_2)_nN^{\bullet}R^2$	1.410	0.539	9.9	3.1
$R^1N=CH_2(CH_2)_nC^{\bullet}HR^2$	1.478	0.565	10.0	3.2
$R^1N=N(CH_2)_nC^{\bullet}HR^2$	1.593	0.609	10.8	4.0

The br_e, E_{e0}, and r_e parameters calculated from the data of Table 12 are presented in Table 13.

Unlike alkyl radicals, cyclisation of aminyl radicals to give a six-membered ring is characterised by lower activation energies E_{e0} than the cyclisation to give a five-membered ring. Obviously, this is due to the strain energy in the ring being formed, as follows from comparison of the E_{e0} and E_{rsc} values (in kJ mol^{-1}).

Table 12. Experimental enthalpies, activation energies and rate constants for cyclisation of aminyl radicals.

A. Experimental enthalpies and activation energies

Reactant	Product	ΔH /kJ mol^{-1}	E_a /kJ mol^{-1}	Ref.
Opening of a three-membered ring				
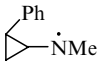	$PhC^{\bullet}HCH_2CH=NMe$	15.0	14.5	122
Opening of a four-membered ring				
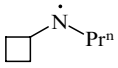	$C^{\bullet}H_2(CH_2)_2CH=NPr^n$	–	43.9	123
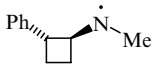	$PhC^{\bullet}H(CH_2)_2CH=NMe$	24.7	13.2	121
Formation of a five-membered ring				
$CH_2=CH(CH_2)_3N^{\bullet}Bu^n$		−49.0	34.0	124
$PhCH=CH(CH_2)_3N^{\bullet}Me$		−70.3	27.6	125
$Ph_2C=CH(CH_2)_3N^{\bullet}Me$	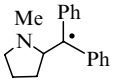	−90.9	26.3	125
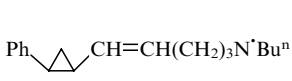	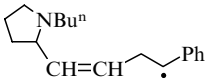	−73.0	38.3	109
$CH_2=CH(CH_2)_2C(O)N^{\bullet}Bu^n$	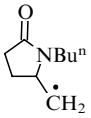	−49.0	38.3	126
Formation of a five-membered ring				
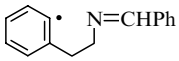	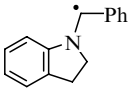	−114.1	17.7	127
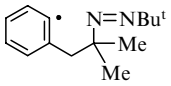	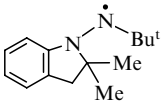	−131.2	6.9	128, 129

B. Experimental rate constants

Reactant	Product	T /K	k /s^{-1}	Ref.
Formation of a six-membered ring				
$Ph_2C=CH(CH_2)_4N^{\bullet}Me$	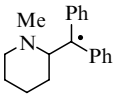	293	7.0×10^3	125
$Ph_2C=CH(CH_2)_4\overset{+}{N}{}^{\bullet}HMe$	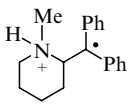	293	9.0×10^7	130
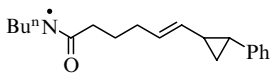	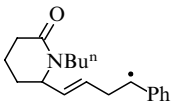	298	1.2×10^7	109
$Ph_2NN=CH(CH_2)_4C^{\bullet}H(CH_2)_3CH=CH_2$	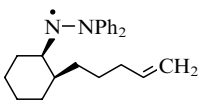	353	9.4×10^5	81

Table 12 (continued).

Reactant	Product	T /K	k /s^{-1}	Ref.
Formation of a six-membered ring				
$Ph_2NN=CH(CH_2)_4C^{\bullet}H(CH_2)_3CH=CH_2$	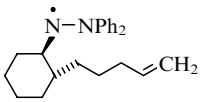	353	9.4×10^5	81
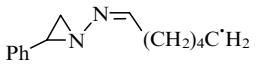	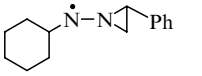	353	4.7×10^6	131
$PhC(O)N=CH(CH_2)_4C^{\bullet}H_2$	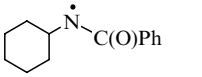	353	6.7×10^5	132
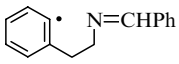	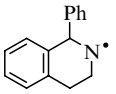	355	1.6×10^8	127
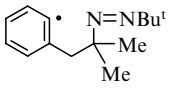	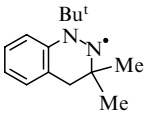	355	2.3×10^9	128, 129
$PhC(O)ON=CH(CH_2)_4C^{\bullet}H_2$	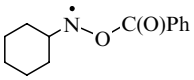	353	2.4×10^6	133
$PhC(O)ON=CH(CH_2)_3CH(C^{\bullet}H_2)(CH_2)_3CH=CH_2$	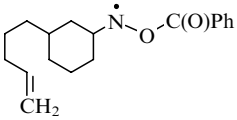	353	4.1×10^6	133

Reaction	E_{e0}	E_{rsc}	E_{e0}(b)
(A)	75.2	26.7	61.0
(B)	61.5	3.1	61.0

The same trend is observed for cyclisations occurring through addition to an N=N bond [$E_{e0}(n=5)$ = 66.7 kJ mol^{-1}, $E_{e0}(n=6)$ = 62.4 kJ mol^{-1}]. It is noteworthy that classical potential barriers to intraradical and bimolecular addition of alkyl radicals to a C=C bond are equal, $E_{e0}(m) = E_{e0}(b)$ (see above).

Table 13. MIP-derived kinetic parameters for cyclisation of radicals containing nitrogen atoms.

Reaction	br_e (see [a])	E_{e0} (see [b])	$10^{10}\,r_e$ (see [c])
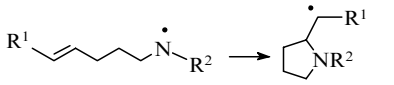	20.90	75.2	0.388
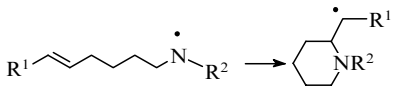	19.44	61.5	0.344
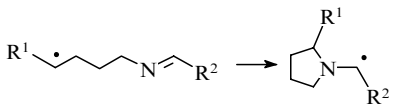	22.00	78.8	0.389
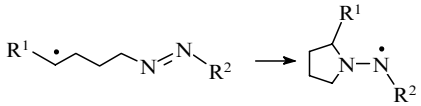	21.18	66.7	0.348
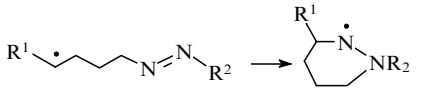	20.49	62.4	0.336

[a] Expressed in (kJ mol^{-1})$^{1/2}$; [b] in kJ mol^{-1}; [c] in m.

VIII. Cyclisation and ring opening in oxygen-containing radicals

As examples, one can consider the cyclisation of oxoalkyl radicals

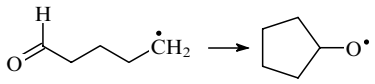

and the reverse ring opening reaction in cycloalkoxyl radicals

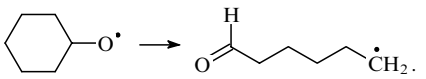

The MIP parameters for cyclisation and ring opening in oxygen-containing radicals are summarised in Table 14. Experimental data for these reactions are given in Table 15. The kinetic parameters found using the MIP relations for various classes of cyclisation and ring opening reactions for these radicals are presented in Table 16.

It can be seen that the E_{e0} values for the forward and reverse reactions coincide to within the error of measurements (±2 kJ mol^{-1}). For a five-membered ring, the activation energy (E_{e0} = 38 kJ mol^{-1}) is higher than that for a six-membered ring (E_{e0} = 32 kJ mol^{-1}). The bimolecular reaction

$$(R^1)^{\bullet} + O=CR^2R^3 \longrightarrow R^1R^2R^3CO^{\bullet}$$

has a higher activation energy (73 kJ mol^{-1}).

Peroxyl radicals undergo cyclisation to give a five-membered ring.[139]

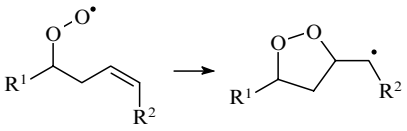

The thermally neutral cyclisation of peroxyl radicals has the activation energy $E_{e0} = 67.4$ kJ mol^{-1} (see Table 16), which is much higher than the E_{e0} value for cyclisation of the oxoalkyl radicals considered above. The bimolecular analogue of these reactions, namely, the addition of $R^1O_2^{\bullet}$ to the double bond of olefins

$$R^1O_2^{\bullet} + CH_2{=}CHR^2 \longrightarrow R^1OOCH_2C^{\bullet}HR^2,$$

is characterised by a much higher potential barrier, $E_{e0} = 90.5$ kJ mol^{-1}.

Ring opening in 1,3-dioxa-2-cycloalkyl radicals, for example,

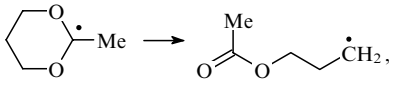

proceeds rather fast and is accompanied by heat evolution (see Table 15). It can be seen from Table 16 that for these reactions, too, $E_{e0}(n = 6) < E_{e0}(n = 5)$; the difference between these values is 47 kJ mol^{-1}. Thus, for all cyclisation and ring opening reactions in oxygen-containing radicals studied, the inequality $E_{e0}(n = 6) < E_{e0}(n = 5)$ also holds.

Table 14. MIP parameters for cyclisation and ring opening of some oxygen-containing radicals.[20]

Reaction	α	$10^{-11}\,b$ /(kJ mol^{-1})$^{1/2}$ m^{-1}	$0.5\,hN_Av$ /kJ mol^{-1}	$0.5\,hN_A(v_i - v_f)$ /kJ mol^{-1}
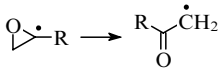	0.637	3.816	6.6	−3.7
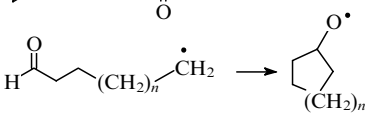	1.336	5.991	10.3	2.1
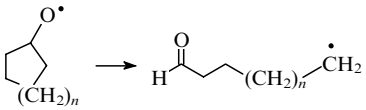	0.748	4.483	8.2	−2.1
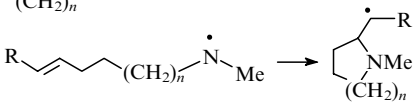	1.410	5.389	9.9	3.1
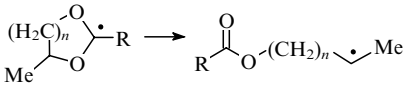	0.655	3.922	6.7	−3.6
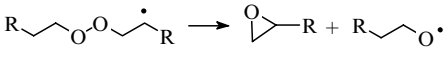	0.826	3.238	5.1	−1.6
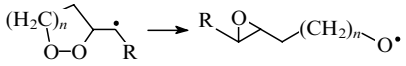	0.826	3.238	5.1	−1.6

Table 15. Experimental kinetic parameters for cyclisation and ring opening of oxygen-containing radicals.

Reactant	Product	$-\Delta H$ /kJ mol^{-1}	E_a /kJ mol^{-1}	br_e (kJ mol^{-1})$^{1/2}$	Ref.
Cyclisation					
$HC(O)(CH_2)_3C^{\bullet}H_2$		−2.3	28.8	14.51	134
$HC(O)(CH_2)_4C^{\bullet}H_2$	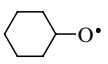	33.2	8.3	13.83	134
Opening of a three-membered ring					
	$Me_2C^{\bullet}HCH(O)$	−113.9	40.1	14.69	102
	$MeC(O)C^{\bullet}H_2$	−118.0	56.7	16.34	102
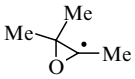	$Me_2C^{\bullet}C(O)Me$	−113.1	47.3	15.37	102
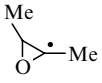	$MeC^{\bullet}HC(O)Me$	−121.0	49.4	15.77	102

Table 15 (continued).

Reactant	Product	$-\Delta H$ /kJ mol^{-1}	E_a /kJ mol^{-1}	br_e (kJ mol^{-1})$^{1/2}$	Ref.
Opening of a three-membered ring					
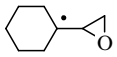	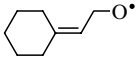	–	19.0	–	135
Opening of a five-membered ring					
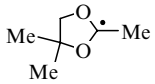	$MeC(O)OCH_2C^{\bullet}Me_2$	127.9	60.2	17.04	122, 136
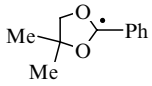	$PhC(O)OCH_2C^{\bullet}Me_2$	49.6	77.4	16.53	122
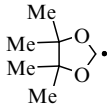	$Me_2C^{\bullet}CMe_2OCH(O)$	93.0	58.7	16.08	136
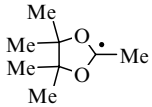	$Me_2C^{\bullet}CMe_2OCMe(O)$	127.9	52.1	16.34	136
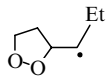	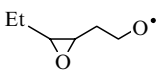	127.6	43.3	17.84	137
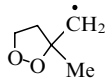	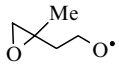	136.5	48.7	18.66	137
	$CH(O)(CH_2)_3C^{\bullet}H_2$	−2.3	27.9	10.30	138
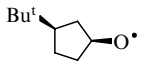	$CH(O)(CH_2)_2CH(Bu^t)C^{\bullet}H_2$	−2.3	33.5	11.11	28
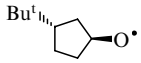	$CH(O)(CH_2)_2CH(Bu^t)C^{\bullet}H_2$	−2.3	32.2	10.93	28
Opening of a six-membered ring					
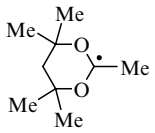	$MeC(O)OCMe_2CH_2C^{\bullet}Me_2$	35.3	35.1	12.04	136
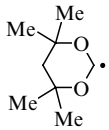	$CH(O)OCMe_2CH_2C^{\bullet}Me_2$	57.0	29.1	12.09	136
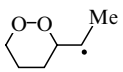	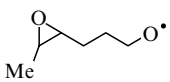	102.3	15.3	13.54	137
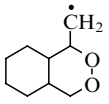	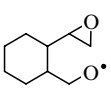	90.6	26.4	14.64	137
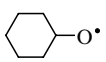	$CH(O)(CH_2)_4C^{\bullet}H_2$	−33.2	38.5	9.58	138
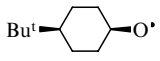	$CH(O)(CH_2)_2CH(Bu^t)CH_2C^{\bullet}H_2$	−33.2	39.4	9.74	28
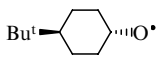	$CH(O)(CH_2)_2CH(Bu^t)CH_2C^{\bullet}H_2$	−33.2	42.2	10.20	28

Table 16. MIP-derived kinetic parameters α, br_e and E_{e0} for various types of cyclisation and ring opening reactions of O-containing radicals.

Reaction	α	br_e (see [a])	E_{e0} (see [b])
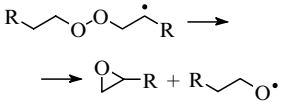	0.826	15.13 ± ± 0.44	68.7 ± 2.0
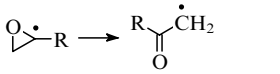	0.637	15.28 ± ± 0.45	87.1 ± 2.2
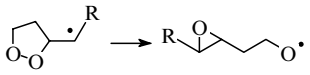	0.826	18.25 ± ± 0.41	99.9 ± 2.2
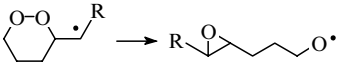	0.826	14.09 ± ± 0.55	59.5 ± 2.3
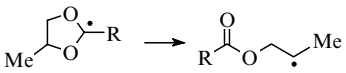	0.655	16.50 ± ± 0.35	99.4 ± 2.1
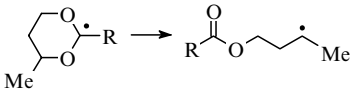	0.655	12.06 ± ± 0.55	53.1 ± 2.5
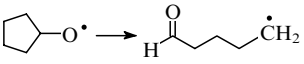	0.748	10.78	38.0
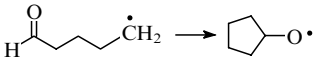	1.336	14.51	38.6
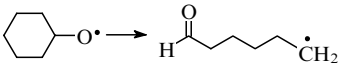	0.748	9.84	31.7
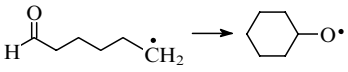	1.336	13.83	35.0

[a] In (kJ mol^{-1})$^{1/2}$; [b] in kJ mol^{-1}.

IX. Decomposition and ring opening in peroxoalkyl radicals to give epoxides

The oxidation of monomers follows a chain mechanism and includes the following chain propagation steps:[11, 12, 23]

$$R^1O_2^{\bullet} + CH_2{=}CHR^2 \longrightarrow R^1OOCH_2C^{\bullet}HR^2,$$

$$R^1OOCH_2C^{\bullet}HR^2 + O_2 \longrightarrow R^1OOCH_2CH(OO^{\bullet})R^2.$$

The last reaction is accompanied by parallel cyclisation of the peroxoalkyl radical, resulting in the epoxide.

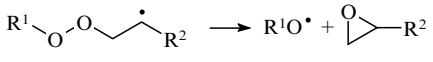

The kinetic data for decomposition of peroxoalkyl radicals with different structures are presented in Table 17.

Decomposition of cyclic peroxoalkyl radicals results in the formation of one (rather than two) alkoxyl radical with an epoxide ring.

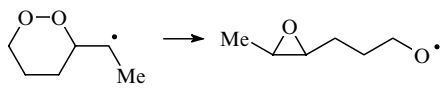

Table 17. Kinetic parameters for decomposition of alkylperoxyl radicals to give epoxides.[10, 31]

Radical	$-\Delta H$ (see [a])	T/K	k/s^{-1}	E_a (see [a])	br_e (see [b])
$ROOMeCHC^{\bullet}HMe$	76.6	363	9.1×10^6	38.3	15.55
$ROOCH_2C^{\bullet}MePr$	70.3	343	9.1×10^6	36.2	15.06
$ROOMe_2CC^{\bullet}HMe$	62.5	333	6.7×10^6	36.0	14.73
$ROOCH_2C^{\bullet}HPh$	31.8	323	7.6×10^3	53.0	15.38
$ROOCH_2C^{\bullet}MePh$	28.1	323	6.8×10^4	47.2	14.57
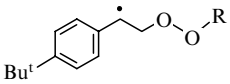	35.0	368	6.6×10^4	53.8	15.60
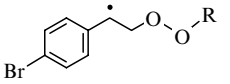	30.4	368	4.7×10^4	54.9	15.53
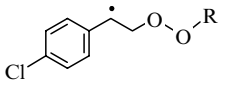	35.5	368	7.6×10^4	53.4	15.58
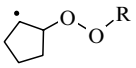	68.5	323	4.5×10^6	36.0	14.97
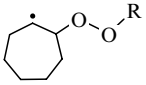	64.5	333	2.9×10^7	32.0	14.32

[a] Expressed in (kJ mol^{-1})$^{1/2}$; [b] in kJ mol^{-1}.

During this reaction, the weak O–O bond is cleaved (D_{O-O} = 162 kJ mol^{-1}) to give a stronger C–O bond. Therefore, such reactions are exothermic. Their enthalpies vary in the range from −28 to −102 kJ mol^{-1} (see Table 17). The br_e parameters calculated for these reactions are very similar (see Table 16). For decomposition of cyclic peroxoalkyl radicals, the br_e and E_{e0} values depend on the ring size, as follows from the data given below.

Radical	$R^1OOCH_2C^{\bullet}HR^2$	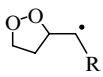	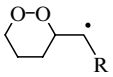
br_e/(kJ mol^{-1})$^{1/2}$	15.13	18.25	14.09
E_{e0}/kJ mol^{-1}	68.7	99.9	59.5
E_{rsc}/kJ mol^{-1}	0	29	10

It can be seen that for this reaction $E_{e0}(n = 5) > E_{e0}(n = 6)$ again. This is consistent with the E_{rsc} value: the higher the ring strain, the higher the activation energy of the thermally neutral reaction.

The bimolecular reaction of the alkyl radical with the peroxide

$$(R^1)^{\bullet} + R^2OOR^2 \longrightarrow R^1OR^2 + R^2O^{\bullet}$$

is characterised by a much higher E_{e0} value (122.7 kJ mol^{-1}).[140] For these reactions, the intraradical attack by the alkyl radical on the peroxy bridge proceeds more easily (with less potential energy required).

X. Migrations of aryl and vinyl groups in alkyl radicals

Alkylaromatic radicals undergo isomerisation accompanied by 1,2-transfer of the aromatic ring,[2] for example,

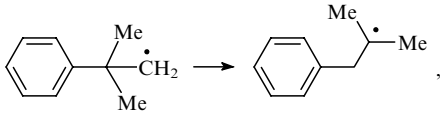

or by 1,4-transfer of the aromatic ring,[2] for example,

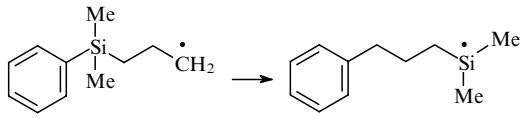

Reactions of this type have also been reported for alkyl radicals with naphthyl, pyridine, vinyl and acetylene fragments in the β-position relative to the carbon atom bearing a free valence. The enthalpies and the rate constants for these reactions are summarised in Table 18.

Table 18. Enthalpies and rate constants for the migration of aryl, vinyl and methylidine groups in alkyl radicals.

Reaction	$-\Delta H$ /kJ mol^{-1}	T /K	k /s^{-1}	Ref.
Migration of the aryl group				
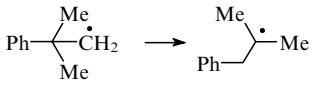	22.0	283–307	$50\times10^{11}\exp(-56/RT)$	141
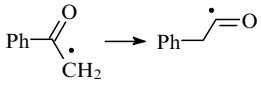	30.8	298–375	$6.3\times10^{11}\exp(-61.5/RT)$	142
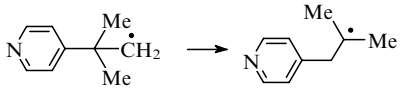	22.0	235–291	$6.3\times10^{11}\exp(-48/RT)$	141
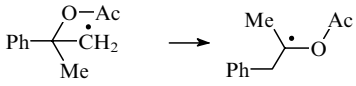	29.7	343	5×10^{3}	143
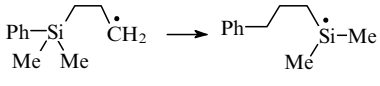	44.0	413	7.3×10^{3}	144
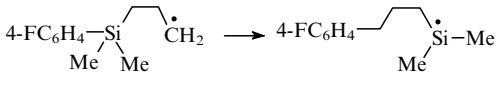	44.0	413	6.1×10^{3}	144
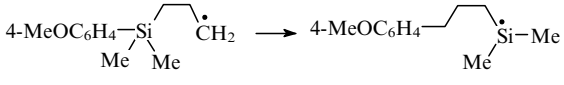	44.0	413	1.9×10^{4}	144
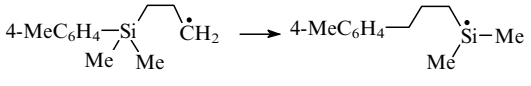	44.0	413	8.3×10^{3}	144
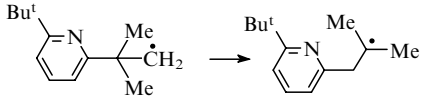	22.0	235–291	$5.0\times10^{11}\exp(-50.1/RT)$	141
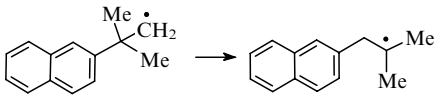	22.0	237–256	$5.6\times10^{11}\exp(-46.0/RT)$	141
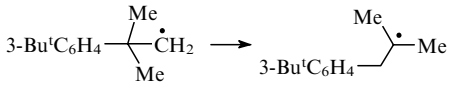	22.0	283–307	$5.0\times10^{11}\exp(-56.4/RT)$	141
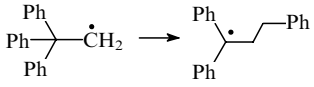	73.2	298–318	$6.3\times10^{11}\exp(-35.6/RT)$	117
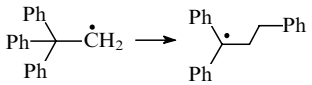	73.2	373	5.0×10^{7}	145
Migration of the vinyl group				
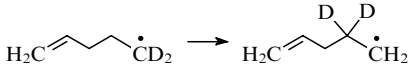	0	298	$1.1\times10^{11}\exp(-38.0/RT)$	51
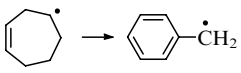	38.0	338	2.5×10^{4}	117
Migration of the methylidine group				
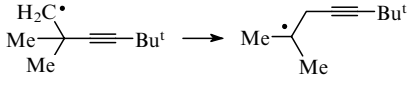	22.0	318–361	$2.5\times10^{12}\exp(-61.1/RT)$	146

The isomerisation reactions presented in Table 18 are exothermic, some of them proceeding very rapidly, for example the fairly exothermic isomerisation of the 2,2,2-triphenylethyl radical. The average pre-exponential factor A for the 1,2-migration is 5.6×10^{11} s^{-1} ($\log A = 11.75 \pm 0.05$). The Ar–C bonds cleaved and formed during this migration are of the same type; therefore $\alpha = 1$ (MIP, see above). Analysis of the experimental data given in Table 18 within the framework of the MIP provided the following parameters for isomerisation reactions accompanied by transfer of a group bearing an unpaired π-electron.

Radical	br_e /(kJ mol^{-1})$^{1/2}$	E_{e0} /kJ mol^{-1}	$10^{10}\, r_e$ /m
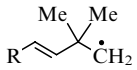	17.00	72.2	0.379
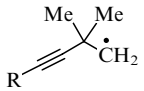	17.21	74.0	0.384
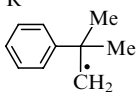	17.04 ± 0.33	72.6 ± 1.4	0.380
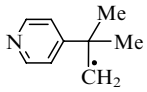	16.36 ± 0.13	66.9 ± 0.5	0.365
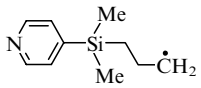	17.46 ± 0.17	76.2 ± 0.7	0.389

It can be seen that the 1,2-migrations of the vinyl, acetylene and phenyl groups are characterised by the same E_{e0} value (72.9 ± 0.8 kJ mol^{-1}). The activation energy for the 1,4-migration of the phenyl group is not much different (E_{e0} = 76.2 kJ mol^{-1}). The potential barrier to the 1,2-migration of pyridine is somewhat lower (66.9 kJ mol^{-1}). Upon comparison of the 1,2-migration of the vinyl group with the cyclisation of radicals containing a vinyl group (see above), one can note that the E_{e0} values for 1,2-migration (72.2 kJ mol^{-1}) and for cyclisation giving a five-membered ring (69.7 kJ mol^{-1}) are similar. Meanwhile the 1,2-migration of groups with π-bonds proceeds much more readily than the addition of the R$^{\bullet}$ radical to a double bond (E_{e0} = 82.6 kJ mol^{-1}).[122]

XI. Conclusion

The material considered in this review provides conclusions concerning the influence of various factors on the kinetic parameters of radical reactions of diverse classes.

The size of the ring formed. This factor is very important for both hydrogen migration and cyclisation or ring opening. First, this affects the reaction enthalpy, as the strain energy of the resulting ring (E_{rsc}) is included with a plus sign in the cyclisation enthalpy and, correspondingly, with a minus sign in the ring opening enthalpy. For three- and four-membered rings, the E_{rsc} value exceeds 100 kJ mol^{-1} (see Section III). Second, as follows from comparison of the activation energies of thermally neutral cyclisation and ring opening reactions, the ring strain influences also the classical potential barrier to the thermally neutral reaction (E_{e0}). For the cyclisation of alkyl radicals, this dependence obeys Eqn (15) (see Section VI): the higher E_{rsc}, the lower E_{e0}. The type of influence involved in the cyclisation of aminyl, iminoalkyl and ω-formyl radicals is different. This can be seen from comparison of the $E_{e0}(n = 6)$ and $E_{e0}(n = 5)$ values presented below (in kJ mol^{-1}) for the above-mentioned radicals.

Radical	$E_{e0}(n = 6)$	$E_{e0}(n = 5)$	$E_{rsc}(n = 5) - E_{rsc}(n = 6)$
$CH_2{=}CH(CH_2)_n\dot{N}R$	68.4	75.1	24
$\dot{C}H_2(CH_2)_nCH{=}CHR$	77.8	66.7	24
$\dot{C}H_2(CH_2)_nCHO$	31.7	38.0	26

A similar regularity is also found for the activation energy (in kJ mol^{-1}) of ring opening in the radicals formed from 1,2- and 1,3-dioxacyclanes (see Section V):

Reaction	$E_{e0}(n = 6)$	$E_{e0}(n = 5)$
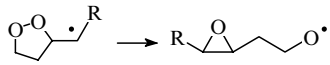	–	99.9
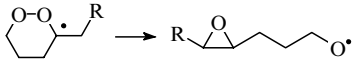	59.5	–
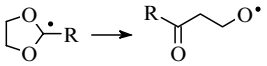	–	54.3
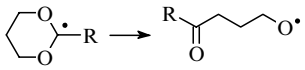	101.6	–

Thus, a different pattern of dependence can be followed for cyclisation of N- and O-containing radicals, namely, the higher the ring strain, the higher the classical potential barrier to the thermally neutral reaction. This also holds for hydrogen migration.

Third, the size of the resulting ring influences the activation entropy and, hence, the pre-exponential factor [see Eqn (17)].

Electronegativity of atoms involved in the ring formation. In radical abstraction reactions

$$X^{\bullet} + HY \longrightarrow XH + Y^{\bullet}$$

the electronegativity (EA) of the atoms X and Y plays an important role by affecting the activation energy E_{e0}.[18] The greater the electronegativity difference (ΔEA) between the atoms X and Y, the lower the E_{e0} value. Does this factor influence also the activation energy of cyclisation? In the cyclisation reactions considered in this review, we were dealing with the the C···C···Y type reaction centres in the TS, where Y = C, N, O. To find out whether or not the electronegativity difference between the C and Y atoms (ΔEA) influences the E_{e0} value for cyclisation, let us juxtapose the kinetic parameters with the ΔEA values for the C···C…C, C…C···N and C···C…O reaction centres. Since the E_{e0} value for addition reactions depends also on the force constants of the reacting bonds,[20] which are different for the C=C, C=N, C=O, C–C, C–O and C–N bonds, we will juxtapose the electronegativity difference ΔEA with the r_e parameter, which does not depend on the force constants of the reacting bonds (underlined) but determines the E_{e0} value [see Eqn (5)].

Radical	Reaction centre	$10^{10}\, r_e$ /m	ΔEA /kJ mol^{-1}
$R^{\bullet}CH(CH_2)_3CH{=}CH_2$	C···C…C	0.378	0
$RCH{=}CH(CH_2)_4\dot{N}R$	C…C···N	0.333	29.5
$CH(O)(CH_2)_4\dot{C}H_2$	C···C…O	0.225	78.5

It can be seen that the r_e value decreases with an increase in the electronegativity difference for the C and Y atoms (Y = N, O). For the three classes of reactions considered, the r_e (in m) and ΔEA (in kJ mol^{-1}) values are correlated satisfactorily through the following relation (Fig. 5):

$$r_e \times 10^{11} = 3.81 \pm 0.06 - (1.91 \pm 0.23) \times 10^{-2}\, \Delta EA. \qquad (19)$$

Thus, the electronegativity of atoms in the reaction centre does really influence the activation energy of cyclisation. The

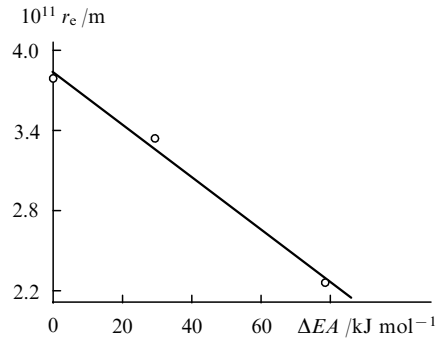

Figure 5. Parameter r_e describing the elongation of the reacting bonds upon cyclisation *vs.* electronegativity of atoms in the reaction centre (ΔEA).

higher the electronegativity difference between the C and Y atoms, the smaller the r_e parameter, and, correspondingly, E_{e0} [see Eqn (5)].

Role of the bending vibrations in the attaining of the activation barrier. According to the transition state theory, bimolecular radical abstraction reactions usually involve a linear configuration of atoms in the reaction centre, *i.e.*, the X···H···Y atoms occur in one straight line. This is confirmed by *ab initio* quantum-chemical calculations.[17] As a rule, the C···H···Y angle in these reactions equals 180° or is close to this value. In the intramolecular migration of the hydrogen atom in the alkyl radical, the corresponding angle in the TS inevitably differs from 180°. Therefore, as noted above, one should expect that $E_{e0}(b) \geqslant E_{e0}(m, n = 6)$ for abstraction reactions. However, it was shown in Section III that this is not really the case.

Reaction	$(R^1)^{\bullet} + R^2H$	$R^1O^{\bullet} + R^2H$	$R^1O_2^{\bullet} + R^2H$
$E_{e0}(m, n = 6)$ /kJ mol^{-1}	46.6	53.4	53.2
$E_{e0}(b)$ /kJ mol^{-1}	74.8	53.2	56.3

It can be seen that for the six-membered ring in the TS, $E_{e0}(m) \leqslant E_{e0}(b)$. This is due to an additional involvement of 'soft' bending vibrations in the radical activation towards isomerisation. A similar situation is observed for the cyclisation reactions resulting in a six-membered ring, namely, $E_{e0}(b) \geqslant E_{e0}(m)$ to within the error of measurements (± 2 kJ mol^{-1}).

Reaction	$E_{e0}(m)$ /kJ mol^{-1}	$E_{e0}(b)$ /kJ mol^{-1}
$R^{\bullet} + C{=}C$	85.7	82.6
$(R^1)^{\bullet} + O{=}CR_2^2$	32	72.9
$RO_2^{\bullet} + C{=}C$	67.4	90.5
$(R^1)^{\bullet} + R^2OOR^2$	59.5	122.7

Obviously, the 'soft' bending vibrations of the C–C bonds in the resulting ring play an important role in the formation of the transition state for cyclisation and for the reverse ring opening reaction and this is responsible for the lower activation energy compared to that for the bimolecular reaction.

Thus, the activation energy of radical isomerisation is determined by, at least, the following four factors: first, the enthalpy; second, the strain energy in the ring in the transition state; third, the electronegativity difference between the atoms forming the reaction centre; and fourth, the involvement of the bending vibrations of bonds in the radical activation.

References

1. N N Semenov *O Nekotorykh Problemakh Khimicheskoi Kinetiki i Reaktsionnoi Sposobnosti* (About Some Problems of Chemical Kinetics and Reactivity) (Moscow: Izd. Akad. Nauk SSSR, 1958)
2. J K Kochi (Ed.) *Free Radicals* Vols 1, 2 (New York: Wiley, 1973)
3. A L J Beckwith, D Griller, J P Lorand *Radical Reaction Rates in Liquids* Vol. 13a (Ed. H Fischer) (Berlin: Springer, 1984)
4. NIST Chemical Kinetics Database NIST, Gaithersburg, 2000
5. K J Laidler, L F Loucks, in *Comprehensive Chemical Kinetics* Vol. 5 (Eds C H Bamford, C F H Tipper) (Amsterdam: Elsevier, 1972) p. 1
6. G C Eastmond, in *Comprehensive Chemical Kinetics* Vol. 14A (Eds C H Bamford, C F H Tipper) (Amsterdam: Elsevier, 1976) p. 104
7. E T Denisov, in *Handbook of Polymer Degradation* (Ed. S H Hamid) (New York: Marcel Dekker, 2000) p. 383
8. T Mill, D G Hendry, in *Comprehensive Chemical Kinetics* Vol. 16 (Eds C H Bamford, C F H Tipper) (Amsterdam: 1980) p. 1
9. E T Denisov, T G Denisova *Handbook of Antioxidants* (Boca Raton, FL: CRC Press, 2000) p. 32
10. R V Kucher, I A Opeida, V I Timokhin, in *Mezhmolekulyarnye Vzaimodeistviya i Mekhanizmy Organicheskikh Reaktsii* (Intermolecular Interactions and Mechanisms of Organic Reactions) (Kiev: Naukova Dumka, 1983) p. 42
11. E T Denisov, V V Azatyan *Inhibition of Chain Reactions* (London: Gordon and Breach, 2000) p. 189
12. N M Emanuel', E T Denisov, Z K Maizus *Tsepnye Reaktsii Okisleniya Uglevodorodov v Zhidkoi Faze* (Chain Reactions of Hydrocarbon Oxidation in Liquid Phase) (Moscow: Nauka, 1965)
13. J W Wilt, in *Free Radicals* Vol. 1 (Ed. J K Kochi) (New York: Wiley, 1973) p. 333
14. D P Curran, N A Porter, B Giese *Stereochemistry of Radical Reactions* (Weinheim: VCH, 1995)
15. C Chatgilialoglu, P Renaud, in *General Aspects of the Chemistry of Radicals* (Ed. Z B Alfassi) (Chichester: Wiley, 1999) p. 501
16. T G Denisova, E T Denisov *Kinet. Katal.* **42** 684 (2001) [a]
17. A F Shestakov, T G Denisova, E T Denisov, N S Emel'yanova *Izv. Akad. Nauk, Ser. Khim.* 559 (2002) [b]
18. T G Denisova, E T Denisov *Izv. Akad. Nauk, Ser. Khim.* 871 (2002) [b]
19. T G Denisova, E T Denisov, A F Shestakov, N S Emel'yanova *Khim. Fiz.* **22** 29 (2003) [c]
20. E T Denisov *Usp. Khim.* **66** 953 (1997) [*Russ. Chem. Rev.* **66** 859 (1997)]
21. E T Denisov *Kinet. Katal.* **32** 461 (1991) [a]
22. E T Denisov, T G Denisova, T S Pokidova *Handbook of Free Radical Initiators* (Hoboken, NJ: Wiley, 2003)
23. E T Denisov, O M Sarkisov, G I Likhtenshtein *Chemical Kinetics* (Amsterdam: Elsevier, 2003)
24. N V Blinova, L V Il'inskaya, N V Kruglova, R G Gasanov *Kinet. Katal.* **31** 1314 (1990) [a]
25. N V Blinova, R G Gasanov *Kinet. Katal.* **31** 524 (1990) [a]
26. R G Gasanov, N V Blinova *Izv. Akad. Nauk SSSR, Ser. Khim.* 2512 (1988) [b]
27. R G Gasanov, L V Ivanova, R Kh Freidina *Izv. Akad. Nauk SSSR, Ser. Khim.* 2810 (1979) [b]
28. A L J Beckwith, K D Raner *J. Org. Chem.* **57** 4954 (1992)
29. G Brunton, D Griller, L R C Barclay, K U Ingold *J. Am. Chem. Soc.* **98** 6803 (1976)
30. P R Marriott, D Griller, *J. Am. Chem. Soc.* **103** 1521 (1981)
31. J A Howard, J C Scaiano *Radical Reaction Rates in Liquids* Vol. 13d (Ed. H Fischer) (Berlin: Springer, 1984)
32. K J Laidler *Chemical Kinetics* (New York: Harper and Row, 1987)
33. E S Domalski, E D Hearing *J. Phys. Chem. Ref. Data* **22** 805 (1993)
34. C Walling, A Padwa *J. Am. Chem. Soc.* **85** 1597 (1963)
35. W R Bergmark, B Beckmann, W Landenberger *Tetrahedron Lett.* 2259 (1971)
36. J A Howard, K U Ingold *Can. J. Chem.* **48** 873 (1970)

37. N A Kravchuk, Abstract of Candidate Thesis in Chemical Sciences, Institute of Physical Chemistry, L'vov, 1987
38. S G Voronina, L V Krutskaya, A L Perkel', B G Freidin *Zh. Prikl. Khim.* **63** 1376 (1990) [d]
39. T Mill, G Montorsi *Int. J. Chem. Kinet.* **5** 119 (1973)
40. M N Schuchmann, C von Sonntag *Z. Naturforsch. B, Chem. Sci.* **42** 495 (1987)
41. D E Van Sickle, T Mill, F R Mayo, H Richardson, C W Gould *J. Org. Chem.* **38** 4435 (1973)
42. I N Demidov, V M Solyanikov *Neftekhimiya* **24** 406 (1986) [e]
43. R K Jensen, S Korcek, L R Mahoney, M Zinbo *J. Am. Chem. Soc.* **103** 1742 (1981)
44. D E Van Sickle *J. Org. Chem.* **37** 755 (1972)
45. I A Opeida, V I Timokhin, V F Galat *Teor. Eksp. Khim.* **14** 554 (1978) [f]
46. E J Hamilton, S Korcek, L R Mahoney, M Zinbo *Int. J. Chem. Kinet.* **12** 577 (1980)
47. A L Perkel', Abstract of Candidate Thesis in Chemical Sciences, Technological Institute, St Petersburg, 1992
48. R K Jensen, S Korcek, M Zinbo *J. Am. Chem. Soc.* **114** 7742 (1992)
49. Z F Sharafutdinova, V S Martem'yanov, I M Borisov *Kinet. Katal.* **29** 553 (1988) [a]
50. A L J Beckwith, V W Bowry *J. Org. Chem.* **54** 2681 (1989)
51. A Effio, D Griller, K U Ingold, A L J Beckwith, A K Serelis *J. Am. Chem. Soc.* **102** 1734 (1980)
52. T A Halgren, J D Roberts, J H Horner, F N Martinez, Ch Tronche, M Newcomb *J. Am. Chem. Soc.* **122** 2988 (2000)
53. E Furxhi, J H Horner, M Newcomb *J. Org. Chem.* **64** 4064 (1999)
54. E C Friedrich, R L Holmstead *J. Org. Chem.* **37** 2550 (1972)
55. P Schmid, K U Ingold *J. Am. Chem. Soc.* **100** 2493 (1978)
56. A L J Beckwith, I A Blair, G Phillipou *Tetrahedron Lett.* **26** 2251 (1974)
57. D Lal, D Griller, S Husband, K U Ingold *J. Am. Chem. Soc.* **96** 6355 (1974)
58. J W Wilt, J Lusztyk, M Peeran, K U Ingold *J. Am. Chem. Soc.* **110** 281 (1988)
59. A L J Beckwith *Tetrahedron* **37** 3073 (1981)
60. A L J Beckwith, T Lawrence, A K Serelis *J. Chem. Soc., Chem. Commun.* 484 (1980)
61. A L J Beckwith, C J Easton, T Lawrence, A K Serelis *Aust. J. Chem.* **36** 545 (1983)
62. A L J Beckwith, C H Schiesser *Tetrahedron* **41** 3925 (1985)
63. C Walling, A Cioffari *J. Am. Chem. Soc.* **94** 6064 (1972)
64. A L J Beckwith, T Lawrence *J. Chem. Soc., Perkin Trans. 2* 1535 (1979)
65. A L J Beckwith, V W Bowry, G Moad *J. Org. Chem.* **53** 1632 (1988)
66. J W Wilt *Tetrahedron* **41** 3979 (1985)
67. A L J Beckwith, G Moad *J. Chem. Soc., Perkin Trans. 2* 1726 (1975)
68. M Newcomb, T R Varick, C Ha, M B Manek, X Yue *J. Am. Chem. Soc.* **114** 8158 (1992)
69. C Ha, J H Horner, M Newcomb, T R Varick, B R Arnold, J Lusztyk *J. Org. Chem.* **58** 1194 (1993)
70. M Newcomb, S Y Choi *J. Org. Chem.* **64** 1225 (1999)
71. C C Johnson, J H Horner, C Tronche, M Newcomb *J. Am. Chem. Soc.* **117** 1684 (1995)
72. M Newcomb, J H Horner, M A Filipkowski, C Ha, S-U Park *J. Am. Chem. Soc.* **117** 3674 (1995)
73. P E Pigou *J. Org. Chem.* **54** 4943 (1989)
74. J W Wilt, S N Massie, R B Dabek *J. Org. Chem.* **35** 2803 (1970)
75. F MacCorquodale, J C Walton *J. Chem. Soc., Perkin Trans. 1* 347 (1989)
76. C Chatgilialoglu, D Chrich, M Komatsu, I Ryu *Chem. Rev.* **99** 1991 (1999)
77. A L J Beckwith, S A Glover *Aust. J. Chem.* **40** 157 (1987)
78. T W Smith, G B Butter *J. Org. Chem.* **43** 6 (1978)
79. A L J Beckwith, I Blair, G Phillipou *J. Am. Chem. Soc.* **96** 1613 (1974)
80. A C Hindson, F MacCorquodale, J C Walton *J. Chem. Soc. Perkin Trans. 2* 871 (1993)
81. C F Sturino, A G Fallis *J. Org. Chem.* **59** 6514 (1994)
82. W R Dolbier *Chem. Rev.* **96** 1557 (1996)
83. A Li, A B Shtarev, B E Smart, Z-Y Yang, J Lusztyk, K U Ingold, A Bravo, W R Dolbier Jr *J. Org. Chem.* **64** 5993 (1999)
84. J W Wilt *J. Am. Chem. Soc.* **103** 5251 (1981)
85. A L J Beckwith, G Moad *J. Chem. Soc., Chem. Commun.* 472 (1974)
86. J Lusztyk, B Maillard, S Deycard, D A Lindsay, K U Ingold *J. Org. Chem.* **52** 3509 (1987)
87. C Chatgilialoglu, C Ferreri, A Sommazzi *J. Am. Chem. Soc.* **118** 7223 (1996)
88. A L J Beckwith, V W Bowry, C H Schiesser *Tetrahedron* **47** 121 (1991)
89. A Phillippon, M Degueil-Castaing, A L J Beckwith, B Maillard *J. Org. Chem.* **63** 6814 (1998)
90. E T Denisov *Usp. Khim.* **69** 166 (2000) [*Russ. Chem. Rev.* **69** 153 (2000)]
91. M Newcomb, A G Glenn *J. Am. Chem. Soc.* **111** 275 (1989)
92. A L J Beckwith, G Moad *J. Chem. Soc., Perkin Trans. 2* 1473 (1980)
93. R Kaptein *J. Am. Chem. Soc.* **94** 6262 (1972)
94. B Maillard, D Forrest, K U Ingold *J. Am. Chem. Soc.* **98** 7024 (1976)
95. L Mathew, J Warkentin *J. Am. Chem. Soc.* **108** 7981 (1986)
96. V W Bowry, J Lusztyk, K U Ingold *J. Am. Chem. Soc.* **113** 5687 (1991)
97. A J Kennedy, J C Walton, K U Ingold *J. Chem. Soc. Perkin Trans. 2* 751 (1982)
98. M Newcomb, A G Glenn, W G Williams *J. Org. Chem.* **54** 2675 (1989)
99. A L J Beckwith, V Bowry *J. Am. Chem. Soc.* **116** 2710 (1994)
100. P S Engel, S-L He, J T Banks, K U Ingold, J Lusztyk *J. Org. Chem.* **62** 1210 (1997)
101. P Burkhard, E Roduner, J Hochmann, H Fischer *J. Phys. Chem.* **88** 773 (1984)
102. H Itzel, H Fischer *Helv. Chim. Acta* **59** 880 (1976)
103. M Newcomb, M B Manek *J. Am. Chem. Soc.* **112** 9662 (1990)
104. M Newcomb, C Johnson, M B Manek, T R Varick *J. Am. Chem. Soc.* **114** 10 915 (1992)
105. J Masnov, E G Samsel, R M Bullock *J. Chem. Soc., Chem. Commun.* 1044 (1989)
106. L J Johnston, J Lusztyk, D D M Wayner, A N Abeywickreyma, A L J Beckwith, J C Scaiano, K U Ingold *J. Am. Chem. Soc.* **107** 4594 (1985)
107. R Hollis, L Hughes, V W Bowry, K U Ingold *J. Org. Chem.* **57** 4284 (1992)
108. M-H Le Tadic-Biadatti, M Newcomb *J. Chem. Soc., Perkin Trans. 2* 1467 (1996)
109. M Newcomb, N Tanaka, A Bouvier, C Tronche, J H Horner, O M Musa, F N Martinez *J. Am. Chem. Soc.* **118** 8505 (1996)
110. M Newcomb, M B Manek, A G Glenn *J. Am. Chem. Soc.* **113** 949 (1991)
111. E W Della, C H Shiesser, D K Taylor, J C Walton *J. Chem. Soc., Perkin Trans. 2* 1329 (1991)
112. B P Branchaud, A G Glenn, H C Stiasny *J. Org. Chem.* **56** 6656 (1991)
113. P S Engel, A M Culotta *J. Am. Chem. Soc.* **113** 2686 (1991)
114. A Effio, D Griller, K U Ingold, J C Scaiano, S J Sheng *J. Am. Chem. Soc.* **102** 6063 (1980)
115. R P Lemieux, P Beak *J. Org. Chem.* **55** 5454 (1990)
116. A A Martin-Esker, C C Johnson, J H Horner, M Newcomb *J. Am. Chem. Soc.* **116** 9174 (1994)
117. A L J Beckwith, G Moad *J. Chem. Soc., Perkin Trans. 2* 1083 (1980)
118. K U Ingold, B Maillard, J C Walton *J. Chem. Soc., Perkin Trans. 2* 970 (1981)
119. F MacCorquodale, J C Walton *J. Chem. Soc., Faraday Trans. 1* **84** 3233 (1988)
120. J C Walton *J. Chem. Soc., Perkin Trans. 2* 231 (1987)
121. G T Binmore, E W Della, G M Elsey, N J Head, J C Walton *J. Am. Chem. Soc.* **116** 2759 (1994)
122. L R C Barclay, D Griller, K U Ingold *J. Am. Chem. Soc.* **104** 4399 (1982)
123. Y Maeda, K U Ingold *J. Am. Chem. Soc.* **102** 328 (1980)

124. M Newcomb, O M Musa, F N Martinez, J H Horner *J. Am. Chem. Soc.* **119** 4569 (1997)
125. O M Musa, J H Horner, H Shahin, M Newcomb *J. Am. Chem. Soc.* **118** 3862 (1996)
126. J L Esker, M Newcomb *J. Org. Chem.* **58** 4933 (1993)
127. A L J Beckwith, B P Hay *J. Am. Chem. Soc.* **111** 2674 (1989)
128. A L J Beckwith, S Wang, J Warkentin *J. Am. Chem. Soc.* **109** 5289 (1987)
129. C P A Kunka, J Warkentin *Can. J. Chem.* **68** 575 (1990)
130. J H Horner, F N Martinez, O M Musa, M Newcomb, H E Shahin *J. Am. Chem. Soc.* **117** 11 124 (1995)
131. S Kim, I S Kee *Tetrahedron Lett.* **34** 4213 (1993)
132. S Kim, K S Yoon, Y S Kim *Tetrahedron Lett.* **38** 73 (1997)
133. A G Fallis, I M Brinza *Tetrahedron* **53** 17 543 (1997)
134. M J Tomaszewski, J Warkentin *Tetrahedron Lett.* **33** 2123 (1992)
135. V Krishnamurthy, V H Rawal *J. Org. Chem.* **62** 1572 (1997)
136. J M Perkins, B P Roberts *J. Chem. Soc., Perkin Trans. 2* 77 (1975)
137. A J Bloodworth, J L Courtneidge, A Davies *J. Chem. Soc., Perkin Trans. 2* 523 (1984)
138. A L J Beckwith, B P Hay *J. Am. Chem. Soc.* **111** 230 (1989)
139. N A Porter, B A Weber, H Weenen, J A Khan *J. Am. Chem. Soc.* **102** 5597 (1980)
140. T S Pokidova, E T Denisov *Neftekhimiya* **38** 269 (1998) [e]
141. B Maillard, K U Ingold *J. Am. Chem. Soc.* **98** 1224 (1976)
142. D Gri1ler, K U Ingold *Acc. Chem. Res.* **13** 317 (1980)
143. A L J Beckwith, C B Thomas *J. Chem. Soc., Perkin Trans. 2* 861 (1973)
144. J W Wilt, W K Chwang, C F Dockus, N M Tomiuk *J. Am. Chem. Soc.* **100** 5534 (1978)
145. K U Ingold, in *Free Radicals* Vol. 1 (Ed. J K Kochi) (New York: Wiley, 1973) p. 37
146. K U Ingold, J Warkentin *Can. J. Chem.* **58** 348 (1980)

[a] — *Kinet. Catal. (Engl. Transl.)*
[b] — *Russ. Chem. Bull., Int. Ed. (Engl. Transl.)*
[c] — *Chem. Phys. Rep. (Engl. Transl.)*
[d] — *Russ. J. Appl. Chem. (Engl. Transl.)*
[e] — *Petrol. Chem. (Engl. Transl.)*
[f] — *Theor. Exp. Chem. (Engl. Transl.)*

Russian Chemical Reviews **73** (11) 1121 – 1141 (2004) © 2004 Russian Academy of Sciences and Turpion Ltd

DOI 10.1070/RC2004v073n11ABEH000869

Chemical physics of decomposition of energetic materials. Problems and prospects

L P Smirnov

Contents

I.	Introduction	1121
II.	Kinetics and mechanism of decomposition of explosives and oxidisers	1121
III.	Polymer networks as binders for solid propellants	1129
IV.	Mathematical modelling of decomposition of energetic materials	1133
V.	Stability prediction of energetic materials	1136
VI.	Conclusion	1137

Abstract. The review is concerned with analysis of the results obtained in the kinetic and mechanistic studies on decomposition of energetic materials (explosives, powders and solid propellants). It is shown that the state-of-the art in this field is inadequate to the potential of modern chemical kinetics and chemical physics. Unsolved problems are outlined and ways of their solution are proposed. The bibliography includes 235 references.

I. Introduction

The kinetic and mechanistic studies of decomposition of energetic materials (explosives, solid propellants and powders; hereafter, EMs) are first of all necessary for solving practical problems. Design of novel EMs, establishment of safe conditions for their synthesis, storage life calculations and control of the stability, combustion and detonation of EMs require knowledge of the mechanism of thermal decomposition and quantitative data for the description of the process over a wide temperature interval and for different states of aggregation. Studies on the kinetics and mechanism of thermal decomposition are necessary to solve not only technical problems but also some fundamental problems of chemical physics, *e.g.*, establishment of interrelations between the structure and reactivity of EMs, development of theoretical concepts of solid-phase reactions, understanding of the mechanism of combustion and detonation of EMs, *etc*.

Intensive research on the kinetics and mechanism of decomposition of explosives and powders began in the 1950s. Investigations on thermal decomposition of particular classes of explosives and model compounds, *viz*., aliphatic nitro compounds,[1] secondary nitramines,[2–4] nitro esters,[3,5] ammonium perchlorate,[6,7] *etc*., have been well documented. The results of thermal decomposition studies of the explosives mentioned above and some other compounds (organic difluoroamino compounds, furazans, furoxans, tetrazoles, ammonium nitrate and metal nitrates, hydrazinium and hydroxyammonium salts, metal perchlorates, nitric acid and perchloric acid) were summarised in a monograph.[8]

High demand for preparation of solid propellants and other polymeric materials including polymeric composite materials (PCMs) for civil purposes gave an impetus to studies on the physical chemistry of polymers. Considerable advances in this field were made by researchers belonging to the scientific schools headed by V A Kargin, N M Emanuel and N S Enikolopov; the most important results were reported earlier.[9–15]

In regard to design of solid propellants, studies on decomposition of explosives and powders were followed by investigations of destruction of polymer networks that are also widely used in national economy. The authors of monographs[9,15] also analysed the results of kinetic and mechanistic studies of molecular destruction of various classes of unfilled polymers (mostly linear carbochain polymers) exposed to heat treatment, various kinds of radiation, mechannical load and corrosive media and formulated the physical and chemical principles of stabilisaiton of these compounds. Studies of destruction processes showed that distinctions between linear polymers and polymer networks cause marked differences in character of molecular destruction of these compounds.[16–31]

In writing this review the author tried to present a critical analysis of the results obtained in the kinetic and mechanistic studies of decomposition of EMs in order to reveal unsolved problems and to compare the state-of-the-art in this field and the potential of modern chemical kinetics and chemical physics. Such a critical assessment for EMs has not been reported as yet, though it would be useful for outlining prospects for the development of this branch of chemical physics and for formulating and planning further research of decomposition of EMs.

II. Kinetics and mechanism of decomposition of explosives and oxidisers

1. Explosives and model compounds

A chemical reaction can be characterised both qualitatively by dividing into elementary stages (mechanism) and quantitatively by determining the corresponding rate constants; therefore, interrelations between the kinetics and mechanism are of great importance. At present, the mechanism of a complex chemical reaction is usually established using experimental data on the composition of the reaction system obtained from thermochemical measurements, while the rate constants for elementary stages of the process are determined from the results of measurements of changes in the concentrations of the starting compounds, inter-

L P Smirnov Institute of Problems of Chemical Physics, Russian Academy of Sciences, 142432 Chernogolovka, Moscow Region, Russian Federation. Fax (7-096) 515 54 20. Tel. (7-096) 522 10 74.
E-mail: lsmirn@icp.ac.ru

Received 12 January 2004
Uspekhi Khimii **73** (11) 1210 – 1232 (2004); translated by A M Raevskiy

mediates and end products in the course of reaction. Usually, the reaction kinetics and mechanisms are studied in relation to the reactant concentrations and state of aggregation, temperature and other external factors. A combination of this approach and modern physicochemical methods (EPR, IR and NMR spectroscopy, gas-phase electron diffraction, gas-phase neutron diffraction, positron annihilation, *etc.*) has been successfully employed in, *e.g.*, studies on thermal destruction and oxidation of linear carbochain polymers.[9,15]

To date, hundreds of explosives and model compounds belonging to various chemical classes have been studied. Usually, the mechanisms of their decomposition are multistage. A characteristic example is provided by the decomposition of 1,1,1-trinitroethane vapours, which involves the following elementary stages:[1,8]

$$CH_3C(NO_2)_3 \longrightarrow CH_3\dot{C}(NO_2)_2 + NO_2, \quad (1)$$

$$CH_3\dot{C}(NO_2)_2 \longrightarrow CH_3\dot{C}O + NO + NO_2, \quad (2)$$

$$CH_3\dot{C}(NO_2)_2 + NO_2 \longrightarrow CH_3\dot{C}O + NO + 2NO_2, \quad (3)$$

$$CH_3\dot{C}(NO_2)_2 + NO \longrightarrow CH_3C(NO)(NO_2)_2, \quad (4)$$

$$CH_3C(NO)(NO_2)_2 \longrightarrow CH_3CN + NO_2 + NO_3, \quad (5)$$

$$CH_3\dot{C}O \longrightarrow \dot{C}H_3 + CO, \quad (6)$$

$$CH_3\dot{C}O + NO_2 \longrightarrow CH_3CO\dot{O} + NO, \quad (7)$$

$$CH_3CO\dot{O} \longrightarrow \dot{C}H_3 + CO_2, \quad (8)$$

$$CH_3CO\dot{O} + RH \longrightarrow \mathbf{CH_3COOH} + \dot{R}, \quad (9)$$

$$CH_3CO\dot{O} + \dot{C}H_3 \longrightarrow \mathbf{CH_3COOCH_3}, \quad (10)$$

$$\dot{C}H_3 + NO_2 \longrightarrow \mathbf{CH_3NO_2}, \quad (11)$$

$$\dot{C}H_3 + NO_2 \longrightarrow CH_3\dot{O} + NO, \quad (12)$$

$$\dot{C}H_3 + NO \longrightarrow CH_3NO, \quad (13)$$

$$CH_3NO \longrightarrow \mathbf{HCN} + H_2O, \quad (14)$$

$$CH_3NO + 2NO \longrightarrow \dot{C}H_3 + N_2 + NO_3, \quad (15)$$

$$CH_3NO + NO_2 \longrightarrow \mathbf{CH_3NO_2} + NO, \quad (16)$$

$$CH_3\dot{O} + RH \longrightarrow \mathbf{CH_3OH} + \dot{R}, \quad (17)$$

$$CH_3\dot{O} + NO_2 \longrightarrow \mathbf{CH_3ONO_2}, \quad (18)$$

$$CH_3\dot{O} + NO_2 \longrightarrow CH_2O + HNO_2, \quad (19)$$

$$CH_3\dot{O} + NO \longrightarrow \mathbf{CH_3ONO}, \quad (20)$$

$$CH_3\dot{O} + NO \longrightarrow CH_2O + HNO, \quad (21)$$

$$2HNO \longrightarrow H_2O + N_2O, \quad (22)$$

$$CH_2O + NO_2 \longrightarrow H_2O + NO + CO_2. \quad (23)$$

However, the actual decomposition mechanism of 1,1,1-trinitroethane vapours is more complex than that described by Eqns (1)–(23). For instance, Eqn (23) is unbalanced and seemingly describes several stages simultaneously. A number of compounds treated as end reaction products in Eqns (1)–(23) (they are given in bold) differ only slightly in stability from the starting compound (similarly to NO_3 and HNO_2) and react with other components of the reaction system (*e.g.*, CH_3OH reacts with NO_3 and HNO_2). According to Refs 1 and 8, at least twenty-six reactions are needed to schematically describe the decomposition of CH_3NO_2 up to ignition, the primary stage being a homolysis of the C–N bond. However, there is no consensus of opinion concerning the decomposition mechanism of even such a simple compound as nitromethane.[32] It was established that at temperatures below 700 °C the initial stage of the reaction involves cleavage of the C–N bond accompanied by rearrangement of CH_3NO_2 to give methyl nitrite and by decomposition of the last-mentioned compound.[33–35]

Decomposition of explosives is usually a complex process that involves at least several tens of elementary stages. Therefore, determination of the true rate constants for all these stages is a complicated task. The compositions of explosives, oxidisers of solid propellants and powders also contain carbon, hydrogen, oxygen and nitrogen and chlorine or fluorine (more rarely; the oxidation states of nitrogen and chlorine can vary over a wide range). The decomposition mechanisms of these compounds are hardly simpler than the destruction and oxidation mechanisms of carbochain polymers. Because of this, studies on decomposition of explosives, oxidisers of solid propellants and powders should be *a priori* carried out using modern methods. Up to date, almost all studies on thermal decomposition of explosives (with few exceptions) are carried out by sufficiently sensitive and simple methods of formal kinetics.[8] Abroad, research in recent ten to fifteen years has been carried out using improved methods of isotope mixing, pulsed laser irradiation, mass spectrometry with modulation of gas beam, fast IR spectroscopy and other dynamical methods of detection of products, which allows the temporal evolution of chemical compounds in the gas phase to be followed.[4]

Studies on the kinetics of thermal decomposition of explosives and model compounds using gas manometric technique involve determination of the pressure of gaseous compounds in the course of a reaction performed in a closed volume. The degree of decomposition of explosives (η) is calculated as the ratio of the current pressure of gases $p(t)$ to the pressure corresponding to complete cessation of the increase in the pressure in the course of decomposition (p_∞),

$$\eta = \frac{p(t)}{p_\infty}.$$

The decomposition of 1,1,1-trinitroethane [see Eqns (1)–(23)] is characterised by a $\sim 35 : \sim 25 : \sim 40$ ratio (in per cent with respect to the total number of stages) between the reaction stages accompanied by an increase in, a decrease in and constancy of the number of moles of gases. This ratio remains nearly the same for other explosives.[1–8] Therefore, the major drawback of the manometric technique is that it introduces an element of uncertainty and provides incomplete kinetic data. This method cannot in principle provide information on the stages proceeding without changing the number of moles of gases. Generally, it can be used to obtain generalised information on the stages accompanied by changes in the number of moles of gases because usually the kinetic curves of decomposition of explosives are described by relatively simple reaction equations (first-order reaction or first-order autocatalysis equations) containing one or two empirical rate constants. Often, a certain equation can describe only a portion of rather than the whole kinetic curve. The temperature interval for kinetic studies of thermal decomposition of explosives is usually no wider than 40–50 °C. The complete gas evolution, ΔV_∞, is related to the pressure p_∞ and is expressed in units of reduced volume (volume of gaseous products evolved under normal conditions per 1 gramme of explosive under study). Usually, the parameter ΔV_∞ is only determined at elevated temperatures in spite of the fact that the ΔV_∞ value considerably increases with temperature. The dependence of ΔV_∞ on temperature and changes in the composition of gaseous products in the course of reaction introduce errors in the determination of the rate constants, activation energy, E_a, and pre-exponent, k_0, in the Arrhenius equation. By and large, the method is characterised by low accuracy so that determination of the activation energy with an error of at most 4 kJ mol^{-1} in a temperature interval of 40 °C requires a series of 10–12 runs.[36]

Solving some practical problems at least requires knowledge of the true rate constant for the initial stage of a complex reaction (k_{in}). Usually, it is believed that k_{in} can be determined using methods of formal kinetics provided that the rate of the overall reaction is limited by the first step[36] or that the k_{in} value much exceeds the rate constants for the subsequent stages. Thus, to determine k_{in}, one should know all the rate constants for the subsequent stages. If the manometric technique is employed, it is also necessary that the initial stage of the reaction be accompanied

by a change in the number of moles of gases and irreversible. Yet another necessary condition is the absence of competing concurrent reactions. However, these conditions are far from being met.[8, 37, 38] For instance, the primary stages of the decomposition of 1,5- and 2,5-disubstituted tetrazoles proceed without evolution of gas.[37, 38] Decomposition of some nitro derivatives of cyclic compounds containing strained bonds also involves no formation of gaseous products in the first step. A conventional assumption that the experimental rate constant (k_{exp}) equals the rate constant for the primary (limiting) step of a successive reaction is qualitative in character. To assess feasibility of this assumption, information on the kinetics and mechanisms of further steps is required, because the accuracy depends on the number of stages and on the corresponding rate constants. However, relations between k_{exp} and the rate constants for elementary stages were established only for relatively simple reactions.[37, 39] An example is provided by the decomposition of 1,5-disubstituted tetrazoles, which involves a reversible formation and decomposition of azidoazomethines:[37]

$$k_{exp} = k_1 k_2 (k_{-1} + k_2)^{-1},$$

where k_1, k_{-1} and k_2 are the rate constants for the direct and reverse formation of azidoazomethine from tetrazole and for the decomposition of azidoazomethine with evolution of N_2, respectively. The rate constants for a concurrent decomposition channel involving no intermediate formation can also contribute to k_{exp}.[37] The rate constant, k_{exp}, for the radical-chain decomposition of 2,4,6-trinitrotoluene can be expressed as the sum:[39]

$$k_{exp} = a_1 k_1 + a_2 k_1 k_2 k_5^{-1} + a_3 k_1 k_3 (k_2 k_5)^{-1},$$

where k_1, k_2, k_3 and k_5 are the rate constants for the chain initiation, propagation, transfer and termination steps, respectively, and a_1, a_2 and a_3 are constants.

The primary step of decomposition of explosives can be directly studied in the gas phase by suppressing secondary reactions. Detection of gaseous products of primary decomposition in the condensed phase is a much more complicated task compared to gas-phase studies, because diffusion even through thin layers of explosives takes a finite time, which is responsible for a finite degree of conversion with respect to secondary reactions.[4] It is believed [8] that the possibility of changing gas-phase reaction conditions over a wide range allows the first monomolecular stage of a complex decomposition reaction to be distinguished and its kinetic characteristics to be determined by the manometric technique. This approach was employed in studies of gas-phase decomposition of nitroaromatic compounds. However, the radical-chain mechanism of these reactions was not proved, the amounts of inhibitors (I_2, NO_2, NO) introduced were comparable with the amounts of compounds under study and the kinetic chain length was not determined. Clearly, the assumption mentioned above is inapplicable to those explosives for which the primary step of decomposition is due to competition between a number of reactions proceeding by a radical or molecular mechanism.

Often, the molecules of energetic compounds contain a number of (different-type) active reaction centres. These atomic groups interact with one another and compete in the initial stages of thermal decomposition reactions. In this connection the most reactive centre must be determined. The interaction of atomic groups causes the electron density to be redistributed between them as a result of the donor–acceptor interaction, which manifests itself in specific properties of complex energetic compounds (structural elasticity and conformational mobility of atomic groups), electron density redistribution in the transition state of a chemical reaction, *etc.*[40, 41] Extensive literature on manifestation of the mutual influence of atomic groups in various complex organic molecules is available. Combining a number of experimental methods (IR and Raman spectroscopy, X-ray diffraction and neutron diffraction, measurements of dipole moments, *etc.*) allows reliable information on the structural features of complex molecules and intramolecular dynamics to be obtained. Unfortunately, interrelations between different characteristics are still poorly studied. Because of this, many correlations can only be applied to structurally similar compounds.[42]

At present, a number of stubborn problems related to the presence of and donor-acceptor interaction between several reaction centres in the molecules of explosives can be solved only experimentally.[36, 43] For instance, the decomposition of compounds $RN(NO_2)CH_2C(NO_2)_2X$ begins with homolysis of the $C-NO_2$ bond ($X = NO_2$) and the $N-NO_2$ bond ($X = F$).[36] The inductive effect of substituents causes a decrease in the bond dissociation energies by 4–8 kJ mol^{-1}. Experiments showed that at least in those cases where the molecules of explosives contain unstable functional groups some rate constants for the subsequent stages of decomposition are comparable with k_{in} in magnitude. This can lead to the formation of rather stable products which can still undergo further decomposition.[43] This phenomenon called a stepwise (two-stage) decomposition has long been known;[44–46] recently, it again attracted considerable attention.[36, 43, 47]

A few studies concerned with comparison of the kinetic parameters of decomposition obtained by methods of formal kinetics and by direct analytical techniques have been reported. For instance, liquid chromatography and UV spectroscopic studies of decomposition of trinitrophenylmethylnitramine (**1**) showed [46] that the concentration of this compound decreases down to zero before the evolution of gaseous products ceases (Table 1). The composition of gaseous products changes in the course of the process, *viz.*, the NO_2 content passes through a maximum and decreases down to zero nearly simultaneously with full consumption of compound **1**, which decomposes into three condensed compounds, *N*-methyltrinitroaniline (**2**), trinitroanizole (**3**) and picric acid (**4**). It seems likely that the primary step of decomposition is characterised by three rate constants, the ratios between them being varied with temperature because the fraction of compound **2** in the condensed phase increases as temperature increases. Products **2** and **3** undergo a slow decomposition to give compound **4**, so the exact rate constants for the primary step of decomposition of compound **1** can be determined by studying not only the kinetics of comsumption of **1** but also the kinetics of accumulation of the condensed products **2**–**4**. Thus, the true rate constant, k_{in}, for the initial stage of decomposition of explosives cannot be determined using methods of formal kinetics.[46] Changes in the ratios between the rates of particular stages of 1,1,1-trinitroethane decomposition are also indicated by the dependence of the composition of decomposition products on the degree of decomposition η (Fig. 1).

Table 1. Composition of reaction system (in moles of product per mole of starting compound) for thermal decomposition of trinitrophenylmethylnitramine at 433 K.[46]

t/min	Gaseous products [a]	Content of system's components			
		1	**2**	**3**	**4**
25	–	0.832	0.030	0.073	0.037
40	0.450 (0.021)	–	–	–	–
50	0.667 (0.018)	–	0.039	0.230	–
55	–	0.494	0.045	0.265	0.094
70	1.118 (0.031)	–	–	0.295	0.113
90	1.550 (0.021)	0.227	0.072	0.412	0.131
110	1.808 (0.016)	–	–	0.503	–
145	2.030 (0.004)	0.029	0.065	0.525	0.160
200	2.149 (0.001)	–	–	–	–
300	–	0.019	0.047	0.478	0.204
400	2.280 (0.000)	–	–	0.463	–
1440	2.674	0	0.031	0.110	0.524

[a] NO_2 is given in parentheses.

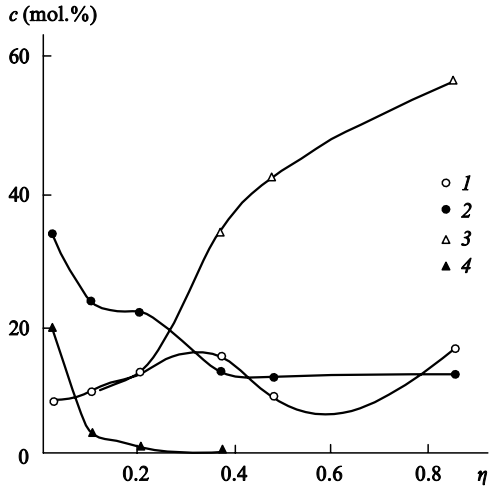

Figure 1. Yield of decomposition products of 1,1,1-trinitroethane at 443 K plotted *vs.* degree of decomposition;[1,8]
CH_3NO_2 (*1*), CH_3ONO_2 (*2*), CH_3CO_2H (*3*), CH_3NO (*4*).

Usually, calorimetric or gravimetric methods of studies on the kinetics of complex chemical reactions are also inappropriate for the determination of true rate constants. Indeed, the decomposition of explosives involves both exothermic and endothermic stages that can strongly differ from one another in thermal effects. Generally, different elementary stages of a complex reaction are accompanied by different changes in the mass of the condensed phase. Despite the fact that methods of formal kinetics do not allow the true rate constants for thermal decomposition to be determined, they can be useful for comparing the stability of functional groups with strongly different reactivities.[48]

However, often the activation parameters (E_a and k_0) determined using methods of formal kinetics differ even for the same compound.[4,8,49] Scatter of data can be explained by inadequacy of procedures employed that makes it impossible to distinguish between the initial steps and catalytic stages and between different phase states of a compound under study and by the influence of side effects on the decomposition. Large scatter of data can be a reason for incorrect conclusions concerning the influence of the structure on the stability of explosives. For instance, the nitramine N–N bonds are only slightly influenced by the inductive effect of substituents; in this case, the geometry of the nitramine group is of great importance, namely, the N–N bond dissociation energy, D(N–N), is 169.5 kJ mol^{-1} for planar nitramine groups and 157.5 kJ mol^{-1} for pyramidal ones. Different degree of structural distortion of pyramidal nitramine group caused by steric strain results in different degree of conjugation between nitrogen atoms in this group, which in turn influences the N–N bond length and, hence, strength. Since it is this bond whose cleavage is the primary step of the decomposition of nitramines, a change in the N–N bond length affects the activation energy, E_a, for the initial stage of the reaction. It was found that the E_a value increases rather than decreases as the N–N bond elongates.[49,50] Thus, it does not always happen that the results obtained by methods of formal kinetics permit estimation of the thermal stability ratios of related compounds.

Usually, it is appropriate to generalise the results of kinetic studies of various classes of explosives and to reveal relations between the reactivity, structure and physical characteristics of explosives using the Hammett–Taft equations that relate different rate constants to one another.[51–53] Correlations between the activation energy, E_a, for decomposition of nitro compounds and their structural characteristics were established using home-made codes.[54,55] These correlations are to some extent useful for systematisation of experimental data on the rate constants; however, detailed analysis of the reactivity problem can be performed only for groups of related reactions. Moreover, interpretation of the physical meaning of the correlation coefficients is arbitrary. In addition, because we don't know with certainty whether the experimental rate constant for decomposition, k_{exp}, is the true rate constant for the primary elementary step, the scientific value of the relations between the structure of explosives and their reactivities characterised by methods of formal kinetics seems to be doubtful.

In solving a number of practically important problems one should know the rate constants for not only initial stages of decomposition. Determination of all the rate constants for multistage reactions is a complicated task. The situation is simplified if the case in point is a study on in-service explosives because decomposition of related explosives involves a number of identical stages. Knowledge of the rate constants for many elementary stages of decomposition of explosives is also necessary to solve other problems.[56,57] Obtaining detailed kinetic information requires the use of modern methods that allow one to monitor changes in the reactant concentrations directly in the reaction system, to establish position of the reaction centre, to obtain information on transient structures, *etc.*[58–62]

However, these techniques are scarcely employed in the decomposition studies of explosives. Because of this, neither the mechanisms of nor rate constants for elementary stages are known even for in-service explosives. In this case, the decomposition of cyclic nitramines near the melting temperature was studied in most detail.[63] Generally, thermal decomposition of 1,3,5-trinitro-1,3,5-triazacyclohexane in the liquid phase can follow four reaction paths in the primary stage. These are HNO_2 release (30%), N–N bond cleavage (10%), formation of a mononitroso compound in the reaction of the explosive with NO (35%) and, finally, autocatalysis of the decomposition of the explosive (or the mononitroso compound) with the end product containing amide groups (25%). A similar composition of products was observed for the decomposition of molten 1,3,5,7-tetranitro-1,3,5,7-tetraazacyclooctane, but the decomposition mechanism of this compound was not established because of the lack of quantitative data.[4] In addition to the reactions considered above there is a number of examples that suggest unreliability of at least particular stages of the decomposition mechanism of explosives and model compounds.[3,4] This can likely be explained by the fact that the mechanism of a complex decomposition reaction of an explosive is usually studied in isolation from the studies on the kinetics of elementary stages of the reaction. For instance, compounds **2** and **3** were not included[8,64] in the scheme of decomposition of compound **1**, though they were experimentally detected among the decomposition products.[46]

Reliability of a reaction mechanism can be established by performing a complex study on the kinetics of elementary stages and by comparing the experimental and calculated kinetic curves plotted for intermediates and end reaction products. In this case, computer simulation can offer considerable advantages (Fig. 2).

Data on the elementary stages and corresponding rate constants for decomposition of explosives in the condensed phase are scarce and less reliable compared to similar data for the gas phase.[3,4,8] For instance, no well-substantiated chemical schemes of liquid-phase decomposition of some classes of explosives are available and there is no consensus of opinion of the reasons for the fact that some nitro compounds decompose in the liquid phase faster than in the gas phase.[39,65] It should be kept in mind that passage from the gas phase to the liquid phase can be accompanied by a change in the reaction mechanism.[3,4] Here, even if the elementary reactions remain unchanged, physics of reactions in the condensed phase is significantly different from physics of gas-phase reactions. Namely, the ratios between the rates of competing processes, the limiting stages and the physical meaning of the kinetic constants are often changed. Studies on the decomposition kinetics in the condensed phase are complicated by the appearance of the gas phase. Differences between the mechanisms of decomposition in different phases and ignoring the distribution of

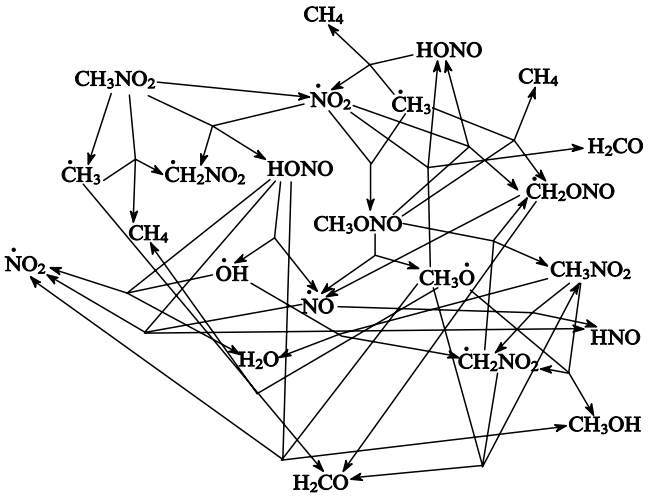

Figure 2. Nitromethane decomposition graph obtained by computer simulation.[32]

reaction products and sometimes reactants between phases cause the reaction kinetics to be dependent on the ratio of the mass, m, of the sample to the volume, V, of the reaction vessel. The influence of experimental conditions on the results of studies carried out using methods of formal kinetics has been the subject of a wide but unsuccessful speculation.

Many explosives are polar compounds. A reason for a possible change in the decomposition mechanism of explosives on going from the gas phase to the liquid phase is intermolecular interaction. Recently, supramolecular chemistry has been intensively developed. The subject of this branch of science is physical chemistry of systems that are (i) more complex than single molecules and (ii) connected to one another through intermolecular (non-covalent) interactions.[66] Supramolecular systems can be characterised by the spatial arrangement and architecture (supramolecular structure) of their components and by types of the intermolecular interactions responsible for interconnection of the components. Liquids whose molecules contain centres of intermolecular interactions can form hydrogen, dipole–dipole and other strong bonds with energies ranging between 10 and 60 kJ mol^{-1}. Association of liquid molecules is a consequence of the formation of labile intermolecular bonds, the equilibrium concentration of which increases as temperature decreases. Association of molecules can influence their reactivities [67] due to (i) a change in the structure of valence electron shells, (ii) such a mutual arrangement of the molecules, which favours (or precludes) a chemical reaction and (iii) a decrease in the molecular mobility. The higher the concentration of intermolecular bonds, the greater the decrease in the molecular mobility in the system on the time scale comparable with the lifetimes of the labile bonds.

Molten trinitrotoluene contains both free molecules and trimolecular associates.[68] Intramolecular oxidation of a CH_3 group proceeds *via* transformation of a transient cyclic complex, resulting in 4,6-dinitroanthranyl. In the associate a CH_3 group of one trinitrotoluene molecule is oxidised owing to NO_2 groups of other molecules in the associate, which are reduced to give azoxy and azo compounds. On going from vapour-phase decomposition to liquid-phase decomposition a number of high-melting thermally stable explosives (nitropyrroles, nitro derivatives of pyridine, pyrazole and triazole, furazans, benzofuroxans and pyridofuroxans) exhibit a dramatic decrease in E_a (by up to 125 kJ mol^{-1}) and in thermal stability (by 50–140 °C). This can be explained by the formation of associates, which allows the radical mechanism of decomposition to be replaced by the molecular mechanism.[69] IR spectroscopic studies revealed self-association in dimethylnitramine [70] and nitroglycerine.[71] At room temperature, nitroglycerine monomers, dimers, trimers and tetramers are in 1 : 1 : 4 : 5.5 ratio.

Despite the fact that association of molecules can affect their reactivities (and, hence, should be taken into account in the kinetic and mechanistic studies of decomposition of explosives), the role of molecular association in the course of decomposition of explosives is still to be clarified. Based on indirect data (feasibility of Trouton's rule), it was assumed[8] that association has no effect on thermal decomposition of explosives, because no association possibly takes place at corresponding elevated temperatures. However, this assumption does not simplify the situation because data obtained at elevated temperatures cannot be used for stability prediction of explosives under the working and storage conditions if uncorrected for molecular association. Self-association of the molecules of explosives both at low and at elevated temperatures has not been studied in detail as yet, though this phenomenon and formation of clusters of associates can be directly quantitatively studied by IR and NMR spectroscopy. If inhomogeneity of a system is due to the presence of associates, an exchange between the associated and non-associated states must affect the transverse magnetisation decay. NMR spectroscopy allows the rate of magnetisation exchange between nuclear spin subsystems with different mobilities and/or different resonance frequencies to be evaluated.[72] This technique can be used in the kinetic studies of complex chemical processes involving transitions from high-populated ground states to less populated but kinetically more active states.[73] To follow structural changes in molecular and supramolecular systems on the picosecond and shorter time scales, a number of multidimensional nonlinear coherent NMR, IR, Raman and EPR spectroscopic techniques were developed.[60–62, 74, 75]

According to modern concepts,[76] multistaginess of the mechanism of a chemical reaction, which involves reversible, concurrent and successive stages and catalysis by gaseous or condensed products, causes the appearance of spatial and temporal dissipative structures (DS). In the former case the distribution of reactants and, hence, the rates of elementary stages and of the overall process is nonuniform in space, the nonuniformity being microheterogeneous in character. In this case, traditional methods of kinetic studies providing volume-averaged values of measured parameters are inapplicable and local methods should be developed. A rather high spatial resolution (a few nanometres) can be obtained in spin diffusion studies.[72, 77]

In the case of temporal DS the concentration of intermediates and the corresponding rates of formation are characterised by oscillations, which can be either regular of chaotic in character. The discovery of oscillations of the heat release rate in studies [78] of thermal decomposition of moist nitrocellulose (Fig. 3) was followed by observations of this phenomenon in the course of decomposition of explosives in the presence of water and in the decomposition of aqueous HNO_3 solutions.[79, 80]

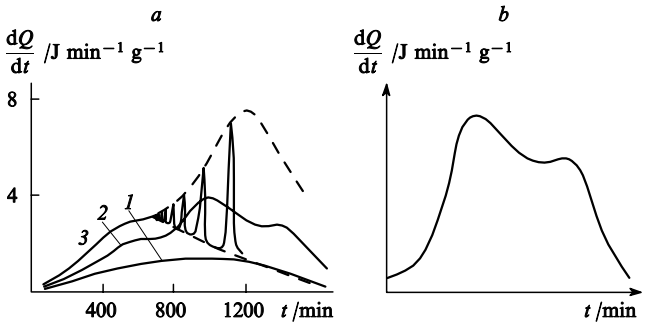

Figure 3. Heat release rate, dQ/dt, plotted *vs.* time for decomposition of nitrocellulose at 423 K (*a*) and total oscillation profile (*b*);[79] open system (*1*); $mV^{-1} = 0.5 \times 10^{-3}$ g cm^{-3}, humidity 1% (*2*); $mV^{-1} = 0.5 \times 10^{-3}$ g cm^{-3}, humidity 23% (*3*).

Detailed studies on the stability of a reaction system require methods that permit the determination of the concentrations of intermediates in the course of reaction and provide a reasonably high temporal (for monitoring) or spatial resolution. A calorimetric technique [78–80] allows the sum of the rates of the changes in the enthalpies due to the occurrence of chemical and physical processes rather than the reactant concentrations to be measured, so oscillations of the total rate of heat release (absorption) can be significantly different from oscillations of the concentrations of intermediates. When using manometric technique, the pressure of gaseous products of decomposition of explosives is usually measured manually in relatively long time intervals (as a rule, tens and hundreds of minutes). Therefore, small pressure oscillations remain undetected in the course of decomposition, though the method permits detection of dramatic changes in pressure in the case of low-frequency, large-amplitude oscillations.

Stability studies of reaction systems are of importance for both elucidation of reaction mechanism and determination of true rate constants for elementary stages of decomposition. If an attempt to describe a self-oscillation reaction using a kinetic model based on a hypothetical mechanism fails, either the reaction mechanism involves no appropriate stages or some constants for the stages under study are incorrect. In this connection theoretical methods [81–83] seems to be promising. For instance, oscillations in the course of decomposition of aqueous HNO_3 solutions cannot be explained in the framework of the mechanism proposed in Ref. 8. Reversibility of HNO_3 decomposition has not been experimentally proved as yet. Probably, the following reactions proceed at rather high temperatures

$$HNO_3 + NO \longrightarrow HNO + NO_3,$$

$$2\,HNO \longrightarrow H_2O + N_2O,$$

therefore, the overall decomposition of HNO_3 is irreversible. The rate constants calculated [8] from the data of calorimetric experiments do not correspond to elementary stages because the calculation procedure ignores the presence of HNO_3 monohydrates and trihydrates in aqueous HNO_3 solutions and the enthalpy changes upon the formation of hydrates.[84] The need of determination of the rate constants for elementary stages of decomposition of HNO_3 and nitrogen oxides is also due to the fact that these compounds are intermediates of decomposition of many explosives.

Experiments showed that solid-phase thermal decomposition of explosives is a spatially inhomogeneous process.[8,85] Corresponding studies of liquid-phase thermal decomposition have not been reported so far. NMR spectroscopy is an efficient method of DS studies in the condensed phase, which allows the appearance of microheterogeneous species to be detected and their size and concentration to be determined.[77,86,87]

Information on the mechanisms of solid-phase decomposition of explosives and oxidisers of solid propellants and corresponding rate constants for elementary stages is scarce. It was repeatedly pointed out that the determination of low degrees of conversion (a few tenths of a per cent) in studies of solid-phase decomposition is precluded by the fact that some products remain solid and cannot thus be determined gravimetrically and manometrically. For instance, it was established [88] that the pressure of gaseous decomposition products in microcavities of ammonium perchlorate crystals reaches 2–3 MPa. It is assumed [89] that accumulation of gaseous products in a crystal having cavities filled with gas leads to the formation of two zones differing in reactivity, namely, a near-surface zone (here, the compound is under tension) and an internal zone where the compound is under uniform compression.

It was proposed to characterise the effect of the lattice of molecular crystals on the reactivity of explosives by the ratio of the apparent rate constants for gas-phase [90] (or liquid-phase [91]) and solid-phase [$k_{exp,(s)}$] decomposition, or the so-called retardation effect of the crystal lattice.[90,91] This effect ignores both the concentration and type of defects. Studies [90,91] were carried out without evaluation of crystal defectivenesses; the $k_{exp,(s)}$ values obtained were low (up to nearly 10^{-12} s^{-1}) and not corrected for dissolution of gases in the explosives under consideration and for the absence of quasi-stationary concentrations of intermediates (this is of importance at low degrees of decomposition), so the parameters $k_{exp,(s)}$ seem to be determined with a low accuracy. In addition, no proofs were presented that the reaction mechanism remains unchanged on going from the gas-phase to the solid-phase reaction, though such a change is possible.[3,68,69] In particular, mention may be made that the energy barrier to interconversion of 1,3,5-trinitro-1,3,5-triazacyclohexane conformers in the gas phase is low (6 to 20 kJ mol^{-1}) and the results of kinetic measurements of gas-phase decomposition of this compound correspond to the dynamically averaged structure.[92] Based on comparison of similar experimental data with the conclusions drawn using an approximate theory that ignores many essential factors, it was concluded [8] that the decomposition of all plastic crystals and compounds with the melting temperatures below 100 °C proceeds as a homogeneous bulk reaction.[8] This conclusion seems to be not proved and the criteria for reaction homogeneity (plasticity of crystals and $T_m < 100$ °C) lack substantiation.

2. Decomposition of explosives under fast initiation

Recently, considerable progress has been made in studies of pre-explosion phenomena under fast initiation of explosives [93–97] due to the use of equipment with submicrosecond and nanosecond time resolutions. The results obtained using fast pulse radiolysis and flash photolysis techniques allowed conclusions about the mechanism of an elementary act of explosive decomposition of metal azides and a chain nature of the process to be drawn.[94] The decomposition of metal azides involves the following stages: hole localisation on a cationic vacany, reconstruction of a reactive site *via* a chemical reaction resulting in the formation of a quasi-local hole state in the valence band, hole delocalisation from the reconstructed reactive site, generation of charge carriers by impact ionisation by 'hot' holes and recovery of the local state in the forbidden band, which provides conditions for repetition of this sequence of stages. Propagation velocity measurements for explosive decomposition of a silver azide whisker were reported.[95] The results obtained ($\sim$1500 m s^{-1}) were associated with the propagation velocity of the diffusion front of holes generated in the course of decomposition.

Pre-explosive phenomena in secondary explosives studied taking 1,3,5-trinitro-1,3,5-triazacyclohexane as an example are characterised by a larger number of stages compared to similar phenomena in metal azides.[96] Initiation of an explosive involves a destruction stage, which is necessary for subsequent efficient supply of energy and is local in character. Energy dissipation occurs in the so-called hot spots. Dislocations or associations of dislocations play an important role in the hot spot nucleation stage. A key feature of this stage are electronic excitations. Local narrowing of the forbidden band near dislocations on compression of explosives dramatically increases the probability of electronic excitation and cleavage of the $N-NO_2$ bond.[4,93]

The decomposition kinetics of explosives under fast initiation was studied by direct detection of gaseous decomposition products on the millisecond time scale using time-resolved mass spectrometers with a performance of up to a hundred of scans per second.[96] More than ten neutral and ionised particles (NO_2, NO, HCN, CN, *etc.*) were detected near the surface of the sample 40 μs after application of a 20 ns pulse of an excimer (KrF) laser with a fluence of 5 J cm^{-2} to a 1,3,5-trinitro-1,3,5-triazacyclohexane single crystal.[96] Photon emission in the near UV and visible regions, delayed by 200 ns to 1.2 μs relative to the laser pulse was also detected. An increase in the laser fluence was accompanied by the appearance of long-lived excited neutral species identified as NO.

In discussing the results of studies on laser-initiated decomposition of explosives it was hypothesised that optical breakdown can compete with chemical decomposition of explosives. Mani-

festation of a particular mechanism is governed by the porosity, dispersion and reactivity of explosives. The problem of extraction of kinetic information from the data obtained under fast initiation of decomposition is still to be solved. In this connection time-resolved magnetic resonance spectroscopy based on detection of the nuclear polarisation of diamagnetic reaction products offers great prospects for research on the spin dynamics and chemical kinetics of short-lived radical species in photochemical reactions.[98]

3. Ammonium perchlorate

Among oxidisers of solid propellants, ammonium perchlorate (AP) has undoubtedly been studied in most detail. Nearly a thousand of publications concerned with the properties of this compound have been reported (see, *e.g.*, Ref. 7 and references cited therein). The results of studies carried out in the 1960s and 1970s changed our concepts of the mechanism of AP decomposition, though researchers still have contradictory opinions of some important issues.[88,99–101] In particular, it was established that the primary act of solid-phase decomposition of AP involves transfer of a proton followed by the formation of ammonia and perchloric acid.

The topographical features of thermal decomposition of AP were studied by optical microscopy.[88] Note that optical microscopy has a limited spatial resolution, which prevents structural elements smaller than 0.2 μm from being observed. The decomposition was accompanied by the appearance of spherical mobile 'nuclei' at depths greater than 5 μm (below dislocation outcrops), which grew until a size of nearly 1 μm. As time passed, the nuclei formed an ellipsoidal decomposition centre elongated along the ⟨010⟩ crystallographic direction. The number of decomposition centres in the crystal can vary over a wide range (from one or two to several tens), being (probably) dependent on uncontrollable factors influencing the sample in the course of preparation; the defectiveness of AP crystals on the nanolevel was not assessed prior to the experiments.

Based on the results of studies on the topographical features of AP decomposition,[88] a dislocation-chain mechanism (DCM) of reaction was proposed.[8] According to this mechanism, dislocations can be generated in the course of reaction under the action of mechanical stress produced on accumulation of gaseous decomposition products in the bulk of the crystal and the motion of dislocations favours the decomposition reaction owing to rearrangement of the AP lattice. This is a phenomenological concept, because experimental data[88] provide no unambiguous proof of the effect of dislocations on the decomposition of AP crystals. For instance, a substantial increase in the starting dislocation density (from 10^2 to 10^6 cm^{-2}) affects only slightly the induction period in the curves of relative mass change in the course of thermal destruction, which becomes nearly three times shorter; however, the change in the dislocation density has no effect on the acceleration stage (Fig. 4).

Preliminary deformation of a crystal to saturate it with dislocations is accompanied by a nearly 105 kJ mol^{-1} increase rather than a decrease in the activation energy for the formation of a decomposition centre. As a result, the induction period of the formation of decomposition centres increases by a factor of nearly 25 even at 230 °C. The increase in the activation energy can be explained by the fact that the formation of a potential nucleation centre in the crystal lattice involves polygonisation and interaction between the newly formed dislocations and is followed by vacancy diffusion from the deformation zone towards the dislocations.[88] Thus, contrary to the basic principles of the DCM concept, the newly formed dislocations are inactive. It is believed that ellipsoidal shape of reaction centres is an argument in favour of the mechanism proposed.[88] [This shape is associated with the fact that the motion and generation of dislocations along the ⟨010⟩ direction occur much easier than in perpendicular directions due to anisotropy of mechanical properties of AP crystals.] For instance,

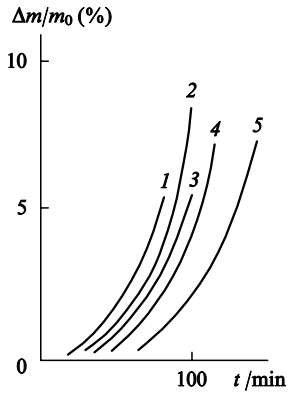

Figure 4. Relative mass change, $\Delta m/m_0$, of ammonium perchlorate crystal in the primary stage of decomposition at 503 K plotted *vs.* time at different dislocation densities.[88]
Initial dislocation density: 10^6 (*1*), 10^5 (*2*), 10^4 (*3*), 10^3 (*4*), 10^2 cm^{-2} (*5*).

it was found that the mechanical characteristics of an AP crystal under tensile stress along the ⟨100⟩ and ⟨001⟩ axes are better than the those of the same AP crystal under tensile stress along the ⟨010⟩ axis. However, it is known that the action of both external forces and the pressure of gases filling microcracks[102] cause the microcracks to grow along the direction perpendicular to the force direction. In other words, growth of the reaction centre along the ⟨010⟩ direction is caused by the forces acting along the ⟨100⟩ and ⟨001⟩ axes. We can agree with the authors of Ref. 100 who said that the available data are insufficient to establish the growth mechanism of an AP decomposition centre. It seems likely that the DCM concept underestimates the role of point defects and overestimates the role of dislocations in the AP decomposition. It should be noted that the starting AP crystals had pores up to 100 nm in diameter, but their prehistory was unknown and the pore size distribution and its evolution in the course of AP decomposition were not characterised.

To gain a better insight into the role of defects in the decomposition of AP and other solid explosives and oxidisers, the formation of vacancy pores of size 1–10 nm and the evolution of the pore size distribution should be studied using, *e.g.*, ^{1}H, ^{15}N or ^{129}Xe NMR spectroscopy (see Refs 103–105). For instance, ^{14}N NMR spectroscopy can be lifted to a level of high usefulness in chemistry and materials science.[105]

The results of studies on AP decomposition indicate an important role played by the kinetic and diffusion factors, exchange with the environment and peculiarities of the crystal structure of AP in localisation of thermal decomposition reaction. A study on topokinetic regularities of low-temperature decomposition of AP crystals as functions of the concentration of additives and temperature suggested that the nucleation rate of decomposition centres is governed by the content of ClO^{3-} impurity ions and by the concentration of free protons, while the growth rate of decomposition centres is nearly independent of the presence of additives.[100] A mechanism of the formation and growth of the AP decomposition centres was proposed.[99] It is assumed that the appearance of spatial and spatial-temporal DS is promoted by the phenomena caused by the pressure of gaseous reaction products. The equation for the reaction front velocity (μm min^{-1}) obtained using a simplest model with allowance for diffusion of perchloric acid has the form

$$u \approx 10^{12.4}\exp\left(-\frac{128\,000}{RT}\right).$$

The results of calculations were found to be similar to the observed 'slow' rates.

4. Hezanitrohexaazaisowurtzitane

Recently, hezanitrohexaazaisowurtzitane (HNIW) first obtained in the USA in 1987 has been the subject of intensive research. This energetic compound belongs to cage-type polynitramines and is of practical interest as a high explosive and a component of solid propellants.[106] The cage structure of HNIW is responsible for high density and enthalpy of formation (ΔH_f = 416 kJ mol^{-1}) and for structural strain. X-Ray diffraction, spectroscopic and quantum-chemical studies revealed [107] violation of the close packing principle in the nitramine crystals. A feature of the polynitramine molecules is the possibility of orbital interaction between the lone electron pairs of amine nitrogens. The variety of interactions of the lone electron pairs in the molecules of conformers is in excellent agreement with the diversity of polymorphs of cyclic and cage-type nitramines. Crystals of the ε-phase are characterised by the highest density (d = 2.062 g cm^{-3}).

The mechanism of thermal decomposition of HNIW has not been established as yet. Data on the kinetics and composition of gaseous decomposition products are contradictory.[108–112] The kinetic parameters of HNIW decomposition exhibit a large scatter (Fig. 5). Solid-phase thermal decomposition of α-, β-, γ- and ε-polymorphs and liquid-phase thermal decomposition of ε-modification were studied in detail by thermogravimetry, manometric technique, IR spectroscopy and optical microscopy.[108, 109] It was shown that decomposition of crystalline HNIW is a pure solid-phase process characterised by self-acceleration due to nucleation and growth of reaction centres. Decomposition follows the phase transitions α → γ, β → γ and ε → γ. The ε → γ transition occurs in the temperature range 180–220 °C and is endothermic in character.[106] The thermal stability of HNIW depends on the initial polymorph state and changes as follows: α < β < γ < ε. The kinetic parameters of decomposition of particular samples are governed by the size, size distribution and crystal morphology. The molecule of a solid product of ε-HNIW decomposition at temperatures below 210 °C contains one of the six nitro groups. The solid product is comprised of transparent microporous particles whose sizes correspond to the sizes of the initial crystals. Heating of the solid product to 600 °C results in a solid residue with a network structure composed mainly of carbon and nitrogen atoms.

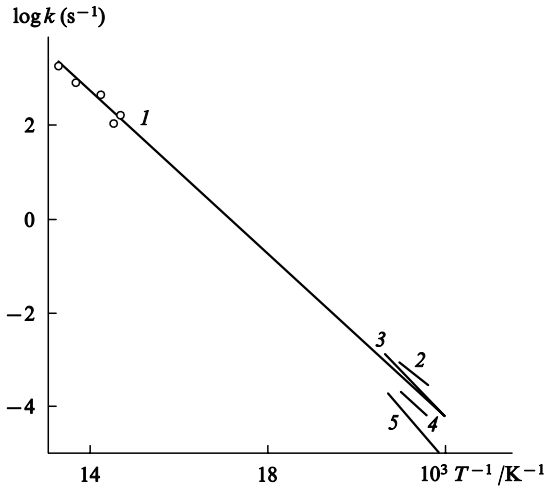

Figure 5. Temperature dependences of the rate constants for decomposition of HNIW.
Rate constants for the leading stage of combustion (open circles) calculated using the Zel'dovich combustion model for a first-order reaction [106] (*1*); rate constants determined from changes in the νNO_2 vibrational intensity in the IR spectrum [110] (*2*) and rate constants for mass change [108, 110] (*3*)–(*5*).

5. Nitrocellulose

Nitrocellulose has a rather complex structure. This is a polymer characterised by some distribution trinitrate, dinitrate and mononitrate units along the polymer chain. Nitro groups can be bonded to both primary and secondary carbon atoms of the monomer unit. A method of assessing structural inhomogeneities in nitrocellulose was developed.[113]

Decomposition of nitrocellulose involves a number of concerted and successive reactions, namely, initial cleavage of the O–NO$_2$ bond, redox interaction between nitrogen oxide (nitrogen dioxide) and macroradicals that are formed in the decomposition of nitrocellulose, hydrolysis of nitrate and glycoside groups, *etc*. However, the mechanism of decomposition has not been completely established as yet. In the early studies carried out in the 1950s and 1960s, the decomposition of nitrocellulose was studied by methods of formal kinetics, *viz*., using the complete gas evolution, loss of the sample mass and formation of the so-called 'condensing' and 'hardly condensing' gases.[114–117] The composition of gaseous products in the initial stage of nitrocellulose decomposition was assessed indirectly;[116, 117] it is inconsistent with the results of more recent mass spectrometric studies.[118] It should be noted that the authors of Refs 116 and 117 pointed that their conclusions about the mechanism of nitrocellulose decomposition are tentative and that the numerical data (E_a and k_0 values) cannot be used in calculating the kinetic parameters of particular stages. The results of IR spectroscopic study of nitrocellulose decomposition are available;[119] however, the reactivity ratios of the primary and secondary ONO$_2$ groups in the dinitrate and trinitrate units was not reported.

The mechanism of decomposition was detailed and the rate constant for the primary step determined in Refs 120–122. Thermal decomposition of nitrocellulose with a nitration degree of 2.7 was studied [120] by UV and IR spectroscopy, gravimetric and photometric methods, gas chromatography and gel permeation chromatography (GPC). It was shown that the reaction begins with cleavage of the O–NO$_2$ bond at a secondary carbon atom in the trinitrate unit. The temperature dependence of the rate constant for loss of secondary nitrate groups in the trinitrate unit (according to IR spectroscopy data) in a system with running medium and the temperature dependence of the rate constant for NO and NO$_2$ formation (according to UV spectroscopy data) in a closed system (at $mV^{-1} \leqslant 5 \times 10^{-4}$ g cm^{-3}) are described by an Arrhenius equation with the same parameters (E_a = 149 kJ mol^{-1} and k_0 = 13.9 s^{-1}). The kinetics and mechanism of subsequent transformations of nitrocellulose are to a great extent determined by conditions for removal of gaseous products. An EPR study of thermal decomposition of nitrocellulose in inert runnimg medium [121] revealed accumulation of free iminoxyl radicals in the primary step. This indicates that the decomposition mechanism involves a stage of formation of a nitroso compound, which subsequently isomerises into an oxime, which then readily decomposes to give an iminoxyl radical.

The average number of breaks of the nitrocellulose polymer chain in the course of decomposition was determined [123] assuming a constant molecular mass. Changes in the molecular mass distribution (MMD) in the course of nitrocellulose decomposition were determined more recently.[120, 122] The conditions for removal of gaseous products from the reaction volume affect the character of the changes in the MMD in the course of thermal decomposition of nitrocellulose. In the system with running medium the MMD becomes narrower due to breakdown of chains with large molecular masses. Terminal macroradicals thus produced undergo partial recombination within the same cage. However, by and large the molecular mass of nitrocellulose decreases due to evolution of gaseous products. In a closed system, the MMD is broadened (Fig. 6) because of production of middle-type macroradicals that recombine to give macromolecules with the molecular masses exceeding that of the starting nitrocellulose.

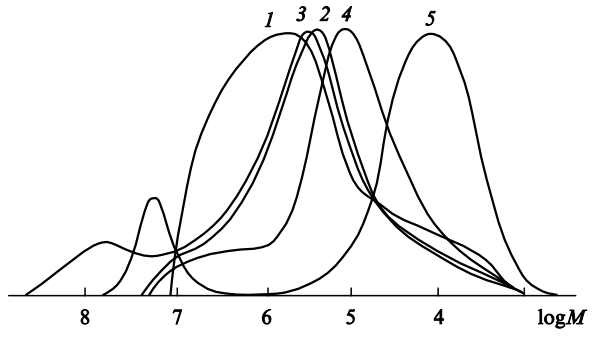

Figure 6. Changes in the MMD of macromolecules in the course of thermal decomposition of nitrocellulose in closed system at $mV^{-1} = 0.02$ g cm^{-3} and $T = 373$ K.[122]
Duration of decomposition /h: 0 (*1*), 48 (*2*), 104 (*3*), 612 (*4*), 1096 (*5*); *M* is the molecular mass of nitrocellulose.

III. Polymer networks as binders for solid propellants

A solid propellant can be treated as a composite material composed of a polymeric binder (10 mass % – 20 mass %), which is usually based on a sparse polymer network containing distributed oxidiser and metal particles of preset dispersion. The compositions of solid propellants depend on the requirements imposed on the specific momentum, stress – strain behaviour, burning rate and the dependence on pressure. A promising way is to prepare binders possessing improved adhesive properties (see Ref. 124).†

1. Structure of polymer networks

A polymer network can be considered as a system comprised of two subsystems, *i.e.*, molecules and the free volume. Each subsystem has a complex multilevel structure.[14] The chemical level of the structure of polymer networks is governed by the structure of the monomer unit. Abstracting of the chemical composition of polymer networks, the topological level of their structure characterises the connectivity of the network structure. The topological structure of a polymer network is characterised by the MMDs of its elements, *viz.*, chain fragments between cross-link points, dangled chains attached to the network through one end, loops formed through end attachment to the initial point of the same chain and free chains. In addition to stable chemical branchings, polymer networks contain labile physical nodes ('entanglements'). The nature of the nodes of physical network and its role in the macromolecular dynamics has been comprehensively reviewed.[126, 127]

The properties of a material are strongly affected by self-organisation on the supramolecular level.[128] This level of structural organisation of polymer networks is characterised by the presence of both highly cross-linked and sparser domains of size of a few nanometres and more. The formation of microheterogeneous domains in polymer networks can be due to various reasons including diffusion and kinetic factors.

The most important operating characteristics of polymer networks including stability and stress – strain characteristics depend not only on the chemical, topological and supramolecular levels of the molecular subsystem but also on the structure of the free volume subsystem. The pore distribution in polymer networks and in other materials with pore sizes from a few tenths of nanometre to a few nanometres can be characterised using positron annihilation method or NMR spectroscopy with hyperpolarised ^{129}Xe or water as probes.[129 – 131]

Some characteristics of the topological structure, *viz.*, the density of cross-links and the average molecular mass of the chain fragments between cross-link points are related to the elastic modulus of a network polymer by a known relation. Direct methods of studies of the supramolecular design of polymers including polymer networks are unavailable as yet. Attempts to construct supramolecular models of linear polymers were reported.[9] Inequality of traditional concepts of the non-crystalline phase of linear polymers as a high-molecular-mass homogeneous liquid disturbed by fluctuations to the task of relevant description of the phase has been exemplified[132] and a framework-micelle model of structural organisation of this phase proposed. QSPR studies of glassy polymers are carried out using principles of synergetics of nonequilibrium systems and fractal analysis.[133] The model of the polymer structure includes a sparse matrix with cross-links represented by entanglements comprised of close-packed segments (the entanglements form a cluster network).

The effect of fillers on polymers manifests itself in variations of the physicomechanical, structural, thermodynamic and chemical properties of binders.[13, 134, 135] Adsorption bonds are formed between the polymeric binder and disperse filler. These bonds are intermediate between the intermolecular and chemical bonds in strength. Filler particles act as polyfuntional nodes; the amount of the 'bound' binder can exceed 40% of the total mass of the binder. A decrease in the molecular mobility of elastomers upon introduction of fillers can be detected by NMR spectroscopy.[135, 136] An NMR-based method of determination of the network structure of filled elastomers135 allows the total concentrations of physical nodes and chemical cross-link points, the fraction of polymer in nearly immobile adsorbed layer at the filler – polymer interface and the fraction of topological nodes that are formed by the polymer chains present between filler particles (Fig. 7) to be determined.

The molecular mass distribution is an important structural characteristic of polymer networks. Methods of determination of the MMDs of linear polymers are based on analysis of the

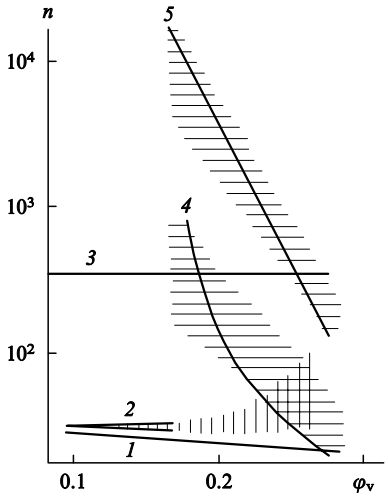

Figure 7. Number, *n*, of repeating units in the chain fragments between cross-link points plotted *vs.* filling degree, φ_v, in polydimethylsiloxane – aerosil mixtures.[135]
Total number of units (*1*); contribution of obstacles created by filler (*2*); contribution of physical nodes (*3*); contribution of adsorption sites (*4*); contribution of cross-links (*5*).

† In contrast to solid propellants, binders for PCMs are usually linear polymers containing 30 mass % – 40 mass % of reinforcing fibres (or mineral filler), antipyrene and other additives.[13] The main operating characteristics of PCMs are improved strength, rigidity, impact strength and incombustibilty. The properties of PCMs depend on particular field of applications.[12, 13] For instance, aviation PCMs must have a heat resistance of 300 – 400 °C and be stable at 500 – 520 °C.[125] For fundamentals of preparation of PCMs with preset properties, see a monograph.[13]

properties of dilute polymer solutions. The MMDs of many insoluble polymers cannot be evaluated using these techniques. Methods based on the degradation of those polymers [137] appeared to be impracticable because they are time-consuming and destructive in character. In this connection recently attempts have been undertaken at using the relaxation properties of polymers for MMD evaluation because the relaxation time spectrum is related to MMD.[16–19, 138–141]

Investigations of the kinetics and mechanism of decomposition of polymer networks and solid propellants based on them are necessary to solve two problems, namely, service life assessment and control of items made of these materials and mathematical modelling of corresponding combustion processes. The service life of the items mentioned above usually depends on the stress–strain properties of polymer networks and solid propellants. Its determination requires knowledge of kinetic data and information on the mechanism responsible for changes in the topological and supramolecular structures of polymer networks and on adhesive properties of solid propellants. Mathematical modelling of combustion of solid propellants requires information on the kinetics and mechanism of thermal decomposition of these compounds.

2. Molecular degradation of polymer networks

Polymer degradation is governed by the chemical and physical transformations of these materials under action of temperature, mechanical stress, aggressive media (water, acids, alkali, oxygen, ozone, *etc.*), various kinds of radiation (photoemission, radioactivity, laser radiation, cosmic rays).[9, 142] In practice, polymeric materials are subject to a number of factors simultaneously. Complexity of studies on the chemical degradation processes is due to diversity of the mechanisms and reactive particles (radicals, ions, unstable molecules) responsible for the development of these processes. The key role in the degradation of linear polymers is played by the radical and radical-chain mechanisms. Ionic mechanisms are of importance for the degradation in acid-base media and in the presence of strong oxidisers; molecular mechanisms are less-common.[9]

Thermal degradation mechanism of polymer networks is to a great extent similar to the degradation mechanism of corresponding linear polymers. For instance, a radical-chain degradation mechanism of polymer networks and the degradation mechanism of linear polymers involve the same elementary stages, *viz.*, chain initiation, propagation, transfer and termination. The molecular mechanism of degradation of polymer networks usually involves a relatively small number of elementary stages. Therefore, studies on the degradation kinetics and the determination of true rate constants for the elementary stages can be performed using methods of formal kinetics. Mathematical formalism developed to analyse the kinetic curves in the case of radical-chain mechanism of degradation of linear polymers [143] can with some variations be applied to polymer networks. When analysing kinetic data for molecular mechanism of degradation, one should take into account that every act of evolution of volatile products (change in the mass of the sample) requires two acts of degradation of chain fragments between cross-link points.

Usually, thermal degradation of polymer networks is studied by simpler methods, namely, thermogravimetry and differential thermal analysis in the dynamic heating regime [144, 145] rather than methods of formal kinetics. Often, assuming a simple one-step degradation mechanism, the thermal stability is characterised by the empirical parameters determined from the experimental data, *viz.*, the degradation onset temperature, maximum mass loss rate temperature and integrated decomposition temperature rather than the activation energy E_a.

The results obtained in studies of the temporal dependence of the charactetistics of the topological structure (*e.g.*, density of cross-links, MMD of chain fragments between cross-link points) can be used for the determination of true rate constants for degradation. In this case, account must be taken of the fact that the chain scission and cross-linking can occur simultaneously.

Mechanical stress is an important factor affecting the rates of chemical reactions of polymers.[15, 142] Often, it is responsible for changes in the reactivities of strained macromolecules, that is, stress influences the kinetics of those reactions that involve structural rearrangements in the reaction centre.[15] If these changes are similar in character to spontaneous structural changes occurring in the course of reaction, the process is accelerated. Otherwise, retardation occurs. Tensile stress causes activation of C–H bonds in the reactions accompanied by proton abstraction.[15] If the hybridisation of a main-chain atom changes, the rate constant, k_σ, for an elementary stage under stress and the rate constant, k, for the same elementary stage in the absence of stress are related as follows

$$k_\sigma = k \exp[\gamma\sigma(RT)^{-1}],$$

where the coefficient γ, or the reaction sensitivity to stress, can be considered as the product of two independent coefficients, $\gamma = \gamma_a\beta$. The coefficient γ_a depends on the energy capacity of the strained structural fragment and on the extent of structural changes in this fragment in the transition state; the sign of the coefficient γ_a depends on the type of stress (tensile or compressive) and on the type of the hybridisation change ($sp^3 \rightarrow sp^2$ or $sp^2 \rightarrow sp^3$). The coefficient β depends on the nonuniformity of stress distribution over the system of bonds. Under tensile stress, chemical reactions accompanied by the $sp^2 \rightarrow sp^3$ rehybridisation of two neighbouring carbon atoms (*e.g.*, addition to the main-chain double bond) are characterised by acceleration of the addition of all reactants to the *trans*-C=C-bond; in the case of addition to the *cis*-isomer, this is only valid for those reagents that have the reaction coordinate $\delta^{\neq} > 0.68$. At $\delta^{\neq} < 0.68$, tensile stress has a retardation effect on the reaction. Compressive stress causes the opposite effect.

The reaction rate sensitivity to mechanical stress can be used to study the reaction mechanism and to determine the constants for elementary reactions.[142] The influence of stress on the reaction kinetics is detected not only in the case of external mechanical stress but also in the presence of internal structural strain in, *e.g.*, polymeric composites, swelled polymer networks, *etc.*

3. Kinetic regularities of decomposition of cross-linked polymers

Kinetic regularities of decomposition of cross-linked polymers have been studied in most detail taking polyurethanes (PUs) as examples.[16–24, 26, 27] Sparse PUs have, on the one hand, a number of valuable service properties typical of elastomers and, on the other hand, a significant drawback, because they are readily degradable at elevated temperatures.

Thermal decomposition of linear PU and model low-molecular-mass urethanes has been the subject of extensive literature. In studies of the degradation of linear PUs the emphasis was placed on analysis of reaction products. Only a few publications concern the degradation kinetics. It was established that the most unstable structural unit of linear PU is the urethane group, which can dissociate into initial alcohol and isocyanate or decompose *via* formation and subsequent decomposition of an intermediate cyclic complex following a molecular or quasi-ionic mechanism.[146–148] Degradation of linear PUs and low-molecular-mass urethanes results in the same products,[149–151] but the data on the degradation kinetics of linear PU are nonsystematic, namely, the Arrhenius equation parameters were usually determined from the rate constants measured at three or four temperatures while the effect of the chemical structure on the thermal stability was characterised using the results obtained only at one temperature.

Calorimetric and gravimetric studies of the degradation kinetics of sparse PUs showed that the parameters, E_a and k_0, of the process depend on the sample synthesis conditions (temperature, presence of catalyst, solvent).[20, 21, 26, 27, 152] This can be explained as follows. Polyurethanes are synthetised in the presence of a catalyst at relatively low temperatures. The process is accompanied by association of reactants, which results in the

formation of nonequilibrium network structures containing systems of strained bonds. Studies on the evolution of structural characteristics of PU networks in the course of PU degradation became possible owing to the use of modern methods of determination of the sol fraction MMD,[21,27] the MMD of chain fragments between cross-link points [16–20] and the microheterogeneity of the sparse polymer networks.[22]

The MMD evolution of the sol fraction in the course of thermal degradation of sparse PU networks was studied by GPC.[21,27] The sol fraction has a trimodal molecular mass distribution with two peaks at $M \approx 300$ and 600 corresponding to the low-molecular-mass fraction and a peak with a maximum at $M \approx 10^4$ corresponding to the 'polymeric' fraction (Fig. 8). It was shown that the urethane groups near cross-link points are the most probable chain scission sites and that the MMD of the 'polymeric peak' of the sol fraction characterises the MMD of the chain fragments between cross-link points in the PU network. The results of computer simulation [27,153] showed that the reactivity of the most stable (urethane) functional group depends on its position in the polymer chain. The formation of a cross-link point of a network based on 1,1,1-trimethylolpropane causes a strong deformation of the neighbouring urethane groups. Steric hindrances to arrangement of three bulky diisocyanate units in the cross-link point lead to the formation of urethane groups with less stable strained bonds compared to the urethane groups in the linear chain fragments. Thus, the primary step of degradation of cross-linked PUs mainly involves breakdown of the urethane groups near the cross-link points.

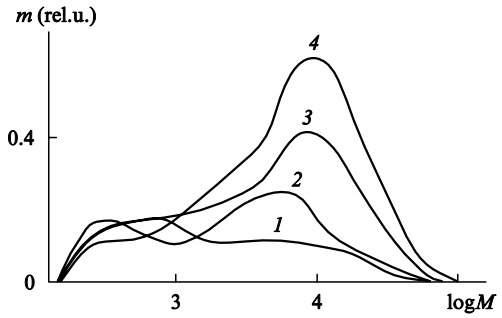

Figure 8. Molecular mass distribution of sol fraction for *in vacuo* thermal destruction of cross-linked polyurethane at 393 K.[21,27]
The amount of the sol fraction in the initial sample was 2.89 mass % and the initial density of cross-links was 2.13×10^4 cm^{-3}. Duration of destruction, days: 0 (*1*), 8 (*2*), 15 (*3*), 35 (*4*); *M* is the molecular mass of the sol fraction.

A theory was developed, which relates the molecular mobility of the chain fragments between cross-link points in sparse polymer networks to the MMD of these chains.[18,24] The MMD evolution of the chain fragments between cross-link points of cross-linked PUs in the course of thermal degradation of these compounds was studied by NMR spectroscopy.[17–20,24] The results obtained are illustrated in Fig. 9. As can be seen, in the initial stage of the process the unimodal MMD is transformed into a broader bimodal MMD and not only longer but also short chain fragments between cross-link points appear; *i.e.*, breakdown of cross-links and cross-linking occur simultaneously. The longest chain fragments between cross-link points are also the most unstable, which is seemingly due to microheterogeneous character of the supramolecular structure of sparse PU networks.[22]

Studies on the MMD evolution of the chain fragments between cross-link points of sparse PU networks under permanent tensile stress or strain showed [17,19] that in this case the network structure changes long before the macroscopic degradation of the sample, the structural changes being similar to those observed in the course of thermal degradation (Fig. 10). Distinctions between

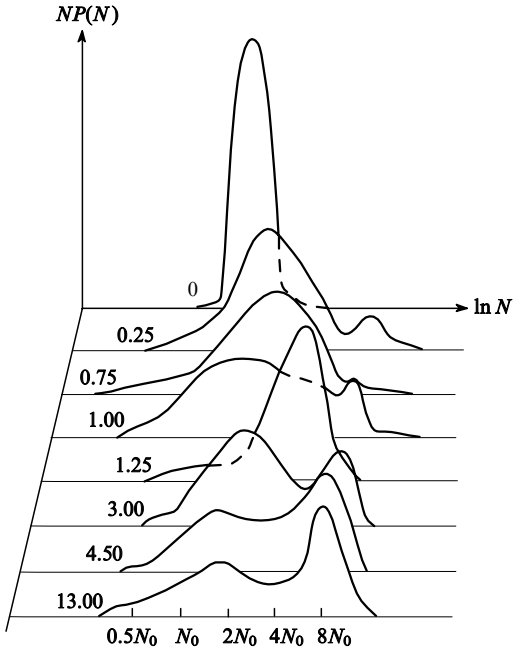

Figure 9. Molecular-mass distribution in the chain fragments between cross-link points for *in vacuo* thermal destruction of cross-linked polyurethane at 498 K.[19]
Figures near curves denote the duration of destruction /h; N_0 is the average length of a chain fragment connecting cross-link points in the starting sample.

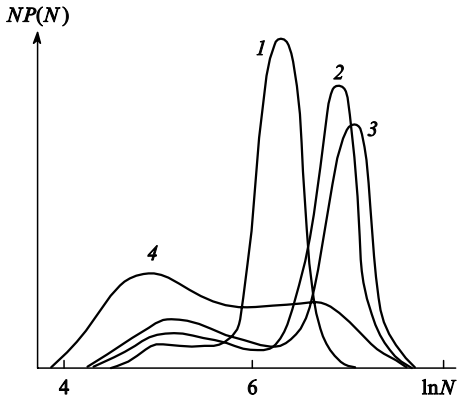

Figure 10. MMD of chain fragment connecting cross-link points in cross-linked PU after storage of the sample for 21 days at 300 K at constant tensile stress σ.[17]
σ /MPa: 0 (*1*), 0.75 (*2*), 1.0 (*3*), 1.25 (*4*).

the character of changes in the MMDs of the chain fragments connecting cross-link points under permanent stress and strain were revealed. The results obtained allowed the degradation mechanism of strained elastomers to be clarified because opposite views of this mechanism were reported.[9,142,154,155]

This nondestructive method of studying the MMD evolution of the chain fragments between cross-link points in the course of thermal degradation of elastomers under stress and strain is of importance for estimation of accumulated defects. However, the technique has not been employed in studies of solid propellants as yet.

The kinetic regularities of the degradation of three highly cross-linked polymers, *viz.*, dimethacrylate triethylene glycol (DMATG), cross-linked and 'hyper-cross-linked' polystyrene (HPS) and poly(epoxyamine) (PEA) have been studied in sufficient detail.[23–26,29,30]

DMATG has a microheterogeneous supramolecular structure formed by highly cross-linked 'granules' distributed in a highly defect matrix. Degradation of DMATG was studies by NMR and gravimetry.[23–26] The kinetic regularities of the degradation depend on the initial degree of conversion (Γ_0) of the sample and dramatically change at $\Gamma_0 = \Gamma_m$ (Γ_m is the degree of conversion at which highly cross-linked granules contact one another and the polymer becomes monolithic). Degradation of the samples with $\Gamma_0 < \Gamma_m$ is characterised by cleavage of the weak, strained matrix bonds and a decrease in the total mass of granules; the density of cross-links remains unchanged. The process proceeds by a radical-chain mechanism and involves partial formation of new cross-links. At $\Gamma_0 > \Gamma_m$, degradation follows the molecular mechanism *via* decomposition of the ester groups of DMATG and formation of polymethacrylic anhydride.

The character of PEA and HPS degradation depends on the density of cross-links.[29,30] The process proceeds by the mechanism of radical-chain depolymerisation at relatively low values of this parameter and by the molecular mechanism in the case of more cross-linked samples. The degradation of the HPS samples with the density of cross-links greater than 40% obeys a more complex pattern and proceeds much lower than in the case of the samples characterised by lower densities of cross-links (Fig. 11). The presence of strained network fragments in HPS affects the shape of the initial portions of the dependences of the specific degradation rate on the degree of degradation. An increase in the thermal stability of the networks with higher density of cross-links can be explained by a decrease in the chain initiation probability and by an increase in the kinetic chain termination probability for radical-chain depolymerisation of the short, and therefore, nearly immobile chain fragments connecting cross-link points. The fact that fullerenes inhibit the degradation of these samples confirms the radical-chain degradation mechanism of the cross-linked polymer networks with a density of cross-links less than 40%.

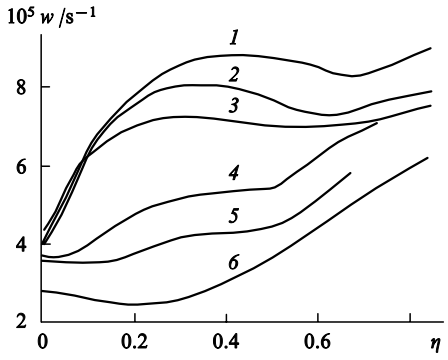

Figure 11. Specific rate of change in mass (w) plotted *vs.* degree of decomposition η for *in vacuo* destruction of cross-linked polystyrene samples at 613 K.[30]
Initial density of cross-links (%): 11 (*1*), 17 (*2*), 25 (*3*), 43 (*4*), 66 (*5*), 100 (*6*).

The formation of polymer networks is usually accompanied by noticeable reaction shrinkage. Sometimes this results in the polymer networks with a large nonequilibrium excess free volume and sometimes causes defect formation (micropores appear and cracking occurs). The kinetic regularities of the PEA degradation are affected by the value of the excess free volume and, in partiular, by the excess free volume distributions over the *n*-defects, clusters and microcavities and across the width of the sample.[31,156]

Degradation of polymeric composite materials based on linear polymers is usually studied by thermogravimetry and differential thermal analysis in the dynamic heating regime. Statistical treatment of experimental data is often carried out assuming a simple one-step kinetics. Because of this, the results obtained and conclusions drawn are, as a rule, qualitative in character. Clearly, the reasons for contradictory results of many studies on thermal and oxidative degradation of PCMs are differences between the experimental methods and procedures employed.[157]

There are a few studies on the degradation of filled polymers based on polymer networks. The decomposition kinetics of these compounds is significantly different from the decomposition kinetics of binders and depends on the type of the filler used (Fig. 12).[28,31] An increase in the decomposition rate in the presence of chemically inert fillers cannot be explained by the chemical interaction between the binder and filler. An increase in the binder decomposition rate can be attributed to the action of internal stress that depends on the type of filler, adhesion strength of the filler and binder, and the difference between the thermal expansion coefficients of the filler and binder. Residual shrinkage stress should also be taken into account because the formation of polymer networks is usually accompanied by noticeable shrinkage. A procedure based on pulsed NQR technique was developed for the determination of internal stress in polymers and polymeric composites.[158]

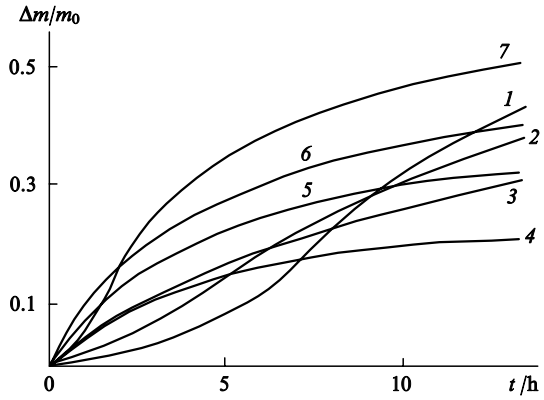

Figure 12. Relative mass change, $\Delta m/m_0$, of PEA samples for *in vacuo* destruction at 543 K.[28,31]
Unfilled samples (*1–3*), filled samples (*4–7*); particles of size 1–2 mm (*1*), film 0.2 mm thick (*2*), particles of size 0.09–0.16 mm (*3*); filler: boron fibre (*4*), organic fibre (*5*), glass fibre (*6*), carbon fibre (*7*).

Highly cross-linked polymers can be considered as best model systems suitable for establishment of the effect of microheterogeneity, restricted molecular mobility of binder with an increase in the density of cross-links, the excess free volume and its distribution over the structural elements and the stressed state of the binder (due to the difference between the thermal expansion coefficients of the binder and filler) on the thermal stability of polymer networks.

4. Effect of decomposition products of solid propellant oxidisers on the degradation of polymeric binder

Often, oxidisers or some other components of solid propellants decompose faster than binders. The decomposition products of a given component can interact with the binder. The kinetics and mechanism of this interaction depend on the nature of the oxidiser decomposition products and on the type of the polymeric binder. Oxidative degradation of linear polymers has been studied in most detail.[9,15] A monograph [15] is concerned with peculiarities of this process, supramolecular and conformational effects in the oxidation kinetics of oriented polyolefins, changes in the structure and properties of polymers under stress and analysis of the degradation regularities of polymers exposed to aggressive media under mechanical stress. Among numerous studies on the ozone ageing of strained cross-linked rubbers based on natural rubber, polyisoprene, polybutadiene, butadiene–styrene or butadiene–acrylonitrile copolymers, *etc.*, most are applied in character and

mainly concern cracking assessment and the time to rupture measurements (see monograph [15] and references cited therein). The critical strain observed during the ozone degradation of elastomers (maximum crack growth rate and minimum sample durability under nearly 20% tensile strain) can be explained [15] by a change in the reactivity of the strained C=C bond.

The kinetics and mechanism of oxidative degradation of the elastomers used as binders for solid propellants have almost not been studied. For instance, studies on the oxidative degradation of a PU elastomer based on polybutadiene containing terminal hydroxyl groups and diisocyanate were aimed at solving practical problems, *viz*., elucidation of the reasons for embrittlement of elastomers and deviation of the experimental data on thermal ageing from the Arrhenius equation.[159–163] The temperature dependences of the oxidation products of the elastomer samples containing and containing no antioxidant was studied by IR and NMR spectroscopy, GPC and oxygen uptake measurements.[162] Dynamic and chemical heterogeneity of size nearly 20 nm was found in the aged samples. The major oxygen-containing products are alcohols (~60%). Ester and acid groups were found but no ketones were detected. It was shown that chain scission is cross-linking of macromolecules occur simultaneously during degradation. The gel content increases from 60% to 90% during the oxidation, the density of cross-links in the gel substantially increases and the sol molecular mass decreases. Nevertheless, the reason for cross-linking was not established. Probably, this is due to radical-chain polymerisation of the polybutadiene fragment at the double bonds.[152]

Undoubtedly, the decomposition products of solid propellant oxidisers that intensely interact with polymeric binder are nitrogen oxides and chlorine oxides, perchloric acid and nitric acid. The interaction of nitrogen oxides and nitric acid with low-molecular-mass organic compounds and polymers was mainly investigated in relation with the kinetic and mechanistic studies of nitration of organic compounds.[164–168] It was shown that nitration of aromatic compounds is an ionic process and that nitration of paraffinic hydrocarbons is a free-radical process initiated by nitrogen dioxide. Nitration of cellulose only proceeds under the action of a nitric acid pseudoform ($HONO_2$) present at HNO_3 concentrations greater than 70%.[168] At concentrations below 60%, HNO_3 is present in the form of a trihydrate which causes oxidative degradation of cellulose. Liquid-phase oxidation of decane by nitrogen dioxide proceeds by the mechanism of degenerate branched-chain reaction.[169] Gas-phase oxidation of glyoxal by nitrogen dioxide follows a radical-chain mechanism.[170]

The effect of nitrogen oxides on polymers was mainly studied in relation with the problem of maintenance of the operating characteristics of polymeric materials exposed to aggressive media (see a review [171] and references cited therein). Degradation of various classes of polymers in NO, NO_2 and $(NO_2)_2$ atmospheres was usually studied phenomenologically without determining the rate constants and parameters of the Arrhenius equation. It was shown that at temperatures similar to room temperature NO_2 is capable of abstracting mobile hydrogen atoms from polymers to produce side nitro and nitrite groups. These processes are accompanied by scission of the main polymer chain. Nitrogen dioxide can also add to the double bonds of carbochain polymers to generate macroradicals and thus initiate free-radical ageing of the polymers. Exposure to nitrogen dioxide causes not only degradation but also cross-linking of polyisoprene and polybutadiene macromolecules. At elevated temperatures ($T \geqslant 373$ K), NO_2 also reacts with less responsive methylene C–H bonds. Interacting with alkyl, alkoxy and peroxy macroradicals, NO_2 can inhibit free-radical transformatins of polymers to give macromolecular products of different thermal stability.

Nitrogen monoxide is much less reactive compared to nitrogen dioxide. It is incapable of abstracting mobile hydrogen atoms from organic molecules and cannot add to isolated double bonds to produce free radicals at temperatures similar to room temperature. Being an efficient acceptor of free radicals, nitrogen monoxide inhibits free-radical processes.

A few phenomenological studies on the oxidation of polymers with the decomposition products of ammonium perchlorate are available.[172–174] It was shown that at high temperatures oxidative pyrolysis of polymers [poly(methyl methacrylate), polystyrene, butyl rubber, polyethylene, SKDN rubber, *etc*.] in perchloric acid vapours and in mixtures with AP becomes the predominant process proceeding with an effective activation energy of 200–240 kJ mol^{-1} (*cf*. 140 kJ mol^{-1} for the decomposition of pure AP). The kinetic and mechanistic aspects of the interaction between the oxidiser decomposition products and the binder on the topological and supramolecular levels, the effect of stress on the kinetics and mechanism of this interaction and the adhesive properties of the binder towards the filler have almost not been studied so far, though this is of great importance for well-warranted stability control of solid propellants. In this context the use of NMR, IR and EPR spectroscopies can play a significant role.[62, 74, 75] For instance, two-dimensional IR Fourier spectroscopy allowed one to study fine details of the oxidative degradation mechanism of polymer networks that cannot be established using one-dimensional spectroscopy in the frequency domain.[62] It is also possible to study the evolution of the structural characteristics of filled polymer networks in the course of binder degradation to reveal the most unstable block in the composite structure. In particular, nanolayer spectroscopy seems to be promising for studies of degradation of filled polymer networks. This method permits measurements of temporal intervals corresponding to the appearance of different types of radicals in nanolayers of a compound and establishment of the sequence of elementary acts of a chemical reaction up to the formation of molecular products.[175] However, these techniques have not been employed in studies of filled polymer networks including solid propellants as yet.

IV. Mathematical modelling of decomposition of energetic materials

1. Modelling of structure – reactivity relations

The strategy of development of weapon systems involves design of new and improvement of the existing EMs. At present, the problem of development of a cheap, efficient and fast method for testing newly designed EMs is topical in connection with enhanced requirements for the service properties of EMs.[176] An improved screening methodology is required to avoid expensive tests of inappropriate materials. This can be realised using methods of mathematical modelling that are divided into two main classes: (1) classical Monte Carlo (MC) simulation and molecular dynamics (MD) modelling and (2) quantum-chemical calculations. Quantum-chemical calculations are based on fundamental principles of quantum chemistry; solving quantum chemistry equations provides a complete and exact description of an atomic system. MD modelling using realistic models allows the reaction dynamics of large atomic systems to be described correctly.

A basic problem of theoretical chemistry is establishment of relations between the electronic structure and reactivities of reactants (rate constant for an elementary reaction can be considered as a measure of reactivity). The methodology and computational procedures employed for calculating the potential energy surfaces, dynamics and rate constants for gas-phase reactions were developed in the 1970s.

At present, quantum-chemical calculations can be carried out only for the simplest explosives and their models.[177–182] The molecular geometries in the equilibrium and transition states, Mulliken atomic charge distributions and electric dipole moments were calculated for, *e.g*., the simplest nitramines.[177, 178] These characteristics, as well as their changes caused by intramolecular motions are of importance in discussing the chemical properties of compounds. Quantum-chemical calculations of the force field,

analysis of vibrational spectra of several nitro compounds and the force constants of stretching vibrations, internuclear distances and spectral characteristics of the simplest nitramines were reported.[179]

Ab initio (including multiconfigurational) quantum-chemical methods were employed to calculate the potential energy surfaces of nitroso compounds in the ground state and in the lowest excited electronic state and to determine the equilibrium geometric parameters, vibrational frequencies and the potential functions of internal rotation of molecules.[180] The structures of nitroso compounds were calculated and the Y—NO (Y = C, N, O, S) bond dissociation energies determined.[57] The bond lengths and bond angles in ammonium dinitramide $NH_4N(NO_2)_2$ in the gas phase were obtained from *ab initio* MO calculations.[181,182]

No substantiated assumptions of the molecular geometries of 1,5- and 2,5-substituted tetrazoles, furazans and furoxans in the transition states of thermal decomposition of these compounds are available; therefore, the principle of least motion cannot be used.[183] For instance, the ground-state parameters characterising those bonds in the heterocycle that are involved in thermal decomposition were used[184] as reactivity indices. The relations established are consistent with the assumptions[37,38] of the mechanism of thermal decomposition of tetrazoles.

Quantum-chemical methods offer great computational potentials and are employed in calculations of the properties of particular molecules. Much less attention has been paid to the interpretation of results obtained in terms of the chemical bonding, molecular structure and mutual influence of molecular fragments. A quantum-chemical procedure for analysis of the electronic structure and physicochemical properties of complex molecules in terms of the interactions between the fragment orbitals was reported.[185] This approach has long been known[186] but was not systematically employed in the analysis of intramolecular interactions in order to distinguish between the key mechanisms of the mutual influence of structural fragments in complex organic molecules (inductive effect, conjugation, *etc.*) and in studies of their relations to the physicochemical properties of compounds.

Using quantum-chemical methods, it is possible to calculate the rate constant for a certain individual reaction;[187] however, generalisaiton of kinetic data for different classes of chemical reactions and the problem of establishing relations between the reactivity and structure (and physical characteristics) of reactants remain unsolved. Two empirical models (a model of intersecting parabolas and a model of intersecting Morse curves) for hydrogen abstraction reactions have been reported.[188] It was shown that the activation energy of such a reaction depends on ten parameters. These models allows the transition-state geometry (interatomic distances in the reaction centre and bond angles) to be calculated from experimental data.[189]

Recently, considerable attention has been paid to studies on the reactions dynamics in the condensed phase. Detailed consideration of the main methods of theory of liquid-phase reactions, *viz.*, numerical simulation by the Monte Carlo and molecular dynamics methods, numerical and analytical studies of the Langevin stochastic equations, Focker–Planck equation and Bohm–Gross kinetic equation has been given.[190–192] The potentials and limitations of moderm methods were exemplified by calculations of the rate constants for particular isomerisation, substitution, addition and electron transfer reactions.

Attempts at calculating the activation energy, E_a, for a dissociation reaction from the IR spectra using a relation between the anharmonicity constant and the dissociation energies of those diatomic molecules in which the interatomic interaction is described by a Morse function were undertaken.[193,194] The dissociation energies of the C—N bond in CH_3NO_2 and of the N—N bond in solid *N*-nitrodimethylamine and in CCl_4 and CH_3NO_2 solutions were calculated.

Studies[195,196] concerned more rigorous mathematical modelling of the primary steps of thermal decomposition of explosives. Density functional calculations of the initial stages of decomposition of 5-nitro-2,4-dihydro-3*H*-1,2,4-triazol-3-one dimer were reported.[195] The reaction is characterised by an activation energy of 369 kJ mol^{-1}; its elementary stages involve the formation of four intermediates and five transition states and result in CO_2 evolution.

The initial decomposition process of urea nitrate were studied by the Hartree–Fock, density functional and second-order Müller–Plesset perturbation theories.[196] Calculations revealed the sequence of elementary stages of urea nitrate decomposition which involves one intermediate and two transition states (TS1 and TS2) with successive formation of NH_3, HNCO and HNO_3. A potential energy profile for the urea nitrate decomposition is shown in Fig. 13 *a*. The decomposition begins with intramolecular proton transfer from one NH_2 group to another to produce NH_3. The optimised geometry of TS1 corresponding to the beginning of intramolecular proton transfer is shown in Fig. 13 *b* (arrows

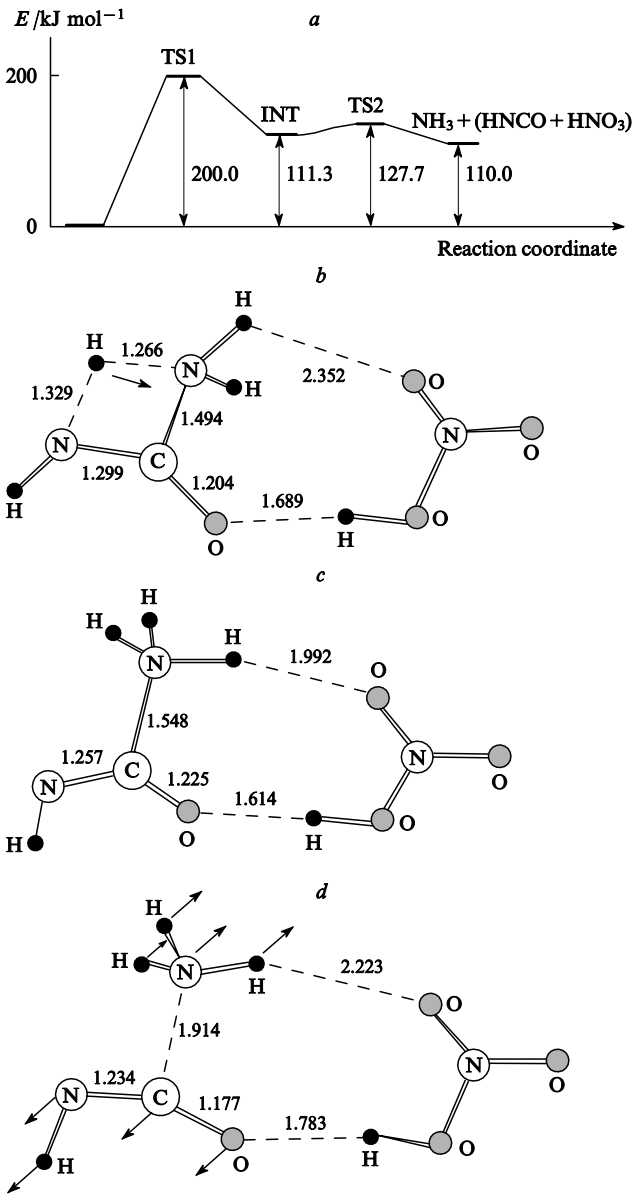

Figure 13. Results of mathematical modelling of primary stages of thermal decomposition of urea nitrate.[196]
Changes in potential energy (*a*), optimised geometry of TS1 and displacement vectors of the normal mode at 1762.7 cm^{-1} (*b*); optimised geometry of (*c*), optimised geometry of TS2 and displacement vectors of the normal mode at 319.2 cm^{-1} (*d*). Bond lengths are given in Å.

denote the displacement vectors). Transition state 1 is a four-membered ring. The intermediate formed after proton transfer goes to TS2. The directions of the displacement vectors in TS2 correspond to the decomposition with production of NH_3, HNCO and HNO_3. Transition state 1 is formed only based on the optimised structure of urea nitrate. In the case of $(NH_2)_2COH^+$, which is the ground state of the crystal structure of urea nitrate, no formation of the four-membered ring N–H–N–C occurs. Therefore, it is assumed that the two-dimensional network of strong hydrogen bonds in the crystal needs to be destroyed by external stimuli (*e.g.*, heat or impact) to begin the decomposition reaction of urea nitrate.

To design new low-sensitive EMs with improved service properties, the effect of mechanical stress on the kinetics and mechanism of their decomposition should be studied.[197] Detailed mathematical modelling of stress action on the reactivity of EMs has been carried out only for polymers.[15]

2. Modelling of solid-phase decomposition

Solid-phase decomposition of EMs can produce some products that form individual phases. Mathematical description of the formation of a new phase has attracted considerable attention.[198, 199] In particular, kinetic concepts of the nucleation and growth of vacancy pores in crystals are based on the kinetic equation of formation of a new phase.[200] According to these concepts, vacancy pores are associations of vacancies that form clusters in the form of vacancy voids (negative crystal), the cluster size varying from tens to hundreds of lattice constants. In the vicinity of each pore there is a nonuniform vacancy distribution, which depends on the vacancy size and can be treated as a vacancy-gas cloud. Diffusive motion of vacancies to a pore and settling on it cause pore motion and growth. The higher the curvature of the pore surface area, the higher the concentration of vacancies above this area.

A closed kinetic equation for the description of radiation-induced evolution of vacancy pores in the coordinate space was derived.[199] The stability regions of the vacancy pore lattice with respect to pore growth and pore displacements from the lattice sites were established. The main processes responsible for changes in the pore distribution in supersaturated vacancy gas are condensation, evaporation and surface diffusion of vacancies and coagulation of pores.

Detailed mathematical modelling of the primary step of solid-phase thermal decomposition of explosives is unavailable as yet. Mathematical treatment of decomposition of a model solid compound involving formation of solid and gaseous products was reported [8, 201] assuming deep stages of conversion where the overall steady-state process is governed by production of the solid product isolated in individual phase. Expressions for the interface propagation velocity, characteristic thickness of the reaction zone and concentration distribution were derived for the simplest idealised case of reversible first-order reaction with allowance for diffusion of the solid product ignoring the stress and strain effects on the reaction rate.

A steady-state mathematical model [8, 202] for reaction front propagation in AP crystal was constructed assuming a dislocation-chain mechanism of AP decomposition ignoring diffusion of reaction products. According to the DCM model, AP decomposes on dislocations, multiplication of dislocations being stress induced. However, the kinetic description of dislocations in this model is phenomenological. The dependences of the dislocation multiplication rate on stress applied and on the concentration of dislocations have no substantiation. The model also ignores such important stages of plastic deformation of the crystalline material as dislocation annihilation, mutual entrapment of dislocations in the intersecting slip planes, dislocation absorption at grain boundaries and dislocation multiplication by double cross sliding.[203, 204] In addition, stress distribution was preset arbitrarily and relations between the stress–strain state and fracture micromechanics of the crystal and the pressure of gaseous products were ignored. Linear dependence of the AP decomposition rate on the dislocation concentration postulated in the model is inconsistent with the experimental data. It should also be noted that evaluation of the model is impossible due to the lack of methods suitable for the determination of the constants appeared in the model equations.

N S Enikolopov and co-workers (see a review [205] and references cited therein) showed that shear deformation causes a substantial (by 3–8 orders of magnitude) increase in the rate of solid-phase reactions compared to the rate of liquid-phase reactions. It was assumed that reactions in the detonation regime proceed isothermally at low temperatures due to immediate conversion of chemical energy into mechanical energy.

Theoretical studies of pre-explosive phenomena under shock-wave initiation showed that the key step of the solid-phase stage of the process are electronic excitations. Narrowing of the forbidden band upon compression of explosives at the reaction wave front was considered.[206] Calculations of the electronic structure of 1,3,5-trinitro-1,3,5-triazacyclohexane revealed [207] a local narrowing of the forbidden band near dislocations and additional narrowing of the forbidden band upon compression in the shock front, which leads to considerable increase in the electronic excitation probability (formation of an exciton) and cleavage of the $N-NO_2$ bond. A molecular dynamics study [176] revealed that metallisation (loss of covalency) upon compression of explosives must be taken into account as the primary step of a sequence of reactions leading to detonation. On the molecular level, a shock-initiated chemical reaction is described [208, 209] as a nonequilibrium non-thermal process whose rate is determined by the average vibrational rate of radical pairs produced *via* molecular decomposition on the 10^{-14}–10^{-12} s time scale. This model is consistent with the results of MD calculatios.[210]

Almost all EMs are heterogeneous in nature, being often composed of a polycrystalline material and a binder. The presence of internal interfaces differs the behaviour of EMs from that of pure materials. Compaction (consolidation), strain and a chemical reaction in a porous explosive was studied using three-dimensional modelling of shock action on an 'array of discrete crystals'.[211] It was shown that fast deformation at contact points induces large-amplitude fluctuations of the strain state characterised by a wavelength of the order of a few particle diameters. Energy localisation causes the appearance of 'hot' spots. Chemical reaction produces multiple wave structures depending on the particle size distribution.

Modelling of thermal decomposition of solid propellants on the mesolevel (oxidiser particle — binder layer) was not performed.

3. Modelling of combustion of energetic materials

Combustion of EMs is a complex physicochemical process, which involves decomposition reactions, heat and mass transfer and strain and decomposition. The complexity of the process makes experimental studies and the development of rigorous quantitative theories of EM combustion difficult. It is believed that elaboration and analysis of simplified combustion models with allowance for particular factors only in order makes possible clarification of the physical picture of combustion and a relatively simple mathematical description. The problem of mathematical modelling of EM combustion goes beyond the scope of this review and should be considered separately due to extensive literature on the problem. However, we will dwell on those aspects of mathematical modelling of the process that are immediately related to the influence of the kinetics and mechanism of EM decomposition on the regularities of their combustion.

A number of simple models of linear combustion with allowance for dispersion, foaming, evaporation and sublimation of the solid compound have been analysed.[212–219] Usually, one-step or two-step reactions are considered ignoring differences between the kinetic regularities of heat release and gas evolution in the course of decomposition. For instance, combustion of highly volatile compounds is analysed using a reaction kinetics scheme

involving two concurrent or two successive steps.[215, 216] Combustion studies of individual explosives were carried out assuming a one-step kinetics with allowance for the difference between the activation parameters for the condensed phase and the gas phase.[217, 218] Combustion of mixed systems was analysed in the homogeneous condensed zone approximation taking into account (i) thermal decomposition and sublimation of oxidiser and (ii) binder degradation and oxidation by the oxidiser decomposition products; however, the corresponding reaction kinetics were described by zero-order reaction equations.[219]

As shown above, the decomposition of EMs proceeds by a complex multistage mechanism. The results of the combustion rate calculations obtained in the analysis of simple combustion models are in good agreement with the experimental data of combustion studies of several oxidisers (NH_4ClO_4, $NH_3OH.ClO_4$, NH_4NO_3, $CH_3NH_3ClO_4$) with complex decomposition mechanisms.[8, 220] Because of this, it may appear that complexity of the EM decomposition kinetics and mechanism is insignificant for mathematical modelling and there is no longer need of detailed studies on the EM decomposition. However, this conclusion is incorrect, because mathematical modelling of combustion of EMs often involves an arbitrary closure of the system of equations by introducing one or two arbitrary parameters, *e.g.*, an additional heat flow from the gas phase to the condensed phase and the degree of dispersion (sublimation). These models ignore the mechanical problem; therefore, a relation between the dispersion and combustion conditions is established based on the simplest estimates.[8] Following this way, the interrelation between the stress–strain state of EMs and the regularities of combustion is reduced to the dependence of the burning rate on pressure.

Note that an increase in pressure has almost no effect on thermal decomposition of binder in the case of radical-chain mechanism. The molecular mechanism is characterised by a decrease in the rate of evaporation of high-molecular-mass degradation products.[221] Consideration of the mechanical problem in combustion modelling is also necessary because combustion of charges with actual geometry requires allowance for not only hydrostatic pressure but also the deviator components of the stress tensor. As shown above, these components can strongly influence the decomposition of solid propellants.

Finally, note that in the early 1960s studies on the macrokinetics of exothermic reactions revealed that the reaction front temperature exceeds the adiabatic temperature (Fig. 14). A part of these results obtained in experimental studies of solid propellant block formation was reported some later.[222] Nevertheless, combustion in the condensed phase is usually modelled assuming that reaction front propagation can be described similarly to gas-phase combustion[8, 223] and the steady-state combustion models ignore experimentally detected excess of enthalpy in the combustion wave, which leads to superadiabatic temperatures.

To some extent the simplified mathematical treatment of EM combustion can be explained by the lack of the kinetic parameters relevant to complexity of the multistage EM decomposition over a wide temperature interval. Nevertheless, note that almost all correctly posed problems can be solved using modern powerful computers and experimental techniques. For instance, a modern strategy of modelling well-developed turbulent flows of multicomponent reactive gases with allowance for interrelations between the chemical kinetics and turbulent transfer was reported.[224]

Recently, advances were also made in studies of combustion of mixed fuels. These studies intensively use computer simulation of processes proceeding in the gas phase and condensed phase. Numerical analysis of combustion of a model fuel based on 1,3,5-trinitro-1,3,5-triazacyclohexane and glycidyl azide polymer has been reported.[225] Four oxidiser and binder decomposition reactions were taken into account for the condensed phase while the kinetic scheme for the gas phase included a total of 532 reactions involving seventy-four compounds.

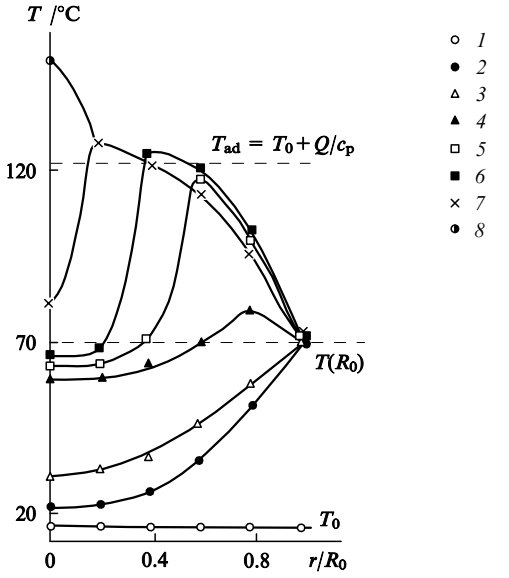

Figure 14. Temperature distribution throughout the cross section of a cylindrical reactor of radius R_0 = 20 cm for polymerisation of a model mixture based on triethylene glycol dimethacrylate.[222]
Dimensionless time, t/t_∞: 0 (*1*), 0.25 (*2*), 0.40 (*3*), 0.86 (*4*), 0.91 (*5*), 0.95 (*6*), 0.99 (*7*), 1.0 (*8*).

V. Stability prediction of energetic materials

Explosives, solid propellants and powders are thermodynamically unstable materials due to occurrence of chemical reactions and physical processes in these substances.[8, 226] This requires the EM service life to be assessed with a rather high accuracy because untimely replacement of items made of EMs causes unreasonable expenditures. Explosive demolition requires that precautions be taken, often being an environmental hazard.

The warranty period of items made of EMs can be determined empirically or semiempirically but mathematical modelling is thought to be more efficient.[9, 226] A scheme of modelling of complex physicochemical processes was first developed to study thermal explosions. It involves phenomenological studies of the process, aimed at identification of the most important factors responsible for the changes in the practically valuable properties of EMs; construction of physicochemical and mathematical models of the process; experimental determination of parameters of particular stages; calculations and comparison of the results obtained with the results of full-scale tests to evaluate the accuracy of prediction, *etc*.

No mathematical model suitable for correct description of all (most important) physicochemical and physicomechanical processes proceeding in the course of production and storage of items made of EMs is available as yet. A relevant procedure for assessment of the warranty period of items made of EMs based on mathematical modelling has also not been elaborated so far. It was proposed[8] to characterise the stabilities of solid fuels and of the cast and pressed charges by the time taken to reach a degree of decomposition of 0.02% during the reprocessing step and storage life of the composition (in this case all gaseous products are dissolved in the condensed phase and development of internal pressure, pore formation and swelling of items are impossible). According to this concept, the extent of changes in the service life of items made of EMs are solely determined by the after-effects of gas evolution in the course of decomposition (increase in internal pressure, pore formation and swelling of items). Calculations of the tolerable degree of decomposition were carried out ignoring gas diffusion and the presence of atmospheric gases dissolved in the condensed phase.

This method of determination of stability criteria for EMs and items made of them has neither practical nor theoretical substantiation. The development of internal pressure, pore formation and swelling of items owing to gas evolution in the course of EM decomposition have not been studied even phenomenologically, the effect of these parameters on the operating characteristics has not been established and no quantitative relationships between them and the degree of decomposition was found, though porosimetry techniques for the condensed phase are well known (*e.g.*, positron annihilation and NMR spectroscopy). A small variation of porosity during decomposition is permissible, because pressed items made of explosives are characterised by a nearly 5% initial porosity. The service life of most solid propellants depends on the changes in their physicomechanical characteristics due to the binder degradation, which often proceeds without gas evolution.[227, 228] If an item made of solid propellants is subject to shrinkage or temperature stress, an increase (within certain limits) in the volume of the solid propellant due to gas evolution and pore formation is useful, because it reduces or even completely relieves stress.

The predictive power of the proposed unexperimented procedure for the determination of stability criterion is low. The authors noted that this criterion can vary within the limits of two orders of magnitude for the same composition. In practice, low accuracy of prediction is to some extent compensated by prolongation of the warranty period based on the results of full-scale tests of the items after expiration date. The 'benefit' from the prolongation of the warranty period is of course imaginary. Nevertheless, for obvious reasons this does not favour improvement of service life assessment procedures.

Temperature is not the sole factor determining the stability of items made of EMs.[226] The rate of a decomposition reaction also depends on different kinds of radiation (X-ray, UV, *etc.*), on the mechanical stress, on the presence of moisture and other compounds in the environment, *etc*. The influence of these factors on the EM decomposition and on the stability of items made of EMs has been studied much poorer than the thermal effects.

Instability of the shape and size of items made of EMs can be due to not only thermal decomposition but also incompleteness of phase separation in the course of crystallisation, thermodynamically nonequilibrium conformation of polymer chains and other physical factors.[226, 229]

Solving the problem of stability prediction for EMs requires a great body of data and takes a long time. For instance, in the USA the service life of rocket engines is evaluated by statistical treatment of the results of accelerated cyclic load tests of engines belonging to groups with different storage lifes. This allows one to attain engine failure in admissible and predictable time.[230, 231] Direct comparison of the results of calculations with the behaviour of the item under operating conditions requires too long time. However, differences between the test results and the life expectancy can be due to not only ignoration of some operation factors but also to a change in the mechanism of the process under operating conditions. For instance, if two competing concurrent processes (breakdown of cross-links and cross-linking) proceed in a polymer network, the dependence of the stress – strain properties on time has the form

$$Y = \alpha\exp(-k_1 t) - \beta\exp(-k_2 t) + Y_0,$$

where k_1 and k_2 are the rate constants for breakdown of cross-links and cross-linking, respectively, and Y_0, α and β are constants. If $k_1 < k_2$ under test conditions, the dependence $Y(t)$ passes through a minimum; otherwise ($k_1 > k_2$), it passes through a maximum. Extrapolation with allowance for the behaviour of the function $Y(t)$ in the initial period of tests can introduce gross errors.[226] Changes in the stress – strain state of the composite due to the difference between the binder and filler thermal expansion coefficients and temperature-induced changes in the mechanism of the interaction between the oxidiser decomposition products and binder can also introduce large errors when using a similar extrapolation.

A combined prediction procedure involving alternate 'placing' of a material or an item under accelerated test conditions and under operating conditions is nearly free from these drawbacks.[9]

At present, NMR imaging techniques have been intensively developed. They permit imaging of internal structure of a material and monitoring of its state immediately under operating conditions.[87, 232–235] NMR images are in essence multidimensional NMR spectra. For instance, NMR imaging permits non-destructive real-time monitoring of the dynamics of physical and chemical processes by measuring the spatial distribution of concentration in any section of the sample. Large objects are studied using surface coils [233] or devices combining an RF coil and a magnetic field source.

VI. Conclusion

The kinetic and mechanistic studies of EM decomposition aimed at solving important practical and theoretical problems are far from being completed. This is to a great extent due to the fact that the scientific and methodological potentials of modern chemical physics (in particular, chemical kinetics) and solid state physics are still little used in the EM decomposition studies. An optimum research strategy must involve joint kinetic and mechanistic studies of complex chemical reactions. This can be done using various efficient methods of determination of the composition of reaction mixtures and the evolution of reactant concentrations in the course of reaction. However, the decomposition mechanism of explosives is usually studied out of the context of the kinetics of elementary decomposition stages while the kinetic parameters are as a rule determined using methods of formal kinetics. However, these methods are little informative and therefore cannot be used for the determination of the rate constants for elementary stages of multistage processes.

Computer simulation of the decomposition of explosives as a means of controlling the mechanism reliability is only coming in practice, being performed taking simple model compounds as examples. The kinetics and mechanism of the decomposition of explosives in the condensed phase are very poorly studied because improved methods of investigation of the supramolecular structure of liquid and solid explosives characterised by rather high spatial and temporal resolution are almost not employed. Information on the supramolecular structure of the condensed phase and its evolution in the course of reaction is ignored. The true rate constants for the primary steps of decomposition (leave alone the rate constants for all elementary stages of the process) have not been determined as yet even for in-service explosives and solid propellant oxidisers and the corresponding decomposition mechanisms are not substantiated. The aforesaid suggests that the available methods of theoretical chemistry have considerable promise for the determination of the kinetics and mechanism of thermal decomposition of EMs. The highest efficiency can be attained in joint studies carried out using these methods and modern experimental techniques.

Usually, solid propellant binders are polymer networks with a complex multilevel structure. The chemical, topological and supramolecular structure of such polymers and composites based on them can be investigated using modern efficient and theoretically substantiated approaches. A number of methods for studying the structure of the free volume subsystem of the polymer network are available. This allows the decomposition kinetics of polymer networks and composites exposed to the action of various external factors to be studied, the most unstable structural blocks to be determined and efficient methods of stability improvement to be elaborated. However, the new techniques are very rarely used in studies of the degradation and stabilisation of solid propellants; the decomposition of solid propellants is studied using methods of formal kinetics.

The most important problem, prediction of stability of EMs, is still to be solved. The proposed criterion for stability of these materials (limitation on the tolerable degree of conversion during the reprocessing time and the storage life to a value of 0.02%) is not substantiated. In this situation the best way is to use of a combined prediction procedure and NMR techniques that allow the state of items made of EMs to be monitored immediately under operating conditions.

Mathematical modelling of combustion is performed using simple steady-state models and a number of essential assumptions. This is due to the lack of kinetic parameters relevant to the actual complexity of EM decomposition over a wide temperature interval. Powerful modern computers allow almost all correctly posed problems in the field of mathematical modelling of EM combustion to be solved.

References

1. G M Nazin, G B Manelis *Usp. Khim.* **63** 327 (1994) [*Russ. Chem. Rev.* **63** 313 (1994)]
2. F I Dubovitskii, B L Korsunskii *Usp. Khim.* **50** 1828 (1981) [*Russ. Chem. Rev.* **50** 958 (1981)]
3. R A Fifer, in *Fundamentals of Solid-Propellant Combustion* Vol. 90 (Eds K Kuo, M Summerfield) (New York: AIAA, 1984) p. 177
4. N E Ermolin, V E Zarko *Fiz. Goren. Vzryva* **33** (3) 10 (1997) [a]
5. R Boshan, R T Merrow, R W Van Dolan *Chem. Rev.* **55** 485 (1955)
6. A G Keenan, R F Siegmund *Quart. Rev.* **23** 430 (1969)
7. G B Manelis (Ed.) *Mekhanizm Termicheskogo Razlozheniya Perkhlorata Ammoniya* (Mechanism of Thermal Decomposition of Ammonium Perchlorate) (Chernogolovka: United Institute of Chemical Physics, 1981)
8. G B Manelis, G M Nazin, Yu I Rubtsov, V A Strunin *Thermal Decomposition and Combustion of Explosives and Propellants* (London, New York: Taylor and Francis, 2003)
9. N M Emanuel, A L Buchachenko *Khimicheskaya Fizika Molekulyarnogo Razrusheniya i Stabilizatsii Polimerov* (Chemical Physics of Molecular Destruction and Stabilisation of Polymers) (Moscow: Nauka, 1988)
10. N A Plate, A V Litmanovich, O V Noa *Makromolekulyarnye Reaktsii* (Macromolecular Reactions) (Moscow: Khimiya, 1977)
11. V A Kabanov, V P Zubov, Yu D Semchikov *Kompleksno-Radikal'naya Polimerizatsiya* (Complex Radical Polymerisation) (Moscow: Khimiya, 1987)
12. A L Volynskii, N F Bakeev *Vysokodispersnoe Orientirovannoe Sostoyanie Polimerov* (Highly Dispersed Directed State of Polymers) (Moscow: Khimiya, 1984)
13. Al Al Berlin, S A Vol'fson, V G Oshmyan, N S Enikolopov *Printsipy Sozdaniya Kompozitsionnykh Polimernykh Materialov* (Principles of Creation of Composite Polymer Materials) (Moscow: Khimiya, 1990)
14. V I Irzhak, B A Rozenberg, N S Enikolopyan *Setchatye Polimery: Sintez, Struktura, Svoistva* (Cross-Linked Polymers: Syntheses, Structure and Properties) (Moscow: Khimiya, 1979)
15. A A Popov, N Ya Rapoport, G E Zaikov *Okislenie Orientirovannykh i Napryazhennykh Polimerov* (Oxidation of Directed and Stressed Polymers) (Moscow: Khimiya, 1987)
16. G I Sandakov, V P Tarasov, N N Volkova, Yu A Ol'khov, L P Smirnov, L N Erofeev, A K Khitrin *Vysokomol. Soedin., Ser. B* **31** 821 (1989) [b]
17. L N Erofeev, G I Sandakov, L P Smirnov, A I Sosikov, K T Summanen, N N Volkova, in *Proceedings of the International Rubber Conference IRC'94, Moscow, 1994* Vol. 2, p. 628
18. G I Sandakov, L P Smirnov, A I Sosikov, K T Summanen, N N Volkova *J. Polym. Sci., Polym. Phys.* **32** 1585 (1994)
19. G I Sandakov, L P Smirnov, K T Summanen, N N Volkova *Prog. Colloid Polym. Sci.* **90** 235 (1992)
20. N N Volkova, G I Sandakov, A I Sosikov, Yu A Ol'khov, L P Smirnov, K T Summanen *Vysokomol. Soedin., Ser. A* **34** 77 (1992) [b]
21. E Sh Nudel'man, G A Gorbushina, Yu A Ol'khov, L P Smirnov *Vysokomol. Soedin., Ser. A* **34** 69 (1992) [b]
22. B E Krisyuk, G I Sandakov *Vysokomol. Soedin., Ser. A* **37** 615 (1995) [b]
23. L P Smirnov, N N Volkova *Prog. Colloid Polym. Sci.* **90** 222 (1992)
24. L P Smirnov *Vysokomol. Soedin., Ser. B* **42** 1775 (2000) [b]
25. N N Volkova, A I Sosikov, M P Berezin, G V Korolev, L N Erofeev, L P Smirnov *Vysokomol. Soedin., Ser. A* **30** 2133 (1988) [b]
26. N N Volkova, Candidate Thesis in Chemical Sciences, United Institute of Chemical Physics, Academy of Sciences of the USSR, Chernogolovka, 1984
27. E Sh Nudel'man, Candidate Thesis in Chemical Sciences, United Institute of Chemical Physics, Academy of Sciences of the USSR, Chernogolovka, 1991
28. N N Volkova, E V Summanen, L P Smirnov, E A Dzhavadyan, T I Ponomareva, B A Rozenberg *Mekh. Kompoz. Mater.* 391 (1990)
29. N N Volkova, L M Bogdanova, E V Summanen, B A Shumm, L N Erofeev, L P Smirnov *Vysokomol. Soedin., Ser. A* **43** 1773 (2001) [b]
30. N N Volkova, E V Summanen, L P Smirnov *Vysokomol. Soedin., Ser. A* **45** 1659 (2003) [b]
31. L P Smirnov, in *Heterophase Network Polymers. Synthesis, Characterization and Properties* (Eds B A Rozenberg, G M Sigalov) (London, New York: Taylor and Francis, 2002) p. 235
32. E V Sokerina, D E Lushnikov, T S Pivina, A A Porollo, V P Ivshin, in *The Proceedings of the 21st International Pyrotechnic Seminar, Moscow, 1995* p. 849
33. M J S Dewar, J P Ritchie, J Alster *J. Org. Chem.* **50** 1031 (1985)
34. A M Wodtke, E J Hintsa, Y T Lee *J. Chem. Phys.* **84** 1044 (1986)
35. A M Wodtke, E J Hintsa, Y T Lee *J. Phys. Chem.* **90** 3549 (1986)
36. B L Korsunskii, V G Matveev, L D Nazina, G M Nazin *Izv. Akad. Nauk, Ser. Khim.* 259 (1998) [c]
37. V G Prokudin, V S Poplavskii, V A Ostrovskii *Izv. Akad. Nauk, Ser. Khim.* 2209 (1996) [c]
38. V G Prokudin, V S Poplavskii, V A Ostrovskii *Izv. Akad. Nauk, Ser. Khim.* 2216 (1996) [c]
39. V V Dubikhin, V G Matveev, G M Nazin *Izv. Akad. Nauk, Ser. Khim.* 1977 (1996) [c]
40. S N Bulusu (Ed.) *Chemistry and Physics of Energetic Materials* (London: Kluwer, 1990)
41. G F Adams, R W Shaw *Annu. Rev. Phys. Chem.* **4** 311 (1992)
42. P P Shorygin, N B Lopatina, B V Lopatin, T E Gorodilova *Izv. Akad. Nauk, Ser. Khim.* 304 (1998) [c]
43. V V Dubikhin, G V Lagodzinskaya, A M Korolev, V G Matveev, G M Nazin *Khim. Fiz.* **22** (7) 28 (2003) [d]
44. R C Farmer *J. Chem. Soc.* **117** 1603 (1920)
45. C N Hinshelwood *J. Chem. Soc.* **119** 721 (1921)
46. F I Dubovitskii, G B Manelis, L P Smirnov *Zh. Fiz. Khim.* **35** 521 (1961) [e]
47. B A Lur'e, V P Sinditskii, S P Smirnov *Fiz. Goren. Vzryva* **39** (5) 55 (2003) [a]
48. G M Nazin, V G Prokudin, G B Manelis *Izv. Akad. Nauk, Ser. Khim.* 231 (2000) [c]
49. V P Sinditskii, V Yu Egoryshev, M V Berezin *Khim. Fiz.* **22** (4) 56 (2003) [d]
50. Z Jalovy, S Zeman, in *The Proceedings of the 30th International Annual Conference ICT, Karlsruhe, 1999* p. 104
51. L P Hammet *Physical Organic Chemistry* (New York: McGraw-Hill, 1940)
52. R W Taft *J. Am. Chem. Soc.* **74** 2729 (1952)
53. R W Taft *J. Am. Chem. Soc.* **74** 3120 (1952)
54. M I Kumskov, S E Peshkova, L A Ponomareva, K I Rezchikova *Izv Akad. Nauk, Ser. Khim.* 1942 (1996) [c]
55. T S Pivina, D V Sukhachev, L K Maslova, V A Shlyapochnikov, N S Zefirov *Dokl. Akad. Nauk* **330** 468 (1993) [f]
56. A R Bulter, D L H Williams *Chem. Soc. Rev.* **22** 233 (1993)
57. Y Fu, Y Mou, B-L Lin, L Lin, Q-X Guo *J. Phys. Chem. A* **106** 12386 (2002)
58. M Schütze, H Herrmann *Phys. Chem. Chem. Phys.* **4** 60 (2002)

59. I V Koptyug, R Z Sagdeev *Usp. Khim.* **72** 183 (2003) [*Russ. Chem. Rev.* **72** 165 (2003)]
60. M Khalil, N Demirdöven, A Tokmakoff *J. Phys. Chem. A* **107** 5258 (2003)
61. R R Ernst, G Bodenhausen, A Wokaun *Principles of Nuclear Magnetic Resonance in One and Two Dimensions* (Oxford: Oxford University Press, 1987)
62. P Musto *Macromolecules* **36** 3210 (2003)
63. S Belusu, R Behrens *Def. Sci. J.* **46** 347 (1996)
64. R S Stepanov, V N Shan'ko, I P Medvedetskaya, L A Kuznetsov, in *Fizicheskaya Khimiya* (Physical Chemistry) Vol. 2 (Krasnoyarsk: Siberian Technological Institute, 1965) p. 3
65. V V Dubikhin, V G Matveev, G M Nazin *Izv. Akad. Nauk, Ser. Khim.* 266 (1995) [c]
66. J-M Lehn *Supramolecular Chemistry. Concepts and Perspectives* (Weinheim: VCH, 1995)
67. H Ratajczak, W J Orville-Thomas *Molecular Interactions* Vol. 2 (New York: Wiley, 1981)
68. Yu Ya Maksimov, E N Kogut *Zh. Fiz. Khim.* **52** 1400 (1978) [c]
69. I F Falyachov, G P Sharnin, N M Safin, I Sh Saifullin, R Kh Fassakhov, in *The Proceedings of the 21st International Pyrotechnic Seminar, Moscow, 1995* p. 187
70. V A Shlyapnikov, L S Khaikin, O E Grikina, N O Cherskaya, L E Maksimova, N F Pyatakov *Izv. Akad. Nauk, Ser. Khim.* 2241 (1998) [c]
71. B Lurie, E Semkiv, in *The Proceedings of the 21st International Pyrotechnic Seminar, Moscow, 1995* p. 547
72. P S Belton, R G Ratcliffe *Prog. Nucl. Magn. Reson. Spectrosc.* **17** 241 (1985)
73. N R Skrynnikov, F W Dahlquist, L E Kay *J. Am. Chem. Soc.* **124** 12 352 (2002)
74. D E Thompson, K A Merchant, M D Fayer *J. Chem. Phys.* **115** 317 (2001)
75. A T Krummel, P Mukherjee, M T Zanni *J. Phys. Chem. B* **107** 9165 (2003)
76. P Gray, S K Scott *Chemical Oscillations and Instabilities. Non-linear Kinetics* (Oxford: Clarendon Press, 1994)
77. M Goldman *Spin Temperature and Nuclear Magnetic Resonance in Solids* (Oxford: Clarendon Press, 1970)
78. L T Abramova, Yu N Rogov, L P Smirnov, in *Tezisy Dokladov Pervogo Vsesoyuznogo Simpoziuma po Makroskopicheskoi Kinetike i Khimicheskoi Gazodinamike, Alma-Ata, 1984* (Abstracts of Reports of the First All-Union Symposium on Macroscopic Kinetics and Chemical Gaz Dynamics, Alma-Ata, 1984) Vol. 2, p. 80
79. L P Smirnov, E V Deyun, E V Summanen, in *Khimicheskaya Fizika Protsessov Goreniya i Vzryva (Tez. Dokl. XII Simpoziuma po Goreniyu i Vzryvu), Chernogolovka, 2000* [Chemical Physics of Combustion and Explosion Processes (Abstracts of Reports of the XXIIth Symposium on Combustion and Explosion), Chernogolovka, 2000] Pt. 3, p. 107
80. L P Smirnov, E V Summanen *Dokl. Akad. Nauk* **386** 359 (2002) [f]
81. A N Ivanova *Kinet. Katal.* **20** 1019 (1979) [g]
82. M Feinberg *Chem. Eng. Sci.* **42** 2229 (1987)
83. M Feinberg, in *Patterns and Dynamics in Reactive Media* Vol. 37 (Eds R Aris, D Ararson, H L Swinney) (Berlin: Springer, 1991) p. 43
84. M J Chedin *J. Chim. Phys. (France)* **49** 109 (1952)
85. Yu Ya Maksimov, E N Kogut *Izv. Vyssh. Uchebn. Zaved., Khim. Khim. Tekhnol.* **20** 349 (1977)
86. I V Koptyug, A A Lysova, V N Parmon, R Z Sagdeev *Kinet. Katal.* **44** 436 (2003) [g]
87. I V Koptyug, R Z Sagdeev *Usp. Khim.* **71** 672 (2002) [*Russ. Chem. Rev.* **71** 593 (2002)]
88. A V Raevskii, in *Mekhanizm Termicheskogo Razlozheniya Perkhlorata Ammoniya* (Mechanism of Thermal Decomposition of Ammonium Perchlorate) (Ed. G B Manelis) (Chernogolovka: United Institute of Chemical Physics, 1981) p. 30
89. S M Ryabykh *Khim. Fiz.* **9** (2) 191 (1990) [d]
90. Yu M Burov, G B Manelis, G M Nazin *Khim. Fiz.* **4** (7) 956 (1985) [d]
91. Yu M Burov, G M Nazin, G B Manelis *Izv. Akad. Nauk, Ser. Khim.* 1261 (1999) [c]
92. T Vladimiroff, B M Rise *J. Phys. Chem. A* **106** 10437 (2002)
93. V I Tarzhanov *Fiz. Goren. Vzryva* **39** (6) 3 (2003) [a]
94. Yu A Zakharov, E D Aluker, B P Aduev *Predvzryvnye Yavleniya v Azidakh Tyazhelykh Metallov* (Preexplosive Effects in Azides of Heavy Metals) (Moscow: TsEI 'Khimmash', 2002)
95. B P Aduev, E D Aluker, A G Krechetov, A Yu Mitrofanov *Fiz. Goren. Vzryva* **39** (6) 104 (2003) [a]
96. J T Dickinson, L C Jensen, D L Doering, R Yee *J. Appl. Phys.* **67** 3641 (1990)
97. B P Aduev, E D Aluker, G M Belokurov, A G Krechetov *Zh. Eksp. Teor. Fiz.* **116** 1676 (1999) [h]
98. E G Bagryanskaya, R Z Sagdeev *Usp. Khim.* **69** 1009 (2000) [*Russ. Chem. Rev.* **69** 925 (2000)]
99. V A Koroban, B S Svetlov, V P Guk, T I Smirnova, in *Mekhanizm Termicheskogo Razlozheniya Perkhlorata Ammoniya* (Mechanism of Thermal Decomposition of Ammonium Perchlorate) (Ed. G B Manelis) (Chernogolovka: United Institute of Chemical Physics, 1981) p. 5
100. E F Khairetdinov, T V Mulina, V V Boldyrev, in *Mekhanizm Termicheskogo Razlozheniya Perkhlorata Ammoniya* (Mechanism of Thermal Decomposition of Ammonium Perchlorate) (Ed. G B Manelis) (Chernogolovka: United Institute of Chemical Physics, 1981) p. 101
101. Yu I Rubtsov, G B Manelis, in *Mekhanizm Termicheskogo Razlozheniya Perkhlorata Ammoniya* (Mechanism of Thermal Decomposition of Ammonium Perchlorate) (Ed. G B Manelis) (Chernogolovka: United Institute of Chemical Physics, 1981) p. 123
102. R V Gol'dshtein, V M Entov, B R Pavlovskii *Dokl. Akad. Nauk SSSR* **237** 828 (1977) [f]
103. Y Ba, D Chagolla *J. Phys. Chem. B* **106** 5250 (2002)
104. V P Shantarovich, Yu A Novikov, Z K Azamatova *Fiz. Tv. Tela* **40** 164 (1998) [i]
105. T Giavani, H Bildsoe, J Skibsted, H J Jakobsen *J. Phys. Chem. B* **106** 3026 (2002)
106. V P Sinditskii, V Yu Egoryshev, M V Berezin, V V Serushkin, Yu M Milekhin, S A Gusev, A A Matveev *Khim. Fiz.* **22** (7) 69 (2003) [d]
107. N I Golovina, G V Shilov, L O Atovmyan, S M Aldoshin, in *Materialy Vserossiiskoi Konferentsii 'Energeticheskie Kondensirovannye Sistemy'* (Materials of All-Russian Conference 'Energetic Condensed Systems') (Chernogolovka, Moscow: Yanus-K, 2002) p. 22
108. B L Korsunskii, V V Nedel'ko, N V Chukanov, T S Larikova, F Fol'k *Izv Akad. Nauk, Ser. Khim.* 815 (2000) [c]
109. V V Nedel'ko, B L Korsunskii, N V Chukanov, T S Larikova, E A Semendyaeva, in *Materialy Vserossiiskoi Konferentsii 'Energeticheskie Kondensirovannye Sistemy'* (Materials of All-Union Conference 'Energetic Condensed Systems') (Chernogolovka, Moscow: Yanus-K, 2002) p. 30
110. D G Patil, N B Brill *Combust. Flame* **87** 145 (1991)
111. S Löbbecke, M A Bohn, A Pfeil, H Krause, in *The Proceedings of the 29th International Annual Conference of ICT*. Karlsruhe 1998. P. 145
112. J C Oxley, A B Kooh, R Szekeres, W Zheng *J. Phys. Chem.* **98** 7004 (1994)
113. V I Kovalenko *Usp. Khim.* **64** 803 (1995) [*Russ. Chem. Rev.* **64** 753 (1995)]
114. L G Browning, G G Gelenter, S R Harris, C M Mason *J. Phys. Chem.* **60** 1260 (1956)
115. G E Kornilova, B A Lur'e, B S Svetlov, in *Trudy MKhTI im. D I Mendeleeva* (Proceedings of D I Mendeleev Moscow Chemical Technology Institute) (Moscow: Vyssh. Shkola, 1969) No. 62, p. 62
116. K K Andreev, B S Samsonov, in *Trudy MKhTI im. D I Mendeleeva* (Proceedings of D I Mendeleev Moscow Chemical Technology Institute) (Moscow: Vyssh. Shkola, 1967) No. 53, p. 7
117. K K Andreev, B S Samsonov, in *Trudy MKhTI im. D I Mendeleeva* (Proceedings of D I Mendeleev Moscow Chemical Technology Institute) (Moscow: Vyssh. Shkola, 1967) No. 53, p. 22
118. V A Mal'chevskii, O F Pozdnyakov, V R Regel', M G Fal'kovskii *Vysokomol. Soedin., Ser. A* **13** 2078 (1971) [b]

119. R W Phillips, C A Orlick, R J Steinberger *Phys. Chem.* **59** 1034 (1955)
120. L P Smirnov, L N Leksina, Yu N Rogov, G A Volkov, in *The Proceedings of the 21st Pyrotechnics Seminar, Moscow, 1995* p. 813
121. V A Silaev, F M Gumerov, V F Sopin, I L Zhuravleva, G N Marchenko *Khim. Fiz.* **10** (1) 70 (1991) [d]
122. Yu N Rogov, L P Smirnov, L N Leksina, V S Ushakova *Vysokomol. Soedin., Ser. A* **31** 352 (1989) [b]
123. B A Lur'e, B S Svetlov, in *Trudy MKhTI im. D I Mendeleeva* (Proceedings of D I Mendeleev Moscow Chemical Technology Institute) (Moscow: Vyssh. Shkola, 1980) No. 112, p. 5
124. A El-ghayoury, H Hofmeier, B de Ruiter, U S Schubert *Macromolecules* **36** 3955 (2003)
125. E N Kablov *Vestn. Ros. Akad. Nauk* **72** (1) 3 (2002) [j]
126. E Ya Davydov, A P Vorotnikov, V P Pustoshnyi, G B Pariiskii *Usp. Khim.* **69** 981 (2000) [*Russ. Chem. Rev.* **69** 899 (2000)]
127. V I Irzhak *Usp. Khim.* **69** 283 (2000) [*Russ. Chem. Rev.* **69** 261 (2000)]
128. Yu D Tretyakov *Usp. Khim.* **72** 731 (2003) [*Russ. Chem. Rev.* **72** 651 (2003)]
129. I L Moudrakovski, V V Terskikh, Ch I Ratcliffe, J A Ripmeester, L-Q Wang, Y Shin, G J Exarhos *J. Phys. Chem. B* **106** 5938 (2002)
130. J H Strang, M Rahman, E G Smith *Phys. Rev. Lett.* **71** 3589 (1993)
131. S G Allen, P C L Stephenson, J H Strange *J. Chem. Phys.* **106** 7802 (1997)
132. Yu A Mikheev, G E Zaikov *Khim. Fiz.* **20** (11) 55 (2001) [d]
133. V U Novikov, G V Kozlov *Usp. Khim.* **69** 572 (2000) [*Russ. Chem. Rev.* **69** 523 (2000)]
134. V P Solomko *Napolnennye Kristallizuyushchiesya Polimery* (Filled Crystallisable Polymers) (Kiev: Naukova Dumka, 1980)
135. V M Litvinov, V G Vasil'ev *Vysokomol. Soedin., Ser. A* **32** 2329 (1990) [b]
136. J W ten Brinke, V M Litvinov, J E G J Wijnhoven, J W M Noordermeer *Macromolecules* **35** 10 026 (2002)
137. H Matsubara, A Yoshido, Y Kondo, Sh Tsuge, H Ohtani *Macromolecules* **36** 4750 (2003)
138. W F Jaeger, A Lungu, D Y Chen, D C Neckers *Macromolecules* **30** 780 (1997)
139. A Lungu, D C Neckers *Macromolecules* **28** 8147 (1995)
140. P E M Allen, G P Simon, D R G Williams, E H Williams *Macromolecules* **22** 809 (1989)
141. T P Kulagina, V M Litvinov, K T Summanen *J. Polym. Sci., Polym. Phys.* **31** 241 (1993)
142. E V Deyun, G B Manelis, E V Polianchik, L P Smirnov *Usp. Khim.* **49** 1574 (1980) [*Russ. Chem. Rev.* **49** 749 (1980)]
143. L Reich, S S Stivala *Elements of Polymer Degradation* (New York: McGraw-Hill, 1972)
144. N A Lavrov, A G Pisarev *Plasticheskie Massy* (1) 28 (2002)
145. S-J Rark, H-C Kim, H-I Lee, D-H Suh *Macromolecules* **34** 7573 (2001)
146. E Dyer, G E Newborn *J. Am. Chem. Soc.* **80** 5495 (1958)
147. E Dyer, G C Wright *J. Am. Chem. Soc.* **81** 2138 (1959)
148. M P Thorne *Can. J. Chem.* **45** 2537 (1967)
149. N Grassie, M Zulfiqar *J. Polym. Sci., Polym. Chem. Ed.* **16** 1563 (1978)
150. N Grassie, M Zulfiqar, M I Guy *J. Polym. Sci., Polym. Chem. Ed.* **18** 265 (1980)
151. S Poti, P Maravigna, G Mantando *J. Polym. Sci., Polym. Chem. Ed.* **19** 1679 (1981)
152. N N Volkova, Yu I Ol'khov, S M Baturin, L P Smirnov *Issledovanie Termicheskogo Razlozheniya Shitykh Poliuretanov* (Investigation of Thermal Decomposition of Cross-Linked Polyurethanes) (Preprint of United Institute of Chemical Physics, Academy of Sciences of the USSR, Chernogolovka, 1983)
153. L P Smirnov, E Sh Nudel'man *Raschet Konfiguratsii Uretanovykh Grupp v Zavisimosti ot ikh Polozheniya v Polimernoi Setke* (Calculation of Configuration of Urethane Groups Depending on Their Position in Polymer Network) (Preprint of Institute of Chemical Physics, Academy of Sciences of the USSR, Chernogolovka, 1991)
154. N N Kausch *Polymer Fracture* (Berlin: Springer, 1978)
155. G M Bartenev *Prochnost' i Mekhanizm Razrusheniya Polimerov* (Strength and Mechanism of Polymer Fracture) (Moscow: Khimiya, 1984)
156. L M Bogdanova, N N Volkova, A V Lankin, L P Smirnov *Vysokomol. Soedin., Ser. A* **40** 297 (1998) [b]
157. M T Bryk *Destruktsiya Napolnennykh Polimernykh Sistem* (Destruction of Filled Polymer Systems) (Moscow: Khimiya, 1989)
158. V P Tarasov, L N Erofeev, E A Dzhavadyan, Yu N Smirnov, B A Rozenberg, in *Heterophase Network Polymers. Synthesis, Characterization and Properties* (Eds B A Rozenberg, G M Sigalov) (London, New York: Taylor and Francis, 2002) p. 301
159. K T Gillen, M Celina, R L Clough, J Wise *Trends Polym. Sci.* **5** 250 (1997)
160. E Földes, J Lohmeijer *Polym. Degrad. Stab.* **66** 31 (1999)
161. G Ahlblad, T Reitberger, B Terselius, P Stenberg *Polym. Degrad. Stab.* **65** 185 (1999)
162. D J Harris, R A Assink, M Celina *Macromolecules* **34** 6695 (2001)
163. M Celina, A C Graham, K T Gillen, R A Assink, L M Minier *Rubber Chem. Technol.* **73** 678 (2000)
164. E D Hughes, C K Ingold, R I Reed *J. Chem. Soc.* 2400 (1950)
165. A V Topchiev *Nitrovanie Uglevodorodov i Drugikh Organicheskikh Soedinenii* (Nitration of Hydrocarbons and Other Organic Compounds) (Moscow: Academy of Sciences of the USSR, 1956)
166. S S Novikov, G A Shveikhgeimer, V V Sevost'yanova, V A Shlyapochnikov *Khimiya Alifaticheskikh Alitsiklicheskikh Nitrosoedinenii* (The Chemistry of Aliphatic and Alicyclic Nitrocompounds) (Moscow: Khimiya, 1974)
167. V A Rafeev, Yu I Rubtsov, T V Sorokina *Izv. Akad. Nauk, Ser. Khim.* 343 (1996) [c]
168. E Farmer *J. Soc. Chem. Ind.* **50** 75 (1931)
169. Yu I Rubtsov, A I Kazakov, E Yu Rubtsova, L P Andrienko, E P Kirpichev *Izv. Akad. Nauk, Ser. Khim.* 1986 (1996) [c]
170. J H Thomas *Trans. Faraday Soc.* **49** 630 (1953)
171. G B Pariiskii, I S Gaponova, E Ya Davydov *Usp. Khim.* **69** 1071 (2000) [*Russ. Chem. Rev.* **69** 985 (2000)
172. O P Korobeinichev, K K Kovalenko, A I Lesnikovich *Fiz. Goren. Vzryva* **13** 550 (1977) [a]
173. E P Goncharov, A G Merzhanov, A S Shteinberg, in *Gorenie i Vzryv. Materialy 3-go Vsesoyuznogo Simpoziuma po Goreniyu i Vzryvu* (Combustion and Explosion. Proceedings of the 3rd All-Union Symposium on Combustion and Explosion) (Moscow: Nauka, 1972) p. 765
174. A P D'yakov, L I Nikolaeva, V A Strunin, G B Manelis *Khim. Fiz.* **22** (5) 70 (2003) [d]
175. A I Pristupa, V A Sharpatyi *Dokl. Akad. Nauk* **387** 643 (2002) [f]
176. B M Rice, J Hare, S V Pai, W Mattson, G Krasko, S F Trevino, D C Sorescu, D L Thompson *Khim. Fiz.* **20** (10) 9 (2001) [d]
177. L S Khaikin, O E Grikina, L V Vilkov, M A Palafoks, J E Boggs *Zh. Strukt. Khim.* **34** 4 (1993) [k]
178. L S Khaikin, O E Grikina, V A Shlyapochnikov, L V Vilkov, Ch V Bok *Izv. Akad. Nauk, Ser. Khim.* 2135 (1995) [c]
179. L S Khaikin, O E Grikina, V I Perevozchikov, S S Kramarenko, V A Shlyapochnikov, J E Boggs *Izv. Akad. Nauk, Ser. Khim.* 1557 (1998) [c]
180. E K Dolgov, V A Bataev, I A Godunov *Izv. Akad. Nauk, Ser. Khim.* 35 (2003) [c]
181. A M Mebel, M C Lin, K Morokuma, C F Melius *J. Phys. Chem.* **99** 6842 (1995)
182. G F Valardez, S Alavi, D L Thompson *J. Chem. Phys.* **119** 6698 (2003)
183. V I Minkin, B Ya Simkin, R M Minyaev *Kvantovaya Khimiya Organicheskikh Soedinenii. Mekhanizmy Reaktsii* (Quantum Chemistry of Organic Compounds. Reaction Mechanisms) (Moscow: Nauka, 1986)
184. Yu Yu Nikishev, I Sh Saifullin, O R Klyuchnikov *Kinet. Katal.* **34** 969 (1993) [g]
185. V M Promyslov, P P Shorygin *Izv. Akad. Nauk, Ser. Khim.* 1835 (2000) [c]

186. E L Mehler *J. Chem. Phys.* **74** 6298 (1981)
187. K J Leidler *Chemical Kinetics* (New York: Harper and Row, 1987)
188. E T Denisov *Usp. Khim.* **66** 953 (1997) [*Russ. Chem. Rev.* **66** 859 (1997)]
189. T G Denisova, N S Emel'yanova *Kinet. Katal.* **44** 485 (2003) [g]
190. M V Bazilevskii, V I Faustov *Usp. Khim.* **61** 1185 (1992) [*Russ. Chem. Rev.* **61** 651 (1992)]
191. B Ya Simkin, I I Sheikhet *Kvantovo-Khimicheskaya i Statisticheskaya Teoriya Rastvorov. Vychislitel'nye Metody i Ikh Primenenie* (Quantum-Chemical and Statistic Theory of Solutions. Numerical Methods and Their Applications) (Moscow: Khimiya, 1989)
192. P Haggi, P Talkner, M Borkovec *Rev. Modern Phys.* **62** 251 (1990)
193. N V Chukanov, B L Korsunskii, F I Dubovitskii, O V Anan'ina *Dokl. Akad. Nauk SSSR* **265** 1445 (1982) [f]
194. N V Chukanov, B L Korsunskii, F I Dubovitskii, O V Anan'ina *Dokl. Akad. Nauk SSSR* **277** 1181 (1984) [f]
195. Y Kohno, O Takahashi, K Saito *Phys. Chem. Chem. Phys.* **3** 2724 (2001)
196. Y Kohno, O Takahashi, R I Hiyoshi, J Nakamura, K Saito *J. Phys. Chem. A* **107** 6444 (2003)
197. P Politzer, H E Alper, in *Computational Chemistry, Reviews of Current Trends* Ch. 6 (Ed. J Leszezynski) (Singapore: World Scientific, 1999) p. 4
198. A I Olemskoi, I V Kaplyk *Usp. Fiz. Nauk* **165** 1105 (1995) [*Physics-Uspekhi* **38** 1061 (1995)]
199. L A Maksimov, A I Ryazanov *Zh. Eksp. Teor. Fiz.* **79** 2311 (1980) [h]
200. Ya B Zel'dovich *Zh. Eksp. Teor. Fiz.* **12** 525 (1942) [h]
201. G B Manelis, V A Strunin *Zh. Fiz. Khim.* **46** 1987 (1972) [e]
202. G B Manelis, E V Polianchik *Sov. Sci. Rev., Chem. Rev. B* **15** 61 (1991)
203. V I Trefilov (Ed.) *Deformatsionnoe Uprochnenie i Razrushenie Kristallicheskikh Materialov* (Deformation Strengthening and Destruction of Crystalline Materials) (Kiev: Naukova Dumka, 1987)
204. V E Panin, V A Likhachev, Yu V Grinyaev *Strukturnye Urovni Deformatsii Tverdykh Tel* (Structure Levels of Deformation of Solids) (Novosibirsk: Nauka, 1985)
205. N S Enikolopov *Usp. Khim.* **60** 586 (1991) [*Russ. Chem. Rev.* **60** 283 (1991)]
206. J J Gilman *Mechanochemistry* **274** 65 (1996)
207. M M Kuklja, E V Stefanovich, A B Kunz *J. Chem. Phys.* **112** 3417 (2000)
208. F E Walker *J. Appl. Phys.* **63** 5548 (1988)
209. F E Uoker *Khim. Fiz.* **14** (12) 47 (1995) [d]
210. B M Rice, W Mattson, J Grosh, S F Trevino *Phys. Rev. E* **53** 611 (1996)
211. M R Baer *Khim. Fiz.* **20** (10) 21 (2001) [d]
212. V A Strunin *Zh. Fiz. Khim.* **39** 433 (1965) [e]
213. E I Maksimov, A G Merzhanov *Dokl. Akad. Nauk SSSR* **157** 412 (1964) [f]
214. G B Manelis, V A Strunin *Combust. Flame* **17** 69 (1971)
215. V A Strunin, G B Manelis *Fiz. Goren. Vzryva* **19** (2) 89 (1983) [a]
216. B I Khaikin, A K Filonenko, S I Khudyaev *Fiz. Goren. Vzryva* **4** 591 (1968) [a]
217. V A Strunin, A N Firsov, K G Shkadinskii, G B Manelis *Fiz. Goren. Vzryva* **22** (1) 3 (1986) [a]
218. V A Strunin, A N Firsov, K G Shkadinskii, G B Manelis *Fiz. Goren. Vzryva* **22** (1) 40 (1986) [a]
219. V A Strunin, G B Manelis *Fiz. Goren. Vzryva* **15** (5) 24 (1979) [a]
220. F I Dubovitskii *Khim. Fiz.* **1** (1) 127 (1982) [d]
221. A A Koptelov, S V Karyazov *Dokl. Akad. Nauk* **389** 643 (2003) [f]
222. G B Manelis, L P Smirnov *Fiz. Goren. Vzryva* **12** 665 (1976) [a]
223. A G Merzhanov, B I Khaikin *Teoriya Voln Goreniya v Gomogennykh Sredakh* (Theory of Combustion Wave in Homogenous Media) (Chernogolovka: Institute of Structural Macrokinetics, Academy of Sciences of the USSR, 1992)
224. A V Kolesnichenko *Matemat. Model.* **14** (7) 81 (2002)
225. E S Kim, V Yang, Y-C Liau *Combust. Flame* **131** 227 (2002)
226. B D Goikhman, T P Smekhunova *Usp. Khim.* **49** 1554 (1980) [*Russ. Chem. Rev.* **49** 748 (1980)]
227. W N Huang, J J Aklonis *Polym. Prepr. (Am. Chem. Soc., Div. Polym. Chem.)* **16** 88 (1975)
228. J Moacanin, J J Aklonis, R F Landel *J. Macromol. Sci., B* **11** 41 (1975)
229. Ch Lin, S B Chun, P T Mather, L Zheng, E H Haley, E B Coughlin *Macromolecules* **35** 9868 (2002)
230. G J Svob, K W Bills *J. Spacecraft Rockets* **21** 162 (1984)
231. K Kishore, V R P Verneker, V Gayathri, K R Shubha, K Sridhara *J. Spacecr. Rockets* **20** 345 (1983)
232. P T Callaghan *Principles of Nuclear Magnetic Resonance Microscopy* (Oxford: Clarendon Press, 1991)
233. I V Koptyug, L Yu Il'ina, V B Fenelonov, A Yu Derevyankin, R Z Sagdeev, V N Parmon *Dokl. Akad. Nauk* **376** 777 (2001) [f]
234. G Eidmann, R Savelsberg, P Blümler, B B Bülmich *J. Magn. Res., A* **122** 104 (1996).
235. J J Ackerman *Concepts Magn. Res.* **2** 33 (1990)

[a] — *Combust. Explos. Shok Waves (Engl. Transl.)*
[b] — *Polym. Sci. (Engl. Transl.)*
[c] — *Russ. Chem. Bull., Int. Ed. (Engl. Transl.)*
[d] — *Chem. Phys. Rep. (Engl. Transl.)*
[e] — *Russ. J. Phys. Chem. (Engl. Transl.)*
[f] — *Dokl. Chem. (Engl. Transl.)*
[g] — *Kinet. Catal. (Engl. Transl.)*
[h] — *J. Exp. Theor. Phys. (Engl. Transl.)*
[i] — *Phys. Solid State (Engl. Transl.)*
[j] — *Herald Russ. Acad. Sci. (Engl. Transl.)*
[k] — *Russ. J. Struct. Chem. (Engl. Transl.)*

Russian Chemical Reviews **73** (12) 1143 – 1172 (2004) © 2004 Russian Academy of Sciences and Turpion Ltd

DOI 10.1070/RC2004v073n12ABEH000875

Modern analytical thermooptical spectroscopy

M A Proskurnin, M Yu Kononets

Contents

I.	Introduction	1143
II.	General characterisation of thermooptical spectroscopy methods	1144
III.	Fields of application of analytical thermooptical spectroscopy	1152
IV.	Study of interfaces in condensed systems	1161
V.	Conclusion	1165

Abstract. The review surveys the main lines of research in thermooptical spectroscopy related directly or indirectly to analytical chemistry. The advantages and drawbacks of thermooptical spectroscopy methods are considered. Particular attention is given to the coupling of thermooptical spectroscopy to chromatography, flow analysis techniques, capillary electrophoresis, *etc*. Prospects for the development of analytical thermooptical spectroscopy are discussed. The bibliography includes 606 references.

I. Introduction

A pioneering study on analytical thermooptical spectroscopy [1] was published 25 years ago. In this time, the development of an analytical method is considerable and its status compared with other methods also change. The characteristic feature of the recent studies in the field of thermooptical spectroscopy is that researchers turn from the 'reproduction' of spectrophotometric procedures to a search for specific thermooptical methods of analysis.[2 – 17] It should be noted that not only the most commonly used thermal lens spectrometry but also such methods as mirage spectroscopy,[2, 5, 7, 8] the thermal prism technique,[4, 5, 16] photothermal refraction spectrometry [2, 4, 7, 8, 10, 11, 16] and photothermal interferometry [4, 17] have attracted increasing attention. In the period from 1997 to 2002, the distribution of methods used in studies in the field of thermooptical spectroscopy was as follows: thermal lens spectrometry, 43%; photothermal deflection, 27%; photothermal radiometry, 12%; photothermal displacement, 9%; photothermal interferometry, 4%; thermal lens microscopy, 4%; photothermal refraction spectrometry, 1%. Hence, it is evident that a new line of investigation, *viz*., analytical thermooptical spectroscopy, has evolved. There is a pronounced tendency to use thermooptical methods in fundamental studies, where their advantages as non-destructive highly sensitive methods of molecular light absorption spectroscopy are most obvious.[6, 15, 17, 18] In the period from 1998 to 2003, the number of studies devoted to thermooptical methods has steadily increased by approximately 300 papers *per annum* (Fig. 1).

In the present review, we analyse state-of-the-art thermooptical spectroscopy and its applications in analytical chemistry and related fields in the last 10 – 15 years. The coupling of thermooptical spectroscopy to other modern analysis methods (primarily, to chromatography, flow analysis methods, capillary electrophoresis, kinetic methods) enables one to extend the range of compounds that can be detected and to enhance the sensitivity of measurements. The review covers new fields of application of thermooptical spectroscopy in analytical chemistry and chemical analysis, such as the design of compact photothermal and photometric devices (chemical microchips and integrated microanalysis systems) on the basis of thermooptical detection, analysis of medical and biological samples and molecular analysis of surface- and volume-absorbing solid substances. In our opinion, the review of the main methods and applications of modern thermooptical spectroscopy will be of interest not only to analytical chemists but also to researchers in physical chemistry, biochemistry, surface chemistry and physics and laser chemistry.

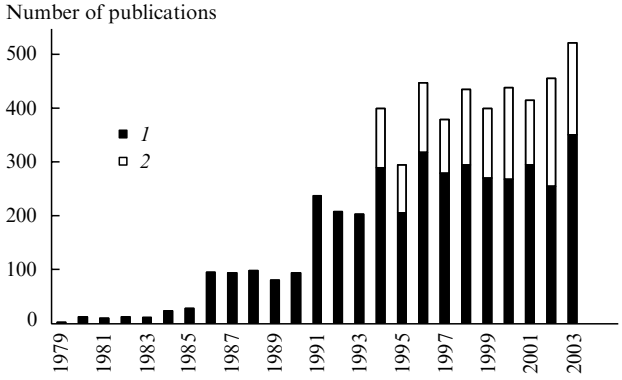

Figure 1. Changes in the number of papers (*1*) in the field of thermooptical spectroscopy in refereed journals in the period from 1979 to 2003 and changes in the number of abstracts of papers (*2*) presented at conferences on thermooptical and photoacoustic spectroscopy, analytical chemistry, chromatography, capillary electrophoresis and microanalytical systems in the period from 1994 to 2003.

M A Proskurnin Department of Chemistry, M V Lomonosov Moscow State University, Leninskie Gory, 119992 Moscow, Russian Federation. Fax (7-095) 939 46 75. Tel. (7-095) 939 35 14.
E-mail: proskurnin@rbcmail.ru
M Yu Kononets Department of Fundamental Medicine, M V Lomonosov Moscow State University, Leninskie Gory, 119992 Moscow, Russian Federation. Fax (7-095) 939 46 75. Tel. (7-095) 932 99 09.
E-mail: kononets@analyt.chem.msu.ru

Received 22 September 2003
Uspekhi Khimii **73** (12) 1235 – 1268 (2004); translated by T N Safonova

II. General characterisation of thermooptical spectroscopy methods

1. Theoretical fundamentals of thermooptical spectroscopy

Methods of thermooptical (photothermal) spectroscopy are based on measurements of refractive index changes induced by electromagnetic radiation absorption (Fig. 2).[2–5,7,8]

All thermooptical methods are based on the conversion of absorbed radiation into heat. Initially, an irradiated sample absorbs radiation which is accompanied by transition of its atoms or molecules into the excited state. Then, the excited state relaxes back to the ground state. Relaxation can follow several paths. For purposes of thermooptical spectroscopy, radiationless non-radiative relaxation accompanied by the conversion of absorbed radiation into heat is of most interest. The spatial temperature distribution in an irradiated sample corresponds to the spatial energy distribution in incident radiation. The temperature distribution, in turn, gives rise to optical anisotropy, *viz*., a non-uniform spatial refractive index distribution. The refractive index distribution causes a change in the optical path length, resulting in the formation of an optical element. The characteristics of this element provide a basis of a photothermal signal.

For thermooptical spectroscopy methods, not only high intensity of laser radiation but also its mode composition, *viz*., a particular spatial energy distribution in the beam, is of considerable importance. In this case, the photothermal effect is regular. In a medium, which is isotropic before irradiation, this effect leads to the formation of an optical element similar in action to a lens, a prism, a diffraction grating, *etc*.[2,4,6,7] Data on thermooptical elements, measured signals, methods of their detection and the fields of application are given in Table 1.

The theory of thermooptical spectroscopy can be divided into three parts describing the following stages:[4]

(1) absorption of excitation radiation to form the temperature field;

(2) formation of the refractive index field in accordance with the temperature distribution;

(3) influence of the thermooptical element on transmitted radiation.

The key problem is to calculate the temperature change, which depends most substantially on the thermooptical properties of a sample and its thermal and optical structure. A calculation of the changes in the probe beam after it passes through a thermooptical element is a trivial problem. Methods for its solution have been developed in detail.[4]

Let us consider a finite thickness sample irradiated with a laser beam in the TEM_{00} mode (the Gaussian intensity distribution across the TEM_{00} mode), *i.e*., with the beam with radial symmetry of intensity. This beam is described by the expression[4]

$$I(r) = \frac{2P_e}{\pi\omega_{0e}^2}\exp\left(-\frac{2r^2}{\omega_{0e}^2}\right), \quad (1)$$

where $I(r)$ and P_e are the intensity at a distance r from the centre of the beam and the total power of the excitation beam, respectively, and ω_{0e} is the excitation-beam waist radius. The spatial heat distribution in the sample in the absence of radiation losses is defined by the three-dimensional differential equation of thermal diffusion

$$C_P\rho\frac{d}{dt}\left[\Delta T(r,z,t)\right] - k\nabla^2\left[\Delta T(r,z,t)\right] = Q(r,z,t). \quad (2)$$

Here C_P is the heat capacity, ρ is the density of the medium, k is the thermal conductivity coefficient, $\Delta T(r,z,t)$ is the change in the sample temperature with respect to the initial level (the temperature of the environmental medium), z is the coordinate along the axis coinciding with the beam propagation direction, t is the time, $Q(r,z,t)$ is the heat released upon absorption of laser radiation in the TEM_{00} mode per unit of volume in a unit of time

$$Q(r,z,t) = 2\pi\alpha(z)I(r)r\mathrm{d}r, \quad (3)$$

where $\alpha(z)$ is the linear absorptivity of the sample.

Various other processes can easily be taken into account by introducing additional terms in the thermal diffusion equation. For a particular experiment, the characteristic features are specified by the boundary conditions necessary for solving the heat transfer equation. By choosing appropriate conditions, one can reduce the dimensionality of the thermal diffusion equation. The solution of this equation is the spatial and time dependences of the temperature rise in the excitation region $\Delta T(r,z,t)$. The solution of the thermal diffusion equation is expressed in terms of Green's function formalism.[4] In studies with the use of pulse lasers, the heat transfer is often ignored because the time of thermal wave propagation is substantially longer than the laser pulse duration. In this case, the spatial temperature distribution in the sample is assumed to be exactly consistent with the spatial energy distribution in the incident pulse.[4] In experiments using a continuous radiation source, the signal is, on the contrary, formed predominantly through heat transfer.

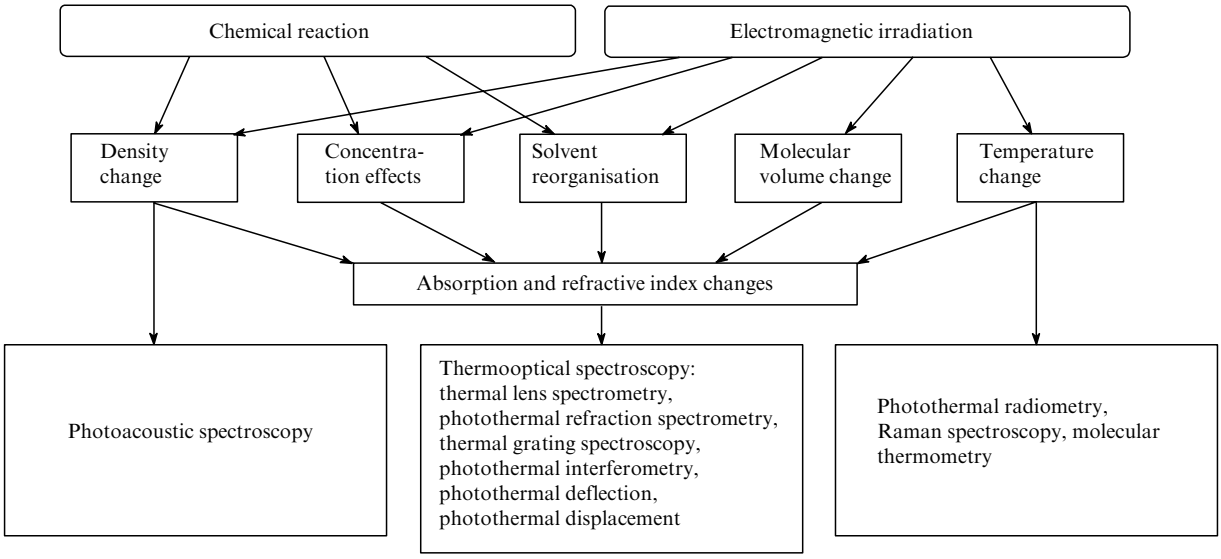

Figure 2. Main photothermal effects, which occur in condensed media irradiated with a laser, and methods for their detection.

Table 1. Main thermooptical methods and their characterisation.

Method	Thermooptical element	Signal	Detector	Objects; fields of application
Thermal lens spectrometry	divergent spherical lens	changes in the probe beam divergence (lens focal distance)	photodiode, photoelectron multiplier or multichannel photodetector	analytical determination of microamounts, detectors in chromatography, remote probing
Time-resolved thermal lens spectrometry	divergent spherical lens	slope of a time evolution curve of a thermal lens	photodiode, photoelectron multiplier	liquids and gases; a detector in chromatography
Photothermal refraction spectrometry	divergent cylindrical lens	changes in the probe beam divergence (lens focal distance)	photodiode, photoelectron multiplier or multichannel photodetector	liquids; probe analysis, analysis of small-volume samples (10^{-12}–10^{-14} litre), detectors in chromatography and capillary electrophoresis
Photothermal deflection (mirage effect)	pseudoprism in a medium in direct contact with a sample	probe-beam deflection	position-sensitive detector	gases, surfaces of condensed media; detectors in capillary electrophoresis
Photothermal displacement	mirror (bending of the sample surface)	spatial probe beam displacement	the same	surface and subsurface flaw detection
Photothermal radiometry	temperature fluctuations on the sample surface	surface thermal radiation	IR detector, lock-in amplifier	remote probing of surfaces, studies of fast processes
Photothermal microscopy	changes in refractive index distribution	amplitude and phase of the probe beam or thermal lens signal	scanning photodetector	microscopic analysis of surfaces, biological cultures and tissues, *in situ* analyses
Thermal grating spectroscopy	spatial diffraction grating	diffraction pattern in probe beam	the same	condensed media; studies of reaction mechanisms
Photothermal interferometry	changes in refractive index distribution	amplitude and phase of probe beam	Mach–Zehnder, Fabry–Perot, Jamin–Lebedev interferometers	flow rate measurements, surface absorption measurements, studies of DNA and proteins

The refractive index distribution $n(r,z,t)$, *i.e.*, the thermooptical element as such, is generally described by the following approximate equation:[19]

$$n(r,z,t) \approx n_0 + \frac{\mathrm{d}n}{\mathrm{d}T}\Delta T(r,z,t), \tag{4}$$

where n_0 is the refractive index of the non-excited sample. In the simplest case, the optical-path length change depends only on the refractive index (for example, in liquids). However, for solid samples, an additional increase in the optical path length due to expansion on heating is sometimes taken into account. In this case, the thermal expansion profile of the sample in the excitation region corresponds to the intensity profile of the incident radiation. This effect is described by a general equation of the optical path length (s) [17, 20]

$$\frac{\mathrm{d}s}{\mathrm{d}Q} = \frac{1}{\rho C_P}\frac{\mathrm{d}s}{\mathrm{d}T}. \tag{5}$$

The temperature dependence of the optical path length is related to the refractive index change $n(T)$ and the sample elongation $l(T)$ by the equation

$$s(T) = n(T)l(T).$$

The distribution of the optical-path length change (or the refractive index change) determines the phase shift of probe electromagnetic radiation passing through the excitation region. The phase shift is accompanied by a change in the radiation intensity distribution in the detector plane. Changes in the probe beam intensity in the detector plane are most accurately estimated by methods of diffraction optics. In this approach, the precise solution is found by solving the Huygens–Fresnel superposition integral. The direct solution of the system of Eqns (2)–(5) is very complex and cumbersome. The simplest expressions can be obtained with the use of the Fresnel and Fraunhofer approximations in diffraction processes, which involve detection in the near-field and far-field regions, respectively. Along with the diffraction model for the photothermal signal, simpler models, for example, a parabolic model [19] and a paraxial aberration model,[4] are sometimes used in thermal lens spectrometry.

From the above it follows that the mathematical apparatus of thermooptical spectroscopy is very complex. Hence, it is generally impossible to deduce an exact, simple and clear expression for a photothermal signal in analytical form. In practice, numerical methods are often used for simulation of a signal.

The theory of thermooptical spectroscopy of solid substances and heterogeneous materials differs substantially from the theory of thermooptical spectroscopy of homogeneous samples. Heat propagates in different layers or regions of solid matter and can also go to the gas or liquid surrounding the sample. To describe the resulting temperature change, it is necessary to simulate thermal diffusion.[4]

The complexity of three-dimensional thermal diffusion and the temperature and refractive-index changes taking place in solid samples forced researchers to search for alternative way to describe of a photothermal signal.[4] It is assumed that, first, spatial anisotropy of the refractive index, responsible for a photothermal signal, is not necessarily determined by the source intensity but depends much more substantially on the anisotropy of the sample. Second, it is generally impossible to obtain an exact solution of the thermal diffusion equation for a given geometry of the optical scheme.[4] To the contrary, this geometry is determined by the heterogeneous nature of the sample and the excitation source. In the next step, the chosen scheme can be used for studying thermal diffusion and the resulting temperature and refractive-index changes according to a standard procedure.[4] The three-dimensional structure of the material under study is revealed using experimental data and information, which is obtained by solving

the equation for specially chosen geometric conditions, rather than by solving thermal diffusion equations for a specific geometry of the optical scheme, which is usually done in studies of homogeneous samples.[4]

2. Thermal lens spectrometry

Of all the thermooptical methods, thermal lens spectrometry has gained the widest acceptance.[1–18, 21–71] This method is based on the periodic formation of a lens-like element in a medium that absorbs laser radiation with the TEM_{00} mode. The focal distance of the resulting thermal lens depends on the absorbance of the sample. The main advantages of this method are as follows: first, it allows one to study samples in different aggregate states and perform remote measurements and, second, it requires relatively simple equipment. The thermal lens signal depends on the temperature gradient of the refractive index and the thermal conductivity coefficient of the medium. The strongest thermal lens effects are observed in non-polar and low-polarity organic liquids.[3] It should be emphasised that this is also typical of other photothermal effects. Physical models of the thermal lens effect have been developed in detail.[54–60]

In conventional thermal lens spectrometry, two laser beams are coaxial (a spherical lens). The scheme of formation and detection of a thermal lens signal is presented in Fig. 3. If the formation of the thermal lens is completed, the stationary thermal lens signal (ϑ) is calculated as either a change in the probe beam intensity at the detector

$$\vartheta \equiv \frac{I_p(0) - I_p(\infty)}{I_p(\infty)}, \tag{6}$$

where $I_p(0)$ is the intensity at the centre of the probe beam reaching the detector at the initial moment $t = 0$, before the formation of the thermal lens; $I_p(\infty)$ is the intensity at the centre of the probe beam after completion of the formation of the thermal lens ($t \to \infty$), or as a relative broadening of the probe beam in the detector plane

$$\vartheta = \frac{\omega_{2p}^2(\infty) - \omega_{2p}^2(0)}{\omega_{2p}^2(\infty)}. \tag{7}$$

Time evolution of the thermal lens in a sample during one cycle of operation of a chopper (a modulator) of the excitation beam (or a single laser pulse) is described by a time-resolved thermal lens signal, which is the instantaneous relative intensity of the probe beam at the centre of the detector, $I_p(t)/I_p(0)$. The probe beam absorption in a sample is assumed to be negligible.

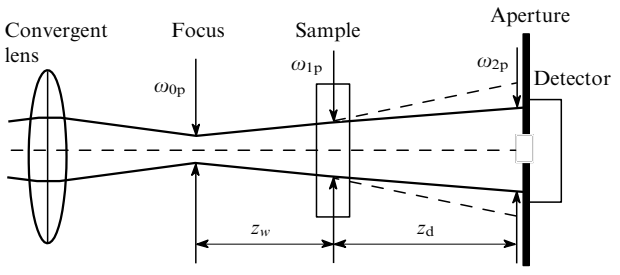

Figure 3. Diagram showing propagation of the probe beam; ω_{0p}, ω_{1p}, ω_{2p} are the radii of the probe beam in the waist, at the sample and in the plane of the detector, respectively; z_w is the distance between the probe laser waist and the sample; z_d is the distance between the sample and the plane of the detector.

In the case of liquids and isotropic solid substances, the thermal lens signal is usually described using the diffraction theory, in terms of which the relation between the thermal lens signal and the absorbance of the sample is expressed as follows:

$$\vartheta = (1 - 2.303AE_0P_eB)^2 - 1, \tag{8}$$

where A is the absorbance of the sample, P_e is the power of excitation radiation, E_0 is the thermal-lens enhancement factor (an increase in sensitivity compared to conventional spectrophotometry) for a unity power of excitation radiation

$$E_0 = -\frac{dn/dT}{\lambda_e k}, \tag{9}$$

(dn/dT is the temperature gradient of the refractive index, λ_e is the wavelength of the excitation laser, k is the thermal conductivity coefficient), B is the geometrical constant of a thermal lens spectrometer

$$B = \frac{1}{2}\operatorname{arctg}\left(\frac{2mV}{1 + 2m + V^2}\right), \tag{10}$$

V is the distance between the probe beam waist and the cell with a sample (in units of confocal distances of the probe laser)

$$V = \frac{z_\omega}{z_{cp}} + \frac{z_{cp}}{z_d}\left[\left(\frac{z_\omega}{z_{cp}}\right)^2 + 1\right], \tag{11}$$

m is the area ratio of the cross-sections of the probe and excitation beams in the sample

$$m = \left(\frac{\omega_{1p}}{\omega_{0e}}\right)^2 = \left(\frac{\omega_{0p}}{\omega_{0e}}\right)^2\left[1 + \left(\frac{z_\omega}{z_{cp}}\right)^2\right]^2, \tag{12}$$

where ω_{0e} and ω_{0p} are the waist radii of the excitation and probe lasers, respectively, z_{cp} is the confocal parameter of the probe laser.

For non-isotropic solid substances, the diffraction model of the thermal lens effect is inapplicable, because an analytical expression for neither a time-resolved lens signal nor a stationary thermal lens signal can be deduced.[72]

Quantitative measurements of the thermal lens effect enable one to evaluate the absorbance up to $y \times 10^{-8}$ and the concentration up to $y \times 10^{-12} - y \times 10^{-10}$ mol litre^{-1} (see Refs 6, 13, 21–43, 58, 62–71, 73–93). On the whole, the sensitivity of thermal lens spectrometry is 2–4 orders of magnitude higher than that of conventional spectrophotometry.

For isotropic samples, the time-resolved thermal lens signal is described in terms of the diffraction model by the following expression:

$$\frac{I_p(t)}{I_p(0)} = \left(1 - \frac{2.303E_0P_eA}{2} \times \right. \tag{13}$$

$$\left. \times \operatorname{arctg}\left\{\frac{2mV}{[(1 + 2m)^2 + V^2]t_c/2t + 1 + 2m + V^2}\right\}\right)^2 +$$

$$+\left(\frac{2.303E_0P_eA}{4}\ln\left\{\frac{[1 + 2m/(1 + 2t/t_c)]^2 + V^2}{(1 + 2m)^2 + V^2}\right\}\right)^2,$$

where t_c is the characteristic time constant of the thermal lens

$$t_c = \frac{\omega_{0e}^2}{4D}, \tag{14}$$

D is the thermal diffusivity of the sample.

Time-resolved thermal lens spectrometry is based on the time evolution of the focal distance of the thermal lens. The response time of the method is 0.1–1 ms, which is approximately an order of magnitude shorter than that achieved in stationary thermal lens measurements.[78, 94–98] Time-resolved thermal lens spectrometry is used for the detection in chromatography or studies of kinetic processes.

Presently, a differential (dual-cell) modification of thermal lens spectrometry is under development. In this method, the background signal is compensated by the formation of a thermal lens in two cells placed sequentially. The second cell containing a reference solution is placed symmetrically in front of the excitation laser waist.[30, 99–105] The thermal lens signal formed in this cell [see Eqn (6)] is proportional to absorption of impurities responsible for the background signal. The thermal lens signal in the second cell can be represented as the sum of the thermal lens signals of the analyte component and the background. The divergent thermal lens formed in this cell can be considered as a superposition of two thermal lenses, whose focal distances depend on absorption of the analyte components and impurities. Hence, the thermal lens effect in the first cell compensates for broadening of the probe beam, which occurs due to absorption of impurities in the second cell containing the solution analysed. In this case, the signal depends only on absorption of the component analysed in the second cell. Advantages of two-cell measurements over the conventional single-cell method is evidenced by the fact that the detection limit of iron(II) by its reaction with 1,10-phenanthroline is five times lower (20 nmol litre^{-1}), and the minimum quantifiable concentration is almost ten times lower (40 nmol litre^{-1}).[99]

3. Photothermal refraction

Crossed-beam thermal lens spectrometry or photothermal refraction is based on the optical scheme of thermal lens measurements, in which the excitation and probe laser beams are mutually perpendicular (a cylindrical lens).[49, 106–111] Although the sensitivity characteristics of this method are analogous to those of thermal lens spectrometry, photothermal refraction makes it possible to detect absolute amounts as low as several tens of molecules of absorbing substances in the volume from $y \times 10^{-18}$ to $y \times 10^{-15}$ litre (a crossing region).

Due to a high spatial resolution, photothermal refraction is used in capillary chromatography, capillary electrophoresis methods and local analysis of liquids.[49, 106–117] However, equipment required for the optical schemes of photothermal refraction are more cumbersome compared to that used in the parallel-beam scheme, and these optical schemes are characterised by a substantially more complex mathematical model, which describes the relationship between the signal recorded and the geometric parameters of the optical scheme. Besides, this mode of recording the thermal lens signal is inconvenient for performing analyses in a volume larger than 0.1 ml, because the energy of the excitation laser beam reaching the crossing region substantially decreases as the absorbance of the sample and the optical path length increase, resulting in narrowing of a region of the linear dependence of the refractometric signal (a linearity region).[118]

The use of the thermal lens detection in the near-field region (the sample-to-detector distance is 10 cm) gave additional impetus to the development of photothermal refraction.[109–111] Further investigation demonstrated that detection under these conditions corresponds to detection in capillaries, because the edge effects caused by interference of the probe laser beam at capillary walls are eliminated, and the measurement reproducibility is substantially improved. In addition, this approach employs compact apparatus, which made it possible to create a detector prototype for capillary electrophoresis (Fig. 4).

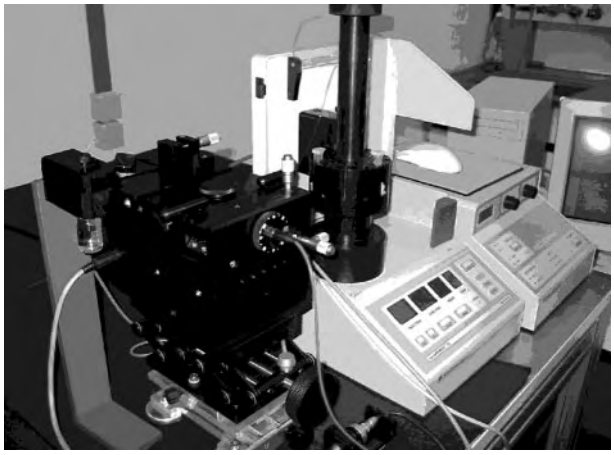

Figure 4. Photograph of a detector prototype for capillary electrophoresis based on photothermal refraction spectrometry.
The photograph courtesy of Drs W Faubel (Karlsruhe Research Centre, Germany) and U Puell (Marburg University, Germany).

4. Total internal reflection thermal lens spectroscopy

Thermal lens spectrometry under conditions of total internal reflection [an analogue of total internal reflection fluorescence spectroscopy] is a powerful tool for studying interfaces (liquid–liquid, liquid–solid, *etc.*) when nanogram amounts of reagents are used.[119, 120] However, this method has little use. The method is based on providing conditions under which the laser beam inducing a thermal lens undergoes total internal reflection from the interface. This allows the detection of photothermal effects, which appear virtually only at the interface. Taking into account that thermal lens spectrometry as a method of molecular absorption spectroscopy is suitable for a larger number of compounds compared to fluorescence, this method has great potential although it is still in its infancy.

5. Photothermal deflection and photothermal displacement

Mirage-effect spectroscopy (thermal deflection spectroscopy, thermal prism)[5, 51, 121–153] and photothermal displacement spectroscopy (thermal mirror)[154–170] are the next most commonly used methods after thermal lens spectrometry. These methods are most widely employed in a purely thermal modification using excitation with IR radiation, which is associated primarily with investigations of semiconducting and polymer materials. These methods are only partially used in experiments on selective excitation in the optical range.

These methods are based on the changes in the optical characteristics of the surface and subsurface layers of the medium caused by heating of a sample with an excitation laser (Fig. 5). In a liquid or gaseous medium, which exists in direct contact with the sample, the thermooptical element is formed. The latter acts as a prism on the radiation propagating along the sample surface. This process is accompanied by thermal deformation of the irradiated surface, resulting in its bending. The probe laser beam, which passes parallel to the surface (a mirage effect) or is incident on the surface at a particular angle (a thermal mirror), is deflected by the thermal prism at a definite angle from the initial direction or is

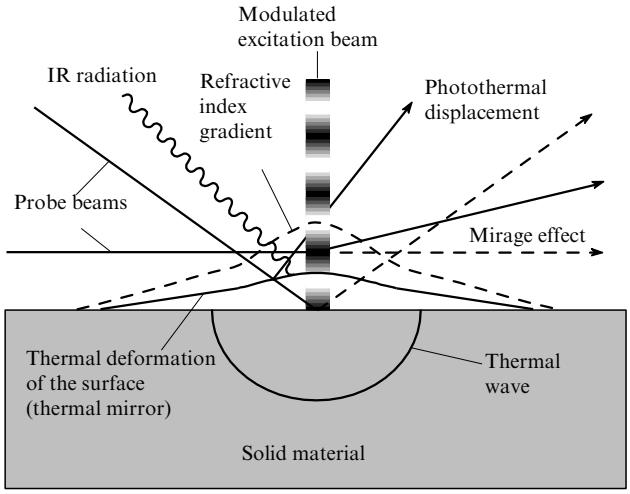

Figure 5. Thermooptical effects under laser excitation of the surface.

reflected from the bent surface and broadened. The perturbations caused by heating are associated with the absorbing ability and thermal properties of the surface under study and depend on the thermal properties (heat capacity, thermal conductivity) of the environmental medium. The scheme of the appearance of the above-described photothermal effects is shown in Fig. 5.

In mirage and photothermal displacement spectroscopy, optical position-sensitive detectors, for example, photodiode matrices and video cameras, are generally used. The angle ϕ (or a distance) at which the probe beam is deflected can serve as an analytical signal. This signal is called the amplitude signal, because it characterises the displacement amplitude of the probe beam relative to the non-excited state of the surface.

There are a number of equations describing the photothermal deflection. The form of these equations depends on the aim of a particular study and the phase state of the medium under study. In investigations of the surfaces of solid materials and gaseous media, the following equation is used:[5]

$$\phi = -\frac{\mathrm{d}n}{\mathrm{d}T}\frac{\alpha l P_\mathrm{e}}{\pi^2\psi\rho C_\mathrm{P}\omega_{\mathrm{e}0}^2}\left(-\frac{2x_0}{\omega_{\mathrm{e}0}^2}\right)\exp\left(-\frac{x_0}{\omega_{\mathrm{e}0}^2}\right). \qquad (15)$$

This equation is valid if the excitation and probe beams are mutually perpendicular (Scheme 1). In studies of weakly absorbing media, the propagation directions of the excitation and probe beams in samples form an acute angle (Scheme 2). In this case, the following equation is valid:[4]

$$\phi = -\frac{\mathrm{d}n}{\mathrm{d}T}\frac{\alpha l P_\mathrm{e}}{2\pi k x_0}\left\{2\exp\left[-\frac{2x_0^2}{\omega_{\mathrm{e}0}^2(1+1/\psi t_\mathrm{c})}\right]- \qquad (16)$$

$$-\exp\left[-\frac{2x_0^2}{\omega_{\mathrm{e}0}^2(1+2/\psi t_\mathrm{c})}\right]-\exp\left(-\frac{2x_0}{\omega_{\mathrm{e}0}^2}\right)\right\}.$$

Here α is the linear absorptivity of the sample layer giving rise to a photothermal signal; l is the thickness of the absorbing layer; ψ is the chopper frequency; x_0 is the so-called interaction distance, *viz*., the distance between the surface of the sample and the parallel-arranged probe beam (displacement of the probe beam) for Scheme 1 or the distance between the optical axes of the beams for Scheme 2.

The refractive index field induced by heating is responsible for the phase change of the displaced beam relative to the incident beam. The observed phase difference is called the phase signal. This signal is recorded by a lock-in amplifier connected to a position-sensitive detector. The spatial resolution of measurements is related to the size of the beam cross-section of the excitation laser, which, in turn, is limited by the wavelength of the excitation beam.

These methods have some specific features. For example, the mirage effect appears in the surrounding medium rather than in the sample. In this connection, measurements by the mirage spectroscopy are not carried out *in vacuo*. The possibilities of determining the concentrations of solid substances in gases, in particular, in air, are limited by their thermooptical characteristics. Hence, an auxiliary liquid possessing appropriate thermooptical properties is often applied on the surface to strengthen the thermal prism. However, this approach has drawbacks associated with the difficulty of choosing such liquids (it is necessary to exclude completely an interaction of the liquid with the material under study).

Of all theoretical models of the formation of a photothermal signal, the model of the mirage effect has been best developed. In the method of photothermal mirror, simulation of the thermal deformation of the surface is a much more complicated problem. In addition, the probe beam deflected by the deformed excited surface can be additionally deflected due to the presence of the refractive index field in the surrounding medium (if measurements are carried out not in vacuum). As a result, calculations become even more complicated.

Nowadays, mirage spectroscopy is one of the most convenient and commonly used thermooptical methods for studying surfaces with very high or very low light absorption. Generally, this method is used for microscopic studies and flaw detection in semiconductors,[171] metals[172,173] and various optical materials.[174–176] Mirage spectroscopy is rarely employed in analytical chemistry as a highly sensitive method of molecular absorption spectroscopy.

Mirage spectroscopy is used in immunoassay adsorption analysis with isolation of a specially coloured antigen–antibody complex on the surface of a solid substrate followed by detection of surface absorption.[177–179] This method is used also in thin-layer chromatography for detection of the absorption profile along the elution profile.[180–182] The new application of mirage spectroscopy for analysis by thin-layer chromatography[183] is limited to measurements with the use of non-selective excitation. However, mirage spectroscopy is not considered as a solo analytical method for the detection of surface absorption. The study[183] was aimed only at estimating the deep concentration profile in the chromatographic zone based on the determination of the surface properties by several thermooptical methods, including mirage spectroscopy. Besides, mirage spectroscopy is used in capillary chromatography.[149–153,184]

6. Photothermal radiometry

Photothermal radiometry is based on measurements of IR radiation from the sample surface after its irradiation with a laser beam (see Fig. 5).[185–214] The amount of emitted energy is proportional to the absorptivity of the sample. In photothermal radiometry, the rate of time evolution of the signal is substantially higher than that in mirage spectroscopy and the thermal-mirror technique, because the time required for evolution of surface deformation and the temperature gradient in the surrounding medium is longer than the thermal relaxation time determining the onset of emission of IR radiation from a heated sample. Semiconducting energy-dispersive detectors are used for rapid and highly sensitive measurements of emitted IR radiation. The possibilities of photothermal radiometry are most evident in studies of semiconducting materials and in IR tomography of biological tissues, including *in vivo* studies. The advantages of photothermal radiometry are the possibility of remote probing, simplicity of experimental equipment and, what is most important, high time resolution (10^{-7}–10^{-8} s). The latter fact allows one to measure absorption spectra of intermediates and study fast processes. Photothermal radiometry is used for determining the absorptivities of thin films, coatings and biological tissues of living organisms.[191,199–206] Theoretical models for photothermal radiometry are constructed on the basis of one-dimensional heat transfer and the law of blackbody radiation. However, the majority of real systems show substantial deviations from the model approximations, which complicates the interpretation of experimental data. These approximations are best suitable for analysis of semiconductors using laser radiation, whose wavelength is larger than the semiconductor band gap. In this case, the signal (thermal radiation) is generated by a plasma wave rather than by a thermal wave, and experiments correspond closely to the model of blackbody radiation.

7. Photothermal microscopy

Photothermal microscopy has been created in the course of the development of thermal lens spectrometry. In this case, the optical set-up of a thermal lens spectrometer is included in the scheme of measurements of an optical microscope.[178,215–232] Photothermal microscopy is used primarily in biological studies as a non-destructive method for investigating cell functioning and in medicine for diagnostic purposes. Depending on the conditions (virus activity, impairment of cellular functions, *etc*.), the optical

characteristics of cytoplasm can differ from those of cell nuclei, which are easily detected with a photothermal microscope.

Photothermal microscopy enables one to study the characteristic features of reaction pathways with the use of nanogram amounts of reagents. This method can be combined with microflow analysis and microchromatography. The further use of the results of these investigations is directly associated with the development of microflow injection analysis, microelectrophoresis and, on the whole, integrated microanalysis systems.[216–231] Photothermal microscopy can also be used for studying reactions under conditions of integrated microanalysis systems (detection of trace concentrations, investigations of mirochannels, microflows, *etc*.) and as a detection method.

8. Photothermal interferometry

Another group of thermooptical spectroscopy methods includes photothermal interferometry and related methods.[189, 233–245] In these methods, a three-dimensional pattern (an amplitude and a phase) of the probe beam recorded on an interferometer (Mach–Zehnder, Fabry–Perot or Jamin–Lebedev) serves as an analytical signal.[239, 246, 247] These methods allow one to determine the local absorption distribution on the surface and in subsurface layers. The sensitivity of photothermal interferometry is the highest of all thermooptical methods (the weakest signal is determined by quantum noise of an interferometer, the absorbance is $y \times 10^{-10}$) and allows the determination of highly absorbing compounds in amounts up to individual molecules. In addition to chemical analysis, photothermal interferometry is employed to study the hydrodynamics of liquids and gases, determine the rates of microflows with high precision, and establish nucleotide sequences in DNA and amino acid sequences in proteins.[242, 245] The amplitude signal in photothermal interferometry is calculated by the equation

$$\phi = \frac{\pi^2}{2}\sqrt{\frac{D}{\psi}}\,\frac{\omega_{e0}^2}{\lambda_p}\,\frac{\partial n}{\partial T}\,\frac{\alpha l}{k}\,P_e\left|\mathrm{erfc}\left(\sqrt{\frac{\psi}{D}\,\frac{\omega_e^2+\omega_{e0}^2}{8}}\;e^{i\pi/4}\right)\right|, \qquad (17)$$

where λ_p is the probe beam wavelength.

Photothermal spectroscopy holds promise for measuring ultralow light absorption in solid materials for laser and fibre-optical techniques, which was confirmed by studies.[239, 240, 248–251] To measure the rates of liquid and gas flows with a sensitivity up to $y \times 10^{-6}$ cm s^{-1}, an optical thermal anemometer was devised.[249–251] An apparatus was created for separate measurements of the bulk and surface light absorption in materials for power optics. This apparatus is successfully used for monitoring low absorption ($y \times 10^{-5}$ cm^{-1}) in ZnSe and ZnSe-based optical elements.

9. Thermal diffraction spectroscopy

Thermal diffraction spectroscopy is based on the spatial periodic refractive index change in a medium caused by the photothermal effect, which is induced by absorption of the excitation beam energy.[252–261] In this case, the thermooptical element behaves as a diffraction grating, and the diffraction pattern produced by the probe beam serves as a signal. This method requires very complex equipment and is used for solving special problems, in particular, for testing the quality of laser optics (spatial distribution of microelements in optical materials) and for studying fast processes (energy transfer in crystals, photochemical processes, structural vibrations of crystal lattices).[254, 257, 260, 262–267]

One promising line of investigation for the use of thermal diffraction spectroscopy is concerned with chemical kinetics and reaction mechanisms. The method allows one to separate diffusion processes and chemical reactions, because the total signal of these processes can be considered as a superposition of short-lived and long-lived diffraction gratings.

A modification of the thermal diffraction method, *viz*., photothermal IR microspectroscopy, employs a microthermometer as a probe, which is used in atomic-force microscopy and thermal microscopy.[268, 269] In a photothermal microscope (unlike an atomic-force microscope), a probe of this type serves both as a thermometer and a heater, which allows the simultaneous detection of surface samples and samples of subsurface layers.[262] The instrument can be use both for measuring photothermal spectra at a given point (region) of samples based on the results of surface scanning in the mode of atomic-force microscopy and for obtaining photothermal samples, in which the signal is proportional to the concentrations of substances that absorb at the excitation wavelength. An important feature of photothermal IR microspectroscopy employing a thermoprobe is that this method, unlike other photothermal methods, is not restricted by the diffraction limit of spatial resolution.[267] Interestingly, photothermal measurements, scanning thermal microscopy, thermomechanometry or thermocalorimetry can be combined in the same instrument, because all these studies are carried out with the use of a Wollaston thermoprobe.[270] Photothermal microscopy provides better spatial resolution compared to conventional measurements using Fourier-transform IR spectroscopy.[267] Such photothermal measurements are used for studying composite materials, biological samples (hair, cells), in particular, for examining microprobing of drugs and the influence of antioxidants on cell functioning.[267–270]

10. Characteristic features of thermooptical spectroscopy methods

The characteristic features of thermooptical spectroscopy methods can be divided into six main groups.

The first group includes characteristics related to high sensitivity. Modern methods for recording the absorbed energy allows the determination of the temperature, volume or refractive-index changes corresponding to absorption of $y \times 10^{-8}$–$y \times 10^{-10}$ absorbance units, which is 4–6 orders of magnitude lower than the sensitivity of conventional spectrophotometric methods.[1–10, 46, 59, 74, 86] In addition to high instrumental sensitivity, thermooptical spectroscopy is characterised by a wide linear dynamic range of measurements (for thermal lens spectrometry, this range is up to 6–8 orders[4, 6, 11, 18, 90]). However, highly sensitive analytical methods have drawbacks, which are associated primarily with the purity of reagents and solvents, the problem of test experiments, laborious sampling, sample preparation, *etc*.

The second group includes characteristics reflecting the distinguishing features of thermooptical spectroscopy as a method of molecular absorption spectroscopy. The advantages of the latter are diversity of substances (including organic compounds) which can be detected, the possibility of investigating samples in different aggregate states, well-developed methods and numerous procedures for sample preparation and non-destructive determination (which allows one to analyse biological samples, for example, living cells), the possibility of performing remote analysis[21] and determinations in flow.[8, 10, 42, 43, 46, 178] However, thermooptical spectroscopy has all drawbacks of conventional spectrophotometry (primarily, spectral non-selectivity).

The third group includes the parameters of thermooptical spectroscopy as calorimetric methods. The common feature of these methods is the extraction of information on the composition and properties of the analyte by recording absorbed radiation and taking into account the attendant changes in the physical and (or) thermodynamic parameters. The absorbed energy can be measured using various modes of detection: acoustic (acoustic wave formation, gas pressure changes), interferometric, refractometric (refractive index changes), optical (measurements of the intensities of transmitted or absorbed radiation), thermometric (contact temperature control), direct calorimetric (direct detection of thermal radiation) or extensometric (changes in the sample size).

The fourth group includes the characteristics of thermooptical spectroscopy, such as power characteristics (the signal is proportional to the incident radiation intensity) and geometric characteristics (the signal depends on the geometry of the optical scheme).

These properties are not unique (recall photoacoustic spectroscopy). The advantage is that the dynamic range can be even more extended (up to 8 – 10 orders of magnitude) by varying the power of the radiation source.[27 – 33, 91 – 93, 271] However, the strong dependence of the thermal lens signal on the geometric parameters (positions of the laser beam waists, cells containing samples and the detector) leads to a serious problem of measurement reproducibility.[55, 58, 59, 80, 272, 273] In addition, not only sensitivity and reproducibility but also the linear range of the signal depends on the geometric parameters of the optical scheme.[59, 274 – 279]

The fifth group of parameters, which characterise the main distinguishing features of thermooptical spectroscopy, is associated with the use of lasers as powerful intense sources of monochromatic coherent radiation. As a result, the number of effects induced by interaction of radiation with an absorbing medium sharply increases. In addition to sample heating, researchers face the photochemical effects (which can play both positive and negative roles), the simultaneous manifestation of the photothermal effect and luminescence, *etc.*[3, 6, 280 – 284] It should be noted that the influence of laser radiation on samples in thermooptical experiments is poorly understood.

The sixth group includes parameters reflecting the unique properties of thermooptical spectroscopy. In relation to this connection, let us mention several important factors.

1. In thermooptical spectroscopy, the laser mode structure is the most important characteristic of laser radiation. Due to regularity of this distribution for the observed photothermal effect, it is possible to construct the precise mathematical model, which relates the strength of the effect (for example, the focal distance of the resulting thermal lens) to the concentration of absorbing components of the system.[6, 55, 56, 239]

2. The solvent plays a decisive role in thermooptical spectroscopy because when a medium is heated its parameter change, for example, refractive index and density. For example, a particular (chemically inert) absorbing compound is characterised by photothermal signals in organic and aqueous media, which differ by several orders of magnitude.[271] Methods of thermooptical spectroscopy are successfully used for determining the above-mentioned characteristics of solvents.[285 – 291]

3. It should be emphasised that the photothermal effects are local in character. They do not cover the overall volume of the sample, but only a small region around the excitation laser beam. This gives rise to strong convection of the liquid, which can lead to blurring and periodic oscillations of the signal.[292] However, the period of convective oscillations can provide important information on the photothermal properties of substances.[293, 294] Another consequence of the local character of the photothermal effects is that chemical processes in the heated portion of the solution can be either accelerated or decelerated (due to heating, photochemical reactions, *etc.*), resulting in a change in the concentration gradient and the formation of diffusion flows of substances.

Evidently, the above classification of the characteristics is tentative, but it gives an insight into the problems associated with the development of analytical thermooptical methods. When describing the features of these methods and classifying these characteristics, we used the principle 'from general to special'. It should be noted that only the first three groups of characteristics were considered in the literature concerned with the problems, advantages and drawbacks of analytical thermooptical spectroscopy, although (strange as it may seem) these characteristics are not unique for thermooptical spectroscopy and are met with in other methods. The last three groups of characteristics are generally ignored considering their well-known drawbacks, which decrease the efficiency of the method, or regarding them as personal techniques used by researchers. As a result, the true place of thermooptical spectroscopy among analytical methods is actually an open question.

In our opinion, this view is incorrect, because specific effects manifested in thermooptical experiments, such as the simultaneous detection of several analytical signals, and the employment of photothermal effects as an active component of the analytical method rather than as a passive mode of detection will presumably provide the basis for a 'special line' of the development of analytical thermooptical spectroscopy. It is encouraging that virtually all most important recent studies have been aimed at developing or, at least, searching for new approaches to methodology, sample preparation and measurements of the signals.[9 – 18, 50 – 54, 58, 112 – 117, 119, 120, 216 – 232, 239, 274, 282, 295 – 297]

11. Apparatus for thermooptical measurements

Dual-laser (dual-beam) optical set-ups have gained wide acceptance in thermooptical spectroscopy. In these schemes, a thermooptical element is formed in a sample under the action of one beam (the excitation beam), and the change in the characteristics of the second (probe) beam serves as an analytical signal.[4 – 10, 54 – 71, 184, 298 – 309] Correspondingly, the excitation laser wavelength is chosen at the absorption maximum, and the probe beam wavelength is, on the contrary, chosen at the absorption minimum. Since thermooptical methods belong to power methods, powerful continuous wave lasers (argon ion, krypton ion, helium cadmium, *etc.*) or pulsed lasers (Nd : YAG, CO, nitrogen, eximer, *etc.*) are used for excitation. It should be noted that thermooptical methods are not limited to the use of laser radiation. However, the use of laser radiation allows one to substantially enhance the effects, which, in fact, appear upon any interaction of radiation with matter. Sources of IR, UV and visible radiation with a continuous spectrum (xenon lamps) are also employed.[295] In this case, the regularity of the intensity profile of excitation radiation is achieved by using absorbing spatial filters.

The basic diagram of thermooptical measurements is shown in Fig. 6. Various methods employ radically different systems for beam focusing and convergence. In all thermooptical methods, the signal depends on the geometry of the optical set-up. Hence, careful adjustment and calibration of a thermooptical spectrometer are required before experiments, and the parameters should be frequently monitored during the course of measurements. A system for synchronisation, which provides synchronisation of the onset of the formation of a thermooptical element and the onset of signal accumulation, most commonly consists of either a mechanical or electromechanical chopper (for beam modulation of an excitation continuous wave laser), a controlling block (a lock-in amplifier or a sampling integrator) and a photodiode. The function of the reference signal is to record the current power of the excitation laser and normalise the signal.

The uniqueness of a thermooptical spectrometer is that the signal contains information only on light absorption of a sample, but the measurement technique allows one to use this instrument simultaneously as, for example, a nephelometer or a refractometer. Hence, a thermooptical spectrometer is a multipurpose instrument, which can provide much more information compared

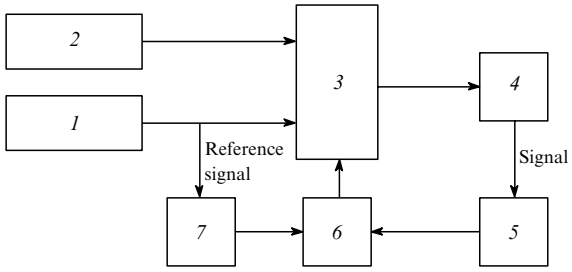

Figure 6. Basic diagram of thermooptical measurements.
(*1*) An excitation laser, (*2*) a probe laser, (*3*) a system for beam modulation, focusing and convergence, (*4*) a sample, (*5*) a photodetector for analytical signal, (*6*) a system for synchronising and recording, (*7*) a photodetector of a reference channel.

to its spectrophotometric analogue. As an example we refer to thermal lens fluorimetric procedures for the determination of picogram amounts of transition metal complexes and a combined thermooptical refractometric detector for liquid chromatography. The merit of the latter is that it can be used for the simultaneous determination of compounds of different nature at nanogram levels (for example, the determination of metal chelates and polysaccharides without their preliminary derivatisation).[239, 248]

Let us consider a typical thermal lens spectrometer[58, 59] (Fig. 7). A thermal lens is induced in a cell with an Innova 90-6 argon ion laser *1* (Coherent, USA) with a lasing wavelength of 514.5 nm (TEM_{00} mode, the maximum power is 1.5 W). An SP-106-1 helium neon laser (Spectra Physics, USA) is used as the probe laser *2* with a lasing wavelength of 632.8 nm (TEM_{00} mode, the power is 10 mW). The beams of both lasers are initially vertically polarised. After an optical rotator *3* (model 310A, Spectra Physics, USA), the horizontally polarised excitation laser beam passes through a mechanical modulator (chopper) *4*. A part of the beam energy is directed to a FD-7K power monitoring photodiode *6* using a plate *5*. An amplifier *7* converts the current from the photodiode into a voltage and directs the signal to the second channel of an analogue-to-digital converter and a digital-to-analogue converter (ADC–DAC) board *8* installed on an IBM PC/AT *9*. To synchronise the detection system with the operation mode of the modulator, a part of the radiation energy of the excitation laser is allocated to a lock-in photodiode *11* using a plate *10*. The signal passes to a synchronisation block *12*. The latter forms a pulse, which coincides with the moment of the opening of the chopper. The pulse passes to the ADC–DAC board of the computer. This pulse corresponds to the onset of the formation of a thermal lens in the cell and serves as a signal for the beginning of a new cycle of data reading. The chopper is controlled by a computer through a converter *8* and a synchronisation block *12*. The excitation laser beam, which is focused by a lens *13*, passes through a plane-parallel plate *14* (which is used for fine tuning of the beams in the cell) and a Glan prism *15* and is directed to a cell *16*. The probe laser beam is sent through a system of mirrors *17* and *18* and a focusing lens *19* to the Glan prism, where it is reflected and goes to the cell. A dichroic mirror *20* serves for the preliminary separation of the excitation and probe laser beams and makes it possible to get rid of an additional thermal lens, which could be induced by a highly absorbing filter *21*. The helium neon laser beam, which bears information on light absorption by the sample, passes through an 2-mm aperture *22* located on an optical axis of the system and falls on a FD-7K photodiode *23*. The signal from the photodiode is converted by an amplifier *24* and goes to an ADC–DAC converter of the computer.

Photothermal detectors for capillary electrophoresis on the basis of photothermal refraction in the near-field region (Fresnel diffraction) have been extensively developed in recent years. A prototype of such detectors for high-performance capillary electrophoresis was devised at the Karlsruhe Research Centre (Germany)[113, 114, 310, 311] (see Fig. 4).

The scheme of a typical instrument for mirage spectroscopy[112–115] is shown in Fig. 8. This instrument consists of a probe monoblock equipped with a position-sensitive recording system (Phototherm Dr. Petry Gmbh, Germany). Excitation is performed with a Nd : YAG laser (ADLAS DPY 321, Germany) at wavelengths of 1064 and 532 nm; the maximum radiation power is 50 mW. A helium neon laser (Melles Griot, USA) with a power of 5 mW and a wavelength of 632.8 nm is used as the probe laser. The scanning system allows one to study samples of sizes of 2×2 cm at 1 μm resolution. The chopper frequency of the excitation source varies from 10 to 1000 Hz, which corresponds to heating of a sample layer with a depth from 1 nm to 1 μm. The signal recording system is equipped with a position-sensitive detector and a lock-in amplifier. The deflection amplitude (the amplitude signal) and the path difference (the phase signal) of the probe beam are recorded.

Photothermal IR microspectroscopy employs a modified Fourier-transform IR spectrometer. To ensure thermooptical measurements, the modulated beam from an IR spectrometer heats a sample. Heating is detected by a thermal probe. The output signal from the spectrometer returns to the input of the spectrometer, which makes it possible to record photothermal interferograms. In the scanning mode, a thermal probe is mounted on a positioning system (most often on an atomic-force microscope).[262]

As mentioned above, the main idea of photothermal interferometry consists of measuring the optical path length changes caused by a photothermal modulation of the refractive index. Compared to other photothermal methods used for detecting thermal perturbations of the optical parameters of a medium, *viz.*, photothermal deflection spectroscopy and thermal lens spectrometry, the phase method provides higher sensitivity and stability of measurements. However, in spite of substantial potential advantages, the phase method has little practical application. This is associated with the fact that commonly used Michelson and Mach–Zehnder interferometers are rather complex instruments, which are very sensitive to the environmental conditions and require tedious tuning. A photothermal detector on the basis of polarisation and fibre-optic interferometers, which has been

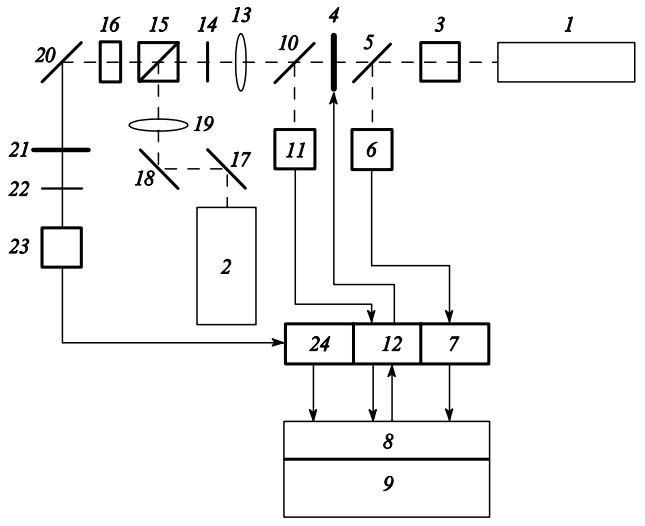

Figure 7. Block diagram of a dual-laser thermal lens spectrometer (for notations see text).[58, 59]

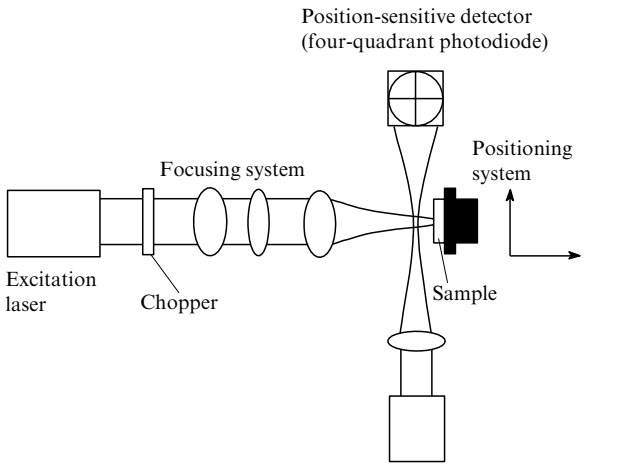

Figure 8. Scheme of a mirage spectrometer.[112–115]

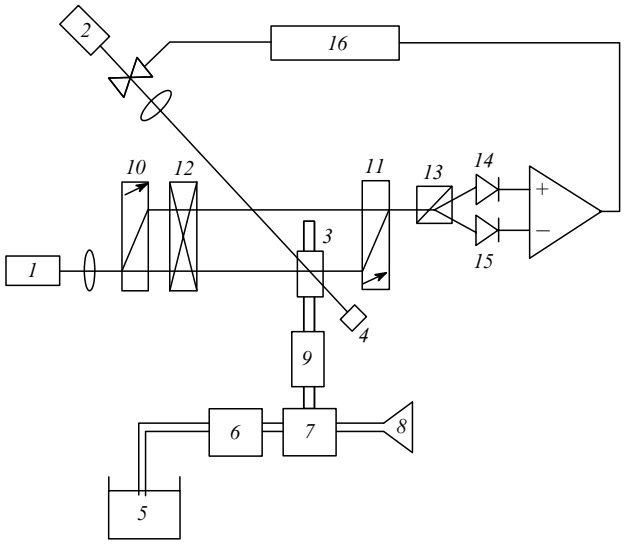

Figure 9. Scheme of a thermooptical polarisation interferometer equipped with an HPLC detector.[239, 240, 248]
(*1*) A probe laser, (*2*) an excitation laser, (*3*) a cell, (*4*) a power metre of an excitation laser, (*5*) an eluent, (*6*) a chromatographic pump, (*7*) an injector, (*8*) an injector port, (*9*) a chromatographic column, (*10*, *11*) Savart plates ($CaCO_3$), (*12*) a 90° optical rotator, (*13*) a Wollaston prism, (*14*, *15*) photodiodes, (*16*) a lock-in amplifier.

Figure 10. Photograph of a commercial thermal lens microscope for measurements in microfluid chips.[314]
The photograph courtesy of Prof. T Kitamori and Dr. M Tokeshi (University of Tokyo, Institute of Microchemical Technology, Japan).

devised in recent years, can be used in liquid chromatography and capillary electrophoresis.[239, 240, 248–251, 312, 313]

A diagram indicating the main features of a thermooptical interferometer based on a Jamin–Lebedev polarisation interferometer is presented in Fig. 9. Doubled-frequency radiation of a Nd:YAG laser *2* (532 nm, 25 mW) is used for excitation. A semiconducting laser *1* (680 nm, 10 mW) serves as a source of probe radiation. The diameter of the probe beam in cell *3* is 100 mm. The detector operates simultaneously in photothermal and refractometric modes. In the latter case, non-periodic changes in the refractive index of a liquid flowing through the detector are measured. The corresponding signal induced by changes in the mobile phase in a chromatographic system *5–9* is formed in a feedback system. In the photothermal mode, the presence of an absorbing analyte in the cell leads to a temperature rise and, consequently, to an increase in the refractive index, whose variations are proportional to the modulation frequency of the excitation beam. This gives rise to an additional phase signal, which modulates the polarisation state in the second Savart plate *11*. This modulation amplitude is analysed using a Wollaston prism *13* and is measured with the use of photodiodes *14* and *15*, which are connected to a lock-in amplifier *16* incorporated into the interferometer.[239, 240, 248, 250, 312, 313]

The results of studies confirmed that this model can serve as a basis for the construction of commercial detectors. The minimum absorbance detected with this instrument is 2×10^{-10}; the sensitivity is 1000–10 000 times higher than that of conventional spectrophotometers and is 10–100 times higher than that of thermal lens spectrometers; the detection limits are about a few picograms per millilitre; the linear dynamic measurement range is about five orders of magnitude.[239, 240, 248, 250, 312, 313]

The first commercial instrument based on integrated microanalysis systems, *viz*., an ITLM-10 thermal lens microscope (Institute of Microchemical Technology, Japan),[314] was specially designed for applications associated with chemical microchips (Fig. 10). The instrument employs a dual-beam parallel scheme of thermal lens measurements involving an excitation laser with a wavelength of 532 nm (50 mW) modulated with a frequency of 1 kHz and a probe laser with a wavelength of 670 nm (1 mW). A silicon photodiode connected to a lock-in amplifier serves as a detector. The dimensions of the instrument are $650 \times 280 \times 550$ mm and its weight is 25 kg. The provisional price of the instrument equipped with accessories (micropumps, microheaters, *etc*.) is ~ $70 000. The IMT Company (Japan) has designed about 300 modifications of glass and plastic chips for the determination of trace amounts of various substances. This instrument finds an ever increasing use in a combination of thermal lens spectrometry with chemical microchips.[314–319] Models for the simultaneous detection of a thermooptical signal and fluorescence and a portable thermal lens microscope are at the development stage.

III. Fields of application of analytical thermooptical spectroscopy

More than a thousand of papers, several monographs[2–5, 297] and numerous reviews[6–17, 115, 116, 220, 278, 279, 308, 320–322] concerned (in one way or another) with applications of thermooptical spectroscopy have been published. More than half of these publications were devoted to studies in the field of analytical and physical chemistry. Thermooptical spectroscopy has various applications regarding signal recording systems, purposes and subjects of investigation.

Analytical studies of gases by thermooptical methods are scarce.[111, 233, 323–336] Photoacoustic methods prove to be much more convenient, sensitive and fast in studies of gaseous media. Because of this, we do not consider this field of application in the present review. The possibilities of thermooptical methods in the determination of physicochemical parameters and the development of analytical applications are most evident in the analysis of condensed media.

Studies of volume-absorbing solids are limited to transparent substances. An important task is to search for and study new laser active media.[337–348] These studies dealt primarily with the balance between the appearance of fluorescence and the thermal lens effect in the solid matter that generates laser radiation. This problem has been considered in detail in several publications.[17, 320, 349]

1. Stages of the development of analytical thermooptical spectroscopy

There are three stages of the development of thermooptical spectroscopy, each next stage being performed at a higher qualitative level and their role in analytical chemistry being increased.

The publication of the classical study [1] can be considered as the beginning of the first stage. It is characterised by the simplest way of using thermooptical spectroscopy in analytical chemistry. In this stage, the available spectrophotometric procedures were simply extended to the thermooptical detection of absorption. During a long period of time, this approach prevailed, because it combined reliable conventional spectrophotometric procedures and high instrumental sensitivity of thermooptical instruments.[2, 7, 8, 272, 350] Nowadays, more than half of thermooptical procedures for analysis are still based on this approach. This approach is very fruitful both for determining various compounds from their own absorption and in the situation where the detection limit cannot be improved due to instrumental characteristics of a spectrophotometric instrument (Refs 1, 4, 7, 8, 21, 22, 63, 73–82, 272, 273, 295, 350–357).

However, by the late 1980s, evidence showed that the available photometric procedures could not be used for detecting compounds, whose concentrations were 2–4 orders of magnitude lower than those, for which these procedures have been designed.[2, 4, 23–26, 83–87] In addition to a serious problem associated with the purity of reagents, it is necessary to take into account changes in the conditions of complex formation and real redox potentials.[18] These changes can give rise to new side processes, which affect the reaction pathway.[4, 7, 27–38, 87–93] Hence, a demand arose for modifications of spectrophotometric methods. This gave impetus to the second stage of the development of thermooptical spectroscopy, which reached its peak in the early 1990s. The main aim of studies carried out at this stage was to enhance the sensitivity by both modifying chemical systems and optimising the optical set-up of an instrument. At the same stage, researchers began to design combined methods (primarily, chromato-thermooptical methods).[4, 16, 23, 36–40]

The modern stage began in the late 1990s. This stage is characterised by the development of unique applications (not necessarily photometric), which employ the combined influence of laser radiation and thermooptical effects on the system under study. The development of this approach is accompanied by an increase in the fraction of applied combined analytical (chromatographic,[41, 42] kinetic,[43, 44] electrophoretic [45, 46]) and non-analytical (for example, highly precise measurements of flow rates or sizes of colloidal particles [47–49]) methods. Growing interest in this line of investigation is evidenced by a large number of studies (in 2003, it reached a record value) and research groups working in this field (about 76 groups in 25 countries, Fig. 11) as well as by a qualitative change in the aims of studies. In 1986, journals publishing research papers in the field of analytical chemistry contained primarily studies devoted to instrumental characteristics of thermooptical measurements, mathematical processing, *etc*., whereas 75% of present-day publications are devoted to applied aspects (Table 2) and are based on specific features of thermooptical spectroscopy.[9, 13, 16, 50–53] In the following sections, we will try to explain the factors responsible for such substantial changes.

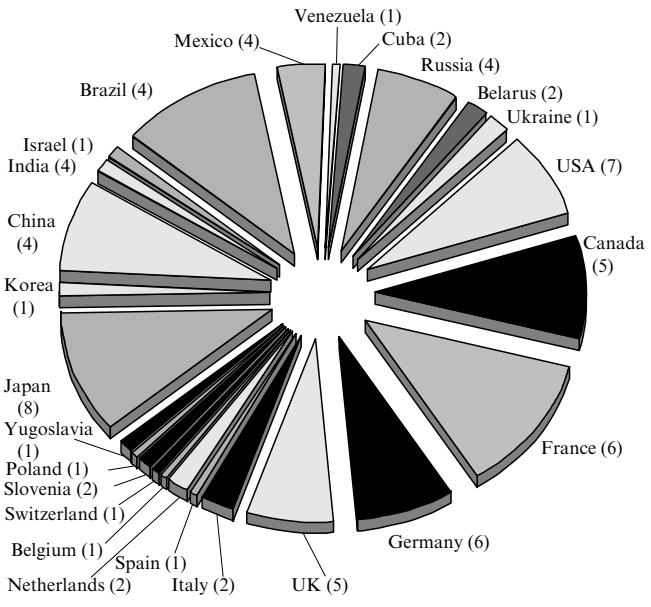

Figure 11. Diagram of the distribution of studies in the field of thermooptical spectroscopy by country in 2002.
The numbers of research groups working with this problem are given in parentheses.

Table 2. Distribution (in %) of studies in the field of thermooptical spectroscopy by main lines of investigation.

Line of investigation	Year		
	1986	1997	2000
Design and optimisation of instruments	39	11	17
Development of methods for analysis	23	41	27
Combined analytical methods	18	22	31
Other applied studies	20	26	25

2. Use of spectrophotometric procedures

Thermooptical spectroscopy allows one to determine optical densities at levels as low as 10^{-8} (see Refs 4–6 and 297). For most compounds, the detection limits are 10^{-10}– 10^{-9} mol litre^{-1} (the absorbance is from $y \times 10^{-7}$ to $y \times 10^{-6}$).[21, 22, 38, 76, 77, 353, 354] Even higher sensitivites (detection limits are from $y \times 10^{-12}$ to $y \times 10^{-10}$ mol litre^{-1}) were achieved in some studies.[355, 356, 358–360] The main advantage of thermooptical methods is the possibility of measuring absorption of ultrasmall amounts of substances in volumes of about $y \times 10^{-15}$–$y \times 10^{-9}$ litre due to small diameters of focused laser beams.[72, 112–116, 167, 189, 191, 239, 261, 321, 322, 361–375] In studies by crossed-beam thermal lens spectrometry, the detection limit of iron(II) involved in the complex with 1,10-phenanthroline was 120 molecules in a volume of 0.2 pl, which was determined by the crossing region of the laser beams in a cell.[356] In addition, a series of recent studies were devoted to the use of thermal lens microscopy in microflow analysis of substances and for the detection in capillary electrophoresis, where the detection limits were as low as zepto- (10^{-21} mol) and yoctomolar (10^{-24} mol) levels (in other words, individual molecules were detected) (Refs 178, 215–227, 296, 325, 376, 377).

Numerous studies were concerned with compounds, which served as models for either estimating the instrumental sensitivity of spectrometers (or signal recording systems),[1, 3, 6, 272, 350–354, 356] or examining the influence of solvents on the thermal lens effect.[1, 73–75, 273, 352–354, 357] For this purpose, the following simple and stable compounds, which are resistant to laser radiation, were chosen: a solution of molecular iodine in carbon tetrachloride,[73, 272, 351, 355, 357, 358, 378] aqueous solutions of presynthesised copper(II) complexes with EDTA [272] and acetylacetone,[77] iron(II) complexes with 1,10-phenanthroline [22, 78, 79, 272, 273, 357] or its analogues [273, 352] and cobalt(II) complexes with 1-(2-pyridylazo)-2-naphthol [77] and ethylenediamine.[73, 351]

Some researchers attempted to apply known spectrophotometric procedures without modifications to thermooptical spec-

troscopy,[22, 26, 85, 108, 354, 356] which led to a decrease in the detection limits, but did not allow the researchers to gain the most benefit from the method. The successive formation of a thermal lens under irradiation at two or more wavelengths made it possible to determine microamounts of compounds, whose maxima of absorption bands differ by 10–20 nm, in the case of their simultaneous presence in the sample.[61, 62, 81]

Thermooptical spectroscopy methods were used for determining various organic compounds, primarily, those containing nitrogen or sulfur.[32–36, 69, 71, 184, 379] In addition to studies of artificial mixtures serving for comparison of different modes of chromatographic separation, several studies were devoted to analysis of natural substances,[21, 26, 36, 37] in particular, to analysis of industrial and household dyes,[306] and examination of the possibility of controlling products of organic synthesis.[25] Studies dealing with the determination of proteins at a level of 1–100 ng[26, 38, 66, 76, 85, 304, 379] and amino acids at concentrations of $y \times 10^{-15}$–$y \times 10^{-12}$ mol litre^{-1} also deserve attention.[108, 301, 380, 381] Procedures were developed for the thermal lens detection of nanogram amounts of particular high-priority biological and medical samples (theophylline,[88, 89] phenols,[382] acetyl choline,[383] *p*-aminophenol[384–386]).

Modifications of the known spectrophotometric procedures taking into account the characteristic features of thermal lens spectrometry is the most rational way of devising analytical thermal lens procedures for the determination of different classes of compounds. In recent years, studies of real substances have become typical of analytical chemistry.

Many studies in the latter field associated with a combination of the thermooptical detection and the known separation and concentration methods are considered below. Here let us mention the following applications of thermal lens spectrometry: the determination of iron(II) in blood plasma using bathophenanthroline at a concentration of $y \times 10^{-7}$ mol litre^{-1};[373] the evaluation of the total concentrations of soluble organic compounds in sea water;[34] the determination of iron(III) and aluminium in natural waters[387, 388] and pesticides in waters, vegetables and food;[389, 390] and the detection of P-, Si-, S- and N-containing compounds in real substances.[54]

Investigations of the characteristic features of the photometric determination of phosphorus and silicon from the formation of heteropoly compounds and application of intracavity thermal lens spectrometry made it possible to detect these elements in various substances (inorganic acids of special purity grade, semiconducting materials, *etc.*) at a level of 50–100 pg ml^{-1}.[2, 24, 86, 87, 298, 353] Procedures were developed for the detection of cobalt, nickel and iron with the use of nitrosonaphthol,[90] dimethylglyoxime[91] and 1,10-phenanthroline.[92] A combination of reliable photometric methods and a universal methodology for devising thermal lens procedures made it possible to achieve the detection limits of 0.2–10 pg ml^{-1} and the quantifiable concentration ranges from 3 to 5 orders of magnitude.

The development of a methodological basis of measurements, a consideration of thermodynamic and kinetic factors, which affect the selectivity and sensitivity of the detection and minimisation of test experiments substantially improve the metrological characteristics of thermal lens procedures for the detection of various compounds.[228, 229, 232, 274, 276, 283, 382, 391–406] These procedures were used for determining molybdenum[27] and copper[401] in sea water, cobalt,[90] nickel[91, 93] and iron[92, 93] in highly pure water, bismuth[28] and cobalt[90, 93] in highly pure metals and nickel in nickel-containing heteropoly compounds, which are used as active compounds in chemical sensor elements for the detection of ammonia in the atmosphere.[407] The use of thermal lens spectrometry allows one to reduce the number of stages of analysis of heteropoly compounds and increase the accuracy of the determination of nickel.

In recent years, new possibilities of thermooptical spectroscopy have attracted considerable attention. Besides, pioneering studies were carried out within the framework of conventional photometric experiments. For example, the advantages and drawbacks of photometric thermooptical measurements compared to classical spectrophotometric measurements were considered by researchers from the University of Lyon (France) (Refs 9, 57, 364, 367, 371, 373, 408–411). In addition to high instrumental sensitivity, thermooptical spectroscopy is characterised by having a substantially smaller dependence on light scattering and the possibility of detecting trace amounts of elements in samples. It should be noted that a photothermal spectrum does not coincide with the corresponding classical absorption spectrum (in particular, in the case of rare-earth metals),[412] which provides the basis for developing more selective and sensitive procedures for the detection of trace amounts of compounds. For example, procedures were designed to detect uranium(VI), neodymium(III) and praseodymium(III) at a level of 10^{-6}–10^{-5} mol litre^{-1} (Refs 24, 30, 413, 414).

Procedures for the determination of trace amounts, which cannot be used within the framework of conventional spectrophotometry (for example, for the determination of metals inolved in aqua complexes), deserve attention.[29, 43, 77, 86, 87, 353, 357] Studies devoted to thermal lens techniques for the detection of individual rare-earth metals and their mixtures[30, 31, 62, 70, 80] are of most interest. In this case, virtually no additional sample preparation is required, because absorption bands of aqua complexes of rare-earth metals are rather narrow, due to which they can be selectively determined in soils,[30] waters[80, 81] and uranium fuel[70] at a level of $y \times 10^{-7}$–$y \times 10^{-6}$ mol ml^{-1}. Dual-beam thermal lens spectrometry made it possible to determine the composition of a mixture of neodymium and erbium involved in aqua complexes at a level of $y \times 10^{-4}$ mol ml^{-1} against the background of a 50-fold excess of nickel glycinate.[62]

Accumulation of thermal energy in the sample under study was demonstrated to play an important role in the thermal lens detection of trace amounts of compounds, which adversely affect the accuracy of the determination.[32] Hence, it is necessary to optimise the set-up of a thermal lens spectrometer compared to the set-up of model measurements to provide the best sensitivity and reproducibility of thermooptical measurements of real samples.[32]

In recent years, successful attempts were made to extend the range of samples investigated by thermooptical spectroscopy. Procedures for the photometric determination of pyrogenic endotoxins from the main functional regions of their molecules (polysaccharides, lipids, the core region) were applied to the thermal lens detection of a total concentration of endotoxins in Pyrogenal and in an endotoxin sample from *E.coli* 0113 : H10, which is used for standardisation of biological assays. The detection limit of lipopolysaccharides is 70 ng ml^{-1}, which is comparable to the sensitivity of biological assays.[415–417] Let us also mention a method for the simultaneous evaluation of the concentration of hydroxy groups, the temperature and flow rate in the flame from the data of one experiment using thermooptical deflection spectroscopy,[418] where other methods do not work.[418]

a. Selectivity change

It is known that an increase in instrumental sensitivity imposes heavier demands upon the sample preparation. This problem, which is associated primarily with non-selective absorption, is typical of all highly sensitive methods. Hence, it is of first importance that the reagents and solvents be pure and the signal of the test experiment be low. However, a change in the reaction conditions in going to nanogram amounts of the reagents can lead to a substantial increase in selectivity of the thermal lens detection compared to the spectrophotometric method.

Let us consider several examples. It is known that the results of the spectrophotometric determination of bismuth by the iodide method are most affected by lead, tin, copper and antimony,[419–422] because poorly soluble iodides and sulfates of these elements are formed under the reaction conditions. The thermal lens detection of bismuth proved to be much more selective. Under new conditions, precipitates of poorly soluble compounds

are not formed and the selectivity is determined by absorption of metal iodide complexes.[423–425] The adverse effect of copper(II) on the determination of bismuth by the thermal lens method is much weaker than that in the case of spectrophotometric measurements and is manifested at concentrations four times as high as those in the case of monovalent copper ions. This effect can be due to the fact that the formation of copper(II) sulfate complexes cannot be ignored in dilute solutions containing sulfuric acid at a concentration of 0.02 mol litre^{-1}. These complexes inhibit reduction of copper(II) with iodide but do not hinder the detection of bismuth. Therefore, copper(II) is masked, which is manifested only in the determination of trace amounts of bismuth by the thermal lens technique.[403] The hindering effect of nickel, which is observed in the case of determination of iron with the use of 1,10-phenanthroline, also vanishes in going from micro- to nanogram concentrations of the reagents. This could be attributable to the fact that the nickel(II) complex is inert and is not formed in a sufficient amount during the sample preparation (20–25 min) at a level of $y \times 10^{-7}$ mol litre^{-1}.[392]

b. Sensitivity change

It is commonly assumed that sensitivity characteristics (detection limits, lowest quantifiable concentrations) depend primarily on the instrumental sensitivity of a thermooptical spectrometer (the laser radiation power and geometry of the optical scheme) as well as on the thermooptical characteristics of the medium [see Eqn (9)].[2, 4, 58, 276–279] However, a change in chemical interactions with decreasing concentration can enhance the sensitivity of the thermooptical determination of compounds in trace amounts.

For example, the lowest concentration of bismuth detectable by spectrophotometric and thermal lens techniques is 600 and 0.5 ng ml^{-1}, *i.e.*, the sensitivity increases by a factor of 1200.[18, 403] The thermal-lens enhancement factor E_0 is 160. The relatively low sensitivity of the spectrophotometric determination could be attributable to the fact that in the vicinity of the determination limit, an excess of potassium iodide is oxidised with atmospheric oxygen to form free iodine, which impairs the measurement reproducibility. In thermal lens measurements (because there is a large excess of ascorbic acid and a smaller amount of iodide), this fact can be ignored.[403]

The sensitivity of thermal lens measurements is additionally increased due to an increase in the degree of completeness of the analytical reaction at nanogram level. The real sensitivity coefficient of the thermal lens determination of phenols with the use of the azo-coupling reaction with *p*-nitrophenyl diazonium[382] increases by a factor of $\sim$100 compared to the spectrophotometric determination, and calculations according to Eqn (9) give an increase by a factor of 35–40. This is associated with the fact that the azo-coupling reaction is not completed under the conditions of spectrophotometric measurements (0.5 mg ml^{-1} of *p*-nitrophenyl diazonium, 0.1–1 μg ml^{-1} of the phenol); the yield of the product is $\sim$50%. Under the conditions of thermal lens measurements (0.01 mg ml^{-1} of *p*-nitrophenyl diazonium, 1–10 ng ml^{-1} of the phenol), the reaction is completed by 95%–99%, because the sensitivity of the determination is additionally increased by a factor of two.[382]

3. Determination of the fundamental characteristics of reactions at trace levels of components

A decrease in the concentration level of the reacting components is accompanied by a substantial change in the reaction conditions and different analytical effects.[27, 28, 32–36, 69, 71, 88–93, 184, 379, 400] This fact can be used for determining the reaction parameters, such as stability constants, acid dissociation constants, *etc*. It should be noted that measurements are carried in substantially more dilute solutions compared to those used in conventional spectrophotometry, which provides better measurement reproducibility.

Data on the thermodynamics and kinetics of the complex formation of nano- and picogram amounts of transition metal complexes with 1,10-phenanthroline, dioximes and diethyl dithiocarbaminates were collected based on the results of thermal lens experiments.[403–407, 426] The methods were developed for calculations of the overall and stepwise stability constants, characteristic rate constants, molar absorptivities (including those of intermediate complexes), acid dissociation constants and other characteristics obtained from thermal lens experiments.[18, 392, 403–407, 426] These studies showed that stability constants determined by thermal lens spectrometry have a higher accuracy, their values being one–two orders of magnitude lower than the stability constants determined by conventional spectrophotometry and potentiometry. When evaluating the stability constants by thermal lens spectrometry, one must take into account the changes in the kinetic characteristics of the reaction under study when changing from micro- to nanogram concentrations of the reacting components.[405, 406]

Thermal lens spectrometry provides a possibility of determining stepwise complexation constants (at concentration levels of components of $y \times 10^{-6}$–$y \times 10^{-8}$ mol litre^{-1}) in systems, where conventional methods do not work.[401, 402] In particular, the characteristic features of the complex formation in the bismuth(III)–iodide system can be judged at nanogram level from the stepwise stability constants evaluated by thermal lens spectrometry. In the case of copper(I) bis(1,10-phenanthrolinate), the stepwise stability constants can be determined by thermal lens spectrometry in more dilute solutions (large relative excesses of a competitive ligand, *viz*., acetonitrile, without changes in the composition of the medium).[401]

4. Kinetic applications

One of the modern trends in the development of thermooptical spectroscopy is the combination of thermooptical, kinetic and catalytic methods of analysis.[43, 44, 376, 427–447] The main advantage of this combination is the formation of a selective chemical analytical signal and its highly sensitive thermooptical detection. Also, the kinetic measurements have better reproducibility compared to stationary thermooptical measurements, because the accuracy of the determination is substantially improved.[44, 432] Another advantage of thermooptical spectroscopy is that it can be used for both the analytical determination and calculation of the kinetic constants.

Studies of the kinetics of interaction of metal ions with natural ligands (fulvic acids, humic acids, zeolites) and various photometric reagents in the presence of these natural ligands are among the most interesting applications.[387, 388] In these studies, procedures were designed for the determination of submicrogram amounts of copper, nickel, iron and aluminium in natural waters. These studies examined also the fundamental parameters of chemical interactions of the components in complex systems at trace levels. In particular, thermal lens spectrometry was used for measuring the characteristic rate constants with an accuracy of $\pm$0.001; the total absorbance change in the system was $>$0.003. The influence of light scattering on the thermooptical determination of metals and organic compounds was demonstrated [388] to be substantially smaller than that in classical photometric experiments. Studies of the reaction mechanisms of iron(II) tetrakis(4-sulfonatophenyl)porphyrin with carbon monoxide by photothermal deflection spectroscopy and the development of a procedure for the determination of carbon monoxide in biological samples[448] are interesting applications of thermooptical spectroscopy. The characteristic rate constants and activation enthalpies of the reaction were evaluated.

It should be emphasised that thermooptical spectroscopy can be used for studying both processes with very low quantum yields of fluorescence and processes characterised by substantial fluorescence of the products or reaction components. In the latter case, the results of thermooptical experiments supplement data

from luminescence spectroscopy, which allows one to characterise the reaction mechanism in much more detail and develop procedures for the simultaneous determination of several compounds in one experiment.[399] Undoubtedly, the main application of thermooptical spectroscopy is its use for enhancing the sensitivity of kinetic methods. The determination of nitrite ions and nitrate reductase by single-laser thermal lens spectrometry (argon laser, 514.5 nm, 800 mW) in an aqueous medium with a detection limit of 9 pg ml^{-1} (9×10^{-10} mass%) deserves attention.[43, 449] Compared to spectrophotometry, the detection limit was reduced by a factor of 20. The conditions of the thermal lens determination of *p*-aminophenol in paracetamol samples provide a detection limit of 100 ng ml^{-1}, which is an order of magnitude better than that obtained in most spectrophotometric and chromatographic procedures. Dual-beam kinetic measurements of a thermal lens signal (the excitation argon ion laser, 514.5 and 457.9 nm, 30 mW; the probe helium neon laser) were used for analysing binary gaseous mixtures.[61] The selectivity is provided by measuring the ratio of signals obtained at different wavelengths. The study,[442] in which the concentrations of heavy metals were determined in ancient animal remains, is yet another illustration of the possibilities of thermooptical spectroscopy.

The iron(II) complex with 1,10-phenanthroline (ferroin) is widely employed as a catalyst in the Belousov–Zhabotinsky oscillatory reaction.[450, 451] Bromide selective electrodes are most often used for monitoring the course of the oscillatory process.[452, 453] The bromate Belousov–Zhabotinsky oscillator, which was created on the basis of malonic acid as an organic substrate and iron(II) 1,10-phenanthrolinate as a catalyst and an indicator of the reaction pathway, was investigated.[391] The dependence of the physicochemical parameters of the reaction (the oscillation period, the lifetime of the system) on the starting concentrations of the reagents and the effect of additives of inhibiting ions on the system were examined. Under new conditions, the oscillation amplitude was demonstrated to increase compared to the oscillation amplitude under the conditions of spectrophotometric studies due to an increase in the fraction of ferroin involved in the reaction (the overall concentration of iron decreases), and the reproducibility of the oscillation period is improved.[391] The kinetics of the Belousov–Zhabotinsky reaction can be reliably monitored by thermooptical spectroscopy at iron concentrations of $y \times 10^{-6}$ mol litre^{-1} (which is impossible in studies using of most other procedures [454]), and the oscillation period can serve as an analytical signal.[391]

In recent years, a number of studies concerned with analytical applications of thermooptical spectroscopy have investigated of the enzyme kinetics. For example, a thermooptical biosensor for pesticides was designed on the basis of acetylcholine esterase.[389, 390] As a result, the time of analysis of organophosphate pesticides (paraoxon, chlorpyrifos, diazinon) and carbamate pesticides (carbaryl, carbofuran) was decreased to 15 min. The detection limits of pesticides were $y \times 10^{-7}$–$y \times 10^{-5}$ g litre^{-1}. The thermal lens method for the determination of pesticides was demonstrated to be rather inexpensive and does not require thorough sample preparation even for such complex substances as agricultural cultures.[390] In the study,[273] thermal lens spectrometry was used in combination with the enzymatic kinetic determination of dopamine with polyphenyl oxidase.

On the whole, the above examples demonstrate that a combination of thermooptical spectroscopy with kinetic methods of analysis holds promise. Particular new methods can be characterised as kinetic methods coupled with the thermooptical detection. In these methods, a detector plays a passive role. In applications which are not limited to the thermooptical detection of absorption, combinations of kinetic and thermooptical methods show unusual possibilities due to the use of thermooptical effects rather than their consequences (absorbance measurements). For example, new signals allow one to solve problems, which are otherwise impossible to solve.

In the diagram showing formation of analytical signals presented in Fig. 12, the following three groups of sources of analytical information can be distinguished: (1) photometric [the formation of coloured products, a usual slope (α) of the initial region of the kinetic curve]; (2) thermooptical (changes in the thermooptical characteristics of the medium, convective oscillations, auto-acceleration of coagulation of colloidal products); (3) sources directly dependent on laser radiation (temperature effects, photoinduced effects, *etc*.). For example, we can go from simple photometric thermooptical measurements, which are described by the equation,

$$\vartheta(c) \propto A\,(c), \tag{18}$$

to

$$\vartheta(c) \propto E_0(c)A(c), \tag{19}$$

where the factor $E_0(c)$ [see Eqn (9)] reflects the dependence of the thermooptical properties of the sample on the concentrations of the reaction products. Hence, $\mathrm{d}E_0(c)/\mathrm{d}t$ is a new analytical signal.

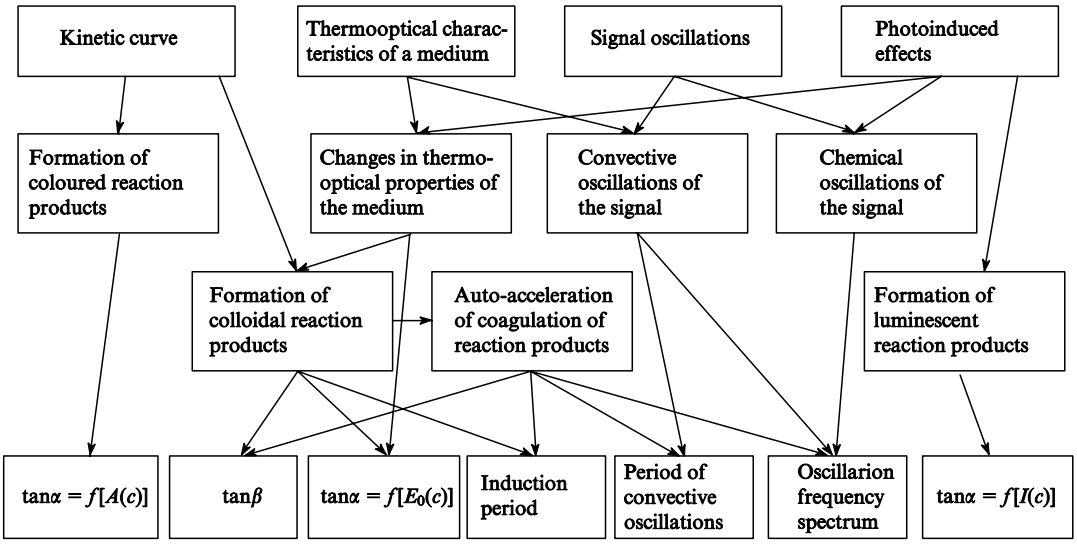

Figure 12. Scheme of formation of analytical signals in the kinetic thermal lens detection.
A is absorbance, α, β are slopes of kinetic curves.

In some cases, the thermooptical sensitivity $E_0(c)$ plays the major role. In particular, the spectrophotometric detection is inapplicable to the simultaneous determination of resorcinol and pyrocatechol by oxidation of bromate ions, because the molar absorptivity of the reaction products of resorcinol is no higher than 500 litre mol^{-1} cm^{-1}. Under the same conditions, the thermal-lens kinetic curves are characterised by good reproducibility and the detection limit of resorcinol in the absence of pyrocatechol is 5×10^{-5} mol $litre^{-1}$. Calculations showed that the factor $E_0(c)$ makes the major contribution to an increase in sensitivity of thermal lens measurements: the rate ratio $E_0(c)/dt : dA(c)/dt$ is 25 : 1. Therefore, the enhancement of sensitivity of thermal lens spectrometry due to changes in the thermooptical properties of the medium makes it possible to determine compounds, which cannot be detected by spectrophotometric methods.[283, 398, 399] In the case of the purely thermooptical detection, the kinetic equation takes the form

$$\vartheta(c) \propto E_0(c)A, \qquad (20)$$

where A = const. In other words, the equation is true if the reaction products do not absorb at the wavelength of the exciting radiation, and only thermooptical characteristics of a sample vary in the course of the reaction. In this case, the sensitivity of thermal lens measurements is provided by the addition of inert absorbing compounds. The range of compounds determined by kinetic methods can be substantially extended.

It was demonstrated that certain effects (changes in the thermooptical characteristics, auto-acceleration of coagulation of colloidal solutions of the reaction products in the region of thermal lens formation, a change in the period of convective oscillations of the thermal lens signal, *etc.*) can be used for determining the reaction components at trace levels. Components of mixtures can be determined by thermal lens spectrometry simultaneously (unlike spectrophotometric methods) due to the appearance of new analytical signals. In spite of an obvious complication of the system, the sensitivity of thermal lens measurements increases with no sacrifice in reproducibility.[384, 398]

Kinetic thermal lens measurements are used for measuring spectra of intermediate states. The changes in the enthalpies of the ketone and enol forms of 7-hydroxyquinone were evaluated by thermal lens spectrometry. The enol form was demonstrated to prevail in the ground state, whereas the ketone form prevails in the excited singlet state.[455] The quantum yield of the formation and the lifetime of the triplet state of pyridine in the liquid phase were measured [456] under two-photon excitation. In both cited studies, information was extracted from the analysis of the fast and slow components of the thermal lens signal after laser pulse absorption. The absolute quantum yield and the lifetime of singlet molecular oxygen sensitised by haematoporphyrin in ethanol were also estimated from the analysis of these components.[457]

Specific effects, which are directly associated with the nature of the thermal lens effect and, primarily, with the changes in the thermooptical and colloidal properties of the medium, are manifested in thermal lens measurements performed in systems involving an oxidiser (bromate or periodate ions), an organic reducing agent (aromatic amines or phenols), a catalyst (vanadium ions) and an activator (phenols, hydroxy acids).[458]

To conclude of this section, let us consider the kinetic effects observed only in thermal lens studies of known analytical reactions. Investigations of the stability of transition metal complexes with 1,10-phenanthroline by thermal lens spectrometry showed that the rate of formation of the iron(II) complex with 1,10-phenanthroline at pH 0–2 decreased substantially,[392] which was not observed in spectrophotometric studies.[459] Even more substantial differences in the results were found in studies of stability of iron(II) tris(1,10-phenanthrolinate) by thermal lens spectrometry and spectrophotometry. In spectrophotometric studies, the pH range for the formation of the complex coincides with the pH range of its decomposition, whereas at iron concentrations of $y \times 10^{-7}$ mol $litre^{-1}$ the complex decomposes at pH 1 only after one day, which differs from dissociation of ferroin at a concentration of $y \times 10^{-5}$ mol $litre^{-1}$.[460–462] A change in kinetic stability of the iron(II) complex with 1,10-phenanthroline at low pH can have an analytical application. Since the iron(III) complex is formed in an even more alkaline medium,[463] iron(II) can be determined in the presence of iron(III).

5. Use of thermooptical methods in flow analysis, high-performance liquid chromatography and capillary electrophoresis

Thermooptical spectroscopy holds considerable promise and is finding rapidly increasing analytical use for detection in HPLC, capillary electrophoresis, continuous flow and flow-injection analysis. The main advantage of this approach is the possibility of combining selective separation of the analyte components and their highly sensitive non-destructive detection in one instrument.

A large number of studies were devoted to the coupling of thermal lens spectrometry with HPLC (Refs 4, 6, 23, 36–43, 49, 106–111, 178, 377–379, 393, 408, 409, 464–480), capillary electrophoresis (Refs 45, 46, 112–116, 310, 311, 380, 381, 481–504) and various modes of flow-injection analysis.[73, 117, 389, 394, 395, 444, 505–510] Several reviews have dealt with these problems.[8, 10, 23, 84, 115, 220, 468, 471]

a. Flow analysis

Flow-injection analysis is an important area of application of thermal lens spectrometry.[73, 117, 394, 444, 505, 507–509] No universal detectors were designed for this analysis, and the choice of the detection method depends primarily on the purpose of a particular investigation. In flow-injection systems, the flow rates are generally 1–5 ml min^{-1}. In these experiments, peristaltic pumps are used instead of plunger pumps, which are employed in HPLC. Hence, noise, which is caused by flow pulsations and masks the thermooptical effect, is the most serious problem associated with the use of photothermal detectors. Nevertheless, due to the highly sensitive detection of absorption in automated analysis of solutions, thermooptical spectroscopy can be considered as one of the most promising detection methods in flow-injection analysis.

Models of changes in the thermal lens signal under flow conditions were proposed.[56, 58, 73, 78, 297] The thermal lens method was devised for the flow determination of Cu(II), Co(II), Fe(III), Bi(III), Nd(III), Pr(III), Al(III), Cr(III), Mn(II), Zn(II) and Pb(II) by the reaction with Xylenol Orange at pH 4.5 in aqueous solutions.[394] The influence of the reactor length and its temperature on the sensitivity and reproducibility of measurements was examined. The detection limits are $y \times 10^{-7}$ mol $litre^{-1}$, the quantifiable concentration ranges are $\sim$1.5 orders of magnitude.[394, 395] The absorbance can be measured in flow up to 1×10^{-6} using a dual-beam scheme (argon laser, 458 nm, 100 mW).[58, 59] The detection limit achieved in the colorimetric determination of iron(II) as a complex with 1,10-phenanthroline was 40 pg of iron in 100 μl of a sample at a flow rate of 0.5 ml min^{-1}. Organic dyes were detected at levels of $y \times 10^{-7}$ mol $litre^{-1}$ by flow-injection analysis coupled with photothermal refraction spectrometry.

b. High-performance liquid chromatography

A large number of combined analytical procedures employ thermooptical methods and HPLC. Universal spectrophotometric methods are widely used for detection in HPLC. In this case, the sensitivity is determined by the optical path length in a detector cell. The sensitivity of such detectors decreases substantially in going to capillary and microcolumn chromatographic systems. If a capillary is several micrometers in length, a conventional photometric detector actually does not work.

On the whole, thermooptical spectroscopy works well in HPLC. The main advantages of this method, *viz.*, high sensitivity and a small detectable volume, have been exploited in the majority of liquid chromatographic methods. As a rule, photothermal detectors decrease the detection limits by two–three orders of

magnitude compared to analogous methods employing the spectrophotometric detection.[11, 16, 58, 297]

A dual-beam optical scheme of thermal lens measurements with a coaxial arrangement of the excitation and probe beams in a detector cell is successfully employed in high-performance liquid chromatography. This method was used for determining various organic and inorganic compounds.[11, 389, 468, 469, 475, 505, 506, 511, 512] The sensitivity achieved in ion chromatography is more than three orders of magnitude higher than that of the photometric detection.[312, 313]

An attempt was made not only to create a model of a thermooptical detector for HPLC but also to devise algorithms of data collection and processing which are specific for the conditions of thermooptical detection in chromatography.[312, 313, 393, 397, 513] The optical set-up of a thermal lens spectrometer was optimised taking into account expert estimates,[274] according to which a substantial gain in spectrometer sensitivity is achieved for all optical schemes.

Most studies performed by thermal lens spectrometry coupled with HPLC were devoted to analysis of organic compounds. A combination of HPLC with the thermal lens detection was used to detect amino acids,[108, 474] nitro derivatives of aromatic compounds,[378, 514, 515] catecholamines[478, 479] and carotenoids (Refs 408, 475, 511). Thermal lens spectrometry, photothermal refraction spectrometry and other thermooptical methods are employed for constructing detectors for chromatographic analysis of organic compounds. The thermooptical detection in capillaries gives better results compared to those obtained with the use of standard cells due to the absence of liquid turbulence in the detection region. Dabsyl derivatives of amino acids were detected by reverse-phase HPLC coupled with photothermal refraction at a level of 10^{-15} mol litre^{-1}. In addition, thermooptical detectors are employed in analysis of dye compositions and for the quality control of products of industrial organic synthesis.

The detection of inorganic compounds has been studied less. After separation, cobalt(II), copper(II), manganese(II), nickel(II), iron(III), zinc(II) and lead(II) cations were determined by ion chromatography according to the post-column reaction with 4-(2-pyridylazo)resorcinol.[516] The influence of noise from a flow reactor on fluctuations of the thermal lens signal was examined.[517] A method was proposed for the determination of trace amounts of elements by HPLC coupled with the thermal lens detection. Procedures were developed for the detection of neodymium and uranium at nanogram levels.[518] Double-beam thermal lens spectrometry was used for detecting chromium(III) and chromium(VI).[42] In this case, pre-column derivatisation of chromium(III) with pyridine-2,6-dicarboxylic acid and of chromium(VI) with diphenylcarbazide was used. The detection limits of chromium(III) and chromium(VI) were 30 and 0.3 ng ml^{-1}, respectively.[42, 512, 519]

Various modifications of the thermal lens technique were used in combination with capillary liquid chromatography.[149–153, 184, 409, 473, 476, 477] In this mode of HPLC, crossed-beam thermooptical systems (photothermal refraction and mirage spectroscopy) are generally used for the detection. A prerequisite to the use of such systems in capillary liquid chromatography is the possibility of measuring the thermooptical characteristics of samples of very small volumes (as small as $y \times 10^{-9}$ litre). This method was used for detecting amino acids as dabsyl derivatives at femtomole levels (10^{-15} mol).[108] Other thermooptical spectroscopy methods were also employed in capillary liquid chromatography. For example, nitropyrene and dinitropyrenes were determined with the use of a pulsed photothermal refractometer as a detection system.[379]

In spite of the large number of studies devoted to applications of thermooptical spectroscopy in HPLC, there are no universal combined methods. Studies dealing with the complex and comprehensive examination of the possibility of combining HPLC with thermooptical detection methods are scarce. Nevertheless, taking into account the characteristic features of both methods,[112–117, 377, 464–467, 469, 472, 475, 480] their combination would be expected to provide a basis for devising a new analytical method.

Thermooptical methods are also used for the highly sensitive detection required in thin-layer chromatography.[33, 500, 520] A photothermal detector for this chromatographic method was constructed on the basis of the mirage effect induced by pulsed laser radiation.[33]

c. Capillary electrophoresis

Nowadays, thermooptical spectroscopy is being extensively employed as a detection method in capillary electrophoresis.[108, 115, 116, 297, 301, 310, 380, 381, 473, 481–491, 493, 496–500] This combined method has a wide application in the detection of amino acids.[108, 116, 301, 380, 381, 482–488] The determination of amino acids as their dabsyl derivatives at a level of 10^{-12} mol litre^{-1} was described.[380] Unlike HPLC and flow analysis, not all detection methods are suitable for this separation method. Thermooptical methods (thermal lens spectrometry, photothermal refraction spectroscopy and the thermal prism method) are among the best detection methods in capillary electrophoresis. After the reaction with 4′-(dimethylamino)azobenzene-4-sulfonyl chloride, amino acids were determined at a level of several attomoles by probe capillary electrophoresis coupled with the thermooptical detection.[381, 501] Twelve amino acids were determined using the thermooptical detection during 13.5 min.[496] The detection limits were $\sim 10^{-7}$ mol litre^{-1} (or 100 fg in an injected volume of 0.6 nl). The authors of the cited study emphasised that the linearity range was substantially larger than that achieved in the spectrophotometric detection and covers more than four orders of magnitude. In the study,[521] traces of amino acids (tryptophane and phenylalanine) were detected without derivatisation at a level of tens of femtomoles by the photothermally induced capillary vibration method at the second harmonic wavelength of an argon ion laser (257.2 nm, 5 mW). In this study, the results of determination of vitamin B_2 were also reported; the detection limit at the excitation wavelength (476 nm) was 80 attomoles (the absorbance was 1.8×10^{-7}), which is three orders of magnitude larger than the detection limits reached with the use of alternative methods for absorption measurements.[521]

Methods of thermooptical spectroscopy are employed also for the detection of other organic and biologically active compounds, such as components of food additives,[466] proteins,[486] nucleotides,[485] metabolism products[492] and pesticides.[243] It should also be noted that thermooptical spectroscopy was used to determine the sequences of amino acids in DNA, peptides, *etc*.[522] In recent years, a number of studies were devoted to the determination of drugs, primarily, of antidepressants.[310, 523]

Methods of thermooptical spectroscopy are widely used also in inorganic analysis, for example, for the simultaneous detection of cations and anions (involved in coloured compounds) at levels of 10^{-12}–10^{-10} mol litre^{-1}.[493] In analysis of real samples, thermal lens spectrometry in the near-field region was employed for the determination of iron and nickel using 1,10-phenanthroline[311] and bathophenanthroline,[524] respectively. For iron, the detection limit was 4×10^{-8} mol litre^{-1}.[310]

As demonstrated above, the main processes attendant on the formation of thermooptical elements (heat transfer and the formation of the temperature profile of the refractive index) are directly related to the thermooptical characteristics of the medium (thermal conductivity, heat capacity, the temperature gradient of the refractive index). Changes in the latter provide the possibility to control the signal. For example, the sensitivity of thermal lens detection in capillary electrophoresis using an aqueous-acetonitrile mixture or an aqueous-methanolic mixture increases by an order or half-order of magnitude, respectively, compared to that achieved in the case of aqueous buffer solutions. The experimental data agree well with the results of calculations. Under the above-considered conditions, the detection limits of a number of organic compounds (phenol and aniline derivatives) are 10^{-8}–10^{-7} mol litre^{-1}.[310]

6. Microanalytical systems

A recent trend is to miniaturise instruments and equipment for chemical analysis and integrate all stages of analysis (sampling, sample preparation, separation, concentration processes, analytical reactions and measurements of an analytical signal) in one small (supercompact) device. Presently, such devices (called 'microanalytical systems' (micro-Total Analysis System, μTAS) or 'laboratories on a chip') are used for solving various problems of analytical chemistry, biochemistry, synthetic chemistry and biotechnology.[220,525] Chemical microchips are generally constructed with the use of state-of-the-art microtechnologies, and they often have a planar geometry. Glasses, quartz, various plastics, silicon and (more rarely) metals serve as materials for microchips. As a rule, a microchip scheme includes reservoirs for reagents, reaction circuits or microvessels, microcolumns or capillaries and communications with linear sizes of $y \times 10^{-9}$–$y \times 10^{-4}$ m.[232,443–445] In addition, micropumps, voltage sources and electrodes can be integrated into a microchip.[525] In some cases, a detector is also integrated into a microchip, although a microchip contains only a detection zone (generally optical) and an interface equipped with an external detector.[525]

A consequence of miniaturisation of analytical detection systems and their integration in a single device is a decrease in the volumes of samples (to $y \times 10^{-10}$ litre), reagents, solvents and wastes (to $y \times 10^{-6}$–$y \times 10^{-7}$ litre) and reduction of the analysis time compared to conventional analytical instruments. In addition, the principal distinguishing features of chemical microchips are that they differ (compared to macrosystems) in the conditions of heat and mass transfer and separation in microchannels, which provides the possibility to construct unique analytical devices and devise new procedures.

Due to a tendency to combine advantages of microchips (integration, compactness, the possibility of using the modern achievements of flow-injection analysis, capillary electrophoresis, HPLC, *etc*.) and detection by thermooptical spectroscopy (sensitivity, locality, high response rate), many studies devoted to microchips were performed with the use of thermooptical spectroscopy (Fig. 13), and the detection limits were declared to be several molecules or tens of molecules.[219,224,325,376,377]

The main fields of application of integrated microanalysis systems are as follows: (1) analytical chemistry (immunoassay methods, capillary electrophoresis, flow-injection analysis, extraction processes, enzymatic catalysis); (2) synthetic chemistry (transfer reactions at the liquid–liquid interface, influence of thermal, electrical and magnetic fields on reactions in microchannels, polymerisation); (3) studies in the field of cell biochemistry. Photothermal deflection spectroscopy, thermal lens microscopy and wavelength-tunable thermal lens microscopy are employed as the main instrumental approaches. The major achievements are associated with the detection of individual molecules, studies of the nanospace and spectroscopy of the liquid–liquid interface. Let us illustrate the above with typical example.

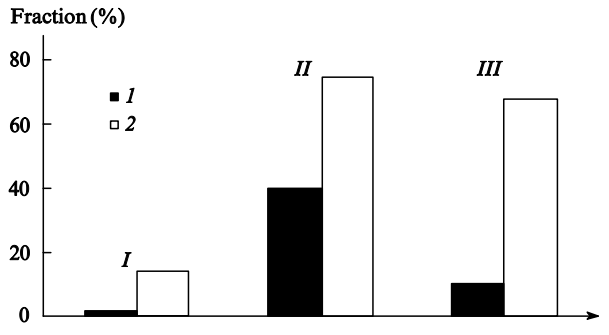

Figure 13. Distribution of studies in the field of thermooptical spectroscopy using macro- (*1*) and microsystems (*2*).
I — applied spectroscopy, *II* — analytical chemistry, *III* — commercial studies.

Methods of thermal lens microscopy were used in microflow-injection analysis of L-ascorbic and dehydroascorbic acids by reduction of iron(III) in the presence of 1,10-phenanthroline[228] and analysis of epinephrine and other catecholamines by their oxidation with sodium periodate.[526] The detection limit of ascorbic acid was 1×10^{-7} mol litre^{-1} (the absolute quantifiable amount of the compound was 3×10^{-20} mol), which is at least one-and-a-half orders of magnitude lower than the determination limit of this acid by capillary electrophoresis coupled with the electrochemical detection[527] and surpasses the known pharmacological method in sensitivity.[528] The procedure was used to determine ascorbic acid in urine and pharmaceutical samples.[228] The sensitivity of detection of catecholamines was as high as $y \times 10^{-6}$ g litre^{-1}, which allows one to use microflow analysis coupled with the thermooptical detection in clinical analysis. The method was employed for the determination of epinephrine, norepinephrine, dopamine and L-dopa in injection samples.[526]

An integrated microanalysis system equipped with a thermal lens detector and an additional IR laser was used for the rapid monitoring of enzyme reactions in flow.[444] Photothermal heating of a liquid flow in a small volume (5 nl) made it possible to heat and cool analyte solutions at rates of 50–60 K s^{-1}, which are an order of magnitude higher than that achieved in conventional heaters and 3–6 times higher than the heating rate of electrothermal microheaters. In enzyme reactions of hydrogen peroxide with 4-aminoantipyrine and *N*-ethyl-(*N*-oxy-3-sulfopropyl)-*m*-toluidine in the presence of horseradish peroxidase, the concentration of substrates can be determined by the thermooptical techniques with a time resolution of 0.6 s at a level of $y \times 10^{-4}$ mol litre^{-1}. In this case, the formation of reaction products depends completely on heating the flow with an IR laser beam and can be determined with high reliability.[444] The minimum reaction volume and the minimum quantifiable amount of the reaction products are 10 nl and 100 fmol, respectively.[445]

A microsystem equipped with a scanning thermal lens microscope deserves attention.[529] This microsystem was employed to study processes in a cell *in vivo*. It should be noted that nonfluorescent reagents can be used, and the detection does not require markers. The spatial resolution of the instrument is 1 μm, and the minimum absolute quantifiable amount of a compound (cytochromes in mitochondria) is 10^{-22} mol.[529]

A microimmunoassay analysis system coupled with the thermooptical detection was used for determining the oncofetal antigen, which serves as a marker of pancreatic cancer.[222] A specially designed microchip, was partially filled with polystyrene granules containing immobilised antibodies to this antigen. A sample of blood plasma with the marker under investigation and a solution containing free antibodies and antibodies immobilised on colloidal gold particles were passed through a microchannel. An interaction gave rise to complexes of the antigen with three antibodies immobilised on the surface of granules, whose concentration was measured on a thermal lens microscope. The determination limit of the oncofetal antigen was an order of magnitude lower than the limit achieved in an immunoassay (ELISA).[530] The results obtained in clinical tests were in good agreement with the results of the determination of the antigen by conventional methods. Analogously, an immunoassay combined with the thermooptical detection on chemical microchips was used for determining human immunoglobulin in blood[446] and gamma interferon.[481] In these experiments, the analysis time was halved due to the use of microanalytical systems. The time of determination of the oncofetal antigen was reduced from 24 to 1 h. In all cases, the detection is characterised by very simple procedures, which are presently under clinical tests.

The possibilities of thermal lens spectrometry coupled with microanalytical fluid devices are also well exemplified by studies of molecular transport in a three-phase water–cyclohexane–water flow system (in a microchannel, the thickness of the organic

phase sandwiched between two aqueous systems, was 64 μm).[510] Under these conditions, the distribution parameters of Methyl Red were determined.[510] Such experiments can be carried out only with the use of integrated microanalysis systems (under these conditions, an organic phase exhibits membrane properties). As in the above-described case, non-fluorescent compounds can be used, which substantially extends the scope of this method. In particular, a theoretical model of molecular transport through a liquid organic membrane under microflow conditions was proposed in the study.[531] This model can find use in biochemical investigations.

A number of recent studies have been aimed at designing microanalytical systems, which combined, for example, flow-injection analysis and immunoassays,[222, 481] capillary electrophoresis and the detection on a microchip by thermal lens microscopy [315] and the detection with the use of interferometer-based microsystems.[532]

Full spectrum lamps were used in the study [315] for inducing a regular thermooptical effect. In this case, a thermooptical element is formed not due to a spatial distribution of the intensity in the incident beam but due to formation of the heat outflow profile as a result of a specially chosen shape of a microchannel in a microchip. In this case, the thermooptical detection is the only possible way of forming an analytical signal, and a thermal lens detector is completely integrated in a microanalysis system.

A combination of thermooptical spectroscopy and integrated microanalysis systems is employed not only in analytical and bioanalytical investigations but also for the synthesis of compounds in a microflow with the thermooptical detection of the products in a real-time mode.[218, 219, 223, 316, 317, 533, 534] These methods are based primarily on two-phase systems under flow conditions giving rise to coloured reaction products at the interface and the thermooptical detection of the compounds in the organic phase. These methods are characterised by high selectivity of reactions at the interface and high sensitivity of thermooptical detection in organic media. In particular, this combination of methods was proposed for use in studies of azo-coupling reactions [218] and alkylation.[317]

Of analytical applications within the framework of this approach, a selective method for the detection of potassium and sodium ions is worthy of notice.[223] This method is based on the formation of a two-phase system in a microchannel. The organic phase in this system contains the ions under study, whereas the organic phase is composed of several solutions of ionophores added successively. The solutions contain also a lipophylic non-selective acid – base indicator. The ionophores selectively interact with the ions (in the case under consideration, valinomycin reacts with potassium ions, and dibenzo-16-crown-5 derivatives react with sodium ions). Interactions of ionophores with the ions lead to extraction of the latter into the organic phase, resulting in a change in the colour of the indicator, and the ions are detected using a thermal lens microscope.[219] In addition to high sensitivity of detection, this approach is fast, which is an obvious advantage over an optrode detector.[535] The thermooptical detection in microchannels is characterised by a short diffusion time and rapid response of the thermooptical detector (the overall time of analysis is 8 s).[219] In the case of an optrode, the system response is rather slow because of slow diffusion of the ions in the optrode membrane. In addition, a micromode of measurements allows one to use substantially smaller amounts of expensive reagents. In particular, the detection of subnanogram amounts of potassium and sodium necessitates 0.5 μl an organic solution of the reagent. For one test, 2 ng of ionophores and 3 ng of an indicator are required. On the whole, the thermooptical detection leads to an increase in the sensitivity of determination of sodium and potassium by an order of magnitude compared to that achieved with the use of an optrode detector.[535]

7. Specific fields of application of thermooptical methods

a. Role of the solvent. Non-photometric thermooptical spectroscopy

The highest sensitivity, *i.e.*, the maximum factor E_0 [see Eqn (9)], can be achieved by choosing a medium characterised by a high temperature refractive index and low thermal conductivity. In this respect, aqueous solutions are inferior to non-polar solvents (benzene, carbon tetrachloride, saturated hydrocarbons) as a medium for thermal lens measurements. For example, low concentrations of 9-nitroanthracene were determined in various solvents, and the detection sensitivity in n-pentane was demonstrated to be twice as high as that in methanol and 40 times higher than that in water.[536]

However, water has a number of advantages, because it is available, can be easily purified and serves as a convenient reaction medium. It should also be taken into account that fluctuations of the thermal lens signal in aqueous solutions are much weaker than those in organic solvents.[93] As a result, the determination limits in aqueous solutions are lower than those in organic solvents.[93, 271]

Aqueous-organic mixtures can be considered as solvents of choice for thermooptical measurements. On the one hand, convenient conditions for both the sample preparation and the photometric reaction in an aqueous medium are provided. On the other hand, high values of the E_0 factor ($3-5$ mW^{-1}) typical of organic liquids are achieved.[396, 537] As an example, Fig. 14 shows the ranges of detectable concentrations of the same compound in aqueous, organic and aqueous-organic media.[271]

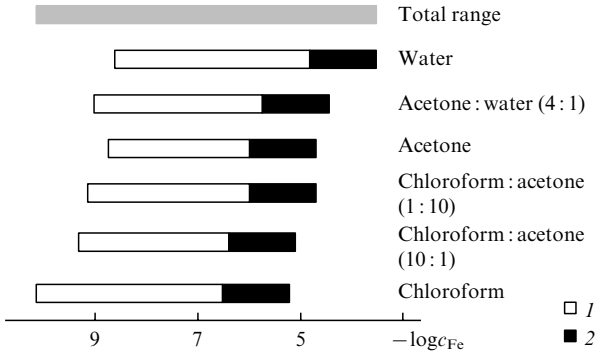

Figure 14. Ranges of quantifiable concentrations of iron(II) tris(1,10-phenanthrolinate) by thermal lens spectrometry in various solvents; the power of laser radiation inducing a thermal lens is 400 (*1*) and 40 mW (*2*).[271]

Due to the fact that the sensitivity of thermooptical measurements depends on the characteristics of the medium, thermooptical spectroscopy can be used for determining characteristics of the medium, such as the thermal conductivity, viscosity, density and the temperature dependence of the refractive index.[285–288] The results of determination of these characteristics for benzene, toluene, carbon disulfide, acetone, methanol and white Burgundy wine from the time evolution of the thermal lens signal correspond to the reference data.[286] Dual-beam thermal lens spectrometry was used to measure the thermal conductivity coefficients of krypton, carbon dioxide, methane, ethane, propane and butane.[288]

It was demonstrated that trace amounts of colourless organic compounds in water can be determined with the use of the thermal lens signal as a function of thermooptical characteristics of a medium (the thermal conductivity, viscosity, density, the temperature dependence of the refractive index, *etc.*) rather than as an analogue of the absorbance. For example, the determination limits of ethanol and DMSO thus determined are 0.05 and 0.04 mass %, respectively.[513]

b. Photochemical thermooptical spectroscopy

The high power and intensity of laser radiation in thermooptical spectroscopy are responsible for initiation of photochemical processes involving reaction products and reagents (Refs 281–284, 411, 430, 440, 538–545). These effects were observed often.[440, 538–540, 542, 543] However, they have attracted considerable attention only in recent years. One of the pioneering series of studies was devoted to photoreduction of complex heteropoly acids of phosphorus and silicon in ethanolic solutions giving rise to bright coloured reduced forms of heteropoly acids (the determination limits $y \times 10^{-9} - y \times 10^{-8}$ g ml^{-1}, see Refs 298 and 546).

Thermal lens spectrometry can be used to study the kinetics of photodecomposition and the formation of radicals in various solvents. For example, the photochemical reaction involving the 2-naphthylmethyl radical was discovered,[430] and the behaviour of benzophenone in acetonitrile and propan-2-ol was investigated.[545]

Photochemical thermooptical spectroscopy is used to determine the thermodynamic characteristics (the enthalpy, entropy and free energy) of chemical processes and to control the parameters of chemical reactions by varying the intensity of excitation laser radiation.[455, 538, 541, 547] Procedures in which the thermooptical detection is coupled with a method for concentrating an analyte component photoinduced by the laser beam,[548] photocatalysis and photocoagulation [398, 399, 549] are similar to the above-described thermooptical measurements.

c. Thermooptical cytometry

Two studies [550, 551] have laid the groundwork for thermooptical cytometry. The method is based on measurements of the response of living cells to short-time heating induced by a laser pulse. Elements of the theory of thermooptical microscopy in a pulsed mode of operation of an excitation laser were developed. The method was used for non-destructive control of living cells,[552–554] control of selective photothermolysis, investigations of DNA and studies of defects and impurities in ultrapure optics and semiconductors. This method can be performed in modes of thermal lens spectrometry, photothermal deflection spectroscopy and photothermal radiometry.

8. Colloidal systems

a. Coarsely dispersed colloidal systems †

Coarsely dispersed systems, *viz*., coarse slurries, suspensions and emulsions, are most often used in thermooptical measurements.[4, 18, 37, 38] Several studies [54, 295, 529, 555, 556] were concerned with measurements of thermooptical deflection of the probe laser beam from the reflecting surface formed by large suspension particles. In the case of spontaneous formation of coarsely dispersed systems, the efficient power of the excitation beam decreases proportionally to the number of reflecting particles and, consequently, the detection sensitivity decreases, which limits the use of these systems in analytical practice.[398, 399]

b. Finely dispersed colloidal systems

Finely dispersed systems with particle sizes $y \times 10^{-7} - y \times 10^{-9}$ m also affect the sensitivity of thermooptical detection. In this respect, surfactants are of considerable interest (Refs 4, 18, 47, 397, 410, 536, 537, 557). A micellar mechanism of modifications of thermooptical properties of a medium involves an increase in the temperature gradient of the refractive index and a decrease in the thermal conductivity coefficient due to disruption of the rigid water structure.[558]

In the study,[557] the concentrations of the hydrophilic salt TbCl were determined using surfactants, which form micelles with the analyte in non-polar solvents. The thermal lens signal corresponding to the absorbance of 1×10^{-7} was recorded. The simultaneous determination by fluorescence spectroscopy and the thermal lens techniques demonstrated that the determination limits of tetracycline in the presence of Triton X-100 are three times lower than those in the absence of the surfactant.[410] The micellar effect in aqueous solutions was examined in the study of 9-nitroanthracene.[536] Being highly soluble both in polar and non-polar solvents at concentrations lower than $y \times 10^{-7}$ mol litre^{-1}, this compound was chosen for testing the validity of the assumption that the change in the thermal lens signal depends only on the thermooptical characteristics of the medium. The mechanism of interaction of this signal with surfactants of different nature was elucidated and it was noted that the thermal lens signal strength is proportional to the degree of hydrophobicity of the environment of the molecule.[536] This fact was confirmed by the data obtained in the study of 9-nitroanthracene derivatives. The presence of long hydrocarbon chains is favourable for higher solubilisation, which leads to a substantial increase in the signal strength.[536]

It was demonstrated [47] that microemulsions can be studied by thermal lens spectrometry. Microemulsions of differently charged particles were studied above and below their percolation threshold. Microemulsions of negatively charged particles are subjected to percolation at rather high concentrations of surfactants (30%), and the thermal lens signal is independent of the water content. Apparently, microemulsions consist of small reverse micelles, and this structure exists both above and below the percolation threshold. In contrast, percolation of microemulsions of positively charged particles occurs at relatively lower concentrations of surfactants (10%), and the thermal lens signal depends on the concentration of water in the system.[47] Consequently, the structure of these microemulsions changes upon percolation, and these microemulsions above the percolation threshold consist of large bound aggregates or two-dimensional structures.[47]

It was proved [557] that an increase in the thermal lens signal upon the addition of surfactants occurs primarily due to an increase in dn/dT of the solution. The influence of surfactants and various dissolved compounds on the water structure can be characterised by the following two parameters: the temperature at which $dn/dT = 0$, and the temperature dependence d^2n/dT^2. These parameters decrease upon the addition of substances disrupting the water structure (for example, of urea), whereas the addition of, for example, *tert*-butyl alcohol leads to an increase in these parameters.[47, 557] The molecular structure of the surfactant plays an important role in the observed effect. A reduction of water structurisation is more pronounced when a surfactant exists in the micellar rather than monomeric form.[557] The disruption of the water structure in the presence of surfactants, such as polyoxyethylene lauric ester (**1**), hexadecyltrimethylammonium bromide (**2**), 3-(*N*-dodecyl-*N*,*N*-dimethylammonium)propane-1-sulfonic acid (**3**) or sodium dodecylsulfate (**4**), was examined. At concentrations of a surfactant lower than the critical micelle concentration, this effect decreases in the series **1** > **2** > **3** > **4**. For micellar solutions, **1** > **2** = **3** = **4**.

The characteristic features of thermooptical non-linearity in cast films of polymer-encapsulated nematic liquid crystals were studied experimentally. The dynamics of changes in the light transmission of the film on heating of liquid crystal drops by a laser radiation pulse was examined.[559]

IV. Study of interfaces in condensed systems

Photothermal methods have wide application in studies of interfaces in condensed heterogeneous systems.[176] They are virtually the only methods suitable for non-contact studies of the thermal and optical properties of condensed phases. The use of photothermal methods in studies of interfaces is dictated primarily by the necessity of solving a number of important problems [158, 173, 560–563] associated with experiment planning. The characteristic features of photothermal methods were efficiently

† This section deals with colloidal systems, in which liquids serve as a dispersion medium. In the case of colloidal systems, thermooptical spectroscopy examines changes in the macroproperties of solutions caused by changes in the number and size of colloidal particles.[4]

used in specific investigations concerned with the dynamics of absorption processes [119, 183, 564–577] and the extraction equilibrium in microspace.[219, 223, 531] Non-transparent solid samples with smooth and rough surfaces [158, 172, 173, 212, 563, 578–586] and transparent substances, including transparent films (Refs 174, 562, 587–594), were also studied by these methods. Modern apparatus allows one to perform two- and even three-dimensional surface imaging.[174, 579, 583, 593]

1. Physical models

Simulation of experiments with consideration for all characteristic features of the system under examination and apparatus employed gives the best results. The main results in this field are concerned with the solid–gas (air) interfaces. The influence of the form of the energy profile in a pulse on the thermal response was examined by the mirage effect method,[158] and the theoretical data were compared with the experimental results with and without considering this form. Investigation of a gold (1.5 μm)/tetrahedral amorphous carbon (80 nm) coating on a silicon substrate demonstrated that the thermal properties of carbon are virtually independent of the pulse form, whereas the correct characterisation of the thermal properties of gold requires that the pulse form of the incident laser radiation be taken into account. This approach simplifies the mathematical apparatus for the description of multilayer structures of semiconducting products.[560, 561]

A model for simulation of the photothermal beam deflection (for a perpendicular crossed-beam configuration of an instrument) in samples, including weakly absorbing thin films on substrates with high light absorption, was considered in the study.[562] The model was employed to determine the thermal conductivity of thin films on substrates. The influence of the intersection angle of the excitation and probe beams at the sample, the modulation frequency of the excitation beam, the thickness and absorption of the thin film and the thermal properties of the substrate on the thermal conductivity of thin films was discussed. This method proved to be suitable for thermal conductivity measurements of thin films with high thermal conductivity, for example, of diamond and diamond-like carbon films deposited on substrates with relatively low thermal conductivity at low modulation frequencies.

The crossed-beam configuration of the optical scheme of photothermal deflection was investigated.[173] Equations describing the probe beam deflection were deduced. In particular, the role of the incident angle of the probe beam [see Eqn (16)] was demonstrated to be analogous to the role of the height at which this beam passes above the surface in photothermal deflection measurements employing the parallel configuration of the probe beam [see Eqn (15)]. An analogy between these two configurations was found by comparing the dependences of the signals on the incident angle and the height at which the probe beam passes. To confirm the results of theoretical calculations, photothermal deflection measurements on invar samples were performed (since this compound has a small thermal expansion coefficient, a thermally induced surface displacement in a limited range of the incident angles can be ignored).

A new model of the laser-induced thermal lens on the surface of semiconducting materials was devised.[563] The model is based on the Fresnel diffraction theory and other photothermal effects, such as photothermal deflection, the thermal lens effect and photoreflection. According to this model, the photothermal reflection makes the major contribution to the detectable signal and the diffraction pattern, but the air-thermal lens effect at low modulation frequencies and the photothermal reflection at high frequencies are also significant. It was demonstrated that the sensitivity can be enhanced by choosing an optimum position of the sample, which depends on the modulation frequency.

2. Adsorption

The surface of a gold film electrode (a polycrystalline gold film of thickness 1 μm on a polymer substrate) was studied [564] by the transient reflecting grating method. The thermal response to both the formation of a double layer and oxidation at anode potentials above +1 V and the acoustic response only to the formation of an oxide film were detected using a cyclic potential scan in 0.05–0.1 M solutions of acids (HCl, HClO). The thickness of the oxide film varied from one to several monolayers. Thermal grating spectroscopy proved to be more sensitive than other photothermal and photoacoustic methods. However, attempts to describe the observed phenomena in terms of a simple model based on enhancement of oxygen adsorption at anode potentials failed.

A highly sensitive method for the detection of antigens on the blood cell surface by thermal lens microscopy was considered in the study.[565] Colloidal gold coated with antibodies was used for staining leukocyte membrane antigens. Human leukocyte antigens on lymphocytes and mononuclear leukocytes were observed by thermal lens microscopy. Antigens of particular chromosomes on lymphocytes were detected and determined for a single cell. Antigen mapping studies were carried out on mononuclear leukocytes. Thermal lens microscopy allows one to perform non-degrading biochemical studies directly on living cell membranes.

Studies of sorption of various classes of model compounds on a series of sorbents showed that thermal lens spectrometry is suitable for investigations of adsorption of nanogram amounts of these compounds by measuring their residual concentrations in solution. The sorption kinetics were studied, adsorption isotherms were constructed and characterised, and the maximum adsorption and the conditional adsorption coefficient were determined.[566]

It was demonstrated that thermal lens spectrometry can be used to study adsorption on low-capacity sorbents (chemical glass and quartz). Thermal lens spectrometry was applied for the direct determination of the concentration of iron(II) tris(1,10-phenanthrolinate) on the quartz surface upon adsorption from aqueous solutions. It is possible to determine quantitatively the concentrations to about pmol litre^{-1} [$\sim$0.01 monolayer for adsorption of iron(II) tris(1,10-phenanthrolinate) on quartz glass] and the absolute amounts of about tens of attomoles.[566, 570] The limiting sensitivity of thermal lens determination is $\sim$100 times higher than that of diffuse reflection measurements under the same conditions. The adsorption characteristics of iron(II) tris(1,10-phenanthrolinate) and nickel(II) dimethylglyoximate from aqueous and aqueous-ethanolic solutions on laboratory glass were evaluated at nanogram levels of the sorbate in solution, and the surface concentrations of irreversible and reversible sorption centres were estimated.[407, 570] The process is most adequately described by the Freundlich equation for monomolecular adsorption.[568]

It was shown that thermal lens spectrometry is suitable for investigating of the continuity and surface concentrations of molecular layers grafted onto the quartz glass surface [567, 569, 595, 596] and for the direct detection of the dye Reactivrot B5A on the glass substrate.[567] The method allows one to perform quantitative determinations up to a monolayer of the grafted dye. Rapid ($\sim$5 min) laser-induced photodestruction of the grafted dye was observed for the first time.[567]

Investigation of adsorption of the dye acridine orange at the quartz glass–water interface by total internal reflection thermal lens spectrometry demonstrated [119] that the thermal lens effect is induced only by the penetrating wave. The adsorption depth profile can be obtained. The determination limit of the dye Sudan II in acetone is 3.0×10^{-5} absorbance units (the 2s criterion, the concentration of the dye was 3.8×10^{-5} mol litre^{-1}), which is hundreds of times lower than that achieved by the attenuated total reflection method. Under these experimental conditions, adsorption of the dye acridine orange on silanol groups of glass was observed. The adsorption isotherm is consistent with the Langmuir model.

Adsorption of diphilic surfactants at the water–hexane interface was studied [571] by surface thermal lens spectrometry. A thin thermal lens was observed for the diphilic molecules of 10-(1-pyrene)decanoic and 4-(1-pyrene)butanoic acids present at the

hexane – phosphate buffer solution interface. This method gives a linear response to the number of molecules; the detection limit is ~ 0.01 monolayer.

A procedure was proposed [572] for studying liquid – liquid interfaces. This method is called total internal reflection optical beam deflection (OBD). A comparison with total internal reflection thermal lens spectrometry [571] demonstrated that the background noise in the OBD method is substantially lower. The fact is that the probe beam in thermal lens measurements should be precisely focused onto the centre of the excitation region at the interface. In this case, even small variations in the conditions affect the background signal. In OBD measurements, the probe beam passes at a particular distance from the interface in an isotropic medium, due to which it is less dependent on the accuracy of tuning and external conditions. The maximum sensitivity is reached when the probe beam passes in dodecane in the vicinity of the interface (due to the higher sensitivity enhancement factor for dodecane compared to that for water). The method was used to examine the complex formation of iron(II) with 4,7-diphenyl-1,10-phenanthroline upon the contact of an aqueous solution of iron with a dodecane solution of the ligand. The detection limit (the 3*s* criterion), which is 750 molecules per 1 μm^2 or 2.8×10^{-6} absorbance units, is ~ 3 orders of magnitude lower than the detection limit provided by total internal reflection thermal lens spectrometry.

Adsorption of asphaltenes on glass substrates was studied by photothermal deflection and displacement spectroscopy.[573, 574] Adsorption isotherms for asphaltenes were measured at room temperature in toluene on a glass substrate.[573, 574] Multilayer adsorption was detected in three experiments, where the time of the contact was longer than 3 days. The isotherms measured during short periods of time show a linear dependence of adsorption on the concentration.[573] In the case of an appropriate ratio of the radii of the excitation and probe beams at the sample surface, an analytical signal can be measured by a single photodiode.[574]

A series of studies by Japanese researchers were concerned with the dynamics of diffusion and isomerisation of coloured compounds. They examined *N*-(4-methoxybenzylidene)-4-*p*-butylaniline (MBBA) in ethanol [575, 576] and other organic solvents,[576] in experiments with total internal reflection of the probe beam and the vertical direction of the excitation beam and studied spiropyran at the water – air [577] and solid – liquid [576] interfaces by the transient reflecting grating method. Surfaces of pure and polystyrene-coated sapphire [575, 576] and porous glass [576] were investigated. In the presence of a molecular layer of spiropyran, diffusion of molecules and their aggregates was demonstrated to occur at the water – air interface (fast and slow components of a biexponential decrease in the signals).[577] Studies with MBBA showed that the surface strongly catalyses isomerisation. This fact was confirmed by measurements in porous glass.[575, 576]

The possibilities of photothermal deflection spectroscopy and photothermal radiometry were examined as applied to characterisation of plates, which are used in thin-layer chromatography to determine the surface and depth distributions of various compounds on a sorbent.[183] Photothermal radiometry proved to be of little use for characterisation of thin-layer chromatograms. The observed low reproducibility of measurements is presumably associated with poor reproducibility of the separation conditions and inhomogeneity of different chromatographic plates.

3. Semiconductors

Semiconducting materials are most often studied by photothermal deflection methods (mirage effect) [578 – 580] and photothermal radiometry.[212, 581, 582] The photothermal reflection technique [583] and surface thermal lens spectrometry are also used for these purposes.[563]

The nature of surface defects in insulator films and defects between a-Si : H and insulator layers were examined [578] by ESR and photothermal deflection spectroscopy. The surface defect densities for a-Si : H, a-$SiN_{1.7}$: H and a-SiO were estimated from the dependence of the ESR signal intensity on the thickness. The surface state density in a-$SiN_{1.7}$: H/a-Si:H and a-SiO_2/a-Si : H was evaluated by analysis of the layered structure of thin layers. For an a-Si : H film, the results obtained by ESR agree well with the results of photothermal deflection spectroscopy. However, defects in a-$SiN_{1.7}$: H and a-SiO_2 films were not observed by the photothermal deflection technique in spite of the fact that their concentrations were virtually equal to that in a-Si : H films. The reason is that the spectral range of excitation of a photothermal spectrometer does not coincide with the absorption range of defects in a-$SiN_{1.7}$: H and a-SiO films. Defects in these structures were demonstrated to appear in the course of the plasma surface reaction and are located on the a-Si:H side of the interface. A combination of these methods holds promise. Thus, the energy distribution of defects can be studied by photothermal deflection spectroscopy, and their chemical environment can be revealed by ESR. Therefore, these methods supplement each other.

Non-contact imaging of the buried structures in air was performed by the photothermal deflection technique.[579] The method was employed to analyse layered CdTe (50 nm)/glass (0.15 mm)/carbon black (10 μm) samples. Photothermal amplitude and phase images of optically nontransparent buried structures were obtained. The phase images were more smooth and regular. The thermal diffusivity and the absorptivity of the material were calculated from the amplitude and phase parameters of the photothermal image. The thermal diffusivity of buried structures can be determined (non-destructively) from the data on photothermal deflections at two modulation frequencies.

The thermal conductivity, adhesion and mechanical stress in diamond films, which were synthesised on a ceramic aluminium nitride substrate, were studied.[580] The thermal conductivity of this composite was examined by photothermal deflection spectroscopy. It was found that this parameter is 73% larger than the thermal conductivity of pure aluminium nitride. Scanning electron microscopy and Raman spectroscopy revealed the influence of a diamond film on the thermal conductivity of samples. Unusual stability and very high adhesion of a diamond film to an aluminium nitride substrate are associated with the formation of an aluminium carbide underlayer in the synthesis of a diamond film. It was noted that diamond-coated aluminium nitride substrates are promising materials for heat removal from semiconducting electronic devices.

Photothermal radiometry was demostrated to be suitable for non-contact temperature measurements of semiconductors.[212] This method can be used to measure the temperature of high-alloy silicon samples, but it is necessary to find experimental conditions to minimise the effect of formation of electron – hole pairs (for example, to use a low modulation frequency of the excitation laser). The latter effect can be eliminated by using a laser, whose wavelength is smaller than the energy gap width of the semiconductor. For semiconductors characterised by a very short lifetime of electron – hole pairs, this effect is insignificant and has virtually no influence on the measurements.

In the study,[581] the non-contact diagnostics of the SiO_2/Si interface was carried out by photothermal radiometry. Two silicon plates containing aluminium and silicon gate metal-oxide-semiconductor structures were analysed by this method. Diffusion of charge carriers, their lifetime and the surface recombination rate were examined. The activation energies measured by two photothermal methods have close values, which are 0.15 – 0.17 and 0.21 eV lower than the lower limit of the conduction band for plates with aluminium and silicon gate devices, respectively.

Three-dimensional photothermal radiometric microscopy was employed in non-contact non-destructive studies of electron transfer in integrated schemes of lithographed silicon plates.[582] The surface resolution was 20 μm. It was demonstrated that scribeline photothermal probing can be efficiently used for non-contact monitoring of local changes in the lifetime of charge

carriers, which provides a way of determining contaminations and plate damage during the manufacture of integrated devices.

The structure of a metal-oxide-semiconductor insulated-gate field-effect transistor (MOSFET) was studied by reflection microscopy.[583] In the optical range for probing of the gate surface, the resolution was ~ 1 μm, and the constituent electro- and thermal reflections were found in the signal. Depending on the configuration of the gate valve, six different types of images with different sharpness can be obtained. In the cited study, it was also demonstrated that this method is suitable for the detection of subsurface effects.

4. Non-transparent films

Electron transitions in C_{60} under the influence of oxygen were investigated.[584] Absorption of atmospheric oxygen was demonstrated to impair dark conductivity and photoconductivity of C_{60} films. Light absorption was measured at 300 and 77 K by the photothermal deflection method. A new method, *viz*., photothermal bending, was described in the literature.[584] Absorption of excitation laser radiation which is incident perpendicular to the film surface leads to expansion of the external absorbing layer of the sample fixed at one end, resulting in bending of the sample, which is accompanied by a change in the reflection angle of the probe laser beam. This method can be used *in vacuo* (this is of considerable importance in studies of materials sensitive to an environmental medium). The method is also sensitive to temperature changes; however, it is applicable only to thin samples.

Two schemes of photothermal deflections were used to study a non-transparent film deposited on Corning 7059 glass substrates.[585] At low modulation frequencies, both schemes give similar results and it is preferable to detect the phase shift, because it is less affected by the thermal thickness of the sample.

The photothermal deflection method was employed for the non-destructive non-contact study of artificial and natural copper patina.[172] This approach is used in non-destructive analysis of ancient copper production.

Photothermal radiometry was used to characterise nickel-pigmented aluminium oxide solar cells.[586] After heating of a sample with a modulated laser beam, thermal radiation emission was measured as a dependence on the modulation frequency in a range from 10 Hz to 10 kHz. The experimental results were described by a simple one-dimensional model, which made it possible to estimate the thermal parameters of light-absorbing coatings. The radiation ability measured by conventional methods was compared with that determined by photothermal radiometry.

5. Weakly absorbing films

The optical and thermal properties of defect polycrystalline boron-doped diamond films were investigated.[587, 588] The absorptivities of thin (< 10 μm) diamond films cannot be determined by conventional methods because of a small film thickness and large scattering due to surface roughness. Both problems can be overcome by determining the absorptivity from the results of measurements of heat adsorbed by the surface using photothermal deflection spectroscopy. The method was used to study defects and impurities in polycrystalline diamond. Absorption, which is caused by local structures that appear upon implantation of polycrystalline diamond films, and reduction after annealing were observed for the first time.

An application of surface thermal lens spectrometry to investigations of weakly absorbing films was proposed in the study.[579] The results were compared with the data from photothermal deflection spectroscopy. Laser-induced deformation is considered as a bent mirror, which either focuses or defocuses the probe beam depending on the geometry used. Surface thermal lens spectrometry does not require the precise tuning of the probe beam and has the same high sensitivity as photothermal deflection spectroscopy. The exact size and shape of the region deformed upon excitation can be observed with a CCD camera. This fact is of considerable importance in studies of thermal expansion and absorbance. The reproducibility of measurements increases by a factor of ~ 5. The spatial resolution depends only on the size of the excitation beam, which can be focused to a submicrometre size by near-field photothermal microscopy. The above advantages were exemplified by studies of adsorption and characterisation of defects of weakly absorbing films of titanium(IV), tantalum(V), zirconium(IV) and silicon(IV) oxides on the surface of BK7 glass. The accuracy of the detection of absorbance is retained down to 2.6×10^{-6}.

Photothermal displacement spectroscopy was used to examine defects and attendant damages of coatings of optical elements under high-power pulsed laser irradiation, for example, in photolithographic devices.[590] Multilayer Al_2O_3/SiO_2 coatings on quartz glass, which reflect strongly at 248 nm, were investigated.

Photothermal deflection spectroscopy was used to study transparent amorphous diamond-like graphite films deposited on the quartz surface.[591] These films are resistant to damages and are transparent in the visible region.

A series of studies [174, 592, 593] were concerned with the properties of polymer materials for waveguides. The photothermal deflection spectra of non-oxidised polyalkylthiophenes containing alkyl side chains of different lengths were measured in the near-field IR region.[592] This field is used in non-linear optical waveguides. Fluorination of polyalkylthiophenes does not lead to a noticeable improvement of the waveguide properties (for example, in a range of 1700–1800 nm). Besides, purification from iron trichloride is required; otherwise, such materials are unsuitable for the construction of non-linear optical devices. The best wavelength range for waveguide materials is about 1300 nm.

Photothermal beam deflection imaging of the refractive index structure was described in the publications.[174, 593] Poly(methyl methacrylate) (PMMA) and polythiophene containing the dissolved dye Disperse Red 1 were studied. A mixture of PMMA with the dye was analysed by the laser photodecomposition technique.[593] The refractive index distribution in the polymer was determined. The method, in essence, is to examine the absorption spectrum changes caused by decomposition and subsequent image contrast reversal due to the corresponding change in the excitation beam wavelength. Images of integrated waveguide devices constructed from PMMA and polythiophene were obtained by photodecomposition and photothermal deflection on a photolithographic instrument. Structures of dimensions > 50 μm were resolved. Attempts to image structures of dimensions < 30 μm by the photothermal deflection technique failed. Photothermal displacement spectroscopy would be expected to overcome this limitation.

Scanning photothermal deflection was compared with scanning photothermal displacement.[174] A 20% solution of the dye Disperse Red 1 in PMMA was examined. Two methods show similar depth resolution. Data on photothermal deflection are rather easy to interpret due to a simple relation between the signal and excitation source power. Due to enhancement of the signal by an auxiliary liquid, images with an acceptable signal/noise ratio can be obtained even at low excitation power. However, immersion of a sample into an auxiliary liquid may be a drawback if the latter cannot be removed after the experiment. Besides, signal accumulation time is large due to a rather low chopping frequency.

To interpret the results of photothermal displacement spectroscopy, numerous factors should be taken into account. The convexity theory is complex and is additionally complicated in the case of focused-beam excitation. For thin samples, a convexity is formed primarily in the substrate. Hence, it is necessary to know the distribution of the thermal and optical properties of the substrate. The advantages are a high rate of signal accumulation (due to a high chopping frequency) and the possibility of performing analysis in air. Hence, it was concluded that the photothermal deflection method is more convenient for studying polymer films (due to higher reproducibility of the results) compared to the photothermal displacement technique.[174]

Amorphous graphite films, which were prepared on polystyrene under its irradiation with He^+ and H^+ ions, were analysed in the study.[594] These films are used in particular types of protective coatings. The photothermal deflection method was employed to record an absorption spectrum in a wavelength range from 1.2 to 2.0 μm. The mechanical, electrical and optical properties of such films depend on the ratio between the contents of the sp^2- and sp^3-hybridised carbon atoms. The changes occurring in the film can readily be observed from evolution of particular overtones in the absorption spectrum in the above-mentioned range.

V. Conclusion

When considering the development of analytical thermooptical spectroscopy, it is necessary to mention a considerable contribution of the research team headed by Professors V I Grishko and I G Yudelevich (A V Nikolaev Institute of Inorganic Chemistry of the Siberian Branch of the Russian Academy of Sciences, Novosibirsk), who laid the groundwork for analytical investigations in the field of thermal lens spectrometry. Initial studies using thermooptical spectroscopy methods have been concerned with chemical interactions at low concentrations of reacting compounds. The metrological characteristics of the method have been comprehensively evaluated, and its possibilities in the determination of traces of organic and inorganic compounds have been examined.[82, 86, 87, 106, 298, 353, 541, 546] In addition, this research team published the only Russian monograph [2] (and the first monograph in the world), which was completely devoted not only to the physics of the thermooptical phenomena but also to instrumental possibilities of thermal lens spectrometry and (which is of most importance) to its analytical applications. The results of the studies performed by this research group in the field of thermooptical spectroscopy were so voluminous that they are still being published (even ten years after the completion of their research).[359]

Nowadays, thermooptical methods for analysis are being developed and used in leading research centres in Russia and Former Soviet Republics, such as M V Lomonosov Moscow State University,[313, 401, 402, 548, 595–600] St Petersburg State University,[218, 229, 232, 443–445, 510, 531] Institute of Physics of Microstructures of the Russian Academy of Sciences (Nizhnii Novgorod),[239, 240, 248–251, 313] A V Lykov Institute of Heat and Mass Transfer (Minsk, Republic of Belarus),[552–554] N E Bauman Moscow State Technical University,[5, 552, 554] L V Kirensky Institute of Physics of the Siberian Branch of the Russian Academy of Sciences (Krasnoyarsk) [559] and Dnepropetrovsk State University (Ukraine).[601] Considerable experience has been gained in the field of thermooptical spectroscopy. Numerous studies were published, many of which made a considerable contribution to the theory and practice of thermooptical investigations.

The section 'Thermooptical Methods' was included in the Handbook 'Analytical Chemistry' (Ed. Yu A Zolotov, Nauka, Moscow, 1998, 2d edition). This is the only example of the inclusion of information a review format on thermooptical methods in a handbook for university students. Nowadays, the fundamentals of thermooptical spectroscopy are included in training courses of the Departments of Physics [602] and Chemistry (the Chair of Analytical Chemistry, the training course 'Analytical Chemistry',[603] and the Chair of Laser Chemistry, the training course 'Introduction to Laser Chemistry' [604]) of Moscow State University, St Petersburg State University (the training course 'Physical Fundamentals of Optical Methods of Analysis of Substances and Materials') [605] and Krasnoyarsk State University (the Chair of Physical Chemistry, the training courses 'Materials Science and Technology of New Materials' and 'Modern Methods of Analysis').[606]

In conclusion, it should be noted that, in addition to high sensitivity, methods of thermooptical spectroscopy provide much more information than spectrophotometric methods. This makes it possible to increase substantially the range of the problems, which can be solved. Apparently, the main advantages of thermooptical methods (the possibility of the simultaneous detection of several analytical signals and the use of specific effects not as a passive way of detecting but as an active component of new analytical methods) will assist the development of analytical thermooptical spectroscopy.

References

1. J M Harris, N J Dovichi *Anal. Chem.* **51** 728 (1979)
2. V I Grishko, V P Grishko, I G Yudelevich *Lazernaya Analiticheskaya Termooptricheskaya Spektrometriya* (Laser Analytical Thermooptical Spectrometry) (Novosibirsk: Institute of Inorganic Chemistry, Siberian Branch of Russian Academy of Sciences, 1992)
3. D S Kliger (Ed.) *Ultrasensitive Laser Spectroscopy* (New York: Academic Press, 1983)
4. S E Bialkowski *Photothermal Spectroscopy Methods for Chemical Analysis* (New York: Whiley, 1996)
5. V P Zharov, V S Letokhov *Lazernaya Optiko-Akusticheskaya Spektroskopiya* (Laser Optic-Acoustic Spectroscopy) (Moscow: Nauka, 1984)
6. R D Snook, R D Lowe *Analyst* **120** 2051 (1995)
7. N J Dovichi *CRC Crit. Rev. Anal. Chem.* **17** 357 (1987)
8. N J Dovichi *Prog. Anal. Spectrosc.* **11** 179 (1988)
9. J Georges *Talanta* **48** 501 (1999)
10. M J Navas, A M Jimenez *CRC Crit. Rev. Anal. Chem.* **33** 77 (2003)
11. M Franko *Talanta* **54** 1 (2001)
12. K Swinney, D Bornhop *CRC Crit. Rev. Anal. Chem.* **30** 1 (2000)
13. K Uchiyama *Bunseki Kagaku* **48** 737 (1999)
14. A Mandelis *Anal. Sci.* **6** 491 (1990)
15. F A McDonald *Can. J. Phys.* **64** 1023 (1986)
16. T de Beer, N H Velthorst, U A T Brinkman *J. Chromatogr. A* **971** 1 (2002)
17. S M Lima, J A Sampaio, T Catunda, A C Bento, L C M Miranda, M L Baesso *J. Non-Cryst. Solids* **273** 215 (2000)
18. M A Proskurnin, V V Chernysh *Zh. Anal. Khim.* **55** 1049 (2000) [a]
19. S J Sheldon, L V Knight, J M Thorne *Appl. Opt.* **21** 1663 (1982)
20. R D Snook, R D Lowe, M L Baesso *Analyst* **123** 587 (1998)
21. K Fujiwara, W Lei, H Uchiki *Anal. Chem.* **54** 2026 (1982)
22. R A Leach, J M Harris *Anal. Chim. Acta* **164** 91 (1984)
23. E S Yeung (Ed.) *Detectors for Liquid Chromatography* (New York: Whiley, 1986)
24. G Bidoglio, G Tanet, P Cavalli, N Omenetto *Inorg. Chim. Acta* **140** 293 (1987)
25. J R Guckert, R W Carr *J. Phys. Chem.* **90** 4286 (1986)
26. T Higashi, T Imasaka, N Ishibashi *Anal. Chem.* **55** 1907 (1983)
27. A G Abroskin, S I Artemova, T V Belyaeva, E K Ivanova, M A Proskurnin *Zh. Anal. Khim.* **47** 545 (1992) [a]
28. M A Proskurnin, A G Abroskin, I V Golovko, E K Ivanova *Zh. Anal. Khim.* **49** 263 (1994) [a]
29. D K Sharma, F Villamagna, C H Langford *Can. J. Spectrosc.* **28** 181 (1983)
30. T Berthoud, N Delorme *Appl. Spectrosc.* **41** 15 (1987)
31. C D Tran, W Zhang *Anal. Chem.* **62** 830 (1990)
32. T Masujima, A Sharda, L B Lloyd, J M Harris, E M Eyring *Anal. Chem.* **56** 2975 (1984)
33. F K Fotiou, M D Morris *Appl. Spectrosc.* **40** 700 (1986)
34. J F Power, C H Langford *Anal. Chem.* **60** 842 (1988)
35. T I Chen, M D Morris *Anal. Chem.* **56** 19 (1984)
36. K Mori, T Imasaka, N Ishibashi *Anal. Chem.* **55** 1075 (1983)
37. C M Phillips, S R Crouch, G E Leroi *Anal. Chem.* **58** 1710 (1986)
38. C D Tran *Appl. Spectrosc.* **41** 512 (1987)
39. S E Bialkowski *Anal. Chem.* **58** 1704 (1986)
40. J Pawliszyn *Anal. Chem.* **58** 243 (1986)
41. Y Martín-Biosca, J J B Baeza, G Ramis-Ramos *Chromatographia* **44** 145 (1997)
42. M Šicovec, M Novi, M Franko *J. Chromatogr. A* **739** 111 (1996)
43. K Fujiwara, H Uchiki, F Shimokoshi, K I Tsunoda, K Fuwa, T Kobayashi *Appl. Spectrosc.* **36** 157 (1982)

44. H T Yan, S K Yang *Chin. Chem. Lett.* **7** 773 (1996)
45. B S Seidel, E Steinle, W Faubel, H J Ache *Proc. SPIE-Int. Soc. Opt. Eng.* **2836** 283 (1986)
46. B S Seidel, W Faubel, H J Ache *J. Biomed. Opt.* **2** 326 (1997)
47. M S Baptista, C D Tran *J. Phys. Chem. B* **101** 4209 (1997)
48. J Pawliszyn, M F Weber, M J Gignam, A Mandelis, R D Venter, S M Park *Anal. Chem.* **58** 236 (1986)
49. J A Sell, R J Cattolica *Appl. Opt.* **25** 1420 (1986)
50. J H Rohling, J Mura, J R D Pereira, A J Palangana, A N Medina, A C Bento, M L Baesso, L C M Miranda *Braz. J. Phys.* **32** 575 (2002)
51. J H Zhao, J Shen, C Hu *Opt. Lett.* **27** 1755 (2002)
52. T Toyoda, M Hayashi, J Sato, Q Shen *J. Therm. Anal. Calorim.* **69** 1037 (2002)
53. E Demirbas, R Devonshire *Spectrosc. Lett.* **35** 603 (2002)
54. Y Martín-Biosca, M C García-Alvares-Coque, G Ramis-Ramos *Trends Anal. Chem.* **16** 342 (1997)
55. J Shen, R D Lowe, R D Snook *Chem. Phys.* **165** 385 (1992)
56. J Shen, A J Soroka, R D Snook *J. Appl. Phys.* **78** 700 (1995)
57. M Fischer, J Georges *Anal. Chim. Acta* **332** 117 (1996)
58. M A Proskurnin, A G Abroskin, D Yu Radushkevich *Zh. Anal. Khim.* **54** 101 (1999) [a]
59. M A Proskurnin, A G Abroskin *Zh. Anal. Khim.* **54** 460 (1999) [a]
60. S E Bialkowski *Appl. Opt.* **24** 2792 (1985)
61. C D Tran, M Franko *J. Phys. E* **22** 586 (1989)
62. M Franko, C D Tran *Appl. Spectrosc.* **43** 661 (1989)
63. W A Weimer, N J Dovichi *J. Appl. Phys.* **59** 225 (1986)
64. M C Gupta, S D Hong, A Gupta, J Moacanin *Appl. Phys. Lett.* **37** 505 (1980)
65. H L Fang, R L Swofford *J. Appl. Phys.* **50** 6609 (1979)
66. J P Haushalter, M D Morris *Appl. Spectrosc.* **34** 445 (1980)
67. D S Kliger *Acc. Chem. Res.* **13** 129 (1980)
68. N J Dovichi, J M Harris *Proc. SPIE-Int. Soc. Ont. Eng.* **228** 372 (1980)
69. C E Buffet, M D Morris *Anal. Chem.* **54** 1824 (1982)
70. J V Beitz, J P Hessler *Nucl. Technol.* **51** 169 (1980)
71. T W Colette, N J Parekh, J H Griffin, L A Carreira, L B Rogers *Appl. Spectrosc.* **40** 164 (1986)
72. S Wu, N J Dovichi *J. Appl. Phys.* **67** 1170 (1990)
73. N J Dovichi, J M Harris *Anal. Chem.* **52** 2338 (1980)
74. T Imasaka, K Nakanishi, N Ishibashi *Anal. Chem.* **59** 1554 (1987)
75. K Miyaishi, T Imasaka, N Ishibashi *Anal. Chem.* **54** 2039 (1982)
76. Y Yang, S C Hall *Appl. Spectrocs.* **42** 72 (1988)
77. Y Deng, R Sheng, M Wang *J. Phys. Colloq. (France)* **44** 565 (1983)
78. W A Weimer, N J Dovichi *Anal. Chem.* **57** 2436 (1985)
79. A Uejima, M Habiro, F Itoga *Anal. Sci.* **2** 389 (1986)
80. T Berthoud, P Mauchien, N Omenetto, G Rossi *Anal. Chim. Acta* **153** 265 (1983)
81. M Franko, C D Tran *Anal. Chem.* **60** 1925 (1988)
82. V I Grishko, I G Yudelevich, V P Grishko, in *Tezisy Dokladov XIX Vsesoyuznogo S'ezda po Spektroskopii, Tomsk, 1983* (Abstracts of Reports of the XIXth All-Union Congress on Spectroscopy, Tomsk, 1983) p. 23
83. M D Morris, K Peck *J. Chromatogr.* **448** 193 (1988)
84. E S Yeung *J. Chromatogr. Libr.* **30** 135 (1985)
85. K Nakanishi, T Imasaka, N Ishibashi *Anal. Chem.* **57** 1219 (1985)
86. V I Grishko, I G Yudelevich, V P Grishko *Zh. Anal. Khim.* **39** 1219 (1984) [a]
87. V I Grishko, I G Yudelevich, V P Grishko *Anal. Chim. Acta* **160** 159 (1984)
88. A G Abroskin, T V Belyaeva, E K Ivanova, S G Mayakova, M A Proskurnin *Zh. Anal. Khim.* **46** 1199 (1991) [a]
89. A G Abroskin, Yu A Barbalat, T V Belyaeva, E K Ivanova, M A Proskurnin, V M Savostina, V A Filichkina *Mendeleev Commun.* **1** 57 (1991)
90. V A Filichkina, A G Abroskin, Yu A Barbalat, T V Belyaeva, M A Proskurnin, V M Savostina *Zh. Anal. Khim.* **47** 503 (1992) [a]
91. V A Filichkina, A G Abroskin, O M Zharikova, M A Proskurnin, V M Savostina *Zh. Anal. Khim.* **47** 660 (1992) [a]
92. V A Filichkina, A G Abroskin, M A Proskurnin, V M Savostina *Zh. Anal. Khim.* **47** 1417 (1992) [a]
93. A G Abroskin, T V Belyaeva, V A Filichkina, E K Ivanova, M A Proscurnin, V M Savostina, Yu A Barbalat *Analyst* **117** 1957 (1992)
94. M Giglio, A Vendramini *Appl. Phys. Lett.* **25** 555 (1974)
95. J Pawliszyn *Anal. Chem.* **60** 766 – 773 (1988)
96. G Eden, W Schroer, W Staude *Opt. Commun.* **63** 135 (1987)
97. S L Nickolaisen, S E Bialkowski *Anal. Chem.* **58** 215 (1986)
98. W A Weimer, N J Dovichi *Appl. Opt.* **24** 2981 (1985)
99. M A Proskurnin, M E Volkov *Vestn. Mosk. Univ., Ser. 2: Khim.* **41** 182 (2000) [b]
100. H Chen, J Du, E Wang *Guangpuxue Yu Guangpu Fenxi* **12** 117 (1992)
101. S R Erskine, D R Bobbitt *Appl. Spectrosc.* **43** 668 (1989)
102. M Franko, D Bicanic *Israel J. Chem.* **38** 175 (1998)
103. V P Kozich, A Marcano, F E Hernandez, J Castillo *Appl. Spectrosc.* **48** 1419 (1994)
104. T K J Pang, M D Morris *Anal. Chem.* **27** 1253 (1985)
105. S R Erskine, D R Bobbitt *Anal. Chem.* **61** 910 (1989)
106. V I Grishko, I G Yudelevich *Zh. Anal. Khim.* **44** 1753 (1989) [a]
107. M J Pelletier, J M Harris *Anal. Chem.* **55** 1537 (1983)
108. T G Nolan, N J Dovichi *Anal. Chem.* **59** 2803 (1987)
109. C D Tran *Appl. Spectrosc.* **40** 1108 (1986)
110. G R Long, S E Bialkowski *Anal. Chem.* **57** 1079 (1985)
111. S E Bialkowski, G R Long *Anal. Chem.* **59** 873 (1987)
112. E Steinle, W Faubel, H J Ache *Anal. Chim. Acta* **353** 207 (1997)
113. B S Seidel, W Faubel *Opt. Eng.* **36** 469 (1997)
114. B S Seidel, W Faubel *J. Chromatogr. A* **817** 223 (1998)
115. A K Malik, W Faubel *Chem. Soc. Rev.* **29** 275 (2000)
116. J M Saz, J C Díez-Masa *J. Liq. Chromatogr.* **17** 499 (1994)
117. G Ramis-Ramos *Anal. Chim. Acta* **283** 623 (1993)
118. T G Nolan, W A Weimer, N J Dovichi *Anal. Chem.* **56** 1700 (1984)
119. T Shimosaka, T Sugil, T Hobo, J B Alexander Ross, K Uchiyama *Anal. Chem.* **72** 3532 (2000)
120. T Shimosaka, T Sugil, K Uchiyama, T Hobo *Bunseki Kagaku* **47** 1099 (1998)
121. H Minato, Y Ishido *Rev. Sci. Instrum.* **72** 2889 (2001)
122. B C Li, R Gupta *Appl. Opt.* **40** 1563 (2001)
123. K Chew, Rusli, S F Yoon, J Ahn, Q Zhang, V Ligachev, E J Teo, T Osipowicz, F Watt *Appl. Phys.* **91** 4319 (2002)
124. K H Jun, R Carius, H Stiebig *Phys. Rev. B* **66** (2002)
125. Z Remez, M Nesladek, C S J Pickles *Phys. Status Solidi A* **186** 297 (2001)
126. T Hoshimiya, K Miyamoto *Jpn. J. Appl. Phys.* **140** 3591 (2001)
127. C Eisele, C E Nebel, M Stutzmann *Solid State Phenomena* **80 – 81** 205 (2001)
128. N A George, C P G Vallablan, V P N Nampoori, P Radhakrishnan *Appl. Opt.* **41** 5179 (2002)
129. E Corona-Organishe, E Lopez-Cruz *Mod. Phys. Lett. B* **15** 613 (2001)
130. L M Wu, A Knoesen *J. Polym. Sci., Polym. Phys. Ed.* **39** 2717 (2001)
131. F Charbonnier, D Fournier *Rev. Sci. Instrum.* **57** 1126 (1986)
132. P K Kuo, M J Lin, C B Reyes, L D Favro, R L Thomas, D S Kim, S Y Zhang, L J Inglehart, D Fournier, A C Boccara, N Yacoubi *Can. J. Phys.* **64** 1165 (1986)
133. J P Roger, F Lepoutre, D Fournier, A C Boccara *Thin Solid Films* **155** 165 (1987)
134. J P Roger, D Fournier, A C Boccara, F Lepoutre *J. Phys. (France)* **50** 295 (1989)
135. D Fournier, B C Forget *J. Phys. IV* **1** 241 (1991)
136. G Savignat, P Bosh, L Pottier, D Vandembroucq, D Fournier *J. Phys. IV* **3** 1267 (1993)
137. G C Pandey, C Boue, D Fournier, A C Boccara *J. Phys. IV* **4** 279 (1994)
138. J P Roger, P Gleyzes, H Elrhaleb, D Fournier, A C Boccara *Thin Solid Films* **261** 132 (1995)
139. A Salazar, A Sanchezlavega, A Ocariz, J Guitonny, J C Pandey, D Fournier, A C Boccara *Appl. Phys. Lett.* **67** 626 (1995)
140. E Anger, A Gicquel, M F Ravet, Z Z Whang, F Rousseaux, J Perriere, F Rossi, D Fournier, K Plamann *Vide, Couches Minces* **51** 139 (1995)
141. K Plamann, D Fournier *Phys. Status Solidi A* **154** 351 (1999)
142. A Salazar, A Sanchezlavega, A Ocariz, J Guitonny, J C Pandey, D Fournier, A C Boccara *J. Appl. Phys.* **79** 3984 (1996)
143. A Ocariz, A Sanchezlavega, A Salazar, D Fournier, A C Boccara *J. Appl. Phys.* **80** 2968 (1996)

144. I Barbereau, B C Forget, D Fournier *Prog. Nat. Sci.* **6** S503 (1996)
145. R A Palmer, A C Boccara, D Fournier *Prog. Nat. Sci.* **6** S3 (1996)
146. J Fantini, D Fournier, A C Boccara, V Plichon *Electrochim. Acta* **42** 937 (1997)
147. A C Boccara, D Fournier, A Kumar, G C Pandey *J. Appl. Polym. Sci.* **63** 1785 (1997)
148. S Tuli, A B Bhattacharrya, B C Forget, D Fournier *Sens. Actuators, A* **64** 203 (1998)
149. J F Bisson, D Fournier *J. Appl. Phys.* **83** 1036 (1998)
150. G C Pandey, A Kumar, A C Boccara, D Fournier *J. Appl. Polym. Sci.* **67** 1249 (1998)
151. J F Bisson, D Fournier *J. Appl. Phys.* **84** 38 (1998)
152. G C Pandey, A Kumar, A C Boccara, D Fournier *Process Control Qual.* **11** 129 (1998)
153. D Fournier, W Coatesworth, J P Roger *Anal. Sci.* **17** S490 (2001)
154. B C Li, L Plottier, J P Roger, D Fournier, K Watari, K Hirao *J. Eur. Ceram. Soc.* **19** 1631 (1999)
155. J A Batista, D Takeuti, A M Mansanares, E C Da Silva *Anal. Sci.* **17** S73 (2001)
156. A Salazar, A Sanchez-Lavega, J M Terron, M Gateshki *Bol. Soc. Esp. Ceram.* **39** 584 (2000)
157. G Chen, P Hui, S Xu *Thin Solid Films* **366** 95 (2000)
158. G Chen, P Hui *Thin Solid Films* **339** 58 (1999)
159. K Kurabayashi, K E Goodson *IEEE Compon. Pack A* **21** 506 (1998)
160. K L Muratikov, I O Usov, H G Walther, H Karge, A V Suvorov *Appl. Phys. Lett.* **71** 3001 (1997)
161. T Tanaka, A Harata, T Sawada *J. Appl. Phys.* **82** 4033 (1997)
162. M Nestoros, B C Forget, A Seas, C Cristofides *Prog. Nat. Sci.* **6** S507 (1996)
163. A M Masanares, T Velinov, Z Bozoki, D Fournier, A C Boccara *J. Appl. Phys.* **75** 3344 (1994)
164. G Chen, C L Tien *J. Appl. Phys.* **73** 3461 (1993)
165. V A Sablikov *J. Appl. Phys.* **70** 1084 (1991)
166. A Mandelis, A A Waard, K T Lee *J. Appl. Phys.* **7** 1086 (1991)
167. A Seas, C Cristofides *Appl. Phys. Lett.* **66** 3346 (1995)
168. G Amato, L Boarino, G Benedetto, R Spagnolo *Thin Solid Films* **255** 111 (1995)
169. G Benedetto, L Boarino, R Spagnolo *Phys. Status Solidi A* **146** 777 (1994)
170. L Fabbri, D Fournier, L Pottier, L Esposito *J. Mater. Sci.* **31** 5429 (1996)
171. T Ikari, J P Roger, D Fournier *Rev. Sci. Instrum.* **74** 553 (2003)
172. S Janssen, G R Hofmann, W Faubel, H J Ache *Fresenius' J. Anal. Chem.* **360** 788 (1998)
173. M Bertolotti, G L Liakhou, R Li Voti, S Paoloni, C Sibilia *Appl. Phys. B* **67** 641 (1998)
174. M J S Kreiter, S S Mittler-Neher *Thin Solid Films* **342** 244 (1999)
175. K Plamann, D Fournier, B C Forget, A C Boccara *Diamond Relat. Mater.* **5** 699 (1996)
176. *Rev. Sci. Instrum.* **74** A13 (2003)
177. M Harada, S Obata, T Kitamori, T Sawada *Anal. Chem.* **65** 2181 (1993)
178. M Harada, K Iwamoto, T Kitamori, T Sawada *Anal. Chem.* **65** 2938 (1993)
179. H Kimura, S Matsuzawa, C-Y Tu, T Kitamori, T Sawada *Anal. Chem* **68** 3063 (1996)
180. F K Fotiou, M D Morris *Anal. Chem.* **59** 185 (1987)
181. F K Fotiou, M D Morris *Anal. Chem.* **59** 1146 (1987)
182. P J Treado, M D Morris *Appl. Spectrosc.* **42** 1487 (1988)
183. J Gibkes, I Vovk, J Bolte, D Bicanic, B Bein, M Franko *J. Chromatogr. A* **786** 163 (1997)
184. T G Nolan, D J Bornhop, N J Dovichi *J. Chromatogr.* **384** 189 (1987)
185. J G Laufer, P C Beard, T N Mills *Rev. Sci. Instrum.* **73** 3345 (2002)
186. H G Walther *Appl. Surf. Sci.* **193** 156 (2002)
187. B Choi, B Majaron, J S Nelson *Laser Surg. Med.* **79** 14 (2002)
188. Y Nagasaka, T Sato, T Ushiki *Meas. Sci. Technol.* **12** 2081 (2001)
189. J H Gu *Prog. Natl. Sci.* **11** S210 (2001)
190. A Mandelis *NDT & E Int.* **34** 277 (2001)
191. L Nikolaides, A Mandelis, C J Beingessner *J. Appl. Phys.* **89** 7879 (2001)
192. C Martinsons, A Levick, G Edwards *Anal. Sci.* **17** S114 (2001)
193. P Xiao, J A Cowen, R E Imhof *Anal. Sci.* **17** S349 (2001)
194. J C Krapez, R Li Voti *Anal. Sci.* **17** S417 (2001)
195. A Levick, G Edwards *Anal. Sci.* **17** S438 (2001)
196. T Zweschper, A Dillenz, G Busse *Insight* **43** 173 (2001)
197. M K Loze, C D Wright *J. Biomed. Opt.* **6** 74 (2001)
198. J S Nelson, B Majaron, K M Kelly *Semin. Cutan. Med. Surg.* **19** 253 (2000)
199. A Mandelis, Y Riopel *J. Vac. Sci. Technol. A* **18** 705 (2000)
200. L Nikolaides, A Mandelis, S H Abrams *J. Biomed. Opt.* **5** 31 (2000)
201. A Mandelis, M Munidasa, L Nicolaides *NDT & E Int.* **32** 437 (1999)
202. W Karpen, D Wu, G Busse *Res. Nondestruct. Eval.* **11** 179 (1999)
203. E M Abdulwafa *J. Phys. D* **32** 1626 (1999)
204. L Fabbri, M Oksanen *J. Therm. Spray Technol.* **8** 263 (1999)
205. T Ikari, A Salnick, A Mandelis *J. Appl. Phys.* **85** 7392 (1999)
206. L Kehoe, P V Kelly, G M Crean *Microsyst. Technol.* **5** 18 (1998)
207. V Scharf, O Eyal, A Katzir *Opt. Eng.* **37** 2784 (1998)
208. D T Wu, G Busse *Rev. Gen. Therm.* **37** 693 (1998)
209. O Eyal, V Scharf, A Katzir *Appl. Opt.* **37** 5945 (1998)
210. A Feldman, N M Bazaretti *Rev. Sci. Instrum.* **69** 2576 (1998)
211. N Hmina, Y Scudeller *Int. J. Heat Mass Transfer* **41** 2781 (1998)
212. G Chen, T Borca-Tascuic *Int. J. Heat Mass Transfer* **41** 2279 (1998)
213. M Munidasa, F Funak, A Mandelis *J. Appl. Phys.* **83** 3495 (1998)
214. L Nicolaides, M Munidasa, A Mandelis *Inverse Probl.* **13** 1413 (1997)
215. T Kitamori, T Matsui, M Sakagami, T Sawada *Chem. Lett.* **4** 2205 (1989)
216. M Tokeshi, T Minagawa, K Uchiyama, A Hibara, K Sato, H Hisamoto, T Kitamori *Anal. Chem.* **74** 1565 (2002)
217. A Hibara, M Nonaka, H Hisamoto, K Uchiyama, Y Kikutani, M Tokeshi, T Kitamori *Anal. Chem.* **74** 1724 (2002)
218. A Hibara, K Sato, H Hisamoto, K Uchiyama, M N Slyadnev, M Tokeshi, T Kitamori *Prog. Nat. Sci.* **11** S237 (2001)
219. H Hisamoto, T Horiuchi, K Uchiyama, M Tokeshi, A Hibara, T Kitamori *Anal. Chem.* **73** 5551 (2001)
220. T Kitamori *Fresenius' J. Anal. Chem.* **371** 89 (2001)
221. M Tokeshi, M Uchida, A Hibara, T Sawada, T Kitamori *Anal. Chem.* **73** 2112 (2001)
222. K Sato, M Tokeshi, H Kimura, T Kitamori *Anal. Chem.* **73** 1213 (2001)
223. H Hisamoto, T Horiuchi, M Tokeshi, A Hibara, T Kitamori *Anal. Chem.* **73** 1382 (2001)
224. A Hibara, M Tokeshi, K Uchiyama, H Hisamoto, T Kitamori *Anal. Sci.* **17** 89 (2001)
225. Z H Zhang, T Kitamori, T Sawada, I Tsuyumoto *Anal. Sci.* **16** 1199 (2000)
226. M Tokeshi, T Minagawa, T Kitamori *J. Chromatogr. A* **894** 19 (2000)
227. K Uchiyama, T Kitamori, T Sawada, I Tsuyumoto *Langmuir* **16** 6597 (2000)
228. H M Sorouraddin, A Hibara, M A Proskurnin, T Kitamori *Anal. Sci.* **16** 1033 (2000)
229. M A Proskurnin, M Tokeshi, M N Slyadnev, T Kitamori *Anal. Sci.* **17** S454 (2001)
230. M Tokeshi, T Minagawa, T Kitamori *Anal. Chem.* **72** 1711 (2000)
231. K Sato, M Tokeshi, T Kitamori, T Sawada *Anal. Sci.* **15** 641 (1999)
232. M N Slyadnev, M A Proskurnin, K Sato, M Tokeshi, T Kitamori, Y Tanaka *Bunseki Kagaku Toronkai Koen Yoshishu* **61** 55 (2001)
233. R S Schley, K L Telschow *Opt. Eng.* **41** 1688 (2002)
234. D Pogany, N Seliger, E Gornik, M Stoisiek, T Lalinsky *J. Appl. Phys.* **84** 4495 (1998)
235. Z Sodnik, H J Tiziani *Opt. Commun.* **58** 295 (1986)
236. B C Li, Y Z Deng, J K Cheng *Rev. Sci. Instrum.* **67** 3649 (1996)

237. B C Li, Y Z Deng, J K Cheng *Prog. Nat. Sci.* **6** S657 (1996)
238. M A Owens, C C Davis, R R Dickerson *Anal. Chem.* **71** 1391 (1999)
239. A Yu Luk'yanov, M A Novikov *Zh. Tekh. Fiz.* **70** 99 (2000) [c]
240. A Yu Luk'yanov *Pis'ma Zh. Tekh. Fiz.* **26** 43 (2000) [d]
241. B S Seidel, W Faubel, J Henningsen, H J Ache *Prog. Nat. Sci.* **6** S614 (1996)
242. W Faubel, B S Seidel, H J Ache *Opt. Eng.* **35** 3555 (1996)
243. B S Seidel, O Dübel, W Faubel, H J Ache *Fresenius' J. Anal. Chem.* **354** 900 (1996)
244. K Haupt, D Bicanic, E Gerkema, A Frandas *Biosci. Biotech. Biochem.* **59** 1044 (1995)
245. M Soltanolkotabi, R Gupta *Appl. Opt.* **37** 7137 (1998)
246. X Zhao, T Suzuki, O Sasaki *Opt. Rev.* **9** 13 (2002)
247. M A Owens, C C Davis, R R Dickerson, in *Lasers and Electro-Optics Society Annual Meeting (LEOS'94), Boston, 1994*
248. A Yu Luk'yanov, G B Vladykin, M A Novikov, Ya I Yashin *Zh. Anal. Khim.* **54** 718 (1999) [a]
249. V V Ivanov, M A Novikov, V M Gelikonov *Pis'ma Zh. Tekh. Fiz.* **25** 34 (1999) [d]
250. A Yu Luk'yanov, G B Vladykin, A A Aratskova, M A Novikov, Ya I Yashin *Zh. Fiz. Khim.* **71** 1497 (1997) [e]
251. A Yu Luk'yanov, M A Novikov, G B Vladykin, Ya I Yashin *Opt. Spektrosk.* **79** 348 (1995) [f]
252. Y Han, Z L Wu, J S Rosenshein, M Thomsen, Q Zhao, K Moncur *Opt. Eng.* **38** 2122 (1999)
253. J F Power, M A Schweitzer *Opt. Eng.* **36** 512 (1997)
254. X R Zhu, J M Harris *Chem. Phys.* **157** 409 (1991)
255. R T Cambron, J M Harris *J. Phys. Chem.* **99** 695 (1995)
256. R T Cambron, J M Harris *Anal. Chem.* **67** 365 (1995)
257. X R Zhu, J M Harris *J. Phys. Chem.* **97** 6650 (1993)
258. X R Zhu, J M Harris *Chem. Phys. Lett.* **186** 183 (1991)
259. K Tanzawa, N Hirota, M Terazima *Bull. Chem. Soc. Jpn.* **70** 2935 (1997)
260. R Miyata, M Terazima *Anal. Sci.* **17** S231 (2001)
261. E Vauthey *J. Photochem. Photobiol. A* **109** 195 (1997)
262. A Hammiche, L Bozec, M J German, J M Chalmers, N J Everall, G Poultier, M Reading, D B Grandy, F L Martin, H M Pollock *Spectrocsopy* **19** 20 (2004)
263. J D Rudnitski, F R McLarnon, E J Cairns, in *Techniques for Characterization of Electrodes and Electrochemical Processes* (Eds R Varna, J R Selman) (New York: Wiley, 1991) p. 127
264. J D Rudnitski, G M Brisard, H A Gasteiger, R E Russo, F R McLarnon, E J Cairns *J. Electronal. Chem.* **362** 55 (1993)
265. O Haas, J Rudnitski, F R McLarnon, E J Cairns *J. Chem. Soc., Faraday Trans.* **87** 939 (1991)
266. http://eetd.lbl.gov/BERC/Page1.html
267. L Bozec, A Hammiche, H M Pollock, M Conroy, J M Chalmers, N J Everall, L Turin *J. Appl. Phys.* **90** 5159 (2001)
268. A Hammiche, H M Pollock, M Reading, M Claybourn, P Turner, K Jewkes *Appl. Spectrosc.* **53** 810 (1999)
269. A Majumdar *Annu. Rev. Mater. Sci.* **29** 505 (1999)
270. R B Dinwiddie, R J Pylkki, P E West, in *Thermal Conductivity 22* (Ed. T W Tong) (Lancaster: Technomics, 1994) p. 668
271. V A Filichkina, Candidate Thesis in Chemical Sciences, Moscow State University, Moscow, 1993
272. J M Harris, N J Dovichi *Anal. Chem.* **52** 695A (1980)
273. T Imasaka, K Miyaishi, N Ishibashi *Anal. Chim. Acta* **115** 407 (1980)
274. M A Proskurnin, V V Kuznetsova *Anal. Chim. Acta* **418** 101 (2000)
275. J Shen, R D Snook *J. Appl. Phys.* **73** 5286 (1993)
276. M A Proskurnin, V V Kuznetsova, M E Volkov, V V Chernysh, in *The 12th International Conference on Photoacoustic and Photothermal Phenomena (Book of Abstracts), Toronto, Canada, 2002* p. 173
277. A Eickmeier, T Bahnes, E Schollmeyer *Angew. Macromol. Chem.* **185** 239 (1991)
278. S E Bialkowski *Trends Anal. Chem.* **17** 520 (1998)
279. R D Snook *Chem. Soc. Rev.* **26** 319 (1997)
280. B B Radak, S S Miljanic *J. Serb. Chem. Soc.* **51** 37 (1986)
281. Y Inoue, H Hori, T Sakurai, Y Tokimoto, J Saito, T Misonou *Opt. Rev.* **9** 75 (2002)
282. D J Qian, A Planner, J Miyake, D Frackowiak *J. Photochem. Photobiol. A* **144** 93 (2001)
283. M A Proskurnin, N V Osipova, V V Kuznetsova, E K Ivanova, A G Abroskin *Analyst* **121** 419 (1996)
284. A Driesenaar, U Schreiber, S Malkin *Photosynth. Res.* **40** 45 (1994)
285. S E Bialkowski *Chem. Phys. Lett.* **105** 448 (1984)
286. P Calmettes, C Laj *Colloq. Int. CNRS* **202** C1 (1972)
287. R T Bailey, F R Cruickshank, D Pugh, A McLeod, W Johnstone *Chem. Phys.* **68** 351 (1982)
288. E Z Gribova, Yu M Sorokin *Kvant. Elektron.* **17** 488 (1990) [g]
289. A D Bishigaev, S M Burkitbaev, E A Manykin, A E Nikitin, P P Poluektov *Kvant. Elektron.* **16** 2153 (1989) [g]
290. N M Danilenko, V I Romanenko, L P Yatsenko *Dokl. Akad. Nauk Ukr.SSR, Geol., Khim. Biol. Nauki* **3** 59 (1989)
291. L S Aslanyan, M A Khurshudyan *Opt. Spektrosk.* **70** 188 (1991) [f]
292. C E Buffett, M D Morris *Appl. Spectrosc.* **37** 455 (1983)
293. W Bai, B S Wong *J. Appl. Phys.* **89** 3275 (2001)
294. C Gruss, U Katscher, B K Bein, J Pelzl *Prog. Nat. Sci.* **6** S305 (1996)
295. A Chartier, S E Bialkowski *Opt. Eng.* **36** 303 (1997)
296. K Uchiyama, A Hibara, H Kimura, T Sawada, T Kitamori *Jpn. J. Appl. Phys.* **39** 5316 (2000)
297. A Mandelis, P Hess (Eds) *Progress in Photothermal and Photoacoustic Science and Technology* Vol. 3 (Washington, DC: Optical Engineering Press, 1997)
298. V P Grishko, V I Grishko, V M Moralev, in *Tezisy Dokladov III Vsesoyuznoi Konferentsii po Novym Metodam Spektral'nogo Analiza, Zaporozh'e, 1983* (Abstracts of Reports of the IIIth All-Union Conference on New Methods of Spectrum Analysis, Zaporozh'e, 1983) p. 55
299. M D Morris *Proc. SPIE-Int. Soc. Ont. Eng.* **426** 116 (1983)
300. N M Amer *J. Phys. Colloq. (France)* **44** 185 (1983)
301. N Teramae, J D Winefordner *Appl. Spectrosc.* **41** 164 (1987)
302. D S Burgi, N J Dovichi *Appl. Opt.* **26** 4665 (1987)
303. H M Chen, Z A Schelly *Chem. Phys. Lett.* **145** 102 (1988)
304. K Peck, T Demana, M D Morris *Appl. Theor. Electrophores.* **1** 41 (1988)
305. K Peck, M D Morris *Appl. Spectrosc.* **42** 513 (1988)
306. C N Renn, R C Synovec *Anal. Chem.* **60** 1188 (1988)
307. M J Pelletier, H R Thorshelm, J M Harris *Anal. Chem.* **54** 239 (1982)
308. R T Bailey, F R Cruickshenk, D Pugh *Chem. Br.* **25** 39 (1989)
309. R L Swofford, J A Morell *J. Appl. Phys.* **49** 3667 (1978)
310. N Ragozina, S Heissler, W Faubel, U Pyell *Anal. Chem.* **74** 4480 (2002)
311. B S Seidel, W Faubel *Fresenius' J. Anal. Chem.* **360** 795 (1998)
312. A Yu Lukyanov, M A Proskurnin, A A Bendryshev, A I Elefterov, O A Shpigun, in *ICAS 2001. IUPAC International Congress Analytical Sciences (Program and Abstracts), Tokyo, 2001* p. 280
313. A Yu Luk'yanov, S N Bendrysheva, M A Proskurnin, A A Bendryshev, A I Elefterov, O A Shpigun *Rev. Sci. Instrum.* **74** 656 (2003)
314. http://www1.odn.ne.jp/imt/english/09.html
315. E Tamaki, A Hibara, M Tokeshi, T Kitamori *J. Chromatogr. A* **987** 197 (2003)
316. H Hisamoto, Y Shimizu, K Uchiyama, M Tokeshi, Y Kikutani, A Hibara, T Kitamori *Anal. Chem.* **75** 350 (2003)
317. M Ueno, H Hisamoto, T Kitamori, S Kobayashi *Chem. Commun.* 936 (2003)
318. M A Proskurnin, M N Slyadnev, M Tokeshi, T Kitamori *Anal. Chim. Acta* **480** 79 (2003)
319. K Uchiyama, A Hibara, K Sato, H Hisamoto, M Tokeshi, T Kitamori *Electrophoresis* **24** 179 (2003)
320. J R D Pereira, A M Masanares, A J Palangana, M L Baesso *Mol. Cryst. Liq. Cryst. A* **332** 3079 (1999)
321. R D Snook *Analyst* **125** 45 (2000)
322. G J Blanchard *Appl. Spectrosc.* **55** 110a (2001)
323. I G Calasso, M Chirtoc, M W Sigrist *Prog. Nat. Sci.* **6** S618 (1996)
324. H S M Devries, M R Vanlieshout, F J M Harren, J Reuss *Infrared Phys. Technol.* **36** 483 (1995)

325. D Y Chen, N J Dovichi *J. Chromatogr. B* **657** 265 (1994)
326. S B Lang *Key Eng. Mater.* **92** 83 (1994)
327. H S M Devries, N Dam, M R Vanlieshout, C Sikkens, F J M Harren, J Reuss *Rev. Sci. Instrum.* **66** 4655 (1995)
328. C T Chen, J L Graham, B Dellinger *Waste Manag.* **15** 159 (1995)
329. M Z Silva, P Forge, F Lepoutre *J. Phys.: Condens. Mater* **7** 9401 (1995)
330. M Martinelli, U Zammit, F Mercuri, R Pizzoferrato *J. Appl. Phys.* **72** 1096 (1992)
331. M Lenzi, E Molinari, G Piciacchia *Chem. Phys.* **173** 291 (1993)
332. N Nakatani *Rev. Sci. Instrum.* **71** 1971 (2000)
333. B C Li, R Gupta *J. Appl. Phys.* **89** 859 (2001)
334. G C Pandey, A Kumar *J. Sci. Ind. Res.* **60** 28 (2001)
335. O Oehler *Anal. Sci.* **17** S436 (2001)
336. R L Thomas *Anal. Sci.* **17** S1 (2001)
337. B Neuenschwander, R Weber, H P Weber *IEEE J. Quantum Electron.* **32** 365 (1996)
338. P K Mukhopadhyay, J George, S K Sharma, K Ranganathan, T P S Nathan *Opt. Laser Technol.* **34** 357 (2002)
339. D Mudge, M Ostermeyer, P J Veitch, J Munch, B Middlemiss, D J Ottaway, M W Hamilton *IEEE J. Sel. Top. Quantum. Electron.* **6** 643 (2000)
340. J L Blows, G W Forbes, J M Dawes *Opt. Commun.* **186** 111 (2000)
341. C V Bindhu, S S Harilal *Anal. Sci.* **17** 141 (2001)
342. T Graf, E Wyss, M Roth, H P Weber *Opt. Commun.* **190** 327 (2001)
343. K X Liu, C J Flood, D R Walker, H M Vandriel *Opt. Lett.* **17** 1361 (1992)
344. S A Chetkin, G V Vdovin, K Ueda *Laser Phys.* **5** 1189 (1995)
345. H J Eichler, A Haase, R Menzel *Int. J. Nonlinear Opt. Phys.* **3** 339 (1994)
346. U J Greiner, H H Klingenberg *Opt. Lett.* **19** 1207 (1994)
347. T Dascalu, N Pavel, V Lupei *J. Phys. IV* **4** 73 (1994)
348. J L Blows, J M Dawes, J A Piper *Opt. Commun.* **162** 247 (1999)
349. J A Sampaio, S M Lima, T Catunda, A N Medina, A C Bento, M L Baesso *J. Non-Cryst. Solids* **304** 315 (2002)
350. Y Yang *Anal. Chem.* **56** 2336 (1984)
351. Y Yang *Anal. Chem.* **58** 1420 (1986)
352. K Miyaishi, T Imasaka, N Ishibashi *Anal. Chim. Acta* **124** 381 (1981)
353. V I Grishko, I G Yudelevich, L Kh Kravchenko, V P Nikitina *Zh. Anal. Khim.* **39** 826 (1984) [a]
354. T Imasaka, K Sakaki, N Ishibashi *Anal. Chim. Acta* **243** 109 (1991)
355. K L Jansen, J M Harris *Anal. Chem.* **57** 2434 (1985)
356. T G Nolan, N J Dovichi *IEEE Circuits Devices Mag.* **2** 54 (1986)
357. T G Nolan, W A Weimer, N J Dovichi *Anal. Chem.* **56** 1704 (1984)
358. G Ramis-Ramos, M C Garcta-Alvares-Coque, B W Smith, N Omenetto, J D Winefordner *Appl. Spectrosc.* **42** 341 (1988)
359. V I Grishko, C D Tran, W W Duley *Appl. Opt.* **41** 5814 (2002)
360. S Luterotti, M Franko, M Šicovec, D Bicanic *Anal. Chim. Acta* **460** 193 (2002)
361. A Kurian, K P Unnikrishnan, P Gopinath, V P N Nampoori, C P G Vallabhan *J. Nonlinear Opt. Phys.* **10** 415 (2001)
362. X L Zhang, H T Yan, G Q Liu *Chin. J. Anal. Chem.* **30** 75 (2002)
363. T Yoshihara, H Shimada, H Shizuka, S Tobita *Phys. Chem. Chem. Phys.* **3** 4972 (2001)
364. N Arnaud, J Georges *Anal. Chim. Acta* **445** 239 (2001)
365. X L Zhang, H T Yan, G Q Liu *Anal. Lett.* **34** 2159 (2001)
366. A Marcano, C Loper, N Melikechi *Phys. Lett.* **78** 3415 (2001)
367. N Arnaud, J Georges *Spectrochim. Acta* **57** 1295 (2001)
368. M Franko, M Šikovec, J Kozar-Logar, D Bicanic *Anal. Sci.* **17** S515 (2001)
369. A S Fontes, A C Bento, L C M Miranda, M L Baesso *Anal. Sci.* **17** S526 (2001)
370. M Ith, M Frenz, H P Weber *Appl. Opt.* **40** 2216 (2001)
371. N Arnaud, J Georges *Spectrochim. Acta* **57** 1085 (2001)
372. S S Gupte, O Marcano, R D Pradhan, C D Desai, N Melikechi *J. Appl. Phys.* **89** 4939 (2001)
373. S Legeai, J Georges *Anal. Lett.* **33** 3153 (2000)
374. D Bicanic, O Dhka, S Luterotti, A Bohren, M Šikovec, B van Veldhuizen, O Berkessy, M Chirtoc, M Franko, G Szabo, M Sigrist *Anal. Sci.* **17** S547 (2001)
375. D A Affonce, A J Fowler *J. Quant. Spectrosc. Radiat. Transfer* **73** 473 (2002)
376. H Hisamoto, T Saito, M Tokeshi, A Hibara, T Kitamori *Chem. Commun.* **24** 2662 (2001)
377. T Imasaka *Anal. Sci.* **9** 329 (1993)
378. Y Yang, S C Hall, M C de la Cruz *Anal. Chem.* **58** 758 (1988)
379. C N Kettler, M J Sepaniak *Anal. Chem.* **59** 1733 (1987)
380. M Yu, N J Dovichi *Microchim. Acta* **3** 27 (1988)
381. M Yu, N J Dovichi *Appl. Spectrosc.* **43** 196 (1989)
382. V V Chernysh, M A Proskurnin, V V Kuznetsova, S V Pakhomova *Anal. Commun.* **34** 291 (1997)
383. M A Proskurnin, A V Pikhtar', V B Ivleva, E K Ivanova *Zavod. Lab.* **67** 12 (2001)
384. N S Evtushenko, M A Proskurnin, N V Orlova, A V Pikhtar', V V Kuznetsova *Vedomosti Nauchnogo Tsentra Ekspertizy i Gosudarstvennogo Kontrolya Lekarstvennykh Sredstv Minzdrava Rossii* (Bulletin of the Scientific Centre of Examination and State Control of Drugs of the Russian Ministry of Health) **3** 84 (2000)
385. M A Proskurnin, N V Orlova, A V Pikhtar', V V Kuznetsova *Vestn. Mosk. Univ., Ser. 2: Khim.* **41** 30 (2000) [b]
386. M A Proskurnin, N V Orlova, V V Kuznetsova, N S Evtushenko, A V Pikhtar', in *VIII Rossiiskii Natsional'nyi Kongress 'Chelovek i Lekarstvo' (Tez. Dokl.), Moskva, 2001* [Russian National Congress 'The Man and Drug' (Abstracts of Reports), Moscow, 2001] p. 705
387. C H Langford, D W Gutzman *Anal. Chim. Acta* **256** 183 (1992)
388. D W Gutzman, C H Langford *Anal. Chim. Acta* **283** 773 (1993)
389. L Poganik, M Franko *Biosens. Bioelectron.* **14** 569 (1999)
390. L Poganik, M Franko *Biosens. Bioelectron.* **18** 1 (2003)
391. M A Proskurnin, D A Nedosekin, V V Kuznetsova *Talanta* **57** 841 (2002)
392. V V Chernysh, M Yu Kononets, M A Proskurnin, S V Pakhomova, V V Komissarov, A I Zatsman *Fresenius' J. Anal. Chem.* **369** 535 (2001)
393. A A Dzyabchenko, M A Proskurnin, A G Abroskin, D V Chaschikhin *J. Chromatogr. A* **827** 13 (1998)
394. M A Proskurnin, V V Chernysh, M A Kurzin *Zh. Anal. Khim.* **56** 38 (2001) [a]
395. M A Proskurnin, M A Kurzin, V V Chernysh *Vestn. Mosk. Univ., Ser. 2: Khim.* **42** 116 (2001) [b]
396. V A Filichkina, A G Abroskin, Yu A Barbalat, I V Golovko, M A Proskurnin, V M Savostina *Zh. Anal. Khim.* **48** 269 (1993) [a]
397. M A Proskurnin, V B Ivleva, N Yu Ragozina, E K Ivanova *Anal. Sci.* **16** 397 (2000)
398. V V Kuznetsova, M A Proskurnin, N Yu Ragozina, S V Pakhomova *Vestn. Mosk. Univ., Ser. 2: Khim.* **41** 178 (2000) [b]
399. V V Kuznetsova, M A Proskurnin, D S Rudelev, A P Smirnova, S N Bendrysheva *Analit. Kontrol* **6** 13 (2002)
400. V V Chernysh, M A Proskurnin, A A Dzyabchenko, E K Ivanova *Zh. Anal. Khim.* **55** 378 (2000) [a]
401. S V Pakhomova, M A Proskurnin, V V Chernysh, M Yu Kononets, E K Ivanova *Zh. Anal. Khim.* **56** 1042 (2001) [a]
402. M A Proskurnin, V V Chernysh, S V Pakhomova, M Yu Kononets, A A Sheshenev *Talanta* **57** 831 (2002)
403. V V Chernysh, I V Nesterova, M A Proskurnin *Talanta* **53** 1073 (2001)
404. M A Proskurnin, V V Chernysh, M Yu Kononets, S V Pakhomova, V V Kuznetsova *Anal. Sci.* **17** S19 (2001)
405. M A Proskurnin, V V Chernysh, S V Pakhomova, M Yu Kononets, A P Smirnova, D A Nedosekin *Anal. Sci.* **17** i1169 (2001)
406. V V Chernysh, Candidate Thesis in Chemical Sciences, Moscow State University, Moscow, 2002
407. V V Chernysh, M A Proskurnin, D A Nedosekin *Zh. Anal. Khim.* **58** 166 (2003) [a]
408. A Chartier, J Georges *Anal. Chim. Acta* **284** 311 (1993)
409. S Chanlon, J Georges *Spectrochim. Acta, Part A* **58** 1607 (2002)
410. J Georges, S Ghazarian *Anal. Chim. Acta* **276** 401 (1993)

411. A Chartier, J Georges, J M Mermet *Spectrochim. Acta, Part A* **47** 1505 (1991)
412. T Sawada, S Oda, H Shimizu, H Kamada *Anal. Chem.* **51** 688 (1979)
413. N Omenetto, P Cavalli, G Rossi, G Bidoglio, G C Turk *J. Anal. At. Spectrom.* **2** 579 (1987)
414. D Rojas, R J Silva, R E Russo *Rev. Sci. Instrum.* **62** 2989 (1992)
415. N V Orlova, M A Proskurnin, V A Samburova, M V Fedyaev, P V Tsvetkov, A V Brusnichkin, in *The 12th International Conference on Photoacoustic and Photothermal Phenomena (Book of Abstracts), Toronto, Canada, 2002* p. 110
416. N V Orlova, M A Proskurnin, V A Samburova, I D Dryagleva, A V Brusnichkin *Rev. Sci. Instrum.* **74** 506 (2003)
417. M A Proskurnin, N V Orlova, P V Tsvetkov, V A Samburova *Zh. Anal. Khim.* **58** 171 (2003) [a]
418. Y Li, R Gupta *Appl. Phys. B* **75** 903 (2002)
419. E B Sandell, H Onishi *Photometric Determination of Traces of Metals* (New York: Wiley, 1985)
420. Z Marzenko *Kolorymetryczne Oznaczanie Pierwiastkow* (Warszawa: Wysdawnictwa Naukowo-Techniczne, 1968)
421. G Norwitz, M Galan *Anal. Chim. Acta* **83** 289 (1976)
422. A A Nemodruk *Analiticheskaya Khimiya Sur'my* (Analytical Chemistry of Antimony) (Moscow: Nauka, 1978)
423. E W McChesney *Ind. Eng. Chem. Anal. Ed.* **18** 146 (1946)
424. A Elkind, K H Gayer, D F Boltz *Anal. Chem.* **25** 1744 (1953)
425. Z Marczenko *Chem. Anal. (Warsaw)* **2** 160 (1957)
426. M A Proskurnin, M Tokeshi, M N Slyadnev, T Kitamori, in *The 10th Russian-Japan Joint Symposium on Analytical Chemistry. Final Program (Book of Abstracts), Moscow, St Petersburg, 2000* p. 93
427. Q Han, H T Yan *Chem. J. Chin. Univ.* **23** 573 (2002)
428. Q Han, H T Yan *Prog. Chem.* **14** 24 (2002)
429. T Suzuki, T Ichimura *Anal. Sci.* **17** S23 (2001)
430. M Nagano, T Suzuki, T Ichimura *Anal. Sci.* **17** S26 (2001)
431. K Takeshita, N Hirota, Y Imamoto, M Kataoka, F Tokunaga, M Terazima *Anal. Sci.* **17** S320 (2001)
432. S Takahashi, I Tsuyumoto, T Kitamori, T Sawada *Electrochim. Acta* **44** 165 (1998)
433. A Mandelis, M E Rodriguez, J A Garsia, V Gorodokin, Y Raskin *Anal. Sci.* **17** S265 (2001)
434. M E Rodriguez, A Mandelis, P J Mendoza, J A Garsia *Anal. Sci.* **17** S273 (2001)
435. A Chartier, S E Bialkowski *Appl. Spectrosc.* **55** 84 (2001)
436. M E Rodriguez, J A Garcia, A Mandelis, C Jean, Y Riopel *Appl. Phys. Lett.* **74** 2429 (1999)
437. M Okamoto, F Tanaka, S Hirayama *J. Phys. Chem. A* **102** 10 703 (1998)
438. T Sakka, T Tsuboi, Y H Ogata *J. Chem. Soc., Faraday Trans.* **93** 1305 (1997)
439. D E Falvey *Photochem. Photobiol.* **65** 4 (1997)
440. D M Laman, D E Falvey *Rev. Sci. Instrum.* **67** 3260 (1996)
441. Y Uchiyama, I Tsuyumoto, T Kitamori, T Sawada *J. Phys. Chem. B* **103** 4663 (1999)
442. H T Yan, S K Yang *Chin. Chem. Lett.* **7** 733 (1996)
443. Y Tanaka, M N Slyadnev, K Sato, M Tokeshi, H B Kim, T Kitamori *Anal. Sci.* **17** 809 (2001)
444. M N Slyadnev, Y Tanaka, M Tokeshi, T Kitamori *Anal. Chem.* **73** 4037 (2001)
445. Y Tanaka, M N Slyadnev, A Hibara, M Tokeshi, T Kitamori *J. Chromatogr. A* **894** 45 (2000)
446. K Sato, M Tokeshi, T Odake, H Kimura, T Ooi, M Nakao, T Kitamori *Anal. Chem.* **72** 1144 (2000)
447. Z H Zhang, I Tsuyumoto, T Kitamori, T Sawada *J. Phys. Chem. B* **103** 5742 (1999)
448. B D Barker, R W Larsen *J. Inorg. Biochem.* **85** 107 (2001)
449. K Fujiwara, K Kishibe, H Uchiki, F Shimokoshi, K Fuwa, T Kobayashi *Anal. Biochem.* **127** 164 (1982)
450. K B Yatsimirskii, P E Strizhak, T S Ivaschenko *Talanta* **40** 1227 (1993)
451. R J Field, M Burger (Eds) *Oscillations and Travelling Waves in Chemical Systems* (New York: Wiley, 1985)
452. J J Jwo, R M Noyes *J. Am. Chem. Soc.* **97** 5422 (1975)
453. V Jayalakshmi, R Ramaswamy *Can. J. Chem.* **75** 547 (1997)
454. M Jiang, Y Li, X Zhou, Z Zhao, J Wang, J Mo *Anal. Chim. Acta* **236** 411 (1990)
455. M Terazima, T Azumi *J. Am. Chem. Soc.* **111** 3824 (1989)
456. M Terazima, T Azumi *Chem. Phys. Lett.* **153** 27 (1988)
457. R W Redmond, K Heihoff, S E Braslavsky, T G Tuscott *Photochem. Photobiol.* **45** 209 (1987)
458. M A Proskurnin, A A Shelepchikov, V V Kuznetsova, O A Sviridova, N V Osipova *Vestn. Mosk. Univ., Ser. 2: Khim.* **41** 247 (2000) [b]
459. G Wilkinson, R D Willard, J A McCleverty (Eds) *Comprehensive Coordination Chemistry* Vols 1–7 (Oxford: Pergamon Press, 1987)
460. J E Dickens, F Basolo, H M Neumann *J. Am. Chem. Soc.* **79** 1286 (1957)
461. T S Lee, I M Koltoff, D L Leussing *J. Am. Chem. Soc.* **70** 3596 (1948)
462. F Basolo, H M Hayes, H M Neumann *J. Am. Chem. Soc.* **76** 3807 (1954)
463. A E Harvey, J A Smart *Anal. Chem.* **27** 26 (1955)
464. S Luterotti, M Franko, D Bicanic *J. Am. Oil Chem. Soc.* **79** 1027 (2002)
465. J K Logar, M Šikovec, A Malej, M Franko *Anal. Bioanal. Chem.* **374** 323 (2002)
466. J J Li, K C Waldron *J. Liq. Chromatogr.* **22** 1919 (1999)
467. I Michler, S E Braslavsky *Photochem. Photobiol.* **74** 624 (2001)
468. A Berthod *Spectrochim. Acta* **13** 11 (1990)
469. B Dvijak, M Franko, M Novič *J. Chromatogr. A* **829** 167 (1998)
470. E S Yeung *Chromatogr. Sci.* **45** 117 (1989)
471. D J Bornhop, J G Wangsgaard *J. Chromatogr. Sci.* **27** 84123 (1989)
472. M S Baptista, C D Tran *Appl. Opt.* **36** 7059 (1997)
473. N J Dovichi, F Zarrin, T G Nolan, D J Bornhop *Spectrochim. Acta, Part B* **43** 639 (1988)
474. T G Nolan, B K Hart, N J Dovichi *Anal. Chem.* **57** 2703 (1985)
475. S Luterotti, M Franko, D Bicanic *J. Pharm. Biomed.* **21** 901 (1999)
476. B G Belen'kii *Zh. Anal. Khim.* **45** 643 (1990) [a]
477. P G Muijselaar, K Otsuka, S Terabe *J. Chromatogr. A* **780** 41 (1997)
478. R M Villanueva-Camanas, J M Sanchis-Mallols, E F Simo-Alfonso *Anal. Lett.* **25** 1425 (1992)
479. J M Sanchis-Mallols, R M Villanueva-Camanas, E F Simo-Alfonso *Chromatogr.* **38** 365 (1994)
480. T Imasaka *Fresenius' J. Anal. Chem.* **355** 216 (1996)
481. K Sato, M Yamanaka, H Takahashi, M Tokeshi, H Kimura, T Kitamori *Electrophores.* **23** 734 (2002)
482. H Salimi-Moosavi, R M Cassidy *J. Chromatogr. A* **790** 185 (1997)
483. M W Briggs, G R Long *Appl. Spectrosc.* **50** 241 (1996)
484. J C Ren, B C Li, Y Z Deng, J K Cheng *Chem. J. Chin. Univ.* **16** 1182 (1995)
485. J M Saz, B Krattiger, A E Bruno, J C Díez-Masa, H M Widmer *J. Chromatogr. A* **699** 315 (1995)
486. B Krattiger, A E Bruno, H M Widmer, R Dandliker *Anal. Chem.* **67** 124 (1995)
487. S Michaelsen, P Moller, H Sorensen *J. Chromatogr. A* **680** 299 (1994)
488. A Hibara, M Tokeshi, T Kitamori *Electrochem.* **69** 620 (2001)
489. M Tokeshi, T Kitamori *Electrochem.* **68** 192 (2000)
490. J J Zheng, T Odake, T Kitamori, T Sawada *Anal. Sci.* **15** 223 (1999)
491. T Odake, T Kitamori, T Sawada *Analysis* **26** M41 (1998)
492. X F Li, S J Carter, N J Dovichi *J. Chromatogr. A* **895** 81 (2000)
493. Y G Hu, J K Cheng, Y Z Deng *Analyst* **122** 1089 (1997)
494. A Zhu *Capillary Electrophores.* **5** 201 (1998)
495. J D Spear, G L Klunder, R E Russo *Rev. Sci. Instrum.* **69** 2259 (1998)
496. K C Waldron, N J Dovichi *Anal. Chem.* **64** 1396 (1992)
497. M A Thompson, J C Ford, G R Long *Appl. Spectrosc.* **46** 945 (1992)
498. L G Hargis, J A Howell *Anal. Chem.* **64** R66 (1992)
499. A E Bruno, A Paulus, D J Bornhop *Appl. Spectrosc.* **45** 462 (1991)

500. P J Treado, L M Briggs, M D Morris *J. Chromatogr.* **511** 341 (1990)
501. M Yu, N J Dovichi *Anal. Chem.* **61** 37 (1989)
502. Y G Hu, Y Z Deng, J K Cheng *Chin. Chem. Lett.* **8** 425 (1997)
503. Y G Hu, Y Z Deng, J K Cheng *Prog. Nat. Sci.* **6** S42 (1996)
504. M Harada, M Shibata, T Kitamori, T Sawada *Anal. Sci.* **15** 647 (1999)
505. L Pogacnik, M Franko *Ann. Chim. (Rome)* **92** 93 (2002)
506. L Pogacnik, M Franko *Talanta* **54** 631 (2001)
507. E F Simo-Alfonso, M C García-Alvares-Coque, G Ramis-Ramos, A C Forteza, M E Ripol, V C Martin *Anal. Lett.* **25** 573 (1992)
508. D I Vaireanu, P R Fielden, R D Snook *Anal. Commun.* **36** 403 (1999)
509. D I Vaireanu, P R Fielden, R D Snook *Anal. Commun.* **36** 407 (1999)
510. M Surmeian, A Hibara, M Slyadnev, K Uchiyama, H Hisamoto, T Kitamori *Anal. Lett.* **34** 1421 (2001)
511. M Franko, P van de Bovenkamp, D Bicanic *J. Chromatogr. B* **718** 47 (1998)
512. M Šikovec, M Franko, M Novič, M Veber *J. Chromatogr. A* **920** 119 (2001)
513. M A Proskurnin, N Yu Ragozina, A P Smirnova, V V Chernysh, in *The 4th International Congress and Trade Fair 'Water: Ecology and Technology' ECWATECH-2000 (Abstracts of Reports), Moscow, 2000* p. 584
514. Z Rosenzweig, E S Yeung *Appl. Spectrosc.* **47** 1175 (1993)
515. Q E Khuen, W Faubel, H J Ache *Fresenius' J. Anal. Chem.* **348** 533 (1994)
516. E F Simo-Alfonso, G Ramis-Ramos, J M Estela-Ripon *Quim. Anal.* **9** 245 (1990)
517. E F Simo-Alfonso, Y Martín-Biosca, M C Garcta-Alvares-Coque *Thermochim. Acta* **219** 53 (1993)
518. N Delorme *Radiochim. Acta* **52–53** 105 (1991)
519. M Šikovec, M Novič, V Hudnik, M Franko *J. Chromatogr. A* **706** 121 (1995)
520. B J Jager, R J G Carr, C R Goward *J. Chromatogr.* **472** 331 (1989)
521. J Q Wu, T Odake, T Kitamori, T Sawada *Anal. Chem.* **63** 2216 (1991)
522. M Chen, K C Waldron, Y Zhao, N J Dovichi *Electrophoresis* **15** 1290 (1994)
523. X F Li, C S Liu, P Roos, E B Hansen Jr, C E Cerniglia, N J Dovichi *Electrophoresis* **19** 3178 (1998)
524. T Yokoyama, K Nakano, M Zenki *Anal. Chim. Acta* **396** 117 (1999)
525. A J de Mello *Lab on a Chip* **1** 7N (2001)
526. H M Sorouraddin, A Hibara, T Kitamori *Fresenius' J. Anal. Chem.* **371** 91 (2001)
527. U Backofen, F M Matysik, C E Lunte *Anal. Chem.* **74** 4054 (2002)
528. *British Pharmacopoeia* (London: HM Stationary Office, 1998) p. 47
529. E Tamaki, K Sato, M Tokeshi, M Aihara, T Kitamori *Anal. Chem.* **74** 1560 (2002)
530. S Matsuzawa, H Kimura, C Y Tu, T Kitamori, T Sawada *J. Immunol. Methods* **161** 59 (1993)
531. M Surmeian, M N Slyadnev, H Hisamoto, A Hibara, K Uchiyama, T Kitamori *Anal. Chem.* **74** 2014 (2002)
532. X D Xu, P K Kuo, S Y Zhang, X J Shui, Z N Zhang *Microwave Opt. Technol. Lett.* **35** 140 (2002)
533. Y Kikutani, A Hibara, K Uchiyama, H Hisamoto, M Tokeshi, T Kitamori *Lab. Chip* **2** 193 (2002)
534. Y Kikutani, A Hibara, K Uchiyama, H Hisamoto, M Tokeshi, T Kitamori *Lab. Chip* **2** 188 (2002)
535. H Hisamoto, S Satoh, K Satoh, M Tsubuku, D Siswanta, Y Shichi, Y Koike, K Suzuki *Anal. Chim. Acta* **396** 131 (1999)
536. C D Tran, T A van Fleet *Anal. Chem.* **60** 2478 (1988)
537. S M Colcombe, R D Snook *Anal. Chim. Acta* **390** 155 (1999)
538. M Franko, C D Tran *Rev. Sci. Instrum.* **62** 2430 (1991)
539. M Havaux, L Lorrain, R M Leblanc *Photosynth. Res.* **24** 63 (1990)
540. U Hempelmann, T Dorfmuller *J. Mol. Liq.* **48** 261 (1991)
541. V I Grishko, V P Grishko, Yu Ya Kuzyakov *Sib. Khim. Zh.* **6** 20 (1991)
542. S R Yeh, D E Falvey *J. Photochem. Photobiol. A* **87** 13 (1995)
543. T Hara, N Hirota, M Terazima *J. Phys. Chem.* **100** 10194 (1996)
544. M Terazima *Chem. Phys. Lett.* **304** 343 (1999)
545. T R Cambron, J M Harris *J. Phys. Chem.* **97** 13598 (1993)
546. V P Grishko, V I Grishko, V M Moralev, in *The XXVth Colloquim Spectrocscopicum Internationale (Abstracts of Papers), Toronto, 1987* p. 120
547. R K Grygier, P A Brugger, D M Bruland *J. Phys. Chem.* **89** 112 (1985)
548. T V Belyaeva, F V Bunkin, V M Savostina, G A Shafeev *Dokl. Akad. Nauk SSSR* **307** 583 (1989) [h]
549. F W Deeg, J Prinsl, C H R Brauchle *J. Phys. Chem.* **90** 5710 (1986)
550. D Lapotko, T Romanovskaya, G Kutchinsky, V Zharov *Cytometry* **37** 320 (1999)
551. D Lapotko, T Romanovskaya *Proc. SPIE-Int. Soc. Ont. Eng.* **3914** 262 (2000)
552. D Lapotko, T Romanovskaya, V Zharov *J. Biomed. Opt.* **7** 425 (2002)
553. D Lapotko, T Romanovskaya, E Gordiyko *Photochem. Photobiol.* **75** 519 (2000)
554. D Lapotko, T Romanovskaya, A Shnip, V Zharov *Laser Surg. Med.* **31** 53 (2002)
555. M A Ruis-Revert, M C García-Alvares-Coque, G Ramis-Ramos *Anal. Chim. Acta* **292** 113 (1994)
556. Y Martín-Biosca, M C García-Alvares-Coque, G Ramis-Ramos *J. Biochem. Biophys. Methods* **29** 1 (1994)
557. M Baptista, C Tran *J. Phys. Chem.* **99** 12952 (1995)
558. C D Tran *Anal. Chem.* **60** 182 (1988)
559. S L Smorgon, V Ya Zyryanov, P G Shkuryaev, V F Shabanov *Opt. Zh.* **64** 51 (1997)
560. F Saadallah, N Yacoubi, A Hfaiedh *Opt. Mater.* **6** 35 (1996)
561. F Saadallah *Opt. Mater.* **12** 163 (1999)
562. B-C Li, S-Y Zhang *Appl. Phys. B* **65** 403 (1997)
563. J W Fang, S Y Zhang *Appl. Phys. B* **67** 633 (1998)
564. A Harata, T Kawasaki, M Ito, T Sawada *Anal. Chim. Acta* **299** 349 (1995)
565. H Kimura, F Nagao, A Kitamura, K Sekiguchi, T Kitamori, T Sawada *Anal. Biochem.* **283** 27 (2001)
566. V V Chernysh, M A Proskurnin, M Yu Kononets, S N Bendrysheva *Talanta* **53** 1221 (2001)
567. M Yu Kononets, S N Bendrysheva, M A Proskurnin, E V Proskurnina, E M Min'kovskii, A R Tarasov, G V Lisichkin *Mendeleev Commun.* **12** 9 (2002)
568. M A Proskurnin, M Yu Kononets, S N Bendrysheva, E V Proskurnina, D A Nedosekin, A D Khrycheva *Rev. Sci. Instrum.* **74** 334 (2003)
569. M A Proskurnin, M Yu Kononets, E M Min'kovskii, E V Proskurnina, S N Bendrysheva, A R Tarasov, G V Lisichkin *Rev. Sci. Instrum.* **74** 740 (2003)
570. M A Proskurnin, M Yu Kononets, S V Bendrysheva, A D Khrycheva *Zh. Anal. Khim.* **58** 382 (2003) [a]
571. H Kawazumi, T Kaieda, T Inoue, T Ogawa *Chem. Phys. Lett.* **282** 159 (1998)
572. M Fujinami, H Murakawa, T Sawada *Rev. Sci. Instrum.* **74** 352 (2003)
573. S Acevedo, J Castillo, A Fernández, S Goncalves, M A Ranaudo *Energy Fuels* **12** 386 (1998)
574. J Castillo, S Goncalves, A Fernández, V Mujica *Opt. Commun.* **145** 69 (1998)
575. M Terazima, Y Kojima, N Hirota *Chem. Phys. Lett.* **259** 451 (1996)
576. N Nakajima, N Hirota, M Terazima *J. Photochem. Photobiol. A* **120** 1 (1999)
577. K Tanzawa, N Hirota, M Terazima *Chem. Phys. Lett.* **274** 159 (1997)
578. I Umezu, K Kitamura, K Maeda *J. Non-Cryst. Solids* **198–200** 778 (1996)
579. T Kawahara, M Miyazaki, A Kimura, Y Okamoto, J Morimoto, T Miyakawa *Appl. Phys. A* **69** 343 (1999)
580. Y Liao, R C Fang, Z Y Ye, N G Shang, S J Han, Q Y Shao, S Z Ji *Appl. Phys. A* **69** 101 (1999)

581. A Salnick, C Jean, A Mandelis *Solid-State Electronics* **41** 591 (1997)
582. M E Rodriguez, A Mandelis, G Pan, J A Garcia, Y Riopel *Solid-State Electronics* **44** 703 (2000)
583. J A Batista, A M Masanares, E C da Silva, M B C Pimentel, N Januzzi, D Fournier *Sens. Actuators, A* **71** 40 (1998)
584. T Gotoh, S Nonomura, S Hirata, S Nitta *Appl. Surf. Sci.* **113–114** 278 (1997)
585. B X Shi, C W Ong, K L Tam *J. Mater. Sci.* **34** 5169 (1999)
586. A Othonos, M Nestoros, D Palmerio, C Christofides, R S Bes, J P Traverse *Sol. Energy Mater. Sol. Cells* **51** 171 (1998)
587. E Gheeraert, A Deneuville, E Bustarret, F Fontaine *Diamond Relat. Mater.* **4** 684 (1995)
588. M Nesládek, M Vaněčk, J Rosa, C Quaeyhaegens, L M Stals *Diamond Relat. Mater.* **4** 697 (1995)
589. Z L Wu, P K Kuo, Y S Lu, S T Gu, R Krupka *Thin Solid Films* **290–291** 271 (1996)
590. M Reichling, A Bodemann, N Kaiser *Thin Solid Films* **320** 264 (1998)
591. T Y Leung, W F Man, S K So, P K Lim, W C Chan, F Gaspari, S Zukotynski *J. Non-Cryst. Solids* **254** 151 (1999)
592. H Einsiedel, M Kreiter, M Leclerc, S Mittler-Neher *Opt. Mater.* **10** 61 (1998)
593. H Einsiedel, S Mittler-Neher *Thin Solid Films* **288** 243 (1996)
594. H Nagavally, K N Madhusoodanan, T M A Rasheed *Appl. Phys. A* **68** 475 (1999)
595. M A Proskurnin, E M Min'kovskii, M Yu Kononets, E V Proskurnina, S N Bendrysheva, A R Tarasov, G V Lisichkin *Anal. Sci.* **17** i73 (2001)
596. M A Proskurnin, M Yu Kononets, E V Proskurnina, S N Bendrysheva, A D Khrycheva, M M Letunovskaya *Anal. Sci.* **17** i1303 (2001)
597. M A Proskurnin, Candidate Thesis in Chemical Sciences, Moscow State University, Moscow, 1993
598. A G Abroskin, M A Proskurnin, Yu A Barbalat, E K Ivanova *Zh. Anal. Khim.* **46** 870 (1991) [a]
599. M A Proskurnin, N V Orlova, M V Fedyaev, V A Samburova, V V Kuznetsova *Anal. Sci.* **17** i1299 (2001)
600. M A Proskurnin, D A Nedosekin, V V Kuznetsova *Rev. Sci. Instrum.* **74** 343 (2003)
601. T V Panchenko *Fiz. Tv. Tela* **49** 452 (1998) [i]
602. http://www.phys.msu.ru/rus/education/students/div-nuclear/chair-optics/
603. http://tls-msu.narod.ru/Teaching_Activities.htm
604. http://www.chem.msu.ru/rus/lab/laspec_k.html
605. http://www.phys.spbu.ru/Education/Magister/Depts/Optics/Courses/lazer.html
606. http://kristall.lan.krasu.ru/Education/Analiz/analiz.html

[a] — *Russ. J. Anal. Chem. (Engl. Transl.)*
[b] — *Moscow Univ. Bull. (Engl. Transl.)*
[c] — *J. Tech. Phys. (Engl. Transl.)*
[d] — *J. Tech. Phys. Lett. (Engl. Transl.)*
[e] — *Russ. J. Phys. Chem. (Engl. Transl.)*
[f] — *Opt. Spectrosc. (Engl. Transl.)*
[g] — *Quantum Electron. (Engl. Transl.)*
[h] — *Dokl. Chem. (Engl. Transl.)*
[i] — *Phys. Solid State (Engl. Transl.)*

Russian Chemical Reviews **73** (12) 1173 – 1209 (2004) © 2004 Russian Academy of Sciences and Turpion Ltd

DOI 10.1070/RC2004v073n12ABEH000801

The central chirality of the metal atom and configurational relations in asymmetric reactions catalysed by metal complexes †

V A Pavlov

Contents

I.	Introduction	1173
II.	Configurational models in asymmetric homogeneous catalysis	1174
III.	Hydrogen-transfer hydrogenation of acetophenone catalysed by metal complexes	1179
IV.	Catalytic hydroformylation of styrene in the presence of metal complexes	1184
V.	Allylic alkylation catalysed by palladium complexes	1184
VI.	Alkylation of benzaldehyde with dialkylzinc catalysed by titanium complexes	1191
VII.	Alkylation of benzaldehyde with dialkylzinc in the presence of amino alcohols and related compounds	1195
VIII.	Complexes with chiral C_2-symmetric ligands as the asymmetry inductors	1199
IX.	Conclusion	1203

Abstract. The recently published data on the dependence of the configuration of the reaction product on the structure of a catalytic metal complex (or an intermediate determining the asymmetric induction) in asymmetric catalytic reactions of hydrogen-transfer hydrogenation of acetophenone, hydroformylation of styrene, allylic alkylation of 1,3-diphenylprop-2-enyl acetate and alkylation of benzaldehyde with dialkylzinc are systematised. The applicabilities of octant and quadrant projections of the complexes are compared in order to establish the relationships between their structures and the enantioselectivities of the reactions. The known mechanisms of asymmetric induction in these reactions are discussed with regard to the C_1 or C_2 symmetry of the catalytic complex. The reasons for a decrease in the enantioselectivities of hydrogen-transfer hydrogenation, hydroformylation and alkylation by dialkylzinc [in the absence of $Ti(OPr^i)_4$] when performed with complexes with chiral C_2-symmetric ligands (as compared with complexes with asymmetric ligands) are considered. The bibliography includes 435 references.

I. Introduction

Asymmetric catalysis is undergoing a period of explosive development as can be evidenced from the increasing number of publications (see the monographs [1–5] and the most recent reviews [6–23]) and financial support of this field of research. The interest of the pharmaceutical industry in asymmetric catalysis stems from its possible use for the preparation of enantiomerically pure drug components. In 1996 – 1998, the annual expenditures for their production increased from US $ 73 bln to 96 bln.[24] The number of publications devoted to the theoretical aspects of asymmetric homogeneous catalysis was steadily increased correspondingly.

Studies into the mechanisms of asymmetric reactions on metal-complex catalysts that yield products with great enantiomeric excess (*ee*) attract special attention. The hydrogenation of enamides of α-acetamidocinnamic acid derivatives, on rhodium phosphine complexes is especially well-studied.[6]

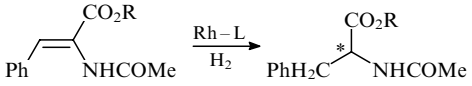

In the 1980's, following a publication by Galpern and Brown (for Ref. 6), it was thought that the predominant mechanism of this reaction is characterised by the following features:

(1) the first reaction step yields two intermediate complexes with the substrate, *viz*., minor and major, the concentration of the former being order of magnitude lower than that of the latter;

(2) the asymmetric induction occurs in the subsequent transformation of the intermediate;

(3) the major enantiomeric product is formed predominantly *via* the minor intermediate, since the rate of its reaction exceeds that *via* the major intermediate by three orders of magnitude.

However, a recently postulated alternative mechanism [25, 26] entails the formation of a hydride complex in the first step, the asymmetric induction as a result of substrate coordination and the formation of the predominant enantiomer of the reaction product *via* the major intermediate.

This discussion is not yet complete, since both mechanisms of reactions on rhodium [27, 28] and ruthenium complexes [28, 29] have advocates of their own. Presumably, the reaction mechanism depends on the nature of the catalytic complex with different phosphine ligands. However, the similarity of the dependences of the product configuration on the structure of the catalytic complex [10] (see Section II) is rather in favour of a single mechanism.

The character of the asymmetric induction step is the key difference between the aforesaid mechanisms. However, even if the asymmetric induction occurs in different reaction steps, this does not always account for the differences in the configurations of the reaction products. The dependence mentioned above is consistent with either mechanism on the assumption of a random coincidence of the product configuration in the case of one or another asymmetric induction step. Formally, only the second mechanism fits well into the most popular concept on the interaction of a chiral complex with a substrate commonly

V A Pavlov N D Zelinsky Institute of Organic Chemistry, Russian Academy of Sciences, Leninsky prosp. 47, 119991 Moscow, Russian Federation. Fax (7-095) 135 53 28. Tel. (7-095) 938 35 02.
E-mail: pvlv@cacr.ioc.ac.ru

Received 17 December 2002
Uspekhi Khimii **73** (12) 1269 – 1307 (2004); translated by R L Birnova

† Dedicated to the memory of Prof. G Snatzke.

known as a 'key–lock' mechanism. The overwhelming majority of configurational models used in asymmetric homogeneous catalysis also fit into this model.

The construction of configurational models, *i.e.*, determination of simple relationships between the configurations of asymmetric catalystic reaction products and those of chiral metal complexes that play the role of the catalysts attracts special attention.

II. Configurational models in asymmetric homogeneous catalysis

Knowles [30] who studied the hydrogenation of α-acetamidoacrylic acid in the presence of the Rh–dipamp complex (**1**) recommended that the so-called quadrant diagram was used to determine the efficient and non-efficient coordination variants of an enamide in a hypothetical transition complex.[6, 10]

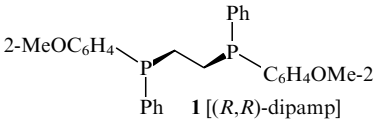

1 [(*R*,*R*)-dipamp]

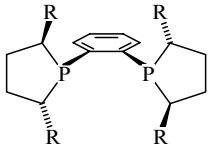

2 [(*R*,*R*)-duphos]

R = Me, Et, Pr^n.

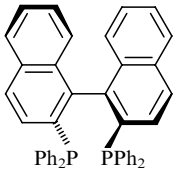

3 [(*R*)-binap]

This diagram is based on the arrangement of the phosphine phenyl groups (with the edge or the plane facing the viewer) in the precursor of the catalytic complex as established by X-ray diffraction spectroscopy. [31] According to this diagram, the substituents of a coordinated substrate that fall into the quadrants blocked by the phenyl groups of the ligand turned edgewise to the viewer encounter with a greater steric hindrance. A similar diagram with two blocked diagonal quadrants (Fig. 1) was used by Burk *et al.*[11, 32, 33] to rationalise the enantioselectivity of enamide hydrogenation in the presence of the Rh–duphos complex (**2**). The results of computations based on this model [27] were in good agreement with the experimental data.

A similar graphical approach based on a sector diagram was developed for the consideration of hydrogenation of β-keto esters,[34, 35] β-keto sulfonates [36] and other β-keto derivatives [7] on the Ru–binap complex (**3**).[10] Whereas the Ru–(*R*)-binap complex catalyses the formation of *R*-alcohols, the Ru–(*S*)-binap complex favours the formation of *S*-hydroxy derivatives. Pfaltz *et al.*[37–39] used a projection of a catalytic complex and a substrate coordinated by this complex, which is similar to the quadrant projection, to establish the preferential coordination of the substrate and, correspondingly, the configuration of the product formed upon reduction of α,β-unsaturated esters and amides with sodium cyanoborohydride in the presence of an *in situ* generated complex $CoCl_2$–**4**.

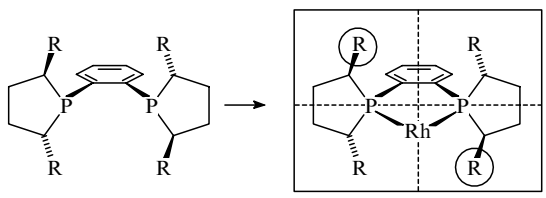

Figure 1. Shielding of diagonal quadrants in a rhodium complex with (*R*,*R*)-duphos in the hydrogenation of enamides.[11, 32]

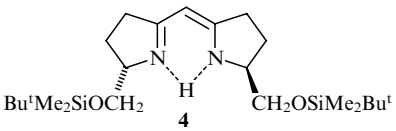

4

The transition-state model [40] of yet another popular asymmetric reaction, *viz.*, hydroformylation on rhodium and palladium complexes (Section IV), is based on the quadrant projection of a chiral complex. Within the framework of this model, asymmetric induction takes place in the substrate coordination step as is tacitly accepted for other intermediates mentioned above. This model is based on the following assumptions:

(1) an activated complex resulting in the formation of a metal–alkenyl intermediate possesses the highest free energy;

(2) in the transitions state, the double bond of the substrate is approximately coplanar with the bond between the metal and hydrogen.

The transition state is displayed as a projection of a complex onto a plane perpendicular to the direction of approach of the substrate to the metal atom. The ligands L and S and the reagent Z differ in size: L > S, Z > H (*e.g.*, Z = CO). The metal–ligand bonds form quadrants differing in the degree of occupation of space with these ligand fragments. The four variants of the distribution patterns of substrate substituents between the quadrants depending on substrate orientation correspond to four intermediate states characterised by different values of free activation energies (Q). The predominant orientation of styrene shown in the scheme corresponds to the arrangement of the ligands and the ratios of Q.

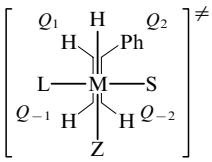

M is metal, $Q_{-1} > Q_{-2} \gg Q_1 > Q_2$.

The distribution of the molecular masses of the ligands between the quandrants, especially for C_2-symmetric bidentate ligands, such as diop (**5**) and dbp-diop (**6**), for which this model has been constructed (for rhodium [40–42] and platinum [41, 43–45] complexes), remains unclear.

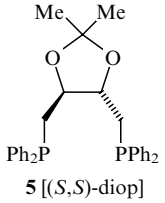

5 [(*S*,*S*)-diop]

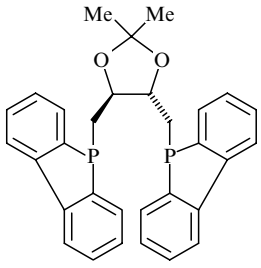

6 [(*S*,*S*)-dbp-diop]

Besides, this model does not take into account the fact that the enantiomeric outcome of the reactions carried out on rhodium and platinum catalysts can be different even if the same ligands are used.[41, 46] The experimental proof of this model showed that the predicted isomeric compositions of the reaction products and the configuration of the chiral product do not often coincide with the experimental data.[47] This fact was also acknowledged by the authors.[40, 41]

In practice, the relative positions of the ligands L and S in the transition state are deduced from the results of hydroformylation of a simple substrate;[47] therefore, the model under consideration is more explanatory than predictive.

A combination of quantum-chemical calculations and the molecular mechanics method was used in the construction of yet

another semiquantitative model of this reaction.[48] Experimental data suggest a trigonal-bipyramidal structure of an intermediate with a coordinated alkene.[49] The admissions underlying this model are very similar to those used in the previous model:

(1) the double bond of the substrate is coplanar with the apical bond M – H;

(2) the substrate coordination step is responsible for the regioselectivity and enantioselectivity;

(3) this step is irreversible.

It has previously been established [48] that this model provides an adequate interpretation of the data on hydroformylation of alkenes in the presence of the Rh – (*R*,*S*)-binaphos complex (**7**).[49]

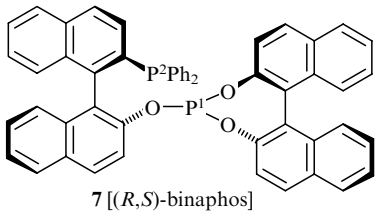

7 [(*R*,*S*)-binaphos]

With styrene as a substrate, four intermediates (**A** – **D**) are possible.

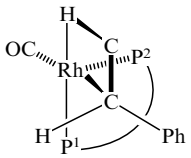

A

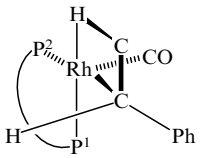

B

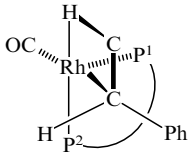

C

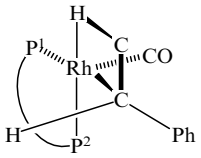

D

The coincidence of the calculated value of *ee* and the product configuration with the experimental results is achieved only with the intermediate **A**. A drawback of this model is that another intermediate can be more preferable for ligands having different structures. The calculated data should be compared each time with the experimental results; hence, this model also has a limited predictive potential.

Simpler literal rules for the dependence of the product configuration on the complex structure have been proposed. The relationship between the configurations of the enamide hydrogenation products and the conformations of the five-membered chelate rings in the rhodium complexes with bis(diphenylphosphine) ligands were simultaneously and independently established by Kagan [50] and by Pavlov and Klabunovskii.[51 – 53]

In this case, the folded conformations, λ and δ, were formed due to the presence, in the ring, of bulky substituents at one or two chiral carbon atoms. The conformation λ of the chelate ring results in (*S*)-, whereas the conformation δ yields the (*R*)-enantiomer of the reaction product.

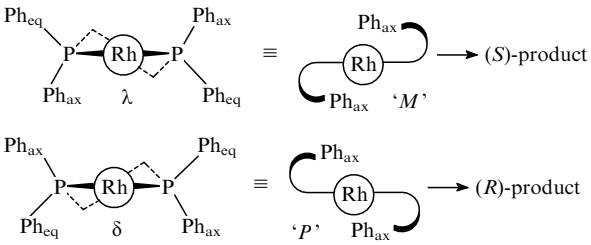

This model was further extended to rhodium complexes used for enamide hydrogenation with seven-membered chelate rings in the λ-twist-chair and δ-twist-chair conformations.[10, 52 – 56] Similar dependences were found for hydrosilylation,[10, 55] cross-coupling [10, 57, 58] and allylic alkylation [59] on Rh, Ni, Pd, *etc.* complexes.

As the enantioselectivity of this reaction is directly related not to the conformation, but rather to the chiral arrangement of the phosphine phenyl groups determined by this conformation,[60, 61] a more general expression for the same dependence which is based on a conventionalised image of a helix loop can be used.‡ In this case, the indices '*P*' and '*M*' describe the chiral arrangement of molecular masses of two pairs of phosphine phenyl groups in the complex.

For simplicity's sake, this regularity can be described by the dependence [10] λ('*M*') – (*S*), δ('*P*') – (*R*). Obviously, it is the use of '*P*'/'*M*'-indices only that is applicable in the case of enamide hydrogenation on rhodium phosphine complexes where the chirality of the ligands is determined either by the chiral phosphorus atoms [(*R* ,*R*)-miniphos (**8**),[62] (*R*,*R*)-bisP* (**9**) [63]] or by four chiral carbon atoms located pairwise in two rings containing phosphorus atoms [(*S*,*S*)-bpe (**10**), (*R*,*R*)-**2**].[32]

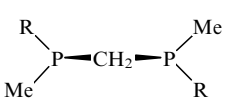

8 [(*R*,*R*)-miniphos]

R = Pr^i, Bu^t, cyclo-C_6H_{11}, Ph.

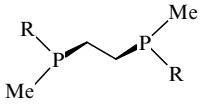

9 [(*R*,*R*)-bisP*]

R = Bu^t, Et_3C, 1-adamantyl, *etc.*

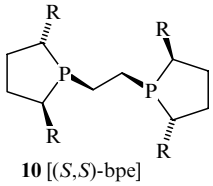

10 [(*S*,*S*)-bpe]

R = Me, Et, Pr^n, Pr^i.

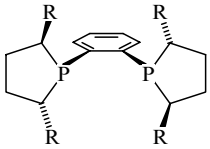

2 (R = Me, Et, Pr^n).

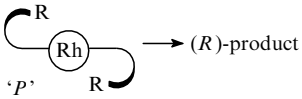

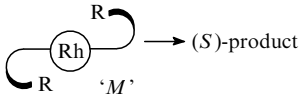

In the case of rhodium complexes with the ligands **8** and **9**, the indices are given with respect to substituents R bulkier than the methyl group, whereas those for the complexes with ligands **10** and **2** are determined from the substituents facing the viewer.

Hydrogenation of methyl α-acetamidocinnamate in the presence of the rhodium complexes with the ligands **10** – **17** and **1** obeys the regularity '*M*' – (*S*), '*P*' – (*R*) (Table 1). Thus, this concept may have a predictive potential.

The enantioselectivities of the hydrogenation reactions of α-acetamidocinnamic acid derivatives in the presence of the complexes Rh – **2**,[32] Rh – **10** and Rh – (**11** – **13**) are virtually the same. Thus, additional chiral carbon atoms in the ligand more remote from the metal atom in the chelate complex than the carbon atoms in the substituents that determine the chirality in the quadrant projection, have no effect on the enantiodiscrimination. The change in the configuration of the chiral donor phosphorus atom in the 'hybrid' ligand **17** has a much more pronounced effect on the value (but not the sign) of the enantioselectivity.

In total, more than 80 structural variants of chiral ligands [10] involved in the hydrogenation of enamides on rhodium complexes have been considered. All of them (with the exception of several deviations which have a specific explanation of their own) obey the above-mentioned regularity. Unfortunately, the involvement of a rhodium complex containing a cyclophane bis(diphenylphos-

‡ Quotation marks are used in this case to denote the helicity indices.

Table 1. Hydrogenation of methyl α-acetamidocinnamate in the presence of Rh complexes with the ligands **10** – **17**.

Ligand	Chirality indices	Product configuration	*ee* (%)	Ref.
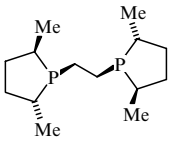 **10** [(*R*,*R*)-bpe]	'*P*'	*R*	98	32
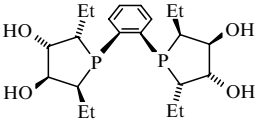 (*S*,*S*,*S*,*S*)-**11**	'*M*'	*S*	> 99	64
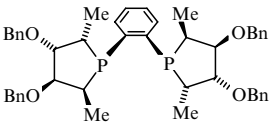 (*S*,*S*,*S*,*S*)-**12**	'*M*'	*S*	96	65
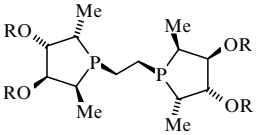 (*S*,*S*,*S*,*S*)-**13** (R = Bu^t, Bn)	'*M*'	*S*	~98	65
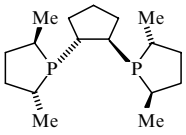 [λ-(*R*,*R*)]-**14**	'*P*'	*R*	73	66
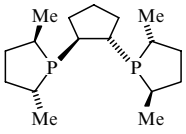 [δ-(*R*,*R*)]-**14**	'*P*'	*R*	95	66
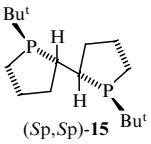 (*S*p,*S*p)-**15**	'*P*'	*R*	> 99	67
(*R*p,*R*p)-**1**	'*M*'	*S*	94	31
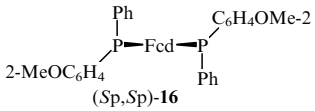 (*S*p,*S*p)-**16**	'*P*'	*R*	96	68
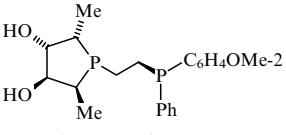 (*S*,*S*,*S*,*S*,*S*p)-**17**	'*M*'/'*P*'	*S*	43	69
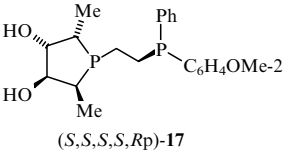 (*S*,*S*,*S*,*S*,*R*p)-**17**	'*M*'	*S*	92	69

Note. Hereinafter Fcd is ferrocenylene.

phine) ligand with planar chirality [70] cannot adequately be analysed due to the lack of X-ray diffraction data.

A model of configurational relationships based on the conformations of the intermediates was employed in the study of allylic alkylation products of 1,3-diphenylprop-2-enyl acetate (Section V) by a diethyl malonate anion in the presence of a bis(diphenylphosphinite) palladium complex.[59, 71]

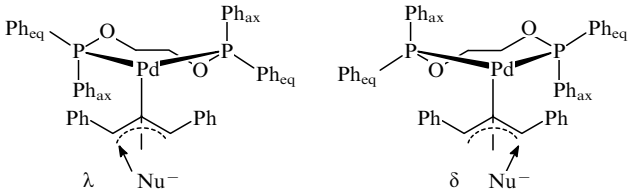

It was found that the λ-conformation of the intermediate favours the formation of the *S*-product, whereas the δ-conformation yields the *R*-enantiomer.

A more general configurational model considers the arrangement of the complex in the space of the quadrant (Fig. 2).[72, 73]

The regions determining the complex chirality are marked by the indices *Pr* (plus region) and *Mr* (minus region); the configuration of the reaction product depends on the region *Pr* or *Mr* where the ligand fragments fall. This model has found experimental support in that the dependence *Mr* – (*R*), *Pr* – (*S*) was observed in the allylic alkylation of 1,3-diphenylprop-2-enyl acetate by a diethyl malonate anion catalysed by palladium complexes with iminophosphine, diphosphine and diamine ligands.[72] However, the choice of this reaction is not quite suitable. In terms of this model, the asymmetric induction occurs in the substrate coordination step (the 'key – lock'-type interaction). However, the asymmetric induction step of this reaction does not coincide with the substrate coordination step (see Section V). Therefore, this model is applicable to such reactions as ketone hydrogen-transfer hydrogenation and to certain enamide hydrogenation, ketone hydrosilylation reactions, *etc*., where the asymmetric induction occurs in the substrate coordination.[6] A drawback of this model is that the space in front of the metal atom is not taken into consideration. The model is inapplicable to complexes with ligands, the bulky fragments of which face the viewer (see Fig. 2) and are nearer to it than the metal atom. Indeed, the complexes with ligands **18** and **19**, **20** and **21** (see Table 2) possess different *Pr*/*Mr*-chiralities, but the configuration of the allylic alkylation product of 1,3-diphenylprop-2-enyl acetate by a diethyl malonate anion is similar in these pairs.§ As a matter of fact, two phenyl groups in the

§ The conformations employed in the construction of complexes using molecular models corresponded to more favourable equatorial positions of bulky substituents in the chelate rings.[76, 77]

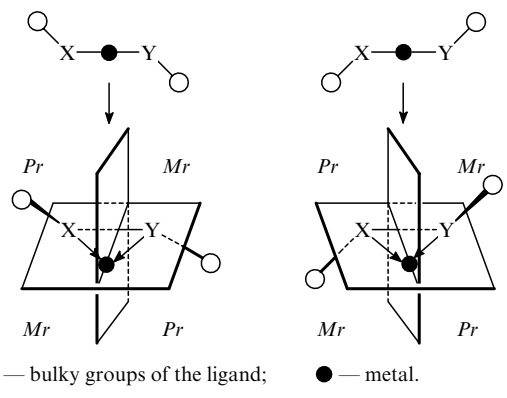

○ — bulky groups of the ligand; ● — metal.

Figure 2. A configurational model of the location of a complex in the quandrant volume.[72, 73]
(*a*) *Pr*-chirality, (*b*) *Mr*-chirality; X, Y = P, S, N.

Table 2. Comparison of the configurational models *Pr*/*Mr* and Pr^{oct}/Mr^{oct} in the allylic alkylation of 1,3-diphenylprop-2-enyl acetate by diethyl malonate anion under the action of palladium complexes with diamines.[74, 75]

Ligand	Complex	*ee* (%) (product configuration)	Location of substituents in octants	Chirality in configurational models	
				Pr/*Mr*	Pr^{oct}/Mr^{oct}
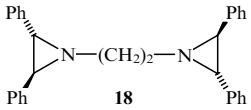 **18**	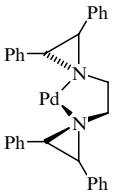	> 99 (*S*)	FL(+), FR(+), RR(+), RL(+)	*Mr*	Pr^{oct}
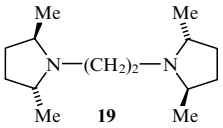 **19**	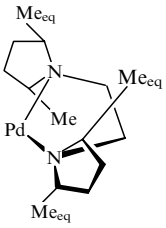	89–91 (*S*)	RL(+), RR(+)	*Pr*	Pr^{oct}
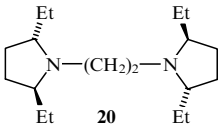 **20**	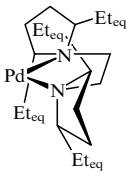	64 (*R*)	RL(−), RR(−)	*Mr*	Mr^{oct}
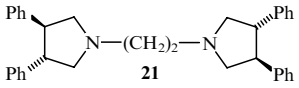 **21**	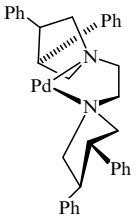	48 (*R*)	FL(−), FR(−), RL(−), RR(−)	*Pr*	Mr^{oct}

Note. Hereinafter, the following designations are used: Mr^{oct} (minus region octants); FL(−), frontal left (−); FR(−), frontal right (−); RL(−), rear left (−); RR(−), rear right (−) octants; Pr^{oct} (plus region octants), FL(+), frontal left (+); FR(+), frontal right (+); RL(+), rear left (+); RR(+), rear right (+) octants.

complexes with ligands **18** and **21** are located beyond quadrants that contain the chelate rings and that are limited by a plane passing through the metal atom perpendicular to the symmetry axis C_2. In the case of complexes with ligands **19** and **20**, the alkyl groups remain within the quadrants. In the framework of the *Pr*/*Mr* model, the complexes Pd–**18** and Pd–**20**, Pd–**19** and Pd–**21** are identical pairwise. Nevertheless, the configurations of the corresponding reaction products are different. It may thus be concluded that the escape of the substituent from the limits of the above-mentioned space changes the chirality sign. However, in this case the octant projection with the opposite signs of the frontal and rear octants¶ (Fig. 3) becomes applicable and the configurational *Mr*/*Pr* model is considered as a particular case of the configurational model based on the octant projection (the Mr^{oct}/Pr^{oct} model) for those complexes with ligands which do not escape the space of the rear octants.

As can be seen from Table 2, the Mr^{oct}/Pr^{oct} model is more adequate to the experimentally determined enantioselectivity of this reaction.

Cycloaddition of cyclopentadiene to methacrolein catalysed by the *in situ* formed complexes Al–**22** and Al–**23** is yet another example of the difference between the models *Mr*/*Pr* and Mr^{oct}/Pr^{oct}.[80]

¶ By analogy with the octant projection used for the description of the chiral environment of the carbonyl chromophore in cyclohexanone based on data from circular dichroism.[78, 79]

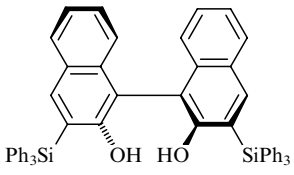
(R_{ax})-**22**

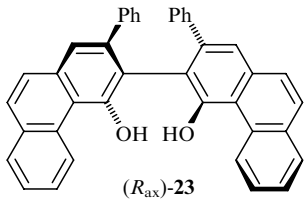
(R_{ax})-**23**

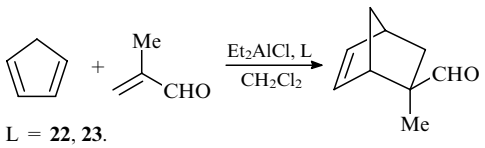

L = **22**, **23**.

Complex	The sign of optical rotation of the cycloaddition product	*ee* (%)	Chirality in configurational models	Location of substituents in octants
(R_{ax})-**22**	−	17	*Pr*, Pr^{oct}	RL(+), RR(+)
(R_{ax})-**23**	+	97	*Mr*, Mr^{oct}	FL(−), FR(−)

The silicon atoms in the octant projection of the molecular model of the Al–**22** complex fall into the rear positive octants close to the plane separating the frontal and rear octants; hence, the low enantiomeric excess of the reaction product is explicable. The terminal fragments of the phenanthrene units of the ligand in

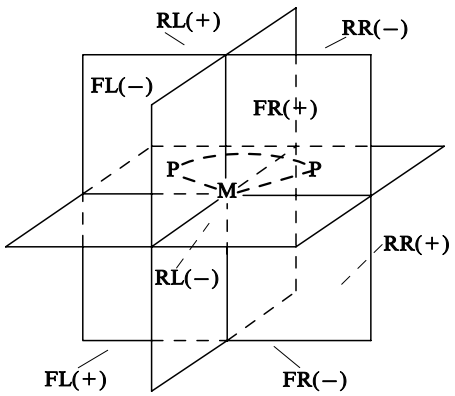

Figure 3. The octant projection of the Pd complexes **18**–**21**. The designations of the types and signs of the octants as in Legend to Table 2.

the projection of the complex Al–**23** lie in the frontal negative octants, which suggests a change in the chirality sign in comparison with the previous case. This observation is consistent with the experimental data[80] and suggests that the results obtained are better rationalised in terms of the Pr^{oct}/Mr^{oct} model than in terms of the Pr/Mr model.

Cyclopropanation of styrene with ethyl diazoacetate in the presence of complexes CuOTf–**24** (see Ref. 81) and CuOTf–**25** (Ref. 82) is yet another illustrative example of the applicability of the octant model to the estimation of enantioselectivity.

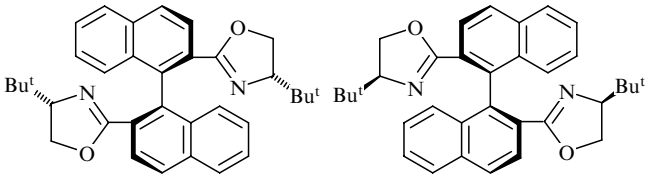

(S_{ax},*S*,*S*)-**24** (R_{ax},*S*,*S*)-**24**

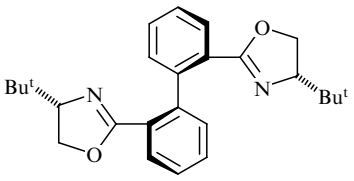

(S_{ax},*S*,*S*)-**25**

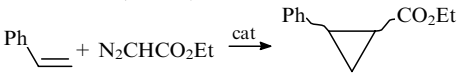

Catalyst	Isomer of ethyl 2-phenylcyclopropanecarboxylate	*ee* (%) (see †)
(S_{ax},*S*,*S*)-**24**	*trans*-(1*R*,2*R*)	87
	cis-(1*R*,2*S*)	86
(R_{ax},*S*,*S*)-**24**	*trans*-(1*S*,2*S*)	3
	cis-(1*S*,2*R*)	3
(S_{ax},*S*,*S*)-**25**	*trans*-(1*R*,2*R*)	71
	cis-(1*R*,2*S*)	84

† Chromatographic analysis of the cyclopropanation products on columns with chiral phases gives the ratio of the enantiomeric pairs *trans*-(1*S*,2*S*)/*trans*-(1*R*,2*R*) and *cis*-(1*S*,2*R*)/*cis*-(1*R*,2*S*). Therefore, the enantioselectivity of the reaction is usually expressed by *ee* values and the total ratio of the *trans*/*cis* products. If the reaction is carried out with chiral esters, the value of the diastereomeric excess [*de* (%)] is sometimes used.

The lateral projections of the first two complexes are shown below. In the projection of the Cu–(S_{ax},*S*,*S*)-**24** complex, the Bu^t_{eq} groups lie in the frontal negative octants (for simplicity's sake, the second dihydrooxazole ring in each complex is omitted). In the projection of the second complex, these groups are localised in the vicinity of the plane separating the frontal octants with the opposite signs. Presumably, such a border location is the reason for the extremely low (3%) enantioselectivity of the reaction catalysed by this complex.

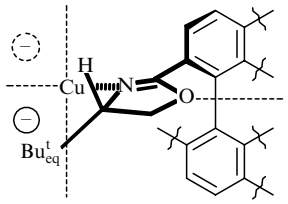

Cu-(S_{ax},*S*,*S*)-**24**

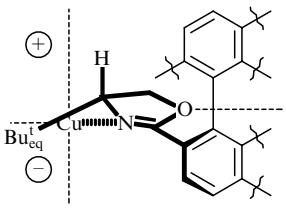

Cu-(R_{ax},*S*,*S*)-**24**

A comparison of the contributions of different types of chirality to the enantioselectivity gives rather controversial results. On the one hand, the dominant role of the axial chirality in the dihydrooxazole ring (in comparison with the central chirality) in the cyclopropanation reaction [Cu–(S_{ax},*S*,*S*)-**24** and Cu–(R_{ax},*S*,*S*)-**24**] leaves no doubt (see Ref. 81). On the other hand, the contribution of the axial chirality caused by the difference between the dinaphthyl and diphenyl systems in analogous complexes Cu–(S_{ax},*S*,*S*)-**24** (see Ref. 81) and Cu–(S_{ax},*S*,*S*)-**25** (see Ref. 82) in the same reaction is very small. As regards the central chirality of the carbon and phosphorus atoms in the complexes[69] Rh–(*S*,*S*,*S*,*S*,*S*p)-**17** and Rh–(*S*,*S*,*S*,*S*,*R*p)-**17** employed for hydrogenation (see Table 1), the data available do not allow an unambiguous conclusion. The dominant role of the axial chirality in comparison with the central chirality in the dihydroxazole fragment in the allylic alkylation of 1,3-diphenylprop-2-enyl acetate can be judged from the example of the palladium complexes with ligands (S_{ax},*S*)-**26** [(*S*), 28%] and (R_{ax},*S*)-**26** [(*R*), 86%].[83, 84]

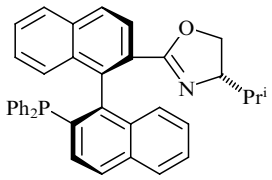

(S_{ax},*S*)-**26**

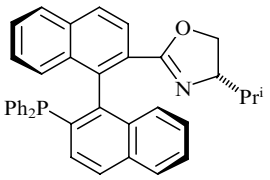

(R_{ax},*S*)-**26**

However, even a qualitative estimation of the contribution of one or another type of chirality is not always possible.[8] Generally speaking, estimation of contributions of different types of chirality of catalytic complexes to enantioselectivity can be regarded as a formal approach to the problem. Enantioselectivity is provided by spatial fixation of bulky groups of the ligand that being nearest to the donor atoms form the chiral environment of the metal atom. In other words, the ligand molecule within a catalytic complex plays the role of a template.

The octant projections and the 'Pr^{oct} (Mr^{oct})–product configuration' relationship cannot be regarded as the quantitative reflection of the stereochemistry of these complexes. These projections simply show the probable distribution of the groups that determine the chirality of the metal environment. These results were obtained from the analysis of molecular models, *viz*., Dreiding stereomodels ('Büchi Laboratoriums-Technik AG') or the published X-ray diffraction data and calculations.

The description of the real stereochemistry of a complex suitable for predicting both the configuration of the product and *ee* is possible only if exact spatial coordinates of the environment of the bulky groups that form the chiral environment of the metal atom under the reaction conditions are known. Unfortunately, X-ray diffraction data, *e.g*., on transition metal chiral chelate

complexes,[61] can hardly be used as a reliable basis in the construction of quantitative models of the type 'structural elements of complex – *ee* and product configuration'. Equalisation of molecular parameters of complexes in crystal to those in solution is probably unjustified. However, this approach gives positive results when using relative values, such as changes in certain complex parameters due to the presence of ligands with similar structures. Thus, it has been found[85] that in the case of an asymmetric Diels–Alder reaction where acrylates react with cyclopentadiene in the presence of the Ti–2,2′-biaryldiol complex the dependence of *ee* of the *endo*-adduct on the torsion angle of the biaryl passes through a maximum. A similar dependence exists between *ee* and the calculated parameter 'chirality content of molecule' (CCM), used as a quantitative measure of chirality of the given chiraphore‡ (in this case, of the biaryl fragment).[86] Correspondingly, a linear dependence exists between CCM and the dihedral angle. This testifies to the non-linear dependence between CCM and the experimentally determined *ee* value of the reaction product.[86] Most probably, the introduction of the parameter CCM[87] opens up a new way of predicting the magnitude and sign of enantioselectivity on the basis of calculations.

The majority of quantitative theoretical approaches dealing with asymmetric homogeneous catalytic reactions catalysed by metal complexes are based on computations that employ different programs and methods for different reactions and catalysts. The correspondence of the calculated parameters to the experimental results is considered as evidence in favour of a suggested mechanism. Recently, calculations have been carried out for the hydrogenation of enamides in the presence of the Rh–**2** complex;[27] for hydrogen-transfer hydrogenation of ketones catalysed by Rh–diamine,[88,89] Ru–*N*-tosylethylenediamine[90] or Ru–amino alcohol complexes,[90–92] for cyclopropanation of styrene on the complex Cu–*N*,*N*′-dimethylmalonaldiimine,[93] *etc*.

Although the use of the configurational models *Pr*/*Mr* or Pr^{oct}/Mr^{oct} is a qualitative approach, it provides a simple tool for predicting the sign of asymmetric induction and its interpretation. Many additional examples in which these models were compared can be mentioned. However, this is more appropriate in the subsequent analysis of the most extensively studied reactions catalysed by metal complexes (see Sections III–VII).

The octant projection localisation of the chiral C_2-symmetric metallacycle containing two identical donor atoms is shown in Fig. 3. The following conditions should be met when octant projections are used. In defining the sign of the octant determining the chirality, preference is given to the substituent nearest to the donor atom. Other conditions being the same, the preference is given to a bulkier substituent ($Bu^t > Pr^i > Pr^n > Et > Me$; $Bu^tCH_2 > Ph > Bn$, *etc*.). For different substituents at the same atom of the metallacycle of the complex not affecting the sign of the asymmetric induction, the complex with a substituent, which ensures the maximum value of *ee* of the reaction product, is allowed for. If the changes in the reaction conditions (*e.g*., solvent, temperature, additional reagent, *etc*.) do not cause any reversal of the product configuration, they are excluded from consideration.

Additional conditions should be met in order to unify the approach to the description of this model. In the octant projection (a view from the metal side) of an asymmetric metallacycle containing two identical donor atoms, the atom with a substituent determining the octant sign (which is closer to the donor atom or is bulkier) occupies a right-sided position; in the presence of two different donor atoms, the inferior (as regards its atomic number) atom takes a right-sided position; preference is given to the substituent or the environment of the left (senior) donor atom.

It is necessary that the last three requirements are met for the standardisation of the subjects that are analysed. The requirement for the unification is extended to the choice of relevant data for a concrete substrate in reactions carried out under maximally similar conditions.

‡ By analogy with the terms 'chromophore' and 'pharmacophore'.

Determination of octant projections of various complexes is based on the use of molecular models or X-ray diffraction data. For example, the octant projections of bis(diphenylphosphine) complexes were obtained on the basis of data on the λ- and δ- as well as λ- and δ-twist-chair conformations of five- and seven-membered rhodium chelate complexes.[10]

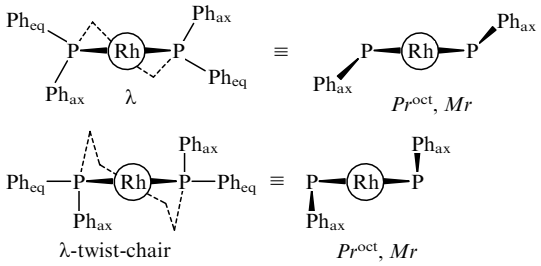

This projection shows only axial phenyl substituents. They fall completely into the corresponding octants, whereas the equatorial substituents lie at the border between two opposite octants. Therefore, the chirality of a complex is determined from the position of the axial substituents in the octants.

III. Hydrogen-transfer hydrogenation of acetophenone catalysed by metal complexes

Hydrogenation of aromatic ketones is one of the simplest asymmetric reactions catalysed by metal complexes with different chiral ligands.[16,94,95]

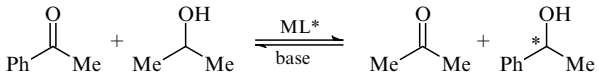

A comparison of the '*Pr*(*Mr*)–product configuration' and '$Pr^{oct}(Mr^{oct})$–product configuration' relationships for the hydrogen-transfer hydrogenation of acetophenone in the presence of rhodium and iridium complexes is presented in Table 3. Those complexes with bidentate ligands are considered where the spatial configurations of the bulky groups adjacent to the metal atom that determine its chiral environment are established on the basis of molecular models or using X-ray diffraction. As can be seen, the relationships Pr^{oct}–(*S*), Mr^{oct}–(*R*) and *Pr*–(*R*), *Mr*–(*S*) are observed in 60% and 53% of cases, respectively. An analysis of other complexes including ruthenium complexes (Table 4) revealed that the relationships Pr^{oct}–(*R*), Mr^{oct}–(*S*) and *Pr*–(*R*), *Mr*–(*S*) are observed in 70% and 80% of cases.

Special attention in Tables 3 and 4 should be paid to the relatively low enantioselectivity of reactions in the presence of complexes with chiral C_2-symmetric ligands. The *ee* values of the reaction product increase significantly on going to complexes with asymmetric ligands. At the first glance, this conclusion is contradictory to the high enantioselectivity of acetophenone hydrogenation catalysed by complexes containing chiral C_2-symmetric tri- and tetradentate ligands **56**–**59**[119–123] (Table 5).§ However, as can be seen from Table 5, the *ee* values and the configurations of the products formed in the presence of complexes with these ligands and of complexes with ligands which represent 'monomeric' analogues of these complexes, are virtually identical, which probably suggests that it is on these asymmetric 'monomeric' fragments that the reaction occurs. Indeed, excessive shielding of the metal atom, which fulfils the catalytic function, with bulky groups of tri- and tetradentate ligands prevents substrate coordination. Besides, the results of molecular model studies suggest that considerable stress is required for the ligand **59** to be coordinated

§ In the presence of some complexes with chiral C_2-symmetric tridentate ligands, this reaction proceeds with low enantioselectivity ($ee_{max} \leqslant 45\%-48\%$).[124,125]

Table 3. Comparison of the configurational models *Pr*/*Mr* and Pr^{oct}/Mr^{oct} in the hydrogen-transfer hydrogenation of acetophenone catalysed by rhodium and iridium complexes.

Ligand	Schematic projection of metallacycle	Location of chirality-determining substituents in octants	Chirality in configurational models		*ee* (%) (configuration of 1-phenylethan-1-ol)	Ref.
			Pr^{oct}/Mr^{oct}	*Pr*/*Mr*		
Complexes with chiral C_2-symmetric ligands						
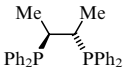 (*S*,*S*)-**27**	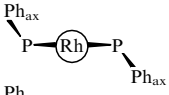	FR(−), FL(−)	Mr^{oct}	*Pr*	< 1	96
(*R*,*R*)-**5**	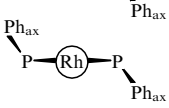	FR(−), FL(−)	Mr^{oct}	*Pr*	< 1	96
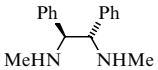 (*S*,*S*)-**28**	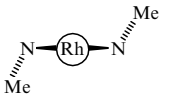 (see [a])	RR(−), RL(−)	Mr^{oct}	*Mr*	67 (*R*)	96
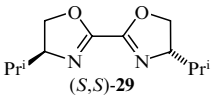 (*S*,*S*)-**29**	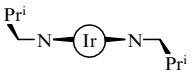	FR(−), FL(−)	Mr^{oct}	*Pr*	58 (*R*)	98
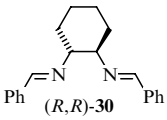 (*R*,*R*)-**30**	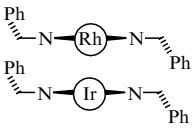	RR(+), RL(+) the same	Pr^{oct} Pr^{oct}	*Pr* *Pr*	48 (*S*) 41 (*S*)	99 99
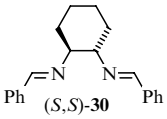 (*S*,*S*)-**30**	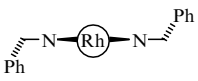	RR(−), RL(−)	Mr^{oct}	*Mr*	45 (*R*)	99
Complexes with asymmetric ligands						
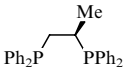 (*R*)-**31**	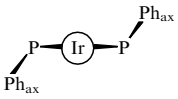	FR(+), FL(+)	Pr^{oct}	*Mr*	58 (*S*)	100
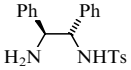 (*S*,*S*)-**32**	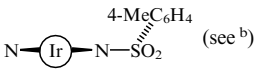 (see [b])	RR(+)	Mr^{oct}	*Mr*	90 (*S*)	102
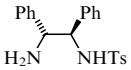 (*R*,*R*)-**32**	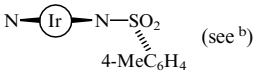 (see [b])	RR(−)	Pr^{oct}	*Pr*	96 (*R*)	103
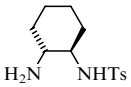 (*R*,*R*)-**33**	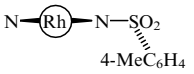	RR(−)	Pr^{oct}	*Pr*	97 (*R*)	103
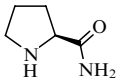 (*S*)-**34**	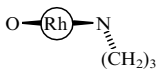	RR(+)	Pr^{oct}	*Pr*	59 (*R*)	104
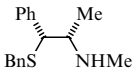 (*R*,*S*)-**35**	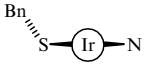	RL(+)	Pr^{oct}	*Pr*	82 (*S*)	105
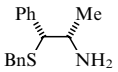 (*R*,*S*)-**36**	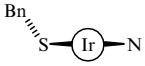	RL(+)	Pr^{oct}	*Pr*	65 (*S*)	105

Table 3 (continued).

Ligand	Schematic projection of metallacycle	Location of chirality-determining substituents in octants	Chirality in configurational models		*ee* (%) (configuration of 1-phenylethan-1-ol)	Ref.
			Pr^{oct}/Mr^{oct}	Pr/Mr		
Complexes with asymmetric ligands						
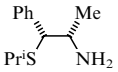 (*R*,*S*)-**37**	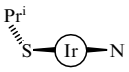	RL(+)	Pr^{oct}	*Pr*	73 (*S*)	105
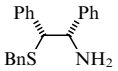 (*R*,*S*)-**38**	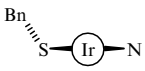	RL(+)	Pr^{oct}	*Pr*	80 (*R*)	105

Note. Here and in the subsequent Tables, a schematic projection of the metallacycle onto the plane perpendicular to the XMY plane passing through the metal atom is given (X and Y are the donor atoms of the ligand; M is metal).
[a] Calculated by the DFT method (see Refs 89 and 97). [b] According to X-ray diffraction data[101] for the complex Rh – [(*S*,*S*)-**32**].

Table 4. Comparison of the configurational models Pr/Mr and Pr^{oct}/Mr^{oct} in the hydrogen-transfer hydrogenation of acetophenone catalysed by ruthenium and zirconium complexes.

Ligand	Schematic projection of metallacycle	Location of chirality-determining substituents in octants	Chirality in configurational models		*ee* (%) (configuration of 1-phenylethan-1-ol)	Ref.
			Pr^{oct}/Mr^{oct}	Pr/Mr		
Complexes with chiral C_2-symmetric ligands						
(*S*,*S*)-**27**	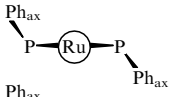	FR(−), FL(−)	Mr^{oct}	*Pr*	1 (*S*), 30(*R*)	106
(*R*,*R*)-**5**	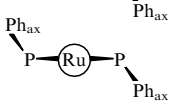	FR(−), FL(−)	Mr^{oct}	*Pr*	2 (*R*), 8 (*S*)	106
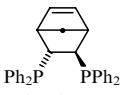 (*R*,*R*)-**39**	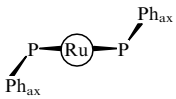	FR(+), FL(+)	Pr^{oct}	*Mr*	28 (*R*)	106
(*R*)-**3**	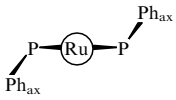	FR(+), FL(+)	Pr^{oct}	*Mr*	30 (*S*)	106
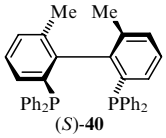 (*S*)-**40**	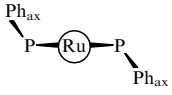	FR(−), FL(−)	Mr^{oct}	*Pr*	15 (*R*)	106
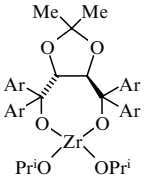 Zr–(*R*,*R*)-**41** (Ar = H, C_6H_4OMe-4)	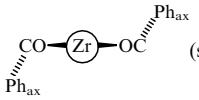 (see [a])	RR(−), RR(−)	Mr^{oct}	*Mr*	40 (*R*)	107
Complexes with asymmetric ligands						
(*R*)-**31**	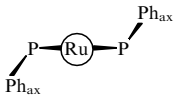	FR(+), FL(+)	Pr^{oct}	*Mr*	52 (*S*)	106
(*S*,*S*)-**32**	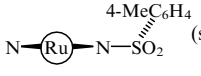 (see [b])	RR(+)	Mr^{oct}	*Mr*	90 – 98 (*S*)	102, 108 – 110
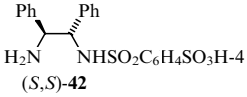 (*S*,*S*)-**42**	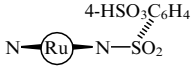	RR(+)	Mr^{oct}	*Mr*	94 (*S*)	111

Table 4 (continued).

Ligand	Schematic projection of metallacycle	Location of chirality-determining substituents in octants	Chirality in configurational models		*ee* (%) (configuration of 1-phenylethan-1-ol)	Ref.
			Pr^{oct}/Mr^{oct}	Pr/Mr		
Complexes with asymmetric ligands						
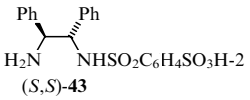 (*S*,*S*)-**43**	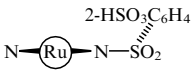	RR(+)	Mr^{oct}	*Mr*	91 (*S*)	111
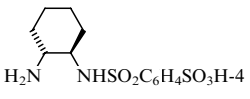 (*R*,*R*)-**44**	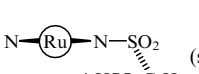 (see [b])	RR(−)	Pr^{oct}	*Pr*	88 (*R*)	111
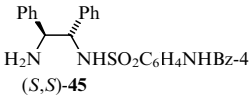 (*S*,*S*)-**45**	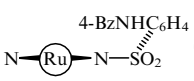 (see [b])	RR(+)	Mr^{oct}	*Mr*	96.5 (*S*)	112
(*S*)-**34**	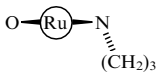	RR(+)	Pr^{oct}	*Pr*	79 (*R*)	104
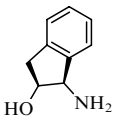 (*S*,*R*)-**46**	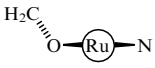	RL(+)	Pr^{oct}	*Pr*	91 (*S*)	113
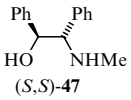 (*S*,*S*)-**47**	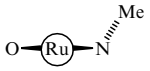	RR(−)	Mr^{oct}	*Mr*	92 (*S*)	114
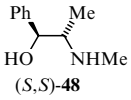 (*S*,*S*)-**48**	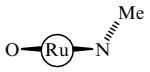	RR(−)	Mr^{oct}	*Mr*	89 (*S*)	114
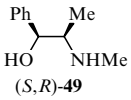 (*S*,*R*)-**49**	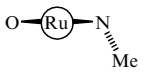	RR(+)	Pr^{oct}	*Pr*	91 (*S*)	114
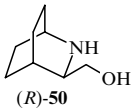 (*R*)-**50**	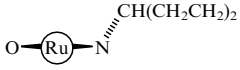	RR(−)	Mr^{oct}	*Mr*	95 (*S*)	115
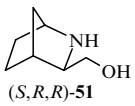 (*S*,*R*,*R*)-**51**		RR(−)	Mr^{oct}	*Mr*	94 (*S*)	115
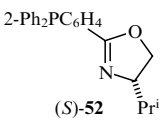 (*S*)-**52**	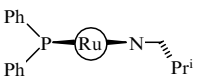	FR(−)	Pr^{oct}	*Pr*	86 (*R*)	116
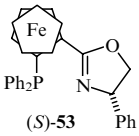 (*S*)-**53**	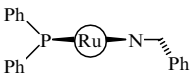	FR(−)	Pr^{oct}	*Pr*	94 (*R*)	117
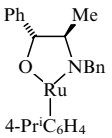 (*R*,*R*)-**54**	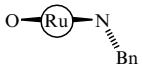	RR(+)	Pr^{oct}	*Pr*	95 (*R*)	92, 118

[a] X-Ray diffraction data of the complex Ti–[(*R*,*R*)-**41**]$_2$ (see Ref. 107). [b] Data from X-ray diffraction analysis.[101]

Table 5. Asymmetric hydrogen-transfer hydrogenation of acetophenone catalysed by complexes with chiral C_1-symmetric bidentate (monomeric) ligands and chiral C_2-symmetric tri- and tetradentate (dimeric) ligands.

Ligand	Complex	*ee* (%)	Product configuration	Ref.
Monomeric ligands				
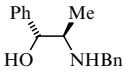 (*R*,*R*)-**55**	Ru–(*R*,*R*)-**55**	95	*R*	92, 118
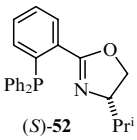 (*S*)-**52**	Ru–(*S*)-**52**	86	*R*	116
(*R*)-**52**	Ru–(*R*)-**52**	86	*S*	116
Dimeric ligands				
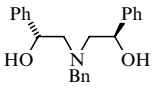 (*R*,*R*)-**56**	Sm–[(*R*,*R*)-**56**]$_2$	96	*R*	119
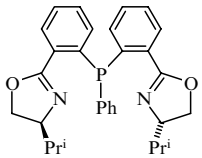 (*S*,*S*)-**57**	Ru–[(*S*,*S*)-**57**]$_2$	79	*R*	120
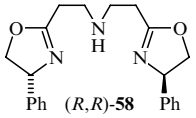 (*R*,*R*)-**58**	Ru–[(*R*,*R*)-**58**]$_2$	97	*S*	121
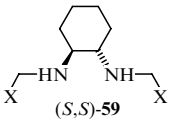 (*S*,*S*)-**59** (X = $C_6H_4PPh_2$-2)	Ru–(*S*,*S*)-**59**	97	*R*	122, 123
(*R*,*R*)-**59**	Ru–(*R*,*R*)-**59**	96	*S*	122, 123

within the complex through all the four donor atoms. A similar assumption based on a larger body of experimental evidence according to which complexes with asymmetric fragments (but not complexes with chiral C_2-symmetric tri- and tetradentate ligands) are involved in the catalytic reaction will be considered in Section VII.

The position of substituents in certain complexes is sometimes difficult to establish with the use of molecular models, although asymmetric hydrogenation of acetophenone on these complexes proceeds with sufficiently high enantioselectivity.[126–134]

Two mechanisms of the hydrogen-transfer hydrogenation of ketones are currently being considered,[6,95,105] *viz*., route *a* (hydride route) and route *b* (direct hydrogen transfer) (Scheme 1).

Route *a* seems to be more substantiated,[97] since the hydride intermediate **B**, which adds the substrate, was detected experimentally.[135] According to DFT calculations,[89] the structure of the metallacycle containing stereogenic nitrogen atoms (the symmetry axis C_2) is the most stable in the case of the chiral C_2-symmetric ligand. By illustration, in the case of (*R*,*R*)-*N*,*N*′-dimethyl-1,2-diphenylethylenediamine (*R*,*R*)-**28** and the catalytic system

Scheme 1

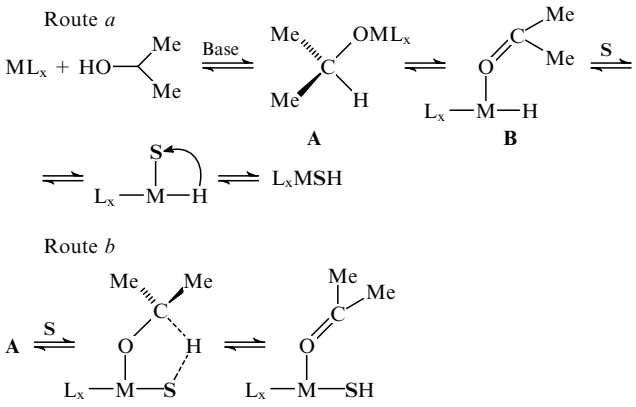

[RhCl(COD)]$_2$–(*R*,*R*)-**28** (COD is cycloocta-1,5-diene) the structures **C** and **D** can be formed.

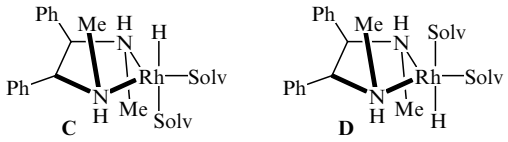

If structures **C** and **D** are at equilibrium and the asymmetric induction in the substrate coordination step proceeds at a slower rate, the substrate can recognise the chiral environment of the metal atom as a C_2-symmetric environment.

We have obtained some experimental evidence[6,99] in favour of the asymmetric induction of hydrogen-transfer hydrogenation of aromatic ketones during their coordination on rhodium and iridium complexes [Rh–(*R*,*R*)-**30**, Rh–(*S*,*S*)-**30**, Ir–(*R*,*R*)-**30**, *etc*.].

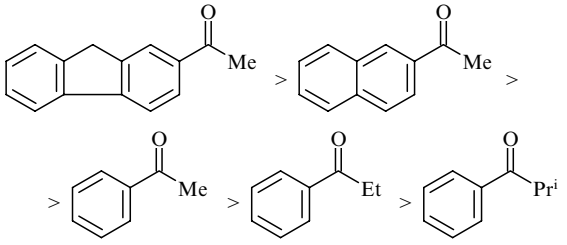

The order of changes in the *ee* values of the reaction products in the ketone series suggests that enantiodiscrimination by catalytic complexes correlates with the molecular sizes of substituents in prochiral aromatic ketones. The direct proportionality between these parameters is in favour of the asymmetric induction in the direct interaction of the catalytic complex with the substrate (ketone), *i.e*., during the coordination of the substrate.

Thus, the enantioselectivity of the hydrogen-transfer hydrogenation of acetophenone on rhodium, iridium and ruthenium complexes depends on the symmetry of a catalytic complex. Complexes with chiral C_1-symmetric (asymmetric) ligands manifest higher enantioselectivity than complexes with chiral C_2-symmetric ligands. Probably, the asymmetric induction takes place in the coordination of the carbonyl group of the ketone by the C_2-symmetric chiral hydride complex (in the case of a C_2-symmetric starting complex). In complexes with asymmetric ligands, the asymmetric induction is controlled by the asymmetric hydride complex. In some other reactions,[6] asymmetric intermediates also ensure high enantioselectivity.

IV. Catalytic hydroformylation of styrene in the presence of metal complexes

Hydroformylation of alkenes on chiral metal complexes is one of the most prominent industrially important reactions in asymmetric catalysis.[3, 47, 136–138] Several types of such reactions exist that differ in the positions of the double bonds in alkenes and the pathway of formation of chiral carbon atoms in the reaction products. Hydroformylation of styrene is especially well studied.

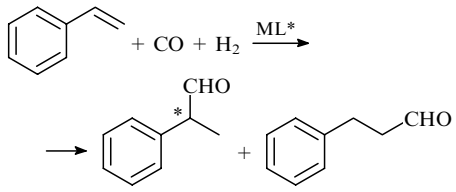

Platinum and rhodium complexes with phosphine and phosphinite ligands as catalysts provide the highest enantioselectivity.

Correlation of the *ee* values and the configurations of the products with the arrangement of the substituents which determine the chiralities of the corresponding complexes in the octants (the octant projection) or quadrants (the quadrant projection) suggests that the regularities $Mr^{oct}-(S)$, $Pr^{oct}-(R)$ and $Pr-(S)$, $Mr-(R)$ are fulfilled similarly in both cases for both platinum [40, 41, 45, 139–145] and rhodium complexes.[41, 46, 146, 147]

A comparison of enantioselectivities in the hydroformylation of styrene catalysed by rhodium complexes with chiral C_2-symmetric ligands and chiral C_1-symmetric (asymmetric) ligands revealed that as in the hydrogen-transfer hydrogenation, complexes containing C_2-symmetric ligands [148–154] are noticeably less enantioselective than complexes with asymmetric ligands [115, 155–162] of the type (*S*,*R*)-**60** (*ee* = 94%) or (*R*,*R*)-**61** (*ee* > 96%).[161, 162]

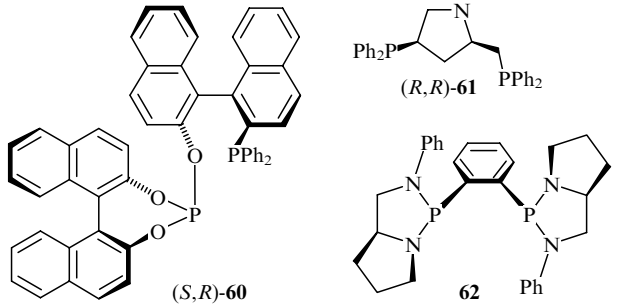

The lack of enantioselectivity in the reaction catalysed by a rhodium complex with the chiral C_2-symmetric ligand **62** (*ee* = 0) is especially surprising.[153] This ligand manifests a virtually ideal C_2-symmetry due to the conformational rigidity of the bicyclic systems at the donor phosphorus atoms.

For complexes with sulfur-containing bidentate ligands [163, 164] or ligands based on donor sulfur and phosphorus atoms,[165] or phosphorus and nitrogen atoms [166, 167] or bis(dialkylphosphine) complexes,[168] the enantioselectivity of styrene hydroformylation is rather low.

The known mechanisms of asymmetric hydroformylation of alkenes on rhodium diphosphine complexes [136, 154] suggest competition between two pairs of diastereomeric intermediates **A** and **B**,[169] which have the shape of trigonal bipyramids.

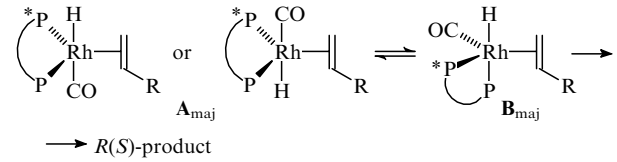

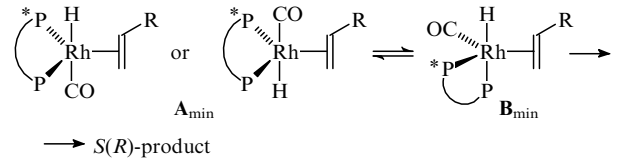

These intermediates determining the direction of the asymmetric induction represent constituents of stereoisomeric minor and major cycles. If the starting compounds represent chiral C_2-symmetric complexes and the equilibrium is established rather quickly, the chiral fragments of the intermediates $\mathbf{A}_{maj}$ and $\mathbf{A}_{min}$ are considered to be C_2-symmetric with respect to the coordination substrate.

Thus, the enantioselectivities of alkene hydroformylation on rhodium diphosphine complexes and hydrogen-transfer hydrogenation of ketones on rhodium, iridium and ruthenium complexes are determined by the symmetry of the catalytic complex. Chiral C_1-symmetric (asymmetric) complexes provide higher enantioselectivity in comparison with chiral C_2-symmetric complexes.[170] Apparently, the asymmetric induction occurs in the coordination of alkenes on chiral C_2-symmetric intermediates, the starting complex being chiral and C_2 -symmetric. In complexes containing asymmetric ligands, the asymmetric induction is effected by the asymmetric intermediate. Similar to other reactions,[6] asymmetric intermediates provide higher enantioselectivity.

V. Allylic alkylation catalysed by palladium complexes

Among other asymmetric allylic alkylation reactions catalysed by palladium complexes,[171–176] the reaction with 1,3-diphenylprop-2-enyl acetate is especially well-studied.

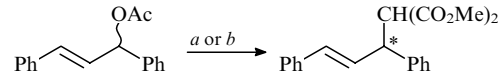

(*a*) $[Ph(\eta^3\text{-}C_3H_5)Cl]_2$/L*, $NaCH(CO_2Me)_2$; (*b*) $[Pd(\eta^3\text{-}C_3H_5Cl]_2$/L*, $CH_2(CO_2Me)_2$, *N,O*-bis(trimethylsilyl)acetamide, AcOK.

Although the reaction product probably does not represent a valuable synthon, this reaction is very popular for a number of reasons. First, large dimensions of both the substrate and the nucleophile molecules ensure a high level of discrimination of the reaction in the presence of a catalytic complex and, as a consequence, its high enantioselectivity. Second, the nature of palladium as a complex-forming metal allows the use of diverse ligands that do not reduce the catalytic properties of the complex in this reaction.

In the allylic alkylation of 1,3-diphenylprop-2-enyl acetate with diethyl malonate in the presence of palladium complexes with several ligands, a series of intermediates with a coordinated allylic substrate was isolated and their structures were established by X-ray diffraction analysis.[177–179] The bulky, spatially extended molecule of the coordinated substrate in these intermediates shifts the ligand fragments to the rear octants (the octant projection). However, such a shift should be considered as a trend rather than a rule. Thus the phenyl substituent in the oxazoline ligand fragment of the complex **B** falls into the frontal octant.[179]

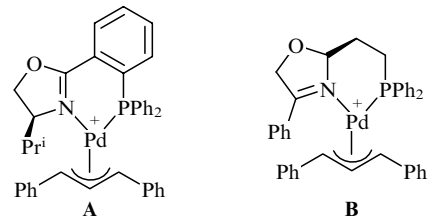

As the asymmetric induction takes place in the attack of the nucleophile on the intermediate containing a coordinated allylic group (see below), the distribution of substituents in the octants should be estimated for these intermediates. The projections and the distributions of substituents in palladium chiral C_2-symmetric diphosphine and diphosphinite complexes in the octants and quadrants as well as *ee* values and the configuration of the allylic alkylation product of 1,3-diphenylprop-2-enyl acetate by diethyl malonate in the presence of these complexes are listed in Table 6. As can be seen, in 70% of cases the formation of allylic alkylation products conforms to the rule: Pr^{oct}–(*S*), Mr^{oct}–(*R*). The configurational model *Pr*/*Mr*–(*S*)/(*R*) is fulfilled with a ~50% probability, *i.e.*, the rule based on quadrant projections is inapplicable to this case.

The enantioselectivity of the reaction catalysed by palladium diphosphinite complexes depends, to a large measure, on the nature of the substituents at the phosphorus atoms of the ligand (see data from the complexes Pd–**66**, Table 6).

The enantioselectivity of this reaction can be explained by steric and electronic factors, *e.g.*, the effects of substituents on the relative activities of two terminal allylic positions attacked by a nucleophile (Scheme 2, routes *a*, *b*) or *syn*,*syn*/*syn*,*anti*-isomerism (Scheme 2, route *c*).[71]

Scheme 2

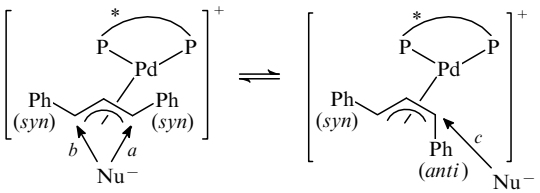

All three routes are associated with changes in the product configuration. The contribution of steric factors due to the energy gain in the case of the equatorial position of bulky substituents in the chelate ring (*cf.* Ref. 77) is presumably [71] compensated for by the effects of electronic factors. It is rather difficult to detect electronic effects in the background of the steric effects in reactions carried out in the presence of complexes with ligands that form seven-membered chelate rings [71] because of the high conformational labilities of these complexes.

Table 6. Allylic alkylation of 1,3-diphenylprop-2-enyl acetate with diethyl malonate in the presence of palladium chiral C_2-symmetric diphosphine and diphosphinite complexes.

Ligand	Schematic projection of metallacycle	Location of chirality-determining substituents in octants	Chirality in configurational models		*ee* (%) (product configuration)	Ref.
			Pr^{oct}/Mr^{oct}	*Pr*/*Mr*		
(*S*,*S*)-**39**	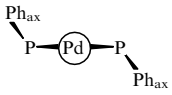	FR(−), FL(−)	Mr^{oct}	*Pr*	81 (*R*)	180
(*S*,*S*)-**27**	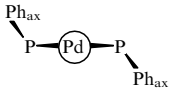	FR(−), FL(−)	Mr^{oct}	*Pr*	90 (*R*)	180
(*S*)-**3**	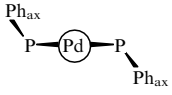	FR(−), FL(−)	Mr^{oct}	*Pr*	30 (*R*)	180
(*R*)-**40**	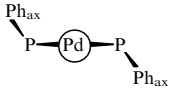	FR(−), FL(−)	Mr^{oct}	*Pr*	90 (*S*)	177
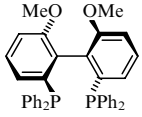 (*S*)-**63**	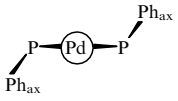	FR(+), FL(+)	Pr^{oct}	*Mr*	87 (*R*)	177
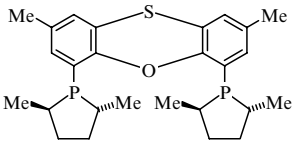 (*R*,*R*,*R*,*R*)-**64**	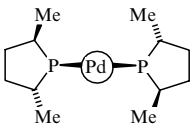	FL(−), FR(−)	Mr^{oct}	*Mr*	97 (*R*)	181
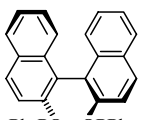 (*R*)-**65**	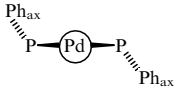 (see [a])	RL(+), RR(+)	Pr^{oct}	*Pr*	63–80 (*R*)	71

Table 6 (continued).

Ligand	Schematic projection of metallacycle	Location of chirality-determining substituents in octants	Chirality in configurational models		*ee* (%) (product configuration)	Ref.
			Pr^{oct}/Mr^{oct}	Pr/Mr		
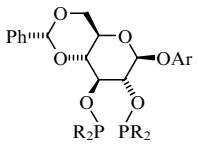 (1*R*,2*S*,3*R*,4*S*,5*R*)-**66**	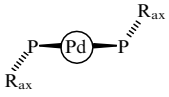 (R = Cy)	RL(−), RR(−)	Mr^{oct}	*Mr*	59 (*R*)	71
	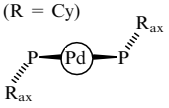 (R = 3,5-$(CF_3)_2C_6H_3$)	RL(−), RR(−)	Mr^{oct}	*Mr*	39 (*R*)	71
	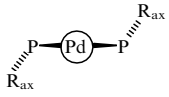 (R = 4-$CF_3C_6H_4$)	RL(−), RR(−)	Mr^{oct}	*Mr*	55 (*R*)	71
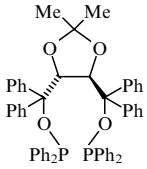 (*R*,*R*)-**67**	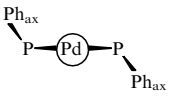 (see [b])	FL(−), FR(−)	Mr^{oct}	*Pr*	76 (*R*)	59, 182

Note. Cy is cyclohexyl. [a] Calculation (see Ref. 182). [b] X-Ray diffraction data.[59]

The ligand **68** forms a palladium complex with a conformationally more rigid five-membered metallacycle; therefore, it represents a more convenient subject for this study.[183]

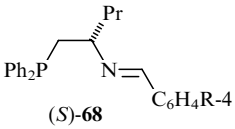

(*S*)-**68**

R	H	CO_2Me	CF_3	Me	OMe	NMe_2
ee, %	52 (*R*)	19 (*R*)	38 (*R*)	74 (*R*)	85 (*R*)	92 (*R*)

It has been found that electron-withdrawing groups decrease enantioselectivity, while electron-donor groups increase it. The effects of purely electronic factors on the enantioselectivity can be judged from a comparison of ligands with 4-CF_3 and 4-Me groups. Their steric effects are virtually similar, but *ee* values are significantly different. Hence, electronic factors influence *ee*, but not the product configuration.

The data on the allylic alkylation of 1,3-diphenylprop-2-enyl acetate by diethyl malonate in the presence of conformationally rigid Pd complexes are summarised in Table 7. The positions of the substituents in the ligands can be determined using molecular models and based on the data for the complexes the structures of which were established by X-ray diffraction analysis or by calculations.

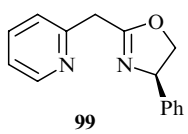

99

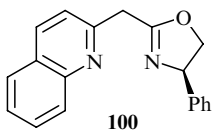

100

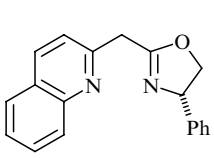

101

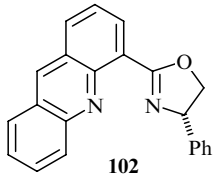

102

Ligand	*ee* (%)	Product configuration
(*R*)-**99**	16	*R*
(*R*)-**100**	78	*S*
(*S*)-**101**	75	*R*
(*S*)-**102**	34	*R*

The sign of enantioselectivity for the complexes with the ligands (*R*)-**100**, (*S*)-**101** and (*S*)-**102**[190] not included in Table 7 is opposite to that expected based on the corresponding data for the complexes Pd–**80** (see Table 7) and Pd–**99**. It is suggested[190] that two diastereomeric intermediates, **A** and **B** (Scheme 3), exist, which are converted into the π-complexes **C**–**F** by four different routes. Different reactivities of these intermediates also contribute to the stereochemistry of the reaction products. The intermediates **C** and **E** are preferable for complexes with ligands of the type **99**, whereas the intermediates **D** or **F** are more typical of complexes with ligands of the type **100**. This is due to the steric interactions of the left chiral centre in the complexes **C** and **E** containing an isoquinoline fragment. The transition from the complex **C** to **D** or from **E** to **F** should be accompanied by configurational changes in the reaction product, which is the case.

As can be seen from Table 7, the dependences Pr^{oct}–(*S*), Mr^{oct}–(*R*) and *Pr*–(*S*), *Mr*–(*R*) are fulfilled in 95% and 80% of cases, respectively. Besides, the model *Pr*/*Mr* is inapplicable in a few cases (see ligands **89**–**91**). Therefore, the octant model is preferable for this reaction.

Table 7. Allylic alkylation of 1,3-diphenylprop-2-enyl acetate with diethyl malonate in the presence of chiral C_2-symmetric and asymmetric palladium complexes.

Ligand	Schematic projection of metallacycle	Location of chirality-determining substituents in octants	Chirality in configurational models		*ee* (%) (product configuration)	Ref.
			Pr^{oct}/Mr^{oct}	Pr/Mr		
Complexes with chiral C_2-symmetric ligands						
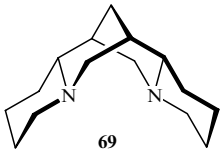 **69**	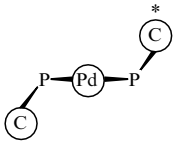	FL(+), FR(+)	Pr^{oct}	Mr	88 (*R*)	184
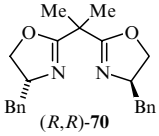 (*R*,*R*)-**70**	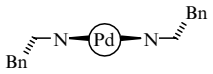 (see [a])	RL(−), RR(−)	Mr^{oct}	Mr	88 (*R*)	186
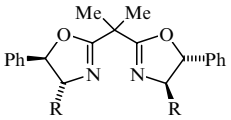 (*R*,*R*,*R*,*R*)-**71** (R = $CH_2OSiMe_2Bu^t$)	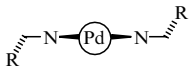 (see [a])	RL(−), RR(−)	Mr^{oct}	Mr	97 (*R*)	185
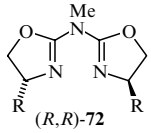 (*R*,*R*)-**72** (R = $CH_2OSiMe_2Bu^t$)	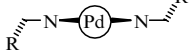 (see [a])	RL(−), RR(−)	Mr^{oct}	Mr	95 (*R*)	186
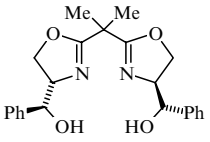 (*R*,*S*,*R*,*S*)-**73**	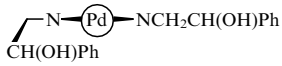 (see [b])	FL(+)	Pr^{oct}	Mr	92 (*S*)	187
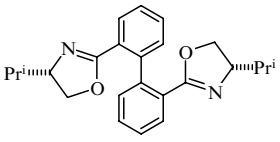 (*S*,*S*)-**74**	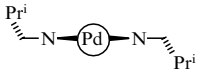	RL(+), RR(+)	Pr^{oct}	Pr	89 (*S*)	188
Complexes with asymmetric ligands						
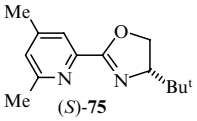 (*S*)-**75**	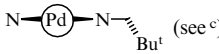 (see [c])	RR(+)	Pr^{oct}	Pr	93 (*S*)	190
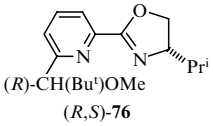 (*R*)-CH(Bu^t)OMe (*R*,*S*)-**76**	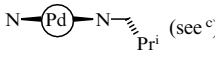 (see [c])	RR(+)	Pr^{oct}	Pr	99 (*S*)	191
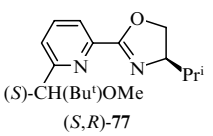 (*S*)-CH(Bu^t)OMe (*S*,*R*)-**77**	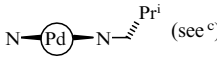 (see [c])	RR(−)	Mr^{oct}	Mr	>99 (*R*)	191, 192
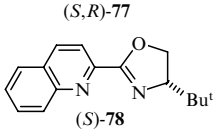 (*S*)-**78**	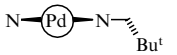	RR(+)	Pr^{oct}	Pr	92 (*S*)	190

Table 7 (continued).

Ligand	Schematic projection of metallacycle	Location of chirality-determining substituents in octants	Chirality in configurational models		*ee* (%) (product configuration)	Ref.
			Pr^{oct}/*Mr*^{oct}	*Pr*/*Mr*		
Complexes with asymmetric ligands						
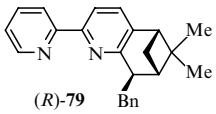 (*R*)-**79**	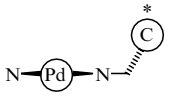	RR(−)	*Mr*^{oct}	*Mr*	89 (*R*)	193, 194
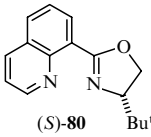 (*S*)-**80**	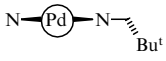	RR(+)	*Pr*^{oct}	*Pr*	77 (*S*)	195
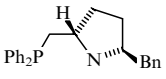 (*S*)-**81**	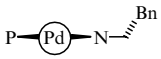	RR(−)	*Mr*^{oct}	*Mr*	74 (*R*)	196
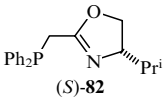 (*S*)-**82**	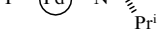	RR(+)	*Pr*^{oct}	*Pr*	73 (*S*)	197
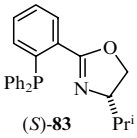 (*S*)-**83**	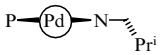 (see [d])	RR(+)	*Pr*^{oct}	*Pr*	98 (*S*)	197–200
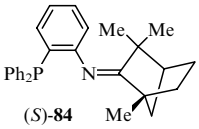 (*S*)-**84**	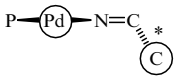	RR(+)	*Pr*^{oct}	*Pr*	53–90 (*S*)	198
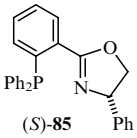 (*S*)-**85**	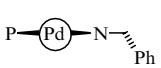 (see [d])	RR(+)	*Pr*^{oct}	*Pr*	99 (*S*) 92 (*S*) 94–99 (*S*)	201 202 203
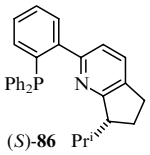 (*S*)-**86**	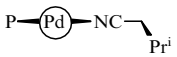	FR(−)	*Mr*^{oct}	*Pr*	98 (*S*)	204, 205
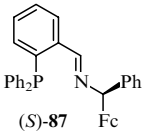 (*S*)-**87**	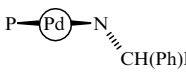 (see [e])	RR(+)	*Pr*^{oct}	*Pr*	87 (*S*)	206
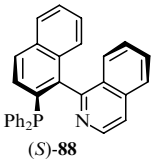 (*S*)-**88**	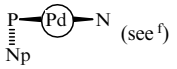 (see [f])	RL(−)	*Mr*^{oct}	*Mr*	98 (*R*)	178
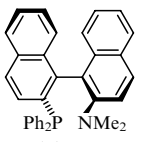 (*R*)-**89**	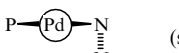 (see [g])	RL(+), RR(+), FL(+), FR(+)	*Pr*^{cot}	*Mr*/*Pr*	71 (*S*) 67(*S*)	207 208

Table 7 (continued).

Ligand	Schematic projection of metallacycle	Location of chirality-determining substituents in octants	Chirality in configurational models		*ee* (%) (product configuration)	Ref.
			Pr^{oct}/Mr^{oct}	Pr/Mr		
Complexes with asymmetric ligands						
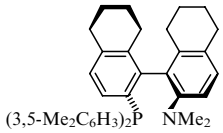 (*R*)-**90**	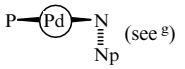 (see [g])	RL(+), RR(+), FL(+), FR(+)	Pr^{oct}	Mr/Pr	84 (*S*)	208
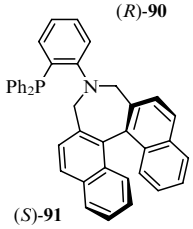 (*S*)-**91**	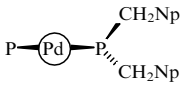	FR(+), RR(+)	Pr^{oct}	Mr/Pr	96 (*S*)	209
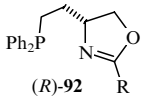 (*R*)-**92**	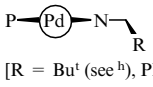 [R = Bu^t (see [h]), Ph]	FR(−)	Mr^{oct}	Pr	98 (*R*)	179
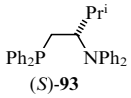 (*S*)-**93**	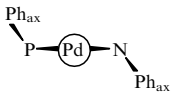	FR(−), FL(−)	Mr^{oct}	Pr	92 (*R*)	210
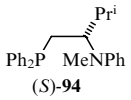 (*S*)-**94**	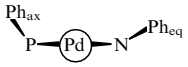	FL(−), FR(+)	Pr^{oct}	Mr	83 (*S*)	210
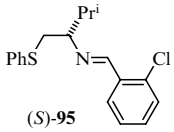 (*S*)-**95**	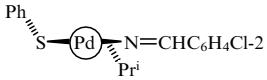 (see [i])	RL(+), RR(+)	Mr^{oct}	Pr	94 (*R*)	211
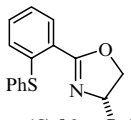	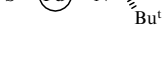	RR(+)	Pr^{oct}	Pr	> 96 (*S*)	202
(*S*)-**96** Bu^t						
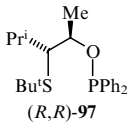 (*R*,*R*)-**97**	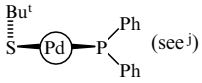 (see [j])	RL(+)	Pr^{oct}	Pr	98 (*S*)	212
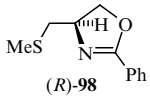 (*R*)-**98**	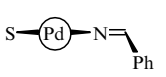	FR(−)	Mr^{oct}	Pr	56 (*R*)	213

Note. Hereinafter, the molecular mass centre of a substituent or a ligand fragment is marked with an asterisk. [a] X-Ray diffraction data (see Ref. 185). [b] X-Ray diffraction data (see Ref. 187). [c] X-Ray diffraction data (see Ref. 189). [d] X-Ray diffraction data (see Refs 179 and 199). [e] Calculation (see Ref. 206). [f] X-Ray diffraction data (see Ref. 178). [g] X-Ray diffraction data (see Ref. 207). [h] X-Ray diffraction data (see Ref. 179). [i] X-Ray diffraction data (see Ref. 211). [j] X-Ray diffraction data (see Ref. 212).

The enantioselectivities of the majority of the complexes with ligands listed in Table 7 are close to 90% or higher. All these ligands confer higher conformational rigidity on the chelate rings formed due to the presence of aromatic or oxazoline substituents in the metallacycle.

For the majority of cases, the higher the enantioselectivity of the reaction in the presence of a complex, the larger is the molecular volume of the chirality-determining substituent in the conformationally rigid chelate ring of the complex (only the most efficient substituents are listed in Table 7).

If a chiral centre is located at the donor atom of the ring, as in the case of the ligands **103**–**105**, the coordination of the ligand by the metal atom results in the formation of two stereoisomeric complexes.

Scheme 3

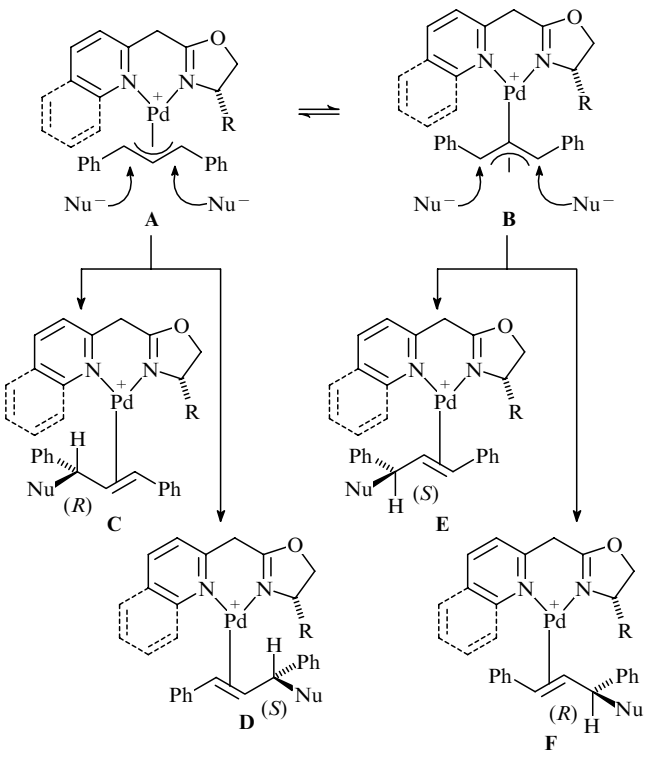

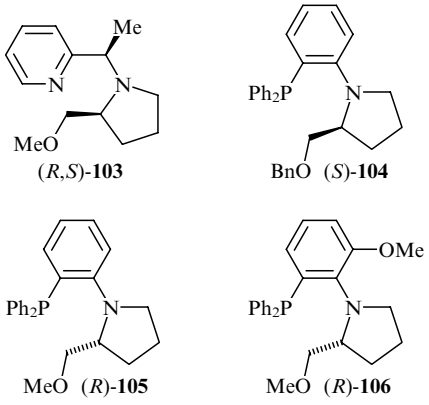

Ligand	*ee* (%)	Product configuration	Ref.
(*R*,*S*)-**103**	6	*S*	214
(*S*)-**104**	36	*S*	215
(*R*)-**105**	49	*R*	215
(*R*)-**106**	85	*R*	216

The substituents in such stereoisomers can fall into octants bearing opposite signs; therefore, it is expected that the reaction enantioselectivity cannot be too high, which is the case. However, the introduction of an additional substituent preventing free rotation around the C–N bond (ligand **106**) causes a sharp increase in the enantioselectivity.

A similar situation is observed for complexes with the ligands **107**–**109**.[215]

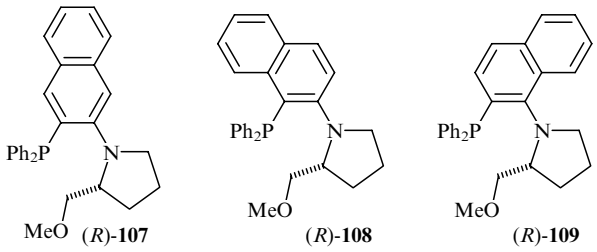

Ligand	*ee* (%)	Product configuration
(*R*)-**107**	24	*R*
(*R*)-**108**	39	*R*
(*R*)-**109**	74	*R*

The arrangement of the naphthyl rings in the ligand **109** hinders the free rotation of the pyrrolidine fragment to the largest extent if compared with compounds **107** and **108**; therefore, the enantioselectivity of the reaction is higher in this case.

Bidentate ligands of the cyclophane [217] and ferrocene [218] series have been described, which appear to be too bulky to allow the analysis of the octant projections of the complexes based on them.

The enantioselectivity of the allylic alkylation catalysed by conformationally rigid palladium complexes depends only slightly on reaction conditions. For example, the *ee* value of the reaction product formed in the presence of the Pd–**84** complex depends only slightly on the nature of the cation in MOAc.[198] The enantioselectivity is virtually independent of either the precursor of the catalytic complex and the solvent or of temperature and reaction time.

Some ligand complexes provide sufficiently high reaction enantioselectivity, but their octant projections are difficult to establish for a number of reasons. For some complexes containing bulky tetradentate C_2-symmetric,[72, 73, 219–223] tridentate asymmetric [72, 196, 224] and tetradentate asymmetric [225] ligands, X-ray diffraction data are lacking. Complexes with some bi- and tridentate ligands [194, 216, 226, 227] manifest rotational isomerism as in the case of the ligands **103**–**109**. Bi-, tri- and tetradentate C_1- and C_2-symmetric ligands of some other complexes [221, 224, 225, 228–236] have too bulky backbones and determination of their octant projections is ambiguous.

The mechanism of allylic alkylation includes oxidative addition of the allylic group to a Pd(0) complex to yield diastereomeric π-allylic intermediates (see Schemes 2 and 3), which are at equilibrium (the π–δ–π-mechanism), and their subsequent attack by a nucleophile from the side opposite to the coordinated palladium.[75, 171, 185, 237–239] The irreversible oxidative addition of the allylic group occurs much faster than the nucleophilic attack. The rate of the epimerisation of π-allylic intermediates is also by one or two orders of magnitude higher.[237] Therefore, the attack by a nucleophile is the limiting and, simultaneously, the asymmetric induction step. The latter is controlled by an asymmetric π-allylic intermediate irrespective of whether the starting palladium complex is asymmetric or chiral C_2-symmetric. The predominant enantiomer of the reaction product, which determines its configuration,[237] is formed *via* a π-allylic intermediate, which is in excess.

An alternative opinion[75, 185] consists of the following: if the starting complex is chiral and C_2-symmetric, the enantiomerism of the major product is determined by the competition between the positions C(1) and C(3) of the coordinated allylic substituents subject to the attack by the nucleophile in a single reaction intermediate. This is exemplified by the complex Pd–(*R*)-**70** (Scheme 4). The square-planar geometry of this intermediate was confirmed by X-ray diffraction analysis.[185] The intermediates

Scheme 4

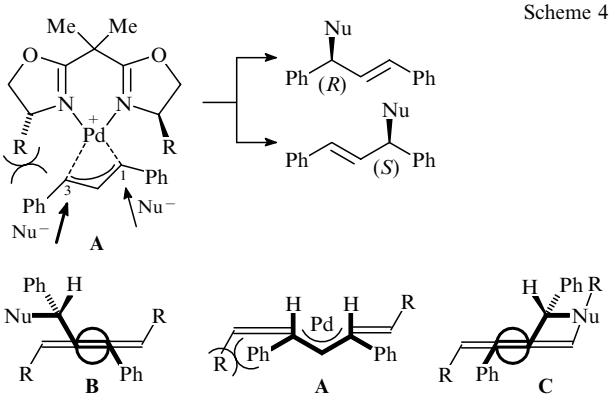

Scheme 5

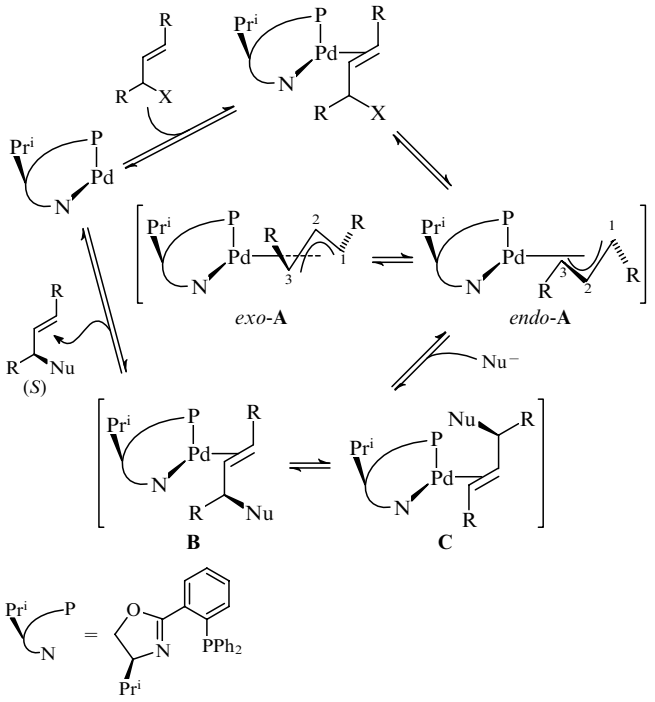

of reactions catalysed by other palladium complexes have similar structures.[174, 200, 240–242] The enantioselectivity is determined by the regioselectivity of the nucleophilic attack on the (1,3-diphenylallyl)palladium intermediate at positions C(3) or C(1). X-Ray diffraction and ^{13}C NMR spectroscopic data suggest that the Pd–C(3) bond is longer than the Pd–C(1) bond, presumably due to the steric interaction of the allylic phenyl group at the C(3) atom with the neighbouring benzyl group (R) in the dihydroxazole ring of the ligand **70**. The elongation of the bond increases the reactivity of the allylic substituent at position C(3) and favours its attack by the nucleophile at this position. The configuration of the reaction product [*ee* = 88% (*R*)] is consistent with this interpretation. Analogous considerations were employed in the analysis of reactions with other chiral C_2-symmetric complexes.[75] However, the concept of the regioselective activation of palladium–allylic bonds differs from that suggesting that the enantioselectivity is determined by the direct interaction of the chiral ligand with the nucleophile.[243–247]

An alternative interpretation of enantioselectivity is based on the differences in the thermodynamic stabilities of the Pd(0) complexes **B** and **C** with the product the existence of which was recently confirmed experimentally (see Scheme 4).[238] As regards stereochemistry, the intermediate **B**, which favours the formation of the (*R*)-product, is undoubtedly more stable than the intermediate **C**.

If asymmetric complexes contain different donor atoms as in, *e.g.*, the complex Pd–**83**, two (1,3-diphenylallyl)palladium intermediates are in equilibrium.[238] The catalytic cycle of the allylic alkylation reaction catalysed by the Pd–**83** complex [R = Ph, X = OAc, Nu = $CH(CO_2Me)_2$] is shown in Scheme 5. The attack by the nucleophile at positions C(1) or C(3) of the intermediates *exo*-**A** and *endo*-**A** corresponds to the four possible reaction routes two of which, *viz.*, the attack at position C(3) of the intermediate *exo*-**A** and at position C(1) of the intermediate *endo*-**A**, should yield the *S*-enantiomer, which is the case. The intermediate **B** was identified experimentally by NMR spectroscopy,[238] therefore, it it assumed that the predominant reaction route involves a nucleophilic attack at the *trans*-position relative to the phosphorus atom in the intermediate *exo*-**A**. This conclusion is in keeping with the allylic alkylation mechanism proposed for reactions catalysed by other asymmetric palladium complexes.[178, 200, 239–248]

Thus, the asymmetric induction in the allylic alkylation catalysed by palladium chiral C_2-symmetric complexes takes place either in the step of the chiral intermediate, which has lost its C_2-symmetry after coordination to the substrate (see Scheme 4, intermediate **A**), or during the conversions of chiral intermediates (see Scheme 5) which are also devoid of the symmetry elements (except for C_1). In this case, palladium complexes containing both chiral C_2-symmetric ligands and chiral C_1-symmetric (asymmetric) ligands ensure high (up to 98%–99%) enantioselectivity of this reaction.

VI. Alkylation of benzaldehyde with dialkylzinc catalysed by titanium complexes

The formation of optically active alcohols in reactions of aldehydes with diethylzinc at low temperatures in the presence of *in situ* generated titanium chiral complexes is a well-studied reaction.[9, 17, 249, 250]

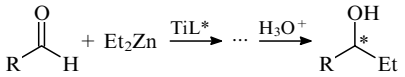

The reaction of benzaldehyde with diethylzinc in the presence of titanium complexes with chiral diols, sulfonamides and phosphoramides has been studied in especially great detail (Table 8). The experimental results suggest that the regularities Pr^{oct}–(*R*), Mr^{oct}–(*S*) and *Pr*–(*R*), *Mr*–(*S*) are fulfilled with a probability of 97%.

The same probability of fulfilment (87%) of the dependences based on the use of octant and quadrant projections [Pr^{oct}–(*S*), Mr^{oct}–(*R*) and *Pr*–(*S*), *Mr*–(*R*)] was also observed in the alkylation of benzaldehyde with diethylzinc in the presence of titanium asymmetric complexes with amino alcohols, *N*-sulfonylamino alcohols and *N*-thiophosphoramido alcohols (Table 9).

A hypothetical catalytic cycle of alkylation of benzaldehyde with diethylzinc in the presence of titanium complexes with *N*-substituted diamines is shown in Scheme 6.[266] Presumably, the intermediate **A** is the key species. This reacts with the aldehyde to give dialkoxytitanate **B**, which regenerates the key intermediate **A** in such a way that the catalytic cycle is closed. According to this scheme, the asymmetric induction takes place in the interaction of the aldehyde with the asymmetric complex irrespective of the symmetry (C_1 or C_2) of the starting catalytic complex. The maximum values of *ee* for the alkylation of benzaldehyde catalysed by Ti complexes with chiral C_2- and C_1-symmetric ligands are nearly identical (up to 98%).

Table 8. Asymmetric alkylation of benzaldehyde (**S**) with diethylzinc in the presence of titanium complexes with chiral diols, sulfonamides and phosphoramides.

Ligand (complex)	Molar ratio of reaction components	T /°C	Schematic projection of metallacycle	Location of chirality-determining substituents in octants	Chirality in configurational models		*ee* (%) (configuration of 1-phenylpropan-1-ol)	Ref.
					Pr^{oct}/Mr^{oct}	Pr/Mr		
Complexes with chiral C_2-symmetric ligands								
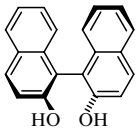 (*S*)-**110**	**S** : L : $Ti(OPr^i)_4$: : Et_2Zn = = 1 : 0.2 : 1.4 : 3	−78	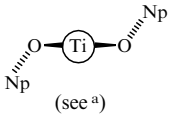 (see [a])	RR(−), RL(−)	Mr^{oct}	Mr	95.6 (*S*) 85 (*S*)	252 253
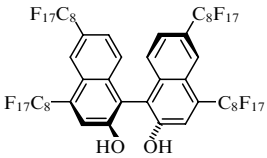 (*S*)-**111**	$Ti(OPr^i)_4$: L = = 1 : 0.2	45	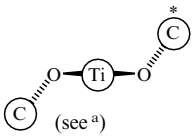 (see [a])	RR(−), RL(−)	Mr^{oct}	Mr	58 (*S*)	254
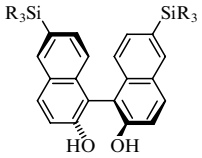 (*R*)-**112** (R = $(CH_2)_2C_6F_{13}$)	L : Et_2Zn : : $Ti(OPr^i)_4$: **S** = = 0.2 : 3 : 1.2 : 1	0	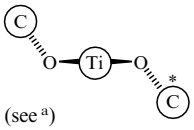 (see [a])	RR(+), RL(+)	Pr^{oct}	Pr	83 (*R*)	255, 256
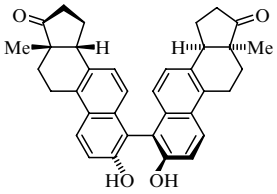 (*R*)-**113**	**S** : Et_2Zn : : $Ti(OPr^i)_4$: L = = 1 : 1.9 : 1.4 : 0.2	−20	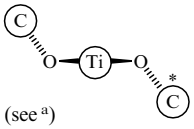 (see [a])	RR(+), RL(+)	Pr^{oct}	Pr	78 (*R*)	257
(*S*)-**113**	**S** : Et_2Zn : : $Ti(OPr^i)_4$: L = = 1 : 1.9 : 1.4 : 0.2	−20	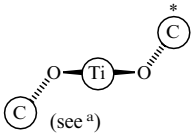 (see [a])	RR(−), RL(−)	Mr^{oct}	Mr	82 (*S*)	257
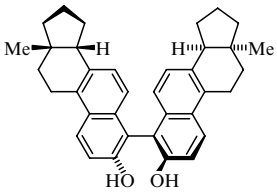 (*R*)-**114**	**S** : Et_2Zn : : $Ti(OPr^i)_4$: L = = 1 : 1.9 : 1.4 : 0.2	−20	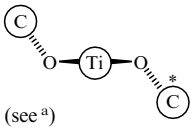 (see [a])	RR(+), RL(+)	Pr^{oct}	Pr	57 (*R*)	257
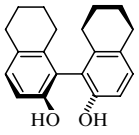 (*S*)-**115**	**S** : L : $Ti(OPr^i)_4$: : Et_2Zn = = 1 : 0.2 : 1.4 : 3	0	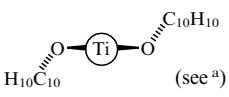 (see [a])	RR(−), RL(−)	Mr^{oct}	Mr	98.5 (*S*)	258
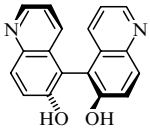 (*R*)-**116**	**S** : L : $Ti(OPr^i)_4$: : Et_2Zn = = 1 : 0.2 : 1.4 : 3	0	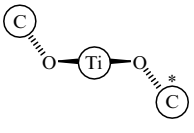	RR(+), RL(+)	Pr^{oct}	Pr	89 (*R*)	259

Table 8 (continued).

Ligand (complex)	Molar ratio of reaction components	T /°C	Schematic projection of metallacycle	Location of chirality-determining substituents in octants	Chirality in configurational models		*ee* (%) (configuration of 1-phenylpropan-1-ol)	Ref.
					Pr^{oct}/Mr^{oct}	Pr/Mr		
Complexes with chiral C_2-symmetric ligands								
$Ti[(R,R)$-**41**$]_2$	**S** : Et_2Zn : : $Ti[(R,R)$-**41**$]_2$ = = 1 : 1.8 : 1.2	0	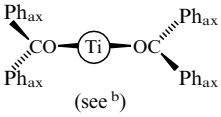 (see [b])	RR(−), RL(−), FR(−), FL(−)	Mr^{oct}	Pr	90 (*R*)	107
$Ti(OPr^i)_2[(R,R)$-**41**]	**S** : Et_2Zn : : $Ti(OPr^i)_4$: : $Ti(OPr^i)_2[(R,R)$-**41**] = = 1 : 1.8 : 1.2 : 0.2	0	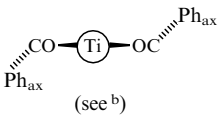 (see [b])	RR(−), RL(−)	Mr^{oct}	Pr	98 (*S*)	107
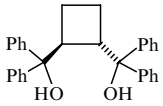 (*S*,*S*)-**117**	**S** : Et_2Zn : : $Ti(OPr^i)_4$: : [Ti/L] = = 1 : 1.8 : 1.2 : 0.2	−25	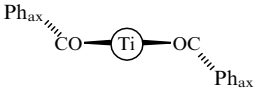	RR(+), RL(+)	Pr^{oct}	Pr	88 (*R*)	260
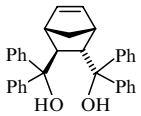 (*S*,*S*)-**118**	**S** : Et_2Zn : : $Ti(OPr^i)_4$: : [Ti/L] = = 1 : 1.8 : 1.2 : 0.2	−25	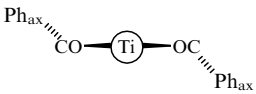	RR(+), RL(+)	Pr^{oct}	Pr	60 (*R*)	260
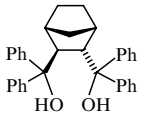 (*S*,*S*)-**119**	**S** : Et_2Zn : : $Ti(OPr^i)_4$: : [Ti/L] = = 1 : 1.8 : 1.2 : 0.2	−25	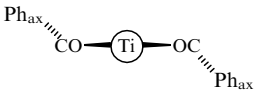	RR(+), RL(+)	Pr^{oct}	Pr	70 (*R*)	260
(*R*,*R*)-**119**	$Ti(OPr^i)_4$: L = = (1.2 − 1.4) : 0.2	−78 to −20	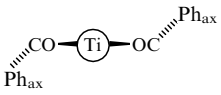	RR(−), RL(−)	Mr^{oct}	Mr	98 (*S*)	261, 262
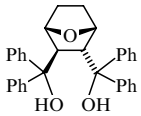 (*S*,*S*)-**120**	**S** : Et_2Zn : : $Ti(OPr^i)_4$: : [Ti/L] = = 1 : 1.8 : 1.2 : 0.2	−25	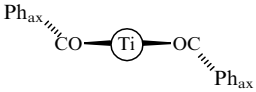	RR(+), RL(+)	Pr^{oct}	Pr	70 (*R*)	260
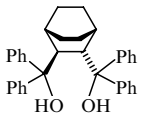 (*R*,*R*)-**121**	$Ti(OPr^i)_4$: L = = (1.2 − 1.4) : 0.2	−78 to −20	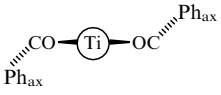	RR(−), RL(−)	Mr^{oct}	Mr	82 (*S*)	261, 262
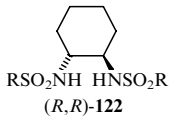 (*R*,*R*)-**122** (R = 4-$MeOC_6H_4$)	**S** : $Ti(OPr^i)_4$: : Et_2Zn : L = = 1 : 1.2 : 1.2 : 0.02	−45	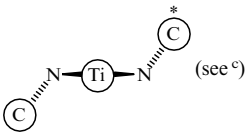 (see [c])	RR(−), RL(−)	Mr^{oct}	Mr	98 (*S*)	264
(*R*,*R*)-**123**	**S** : $Ti(OPr^i)_4$: : Et_2Zn : L = = 1 : 1.2 : 1.2 : 0.02	−30	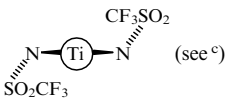 (see [c])	RR(−), RL(−)	Mr^{oct}	Mr	99 (*S*)	265
(*S*,*S*)-**123**	**S** : $ZnEt_2$: : $Ti(OPr^i)_4$: L = = 1 : 1.2 : 0.048 : 0.04	0	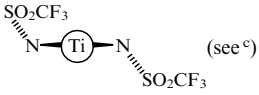 (see [c])	RR(+), RL(+)	Pr^{oct}	Pr	98 (*R*)	266

Table 8 (continued).

Ligand (complex)	Molar ratio of reaction components	T /°C	Schematic projection of metallacycle	Location of chirality-determining substituents in octants	Chirality in configurational models		*ee* (%) (configuration of 1-phenylpropan-1-ol)	Ref.
					Pr^{oct}/Mr^{oct}	Pr/Mr		
Complexes with chiral C_2-symmetric ligands								
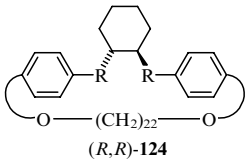 (R,R)-**124** (R = $NHSO_2$)	**S** : $Ti(OPr^i)_4$: : Et_2Zn : L = = 1 : 1.2 : 1.2 : 0.02	−45	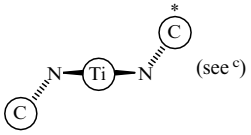 (see [c])	RR(−), RL(−)	Mr^{oct}	Mr	89 (*S*)	264
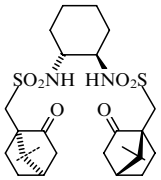 (R,R)-**125**	**S** : L : $Ti(OPr^i)_4$: : Et_2Zn = = 1 : 0.2 : 1.4 : 3	−20	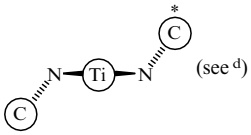 (see [d])	RR(−), RL(−)	Mr^{oct}	Mr	91 (*S*)	267
(S,S)-**125**	**S** : L : $Ti(OPr^i)_4$: : Et_2Zn = = 1 : 0.2 : 1.4 : 3	−20	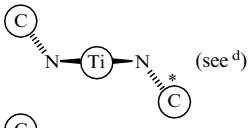 (see [d])	RR(+), RL(+)	Pr^{oct}	Pr	57 (*R*)	267
(S,S)-**126**	**S** : L : $Ti(OPr^i)_4$: : Et_2Zn = = 1 : 0.01 : 1.2 : 1.2	−40	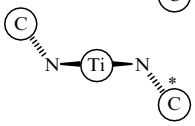	RR(+), RL(+)	Pr^{oct}	Pr	98 (*R*)	268
(R,R)-**127** (R = C_6H_2-3,5-Cl_2-2-OH)	**S** : L : $Ti(OPr^i)_4$: : Et_2Zn = = 1 : 0.2 : 1.4 : 1.8	−23	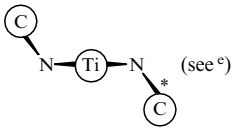 (see [e])	FR(−), FL(−)	Mr^{oct}	Pr	99 (*S*)	269, 270
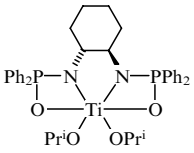 (R,R)-**128**	**S** : L : $Ti(OPr^i)_4$: : Et_2Zn = = 1 : 0.2 : 1.4 : 1.8	−50 to −20	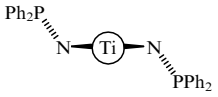	RR(+), RL(+)	Pr^{oct}	Pr	81 (*R*)	271
Complexes with asymmetric ligands								
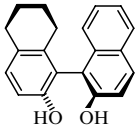 (*R*)-**129**	**S** : L : $Ti(OPr^i)_4$: : Et_2Zn = = 1 : 0.2 : 1.4 : 3	0	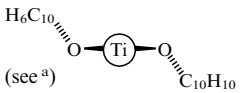 (see [a])	RR(+), RL(+)	Pr^{oct}	Pr	91 (*R*)	272
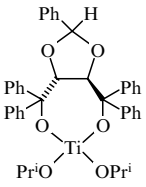 (R,R)-**130**	**S** : Et_2Zn : : $Ti(OPr^i)_4$: : $Ti(OPr^i)_2$[(R,R)-**130**] = 1 : 1.8 : 1.2 : 0.2	−20	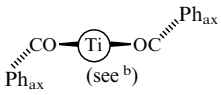 (see [b])	RR(−), RL(−)	Mr^{oct}	Mr	98 (*R*)	107

[a] X-Ray diffraction data (see Ref. 251). [b] X-Ray diffraction data (see Ref. 107). [c] X-Ray diffraction data (see Ref. 263). [d] X-Ray diffraction data (see Ref. 267). [e] Calculation (see Ref. 269).

It is of note that the feasibility of the configurational model (Pr^{oct}/Mr^{oct} or Pr/Mr) in the alkylation of benzaldehyde in the presence of titanium complexes with various chiral C_1- and C_2-symmetric ligands is very high (up to 93%). This testifies to a similarity of the reaction mechanisms in both cases and corrobo-

Table 9. Asymmetric alkylation of benzaldehyde (**S**) with diethylzinc in the presence of titanium asymmetric complexes with amino alcohols, *N*-sulfonylamino alcohols and *N*-phosphorothioamido alcohols.

Ligand	Molar ratio of reaction components	T /°C	Schematic projection of metallacycle	Location of chirality-determining substituents in octants	Chirality in configurational models		*ee* (%) (product configuration)	Ref.
					Pr^{oct}/Mr^{oct}	Pr/Mr		
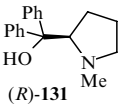 (*R*)-**131**	**S** : L : $Ti(OPr^i)_4$: : $(cyclo\text{-}C_3H_5)_2Zn$ = = 1 : 0.05 : 1.2 : 3	−18	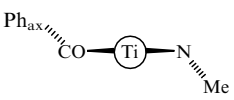	RR(+), RL(+)	Pr^{oct}	Pr	84 (*S*)[a]	273
(*S*)-**131**	**S** : L : $Ti(OPr^i)_4$: : $(cyclo\text{-}C_3H_5)_2Zn$ = = 1 : 0.2 : 1.2 : 3	0	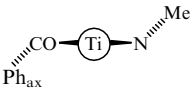	RR(−), RL(−)	Mr^{oct}	Mr	86 (*R*)[a]	273
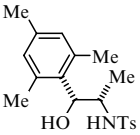 (*R*,*S*)-**132**	**S** : L : $Ti(OPr^i)_4$: : Et_2Zn = = 1 : 0.05 : 1.2 : 2	0	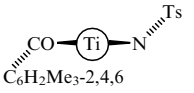	RR(−), RL(−)	Mr^{oct}	Mr	84 (*S*)[b]	274
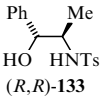 (*R*,*R*)-**133**	**S** : L : $Ti(OPr^i)_4$: : Et_2Zn = = 1 : 0.05 : 1.2 : 2	0	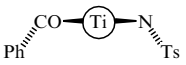	RR(+), RL(−)	Pr^{oct}/Mr^{oct}	Mr/Pr	0	274
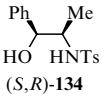 (*S*,*R*)-**134**	**S** : L : $Ti(OPr^i)_4$: : Et_2Zn = = 1 : 0.05 : 1.2 : 2	0	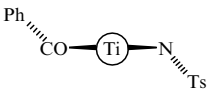	RR(+), RL(+)	Pr^{oct}	Pr	83 (*S*)[b]	274
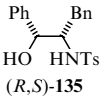 (*R*,*S*)-**135**	20 mol.% [L], 1 mmol $Ti(OPr^i)_4$	0	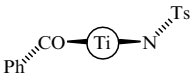	RR(−), RL(−)	Mr^{oct}	Mr	>99 (*R*)[b]	275
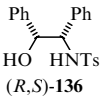 (*R*,*S*)-**136**	10 mol.% [L], 0.5 mmol $Ti(OPr^i)_4$	0	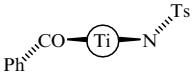	RR(−), RL(−)	Mr^{oct}	Mr	90 (*R*)[b]	275
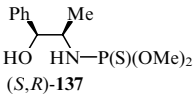 (*S*,*R*)-**137**	**S** : L : $Ti(OPr^i)_4$: : Et_2Zn = = 1 : 0.05 : 1.5 : 1.5	−30	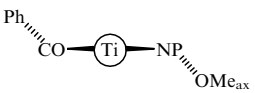	RR(+), RL(+)	Pr^{oct}	Pr	97 (*S*)[b]	276
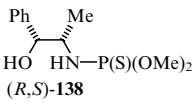 (*R*,*S*)-**138**	**S** : L : $Ti(OPr^i)_4$: : $(cyclo\text{-}C_3H_5)_2Zn$ = = 1 : 0.15 : 1.2 : 3	−30	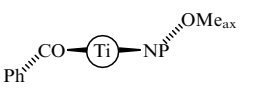	RR(−), RL(−)	Mr^{oct}	Mr	96 (*R*)[a]	273

[a] The reaction product is cyclo-$C_3H_5CH(OH)Ph$. [b] The reaction product is 1-phenylpropan-1-ol.

rates the conclusion that the maximum enantioselectivity of this reaction does not depend on the symmetry of the ligand.

Scheme 6

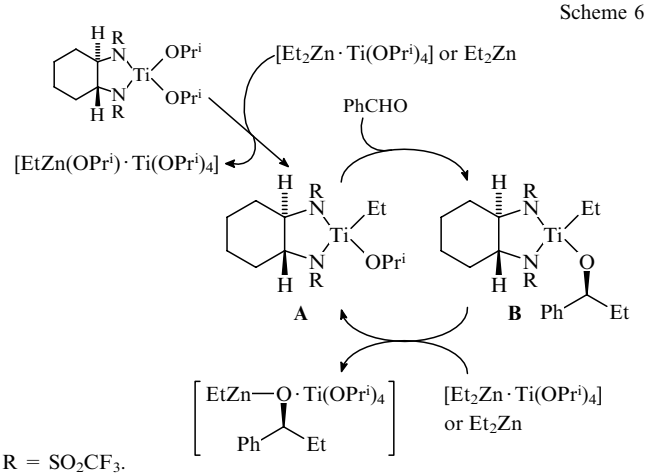

R = SO_2CF_3.

VII. Alkylation of benzaldehyde with dialkylzinc in the presence of amino alcohols and related compounds

In the asymmetric alkylation of aldehydes with dialkylzinc (see Refs 9, 17, 249 and 250), chiral amino alcohols, amido alcohols, diamines, diols, amino thiols, disulfides and diselenides represented components of *in situ* generated catalytic systems. The reaction of benzaldehyde with diethylzinc is a standard reaction, but in this case it is carried out in the absence of $Ti(OPr^i)_4$. As can be judged from the number of compounds tested as chiral ligands, this reaction seems to be a leader among other asymmetric reactions.

Experimental and theoretical studies into the mechanism of the reaction of dialkylzinc with benzaldehyde in the presence of amino alcohols have made it possible to establish the order of formation of intermediates [3, 9, 277–281] (Scheme 7). The first step includes the formation of the chelate zinc complex **A** with an amino alcohol, which determines the stereochemistry of its further conversions. The configurational relationships between the

Scheme 7

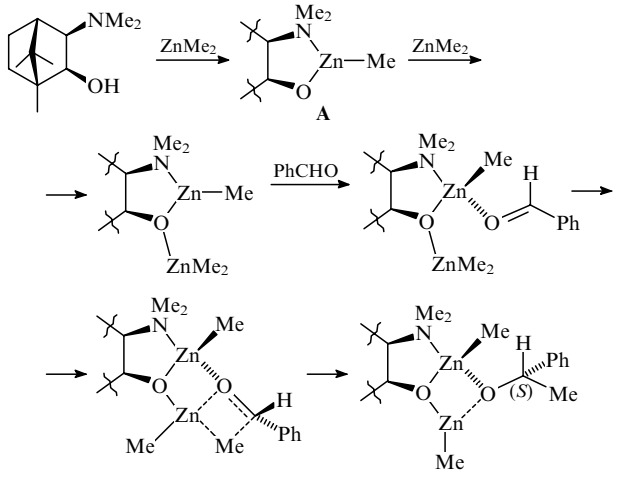

amino-alcohol ligand and the reaction product are described by the scheme (Scheme 8) proposed by Noyori *et al.*[249]

Scheme 8

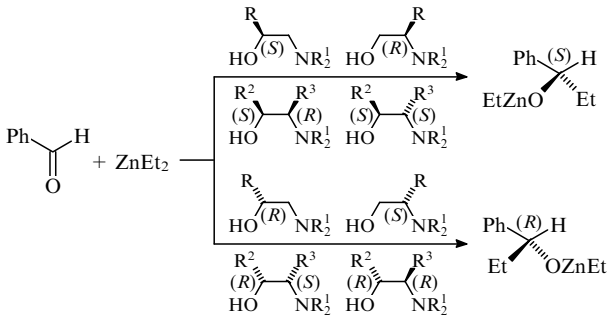

This scheme is based on a large body of experimental evidence [282–344] and reflects adequately the relationship between the product and ligand configurations. A comparison of configurational models for the reaction of dialkylzinc with benzaldehyde in the presence of amino alcohols,[304–316, 333] which provide the maximum enantioselectivity of the reaction, is given in Table 10. The data from Table 10 and the analysis of experimental data [282–344] suggest that the regularities $Pr^{oct} \rightarrow (S)$, $Mr^{oct} \rightarrow (R)$ and $Pr \rightarrow (S)$, $Mr \rightarrow (R)$ are equally observed in nearly 93% of cases. However, in contrast to the octant model, the quadrant

Table 10. Alkylation of benzaldehyde with diethylzinc catalysed by *in situ* generated zinc complexes with chiral (bidentate) amino alcohols.

Ligand (complex)	Schematic projection of metallacycle	Location of chirality-determining substituents in octants	Chirality in configurational models		*ee* (%) (product configuration)	Ref.
			Pr^{oct}/Mr^{oct}	Pr/Mr		
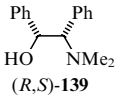 (*R*,*S*)-**139**	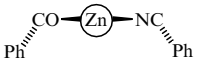	RR(+), RL(−) [a]	$\sum Mr^{oct}$	*Mr*	97 (*R*)	282
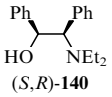 (*S*,*R*)-**140**	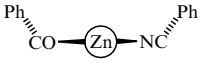	RR(−), RL(+) [a]	$\sum Pr^{oct}$	*Pr*	94 (*S*)	283
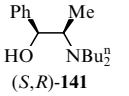 (*S*,*R*)-**141**	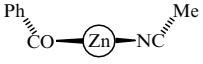	RR(−), RL(+) [a]	$\sum Pr^{oct}$	*Pr*	90 (*S*)	283–286
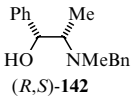 (*R*,*S*)-**142**	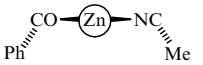	RR(+), RL(−) [a]	$\sum Mr^{oct}$	*Mr*	86 (*R*)	287
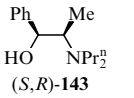 (*S*,*R*)-**143**	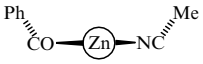	RR(−), RL(+) [a]	$\sum Pr^{oct}$	*Pr*	92 (*S*)	288
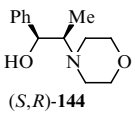 (*S*,*R*)-**144**	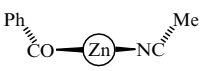	RR(−), RL(+) [a]	$\sum Pr^{oct}$	*Pr*	88 (*S*)	288
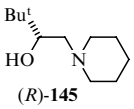 (*R*)-**145**	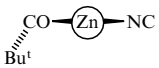	RL(−)	Mr^{oct}	*Mr*	98 (*R*)	282
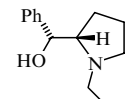 (*R*,*S*)-**146**	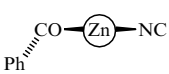	RL(−)	Mr^{oct}	*Mr*	100 (*R*)	289
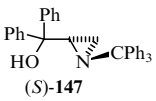 (*S*)-**147**	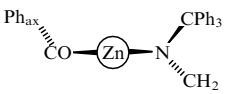	RR(+), RL(+), FR(+)	Pr^{oct}	*Pr*	99 (*S*)	301, 302

Table 10 (continued).

Ligand (complex)	Schematic projection of metallacycle	Location of chirality-determining substituents in octants	Chirality in configurational models		*ee* (%) (product configuration)	Ref.
			Pr^{oct}/Mr^{oct}	Pr/Mr		
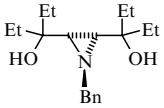 (*S*,*S*)-**148**	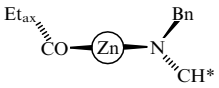	RR(+), RL(+), FR(+)	Pr^{oct}	Pr/Mr	94 (*S*)	303
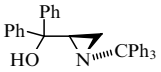 (*R*)-**149**	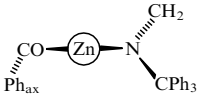	RR(−), RL(−), FR(−)	Mr^{oct}	Mr/Pr	99 (*R*)	302
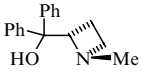 (*S*)-**150**	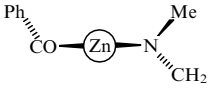	RR(+), RL(+), FR(+)	Mr^{oct}	Pr/Mr	98 (*S*)	304
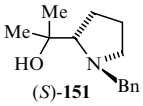 (*S*)-**151**	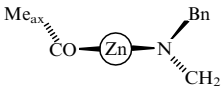	RR(+), RL(+), FR(+)	Pr^{oct}	Pr/Mr	99 (*R*)	305
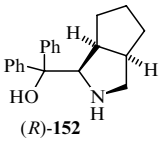 (*R*)-**152**	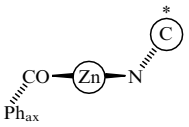	RR(−), RL(−)	Mr^{oct}	*Mr*	99 (*R*)	306–312
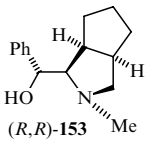 (*R*,*R*)-**153**	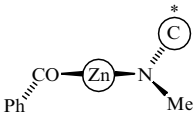	RR(−), RL(−), FR(−)	Mr^{oct}	Mr/Pr	68 (*R*)	306–312
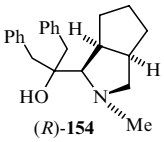 (*R*)-**154**	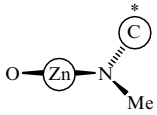	RR(−), RL(−)	Mr^{oct}	Mr/Pr	90 (*R*)	306–312
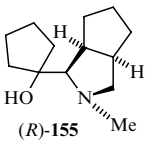 (*R*)-**155**	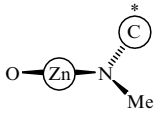	RR(−), FR(−)	Mr^{oct}	Mr/Pr	99 (*R*)	306–312
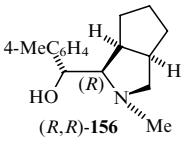 (*R*,*R*)-**156**	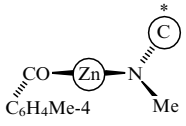	RR(−), RL(−), FR(−)	Mr^{oct}	Mr/Pr	91 (*R*)	306–312
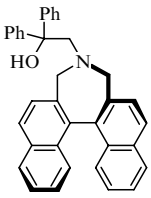 (*S*)-**157**	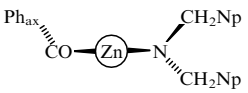	FR(+), RR(+), RL(+)	Pr^{oct}	Pr/Mr	87 (*S*)	318

Note. The sign $\sum$ designates the predominant contribution of the given type of chirality. [a] A substituent at the left senior atom has preference.

projection model can be applied to a limited number of ligands only. The quadrant model is inapplicable to reactions in the presence of complexes with the ligands **148**–**151** and **153**–**157** due to location of coordinated ligand fragments in the quadrants with opposite signs.

Here, as in other cases (see, *e.g.*, Tables 3–7), the overwhelming majority of complexes that ensure high enantioselectivity of the reaction possess conformational rigidity. These include five-membered chelate complexes with bulky substituents (Ph, Bu^t, Pr^i) the conformational rigidity of the chelate ring which is

Table 11. Asymmetric alkylation of benzaldehyde with diethylzinc catalysed by 'monomeric' chiral C_1-symmetric and 'dimeric' C_2-symmetric ligands (toluene, 20 °C).

'Monomeric' ligand	*ee* (%) (product configuration)	Ref.	'Dimeric' ligand	*ee* (%) (product configuration)	Ref.
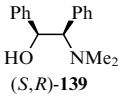 (*S*,*R*)-**139**	73 (*S*)	282	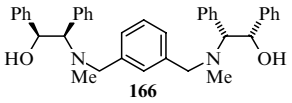 **166**	75 (*S*)[a]	355
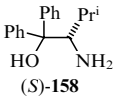 (*S*)-**158**	88 (*R*)	290	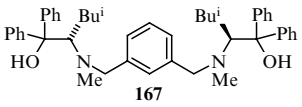 **167**	87 (*R*)[a]	355
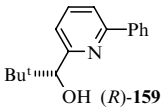 (*R*)-**159**	93 (*R*)	320, 321	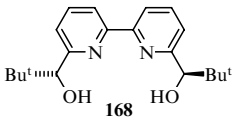 **168**	97 (*R*)	320, 321
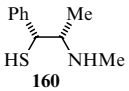 **160**	80 (*R*)	345 – 347	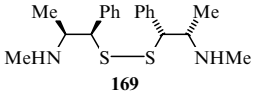 **169**	86 (*R*)	345 – 347
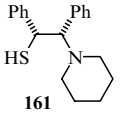 **161**	99 (*R*)	348 – 350	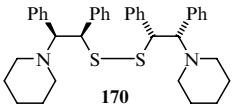 **170**	99 (*R*)	348 – 350
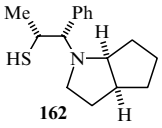 **162**	90 (*R*)	306	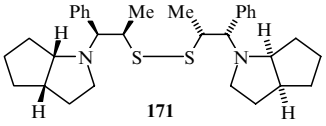 **171**	86 (*R*)	306
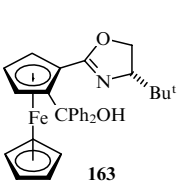 **163**	93 (*R*)	338, 342, 343	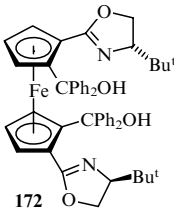 **172**	91 (*R*)	342
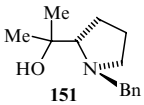 **151**	99 (*R*)	305	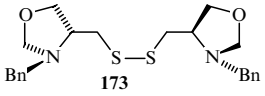 **173**	> 99 (*R*)	356
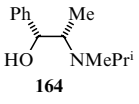 **164**	80 (*R*)	286	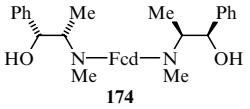 **174**	70 (*R*)	357
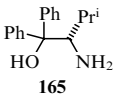 **165**	88 (*R*)	290	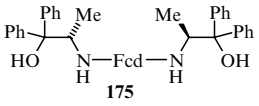 **175**	83 (*R*)	357

[a] This reaction occurs in the presence of 4-ClC_6H_4CHO.

provided by a more advantageous equatorial position of the substituent [77] (complexes with the ligands **139** – **145**). The conformational rigidities of many efficient complexes are enhanced owing to the incorporation of one of the bonds of the first chelate ring into the second ring (complexes with the ligands **146** – **156**). Complexes with atropoisomeric ligands (*e.g.*, the ligand **157**) constitute a special group.

Octant projections can be constructed for a small group of complexes with chiral amino thiols, which represent thio analogues of the ligands **139** – **143** and **145**.[306, 326, 345 – 354] All of them have the same structural features as the amino alcohol-containing complexes. It is therefore not surprising that reactions catalysed by these complexes follow the same regularities, *viz.*, $Pr^{oct}\rightarrow(S)$, $Mr^{oct}\rightarrow(R)$ and $Pr\rightarrow(S)$, $Mr\rightarrow(R)$, with a high degree of probability (~90%).

A comparison of chiral C_2-symmetric tetradentate ligands (which are rather few in number) (Table 11) with their asymmetric 'monomeric' bidentate counterparts has shown that the involvement of all these ligands in the reaction is largely due to the involvement of their 'monomeric' asymmetric fragments. A comparison of the experimental results obtained with the complexes with both 'monomeric' and the corresponding 'dimeric' ligands revealed a virtually complete coincidence of the *ee* values and the

Table 12. Asymmetric alkylation of benzaldehyde with diethylzinc in the presence of chiral C_2-symmetric tridentate ligands and their asymmetric analogues.[358]

Chiral C_2-symmetric ligand	*ee* (%) (product configuration)	Asymmetric ligand	*ee* (%) (product configuration)
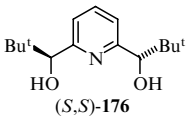 (*S*,*S*)-**176**	65 (*S*)	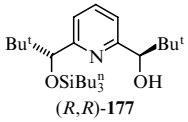 (*R*,*R*)-**177**	67 (*R*)
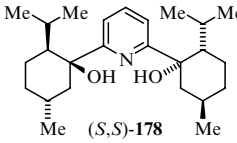 (*S*,*S*)-**178**	55 (*S*)	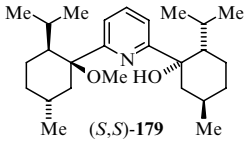 (*S*,*S*)-**179**	35 (*S*)
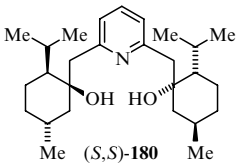 (*S*,*S*)-**180**	93 (*S*)	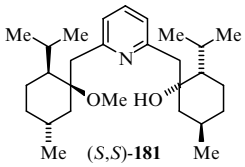 (*S*,*S*)-**181**	95 (*S*)

product configurations, which provides convincing evidence in favour of this conclusion.

An analysis of the data summarised in Table 12, which compares the results obtained in the presence of chiral C_2-symmetric tridentate ligands and their asymmetric analogues, corroborated this conclusion. The similarity of the *ee* values and the coincidence of the product configurations were observed in the majority of cases. This provides additional evidence in favour of the fact that the reaction in the presence of chiral C_2-symmetric tri- and tetradentate ligands involves their asymmetric bidentate fragments.

Thus, it is only asymmetric ligands that are effective in the asymmetric alkylation of benzaldehyde with diethylzinc in the absence of $Ti(OPr^i)_4$.

Successful implementation of asymmetric reactions in the presence of chiral C_2-symmetric ligands requires the presence of $Ti(OPr^i)_4$ in the catalytic system (see Table 8).

Unfortunately, the applicability of the above-described regularities to a large number of complexes cannot be estimated because their octant projections are too difficult to establish.

In some cases,[359–365] the problem arises as to whether the chiral centre is located in the side chain of the ligand or the complex contains a ring spiro-fused to the metallacycle.[319,366–373] Because of the ambiguity of determination of the octant projection, complexes with bulky tri- and tetradentate ligands cannot be considered.[362,368,371,374–388] However, the tetradentate C_2-symmetric ligands **166**–**175** were included in Table 11, because there is evidence that their bidentate fragments are involved in the catalysis as components of the corresponding complexes. For complexes with ligands containing bulky fragments[306,383] that rotate around the C–C bond in their side chains, the octant projection cannot be established at all. Complexes with several seven-membered metallacycles[389–392] contain $(CH_2)_2$ fragments, and their octant projections cannot be unambiguously determined because of the conformational lability of the coordinated ligand. The octant projections of the complexes the ligands in which form eight-membered (and larger-sized) metallacycles[393,394] as well as of some other complexes[285,372,376,395–397] cannot be reliably determined either.

The mechanism of asymmetric induction in the alkylation of benzaldehyde with diethylzinc in the presence of chiral C_2-symmetric ligands will be discussed in the next Section.

VIII. Complexes with chiral C_2-symmetric ligands as the asymmetry inductors

Previously, it was concluded[6] that the intermediate responsible for the asymmetric induction in some asymmetric reactions is asymmetric irrespective of the symmetry of the starting complex. This conclusion was made in the analysis of mechanisms of such reactions as hydrogenation of amino acid precursors and hydrosilylation of ketones in the presence of chiral metal complexes. In other words, in the catalysis by complexes containing C_2-symmetric ligands the C_2-symmetry is lost in the step preceding the asymmetric induction. High enantioselectivity can be achieved with the use of complexes with both asymmetric and chiral C_2-symmetric ligands as catalysts. A similar conclusion was made in the analysis of allylic alkylation, cyclopropanation, the Diels–Alder reactions and benzaldehyde alkylation with dialkylzinc on titanium complexes.

Complexes with chiral C_2-symmetric and asymmetric ligands manifest different efficiencies in the hydrogen-transfer hydrogenation of acetophenone and hydroformylation of styrene. Complexes with asymmetric ligands provide higher enantioselectivities (see Sections III and IV). Presumably, this can be related to the C_2-symmetry of the intermediate responsible for the asymmetric induction (in the case of chiral C_2-symmetric complexes).

The presence or the absence of titanium complexes in the catalytic system influences significantly the enantioselectivity of the alkylation of benzaldehyde with dialkylzinc in the presence of chiral C_2-symmetric ligands (Table 13). In all the cases studied,

Table 13. Asymmetric addition of diethylzinc to benzaldehyde in the presence of chiral C_2-symmetric ligands and complexes of $Ti(OPr^i)_4$ with these ligands.

In the absence of $Ti(OPr^i)_4$			In the presence of $Ti(OPr^i)_4$		
Ligand	*ee* (%) (product configuration)	Ref.	Ligand	*ee* (%) (product configuration)	Ref.
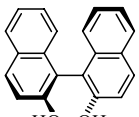 (*S*)-**110**	no reaction	253	(*S*)-**110**	92 (*S*)	253
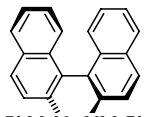 (*R*)-**182**	8 (*R*)	339	–	–	–
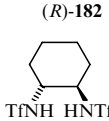 (*R*,*R*)-**123**	54 (*S*)	266, 267, 268	(*R*,*R*)-**123**	99 (*S*)	266, 267, 269
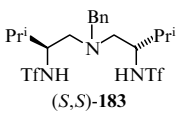 (*S*,*S*)-**183**	15 (*S*)[a]	398	(*S*,*S*)-**183**	72 (*S*)[b]	398
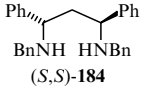 (*S*,*S*)-**184**	15[c] 0[d]	399 399	– –	– –	– –

[a] In the presence of molecular sieves MS 4 Å. [b] The reaction with 4-$CF_3C_6H_4CHO$. [c] The configuration is not indicated. [d] The reaction with 4-MeC_6H_4CHO.

the enantioselectivity is highly enhanced in the presence of $Ti(OPr^i)_4$ in the catalytic system.

The data on the addition of diethylzinc to benzaldehyde in the presence of chiral ligands with a C_2-symmetry axis passing through the donor nitrogen atom are presented in Table 14. In C_2-symmetric fragments of the ligands **188**–**190**, one of the oxygen atoms can be coordinated with the catalyst (in contrast to the ligands **185** and **186** which are devoid of such an ability due to the shielding of the oxygen atoms by bulky groups). As a result, the *ee* value increases from 10(20)% to 90(95)% (the ligand **187** [400, 401] occupies an intermediate position). An analysis of molecular models revealed that the zinc atom can coordinate not only the donor atoms of the ligands [O(S) and N], but also the oxygen atom of one of two identical and C_2-symmetric groups in the nitrogen-containing ring. Under these conditions, the second group becomes inaccessible for the coordination. The C_2-symmetry of the catalytic complex is lost as a result of additional coordination of the oxygen atom of only one of the chiral C_2-symmetric groups of the ligand by the zinc atom. Complexes with similar ligands that are incapable of such coordination and therefore manifest higher symmetry appear to be less enantioselective as catalysts.

The reaction catalysed by chiral C_2-symmetric titanium complexes proceeds *via* the asymmetric intermediate **A** (see Scheme 7). Based on calorimetric studies, a catalytic model has been proposed for the reaction catalysed by complexes with asymmetric ligands of the type **191** and **192** (Scheme 9). According to this scheme, the asymmetric induction is realised in the **A** → **B** conversion step.

Table 14. Addition of diethylzinc to benzaldehyde in the presence of chiral ligands with a C_2-symmetry axis passing through the donor nitrogen atom.

Ligand	*ee* (%) (product configuration)	Ref.
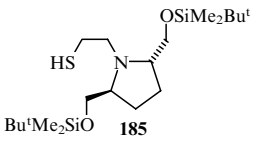 **185**	10 (*R*)	363
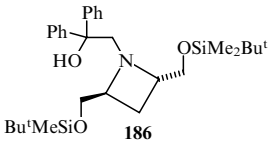 **186**	20 (*S*)	361
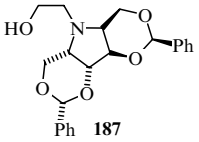 **187**	40 (*S*)	400, 401
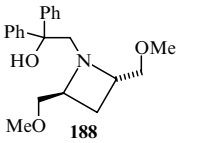 **188**	~90 (*S*)	361
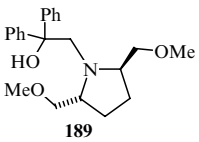 **189**	~90 (*R*)	362, 363
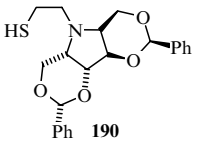 **190**	95 (*S*)	400, 401

Scheme 9

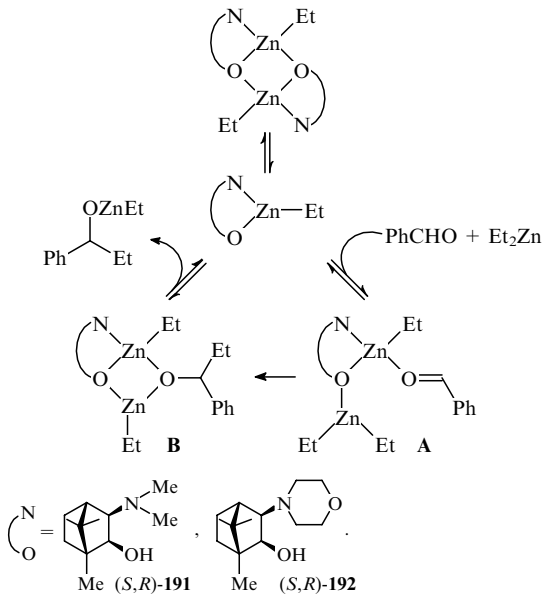

Extrapolation of this model to a reaction catalysed by complexes with chiral C_2-symmetric ligands of the type **123**, **182**–**184** (Scheme 10) demonstrates that in this case, too, the **A** → **B** step is responsible for asymmetric induction. The structures **C** and **D** determining the asymmetric induction are diastereomeric, but the immediate environments of the coordinated aldehyde in each of these intermediates represent enantiomeric species. Presumably, the difference in the concentrations of the diastereomers **E** and **F**, which favour the formation of different enantiomers of the reaction product, is small; therefore, the enantioselectivity of the reaction should be low which actually is the case.

Thus, the increase in enantioselectivity on going from a reaction in the presence of chiral C_2-symmetric ligands to a reaction catalysed by titanium complexes with these ligands (see Table 13), is due to the loss of C_2-symmetry by the intermediate. A deviation from this rule, which is manifested in moderate enantioselectivity in the presence of the chiral C_2-symmetric ligand **123** [*ee* = 54% (*S*)], can be attributed to the fact that the ideal C_2-symmetry is not realised in this case, presumably due to, *e.g.*, conformational distortions in the six-membered ring.

The reduction of acetophenone with borane in the presence of chiral C_2-symmetric atropoisomeric ligands becomes enantioselective upon the addition of $Al(OPr^i)_3$ to the reaction system (Table 15).[402]

Scheme 10

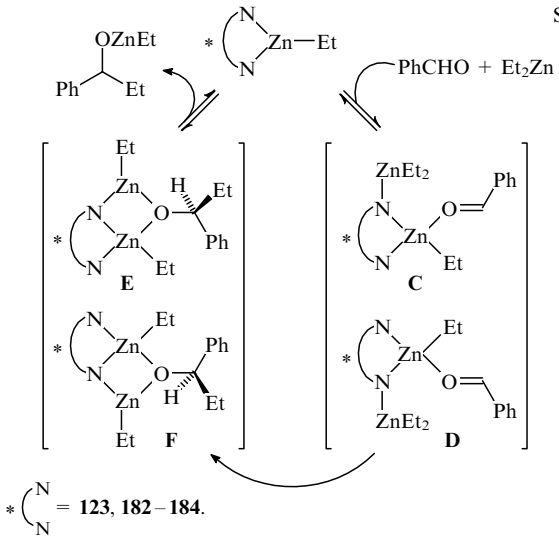

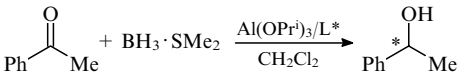

The enhancement of the enantioselectivity of this reaction can be due to the same factors as in the alkylation of benzaldehyde with dialkylzinc in the presence of $Ti(OPr^i)_4$ and without it (see Table 13). Apparently, in contrast to the chiral C_2-symmetric reducing reagent based on borane and a ligand, the catalytic system generated *in situ* from borane, a chiral C_2-symmetric ligand and $Al(OPr^i)_3$, is asymmetric.

The loss of C_2-symmetry in the series of chiral ligands of the same type is accompanied by a drastic enhancement of the enantioselectivity of certain catalytic reactions. The allylation of aldehydes is an example.[403]

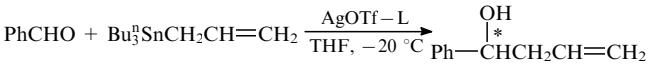

L	*ee* (%)	Product configuration
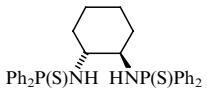 (*R*,*R*)-**195**	9	*R*
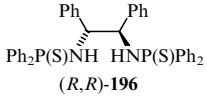 (*R*,*R*)-**196**	15	*R*
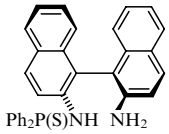 (*R*)-**197**	52	*R*

The oxidation of sulfides is a striking example of high sensitivity of the enantioselectivity of a catalytic reaction to the C_2-symmetry of the chiral ligands.

Table 15. Asymmetric reduction of acetophenone with borane catalysed by chiral C_2-symmetric ligands in the presence and in the absence of $Al(OPr^i)_3$ (CH_2Cl_2, 20 °C).[402]

Ligand	Reaction in the absence of $Al(OPr^i)_3$		Reaction in the presence of $Al(OPr^i)_3$	
	yield (%)	*ee* (%)	yield (%)	*ee* (%)
(*R*)-**110**	78	0	97	60 (*S*)
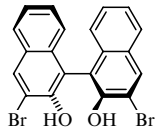 (*R*)-**193**	90	0	94	46 (*R*)
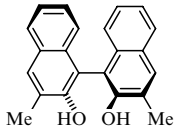 (*R*)-**194**	93	0	97	10 (*R*)
(*R*)-**115**	91	0	95	71 (*S*)

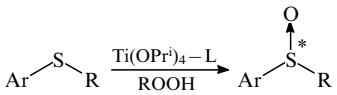

As can be seen from Table 16, the enantioselectivity of this reaction depends on the structures of chiral diols as the ligands. A comparison of conformational rigidities of such ligands revealed that the possible conformational deviations from the ideal C_2-symmetry decrease in the following order: **198** < **199** ≪ **200** ≈ **201**. For the latter two ligands, the deviations are the greatest due to the free rotation of the Bu^t and Ph groups at the chiral carbon atoms around the C–C bond. This order coincides with the order of changes in *ee* of the reaction product formed in the presence of the same ligands (Table 16). Thus, in the sulfide oxidation these parameters are linearly interrelated.

The existence of such a relationship is confirmed by an analysis of numerous published data on asymmetric catalytic reactions. Contrary to expectations, the transition from a conformationally labile six-membered metallacycle to a more rigid seven-membered ring results in a radical decrease in the enantioselectivity of aldol condensation.[407]

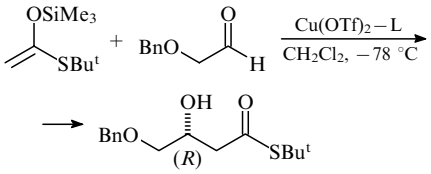

Ligand L	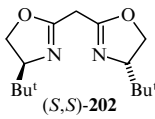 (*S*,*S*)-**202**	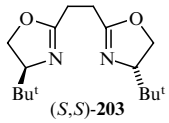 (*S*,*S*)-**203**
ee (%) (product configuration)	64 (*R*)	0

In this case, this can be attributed to a more perfect C_2-symmetry of the complex with a seven-membered metallacycle. Similarly, lower enantioselectivity of aldehyde allylation corre-

Table 16. Dependence of the enantioselectivity of oxidation of methyl *p*-tolyl sulfide and benzyl phenyl sulfide on the ligand structure.

Ligand (L)	Composition of reaction mixture and temperature	*ee* (%) (product configuration)		Ref.
		p-Tol–S–Me	Ph–S–Bn	
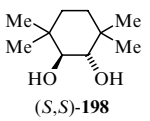 (*S*,*S*)-**198**	$Ti(OPr^i)_4$–L, 4-$Pr^nC_6H_4O_2H$, MS 4Å, toluene, −20 °C	0	0	404
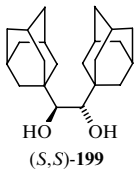 (*S*,*S*)-**199**	$Ti(OPr^i)_4$–L, 4-$Pr^nC_6H_4O_2H$, MS 4Å, toluene, −20 °C	7 [a]	14 [a]	404
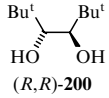 (*R*,*R*)-**200**	$Ti(OPr^i)_4$–L, 4-$Pr^nC_6H_4O_2H$, MS 4Å, toluene, −20 °C	–	95 (*S*)	405
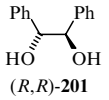 (*R*,*R*)-**201**	$Ti(OPr^i)_4$–L, Bu^tO_2H, CCl_4, 0 °C	80 (*S*)	>99 (*S*)	406

[a] The configuration is not indicated.

sponds to a more perfect C_2-symmetry of the complex $RhCl_2[(S,S)$-**204**$]\cdot H_2O$ (R = Ph) (in comparison with the symmetry of the same complex containing a benzyl substituent).[408]

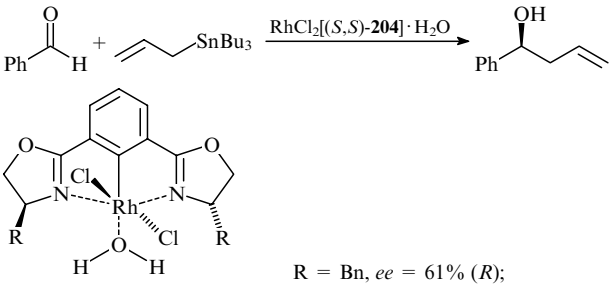

$RhCl_2[(S,S)$-**204**$]\cdot H_2O$

R = Bn, *ee* = 61% (*R*);
R = Ph, *ee* = 6% (*R*).

And, finally, there is evidence that the enhancement of enantioselectivity can be due to the loss, by the chiral C_2-symmetric catalytic complex, of the symmetry axis C_2. Numerous findings suggest that the enantioselectivity is enhanced upon addition of monodentate achiral auxiliary ligands (additives or co-catalysts) to the reaction mixture.[409] The cyanosilylation of aldehydes in the presence of Lewis acids as catalysts is a typical example of such a reaction.

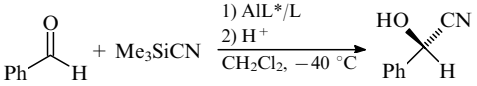

For example, the reaction catalysed by the aluminium complex AlCl[(*S*)-**205**] in the presence of an achiral ligand proceeds with a much higher enantioselectivity.[410]

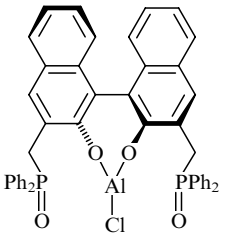

AlCl[(*S*)-**205**]

Substrate	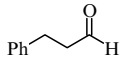		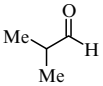	
Achiral ligand L	without ligand	$Bu_3P(O)$	without ligand	$Bu_3P(O)$
ee (%) (product configuration)	9 (*S*)	97 (*S*)	25 (*S*)	90 (*S*)

It is known that the intermediate **A**, which has the structure of a trigonal bipyramid, is formed in the presence of an achiral ligand.[411, 412]

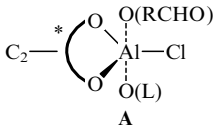

A

In contrast to the complex formed in the absence of an additional ligand, in the intermediate **A** the symmetry axis C_2 is lost. Consequently, the enhancement of the enantioselectivity can be explained by the asymmetry of the intermediate **A**. A similar effect in the Mannich reaction is induced by an additional ligand.[413] A weaker effect is observed in the allylic alkylation reaction,[414] *etc.*[415] upon introduction of an achiral ligand. Numerous examples of the use of molecular sieves (MS 4 Å) for enhancement of the enantioselectivity of a catalytic reaction in the presence of chiral C_2-symmetric metallocomplexes are known (for more recent publications, see Refs 416 and 417). This effect can also be due to the loss of the C_2-symmetry by chiral C_2-symmetric complexes upon chemisorption on the surface of aluminosilicate. As a result, the asymmetric induction is realised in the step involving the asymmetric intermediate, *i.e.*, that devoid of any symmetry elements other than C_1.

Thus, the opinion[418] that chiral C_2-symmetric ligands are the most efficient asymmetry inductors should probably be considered in the context of a concrete reaction mechanism. For example, in such reactions as hydrogen-transfer hydrogenation of ketones, hydroformylation of styrene or alkylation of aldehydes with dialkylzinc [without the involvement of $Ti(OPr^i)_4$ or analogous complexes], these ligands are less efficient than asymmetric ligands. In reactions like sulfide oxidation, complexes with a chiral C_2-symmetric ligand act as asymmetry inductors, most probably due to the deviation from the ideal C_2-symmetry. Actually, in such cases it is the intermediate that becomes asymmetric due to the loss of the symmetry axis C_2 that is responsible for the asymmetric induction.

The abnormal inefficiency of complexes with chiral C_2-symmetric ligands as asymmetry inductors was observed earlier, *e.g.*, in hydroformylation reactions.[170] This was rationalised by the peculiarities of this reaction, but the true reason for this phenomenon seems to be more fundamental. Presumably, this effect is not confined to catalytic reactions only. Thus, our findings[419–421] and the results by other investigators[422–425] point to an abnormally low enantioselectivity of acetophenone reduction by lithium chiral dihydrides $[(O\ O)LiH_2]$¶ modified by the atropoisomeric ligands **41**, **110**, and **206**–**208**.

Ligand	*ee* (%) (product configuration)	Ref.	Ligand	*ee* (%) (product configuration)	Ref.
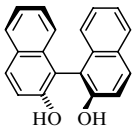 (*R*)-**110** (binol)	2 (*R*) 0	422 420	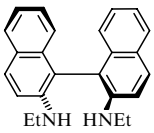 (*R*)-**208**	43 (*R*)	423
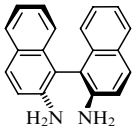 (*R*)-**206**	9 (*R*)	423	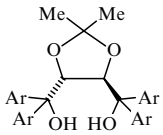 (*R*,*R*)-**41** (Ar = H, C_6H_4OMe-4)	78 (*R*)	425
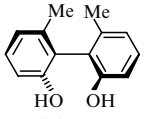 (*R*)-**207**	2 (*R*)	424			

Since the aluminium atom in $LiAlH_4$ has a tetrahedral environment, the structure of the dihydride anion based on these chiral C_2-symmetric ligands is close to ideal C_2-symmetric. The introduction of an ethyl group into the ligand **206** (giving the ligand **208**) increases the deviation of its C_2 symmetry from the ideal in comparison with the ligands **110**, **206** and **207**. It is this factor that is responsible for the moderate enantioselectivity of the dihydride containing the ligand **208**. Further enhancement of the enantioselectivity is observed upon transition to the ligand **41**,

¶ It was suggested[422] that the disproportionation of $Li(binol)AlH_2$ to $LiAlH_4$ and $LiAl(binol)_2$ was the reason for the low enantioselectivity of the reduction of ketones with this dihydride. Our experiments[420] showed that this was not the case: no disproportionation took place under the reaction conditions.

which has four phenyl groups that rotate around the $C-C_{Ph}$ bond and thus disturb the C_2-symmetry.

Both the non-modified hydrides $LiAlH_4$ and $NaAlH_4$ and diol-modified hydrides react with ketones in THF or diglyme, predominantly as contact and dissociated ion pairs.[426]

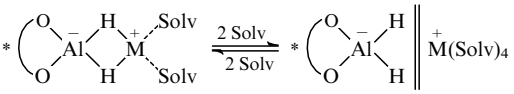

Solv is solvent.

Since the Li^+ cation is a stronger acid than Na^+, it can be expected that the bridging ring is more rigid in the case of Li; therefore, the violation of the C_2-symmetry in the case of lithium dihydride is less pronounced. In turn, the ring formed by the ligand in a planar monohydride based on AlH_3 is more strained than that in the dihydride based on $NaAlH_4$. Therefore, the C_2-symmetry of the latter is less perfect. We found that the *ee* values of the reduction products of substrates containing C=O and C=N groups are higher in the case where the C_2-symmetry of the hydride is violated to a greater extent [the ligand **209** represents an analogue of the ligand **41** (Ar = C_6H_4OMe-4)] (Table 17).

Table 17. Enantioselectivity in reduction with aluminium hydrides.[420, 421]

Substrate	Complex with aluminium hydride	Cation	*ee* (%)	Product configuration
PhCOMe	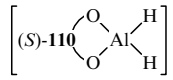	Na	38	(*S*)
		Li	0	–
PhCMe ‖ NP(O)Me_2	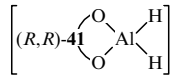	Na	78	(*R*)
		Li	30	(*R*)
PhC(O)Pr^i	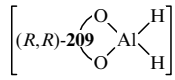	Na	73	(*S*)
	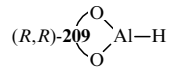	–	7	(*S*)
	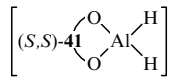	Na	76	(*R*)
	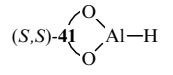	–	36	(*R*)

These data suggest that this phenomenon is versatile and is not confined to catalytic reactions.

IX. Conclusion

A comparison of the configurational models Mr^{oct}/Pr^{oct} and Mr/Pr, in the example of catalytic hydrogen-transfer hydrogenation, hydroformylation, allylic alkylation and alkylation of aldehydes with dialkylzinc and some other reactions, suggests that preference should be given to the former based on the octant projection.

The configurational relationships 'catalytic complex – reaction product' considered in this review are based on the analysis of octant and quadrant projections obtained from consideration of molecular models, X-ray diffraction data or calculations for certain structures. It is of note that both X-ray diffraction data and numerous calculations (to say nothing of molecular models) give purely probabilistic patterns of spatial arrangements of molecular fragments in real intermediates, especially under the reaction conditions. However, the accuracy of the estimation of the fulfillment of the regularity $Pr^{oct}-(S)$, $Mr^{oct}-(R)$ [or $Pr^{oct}-(R)$, $Mr^{oct}-(S)$] increases manifold with an increase in the number of variants under study. Having established such a regularity relative to a concrete substrate and a concrete reaction and knowing the configuration of the reaction product, its *ee* and reaction mechanism, one can get a better insight into the structure of an intermediate responsible for the asymmetric induction, especially if we take into consideration the fact that such an intermediate can be isolated and studied instrumentally in only a few catalytic reactions.

Thus, the judgement on the absolute configuration of the intermediate determining the asymmetric induction in the hydrogenation of enamides on rhodium bis(diphenylphosphine) complexes can be made exclusively by analogy with the structure of a stable diastereomeric intermediate present in excess in the reaction mixture. X-Ray diffraction analysis of the latter requires its preliminary isolation at low temperature,[427] *i.e.*, under the conditions where the ratio of the conformers changes drastically as can be evidenced from low-temperature circular dichroism data.[428] Moreover, the results of X-ray diffraction analysis of the complex in crystal from do not provide any relevant information about conformations of complexes in solution, since crystallisation forces are stronger than forces responsible for conformational changes. For example, the conformations of the ligand diop in crystals of the complexes Ir[(*S*,*S*)-(+)-diop](COD)Cl (see Ref. 429) and [(*R*,*R*)-(−)-diop]$NiCl_2$ (see Ref. 430) differ from the ideal twist-chair-λ and twist-chair-δ conformations which are more favourable. In the latter crystal, the distortions are so strong that the array of the phenyl groups determining the complex chirality becomes virtually symmetric with respect to the metal (the symmetry plane). If a complex retained such a conformation in solution in the asymmetric induction step, it would contradict the well-known rule of asymmetric catalysis ('no asymmetry without asymmetry'), since the cross-coupling in the presence of the same complex, [(*R*,*R*)-(−)-diop]$NiCl_2$, occurs enantioselectively.[431, 432]

It is of note that the interpretation of effects of metal complexes on the enantioselectivity in catalytic reactions using models Pr^{oct}/Mr^{oct} or Pr/Mr is based on static factors. These effects are steric in nature. An alternative explanation based on dynamic factors also exists. A recently proposed theory[433, 434] of the so-called chiral molecular recognition and induction is based on helical electronic effects in the chiral metallocomplex (catalyst) and the coordinating substrate. 'Handedness matching' of the signs of helical polarisability of a chiral catalyst and a coordinating substrate in enantioselective reactions should be met.

An optimistic prognosis of applicability of chiral C_2-symmetric compounds as asymmetry inductors has been made in the review[418] devoted to the phenomenon of asymmetric induction. The analysis made in the present review suggests that these prospects refer only to such reactions as enamide hydrogenation, allylic alkylation, alkylation with diethylzinc in the presence of $Ti(OPr^i)_4$ as well as cyclopropanation and the Diels–Alder reactions not considered in this review. It should also be noted that the use of the term 'chiral induction'[435] instead of the generally accepted term 'asymmetric induction' is incorrect, since the highest value of asymmetric induction is observed in the step of an asymmetric intermediate, *i.e.*, that devoid of any elements of symmetry (exception for C_1).

References

1. E N Jacobsen, A Pfaltz, H Yamamoto (Eds) *Comprehensive Asymmetric Catalysis* Vols 1–3 (Berlin: Springer, 1999)
2. M P Doyle, M A McKervey, T Ye *Modern Catalytic Methods for Organic Synthesis with Diazo Compounds* (New York: Wiley, 1998)
3. R Noyori *Asymmetric Catalysis in Organic Synthesis* (New York: Wiley, 1994)
4. H Brunner, W Zettlmeier *Handbook of Enantioselective Catalysis with Transition Metal Complexes* Vols 1, 2 (Weinheim: VCH, 1993)

5. I Ojima (Ed.) *Catalytic Asymmetric Synthesis* (New York: VCH, 1993)
6. V A Pavlov *Usp. Khim.* **71** 39 (2002) [*Russ. Chem. Rev.* **71** 33 (2002)]
7. R Noyori, T Ohkuma *Angew. Chem., Int. Ed.* **40** 40 (2001)
8. M McCarthy, P J Guiry *Tetrahedron* **57** 3809 (2001)
9. L Pu, H-B Yu *Chem. Rev.* **101** 757 (2001)
10. V A Pavlov *Usp. Khim.* **70** 1175 (2001) [*Russ. Chem. Rev.* **70** 1037 (2001)]
11. M J Burk *Acc. Chem. Res.* **33** 363 (2000)
12. K Muniz, C Bolm *Chem.-Eur. J.* **6** 2309 (2000)
13. T D Machajewski, C-H Wong *Angew. Chem., Int. Ed.* **39** 1352 (2000)
14. G Helmchen *J. Organomet. Chem.* **576** 203 (1999)
15. A Pfaltz *Synlett* 835 (1999)
16. M J Palmer, M Wills *Tetrahedron: Asymmetry* **10** 2045 (1999)
17. K Soai, T Shibata, in *Comprehensive Asymmetric Catalysis* Vol. 2 (Eds E N Jacobsen, A Pfaltz, H Yamamoto) (Berlin: Springer, 1999) p. 911
18. Y N Ito, T Katsuki *Bull. Chem. Soc. Jpn.* **72** 603 (1999)
19. T Naota, H Takaya, S-I Murahashi *Chem. Rev.* **98** 2599 (1998)
20. M P Doyle, M N Protopopova *Tetrahedron* **54** 7919 (1998)
21. A K Ghosh, P Mathivanan, J Cappiello *Tetrahedron: Asymmetry* **9** 1 (1998)
22. O Piccolo *Chim. Ind. (Milan)* **80** 1177 (1998)
23. P Knochel, J J A Perea, P Jones *Tetrahedron* **54** 8275 (1998)
24. S C Stinson *Chem. Eng. News* 101 (1999)
25. I D Gridnev, N Higashi, K Asakura, T Imamoto *J. Am. Chem. Soc.* **122** 7183 (2000)
26. I D Gridnev, M Yasutake, N Higashi, T Imamoto *J. Am. Chem. Soc.* **123** 5268 (2001)
27. C R Landis, S Feldgus *Angew. Chem., Int. Ed.* **39** 2863 (2000)
28. K Rossen *Angew. Chem., Int. Ed.* **40** 4611 (2001)
29. J A Wiles, S H Bergens *Organometallics* **18** 3709 (1999)
30. W S Knowles *Acc. Chem. Res.* **16** 106 (1983)
31. B D Vineyard, W S Knowles, M J Sabacky, G L Bachman, D J Weinkauff *J. Am. Chem. Soc.* **99** 5946 (1977)
32. M J Burk, J E Feaster, W A Nugent, R L Harlow *J. Am. Chem. Soc.* **115** 10 125 (1993)
33. M J Burk, A Pizzano, J A Martin, L M Liable-Sands, A L Rheingold *Organometallics* **19** 250 (2000)
34. R Noyori *Acta Chem. Scand.* **50** 380 (1996)
35. R Noyori, M Tokunaga, M Kitamura *Bull. Chem. Soc. Jpn.* **68** 36 (1995)
36. M Kitamura, M Yoshimura, N Kanda, R Noyori *Tetrahedron* **55** 8769 (1999)
37. U Leutenegger, A Madin, A Pfaltz *Angew. Chem., Int. Ed. Engl.* **28** 60 (1989)
38. P A Pfaltz *Tetrahedron: Asymmetry* **2** 691 (1991)
39. A Pfaltz *Acc. Chem. Res.* **26** 339 (1993)
40. G Consiglio, P Pino *Top. Curr. Chem.* **105** 77 (1982)
41. G Consiglio, F Morandini, M Scalone, P Pino *J. Organomet. Chem.* **279** 193 (1985)
42. S Gladiali, L Pinna *Tetrahedron: Asymmetry* **2** 623 (1991)
43. L Kollar, G Consiglio, P Pino *J. Organomet. Chem.* **330** 305 (1987)
44. G Consiglio, L Kollar, R Klliker *J. Organomet. Chem.* **396** 375 (1990)
45. G Consiglio, S C A Nefkens, A Borer *Organometallics* **10** 2046 (1991)
46. T Hayashi, M Tanaka, Y Ikeda, I Ogata *Bull. Chem. Soc. Jpn.* **52** 2605 (1979)
47. F Agbossou, J-F Carpentier, A Mortreux *Chem. Rev.* **95** 2485 (1995)
48. D Gleich, R Schmid, W Herrmann *Organometallics* **17** 2141 (1998)
49. K Nozaki, N Sakai, T Nanno, T Higashijima, S Mano, T Horiuchi, H Takaya *J. Am. Chem. Soc.* **119** 4413 (1997)
50. H B Kagan, in *Comprehensive Organometallics Chemistry* Vol. 8 (Eds G Wilkinson, F G A Stone, E W Abel) (Oxford: Pergamon Press, 1982) p. 463
51. V A Pavlov, in *Koordinatsionnoe Soveshchanie po Asimmetricheskomu Katalizu (Tez. Dokl.), Borzhomi, 1982* [Coordination Meeting on Asymmetrical Catalysis (Abstracts of Reports), Borzhomi, 1982] p. 31
52. V A Pavlov, E I Klabunovskii *Dokl. Akad. Nauk SSSR* **269** 856 (1983) [a]
53. V A Pavlov, E I Klabunovskii *Izv. Akad Nauk SSSR, Ser. Khim.* 2015 (1983) [b]
54. V A Pavlov, A A Bagatur'yants, V B Kazanskii, E I Klabunovskii *Izv. Akad. Nauk SSSR, Ser. Khim.* 508 (1987) [b]
55. V A Pavlov, E I Klabunovskii, Y T Struchkov, A A Voloboev, A I Yanovsky *J. Mol. Catal.* **44** 217 (1988)
56. T V RajanBabu, B Radetich, K K You, T A Ayers, A L Casalnuovo, J C Calabrese *J. Org. Chem.* **64** 3429 (1999)
57. V A Pavlov, E Yu Zhorov, A A Voloboev, E I Klabunovskii *J. Mol. Catal.* **59** 119 (1990)
58. V A Pavlov, E A Misrtyukov, H Duddeck, M G Vinogradov, G Snatzke *J. Mol. Catal.* **79** 55 (1993)
59. D Seebach, E Devaquet, A Ernst, M Hayakawa, F N M W B Schweizer, B Weber *Helv. Chim. Acta* **78** 1636 (1995)
60. M D Fryzuk, B Bosnich *J. Am. Chem. Soc.* **100** 5491 (1978)
61. H Brunner, A Winter, J Breu *J. Organomet. Chem.* **553** 285 (1998)
62. Y Yamanoi, T Imamoto *J. Org. Chem.* **64** 2988 (1999)
63. T Imamoto, J Watanabe, Y Wada, H Masuda, H Yamada, H Tsuruta, S Matsukawa, K Yamaguchi *J. Am. Chem. Soc.* **120** 1635 (1998)
64. W Li, Z Zhang, D Xiao, X Zhang *J. Org. Chem.* **65** 3489 (2000)
65. J Holz, M Quirmbach, U Schmidt, D Heller, R Sturmer, A Borner *J. Org. Chem.* **63** 8031 (1998)
66. E Fernandez, A Gillon, K Heslop, E Horwood, D J Hyett, A G Orpen, P G Pringle *Chem. Commun.* 1663 (2000)
67. W Tang, X Zhang *Angew. Chem., Int. Ed.* **41** 1612 (2002)
68. F Maienza, M Worle, P Steffanut, A Mezzetti, F Spindler *Organometallics* **18** 1041 (1999)
69. D Carmichael, H Doucet, J M Brown *Chem. Commun.* 261 (1999)
70. P J Rye, K Rossen, R A Reamer, N N Tsou, R P Volante, P J Reider *J. Am. Chem. Soc.* **119** 6207 (1997)
71. D S Clyne, Y C Mermet-Bouvier, N Nomura, T V RajanBabu *J. Org. Chem.* **64** 7601 (1999)
72. A Saitoh, A Achiwa, K Tanaka, T Morimoto *J. Org. Chem.* **65** 4227 (2000)
73. A Saitoh, T Uda, T Morimoto *Tetrahedron: Asymmetry* **11** 4049 (2000)
74. D Tanner, P G Andersson, A Harden, P Somfai *Tetrahedron Lett.* **35** 4631 (1994)
75. H Kubota, M Nakajima, K Koga *Tetrahedron Lett.* **34** 8135 (1993)
76. E L Eliel, N L Allinger, S J Angyal, G A Morrison *Conformational Analysis* (New York, London, Sydney: Interscience-Wiley, 1965)
77. E J Corey, J C Bailar *J. Am. Chem. Soc.* **81** 2620 (1959)
78. W Moffitt, R B Woodward, A Moscowitz, W Klyne, C Djerassi *J. Am. Chem. Soc.* **83** 4013 (1961)
79. G Snatzke (Ed.) *Optical Rotatory Dispersion and Circular Dichroism in Organic Chemistry* (London: Heyden, 1967)
80. J Bao, W D Wulff *J. Am. Chem. Soc.* **115** 3814 (1993)
81. Y Uozumi, H Kyota, E Kishi, K Kitayama, T Hayashi *Tetrahedron: Asymmetry* **7** 1603 (1996)
82. Y Imai, W Zhang, T Kida, Y Nakatsuji, I Ikeda *J. Org. Chem.* **65** 3326 (2000)
83. M Ogasawara, K Yoshida, H Kamei, K Kato, Y Uozumi, T Hayashi *Tetrahedron: Asymmetry* **9** 1779 (1998)
84. Y Imai, W Zhang, T Kida, Y Nakatsuji, I Ikeda *Tetrahedron Lett.* **39** 4343 (1998)
85. T Harada, M Takeuchi, M Hatsuda, S Ueda, A Oku *Tetrahedron: Asymmetry* **7** 2479 (1996)
86. D Gao, S Schefzick, K B Lipkowitz *J. Am. Chem. Soc.* **121** 9481 (1999)
87. K B Lipkowitz, D Gao, O Katzenelson *J. Am. Chem. Soc.* **121** 5559 (1999)
88. V Guiral, F Delbecq, P Sautet *Organometallics* **20** 2207 (2001)
89. M Bernard, F Delbecq, P Sautet, F Fache, M Lemaire *Organometallics* **19** 5715 (2000)
90. M Yamakawa, H Ito, R Noyori *J. Am. Chem. Soc.* **122** 1466 (2000)

91. D A Alonso, P Brandt, S J M Nordin, P G Andersson *J. Am. Chem. Soc.* **121** 9580 (1999)
92. D G I Petra, J N H Reek, J-W Handgraaf, E J Meijer, P Dierks, P C J Kamer, J Brussee, H E Schoemaker, P W N M van Leeuwen *Chem.-Eur. J.* **6** 2818 (2000)
93. J M Fraile, J I Garsia, V Martinez-Merino, J A Mayoral, L Salvatella *J. Am. Chem. Soc.* **123** 7616 (2001)
94. R Noyori, S Hashigushi *Acc. Chem. Res.* **30** 97 (1997)
95. G Zassinovich, G Mestroni, S Gladiali *Chem. Rev.* **92** 1051 (1992)
96. P Gamez, F Fache, P Mangeney, M Lemaire *Tetrahedron Lett.* **34** 6897 (1993)
97. M Bernard, V Quiral, F Delbecq, F Fache, P Sautet, M Lemaire *J. Am. Chem. Soc.* **120** 1441 (1998)
98. D Muller, G Umbricht, B Weber, A Pfaltz *Helv. Chim. Acta* **74** 232 (1991)
99. V A Pavlov, M G Vinogradov, E V Starodubtseva, G V Chel'tsova, V A Ferapontov, O R Malyshev, G L Kheis *Izv. Akad. Nauk, Ser. Khim.* 704 (2001) [b]
100. R Spogliarich, J Kaspar, M Graziani, F Morandini *J. Organomet. Chem.* **306** 407 (1986)
101. K-J Haack, S Hashiguchi, A Fujii, T Ikariya, R Noyori *Angew. Chem., Int. Ed. Engl.* **36** 285 (1997)
102. K Mashima, T Abe, K Tani *Chem. Lett.* 1199 (1998)
103. K Murata, T Ikariya, R Noyori *J. Org. Chem.* **64** 2186 (1999)
104. J W Faller, A R Lavoie *Organometallics* **20** 5245 (2001)
105. D G I Petra, P C J Kamer, A L Spek, H E Schoemaker, P W N M van Leeuwen *J. Org. Chem.* **65** 3010 (2000)
106. J-P Genet, V Ratovelomanana-Vidal, C Pinel *Synlett* 478 (1993)
107. D Seebach, D A Plattner, A K Beck, Y M Wang, D Hunziker, W Petter *Helv. Chim. Acta* **75** 2171 (1992)
108. S Hashiguchi, A Fujii, J Takehara, T Ikariya, R Noyori *J. Am. Chem. Soc.* **117** 7562 (1995)
109. A Fujii, S Hashiguchi, N Uematsu, T Ikariya, R Noyori *J. Am. Chem. Soc.* **118** 2521 (1996)
110. K Mashima, H Kaneyoshi, S Kaneko, A Mikami, K Tani, A Nakamura *Organometallics* **16** 1016 (1997)
111. C Bubert, J Blacker, S M Brown, J Crosby, S Fitzjohn, J P Muxworthy, T Thorpe, J M J Williams *Tetrahedron Lett.* **42** 4037 (2001)
112. Y-C Chen, T-F Wu, J-G Deng, H Liu, Y-Z Jiang, M C K Choi, A S C Chan *Chem. Commun.* 1488 (2001)
113. M Palmer, T Walsgrove, M Wills *J. Org. Chem.* **62** 5226 (1997)
114. J Takehara, S Hashiguchi, A Fujii, S Inoue, T Ikariya, R Noyori *J. Chem. Soc., Chem. Commun.* 233 (1996)
115. D A Alonso, S J M Nordin, P Roth, T Tarnai, P G Andersson, M Thommen, U Pittelkow *J. Org. Chem.* **65** 3116 (2000)
116. T Langer, G Helmchen *Tetrahedron Lett.* **37** 1381 (1996)
117. T Sammakia, E L Stangeland *J. Org. Chem.* **62** 6104 (1997)
118. D G I Petra, P C J Kamer, P W N M van Leeuwen, K Goubitz, A M van Loon, J G de Vries, H E Schoemaker *Eur. J. Inorg. Chem.* **12** 2335 (1999)
119. D A Evans, S G Nelson, M R Gagne, A R Muci *J. Am. Chem. Soc.* **115** 9800 (1993)
120. Y Jiang, Q Jiang, G Zhu, X Zhang *Tetrahedron Lett.* **38** 215 (1997)
121. Y Jiang, Q Jiang, X Zhang *J. Am. Chem. Soc.* **120** 3817 (1998)
122. J-X Gao, X-D Yi, P-P Xu, C-L Tang, H-L Wan, T Ikariya *J. Organomet. Chem.* **592** 290 (1999)
123. J-X Gao, T Ikariya, R Noyori *Organometallics* **15** 1087 (1996)
124. Q Jiang, D Van Plew, S Murtuza, X Zhang *Tetrahedron Lett.* **37** 797 (1996)
125. P Braunstein, F Naud, A Pfaltz, S J Rettig *Organometallics* **19** 2676 (2000)
126. S Gladiali, L Pinna, G Delogu, S De Martin, G Zassinovich, G Mestroni *Tetrahedron: Asymmetry* **1** 635 (1990)
127. G Zassinovich, R Bettella, G Mestroni, N Bresciani-Pahor, S Geremia, L Randaccio *J. Organomet. Chem.* **370** 187 (1989)
128. P Gamez, B Dunjic, M Lemaire *J. Org. Chem.* **61** 5196 (1996)
129. F Touchard, F Fache, M Lemaire *Tetrahedron: Asymmetry* **8** 3319 (1997)
130. L Schwink, T Ireland, K Puntener, P Knochel *Tetrahedron: Asymmetry* **9** 1143 (1998)
131. L Schwink P Knochel *Tetrahedron Lett.* **37** 25 (1996)
132. K Puntener, L Schwink, P Knochel *Tetrahedron Lett.* **37** 8165 (1996)
133. H Yang, M Alvarz-Gressier, N Lugan, R Mathieu *Organometallics* **16** 1401 (1997)
134. S Inoue, K Nomura, S Hashiguchi, R Noyori, Y Izawa *Chem. Lett.* 957 (1997)
135. C Bianchini, E Farnetti, L Glendenning, M Graziani, G Nardin, M Peruzzini, E Roccini, F Zanobini *Organometallics* **14** 1489 (1995)
136. S Gladiali, J C Bayon, C Claver *Tetrahedron: Asymmetry* **6** 1453 (1995)
137. G Consiglio, in *Catalytic Asymmetric Synthesis* (Ed. I Ojima) (New York: VCH, 1993) p. 273
138. C Botteghi, S Paganelli, A Schionato, M Marchetti *Chirality* **3** 355 (1991)
139. C U Pittman, Y Kawabata, L I Flowers *J. Chem. Soc., Chem. Commun.* 473 (1982)
140. G Parrinello, R Deschenaux, J K Stille *J. Org. Chem.* **51** 4189 (1986)
141. G Consiglio, P Pino, L I Flowers , C U Pittman *J. Chem. Soc., Chem. Commun.* 612 (1983)
142. G Consiglio, S C A Nefkens *Tetrahedron: Asymmetry* **1** 417 (1990)
143. L Kollar, P Sandor, G Szalontai *J. Mol. Catal.* **67** 191 (1991)
144. L Kollar, J Bakos, I Toth, B Heil *J. Organomet. Chem.* **350** 277 (1988)
145. S Naili, I Suisse, A Mortreux, F Agbossou-Niedercorn, G Nowogrocki *J. Organomet. Chem.* **628** 114 (2001)
146. T Hayashi, M Tanaka, I Ogata, T Kodama, T Takahashi, Y Uchida, T Uchida *Bull. Chem. Soc. Jpn.* **56** 1780 (1983)
147. A M Masdeu-Bulto, A Orejon, A Castellanos, S Castillon, C Claver *Tetrahedron: Asymmetry* **7** 1829 (1996)
148. G J H Buisman, E J Vos, P C J Kamer, P W N M van Leeuwen *J. Chem. Soc., Dalton Trans.* 409 (1995)
149. G J H Buisman, L A van der Veen, A Klootwijk, W G J de Lange, P C J Kamer, P W N M van Leeuwen, D Vogt *Organometallics* **16** 2929 (1997)
150. Y Jiang, S Xue, Z Li, J Deng, A Mi, A S C Chan *Tetrahedron: Asymmetry* **9** 3185 (1998)
151. S Cserepi-Szucs, G Huttner, L Zsolnai, J Bakos *J. Organomet. Chem.* **586** 70 (1999)
152. S Claver, S Castillon, N Ruiz, G Delogu, D Fabbri, S Gladiali *J. Chem. Soc., Chem. Commun.* 1833 (1993)
153. S Breeden, D J Cole-Hamilton, D F Foster, G J Schwarz, M Wills *Angew. Chem., Int. Ed.* **39** 4106 (2000)
154. U Nettekoven, P C J Kamer, M Widhalm, P W N M van Leeuwen *Organometallics* **19** 4596 (2000)
155. N Sakai, K Nozaki, S Mano, H Takaya *J. Am. Chem. Soc.* **115** 7033 (1993)
156. N Sakai, K Nozaki, H Takaya *J. Chem. Soc., Chem. Commun.* 395 (1994)
157. G Francio, W Leitner *Chem. Commun.* 1663 (1999)
158. T Higashizima, N Sakai, K Nozaki, H Takaya *Tetrahedron Lett.* **35** 2023 (1994)
159. M Dieguez, O Pamies, A Ruiz, S Castillon, C Claver *Chem. Commun.* 1607 (2000)
160. F A Rampf, W Herrmann *J. Organomet. Chem.* **601** 138 (2000)
161. G Parrinello, J F Stille *J. Am. Chem. Soc.* **109** 7122 (1987)
162. J F Stille, H Su, P Brechot, G Parrinello, L S Hegedus *Organometallics* **10** 1183 (1991)
163. O Pamies, M Diegues, G Net, A Ruiz, C Claver *Organometallics* **19** 1488 (2000)
164. A M Masdeu-Bulto, A Orejon, A Ruiz, S Castillon, C Claver *J. Mol. Catal.* **94** 149 (1994)
165. S Gladiali, A Dore, D Fabbri *Tetrahedron: Asymmetry* **5** 1143 (1994)
166. C Basoli, C Botteghi, M A Cabras, G Chelucci, M Marchetti *J. Organomet. Chem.* **488** C20 (1995)
167. C G Arena, F Nicolo, D Drommi, G Bruno, F Faraone *J. Chem. Soc., Chem. Commun.* 2251 (1994)
168. G Consiglio, F Rama *J. Mol. Catal.* **66** 1 (1991)
169. M Dieguez, A Ruiz, C Claver *Tetrahedron: Asymmetry* **12** 2827 (2001)

170. D Gleich, W A Herrmann *Organometallics* **18** 4354 (1999)
171. B M Trost, D L Van Vranken *Chem. Rev.* **96** 395 (1996)
172. B M Trost *Acc. Chem. Res.* **29** 355 (1996)
173. T Hayashi, in *Catalytic Asymmetric Synthesis* Vol. 1 (Ed. I Ojima) (New York: VCH, 1993) p. 325
174. C G Frost, J Howarth, J M J Williams *Tetrahedron: Asymmetry* **3** 1089 (1992)
175. S A Godleski, in *Comprehensive Organic Synthesis* Vol. 4 (Ed. B M Trost) (Oxford: Pergamon Press, 1991) p. 585
176. G Consiglio, R Waymouth *Chem. Rev.* **89** 257 (1989)
177. P Barbaro, P S Pregosin, R Salzmann, A Albinati, R W Kunz *Organometallics* **14** 5160 (1995)
178. J M Brown, D I Hulmes, P J Guiry *Tetrahedron* **50** 4493 (1994)
179. D-R Hou, J H Reibenspies, K Burgess *J. Org. Chem.* **66** 206 (2001)
180. M Yamaguchi, T Shima, T Yamagishi, M Hidai *Tetrahedron: Asymmetry* **2** 663 (1991)
181. P Dierkes, S Ramdeehul, L Barloy, A D Cian, J Fischer, P C J Kamer, P W N M van Leeuwen, J A Osborn *Angew. Chem., Int. Ed.* **37** 3116 (1998)
182. B Weber, D Seebach *Tetrahedron* **50** 7473 (1994)
183. A Saitoh, M Misawa, T Morimoto *Synlett* 483 (1999)
184. J Kang, W O Cho, H G Cho *Tetrahedron: Asymmetry* **5** 1347 (1994)
185. P G C Lloyd-Jones A B E Mindis, A Pfaltz, L Macko, M Neuburger, M Zehnder, H Ruegger, P S Pregosin *Helv. Chim. Acta* **78** 265 (1995)
186. U Leutenegger, G Umbricht, C Fahrni, P von Matt, A Pfaltz *Tetrahedron* **48** 2143 (1992)
187. O Hoarau, H Ait-Haddou, J-C Daran, D Cramailere, G G A Balavoine *Organometallics* **18** 4718 (1999)
188. M Gomer, S Jansat, G Muller, M A Maestro, J Mahia *Organometallics* **21** 1077 (2002)
189. J M Canal, M Gomez, F Jimenez, M Rocamora, G Muller, E Dunach, D Franco, A Jimenez, F H Cano *Organometallics* **19** 966 (2000)
190. G Chelucci, G A Pinna, A Saba, R Valenti *Tetrahedron: Asymmetry* **11** 4027 (2000)
191. K Nordstrom, E Macedo, C Moberg *J. Org. Chem.* **62** 1604 (1997)
192. U Bremberg, F Rahm, C Moberg *Tetrahedron: Asymmetry* **9** 3437 (1998)
193. G Chelucci, A Saba, G Sanna, F Soccolini *Tetrahedron: Asymmetry* **11** 3427 (2000)
194. G Chelucci, A Saba *Tetrahedron: Asymmetry* **9** 531 (1998)
195. G Chelucci, S Gladiali, A Saba *Tetrahedron: Asymmetry* **10** 1393 (1999)
196. K Hiroi, Y Suzuki, I Abe *Tetrahedron: Asymmetry* **10** 1173 (1999)
197. J Sprinz, G Helmchen *Tetrahedron Lett.* **34** 1769 (1993)
198. Y Suzuki, Y Ogata, K Hiroi *Tetrahedron: Asymmetry* **10** 1219 (1999)
199. S Lee, C W Lim, C E Song, K M Kim, C H Jun *J. Org. Chem.* **64** 4445 (1999)
200. J Sprinz, M Kiefer, G Helmchen, M Reggelin, G Huttner, O Walter, L Zsolnai *Tetrahedron Lett.* **35** 1523 (1994)
201. P von Matt, A Pfaltz *Angew. Chem., Int. Ed. Engl.* **32** 566 (1993)
202. G J Dawson, C G Frost, J M J Williams, S J Coote *Tetrahedron Lett.* **34** 3149 (1993)
203. N K Anand *Synlett* 924 (2000)
204. K Ito, R Kashiwagi, K Iwasaki, T Katsuki *Synlett* 1563 (1999)
205. B M Trost, A C Krueger, R C Bunt, J Zambrano *J. Am. Chem. Soc.* **118** 6520 (1996)
206. T Fukuda, A Takehara, M Iwao *Tetrahedron: Asymmetry* **12** 2793 (2001)
207. S Vyskocil, M Smrcina, V Hanus, M Polasek, P Kocovsky *J. Org. Chem.* **63** 7738 (1998)
208. Y Wang, H Guo, K Ding *Tetrahedron: Asymmetry* **11** 4153 (2000)
209. P Wimmer, M Widhalm *Tetrahedron: Asymmetry* **6** 657 (1995)
210. J C Anderson, R J Cubbon, J D Harling *Tetrahedron: Asymmetry* **12** 923 (2001)
211. H Adams, J C Anderson, R Cubbon, D S James, J P Mathias *J. Org. Chem.* **64** 8256 (1999)
212. D A Evans, K R Campos, J S Tedrow, F E Michael, M R Gagne *J. Am. Chem. Soc.* **122** 7905 (2000)
213. G J Dawson, C G Frost, C J Martin, J M J Williams, S J Coote *Tetrahedron Lett.* **34** 7793 (1993)
214. J Uenishi, M Hamada *Tetrahedron: Asymmetry* **12** 2999 (2001)
215. Y Suzuki, I Abe, K Hiroi *Heterocycles* **50** 89 (1999)
216. T Mino, Y Tanaka, M Sakamoto, T Fujita *Tetrahedron: Asymmetry* **12** 2435 (2001)
217. X-L Hou, X-W Wu, L-X Dai, B-X Cao, J Sun *Chem. Commun.* 1195 (2000)
218. S-L You, X-L Hou, L-X Dai, Y-H Yu, W Xia *J. Org. Chem.* **67** 4684 (2002)
219. G Chelucci *Tetrahedron: Asymmetry* **8** 2667 (1997)
220. A Zhang, Y Feng, B Jiang *Tetrahedron: Asymmetry* **11** 3123 (2000)
221. W Zhang, T Shimanuki, T Kida, Y Nakatsuji, I Ikeda *J. Org. Chem.* **64** 6247 (1999)
222. M Sauthier, J Fornies-Camer, L Toupet, R Reau *Organometallics* **19** 553 (2000)
223. T Mino, W Imiya, M Yamashita *Synlett* 583 (1997)
224. A I Polosukhin, O G Bondarev, S E Lyubimov, A V Korostylev, K A Lyssenko, V A Davankov, K N Gavrilov *Tetrahedron: Asymmetry* **12** 2197 (2001)
225. X Dai, S Virgil *Tetrahedron Lett.* **40** 1245 (1999)
226. M-J Jin, J-A Jung, S-H Kim *Tetrahedron Lett.* **40** 5197 (1999)
227. Y Okuyama, H Nakano, H Hongo *Tetrahedron: Asymmetry* **11** 1193 (2000)
228. T Kohara, Y Hashimoto, K Saigo *Synlett* 517 (2000)
229. H Kodama, T Taiji, T Ohta, I Furukawa *Tetrahedron: Asymmetry* **11** 4009 (2000)
230. T Hashizume, K Yonehara, K Ohe, S Uemura *J. Org. Chem.* **65** 5197 (2000)
231. M Dieguez, S Jansat, M Gomez, A Ruiz, G Muller, C Claver *Chem. Commun.* 1132 (2001)
232. H Nakano, Y Okuyama, M Yanagida, H Hongo *J. Org. Chem.* **66** 620 (2001)
233. W-P Deng, X-L Hou, L-X Dai, Y-H Yu, W Xia *Chem. Commun.* 285 (2000)
234. J Clayden, L W Lai, M Helliwell *Tetrahedron: Asymmetry* **12** 695 (2001)
235. T Mino, M Shiotsuki, N Yamamoto, T Suenaga, M Sakamoto, T Fujita, M Yamashita *J. Org. Chem.* **66** 1795 (2001)
236. L F Tietze, J K Lohmann *Synlett* 2083 (2002)
237. P B Mackenzie, J Whelan, B Bosnich *J. Am. Chem. Soc.* **107** 2046 (1985)
238. H Steinhagen, M Reggelin, G Helmchen *Angew. Chem., Int. Ed. Engl.* **36** 2108 (1997)
239. D A Evans, K R Campos, J S Tedrow, F E Michael, M R Gagne *J. Org. Chem.* **64** 2994 (1999)
240. J V Allen, S J Coote, G J Dawson, C G Frost, C J Martin, J M J Williams *J. Chem. Soc., Perkin Trans. 1* 2065 (1994)
241. B Akermark, S Hansson, B Krakenberger, A Vitagliano, K Zetterberg *Organometallics* **3** 679 (1984)
242. B Akermark, B Krakenberger, S Hansson, A Vitagliano *Organometallics* **6** 620 (1987)
243. B M Trost, D J Murphy *Organometallics* **4** 1143 (1985)
244. T Hayashi, A Yamamoto, T Hagihara, Y Ito *Tetrahedron Lett.* **27** 191 (1986)
245. T Hayashi, A Yamamoto, Y Ito, E Nishioka, H Miura, K Yanagi *J. Am. Chem. Soc.* **111** 6301 (1989)
246. B M Trost, B Breit, M G Organ *Tetrahedron Lett.* **32** 5817 (1994)
247. M Sawamura, Y Ito *Chem. Rev.* **92** 857 (1992)
248. P S Pregosin, R Salzmann, A Togni *Organometallics* **14** 842 (1995)
249. R Noyori, M Kitamura *Angew. Chem., Int. Ed. Engl.* **30** 49 (1991)
250. K Soai, S Niwa *Chem. Rev.* **92** 833 (1992)
251. K Mikami, M Terada, S Narisawa, T Nakai *Synlett* 255 (1992)
252. F-Y Zhang, C-W Yip, R Cao, A S C Chan *Tetrahedron: Asymmetry* **8** 585 (1997)
253. M Mori, T Nakai *Tetrahedron Lett.* **38** 6233 (1997)
254. Y Tian, K S Chan *Tetrahedron Lett.* **41** 8813 (2000)

255. Y Nakamura, S Takeuchi, Y Ohgo, D P Curran *Tetrahedron Lett*. **41** 57 (2000)
256. H Kodama, J Ito, A Nagaki, T Ohta, I Furukawa *Appl. Organometal. Chem*. **14** 709 (2000)
257. K Kostova, M Genov, I Philipova, V Dimitrov *Tetrahedron: Asymmetry* **11** 3253 (2000)
258. F-Y Zhang, A S C Chan *Tetrahedron: Asymmetry* **8** 3651 (1997)
259. Y-X Chen, L-W Yang, Y-M Li, Z-Y Zhou, K-H Lam, A C S Chan, H-K Kwong *Chirality* **12** 510 (2000)
260. Y N Ito, X Ariza, A K Beck, A Bohac, C Ganter, R E Gawley, F N M Kuhnle, J Tuleja, Y M Wang, D Seebach *Helv. Chim. Acta* **77** 2071 (1994)
261. C Dreisbach, U Kragl, C Wandrey *Synthesis* 911 (1994)
262. H Waldmann, M Weigerding, C Dreisbach, C Wandrey *Helv. Chim. Acta* **77** 2111 (1994)
263. S Pritchett, D H Woodmansee, P Gantzel, P J Walsh *J. Am. Chem. Soc*. **120** 6423 (1998)
264. J Balsells, J M Betancort, P J Walsh *Angew. Chem., Int. Ed*. **39** 3428 (2000)
265. H Takahashi, T Kawakita, M Yoshioka, S Kobayashi, M Ohno *Tetrahedron Lett*. **30** 7095 (1989)
266. H Takahashi, T Kawakita, M Ohno, M Yoshioka, S Kobayashi *Tetrahedron* **48** 5691 (1992)
267. C-D Hwang, B-J Uang *Tetrahedron: Asymmetry* **9** 3979 (1998)
268. L A Paquette, R Zhou *J. Org. Chem*. **64** 7929 (1999)
269. X Zhang, C Guo *Tetrahedron Lett*. **36** 4947 (1995)
270. C Guo, J Qiu, X Zhang, D Verdugo, M L Larter, R Christie, P Kenney, P J Walsh *Tetrahedron* **53** 4145 (1997)
271. M Shi, W-S Sui *Tetrahedron: Asymmetry* **10** 3319 (1999)
272. X Shen, H Guo, K Ding *Tetrahedron: Asymmetry* **11** 4321 (2000)
273. T Shibata, H Tabira, K Soai *J. Chem. Soc., Perkin Trans. 1* 177 (1998)
274. K Ito, Y Kimura, H Okamura, T Katsuki *Synlett* 573 (1992)
275. J-S You, M-Y Shao, H-M Gau *Tetrahedron: Asymmetry* **12** 2971 (2001)
276. K Soai, Y Hirose, Y Ohno *Tetrahedron: Asymmetry* **4** 1473 (1993)
277. R Noyori, S K Kawai, S Okada, M Kitamura *Pure Appl. Chem*. **60** 1597 (1988)
278. M Yamakawa, R Noyori *J. Am. Chem. Soc*. **117** 6327 (1995)
279. M Yamakawa, R Noyori *Organometallics* **18** 128 (1999)
280. B Goldfuss, K N Houk *J. Org. Chem*. **63** 8998 (1998)
281. B Goldfuss, M Steigelmann, S I Khan, K N Houk *J. Org. Chem*. **65** 77 (2000)
282. S J Li, Y Jiang, A Mi *Tetrahedron: Asymmetry* **3** 1467 (1992)
283. R Noyori, S Suga, K Kawai, S Okada, M Kitamura, N Oguni, M Hayashi, T Kaneko, Y Matsuda *J. Organomet. Chem*. **382** 19 (1990)
284. K Soai, S Yokoyama, K Ebihara, T Hayasaka *J. Chem. Soc., Chem. Commun*. 1690 (1987)
285. G Muchow, Y Vannoorenberge, G Buono *Tetrahedron Lett*. **28** 6163 (1987)
286. P A Chaloner, S A R Perera *Tetrahedron Lett*. **28** 3013 (1987)
287. S Itsuno, J M J Frechet *J. Org. Chem*. **52** 4140 (1987)
288. K Soai, T Hayase, K Takai, T Sugiyama *J. Org. Chem*. **59** 7908 (1994)
289. K Soai, A Ookawa, T Kaba, K Ogawa *J. Am. Chem. Soc*. **109** 7111 (1987)
290. P Delair, C Einhorn, J Einhorn, J L Luche *Tetrahedron* **51** 165 (1995)
291. J Beliczey, G Giffels, U Kragl, C Wandrey *Tetrahedron: Asymmetry* **8** 1529 (1997)
292. Y Kawanami, T Mitsuie, M Miki, T Sakamoto, K Nishitani *Tetrahedron* **56** 175 (2000)
293. L Sola, K S Reddy, A Vidal-Ferran, A Moyano, M A Pericas, A Riera, A Alvarez-Larena, J-F Piniella *J. Org. Chem*. **63** 7078 (1998)
294. K S Reddy, L Sola, A Moyano, M A Pericas, A Riera *J. Org. Chem*. **64** 3969 (1999)
295. A Vidal-Ferran, A Moyano, M A Pericas, A Riera *J. Org. Chem*. **62** 4970 (1997)
296. A Vidal-Ferran, A Moyano, M A Pericas, A Riera *Tetrahedron Lett*. **38** 8773 (1997)
297. M R Paleo, I Cabeza, F J Sardina *J. Org. Chem*. **65** 2108 (2000)
298. C M Bellucci, A Bergamini, P G Cozzi, A Papa, E Tagliavini, A Umani-Ronchi *Tetrahedron: Asymmetry* **8** 895 (1997)
299. L Sola, A Vidal-Ferran, A Moyano, M A Pericas, A Riera *Tetrahedron: Asymmetry* **8** 1559 (1997)
300. L Sola, A Vidal-Ferran, A Moyano, M A Pericas, A Riera *Tetrahedron: Asymmetry* **8** 3985 (1997)
301. K Kimura, E Sugiyama, T Ishizuka, T Kunieda *Tetrahedron Lett*. **33** 3147 (1992)
302. C F Lawrence, S K Nayak, L Thijs, B Zwanenburg *Synlett* 1571 (1999)
303. D Tanner, H T Korno, D Guijarro, P G Andersson *Tetrahedron* **54** 14213 (1998)
304. W Behnen, T Mehler, J Martens *Tetrahedron: Asymmetry* **4** 1413 (1993)
305. X Yang, J Shen, C Da, R Wang, M C K Choi, L Yang, K Wong *Tetrahedron: Asymmetry* **10** 133 (1999)
306. M Kossenjans, M Soeberdt, S Wallbaum, K Harms, J Martens, H G Aurich *J. Chem. Soc., Perkin Trans. 1* 2353 (1999)
307. S Wassmann, J Wilken, J Martens *Tetrahedron: Asymmetry* **10** 4437 (1999)
308. J Wilken, M Kossenjans, H Groger, J Martens *Tetrahedron: Asymmetry* **8** 2007 (1997)
309. J Eilers, J Wilken, J Martens *Tetrahedron: Asymmetry* **7** 2343 (1996)
310. J Wilken, H Groger, M Kossenjans, J Martens *Tetrahedron: Asymmetry* **8** 2761 (1997)
311. S Wallbaum, J Martens *Tetrahedron: Asymmetry* **4** 637 (1993)
312. K Stingl, J Martens *Liebigs. Ann. Chem*. 491 (1994)
313. E J Corey, F J Hannon *Tetrahedron Lett*. **28** 5237 (1987)
314. M Kitamura, S Suga, K Kawai, R Noyori *J. Am. Chem. Soc*. **108** 6071 (1986)
315. W A Nugent *Chem. Commun*. 1369 (1999)
316. J Kang, H Y Kim, J H Kim *Tetrahedron: Asymmetry* **10** 2523 (1999)
317. J V Allen, C G Frost, J M J Williams *Tetrahedron: Asymmetry* **4** 649 (1993)
318. S Superchi, T Mecca, E Giorgio, C Rosini *Tetrahedron: Asymmetry* **12** 1235 (2001)
319. G Chelucci, F Soccolini *Tetrahedron: Asymmetry* **3** 1235 (1992)
320. C Bolm, G Schlingloff, K Harms *Chem. Ber*. **125** 1191 (1992)
321. C Bolm, M Zehnder, D Bur *Angew. Chem., Int. Ed. Engl*. **29** 205 (1990)
322. M Falorni, C Collu, S Conti, G Giacomelli *Tetrahedron: Asymmetry* **7** 293 (1996)
323. H-L Huang, Y-C Lin, S-F Chen, C-L J Wang, L T Liu *Tetrahedron: Asymmetry* **7** 3067 (1996)
324. M Okaniwa, R Yanada, T Ibuka *Tetrahedron Lett*. **41** 1047 (2000)
325. B T Cho, Y S Chun *Tetrahedron: Asymmetry* **9** 1489 (1998)
326. B T Cho, Y S Chun, W K Yang *Tetrahedron: Asymmetry* **11** 2149 (2000)
327. N Ikota, H Inaba *Chem. Pharm. Bull*. **44** 587 (1996)
328. S Bastin, J Brocard, L Pelinski *Tetrahedron Lett*. **41** 7303 (2000)
329. R Ruzziconi, O Piermatti, G Ricci, D Vinci *Synlett* 747 (2002)
330. S H Lee, D S Im, C S Cheong, B Y Chung *Heterocycles* **51** 1913 (1999)
331. K Stingl, J Martens *Synth. Commun*. **22** 2745 (1992)
332. C Cardellicchio, G Ciccarella, F Naso, F Perna, P Tortorella *Tetrahedron* **55** 14685 (1999)
333. G Palmieri *Eur. J. Org. Chem*. 805 (1939)
334. J Palmieri *Tetrahedron: Asymmetry* **11** 3361 (2000)
335. H Zhang, K S Chan *J. Chem. Soc., Perkin Trans. 1* 381 (1999)
336. H Zhang, F Xue, T C W Mak, K S Chan *J. Org. Chem*. **61** 8002 (1996)
337. S Dahmen, S Brase *Chem. Commun*. 26 (2002)
338. C Bolm, K Muniz-Fernandez, A Seger, G Raabe, K Gunther *J. Org. Chem*. **63** 7860 (1998)
339. S Vyskocil, S Jaracz, M Smrcina, M Sticha, V Hanus, M Polasek, P Kocovsky *J. Org. Chem*. **63** 7727 (1998)

340. M Uemura, R Miyake, K Nakayama, M Shiro, Y Hayashi *J. Org. Chem.* **58** 1238 (1993)
341. M Watanabe *Synlett* 1050 (1995)
342. W Zhang, H Yoshinaga, Y Imai, T Kida, Y Nakatsuji, I Ikeda *Synlett* 1512 (2000)
343. C Bolm, K Muniz-Fernandez, A Seger, G Raabe *Synlett* 1051 (1997)
344. E J Corey, P-W Yuen, F J Hannon, D A Wierda *J. Org. Chem.* **55** 784 (1990)
345. M A Poelert, R P Hof, N C M W Peper, R M Kellogg *Heterocycles* **37** 461 (1994)
346. R P Hof, M A Poelert, N C M W Peper, R M Kellogg *Tetrahedron: Asymmetry* **5** 31 (1994)
347. K Fitzpatrick, R Hulst, R M Kellogg *Tetrahedron: Asymmetry* **6** 1861 (1995)
348. J Kang, J W Kim, J W Lee, D S Kim, J I Kim *Bull. Korean Chem. Soc.* **17** 1135 (1996)
349. J Kang, D S Kim, J I Kim *Synlett* 842 (1994)
350. J Kang, J W Lee, J I Kim *J. Chem. Soc., Chem. Commun.* 2009 (1994)
351. C L Gibson *Tetrahedron: Asymmetry* **10** 1551 (1999)
352. J C Anderson, M Harding *Chem. Commun.* 393 (1998)
353. M-J Jin, S-J Ahn, K-S Lee *Tetrahedron Lett.* **37** 8767 (1996)
354. H G Aurich, M Soeberdt *Tetrahedron Lett.* **39** 2553 (1998)
355. J M Andres, M A Martinez, R Pedrosa, A Perez-Encabo *Tetrahedron: Asymmetry* **5** 67 (1994)
356. A L Braga, H R Appelt, P H Schneider, C C Silveira, L A Wessjohann *Tetrahedron: Asymmetry* **10** 1733 (1999)
357. S Bastin, N Delebecque, F Agbossou, J Brocard, L Pelinski *Tetrahedron: Asymmetry* **10** 1647 (1999)
358. D Le Goanvic, M Holler, P Pale *Tetrahedron: Asymmetry* **13** 119 (2002)
359. C A de Parrodi, E Juaristi, L Quintero-Cortes, P Amador *Tetrahedron: Asymmetry* **7** 1915 (1996)
360. A Iuliano, D Pini, P Salvadori *Tetrahedron: Asymmetry* **6** 739 (1995)
361. M Shi, J-K Jiang *Tetrahedron: Asymmetry* **10** 1673 (1999)
362. M Shi, Y Satoh, T Makihara, Y Masaki *Tetrahedron: Asymmetry* **6** 2109 (1995)
363. M Shi, Y Satoh, T Makihara *J. Chem. Soc., Perkin Trans. 1* 2547 (1998)
364. Y-J Cherng, J-M Fang, T-J Lu *J. Org. Chem.* **64** 3207 (1999)
365. S Cicchi, S Crea, A Goti, A Brandi *Tetrahedron: Asymmetry* **8** 293 (1997)
366. K S Reddy, L Sola, A Moyano, M A Pericas, A Riera *Synthesis* 165 (2000)
367. M Genov, K Kostova, V Dimitrov *Tetrahedron: Asymmetry* **8** 1869 (1997)
368. H-L Kwong, W-S Lee *Tetrahedron: Asymmetry* **10** 3791 (1999)
369. S Panev, A Linden, V Dimitrov *Tetrahedron: Asymmetry* **12** 1313 (2001)
370. S Malfait, L Pelinski, J Brocard *Tetrahedron: Asymmetry* **9** 2595 (1998)
371. S Malfait, L Pelinski, J Brocard *Tetrahedron: Asymmetry* **7** 653 (1996)
372. H G Aurich, F Biesemeier, M Geiger, K Harms *Liebigs Ann. Recl.* 423 (1997)
373. B Goldfuss, M Steigelmann, F Rominger *Eur. J. Org. Chem.* 1785 (2000)
374. O Legrand, J-M Brunel, G Buono *Tetrahedron Lett.* **39** 9419 (1998)
375. W-M Dai, H J Zhu, X-J Hao *Tetrahedron Lett.* **37** 5971 (1996)
376. J-M Brunel, T Constantieux, O Legrand, G Buono *Tetrahedron Lett.* **39** 2961 (1998)
377. E Macedo, C Moberg *Tetrahedron: Asymmetry* **6** 549 (1995)
378. Y Wu, H Yun, Y Wu, K Ding, Y Zhou *Tetrahedron: Asymmetry* **11** 3543 (2000)
379. H Yun, Y Wu, Y Wu, K Ding, Y Zhou *Tetrahedron Lett.* **41** 10263 (2000)
380. H Kotsuki, H Hayakawa, H Tateishi, M Wakao, M Shiro *Tetrahedron: Asymmetry* **9** 3203 (1998)
381. W-M Dai, H-J Zhu, X-J Hao *Tetrahedron: Asymmetry* **6** 1857 (1995)
382. W-M Dai, H J Zhu, X-J Hao *Tetrahedron: Asymmetry* **11** 2315 (2000)
383. P Collomb, A von Zelewsky *Tetrahedron: Asymmetry* **9** 3911 (1998)
384. Y Imai, S Matsuo, W Zhang, Y Nakatsuji, I Ikeda *Synlett* 239 (2000)
385. P G Cozzi, A Papa, A Umani-Ronchi *Tetrahedron Lett.* **37** 4613 (1996)
386. Y Furusho, A Tsunoda, T Aida *J. Chem. Soc., Perkin Trans. 1* 183 (1996)
387. D E Ho, J M Betancort, D H Woodmansee, M L Larter, P J Walsh *Tetrahedron Lett.* **38** 3867 (1997)
388. M Kossenjans, J Martens *Tetrahedron: Asymmetry* **9** 1409 (1998)
389. N Hanyu, T Mino, M Sakamoto, T Fujita *Tetrahedron Lett.* **41** 4587 (2000)
390. N Hanyu, T Aoki, T Mino, M Sakamoto, T Fujita *Tetrahedron: Asymmetry* **11** 2971 (2000)
391. M Knollmuller, M Ferencic, P Gartner, K Mereiter, C R Noe *Tetrahedron: Asymmetry* **9** 4009 (1998)
392. M Knollmuller, M Ferencic, P Gartner *Tetrahedron: Asymmetry* **10** 3969 (1999)
393. G Bringmann, M Breuning *Tetrahedron: Asymmetry* **9** 667 (1998)
394. X-W Wu, X-L Hou, L-X Dai, J Tao, B-X Cao, J Sun *Tetrahedron: Asymmetry* **12** 529 (2001)
395. B T Cho, N Kim *J. Chem. Soc., Perkin Trans. 1* 2901 (1996)
396. B T Cho, N Kim *Synth. Commun.* **25** 167 (1995)
397. B T Cho, N Kim *Tetrahedron Lett.* **35** 4115 (1994)
398. F Lake, C Moberg *Tetrahedron: Asymmetry* **12** 755 (2001)
399. D Pini, A Mastantuono, G Uccello-Barretta, A Juliano, P Salvadori *Tetrahedron* **49** 9613 (1993)
400. Y Masaki, Y Satoh, T Makihara, M Shi *Chem. Pharm. Bull.* **44** 454 (1996)
401. Y Masaki, H Oda, K Kazuta, A Usui, A Itoh, F Xu *Tetrahedron Lett.* **33** 5089 (1992)
402. Y-M Lin, I-P Fu, B-J Uang *Tetrahedron: Asymmetry* **12** 3217 (2001)
403. M Shi, W-S Sui *Tetrahedron: Asymmetry* **11** 773 (2000)
404. T Takeda, T Imamoto *Tetrahedron: Asymmetry* **10** 3209 (1999)
405. Y Yamanoi, T Imamoto *J. Org. Chem.* **62** 8560 (1997)
406. M I Donnoli, S Superchi, C Rosini *J. Org. Chem.* **63** 9392 (1998)
407. H Matsunaga, Y Yamada, T Ide, T Ishizuka, T Kunieda *Tetrahedron: Asymmetry* **10** 3095 (1999)
408. Y Motoyama, H Narusawa, H Nishiyama *Chem. Commun.* 131 (1999)
409. E M Vogl, H Groger, M Shibasaki *Angew. Chem., Int. Ed.* **38** 1570 (1999)
410. Y Hamashima, D Sawada, M Kanai, M Shibasaki *J. Am. Chem. Soc.* **121** 2641 (1999)
411. T Ooi, N Kagoshima, K Maruoka *J. Am. Chem. Soc.* **119** 5754 (1997)
412. M Murakata, T Jono, Y Mizuno, O Hoshino *J. Am. Chem. Soc.* **119** 11 713 (1997)
413. H Ishitani, M Ueno, S Kobayashi *J. Am. Chem. Soc.* **122** 8180 (2000)
414. B M Trost, G M Schroeder *J. Org. Chem.* **65** 1569 (2000)
415. T Ikeno, M Sato, H Sekino, A Nishizuka, T Yamada *Bull. Chem. Soc. Jpn.* **74** 2139 (2001)
416. A Ishii, V A Solozhonok, K Mikami *J. Org. Chem.* **65** 1597 (2000)
417. O Jacques, S J Richards, R F W Jackson *Chem. Commun.* 2712 (2001)
418. J K Whitesell *Chem. Rev.* **89** 1581 (1989)
419. V A Pavlov, Doctoral Thesis in Chemical Sciences, Institute of Organic Chemistry, Russian Academy of Sciences, Moscow, 2000
420. M G Vinogradov, L S Gorshkova, V A Pavlov, O V Mikhalev, G V Chel'tsova, I V Razmanov, V A Ferapontov, O R Malyshev, G L Kheis *Izv. Akad. Nauk, Ser. Khim.* 459 (2000) [b]

421. M G Vinogradov, L S Gorshkova, G V Chel'tsova, V A Pavlov, I V Razmanov, V A Ferapontov, O R Malyshev, G L Kheis *Izv. Akad. Nauk, Ser. Khim.* 450 (2003) [b]
422. R Noyori, I Tomino, Y Tanimoto, M Nashizawa *J. Am. Chem. Soc.* **106** 6709 (1984)
423. K Kabuto, T Yoshida, S Yamaguchi, S Miyano, H Hashimoto *J. Org. Chem.* **50** 3013 (1985)
424. H Suda, S Kanoh, N Umeda, M Ikka, M Motoi *Chem. Lett.* 899 (1984)
425. Jpn. P. 6 219 542; *Chem. Abstr.* **107** 175 489 (1987)
426. E C Ashby, F R Dobbs, H P Hopkins *J. Am. Chem. Soc.* **95** 2823 (1973)
427. A S C Chan, J J Pluth, J Halpern *J. Am. Chem. Soc.* **102** 5952 (1980)
428. M Legrand, in *Fundamental Aspects and Recent Developments in Optical Rotatory Dispersion and Circular Dichroism* (Eds F Ciardelli, P Salvadori) (London: Heyden, 1973) p. 285
429. S Brunie, J Mazan, N Langlois, H B Kagan *J. Organomet. Chem.* **114** 225 (1976)
430. V Gramlich, C Salomon *J. Organomet. Chem.* **73** C61 (1974)
431. Y Kiso, K Tamao, N Miyake, K Yamamoto, M Kumada *Tetrahedron Lett.* 3 (1974)
432. G Consiglio, C Botteghi *Helv. Chim. Acta* **56** 460 (1973)
433. D Z Wang, URL: http://preprint chemweb com/orgchem/0403001
434. D Z Wang, URL: http://preprint chemweb com/orgchem/0403002
435. J W Faller, A R Lavoie, J Parr *Chem. Rev.* **103** 3345 (2003)

[a] — *Dokl. Chem. (Engl. Transl.)*
[b] — *Russ. Chem. Bull., Int. Ed. (Engl. Transl.)*

Russian Chemical Reviews **73** (12) 1211 – 1238 (2004) © 2004 Russian Academy of Sciences and Turpion Ltd

DOI 10.1070/RC2004v073n12ABEH000833

Methodological, applied and thermodynamic aspects of hydrogen sorption by graphite and related carbon nanostructures

Yu S Nechaev, O K Alekseeva

Contents

I.	Introduction	1211
II.	Experimental studies of hydrogen sorption by carbon nanostructures	1212
III.	Theoretical studies of physisorption and chemisorption	1220
IV.	A thermodynamic analysis of the experimental data	1224
V.	Conclusion	1235

Abstract. Results of the experimental and theoretical investigations into hydrogen sorption by various carbon nanostructures, including fullerenes, single-walled and multi-walled nanotubes, nanofibres, nanographite and nanographite-based composites are surveyed. Results of a thermodynamic analysis of the most significant experimental data are presented. The emphasis is placed on the studies reporting the extremum sorption parameters. The thermodynamic and kinetic (diffusion) parameters and equations describing the sorption processes are refined. The prospects of the applications of new carbon nanomaterials for hydrogen storage in the automotive industry are discussed. The bibliography includes 206 references.

I. Introduction

Hydrogen represents a unique energy-rich fuel and highly efficient energy carrier.[1] The modern trends in the development of large-scale production of energy carriers and the automotive industry imply gradual replacement of non-renewable hydrocarbon fuels with hydrogen as an environmentally friendly processing product of water and biomass (which are renewable natural resources). This may only be achieved if either the problem of hydrogen storage and transportation † is successfully solved or autonomous systems for its *in situ* production are designed.

The governments of several countries have approved federal programmes aimed at the development of hydrogen-driven mobile motor vehicles. In the U.S., president Bush's initiative[2] has given a high priority to this programme. At the end of November 2003, the International Partnership for the Hydrogen Economy (IPHE) was founded, which joined 15 countries, including Russia. One of the major goals declared by the IPHE is the design of competitive affordable electric vehicles operated with hydrogen fuel cells by 2020. In December 2003, the Complex program of R&D activities in the field of hydrogen energetics and fuel cells was approved in Russia.[3] A prerequisite for all these programmes is the development of compact systems of hydrogen storage that would provide sufficiently fast desorption of hydrogen in a technically reasonable temperature range.[2,4–8]

According to the basic qualifying standards of the U.S. Department of Energy (DOE), the prospective stand-alone systems should store no less than 6.5 mass % or 62 kg m^{-3} of hydrogen (to guarantee a haul of $\sim$500 km) ‡ and operate with in the technologically acceptable temperature and time regimes to be commercially justified.§

The potential utility of carbon-based light sorbents for hydrogen storage was pointed out as early as in the 1960s. The best performance for cryoadsorption storage has been achieved for adsorbents based on low-density high-surface-area activated carbons, which also enabled purification of molecular hydrogen from admixtures. In particular, porous carbon AX-21, which is characterised by a specific surface area of 3000 m^2 g^{-1}, adsorbs up to 10 mass % (or 32 kg m^{-3}) of hydrogen at 77 K and 5 MPa (50 atm). However, the adsorption capacity of this material as well as of other activated carbons drops down to 0.5 mass % at room temperature and 7 MPa,[9,10] which is hardly acceptable for the automotive industry.

The interest of researchers in the hydrogen sorption by carbon materials has been rekindled following the discovery of new allotropic forms of carbon, *viz*., fullerenes, nanotubes, graphite nanofibres and other nanostructured carbon materials.[11–13] These carbon materials are composed of quasi-sp^2-hybridised carbon atoms assembled into closed spherical (fullerenes), non-spherical clusters or quasi-one-dimensional tubes seamlessly rolled-up from graphene sheets. Nanotubes are subdivided into single-walled (with a diameter of 1 – 2 nm) and multi-walled (with a diameter of 10 – 40 nm) species.[12,14–17] The latter may contain from 2 to 50 graphene layers. Graphite nanofibres are built up of graphite platelets stacked at different angles with respect to the

Yu S Nechaev G V Kurdjumov Institute of Metals Science and Physics, State Research Centre of the Russian Federation, I P Bardin Central Research Institute of Ferrous Metallurgy, 2-ya Baumanskaya ul. 9/23, 105005 Moscow, Russian Federation. Fax (7-095) 777 93 50. E-mail: nechaev@online.ru
O K Alekseeva Institute of Hydrogen Energy and Plasma Technology, Russian Research Centre 'Kurchatov Institute', pl. Kurchatova 1, 123182 Moscow, Russian Federation. Fax (7-095) 196 62 78. Tel. (7-095) 196 73 90. E-mail: alex@hepti.kiae.ru

Received 14 July 2003
Uspekhi Khimii **73** (12) 1308 – 1337 (2004); translated by Ya V Zubavichus

† According to estimates,[1] the long-distance transportation of hydrogen through the pipe lines at a pressure of 7 – 8 MPa (70 – 80 atm) is less expensive than the electric power transmission through the high-voltage lines.

‡ A typical motor vehicle requires $\sim$0.04 m^3 of a hydrocarbon fuel to travel 500 km, whereas an electric vehicle driven by a hydrogen fuel cell requires 2 – 4 kg of H_2 for the same haul.[4–6]

§ Networked or autonomous hydrogen storage systems should conform to common qualifying standards: ignition time $\sim$15 s, refueling time $<$ 5 min, working lifetime (no less than 500 cycles) at a fuel regeneration level no lower than 90%.

fibre axis (*i.e.*, parallel, perpendicular or in a herringbone arrangement). Typically, the fibres possess lengths of 5 – 100 μm and diameters of 1 – 500 nm.

The first experimental results reporting increased hydrogen sorption (5 mass % – 10 mass % under normal conditions) by a material consisting of single-walled carbon nanotubes were published in 1997.[18] Numerous investigations into hydrogen sorption by various carbon nanomaterials and their metal-doped modifications that followed have demonstrated that the required sorption capacity at room temperature and a reasonable pressure is difficult to achieve but is attainable, in principle.[4, 18 – 26] For instance, nanographite adsorbs hydrogen sufficiently well but its applications are hampered by typically high desorption temperatures.[22, 27 – 31] Furthermore, it turned out that the sorption capacities could be different by as much as two – three orders of magnitude even for closely related materials. In 1998, exceptionally high hydrogen sorption (up to 67 mass %) by graphite nanofibres (GNF) at room temperature and 12 MPa was reported.[32, 33] These communications evoked both great interest and many critical comments.[34 – 37]

Several factors can be responsible for the observed scatter in the experimental hydrogen sorption capacities by different carbon nanomaterials. The major reasons for the discrepancies in quantitative estimates of sorption properties of carbon nanomaterials include difficulties in the preparation of pure sorbents with a strictly defined microstructure, the lack of commonly adopted techniques for their attestation, complexity of physical and chemical processes in their interactions with hydrogen and dependence of these processes on the experimental conditions.[14, 34, 38 – 40] These, as well as a number of other aspects of the interactions of carbon sorbents with hydrogen, became a subject of vivid discussion at conferences during 2001 – 2004.[41 – 51] The same issues were analysed in a number of reviews devoted to fullerenes,[52] fullerites,[52, 53] carbon nanotubes, graphite nanofibres[14, 52, 54 – 57] and other carbon nanostructures[4, 14, 22, 58 – 62] (see also http://asyncbrain.baf.cz/sanatorium/1/h2fuel/).

Although some sceptics have pointed out that 'reliable data on carbon nanostructures are lacking and the experimental results are characterised by poor reproducibility', many researchers (for instance, see Refs 10, 14, 42 – 47, 51, 63 – 65) share the opinion that all aspects of the problem deserve a more accurate and thorough consideration and soundly propose to continue investigations within the scope of an international project 'Physicochemical fundamentals and prospects in the use of new carbon materials for hydrogen storage in automotive industry'.[48] The present review describes for the first time an original constructive analysis of thermodynamic and diffusion parameters as applied to a series of hydrogen – carbon sorbent systems that are characterised by the extremum characteristics of the sorption processes.

II. Experimental studies of hydrogen sorption by carbon nanostructures

Table 1 summarises experimental data on sorption (and storage) of hydrogen by various carbon nanomaterials (CNM), such as fullerenes, single- and multi-walled nanotubes (SWNT and MWNT, respectively), carbon and graphite nanofibres (CNF and GNF, respectively), nanographite and composites on its base and new types of nanostructures, such as fullerene-filled nanotubes ('peas in the pod'), nanobells, *etc*. Micrographs of some of these nanostructures are shown in Fig. 1. An analysis of the factors influencing the results of sorption capacity determination indicates that even carbon materials belonging to one type differ strongly from each other. For example, nanotubes synthesised using different methods can differ in purity, diameter, length, specific surface area, *etc*. The apparent sorption capacity of such materials is also strongly affected by the character of the chemical or thermal pretreatment of the samples and purity of hydrogen.[106]

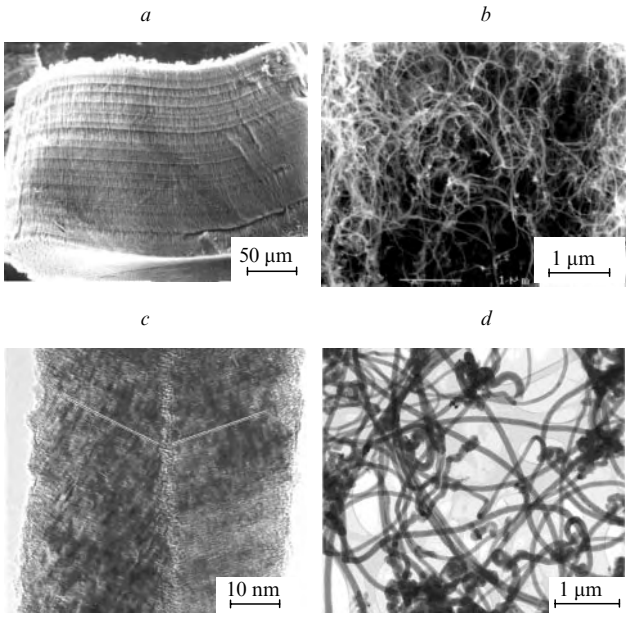

Figure 1. Micrographs of some carbon nanostructures.[32, 91] (*a*) A dense block of aligned (straightened) carbon nanotubes prepared by catalytic pyrolysis of ferrocene on a quartz support, (*b*) randomly oriented carbon nanotubes, (*c*) GNF composed of graphite platelets oriented at 45° (herringbone-type) with respect to the fibre axis, (*d*) GNF prepared by catalytic decomposition of an ethylene – hydrogen mixture.

Quantitative estimates of the sorption capacities discussed in the present review are based on several experimental techniques, such as volumetric analysis (VA), thermogravimetric analysis (TGA), temperature-programmed desorption (TPD) and thermodesorption spectroscopy (TDS). The apparent values of the sorption capacity of carbon nanomaterials can differ from the real ones if possible sources of the experimental errors are neglected.¶

In particular, in the case of volumetric analysis (*i.e.*, when a change in the volume or pressure of hydrogen due to sorption or desorption is measured), the following factors should be taken into account:

— temperature effects (that are especially significant for high-pressure experiments),

— thermal effects due to compression/decompression of the sorbent upon sorption/desorption of hydrogen,

— thermal effects due to nuclear spin transitions (changes in the ratio of ortho/para modifications of molecular hydrogen),

— the actual equilibration time,

— possible leaks in the experimental setup (which can strongly decrease the accuracy of determination of small changes in pressure).

Tibbetts *et al.*[38] studied sorption of hydrogen at 300 K and 10 MPa and estimated that a decrease in the temperature by 1° for a sample with a mass of 1 g in a volume of 1 litre necessitates that the pressure was increased by 33.3 kPa, which results in an apparent increase in the amount of absorbed hydrogen by 2.6 mass %. They found that filling of the chamber with hydrogen was accompanied by a jump-like increase in temperature by more than 25 °C and the system required about 100 min to equilibrate.

TGA and TDS data can become less accurate due to admixtures of water vapour and other gases in hydrogen (*e.g.*, sample No. 26 in Table 1).[39, 40] The experimental errors are often aggravated by insufficient purity of sorbents themselves (in particular, due to admixtures of catalysts).

¶ For a discussion concerning potential sources of the experimental errors, see, for instance, Refs 1, 34, 38, 56.

Table 1. Results of experimental studies of hydrogen sorption by carbon nanomaterials.

No	Sorbent and its characteristics	Sample mass /mg	Sorbent preparation method	Sorbent pretreatment method	T /K [a]	P /MPa	H_2 (mass %) (sorption)	Measurement method [b] (hydrogen purity)	Comments	Ref.
Porous carbon										
1	AX-21, $S_{sp} = 3000\ m^2\ g^{-1}$				77 300	5 7	10 0.5			9
	AX-21, $S_{sp} = 2000\ m^2\ g^{-1}$				77	3.5	5.3			66
2	Saran, $S_{sp} = 1600\ m^2\ g^{-1}$		pyrolysis of poly(vinylidene chloride)		77 300	0.3 16	2.4 0.4	VM		35
3	Nanoporous carbon (total porosity ~70%), mean pore size ~0.8 nm, $S_{sp} = 1200\ m^2\ g^{-1}$				520–970	20	1.3	TPD, MS, electroresistance	sorption and desorption kinetics were studied	67
4	Pyrolytic graphite				323–363	30–50	~0.1	TPD		68, 69
Carbon nanotubes										
5	SWNT, diameter of 1.3 nm (contains 90% of amorphous carbon)		electric arc	milling in a ball mill for 24 h in Ar	RT	0.08	<0.1	TPD		34
6	SWNT ropes, diameter of 13 nm, $S_{sp} = 285\ m^2\ g^{-1}$	200	laser ablation	sonication	80	12	8.25	VM (H_2 99.9999%)	the isotherms pressure *vs.* composition were measured	70
7	SWNT, diameter of 1.85 nm	500	electric arc (hydrogen)	no treatment	RT	12–10	2.4	VM (H_2 99.999%)		71
				chemical treatment	RT	12–10	2.8			
				chemical treatment and annealing in vacuum	RT	12–10	4.2 [c]			
8	SWNT	160–350	catalytic decomposition of acetylene	heating in NaOH acidic treatment	RT RT	10 10	5.15 2.67	hydrogen adsorption	effects of surface treatment were observed	23
9	SWNT, $S_{sp} = 263\ m^2\ g^{-1}$	10	DEL (Dynamic Enterprises Limited)	cold compacting with Au powder	293		0.9	ECM		72
				cold compacting	78	0.2	0.6	TPD		72
10	SWNT (long bundles), diameter of 1.69 nm	500	catalytic decomposition of hydrocarbons	no treatment chemical treatment chemical treatment and annealing in vacuum	RT RT RT	11 11 11	2.4 2.8 4.2	VM		24

Table 1 (continued).

No	Sorbent and its characteristics	Sample mass /mg	Sorbent preparation method	Sorbent pretreatment method	T /K [a]	P /MPa	H_2 (mass %) (sorption)	Measurement method [b] (hydrogen purity)	Comments	Ref.
Carbon nanotubes										
11	SWNT		laser ablation	sonication, purification	RT	0.1	7	TPD, VM		4, 25, 73
12	SWNT in the form of peapods, bundles (C_{60}@SWNT)		Nd : YAG, laser ablation, Ni/Co catalyst	chemical and thermal purification	RT	6		TPD	a peak of H_2 desorption is observed at 350 K	74
				additional treatment with NaOH	RT	6				
13	SWNT in the form of peapods, bundles (C_{60}@SWNT)		the same	chemical treatment with NaOH	RT	6		TPD	adsorption of molecular hydrogen at 365 K	75
14	SWNT ropes, bundles (mats), diameter of tubes 1.4 nm, diameter of bundles 15 nm		electric arc (Carbolex, Inc.)	no treatment	500	0.1		thermo-EMF		76
				the same	77	0.2 – 0.3	1.2	TGA, thermo-EMF, electroresistance (H_2 99.999%)		76
				oxidation and chemical treatment with						
				4.0 M HCl	77	0.2 – 0.3	3.5			
				HNO_3	77	0.2 – 0.3	6.5			
15	Purified SWNT (purity of 90 mass % – 95 mass %), diameter of 1.38 nm	1000	laser ablation, Ni/Co catalyst	chemical and thermal treatment	295	9	0.32	TPD	activation energy of desorption was estimated (E_d = 9.6 kJ mol^{-1})	77
16	CNT									
	aligned bundles, S_{sp} = 61 m^2 g^{-1}		catalytic pyrolysis	no treatment	RT	10	3.5	VM (H_2 > 99.999%)	a new compact structure was formed under the action of hydrogen	78
	random ordered bundles		the same	the same	RT	10	0.5			
17	CNT ('amorphous', diameter of 10 – 60 nm)	200	floating catalyst method	no treatment	RT	10	1.3	VM (H_2 99.999%)	adsorption during 24 h; structure of the samples was similar to GNF (herringbone-type)	79
				annealing at						
				1700 °C			1.6			
				1900 °C			2.2			
				2000 °C			2.3			
				2200 °C			4.0			
18	SWNT, bundles	500	laser ablation, Ni/Co catalyst	no treatment	200		0.05	inelastic neutron scattering	hydrogen storage below 200 K does not require external pressure; hydrogen desorbs at T > 200 K	80
				chemical treatment	200		1.2			
19	SWNT		electric arc, Co/Ni, YNi_2 catalysts	purification	123	2.5	2.4	VM, TPD (H_2 99.9999%)	H_2 desorbs at 723 K (0.24% of H_2 adsorbs reversibly)	81

Table 1 (continued).

No	Sorbent and its characteristics	Sample mass /mg	Sorbent preparation method	Sorbent pretreatment method	T /K [a]	P /MPa	H_2 (mass %) (sorption)	Measurement method [b] (hydrogen purity)	Comments	Ref.
Carbon nanotubes										
20	SWNT	1000	HiPco, Carbon Nanotechnologies, Inc.	thermal treatment	RT	8	0.43	VM		82
21	SWNT, aligned long ropes	500 – 800	electric arc	cold pressed into pellets (without binder)	295	11	4.0 [d]	VM	70% of H_2 desorbs upon release of high pressure; the sample meets the requirements for automotive industry	83
22	SWNT	30 – 50	Tubes@Rice	no treatment	RT	4.8	0.4	microbalance	chemical treatment increases the sorption by a factor of 3	84
				mild oxidation in CO_2 and thermal treatment	RT	4.8	1.2			
23	SWNT, diameter of 1.3 nm				295	0.1	0.94			85
					77	0.1	2.37			
24	CNT, diameter of 20 – 30 nm	200	pyrolysis of acetylene, catalysts:					VM		86
			AB_5 hydrides	no treatment	298	10	2.4			
				purification	298	10	3.3			
			AB_2 hydrides	no treatment	298	10	2.3			86
				purification	298	10	3.1			
25	CNT doped with transition metals				RT		0.5 – 1.0	TGA	preliminary results	87
26	K-MWNT, S_{sp} = 148 $m^2\ g^{-1}$	10	catalytic decomposition of methane	chemical and thermal treatment in He	293 – 373	0.1	1.8 [e]	TGA, TPD (H_2 99.999%)		39
							12			
	Li-MWNT, S_{sp} = 148 $m^2\ g^{-1}$	10	the same	the same	293 – 373	0.1	2.5 [e]			
							21			
27	MWNT (aligned, cone-shaped), diameter of 50 – 100 nm	1	CVD [f]	no treatment	RT	0.2	0	TPD (H_2 99.999%)		88
				the same	RT	1	5 – 7			
				thermal treatment	RT	0.2	7.8			
				thermal and chemical treatment	RT	1	8.8 – 13.8 [g]			
28	MWNT in the form of curls, S_{sp} = 263 $m^2\ g^{-1}$, internal diameter of 5 – 15 nm, external diameter of 10 – 30 nm	2	CVD [f]	no treatment	300	4	0.67	TPD (H_2 99.999%)		89
	Aligned MWNT, S_{sp} = 877 $m^2\ g^{-1}$, internal diameter of 8 nm, external diameter of 20 nm	2	CVD [f]	the same	300	4	1.97	TPD (H_2 99.999%)		89

Table 1 (continued).

No	Sorbent and its characteristics	Sample mass /mg	Sorbent preparation method	Sorbent pretreatment method	T /K [a]	P /MPa	H_2 (mass %) (sorption)	Measurement method [b] (hydrogen purity)	Comments	Ref.
Carbon nanotubes										
29	MWNT samples with cracks in external walls	100	catalytic synthesis	no treatment	RT	10	1.3	VM	hydrogen sorption	90
				annealing	RT	10	4.0	(H_2 99.999%)	during 24 h	
	MWNT samples without cracks	100	the same	no treatment	RT	10	0.73			
				annealing	RT	10	0.81			
30	Highly-oriented closed MWNT, diameter of 10 – 40 nm, S_{sp} = 60 m^2 g^{-1}	100	catalytic pyrolysis	heeting to 373 K, 24 h	290	10	2.4	VM	adsorption of H_2 results in formation of microchannels	91
	randomly oriented closed MWNT, S_{sp} = 27 m^2 g^{-1}	100	the same		290	10	0.68			
31	MWNT, open	200 – 500	template synthesis	thermal and chemical treatment, annealing in vacuum	77	10	6.46	VM	sorption of H_2 in subnanopores	92
					RT	10	1.12	(H_2 99.999%)		
Carbon and graphite nanofibres										
32	GNF, tubular structure	21.4	catalytic decomposition of hydrocarbons	chemical treatment for removal of metal particles of the catalyst	RT	12	11.26	VM		33
	GNF, herringbone structure	318.8	the same	the same	RT	12	57.85			
		291.4	"	"	RT	12	67.55 [h]			
		103.7	"	"	RT	12	60.58			
	GNF, platelet structure	103.2	"	"	RT	12	53.68			
		101.4	"	"	RT	12	43.63			
33	GNF	> 1000	catalytic decomposition of hydrocarbons	annealing in vacuum (423 K, 5 h)	RT	12	40	VM	reversible changes in the crystal lattice parameters are possible (d increases from 0.340 nm to 0.347 nm)	93
34	GNF	500 – 1000	catalytic decomposition of a $C_2H_4 - CO - H_2$ mixture	annealing in an inert atmosphere *in situ*	RT	12	40	VM, TGA, TPD, XRD		32
	GNF	500 – 1000	the same	no treatment	RT	12	2			
35	GNF, S_{sp} = 25 m^2 g^{-1}	300	catalytic decomposition of ethylene	annealing in vacuum at 1173 K	77	0.45	0.17	VM		35
					300	16	0.25			
	GNF, S_{sp} = 23 m^2 g^{-1}	300	the same	the same	77	0.45	–			
					300	16	0.2			

Table 1 (continued).

No	Sorbent and its characteristics	Sample mass /mg	Sorbent preparation method	Sorbent pretreatment method	T /K [a]	P /MPa	H_2 (mass %) (sorption)	Measurement method [b] (hydrogen purity)	Comments	Ref.
Carbon and graphite nanofibres										
36	CNF, $S_{sp} = 300\ m^2\ g^{-1}$ CNF, $S_{sp} = 2290\ m^2\ g^{-1}$		commercial product the same	without activation activation	300 300	6 6	0.1 0.6	VM		94
37	GNF	1750	catalytic decomposition of ethylene	annealing in vacuum at 423 K activation	290 290	12 12	10 15	VM, XRD	the $P-C-T$ phase diagram was determined, several sorption – desorption cycles were completed	95 – 97
38	GNF		pyrolysis	no treatment pretreatment	RT RT	12 12	4.18 6.54			20
39	CNF, herringbone structure, diameter of 200 – 500 nm	10 – 20	catalytic decomposition of ethylene	no treatment doping with KNO_3	303 303	0.1 0.1	0.34 4.9	TGA/QMS, XRD (H_2 99.999%)	doping with KNO_3 increases concentration of H_2 by < 0.3 mass %	98
40	CNF	300 – 1000	catalytic pyrolysis	thermal treatment in Ar thermal treatment in vacuum washing with deionised water	RT RT RT	11 11 11	3.4 4.5 5.7	VM	$LaNi_5$ was used as a standard	24
41	Activated CNF		commercial samples	–	77	2	2.8	VM	reversible physisorption in subnanopores	99
42	CNF, herringbone structure	500	catalytic decomposition of CH_4, catalyst Ni – MgO	thermal treatment in N_2 at 1473 K	298	12	1.4	VM (H_2 99.999%)		36
Miscellaneous carbon nanomaterials										
43	SWNH, nanohorns, $S_{sp} = 1006\ m^2\ g^{-1}$ (SWNH content 95%)		laser ablation	oxidation at 693 K	77 77 196 303	0.1 2 – 3 6.5 6.5	0.5 2.5 0.95 0.3	gravimetry (a balance with a precision within 0.1 μg)		100
44	Multi-walled nanobarrels	471.7	reaction of Al_4C_3 with halogens (gas)		77 300	10 10	6.2 3.2	(H_2 99.999%)		101
45	C-N-Nanobells (oriented), diameter of 15 nm, length of 50 nm		CVD [f]	treatment with N_2 plasma + chemical treatment	RT	1	8	QMS, TGA (H_2 99.999%)	ten cycles were completed	21
46	Nanographite, $S_{sp} = 10\ m^2\ g^{-1}$		mechanochemical synthesis in a ball mill at $P_{H_2} \approx 1$ MPa and 300 K		373	1	7.4	TPD, NMR, neutron diffraction	hydrogen desorbs at an elevated temperature	27 – 31

Table 1 (continued).

No	Sorbent and its characteristics	Sample mass /mg	Sorbent preparation method	Sorbent pretreatment method	T /K [a]	P /MPa	H_2 (mass %) (sorption)	Measurement method [b] (hydrogen purity)	Comments	Ref.
Miscellaneous carbon nanomaterials										
47	Nanographite, $S_{sp} = 780\ m^2\ g^{-1}$	1000	mechanochemical synthesis in a ball mill in vacuum	thermal treatment	RT	6.0	0.20 – 0.25	VM (H_2 99.99999%)	five sorption – desorption cycles were completed (formation of pores with $d < 1.0$ nm was observed)	102
	Initial graphite, $S_{sp} = 7\ m^2\ g^{-1}$	1000	the same	the same	RT	6.0	0.02			
48	Nitrogen-doped nanographite		CVD [f]	plasma treatment	RT	7	0.7 – 0.8	TGA		64
49	Fullerites C_{60}, C_{60}/C_{70}			liquid phase hydrogenation	453	2.4 – 2.8	6	pressure change		103
50	Fullerites C_{60}				723 – 773	3000 – 7000	5.0 – 7.9			19
51	Films of nanostructured carbon, $S_{sp} = 665\ m^2\ g^{-1}$	1.25	ultrasound-assisted cluster deposition	annealing in an Ar flow (150 °C, 1 h)	RT	0.1	1.1	TPD , NEXAFS		104, 105

[a] RT is room temperature. [b] Adopted acronyms: VM is volumometry, TPD is temperature-programmed desorption, MS is mass spectrometry, ECM is electrochemical methods, TGA is thermogravimetric analysis, XRD is X-ray diffraction, QMS is quadrupole mass spectrometry, NEXAFS is Near-edge X-ray absorption fine structure. [c] Total amount of desorbed H_2 is 4.2 mass % (3.3 mass % at RT and 0.9 mass % upon heating). [d] Volume capacity is 68 kg m^{-3}. [e] Corrected data from Ref. 40, which reported overestimated values due to utilisation of humid hydrogen for similar samples. [f] CVD stands for chemical vapour deposition. [g] Desorption of hydrogen occurs upon heating to 573 K. [h] Total amount of desorbed H_2 is 45.09 mass %.

As can be seen from Table 1, DOE requirements to the parameters of hydrogen sorption by carbon nanostructures have been met in several cases (*e.g.*, sample Nos 11, 27, 32–34, 37, Table 1). In particular, hydrogen sorption capacity at room temperature and 12 MPa (measured using a Sieverts-type apparatus) has reached ~67 mass % (!) for specific GNF samples prepared by metal-catalysed (typically, Ni, Fe) pyrolysis of hydrocarbons at 723–1023 K (sample No. 32).[33] These fibres were composed of graphite platelets with lengths of 10–100 μm and thicknesses of 3–50 nm oriented parallel (tubular-type fibres), perpendicular (platelet-type fibres) and at an acute angle (herringbone-type fibres) with respect to the fibre axis; the minimum distance between the platelets was 0.335 nm. The authors of this study suggested [33] that the structures of these materials are ideally suited for hydrogen storage. Desorption occurred within 5–10 min. Later, the same authors in response to criticism from other researchers, noted [32] that a special thermal pretreatment of the fibres aimed at the removal of chemisorbed gases and water is necessary to provide reproducible results. Sorption capacity of the samples increased from 2 mass % to 40 mass % (sample No. 34, Table 1) as a result of an *in situ* thermal treatment in an inert gas.[32]

Attempts undertaken by several other research groups to reproduce these results failed despite the experimental conditions being strictly observed.[35, 36, 94, 107] Nevertheless, attainability of high sorption capacities for similar structures has been confirmed in other studies [20, 24, 95–97] (sample Nos 37, 38, 40, Table 1).

Recently, a continuous process for the synthesis of MWNT using hot-filament plasma-assisted chemical vapour deposition has been developed.[88] The structure of MWNT prepared using this method (sample No. 27, Table 1) differs from the ideal one and resembles to a certain extent that of the graphite nanofibres having graphite platelets with open ends. These materials are characterised by relatively high and reproducible sorption capacity (5 mass % – 7 mass %) at room temperature and moderate pressures (1 MPa). Annealing of the samples at 573 K and removal of admixtures of catalysts gave rise to an increase in the sorption capacity up to 13.8 mass %.

Note that volume density of hydrogen is also of importance for applications: it should be no less than 62 kg m^{-3}. According to estimates,[5] volume density of hydrogen sorbed by an array of nanotubes with a diameter of 2 nm can reach 54 kg m^{-3} assuming that density of the original nanotubes is ~1000 kg m^{-3}. Indeed, density of the standard carbon adsorbents lies in the range of 500–1000 kg m^{-3}, but that of CNT is typically significantly lower, *viz.*, 100–200 kg m^{-3}. Only pressed bundles of nanotubes had a density of ~330 kg m^{-3}, which corresponded to the volume density of absorbed hydrogen of 10–33 kg m^{-3} at a sorption capacity of 10 mass %. Recently developed methods for the compaction of CNT enable preparation of materials with a density of as high as ~800 kg m^{-3} (see Ref. 56) and even 1700 kg m^{-3} (see Ref. 83). In the latter case, promising results with respect to hydrogen sorption have been obtained: the volume density of hydrogen reached 68 kg m^{-3} at a sorption capacity of 4 mass % (sample No. 21, Table 1).

Not all the experimental results look so promising (see, for instance, data for sample Nos 5, 15, 20, 35, 36, Table 1). According to measurements [38] performed in a temperature and pressure range of 193–773 K and 3.5–11 MPa for nine samples including graphite flakes, activated carbon G-60 with a specific surface area of 700 m^2 g^{-1}, carbon wires (grown on a FeNiCu composite), graphitised carbon fibres, PYROGRAF fibres and MWNT with different diameters, the hydrogen sorption capacity at room temperature did not exceed 0.1 mass % at 3.5 MPa and 0.5 mass % at 11 MPa. All attempts to activate the samples did not give positive results. A study of hydrogen sorption by purified SWNT samples as well as by differently pretreated samples of SWNT, MWNT and GNF prepared using the CVD method [37] has given similar results: the maximum hydrogen uptake did not exceed 0.63 mass % at room temperature and 4.5 MPa.

One possible route to enhance sorption capacity of carbon nanomaterials is development of alternative synthetic approaches. A series of experimental studies (see, for instance, reviews [108, 109]) has shown that a high sorption capacity can be achieved by implantation of atoms or ions of hydrogen isotopes with a kinetic energy on the order of 10 keV into graphite or by sputtering of graphite (or another graphite material) with a hydrogen plasma. In the latter case, amorphous 'a-C : H' films are deposited onto metallic walls of the plasmatron. Such films are characterised by a high tritium content (T/C ≈ 0.5–0.7), which corresponds to a sorption capacity of 4.2 mass % – 5.8 mass % (recalculated for the same protium content).

The prospects of the application of less typical forms of nanostructured carbon as hydrogen sorbents were recently discussed by Rawat *et al.*[110] They synthesised liquid crystals of carbon doped with carbon nanofibres and found that sorption of hydrogen by the material increased linearly in a pressure range of 0.3–0.6 MPa (at 77 K) and reached 3.5 mass % at 0.6 MPa (that is the maximum pressure achievable with their experimental setup); extrapolation of the experimental results to a pressure of 2.5 MPa gave a sorption capacity of 6.5 mass %. A new class of 'pillared' materials based on nanographite and nanotubes doped with lithium was proposed [111] as potential hydrogen sorbents. These materials are characterised by an increased separation between layers of graphite or walls of nanotubes, which can enhance their sorption capacity. Unfortunately, for the moment, these materials exist only in theory although the authors proposed possible routes to their synthesis. According to estimates,[111] the hydrogen sorption capacity of these materials at room temperature and 2–5 MPa can reach as high as 6.0 mass % – 6.5 mass % (or 61.7–62.9 kg m^{-3}), depending on the exact structure.

Investigations into the electrochemical accumulation of hydrogen in carbon nanomaterials are also of great interest.[65, 72, 112–121] In the majority of cases, the measurements were conducted in a system of half-cells filled with 6–7 M KOH (as an electrolyte) at room temperature with the working electrode made of the respective metallised carbon nanomaterial. In this case, the charge/discharge processes, which occur on the working electrode, can be represented as:

$$\mathrm{CNM} + x\,\mathrm{H_2O} + \mathrm{e^-} \underset{\text{discharge}}{\overset{\text{charge}}{\rightleftharpoons}} (\mathrm{CNM} + x\,\mathrm{H}) + x\,\mathrm{OH^-}\,.$$

A series of carbon materials including various CNT, SWNT and MWNT have been studied with respect to the electrochemical accumulation of hydrogen.[112] In this case, the hydrogen sorption capacity can reach 2.0 mass % at 298 K, partly due to metallic admixtures. For an SWNT sample, a discharge capacity of 316 mA h g^{-1} was achieved,[112] which corresponds to a hydrogen sorption capacity of 1.2 mass %. The capacity was virtually independent of the number of charge–discharge cycles. The most significant experimental and theoretical studies on the electrochemical sorption of hydrogen by carbon nanotubes (CNT) have been recently surveyed.[113] Good results were obtained for the CNF decorated with Ni–P alloy particles.[114] A high discharge capacity of 1625 mA h g^{-1} (which corresponds to a hydrogen sorption capacity of 5.7 mass %) was also obtained for the electrodes prepared by compacting a mixture of CNT, copper powder and polymer binder (polytetrafluoroethylene, or PTFE) taken in a mass proportion 1 : 5 : 3 into a nickel collector.[116] No doubt, the electrochemical accumulation of hydrogen in systems with carbon electrodes will find applications in the future,[65, 72] although development of the electrodes on the basis of less expensive activated carbons seems more promising due to a high cost of CNT.[119]

Different physical methods, such as NMR (see Refs 122–125), neutron scattering,[80, 126–135] ESR,[136] Raman scattering, are normally applied to elucidate the mechanisms of hydrogen accumulation in the storage systems under development.[137] In particular, it has been demonstrated that physisorption of hydro-

gen molecules by SWNT bundles at 200 K occurred predominantly in the internal channel-cavities,[128] although sorption centres were observed on the external surfaces of SWNT as well.[129] The ^{1}H NMR data [125] supported the presence of sorption centres both on the external surfaces of SWNT and in the internal channels (the authors observed mutual diffusion of hydrogen molecules between the two types of the centres). An analysis of the ESR spectra indicates that hydrogen adsorbs dominantly on admixtures since the signal caused by admixtures attenuates upon hydrogen adsorption. In the case of an MWNT sample synthesised without metal catalysts, the experimental data were interpreted as evidence for the direct interaction of hydrogen with the walls of the tubes.[136] An analysis of the Raman scattering spectra for an H_2–MWNT system has revealed an influence of the method used for the synthesis of the MWNT on the hydrogen uptake and confirmed that hydrogen can be adsorbed not only in the molecular form but in the dissociated atomic form as well.[137]

III. Theoretical studies of physisorption and chemisorption

The great interest to the problems of hydrogen storage has promoted numerous theoretical investigtions into the interactions of molecular and atomic hydrogen with carbon nanostructures. This interest was to a large extent stimulated by impressive results obtained in the field of spherical carbon clusters and nanosized tubes [12, 15, 16] as well as by the relative simplicity of the species being adsorbed and availability of efficient computational methods (advantages and disadvantages of the modern computational approaches have been analysed elsewhere [138, 139]). Table 2 summarises the theoretical results obtained using different models, which are of greatest importance for the following discussion. Supplementary information may be found elsewhere,[4, 14, 56, 57, 61] in particular, in two recent reviews (Refs 138, 152).

All theoretical studies can be formally subdivided into two main groups. The first group of studies analyses idealised models of physisorption of molecular hydrogen whereas the second group elucidates the mechanisms of chemisorption of molecular and atomic hydrogen.

1. Physisorption of molecular hydrogen by carbon nanomaterials

The Monte Carlo method, classical molecular mechanics algorithms and approved sets of empirical potentials were applied to simulate physisorption of hydrogen by carbon nanostructures.[57, 94, 140, 142, 144, 153–155] Additionally, some of the simulations explicitly took into account the quantum effects.[139, 141, 144, 155] Virtually in all simulations, calculated sorption capacities of isolated ideal single-walled nanotubes with cylindrical pores as well as of graphite nanofibers with slot-like pores agree with the experimental data at 77 K but do not support the possibility of detection of a high sorption capacity at 300 K (see Table 2).

Figure 2 depicts schematically different areas of a bundle of SWNT available to adsorption of molecular hydrogen.[155, 156]

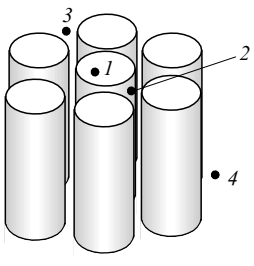

Figure 2. Sorption of hydrogen by an SWNT bundle.[155, 156]
(*1*) Inside the nanotube, (*2*) in the channels between the nanotubes, (*3*) in a 'groove', (*4*) on the outer surface of the bundle.

According to calculations of sorption of molecular hydrogen within the density functional theory (DFT), the inner space of the nanotubes, their outer surfaces and channels between them can be involved in the sorption process.[157] Adsorption in channels and slots is favoured over the adsorption on individual nanotubes.[156] An explicit account for the curvature of the surface of SWNT (which is of especially great importance for nanotubes with small diameters) indicates [158] that adsorption on the internal surface of the tube is energetically less favourable than that on the external surface. The probability of adsorption in extremely narrow channels between the tubes is also quite low (sample No. 9, Table 2).[135]

An increase in the sorption capacity can be achieved by optimising the size of the nanotubes and their arrangement within bundles.[140, 144, 145] Two typical types of arrangement of CNT in a bundle are shown in Fig. 3 [142] (samples No. 3, 9, 10, 11, Table 2). Probably, the arrangement of CNT giving rise to bundles with a triangular cross-section can ensure fairly high sorption levels even at room temperature provided that some specific conditions are met (sample No. 11, Table 2).[145] Changes in the parameters of the lattice formed by parallel bundles of single- or multi-walled nanotubes due to hydrogen sorption have been analysed by Cabli *et al.*[159, 160] and Gordilio *et al.*[161] Sorption capacity of SWNT bundles at 298 K and 12 MPa can be enhanced by 40% by doping them with alkali metals (sample No. 12, Table 2).[57]

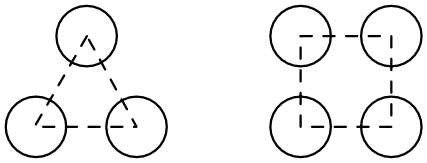

Figure 3. Bundles of CNT with triangular and square cross-sections.[142]

The results of simulations of molecular hydrogen sorption inside SWNT in a wide temperature (20–300 K) and pressure (up to 20 MPa) ranges [139] are of special note. An analysis of the computational data obtained within the density functional theory showed that changes in the external pressure can induce a series of first-order phase tranitions accompanied by abrupt changes in the density of adsorbed hydrogen. According to estimates,[139] the amount of adsorbed hydrogen at 290 K and 10 MPa does not exceed 0.42 mass % (sample No. 6, Table 2). A simulation of the interactions in the system H_2–SWNT using molecular dynamics methods and density functional theory has confirmed that molecular hydrogen adsorbed inside SWNT can undergo condensation to form quasi-one-dimensional crystal lattices at low temperature or one-dimensional associates with a variable density at high temperature.[162]

Recently, the effects exerted by a surface chemical modification of SWNT on hydrogen physisorption have been elucidated [143] (sample No. 8, Table 2). According to simulations based on a combination of the Monte Carlo and molecular dynamics methods, oxidation (which opens holes in the walls of the nanotubes) increases the sorption capacity whereas the presence of the surface C–H groups results in its decrease.

In summary, the above investigations clearly indicate that physisorption alone cannot be responsible for the high values of sorption capacities at high temperatures observed experimentally.

2. Interaction of atomic hydrogen with carbon nanostructures

There are a number of experimental facts that imply that the interaction of hydrogen with graphite and related carbon nanostructures cannot be reduced to a mere physisorption of molecular hydrogen and a more complex process has to be considered. These include an unexpectedly low rate of sorption, stepwise desorption occurring with an increase in temperature and evident effects of

Table 2. Selected theoretical estimates of parameters of hydrogen sorption on carbon nanomaterials.

No	Sorbent	Sorbent's basic parameters [a]	T /K	P /MPa	H_2 (mass %)	H_2 /kg m^{-3}	Computational methods [b] (comments)	Ref.
Physisorption								
1	Nanotubes	d = 2 nm			5.1		simple geometrical estimate	4
2	Nanotubes	d /nm					GCMC, Lennard-Jones potential	94
		0.7	300	10	0.8	10		
		0.7	300	30	0.5	14		
		1.0	300	10	0.6	9		
		1.0	300	30	1.1	15		
	Slitpores	h /nm						
		0.7	300	6	0.7			
		0.7	300	10	1.1			
		1.0	300	30	1.8			
		1.0	300	30	2.5			
3	Nanotubes (open), in a densely packed BTCS [c] configuration	d = 1.33 nm, $l \approx 0.6$ nm	298	1	0.15	1.45	the same	140
			298	10	1.0	10.4		
			298	20	1.6	16.5		
4	SWNT	d /nm					GCMC, Silvera – Goldman potential for the H – H and Crowell – Brown potential for the H – C interactions	141
	isolated	2.4	77	10	15.5	–		
		2.4	77	4	11	–		
		1.2	77	10	15	40		
		1.2	77	4	10	35		
	arrays	2.4	77	10	4.5	8		
		2.4	77	4	3.6	4		
		2.4	298	10	0.85	6		
		2.4	298	4	0.4	3		
		1.2	298	10	0.4			
		1.2	298	4	0.2			
	Slitpores	h /nm						
		0.6	98	10	0.2			
		0.9	298	10	0.45			
		1.2	298	10	0.40			
		2.0	298	10	0.36			
5	SWNT	d /nm					DFT (data on overall H_2 sorption inside and outside the nanotubes are given)	142
	isolated	1.225	77	4	8.1			
		2.04	77	4	9.5			
		2.719	77	4	9.6			
		a mixture	300	16	< 1			
	arrays	1.225	77	4.2	4.2			
		2.04	77	3.8	6.3			
		2.719	77	4	7.1			
		a mixture	300	16	< 1			
6	SWNT (isolated)	d = 0.4 nm	290	10	0.42		DFT	139
7	SWNT	S_{sp} /m^2 g^{-1}					GCMC, Silvera – Goldman potential for the H – H interactions and Lennard-Jones potential for the C – H_2 interactions (S_{sp} values were calculated)	115
	isolated (10.10)	2676	77	10	9.6			
		2676	300	10	1.3			
	bundles of 3 parallel tubes	2070	77	10	7.0			
		2070	300	10	1			
	bundles of 19 parallel tubes	1333	77	10	4.3			
		1333	300	10	0.6			
8	Defectless SWNT						GCMC, MD (effects of a surface chemical modification were estimated)	143
	(15,0) SWNT		77	20	6.8	60		
			77	40	7.1	62		
			293	20	2	15		
			293	40	3.1	25		
	(15,0) SWNT containing 10% of surface C – H groups		77	20	6.5	57		
			77	40	6.9	60		
			293	20	1.9	14		
			293	40	3	24		

Table 2 (continued).

No	Sorbent	Sorbent's basic parameters [a]	T /K	P /MPa	H_2 (mass %)	H_2 /kg m^{-3}	Computational methods [b] (comments)	Ref.
Physisorption								
8	Defectless SWNT						GCMC, MD (effects of a surface chemical modification were estimated)	143
	(6,6) SWNT		77	20	6.0	55		
			77	40	6.5	57		
			293	20	1.8	15		
			293	40	2.6	22		
	(6,6) SWNT after oxidation of 40% of the surface		77	20	8.0	60		
			77	40	8.6	65		
			293	20	2.0	15		
			293	40	3.4	23		
9	SWNT in a densely packed BTCS [c] configuration	d = 1.35 nm, $l \approx$ 0.21 nm	77	1	0.54		DFT	135
			300	53	0.54			
10	SWNT in a densely packed BSCS [d] configuration	d = 2.2 nm, $l \approx$ 1.1 nm	77	10	11.24	60	GCMC, Lennard-Jones potentials	144
11	SWNT (open), arrays in a BTCS [c] configuration	d = 0.6 nm, $l \approx$ 3 nm	77	7	33		the same	145
		d = 6 nm, $l \approx$ 1 nm	298	10	4.7			
	Slitpores	h = 0.6 nm	77	7	4.2 – 15.3			
			298	7	0.5 – 1.9			
12	SWNT (bundles) doped with alkali metals		298	12	2		GCMC, Silvera – Goldman potential for the H – H interactions and Lennard-Jones potential for the C – H_2 interactions	57
	dopant-free		298	12	1.4			
Chemisorption								
13	(5,5), (9,0) and (10,0) CNT (closed)				8		DFT/MM (in a stable configuration with 50% of H atoms inside and 50% thereof outside the tubes)	146
14	Isolated (10,10) SWNT				14	160	DFT with periodic boundary conditions	147
	MWNT				7.7			
15	(5,5) SWNT (capsule)				3.5	142	MD, Tersoff – Brenner and Lennard-Jones potentials; a selected part [atomic H (16 – 25 eV) inside the SWNT] *ab initio*	148 – 150
	(9,0) SWNT (capsule)				5.0	172		
	(10,10) SWNT (capsule)				9.1	177		
16	Carbon nanostructures				7.7		DFT (the maximum possible value for chemisorption, contribution of physisorption is insignificant)	151

[a] Notations used: d is a diameter of the nanotube, h is a pore size, l is the minimum distance between walls of the nanotubes. [b] Acronyms used: GCMC is Grand Canonical Monte Carlo, DFT is Density Functional Theory, MD is Molecular Dynamics, MM is Molecular Mechanics. [c] BTCS is bundles with a triangular cross-section. [d] BSCS is bundles with a square cross-section.

catalysts (for instance, Fe, Co or Ni), structural defects and other factors favouring dissociation of hydrogen molecules.[163, 164]

The use of the *ab initio* methods to study chemisorption is quite difficult due to the fact that a correct representation of the carbon nanostructure (*e.g.*, SWNT) requires a model containing approximately 200 atoms.[138] There are two principal ways to overcome this difficulty. The first one is based on the periodicity of the structure of SWNT, which makes it possible to adapt *ab initio* and DFT methods suitable for small systems to larger extended structures using periodic boundary conditions.[147, 165] The second way exploits the two-level approach, in which a relatively small but essential part of the system (*i.e.*, its active site) is simulated at a high quantum-mechanical level, while the remainder is treated at a lower level (for example, using molecular mechanics methods). For instance, the active site of a closed SWNT was simulated by DFT using only 24 carbon atoms [146, 166] (sample No. 13, Table 2).

The first DFT calclulations [147] showed that sorption of hydrogen atoms occurs both inside and outside the SWNT (Fig. 4). Hydrogen atoms adsorbed inside the SWNT can assemble to molecules. Sorption capacity increases linearly with an increase in the diameter of nanotubes. Gravimetric capacity of the system H_2 – (10,10) SWNT † amounts to 14 mass % whereas volume capacity is 160 kg H_2 m^{-3}. Sorption capacity of the system

† The so-called chirality indices of nanotubes (n,m), which define orientation of the axes of a graphene sheet rolled-up into a nanotube with respect to the axes of the tube formed (for details, see, for instance, reviews [12, 15, 16]).

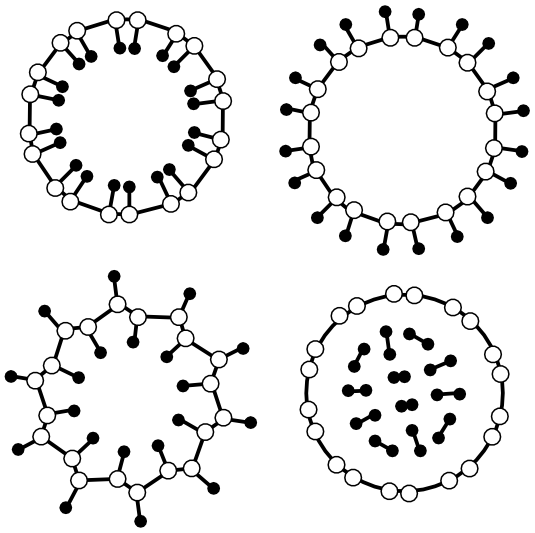

Figure 4. Hydrogen chemisorption centres in SWNT (a model representation, see text).[147]

H_2–MWNT is 7.7 mass % (sample No. 14, Table 2), which is close to the maximum theoretical value.

Bonding energies of an H atom to external surfaces of three types of SWNT, *i.e.*, (9,0), (5,5) (Fig. 5) and (10,0), for their coverage with hydrogen by 50% and 100% were calculated using DFT. It turned out that the hydrogen bonding energies are similar for all the three types of SWNT. For the (10,0) SWNT, another filling pattern, *i.e.*, 50% of H atoms bound to the internal surface and 50% bound to the external surface, was simulated. This filling mode proved to be the optimum one whereas the exclusive filling of the external surface was energetically unfavourable. It remains unclear, to what extent such a model can be achieved in practice, since no methods for the hydrogen insertion and extraction have been developed so far. The authors suggested[146, 166] that these stages can be accomplished using *ad hoc* catalysts initiating cleavage of the H—H and C—H bonds.

Similarly, according to calculations,[167] the system nanotube–H_2 has to be initiated catalytically or electrochemically prior to hydrogen sorption. Hydrogen chemisorption depends on the radius and chirality of the nanotube, as evidenced by the DFT simulation.[167] The threshold radius for the stability of nanotubes with hydrogen adsorbed on their external surface is 0.625 nm [note that it is nanotube (8,8) that have a close radius]. Measurements of photoinduced desorption of hydrogen from SWNT treated with atomic hydrogen[168] confirmed that the critical radii of curvature for chemisorption is $\sim$0.6 nm.

Figure 5. A model of a (5,5) SWNT with 50% coverage (as compared to the ultimate 'carbohydride' filling) with hydrogen (a stable structure).[146, 166]

Calculations at the DFT level have shown that a mechanical deformation of the nanotubes substantially affects the energy of their interaction with hydrogen atoms. An increase in the ellipticity of a nanotube (or a decrease in its radii of curvature) decreases the hydrogen bonding energy to a value typical of hydrogen sorption on a graphene sheet.[163, 169] A certain analogy between hydrogen sorption on a CNT and the basal plane of graphite was derived from *ab initio* calculations[163] (these results will be considered in more detail in the following section).

According to *ab initio* data,[170] dissociative chemisorption of molecular hydrogen from the gas phase on the surface of individual nanotubes is characterised by vanishingly low probability but in the case of a solid phase composed of bundles of nanotubes at a high hydrogen pressure, hydrogen molecules can dissociate forming simultaneously two C—H bonds on adjacent nanotubes. The adsorption is reversible: hydrogen desorbs if the high pressure is released. The experimental studies[19, 78] of hydrogen sorption by arrays of CNT have shown that the complete desorption requires at least 573 K.

In a series of papers,[148–150, 171–173] Ma and coworkers suggested a model describing the interactions of low-kinetic-energy hydrogen atoms (0.5–30 eV) with SWNT based on the molecular dynamics and, partially, *ab initio* calculations. According to their findings, the energy range of 1–3 eV is optimum for the sorption of hydrogen atoms on the external walls of the SWNT; hydrogen atoms with an energy of 4–14 eV are reflected from the walls whereas those with an energy of 16–25 eV are characterised by a high probability of penetrating through the side faces of the closed single-walled nanotubes and accumulating inside these capsules in the form of hydrogen molecules (Fig. 6). Owing to the high mechanical strength of nanotubes, hydrogen molecules can be concentrated therein up to densities exceeding by far that observed upon capillary condensation (sample No. 15, Table 2). According to estimates,[173] pressure of molecular hydrogen embedded into SWNT can reach as high values as 60 GPa. This hydrogen condensate inside individual SWNT, depending on hydrogen density and pressure, can undergo several phase transitions giving rise to different crystal lattices built up of hydrogen molecules.[172] If the pressure of hydrogen inside a (5,5) SWNT is 37.4 GPa, the bulk sorption capacity can reach 0.63 g cm^{-3}, which meets the requirements of the automotive industry. Potential ways to

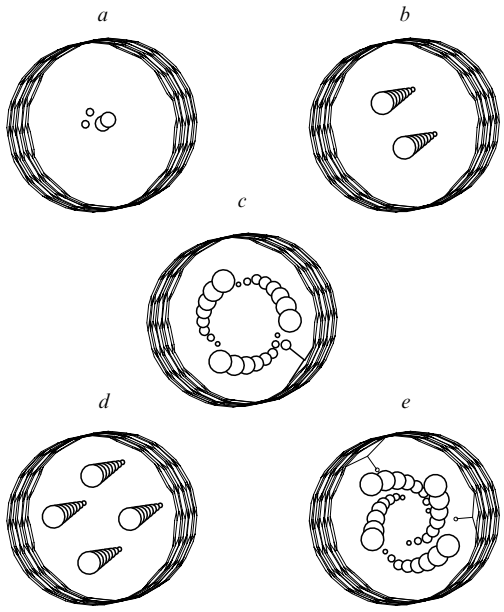

Figure 6. Arrangements of H_2 molecules inside a (5,5) SWNT at different volume densities of hydrogen.[148]
Volume density of hydrogen /kg m^{-3}: (*a*) 20, (*b*) 51, (*c*) 90, (*d*) 125, (*e*) 142.

practical achieving of such high hydrogen sorption levels by bundles of closed SWNT have been suggested as well as methods for hydrogen withdrawal through the walls of the nanotubes.[150, 174]

Recently, the first results of a semi-empirical study on the chemisorption of atomic hydrogen on a graphite sheet with structural defects have been published.[175] The authors used a modified (*i.e.*, not self-consistent) tight-binding model, which, in their opinion, described the chemical bonding between H and C atoms in real complex systems with sufficient accuracy and, at the same time, was simple enough to enable computer simulations.

In general, as correctly pointed out by Froundakis [138] and Tada *et al.*,[176] computer simulations of hydrogen adsorption on carbon nanomaterials conducted so far were successful only in rationalising a few first elementary steps of the overall process. Therefore, any step beyond the bounds of the idealised models would be indeed interesting but its practical implementation is challenging due to the necessity of bulk calculations. A search for conditions that would provide the optimum combination of thermodynamic and kinetic parameters of physisorption and chemisorption, is a current task for the development of hydrogen storage systems.[57, 59]

IV. A thermodynamic analysis of the experimental data

1. Methodology of the analysis

The similarity between the basic chemical structure elements of carbon nanomaterials under consideration and those of graphite implies that their interactions with hydrogen should obey some common rules. In order to elucidate these rules and factors governing the sorption capacities of the respective materials we applied the methods of thermodynamics of reversible processes and formal kinetics (the linear approximation of thermodynamics of irreversible processes). Earlier, we applied this methodology to an analysis of similar problems.[63, 177–180] The proposed methodology includes a new (simplified) procedure [63] for the evaluation of the diffusion coefficient based on the corresponding parameters of the thermodesorption peak and the characteristic length of the diffusion path. The proposed interpretation of the thermodynamic and kinetic (diffusion) parameters calculated in this way takes into account the results of theoretical studies of atomic hydrogen chemisorption by graphite and carbon nanostructures.[163]

2. Solubility, sorption and diffusion of deuterium in isotropic and pyrolytic graphites

Synthetic graphites are usually not single-crystalline materials. They are composed of small polycrystalline granules. One of the models proposed for such a spherical granule of isotropic graphite [181] is shown in Fig. 7. This granule has a size of ~ 2 μm (r_{gg}) and contains crystallite grains with sizes (r_{cg}) ranging from 0.03 μm to 0.2 μm.[182]

The equilibrium solubility of gaseous deuterium in the high-density ($\rho = 1.90$ g cm^{-3}) isotropic graphite ISO-880U (for the measurements, plates with a thickness of $l = 1$ mm were taken) at 1123–1323 K and 2.6–12.7 kPa is described by the following expression (the Sieverts isotherm)

$$x = \frac{D}{C} = 2.0 \times 10^{-7} \left(\frac{P_{D_2}}{P^{\circ}_{D_2}}\right)^{1/2} \exp\left(-\frac{\Delta H}{RT}\right), \quad (1)$$

where $\Delta H = -19 \pm 2$ kJ mol^{-1} is the standard enthalpy of dissolution of 0.5 mol of gaseous deuterium in graphite (the mean value for the above temperature range); P_{D_2} and $P^{\circ}_{D_2}$ are equilibrium and standard pressures of gaseous molecular deuterium at a specific temperature (expressed in Pa), respectively; $P^{\circ}_{D_2} = 1$ Pa.

Making use of the results obtained elsewhere [177, 179, 180] we can show that the expression (1) corresponds to the approximations of the ideal gas phase (hydrogen, deuterium) and the ideal solid solution, for which the infinitely dilute solution ($x^{\circ} \to 0$) can be taken as the standard state. Appropriateness of the approximation for the gas phase (within the temperature and pressure ranges of interest) can be verified using the semi-empirical equations of states for hydrogen.[1, 183] The applicability of the aforementioned approximation for the solid phase (*i.e.*, graphite and carbon nanomaterials) as well as effects of internal stresses and local deformations,[154, 184–187] which emerge upon dissolution of the gas in an inhomogeneous (defect-rich) solid phase, on the apparent solubility of the gas will be considered in the following sections as a part of the experimental data analysis.

Let us first consider the process of deuterium desorption from samples of isotropic graphite with a thickness of 1 mm. In the case of samples of isotropic graphite exposed to deuterium at $P_{D_2} = 60$ kPa and $T = 1173$ K (samples A) or 973 K (samples B) for 5 h, the temperature-programmed desorption curves (TPD) for a heating rate of $\upsilon = 0.17$ K s^{-1} manifest [63, 181] three peaks ‡ (Fig. 8) centred at $T_I \approx 445$ K, $T_{II} \approx 727$ K and $T_{III} \approx 1239$ K and at $T_I \approx 445$ K, $T_{II} \approx 760$ K and $T_{III} \approx 1193$ K for the samples A and B, respectively.

‡ However, one more peak *IV* ($T_{IV} \approx 973$ K) can be revealed, which is especially distinct for the samples deuterated at 673 K and 1173 K (Fig. 8). Also note that two peaks around T_I can be resolved for the samples deuterated at 673 K.

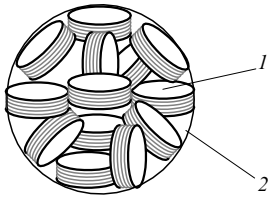

Figure 7. A model of a spherical granule of isotropic graphite [182] composed of independent crystallite grains.
(*1*) A crystallite grain, (*2*) a granule of isotropic graphite.

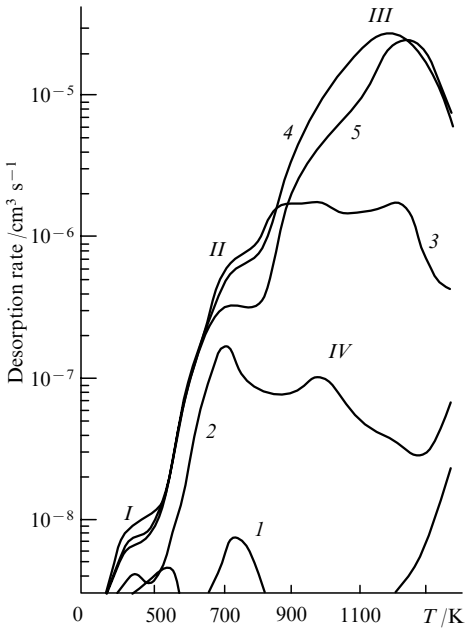

Figure 8. Temperature-programmed desorption of deuterium from isotropic graphite hydrogenated at different temperatures (curves *1* – *5*) (60 kPa, 5 h).[181]
Hydrogenation temperature /K: 473 (*1*), 673 (*2*), 773 (*3*), 973 (*4*) and 1173 (*5*) (for assignment of the TPD peaks *I*–*IV*, see text).

It was suggested [63, 181] that the peak *I* is due to desorption of deuterium molecules adsorbed on the surface of graphite granules, the peak *II* is due to deuterium molecules adsorbed on the surface of crystallite grains and the peak *III* is due to deuterium atoms absorbed (dissolved) in the crystallite grains. This assignment was based on the TPD data [181] obtained for isotropic graphite deuterated at 973 K, which showed that the amount of deuterium (x) desorbed during stages *I* and *II* was proportional to P_{D_2} whereas that desorbed during stage *III* was proportional to $(P_{D_2})^{1/2}$.

Furthermore, the amount of deuterium desorbed from the samples deuterated at 973 K and 60 kPa in the region corresponding to T_{III} was of the same order of magnitude as the equilibrium solubility ($x_{III} \approx 0.6\,x$); the amount of deuterium desorbed in the regions corresponding to T_{II} and T_I was smaller by two and four orders of magnitude, respectively. The equilibrium bulk solubility of deuterium in graphite was achieved only for the samples deuterated at 1173 K and 60 kPa (Fig. 8):[181] $x_{III} \approx x$, $x_{IV} \approx 1.1\times10^{-1}\,x$, $x_{II} \approx 1.5\times10^{-2}\,x$, $x_I \approx 3\times10^{-4}\,x$.

Taking into account that the position of the peak *II* (T_{II}) shifts depending on the thickness of the sample from 760 K (for a sample with a thickness of 1 mm) to 710 K (for a thinner sample with a thickness of $l = 0.45$ mm), annealing of the samples at 573–1173 K has a stepwise character and x_{II} linearly depends on P_{D_2}, Atsumi *et al.*[181] suggested that the peak *II* is due to one-dimensional diffusion of deuterium molecules from the adsorbed nanolayers on the surface of crystallite grains along the nanolayers towards the free external surface of the sample.

The diffusion coefficient as a function of temperature obeys the Arrhenius equation [181]

$$D_{II} = (D_0)_{II}\exp\left(-\frac{Q_{II}}{RT}\right)$$

with a preexponential factor $(D_0)_{II} = 1800$ cm^2 s^{-1} and an activation energy $Q_{II} = 120\pm5$ kJ mol^{-1}.

Taking into account that the peak *III* (in contrast to the peak *II*) does not shift with a decrease in the thickness of graphite samples, annealing of the samples has a stepwise character, x_{III} is proportional to $(P_{D_2})^{1/2}$ (see Ref. 181) and other experimental evidence, in particular, parameters of the bulk diffusion of hydrogen in graphite [188] and data on the sizes of polycrystalline granule grains (r_{gg}) and crystallite grains within these granules (r_{cg}),[108, 181, 182, 189] one may assume that the peak *III* is due to bulk diffusion (*i.e.*, diffusion occuring between the graphene sheets) of deuterium atoms dissolved in graphite crystallite micrograins towards the nearest boundaries of these grains. Temperature dependence of the diffusion coefficient D^*_{III} of hydrogen atoms in crystallite grains of isotropic graphite corrected as compared to the value given by Atsumi *et al.*[181] (see Ref. 188) can be represented in the following form:

$$D^*_{III} = (D^*_0)_{III}\exp\left(-\frac{Q_{III}}{RT}\right),$$

where $(D^*_0)_{III} \approx 3\times10^{-3}$ cm^2 s^{-1}, $Q_{III} = 250\pm10$ kJ mol^{-1}.

It should be stressed that in Ref. 188 (in contrast to Ref. 181) the diffusion coefficient was determined from the experimental data on the characteristic length of diffusion path. Therefore, we find it appropriate to correct the preexponential factor $(D_0)_{III} = 1.7$ cm^2 s^{-1} given in Ref. 181 using the data from Ref. 188. The uncorrected former value corresponds to a mean radius of the polycrystalline granule rather than the crystallite grains. The corrected $(D^*_0)_{III}$ is given by the following formula: $(D^*_0)_{III} = (D_0)_{III}\,(r_{cg}/r_{gg})^{1/2}$.

The characteristic length of diffusion path travelled by a deuterium molecule (L_{II}) corresponding to the peak *II* can be estimated using the following expression:

$$L_{II} \approx (D_{II}\,t)^{1/2} \approx \left(\frac{D_{II}\Delta T_{II}}{\upsilon}\right)^{1/2}, \qquad (2)$$

where $D_{II} = 4.3\times10^{-6}$ cm^2 s^{-1} (for $T_{II} = 727$ K); $t = \Delta T_{II}/\upsilon$ is the diffusion time [$\Delta T_{II} \approx 182$ K is the full width at half maximum of peak *II* (Fig. 8); $\upsilon = 0.17$ K s^{-1} (see Ref. 181)].

Substitution of these values for D_{II} and ΔT_{II} in Eqn (2) gives rise to the value of L_{II}, which agrees with the thickness of the samples (l)§ reported in Ref. 181. In this case, one may consider that the characteristic length of diffusion path (L) was determined experimentally based on the dependence of T_{II} on l.[181]

The apparent sizes of crystallite grains in polycrystalline granules, which correspond to the characteristic length of diffusion path travelled by deuterium atoms from a crystallite grain to its surface (peak *III*), can be estimated using the following expression:

$$L_{III} \approx r_{cg} \approx \left(\frac{D^*_{III}\Delta T_{III}}{\upsilon}\right)^{1/2}, \qquad (3)$$

where $D^*_{III} \approx 1\times10^{-13}$ cm^2 s^{-1} (for $T_{III} = 1239$ K), $\Delta T_{III} \approx 210$ K is the full width at half maximum of the peak *III*. The value of $r_{cg} \approx 0.1$ μm calculated in this way is in accord with the experimental data [108, 182] on the sizes of crystallite grains. These values of structural parameters $r_{cg} \approx 0.1$ μm and $r_{gg} \approx 2$ μm (from Ref. 189) are used below in the analysis and interpretation of the results by Atsumi *et al.*[181]

According to thermodynamic data (for $T \approx 1200$ K), experimental data on equilibrium solubility of deuterium in graphite [$x \approx x_{III} \sim (P_{D_2})^{1/2}, \Delta H$] [181] and diffusion parameters corresponding to the peak *III* [Q_{III}, $(D^*_0)_{III}$, L_{III}], the process of dissolution of gaseous molecular deuterium in graphite crystallite grains can be represented with the following scheme (dissociative chemisorption):[63, 181]

$$0.5\,D_2(\text{gas}) \rightleftharpoons D - 224\ \text{kJ mol}^{-1}, \qquad (4)$$

$$D \longrightarrow D(\text{gr.latt.}), \qquad (5)$$

$$D(\text{gr.latt.}) + C(\text{gr.ch.c.}) \rightleftharpoons DC(\text{gr.abs.}), \qquad (6)$$

$$0.5\,D_2(\text{gas}) + C(\text{gr.ch.c.}) \longrightarrow DC(\text{gr.abs.}) + 19\ \text{kJ mol}^{-1}, \qquad (7)$$

where D is a deuterium atom on the surface of a crystallite grain; D(gr.latt.) is a deuterium atom in the graphite lattice (away from chemisorption centres); C(gr.ch.c.) is an internal carbon chemisorption centre for deuterim in the graphite lattice capable of forming a chemisorbed complex DC; DC(gr.abs.) is a deuterim atom absorbed in the graphite lattice. The total process (7) is characterised by an enthalpy change $\Delta H_{(7)III} = \Delta H \approx -19$ kJ mol^{-1}.

The law of mass action for the reaction (7)

$$K_{III} = \frac{x_{III}/(x_{III})_{max}}{(P_{D_2}/P^\circ_{D_2})^{1/2}[1 - x_{III}/(x_{III})_{max}]} \qquad (8)$$

is transformed into the Sieverts–Langmuir adsorption isotherm:[177, 179]

$$\frac{x_{III}}{(x_{III})_{max}} = \frac{K_{III}(P_{D_2}/P^\circ_{D_2})^{1/2}}{1 + K_{III}(P_{D_2}/P^\circ_{D_2})^{1/2}}, \qquad (9)$$

where equilibrium constant (K_{III}) for the reaction (7) is given by:

$$K_{III} = \exp\left(\frac{\Delta S}{R}\right)\exp\left(-\frac{\Delta H}{RT}\right). \qquad (10)$$

Here, $(x_{III})_{max}$ denotes the maximum possible D/C ratio (or the fraction of internal chemisorption centres), $\Delta H = \Delta H_{(7)III} \approx -19$ kJ mol^{-1}, $\Delta S = \Delta S_{(7)III}$ is the standard change of entropy

§ A similar value $L_{II} \approx l$ is obtained if the diffusion problem is reformulated to an isothermal case (using the value of Q_{II} from Ref. 181).[190, 191]

for the reaction (7). If $x_{III} \ll (x_{III})_{max}$, Eqns (8)–(10) are transformed into the expression (1), *i.e.*, the Sieverts isotherm.

As follows from Eqns (1) and (8)–(10), $(x_{III})_{max} \exp(\Delta S/R) \approx 2 \times 10^{-7}$. For the ultimate (carbohydride) values of concentration $(x_{III})_{max} = 0.5$ (or 1.0),[146] $\Delta S/R \approx -14.7$ (or -15.4), which means that $\Delta S = \Delta S_{(7)III} \approx -122$ (or -128) J K^{-1} mol^{-1} [the latter value is close to the values of ΔS known for reactions similar to (7), see reference books [192–194]]. Within this approximation, the standard enthalpy ($\Delta H_{(7)III}$) and entropy ($\Delta S_{(7)III}$) of absorption for the reaction (7) are independent of the concentration of absorbed deuterium. Note that in this case, it is the concentrated solution ($x^{\circ}/x_{max} = 0.5$) that can be chosen as the standard state for the solid phase, then $\Delta H_{(7)III}$ and $\Delta S_{(7)III}$ in the expression (10) are constants.[177, 179]

Assuming that dissolution of deuterium atoms in the graphite lattice without involvement of chemisorption centres in stage (5) does not modify the enthalpy of the system [*i.e.*, $\Delta H_{(5)III} \approx 0$], the value of enthalpy determined from Eqns (4)–(7) is $\Delta H_{(6)III} \approx -243$ kJ mol^{-1}.

The factors essential for understanding of the mechanism underlying deuterium dissolution in crystallite grains are listed below:

— The calculated value of $\Delta H_{(6)III}$ is close in absolute value to the activation energy of bulk diffusion of deuterium atoms through the graphite crystallite grains but has the opposite sign ($Q_{III} = 250$ kJ mol^{-1}) (see Refs. 181, 188).

— The value of $\Delta H_{(6)III}$ is close to the energy of interaction of hydrogen atoms with the external surface of nanotubes belonging to types (5,5), (10,10), (10,0) and (9,0) calculated using the DFT method.[146, 147]

— The value of $\Delta H_{(6)III}$ is by 48 kJ mol^{-1} larger than the energy of interaction of hydrogen atoms with the graphene surface calculated using the DFT method [195] and the energy of hydrogen sorption on the basal plane of graphite according to the model F (Fig. 9, $\Delta H_F = -195$ kJ mol^{-1}) calculated using the *ab initio* molecular orbitals method.[163] Presumably, the discrepancies between the experimental and theoretical values of $\Delta H_{(6)III}$ are related to large errors associated with theoretical determination of the C–H bonding energy.

Furthermore, estimates for the chemisorption energy of hydrogen on the (0001) basal plane of graphite (models E and F) and on cleaved C–C bonds at (1010) zigzag-like (models D and H) and (1121) chair-like (models C and G) side planes of graphite (Fig. 9)¶ are available, which are sufficiently accurate and can be used to rationalise some parameters of the sorption processes corresponding to peaks *I*–*IV* (see Fig. 8).†

The aforementioned data clearly indicate that both bulk dissolution of D_2 and bulk diffusion of deuterium atoms through the crystallite grains of isotropic graphite (peak *III* in Fig. 8) contribute to the dissociative chemisorption of deuterium on active carbon sites with the absorption enthalpy of $\Delta H_{(abc)III} = \Delta H_{(6)III} \approx -Q_{III}$.

A model [177] of diffusion of hydrogen atoms through the graphite lattice accompanied by reversible capture of the diffusant by internal carbon chemisorption centres yields similar values of the thermodynamic ($\Delta H_{(6)III}$) and kinetic ($-Q_{III}$) parameters of the hydrogen absorption process. In this case, the diffusion activation energy is consumed predominantly to cleavage of the chemisorption bonds formed by the diffusant.

It might be assumed [63] that sorption of two hydrogen atoms on two adjacent centres on the basal plane (model F) generates

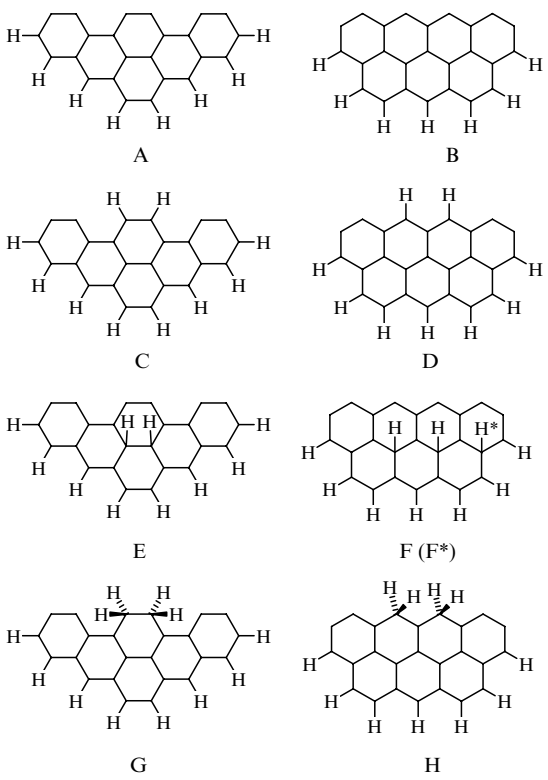

Figure 9. Models of hydrogen chemisorption on graphite (for description of the models, see text).[163]

new potential chemisorption centres for the next hydrogen atoms (third, fourth, *etc.*) on proximate carbon atoms of the graphene layer (model F*, Fig. 9). The energy of chemisorption for the additional hydrogen atoms on adjacent carbon atoms of the graphene layer (model F*) is likely characterised by a value similar to ΔH_F. For the model F*, according to results of Ref. 146 (sample No. 13, Table 2), $(x_{III})_{max} \approx 0.5$ [or $(x_{III})_{max} \approx 1.0$, if both sides of a graphene layer are considered]. The validity of such a model is justified by experimental data on the realisation of a high content of hydrogen isotopes in implanted graphite layers in the case of a-C : H-films (H/C $\approx 0.5-0.7$) [108, 109] and fullerites (H/C $\approx 0.6-0.95$).[19, 103]

Taking into account that the C–H (C–D) chemical bonds are characterised by saturability, directionality and localisation, it might be assumed that the expressions (8) and (9) can remain valid even for deuterium concentrations approaching the ultimate carbohydride values $(x_{III})_{max} \approx 0.5$ (or 1.0). An analysis of the experimental data on the amount of hydrogen isotopes absorbed in nanocrystalline graphite synthesised mechanochemically (see Section IV.6),[27, 29, 30] and on the hydrogen content in graphite nanofibres (see Section IV.9) [32, 33, 196] support the applicability of the model of chemisorption centres and ultimate concentrations $(x_{III})_{max}$ corresponding to a specific bulk carbohydride phase (H/C = 0.5–1.0) [146] to the description of hydrogen sorption by these materials.

Within the model [177] of bulk diffusion of deuterium (hydrogen) atoms through the graphite lattice accompanied by reversible capture of the diffusant by internal chemisorption centres [provided that the predominant fraction of the diffusant is localised in the absorption centres and $x_{III}/(x_{III})_{max} \ll 1$], the apparent diffusion coefficient (D^*_{III}) and activation enthalpy (energy) (Q_{III}) can be written as:

$$D^*_{III} \approx \frac{AD_{latt}}{K_{(6)III}}, \qquad (11)$$

¶ The model A in Fig. 9 corresponds to the basal plane with empty chair-like edge centres, the model B corresponds to the basal plane with empty zigzag-like edge centres.

† A comparison of the experimental values of ΔH (for peaks *I*–*IV*) with the theoretical values of E_{ad} makes it possible the most appropriate model (models C–H, Fig. 9) for description of the sorption process attributed to specific TPD peaks.

$$Q_{III} \approx Q_{\text{latt}} - \Delta H_{(6)III}, \quad (12)$$

where A = const, D_{latt} and Q_{latt} are the diffusion coefficient and the activation enthalpy (energy) for the diffusion of deuterium (hydrogen) atoms through the graphite lattice in the absence of capturing chemisorption centres, respectively; $K_{(6)III}$ is the equilibrium constant of the reaction (6) as applied to peak *III*. Here,

$$D_{\text{latt}} \approx (D_0)_{\text{latt}} \exp\left(-\frac{Q_{\text{latt}}}{RT}\right),$$

$$K_{(6)III} \approx B \exp\left(-\frac{\Delta H_{(6)III}}{RT}\right),$$

where $(D_0)_{\text{latt}}$ and B are preexponential factors.

The activation energy of diffusion of hydrogen atoms in nanostrucured graphite was estimated both experimentally [28] for a temperature range of 300–425 K ($Q_{\text{exp}} \approx 9.6$ kJ mol^{-1}) and theoretically [197] ($Q_{\text{theor}} \approx 1.5$ kJ mol^{-1}). The diffusion activation energy (Q) can be characterised by that small value only if the chemisorption centres are either absent or almost completely occupied, *i.e.*, if $Q = Q_{\text{latt}}$. Provided that Q_{latt} acquires such a value, the activation energy of diffusion of deuterium atoms through the graphite lattice [the expression (12)] approaches the enthalpy of desorption of deuterium atoms from graphite, *i.e.*, $Q_{III} \approx -\Delta H_{(6)III} = -\Delta H_{(\text{abs})III}$.

Taking into account the linear dependence of x_{II} on P_{D_2} and values of Q_{II} (as reported in Ref. 181), it might be assumed that the diffusion processes of deuterium sorption on graphite [181] associated with peak *II* are described by the following reactions:

$$D_2(\text{gas}) \longrightarrow D_2(\text{graph.}), \quad (13)$$

$$D_2(\text{graph.}) \rightleftharpoons 2D(\text{graph.}), \quad (14)$$

$$2D(\text{graph.}) + C(\text{ch.c.}) \rightleftharpoons D_2C(\text{ads.}), \quad (15)$$

$$D_2(\text{gas}) + C(\text{ch.c.}) \longrightarrow D_2C(\text{ads.}), \quad (16)$$

where D_2(graph.) and D(graph.) denote, respectively, a deuterium molecule or atom on the surface of graphite crystallite grains (away from chemisorption centres); C(ch.c.) is a carbon chemisorption centre that binds two deuterium atoms in graphite (potential formation of a D_2C complex) localised at the surface of the crystallite grains; D_2C(ads.) is a couple of deuterium atoms adsorbed on a carbon centre on the surface of the crystallite grains.

Our analysis shows that in many cases the rate of the first stage (13) of the process is diffusion-limited.

There is some evidence (see Refs 28, 197) suggesting that the activation energy for diffusion of deuterium molecules becomes negligibly small as compared to Q_{II} in the absence of chemisorption centres on the surface of crystallite grains.[181] In such a case, the apparent activation enthalpy (energy) for the diffusion of deuterium molecules along the surface of graphite crystallite grains (Q_{II}) should be similar to the standard change of enthalpy for the desorption of deuterium molecules from the surface of crystallite grains, which is the thermodynamic characteristics of a reaction reversed with respect to the reaction (16).

$$\Delta H_{(\text{ads})II} = \Delta H_{(16)II} \approx -Q_{II} = -120 \text{ kJ mol}^{-1}.$$

A similar situation is typical, for instance, of gas chromatography.[198]

The standard change of enthalpy for the reaction (14) at a temperature close to T_{II} can be written as $\Delta H_{(14)} \approx 2\Delta H_{(4)} \approx 450$ kJ mol^{-1} (see Refs 192–194), whereas the standard change of enthalpy for the reaction (15) can be written as $\Delta H_{(15)II} = \Delta H_{(16)II} - \Delta H_{(14)} - \Delta H_{(13)II} \approx -570 \pm 8$ kJ mol^{-1} [provided that $\Delta H_{(13)II} \approx 0$]. The experimentally measured value of $\Delta H_{(15)II}$ is similar to the theoretical value of energy of chemisorption of two hydrogen atoms on a zigzag-like edge carbon centre: $\Delta H_{\text{H}} = -540$ kJ mol^{-1} (model H, Fig. 9).[163] Taking into account that a zigzag-like edge carbon centre cannot adsorb an H_2 molecule, a scheme describing the process of chemisorption of two hydrogen atoms on such a centre should include stages (14) and (15), which correspond to a dissociative-associative adsorption.

The enthalpy of adsorption of deuterium molecules in intergranule nanoareas of graphite can be estimated from the experimental dependence of the area under the peak *I* (that is respective concentration) on deuteration temperature (1173 K and 973 K, Fig. 8) using the Henry adsorption isotherm equation.[181] The standard change of enthalpy for the reaction (16) as applied to the peak *I* is $\Delta H_{(16)I} = \Delta H_{(\text{abc})I} \approx -20 \pm 5$ kJ mol^{-1}, whereas the standards change of enthalpy for the reaction (15) is $\Delta H_{(15)I} = \Delta H_{(16)I} - \Delta H_{(14)} - \Delta H_{(13)I} \approx -465 \pm 7$ kJ mol^{-1} [provided that $\Delta H_{(14)} \approx 445$ kJ mol^{-1} (see Refs 192–194) and $\Delta H_{(13)I} \approx 0$]. The value of $\Delta H_{(15)I}$ obtained in this way is close to the theoretical value of energy of chemisorption of two hydrogen atoms on a chair-like edge carbon centre, which is $\Delta H_{\text{G}} = -480$ kJ mol^{-1} (model G, Fig. 9).[163] Taking into account that the chair-like centre cannot adsorb an H_2 (or D_2) molecule, the stages (14) and (15), which correspond to a dissociative-associative adsorption, should be included in the total chemisorption process.

Probably, any two nearest carbon atoms of graphene layers located at the surface of granules can also act as adsorption centres. Chemisorption of two hydrogen atoms on such a centre is characterised by an energy change of $\Delta H_{\text{F}} = -390$ kJ mol^{-1} (model F, Fig. 9),[163] which is in reasonable agreement with the experimental value of $\Delta H_{(15)I}$.‡ Formally, these centres correspond to potential chemisorbed complexes D_2C_2 (or H_2C_2). Taking this into account, Eqn (15) should be rewritten as:

$$2D(\text{graph.}) + 2\,C(\text{ch.c.}) \rightleftharpoons D_2C_2(\text{ads}). \quad (15a)$$

Since $T_I \ll T_{II}$ and processes associated with peaks *I* and *II* are characterised by identical lengths of diffusion path (L = 1 mm), it might be expected that [according to Eqn (2)] $Q_I < Q_{II}$.[181] The value of Q_I should be close to the standard change of enthalpy of desorption of deuterium molecules from the surface of granules, *i.e.*, $Q_I \approx \Delta H_{(\text{desorb})I} = -\Delta H_{(16)I} \approx 20$ kJ mol^{-1}. Within this formalism, the peak *I* corresponds to diffusion transfer of deuterium molecules from the surface of granules to the external surface of the sample accompanied by their reversible capture by carbon chemisorption centres (to form complexes D_2C or D_2C_2) in nanocavities between granules. The following equations can be applied to calculate the apparent diffusion coefficient of deuterium molecules (D_I) and effective solubility of deuterium ($x_I \approx$ D/C, where C is the total number of carbon atoms in the sample) on the surface of granules:

$$D_I = (D_0)_I \exp\left(-\frac{Q_I}{RT}\right) \approx \frac{AD_{\text{surf}}}{K_{(16)I}}, \quad (17)$$

$$x_I \approx 6\,\frac{\Delta r_I}{r_{\text{gg}}} x_{D_2 I}, \quad (18)$$

$$Q_I \approx -(\Delta H_{(14)I} + \Delta H_{(15)I}) \approx -\Delta H_{(16)I}, \quad (19)$$

$$K_{(16)I} = \frac{x_{D_2 I}/(x_{D_2 I})_{\max}}{(P_{D_2}/P^{\circ}_{D_2})[1 - x_{D_2 I}/(x_{D_2 I})_{\max}]}, \quad (20)$$

$$K_{(16)I} = \exp\left(\frac{\Delta S_{(16)I}}{R}\right)\exp\left(-\frac{\Delta H_{(16)I}}{RT}\right). \quad (21)$$

Here, A = const, D_{surf} is the diffusion coefficient of hydrogen molecules within the surface layer of granules in the absence of chemisorption centres, Δr_I is the effective thickness of the chem-

‡ A similar conclusion was derived from a comparison of the theoretical values of ΔH_{ads} (the models F and F*, Fig. 9) with the experimental values of $\Delta H_{(6)III}$.

isorbing layer on the surface of granules, $x_{D_2 I}$ is the local concentration of D_2 molecules (the ratio D_2/C^*, where D_2 and C^* are numbers of D_2 molecules and carbon atoms in the chemisorbing layer, respectively) on the surface of granules, $(x_{D_2 I})_{max}$ is the maximum concentration of D_2 molecules, $\Delta H_{(14)I}$ and $\Delta H_{(15)I}$ are the standard changes of enthalpy for the reactions (14) and (15), respectively, $\Delta H_{(16)I}$ and $\Delta S_{(16)I}$ are the standard changes of enthalpy and entropy for the reaction (16), respectively, $K_{(16)I}$ is the equilibrium constant for the reaction (16). The equation (20) represents the Henry–Langmuir adsorption isotherm. In the proximity of T_I ($T_I \approx 445$ K), the condition $D_I \approx L_I^2 \upsilon/\Delta T_I$ is met [equation similar to (2)], where $L_I \approx l = 1$ mm (the thickness of the samples).[181] If $x_{D_2 I}/(x_{D_2 I})_{max} \ll 1$, Eqn (20) is reduced to the Henry adsorption isotherm equation.

Substituting $Q_I \approx 20$ kJ mol^{-1} in Eqn (17) and using the expression $D_I \approx L_I^2 \upsilon/\Delta T_I$, one gets $(D_0)_I \approx 3 \times 10^{-3}$ cm^2 s^{-1}.

In order to estimate $x_{D_2 I}$ in the samples of isotropic graphite[181] after their exposure to hydrogen at $P_{D_2} = 60$ kPa and $T = 1173$ K, one can utilise the experimental value of $x_I(D/C) \approx 3 \times 10^{-4} x = 1.0 \times 10^{-7}$. Provided that $r_{gg} \approx 2$ μm and $\Delta r_I \approx$ 0.3 nm, Eqn (18) gives rise to the value $x_{D_2 I} \approx 1.3 \times 10^{-4}$. Within the model G (Fig. 9) for sorption complexes D_2C corresponding to the peak I,[181] it can be taken that $(x_{D_2 I})_{max} \approx 0.5$. Substituting $\Delta H_{(16)I} \approx -20$ kJ mol^{-1} in Eqns (20) and (21), one gets $\Delta S_{(16)I} \approx -180$ J K^{-1} mol^{-1} [the latter value is typical of chemical reactions similar to (16)[192–194]]. It might be assumed that for the D_2C_2 centres of type F (Fig. 9) at $(x_{D_2 I})_{max} \approx 0.25$, $\Delta S_{(16)I} \approx -170$ J K^{-1} mol^{-1}.

The respective expressions for the desorption process corresponding to the peak II can be written as:

$$D_{II} = (D_0)_{II} \exp\left(-\frac{Q_{II}}{RT}\right) \approx \frac{A' D'_{surf}}{K_{(16)II}}, \quad (22)$$

$$x_{II} \approx 6 \frac{\Delta r_{II}}{r_{cg}} x_{D_2 II}, \quad (23)$$

$$Q_{II} \approx -(\Delta H_{(14)II} + \Delta H_{(15)II}) \approx -\Delta H_{(16)II}, \quad (24)$$

$$K_{(16)II} = \frac{x_{D_2 II}/(x_{D_2 II})_{max}}{(P_{D_2}/P^{\circ}_{D_2})[1 - x_{D_2 II}/(x_{D_2 II})_{max}]}, \quad (25)$$

$$K_{(16)II} \approx \exp\left(\frac{\Delta S_{(16)II}}{R}\right) \exp\left(-\frac{\Delta H_{(16)II}}{RT}\right), \quad (26)$$

where respective parameters have similar physical meanings to those in the formulas (17)–(21) but correspond to peak II and $\Delta H_{(16)II} \approx -Q_{II} = -120$ kJ mol^{-1}.

Using the experimental value $x_{II} \approx 1.5 \times 10^{-2} x = 5.2 \times 10^{-6}$ and assuming that $r_{cg} \approx 0.1$ μm and $\Delta r_{II} \approx 0.3$ nm, one gets from Eqn (23) that $x_{D_2 II} \approx 4.0 \times 10^{-4}$. Similarly, using the values $\Delta H_{(16)II} \approx -120$ kJ mol^{-1} and $(x_{D_2 II})_{max} \approx 0.5$, one gets from Eqns (25) and (26) that $\Delta S_{(16)II} \approx -250$ J K^{-1} mol^{-1}.

According to our analysis, parameters of sorption and diffusion of deuterium in isotropic graphite,[181] which correspond to the peak IV (Fig. 8) are in satisfactory agreement with the respective parameters of sorption and diffusion of tritium in pyrolytic graphite§ (data from the review by Causey[109]).

In particular, the apparent enthalpy of activation of tritium diffusion[109] ($Q = 365 \pm 50$ kJ mol^{-1}) is close in absolute value (but opposite in sign) to the theoretical value of energy of chemisorption of a hydrogen atom on a chair-like ($\Delta H_C = -360$ kJ mol^{-1}, model C, Fig. 9)[163] or zigzag-like ($\Delta H_D = -380$ kJ mol^{-1}, model D, Fig. 9) edge carbon centre. The experimentally measured value of tritium dissolution enthalpy[109] ($\Delta H \approx -140$ kJ mol^{-1}) is close to the value of ΔH calculated for the reactions (4)–(7) based on the models C and D assuming that $\Delta H_{(4)} \approx 228$ kJ mol^{-1}: $\Delta H = \Delta H_{(7)IV} \approx \Delta H_{(4)} + \Delta H_{C(D)} \approx -132$ kJ mol^{-1} and -152 kJ mol^{-1} for the models C and D, respectively (see Refs 192–194). Thus, the experimental results[109] can be interpreted on the basis of Eqns (4)–(12) for the chemisorption centres belonging to types C and D (Fig. 9).

Assuming that the experimental data[181] corresponding to the peak IV (Fig. 8) for isotropic graphite can be described in a similar way, one can write:

$$\Delta H_{(7)IV} \approx \Delta H_{(4)} + \Delta H_{(6)IV}, \quad (27)$$

$$Q_{IV} \approx Q_T \approx -\Delta H_{(6)IV} \approx -\Delta H_C \approx -\Delta H_D, \quad (28)$$

where $\Delta H_{(7)IV}$ and $\Delta H_{(6)IV}$ are the standard enthalpy changes for the reactions (7) and (6) as applied to peak IV (Fig. 8); Q_{IV} is the apparent activation enthalpy (energy) for the diffusion process.

The effective diffusion coefficient of deuterium (tritium) atoms in graphite corresponding to the peak IV can be calculated according to the following equation:

$$D_{IV} \approx D_T = (D_0)_{IV} \exp\left(-\frac{Q_{IV}}{RT}\right),$$

where $(D_0)_{IV} \approx 620$ cm^2 s^{-1}, $Q_{IV} \approx Q_T \approx 365$ kJ mol^{-1} (data from Ref. 109).

For the graphite samples,[181] the desorption peak IV is characterised by the following values of parameters (Fig. 8): $T_{IV} \approx 973$ K, $\Delta T_{IV} \approx 140$ K, $x_{IV} \approx 0.11x \approx 3 \times 10^{-5}$. Substituting these values into the equation

$$L_{IV} \approx \left(\frac{D_{IV} \Delta T_{IV}}{\upsilon}\right)^{1/2}$$

it is possible to estimate the characteristic length of diffusion path of deuterium atoms ($L_{IV} \approx 1$ nm).

Sorption and diffusion parameters of the process corresponding to the peak IV are described by equations analogous to Eqns (8)–(12) for the peak III, thus giving rise to

$$\Delta S = \Delta S_{(7)IV}, \Delta H = \Delta H_{(7)IV} \approx -140 \text{ kJ mol}^{-1},$$

$$\Delta H_{(6)IV} \approx \Delta H_{C(D)} \approx -370 \text{ kJ mol}^{-1},$$

$$x_{IV} \approx \left(\frac{3 L_{IV}}{r_{cg}}\right) x_{DIV},$$

where x_{DIV} is the local concentration of deuterium atoms (D/C) absorbed in the graphite layer with the thickness L_{IV} in the proximity of boundaries of the crystallite grains, $(x_{DIV})_{max} \leqslant 0.5$.

It should be noted that the parameters calculated in this way for the peak IV (Fig. 8) require further refinement. However, even within the current approximation they give satisfactory explanation for the abrupt slowing-down of the diffusion process[181] upon isothermal deuteration of isotropic graphite at 473–773 K and 60 kPa as compared to the rate of deuterium desorption upon annealing of the samples hydrogenated at 973–1173 K extrapolated to the respective temperatures (Fig. 8).

In order to refine the parameters of the TPD peaks I–IV (Fig. 8) it would be reasonable to analyse a large array of the experimental data on sorption and diffusion of hydrogen in various graphite materials including graphite layers ion-implanted with hydrogen followed by neutron irradiation and a-C : H films.[108, 109]

Typically, absorption of hydrogen in graphite, *i.e.*, dissolution of hydrogen atoms in the graphite lattice (a bulk phenomenon) is contrasted[100] to hydrogen chemisorption on cleaved σ-bonds on the surface of the crystal, grain boundaries and dislocations

§ Pyrolytic graphite is routinely synthesised by pyrolysis of hydrocarbons. Depending on the experimental conditions and composition of the starting gas, crystals with different sizes and orientations can be prepared.

Table 3. Basic results of the analysis of data on sorption and diffusion of hydrogen (deuterium) in isotropic [181] and pyrolytic [109] graphites.

Experimental data (Fig. 8)	Models of		Reactions	Parameters of processes		Equations used for the calculations	Type of the adsorption isotherm
	sorption (Fig. 9)	diffusion		sorption	diffusion		
Peak *III*	Dissociative chemisorption (model F*)	Diffusion of deuterium atoms through the crystallite grains	(4)–(7)	$\Delta H = \Delta H_{(7)III} \approx -19$ kJ mol^{-1}, $\Delta S/R \approx -14.7$ (-15.4) for $(x_{III})_{max} = 0.5$ (1.0)	$(D_0^*)_{III} \approx 3 \times 10^{-3}$ cm^2 s^{-1}, $Q_{III} \approx$ 250 kJ mol^{-1}	(3), (8)–(12)	Sieverts–Langmuir [Eqns (8), (9)]
Peak *II*	Dissociative–associative chemisorption (model H)	Diffusion of deuterium molecules along the boundaries of the crystallite grains	(13)–(16)	$\Delta H_{(16)II} \approx -120$ kJ mol^{-1}, $\Delta S_{(16)II}/R \approx -30.0$ for $(x_{D_2II})_{max} = 0.5$	$(D_0)_{II} \approx$ 1800 cm^2 s^{-1}, $Q_{II} \approx$ 120 kJ mol^{-1}	(2), (22)–(26)	Henry–Langmuir [Eqn (25)]
Peak *I*	Dissociative-associative chemisorption (models G and/or F)	Diffusion of deuterium molecules along the boundaries of the granules	(13)–(16)	$\Delta H_{(16)I} \approx -20$ kJ mol^{-1}, $\Delta S_{(16)I}/R \approx -21.3$ for $(x_{D_2I})_{max} = 0.5$	$(D_0)_I \approx 3 \times 10^{-3}$ cm^2 s^{-1}, $Q_I \approx$ 20 kJ mol^{-1}	(17)–(21)	Henry–Langmuir [Eqn (20)]
Peak *IV*	Dissociative chemisorption (models C and/or D)	Diffusion of deuterium and tritium atoms through the intergrain nanoregions	(4)–(7)	$\Delta H_{(7)IV} \approx -140$ kJ mol^{-1}	$(D_0)_{IV} \approx$ 620 cm^2 s^{-1}, $Q_{IV} \approx$ 365 kJ mol^{-1}	(27), (28)	Sieverts–Langmuir [Eqns (8), (9)]

(surface phenomena). For this, it should be stressed that the peak *III* for isotropic graphite (see Fig. 8) corresponds to chemisorption of hydrogen atoms on the internal carbon centres located at the graphite ¶ basal planes.

The process of desorption [stage (6)] of single hydrogen (or deuterium) atoms dissolved between the graphene sheets within the graphite crystallite grains [181] corresponding to the peak *III* is not accompanied by abstraction of carbon atoms from the graphene sheets, since the desorption energy of a hydrogen atom [$-\Delta H_{(6)III} \approx 243$ kJ mol^{-1}] is three times smaller than the energy required to abstract a carbon atom from its three carbon neighbours in a graphene layer [$-3/2\,\Delta H_{(C-C)} \approx 730$ kJ mol^{-1}, model F*, Fig. 9].

In the case of peaks *I* and *IV* for graphite,[181] the desorption energy of hydrogen atoms [stages (15) or (6) $-\Delta H_{(15)I} \approx$ 465 kJ mol^{-1} (models G, F) or $-\Delta H_{(6)IV} \approx 370$ kJ mol^{-1} (models C, D)] are also smaller than the energy required to abstract a carbon atom from its neighbours (485 kJ mol^{-1} or 1460 kJ mol^{-1} for the peak *I* and 485 kJ mol^{-1} for the peak *IV*).

The opposite situation is observed in the case of the desorption of two hydrogen (deuterium) atoms adsorbed on the surface of the graphite crystallite grains [stage (15)][181] corresponding to the peak *II*, since the desorption energy of two hydrogen atoms [$-\Delta H_{(15)II} \approx 570$ kJ mol^{-1}, model H, Fig. 9] is larger than the abstraction energy of a carbon atoms from its two neighbours (485 kJ mol^{-1}). In this case, the desorption of hydrogen atoms can be accompanied by abstraction of carbon atoms followed by formation and desorption of hydrocarbon molecules (CH_4, C_2H_4, *etc*.).

* * *

This is supported by mass-spectrometric data,[181] which reveal concomitant liberation of methane (CD_4) from hydrogenated graphite samples. The total amount of liberated methane is three orders of magnitude smaller than the total amount of desorbed deuterium and constitutes ~10% of deuterium desorbed at T_{II}. Liberation of small amounts of hydrocarbons has also been detected in the course of hydrogen desorption from nanostructured graphite and carbon nanofibres (see Sections IV.6 and IV.9).

Thus, the following equation should be utilised in order to determine the effective deuterium (hydrogen) concentration in isotropic graphite [181] hydrogenated at a temperature and exposure sufficiently high to achieve the equilibrium state both inside the crystallite grains and granules and at their boundaries:

$$x_\Sigma(\mathrm{D/C}) = x_I + x_{II} + x_{III} + x_{IV}. \quad (29)$$

Relaxation times (τ_I, τ_{II}, τ_{III}, τ_{IV}) of diffusion processes corresponding to the TPD peaks *I*–*IV* for graphite [181] can be estimated on the basis of D_I, D_{II}, D^*_{III}, D_{IV} and characteristic lengths of diffusion path L_I, L_{II}, L_{III} and L_{IV}.

The major results concerning the analysis and interpretation of data on the sorption of hydrogen in isotropic [181] and pyrolytic [109] graphites are summarised in Table 3. These results are used below to analyse and rationalise some published data on hydrogen sorption by other carbon nanomaterials.

3. High-temperature sorption and diffusion of hydrogen in nanoporous carbon

This section analyses experimental data [67, 199, 200] on high-temperature hydrogen sorption by nanoporous carbon (NPC) composed of graphite-like microfragments joined together by a pyrocarbon binder.

The overall porosity of one of the investigated materials [67] reached ~70% (~40% of porosity was due to nanopores with a mean diameter of ~0.8 nm and the remaining 30% of porosity was due to pores with sizes in the range 0.2–1 μm), specific surface area of this sample (S_{sp}) was ~1200 m^2 g^{-1}.

For the temperature-programmed desorption measurements,[199] samples with a thickness of $l = 1$ mm (exposed to hydrogen at $P_{H_2} = 7.1$ MPa and $T = 523$ K for 3 h) were heated at a rate of $\upsilon = 7.5 \times 10^{-2}$ K s^{-1}. The TPD curves manifest three peaks (Fig. 10) centred at 753 K (peak *I*′), 923 K (peak *II*′) and 1193 K (peak *III*′). The total hydrogen concentration x_Σ in the studied samples was up to 0.16.

The peak *I*′ is comparable in its origin and parameters of the sorption and diffusion processes to those of the peak *II* (Table 3)

¶ Essentially, chemisorption can be involved also in the cases of nanostructured graphite and carbon nanofibres. For high concentrations of chemisorbed hydrogen in such materials, the interlayer separation between graphite layers is substantially increased, which is supported by the experimental X-ray diffraction data (see Sections IV.6 and IV.9).

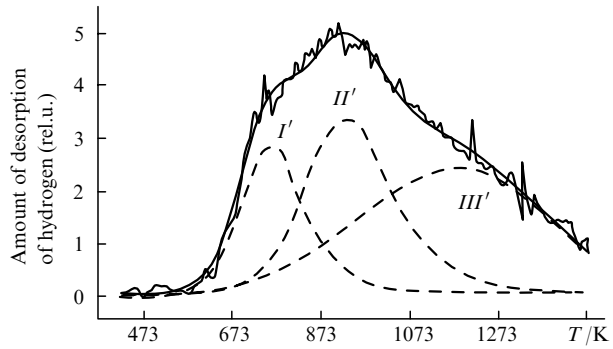

Figure 10. Temperature-programmed desorption of hydrogen from nanoporous carbon hydrogenated at 523 K and P_{H_2} = 7.1 MPa for 3 h (for assignment of the TPD peaks, see text).[199]
The experimental curve shown as a solid line, its components are shown as dashed lines.

for isotropic graphite discussed above.[181] Substitution of the experimental values of $T_{I'}$, $D_{II}(T_{I'})$, υ and $\Delta T_{I'}$ into Eqn (2) yields the length of diffusion path of hydrogen molecules ($L_{I'} \approx 1$ mm), which is in agreement with the thickness of the samples.[199] The hydrogen concentration corresponding to the peak I' [$x_{I'} \approx x_\Sigma(S_{I'}/S_\Sigma) \approx 0.04$] can be described with the expression (23) as well as expressions (25) and (26) (for 523 K and 7.1 MPa). Assuming $x_{II} \approx x_{I'}$ and $\Delta r_{II} \approx 0.3$ nm, the mean size (radius) of a nanograin in the NPC samples can be estimated as $r_{cg} \approx 10$ nm.[199]

The peak II' on the TPD curve for hydrogen desorption from NPC [199] is analogous to the peak *III* (Table 3) for isotropic graphite.[181] The mean size of nanograins for the NPC samples [199] estimated using Eqn (3) is 4 nm ($L_{III'}$) in satisfactory agreement with the aforementioned value of r_{cg}. The concentration of hydrogen corresponding to the peak II' [$x_{II'} \approx x_\Sigma(S_{II'}/S_\Sigma) \approx 0.06$] can be described using the expressions (8)–(10) (for 523 K and 7.1 MPa).

Presumably, the peak III' for NPC (see Ref. 199) is analogous to the peak *IV* (Table 3) for isotropic graphite.[181] Based on the equation similar to (3) and experimental values of $T_{III'}$, $D_{IV}(T_{III'})$, υ and $\Delta T_{III'}$, a value $L_{III'} \approx 190$ nm can be derived, which should characterise the mean linear size of areas of localisation of the corresponding chemisorption centres in the NPC samples.[199]

4. Parameters of hydrogen diffusion in nanostructured pyrolytic graphite

Recently,[68, 69, 201] experimental results on hydrogen thermodesorption from highly oriented pyrolytic graphite [108] exposed to atomic hydrogen at 323–363 K have been reported. This treatment resulted in emergence of surface nanohillocks with heights of 3–5 nm and diameters of 40–75 nm, which can be considered as a sort of nanostructuring of graphite. The nanohillocks disappeared after hydrogen desorption that proceeded as a first-order reaction.[69, 201] Probably, the nanohillocks are formed due to filling of nanocavities with gaseous molecular hydrogen at a high pressure ($P_{H_2} \approx 30$–50 MPa [68]). The TPD measurements (at a heating rate of υ = 25 K s^{-1}) revealed [69, 201] two dominant peaks: a peak α centred at $T_\alpha \approx 1123$ K ($\Delta T_\alpha \approx 180$ K, $S_\alpha/S_\Sigma \approx 0.45$, the activation energy of the process is $Q_\alpha \approx 230$ kJ mol^{-1}) and a peak β centred at $T_\beta \approx 1523$ K ($\Delta T_\beta \approx 250$ K, $S_\beta/S_\Sigma \approx 0.55$, $Q_\beta \approx 385$ kJ mol^{-1}).

The peak α can be attributed to bulk diffusion of hydrogen atoms dissolved in graphite through the nanocavities towards the external free surface of the samples.[68] It should be correlated with the peak *III* for isotropic graphite.[181] The length of the diffusion path (which, in this case, means the width of the nanocavity) is calculated based on Eqn (3), $L_\alpha \approx 4$ nm.

The peak β is analogous to the peak *IV* for isotropic graphite.[181] Using Eqn (3), the length of the diffusion path can be estimated as $L_\beta \approx 300$ nm, this value, effectively, characterises the mean linear size of the areas of localisation of the corresponding chemisorption centres in the samples.[69, 201]

5. Parameters of hydrogen diffusion and sorption in films of nanostructured carbon

Let us now consider experimental data [104, 105] on hydrogen sorption by films of nanostructured carbon prepared using ultrasound-assisted deposition of carbon clusters. The films had porous structures where the size distribution of pores peaked at 3.4 nm and the specific surface area of the samples was 665 m^2 g^{-1} (while volume of the samples was $\sim$0.9 mm^3). The samples hydrogenated at $T \approx 298$ K and P_{H_2} = 100 kPa revealed two dominant peaks in TPD (measured with a heating rate of υ = 0.33 K s^{-1}) with the following characteristics: peak α ($T_\alpha \approx 513$ K, $\Delta T_\alpha \approx 220$ K, $x_\alpha \approx 6 \times 10^{-2}$) and peak γ ($T_\gamma \approx 970$ K, $\Delta T_\gamma \approx 150$ K, $x_\gamma \approx x_\alpha$).

These values assume that peaks α and γ for nanostructured carbon [104, 105] are analogous to peaks *II* and *III* for isotropic graphite.[181] The lengths of diffusion path for hydrogen molecules and atoms can be derived from Eqns (2) and (3). The values obtained in this way, $L_\alpha \approx 9$ μm and $L_\gamma \approx 3$ nm, most probably characterise the mean thickness of the film [104, 105] and the size of the crystallite grains, respectively. The expressions (9), (10), (23), (25) and (26) (for $\sim$298 K and 100 kPA) give rise to the values of $x_{III} \approx 0.1$, which is close to x_γ, and the characteristic size of the crystallite grains $r_{cg} \approx 10$ nm, which is close to L_γ.

* * *

The analysis conducted above indicates that the parameters and equations (Table 3) proposed for characterisation of processes of hydrogen desorption from isotropic graphite [181] give a satisfactory description of the processes corresponding to analogous TPD peaks for a range of nanostructured carbon materials.[67–69, 104, 105, 199–201]

6. Parameters of hydrogen diffusion and sorption in mechanochemically synthesised nanocrystalline graphite

Let us now turn to experimental data [27, 29, 30] on hydrogen and deuterium sorption by mechanochemically synthesised nanocrystalline graphite. The starting material [27, 29] represented graphite powder composed of microgranules with a diameter of $l_{mg} \approx 200$ μm. The graphite powder was saturated with hydrogen (or deuterium) during its milling in a ball mill for 80 h at $T \approx 300$ K and $P_{H_2(D_2)}$ = 1.0 MPa. As a result, a material containing $x_\Sigma \approx 0.96$ of hydrogen was produced. The specific surface area of this sample after milling for 80 h was $S_{sp} \approx 10$ m^2 g^{-1}, which was close to its starting value.[27] For the graphite microgranules after milling for 2 hours, the linear size of nanocrystallites in the direction perpendicular to the graphene layers estimated from the width of peak (002) in the diffraction pattern was $l \approx 40$ nm.[29] The linear size of nanocrystallites ('nanograins') along the graphene layers for the microgranules after milling for 20–80 h was $l_{cg} \leqslant 4$ nm according to Raman scattering and neutron diffraction data.[29] The TPD curves measured for desorption of hydrogen (or deuterium) from these samples upon heating at a rate of υ = 0.33 K s^{-1} revealed two peaks (Fig. 11): a peak α ($T_\alpha \approx$ 730 K, $\Delta T_\alpha \approx$ 130 K, $S_\alpha/S_\Sigma \approx$ 0.8–0.6) and a peak β ($T_\beta \approx 1000$ K, $\Delta T_\beta \approx 30$ K, $S_\beta/S_\Sigma \approx 0.2$–$0.4$). Minor desorption peaks of hydrocarbons with masses of 16 (CH_4) and 28 (C_2H_4) were also detected [29] around T_α (Fig. 11 *a*). No extra peaks were detected around T_β. It is noteworthy that the peak β appears at the same temperature as the peak observed by differential thermal analysis (DTA) and attributed to recrystallisation of nanostructured graphite, which is characterised by the activation enthalpy of $Q_{recr} \approx 244$ kJ mol^{-1}.

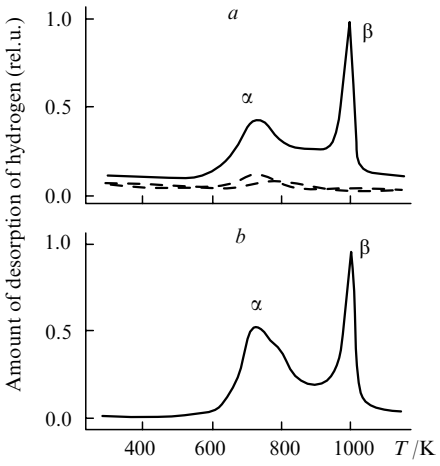

Figure 11. Temperature-programmed desorption of hydrogen (*a*) and deuterium (*b*) (solid lines) from nanocrystalline graphite saturated with hydrogen (or deuterium) during mechanochemical synthesis (1.0 MPa, 300 K, 80 h).[29]
The desorption curves of CH_4 and C_2H_4 are shown as dashed lines.

On the basis of neutron diffraction and Raman scattering data, Orima *et al.* suggested[27,29,30] that the peak α is due to desorption of chemically bound hydrogen (deuterium) whereas the peak β is due to desorption of hydrogen (deuterium) from the interlayer space of the crystallite grains. Therefore, peak β is analogous to peak *III* for isotropic graphite.[181] The length of diffusion path, which corresponds to the linear size of the crystallite grains or nanograins (l_{cg}), determined using Eqn (3) is $L_\beta \approx 2$ nm. This value agrees with the value $l_{cg} \leqslant 4$ nm found experimentally[29].

The calculated concentration of hydrogen $x_\beta \approx (S_\beta/S_\Sigma)x_\Sigma \approx 0.2-0.4$ is in agreement with the value $x_{III} \approx 0.2-0.3$ determined using Eqns (9) and (10) at $P_{D_2} = 1$ MPa and $T = 300$ K, which assumes that under the experimental conditions, the equilibrium bulk solubility of hydrogen (deuterium) in the graphite lattice is reached.[27,29]

The experimental and calculated values of bulk solubility of hydrogen (deuterium) in the graphite lattice[27,29] ($x_\beta \approx x_{III} \approx 0.2-0.4$) approach the ultimate (carbohydride) values of concentrations of occupied chemisorption DC centres in the graphene layers (Table 3).

Evidently, the peak α is due to diffusion of hydrogen (deuterium) molecules from the surface of the crystallite grains towards the external surface of the granules, *i.e.*, it corresponds to the peak *II* (Table 3) for isotropic graphite.[181]

The length of diffusion path L_α estimated using Eqn (2) is comparable to the diameter of graphite microgranules ($l_{mg} \approx 200$ μm) within the samples.[27,29]

The local concentration of hydrogen (deuterium) molecules $x_{D2\alpha}$ on the surface of the crystallite grains can be calculated using the following formula:

$$x_\alpha \approx 12\left(\frac{\Delta r}{l_{cg}}\right)x_{D_2\alpha}\,, \qquad (23a)$$

and the value $x_\alpha \approx (S_\alpha/S_\Sigma)x_\Sigma \approx 0.6-0.8$. Substitution of $\Delta r \approx 0.3$ nm and $l_{cg} \approx 3$ nm[29] in (23a) gives rise to the value of $x_{D2\alpha}$, which is close to the ultimate values of concentration of the chemisorption centres D_2C (model H, Fig. 9), which correspond to formation of a carbohydride adsorbed nanophase on the surface of the crystallite grains.

The above results, in particular, imply that the nanoareas at boundaries of the crystallite grains in nanostructured graphite[27,29] are similar to a certain extent to those of the crystallite micrograins in polycrystalline microgranules of isotropic graphite.[181]

It would be useful to note that such nanoareas at boundaries of crystallite grains are evidently formed upon milling of graphite[27,29] in a ball mill, *i.e.*, upon periodic high-speed plastic deformation of graphite, which results[178] in emergence of a high stationary dislocation density in the material being deformed. These dislocations apparently accelerate diffusion mass transfer of hydrogen in grapite during mechanochemical synthesis of these materials in the atmosphere of hydrogen.[27,29]

Kinetics of hydrogenation of graphite milled in a ball mill (*i.e.*, synthesised mechanochemically) can be formally described as a first-order reaction (Fig. 12):[63,178,202]

$$x_{\Sigma(t)} \approx x_{\Sigma 0}\left[1 - \exp\left(-\frac{t}{\tau_\Sigma}\right)\right]. \qquad (30)$$

Here, $x_{\Sigma(t)}$ is the mean deuterium concentration in the material subjected to milling (mechanochemical synthesis) for a time t; $x_{\Sigma 0}$ is the saturation concentration of deuterium in nanocrystalline graphite; τ_Σ is the relaxation time of diffusion process within the material during mechanochemical hydrogenation ($\tau_\Sigma \approx L_\Sigma^2/D_\Sigma$), where L_Σ is the distance travelled by deuterium in graphite upon mechanochemical synthesis, D_Σ is the apparent deuterium diffusion coefficient in graphite, $\tau_\Sigma \approx 16$ h. This yields a value $D_\Sigma \approx (L_\Sigma^2/\tau_\Sigma)$ that is larger by many orders of magnitude than D^*_{III} and by several orders of magnitude than D_{II}, estimated using the respective equations (see Table 3). Therefore, deuterium diffusion in graphite is abnormally accelerated during mechanochemical synthesis.

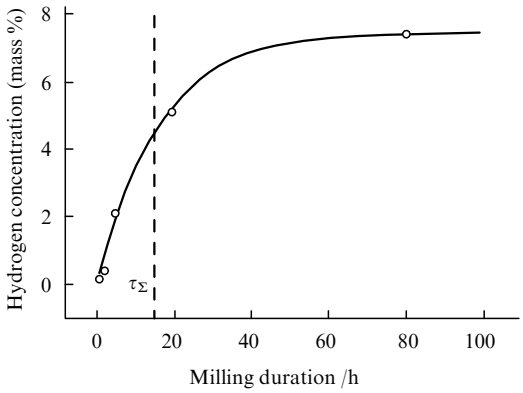

Figure 12. The kinetics of hydrogenation of nanostructured graphite during mechanochemical synthesis [$P_{D_2(H_2)} = 1$ MPa, $T = 300$ K].[27,29]

A series of samples of mechanochemically nanostructured graphite[27,28,124] hydrogenated up to $x_\Sigma \approx 0.96$ (according to Ref. 28) and $x_\Sigma \approx 0.24$, 0.31 and 0.96 (according to Ref. 124) has been studied using NMR. NMR spectra of the samples with $x_\Sigma \approx 0.96$ manifested two peaks suggestively attributed[27,28,124] to chemisorption of deuterium on defect areas (peak *1*) and physisorption of deuterium in the interlayer space (peak *2*).

Additionally, spin–lattice relaxation times of hydrogen atoms were measured[28,124] for the samples of mechanochemically nanostructured graphite (with $x_\Sigma \approx 0.96$, 0.31, 0.24) at 67.7 MHz in a temperature range of 300–425 K (the peak had the maximum intensity at ~390 K). Based on these experimental data, the enthalpy of activation of hydrogen diffusion in graphite (ΔH_a) was estimated as 9.6 kJ mol^{-1}. The authors attributed this 'suprisingly low' value of H_a to diffusion of hydrogen physisorbed between the graphene layers.

Taking into account the specific character of the NMR procedure utilised in the above studies[28,124], theoretical results (MD simulation)[197] concerning hydrogen diffusion between the graphene layers (in the absence of chemisorption centres) as well as the results of our analysis of published data,[27,29,30] it might be

assumed that the above value $\Delta H_a \approx 9.6$ kJ mol^{-1} characterises the enthalpy of activation [Q_{latt} in Eqn (12)] of diffusion of those hydrogen atoms located between the graphene layers, which have not been captured by the chemisorption centres. There are some reasons to suggest that the chemisorption centres capable of capturing the diffusant appeared completely occupied (up to the ultimate hydrocarbon concentrations H/C $\approx$ 1) under the experimental conditions.[28] This situation is equivalent to the lack of the chemisorption centres.[177, 203] The diffusion coefficient determined under such conditions should be close to D_{latt} [expression (11)]. Furthermore, it might be suggested that peaks *1* and *2* in the NMR spectra [28, 124] characterise the same processes as TPD the peaks α and β, respectively.[29, 31]

7. Hydrogen sorption and diffusion in bundles of single-walled carbon nanotubes

Hydrogen sorption by soot containing ~0.01 mass % – 0.02 mass % of SWNT bundles has been studied.[18] The bundles were composed of 7 – 14 SWNT (each tube had a diameter of ~ 1.2 nm and a length of ~ 5 μm). The soot samples (with a mass of ~1 mg) were exposed to hydrogen for 10 min at $P_{H_2} = 40$ kPa and $T = 273$ K (followed by quenching for 3 min at 133 K), then they were heated at a rate of $\upsilon = 1$ K s^{-1}. The TPD curves revealed two peaks (α and β) centred at ~150 K (peak α) and ~288 K (peak β characterised by the following parameters: $\Delta T_\beta = 50$ K, $x_\beta \approx 0.6 - 1.2$).† Based on additional TPD measurements with $\upsilon = 0.3 - 30$ K s^{-1}, the activation enthalpy of the process was determined ($Q_\beta = 19.6$ kJ mol^{-1}, peak β) according to the Kissinger procedure. The process was considered to be a first-order reaction.

The similarity between Q_β and Q_I (see Table 3) allows one to suggest that the diffusion process corresponding to the peak β is analogous to that attributed to the peak *I* for isotropic graphite.[181] Therefore, in order to estimate the length of diffusion path, Eqn (2) can be used, which yields $L_\beta \approx 70$ μm. This value is close to the thickness of the sample. Evidently, in this case, diffusion of hydrogen adsorbed by carbon nanotubes towards the external surface of the sample is accompanied by reversible capture of the diffusant by the chemisorption centres (traps) located on the nanotubes. Within this model, the apparent diffusion coefficient is described by the expression $D_{SWNT} \approx AD_{cap}/K_{(16)I} \approx D_I$ (A = const, D_{cap} is the capillary diffusion coefficient of hydrogen in the absence of chemisorbing traps) similar to Eqn (17).

Taking into account that the experimental values of specific surface area of SWNT samples [76, 204] are typically three – four times smaller than the theoretical value ($S_{sp} \approx 1300$ m^2 g^{-1}),[72] the experimental value x_β should be written in a modified form:

$$x_\beta \approx 2\,\Delta r\, S_{sp}\, \rho\, x_{H_2\beta} \qquad (18a)$$

Substitution of $S_{sp} \approx 400$ (or 1300 m^2 g^{-1}), $x_\beta \approx 0.6 - 1.2$, $\Delta r \approx 0.3$ nm and $\rho \approx 2$ g cm^{-3} (density of the material) [72, 192] into Eqn (18a) gives rise to $x_{H_2\beta} \approx 1.2 - 2.4$ (or 0.4 – 0.8).

For the sorption process corresponding to the peak *I*, Eqns (20) and (21) for $T = 273$ K and $P_{D_2} = 40$ kPa yield $x_{D_2 I} \approx 0.075$, which is substantially smaller than $x_{H_2\beta}$. Thus, it might be assumed that it is physisorption of hydrogen (*i.e.*, condensation of the adsorbate) that dominates in the SWNT samples [18] (peak β) rather than chemisorption as in the case of graphite [181] (peak *I*); to a certain extent, this could be promoted by additional quenching of the SWNT samples at 133 K.

A totally different situation occurs upon hydrogen adsorption on SWNT samples ($x_{SWNT} \approx 0.01$) and graphite powder ($x_{graph} \approx 0.01$) hydrogenated at $T = 295$ K and $P_{H_2} =$ 107 kPa.[85] In a pressure range from 5 kPa to 107 kPa (P_{H_2}), the adsorption process is described by the Henry isotherm, which represents a reduced form of the Henry – Langmuir isotherm [Eqn (20)] at near-zero filling of the sorption centres.

Substitution of the experimental values [85] S_{sp}(SWNT) $\approx$ 504 m^2 g^{-1} and S_{sp}(graph.) $\approx$ 60 m^2 g^{-1} into (18a) yields x_{H_2}(SWNT) ≈ 0.16 and x_{H_2}(graph) ≈ 0.12. Similarly, from Eqns (20) and (21) for $T = 295$ K and $P_{H_2} = 107$ kPa, it follows that $x_{D_2 I} \approx 0.09$, which is close to x_{H_2}(SWNT) and x_{H_2}(graph.). This implies that the mechanism and parameters of hydrogen (deuterium) adsorption by the SWNT and graphite samples [85] studied at a pressure of ~10 – 100 kPa and room temperature are similar to those of the chemisorption process attributed to the peak *I* (Table 3) for isotropic graphite.[181]

The sorption capacity of the graphite sample [85] at 295 K and 107 kPa recalculated for $S_{sp} = 1000$ m^2 g^{-1} is $c_S \approx 1.3$ mass %; the respective sorption capacity of the SWNT samples [85] at the same temperature and hydrogen pressure is $c_S \approx 1.9$ mass %. A similar value $c_S = 1.5 \pm 0.2$ mass % was obtained [72] for electrochemically hydrogenated SWNT and graphite samples with a specific surface area from 50 to 1200 m^2 g^{-1}, which strongly supports the surface character of the sorption processes.

Note that a significantly larger sorption capacity $c_S \approx 10$ mass % – 20 mass % (at 273 K and 40 kPa) was reported for another series of SWNT samples.[18] The reason for this discrepancy is either a strong overestimation of the experimental sorption capacity (by an order of magnitude) or localisation of the dominant fraction of the adsorbate in nanocavities between the tubes, *i.e.*, involvement of the physical mechanism of hydrogen sorption (condensation) under the experimental conditions. (It should also be kept in mind that the SWNT samples [18] were heavily contaminated with soot and subjected to an additional hydrogenation step at 133 K.)

Kinetics of hydrogenation (at $P_{H_2} = 0.1$ MPa and $T = 500$ K) and isothermal hydrogen desorption in a vacuum (at $T = 500$ K) were measured on pads (with a thickness of ~1 mm) composed of tangled bundles of SWNT (50 vol.% – 70 vol.%, diameter of bundles ~15 nm, diameter of nanotubes ~1.4 nm, $S_{sp} \approx 250 - 470$ m^2 g^{-1}, residual content of the catalyst 0.2, 2 and 6%) using the thermo-EMF method.[76] Both processes proceeded as first-order reactions with a relaxation time of $\tau \approx 1$ h. Assuming that the rate-limiting step of the process is diffusion of hydrogen molecules from the surface of the samples to the bulk with the parameters similar to those corresponding to the peak *I* for graphite [181] (Table 3), the estimated length of diffusion path [$L_I \approx (D_I \tau)^{1/2}$] appears similar to the thickness of the pads.

Kinetics of isothermal desorption of hydrogen from electrochemically hydrogenated cylindrical samples ($d = 7$ mm) prepared by cold compacting of a SWNT material (10 mg) mixed with gold powder (90 mg) was studied.[72] Hydrogen content in these SWNT samples reached 0.9 mass %. At 293 K, about half of the total hydrogen amount desorbs during first 10 h whereas the remaining part desorbs for $t_\Sigma \approx 200$ h.[72]

On the basis of diffusion parameters corresponding to the TPD peak *I* for isotropic graphite [181] (Table 3), one can estimate the diffusion coefficient at 293 K to be $D_I = 7.1 \times 10^{-7}$ cm^2 s^{-1}, which is close to $(d^2/t_\Sigma) \approx 6.8 \times 10^{-7}$ cm^2 s^{-1}. This means that it gives a satisfactory description for the process of hydrogen diffusion in such materials.[72]

The same study [72] reported results on hydrogen desorption from SWNT samples hydrogenated at 78 K and 0.2 MPa upon their heating with a rate of $\upsilon \approx 0.067$ K s^{-1} (in a temperature range from 78 K to 800 K) and from graphite samples hydrogenated at room temperature and 2 MPa (for 30 min) upon their cooling to 78 K. For both SWNT and graphite samples, three peaks were revealed [72] at ~105 K, ~136 K and ~300 K. The two latter peaks correspond evidently to peaks α (~150 K) and β (~288 K) observed for the aforementioned SWNT samples studied in Ref. 18. Additional peaks were revealed [72] at ~800 K for the SWNT samples and at ~650 K for the graphite samples,

† In the estimate [18] of sorption capacity of the SWNT samples, a possible involvement of soot and amorphous graphite abundant in the samples (their content reached 99.9 mass % – 99.8 mass %) was not taken into account, peak α was also neglected.

which, probably, can be correlated with peaks *II* and/or *IV* (Fig. 8) for isotropic graphite.[181]

Measurements of hydrogen desorption from samples composed of SWNT bundles, amorphous carbon and particles of a metal catalyst were reported.[34] The samples were first milled in a ball mill (for 24 h in an argon atmosphere) and then exposed to hydrogen for 15 min at $P_{D_2} = 80$ kPa and room temperature. According to electron microscopy,[34] the milling process results in the emergence of deformed areas (defects) in the structure of SWNT bundles and the formation of strongly bent or broken SWNT fibres. TPD curves of the hydrogenated SWNT samples treated in this way (measured at a heating rate of $\upsilon \approx 0.3$ K s^{-1} from $\sim$400 K to $\sim$850 K) reveal a single peak at $\sim$590 K, ($\Delta T \approx 75$ K, $x \approx 0.01$). Based on TPD measurements at different heating rates (from 0.03 to 0.3 K s^{-1}), the activation energy of the process was determined to be $Q_{SWNT} = 145 \pm 20$ kJ mol^{-1}.

The similarity between Q_{SWNT} and Q_{II} implies that the parameters of the diffusion process corresponding to the peak of hydrogen desorption from SWNT bundles[34] are analogous to those of the peak *II* for graphite (Table 3).[181] The length of diffusion path, which characterises the thickness of the samples, estimated from Eqn (2) is L(SWNT) $\approx$ 30 μm.

Within such a model, the apparent diffusion coefficient of hydrogen within the deformed SWNT bundles[34] upon their heating in a vacuum can be described using the following equation: $D_{SWNT} \approx AD_{cap}/K_{(16)II} \approx D_{II}$.

The value $x_{D2II} \approx 0.5$, calculated using Eqns (25) and (26) for 295 K and 80 kPa, can be further used to estimate the atomic (volume) fraction of the deformed areas (η_{II}) within the structure of SWNT bundles. From the expression $x \approx 2\eta_{II} x_{D2II}$, it follows that $\eta_{II} \approx 10^{-2}$. [Most probably, it is the H_2C chemisorption centres of type H (Fig. 9) that are localised in these deformed areas of the SWNT samples.[34]]

Another study[34] was devoted to SWNT, GNF and graphite samples hydrogenated using mechanochemical synthesis in a deuterium atmosphere (in a ball mill at $P_{D_2} =$ 0.9 MPa for 24 h). TPD measurements at a heating rate of $\upsilon \approx 0.08$ K s^{-1} in a temperature range from $\sim$300 K to $\sim$900 K, revealed[34] a peak centred at 740 K (that was distinct in the cases of SWNT and GNF samples but poorly resolved for the graphite samples) and a leading edge of a second peak (especially pronounced for the GNF samples) apparently centred in the range of 900–1100 K. Temperature positions of these peaks are close (taking into account different heating rates υ) to those of peaks α and β observed for the samples of nanostructured graphite[27,29] prepared mechanochemically in a deuterium atmosphere.

It would be useful to consider the experimental results[83] on volume (68 kg m^{-3}) and gravimetric ($x_{exp} \approx 0.48$) hydrogen sorption capacities of SWNT samples (pellets) characterised by S_{sp}(SWNTC) $\approx$ 110 m^2 g^{-1} hydrogenated at $\sim$11 MPa and 295 K. For these conditions, Eqn (18a) gives rise to the value x_{H_2}(SWNT) $\approx$ 3.6 (provided that $S_{sp} = 110$ m^2 g^{-1}) while Eqns (20) and (21)give rise to the value $x_{D_2I} \approx 0.48$, which is close to the ultimate (carbohydride) value (0.5). This discrepancy may be, firstly, due to strongly underestimated experimental specific surface area S_{sp}, which is smaller than the theoretical value by an order of magnitude (see Ref. 72); secondly, it may indicate condensation of the predominant fraction of the adsorbate in the nanocavities between the nanotubes, which is possible at such a high pressure.

Similar values of sorption capacity ($x \approx 0.5$–0.6) were reported in other studies[23,71] for the SWNT samples hydrogenated at 10 MPa and room temperature, which can thus be interpreted analogously.

The interaction of gaseous molecular hydrogen with purified SWNT samples (content of SWNT bundles was $\sim$90 mass %–95 mass %, diameter of the tubes was $\sim$1.38 nm) with the ends open using a chemical treatment with an NaOH aqueous solution was elucidated.[77] The samples with a mass of $\sim$1 g and volume of $\sim$1 cm^3 were hydrogenated at 1.5–9.0 MPa and room temperature ($\sim$295 K). The sorption capacity of the SWNT samples[77] in the case of hydrogenation at 9 MPa and 295 K was x(H/C) = 0.038. The experimental data[77] at $P_{H_2} =$ 1.5–9.0 MPa and $T = 295$ K are described by the Henry adsorption isotherm. TPD measurements with heating rates of $\upsilon = 0.17$ K s^{-1} and 0.017 K s^{-1} revealed peaks centred at $T \approx 508$ K and 374 K, respectively. The enthalpy of activation of the process (Q) determined using the Kissinger procedure was 20 kJ mol^{-1}.

Since the above value of Q coincides with the value of Q_I determined in an analysis of hydrogen desorption from the purified SWNT samples,[77] it is reasonable to utilise the diffusion and sorption parameters corresponding to the peak *I* for graphite (see Table 3).[181] The length of diffusion path calculated using the expression (2) is $L \approx 1$ mm, which corresponds to the thickness of the SWNT samples.[77] Similarly, sorption capacity can be estimated based on Eqns (20) and (21) for 295 K and 9 MPa as $x_{D_2I} \approx 0.47$, which approaches the ultimate (carbohydride) value.

The value x_{H_2}(SWNT) ≈ 0.08 calculated from Eqn (18a) using a typical value of S_{sp}(exp.) = 400 m^2 g^{-1} is substantially smaller than the aforementioned x_{D_2I}. This means that hydrogen sorption on the SWNT samples[77] cannot be described on the basis of the sorption parameters (Table 3) corresponding to the peak *I* for isotropic graphite.[181]

Hydrogen sorption on a new carbon nanomaterial, *viz*., single-walled nanotubes with cone-shaped (horn-like) ends, or nanohorns (SWNH), was studied.[100] The content of SWNH in the samples exceeded 95 mass % while metal catalysts and soot were virtually absent. The original SWNH samples ($S_{sp} \approx 308$ m^2 g^{-1}) and those treated with oxygen at 693 K for 10 min ($S'_{sp} \approx 1006$ m^2 g^{-1}) were tested. Both samples were hydrogenated at $\sim$0.1–6.5 MPa and 303 K. In both cases, the hydrogenation process obeyed the Henry adsorption isotherm (similar to Ref. 77). The sorption capacity of the oxidised samples at 6.5 MPa was $x_{ox} \approx 0.038$ whereas that of the original samples was $x_{init} \approx 0.014$. Substitution of typical experimental values of specific surface area for similar samples into the expression (18a) yields x_{H_2}(ox.) = 0.032 and x_{H_2}(init.) = 0.038. On the other hand, the value calculated using Eqns (20) and (21) for 303 K and 6.5 MPa, $x_{D_2I} = 0.46$ [which is close to the ultimate (carbohydride) value of 0.5], is larger than the above x_{H_2}(ox.) and x_{H_2}(init.) values by an order of magnitude.

These results are similar to those obtained in the above analysis of the experimental data from Ref. 77 but drastically different from those of Ref. 83. The latter results were obtained at a similarly high pressure for the SWNT samples that have not been purified from soot, amorphous carbon and particles of metal catalysts. Therefore, the presence of soot, amorphous carbon and metal catalyst in the SWNT samples strongly affects the overall sorption process.

8. Sorption and diffusion of hydrogen in multi-walled carbon nanotubes

Sorption of hydrogen by two types of MWNT samples (with a mass of $\sim$2 mg) having different structures were studied by Lee *et al*.[89] The samples were exposed to hydrogen for 5 h at 4 MPa and 300 K (with subsequent cooling down to 80 K) and then studied using TPD (at $\upsilon = 0.03$–0.08 K s^{-1}).

The first type (A) of the samples were composed of strongly bent nanotubes with strongly distorted graphene layers and partially blocked nanoholes. Side faces of the majority of the tubes were closed. External and internal diameters of the tubes were estimated[89] to be 10–30 nm and 5–15 nm, respectively, and the specific area amounted to S_{sp}(A) $\approx$ 174 m^2 g^{-1}. The samples A manifested two TPD peaks: a peak α_1 around 312 K ($\Delta T_{\alpha 1} \approx 18$ K, $\upsilon = 0.05$ K s^{-1}, $Q_{\alpha 1} \approx 18.5$ kJ mol^{-1}, $x_{\alpha 1} \approx 7.7 \times 10^{-2}$) and a peak β_1 around 419 K ($\Delta T_{\beta_1} \approx 8$ K, $\upsilon = 0.05$ K c^{-1}, $Q_{\beta 1} \approx 124.4$ kJ mol^{-1}, $x_{\beta 1} \approx 3.6 \times 10^{-3}$). The peak α_1 reappeared upon several consecutive cycles of hydro-

genation and heating of the samples whereas the peak β_1 did not reappear.

The samples B were composed of straightened, aligned MWNT with a less distorted structure as compared to the samples A. Nanoholes within the samples B were assembled into pores and side faces of the tubes remained open. The external and internal diameters of the tubes were $\sim$20 nm and $\sim$8 nm, respectively; specific surface area $S_{sp}(B) \approx 877$ m^2 g^{-1} [this value is several times larger than the theoretical value of the specific surface area (263 m^2 g^{-1}) [72] for ten-walled nanotubes]. The samples B manifested only one TPD peak (α_2) around 313 K ($\Delta T_{\alpha 2} \approx 7$ K, $\upsilon = 0.05$ K c^{-1}, $Q_{\alpha 2} \approx 16.5$ kJ mol^{-1}, $x_{\alpha 2} \approx 0.24$).[89]

The similarity between $Q_{\alpha 1}$ and $Q_{\alpha 2}$, on the one hand, and Q_I in graphite,[181] on the other hand, indicates that the parameters characterising the TPD peak *I* (Table 3) for isotropic graphite [181] can be used to describe peaks α_1 and α_2 for the MWNT samples.[89] The lengths of diffusion path $L_{\alpha 1}$ and $L_{\alpha 2}$, which characterise thickness of the samples, calculated on the basis of Eqn (2) are 130–200 μm.

The ratio $x_{\alpha 2}/x_{\alpha 1}$ is close to the ratio $S_{sp}(A)/S_{sp}(B)$, which is in agreement with the published results.[72, 81] The local concentration of hydrogen molecules within the adsorbed layers on the walls of the nanotubes calculated using Eqn (18a) is $\sim$0.2–0.3. For the experimental conditions used in Ref. 89, Eqns (20) and (21) yield $x_{D_2 I} \approx 0.4$. This value of $x_{D_2 I}$ is close to $x_{H_2 \alpha}$ calculated from the experimental data [*i.e.*, $x_{\alpha 1}$, $S_{sp}(A)$, $x_{\alpha 2}$, $S_{sp}(B)$] for the MWNT samples.[89]

The similarity between $Q_{\beta 1}$ and Q_{II} assumes that the peak β_1 for the samples A is analogous (with regard to diffusion parameters) to the peak *II* (Table 3) for isotropic graphite.[181] The absence of the peak β_1 in subsequent cycles of hydrogenation and annealing of the samples A [89] can be explained by curing of the deformational structural defects in these samples upon their first annealing. The length $L_{\beta 1} \approx 0.2$ μm calculated using Eqn (2) probably characterises the diffusion dimension of the distorted areas within the samples A.[89] The volume fraction of such distorted areas within the samples A with chemisorbing carbon 'centres' can be estimated using the equation $x_{\beta 1} = 2\eta_{\beta 1} x_{D_2 II}$, where $x_{D_2 II} \approx 0.5$ [as determined from the expressions (25) and (26)] to $\eta_{\beta 1} \approx 4 \times 10^{-3}$.

Sorption of hydrogen by MWNT samples at 10 MPa and room temperature was studied by Li *et al.*[90] They used two types of samples: one type of the samples (A) was characterised by numerous cracks in the external graphene layers (walls) of nanotubes even after annealing at 2473 K (for 2 h); another type (B) was characterised by crack-less graphene layers (walls) both before and after annealing at 2473 K (for 2 h). Sorption capacities (x) of the non-annealed samples A and B were 0.1 and 0.09, respectively whereas those of the annealed samples were 0.5 and 0.1, respectively.

Specific surface areas of the samples A and B [90] calculated using Eqns (18a), (20) and (21) are $\sim$520 m^2 g^{-1} and $\sim$110 m^2 g^{-1}, respectively. These calculated values of S_{sp} are within the range of typical values found experimentally for such materials, which implies that the process of hydrogen sorption on the MWNT samples [90] can be described using the parameters corresponding to the peak *I* for graphite.[181]

Sorption of hydrogen by MWNT samples with a diameter of 10–40 nm (predominantly with closed side faces) at 290 K and $P_{H_2} = 3$–10 MPa was studied by Cao *et al.*[91] They used two types of samples: samples A composed of straightened highly oriented nanotubes [tube density was up to $\sim 10^8$ mm^{-2}, thickness of some tube blocks was $h \approx 250$ μm, $S_{sp}(A) \approx 60$ m^2 g^{-1}] and samples B characterised by a random arrangement of the nanotubes [and variable nanoporosity, $S_{sp}(B) \approx 27$ m^2 g^{-1}].

For both types of the MWNT samples (A and B), the hydrogen uptake increased linearly with an increase in pressure P_{H_2} from 3 to 10 MPa.[91] Sorption capacities (x) of the samples A and B at 290 K and 10 MPa were $\sim$0.29 and $\sim$0.082, respectively. Hydrogenation of the samples A resulted in disappearance of pores in the size range of 10–100 nm and an increase in the number of pores in the size range of 2–10 nm, which can be due to development of local strains and deformations.[154, 184–187]

Sorption capacity x_{H_2}, determined using the expression (18a) and experimental values of $x(A)$, $x(B)$, $S_{sp}(A)$ and $S_{sp}(B)$ is 2.2–3.6, which is significantly larger than $x_{D_2 I} \approx 0.46$, estimated on the basis of Eqns (20) and (21) for 290 K and 10 MPa. Presumably, this discrepancy is due to inaccurate determination of the specific surface areas of the MWNT samples [91] (the experimental values of S_{sp} were measured using the BET adsorption isotherms of nitrogen rather than hydrogen at 77 K and thus were underestimated). The high values of x_{H_2} can be also explained by condensation of a large fraction of the adsorbate in the nanocavities between the tubes of the MWNT samples,[91] *i.e.*, domination of physisorption over chemisorption with the parameters corresponding to the peak *I* for graphite.[181]

Characteristics of hydrogen sorption on straightened (aligned) multi-walled nanotubes with a diameter of 50–100 nm and density of $\sim 10^8$–10^9 mm^{-2} were reported by Chen *et al.*[88] The samples were hydrogenated at $\sim$295 K and $\sim$0.1 MPa (or $\sim$1.0 MPa) up to hydrogen concentration $x_{exp} \approx 0.60$–0.84 (or 1.08–1.56), then treated with nitric acid and annealed at 673 K.

Upon heating of the hydrogenated samples (with a mass of $\sim$1 mg) from $\sim$295 K to 573 K with a rate of $\upsilon \approx 0.083$ K s^{-1}, several hydrogen desorption peaks were detected by mass spectrometry.[88] The major peak (about 90%) was centred at $T \approx 540$ K with a width at half maximum of $\Delta T \approx 45$ K, *i.e.*, the dominant fraction of adsorbed hydrogen was liberated from the MWNT samples at 500–600 K.[88]

The length of diffusion path of hydrogen estimated using Eqn (2) is $L \approx 15$ μm. This value is comparable with the mean length of the nanotubes and thickness of the MWNT samples.[88] This indicates that the diffusion process corresponding to the peak at 540 K for the MWNT samples [88] is characterised by parameters similar to those attributed to the peak *II* for graphite.[181]

Substitution of $x_{D_2 II} \approx 0.5$ calculated using Eqns (25) and (26) and the experimental value $0.9\,x_{exp} \approx 0.54$–0.76 into Eqn (18a) gives rise to $S_{sp} \approx 500$–700 m^2 g^{-1}, which is significantly larger than the ultimate theoretical value.[72] Therefore, it might be assumed that in this case, the dominant part of the adsorbate undergoes condensation in the nanocavities between the tubes of the MWNT samples.[88]

Chen et al. [88] noted that the cone-shaped structure of studied samples was different from that typical of ideal MWNT samples and rather similar to GNF samples.[32, 33, 205]

9. An analysis of abnormal data concerning hydrogen sorption by graphite nanofibres

In 1998, Chambers *et al.* published a sensational paper [33] on the possibility of hydrogen storage in a new materials, *viz.*, graphite nanofibres‡ with a specific structure. They reported that GNF samples with an oriented (at $\sim$45°) nanostructure are capable of sorbing an abnormally high amount of hydrogen ($x_\Sigma \approx 18.5$) at $P_{H_2} \approx 9.6$ MPa (final value) and $T = 298$ K.

Hydrogenation of the GNF samples lasted for 20 h (τ_Σ). Upon release of the pressure, the dominant fraction of adsorbed hydrogen ($x \approx 9.8$) desorbed during $\tau \approx 5$–10 min.

Chambers *et al.* [33] also hydrogenated a series of other materials, including palladium powder (up to final composition of $PdH_{2.2}$, which differs from the stoichiometry of stable Pd_2H and metastable $PdH_{1.1-1.3}$ palladium hidrides [177]) and $LaNi_5$. The sorption capacities of these materials were overestimated as well,

‡ The nanofibres with a length of $\sim$10–100 μm were composed of stacks of strictly oriented (parallel, perpendicular, or at an angle of $\sim$45° with respect to the stack axis) graphene platelets with a distance between the graphene sheets of $\geqslant$0.335 nm (which is close to the interlayer separation in graphite [181]) and a cross-section area of $\sim$0.3–5.0 nm^2. This material represented a system of spot-like nanopores with open ends.[33]

which, according to Nishimiya *et al.*,[85] can be considered as additional evidence for a systematic error in the measurements of hydrogen sorption by GNF performed by Chambers *et al.*[33] Results regarding hydrogenation of graphite (at $\sim$11 MPa and 298 K for $\sim$40 h) up to a concentration of $x_\Sigma \approx 0.57$ and activated carbon 'Norite' characterised by $S_{sp} \approx 1000$ m^2 g^{-1} up to a concentration of $x_\Sigma \approx 0.20$ were also significantly different from those reported by other groups.[35, 38, 72, 85, 141]

In a subsequent study of hydrogen sorption by GNF samples, the same group of authors [32] reported much lower values $x_\Sigma \approx 8.0$ (hydrogenation was performed at $P_{H_2} \approx 11.2$ MPa and 298 K for 24 h).§ Furthermore, the authors noted that achievement of such a high value of x_Σ required an additional short *in situ* annealing of the GNF samples at 473 K.

Followed by release of the high pressure and retention of the hydrogenated samples at 298 K for $\tau_\alpha \geqslant 10$ min giving rise to desorption of the dominant fraction of hydrogen ($x_\alpha \approx 5.9$, peak α), the GNF samples were heated again to $\sim$1223 K at a rate of $\upsilon \approx 0.17$ K s^{-1}. Upon this second heating, the TPD curve (Fig. 13) revealed two peaks (β and γ) centred at 880 K ($\Delta T_\beta \approx 245$ K, $x_\beta \approx 1.2$) and 1140 K ($\Delta T_\gamma \approx 205$ K, $x_\gamma \approx 0.9$). Around T_β, a concomitant liberation of gaseous hydrocarbons (CH_4, *etc.*) was detected.

A comparison of the TPD curves (Fig. 13) for the GNF samples hydrogenated at 11 MPa (curve *1*) and 0.1 MPa (curve *2*) shows that the sorption process corresponding to the peak β is described by the Henry – Langmuir adsorption isotherm and that corresponding to the peak γ is described by the Sieverts – Langmuir isotherm. The peak β is analogous to the peak *II* in the case of isotropic graphite,[181] whereas the peak γ is analogous to the peak *III*. Therefore, in order to calculate the respective length of diffusion path of hydrogen in the GNF samples (for peak β), one can utilise Eqn (2). The value $L_\beta \approx 0.4$ cm determined in this way corresponds to the linear size of the GNF sample ($l \approx 0.6 - 0.8$ cm).[32]

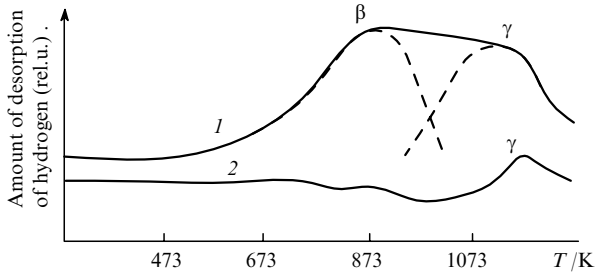

Figure 13. Temperature-programmed desorption of hydrogen from the GNF samples hydrogenated at 11.2 MPa (*1*) and 0.1 MPa (*2*) (for assignment of the TPD peaks, see text).
The experimental curves are shown as solid lines, individual components of the curve (*1*) are shown as dotted lines.

The value of sorption capacity $x_{H_{2\beta}}$ calculated using the equation $x_\beta \approx 12\,(\Delta r/d_{GNF})x_{H_2\beta}$ ($\Delta r \approx 0.2$ nm, $d_{GNF} \approx 1$ nm)[32] is $\sim$0.5. A similar value is obtained for x_{D_2II} on the basis of Eqns (25) and (26).

The experimental value x_γ is in fair agreement with the value $x_{III} \approx 0.6$ calculated using Eqns (9) and (10) for the peak *III* (Table 3). Also note that the values of x_γ, x_{III}, $x_{H_2\beta}$ and x_{D_2II} are close to the ultimate (carbohydride) values of $(x_{III})_{max}$ and $(x_{II})_{max}$.

The length of diffusion path ($L_\gamma \approx 50$ nm) estimated on the basis of parameters of the peak γ (for the GNF samples) according to Eqn (3) using D_{III} (Table 3) is significantly larger than $d_{GNF} \approx 1$ nm.[32, 33] There are two possible reasons for the difference between L_γ and d_{GNF}: either the value of diffusion coefficient used in the calculation of L_γ is overestimated ¶ or the value of d_{GNF} as determined in Ref. 32 is incorrect.† This can be due to the formation of a specific substructure (with a characteristic linear size of $\sim$1 – 3 nm) in the hydrogenated GNF samples [32] (having a fibre diameter of $\sim$50 nm), which disappears (due to curing) upon heating of the samples in the course of the TPD measurements. This suggestion is supported by the results of other studies,[32, 91] which revealed an abrupt decrease in the hydrogen concentration and a change in the size of nanopores within the hydrogenated GNF and MWNT samples and their reappearance upon heating.

It should be emphasised that the parameters of sorption and diffusion processes corresponding to peaks β and γ for the GNF samples [32] agree with those of processes corresponding to peaks α and β for nanocrystalline graphite [29] and are satisfactorily described by the parameters of peaks *II* and *III* for isotropic graphite (Table 3).[181]

The apparent diffusion coefficient of hydrogen in the GNF samples,[32] which characterises the process of desorption of the dominant fraction (x_α) of hydrogen at 298 K (peak α that appears just after release of the high pressure), can be estimated as $D_\alpha \approx (L^2/\tau_\alpha) \approx 2 \times 10^{-3}$ cm^2 s^{-1}. This value is larger by 3.5 orders of magnitude than D_I (peak *I*, Table 3) typical of graphite.[181] This strongly assumes different mechanisms of hydrogen sorption on GNF [32] and graphite [181] around T_α and T_I.

The sorption capacity corresponding to the peak α cannot be described using the parameters attributed to the peak *I* for isotropic graphite.[181] Thus, there are serious reasons validating the suggestion [32, 33] that the desorption process corresponding to the peak α is essentially due to the removal of hydrogen condensate from the nanocavities of the graphite nanofibres. Additionally, this is supported by the neutron diffraction data [4, 32] on abnormally high packing density (which exceeds that of hydrogen molecular crystals) of the adsorbate on the graphite surface and X-ray diffraction data [26] on an abnormally large increase (by 40%) in the interplane separation observed for the GNF samples hydrogenated at 9 GPa.

V. Conclusion

The comparative and constructive thermodynamic analyses of the experimental and theoretical data on the sorption of hydrogen by carbon nanomaterials in technically reasonable ranges of pressure and temperature confirm that the abnormally large scatter (up to three orders of magnitude) and poor reproducibility (or even lack of reproducibility) of the measurements of sorption capacities of these materials is caused by a number of factors, including complexity of the objects under study, variations in the microstructure (that strongly depends upon method used for the preparation of the sorbents) and conditions of physicochemical pretreatment and modes of hydrogenation of the samples, etc. The state-of-the-art in investigations into the interactions of hydrogen with graphite and carbon nanomaterials makes it possible to deliberately optimise synthetic conditions and modes of hydrogenation for such materials, which is an absolute prerequisuite for advancement towards creation of superadsorbents for hydrogen.

The authors are grateful to their colleagues, A K Chernysheva and E V Borisov, for the fruitful discussion of the results.

§ These data were neither confirmed by other researchers.

¶ It might be assumed that the diffusion coefficient of hydrogen atoms in the 'hydrocarbon phase' of GNF is smaller than that in the graphite lattice [181] with partially occupied carbon chemisorption centres, therefore, the value of D_{III} should not be used in a calculation of L_γ.

† There is experimental evidence [35, 71, 141, 142, 206] that the graphite nanofibres were characterised by a larger diameter ($d_{GNF} \approx 10 - 100$ nm) than that reported in Ref. 32.

References

1. D Yu Gamburg, M F Dubovkin *Vodorod. Svoistva, Poluchenie, Khranenie, Transportirovanie, Primenenie. Spravochnoe Izdanie* (Hydrogen. Properties, Production, Storage, Transport, Applications. Handbook) (Moscow: Khimiya, 1989)
2. P M Grant *Nature* (*London*) **424** 129 (2003)
3. *Poisk* (3) (765) 15 (2004); http://www.poisknews.ru/-ingz/arkiv.asp
4. A C Dillon, M J Heben *Appl. Phys. A* **72** 133 (2001)
5. L Schlapbach, A Züttel *Nature* (*London*) **414** 353 (2001)
6. S Hynek, W Fuller, J Bentley *Int. J. Hydrogen Energy* **22** 601 (1997)
7. M Junker, L Bocquet, M Bendif, D Karboviac *Ann. Chim. Sci. Mat.* **26** 117 (2001)
8. M Schrope *Nature* (*London*) **414** 682 (2001)
9. R Chahine, T K Bose *Int. J. Hydrogen Energy* **19** 161 (1994)
10. E Poirier, R Chahine, P Bénard, D Cossement, L Lafi, E Mélancon, T K Bose, S Désilets *Appl. Phys. A* **78** 961 (2004)
11. S Iijima *Nature* (*London*) **354** 56 (1991)
12. A V Eletskii, B M Smirnov *Usp. Fiz. Nauk* **163** 33 (1993) [a]
13. M Inagaki, L R Radovic *Carbon* **40** 2279 (2002)
14. B P Tarasov, N F Goldshdeger, A P Moravsky *Usp. Khim.* **70** 149 (2001) [*Russ. Chem. Rev.* **70** 131 (2001)]
15. A L Ivanovskii *Usp. Khim.* **68** 119 (1999) [*Russ. Chem. Rev.* **68** 103 (1999)]
16. A L Ivanovskii *Usp. Khim.* **71** 203 (2002) [*Russ. Chem. Rev.* **71** 175 (2002)]
17. B M Smirnov *Khimiya Nanostruktur. Sintez, Stroenie, Svoistva* (The Chemistry of Nanostructures. Synthesis, Structure, Properties) (St Petersburg: St Petersburg State University, 1996)
18. A C Dillon, K M Jones, T A Bekkedahl, C H Kiang, D S Bethune, M J Heben *Nature* (*London*) **386** 377 (1997)
19. I O Bashkin, in *International Symposium on Metal Hydrogen Systems (Abstracts of Reports), Annecy, France, 2002* p. 28
20. D J Browning, M L Gerrard, J B Laakeman, I M Mellor, R J Mortimer, M C Turpin, in *Proceedings of the 13th World Hydrogen Energy Conference, Beijing, China, 2000* p. 580
21. X D Bai, D Zhong, G Y Zhang, X C Ma, S Liu, E G Wang, Y Chen, D T Shaw *Appl. Phys. Lett.* **79** 1552 (2001)
22. M Hirscher, M Becher, M Halushka, F Zeppelin, X Chen, U Dettlaff-Weglikowska, S Roth *J. Alloys Compd.* **356-357** 433 (2003)
23. H W Zhu, A Chen, Z Q Mao, C L Xu, X Xiao, B Q Wei, J Liang, D H Wu *J. Mater. Sci. Lett.* **19** 1237 (2000)
24. H M Cheng, C Liu, Y Y Fan, F Li, G Su, L L He, M Liu *Z. Metallkd.* **91** 306 (2000)
25. A C Dillon, P A Parilla, K M Jones, G Riker, M J Heben, in *Proceedings of the 1998 U.S.DOE Hydrogen Program Review*. NREL/CP-570-25315
26. I O Bashkin, V E Antonov, A V Bazhenov, I K Bdikin, D N Borisenko, E P Krinichnaya, A P Moravskii, A I Kharkunov, Yu M Shul'ga, Yu A Osip'yan, E G Ponyatovskii *Pisma Zh. Eksp. Teor. Fis.* **79** 280 (2004) [b]
27. S Orimo, G Majer, T Fukunaga, A Züttel, L Schlapbach, H Fujii *Appl. Phys. Lett.* **75** 3093 (1999)
28. G Majer, U Eberle, F Kimmerle, E Stanik, S Orimo *Physica B* **328** 81 (2003)
29. S Orimo, T Matsushima, H Fujii, T Fukunaga, G Majer *J. Appl. Phys.* **90** 1545 (2001)
30. T Fukunaga, K Itoh, S Orimo, M Aoki, H Fujii *J. Alloys Compd.* **327** 224 (2001)
31. H Fujii, S-i Orimo *Physica B* **328** 77 (2003)
32. C Park, P E Anderson, A Chambers, C D Tan, R Hidalgo, N M Rodrigues *J. Phys. Chem. B* **103** 10572 (1999)
33. A Chambers, C Park, R T K Baker, N M Rodriguez *J. Phys. Chem. B* **102** 4253 (1998)
34. M Hirscher, M Becher, M Galuska, A Quintel, V Skakalova, Y-M Choi, U Dettlaff-Weglikowska, S Roth, I Stepanek, P Bernier, A Leonhardt, J Fink *J. Alloys Compd.* **330-332** 654 (2002)
35. C C Ahn, Y Ye, B V Ratnakumar, C Witham, R C Bowman Jr, B Fultz *Appl. Phys. Lett.* **73** 3378 (1998)
36. J Y Hwang, S H Lee, K S Sim, J W Kim *Synth. Met.* **126** 81 (2002)
37. M Ritschell, M Uhlemann, O Gutfleish, A Leonhardt, A Graff, Ch Tuschner *Appl. Phys. Lett.* **80** 2985 (2002)
38. G G Tibbetts, G P Meisner, Ch H Olk *Carbon* **39** 2291 (2001)
39. R T Yang *Carbon* **38** 623 (2000)
40. P Chen, X Wu, J Lin, K L Tan *Science* **285** 91 (1999)
41. O K Alexeeva, in *Proceedings of the VIIth International Conference 'Hydrogen Materials Science'* (Kiev: ADEF-Ukraine, 2001) p. 672
42. Yu S Nechaev, D V Iourtchenko, T N Veziroglu, in *Proceedings of the International Conference of American Carbon Society 'Carbon 2004', Providence, RI, 2004* p. 250
43. Yu S Nechaev, O K Alekseeva, in *Materialy Nauchno-Prakticheskoi Konferentsii Materialovedcheskikh Obshchestv Rossii 'Novye Funktsional'nye Materialy i Ekologiya', Moskva, 2002* (Proceedings of the Scientific and Practical Conference of Materials Science Societies 'New Functional Materials and Ecology', Moscow, 2002) p. 75
44. Yu S Nechaev, D V Iourtchenko, T N Veziroglu, in *Proceedings of the 15th World Hydrogen Energy Conference, Yokohama, Japan, 2004* p. 310
45. Yu S Nechaev, D V Iourtchenko, T N Veziroglu, in *Proceedings of the VIIIth World Renewable Energy Congress, Denver, CO, 2004* p. 270
46. Yu S Nechaev, O K Alekseeva, in *Sbornik Tezisov Dokladov II Mezhdunarodnogo Simpoziuma 'Bezopasnost' i Ekonomika Vodorodnogo Transporta', Sarov, 2003* (Abstracts of Reports of the IIth International Symposium 'Safety and Economics of Hydrogen Transport', Sarov, 2003) p. 138
47. Yu S Nechaev, O K Alekseeva, in *Sbornik Rasshirennykh Tezisov Dokladov VIII Mezhdunarodnoi Konferentsii 'Vodorodnoe Materialovedenie i Khimiya Uglerodnykh Nanomaterialov' (ICHMS'2003), Sudak, 2003* [Expanded Abstracts of the VIIIth International Conference 'Hydrogen Materials Science and Chemistry of Carbon Nanostructures (ICHMS'2003)', Sudak, Ukraine, 2003] p. 774
48. Yu S Nechaev, O K Alexeeva, J G Hirschberg, T N Veziroglu, in *The Vth International Conference 'Hydrogen Power Theoretical and Engineering' (Abstracts of Reports), Porto Conte, 2003* p. 97
49. M Hirscher, M Becher, M Haluska, X Chen, U Dettlaff-Weglikowska, S Roth, in *International Symposium on Metal Hydrogen Systems (Abstracts of Reports), Annecy, France, 2002* p. 29
50. S Orimo, T Matsushima, P Wang, H Fujii, T Fukunaga, G Majer, A Züttel, L Schlapbach, in *International Symposium on Metal Hydrogen Systems (Abstracts of Reports), Annecy, France, 2002* p. 28
51. B P Tarasov, in *Sbornik Tezisov Dokladov II Mezhdunarodnogo Simpoziuma 'Bezopasnost' i Ekonomika Vodorodnogo Transporta', Sarov, 2003* (Abstracts of Reports of the IIth International Symposium 'Safety and Economics of Hydrogen Transport', Sarov, 2003) p. 38
52. B P Tarasov, N F Goldshleger *Al'ternat. Energ. Ekol.* **3** 20 (2001)
53. D V Schur, B P Tarasov, Y M Shul'ga, S Yu Zaginaichenko, Z A Matysina, A P Pomytkin *Carbon* **41** 1331 (2003)
54. H-M Cheng, Q-H Yang, C Liu *Carbon* **39** 1447 (2001)
55. Z Liu, X-H Chen, H-H Song *New Carbon Mater.* **17** 73 (2002)
56. F Darkrim, P Malbrunot, G P Tartaglia *Int. J. Hydrogen Energy* **27** 193 (2002)
57. V V Simonyan, J K Johnson *J. Alloys Compd.* **330-332** 659 (2002)
58. E G Rakov *Usp. Khim.* **70** 934 (2001) [*Russ. Chem. Rev.* **70** 827 (2001)]
59. S Orimo, A Züttel, L Schlapbach, G Majer, T Fukunaga, H Fujii *J. Alloys Compd.* **356-357** 716 (2003)
60. J Conard *Ann. Chim. Sci. Mat.* **26** 107 (2001)
61. M S Dresselhaus, K A Williams, P C Eklund *MRS Bull.* **24** 145 (1999)
62. Z-Q Yang, Z-L Xie, Y-S He *New Carbon Mater.* **18** 75 (2003)
63. Yu S Nechaev, O K Alexeeva *Int. J. Hydrogen Energy* **28** 1433 (2003)

64. A Badzian, T Badzian, E Breval, A Piotrowski *Thin Solid Films* **398-399** 170 (2001)
65. L Schlapbach, A Züttel, P Grlning, O Gröning, P Aebi *Appl. Phys. A* **72** 245 (2001)
66. P Bénard, R Chahine *Langmuir* **17** 1950 (2001)
67. E A Evard, A P Voit, S K Gordeev, I E Gabis *Fiz.-Khim. Mekh. Mater*. **36** 23 (2000)
68. E A Denisov, T N Kompaniets, I V Makarenko, Z Vakar, A N Titkov *Materialovedenie* (2) 45 (2002)
69. E A Denisov, T N Kompaniets, A A Kurdyumov *NATO Sci. Ser. II, Math., Phys., Chem*. **1** 273 (2000)
70. Y Ye, C C Ahn, C Witham, B Fultz, J Liu, A G Rinzier, D Colbert, K A Smith, R E Smalley *Appl. Phys. Lett*. **74** 2307 (1999)
71. C Liu, Y Y Fan, M Liu, H T Cong, M S Dresselhaus *Science* **286** 1127 (1999)
72. A Züttel, P Sudan, Ph Mauron, Ph Mauron, T Kiyobaushi, Ch Emmenegger, L Schlapbach *Int. J. Hydrogen Energy* **27** 203 (2002)
73. A C Dillon, K E H Gilbert, P A Parilla, J L Alleman, G L Hornyak, K M Jones, M J Heben, in *Proceedings of the 2002 U.S. DOE Hydrogen Program Review NREL/CP-610-32405, Golden, CO, 2002*
74. M Shiraishi, T Takenobu, A Yamada, M Ata, H Kataura *Chem. Phys. Lett*. **358** 213 (2002)
75. T Takenobu, M Shiraishi, A Yamada, M Ata, H Kataura, Y Iwasa *Synth. Met*. **135-136** 787 (2003)
76. B K Pradhan, G U Sumanasekera, K W Adu, H E Romero, K A Williams, P C Eklund *Physica B* **323** 115 (2002)
77. M Shiraishi, T Takenobu, M Ata *Chem. Phys. Lett*. **367** 633 (2003)
78. H W Zhu, A Y Cao, X S Li , C L Xu, Z Q Mao, D B Ruan, J Liang, D H Wu *Appl. Surf. Sci*. **178** 50 (2001)
79. L Ci, H Zhu, B Wei, C Hu, D Wu *Appl. Surf. Sci*. **205** 39 (2003)
80. B Renker, H Schober, P Schweiss, S Lebedkin, F Henrich *Condens. Mater*. **1** 1266 (2003)
81. B P Tarasov, J P Maehlen, M V Lototsky, V E Muradyan, V A Yartys *J. Alloys Compd*. **356-357** 510 (2003)
82. H Kajiura, S Tsutsui, K Kadono, M Kakuta, M Ata, Y Murakami *Appl. Phys. Lett*. **82** 1105 (2003)
83. C Liu, Q H Yang, Y Tong, H T Cong, H M Cheng *Appl. Phys. Lett*. **80** 2389 (2002)
84. M R Smith Jr, E W Bittner, W Shi, J K Johnson, B C Bockrath *J. Phys. Chem. B* **107** 3752 (2003)
85. N Nishimiya, K Ishigaki, H Takikawa, M Ikeda, Y Hibi, T Sakakibara, A Matsumoto, K Tsutsumi *J. Alloys Compd*. **339** 275 (2002)
86. M M Shaijumon, S Ramaprabhu *Chem. Phys. Lett*. **374** 513 (2003)
87. R Zidan, A M Rao, in *Proceedings of the 2002 U.S. DOE Hydrogen Program Review NREL/CP-610-32405, Golden, CO, 2002*
88. Y Chen, D T Shaw, X D Bai, E J Wang, C Lund, W M Lu, D D L Chung *Appl. Phys. Lett*. **78** 2128 (2001)
89. H Lee, Y-S Kang, S-H Kim, J-Y Lee *Appl. Phys. Lett*. **80** 577 (2002)
90. X Li, H Zhu, L Ci, C Xu, Z Mao, B Wei, J Liang, D Wu *Carbon* **39** 2077 (2001)
91. A Cao, H Zhu, X Zhang, X Li, D Ruan, C Xu, B Wei, J Liang, D Wu *Chem. Phys. Lett*. **342** 510 (2001)
92. H Gao, X B Wu, J T Li, G T Wu, J Y Lin, K Wu, D S Xu *Appl. Phys. Lett*. **83** 3389 (2003)
93. C Park, C D Tan, R Hidalgo, A Chambers, R T K Baker, N M Rodriguez, in *Proceedings of the 1998 U.S. DOE Hydrogen Program Review NREL/CP-570-25315*
94. M Rzepka, P Lamp, M A de la Casa-Lillo *J. Phys. Chem. B* **102** 10894 (1998)
95. B K Gupta, O N Srivastava *Int. J. Hydrogen Energy* **25** 825 (2000)
96. B K Gupta, O N Srivastava *Int. J. Hydrogen Energy* **26** 857 (2001)
97. B K Gupta, in *Extended Abstracts of the VIIIth International Conference 'Hydrogen Materials Science and Chemistry of Carbon Nanostructures (ICHMS'2003)', Sudak, Ukraine, 2003* p. 794
98. K Hanada, H Shiono, K Matsuzaki *Diamond Relat. Mater*. **12** 874 (2003)
99. K Kadono, H Kajiura, M Shiraishi *Appl. Phys. Lett*. **83** 3392 (2003)
100. K Murata, K Kaneko, H Kanoh, D Kasuya, K Takahashi, F Kokai, M Yudasaka, S Iijima *J. Phys. Chem. B* **106** 11132 (2002)
101. E Johansson, B Hjorvarsson, T Ekstrom, M Jacob *J. Alloys Compd*. **330-332** 670 (2002)
102. H Kajiura, K Kadono, S Tsutsui, Y Murakami *Appl. Phys. Lett*. **82** 1929 (2003)
103. J C Wang, R W Murphy, F C Ten, R O Loutfy, E Veksler, W Li, in *Proceedings of the 1998 U.S.DOE Hydrogen Program Review NREL/CP-570-25315*
104. C Lenardi, E Barborini, V Briois, L Lucarelli, P Piseri, P Milani *Diamond Relat. Mater*. **10** 1195 (2001)
105. P Milani, P Piseri, E Barborini, C Lenardi, M Marino, S Maffi, V Briois, in *Proceedings of the VIIth International Conference 'Hydrogen Materials Science'* (Kiev: ADEF-Ukraine, 2001) p. 502
106. H Takagi, H Hatori, Y Soneda, Y Yamada *TANSO* (205) 231 (2002)
107. D Lupu, A R Biris, I Misan, A Jianu, G Holzhuter, E Burkel *Int. J. Hydrogen Energy* **29** 97 (2004)
108. W Muller *J. Nucl. Mater*. **162-164** 138 (1989)
109. R A Causey *J. Nucl. Mater*. **162-164** 151 (1989)
110. D S Rawat, S Talapatra, K Lafdi, A D Migone *Appl. Phys. A* **78** 969 (2004)
111. W-Q Deng, X Xu, W Goddard *Phys. Rev. Lett*. **92** 166103 (2004)
112. A Züttel, Ch Nutzenadel, P Sudan, Ph Mauron, Ch Emmenegger, S Rentsch, L Schlapbach, A Weidenkaff, T Kiyobayashi *J. Alloys Compd*. **330-332** 676 (2002)
113. G-P Dai, M Liu, M-Z Wang, H-M Cheng *New Carbon Mater*. **17** 70 (2002)
114. X Yan, X Gao, Y Li, Z Liu, F Wu, Y Shen, D Song *Chem. Phys. Lett*. **372** 336 (2003)
115. M Miranda-Hernández, J-A Ayala, M E Rincón *J. Solid State Electrochem*. **7** 264 (2003)
116. D Hao, H Zhu, X Zhang, Y Li, C Xu, Z Mao, J Liu, D Wu *Chin. Sci. Bull*. **48** 538 (2003)
117. C Nutzenadel, A Züttel, D Chartouni, L Schlapbach *Electrochem. Solid-State Lett*. **2** 30 (1999)
118. G-P Dai, M Liu, D M Chen, P X Hou, Y Tong, H-M Cheng *Electrochem. Solid-State Lett*. **5** E13 (2002)
119. E Frackowiak, F Béguin *Carbon* **40** 1775 (2002)
120. K Jurewicz, E Frackowiak, F Béguin *Appl. Phys. A* **78** 981 (2004)
121. L Lombardi, M Bestetti, C Mazzocchia, P L Cavalotti, U Ducati *Electrochem. Solid-State Lett*. **7** A115 (2004)
122. M Schmid, S Kramer, C Goze, M Mehring, S Roth, P Bernier *Synth. Met*. **135-136** 727 (2003)
123. I Yu, J Lee, S G Lee *Physica B* **329-333** 421 (2003)
124. G Majer, E Stanik, S Orimo *J. Alloys Compd*. **356-357** 617 (2003)
125. K Shen, T Pietra *Appl. Phys. Lett*. **84** 1567 (2004)
126. D G Narehood, J V Pearce, P C Eklund, P E Sokol, R E Lechner, J Pieper, J R D Copley, J C Cook *Phys. Rev. B* **67** 205 409 (2003)
127. D G Narehood, M K Kostov, P C Eklund, M W Cole, P E Sokol *Phys. Rev. B* **65** 233 401 (2002)
128. Y Ren, D L Price *Appl. Phys. Lett*. **79** 3684 (2001)
129. C M Brown, T Yildirim, D A Neumann, M J Heben, T F Gennet, A C Dillon, J L Allemen, J E Fischer *Chem. Phys. Lett*. **329** 311 (2000)
130. S Challet, R Azais, R J-M Pellenq, L Duclaux *Chem. Phys. Lett*. **377** 544 (2003)
131. P A Georgiev, D K Ross, A De Monte, U Montaretto-Marullo, R A H Edwards, A J Ramirez-Cuesta, D Colognesi *J. Phys.: Condens. Matter* **16** L73 (2004)
132. A Burian, J C Dore, H E Fischer, J Sloan *Phys. Rev. B* **59** 1665 (1999)
133. K Itoh, Y Miyahara, S-i Orimo, H Fujii, T Kamiyama, T Fukunaga *J. Alloys Compd*. **356-357** 608 (2003)
134. V P Glazkov, V P Zhukov, V N Ivanova, V A Somenkov, S Sh Shil'shtein *Poverkhnost'* (6) 52 (2001)
135. H G Schimmel, G J Kearley, M G Nijkamp, C T Visser, K P de Jong, F M Mulder *Chem.-Eur. J*. **9** 4764 (2003)
136. K Shen, D L Tierney, T Pietra *Phys. Rev. B* **68** 165 418 (2003)
137. H-B Zhang, G-D Lin, Z-H Zhou, X Dong, T Chen *Carbon* **40** 2429 (2002)

138. G E Froundakis *J. Phys.: Condens. Matter* **14** R453 (2002)
139. A S Fedorov, S G Ovchinnikov *Fiz. Tv. Tela* **46** 563 (2004) [c]
140. D Levesque, A Gicquel, F Lamari Darkrim, S Beyaz Kayiran *J. Phys.: Condens. Matter* **14** 9285 (2002)
141. Q Wang, J K Johnson *J. Chem. Phys.* **110** 577 (1999)
142. X Zhang, D Cao, J Chen *J. Phys. Chem. B* **107** 4942 (2003)
143. M Volpe, F Cleri *Chem. Phys. Lett.* **371** 476 (2003)
144. F Darkrim, D Levesque *J. Phys. Chem. B* **104** 6773 (2000)
145. Y F Yin, T Mays, M McEnaney *Langmuir* **16** 10 521 (2000)
146. C W Bauschlicher Jr, Ch R So *Nano Lett.* **2** 337 (2002)
147. S M Lee, Yo H Lee *Appl. Phys. Lett.* **76** 2877 (2000)
148. Y C Ma, Y Xia, M Zhao, M Ying *Chem. Phys. Lett.* **357** 97 (2002)
149. Y C Ma, Y U Xia, M W Zhao, R Wang, L Mei *Phys. Rev. B* **63** 115 422 (2001)
150. Y Ma, Y Xia, M Zhao, M Ying *Phys. Rev. B* **65** 155430 (2002)
151. J Li, T Furuta, H Goto, T Ohashi, Y Fujiwara, S Yip *J. Chem. Phys.* **119** 2376 (2003)
152. Q Y Wang, J K Johnson *J. Phys. Chem. B* **103** 277 (1999)
153. K A Williams, P C Eklund *Chem. Phys. Lett.* **320** 352 (2000)
154. V Meregalli, M Parrinello *Appl. Phys. A* **72** 143 (2001)
155. T Yildrim, A B Harris *Phys. Rev. B* **67** 245 413 (2003)
156. J Zhao, A Buldum, J Han, J P Li *Nanotechnology* **13** 195 (2002)
157. Y Akai, S Saito *Jpn. J. Phys.* **42** 640 (2003)
158. M K Kostov, H Cheng, A C Cooper, G P Pez *Phys. Rev. Lett.* **89** 146105 (2002)
159. M M Cabli, F Toigo, M W Cole *Phys. Rev. Lett.* **86** 5062 (2001)
160. M M Cabli, F Toigo, M W Cole *J. Low Temp. Phys.* **126** 179 (2002)
161. M C Gordilio, J Boronat, J Casulleras *Phys. Rev. B* **68** 125 421 (2003)
162. M-J Ying, Y-Y Xia, M-W Zhao, X-D Liu, F Li, B-D Huang, Z-Y Tan *Chin. Phys. Lett.* **20** 550 (2003)
163. F H Yang, R T Yang *Carbon* **40** 437 (2002)
164. P-H Hou, S-T Xu, Z Ying, Q-H Yang, C Liu, H-M Cheng *Carbon* **41** 2471 (2003)
165. S M Lee, K H An, W S Kim, Y H Lee, Y S Park, G Seifert, T Frauenheim *Synth. Met.* **121** 1189 (2001)
166. C W Bauschlicher *Nano Lett.* **1** 223 (2001)
167. T Yildirim, O Gulseren, S Ciraci *Phys. Rev. B* **64** 075 404 (2001)
168. P Ruffieux, O Groning, M Bielmann, P Mauron, L Schlabach, P Groning *Phys. Rev. B* **66** 245 416 (2002)
169. D Stojkovic, P Zhang, P E Lammert, V H Crespi *Phys. Rev. B* **68** 195 406 (2003)
170. S-P Chan, G Chen, X G Gong, Z-F Liu *Phys. Rev. Lett.* **87** 205 502 (2001)
171. Y C Ma, Y Xia, M Zhao, M Ying X Liu, P Liu *Phys. Lett. A* **288** 207 (2001)
172. Y Xia, M Zhao, Y C Ma, X Liu, M Ying, L Mei *Phys. Rev. B* **67** 115 117 (2003)
173. Y Y Xia, M W Zhao, Y C Ma, M J Ying, X D Liu, P J Liu, L Mei *Phys. Rev. B* **65** 155 415 (2002)
174. S M Lee, K H An, Y N Lee, G Seifert, T Frauencheim *J. Am. Chem. Soc.* **123** 5059 (2001)
175. M Volpe, F Cleri *Surf. Sci.* **544** 24 (2003)
176. K Tada, S Furuya, K Watanabe *Phys. Rev. B* **63** 155 405 (2001)
177. Yu S Nechaev *Usp. Fiz. Nauk* **171** 1251 (2001) [*Physics-Uspekhi* **44** 1189 (2001)]
178. Yu S Nechaev *Izv. Akad. Nauk, Ser. Fiz.* **65** 1507 (2001)
179. L A Andreev, Yu S Nechaev, E A Kalashnikova, N T Konovalov, V A Lykhin, Yu A Minaev, N A Olshevskii *Phys. Status Solidi B* **163** 221 (1991)
180. Yu S Nechaev, A V Omel'chenko *Zh. Fiz. Khim.* **69** 1765 (1995) [d]
181. H Atsumi, S Tokura, M Miyake *J. Nucl. Mater.* **155-157** 241 (1988)
182. H Atsumi, K Tauchi *J. Alloys Compd.* **356-357** 705 (2003)
183. H P van Leeuwen, in *Hydrogen Degradation of Ferrous Alloys* (Eds A Oriani, J P Hirth, M Smialowski) (Park Ridges, NJ: Noyes Publ., 1985) p. 16
184. V A Bakaev, Doctoral Thesis in Physical Mathematical Sciences, Moscow State University, Moscow, 1989
185. Yu S Nechaev *Defect Diffus. Forum* **194-199** 1713 (2001)
186. V I Kostikov, Yu S Nechaev, G Ya Kul'ga *Zh. Fiz. Khim.* **76** 1583 (2002) [d]
187. Yu S Nechaev, in *Hydrogen Materials Science and Chemistry of Metal Hydrides* (Ed. N Veziroglu) (Dordrecht: Kluwer Academic, 2002) p. 161
188. M Saeki *J. Nucl. Mater.* **131** 32 (1985)
189. H Atsumi, M Iseki *J. Nucl. Mater.* **283-287** 1053 (2000)
190. J Klatte, W Ruth, W Ebenhlh *Scr. Met.* **15** 591 (1981)
191. Yu S Nechaev, S A Vladimirov, N A Olshevskii *Phys. Status Solidi* **94** 553 (1986)
192. A I Efimov, L P Belorukova, I V Vasil'kova, V P Chechev *Svoistva Neorganicheskikh Soedinenii. Spravochnik* (Properties of Inorganic Compounds. Handbook) (Leningrad: Khimiya, 1983)
193. M Kh Karapet'yants, M L Karapet'yants *Osnovnye Termodinamicheskie Konstanty Neorganicheskikh i Organicheskikh Veshchestv* (Fundamental Thermodynamic Constants of Inorganic and Organic Substances) (Moscow: Khimiya, 1968)
194. I Barin, O Knacke *Thermochemical Properties of Inorganic Substances* (Berlin: Springer, 1973)
195. M-W Zhao, Y-Y Xia, Y-C Ma, M-J Ying, X-D Liu, L-M Mei *Chin. Phys. Lett.* **19** 1498 (2002)
196. I O Bashkin, V E Antonov, E G Ponyatovskii, in *Extended Abstracts of the VIIIth International Conference 'Hydrogen Materials Science and Chemistry of Carbon Nanostructures (ICHMS'2003)', Sudak, Ukraine, 2003* p. 796
197. A Shimizu, H Tachikawa *J. Phys. Chem. Solids* **64** 419 (2003)
198. A A Zhukhovitskii, L A Shvartsman *Fizicheskaya Khimiya* (Physical Chemistry) (Moscow: Metallurgiya, 1987)
199. I E Gabis, E A Evard, A P Voit, S K Gordeev, in *Proceedings of the VIIth International Conference 'Hydrogen Materials Science'* (Kiev: ADEF-Ukraine, 2001) p. 700
200. E A Evard, A P Voit, S K Gordeev, I E Gabis *Mater. Sci.* **36** 499 (2000)
201. E A Denisov, T N Kompaniets *Zh. Tekhn. Fiz.* **71** 111 (2001) [e]
202. P G Shewman *Diffusion in Solids* (New York, London: Wiley, 1962)
203. Yu S Nechaev, K H G Egziabher *Phys. Status Solidi A* **106** 399 (1988)
204. M Cinke, J Li, B Chen, A Cassell, L Delzeit, J Han, M Meyyappan *Chem. Phys. Lett.* **365** 69 (2002)
205. US P. 5 653 951 (1997)
206. A Chambers, T Nemes, N M Rodriguez, T K Baker *J. Phys. Chem. B* **102** 2251 (1998)

[a] — *Physics-Uspekhi (Engl. Transl.)*
[b] — *J. Exp. Theor. Phys. Lett. (Engl. Transl.)*
[c] — *Phys. Solid State (Engl. Transl.)*
[d] — *Russ. J. Phys. Chem. (Engl. Transl.)*
[e] — *J. Techn. Phys. (Engl. Transl.)*